Encyclopedia of Sustainability Science and Technology

Robert A. Meyers (Ed.)

Encyclopedia of Sustainability Science and Technology

With 5917 Figures and 1553 Tables

Springer

Editor
Robert A. Meyers
RAMTECH LIMITED
Larkspur, CA, USA

ISBN 978-0-387-89469-0 ISBN 978-1-4419-0851-3 (eBook)
ISBN 978-1-4419-0852-0 (print and electronic bundle)
DOI 10.1007/978-1-4419-0851-3
Springer New York Dordrecht Heidelberg London

Library of Congress Control Number: 2012944368

© Springer Science+Business Media, LLC 2012
This work is subject to copyright. All rights are reserved by the Publisher, whether the whole or part of the material is concerned, specifically the rights of translation, reprinting, reuse of illustrations, recitation, broadcasting, reproduction on microfilms or in any other physical way, and transmission or information storage and retrieval, electronic adaptation, computer software, or by similar or dissimilar methodology now known or hereafter developed. Exempted from this legal reservation are brief excerpts in connection with reviews or scholarly analysis or material supplied specifically for the purpose of being entered and executed on a computer system, for exclusive use by the purchaser of the work. Duplication of this publication or parts thereof is permitted only under the provisions of the Copyright Law of the Publisher's location, in its current version, and permission for use must always be obtained from Springer. Permissions for use may be obtained through RightsLink at the Copyright Clearance Center. Violations are liable to prosecution under the respective Copyright Law.
The use of general descriptive names, registered names, trademarks, service marks, etc. in this publication does not imply, even in the absence of a specific statement, that such names are exempt from the relevant protective laws and regulations and therefore free for general use.
While the advice and information in this book are believed to be true and accurate at the date of publication, neither the authors nor the editors nor the publisher can accept any legal responsibility for any errors or omissions that may be made. The publisher makes no warranty, express or implied, with respect to the material contained herein.

Printed on acid-free paper

Springer is part of Springer Science+Business Media (www.springer.com)

Preface

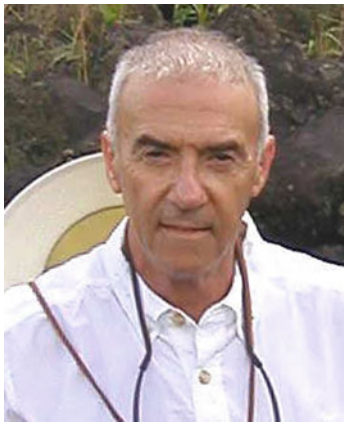

Editor in chief Bob Meyers at the Aranal Volcano in Costa Rica

Our team consisted of nearly 1,000 chemists, biologists, environmentalists, agronomists, physicists, mathematicians, and engineers who have prepared, supervised, or peer reviewed the content of this *Encyclopedia*. Our magnum opus is a 18-volume 12555-page resource available in both print and online, of over 550 peer-reviewed, detailed articles defining the science and technology basis for providing for the sustainability of the earth as global population and the needs of that population increase dramatically. We plan to continually update our articles as new technology and data become available such that this *Encyclopedia* will remain the most up-to-date compendium of sustainability science and technology available. This encyclopedic treatment has been prepared by scientists and engineers for other scientists and engineers as well as planners and evaluators, in a format which allows experts in one field to easily understand detailed treatments of fields not within their area of expertise. These entries form a scientific basis for the huge volume of sustainability evaluations and studies as well as research and business decisions, being performed within thousands of institutions worldwide. This new *Encyclopedia* is a natural follow-on and is symbiotic with our recently completed *Encyclopedia of Complexity and Systems Science*, which provides key mathematical and modeling tools for understanding such diverse complex systems as cosmology, earthquakes, volcanoes, tsunamis, molecular biology, traffic management, and robotics as well as econometrics and sustainability of the earth.

We have established an advisory board of nineteen of the most prominent experts in sustainability which includes five Nobel Laureates and a co-recipient of the Nobel Peace Prize for climate change research, as well as a group of 41 section editors who have overseen the content of each of the 38 topical areas and coordinated the near 1,000 authors and peer reviewers who prepared and reviewed the entries.

The content of the *Encyclopedia* includes:

- Solar energy (thermal, photovoltaic, thermal electric)
- Renewables (wind, ocean thermal, biomass, ethanol, and other biofuels)
- Geothermal
- Fossil energy technologies (extraction, production, storage, transport)
- Nuclear energy
- Electrical generation and transmission

- Green chemistry and engineering
- Transportation
- Conservation
- Science and technology of the sustainable built environment
- Pollution sources, statistics, measurement, and control
- Natural resources
- Food production and technology
- Oceans farming and oceans and human health
- Fresh water resources, water purification, and desalinization
- Social ecological systems
- Biological ecological systems
- Green practices
- Climate change data, mitigation, and modeling
- Earth system monitoring
- Earth system modeling and economics
- Health and infectious diseases and epidemiology

This list of topics clearly sets our project apart from compendia and publications which now exist, in both extent and depth. In fact, current compendia of the science and technology of several of these topics do not presently exist and yet the content is crucial to any evaluation and planning for the sustainability of the earth.

Vital scientific issues include: human and animal ecological support systems, energy supply, and effects; the planet's climate system; systems of agriculture, industry, forestry, and fisheries; the ocean, fresh water, and human communities; waste disposal, transportation, and the built environment in general and the various systems on which they depend; and the balance of all of these with sustainability. In this context, sustainability is a characteristic of a process or state that can be maintained at a certain level indefinitely even as global population increases toward 9 billion by 2050. The population growth, and the hope for increase in wealth, implies something like a 50% increase in food demand by as early as 2030. At the same time, the proportion of the population that lives in an urban environment will go up from about 47 to 60%. Global economic activity is expected to grow 500%, and global energy and materials use is expected to increase by 300% over this period. That means there are going to be some real problems for energy, agriculture, and water, and it is increasingly clear that conflicting demands among biofuels, food crops, and environmental protection will be difficult to reconcile. The "green revolution" was heavily dependent on fertilizers which are manufactured using increasingly expensive and diminishing reserves of fossil fuels. In addition, about 70% of available freshwater is used by agriculture. Clearly, many natural resources will become either depleted or scarce relative to population. This *Encyclopedia* is founded on two major assumptions. First, we acknowledge that any true measure of sustainability must include some consideration of the number of people to be supported and at what standard of living. In this respect, population is a linchpin in attempts to understand and achieve sustainability. While top-down approaches to controlling population growth, maintaining biodiversity, etc., certainly do exist, science and technology and the resulting innovation economy is a bottom-up affair involving individuals and teams of individuals in publicly funded scientific laboratories and private corporations. This process is essentially unpredictable, resulting in a great range of promising technologies that are individually dwarfed by the scope of the challenge but represent essential contributions to sustainability.

While there are many Web-based and even some print encyclopedic treatments of sustainability science in the broad sense, none are comprehensive and rise to the university or professional scientist and engineer level needed to support real progress from the bottom up. The emphasis for the *Encyclopedia of Sustainability Science and Technology* team is on science and technology and not on policy and positions. Rather, this *Encyclopedia* is a comprehensive and authoritative resource for policy makers who want to understand how scientific and technological innovations

in all fields map onto the true scope of the sustainability challenge and will also be a major resource for scientists and engineers in developing new technologies and for applying existing technologies to sustainability. Further, we plan to maintain our 1,000-scientist and engineer team to continually update our content.

Among the topics covered are: the chemistry, physics, modeling, and engineering of green chemistry for industry, water use, and recovery; crop production including precision farming, genetic modification of crops, with forest maintenance; all types of energy production, electric utility as well as small-scale electric generation (fossil fuel as well as nuclear fission and fusion, solar electric and thermal and renewable) and mass and personal transportation with fuel modification, power source variation, pollution control, and waste disposition; solid waste utilization, recycle, and disposition; urban planning and the built environment; environmental quality; engineering mitigation, adaptation, and forecasting of global warming, and any possible cooling due to solar-earth insolation dimming; geoengineering and greenhouse effect mitigation measures; measurement and observation systems (terrestrial and from space); analytical chemistry methods for the biosphere, including indoor pollution and industrial hygiene; disease prevention and treatment; and catastrophic event (e.g., volcanic eruption, tsunamis, cyclones, tornadoes) measurement and mitigation.

RAMTECH LIMITED
Larkspur, CA, USA

Robert A. Meyers
Editor in Chief
August 2012

Acknowledgments

I wish to thank David Packer, executive editor, who worked with me to define the scope of the project and then provided invaluable counsel in performance of many elements of the publication process. I also wish to express our profound gratitude to Lydia Mueller, Anil Chandy and Sara Kate Heukerott for their project management skills as well as Neha Thapa, associate editor, and Sunali Mull, editorial assistant, for their outstanding efforts in producing this *Encyclopedia*. Their interaction with our team of authors, section editors, and board members was highly professional, courteous, pleasant, and yet firm, which was integral in obtaining high quality and timely delivery of our manuscripts. Their mastery of formal as well as idiomatic English facilitated many of these interactions.

Topical Table of Contents

Air Pollution Sources, Statistics and Health Effects, Section Editor: Roy M. Harrison

Aerosol in Global Atmosphere
Air Pollution Monitoring and Sustainability
Air Pollution Sources, Statistics and Health Effects, Introduction
Air Quality Guidelines and Standards
Air Quality, Surface Transportation Impacts on
Aviation and Atmosphere
Regional Air Quality
Stratospheric Pollution
Urban Air Quality: Meteorological Processes
Urban Air Quality: Sources and Concentrations
Urban Atmospheric Composition Processes

Animal Breeding and Genetics, Section Editor: Ignacy Misztal

Animal Breeding and Genetics, Introduction
Animal Breeding Methods and Sustainability
Animal Breeding, Foundations of
Animal Breeding, Long-Term Challenges
Animal Breeding, Modeling in
Animal Genetic in Environment Interaction
Animal Molecular Genetics from Major Genes to Genomics
Breeding in Beef Cattle
Breeding in Developing Countries and Tropics
Breeding in Horses
Dairy Cattle Breeding
Pig Breeding for Increased Sustainability
Poultry Breeding
Socially Affected Traits, Inheritance and Genetic Improvement

Batteries, Section Editor: Ralph J. Brodd

Batteries, Introduction
Battery Cathodes
Battery Components, Active Materials for
Electrochemical Supercapacitors and Hybrid Systems
Lead Acid Battery Systems and Technology for Sustainable Energy
Lithium Battery Electrolyte Stability and Performance from Molecular Modeling and Simulations
Lithium-Ion Batteries, Electrochemical Reactions in
Lithium-Ion Batteries, Safety
Lithium-Ion Battery Systems and Technology

Medical Device Batteries
Nanocarbons for Supercapacitors
Nickel-Based Battery Systems
Olivine Phosphate Cathode Materials, Reactivity and Reaction Mechanisms
Rechargeable Batteries, Separators for
Silicon-Based Anodes for Li-Ion Batteries

Climate Change Modeling Methodology, Section Editor: Philip J. Rasch

Atmospheric General Circulation Modeling
Climate Change Modeling Methodology, Introduction
Climate Change Projections: Characterizing Uncertainty Using Climate Models
Climate Predictions, Seasonal-to-Decadal
Coupled Climate and Earth System Models
Cryosphere, Modeling of
Earth System Model, Modeling the Land Component of
Integrated Assessment Modeling
Monsoon Systems, Modeling of
Oceanic General Circulation Models
Regional Climate Models
Weather Prediction Models

Climate Change Remediation, Section Editor: Timothy M. Lenton and Naomi E. Vaughan

Biochar, Tool for Climate Change Mitigation and Soil Management
Carbon Dioxide Sequestration, Weathering Approaches to
Climate Change Remediation, Introduction to
Geoengineering Policy and Governance Issues
Ocean Fertilization for Sequestration of Carbon Dioxide from the Atmosphere
Solar Radiation Management, Cloud Albedo Enhancement
Stratospheric Aerosols for Solar Radiation Management
Sunshades for Solar Radiation Management

Crop Science and Technology, Section Editor: Paul Christou and Roxana Savin

Abiotic Stress Tolerant Crops: Genes, Pathways and Bottlenecks
Agroecological Basis for Managing Biotic Constraints
Agronomic Interactions with CO_2 Sequestration
Biomass Crops for Biofuels and Bio-based Products
Biotechnology and Nutritional Improvement of Crops
Commercialisation of GM Crops: Comparison of Regulatory Frameworks
Crop Breeding for Sustainable Agriculture, Genomics Interventions in
Crop Development Related to Temperature and Photoperiod
Crop Diseases, Management and Control of
Crop Plants Transformation Methods
Crop Radiation Capture and Use Efficiency
Crop Responses to Available Soil Water

Crop Responses to Nitrogen
Crop Science and Technology, Introduction
Crop Traits: Gene Isolation
Crop Yields Around the World: Closing the Gap and Raising the Potential
Cropping Systems: Shaping Nature
Fertilizer Science and Technology
Genetic Engineering of Crops for Insect Resistance
Genotype by Environment Interaction and Adaptation
Global Economic Impact of Transgenic/Biotech Crops (1996–2008)
GM Crop Risk Debate, Science and Socioeconomics
Grain Quality in Oil and Cereal Crops
Increasing Salinity Tolerance of Crops
Integrated Pest Management
Irrigation Management for Efficient Crop Production
Lodging Resistance in Cereals
Marker-Assisted Breeding in Crops
Medicinal Plants, Engineering of Secondary Metabolites in Cell Cultures
Molecular Breeding Platforms in World Agriculture
Plant Breeding Under a Changing Climate
Plant Molecular Pharming, Industrial Enzymes
Plant Molecular Pharming, Pharmaceuticals for Human Health
Plant Molecular Pharming, Veterinary Applications
Roots and Uptake of Water and Nutrients
Seed Dormancy and Agriculture, Physiology
Simulation Models as Tools for Crop Management
Spatial Crop Structure in Agricultural Systems
Sustainable Herbicide-Resistant Crops
Sustainable Productivity, Heat Tolerance for
Transgene Expression in Plants, Control of
Transgenic Crops Resistant to Fungal, Bacterial, and Viral Pathogens
Transgenic Crops, Environmental Impact
Transgenic Crops, Next Generation
Transgenic Crops, Risk Assessment and Regulatory Framework in the European Union

Earth System Monitoring, Section Editor: John Orcutt

Airborne and Space-borne Remote Sensing of Cryosphere
Aircraft and Space Atmospheric Measurements Using Differential Absorption Lidar (DIAL)
Contemporary Sea Level Variations, Observations and Causes
Coral Reef Ecosystems
Earth System Environmental Literacy
Earth System Monitoring, Introduction
Gravity Recovery and Climate Experiment (GRACE): Detection of Ice Mass Loss, Terrestrial Mass Changes, and Ocean Mass Gains
Heat Content and Temperature of the Ocean
Hurricane and Monsoon Tracking with Driftsondes

Large-Scale Ocean Circulation: Deep Circulation and Meridional Overturning
Long-Term Ecological Research Network
Ocean Acidification
Ocean Evaporation and Precipitation
Ocean Observatories and Information: Building a Global Ocean Observing Network
Oil Spill Remote Sensing
Remote Sensing of Natural Disasters
Remote Sensing of Ocean Color
Volcanoes, Observations and Impact

Ecological Systems, Section Editor: Rik Leemans

Atmospheric Biogeochemistry
Ecological Succession and Community Dynamics
Ecological Systems, Introduction
Ecosystem Engineers, Keystone Species
Ecosystem Flow Analysis
Ecosystem Services
Ecosystems and Spatial Patterns
Ecosystems, Adaptive Management
Ecotones and Ecological Gradients
Invasive Species
Landscape Ecology
Marine Biogeochemistry
Species Competition and Predation
Species Diversity Within and Among Ecosystems
Urban Ecology

Electric, Hybrid, and Fuel Cell Vehicles, Section Editor: Mehrdad Ehsani

AC Machines: Permanent Magnet Synchronous and Induction Machines
Batteries, Battery Management, and Battery Charging Technology
Battery Technologies
Electric, Hybrid, and Fuel Cell Vehicles, Introduction
Electric, Hybrid Electric and Fuel cell Vehicles, Architectures of
Energy Storage: Ultracapacitor
Fuel-Cell-Powered Hybrid electric vehicle HEV Design and Control
Hybrid Electric and Hydraulic Technology Applications in Off-Road Vehicles
Hybrid Energy Storage Systems for Vehicle Applications
Internal Combustion Engines, Alternative Fuels for
PHEVs and BEVs in Coupled Power and Transportation Systems
Plug-in Hybrid Electric Vehicles
Regenerative Braking
Sustainable Transportation
Sustainable Vehicle Fuels, Well-to-Wheel Analysis
Switched Reluctance Motor Drives for Propulsion and Regenerative Braking in EV and HEV
Vehicle Biofuels

Vehicle Dynamics and Performance
Vehicle Energy Storage: Batteries
Vehicle Traction Motors

Electrical Transmission Systems and Smart Grids, Section Editor: Miroslav M. Begovic

Distribution Systems, Substations, and Integration of Distributed Generation
Electrical Transmission Systems and Smart Grids, Introduction
Energy and Water Interdependence, and Their Implications for Urban Areas
Renewable Generation, Integration of
Smart Grids, Distributed Control for
Sustainable Smart Grids, Emergence of a Policy Framework
Transmission Blackouts: Risk, Causes, and Mitigation
Underground Cable Systems
Wide Area Monitoring, Protection and Control

Environmental Geology, Section Editor: James W. LaMoreaux

Construction Planning, Environmental Impact of Foundation Studies and Earthquake Issues
Dam Engineering and Its Environmental Aspects
Desertification and Impact on Human Systems
Dredging Practices and Environmental Considerations
Earthquake Faulting, Ground Motions and Deformations
Environmental Geology, Introduction
Geochemical Modeling in Environmental and Geological Studies
Geologic Carbon Sequestration: Sustainability and Environmental Risk
Groundwater Impacts of Radioactive Wastes and Associated Environmental Modeling Assessment
Groundwater Salinity Due to Urban Growth
Karst Terrane and Transportation Issues
Land Subsidence in Urban Environment
Marine Life Associated with Offshore Drilling, Pipelines, and Platforms
Mining and Its Environmental Impacts
Natural Resource Flows and Sustainability in Urban Areas
Volcanoes of Mexico

Environmental Radioactivity and Ecotoxicology of Radioactive Substances, Section Editor: Glen A. Bird

Environmental Countermeasures and Restoration
Environmental Radioactivity and Ecotoxicology of Radioactive Substances, Introduction to
Fallout Radionuclides and the Study of Erosion and Sedimentation
Ionizing Radiation on Nonhuman Biota, Effects of Low Levels of
Nuclear Accidents, Chernobyl Fallout in Scandinavian Watersheds
Radioactivity in the Marine Environment
Radiation Assessment, Use of Transfer Parameters
Radiation Effects on Caribou and Reindeer
Radiation in the Environment, Sources of
Radionuclide Fate and Transport in Terrestrial Environments

Radionuclide Migration from Catchments, Modeling
Radionuclides as Tracers of Ocean Currents
Speciation of Metals, Effects on Aquatic Biota
Tritium in the Environment
Tritium, Health Effects and Dosimetry
Uranium in the Environment: Behavior and Toxicity

Environmental Toxicology, Section Editor: Edward A. Laws

Airborne Toxic Chemicals
Bioaccumulation/Biomagnifications in Food Chains
Biomarkers and Metabolomics, Evidence of Stress
Bioremediation and Mitigation
Biosensors and Bioassays for Ecological Risk Monitoring and Assessment
CERCLA, Sustainability and Public and Environmental Health
Ecological and Health Risks at Low Doses
Ecological Risk Assessment and Animal Models
Environmental Toxicology, Introduction
Environmental Toxicology: Carcinogenesis
Environmental Toxicology: Children at Risk
Environmental Toxicology: Oxidative Stress
Microbial Risk Assessment of Pathogens in Water
Pathogen and Nutrient Transfer Through and Across Agricultural Soils
Recreational Water Risk: Pathogens and Fecal Indicators
Science, Policy, and Risk Management: Case of Seafood Safety
Toxic Chemical Risks
Xenobiotic Protection/Resistance Mechanisms in Organisms

Fossil Energy, Section Editor: Ripudaman Malhotra

Alaska Gas Hydrate Research and Field Studies
CO_2 Capture and Sequestration
CO_2 Reduction and Coal-Based Electricity Generation
Coal and Peat: Global Resources and Future Supply
Coal Preparation
Coal to Liquids Technologies
Fossil Energy, Introduction
Gas to Liquid Technologies
Internal Combustion Engines, Developments in
Mining Industries and Their Sustainable Management
Natural Gas Power
Oil and Natural Gas: Global Resources
Oil Shale Processing, Chemistry and Technology
Petroleum and Oil Sands Exploration and Production
Petroleum Refining and Environmental Control and Environmental Effects
Pulverized Coal-Fired Boilers and Pollution Control

Fuel Cells, Section Editor: Klaus-Dieter Kreuer

Alkaline Membrane Fuel Cells
Direct Hydrocarbon Solid Oxide Fuel Cells
Fuel Cell Comparison to Alternate Technologies
Fuel Cell Types and Their Electrochemistry
Fuel Cells (SOFC): Alternative Approaches (Electroytes, Electrodes, Fuels)
Fuel Cells, Introduction
Membrane Electrolytes, from Perfluoro Sulfonic Acid (PFSA) to Hydrocarbon Ionomers
Molten Carbonate Fuel Cells
PEM Fuel Cell Materials: Costs, Performance and Durability
PEM Fuel Cells and Platinum-Based Electrocatalysts
PEM Fuel Cells, Materials and Design Development Challenges
Phosphoric Acid Fuel Cells for Stationary Applications
Polybenzimidazole Fuel Cell Technology
Polymer Electrolyte (PE) Fuel Cell Systems
Polymer Electrolyte Membrane (PEM) Fuel Cells, Automotive Applications
Polymer Electrolyte Membrane Fuel Cells (PEM-FC) and Non-noble Metal Catalysts for Oxygen Reduction
Proton Exchange Membrane Fuel Cells: High-Temperature, Low-Humidity Operation
Solid Oxide Fuel Cell Materials: Durability, Reliability and Cost
Solid Oxide Fuel Cells
Solid Oxide Fuel Cells, Marketing Issues
Solid Oxide Fuel Cells, Sustainability Aspects

Geothermal Power Stations, Section Editor: Lucien Y. Bronicki

Engineered Geothermal Systems, Development and Sustainability of
Geothermal Energy Utilization
Geothermal Energy, Nature, Use, and Expectations
Geothermal Energy, Geology and Hydrology of
Geothermal Field and Reservoir Monitoring
Geothermal Power Capacity, Sustainability and Renewability of
Geothermal Power Conversion Technology
Geothermal Power Economics
Geothermal Power Stations, Introduction to
Geothermal Resources Worldwide, Direct Heat Utilization of
Geothermal Resources, Drilling for
Geothermal Resources, Environmental Aspects of
Hydrothermal Systems, Geochemistry of
Reservoir Engineering in Geothermal Fields

Green Chemistry and Chemical Engineering, Section Editor: Paul T. Anastas and Julie B. Zimmerman

Gas Expanded Liquids for Sustainable Catalysis
Green Catalytic Transformations
Green Chemistry and Chemical Engineering, Introduction

Green Chemistry Metrics: Material Efficiency and Strategic Synthesis Design
Green Chemistry with Microwave Energy
Nanotoxicology in Green Nanoscience
New Polymers, Renewables as Raw Materials
Organic Batteries
Oxidation Catalysts for Green Chemistry
Supercritical Carbon Dioxide (CO_2) as Green Solvent

Hazardous Waste, Section Editor: Mervin Fingas

Contaminated Soil, Remediation of
Hazardous Materials Characterization and Assessment
Hazardous Waste Incineration Ashes and Their Utilization
Hazardous Waste Incinerator Emissions
Hazardous Waste, Introduction
Incineration Technologies
Non-flame Incineration
Vitrification of Waste and Reuse of Waste-Derived Glass

Hydrogen Production Science and Technology, Section Editor: Timothy E. Lipman

Electrochemical Hydrogen Production
Hydrogen Production from High-Temperature Fuel Cells
Hydrogen Production Science and Technology
Hydrogen via Direct Solar Production
Photo-catalytic Hydrogen Production

Infectious Diseases, Section Editor: Phyllis J. Kanki

Antibiotics for Emerging Pathogens
HIV/AIDS Global Epidemic
Infectious Disease Modeling
Infectious Diseases, Climate Change Effects on
Infectious Diseases, Introduction
Infectious Diseases, Vibrational Spectroscopic Approaches to Rapid Diagnostics
Malaria Vaccines
Polio and Its Epidemiology
Tropical Health and Sustainability
Tuberculosis, Epidemiology of
Waterborne Infectious Diseases, Approaches to Control

Intelligent Vehicle Technology, Section Editor: Fei-Yue Wang

Unscented Kalman Filter in Intelligent Vehicles
3D Pose Estimation of Vehicles Using Stereo Camera
Active Multifocal Vision System, Adaptive Control of
Active Pedestrian Protection System, Scenario-Driven Search Method for
Cooperative Group of Vehicles and Dangerous Situations, Recognition of

Driver Assistance System, Biologically Inspired
Driver Assistance Systems, Automatic Detection and Site Mapping
Driver Behavior at Intersections
Driver Characteristics Based on Driver Behavior
Driver Inattention Monitoring System for Intelligent Vehicles
Driving Under Reduced Visibility Conditions for Older Adults
Dynamic Environment Sensing Using an Intelligent Vehicle
Intelligent Vehicles Technology, Introduction
Night Vision Pedestrian Warning in Intelligent Vehicles
True Color Night Vision Video Systems in Intelligent Vehicles
Vehicle Detection, Tightly Coupled LIDAR and Computer Vision Integration for
Vehicular Ad Hoc Networks, Enhanced GPSR and Beacon-Assist Geographic Forwarding in

Mass Transit Science and Technology, Section Editor: Gary L. Brosch

Advanced Public Transport Systems, Simulation-Based Evaluation
Bicycle Integration with Public Transport
Bus Rapid Transit and Light Rail Transit Systems: State of Discussion
Bus Rapid Transit, Institutional Issues Related to Implementation
Bus Rapid Transit: Worldwide History of Development, Key Systems and Policy Issues
Bus Versus Rail Implications for Transit-Oriented Development
Bus Rapid Versus Light Rail Transit: Service Quality, Economic,
Environmental, and Planning Aspects
High Speed Rail, Technology Development of
High-Occupancy Vehicle and Toll Lanes
HOT Lanes/Value Pricing: Planning and Evaluation of Multiclass Service
Light Rail Transit in the US and Abroad, Examination of History and Innovations
Light Rail Transit, Shared Infrastructural Issues
Light Rail Transit, Systemic Viability
MAGLEV Technology Development
Mass Transit Science and Technology, Introduction
Personal Rapid Transit and Its Development
Transit-Oriented Development and Land Use

Nuclear Energy, Section Editor: Nicholas Tsoulfanidis

Dosimetry
Fission Reactor Physics
GEN-IV Reactors
Health Physics
Ionizing Radiation Detectors
Isotope Separation Methods for Nuclear Fuel
Modern Nuclear Fuel Cycles
Nuclear Energy, Introduction
Nuclear Facilities, Decommissioning of
Nuclear Fission Power Plants
Nuclear Fuel, Reprocessing of

Nuclear Fusion
Nuclear Power, Economics of
Nuclear Reactor Materials and Fuels
Nuclear Safeguards and Proliferation of Nuclear Weapons Materials
Radiation Shielding
Radiation Sources
Radioactive Waste Management: Storage, Transport, Disposal
Uranium and Thorium Resources

Ocean Energy, Section Editor: Luis A. Vega

Marine and Hydrokinetic Energy Environmental Challenges
Ocean Energy, Introduction
Ocean Thermal Energy Conversion
Offshore Wind Energy Technology Trends, Challenges, and Risks
Tidal Energy

Ocean Farming and Sustainable Aquaculture Science and Technology, Section Editor: Barry A. Costa-Pierce

Aquaculture and Renewable Energy Systems, Integration of
Aquaculture, Ecological
Aquaculture, Integrated Multi-trophic (IMTA)
Aquaculture, Sustainability Science in
Aquapod Systems for Sustainable Ocean Aquaculture
Carrying Capacity for Aquaculture, Modeling Frameworks for Determination of
Carrying Capacity for Sustainable Bivalve Aquaculture
Environmental Impacts of an Open Ocean Mariculture Operation in Kona, Hawaii
Life Cycle Assessments and Their Applications to Aquaculture Production Systems
Mariculture Systems, Integrated Land-Based
Marine Aquaculture in the Mediterranean
Marine Fisheries Enhancement, Coming of Age in the New Millennium
Mussel Culture, Open Ocean Innovations
Ocean Farming and Sustainable Aquaculture Science and Technology, An Introduction to
Polyculture in Aquaculture
Seaweed Aquaculture for Human Foods in Land-Based and IMTA Systems
Shellfish Aquaculture, Methods of Sustainable
Sustainable Ecological Aquaculture

Oceans and Human Health, Section Editor: Darrell Jay Grimes

Coastal Ecosystems, Sustainable Management
Drug Discovery in Ocean
Harmful Algal Blooms
Human Bacterial Diseases from Ocean
Living Ocean, An Evolving Oxymoron
Marine and Freshwater Fecal Indicators and Source Identification
Oceans and Human Health, Introduction

Oceans and Human Health, Social and Economic Impacts
Remote Sensing Applications to Ocean and Human Health
Sentinel Species in Oceans and Human Health
Waterborne Diseases of the Ocean, Enteric Viruses
Waterborne Parasitic Diseases in Ocean

Photovoltaics, Section Editor: Daniel Lincot

CdTe Solar Cells
Mesoscopic Solar Cells
Organic Solar Cells
Photovoltaic Energy, Introduction
Photovoltaics, Status of
PV Policies and Markets
Silicon Solar Cells, Crystalline
Silicon Solar Cells, Thin-film
Solar Cells, Chalcopyrite-Based Thin Film
Solar Cells: Very High Efficiencies Approaches
Solar Cells: Energy Payback Times and Environmental Issues

Renewable Energy from Biomass, Section Editor: Martin Kaltschmitt

Algae, a New Biomass Resource
Biodiesel
Bioethanol from Celluloses
Bioethanol from Starch
Bioethanol from Sugar: the Brazilian Experience
Biofuels: A Technical, Economic and Environmental Comparison
Biofuels: Upgraded New Solids
Biogas for Electricity Generation, Hi-tech Applications
Biogas Production and Energy crops
Biogas Production Developing Countries
Biogas Substrates from Municipalities and Industries
Biomass as Renewable Source of Energy, Possible Conversion Routes
Biomass Combustion for Electricity Generation
Biomass Energy Heat Provision for Cooking and Heating in Developing Countries
Biomass Energy Heat Provision in Modern Large-Scale Systems
Biomass Energy Heat Provision in Modern Small-Scale Systems
Biomass Energy Small-Scale Combined Heat and Power Systems
Biomass Gasification for Electricity and Fuels, Large Scale
Biomass Gasification for Rural Electrification, Small Scale
Biomass Production
Biomass Provision and Use, Sustainability Aspects
Biomass Pyrolysis
Biomass Resources, Worldwide
Biomass to Liquid (BtL), Concepts and Their Assessment
Biomass Use on a Global Scale
Biomethane from Anaerobic Processes

Biosynthetic Natural Gas
Co-combustion of wood in Coal-Fired Large-Scale Power Plants
Hydrogen from Biomass
Lignocellulosic Energy Crops, Production and Provision
Plant Oil Fuels Combined Heat and Power (CHP)
Renewable Energy from Biomass, Introduction
Solid Biofuels, Fuels and Their Characteristics

Solar Radiation, Section Editor: Christian A. Gueymard

Daylight, Indoor Illumination, and Human Behavior
Photosynthetically Active Radiation: Measurement and Modeling
Solar Constant and Total Solar Irradiance Variations
Solar Irradiance, Global Distribution
Solar Radiation and Human Health
Solar Radiation for Solar Energy Utilization
Solar Radiation Spectrum
Solar Radiation versus Climate Change
Solar Radiation, Introduction
Solar Radiation, Spatial and Temporal Variability
Solar-Induced Climate Effects
Topographic Solar Radiation Modeling for Environmental Applications
Ultraviolet Radiation: Distribution and Variability
UV Effects on Living Organisms

Solar Thermal Energy, Section Editor: Christoph Richter

Concentrating Receiver Systems (Solar Power Tower)
Linear Fresnel Collectors
Parabolic Trough Solar Technology
Solar Collectors, Non-concentrating
Solar Cookers and Dryers to Conserve Human and Planet Health
Solar Cooling Systems
Solar Detoxification and Disinfection of Water
Solar Energy in Thermochemical Processing
Solar Thermal Desalination
Solar Thermal Energy, Introduction
Solar Updraft Towers
Thermal Energy Storage

Solid Waste Disposal and Recycling, Section Editor: Ronald L. Mersky

Construction and Demolition Wastes
Electronic Waste and Its Regulation
Fly Ash
Land Disposal
Landfill Bioreactors
Landfill Closure and Reuse of Land

Landfill Leachate Control
Mining Solid Wastes
Recycling Collection and Materials Separation
Recycling Technologies
Solid Waste Disposal and Recycling, Environmental Impacts
Solid Waste Disposal and Recycling, Introduction
Solid Waste Generation and Characterization
Solid Waste Public Involvement and Education
Waste Collection and Transport
Waste Diversion
Waste Materials in Construction, Utilization of

Sustainability in Water, Section Editor: Jeaweon Cho

Climate Change and Global Water Sustainability
Climate Change Impacts on Emerging Contaminants
Community-Owned Water Resource and Climate Change, Quality Management
Desalination Technology for Sustainable Water Resource
Groundwater Remediation, Environmental and Economic Assessment
Rainwater Harvesting
Stormwater Harvesting and Reuse
Sustainability in Water, Introduction
Sustainable Remediation Methods for Metals and Radionuclides
Sustainable Remediation: Integrating Risk, Science, and Sustainability Principles
Sustainable Water Treatment Using Nanofiltration and Tight Ultrafiltration Membranes
Wastewater Reclamation
Wastewater Treatment and Control through Wetlands
Wastewater Treatment Plant: Anthropogenic Micropollutant Indicators for Sustainable River Management
Water and Energy Nexus
Water and Wastewater Operation: Instrumentation, Monitoring, Control and Automation
Water Reclamation System and Micropollutants

Sustainable Built Environment, Section Editor: Vivian Loftness

Bioclimatic Design
Biofuels and Sustainable Buildings
Daylighting Controls, Performance and Global Impacts
Facades and Enclosures, Building for Sustainability
Geothermal Conditioning: Critical Sources for Sustainability
Indoor Environmental Quality and Health Improvement, Evidence-Based Design for
Natural Ventilation in Built Environment
Passive House (Passivhaus)
Passive Solar Heating in Built Environment
Rating Systems for Sustainability
Regenerative Development and Design

Resource Repletion, Role of Buildings
Sustainability Performance Simulation Tools for Building Design
Sustainable and Healthy Built Environment
Sustainable Built Environment, Introduction
Sustainable Design and Construction, Integrated Delivery Processes and Building Information Modeling
Sustainable Heating Ventilation and Air Conditioning

Sustainable Landscape Design, Urban Forestry and Green Roof Science and Technology, Section Editor: Dagmar Haase

Biodiversity in Cities, Reconnecting Humans with Nature
Green Infrastructure and Climate Change
Green Roof Infrastructures in Urban Areas
Green Roof Planning in Urban Areas
Green Roofs, Ecological Functions
Landscape Planning for Minimizing Land Consumption
Landscape Planning for Sustainable Water Usage
Landscape Planning/Design of Shrinking Landscapes
Sustainable Landscape Design, Urban Forestry, and Green Roof Science and Technology, Introduction
Sustainable Landscapes
Urban Forest Function, Design and Management
Urban Redevelopment and Quality of Open Spaces

Transgenic Livestock for Food Production, Section Editor: C. Bruce A. Whitelaw

Avian Specific Transgenesis
Disease-Resistant Transgenic Animals
Livestock Somatic Cell Nuclear Transfer
Nuclear Transfer to Produce Transgenic Mammals
Transgenic Fishes: Applications, State of the Art, and Risk Concerns
Transgenic Livestock for Food Production, Introduction
Transgenic Livestock Technologies
Transgenic Livestock, Decreasing Environmental Impact of
Transgenic Livestock, Enhanced Nutritional Quality in
Transgenic Livestock, Ethical Concerns and Debate
Transgenic Technologies and Increased Livestock Fertility
Transgenics: Alternative Gene Transfer Methods

Transport and Fate of Chemicals in the Environment, Section Editor: John S. Gulliver

Atmosphere-Water Exchange
Chemicals in the Environment, Diffusive Transport
Chemicals in the Environment, Dispersive Transport
Chemicals in the Environment, Turbulent Transport
Lake and Reservoir Fate and Transport of Chemicals
Oceanic Fate and Transport of Chemicals
River Fate and Transport
Sediment-Water Interfaces, Chemical Flux at

Subsurface Fate and Transport of Chemicals
Toxic Organic Chemicals
Transport and Fate of Chemicals in the Environment, Introduction
Transport in the Environment
Transport with Jets and Plumes of Chemicals in the Environment

Waste to Energy, Section Editor: Nickolas J. Themelis

Gasification and Liquefaction Alternatives to Incineration in Japan
Greenhouse Gas Emission Reduction by Waste-to-Energy
Hitachi Zosen Inova Technology
Incinerator Grate Combustion Phenomena
Life Cycle Comparison of Waste-to-Energy to Sanitary Landfill
Martin Waste-to-Energy Technology
Plasma-Assisted Waste-to-Energy Processes
Thermal Treatment of Waste: Key Element for Sustainable Waste Management
Waste Management for Sustainable Society
Waste-to Energy: Decreasing the Entropy of Solid Wastes and Increasing Metal Recovery
Waste-to-Energy Ash Management in Europe
Waste-to-Energy Ash Management in the United States
Waste-to-Energy Facilities as Power Plants
Waste-to-Energy for District Heating
Waste-to-Energy Using Refuse-Derived Fuel
Waste-to-Energy, Introduction
Waste-to-Energy: Energy Resource in Solid Wastes
Waste-to-Energy: Fluidized Bed Technology

Wind Power, Section Editor: Lennart Söder

Electricity Generation with Small Wind Turbines
Global Wind Power Installations
Meterology and Wind Power
Offshore Wind Power
Wind Power Balancing
Wind Power Generator Systems and Local Power System Interconnection
Wind Power Grid Integration: Transmission Planning
Wind Power, Aerodynamics and Blade Technology
Wind Power, Introduction
Wind Power: Basic Challenge Concerning Social Acceptance
Wind Power: Economy, Market, Subsidies, Payment Mechanisms, and Capacity Credit
Wind Turbine Noise Emissions

About the Editor-in-Chief

Robert A. Meyers
Dr. Meyers has just completed serving as editor in chief for the Springer *Encyclopedia of Complexity and Systems Science*
President: RAMTECH Limited
Manager, Energy and Environmental Projects, TRW Inc.,
Postdoctoral Fellow and Member of the Faculty, California Institute of Technology
Ph.D. Chemistry, University of California at Los Angeles
B.A., Chemistry with minor in mathematics, California State University, San Diego
Email robert.meyers@ramtechlimited.org

BIOGRAPHY
Dr. Meyers has worked with more than 20 Nobel laureates during his career. The photo of Dr. Meyers at the Continental Divide was taken during a tour of Colorado earth sciences, environmental and solar energy facilities.

EDUCATION
Postdoctoral Fellow, California Institute of Technology
Ph.D. in Organic Chemistry, University of California at Los Angeles
B.A., Chemistry with minor in Mathematics, California State University, San Diego

RESEARCH
Dr. Meyers was manager of Energy and Environmental Projects at TRW (now Northrop Grumman) in Redondo Beach, CA, and is now president of RAMTECH Limited. He is coinventor of the Gravimelt process for desulfurization and demineralization of coal for air pollution and water pollution control and was manager of the Department of Energy project leading to the construction and successful operation of a first-of-a-kind Gravimelt Process Integrated Test Plant. Dr. Meyers is the inventor of and was project manager for the DOE-sponsored Magnetohydrodynamics Seed Regeneration Project which has resulted in the construction and successful operation of a pilot plant for production of potassium formate, a chemical utilized for plasma electricity generation and

air pollution control. He also managed TRW efforts in magnetohydrodynamics electricity generating combustor and plasma channel development. Dr. Meyers managed the pilot-scale DoE project for determining the hydrodynamics of synthetic fuels. He is a coinventor of several thermo-oxidative stable polymers which have achieved commercial success as the GE PEI, Upjohn Polyimides, and Rhone-Polenc bismaleimide resins. He has also managed projects for photochemistry, chemical lasers, flue gas scrubbing, oil shale analysis and refining, petroleum analysis and refining, global change measurement from space satellites, analysis and mitigation (carbon dioxide and ozone), hydrometallurgical refining, soil and hazardous waste remediation, novel polymers synthesis, modeling of the economics of space transportation systems, space rigidizable structures, and chemiluminescence-based devices.

He is a senior member of the American Institute of Chemical Engineers, member of the American Physical Society, member of the American Chemical Society, and serves on the UCLA Chemistry Department Advisory Board. He was a member of the joint USA-Russia working group on air pollution control and the EPA-sponsored Waste Reduction Institute for Scientists and Engineers.

Dr. Meyers has more than 20 patents and 50 technical papers in the fields of photochemistry, pollution control, inorganic reactions, organic reactions, luminescence phenomena, and polymers. He has published in primary literature journals including *Science* and the *Journal of the American Chemical Society*, and is listed in *Who's Who in America* and *Who's Who in the World*. Dr. Meyers' scientific achievements have been reviewed in feature articles in the popular press in publications such as *The New York Times Science Supplement* and *The Wall Street Journal* as well as more specialized publications such as *Chemical Engineering* and *Coal Age*. A public service film was produced by the Environmental Protection Agency of Dr. Meyers' chemical desulfurization invention for air pollution control.

SCIENTIFIC BOOKS

Dr. Meyers is the author or editor in chief of 12 technical books including the *Handbook of Chemical Production Processes*; *Handbook of Synfuels Technology and Handbook of Petroleum Refining Technology (McGraw-Hill)*; *and The Handbook of Energy Technology and Economics*, published by John Wiley & Sons*; Coal Structure*, published by Academic Press; and *Coal Desulfurization* as well as the *Coal Handbook* published by Marcel Dekker. He served as chairman of the advisory board for *A Guide to Nuclear Power Technology*, published by John Wiley & Sons, which won the Association of American Publishers Award as the best book in technology and engineering.

ENCYCLOPEDIAS

Dr. Meyers conceived and has served as editor in chief of the Academic Press (now Elsevier) *Encyclopedia of Physical Science and Technology*. This is an 18-volume publication of 780 twenty-page articles written to an audience of university students and practicing professionals. This encyclopedia, first published in 1987, was very successful, and because of this, was revised and reissued in 1992 as a second edition. The Third Edition was published in 2001 and is now available online. Dr. Meyers has completed two editions of the *Encyclopedia of Molecular Cell Biology and Molecular Medicine* for Wiley VCH publishers (1995 and 2004). These cover molecular and cellular level genetics, biochemistry, pharmacology, diseases, and structure determination as well as cell biology. His eight-volume *Encyclopedia of Environmental Analysis and Remediation* was published in 1998 by John Wiley & Sons and his 15-volume Encyclopedia of *Analytical Chemistry* was published in 2000, also by John Wiley & Sons.

Editorial Board Members

Rita R. Colwell
Center for Bioinformatics and Computational Biology
University of Maryland
College Park, MD
USA

Donald A. Glaser
Glaser Lab, University of California
Berkeley
Department of Molecular & Cell Biology
Berkeley, CA
USA

Andreas Fischlin
Terrestrial Systems Ecology, ETH-Zentrum
Zürich
Switzerland

Timothy L. Killeen
National Science Foundation
Arlington, VA
USA

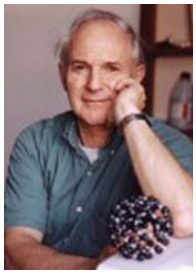

Harold W. Kroto
Department of Chemistry and Biochemistry
The Florida State University
Tallahassee, FL
USA

Daniel L. McFadden
Econometrics Laboratory
University of California
Berkeley, CA
USA

Amory B. Lovins
Rocky Mountain Institute
Snowmass, CO
USA

Thomas C. Schelling
Department of Economics
University of Maryland
College Park, MD
USA

Lord Robert May
Department of Zoology
University of Oxford
Oxford
UK

Charles H. Townes
University of California
Berkeley, CA
USA

Emilio Ambasz
Emilio Ambasz & Associates, Inc.
New York, NY
USA

Mehrdad Ehsani
Department of Electrical & Computer Engineering
Texas A&M University
College Station, TX
USA

Clare Bradshaw
Department of Systems Ecology
Stockholm University
Stockholm
Sweden

Ali Emadi
Electrical and Computer Engineering Department
Illinois Institute of Technology
Chicago, IL
USA

Terry Coffelt
Research Geneticist
Arid Land Agricultural Research Center
Maricopa, AZ
USA

Charles A. S. Hall
College of Environmental Science & Forestry
State University of New York
New York
USA

Rik Leemans
Environmental Systems Analysis Group
Wageningen University
Wageningen
The Netherlands

Timothy D. Searchinger
Woodrow Wilson School
Princeton University
Princeton, NJ
USA

Keith Lovegrove
Department of Engineering
The Australian National University
Canberra
Australia

Section Editors

Air Pollution Sources, Statistics and Health Effects

Roy M. Harrison
Division of Environmental Health and Risk Management, School of Geography, Earth and Environmental Sciences
The University of Birmingham
Edgbaston, Birmingham
UK

Batteries

Ralph J. Brodd
Broddarp of Nevada
Henderson, NV
USA

Animal Breeding and Genetics

Ignacy Misztal
Breeding and Genetics, University of Georgia
Department of Animal and Dairy Science
Athens, GA
USA

Climate Change Modeling Methodology

Philip J. Rasch
Pacific Northwest National Laboratory
Richland, WA
USA

Climate Change Remediation

Timothy M. Lenton
University of Exeter, Hatherly Laboratories
Biosciences College of Life and Environmental Sciences
Exeter
UK

and

Naomi E. Vaughan
School of Environmental Sciences
University of East Anglia
Norwich
UK

Crop Science and Technology

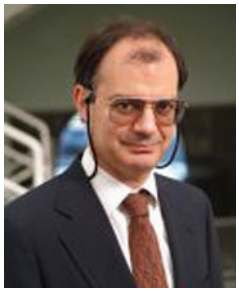

Paul Christou
Department de Produccio Vegetal i Ciencia Forestal
Universitat de Lleida/ICREA
Lleida
Spain
and
Institució Catalana de Recerca i Estudis Avançats (ICREA)
Barcelona
Spain

and

Roxana Savin
Department of Crop and Forest Sciences
University of Lleida
Lleida
Spain

Earth System Monitoring

John Orcutt
Scripps Institution of Oceanography
University of California, San Diego
La Jolla, CA
USA

Electric, Hybrid, and Fuel Cell Vehicles

Mehrdad Ehsani (also one of the board members)
Department of Electrical & Computer Engineering
Texas A&M University
College Station, TX
USA

Ecological Systems

Rik Leemans (also one of the board members)
Environmental Systems Analysis Group
Wageningen University
Wageningen
The Netherlands

Electrical Transmission Systems and Smart Grids

Miroslav M. Begovic
School of Electrical and Computer Engineering
Georgia Institute of Technology
Atlanta, GA
USA

Environmental Geology

James W. LaMoreaux
P.E. LaMoreaux & Associates
Tuscaloosa, AL
USA

Environmental Toxicology

Edward A. Laws
Louisiana State University
School of the Coast and Environment
Baton Rouge, LA
USA

Environmental Radioactivity and Ecotoxicology of Radioactive Substances

Glen A. Bird
EcoMetrix Incorporated
Mississauga, ON
Canada

Fossil Energy

Ripudaman Malhotra
Chemistry and Chemical Engineering Laboratory
Pure and Applied Physical Sciences Division
SRI International
Menlo Park, CA
USA

Fuel Cells

Klaus-Dieter Kreuer
Max-Planck-Institut für Festkörperforschung
Stuttgart
Germany

Green Chemistry and Chemical Engineering

Paul T. Anastas
Center for Green Chemistry and Green Engineering
Yale University
New Haven, CT
USA

and

Geothermal Power Stations

Lucien Y. Bronicki
Ormat Technologies, Inc.
Reno, NV
USA

Julie B. Zimmerman
Department of Chemical Engineering
Environmental Engineering Program
Yale University
New Haven, CT
USA

Hazardous Waste

Mervin Fingas
Spill Science
Edmonton, AB
Canada

Infectious Diseases

Phyllis J. Kanki
Department of Immunology and Infectious Diseases
Harvard School of Public Health
Boston, MA
USA

Hydrogen Production Science and Technology

Timothy E. Lipman
Institute of Transportation Studies
University of California – Berkeley
Berkeley, CA
USA

Intelligent Vehicles Technology

Fei-Yue Wang
Institute of Automation
Chinese Academy of Sciences
Beijing
China

Mass Transit Science and Technology

Gary L. Brosch
Center for Urban Transportation Research
University of South Florida
Tampa, FL
USA

Ocean Energy

Luis A. Vega
Hawaii Natural Energy Institute
School of Ocean And Earth Science And Technology
University of Hawaii at Manoa
Honolulu, HI
USA

Nuclear Energy

Nicholas Tsoulfanidis
Department of Nuclear Energy
Missouri University of Science and Technology
Rolla, MO
USA

Ocean Farming and Sustainable Aquaculture Science and Technology

Barry A. Costa-Pierce
Graduate School of Oceanography, Rhode Island Sea Grant College Program
University of Rhode Island, URI Bay Campus
Narragansett, RI
USA

Oceans and Human Health

Darrell Jay Grimes
Department of Coastal Sciences
The University of Southern Mississippi
Ocean Springs, MS
USA

Renewable Energy From Biomass

Martin Kaltschmitt
German Biomass Research Centre
Leipzig
Germany
and
Institute of Environmental Technology and Energy Economics
Hamburg University of Technology
Hamburg
Germany

Photovoltaics

Daniel Lincot
Institute of Research and Development of Photovoltaic Energy
Chatou Cedex
France

Solar Radiation

Christian A. Gueymard
Solar Consulting Services
Colebrook, NH
USA

Solar Thermal Energy

Christoph Richter
Plataforma Solar de Almeria
Institute of Solar Research
DLR – German Aerospace Centre
Germany

Sustainability in Water

Jaeweon Cho
Gwangju Institute Science and Technology (GIST)
Department of Environmental Science and Engineering, Natural Organic Matter Lab
Gwangju
Korea

Solid Waste Disposal and Recycling

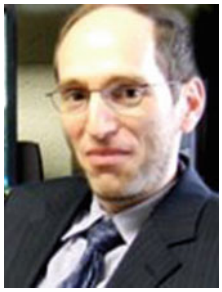

Ronald L. Mersky
Department of Civil Engineering
Widener University
Chester, PA
USA

Sustainable Built Environment

Vivian Loftness
Center for Building Performance and Diagnostics
Carnegie Mellon University
Pittsburgh, PA
USA

Sustainable Landscape Design, Urban Forestry and Green Roof Science and Technology

Dagmar Haase
Department of Geography
Humboldt University Berlin
Berlin
Germany
and
Department of Computational Landscape Ecology
Helmholtz Center for Environmental Research – UFZ
Leipzig
Germany

Transport and Fate of Chemicals in the Environment

John S. Gulliver
Department of Civil Engineering
University of Minnesota
Minneapolis, MN
USA

Transgenic Livestock for Food Production

C. Bruce A. Whitelaw
The Roslin Institute and Royal (Dick) School of Veterinary Studies
Division of Developmental Biology, University of Edinburgh
Midlothian, Scotland
UK

Waste to Energy

Nickolas J. Themelis
Earth Engineering Center
Columbia University
New York, NY
USA

Wind Power

Lennart Söder
Royal Institute of Technology
Electric Power Systems
Stockholm
Sweden

List of Contributors

Magdy Abdelrahman
Department of Civil Engineering (CIE 201F)
North Dakota State University
North – Fargo, ND
USA

Mats Åbom
KTH Royal Institute of Technology, KTH-The Marcus Wallenberg Laboratory for Sound and Vibration Research
Stockholm
Sweden

Thomas Ackermann
Energynautics GmbH
Langen
Germany

William J. Adams
Rio Tinto
Murray, UT
USA

Vinayak Agarwal
Center for Biophysics and Computational Biology
University of Illinois at Urbana-Champaign
Urbana, IL
USA

A. Alonso Aguirre
Department of Environmental Science and Policy
George Mason University
Fairfax, VA
USA
and
Smithsonian-Mason School of Conservation
C/O Smithsonian Conservation Biology Institute
Front Royal, VA
USA

Motoyuki Akamatsu
Human Technology Research Institute, National Institute of Advanced Industrial Science and Technology (AIST)
Tsukuba-shi, Ibaraki
Japan

Haluk Akgün
Department of Geological Engineering
Middle East Technical University (METU)
Ankara
Turkey

Ramon Albajes
Department of Plant Production and Forest Sciences
Universitat de Lleida, Centre UdL-IRTA
Lleida
Spain

Spiros Alexopoulos
Solar-Institut Jülich (SIJ), FH Aachen
Aachen University of Applied Sciences
Jülich
Germany

Craig R. Allen
U.S. Geological Survey, Nebraska Cooperative Fish and Wildlife Research Unit, School of Natural Resources
University of Nebraska
Lincoln, NE
USA

Klaus Ammann
Botanical Garden
University of Bern
Bern
Switzerland

Stefan Anderberg
Lund University Centre for Sustainability Studies
Lund University
Lund
Sweden

John Andraos
Department of Chemistry
York University
Toronto, ON
Canada

Dror L. Angel
Leon Recanati Institute for Maritime Studies
University of Haifa
Mt Carmel, Haifa
Israel

J. F. Angus
CSIRO Plant Industry
Canberra, ACT
Australia

Shamindri M. Arachchige
Department of Chemistry
Virginia Polytechnic Institute and State University
Blacksburg, VA
USA

Víctor Arellano
Instituto de Investigaciones Eléctricas
Cuernavaca, Morelos
Mexico

Thorvaldur Árnason
Agricultural University of Iceland
Borgarnes
Iceland
and
International Horse Breeding Consultant
Morgongava
Sweden

Jon A. Arnot
Department of Physical and Environmental Sciences
University of Toronto Scarborough
Toronto, ON
Canada

M. Arrott
Scripps Institution of Oceanography & Calit2
University of California at San Diego
La Jolla, CA
USA

Marianna Asaro
SRI International
Menlo Park, CA
USA

Cheryl J. Ashworth
The Roslin Institute and Royal (Dick) School of Veterinary Studies
University of Edinburgh
Scotland
UK

A. Atkinson
Department of Materials
Imperial College London
London
UK

Ömer Aydan
Geomechanics and Geoengineering
Tokai University, Ocean Research Institute
Shizuoka
Japan

Azizan Aziz
Center for Building Performance and Diagnostics
Carnegie Mellon University
Pittsburgh
USA

Antje Backhaus
Forest and Landscape Denmark
University of Copenhagen
Frederiksberg C
Denmark

Julio T. Bacmeister
NCAR Earth System Laboratory
National Center for Atmospheric Research
Boulder, CO
USA

Brian Bahor
Covanta Energy Corporation
Morristown, NJ
USA

Chao Bai
Department of Vegetal Production and Forestry Science, ETSEA
University of Lleida
Lleida
Spain

Jonathan E. M. Baillie
Zoological Society of London
London
UK

Lisa J. Bain
Department of Biological Sciences
Clemson University
Clemson, SC
USA

Nina Baird
Center for Building Performance & Diagnostics
Carnegie Mellon University
Pittsburgh, PA
USA

J. Kevin Baird
Eijkman–Oxford Clinical Research Unit
Jalan Diponegoro
Jakarta
Indonesia
and
Centre for Tropical Medicine, Nuffield Department of Medicine
University of Oxford
Oxford
UK

Michael C. Baker
Advanced Nuclear Technology Group, Nuclear Nonproliferation Division
Los Alamos National Laboratory
Los Alamos, NM
USA

Miriam Balaban
European Desalination Society (EDS)
Tel Aviv
Israel

Robert S. Balog
Department of Electrical and Computer Engineering
Texas A & M University
College Station, TX
USA

Frédéric Baret
INRA
UMR Environnement Méditerranéen et Modélisation des Agro-Hydrosystèmes, EMMAH
Avignon
France

Roy Baria
EGS Energy Ltd
Penance Cornwall
UK

Morton A. Barlaz
Civil, Construction and Environmental Engineering
North Carolina State University
Raleigh, NC
USA

Frank Barnes
Electrical, Computer, and Energy Engineering Department
University of Colorado
Boulder, CO
USA

Brian Barnett
TIAX LLC
Lexington, MA
USA

Rosa María Barragán
Instituto de Investigaciones Eléctricas
Cuernavaca, Morelos
Mexico

Frank T. Barranco, Jr.
EA Engineering, Science, and Technology, Inc.
Sparks, MD
USA

Björn Barrois
EvoBus GmbH
Neu-Ulm
Germany

Matthew Barth
Department of Electrical Engineering
University of California
Riverside, CA
USA

Michael E. Bartkow
Seqwater
c/- National Research Centre for Environmental Toxicology (Entox)
Queensland
Australia

Roberto Bassi
Dipartimento di Biotecnologie
Università di Verona
Verona
Italy

Diego Batlla
IFEVA – Cátedra de Cerealicultura/
CONICET-Universidad de Buenos Aires
Buenos Aires
Argentina

Thomas Batz
Department Information Management
Fraunhofer Institute of Optronics, System Technologies and Image Exploitation IOSB
Karlsruhe
Germany

Ausilio Bauen
Centre for Energy Policy and Technology
Imperial College
London
UK

Thomas Bauer
Institute of Technical Thermodynamics
German Aerospace Center
Stuttgart
Germany

Charlene W. Bayer
Georgia Tech Research Institute
Georgia Institute of Technology
Atlanta, GA
USA

Matthew Baylis
LUCINDA Group, Institute of Infection and Global Health
University of Liverpool
Neston, Cheshire
UK

G. Beardsmore
Hot Dry Rocks Pty Ltd
South Yarra, Victoria
Australia

Barry Beck
Karst
P.E. LaMoreoux, Inc.
Oak Ridge, TN
USA

Miroslav M. Begovic
School of Electrical and Computer Engineering
Georgia Institute of Technology
Atlanta, GA
USA

François Béguin
Research Centre on Divided Matter
CRMD-CNRS & Orléans University
Orléans
France

Simon Bell
OPENspace Research Centre
Edinburgh College of Art
Edinburgh
UK
and
Estonian University of Life Sciences
Tartu
Estonia

Moshe Ben-Akiva
Department of Civil and Environmental Engineering
MIT
Cambridge, MA
USA

Roberto L. Benech-Arnold
IFEVA – Cátedra de Cultivos Industriales/CONICET-Universidad de Buenos Aires
Buenos Aires
Argentina

Brian C. Benicewicz
Department of Chemistry and Biochemistry
University of South Carolina
Columbia, SC
USA

János Beér
MIT
Cambridge, MA
USA

Nicholas A. Beresford
Radioecology Group
Centre for Ecology & Hydrology – CEH Lancaster
Lancaster Environment Centre
Bailrgg, Lancaster
UK

Peer Berg
Faculty of Agricultural Sciences
Aarhus University
Tjele
Denmark

Rudolf Bergermann
Schlaich Bergermann Solar GmbH
Stuttgart
Germany

Bob Berkebile
FAIA
BNIM – Berkebile Nelson Immenschuh McDowell Architects
Kansas City, MO
USA

Enrico Bernardo
Department of Mechanical Engineering – Materials Division
University of Padova
Padova
Italy

Pete M. Berry
Sustainable Crop Management
ADAS UK Ltd
Malton, North Yorkshire
UK

Ruggero Bertani
Enel
Rome
Italy

Srinivas Bettadpur
Center for Space Research
University of Texas-Austin
Austin, TX
USA

Frederik Betz
Affiliated Engineers, Inc
Madison, WI
USA

Eda Beyazit
Transport Studies Unit
School of Geography and the Environment
University of Oxford
Oxford
UK

H. G. Beyer
Department of Engineering
University of Agder
Grimstad
Norway

Jürgen Beyerer
Fraunhofer Institute of Optronics, System Technologies and Image Exploitation IOSB
Karlsruhe
Germany
and
Institute for Anthropomatics, Vision and Fusion Laboratory
Karlsruhe Institute of Technology
Karlsruhe
Germany

Friedrich Biedermann
Bios Bioenergiesysteme GmbH
Graz
Austria
and
BIOENERGY 2020+ GmbH
Graz
Austria

Paul K. Bienfang
Oceanography Department
School of Ocean and Earth Science and Technology (SOEST)
University of Hawaii
Honolulu, HI
USA

Piter Bijma
Animal Breeding and Genomics Centre
Wageningen University
Wageningen
The Netherlands

Bernd Bilitewski
Institute of Waste Management and Contaminated Site Treatment
Technical University of Dresden
Pirna
Germany

Glen A. Bird
EcoMetrix Incorporated
Mississauga, ON
Canada

Lori Bird
National Renewable Energy Laboratory
Golden, CO
USA

K. U. Birnbaum
Institute of Energy Research
Forschungszentrum Jülich
Juelich
Germany

Cecilia M. Bitz
Atmospheric Sciences Department
University of Washington
Seattle, WA
USA

Jason J. Blackstock
Kennedy School of Government
Cambridge, MA
USA

Agustin Blasco
Institute of Animal Science and Technology
Universidad Politécnica de Valencia
Valencia
Spain

William Bloss
School of Geography, Earth & Environmental Sciences
University of Birmingham
Birmingham
UK

Alexandria B. Boehm
Environmental and Water Studies
Department of Civil and Environmental Engineering
Stanford University
Stanford, CA
USA

Peter Bogdanoff
Helmholtz-Zentrum Berlin für Materialien und Energie GmbH (HZB)
Institut für Solare Brennstoffe und Energiespeichermaterialien
Berlin
Germany

John T. Bolan
Paulus, Sokolowski and Sartor, LLC
Warren, NJ
USA

Karl Bolin
KTH Royal Institute of Technology, KTH-The Marcus Wallenberg Laboratory for Sound and Vibration Research
Stockholm
Sweden

Giuseppe Bonifazi
Dipartimento di Ingegneria Chimica Materiali Ambiente Sapienza
Università di Roma Via Eudossiana
Rome
Italy

David Bonnett
CIMMYT Int
Mexico D.F
Mexico

Oleg Borodin
Department of Materials Science and Engineering
University of Utah
Salt Lake City, UT
USA
and
Electrochemistry Branch, SEDD, AMSRD–ARL–RDRL–SED–C
Adelphi, MD
USA

Lucas Borrás
CONICET, National Council of Scientific and Technical Research
Buenos Aires
Argentina
and
Departamento de Producción Vegetal
Universidad Nacional de Rosario
Zavalla, Santa Fe
Argentina

Gisela Borràs-Gelonch
Department of Crop and Forest Sciences
University of Lleida
Lleida
Spain

Michael van den Bossche
Department of Chemical Engineering
University of Virginia
Charlottesville, VA
USA

Paul Boulter
PAEHolmes
Sydney
Australia

Philip W. Boyd
Department of Chemistry
NIWA Centre for Chemical and Physical Oceanography
University of Otago
Dunedin
New Zealand

Bert Bras
George W. Woodruff School of Mechanical Engineering
Georgia Institute of Technology
Atlanta, GA
USA

Michael Braungart
EPEA Internationale Umweltforschung GmbH
Hamburg
Germany
and
Academic Chair Cradle to Cradle for Innovation and Quality, Rotterdam School of Management, Erasmus University
Rotterdam
The Netherlands

Stephan Brenneisen
Life Sciences und Facility Management
Wädenswil
Switzerland

Karen J. Brewer
Department of Chemistry
Virginia Polytechnic Institute and State University
Blacksburg, VA
USA

Kevin V. Brix
University of Miami, RSMAS, Marine Biology and Fisheries
Miami, FL
USA

Ralph J. Brodd
Broddarp of Nevada
Henderson, NV
USA

Alberto Broggi
VisLab – Dipartimento di Ingegneria dell'Informazione
Università degli Studi di Parma
Parma
Italy

Egbert Broßmann
Vattenfall Europe Wärme AG
Berlin
Germany

Christopher Bromley
GNS Science
Wairakei Research Centre
Taupo
New Zealand

Lucien Y. Bronicki
Ormat Technologies, Inc.
Reno, NV
USA

Jeffrey R. Brook
Department of Chemical Engineering and Applied Chemistry
University of Toronto
Toronto, ON
Canada
and
Air Quality Research Division, Atmospheric Science and Technology Directorate
Environment Canada
Toronto, ON
Canada

Graham Brookes
Agricultural Economist, PG Economics Ltd
Dorset
UK

Gary L. Brosch
Center for Urban Transportation Research
University of South Florida
Tampa, FL
USA

Jacob Brouwer
National Fuel Cell Research Center
University of California
Irvine, CA
USA

Jeffrey R. Brown
Department of Urban and Regional Planning
Florida State University
Tallahassee, FL
USA

Carl Brown
Emergencies Science and Technology Section
Environment Canada
Ottawa, ON
Canada

Marilyn A. Brown
School of Public Policy
Georgia Institute of Technology
Atlanta, GA
USA

Peter Brownsort
UK Biochar Research Centre (UKBRC)
School of GeoSciences
Science and Engineering at The University of Edinburgh
Edinburgh, Scotland
UK

A. de Frank Bruijn
Energy Research Centre of the Netherlands
Petten
The Netherlands
and
Energy and Sustainability Research Institute Groningen
University of Groningen
The Netherlands

Paul H. Brunner
Institute for Water Quality, Resource and Waste Management
Vienna University of Technology
Vienna
Austria

Ruth Brunstermann
Department of Urban Water and Waste Management
University of Duisburg-Essen
Essen
Germany

Eric C. Bruun
Department of Electrical & Systems Engineering
University of Pennsylvania
Philadelphia, PA
USA

Ian G. Bryden
Head of Institute for Energy Systems
School of Engineering
The University of Edinburgh
Edinburgh
UK

Daniel Büchner
German Biomass Research Centre (DBFZ)
Leipzig
Germany

Bela H. Buck
Biological Sciences – Marine Aquaculture
Alfred Wegener Institute for Polar and Marine Research (AWI)
Bremerhaven
Germany
and
Marine Aquaculture for Sustainable Fisheries
Institute for Marine Resources (IMARE)
Bremerhaven
Germany
and
Maritime Technologies – Applied Marine Biology
University for Applied Sciences
Bremerhaven
Germany

Stephan Buecheler
Laboratory for Thin Films and Photovoltaics
EMPA – Swiss Federal Laboratory for Materials Science and Technology
Duebendorf
Switzerland

Ralph Buehler
School of Public and International Affairs
College of Architecture and Urban Studies Virginia Tech
Alexandria, VA
USA

Alfons Buekens
Vrije Universiteit Brussel, VUB
Brussels
Belgium
and
Zhejiang University
Hangzhou
China

Kathryn R. Bullock
President, Coolohm, Inc.
Blue Bell, PA
USA

Kevin Bundy
Directorate of Environmental and Radiation Protection and Assessment
Canadian Nuclear Safety Commission
Ottawa, ON
Canada

Walter W. Burke
Paulus, Sokolowski and Sartor, LLC
Warren, NJ
USA

Andrew F. Burke
Institute of Transportation Studies
University of California-Davis
Davis, CA
USA

Julie Burtt
Directorate of Environmental and Radiation Protection and Assessment
Canadian Nuclear Safety Commission
Ottawa, ON
Canada

G. J. W. van Bussel
Aerospace Engineering Section Wind Energy
Delft University of Technology
Delft
The Netherlands

Jorge Cabrera Medaglia
Centre for International Sustainable Development Law, Lead Counsel on Biodiversity and Biosafety
Montreal, Canada
University of Costa Rica
San Rafael de Heredia
Costa Rica

Mary L. Cadenasso
Department of Plant Sciences
University of California
Davis, CA
USA

Katherine V. Calvin
Joint Global Change Research Institute (JGCRI)
Pacific Northwest National Laboratory (PNNL)
College Park, MD
USA

Keith H. S. Campbell
School of Biosciences
University of Nottingham
Sutton Bonington, Loughborough, Leicestershire
UK

Teresa Capell
Department of Vegetal Production and Forestry Science, ETSEA
University of Lleida
Lleida
Spain

J. J. Carrillo-Rivera
Instituto de Geografía
UNAM
CU México, DF
Mexico

Maria J. Carroquino
Instituto de Salud Carlos III
Madrid
Spain

David Carruthers
Cambridge Environmental Research Consultants
Cambridge
UK

Anny Cazenave
LEGOS
Laboratoire d'Etudes en Geophysique et
Oceanographie Spatiales
Toulouse
France

Pietro Cerri
VisLab – Dipartimento di Ingegneria
dell'Informazione
Università degli Studi di Parma
Parma
Italy

Robert Cervero
Department of City and Regional Planning
University of California
Berkeley, CA
USA

G. G. Tushara Chaminda
The University of Tokyo
Bunkyo-ku, Tokyo
Japan

C. C. Chan
Department of Electrical and Electronic Engineering
University of Hong Kong
Hong Kong
China

Jess Chandler
School of Public Policy
Georgia Institute of Technology
Atlanta, GA
USA

Michael Chang
Brook Byers Institute for Sustainable Systems
Department of Civil & Environmental Engineering
Georgia Institute of Technology
Atlanta, GA
USA

Y. Chao
Jet Propulsion Laboratory
Pasadena, CA
USA

Devamita Chattopadhyay
CH2M Hill
Dayton, OH
USA

Sandip Chattopadhyay
Tetra Tech Inc
Cincinnati, OH
USA

Manuela M. Chaves
Plant Molecular Ecophysiology Laboratory (LEM)
Instituto de Tecnologia Química e Biológica
Universidade Nova de Lisboa
Oeiras
Portugal
and
Instituto Superior de Agronomia
Universidade Técnica de Lisboa
Lisbon
Portugal

Zhewen Chen
Centre for International Governance Innovation
Waterloo, ON
Canada

Yongsheng Chen
Department of Civil & Environmental Engineering
Georgia Institute of Technology
Atlanta, GA
USA

Ming Cheng
School of Electrical Engineering
Southeast University
Nanjing
China

Peter Chesson
Department of Ecology and Evolutionary Biology
The University of Arizona
Tucson, AZ
USA

Mohit Chhabra
Electrical Engineering
University of Colorado
Boulder, CO
USA

Steve Chien
Jet Propulsion Laboratory
California Institute of Technology
Pasadena, CA
USA

Martyn P. Chipperfield
Institute for Climate and Atmospheric Science
School of Earth and Environment
University of Leeds
Leeds
UK

Jaeweon Cho
Gwangju Institute Science and Technology (GIST)
Department of Environmental Science and Engineering, Natural Organic Matter Lab
Gwangju
Korea

Daiwon Choi
Pacific Northwest National Laboratory
Richland, WA
USA

Thierry Chopin
Canadian Integrated Multi-Trophic Aquaculture Network (CIMTAN)
University of New Brunswick
Saint John, NB
Canada

Mei-In Melissa Chou
Illinois State Geological Survey-Prairie Research Institute and Department of Natural Resources and Environmental Sciences
University of Illinois at Urbana-Champaign
Champaign, IL
USA

Niels Christiansen
Topsoe Fuel Cell A/S
Lyngby
Denmark

Paul Christou
Department de Produccio Vegetal i Ciencia Forestal
Universitat de Lleida/ICREA
Lleida
Spain
and
Institució Catalana de Recerca i Estudis Avançats (ICREA)
Barcelona
Spain

Peter Chromec
Hitachi Zosen Inova U.S.A. LLC
Norcross, GA
USA

James H. Clark
Department of Chemistry
University of York
Heslington, York
UK

Leon E. Clarke
Joint Global Change Research Institute (JGCRI)
Pacific Northwest National Laboratory (PNNL)
College Park, MD
USA

Andrew Michael Clements
Green Roof Greece
Athens
Greece

Derek J. Clements-Croome
School of Construction Management and Engineering
University of Reading
Reading
UK

Philippe Clergeau
Department of Ecology and Biodiversity Management
National Museum of Natural History
Paris
France

SWP Cloete
Department of Animal Sciences
University of Stellenbosch
Matieland
South Africa
and
Institute for Animal Production
Elsenburg
South Africa

Philippe Cocquerez
Sous-direction Ballon
Centre National d'Études Spatiales
Toulouse
France

Suani Teixeira Coelho
CENBIO – The Brazilian Reference Center o Biomass
University of São Paulo
São Paulo
Brazil

Raymond J. Cole
School of Architecture & Landscape Architecture
University of BC
Vancouver, BC
Canada

Tracy K. Collier
National Oceanic and Atmospheric Administration
National Ocean Service
Oceans and Human Health Initiative
Silver Spring, MD
USA

Paolo Colombo
Department of Mechanical Engineering – Materials Division
University of Padova
Padova
Italy

James W. Comerford
Department of Chemistry
University of York
Heslington, York
UK

Udo Conrad
Leibniz Institute of Plant Genetics and Crop Plant Research (IPK), Phytoantibodies
Gatersleben
Germany

Andrea E. Copping
Marine Sciences Laboratory
Pacific Northwest National Laboratory
Seattle, WA
USA

Barry A. Costa-Pierce
Graduate School of Oceanography, Rhode Island Sea Grant College Program
University of Rhode Island, URI Bay Campus
Narragansett, RI
USA

Gordon M. Cragg
Natural Products Branch Developmental Therapeutics Program
National Cancer Institute, NCI-Frederick
Frederick, MD
USA

Wendy Craig
Biosafety Unit
International Centre for Genetic Engineering and Biotechnology (ICGEB)
Trieste
Italy

Alan T. Critchley
Acadian Seaplants Limited
Dartmouth, NS
Canada

John C. Crittenden
Georgia Institute of Technology
Atlanta, GA
USA

Stephen F. Cross
Coastal Aquaculture Research & Training (CART) Network, Department of Geography
University of Victoria
Victoria, BC
Canada
and
SEA–Vision Group of Companies
Courtenay, BC
Canada

Andrew Cross
UK Biochar Research Centre (UKBRC), School of GeoSciences
Science and Engineering at The University of Edinburgh
Edinburgh, Scotland
UK

Edward Cussler
Department of Chemical Engineering
University of Minnesota
Minneapolis, MN
USA

Jaak J. K. Daemen
Department of Mining Engineering
University of Nevada
Reno, NV
USA

Lisa Dahlén
Civil, Mining and Environmental Engineering
Waste Science and Technology
Luleå University of Technology
Luleå
Sweden

Gretchen C. Daily
The Natural Capital Project
Department of Biology and Woods Institute
Stanford University
Stanford, CA
USA
and
Department of Biological Sciences
Stanford University
Stanford, CA
USA

Göran Dalén
WPD Scandinavia AB
Stockholm
Sweden

Gordon Danby
Maglev-2000 Corporation
Wading River, NY
USA

A. Y. Dandekar
Institute of Northern Engineering
University of Alaska Fairbanks
Fairbanks, AK
USA

Svetlana Dashevskaya
Department of Vegetal Production and Forestry Science
ETSEA University of Lleida
Lleida
Spain

Philip A. Davis
AECL
Chalk River, ON
Canada

Ali Davoudi
University of Texas
Arlington, TX
USA

Sylvie De Buck
Department of Plant Biotechnology and Genetics
Ghent University
Ghent
Belgium

Annelies De Paepe
Department of Plant Systems Biology
Flanders Institute for Biotechnology VIB
Ghent
Belgium

Russell De Young
NASA Langley Research Center
Hampton, VA
USA

Joseph F. DeCarolis
Civil, Construction and Environmental Engineering
North Carolina State University
Raleigh, NC
USA

M. R. Deinert
Department of Mechanical Engineering
The University of Texas at Austin
Austin, TX
USA

Xavier Delannay
Integrated Breeding Platform
Consultative Group on International Agricultural Research, Generation Challenge Programme, c/o CIMMYT
Texcoco
Edo. Mexico

Paul Denholm
Energy Forecasting and Modeling Group
National Renewable Energy Laboratory
Golden, CO
USA

Ann Depicker
UGent Vakgroep Plantenbiotechnologie en Genetica, VIB Plant Systems Biology Department
Ghent University
Ghent
Belgium

Dimitris Dermatas
Department of Water Resources and Environmental Engineering, School of Civil Engineering
National Technical University of Athens
Zografou
Greece

Reginald Desroches
Department of Civil & Environmental Engineering
Georgia Institute of Technology
Atlanta, GA
USA

Shivakumar P. Devaiah
Arkansas Biosciences Institute
Arkansas State University
Jonesboro, AR
USA

Yann Devos
GMO Unit
European Food Safety Authority (EFSA)
Parma
Italy

Silvana Di Sabatino
Dipartimento di Scienza dei Materiali
Università del Salento
Lecce
Italy

Heidi M. Dierssen
Department of Marine Sciences
University of Connecticut
Groton, CT
USA

Klaus C. J. Dietmayer
Institute of Measurement, Control, and Microtechnology
University of Ulm
Ulm
Germany

Deepak Divan
School of Electrical and Computer Engineering
Georgia Institute of Technology
Atlanta, GA
USA

Marca M. Doeff
Environmental Energy Technologies Division, Lawrence Berkeley National Laboratory
University of California
Berkeley, CA
USA

A. Doerenbecher
Centre National de Recherches Météorologiques
Météo-France/CNRS
Toulouse
France

Thomas J. Dolan
Department of Nuclear, Plasma, and Radiological Engineering
University of Illinois
Urbana, IL
USA

José L. Domingo
Laboratory of Toxicology and Environmental Health
School of Medicine, IISPV
Universitat Rovira i Virgili
Reus, Catalonia
Spain

F. Xavier Donadeu
The Roslin Institute and Royal (Dick) School of Veterinary Studies
University of Edinburgh
Scotland
UK

Yanchao Dong
Graduate School of Science and Technology
Kumamoto University
Kumamoto
Japan

Moustapha Doumiati
B2i Automotive Engineering Company
Massy
France

M. Fernanda Dreccer
CSIRO Plant Industry Cooper Laboratory
Gatton, QLD
Australia

Jeremy D. Driskell
Department of Infectious Diseases, College of Veterinary Medicine, Animal Health Research Center
University of Georgia
Athens, GA
USA

Philippe Drobinski
Institut Pierre Simon Laplace/Laboratoire de Météorologie Dynamique
École Polytechnique/UPMC/ENS/CNRS
Palaiseau
France

Anita Drumond
Environmental Physics Laboratory (EPhysLab)
Universidade de Vigo
Ourense
Spain

Sébastien Dubois
INES-CEA
Le Bourget du Lac
France

Ana María Durán-Quesada
Environmental Physics Laboratory (EPhysLab)
Universidade de Vigo
Ourense
Spain

Thomas Dyer
Division of Civil Engineering
University of Dundee
Dundee
UK

James A. Edmonds
Joint Global Change Research Institute (JGCRI)
Pacific Northwest National Laboratory (PNNL)
College Park, MD
USA

Martin G. Edwards
School of Biology
Newcastle Institute for Research on Sustainability
Newcastle University
Newcastle upon Tyne
UK

Fred van Eeuwijk
Biometris
Wageningen University and Research Centre
Wageningen
The Netherlands

Mehrdad Ehsani
Department of Electrical & Computer Engineering
Texas A&M University
College Station, TX
USA

Yoav Eitan
Department of Genetics
The Silberman Life Sciences Institute
The Hebrew University of Jerusalem
Jerusalem
Israel

Okechukwu Ekenna
Singing River Health System
Pascagoula, MS
USA
and
University of South Alabama
Mobile, AL
USA

Erik Ela
Transmission and Grid Integration Group
National Renewable Energy Laboratory
Golden, CO
USA

Amgad Elgowainy
Center for Transportation Research
Argonne National Laboratory
Argonne, IL
USA

John F. Elter
Sustainable Systems, LLC
Latham, New York
USA

Michaela Ernst
IBG-2: Plant Science
Forschungszentrum Jülich
Jülich
Germany

Greg J. Evans
Department of Chemical Engineering and Applied Chemistry
University of Toronto
Toronto, ON
Canada

Jess W. Everett
Civil and Environmental Engineering
Rowan University
Glassboro, NJ
USA

André Faaij
Copernicus Institute
Department of Science, Technology and Society
Utrecht University
Utrecht
The Netherlands

Babak Fahimi
University of Texas
Arlington, TX
USA

Xing Fang
Department of Civil Engineering
Auburn University
Auburn, AL
USA

Gemma Farre
Department of Vegetal Production and Forestry Science, ETSEA
University of Lleida
Lleida
Spain

José I. Farrán
Adavant Consulting
San Francisco, CA
USA

Brian D. Fath
Biology Department
Towson University
Towson, MD
USA
and
Advanced Systems Analysis Program
International Institute for Applied Systems Analysis
Laxenburg
Austria

Richard E. Faw
Department of Mechanical & Nuclear Engineering
Kansas State University
Winston Salem, NC
USA

Audeen W. Fentiman
School of Nuclear Engineering
Purdue University
West Lafayette, IN
USA

Alan Fenwick
Department of Infectious Disease Epidemiology
Schistosomiasis Control Initiative
Imperial College London
London
UK

Elías Fereres
Institute for Sustainable Agriculture
IAS-CSIC and University of Cordoba
Cordoba
Spain

P. Fernández-Ibáñez
Plataforma Solar de Almería (CIEMAT)
Tabernas, Almería
Spain

Joao G. Ferreira
Departamento de Ciências e Engenharia do Ambiente
Faculdade de Ciências e Tecnologia Universidade Nova de Lisboa
Monte Caparica
Portugal

Natalie Ferry
School of Biology
Newcastle Institute for Research on Sustainability, Newcastle University
Newcastle upon Tyne
UK
and
School of Environment and Life Sciences
University of Salford
Salford
UK

Sergey V. Fesenko
Department of Nuclear Sciences and Applications
IAEA Environment Laboratories
International Atomic Energy Agency
Vienna
Austria

Marc Fibla
Department of Vegetal Production and Forestry Science, ETSEA
University of Lleida
Lleida
Spain

Sebastian Fiechter
Helmholtz-Zentrum Berlin für Materialien und Energie GmbH (HZB)
Institut für Solare Brennstoffe und Energiespeichermaterialien
Berlin
Germany

Mervin Fingas
Spill Science
Edmonton, AB
Canada

John T. Finger
Sandia National Laboratories, retired
Albuquerque, NM
USA

Sari Fink
Exeter Associates
Columbia, Maryland
USA

R. A. (Tony) Fischer
CSIRO Plant Industry
Canberra City
Australia

Doreen M. Floss
Institute of Biochemistry and Molecular Biology II
Heinrich-Heine-University Düsseldorf
Düsseldorf
Germany

Byron Flynn
GE Energy, Digital Energy
Norcross, GA
USA

Joseph J. Fontaine
U.S. Geological Survey, Nebraska Cooperative Fish and Wildlife Research Unit
School of Natural Resources
University of Nebraska
Lincoln, NE
USA

Christy M. Foran
Engineer Research and Development Center-Environmental Lab
Concord, MA
USA

Cinzia Formighieri
Dipartimento di Biotecnologie
Università di Verona
Verona
Italy

Cecil W. Forsberg
Department of Molecular and Cellular Biology
University of Guelph
Guelph, ON
Canada

Marie-Josée Fortin
Department of Ecology and Evolutionary Biology
University of Toronto
Toronto, ON
Canada

Stefan Fortuin
Division Solar Thermal and Optics
Fraunhofer-Institut für Solare Energiesysteme ISE
Freiburg
Germany

Jennifer Fosket
Social Green
Berkeley, CA
USA

M. J. Foulkes
Division of Plant and Crop Sciences
School of Biosciences
University of Nottingham
Loughborough
UK

Matthew J. Franchetti
Department of Mechanical, Industrial, and Manufacturing Engineering
University of Toledo
Toledo, OH
USA

Steve French
Center for Geographic Information Systems and the School of City and Regional Planning
Georgia Institute of Technology
Atlanta, GA
USA

Michael French
Department of Infectious Disease Epidemiology
Schistosomiasis Control Initiative
Imperial College London
London
UK

Christian Frese
Institute for Anthropomatics, Vision and Fusion Laboratory
Karlsruhe Institute of Technology
Karlsruhe
Germany

Anton Friedl
Vienna University of Technology
Vienna
Austria

S. Julio Friedmann
Lawrence Livermore National Laboratory
Livermore, CA
USA

Claus Fröhlich
PMOD/WRC
Davos
Switzerland

Ole Fryd
Forest and Landscape Denmark
University of Copenhagen
Frederiksberg C
Denmark

Vasilis Fthenakis
National Photovoltaic Environmental Research Center, Brookhaven National Laboratory
Upton, NY
USA
and
Center of Life Cycle Analysis
Columbia University
New York, NY
USA

Clement E. Furlong
Departments of Medicine-Division of Medical Genetics and Genome Sciences
University of Washington
Seattle, WA
USA

Hiroaki Furumai
Department of Urban Engineering
The University of Tokyo
Bunkyo-ku, Tokyo
Japan

Albis Francesco Gabrielli
Department of Control of Neglected Tropical Diseases
World Health Organization
Geneva
Switzerland

Mats Galbe
Department of Chemical Engineering
Lund University
Lund
Sweden

Dan C. Galeriu
Life and Environmental Physics Department
"Horia Hulubei" Institute for Physics and Nuclear Engineering
Bucharest-Magurele
Romania

Cesare Galli
Avantea, Laboratorio di Tecnologie della Riproduzione
Cremona
Italy
and
Clinical Veterinary Department
University of Bologna
Italy

Simanga Gama
Canadian Centre for Environmental Modelling and Chemistry
Trent University
Peterborough, ON
Canada

Yimin Gao
Department of Electrical and Computer Engineering
Texas A&M University
College Station, TX
USA

Margarita García-Vila
Institute for Sustainable Agriculture
IAS-CSIC and University of Cordoba
Cordoba
Spain

Vijay K. Garg
Dublin, OH
USA

Ahjond S. Garmestani
U.S. Environmental Protection Agency
National Risk Management Research Laboratory
Cincinnati, OH
USA

Hubert A. Gasteiger
Department of Chemistry
Technische Universität München
Munich
Germany

John A. Gatehouse
School of Biological and Biomedical Sciences
Durham University
Durham
UK

Angharad M. R. Gatehouse
School of Biology
Newcastle Institute for Research on Sustainability
Newcastle University
Newcastle upon Tyne
UK

Marek Gawor
German Biomass Research Centre (DBFZ)
Leipzig
Germany

Dusty Gedge
Livingroofs.org Ltd
London
UK

Peter R. Gent
Oceanography Section
National Center for Atmospheric Research
Boulder, CO
USA

Sergio D. German
School of Biosciences
University of Nottingham
Sutton Bonington, Loughborough, Leicestershire
UK

Joseph Germano
Germano & Associates, Inc.
Bellevue, WA
USA

Claudio M. Ghersa
IFEVA-CONICET, Depto. de Recursos Naturales y Ambiente
Universidad de Buenos Aires (UBA)
Buenos Aires
Argentina

Stefano Ghidoni
Intelligent Autonomous System Laboratory (IAS-Lab), Department of Information Engineering
University of Padua
Padova
Italy

Luis Gimeno
Environmental Physics Laboratory (EPhysLab)
Universidade de Vigo
Ourense
Spain

Moshe Givoni
Transport Studies Unit, School of Geography and the Environment
University of Oxford
Oxford
UK

Mickey Gjerris
Danish Centre for Bioethics and Risk Assessment
Institute of Food and Resource Economics
University of Copenhagen
Frederiksberg
Denmark

William E. Glassley
Energy Institute
University of California
Davis, CA
USA
and
Geologisk Institut
University of Aarhus
Aarhus
Denmark

S. M. Glenn
Coastal Ocean Observation Lab, Institute of Marine and Coastal Sciences, School of Environmental and Biological Sciences
Rutgers University
New Brunswick, NJ
USA

Lisa Goddard
Forecasting and Prediction Group
International Research Institute for Climate Society (IRI), The Earth Institute of Columbia University
Palisades, NY
USA

José Goldemberg
CENBIO – The Brazilian Reference Center o Biomass
University of São Paulo
São Paulo
Brazil

Barry Goldstein
Pirsa Petroleum Group
Adelaide, SA
Australia

Serguei P. Golovan
Department of Animal and Food Science
University of Delaware
Newark, DE
USA

Sonia Gomez-Galera
Department of Vegetal Production and Forestry Science, ETSEA
University of Lleida
Lleida
Spain

J. B. Goodenough
Texas Materials Institute, Mechanical Engineering
University of Texas
Austin, TX
USA

Michael Evan Goodsite
Department of Atmospheric Environment
National Environmental Research Institute
Aarhus University
Roskilde
Denmark

Regiane Gorren
CENBIO – The Brazilian Reference Center o Biomass
University of São Paulo
São Paulo
Brazil

Jim Gover
Department of Electrical Engineering
Kettering University
Flint, MI
USA

Eric Daniel Głowacki
Linz Institute for Organic Solar Cells (LIOS)
Johannes Kepler University
Linz
Austria

Gordon L. Graff
Pacific Northwest National Laboratory
Richland, WA
USA

Jon Grant
Department of Oceanography
Dalhousie University
Halifax, NS
Canada

Hartmut Grassl
Max Planck Institute for Meteorology
Hamburg
Germany

Michael Grätzel
Laboratory of Photonics and Interfaces, Institute of Chemical Science and Engineering
Ecole Polytechnique Fédérale de Lausanne (EPFL)
Lausanne
Switzerland

Steve G. Greenbaum
Department of Physics and Astronomy
Hunter College of CUNY
New York, NY
USA

Ruediger Greinert
Centre of Dermatology
Elbe Kliniken Buxtehude
Buxtehude
Germany

Jonathan Gressel
Plant Sciences Department
Weizmann Institute of Science
Rehovot
Israel

Darrell Jay Grimes
Department of Coastal Sciences
The University of Southern Mississippi
Ocean Springs, MS
USA

Paolo Grisleri
VisLab – Dipartimento di Ingegneria dell'Informazione
Università degli Studi di Parma
Parma
Italy

Renata Grisoli
CENBIO – The Brazilian Reference Center o Biomass
University of São Paulo
São Paulo
Brazil

Julian Gröbner
European Ultraviolet Calibration Center
Physikalisch-Meteorologisches Observatorium
Davos, World Radiation Center
Davos Dorf
Switzerland

Paul G. Grothaus
Natural Products Branch Developmental Therapeutics Program
National Cancer Institute, NCI-Frederick
Frederick, MD
USA

Patricia Guardabassi
CENBIO – The Brazilian Reference Center o Biomass
University of São Paulo
São Paulo
Brazil

Anne Guerry
The Natural Capital Project
Department of Biology and Woods Institute
Stanford University
Stanford, CA
USA

Christian A. Gueymard
Solar Consulting Services
Colebrook, NH
USA

Jean-François Guillemoles
Institut de Recherche et Developpement sur l'Energie Photovoltaique
Chatou
France

S. Can Gülen
GE Infrastructure-Energy
Schenectady, NY
USA

Frances M. Gulland
The Marine Mammal Center
Sausalito, CA
USA

John S. Gulliver
Department of Civil Engineering
University of Minnesota
Minneapolis, MN
USA

Luis Gutierrez-Negrin
Mexican Geothermal Association
Mexico

Jens Gutzmer
TU Bergakademie Freiberg, Institute of Mineralogy and Helmholtz Institute Freiberg for Resource Technology
Freiberg, Saxony
Germany

Dagmar Haase
Department of Geography
Humboldt University Berlin
Berlin
Germany
and
Department of Computational Landscape Ecology
Helmholtz Center for Environmental Research – UFZ
Leipzig
Germany

Andreas Häberle
PSE AG
Freiburg
Germany

Paul W. Hadley
Department of Toxic Substances Control
California EPA
Sacramento, CA
USA

Lars Håkanson
Department of Earth Sciences
Uppsala University
Uppsala
Sweden

Suvi T. Häkkinen
VTT Technical Research Centre of Finland
Espoo
Finland

Anthony E. Hall
Department of Botany and Plant Sciences
University of California Riverside
Quincy, CA
USA

Eric M. Hallerman
Department of Fisheries and Wildlife Sciences
Virginia Polytechnic Institute and State University
Blacksburg, VA
USA

Mark T. Hamann
Department of Pharmacognosy
The University of Mississippi
University, MS
USA
and
Department of Chemistry and Biochemistry
The University of Mississippi
University, MS
USA
and
Department of Pharmacology
The University of Mississippi
University, MS
USA
and
Institute of Marine and Environmental Technology
University of Maryland Center for Environmental Science
Baltimore, MD
USA

Annette Hammer
Energy Meteorology Group, Energy and Semiconductor Research Laboratory
Institute of Physics
University of Oldenburg
Oldenburg
Germany

Jim Hammond
UK Biochar Research Centre (UKBRC)
School of GeoSciences
Science and Engineering at The University of Edinburgh
Edinburgh, Scotland
UK

Nigel Hampton
National Electric Energy Test Research and Application Centre (NEETRAC)
Forrest Park, GA
USA

Steven J. Hamrock
Fuel Cell Components Program
3M Company
St Paul, MN
USA

Buxing Han
Institute of Chemistry
Chinese Academy of Sciences
Beijing
China

Martin O. L. Hansen
DTU Mechanical Engineering
Technical University of Denmark
Lyngby
Denmark

Katja Hansen
EPEA Internationale Umweltforschung GmbH
Hamburg
Germany
and
Academic Chair Cradle to Cradle for Innovation and Quality, Rotterdam School of Management, Erasmus University
Rotterdam
The Netherlands

John Bøgild Hansen
Haldor Topsøe A/S
Lyngby
Denmark

Paul Hardisty
WorleyParsons
Perth, WA
Australia

Roy M. Harrison
Division of Environmental Health and Risk Management
School of Geography, Earth and Environmental Sciences
The University of Birmingham
Edgbaston, Birmingham
UK

Volker Hartkopf
Center for Building Performance and Diagnostics
Carnegie Mellon University
Pittsburgh
USA

Gregory Hartman
Hartman Associates Inc, Waterway Engineering & Sediment Remediation
Port Orchard, WA
USA

Hans Hartmann
Technologie- und Förderzentrum im Kompetenzzentrum für Nachwachsende Rohstoffe (TFZ)
Straubing, Bavaria
Germany

Shuichi Hasegawa
Department of Systems Innovation
School of Engineering
The University of Tokyo
Tokyo
Japan

Floyd Hasselriis
Hasselriis Associates
Forest Hills, NY
USA

Robert Hastings
AEU Ltd. Architecture, Energy & Enviornment
Wallisellen
Switzerland

Stuart Haszeldine
UK Biochar Research Centre (UKBRC), School of GeoSciences
Science and Engineering at The University of Edinburgh
Edinburgh, Scotland
UK

Hideki Hatanaka
West Japan Engineering Consultants, Inc
Chuou-ku, Fukuoka
Japan

Louise A. Heathwaite
Centre for Sustainable Water Management
Lancaster Environment Centre
Lancaster University
Lancaster
UK

Jörgen Held
Swedish Gas Centre
Malmö
Sweden

Cliff Henke
Parsons Brinckerhoff
Newark, NJ
USA

Hans-Martin Henning
Department of Thermal Systems and Buildings
Fraunhofer Institute for Solar Energy Systems ISE
Freiburg
Germany

Patrik J. G. Henriksson
Institute of Environmental Sciences
Leiden University
Leiden
The Netherlands

and
Department of System Ecology
Stockholm University
Stockholm
Sweden

J. Stephen Herring
Idaho National Laboratory
Idaho Falls, ID
USA

Andrew M. Herring
Department of Chemical Engineering
Colorado School of Mines
Golden, CO
USA

Dirk Hertel
Quincy, MA
USA

Ole Hertel
Department of Atmospheric Environment
National Environmental Research Institute, Aarhus University
Roskilde
Denmark

J. Patrick A. Hettiaratchi
Department of Civil Engineering and CEERE
University of Calgary
Calgary, AB
Canada

Dario Hidalgo
EMBARQ, The World Resources Institute Center for Sustainable Transport
Washington, DC
USA

Gerardo Hiriart
Energías Alternas
Estudios y Proyectos
Mexico

Katsumi Hirose
Faculty of Science and Technology
Sophia University
Chiyodaku, Tokyo
Japan

April Hiscox
Department of Geography
The University of South Carolina
Columbia, SC
USA

Terrence Hock
Atmospheric Technology Division
National Center for Atmospheric Research
Boulder, CO
USA

Bri-Mathias Hodge
Transmission and Grid Integration Group
National Renewable Energy Laboratory
Golden, CO
USA

Hermann Hofbauer
Institute of Chemical Engineering
Vienna University of Technology
Vienna
Austria

Bernhard Hoffschmidt
Solar-Institut Jülich (SIJ), FH Aachen
Aachen University of Applied Sciences
Jülich
Germany

Eileen E. Hofmann
Center for Coastal Physical Oceanography
Old Dominion University
Norfolk, VA
USA

Hannele Holttinen
Technical Research Centre of Finland VTT
VTT
Finland

Mark Holtzapple
Department of Chemical Engineering
Texas A&M University
College Station, TX
USA

Rick Q. Honaker
Department of Mining Engineering
Mining & Mineral Resources Engineering
University of Kentucky
Lexington, KY
USA

Seungkwan Hong
Department of Civil, Environmental & Architectural Engineering
Korea University
Sungbuk-gu, Seoul
Republic of Korea

Elizabeth E. Hood
College of Agriculture and Technology
Arkansas State University, AR Biosciences Institute
Jonesboro, AR
USA

Mikael Höök
Global Energy Systems
Uppsala University
Uppsala
Sweden

Teruhisa Horita
National Institute of Advanced Industrial Science and Technology (AIST)
Tsukuba, Ibaraki
Japan

Andreas Hornung
European Bioenergy Research Insitute – EBRI
Aston University
Aston Triangle, Birmingham
UK

Colin P. Horwitz
GreenOx Catalysts, Inc
Pittsburgh, PA
USA

Louis-Marie Houdebine
Biologie du Développement et Reproduction
Institut National de le Recherche Agronomique
Jouy en Josas
France

Martin Hovland
Centre for Geobiology
University of Bergen
Bergen
Norway
and
Statoil ASA
Stavanger
Norway

Brenda J. Howard
Centre for Ecology and Hydrology
Lancaster Environment Centre
Bailrigg, Lancaster
UK

John Howard
Applied Biotechnology Institute
San Luis Obispo, CA
USA

Jiang Yong Hu
Division of Environmental Science and Engineering
National University of Singapore
Singapore

Zhencheng Hu
Graduate School of Science and Technology
Computer Science Department
Kumamoto University
Kumamoto
Japan

Lili Huang
Department of Electrical Engineering
University of California, Riverside
Riverside, CA
USA

Elisabeth-Maria Huba
Technologies for Economic Development
Maseru
Lesotho

Reinhard Huber
Laboratory Animal Science Group
IBMC – Instituto de Biologia Molecular e Celular
Universidade do Porto
Porto
Portugal

Ernst Huenges
GFZ-Potsdam
Germany

Yu-Jeong Huh
Yeongsan River Environment Research Center
Buk-gu, Gwangju
South Korea

Julian Hunt
University College London
London
UK

Trevor M. Hunt
GNS Science
Wairakei Geothermal Research Centre
Taupo
New Zealand

Kevin Hydes
Integral Group
Oakland, CA
USA

Kent M. Hymel
US Department of Transportation
Volpe National Transportation Systems Center
Cambridge, MA
USA

Rodrigo Ibarrola
UK Biochar Research Centre (UKBRC), School of GeoSciences
Science and Engineering at The University of Edinburgh
Edinburgh, Scotland
UK

Maria Debora Iglesias-Rodriguez
School of Ocean and Earth Science, National Oceanography Centre
University of Southampton
Southampton
UK

A. Irwin
Mount Allison University
Sackville, NB
Canada

Timothy J. Jacobs
Department of Mechanical Engineering
Texas A&M University
College Station, TX
USA

Arnulf Jäger-Waldau
European Commission, DG Joint Research Centre
Institute for Energy and Transport
Renewable Energy Unit
Ispra (VA)
Italy

Bernd Jähne
Institute for Environmental Physics and Heidelberg Collaboratory for Image Processing (HCI)
University of Heidelberg
Heidelberg
Germany

Patrick M. A. James
Department of Biological Sciences
University of Alberta
Edmonton, AB
Canada

Jean-Ann James
Brook Byers Institute for Sustainable Systems and the
Department of Civil & Environmental Engineering
Georgia Institute of Technology
Atlanta, GA
USA

Anthony C. Janetos
Joint Global Change Research Institute (JGCRI)
Pacific Northwest National Laboratory (PNNL)
College Park, MD
USA

Gaby J. M. Janssen
Energy Research Centre of the Netherlands
Petten
The Netherlands

Hofierka Jaroslav
Department of Geography and Regional
Development
University of Presov
Presov
Slovakia

Marina Bergen Jensen
Forest and Landscape Denmark
University of Copenhagen
Frederiksberg C
Denmark

Hyunju Jeong
Brook Byers Institute for Sustainable Systems and the
Department of Civil & Environmental Engineering
Georgia Institute of Technology
Atlanta, GA
USA

Robert Davis Jewett
Department of Environmental Sciences
Louisiana State University
Baton Rouge, LA
USA

Kenneth C. Jezek
Byrd Polar Research Center, School of Earth Sciences
The Ohio State University
Columbus, OH
USA

Zhen-Gang Ji
Minerals Management Service
Herndon, VA
USA

M. A. H. Johir
University of Technology
Sydney, NSW
Australia

Dean P. Jones
Division of Pulmonary, Allergy and Critical Care
Medicine, Department of Medicine
Emory University School of Medicine
Atlanta, GA
USA

Ho Gi Jung
The School of Mechanical Engineering
Hanyang University
Seondong-gu, Seoul
South Korea

Niels Jungbluth
ESU-services
Uster
Switzerland

Martin Kaltschmitt
German Biomass Research Centre
Leipzig
Germany
and

Institute of Environmental Technology and Energy Economics
Hamburg University of Technology
Hamburg
Germany

Bettina Kamuk
Ramboll Energy – Waste-to-Energy
København S
Denmark

J. Kandasamy
University of Technology
Sydney, NSW
Australia

Phyllis J. Kanki
Department of Immunology and Infectious Diseases
Harvard School of Public Health
Boston, MA
USA

Sridhar V. Kanuri
UTC Power
South Windsor, CT
USA

P. Ozge Kaplan
National Risk Management Research Laboratory,
Office of Research and Development
U.S. Environmental Protection Agency
Research Triangle Park, NC
USA

Salit Kark
The Biodiversity Research Group, Department of
Ecology, Evolution, and Behavior
The Hebrew University of Jerusalem
Jerusalem
Israel
and
ARC Centre for Environmental Decisions (CEED)
School of Biological Sciences
The University of Queensland
St Lucia, QLD
Australia

Asadullah Kazi
Isra University
Hyderabad
Pakistan

Craig Kedrowski
Hitachi Zosen Inova U.S.A. LLC
Norcross, GA
USA

Christopher Kellner
Water and Sanitation Association of Zambia
Lusaka
Zambia

Christopher J. Kennedy
Department of Biological Sciences
Simon Fraser University
Burnaby, BC
Canada

Herman van Keulen
Chairgroup Plant Production Systems
Wageningen University
Wageningen
The Netherlands
and
Business Unit Agrosystems Research, Plant Research
International
Wageningen University and Research Centre
AK Wageningen
The Netherlands

Young Soo Keum
Division of Applied Life Sciences
Konkuk University, College of Life and
Environmental Science
Seoul
South Korea

Mladen Kezunovic
Department of Electrical and Computer Engineering
Texas A&M University
College Station, TX
USA

Saifullah Khan
Plant Biotechnology Section
International Center for Chemical and Biological Sciences, HEJ research Institute
University of Karachi
Karachi
Pakistan

S. Khataniar
Institute of Northern Engineering
University of Alaska Fairbanks
Fairbanks, AK
USA

Manfred Köhler
University of Applied Sciences
Neubrandenburg
Germany

J. A. Kilner
Department of Materials
Imperial College London
London
UK

In S. Kim
Center for Seawater Desalination Plant
Gwangju Institute of Science and Technology (GIST)
Buk-gu, Gwangju
Republic of Korea

Taek K. Kim
Nuclear Engineering Division
Argonne National Laboratory
Argonne, IL
USA

Reeho Kim
Department of Water Resources and Environmental Research
Korea Institute of Construction Technology
Goyang-Si, Gyeonggi-Do
Republic of Korea

Son H. Kim
Joint Global Change Research Institute (JGCRI)
Pacific Northwest National Laboratory (PNNL)
College Park, MD
USA

Yunah Kim
Department of Environmental Science and Engineering
Gwangju Institute of Science and Technology (GIST)
Buk-gu, Gwangju
South Korea

Jeong-Han Kim
Department of Agricultural Biotechnology
Seoul National University
Seoul
South Korea

Kap-Soon Kim
Yeongsan River Environment Research Center
Buk-gu, Gwangju
South Korea

Insu Kim
School of Electrical and Computer Engineering
Georgia Institute of Technology
Atlanta, GA
USA

Joon Ha Kim
School of Environmental Science & Engineering
Gwangju Institute of Science & Technology (GIST)
Gwangju
South Korea
and
Sustainable Water Resource Technology Center (SWRTC)
Gwangju
South Korea

Alexander Kind
Chair of Livestock Biotechnology
Technical University of Munich
Freising
Germany

Brendan Kirby
National Renewable Energy Laboratory
Golden, CO
USA

Claudia Kirsten
Deutsches BiomasseForschungsZentrum GmbH
German Biomass Research Centre (DBFZ)
Leipzig
Germany

Jamie P. Kizewski
Department of Chemistry
University of Surrey
Guildford
UK

Jean-Paul Kleider
LGEP
Paris
France

Marco Klemm
German Biomass Research Centre (DBFZ)
Leipzig
Germany

Katrin Klingenberg
Passive House Institute US
Urbana, IL
USA

Pieter W. Knap
PIC International Group
Schleswig
Germany

Ronald Allen Knief
Sandia National Laboratories
Albuquerque, NM
USA

Andrew Knox
Department of Chemical Engineering and Applied Chemistry
University of Toronto
Toronto, ON
Canada

Reto Knutti
Institute for Atmospheric and Climate Science
ETH
Zürich
Switzerland

Marc Koch
Vattenfall Europe Wärme AG
Berlin
Germany

Shyam S. Kocha
Hydrogen Technologies and Systems Center
National Renewable Energy Laboratory
Golden, CO
USA
and
Fuel Cell Laboratory
Nissan Technical Center North America
Farmington Hills, MI
USA

Cecil C. Konijnendijk
Danish Centre for Forest, Landscape and Planning
University of Copenhagen
Frederiksberg C
Denmark

Marc T. M. Koper
Leiden Institute of Chemistry
Leiden University
Leiden
The Netherlands

Ralf Koralewska
Martin GmbH für Umwelt- und Energietechnik
Munich
Germany

Helmut Köster
Köster Lichtplanung
Frankfurt am Main
Germany

Haris N. Koutsopoulos
Department of Transport Sciences
The Royal Institute of Technology, KTH
Stockholm
Sweden

Jed Kraiem
Apollon Solar
Lyon
France

Ulrike I. Kramm
Brandenburg University of Technology
Applied Physics and Sensors
Cottbus
Germany

Lukas Kranz
Laboratory for Thin Films and Photovoltaics
EMPA – Swiss Federal Laboratory for Materials
Science and Technology
Duebendorf
Switzerland

Gesche Krause
Leibniz Center for Tropical Marine Ecology (ZMT)
Bremen
Germany

Ben Kravitz
Department of Global Ecology
Carnegie Institution for Science
Stanford, CA
USA

Frank Kreikebaum
Georgia Institute of Technology
Atlanta, GA
USA

Klaus-Dieter Kreuer
Max-Planck-Institut für Festkörperforschung
Stuttgart
Germany

Wm. David Kulp, III
Mechanical Engineering
Georgia Institute of Technology
Atlanta, GA
USA

Pawan L. Kulwal
State Level Biotechnology Centre
Mahatma Phule Agricultural University
Rahuri, Maharashtra
India

Julia Kunze
Institute for Advanced Study (IAS)
Garching
Germany
and
Department of Physics
Technische Universität München
Garching
Germany

B. Kus
University of Technology
Sydney, NSW
Australia

Rena Kuwahata
Energynautics GmbH
Langen
Germany

Tanguy Lafarge
CIRAD, UMR AGAP
Montpellier
France
and
IRRI, CESD
Los Baños
Philippines

Anders Lagerkvist
Civil, Mining and Environmental Engineering
Waste Science and Technology
Luleå University of Technology
Luleå
Sweden

Götz Laible
AgResearch, Ruakura Research Centre
Hamilton
New Zealand

Doerte Laing
Institute of Technical Thermodynamics
German Aerospace Center
Stuttgart
Germany

Rattan Lal
OARDC/FAES Kottman Hall
Carbon Management and Sequestration Center
The Ohio State University
Columbus, OH
USA

Khee Poh Lam
Center for Building Performance and Diagnostics
School of Architecture
Carnegie Mellon University
Pittsburgh, PA
USA

Carl W. Lam
Department of Chemical Engineering and Materials Science
University of California
Davis, CA
USA

James W. LaMoreaux
P.E. LaMoreaux & Associates
Tuscaloosa, AL
USA

Judith Lancaster
Division of Earth and Ecosystem Sciences
Desert Research Institute
Reno, NV
USA

Felix W. Landerer
Jet Propulsion Laboratory
California Institute of Technology
Pasadena, CA
USA

P. J. Landrigan
Department of Preventive Medicine
Mount Sinai School of Medicine
New York, NY
USA

Thomas Landry
Fisheries and Oceans Canada
Gulf Fisheries Centre
Moncton, NB
Canada

Rachel Lane
Directorate of Environmental and Radiation Protection and Assessment
Canadian Nuclear Safety Commission
Ottawa, ON
Canada

Richard Langan
Atlantic Mariner Aquaculture Center
University of New Hampshire
Durham, NH
USA

Jesper Lassen
Danish Centre for Bioethics and Risk Assessment,
Institute of Food and Resource Economics
University of Copenhagen
Frederiksberg
Denmark

Caroline Lassnig
Institute of Animal Breeding and Genetics & Biomodels Austria
University of Veterinary Medicine Vienna
Vienna
Austria

William K. M. Lau
Laboratory for Atmospheres
NASA Goddard Space Flight Center
Greenbelt, MD
USA

C. Lavaysse
Institut Pierre Simon Laplace/Laboratoire de Météorologie Dynamique
École Polytechnique/UPMC/ENS/CNRS
Palaiseau
France

Jack D. Law
Fuel Cycle Science and Technology Division
Idaho National Laboratory
Idaho Falls, ID
USA

Edward A. Laws
Louisiana State University
School of the Coast and Environment
Baton Rouge, LA
USA

Giovanna Lazzari
Avantea, Laboratorio di Tecnologie della Riproduzione
Cremona
Italy

Nam Le Quang
Photowatt International S.A
Bourgoin Jailleu
France

Kenneth M. Leber
Center for Fisheries Enhancement
Mote Marine Laboratory
Sarasota, FL
USA

Daniel Lechner
Department of Accident Mechanism Analysis
IFSTTAR-MA Laboratory
Salon de Provence
France

Choong-Gon Lee
Department of Chemical Engineering
Hanbat National University
Yuseong-gu, Daejeon
South Korea

Colin J. Lee
Department of Chemical Engineering and Applied Chemistry
University of Toronto
Toronto, ON
Canada

Douglass B. Lee, Jr.
US Department of Transportation
Volpe National Transportation Systems Center
Cambridge, MA
USA

Eunkyung Lee
Department of Environmental Science and Engineering
Gwangju Institute of Science and Technology (GIST)
Buk-gu, Gwangju
South Korea

Sungyun Lee
Department of Environmental Science and Engineering
Gwangju Institute of Science and Technology (GIST)
Buk-gu, Gwangju
South Korea

Sangho Lee
Department of Water Resources and Environmental Research
Korea Institute of Construction Technology
Goyang-Si, Gyeonggi-Do
Republic of Korea

Rik Leemans
Environmental Systems Analysis Group
Wageningen University
Wageningen
The Netherlands

Gilles Lemaire
INRA
Lusignan
France

Mustapha Lemiti
INL-INSA
Lyon
France

Timothy M. Lenton
University of Exeter
Hatherly Laboratories Biosciences
College of Life and Environmental Sciences
Exeter
UK

Volker Lenz
German Biomass Research Centre (DBFZ)
Leipzig
Germany

Laura Lesniewski
AIA
BNIM – Berkebile Nelson Immenschuh McDowell Architects
Kansas City, MO
USA

L. Ruby Leung
Atmospheric Sciences and Global Change Division
Pacific Northwest National Laboratory
Richland, WA
USA

Claude Levy-Clement
CNRS
Thiais
France

Iris Lewandowski
Department of Biobased Products and Energy Crops
Institute for Crop Science
Hohenheim University
Stuttgart
Germany

Ke Li
Department of Biological and Agricultural Engineering
University of Georgia
Atlanta, GA
USA

Xiaolin Li
Pacific Northwest National Laboratory
Richland, WA
USA

Keqiang Li
State Key Laboratory of Automotive Safety and Energy
Tsinghua University
Beijing
China

Zifu Li
Centre for Sustainable Environmental Sanitation
University of Science and Technology
Beijing
China

Qing X. Li
Department of Molecular Biosciences and Bioengineering
University of Hawaii
Honolulu, HI
USA

Joseph J. Lifrieri
Paulus, Sokolowski and Sartor, LLC
Warren, NJ
USA

Enrique Lima
West Japan Engineering Consultants, Inc
Chuou-ku, Fukuoka
Japan

Daniel Lincot
Institute of Research and Development of Photovoltaic Energy
Chatou, Cedex
France

Timothy E. Lipman
Institute of Transportation Studies
University of California – Berkeley
Berkeley, CA
USA

Rongfang Rachel Liu
Department of Civil and Environmental Engineering
New Jersey Institute of Technology
Newark, NJ
USA

Fuqiang Liu
Department of Information and Communication Engineering
Tongji University
Shanghai
China

Yiming Liu
Key Lab of Machine Perception (MOE)
Peking University
Beijing
China

Jun Liu
Pacific Northwest National Laboratory
Richland, WA
USA

Chongxuan Liu
Pacific Northwest National Laboratory
Richland, WA
USA

Mike Lockwood
Department of Meteorology
University of Reading
Reading
UK
and
RAL Space
Rutherford Appleton Laboratory
Oxfordshire
UK

Vivian Loftness
Center for Building Performance and Diagnostics
Carnegie Mellon University
Pittsburgh, PA
USA

Otto Löhlein
Machine Perception Systems and Reliability
Environment Perception Daimler AG
Ulm
Germany

Sarah Loker
Department of Animal and Poultry Science
University of Guelph
Guelph, ON
Canada

Rafael J. López-Bellido
Departamento de Ciencias y Recursos Agrícolas y Forestales
University of Córdoba
Córdoba
Spain

Luis López-Bellido
Departamento de Ciencias y Recursos Agrícolas y Forestales
University of Córdoba
Córdoba
Spain

Raoul Lopez-Lozano
INRA
UMR Environnement Méditerranéen et Modélisation des Agro-Hydrosystèmes, EMMAH
Avignon
France

Jeffrey M. Lotz
Department of Coastal Sciences, Ecology and Epidemiology of Parasites and Pathog
Gulf Coast Research Laboratory
The University of Southern Mississippi
Ocean Springs, MS
USA

Sean Low
Centre for International Governance Innovation
Waterloo, ON
Canada

Margaret Lowman
Nature Research Center, NC Museum of Natural Sciences and Professor
North Carolina State University
Raleigh, NC
USA
and
TREE Foundation
Sarasota, FL
USA

Zhongming Lu
Brook Byers Institute for Sustainable Systems and the Department of Civil & Environmental Engineering
Georgia Institute of Technology
Atlanta, GA
USA

Xiaojia Lu
China Agricultural University
Beijing
China

Franco Lucchini
Centro Ricerche Biotecnologiche
Università Cattolica del Sacro Cuore
Cremona
Italy

John W. Lund
Geo-Heat Center
Oregon Institute of Technology
Klamath Falls, OR
USA

Daniel J. Lunt
School of Geographical Sciences
University of Bristol
Bristol
UK

Nguyen Gia Luong
Biogas Technology Centre (BTC) of the Vietnam Union of Science and Technology Association (VUSTA)
Hanoi
Vietnam

Eckhard Lüpfert
DLR Deutsches Zentrum für Luft- und Raumfahrt
German Aerospace Center
Institute of Technical Thermodynamics
Solarforschung
Koeln/Cologne
Germany

Gerald H. Luttrell
Department of Mining and Minerals Engineering
Holden Hall Virginia Polytechnic Institute & State University
Blacksburg, VA
USA

Rui Ma
Department of Geological Sciences
University of Alabama
Tuscaloosa, AL
USA
and
China University of Geosciences
Wuhan
China

Po-Lun Ma
Atmospheric Science and Global Change Division
Pacific Northwest National Laboratory
Richland, WA
USA

Mark Macauda
Health Promotion, Education, and Behavior
University of South Carolina
Columbia, SC
USA

Don Mackay
Canadian Centre for Environmental Modelling and Chemistry
Trent University
Peterborough, ON
Canada

D. J. Macquarrie
Department of Chemistry
University of York
Heslington, York
UK

Ondřej Mašek
UK Biochar Research Centre (UKBRC)
School of GeoSciences
Science and Engineering at The University of Edinburgh
Edinburgh, Scotland
UK

Peter Hauge Madsen
Wind Energy Division, Risø DTU National Laboratory for Sustainable Energy
Technical University of Denmark
Roskilde
Denmark

Ramakrishnan Mahadevan
Telecommunications
University of Colorado
Boulder, CO
USA

Patrick F. Mahoney
Energy Answers International, Inc.
Albany, NY
USA

Natalie M. Mahowald
Department of Earth and Atmospheric Sciences
Atkinson Center for Sustainable Future
Cornell University
Ithaca, NY
USA

Stefan Majer
German Biomass Research Centre Non Profit Research Company (DBFZ)
Leipzig
Germany

Asko Mäki-Tanila
Biotechnology and Food Research
MTT Agrifood Research Finland
Jokioinen
Finland

Sixto Malato
Plataforma Solar de Almería (CIEMAT)
Tabernas, Almería
Spain

M. I. Maldonado
Plataforma Solar de Almería (CIEMAT)
Tabernas, Almería
Spain

Ripudaman Malhotra
Chemistry and Chemical Engineering Laboratory
Pure and Applied Physical Sciences Division
SRI International
Menlo Park, CA
USA

Heinz-Peter Mang
German Society for sustainable Biogas and Bioenergy Utilization
Freudenberg-Boxtal, Baden-Wuerttemberg
Germany

Pamela Mang
Regenesis Group and Story of Place Institute
Santa Fe, NM
USA

James F. Manwell
Department of Mechanical and Industrial Engineering
University of Massachusetts
Amherst, MA
USA

Fuchs Marc
Department of Plant Pathology and Plant-Microbe Biology
Cornell University, New York State Agricultural Experiment Station
Geneva, NY
USA

John Mardaljevic
Institute of Energy and Sustainable Development
De Montfort University
Leicester
UK

Pere Margalef
National Fuel Cell Research Center
University of California
Irvine, CA
USA

Montse Mari
Laboratory of Toxicology and Environmental Health
School of Medicine, IISPV
Universitat Rovira i Virgili
Reus, Catalonia
Spain

Shawn J. Marshall
Department of Geography
Earth Sciences
University of Calgary
Calgary, AB
Canada

Johannes J. E. Martin
Martin GmbH für Umwelt- und Energietechnik
Munich
Germany

Santo Martinuzzi
Formerly University of Marseilles
Marseilles
France

Robert P. Mason
Department of Marine Sciences & Chemistry
University of Connecticut
Groton, CT
USA

M. Abul Masrur
College of Engineering & Science
University of Detroit Mercy
Detroit, MI
USA

Juliane Mathey
Leibniz Institute of Ecological and Regional Development (IOER)
Dresden
Germany

Jörg Matschullat
TU Bergakademie Freiberg, Institute of Mineralogy and Helmholtz Institute Freiberg for Resource Technology
Freiberg, Saxony
Germany

Peter J. McCabe
School of Earth, Environmental and Biological Sciences
Queensland University of Technology
Brisbane, QLD
Australia

Roger O. McClellan
Toxicology and Health Risk Analysis
Albuquerque, NM
USA

John D. McDonald
GE Energy, Digital Energy
Atlanta, GA
USA

Shannon S. McDonald
Southern Illinois University
Carbondale, Il
USA

James C. McGeer
Department of Biology
Wilfrid Laurier University
Waterloo, ON
Canada

Michael J. McGrew
Avian Germ Cell Laboratory, Division of Developmental Biology
The Roslin Institute and Royal (Dick) School of Veterinary Studies, University of Edinburgh
Roslin, Midlothian
UK

Thomas McIlwain
Gulf Coast Research Laboratory
The University of Southern Mississippi
Ocean Springs, MS
USA

Steven McIntosh
Department of Chemical Engineering
University of Virginia
Charlottesville, VA
USA
and
Department of Chemical Engineering
Lehigh University
Bethlehem, PA
USA

Haewon C. McJeon
Joint Global Change Research Institute (JGCRI)
Pacific Northwest National Laboratory (PNNL)
College Park, MD
USA

Richard McKenzie
National Institute for Water and Atmospheric Research (NIWA)
Lauder
New Zealand

Christopher W. McKindsey
Ocean and Environmental Sciences Division
Fisheries and Oceans Canada
Institut Maurice-Lamontagne Fisheries and Oceans Canada
Mont-Joli, Québec
Canada

Graham McLaren
Integrated Breeding Platform
Consultative Group on International Agricultural Research, Generation Challenge Programme, c/o CIMMYT
Texcoco
Edo. Mexico

Angela R. McLean
Zoology Department
Institute of Emerging Infections
University of Oxford
Oxford
UK

Timothy I. McLean
Department of Biological Sciences
University of Southern Mississippi
Hattiesburg, MS
USA

Sandra L. McLellan
School of Freshwater Sciences
University of Wisconsin-Milwaukee
Milwaukee, WI
USA

Keith McManamen
University of Waterloo
Waterloo, ON
Canada

Gregory S. McMaster
USDA-ARS, Agricultural Systems Research Unit
Fort Collins, CO
USA

Gertjan Medema
Water Quality & Health
KWR Watercycle Research Institute
Nieuwegein
The Netherlands
and
Sanitary Engineering
Delft University of Technology
Delft
The Netherlands

Tamás Meggyes
University of Wolverhampton, UK and ICP Hungária
Budapest
Hungary
and
BAM Federal Institute for Materials Research and Testing
Berlin
Germany

Anton Meier
Solar Technology Laboratory, Department of General Energy Research
Paul Scherrer Institute
Villigen PSI
Switzerland

Bashir Memon
P.E. LaMoreaux & Associates
Tuscaloosa, AL
USA

Sylvain Merel
Department of Chemical and Environmental Engineering
University of Arizona
Tucson, AZ
USA

Ronald L. Mersky
Department of Civil Engineering
Widener University
Chester, PA
USA

Claus R. Mertes
Geschäftsbereich Energie/Business Group Energy
Borsteler Chausse
Poyry Deutschland GmbH
Hamburg
Germany

Michael Metzlaff
Bayer BioScience N.V
Ghent
Belgium

Damaris A. F. Meujo
Department of Pharmacognosy
The University of Mississippi
University, MS
USA

Scott A. Miers
Mechanical Engineering
Michigan Technological University
Houghton, MI
USA

Filippo Miglior
Guelph Food Research Centre, Agriculture and Agri–Food Canada
ON
Canada
and
Canadian Dairy Network
Guelph, ON
Canada

Petar T. Milanović
Belgrade
Serbia

Mark A. Miller
California Partners for Advanced Transit and Highways (PATH) Program
Institute of Transportation Studies
University of California
Berkeley, CA
USA
and
Institute of Transportation Studies, School of Public Affairs
University of California
Los Angeles, CA
USA

Michael Milligan
National Renewable Energy Laboratory
Golden, CO
USA

Liz Minne
Environmental Engineering
Brook Byers Institute for Sustainable Systems
Georgia Institute of Technology
Atlanta, GA
USA

Ignacy Misztal
Department of Animal and Dairy Science
Breeding and Genetics, University of Georgia
Athens, GA
USA

Martin Mittelbach
Institute of Chemistry
Karl-Franzens-University of Graz
Graz
Austria

Kenji Miyatake
Clean Energy Research Center
University of Yamanashi
Kofu
Japan

M. A. Moline
Center for Marine and Coastal Sciences
California Polytechnic State University
San Luis Obispo, CA
USA

Max Molleo
Department of Chemistry and Biochemistry
University of South Carolina
Columbia, SC
USA

Mike Mongillo
GNS Science
Wairakei Research Centre
Taupo
New Zealand

Paul S. Monks
Department of Chemistry
University of Leicester
Leicester
UK

Remi Monna
INES-CEA
Le Bourget du Lac
France

Luigi Monte
ENEA, CR Casaccia
Rome
Italy

Harry Moore
Tennessee Department of Transportation, Retired
Blaine, TN
USA

Nigel Moore
Centre for International Governance Innovation
Waterloo, ON
Canada

Marc Moragues
Department of Soil and Crop Sciences
Colorado State University
Fort Collins, CO
USA

L. Mortimer
Hot Dry Rocks Pty Ltd
South Yarra, Victoria
Australia

Anna Mosby
Department of Biological Sciences
Virginia Institute of Marine Science
College of William & Mary
Gloucester Pt, VA
USA

Matti Mõttus
Department of Geosciences and Geography
University of Helsinki
Helsinki
Finland

Sathya Motupally
UTC Power
South Windsor, CT
USA

David Mouat
Division of Earth and Ecosystem Sciences
Desert Research Institute
Reno, NV
USA

David K. Moyeda
GE Energy
Irvine, CA
USA

Richard W. Mueller
Deutscher Wetterdienst
Offenbach
Germany

Franziska Mueller-Langer
German Biomass Research Centre gGmbH (DBFZ)
Leipzig
Germany

Douglas Mulhall
EPEA Internationale Umweltforschung GmbH
Hamburg
Germany
and
Academic Chair Cradle to Cradle for Innovation and Quality, Rotterdam School of Management, Erasmus University
Rotterdam
The Netherlands

Mathias Müller
Institute of Animal Breeding and Genetics & Biomodels Austria
University of Veterinary Medicine Vienna
Vienna
Austria

Frank E. Muller-Karger
College of Marine Science
University of South Florida
St. Petersburg, FL
USA

Michio Murakami
The University of Tokyo
Bunkyo-ku, Tokyo
Japan

Hirofumi Muraoka
National Institute of Advanced Industrial Science and Technology
Institute for Geo-Resources and Environment (GREEN)
Tsukuba, Ibaraki
Japan

Erik Murchie
Division of Plant and Crop Sciences
School of Biosciences
University of Nottingham
Sutton Bonington
UK

Daryl R. Myers
Resource Information and Forecasting Group
Electricity, Resources, and Building Systems Integration Center
National Renewable Energy Laboratory
Golden, CO
USA

Martí Nadal
Laboratory of Toxicology and Environmental Health, School of Medicine, IISPV
Universitat Rovira i Virgili
Reus, Catalonia
Spain

R. Naidu
CRC Care, University of South Australia
Adelaide
Australia

Satish K. Nair
Department of Biochemistry and Center for Biophysics and Computational Biology
University of Illinois at Urbana-Champaign
Urbana, IL
USA

Shyam S. Nandwani
Laboratorio de Energia Solar, Department of Physics
Universidad Nacional
Heredia
Costa Rica

Katsuhiko Naoi
Institute of Symbiotic Science and Technology
Tokyo University of Agriculture & Technology
Koganei, Tokyo
Japan

Shaista Naqvi
Department of Vegetal Production and Forestry Science, ETSEA
University of Lleida
Lleida
Spain

Michael Natelson
Retired from the Bettis Atomic Power Laboratory
West Mifflin, PA
USA

Michael Nelles
Department Waste Management
University of Rostock
Rostock
Germany

Franz P. Neubacher
UV&P Environmental Engineering M.S. Chemical Engineering (T.U. Graz) M.S. Technology & Policy (M.I.T)
Vienna
Austria

Martina Newell-McGloughlin
Department of Plant Pathology
University of California Davis
Davis, CA
USA

David J. Newman
Natural Products Branch Developmental Therapeutics Program
National Cancer Institute, NCI-Frederick
Frederick, MD
USA

Rui Ni
Department of Psychology
Wichita State University
Wichita, KS
USA

Anders Busse Nielsen
Department of Landscape Management, Design and Construction
Swedish University of Agricultural Sciences
Alnarp
Sweden

Raquel Nieto
Environmental Physics Laboratory (EPhysLab)
Universidade de Vigo
Ourense
Spain

David Nieva
Instituto de Investigaciones Eléctricas
Cuernavac, Morelos
Mexico

Kjell Nilsson
Danish Centre for Forest, Landscape and Planning
University of Copenhagen
Frederiksberg C
Denmark

Hiroyuki Nishide
Department of Applied Chemistry
Waseda University
Tokyo
Japan

Guo-Yue Niu
Biosphere 2
University of Arizona
Oracle, AZ
USA

Y. Nojiri
International Research Center for Hydrogen Energy
Kyushu University
Fukuoka
Japan

Douglas Noonan
School of Public Policy
Georgia Institute of Technology
Atlanta, GA
USA

Damir Novosel
Quanta Technology, LLC
Raleigh, NC
USA

Henning Nuissl
Geographical Institute
Humboldt-Universität zu Berlin
Berlin
Germany

Francis X. O'Beirn
Marine Institute
Galway
Ireland

Ingwald Obernberger
Bios Bioenergiesysteme GmbH
Graz
Austria
and
BIOENERGY 2020+ GmbH
Graz
Austria
and
Institute for Process and Particle Engineering
Graz University of Technology
Graz
Austria

Colin O'Dowd
School of Physics & Centre for Climate and Air Pollution Studies
Ryan Institute, National University of Ireland Galway
Galway
Ireland

David Ofer
TIAX LLC
Lexington, MA
USA

Byung Soo Oh
Center for Seawater Desalination Plant
Gwangju Institute of Science and Technology (GIST)
Buk-gu, Gwangju
Republic of Korea

Vahur Oja
Department of Chemical Engineering
Tallinn University of Technology
Tallinn
Estonia

Frederick Okono
Integrated Breeding Platform
Consultative Group on International Agricultural Research, Generation Challenge Programme, c/o CIMMYT
Texcoco
Edo. Mexico

K.-M. Oksman-Caldentey
VTT Technical Research Centre of Finland
Espoo
Finland

Curtis M. Oldenburg
Earth Sciences Division
Lawrence Berkeley National Laboratory
Berkeley, CA
USA

David M. Oliver
Biological & Environmental Sciences, School of Natural Sciences
University of Stirling
Stirling
UK
and
Centre for Sustainable Water Management
Lancaster Environment Centre
Lancaster University
Lancaster
UK

M. Oliver
School of Marine Science and Policy, College of Earth, Ocean and Environment
University of Delaware
Lewes, DE
USA

I. Oller
Plataforma Solar de Almería (CIEMAT)
Tabernas, Almería
Spain

Gustaf Olsson
Industrial Electrical Engineering and Automation (IEA)
Lund University
Lund
Sweden

I Anna S. Olsson
Laboratory Animal Science Group
IBMC – Instituto de Biologia Molecular e Celular
Universidade do Porto
Porto
Portugal

John Orcutt
Scripps Institution of Oceanography
University of California, San Diego
La Jolla, CA
USA

M. Adrián Ortega-Guerrero
Centro de Geociencias, UNAM Juriquilla
Querétaro
Mexico

Dale Osborn
Midwest ISO
Columbus, OH
USA

S. Ouysse
Cadi Ayyad University
Marrakech
Morocco

Ralph P. Overend
Golden, CO
USA

Robin M. Overstreet
Department of Coastal Sciences
Gulf Coast Research Laboratory
University of Southern Mississippi
Ocean Springs, MS
USA

Micheal D. K. Owen
Department of Agronomy
Iowa State University
Ames, IA
USA

Kenichi Oyaizu
Department of Applied Chemistry
Waseda University
Tokyo
Japan

Ece Ozdemiroglu
Economics for the Environment Consultancy (EFTEC)
London
UK

Carvalho P.
Division of Plant and Crop Sciences, School of Biosciences
University of Nottingham
Loughborough
UK

Stephen J. Paddison
Department of Chemical & Biomolecular Engineering
University of Tennessee
Knoxville, TN
USA

Glenn G. Page
SustainaMetrix, LLC
Johns Hopkins University
Baltimore, MD
USA

Stephen H. Page
Ocean Farm Technologies, Inc.
Morrill, ME
USA

Wolfgang Palz
Former EU Commission Official
World Council for Renewable Energy (WCRE)
Brussels
Belgium

Iraklis Panagiotakis
ENYDRON - Environmental Protection Services
Athens
Greece

Arka Pandit
Brook Byers Institute for Sustainable Systems and the Department of Civil & Environmental Engineering
Georgia Institute of Technology
Atlanta, GA
USA

Se-Keun Park
Division of Environmental Science and Engineering
National University of Singapore
Singapore

Kiho Park
Environment & Energy Research Team
Daewoo Institute of Construction Technology
Suwon, Gyeonggi-do
South Korea

Minho Park
Environment & Energy Research Team
Daewoo Institute of Construction Technology
Suwon, Gyeonggi-do
South Korea

D. Parsons
Atmospheric Technology Division
National Center for Atmospheric Research
Boulder, CO
USA

Odysseas Paschos
Department of Physics
Technische Universität München
Garching
Germany

Puneet Pasrich
Electrical, Computer, and Energy Engineering Department
University of Colorado
Boulder, CO
USA

S. L. Patil
Institute of Northern Engineering
University of Alaska Fairbanks
Fairbanks, AK
USA

Tennant Paula
Department of Life Sciences
University of the West Indies
Mona, Kingston, WI
Jamaica

Stephan Pauleit
Center of Life and Food Sciences Weihenstephan
Technical University of Munich
Freising
Germany

Nathan L. Pelletier
Dalhousie University
Halifax, Nova Scotia
Canada

Rui Pereira
CIMAR/CIIMAR – Centre for Marine and Environmental Research
University of Porto
Porto
Portugal

Andy Pereira
University of Arkansas
Fayetteville, AR
USA

Isabelle Périchaud
University of Marseilles
Marseilles
France

Anastasios Perimenis
German Biomass Research Centre Non Profit Research Company (DBFZ)
Leipzig
Germany

Josh Perkel
National Electric Energy Test Research and Application Centre (NEETRAC)
Forrest Park, GA
USA

Andrea Perota
Avantea, Laboratorio di Tecnologie della Riproduzione
Cremona
Italy

Julian Perrenoud
Laboratory for Thin Films and Photovoltaics
EMPA – Swiss Federal Laboratory for Materials Science and Technology
Duebendorf
Switzerland

Erik Lundtang Petersen
Wind Energy Division, Risø DTU National Laboratory for Sustainable Energy
Technical University of Denmark
Roskilde
Denmark

Arun G. Phadke
Bradley Department of Electrical and Computer Engineering
Virginia Polytechnic Institute and State University
Blacksburg, VA
USA

S. T. A. Pickett
Cary Institute of Ecosystem Studies
Millbrook, NY
USA

Lisa W. Plano
Departments of Pediatrics & Department of Microbiology and Immunology
Miller School of Medicine, University of Miami
Miami, FL
USA

Christopher V. Plowe
Howard Hughes Medical Institute/Center for Vaccine Development
University of Maryland School of Medicine
Baltimore, MD
USA

Rui M. Ponte
Atmospheric and Environmental Research, Inc
Lexington, MA
USA

Martina de Mantopi Porres Lebofa
Technologies for Economic Development
Maseru
Lesotho

Kevin Porter
Exeter Associates
Columbia, Maryland
USA

Ralph J. Portier
Department of Environmental Sciences
School of the Coast & Environment
Louisiana State University
Baton Rouge, LA
USA

M. Posada
Instituto de Salud Carlos III
Madrid
Spain

John W. Poston, Sr.
Department of Nuclear Engineering
Texas A & M University
College Station, TX
USA

Pavel P. Povinec
Faculty of Mathematics, Physics and Informatics
Comenius University
Bratislava
Slovakia

James R. Powell
Maglev-2000 Corporation
Shoreham, NY
USA

Simon D. Poynton
Department of Chemistry
University of Surrey
Guildford
UK

Stephanie Prejean
Seismology
USGS Volcano Science Center
Alaska Volcano Observatory
Anchorage, AK
USA

Miranda Prendergast-Miller
UK Biochar Research Centre (UKBRC), School of GeoSciences
Science and Engineering at The University of Edinburgh
Edinburgh, Scotland
UK

Catherine H. Price
Department of Casino, Hospitality, Tourism Management
College of Business
The University of Southern Mississippi
Hattiesburg, MS
USA

John Pucher
Bloustein School of Planning and Public Policy
Rutgers University
New Brunswick, NJ
USA

Arni Ragnarsson
Iceland Geosurvey
Reykjavik
Iceland

Vidya Rajan
Applied Biotechnology Institute
San Luis Obispo, CA
USA

Nallamuthu Rajaratnam
Department of Civil and Environmental Engineering
University of Alberta
Edmonton, AB
Canada

Premanand Ramadass
Celgard, LLC
Charlotte, NC
USA

Juan Antonio López Ramínez
Departamento de Tecnologias del Medio Ambiente
Centro Andaluz Superior de Estudios Marinos
CASEM
Universidad de Cádiz
Cadiz
Spain

Kaylan Randolph
Department of Marine Sciences
University of Connecticut
Groton, CT
USA

A. H. Ranjbar
Department of Electrical Engineering
Amirkabir University of Technology
Tehran
Iran

Philip J. Rasch
Pacific Northwest National Laboratory
Richland, WA
USA

Mario C. Raviglione
STOP TB Department (STB), HIV/AIDS, TB & Malaria Cluster (HTM)
World Health Organization
Geneva
Switzerland

Encarnación Raymundo-Piñero
Research Centre on Divided Matter
CRMD-CNRS & Orléans University
Orléans
France

Helmut Rechberger
Institute of Water Quality, Resource and Waste Management
Vienna University of Technology
Vienna
Austria

J. L. Redelsperger
Centre National de Recherches Météorologiques
Météo-France/CNRS
Toulouse
France

Bill Reed
Regenesis Group and Story of Place Institute
Arlington, MA
USA

L. Reijnders
Institute for Biodiversity and Ecosystem Dynamics
University of Amsterdam
Amsterdam
The Netherlands

Isabelle Périchaud
University of Marseilles
Marseilles
France

Dieter O. Reimann
Confederation of European Waste-to-Energy Plants (CEWEP)
Bamberg
Germany

Anu Reinart
Tartu Observatory, Tõravere
Tartumaa
Estonia

Matthew Reynolds
International Maize and Wheat Improvement Centre (CIMMYT)
Mexico DF
Mexico

Mary Rezai
Natural Resources Institute
University of Manitoba
Winnipeg, MB
Canada

Jean-Marcel Ribaut
Integrated Breeding Platform
Consultative Group on International Agricultural Research, Generation Challenge Programme, c/o CIMMYT
Texcoco
Edo. Mexico

Anthony Ricciardi
Redpath Museum & McGill School of Environment
McGill University
Montreal, QC
Canada

Christoph Richter
Project Manager Solar Research
Plataforma Solar de Almeria
Institute of Solar Research
DLR – German Aerospace Centre
Germany

Caryn Riley
National Electric Energy Test Research and Application Centre (NEETRAC)
Forrest Park, GA
USA

Dieter Rink
Helmholtz Centre for Environmental Research (UFZ)
Leipzig
Germany

Stephen R. Rintoul
Antarctic Climate and Ecosystems Cooperative Research Centre, Wealth from Oceans National Research Flagship
CSIRO Marine and Atmospheric Research
Hobart, TAS
Australia

Heiko Rischer
VTT Technical Research Centre of Finland
Espoo
Finland

Claire Risley
LUCINDA Group, Institute of Infection and Global Health
University of Liverpool
Neston, Cheshire
UK

Anneli Ritala
VTT Technical Research Centre of Finland
Espoo
Finland

Kimberly A. Roberts
Radiological Performance Assessment
Savannah River National Laboratory
Aiken, SC
USA

M. Verónica Rodriguez
IFEVA – Cátedra de Fisiología Vegetal/CONICET-Universidad de Buenos Aires
Buenos Aires
Argentina

Benoit Roig
Environment and Health Research Laboratory
French School of Public Health
Rennes
France

Eduard Rojas
Department of Vegetal Production and Forestry Science, ETSEA
University of Lleida
Lleida
Spain

Ignacio Romagosa
Department of Crop and Forest Sciences
University of Lleida
Lleida
Spain

Déborah P. Rondanini
Department of Crop Production
University of Buenos Aires
Buenos Aires
Argentina
and
CONICET, National Council of Scientific and Technical Research
Buenos Aires
Argentina

Stefan Rönsch
German Biomass Research Centre (Deutsches BiomasseForschungsZentrum gemeinnützige GmbH)
Leipzig
Germany

Michael J. Root
Cardiology, Rhythm and Vascular Research and Development
Boston Scientific Corp.
St. Paul, MN
USA

Guilherme J. M. Rosa
Departments of Animal Sciences, Biostatistics & Medical Informatics, Dairy Science
University of Wisconsin
Madison, WI
USA

Stuart J. Roy
Australian Centre for Plant Functional Genomics
University of Adelaide
Adelaide, SA
Australia

C. de Peter Ruiter
Biometris, Wageningen UR
Wageningen
The Netherlands

Ladislaus Rybach
Geowatt AG
Switzerland

Samantha L. Saalfield
EA Engineering, Science, and Technology, Inc.
Sparks, MD
USA

Arash Saboori
Department of Civil Engineering (CIE 201F)
North Dakota State University
North – Fargo, ND
USA

Stephen H. Salter
Institute for Energy Systems, School of Engineering
The University of Edinburgh
Scotland
UK

Georgina Sanahuja
Department of Vegetal Production and Forestry Science, ETSEA
University of Lleida
Lleida
Spain

Ben Sanderson
National Center for Atmospheric Research
Boulder, CO
USA

Paul A. Sandifer
National Oceanic and Atmospheric Administration
National Ocean Service
c/o Hollings Marine Laboratory
Charleston, SC
USA

Peter Sandøe
Danish Centre for Bioethics and Risk Assessment
Institute of Food and Resource Economics
University of Copenhagen
Frederiksberg
Denmark

Shriram Santhanagopalan
Celgard, LLC
Charlotte, NC
USA

Subir K. Sanyal
GeothermEx, Inc
Richmond, CA
USA

Niyazi Serdar Sariciftci
Linz Institute for Organic Solar Cells (LIOS)
Johannes Kepler University
Linz
Austria

K. Sasaki
International Research Center for Hydrogen Energy
Kyushu University
Fukuoka
Japan
and
International Institute for Carbon–Neutral Energy Research (WPI)
Kyushu University
Fukuoka
Japan
and
Faculty of Engineering
Kyushu University
Fukuoka
Japan

Toshihisa Sato
Human Technology Research Institute, National Institute of Advanced Industrial Science and Technology (AIST)
Tsukuba-shi, Ibaraki
Japan

Emilio H. Satorre
Cátedra de Cerealicultura
University of Buenos Aires
Buenos Aires
Argentina
and
CONICET (National Research Council)
University of Buenos Aires
Buenos Aires
Argentina
and
AACREA
Buenos Aires
Argentina

Roxana Savin
Department of Crop and Forest Sciences
University of Lleida
Lleida
Spain

Lorenzo Savioli
Department of Control of Neglected Tropical Diseases
World Health Organization
Geneva
Switzerland

Giovanni Scarinci
Department of Mechanical Engineering – Materials Division
University of Padova
Padova
Italy

Lawrence R. Schaeffer
Department of Animal and Poultry Science
Centre for Genetic Improvement of Livestock
University of Guelph
Guelph, ON
Canada

Günther Schauberger
WG Environmental Health
University of Veterinary Medicine
Vienna
Austria

Günther G. Scherer
Paul Scherrer Institut
Electrochemistry Laboratory
Villigen
Switzerland

Joachim Schiemann
Julius Kühn Institute (JKI), Federal Research Centre for Cultivated Plants, Institute for Biosafety of Genetically Modified Plants
Quedlinburg
Germany

Andreas Schiermeyer
Department of Plant Biotechnology
Fraunhofer IME
Aachen
Germany

Stefan Schillberg
Department of Plant Biotechnology
Fraunhofer IME
Aachen
Germany

Jörg Schlaich
Schlaich Bergermann Solar GmbH
Stuttgart
Germany

Alois W. Schmalwieser
WG Environmental Health
University of Veterinary Medicine
Vienna
Austria

Ralf Schmersahl
Deutsches BiomasseForschungsZentrum GmbH
German Biomass Research Centre (DBFZ)
Leipzig
Germany
and
Institute of Agricultural Engineering Bornim e.V. (ATB)
Potsdam
Germany

Ralf Schmersahl
German Biomass Research Centre (DBFZ)
Leipzig
Germany

Thomas J. Schmidt
General Energy Research, Lab. of Electrochemistry
Paul Scherrer Institute
Villigen-PSI
Switzerland

Erika von Schneidemesser
Department of Chemistry
University of Leicester
Leicester
UK

Roland Schnell
Graskraft Ltd
Berlin
Germany

Angelika Schnieke
Chair of Livestock Biotechnology
Technical University of Munich
Freising
Germany

Hans-Werner Schock
Institut Technologie, Solar Forschung Division
Helmholtz Zentrum für Materialien und Energie
Berlin
Germany

Julie M. Schoenung
Department of Chemical Engineering and Materials Science
University of California, Davis
Davis, CA
USA

O. Schofield
Coastal Ocean Observation Lab, Institute of Marine and Coastal Sciences, School of Environmental and Biological Sciences
Rutgers University
New Brunswick, NJ
USA

Frank Scholwin
University Rostock
Germany

Marta Schuhmacher
Laboratory of Toxicology and Environmental Health, School of Medicine, IISPV
Universitat Rovira i Virgili
Reus, Catalonia
Spain

R. D. Schuiling
Department of Earth Sciences – Geochemistry
Institute of Geosciences
Utrcht University
Utrecht
The Netherlands

Ulrich Schurr
IBG-2: Plant Science
Forschungszentrum Jülich
Jülich
Germany

Lori H. Schwacke
NOAA Center for Excellence in Oceans and Human Health
National Oceanic and Atmospheric Administration's Hollings Marine Laboratory
Charleston, SC
USA

Dishna Schwarz
Deutsche Gesellschaft für Internationale Zusammenarbeit GmbH
Eschborn
Germany

John C. Seaman
Environmental Geochemistry, Savannah River Ecology Laboratory
The University of Georgia
Aiken, SC
USA

Gunther Seckmeyer
Institute of Meteorology and Climatology
Leibniz University of Hannover
Hannover
Germany

Michael Seiffert
German Biomass Research Centre (Deutsches BiomasseForschungsZentrum gemeinnützige GmbH)
Leipzig
Germany

Johannes Selke
International Biogas & Bioenergy Centre of Expertise (IBBK GmbH)
Stuttgart
Germany

Matthias Serfling
Machine Perception Systems and Reliability
Environment Perception Daimler AG
Ulm
Germany

Silvia Serranti
Dipartimento di Ingegneria Chimica Materiali Ambiente Sapienza
Università di Roma Via Eudossiana
Rome
Italy

Ulrike Seyfert
German Biomass Research Centre
Leipzig
Germany

Simon Shackley
UK Biochar Research Centre (UKBRC), School of GeoSciences
Science and Engineering at The University of Edinburgh
Edinburgh, Scotland
UK

Orin C. Shanks
National Risk Management Research Laboratory
United States Environmental Protection Agency
Cincinnati, OH
USA

Roger D. Shanks
Department of Animal Sciences
University of Illinois
Urbana, IL
USA

Vida N. Sharifi
Energy and Environment Engineering (EEE)
Sheffield University
Sheffield
UK
and
EEE Group, Chemical and Biological Engineering
Sheffield University
Sheffield
UK

Brian P. Shedd
EA Engineering, Science, and Technology, Inc.
Sparks, MD
USA

Y. Shiratori
International Research Center for Hydrogen Energy
Kyushu University
Fukuoka
Japan
and
International Institute for Carbon–Neutral Energy Research (WPI)
Kyushu University
Fukuoka
Japan
and
Faculty of Engineering
Kyushu University
Fukuoka
Japan

Hokyong Shon
School of Civil and Environmental Engineering
University of Technology, Sydney (UTS)
Broadway, NSW
Australia

H. K. Shon
School of Civil and Environmental Engineering
University of Technology, Sydney
Broadway, NSW
Australia

Muki Shpigel
Israel Oceanographic and Limnological Research, National Center for Mariculture
Eilat
Israel

Wenjie Shu
Department of Information and Communication Engineering
Tongji University
Shanghai
China

Herman H. (Hank) Shugart
Department of Environmental Sciences
The University of Virginia
Charlottesville, VA
USA

Lester M. Shulman
Central Virology Laboratory, Laboratory of Environmental Virology at Sheba Medical Center
Public Health Services, Israel Ministry of Health
and
Department of Epidemiology and Preventive Medicine
School of Public Health, Sackler Faculty of Medicine, Tel Aviv University
Tel Aviv
Israel

J. Kenneth Shultis
Department of Mechanical & Nuclear Engineering
Kansas State University
Manhattan, KS
USA

Paul J. Sideris
Department of Physics and Astronomy
Hunter College of CUNY
New York, NY
USA

Stefan Siedentop
Institute of Regional Development Planning
University of Stuttgart
Stuttgart
Germany

Franz-Georg Simon
Department Material and Environment
BAM Federal Institute for Materials Research and Testing
Berlin
Germany

Michael F. Simpson
Fuel Cycle Science and Technology Division
Idaho National Laboratory
Idaho Falls, ID
USA

Neil Anthony Sims
Kona Blue Water Farms, Inc
Kailua-Kona, HI
USA

Geoffrey A. Sinclair
DeFelice Marine Center
Louisiana Universities Marine Consortium
Chauvin, LA
USA

G. Singh
University of Technology
Sydney, NSW
Australia

S. J. Skinner
Department of Materials
Imperial College London
London
UK

Raphael Slade
Centre for Energy Policy and Technology
Imperial College
London
UK

Robert C. T. Slade
Department of Chemistry
University of Surrey
Guildford
UK

Gustavo Slafer
Department of Crop and Forest Sciences
University of Lleida
Lleida
Spain

Abdelillah Slaoui
CNRS-INESS
Strasbourg
France

Raub W. Smith
GE Infrastructure-Energy
Schenectady, NY
USA

D. Scott Smith
Department of Chemistry
Wilfrid Laurier University
Waterloo, ON
Canada

Ronald M. Smith
SRI Consulting
Menlo Park, CA
USA

Grant D. Smith
Department of Materials Science and Engineering
University of Utah
Salt Lake City, UT
USA

Walker O. Smith, Jr.
Department of Biological Sciences
Virginia Institute of Marine Science, College of William & Mary
Gloucester Pt, VA
USA

Robbert P. H. Snep
Alterra
Wageningen University and Research Center
Wageningen
The Netherlands

Megan Snyder
School of Architecture and Center for Building Performance & Diagnostics
Carnegie Mellon University
Pittsburgh, PA
USA

Shane A. Snyder
Department of Chemical and Environmental Engineering
University of Arizona
Tucson, AZ
USA

Lennart Söder
Royal Institute of Technology
Electric Power Systems
Stockholm
Sweden

Scott D. Soelberg
Departments of Medicine-Division of Medical Genetics and Genome Sciences
University of Washington
Seattle, WA
USA

Saran Sohi
UK Biochar Research Centre (UKBRC), School of GeoSciences
Science and Engineering at The University of Edinburgh
Edinburgh, Scotland
UK

Morris Soller
Department of Genetics, The Silberman Life Sciences Institute
The Hebrew University of Jerusalem
Jerusalem
Israel

Jeffrey A. Soller
Soller Environmental, LLC
Berkeley, CA
USA

Giovanni Sotgiu
Epidemiology and Biostatistics Unit, Department of Biomedical Sciences
University of Sassari
Sassari
Italy

Matthew L. Spangler
Department of Animal Science
University of Nebraska
Lincoln, NE
USA

James G. Speight
CD&W Inc
Laramie, WY
USA

Suresh Sriramulu
TIAX LLC
Lexington, MA
USA

Richard M. Stanger
Los Angeles, CA
USA

Heinz G. Stefan
St. Anthony Falls Laboratory, Department of Civil Engineering
University of Minnesota
Minneapolis, MN
USA

R. Steinberger-Wilkens
Institute of Energy Research, Forschungszentrum Jülich
Juelich
Germany

Aldo Steinfeld
Institute of Energy Technology, Department of Mechanical and Process Engineering
ETH Zurich
Zurich
Switzerland

Wolf-Dieter Steinmann
Institute of Technical Thermodynamics
German Aerospace Center
Stuttgart
Germany

Robert R. Stickney
Texas Sea Grant College Program
Texas A&M University
College Station, TX
USA

Ulrich Stimming
Institute for Advanced Study (IAS)
Garching
Germany
and
Department of Physics
Technische Universität München
Garching
Germany

Erling Strandberg
Department of Animal Breeding and Genetics
Swedish University of Agricultural Sciences
Uppsala
Sweden

Christoph Strauß
Plant Production and Agricultural Ecology
Thuringian State Institute for Agriculture
Dornburg
Germany

Richard Stringfellow
TIAX LLC
Lexington, MA
USA

Gerhard Stryi-Hipp
Division Solar Thermal and Optics
Fraunhofer-Institut für Solare Energiesysteme ISE
Freiburg
Germany

Muthukumar Subrahmanyam
Center for Geographic Information Systems and the
School of City and Regional Planning
Georgia Institute of Technology
Atlanta, GA
USA

Bala Subramaniam
Department of Chemical and Petroleum Engineering
The Center for Environmentally Beneficial Catalysis
University of Kansas
Lawrence, KS
USA

Madis Sulev
Tartu Observatory, Tõravere
Tartumaa
Estonia

Eric M. Suuberg
Division of Engineering
Brown University
Providence, RI
USA

J. Swithenbank
Energy and Environment Engineering (EEE)
Sheffield University
Sheffield
UK

Heather Tallis
The Natural Capital Project, Department of Biology
and Woods Institute
Stanford University
Stanford, CA
USA

Rainer Tamme
Institute of Technical Thermodynamics
German Aerospace Center
Stuttgart
Germany

Yongrui Tan
Applied Research and Development Center
Southern Nevada Water Authority
Las Vegas, NV
USA

Ching W. Tang
Department of Chemical Engineering
University of Rochester
Rochester, NY
USA

Robert L. Tanguay
Department of Environmental and Molecular Toxicology
Environmental Health Sciences Center, Oregon State University
Corvallis, OR
USA

S. Taniguchi
International Research Center for Hydrogen Energy
Kyushu University
Fukuoka
Japan

Veerachai Tanpipat
Forest Fire Control Division
National Park, Wildlife and Plant Conservation Department of Thailand
Chatuchak, Bangkok
Thailand

Nick G. H. Taylor
Cefas Weymouth Laboratory
Weymouth, Dorset
UK

Philip H. Taylor
Environmental Engineering Group
University of Dayton Research Institute
Dayton, OH
USA

Suzanne Tegen
National Renewable Energy Laboratory
Golden, CO
USA

Frederick J. Tenbus
EA Engineering, Science, and Technology, Inc.
Sparks, MD
USA

Keat (Thomas) Teoh
Arkansas Biosciences Institute
Arkansas State University
Jonesboro, AR
USA

Mark Tester
Australian Centre for Plant Functional Genomics
University of Adelaide
Adelaide, SA
Australia

Jeff Tester
Energy Institute, Cornell University
Ithaca, NY
USA

Elisa Thébault
CNRS, UMR 7618 "Biogéochimie et écologie des milieux continentaux"
Paris
France

Nickolas J. Themelis
Earth Engineering Center
Columbia University
New York, NY
USA

Bertrand Thériault
Directorate of Environmental and Radiation Protection and Assessment
Canadian Nuclear Safety Commission
Ottawa, ON
Canada

Louis J. Thibodeaux
Cain Department Chemical Engineering
Louisiana State University
Baton Rouge, LA
USA

Torbjörn Thiringer
Department of Energy and Environment, Division of Electric Power Engineering
Chalmers University of Technology
Göteborg
Sweden

McOwiti O. Thomas
Long Term Ecological Research Network Office
Albuquerque, NM
USA

Olivier Thomas
Environment and Health Research Laboratory
French School of Public Health
Rennes
France

Shirley Thompson
Natural Resources Institute
University of Manitoba
Winnipeg, MB
Canada

Gregory L. Thompson
Department of Urban and Regional Planning
Florida State University
Tallahassee, FL
USA

Patsy Thompson
Directorate of Environmental and Radiation Protection and Assessment
Canadian Nuclear Safety Commission
Ottawa, ON
Canada

Shirley Thompson
Natural Resources Institute
University of Manitoba
Winnipeg, MB
Canada

James S. Thorp
Bradley Department of Electrical and Computer Engineering
Virginia Polytechnic Institute and State University
Blacksburg, VA
USA

Daniela Thrän
German Biomass Research Centre (DBFZ)
Leipzig
Germany
and
Helmholtz–Centre for Environmental Research (UFZ)
Leipzig
Germany

Mahendar Thudi
Centre of Excellence in Genomics (CEG)
International Crops Research Institute for the Semi-Arid Tropics (ICRISAT)
Patancheru, Hyderabad, AP
India

Klaus Thuneke
Technologie- und Förderzentrum im Kompetenzzentrum für Nachwachsende Rohstoffe (TFZ)
Straubing
Germany

Clifford Thurber
Department of Geoscience
University of Wisconsin-Madison
Madison, WI
USA

Keith B. Tierney
Department of Biological Sciences
University of Alberta
Edmonton, AB
Canada

Ayodhya Nath Tiwari
Laboratory for Thin Films and Photovoltaics
EMPA – Swiss Federal Laboratory for Materials Science and Technology
Duebendorf
Switzerland

Lasse Tobiasen
Ramboll Energy – Waste-to-Energy
København S
Denmark

Hiroyuki Tokita
West Japan Engineering Consultants, Inc
Chuou-ku, Fukuoka
Japan

Bliss L. Tracy
Radiation Protection Bureau
Health Canada 6604C
Ottawa, ON
Canada

Henry Trapido-Rosenthal
Center for Marine Microbial Ecology and Diversity,
School of Ocean and Earth Science and Technology
University of Hawaii
Honolulu, HI
USA

Christian Trassy
CNRS
Grenoble
France

Kurniawan Rudi Trijatmiko
International Rice Research Institute
Manila
Philippines

Ralph A. Tripp
Department of Infectious Diseases, College of
Veterinary Medicine, Animal Health Research Center
University of Georgia
Athens, GA
USA

Max Troell
The Royal Swedish Academy of Sciences
The Beijer Institute of Ecological Economics
Stockholm
Sweden
and
Stockholm Resilience Centre
Stockholm University
Stockholm
Sweden

Juli M. Trtanj
National Oceanic and Atmospheric Administration,
National Ocean Service
Oceans and Human Health Initiative
Silver Spring, MD
USA

Nicholas Tsoulfanidis
Department of Nuclear Energy
Missouri University of Science and Technology
Rolla, MO
USA

Roberto Tuberosa
Department of Agroenvironmental Science and
Technology
University of Bologna
Bologna
Italy

James S. Tulenko
Laboratory for Development of Advanced Nuclear
Fuels and Materials
University of Florida
Gainesville, FL
USA

Katherine F. Turnbull
Department of Landscape Architecture & Urban
Planning, Texas Transportation Institute
College of Architecture – The Texas A&M University
System
College Station, TX
USA

David R. Turner
Geosciences and Engineering Division
Southwest Research Institute
San Antonio, TX
USA

Laura Tutusaus Codony
Department of Vegetal Production and Forestry
Science, ETSEA
University of Lleida
Lleida
Spain

Richard M. Twyman
Department of Biological Sciences
University of Warwick
Coventry
UK

Peter H. Tyedmers
Dalhousie University
Halifax, Nova Scotia
Canada

Etim U. Ubong
Center for Fuel Cell Research and Powertrain Integration, Electrical & Computer Eng
Kettering University
Flint, MI
USA

James W. Udy
Seqwater
Queensland
Australia

Alois Unterholzner
Institute for Autonomous Systems Technology, Department of Aerospace Engineering
University of the Bundeswehr Munich
Neubiberg
Germany

Karolyn Upham
Zoological Society of London
London
UK

Jeff Valdivia
Natural Resources Institute
University of Manitoba
Winnipeg, MB
Canada

Yamille Del Valle
National Electric Energy Test Research and Application Centre (NEETRAC)
Forrest Park, GA
USA

M. A. J. (Marcel) van Berlo
Free University of Amsterdam and AEB-Amsterdam
Amsterdam
The Netherlands

Michael Van Brunt
Covanta Energy Corporation
Morristown, NJ
USA

Korneel Vandenbroucke
Bayer BioScience N.V
Ghent
Belgium

Siva Reddy Vanga
ICGEB, Plant Biology: Plant Transformation Group
New Delhi
India

John R. Varcoe
Department of Chemistry
University of Surrey
Guildford
UK

Armelle M. Vardelle
Laboratoire Sciences des Procédés Céramiques et de Traitements de Surface
University of Limoges
Limoges Cedex
France

Nick Varley
Centre of Exchange and Research in Volcanology
Universidad de Colima
Col. Villas San Sebastián, Colima
Mexico

Rajender S. Varma
Sustainable Technology Division
National Risk Management Research Laboratory, U.S. Environmental Protection Agency
Cincinnati, OH
USA

Rajeev K. Varshney
Centre of Excellence in Genomics (CEG)
International Crops Research Institute for the Semi–Arid Tropics (ICRISAT)
Patancheru, Hyderabad, AP
India
and

Genomics Towards Gene Discovery Sub programme,
Generation Challenge Programme (GCP)
Generation Challenge Programme (GCP) c/o CIMMYT
Mexico, DF
Mexico
and
School of Plant Biology, Faculty of Natural and Agricultural Sciences
The University of Western Australia
Crawley, WA
Australia

N. C. Vasuki
RGM
Dover, DE
USA

Naomi E. Vaughan
School of Environmental Sciences
University of East Anglia
Norwich
UK

Luis A. Vega
Hawaii Natural Energy Institute
School of Ocean And Earth Science And Technology
University of Hawaii at Manoa
Honolulu, HI
USA

Juergen Vehlow
Karlsruhe Institute for Technology, Institute for Technical Chemistry
Karlsruhe
Germany

David W. Verner-Jeffreys
Cefas Weymouth Laboratory
Weymouth, Dorset
UK

Yves Veschetti
INES-CEA
Le Bourget du Lac
France

Armin Vetter
Plant Production and Agricultural Ecology
Thuringian State Institute for Agriculture
Dornburg
Germany

Deborah Vicuna Requesens
Arkansas Biosciences Institute
Arkansas State University
Jonesboro, AR
USA

S. Vigneswaran
University of Technology
Sydney, NSW
Australia

Sanne de Visser
Community and Conservation Ecology group
University of Groningen
Groningen
The Netherlands

Jordi Vives i Batlle
Biosphere Impact Studies Unit
Belgian Nuclear Research Centre
Mol
Belgium

Craig Vogt
Craig Vogt Inc
Hacks Neck, VA
USA

Martin Volk
Department of Computational Landscape Ecology
UFZ Helmholtz Centre for Environmental Research
Leipzig
Germany

Ilia Voloh
GE Energy, Digital Energy
Norcross, GA
USA

A. Von Felde
Energy Plants
KWS SAAT AG
Einbeck
Germany

Vukan R. Vuchic
Department of Electrical & Systems Engineering
University of Pennsylvania
Philadelphia, PA
USA

Jan Vymazal
Department of Landscape Ecology
Czech University of Life Sciences Prague
Kostelec nad Černými lesy, Prague
Czech Republic
and
ENKI, o.p.s.
Třeboň
Czech Republic

Robert B. Waide
Long Term Ecological Research Network Office
Albuquerque, NM
USA

Edward J. Waller
University of Ontario Institute of Technology
Oshawa, ON
Canada

S. Travis Waller
Department of Civil Engineering
The University of Texas at Austin
Austin
USA

Desmond E. Walling
Department of Geography
College of Life and Environmental Sciences
University of Exeter
Exeter
UK

Thomas Wallner
Energy Systems Division
Argonne National Laboratory
Argonne, IL
USA

Achim Walter
IBG–2: Plant Science
Forschungszentrum Jülich
Jülich
Germany
and
ETH Zürich
Institute of Plant, Animal and Agroecosystem
Sciences, Professorship of Crop Science
Zurich
Switzerland

Dale R. Walters
Crop & Soil Systems Research Group
Scottish Agricultural College
Edinburgh
UK

Chien Wang
Department of Earth, Atmospheric, and
Planetary Sciences
Massachusetts Institute of Technology
Cambridge, MA
USA

Deyu Wang
Pacific Northwest National Laboratory
Richland, WA
USA

Wei Wang
Pacific Northwest National Laboratory
Richland, WA
USA

Jianqiang Wang
State Key Laboratory of Automotive Safety
and Energy
Tsinghua University
Beijing
China

Fei-Yue Wang
Institute of Automation
Chinese Academy of Sciences
Beijing
China

Ping Wang
Department of Information and Communication Engineering
Tongji University
Shanghai
China

Michael Wang
Center for Transportation Research
Argonne National Laboratory
Argonne, IL
USA

Scott D. Warner
AMEC
Oakland, CA
USA

Michael W. Wascom
Department of Environmental Sciences
Louisiana State University
Baton Rouge, LA
USA

Michael M. Watkins
Jet Propulsion Laboratory
California Institute of Technology
Pasadena, CA
USA

Donald Watson
FAIA
Trumbull, CT
USA

Kym Watson
Department Information Management
Fraunhofer Institute of Optronics, System Technologies and Image Exploitation IOSB
Karlsruhe
Germany

E. Scott Weber III
Medicine and Epidemiology: Vet Med Center for Aquatic Biology and Aquaculture
University of California, Davis
Davis, CA
USA

Leah Wehmas
Department of Environmental and Molecular Toxicology
Environmental Health Sciences Center, Oregon State University
Corvallis, OR
USA

Philipp Weihs
University of Natural Resources and Applied Life Sciences
Vienna
Austria

Gerhard Weinrebe
Schlaich Bergermann Solar GmbH
Stuttgart
Germany

Nadja Weller
Deutsches BiomasseForschungsZentrum GmbH
German Biomass Research Centre (DBFZ)
Leipzig
Germany

Susan White
NOAA Center for Excellence in Oceans and Human Health
National Oceanic and Atmospheric Administration's Hollings Marine Laboratory
Charleston, SC
USA

C. Bruce A. Whitelaw
The Roslin Institute and Royal (Dick) School of Veterinary Studies
Division of Developmental Biology
University of Edinburgh
Midlothian, Scotland
UK

Renatus Widmann
Department of Urban Water and Waste Management
University of Duisburg-Essen
Essen
Germany

Andreas Wiese
Energy Division
Lahmeyer International GmbH
Bad Vilbel
Germany

Martin Wild
Institute for Atmospheric and Climate Science
ETH Zurich
Zurich
Switzerland

Kristine L. Willett
Department of Pharmacology and Environmental Toxicology Research Program
University of Mississippi School of Pharmacy
University, MS
USA

Eric Williams
Golisano Institute of Sustainability
Rochester Institute of Technology
Rochester, NY
USA

Vincent L. Wilson
Department of Environmental Sciences
Louisiana State University
Baton Rouge, LA
USA

Andreas Wimmer
Institute of Measurement, Control, and Microtechnology
University of Ulm
Ulm
Germany

Marshall A. Wise
Joint Global Change Research Institute (JGCRI)
Pacific Northwest National Laboratory (PNNL)
College Park, MD
USA

Christian Wöhler
Image Analysis Group
Dortmund University of Technology
Dortmund
Germany

Bartosz Wojszczyk
GE Energy, Digital Energy
Norcross, GA
USA

Maarten Wolsink
Department of Geography, Planning and International Development Studies
University of Amsterdam
Amsterdam
The Netherlands

Y. S. Wong
State Grid Energy Research Institute
State Grid Corporation of China
China

Jacquelina W. Woods
US Food and Drug Administration
Center for Food Safety and Applied Nutrition
Gulf Coast Seafood Lab
Dauphin Island, AL
USA

Richard P. Wool
Department of Chemical Engineering, Center for Composite Materials, Affordable Composites from Renewable Sources (ACRES)
University of Delaware
Newark, DE
USA

Christopher R. Wronski
Electrical Engineering Department
Center for Thin Film Devices
Pennsylvania State University
University Park, PA
USA

Tianbin Wu
Institute of Chemistry, Chinese Academy of Sciences
Beijing
China

Jianguo (Jingle) Wu
School of Life Sciences and Global Institute of Sustainability
Arizona State University
Tempe, AZ
USA

Hans-Joachim Wuensche
Institute for Autonomous Systems Technology
Department of Aerospace Engineering
University of the Bundeswehr Munich
Neubiberg
Germany

Christoph Wünsch
Institute of Waste Management and Contaminated Site Treatment
Technical University of Dresden
Pirna
Germany

Nicolas Wyrsch
Photovoltaics and Thin-film Electronics Laboratory
Institute of Microengineering (IMT), Ecole Polytechnique Fédérale de Lausanne (EPFL)
Neuchâtel
Switzerland

Jie Xiao
Pacific Northwest National Laboratory
Richland, WA
USA

Long Xiong
Key Lab of Machine Perception (MOE)
Peking University
Beijing
China

Wenqiang Xu
Department of Information and Communication Engineering
Tongji University
Shanghai
China

Wu Xu
Pacific Northwest National Laboratory
Richland, WA
USA

Ming Xu
School of Natural Resources and Environment
University of Michigan
Ann Arbor
USA

Atsuo Yamada
Department of Chemical System Engineering
The University of Tokyo
Tokyo
Japan

Tong Yang
Department of Civil and Building Engineering
Loughborough University
Leicestershire
UK

Gary Yang
Pacific Northwest National Laboratory
Richland, WA
USA

Helen T. Yap
The Marine Science Institute
University of the Philippines
Quezon City
Philippines

Charles Yarish
Departments of Ecology & Evolutionary Biology and Marine Sciences
University of Connecticut
Stamford, CT
USA

Harumi Yokokawa
Advanced Research Laboratories
Tokyo City University
Tokyo
Japan
and
National Institute of Advanced Industrial Science and Technology (AIST)
Tsukuba, Ibaraki
Japan

Jin-Ho Yoon
Atmospheric Science and Global Change Division
Pacific Northwest National Laboratory
Richland, WA
USA

Seokmin Yoon
Environment Research Division
Research Institute of Industrial Science and Technology (RIST)
Pohang
Republic of Korea

Kunio Yoshikawa
Frontier Research Center
Tokyo Institute of Technology
Yokohama
Japan

Dawei Yuan
Department of Vegetal Production and Forestry Science, ETSEA
University of Lleida
Lleida
Spain

Guido Zacchi
Department of Chemical Engineering
Lund University
Lund
Sweden

A. Zapata
Plataforma Solar de Almería (CIEMAT)
Tabernas, Almería
Spain

P. Zapp
Institute of Energy Research, Forschungszentrum Jülich
Juelich
Germany

O. Zarrouk
Plant Molecular Ecophysiology Laboratory (LEM)
Instituto de Tecnologia Química e Biológica
Universidade Nova de Lisboa
Oeiras
Portugal

Rong Zeng
Department of Chemistry
University of Surrey
Guildford
UK

Xubin Zeng
The Department of Atmospheric Sciences
University of Arizona
Tucson, AZ
USA

Hongbin Zha
Key Lab of Machine Perception (MOE)
Peking University
Beijing
China

Junliang Zhang
Electrochemical Energy Research Laboratory
General Motors Global R&D
Honeoye Falls, NY
USA

Ming Zhang
Graduate Program in Community and Regional Planning
School of Architecture, The University of Texas at Austin
Austin, TX
USA

Harry X. Zhang
Associate Editor on Sustainability, Journal of Water Science and Technology, IWA
Reston, VA
USA

Ji-Guang Zhang
Pacific Northwest National Laboratory
Richland, WA
USA

Zhengming (John) Zhang
Celgard, LLC
Charlotte, NC
USA

Wenming Zhang
Department of Civil and Environmental Engineering
University of Alberta
Edmonton, AB
Canada

Lei Zhang
State Key Laboratory of Automotive Safety and Energy
Tsinghua University
Beijing
China

Huijing Zhao
Key Lab of Machine Perception (MOE)
Peking University
Beijing
China

Yipu Zhao
Key Lab of Machine Perception (MOE)
Peking University
Beijing
China

Chunmiao Zheng
Department of Geological Sciences
University of Alabama
Tuscaloosa, AL
USA

Shan Zhou
School of Public Policy
Georgia Institute of Technology
Atlanta, GA
USA

Chen Zhu
Department of Geological Sciences
Indiana University
Bloomington, IN
USA

Xiaolong Zhu
Key Lab of Machine Perception (MOE)
Peking University
Beijing
China

Changfu Zhu
Department of Vegetal Production and Forestry Science, ETSEA
University of Lleida
Lleida
Spain

David Z. Zhu
Department of Civil and Environmental Engineering
University of Alberta
Edmonton, AB
Canada

Jiefang Zhu
Department of Materials Chemistry
Ångström Laboratory
Uppsala University
Uppsala
Sweden

Matteo Zignol
STOP TB Department (STB), HIV/AIDS, TB & Malaria Cluster (HTM)
World Health Organization
Geneva
Switzerland

Armin Zittermann
Clinic for Thoracic and Cardiovascular Surgery, Heart Center North Rhine-Westphalia
Ruhr University Bochum
Bad Oeynhausen
Germany

Victor Zlotnicki
Climate, Oceans and Solid Earth Science Section
Jet Propulsion Laboratory
California Institute of Technology
Pasadena, CA
USA

Uxue Zorrilla
Department of Vegetal Production and Forestry Science, ETSEA
University of Lleida
Lleida
Spain

Vladimir Zui
Belarusian Research Geological Prospecting Institute
Belarus

Peer Reviewers Assisting the Section Editors

Paul Erickson

Andreas Fischlin

Lois D. George

Jonathan Levine

Colin Macdonald

Paul McDonald

Nancy McIntyre

Bashir A. Memon

Curtis Oldenburg

Arthur Pettit

Mike Poland

Marc Portnoff

Susan Roe

David Rowan

Alvin J. Salkind

Michael Schrader

Jerry Schuett

John Smith

James Tatone

Bliss Tracy

Kwok Tsang

Mike Walters

How to Access the Articles

Each Section Editor prepared an introductory article describing their field, the articles comprising the section and the interrelationship of the articles. Thus, our readership can utilize each section introduction as the reference point to the individual articles or can look up individual articles by alphabetical entry. The introductory articles occur alphabetically, under the section name, among the 578 alphabetically listed entries.

A

Abiotic Stress Tolerant Crops: Genes, Pathways and Bottlenecks

Korneel Vandenbroucke, Michael Metzlaff
Bayer BioScience N.V, Ghent, Belgium

Article Outline

Glossary
Definition of the Subject
Introduction
Abiotic Stress-Tolerant Crops
Limitations of Genetic Engineering for Stress Tolerance
Systematic Phenotyping of Plants
Future Directions
Bibliography

Glossary

Abiotic stress Any negative impact on a living organism caused by a nonliving factor in the environment in which the organism is present.

Biological modeling *In silico* description of a biological process to generate predictions for experimental validation.

Conventional breeding Development of new plant varieties by selection after natural reproduction.

Epigenetics The study of inherited changes in phenotype or gene expression caused by mechanisms other than changes in the DNA sequence.

Genetic engineering Development of a new plant variety through genetic modification by using recombinant DNA technology.

Phenotype Observable trait or characteristic (i.e., appearance) of an organism in a specific environment.

Phenome Collection of phenotypes of an organism in all possible environments.

Phenotyping Process of studying the phenotype.

Plant productivity Ability of a plant to produce a certain amount of biomass, either as green tissue and/or as seeds (yield).

Quantitative trait locus (QTL) Stretches of DNA that are closely linked to the genes that underlie the trait in question.

Regulon biotechnology Genetic engineering by targeting genes encoding proteins with regulatory function, often transcription factors.

Trait Characteristic of an object.

Definition of the Subject

World food and feed security is increasingly dependent on continuous crop improvement and, in particular, the development of crops with increased resistance to abiotic stresses. This economical and social challenge has attracted the global community of plant breeders and scientists and many potential solutions have been put forward. Our understanding of the response of plants to abiotic stress has significantly improved over the last year. However, abiotic stress tolerance is a complex trait that can be affected by many external factors. Abiotic stress tolerance involves many processes that are not yet completely understood and several limitations still need to be overcome. Recent advances in many areas of plant research, including phenotyping, make scientists optimistic that valuable solutions will be found to allow deployment/commercialization of plants better able to tolerate abiotic stresses.

Introduction

A growing world population with increased living standards combined with the urgent need for a more sustainable agriculture demands the development of crop varieties which are able to cope with fluctuating and adverse environmental conditions limiting plant growth and productivity, referred to as abiotic stresses [1]. Further global warming is expected to aggravate the negative impact of abiotic stresses. Low water

Robert A. Meyers (ed.), *Encyclopedia of Sustainability Science and Technology*, DOI 10.1007/978-1-4419-0851-3,
© Springer Science+Business Media, LLC 2012

availability (drought stress), high salinity (salt stress), and high temperatures (heat stress) are considered to be among the most threatening abiotic stresses, which can compromise up to 80% of the attainable yield [2]. New technologies for plant improvement that aim to overcome the negative impact of these stresses therefore need to be urgently identified and implemented. Abiotic stresses and their effects on plant productivity have attracted academic scientists as well as large and small Ag biotech companies. This is reflected by increasingly more publications in peer-reviewed journals (including recent issues in plant physiology and functional plant biology dedicated to abiotic stress), online centralization of relevant information (www.plantstress.com; www.yieldbooster.org) and numerous patent applications protecting potential new solutions (Fig. 1).

Plants respond to abiotic stresses at different levels in an avoidance-tolerance mode, which includes physiological and molecular changes (Fig. 2). An important interest of plant biologists aims not only to better understand the adaptive response of plants to abiotic stress, but also to exploit this knowledge for the production of varieties that are better protected against the detrimental effects. Before the genomics era, classical or conventional breeding of plants with improved physiological characteristics was the only way to improve crop productivity. In the last 20 years, mapping of quantitative trait loci (QTL), genetic engineering, and their implementation in marker-assistant (molecular) breeding have become increasingly important [3–5]. Such genomics-based approaches rely on the identification of genes (gene discovery) that may be valuable candidates for crop improvement and were empowered by the advent of state-of-the-art molecular tools, such as DNA sequencing and expression profiling [6].

In this entry, some of the recent genomics-based advances in engineering stress-tolerant crops are summarized, existing limitations associated with these approaches are described, and some emerging trends facilitating better evaluation of crop performance in the greenhouse and in the field are outlined.

Abiotic Stress-Tolerant Crops

Plants protect themselves from the detrimental effects of abiotic stresses by increasing the expression of

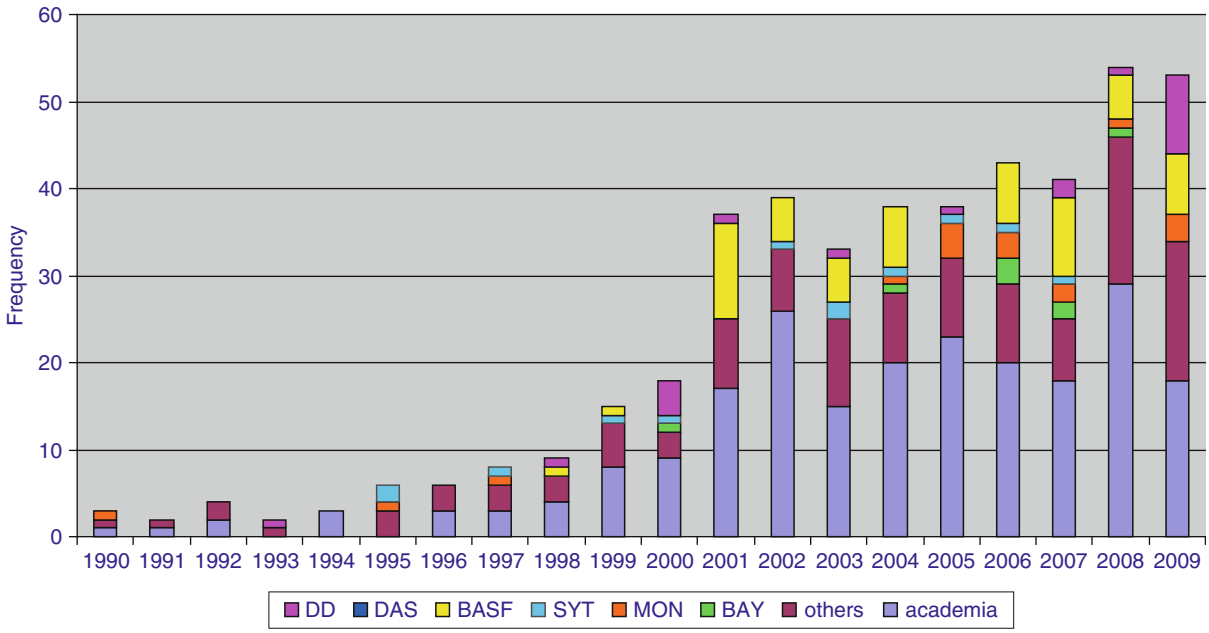

Abiotic Stress Tolerant Crops: Genes, Pathways and Bottlenecks. Figure 1
Abiotic stress-related publications of international patent applications by academia and agbiotech companies (provided by Rolf Deblaere). *BAY* Bayer, *MON* Monsanto, *SYT* Syngenta, *DD* Dupont, *DAS* Dow AgroSciences

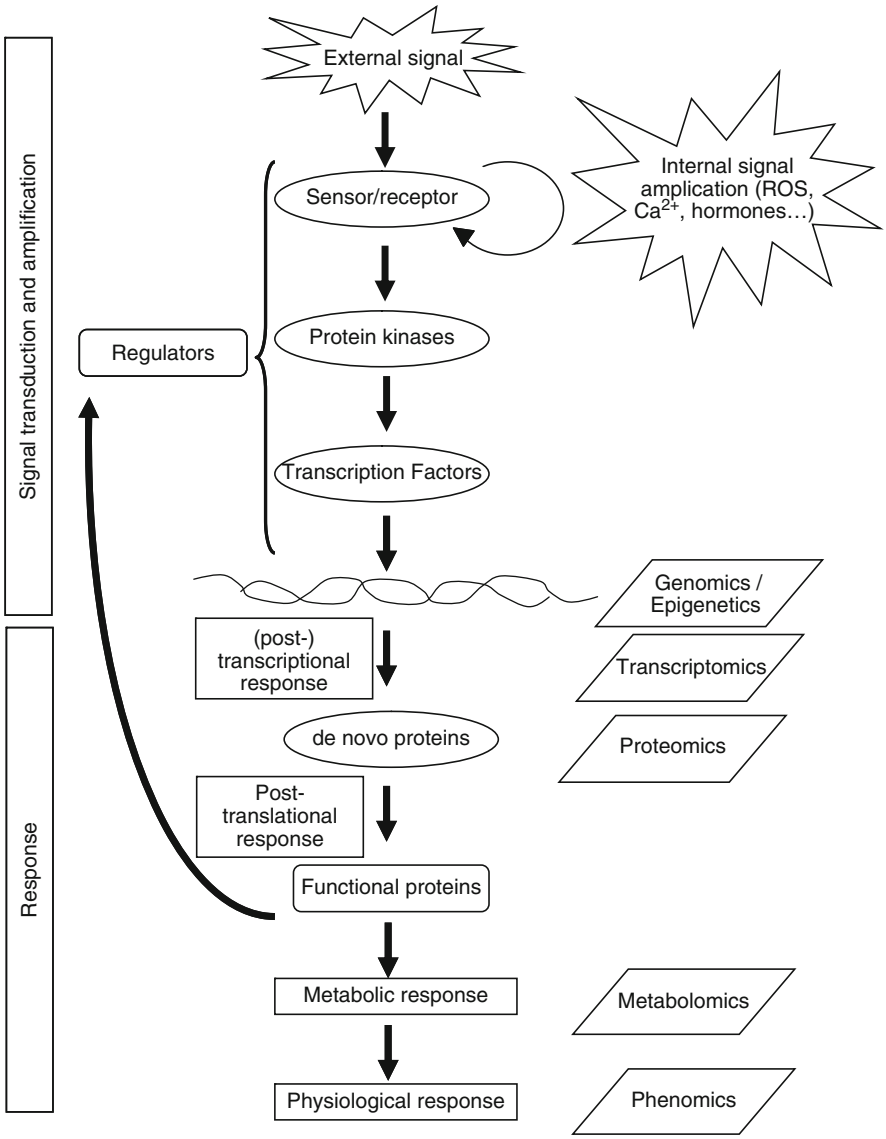

Abiotic Stress Tolerant Crops: Genes, Pathways and Bottlenecks. Figure 2
Signal transduction and response of plants to abiotic stress with the corresponding evaluation platforms

defense or stress tolerance genes. Plant varieties that evolved to have constitutive or high(er) expressed levels of such genes are better adapted to abiotic stress conditions. Genes with potential value for genetic engineering of stress tolerance have been ever more discovered either indirectly by genetic dissection of identified QTLs in stress-tolerant varieties, or directly through their changed expression in plants exposed to stress. Introduction of selected genes seems to be the favored way to improve plants in the future [1]. Plant biotechnologists have been reporting genetically engineered plants with increased stress tolerance for almost 2 decades. Many genes have already been directly employed to improve stress tolerance of higher plants using a wide variety of approaches [7].

One attractive approach for engineering stress tolerance in crops has been the constitutive overexpression of stress genes from bacteria, yeast, or model plant species, such as *Arabidopsis thaliana (Arabidopsis)*. Such a heterologous gene approach

worked particularly well when the genes encode proteins with single biological functions that are often absent or only expressed at low levels in the target plant. Such genes are often referred to as functional genes and can encode molecular protectants, detoxifying proteins, or ion transporters. A second group is comprised of regulatory proteins with often multiple biological functions, including enzymes involved in (phospho)lipid signaling, protein kinases, protein phosphatases, calcium/calmodulin-binding proteins, and various transcription factors (TFs) [8]. With the emergence of large-scale genome sequencing in crops, several crop orthologues of stress genes could be identified and increasingly be used to engineer stress tolerance in crops. Here some of the approaches for engineering stress tolerance using genes involved in different cellular processes or pathways are summarized, including detoxification, protein stabilization, osmoregulation, transport, lipid metabolism, transcription and signaling, and posttranscriptional, and (post-) translational regulation. However, genetic engineering for stress tolerance in crops is not limited to these gene classes as recently shown for mustard annexin Bj1, a gene encoding a calcium-dependent phospholipid and cytoskeleton binding protein that is involved in golgi-mediated secretion, which resulted in stress tolerance when expressed in cotton [9].

Detoxifying Genes

Most, if not all, abiotic stresses induce the accumulation of reactive oxygen species (ROS), which in turn cause oxidative stress [10, 11]. ROS are extremely reactive, and therefore can undergo uncontrollable and damaging reactions with cellular components, including DNA, lipids, and proteins. This can aggravate the detrimental effects of the initial stress and can even lead to cell death [12, 13]. To protect against oxidative stress, plant cells possess an extensive ROS scavenging network, which involves nonenzymatic antioxidants, including vitamin C, vitamin E, glutathione, carotenoids, and flavonoids, as well as numerous enzymatic mechanisms such as multiple superoxide dismutases (SOD), catalases (CAT), ascorbate peroxidases (APX), glutathione peroxidases (GPX), glutathione-S-transferases (GST), alternative oxidases, and peroxiredoxines [12]. It was hypothesized that alleviation of oxidative damage by the use of ROS scavengers would enhance plant resistance. This was confirmed by a number of transgene transfers using this detoxification strategy. Stress tolerance could be improved by either direct scavenging of ROS or by enhanced removal of oxidative damaged and hazardous components accumulating in the cell. Since the accumulation of ROS and derivatives thereof is a common theme during most, if not all, abiotic stresses, the detoxification strategy enabled the generation of transgenic plants with simultaneous tolerance to multiple stresses [14–22].

In crops, enhanced stress tolerance was achieved by increasing the level of typical scavenging enzymes such as GST, different SOD isoforms, APX, and CAT [23–28]. Overexpression of a GST enzyme in rice resulted in increased protection against salt, low temperature, and oxidative stress [23]. SOD catalyzes the dismutation of superoxide into oxygen and hydrogen peroxide (H_2O_2). Transgenic rice plants expressing a manganese SOD from pea were more tolerant to drought stress [26]. Similarly, transgenic oilseed plants ectopically expressing a wheat manganese SOD were tolerant to oxidative and heavy metal stress [15]. A copper/zinc SOD was shown to be effective to protect rice plants against drought, salt, and oxidative stress [28]. Excess H_2O_2, produced either as by-product of superoxide detoxification by SOD or directly by metabolic processes, can be removed by APX, which catalyzes the reduction of H_2O_2 to water. Cotton plants with high levels of an APX isolated from pea were tolerant to low temperature stress [24]. Because of their complementary functions (i.e., removal of superoxide and H_2O_2), also the combination of SOD and APX resulted in enhanced stress tolerance [27]. As APX, also CAT protects plants from toxic H_2O_2 molecules. Hence, expression of a wheat CAT enzyme in rice protected these plants against low temperature stress by reducing the levels of H_2O_2 [25].

Engineering tolerance to oxidative stress is not limited to the use of the traditional ROS detoxifying enzymes. Significant improvement of stress tolerance in tobacco plants was achieved by overexpressing a stress-responsive aldehyde dehydrogenase gene from maize [29]. Recently, it was also shown that ectopic expression of the cotton stress-responsive MT3a gene in tobacco increased tolerance to salt, drought, and low temperature [30]. MT3a belongs to the

metallothionein family that has numerous cellular functions including the regulation of metal homeostasis and oxidative stress. Another gene that can protect plants from abiotic stress-induced ROS is the mitochondrial alternative oxidase (AOX), the terminal oxidase in the alternative respiratory pathway of plants [31]. For example, tobacco AOX1a is necessary for survival against oxidative stress when the cytochrome pathway is dysfunctional [32].

Protein Stabilization by Molecular Chaperones

One major detrimental effect of abiotic stresses is that they usually cause protein dysfunction through denaturation and aggregation of nonfunctional or aberrant proteins. Maintaining proteins in their functional conformation is therefore important for cell survival under stress. This can be accomplished, for example, through transcriptional induction of genes encoding heat shock proteins (HSPs, [33]). HSPs control the correct folding and conformation of both structural (e.g., cell membrane) and functional (e.g., enzymes) proteins. This important function has prompted researches to create transgenic lines with increased HSP levels. Studies on HSP proteins in plants have mostly focused on heat stress [34–42]. Although most of the evidence is limited to *Arabidopsis*, the protective capacities of HSP proteins and their potential economical value for crop engineering for heat stress tolerance was proven in tomato [42]. Recently, it was demonstrated that constitutive expression of a cotton HSP, GHSP26, enhanced drought tolerance in transgenic cotton plants [43].

In addition to HSPs, also LEA-type proteins can confer molecular protection of cellular components during abiotic stress [44]. LEA-type proteins are encoded by RD (responsive to dehydration), ERD (early responsive to dehydration), KIN (cold inducible), COR (cold regulated), and RAB (responsive to abscisic acid) genes in different plant species [45, 46]. As HSPs are typically induced by high temperatures, LEA proteins accumulate in response to dehydration (drought, osmotic, and/or cold stress). The actual functions of these proteins remain however largely unknown. Their hydrophilic nature suggest that LEA proteins act as water-binding proteins, but additional functions, including ion sequestration and protein and membrane stability, have also been proposed [47, 48]. Few examples for the use of LEA proteins to engineer stress tolerance in crop exist. Increasing the levels of endogenous LEA3 through genetic engineering of rice made these plants more tolerant to drought stress [47]. Ectopic expression of barley HVA1 in oat resulted in enhanced salt and osmotic stress tolerance [49].

Osmoregulation and Protection by Genes Involved in Metabolite Biosynthesis

Plants respond to drought stress by producing organic compounds to avoid water loss from cells (dehydration) and damage to essential components (osmotic stress). Therefore, one of the earliest approaches for genetic engineering of stress tolerance in plants (reports dating from the early 1990s) consists in enhanced synthesis of such metabolites, called osmoprotectants [50, 51]. Osmoprotectants include sugars and sugar alcohols (e.g., mannitol, trehalose, and galactinol), amines (e.g., polyamines and glycine betaine), and amino acids (e.g., proline) [52, 53]. These molecules normally do not interfere with cellular functions and are therefore often referred to as compatible solutes. Many plant species lack the ability to synthesize the special osmoprotectants that naturally accumulate in stress-tolerant species. Therefore, several transgenic approaches to increase the synthesis of osmoprotectants used bacterial biosynthetic genes, such as CodA and BetA (glycine betaine), MtlD (mannitol), and genes from the ectoine or trehalose biosynthesis operon [54–59]. Alternatively, key biosynthetic genes, including betaine aldehyde dehydrogenase and choline monooxygenase (glycine betaine biosynthesis), and pyrroline carboxylate synthase (proline synthesis), were isolated from specific plant species, such as *Vigna aconitifolia* and *Spinacia oleracea* and used to induce drought and salt tolerance in wheat and rice respectively [60, 61]. Although the accumulation of compatible solutes during stress is mainly important for osmoregulation and for maintaining correct protein structures, this may also be important for reducing or preventing the damaging effects of ROS [62, 63].

Transport Proteins

Ion transport proteins are involved in reestablishing ionic homeostasis after salt stress either by increasing ion storage in the vacuole, or by improving ion

excretion from the cells [64]. Different types of ion transporters, depending on their localization and selectivity, have been the target of genetic engineering. These include both vacuolar and membrane Na^+/H^+ antiporters, vacuolar Ca^{2+}/H^+ antiporter, and Mg^{2+}, Na^+/K^+, and Ca^{2+} transporters [43, 64]. Known salt stress tolerance genes encoding ion transporters isolated from crops include NHX1 (rice), KAT1 (rice), and HKT1 (wheat) [65–67]. Plasma membrane cation/proton antiporters cause alkalinization of the apoplast, thereby changing the activity and conformation of membrane proteins, which might serve as a signal to mediate gene regulation and induce a general stress response [68]. Besides using ion transporters to induce tolerance to salt stress, tolerance to osmotic stresses was engineered by increasing the levels of proteins involved in water transport [69]. Tolerance to heavy metal stress was achieved by constitutive expression of heavy metal transport proteins, including wheat ALMT1 [70–72].

Lipid Metabolism

Adaptation of living cells to low temperatures involves alterations in the membrane lipid composition, for example, by decreasing membrane fluidity through fatty acid unsaturation. It was demonstrated that increasing the number of unsaturated fatty acids by genetic engineering could improve stress tolerance in plants [73–77]. Overexpression of a spinach glycerol-3-phosphate acyltransferase (GPAT) in rice increased tolerance to low temperature whereas downregulation of a fatty acid desaturase in rice increased tolerance to high temperatures [73, 78]. Upon overexpression, tomato GPAT also increased the tolerance of tomato plants to low temperature stress [76].

Stress Sensing and Signal Transduction

The first and probably most important step in the response of plants to abiotic stress is the sensing or detection of the external stimuli by receptors, typically located in the cellular membranes. The identification of important stress receptors has been a difficult challenge and until recently, there was no report on their use in engineering stress tolerance. Overexpression of *Arabidopsis* membrane-bound receptor-like protein kinase 1 and a membrane located calcium/calmodulin-binding receptor-like kinase from soybean in transgenic *Arabidopsis* resulted in enhanced plant tolerance to drought and salt stress, respectively [79, 80]. In rice, overexpression of SIK1 resulted in higher tolerance to salt and drought stresses [81]. Other receptors operate in the cytosol and react to internal stimuli that amplify abiotic stress signals, such as calcium and ROS, as well as various hormones and other small molecules. The best-studied stress hormone is abscisic acid (ABA), which is involved in stomatal closure and plays a crucial role in tolerance against drought stress by preventing transpiration and water loss from stomata [82]. ABA also has an essential role in activating signal transduction pathways involved in tolerance to drought, cold, and salt stress. Recently, an important ABA receptor protein family has been identified [83, 84].

Stress receptors or sensors transduce external and internal signals into an intracellular response, for example, through phosphorylation and dephosphorylation cascades controlled by protein kinases and phosphatases. Genes encoding protein kinases were successfully exploited to engineer stress-tolerant crops. Modification of normal endogenous levels of GSK1, SAPK4, CDPK7, CIPK03, CIPK12, and CIPK15 in rice protected the plants against various abiotic stresses, including drought, salt, and low temperature stress [85–88]. Expression of tobacco mitogen-activated protein kinase, NPK1, in maize resulted in drought and low temperature stress tolerance [89]. Constitutive overexpression of a stress-inducible small GTP-binding protein PgRAB7 from *Pennisetum glaucum* enhances abiotic stress tolerance in transgenic tobacco [90].

Transcriptional Regulation

In the last decade, the most widely used and probably most important strategy for engineering abiotic stress tolerance in plants relied on the expression of genes that are involved in signaling and regulatory pathways [91, 92]. The use of TFs for tailoring stress tolerance is often referred to as regulon biotechnology because it affects the expression of many target genes in parallel [93, 94]. One of the reasons for their popularity is that TFs are believed to mediate durable tolerance to multiple stresses. Most TFs that control stress tolerance in plants belong to (large) protein families based on the

presence of common DNA binding motifs and selectivity toward certain cis-regulatory elements in the promoters of target genes. These families include APETALA2/ ethylene responsive element binding proteins (AP2/EREBP) such as ethylene responsive factors (ERF), the DREB/CBF (drought-responsive element binding/cold-responsive element binding factor) proteins, basic domain leucine-zipper (bZIP) proteins such as ABFs (abscisic acid (ABA)-responsive element binding factor), basic helix-loop-helix proteins (including MYC proteins), NAC (petunia NAM *Arabidopsis* ATAF1/2, and CUC2-domain) proteins, MYB-related proteins, as well as different families of zinc-fingers domain-containing proteins, such as WRKY binding factors, C_3H- and C_2H_2-type TFs. In recent years, many excellent reviews have been published on the role and use of TFs for engineering of stress tolerance in plants [48, 93–96].

Many AP2/EREBP–type TFs, the best studied being DREB/CBF proteins, have been used to engineer stress-tolerant crops. Transgenic rice plants with higher levels of CBF1/DREB1B and CBF3/DREB1A were more resistant to drought, salt, and low temperature stress [97]. A similar approach with CBF15 and CBF17 in oilseed and NF-YB2 in maize resulted in increased tolerance to low temperature and drought stress, respectively [98, 99]. Potato plants with increased levels of endogenous EREBP1 were more tolerant to salt stress and low temperatures [100]. Ectopic expression of the soybean ERF3 gene in transgenic tobacco plants gave tolerance to drought and salt stress [101]. Similarly, ectopic expression of an *Arabidopsis* AP2/ERF TF, HARDY, in rice also induced tolerance to drought and salt [102]. Expression of TERF1 in rice regulates expression of stress-responsive genes and enhances tolerance to drought and high salinity [103].

However, not only the AP2/EREBP-type TFs have been exploited to engineer stress-tolerant crops. For example, in rice, it was shown that constitutive expression of proteins from various other TF types, including bZIP23, zinc-finger protein 245, TIFY11, MYB3R-2, IRO2, NAC6, SNAC1, and PF1 TFs, could induce tolerance to drought, salt, low temperature, and nutrient deficiency [104–111], and the rice dst mutant, DST encoding a novel C_2H_2-type TF, showed increased tolerance to drought and salt [112]. In tomato, ectopic expression of rice MYB4 and pepper PIF1 induced low temperature and drought stress tolerance, respectively [113, 114]. Also in tomato, constitutive expression of SlAREB, a bZIP TF with affinity for ABA-responsive elements, increased tolerance to drought and salt stress [115]. Ectopic expression of cotton ZFP1, encoding a CCCH-type zinc-finger protein, and rice ZFP177, an A20/AN1-type zinc finger, enhanced stress tolerance in tobacco [116, 117].

Posttranscriptional and (Post-)Translational Regulation

Posttranscriptional control of stress gene expression is mediated by proteins that are involved in splicing, export, and degradation of gene transcripts, which contributes to correct function of the encoded proteins. In the last years, it has become evident that nonprotein coding RNA molecules, including microRNA and other small RNA molecules, play a very important role in posttranscriptional regulation of plant stress responses [118]. miRNA-mediated posttranscriptional control of antioxidant gene expression seems very important in plants, as shown for APX during programmed cell death and drought stress, and for Cu/Zn SOD during tolerance against oxidative stress [21, 119, 120]. ROS-induced stabilization of SOS1 mRNA transcripts is essential for SOS1-dependent salt tolerance [68].

Several genes that encode proteins involved in RNA processing were discovered to be involved in stress tolerance processes [121–125]. In addition, also proteins that control translation (deoxyhypusine synthase, DHS), posttranslational modification (peptide methionine sulfoxide reductase, PMSR4), and protein degradation (SDIR1) are interesting candidates for engineering stress tolerance in plants [126–128]. However, the above examples resulted only from *Arabidopsis* research and much less information on the importance of such processes is available for crops. Recently, it was shown that transgenic rice plants with increased levels of methione sulfoxide reductases, MSRA and MSRB, are more tolerant to salt stress [129]. Two other approaches were reported to work in both *Arabidopsis* and oilseeds. Wang and coworkers (2005) reported that loss-of-function of farnesyl transferase (FTA and FTB) increased tolerance to drought stress [130]. Similarly, reduction of poly-ADP-ribose

polymerase (PARP) activity improved drought tolerance by increasing energy use efficiency [131]. PARP is involved in the modification of nuclear genes, such as histones. Downregulation of PARP resulted in the deregulation of the expression of genes in response to stress [132]. Processes that control stress tolerance and general fitness of plants in the field, such as energy use efficiency, can even be controlled by an epigenetic component [133]. By starting with an isogenic canola line, Hauben and coworkers could separate in subsequently selfed generations "good" and "bad" performing plants, which only differed in epigenetic parameters but remained genetically identical.

All these examples show that the plant response to abiotic stress is not only dependent on transcriptional changes, but also on RNA processing, translation, post-translational processes, and epigenetics, which are nearly unexploited until today. The lack of understanding these processes is a limiting factor in engineering stress tolerance in crops.

Limitations of Genetic Engineering for Stress Tolerance

Because conventional breeding is a very time-consuming process, genetic engineering is now an important technology for many commercial applications aiming at plant improvement [1]. Today this mainly includes the production of plants with engineered herbicide or insect tolerance. However, it has been and still is extremely challenging to progress engineered plants with reported abiotic stress tolerance from research to field applications for farmers [134]. The main factors hampering the production of commercial solutions for the abiotic stress-related problems in agriculture are related to: (1) the availability of sequence information and transformation protocols, (2) the genetic diversity between model species and crop, (3) the multigenic character of stress tolerance, (4) the definition of stress tolerance and (5) the methods for the evaluation of stress tolerance [53, 135].

The first requirements for genetic engineering of plants include the availability of sequence information and transformation protocols. This important information is still lacking for many agricultural crops. For long time, this has limited (academic) research to model plant species. Although the use of model species such as *Arabidopsis* has proven its value, the genetic diversity within higher plants is the main factor that limits translatability of results obtained in model species into commercial crops. Even in those cases where the research is conducted in a more closely related model crop, it remains to be a challenge to translate the results into genetically diverse elite varieties used for commercialization.

Another factor limiting translatability from model species to crops is the complex, multigenic character of stress tolerance mechanisms. Despite the use of single genes for engineering stress tolerance, efficient and sustainable stress tolerance requires the cooperative action of many genes that are involved in various cellular processes that are not completely understood. Due to the initial success of transcriptomics, it has been accepted for long time that responses to abiotic stresses were almost exclusively regulated at the transcriptional level by a small set of core transcription factors. However, it is now clear that many other regulatory processes such as posttranscriptional control, translation, posttranslational, and epigenetic effects play an important role. In addition, some of these processes might not always be evolutionarily conserved but rather genetically diverse.

The early availability of the full genome sequence and many molecular analysis tools has turned *Arabidopsis* into the primary model species of choice for academic research in general, and for studying the response of plants to abiotic stresses in particular. However, the methods for evaluation of stress tolerance using *Arabidopsis* plants grown in a laboratory environment and agricultural crops in the field can be quite diverse. From an agronomic point of view, it is more relevant to study the effects of abiotic stresses on plant growth and yield over longer periods which cover the life span of a crop under field conditions. Appropriate field tests are therefore highly important because they allow studying plants in their natural environment in which they are exposed to combination of multiple stresses or cycles of the same stress [136]. In contrast to the field situation for crops, most studies on abiotic stress in *Arabidopsis* focus on short-term and strong stress treatments. Therefore, evaluation of stress tolerance is often focused on survival which is easier to screen. In contrast, yield-related traits are more difficult to measure but much more important for

crops. Abiotic stress tolerance of crops should therefore be defined as the potential to produce high yields when exposed to mild(er), multiple stresses instead of the ability to survive a single, lethal stress.

Another limiting factor for successful field applications of plants with engineered protection against stress is the seemingly mutual exclusive characteristic of high yield under normal conditions and high stress tolerance. Most reported experiments focused either on abiotic stress tolerance or on yield rather than including detailed analysis of both traits. More in-depth analysis of stress-tolerant plants under "normal" conditions often revealed a negative effect on growth, development, and yield traits. On the other hand, engineered plant with improved growth features, for example, by boosting a metabolic process, can be less adapted to maintain growth under abiotic stress conditions. Negative effects, often referred to as yield penalty, can be (at least partially) circumvented by temporally and spatially controlled expression of the target gene [137]. However, the availability of suitable promoters is still limited. Improved sequencing and bioinformatic tools for identification and construction of promoters allowing the expression of genes in a spatially and temporally controlled manner can overcome this bottleneck.

Phenotyping experiments with a set of genetically defined plants are often difficult to repeat because plants are largely influenced by the environment in which they grow. In fact, growth and yield (i.e., performance) of a plant under normal or stress conditions is the output of all integrated physiological processes in the plant. It is therefore not surprising that different laboratories often obtain different results for plant performance [138]. More effort is needed to describe and standardize the design of the experiments, of protocols for measuring traits, and of the growing conditions. Different methods to evaluate stress tolerance in *Arabidopsis* and a conceptual framework for phenotyping during breeding for drought tolerance have already been proposed, including defining the minimal information needed for carrying out a drought stress experiment [139, 140]. Improved and systematic phenotyping of plants will greatly contribute to overcome the limitations associated with the methods to evaluate stress tolerance.

Systematic Phenotyping of Plants

In the last decades, it has become clear that there is a substantial need for automation of research processes [141]. Automation not only allows increasing throughput, but also ameliorates standardization, reproducibility, and therefore the overall quality of an experiment. Automation increases the research value and also reduces "cost to practice" for companies aiming to apply the research findings toward the development of a superior and sustainable product. It can therefore be assumed that automation will help to improve the translation of research findings into valuable products for the customer.

Plant research has already embraced the development of high-throughput screening experiments that were used for drug or herbicide discovery. Such experiments focused on assessment of certain molecular function. Next to these screens, also high-content screening protocols were developed to asses such molecules in a biological assay. Although these technologies have proven value for single trait discovery, the efficient development of plants with complex, multifactorial traits such as increased tolerance to abiotic stresses is fully dependent on protocols and methods to automatically phenotype at the plant level. The performance of whole plants is assessed by studying their physiology or phenotype in tissue culture, environmentally controlled growth chambers, greenhouse, or the field. Various methods for automated phenotyping of plants or plant parts in well-defined environments have been published [141]. After the establishment of genomics, transcriptomics, proteomics, and metabolomics in plant sciences, which all greatly contributed to gene or lead discovery in the field of abiotic stress, plant phenomics needs to be developed and implemented [142–144].

Plant phenomics is expected to enable the efficient and reliable evaluation of a new trait solution and thereby enhance breeding for stress-tolerant varieties. Large, dedicated plant phenotyping centers such as the ACPFG in Adelaide (Plant Accelator™; http://www.plantaccelerator.org.au/), the CSIRO Plant Industry in Canberra (High Resolution Plant Phenomics Centre; http://www.plantphenomics.org.au/HRPPC), or the Research Centre in Jülich (Jülich Phenomics Centre; http://www.fz-juelich.de/icg/icg-3/jppc/) have been

created. These research institutions can act as service providers for academia and industry by centralizing both high-tech infrastructure and highly skilled researchers with different background, including engineering, mathematics, computer science, and plant physiology/biology. An important biological question that probably can be answered by automated phenomics studies is which phenotypes or combination of multiple phenotypes need or do not need to be collected in order to be able to correctly evaluate plant performance in the environment of interest. Moreover, parallel phenotyping of plants in one or multiple environments allows detection of associations between traits [145]. Identification of redundant information from (highly) associated phenotypes will help to reduce complexity and focus on essential phenotypes.

Well-described examples of automated platforms from academia or private companies to study the phenotype of model plants or crops include phenopsis, phenodyn, GROWSCREEN, TraitMill™, PlaRoM, and various LemnaTec products. Phenopsis is a phenotying platform for *Arabidopsis* that allows measuring multiple parameters, including plant growth, water use, and transpiration rates, which are associated to plant performance under normal and drought stress conditions [146]. Phenodyn was specifically constructed to perform similar experiments with monocots such as maize and rice [147]. GROWSCREEN is an automated method for growth analysis of a limited set of small seedlings [148]. TraitMill™, one of the first automated phenotyping systems, was developed to study traits in rice [149]. LemnaTec offers commercialized phenotyping systems for different purposes and has customers from both academia and industry all over the world (http://www.lemnatec.com). Although most phenotyping platforms focus on the shoot of the plant, several systems for root phenotyping were also developed [150, 151]. By using large field scanners, it is even possible to use similar approaches during field trials.

One common feature of all automated phenotyping systems is the use of digital cameras for imaging. The use of digital imaging has many advantages over traditional plant phenotyping efforts. While traditional experiments were often dependent on subjective visual scoring of plant traits or on labor-intensive, often destructive manual sampling, for example, for fresh and dry weight measurements, automated phenotyping by digital imaging is nondestructive, and therefore allows following the development of a single plant over time [152]. Another important advantage of digital imaging is that the raw data (digital images) can be easily stored and accessed later on for reanalysis, providing there is a good database in place. Obviously, adequate image analysis software is an essential feature in the concept of automated phenotyping. Several (semi-automated) image analysis tools are based on the free-ware ImageJ software, but other, more sophisticated software, for 2D or 3D analysis, were designed for measurement of leaf shape (LAMINA, [153]), root growth (GROWSCREEN_ROOT, [154]; ROOTEDGE, [155]; RHIZOSCAN, [156]; [157]; EZ-Rhizo, [158]); and hypocotyl growth and shape (HYPOTrace, [159]). The challenge is to find the most appropriate software that can extract the information relevant for the biological questions driving the experiment. Depending on the type of digital camera and the image analysis software, different types of information that describe the phenotype of the plant can be extracted: morphological or physiological and quantitative or qualitative. For example, conventional imaging can be used to measure color, shape, length, width, and size. Video imaging or consecutive imaging of the same plant or plant part over time even allows calculating plant growth. Thermal imaging (infrared thermography) is used to measure temperature and transpiration, while fluorescence and reflectance imaging allows measuring photosynthetic activity of a plant leaf or canopy. Leaf density in the canopy can be analyzed using light detection and ranging imaging that is based on laser scanning. It is now also possible to use typical clinical imaging applications, for example, magnetic resonance imaging (MRI, alternatively called nuclear magnetic resonance) for studying plant hydraulics (water or sap flow) and carbon biomass production [160]. X-ray computed tomography and a combined analysis using MRI and positron emission tomography allow the nondestructive analysis of root growth in soil environments [154]. All these types of image-derived information can be relevant to study abiotic stress tolerance mechanisms, but temperature and photosynthetic activity of leaves are among the most widely studied phenotypes in the response to abiotic stresses.

Imaging is particularly useful for the rapid, early-stage detection of abiotic stress in a plant because it allows detecting changes in the plant performance beyond the naked eye. It is therefore a unique way to diagnose plants. Understanding how plants sense stresses can be considered as a prerequisite for engineering stress tolerance. It can be assumed that plants that have reduced stress-sensing capacities will continue to grow in mild stress conditions for longer time and thereby produce higher yields. In contrast, when subjected to severe or lethal stresses, the same plants could have a disadvantage because the investment into energy-demanding processes such as growth is high and tolerance mechanisms may be induced only late. Therefore, when exposed to severe stress conditions, plants ideally should be able to increase their stress-sensing ability.

Future Directions

Increased protection of plants against abiotic stresses involves a complex regulatory network controlling morphological, physiological, biochemical, and molecular changes. Understanding such changes has been of key importance in breeding. Breeding crop varieties with improved performance under suboptimal growing conditions is now one of the ambitious, but crucial objectives in modern plant biotechnology. Despite the great progress in the last decade, it is now apparent that abiotic stress tolerance is a complex trait involving genes with different biological functions. However, the number of genes that were actually successfully used to improve crop performance in the field is still low. Although many types of genes or processes have been the target of genetic engineering, certain areas are still unexplored. Interesting developments were recently made in the field of miRNA regulation and epigenetics [161]. Another unexplored field is that of small peptides and their role during abiotic stress signaling.

It is very unlikely that there will be one or a few solutions for current agronomic challenges caused by abiotic stresses, but rather specific solutions for specific cases. Most of the current findings originate from work in model plant species, but much more work is needed to translate such basic research findings to crops. Because of the complex nature of abiotic stress tolerance in plants, it appears that modifying one gene to induce stress tolerance will be in many cases not sufficient. Hence, the approach of using regulon biotechnology for crop improvement, modifying a functional process or even multiple interconnected functional processes instead of one single function, appears to be the way forward. However, this approach is often limited by the lack of knowledge on the network of molecular mechanisms underpinning stress tolerance. Conventional approaches were also hampered by experimental limitations, which can now (partially) be overcome by the advent of automated phenotyping platforms for both model and crop species. Based on the efforts made for phenotyping of *Arabidopsis* plants, it can be anticipated that this small weed will remain the primary model system of choice for academic/basic research in near future. However, "omics" platforms for crop species are becoming available and it will not take too long before research in model crop species will become intensified. Validation of results obtained in *Arabidopsis* in (model) crops will increase the value of the lead technologies and justify the large investments for field trials.

After the development of high-throughput, automated platforms to study plant phenotypes in various environments, it will be essential to combine the data obtained from the various "omics" platforms to intensify biological modeling. Modeling has proven to be useful to study specific processes, such as root growth and flowering. Efforts are now being made to model abiotic stress tolerance in plants [162]. Improved phenotyping technologies will not only allow better experimental validation of predictions drawn from such biological models, but also to improve existing models by including knowledge on the impact of external factors such as abiotic stresses. By including modeling in biological studies, our understanding of the plants' response to abiotic stress will reach a systems biology level, a new quality in plant sciences, which will accelerate the breeding process toward abiotic stress tolerance in all our major crops.

Bibliography

1. Fedoroff NV, Battisti DS, Beachy RN, Cooper PJ, Fischhoff DA, Hodges CN, Knauf VC, Lobell D, Mazur BJ, Molden D, Reynolds MP, Ronald PC, Rosegrant MW, Sanchez PA, Vonshak A, Zhu JK (2010) Radically rethinking agriculture for the 21st century. Science 327:833–834

2. Buchanan BB, Gruissem W, Jones RL (eds) (2000) Biochemistry and molecular biology of plants. American Society of Plant Physiologists, Rockville
3. Ribaut JM, Ragot M (2007) Marker-assisted selection to improve drought adaptation in maize: the backcross approach, perspectives, limitations, and alternatives. J Exp Bot 58:351–360
4. Sreenivasulu N, Sopory SK, Kavi Kishor PB (2007) Deciphering the regulatory mechanisms of abiotic stress tolerance in plants by genomic approaches. Gene 388:1–13
5. Witcombe JR, Hollington PA, Howarth CJ, Reader S, Steele KA (2008) Breeding for abiotic stresses for sustainable agriculture. Philos Trans R Soc Lond B Biol Sci 363:703–716
6. Vij S, Tyagi AK (2007) Emerging trends in the functional genomics of the abiotic stress response in crop plants. Plant Biotechnol J 5:361–380
7. Bhatnagar-Mathur P, Vadez V, Sharma KK (2008) Transgenic approaches for abiotic stress tolerance in plants: retrospect and prospects. Plant Cell Rep 27:411–424
8. Shinozaki K, Yamaguchi-Shinozaki K (2007) Gene networks involved in drought stress response and tolerance. J Exp Bot 58:221–227
9. Divya K, Jami SK, Kirti PB (2010) Constitutive expression of mustard annexin, AnnBj1 enhances abiotic stress tolerance and fiber quality in cotton under stress. Plant Mol Biol 73:293–308
10. Apel K, Hirt H (2004) Reactive oxygen species: metabolism, oxidative stress, and signal transduction. Annu Rev Plant Biol 55:373–399
11. Laloi C, Apel K, Danon A (2004) Reactive oxygen signalling: the latest news. Curr Opin Plant Biol 7:323–328
12. Halliwell B (2006) Reactive species and antioxidants Redox biology is a fundamental theme of aerobic life. Plant Physiol 141:312–322
13. Van Breusegem F, Dat JF (2006) Reactive oxygen species in plant cell death. Plant Physiol 141:384–390
14. Badawi GH, Kawano N, Yamauchi Y, Shimada E, Sasaki R, Kubo A, Tanaka K (2004) Over-expression of ascorbate peroxidase in tobacco chloroplasts enhances the tolerance to salt stress and water deficit. Physiol Plant 121:231–238
15. Basu U, Good AG, Taylor GJ (2001) Transgenic Brassica napus plants overexpressing aluminium- induced mitochondrial manganese superoxide dismutase cDNA are resistant to aluminium. Plant Cell Environ 24:1269–1278
16. Gaber A, Yoshimura K, Yamamoto T, Yabuta Y, Takeda T, Miyasaka H, Nakano Y, Shigeoka S (2006) Glutathione peroxidase-like protein of Synechocystis PCC 6803 confers tolerance to oxidative and environmental stresses in transgenic Arabidopsis. Physiol Plant 128:251–262
17. Gong H, Jiao Y, Hu WW, Pua EC (2005) Expression of glutathione-S-transferase and its role in plant growth and development in vivo and shoot morphogenesis in vitro. Plant Mol Biol 57:53–66
18. Yoshimura K, Miyao K, Gaber A, Takeda T, Kanaboshi H, Miyasaka H, Shigeoka S (2004) Enhancement of stress tolerance in transgenic tobacco plants overexpressing Chlamydomonas glutathione peroxidase in chloroplasts or cytosol. Plant J 37:21–33
19. Murgia I, Tarantino D, Vannini C, Bracale M, Carravieri S, Soave C (2004) Arabidopsis thaliana plants overexpressing thylakoidal ascorbate peroxidase show increased resistance to Paraquat-induced photooxidative stress and to nitric oxide-induced cell death. Plant J 38:940–953
20. Oberschall A, Deák M, Török K, Sass L, Vass I, Kovács I, Fehér A, Dudits D, Horváth GV (2000) A novel aldose/aldehyde reductase protects transgenic plants against lipid peroxidation under chemical and drought stresses. Plant J 24:437–446
21. Sunkar R, Kapoor A, Zhu JK (2006) Posttranscriptional induction of two Cu/Zn superoxide dismutase genes in Arabidopsis is mediated by downregulation of miR398 and important for oxidative stress tolerance. Plant Cell 18:2051–2065
22. Yamamoto A, Bhuiyan MN, Waditee R, Tanaka Y, Esaka M, Oba K, Jagendorf AT, Takabe T (2005) Suppressed expression of the apoplastic ascorbate oxidase gene increases salt tolerance in tobacco and Arabidopsis plants. J Exp Bot 56:1785–1796
23. Zhao F, Zhang H (2006) Expression of Suaeda salsa glutathione S-transferase in transgenic rice resulted in a different level of abiotic stress resistance. J Agric Sci 144:547–554
24. Kornyeyev D, Logan BA, Payton P, Allen RD, Holaday AS (2001) Enhanced photochemical light utilization and decreased chilling-induced photoinhibition of photosystem II in cotton overexpressing genes encoding chloroplast-targeted antioxidant enzymes. Physiol Plant 113:323–331
25. Matsumura T, Tabayashi N, Kamagata Y, Souma C, Saruyama H (2002) Wheat catalase expressed in transgenic rice can improve tolerance against low temperature stress. Physiol Plant 116:317–327
26. Wang FZ, Wang QB, Kwon SY, Kwak SS, Su WA (2005) Enhanced drought tolerance of transgenic rice plants expressing a pea manganese superoxide dismutase. J Plant Physiol 162:465–472
27. Lee SH, Ahsan N, Lee KW, Kim DH, Lee DG, Kwak SS, Kwon SY, Kim TH, Lee BH (2007) Simultaneous overexpression of both CuZn superoxide dismutase and ascorbate peroxidase in transgenic tall fescue plants confers increased tolerance to a wide range of abiotic stresses. J Plant Physiol 164:1626–1638
28. Prashanth SR, Sadhasivam V, Parida A (2008) Over expression of cytosolic copper/zinc superoxide dismutase from a mangrove plant Avicennia marina in indica rice var Pusa Basmati-1 confers abiotic stress tolerance. Transgenic Res 17:281–291
29. Huang W, Ma X, Wang Q, Gao Y, Xue Y, Niu X, Yu G, Liu Y (2008) Significant improvement of stress tolerance in tobacco plants by overexpressing a stress-responsive aldehyde dehydrogenase gene from maize (Zea mays). Plant Mol Biol 68:451–463
30. Xue T, Li X, Zhu W, Wu C, Yang G, Zheng C (2009) Cotton metallothionein GhMT3a, a reactive oxygen species scavenger, increased tolerance against abiotic stress in transgenic tobacco and yeast. J Exp Bot 60:339–349

31. Van Aken O, Giraud E, Clifton R, Whelan J (2009) Alternative oxidase: a target and regulator of stress responses. Physiol Plant 137:354–361
32. Zhang Y, Xi D, Wang J, Zhu D, Guo X (2009) Functional analysis reveals effects of tobacco alternative oxidase gene (NtAOX1a) on regulation of defence responses against abiotic and biotic stresses. Biosci Rep 29:375–383
33. Wang W, Vinocur B, Shoseyov O, Altman A (2004) Role of plant heat shock proteins and molecular chaperones in the abiotic stress response. Trends Plant Sci 9:244–252
34. Katiyar-Agarwal S, Agarwal M, Grover A (2003) Heat-tolerant basmati rice engineered by over-expression of hsp101. Plant Mol Biol 51:677–686
35. Guo S-J, Zhou H-Y, Zhang XS, Li X-G, Meng Q-W (2007) Overexpression of CaHSP26 in transgenic tobacco alleviates photoinhibition of PSII and PSI during chilling stress under low irradiance. J Plant Physiol 164:126–136
36. Hong S-W, Vierling E (2000) Mutants of Arabidopsis thaliana defective in the acquisition of tolerance to high temperature stress. Proc Natl Acad Sci USA 97:4392–4397
37. Lee JH, Schöffl F (1996) An Hsp70 antisense gene affects the expression of HSP70/HSC70, the regulation of HSF, and the acquisition of thermotolerance in transgenic Arabidopsis thaliana. Mol Gen Genet 252:11–19
38. Malik MK, Slovin JP, Hwang CH, Zimmerman JL (1999) Modified expression of a carrot small heat shock protein gene, hsp17. 7, results in increased or decreased thermotolerance. Plant J 20:89–99
39. Park SM, Hong CB (2002) Class I small heat-shock protein gives thermotolerance in tobacco. J Plant Physiol 159:25–30
40. Queitsch C, Hong SW, Vierling E, Lindquist S (2000) Heat shock protein 101 plays a crucial role in thermotolerance in Arabidopsis. Plant Cell 12:479–492
41. Rhoads DM, White SJ, Zhou Y, Muralidharan M, Elthon TE (2005) Altered gene expression in plants with constitutive expression of a mitochondrial small heat shock protein suggests the involvement of retrograde regulation in the heat stress response. Physiol Plant 123:435–444
42. Yang JY, Sun Y, Sun AQ, Yi SY, Qin J, Li MH, Liu J (2006) The involvement of chloroplast HSP100/ClpB in the acquired thermotolerance in tomato. Plant Mol Biol 62:385–395
43. Maqbool A, Abbas W, Rao AQ, Irfan M, Zahur M, Bakhsh A, Riazuddin S, Husnain T (2010) Gossypium arboreum GHSP26 enhances drought tolerance in Gossypium hirsutum. Biotechnol Prog 26:21–25
44. Wang W, Vinocur B, Altman A (2003) Plant responses to drought, salinity and extreme temperatures: towards genetic engineering for stress tolerance. Planta 218:1–14
45. Shinozaki K, Yamaguchi-Shinozaki K (2000) Molecular response to dehydration and low temperature: Differences and cross-talk between two stress signaling pathways. Curr Opin Plant Biol 3:217–223
46. Zhu JK (2002) Salt and drought stress signal transduction in plants. Annu Rev Plant Biol 53:247–273
47. Thomashow MF (1998) Role of cold-responsive genes in plant freezing tolerance. Plant Physiol 118:1–8
48. Thomashow MF (1999) Plant cold acclimation: freezing tolerance genes and regulatory mechanisms. Annu Rev Plant Physiol Plant Mol Biol 50:571–599
49. Xiao B, Huang Y, Tang N, Xiong L (2007) Over-expression of a LEA gene in rice improves drought resistance under the field conditions. Theor Appl Genet 115:35–46
50. Delauney AJ, Verma DPS (1993) Proline biosynthesis and osmoregulation in plants. Plant J 4:215–223
51. Tarczynski MC, Jensen RG, Bohnert HJ (1993) Stress protection of transgenic tobacco by production of the osmolyte mannitol. Science 259:508–510
52. Hasegawa PM, Bressan RA, Zhu JK, Bohnert HJ (2000) Plant cellular and molecular responses to high salinity. Annu Rev Plant Physiol Plant Mol Biol 51:463–499
53. Vinocur B, Altman A (2005) Recent advances in engineering plant tolerance to abiotic stress: achievements and limitation. Curr Opin Biotechnol 16:123–132
54. Kathuria H, Giri J, Nataraja KN, Murata N, Udayakumar M, Tyagi AK (2009) Glycinebetaine-induced water-stress tolerance in codA-expressing transgenic indica rice is associated with up-regulation of several stress responsive genes. Plant Biotechnol J 7:512–526
55. Jang IC, Oh SJ, Seo JS, Choi WB, Song SI, Kim CH, Kim YS, Seo HS, Choi YD, Nahm BH, Kim JK (2003) Expression of a bifunctional fusion of the Escherichia coli genes for trehalose-6-phosphate synthase and trehalose-6-phosphate phosphatase in transgenic rice plants increases trehalose accumulation and abiotic stress tolerance without stunting growth. Plant Physiol 131:516–524
56. Garg AK, Kim J-K, Owens TG, Ranwala AP, Choi YD, Kochian LV, Wu RJ (2002) Trehalose accumulation in rice plants confers high tolerance levels to different abiotic stresses. Proc Natl Acad Sci USA 99:15898–15903
57. Quan R, Shang M, Zhang H, Zhao Y, Zhang J (2004) Engineering of enhanced glycine betaine synthesis improves drought tolerance in maize. Plant Biotechnol J 2:477–486
58. Park EJ, Jeknić Z, Pino MT, Murata N, Chen TH (2007) Glycinebetaine accumulation is more effective in chloroplasts than in the cytosol for protecting transgenic tomato plants against abiotic stress. Plant Cell Environ 30:994–1005
59. Abebe T, Guenzi AC, Martin B, Cushman JC (2003) Tolerance of mannitol-accumulating transgenic wheat to water stress and salinity. Plant Physiol 131:1748–1755
60. Vendruscolo EC, Schuster I, Pileggi M, Scapim CA, Molinari HB, Marur CJ, Vieira LG (2007) Stress-induced synthesis of proline confers tolerance to water deficit in transgenic wheat. J Plant Physiol 164:1367–1376
61. Shirasawa K, Takabe T, Takabe T, Kishitani S (2006) Accumulation of glycinebetaine in rice plants that overexpress choline monooxygenase from spinach and evaluation of their tolerance to abiotic stress. Ann Bot 98:565–571
62. Diamant S, Eliahu N, Rosenthal D, Goloubinoff P (2001) Chemical chaperones regulate molecular chaperones in vitro and in

cells under combined salt and heat stresses. J Biol Chem 276:39586–39591
63. Hare PD, Cress WA, Van Staden J (1998) Dissecting the roles of osmolyte accumulation during stress. Plant Cell Environ 21:535–553
64. Tuteja N (2007) Mechanisms of high salinity tolerance in plants. Methods Enzymol 428:419–438
65. Obata T, Kitamoto HK, Nakamura A, Fukuda A, Tanaka Y (2007) Rice shaker potassium channel OsKAT1 confers tolerance to salinity stress on yeast and rice cells. Plant Physiol 144:1978–1985
66. Fukuda A, Chiba K, Maeda M, Nakamura A, Maeshima M, Tanaka Y (2004) Effect of salt and osmotic stresses on the expression of genes for the vacuolar H+-pyrophosphatase, H+-ATPase subunit A, and Na+/H+antiporter from barley. J Exp Bot 55:585–594
67. Laurie S, Feeney KA, Maathuis FJ, Heard PJ, Brown SJ, Leigh RA (2002) A role for HKT1 in sodium uptake by wheat roots. Plant J 32:139–149
68. Chung JS, Zhu JK, Bressan RA, Hasegawa PM, Shi H (2008) Reactive oxygen species mediate Na^+-induced SOS1 mRNA stability in Arabidopsis. Plant J 53:554–565
69. Lian HL, Yu X, Ye Q, Ding X, Kitagawa Y, Kwak SS, Su WA, Tang ZC (2004) The role of aquaporin RWC3 in drought avoidance in rice. Plant Cell Physiol 45:481–489
70. Pereira JF, Zhou G, Delhaize E, Richardson T, Zhou M, Ryan PR (2010) Engineering greater aluminium resistance in wheat by over-expressing TaALMT1. Ann Bot 106:205–214
71. Sasaki T, Yamamoto Y, Ezaki B, Katsuhara M, Ahn SJ, Ryan PR, Delhaize E, Matsumoto H (2004) A wheat gene encoding an aluminum-activated malate transporter. Plant J 37:645–653
72. Delhaize E, Ryan PR, Hebb DM, Yamamoto Y, Sasaki T, Matsumoto H (2004) Engineering high-level aluminum tolerance in barley with the ALMT1 gene. Proc Natl Acad Sci USA 101:15249–15254
73. Ariizumi T, Kishitani S, Inatsugi R, Nishida I, Murata N, Toriyama K (2002) An increase in unsaturation of fatty acids in phosphatidylglycerol from leaves improves the rates of photosynthesis and growth at low temperatures in transgenic rice seedlings. Plant Cell Physiol 43:751–758
74. Khodakovskaya M, McAvoy R, Peters J, Wu H, Li Y (2006) Enhanced cold tolerance in transgenic tobacco expressing a chloroplast omega-3 fatty acid desaturase gene under the control of a cold-inducible promoter. Planta 223:1090–1100
75. Orlova IV, Serebriiskaya TS, Popov V, Merkulova N, Nosov AM, Trunova TI, Tsydendambaev VD, Los DA (2003) Transformation of tobacco with a gene for the thermophilic acyl-lipid desaturase enhances the chilling tolerance of plants. Plant Cell Physiol 44:447–450
76. Sui N, Li M, Zhao SJ, Li F, Liang H, Meng QW (2007) Overexpression of glycerol-3-phosphate acyltransferase gene improves chilling tolerance in tomato. Planta 226:1097–1108
77. Zhang M, Barg R, Yin M, Gueta-Dahan Y, Leikin-Frenkel A, Salts Y, Shabtai S, Ben-Hayyim G (2005) Modulated fatty acid desaturation via overexpression of two distinct ω-3 desaturases differentially alters tolerance to various abiotic stresses in transgenic tobacco cells and plants. Plant J 44:361–371
78. Sohn SO, Back K (2007) Transgenic rice tolerant to high temperature with elevated contents of dienoic fatty acids. Biol Plant 51:340–342
79. Osakabe Y, Mizuno S, Tanaka H, Maruyama K, Osakabe K, Todaka D, Fujita Y, Kobayashi M, Shinozaki K, Yamaguchi-Shinozaki K (2010) Overproduction of the membrane-bound receptor-like protein kinase 1, RPK1, enhances abiotic stress tolerance in Arabidopsis. J Biol Chem 285:9190–9201
80. Yang L, Ji W, Zhu Y, Gao P, Li Y, Cai H, Bai X, Guo D (2010). GsCBRLK, a calcium/calmodulin-binding receptor-like kinase, is a positive regulator of plant tolerance to salt and ABA stress. J Exp Bot 61:2519–2533
81. Ouyang SQ, Liu YF, Liu P, Lei G, He SJ, Ma B, Zhang WK, Zhang JS, Chen SY (2010) Receptor-like kinase OsSIK1 improves drought and salt stress tolerance in rice (Oryza sativa) plants. Plant J 62:316–329
82. Raghavendra AS, Gonugunta VK, Christmann A, Grill E (2010) ABA perception and signaling. Trends Plant Sci 15:395–401
83. Melcher K, Ng LM, Zhou XE, Soon FF, Xu Y, Suino-Powell KM, Park SY, Weiner JJ, Fujii H, Chinnusamy V, Kovach A, Li J, Wang Y, Li J, Peterson FC, Jensen DR, Yong EL, Volkman BF, Cutler SR, Zhu JK, Xu HE (2009) A gate-latch-lock mechanism for hormone signalling by abscisic acid receptors. Nature 462:602–608
84. Santiago J, Dupeux F, Round A, Antoni R, Park SY, Jamin M, Cutler SR, Rodriguez PL, Márquez JA (2009) The abscisic acid receptor PYR1 in complex with abscisic acid. Nature 462:665–668
85. Koh S, Lee SC, Kim MK, Koh JH, Lee S, An G, Choe S, Kim SR (2007) T-DNA tagged knockout mutation of rice OsGSK1, an orthologue of Arabidopsis BIN2, with enhanced tolerance to various abiotic stresses. Plant Mol Biol 65:453–466
86. Diédhiou CJ, Popova OV, Dietz KJ, Golldack D (2008) The SNF1-type serine-threonine protein kinase SAPK4 regulates stress-responsive gene expression in rice. BMC Plant Biol 28(8):49
87. Saijo Y, Hata S, Kyozuka J, Shimamoto K, Izui K (2000) Over-expression of a single Ca2+-dependent protein kinase confers both cold and salt/drought tolerance on rice plants. Plant J 23:319–327
88. Xiang Y, Huang Y, Xiong L (2007) Characterization of stress-responsive CIPK genes in rice for stress tolerance improvement. Plant Physiol 144:1416–1428
89. Shou H, Bordallo P, Wang K (2004) Expression of the Nicotiana protein kinase (NPK1) enhanced drought tolerance in transgenic maize. J Exp Bot 55:1013–1019
90. Agarwal PK, Agarwal P, Jain P, Jha B, Reddy MK, Sopory SK (2008) Constitutive overexpression of a stress-inducible small GTP-binding protein PgRab7 from Pennisetum glaucum enhances abiotic stress tolerance in transgenic tobacco. Plant Cell Rep 27:105–115
91. Seki M, Kamei A, Yamaguchi-Shinozaki K, Shinozaki K (2003) Molecular responses to drought, salinity and frost: common and different paths for plant protection. Curr Opin Biotechnol 14:194–199

92. Shinozaki K, Yamaguchi-Shinozaki K, Seki M (2003) Regulatory network of gene expression in the drought and cold stress responses. Curr Opin Plant Biol 6:410–417
93. Nakashima K, Yamaguchi-Shinozaki K (2005) Molecular studies on stress-responsive gene expression in Arabidopsis and improvement of stress tolerance in crop plants by regulon biotechnology. Jpn Agr Res Q 39:221–229
94. Umezawa T, Fujita M, Fujita Y, Yamaguchi-Shinozaki K, Shinozaki K (2006) Engineering drought tolerance in plants: discovering and tailoring genes to unlock the future. Curr Opin Biotechnol 17:113–122
95. Agarwal PK, Agarwal P, Reddy MK, Sopory SK (2006) Role of DREB transcription factors in abiotic and biotic stress tolerance in plants. Plant Cell Rep 25:1263–1274
96. Yamaguchi-Shinozaki K, Shinozaki K (2006) Transcriptional regulatory networks in cellular responses and tolerance to dehydration and cold stresses. Annu Rev Plant Biol 57:781–803
97. Ito Y, Katsura K, Maruyama K, Taji T, Kobayashi M, Seki M, Shinozaki K, Yamaguchi-Shinozaki K (2006) Functional analysis of rice DREB1/CBF-type transcription factors involved in cold-responsive gene expression in transgenic rice. Plant Cell Physiol 47:141–153
98. Savitch LV, Allard G, Seki M, Robert LS, Tinker NA, Huner NP, Shinozaki K, Singh J (2005) The effect of overexpression of two Brassica CBF/DREB1-like transcription factors on photosynthetic capacity and freezing tolerance in Brassica napus. Plant Cell Physiol 46:1525–1539
99. Nelson DE, Repetti PP, Adams TR, Creelman RA, Wu J, Warner DC, Anstrom DC, Bensen RJ, Castiglioni PP, Donnarummo MG, Hinchey BS, Kumimoto RW, Maszle DR, Canales RD, Krolikowski KA, Dotson SB, Gutterson N, Ratcliffe OJ, Heard JE (2007) Plant nuclear factor Y (NF-Y) B subunits confer drought tolerance and lead to improved corn yields on water-limited acres. Proc Natl Acad Sci USA 104:16450–16455
100. Lee HE, Shin D, Park SR, Han SE, Jeong MJ, Kwon TR, Lee SK, Park SC, Yi BY, Kwon HB, Byun MO (2007) Ethylene responsive element binding protein 1 (StEREBP1) from Solanum tuberosum increases tolerance to abiotic stress in transgenic potato plants. Biochem Biophys Res Commun 353:863–868
101. Zhang G, Chen M, Li L, Xu Z, Chen X, Guo J, Ma Y (2009) Overexpression of the soybean GmERF3 gene, an AP2/ERF type transcription factor for increased tolerances to salt, drought, and diseases in transgenic tobacco. J Exp Bot 60:3781–3796
102. Karaba A, Dixit S, Greco R, Aharoni A, Trijatmiko KR, Marsch-Martinez N, Krishnan A, Nataraja KN, Udayakumar M, Pereira A (2007) Improvement of water use efficiency in rice by expression of HARDY, an Arabidopsis drought and salt tolerance gene. Proc Natl Acad Sci USA 104:15270–15275
103. Gao S, Zhang H, Tian Y, Li F, Zhang Z, Lu X, Chen X, Huang R (2008) Expression of TERF1 in rice regulates expression of stress-responsive genes and enhances tolerance to drought and high-salinity. Plant Cell Rep 27:1787–1795
104. Xiang Y, Tang N, Du H, Ye H, Xiong L (2008) Characterization of OsbZIP23 as a key player of the basic leucine zipper transcription factor family for conferring abscisic acid sensitivity and salinity and drought tolerance in rice. Plant Physiol 148:1938–1952
105. Huang J, Sun SJ, Xu DQ, Yang X, Bao YM, Wang ZF, Tang HJ, Zhang H (2009) Increased tolerance of rice to cold, drought and oxidative stresses mediated by the overexpression of a gene that encodes the zinc finger protein ZFP245. Biochem Biophys Res Commun 389:556–561
106. Ye H, Du H, Tang N, Li X, Xiong L (2009) Identification and expression profiling analysis of TIFY family genes involved in stress and phytohormone responses in rice. Plant Mol Biol 71:291–305
107. Ma Q, Dai X, Xu Y, Guo J, Liu Y, Chen N, Xiao J, Zhang D, Xu Z, Zhang X, Chong K (2009) Enhanced tolerance to chilling stress in OsMYB3R-2 transgenic rice is mediated by alteration in cell cycle and ectopic expression of stress genes. Plant Physiol 150:244–256
108. Ogo Y, Itai RN, Nakanishi H, Kobayashi T, Takahashi M, Mori S, Nishizawa NK (2007) The rice bHLH protein OsIRO2 is an essential regulator of the genes involved in Fe uptake under Fe-deficient conditions. Plant J 51:366–377
109. Nakashima K, Tran LS, Van Nguyen D, Fujita M, Maruyama K, Todaka D, Ito Y, Hayashi N, Shinozaki K, Yamaguchi-Shinozaki K (2007) Functional analysis of a NAC-type transcription factor OsNAC6 involved in abiotic and biotic stress-responsive gene expression in rice. Plant J 51:617–630
110. Yi SY, Kim JH, Joung YH, Lee S, Kim WT, Yu SH, Choi D (2004) The pepper transcription factor CaPF1 confers pathogen and freezing tolerance in Arabidopsis. Plant Physiol 136:2862–2874
111. Hu H, Dai M, Yao J, Xiao B, Li X, Zhang Q, Xiong L (2006) Overexpressing a NAM, ATAF, and CUC (NAC) transcription factor enhances drought resistance and salt tolerance in rice. Proc Natl Acad Sci USA 103:12987–12992
112. Huang XY, Chao DY, Gao JP, Zhu MZ, Shi M, Lin HX (2009) A previously unknown zinc finger protein, DST, regulates drought and salt tolerance in rice via stomatal aperture control. Genes Dev 23:1805–1817
113. Vannini C, Campa M, Iriti M, Genga A, Faoro F, Carravieri S, Rotino GL, Rossoni M, Spinardi AM (2007) Evaluation of transgenic tomato plants ectopically expressing the rice Osmyb4 gene. Plant Sci 173:231–239
114. Seong ES, Baek K-H, Oh S-K, Jo SH, Yi SY, Park JM, Joung YH, Lee S, Cho HS, Choi D (2007) Induction of enhanced tolerance to cold stress and disease by overexpression of the pepper CaPIF1 gene in tomato. Physiol Plant 129:555–566
115. Hsieh TH, Li CW, Su RC, Cheng CP, Sanjaya TYC, Chan MT (2010) A tomato bZIP transcription factor, SlAREB, is involved in water deficit and salt stress response. Planta 231:1459–1473
116. Guo YH, Yu YP, Wang D, Wu CA, Yang GD, Huang JG, Zheng CC (2009) GhZFP1, a novel CCCH-type zinc finger protein from cotton, enhances salt stress tolerance and fungal disease resistance in transgenic tobacco by interacting with GZIRD21A and GZIPR5. New Phytol 183:62–75

117. Huang J, Wang MM, Jiang Y, Bao YM, Huang X, Sun H, Xu DQ, Lan HX, Zhang HS (2008) Expression analysis of rice A20/AN1-type zinc finger genes and characterization of ZFP177 that contributes to temperature stress tolerance. Gene 420:135–144
118. Shukla LI, Chinnusamy V, Sunkar R (2008) The role of microRNAs and other endogenous small RNAs in plant stress responses. Biochim Biophys Acta 1779:743–748
119. Mittler R, Feng X, Cohen M (1998) Post-transcriptional suppression of cytosolic ascorbate peroxidase expression during pathogen-induced programmed cell death in tobacco. Plant Cell 10:461–473
120. Mittler R, Zilinskas BA (1994) Regulation of pea cytosolic ascorbate peroxidase and other antioxidant enzymes during the progression of drought stress and following recovery from drought. Plant J 5:397–405
121. Forment J, Naranjo MA, Roldán M, Serrano R, Vicente O (2002) Expression of Arabidopsis SR-like splicing proteins confers salt tolerance to yeast and transgenic plants. Plant J 30:511–519
122. Kant P, Kant S, Gordon M, Shaked R, Barak S (2007) STRESS RESPONSE SUPPRESSOR1 and STRESS RESPONSE SUPPRESSOR2, two DEAD-box RNA helicases that attenuate Arabidopsis responses to multiple abiotic stresses. Plant Physiol 145:814–830
123. Gong Z, Dong CH, Lee H, Zhu J, Xiong L, Gong D, Stevenson B, Zhu JK (2005) A DEAD box RNA helicase is essential for mRNA export and important for development and stress responses in Arabidopsis. Plant Cell 17:256–267
124. Kim YO, Kim JS, Kang H (2005) Cold-inducible zinc finger-containing glycine-rich RNA-binding protein contributes to the enhancement of freezing tolerance in Arabidopsis thaliana. Plant J 42:890–900
125. Kim YO, Pan S, Jung C-H, Kang H (2007) A zinc finger-containing glycine-rich RNA-binding protein, at RZ-1a, has a negative impact on seed germination and seedling growth of Arabidopsis thaliana under salt or drought stress conditions. Plant Cell Physiol 48:1170–1181
126. Romero C, Belles JM, Vaya JL, Serrano R, Culianez-Macia FA (1997) Expression of the yeast trehalose-6-phosphate synthase gene in transgenic tobacco plants: pleiotropic phenotypes include drought tolerance. Planta 201:293–297
127. Zhang Y, Yang C, Li Y, Zheng N, Chen H, Zhao Q, Gao T, Guo H, Xie Q (2007) SDIR1 is a RING finger E3 ligase that positively regulates stress-responsive abscisic acid signaling in Arabidopsis. Plant Cell 19:1912–1929
128. Zhang YY, Li Y, Gao T, Zhu H, Wang DJ, Zhang HW, Ning YS, Liu LJ, Wu YR, Chu CC, Guo HS, Xie Q (2008) Arabidopsis SDIR1 enhances drought tolerance in crop plants. Biosci Biotechnol Biochem 72:2251–2254
129. Guo X, Wu Y, Wang Y, Chen Y, Chu C (2009) OsMSRA4.1 and OsMSRB1.1, two rice plastidial methionine sulfoxide reductases, are involved in abiotic stress responses. Planta 230:227–238
130. Wang Y, Ying J, Kuzma M, Chalifoux M, Sample A, McArthur C, Uchacz T, Sarvas C, Wan J, Dennis DT, McCourt P, Huang Y (2005) Molecular tailoring of farnesylation for plant drought tolerance and yield protection. Plant J 43:413–424
131. De Block M, Verduyn C, De Brouwer D, Cornelissen M (2005) Poly(ADP-ribose) polymerase in plants affects energy homeostasis, cell death and stress tolerance. Plant J 41:95–106
132. Vanderauwera S, De Block M, Van de Steene N, van de Cotte B, Metzlaff M, Van Breusegem F (2007) Silencing of poly(ADP-ribose) polymerase in plants alters abiotic stress signal transduction. Proc Natl Acad Sci USA 104:15150–15155
133. Hauben M, Haesendonckx B, Standaert E, Van Der Kelen K, Azmi A, Akpo H, Van Breusegem F, Guisez Y, Bots M, Lambert B, Laga B, De Block M (2009) Energy use efficiency is characterized by an epigenetic component that can be directed through artificial selection to increase yield. Proc Natl Acad Sci USA 106:20109–20114
134. Mittler R, Blumwald E (2010) Genetic engineering for modern agriculture: challenges and perspectives. Annu Rev Plant Biol 61:443–462
135. Yamaguchi T, Blumwald E (2005) Developing salt-tolerant crop plants: challenges and opportunities. Trends Plant Sci 10:615–620
136. Mittler R (2006) Abiotic stress, the field environment and stress combination. Trends Plant Sci 11:15–19
137. Pino MT, Skinner JS, Park EJ, Jeknić Z, Hayes PM, Thomashow MF, Chen TH (2007) Use of a stress inducible promoter to drive ectopic AtCBF expression improves potato freezing tolerance while minimizing negative effects on tuber yield. Plant Biotechnol J 5:591–604
138. Massonet C, Vile D, Fabre J, Hannah MA, Caldana C, Lisec J, Beemster GT, Meyer RC, Messerli G, Gronlund JT, Perkovic J, Wigmore E, May S, Bevan MW, Meyer C, Rubio-Diaz S, Weigel D, Micol JL, Buchanan-Wollaston V, Fiorani F, Walsh S, Rinn B, Gruissem W, Hilson P, Hennig L, Willmitzer L, Granier C (2010) Plant Physiol 152:2142–2157
139. Verslues PE, Agarwal M, Katiyar-Agarwal S, Zhu J, Zhu JK (2006) Methods and concepts in quantifying resistance to drought, salt and freezing, abiotic stresses that affect plant water status. Plant J 45:523–539
140. Salekdeh GH, Reynolds M, Bennett J, Boyer J (2009) Conceptual framework for drought phenotyping during molecular breeding. Trends Plant Sci 14:488–496
141. Kolukisaoglu Ü, Thurow K (2010) Future and frontiers of automated screening in plant sciences. Plant Sci 178:476–484
142. Urano K, Kurihara Y, Seki M, Shinozaki K (2010) 'Omics' analyses of regulatory networks in plant abiotic stress responses. Curr Opin Plant Biol 13:132–138
143. Mochida K, Shinozaki K (2010) Genomics and bioinformatics resources for crop improvement. Plant Cell Physiol 51:497–523
144. Finkel E (2009) Imaging. With 'phenomics', plant scientists hope to shift breeding into overdrive. Science 325:380–381
145. Saint Pierre C, Crossa J, Manes Y, Reynolds MP (2010) Gene action of canopy temperature in bread wheat under diverse environments. Theor Appl Genet 120:1107–1117
146. Granier C, Aguirrezabal L, Chenu K, Cookson SJ, Dauzat M, Hamard P, Thioux JJ, Rolland G, Bouchier-Combaud S,

Lebaudy A, Muller B, Simonneau T, Tardieu F (2006) PHENOPSIS, an automated platform for reproducible phenotyping of plant responses to soil water deficit in Arabidopsis thaliana permitted the identification of an accession with low sensitivity to soil water deficit. New Phytol 169:623–635
147. Sadok W, Naudin P, Boussuge B, Muller B, Welcker C, Tardieu F (2007) Leaf growth rate per unit thermal time follows QTL-dependent daily patterns in hundreds of maize lines under naturally fluctuating conditions. Plant Cell Environ 30:135–146
148. Walter A, Scharr H, Gilmer F, Zierer R, Nagel KA, Ernst M, Wiese A, Virnich O, Christ MM, Uhlig B, Jünger S, Schurr U (2007) Dynamics of seedling growth acclimation towards altered light conditions can be quantified via GROWSCREEN: a setup and procedure designed for rapid optical phenotyping of different plant species. New Phytol 174:447–455
149. Reuzeau C, Pen J, Frankard V, de Wolf J, Peerbolte R, Broekaert W, van Camp W (2005) TraitMill: a discovery engine for identifying yield-enhancement genes in cereals. Mol Plant Breed 3:753–759
150. Gregory PJ, Hutchison DJ, Read DB, Jenneson PM, Gilboy WB, Morton EJ (2003) Non-invasive imaging of roots with high resolution X-ray micro-tomography. Plant Soil 255:351–359
151. Yazdanbakhsh N, Fisahn J (2010) Analysis of Arabidopsis thaliana root growth kinetics with high temporal and spatial resolution. Ann Bot 105:783–791
152. Chaerle L, Lenk S, Leinonen I, Jones HG, Van Der Straeten D, Buschmann C (2009) Multi-sensor plant imaging: towards the development of a stress-catalogue. Biotechnol J 4:1152–1167
153. Bylesjö M, Segura V, Soolanayakanahally RY, Rae AM, Trygg J, Gustafsson P, Jansson S, Street NR (2008) LAMINA: a tool for rapid quantification of leaf size and shape parameters. BMC Plant Biol 22(8):82
154. Nagel KA, Kastenholz B, Jahnke S, van Dusschoten D, Aach T, Mühlich M, Truhn D, Scharr H, Terjung S, Walter A, Schurr U (2009) Temperature responses of roots: impact on growth, root system architecture and implications for phenotyping. Funct Plant Biol 36:947–959
155. Kasper TC, Ewing RP (1997) ROOTEDGE: software for measuring root length from desktop scanner images. Agron J 89:932–940
156. Berzin I, Cohen B, Mills D, Dinstein I, Merchuk JC (2000) RHIZOSCAN: a semiautomatic image processing system for characterization of the morphology and secondary metabolite concentration in hairy root cultures. Biotechnol Bioeng 70:17–24
157. French A, Ubeda-Tomás S, Holman TJ, Bennett MJ, Pridmore T (2009) High-throughput quantification of root growth using a novel image-analysis tool. Plant Physiol 150:1784–1795
158. Armengaud P (2009) EZ-Rhizo software: the gateway to root architecture analysis. Plant Signal Behav 4:139–141
159. Wang L, Uilecan IV, Assadi AH, Kozmik CA, Spalding EP (2009) HYPOTrace: image analysis software for measuring hypocotyl growth and shape demonstrated on Arabidopsis seedlings undergoing photomorphogenesis. Plant Physiol 149:1632–1637
160. Van As H (2007) Intact plant MRI for the study of cell water relations, membrane permeability, cell-to-cell and long distance water transport. J Exp Bot 58:743–756
161. Jia X, Mendu V, Tang G (2010) An array platform for identification of stress-responsive MicroRNAs in plants. Methods Mol Biol 639:253–269
162. Tardieu F, Tuberosa R (2010) Dissection and modelling of abiotic stress tolerance in plants. Curr Opin Plant Biol 13:206–212

AC Machines: Permanent Magnet Synchronous and Induction Machines

A. H. Ranjbar[1], Babak Fahimi[2]
[1]Department of Electrical Engineering, Amirkabir University of Technology, Tehran, Iran
[2]University of Texas, Arlington, TX, USA

Article Outline

Glossary
Definition of the Subject
Introduction
Permanent Magnet Motor Drives
AC Induction Machines
Fundamental Equations of Induction Machine
Power Electronic Inverter
IM Drive in Synchronous Reference Frame
Fundamental Equations of the IM Drive Under Field-Oriented Control
Field-Oriented Control Implementations
Future Directions
Bibliography

Glossary

Permanent magnet synchronous machine (PMSM) PMSM is an electromechanical energy conversion device that forms as an important category of electric machines. This machine comprises an AC stator and a brushless rotor that houses permanent magnet. Since the frequency of the excitation in the stator winding is proportional to the mechanical speed of the rotor, this family of machines is called "synchronous." PMSM is being

considered for variety of applications including electric propulsion of modern vehicles.

Surface-mounted PMSM (SM-PMSM) A type of PMSM where permanent magnets are placed on the surface of the rotor, making it easy to build, and skewed poles are easily magnetized on this surface-mounted type to minimize cogging torque.

Interior permanent magnet (IPM) A type of PMSM where, unlike SM-PMSM, permanent magnets are mounted such that a magnetic saliency is established.

Induction machine (IM) A type of electrical machines that operates based on the principle of induction. While stator is formed by a multiphase AC winding, the rotor houses is (a) a series of short-circuited bars in the form of a squirrel cage or (b) a multiphase AC winding. The latter rotor form will allow for external injection of the current. In this family of electric machines, speed of the rotor is not an integer multiple of the stator frequency, and as such, they are named asynchronous machines.

Permanent magnet material Permanent magnet used in PMSM is a piece of magnetic material which, once magnetized or "charged" by an external magnetic field, retains a usefully large magnetic moment after the magnetizing force is removed. Thus, a permanent magnet becomes a source of magnetic field in the rotor.

Field-oriented control Field-oriented control was introduced in the beginning of 1970s. It demonstrated that an induction motor or synchronous motor could be controlled similar to that of a separately excited DC motor by the orientation of the stator mmf or current vector in relation to the rotor flux to achieve a fast dynamic response in the electromagnetic torque.

Definition of the Subject

Electrical machines can be viewed as electromechanical energy converters where at least two magnetic fields interact with each other to produce torque. There are different types of electrical machines including: brushed DC machines, brushless DC machines, permanent magnet synchronous machines (PMSM), AC induction machines (IM), switched reluctance machines (SRM), and etc.

In 1886, the first practical DC motor was invented by Frank Julian Sprague. It was a motor capable of constant speed under variable loads. Brushes were used inevitably for this family of electric machinery which played a dominant role for a good part of the nineteenth century and early decades of the twentieth century.

In 1882, Nikola Tesla discovered the rotating magnetic field and pioneered the use of a rotary field of force to operate machines. Later on, he suggested that the commutators could be removed from a machine, and the device could operate on a rotary field of force. In 1888, Nikola Tesla invented the first AC motor, and, consequently, the polyphase power transmission system was developed. With the advent of AC machine and the effective use of the rotating magnetic field, development of brushless electric machinery attracted significant attention.

This chapter is dedicated to analysis of AC machines including induction machines (IM) and permanent magnet synchronous machines (PMSM). Both IM and PMSM take advantage of the rotating magnetic field that is produced by their multiphase stator windings. Permanent magnet synchronous machines (PMSM) also known as brushless DC machines (BLDC) form an important group of electric machinery that are being considered for variety of applications including electric propulsion of modern vehicles. Due to their high efficiency, compact structure, high torque-to-current and torque-to-volume ratios, fast dynamic response, simple mechanical construction, absence of moving contact, and easy maintenance, PMSMs are widely used in many industrial applications. However, induction motors are now the preferred choice for industrial motors due to their rugged construction, absence of brushes compared to DC machines, absence of permanent magnets (PM) compared to PMSM, and the simplicity of speed control. Induction motor is considered most suitable for almost every application because of its robust and rugged construction and reliability. Moreover, its maintenance is easy, and costs are relatively lesser. It has widespread use in industrial, commercial, and domestic applications.

Introduction

Electromechanical energy conversion can be viewed as an interaction between at least two magnetic fields.

These fields can be constituted by (1) electric current, (2) induced magnetization in ferromagnetic materials, and (3) permanent magnets. To sustain a productive electromechanical energy conversion, the following requirements should be met:

1. At least one of the magnetic fields must be caused by a controllable current.
2. The two interacting magnetic fields should be perpendicular to each other. They can be stationary in space (i.e., DC-brushed machines) or rotating together at the same angular speed (i.e., AC machines).

In order to understand the operation of AC machines, a quick review of DC-brushed machines is helpful. Rotor and stator of a typical two-pole DC machine are shown in Fig. 1. To compensate for the motion of the rotor, the resulting field of the rotor should be continuously kept in a stationary location. This is accomplished by the virtue of the mechanical commutator. Field of the stator can be produced by permanent magnets or fixed coils which are fed with DC current. Injection of the current to a moving member requires a continuous contact between the armature and the external supply of the direct current. This makes the use of brushes inevitable for this family of electric machinery which played a dominant role for a good part of the nineteenth century and early decades of the twentieth century.

With the advent of induction machine and the effective use of the rotating magnetic field, development of brushless electric machinery attracted significant attention. However, ease of control has made DC machines more popular in applications that require a wide range of motor speeds. DC-brushed machines are still among the most popular electromechanical energy converters especially for low powers where the use of permanent magnets is prominent.

This chapter is dedicated to the analysis of AC machines including induction machine (IM) and permanent magnet synchronous machine (PMSM) that are shown in Figs. 2 and 3, respectively. As shown in Figs. 2 and 3, both IM and PMSM take advantage of the rotating magnetic field that is produced by their three-phase stator windings.

Since the magnetic field caused by the multiphase stator windings rotates with a frequency equal to supply frequency, the corresponding field of the rotor has to maintain an adequate speed and orientation to establish a relative stationary displacement with respect to the field of the stator. This can be established by rotating the rotor at a speed whose addition to the supply frequency of the rotor field (at stand still) equates that of the stator supply. While this mechanism automatically happens in a squirrel-cage induction machine, special tuning of the rotor currents in doubly fed electric machinery turns into a necessity which is properly handled by using power electronic converters. Following this design philosophy, one can intuitively expect that existence of a DC field on the rotor necessitates a mechanical speed which is proportional to that of the stator frequency. In a two-pole machine, if two

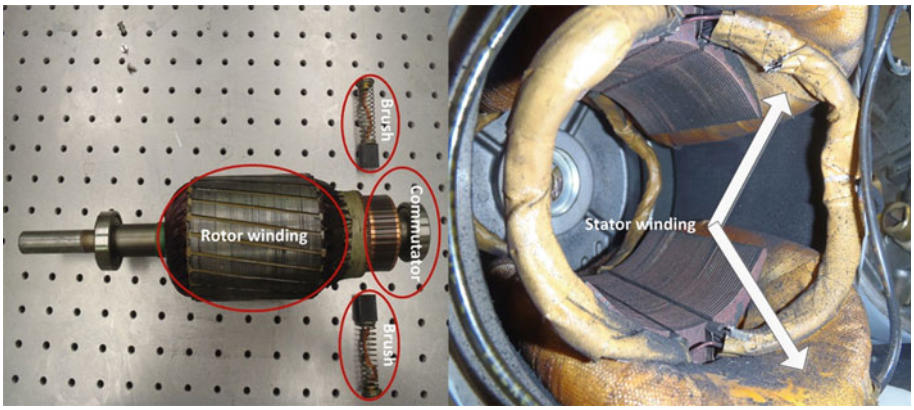

AC Machines: Permanent Magnet Synchronous and Induction Machines. Figure 1
Rotor and stator of a two-pole DC machine

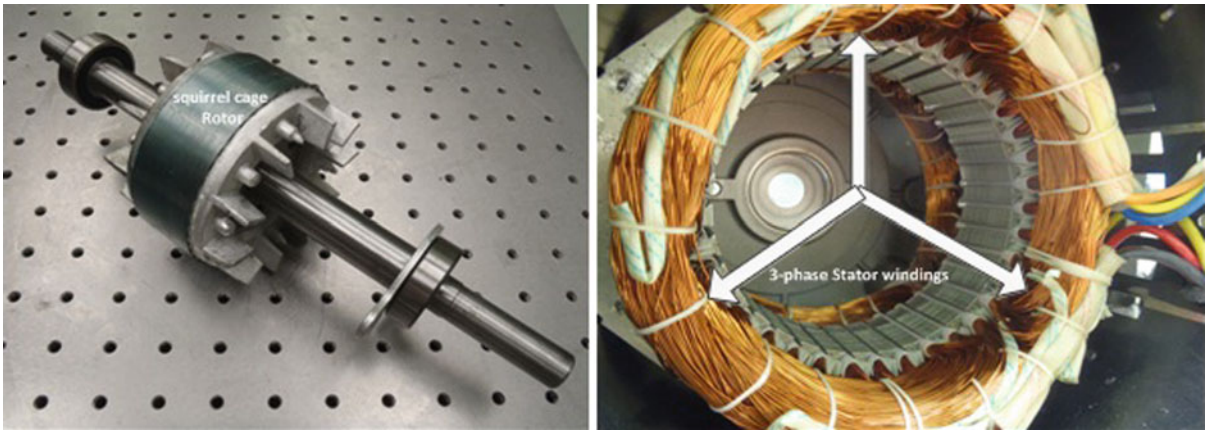

AC Machines: Permanent Magnet Synchronous and Induction Machines. Figure 2
Stator and rotor of a squirrel-cage induction machine

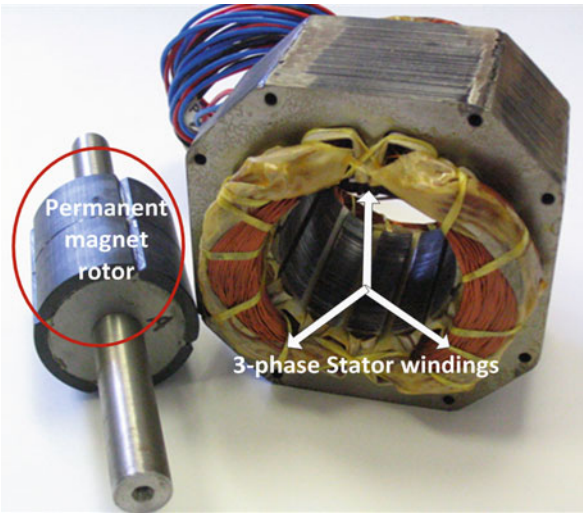

AC Machines: Permanent Magnet Synchronous and Induction Machines. Figure 3
Stator and rotor of a three-phase four-pole surface-mounted permanent magnet synchronous machine

sources of magnetic field (i.e., electric currents) with frequencies of f_1 and f_2 rotate at angular speeds of ω_{m1} and ω_{m2} respectively, then the following relationship must be held at all time to maintain synchronism between the two fields (i.e., $f_1 + \frac{\omega_{m1}}{2\pi} = f_2 + \frac{\omega_{m2}}{2\pi}$).

Employment of permanent magnets as the source of DC magnetic field on the rotor elevates the use of slip rings and brushes which are otherwise used for injection of current in a rotating circuit, hence, resulting in a brushless configuration. Low conductivity of the permanent magnets will prohibit the appearance of appreciable induced currents at low speeds and effectively eliminates the need for providing reactive power for magnetization of the magnetic circuit. These attributes have turned permanent magnet synchronous machines into attractive alternatives for a wide range of applications with power ranging from a few watts into several megawatts.

Yet cooling, mechanical integrity, and operation under harsh ambient conditions have been reportedly impeding a universal takeover of the PMSM drives. Besides, the issue of supply chain and lower efficiency at higher speeds when field weakening has to be done are among other reasons which have raised concern over the use of PMSM in even larger scales. Yet, PMSM drives have been considered as main contenders for many applications among which electric propulsion of modern electrified automobiles, advanced renewable energy harvesting apparatus, and high-performance precision equipments stand out. The compact, relatively low-cost, and optimally sized power electronic converters pave the way for the massive integration of PMSM drives for many applications. The invention of affordable temperature-resilient high-energy permanent magnet materials (rare-earth permanent magnet) has undoubtedly accelerated the integration of PMSM into many industries.

The continued growth of automotive market for PMSM, in large part, depends on efficient operation

in the field-weakening region. The existence of permanent magnets as a steady source of magnetic field can potentially lead to supply of fault currents even when the source is disconnected leading to unsafe operating conditions. For the foreseeable future, PMSM drives continue to enjoy the affordable cost of high-energy permanent magnets and research and development will continue on development of novel magnetic configurations which can increase the efficiency of the electromechanical energy conversion and improve the reliability of this family of actuators.

Rotating Magnetic Field Versus Stationary Magnetic Field

As mentioned earlier, both IM and PMSM contain multiphase stator windings. These multiphase stator windings produce a rotating magnetic field. In this section, a three-phase arrangement for the stator winding is considered although the same conclusion can be derived for higher number of stator phases. The rotating magnetic field produced by the three-phase AC windings in IM and PMSM can also be produced by a set of two-phase AC windings that is stationary and 90° apart with respect to each other. This rotating field can be symbolically represented as:

$$MMF_s = kCos(\omega_s t - \phi_s) \tag{1}$$

In which ω_s and ϕ_s denote the frequency of current and displacement of an arbitrary point on the stator. If the frame of reference is rotating at a speed of ω_{m1} then for an observer located at another frame of reference which has a mechanical speed of ω_{m2} (in the same direction), the rotating field will be seen as:

$$MMF_s = kCos((\omega_s + \omega_{m1} - \omega_{m2})t - \phi_s) \tag{2}$$

This suggests that if the stator is excited with a frequency of ω_s, an observer in the air gap will sense the rotating field at a speed of ω_s; while for an observer on the rotor (rotor rotates with a speed of ω_m in counterclockwise direction), the sensed frequency of the rotating field due to stator excitation will be $\omega_s - \omega_m$. Notably, the two-phase AC windings mentioned above can be replaced by two-phase DC windings that are rotating (at an angular speed equal to the AC supply) and are 90° apart with respect to each other. Therefore, instead of analyzing the magnetic field produced by the stationary three-phase AC windings, one can imagine the rotating two-phase DC windings that are 90° apart with respect to each other. This can be a physical interpretation of Park's transformation that is a mathematical transformation used to simplify the analysis of three-phase systems.

In the case of balanced three-phase systems, the application of Park's transformation reduces the three AC quantities to two DC quantities. Simplified calculations can then be carried out on these transformed quantities before performing the inverse transform to recover the actual three-phase AC quantities. This is often used in order to simplify the analysis of three-phase synchronous machines and to simplify calculations for the control of three-phase inverters. The unique characteristic of Park's transformation is that it eliminates all time-varying inductances from the voltage equations of the machine. These time-varying inductances can originate from motion or varying magnetic reluctance. Park's transformation is expressed by Eq. 3 where f can be voltage, current, or flux linkage of a synchronous machine. Park's transformation is a special case of the reference-frame theory (also referred to as direct-quadrature (*dq0*) transformation). In the case of balanced three-phase circuits, application of the *dq0* transform reduces the three AC quantities in the *abc* frame of references to two DC quantities in *dq* frame of references.

$$f_{qd0S} = K_S(\theta).f_{abcS} \tag{3}$$

where

$$\left(f_{dqoS}\right)^T = \left[f_{qS} \quad f_{dS} \quad f_{oS}\right] \tag{4}$$

$$\left(f_{abcS}\right)^T = \left[f_{aS} \quad f_{bS} \quad f_{cS}\right] \tag{5}$$

$$K_S(\theta) = \frac{2}{3}\begin{bmatrix} \cos\theta & \cos(\theta - \frac{2\pi}{3}) & \cos(\theta + \frac{2\pi}{3}) \\ \sin\theta & \sin(\theta - \frac{2\pi}{3}) & \sin(\theta + \frac{2\pi}{3}) \\ \frac{1}{2} & \frac{1}{2} & \frac{1}{2} \end{bmatrix} \tag{6}$$

$$\omega = \frac{d\theta}{dt} \tag{7}$$

In Eq. 7, ω and θ are supply frequency and rotor position, respectively. Thus, the definite integral form Eq. 7 can be written as Eq. 8, where $\theta(0)$ is the initial rotor position.

$$\theta = \int_0^t \omega(\xi)\, d\xi + \theta(0) \tag{8}$$

It can be shown that for the inverse transformation, the following form can be used:

$$(K_S)^{-1} = \frac{2}{3}\begin{bmatrix} \cos\theta & \sin\theta & 1 \\ \cos(\theta - \frac{2\pi}{3}) & \sin(\theta - \frac{2\pi}{3}) & 1 \\ \cos(\theta + \frac{2\pi}{3}) & \sin(\theta + \frac{2\pi}{3}) & 1 \end{bmatrix} \tag{9}$$

Torque Production in Electrical Machines

The magnetic field of stator in both IM and PMSM is produced by the virtue of three-phase stator windings which are distributed 120° apart from each other [1]. However, the source of magnetic field for the rotor in PMSM is different from that of IM. Assuming the squirrel-cage IM, as shown in Fig. 2, the magnetic field of the rotor originates from the voltage that is induced on the rotor bars. Since these bars are short circuited through the end ring, the voltage induced on their terminals translates into significant currents that originate the magnetic field of the rotor. Consequently, the magnetic field of the stator interacts with the magnetic field produced by rotor currents to produce torque in IM. It must be kept in mind that the resulting field of the rotor rotates at the synchronous speed in the air gap.

Unlike magnetic field of the rotor in IM that is dependent on the voltage induced by stator windings on the rotor, magnetic field of PMSM is generated by permanent magnets that are placed on the rotor. As a result, the electromagnetic torque in the PMSM results from interaction between the magnetic field of the stator (i.e., an electromagnet) and the magnetic field of the permanent magnets on the rotor. The electromagnetic torque that is the cause of rotation in electrical machines can also be defined in terms of electromagnetic co-energy. The electromagnetic co-energy that is stored in the coupling field of unsaturated electrical machines can be expressed as Eq. 10.

$$W^c = \Lambda^t(\theta_r).I \tag{10}$$

where

$$I = \begin{bmatrix} I_S \\ I_R \end{bmatrix} \tag{11}$$

$$\Lambda = \begin{bmatrix} \Lambda_S(\theta_r) \\ \Lambda_R(\theta_r) \end{bmatrix} = \begin{bmatrix} \Lambda_{SS}(\theta_r) + \Lambda_{SR}(\theta_r) \\ \Lambda_{RR}(\theta_r) + \Lambda_{RS}(\theta_r) \end{bmatrix} \tag{12}$$

The electromagnetic torque is defined as the derivative of electromagnetic energy with respect to rotor position and is expressed by Eq. 13.

$$\begin{aligned} T = \frac{\partial W^c}{\partial \theta_r} = \frac{\partial \Lambda^t{}_{SS}}{\partial \theta_r}.I_S + \frac{\partial \Lambda^t{}_{SR}}{\partial \theta_r}.I_S \\ + \frac{\partial \Lambda^t{}_{RR}}{\partial \theta_r}.I_R + \frac{\partial \Lambda^t{}_{RS}}{\partial \theta_r}.I_R \end{aligned} \tag{13}$$

Based on Eq. 13, in order to have nonzero torque, the electromagnetic energy in the coupling field of the electrical machine should vary with respect to rotor position. Considering Eq. 10, since rotor and stator currents are not dependent on the rotor position, the electromagnetic torque can only be produced whenever the self-/mutual inductance of the windings changes with respect to rotor position. Therefore, the electromagnetic torque can be expressed as Eq. 14.

$$T = \frac{\partial w_f}{\partial \theta_r} = \frac{1}{2} I^T . \frac{\partial}{\partial \theta_r}\begin{bmatrix} L_{SS} & L_{SR} \\ L_{RS} & L_{RR} \end{bmatrix}.I \tag{14}$$

$$T = \frac{1}{2}\left\{ I_s^t \frac{\partial L_{ss}(\theta_r)}{\partial \theta_r} I_s + I_r^t \frac{\partial L_{rs}(\theta_r)}{\partial \theta_r} I_s + I_s^t \frac{\partial L_{sr}(\theta_r)}{\partial \theta_r} I_r + I_r^t \frac{\partial L_{rr}(\theta_r)}{\partial \theta_r} I_r \right\} \tag{15}$$

IPM

IM

SM-PMSM

In Eq. 15, the torque that is produced by change of self-inductance with respect to rotor position is called "reluctance torque," and the torque that is produced by change of mutual inductance with respect to rotor position is called "reaction torque." Therefore, depending on the specific structure of the machine, any of these two torque components or both of them may exist. Considering the rotor and stator structures in the IM and PMSM, as shown in Figs. 2 and 3, it can be seen that the self-inductances do not change with respect to rotor position since the air gap between rotor

and stator is fixed. So, the rotation in the squirrel-cage IM and surface-mounted (SM) PMSM is due to the reaction torque.

When the rotor magnets are placed inside the rotor iron in PMSM, the machine is called interior permanent magnet (IPM). In this case, the magnetic reluctance is not uniform as it was for SM-PMSM. So, the self-inductance value of the stator will depend on the rotor position and, consequently, there will be nonzero reluctance torque in addition to the reaction torque. Therefore, an IPM has high efficiency and torque density because the motor can utilize both reaction and reluctance torque due to the magnetic saliency [2]. The interior permanent magnet motors have demonstrated attractive performance in the field-weakening region as well. This is accomplished by the virtue of the reluctance torque which allows for an extended speed range in the constant power region. Table 1 briefly compares PMSM and IM in terms of important characteristics including torque, cooling, fault tolerance, supply chain, speed ratio, and noise.

Equation 13 also suggests that the electromagnetic torque can be expressed symbolically as:

$$T = \sum_i f_i(I_s, I_r) g_i(\theta_r) \tag{16}$$

The above equation illustrates the impact of power electronic-based control (i.e., $f(.,.)$) and magnetic design (i.e., $g(.)$). Power electronic-based control allows for injection of a desired waveform for electric current and, as such, many researchers have tried to obtain optimal waveforms which results in maximum torque, minimum torque pulsation, maximum torque per ampere, etc. For instance, in the case of PMSM, a maximum torque production has pointed toward the following relationship:

$$i_s \propto \frac{\partial \lambda_{pm}}{\partial \theta_r} \tag{17}$$

where λ_{pm} represents the flux linkage in the stator phase due to permanent magnets. Similarly, in switched reluctance drives, the stator current is found to be optimal when the following condition is met:

$$i_s^2 \propto \frac{\partial L_s}{\partial \theta_r} \tag{18}$$

where L_s represents the self-inductance of the stator phase. In general, the problem can be mathematically formulated as the following optimization task:

$$(I_s, I_r) = Arg\left(Max\left(\int_0^{\pi} \sum_i f_i(I_s, I_r).g_i(\frac{P}{2}\theta_r) d\theta_r \right)\right) \tag{19}$$

where P represents the number of magnetic poles. The boundary conditions imposed by the available DC-link voltage, time constants of the circuit, and power electronic circuits have to be taken account in this optimization process. Similar expressions can be found for other objective functions. It is clear that magnetic configuration of the electromechanical energy conversion device plays a central role in this process. In particular, it influences the room for optimization using power electronic converter.

Permanent Magnet Motor Drives

Classification

Permanent magnet synchronous machines (PMSM) also known as brushless DC machines (BLDC) form an important group of electric machinery that are being considered for variety of applications including electric propulsion of modern vehicles. PMSM is an electromechanical energy conversion device formed by

AC Machines: Permanent Magnet Synchronous and Induction Machines. Table 1 Comparison of characteristics in PMSM and IPM

	[N-m/kg]	[W/kg]	Cooling	Fault tolerance	Supply chain	Speed ratio	Noise
IPM	++	++	–	–	––	+	+
SM-PMSM	++	+	–	–	––	–	+
IM	+	+	––	–	++	+	+

a conventional AC stator (i.e., sinusoidally distributed multiphase winding fed with a balanced set of currents). In this class of machines, permanent magnets are mounted on the rotor which then removes the need for injection of the current to a moving component. Special magnetic arrangement for the rotor provides the advantages of (a) brushless operation, (b) controllability of a DC machine, (c) high power density in constant torque region and also (d) compatibility with the commonly used multiphase inverters. The magnets can be placed in number of ways on the rotor. Depending on the placement, they are called either a surface-mounted PMSM (SM-PMSM) or an interior PMSM (IPM). In SM-PMSM, permanent magnets are placed on the rotor surface, making it easy to build, and skewed poles are easily magnetized on this surface-mounted type to minimize cogging torque.

This configuration is used for low-speed applications because of the limitation that the magnets may fly apart if they are used in high-speed applications. Introduction of container shields to protect the permanent magnets will effectively increase the air gap length which undermines an efficient use of permanent magnets. These motors are considered to have small saliency, thus having practically equal inductances in both direct and quadrature axes. Besides, the relatively small self-inductance of SM-PMSM will result in a small electrical time constant which in turn requires fast switching for direct control of the current. Notably, in SM-PMSM, reluctance torque is almost nonexistent and reaction torque is the main source of motion. The permeability of the permanent magnet is almost that of the air, thus for calculation of self-inductances, the magnetic material should be treated as an extension of the air gap. In SM-PMSM, the rotor has an iron core that may be made of punched laminations for simplicity in manufacturing. Thin permanent magnets are mounted on the surface of this core using adhesives. Alternating magnets of the opposite magnetization direction produce radially directed flux density across the air gap. The magnetic field produced by these PMs then interacts with magnetic field produced by the stator current to produce torque. Figure 4 shows how magnets are placed in SM-PMSM [3].

Interior PMSMs have embedded permanent magnets which are mounted inside rotor as shown in Fig. 5 [3]. Unlike SM-PMSM, each PM is mounted inside the rotor in IPM. This will make IPM a good candidate for high-speed applications. There is inductance variation for this type of rotor because the permanent magnet is equivalent to air in the magnetic circuit calculation. The use of axial lamination will further intensify the magnetic saliency for this family of machines. These machines are considered to have magnetic saliency in the sense that q-axis inductance is greater than the

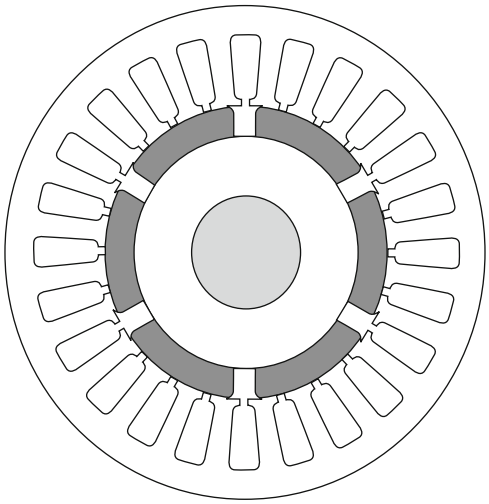

AC Machines: Permanent Magnet Synchronous and Induction Machines. Figure 4
Cross-sectional area of an SM-PMSM

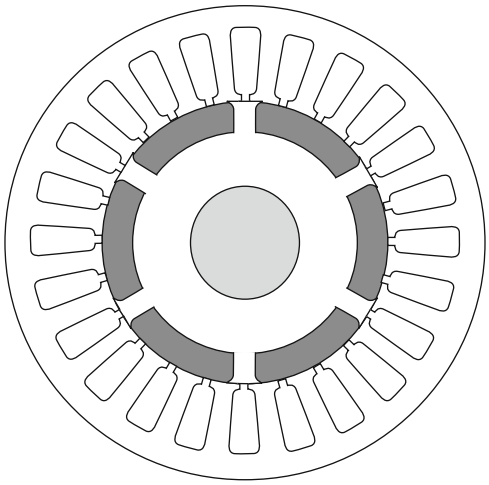

AC Machines: Permanent Magnet Synchronous and Induction Machines. Figure 5
Cross-sectional area of an IPM

d-axis inductance. The q and d axes represent the quadrature and direct axes values, respectively. This frame of references rotate with the mechanical speed of the motor and as such a DC current in q and d axes can produce the same field as in the stationary AC windings of the machine. Since the PMs are not uniformly distributed on the rotor surface, the effective air gap between rotor and stator is not constant. As a result, the stator self-inductance varies with respect to rotor position. Consequently, in IPM, both reaction torque and reluctance torque contribute to the motion.

PMSM machines have recently attracted considerable attention from various sectors of industry due to their compact, efficient, and maintenance-free operation. Recent advancements in manufacturing of magnets have enabled the use of such machines in a wide range of applications. This in turn, has initiated many new opportunities for this family of electric machines.

These machines can further be classified into either sinusoidal type or trapezoidal type according to the type of flux produced in the air gap by the magnets. The difference is created by the way the magnets are magnetized initially before mounting on the rotor. Machines with sinusoidal back-emf can be controlled to achieve ripple-free torque whereas machines with nonsinusoidal back-emf offer lower inverter size and a reduction in losses.

Permanent Magnet Material

Permanent magnet used in PMSM is a piece of magnetic material which, once magnetized or "charged" by an external magnetic field, retains a usefully large magnetic moment after the magnetizing force is removed. Thus, a permanent magnet becomes a source of magnetic field in the rotor which can interact with the magnetic field generated by stator currents to produce torque. For a magnet to be technologically useful, this magnetization must persist in the presence of fairly high-opposing fields (the permanent magnet must have a high "coercive force") and often at elevated and sometimes at very cold temperatures. Its magnetic properties must be reasonably stable for long periods of time in adverse environments.

NdFeB magnets set a vivid example of this trend by offering an impressive energy density of about 200–440 $\frac{kJ}{m^3}$. In addition, highly efficient performances, more compact geometry, lower weight, and shorter electrical time constants are among other attractive attributes of these technologies.

Permanent magnets are described by their demagnetization characteristic. This is a portion of the hysteresis cycle located in the second quadrant of the flux density vs. field intensity (B-H) plane. Figure 6 shows demagnetization characteristics of various magnets at rated temperature (20°C) [5]. As can be observed, the demagnetization curve of a permanent magnet can be fully characterized by the following parameters:

1. Remanent magnetism (B_r), where characteristic crosses the B-axis. B_r is the magnetic flux density remaining in a material, especially a ferromagnetic material, after removal of the magnetizing field.
2. Coercive field intensity (H_c), where characteristic crosses the H-axis. H_c shows the material's resistance to becoming demagnetized.
3. Curvature connecting these two points, mostly one or two linear segments.

In fact, the second linear region that is close to the H-axis is considered as an unstable region.

Therefore a proper operating point will be located in the first linear part, which is expressed as:

$$B = B_r + \mu_0 \mu_r H \tag{20}$$

where μ_r and μ_0 stand for relative and air permeability, respectively. It must be noted that in permanent magnets, μ_r is very close to 1 (relative permeability of the air). Accordingly, the energy density of a permanent magnet (assuming a linear characteristic) can be computed as:

$$E = B.H \Rightarrow E_{Max} = \frac{{B_r}^2}{4\mu_0\mu_r}\left[\frac{kJ}{m^3}\right]. \tag{21}$$

Figure 7 illustrates the constant energy loci along with demagnetization characteristics of various permanent magnets [5]. AlNiCo alloys, the hexaferrites, and the rare earth permanent magnets are the three types of magnets that are used in electrical machines among which rare earth PMs have attracted more attention in PMSM applications.

Chemically, the AlNiCos are iron–cobalt–nickel–based alloys with minor additions of aluminum and copper, and in some grades titanium. The ferrites have

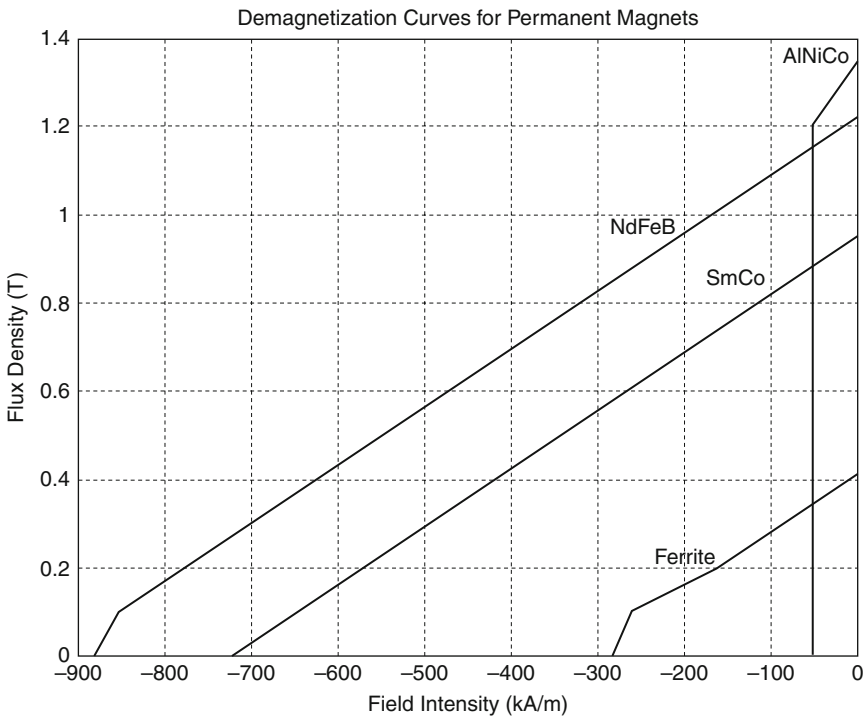

AC Machines: Permanent Magnet Synchronous and Induction Machines. Figure 6
Demagnetization characteristics for various permanent magnets

some peculiar properties setting them apart from other magnets, for better and worse. As oxides, they are electrical insulators, which eliminate eddy currents. (Most permanent magnet materials, being metals, are fairly good conductors.) This is advantageous under dynamic operating conditions as in electric motors and also facilitates pulsed field charging. They are chemically inert, so the production steps of milling, pressing, and surface grinding can be done in air and with water lubrication; they also have no corrosion problems in use even at high temperatures, but the magnetization in ferrites drops more rapidly in the presence of heating.

Developed in the 1970s and 1980s, rare earth magnets are the strongest type of permanent magnets made, substantially stronger than ferrite or AlNiCo magnets. The magnetic field typically produced by rare-earth magnets can be in excess of 1.4 T, whereas ferrite or ceramic magnets typically exhibit fields of 0.5–1 T. There are two types of rare-earth PMs: neodymium magnets ($Nd_2Fe_{14}B$) and samarium–cobalt (SmCo magnets). The newest family of hard magnetic alloys, rare-earth PM, includes not only the well-known samarium–cobalt and neodymium–iron–boron magnets but also many other related materials. All are based on intermetallic compounds formed when 3d-transition metals (TM), notably the strongly magnetic Co and Fe, are alloyed with rare-earth elements (RE) of the 4f-transition series, (i.e., the "lanthanides" Ce, Pr, Nd, Sm, Gd, Dy, and others,) or their close chemical relatives La and Y. Addition of still another element, such as B, C, Si, or Ti, often helps form ternary compounds [4]. Addressing different types of permanent magnet in the above graphs, it must be mentioned that ferrite magnets represent a low-cost solution while offering a limited flux density. AlNiCo magnets, which are more expensive as compared to ferrite magnets, demonstrate a very high remanent magnetism. This, however, is undermined by very limited coercive field intensity. The most expensive SmCo magnets represent quality in every aspect including high remanent magnetism, large coercive field intensity, and a fully linear demagnetization characteristic. They also are known as highly stable in the presence of high-temperature variation. Finally, the

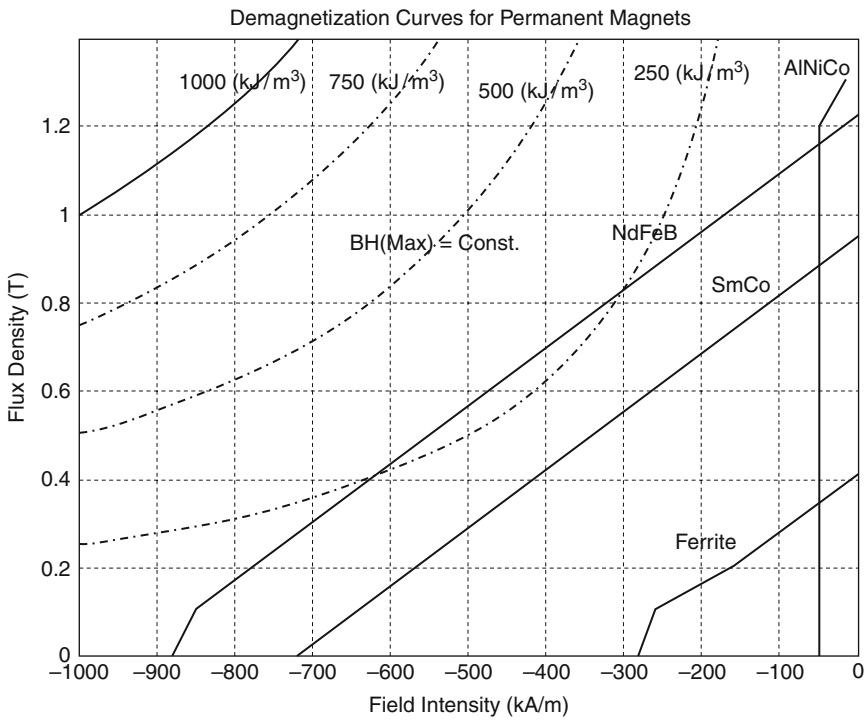

AC Machines: Permanent Magnet Synchronous and Induction Machines. Figure 7
Constant energy loci and demagnetization curves of various PM

NdFeB magnets demonstrate very high-energy density at room temperature. Furthermore, the cost associated with NdFeB is much less than SmCo magnets. However, coercive field intensity in NdFeB magnets is highly sensitive to temperature changes. This, in turn, results in an inadequate performance at high temperatures.

In general, the main objectives in selecting a permanent magnet for motor drive application can be summarized as:

- High-energy density
- A linear demagnetization characteristic in the entire vicinity of the second quadrant (B-H plane)
- High stability with respect to temperature
- High specific resistance to mitigate eddy currents
- Durability against corrosion and demagnetization
- Low cost

Although achieving all these attributes in a single magnet is not possible, proper design can help in optimizing the performance of the drive in the context of the application.

Table 2 summarizes the magnetic characteristics of four families of the permanent magnets.

Comparing various properties of permanent magnets, the following observation can be made:

- A rise in temperature will reduce the remanent magnetism in all magnet types. On a percentage basis, ferrite magnets seem to be the most sensitive magnets, while SmCo demonstrates the least sensitivity.
- Coercive field intensity portrays different behavior for various materials. While an increase in temperature results in significant decrease of coercive field in NdFeB, an opposite response is seen in ferrite magnets. Overall, SmCo offers the least sensitivity to temperature.
- SmCo is the heaviest and the most expensive alternative among all candidates. It also presents one of the lowest specific resistances, which translates to high eddy-current losses.
- AlNiCo offers the highest remanent magnetism. This, however, is mainly undermined by a very

AC Machines: Permanent Magnet Synchronous and Induction Machines. Table 2 Summary of attributes for various permanent magnets

Parameters at 20°C	Ferrite	AlNiCo	SmCo5	NdFeB
Remanent magnetism (B_r [T])	0.38...0.42	0.61...1.35	0.85...1.0	1.0...1.23
Coercive field intensity (H_c [KA/m])	390...280	59...50	1000...1200	1600...960
Max. energy density (BH_{max} [kJ/m^3])	28...34	13...62	140...200	195...280
Temperature coefficient (K_B [%/C])	−0.2... − 0.23	−0.02	−0.04... − 0.05	−0.11... − 0.13
Temperature coefficient (K_H [%/C])	+0.4... + 0.22	+0.03... − 0.07	−0.25	−0.6... − 0.8
Reversible permeability (μ_{rev})	1.05	< 5	1.05	< 1.2
Density $[\rho/(kg/dm^3)]$	4.6...4.9	6.7...7.3	8.1...8.3	7.3...7.4
Specific electric resistance $[\rho/\mu\Omega cm]$	$10^{12}...10^{16}$	40...70	50...60	140
Cost (%)	10...15	40...60	600...800	200...300

limited coercive field intensity and extremely high conductivity.

- The reversible permeability in most cases is close to 1.

Impact of Temperature on Performance of PMSM

Temperature variations are an inevitable attribute of many industrial applications such as automotive products. In fact, in some automotive applications, a temperature range of −40 – 150°C is reported. This, in turn, can alter the properties of permanent magnets used in PMSM. Figures 8 and 9 show demagnetization curves for NdFeB and ferrite magnets at various temperatures. As can be seen, a rise in temperature reduces the remanent magnetism in both cases. However, a severe reduction in coercive field in NdFeB poses a real limitation for armature currents at high temperatures. This will clearly undermine the practicality of using NdFeB magnets at very high temperatures. It must be noted that a modest range of temperature, below 40°C, can be appropriate for employing the NdFeB. The ferrite magnets, on the other hand, depict a reverse behavior at high temperatures; they tend to have larger coercive fields. This, however, at very low temperatures may cause a problem. According to Table 2, some rare-earth permanent magnets demonstrate a superior performance in terms of temperature stability. However, this comes with a significantly higher cost. Therefore, if a modest range of temperatures can be accommodated, employment of NdFeB magnets is recommended.

In order to quantify the effects of temperature change, the linear (stable) part of demagnetization characteristics is expressed as follows:

$$B = f(H) \cong B_r + \mu_0 \mu_r H \tag{22}$$

$$B_r \approx B_{ro}(1 + k_B T/100) \tag{23}$$

$$H_K \approx H_{k0}(1 + k_H T/100) \tag{24}$$

The no-load operating points are as follows:

$$B_{M0} \cong \frac{B_r}{1 + \left(\frac{\sigma}{h_M}\right)} = \frac{(B_{r0}(1 + k_B T/100))}{1 + \left(\frac{\sigma}{h_M}\right)} \tag{25}$$

in which σ and h_M represent air gap length and radial thickness of permanent magnets, respectively. A change in the temperature, therefore, directly shifts the location of operating point. This will affect the allowed armature current as the maximum coercive field has also been changed. This is expressed as:

$$\Delta H_M \leq H_{M0} - H_k = \frac{-B_r}{\mu_0(1 + h_M/\sigma)} - H_k = \frac{-(B_{r0}(1 + k_B T/100))}{\mu_0(1 + h_M/\sigma)} - (H_{k0}(1 + k_H T/100)) \tag{26}$$

One can say that an increase in temperature will reduce remanent magnetism and, hence, will reduce the torque productivity of the machine by a factor of:

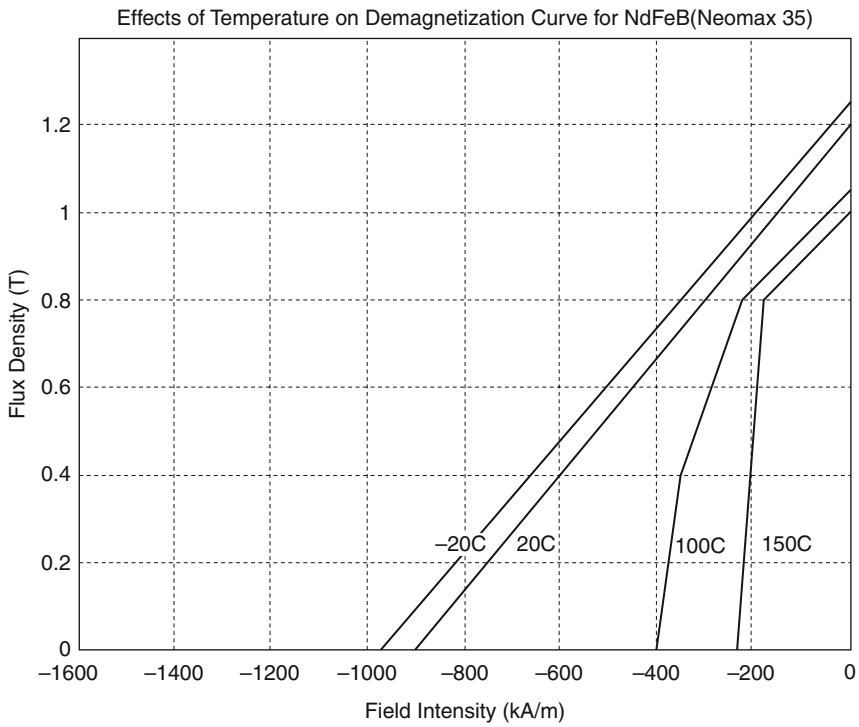

AC Machines: Permanent Magnet Synchronous and Induction Machines. Figure 8
Thermal behavior of NdFeB magnets

$$\frac{\partial B}{\partial T} = \left(\frac{(k_B)}{1 + (\sigma/h_M)}\right)\frac{B_{r0}}{100} \tag{27}$$

where T stands for temperature in degree Celsius. Table 2 provides a range of k_B values for various permanent magnets. At the same time, the permitted armature field to maintain a stable operation is limited by:

$$\frac{\partial B}{\partial T} = \left(\frac{-k_B B_{r0}}{\mu_0(1 + h_M/\sigma)} - k_H H_{K0}\right)\frac{1}{100} \tag{28}$$

It must be noted that a more strict limit on the armature excitation will further impact the torque generation of the permanent magnet synchronous motor drive. Table 2 provides a range of k_H values for various permanent magnets. In order to illustrate the effects of temperature, the following example is given. Table 3 shows three various designs (two-pole design is assumed) using ferrite, SmCo, and NdFeB permanent magnets.

Once the air gap flux density and armature mmf are known, the following equation can be used to estimate electromagnetic torque:

$$T \propto \frac{\pi}{3} HBD^2 l \tag{29}$$

in which D and l represent outer diameter of the rotor and effective stack length of the machine, respectively. Using Eq. 29, one can select the stack length such that a total torque of 5 N - m is achieved. Table 4 shows the results of torque calculation.

In the next step, using the above method, operating points and the electromagnetic torque at −20, 20, 100, and 150°C are computed and listed in Table 5. Please note that the stack length of machines is kept constant in this exercise.

The results of this study are graphically shown in Fig. 10 [5]. As can be seen, reduction in remanent magnetism, due to temperature variations, is the main cause for reduction in torque. At high temperatures, despite the relatively low armature mmf, low coercive/knee point field intensity also contributes to

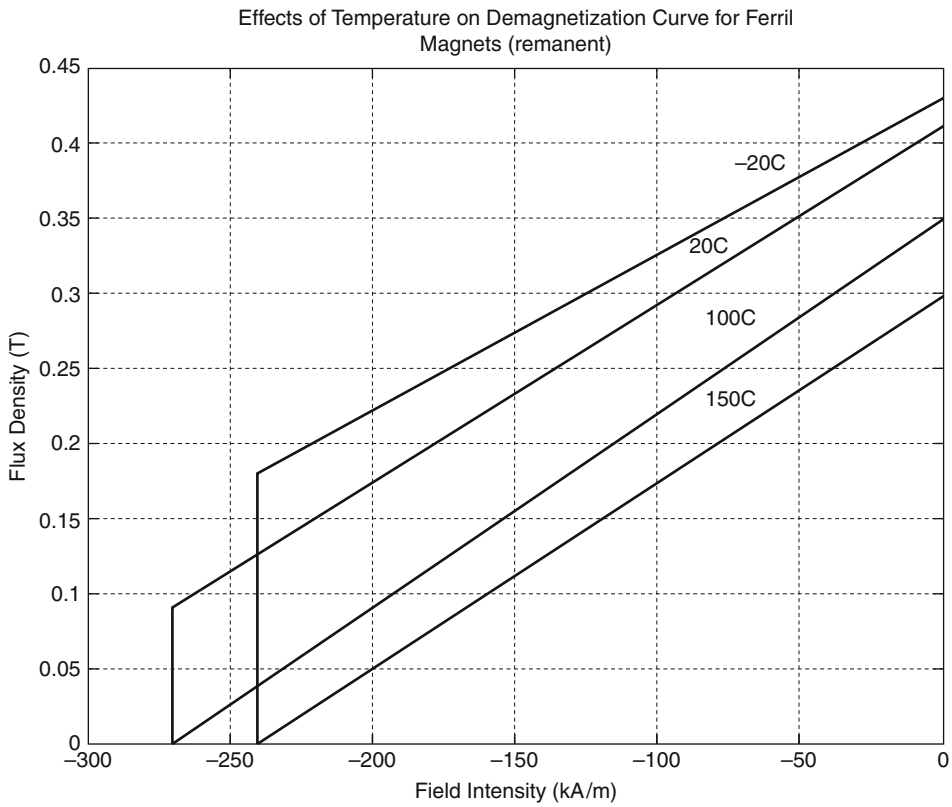

AC Machines: Permanent Magnet Synchronous and Induction Machines. Figure 9
Thermal behavior of ferrite magnets

AC Machines: Permanent Magnet Synchronous and Induction Machines. Table 3 Example design for illustration of temperature effects

Type	σ (mm)	h_M (mm)	D (mm)
Ferrite	0.5	4.5	50
SmCo	0.5	1	50
NdFeB	0.5	2	50

AC Machines: Permanent Magnet Synchronous and Induction Machines. Table 4 Operational condition at 20°C

Type	B_r (T) @ 20°C	H_A (kA/m) @ 20°C	Stack length	Torque (N-m)
Ferrite	0.42	30	165	5
SmCo	1	30	96	5
NdFeB	1.23	30	64	5

this reduction. It is therefore expected that a higher armature mmf would result in yet higher reduction in torque under this design. It must also be noted that SmCo depicts the most stable operation; however, with a reasonable range of temperatures, employment of NdFeB magnets seems to be the most appropriate choice. NdFeB magnets not only are better economic choices, they also offer higher specific resistance at a lower weight compared to SmCo magnets. This in turn minimizes the effects of high-frequency eddy-current losses caused by slot harmonics.

Voltage and Torque Equations for SM-PMSM

Since SM-PMSM is more popular than IPM, this part is dedicated to describing dynamic equations of a typical two-pole three-phase SM-PMSM depicted in

AC Machines: Permanent Magnet Synchronous and Induction Machines. Table 5 Effects of temperature on operational characteristics of PMSM

Type		B_r (T)	H_k (kA/m)	$B_{air\ gap}$ (T)	H_M (kA/m)	Torque (N-m)
Ferrite	−20	0.46	−246	0.414	−36	5.36
	20	0.42	−280	0.378	−33	5
	100	0.34	−246	0.306	−27	3.57
	150	0.29	−280	0.261	−23	2.6
SmCo	−20	1.02	−1,320	0.68	−270	5.12
	20	1	−1,200	0.667	−265	5
	100	0.96	−960	0.64	−254	4.83
	150	0.94	−810	0.627	−250	4.73
NdFeB	−20	1.29	−980	1.032	−205	5.18
	20	1.23	−900	0.984	−196	5
	100	1.1	−220	0.88	−175	4.42
	150	1.02	−190	0.816	−162	3.82

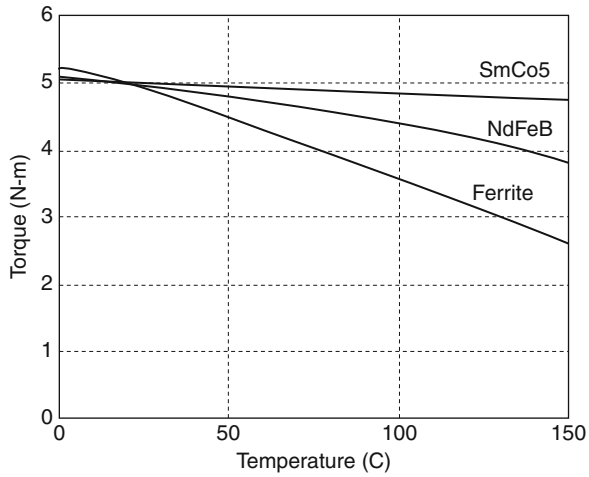

AC Machines: Permanent Magnet Synchronous and Induction Machines. Figure 10 Effects of temperature on electromagnetic torque in brushed DC motor drives

Fig. 11 [6]. In this figure, stator includes three sinusoidally distributed windings placed 120° apart from each other. Each winding has N_s equivalent turns and resistance r_s. In this section, the voltage and torque equations that are used to describe the dynamic behavior of the PMSM will be established.

Voltage equations in machine variables are expressed through Eqs. 30–32

$$V_{as} = r_s i_{as} + p\lambda_{as} \tag{30}$$

$$V_{bs} = r_s i_{bs} + p\lambda_{bs} \tag{31}$$

$$V_{cs} = r_s i_{cs} + p\lambda_{cs}. \tag{32}$$

Writing stator voltage equations in matrix format results in Eq. 33.

$$V_{abcs} = r_s i_{abcs} + p\lambda_{abcs} \tag{33}$$

where

$$(f_{abcs})^T = [f_{as} \quad f_{bs} \quad f_{cs}] \tag{34}$$

$$r_s = diag[r_s \quad r_s \quad r_s] \tag{35}$$

The flux linkage can be written as:

$$\lambda_{abcs} = L_s i_{abcs} + \lambda'_m \tag{36}$$

where L_s is the stator inductance matrix and is expressed by Eq. 37. Also, λ'_m is the flux linkage established by the PMs on the rotor as viewed from stator windings and is expressed by Eq. 38. Where λ'_m is the flux linkage amplitude produced by the PMs as viewed from stator phase winding.

$$L_s = \begin{bmatrix} L_{aa} & L_{ab} & L_{ac} \\ L_{ba} & L_{bb} & L_{ab} \\ L_{ca} & L_{cb} & L_{cc} \end{bmatrix} \tag{37}$$

Where;

$$L_{ab} = L_{ba}$$
$$L_{ac} = L_{ca}$$
$$L_{bc} = L_{cb}$$

And;

$$L_{aa} = L_{ls} + L_A - L_B \cos 2\theta_r$$

$$L_{ab} = -\frac{1}{2}L_A - L_B \cos 2\left(\theta_r - \frac{\pi}{3}\right)$$

$$L_{ac} = -\frac{1}{2}L_A - L_B \cos 2\left(\theta_r + \frac{\pi}{3}\right)$$

$$L_{bb} = L_{ls} + L_A - L_B \cos 2\left(\theta_r - \frac{2\pi}{3}\right)$$

$$L_{bc} = -\frac{1}{2}L_A - L_B \cos 2(\theta_r + \pi)$$

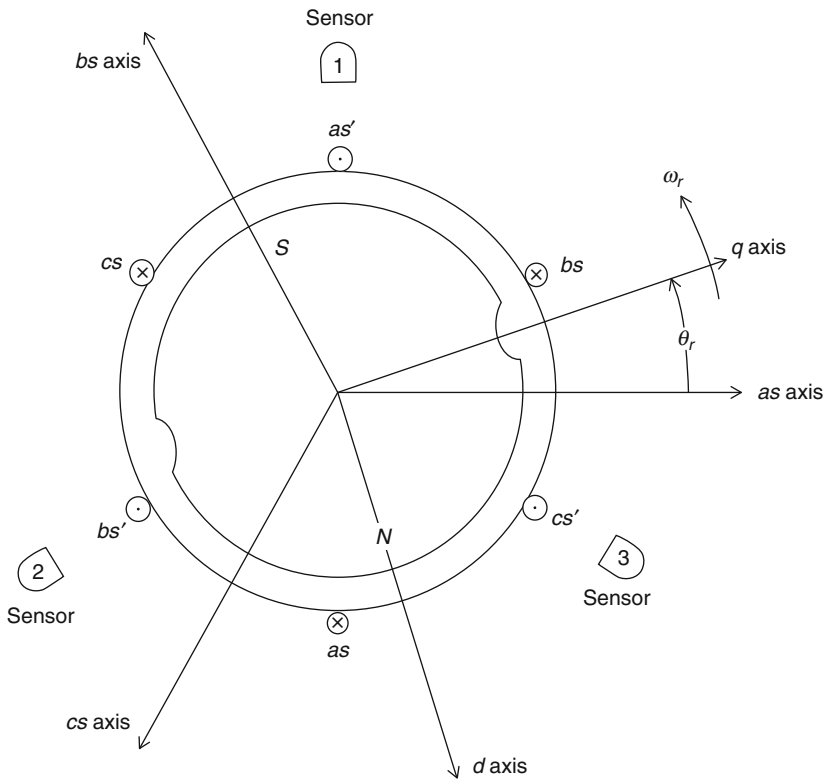

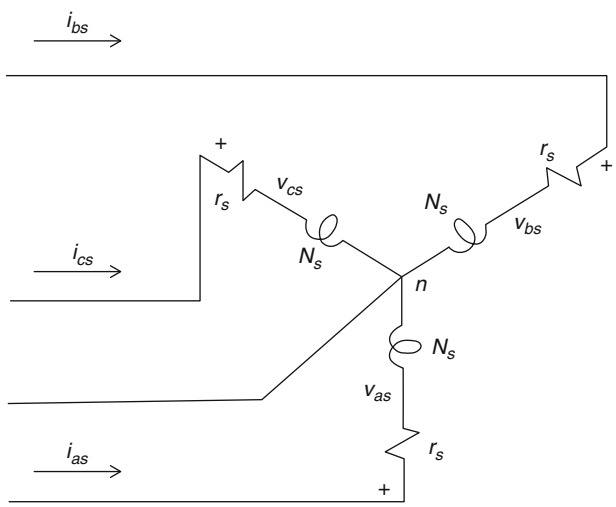

AC Machines: Permanent Magnet Synchronous and Induction Machines. Figure 11
A two-pole three-phase SM-PMSM

$$L_{cc} = L_{ls} + L_A - L_B \cos 2\left(\theta_r + \frac{2\pi}{3}\right)$$

$$\lambda'_m = \lambda'_m \begin{bmatrix} \sin\theta_r \\ \sin(\theta_r - \frac{2\pi}{3}) \\ \sin(\theta_r + \frac{2\pi}{3}) \end{bmatrix} \tag{38}$$

So, $p\lambda'_m$ would be the open-circuit voltage induced in each stator phase winding. In Eq. 38, it is assumed that the voltages induced by PMs on the stator windings are sinusoidal.

The electromagnetic torque in machine variables can be expressed by Eq. 39.

$$\begin{aligned} T_e = \left(\frac{P}{2}\right)\Bigg\{ & \frac{(L_{md} - L_{mq})}{3} \\ & \times \Bigg[\left(i_{as}^2 - \frac{1}{2} i_{bs}^2 - \frac{1}{2} i_{cs}^2 - i_{as} i_{bs} - i_{as} i_{cs} + 2 i_{bs} i_{cs}\right) \sin 2\theta_r \\ & + \frac{\sqrt{3}}{2}(i_{bs}^2 i_{cs}^2 - 2 i_{as} i_{bs} + 2 i_{as} i_{cs}) \cos 2\theta_r \Bigg] \\ & + \lambda'_m \Bigg[\left(i_{as} - \frac{1}{2} i_{bs} - \frac{1}{2} i_{cs}\right) \cos\theta_r \\ & + \frac{\sqrt{3}}{2}(i_{bs} - i_{cs}) \sin\theta_r \Bigg]\Bigg\} \end{aligned} \tag{39}$$

The dynamic *dq0* modeling is used to study the motor during transient and steady state. This can be done by the virtue of Park's transformation. As discussed earlier, Park's transformation converts the three-phase voltage, current, and flux variables into *dq0* variables. Park's transformation for the three-phase stator voltages can be expressed as Eq. 40. Consequently, voltage equations in *dq0* frame are expressed as Eq. 41.

$$\begin{bmatrix} V_q \\ V_d \\ V_0 \end{bmatrix} = \frac{2}{3} \begin{bmatrix} \cos\theta_r & \cos(\theta_r - 120) & \cos(\theta_r + 120) \\ \sin\theta_r & \sin(\theta_r - 120) & \sin(\theta_r + 120) \\ \frac{1}{2} & \frac{1}{2} & \frac{1}{2} \end{bmatrix} \begin{bmatrix} V_a \\ V_b \\ V_c \end{bmatrix} \tag{40}$$

$$V_{dq0s} = r_s i^r_{dq0s} + \omega_r \lambda^r_{dqs} + p\lambda^r_{dq0s} \tag{41}$$

where

$$\left(\lambda^r_{dqs}\right)^T = \left[\lambda^r_{ds} \quad -\lambda^r_{qs} \quad 0\right] \tag{42}$$

$$\lambda^r_{dq0s} = \begin{bmatrix} L_{ls} + L_{mq} & 0 & 0 \\ 0 & L_{ls} + L_{md} & 0 \\ 0 & 0 & L_{ls} \end{bmatrix} \begin{bmatrix} i^r_{qs} \\ i^r_{ds} \\ i_{0s} \end{bmatrix} + \lambda'^r_m \begin{bmatrix} 0 \\ 1 \\ 0 \end{bmatrix} \tag{43}$$

Expanding these equations,

$$v^r_{qs} = r_s i^r_{qs} + \omega_r \lambda^r_{ds} + p\lambda^r_{qs} \tag{44}$$

$$v^r_{ds} = r_s i^r_{ds} - \omega_r \lambda^r_{qs} + p\lambda^r_{ds} \tag{45}$$

$$v_{0s} = r_s i_{0s} + p\lambda_{0s} \tag{46}$$

where

$$\lambda^r_{qs} = L_q i^r_{qs} \tag{47}$$

$$\lambda^r_{ds} = L_d i^r_{ds} + \lambda'^r_m \tag{48}$$

$$\lambda_{0s} = L_{ls} i_{0s} \tag{49}$$

where $L_q = L_{ls} + L_{mq}$ and $L_d = L_{ls} + L_{md}$.

Substituting Eq. 47 to Eq. 49 into Eq. 43 to Eq. 46, results in:

$$v^r_{qs} = (r_s + pL_q) i^r_{qs} + \omega_r L_d i^r_{ds} + \omega\lambda'^r_m \tag{50}$$

$$v^r_{ds} = (r_s + pL_d) i^r_{ds} - \omega_r L_d i^r_{qs} \tag{51}$$

$$v_{0s} = (r_s + pL_{ls}) i_{0s} \tag{52}$$

The expression for electromagnetic torque in *dq0* reference frame is then written as Eq. 53).

$$T_e = \left(\frac{3}{2}\right)\left(\frac{P}{2}\right)(\lambda^r_{ds} i^r_{qs} - \lambda^r_{qs} i^r_{ds}) \tag{53}$$

Substituting Eq. 47 and Eq. 48 into Eq. 53, Eq. 54 is achieved as the final expression for the electromagnetic torque in *dq0* reference frame.

$$T_e = \left(\frac{3}{2}\right)\left(\frac{P}{2}\right)\left[\lambda'^r_m i^r_{qs} + (L_d - L_q) i^r_{qs} i^r_{ds}\right] \tag{54}$$

The second term in Eq. 54 denotes the reluctance torque which is not significant in SM-PMSM, and therefore, the equation for the electromagnetic torque in SM-PMSM can be simplified to:

$$T_e = (\frac{3}{2})(\frac{P}{2})\lambda'_m i^r_{qs} \tag{55}$$

In which P, λ'_m, and i^r_{qs} represent number of magnetic poles, flux linkage due to permanent magnet as observed by the coils on the new frame of reference

(which is mounted on the rotor), and the quadrature component of the new two-phase system mounted on the rotor, respectively. This equation resembles that of a separately excited DC machine in which the armature current is replaced with. Although there is a difference between the separately excited brushed machine and SM-PMSM in the new frame of references and that is the fact illustrated in Eq. 50 and Eq. 51. As can be seen, the current in *d*-axis will influence the voltage equation in *q*-axis and visa verse. In separately excited brushed machine, the flux generated by the armature current does not link the field windings and as such does not appear in the phase voltage equation. From Eq. 55, it is evident that increasing the *d*-axis current does not contribute to the torque generation, and therefore, it is usually regulated around zero. However, to extend the constant power region of the machine, a negative value of the direct axis current can counteract the field of the permanent magnets leading to a smaller motional back-emf. This will allow for regulation of the current in stator phases with a penalty on efficiency. The second term in Eq. 54 represents the reluctance torque and only exists in interior permanent magnet machines. In this case, direct and quadrature axis current will both contribute to the formation of electromagnetic torque, and as such, they have to be optimally controlled to ensure a maximum torque per ampere operation. Due to the presence of the reluctance torque component, an extended operation in the constant power region is feasible. The latter makes IPM an attractive candidate for electric propulsion of electrified power trains. Figure 12 illustrates a graphical interpretation of change in frame of references in SM-PMSM.

Field-Oriented Control in PMSM

Field-oriented control was introduced in the beginning of 1970s. It demonstrated that an induction motor or synchronous motor could be controlled similar to that of a separately excited DC motor by the orientation of the stator mmf or current vector in relation to the rotor flux to achieve a desired objective. The stator windings of the PMSM are fed by an inverter that generates a variable frequency and variable voltage magnitude. In field-oriented control of PMSM, instead of controlling the inverter frequency independently, the frequency and phase of the output wave are controlled using position sensors that are shown in Fig. 11 [4].

In order for the motor to behave like DC motor, the controller needs to know the position of the instantaneous rotor flux or rotor position of PMSM. This can be accomplished using an optical encoder. Having continuous access to the rotor position, the three-phase currents can be calculated.

There are generally two control modes for controlling PMSM. These control modes correspond to constant torque and flux weakening. These modes are determined by the physical limitation of the motor and the inverter. The limit is established by the rated speed of the motor, at which the constant torque operation finishes (i.e., back-emf partially exceeds the available inverter-phase voltage) and the flux weakening starts as shown in Fig. 13.

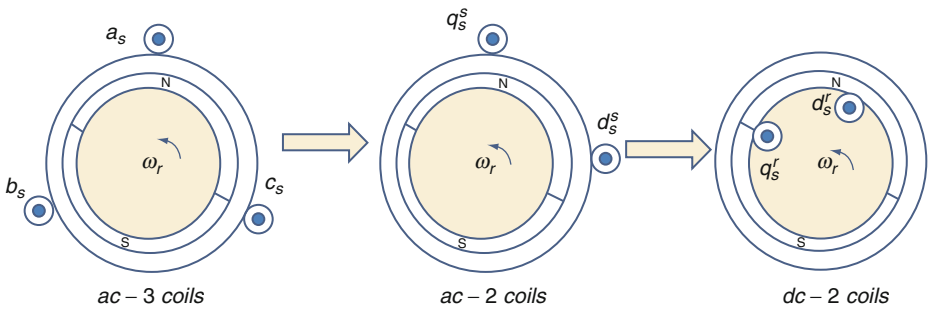

AC Machines: Permanent Magnet Synchronous and Induction Machines. Figure 12
Consecutive change in frame of references to reach a field-oriented arrangement with DC currents in quadrature and direct axes

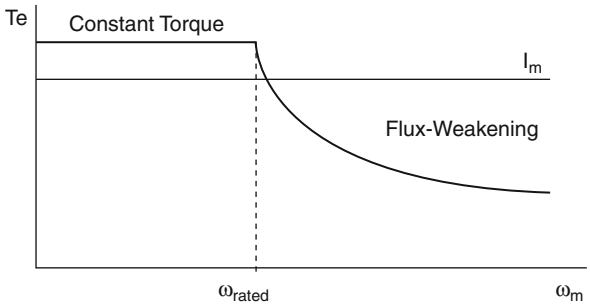

AC Machines: Permanent Magnet Synchronous and Induction Machines. Figure 13
Torque versus speed characteristics of a PMSM

The field-oriented control of PMSM is also called vector control due to the fact that the direct and quadrature components of the current are controlled simultaneously. As shown in Fig. 14, accurate measurement of three-phase currents and rotor position is an integral part of this control strategy. Once the transformation to the synchronous frame of references (tied to the rotor) is completed, the desired values of the direct and quadrature current will be compared to the computed values of these DC quantities. The existing error will be then processed by a proportional + integral (i.e., PI) controller, and the controlled variable is then transformed back to the physical quantities (AC quantities) which are fed to the inverter control. According to Equation 55, the quadrature axis current of the stator will be controlled directly to achieve the desired torque in constant torque region. The direct axis current will be kept at zero to maximize the torque per ampere and to eliminate any need for reactive power [7].

In order to increase the speed range in PMSM, the flux in the *d*-axis current can be used to reduce the net flux generated by the permanent magnet. This action is called flux weakening.

For any given DC-link voltage, there exist a unique angular speed beyond which, at least for a nonzero portion of one electrical cycle, the induced back-emf (at rated constant torque) in each phase will exceed the available phase voltage. This speed is defined as base speed beyond, which regulation of the current waveform will necessitate a net reduction in the back-emf. This can be accomplish by application of a negative direct axis current which will effectively reduce the flux originated from permanent magnet, thereby reducing the motional back-emf. This method, however, introduces additional loss in the stator and cannot be practiced indefinitely, especially at high stator currents which may lead to partial demagnetization of the permanent magnets. The appearance of direct axis current will introduce the need for reactive power and a reduction in torque per ampere. This can be interpreted from the following equations:

$$\alpha = \tan^{-1}\left(\frac{i_q}{i_d}\right) \tag{56}$$

It is also known that:

$$I_m = \sqrt{{i_d}^2 + {i_q}^2} \tag{57}$$

AC Induction Machines

The induction machine is widely used in the industry for a variety of applications for converting electrical energy into mechanical work. Until the early 1970s, they had been mostly operated in the constant-voltage, uncontrolled mode which even today is the most common approach in practice.

The advent of thyristors and, consequentially, the development of variable-frequency converters allowed the wide-range speed control of induction motors. The scalar control method (e.g., Volts/Hertz control method) requires the simultaneous adjustments of the frequency and the magnitude of the sinusoidal voltage or current supplied to the motor. This allows making steady-state operating characteristics of an induction motor similar to those of a DC motor. Adjustable-speed AC drive systems, employing scalar control principles have been replacing DC drives in numerous industrial applications, such as pumps, fans, compressors, etc. Induction machines are extensively preferred as they are less expensive and more robust.

The scalar control of an induction motor does not make it dynamically equivalent to a DC motor. For instance, in an induction machine accurate position, control is not possible since precise control of the instantaneous torque is needed to obtain the required speed trajectory. This, in turn, means that it is the instantaneous stator current which needs to be controlled. Scalar control applies to steady-state operation of the motor only, while no particular control strategies are involved for the transient operating conditions.

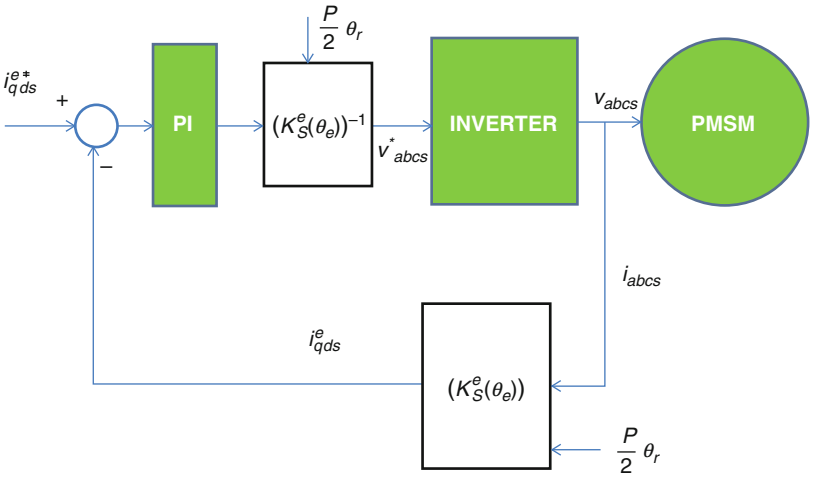

AC Machines: Permanent Magnet Synchronous and Induction Machines. Figure 14
Block diagram of the field-oriented (vector-controlled) control of SM-PMSM drive

The separately excited DC motor has physically separated armature and field windings whose mmfs are orthogonally displaced from each other in space. The armature current can be controlled without affecting the field current. Therefore, a decoupled control of torque and flux is possible, which results in fast torque and speed response. This is not the case in induction motors. To obtain the optimal torque from an induction motor, an algorithmic equivalent of the DC motor has to be established to obtain an appropriate decoupling between the stator and rotor flux. The control technique used to obtain such a stator–rotor physical link is named as field-oriented control or vector control.

The Field Orientation Principle was first formulated by Haase in 1968 and Blaschke in 1970. At that time, due to inadequate means to implement this mode, the concept of vector control seemed impractical. The advent of microprocessors made vector control of AC drives increasingly acceptable in the 1980s. Vector-controlled AC drive systems have proved to provide better dynamic performance than DC drive systems because of higher allowable speeds and shorter time constants of AC motors.

The typical induction motor is supplied by three alternating currents displaced by 120° which are then applied to a set of stationary coils. The resulting flux from the stator induces alternating currents in the "squirrel-cage" conductors of the rotor to create its own field. These fields interact to create torque. Thus the rotor currents in an AC induction motor cannot be directly controlled from an external source. As a result, the torque, which is dependent on the interaction of the stator field and the consequential rotor current, cannot be inherently controlled to obtain a desirable torque.

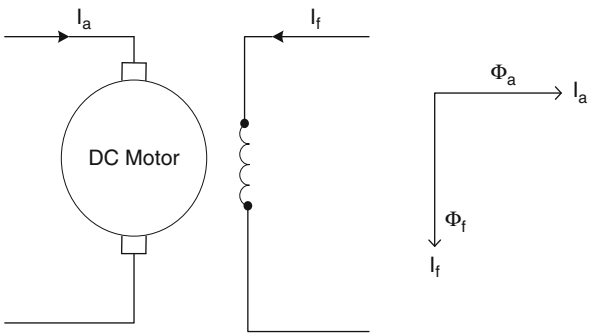

AC Machines: Permanent Magnet Synchronous and Induction Machines. Figure 15
DC machine

Vector control or field-oriented control of an AC induction motor is analogous to the control of a separately excited DC motor. In a DC motor, as shown in Fig. 15, the field flux Φ_f is produced by the field current I_f. I_a is the armature current which produces the armature flux Φ_a. The field flux Φ_f and the armature flux Φ_a are perpendicular to each other. Thus

the fields are decoupled and stationary with respect to each other. The armature current is controlled to control torque. The field flux is unaffected thus allowing a fast-transient response.

The purpose of field-oriented control is to recreate these orthogonal components in the AC machine so as to control the torque-producing current separately from the magnetic flux-producing current in order to achieve the responsiveness of a DC machine.

Fundamental Equations of Induction Machine

A two-pole, three-phase wye-connected symmetrical induction machine is considered for the purpose, as shown in Fig. 16 [6]. The stator windings are identical, sinusoidally distributed displaced by 120° from each other with N_s equivalent turns and resistance r_s. The rotor windings are also considered to be three identical sinusoidally distributed displaced by 120° from each other with N_r equivalent turns and resistance r_r.

The voltage equations for the stator and rotor circuits can be written as:

$$V_{as} = r_s i_{as} + p\lambda_{as} \tag{58}$$

$$V_{bs} = r_s i_{bs} + p\lambda_{bs} \tag{59}$$

$$V_{cs} = r_s i_{cs} + p\lambda_{cs} \tag{60}$$

V_{as}, V_{bs}, and V_{cs} are the three-phase balanced voltages which rotate at supply frequency. λ_{as}, λ_{bs}, and λ_{cs} are the stator flux linkages.

$$V_{ar} = r_r i_{ar} + p\lambda_{ar} \tag{61}$$

$$V_{br} = r_r i_{br} + p\lambda_{br} \tag{62}$$

$$V_{cr} = r_r i_{cr} + p\lambda_{cr} \tag{63}$$

V_{ar}, V_{br}, and V_{cr} are the rotor voltages and the rotor flux linkages which rotate at rotor speed, ω_r.

The above equations can be written in short as:

$$V_{abcs} = r_s i_{abcs} + p\lambda_{abcs} \tag{64}$$

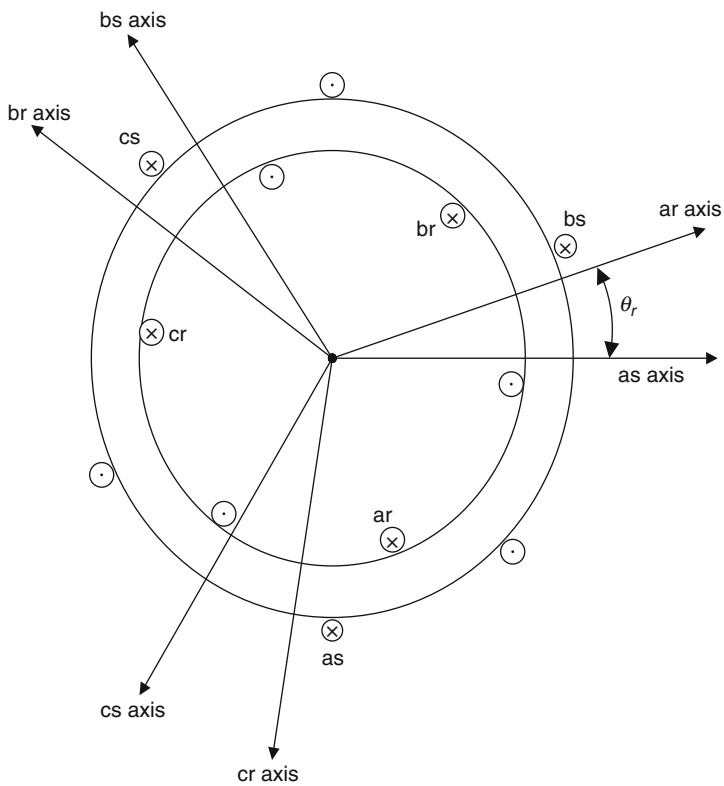

AC Machines: Permanent Magnet Synchronous and Induction Machines. Figure 16
Two-pole, three-phase symmetrical induction machine

$$V_{abcr} = r_s i_{abcr} + p\lambda_{abcr} \tag{65}$$

where

$$(V_{abcs})^T = [V_{as}\ V_{bs}\ V_{cs}] \tag{66}$$

$$(V_{abcr})^T = [V_{ar}\ V_{br}\ V_{cr}] \tag{67}$$

The subscripts "s" and "r" denote that the variables and parameters are associated with the stator and the rotor, respectively. The flux linkages may be written as:

$$\begin{bmatrix} \lambda_{abcs} \\ \lambda_{abcr} \end{bmatrix} = \begin{bmatrix} L_s & L_{sr} \\ (L_{sr})^T & L_r \end{bmatrix} \begin{bmatrix} i_{abcs} \\ i_{abcr} \end{bmatrix} \tag{68}$$

L_s and L_r are the winding inductance matrices of the stator and the rotor, respectively. L_{sr} is the mutual inductance of the stator and rotor windings. The inductance matrix for the stator can be written as following:

$$L_s = \begin{bmatrix} L_{ls} + L_{ms} & -1/2L_{ms} & -1/2L_{ms} \\ -1/2L_{ms} & L_{ls} + L_{ms} & -1/2L_{ms} \\ -1/2L_{ms} & -1/2L_{ms} & L_{ls} + L_{ms} \end{bmatrix} \tag{69}$$

L_{ls} and L_{ms} are the leakage and magnetizing inductances of the stator winding, respectively.

Similarly, the inductance matrix of the rotor winding is written as:

$$L_r = \begin{bmatrix} L_{lr} + L_{mr} & -1/2L_{mr} & -1/2L_{mr} \\ -1/2L_{mr} & L_{lr} + L_{mr} & -1/2L_{mr} \\ -1/2L_{mr} & -1/2L_{mr} & L_{lr} + L_{mr} \end{bmatrix} \tag{70}$$

L_{lr} and L_{mr} are the leakage and magnetizing inductances of the rotor winding, respectively.

The mutual inductance matrix can be written as:

$$L_{sr} = L_{sr} \begin{bmatrix} Cos(\theta_r) & Cos(\theta_r + \frac{2\pi}{3}) & Cos(\theta_r - \frac{2\pi}{3}) \\ Cos(\theta_r - \frac{2\pi}{3}) & Cos(\theta_r) & Cos(\theta_r + \frac{2\pi}{3}) \\ Cos(\theta_r + \frac{2\pi}{3}) & Cos(\theta_r - \frac{2\pi}{3}) & Cos(\theta_r) \end{bmatrix} \tag{71}$$

L_{sr} is the amplitude of the mutual inductance between the stator and rotor windings. θ_r is the rotor position. For a machine with P number of poles,

$$\theta_r = \frac{P}{2}\theta_{rm} \tag{72}$$

where, θ_{rm} is the mechanical rotor position. The speed ω_r in terms of the rotor mechanical speed ω_{rm} for a P-pole induction machine may therefore be expressed as:

$$\omega_r = \frac{P}{2}\omega_{rm} \tag{73}$$

It is convenient to express the physical variables of the rotor referred to the stator variables by appropriate turns-ratios:

$$V'_{abcr} = \frac{N_s}{N_s} V_{abcr} \tag{74}$$

$$i'_{abcr} = \frac{N_s}{N_r} i_{abcr} \tag{75}$$

$$\lambda'_{abcr} = \frac{N_s}{N_r} \lambda_{abcr} \tag{76}$$

The resistive and inductive elements of the rotor coil as referred to the stator windings may be written as:

$$L_{ms} = \frac{N_s}{N_r} L_{sr} \tag{77}$$

$$L'_{sr} = \frac{N_s}{N_r} L_{sr} \tag{78}$$

Thus, one can conclude that:

$$L'_{sr} = L_{ms} \begin{bmatrix} Cos(\theta_r) & Cos(\theta_r + \frac{2\pi}{3}) & Cos(\theta_r - \frac{2\pi}{3}) \\ Cos(\theta_r - \frac{2\pi}{3}) & Cos(\theta_r) & Cos(\theta_r + \frac{2\pi}{3}) \\ Cos(\theta_r + \frac{2\pi}{3}) & Cos(\theta_r - \frac{2\pi}{3}) & Cos(\theta_r) \end{bmatrix} \tag{79}$$

$$r'_r = \left(\frac{N_s}{N_r}\right)^2 r_r \tag{80}$$

$$L_{mr} = \left(\frac{N_s}{N_r}\right)^2 L_{ms} \tag{81}$$

$$L'_r = \left(\frac{N_s}{N_r}\right)^2 L_r \tag{82}$$

One may therefore write:

$$L'_r = \begin{bmatrix} L'_{lr} + L_{ms} & -1/2L_{ms} & -1/2L_{ms} \\ -1/2L_{ms} & L'_{lr} + L_{ms} & -1/2L_{ms} \\ -1/2L_{ms} & -1/2L_{ms} & L'_{lr} + L_{ms} \end{bmatrix} \tag{83}$$

where

$$L'_{lr} = \left(\frac{N_s}{N_r}\right)^2 L_{lr} \tag{84}$$

Thus the flux linkages may be written as:

$$\begin{bmatrix} \lambda_{abcs} \\ \lambda'_{abcr} \end{bmatrix} = \begin{bmatrix} L_{s} & L'_{sr} \\ (L'_{sr})^T & L_r \end{bmatrix} \begin{bmatrix} i_{abcs} \\ i'_{abcr} \end{bmatrix} \tag{85}$$

Power Electronic Inverter

The inverter consists of six switching devices which produce three-phase AC power from a DC source. Figure 17 displays the inverter topology.

The DC voltage is assumed to be constant, and the transistors are assumed to be ideal switches. From Fig. 17 and Kirchhoff's Voltage Law.

$$V_{ag} = V_{as} + V_{ng} \tag{86}$$

$$V_{bg} = V_{bs} + V_{ng} \tag{87}$$

$$V_{cg} = V_{cs} + V_{ng} \tag{88}$$

Adding equations Eq. 86 to Eq. 88 yields,

$$V_{ag} + V_{bg} + V_{cg} = V_{as} + V_{bs} + V_{cs} + 3V_{ng} \tag{89}$$

By Kirchhoff's Current Law,

$$i_{as} + i_{bs} + i_{cs} = 0 \tag{90}$$

which implies,

$$\frac{di_{as}}{dt} + \frac{di_{as}}{dt} + \frac{di_{as}}{dt} = 0 \tag{91}$$

Thus, adding Eqs. 58 to 60 and substituting Eqs. 90 and 91 into this sum results in:

$$V_{as} + V_{bs} + V_{cs} = 0 \tag{92}$$

Thus Eq. 89 reduces to:

$$V_{ag} + V_{bg} + V_{cg} = 3V_{ng} \tag{93}$$

Solving Eq. 93 for V_{cg} and substituting this result into Eqs. 86–88 yields:

$$V_{as} = \frac{2}{3}V_{ag} - \frac{1}{3}V_{bg} - \frac{1}{3}V_{cg} \tag{94}$$

$$V_{bs} = \frac{2}{3}V_{bg} - \frac{1}{3}V_{ag} - \frac{1}{3}V_{cg} \tag{95}$$

$$V_{cs} = \frac{2}{3}V_{cg} - \frac{1}{3}V_{ag} - \frac{1}{3}V_{bg} \tag{96}$$

Thus, the given inverter line-to-ground voltages, the machine line-to-neutral voltages may be calculated using Eqs. 94–96.

IM Drive in Synchronous Reference Frame

To reduce the complexity involved in analysis with these differential equations, one can apply the reference-frame theory to transform the variables and equations associated with the stator and the rotor to the synchronous reference frame. In the case of a synchronous reference frame, the reference frame rotates with the same frequency as the supply frequency ω_e (see Fig. 18).

The transformation of variables to the synchronous reference frame can be obtained by using a transformation matrix $K_s(\theta_e)$ such that:

$$f_{qd0} = K_s(\theta_e) f_{abc} \tag{97}$$

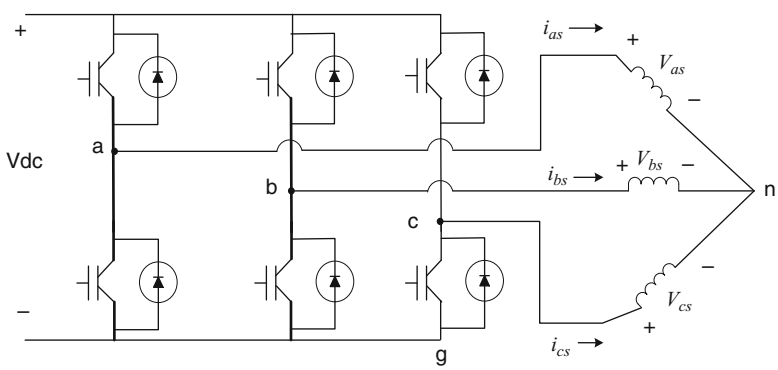

AC Machines: Permanent Magnet Synchronous and Induction Machines. Figure 17
Inverter drive

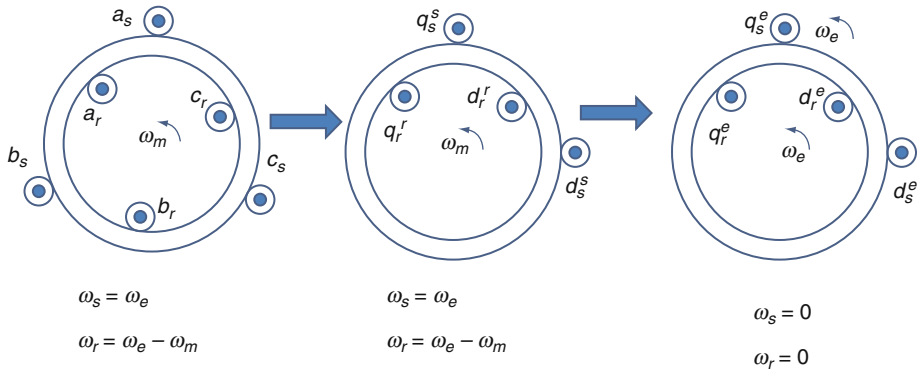

AC Machines: Permanent Magnet Synchronous and Induction Machines. Figure 18
Change in frame of references applied to three-phase induction machine

where f can be any of the variables V, i, or λ and $K_s(\theta_e)$ can be expressed as:

$$K_s(\theta_e) = \frac{2}{3}\begin{bmatrix} Cos(\theta_e) & Cos(\theta_e - \frac{2\pi}{3}) & Cos(\theta_e + \frac{2\pi}{3}) \\ Sin(\theta_e) & Sin(\theta_e - \frac{2\pi}{3}) & Sin(\theta_e + \frac{2\pi}{3}) \\ \frac{1}{2} & \frac{1}{2} & \frac{1}{2} \end{bmatrix} \tag{98}$$

where $\theta_e = \int_0^t \omega_e(\xi)\, d\xi + \theta_{eo}$ and θ_{eo} is the initial angle of the reference frame.

Applying this transformation to the stator voltage equations, one gets a set of equations transformed into the synchronous frame of reference which can be expressed as follows:

$$V_{qs} = r_s i_{qs} + p\lambda_{qs} + \omega_e \lambda_{ds} \tag{99}$$

$$V_{ds} = r_s i_{ds} + p\lambda_{ds} - \omega_e \lambda_{qs} \tag{100}$$

$$V_{os} = r_s i_{os} + p\lambda_{os} \tag{101}$$

Similarly, applying the transform to the rotor voltage equations, one obtains a set of equations transformed into the synchronous frame of reference which can be expressed as follows:

$$V'_{qr} = r'_r i'_{qr} + p\lambda'_{qr} + (\omega_e - \omega_r)\lambda'_{dr} \tag{102}$$

$$V'_{dr} = r'_r i'_{dr} + p\lambda'_{dr} + (\omega_e - \omega_r)\lambda'_{qr} \tag{103}$$

$$V'_{or} = r'_r i'_{or} + p\lambda'_{or} \tag{104}$$

In Eq. 99 to Eq. 101, V_{qs}, i_{qs}, and λ_{qs} are q-axis stator variables. V_{ds}, i_{ds}, and λ_{ds} are the d-axis stator variables and V_{os}, i_{os}, and λ_{os} are the zero-axis stator variables. Under balanced normal operating conditions, the zero-axis variables have zero values. Similarly, the variables with subscript "r" are the corresponding rotor variables.

The flux linkage equation after transformation may be expressed in the qdo-axis as:

$$\begin{bmatrix} \lambda_{qdos} \\ \lambda_{abcr} \end{bmatrix} = \begin{bmatrix} K_s L_s K_s^{-1} & K_s L_{sr} K_s^{-1} \\ K_s (L_{sr})^T K_s^{-1} & K_s L_r K_s^{-1} \end{bmatrix} \begin{bmatrix} i_{qdos} \\ i_{qdor} \end{bmatrix}. \tag{105}$$

The terms of the matrix in Eq. 105 can be evaluated to obtain the following forms:

$$K_s L_s K_s^{-1} = \begin{bmatrix} L_{ls} + L_M & 0 & 0 \\ 0 & L_{ls} + L_M & 0 \\ 0 & 0 & L_{ls} \end{bmatrix} \tag{106}$$

where

$$L_M = \frac{3}{2} L_{ms} \tag{107}$$

$$K_s L_r K_s^{-1} = \begin{bmatrix} L_{lr}' + L_M & 0 & 0 \\ 0 & L_{lr}' + L_M & 0 \\ 0 & 0 & L_{lr}' \end{bmatrix} \tag{108}$$

$$K_s L_{sr} K_s^{-1} = \begin{bmatrix} L_M & 0 & 0 \\ 0 & L_M & 0 \\ 0 & 0 & 0 \end{bmatrix} \tag{109}$$

Thus the flux linkage equations in the synchronous frame are expressed as:

$$\lambda_{qs} = L_{ls} i_{qs} + L_M (i_{qs} + i'_{qr}) \tag{110}$$

$$\lambda_{ds} = L_{ls} i_{ds} + L_M (i_{ds} + i'_{dr}) \tag{111}$$

$$\lambda_{os} = L_{ls} i_{os} \tag{112}$$

$$\lambda'_{qr} = L'_{lr} i'_{qr} + L_M (i_{qs} + i'_{qr}) \tag{113}$$

$$\lambda'_{dr} = L'_{lr} i'_{dr} + L_M (i_{ds} + i'_{dr}) \tag{114}$$

$$\lambda'_{or} = L'_{lr} i'_{or} \tag{115}$$

The expression for the electromagnetic torque in terms of the reference frame variables can be written as:

$$T_e = \left(\frac{3}{2}\right)\left(\frac{P}{2}\right) L_M (i_{qs} i'_{dr} - i_{ds} i'_{qr}) \tag{116}$$

The electromagnetic torque in terms of flux linkages can be written as:

$$T_e = \left(\frac{3}{2}\right)\left(\frac{P}{2}\right) (\lambda'_{qr} i'_{dr} - \lambda'_{dr} i'_{qr}) \tag{117}$$

$$T_e = \left(\frac{3}{2}\right)\left(\frac{P}{2}\right) (\lambda_{ds} i_{qs} - \lambda_{qs} i_{ds}) \tag{118}$$

Fundamental Equations of the IM Drive Under Field-Oriented Control

To understand the concept of vector control in an induction machine, a current loop consisting of a coil of length L, radius r, and with N number of turns carrying a current i in the presence of a flux density B, as shown in Fig. 19, is considered.

According to the Lorenz force equation, the torque acting on the current loop is given by:

$$T_e = -2BiNLr \sin\theta \tag{119}$$

Thus, the magnitude of the torque is maximum when the current vector is perpendicular to the direction of flux density, B. The same concept maybe extended to an induction machine. Consider Fig. 20 representing an induction machine torque production phenomenon. The rotor current and flux linkage vectors respectively are:

$$i'_{qdr} = \begin{bmatrix} i'_{qr} & i'_{dr} \end{bmatrix}^T \tag{120}$$

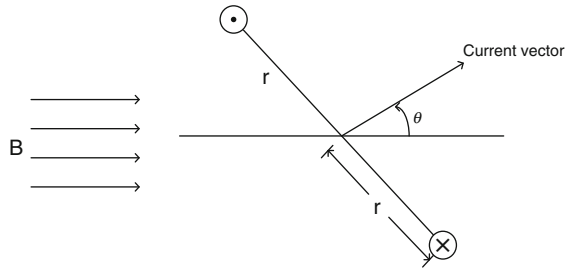

AC Machines: Permanent Magnet Synchronous and Induction Machines. Figure 19
Current loop

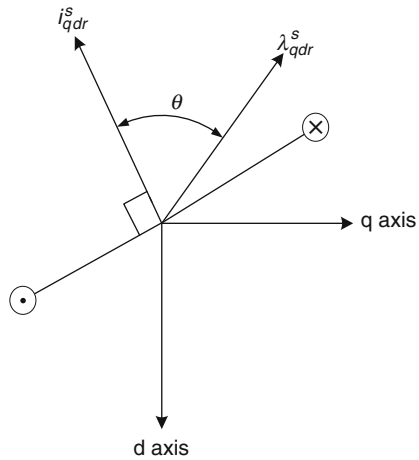

AC Machines: Permanent Magnet Synchronous and Induction Machines. Figure 20
Induction machine torque production phenomenon

and

$$\lambda'_{qdr} = \begin{bmatrix} \lambda'_{qr} & \lambda'_{dr} \end{bmatrix}^T \tag{121}$$

It is also known from Eq. 117

$$T_e = \left(\frac{3}{2}\right)\left(\frac{P}{2}\right)\left(\lambda'_{qr} i'_{dr} - \lambda'_{dr} i'_{qr}\right) \tag{122}$$

this may be expressed as:

$$T_e = \left(\frac{3}{2}\right)\left(\frac{P}{2}\right)\left|\lambda'_{qdr}\right|\left|i'_{qdr}\right| \sin\theta \tag{123}$$

This is analogous to Eq. 117. Thus, one can conclude that for a given magnitude of flux linkage, torque is maximum in the case when the rotor current vectors

are perpendicular to the flux linkage vectors. In vector control, the method to achieve the condition that the rotor flux and rotor current vectors are always perpendicular is twofold. The first condition is that:

$$\lambda'^{e}_{qr} = 0 \tag{124}$$

This condition can be satisfied by choosing a suitable θ_e on an instantaneous basis such that all the rotor flux is in the d-axis. The second condition is that:

$$i'^{e}_{dr} = 0 \tag{125}$$

This condition can be achieved if the d-axis stator current is held constant.

Combining the d-axis stator and rotor flux linkage equations and the condition $i'^{e}_{dr} = 0$ results in:

$$\lambda^{e}_{ds} = L_{ss} i^{e}_{ds} \tag{126}$$

where

$$L_{ss} = L_{ls} + L_M \tag{127}$$

and

$$\lambda'^{e}_{dr} = L_M i^{e}_{ds}. \tag{128}$$

Combining Eqs. 107 and 114, the torque equation may now be expressed as:

$$T_e = -\left(\frac{3}{2}\right)\left(\frac{P}{2}\right)\left(\lambda'^{e}_{dr}\, i'^{e}_{qr}\right) \tag{129}$$

Since $\lambda'^{e}_{qr} = 0$, from the q-axis rotor flux linkage equation, it is known that:

$$i'^{e}_{qr} = -\frac{L_M}{L_{rr}} i^{e}_{qs} \tag{130}$$

where

$$L_{rr} = L_{lr} + L_M \tag{131}$$

Combining Eqs. 129 and 130 results in Eq. 132.

$$T_e = -\left(\frac{3}{2}\right)\left(\frac{P}{2}\right)\left(\frac{L_M}{L_{rr}}\right)\left(\lambda'^{e}_{dr} i^{e}_{qs}\right) \tag{132}$$

Equations 126–132 are the equations of the IM drive under rotor flux-oriented control.

Field-Oriented Control Implementations

The basis of the field orientation algorithm is to use the flux angle, usually the rotor flux angle, to decouple the torque and flux components of the stator current. The most challenging feature of field orientation is the estimation or measurement of the flux angle. The direct field-oriented method, in which direct measurement of flux is performed using flux sensing coils and Hall-effect devices, proved to be impractical for general use. The indirect field-oriented control (IFOC) method has become more common. In this case, the flux angle is not measured directly but is estimated from the equivalent circuit model and from measurements of rotor speed, stator current, and the voltage. Given sufficiently correct current and position sensors, this method performs reasonably well over the entire speed range.

Direct Field-Oriented Control

In direct field-oriented control, the magnitude and angular position of the reference flux vector are either measured or estimated from the stator voltage and currents using flux observers. Hall sensors can be used to measure magnetic fields. If the position of the stationary reference frame is set to zero then the rotor flux linkage in the q-d-axes of the synchronous reference frame may be written as:

$$\begin{bmatrix} \lambda'^{e}_{qr} \\ \lambda'^{e}_{dr} \end{bmatrix} = \begin{bmatrix} Cos\,\theta_e & -Sin\,\theta_e \\ Sin\,\theta_e & Cos\,\theta_e \end{bmatrix} \begin{bmatrix} \lambda'^{s}_{qr} \\ \lambda'^{s}_{dr} \end{bmatrix} \tag{133}$$

In order to achieve $\lambda'^{e}_{qr} = 0$, the position of the synchronous reference frame can be defined as:

$$\theta_e = angle(\lambda'^{s}_{qr} - j\lambda'^{s}_{dr}) + \frac{\pi}{2} \tag{134}$$

$$\lambda'^{e}_{dr} = \sqrt{\left(\lambda'^{s}_{qr}\right)^2 + \left(\lambda'^{s}_{dr}\right)^2} \tag{135}$$

The mutual flux linkages λ'^{s}_{qm} and λ'^{s}_{dm} may be regarded as measurable. The mutual flux linkage in the q-axis may be expressed as:

$$\lambda'^{s}_{qm} = L_M(i^{s}_{qs} + i'^{s}_{qr}) \tag{136}$$

Also, the q-axis rotor flux linkage may be written as:

$$\lambda'^{s}_{qr} = L_{lr} i'^{s}_{qr} + L_M (i^s_{qs} + i'^{s}_{qr}) \tag{137}$$

From the Eqs. 134 and 135, the expression Eq. 138 is obtained.

$$\lambda'^{s}_{qr} = \frac{L'_{rr}}{L_M} \lambda^s_{qm} - L'_{lr} i^s_{qs} \tag{138}$$

Similarly, for d-axis, the following equation is achieved:

$$\lambda'^{s}_{dr} = \frac{L'_{rr}}{L_M} \lambda^s_{dm} - L'_{lr} i^s_{ds} \tag{139}$$

The block diagram of a vector control system for an induction motor employing direct flux-oriented control is shown in Fig. 21.

Indirect Field-Oriented Control

In the direct field orientation scheme, the angular position θ_r of the rotor flux vector is measured directly, using the air gap flux sensors. The indirect approach on the other hand is based on the calculation of slip speed, ω^*_r required for correct field orientation, and the imposition of this speed on the motor.

From the q-axis rotor voltage equation of the induction machine, Eq.140 is obtained.

$$0 = r_r i_{qr} + p\lambda_{qr} + (\omega_e - \omega_r)\lambda_{dr} \tag{140}$$

Applying the condition of vector control $\lambda'^{e}_{qr} = 0$ Eq. 138 becomes:

$$\omega_e = \omega_r - r_r' \frac{i'^{e}_{qr}}{\lambda'^{e}_{dr}} \tag{141}$$

Using Eqs. 117 and 114 will result in Eq. 142.

$$\omega_e = \omega_r + \frac{r_r'}{L'_{rr}} \frac{i^e_{qs}}{i^e_{ds}} \tag{142}$$

which can also be written in terms of rotor time constant τ_r, as:

$$\omega_e = \omega_r + \frac{1}{\tau_r} \frac{i^e_{qs}}{i^e_{ds}} \tag{143}$$

Thus, field-oriented control can be established by imposing the speed on the machine as calculated by the Eq. 143. A vector control system for an induction motor based on the indirect vector control technique is shown in Fig. 22.

The rotor flux and the torque are controlled in a feed-forward manner. As a result, the performance of the system strongly depends on the accurate knowledge of the motor parameters, that is, the rotor time constant. The advantage of this method is that a standard motor can be used whose rotor position can be easily measured by an external sensor.

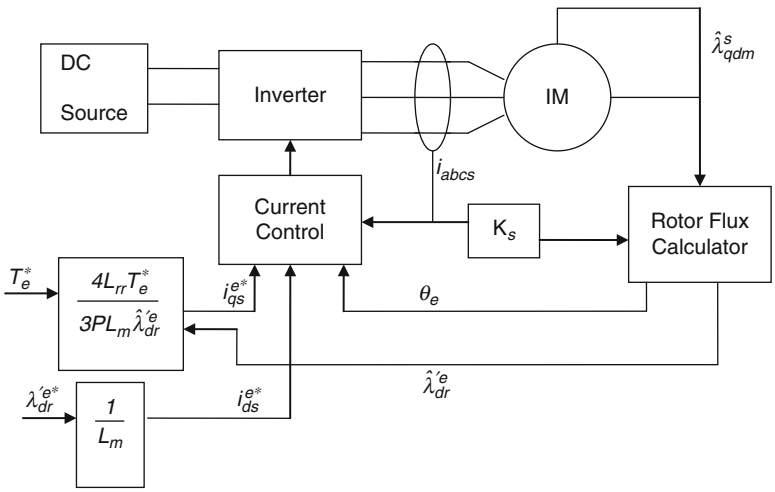

AC Machines: Permanent Magnet Synchronous and Induction Machines. Figure 21
Direct field-oriented control

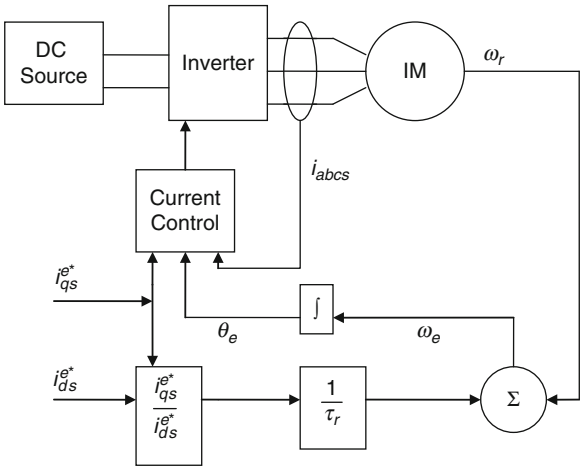

AC Machines: Permanent Magnet Synchronous and Induction Machines. Figure 22
Indirect field-oriented control

Future Directions

Induction motors are subject to many kinds of different internal and external faults during their operation [8]. Often the motor can run with these faults but ultimately it results in performance degradation of the machine, production shutdowns of the industrial process and sometimes permanent burnouts of the motor. Such shutdowns are costly in terms of lost production time, maintenance costs, and wasted raw materials. Therefore, schemes and methods for the diagnosis and detection of the external faults of IMs are major areas of research. Stator faults are one of the most commonly reported faults. Almost 30–40% of all reported faults are related to stator [9]. Stator faults are essentially insulation failures, which ultimately lead to commonly known line-to-ground or line-to-line faults. The primary causes for stator faults are high stator core or winding temperatures; slack core lamination; slot wedges and joints; loose bracing for end winding; contamination due to oil, moisture, and dirt; short-circuit or starting stresses; electrical discharges; and leakage in cooling systems, to name a few. Still, quite a few techniques are available to detect stator faults. So, detection of stator faults in induction machines has attracted much attention in recent years.

Fault-tolerant control for induction machine drives is another interesting issue since it enhances the reliability of the drive without inducing high-cost investment. Improving reliability of electric motor drives can be achieved by improving the fault tolerance of converter switch modules and the fault tolerance of the motor control algorithm. Field-oriented fault-tolerant control algorithms and PWM strategies under fault conditions have been recently introduced, and their performances are studied [10].

Accurate assessment of the electro-magneto-mechanical energy conversion process is another significant field of research which usually requires a Multiphysics Finite Element (FEA) analysis [11]. Since FE analysis is a time-consuming numerical process, lumped parameter models, simplified equivalent magnetic circuits, and separated field analysis are usually used for design and control of electric motor and generator drives. This computational burden is particularly visible in the design of generators for wind energy harvest and motors for propulsion of electric and plug-in hybrid electric vehicles where significant field statistics are often used in the design process. Field reconstruction method (FRM) is a technique in which a minimal set of field analysis is used to establish basis functions for the magnetic flux densities in the machine. Once the basis functions are established, the performance of the machine is predicted under arbitrary speed and excitation. It has been shown that the FRM can reduce the computational time by two or three orders of magnitude while maintaining the same level of precision that is usually accomplished in a two-dimensional FE analysis. Due to its high computational efficiency, FRM has created new opportunity for health monitoring, fault-tolerant operation, and multiphysics design of electric machines. Over the past 6 years, this technique has been successfully applied to different types of machines [11]. This method still needs more researches.

The main disadvantage of PMSMs is nonuniformity in the developed torque (torque ripple) [12]. These torque pulsations vary periodically with rotor position and are reflected as speed ripple. This ripple is parasitic, and can lead to mechanical vibration, acoustic noise, and drive system problems. Therefore, minimizing the torque ripple is of great importance for PMSM design. Cogging torque is the consequence of interaction (magnetic attraction) between rotor-mounted permanent magnets field and the stator teeth, which produces reluctant variations

depending on the rotor position; it is stator current independent.

In the literature, numerous methods for reducing cogging torque, such as employing a fractional number of slots per pole, skewing of magnets or stator lamination stack (slots), displacing and shaping the magnets, optimizing magnet pole-arc-to-pole-pitch ratio, introducing auxiliary slots or teeth, etc., have been proposed.

Reducing acoustic noise in an interior permanent magnet motor during the design stage is another major issue related to IPMs [13]. Noise sources in electric machines are broadly categorized as magnetic, mechanical, electronic, and aerodynamic sources. Generally, the mechanical and magnetic sources are considered as main noise sources of electric motors because the interaction between the harmonic of magnetic forces and the resonant frequency of mechanical structure is the major cause of vibration which produces the noise. So, when designing high-speed permanent magnet (PM) machine, an effort to obtain eddy-current losses reduction in the magnets is necessary in order to improve their performances and diminish the risk of demagnetization. The iron losses in machines however, are strongly affected by the frequency of the excitation, which is proportional to the speed of the machine. In order to reduce iron losses, it is important to consider using alternative magnetic materials in the core of the machines [14]. So, optimal design of PMSMs which still is an open area of research can be translated into minimization of the loss while reducing the flux and torque ripples.

Bibliography

Primary Literature

1. Fahimi B (2007) Qualitative approach to electromechanical energy conversion: reinventing the art of design in adjustable speed drives. In: ICEMS international conference on electrical machines and systems, Beijing, pp 432–439
2. Jiang W, Moallem M, Fahimi B, Pekarek S (2006) Qualitative investigation of force density components in electromechanical energy conversion process. In: IEEE industrial electroniocs, IECON 2006 – 32nd annual conference, Paris, pp 1113–1118
3. Arroyo ELC (2006) Modeling and simulation of permanent magnet synchronous motor drive system. Master thesis in electrical engineering, University of Puerto Rico
4. Strnat KJ (1990) Modern permanent magnets for applications in electro-technology. Proc IEEE 78(6):923
5. Fahimi B (2002) Fault tolerant motor drives. In: Jurgen RK (ed) Handbook of automotive electronics. CRC Press, Boca Raton
6. Krause PC, Wasynczuk O, Sudhoff SD (2002) Analysis of electric machinery and drive systems, 2nd edn. Wiley Inter-Science, New York
7. Rahman MF, Haque ME, Tang L, Zhong L (2004) Problems associated with the direct torque control of an interior permanent magnet synchronous motor drive and their remedies. IEEE Trans Ind Electron 51(4):799–809
8. Yu H, Fahimi B (2008) A novel detection technique of non-uniform airgap in frictionless linear induction transportation systems. In: IEEE VEHICLE POWER AND PROPULSION CONFERENCE (VPPC), Harbin, 3–5 Sept 2008
9. Nandi S (2006) Detection of stator faults in induction machines using residual saturation harmonics. IEEE Trans Ind Appl 42(5):1201–1208
10. Bennani ABA, Ghodbane Cherif M, Belkhodja IS (2008) New fault tolerant DTC control for induction machine drives. In: 13th power electronics and motion control conference (EPE-PEMC), Poznan
11. Fahimi B, Pekarek S (2010) Design and control of electric machines utilizing a field reconstruction method (FRM). In: 36th annual conference on IEEE industrial electronics society, IECON, Glendale
12. Guemes JA, Iraolagoitia AM, Del Hoyo JI, Fernandez P (2011) Torque analysis in permanent-magnet synchronous motors: a comparative study. IEEE Trans Energy Convers 26(1):55–63
13. Lee S, Hong J, Hwang SM, Lee WT, Lee JY, Kim YK (2009) Optimal design for noise reduction in interior permanent-magnet motor. IEEE Trans Ind Appl 45(6):1954–1960
14. Liew GS, Ertugrul N, Soong WL, Gayler J (2006) An investigation of advanced magnetic materials for axial field brushless permanent magnet motor drives for automotive applications. In: 37th IEEE power electronics specialists conference (PESC '06), Jeju

Books and Reviews

Belahcen A (1999) Overview of the calculation methods for forces in magnetized iron cores of electrical machines. Presented at the Seminar on modeling and simulation of multi-technological machine systems, vol 29, pp 41–47

Desai PC, Krishnamurthy M, Schofield N, Emadi A (2010) Novel switched reluctance machine configuration with higher number of rotor poles than stator poles: concept to implementation. IEEE Trans Ind Electron 57(2):469–476

Edrington CS, Kaluvagunta DC, Joddar J, Fahimi B (2005) Investigation of electromagnetic force components in SRM under single and multiphase excitation. IEEE Trans Ind Appl 41(4):978–988

Hayashi H, Nakamura K, Chiba A, Fukao T, Tungpimolrut K, Dorrell DG (2009) Efficiency improvements of switched reluctance motors with high-quality iron steel and enhanced conductor slot fill. IEEE Trans Energy Convers 24(4):819–825

Holtz J (1996) Methods for speed sensorless control of AC drives. In: Rajashekara K, Kawamura A, Matsuse K (eds) Sensorless control of AC motor drives. IEEE Press, Piscataway

Hwu KI, Liaw CM (2003) Intelligent tuning of commutation for maximum torque capability of a switched reluctance motor. IEEE Trans Energy Convers 18(1):113–120

Khoobroo A, Fahimi B, Pekarek S (2008) A new field reconstruction method for permanent magnet synchronous machines. In: IECON international conference on industrial electronics, Orlando, pp 2009–2013

Kioskeridis I, Mademlis C (2006) Optimal efficiency control of switched reluctance generators. IEEE Trans Energy Convers 21(4):1062–1071

Krishnan R (2001) Switched reluctance motors drives: modeling simulation, analysis, design, and applications. CRC Press, Boca Raton

Lin F, Yang S (2007) Instantaneous shaft radial force control with sinusoidal excitations for switched reluctance motors. IEEE Trans Energy Convers 22(3):629–636

Mao SH, Tsai MC (2005) A novel switched reluctance motor with C-core stators. IEEE Trans Magn 41(12):3334–3336

Mecrow C, El-Kharashi EA, Finch JW, Jack AG (2004) Preliminary performance evaluation of switched reluctance motors with segmental rotors. IEEE Trans Energy Convers 19(4):679–686

Zhu W, Fahimi B, Pekarek S (2006) A field reconstruction method for optimal excitation of permanent magnet synchronous machines. IEEE Trans Energy Convers 21(2):305–313

Active Multifocal Vision System, Adaptive Control of

Alois Unterholzner, Hans-Joachim Wuensche
Institute for Autonomous Systems Technology, Department of Aerospace Engineering, University of the Bundeswehr Munich, Neubiberg, Germany

Article Outline

Glossary
Definition of the Subject
Introduction: The Human Eye as a Template
Related Work
Design of the Visual Sensor
Realizing Visual Motor Routines
Saccades and Smooth-Pursuit Movements
Vestibulo-Ocular Reflex
Future Directions: The Importance of Visual Perception
Bibliography

Glossary

Adaptive control The adaptation of the control mechanism to unknown or changing plant characteristics.

Multifocal vision system A set of cameras with different focal length. Potentially the orientation of the cameras can be actively changed. Equivalent to camera platform.

Saccade Rapid, abrupt sensor movement to bring an interesting object into the sensor focus.

Selective attention Selecting the most informative parts within the sensor's field of view for further exploration.

Smooth-pursuit movement Slow sensor movement to keep an object centered in the field of view.

Vestibulo-ocular reflex Sensor movement to compensate disturbing motions of the sensor carrier.

Visual odometry Determining the position and orientation of a moving camera by analyzing the camera images.

Definition of the Subject

The perception of the environment is crucial for autonomous systems and visual perception in particular is a substantial source of information for intelligent vehicles. For a visual perception system of an intelligent vehicle high measurement accuracy combined with a large field of view is essential. Since these are contradictory requirements for a single camera, multifocal vision systems – equipped with tele- and wide-angle cameras – are frequently used. However, due to their small aperture angles high resolution telecameras have to be actively directed toward scene regions of interest. Moreover active inertial gaze stabilization is required since telecameras are highly sensitive to rotational vehicle motions. Gaze stabilization as well as adjusting the orientation of the telecamera requires control of the vision system. The use of adaptive control allows for varying camera configurations and thereby further enhances the applicability of multifocal vision systems.

Introduction: The Human Eye as a Template

Visual perception is one of the most important senses for biological as well as for technical systems. However for technical systems it is still challenging to extract meaningful information from visual sensor input.

Due to its impressive performance in interpreting visual scenes, the human sense of vision may serve as a template for an artificial visual sense.

Similar to a camera in technical systems the eye is the sensor of the human visual system. The human eye provides high visual acuity in the central region of the retina – the fovea – close to the optical axis. Simultaneously the eye offers a wide field of view due to a large but low-resolution peripheral area surrounding the fovea. Therefore peripheral vision delivers highly compressed but less detailed data compared to the high-resolution foveal vision. Since data compression already takes place in the sensor, there is the need for a selection stage – often referred to as selective attention – that decides which parts of the environment are most informative and therefore should be discovered in more detail.

Selective attention combined with high-resolution foveal vision in turn requires directing the fovea actively toward selected regions of interest (ROI). Moreover during the measurement process the ROI shall be kept foveated despite relative motions of the ROI with respect to the sensor. Shifting the fovea toward a ROI as fast as possible is called a saccade. Smooth-pursuit movements keep the selected ROI within the fovea based on visual feedback. However visual feedback is subject to large latencies and therefore smooth-pursuit movements are inappropriate to compensate for, e.g., fast head motions. The vestibulo-ocular reflex (VOR) inertially stabilizes the image on the retina based on measurements of the vestibulo organ located in the inner ear. The combination of the vestibulo-ocular reflex and smooth-pursuit movements ensures stable tracking of selected ROIs. Binocular vision additionally requires vergence movements – simultaneous movements of both eyes in opposite directions – to keep a selected ROI foveated in both eyes.

In summary the visual properties of the human eye in combination with selective attention lead to decreased data rates with increased information density compared to a sensor with high resolution in the whole field of view.

An artificial visual sensor for intelligent vehicles mimicking the desirable visual properties of the human eye implies the need for a multifocal vision system comprising at least one tele- and one wide-angle camera. Such a sensor should be active and provide the visual motor routines: saccade, smooth-pursuit movement, and vestibulo-ocular reflex. The need for vergence movements decreases with the increasing distance of the observed features. Therefore the capability of vergence movements is not essential for intelligent vehicles and can be omitted in favor of a considerable reduction of the mechanical complexity of the resulting multifocal vision system.

Before going into the details of the design and control of active multifocal vision systems, this entry gives a brief overview on related work. The design of visual sensors for intelligent vehicles is discussed in the subsequent section. In the following sections the realization of the visual motor routines is presented. The entry finally concludes with a discussion of possible future research directions.

Related Work

This entry is mainly on the design and control of multifocal vision systems. Yet to provide a more general overview on the subject, literature on the human visual sense is presented first.

A profound discussion of the human visual sense including eye movements and visual attention is given in [1]. A more general treatment of human perception is presented in the textbooks [2] and [3]. Recent findings regarding human gaze control and visual attention can be found, e.g., in the reviews [4–9]. Human visual perception during driving is investigated in [10–16], for example.

Several approaches exist to the design and control of active vision systems. Most of them are more or less inspired by the human eye, mimicking to some extent its sensing properties and visual motor routines. Vision systems for robots – including humanoids – are described, e.g., in [17–27]. Simulating human binocular vision is the purpose of the vision system presented in [28]. The design and control of vision systems for autonomous ground vehicles is discussed in [29–38].

The research on computational realizations of visual attention may be divided into two – partially overlapping – groups:

The first group deals mainly with computational models of visual attention with the purpose of identifying interesting scene regions and possibly

directing a camera toward this region. These models mainly result in the computation of saliency maps based on bottom-up feature extraction and top-down weighting of these features, e.g., to find a certain object of interest. However up to now these approaches are not or rarely used for tracking applications. The publications [39–58] provide by no means a complete overview. Michalke et al. [59] present an application of this approach in the context of intelligent driver assistance systems.

In the second group the possibility of camera motions is utilized to enhance the capabilities of a robotic system. Some of the pioneering work on what is commonly referred to as "active perception" or "active vision" is presented in [60–64]. Dickmanns [65] presents an early approach to vision-based vehicle guidance. A lot of research is concerned with active vision or gaze control respectively to improve self-localization or obstacle avoidance of (humanoid) robots: [66–76]. There are also some works on simultaneous localization and mapping (SLAM): [77–79]. Gaze control for autonomous vehicles is presented, e.g., in [80–82] and [29]. Most of these works are based on simulations or were conducted in comparably simple structured and almost static environments.

Design of the Visual Sensor

Active multifocal vision systems – or equivalently camera platforms – are able to provide simultaneously a wide field of view, high resolution, and stereo vision.

A wide field of view is desirable to scan simultaneously as much of the vehicle's environment as possible. A high resolution provides detailed images of points of interest in the vehicle's surrounding. Moreover telecameras are required for early detection of distant objects, since the maximum range of object detection limits the maximum speed of the vehicle. Stereo vision is used to gather 3D information of the environment.

Active vision systems that are pivotable in pitch and yaw axis enable the exploitation of the high measurement accuracy offered by telecameras within the entire field of view of the vision system. Moreover the visual field of the intelligent vehicle is enlarged this way. However telecameras are more sensitive to disturbances than wide-angle cameras and therefore active gaze stabilization is required to obtain stable images and to keep objects of interest within camera scope.

For a sound discussion of these requirements and the resulting design of multifocal vision systems refer to [29] or [30]. According to [30], platforms pivotable in pitch and yaw axis and equipped with several cameras, that either provide a wide field of view or a high resolution, offer a good compromise to meet the needs of visual perception in autonomous ground vehicles. Figure 1 depicts one possible multifocal camera arrangement following the recommendations given in [29].

Although multifocal vision systems offer a good compromise covering more or less the needs of each visual perception module of an intelligent vehicle, the optimal camera configuration for a single perception module can differ from the currently utilized camera arrangement. To detect, e.g., lane markings black/white cameras might be best; to detect drivable areas in off-road terrain color cameras might be better. Divergent cameras offer a wide field of view. Parallel cameras, on the contrary, increase the range where stereo vision is possible. Depending on their range of interest different perception modules require different focal lengths of camera lenses. Therefore software designers prefer to use the camera configuration that suits best their application's demands. For this reason the configuration of the multifocal vision system of an intelligent vehicle may be frequently changed during the development process.

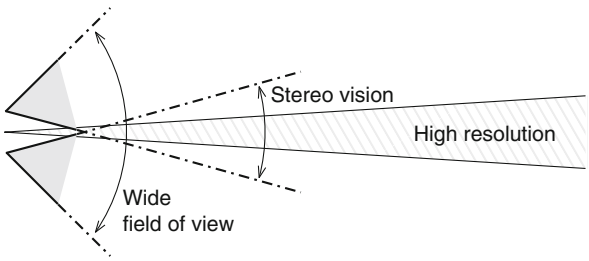

Active Multifocal Vision System, Adaptive Control of. Figure 1
A multifocal vision system offering a wide field of view combined with a high-resolution central area. Stereo vision is possible within the intersection of the field of view of the two wide-angle cameras

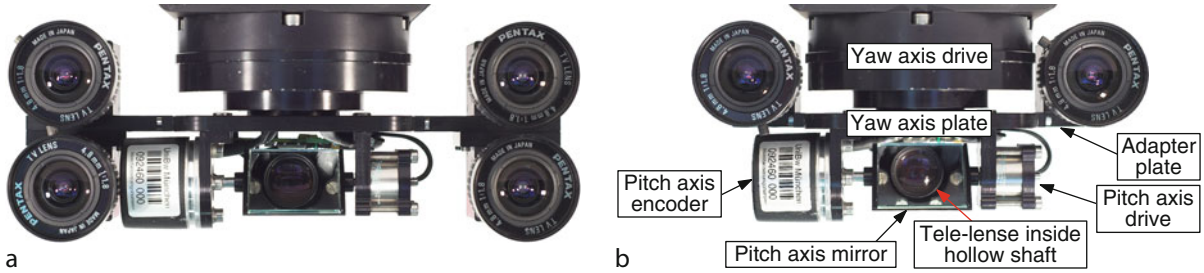

Active Multifocal Vision System, Adaptive Control of. Figure 2
Two possible configurations of the proposed multifocal vision system

With every change of the cameras the extrinsic camera parameters are lost and recalibration is required. Moreover exchanging cameras may alter camera platform dynamics due to different camera masses, which in turn alters platform inertia leading to reduced motion control performance of the multifocal vision system.

To overcome these problems the presented multifocal vision system not only follows the design recommendations given in [29], but additionally offers the possibility to exchange cameras while retaining camera calibration for later reuse of this configuration as suggested in [83]. Two possible system configurations are shown in Fig. 2. For easy exchange of the cameras they are mounted on adapter plates (Fig. 2b). These plates are attached to the yaw axis plate. For high repeat accuracy the plates are positioned with adjust pins relative to the yaw axis plate. Thus camera calibration is preserved as long as the cameras remain fixed to the adapter plates. Pitch axis drive and position sensor are mounted below the yaw axis plate. The pitch axis camera is placed in the hollow shaft of the yaw axis drive. A mirror is used to reflect the horizontal view toward the camera in the hollow shaft. Inertia of the pitch axis is kept low this way since only the mirror has to be rotated. Thus the weight of the pitch axis drive can also be kept to a minimum, which in turn reduces the inertia of the yaw axis. Placing the pitch axis camera in the center of rotation of the yaw axis further reduces yaw axis inertia.

Realizing Visual Motor Routines

An active multifocal vision system implies the need for visual motor routines like saccades, smooth-pursuit movement, and the vestibulo-ocular reflex.

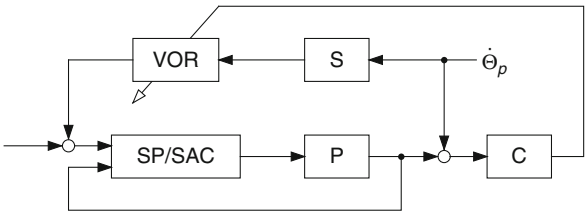

Active Multifocal Vision System, Adaptive Control of. Figure 3
Control of the multifocal vision system comprising three distinct controllers for saccades, smooth-pursuit movements, and the vestibulo-ocular reflex

Saccades are fast movements to a given reference position. Smooth-pursuit movements are used to track objects of interest or equivalently to keep selected regions of interest foveated. Saccades and smooth-pursuit movements require reference values either from a single visual perception module, e.g., a vehicle tracker or – based on the current situational context – from an attention module. Both saccades (SAC) and smooth-pursuit movements (SP) are based on feedback control that directs the plant P – which is the multifocal vision system – to a given reference position (Fig. 3).

The vestibulo-ocular reflex (VOR) provides active gaze stabilization based on inertial measurements of disturbing platform motions. A MEMS (micro-electro-mechanical system) sensor S is placed on the yaw axis plate of the multifocal vision system to measure the angular velocity $\dot{\Theta}_p$ of the pitch axis induced by vehicle rotations. Visual feedback from the camera C is used to calibrate this open-loop gaze stabilization.

Due to the different control objectives, the realization of saccades, smooth-pursuit movements, and the

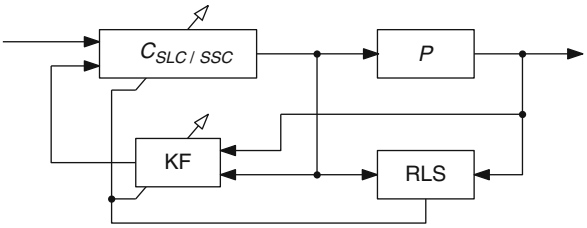

Active Multifocal Vision System, Adaptive Control of. Figure 4
Block diagram control of saccade and smooth pursuit

vestibulo-ocular reflex requires three distinct controllers (Fig. 3). The controllers for saccades and smooth-pursuit movements are implemented for both the yaw and the pitch axis of the multifocal vision system. The vestibulo-ocular reflex is only realized for the platform pitch axis, since disturbances like bumps, braking, or accelerating mainly induce vehicle pitch rotations.

Saccades and Smooth-Pursuit Movements

Saccades can be considered to be a time-optimal control problem. Therefore a near time-optimal sliding-mode control law (C_{SLC}) is proposed for saccades (Fig. 4). The smooth-pursuit movements are governed by a state-space controller (C_{SSC}) that is designed to provide good tracking behavior. Both controllers share a Kalman filter (KF) to derive full state information and a recursive least squares (RLS) parameter estimator for online identification of the parameters of the dynamic model of plant *P*. The RLS estimator is necessary since altering the camera configuration of the multifocal vision system may lead to a change in the platform dynamics – which is obvious from Fig. 2a and b. The parameter estimates of the RLS estimator are used to adapt the Kalman filter KF as well as the control laws C_{SLC} and C_{SSC}. Based on the control error a switch determines which control law is applied.

Dynamic Model

The dynamic plant models of platform yaw and pitch axis differ only slightly. Since the pitch axis model emerges from the yaw axis model, the yaw axis model is derived first. Plant dynamics is modeled as a nonlinear second-order differential equation as in [83] and [84]:

$$J \cdot \ddot{\varphi} = k_m \cdot I - \tau_\varphi - \tau_{\dot{\varphi}} \tag{1}$$

I is the torque generating motor current, k_m the motor torque constant, and J the inertia of the platform yaw axis. The angular velocity-dependent disturbance torque $\tau_{\dot{\varphi}}$ is described by

$$\tau_{\dot{\varphi}} = \tau_c \cdot sgn(\dot{\varphi}) + d \cdot \dot{\varphi} \tag{2}$$

with τ_c representing Coulomb and d representing viscous friction coefficient, with $sgn(\dot{\varphi})$ being the signum function. The angular position-dependent disturbance torque τ_φ results from twisted cables and from the unbalanced mass m with respect to the platform yaw axis:

$$\tau_\varphi = r \cdot m \cdot g \cdot sin(\theta_p) \cdot cos(\varphi) + c \cdot \varphi \tag{3}$$

The torsion-spring model $c \cdot \varphi$ describes the torque resulting from twisted cables. The term $r \cdot m \cdot g \cdot sin(\theta_p) \cdot cos(\varphi)$ represents the disturbance torque resulting from the unbalanced mass, with r being the distance from the center of gravity of the unbalanced mass m to the center of rotation of the platform yaw axis, g being the gravitational acceleration, and θ_p being the adjustable pitch angle of the platform yaw axis. The unbalanced mass results from the pitch axis encoder outweighing the pitch axis drive and any mass differences of the used camera/lens combinations. Defining $r \cdot m \cdot g \cdot sin(\theta_p) =: \tau_u$, the disturbance torque τ_φ can be written as

$$\tau_\varphi = \tau_u \cdot cos(\varphi) + c \cdot \varphi \tag{4}$$

With (2) and (4) the plant dynamics (1) can be summarized to:

$$J \cdot \ddot{\varphi} = k_m \cdot I - d \cdot \dot{\varphi} - c \cdot \varphi - \tau_c \cdot sgn(\dot{\varphi}) - \tau_u \cdot cos(\varphi) \tag{5}$$

The dynamic plant model of the platform pitch axis can be derived from the yaw axis model by neglecting the angular position-dependent disturbance torque (4) in (5).

Parameter Estimation

Since the model parameters J, d, c, τ_c, and τ_u are unknown, a parameter estimator is used to get the estimates $\hat{J}, \hat{d}, \hat{c}, \hat{\tau}_c$, and $\hat{\tau}_u$ respectively. Discretizing (5) using the forward differences as suggested in [85]

$$\dot{\varphi} = (\varphi_{k+1} - \varphi_k)/T \tag{6}$$

a discrete time plant model

$$\begin{aligned}\varphi_k = &- a_1 \cdot \varphi_{k-1} - a_2 \cdot \varphi_{k-2} + b_2 \cdot I_{k-2} \\ &- \delta_1 \cdot sgn\left(\frac{\varphi_{k-1} - \varphi_{k-2}}{T}\right) - \delta_2 \cdot cos(\varphi_{k-2})\end{aligned} \tag{7}$$

is derived which is linear in the parameters:

$$\begin{aligned} a_1 &= \tfrac{Td}{J} - 2, \quad a_2 = 1 - \tfrac{Td}{J} + \tfrac{cT^2}{J}, \quad b_2 = \tfrac{k_m T^2}{J} \\ \delta_1 &= \tfrac{\tau_c T^2}{J}, \qquad \delta_2 = \tfrac{\tau_u T^2}{J} \end{aligned} \tag{8}$$

Then (7) can be written as linear regression which is suitable for the application of a RLS parameter estimator. Parameter projection is used to constrain the parameter estimates to stay within reasonable limits as outlined in [86] and [83].

State Estimation

Both state-space control and sliding-mode control require full state information. Therefore, analog to [83] and [84], a state estimator is applied, using the angular position φ as measurement input. Since the plant model (5) is nonlinear, the parameter estimates $\hat{\tau}_c$ and $\hat{\tau}_u$ are used to compensate for the nonlinear disturbance terms in (5) with the disturbance feedforward:

$$I_{ff} = k_m^{-1} \cdot (\hat{\tau}_c \cdot sgn(\dot{\varphi}) + \hat{\tau}_u \cdot cos(\varphi)) \tag{9}$$

In [85], a similar approach is suggested for adaptive friction compensation. The plant input current I can be written as:

$$I = I_{ff} + I_{fb} + I_{ref} \tag{10}$$

with I_{ff} resulting from feedforward control, I_{fb} resulting from feedback control, and I_{ref} resulting from the reference input r of the axis controller. By inserting feedforward control (9) in the plant model (5) the equation

$$\begin{aligned} J \cdot \ddot{\varphi} = &k_m \cdot (I_{fb} + I_{ref}) - d \cdot \dot{\varphi} - c \cdot \varphi \\ &- (\tau_c - \hat{\tau}_c) \cdot sgn(\dot{\varphi}) - (\tau_u - \hat{\tau}_u) \cdot cos(\varphi) \end{aligned} \tag{11}$$

is derived.

Summarizing the remaining disturbance torques resulting from parameter estimation errors $\tau_u - \hat{\tau}_u$ and $\tau_c - \hat{\tau}_c$, as well as from unmodeled disturbances in one disturbance torque τ_d, (11) can be written as

$$J \cdot \ddot{\varphi} = k_m \cdot (I_{fb} + I_{ref}) - d \cdot \dot{\varphi} - c \cdot \varphi - \tau_d \tag{12}$$

$\ddot{\tau}_d = 0$ is used as a disturbance model, as this is found in [87] to be a good compromise between model complexity and estimation accuracy in the context of friction compensation.

Using the continuous time state-space formulation

$$\begin{aligned} &\dot{x} = Fx + G\bar{u}, y = Cx, \text{with} \\ &x = (\varphi,\ \dot{\varphi},\ \tau_d,\ \dot{\tau}_d)^T,\ \bar{u} = I_{fb} + I_{ref} \end{aligned} \tag{13}$$

from (12) and disturbance model $\ddot{\tau}_d = 0$ the state-space description

$$\begin{aligned} &F = \begin{pmatrix} 0 & 1 & 0 & 0 \\ -\frac{c}{J} & -\frac{d}{J} & -\frac{1}{J} & 0 \\ 0 & 0 & 0 & 1 \\ 0 & 0 & 0 & 0 \end{pmatrix},\ G = \begin{pmatrix} 0 \\ \frac{k_m}{J} \\ 0 \\ 0 \end{pmatrix}, \\ &C = (1,\ 0,\ 0,\ 0) \end{aligned} \tag{14}$$

can be derived. As a discrete time Kalman filter is used for state estimation, a discrete time description

$$\begin{aligned} &x_{k+1} = Ax_k + B\,\bar{u}_k, y_k = Cx_k, \ \text{with} \\ &x_k = (\varphi_k, \dot{\varphi}_k, \tau_{dk}, \dot{\tau}_{dk})^T \end{aligned} \tag{15}$$

of (14) is needed. Using (6) for discretization yields

$$\begin{aligned} &A = \begin{pmatrix} 1 & T & 0 & 0 \\ -\frac{cT}{J} & \frac{J-Td}{J} & -\frac{T}{J} & 0 \\ 0 & 0 & 1 & T \\ 0 & 0 & 0 & 1 \end{pmatrix}, B = \begin{pmatrix} 0 \\ \frac{k_m T}{J} \\ 0 \\ 0 \end{pmatrix} \\ &C = (1,\ 0,\ 0,\ 0) \end{aligned} \tag{16}$$

Replacing parameters J, c, and d at every time step k with their estimates $\hat{J}_k$, $\hat{c}_k$, and $\hat{d}_k$ results in $\hat{A}_k$ and $\hat{B}_k$ as state and input matrices respectively.

State-Space Control

State-space control is used for smooth-pursuit movements that demand a good tracking behavior. Therefore the reference r is designed to track the desired axis angle φ_{ref} up to a ramp signal without steady-state error. Thus r is a linear combination of φ_{ref} and its

time derivative $\dot{\varphi}_{ref}$ with gains w_1 and w_2:

$$r = w_1 \cdot \varphi_{ref} + w_2 \cdot \dot{\varphi}_{ref} \tag{17}$$

Following the controller design in [83] and [84], the steady-state error of the discrete time tracking error $\varphi_{ref}(z) - \varphi(z)$ is calculated by applying the final value theorem. Provided $\hat{c}$ and $\hat{d}$ approach their true values, the steady-state tracking error becomes zero if w_1 and w_2 are chosen as follows:

$$w_1 = k_1 + \frac{\hat{c}}{k_m} \text{ and } w_2 = k_2 + \frac{\hat{d}}{k_m} \tag{18}$$

Using the estimated state vector $\hat{x}_k$ and the disturbance feedforward I_{ff} together with the discrete time reference input r_k yields the control law:

$$\begin{aligned} u_k = r_k - k_{1_k}\hat{\varphi}_k - k_{2_k}\dot{\hat{\varphi}}_k + \frac{\hat{\tau}_{d_k}}{k_m} \\ + \frac{\hat{\tau}_{c_k}}{k_m} sgn(\dot{\hat{\varphi}}_k) + \frac{\hat{\tau}_{u_k}}{k_m} cos(\hat{\varphi}_k) \end{aligned} \tag{19}$$

Applying the control law (19) to the plant (5), results in a second-order closed-loop system. As described in [83], the controller gains k_1 and k_2 are determined by the comparison of coefficients with the desired second-order closed-loop characteristic polynomial. The derived gains are

$$k_1 = (\hat{J}\omega_0^2 - \hat{c})/k_m \text{ and } k_2 = \left(2\zeta\omega_0\hat{J} - \hat{d}\right)/k_m \tag{20}$$

with closed-loop natural frequency ω_0 and damping ζ. Damping is chosen $\zeta > 1$ to avoid overshoot and ω_0 is calculated as follows [83, 88]:

$$\omega_0 = \frac{4.6}{\eta\zeta\sqrt{\hat{J}}} \tag{21}$$

The constant η is used to adjust the influence of the estimated inertia $\hat{J}$ on the desired closed-loop dynamics ω_0.

Sliding-Mode Control

Saccadic movements are a typical application for time-optimal control. Time-optimal control problems can be solved using Pontryagin's minimum principle [89], but the solution is sensitive to unknown plant dynamics or disturbances. Moreover it is difficult to derive a solution analytically for nonlinear systems.

Sliding-mode control on the contrary is an inherently robust method to cope with uncertain plant dynamics. If the controlled system has reached the sliding-mode, it is insensitive to disturbances and system motion is determined by the sliding-surface only [90, 91].

There are several approaches that try to utilize the robustness properties of sliding-mode control, while simultaneously attaining near time-optimal control performance, e.g., [92–94].

These control law design methods are offline methods and therefore the derived controllers are not suitable for online adaptation. The design of the presented saccade controller is based on the minimum time sliding-mode control law for second-order systems derived in [94]. However the sliding-line proposed in [94] is subject to stability constraints that prevent the control from being time-optimal. Analog to [84], the proposed sliding-line is designed to relax these constraints and thus achieve near time optimality.

The system motion of a system under sliding-mode control consists of two modes: the *reaching-mode* and the *sliding-mode* [91]. During the *reaching-mode* the phase trajectory of the system (Fig. 5) starts from anywhere in the phase plane and moves toward the sliding-line $s = 0$. After reaching the sliding-line $s = 0$ the phase trajectory will stay on it, provided the *reaching condition* is satisfied. Then the system is in the so-called sliding-mode and the system motion is only governed by the differential equation $s = 0$. With the system under control

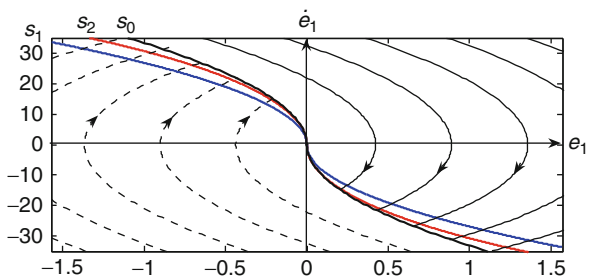

Active Multifocal Vision System, Adaptive Control of. Figure 5
Phase trajectories and sliding-lines [84]

$$u = -K\, sgn(s),\ K > 0 \tag{22}$$

and using the Lyapunov function candidate

$$V(s) = \frac{1}{2}s^2 \tag{23}$$

a global reaching condition [91, 94] is given by:

$$\dot{V}(s) = s\dot{s} < 0,\ s \neq 0 \tag{24}$$

That means $s > 0$ indicates $\dot{s} < 0$ and vice versa. Thus the phase trajectories will always move toward and stay on $s = 0$ after reaching it.

In order to apply sliding-mode control, plant dynamics (5) is rewritten as a set of first-order differential equations. Defining the control error $\varphi - \varphi_{ref} := e_1$ and noting that φ_{ref} is constant yields

$$\begin{aligned} \dot{e}_1 &= e_2 \\ \dot{e}_2 &= (f(\dot{\varphi}) + g(\varphi) + h(\varphi, \dot{\varphi}) + u)/J \end{aligned} \tag{25}$$

with $\dot{e}_1 = \dot{\varphi}$ and $\dot{e}_2 = \ddot{\varphi}$. The disturbance torque is separated into three categories: $f(\dot{\varphi})$describes the friction torque, with the property $f > 0$ if $\dot{\varphi} < 0$ and vice versa. Secondly $g(\varphi)$ is a spring torque and is assumed to be monotonically decreasing, i.e., $\partial g/\partial\varphi < 0 \forall\varphi$. Finally, $h(\varphi, \dot{\varphi})$ sums up the remaining disturbance torques that cannot be described by f or g. u is the plant input torque.

For a second-order system the nonlinear switching surface

$$s = \alpha e_1 + |e_2|e_2 = 0 \tag{26}$$

is proposed in [94]. Solving the differential equation (26) for constant α, the time span t needed to approach $e_1 = 0$ is calculated as follows:

$$t = 2\sqrt{|e_1(t = 0)|/\alpha} \tag{27}$$

Provided that (24) is satisfied, it is obvious from (27) that the resulting transient response is faster for higher α. Thus α has to be maximized to reach near time-optimal control. For a double-integrator plant the sliding-line (26) becomes identical to the time-optimal switching-line for $\alpha \rightarrow 2K$ [94], with K being the maximum control torque. In [94] it is argued that if the plant is not a pure double integrator but subject to disturbances as, e.g., system (25), the maximum values of the disturbances have to be considered in the calculation of α. Otherwise there are no resources left to compensate for the disturbances. Following this argumentation, it can be shown that the *reaching condition* (24) is satisfied for system (25) with control (22) and switching surface (26) for

$$\alpha < \frac{2}{J}(K - f_{max} - g_{max} - h_{max}) \tag{28}$$

But supposing that, e.g., f describes viscous friction $f = d\,\dot{\varphi}$, f_{max} depends linearly on the largest possible angular velocity $\dot{\varphi}_{max}$. Thus α is too conservative for $\dot{\varphi} \ll \dot{\varphi}_{max}$.

The proposed approach utilizes the properties of the disturbance torques f and g to increase α, leading to a faster transient response of the control loop:

$$\alpha < \frac{2}{J}(K + g \cdot sgn(e_1) - h_{max}) \tag{29}$$

The term $g{\cdot}sgn(e_1)$ is chosen such that α increases if g reduces acceleration or supports deceleration. On the contrary α decreases if g supports acceleration or reduces deceleration. The friction torque f always counteracts the actuator torque and can thus be neglected in the calculation of α. Therefore α is independent from f_{max} and g_{max}, which is a desirable property. Figure 5 depicts some switching surfaces of system (25) with $\varphi_{ref} = 0$. The time-optimal switching-line is s_0. s_1 and s_2 are the switching-lines from (26) with α according to (28) or (29) respectively. s_2 lies in between s_0 and s_1, indicating that using (29) to calculate α yields a faster transient response than using (28).

Comparing system (25) with the plant dynamics (5), one derives

$$\begin{aligned} f &= -d \cdot \varphi - \tau_c \cdot \mathrm{sgn}(\dot{\varphi}) \\ g &= -c \cdot \varphi \\ h &= -\tau_u \cdot cos(\varphi) \end{aligned} \tag{30}$$

for the disturbance torques f, g, and h. The maximum control torque K in (22) corresponds to the maximum actuator torque $k_m \cdot I_{max}$.

Since the plant parameters are not known in advance, the parameter estimates derived from the RLS parameter estimator are used (cf. section "Parameter Estimation") for the calculation of the sliding-line. Moreover the state estimates are obtained from the Kalman filter introduced in section "State Estimation." Thus the sliding-line is

$$s = \alpha\left(\hat{\varphi}k - \varphi_{ref}\right) + |\dot{\hat{\varphi}}_k|\dot{\hat{\varphi}}_k \tag{31}$$

with

$$\alpha < \frac{2}{\hat{J}}\left(K - \hat{c}\cdot\hat{\varphi}_k \cdot sgn\left(\hat{\varphi}_k - \varphi_{ref}\right) - |\hat{\tau}_u|\right) \tag{32}$$

Switching Strategy

To switch between state-space control and sliding-mode control the simple hysteresis

$$\text{IF } \left|\varphi_{ref} - \varphi\right| > \varepsilon_u \text{ THEN saccade} = \textit{true}$$
$$\text{IF } \left|\varphi_{ref} - \varphi\right| > \varepsilon_l \text{ THEN saccade} = \textit{false}$$

is used, with $\varepsilon_u > \varepsilon_l > 0$. If the control error $\varphi_{ref} - \varphi$ exceeds the upper threshold ε_u, a saccade is carried out and sliding-mode control is active. If the control error goes below the lower threshold ε_l, state-space control becomes active until the control error exceeds ε_u again.

Experimental Results

Some experimental results described in [84] demonstrate the validity of the presented saccade and smooth-pursuit control laws. The two configurations of the multifocal vision system shown in Fig. 2 were used for the experiments. These configurations equipped with three (Fig. 2b) and five cameras (Fig. 2a) are called 3c- and 5c-configuration respectively. Saccades with three different step sizes were conducted. For every step size the results of the sliding-mode control are compared with the state-space control, this way demonstrating the superior performance of the proposed near time-optimal sliding-mode control over state-space control with respect to saccades. The step sizes were ±10°, ±20°, and ±30° (Fig. 6). Every plot of Fig. 6 depicts four saccades: two for each platform configuration, resulting from sliding-mode control and state-space control respectively.

For fast saccades maximum acceleration followed by maximum deceleration is required. Sliding-mode control design is explicitly based on the maximum achievable acceleration and deceleration. That is why sliding-mode control suits saccadic movements better than state-space control.

From Fig. 6 it is obvious that saccades under state-space control are either too slow or result in overshoot.

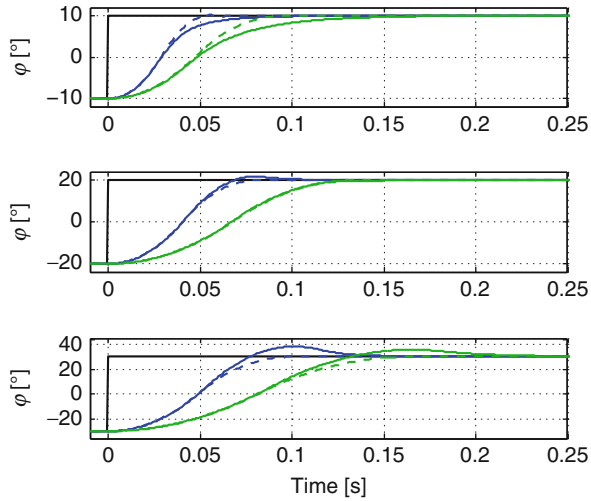

Active Multifocal Vision System, Adaptive Control of. Figure 6
Saccades [84]: *Black lines* are reference values. *Blue lines* correspond to the 3c-configuration, *green lines* to the 5c-configuration. *The dashed lines* result from the sliding-mode control, the solid lines from state-space control

The results for sliding-mode and state-space control are similar only for a small operating range as can be seen from the ±20°-saccade.

Figure 7 depicts the controller output corresponding to the saccades of the 5c-configuration shown in Fig. 6. For the ±20°-saccade the controller output of state-space control and sliding-mode control overlap to a large extent. In particular the switching from acceleration to deceleration and vice versa takes place at nearly identical points in time. Therefore the resulting saccades are also similar. During the ±30°-saccade the state-space control output changes from acceleration to deceleration later than the sliding-mode control output. Also the deceleration phase is finished later, resulting in considerable overshoot. For the ±10°-saccade the state-space controller starts decelerating earlier than the sliding-mode controller and thus the corresponding saccade is finished later.

The switching activity (chattering) of the sliding-mode controller is low, indicating that the control performance is close to time-optimal. For practical applications, however, it is preferable to avoid chattering completely, since it may cause increased hardware attrition and induces audible noise.

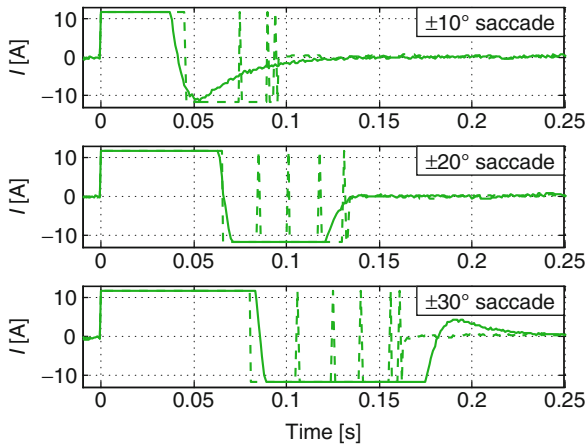

Active Multifocal Vision System, Adaptive Control of. Figure 7
Controller output for saccades of the 5c-configuration [84]: *Solid lines* correspond to state-space control, *dashed lines* to sliding-mode control

Replacing the signum function in (22) with the saturation function

$$u = K\,sat(s) = \begin{cases} -\dfrac{K}{l}s & \text{for } s \le |l| \\ -K\,sgn(s) & \text{for } s > |l| \end{cases} \tag{33}$$

is a possible alternative. The saturation function introduces a boundary layer around the sliding-line s. Outside the boundary layer the saturation function equals the signum function. Inside the boundary layer the sliding-mode control is replaced by a high-gain proportional control, thereby avoiding the discontinuity of the signum function for $s = 0$.

The sliding-lines for the 3c- and 5c-configuration are shown in Fig. 8. Note that the slope of the sliding-line of the 3c-configuration is higher than the slope of the 5c-configuration. This results mainly from the influence of the estimated inertia $\hat{J}$ on the calculation of α in (32). Obviously the inertia of the 3c-configuration is smaller than the inertia of the 5c-configuration.

Moreover the resulting phase trajectories of the $\pm 20°$-saccade for the 3c-configuration and the $\pm 30°$-saccade for the 5c-configuration are depicted in Fig. 8. After reaching the sliding-line, the trajectories stay in a small vicinity of the sliding-line, due to the nonideal components of a real-world control loop.

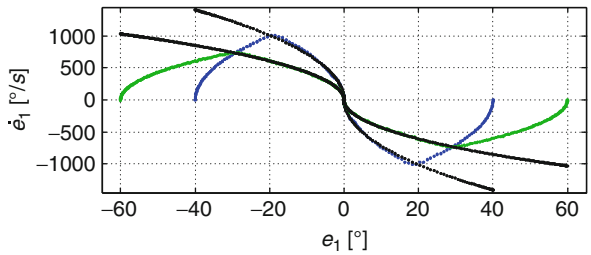

Active Multifocal Vision System, Adaptive Control of. Figure 8
Sliding surfaces and phase trajectories [84]: The *blue line* corresponds to the phase trajectory of the 3c-configuration, the *green line* to the trajectory of the 5c-configuration. The *black lines* are the corresponding sliding surfaces

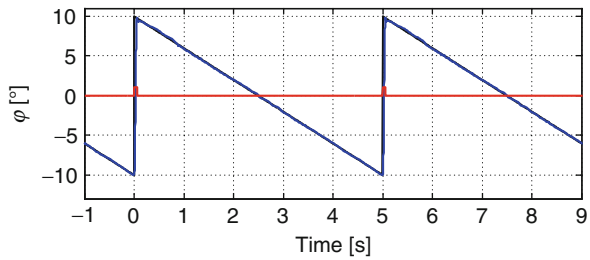

Active Multifocal Vision System, Adaptive Control of. Figure 9
Saccades and smooth-pursuit movements [84]: The *black line* is the reference value. The *blue line* corresponds to the 3c-configuration. The *red line* states which control law is active: state-space or sliding-mode control

A sawtooth signal is used as position reference to test the switching between sliding-mode control and state-space control (Fig. 9). With the sawtooth signal saccades and smooth-pursuit movements can be simulated since it offers fast (saccade like) changes as well as continuous change over time with a constant slope. The output of the switching hysteresis proposed in section "Switching Strategy" is depicted in red. Both smooth-pursuit movements and saccades show satisfactory control behavior. Furthermore the switching between both controllers is smooth and without noticeable influence on the control performance.

Vestibulo-Ocular Reflex

The use of high resolution telecameras enhances the perceptional capabilities of autonomous vehicles. It enables both the early detection of distant objects and provides detailed images of points of interest in the vehicles surrounding. But telecameras are more sensitive to disturbances – especially rotational vehicle motion – than wide-angle cameras.

To obtain stable images and keep objects of interest within camera scope active gaze stabilization is necessary. In [29, 33], inertial measurements of the rotational vehicle motion are used for active image stabilization in autonomous vehicles.

This is a pure feedforward control, since image-based information is not used for the stabilization. Residual image motion may be induced by errors of the inertial angular-rate sensor, such as sensor offset, wrong or changing sensor sensitivity, errors in the mounting position of the sensor, or imperfections in the control loop of the stabilizing actuator.

Therefore in more recent works visual information is incorporated in the stabilization process. Either information from inertial sensors and vision is fused as, e.g., in [24], or the inertial sensors are calibrated based on visual information as in [27, 36, 37]. The latter approach is similar to the vestibulo-ocular reflex (VOR) that many vertebrates use for gaze stabilization. The VOR not only stabilizes the image on the retina, but also continuously adapts to erroneous measurements of the vestibular organ located in the inner ear [37]. This adaptation process is based on visual feedback.

In [27, 36, 37] sensor and actuator errors are compensated by means of an adaptive FIR (finite impulse response) filter as suggested in [95]. The filter adaptation is driven by optical flow. The camera platform in [27] executes only rotational motions in an indoor environment. Thus optical flow results solely from rotational motion. In [36, 37] the camera platform is mounted behind the windshield of a car. Optical flow computation is based on distant features. This way the translational platform motion has little impact on the resulting optical flow. But calculating the optical flow by utilizing distant features only is not always possible, consider, e.g., a car driving on a forest track or in an inner-city environment.

The presented active inertial gaze stabilization is inspired by the vestibulo-ocular reflex too. In contrast to the aforementioned works, however, the sensor and actuator errors are modeled explicitly. From those error models a filter transfer function is derived that is suitable to modify the sensor signal such as to compensate for the overall stabilization error. The adaptation of the unknown filter parameters is driven by the residual camera motion.

Calibrating the Inertial Gaze Stabilization

Analog to [96], the realization of the vestibulo-ocular reflex includes the open-loop gaze stabilization based on an MEMS angular-rate sensor and the calibration of this sensor driven by visual feedback (Fig. 10).

The angular-rate sensor S measures the pitch velocity $\dot{\Theta}_p$ of the camera platform. After passing the filter

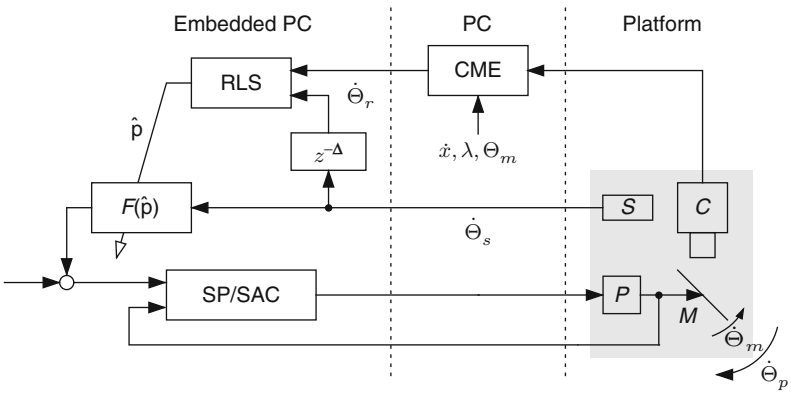

Active Multifocal Vision System, Adaptive Control of. Figure 10
Block diagram of the inertial gaze stabilization and its calibration

$F(\hat{\mathbf{p}})$ the sensor signal $\dot{\Theta}_s$ is the reference value for the control (SP/SAC) of the gaze stabilizing plant P. A mirror together with an actuator is used for gaze stabilization. In fact the reference value for the control of P is half the size of the filtered sensor signal, since for a mirror the incident angle equals the emergent angle.

Image correspondences computed from already stabilized images from camera C together with the vehicle velocity $\dot{x}$ and the vehicle steering angle λ serve as measurements for the camera motion estimation (CME) based on an unscented Kalman filter (UKF) [97]. The CME is used to estimate the residual pitch velocity $\dot{\Theta}_r$, which is the difference between the real platform velocity $\dot{\Theta}_{pl}$ and two times the mirror velocity $\dot{\Theta}_m$. $\dot{\Theta}_r$ again is used as an error signal for a recursive least squares (RLS) parameter estimator that estimates the parameters $\hat{\mathbf{p}}$ of the filter $F(\hat{\mathbf{p}})$ in a way that the residual image motion is minimized. To consider the latencies Δ resulting from image processing in the parameter estimation process, the sensor signal $\dot{\Theta}_s$ is artificially delayed by Δ before entering the RLS parameter estimator.

Compensating the Open-Loop Errors

To derive an adaptive filter that compensates for the open-loop errors of the inertial gaze stabilization, the sensor and actuator characteristics are modeled explicitly as in [96].

The MEMS angular-rate sensor signal

$$\dot{\Theta}_s = k_s \dot{\Theta}_{pl} + \delta_s \tag{34}$$

is considered to be biased resulting from an offset δ_s. Moreover the sensor is thought to have a sensitivity k_s differing from the nominal sensitivity. Please note that the sensitivity k_s may also be influenced by the mounting position of the sensor, e.g., when the sensor is not exactly aligned with the axis of rotation of the mirror.

The stabilizing mirror and its control are modeled as a first-order transfer function in the Laplace domain

$$\dot{\Theta}_m = \frac{0.5 k_a}{\tau_a s + 1} \dot{\Theta}_s \tag{35}$$

with the time constant τ_a describing the bandwidth of the control loop and the gain k_a. The gain k_a describes the steady-state deviation of the mirror velocity $\dot{\Theta}_m$ from half of the measured sensor value $\dot{\Theta}_s$.

The goal of the adaptive filter design is to reconstruct the real platform pitch velocity $\dot{\Theta}_p$ from the sensor signal $\dot{\Theta}_s$ and to compensate the influence of the actuator control loop on the gaze stabilization. The filter equation is chosen as follows:

$$\dot{\Theta}_F = F(\hat{\mathbf{p}}) = \frac{\hat{\tau}_a s + 1}{\hat{k}_a \hat{k}_s} (\dot{\Theta}_s - \hat{\delta}_s) \tag{36}$$

Using the output of filter (36) as input to the mirror control loop (35) and inserting (34) in (36) results in

$$\dot{\Theta}_m = \frac{0.5 k_a}{\tau_a s + 1} \frac{\hat{\tau}_a s + 1}{\hat{k}_a \hat{k}_s} (k_s \dot{\Theta}_p + \delta_s - \hat{\delta}_s) \tag{37}$$

If the estimated parameters $\hat{\mathbf{p}} = [\hat{\tau}_a, \hat{k}_a, \hat{k}_s, \hat{\delta}_s]^T$ approach their true values $\mathbf{p} = (\tau_a, k_a, k_s, \delta_s)^T$ (37) reduces to

$$\dot{\Theta}_m = 0.5 \dot{\Theta}_p \tag{38}$$

which is the desired optimal gaze stabilization.

To get estimates $\hat{\mathbf{p}}$ of the unknown parameters $\mathbf{p}$ with a discrete time RLS parameter estimator (Fig. 10), the filter equation (36) has to be discretized. Since the sampling interval T is small compared to the vehicle's pitch dynamics, backward differences $\dot{x}(k) = \frac{x(k) - x(k-1)}{T}$ can be used for discretization:

$$\dot{\Theta}_F(k) = \frac{\hat{\tau}_a + T}{\hat{k}_a \hat{k}_s T} \dot{\Theta}_s(k) - \frac{\hat{\tau}_a}{\hat{k}_a \hat{k}_s T} \dot{\Theta}_s(k-1) - \frac{\hat{\delta}_s}{\hat{k}_a \hat{k}_s} \tag{39}$$

The resulting discretized filter equation (39) is linear in its parameters and can be written as a linear regression

$$\begin{aligned} \dot{\Theta}_F(k) &= \left[\dot{\Theta}_s(k), \dot{\Theta}_s(k-1), 1\right]^T \begin{bmatrix} \hat{b}_0 \\ \hat{b}_1 \\ \hat{d} \end{bmatrix} \\ &=: \phi^T(k-1)\hat{\theta} \end{aligned} \tag{40}$$

which is suitable for the RLS parameter estimation [86].

Usually the RLS parameter update is driven by the difference of a measured signal y and a prediction $\hat{y}$ of y based on the estimated parameters $\hat{\theta}$. The difference $y - \hat{y}$ is a measure for the RLS parameter estimation error. The residual camera pitch velocity $\dot{\Theta}_r$ can also be considered to be a measure for the parameter

estimation error. Unless $\dot{\Theta}_r = 0$ the estimated parameters $\hat{\mathbf{p}}$ of filter $F(\hat{\mathbf{p}})$ are not equal to their true values $\mathbf{p}$. Therefore equation

$$\hat{\theta}(k+1) = \hat{\theta}(k) + K(k)\,\dot{\Theta}_r \tag{41}$$

can be used for the parameter update, with $K(k)$ being the parameter update gain of the RLS parameter estimator.

Camera Motion Estimation

The estimation of the unknown residual camera motion (CME) is based on image data. This is commonly referred to as *visual odometry*. The estimation of non-holonomic vehicle motion in real time was presented, e.g., in [98, 99]. An overview on the relevant literature is also given therein. *Visual odometry* relies on the calculation of image correspondences between consecutive image frames. A method to calculate these correspondences in real time is given in [100].

Most works on *visual odometry* aim at estimating the camera motion from visual data only. However to enhance the robustness of the CME the vehicle velocity and the vehicle steering angle are incorporated in the estimation process as suggested in [96]. These measurements are available on most ground-moving vehicles.

One fundamental problem in *visual odometry* is the determination of the depth of image keypoints. To circumvent this, the drivable area in front of the vehicle is assumed to be an ideal ground plane. Considering only image correspondences corresponding to that ground plane implicitly determines the depth of the image keypoints due to the known camera position relative to the ground plane.

As a tribute to computation speed, the calculated image correspondences include some *false positives* [100]. Thus a preselection of valid correspondences is necessary; otherwise the estimation performance may be corrupted.

The gaze stabilization is independent of the camera motion estimation. Only the calibration of the angular-rate sensor is based on the estimated camera motion. But the calibration can be switched off, whenever the estimated camera motion seems to be unreliable. This may be the case, e.g., if too little image correspondences are available or if the ground plane assumption is invalid.

The calibration of the gaze stabilization is driven by the estimated residual camera motion. However this estimation is not the main purpose of this entry. The interested reader may refer to [96] for a more detailed description of the applied camera motion estimation or to the literature on *visual odometry* for alternative approaches.

Experimental Results

The proposed gaze stabilization was evaluated during several test runs on a bumpy dirt road as described in [96]. Figure 11 gives some impressions of the test track.

The red rectangles in Fig. 11a–c mark the region of interest of the feature correspondence algorithm. Feature correspondences are only computed within this region. According to the ground plane assumption the ROI corresponds to the drivable area in front of the vehicle. The green lines in Fig. 11a–c mark correspondences that were accepted as measurements for the camera motion estimation. The red lines depict correspondences that were considered to be false positives.

The proposed vision-based online-calibration of the MEMS angular-rate sensor was tested during three consecutive runs along the test track with activated sensor calibration and gaze stabilization. Figure 12 depicts the estimated gain $\hat{k}_f = \frac{1}{\hat{k}_a \hat{k}_s}$ of the filter $F(\hat{\mathbf{p}})$. For evaluation purposes the filter gain was artificially reduced from 1 to 0.5. During parameter estimation the gain rose from $\hat{k}_f = 0.5$ to $\hat{k}_f \approx 0.88$, which is beneath the nominal gain 1.

The estimated time constant $\hat{\tau}_a$ remained close to its initial value zero. This indicates that the bandwidth of the actuator control loop is sufficiently large and no phase-delay occurs during stabilization. The estimated residual pitch velocity $\dot{\Theta}_r$ was biased and had to be high-pass filtered to avoid parameter drift, therefore the offset δ_s was estimated to be zero too.

To further evaluate the proposed gaze stabilization, the estimated residual camera motion $\dot{\Theta}_r$ was compared for the following three runs on the test track: One with deactivated gaze stabilization, another one with activated stabilization but uncalibrated sensor ($\hat{k}_f = 1$), and finally the one with activated gaze stabilization and calibrated sensor ($\hat{k}_f \approx 0.88$). During this last run the calibration was active, but the parameters had already converged.

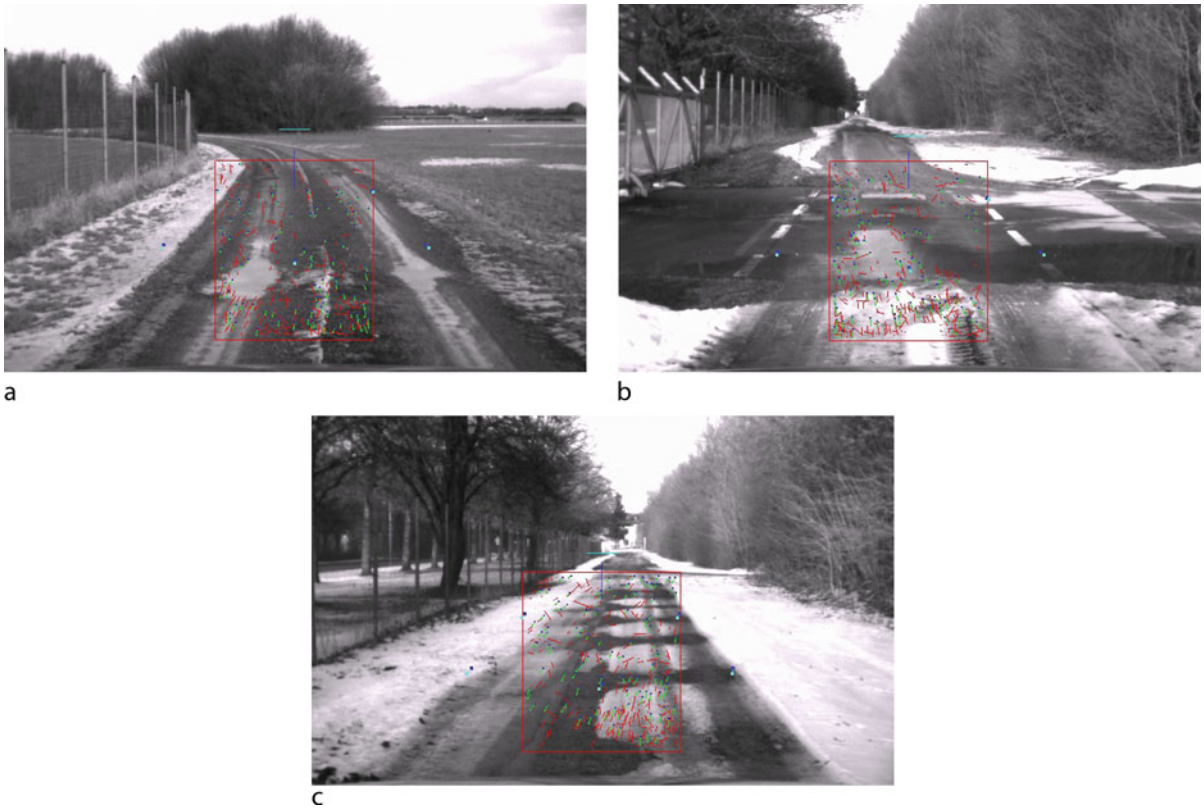

Active Multifocal Vision System, Adaptive Control of. Figure 11
Selected images from the test track [96]

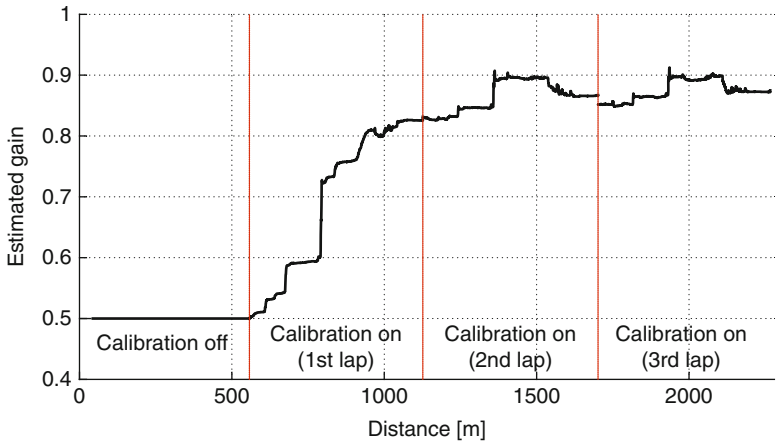

Active Multifocal Vision System, Adaptive Control of. Figure 12
Estimated gain of the filter $F(\hat{\mathbf{p}})$ [96]

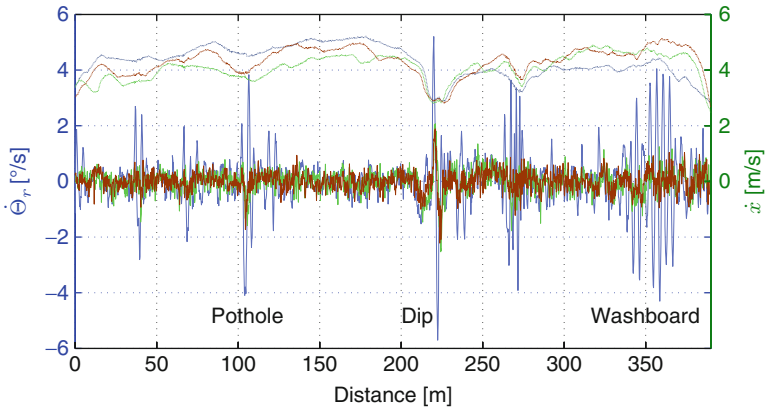

Active Multifocal Vision System, Adaptive Control of. Figure 13
Gaze stabilization results [96]: The *blue lines* correspond to the deactivated stabilization, the *green lines* to the activated stabilization, and the *dark red lines* to the calibrated stabilization. *Solid lines* correspond to the residual camera motion $\dot{\Theta}_r$, *dotted lines* to the vehicle velocity $\dot{x}$

The stabilization results are plotted in Fig. 13. It gives an overview of the resulting estimated camera pitch velocities $\dot{\Theta}_r$ during the test runs. The labels "pothole," "dip," and "washboard" mark peaks in the pitch velocities $\dot{\Theta}_r$ that originate from passing the track sections depicted in Fig. 11a–c.

The gaze stabilization based on the uncalibrated MEMS sensor already showed good results. Therefore for better evaluation the rms-value of $\dot{\Theta}_r$ was calculated as a measure for the stabilization error (Fig. 14). The resulting rms-value was normalized with respect to the rms-value of $\dot{\Theta}_r$ in case of the unstabilized camera. The normalized rms-error for the unstabilized camera is then 100%. It turns out that the rms-error corresponding to the calibrated gaze stabilization is smaller than the rms-error corresponding to the uncalibrated gaze stabilization.

The rms-error for the calibrated stabilization is approximately 12% smaller than the rms-error resulting from the uncalibrated stabilization. This can be considered to be the average reduction of the stabilization error, resulting from an increasing or a decreasing filter gain $\hat{k}_f$. The reduction of the rms-error corresponds to the magnitude of change of the filter gain.

The test runs were carried out at similar but not equal velocities (Fig. 13). However, the velocity during the test run with calibrated stabilization (dark red) was almost always higher than the velocity corresponding to the test run with active but uncalibrated stabilization (green). Although higher vehicle velocities are assumed to induce higher camera pitch velocities, the calibrated stabilization still beats the uncalibrated stabilization.

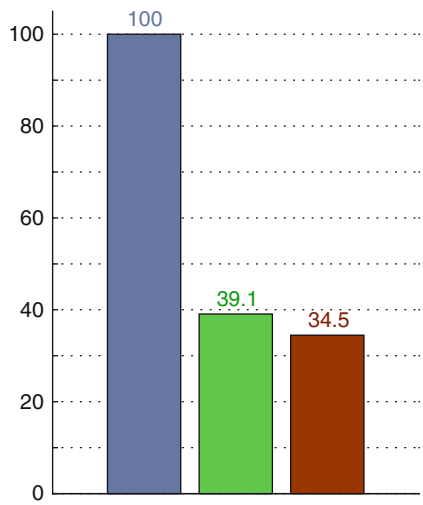

Active Multifocal Vision System, Adaptive Control of. Figure 14
The normalized rms-error of the gaze stabilization (based on $\dot{\Theta}_r$) [96]. The *blue bar* corresponds to the deactivated stabilization, the *green bar* to the activated stabilization, and the *dark red bar* to the calibrated stabilization

Future Directions: The Importance of Visual Perception

Perception of the environment for intelligent vehicles should cover large parts of their surrounding with sufficient accuracy. One possible realization for the visual sensory system is a multifocal vision system simultaneously offering a wide field of view and high resolution. Obviously such a system has to be active, since the high visual acuity is limited to the small aperture angles of the tele-lenses. Saccades, smooth-pursuit movements, and the vestibulo-ocular reflex are therefore essential capabilities to be able to fully exploit the possibilities offered by an active multifocal vision system.

However multifocal vision systems are only beneficial if there is a competition for sensing resources, be it either to observe characteristic parts of an object in more detail or to observe regions of interest that are not in the current sensor view. Then, similar to human selective attention, a selection stage is necessary that decides which gaze direction is most appropriate to the task at hand.

The outcome of most current computational models of visual attention are saliency maps of interesting scene regions. These maps can be used to direct the telecamera of a multifocal vision system toward this salient region to obtain high-resolution images thereof. If top-down cues are incorporated in the map calculation they can be used, e.g., for object detection of previously known objects. However, if at all, up to now saliency maps are only rarely used for object tracking.

Multifocal object tracking requires object recognition based on the identification and tracking of a set of characteristic object features, e.g., the lights, the tires, or the license plate of a car. After identifying these features in the image frame of a wide-angle camera they could be successively observed with a high resolution tele-lense. This kind of object tracking is subject to current research and therefore it is developed for a single camera first.

Apart from the computation of saliency maps, there exist some approaches to gaze control that are used to track multiple objects, landmarks, or road networks. These approaches either try to predict the most informative viewing direction(s) based on information theoretic concepts or to plan a sequence of gaze directions ensuring an optimal viewing behavior considering the needs of several distributed visual perception modules with respect to the visibility of interesting scene regions. However these existing gaze control approaches were not employed in dynamic environments like inner-city traffic scenes.

Providing visual perception for intelligent vehicles, capable of reliable and robust multiple object tracking together with the detection and tracking of intersections, roads, traffic signs, and so on, is a major challenge in future research. Multifocal object tracking and computational models of visual attention may contribute to this by no means trivial task. Such advanced perceptual capabilities give rise to a competition for sensing resources. Then the intelligent selective gaze control – based on the current context – choosing the appropriate gaze directions will be inevitable.

Bibliography

1. Palmer SE (1999) Vision science. MIT Press, Cambridge, MA
2. Kolb B, Whishaw IQ (2009) Fundamentals of human neuropsychology, 6th edn. Worth, New York
3. Kandel ER, Schwartz JH, Jessell TH (1995) Essentials of neural science behavior, 1st edn. Prentice Hall International, London
4. Henderson JM (2003) Human gaze control during real-world scene perception. Trends Cogn Sci 7(11):498–504, November
5. Treue S (2003) Visual attention: the where, what, how and why of saliency. Curr Opin Neurobiol 13:428–432
6. Chun MM, Marois R (2002) The dark side of visual attention. Curr Opin Neurobiol 12:184–189
7. Krauzlis RJ (2005) The control of voluntary eye movements: new perspectives. Neuroscientist 11(2):124–137
8. Knudsen EI (2007) Fundamental components of attention. Annu Rev Neurosci 30:57–78
9. Summerfield C, Egner T (2009) Expectation (and attention) in visual cognition. Trends Cogn Sci 13(9):403–409
10. Land MF, Lee DN (1994) Where we look when we steer. Nature 369:742–744
11. Chapman PR, Underwood G (1998) Visual search of driving situations: danger and experience. Perception 27:951–964
12. Olson PL, Battle DS, Aoki T (1989) Driver eye fixations under different operating conditions, University of Michigan, Ann Arbor, Transportation Research Institute, Technical Report
13. Wann JP, Wilkie RM (2004) How do we control high speed steering. In: Optic flow and beyond. Kluwer, Norwell, pp 401–419, ch 18
14. Falkmer T, Gregersen NP (2005) A comparison of eye movement behavior of inexperienced and experienced drivers in real traffic environments. Optom Vis Sci 82(8):732–739

15. Metz B (2009) Worauf achtet der Faherer? steuerung der aufmerksamkeit beim fahren mit visuellen nebenaufgaben. Ph.D. dissertation, Julius-Maximilians-Universität Würzburg
16. Doshi A, Trivedi MM (2009) On the roles of eye gaze and head dynamics in predicting driver's intent to change lanes. IEEE Trans Intell Transp Syst 10(3):453–462
17. Kühnlenz K (2007) "Aspects of multi-focal vision," ser. Mess-, Steuerungs- und Regelungstechnik.VDI Verlag 8(1129)
18. Kühnlenz K, Bachmayr M, Buss M (2006) A multi-focal high-performance vision system. In: Proceedings of the 2006 IEEE international conference on robotics and automation, Orlando, pp 150–155
19. Ude A, Gaskett C, Cheng G (2006) Foveated vision systems with two cameras per eye. In: Proceedings of the 2006 IEEE international conference on robotics and automation (ICRA 2006), Orlando
20. Roca X, Vitrià J, Vanrell M, Villanueva JJ (1999) Gaze control in a binocular robot systems. In: Proceedings of the 1999 IEEE international conference on emerging technologies and factory automation (ETFA 1999), Spain
21. Peng J, Srikaew A, Wilkes M, Kawamura K, Peters A (2000) An active vision system for mobile robots. In: Proceedings of the 2000 IEEE international conference on systems, man and cybernetics (ICSMC 2000), Nashville
22. Yamato J (1999) A layered control system for stereo vision head with vergence. In: Proceedings of the 1999 IEEE international conference on systems, man and cybernetics (ICSMC 1999), Tokyo
23. Panerai F, Metta G, Sandini G (2000) Adaptive image stabilization: a need for vision-based active robotic agents. In: Proceedings of the international conference on the simulation of adaptive behavior (SAB 2000), Paris
24. Lobo J, Ferreira JF, Dias J (2008) Robotic implementation of biological Bayesian models towards visuo-inertial image stabilization and gaze control. In: Proceedings of the 2008 IEEE international conference on robotics and biomimetics, Bangkok
25. Suppa M, Kielhöfer S, Langwald J, Hacker F, Strobl KH, Hirzinger G (2007) The 3D-modeller: a multi-purpose vision platform. In: Proceedings of the 2007 IEEE international conference on robotics and automation (ICRA 2007), Roma
26. Vilgrattner T, Ulbrich H (2011) Design and control of a compact high-dynamic camera-orientation system. IEEE-ASME T Mech 16(2):221–231
27. Lenz A, Balakrishnan T, Pipe AG, Melhuish C (2008) An adaptive gaze stabilization controller inspired by the vestibulo-ocular reflex. Bioinspir Biomim 3(3):035001
28. Zhang X, Tay ALP (2009) A physical system for binocular vision through saccade generation and vergence control. Cybernet Syst 40:549–568
29. Dickmanns ED (2007) Dynamic vision for perception and control of motion. Springer, London
30. Dickmanns ED (2003) An advanced vision system for ground vehicles. In: Proceedings of the 1st international workshop on in-vehicle cognitive computer vision systems, Graz
31. Schiehlen J, Dickmanns ED (1994) A camera platform for intelligent vehicles. In: Proceedings of the 1994 IEEE intelligent vehicles symposium (IV 1994), Paris
32. Schiehlen J, Dickmanns ED (1994) Design and control of a camera platform for machine vision. In: Proceedings of the 1994 IEEE international conference on intelligence in robotics and autonomous systems (IROS 1994), Neubiberg
33. Schiehlen J (1995) Kameraplattformen für aktiv sehende fahrzeuge ser. Mess-, Steuer- und Regelungstechnik. VDI Verlag 8(514)
34. Günthner W, Wagner P, Ulbrich H (2006) An inertially stabilised vehicle camera system – hardware, algorithms, test drives. In: Proceedings of the 2006 IEEE international conference on industrial electronics (IECON 2006), Paris
35. Günthner W, Glasauer S, Wagner P, Ulbrich H (2006) Enhancing inertial measurement units by multi-sensor fusion with visual data for active camera stabilization. In: Proceedings of joint conference of the 37th international symposium on robotics ISR 2006 and the German conference on robotics, Munich
36. Guenthner W, Glasauer S, Wagner P, Ulbrich H (2007) Biomimetic control for adaptive camera stabilization in driver-assistance systems. J Mech Sci Technol 21(6):930–934
37. Günthner W (2008) Enhancing cognitive assistance systems with inertial measurement units. Springer, Berlin
38. Ducrocq Y, Bahrami S, Duvieubourg L, Cabestaing F (2008) An effective active vision system for gaze control. In: Advances in visual computing, ser. Lecture notes in computer science, vol 5359. Springer, Berlin, pp 267–277
39. Koch C, Ullman S (1985) Shifts in selective visual attention: towards the underlying neural circuitry. Hum Neurobiol 4:219–227
40. Itti L, Koch C, Niebur E (1998) A model of saliency-based visual attention for rapid scene analysis. IEEE Trans Pattern Anal Mach Intell 20(11):1254–1259
41. Driscoll JA, Peters RA II, Cave KR (1998) A visual attention network for a humanoid robot. In: Proceedings of the 1998 IEEE/RSJ international conference on intelligent robotic systems (IROS 1998), Victoria
42. Backer G, Mertsching B, Bollmann M (2001) Data- and model-driven gaze control for an active-vision system. IEEE Trans Pattern Anal Mach Intell 23(12):1415–1429
43. Breazeal C, Scassellati B (1999) A context-dependent attention system for a social robot. In: Proceedings of the sixteenth international joint conference on artificial intelligence (IJCAI 1999), Stockholm
44. Vijayakumar S, Conradt J, Shibata T, Schaal S (2001) Overt visual attention for a humanoid robot. In: Proceedings of the 2001 IEEE international conference on intelligence in robotics and autonomous systems (IROS 2001), Hawaii
45. Sprague N, Ballard D (2003) Eye movements for reward maximization. In: Advances in neural information processing systems 15. MIT Press, Cambridge, MA
46. Choi SB, Jung BS, Ban SW, Lee M (2004) Trainable attention model based vergence control for active stereo vision system. In: Proceedings of the 2004 IEEE international conference on

intelligent sensors, sensor networks and information processing (ISSNIP 2004), Melbourne
47. Navalpakkam V, Itti L (2005) Modeling the influence of task on attention. Vis Res 45:205–231
48. Orabona F, Metta G, Sandini G (2005) Object-based visual attention: a model for a behaving robot. In: Proceedings of the 2005 IEEE computer society conference on computer vision and pattern recognition (CVPR 2005), San Diego
49. Ude A, Wyart V, Lin LH, Cheng G (2005) Distributed visual attention on a humanoid robot. In: Proceedings of the 2005 IEEE-RAS international conference on humanoid robots, Tsukuba
50. Frintrop S (2006) VOCUS: a visual attention system for object detection and goal-directed search. Lecture notes in computer sciences ed., ser. (Lecture notes in artificial intelligence), vol 3899. Springer, Heidelberg
51. Begum M, Mann GKI, Gosine RG (2006) A biologically inspired Bayesian model of visual attention for humanoid robots. In: Proceedings of the 2006 IEEE-RAS international conference on humanoid robots (HUMANOIDS 2006), Genova
52. Yu Y, Mann GKI, Gosine RG (2008) An object-based visual attention model for robots. In: Proceedings of the 2008 IEEE international conference on robotics and automation (ICRA 2008), Pasadena
53. Vogel J, de Freitas N (2007) Target-directed attention: sequential decision-making for gaze planning. In: Proceedings of the 2007 IEEE international conference on robotics and automation (ICRA 2007), Pasadena
54. Borji A, Ahmadabadi MN, Araabi BN (2009) Learning sequential visual attention control through dynamic state space discretization. In: Proceedings of the 2009 IEEE international conference on robotics and automation (ICRA 2009), Kobe
55. Xu T, Kühnlenz K, Buss M (2008) Information-based gaze control adaptation to scene context for mobile robots. In: Proceedings of the 2008 IEEE international conference on pattern recognition (ICPR 2008), Tampa
56. Xu T, Wu H, Zhang T, Kühnlenz K, Buss M (2009) Environment adapted active multi-focal vision system for object detection. In: Proceedings of the 2009 IEEE international conference on robotics and automation (ICRA 2009), Kobe
57. Itti L, Baldi P (2009) Bayesian surprise attracts human attention. Vis Res 49(10):1295–1306, June
58. Xu T, Zhang T, Kühnlenz K, Buss M (2010) Attentional object detection with an active multi-focal vision system. Int J Hum Robot 7(2):223–243
59. Michalke T, Kastner R, Adamy J, Bone S, Waibel F, Gayko MKA, Gepperth A, Fritsch J, Goerick C (2008) An attention-based system approach for scene analysis in driver assistance. Automatisierungstechnik 56(11):575–584
60. Aloimonos JY, Weiss I, Bandyopadhyay A (1988) Active vision. Int J Comput Vision 7:333–356
61. Bajcsy R (1988) Active perception. Proc IEEE 76(8):966–1005, Invited Paper
62. Aloimonos JY (1990) Purposive and qualitative active vision. In: Proceedings of the 1990 IEEE international conference on pattern recognition, Atlantic
63. Ballard DH (1991) Animate vision. Artif Intell 48:57–86
64. Aloimonos Y (ed) (1993) Active perception. Lawrence Erlbaum, Hillsdale
65. Dickmanns ED (1988) An integrated approach to feature based dynamic vision. In: Proceedings of the 1988 IEEE computer society conference on computer vision and pattern recognition (CVPR 1988), Ann Arbor
66. Davison AJ (1998) Mobile robot navigation using active vision. PhD Thesis, University of Oxford
67. Davision AJ, Murray DW (1998) Mobile robot localisation using active vision. In: Proceedings of the 5th European conference on computer vision (ECCV 1998), Freiburg
68. Seara JF, Strobl KH, Schmidt G (2002) Information management for gaze control in vision guided biped walking. In: Proceedings of the 2002 IEEE international conference on intelligent robots and systems (IROS 2002), Lausanne
69. Seara JF, Strobl H, Schmidt G (2003) Path-dependent gaze control for obstacle avoidance in vision guided humanoid walking. In: Proceedings of the 2003 IEEE international conference on robotics and automation (ICRA 2003), Taipei
70. Seara JF, Strobl KH, Martín E, Schmidt G (2003) Task-oriented and situation-dependent gaze control for vision guided humanoid walking. In: Proceedings of the 2003 IEEE-RAS international conference on humanoid robots (HUMANOIDS 2003), Munich
71. Seara JF (2004) Intelligent gaze control for vision-guided humanoid walking, ser. Mess-, Steuer- und Regelungstechnik.VDI Verlag 8(1044)
72. Seara JF, Schmidt G (2005) Gaze control strategy for vision-guided humanoid walking. Autmatisierungstechnik 53(2):49–58
73. Lidoris G, Kühnlenz K, Wollherr D, Buss M (2007) Combined trajectory planning and gaze direction control for robotic exploration. In: Proceedings of the 2007 IEEE international conference on robotics and automation (ICRA 2007), Rome
74. Kühnlenz K, Lidoris G, Wollherr D, Buss M (2007) On foveated gaze control and combined gaze and locomotion planning. In: de Pina ACF (ed) Humanoid robots: new developments. I-Tech Education and Publishing, Vienna
75. Kühnlenz K, Buss M (2008) Multi-focal vision and gaze control improve navigation performance. J Hum 1(1):33–44
76. Xu T, Kühnlenz K, Buss M (2008) A view direction planning strategy for a multi-camera vision system. In: Proceedings of the 2008 IEEE international conference on information and automation (ICIA 2008), Zhangjiajie
77. Davison AJ, Kita N (2001) 3D simultaneous localisation and map-building using active vision for a robot moving on undulating terrain. In: Proceedings of the 2001 IEEE computer society conference on computer vision and pattern recognition (CVPR 2001), Lihue
78. Davison AJ, Murray DW (2002) Simultaneous localization and map-building using active vision. IEEE Trans Pattern Anal Mach Intell 24:865–880
79. Lidoris G, Kühnlenz K, Wollherr D, Buss M (2006) Information-based gaze direction planning algorithm for slam.

In: Proceedings of the 2006 IEEE-RAS international conference on humanoid robots (HUMANOIDS 2006), Genova
80. Pellkofer M, Dickmanns ED (2000) EMS-vision: gaze control in autonomous vehicles. In: Proceedings of the 2000 IEEE intelligent vehicles symposium (IV 2000), Dearborn
81. Pellkofer M (2003) Verhaltensentscheidung für autonome fahrzeuge mit blickrichtungssteuerung. Dissertation, Universität der Bundeswehr München
82. Dickmanns ED (2004) Three-stage visual perception for vertebrate-type dynamic machine vision. In: Proceedings of the conference on engineering of intelligent systems (EIS 2004), Madeira
83. Unterholzner A, Wuensche HJ (2009) Adaptive state space control of a camera platform for an autonomous ground vehicle. In: Proceedings of the 2009 IEEE intelligent vehicles symposium (IV 2009), Xi'an
84. Unterholzner A, Wuensche HJ (2010) Hybrid adaptive control of a multi-focal vision system. In: Proceedings of the 2010 IEEE intelligent vehicles symposium (IV 2010), San Diego
85. Canudas C, Åström KJ, Braun K (1987) Adaptive friction compensation in DC-motor drives. IEEE J Robotic Autom RA-3(6):681–685
86. Goodwin GC, Sin KS (1984) Adaptive filtering prediction and control, Information and system sciences. Prentice-Hall, Englewood Cliffs
87. Ramasubramanian A, Ray LR (2007) Comparison of EKBF-based and classical friction compensation. J Dyn Syst Meas Contr 129:236–242
88. Franklin GF, Powell JD, Emami-Naeini A (2002) Feedback control of dynamic systems, 4th edn. Prentice Hall, Upper Saddle River
89. Athans M, Falb PL (1966) Optimal control: an introduction to the theory and its applications. McGraw-Hill, New York
90. Utkin VI (1977) Variable structure systems with sliding modes. IEEE Trans Autom Control AC-22(2):212–222
91. Hung JY, Gao W, Hung JC (1993) Variable structure control: a survey. IEEE Trans Ind Electron 40(1):2–22, February
92. Chatchanayuenyong T, Parnichkun M (2008) Time optimal hybrid sliding mode-PI control for an autonomous underwater robot. Int J Adv Rob Syst 5(1):91–98
93. You KH, Lee EB (2000) Robust, near time-optimal control of nonlinear second order systems with model uncertainty. In: Proceedings of the 2000 IEEE international conference on control applications, Anchorage, Alaska
94. Iliev B, Kalaykov I (2004) Minimum-time sliding mode control for second-order systems. In: Proceedings of the 2004 American control conference, Boston
95. Dean P, Porrill J, Stone JV (2002) Decorrelation control by the cerebellum achieves oculomotor plant compensation in simulated vestibulo-ocular reflex. Proc R Soc Lond Biol Sci 269(1503):1895–1904, August
96. Unterholzner A, Rohland M, Schweitzer M, Wuensche HJ (2010) Vision based online-calibration of inertial gaze stabilization. In: Proceedings of the 2010 IEEE intelligent vehicles symposium (IV 2010), San Diego
97. Julier SJ, Uhlmann JK (2004) Unscented filtering and nonlinear estimation. Proc IEEE 92(3):410–422, Invited Paper
98. Schweitzer M, Wuensche HJ (2010) Real-time visual odometry for ground moving robots using GPUs. In: Proceedings of the international conference on computer vision theory and applications (VISAPP 2010), Angers
99. Scaramuzza D, Fraundorfer F, Pollefeys M, Siegwart R (2009) Absolute scale in structure from motion from a single vehicle mounted camera by exploiting nonholonomic constraints. In: Proceedings of the IEEE international conference on computer vision (ICCV 2009), Kyoto
100. Schweitzer M, Wuensche HJ (2009) Efficient keypoint matching for robot vision using GPUs. In: Proceedings of the fifth IEEE workshop on embedded computer vision at ICCV 2009, Kyoto

Active Pedestrian Protection System, Scenario-Driven Search Method for

Alberto Broggi[1], Pietro Cerri[1], Stefano Ghidoni[2], Paolo Grisleri[1], Ho Gi Jung[3]
[1]VisLab – Dipartimento di Ingegneria dell'Informazione, Università degli Studi di Parma, Parma, Italy
[2]Intelligent Autonomous System Laboratory (IAS-Lab), Department of Information Engineering, University of Padua, Padova, Italy
[3]The School of Mechanical Engineering, Hanyang University, Seondong-gu, Seoul, South Korea

Article Outline

Glossary
Definition of the Subject and Its Importance
Introduction
Why Are ADAS Related to Sustainability?
Innovation of This Method
State of the Art
Setup
Focus of Attention
Vision Fusion
Automatic Braking
Results
Future Directions
Bibliography

Glossary

ADAS *Advanced Driver Assistance Systems* are complex systems to help the driver during specific maneuvers, or during normal driving.

Laser scanner Laser scanner is an optical sensor based on *LIDAR* (Light Detection And Ranging) technology that measures the distance of targets measuring the time delay between transmission of a pulse and detection of the reflected signal.

NIR Near InfraRed (0.75–1.4 μm) is the wavelength closest to visible that is often used in image processing for night vision, together with specific illuminators.

Definition of the Subject and Its Importance

This paper presents an application of a pedestrian detection system aimed at localizing potentially dangerous situations in specific urban scenarios. The approach used in this work differs from the ones implemented in traditional pedestrian detection systems, which are designed to localize all pedestrians in the area in front of the vehicle. Conversely this approach searches for pedestrians in critical areas only.

The great advantages of such an approach are that pedestrian recognition is performed on limited image areas – therefore boosting its time-wise performance – and no assessment on the danger level is finally required before providing the result to either the driver or an onboard computer for automatic maneuvers. A further advantage is the drastic reduction of false alarms, making this system robust enough to control nonreversible safety systems.

Introduction

This paper presents an innovative approach to the detection of pedestrians, explicitly designed to work in a particularly challenging urban scenario, which represents a particularly critical environment for traditional pedestrian detection approaches. The aim of the system is to trigger reversible and nonreversible driving assistance system.

This work was developed by VisLab at Parma University and funded by MANDO Corporation, Korea.

Why Are ADAS Related to Sustainability?

In his book *May Contain Nuts* [1] John O'Farrell depicts a mother terrified by modern world's dangers. In order to show how dangerous the road where vehicles are running can be, she builds a puppet, and throws it onto the road, letting it come out between two parked cars.

The description of that particular "experiment" intended to highlight two points, among others: first of all, the (motivated) worries people have about the road environment, especially when dealing with children, which cannot correctly evaluate risks; the second observation is that road safety relies, in some cases, on a very strong hypothesis, that is, everyone is following road traffic laws. Of course, this should normally be the case, but an important point is to understand whether there are margins, in order to recover for other road users' illegal behaviors. This applies mainly to drivers, since they are the strong road users. When a car hits a pedestrian, even if this is due to a pedestrian fault, the driver could, in principle, take actions that may avoid or, at least, mitigate the collision consequences. This is, then, the difference. It is difficult, if not impossible, for a pedestrian to take actions that can recover from a driver's fault; on the contrary, it is often possible for a driver to cope with pedestrians' faults.

Road dangers are caused by several factors. At the very beginning, vehicles were slow, and few of them were running on roads – traffic also was an unknown problem! Then, the number of vehicles dramatically increased, but not enough care was dedicated to the protection of pedestrians and bicycles mobility, either because of economic factors, or because the problem itself is really difficult to face.

Whatever the reason, traffic and related pedestrian injuries have now become an important issue that has been on the agenda of several governments and public institutions for many years. The reasons for this change can be found, again, in economic factors – every injury brings a high social cost – but, also, human society underwent substantial changes during the last few decades. After more than a century of economic and technical growth, the capability of mankind to deeply influence the environment had become so high, and the available technology so powerful, that it became clear it is mandatory to keep them under control. In other words, it became clear that growth could not continue without limits, but rather, it had to face a new issue: the capacity to endure, that is, sustainability.

Sustainability is a complex and wide concept, which includes the capability of reducing as much as possible

the negative impact on the environment that the use of almost every new technology involves. Therefore sustainability deeply deals also with all transportation systems, because they pollute, they can be dangerous, they impact on people's everyday life, and, above all, they are essential.

Several studies on countermeasures aimed at reducing traffic injuries have been undertaken. Car manufacturers deeply increased the safety levels available inside cars. Back to the 1970s, objects like the steering wheel or the pedals, or, more generally, every part of a car's interior, could cause severe injuries in case of accidents, because they could hit the driver or passengers in an uncontrolled way. Car manufacturers then invested a considerable amount of money to reduce fatalities, and studied the problem. Nowadays, the steering wheel itself is not only able to avoid dangers in case of accidents, but also contains a safety system, the airbag, that sensibly reduces the consequences of a car accident.

Unfortunately, increasing road safety in the case of accidents involving pedestrians is sensibly more difficult. The EuroNCAP institution is involved in a number of projects related to this field (see www.euroncap.com for an overview). Some of them aim at mitigating the consequences for a pedestrian being hit by a vehicle, for instance by modifying the shape of the car front, a sort of outer passive safety system. Similar ideas are under development since decades. Some patents regarding systems capable of mitigating collisions with a pedestrian date back to the beginning of the 1980s [2].

Following the idea of mitigating the impact energy, external airbags were also proposed. Several patents were submitted by the end of the 1990s [3, 4]. Such airbags should inflate in case the car hits a pedestrian, but still the problem of the collision sensor is open and hard to solve. Such sensors should detect collisions that are relatively soft, since the mass of a pedestrian is sensibly lower than that of a vehicle. Moreover, the sensor is required to be extremely fast and precise, because each false positive leads to the need of expensive service for restoring the external airbag system.

Together with passive safety systems, active systems were studied and developed in the last years. Since active safety systems should predict an imminent collision, they need sophisticated sensors and collision detection systems. The task of preventing accidents from happening is extremely difficult, because it requires that the safety system understands the road scene at a high level, detecting potentially dangerous conditions. Such an understanding can be provided only by a computer system connected to sensors. The need for safety systems has therefore caused computer science to deeply enter into the automotive world, a process that had started with the very first electronic active safety systems, like ABS, few decades before.

Car manufacturers, together with public institutions, are still investing a huge amount of money in the study and development of such active systems. Several research groups are addressing the high number of problems that are related to road safety. Yet a system capable of a complete understanding of a generic road scene is not available, but technology is evolving rapidly, and now several systems exist that can analyze cars' or pedestrians' behavior over time, thus getting a high-level understanding of the road scene, even if limited to some aspects.

In order to achieve brilliant results, highly effective sensors should be used; possible selections include radars, laser scanners, cameras, or a combination of them. The number of solutions proposed so far is really huge, and substantial differences can be found in a number of design choices. This is clear even by just having a look at the various prototype vehicles that have been developed. Some of them are full of sensors, mounted in a fashion that is not realistic for an off-the-shelf car. Such vehicles are useful for experimenting with new solutions, understanding their possible advantages over more well-known system designs, without the effort of caring too much about the feasibility of the solution itself. On the other hand, vehicles designed with a high level of integration are vital to design systems that can be really installed onto a vehicle in the future. It often happens, in fact, that restrictions even on the hardware placement affect software algorithms dedicated to road scene understanding.

An example of the coexistence of these two kinds of design philosophy was clearly visible during the DARPA Urban Challenge [5], a competition for unmanned vehicles. Each vehicle had to complete a series of tasks, each one consisting in reaching a destination point driving inside an urban environment, dealing with traffic and intersections, and also

the other unmanned vehicles. Even if, in principle, no limitations were imposed on system design and number and type of sensors, vehicles that attended the race can be divided into the two categories described above.

Despite the high number of developed systems, as noted above, they are all exploiting, with few exceptions, the same types of sensor: radars, laser scanners, and cameras. Cameras can be further divided into three categories, depending on which part of the electromagnetic spectrum they are sensing: visible light, near infrared, or far infrared. They can be considered three different kinds of sensors since the data they provide have completely different characteristics, and usually undergo different processing.

Thanks to the high number of research groups working on road safety systems, a huge amount of algorithms has been developed for analyzing all kinds of data provided by the sensors described above. Also, due to the fact that those sensors are characterized by different and somehow complementary features, they are often used together. This led to the need for sensor fusion techniques, that is, techniques that, by exploiting measurements provided by more than one sensor, derive a single measurement. Such final result is more reliable than that provided by each sensor, as sensor fusion techniques know the feature of each sensor, and their reliability intervals.

As it has been described so far, computer vision applied to the automotive field is a really hot topic, and systems are being developed that successfully achieve a high and rather precise level of road scene understanding. However, beside system development, possible applications should be taken into consideration. The introduction of active safety systems based on such complex equipments into off-the-shelf vehicles is advancing at a rate that is sensibly slower compared with the advances in technology gained by research groups operating worldwide. Beside people acceptance of such systems, and legal issues, the requirements of the automotive world are extremely difficult to be met. If a system is capable of interfering with commands issued by a human driver, its acceptable fault rate will be extremely low, if not at no fault level. It is straightforward, on the other hand, that such a reliability level is really hard to be achieved, when dealing with such complex environment. The scenario is definitely challenging.

To understand how this kind of technology could develop, consider that still for a long time systems will not be able to reliably tackle the whole problem. Instead, some systems are already on the market, as equipment of luxury cars, which reliably perform simple and noninvasive tasks. As an example, some already available systems are meant to detect possible conflicts with overtaking vehicles when a lane change maneuver is undertaken by the driver. In this case the system issues a warning, like an acoustic signal. Some sporadic false positives do not have a strong impact; however, the driver will tend to ignore the system hints if failure rate is not extremely low. This kind of systems, that is, whose failure is not dangerous, but rather may be annoying, seems to be the next step on the roadmap of the introduction of active vision systems into the automotive world.

Given the previous considerations about the need to reduce accidents and the overview on future active safety systems, it is now worth analyzing into more detail which are the road scenarios causing a high number of fatalities or injuries. Several papers and reports exist on this topic; moreover, specific studies addressed the problem of accidents involving children [6]. This last problem is particularly alarming, since it involves people of very young age, whose perception of danger and understanding of road traffic rules is rather low due to their very young age. The danger comes from the fact that young children turn out to be often living in environments that are designed for adults. However, in the last decades modern societies started to invest in the safety of new generations, which is directly related to the sustainability of the societies themselves.

Describing the causes of pedestrian fatalities is, of course, an extremely complex task, and it also leads to subjective conclusions. For instance, the effect of car speed is debated. It seems to be a key factor in some studies, like [7]. On the other hand, in other studies related to children [6] it is stated that "higher vehicular speeds [...] were not associated with child pedestrian injury indicating that residential streets that had vehicles travelling at higher speeds were not at increased risk in the absence of other environmental risk factors." Both studies point out that a main cause of accidents is the sudden appearance of the pedestrian in the road scene, as it often happens when a pedestrian comes

onto the street between two parked cars. This scenario is quite common, especially in residential areas, where, despite the low speed limits, a high number of pedestrian injuries happen. In most cases, the driver did not see the pedestrian before the accident occurred.

Investigating on main accident causes leads to a set of countermeasures that can be undertaken. In [7], three main actions are reported: "speed control, separation of pedestrians from vehicles, and measures that increase the visibility and conspicuity of pedestrians." These involve road infrastructure, including some important details like the way cars are parked. The implementation of diagonal parking improves the visibility of pedestrians going toward the street, because it makes them walk in a diagonal direction, which is more easily seen from a driver's perspective. This last example points out that protecting pedestrians does not necessarily mean the need for huge and expensive actions, but rather, that in some cases simple and well-thought expedients can be extremely effective.

Besides the modification of road infrastructure, improvement of pedestrian visibility can also be achieved by the active safety systems that were mentioned above. They seem to be the ultimate solution to the problem, because they are the only countermeasure to one of the major issues of the human drivers, that is, the tendency to get distracted, especially after driving for a long time. The activity of driving would require, in principle, a high and constant level of attention that a human driver can hardly provide. In particular, a driver usually cares about issues he is expecting, like a traffic light, but handles with much more difficulty a totally unexpected event, like a child darting into the street. For this kind of events, only the quick response of an active safety system can represent the final solution.

Innovation of This Method

Instead of searching for pedestrians in a large area in front of the vehicle making no assumption on the external environment, the system presented in this work focuses on a specific urban scenario in which not only the detection of a pedestrian is of basic importance, but the danger of the situation can be clearly assessed as well.

In fact, in an advanced driving assistance system, a correct detection must be followed by the estimation of its position with respect to the vehicle and the environment.

As an example, a pedestrian detection system able to correctly localize all pedestrians present in the scene provides a huge amount of information that still needs to be filtered in order to be useful to either the driver or the onboard computer in charge of automatic maneuvers.

A possible filter may be implemented by fusing information coming from other systems, such as lane detection or other situation analysis engines, and CAN data. A pedestrian exactly in front of the vehicle may or may not be considered dangerous depending on the surrounding environment, as shown in Fig. 1.

This work is based on a totally different approach. Instead of detecting all possible candidates and assess their danger level, the system first analyzes the scenario, and then searches for possible pedestrians in specific positions for that particular scenario. This approach is called *scenario-driven search* or *SDS*. In this way, all detected pedestrians represent possible threats and no further filtering is needed (apart from a validation and a possible final tracking step).

The scenarios that are considered here refer to the most common urban situations in which the presence of a pedestrian causes a serious problem that could be mitigated by an early detection. In particular, when vehicles are moving on an urban road, the most common threat that a pedestrian may pose – therefore requiring a successful detection – is road crossing. Stopped vehicles on the road or on the road edges may occlude visibility, thus making the detection of the pedestrian more complex and requiring a real-time reaction.

The application of the *SDS* approach to this specific scenario is based on the localization of stopped vehicles followed by the search for pedestrians in their close proximity or in the areas partly hidden by them.

Stopped vehicles, whose edges trigger the search for pedestrians, may be parked cars on the road edge, vehicles temporarily stopped on the road, or vehicles queued in a line in front of a traffic light, zebra crossing, or simply jammed cars.

The first row of Fig. 2 shows some examples of situations in which the visibility of a crossing pedestrian is partly or completely occluded by stopped

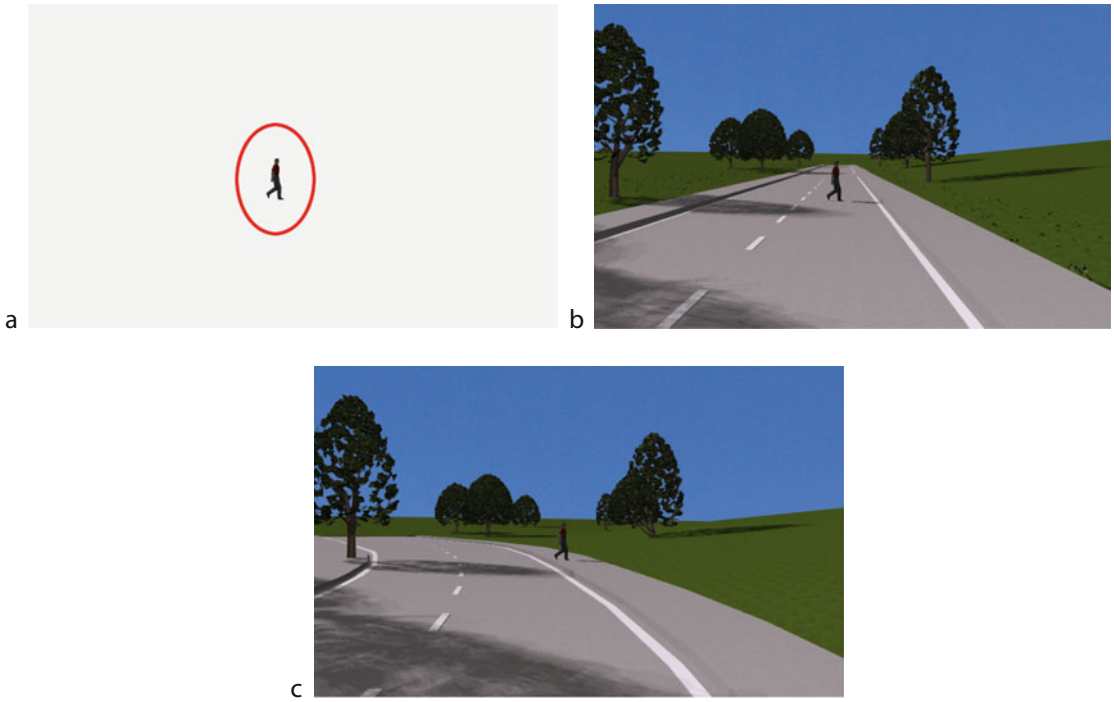

Active Pedestrian Protection System, Scenario-Driven Search Method for. Figure 1
When a pedestrian is localized but no reference with respect to the environment is provided like in (**a**), the detector is not able to assess the danger level. When environmental information are available, the very same pedestrian may become a threat (**b**), or may be in a safe position (**c**)

vehicles. The second row of Fig. 2 highlights, for each situation, the areas on which the system will perform a check for the presence of a possible pedestrian.

In other words, the approach is to focus on the detection of pedestrians appearing from behind occluding obstacles; pedestrians that are clearly visible in the frontal area of the vehicle need also to be detected. This function is also available on other systems [8, 9].

The idea of focusing on a specific scene or scenario (referring to a dynamic or a static environment, respectively) is not new to pedestrian detection systems. In 2002, Franke and Heinrich [10] developed a module able to detect balls (which are usually a strong signature of the presence of a child).

Another example of very specific systems is the one developed by Curio et al. [11] which was based on the visual localization of the specific moving pattern of human legs.

It is known [7] that parked vehicles, blocking the visibility of pedestrians, are one of the main causes of accidents. Agran et al. [6] show that the number of parked vehicles along a street is the strongest risk factor for pedestrian injuries occurring in residential areas.

Although in these areas parking spaces should be arranged diagonally, there are situations, as shown in Fig. 2, in which vehicles stop temporarily on the road and their position cannot be predetermined and carefully controlled as in the case of parking lots. Although some of the situations of Fig. 2 refer to specific urban areas (i.e., zebra crossings and bus stops) that could be specifically enhanced by intelligent infrastructures aimed at warning oncoming vehicles, other situations can happen in any part of the road network, making the installation of specific warning infrastructures impractical.

The main characteristics required by a system like this are:

- To detect pedestrians quickly, given the short sensing range and the particularly high risk of a collision

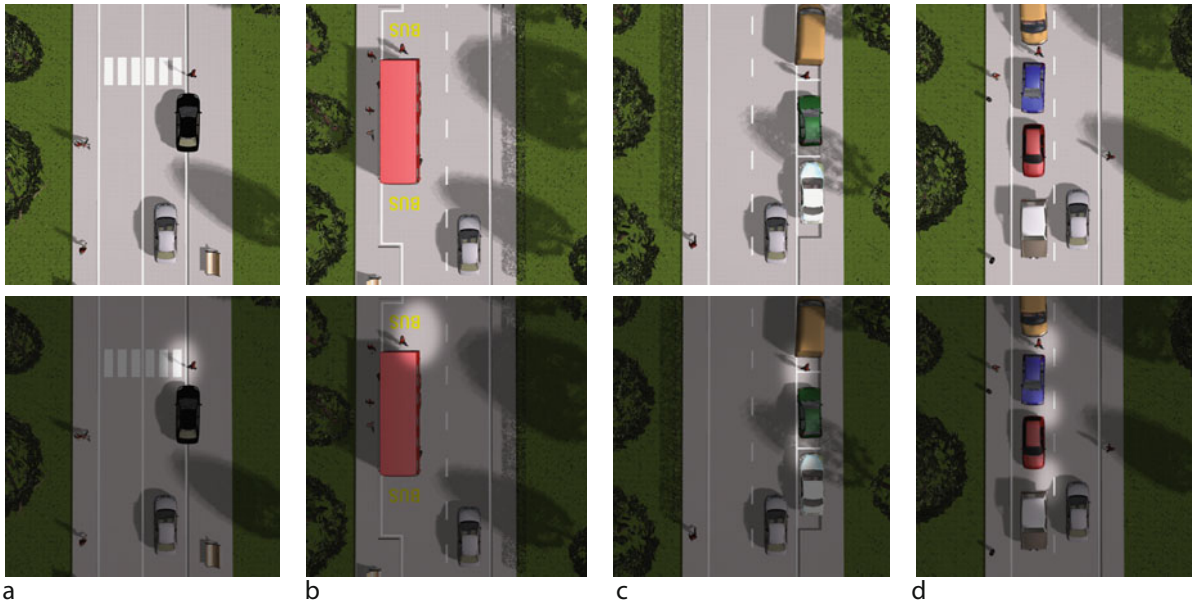

Active Pedestrian Protection System, Scenario-Driven Search Method for. Figure 2
Situations considered in this work (*first row*) and areas of interest considered for the detection of a possible pedestrian (*second row*). (**a**) A crossing pedestrian is hidden by a parked vehicle. (**b**) A pedestrian is crossing the road behind a stopped bus. (**c**) A pedestrian is appearing between two parked vehicles. (**d**) A pedestrian is crossing the road between two vehicles stopped on the other side of the road

with a pedestrian suddenly appearing behind an obstacle

- To detect pedestrians as soon as they appear, therefore even when they are still partly occluded
- To limit the search to specific areas, determined by a quick preprocessing

Figure 3 shows the coverage of different sensing technologies (laser and vision) in a specific scenario considered in this work.

The fusion of a laser scanner and vision can provide a quick and robust detection in case of suddenly appearing pedestrians. The laser scanner provides a list of areas in which a pedestrian may appear, while the camera is able to detect the pedestrian even when he/she is not yet visible to the laser scanner.

A remarkable improvement of road safety can be obtained thanks to the use of both reversible and nonreversible driving assistance systems. Three levels of intervention are defined:

- Once the pedestrian is detected with a sufficiently high confidence level, a warning is sent to the driver.
- Should the driver not react promptly to the warning, the system would issue a second level of warning by blowing the vehicle's horn. This second warning is still considered a reversible system, although it is much more invasive than the former. The aim of this loud warning is to attract the attention of both the pedestrian itself and – once again – the driver.
- In case the danger level is not reduced thanks to a prompt reaction of the driver (or the pedestrian), the intelligent vehicle will jump into the third level and trigger a nonreversible system. In this case it is automatic braking.

This being a nonreversible and very invasive system, its triggering must be preceded by an extremely careful analysis of the danger level and requires the complete processing to be thoroughly tested with respect to false detections. In the case of nonreversible systems, the number of false positives is even more important than the number of correct detections.

In the literature [12] many different pedestrian detection systems have been surveyed, and a large

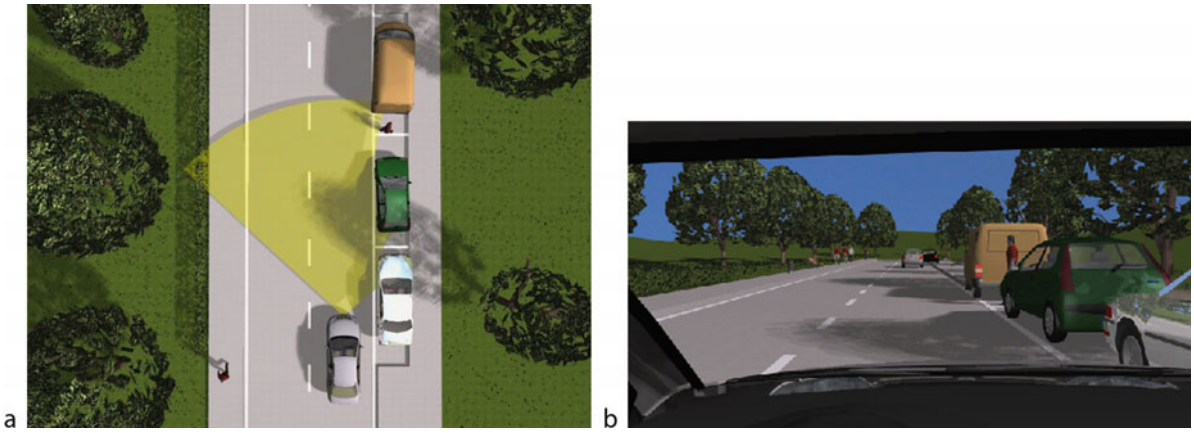

Active Pedestrian Protection System, Scenario-Driven Search Method for. Figure 3
A pedestrian partially hidden by parked cars may not be detected by a laser scanner positioned in the front bumper but can be detected using vision, even if partially occluded

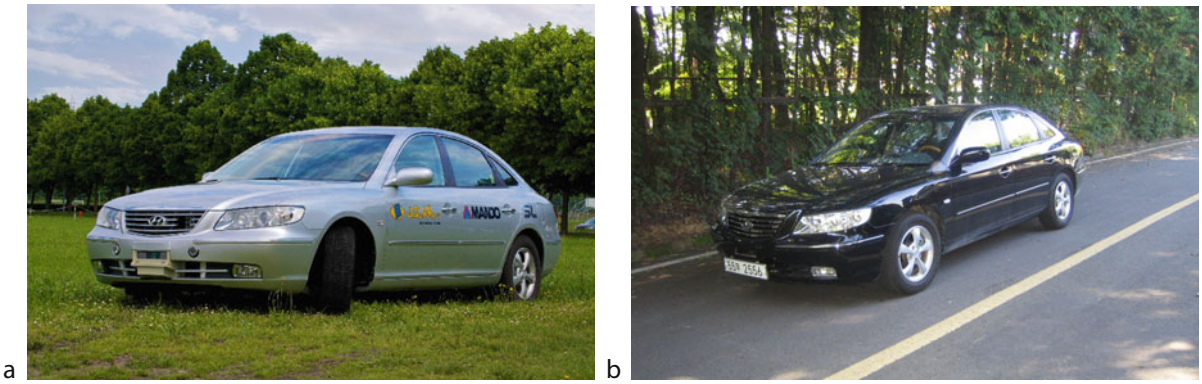

Active Pedestrian Protection System, Scenario-Driven Search Method for. Figure 4
The Hyundai Grandeur test vehicle equipped in Parma, Italy (**a**), and the replica in Seoul, Korea (**b**)

number of test methods for pedestrian detection systems have been proposed, which are based on single frame analysis, temporal analysis of continuous video streams, or event based.

Their performance is still far from the ideal system; this is the reason why the approach proposed in this paper is regarded as an alternative to conventional systems. Pedestrians are searched in situations of clear danger by limiting the search to specific areas. Besides being quicker than other systems, this method aims also at reducing the number of false detections to zero.

The system presented in this work has been developed and tested by VisLab in Parma on a Hyundai Grandeur prototype vehicle; Mando is using an exact replica of this system in Korea (see Fig. 4) to double testing time.

State of the Art

As long-time pursued advanced driver assistance systems (ADAS) and active safety vehicles (ASV) such as lane departure warning (LDW), blind spot detection (BSD), adaptive cruise control (ACC), precrash safety (PCS), and collision warning/avoidance (CW/CA) become commercialized [13–15], interest of research groups and transportation authorities moves to newly

emerging technologies or candidate projects such as intersection accident prevention [16], intelligent parking assist system [17], and active pedestrian protection system (APPS). Particularly, APPS attracts a great interest because it is directly related with a vulnerable road user who holds a significant portion of traffic accident fatalities. The success of ACC, PCS, and CW/CA does not guarantee the success of APPS because the pedestrian is relatively small and their appearance is various and continuously changing. However, they are expected to provide abundant elementary technologies and economic backgrounds. In particular, progress of electronics and sensors, such as high performance embedded processor, monolithic microware-integrated circuit (MMIC)-based compact radar, multilayer scanning laser radar, and high dynamic range CMOS (HDRC) camera, are regarded as the enabling technologies for APPS.

Recently, Gandhi and Trivedi provided a great survey of pedestrian protection systems [12]. They classified pedestrian protection approaches into four categories: infrastructure design enhancement, passive safety system involving vehicle design, active safety system based on pedestrian detection, and collision prediction. The pedestrian protection system designed to be installed on board can be divided into passive and active approaches according to whether the operation time is before or after vehicle–pedestrian collision. If a system is designed to prevent the collision or mitigate its damage, it is categorized as an active approach. Contrarily, if a system is designed to minimize the pedestrian's damage after the collision, it is categorized as a passive approach. The collision prediction could be differentiated from the active safety system in the point that the sensing devices are installed on infrastructure rather than on board.

Infrastructure enhancement to reduce pedestrian-related accidents is supposed to be the most traditional approach. The approach can be divided into three categories of countermeasures: speed control, pedestrian vehicle separation, and measures to increase visibility and conspicuity of the pedestrian [12].

The first and second could be easily understood by investigating traffic calming which is a kind of movement or concept [18]. Definitions of traffic calming vary, but they all share the goal of reducing vehicle speeds, improving safety, and enhancing the quality of life. Traffic-calming measures can be separated into two groups based on the main impact intended. Volume control measures are primarily used to address cut-through traffic problems by blocking certain movements, thereby diverting traffic to streets better able to handle it. Volume control measures also include divertive or restrictive measures such as full closures, half closures, diagonal diverters, and median barriers. Speed control measures are primarily used to address speeding problems by changing vertical alignment, changing horizontal alignment, or narrowing the roadway. Vertical deflection includes speed humps, speed tables, raised crosswalks, raised intersections, and textured pavements. Horizontal deflection includes traffic circles, roundabouts, chicanes, and realigned intersections. Horizontal narrowing includes neckdown, center-island narrowing, and chokers. US DoT (Department of Transportation) FHWA (Federal Highway Administration) reports [19, 20] show that well-designed and implemented traffic-calming techniques can have a number of beneficial impacts for bicyclists and pedestrians. The reduced vehicle speeds associated with such projects can reduce both the severity and incidence of motor vehicle/bicycle/pedestrian crashes and can make bicyclists and pedestrians feel more comfortable in traffic.

Pedestrian visibility can be increased by improving roadway lighting since a majority of pedestrian fatalities occur at nighttime. Since parked vehicles block the vision of drivers as well as pedestrians, removing on-street parking and implementing diagonal parking in residential streets would help in reducing accidents especially involving children [12].

According to the analysis of vehicle impact zones in pedestrian–vehicle collisions, vehicle front is responsible for most pedestrian injuries: 71.1% according to US national highway traffic safety administration (NHTSA) data. Almost 80% of the fatalities occur when the pedestrian is struck by vehicle front, whereas most of the remaining fatalities occur when the pedestrian is hurled to the street [21]. Accident analysis also proved the importance of head injury [22, 23]. Although upper and lower extremities, as well as head, are the most frequently injured body regions in passenger car-to-pedestrian accidents, 62% of the pedestrian fatalities were caused by head injuries. Pedestrian head suffers both a direct impact with stiff

vehicle structures and a large degree of rotational accelerations [24]. In particular, stiff structure of windshield including A-pillar should not be overlooked. An analysis of all vehicle parts which caused head injuries shows that impact on the windshield causes 44.3% of head injuries. Impact on the windshield causes twice as often head injuries as at the bonnet, and three times often for severe head injuries. Head impact on the A-pillar causes severe injuries in 82% of the cases. Other vehicle parts mostly cause only slight injuries [24].

Therefore, passive safety measures are being developed by installing energy-absorbing devices in the vehicle front structures, on which pedestrian head hits, such as hood (bonnet), windshield lower part, and A-pillar. A passive pedestrian protection system includes an impact-reducing front structure, active bumper, active hood (hood lifting, active bonnet), and pedestrian airbag. Active bumper is designed to provide the appropriate stiffness to cushion the impact while at the same time providing support of all parts of the limb to limit knee joint lateral bending [25]. Cushioning method of active bumper includes foam energy absorber, molded plastic energy absorbers, air-filled energy absorbers, flexible plastic beam, bumper deploying, crush cans, outside additional structure, foam-encapsulated metal, and steel energy absorber [25]. Active hood system detects vehicle–pedestrian collision using bumper-installed pedestrian crash sensor and acceleration sensor, and then two actuators lift the rear part of the bonnet approximately 100 mm within 60–70 ms after the leg-to-bumper impact [26]. Pedestrian protection airbag deploys an airbag through a gap between windshield lower part and bonnet lifted by the active hood system [27]. The airbag is deployed in U-character shape and covers the windshield lower part and A-pillar lower part. When up-lifting bonnet and airbag are used simultaneously, the impact absorbing effect is significantly larger than when only one measure is used. It is because vehicle front regions critical to pedestrian head impact cannot be effectively covered with only one measure [24]. Intelligent Vehicle Safety System (IVSS) seems to be a good example: Active bumper, active hood, and pedestrian protection airbag is developed simultaneously and they are expected to operate as a suite of tools [27]. Autoliv also developed and provided active hood and pedestrian protection airbag as a pedestrian protection tool chain [28, 29].

Such a development of passive safety measure is supposed to have been significantly influenced and encouraged by the reinforced requirement of pedestrian–vehicle collision. The European Enhanced Vehicle Safety Committee (EEVC) Working Group (WG) 10 and WG 17 have developed test procedures to assess the level of pedestrian protection for vehicle fronts. Based on the EEVC WG 17 report, legal requirements have been derived. The European directive (2003/102/EC) consists of head impact, upper leg impact, and lower leg impact. The requirement was scheduled to be enforced in two phases, that is, 2005 and 2010 [30]. The EU test levels are 1,000 head-injury criteria (HIC) for 2/3 of the hood surface and 2,000 HIC for the remaining 1/3. HIC is an internationally accepted acceleration-based measurement for violence against the head. HIC values under 1,000 imply that the risk of life-threatening injury is 15% or less. However, the curve rises sharply; at 2,000 HIC, the fatality risk is almost 90% [28].

Active safety systems are based on pedestrian detection and collision avoidance measures. Considerable research is being conducted by various groups for designing pedestrian detection systems. Such systems can employ various types of sensors and computer vision algorithms in order to detect pedestrians and predict the possibility of collisions. The output of the systems can be used to generate appropriate warnings for the driver or to perform autonomous braking or maneuvering in case of imminent collision [12]. Naturally, if impending collision could not be avoided, the fact can be sent to the passive pedestrian protection measures and precrash safety system to help their preparations. Even when the autonomous braking cannot prevent collision, it can mitigate the pedestrian's damage. The reduction of collision speed leads to a reduction of the induced head accelerations and results in a shift of the relevant head impact regions away from stiff windshield lower parts. The core technology of active pedestrian protection system is pedestrian detection because the active braking function is already implemented by several active safety systems such as PCS, CW/CA, and full-range ACC [13, 14].

Pedestrian detection can be divided into five categories according to the used sensors: thermal infrared camera-based, visible camera-based including near infrared camera, millimeter wave radar-based,

communication-based, and sensor fusion-based. Even though scanning laser radar is frequently used by pedestrian detection system, it is not considered in a separate category because it is not used as a standalone sensor but as a participator in sensor fusion with visible camera.

Thermal infrared camera-based is specialized for nighttime pedestrian detection, for example, night vision, and is based on the point that the human body temperature is higher than ambient temperature. Although it can easily detect pedestrians even in dark illumination conditions, it loses the advantage in daytime and its cost is comparatively high for all grades of vehicle.

David Gernóimo et al. provide a great survey of visible camera-based pedestrian detection [31]. They propose a general architecture of a visible camera-based pedestrian detection system consisting of six phases: preprocessing, foreground segmentation, object classification, verification, tracking, and application. Preprocessing, foreground segmentation, and appearance-based object classification are very similar to vehicle detection case [32]. Foreground segmentation for candidate generation can be performed using knowledge-based, stereo-based or motion-based methods. Appearance-based object classification uses generally proven learning algorithms such as support vector machine (SVM), AdaBoost, and neural networks. Characteristic approaches are contour tree-based template matching devised by D. Gavrila and part detection-based to cope with the pedestrian's continuously changing contour and appearance. What kind of feature and classifier is the best for pedestrian detection is a problem under fierce discussion. To answer the question, Mohamed Hussein et al. compared performances of two promising features, that is, histograms of oriented gradients (HOG) and region covariance (COV), while the total system was implemented by a rejection cascade of boosted feature regions [33]. Markus Enzweiler and Dariu M. Gavrila compared four state-of-the-art pedestrian detection systems: wavelet-based AdaBoost cascade, linear SVM with HOG, neural network (NN) with local receptive field (LRF), and hierarchical shape matching combined with texture-based NN/LRF classification [34].

Prof. Hermann Rohling's team of Hamburg University of Technology developed distinctive pedestrian detection systems using only automotive millimeter wave radar [35, 36]. They discovered a fact that radar echo signals from a walking pedestrian contain characteristic information that differs from other backscattering objects like cars and trucks. Automotive radar sensor can measure not only target range with high resolution but also velocity with an accuracy of a few centimeters per second. When the location and velocity of target are measured, the pedestrian has a narrow location range and a wide velocity range because of its moving arms and legs while the vehicle and pillar have a narrow velocity range with a wide and a narrow location range, respectively. Furthermore, the tracked velocity of pedestrian shows regular oscillation with a certain low frequency, which is a strong indicator and a signal feature to distinguish between pedestrian and car. Using features extracted from radar signal, the pedestrian can be classified from moving vehicle and stationary objects.

Communication-based pedestrian detection is the newest approach. It is derived from the idea that radio-based communication does not need line of sight and could solve hidden pedestrian problems. Although the feasibility of mobile communications such as global system for mobile communication (GSM) and universal mobile telecommunications system (UMTS) was studies, they have many disadvantages. Every node should have a precise global positioning system (GPS) and peer-to-peer communication should be added to meet latency requirement [37]. EU project WATCH-OVER and German project AMULETT investigate the possibility of short-range communication for pedestrian protection [38, 39]. In this approach, vehicles transmit interrogations and transponders embedded into vulnerable user's accessories such as school bag, bicycle, and motor bicycle return identification messages. With the multi-antenna system, the vehicles can recognize the directions and distances of the transponders. Furthermore, the identification message can provide a user's information such as agility, age, and moving pattern. Candidate short communication technologies include IEEE 802.15.4 (Zig-Bee), radio frequency identification (RFID), and IEEE 802.15.3a ultra wide band (UWB) radio. Even if this last approach is very interesting, it is based on the strong assumption that all road users have transponders: at present this is unrealistic.

Setup

This section describes the setup, starting from the perception technologies, going through the sensor suite and actuators, and concluding with the processing system.

Being designed to address an urban scenario in which the prototype vehicle is running close to stopped vehicles, a limitation on vehicle speed and detection range can be accepted. Low-to-medium vehicle speeds up to 50 km/h and a detection range of about 40 m can be considered as a safe choice.

One of the constraints of this problem is the detection of stopped vehicles and other standing obstacles to be detected; a laser-based solution sufficiently fit this requirement robustly enough supplying both distance measurement and shape classification. The speed information is commonly missing in laser data. However, some laser scanners, like the one selected for this application, can provide interlaced data. For these devices, a number of interlaced scans, taken at different times, are grouped together in a single, high-resolution scan. Obstacles speed can be estimated by analyzing these interlaced data together with vehicle inertial information. Using obstacle speed a classification between standing and moving obstacles is straightforward.

Vision, is the key technology to detect pedestrians even if they are partially occluded. Since distance measurements are already available from the laser and no further 3D reconstruction is required, a single NIR camera satisfies the requirements for both daylight and night scenario.

The camera selected for this system is an AVT Guppy F-036B. Its sensor of 752×480 pixels has a wide aspect ratio which is beneficial for automotive applications since relevant information is often contained in lateral area. The sensitivity covers both the visible and the NIR spectra. During the night, object detection is improved combining the high response in the NIR domain using and specific illumination. Additional headlamps are mounted in front of the vehicle. A NIR LED headlight with 25° of aperture is mounted in front of the radiator, while the headlamp blocks customized by SL can illuminate in the visible domain, using a bifunctional lamp (low-beams and high-beams), and in the NIR domain using additional specific lamp.

The laser scanner is a SICK LMS 211–30206. This laser has a horizontal scanning angle of 100° with angular resolution selectable from a minimum of 0.25°; the detection range goes up to 80 m; a fog correction feature is also available.

All these characteristics well fit the application requirements, as a lot of commercially available lasers. But this one also features interlacing. Selecting 1° of resolution and a phase-gap of 0.25°, four subsequent rotations are included in the same scan. Four rotations are performed in 53.28 ms, thus every rotation takes 13.32 ms. This time is comparable with that of the events occurring in a driving scenario. This means the scans deformed mainly depending on the vehicle movement. This effect becomes more evident using the interlacing feature.

Since the camera and the laser scanner are not synchronized, there is a continuously variable time shift between the two captured sample streams; however the displacement due to the non-synchronization is considered negligible due to ratio between the vehicle speed, which is low, and the processing rate, which is high.

The laser scanner and NIR headlamps are integrated in the front bumper, as shown in Fig. 5. The NIR camera is placed inside the driving cabin near the rearview mirror as shown in Fig. 6.

An industrial grade Mini-ITX PC running an Intel Core 2 Duo–based CPU is fixed in the boot. The camera is connected through a FireWire A controller integrated on the motherboard, while an external RS422 to USB adapter is used to connect laser. Inertial data

Active Pedestrian Protection System, Scenario-Driven Search Method for. Figure 5
A detail of the front bumper showing the laser scanner integration and the headlights

produced by off-the-shelf sensors are gathered through the CAN bus using a USB adapter.

On the actuator side, the braking system installed on the test vehicle was replaced with Mando's MGH-40 ESC plus. The braking strength can be controlled by sending appropriate CAN messages to this ECU. In this unit is also available a deceleration control interface (DCI) used for high-level functions, such as adaptive cruise control (ACC) and precrash safety (PCS). The DCI may receive multiple deceleration commands. The desired deceleration is selected depending on priorities and vehicle status. A feed-forward controller uses the deceleration output as control signal in a feedback loop to physically operate on wheel brake pressures. The braking strength can be controlled in the range [0, 1.0] g with a resolution of 0.01 g, a stable error lower than 0.05 g, and response time of 0.3 s. Deceleration is controlled by the DCI in cooperation with other active control system Electronic Brake Distribution (EBD), Anti-lock Brake System (ABS), and Electronic Stability Control (ESC).

Active Pedestrian Protection System, Scenario-Driven Search Method for. Figure 6
How the camera is installed inside the cabin

The horn has been modified to receive a control signal from both the manual command and a USB I/O board (see Fig. 7a) connected to the processing unit and detected as a serial port.

A new 100 Hz yaw rate sensor, manufactured by Siemens VDO and Mando, is connected through the processing system via CAN bus. This sensor provides yaw rate with an accuracy of 0.0625°/s and also lateral acceleration. Figure 7b shows the sensor.

Focus of Attention

Two methods for laser data classifications are developed to improve algorithm robustness. Pulses are first clustered into straight lines for both methods; then the

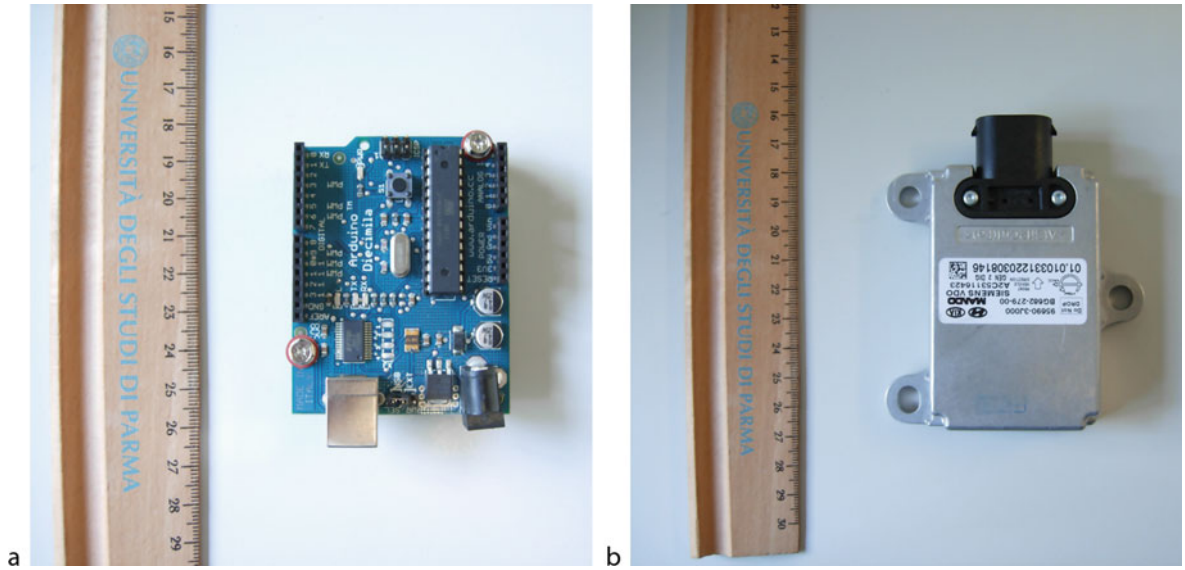

Active Pedestrian Protection System, Scenario-Driven Search Method for. Figure 7
(**a**) The USB I/O board used to control the horn, and (**b**) the special yaw rate sensor

first one classifies obstacles only considering the last scan, while the second one verifies the obstacle position and speed using subsequent scans.

Significant shifts between subsequent laser scanner measurements affect the measured obstacle shape as a distortion, and cause clustering or classification problems.

Vehicle movement in terms of rotation and translation is measured using the ESP CAN box. Having this information available, each pulse in the scan can be corrected removing the shape distortion.

Translation is corrected using vehicle speed, while using the steering wheel angle to compute the yaw rate allows to completely specify the rotation correction matrix.

Yaw rate can be computed as follows:

$$\text{Yawrate} = (V_{\text{fr}} + V_{\text{fl}})/(t_{\text{w}} \cos \delta)$$

where V_{fr} and V_{fl} are front right and front left wheels speeds, respectively, δ indicates the wheel angle, and t_{w} is the vehicle front track.

The additional yaw rate sensor installed on the vehicle is used to measure directly this value, since indirect computation is highly affected by noise.

Figure 8 shows raw and corrected laser data referring to nonmoving obstacles. The four laser rotations that create a scan are clearly visible before the correction, while the obstacle appears as a single line after the correction.

After data correction, moving obstacles captured from interlaced scans are characterized by four parallel lines, as shown in Fig. 9. Obstacle classification is performed relying on this information.

Pulses belonging to the same rotation are connected together as a first step forming chains of segments or cluster. Points which are not joinable to any chain of the same rotation are checked for merging with points of other rotations considering proximity only. Points not connected to other points or close to the limit of the laser scanner range (about 80 m) are permanently discarded.

After clustering, moving obstacles are classified by identifying four different and parallel clusters, while standing obstacles are detected when the clusters are overlapped.

Up to this step, chains of segments are created by joining pulses without any additional information.

Active Pedestrian Protection System, Scenario-Driven Search Method for. Figure 8
Laser data: (**a**) without correction and (**b**) with correction

Active Pedestrian Protection System, Scenario-Driven Search Method for. Figure 9
After data correction a moving obstacle is still represented by four different lines

When adjacent segments have approximately the same orientation, they are merged into a longer segment, preserving the obstacle shape, but reducing the amount of information supplied by the sensor. Straight lines connecting the chain start and end points are obtained merging a chain of adjacent segments.

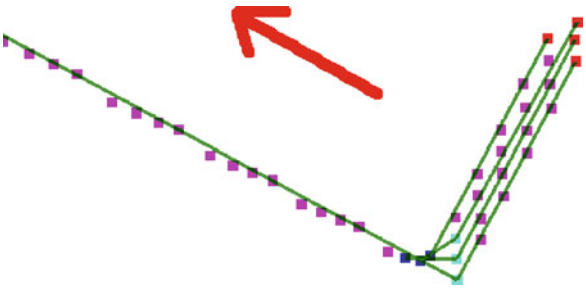

Active Pedestrian Protection System, Scenario-Driven Search Method for. Figure 10
A moving vehicle and its motion direction: the four *parallel lines* correspond to its rear bumper, while the *single line* corresponds to its left side. *Blue points* are polylines start points, *cyan points* are corner points, *red points* are polylines end points, and *violet points* are generic line points

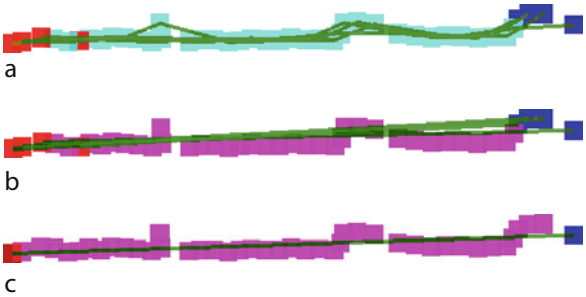

Active Pedestrian Protection System, Scenario-Driven Search Method for. Figure 11
The steps of the algorithm: (**a**) data clustering, (**b**) approximation using polylines, and (**c**) lines merging: all the points are merged into a single line; in order to simplify the following steps, small drifts are ignored

The distances between a line and all its internal points are computed and, if the maximum between these distances is larger than a threshold, the line is split into two separate lines.

These steps are iterated while the maximum distance is larger than a threshold. The result is that each chain is therefore finally segmented into a polyline.

Figure 10 shows a moving vehicle: The rear bumper is framed as four parallel lines, while its side – parallel to the vehicle movement direction – is marked by a single line.

After data correction, points clustering and segment merging, each obstacle detected in the laser scanner field of view, is identified by four lines, one for each laser rotation that composes the whole high-resolution scan. Static and moving obstacles can be located and classified in a robust way using the following observation. A static object has four lines that are overlapped on a single shape, while a moving obstacle has the lines parallel but not overlapped. Figure 11 shows the algorithm steps.

Although this process is very simple and effective, when vehicle pitch is significant, false negatives are possible.

Polylines obtained so far can only be classified thanks to their size and shape. Obstacles can be divided in four categories:

- Possible pedestrian
- Road infrastructure
- L-shaped obstacle
- Generic obstacle

Obstacles with limited size are classified as pedestrians, while obstacles almost parallel to the vehicle and with a large size are classified as road edges (guard-rails, buildings, road infrastructures, etc.).

L-shaped obstacle patterns are detected using a simple and fast method, based on line orientations. All obstacles not yet classified are tagged as generic obstacles; Fig. 12 shows an example.

Information about obstacle movement – already estimated in the previous step – is also stored for further usage.

The procedure described in the previous subsection classifies all small obstacles as possible pedestrians. However a number of false positives may indeed be present under unfavorable conditions.

Parked vehicles and other fixed obstacles along the road are used to identify critical areas in front of the vehicle, to focus the detection in the immediate proximity of these areas where pedestrians can suddenly appear and become dangerous.

Ego-motion information is used to align and roto-translate polylines provided by previous scans; a check on the overlapping between polylines identified in current and in previous frames is then performed to assign a category to the object between: moving obstacle, static obstacle, changing shape obstacle, and new obstacle.

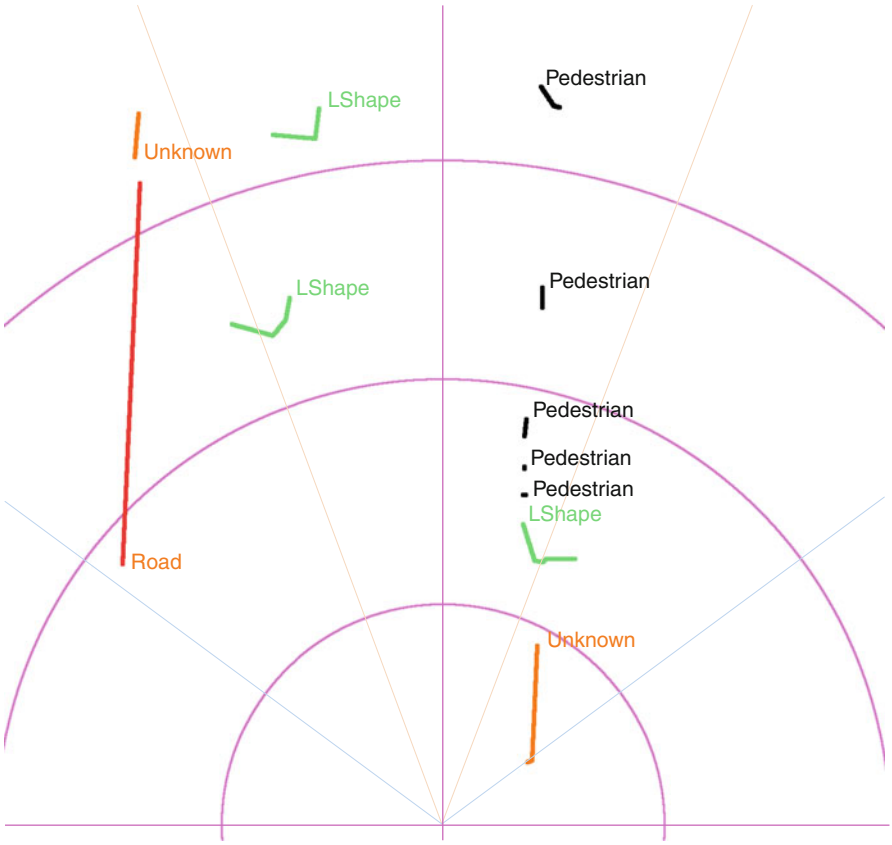

Active Pedestrian Protection System, Scenario-Driven Search Method for. Figure 12
Obstacle classification: all possible classifications based on shape are represented in the image

Moving obstacles have small spatial overlapping if the time window is large.

If no correspondence is found between the current polyline and those from the past, the object is classified as a *new obstacle*.

The areas of interest in which vision will search for pedestrians is determined using static obstacles; obstacles whose shape is changing over time are also of basic importance. They may contain a pedestrian in a smaller region of their shape.

The centroid of each polyline is computed to track obstacles over time. Centroids are used as representative points to simplify the computation. A description of a more complex laser scanner data processing based on comparison between each point of polylines can be found in [40]. A different classification is also made using distances between the centroid of the last and previous scans.

Polylines are labeled using the information contained in the distances between the current centroid and all the past ones as follows:

- Fixed obstacle: if all distances are below a certain threshold. This threshold, to detect, is increased according to the distance of the obstacle (to compensate for a decreasing accuracy) and the time gap (to partly compensate for errors in ego-motion reconstruction).
- Moving obstacle: if the distances grow over time.
- Unknown obstacle: this label is given if the object can neither be labeled as fixed nor moving. This may happen the first time an obstacle appears or when the detection is not stable due to bad reflections of the lasers beam.

The three previous classification results are considered to compensate for laser data processing

inaccurate results. The polyline is classified with the most frequent one.

Example results are shown in Fig. 13 with an estimation of the object speed.

The following steps of the algorithm use the processing results on the labeled polylines. This information is used to sense the static (obstacles and vehicles) position and moving (pedestrians and vehicles) obstacles in the environment. When obstacles are identified as static by the second classification stage, they are used to define the environment structure. Driving corridor is defined as the area that may be reached by the vehicle in the near future. Fixed obstacles are used to build the driving corridor, namely, as shown in Fig. 14.

The driving corridor may have multiple paths or branches, each with a minimum width larger than the vehicle one; branches with a width narrower than this threshold are discarded as closed. The corridor does not necessarily correspond to the free space in front of the vehicle, since it is built considering fixed obstacles only, and may also include moving obstacles.

This algorithm is focused on the detection of suddenly appearing pedestrians; the detection is concentrated on areas hidden by a static obstacle or

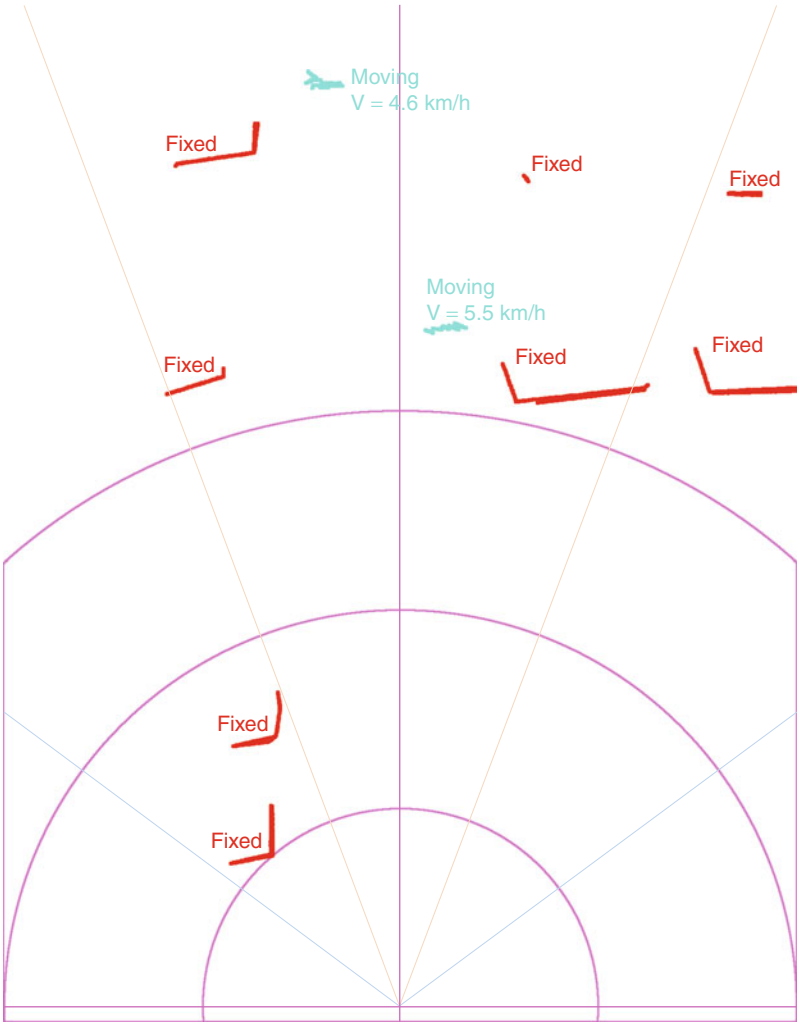

Active Pedestrian Protection System, Scenario-Driven Search Method for. Figure 13
Obstacle classification: all possible classifications based on movement are shown. Note that moving polylines change their position in world coordinates

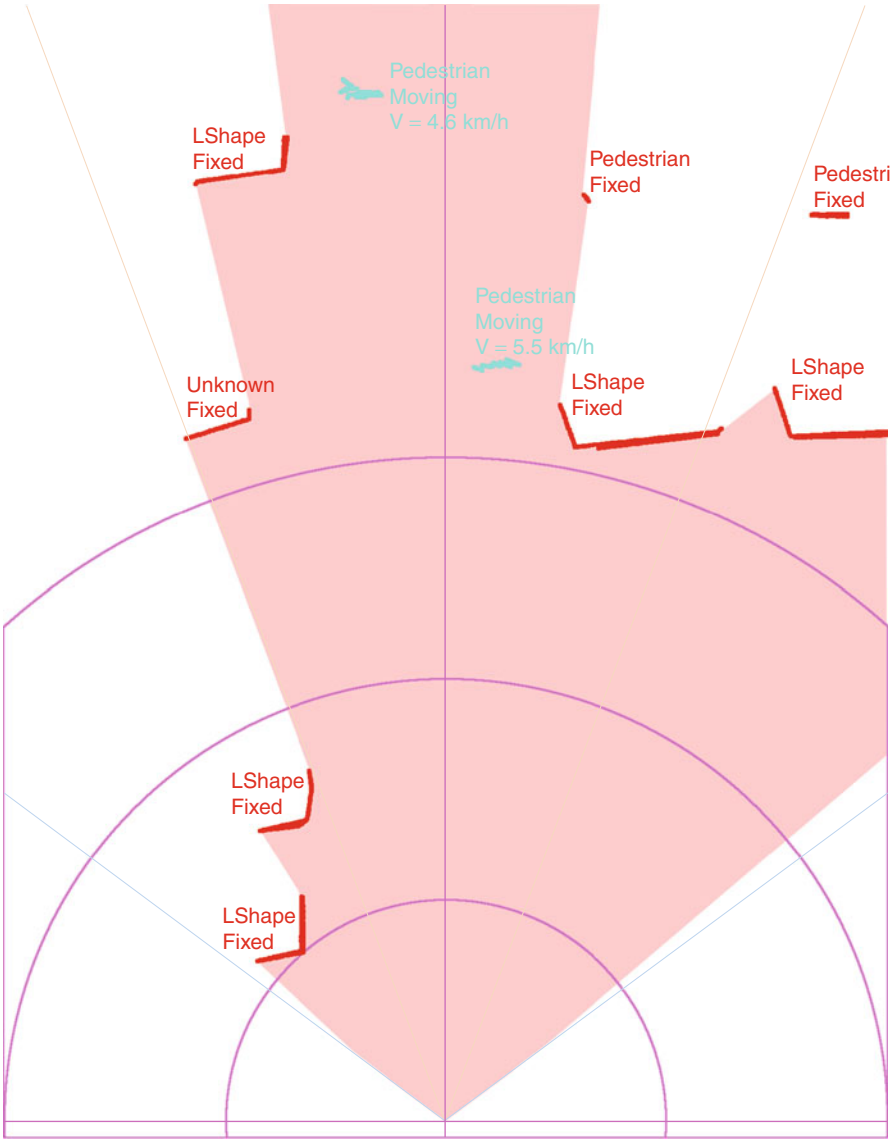

Active Pedestrian Protection System, Scenario-Driven Search Method for. Figure 14
The pink zone represents the driving corridor. Obstacles moving inside the corridor, or near its edges, with a speed and a size typical of a pedestrian, are tagged as possible pedestrians

between two static obstacles. These areas are usually located along the corridor edges. Static obstacles are used to build the corridor, and also to identify dangerous areas, that is, areas in which pedestrians may appear. Dangerous areas are located behind the furthest point of each static polyline as shown in Fig. 15.

Obstacles moving inside the corridor, or near its edges, with a speed and a size typical of a pedestrian, are tagged as possible pedestrians.

Vision Fusion

The regions of interest are 2D areas in world coordinates; their corresponding areas in the image are then located thanks to camera calibration and perspective mapping.

Once the areas of attention are located, the search for pedestrians is triggered in these areas. Specific image windows are defined using a perspective

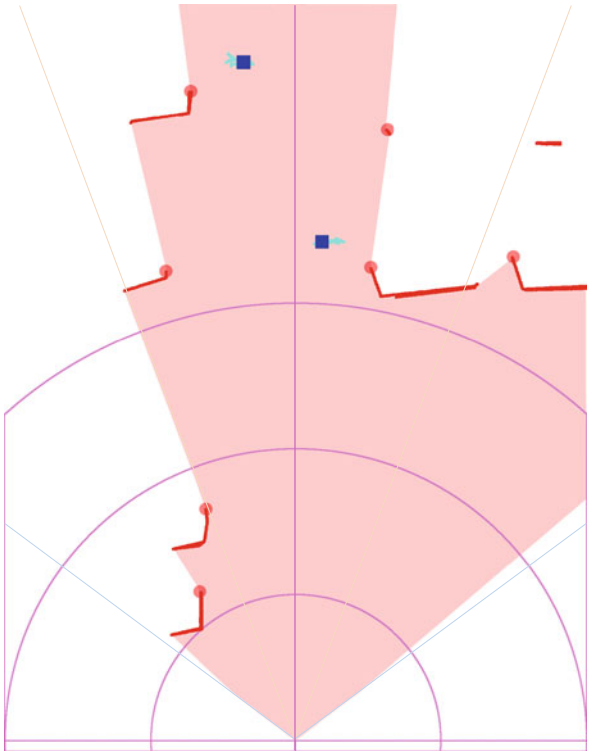

Active Pedestrian Protection System, Scenario-Driven Search Method for. Figure 15
Dangerous areas and possible pedestrians: *red circles* represent dangerous areas, while *blue boxes* identify possible pedestrians

mapping transformation, considering 90 cm as pedestrian width and 180 cm as pedestrian height. These image areas are resampled to a fixed size (24 × 48 pixels).

In order to reach good classification during both day and night, two different systems are developed. The idea is to use a simple and specific classifier for nighttime images, in which pedestrians' shapes clearly appear, and to use more complex classifiers (based on cascade methods) for the day.

The nighttime algorithm is based on the assumption that, thanks to NIR illuminators, pedestrians and other standing objects represent the brightest areas in the image with the exception of light sources. Therefore, after removing light sources, it is possible to detect obstacles with a binarization process and classify them according to their shape.

At the end of the preprocessing steps, a binarized image is obtained. The standing objects (including pedestrians) are remapped as white, while the background is remapped as black. As the NIR headlamps illuminate more the legs of the pedestrian, these first phases are operated separately for the upper and lower part of the image.

After these operations, the procedure continues to check for pedestrian trunks and legs by respectively analyzing the upper and lower half of the image. First of all open legs are searched for; if open legs are not found, an algorithm that checks for closed legs is applied, and, finally a trunk presence check is performed.

The open legs search is based on striped skeletonization. For each row of the image, the white areas present are narrowed to a single point. In such a way it is possible to remap legs as lines. Obtained lines can be transformed to straight lines, and the position of these lines can be finally studied to identify legs.

Search for trunk and closed legs are very similar, differing only in some details and thresholds. The captured images contain a very low level of detail and it is often inadequate for a complex analysis. For this reason a simple procedure is implemented that tries to make the most of the few details that characterize the pedestrian. The algorithm searches for white areas and considers their aspect ratio to confirm the presence of trunk or closed legs.

At the end of the algorithm four rates are assigned, which range from 0 to 1. The votes are:

- Vote of the trunk according to the correspondence with a model and to dimension.
- Vote of the legs according to the correspondence with a model and to dimension.
- Open legs rate which is obtained with the ratio between feet position distance and maximum feet distance.
- Pedestrian vote which is obtained making an average of the body and legs vote. The vote of the legs has more weight if they are open because it is a dominant characteristic of a pedestrian.

All these ratings will be analyzed at a later stage of the application to properly determinate if the figure is recognized as a pedestrian.

AdaBoost (a short for Adaptive Boosting) is a machine-learning meta-algorithm. It is used to select the combination of a weak classifier to obtain a precise classification.

Using an appropriate training set it is possible to compute the correct weight to be set to each classifier and obtain a robust classification. AdaBoost is a technique widely used for the classification of pedestrians [41]. Haar features are firstly chosen for the weak classifier [42]. Different Haar features are selected for each iteration, as suggested by Viola and Jones [43]. Haar features are very simple features that can be used, together with a meta-algorithm similar to AdaBoost, to classify a lot of objects. They consist of a very simple pattern that can be moved and stretched on the image to be compared to image integral, in order to obtain an accurate classification.

As Haar features are very generic, the idea is to develop other features, specific for pedestrians, in order to reach a better classification using AdaBoost again. These features are based on a typical pedestrian shape and body parts aspect. To detect a pedestrian, the algorithm provides a vote to each feature of the following list:

- Open legs shape
- Left step legs, little mask
- Right step legs, little mask
- Left step legs, big mask
- Right step legs, big mask
- Head top, little mask
- Head top, big mask
- Head, with circle formula
- Pedestrian's M function
- Horizontal border function
- Tree and pole search function

To increase the potential and the recognition performance, an additional stage, called AdaBoost cascade, is developed.

In this stage the votes from the classifier implemented with Haar features, with ad hoc ones, and nighttime classifier are merged and combined to obtain an additional level of classification. The votes provided by the previously described algorithms are used as input to make a second kind of AdaBoost classifier.

As the number of outputs from previous classifiers is very low, and some tests pointed out that they cannot be used to reach an efficient classification process by their own, nonlinear combinations of these values are added as input of AdaBoost algorithm.

According to the classic voting approach, a final hypothesis resulting formula is implemented: The final vote is computed as the weighted sum of the classifiers selected by the AdaBoost training stage.

Instead of using two classes only (pedestrians and non-pedestrians) three classes are here used:

- Pedestrians
- Non-pedestrians
- Appearing pedestrians

Appearing pedestrians are pedestrians that are initially not completely visible, that is, partially occluded by obstacles, so only a part of the pedestrian's shape can be framed – the upper or side part only.

AdaBoost was trained using image windows determined by the previous steps of the algorithm. Candidate selection is a complex and critical step for the AdaBoost training process [16]. Both normal and flipped samples are used in the training process. If two or more images are very similar (i.e., the pixel-wise difference is less than a threshold) only one of them is used in the training process. Images framed in Italy, the Netherlands (during tests before the IEEE Intelligent Vehicle Symposium 2008 demonstration), and Korea were used in the training process.

Once a pedestrian partly hidden by a vehicle is detected – by the vision system only – the system issues an internal alert. In this case no warning is provided to the driver because the danger level is not yet determined.

When an alert is issued, the search continues in the same zone and tracking is started. As soon as a tracked pedestrian becomes visible also to the laser scanner, the direction of its movement is considered. If a pedestrian moving from the corridor's edge to the corridor's center is detected, a warning is then issued to the driver. Figure 16 shows an alert and its following warning.

It is of basic importance to note that the driver is warned only when the pedestrian is completely visible, like in other systems. However, the system presented in this work is more reactive than others, since the tracking starts when the pedestrian is only partially visible by one of the sensors. In an urban situation like this, promptness is an important key to the success of the system.

Active Pedestrian Protection System, Scenario-Driven Search Method for. Figure 16
Two subsequent frames of a sequence: (**a**) the system detects the partly occluded pedestrian and issues an internal *alert*, but no warning to the driver. (**b**) When a detection of a fully visible pedestrian follows the internal *alert*, a *warning* is promptly sent to the driver

Figure 17 shows some results obtained in complex conditions (bad weather condition, poor light condition) and a misclassification: a suddenly appearing pedestrian detected as a normal pedestrian.

Automatic Braking

Previous works have introduced the Region of No Escape (RONE [44]) as the area that will be anyway occupied by the vehicle in the near future even if the driver steers away or brakes.

Like traditional pedestrian detection systems, pedestrians present in the RONE are here detected by laser and vision fusion; the presence of a pedestrian in the RONE triggers the automatic braking, as a Collision Mitigation system (i.e., when the accident is unavoidable).

The RONE is indeed important to detect an inevitable crash, but its size and shape are defined assuming an optimal driver maneuver. Most drivers, anyway, have (1) longer reaction times and (2) suboptimal skills; therefore an extension of the RONE is mandatory in order to act as a driving aid (avoid the crash) rather than a collision mitigation system.

It has to be understood, though, that any extension of the RONE will include areas in which the vehicle has a high probability to move, but it is not 100% sure to be occupied by the vehicle in the near future (e.g., in case of a very skilled driver implementing an optimal avoidance maneuver).

The system presented in this work defines the *deceleration area* as a suitable RONE extension designed for the specific scenario addressed by this project. In fact, pedestrians appearing from behind an obstacle might induce a reaction time longer than the time required by a driver to locate a clearly visible pedestrian. Therefore, still assuming that the driver is not distracted and has optimal driving skills, longer reaction times would enlarge the RONE.

The deceleration area width is defined to be equal to vehicle width and its length proportional to vehicle speed, but anyway bounded to 40 m, while yaw is considered constant for the trajectory computation.

Whenever a pedestrian appearing from behind an obstacle crosses the road and enters in the deceleration area, the system will activate the automatic braking, even if a skilled driver might be capable of avoiding it. This is why it is extremely important to be able to issue a warning to the driver well in advance, and provide sufficient time to perform a manual maneuver. The driver has indeed a more subtle and deeper perception of the pedestrian behavior and a manual countermeasure might be more effective than an automatic one.

In this section the concepts of driving corridor, RONE, and deceleration area are introduced. It is important to note the difference between these three areas in front of the vehicle, which are used for different purposes. As shown in Fig. 18, the driving corridor is a jagged area edged by static obstacles present in front

Active Pedestrian Protection System, Scenario-Driven Search Method for. Figure 17
Some suddenly appearing pedestrians correctly detected: (**a**) in an underground parking, (**b**) in the rain, (**c**) behind a misaligned vehicle, (**d**) behind a wall, (**e**) at night; and (**f**) a suddenly appearing pedestrian detected as non-dangerous pedestrian (false negative)

of the vehicle and represents the area where the vehicle can move.

The deceleration area is a smoother area that represents the positions where the vehicle should move considering a fixed yaw rate.

The RONE represents the area where the vehicle will move in the near future.

Results

During the development of an ADAS it is important to consider different aspects for the results assessment: The first aspect is the precision of results, while the second one is the time that is needed to process the information; this second aspect is very important because the whole data processing must be operated real time.

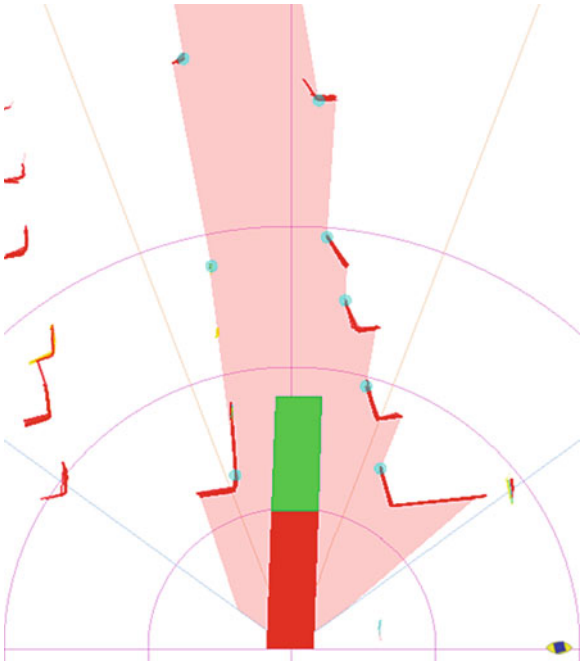

Active Pedestrian Protection System, Scenario-Driven Search Method for. Figure 18
Driving corridor, RONE, and deceleration area: the *pink area* represents the driving corridor, the *red area* represents the RONE, and the *green area* represents the deceleration area

To evaluate the obtained results the parts of the system can be considered separately, in order to assess the performance of each part and to plan following developments.

The system can be divided into two parts, the first one is the regions of interest localization, while the second one is the search for pedestrians inside the region of interest.

The first part is simpler, and the results are only qualitatively evaluated. Regions of interest can be correctly detected with an appropriate precision up to a distance of about 40 m. Unfortunately some errors can occur due to strong vehicle pitch variation. If the laser orientation varies too much, the framed shape does not correspond to a significant representation of the environment. This problem is solved using a pitch rate sensor. If the pitch variation is too big, the whole system is disabled, because the first part of the algorithm is not able to get correct results. Anyway generally high pitching is time limited, therefore the system is blinded for a short time interval.

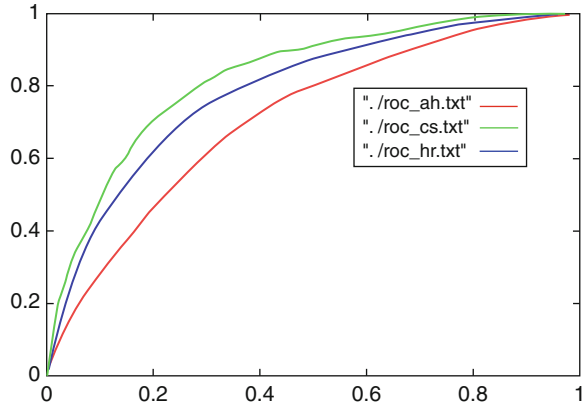

Active Pedestrian Protection System, Scenario-Driven Search Method for. Figure 19
ROC curves for daytime classifier algorithm

Search for pedestrians inside regions of interest is tested with three different test sets: one for daytime scenes, one for nighttime scenes with poorly illuminated environments, and one for nighttime scenes with proper illumination.

Figure 19 shows ROC curves for ad hoc features, Haar features, and cascade method. The algorithms based on Haar features reach more precise results than algorithms based on ad hoc features, but it is important to note that the cascade method, that merges the two methods, can reach a good classification rate. Results obtained on nighttime scenes with proper environmental lighting are similar to the previous one. Some tests also pointed out that the use of specific nighttime algorithms produce worse results.

The nighttime search, based on skeletonization, reaches good results without any further processing, as shown in Fig. 20.

Even if these results are important to develop the system, the final goal of the algorithm is not the detection of all pedestrians present in the scene, but the detection of dangerous pedestrians only. It is not important to detect a pedestrian normally walking on the sidewalk, while it is mandatory to detect a pedestrian that suddenly appears in front of the vehicle; therefore the results must be assessed considering the dangerous situations only.

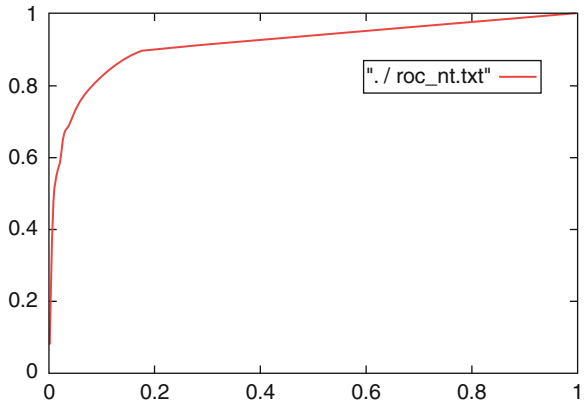

Active Pedestrian Protection System, Scenario-Driven Search Method for. Figure 20
ROC curves for daytime classifier algorithm

A set of sequences were considered for extensive performance assessment, for a total driving time of about 10 h in complex urban scenarios. A total of 236 km were driven during day and night, in different weather conditions (sunny, cloudy, rain, fog). Various scenarios were included: downtown, large and narrow roads, underground car parks, highways, and rural roads. During night tests, scenarios with and without external illumination were acquired. During night tests the NIR illuminators were always turned on. To complete the test sets some specific situations were staged (such as very dangerous pedestrian crossings), but a number of dangerous scenarios were anyway framed in normal driving.

In the tests, the following performance indexes were considered:

(a) Number of pedestrians suddenly appearing in front of the vehicle (that must generate warnings to the driver)
(b) Number of pedestrians appeared in front of the vehicle that have been successfully tracked and which can be hit by the vehicle (that must trigger the automatic brake)
(c) Number of fully visible pedestrians which can be hit by the vehicle (that must trigger the automatic brake)

For each performance index the number of correct detections, false positives, and false negatives were computed.

Performance index	Correct detections	False negatives	False positives
A	24	11	1
B	5	0	0
C	8	0	0

Results of a 10-h drive (~236 km, ~540,000 images)

A total of 24 suddenly appearing pedestrians were correctly detected in the tests (case A). Only one false positive is present.

Only 1 missed warning out of 11 is due to a pedestrian miss-detection; the others are caused by either alert misses or delayed detections, but in these cases, even if the warning signal is not promptly issued to the driver, the automatic brake would have stopped the vehicle avoiding the crash if the pedestrian would have been in a dangerous situation. All pedestrians into the deceleration area are localized (no false negatives): five fall into case B, while eight fall into case C.

No false positives are present, thanks to the special attention paid to develop this *SDS* approach.

Anyway it is important to note that, for safety reasons – given that the tests were performed in real traffic – the size of the deceleration area was increased but, nevertheless, the system behaved very satisfactorily.

The limited number of dangerous events requiring the intervention of the safety system is not surprising. During normal driving dangerous situations are not frequent; plus, some of them are staged in order to challenge the system.

The analysis of the results obtained during the test highlighted good results also in case of rain, when pedestrian with umbrellas were detected as well. The system is anyway not able to discriminate between multiple pedestrians moving together or in situations in which the laser scanner is not able to obtain a clear picture, for example, when pedestrians hold bags or other large objects; moreover suddenly appearing pedestrians walking very slowly or pedestrians under very critical lighting conditions can be missed.

A particular attention was paid to the processing time. A system that it is not able to process the data real time is useless for automotive applications.

The great benefit of the *SDS* method is the reduction of the regions of interest that must be considered

by the vision system. Some tests focused that the number of considered areas is almost half of the ones considered using a traditional system. As the image processing is the most time-consuming part of the algorithm, the system can reach a significant reduction of global processing time.

Considering that the system is designed to work in urban and rural street, where the vehicle speed must be lower than 50 km/h, a processing frequency of 10 Hz can be considered sufficient.

Frame processing time changes according to the chosen method (nighttime method is quicker) and to the number of regions of interest which are analyzed. Anyway, the execution time on a good performing PC is always lower than 70 ms/frame (about 14 Hz), considering the whole system.

Future Directions

An important concept in road safety aimed at avoiding collisions with vulnerable road users was presented. Instead of implementing a traditional pedestrian detection system followed by both a validation step and the assessment of the danger level, it was proposed an innovative approach. Whenever a specific environmental scenario is detected (i.e., stopped vehicles that may hide pedestrians), the possible presence of pedestrians is checked for in well-defined areas only, focusing on a particularly critical environment, typical of urban accidents.

Besides directly detecting dangerous situations, it also boosts timing performance, since the computationally intensive part – vision-based pedestrian recognition – is performed only on limited portions of the image.

The system was developed to tackle a very specific yet very common scenario, while it does not cover the whole set of dangerous situations that may occur in an urban environment.

The search for all the pedestrians present inside the so-called driving corridor can generalize the system, yet maintaining a scenario-driven approach, as the search is performed only in a corridor dynamically built using laser scanner data.

As a conclusion, the proposed approach offers the following advantages over traditional pedestrian detection systems.

- The system looks for specific spots in the 3D scene that might contain pedestrians (even partly occluded ones); in these areas the search for pedestrians is performed by vision; vision is therefore activated only in selected areas providing a lower number of false detections and a faster processing.
- Once a partly occluded pedestrian is detected, an internal alert is issued; when the pedestrian becomes completely visible, the initial alert is followed by a warning to the driver. Therefore the system reacts very quickly to the sudden appearance of a pedestrian, since tracking already started when the pedestrian was partly occluded and visible only to one of the sensors (vision).

This work was developed as a feasibility study aimed at determining whether the deployment of nonreversible systems might be a viable solution for real implementations. Nonreversible systems have always been considered extremely critical, since their robustness and effectiveness has to reach 100% to allow their integration on real vehicles. No sudden stops or irreversible maneuvers have to be triggered by false positives in the detection. Unfortunately, reaching a correct interpretation of all scenes and scenarios is as desirable as improbable and a lot of testing must be performed to evaluate possible failures in the detection.

Bibliography

1. O'Farrell J (2006) May contain nuts. Black Swan, London
2. Lucchini E, Kramer M (1981) Safety device for the protection of pedestrians. Patent
3. Matsuura Y, Maki T (2001) Device for reducing the impact of pedestrians. Patent
4. Myrholt H, Ericsson M (2002) Deployable A-pillar covers for pedestrian protection. Patent
5. Buehler M, Iagnemma K, Singh S (eds) (2010) The DARPA urban challenge. Springer, Berlin
6. Agran PF, Winn DG, Anderson CL, Tran C, Del Valle CP (1996) The role of the physical and traffic environment in child pedestrian injuries. Pediatrics 1996(98):1096–1103
7. Retting RA, Ferguson SA, McCartt AT (2003) A review of evidence-based traffic engineering measures designed to reduce pedestrian-motor vehicle crashes. J Public Health 2003(93):1456–1463
8. Premebida C, Monteiro G, Nunes U, Peixoto P (2007) A lidar and vision-based approach for pedestrian and vehicle detection and tracking. In: Proceedings of IEEE international conference on intelligent transportation systems, Seattle, pp 1044–1049

9. Hwang JP, Cho SE, Ryu KJ, Park S, Kim E (2007) Multi-classifier based LIDAR and camera fusion. In: Proceedings of the IEEE international conference on intelligent transportation systems, Seattle, pp 467–472
10. Franke U, Heinrich S (2002) Fast obstacle detection for urban traffic situations. IEEE Trans Intell Transport Syst 3(3):173–181
11. Curio C, Edelbrunner J, Kalinke T, Tzomakas C, Von Seelen W (2000) Walking pedestrian recognition. IEEE Trans Intell Transport Syst 1(3):155–163
12. Gandhi T, Trivedi MM (2007) Pedestrian protection systems: issues, survey, and challenges. IEEE Trans Intell Transport Syst 8(3):413–430
13. Hodzic M (2008) Distronic plus and brake assist plus reduce rear-end collisions by 20%. http://www.benzinsider.com/2008/06/distronic-plus-and-brake-assist-plus-reduce-rear-end-collisions-by-20/. Accessed 30 May 2010
14. The Motor report (2010) Toyota Prius To ship with advanced safety gear. http://www.themotorreport.com.au/29611/2010-toyota-prius-to-ship-with-advanced-safety-gear. Accessed 30 May 2010
15. Juliussen E (2010) Driver assist systems. http://www.autofocusasia.com/electrical_electronics/driver_assist_systems.htm. Accessed 30 May 2010
16. http://www.prevent-ip.org/en/prevent_subprojects/intersection_safety/intersafe/
17. BBC News (2010) Self-parking car hits the shops. http://news.bbc.co.uk/2/hi/technology/3198619.stm. Accessed 31 May 2010
18. www.trafficcalming.org
19. Clarke A, Dornfeld M J (1994) Traffic calming, auto-restricted zones and other traffic management techniques: their effects on bicycling and pedestrians. national bicycling and walking study, Case Study No. 19, Federal Highway Administration 1994
20. Huang HF, Cynecki MJ (2001) The effects of traffic calming measures on pedestrian and motorist behavior. Research report FHWA-RD-00-104, Federal Highway Administration, U.S. Department of Transportation
21. Crandall JR, Bhalla KS, Madeley NJ (2002) Designing road vehicles for pedestrian protection. Brit Med J 324(7346):1145–1148
22. Yao J, Yang J, Otte D (2008) Investigation of head injuries by reconstructions of real-world vehicle-versus-adult-pedestrian accidents. Saf Sci 46(7):1103–1114
23. Koch W, Howard M (2003) Comprehensive approach to increased pedestrian safety in pedestrian – Car accidents. Proc Inst Mech Eng Part D J Automobile Eng 217:513–519
24. Fröming R, Schindler V, Kühn M (2006) Requirement engineering for active safety pedestrian protection systems based on accident research. In: Advanced microsystems for automotive applications, New York, pp 79–106
25. Schuster PJ (2006) Current trends in bumper design for pedestrian impact. SAE Paper No.: 2006-01-0464
26. Fredriksson R, Håland Y, Yang J (2010) Evaluation of a new pedestrian head injury protection system with a sensor in the bumper and lifting of the bonnet's rear part. http://www.autoliv.com/wps/wcm/connect/5f997a004ce4f3f8ac68eef594aebdee/Pedestrian.pdf?MOD=AJPERES. Accessed 30 May 2010
27. http://www.ivss.se/
28. Broge JL (2010) Autoliv actively saving lives. http://www.sae.org/automag/techbriefs/11-2001/page2.htm. Accessed 30 May 2010
29. Autoliv (2010) Pedestrian protection. http://www.autoliv.com/wps/wcm/connect/autoliv/Home/What+We+Do/Recent%20Innovations/Pedestrian%20Protection. Accessed 30 May 2010
30. Kerkeling C, Schäfer J (2005) Structural hood and hinge concepts for pedestrian protection. In: Proceedings of 19th international technical conference on enhanced safety, Washington, DC, pp 379–389
31. Gernóimo D, López AM, Sappa AD, Graf T (2010) Survey of pedestrian detection for advanced driver assistance systems. IEEE Trans Pattern Anal Mach Intell 32(7):1239–1258
32. Sun Z, Bebis G, Miller R (2006) On-road vehicle detection: a review. IEEE Trans Pattern Anal Mach Intell 28(5):1–18
33. Hussein M, Porikli F, Davis L (2009) A comprehensive evaluation framework and a comparative study of human detector. IEEE Trans Intell Transport Syst 10(3):417–427
34. Enzweileer M, Gavrila DM (2009) Monocular pedestrian detection: survey and experiments. IEEE Trans Pattern Anal Mach Intell 31(2):2179–2195
35. Folster F, Rohling H, Meinecke M-M (2005) Pedestrian recognition based on automotive radar sensors. In: 5th European congress and exhibition on ITS and services, Hanover
36. Ritter H, Rohling H (2007) Pedestrian detection based on automotive radar. In: Proceedings of the international conference on radar systems, Edinburgh
37. David K, Flach A (2010) CAR-2-X and pedestrian safety. IEEE Veh Technol Mag 3:70–76
38. http://www.watchover-eu.org/
39. http://www.project-amulette.de/
40. Broggi A, Cerri P, Ghidoni S, Grisleri P, Jung HG (2008) Localization and analysis of critical areas in urban scenarios. In: Proceedings of IEEE intelligent vehicles symposium, Eindhoven, pp 1074–1079
41. Leyrit L, Chateau C, Tournayre C, Lapresté J-T (2008) Association of Adaboost and kernel based machine learning methods for visual pedestrian recognition. In: Proceedings of IEEE intelligent vehicles symposium, Eindhoven, pp 67–72
42. Geismann P, Schneider G (2008) A two-staged approach to vision- based pedestrian recognition using Haar and HOG features. In: Proceedings of IEEE intelligent vehicles symposium, Eindhoven, pp 554–559
43. Viola P, Jones M (2001) Rapid object detection using a boosted cascade of simple features. In: Proceedings of the international conference on computer vision and pattern recognition, vol 1. Hawaii, pp 511–518
44. Fuerstenberg K, Schulz R (2006) Laserscanners for driver assistance. In: Proceedings of the international workshop on intelligent transportation, Hamburg, pp 155–159

Advanced Public Transport Systems, Simulation-Based Evaluation

Haris N. Koutsopoulos[1], Moshe Ben-Akiva[2]
[1]Department of Transport Sciences, The Royal Institute of Technology, KTH, Stockholm, Sweden
[2]Department of Civil and Environmental Engineering, MIT, Cambridge, MA, USA

Article Outline

Glossary
Definition of the Subject and Its Importance
Introduction
Advanced Public Transportation Systems (APTS)
Simulation-Based Modeling of APTS
Microscopic Transit Simulation Example: MITSIMLab
Mesoscopic Transit Simulation Example: BusMEZZO
Future Directions
Bibliography

Glossary

APTS *Advanced public transportation systems* is the transit component of Intelligent Transportation Systems (ITS). It refers to technologies for the collection, communication, and processing of data useful for the management of transit systems.

AVL *Automated vehicle location* systems combine vehicle location and communications technologies to automatically track the locations of a fleet of vehicles. AVL is an integral component of automated vehicle monitoring and control, fleet management, traffic signal priority, and other transit applications. AVL can be used to monitor schedule adherence, estimate arrival times, and communicate location data to a transit operations control center (TOC) or to field-installed devices that require real-time vehicle location data.

APC *Automatic passenger counters* are systems that count passengers as they board and alight the vehicle at a stop. APCs may be used with AVL systems in order to record the spatial distribution of passenger demand along a vehicle's route. APC technologies include treadle mats, infrared beams, and emerging computer imaging (still at early stage of development). APC records the stop location, the time and date of arrival at the stop, the time the doors open and close, the number of passengers boarding and the number of passengers alighting.

BRT *Bus rapid transit* is an evolving transit concept aiming at combining the quality and capacity of rail transit and the flexibility of bus transit.

Electronic fare payment *Electronic fare payment* includes a range of technologies, such as smart cards, designed to reduce costs associated with fare collection and to improve customer convenience (also known as Automated Fare Collection (AFC) systems).

Fleet management *Fleet management* applications refer to "vehicle-based" technologies that may be used to improve vehicle planning, scheduling, and operations.

ITS *Intelligent transportation systems* is an umbrella term referring to sensor, communication, and computing technologies for improved management of transportation systems. ITS relates to all transportation modes.

Simulation "... the process of designing a model of a real system and conducting experiments with this model for the purpose of understanding the behavior of the system or evaluating various strategies for the operation of the system" [1].

Signal priority Transit *signal priority* involves the modification of a traffic signal's regular timing plan to give preference to transit vehicles. Signal priority is designed to reduce transit vehicle delays at signalized intersections.

Traveler information *Traveler information* refers to technologies designed to provide pre-trip and en route information to travelers to allow them to make informed trip-making decisions.

Transportation demand management *Transportation demand management* refers to systems aimed at improving the utilization of existing transportation network infrastructure, through influencing the demand characteristics.

Definition of the Subject and Its Importance

According to the latest UN report on urbanization, more that 50% of the world's population lives in cities [2]. In Europe and the USA, it approaches 70%.

In part due to developments like these, congestion in urban areas continues to grow and create a number of negative impacts, including worsening air quality and noise pollution, consumption of scarce resources, lost productivity.

Public transportation is an important component of the transportation system and potentially a critical element of any strategy toward sustainable mobility in urban areas. The importance of improved public transportation services toward sustainable and efficient transportation systems is well recognized. With the emergence of Intelligent Transportation Systems (ITS), advanced sensor, communications, and computing technologies have been introduced to facilitate better planning, management, and control of public transportation systems [3]. Known as Advanced Public Transportation Systems (APTS), these technologies aim at developing public transportation systems that are more reliable and responsive to passenger needs, and hence, public transportation systems that offer higher level of service [4, 5].

APTS can be quite complex, with dynamic interactions among the various components. For that reason, simulation-based models that incorporate all the dynamic aspects, as well uncertainty inherent in the operations of public transportation systems, have drawn a lot of interest for evaluation and design of APTS.

Introduction

APTS are ITS technologies applied to public transit in order to improve operational efficiency, cost savings, safety, quality of service, and other transit measures of performance. Some APTS applications offer potential for improving service by providing greater leverage to service providers for managing and controlling bus transit operations. Other APTS applications provide benefits in terms of speed, security, and convenience directly to the customer. APTS have the potential to significantly change the way transit services are provided and the way customers use them. Increasingly, popular technologies such as Automated Vehicle Location (AVL) systems, Automatic Passenger Counters (APC), and Electronic Fare Payment already have a wide range of impacts on bus transit operations.

The first examples of APTS date back to the late 1960s and early 1970s with the introduction of Automated Vehicle Monitoring (AVM) systems. The majority of these vehicle location technologies were signpost-based systems (with stationary signposts along bus routes). The signposts were equipped with electronic transmitters that emit unique identification codes. When a bus passed the signpost, an in-vehicle unit received the signpost's identification code and record the time and date, the difference between the current odometer reading and the last (recorded at the previous signpost), and the vehicle's identification code. The bus sent the information to the TOC via radio or other medium periodically or when prompted by the transit operations control center (TOC). Early implementations of APTS were expensive to install, operate, and maintain. Since then, new locations and communication technologies (e.g., GPS) have emerged and led to both improved performance and reduced costs.

Advanced Public Transportation Systems (APTS)

Existing and emerging APTS applications of interest to this report can be grouped into [4, 5]:

- Fleet Management
- Traveler Information
- Electronic Fare Payment
- Transportation Demand Management

Fleet Management strategies focus on improving the planning, scheduling, and operations of a fleet of vehicles [6, 7]. The related strategies aim at improved service reliability, safety, and operating efficiency (e.g., reduced nonrevenue time, increased productivity) and faster service disruption recovery. In general, fleet management includes technologies that collect and make available vehicle performance data (e.g., vehicle location), and technologies that use that data for real-time control or for planning and scheduling. Important technologies used for fleet management purposes include: Communications Systems, Geographic Information Systems (GIS), Automated Vehicle Location Systems (AVL), Automatic Passenger Counters (APC), Transit Operations Software, and Traffic Signal Priority [8].

Traveler Information in transit applications refers to technologies used to provide travel information to passengers in order to assist their trip-making decision. The information provided may range from static route, schedule, and fare information to real-time vehicle location and/or estimated arrival time. AVL systems are the enabler for the provision of real-time information. Traveler information may be disseminated through various means, for example, web-based itinerary planning services, smart phones, in-vehicle units, etc. Traveler information is generally expected to improve the quality of transit service by improving the passenger experience. Traveler information may give passengers a better sense of control over their trip-making decisions and/or enable them to take action to minimize waiting times at stops, plan transfer connections, and thus reduce overall travel time. Information may be provided prior to departure (e.g., by phone, internet), at the terminal or stop, or in the transit vehicle. Information influences passenger trip-making decisions, for example, route, stop, departure time choice, etc. The attractiveness of transit alternatives is a function of waiting time, in-vehicle travel time, transfer time to the connecting trip, number of transfers, onboard comfort (crowding), etc. Information systems can provide timely information regarding many of these attributes [9, 10].

Electronic Fare Payment technologies forego cash and token payment with the aim of reducing the operating costs of fare collection systems, increasing safety and security on the vehicle, improving data collection, and increasing customer convenience [11, 12]. There are several electronic fare payment technologies, including magnetic stripe cards, and smart cards. Electronic fare payment technologies can have significant impacts on transit operations. The most obvious of the potential impacts on operations occur at the bus stop, where passengers board and alight from the vehicle. Depending on the type of electronic fare payment technology, considerable gains can be realized in terms of lower dwell times at stops through increased transaction speeds. Contact card technologies, where the card is physically swiped through a card reader, and contactless card technologies, where the card and card reader communicate without physical contact but rather via an electromagnetic signal, affect passenger boarding rates differently. Boarding rates increase to a greater extent with contactless card technologies.

Transportation Demand Management is the application of technology to alter the usage patterns of the transportation network, with an emphasis on encouraging users to travel by transit. There is a broad range of technologies designed to better coordinate various transit services, and provide forums for organized carpooling and carsharing. In general, approaches to managing transportation demand aim at increasing the number of high occupancy vehicles in congested transportation networks, promote travel in off-peak hours, and implementing transit incentive programs. Examples include dynamic ridesharing and automated service coordination [13].

Simulation-Based Modeling of APTS

Overview

From the previous discussion, it is clear that evolving information, communications, and sensor technologies and innovative transit operations control strategies are becoming critical elements of viable, competitive public transit systems. APTS, through a variety of data collection and communication capabilities, support improved operations planning and real-time transit operations management. APTS, for example, provide valuable input to planning applications that may lead to better transit system design (e.g., improved scheduling and route planning). APTS also enable a variety of real-time operational strategies (e.g., holding and dispatching) that aim at schedule maintenance and schedule restoration (after major disturbances). Additionally, APTS allow the sharing of real-time performance information with travelers to influence demand and improve passenger level of service.

As innovative technological solutions are integrated with transit services and becoming more common, it is important to have appropriate tools for evaluating and refining the corresponding operating strategies prior to deployment. Because of the complexity of the system, both from the supply and demand sides, simulation is an appropriate tool to evaluate, refine, and design APTS strategies. Simulation allows the representation of the dynamic aspects of transit operations as well as capturing of the stochastic behavior of the system. Hence, simulation enables representation of complex

interactions between the network components: general traffic, transit vehicles and passengers, and comparison of various scenarios and alternatives under realistic and consistent conditions.

In the context of general traffic operations, simulation models have been developed and used for evaluation and design since early on [14]. Traffic simulation models, based on their level of detail, are characterized as macroscopic, mesoscopic, or microscopic. Macroscopic models use a fluid approximation to capture traffic dynamics with a continuous representation of traffic flows [15, 16]. Mesoscopic models represent individual vehicles (which have travel behavior associated with them, e.g., route choice) [17–19]. However, the modeling of traffic dynamics is rather aggregate through speed-density relationships and queuing theory considerations. Microscopic models represent individual vehicles which in addition to travel behavior also have driving behavior. The network is represented in detail, and vehicles make acceleration/deceleration and lane-changing decisions based on traffic conditions, information, and overall travel plans [20, 21]. Hybrid simulation models have also been developed that represent different parts of the network and the associated operations at different levels of details. They combine micrsoscopic simulation at small areas of interest, while the remaining network is represented at a mesoscopic level of detail [22].

Transit simulation has not been developed at the same pace as pure traffic simulation models. Although simulation models can have many advantages for public transportation research and applications, comprehensive transit simulation models are still at an early stage of development. An extensive review of 32 microscopic traffic simulation models report that only 52% represent public transportation at all, 42% model transit priority, and only 6% model transit traveler information systems. At the same time, the majority of users they interviewed were interested in large-scale applications at the urban or regional context, and that these users ranked modeling of public transportation the second most important capability in traffic simulation models [23]. Another review of a representative group of microscopic simulation models concluded that a detailed representation of bus operations and the interactions between buses and other vehicles has been largely ignored or unrealistically simplified [24].

In the context of microscopic simulation models, most of the early advances related to transit systems have focused on implementation of transit signal priority [25–28] or operations of bus stops [24, 26, 29]. For example, in [26], the microscopic simulation model DRACULA was enhanced, mostly from the traffic point of view. The transit modeling was limited, and it did not include the representation of schedules (arrival and departure times at each stop). Passenger arrival rate was drawn from a normal distribution with a stop-specific average value and fixed variance. The dwell time was a function of the number of boarding passengers only. Targeted applications included the evaluation of roadside vs. bay stops, reserved bus lanes vs. guide ways (special ways for guided buses), and bus signal priority.

Recently, several microscopic traffic simulation models have significantly enhanced or extended their transit capabilities, indicating a shift away from traditional, simplistic bus transit modeling and an increased emphasis on realistic bus transit operations simulation. The microscopic traffic simulation model MITSIMLab was systematically extended to represent in detail APTS operations [30]. Earlier work with DRACULA was extended by integrating a transportation planning tool [31, 32]. The simulation includes supply and demand submodels that interact according to a learning algorithm, where the demand (in terms of drivers' route choice) for each day is affected by the cost experienced in the preceding day. The simulation is based on two loops: external (day-to-day) iterations of the demand loop and internal (within-day) iterations of the supply loop.

Similarly, commercial packages such as Transmodeler [33] and VISSIM [34] have added extensive transit simulation capabilities. A number of more specialized systems have also been built on top of available commercial traffic simulation tools. For example, as Bus Rapid Transit (BRT) systems gain in popularity, simulation models of their operations have also appeared in the literature [35]. SmartBRT, a microscopic simulation model for evaluating BRT performance, is built on top of PARAMICS [36]. PARAMICS is a microscopic traffic simulation model [37]. The level of transit integration is rather low since the SmartBRT entities, including bus stops and passengers, do not interact directly with corresponding

PARAMICS entities. This can create considerable complications and inaccuracies in transit modeling and is indicative of the difficulties in integrating successfully transit capabilities on top of existing tools. The model has the capability to represent bus signal priority, various fare collection mechanisms, and detailed dwell-time functions.

MISTRANSIT (Microscopic Simulation Transit) is a PARAMICS API for modeling transit operations [38, 39]. In general, the movement of the buses is run by PARAMICS, while MISTRANSIT operates control strategies and collects transit-related measures of performance. Detailed representation of dwell times at stops as a function of vehicle design parameters, and boarding and alighting passengers are included. Demand is represented through origin–destination flows between stops resulting to individual passengers with attributes, such as stop arrival time, and transfer parameters. MISTRANSIT was used to evaluate holding strategies, operations at bus stops nearby traffic signals, bus signal priority, and capacity of busways with skip–stop operations and interchanges between various public transportation components.

MILATRAS is another API that adds dynamic transit assignment capabilities to PARAMICS [40–42]. It aims at analyzing transit system performance and level of service under real-time information, as well as evaluation of BRT and LRT systems. Given that the underlying platform is a microscopic simulation model, MILATRAS is suited for the analysis of medium-size networks with medium to low frequencies. The model adds dynamic representation of individual passengers and their learning process as they adjust their behavior in response to changes in transit system's performance. The transit path choice problem is modeled as a Markov decision process with each path decision (departure time, boarding and alighting decisions) expressed as a state-action pair. While the overall model does not seek an equilibrium solution, the Markov decision process fulfills the conditions for convergence to a unique and optimal solution (in terms of passenger state-action choices).

Microscopic models are limited when applied to large-scale applications because of the level of detail and extensive computational effort they require. In contrast, mesoscopic simulation models, which represent individual vehicles but avoid detailed modeling of their second-by-second movement, are more appropriate for system-wide evaluation of transit operations and APTS, as they are for general traffic. Research in this area is also limited, especially with respect to APTS applications with large-scale networks [43].

However, activity has recently increased with research focusing on both representation of APTS in mesoscopic simulation models and development of demand models that capture transit-related travel behavior. In contrast to microscopic models, mesoscopic models have a greater need for detailed representation of passenger demand. In this respect, dynamic transit assignment capabilities are an important feature of mesoscopic transit models. In order to evaluate the long-term effects of bus signal priority strategies on drivers' route choice and modal shift, a simulation-based dynamic traffic assignment model within DYNASMART was developed [44]. As a mesoscopic traffic model, DYNASMART represents individual vehicles and uses speed-density relationships to capture traffic dynamics [18]. Transit vehicles are generated deterministically, and dwell times are not calculated explicitly but taken as a fixed delay on the link capacity. Passengers are generated according to time-dependent origin–destination zone demands. Passengers have individual preferences and characteristics that impact their behavior.

A comprehensive transit modeling framework was proposed in [45]. The framework uses a multi-agent approach to transit simulation, focusing on improving the representation of travelers' behavior. The public transportation system consists of three components: passenger behavior, road traffic dynamics, and specific bus-network operations, which include the interactions between the buses, passengers, and road traffic. The network representation is multimodal including pedestrian, road, and bus networks. The multi-agent approach considers the roles that each agent plays: a bus plays two roles simultaneously (vehicle and transportation service), while a traveler plays two roles alternately (as a pedestrian and as a bus passenger). While the vehicles' schedules and travelers' routes are predetermined, their progression is determined by the interaction between the three components of the system. The simulation implementation uses a hybrid approach, where buses and travelers are simulated at a microscopic level of detail and

remaining vehicles are simulated at a macroscopic level of detail.

Another comprehensive framework for mesoscopic transit simulation is BUSMezzo [46, 47], capable of modeling transit operations, and evaluating and designing APTS at the network level. The transit simulation model is fully integrated within the platform of Mezzo, a mesoscopic traffic simulation model [48]. Mezzo is an event-based simulator and is designed with hybrid capabilities (to interface with microscopic models).

General Requirements for Effective Transit Simulation

In order to simulate APTS applications, it is necessary to represent bus transit operations at a level of detail that supports the operational characteristics of the technology or system of interest. For example, AVL systems that monitor bus performance and determine holding and dispatching solutions to schedule deviation problems cannot be simulated in a model that does not represent explicitly bus schedules. Figure 1 summarizes various APTS technologies and the implications they have on bus transit operations and their representation in a simulation framework. In general, APTS

- Enable a variety of real-time operational strategies (e.g., holding and dispatching) that directly affect transit vehicle movements
- Provide valuable input to planning applications that lead to better transit system design (e.g., improved scheduling and route planning)
- Allow the sharing of real-time performance information with travelers to influence demand and improve passenger level of service (e.g., route choice)

In order to simulate APTS applications, the simulation model should be based on a detailed representation of bus transit operations. Bus operations are subject to a number of incidental and controlling forces, including service schedule design, passenger demand, and dispatcher control and intervention. A simulator capable of capturing the behavior of these interacting components should have the following elements:

1. *Transit Supply* representation at the appropriate level of detail. Transit supply refers broadly to the system level components of bus transit operations that are generally under the control of the transit service provider. The transit supply includes the transit network, schedules, and fleet assignments. It also includes the vehicle movements and interactions with the remaining traffic, as well as the representation of APTS. APTS representation is crucial and includes surveillance and monitoring systems that generate and distribute real-time information, the application of that data to real-time control strategies, etc.
2. *Demand representation.* Transit demand refers to the passengers and their behavior with regard to use of the system, including en route and pre-trip decisions, such as route choice, as well as behavior at bus stops and transfer points.
3. *Measures of effectiveness* (*MOE*). MOEs include the indicators, levels of service, and other measures that are used to evaluate the performance of a transit system or an APTS strategy.

The model requirements may be incorporated into a simulation model by providing system variables and parameters as input to the model and/or modeling internally the effects of APTS on system variables. Some transit system variables, such as routes, schedules and passenger demand, are strongly influenced by operations planning or passenger trip planning applications and do not generally vary during the course of a simulation period. These variables are typically represented as static inputs to the model. APTS that interact with real-time operations, on the other hand, should be represented using models that capture interactions between:

- Buses and other modes
- Buses and passengers
- Buses and field-installed control devices
- Bus operators and the operations control center
- Passengers and traveler information systems

Microscopic Transit Simulation Example: MITSIMLab

Microscopic simulation models are very detailed and appropriate for evaluation of APTS strategies at the operational level, including the detailed representation of various design aspects and parameters. MITSIMLab

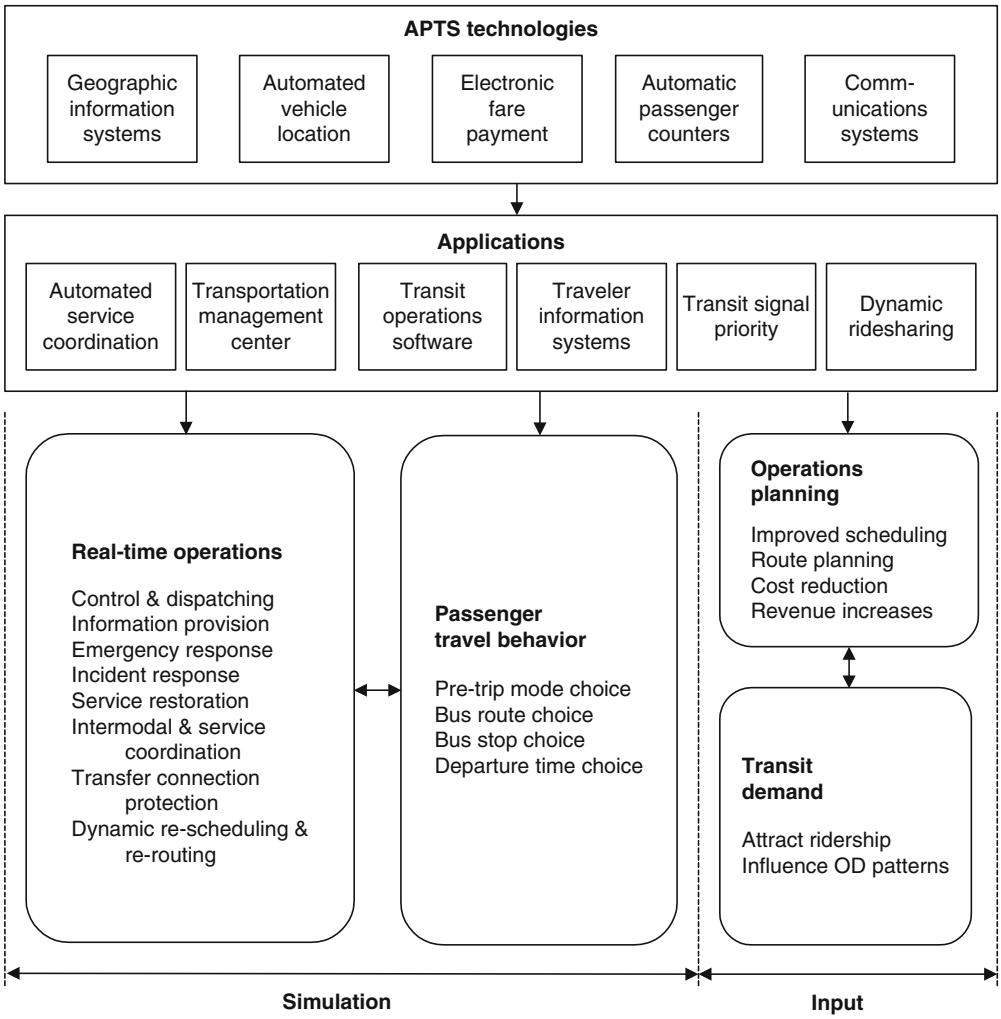

Advanced Public Transport Systems, Simulation-Based Evaluation. Figure 1
APTS impacts on transit operations and implications for simulation (source: [30])

is an example of a general microscopic traffic simulation laboratory that models APTS in detail [30].

Transit System Simulation

MITSIMLab was originally developed for the design and evaluation of advanced traffic management systems (ATMS) and advanced traveler information systems (ATIS) [49, 50]. It is based on sophisticated behavioral models, including driving behavior and travel behavior (e.g., route choice), that capture the complex decisions that drivers make before departing and en route to their destination. MITSIMLab has a modular structure, which facilitates the addition of new functionality to the model.

The objectives of the overall bus transit model are to simulate, at a high level of accuracy and detail, the continuous and complex interactions between vehicles of various types, surveillance technologies, traffic management strategies and control, and information dissemination devices in the network. The modular framework of MITSIMLab, enhanced with bus transit simulation, is illustrated in Fig. 2 with its two main components: MITSIM and TMS.

MITSIM represents the physical road network and simulates the movements of individual vehicles of all

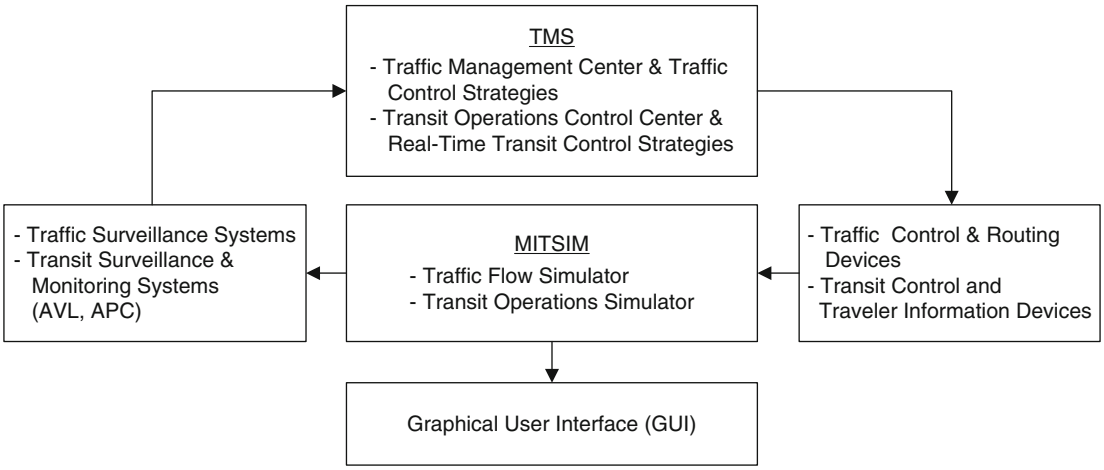

Advanced Public Transport Systems, Simulation-Based Evaluation. Figure 2
Bus transit and APTS modeling framework (source: [30])

types through the network. As such, MITSIM represents the physical portions of the transit network (e.g., bus stops and bus lanes) and simulates the movements of transit vehicles and the interactions between transit and non-transit vehicles. MITSIM requires detailed input describing the transit and traffic network, bus operations, and travel demand (transit and car).

Transit Supply Representation The components of the transit system (transit network, schedule design, and fleet assignment) are generally considered to be static information, provided as input. A detailed representation of routes and schedules is used such that transit and traffic operations in the simulated network are sensitive to the variation in the route and schedule inputs. The transit system representation is based on the following inputs: network, vehicle movements, transit surveillance and monitoring, and transit operations control center.

Transit Network. The transit network representation describes the elements of a transit network, including bus stops and road segments that are used by transit routes. Routes are defined as sequence of links that make up the path and a list of bus stops along the path. Additionally, the transit network representation supports the simulation of deadheading trips, trips between depots and terminals, and other vehicle movements.

- *Schedule Definition.* The schedule definition input describes trips on a route and their timing. When the schedule definition input is read, trips are created. Trips have a single assigned route and a series of scheduled arrival times at the stops or time points along that route. The representation of the schedule is flexible to allow the simulation of different types of routes (e.g., high frequency, express, etc.).
- *Run Definition.* The run definition input specifies the series of trips to which a bus may be assigned. When the run definition file is read, runs are created as a sequence of trips to which the bus is assigned. The representation of runs is generic to allow the simulation of interline, deadheading, and other nonrevenue trips.
- *Fleet Assignment.* The bus assignment input defines the run to which each bus in the fleet is assigned, the type of bus (e.g., articulated), and the departure rate, or time, at which buses enter the network to begin their assignments.

Transit vehicle movements. A set of models capture bus operator behavior which may be different than other drivers in the network. For example, bus operator travel behavior is a function of the route and schedule input rather than merely an origin and a destination. Similarly, bus operator driving behavior includes maneuvers and decision-making processes that are unique to bus operators. Bus operators may accelerate,

decelerate, change lanes, and perform other maneuvers in order to arrive at a bus stop, reenter the traffic stream from a bus stop, and achieve a variety of other objectives that do not pertain to other drivers. Furthermore, other drivers may change their behavior in the presence of buses. Some of the more important elements of vehicle movement and interactions that are modeled include:

- *Behavior between stops.* Operator behavior between stops refers to driving behavior that controls the vehicle's trajectory from one stop to the next. Some of the tasks of bus operators between stops include mandatory lane changing to arrive at bus stops, discretionary lane changing when the bus is far from the downstream stop, and lane choice when bus lanes are present. Furthermore, some bus operator characteristics capture the fact that bus operators generally know their routes very well and are familiar with the network.
- *Behavior approaching stops.* This pertains to both car drivers and bus drivers. The tendency of private auto drivers to overtake buses when traveling behind a bus in a lane that contains stops downstream as an important element of general driving behavior near stops was reported in [24]. It is postulated that drivers anticipate the bus' eventual deceleration to a stop to serve passengers and thus will change lanes or "squeeze" around the bus in the same lane in order to pass. This suggests that general car-following acceleration models do not capture the interactions between buses and other modes correctly. Accordingly, in MITSIMLab, drivers have a high probability of changing lanes when traveling behind a bus in a lane that contains bus stops downstream. That probability increases when the bus is actively decelerating to pull into a stop.
- *Behavior at Stops.* Behavior at stops deals mostly with dwell time, the time the bus operator spends stopped with the doors closed, the time the operator takes to open and close the doors, and the time it takes to serve passengers while the doors are open. The most common dwell-time models assume dwell time to be a linear function of the number of boarding and alighting passengers. A wide variety of dwell-time models have been proposed in the literature, including models that account for fare collection type, bus type (e.g., low-floor, number of doors), and other factors [51–53]. The default dwell-time model in MITSIMLab is the one suggested in [53], the Transit Capacity and Quality of Service Manual (TCQSM).

  $$T = \gamma + \alpha A + \beta B + \varepsilon,$$

  where A is the number of alighting passengers, B is the number of boarding passengers, and ε is a random term. The values of parameters α, β, and γ depend on bus type and design, fare payment strategy, and passenger characteristics, etc. A crowding factor may also be added when there are standing passengers on the bus [52].
- *Behavior departing from stops.* The critical bus operator maneuver near wayside bus stops is the departure from the stop. When a steady traffic stream occupies the general traffic lane into which the bus must enter, the operator must locate a gap into which it may accelerate from a standstill. General lane-changing models might not capture this behavior realistically. In most lane-changing models, the acceptable gap into which the subject vehicle will merge is a function of its position relative to the lead and lag vehicles and its speed relative to the lag vehicle in the target lane. For a bus departing from a stop, where its speed is zero, such a lane-changing model may not be adequate and could lead to unrealistic delays. Specially adjusted gap acceptance models are used to capture this behavior.

Traffic surveillance and monitoring. The systems in place to collect information on the status of the transit operations are simulated in detail (to the level of functional characteristics, e.g., measurement errors). Surveillance is a generic term that refers to various detection and sensing technologies located in the transportation network or onboard vehicles. Some APTS surveillance technologies include automatic vehicle location (AVL) and automatic passenger counters (APC). The communication between MITSIM and TMS is used to mimic the transmission of vehicle location and passenger load information between vehicles (MITSIM) and the transit operations control center or field-installed devices (Fig. 2).

There are three issues related to real-time bus transit surveillance data that are taken into consideration: ownership, storage, and distribution. *Ownership* refers to the entity (e.g., bus) that has possession of the data. For example, to emulate APC technologies, buses store passenger load information as passengers board and alight, and the user may specify input parameters to capture the random error in APC counts. *Storage* refers to the length of time an entity keeps the data before purging it, deleting it, or sending it to another entity. For instance, buses keep track only of their most current schedule information, which is updated each time they arrive at a stop. When a bus arrives at a sensor upstream of a signal equipped for priority, the sensor collects the schedule adherence information and relays it to the signal controller in TMS to determine whether priority should be granted. Finally, data *distribution* deals with when and between which entities the information is shared. If bus load and location information is collected periodically, as through AVL systems, then this information is reported to TMS according to the system logic. Through an accurate representation of data ownership, storage, and distribution, MITSIMLab is able to represent any underlying AVL or other bus surveillance system.

Transit operations control (TOC) center activities. The operations control strategies as well as decentralized field-deployed strategies are simulated in TMS. TMS mimics the logic of the strategy under evaluation, and may use real-time traffic and transit data from the surveillance system as input to that logic. As a TOC simulator, TMS handles incoming transit surveillance data and executes APTS operations that take place in a TOC.

Device-based control strategies, such as signal priority, are also simulated. The information regarding approaching buses received from the surveillance system is used to trigger the corresponding strategy which calculates appropriate actions and sends the signal timing data to the signal controller in TMS. TOC-based strategies, on the other hand, can be simulated by direct control of vehicle movements. For instance, stop-based control strategies, like holding of a bus if it is ahead of schedule, are simulated by placing conditions on bus departures from a stop. APTS control strategies can vary widely in design and implementation from agency to agency and from application to application. The modular structure of the simulation model facilitates the testing of a large number of control strategies.

Demand Representation The representation of the passenger demand is an important element of a simulation model. Passenger demand in MITSIMLab is modeled at two levels of detail (in increasing order of data requirements):

- Dwell times are randomly generated independently for each stop according to probabilistic distributions. However, such a simplified representation of demand, although efficient in terms of input requirements, ignores the impact that dwell times at one stop may have on the headway and, hence, dwell times at downstream stops.
- Arrival rates and alighting rates (e.g., as a percentage of the bus load) at stops. The model assumes that passengers arrive according to some probabilistic distribution and generates randomly the number of passengers waiting to board the incoming bus based on the actual headway from the previous bus. Likewise, the percentage of the bus load alighting at a stop determines the number of alighting passengers. In this representation, passengers are generated in aggregate and have no identifying characteristics, origins, or destinations.

For the last representation of demand, it is important to model the way passengers arrive at bus stops. Three categories of transit passengers have been reported in the literature: those who arrive coincidentally with the bus and thus have no waiting time, those who are familiar with the schedule and arrive close to the vehicle arrival time, and those who arrive randomly [54]. The fraction of the passengers in each category depends on the frequency of service. For example, for high-frequency routes, it is reasonable to assume that passengers arrive randomly. The model uses an aggregate representation of demand with time-dependent arrival rates. The default arrival model assumes that passenger arrivals have a Poisson distribution:

$$P[B(t, t+T) = k] = \frac{(\lambda(t)T)^k e^{-\lambda(t)T}}{k!}$$

where $P[B(t, t+T) = k]$ is the probability that k passengers arrive in the interval of length T and $\gamma(T)$

is the average arrival rate during the corresponding interval.

Measures of Effectiveness An important requirement for any transit simulation model is the generation of appropriate measures of effectiveness (MOEs). In general, simulation allows the collection of a considerable amount of output data, including vehicle trajectories, sensor readings, and segment and link statistics. MITSIMLab collects detailed information (e.g., passenger load, speed, mileage) about each bus and at stops (e.g., dwell times, passengers boarding, alighting and left behind) at user-specified intervals during a simulation. From the detailed data, a number of MOEs can be generated to characterize the performance of the system as dictated by the nature of the application. These MOEs are organized around five levels: system, route segment, stop, vehicle, and passenger.

Case Study: Evaluation of Transit Signal Priority

The purpose of this study is to evaluate the effectiveness of transit signal priority using the MITSIMLab laboratory (more information can be found in [30] and [55]). ITS, with the associated advances in sensor technologies, has enabled the development of interesting transit signal priority strategies [56–59]. Traffic signal priority is designed to reduce transit vehicle delays at signalized intersections. Reduced delay at intersections may also reduce overall travel time, aid schedule adherence and headway maintenance, and increase person throughput at the intersection.

Transit signal priority strategies are varied: they can be passive or active, and unconditional or conditional. Passive priority requires no communication between vehicle and controller, and involves the development of a signal timing plan that reduces delay on the transit vehicle's approach. Passive priority can be achieved by allotting more green time to the transit vehicle's approach, coordinating signals to improve progression along a bus corridor. Active signal priority dynamically adjusts the signal timing when the transit vehicle is detected. This is accomplished by extending the green interval in the current phase, terminating the current phase to start an early green interval for the transit vehicle's approach, or by inserting an extra green phase on the vehicle's approach. As such, active priority requires sensors that identify approaching buses. Depending on the implementation, a communications system may also be needed to convey the sensor information to the traffic signal controller. The signal controller uses the information to adjust the timing of the signal plan to favor the movement of the approaching bus.

Active traffic signal priority can be unconditional or conditional. Unconditional strategies give priority to every qualified vehicle that approaches the intersection regardless of the vehicle's schedule or the impacts on the conflicting approaches. Conditional priority grants priority to approaching transit vehicles only if the vehicle meets some predetermined condition(s). In general, the condition for priority depends on the vehicle's current performance. Based on the available information, it can take various forms. For example, in the simplest case, the condition is based on the schedule (i.e., whether the vehicle is ahead of or behind schedule according to the timetable). However, as APTS facilitates the monitoring of the system in greater detail, other, more advanced, conditions can also be envisioned (based for example on the passenger load on the vehicle, headway from preceding bus, or other measurements or combination of criteria). Thus, communications and controller technologies that support conditional signal priority must be able to transmit and manipulate different pieces of data for evaluating priority eligibility.

In this case study, a number of conditional and unconditional signal priority strategies in an urban network in Stockholm, Sweden, are considered. The study network is located at the western end of Södermalm, one of a cluster of islands in inner Stockholm. The simulated time period of interest is the 7:30–8:30 a.m. morning peak hour. The study network is dominated by the Hornstull intersection that joins three major arterials: Liljeholmsbron, Långholmsgatan, and Hornsgatan (Fig. 3). There are six signalized intersections and one signalized pedestrian and bicycle crossing in the network. Three local bus routes and one BRT route operate within the study area. Buses that serve the local bus routes have 15-min headways during the peak periods, and the BRT buses operate at 7.5-min headways. BRT and local buses share all bus stops. The cross-street traffic in the study network is relatively low compared to traffic on the three arterials

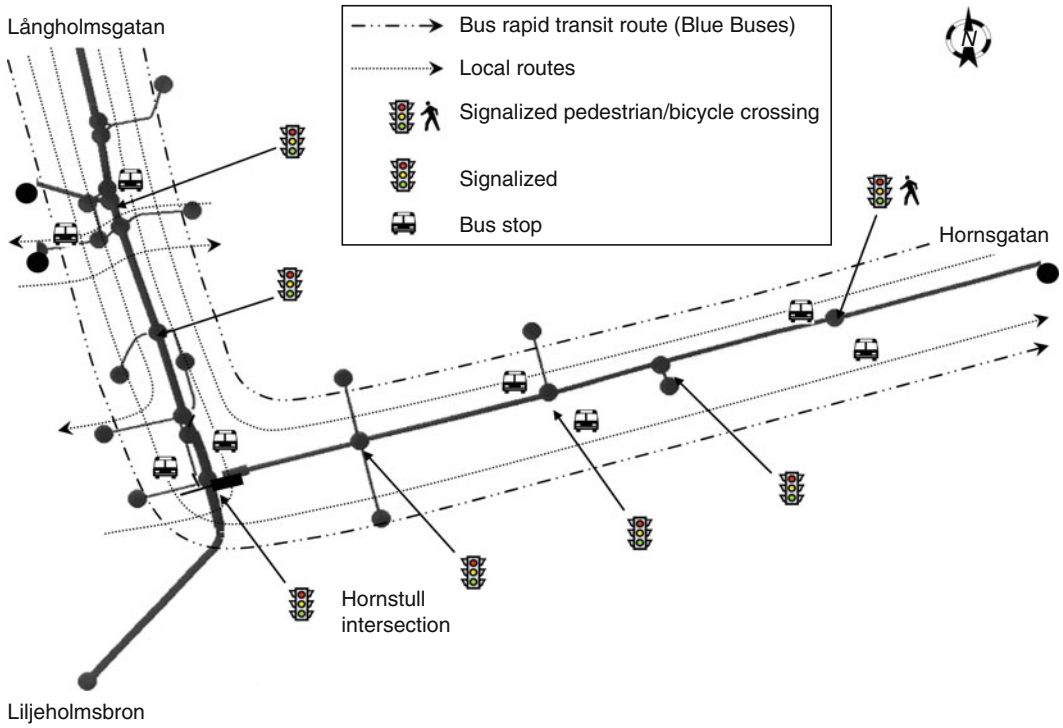

Advanced Public Transport Systems, Simulation-Based Evaluation. Figure 3
Bus routes in the study network (source: [30])

due mostly to street closures that prevent drivers from using alternate routes to avoid congestion.

Only BRT buses are equipped to communicate with sensors to request priority. The objectives of the study are to evaluate the effects of various transit signal priority strategies on transit service and network performance. Four priority implementations are compared in the case study:

- No priority (base case)
- Unconditional priority
- Headway-based conditional priority
- Load-based conditional priority

For headway-based conditional priority, the time headway between the bus requesting priority and the bus before it must be equal to or greater than a minimum headway threshold in order for priority to be granted. A load-based conditional priority strategy gives priority to buses only when the number of the passengers onboard (load) exceeds a threshold. With the use of automated passenger counters (APC), such a strategy is feasible under APTS.

The analysis considers two benefits from each strategy: improved person throughput and reduced transit travel times. However, while it is of interest to assess the extent to which different signal priority strategies achieve these objectives, it is also important to evaluate other impacts, especially to the vehicles entering the network from the side streets. Hence, the measures of effectiveness include average vehicle travel time and total person travel time for all vehicles, BRT buses alone, and side-street vehicles alone. Impact on travel-time variability is also considered.

A sensitivity analysis designed to explore the effects of increased side-street demand is also conducted. Furthermore, given that APC technologies may suffer from measurement errors, the impact of such errors on the performance of signal priority was examined.

Vehicle travel time, total person travel time, and travel-time variability results for the priority strategies as well as the base case were collected using the outcome from several independent simulation replications. A priori, it is expected that BRT vehicles should experience greater travel-time savings, while non-priority

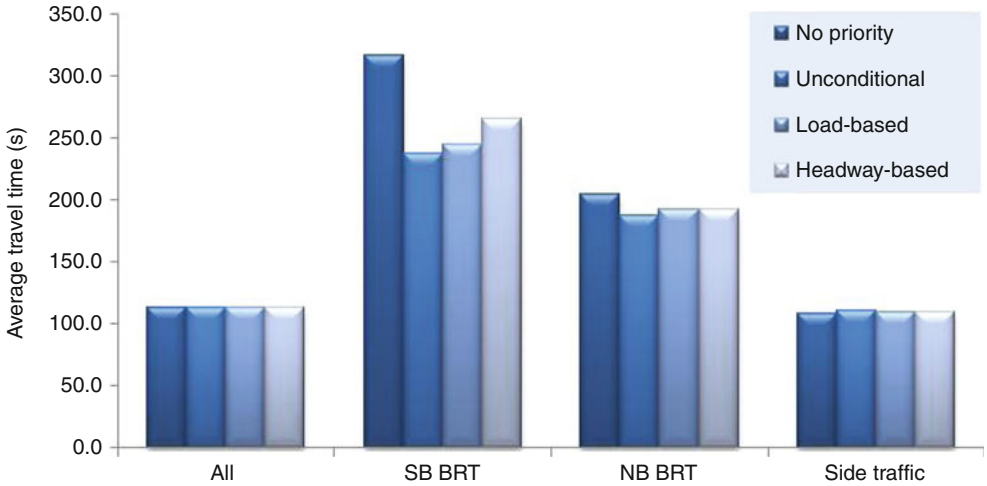

Advanced Public Transport Systems, Simulation-Based Evaluation. Figure 4
Signal priority impact on travel times (source: [55])

movements (i.e., side-street traffic) should experience higher travel times as the conditions for signal priority become less restrictive.

Figure 4 summarizes the main results. Average BRT travel times decrease as the priority conditions become less restrictive, with the lowest average travel times occurring under unconditional priority. Since the demand on the side streets in the study network is very low, the impact on non-transit, non-priority vehicles entering the network from the side origins is not substantial.

Interestingly, the results also indicate that conditional priority strategies can achieve similar benefits as the unconditional priority strategy without granting priority quite as often. Under conditional priority about 70% of the buses receive priority. This tends to indicate that conditional priority strategies also have less impacts on the side traffic. However, due to the low demand on the side streets in this case, the change in average travel time for side-street vehicles for different priority strategies is too low to draw general conclusions about the trade-off between transit travel-time savings and side-street travel-time penalties.

Total person travel time is the total time spent by all commuters in the system. The results show that under conditional priority, particularly load-based conditional priority, the difference between conditional and unconditional priorities is very small (compared to the difference with respect to average travel time per vehicle). For example, the total passenger travel time for the load-based conditional priority is only 1.5% higher than the unconditional priority case.

Travel-time variability is an important measure of performance from the standpoint of traveler level of service. The results from the simulation study indicate that travel-time variability for BRT vehicles was also reduced under signal priority. Furthermore, conditional priority yielded almost similar benefits in that regard, as unconditional priority.

A major advantage of simulation is that it allows testing of a large number of different scenarios and facilitates sensitivity analysis with respect various operating and design parameters. In this case study, the transit simulation laboratory is used to evaluate the impact of increased demand levels as well as the impact of the accuracy of the APC equipment used to count boarding and alighting passengers.

Effective signal priority strategies should balance the benefits for the transit vehicles with the negative impacts on the side traffic. Since the side-street volumes in the study network are not substantial to show marked changes in travel time for non-priority vehicles, three priority strategies (no priority, unconditional priority, load-based conditional priority) were also evaluated assuming a 40% increase in the demand entering the network from the side arterial Liljeholmsbron. Figure 5 summarizes the results with respect to average travel times. Load-based conditional priority strategies yield

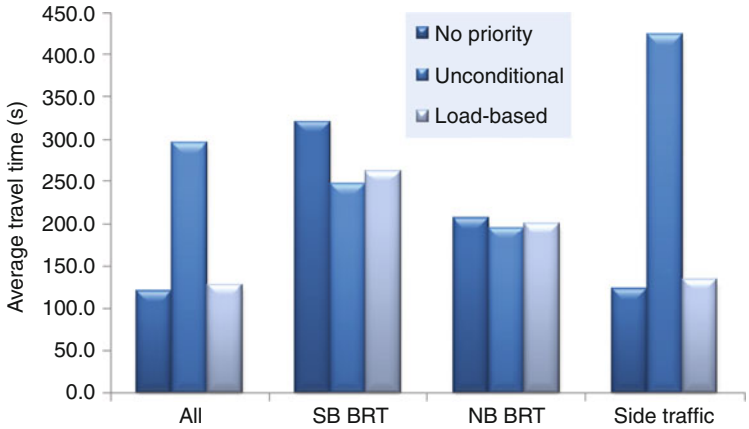

Advanced Public Transport Systems, Simulation-Based Evaluation. Figure 5
Signal priority impact on travel times with increased side-street demand (source: [55])

similar benefits as unconditional priority. More importantly, the improvements in transit vehicle performance under conditional priority can be achieved with considerably less adverse impact on the side-street traffic. The results are consistent with those reported in a field study of schedule-based conditional priority in Eindhoven, the Netherlands [56]. The study, using data collected in the field, showed increases in side-street travel times of 100–300% at some intersections under unconditional priority, while the schedule-based conditional priority strategy produced significant reduction in transit travel times with only a minor impact on non-priority vehicles.

Automatic passenger counters (APC) may have measurement errors. For example, studies indicate that infrared APC systems on buses in Oregon have the tendency to overestimate passenger load, citing errors as high as 10% [60]. Thus, another scenario is simulated to determine whether passenger loads measured by APC with error might affect the performance of load-based conditional priority. Assuming that the APC count varies between 5% below and 15% above the true load, the rate of priority (% of buses receiving priority) increases from 66% (with no error) to 68% (with error). BRT buses experience travel times which on the average are slightly lower than with the same load-based strategy assuming no APC error. Furthermore, there was no effect on the side-street travel times. Hence, the strategy appears robust even under the assumed measurement errors. This analysis illustrates another useful application of simulation. A simulation model, at the level of detail described in this paper, can be used to refine APTS strategies by explicitly modeling all aspects and characteristics of the technologies involved (including operating characteristics, such as measurements errors).

Mesoscopic Transit Simulation Example: BusMEZZO

Mesoscopic transit simulation models are more appropriate for the analysis of the operations of transit systems at the network level. BusMEZZO is an example of such a model. The transit simulation component is directly integrated within the platform of Mezzo, a mesoscopic traffic simulation model [48]. Mezzo is an event-based simulator, which models vehicles individually. Links are divided into two parts: a running part, which contains vehicles that are not delayed by the downstream capacity limit, and a queuing part, which extends upstream from the end of the link when capacity is exceeded. The boundaries between the running and queuing parts are dynamic and depend on the extent of the queue. Vehicles have travel behavior and make route-choice decisions based on prior experience, available traffic information, etc.

Simulating Transit Operations

Mesoscopic transit simulation requires similar functionalities as microscopic models. However, the level

of detail in the representation of some components, especially on the supply side, is lower.

Supply Representation The supply representation includes the transit network, the movement of vehicles and interactions with other traffic, the representation of the surveillance system, and the functionality of the transit operations control center.

Transit network, schedules, and runs are defined in a similar fashion as in the microscopic model presented in the previous section. However, vehicle movements and interactions are represented in simplified way. Buses enter the network according to the provided schedule, interact with the car traffic, and move according to prevailing conditions on the link (based on speed-density relationships). They stop at stops according to a dwell time that is calculated using models similar to the ones in microscopic simulation. Buses depart from stops according to the calculated dwell time or other considerations, such as timetable constraints for the specific route, or real-time control strategies that are implemented to improve the reliability of the route. Upon arrival at the end terminal, a bus either enters the next trip in its schedule or exits the network. With this process, delays encountered by buses on one trip influence its ability to perform the next trip on time. Hence, the model captures the propagation of delays along the route and is capable of producing the occurrence of bunching.

An important aspect in modeling transit supply is the representation of APTS both in terms of the sensor technology in place to collect data and the operating strategies. As in micrsoscopic simulation, the model keeps track of data routinely collected by the APTS in place (AVL, APC, etc.). This data is processed in combination with schedule information preceding and following vehicles' data in order to generate information about the bus performance (e.g., schedule adherence and actual headways). This information, in turn, is used to trigger real-time strategies in order to improve operations. The model is capable of simulating a wide range of transit operations control strategies so that they can be evaluated and refined.

Strategies that are used to improve transit service reliability are of particular importance. Service reliability is often connected to headway variability. Headway variability impacts a number of important measures of level of service for the passengers, such as waiting times, uncertainty with respect to arrival times at destinations, and passenger loads. Reliability also impacts utilization of resources. In this context, the model can be used to both assess the causes of unreliable service and develop strategies for effectively dealing with it. Service reliability has been the subject of many studies, including the comprehensive work reported in [61, 62]. A number of studies also exist that investigate the manifestation of service reliability using data collected through APTS technologies (e.g., [63–65]).

Real-time operations control has always been used as means to improve service reliability. Figure 6 illustrates a taxonomy of the various types of real-time control strategies [66]. A strategy may be applied at the station, route/intersection, or at the fleet level. Station-based strategies are either holding (vehicles held at stops for service restoration) or skipping strategies (where stations may be temporarily skipped during a particular trip). Skipping stops may take several forms, such as deadheading or expressing.

Holding is a particularly popular strategy because of the relative ease of implementation. A number of theoretical models have appeared that cover various aspects of the problem and apply them to both real and idealized scenarios. Originally, most of the work focused on simple network configurations with limiting assumptions and simplifications to make the problem tractable. Early research attempted to provide an understanding of the impact of holding strategies on passenger waiting times, with classic papers such as [67–69] leading the way in this direction. Recent work in the area includes [66, 70–73] and focuses on both evaluation of impacts and development of methods to design optimal strategies. Real-time control of buses for schedule coordination at terminals is studied in [74].

Because of the difficulties in obtaining analytical solutions to the problem, many studies relay on simulation to evaluate the developed strategies. For example, a simulation model of a single direction bus route was used to test several strategies, including holding, skipping, loading (but not unloading) passengers, and signal priority in [74]. Similarly, in [75], simulation was used to evaluate different real-time control strategies. BusMEZZO provides a platform where existing

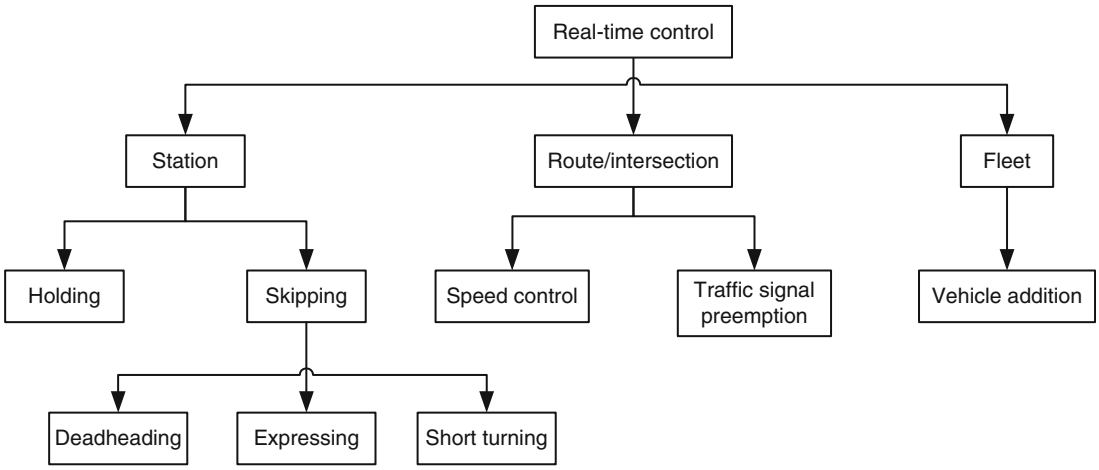

Advanced Public Transport Systems, Simulation-Based Evaluation. Figure 6
Real-time operations control strategies (source: [66])

strategies can be evaluated, and new approaches developed.

Demand Representation Passenger demand is modeled at various levels of detail (more information can be found in [76]):

- Arrival and alighting rates as discussed in section "Transit System Simulation."
- Passenger origin–destination flows and related travel choices and travel behavior. The model can simulate individual passengers with attributes (e.g., age, income), origins, and destinations (assuming that he required information is available). A demand simulator component has been developed to deal with the diverse requirements of transit demand representation. Passengers are explicitly represented. Their behavior is captured dynamically as they make station and route (bus line) decisions based on experience, real-time transit information, and other service attributes. As mentioned in the previous section, in the context of mesoscopic models, transit assignment functionally is an important requirement. A dynamic transit assignment component is implemented based on two submodels: choice-set generation and path choice process. The generation of the choice set aims at reproducing the set of alternatives considered by passengers. The choice-set generation model is based on the transit network attributes – transit routes, timetables, transferring stops and links, as well as access and egress links. However, in order to narrow the set of all available paths to a reasonable choice set, a number of filtering rules are used which apply logical and behavioral constraints.

Once the set of alternative paths has been generated, the path choice model determines how passengers choose between their alternatives. The path choice model takes into account traveler preferences and decision rules. A dynamic representation of the transit system facilitates the explicit modeling of capacity constraints. Moreover, passenger travel experiences and real-time information are important inputs to the path choice decisions. The dynamic assignment model considers the path choice as a decision process that consists of a sequence of dependent decisions. In general, there are two distinctive types of decisions: (a) stop-related decisions (origin stop choice, transfer stop choice, and destination stop choice) and (b) route-related decisions (choice among alternative transit routes). A discrete choice framework is used to model the various decisions [77].

Measures of Effectiveness Outputs from the simulation include stop level statistics, such as early and late arrivals, dwell times, numbers of boarding and alighting, bus loads, and travel times between stops. Aggregations at the level of the trip, the vehicle, or the line,

such as schedule adherence, headway and passenger wait time distributions, load profiles, and other level of service measures, are also computed.

Case Study: Evaluation of Real-Time Holding Strategies

The mesoscopic model described in the previous section is used to evaluate holding strategies to improve service reliability of a busy urban route in Tel-Aviv, Israel (for more information see [78]). This high-demand route connects a dense suburb to the CBD. The scheduled headway during the peak period is 8 min, and the average running time is 49 min inbound and 41 min outbound.

The study compares the base case of no holding to two scenarios with holding strategies. In designing holding strategies, the main aspects of interest are the amount of time the bus is held, and the location of the stops (time points) where holding may be applied. In general, holding strategies are either schedule-based or headway-based. Schedule-based strategies apply control in order to ensure that buses run according to the timetable. Headway-based strategies aim at improving service by regulating the headways at stops.

Headway-based control is more appropriate for lines that have very frequent service (since in those cases, according to [54], passengers arrive at the stop randomly and do not plan their arrival according to schedule). Schedule-based strategies are more appropriate for low frequency routes with passengers coordinating their arrival with the schedule. Another important difference between the strategies is the amount of information required for their implementation. Schedule-based strategies require minimum information (a static timetable), while headway-based strategies require real-time information (that may vary depending on the exact nature of the strategy). In general, it is expected that more information should help the system perform better. A comparison between holding control strategies that rely only on local information to APTS-based strategies that incorporate more information was conducted in [75] in the context of coordination at transfer points. Not surprisingly, the study concluded that the best holding control strategy was the one that used all available information, including predicted arrival times of connecting buses, number of transferring passengers, and expected number of boarding passengers at downstream stops.

Schedule-based strategies hold buses that arrive early at a time point until a predefined time from their scheduled departure time is reached. Depending on the available information, more or less sophisticated headway-based control strategies can be implemented. For example, if only information regarding the preceding bus is available, the strategy takes the form of holding a bus until a certain threshold with respect to the scheduled headway is reached. If information is available with respect to both the preceding and following buses, then the holding strategy may take into account the headway with both buses and hold the subject vehicle until headways between them are equal (mean-headway strategy) or until a maximum holding time is reached [79, 80].

Regarding the location of the time points, strategies are typically applied at a subset of stops along a route [81]. Several studies (e.g., [82–85]) suggest that time-point stops should be located at the beginning of a sequence of high-demand stops. In contrast, [72] found that there are no significant benefits from defining time points along bus routes, except the origin terminal.

Following the recommendations in the literature, the design of the holding strategies that were tested had the following characteristics. The time points were located at three stops upstream of a sequence of high-demand stops. The holding time at each time was based on two strategies: a strategy that aims at equalizing the headway (when possible) between the subject bus and the preceding and following buses (mean headway), and a schedule-based holding. Therefore, the two strategies represent two rather opposite cases of information availability: minimum information (timetable) and relative high (arrivals of preceding and following buses at the time point).

Figure 7 illustrates the impact of control using a time-space diagram of the trajectories of three buses, each performing four chained trips. Sloped segments represent running time between stops, and vertical segments indicate dwell times and holding times at time points. Recovery times between trips at both terminals are also shown. Figure 7a illustrates the base case of no control, while Fig. 7b corresponds to the case of mean-headway control. Buses are experiencing

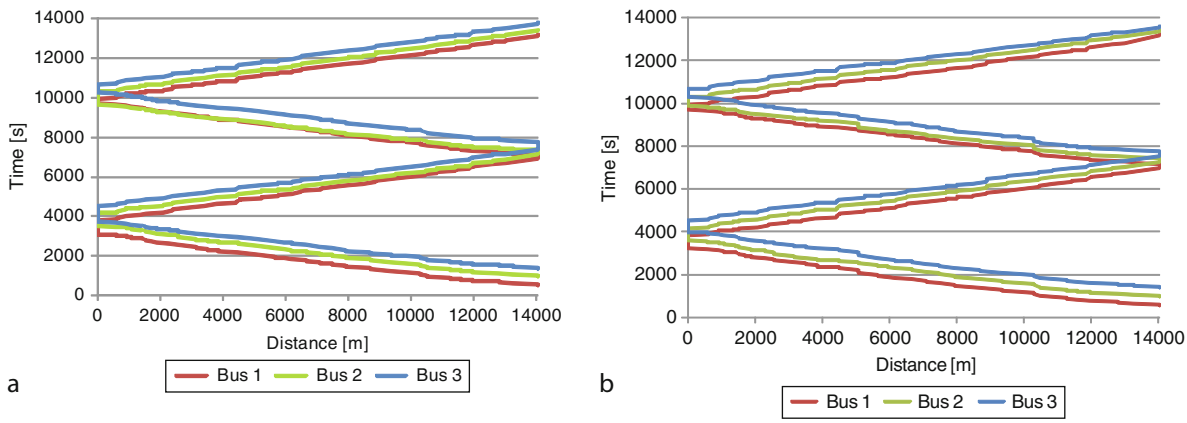

Advanced Public Transport Systems, Simulation-Based Evaluation. Figure 7
Time-space diagram of buses with no control (**a**) and mean-headway control (**b**) (source: [78])

bunching when there is no control, while the holding strategy is effective in preventing this by creating even headways at time points. For example, on the third trip, bus 2 is getting increasingly bunched with bus 1 under (a), a situation that is largely remedied when holding is applied.

At the system level, several measures of performance were calculated for each scenario, including average passenger waiting time, travel-time, and on-time performance. The schedule-based strategy resulted in very small benefits with respect to average waiting time for the passengers. In general, it had practically the same performance as the base case of no control with respect to all measures. The reason for this is that, with the timetable used for the route, only a small number of trips were ahead of schedule, and therefore the schedule-based strategy was used very infrequently. The mean-headway strategy reduced headway variability, as measured by the coefficient of variation, by as much as 30%. The average waiting time deceased by 5%. However, the mean-headway strategy results in service regularity gains at the expense of higher travel times and deterioration of on-time performance.

Future Directions

Transportation systems are highly complex, and researchers, planners, and engineers often use simulation to study their performance, analyze and design possible system improvements, and develop decision support systems to aid with their management. Over the past several years (motivated in part by the introduction of Intelligent Transportation Systems and APTS), transit simulation models have seen a lot of advances. As technology and policy innovations are constantly introduced, the required functionalities of transit simulation models also need to be expanded to satisfy the diverse needs of operations, planning, and policy evaluation. Information technology, for example, has created and will continue to create many opportunities for transit systems. These opportunities are twofold: (a) advances in sensor technologies allow operators to collect a lot of data and information about the system and (b) advances in communications technologies facilitate the dissemination of useful information to passengers, even personalized information on demand. In order to provide the functionality needed to support the new application foci, developments in the context of both microscopic models and mesoscopic models are needed.

On the microscopic side, seamless integration of traffic and transit driving behavior (at the individual vehicle level) needs to be further developed to reliably model APTS at the operational level. On the mesoscopic side, transit simulation needs to be closely integrated with developments in the area of simulation-based dynamic traffic assignment. Integrated, multimodal models that represent demand and supply at a consistent, disaggregate level, and capture the demand–supply interactions are important for the evaluation of future strategies to deal with sustainable

transportation systems. Multimodal models need to be sensitive to changes in the system introduced by policy and technological innovations. In this respect, better integration of demand and supply representations at a consistent level of detail is important and should be organized in modules with the following characteristics: (a) a demand module with disaggregate, dynamic, activity-based representation of the choices of individual travelers; (b) a supply module, with detailed, disaggregate, dynamic modeling of multimodal network performance through vehicle-based traffic simulation; and (c) a demand–supply interactions module with integration between the demand and supply modules through appropriate algorithms.

Integrated, simulation-based, dynamic, and disaggregate models have the potential to provide increased realism in capturing both travel behavior and network performance and so provide considerable flexibility in representing a wide range of systems and predicting their impacts. A number of challenges, both theoretical and practical, need to be resolved before such models become operational. Important challenges include the development of appropriate demand–supply algorithms that are able to predict the resulting behavior of the system, data and approaches for development and estimation of the constituent models, and the systematic validation and calibration of the overall model, and approaches to deal with the computational requirements of such large-scale models (more information about such a disaggregate, dynamic multimodal modeling of transportation systems can be found in [86]).

Bibliography

Primary Literature

1. Shannon RE (1975) Systems simulation: the Art and science. Prentice-Hall, Englewood Cliffs
2. United Nations Population Fund (2010) State of world population 2007. http://www.unfpa.org/swp/2007/english/introduction.html
3. Miles J, Chen K (2004) ITS handbook, 2nd edn. PIARC, Paris
4. Casey RF, Labell LN, Moniz L et al (2000) Advanced public transportation systems – the state of the art: update 2000. U.S. Department of Transportation, Federal Transit Administration (FTA), Washington, DC
5. Hwang M, Kemp J, Lerner-Lam E, Neuerburg N, Okunieff P (2006) Advanced public transportation systems: state of the art update 2006, FTA-NJ-26-7062-06.1. Federal Transit Administration (FTA), Washington, DC
6. Furth P, Hemily B, Muller T, Strahman J (2006) Using archived AVL-APC data to improve transit performance and management, TCRP report 113. Transportation Research Board, Washington, DC
7. Furth P (2000) Data analysis for bus planning and monitoring, TCRP synthesis 34. Transportation Research Board, Washington, DC
8. Smith H, Hemily B, Ivanovic M (2006) Transit signal priority (TSP): a planning and implementation handbook. ITS America and US Department of Transport, Washington, DC
9. Hickman MD, Wilson NHM (1995) Passenger travel time and path choice implications of real-time transit information. Transp Res C 3(4):211–226
10. Nuzzolo A, Russo F, Crisalli U (2001) A doubly dynamic schedule-based assignment model for transit networks. Transp Sci 35(3):268–285
11. Wilson NHM, Zhao J, Rahbee A (2004) The potential impact of automated data collection systems on urban public transport planning. In: Wilson NHM, Nuzzolo A (eds) Schedule-based dynamic transit modeling: theory and applications. Academic, Dordrecht, pp 74–99
12. Vandebona U, Richardson AJ (1985) The effects of fare-collection strategies on transit level of service. Transp Res Rec 1036:79–87
13. Transportation Demand Management User Service (2005) National ITS architecture. US Department of Transportation, Washington, DC. www.iteris.com/itsarch/html/user/usr18.htm
14. Barceló J (ed) (2010) Fundamentals of traffic simulation, vol 145, International series in operations research & management science. Springer, New York
15. Daganzo C (1994) The cell transmission model: a dynamic representation of highway traffic consistent with the hydrodynamic theory. Transp Res B 28(4):269–287
16. Messmer A, Papageorgiou M (1990) METANET: a macroscopic simulation program for motorway networks. Traffic Eng Control 31(9):466–470
17. Ben-Akiva M, Bierlaire M, Burton D, Koutsopoulos HN, Mishalani R (2001) Network state estimation and prediction for real-time transportation management applications. Netw Spat Econ 1(3/4):293–318
18. Ben-Akiva M, Koutsopoulos HN, Antoniou C, Balakrishna R (2010) Traffic simulation with DynaMIT (chap 10). In: Barcelo J (ed) Fundamentals of traffic simulation. Springer, New York
19. Mahmassani HS (2001) Dynamic network traffic assignment and simulation methodology for advanced systems management applications. Netw Spat Econ 1(3/4):267–292
20. Yang Q, Koutsopoulos HN (1996) A microscopic traffic simulator for evaluation of dynamic traffic management systems. Transp Res 4C:113–129
21. Ben-Akiva M, Koutsopoulos HN, Toledo T, Yang Q, Choundhury C, Antoniou C, Balakrishna R (2010) Traffic simulation with MITSIMLab (chap 6). In: Barcelo J (ed) Fundamentals of traffic simulation. Springer, New York

22. Burghout W, Koutsopoulos HN, Andreasson I (2005) Hybrid mesoscopic-microscopic traffic simulation. Transp Res Rec 1934:218–225
23. Algers S, Bernauer E, Boero M, Breheret L, Dougherty M, Fox K, Gabard JF (1997) Review of microsimulation models. In: SMARTEST project deliverable D3, EU, Institute for Transport Studies, University of Leeds, Leeds. Available at: http://www.its.leeds.ac.uk/projects/smartest/deliv3f.html
24. Silva PCM (2001) Modelling interactions between bus operations and traffic flow. Doctoral dissertation, University College London
25. Khasnabis S, Karanti RR, Rudraraju RK (1996) NETSIM-based approach to evaluation of bus preemption strategies. Transp Res Rec 1554:80–89
26. Liu R, Clark S, Montgomery F, Watling D (1999) Microscopic modelling of traffic management measures for guided bus operation. In: Proceedings of eighth world conference on transport research, Antwerp
27. Chang J, Collura J, Dion F, Rakha H (2003) Evaluation of service reliability impacts of traffic signal priority strategies for bus transit. Transp Res Rec 1841:23–31
28. Lee J, Shalaby A, Greenough J, Bowie M, Hung S (2005) Advanced transit signal priority control using on-line microsimulation-based transit prediction model. In: Preprints of the transportation research board 84th annual meeting, Washington, DC
29. Ding Y, Chien S, Zayas A (2001) Simulating bus operations with enhanced corridor simulator. Transp Res Rec 1731:104–111
30. Morgan DJ (2002) A microscopic simulation laboratory for advanced public transport system evaluation. Master thesis, Massachusetts Institute of Technology
31. Liu CL, Pai TW (2006) Methods for path and service planning under route constraints. Int J Comput Appl Technol 25 (1):40–49
32. Liu R, Van Vliet D, Watling D (2006) Microsimulation models incorporating both demand and supply dynamics. Transp Res A 40:125–150, Washington, DC
33. http://www.caliper.com/
34. http://www.ptvag.com/index.php?id=345
35. BRT. http://www.cfte.org/trends/brt.asp
36. Werf JV (2004) SmartBRT: a tool for simulating, visualizing and evaluating bus rapid transit systems. California PATH Research Report, Institute of Transportation Studies, University of California, Berkeley
37. http://www.paramics.com/
38. Cortes CE, Fernandez R, Burgos V (2007) Modeling passengers, buses and stops in traffic microsimulators. The MISTRANSIT approach on the PARAMICS platform. In: Proceedings of the 86th transportation research board annual meeting, Washington, DC
39. Fernandez R, Cortes CE, Burgos V (2010) Microscopic simulation of transit operations: policy studies with the MISTRANSIT application programming interface. Transp Plann Technol 33(2):157–176
40. Wahba M, Shalaby A (2006) A general multi-agent modelling framework for the transit assignment problem – a learning-based approach. In: Innovative internet community systems. Springer, Berlin, pp 276–295
41. Wahba M, Shalaby A (2006) MILATRAS: a microsimulation platform for testing transit-ITS policies and technologies. In: Proceedings of the IEEE ITSC, Canada
42. Wang J, Wahba M, Miller EJ (2010) A comparison of an agent-based transit assignment procedure (MILATRAS) with conventional approaches. In: Proceedings of the 89th transportation research board annual meeting, Washington, DC
43. Boxill SA, Yu L (2000) An evaluation of traffic simulation models for supporting ITS development. Center for Transportation Training and Research, Texas Southern University
44. Abdelghany KF, Abdelghany AF, Mahmassani HS, Abdelfatah AS (2006) Modeling bus priority using intermodal dynamic network assignment-simulation methodology. J Public Transp 9(5):1–22
45. Meignan D, Simonin O, Koukam A (2007) Simulation and evaluation of urban bus-networks using a multiagent approach. Simul Model Pract Theory 15:659–671
46. Cats O, Toledo T, Burghout W, Koutsopoulos HN (2010) Mesoscopic modeling of bus public transportation. In: Proceedings and CD of the 89th transportation research board (TRB) annual meeting, Washington, DC
47. Toledo T, Cats O, Burghout W, Koutsopoulos HN (2010) Mesoscopic simulation for transit operations. Transp Res C 18(6):896–908. doi:10.1016/j.trc.2010.02.008
48. Burghout W (2004) Hybrid microscopic-mesoscopic traffic simulation. Doctoral dissertation, Royal Institute of Technology, Stockholm
49. Yang Q (1997) A simulation laboratory for evaluation of dynamic traffic management systems. Ph.D. thesis, Department of Civil and Environmental Engineering, Massachusetts Institute of Technology
50. Yang Q, Koutsopoulos HN, Ben-Akiva M (2000) A simulation laboratory for evaluating dynamic traffic management systems. Transp Res Rec 1710:122–130
51. Levinson HS (1983) Analyzing transit travel time performance. Transp Res Rec 915:1–6
52. Lin T, Wilson NHM (1992) Dwell time relationships for light rail systems. Transp Res Rec 1361:287–295
53. TCRP Report 100 (2003) Transit capacity and quality of service manual (TCQSM), 2nd edn. Transportation Research Board, Washington, DC
54. Jolliffe JK, Hutchinson TP (1975) A behavioral explanation of the association between Bus and passenger arrivals at a bus stop. Transp Sci 9(3):248–282
55. Morgan D, Koutsopoulos HN, Ben-Akiva M (2003) Simulation-based evaluation of advanced public transportation systems. In: Wilson NHM, Nuzzolo A (eds) Schedule-based dynamic traffic modeling: theory and applications. Series in operations research/computer science interfaces, vol 28, chap 6. Academic, Boston, pp 95–102
56. Furth PG, Muller THJ (2000) Conditional bus priority at signalized intersections: better service quality with less traffic disruption. Transp Res Rec 1731:23–30

57. Chang J, Collura J, Dion F, Rakha H (2003) Evaluation of service reliability impacts of traffic signal priority strategies for bus transit. Transp Res Rec 1841:23–31
58. Kim W, Rilett LR (2005) An improved transit signal priority system for networks with nearside bus stops. Transp Res Rec 1925:205–214
59. Lee J, Shalaby A, Greenough J, Bowie M, Hung S (2005) Advanced transit signal priority control using on-line microsimulation based transit prediction model. Transp Res Rec 1925:185–194
60. Kimpel T, Strathman J (Apr 2002) Automatic passenger counter evaluation: implications for national transit database reporting. http://www.upa.pdx.edu/CUS/PUBS/docs/PR124.pdf
61. Abkowitz M, Slavin H, Waksman R, Englisher L, Wilson N (1978) Transit service reliability. Report UMTA-MA-06-0049-78-1. USDOT Transportation Systems Center, Cambridge
62. Abkowitz M, Tozzi J (1987) Research contributions to managing transit service reliability. Adv Transp J 21:47–65
63. Strathman JG, Dueker KJ, Kimpel T, Gerhart R, Turner K, Taylpr P, Callas S, Griffin D, Hopper J (1999) Automated bus dispatching, operations control and service reliability. Transp Res Rec 1666:28–36, Washington, DC
64. Strathman JG, Kimpel TJ, Dueker KJ, Gerhart RL, Turner K, Griffin D, Callas S (2001) Bus transit operations control: review and experience involving Tri-Met's automated bus dispatching system. In: Transportation Research Board, 80th Annual Meeting, Washington, DC
65. Strathman JG, Kimpel TJ, Dueker KJ, Gerhart RL, Callas S (2002) Evaluation of transit operations: data applications of Tri-Met's automated bus dispatching system. Transportation 29:321–345
66. Eberlein XJ (1995) Real time strategies in transit operations: models and analysis. Ph.D. dissertation, Department of Civil Engineering, MIT
67. Osuna EE, Newell GF (1972) Control strategies for an idealized public transportation system. Transp Sci 6:52–72
68. Barnett A (1974) On controlling randomness in transit operations. Transp Sci 8(2):102–116
69. Barnett A (1978) Control strategies for transport systems with nonlinear waiting costs. Transp Sci 12(2):119–136
70. O'Dell S, Wilson N (1997) Optimal real-time control strategies for rail transit operations during disruption. In: Wilson N (ed) Computer aided transit scheduling, vol 471, Lecture note in economics and mathematical systems. Springer, Berlin, pp 299–323
71. Hickman M (2001) An analytic stochastic model for the transit vehicle holding problem. Transp Sci 35(3):215–237
72. Eberlein XJ, Wilson NHM, Bernstein D (2001) The holding problem with real-time information available. Transp Sci 35(1):1–18
73. Shen S, Wilson NHM (2001) Optimal integrated real-time disruption control model for rail transit systems. In: Voss S, Daduna J (eds) Computer-aided scheduling of public transport, vol 505, Lecture notes in economics and mathematical systems. Springer, Berlin, pp 335–364
74. Koffman D (1978) A simulation study of alternative real-time Bus headway control strategies. Transp Res Rec 663:41–46
75. Dessouky M, Hall R, Zhang L, Singh A (2003) Real-time control of buses for schedule coordination at a terminal. Transp Res A 37:145–164
76. Cats O, Koutsopoulos HN, Burghout W, Toledo T (2011) Effect of real-time transit information on dynamic passenger path choice. Transportation Research Record. J Transp Res B (in press)
77. Ben-Akiva M, Lerman S (1985) Discrete choice analysis. Theory and application to travel demand. MIT Press, Cambridge, MA
78. Cats O, Burghout W, Toledo T, Koutsopoulos HN (2010) Evaluation of real-time holding strategies for improved bus service reliability. Submitted for presentation and publication at the 2010 13th international IEEE conference on intelligent transportation systems (ITSC 10), Madeira Island
79. Koutsopoulos HN, Wang Z (2007) Simulation of urban rail operations. Transp Res Rec 2006:84–91
80. Daganzo CF (2009) A headway-based approach to eliminate bus bunching: systematic analysis and comparisons. Transp Res B 43:913–921
81. Abkowitz M, Lepofsky M (1990) Implementing headway-based reliability control on transit routes. J Transp Eng 116(1):49–63
82. Liu G, Wirasinghe SC (2001) A simulation model of reliable schedule design for a fixed transit route. J Adv Transp 35(2):145–174
83. Abkowitz M, Engelstein I (1984) Methods for maintaining transit service regularity. Transp Res Rec 961:1–8
84. Turnquist MA, Blume SW (1980) Evaluating potential effectiveness of headway control strategies for transit systems. Transp Res Rec 746:25–29, Washington, DC
85. Wirasinghe SC, Liu G (1995) Determination of the number and locations of time points in transit schedule design – case of a single run. Ann Oper Res 60:161–191
86. Ben-Akiva M, Bottom J, Gao S, Koutsopoulos HN, Wen Y (2007) Towards disaaggregate dynamic travel forecasting models. Tsinghua Sci Technol 12(2):115–130

Books and Reviews

Ceder A (2007) Public transit planning and operation: theory, modeling and practice. Elsevier, Burlington

Chung E, Dumont A (eds) (2009) Transport simulation: beyond traditional approaches. EPFL Press, Lausanne

Sussman J (2005) Perspectives on intelligent transportation systems (ITS). Springer, New York

Vuchik V (2005) Urban transit: operations, planning, and economics. Wiley, Hoboken

Vuchik V (2007) Urban transit systems and technology. Wiley, Hoboken

Wilson NHM, Nuzzolo A (eds) (2004) Schedule-based dynamic transit modeling: theory and applications. Academic, Dordrecht

Aerosol in Global Atmosphere

Colin O'Dowd
School of Physics & Centre for Climate and Air Pollution Studies, Ryan Institute, National University of Ireland Galway, Galway, Ireland

Article Outline

Glossary
Definition of the Subject
Introduction: The Nature and Impacts of Atmospheric Aerosols
Aerosol Formation, Dimensions, and Removal
Global Aerosol Budgets, Burdens, and Spatial Distributions
Water Uptake by Aerosols
Aerosols, Global Radiative Budget, Precipitation, and Climate
Aerosols and Air Pollution
Future Directions: Interactions Between Aerosol Air Pollution and Climate
Bibliography

Glossary

Aerosol A suspension of liquid or solid particles in a fluid (in this context air). Also referred to as particulate matter (PM).

Homogeneous nucleation Spontaneous formation of an aerosol particle from vapor phase precursors through a phase transition, without need of a particle nucleus.

Hygroscopicity The ability to absorb water from the atmosphere.

Cloud droplet activation Spontaneous condensation growth of a wettable aerosol particle into a cloud droplet.

Aerosol optical depth Quantitative measure of the extinction of solar radiation by aerosol scattering and absorption between the point of observation and the top of the atmosphere.

Radiative forcing The radiative forcing of the surface-troposphere system due to the perturbation in or the introduction of an agent (say, a change in greenhouse gas concentration) is defined as the change in net (down minus up) irradiance (solar plus longwave in Wm^{-2}) at the tropopause.

Climate Mean values of meteorological parameters in a given region over relatively long periods of time.

Definition of the Subject

Atmospheric aerosols are airborne liquid or solid particles, varying in size from nanometers to hundreds of microns. Atmospheric aerosols are formed from both natural and anthropogenic sources and can have complex chemical speciation and shape. They are formed from mechanical breakup of a parent material, such as dust or sea spray (so-called primary aerosol formation), or from gas-to-particle conversion processes, such as condensation of semivolatile organic compounds (VOCs) or chemical reactions in the aerosol phase such as oxidation of SO_2 to SO_4 (so-called secondary aerosol formation). These tiny airborne particles can form haze and cloud layers that influence the Earth's climate: aerosols directly reflect incoming solar radiation back out to space, providing a direct radiative effect on climate, some of which act as cloud condensation nuclei in the cloud formation process where they determine cloud microphysical and radiative properties, ultimately determining cloud reflectance providing an indirect radiative effect. The net climatic impact of atmospheric aerosols is to provide a cooling effect that partially offsets greenhouse gas-induced global warming. Aerosols also contribute to poor air quality and adverse health effects, typically resulting in reduced life span and increased mortality rates in the most polluted environments.

Introduction: The Nature and Impacts of Atmospheric Aerosols

Atmospheric aerosols are tiny airborne liquid or solid droplets or particles, ranging from nanometers to tens or even hundreds of microns in size. They are diverse in shape and chemical composition and can posses varying optical properties and hygroscopic (water uptake) properties. Particle shape ranges from the most simple to characterize, that is, spherical, to complex fractal agglomerates with similar diversity in aerosol density. Chemical composition ranges from relatively simple inorganic composition to very complex organic matter

composition and mixtures thereof. The vast majority of organic chemical species have not, to date, even been identified. The aerosol population is a dynamic physical and chemical evolving system with fresh aerosol plumes often being externally mixed in terms of chemical composition, evolving with time into more complex internal mixtures. Primary aerosol production is the breakup of a parent material or incomplete combustion and results in the direct injection of aerosol particles into the atmosphere. Secondary aerosol production is the formation of aerosol phase products from nucleation, condensation, and multiphase chemical reactions resulting in aerosol production in the atmosphere itself as opposed to injection into the atmosphere. Aerosol particles in the size range from 100 nm to 1 μm are particularly efficient at scattering, and depending on the chemical composition, absorption of solar radiation. Sea-salt, sulfate, and nitrate are all efficient scatters, while soot or black carbon and dust are efficient absorbers. These important optical properties lead to a reduction of visibility from aerosol haze layers under conditions of high aerosol concentrations and such haze layers are responsible for a number of atmospheric optical phenomena such as beautiful sunsets often seen under clear sky conditions. Aerosol particles also act as condensation nuclei for cloud droplets to form on. Without condensation nuclei, it would be virtually impossible for clouds to form, therefore aerosols also play an important role in the hydrological cycle. Cloud drops are also efficient scatters of solar radiation and consequently, both aerosol haze and cloud layers play an important role in the global radiative budget through contributing to 50% or more of the Earth's albedo. The significant contribution to global albedo necessitates an important role in climate, and in terms of a changing global aerosol population, a role in climate change also exists. Aerosols are both natural and anthropogenic, the former produced by the biosphere (sulfate and organics) and wind interaction at the Earth's surface (sea spray and dust production), the latter produced by industrial, transport, and combustion emissions (sulfate, nitrate, soot, and organics). Biosphere emissions are connected to climate change feedbacks and virtually impossible to control while anthropogenic emissions can be controlled to a certain extent. Although some aerosol species absorb solar radiation, partially contributing to global warming, the predominant climate effect is one of net global cooling. Since the start of the industrial era, aerosol-related air pollution has, to a significant degree, been masking the global warming impact of greenhouse gases and has been slowing the rate of global warming. The effect on climate can be considered as a welcome impact of atmospheric aerosols; however, micron-sized and submicron-sized aerosol also have a high penetration efficiency through the human respiratory system leading to increased respiratory and cardiovascular health impacts. The adverse health impacts lead to increased mortality rates and reduced life span. For example, the London black smoke pollution events in the 1950s resulted in thousands of excess deaths over periods lasting the order of several days. To counteract the adverse health impacts of atmospheric aerosols, various clean air acts have been introduced in various continents, particularly developed industrial continents. Such legislation, while having the required successful impact on air quality and public health, has had a negative impact on global warming in that the reflective haze and cloud layers have become less reflective with the effect of reducing the masking effect on global warming. Particularly over the last two to three decades, cleaner air has resulted in a remarkable increase in the rate of global temperature increase as greenhouse gas concentrations in the atmosphere continue to rise. The coupling between air pollution, air quality, and climate change has led to the synergetic development of air pollution and climate change policy to achieve optimal effect in attempting to mitigate and abate climate change while simultaneously striving for clean air.

The challenge, however, is great in terms of producing accurate assessments of aerosol impacts, particularly those relating to climate change because the atmospheric aerosol system is incredibly complex and this complex system needs to be incorporated into large-scale and global climate assessment and prediction models. From the emission and formation stage of the aerosol life cycle, through its evolution, interaction with clouds and radiation, to its removal from the atmosphere is a highly complex non-linear system spanning spatial and temporal scales from nanometers and seconds (in terms of nucleation of new particles, to global and decadal scales, respectively, in terms of climatic impacts. The complexity is further compounded

by the diverse and even incomplete quantification of the chemical speciation of atmospheric aerosol particles. This article summarizes the nature, formation, transformation, distribution and impacts of aerosols in the global atmosphere and documents the recent advances in the knowledge relating to atmospheric aerosols and their impacts.

Aerosol Formation, Dimensions, and Removal

Aerosols are produced via two generic mechanisms: (1) primary aerosol formation and (2) secondary aerosol formation. Primary aerosols are formed from the mechanical breakup of a parent material, with the resultant aerosol inheriting the chemical properties of the parent bulk material. In addition, primary aerosol production can result from incomplete combustion processes. These processes result in the direct emission of aerosols into the atmosphere. Secondary aerosols, on the other hand, are formed via gas-to-particle conversion processes such as oxidation or other means of chemical reduction of volatile precursor gases, condensation of low-volatility gases onto existing aerosol, homogeneous nucleation (phase-transition) producing new aerosol particles, aqueous phase reactions of dissolved gases producing stable aerosol phase species, or chemical reactions on aerosol surfaces leading to an increase in the condensed aerosol mass. In contrast to direct ejection of primary aerosols into the atmosphere, which necessitates a surface source for primary aerosol (excluding aviation emissions), secondary aerosols are formed in situ in the atmosphere, although many of their precursors are likely to originate at the surface. The formation of secondary aerosols can occur at all levels in the atmosphere, from the boundary layer in the lower troposphere to above the stratosphere.

Once formed, an aerosol particle may undergo physical and chemical transformation, but generally there are only two main sinks – that is through dry deposition at the surface, or wet deposition involving washout by precipitation. Dry deposition is the transport of aerosol particles from the atmosphere to the surface in the absence of precipitation. The level of turbulence in the atmosphere, particularly that close to the ground, determines the rate at which particles are deposited [1]. The deposition rate depends on surface type (i.e., roughness) and particle size since there also is a gravitational settling component to dry deposition. Combining both wet and dry deposition removal processes, on average, submicron particles reside in the boundary layer for up to ~4–8 days [2] depending on precipitation, while supermicron particles, depending on the size, have lifetimes from an hour to 1–2 days. For example, a 100-nm particle takes approximately 36 years to fall 1 km whereas a 10-μm particle takes 3.6 days. Clearly, if particles are vertically transported to the free troposphere or the stratosphere, their lifetime in the atmosphere is greatly increased even to timescales of a year or more in the stratosphere. Removal in the atmospheric boundary layer is increased due to turbulent effects. In terms of aerosol-related air pollution, effects are more so on a local-to-regional scale rather than on a global scale due to removal timescales; however, as it will be seen later, in a climate context, a small amount of aerosol pollution transported to very remote regions can have a notable impact, despite relatively short atmospheric residence timescales. Physical transformations include condensation growth and coagulation (collisions of two particles resulting in one larger particle), while chemical transformations include changes in chemical composition from chemical reactions (e.g., oxidation), along with condensation of different vapors to that already in the aerosol phase. These transformations result in the aerosol population becoming "internally mixed" at long distances from source regions as opposed to "externally mixed" near source regions.

Primary production results typically in larger-micron- or supermicron-sized particles, while secondary production results in nanometer- to submicron-sized particles, leading to size distributions spanning many orders of magnitudes. In Fig. 1, a typical number size distribution is displayed. The peak in the number frequency distribution is in submicron sizes; however, for the same distribution, the volume or mass distribution is more often than not in supermicron sizes, even though the contribution of supermicron particles generally only comprises less than 1% of the total number concentration. Similarly, the mass of particles where the peak concentration occurs contribute less than 1% of the total mass. The peak in aerosol surface area (not shown) usually lies between the number concentration and volume peaks. The size

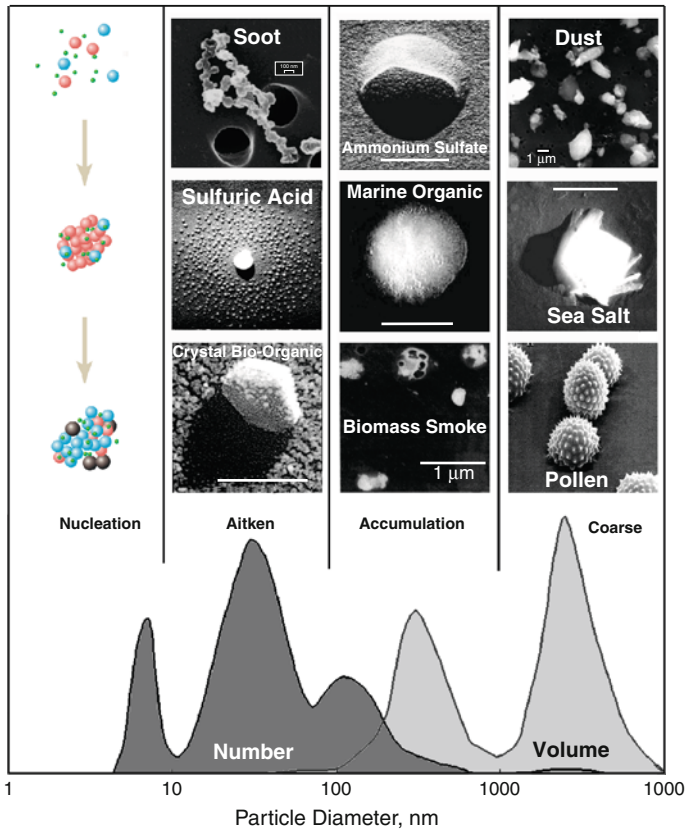

Aerosol in Global Atmosphere. Figure 1
A typical aerosol size distribution covering 4 orders of magnitude in size. Two moments of the size distribution are shown: number and volume. Also shown is a variety of different aerosol types from scanning electron microscope images (Copyright Springer. Modified from [3])

distribution comprises a number of "log-normal" modes reflecting different formation and transformation processes. At the smallest sizes is the nucleation mode where new particles, nanometers in size, are formed from nucleation of condensable vapors. As the nucleation mode grows through further condensation, an Aitken mode (called after the Scottish Scientist John Aitken) of a few tens of nanometers is formed. Through further transformations and growth processes, the Aitken mode grows into an accumulation mode of between about 100 and 200 nm. Generally, the coarse or supermicron mode arises from the direct injection of primary particles. The accumulation mode is termed so as removal processes are least efficient at these sizes and particles tend to accumulate there. Both smaller particles (in the nucleation and Aitken modes) and larger (supermicron mode) particles have notably shorter lifetimes than that associated with accumulation mode particles but for different reasons. Smaller particles are highly diffusive and either self-coagulate to form a larger particle, or they coagulate with larger particles (with a high surface area) where they are effectively removed from the size distribution. Their mass is so small that gravitational settling is negligible. In contrast, larger particles have a negligible diffusion coefficient, but significant mass so that gravitational settling determines their lifetime. Also shown in Fig. 1 are scanning electron micrographs of various aerosol types such as soot (black) carbon, marine organic, sulfate, and bioaerosol particles. These images demonstrate the complexity of atmospheric aerosols in terms of shape, chemistry, and resultant

density, and this complexity is propagated through measurement and modeling challenges associated with quantification of aerosol properties and effects.

Primary Aerosol Formation

In the atmosphere, the most important natural primary aerosol types result from the interaction of wind with terrestrial or oceanic surfaces. For terrestrial primary aerosols, wind interaction with agricultural and desert soils lifts loose fragments of the parent material through saltation and suspension processes resulting in airborne dust particles [4]. These primary dust particles are typically supermicron in size, comprising low number concentration, but high surface area and mass concentrations. The most dramatic example of this is the vertical uplifting of large amounts of desert dust into aerosol plumes that can extend for thousands of kilometers (Fig. 2). These plumes often are transported and deposited into oceanic regions where they can provide an important source of nutrients for the marine biota [5].

Wind interaction with terrestrial vegetation can also trigger the release and dispersion of bioaerosol such as pollen and seeds as well as waxlike and leaf-fragment debris. Humic matter, plant decomposition products, fungi, and microbes are also released from plants. Fungi, in turn, release spores through a variety of ejection processes [6]. Primary bioaerosols also include entire organisms such as bacteria, fungi, and viruses as well as debris [7, 8].

Over oceanic water surfaces, wind stress at the air–sea interface leads to breaking waves and the entrainment of air into the water column, producing whitecaps [9, 10]. Whitecaps are ensembles of bubbles of entrained air rising to the surface where they burst due to the pressure differential inside and outside of the bubble. When the bubble film bursts, it breaks up into hundreds of individual seawater drops that rapidly equilibrate to ambient humidity leaving behind sea-salt "film" droplets, 0.01–1 μm in size and comprising a concentrated solution of the ionic compounds found in sea-salt and water. After the film bursts, the cavity remaining collapses through instabilities leading to the formation of an upward movement of a water jet which fragments into a few jet droplets, typically 1–10 μm in size, of similar composition to film drops [11]. Film and jet drops are produced at wind speeds greater than 3–4 m s^{-1} which is observed to be the threshold for the onset of whitecaps. At wind speeds of 8–10 m s^{-1}, the wind stress is sufficient to tear off the crests of waves and produce spume droplets, typically 10–100 μm in size. The flux of sea spray follows a power-law

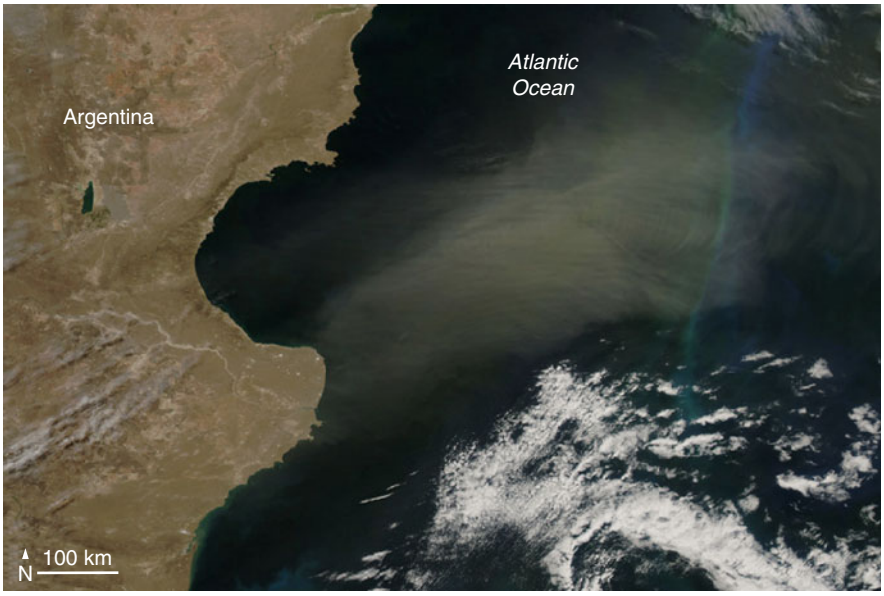

Aerosol in Global Atmosphere. Figure 2
Patagonian dust over the Atlantic Ocean (Courtesy of NASA-MODIS)

dependency on wind speed [12]. In biologically active waters, organic matter tends to become concentrated at the ocean surface and at the bubble–water interface. This organic matter displaces seawater in the bubble film, ultimately displacing the ionic sea-salt in the film and jet drops produced, leading to the enrichment of organic matter in sea-spray aerosol [13]. The enrichment is observed to increase with decreasing particle size. The vast bulk of the organic matter enriched in sea-spray aerosol is water-insoluble organic matter. The chemical composition of marine aerosol is shown in Fig. 3 for periods of low and high biological activity over the North Atlantic as illustrated by oceanic chlorophyll-a concentrations. Supermicron sizes contain predominantly sea-salt, while for submicron sizes, the enrichment of water-insoluble organic matter is linked to biological activity in the ocean (the water-soluble organic matter in the figure is also thought to be marine biogenic in origin but formed from secondary processes).

In terms of anthropogenic sources of primary aerosol, incomplete combustion (mainly from fossil fuel, but also from biomass burning and cooking) results in pyrogenic aerosols in the form of primary organic matter and soot (black) carbon particles. Fossil fuel emissions result from industrial, power plant, transport, and

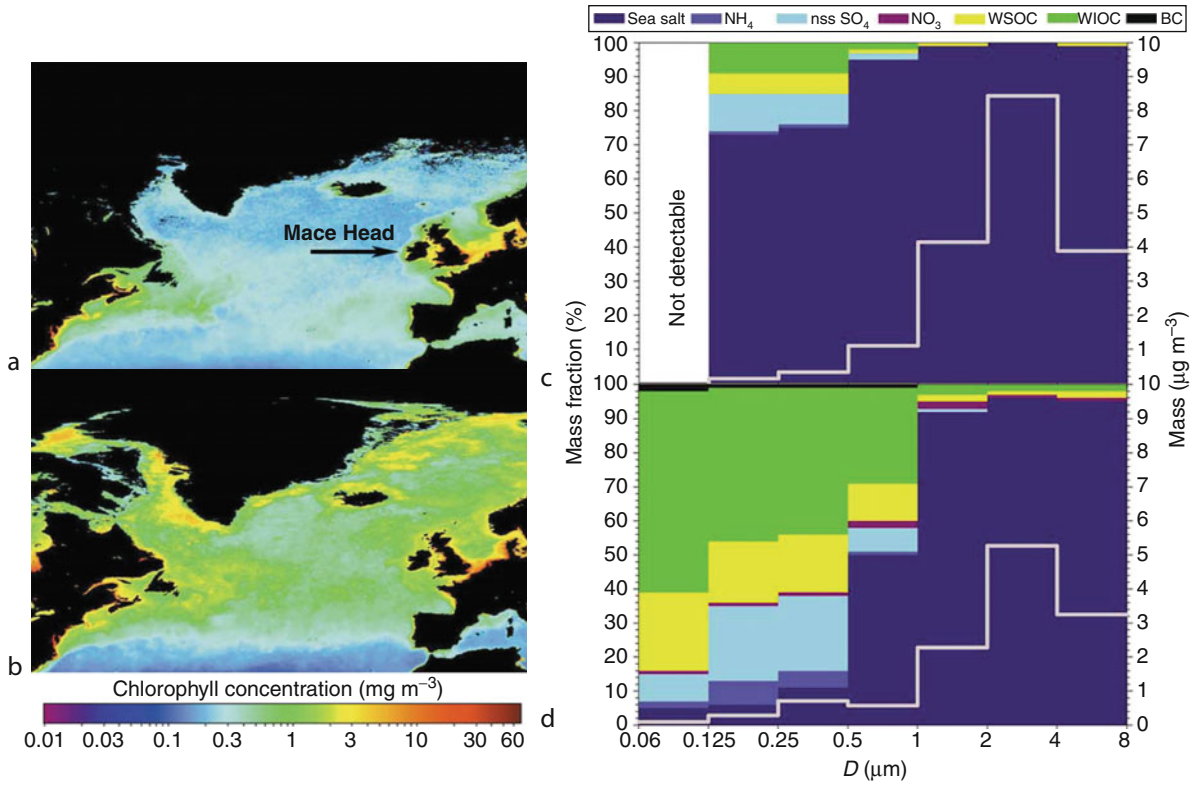

Aerosol in Global Atmosphere. Figure 3

Left: Organic matter in sea-surface waters. SeaWiFS-derived seasonal average sea-surface chlorophyll-*a* concentrations in winter (**a**) and spring (**b**), illustrating low biological activity in North Atlantic waters during low and high biologically active periods (courtesy of SeaWiFS Project, NASA/Goddard Space Flight Center and ORBIMAGE). The location of Mace Head is shown in (**a**). Marine air masses arrive at Mace Head after at least 96 h transit over the ocean from the Arctic and northwest Atlantic. *Right*: Chemical composition of marine aerosols. Shown are average size-segregated chemical compositions and absolute mass concentrations for North Atlantic marine aerosols sampled with a Berner Impactor, for low biologically active periods (**c**) and high biologically active periods (**d**). The concentrations of water-soluble organic carbon, water-insoluble organic carbon, and black carbon are reported as mass of organic matter (Reprinted from [13])

residential heating sources and the resulting aerosol chemical composition varies according to the fuel type and the combustion technology used [14, 15]. Coal combustion results in the emission of supermicron fly-ash particles, while petroleum combustion results in predominantly submicron carbonaceous aerosols comprising soot carbon and organic material [16]. In addition to primary emissions, secondary aerosol precursors such as SO_2, NO_x, and hydrocarbons are also emitted from combustion sources.

Secondary Aerosol Formation via Nucleation

Homogeneous nucleation is the term used for the spontaneous formation of an aerosol particle from vapor phase precursors through a phase transition. Homogeneous-homomolecular nucleation is the self-nucleation of a single species, while homogeneous-heteromolecular nucleation is the self-nucleation of two or more species. Homogeneous nucleation occurs in a supersaturated vapor phase where the saturation ratio (S) of a species in air is the ratio of the species' partial pressure to the saturation vapor pressure in equilibrium with its liquid phase at a given temperature. The Classical Theory of nucleation is based on rate equations relating to the random formation of vapor clusters of more than one vapor molecule and the evaporation of these clusters [1]. The majority of these clusters evaporate as quickly as they form since they are generally thermodynamically unstable. If a sufficient number of the right low-vapor pressure molecules collide, the cluster can achieve a critical radius and achieve thermodynamic equilibrium (i.e., where the evaporation rate is zero). The nucleation rate is the net number of clusters per unit time that will grow past the critical size.

In addition to the kinetic aspect of forming clusters, the thermodynamics of the phase change has to be considered. In a thermodynamic process, such as a phase change resulting in chemical potential equilibrium of the molecular components, the change in the Gibbs free energy (G) must be zero or negative. This condition must also hold for a curved surface of an aerosol particle or droplet. The curved surface will affect the equilibrium vapor pressure in a manner that a higher vapor pressure is required to maintain equilibrium for a smaller droplet (i.e., higher curvature effect). The change in Gibb's free energy ΔG associated with the formation of a single drop of a pure substance or radius R_p is given by:

$$\Delta G = \Delta G_{droplet} - \Delta G_{pure_vapor}$$

which after expanding and rearranging, the right-hand side terms become:

$$\Delta G = -\frac{4}{3}\pi R_p^3 \frac{kT}{v_l} \ln S + 4\pi R_p^2 \sigma$$

The second term on the right-hand side is the free energy associated with an interface with radius of curvature R_p, v_l is the volume occupied by a molecule in the liquid phase, S is the supersaturation, T is the temperature, and σ is the surface tension. The first term is a function of the change in free energy for a molecule going from the gas phase to the liquid phase (ultimately a function of the saturation ratio, S) and the particle volume. It is seen, in Fig. 4, that if $S < 1$, both terms are positive and ΔG increases monotonically. However, if $S > 1$, ΔG contains both positive and negative terms and for small droplet radii the second term dominates with ΔG increasing as for the scenario for $S < 1$. As the radius increases, the first term (providing a reduction in ΔG) progressively becomes more important until ΔG reaches a maximum at ΔG^*, corresponding to a critical radius of $R_p{}^*$. Above $R_p{}^*$, the first term starts to dominate, resulting in a reduction in ΔG. The critical radius can be determined by setting the derivative of $\Delta G = 0$ and solving, resulting in:

$$R_p^{*=} = \frac{2\sigma v_l}{kT \ln S}$$

ΔG^* represents a metastable equilibrium state where if one molecule evaporates from the droplet of critical radius, the droplet will continue to evaporate and shrink, while if one molecule is added to the droplet, the droplet will continue to grow. ΔG^* represents a free energy barrier that the system has to overcome in order to grow and become stable.

Rearranging the previous equation gives the so-called Kelvin equation that describes the equilibrium vapor pressure of a vapor over a droplet relative to that over a flat surface:

$$S = \exp\left(\frac{2\sigma v_1}{kTR_p}\right) \qquad p_A = p_A^0 \exp\left(\frac{2\sigma M}{RT\rho_1 R_p}\right)$$

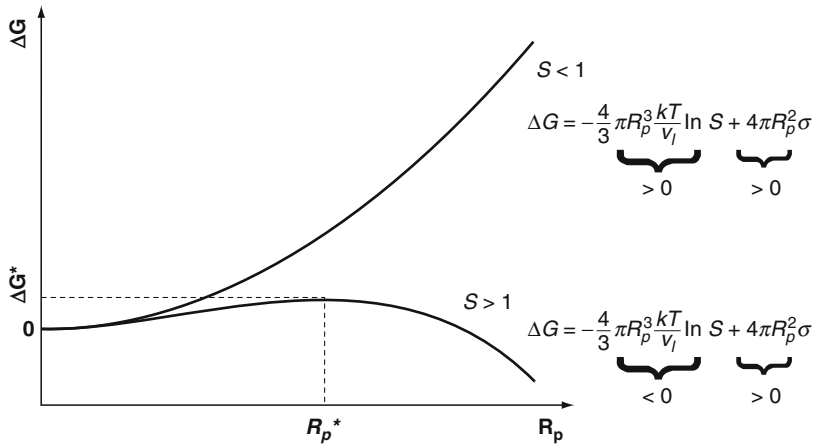

Aerosol in Global Atmosphere. Figure 4
Gibbs free energy change for formation of a droplet of radius R_p from a vapor with saturation ratio S

where M is the molecular weight of the substances and ρ_l is the liquid phase density.

The Kelvin equation demonstrates an exponentially increasing equilibrium vapor pressure with decreasing particle size. From this equation, a saturation ratio of the order of 10 is required for the smallest water vapor clusters to be thermodynamically stable and grow. The critical radius in this case comprises of the order of 20 water molecules. For realistic supersaturations encountered in the atmosphere (e.g., $S = 1.01\%$), the critical radius is 0.12 μm and contains $>10^8$ molecules. As a result, it is seen that water vapor does not participate in homogeneous nucleation in the atmosphere.

For homogeneous-homomolecular nucleation, supersaturation with respect to the species is required. In contrast, this is not the case for heteromolecular nucleation where nucleation can take place when the individual species are subsaturated with respect to the pure substances but supersaturated with respect to the resulting solution droplet containing these substances. Binary homogeneous nucleation is a process typically considered to occur in the atmosphere and the theory is an extension of homogeneous-homomolecular nucleation to account for two species.

Air contains many rapidly moving and colliding trace gases of varying vapor pressures. Those with low saturation vapor pressures, given the right conditions, prefer to be in the liquid solution phase or the solid phase from a thermodynamic perspective. The random collisions of this soup of molecules result in the continuous formation of clusters of a few to tens of molecules. Such stable clusters will then grow in size with each subsequent collision of a low vapor pressure molecule. The size of a critical cluster is of the order of 0.5 nm; however, at this size, the cluster has a very high diffusion coefficient and unless it grows rapidly, it will be scavenged by diffusion to larger, preexisting aerosol particles. For example, if the cluster can grow to 3 nm, its diffusion coefficient is reduced by a factor of 10 and if it grows to 6 nm, it is reduced further by a factor of 10 [17]. In other words, if the cluster can grow to 6 nm, its probability of survival is increased by a factor of 100.

In the atmosphere, very few vapors can participate in homogeneous nucleation. The best candidate is sulfuric acid, which in conjunction with water vapor can participate in binary homogeneous nucleation. It should be noted that the probability of stable cluster formation (or nucleation) is exponentially inversely dependent on temperature, and as a result, binary nucleation of sulfuric acid and water vapor is likely to occur only in the upper troposphere and the stratosphere where temperatures are sufficiently low to promote nucleation under atmospheric concentrations of sulfuric acid. In the troposphere, a different mechanism is required for nucleation to proceed under atmospheric concentrations of sulfuric acid concentrations (typically 10^6–10^7 molecules cm^{-3}). In the presence of ammonia, classical theory predicts that ternary nucleation of ammonia, sulfuric acid, and water can readily

proceed to more readily produce thermonynamically stable clusters under tropospheric conditions. The presence of ammonia lowers the thermodynamic barrier which has to be overcome to form an embryo. In classical theory, whether binary or ternary nucleation, the number of molecules in a critical cluster is of the order of 10 or more.

According to the nucleation theorem [18], the slope of the relationship between the nucleation rate and sulfuric acid concentration corresponds to the number of molecules in a critical cluster:

$$N_{\text{crit}} = d(\ln J)/d(\ln[H_2SO_4])$$

Atmospheric measurements of the nucleation rate versus sulfuric acid concentration reveal a slope of between 1 and 2 [19, 20] as do the most recent laboratory studies of nucleation. A slope of 2 can be explained by collision controlled or kinetic nucleation [21] while a slope of 1 can be explained by two processes: one being the requirement of an additional stabilizing or condensing vapor participating in the initial growth of the clusters; the other being activation of clusters by a supersaturated vapor [22, 23]. It is thought that the acid clusters are activated into aerosol particles in the presence of a supersaturated organic vapor field in the same way that cloud nuclei are activated into cloud droplets in a supersaturated water vapor field (the theory behind activation will be discussed later in the section on aerosol–cloud interactions). Recently, the formation of organosulfate clusters was suggested to explain the chemistry behind the cluster activation or kinetic mechanisms and thus atmospheric nucleation [24]. The aforementioned analysis reveals a critical cluster diameter of 0.8 nm and 1–2 sulfuric acid molecules in the cluster. The most recent laboratory studies [25] reveal that nucleation occurs at H_2SO_4 concentrations similar to those found in the ambient atmosphere during nucleation events and that the measured particle formation rates are proportional to the product of the concentrations of H_2SO_4 and an organic molecule. This suggests that only one H_2SO_4 molecule and one organic molecule are involved in the rate-limiting step of the observed nucleation process.

Indirect measurements of 3–10 nm particle chemical composition immediately after a natural new particle production event over forested regions reveal that the chemical composition of newly formed particles are not sulfuric acid or aerosol sulfate [26], but comprise more so of condensed organic matter. Calculations also reveal that there is insufficient sulfuric acid to nucleate new clusters and to grow these into aerosol particles larger than 3 nm. Whereas sulfuric acid appears to drive the nucleation of new clusters, an additional species is required to grow the clusters into aerosol particles. Under very polluted conditions, there is typically sufficient availability of sulfuric acid to both form stable clusters and to grow these clusters into aerosol particles tens to hundreds of nanometers in size. During particle production events in background air, the aerosol population typically increases from concentrations of ~1,000 to ~100,000 cm^{-3}, while in polluted air concentrations increase from ~10,000 to ~100,000 cm^{-3} [22, 23].

The most dramatic and intense nucleation events occur in coastal air where background concentrations increase from ~500 to ~1,000,000 cm^{-3} [26, 27]. These events occur when seaweed beds are exposed during low tide conditions. The algae emit I_2 and CH_2I_2 which are rapidly photolyzed and oxidized by O_3 resulting in the formation of iodine oxides which readily nucleate into stable clusters. In addition, there is sufficient iodine oxide produced to account for the rapid growth of the clusters into aerosol particles of 100 nm [28].

Multiphase Secondary Aerosol Production

The vast majority of secondary aerosol mass is not produced through the nucleation process but through condensation, aqueous phase reactions, and multiphase processes. Condensation typically involves both inorganic low-volatility gases, such as sulfuric acid and nitric acid, and a vast range of condensable organic species. Sulfuric acid results from the oxidation of SO_2 by the OH radical, while nitric acid results from the oxidation of NO_2 in the atmosphere. NH_3 can also condense on acidic particles resulting in fully or partially neutralized particles. Nitric acid is regarded as a semivolatile condensable gas that can be thermodynamically stable in either the gas phase or the aerosol phase, depending on environmental conditions. At lower temperatures and higher relative humidities, nitric acid is more likely to be found in the condensed aerosol phase, while at warmer temperatures and lower

humidities, it is more likely to evaporate. The chemistry of the preexisting aerosol also influences the gas phase partitioning of nitric acid. For example, in the presence of alkaline aerosol species such as sea-salt and dust, nitric acid will preferentially condense to these aerosol types. Since the bulk of sea-salt and dust aerosol are found in supermicron size ranges, it is in these size ranges where nitric acid can also be found. However, in polluted regions, and in the absence of sea-salt and dust, nitric acid is also found in significant amounts in submicron-sized aerosol. Nitric acid and sulfate aerosol are generally sourced from pollution sources; however, in marine regions, the oxidation of dimethylsulfide, a waste product from plankton activity, can provide a significant source of natural SO_2 and methane sulfonic acid, leading to natural aerosol production.

Aqueous phase reactions can occur in liquid aerosol particles but typically, the majority of aqueous phase production occurs in cloud droplets. It is estimated that between 75% and 90% of aerosol sulfate (SO_4^{--}) is produced through this pathway. In cloud, the droplet surface area and volume of the cloud droplets promote the dissolution of SO_2 into the aqueous phase where it can be rapidly oxidized by ozone and/or hydrogen peroxide [29]. The oxidation route by ozone is highly pH dependent and dominant in alkaline drops such as those formed on sea-salt aerosol, while the hydrogen peroxide route dominates at lower pH values [30]. When sea-salt is present in cloud nuclei, the cloud behaves as a virtual buffer, increasing alkalinity and accelerating ozone-driven aqueous phase oxidation of SO_2 to produce sulfate [30]. This sulfate formation route led to the significant production of acidic sulfate aerosol in polluted air and was the primary cause of the acid-rain problem in the 1970s–1980s.

Oxidation of volatile organic compounds (VOCs) leads to the production of condensable organic vapors, ultimately producing secondary organic aerosol (SOA). The major oxidizing species are the OH radical, ozone, and the nitrate radical (NO_3). Like in the case of nitric acid, some of these condensable vapors can be semivolatile. There are both natural VOCs (biogenic: BVOCs) and anthropogenic VOCs (AVOCs), although it is estimated that the BVOC emissions are of the order of ten times that of AVOC emissions. Some modeling studies suggest that in certain heavily populated regions, AVOCs can contribute significantly to total organic carbon levels [31]; other studies using carbon isotope analysis suggest that BVOC oxidation products contributed to the majority of SOA even in urban regions [32]; however, it should be noted that even BSOA production is somewhat linked to anthropogenic activity as the main VOC oxidants are associated with anthropogenic emissions.

For BVOC emissions, terpenes and sesquiterpenes from terrestrial vegetation emissions, are thought to be the dominant precursors of BSOA, and to a lesser extent isoprene (particularly under high NOx conditions [33]), while aromatic compounds such as toluene, xylene, and trimethyl benzene are thought to account for the majority of ASOA formation. There has been considerable effort to identify the composition of SOA in recent years; however, the vast majority of compounds remain unidentified due to complex mixtures of compounds often with few distinguishing features. SOA is generally oxygenated and water soluble, in contrast to hydrocarbon-like water-insoluble POA. Various approaches have been taken to speciate the organic mass found in SOA. For example, ^{1}H nuclear magnetic resonance (HNMR) techniques have been applied to evaluate functional groups in water-soluble OA for different aerosol source regimes [34]. The technique readily detects four main functional groups in atmospheric water-soluble OA: unfunctionalized alkyls (H–C); aliphatic carbons bound to an unsaturated carbon atom (H–C–C=); aliphatic alcohols, ethers, and esters (H–C–O; and aromatic rings (H–Ar). Additionally, formylic (H–C=O), acetalic (O–CH−O), and sulfonic (H–C–S=O) groups are detected. Water-soluble OA samples from the boreal forest in Finland (terrestrial biogenic), biomass burning events in Brazil, rural UK, and the Northeast Atlantic (marine) were analyzed for functional groups using this approach. Figure 5 illustrates, on the vertical axis, the aliphatic carbon fraction (carbonylic/carboxylic, HC–C=O groups) and, on the horizontal axis, the fraction of aliphatic carbon accounted for by hydroxyl groups for a range of standard SOA compounds (levoglucosan, succinic acid, adipic acid, pinonic acid, glutaric acid, and nonanoic acid) alongside the diverse atmospheric samples. The analysis show that marine

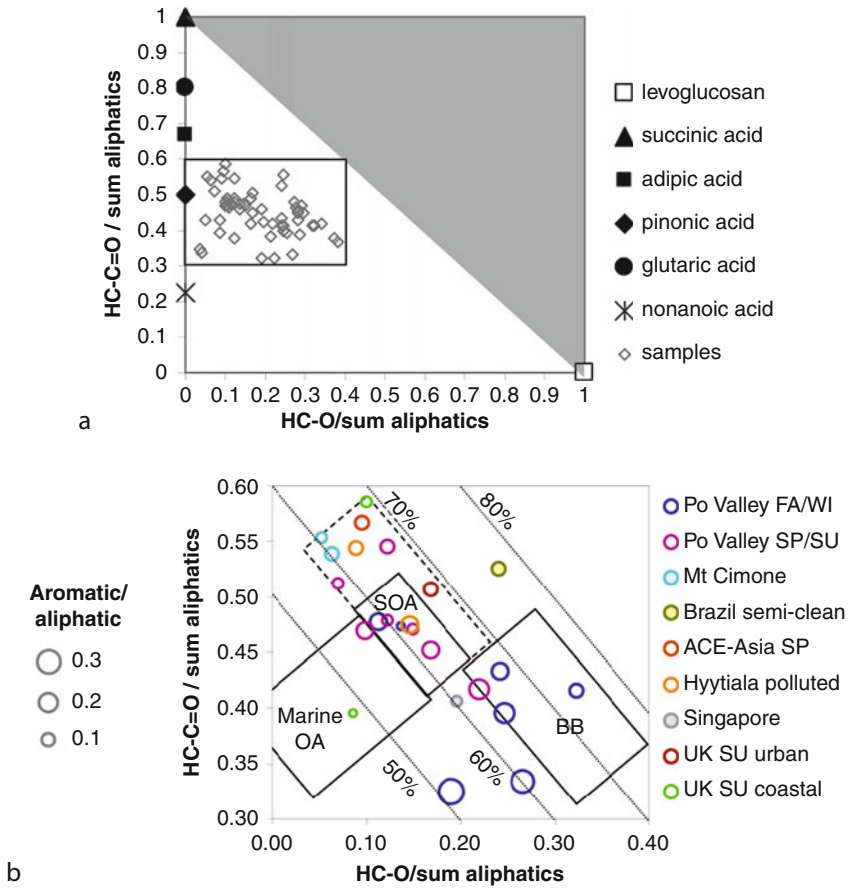

Aerosol in Global Atmosphere. Figure 5

(**a**) Functional group distributions of standards of water-soluble organic compounds. The area including the composition of the real atmospheric samples is also indicated. (**b**) Functional group distribution of WSOCs samples characteristic of specific aerosol sources. Diagonal lines represent the percentage fraction of total oxygenated groups (H–C–O + HC–C=O) (Copyright American Chemical Society 2007. Reprinted from [34])

and terrestrial biogenics are characterized by relatively high H–C and low H–C–O groups which partly overlap; however, the marine samples have a significantly lower aromatic content. The functional composition of biogenic OA and that of rural anthropogenic OA are relatively close with the rural samples having a higher H–C–O content. Both also contain high fractions of aliphatic carbonyls. The biomass burning water-soluble OA contained the highest content of hydroxyls and the lowest amount of alkylic groups.

The formation of SOA is not always via the gas phase formation of condensable vapors. In the case of isoprene-related SOA production, its relatively high vapor pressure oxidation products suggest little contribution to SOA; however, alternative routes have been suggested, which produce low-volatility aerosol phase products. For example, tetrols with the same backbone as isoprene have been observed in atmospheric aerosols [35] possibly formed by the heterogeneous acid-catalyzed oxidation of isoprene in the presence of peroxides [36]. Additionally, heterogeneous reaction of isoprene under highly acidic conditions was also observed to lead to the formation of polymeric, humic-like substances [37]. Other studies showed that some high-volatility carbonylic oxidation products can contribute to SOA through the interaction

with highly acidic inorganic preexisting aerosols [38], while polymerization of second-generation products has been suggested to contribute to SOA growth [39]. Cloud modeling studies [40] also predict that low-volatility water-soluble oxidation products of isoprene can be oxidized in the aqueous phase in clouds to produce dicarboxylic acids.

Once SOA is formed, it contributes to a dynamic thermodynamic and chemical evolution system. SOA species can be repartitioned to the gas phase and undergo polymerization and oxidation leading to significant changes in the chemical nature of SOA. The evolution of SOA is well illustrated through the examination of SOA mass spectral properties moving from strong urban source regions to remote continental regions. Aerosol mass spectrometry (particularly using the Aerodyne Aerosol Mass Spectrometer – AMS) delivers increased speciation capability on both POA and SOA. This technology splits the organic aerosol into three generic types – an oxygenated organic aerosol (OOA), a hydrogenated fossil-fuel-derived organic aerosol (HOA), and a biomass burning organic aerosol (BBOA). OOA is characterized by its highly oxidized state with atomic O:C ratios between 0.25 and 1 and can be further categorized into two subgroups based on volatility and O:C ratio. Low-volatility OOA ($\sim C_8O_{5.5}H_{10}$) has a high O:C ratio and is frequently correlated to other secondary species such as sulfate aerosol and is consistent with an aged aerosol. Semivolatile OOA ($\sim C_8O_3H_{10}$) has a lower O:C ratio and is better correlated with other semivolatile species such as nitrates and is consistent with a partially photochemically aged aerosol.

A compilation [41] of measurements of HOA and OOA types, along with major inorganic species, at different urban, urban downwind, and remote rural locations, is shown in Fig. 6. What is clearly evident from the suite of measurements is that organic matter comprises a significant fraction of the aerosol mass at all locations; however, the further from pollution sources, the more oxygenated the organic aerosol is (i.e., the ratio of OOA/HOA increases) and the more aged, or distant from pollution sources, the higher fraction of OOA is low-volatility OOA. This study also reports the evolution of the Mexico City pollution plume within which there is intense SOA formation. They found that near the plume source region, semivolatile OOA dominated the organic aerosol signal; however, as the plume advected and aged downwind, the fraction of low-volatility OOA and the O:C ratio increased. Laboratory studies on the evolution of biogenic SOA (from α-pinene oxidation), biomass burning smoke, and the POA surrogate squalane also exhibit similar aging patterns as in the reported atmospheric plumes. The laboratory results demonstrate that in the early stages of SOA production, the OA mass spectrum resembles that associated with the respective source, but as oxidation and aging proceeds, the SOA spectra evolve into initially semivolatile OOA spectra and ultimately into low-volatility OOA spectra. The combined atmospheric and laboratory studies suggest that with atmospheric oxidation, most types of OA converge to a final state of low-volatility OOA, irrespective of the original source. It should, however, be noted that primary and secondary marine aerosol aging was not evaluated and that these, potentially, could behave differently to the terrestrial biogenic and anthropogenic OA types.

The previous study developed, on the basis of the mentioned experimental studies, a simple 2D basis (2D-VBS) model encapsulating the evolution of OA volatility (determined as saturation concentration C^* at 298K) and oxidation state (O:C ratio) to describe the evolution of OA in the atmosphere [41]. These two properties can be measured in real time and are thus used to constrain the model with experimental field data. The model incorporates photochemical aging using a branching ratio between functionalization and fragmentation kernels and homogeneous and heterogeneous oxidation by OH, and where the first generation of oxidation is explicitly modeled while the second generation is phenomenologically modeled. The conceptual framework was applied to SOA production from α-pinene ozone-driven oxidation and was found to predict first-generation products with $1 < C^* < 10^7$ μg m^{-3} and $0.1 < O{:}C < 0.4$. Given that generally organics with $C^* < 10$ μg m^{-3} will partition into the aerosol phase, it is evident that most of the oxidation products remain as volatile gases. The first-generation products can then functionalize through OH reactions resulting in a tripling of SOA mass production after second-generation oxidation. The model is able to predict the evolution of SOA in the 2D volatility and O:C space, remaining consistent with the production key

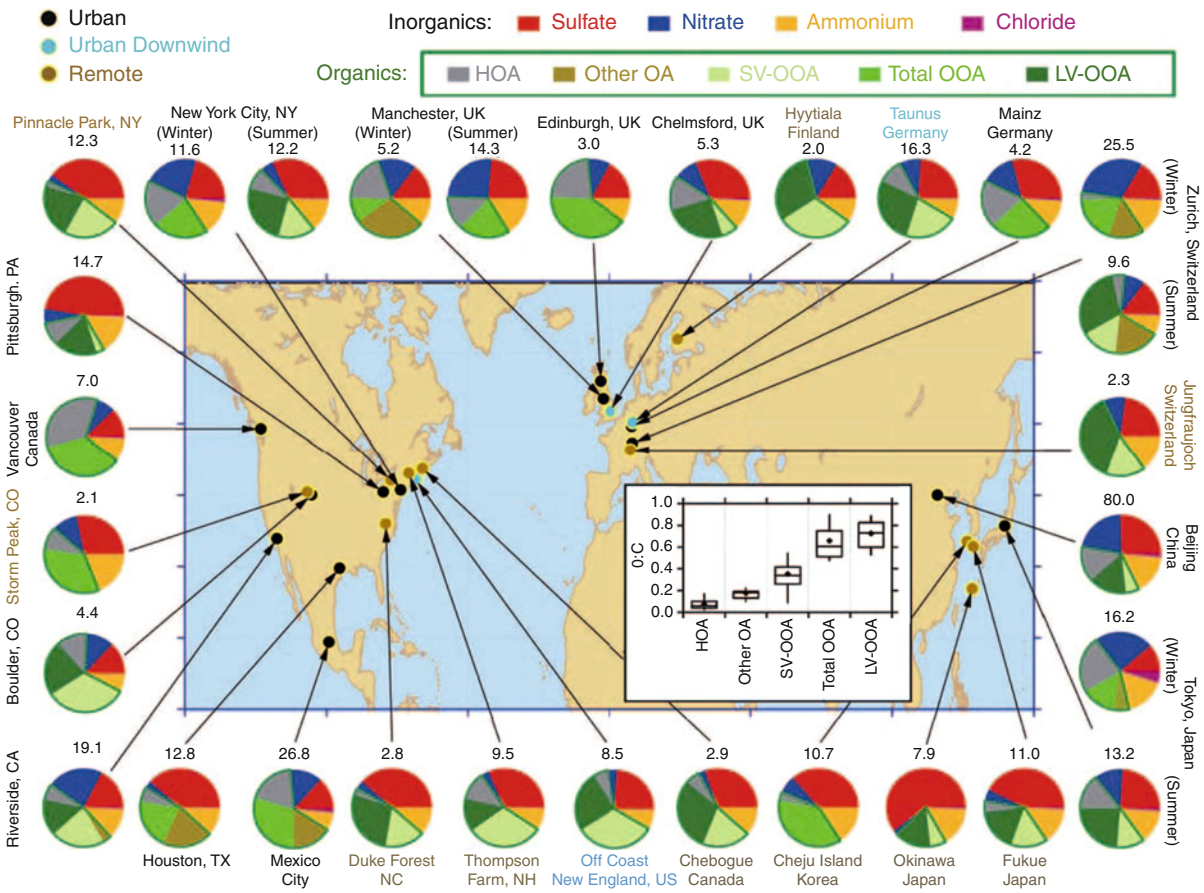

Aerosol in Global Atmosphere. Figure 6

Total mass concentration (in micrograms per cubic meter) and mass fractions of nonrefractory inorganic species and organic components in submicrometer aerosols measured with the AMS at multiple surface locations in the Northern Hemisphere (21). The organic components were obtained with FA-AMS methods (3, 15–17). In some studies, the FA-AMS methods identified one OOA factor, whereas in other locations, two types, SV-OOA and LV-OOA, were identified. HOA is a surrogate for urban primary OA, and Other OA includes primary OAs other than HOA that have been identified in several studies, including BBOA (Reprinted from [41])

products such as the first-generation cis-pinonic acid, regarded as a semivolatile OOA, and second-generation products such as α,α-dimethyltricarballylic acid, a low-volatility OOA. Similar evolution was found for other SOA sources like evaporated diesel and biomass burning. This 2D volatility and O:C conceptual has made considerable advances in simplifying the treatment of an incredibly complex system and can be further developed and extended to include other key processes such as oligomerization. The combined perspective to emerge from the recent mass spectral measurements and the modeling framework is that most OA appears to be an intermediate or transition state between primary emissions and highly oxidized volatile gases such as CO and CO_2.

Global Aerosol Budgets, Burdens, and Spatial Distributions

The diverse nature of aerosol sources from natural and anthropogenic emissions, different formation and removal processes, and different transport mechanisms results in great inhomogeneity in annual emission budgets, atmospheric burdens, and spatial distributions of individual aerosol species. The result is ultimately

significant variability in radiative forcing and air pollution on regional scales. To quantify budgets and distributions, general circulation (climate) models or chemical transport models, are used in conjunction with emission inventories. These models contain aerosol–cloud chemistry formation and evolution modules along with deposition schemes and are underpinned by field and laboratory studies into key processes. In addition, quantification is achieved by long-term observations of atmospheric composition at various point locations around the globe. Remote sensing of aerosol parameters from surface and space-borne platforms also provide added information on horizontal and vertical distributions.

Global Budgets

Atmospheric aerosols are derived from both natural and anthropogenic sources. Natural sources include sulfate and sea spray (sea-salt and primary organic matter) from the oceans, dust from desert regions, particulate organic matter from biogenic sources (both terrestrial and oceanic), and sulfate and silicates from volcanoes. Anthropogenic sources include sulfate, black carbon and primary and secondary organic matter from fossil fuel combustion and biomass burning, dust from industrial sources, and nitrates mainly from transport emissions. The best estimated emissions and resulting atmospheric mass and number burdens are displayed in Table 1 [42]. The largest natural emission is that of sea-salt with a "best guess" of 10,130 Tg a^{-1}, followed by dust with a best guess emission of 1,600 Tg a^{-1}. Biogenic secondary organic emissions are 25 Tg a^{-1}, compared to 3.5 Tg a^{-1} for anthropogenic emissions. For sulfate aerosol, anthropogenic emissions (122 Tg a^{-1}) dominate over natural biogenic (57 Tg a^{-1}) and volcanic (21 Tg a^{-1}) emissions and for primary organic aerosol, anthropogenic emissions amount to 95 Tg a^{-1} while natural oceanic primary organic aerosol (not shown in Table 1) is estimated to be 16 Tg a^{-1} [56]. Black carbon emissions from fossil fuel amount to 4.5 Tg a^{-1}.

Global Burdens

The spatial distribution of total aerosol mass is shown in Fig. 7. The distribution is a medium mass composite from 10 global atmospheric climate (general circulation) models and chemical transport models for the year 2000. From the model output, the global average column burden for all aerosol types is ~50 mg m^{-2}, with regional loadings exceeding 500 mg m^{-2}, in places such as North Africa and Asia. These plumes of high aerosol burdens extend out into ocean regions (e.g., the African plume is seen to extend out west into the Atlantic). North America and Europe exhibit moderate levels of aerosol burden, while somewhat higher burdens are seen over South America and Australia. Significant burdens are also seen over remote oceanic regions such as the south Pacific and Indian Ocean. The dominant source regions for different species are revealed when burden distribution maps are examined for individual aerosol species. For black carbon, the global burden is 0.36 mg m^{-2}, with values exceeding 5 mg m^{-2} occurring over China and burdens of 1–2 mg m^{-2} occurring over regions such as Africa and South America, with slightly lower burdens occurring over Europe and North America. Significant black carbon plumes are seen to advect out over the Atlantic and Indian Oceans from the two aforementioned highest burden regions.

For dust, the global average burden is ~25 mg m^{-2}, with peak burdens exceeding 500 mg m^{-2} occurring over the Sahara desert in Northwest Africa. East Europe and Asia are also seen as significant dust source regions, and to a lesser degree, western USA and central Australia. For Particulate Organic Matter, the spatial distribution of the column burden is similar to that of black carbon, but with a significantly higher column burden of 3 mg m^{-2}. Peak values approach 50 mg m^{-2} and the main source regions are the southwestern African Continent, South America, Europe, India and China, northern Australia, and southeast USA. Significant levels of the order of 1 mg m^{-2} are also seen over most oceanic regions. Non-sea-salt sulfate exhibits a global average burden of ~3.5 mg m^{-2}, with peak values of the order of 50 mg m^{-2}. Again, the main developed and developing countries with significant population densities appear as burden "hot spots" as for the other anthropogenic aerosol types (e.g., black carbon and particulate organic matter). In contrast to other anthropogenic sources, there are notable burdens over remote oceanic regions, reflecting also its natural oceanic source.

Aerosol in Global Atmosphere. Table 1 Particle emission/production and burdens estimated for the year 2000 (Copyright Elsevier 2008. Reprinted from [42])

	Mass emission			Mass burden	Number prod.	
		Min	Max			
	"Best guess"	Tg a^{-1}		Tg	a^{-1}	Number burden
Carbonaceous aerosols						
Primary organic (0–2 μm)	95	40	150	1.2	–	$310 \cdot 10^{24}$
Biomass burning	54	26	70	–	$7 \cdot 10^{27}$	–
Fossil fuel	4	3	9	–	–	–
Biogenic	35	15	70	0.2	–	–
Black carbon (0–2 μm)	10	8	14	0.1	–	$270 \cdot 10^{24}$
Open burning and biofuel	6	5	7	–	–	–
Fossil fuel	4.5	3	6	–	–	–
Secondary organic	28	2.5	83	0.8	–	–
Biogenic	25	2.5	79	0.7	–	–
Anthropogenic	3.5	0.05	4.0	0.08	–	–
Sulfates	200	107	374	2.8	$2 \cdot 10^{28}$	–
Biogenic	57	28	118	1.2	–	–
Volcanic	21	9	48	0.2	–	–
Anthropogenic	122	69	214	1.4	–	–
Nitrates	18	12	27	0.49	–	–
Industrial dust etc.	100	40	130	1.1	–	–
Sea-salt						
$d < 1$ μm	180	60	500	3.5	$7.4 \cdot 10^{26}$	–
$d = 1$–16 μm	9,940	3,000	20,000	12	$4.6 \cdot 10^{26}$	–
Total	10,130	3,000	20,000	15	$1.2 \cdot 10^{27}$	$27 \cdot 10^{24}$
Mineral (soil) dust						
<1 μm	165	–	–	4.7	$4.1 \cdot 10^{25}$	–
1–2.5 μm	496	–	–	12.5	$9.6 \cdot 10^{25}$	–
2.5–10 μm	992	–	–	6	–	–
Total	1,600	1,000	2,150	18 ± 5	$1.4 \cdot 10^{26}$	$11 \cdot 10^{24}$

Range reflects estimates reported in the literature. The actual range of uncertainty may encompass values both larger and smaller than those reported here. Values are based on the following publications: [31, 43–55])

Finally, the sea-salt burden is 13.5 mg m^{-2}, with peak burdens of ~50 mg m^{-2}. The peak burdens occur at midlatitudes, or the "roaring 40s," north and south of the equator, and are associated with regions of intensive cyclonic activity.

It is interesting to note that in Table 1, sea-salt was highlighted as being the single most important aerosol emission type, but it had a mass burden slightly lower than dust which had significantly lower emissions than sea-salt. In the AEROCOM (http://dataipsl.ipsl.jussieu.

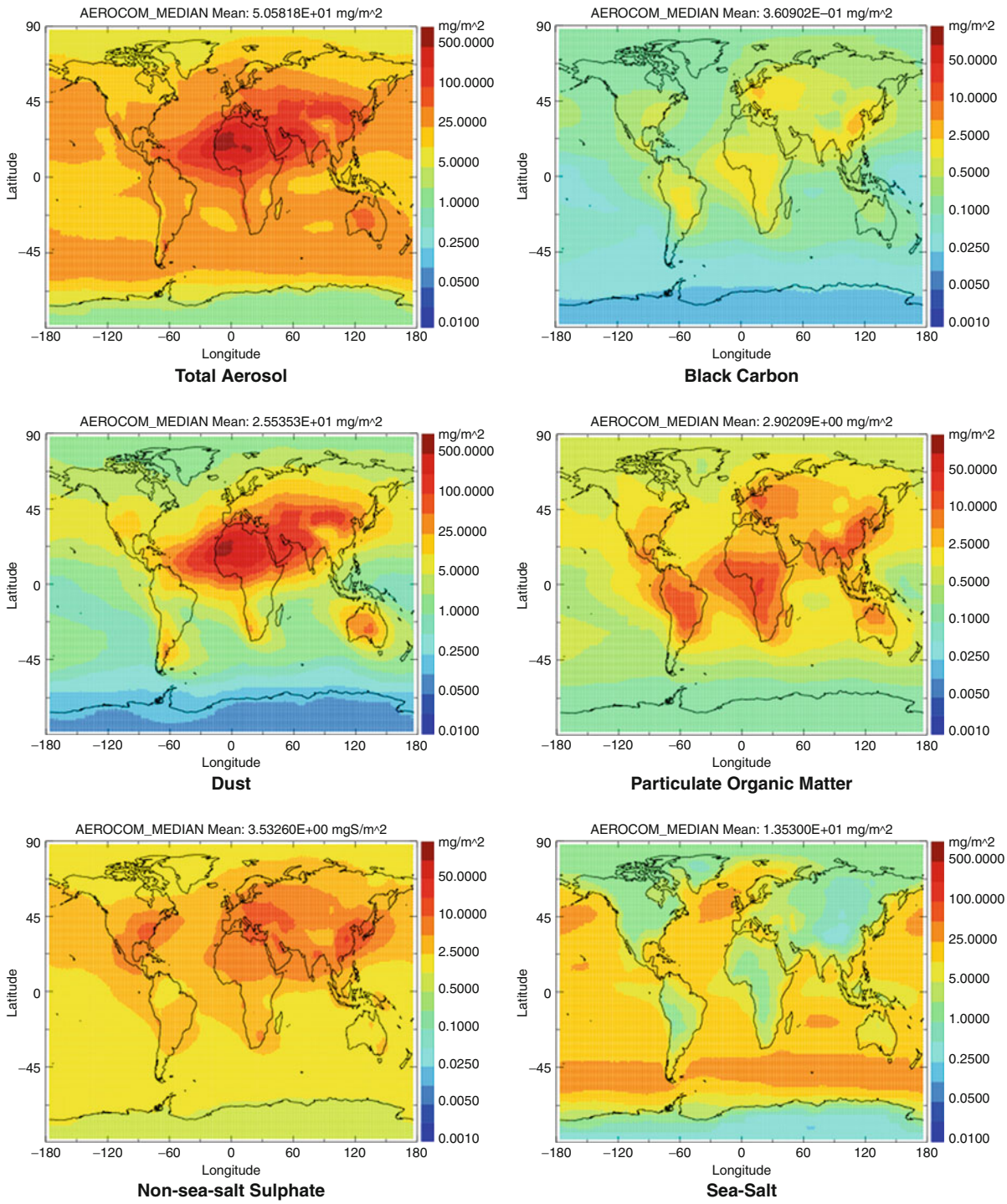

Aerosol in Global Atmosphere. Figure 7

Median global distribution of aerosol column mass, total and per aerosol species, derived from 10 AEROCOM models for the year 2000 (Copyright European Geophysical Union 2006. Reprinted from [57])

fr/AEROCOM; [57]) study, dust also has a higher burden for generally lower emissions. The explanation is that significant dust plumes are vented into the Free Troposphere where removal rates are slower and residence times are longer than in the marine boundary layer where removal rates are likely higher due to higher precipitation rates and, for the larger-sized particles, shorter gravitational settling timescales (i.e., sea-salt is not injected at as high altitudes as dust, so they settle out more rapidly).

At any one location, the chemical composition of atmospheric can vary significantly depending on the air mass back trajectory arriving at that location. An example of the chemical variability encountered is demonstrated for the Northeast Atlantic region where clean marine and polluted continental air masses are frequently encountered at the Mace Head Atmospheric Research Station, which is representative of the region. Figure 8 illustrates the absolute chemical composition and the relative chemical composition observed in two contrasting air masses (continental polar, maritime polar) of different origin over the Northeast Atlantic. Typically, the main ionic compounds such as sodium, chloride, nitrate, sulfate, and ammonium are easily detected; however, it is also possible to quantify the water-soluble and water-insoluble organic component. It is readily seen that the absolute and relative contributions of the above species varies greatly with air mass, or source origin [58]. Peak submicron mass loadings occur for the continental air, while peak supermicron masses occur for marine air. In marine polar air, the supmicron sizes are almost exclusively composed of sea-salt, while submicron sizes are marginally dominated by nss-sulfate, with the second largest contribution derived from sea-salt. Small amounts of ammonia, water-soluble organic matter and water-insoluble organic matter are also evident. By contrast, in the continental air, sea-salt and nitrate are the two dominant species in supermicron sizes, with smaller amounts of organic matter visible and in the submicron sizes, nss-sulfate and water-soluble organic matter dominate. It should be noted that marine aerosol can be significantly enriched in organic matter depending on the degree to which air masses pass over biologically rich waters.

Mass is only one important parameter of an aerosol size distribution. Perhaps the other most important parameter is the number concentration, and in particular, the concentration in the so-called accumulation mode (100–500 nm diameter). This size range is not only important for scattering and radiative effects of atmospheric aerosols, it is crucially important in terms of influencing the number concentration of cloud condensation nuclei. Figure 9 illustrates the horizontal and vertical (zonal) average concentration in the accumulation mode size range [59]. It can be seen that the highest number concentration of aerosols ($N = 3{,}000$–$5{,}000\ \mathrm{cm}^{-3}$) occurs over regions in Europe such as the Netherlands and Northern Italy, China, India, and Brazil.

Vertical Distributions

The vertical distribution of aerosol particles, measured as aerosol backscatter using a LiDAR (Light Detection And Ranging), typically reveals maximum particle mass and number concentrations in the atmospheric boundary layer (lower ~1,000–2,000 m) as shown in Fig. 10. In this figure, the attenuated atmospheric aerosol backscatter profiles illustrate the vertical aerosol structure [58]. In the case shown, the main boundary layer temperature inversion is at ~1,500 m and within the boundary layer there is a surface-mixed layer at 500 m. The peak aerosol burden occurs in the surface-mixed layer and corresponds to a European pollution plume advecting out into the Atlantic. Significant aerosol backscatter (and hence aerosol loading) is seen in the residual boundary layer between 1,000 and 2,000 m. Above 2,000 m, in the free troposphere, very clean aerosol levels are seen.

Figure 11 displays a 10-year climatology of accumulation mode zonal vertical distributions demonstrating that the Northern Hemisphere from 60°N to 20° into the Southern Hemisphere contains the highest particle number concentrations (~700 cm^{-3}). The cleanest concentrations occur in and around Antarctica, while the second cleanest is in the upper troposphere–stratosphere region.

Vertical profiles of total number of concentrations (historically defined as condensation nuclei, or CN, typically larger than 10 nm), and size-resolved concentration measurements (with radius > 0.15 μm to sizes greater than 2 μm) up to the higher stratosphere are shown in Fig. 12 (taken from [60]). In this figure,

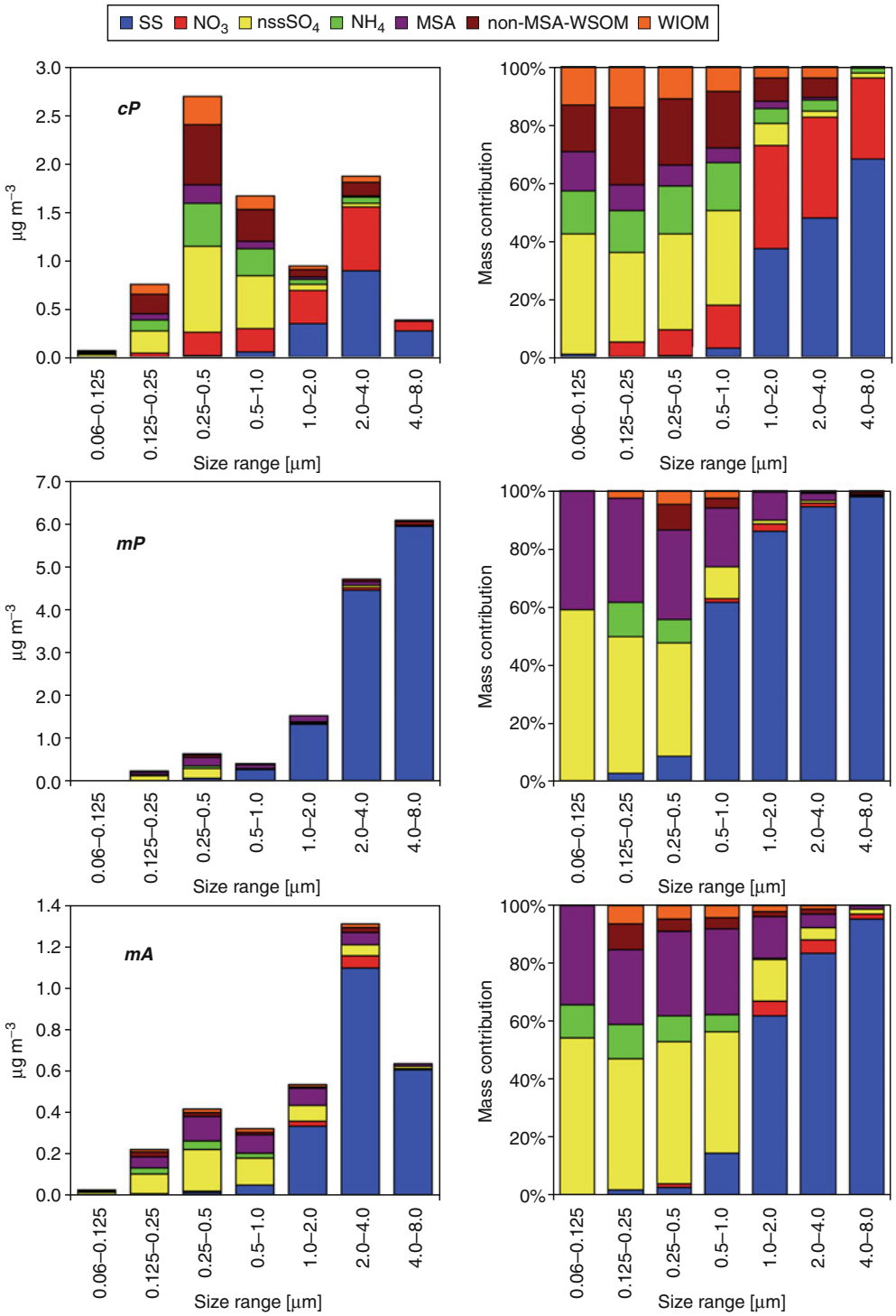

Aerosol in Global Atmosphere. Figure 8

Absolute (*left panel*) and relative (*right panel*) chemical composition of the aerosol samples collected in continental polar (*cP*), maritime polar (*mP*), and maritime Arctic (*mA*) air masses measured at Mace Head, Northeast Atlantic, during June 2008 (Copyright European Geophysical Union 2009. Reprinted from [58])

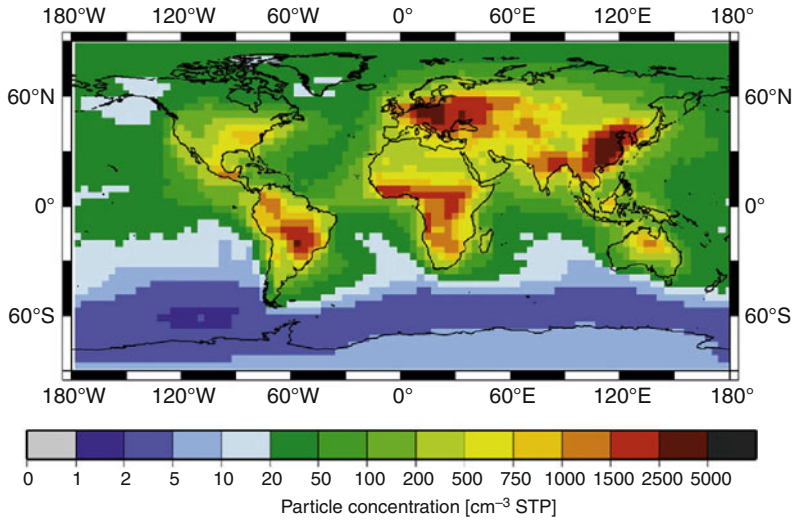

Aerosol in Global Atmosphere. Figure 9
Climatological annual means of simulated accumulation mode aerosol particle concentration obtained from a 10-year integration. The geographical distribution is of the lowermost model layer, which is about 60 m thick (Copyright European Geophysical Union 2006. Reprinted from [59])

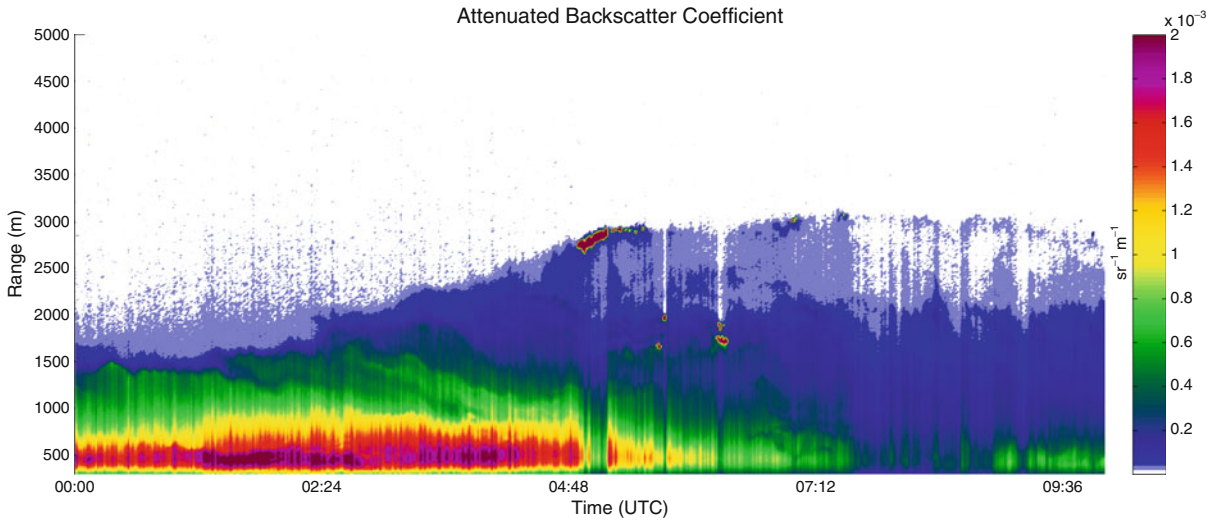

Aerosol in Global Atmosphere. Figure 10
LIDAR aerosol attenuated backscatter vertical profiles of the atmospheric boundary layer and free troposphere. Measurements were taken at the Mace Head Atmospheric Research Station on the Irish Atlantic coastline. Measurements were taken during polluted continental air outflow from Europe into the Atlantic region

concentrations are shown for 1 year and 15 years after the Mt. Pinatubo eruption. What is evident is that total aerosol, or CN, concentration at the surface is between 500 cm^{-3} (typical of clean background continental air masses) and 3,000 cm^{-3} (typical of polluted continental air masses) and that free troposphere, or upper free tropospheric concentrations are relatively constant at a concentration of the order of 500 cm^{-3}. Above 15 km, in the stratospheric layer, CN concentrations are typically 1–10 cm^{-3}, despite the volcanic

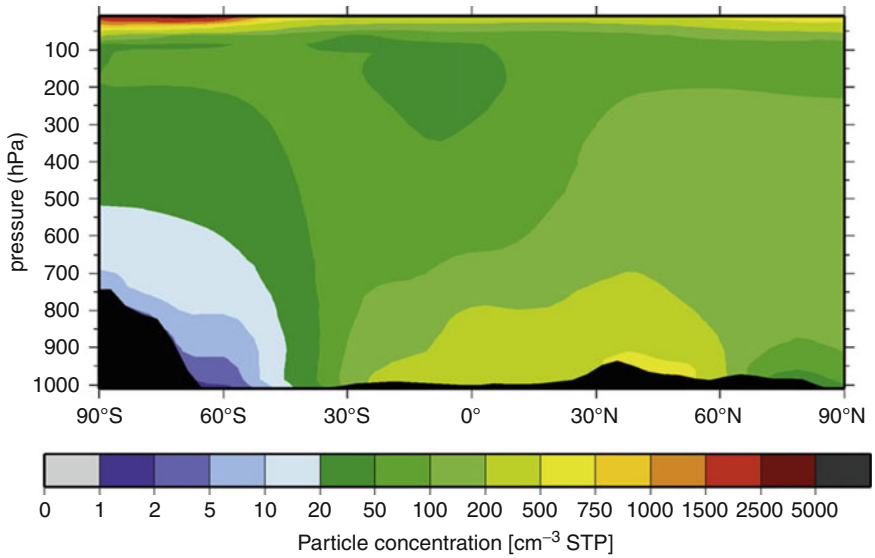

Aerosol in Global Atmosphere. Figure 11
Climatological annual means of simulated zonally averaged vertical cross-section accumulation mode aerosol particle concentration obtained from a 10-year integration. The concentrations are given at STP conditions (Copyright European Geophysical Union 2006. Reprinted from [59])

eruption. However, what is evident in the difference in time lapse following the eruption is that there is a significant increase in aerosol concentration (at least an order of magnitude) at sizes greater than 0.15 μm radius 1 year after the eruption compared to what is considered the background stratospheric aerosol burden 15 years after the eruption. Clearly, volcanic eruptions are a major source of stratospheric aerosols with injections to the tune of 30 Tg SO_2 for intense eruptions such as Pinatubo, producing the main precursor for stratospheric aerosol formation. In terms of stratospheric aerosol chemical composition, the majority of stratospheric aerosol is composed of 75% sulfuric acid and 25% water, formed from binary homogeneous nucleation and subsequent condensation of sulfuric acid as suggested by boiling point measurements of the stratospheric aerosol [61]. Other sources of stratospheric aerosols include organic carbonyl sulfide, particularly above altitudes of 25 km, and meteoritic material, rocket exhaust, and aircraft emissions are regarded as having minimal influence on the stratospheric aerosol layer [[60] and references therein.].

A particularly interesting stratospheric aerosol is aerosol forming polar stratospheric clouds (PSCs). These aerosol haze layers, or more often known as cloud layers, have been the subject of intense interest after the discovery of their role in stratospheric ozone loss through converting chlorine inactive to active chlorine and denitrifying the stratosphere. Observational, laboratory, and theoretical work has since shown that PSC particles above the ice point are either solid nitric acid trihydrate (NAT) particles or liquid ternary aerosol (LTA), droplets composed of nitric acid, sulfuric acid, and water. The composition and phase of the particles determines the threshold temperatures at which they occur and persist – specifically, NAT will exist at temperatures 3–5 K above LTA temperatures, while LTA will begin to appear about 3 K above the ice point for polar stratospheric levels of gaseous nitric acid and water [62, 63]. Particle phase also controls the development of particle size, which plays a large role in the extent and rate of dehydration/denitrification, thus determining the time frame during which chlorine will remain active, and ultimately determining the fundamental processes associated with ozone depletion in the polar stratosphere.

The main open question concerning the formation of PSCs is the process by which NAT forms. LTA growth is strictly a function of gas-phase-mixing ratios and temperature, as the vapor pressures of sulfuric acid,

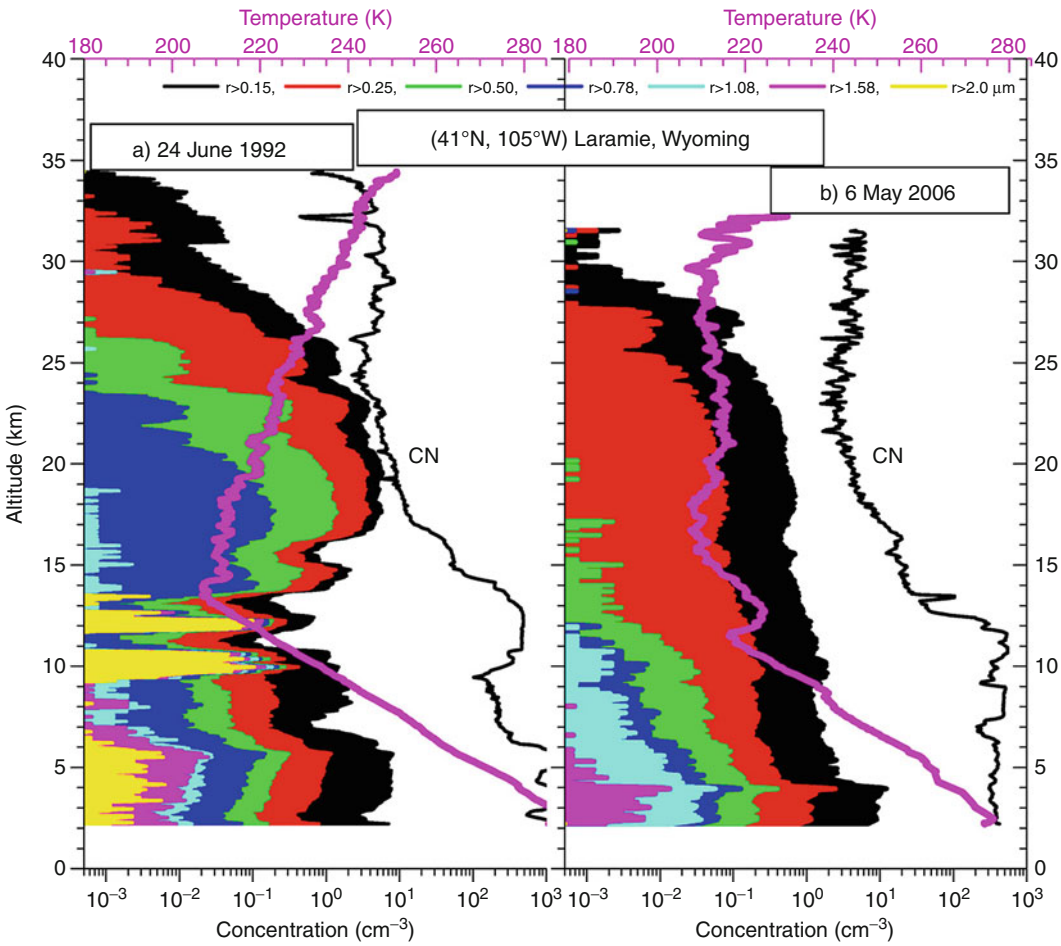

Aerosol in Global Atmosphere. Figure 12

Stratospheric aerosol profiles above Laramie Wyoming (41°N,106°W) indicating the concentration of condensation nuclei (CN) and aerosol with radii greater than 0.15, 0.25, 0.50, 0.78, 1.08, 1.58, and 2.0 μm. Temperature with scale at the top is also shown. These profiles were measured in (**a**) June 1992, 1 year after the Pinatubo eruption and (**b**) May 2006, 15 years after Pinatubo (Copyright Elsevier 2008. Reprinted from [60])

nitric acid, and water adjust to environmental temperature and molecular collisions. LTA begins to grow on the SA as soon as temperatures reach about 3 K above the ice point. At these temperatures, the concentration of NAT particles is often at best only 0.001 of the aerosol population [64–66] indicating clearly a nucleation barrier which is not well understood. Laboratory investigations suggest that LTA must be significantly supercooled for NAT nucleation. Arctic PSC observations in the early 2000s suggest the importance of a small population of NAT particles and that such a population forms at temperatures just a few degrees below the NAT point in both leewaves [64] and synoptic situations [66]. These latter observations are the clearest evidence yet indicating that NAT forms readily on a small fraction (10^{-4}–10^{-5}) of SA through heterogeneous nucleation.

Water Uptake by Aerosols

One of the most important gases in the atmosphere is water vapor as it not only contributes predominantly to the natural greenhouse effect, resulting in a livable global average temperature, in its condensed liquid and ice phases, it forms aerosol haze and cloud layers which contribute to approximately 50% of the planetary albedo. Many aerosol types have an affinity to

water and, under the right humidity conditions, they can become solution droplets, larger than the dry aerosol size, by uptake of water vapor from the air around it. Aerosol humidification has implications for optical scattering, condensation processes, and chemical interactions on and within aerosol particles. Liquid water clouds are extensive in the atmosphere, but as was shown above, pure water droplets cannot form under atmospheric conditions. Condensation nuclei are required for the formation of cloud droplets. Cloud droplets are aerosol particles that have rapidly grown to 10–100 times the size of the initial nucleus, corresponding to more than 1,000 times increase in mass, almost solely through water uptake.

Aerosol Hygroscopicity

A large fraction of the atmospheric aerosol population is water soluble or partially water soluble. The soluble aerosols are typically salts such as sea-salt or ammonium sulfate which readily dissociates in water to form an electrolyte solution droplet. In subsaturated air (relative humidity $< 100\%$), these solution droplets can exist due to the lowering of the equilibrium vapor pressure above the droplet surface by the presence of the dissolved ions (known as the Roault Effect). As a result, soluble aerosol particles, depending on the chemical composition, readily form solution drops with a water fraction dependent on relative humidity. This means that the "wet" aerosol equilibrium size responds to, and is dependent on, ambient relative humidity. The "wet" aerosol size will grow with increasing humidity and shrink with reducing humidity. Since the optical properties (e.g., scattering) of aerosols is size dependent (and proportional to cross-sectional area), relative humidity can significantly influence the hazing, or optical extinction effect of aerosol layers. A measure of this effect is the hygroscopic growth factor, normally defined as the change in aerosol diameter from a low relative humidity (e.g., 40%) corresponding to a dehydrated dry-size diameter to a high relative humidity (normally 90%) with significant hydration. Salts like ammonium sulfate and sea-salt have a growth factor of 1.8 and 2.2, respectively, over this humidity range, while organic aerosol possesses a growth factor typically from 1 to 1.4 depending on the degree of solubility.

Cloud Droplet Activation

In supersaturated environment, a subset of the aerosol can grow to a critical size which becomes metastable, and with an infinitesimal further increase in humidity, the droplet will become unstable and spontaneously grow to sizes of the order of 10 μm and become a cloud droplet. This process is called cloud droplet activation. The description of the equilibrium size of a droplet with water saturation ratio, founded on the early work of Kőhler [67], is now well established and can be readily derived from the *Clausius–Clapeyron* equation modified to give a general equilibrium relation between an aqueous salt solution droplet and water vapor (known as the Kőhler curve):

$$S = a_w \exp\left(\frac{2v_w\sigma}{RTr}\right)$$

S, is known as the saturation ratio, a_w is the water activity, the term within the brackets is the Kelvin factor, v_w is the partial molar volume of water, σ is the surface tension of the solution at the composition of the droplet, R is the universal gas constant, T is the droplet temperature, and r is the particle radius.

This form of the Kohler equation can be simplified to [1, 68–72]

$$S = 1 + \frac{A}{r_c} - \frac{B}{{r_c}^3} \quad A = \frac{2\sigma}{n_w kT} \quad B = \frac{vmM_w}{M_s 4/3\pi\rho_w}$$

where v is the number of dissociated ions per solute molecule, m_s is the solute mass, and subscripts "s" and "w" relate to solute and water properties, respectively. The term in A is denoted the Kelvin or curvature term, and the term in B, is known as the Raoult or solute term. The curvature term results in an increase in equilibrium vapor pressure with reducing particle size, while the solute term results in a reduction in equilibrium vapor pressure with increasing solute mass.

Figure 13 shows the contribution of the Kelvin and Raoult terms to equilibrium vapor pressure and equilibrium droplet size for a 200 nm dry diameter ammonium sulfate particle in a subsaturated and supersaturated regime [73]. This form of the expression shows a single characteristic maximum in supersaturation for a given dry composition and size, known as the critical supersaturation, S_c, associated with

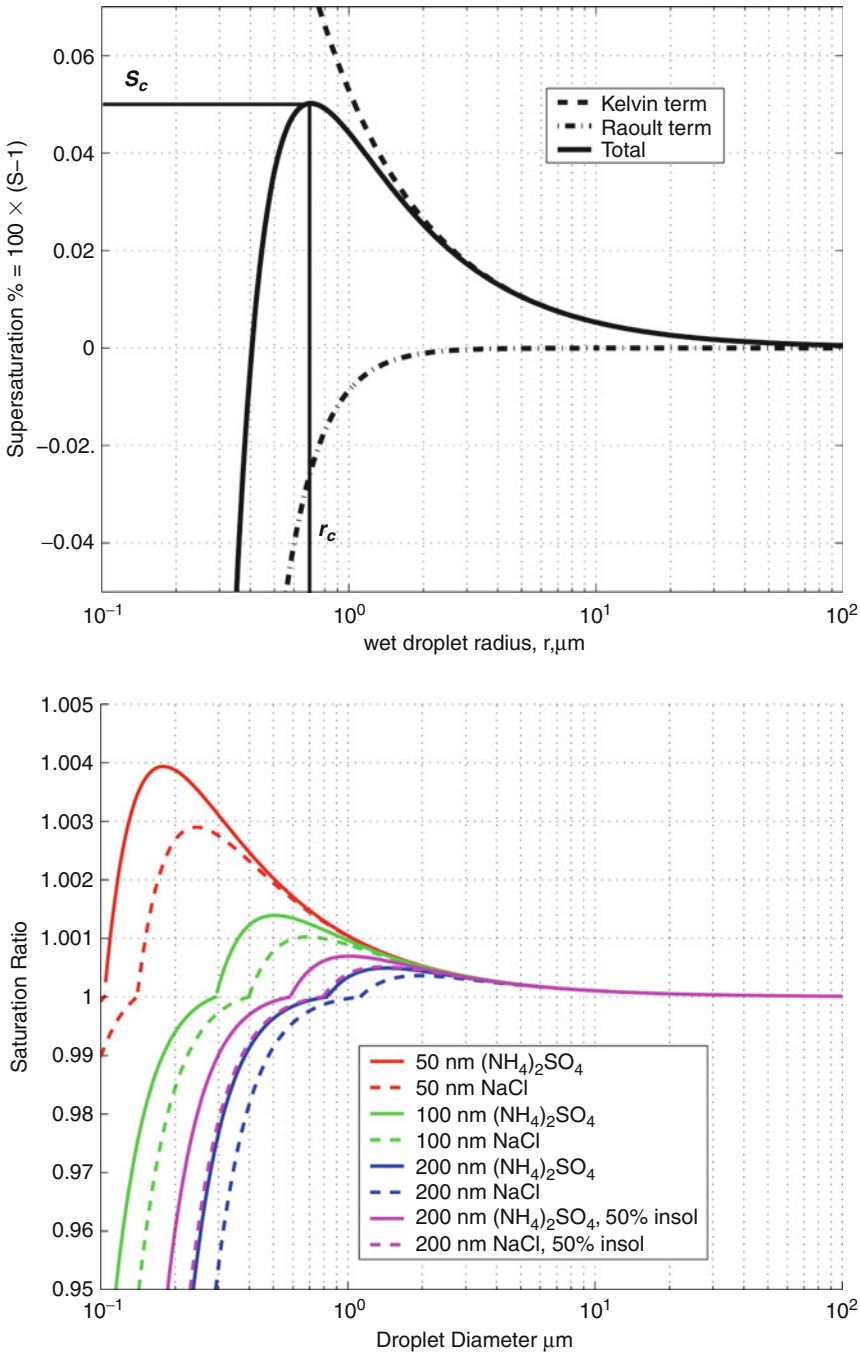

Aerosol in Global Atmosphere. Figure 13

Top: The Kőhler equation can be envisaged as the competition between the curvature (Kelvin) and solute (Raoult) terms. *Bottom*: Activation curves for a range of dry diameter of salt ($(NH_4)_2SO_4$ – solid, NaCl – dashed) particles (red, green and blue curves) and for 200 nm particles containing 50% by mass insoluble core (magenta) (Copyright European Geophysical Union 2006. Reprinted from [73])

a unique size, denoted by the critical radius, r_c. Using the simplified Kőhler curve expression, the analytical solutions for the critical quantities are:

$$r_c = \sqrt{\frac{3B}{A}} \quad S_c = \left(\frac{4A^3}{27B}\right)^{\frac{1}{2}}$$

For an increasing environmental value of S below S_c, there is a unique equilibrium droplet size. Once the droplet grows beyond its critical size (i.e., as the environmental S increases above S_c), the droplet will exhibit unimpeded growth unless the environmental S reduces below the equilibrium value of S_c at the instantaneous value of r_c. In this case, with no further change in S, the droplet will evaporate to its subcritical equilibrium size.

The Kőhler expression can be envisaged as the competition between the two expressions of component properties determining activation of particles: the curvature term and the solute term. The solute terms depend first on the number of solution molecules and then on the dissociation of these molecules. The effect can be illustrated for two frequently assumed cloud condensation nuclei types: ammonium sulfate and sodium chloride. $(NH_4)_2SO_4$ has a molecular weight of 132 g Mol^{-1}, while that of NaCl is 58.5 g Mol^{-1}. Thus, in the absence of dissociation, a given mass of NaCl in solution would yield 2.26 times more dissolved molecules than $(NH_4)_2SO_4$. Assuming full dissociation (infinite dilution), $(NH_4)_2SO_4$ yields three ions while NaCl yields two, so the net effect of the molecular mass and dissociation is that NaCl is 2.26/1.5 = 1.5 times more active than $(NH_4)_2SO_4$ for the same dry mass of particle (the S_c ratio for the two species is around 1.22 due to the square root dependence). This is illustrated in Fig. 13 where the peak supersaturation is plotted versus dry diameter for particles comprising each electrolyte. This figure directly illustrates the significant differences in the critical supersaturation as a function of both the chemical composition and dry size of a particle (Raoult and Kelvin effects). Additionally, in this figure is illustrated the effect of nuclei containing an insoluble core. The effect of an insoluble core is to increase the critical supersaturation required for activation. Cloud nuclei can comprise more complex composition compared to the above cases which will require modifications to the Kőhler expression. For example, nuclei can contain limited solubility components, immiscible liquid phases, and surface-active components. In the latter case, nuclei containing surface active components which alter the droplet surface tension (i.e., reduce surface tension) will have a reduced contribution from the Kelvin term in the Kőhler equation and consequently will require a lower critical supersaturation for activation. However, critical supersaturation is not always decreased since the surfactant may not dissociate into as many ions and while the Kelvin term may be reduced, so may the Raoult effect to an even greater amount. This effect for an ammonium sulfate nuclei (which dissociates into three ions) enriched with 30% mass fraction by the surfactant stearic acid (single ion) is that the critical supersaturation is actually increased. Supersaturations in natural clouds are of the order of 0.1–0.5% for stratiform clouds and below 1% for most convective clouds. This provides a lower limit to the size of particles that can act as cloud nuclei, namely, 30–50 nm, but more commonly, aerosols larger than 100 nm provide the majority of cloud nuclei. Nitric acid can also influence cloud nucleus activation in that it can temporarily partition into the aerosol phase as a nucleus takes up water vapor in the rising humidity field below cloud base. The uptake of nitric acid into the solution droplet increases the solute mass and, as a result, lowers the critical supersaturation required for the nucleus.

Ice nuclei are also important cloud nuclei but produce cloud particles in a very different manner and are comprised of very different chemical composition. Typically, they comprise non-water-soluble matter such as mineral dust and certain primary biogenic aerosol particles. Ice particles are formed either by heterogeneous nucleation in a supersaturated (with respect to ice) environment or homogeneous freezing of supercooled liquid droplets [74]. Far less is known about the nature of ice nuclei than what is known about cloud condensation nuclei.

Aerosols, Global Radiative Budget, Precipitation, and Climate

Aerosols affect the global radiative budget, and hence the global climate, directly through the scattering and/or absorption of incoming solar radiation (and for some aerosol species generally of supermicron size, outgoing infrared radiation) and indirectly

through the modification of cloud microphysics and radiative properties. The former effect is called the direct aerosol radiative forcing effect and the latter, the indirect radiative forcing effect where radiative forcing is defined as "The radiative forcing of the surface-troposphere system due to the perturbation in or the introduction of an agent (say, a change in greenhouse gas concentrations) is the change in net (down minus up) irradiance (solar plus longwave in Wm^{-2}) at the tropopause after allowing for stratospheric temperatures to readjust to radiative equilibrium, but with surface and tropospheric temperatures and state held fixed at the unperturbed values." In simple terms, it is "the rate of energy change per unit area of the globe as measured at the top of the atmosphere" and often it refers to the change since preindustrial conditions (year 1750). Radiative forcing affects the climate, while alterations in aerosol availability and radiative forcing can affect precipitation.

Direct Effect

Rayleigh scattering describes the irradiance scattered by a sphere as small compared to the incident wavelength and proportional to $1/\lambda^4$, while Rayleigh absorption is proportional to $1/\lambda^4$ [75]. When particles are comparable to the incident wavelength, Mie scattering must be invoked where scattering is strongly dependent on particle size, shape, composition (via refractive index), and orientation relative to the incident radiation. For particles large relative to the wavelength, the extinction efficiency converges at 2 (the extinction paradox where twice the energy is removed compared to that derived using geometrical optics). For particles with a complex refractive index, some fraction of the incident radiation is absorbed. The extinction efficiency is defined as the sum of the scattering and absorption efficiency and the single scattering albedo (ω) is the ratio of the scattering coefficient to the extinction coefficient. One parameter used to quantify scattering extinction is the mass scattering and mass absorption efficiency, which quantifies scattering and extinction in terms of the aerosol mass distribution function. Both the mass scattering and mass absorption efficiencies as a function of particle size exhibit peak scattering and absorption efficiencies at sizes between 0.1 and 1 μm for typical atmospheric aerosol chemical compositions pointing to this size range as being the most important size range for aerosol optical properties. Efficient aerosol scattering types are sulfates and sea-salt, while efficient absorption types are black carbon and dust constituents such as hematite.

One of the more important parameters associated with the direct radiative effect is aerosol optical depth (AOD) which describes the extinction of radiation as it propagates through the atmosphere:

$$I/I_0 = e^{-\tau}$$

and

$$\tau = \sigma_{\text{ext}} H,$$

where σ_{ext} is the extinction coefficient of radiation propagating through an aerosol layer of height H.

In terms of radiative forcing, an aerosol layer can either cause a negative or positive sign change to planetary albedo, leading to a cooling or warming effect. ω is the key parameter, along with the albedo of the underlying surface, that determines whether an aerosol layer leads to heating or cooling. Over dark surfaces like the ocean, and regardless of the degree of absorption, albedo will be increased primarily due to the upscatter of incoming radiation. In contrast, over bright surfaces such as snow and desert surfaces, an absorbing component will reduce the amount of surface-reflected radiation radiated back out to space. An additional important factor related to absorbing aerosol layers is that they warm as they absorb radiation, leading to increased atmospheric stability and reduced convection. This effect, it will be seen later, can have important implications for cloud formation.

The global distribution of AOD for total aerosol types and individually for black carbon, particulate organic carbon, sulfate, dust, and sea-salt is shown in Fig. 14. The global average AOD, derived from the medium of the 10 AEROCOM models, is 0.12 (compared to 0.137 derived from satellites and sunphotometers) [57]. Peak AOD values of >0.6 are encountered over Northwest Africa and the Asian continent, and to a lesser degree, over Europe, the USA, and South America. The lowest AOD values of ~0.01–0.02 occur over Antarctica. Black carbon is seen to contribute 0.0036 to the global AOD, with hot spots over Europe and China where black carbon contributes 0.05 to AOD. Dust contributes 0.025 to global AOD with

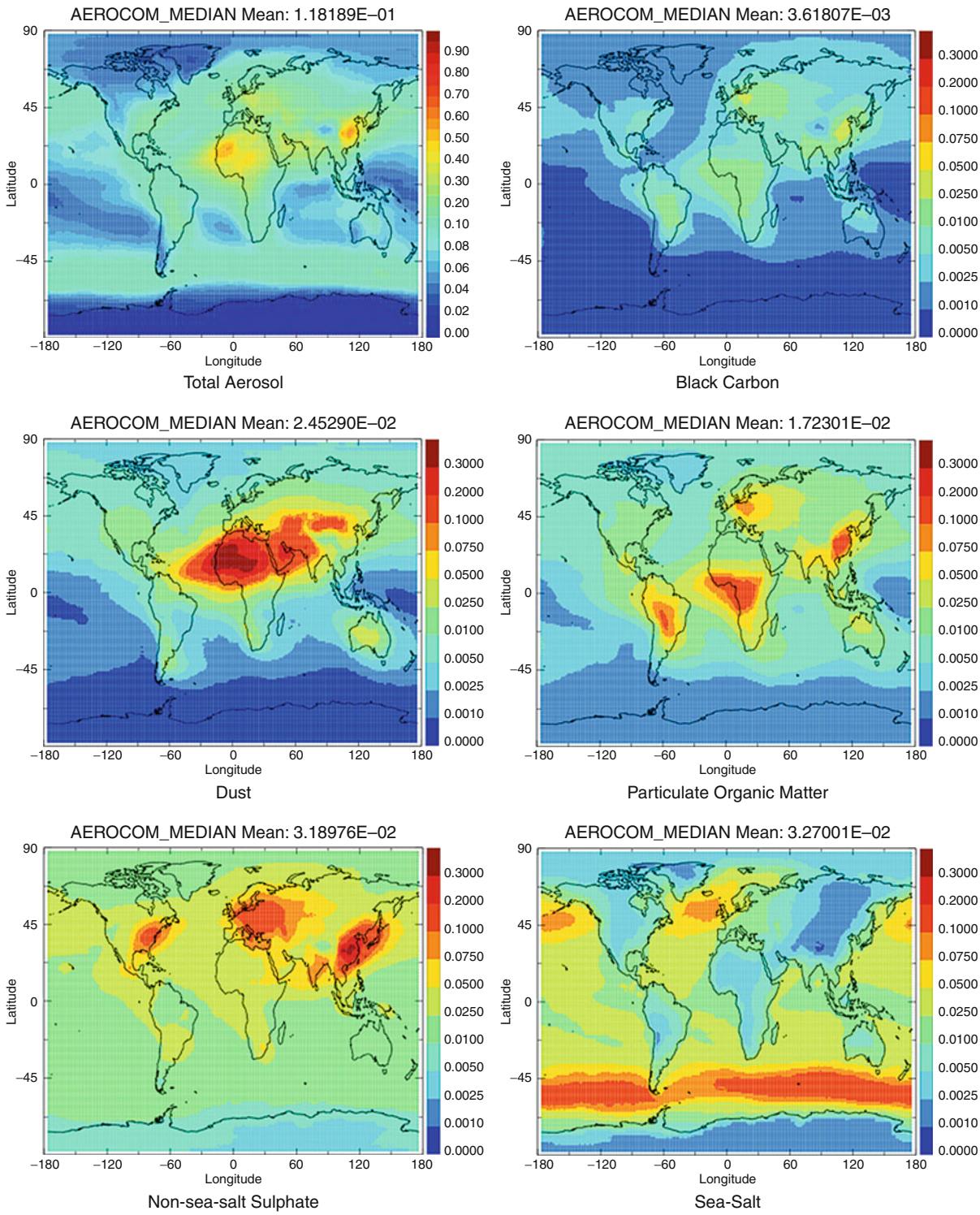

Aerosol in Global Atmosphere. Figure 14

Median global distribution of aerosol AOD, total and per aerosol species, derived from 10 AEROCOM models for the year 2000 (Copyright European Geophysical Union 2006. Reprinted from [57])

peak contributions of 0.3 arising over Northwest Africa, and 0.2 of Asia. Particulate Organic Matter contributes 0.017 to global AOD, with hot spots in midwest Africa (from biomass burning), South America, some regions in Europe and China contributing AOD greater than 2. Sulfate contributes 0.032 to the global AOD, with Europe, east Asia, and east USA contributing to hot spots with AOD about 0.3. Sea-salt contributes 0.033 to the global AOD, with values up to 0.2 seen in some oceanic regions were wind speeds are generally high (i.e., midlatitudes).

The AEROCOM models predict [76] that, for anthropogenic aerosols, a harmonized estimate for the aerosol direct radiative forcing under all-sky conditions, on a global annual basis, is -0.22 Wm^{-2}, ranging from +0.04 to -0.41 Wm^{-2}, with a standard deviation of ± 0.16 Wm^{-2}. Anthropogenic nitrate, secondary organic aerosol, and dust were not, however, included in the estimate. By comparison, the IPCC AR4 [100] reported a direct aerosol radiative effect best estimate of -0.5 W m^{-2} with an uncertainty of -0.9 to -0.1 W m^{-2}. The global annual mean aerosol surface radiative forcing is illustrated in Fig. 15 where it can be seen in the regions with highest aerosol loadings, negative forcings as high as -10 W m^{-2} are encountered. More recent estimates, using a combination of satellite data with a global model [77] suggested a value of -0.65 W m^{-2}. The diversity in model estimates stems more from different model approaches to transport processes, removal mechanisms, and microphysics treatment rather than aerosol emission inventories.

Indirect Effect

There are a number of indirect aerosol radiative effects whereby aerosol fields modify the cloud microphysics, structure, or lifetime, all of which have albedo impacts. The first indirect effect (typically associated with "warm" or water clouds of fixed liquid water content), results from an increase in cloud condensation nuclei leading to a higher number of smaller cloud droplets which ultimately, through an increase in number of droplets, and the increased scattering associated with

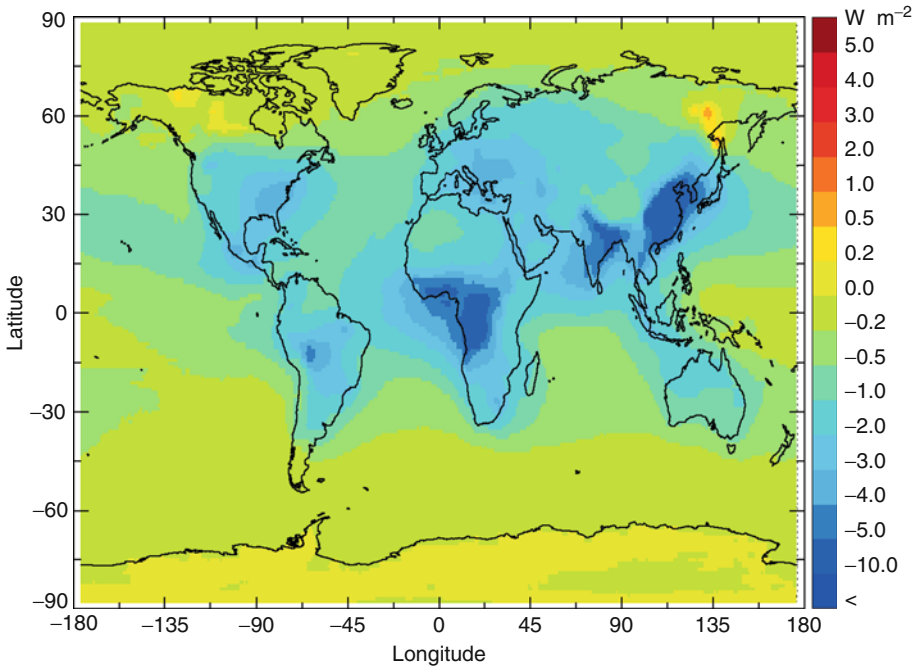

Aerosol in Global Atmosphere. Figure 15
Aerosols in the Global AtmosphereGlobal annual mean aerosol surface radiative forcing from AEROCOM models (Copyright European Geophysical Union 2006. Reprinted from [76])

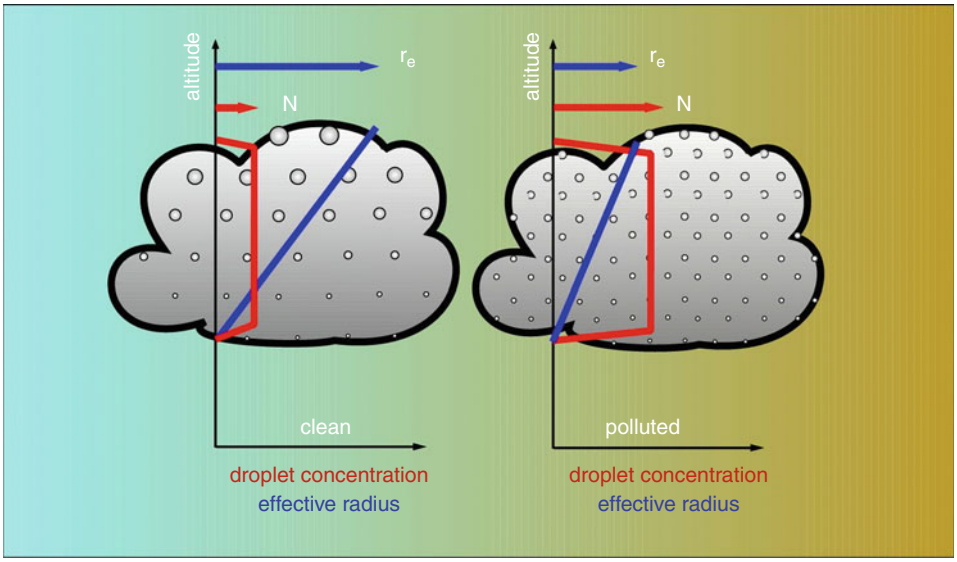

Aerosol in Global Atmosphere. Figure 16
Illustration of changes in cloud microphysics resulting from low (clean) and high (polluted) aerosol fields. For a cloud with the same available liquid water content. With more cloud nuclei available for droplets to form on, the resulting droplets are necessarily smaller in size. The cloud's effective radius is thus smaller and smaller droplets are more efficient scatters of visible radiation. This, combined with an increase in the number of scattering droplets, results in a more reflective cloud (Courtesy L. Schüller and J.L. Brenguier)

smaller droplets, leads to an albedo increase [72, 74]. Figure 16 illustrates this effect. A cloud is generally formed by rising air parcels which eventually become supersaturated. Cloud droplets are activated at cloud base and continue to grow as the air parcel containing the droplets rise to the top of cloud. Even for a fixed number of droplets, their size and liquid water content increases with increasing height into the cloud. A parameter used to describe an effective radius in such a changing field is the cloud drop effective radius defined as the weighted mean of the size distribution of the cloud droplets. This amounts to the ratio of the volumetric distribution to the surface area distribution – or the ratio of the third moment of the distribution to the second moment. Take the two cases of clouds forming under the same environmental conditions (and hence the same available liquid water content), but under different aerosol fields, one clean containing a low number of cloud nuclei, and the other polluted, containing a high number of cloud nuclei. The same amount of liquid water has to be shared out to different nuclei concentrations entering into cloud base. The result is that the clean cloud with a low nuclei and droplet concentration ($N \sim 50$ cm^{-3}) leads to a relatively large effective radius (of the order of 15 μm), while the polluted cloud with high nuclei and droplet concentration ($N \sim 300$ cm^{-3}) leads to a relatively low effect radius (of the order of 5 μm). The net effect is a higher cloud albedo seen at cloud top. An excellent example of this effect is seen in Fig. 17, which displays a satellite image of a Pacific Ocean stratocumulus cloud deck off the west US coast. Seen within the cloud deck are numerous tracks more visible than the background cloud. These tracks are called ship tracks and result from ship stack emissions, rich in cloud nuclei, rising into cloud and modifying cloud microphysics as described above. These tracks are easily visible since the tracks have produced regions of increased reflectance relative to the "clean" regions of the cloud. While ship tracks do not necessarily have a climate impact, they are excellent illustrative examples of the first indirect aerosol effect.

The first indirect effect is particularly important over oceans (where surface albedo is low and clouds

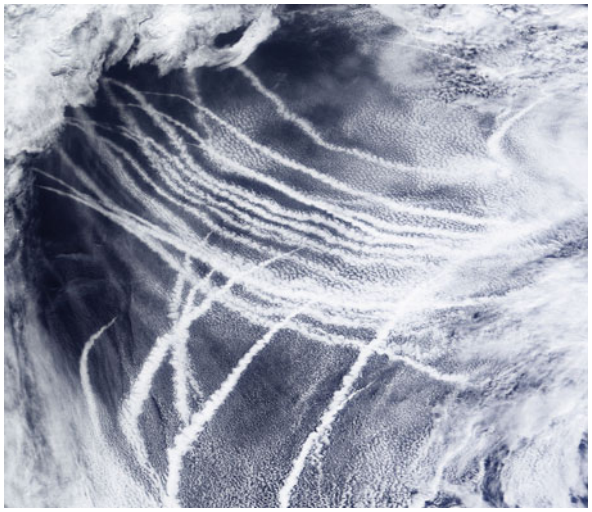

Aerosol in Global Atmosphere. Figure 17
AVHRR satellite image of a stratocumulus cloud deck off the US Washington coast. The tracks are ship tracks produced by ship stack emissions mixing into cloud, resulting in an increase in cloud droplet concentration and reflectance

are very susceptible to changes in aerosol or nuclei availability) and in regions where persistent and extensive stratocumulus cloud decks occur. It is in these regions that the radiative forcing associated with the indirect effect is at its maximum.

The second indirect effect relates to the cloud lifetime effect [78], and relates to a suppression of precipitation due to the smaller mean droplet sizes. The smaller drops have reduced collision-coalescence efficiency and as a result the onset of precipitation can be delayed or even shut down. Given that precipitation is one important process in shortening the lifetime of a cloud, lack of precipitation can increase cloud lifetime and at times, vertical and horizontal extent. Longer lifetimes or greater extent of clouds effectively increases the albedo since cloud optical depth is always greater than aerosol optical depth.

The semi-indirect effect results from aerosol with a significant absorbing component, which heats the atmospheric layer in which the absorbing aerosol resides [79]. This can inhibit cloud formation by reducing stability and reducing relative humidity through increasing the layer temperature and reducing surface water vapor evaporation. It can also lead to increased evaporation rates for existing clouds. The sign of the effect is, however, a matter of debate. Some studies [80] support the warming effect of absorbing aerosols through decreased low-level cloud cover and other studies found that cooling effects through increased cloud coverage [81, 82]. The height of the absorbing layer seems to impact on the sign of the effect.

Other effects include the cloud glaciation effect where an increase in anthropogenic ice nuclei can lead to an increase in cloud glaciation [83], the deactivation effect where anthropogenic sulfate coats ice nuclei making them inactive [84], and the thermodynamic effect where smaller droplets freeze less efficiently than larger droplets [85].

From the IPCC AR4, the most recent consensus on the first indirect effect of warm clouds [86] estimated a range between -0.22 and -1.85 W m^{-2}, with a best estimate of -0.7 W m^{-2}. The combined first and second indirect effect was estimated to have a radiative forcing between -0.2 and -2.3 W m^{-2}, illustrating the difficulties in achieving convergence of these models as the level of complexity increases.

Aerosol–Cloud–Precipitation Interactions

Although the second indirect effect, through changes in cloud microphysics, has been demonstrated to reduce precipitation with increased anthropogenic aerosol, this effect typically applies to warm stratiform clouds and shallow cumulus clouds. Similarly, the radiative effects generally act to suppress precipitation through decreasing the amount of solar radiation reaching the surface thereby reducing the amount of energy available to evaporate water and energize convective clouds. The radiation not reflected back to space is partly absorbed in the atmosphere in the presence of absorbing carbonaceous aerosol leading to a warming of the air above the surface. This warming stabilizes the lower atmosphere and suppresses convection and the generation of convective clouds.

Some studies have also shown [87] that increases in cloud nuclei can invigorate deep convective rain clouds with warm cloud bases ($T > 15°$C). In such clouds, the auto-conversion processes (coalescence of droplets into raindrop sizes) are delayed and hence the onset of precipitation in the cloud is also delayed. This results in more water ascending to higher altitudes and colder

temperatures ($T < 0°C$). Through the delay of precipitation, the additional latent heat release invigorates the cloud. In addition, by not raining early, the condensed water can form ice precipitation particles that release the latent heat of freezing aloft and these reabsorb heat at lower levels where they melt after falling [88]. This process leads to consumption of more convective available potential energy (CAPE) which would then be converted to an equally greater amount of released kinetic energy that could invigorate convection and lead to a greater convective overturning, more precipitation, and deeper depletion of the static instability.

The increased amount of aerosol has two competing effects: one radiative, which suppresses convection (and consequently rainfall) through absorption and warming of atmospheric layers relative to the surface, and the other, which can lead to invigoration of updrafts, leading to an increase in precipitation. These two processes have typically been treated separately leading to opposing views on the impact of aerosols on precipitation. This competing effect was elucidated recently [89] by looking at the combined effect of increasing aerosol and cloud condensation nuclei concentrations on both microphysical and radiative properties. They modeled typical warm tropical convective clouds and found that the microphysical invigoration effect was at a maximum for moderate cloud condensation nuclei concentrations, above which the impact of additional nuclei was reduced. However, as the cloud condensation nuclei concentrations were linearly correlated to AOD, AOD progressively increased with increasing cloud condensation nuclei concentrations which reduced the solar flux which in turn energized convection reaching the surface. As a result, with increasing aerosol loads beyond the optimum, the weakening of the microphysical invigoration is reinforced by the suppressive effect of reduced surface heating. This conceptual model is illustrated in Fig. 18 where it is seen that starting out with clean (low) nuclei concentrations ($N \sim 100$ cm^{-3}), the addition of more nuclei has the effect of increasing the released convective energy up to a maximum point corresponding to a cloud condensation nuclei concentration of the order of 1,200 cm^{-3}. At this point, AOD is a moderate 0.25. Further increases in cloud condensation nuclei result in a reduction of released convective energy with CAPE dropping rapidly at concentrations over 5,000 cm^{-3}, but AOD continues to rise, reaching 1 for extreme nuclei concentrations of 10,000 cm^{-3} (corresponding to 2,000 cm^{-3} cloud droplets. The slope of the CAPE curve represents the effect of aerosols on precipitation. For increasing CAPE release with increasing aerosol concentrations, an increase in precipitation is expected. This trend reverses for moderate levels of aerosol pollution, above which suppression of precipitation is associated with increasing aerosol concentrations.

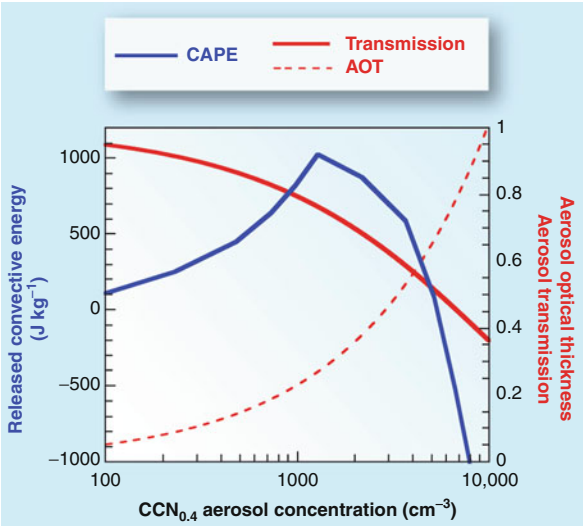

Aerosol in Global Atmosphere. Figure 18
Illustration of the relations between the aerosol microphysical and radiative effects. The aerosol optical (dept) thickness (AOT) is assumed to reach 1 at $CCN_{0.4} = 10^4$ cm^{-3} (dashed red line), which corresponds to nucleation of 2,000 cloud drops cm^{-3}. The related transmission of radiation reaching the surface is shown by the solid red line. The vigor of the convection is shown by the blue line, which provides the released convective available potential energy (CAPE) of a cloud parcel that ascends to the cloud top near the tropopause. Note that a maximum in CAPE occurs at $CCN_{0.4} \approx 1{,}200$ cm^{-3}, which corresponds to the maximum cloud invigoration. The AOT corresponding to the $CCN_{0.4}$ at the microphysical optimum is only 0.25. Adding aerosols beyond this point substantially decreases the vigor of the cloud because both microphysical and radiative effects work in the same direction: smaller release of convective energy aloft and less radiative heating at the surface (Reprinted from [89])

Aerosol–Climate Interactions

The IPCC AR4 concluded that the combined aerosol radiative forcing was negative and partly offset the warming, or positive forcing, by greenhouse gases. This suggests that aerosols, perhaps, have been masking the true rate of global warming, or the climate-temperature sensitivity to CO_2-induced global warming. Over the past 40 years, there has been both observed dimming and brightening trends that point to a direct aerosol influence on climate. Global dimming is a term associated with a decadal decrease in surface solar radiation, while global brightening refers to an increase in surface solar radiation. Studies [90–92] have shown a widespread decrease in surface solar radiation at a variety of locations worldwide between 1960 and 1990. Increasing aerosol concentrations associated with increased air pollution over the period are considered responsible for the dimming [93]. Changes in cloud reflectance and cloud amount contribute to the dimming [90]; however, in a particular study over Europe [94], it was concluded that cloud amount could not explain the dimming and that the aerosol direct and indirect effect was the predominant cause for the trend. The period from 1990 to the present shows a reversal of the trend into a brightening trend [95]. The dimming effect appeared to have been masking, or suppressing, greenhouse warming with reduced or even negative trends on global temperatures over the period as greenhouse gases continued to accumulate. As the trend reversed from dimming to brightening, rapid temperature rises became evident since the mid-1980s. Since the mid-1980s, the decadal rise in temperature has been +0.38°C per decade (Fig. 19), significantly higher than any other period since the preindustrial era [96]. The brightening has been associated with reduced aerosol pollution since the 1980s as developed countries implemented policies to clean up air pollution.

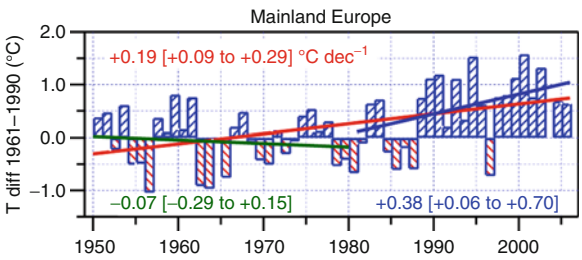

Aerosol in Global Atmosphere. Figure 19
Temperature rise over mainland Europe since 1950. Annual temperature differences for the period 1950 to 2005 with respect to the 1961–1990 climatological mean for mainland Europe (45_–55_N; 5_–15_E). Linear regression lines and decadal trends with 95% confidence interval show the temperature decline from 1950 to 1980 (green), and the temperature rise to be twice as large for the period 1981 to 2005 (blue) than for the whole period 1950 to 2005 (red) (Copyright American Geophysical Union 2009. Reprinted from [96])

Aerosols and Air Pollution

Aerosol is one atmospheric constituent regarded as an air pollutant. In Air Quality communities, aerosol particles are termed particulate matter (PM). Aerosol air pollution is typically measured as the total mass less than a particular cutoff size (e.g., 10 μm for PM_{10}, 2.5 μm for $PM_{2.5}$, and 1 μm for PM_1). Air quality is regulated in terms of exposure to a particular PM standard. Air pollution has been a serious problem since the eighteenth century with the invention of the steam engine which increased the amount of coal burning. Prior to that, air pollution was still a problem due to wood and coal burning although not as severe. In 1905, the term "smog" was coined and it described the combination of smoke and fog that was visible in many industrialized cities. London experienced the most frequent and severe smog events resulting in many "excess" deaths. The worst of these occurred in December 1952 when there were 4,000 excess deaths during the London-type event. During this period, smoke mass concentrations reached 4,460 μg m^{-3}. This is to be compared with a current EU yearly exposure of 25 μg m^{-3} for $PM_{2.5}$ and 50 μg m^{-3} sustained over 24 h 35 times in 1 year for PM_{10}. The events typically occur in winter and during high pressure weather systems.

High pressure systems generally are accompanied by colder temperatures resulting in increased coal burning. In addition to the colder temperatures are stable atmospheric boundary layers, which suppress the dispersion of pollution. Further exasperating the situation are very stable surface-mixing layers 100–200 m deep, which trap the pollution and confine the pollution to a thick layer close to the ground.

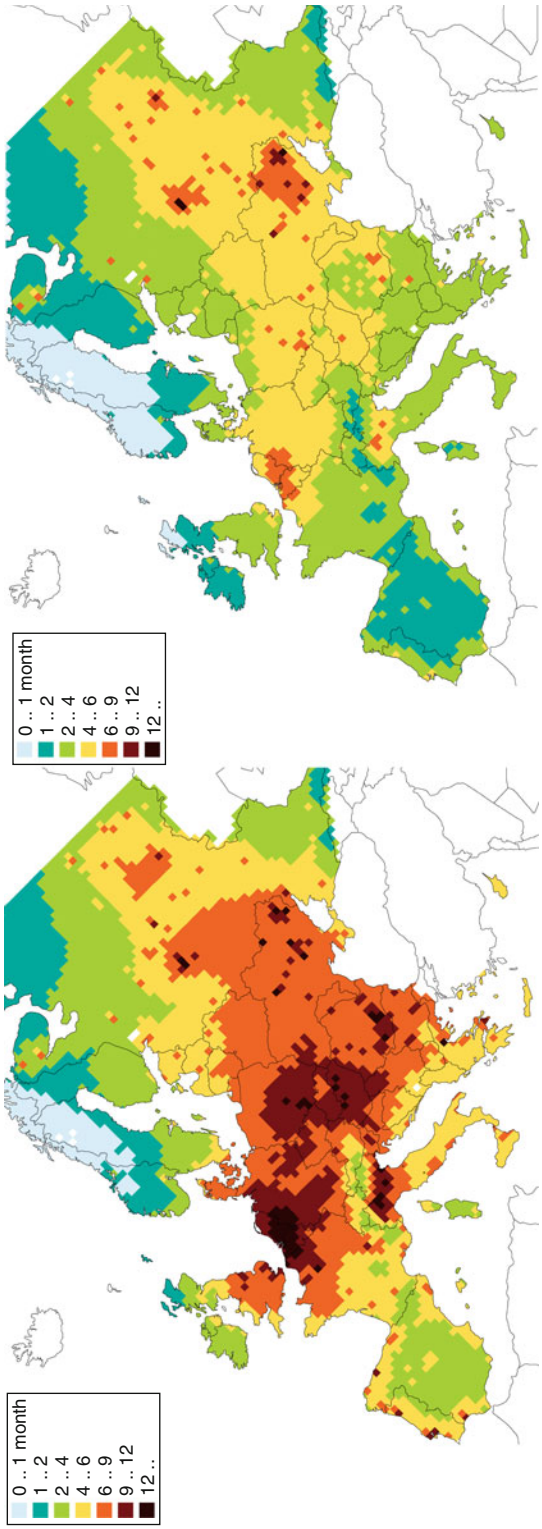

Aerosol in Global Atmosphere. Figure 20
Estimated loss in life expectancy attributable to exposure to fine particulate matter ($PM_{2.5}$) from anthropogenic emissions for the year 2000 (*left*) and projected reduced emissions for the year 2020 (*right*) (Modified from EEA Report No2/2007. Courtesy of Zbigniew Klimont and Markus Amann)

In addition to the London-type smog, there is a chemically produced smog known as photochemical smog. Photochemical smog is produced through gas phase reactions typically involving hydrocarbons, NO, and ozone and is a frequent phenomenon encountered in many megacities such as Los Angeles, Mexico City, Tokyo, Beijing, Johannesburg, and Athens.

The main health impacts of PM relate to respiratory and cardiovascular effects and, additionally, some of the smoke products are considered carcinogenic, all potentially resulting in premature mortality. The European Union's Clean Air for Europe Programme estimated that 348,000 premature deaths occur in Europe due to exposure to $PM_{2.5}$. Figure 20 illustrates the

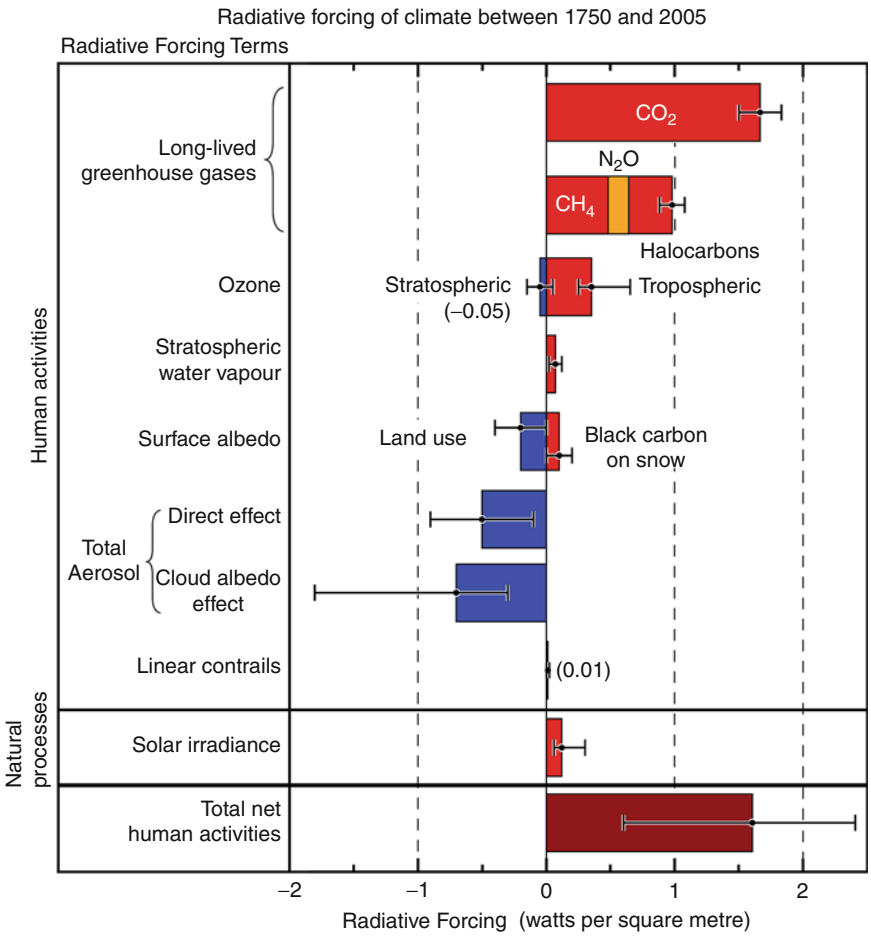

Aerosol in Global Atmosphere. Figure 21
Summary of the principal components of the radiative forcing of climate change. All these radiative forcings result from one or more factors that affect climate and are associated with human activities or natural processes as discussed in the text. The values represent the forcings in 2005 relative to the start of the industrial era (about 1750). Human activities cause significant changes in long-lived gases, ozone, water vapor, surface albedo, aerosols, and contrails. The only increase in natural forcing of any significance between 1750 and 2005 occurred in solar irradiance. Positive forcings lead to warming of climate and negative forcings lead to a cooling. The thin black line attached to each colored bar represents the range of uncertainty for the respective value (Reprinted from the Intergovernmental Panel on Climate Change Assessment Report 4)

estimated losses in life expectancy attributable to exposure to $PM_{2.5}$ from anthropogenic emissions in Europe [97]. The data are calculated for emissions for the year 2000 and for targeted emission reductions by the year 2020.

While air pollution, particularly aerosol air pollution, has been steadily reducing in the developed world, it has become an increasing problem in developing countries, not only on urban megacity scales but also on regional and almost hemispheric scales. Intercontinental and hemispheric transport of pollution is now regarded as a serious concern, impacting on local- and regional-scale air quality.

Future Directions: Interactions Between Aerosol Air Pollution and Climate

Atmospheric aerosol has played an important role in partly offsetting global warming due to greenhouse gases. The IPCC AR4 quantifies the best atmospheric composition component estimates of radiative forcing since 1750 to 2005 (Fig. 21). From this assessment, the combined direct and indirect effect amounts to ~ -1.2 W m^{-2}, which effectively can be regarded as a reduction in the positive forcing by greenhouse gases to an equivalent amount. The IPCC estimate the net forcing due to anthropogenic activities as $\sim +1.5$ W m^{-2}. This positive forcing has led to a global temperature increase of the order of 0.8°C. The European Union, leading the way in climate policy development, have set a long-term (i.e., by year 2050) target of an upper limit of 2°C to the increase in global temperature.

Until recent times, climate policy has been handled separately to air pollution problems, where in the latter case, adverse health effects from PM and ecosystem damage have been the biggest drivers of policies to improve air quality. What has become evident is that the air pollution policies in recent decades have impacted on global warming in a manner that has accelerated temperature rise as dirty air was cleaned up. The current decadal rate of temperature increase is estimated to be 0.3–0.4°C per decade. As a result, by the year 2030, the predicted temperature increase is ~1.9°C – that is,

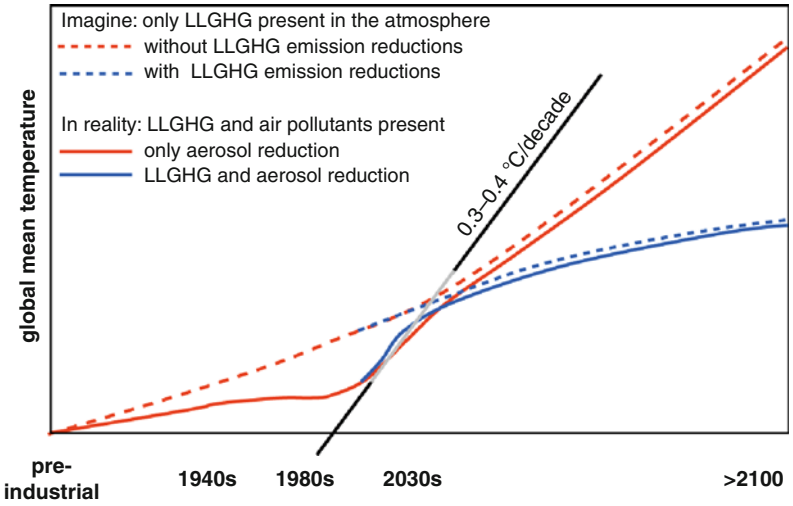

Aerosol in Global Atmosphere. Figure 22
The figure shows schematically the climate consequences of climate change and air pollution abatement strategies. The only way to reach global temperature stabilization is through LLGHG reductions. Such stabilization would be achieved according to the timescales mainly related to the several decade lifetime of LLGHG in the atmosphere. Reduction of air pollution (including that resulting from LLGHG emission reductions) would have a more immediate impact on global warming. Air pollutants have lifetimes of weeks to months, and the climate system would realize, in about 5 years, 50% of the global warming caused by their reduction [98]. Air pollutant reductions are expected to accelerate the increase in global mean temperature in the short term (<30 years), on the way to eventual long-term (>100 years) climate stabilization (Copyright Elsevier 2009. Reprinted from [99])

almost reaching the long-term target limit. Figure 22 illustrates the problem [99]. If there were only long-lived greenhouse gases (LLGHG), the past temperature increase would have been approximately double the actual increase since the preindustrial era. Without emission reductions, looking into the future, temperature will increase by about 0.2°C per decade. However, taking account of the presence of aerosols, the approximate 50% masking of temperature increase is evident up until the 1990s and then the current day and near future rapid rise in temperature from aerosol emission controls is evident, rapidly approaching the increase seen by treating the system as only containing LLGHG. With both a reduction on aerosol emissions and LLGHG, only then can the dual target of clean air and minimal temperature rise be achieved. Such combined policy development, while in the near term will accelerate temperature rise, in the long term, a sustainable temperature rise can be expected.

The development of sophisticated policy development is underpinned by the development of sophisticated climate and air pollution assessment models. Current climate models do not possess treatments of aerosol emissions, formation, transformations, and radiative effects to a high enough level of sophistication yet. This limitation results from the aerosol life cycle being one of the most complex systems to model and the challenges of modeling the formation of nanoclusters to global-scale radiative impacts and interactions with clouds will remain for some time. Nevertheless, the advances in recent years have been immense, most notably in the current day improved understanding of the highly complex nucleation processes and in the characterization of organic aerosols, their properties, and their life cycle.

Bibliography

1. Seinfeld JH, Pandis SN (1998) Atmospheric chemistry and physics: from air pollution to climate change. Wiley, New York/Chichester, air pollution to climate, 1998
2. Jaenicke R (1998) Atmospheric aerosol size distribution. In: Harrison RM, van Grieken RE (eds) Atmospheric particles. Wiley, Chichester, UK/New York
3. Brasseur GP, Prinn RG, Pszenny AAP (eds) (2003) Tropospheric aerosols. Atmospheric chemistry in a changing world – an integration and synthesis of a decade of tropospheric chemistry research. Springer-Verlag, Berlin, Heidelberg. ISBN: 3-540-43050-4
4. Gillette DA (1979) Environmental factors affecting dust emission by wind erosion. In: Morales C (ed) Saharan Dust, SCOPE 14. Wiley, New York, pp 71–91
5. Bishop JKB, Davis RE, Sherman JT (25 October 2002) Robotic observations of dust storm enhancement of carbon biomass in the North Pacific. Science 298(5594):817–821
6. Elbert W, Taylor PE, Andreae MO, Pöschl U (2007) Contribution of fungi to primary biogenic aerosols in the atmosphere: wet and dry discharged spores, carbohydrates, and inorganic ions. Atmos Chem Phys 7:4569–4588
7. Després VR et al (2007) Characterization of primary biogenic aerosol particles in urban, rural, and high-alpine air by DNA sequence and restriction fragment analysis of ribosomal RNA genes. Biogeosciences 4:1127–1141
8. Möhler O, DeMott PJ, Vali G, Levin Z (2007) Microbiology and atmospheric processes: the role of biological particles in cloud physics. Biogeosciences 4:1059–1071
9. Lewis ER, Schwartz SE (2004) Sea salt aerosol production: mechanisms, methods, measurements and models – a critical review, vol 152, Geophysical monograph. American Geophysical Union, Washington, DC
10. Monahan EC, Spiel DE, Davidson KL (1986) A model of marine aerosol generation via whitecaps and wave disruption. In: Monahan EC, MacNiocaill G (eds) Oceanic whitecaps and their role in air-sea exchange processes. Reidel, Dordrecht, pp 167–174
11. Blanchard DC (1963) The electrification of the atmosphere by particles from bubbles in the sea. Progr Oceanogr 1:71–202
12. O'Dowd CD, Lowe JA, Smith MH (1997) Marine aerosol, sea-salt, and the marine sulphur cycle: a short review. Atmos Environ 31:73–80
13. O'Dowd CD, Facchini MC, Cavalli F, Ceburnis D, Mircea M, Decesari S, Fuzzi S, Yoon YJ, Putaud J-P (2004) Biogenically-driven organic contribution to marine aerosol. Nature. doi:10.1038/nature02959
14. IEA (1998a) Energy statistics of OECD countries. International Energy Agency, Paris
15. IEA (1998b) Energy statistics of non-OECD countries. International Energy Agency, Paris
16. Watson JG et al (1994) Differences in the carbon composition of source profiles for diesel-powered and gasoline-powered vehicles. Atmos Environ 28(15):2493–2505
17. O'Dowd CD, Aalto P, Hämeri K, Kulmala M, Hoffmann T (2002) Atmospheric particles from organic Vapours. Nature 416: 497–498
18. Oxtoby DW, Kashchiev D (1994) A general relation between the nucleation work and the size of the nucleus in multicomponent nucleation. J Chem Phys 100(10):7665–7767
19. Riipinen I et al (2007) Connections between atmospheric sulphuric acid and new particle formation during QUEST III–IV campaigns in Heidelberg and Hyytiälä. Atmos Chem Phys 7(8):1899–1914
20. Weber RJ et al (1997) Measurements of new particle formation and ultrafine particle growth rates at a clean continental site. J Geophys Res-Atmos 102(D4):4375–4385

21. McMurry PH, Friedlander SK (1979) New particle formation in the presence of an aerosol. Atmos Environ 13(12):1635–1651
22. Kulmala M et al (2004) Formation and growth rates of ultrafine atmospheric particles: a review of observations. J Aerosol Sci 35(2):143–176
23. Kulmala M, Kerminen V-M, Anttila T, Laaksonen A, O'Dowd CD (2004) Organic aerosol formation via sulphate cluster activation. J Geophys Res 109:D04205. doi:10.1029/2003JD003961
24. Bonn B, Kulmala M, Riipinen I, Sihto SL, Ruuskanen TM (2008) How biogenic terpenes govern the correlation between sulfuric acid concentrations and new particle formation. J Geophys Res-Atmos 113:D12209. doi:10.1029/2007JD009327
25. Metzger A, Verheggen B, Dommena J, Duplissya J, Prevota ASH, Weingartner E, Riipinen I, Kulmala M, Spracklen DV, Carslaw KS, Baltensperger U (2010) Evidence for the role of organics in aerosol particle formation under atmospheric conditions. Proc Natl Acad Sci USA. doi:/10.1073/pnas.0911330107
26. O'Dowd CD, Jimenez JL, Bahreini R, Flagan RC, Seinfeld JH, Pirjola L, Kulmala M, Jennings SG, Hoffmann T (2002) Marine particle formation from biogenic iodine emissions. Nature 417:632–636
27. O'Dowd CD, Geever M, Hill MK, Jennings SG, Smith MH (1998) New particle formation: spatial scales and nucleation rates in the coastal environment. Geophys Res Lett 25:1661–1664
28. O'Dowd CD (2001) Biogenic coastal aerosol production and its influence on aerosol radiative properties. J Geophys Res 106:1545–1550
29. Hegg DA, Hobbs PV (1982) Measurement of sulphate production in natural clouds. Atmos Environ 16:2663–2668
30. O'Dowd CD, Lowe JA, Clegg N, Clegg SL, Smith MH (2000) Modelling heterogeneous sulphate production in maritime stratiform clouds. J Geophys Res 105:7143–7160
31. Henze DK, Seinfeld JH (2007) Global modeling of secondary organic aerosol formation from aromatic hydrocarbons: high- vs low-yield pathways. Atmos Chem Phys Discuss 7:14569–14601
32. Szidat S, Jenk TM, Synal HA, Kalberer M, Wacker L, Hajdas I, Kasper-Giebl A, Baltensperger U (2006) Contributions of fossil fuel, biomass-burning, and biogenic emissions to carbonaceous aerosols in Zurich as traced by 14C. J Geophys Res 111:D07206. doi:10.1029/2005JD006590
33. Kroll JH, Ng NL, Murphy SM, Flagan RC, Seinfeld JH (2005) Secondary organic aerosol formation from isoprene photooxidation under high-NOx conditions. Geophys Res Lett 32:L18808. doi:10.1029/2005GL023637
34. Decesari S, Mircea M, Cavalli F, Fuzzi S, Tagliavini E, Facchini MC (2007) Source attribution of water-soluble organic aerosol by nuclear magnetic resonance spectroscopy. Environ Sci Technol 41:2479–2484. doi:10.1021/es061711l
35. Claeys M et al (2004a) Formation of secondary organic aerosol through photooxidation of isoprene. Science 303:1173–1176
36. Claeys M, Wang W, Ion AC, Kourtchev I, Gelencsér A, Maenhaut W (2004b) Formation of secondary organic aerosols from isoprene and gas-phase oxidation products through reaction with hydrogen peroxide. Atmos Environ 38:4093–4098
37. Limbeck A, Kulmala M, Puxbaum H (2003) Secondary organic aerosol formation in the atmosphere via heterogeneous reaction of gaseous isoprene on acidic particles. Geophys Res Lett 30(19):1996. doi:10.1029/2003GL017738
38. Jang M, Czoschke NM, Lee S, Kamens RM (2002) Heterogeneous atmospheric aerosol production by acid-catalyzed particle phase reactions. Science 298:814
39. Kalberer M et al (2004) Identification of polymers as major components of atmospheric organic aerosols. Science 303:1659–1662
40. Ervens B, Feingold G, Frost GJ, Kreidenweis SM (2004) A modeling study of aqueous production of dicarboxylic acids: 1. Chemical pathways and speciated organic mass production. J Geophys Res 109:D15205. doi:10.1029/2003JD004387, 2004
41. Jimenez JL et al (2009) Evolution of organic aerosols in the atmosphere. Science 326:1525. doi:10.1126/science.1180353
42. Andreae, MO, Rosenfeld D (2008) Aerosol–cloud–precipitation interactions. Part 1, The nature and sources of cloud-active aerosols. Earth-Sci Rev, doi:10.1016/j.earscirev.2008.03.001
43. Andreae MO (1995) Climatic effects of changing atmospheric aerosol levels. In: Henderson-Sellers A (ed) World survey of climatology, vol 16, Future climates of the world. Elsevier, Amsterdam, pp 341–392
44. Andreae MO, Merlet P (2001) Emission of trace gases and aerosols from biomass burning. Glob Biogeochem Cycles 15:955–966
45. Bauer SE et al (2007) Nitrate aerosols today and in 2030: a global simulation including aerosols and tropospheric ozone. Atmos Chem Phys 7:5043–5059
46. Bond TC et al (2004) A technology-based global inventory of black and organic carbon emissions from combustion. J Geophys Res 109(D14):D14203. doi:10.1029/2003JD003697
47. Guelle W, Schulz M, Balkanski Y, Dentener F (2001) Influence of the source formulation on modeling the atmospheric global distribution of sea salt aerosol. J Geophys Res 106(D21):27,509–27,524
48. Gong SL, Barrie LA, Lazare M (2002) Canadian Aerosol Module (CAM): a size segregated simulation of atmospheric aerosol processes for climate and air quality models – 2. Global sea-salt aerosol and its budgets. J Geophys Res 107(D24):4779. doi:10.1029/2001JD002004
49. Ito A, Penner JE (2005) Historical emissions of carbonaceous aerosols from biomass and fossil fuel burning for the period 1870–2000. Glob Biogeochem Cycles 19:GB2028. doi:10.1029/2004GB002374
50. Junker C, Liousse C (2006) A global emission inventory of carbonaceous aerosol from historic records of fossil fuel and biofuel consumption for the period 1860–1997. Atmos Chem Phys Discuss 4:4897–4927
51. Luo C, Mahowald NM, del Corral J (2003) Sensitivity study of meteorological parameters on mineral aerosol mobilization, transport, and distribution. J Geophys Res 108(D15):4447. doi:10.1029/2003JD003483
52. Liousse C et al (2004) Deriving global quantitative estimates for spatial and temporal distributions of biomass burning

emissions. In: Granier C, Artaxo P, Reeves CE (eds) Emissions of atmospheric trace compounds. Kluwer, Dordrecht, pp 71–113
53. Penner JE et al (2001) Aerosols, their direct and indirect effects. In: Houghton JT et al (eds) Climate change 2001: the scientific basis. Contribution of Working Group I to the Third Assessment Report of the Intergovernmental Panel on Climate Change. Cambridge University Press, Cambridge, pp 289–348
54. Stier P et al (2005) The aerosol–climate model ECHAM5-HAM. Atmos Chem Phys 5:1125–1156
55. Zender CS, Miller RL, Tegen I (2004) Quantifying mineral dust mass budgets: terminology, constraints, and current estimates. Eos Trans AGU 85(48):509–512
56. Vignati E, Facchini MC, Rinaldi M, Scannell C, Ceburnis D, Sciare J, Kanakidou M, Myriokefalitakis S, Dentener F, O'Dowd CD (2010) Global scale emission and distribution of sea spray aerosol: sea-salt and organic enrichment. Atmos Environ 44:670–677
57. Kinne S, Schulz M, Textor C, Guibert S, Bauer S, Berntsen T, Berglen T, Boucher O, Chin M, Collins W, Dentener F, Diehl T, Easter R, Feichter J, Fillmore D, Ghan S, Ginoux P, Gong S, Grini A, Hendricks J, Herzog M, Horowitz L, Isaksen I, Iversen T, Koch D, Krol M, Lauer A, Lamarque JF, Lesins G, Liu X, Lohmann U, Montanaro V, Myhre G, Penner J, Pitari G, Reddy S, Seland O, Stier P, Takemura T, Tie X (2006) An AeroCom initial assessment – optical properties in aerosol component modules of global models, /ACP, 6,/ 1-22
58. Dall'Osto M, Ceburnis D, Martucci G, Bialek J, Dupuy R, Jennings SG, Berresheim H, Wenger JC, Healy RM, Facchini MC, Rinaldi M, Giulianelli L, Finessi E, Worsnop D, Ehn M, Mikkilä J, Kulmala M, Sodeau J, O'Dowd CD (2010) Aerosol properties associated with air masses arriving into the North East Atlantic during the 2008 Mace Head EUCAARI intensive observing period: an overview. Atmos Chem Phys 10:8413–8435. doi:10.5194/acp-10-8413-2010
59. Lauer A, Hendricks J (2006) Simulating aerosol microphysics with the ECHAM/MADE GCM – Part II: results from a first multiannual integration. Atmos Chem Phys 6:5495–5513
60. Deshler T (2008) A review of global stratospheric aerosol: measurements, importance, life cycle, and local stratospheric aerosol. Atmos Res 90:223–232. doi:10.1016/j.atmosres.2008.03.016
61. Rosen JM (1971) The boiling point of stratospheric aerosols. J Appl Meteorol 10:1044–1046
62. Carslaw KS, Luo BP, Clegg SL, Peter Th, Brimblecombe P, Crutzen PJ (1994) Stratospheric aerosol growth and HNO3 and water uptake by liquid particles. Geophys Res Lett 21:2479–2482
63. Hanson DR, Mauersberger K (1988) Laboratory studies of the nitric acid trihydrate: implication for the south polar stratosphere. Geophys Res Lett 15:855–858
64. Deshler T, Larsen N, Weisser C, Schreiner J, Mauersberger K, Cairo F, Adriani A, Di Donfrancesco G, Ovarlez J, Ovarlez H, Blum U, Fricke KH, Dörnbrack A (2003b) Large nitric acid particles at the top of an Arctic stratospheric cloud. J Geophys Res 108(D16):4517. doi:10.1029/2003JD003479
65. Fahey DW et al (2001) The detection of large HNO_3-containing particles in the winter Arctic stratosphere. Science 291: 1026–1031
66. Larsen N, Knudsen BM, Svendsen SH, Deshler T, Rosen JM, Kivi R, Weisser C, Schreiner J, Mauersberger K, Cairo F, Ovarlez J, Oelhaf H, Schmidt A (2004) Formation of solid particles in synoptic-scale Arctic PSCs in early winter 2002/2003. Atmos Chem Phys 4:2001–2013
67. Kőhler H (1936) The nucleus in and the growth of hygroscopic droplets. Trans Farad Soc 32:1152–1161
68. Chylek P, Wong JGD (1998) Erroneous use of the modified K¨ohler equation in cloud and aerosol physics application. J Atmos Sci 55:1473–1477
69. Pruppacher H, Klett J (1997) Microphysics of clouds and precipitation, atmospheric and oceanographic sciences library; v. 18, Kluwer, Dordrecht; London, includes bibliographical references and index Previous ed.: 1978 "With an introduction to cloud chemistry and cloud electricity"
70. Rogers RR, Yau MK (1989) A short course in cloud physics, vol. 113, International Series in Natural Philosophy, 3rd edn. Butterworth- Heinemann, Woburn, MA
71. Twomey S (1977) The influence of pollution on shortwave albedo of clouds. J Atmos Sci 34:1149–1152
72. Twomey S (1977) Atmospheric aerosols. Elsevier, New York
73. McFiggans G, Artaxo P, Baltensperger U, Coe H, Facchini MC, Feingold G, Fuzzi S, Gysel M, Laaksonen A, Lohman U, Mentel TF, Murphy DM, O'Dowd CD, Snider JR, Weingartner E (2006) The effect of physical and chemical aerosol properties on warm cloud droplet activation. Atmos Chem Phys 6: 2593–2649
74. Vali G (1996) Ice nucleation – a review. In: Kulmula M, Wagner P (eds) Nucleation and atmospheric aerosols. Pergamon, Oxford, pp 271–279
75. Bohren CF, Huffman D (1983) Absorption and scattering of light by small particles. Wiley, New York
76. Schulz M, Textor C, Kinne S, Balkanski Y, Bauer S, Berntsen T, Berglen T, Boucher O, Dentener F, Guibert S, Isaksen ISA, Iversen T, Koch D, Kirkevåg A, Liu X, Montanaro V, Myhre G, Penner JE, Pitari G, Reddy S, Seland Ø, Stier P, Takemura T (2006) Radiative forcing by aerosols as derived from the AeroCom present-day and pre-industrial simulations. Atmos Chem Phys 6:5225–5246
77. Bellouin N, Jones A, Haywood J, Christopher SA (2008) Updated estimate of aerosol direct radiative forcing from satellite observations and comparison against the Hadley Centre Climate Model. J Geophys Res 113(D10): D10205
78. Albrecht BA (1989) Aerosols, cloud microphysics, and fractional cloudiness. Science 245:1227–1230
79. Hansen J, Sato M, Ruedy R (1997) Radiative forcing and climate response. J Geophys Res 102:6831–6864
80. Jacobson MZ (2002) Control of fossil fuel particulate black carbon and organic matter, possibly the most effective method of slowing global warming. J Geophys Resh 107. doi:10.1029/2001JD001376

81. Menon S, Hansen J, Nazarenko L, Luo Y (2002) Climate effects of black carbon aerosols in China and India. Science 297:2250–2252
82. Penner JE, Zhang SY, Chuang CC (2003) Soot and smoke aerosols may not warm climate. J Geophys Res 108(21):4657. doi:10.1029/2003JD003409
83. Lohmann U (2002) Possible aerosol effects on ice clouds via contact nucleation. J Atmos Sci 59:647–656
84. Girard E, Blanchet J-P, Dubois Y (2004) Effects of arctic sulphuric acid aerosols on wintertime low-level atmospheric ice crystals, humidity and temperature at Alert, Nunavut. Atmos Res 73:131–148
85. Rosenfeld D, Woodley WL (2000) Deep convective clouds with sustained supercooled liquid water down to −37.5°C. Nature 405:440–442
86. Forster P, Ramaswamy V, Artaxo P, Berntsen T, Betts R, Fahey DW, Haywood J, Lean J, Lowe DC, Myhre G, Nganga J, Prinn R, Raga G, Schulz M, Van Dorland R (2007) Changes in atmospheric constituents and in radiative forcing. In: Solomon S, Qin D, Manning M, Chen Z, Marquis M, Averyt KB, Tignor M, Miller HL (eds) Climate change 2007: the physical science basis. Contribution of Working Group I to the Fourth Assessment Report of the Intergovernmental Panel on Climate Change. Cambridge University Press, Cambridge, UK/New York
87. Rosenfeld D, Kaufman YJ, Koren I (2006) Switching cloud cover and dynamical regimes from open to closed Benard cells in response to the suppression of precipitation by aerosols. Atmos Chem Phys 6:2503–2513
88. Rosenfeld D (2006) Aerosol–cloud interactions control of earth radiation and latent heat release budgets. Space Sci Rev 125:149–157
89. Rosenfeld D, Lohmann U, Raga GB, O'Dowd CD, Kulmala M, Fuzzi S, Reissell A, Andreae MO (2008) Flood or drought: how do aerosols affect precipitation? Science 231. doi:10.1126/science.1160606
90. Liepert BG (2002) Observed reductions of surface solar radiation at sites in the United States and worldwide from 1961 to 1990. Geophys Res Lett 29. doi:10.1029/2002GL014910
91. Wild M, Ohmura A, Gilgen H, Rosenfeld D (2004) On the consistency of trends in radiation and temperature records and implications for the global hydrological cycle. Geophys Res Lett 31:L11201. doi:10.1029/2003GL019188
92. Wild M (2009) Global dimming and brightening: a review. J Geophys Res 114:D00D16. doi:10.1029/2008JD011470
93. Stanhill G, Cohen S (2001) Global dimming: a review of the evidence for a widespread and significant reduction in global radiation. Agric Forest Meteorol 107:255–278
94. Norris JR, Wild M (2007) Trends in aerosol radiative effects over Europe inferred from observed cloud cover, solar "dimming" and solar "brightening". J Geophys Res 112:D08214. doi:10.1029/2006JD007794
95. Wild M, Gilgen H, Roesch A, Ohmura A, Long CN, Dutton EG, Forgan B, Kallis A, Russak V, Tsvetkov A (2005) From dimming to brightening: decadal changes in surface solar radiation. Science 308:847–850
96. Philipona R, Behrens K, Ruckstuhl C (2009) How declining aerosols and rising greenhouse gases forced rapid warming in Europe since the 1980s. Geophys Res Lett 36:L02806. doi:10.1029/2008GL036350
97. EEA (2007) Air pollution in Europe 1990–2004. EEA Report No 2/2007. European Environment Agency, Copenhagen
98. Ming Y, Ramaswamy V (2009) Nonlinear climate and hydrological responses to aerosol effects. J Clim 22:1329–1339
99. Raes F, Seinfeld JH (2009) New directions: climate change and air pollution abatement: a bumpy road. Atmos Environ. doi:10.1016/j.atmosenv.2009.06.001
100. IPCC (2007) The Physical Science Basis. Contribution of Working Group I to the Fourth Assessment Report of the Intergovernmental Panel on Climate Change. Cambridge University Press, Cambridge, UK/New York

Agroecological Basis for Managing Biotic Constraints

Claudio M. Ghersa
IFEVA-CONICET, Depto. de Recursos Naturales y Ambiente, Universidad de Buenos Aires (UBA), Buenos Aires, Argentina

Article Outline

Glossary
Definition of the Subject
Introduction
Agroecosystems and Biological Constraints to Production
System Management
Conclusions
Future Directions
Bibliography

Glossary

Abiotic factor A nonliving component of the environment, such as soil, nutrients, light, fire, or moisture.

Adaptation (1) Any aspect of an organism or its parts that is of value in allowing the organism to withstand the conditions of the environment. (2) The evolutionary process by which a species' genome and phenotypic characteristics change over time in response to changes in the environment.

Agroecology The science of applying ecological concepts and principles to the design and management of sustainable agroecosystems.

Agroecosystem An agricultural system understood as an ecosystem.

Agroforestry The practice of including trees in crop- or animal-production agroecosystems.

Allelopathy An interference interaction in which a plant releases into the environment a compound that inhibits or stimulates the growth or development of other plants.

Beneficial insects – arthropods Beneficial insects are predators, parasites, or competitors of insect pests, helping to regulate pest populations without harm to crops.

Biomass The mass of all the organic matter in a given system at a given point in time.

Biotic factor An aspect of the environment related to organisms or their interactions.

Competition An interaction in which two organisms remove from the environment a limited resource that both require, and both organisms are harmed in the process. Competition can occur between members of the same species and between members of different species.

Consumer An organism that ingests other organisms (or their parts or products) to obtain its food energy.

Decomposer A fungal or bacterial organism that obtains its nutrients and food energy by breaking down dead organic and fecal matter and absorbing some of its nutrient content.

Disturbance An event or short-term process that alters a community or ecosystem by changing the relative population levels of at least some of the component species.

Diversity (1) The number or variety of species in a location, community, ecosystem, or agroecosystem. (2) The degree of heterogeneity of the biotic components of an ecosystem or agroecosystem (*see ecological diversity*).

Domestication The process of altering, through directed selection, the genetic makeup of a species so as to increase the species' usefulness to humans.

Dominant species The species with the greatest impact on both the biotic and abiotic components of its community.

Ecosystem A functional system of complementary relations between living organisms and their environment within a certain physical area.

Generalist A species that tolerates a broad range of environmental conditions; a generalist has a broad ecological niche.

Habitat The particular environment, characterized by a specific set of environmental conditions, in which a given species occurs.

Herbaceous Nonwoody.

Herbivore An animal that feeds exclusively or mainly on plants. Herbivores convert plant biomass into animal biomass.

Host An organism that provides food or shelter for another organism.

Intercropping Planting more than one crop in a field using a regular pattern that interleaves each crop in some pattern. A form of polyculture.

Integrated pest management Pest control using an array of complementary approaches including natural predators, parasites, pest-resistant varieties, pesticides, and other biological and environmental control practices.

Legume A plant in the Leguminosae (Fabaceae) family. Most species in this family can fix nitrogen.

Microclimate The environmental conditions in the immediate vicinity of an organism.

Multi-trophic relationships The organization of feeding and energy-transfer relationships that determine the path of energy flow through a community or ecosystem that involves organisms of different levels.

Mycorrhizae Symbiotic fungal connections with plant roots through which a fungal organism provides water and nutrients to a plant and the plant provides sugars to the fungi.

Organic matter Material containing molecules based on Carbon, usually referring to soil organic matter.

Parasite An organism that uses another organism for food and thus harms the other organism.

Parasitism An interaction in which one organism feeds on another organism, harming (but generally not killing) it.

Parasitoid A parasite that feeds on predators or other parasites.

Patchiness A measurement of the diversity of successional stages present in a specific area.

Patchy landscape A landscape with a diversity of successional stages or habitat types.

Phenotype The physical expression of the genotype; an organism's physical characteristics. Phenology is the study of periodic plant and animal life-cycle events and how these are influenced by seasonal and interannual variations in climate

Polyculture Cropping systems in which different crop species are grown in mixtures in the same field at the same time.

Predation An interaction in which one organism kills and consumes another.

Predator An animal that consumes other animals to satisfy its nutritive requirements.

Primary production The amount of light energy converted into plant biomass in a system.

Productivity The ecological processes and structures in an agroecosystem that enable production.

Seed bank The total seed presence in the soil.

Shifting agriculture Farming systems that alternate periods of annual cropping with extended fallow periods. "Slash and burn" systems of shifting cultivation use fire to clear fallow areas for cropping.

Species richness The number of different species in a community or ecosystem.

Successional stages A condition characterized by a particular community of a succession, which is the process by which one community gives way to another.

Definition of the Subject

Agroecology provides guidelines to develop diversified agroecosystems that take advantage of the effects of the integration of plant and animal biodiversity. From a management perspective, the agroecological objective is to provide balanced environments, sustained yields, biologically mediated soil fertility, and natural pest regulation through the design of diversified agroecosystems and the use of low-input technologies.

Introduction

Constraints to agricultural production may be classified into four basic categories: abiotic, biotic, socioeconomic, and those related to crop management. The origin and importance of each constraint, their associated losses, and opportunities to alleviate them will vary for the crop, the input and management levels employed, and the environmental and socioeconomic characteristics of the broader farming system in which the crop is grown. Agronomists and plant protectionists usually address production constraints by focusing on management and input issues to alleviate yield losses caused by particular biotic factors (weed, pest, or disease) that are frequently overestimated, and when added up, exceed crops' yield potential. Moreover, plant breeders, especially with the recent addition of bioengineering and biotechnological tools, have assumed that better varieties alone are able to alleviate the impact of factors curtailing production. From an appreciation of constraints and losses, solutions or opportunities have been proposed, prioritized, and placed into an agenda for action involving technology experimentation, training, socioeconomic and policy support, among other types of intervention. However, there is a need for broader more holistic integration that would jointly assess four broad categories of constraint: biotic, abiotic, management, and socioeconomic. In addition, it is important to focus on how, or through which process constraints to production are generated.

A concern with constraints studies that attempt to average out problems and losses over farms, villages, watersheds, or farming systems is the spatial variation encountered in the types and severity of constraints, in their associated losses, and achieved yields. Variation is often substantial and at a small scale (e.g., parts of the same small field and across field types on a farm). This is especially evident for smallholder farming systems that frequently exhibit historically variable and targeted inputs (e.g., fertilizers) and management superimposed on variability in biophysical factors such as soil types, water availability, weed and pest distribution [1].

Agroecology provides the basic ecological principles needed for studying, designing, and managing agroecosystems that are both productive and that are culturally sensitive, socially just, and economically viable. Instead of focusing on one particular component of the agroecosystem, agroecology emphasizes the interrelatedness of all of its components and the complex dynamics of ecological processes including all environmental and human elements. This approach is based on enhancing the habitat both aboveground and in the soil to produce strong and healthy plants

by promoting beneficial organisms while adversely affecting crop pests (weeds, insects, diseases, and nematodes). From a management perspective, the agroecological objective is to provide balanced environments, sustained yields, biologically mediated soil fertility, and natural pest regulation through the design of diversified agroecosystems and the use of low-input technologies [2, 3].

Agroecologists recognize that intercropping, agroforestry, and other diversification methods mimic natural ecological processes, and that the sustainability of complex agroecosystems lies in the ecological models they follow. By designing farming systems that mimic nature, optimal use can be made of sunlight, soil nutrients, and rainfall [4]. The assumption is that by assembling a functional biodiversity, it is possible to subsidize key processes in the agroecosystem that impact on ecological services, such as the activation of soil biology, the recycling of nutrients, the enhancement of beneficial arthropods and antagonists (Table 1) [5]. Altieri [6] argues that there is evidence supporting that promotion of biodiversity within agricultural systems is the cornerstone strategy of system redesign, since: (1) higher diversity (genetic, taxonomic, structural, and resource) within the cropping system leads to higher diversity in associated biota, (2) increased biodiversity leads to more effective pest control and pollination, and (3) increased biodiversity leads to tighter nutrient cycling.

There is evidence that agroecological diversified agrosystems improve their adaptive capacity and reduces vulnerability to natural disasters, climate change impacts, and new and emerging environmental and economic system stresses and shocks. This ability of withstanding the impact of factors that may reduce agroecosystem sustainability (systems resilience) can be accomplished through physical, biological, sociocultural, and political means. Aspects such as habitat and crop diversification, in situ conservation of local/indigenous seed and germplasm diversity, maintenance of natural enemies' species diversity, increased carbon sequestration, improved water capture and retention, etc., and diversification of farming systems and local economies; technical, legal, and social support networks for small-scale farmers, rural communities, and indigenous people that reduce socioeconomic vulnerability and strengthen adaptive knowledge processes, etc., can be listed as means to increase sustainability. A study of 208 agroecologically based projects and/or initiatives throughout the developing world documented clear increases in food production over some 29 million hectares, with nearly 9 million households benefiting from increased food diversity and security. Promoted sustainable agriculture practices led to 50–100% increases in per hectare food production (about 1.71 t per year per household) in rain-fed areas typical of small farmers living in marginal environments; that is an area of about 3.58 million hectares, cultivated by about 4.42 million farmers. Such yield enhancements are a true breakthrough for achieving food security among farmers isolated from mainstream agricultural institutions [7].

Crop rotations, polyculture cover crops; intercropping, crop/livestock mixtures are some of the strategies that have been recognized as useful to restore agricultural diversity in both time and space. These strategies exhibit ecological features that have been recognized by different studies. For example, crop rotations incorporate temporal diversity into cropping systems, providing crop nutrients and breaking the life cycles of several insect pests, diseases, and weed life cycles [8]. Polycultures are complex cropping systems in which more than two crop species are planted within sufficient spatial proximity to result in competition or complementation, thus enhancing yields [9, 10]. Intercropping may include trees and animals creating agroforestry systems or mixed crop/livestock mixtures resulting in enhanced complementary relations between components increasing multiple use of the agroecosystem [11]. Moreover, animal integration in

Agroecological Basis for Managing Biotic Constraints.
Table 1 Ecological processes to optimize in agroecosystems

• Strengthen natural pest-control system
• Decrease toxicity through elimination of agrochemicals
• Optimize metabolic function (organic matter decomposition and nutrient cycling)
• Balance regulatory systems (nutrient cycles, water balance, energy flow, population regulation, etc.)
• Enhance conservation and regeneration of soil-water resources and biodiversity
• Increase and sustain long-term productivity

agroecosystems aids in achieving high biomass output and optimal recycling [12]. Cover crops based on the use of pure or mixed stands of legumes or other annual plant species under fruit trees improve soil fertility, enhance biological control of pests, and modify the orchard microclimate [13]. Altieri and Rosset [14] argue that including these, strategies in farming provide for diversified forms of agroecosystems that share the following features:

(a) Maintain vegetative cover as an effective soil and water conserving measure
(b) Provide a regular supply of organic matter adding manure, compost, and promotion of soil biotic activity
(c) Enhance nutrient recycling mechanisms with livestock systems based on legumes, etc.
(d) Promote pest regulation enhancing the activity of biological control agents achieved by introducing and/or conserving natural enemies and antagonists

Agroecosystems and Biological Constraints to Production

Plant and animal domestication and technological innovation processes, occurring at different rates depending on ecological and social factors during the expansion of agricultural land use, resulted in the development of sophisticated agricultural systems, which included various types of fallow-crop rotation farming, irrigation, land terracing, soil amendment and fertilizing [15, 16]. In these man-made systems tuned in novel ecosystems, farming became increasingly dependent on labor and capital (technological developments) as intensification maintained or even increased outputs. The population density of domestic animals and humans (slaves and peasants) available to satisfy production needs, such as planting, harvesting, and controlling weeds, became an important factor limiting yields and an important destination for agricultural products. Therefore food and fiber demands were not only driven by the nonagricultural fraction of the society, but were also increasingly demanded as labor populations grew to intensify land production. The social structural changes together with modern technological developments, such as steam and internal combustion engines that occurred since the beginning of industrialization made possible the replacement of animal and human labor by machinery and traditional by scientific agriculture. Mechanization of farming reduced the time needed to perform activities and was the means for augmenting the loads of energy inputs to the agricultural system in a way that increased productivity as never seen before. Postindustrial intensification that occurred during the twentieth century in most of the more developed countries, known as "The Green Revolution," became so efficient that the continuous increase in demands for food and fiber by the world's population could be satisfied despite that during the century's last decades agricultural land shrank [16].

Food supply and human population growth are related, therefore farming intensification process can be seen as following predator prey pattern of change over time, in which population grows following the increase in food supply, and food supply follows labor/energy inputs to the agroecosystem. However, studies on agricultural development have shown that as society builds up its knowledge base through science and other methods to produce technological innovations, they may further increase yield through intensification of farming practices, even when food demands were well below supply, so intensive farming can be pushed just by technological developments [16]. Paradoxically, once expansion of agriculture stops and technological developments give way to intensification of production, technology innovation may at the same time reestablish the expansion model for agricultural production.

This traditional expansion–intensification model has typified agricultural production systems for the first 75 years of the last century. Gain of agricultural land to the sea by means of polders and drainage systems, the use of river damming to build irrigation oasis into desert lands, transformation of tropical rain forests into coffee, tea, sugar cane, and soybean areas, wetland drainage to produce annual crops are all examples on how technology expanded cropped lands. Perhaps the most interesting example on how technology may help in reestablishing the expansion model is the development of improved cultivars by means of plant breeding programs aimed at increasing crop tolerance to stress factors such as high or low temperatures, drought, pests, and disease and soil salinity. Once these characteristics are bread into crops, there is an

expansion in the environmental ranges in which the crops are planted. Shifting agriculture and expansion of agricultural frontiers enabled the incorporation of highly fertile lands into production. These activities molded self-designed novel ecosystems [17, 18], the agroecosystems, which compensated and many times overcompensated the yield reductions due to soil erosion and increase in problems related to biotic constraints to production (weeds, pests, and diseases) that appeared in sites with longer agricultural histories [19, 20]. When settlements became fixed and expansion rate was reduced, intensification originally depended on the generation of spontaneous technological developments. Later, and especially in modern farming, agricultural and agronomy schools became nodal institutions integrating different and somehow related disciplines to generate the technological solutions to the continually emerging problems for agricultural production. Technological approaches tend to engineer and construct new systems, which use practices, like soil plowing, to destroy the natural vegetation and weeds creating the conditions for crop establishment and growth.

As discussed before, these new systems induced important modifications in the human social and economical structures. Individual and collective reactions to these changes repeatedly appeared in different sites and historical times, sometimes sustained on religious dogmas, others on philosophical views, as naturalism, or on scientific disciplines, such as ecology, that became important for modern societies. Integrated pest management (IPM) and agroecology originated as a reaction challenging the modern industrial farming practices. It emerged as a scientific-based philosophical view that questions the modern expansion–intensification agricultural model and its associated dogma of production at any cost. In the last decades, hundreds of research projects and technological development attempts, aimed at environmentally prone management, have taken place delivering significant information. However, the thrust is still highly technological, and focus is on alleviation or suppression of limiting factors or the symptoms disregarding malfunction of the agroecosystem.

Biotic constraints to agricultural production are broadly identified as weeds (plants), pests (animals), and diseases (fungi and bacteria), and their related biological interactions (namely, competition, herbivory, and predation and parasitism), which cause reductions in physical yields or yield quality. The prevalent philosophy is that pests, nutrient deficiencies, or other factors are the cause of low productivity, as opposed to the view that pests or nutrients only become limiting if conditions in the agroecosystem are not balanced [21]. This understanding of how production is sustained has diverted agriculturists from realizing that limiting factors only represent symptoms of a more systemic disease inherent to unbalances within the agroecosystem and from an appreciation of the context and complexity of agroecological processes thus underestimating the root causes of agricultural limitations [6].

Pest, disease, and weed problems are strong site- and time-specific imposing a biotic constraint on a crop dimensions. The crop-loss impacts of one organism growing in a location may be entirely different from the losses incurred by the same organism on the same crop in other locales. Further, organism population dynamics, migration, invasion, and damage are driven by local conditions, such as temperature and rainfall, but also by the ecosystem and community complexities. Recognition of the systemic dimensions of biological constraints to production is needed to understand how climate–soil interactions, topography, natural, ecological, and land-use complexity, agricultural history, and cropping practices may determine their occurrence, importance, and frequency [22].

Agroecosystems that have evolved in tropical and subtropical climates have high levels of complexity, including many organisms and multi-trophic interactions. Those that have evolved under temperate or Mediterranean climates may also show complexity, but frequently are structurally simpler and may show strong seasonal variation caused by changes in resource availability during the cold/dry season that stops primary productivity. Topography may cause environmental gradients or patchiness adding complexity at regional and landscape scales. Agricultural land-use history, however, at both regional and landscape scales are important drivers of the agroecosystem complexity and organization of the communities that occur in the different crops. Agriculture in many regions of Europe, Middle-East, Asia, Andean regions in South America, and Central America has been practiced in the same sites through millennia, while in others, covering large

extensions of Australia, South and North America, expansion of agriculture has occurred within the last centuries. During the last decades, land under agriculture in some of these regions with relatively new agroecosystems has shrunk, and intensification occurred in those areas that remained under cropping. In other regions, such as those in the Mato Grosso, Cerrado, and Chaco from Brasil, Paraguay, and Argentina, natural systems have been turned into cropland recently, and this transformation is still happening. These differences in agricultural histories are related to important differences in the organization of the biotic interactions in the agroecosystem. Different selection pressures occurring in agroecosystems select for different adaptations, which include coevolution of crops and organisms that challenge them as well as cropping practices [23]. Therefore, arable land complex communities have evolved in regions with long agricultural histories. These communities have strong interactions among organisms. Communities that were assembled in apparently homogeneous agroecosystems under long periods of monocultures can reach high levels of complexity. For example, Javanese rice fields, which are cropped as simple rice monocultures, can support large numbers of arthropods summed by 765 species that are important for biocontrol [24]. Vegetationally simple cropping systems in the UK have been shown to develop complex belowground biodiversity that may include 100 species of bacteria, 350 species of protozoa, 140 species of nematodes, and 24 distinct types of arbuscular mycorrhizae [25].

Size and variability in the above- and belowground community structures that functionally support the agroecosytem is important to discuss biotic constraints to production and the agroecological basis for managing them. The more complex and diverse ecosystems may sustain greater productivity and stability in ecosystem functions since they are supported by more than one species, and are then less vulnerable to changes in the populations of a particular species due to environmental stress or pest attack. However, complex biotic systems may also deliver more organisms, which may challenge the crop increasing the importance and stability of biotic constraints [26]. There are numerous studies showing that increased plant diversity enhances biological pest control [27, 28], but counter examples also exist where pests or disease levels increase due to the provision of highly palatable species or changes in canopy microclimate [27–30].

Many of the species originated in regions with long histories of agriculture, and even whole communities have migrated into regions in which crops and agroecosystems have recently expanded. In this way, the flora and fauna of the new agricultural areas of the world such as those in the Argentinean Pampas are dominated by species from the Mediterranean-European agricultural communities. In these new areas, arable land communities may show instability due to the continuous introduction of new organisms and species shifts [18, 31, 32]. Changes in trading systems, land use, and cropping practices, experienced by many regions with long agricultural history, are enhancing instability of biotic communities caused by addition of organisms (*biotic invasions*), extinctions, and species shifts due to change in landscape [33]. The impacts of biotic complexity have significance, especially when cropping systems are simplified to monocultures, as many organisms would impose biotic limitations to production. Diverse cropping systems are typical of many traditional agricultural systems found around the world, particularly in risk-prone environments, but also with long histories of agricultural production [6]. It is also in these regions, primarily in the developing world, where the greatest emphasis on improving diverse production systems through intercropping and agroforestry is found. It is clear that there are trade-offs with more diverse agricultural systems, and that the kind of diversity matters greatly, but the question is how to design diverse systems that can meet multiple goals in an acceptable way [22].

System Management

As discussed previously, cultural and technological changes that took place during the second half of the twentieth century impacted on land-use patterns and agroecosystem design especially driven by the adoption of industrialized production technologies and reliance on increasing input loads of agrochemicals to alleviate agricultural production constraints. Despite the success in achieving significant increases in global food and fiber yields and yield stability, paradoxically, increasing environmental damage, loss of biodiversity, and associated traditional knowledge were often experienced in the new

agroecosystems. In high-external input agriculture intensification of production due to technological development has increased by augmenting input levels that resulted in increased (biomass) production per unit of land and uniformity of the produce. In many cases, this intensification led to reductions in output stability and resource-use efficiency, and has enhanced overexploitation of natural resource base, and consequently reduced sustainability of agroecosystems [34]. There are many examples of reduction in sustainability by the elimination of growth limitations and of yield reduction factors that induced environmental homogenization and a decrease in genetic variation. Noteworthy are the studies showing that application of biocides to reduce biotic constraints to production impact negatively on organisms that are directly or indirectly beneficial for crop growth [34, 35] and, due to their effects on natural enemies of pests and diseases, further increase the need for biocides control [1].

Agroecological bases for reducing biological constraints to crop production depends on the possibility of managing diversity and disturbance at multiple spatial and temporal scales to use biotic interactions to provide desired agroecosystem service.

Arable Land Biotic Community Constraints

Small Scale Soil disturbance caused by plows and other cultivating devices have been used for centuries in different parts of the world to reduce weed competition as well as for reduction of some pests and diseases. Particular traits are selected by cultural practices in many organisms that survive and reproduce in arable lands and show functional patterns that can be identified [36]. Selection pressures imposed by agricultural practices may be sufficiently strong over extended periods of time so that weed populations can evolve into more competitive populations better adapted to agricultural field conditions than populations from nonagricultural areas [37] or populations from agricultural areas submitted to other type of management. In recent times, management approaches that include reduced tillage have strong impacts on the soil biota of plowed soils. It favors fungal food webs, increases abundance and diversity of predators that can reduce soils weed seed banks, and increases control of pests and diseases. It also changes the environmental conditions reducing germination of seed of many weeds or changing ontogenic processes and phenology of pests and diseases adapted to plowed-cultivated soil conditions. These effects may alleviate biotic constraints especially caused by weeds; its effects are not stable, and shifts in species happen after this practice is adopted for some time. The design and management of the agroecosystems complexity requires an understanding of general system behavior combined with species- and site-specific knowledge.

The performance of agroecological management could be improved since crops were selected in the ecological conditions likely to occur in the low-input farming. Adaptation to these conditions in which biotic interactions are expected to occur and characteristics such as increased competitiveness to weeds, disease, and pest resistance, enhanced ability to support beneficial rhizosphere microorganisms, and improved capacity to access soil nutrients could all potentially benefit crop growth. Noteworthy is that selecting for such traits and acquiring the necessary knowledge to understand the structure of particular agroecosystem structure dynamics can only be accomplished with long agricultural history to provide for coevolution and the existence of relatively strong interactions. In addition to this, if such a mix of characteristics can be identified, selecting it would be difficult and time consuming. Probably a more practical alternative to adaptation of a single crop to a complex biotic system would be the use of mixtures of cultivars within a field to improve crop production and disease management [38, 39].

Cropping systems may include crop sequences to favor beneficial biotic interactions, such as the use of crops that enhance the populations of beneficial rhizobacteria that reduce diseases and nematodes [40], accompanied by soil cultivation, fallow, and residue management practices aimed at maintaining soil cover and organic matter as well as arbuscular michorrhiza populations [41] and weed suppression [42]. Competitive crops species or mixtures may be used to reduce the impact of weeds on crop yields. However, holistic management approaches aimed at reducing weeds may integrate the use of other strategies such as manipulating crop seeding density and spatial arrangement, tillage, intercropping, use of allelopathic residues and suppressive mulches, and targeted use of biocontrol agents that reduce weed growth and fecundity during

the growth cycle may be integrated in holistic weed management approaches. Also, various soil management techniques aimed at reducing weed seed survival such as reduced tillage, residue management, and organic matter inputs can be used and integrated with the use of weed-suppressive crop rotations that may also impact on seed survival due to enhanced seed predation or infection by pathogens [39].

In agricultural systems, species are selected to obtain yields but can also be used to manage diversity aiming at encouraging beneficial interactions and minimizing undesired ones [43]. For intercropping systems, species are usually chosen considering species or varieties that differ in rooting patterns, canopy types, phenology, etc., to avoid or reduce negative interference or that have positive interactions such as with the introduction of a legume. Well-designed intercrops can increase overall productivity [10, 44] and potentially reduce risk to farmers. A regional-scale field experiment with rice production in China shows how even a small increase in diversity can have a large impact on system function. In that experiment, simply interplanting two varieties of rice, rather than planting them in separate fields, led to a dramatic reduction in pest problems and pesticide use [45].

Large Scale As scale increases, so does the relative importance of species richness because greater numbers of species are needed for the maintenance of ecosystem functions [26]. Loss of diversity in agricultural landscapes has been linked to the disruption of ecological functions such as pest management, pollination services, resistance to plant invasion [46]. Spatial scale is particularly important for both occurrence of pest-related yield constraints to production and for management, because landscape features affect species interactions, microclimates, and weather patterns [24, 46–48]. Landscape structure and dynamics can have notable effects on pests by changing habitat patterns and immigration rates [46, 49–53]. In many regions of the world, agriculture shares space with other land uses forming structural mosaic of habitats with insects and other mobile organisms moving between them [33]. The development of multi-trophic arthropod communities depends on spatial processes (dispersal and foraging) that occur at larger scales than the farm, as well as temporal processes such as overwintering and reproduction. Habitat fragmentation caused by farming can disrupt both types of process and isolate small natural enemy populations from one another, increasing local extinctions [54].

Several biotic constraints to production could be alleviated if biological control maintained following several strategies that help to enhance indigenous populations of beneficial insects by providing food resources (host prey, pollen and nectar, alternate prey) and shelter for overwintering. Habitat management involves vegetation diversification at multiple scales [55]. Use of insectary plantings or leaving strips of unharvested plants are examples of infield strategies, whereas wildflower borders, grassy buffer strips, windbreaks, and hedgerows are examples of field margin diversification techniques. Larger-scale distribution and connectivity of landscape features such as hedgerows, habitat fragments, and riparian vegetation can also impact levels of biological control as well as provide biodiversity conservation benefits [56]. Interplanting crops with flowering herbaceous plants is promoted as a farmscaping technique since pollen and nectar are essential to the fecundity and longevity of several natural enemy species [57, 58]. Planting of multispecies hedgerows along the edges of farm fields can provide stable habitat and resources for beneficials while fields are bare or crops are young. Biological control may not be enhanced by hedgerows if the availability of pollen and nectar is so high within the hedgerows so that natural enemies do not disperse into adjacent agricultural fields to feed on crop pests [59]; or if the hedgerow attracts new pests, non-pest prey that natural enemies prefer over the crop pest; or top predators that prey on the natural enemies of interest [60–63].

Natural enemy dispersal ranges, which can vary from a few meters to over a kilometer for some parasitoid species [64], will determine the effectiveness of various habitat patterns at enhancing biological control. Blackberry and prune trees provide habitat for alternative hosts of the parasitic wasp, *Anagros epos*, which later preys upon the vineyard leafhopper pest, *Erythroneura elegantula* [65, 66], but connecting border plantings to infield floral corridors may encourage greater natural enemy movement and biological control in vineyards [63]. Successful conservation

biological control relies upon matching vegetational scale and pattern to the movement range of desired natural enemies in relation to their primary food sources. This requires an expansion beyond habitat management at the field level to incorporate larger landscape patterns and processes, a still relatively unexplored area. In addition to the size and distance between habitat patches, the "matrix" between patches is important for insect movement [67]. Many species that live in habitat patches also utilize resources outside the habitat patch, which is a desirable attribute for biological control allowing for natural enemies to migrate into agricultural fields. Structurally complex landscapes have been found to lead to higher levels of parasitism and lower crop damage [68, 69]; but this is not always the case even within the same region if parasitism rates also depend upon the presence of particular species or plant communities [70, 71].

Various strategies for increasing vegetation diversity within crop fields, including tolerating low levels of weed infestation and intercropping, have been exploited to reduce the density of herbivores attacking crops. Crops within diverse assemblages can be "harder to find and easier to lose" by herbivores, and better protected by natural enemies [72]. Diversified vegetation in field margins and mosaic patches across landscapes can support natural enemies that move into crop fields and provide biocontrol of pest herbivores [71]. Vegetation diversity may also affect management of phytopathogens.

Weed consumption by herbivores could be increased by reducing chemical pesticides to control agricultural pest and weeds, and then adopting resistant or repellent crops to generalist consumers found in agroecosystems. This management practice has been successful with some crop species toxic or deterrent to insects, negatively impacting weeds mainly consumed by herbivores [73]. This also is a good example on how food webs may be reorganized in response to human intervention. Native species of insects, rodents, birds, and other organisms can consume large numbers of weed seeds and promote reductions in requirements for chemical control tactics [74]. Interspersed strips of diverse, phenologically dissimilar crops may better conserve populations of weed seed consumers than crop monocultures [75]. Specialist pathogens have been used to suppress several weed species in pasture and rangelands, but in annual crops, the difficulty of maintaining appropriate environmental conditions for host infection and the need to achieve rapid weed suppression in a narrow time window has impeded the use of this approach [76].

Meadow strips enhanced pollinator diversity and plant reproductive success in adjacent fields in Switzerland [77]. Similarly, in Costa Rica, proximity to forested areas increased pollination and yield in coffee orchards [78]. Weeds in crop fields supply food for many bird species [79], and hedgerows and other forms of field margin vegetation supply both habitat and food for wildlife species [80].

Timing and intensity of agricultural management such as the way in which soil cropping or irrigating activities are designed may alter habitat distribution and connectivity across the landscape that are very important for maintaining viable populations of different organisms [59, 61, 81]. For example, asynchronous tillage is important for maintaining beetle populations in arable cropland [82] as well as asynchronous flooding is important for sustaining natural enemy populations in rice fields [24]. Initial studies also found that creating a mosaic of crop fields and wetlands in different successional stages had great promise as a strategy for improving waterfowl habitat and sustaining crop production in a multiuse landscape [83]. Interestingly, maintaining rice fields flooded through the winter for waterfowl foraging habitat also provided beneficial agronomic impacts by increasing decomposition of rice straw and reducing grassy weed biomass [84]. Further, numerous studies have shown the interactive effects of landscape complexity and the impacts of agricultural management practices, with more benign practices (such as organic farming) having the greatest effects on increased biodiversity in simple landscapes [46, 85, 86].

Conclusions

Our understanding of biotic interactions taking place in agroecosystems and how they relate to production constraints is growing rapidly, aided by agroecological approaches and the integration of ecological methodologies and ecologists into agricultural research. Numerous

studies provide data allowing for the characterization of agrosystems that reduce the importance of biological constraints to production. They include great spatiotemporal diversity of crops, discontinuity in monoculture (rotations, early varieties, etc.), a mosaic of small fields to ensure the juxtaposition of cultivated and noncultivated land, the presence of a dominant perennial crop (especially orchards), crops grown with high sowing density to limit weed populations, great genetic diversity in the crops (varieties grown in mixed or alternate rows of crops). Based on them, recommendations can be made concerning the management of cultivated plants and the choice of cropping techniques that consider the spatiotemporal dimension of cropping lands, the composition and abundance of the indigenous flora in and around the fields, soil type, the nature of the environment, and the type of farm.

Future Directions

It is clear that agroecosystems are self-designed, and their outputs are controlled and depend on the biotic interactions that evolve as they exist. If managing biotic constraints for crop production is to be sustained on agroecological bases, there is a need to understand how agricultural communities are structured taking into consideration the effects of diversity, species composition, and food web structure on ecosystem processes; the impacts of timing, frequency, and intensity of disturbance (at different complexity levels, i.e., whole ecosystem, community, population); and the importance of multi-trophic interactions. All of these aspects have to be observed and explicitly integrated at multiple spatial and temporal scales. The potential for a greater use of agroecological management approaches is high. However, given the variability of biological phenomena, the implementation of the agroecological strategy requires a planned spatiotemporal farm management. However, owing to the nature of these self-assembled ecosystems, there is some inherent unpredictability about responses to different management interventions. Effective synthesis of complex and often apparently contradictory information is still needed. Field-based research that includes monitoring of species performance, along with social learning mediated by farmer-researcher collaborations may help in this task.

Bibliography

1. Almekinders CJM, Fresco LO, Struik PC (1995) The need to study and manage variation in agro ecosystems. Neth J Agric Sci 43:127–142
2. Gliessman SR (1998) Agroecology: ecological processes in sustainable agriculture. Ann Arbor Press, Michigan
3. Altieri MA (1999) The ecological role of biodiversity in agroecosystems. Agric Ecosyst Environ 74:19–31
4. Pretty JN (1994) Regenerating agriculture. Earthscan, London
5. Altieri MA, Nicholls CI (1999) Biodiversity, ecosystem function and insect pest management in agroecosystems. In: Collins WW, Qualset CO (eds) Biodiversity in agroecosystems. CRC Press, Boca Raton, pp 69–84
6. Altieri MA (2002) Agroecology: the science of natural resource management for poor farmers in marginal environments. Agric Ecosyst Environ 93:1–24
7. Pretty J, Hine R (2000) Feeding the world with sustainable agriculture: a summary of new evidence: final report from "Safe-World" Research Project. University of Essex, Colchester
8. Sumner DR (1982) Crop rotation and plant productivity. In: Recheigl M (ed) CRC handbook of agricultural productivity, vol I. CRC Press, Boca Raton
9. Francis CA (1986) Multiple cropping systems. Macmillan, New York
10. Vandermeer J (1989) The ecology of intercropping. Cambridge University Press, Cambridge/London
11. Nair PKR (1982) Soil productivity aspects of agroforestry. ICRAF, Nairobi
12. Pearson CJ, Ison RL (1987) Agronomy of grassland systems. Cambridge University Press, Cambridge
13. Finch CV, Sharp CW (1976) Cover crops in California orchards and vineyards. USDA Soil Conservation Service, Washington, DC
14. Altieri MA, Rosset P (1996) Agroecology and the conversion of large-scale conventional systems to sustainable management. Int J Environ Stud 50:165–185
15. Chambers R (1983) Rural development: putting the last first. Longmans Scientific and Technical/Wiley, Essex, England/New York, p 218
16. Vasey DE (1992) An ecological history of agriculture 10, 000 BC–AD 10, 000. Iowa State University Press, Ames
17. Jorgensen SE, Nielsen SN (1996) Application of ecological engineering principles in agriculture. Ecol Eng 7:373–381
18. Hobbs RJ, Salvatore A, Aronson J, Baron JS, Bridgewater P, Cramer VA, Epstein PR, Ewel JJ, Klink CA, Lugo D, Norton DO, Richardson DM, Sanderson ES, Valladares F, Villa M, Zamora R, Zobel M (2006) Novel ecosystems: theoretical and management aspects of the new ecological world order. Glob Ecol Biogeogr 15:1–7
19. Cox GW, Atkins MD (1979) Agricultural ecology: an analysis of world food production systems. W. H. Freeman, San Francisco, p 731
20. Cox CM, Garrett KA, Bockus WW (2005) Meeting the challenge of disease management in perennial grain systems. Renewable Agric Food Syst 20:15–24

21. Carrol CR, Vandermeer JH, Rosset PM (1990) Agroecology. McGraw-Hill, New York
22. Shennan C (2008) Biotic interactions, ecological knowledge and agriculture. Philos Trans R Soc Lond B Biol Sci 363:717–739
23. Ghersa CM, Roush ML, Radosevich SR, Cordray SM (1994) Coevolution of agroecosystems and weed management. Bioscience 44:85–94
24. Settle WH, Ariawan H, Astuti EH, Cahyana W, Hakim AL, Hindayana D, Lestari AS (1996) Managing tropical rice pests through conservation of generalist natural enemies and alternative prey. Ecology 77:1975–1988
25. Fitter AH, Gilligan CA, Hollingworth K, Kleczkowski A, Twyman RM, Pitchford JW (2005) Biodiversity and ecosystem function in soil. Funct Ecol 19:369–377
26. Hooper DU, Chapin FS III, Ewel JJ, Hector A, Inchausti P, Lavorel S, Lawton JH, Lodge DM, Loreau M, Naeem S, Schmid B, Setälä H, Symstad AJ, Vandermeer J, Wardle DA (2005) Effects of biodiversity on ecosystem functioning: a consensus of current knowledge. Ecol Monogr 75:3–35
27. Andow DA (1991) Yield loss to arthropods in vegetationally diverse agroecosystems. Environ Entomol 20:1228–1235
28. Andow DA (1991) Vegetational diversity and arthropod population response. Annu Rev Entomol 36:561–586
29. Brown BJ, Ewel JJ (1987) Herbivory in complex and simple tropical successional ecosystems. Ecology 68:108–116
30. Prieur-Richard AH, Lavorel S, Linhart YB, Dos Santos A (2002) Plant diversity, herbivory and resistance of a plant community to invasion in Mediterranean annual communities. Oecologia 130:96–104
31. Ghersa CM, León RJC (1999) Succesional changes in the agroecosystems of the rolling pampas. In: Walker LR (ed) Ecosystems of disturbed ground. Elsevier, Amsterdam, pp 487–502
32. Radosevich SR, Holt JS, Ghersa CM (2007) Ecology of weeds and invasive plants. Wiley, New York
33. Baudry J, Poggio SL, Laurent C (2010) Agricultural landscape changes through globalisation and biodiversity effects. In: Primdahl J, Swaffied S (eds) Globalisation and agricultural landscapes: change patterns and policy trends in developed countries. Cambridge University Press, Cambridge, UK, pp 58–70
34. Edwards CA (1990) The importance of integration in sustainable agricultural systems. In: Edwards CA, Lal R, Madden P, Miller RH, House G (eds) Sustainable agricultural systems. Soil and Water Conservation Society, Ankeny, pp 249–264
35. Altieri MA (1987) Agroecology: the scientific basis of alternative agriculture. Westview, Boulder
36. Freckleton RP, Watkinson AR (2002) Are weed population dynamics chaotic? J Appl Ecol 39:699–707
37. Weinig C (2005) Rapid evolutionary responses to selection in heterogeneous environments among agricultural and nonagricultural weeds. Int J Plant Sci 166:641–647
38. Mundt CC (2002) Use of multiline cultivars and cultivar mixtures for disease management. Annu Rev Phytopathol 40:381–400
39. Shennan C (2008) Biotic interactions in agroecosystems. Philos Trans R Soc Lond B Biol Sci 363:717–739
40. Welbaum GE, Sturz AV, Dong ZM, Nowak J (2004) Managing soil microorganisms to improve productivity of agro-ecosystems. Crit Rev Plant Sci 23:175–193
41. Gosling P, Hodge A, Goodlass G, Bending GD (2006) *Arbuscular mycorrhizal* fungi and organic farming. Agric Ecosyst Environ 113:17–35
42. Anderson RL (2004) Sequencing crops to minimize selection pressure for weeds in the central great plains. Weed Technol 18:157–164
43. Moonen AC, Bàrberi P (2008) Functional biodiversity: an agroecosystem approach. Agric Ecosyst Environ 127:7–21
44. Mead R, Riley J, Dear K, Singh SP (1986) Stability comparison of intercropping and monocropping systems. Biometrics 42: 253–266
45. Zhu Y, Fen H, Wang Y, Li Y, Chen J, Hu L, Mundt CC (2000) Genetic diversity and disease control in rice. Nature 406:718–772
46. Tscharntke T, Klein AM, Kruess A, Steffan-Dewenter I, Thies C (2005) Landscape perspectives on agricultural intensification and biodiversity—ecosystem service management. Ecol Lett 8:857–874
47. Shennan C, Pisani Gareau T, Sirrine JR (2004) Agroecological approaches to pest management in the US. In: Pretty J (ed) The pesticide detox, solutions for safe agriculture. Earthscan, London, pp 193–211
48. Wilby A, Thomas MB (2002) Natural enemy diversity and pest control, patterns of pest emergence with agricultural intensification. Ecol Lett 5:353–360
49. Colunga GM, Gage SH, Dyer LE (1998) The insect community. In: Cavigelli MA, Deming SR, Probyn LK, Harwood RR (eds) Michigan field crop ecology, managing biological processes for productivity and environmental quality, Michigan State University Extension Bulletin E-2646. Michigan Agricultural Experiment Station, East Lansing, pp 59–70
50. Purtauf T, Roschewitz I, Dauber J, Thies C, Tscharntke T, Wolters V (2005) Landscape context of organic and conventional farms, influences on carabid beetle diversity. Agric Ecosyst Environ 108:165–174
51. Roschewitz I, Hucker M, Tscharntke T, Thies C (2005) The influence of landscape context and farming practices on parasitism of cereal aphids. Agric Ecosyst Environ 108:218–227
52. Roschewitz I, Gabriel D, Tscharntke T, Thies C (2005) The effects of landscape complexity on arable weed species diversity in organic and conventional farming. J Appl Ecol 42:873–882
53. Schmidt MH, Roschewitz I, Thies C, Tscharntke T (2005) Differential effects of landscape and management on diversity and density of ground-dwelling farmland spiders. J Appl Ecol 42:281–287
54. Kalkhoven JTR (1993) Survival of populations and the scale of the fragmented agricultural landscape. In: Bunce RGH, Ryszkowski L, Paoletti MG (eds) Landscape ecology and agroecosystems. Lewis, Boca Raton, pp 83–90

55. Landis DA, Menalled FD, Costamagna AC, Wilkinson TK (2005) Manipulating plant resources to enhance beneficial arthropods in agricultural landscapes. Weed Sci 53: 902–908
56. Burel F, Baudry J, Butet A, Clergeau P, Delettre Y, Le Cœur D, Dubs F, Morvan N, Paillat G, Petit S, Thenail C, Brunel E, Lefeuvre JC (1998) Comparative biodiversity along a gradient of agricultural landscapes. Acta Oecol 19:47–60
57. Jervis MS, Kidd MAC, Fitton MD, Huddleson T, Dawah HA (1993) Flower visiting by hymenopteran parasitoids. J Nat Hist 27:287–294
58. Idris AB, Grafius E (1995) Wildflowers as nectar sources for *Diadegma insulare* (Hymenoptera, Ichneumonidae), a parasitoid of diamondback moth (Lepidoptera, Ypono- meutidae). Environ Entomol 24:1726–1735
59. Bugg RL, Ehler LE, Wilson LT (1987) Effect of common knotweed (*Polygonum aviculare*) on abundance and efficiency of insect predators of crop pests. NAL/USDA Report, Belsville
60. Pollard E (1971) Hedges. VI. Habitat diversity and crop pests, a study of Brevicoryne brassica and its syrphid predators. J Appl Ecol 8:751–780
61. Bugg RL, Pickett CH (1998) Introduction, enhancing biological control—habitat management to promote natural enemies of agricultural pests. In: Pickett CH, Bugg RL (eds) Enhancing biological control: habitat management to promote natural enemies of agricultural pests. The Regents of the University of California, Berkeley, pp 1–23
62. Rosenheim JA, Limburg DD, Colfer RG (1999) Impact of generalist predators on a biological control agent, *Chrysoperla carnea*, direct observations. Ecol Appl 9:409–417
63. Nicholls CI, Parrella M, Altieri MA (2001) The effects of a vegetational corridor on the abundance and dispersal of insect biodiversity within a northern California organic vineyard. Landscape Ecol 16:133–146
64. Corbett A (1998) The importance of movement in the response of natural enemies to habitat manipulation. In: Pickett CH, Bugg RL (eds) Enhancing biological control, habitat management to promote natural enemies of agricultural pests. University of California Press, Berkeley, pp 25–48
65. Doutt RL, Nakata J (1973) The Rubus leafhopper and its egg parasitoid, an endemic biotic system useful in grape pest mangement. Environ Entomol 2:381–386
66. Murphy BC, Rosenheim JA, Granett J, Pickett CH, Dowell RV (1998) Measuring the impact of a natural enemy refuge, the prune tree/vineyard example. In: Pickett CH, Bugg RL (eds) Enhancing biological control, habitat management to promote natural enemies of agricultural pests. University of California Press, Berkeley, pp 297–309
67. Ricketts TH, Daily GC, Ehrlich PR, Michener CD (2004) Economic value of tropical forest to coffee production. Proc Natl Acad Sci USA 101:12579–12582
68. Thies C, Tscharntke T (1999) Landscape structure and biological control in agroecosystems. Science 285:893–895
69. Pullaro TC, Marino PC, Jackson DM, Harrison HF, Keinath AP (2006) Effects of killed cover cropmulch on weeds, weed seeds, and herbivores. Agric Ecosyst Environ 115:97–104
70. Menalled FD, Marino PC, Gage SH, Landis D (1999) Does agricultural landscape structure affect parasitism and parasitoid diversity? Ecol Appl 9:634–641
71. Landis DA, Wratten SD, Gurr GA (2000) Habitat management to conserve natural enemies of arthrop pests in agriculture. Annu Rev Entomol 45:175–201
72. Gurr GM, Wratten SD, Altieri MA (eds) (2004) Ecological engineering for pest management: habitat manipulation for Arthropods. CSIRO, Collingwood, p 244
73. Liebman M, Davis AS (2000) Integration of soil, crop and weed management in low-external-input farming systems. Weed Res 40:27–47
74. Westerman P, Liebman M, Menalled FD, Heggenstaller AH, Hartzler RG, Dixon PM (2005) Are many little hammers effective?—velvetleaf (*Abutilon theophrasti*) population dynamics in two- and four-year crop rotation systems. Weed Sci 53:382–392
75. Heggenstaller AH, Menalled FD, Liebman M, Westerman PR (2006) Seasonal patterns in post-dispersal seed predation of *Abutilon theophrasti* and *Setaria faberi* in three-cropping systems. J Appl Ecol 43:999–1010
76. Ghorbani R, Leifart C, Seel W (2005) Biological control of weeds with antagonistic plant pathogens. Adv Agron 86: 191–225
77. Albrecht M, Duelli P, Muller C, Kleijn D, Schmid B (2007) The Swiss agri-environment scheme enhances pollinator diversity and plant reproductive success in nearby intensively managed farmland. J Appl Ecol 44:813–822
78. Ricketts TH, Daily GC, Ehrlich PR, Fay JP (2001) Countryside biogeography of moths in a fragmented landscape, biodiversity in native and agricultural habitats. Conserv Biol 15: 378–388
79. Marshall EJP, Brown VK, Boatman ND, Lutman PJW, Squire GR, Ward LK (2003) The role of weeds in supporting biological diversity within crop fields. Weed Res 43:77–89
80. Marshall EJP, Moonen AC (2002) Field margins in northern Europe: their functions and interactions with agriculture. Agric Ecosyst Environ 89:5–21
81. Baudry J, Papy F (2001) The role of landscape heterogeneity in the sustainability of cropping systems. In: Nösberger J, Geiger HH, Struik PC (eds) Crop science – progress and prospects. CABI, Oxon
82. Holland JM, Thomas CFG, Birkett T, Southway S, Oaten H (2005) Farm-scale spatiotemporal dynamics of predatory beetles in arable crops. J Appl Ecol 42:1140–1152
83. Shennan C, Bode CA (2002) Integrating wetland habitat with agriculture. In: Jackson LL, Jackson D (eds) The farm as a natural habitat. Island, Washington, DC, pp 189–204
84. van Groenigen JW, Burns EG, Eadie JM, Horwath WR, van Kessel C (2003) Effects of foraging waterfowl in winter flooded rice fields on weed stress and residue decomposition. Agric Ecosyst Environ 95:289–296

85. Benton TG, Vickery JA, Wilson JD (2003) Farmland biodiversity: is habitat heterogeneity the key? Trends Ecol Evol 18:182–188
86. Bengtsson J, Ahnstrom J, Weibull AC (2005) The effects of organic agriculture on biodiversity and abundance, a meta-analysis. J Appl Ecol 42:261–269

Agronomic Interactions with CO_2 Sequestration

Rattan Lal
OARDC/FAES Kottman Hall, Carbon Management and Sequestration Center, The Ohio State University, Columbus, OH, USA

Article Outline

Glossary
Definition of the Subject
Introduction
Soil Carbon Budget
Hidden Carbon Costs
Farming Carbon
Ecosystem Services and Soil Carbon Sequestration
Carbon Sequestration and Agronomic Production
Future Directions
Conclusions
Bibliography

Glossary

Carbon sequestration Transfer of atmospheric CO_2 into long-lived reservoirs

Mean residence time The duration during which CO_2-C resides in a specific pool (pool)

Soil quality Capacity of a soil to perform ecosystem services

Definition of the Subject

Atmospheric concentration of carbon dioxide (CO_2) can be stabilized, if not reduced, by reducing anthropogenic emissions, sequestering emissions, or both. Emission reduction implies identifying and using no-carbon (C) or low-C energy sources such as alternatives to fossil fuel including wind, solar, hydro, geo-thermal, biofuels, etc. Reductions in gaseous emissions can also be achieved by enhancing the energy use efficiency. In agronomic systems, involving practices to raise crops and livestock, enhancing energy efficiency implies a range of practices which increase agricultural productivity per unit input of energy-based resources (i.e., fertilizers, pesticides, irrigation). Another strategy is elimination or reduction in frequency and intensity of tillage operations and converting plow-based tillage to no-till farming or conservation agriculture. Use of solar and wind energy for grain drying, water pumping, and heating buildings can also reduce emissions.

Agricultural soils and ecosystems can also be used for sequestration of atmospheric CO_2 by enhancing photosynthesis, increasing net primary productivity (NPP), and converting some of the NPP into stable biomass (forest products) and the soil C pool. The biomass in forest, with a long mean residence time (MRT), has two distinct but related components: the above-ground biomass and the below-ground biomass. The above-ground biomass can be alive or the detritus material. The photosynthates transferred deep into the subsoil through a tap root system have a long MRT. Agroforestry systems, growing crops and raising livestock in combination with perennials (tree species), can enhance the ecosystem C pool by increasing both biomass-C and soil-C components.

Sequestering C in soil entails increasing soil organic C (SOC) pool and also the soil inorganic C (SIC) pool. The SOC pool has three related components: labile/active pool, intermediate pool, and the passive/recalcitrant pool with MRT of < year, <decades to a century, and several millennia, respectively. The goal is to transfer the labile pool into intermediate and preferably passive pools through conversion to conversion tillage, use of manure/compost and other biosolids (biochar), and complex cropping/farming systems. Sequestration of SIC occurs through formation of secondary carbonates. In irrigated systems, however, leaching of bicarbonates is also an important mechanism of SIC transfer into the groundwater. Agronomic practices strongly interact with strategies of reducing emissions and sequestrating CO_2 in soils and biota. Therefore, the strategy of agronomic management is to identify the interactive agronomic practices which enhance ecosystem (biotic and pedologic) C pools.

Introduction

Limiting global warming to 2°C necessitates identification and adoption of diverse strategies which reduce the net anthropogenic emissions of greenhouse gases (GHGs). Agriculture, hitherto a major source of GHGs, is an important industry which can be made more energy-efficient. Importance of improving agricultural production, by as much as 70% between 2010 and 2050, cannot be overemphasized in view of the need to reduce hunger, malnutrition, and poverty. Although a major challenge, making agriculture emission-neutral is a prudent long-term strategy. It is in this context that understanding of the agronomic interactions with CO_2 sequestration in soil is important.

Agronomic systems are defined as site-specific management of soils and crops on the basis of eco-regional and physiographic characteristics, and in the context of socioeconomic and policy environments. These systems are strong determinants of agricultural production, sustainable use of resources, and their environmental impact. Pertinent examples of the environmental impacts of agronomic systems include accelerated soil erosion, nonpoint source pollution, emission of GHGs, and alterations in ecosystem and soil C pools. Most soils of agricultural ecosystems (i.e., croplands, grazing lands) are depleted of their SOC pool. In comparison with the natural/climax vegetation, the remaining SOC pool in agricultural soils may be 20–50% of the antecedent pool under undisturbed conditions [1]. The magnitude of loss is large in soils characterized by high than low antecedent pool, coarse than fine texture, in warm than cold climates, and in degraded/eroded than favorable quality. Furthermore, the magnitude of loss is more from soils managed by extractive farming than of intensive/science-based agriculture. The historic loss is also equivalent to the potential soil C sink capacity, a part of which can be realized through conversion to a restorative land use and adoption of recommended management practices (RMPs).

Sequestration of CO_2 in agroecosystems implies transfer of atmospheric CO_2 into biota and soils through photosynthesis and NPP in a manner such that the biomass-C is neither readily nor immediately returned back to the atmosphere. The strategy is to enhance the MRT of C in biota and soils. Principal determinants of MRT comprise of a wide range of factors including soil processes and plant/biomass characteristics. Important among soil processes are formation of: (1) stable micro-aggregates, (2) organo-mineral complexes including absorption on clay surfaces, and (3) recalcitrant organic polymers involving physical, chemical, and biological protection of soil organic matter (SOM). Another process of physical protection is transfer of SOM into the subsoil by illuviation as dissolved organic (DOC) such that it is away from the surface layer prone to accelerated erosion, intense mineralization, and other natural and anthropogenic perturbations. Important among plant characteristics which increase MRT are: (1) a deep root system and (2) a high concentration of recalcitrant compounds. This chapter is aimed at describing the processes and practices which moderate the agronomic interactions with CO_2 sequestration in soil as a recalcitrant humus of a long MRT.

Soil Carbon Budget

The strategy is to create a positive SOC budget so that input of biomass-C exceeds the losses. Important among agronomic practices which create a positive C budget (Fig. 1) are mulch farming, no-till/conservation agriculture, integrated nutrient management (INM) including slow release formulation of chemical fertilizers and biofertilizers, conservation and management of soil water to reduce losses by surface runoff and evaporation and increase soil-water storage, and use of complex cropping/farming systems including agroforestry and mixed farming systems. The strategy is to replace extractive farming practices, which deplete soil fertility and SOC pool, by science-based agriculture involving the widespread adoption of RMPs. Some RMPs outlined in Fig. 1 are generic, and no one practice is universally applicable because of the extreme diversity of soil types, ecoregions, and the human dimensions related to socioeconomic and political consideration. Site/soil-specific validation and adaption through fine-tuning of RMPs is essential.

While increasing the input of biomass-C, it is equally important to reduce its losses. Agronomic/soil

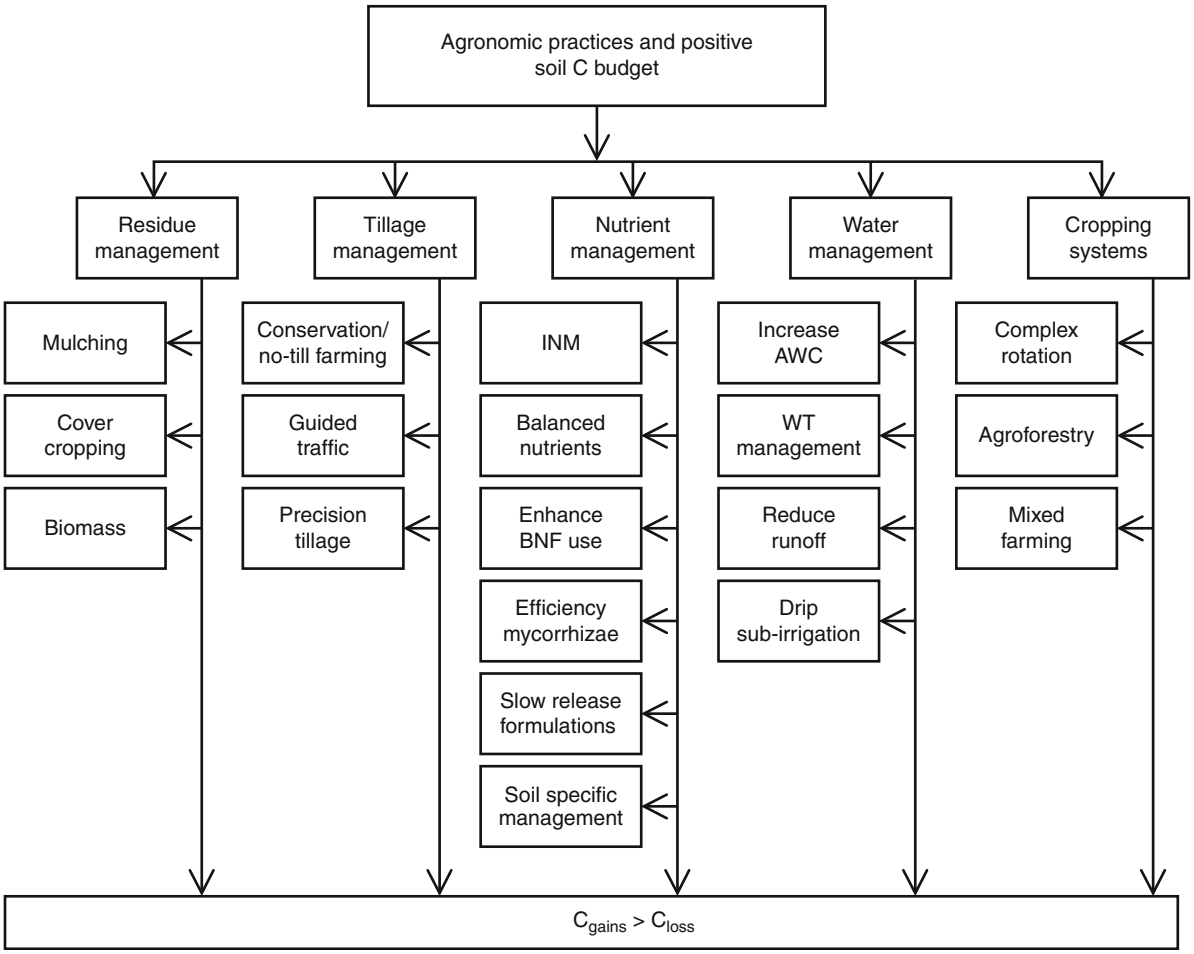

Agronomic Interactions with CO_2 Sequestration. Figure 1
Agronomic interactions which cause positive carbon budget (*INM* integrated nutrient management, *AWC* available water capacity, *WT* water table, *BNF* biological nitrogen fixation)

processes which deplete the SOC pool are outlined in Fig. 2. The SOC pool is strongly depleted by accelerated soil erosion. The preferential/selective removal of SOC by runoff and erosion, as indicated by an enrichment ratio of C in sediments ranging from 5 to 30 depending on soil/land and climate, is attributed to: (1) low density of SOC, (2) high concentration (stratification) in the surface layer, and (3) absorption on clay and thus removal along with the clay particles. Soil erosion is exacerbated by plowing, residue removal, uncontrolled and excessive grazing, and management practices which degrade soil structure and accentuate its vulnerability to climatic erosivity.

The SOC pool is also depleted by increase in the rate of mineralization. The latter increases with increase in soil temperature and changes in soil moisture regime. Conversion of natural to managed/agricultural ecosystems alters both the soil temperature and moisture regimes and accentuates the rate of mineralization. The latter, being a biochemical reaction, is approximately doubled with every 10°C increase in temperature (Vant Hoff rule). There is an optimal soil moisture regime for the mineralization/decomposition. Water table management and drainage of excessively wet soils increase the rate of mineralization. Excessive wetness increases methanogenesis and denitrification with an

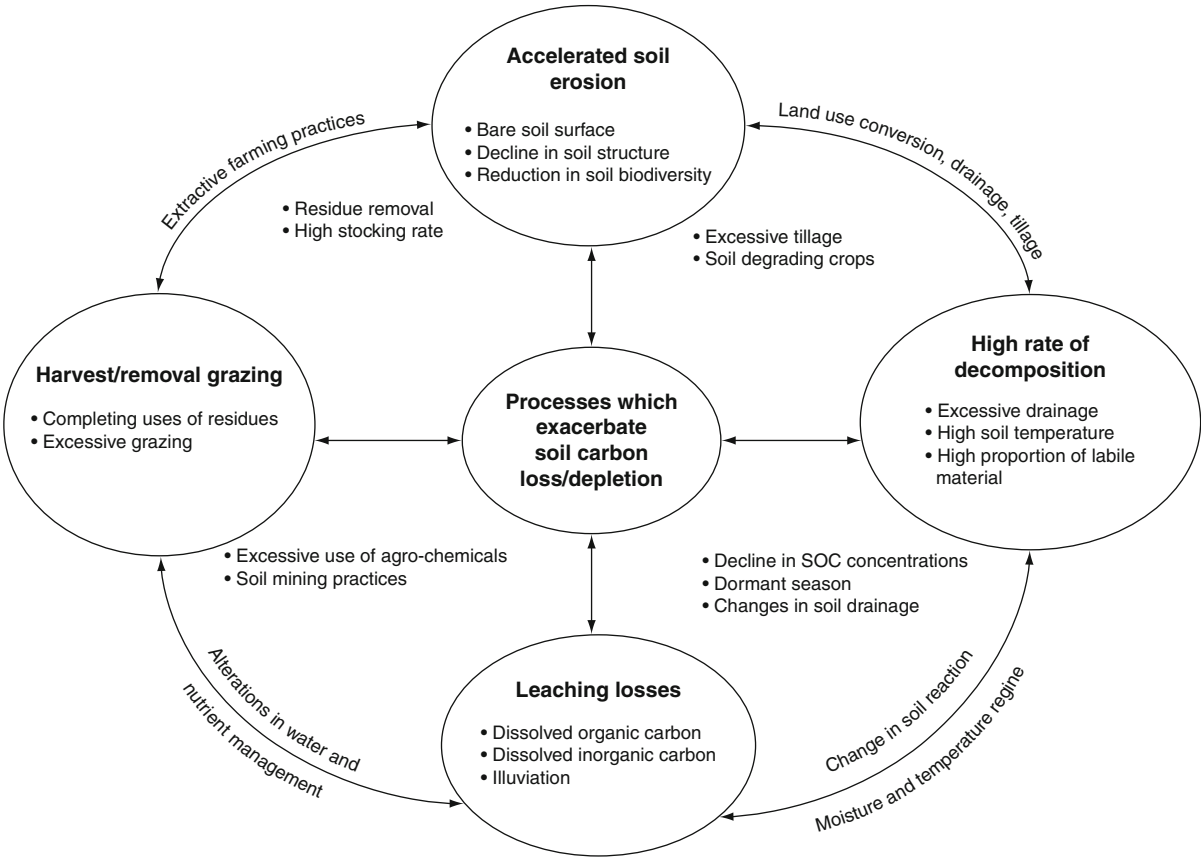

Agronomic Interactions with CO_2 Sequestration. Figure 2
Agronomic soil processes which deplete the soil carbon pool

attendant increase in emissions of CH_4 and N_2O. In contrast, supplemental irrigation in arid and semi-arid climates can also accentuate mineralization and denitrification. In general, therefore, emissions of GHGs may be more from agricultural soils than those under natural ecosystems.

Hidden Carbon Costs

Most agronomic inputs, especially in intensively managed systems, are based on use of fossil fuel combustion. Important among these are tillage operations, harvesting, drying, application of fertilizers, and other chemicals (pesticides) and irrigation. The hidden C cost (HCC) of these inputs are listed in Table 1. Agronomic practices with a significant input of HCC are tillage systems, and agricultural chemicals. Thus, a complete Life Cycle Analysis (LCA) is needed to determine the ecosystem C budget and assess the net C gains. The latter can be described by Eq. 1:

$$\text{Net C gain} = C_{input} - (C_{loss} + HCC) \quad (1)$$

C_{input} includes biomass addition such as shoot, leaves, detritus materials, roots, compost, manure, deposition through wind and water, etc. C_{loss} occurs mainly through erosion, decomposition, and leaching. Principal components of HCC are the energy-based inputs. Quantification of each of these components is essential to conducting LCA for specific soil, crop, ecoregion, and other site-specific factors.

It is often argued that HCC should not be deducted from the gross C gains because agronomic inputs (i.e., fertilizers, tillage, pesticides, manure, irrigation, and harvesting) are not used for C sequestration but for

Agronomic Interactions with CO_2 Sequestration.
Table 1 Hidden carbon costs of agronomic practices (Adapted from [2])

Agronomic practice		Carbon cost
I.	*Tillage (kg CE/ha)*	
	Moldboard plowing	15.2 ± 4.1
	Chisel plowing	7.9 ± 2.3
	Disking	8.3 ± 2.5
	Cultivation	4.0 ± 1.9
	Rotary hoeing	2.0 ± 0.9
II.	*Fertilizers (kg CE/kg)*	
	Nitrogen	1.3 ± 0.3
	Phosphorus	0.2 ± 0.06
	Potassium	0.15 ± 0.06
	Lime	0.16 ± 0.11
III.	*Pesticides (kg CE/kg)*	
	Herbicides	6.3 ± 2.7
	Insecticides	5.1 ± 3.0
	Fungicides	3.9 ± 2.2
IV.	*Irrigation (kg CE/ha/year)*	
	Surface	9.4–24.6
	Sprinkler	16.3–121.3
	Trickle	84.9

achieving food security to meet the food and other demands (i.e., feed, fiber, and raw materials) of the growing population. If HCCs are also considered, land managers/farmers are not adequately rewarded by payments through C trading.

Farming Carbon

The term "farming carbon" implies growing/increasing C pool in soils and biota (trees) of managed ecosystems (agriculture, forestry, urban lands, wetlands) so that any increase in the ecosystem C pool can be traded in the market as a farm produce. Agronomic interactions, practices which enhance soil and the biotic C pools, are strong determinants of the C gains (or losses) from the ecosystem. Changes in the ecosystem C pool must be monitored by a standardized procedure so that the data are credible, reproducible, and verifiable by other procedures. A protocol for measurement, monitoring, and verification (MMV) is essential to implement C trading.

Ecosystem Services and Soil Carbon Sequestration

Sequestration of C in soils and biota generates and enhances numerous ecosystem services (Fig. 3). Important among these are: (1) providing materials of use to human (i.e., food), (2) moderating the environment (i.e., climate), (3) enhancing support, and (4) archiving human and planetary history [3, 4]. Soil and the ecosystem C pools are strong determinants of these services directly and indirectly. For example, quantity and quality of the SOC pool affect soil functions through (1) increasing soil aggregation and improving soil tilth, (2) increasing nutrient retention and availability, (3) moderating water retention and availability, (4) improving infiltration and reducing water runoff, (5) reducing soil erosion and nonpoint source pollution, (6) providing energy source and food to soil biota, (7) enhancing nutrient/elemental cycling, (8) accentuating use efficiency of input, (9) enhancing rhizospheric processes and micro-climatic environment, and (10) improving GPP and NPP.

Carbon Sequestration and Agronomic Production

It is because of numerous positive effects of organic carbon concentration in the root zone on soil quality that it is a strong determinant of the use efficiency of agronomic input and of crop growth and yield. Depending upon soil type and crop characteristics, there is a threshold value of 15–20 g/kg of SOC concentration in the root zone [5]. Crop growth and yield are strongly reduced when SOC concentration is below the threshold level (Fig. 4, [6, 7]). The yield response to SOC concentration in the root zone also depends on the management. The crop response (i.e., growth and yield) is generally stronger in agronomic practices based on low than high external inputs such as fertilizers, manure/compost, irrigation, etc. Indeed, the yield potential of elite varieties cannot be realized

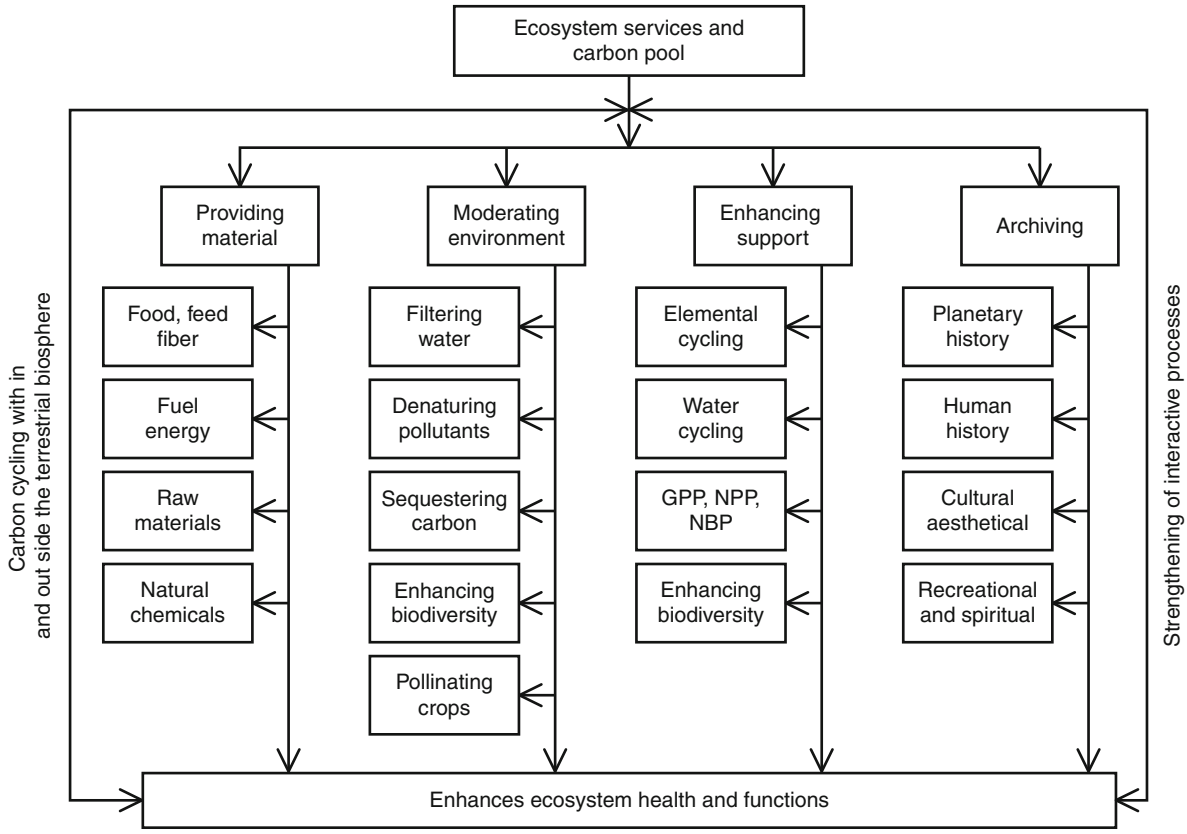

Agronomic Interactions with CO_2 Sequestration. Figure 3
Ecosystem services enhanced by soil carbon sequestration (*GPP* gross primary productivity, *NPP* net primary productivity, *NBP* net biome productivity)

unless soil quality and the related agronomic interactions are optimized. Therefore, enhancing SOC concentration to above the threshold level is essential to improving agronomic yield in depleted/degraded soils of sub-Saharan Africa, South and Central Asia, and elsewhere in regions with low crop yields.

Future Directions

There is a strong need to understand the following:

- Soil processes and agronomic practices which create a positive C budget for diverse ecoregions
- Rate of C sequestration in relation to soil type, climate, and management
- Relationship between soil C pool/concentration and soil quality parameters, and agronomic yield
- Process, factors, and causes which enhance the mean residence time of C in soil
- Threshold value of C concentration for predominant soil type and crops
- Policy interventions to promote "carbon farming"

Conclusions

Creating a positive budget of C (and N) is important to C sequestration in the soil. Agronomic practices to create a positive C budget are those which enhance the inputs of biomass-C. Important among these are conservation/no-till agriculture, mulch farming, cover cropping, integrated nutrient management, harvesting/recycling of water, complex farming systems, and perennial culture. Restoration of eroded/degraded soils and ecosystems is important to C sequestration in the soil. Energy-based inputs (i.e., fertilizers, pesticides, and tillage) have high hidden C costs. The strategy is to minimize losses of these

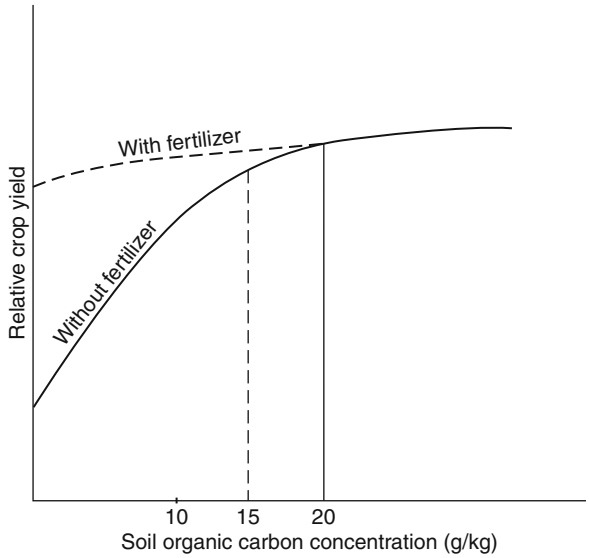

Agronomic Interactions with CO_2 Sequestration. Figure 4
A generalized response curve of agronomic yield response of crops to concentration of soil organic matter in the root zone

inputs by erosion, leaching, volatilization, etc. Increase in soil organic C pool above the threshold level can enhance crop yield. Improvement in soil quality through increase in SOC pool is essential to increasing crop yields and agronomic production of soils in African, Asian, Caribbean, and the Andean regions.

Bibliography

1. Lal R (1999) Soil management and restoration for C sequestration to mitigate the greenhouse effect. Prog Env Sci 1:307–326
2. Lal R (2004) Carbon emissions from farm operations. Environ Int 30:981–990
3. Daily GC (1997) Nature's services: societal dependence on natural ecosystems. Island Press, Washington DC, 392 pp
4. MEA (2005) Ecosystems and human wellbeing: synthesis, Millennium ecosystem assessment. Island Press, Washington, DC, 155 pp
5. Aune JB, Lal R (1997) Agricultural limits in the tropics and critical limits of properties of Oxisols, Ultisols and Alfisols. Trop Agric (Trinadad) 74:96–103
6. Lal R (2010) Beyond Copenhagen: mitigating climate change and achieving food security through soil carbon sequestration. Food Security 2(2):169–177
7. Lal R (2010) Enhancing eco-efficiency in agroecosystems through soil C sequestration. Crop Sci 50:S120–S131

Air Pollution Monitoring and Sustainability

Andrew Knox[1], Greg J. Evans[1], Colin J. Lee[1], Jeffrey R. Brook[1,2]
[1]Department of Chemical Engineering and Applied Chemistry, University of Toronto, Toronto, ON, Canada
[2]Air Quality Research Division, Atmospheric Science and Technology Directorate, Environment Canada, Toronto, ON, Canada

Article Outline

Glossary
Definition of the Subject
Introduction
Air Pollutants
Currently Recognized Air Pollution Problems
Motivations Behind Monitoring Air Pollution
Current Air Pollution Monitoring Practices
Past and Ongoing Success in Air Pollution Mitigation
Outstanding Problems and Challenges
Current Air Pollution Monitoring and Sustainability
Future Directions: Monitoring to Promote Greater Sustainability
Conclusion
Bibliography

Glossary

Acid deposition Settling on land or water of acidic air pollutants or air pollutants capable of becoming acidic once settled.

Acid neutralizing capacity (ANC) The ability of a medium (e.g., soil) to neutralize acidic pH, generally indicated by concentration of base cations.

Adaptive capacity The capacity to adjust to new circumstances such that successful functioning can continue.

Aerodynamic diameter The diameter of a spherical particle of unit density with a terminal velocity equal to the particle being considered.

Aerosol Liquid- or solid-phase particles suspended in a gas.

Aerosol optical depth Total extinction of light due to scattering and absorption by particles suspended in air between the point considered, the light's origin, and the point of observation.

Air pollution monitoring The use of scientific instruments and methods to assess the concentrations or rates of emission of air pollution in various environments.

Air pollution policy Legal guidelines governing allowable emissions of pollutants to air, allowable concentrations of pollutants in air, and air quality remediation efforts.

Air quality monitoring Observation of features of air that relate to the air's quality over some time period. Said features include concentrations of pollutants.

Air quality The degree to which air is an ideal supporter of life.

Background level The concentration of a substance or pollutant that remains regardless of short-term, local changes in emissions patterns. Background concentrations are not static, but changes in background concentration happen over the relatively long term.

Best available technology (BAT) A term relating to emissions standards set based on the ability of existing pollution abatement technology to mitigate the release of pollutants.

Biogenic Produced by biological organisms or systems.

Biosphere All life and ecosystems on Earth.

Chlorofluorocarbons (CFCs) A class of chlorine or fluorine containing organic compounds.

Climate change A long-term change in regional and global meteorological mean state or the variability of that mean state.

Command and control A strategy for limiting emissions by assigning specific emissions maximums to pollution sources or otherwise imposing pollution limiting rules and enforcing those rules.

Concentration-response functions (CRFs) The mathematical relationships between the environmental concentration of a pollutant and an effect of the pollutant. Effects, or responses, could include health effects such as premature mortality.

Consolidated sustainability metrics Summative statistics that are a function of a number of data on different species of pollutants and atmospheric conditions. Consolidated metrics are based on a prior judgment of the relative importance of all the data in their calculation. They are designed to give an overall picture and convey a great deal of information in a single number or index.

Critical load The maximum amount of pollution an ecosystem can tolerate without suffering significant harmful effects, as far as can be understood given the present understanding.

Critical natural capital Natural capital that cannot be lost without irreparable terminal damage to ecosystems.

Ecosystem A system supporting life, including living and nonliving components and the interactions between its components.

Enforcement Action taken or penalties imposed to correct situations in which emissions or concentrations of pollutants are above the legal limit.

Exposure A time-integrated concentration metric reflecting the potential for intake of pollutants.

Greenhouse gas Gas which, when in the atmosphere, induces a climate forcing via its ability to absorb light and convert it to thermal energy.

Hazardous air pollutants (HAPs) Individual or families of compounds that can potentially induce adverse health impacts, including but not limited to cancer, reproductive effects, or adverse environmental effects.

Holism The view that systems cannot be understood in exclusion of other systems but must be understood in relation to the larger whole that affects all parts within itself.

Mortality A statistical measure quantifying the number or fraction of deaths among populations.

Multipollutant monitoring Monitoring with attention to the effects of pollution arising from the interaction of different species of pollutants.

Natural capital The natural systems that produce goods such as clean air and provide services such as life support to the biosphere.

Ozone layer A lower stratospheric region of more concentrated ozone, which absorbs much of the ultraviolet radiation from the sun.

Particulate matter Solid or liquid particles suspended in air. PM is not a term that distinguishes particles by chemical species, and individual PM

particles can contain a variety of species. Particulate Matter is often written as PM_{10} or $PM_{2.5}$ with the number in subscript denoting the maximum aerodynamic diameter in micrometers of the particles being described. The subscripts (e.g., "2.5") indicate that the PM considered is less than the subscript's value in micrometers (μm). Particles smaller than about 10 μm are generally considered inhalable with smaller particles reaching deeper into the lung.

Pedestrian-oriented development Construction or reconstruction of the urban form designed to facilitate walking as a primary means of personal transportation.

Point sources Localized emitters of large amounts of pollution.

Population exposure A statistic accounting for a population's distribution throughout the area it inhabits, the pollution concentration distribution over that area, and the changes in those distributions over time to represent the macro-level (population-level) exposure of the population to a pollutant or set of pollutants.

Primary pollutants Pollutants released from a source directly into the environment in the given form.

Primary standards US EPA Air pollution standards set to protect public health.

Radiative balance The net radiation to or from an object or system accounting for total incoming and outgoing radiation. A positive radiative balance will lead to the warming of the system considered, while a negative radiative balance will lead to cooling, assuming no non-radiative energy flows are at work.

Resilience The ability of a system to renew and reorganize itself after a shock or major socio-ecological shift.

Risk-based policy Policy based on the quantification and understanding of the probabilities of damages incurred. In risk-based policy, allowable pollutant concentrations are set with the knowledge and acceptance of the damage likely to be realized.

Secondary pollutants Pollutants not released directly from sources but formed in the environment via chemical reactions among primary pollutants facilitated by atmospheric conditions such as moisture, temperature, and sunlight.

Secondary standards US EPA Air pollution standards set to mitigate regional environmental problems.

Socio-ecological justice Fairness concerning both the social realm (e.g., fairness among social classes) and the ecological realm (e.g., distribution schemes, including ecosystems as stakeholders), and the interaction between the two realms.

Source apportionment Attributing the pollutants in a region or at a receptor site to their sources, for example, quantification of the portion of ambient NO_x originating from the transportation sector versus the industrial sector.

Target load The pollution burden aimed for in policy. The load deemed achievable once "other factors (such as ethics, scientific uncertainties, and social and economic effects) are balanced with environmental considerations." [96]

Transit-oriented development Construction or reconstruction of the urban form designed to facilitate use of public transportation vehicles as a primary means of medium to long-distance personal transportation.

Troposphere The layer of the atmosphere closest to the Earth's surface, where human exposure to air pollutants occurs.

Urban form The physical shape and design of cities, their structures, and their infrastructure.

Definition of the Subject

Air pollution monitoring is the use of scientific and mathematical tools and methods to assess the concentrations or rates of emission of air pollution in various environments. Monitoring is usually performed at ground level in populated areas, where humans exposure tends to occur but can also include measurements at other altitudes, in other spheres of the atmosphere, or in unpopulated areas. Monitoring data is often an important input into air pollution research projects.

Introduction

Air pollution monitoring is concerned with collecting evidence about the emissions, concentrations, and effects of air pollutants. There are a number of effects of air pollution. Those most commonly recognized are negative impacts on human health, ecosystems, and the economy. Current air pollution monitoring assesses

the properties of air pollution in the atmosphere by monitoring ambient air, monitoring emissions from pollution sources, remotely sensing air pollution indicators via satellite, and through the use of numerical models. Monitoring efforts allow for air quality warnings, tracking trends over time, air pollution research, and policy development, including pollutant concentration and emissions standards. While air pollution monitoring has led to many substantial successes in the reduction of impacts from air pollution, many air pollution problems are still outstanding.

Air pollution monitoring is an essential activity in the assessment of environmental quality and provides information without which acting to promote sustainability would be impossible. However, air pollution monitoring must be expanded in breadth and depth if societies are to progress toward sustainability. Monitoring must extend the information provided in service of more diverse goals. These goals should include facilitating urban design for air quality, socio-ecological justice, methods for acceleration of air pollution research, resilience, and preservation of natural capital. Work that crosses intellectual disciplines would also help, as would public involvement in monitoring. Immediate steps the air pollution monitoring community could take to improve its routine practice include the development of multipollutant impact assessments, greater consideration of consolidated metrics, more and better use of satellite-derived observations, routine use of available design methodologies in the design of monitoring networks, adhering to suggestions in existing literature to improve routine practice, and beginning to address some of the previously necessary oversimplifications involved in conventional monitoring. While the air pollution monitoring community has a historical record of promoting sustainability and should be applauded, a paradigm shift is needed if it is to address these expanded goals.

Air Pollutants

Air pollution monitoring is concerned with air pollutants, substances which have negative effects on life. Some air pollutants are prevalent in most urban areas, and their effects are widespread. Other air pollutants tend to be less concentrated, or are only concentrated in specific areas, but have gained attention for being especially problematic or acutely toxic. In the USA and in Canada, pollutants of this first type are classified as "criteria" pollutants. (In the USA, the label "criteria" is applied to common pollutants. The EPA regulates these pollutants by setting permissible levels based on human health or environmental considerations [1], whereas in Canada, pollutants fall into the "criteria" category as a result of sharing common sources, mostly notably, fossil-fuel combustion [2].) The second type of air pollutant, the type capable of causing problems despite relatively low average emissions rates, have been classified by the US EPA (US Environmental Protection Agency) as "Hazardous Air Pollutants" (HAPs) for the particular hazards they present. One hundred and eighty-nine HAPs are officially recognized by the US EPA [5]. Criteria pollutants and HAPs are discussed below, and classifications by different authorities are given in Table 1. Typical ranges for many non-HAP pollutants in the USA are given in Table 2. Table 3 summarizes the sources and effects of pollutants.

What Are the Criteria Pollutants?

Criteria pollutants include carbon monoxide (CO), nitrogen oxides (NO_x), and sulfur dioxide (SO_2) [1]. Tropospheric ozone (O_3) and Particulate Matter (PM) are also criteria pollutants. Most species of harmful Volatile Organic Compounds (VOCs) that are not acutely toxic enough to be specifically identified as HAPs are included in the criteria air contaminants in Canada [2]. Table 3 shows the common sources of the criteria pollutants mentioned and comments on some of their effects.

Emissions of CO are the result of the incomplete combustion of carbonaceous fuels. Any use of fossil fuels can result in emissions of CO, but vehicles are the dominant source [6]. In motor vehicles, catalytic converters are often used to mitigate CO emissions. CO's effects include human health impacts and contribution to the formation of tropospheric ozone [7].

NO_x is the sum of NO and NO_2. Atmospheric nitrogen (N_2) is oxidized during combustion to form NO_x. NO_x is similar to CO in that it can lead to health effects and the production of tropospheric ozone, its main source in many locations is emissions from vehicles, and catalytic converters are used to minimize these

Air Pollution Monitoring and Sustainability. Table 1 Pollutants and their classification by different systems. Pollutants are described in detail below. The more acutely hazardous pollutants given here (those classified as HAPs by the US system, for example) are only examples and not an extensive representation of the full range of hazardous pollutants. PM_{10} and $PM_{2.5}$ are classified here as CACs by the Canadian classification and Criteria Pollutants by the US EPA classification, as Environment Canada and the US EPA classify "particulate matter" in general as CACs and Criteria Pollutants, respectively [2]. Certain species of dioxins and furans are classified as HAPs by the EPA, but not all are covered. CAC stands for criteria air contaminant, AQSP stands for air quality strategy pollutant, POP stands for persistent organic pollutant [3], HAP stands for hazardous air pollutant

Pollutant	Canadian classification [2]	UK classification [4]	US classification [5]
CO	CAC	AQSP	Criteria pollutant
NO_x	CAC	AQSP	Criteria pollutant
SO_2	CAC	AQSP	Criteria pollutant
NH_3	CAC		
O_3	CAC	AQSP	Criteria pollutant
VOC	CAC		
PM_{10}	CAC	AQSP	Criteria pollutant
$PM_{2.5}$	CAC	AQSP	Criteria pollutant
Dioxins and Furans	POP		HAP
1,3-butadiene		AQSP	
Benzene		AQSP	
Lead		AQSP	Criteria pollutant
Arsenic			HAP
Cadmium			HAP
Mercury			HAP
Nickel			HAP

emissions. Other high-temperature combustion processes also contribute. Emissions of NO_x can indirectly lead to acid deposition (or "acid rain").

Combustion of fossil fuels containing sulfur leads to emissions of SO_2. Refining and production of fuels and minerals (e.g., lead smelting, aluminum refining) also emits substantial amounts of SO_2. SO_2 negatively impacts human health, contributes to acid deposition, and can promote aerosol formation and growth. Sulfate formed from SO_2 is a major contributor to aerosol mass in some regions. Aerosol produced through historic emissions of SO_2 is believed to have caused a negative climate forcing that suppressed temperature rise in the second half of the last century. Using fuels that contain only trace amounts of sulfur, such as natural gas, or that contain less sulfur, such as low-sulfur coal, results in less emission of SO_2. There are also downstream options such as flue-gas desulphurization [6].

Tropospheric ozone (O_3) is a major irritant to human health and vegetation. O_3 is a secondary pollutant, meaning that O_3 is rarely directly emitted from point sources but is formed via chemical reactions involving other air pollutants such as NO_x and VOCs.

There is a multitude of volatile organic carbon (VOC) species both biogenic and anthropogenic. Many have been identified as particular hazards, and they are discussed in the section below on HAPs. Some anthropogenic VOCs have been associated with causing cancer in humans [8]. Anthropogenic sources include vehicle emissions, petroleum product manufacture and use, biomass burning, landfill gas, sewage treatment [9],

Air Pollution Monitoring and Sustainability. Table 2
Typical concentrations of pollutants in the USA [12]

Pollutant	US average range	US typical peak[c]
CO[a]	0.1–5 ppm	20 ppm
NO_2[a]	0.5–50 ppb	200 ppb
NO[a]	0–100 ppb	200 ppb
HNO_3[a]	0–5 ppb	10 ppb
SO_2[a]	0.1–50 ppb	150 ppb
$PM_{2.5}$ Lead[b]	0.5–5 ng/m^3	150 ng/m^3
O_3[a]	0–125 ppb	200 ppb
(VOC)[b]	20–100 μg/m^3	250 μg/m^3
PM_{10}[b]	10–100 μg/m^3	300 μg/m^3
$PM_{2.5}$[b]	5–50 μg/m^3 (mean = 13.4 ± 5.6)	100 μg/m^3
UFP[a]	1,000–20,000/cm^3	100,000/cm^3

[a]Typical hourly average concentrations reached in US cities
[b]Typical 24 h average concentrations
[c]Generally not in concentrated plumes or locations of direct source emission impact

and off-gassing from building materials. Biogenic VOCs can be the result of the natural metabolic processes of life forms [10] and natural decomposition. VOCs play a crucial role in the formation of tropospheric ozone [11].

PM (particulate matter) is a term that covers a wide variety of liquid and solid particles suspended in the atmosphere. PM is classified by size (according to aerodynamic diameter) and various chemical species of PM exist, even within single particles. Size classifications are typically given as PM_{10} (particles with aerodynamic diameters less than 10 μm), $PM_{2.5}$ (particles with aerodynamic diameters less than 2.5 μm), and Ultrafine Particles (UFP, particles with aerodynamic diameters less than 0.1 μm). Particulate species include sulfate (SO_4^{2-} and containing particles), nitrate (NO_3^-), ammonium (NH_4^+), Organic Matter (OM), and Black Carbon (BC). Long-term exposure to $PM_{2.5}$ is one of the major immediate human health risks from air pollution [13]. Specific health effects are varied but include cardiovascular and pulmonary complications. Other effects of PM include the ability to alter the radiative balance of the Earth [14].

What Are the HAPs?

Specific VOCs are very hazardous to human health. These include benzene, PAHs (polycyclic aromatic hydrocarbons), 1,3-butadiene, ethane, propene, and some aldehydes [6]. Hazardous VOCs share sources with the bulk of VOCs.

Dioxins and furans are chlorine containing chemicals with similar chemical structural elements [15]. Their health effects can be extreme and of a wide variety, including cancer and reproductive abnormalities [15]. Dioxins and furans tend to accumulate in soils and sediments, but their sources include sources of air pollution such as municipal waste incinerators [15] and pyrotechnics [16]. They are bioaccumulative [17], meaning that they remain within the bodies of plants and animals that absorb them.

Heavy metals such as arsenic and nickel are not very prevalent in the atmosphere, other than near their industrial sources, but even at low concentrations they can produce serious health effects [6]. These metalloids, metals and their compounds are classified as HAPs. Some lighter metals are also classified as HAPs such as beryllium and cobalt [5].

Lead (Pb) is a HAP [5] worthy of note for its relative abundance. Lead emissions are the source of a wide range of human health problems [18, 19]. While lead as a fuel additive has largely been phased out in the Western world, there are many regions where it is still in use and continues to exist in high concentrations in the atmosphere [6]. Lead is classified both as a HAP [5] and a criteria pollutant in the USA [1].

Mercury (Hg) is a HAP [5] with a number of industrial applications, many still in use today [20] and is a component of compact fluorescent light bulbs. Coal combustion–based electricity generation is one of mercury's major atmospheric emission sources. Mercury is toxic to humans and, once in the environment, can be methylated, whereupon it can easily bind to proteins and enter the food chain [20].

Currently Recognized Air Pollution Problems

Before resources can be committed to monitoring air pollution, the nature and extent of the problems air pollution creates must be understood. Fenger [6] cites three types of air pollution problems. These are local problems such as health effects and damage to goods

Air Pollution Monitoring and Sustainability. Table 3 Criteria pollutants, HAPs, their common sources, and effects. (VOCs are considered CACs in Canada but are not on EPA list of Criteria Pollutants)

Substance	Sources	Effects
Criteria pollutants		
Carbon Monoxide (CO)	Combustion of fossil fuels, especially in motor vehicles	Health effects, smog (Ozone) formation
Nitrogen Oxides (NO_2)	Combustion of fossil fuels	Health effects, smog (Ozone and $PM_{2.5}$) formation, and acid deposition
Sulfur Dioxide (SO_2)	Combustion of sulfur containing fossil fuels and industrial activities (e.g., fuel refining, metal production)	Health effects, acid deposition, smog ($PM_{2.5}$) formation, changes in radiative balance
Tropospheric Ozone (O_3)	Chemical reactions involving other pollutants in the atmosphere	Health effects, damage to vegetation, damage to materials
Volatile organic compounds (VOCs)	Biogenic, vehicle emissions, petroleum products, biomass combustions, landfill gas, sewage treatment, off-gassing of building materials	Health effects, smog (Ozone and $PM_{2.5}$) formation
Particulate Matter (PM)	Varies by species, includes combustion emissions (especially of biomass in wildfires and for fuel), secondary chemistry involving gaseous air pollutants	Health effects, visibility, changes in radiative balance
HAPs		
Hazardous VOCs	Varies by VOC species	Health effects, including cancer, smog (Ozone and $PM_{2.5}$) formation
Hazardous Metals (excluding lead) and their compounds	Industrial sources	Health Effects, soil contamination
Lead	Fuels with lead additives, industrial sources	Health Effects, soil contamination

and capital, regional problems such as acidification, and global problems such as climate change. As air pollution problems scale up in physical area (from regional to global, for example), their effects tend to scale up in terms of time. For example, an air quality episode may aggravate asthma in a population over the course of the episode (hours to days), whereas acidification will impact the environment for decades and climate change will have impacts potentially lasting millennia [21]. The problems receiving the most government recognition are the local problems. Regional problems are recognized by most governments, while some global problems are only recently appearing on the air pollution agenda of some authorities (for example, the US EPA only gained powers to regulate CO_2 emissions as of December, 2009).

Nowhere is the hierarchy of air pollution problems more apparent than in the US EPA's division between primary and secondary air quality standards. Primary standards are set to protect public health, while secondary standards are set to mitigate regional problems, such as acidification, and biosphere damage [1]. There are no tertiary standards set to mitigate global problems. However, in Europe, the "EU Focus on Clean Air" [22] lists climate change and the destruction of the ozone layer among air pollution issues, placing global problems alongside childhood asthma and acidification of forests.

In addition to human health and regional problems, the economic problems caused by air pollution are recognized by governments. For example, Environment Canada recognizes that illness and mortality resulting from air pollution can cause workers to miss work and

thereby have an adverse affect on the productivity of industry [23]. Economic problems arising from air pollution are discussed below along with other problems currently recognized by government agencies.

Health

Human health is often the primary concern related to air pollution, and a great deal of work has been done to connect various air pollutants to health risks. Table 4 identifies some of the health problems associated with the different air pollutants. The references given are examples of studies that have made connections between pollutants and health problems. Thus, Table 4 should not be interpreted as an exhaustive and critical review of the current state of knowledge regarding air pollutant health effects. In some cases, many more studies have confirmed these connections. However, in many cases, the underlying mechanisms that would conclusively demonstrate a cause and effect relationship have yet to be identified. At the present time, $PM_{2.5}$ is considered to be one of the pollutants of greatest concern [12, 32, 42], but it is made up of thousands of chemicals that can each have different types of effects. Ultrafine particles are a subsize of $PM_{2.5}$, and they warrant further study to better understand the range of impacts on health they may cause.

The health effects of air pollution are usually more pronounced in urban populations [6]. Urban settings tend to host more combustion (of transportation and heating fuels, for example) per area, leading to more emission of air pollution per area than in rural settings.

Air Pollution Monitoring and Sustainability. Table 4 Air pollutants and their health effects. COPD stands for chronic obstructive pulmonary disease. This table

Pollutant	Associated health problems	Reference
NO_2	COPD, allergic response, increase in respiratory illness, increased airway responsiveness to stimuli, lung inflammation, decreased pulmonary function, immunological changes, eye irritation	[19, 24, 25]
SO_2	COPD, respiratory symptoms	[19, 24]
CO	COPD, Congestive heart failure, decreased time to onset of angina, behavioral effects, developmental effects	[19, 24]
O_3	Lung inflammation, COPD, aggravation of asthma, eye and nose irritation, pneumonia, increased airway responsiveness to stimuli, centroacinar fibrosis, immunological changes, excess mortality	[19, 24, 26–28]
PM_{10}	Exacerbation of cardiac disease, lung cancer, allergic response, infant mortality	[25, 29–32]
$PM_{2.5}$	Acute and chronic cardiovascular effects, increased incidence of allergies, excess mortality, lung cancer	[12, 32–34]
Ultrafine PM	Cardiorespiratory mortality, pulmonary stress, mitochondrial and DNA damage, potentially other effects as yet proven	[35–39]
Manganese (Mn)	Parkinson's Disease	[40]
Mercury (Hg)	Nervous system damage	[41]
Lead (Pb)	Reproductive problems, behavioral deficiencies in offspring, damage to lungs, nervous system damage, lowered IQ, hypertension, coronary heart disease, reproductive effects in women	[18, 19]
Volatile organic compounds (VOC)s	Cancer	[8]
Dioxins and furans	Cancer, deficiencies in the immune system, reproductive and developmental abnormalities, nervous system damage, endocrine disruption, pulmonary problems including bronchitis, altered testosterone levels, nausea, loss of appetite, rashes, liver damage, and many others	[15]

The higher population densities of urban settings results in greater air pollution population exposure. With over half of all people currently living in cities and the urban population expected to grow to 70% of all people by 2050 [42], the health impacts of air pollution will continue to be a challenge. Long-range transportation of air pollution and local point sources can make the health effects of air pollution a significant risk in rural settings as well.

A cohort study of six US cites started in 1974 and followed up through the present time, the "Harvard Six Cities Study," found that the average life expectancy in the dirtiest city studied (corrected for individual risk factors) was 2 years lower than in the least dirty city [43]. This 2 year gain in average life expectancy is equivalent to what would be expected if all forms of cancer in the USA were eliminated [43]. Indeed, as air quality has improved across the USA in recent decades, life expectancy has risen [44]. Thus it can be seen that the health effects of air pollution pose a substantial problem while mitigation can offer substantial benefits.

Regional Problems

Regional air pollution problems impact large areas and substantially alter ecologies. Regional problems that have been recognized by governments include acid deposition, damage to wildlife and ecosystems, and reduced visibility. In some areas of the globe, many of these problems have been substantially mitigated by changes in practice.

Acid Deposition Acid deposition is the settling of acidic air pollutants on land or water. The pollutants contributing most significantly to acid deposition are oxidized sulfur and nitrogen compounds. When "wet deposited" (deposited on land by precipitation after being taken up in cloud droplets) sulfur is usually in the form of SO_4^{2-} due to oxidation of SO_2 during atmospheric transport. When "dry deposited" (directly deposited from air onto Earth's surface), it is usually in the forms of SO_2 and particulate SO_4^{2-} [45]. NO_x reacts with water to form acids either while airborne or after dry deposition.

On a regional scale, farther downwind from emission sources, wet deposition is the major acid deposition mechanism and has earned acid deposition the popular name "acid rain," though dry deposition makes substantial contributions to ecosystem acidification [45]. Acid deposition reduces ecosystem Acid Neutralizing Capacity (ANC) [46], making future influxes of acids more difficult to cope with. It also has deleterious effects on soils, vegetation, and aquatic ecosystems.

Leaching of soil nutrients is a major impact of acid deposition. Acids deposited in soil react with the soil's base cations (largely Ca^{2+} but also Mg^{2+} and K^+) and increase their mobility in soils, causing them to leach out of soils and making them unavailable for plant uptake [46]. Base cations can be the limiting factor in forest development and their loss has been identified as the source of decline in many forests [47]. Increased acidity in soils also negatively impacts the microbial community in the soil, on which plant life depends, notably decreasing biological nitrogen fixation rates [48]. Acid deposition stresses plant root systems and leaves [49] and can leach nutrients (Ca, Mg, and K) from leaves just as it does from soils [50]. Acid and/or nitrogen deposition have also been seen to increase risk of winter injury in Red Spruce [51]. Acid deposition lowers the pH of lakes and streams, negatively affecting organisms at all levels of the aquatic biosphere in terms of production and growth in lakes with low natural ANC [52]. Acute mortality and reproductive failure has been a result among fish and some species have even been lost entirely [52].

Governments in North America and Europe have addressed acid deposition by limiting the use of sulfur-rich fuels and introducing technologies to reduce emissions of chemicals that eventually result in acid deposition. Acid deposition has been substantially reduced as a result of these strategies, though many of its effects persist. China has not yet addressed acid rain to the extent that North American and European governments have, and today almost 30% of China's area suffers from acid rain [53]. Given the transboundary nature of acid deposition, it is likely that much more area is threatened.

Damage to the Biosphere In addition to the damages to forests and wildlife caused by acid deposition, there are other damages caused by other forms of air pollution. Grantz et al. [54] provides Guderian's categories of effects of air pollutants on ecosystems:

- Accumulation of pollutants in plants and other ecosystem components (e.g., soil, water)
- Damage to humans as a result of pollutant accumulation
- Shifts in competition causing changes in species diversity
- Disruption of biogeochemical cycles
- Disruption of stability and reduction in self-regulation capabilities
- Breakdown of stands and associations
- Expansion of denuded zones

Many of these types of impacts have been observed and linked to particular pollutants. For example, mercury has been shown to be toxic to microorganisms, plants, and animals [55], and toxicity of other heavy metals such as lead has also been confirmed [18]. By binding to proteins, mercury can also accumulate in organisms and ecosystems [20].

Ground-level ozone (O_3) is a known hazard, leading to reduced production of fine roots in some trees [56], reduced tree growth [57], and damage to a plant's photosynthetic systems [58]. The reduced activity of plant life as a result of ozone will reduce an ecosystem's ability to store carbon and thereby exacerbates climate change [59]. Damage and reduced yields of plants will reduce the availability of food for wild animals, stressing those populations as well.

Visibility

Air Pollution (mostly particles) can reduce visibility. Severe visibility problems arising from poor air quality have recently been experienced in some Chinese cities [60]. Human enjoyment of the environment is impeded by poor visibility and in extreme cases poor visibility poses a safety hazard in aviation.

Economy

Restricted activity and lost work days due to illness incurred by air pollution are included in the costs of poor air quality [19]. These are costs both to the individual suffering the illness (in terms of income) and to industry (in terms of lost productivity). Time lost by caregivers, for example, the parents that miss work to care for an ill child, also results in financial costs [61]. Healthcare costs, including the fees of healthcare professionals and operating costs, are also a problem. Pain and suffering has a cost that can be estimated by the price an individual is willing to pay to avoid experiencing it [61]. Similarly, the amount people are willing to pay to avoid risk of premature death can be used to estimate the cost of mortality [62].

Loss of detail in carvings, discoloration of materials, failure of protective coatings, and structural failure are some of the outcomes of material damage from air pollution [63]. These outcomes are the result of acid deposition on materials and oxidation from pollutants like ozone. Delucchi's [64] review of cost estimates in the literature yielded an estimate of \$0.1–3 billion in material damage annually in the USA from ozone. SO_x and PM are estimated to do at least as much damage as ozone [64]. Mayerhofer et al. [63] estimated that the damage from 1995 levels of air pollution cost Europe 2.3–5.3 trillion European Currency Units (ECU, 1995 value) in that year. Calcareous rock (marble and limestone) is vulnerable to air pollution [65], and many historical monuments and structures are made of such materials.

Ozone can enter plant leaves and damage enzymes critical to photosynthesis, reducing the metabolism of plants and limiting plant growth [66, 67]. Ozone, other oxidants, SO_x, and NO_x are thought to be responsible for 90% of damage to plants from air pollution [67]. Damage to crops results in less revenue for agricultural producers. Murphy et al. [66] estimate that in 1990, anthropogenic ozone caused \$2.8–5.8 billion in damage to 8 major crops in the USA (corn, soybeans, wheat, alfalfa hay, cotton, grain sorghum, rice, barley). Barley and soybeans are particularly sensitive to damage from SO_2 [66]. Subsidies to these crops in the USA are on the order of billions [68], meaning that American taxpayers are providing substantial economic recompense for air pollution's damage to crops.

There are a number of services of economic value delivered by ecological systems, including dilution and treatment of wastes, employment, sequestration of carbon, provision of oxygen, and production of goods such as timber, potable water, and irrigation water [54]. The US EPA, 1997 [19] adds pesticides and drugs to the list of products derived from ecosystems as well as recreation, reduced runoff, and reduced erosion to the list of services of economic value. Efforts have been made to estimate some of the economic effects of air pollution's impacts on ecosystems such as wetlands, forests, and

aquatic ecosystems, but realistic estimates are difficult to reach [19]. Both the data and the tools to make complete estimates are lacking [19], as is the discourse to address some forms of ecosystem damage. The effects of local wilderness areas on property value are easier to estimate and work has been done in this area [69]. Such estimates can quantify some portion of the costs of the expansion of denuded zones and the limitations to ecosystem development discussed above. However, property values are just one of many economic impacts associated with pollution, leaving complete costs figures out of reach.

An evaluation of the cost-effectiveness of the Clean Air Act (USA) over the 1970–1990 period showed that the cost of compliance with the act was $523 billion and gave the central estimate of the economic benefits as $22.2 trillion [19]. This estimate of benefits does not include complete evaluations of ecosystem benefits. The 1990 amendments to the Clean Air Act created market-based mechanisms for trading of SO_2 in an effort to reduce emissions and emissions were reduced by 40% between 1990 and 2007. Over the same period, 25 member countries of the EU reduced SO_2 emissions by 70% using conventional, non-market-based legislation [70].

Global Problems

Air pollution and its effects do not respect national boundaries. Regardless of the location of the point of emission, some problems arising from air pollution affect multiple countries. Some, like the destruction of the ozone layer and climate change, are a problem for all life on Earth.

Ozone Layer Destruction While tropospheric ozone can be harmful, the stratospheric ozone layer prevents much of the sun's ultraviolet radiation from reaching the Earth's surface. Anthropogenic chlorofluorocarbons (CFCs) emitted to the atmosphere can act to convert stratospheric ozone into oxygen through a series of reactions. Once the reactions are complete, the destructive capacity of the CFCs is left intact. The reaction series is able to begin again, destroying more ozone through a catalytic process [71]. In the mid-1980s, a large hole in the ozone layer above the Antarctic was documented, as was the general depletion of stratospheric ozone. The damage to the ozone layer led to the Montreal Protocol, which legislated reductions in the production of ozone-depleting substances such as CFCs [72]. While existing ozone-depleting substances will, over decades, be removed from the atmosphere [71], other factors affecting stratospheric ozone chemistry, many of which are anthropogenic, make for some uncertainty about whether the ozone layer will ever return to the pre-1980s levels [72].

Climate Change Air pollutants such as methane and nitrous oxide are greenhouse gases and, as such, act to increase the Earth's trapping of electromagnetic radiation, leading to the increase in global average temperatures often referred to as global warming or climate change. Some Greenhouse Gases (GHGs) are affected by air pollution through chemical reactions [73], and GHGs such as CO_2 are co-emitted with primary pollutants, especially during fossil fuel combustion. Ozone in particular affects the lifetime of GHGs [73]. Other effects of climate change include such global problems as rising sea levels, likely extinction of 15–30% of species (with a 2°C increase in global average temperatures), reduced agricultural productivity, and fresh-water shortages [74].

Summary of Air Pollution Problems

The motivating factors behind air pollution monitoring include understanding air pollution's impacts on human health, regional problems including economic costs, and global problems. Effects on health and the global economy are far from negligible, and the urgency of regional and global environmental problems is apparent. None of these problems at their current magnitude are compatible with sustainability. If the Earth's growing civilization is to be sustainable, understanding air pollution in an effort to minimize its direct and indirect impacts must be a priority.

Motivations Behind Monitoring Air Pollution

Immediate benefits of air pollution monitoring include knowledge of when and where standards are violated and the ability to communicate health risks. Communication of health risk can be accompanied by warnings that can guide behavior of individuals, populations, and industry and reduce human exposure to air pollution.

While minimizing health problems and ensuring that standards are adhered to are important, there are deeper motivations for the monitoring of air pollution. Establishing and quantifying connections between air pollution and the related impacts depends on measurements such as those made through monitoring and related air pollution research. For example, epidemiological studies of associations between air pollution and related hospital admissions could not occur without air pollution monitoring. By proving connections between air pollution and problems, monitoring and the related research influence air pollution policy. It is anticipated, but not guaranteed, that continued improvement of policy will drive improved mitigation efforts and hence avoidance of the problems associated with air pollution.

Air Quality Warnings

Monitoring of air pollution yields data on present air quality conditions that can be used to provide health warnings. For example, Canada's Air Quality Health Index (AQHI) combines data on ozone, PM, and NO_2 to produce an AQHI value ranging from 1 to 10+. Advice associated with the AQHI is given in Table 5 and ranges from "Enjoy" usual activity to "Avoid" strenuous outdoor activity.

Ideally, this health advice, if followed, would reduce the impact of air pollution by reducing the rate of exposure. Air Quality Indices designed to inform the public and potentially alter behavior exist in the USA, China, Europe, and other areas of the globe [13].

Research

Research serves the function of improving the understanding of air pollution, how it behaves, its sources, and its connection to the problems it causes. It can also lead to advancement of monitoring techniques. In an effort to classify research questions typically asked in the field of air pollution research, a survey of research questions from 40 articles pertaining to air pollution published in early 2010 in peer reviewed journals was performed. Research questions appearing in this snapshot of the literature tend to be related to the following broad questions:

1. What is the nature of a given pollutant or set of pollutants (in terms of pollutant properties, distribution, and transport patterns in the atmosphere)?
2. Can we improve our understanding of the factors influencing air quality (e.g., meteorological factors)?
3. What chemical or physical mechanisms explain some yet unexplained observations?
4. At what rate and by what process is a given pollutant rendered benign in the environment?
5. What are the health effects of a specific pollutant or set of pollutants?

Air Pollution Monitoring and Sustainability. Table 5 Canadian air quality health index (AQHI) and related health advice [75]

Air quality health index	Health advice	
	At risk populations	General population
1–3	*Enjoy* your usual outdoor activities	*Ideal* air quality for outdoor activities
4–6	*Consider reducing* or rescheduling strenuous activities outdoors if you are experiencing symptoms	*No need to modify* your usual outdoor activities unless you experience symptoms such as coughing and throat irritation
7–10	*Reduce* or reschedule strenuous activities outdoors. Children and the elderly should also take it easy	*Consider reducing* or rescheduling strenuous activities outdoors if you experience symptoms such as coughing and throat irritation
10+	*Avoid* strenuous activities outdoors. Children and the elderly should also avoid outdoor physical exertion	*Reduce* or reschedule strenuous activities outdoors, especially if you experience symptoms such as coughing and throat irritation

6. What is a population's or an individual's exposure to a specific pollutant or set of pollutants?
7. What are the effects of a specific pollutant or set of pollutants on outcomes other than health?
8. What is a given practice's effect on air pollution levels (e.g., how does highway driving affect air pollution levels)?
9. How are levels of air pollutants changing (are they decreasing as expected given current policies or are they rising in particular regions)?
10. How does a specific instrument, method, or type of analysis perform?

Investigations of these questions inform the air quality monitoring community, are informed by the data collected by said community, and guide interpretations of data. They provide information on the nature of air pollution, the connections between air pollution and problems, and the effects of human behavior on air pollution. They also allow progress in the air pollution monitoring field.

Questions Regarding the Nature of Air Pollution Research questions of types 1–4 are important to the development of the understanding of the nature of air pollution and specific pollutants. Fundamental questions such as these aid in design of mitigation strategies, monitoring strategies and technologies, and can inform policy. They can also suggest reasons why pollution is a problem and which kinds of problems can be expected from particular pollutants.

Questions of type 4 are directly relevant to sustainability. *A sustainable system would not involve emissions rates higher than the rate at which pollutants are rendered benign. Answers to questions of type 4 should inform allowable rates of emissions.*

Questions Connecting Air Pollution to Problems Question types 5–7 help to establish connections between air pollution and the problems that make air pollution a subject of concern and make monitoring a necessary mitigation strategy. Without questions such as these, other types of air pollution questions loose much of their practical application. These questions are central in "risk-based" air pollution management strategies, which frame acceptable levels of pollution in terms of the degree to which their effects are deemed acceptable.

Examination of these questions shows how established air pollution objectives affect the research agenda. As has been discussed, governments tend to emphasize the impacts of air pollution on health, some selected environmental issues, and the economy. As a result, research questions of types 5–7 more frequently attempt to make connections to these issues as opposed to issues given less attention such as the effects of air pollution on overall quality of life or the health of other species. (Climate change is a notable exception, however, and does receive much attention).

Question 7 covers a broad area of research and is often split into several questions investigating the effects of air pollution on climate change, acidification, ozone depletion, economic damages, and other unintended consequences of air pollution. *If the focus of air pollution monitoring is to shift toward sustainability, these types of questions will join health-related questions as questions of central importance.*

Questions connecting air pollution to impacts require continual study. Previously unrecognized or underappreciated issues may be found to be of great importance, thus warranting a change in monitoring. Furthermore, relationships between air pollution and its impacts can change over time, meaning that the nature of established relationships requires continual monitoring. Weatherhead and Anderson's 2006 [72] study is an example of the understanding of a relationship changing as a result of continued questioning. The assumption was that the ozone layer would regain its former abilities as CFC concentrations declined. However, other anthropogenic factors are playing a role in reducing the rate of recovery, despite a decline in CFCs [72]. Airborne PM is another example. Monitoring first dictated that total suspended particulate (TSP) be measured. However, monitoring evolved with increased understanding of health effects and the nature of PM. This increased understanding, itself facilitated by monitoring, recommended that attention be paid to specific size fractions of PM, first PM_{10}, and later $PM_{2.5}$. If connections to problems are not continually reviewed, monitoring can lose it relevance to its objectives.

Research Questions and the Development of Air Pollution Monitoring Questions about the nature of air pollution can aid development of new monitoring technologies and deployment strategies. For example, Miffre, et al. [84] reveals information about the differences between air pollution concentrations at ground level and at 50 m above ground. The findings show when it is valid to assume that ground-level monitoring is sufficient in estimating concentrations at higher elevations and when it is not. This study and studies asking similar questions directly inform how much information can be taken from a given monitoring practice and when more monitoring is necessary, increasing the potential for optimally efficient monitoring. Questions connecting air pollution to problems can guide monitoring so that it is more likely to take place at the point in a pollutants life-cycle that is most directly related to the problems of concern. If monitoring can take place, where it is most relevant to problems arising from air pollution, it will be more efficient and will yield the most relevant and useful results.

Questions of type 8 can direct monitoring to the areas where there is likely to be air pollution by developing an understanding of which practices are likely to create the most pollution and which are relatively benign, requiring less monitoring. Questions of type 9 bring about understanding of how changes in practice impact air pollution concentrations and whether current policies are effective. Type 10 questions can lead to development of new technologies and strategies for monitoring, as well as improvements to existing techniques.

Current Air Pollution Monitoring Practices

Common pollutants (Criteria pollutants, CACs) are routinely monitored in the USA, Canada, Europe, throughout Asia, and elsewhere. Networks of in situ monitoring stations in these regions provide constant measures of air quality and help governments and concerned organizations determine how close they are to meeting their air quality goals. Precipitation chemistry monitoring also provides data on pollutants in air. Satellite remote sensing and air quality models complement the data collected by monitoring stations to form a more complete picture of air quality and can offer the advantage of consistent methods across the globe. Stack emissions for point sources are occasionally monitored in some countries to complement the ambient concentration data collected by monitoring networks, though more often large emitters estimate their emissions using mass-based flow balances for their site and rates of activity. Numerical modeling of air pollution can be a stand-in when measured data are sparse, it can be used in conjunction with other forms of monitoring, and can help predict the effects of changes in emissions patterns. Craig et al. [13] list the outcomes of monitoring air pollution as follows:

- Ability to describe risks and detect potential future risks.
- Documentation of trends, which can demonstrate the impacts of policies.
- Inputs for the further development of models which can improve predictive capacity.
- Information necessary to prove links between pollution concentrations and effects.

Typical observations made during monitoring include concentrations in ambient air (in ppm, $\mu g/m^3$, particles/m^3, mol/L, etc.), rates of emission, typical concentration ranges, rates of change of concentration, and concentration profiles. It is in terms of ambient concentration that pollution standards are set. For example, the European standard for ozone is set such that the maximum concentration of ozone averaged over any 8 h period of the day should not exceed 120 $\mu g/m^3$. Thus, it can be seen that monitoring is important to ensuring that air quality standards are adhered to, and that public health and the environment are protected.

In Situ Monitoring

Air quality monitoring stations exist in the hundreds in some countries and in the thousands globally, covering continental areas and forming networks that contribute the bulk of information to assessments of outdoor air quality. Instruments capable of detecting specific pollutants (NO_x, SO_x, $PM_{2.5}$, etc.) draw in ambient air and accurately measure the pollutant mass per standard volume of air. This type of monitoring, referred to as in situ monitoring, results in the least uncertainty as compared to satellite remote sensing and model estimates. It is important to recognize that the in situ data

from a given monitoring location are only for the specific geographic location and, thus, during the process of site selection, the issue of spatial representativeness must be considered in the context of monitoring objectives.

Most existing stations measure near ground level (∼3–10 m) so that air pollution at the exposure height of the general populace can be quantified. Figure 1 shows the location of ozone monitoring stations throughout North America. It is largely through such networks of stations that an area's compliance with current air quality standards is determined. Networks are also a primary tool in the tracking of progress toward air quality goals, and they provide the necessary baseline measurements for judging whether progress is occurring [87]. Despite there being over 1,000 stations in Fig. 1, there are relatively large unmonitored areas. Network design to minimize the impact of this inevitable incomplete coverage remains an ongoing challenge and, as described below, models and remotely sensed observations are helping to fill in the gaps.

Precipitation Chemistry Monitoring

By collecting and analyzing precipitation, stations and networks in North America (e.g., CAPMoN, NADP [76]), Asia (e.g., EANET [77]), throughout other continents, and over the Ocean [78] can collect data on air pollution. Precipitation samples can provide

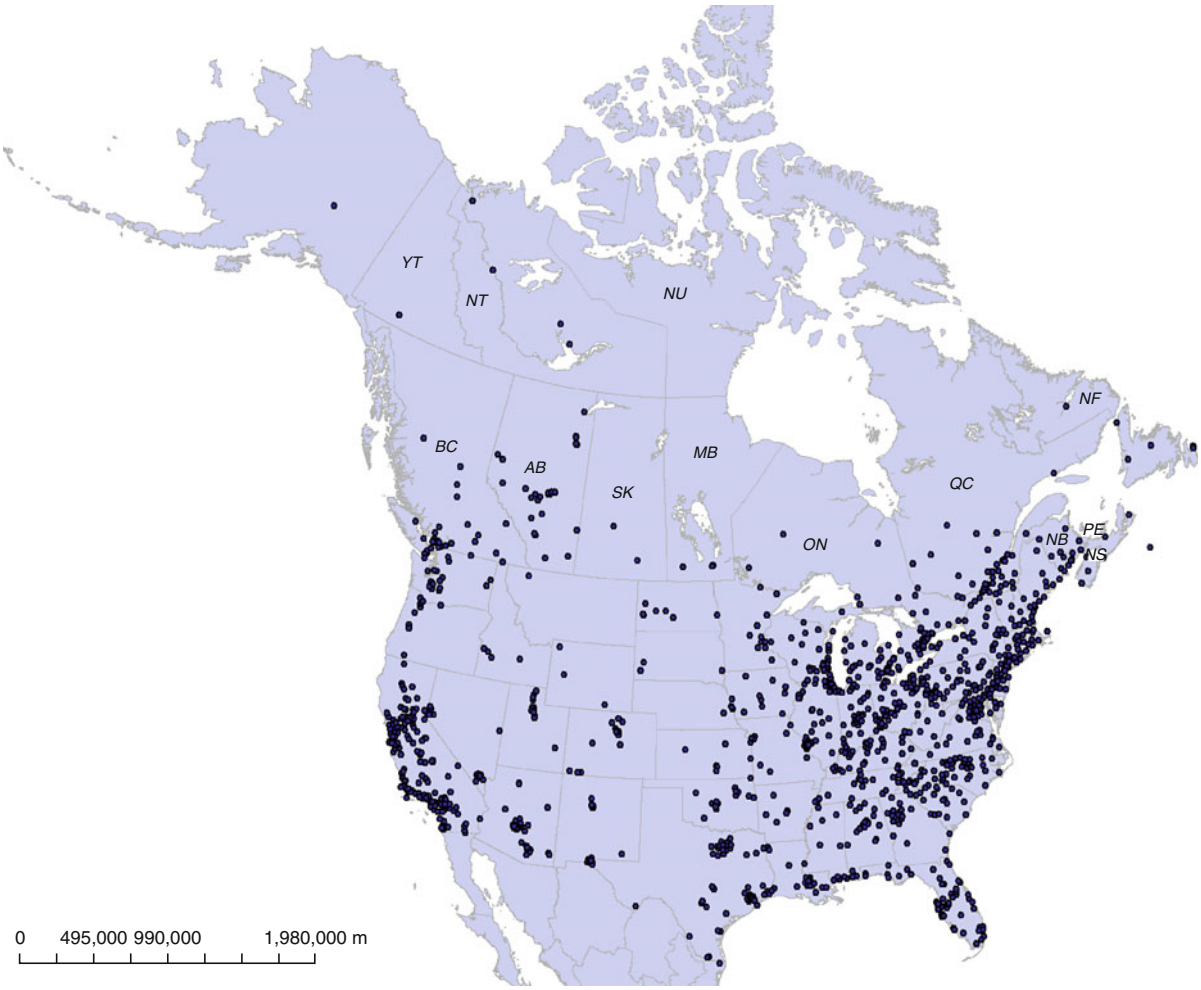

Air Pollution Monitoring and Sustainability. Figure 1
Ozone monitoring station locations throughout North America

information on pH and the mass of various ions such as SO_4^{2-}, NO_3^-, Ca^{2+}, and Na^+ [76]. These data are valuable in tracking the acidity of rain over time and in studying wet deposition. The identity and concentrations of ions discovered through precipitation chemistry monitoring can also provide information about the sources of pollutants, as in Thepanondh et al. [78]. By monitoring the concentration of wet-deposited air pollutants in precipitation, precipitation chemistry monitoring acts as a valuable element of air pollution monitoring.

Satellite Remote Sensing

Satellites can observe electromagnetic radiation from the atmosphere and Earth's surface to infer information about concentrations of aerosols and trace gases in the atmosphere. Pollutants that can be observed by satellites include PM, tropospheric O_3, NO_2, CO, HCHO, and SO_2 [88]. Figure 2 shows satellite-observed NO_2 concentrations in Eastern China.

Satellites can be used to analyze and forecast air quality, provide information on tropospheric air pollution, and be used in conjunction with computer models. Analyses made possible by satellites include observation of events too large in scale to be appreciated using monitoring stations on Earth's surface. Such events include the difference in regional NO_2 concentrations between average conditions in China and the period surrounding Chinese New Year illustrated by Fig. 2. Many spatial features related to typical emissions and those resulting from the change in emissions are better characterized and hence understood using the satellite observations. Forecasting is made possible by observation of synoptic scale meteorology. Observations of surface air quality can be combined with other observations such as those from monitoring stations and point source emissions monitoring to increase certainty of pollutant concentration measurements. Computer modeling aided by satellite remote sensing allows for pollution source apportionment by working backward from present pollutant concentrations and distributions to identify sources [88]. Point source data can be used to model forward in time to obtain estimates of future pollutant concentration. Together, satellite observation and computer modeling

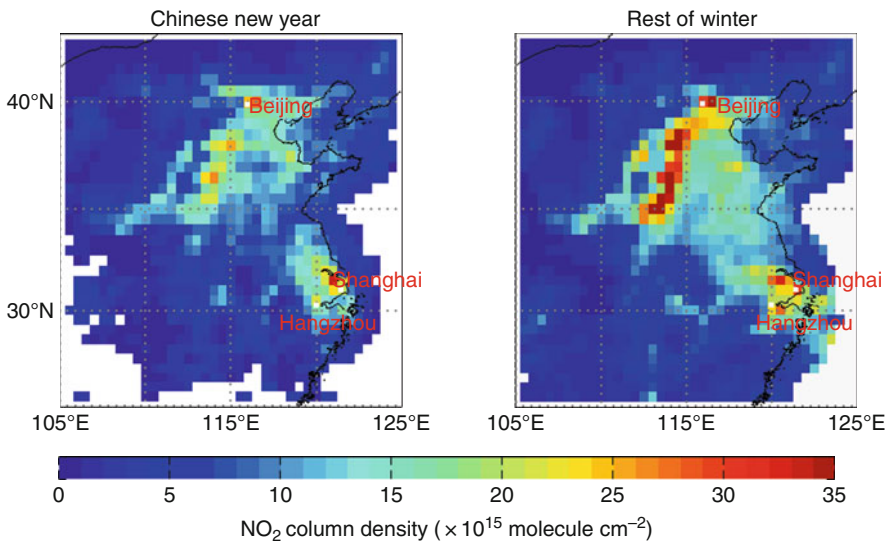

Air Pollution Monitoring and Sustainability. Figure 2
Ozone Monitoring Instrument retrieved NO_2 columns over Eastern China. All data for January 25 to March 5 were averaged for years 2005–2010. The *left* image shows only overpasses taken between Chinese New Year and 2 weeks after Chinese New Year. The right image shows columns from all other days during the period in question. Satellite measurement can show regional scale effects which would be difficult to discern with a surface monitoring network. Free use of tropospheric NO_2 column data from the OMI sensor from www.temis.nl is acknowledged [89]

can increase the certainty of air quality estimates [85] and the attribution of pollutants to specific sources. Satellite observations can also achieve spatial resolution of pollutant concentration over an area that could only be replicated by a large number of ground-based monitoring stations, a number that could only come at great cost [85].

Another advantage of satellite observations is global uniformity. Satellites should ideally be able to measure regions equally well across the globe, in developed and developing countries, using the same measurement techniques and producing data in a uniform format. In reality, differences in surface albedo, vertical mixing, aerosol optical depth, and other factors create inconsistencies in the surface concentrations estimated from satellite data for different regions. However, once these technical challenges have been overcome, this global uniformity should facilitate simpler international cooperation in studies and provide a standard set of data for the comparison of global cities' air pollution footprints. Satellite observations also allow for the tracking of these city footprints over time, allowing for a record of the trend toward sustainability. These advantages make satellite observation an important evolving tool in global cooperation in the pursuit of sustainability. Developing methods for using satellite-derived data to provide information on sustainability should be a priority in future.

Emissions Monitoring

Emissions monitoring provides data on the rates of emissions from pollution sources. These data make for strong inputs into air quality models [87], can ensure that emissions are not exceeding permitted values (either legally permitted or permitted with respect to sustainability), and lead to confirmation that emissions are decreasing over time in compliance with regulations. Emissions trading schemes are dependent on emissions monitoring. Figure 3 shows a Google Earth image of point sources of air pollution in North America.

Continuous Emissions Monitoring Systems (CEMS) quantify gas or particulate emissions by taking measurements as pollution is released. CEMS are common for some major stationary sources in the USA and Europe, where their use is mandated by legislation [79, 80]. PEMS (Predictive Emissions Monitoring Systems) use emissions factors and activity indicators (e.g., fuel use, engine types, duty cycles) in calculations that estimate emissions without measuring them. CEMS and PEMS are commonly applied to stationary sources or point sources, but emissions monitoring can also be applied to mobile sources such as locomotives [81] and ships [82]. Sources too numerous to be monitored as individual sources are often treated as "area sources" [83]. To treat sources such as residential furnaces or urban fuel stations as single sources would not be practical, so emissions from these sources are often calculated and treated as emissions not from the individual sources but from the bulk of those sources of a given type over an area. Agricultural sources such as livestock operations and emissions of N_2O from fertilizers would be considered area sources, and it is sometimes useful to think of vehicle emissions as arising from area (or line) sources. Monitoring emissions from any of these sources requires cooperation from industry and government [87]. Efforts made toward achieving sustainability will rely on accurate and timely emissions monitoring data both to inform model-based decision making and to ensure that emission reduction goals are achieved.

Numerical Modeling

Air quality models use input from meteorological models and emissions from point and area sources to estimate air pollutant levels and deposition amounts based upon current understanding of relevant chemical and physical processes. Models can predict chemical changes in air pollutants over time [13], clarifying links between secondary pollutants and sources. Models can estimate changes in air pollution concentrations that would result from changes in practice (i.e., emissions), making modeling a valuable tool in policy design and analysis of proposed policy [87]. While originally developed mainly for this purpose, models are increasingly being used to provide optimal estimates of air pollutant concentrations over areas where data do not exist. Approaches for using models in conjunction with in situ monitoring data and satellite data are rapidly evolving [85, 86]. This practice can lead to the most complete, consistent spatial-temporal picture of air pollutant levels on the regional to global scale and is

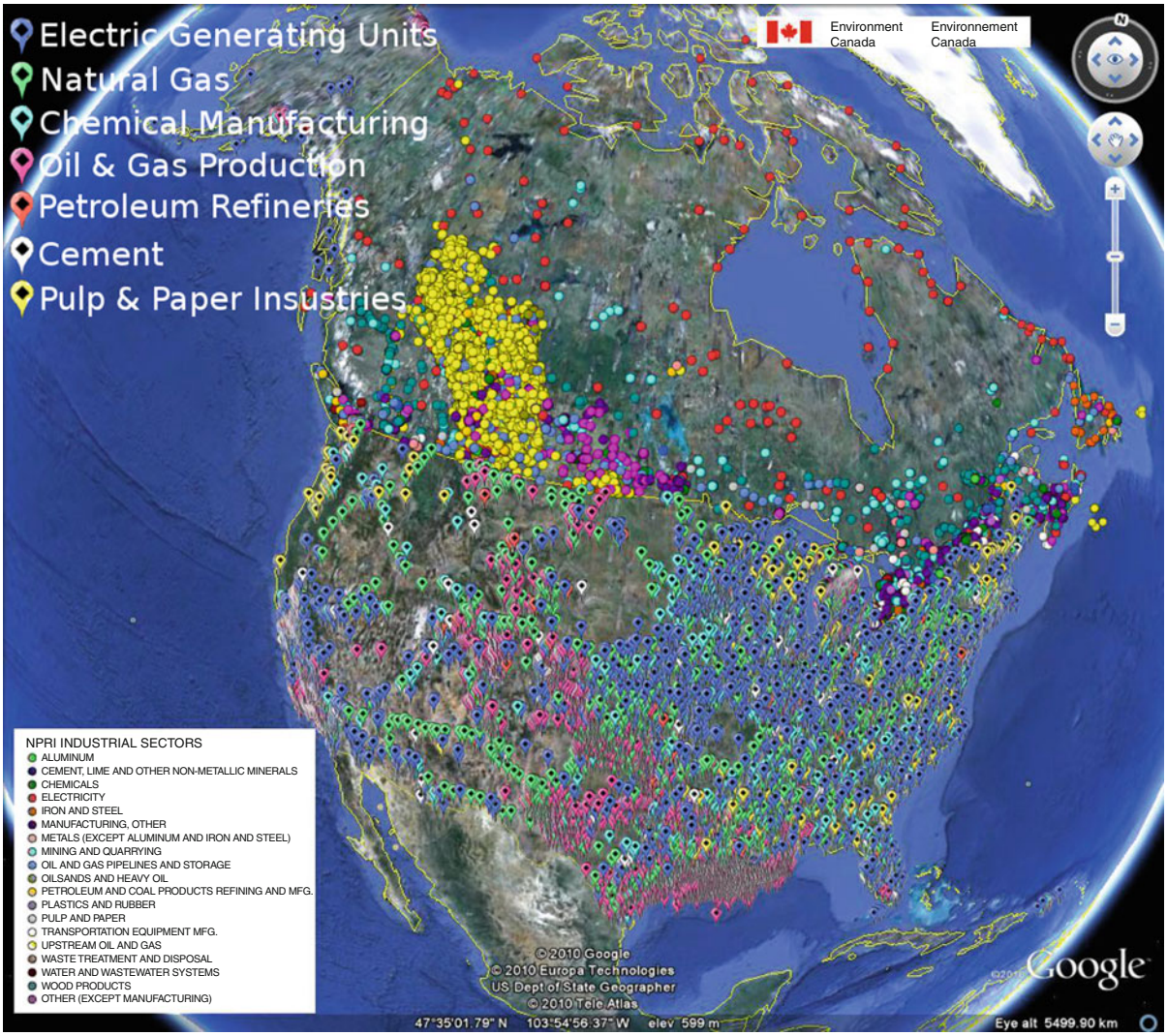

Air Pollution Monitoring and Sustainability. Figure 3
Google Earth image showing point sources of air pollution in North America. USA layer available from the US EPA at http://www.epa.gov/air/emissions/where.htm. Canadian layer available from Environment Canada's National Pollutant Release Inventory (NPRI) at http://www.ec.gc.ca/inrp-npri/default.asp?lang=En&n=1D892B9F-1#npri. Both include source specific data on tonnage of criteria pollutants emitted. Legend for USA sites at *top left*, legend for Canadian sites at *bottom left*

also valuable for identifying weaknesses in current emission inventories. These "fused" data (data derived from multiple types of observations) can extend estimates of the impact of air pollution has on health and the environment, helping to better document problems and improve research. Increasing interest in providing the public with future air quality information, which as described above can help reduce impacts, has led to models that are optimized for forecasting on a daily basis.

Regardless of their application, air quality models require evaluation to assess the reliability of their results. Any model being used to inform policy should have each of its aspects verified, including its design,

methods for representing processes, input data (e.g., emissions), and numerical methods [87]. When supported by detailed measurements, evaluation exercises also identify specific weaknesses in models and possible ways to improve future versions.

Policy and Air Pollution Standards

Air pollution policy is a major influence on monitoring and monitoring is a major influence on policy. Policies determine legally acceptable concentrations of air pollutants. Monitoring shows which pollutants must be subject to improved standards and which areas require the most pollution-abatement planning.

Policies on air pollution centre on concentration standards and emission standards. Standards are often set based on concentrations deemed achievable using the Best Available Technology (BAT) for emissions reduction (an example of a "command and control" strategy), the effects of air pollution deemed acceptable (an example of "risk-based" strategy), or a hybrid of the two strategies [90].

While monitoring and the related science is one influence on policy and standards, it is not the only influence. Political and economic considerations also play a role and can make for situations where environmental damage is accepted despite preventability. Monitoring alone cannot deliver sustainability without policy and practices in accordance with the information it yields.

Concentration Standards Assessing compliance with standards is the primary goal of the majority of air pollution monitoring [91]. These standards are in the form of maximum allowable concentrations of air pollutants. Table 6 gives standards for some major world regions, which are often expressed as an average concentration over a specific time period, for some major world regions.

Emissions Standards Figure 4 shows how emissions reduction programs play a part in achieving concentration standards once air quality goals are established. Emission reduction programs can involve encouragement of energy efficiency, changes in practices (e.g., switching to cleaner fuels, use of emissions controls technology), and redesign of processes. They can also include setting of emissions standards, which limit emissions from particular sources or classes of sources. For example, vehicles in Europe must not exceed the allowable emissions under the "Euro" class of emissions standards for CO, NO_x, certain classes of hydrocarbons, and PM [94].

Monitoring is integral to the "Establishment of Air Quality Goals" and "Track and Evaluate Progress" stages of Fig. 4 and informs the understanding of "Current Ambient Air Quality." Monitoring not only informs policy development, but also the assessment of policy effectiveness.

Non-environmental Considerations in the Setting of Standards Air pollution monitoring is one influence on policy and concentration standards, but politics, economics, and other considerations also play a role [13]. There are at times differences between what the scientific data recommend as the concentration standard and what the concentration standard is in law. The usage of "critical loads" and "target loads" in the in the Eastern Canada Acid Rain Programs is a telling example of the difference between the two terms. A critical load is what has been determined to be close to the maximum amount of pollution an ecosystem can tolerate. (In the case of Environment Canada's Acid Rain critical loads, the aim is to protect 95% of lakes, based on surface area, from acidification beyond critical levels.). A target load, the pollutant load aimed for in policy, is the load deemed achievable once "other factors (such as ethics, scientific uncertainties, and social and economic effects) are balanced with environmental considerations."[96]. Though the Canada-Wide Acid Rain Strategy for Post-2000 set the long-term goal of meeting the critical load, in the short term this system of standard setting determines a level of pollution slightly more than what could be sustained (the critical load) and aims to allow more pollution than that (by aiming for the target load). The critical and target load system has also been applied in areas of Europe. The different grades of Chinese air quality standards in Table 6 are another example of standards not based on the recommendations of the air pollution monitoring community or on the basis of sustainability. The different grades are assigned based on land use (e.g., residential vs industrial) and the economic realities of those areas, not on changes in the definition of

Air Pollution Monitoring and Sustainability. Table 6 Air quality standards by world region

Pollutant	Averaging period	Standards				
		Europe [92]	USA primary standards [93]	China [53]		
				Grade 1	Grade 2	Grade 3
		Conc.	Conc.	Conc.	Conc.	Conc.
CO	1 h		35 ppm	10 μg/m^3	10 μg/m^3	20 μg/m^3
CO	8 h	10,000 μg/m^3	9 ppm			
CO	24 h			4 μg/m^3	4 μg/m^3	6 μg/m^3
NO_2	1 h	200 μg/m^3		120 μg/m^3	240 μg/m^3	240 μg/m^3
NO_2	24 h			80 μg/m^3	120 μg/m^3	120 μg/m^3
NO_2	1 year	40 μg/m^3	0.053 ppm	40 μg/m^3	80 μg/m^3	80 μg/m^3
SO_2	1 h	350 μg/m^3	0.075 ppm	150 μg/m^3	500 μg/m^3	700 μg/m^3
SO_2	24 h	125 μg/m^3	0.14 ppm	50 μg/m^3	150 μg/m^3	250 μg/m^3
SO_2	1 year		0.03 ppm	20 μg/m^3	60 μg/m^3	100 μg/m^3
Lead (Pb)	3 months		0.15 μg/m^3			
Lead (Pb)	1 year	0.5 μg/m^3				
O_3	1 h			160 μg/m^3	200 μg/m^3	200 μg/m^3
O_3	8 h	120 μg/m^3	0.075 ppm			
Benzene	1 year	5 μg/m^3				
PAHs	1 year	1 ng/m^3				
PM_{10}	24 h		150 μg/m^3	50 μg/m^3	150 μg/m^3	250 μg/m^3
PM_{10}	1 year			40 μg/m^3	100 μg/m^3	150 μg/m^3
$PM_{2.5}$	24 h		35 μg/m^3			
$PM_{2.5}$	1 year	25 μg/m^3	15 μg/m^3			
Arsenic (As)	1 year	6 ng/m^3				
Cadmium (Cd)	1 year	5 ng/m^3				
Nickel (Ni)	1 year	20 ng/m^3				

sustainability from area to area. Policy-makers consider much more than what is sustainable when setting standards, and when doing so, the tendency is to make standards less stringent, meaning sustainability is sacrificed further.

Polluters can also play a role in affecting air quality standards. There are concerns that setting stringent air pollution standards will cause polluting industries to relocate to "pollution haven" countries where standards are more lax, though the idea that moving to one of these havens actually benefits businesses is dubious [97]. Fear of such moves can erode the economic base of a policy-maker's purview, providing an incentive to weaken standards. Fredriksson and Gaston [98] review a number of cases in which environmental policy was weakened by business lobbies representing polluters. Clearly, pollution policy making is the result of many disparate influences. Amid social, political, and economic debates involving varying interests, the goal of sustainability is often minimized or even lost.

Violations of Concentration Standards Unfortunately, standards are targets, not guarantees of

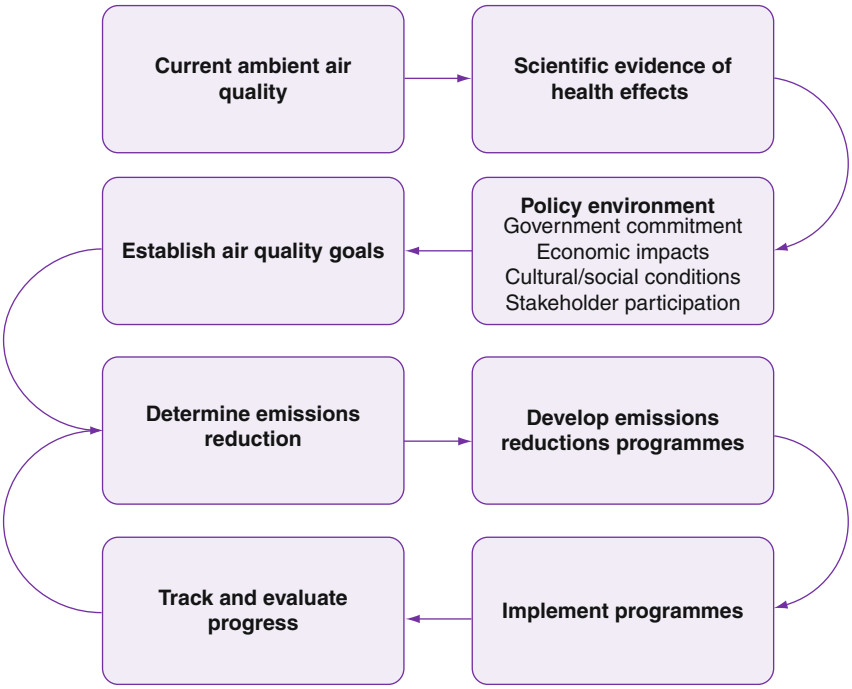

Air Pollution Monitoring and Sustainability. Figure 4
Steps in the emissions reduction cycle including policy lead-up. Figure is based on [95] and [13]

maximum concentrations. As of 2004, 20.2% of Chinese cities exceeded Grade III standards, though this rate was an improvement over the 53.8% of cities exceeding Grade III standards in 1991 and was part of an overall trend of decreasing concentrations [53]. In the case of the USA, it must be noted that the trend in average concentrations of most criteria air pollutants is downward [99]. However, in the USA, in 2007, 21% of sites monitoring $PM_{2.5}$ exceeded the 24 h standard of 35 μg/m^3, 23% of sites monitoring lead showed concentrations in excess of the 0.15 μg/m^3 standard, and 57% of sites monitoring O_3 exceeded the 0.075 ppm standard [95]. The UK's ozone standard is exceeded several times each year [83]. In recording exceedences of standards, air pollution monitoring demonstrates the need for continued improvements in emissions abatement and shows where the need is greatest. It also demonstrates that standards and monitoring alone cannot lead to sustainability. Strong enforcement of standards must make air pollution a consideration in the development and uptake of technologies.

The Effects of Air Pollution Science on Policy Air pollution policy, like all environmental policy, is dependent on research and the state of science. If science has not developed the discourse to describe an air pollution issue, there are no grounds or even terms to support policy-based mitigation. For example, it is believed that different species of air pollutants may act together to produce more severe health impacts than either species would produce if acting alone, but the current understanding of synergistic interactions is inadequate to support this level of policy development [101].

Air pollution science is also critical in identifying the most significant contributors to pollution [101] and can use this and other information to recommend optimally cost-effective solutions to air pollution problems [102]. The concept of critical load is an example of a scientific tool that aids air pollution problem solving [102]. It is also an example, as discussed above, of scientific knowledge being used as a framework but not being fully respected by the political process. While science is the basis of policy's discourse, as well

as the basis for policy evolution, there is room for improvement in how science and policy cooperate in achieving sustainability.

Policy and Air Pollution Standards: Conclusion Policy sets standards by which the results of air pollution monitoring are judged. Concentration standards indicate accepted levels of air pollution in ambient air, and emissions standards are measures of how much any source can contribute to air pollution. Political, social, and economic considerations often influence standards and result in more lax standards than science or sustainability would recommend. Even in these cases of standards not consistent with sustainability, standards are often exceeded. Much of air pollution monitoring is designed to assess compliance with standards [91], but neither standards nor standards-oriented monitoring alone will ensure sustainability.

The current air pollution monitoring establishment can contribute to ultimate sustainability through ongoing scientific assessment in support of increasingly appropriate concentration standards. Monitoring and the related research can show, and have shown, that in many cases lower ambient air pollution concentrations are possible, necessary, and cost effective. Thus, new policy and better standards are encouraged through the results of monitoring. Translating air pollution monitoring into policies that support sustainability may be a considerable challenge. Hurdles may include political and economic dampening of the recommendations of science, and ongoing violations of existing standards. However, progress is essential as without monitoring sustainability becomes virtually impossible to verify. Further, if monitoring is to verify sustainability, it needs to be based on goals and policies that balance the social, environmental and economic aspects of sustainability. The monitoring community can play an important role in establishing such holistic standards for air quality.

Past and Ongoing Success in Air Pollution Mitigation

In general, OECD countries have seen concentrations of most major (or criteria) air pollutants decrease since the introduction of pollution management programs. One of the biggest victories has been sulfur emissions, which were the focus of acid rain reduction programs. Sulfur emissions, again, in OECD countries, are much lower than they were in the past [6]. Acid rain is decreasing in the USA [95], Canada [99], and elsewhere. NO_2, thanks largely to the use of catalytic converters in vehicles, is on the decline in most European cities [6], throughout the USA [95], and Canada [100]. Limitations on lead in gasoline have led to substantial reductions of lead in air. Concentrations of lead are consistently below the WHO concentration guidelines throughout Western Europe and, in Canada, lead is almost undetectable in the atmosphere [6]. Regulations controlling particulate were the most cost-effective regulations the US government put into force [43], and human life expectancy has increased as air quality has improved in the USA [44].

Countries managing air pollution have seen a decline in ambient HAP concentration, with benzene, 1,3-butadiene, styrene, xylenes, and toluene concentrations decreasing by at least 5% per year in the USA from 2000 to 2005 [95]. A major factor in this success was the control of emissions from chemical plants, dry cleaners, coke ovens, and incinerators. The continued reduction in CFCs discussed above is a landmark success in air quality policy and international policy in general.

In many cases, serious efforts to reduce the presence of a pollutant in the environment can succeed. Air pollution monitoring brings problems to attention so that these efforts can be made. It also tracks the impacts of pollution mitigation strategies, indicating success when it is achieved and allowing for comparison of the effectiveness of different strategies. If not for monitoring, the successes mentioned here would be impossible to quantify or prove. Adaptive management strategies would also be impossible.

Outstanding Problems and Challenges

The successes mentioned above are not unmitigated. pH and ANC in ecosystems damaged by acid rain are not recovering in proportion to decreases in acidifying emissions [46]. The Ozone layer's recovery is not proceeding in proportion to decreases in CFC emissions but is being retarded by other anthropogenic air pollutants [72]. Catalytic converters used to decrease NO_2 emissions cause a net increase in fuel use, prompting Fenger [6] to comment we may have mitigated one

problem by aggravating another. Reduction in NO_2 emissions have not led to the reductions in tropospheric ozone that were hoped for [11].

The story of lead as a gasoline additive is an example of how reduction of a pollutant does not always result in greater sustainability. With lead no longer an acceptable fuel additive, methyl *tert*-butyl ether (MTBE) was used to perform its function. However, MTBE was later found to be a powerful contaminant of water and a likely carcinogen [103]. Now bio-ethanol is being discussed as a less poisonous fuel octane booster than MTBE, but it introduces its own risks of soil and groundwater contamination and can lead to increased emissions of NO_x and organics [104], not to mention stresses on global food supplies and agricultural resources (i.e., land and water). While legislation such as the USA's Clean Air Act was successful in reducing emissions from gasoline, it did not eliminate the environmental threat of fuel oxygenates. More holistic systems and policies, rather than the reactionary phasing out of particular pollutants, are necessary to truly solve the problem. Further, when implementing such policies, we need to anticipate potential associated consequences and be prepared for follow-up monitoring so that we can detect any resulting impacts.

In addition to the problems remaining after emissions and ambient concentrations of pollutants have been reduced, there are instances where reductions in concentrations elude the efforts of policy, technology, and behavioral changes. Over half of the population of the USA lives in counties where air quality standards are exceeded [95]. O_3 in populated areas such as those in Southern Ontario is continuing a long-term trend of increasing concentrations [105] despite decreases in concentration of precursors, leading to questioning of the fundamental scientific assumptions surrounding tropospheric ozone concentrations [106]. Background ozone is increasing in parts of the northern hemisphere, and this increase may be linked to intercontinental transport of pollutants [107]. Ozone and PM concentrations also continue to be challenges throughout the USA [95].

Despite the effort and advances made in research, policy, and environmental practice, air pollution is still a health problem, a visibility problem, and an economic problem. Further, only weak links exist between air quality objectives and sustainability. Concentration and emissions standards are not set to serve sustainability. Air quality objectives that will allow the eventual recognition of sustainability once it has been achieved, or even how far away sustainability currently is, are lacking. The biosphere is still being damaged by air pollution. Acid rain is declining in developed countries, but is still beyond the critical load, is increasing in some regions, and totally unmonitored in others. Thus, despite progress in recent decades, there is little reason to believe that we currently have a sustainable burden of pollutants in our atmosphere. Thus, there are considerable challenges remaining for the air pollution monitoring community in relation to sustainability.

Current Air Pollution Monitoring and Sustainability

Diverse techniques contribute to the monitoring of pollution in the atmosphere. This monitoring allows for air quality advisories, research into the nature and sources of air pollution, evaluation of the conformity with standards, and assessment of the need for additional or alternate regulations or policies. All of these outcomes of air pollution monitoring reduce the burden of air pollution on human society and the environment. Unfortunately, what is learned and understood is not proportionate to action taken. Pollution is still eroding the capacity for sustainability. Improvements on all fronts are necessary, including improvements in air pollution monitoring, the associated science, practices, the thinking that underpins them, and the social response they receive. Determination of what constitutes a sustainability standard or threshold will also require further work.

Future Directions: Monitoring to Promote Greater Sustainability

In redesigning the air pollution monitoring community and the larger air pollution establishment for sustainability, there are a number changes to be made to current practices. There are both broad, or institutional, changes and specific changes to be made. The institutional changes will be more difficult to affect in that they require overcoming current inertia. These changes are discussed immediately below. Specific changes are discussed in the "Monitoring More

Effectively" section. Both types of change will help the science of air pollution monitoring encourage sustainability.

Changes in Institutional Practices

Institutional changes that would make air pollution monitoring more relevant to sustainability include the expansion of the conventional goals of air pollution monitoring, working across intellectual disciplines, and involving the general public in the monitoring process.

Expansion of Goals Air pollution monitoring practices are largely determined by the goals underlying air pollution mitigation strategies. When assessment of health impacts is the goal, more monitoring happens in populated urban areas. The hierarchy of goals in current air pollution mitigation tends to prioritize human health, then visibility, then ecosystems [54], then possibly the prevention of economic damage from air pollution, or even climate stability in rare cases. Often studies are oriented toward only one of these goals.

Sustainability requires holistic thinking and if sustainability is the aim, prioritizing based on a hierarchy of problems alone can reduce the potential benefits. Prioritizing air pollution impacts immediately affecting humans (e.g., health effects) over environmental impacts is self-defeating. In the long term, it is possible that the loss of ecosystem services arising from these lower-priority environmental effects may be the greater consequence to humans [54]. Holistic thinking would take into account many more goals in air pollution mitigation than health, visibility, ecosystem damage, economic loss, and climate. A holistic system would involve monitoring air pollution with goals such as the development of natural capital, resilience in human and natural systems, environmental justice, improved urban form, and accelerated learning and research. Studies with these goals in mind have been performed infrequently, and they are fertile ground for new research.

Natural Capital Natural capital is a metaphor used to describe the natural features of ecosystems that do work or provide services for humans and the biosphere. It is useful in that it draws attention to these features and their indispensable services such as clean air, potable water, food, and building materials while drawing comprehensible analogs to economic concepts. Pollution that makes air a health risk, destruction of the ozone layer by air pollutants, acidification of ecosystems via acid rain, and alteration to the climate by air pollutants such as black carbon aerosol are all examples of air pollution destroying natural capital. All of Guderian's categories [54] ("Damage to the Biosphere" section) are ways in which air pollution depletes natural capital. Natural capital is often extended to include the capacity of systems to assimilate waste, such as the atmosphere's capacity to assimilate air pollution, and the life support functions provided by ecosystem components, such as the ozone layer's UV blocking capabilities [108].

The assessment of the cost-effectiveness of the US Clean Air Act, as mentioned, gave a mid-value of the benefits of the Act of $22.2 trillion but could not include the further benefits of preservation of natural capital [19]. All production and consumption in the human economy depends on natural capital [108, 109]. Minimum estimates of the value of natural capital and ecosystem services exceed the value of the human economy [110, 111]; yet, the discourse for the quantification of natural capital has yet to be fully developed. Furthermore, efforts to monitor and quantify pollution's impact on natural capital are rare [112], making the inclusion of natural capital loss in the Clean Air Act's benefits or in the cost-benefit analysis of new air quality policy options near impossible. Data on natural capital are limited and thus far unsatisfactory, and types of natural capital, such as types more vulnerable to air pollution versus types more vulnerable to other damages, have yet to be disaggregated [113]. Assessment of loss of natural capital must become a priority for the air pollution monitoring community, as should the categorization of types of natural capital vulnerable to air pollutants. Mechanisms to ensure that natural capital is fairly recognized in policy development need to be installed at the international level.

Critical natural capital, natural capital that cannot be lost without irreparable terminal damage to ecosystems and thereby similar damage to the human economy, must also be considered. This critical natural capital cannot be lost or exchanged and, therefore, is literally priceless [108]. Criticality of natural capital can

be judged in terms of source and sink functions (sources of ecosystem services and pollution sinks) and life support functions [114]. Examples of critical natural capital would be keystone species or keystone processes [108], which can be affected by air pollution. There is a certain level of natural capital that must be maintained to preserve the biosphere and hence humanity. Unfortunately, where this level lies is not yet understood, especially in terms of atmospheric aerosol loading and chemical pollution [115], two areas directly relevant to the air pollution monitoring community. Air pollution monitoring and air pollution science must be oriented toward defining where atmospheric natural capital becomes critical, how air pollution is damaging natural capital, and the quantification of natural capital savings from emissions reductions. Air pollution monitoring could also provide data on the development and redevelopment of natural capital.

Resilience A sustainable system must be resilient to external shocks and major changes, but the socio-ecological concept of resilience encompasses more than an expectation of a return to business as usual. Socio-ecological resilience is not only the ability of a system to retain basic functions despite a shock. It is also the capacity for renewal, reorganization, and development [109]. Air pollution monitoring should accept the possibility of major system changes and monitor for gradual atmospheric change as early warning signs of upcoming system shifts [114, 116]. Early warnings would allow for preparation for adaptation at worst, possibly allow for avoidance of the worst consequences of system shocks, and expose opportunities to take advantage of upcoming changes at best. The development of appropriate atmospheric indicators of ecological system shifts would be a major research project and require much innovative air pollution monitoring. One aspect of such indicators would be placing the concentration of air pollutants in the context of the capacity of systems to continue to absorb more pollution without major changes in their behavior [114]. Indicators could also include how the dynamic capacity (ability to reorganize around changes) of environmental sinks (e.g., the atmosphere) are affected by continued pollution [114]. These types of indicators would be along the lines of damage-oriented metrics used in life-cycle assessment methods.

Resilient systems are contrasted with vulnerable systems, in which small changes can cause disastrous consequences. The resilience of the human population is a sustainability-relevant metric to be developed. Resilience in this population comes under fire when exposure to pollution increases human vulnerability to disease, as has been shown to be a likely outcome of exposure to some air pollutants [117, 118]. Monitoring to expose the development of vulnerabilities would be a useful endeavor in the promotion of resilience. It would also be useful to show how the allocation of the most polluted land to the most vulnerable populations (babies, young people), as in Mitchell and Dorling [119], and the associated increases in asthma, other respiratory illnesses, and allergies are affecting the ability of humans to reorganize around potential atmospheric changes. Development of such indicators will rely on air pollution monitoring data.

Socio-ecological Justice The social justice of environmental protection is a fundamental tenet of sustainable development [119]. Environmental justice is concerned with equal access to a clean environment and equal protection from risks associated with environmental impurities [119]. Currently, economically disadvantaged communities are often more exposed to air pollution than more affluent communities [117]. Poorer individuals are more likely to live near roadways, resulting in greater exposure [117]. In their study of London, MacKerron and Mourato [120] observed that communities with the least car ownership are exposed to the highest concentration of pollutants, while the cleanest air tends to be in communities where car ownership is greatest. Marshall et al. [121] shows that lower-income neighborhoods tend to have higher walkability (resulting in less auto emissions), but also higher NO concentrations, while higher income neighborhoods tend to have lower NO and O_3 concentrations. In these cases, the injustice is that the people polluting the most impose the cost of their pollution on those polluting least. Identification of such injustices should be a focus of air pollution monitoring.

Routine increased exposure itself may enhance the impacts of air pollution on socioeconomically

disadvantaged groups by weakening normal biological resistance [117] or promoting atherosclerosis [118]. Housing stock in poorer neighborhoods can have higher rates of off-gassing of some allergens and expose occupants to other risk factors of asthma sensitization and exacerbation [117]. These phenomena require greater documentation by air pollution monitoring agencies so that they can be addressed.

Often young families cannot afford to live in more affluent neighborhoods and must purchase lower cost housing. This situation has lead to findings such as those of Mitchell and Dorling [119], that pollution in London is most concentrated where young children and their parents live. London wards with a high proportion of all babies in the city tend to have much higher than average concentrations of NO_2. This injustice is exposing pregnant women, children, and babies (segments of the population very vulnerable to the health effects of air pollution) to greater air pollution concentrations than those more resistant.

Much environmental justice work has been done in the USA to attempt to redress the effects of the frequent location of landfills and polluting industries in black and indigenous communities. A lack of empirical evidence led to failure of many of the class actions meant to address environmental injustice [119]. Air pollution monitoring should be used to supply empirical evidence where environmental injustice exists. As O'Neill et al. [117] state, "Science and public policy would benefit from additional research that integrates the theory and practice from both air pollution and social epidemiologies to gain a better understanding of this issue."

Improved Urban Form Design of urban form can mitigate exposure and reduce emissions [6]. Urban sprawl results in increased automobile dependency and the associated emissions [122]. Many studies have witnessed the negative correlation between urban density and per capita transportation emissions [123]. Frank et al. [124] makes the connection between neighborhood walkability and reduced vehicle emissions. The US EPA has acknowledged the relationship between urban form and emissions through its program of offering urban nonattainment areas emissions credits for "smart growth" development practices [123]. Conventionally, air pollution mitigation has been technology oriented, and Stone [123] claims that the EPA's program of emissions credits for intelligent urban design is an acknowledgement that the technological approach alone is not sufficient to solve air pollution problems. This recognition reinforces the point that sustainable solutions must be holistic and that no single avenue leads to sustainability. Air pollution problems cannot be solved by dealing with the emission sources alone, there must be systemic redesign of the landscapes that create demand for emitting activities.

The air pollution monitoring community can play a role in urban design for emissions reduction. One major contribution would be taking stock of various types of urban forms that exist and the contribution of those forms to emissions. Tang and Wang [125] look at the four different urban forms on the Macau peninsula and associate form with emissions and air pollution. Observations connecting road width, road curvature, and congestion with emissions were made, and it was seen that features such as urban canyons can lead to increased pollution in areas of cities least responsible for total emissions. Other features Tang and Wang [125] recommend for study include street orientation in relation to wind direction, interactions between urban form and wind speed, building design, green spaces, and traffic control schemes. All of these aspects of urban design require further research to determine their impact on air pollution, while data from monitoring will help to substantiate the understanding thereby derived.

Designing urban areas for walkability and public transit will also impact emissions of air pollution. PODs (Pedestrian-Oriented Development) and TODs (Transit-Oriented Development) such as those discussed in Newman et al. [126], can lower transportation energy demand and thereby reduce emissions from vehicles. A study of walkability in Vancouver showed that urban design had a substantial impact on walkability and air pollution exposure, and proved an effective method for connecting air pollution monitoring to urban design and possible future development [127]. Designing for less dependence on automobiles is a very effective strategy for using urban form to mitigate air pollution, and such design has other sustainability benefits such as improved health from physical

activity [127]. Of course, designing for urban density will result in more instances of exposure to urban air pollution, providing additional incentive to minimize emissions.

The air pollution monitoring community can also contribute to improved urban form by uniting air pollution models with urban design models. Involving the air pollution monitoring community in an integrated design process for cities could lead to reductions in emissions and exposure in existing areas by designing new developments to decrease the negative impacts of stagnant air within urban canyons. A stronger air quality perspective on urban design could result in more sustainable places to live.

Acceleration of Learning and Research The majority of investment in air pollution monitoring is directed not toward research or improvement of research capabilities but toward assessing compliance with existing air pollution concentrations standards [91]. The focus on compliance to the exclusion of other objectives reduces the value of data acquired in that the data could also be used for source apportionment, chemical transport modeling, assessment of background levels, and relationships between pollutants and other effects [91]. The link between air pollution and urban form could also be better established if available data were used for that purpose. If priority continues to be given to compliance over other uses of data, few of the other goals discussed herein will be easily pursued. Chow and Watson [91] give specific practices that can be implemented to shift emphasis toward research, including calibrating instruments to detect lower concentrations, decreasing time resolution of sampling, and reporting data to the level of detection rather than rounding to convenient orders of magnitude. Policy recommendations are also made, including periodic reviews of instrument performance. Acceleration of learning, of which research is a fundamental part, should be more of a focus in routine monitoring. Thus resources need to be allocated to ongoing analysis and interpretation of monitoring data.

Folke et al. [116] discuss the relationship between adaptive capacity and sustainability. To lay claim to sustainability, a society must be able to manage adaptively to socio-ecological changes. This capacity, Folke et al. [116] argue, requires mechanisms that allow governments to learn, meaning that the institutional capacity to learn must be optimized. It is not optimized in the current situation as described by Chow and Watson [91], wherein data are primarily oriented toward fulfilling routine functions. Adaptive capacity also requires spaces for institutional collaboration [116]. Data that are conventionally less informative than they could be, as air pollution monitoring data commonly are [91], are not optimally suited for collaborative purposes. The case of the need for fine spatial resolution in the MacKerron and Mourato [120] study of socioeconomic distribution of air pollution is an example where routine data would not have served the study's interdisciplinary purpose. The capacity to adapt requires not only strong data, but the ability to extract maximum information from that data. Adaptive capacity, and therefore sustainability, would be served by the improvements suggested by Chow and Watson [91], and like improvements concerning the acceleration of learning.

Chow and Watson [91] and Folke et al. [116] are effectively calling for continual improvement in capacity to learn on the job. In doing so, they are highlighting two essential components of sustainability: learning and continual improvement. Routine monitoring must cease to focus solely on compliance. It must ensure that research and improvement in the capacity for research are served. Clearly, development of best practices to ensure sustainability needs to be a priority in this learning.

Expansion of Goals: Conclusion The conventional goals of air pollution monitoring influence monitoring practice. Practices thus serve these goals more than others. There is a need to expand the set of goals and expand practices accordingly. Monitoring to understand impacts on natural capital is not only essential to sustainability but will improve the economic future of humanity. Resilience is a concept the air pollution monitoring community can study and apply further. The environmental injustice of air pollution's distribution must be addressed for the sake of justice and for the health of younger populations. Given the strong links between air quality and urban form, air pollution issues should not be ignored in the design of cities nor urban form

ignored in pollution studies. Acceleration of learning and research have the potential to increase the efficiency of monitoring as well as improve understanding of air pollution's effects and optimal concentrations. All of these goals must be adopted if air pollution monitoring is to holistically pursue sustainability, and sustainability will continue to be elusive if approaches are not holistic.

Multidisciplinary Work Attitudes fostering sustainable levels of air pollution in the coming decades will value contributions from intellectual disciplines other than air pollution science. Urban planning work can mitigate exposure to air pollution, and it is clear that improved energy efficiency will reduce emissions from fossil fuels [53, 73]. Folke et al. [116] call for consultations with communities with local ecological knowledge [116] such as neighborhoods and Aboriginal networks. Yi et al. [53] comment that sustainable consumption and production will reduce air pollution, which suggests collaboration with business. Agricultural practices are major sources of air pollution [73], suggesting collaboration opportunities with the agricultural sector. Further, collaboration between air pollution and climate change mitigation efforts can deal with major air pollutants that are also contributors to imbalanced radiative forcing [13, 73] while discouraging the implementation of climate strategies that increase air pollution [73]. Failing to collaborate will make air pollution research more difficult and less rewarding, while collaborating will open new areas that will inform monitoring priorities.

Public Involvement Public involvement and consultation with the general public can be of substantial benefit to science but are rarely taken advantage of. At some levels, there is an aversion to such involvement as illustrated by a survey taken by the British Royal Society which showed that 20% of scientists believed that those scientists seen to engage with the public were less well regarded by their peers [128]. Much value is overlooked when air pollution scientists do not engage with communities they intend to monitor, including sophisticated understanding of local sources of air pollution, how local air pollution changes with weather, and health effects being experienced (even if the sophistication of the knowledge is not of the same kind that air pollution scientists generally regard as sophistication) [120]. Citizens often have or believe they have information that monitoring bodies do not have and, even if this information is incorrect, it may affect the ability to implement policy based on results from air pollution monitoring [129]. Thus, it is a good idea to at least understand how a community feels about its local air pollution before policy, and possibly even monitoring campaigns are designed. When communities do take air quality problems seriously, opportunities for progress on air quality issues arise [13].

Yearly [129] performed two case studies on air pollution and public involvement that illustrate the value of community input. The first was in Sheffield, UK, where the local government had implemented a computer model to study the local air quality. Public consultation showed that the pubic of Sheffield was not satisfied with the model [129]. The public criticized the model on several points, and councilors and researchers felt that the community's and citizen's groups' comments were much more detailed, reasoned, and well supported than expected [129]. Comments were acknowledged by those running the model as insightful and well founded [129]. Issues added to the agenda by the suggestion of the citizen's groups included an inquiry into the extent to which the local council was affected by what the model presented, and consideration of the "value-for-money" associated with the modeling strategy [129], as opposed to a pollution mitigation strategy.

The second case study was in Bristol, UK. Community members were asked to use markers to develop a color-coded map of Bristol that would reflect typical air pollution in the city. Not only was the resulting map a reasonable reflection of actual air pollution in Bristol, there was valuable information to be found in a comparison of Bristol's air pollution model and the community's map in areas where the two disagreed [129]. Both studies were valuable and acted as a kind of extended peer review on the policy-related science [129].

Development of scientific material for public consumption forces scientists to develop understandings of other fields, and does not remove rigor from the work but does demand skill [130]. Communication with the public is a sustainability issue in that emissions reductions recommended by the results of monitoring are easier to implement with an informed public

supporting policies they feel they helped create [130]. Alternatively, an ill-informed public can pressure governments to adopt policy for the wrong reasons, potentially leading to unsustainable environmental impacts. O'Neill et al. [117] recommends that research not only be communicated to the public, but that air pollution research should be developed in collaboration with the affected communities.

Only rarely when scientists are asked about interaction with the public do they imagine anything other than a public lecture [130]. This mistake is an extreme example of the idea that one way communication is the only way to involve the public. Sather et al. [131] shows that the public can be directly involved in research activities. The Sather et al. [131] study covered a large area (~25,000 km^2 of the Dallas-Fort Worth Metroplex) and help from volunteers, including volunteer EPA personnel, 4-H club members, Master Gardeners, and retired farmers, was required. At *each* network site, volunteers were able to correctly operate instruments and collect data of quality. Such involvement is surely replicable in other settings, would increase the range and cost-effectiveness of monitoring, and would have positive impacts on a community's will to reduce air pollution. In addition to sharing of information, public involvement can result in substantial, competent aid in air pollution monitoring. Widespread, hands-on public involvement would be one aspect of a more effective effort to communicate risks associated with air pollution to the public, as called for in Craig et al. [13].

Institutional Changes: Conclusion In order to accelerate the progress of the air pollution monitoring community toward sustainability, there are changes the monitoring community must make. Goals must be expanded beyond the conventional goals of human health, visibility, and documentation of ecosystem damage. Work must cross the boundaries of conventional intellectual disciplines to further develop the implications of monitoring data and the tools and metrics used in monitoring. Public involvement will improve research goals in many cases, bring public support to air pollution mitigation and, in some cases, aid the research process itself. Making changes in these directions will help to promote sustainability in air pollution monitoring.

Monitoring More Effectively

Changes that can be made to standard monitoring practice discussed here are based on current trends or suggested modifications to practices. They include development of the understanding of multipollutant impacts, monitoring for universal consolidated sustainability metrics, improvements to the use of satellite observations (partially through new instrumentation), use of design methodologies for monitoring networks, and removing some of the oversimplifications routinely made in conventional monitoring. These changes can form initial steps toward improving the air pollution monitoring community's contribution to sustainability.

Multipollutant Monitoring and Science Health risks from air pollution are almost exclusively assessed on a single pollutant basis [101]. Health risks from, for example, ozone, are assessed separately from health risks from NO_x. In reality, however, people are exposed to many pollutants at one time. Pollutants can have synergistic effects that exacerbate health impacts beyond the sum of the health impacts they would have individually [101]. Air pollution research and the US EPA are moving toward multipollutant research and legislation, but available data are inadequate to create legislative models [101]. To develop the required data, more and better monitoring, as well as improved exposure modeling and data processing are required [101]. The necessary changes will take time; however, development in this direction is required for accurate assessment of the health impacts of air pollution.

Design for Consolidated Sustainability Metrics Environment Canada's Air Quality Health Index (AQHI) and the US EPA's Air Quality Index (AQI) are examples of consolidated metrics. They incorporate a number of data on different species of pollutants and atmospheric conditions and weight the importance of these data in the calculation of a single summative statistic. These metrics are useful in that they can quickly communicate a great deal of information in a form more easily understood by the public than raw air quality data [87]. Consolidated metrics can also change behavior in ways that minimize the impacts of air pollution, as demonstrated by AQHI-informed decisions to limit personal exposure [87].

The Environmental Performance Index (EPI) is an example of a consolidated metric that can be used in service of sustainability. The EPI is the a function of indicators such as urban particulates, SO_x and NO_x emissions, water stress, habitat protection, pesticide regulation, agricultural water intensity, and GHG emission per capita [131]. It has been applied to rank countries in terms of the state and treatment of their environment, and it can help countries define goals and track progress. It was created in response to a feeling that the environmental goals of the United Nations Millennium Development Goals were poorly defined and that progress toward these goals was difficult to quantify [131]. A remedy to these complaints is exactly what consolidated metrics and monitoring designed with these metrics in mind can provide. How well the EPI can describe a country's environmental status is limited by the data available [131]. The EPI can only incorporate data for which there is already a strong history and temporal trend, making it difficult to represent recently recognized sustainability issues. Nevertheless, the EPI provides countries with an evaluation as to where they stand relative to their peers, a method for tracking progress, and a databased framework to guide decision making.

The discipline of life-cycle assessment (LCA) contains many examples of consolidated metrics, similar to the EPI. LCA method and metrics can be used in attempts to quantify sustainability [133]. Eco-Indicator 99, for example, quantifies the impacts of activities and pollutant releases; translates these impacts into three metrics related to health, ecosystem damages, and depletion of resources; and combines these three metrics into a single indicator [134]. The weighting systems that allow LCA methods such as these to combine disparate data into a single number would encourage the quantification of the relative impacts of various air pollutants. Were that accomplished, data on different pollutants, pollutants with very different behavior and effects, could be compared on the same scale.

Designing air pollution monitoring and monitoring campaigns to serve consolidated sustainability metrics means not only providing data for metrics like the EPI and Eco-indicator 99, but also developing novel data sets to strengthen such metrics. Novel data sets would make it possible for such a metric to be influenced by sustainability issues for which sufficient data do not yet exist. Collecting data so that loss of resilience, for example, could be incorporated into a metric like the EPI would encourage nations to take action on previously ignored sustainability issues and provide governments with the information necessary to do so. It must be borne in mind, however, that there are many pitfalls in the design of consolidated metrics [132], and only a correctly designed metric will lead to sound decision making.

A standardized set of data for use with widely accepted consolidated metrics would clarify the design goals of monitoring campaigns, which is important to the cost-efficiency of monitoring [13]. Information derived would be more similar from campaign to campaign, allowing monitoring groups to more easily share data. Further development of consolidated metrics in the direction of sustainability and the design of monitoring efforts to serve this development would allow the air pollution monitoring community to come to a consensus on the types of data to be counted in the metrics and the weighting of these data.

Development of Satellite Observations Satellite observations can be used in combination with models and in situ measurements to reduce statistical uncertainty in estimates [85]. Recent work by van Donkelaar et al. [86] has made possible the reliable estimation of long-term average $PM_{2.5}$ concentration based on satellite-derived data. Aerosol Optical Depth (AOD) measurements made by the MODIS (Moderate Resolution Imaging Spectroradiometer) and MISR (Multiangle Imaging Spectrometer) instruments on the Terra satellite were combined with estimates of aerosol distribution from the Goddard Earth Observing System chemical transport model (GEOS-chem). Previously, variations in meteorology, aerosol composition, and distribution have prevented accurate estimates by satellite observation beyond small regions, but with the GEOS-Chem model, reliable estimates were obtained across all midlatitude areas of the globe. The concentration estimates with 10 km^2 spatial resolution were obtained.

Many epidemiological studies of $PM_{2.5}$ exposure are limited by a dearth of monitoring data, and the improved satellite estimates from the van Donkelaar at al. 2010 work [86], can now provide some of these

needed data [86]. The lack of data is more pronounced in developing countries, and these countries often have pronounced $PM_{2.5}$ management problems, making these estimates particularly useful. van Donkelaar et al. [86] also suggest that increased satellite coverage could further improve the identification of temporal or spatiotemporal trends. In contrast, other recent attempts to estimate $PM_{2.5}$ concentrations using satellite-observed AOD with fine spatial resolution determined that AOD is a poor tool for assessing spatial $PM_{2.5}$ patterns [135], supporting previous suggestions that current satellite spatial resolution is not sufficient for the intra-urban scale [88]. AOD was also found to contribute little additional information when incorporated into a predictive model that was already accounting for land use, emissions sources, meteorology, and regional variability [135]. Thus, the most effective role of satellite data is still being established, but this tool has the potential to become a valuable and routine part of air pollution monitoring, providing data where there otherwise may be few and improving data where routine rigorous monitoring is taking place.

Martin [88] reviews the many recent improvements in the application of satellite observations to assessments of air quality but includes a number of limitations in obtaining accurate pollutant concentrations. Limitations included the need for more ground-level NO_2 measurement to validate satellite-observed NO_2 data and difficulty in obtaining high-quality O_3 concentration estimates. Martin's work asserts that in terms of instrumentation, air quality monitoring via the current satellites is at a peak but that substantial progress could be made with a new generation of instruments, with more satellites in a variety of orbits (as opposed to all satellites being in sun-synchronous orbit as is currently the case). Specific instrument improvements include a minimization of pixel size, which will reduce the number of pixels obscured by clouds. Work that can be accomplished without additional satellites and a new generation of instrumentation includes the improvement of models critical to the interpretation of satellite observations. Better estimations from these models will improve information derived [88]. If the suggested developments can be made, satellite observations will move closer to delivering spatial and temporal data on a scale that better relates to ground-level monitoring.

Design Methodologies for Monitoring Networks All monitoring techniques, from measurement of ambient pollution levels to computer modeling, rely on some assumptions and estimates in the assessment of pollutant concentrations, exposure to pollution, risk, and damages from pollution. Sophisticated design methodologies for monitoring networks and campaigns have been developed to ensure that the uncertainties are minimized. These methodologies help to ensure that the most useful information can be extracted from what are often limited data.

Established design methodologies include kriging, the use of indices of multivariate effectiveness [136], and the location-allocation method [137]. Each method requires an established area to be monitored and attempts to optimally cover that area with a given number of monitoring stations. Kriging involves placing monitoring stations such that mean square prediction error is minimized [137]. The method employing indices of multivariate effectiveness is based on Shannon's [138] information theory, as used by Silva and Quiroz [136] which tests various configurations of monitors to optimize the information content of data collected. The location-allocation method begins with the creation of a "demand surface," a surface representing the area to be studied, with higher demand areas represented by peaks in the surface. Values on the demand surface are increased by variability in pollution concentrations and by proximity to sensitive populations [137]. To inform the demand surface, an initial pollution surface (representing the distribution of pollution over an area) must exist based on previous or ongoing monitoring. Once the demand surface is finalized, monitoring stations can be placed at the highest demand locations in the area.

Design methodologies for monitoring networks and sampling campaigns are a relatively new development, with many previous networks and campaigns set up in a subjective manner. However, past campaigns and networks lacking rigorous design principles have been effective in that they led to the first generations of information and significant discoveries relating to air pollution (and thereby led much of the effective legislation on air pollution). Further, these campaigns provided information that is necessary for the implementation of some of the newer design methodologies such as the location-allocation methodology,

and they have brought the state of air pollution science to the point where monitoring system design methodologies can be created. However, now that design methodologies have been established, their routine employment can improve the information content of monitoring data and the cost-effectiveness of monitoring efforts.

Overcoming Oversimplifications in Monitoring Often, the practicalities of air pollution monitoring necessitate compromises in aspects such as increased time resolution, assumptions about population behavior, and assumptions of relative uniformity over areas. As methods become more sophisticated, some of these assumptions can be eliminated.

Conventional studies usually assume that the basis of exposure to air pollution is the concentration in a given location, often outdoors. However, people move through various exposure situations in their daily lives, from indoors to "hotspot" intersections and through areas of differing land use. A dynamic activity-based population model has been suggested to develop a more realistic sense of actual individual exposure [139]. Use of this model captures exposure resulting from people's travel in and out of urban areas, rather than assuming a constant number of people within cities, as has been the case in conventional studies [139]. Beckx et al. [139] use of this model showed that conventional static modeling of exposure is underestimating population exposure to air pollution.

Some very small areas in cities, such as high traffic intersections, can have much higher pollution concentrations than the bulk concentrations in the wider area being monitored through conventional means. Gokhale and Khare [141] discuss a model for determining the likelihood of air pollution concentration exceedances over norms at intersections and other areas, where exceedances are likely. The model provides the opportunity to probabilistically manage air pollution on a very fine spatial scale by designing for a minimization of exceedances. Models such as those of Beckx et al. [139], Burke et al. [140] and Gokhale and Khare [141] can provide means for addressing some of the simplifying assumptions in air pollution monitoring. Since their approaches primarily involve modeling, they need not increase the cost of air pollution management excessively.

Monitoring More Effectively: Conclusion

There are a number of changes to air pollution monitoring suggested in the literature and, in many cases, already under way. These changes, the development of multipollutant science, monitoring for consolidated metrics, improvements to satellite-based monitoring, using monitoring network design methodologies, and dealing with routine oversimplifications will improve the operation of the monitoring community and the quality of results. Information, as a common first step toward sustainability and a necessary support for sustainability policy, will help the air pollution community serve sustainability. Hopefully, these changes will be only the first set of changes in a more fundamental shift toward sustainability.

Conclusion

Air pollution is often seen as a negative but unavoidable consequence of human activity. While air pollutants are well classified and there are a number of commonly recognized problems they create, including negative impacts on human health, environmental damage, and economic losses, the establishments designed to mitigate these problems often have a mandate to also pursue sustainability.

The recommendations made herein regarding a shift toward sustainability are largely complimentary. Pursuing one of the goals described would serve other sustainability goals. That complementarity may be one of the most convincing arguments that these goals actually will promote sustainability. While sustainability is difficult to define, it must connote that solutions to one problem do not exacerbate other problems, but contribute to other solutions.

Holism, then, must be an aspect of sustainability, and the lack of holism in the current air pollution monitoring community may underlie its current shortcomings. Not only is there a need for more holistic viewpoints encompassing ideas from other intellectual disciplines, but there is a need for air pollution mitigation to go beyond promoting primarily technology-based solutions to only the immediate impacts. Solutions offered today do not address all aspects of the air pollution problem.

To a very large extent, the lack of holism is not a function of a failing of the air pollution monitoring community, but a result of that community having strategically chosen battles in the past. Dockery [43]

shows how hard advocates of air pollution mitigation were forced to struggle for any political action on air pollution in the early days of air pollution science, and how the battles were won by presenting irrefutable, solely technical and solely scientific evidence proving the very immediate and anthropocentric effects of air pollution. It is only now that less obvious, though arguably more dire, effects on humans, the systems they rely on for sustenance, and on nonhuman stakeholders are gaining more than a slight foothold within the political agenda.

Dockery [43] also shows the great extent to which the burden of proof was on those trying to defend people and ecosystems from the damages of pollution, and not on the polluters. This burden is still in place, and problems must be proven in terms polluters cannot ignore, such as dollar figures and mortality. To a large extent, evidence will need to continue to be in these terms, and monitoring must be expanded in volume, scope, and abilities to continue to prove the damages from air pollution in the normally accepted terms. However, the body of evidence will be more compelling and complete if the terms are expanded to include goals discussed in this article. The terms have been set as a reaction to refusals of those challenging the need for, or priority of, air pollution management, and reactionary strategies do not promote sustainability. If monitoring continues in this way, sustainability will remain elusive. If monitoring is performed to serve sustainability, sustainability will be served.

Bibliography

Primary Literature

1. US EPA (2010) What are the six common air pollutants? http://www.epa.gov/air/urbanair/. Accessed 24 Oct 2010
2. Environment Canada (2010) Criteria air contaminants and related pollutants. http://www.ec.gc.ca/air/default.asp?lang=En&n=7C43740B-1. Accessed 24 Oct 2010
3. Environment Canada (2010) Backgrounder: persistent organic pollutants. http://www.ec.gc.ca/lcpe-cepa/default.asp?lang=En&n=135D347F-1. Accessed 9 Dec 2010
4. Harrison RM (2001) Air pollution: sources, concentrations and measurements. In: Harrison RM (ed) Pollution: causes, sources and control, 4th edn. Royal Society of Chemistry, Cambridge, pp 169–193
5. US EPA (2008) Technology transfer network air toxics website. http://www.epa.gov/ttn/atw/188polls.html. Accessed 19 Oct 2010
6. Fenger J (1999) Urban air quality. Atmos Environ 33:4877–4900
7. Sillman S, Logan JA, Wofsy SC (1990) The sensitivity of ozone to nitrogen oxides and hydrocarbons in regional ozone episodes. J Geophys Res 95:1837–1851
8. Mølhave L, Nielson GD (1992) Interpretation and limitations of the concept "total volatile organic compounds" (TVOCs) as an indicator of human responses to exposures of volatile organic compounds (VOC) in indoor air. Indoor Air 2:65–77
9. Wang DK, Austin CC (2006) Determination of complex mixtures of volatile organic compounds in ambient air: an overview. Anal Bioanal Chem 386:1089–1098
10. Kesselmeier J, Staudt M (1999) Biogenic volatile organic compounds (VOC): an overview on emission, physiology and ecology. J Atmos Chem 33:23–88
11. Geddes JA, Murphy JG, Wang DK (2009) Long term changes in nitrogen oxides and volatile organic compounds in Toronto and the challenges facing local ozone control. Atmos Environ 43:3407–3415
12. Brook RD, Rajagopalan S, Pope CA III, Brook JR, Bhatnagar A, Diez-Roux AV, Holguin F, Hong Y, Luepker RV, Mittleman MA, Peters A, Siscovick D, Smith SC Jr, Whitsel L, Kaufman JD (2010) Particulate matter air pollution and cardiovascular disease: an update to the scientific statement from the American heart association. Circulation 121(21):2331–2378
13. Craig L, Brook JR, Chiotti Q, Croes B, Gower S, Hedley A, Krewski D, Krupnick A, Krzyzanowski M, Moran MD, Pennel W, Samet JM, Schneider J, Shortreed J, Williams M (2008) Air pollution and public health: a guidance document for risk managers. J Toxicol Environ Health A 71:588–698
14. Haywood JM, Shine KP (1995) The effect of anthropogenic sulfate and soot aerosol on the clear sky planetary radiation budget. Geophys Res Lett 22:603–606
15. Schecter A, Birnbaum L, Ryan JJ, Constable JD (2006) Dioxins: an overview. Environ Res 101:419–428
16. Fleischer O, Wichmann H, Lorenz W (1999) Release of polychlorinated dibenzo-p-dioxins and dibenzofurans by setting off fireworks. Chemosphere 39:925–932
17. Kampa M, Castanas E (2008) Human health effects of air pollution. Environ Pollut 151:362–367
18. WHO (World Health Organization) (1977) Environmental health criteria 3: lead. WHO, Geneva
19. US EPA (Environmental Protection Agency) (1997) The benefits and costs of the clean air act, 1970 to 1990. US EPA, Washington, DC
20. Crathorne B, Rees YJ, France S (2001) Chemical pollution of the aquatic environment by priority pollutants and its control. In: Harrison RM (ed) Pollution: causes, sources and control, 4th edn. Royal Society of Chemistry, Cambridge, pp 1–31
21. Gillett NP, Arora VK, Zickfeld K, Marshall SJ, Marryfield WJ (2011) Ongoing climate change following a complete cessation of carbon dioxide emissions. Geoscience, Nature. doi:10.1038/NGE01047
22. European Commission (1999) Directorate General, environment, nuclear safety and civil protection. EU Focus on Clean Air, Germany. http://ec.europa.eu/environment/air/pdf/clean_air.pdf

23. Environment Canada (2010) Impacts of air pollution. http://ec.gc.ca/indicateurs-indicators/default.asp?lang=en&n=D189C09D-1. Accessed 17 Jan 2011
24. Yang W, Omaye ST (2009) Air pollutants, oxidative stress and human health. Mutat Res 674:45–54
25. Saxon A, Diaz-Sanchez D (2005) Air pollution and allergy: you are what you breathe. Nat Immunol 6:223–226
26. Mortimer KM, Neas LM, Dockery DW, Redline S, Tager IB (2002) The effect of air pollution on inner-city children with asthma. Eur Respir J 19:699–705
27. Lee SC, Lam S, Fai HK (2001) Characterization of VOCs, ozone, and PM_{10} emissions from office equipment in an environmental chamber. Build Environ 36:837–842
28. Jerret M, Burnett RT, Pope A III, Ito K, Thurston G, Krewski D, Shi Y, Calle E, Thun M (1995) Long-term ozone exposure and mortality. N Engl J Med 360:1085–1095
29. Schwartz J, Morris R (1995) Air pollution and hospital admissions for cardiovascular disease in Detroit, Michigan. Am J Epidemiol 142:23–35
30. Beeson WL, Abbey DE, Knutsen SF (1998) Long-term concentrations of ambient air pollutants and incident lung cancer in California adults: results from the AHSMOG study. Environ Health Perspect 106:813–823
31. Woodruff TJ, Grillo J, Schoendorf KC (1997) The relationship between selected causes of postneonatal infant mortality and particulate air pollution in the United States. Environ Health Perspect 105:608–612
32. Pope CA III, Dockery DW (2006) Health effects of fine particulate air pollution: lines that connect. J Air Waste Manage Assoc 56:709–742
33. Pope CA III, Thun MJ, Namboodiri MM, Dockery DW, Evans JS, Speizer FE, Heath CW Jr (1995) Particulate air pollution as a predictor of mortality in a prospective study of US adults. Am J Respir Crit Care Med 151:669–674
34. Pope CA III, Burnett RT, Thun MJ, Calle EE, Krewski D, Ito K, Thurston GD (2002) Lung cancer, cardiopulmonary mortality, and long-term exposure to fine particulate air pollution. J Am Med Assoc 287:1132–1141
35. Stölzel M, Breitner S, Cyrys J, Pitz M, Wölke G, Kreyling W, Heinrich J, Wichmann H-E, Peters A (2007) Daily mortality and particulate matter in different size classes in Erfurt, Germany. J Expo Sci Environ Epidemiol 17:458–467
36. Delfino RJ, Sioutas C, Malik S (2005) Potential role of ultrafine particles in associations between airborne particle mass and cardiovascular health. Environ Health Perspect 113:934–946
37. Li N, Sioutas C, Cho A, Schmitz D, Misra C, Sempf J, Wang M, Oberley T, Froines J, Nel A (2003) Ultrafine particulate pollutants induce oxidative stress and mitochondrial damage. Environ Health Perspect 111:455–460
38. Vinzents PS, Møller P, Sørensen M, Knudsen LE, Hertel O, Jensen FP, Schibye B, Loft S (2005) Personal exposure to ultrafine particles and oxidative DNA damage. Environ Health Perspect 113:1485–1490
39. Knol A, de Hartog JJ, Boogaard H, Slottje P, van der Sluijs JP, Lebret E, Cassee FR, Wardekker A, Ayres JG, Brom PJ, Brunekreef B, Donaldson K, Forastiere F, Holgate ST, Kreyling WG, Nemery B, Pekkanen J, Stone V, Wichmann H-E, Hoek G (2009) Expert elicitation on ultrafine particles: likelihood of health effects and causal pathways. Part Fibre Toxicol 6:19. doi:10.1186/1743-8977-6-19
40. Finkelstein MM, Jerrett M (2007) A study of the relationships between Parkinson's disease and markers of traffic-derived and environmental manganese air pollution in two Canadian cities. Environ Res 104:420–432
41. Ewan KB, Pamphlett R (1996) Increased inorganic mercury in spinal motor neurons following chelating agents. Neurotoxicology 17:343–349
42. WHO (World Health Organization) (2010) Urbanization and Health. Bull World Health Organ 88:245–246
43. Dockery DW (2009) Health effects of particulate air pollution. Ann Epidemiol 19:257–263
44. Pope CA, Ezzati M, Dockery DW (2009) Fine-particulate air pollution and life expectancy in the United States. N Engl J Med 360:376–386
45. Likens GE, Driscoll CT, Buso DC, Mitchell MJ, Lovett GM, Bailey TG, Reiners WA, Alewell C (2002) The biogeochemistry of sulfur at Hubbard brook. Biogeochemistry 60:235–315
46. Likens GE, Driscoll CT, Buso DC (1996) Long-term effects of acid rain: response and recovery of a forest eco-system. Science 272:244–246
47. Tomlinson GH (2003) Acidic deposition, nutrient leaching and forest growth. Biogeochemistry 65:51–81
48. Rechcigl JE, Sparks DL (1985) Effects of acid rain on the soil environment: a review. Commun Soil Sci Plant Anal 16:653–680
49. Koricheva J, Roy S, Vranjic JA, Haukioja E, Hughes PR, Hanninen O (1997) Antioxidant responses to simulated acid rain and heavy metal deposition in birch seedlings. Environ Pollut 95:249–258
50. Kratky BA, Fukunaga ET, Hylin JW, Nakano RT (1974) Volcanic air pollution: deleterious effects on tomatoes. J Environ Qual 3:138–140
51. Lazarus BE, Schaberg PG, Hawley G, DeHayes DH (2006) Landscape-scale spatial patterns of winter injury to red spruce foliage in a year of heavy region-wide injury. Can J For Res 36:142–152
52. Haines TA (1981) Acidic precipitation and its consequences for aquatic ecosystems: a review. Trans Am Fish Soc 110:669–707
53. Yi H, Hao J, Tang X (2006) Atmospheric environmental protection in China: current status, developmental trend and research emphasis. Energy Policy 35:907–915
54. Grantz DA, Garner JHB, Johnson DW (2003) Ecological effects of particulate matter. Environ Int 29:213–239
55. WHO (World Health Organization) (1991) Environmental health criteria 118: inorganic mercury. World Health Organization, Geneva
56. Kelting DL, Burger JA, Edwards GS (1995) The effects of ozone on the root dynamics of seedlings and mature red oaks (*quercus rubra L.*). For Ecol Manage 79:197–206
57. Lefohn AS, Jackson W, Shadwick DS, Knudsen HP (1997) Effect of surface ozone exposures on vegetation

grown in the southern Appalachian Mountains: identification of possible areas of concern. Atmos Environ 31: 1695–1708
58. Laurence JA (1998) Ecological effects of ozone: integrating exposure and response with ecosystem dynamics and function. Environ Sci Policy 1:179–184
59. Ren W, Tian H, Liu M, Zhang C, Chen G, Pan S, Felzer B, Xu X (2007) Effects of tropospheric ozone pollution on net primary productivity and carbon storage in terrestrial ecosystems of China. J Geophys Res 112:D22S09. doi:10.1029/2007JD008521
60. Zhang Y, Zhu X, Slanina S, Shao M, Zeng L, Hu M, Bergin M, Salmon L (2004) Aerosol pollution in some Chinese cities. Pure Appl Chem 76:1227–1239
61. OMA (Ontario Medical Association) (2005) The illness costs of air pollution: 2005–2026 health & economic damage estimates. OMA, Toronto
62. Krupnick A, Alberini A, Cropper M, Simon N, O'Brien B, Goeree R, Heintzelman M (2002) Age, health and the willingness to pay for mortality risk reductions: a contingent valuation survey of Ontario residents. J Risk Uncertain 24:161–186
63. Mayerhofer P, Weltschev M, Trukenmuller A, Friedrich R (1995) A methodology for the economic assessment of material damage caused by SO_2 and NO_x emissions in Europe. Water Air Soil Pollut 85:2687–2692
64. Delucchi MA (2000) Environmental externalities of motor-vehicle use in the US. J Transp Econ Policy 34:135–168
65. Metallo MC, Poli AA, Diana M, Persia F, Cirillo MC (1995) Air pollution loads on historical monuments: an air quality model application to the marble arch of Titus in Rome. Sci Total Environ 171:163–172
66. Murphy JJ, Delucchi MA, McCubbin DR, Kim HJ (1999) The cost of crop damage caused by ozone air pollution from motor vehicles. J Environ Manage 55:273–289
67. Skärby L, Selldén G (1984) The effects of ozone on crops and forests. Ambio 13:68–72
68. USDA, (United States Department of Agriculture) (2008) Budget summary and annual performance plan. USDA, Washington, DC
69. Rasker R (1994) A new look at old vistas: the economic role of environmental quality in western public lands. Univ Colo Law Rev 65:369–399
70. Gilbertson T, Reyes O (2009) Carbon trading: how it works and why it fails. Dag Hammarskjöld, Uppsala
71. Solomon S (1999) Stratospheric ozone depletion: a review of concepts and history. Rev Geophys 37:275–316
72. Weatherhead EC, Anderson SB (2006) The search for signs of recovery of the ozone layer. Nature 441(7089):39–45. doi:10.1038/nature04746
73. Swart R, Amann M, Raes F, Tuinstra W (2004) A good climate for clean air: linkages between climate change and air pollution. Clim Change 66:263–269
74. Harvey LD (2010) Energy and the new reality 1 – energy efficiency and the demand for energy. Earthscan, London. ISBN 10: 1849710724
75. Environment Canada (2009) About the air quality health index. http://www.ec.gc.ca/cas-aqhi/default.asp?Lang=En&n=065BE995-1. Accessed 13 Mar 2010
76. Wetherbee GA, Shaw MJ, Latysh NE, Lehmann MB, Rothert JE (2010) Comparison of precipitation chemistry measurements obtained by the Canadian air and precipitation monitoring network and national atmospheric deposition program for the period 1995–2004. Environ Monit Assess 164:111–132
77. Acid Deposition Monitoring Network in East Asia (EANET) (2000) Technical manual for wet deposition monitoring in East Asia. http://www.eanet.cc/product/techwet.pdf
78. Thepanondh S, Ayers GP, Hooper MA (2005) Analysis of precipitation chemistry in northern Thailand. Clean Air Environ Qual 39:43–47
79. Jankhe JA (2000) Continuous emissions monitoring, 2nd edn. Wiley, New York. ISBN 0471292273
80. Environment Agency (UK) (2008) Technical guidance note (monitoring) M20 – quality assurance of continuous emission monitoring systems – application of BS EN 14181 and BS EN 13284–2. http://publications.environment-agency.gov.uk/pdf/GEHO1105BJXZ-e-e.pdf
81. Environment Canada (2005) Locomotive emissions monitoring program 2004. http://www.railcan.ca/documents/publications/1118/2006_04_12_LemReport2004_en.pdf
82. Cooper DA, Ekström M (2005) Applicability of the PEMS technique for simplified NO_x monitoring on board ships. Atmos Environ 39:127–137
83. Williams ML (2001) Atmospheric dispersal of pollutants and the modeling of air pollution. In: Harrison RM (ed) Pollution: causes, sources and control, 4th edn. Royal Society of Chemistry, Cambridge, pp 246–267
84. Miffre A, Chacra MA, Geffroy S, Rairoux P, Soulhac L, Perkins RJ, Frejafon E (2010) Aerosol load study in urban area by Lidar and numerical model. Atmos Environ 44:1152–1161
85. Sarigiannis DA, Soulakellis NA, Sifakis NI (2004) Information fusion for computational assessment of air quality and health effects. Photogramm Eng Remote Sens 70: 235–245
86. van Donkelaar A, Martin RV, Brauer M, Kahn R, Levy R, Verduzco C, Villeneuve PJ (2010) Global estimates of ambient fine particulate matter concentrations from satellite-based aerosol optical depth: development and application. Environ Health Perspect 118(6):847–855
87. Brook JR, Moran MD, Pennell W, Craig L (2010) Elements of air quality management: atmospheric science tools for developing effective policy. In: Gurjar BR, Molina LT, Ojha CSP (eds) Air pollution: health and environmental impacts. Taylor & Francis, Boca Raton, pp 363–418
88. Martin RV (2008) Satellite remote sensing of surface air quality. Atmos Environ 42:7823–7843
89. Boersma KF, Eskes HJ, Veefkind JP, Brinksma EJ, van der A RJ, Sneep M, van den Oord GHJ, Levelt PF, Stammes P, Gleason JF, Bucsel EJ (2007) Near-real retrieval of troporspheric NO_2 from OMI. Atmos Chem Phys 7:2013–2128

90. Bachmann J (2007) Will the circle be unbroken: a history of the U.S. national ambient air quality standards. J Air Waste Manage Assoc 57:652–697
91. Chow JC, Watson JG (2008) New directions: beyond compliance air quality measurements. Atmos Environ 42:5166–5168
92. European Commission (2008) Air quality standards. http://ec.europa.eu/environment/air/quality/standards.htm. Accessed 19 Jan 2010
93. US EPA (Environmental Protection Agency) (2010) National ambient air quality standards (NAAQS). http://www.epa.gov/air/criteria.html. Accessed 19 Jan 2010
94. European Commission (2008) Commission regulation (EC) no. 692/2008, O.J. L 199/1
95. US EPA (Environmental Protection Agency) (2008) National air quality: status and trends through 2007. US EPA Office of Air Quality Planning and Standards, Air Quality Assessment Division, Research Triangle Park
96. Environment Canada (2005) Acid rain and the facts. http://www.ec.gc.ca/AcidRain/acidfact.html. Accessed 25 Jan 2010
97. Wheeler D (2001) Racing to the bottom? Foreign investment and air pollution in developing countries. J Environ Dev 10:225–245
98. Fredriksson PG, Gaston N (2007) Evironmental governance in federal systems: the effects of capital competition and lobby groups. Econ Inq 38:501–514
99. Hidy GM, Brook JR, Demerjian KL, Molina LT, Pennell WT, Scheffe RD (eds) (2011) Technical challenges of multipollutant air quality management. Springer, Dordrecht. ISBN 9789400703032
100. Canada. Environment Canada and Health Canada (2011) Canadian smog science assessment (Unpublished)
101. Dominici F, Peng RD, Barr CD, Bell ML (2010) Protecting human health from air pollution: shifting from a single-pollutant to a multipollutant approach. Epidemiology 21:187–194
102. Sundqvist G, Letell M, Lidskog R (2002) Science and policy in air pollution abatement strategies. Environ Sci Policy 5:147–156
103. Fayolle F, Vandecasteele J-P, Monot F (2001) Microbial degradation and fate in the environment of methyl *tert*-butyl ether and related fuel oxygenates. Appl Microbiol Biotechnol 56:339–349
104. Rass-Hansen J, Falsig H, Jørgensen B, Christensen C (2007) Bioethanol: fuel or feedstock? J Chem Technol Biotechnol 82:329–333
105. Statistics Canada (2007) Canadian environmental sustainability indicators: air quality indicators: data sources and methods. Statistics Canada, Ottawa
106. Brook JR, Demerjian KL, Hidy G, Molina L, Pennell W, Scheffe R (2009) New directions: results-oriented multi-pollutant air quality management. Atmos Environ 43:2091–2093
107. Law K (2010) Atmospheric chemistry: more ozone over North America. Nature 463:307–308
108. MacDonald DV, Hanley N, Moffat I (1999) Applying the concept of natural capital criticality to regional resource management. Ecol Econ 29:73–87
109. Folke C (2006) Resilience: the emergence of a perspective for social-ecological systems analyses. Glob Environ Change 16:253–267
110. Costanza R, d'Arge R, de Groot R, Farber S, Grasso M, Hannon B, Limburg K, Naeem S, O'Neill R, Paruelo J, Raskin RG, Sutton P, van den Belt M (1997) The value of the world's ecosystem services and natural capital. Nature 387:253–260
111. Pimm SL (1997) The value of everything. Nature 387:231–232
112. Daily GC, Söderqvist T, Aniyar S, Arrow K, Dasgupta P, Ehrlich PR, Folke C, Jansson A, Jansson B-O, Kautsky N, Levin S, Lubchenco J, Mären K-G, Simpson D, Starret D, Tilman D, Walker B (2000) The value of nature and the nature of value. Science 289:395–396
113. Engelbrecht H-J (2009) Natural capital, subjective well-being, and the new welfare economics of sustainability: some evidence from cross-country regions. Ecol Econ 69:380–388
114. Deutsch L, Folke C, Skanberg K (2003) The critical natural capital of ecosystem performance as insurance for human well-being. Ecol Econ 44:205–217
115. Rockstrom J, Steffen W, Noone K, Persson Å, Chapin FS III, Lambin EF, Menton TM, Scheffer M, Folke C, Schellnhuber HJ, Nykvist B, de Wit CA, Hughes T, van der Leeuw S, Rodhe H, Sörlin S, Snyder PK, Costanza R, Svedin U, Falkenmark M, Karlberg L, Corell RW, Fabry VJ, Hansen J, Walker B, Liverman D, Richardson K, Crutzen P, Foley JA (2009) A safe operating space for humanity. Nature 461:472–475
116. Folke C, Carpenter S, Elmqvist T, Gunderson L, Holling CS, Walker B (2002) Resilience and sustainable development: building adaptive capacity in a world of transformations. Ambio 31:437–440
117. O'Neill MS, Jerret M, Kawachie I, Levy JI, Cohen AJ, Gouveia N, Wilkinson P, Fletcher T, Cifuentes L, Schwartz J (2003) Health, wealth and air pollution: advancing theory and methods. Environ Health Perspect 111:1861–1870
118. Künzli N, Jerret M, Mack WJ, Beckerman B, LaBree L, Gilliland F, Thomas D, Peters J, Hodis HN (2005) Ambient air pollutin and atherosclerosis in Los Angeles. Environ Health Perspect 113:201–206
119. Mitchell G, Dorling D (2003) An environmental justice analysis of British air quality. Environ Plann A 35:909–929
120. MacKerron G, Mourato S (2009) Life satisfaction and air quality in London. Ecol Econ 68:1441–1453
121. Marshall JD, Brauer M, Frank LD (2009) Healthy neighbourhoods: walkability and air pollution. Environ Health Perspect 117:1752–1759
122. Dannenberg AL, Jackson RJ, Frumkin H, Schieber RA, Pratt M, Kochtitsky C, Tilson HH (2003) The impact of community design and land-use choices on public health: a scientific research agenda. Am J Public Health 93:1500–1508
123. Stone B Jr (2003) Air quality by design: harnessing the clean air act to manage metropolitan growth. J Plann Educ Res 23:177–190
124. Frank LD, Sallis JF, Conway TL, Chapman JE, Saelens BE, Bachman W (2009) Many pathways from land use to health. J Am Plann Assoc 72:75–87

125. Tang UW, Wang ZS (2007) Influences of urban form on traffic-induced noise and air pollution: results from a modelling system. Environ Modell Softw 22:1750–1764
126. Newman P, Beatley T, Boyer H (2008) Resilient cities: responding to peak oil and climate change. Island Press, Washington, DC. ISBN 9781597264990
127. Marshall JD, Brauer M, Frank LD (2009) Health neighbourhoods: walkability and air pollution. Environ Health Perspect 117:1752–1759
128. Royal Society (2006) Survey of factors affecting science communication by scientists and engineers. http://royalsociety.org/uploadedFiles/Royal_Society_Content/Influencing_Policy/Themes_and_Projects/Themes/Governance/Final_Report_-_on_website_-_and_amended_by_SK_no_navigation.pdf. Accessed 31 Mar 2010
129. Yearly S (2006) Bridging the science – policy divide in urban air-quality management: evaluating ways to make models more robust through public engagement. Environ Plann C Gov Policy 24:701–714
130. Pereira AG, Raes F, TdeS P, Rosa P, Broderson S, Jorgensen MS, Ferreira F, Querol X, Rea J (2009) Atmospheric composition change research: time to go post-normal? Atmos Environ 43:5423–5432
131. Sather ME, Varns JL, Mulik JD, Glen G, Smith L, Stallings C (2001) Passive ozone network of Dallas: a modeling opportunity with community involvement 2. Environ Sci Technol 35:4426–4435; Emerson J, Esty DC, Kim C, Srebotnjak T, Levy MA, Mara V, de Sheribinin A, Jaiteh M (2010) 2010 environmental performance index. Yale Center for Environmental Law & Policy. http://epi.yale.edu/file_columns/0000/0157/epi2010_report.pdf
132. Swamee PK, Tyagi A (2007) Improved method for aggregation of water quality Subindices. J Environ Eng 133:220–225
133. Azapagic A (2006) Life cycle assessment as an environmental sustainability tool. In: Dewulf J, Van Langhove H (eds) Renewables-based technology: sustainability assessment. Wiley, Chichester, pp 87–110
134. Goedkoop M, Spriensma R (2001) The Eco-indicator 99: a damage oriented method for life cycle assessment – methodology report, 3rd edn. Pré Consultants, Amersfoort, The Netherlands
135. Paciorek CJ, Liu Y (2009) Limitations of remotely sensed aerosol as a spatial proxy for fine particulate matter. Environ Health Perspect 117:904–909
136. Silva C, Quiroz A (2003) Optimization of the atmospheric pollution monitoring network at santiago de chile. Atmos Environ 37:2337–2345
137. Kanaroglou PS, Jerret M, Morrison J, Beckerman B, Arain MA, Gilbert NL, Brook JR (2005) Establishing an air pollution monitoring network for intra-urban population exposure assessment: a location-allocation approach. Atmos Environ 39:2399–2409
138. Shannon CE (1948) A mathematical theory of communication. Mobile Comput Commun Rev 5:3–55
139. Beckx C, Panis LI, Arentze T, Jansenn D, Torfs R, Broekx S, Wets G (2009) A dynamic activity-based population modelling approach to evaluate exposure to air pollution: methods and application to a Dutch urban area. Environ Impact Assess Rev 29:179–185
140. Burke JM, Zufall MJ, Ozkaynak H (2001) A population exposure model for particulate matter: case study results for $PM_{2.5}$ in Philadelphia, PA. J Expo Anal Environ Epidemiol 11:470–489
141. Gokhale S, Khare M (2007) A theoretical framework for the episodic-urban air quality management plan (*e*-UAQMP). Atmos Environ 41:7887–7894

Books and Reviews

Young TK (2005) Population health: concepts and methods, 2nd edn. Oxford University Press, New York. ISBN 0-19-515854-7

Air Pollution Sources, Statistics and Health Effects, Introduction

Roy M. Harrison
Division of Environmental Health and Risk Management, School of Geography, Earth and Environmental Sciences, The University of Birmingham, Edgbaston, Birmingham, UK

Air pollution has been a topical subject for many centuries. There are records of the nuisance effects of coal burning in London going back for hundreds of years, and the association of high air pollution levels with effects on human health has been recognized for almost as long. Urban pollution in the form of smogs arising from coal burning and industrial emissions, most notably in London, Donora (Pennsylvania), and the Meuse Valley in Belgium, was associated with marked increases in daily mortality and led to legislation which has, in the main, been very effective at improving air quality. Nonetheless, research over the last 2 decades has led to a change in paradigm in our understanding of the health effects of air pollutants. Whereas previously it was assumed that there were no-effect thresholds, i.e., concentrations below which adverse effects on health would not be observed, it is now recognized that for most toxic air pollutants, there is no recognizable no-effect threshold concentration, and effects are seen in the most sensitive members of the population at extremely low concentrations. The most influential studies of pollutants such as airborne

particulate matter have failed to reveal no-effect thresholds, and consequently, air quality management now seeks to limit rather than wholly eliminate adverse effects on the population. The pollutant generally accepted as having the greatest public health impact is particulate matter. Both short-term (acute) and long-term (chronic) exposures have effects upon health. The best quantified information relates to mortality and hospital admissions. Exposure to particulate matter in the PM_{10} size range is associated with an increase of around 0.6% in mortality for a 24-h increase of 10 μg m^{-3}. The impacts of chronic exposure are of greater public health significance with an increase of around 4% in mortality for a 10 μg m^{-3} increase in particles in the $PM_{2.5}$ size range. The impact on life expectancy is a reduction of between a few months and several years across Europe depending upon the local $PM_{2.5}$ concentrations. Adverse effects on human health have been the main driver of scientific research on the emission, atmospheric behavior, and health effects of toxic pollutants referred to as "locally acting" pollutants. Strict *air quality guidelines and standards*, including limit values, have been adopted in most countries in order to limit the adverse effects of exposure to a range of pollutants, most typically including particulate matter, sulfur dioxide, nitrogen dioxide, ozone, lead, and carcinogenic pollutants such as benzene and the polycyclic aromatic hydrocarbons.

The other main driver of science in the air pollution field has been the recognition that air pollutants have an effect upon global climate and that some of the locally acting air pollutants also have the capacity to influence climate locally, regionally, and globally; for example, black carbon from combustion sources has much the same effect as a greenhouse gas, although the precise mechanisms are different. Airborne particles also affect radiative transfer in the atmosphere and provide one of the largest uncertainties in estimating the anthropogenic influences upon climate change. White particles such as ammonium sulfate are reflective and have a net cooling effect by reflecting incoming solar radiation back to space. Water-soluble particles can act as cloud condensation nuclei affecting the albedo (reflectivity) of clouds leading to a reduction in land surface warming.

The majority of the world's population now lives within urban areas which are also a focus for road traffic activity and frequently also for power plants and industry. In this context, urban areas are often more polluted than the regional atmosphere surrounding them, and because of their high concentration of population, this is where a large part of human exposure to locally acting pollutants occurs. The entry ► Urban Air Quality: Sources and Concentrations considers the sources of pollutants influencing urban areas, reviews the measured concentrations within cities internationally, and describes some of the approaches to air quality management. The determinants of urban concentrations of pollutants are the rates of emission of primary pollutants (those emitted directly from sources such as factory chimneys and engine exhaust), the meteorological processes that determine the mixing of the emissions within the atmosphere and the transport both horizontally and vertically away from the source, and the atmospheric chemistry, which can both cleanse the atmosphere of toxic substances but also lead to the formation of secondary pollutants, a term describing pollutants formed within the atmosphere itself. The meteorological processes leading to the vertical mixing of pollutants away from sources and the horizontal transport by the wind (termed advection) are described in the entry ► Urban Air Quality: Meteorological Processes. Computational models used to describe these processes are also included. The complementary entry ► Urban Atmospheric Composition Processes describes the key chemical reactions which serve both to limit the concentrations of toxic pollutants and also to control concentrations of secondary pollutants such as ozone and secondary airborne particles which are very important in relation to both human health and regional pollution. Both photochemical and thermal reactions in the atmosphere can lead to formation of reactive free radical species which degrade organic compounds, sulfur dioxide, nitrogen dioxide, and many other toxic species. However, in doing so, they form secondary products, some of which can also have important consequences for health and climate. For example, oxidation of sulfur dioxide and nitrogen dioxide lead ultimately to the formation of ammonium sulfate and ammonium nitrate which in turn lead to increased concentrations of particulate matter and cloud condensation nuclei. As air pollutants are advected from urban areas, they are subject to atmospheric transport leading to impacts upon

► *regional air quality* which are important in relation both to human health effects and ecosystem effects described in the entry of this name. Transboundary air pollution, in which pollutants cross national boundaries is an important aspect of regional pollution. Chemistry-transport models, which simulate the processes involved in regional transport of pollution and are very important in policy development, are also described.

Most developed countries have achieved considerable success in improving air quality. This has depended upon an advanced approach to air quality management, which requires a number of key components dealt with in subsequent entries. One of the keys to the management of air pollution is high-quality monitoring of airborne concentrations. This is normally carried out with fixed ground-level monitors located so as to reflect outdoor exposures of the public. The entry ► Air Pollution Monitoring and Sustainability discusses the design of monitoring networks and how monitoring data can inform urban design and air quality management policy. In addition to traditional monitoring networks, the monitoring of source emissions and also regional remote sensing of atmospheric composition from space have an important role to play. In addition to monitoring, air quality management also depends upon ► *air quality guidelines and standards*. The original intention of air quality guidelines was to provide no-effect concentrations which could be used as targets in air quality management. As explained above, many pollutants are now recognized as not having a demonstrable no-effect threshold, and consequently, air quality guidelines and standards are designed to limit adverse effects to a very low level, and the implementation of abatement policies is frequently based on cost-benefit analysis. One of the main sources of urban and regional pollution has been surface transportation and especially road traffic. More recently, there has been recognition of the impacts of shipping and railways on emissions and air quality, and the entry ► Air Quality, Surface Transportation Impacts on seeks to quantify the issues and place them in context. Abatement measures applied to road transport have been extremely effective in the developed world in limiting the harmful effects of pollutants emitted from vehicle exhausts, but much remains to be done to achieve full sustainability of the transport fleet. Aviation is also a significant source of pollutant emissions, but because of the altitude at which most of the emissions occur, the effects on ground-level air quality are modest, and the main concern is over climate impacts arising from emissions from greenhouse gases and water vapor which are described in the entry ► Aviation and Atmosphere. Release of long-lived pollutants at ground-level as well as aircraft emissions lead to ► *stratospheric pollution* with consequences for stratospheric ozone concentrations, penetration of UV radiation to ground-level, and for global climate.

Air pollutants comprise both gases and particles. The latter are tiny airborne liquid or solid droplets ranging from nanometers to tens or even hundreds of micrometers in size. In relation to locally acting pollution, they are typically referred to as particulate matter, but in the context of the global atmosphere, they are referred to as aerosol. The impacts of ► *aerosol in global atmosphere* of greatest concern are those upon climate. These are numerous and complex, and aerosol in the global atmosphere may have both warming and cooling effects upon climate. There are sometimes policy tensions between global and local pollution in that the abatement of some kinds of local pollution may worsen global warming problems. This entry deals with the sources and properties of aerosols in the global atmosphere.

Taken together, these contributions by eminent authors give a broad and rather comprehensive view of air pollution, extending from key urban sources and processes through the regional scale to the global, with close attention given to key sources such as road and air transportation.

Air Quality Guidelines and Standards

Roger O. McClellan
Toxicology and Health Risk Analysis, Albuquerque, NM, USA

Article Outline

Glossary
Definition of the Subject
Introduction
Air Quality Management Framework
Context for Air Quality Impacts
The US Legal Framework for Air Quality Standards

National Ambient Air Quality Standards
US Process for Setting National Ambient Air Quality Standards
Paradigm Shift
WHO Process for Setting Air Quality Guidelines
Assessing Hazards and Risks
Sources of Information for Setting Standards and Guidelines
Particulate Matter as an Example
Ozone
Current Air Quality Standards and Guidelines
Future Directions
Bibliography

Glossary

Adverse health effect Alteration in the health status of individuals or populations.

Aerodynamic diameter The diameter of a spherical particle of unity density with a terminal velocity equal to the particle being sampled.

Aerosol Relatively stable suspension of particles or droplets in a gaseous media.

Air quality guidelines AQG, established by World Health Organization to provide guidance to the public and government on levels of air pollutant that will improve air quality.

Air quality monitoring Measurement of the concentration of various pollutants in air for regulatory compliance or research purposes.

Ambient air Air found out of doors, which is a mixture of gases and suspended particles and droplets.

Ambient concentration-response function A mathematical description of the relationship between ambient air concentrations and associated morbidity or mortality indicators, usually expressed as increased risk for a defined increment of increased pollutant.

Anthropogenic Causal by humans, man-made.

Background levels The concentration of a pollutant in the air after accounting for all local or regional emissions.

Biogenic Produced by biological processes.

Carbon monoxide The chemical, CO, that is a product of incomplete combustion. It is regulated as a Criteria Air Pollutant or Common Air Pollutant.

Emissions The quantities of pollutants emitted by a particular source or multiple sources.

Excess risk Risk associated with exposure to an agent over and above the baseline risk.

Exposure Taking materials into the body via inhalation, ingestion, or absorption through the skin.

Guidelines Guidance provided for use by the public or government officials.

Hazardous The property of having the potential to cause adverse health effects with sufficient duration and concentration of exposure.

Lead Pb, an element that occurs naturally and found many uses including as a paint additive and as tetraethyl Lead added to gasoline to enhance engine performance. Regulated as a Criteria Air Pollutant or Hazardous Air Pollutant.

Mobile sources Mobile sources, such as vehicles, of air pollution emissions.

Morbidity A statistical measure of number of fractions of indicators of illness.

Mortality A statistical measure of number or fraction of deaths.

National Ambient Air Quality Standards NAAQS, established under the US Clean Air Act to protect health and welfare.

Nitrogen oxides NO_x, a mixture of NO and NO_2 produced in high-temperature combustion processes. Regulated as a Criteria Air Pollutant or Common Air Pollutant.

Ozone O_3, a molecule with three atoms of oxygen. It is highly reactive with other chemicals and biological systems. It is regulated as a Criteria Air Pollutant or Common Air Pollutant.

Particulate matter Airborne solid material, unspecified as to chemical composition, regulated as a Criteria Pollutant or Common Air Pollutant.

Particulate matter, 10 μm PM_{10}, airborne particulate material included in sampled air size fraction with aerodynamic size of 10 μm and less.

Particulate matter, 2.5 μm $PM_{2.5}$, particulate material included in sampled air size fraction with an aerodynamic size of 2.5 μm or less.

Primary standards or guidelines Air Quality Standards or Guidelines for Criteria or Common Pollutants set to protect public health.

Risk The probability of an adverse health outcome associated with exposure to a hazardous material for a defined period of time and exposure level. Usually expressed as a level of adverse effect, morbidity, or mortality, over and above background.

Risk assessment The analytical process of evaluating exposure and the hazard potential of a material to estimate risk.

Secondary standards or guidelines Air Quality Standards or Guidelines for Criteria or Common Air Pollutants set to protect public welfare such as visibility or effects on plants.

Standards Regulations that are legally binding.

Stationary sources Fixed sources of air pollution emissions such as power plants.

Sulfur dioxide SO_2, released from combustion of sulfur-containing fossil fuels. It is regulated as a Criteria Air Pollutant or Common Air Pollutant.

Definition of the Subject

Air quality is the state of the atmosphere in which humankind lives and works. The air consists of a complex mixture of gases and suspended droplets and particles. Some of the gases, such as oxygen and carbon dioxide, within rather tight concentration limits, are essential for sustaining the life of all living things. Some of the gases and aerosol particles and droplets, when certain concentrations are exceeded and with sufficient duration of exposure, may have adverse effects on humans and other living things, including vegetation. Various governmental agencies around the world have developed air quality guidelines and standards for ambient or outdoor air quality. These guidelines or standards, when achieved or attained, are intended to be protective of human health and minimize the potential for other effects such as impacts on visibility or plants. Some government entities and statutes characterize the guidelines as goals to be attained, while other government entities and statutes treat them as rigid standards which are legally enforced. Guidelines or standards, when attained, are intended to improve the quality and sustainability of human life.

Introduction

The quality of the air that people live in and breathe has no doubt been of concern to people since early in the evolution of humans. This concern, which must have preceded recorded history, likely coincided with man's use of purposeful combustion, fire, for cooking and heating and ultimately, for manufacturing and other activities, including transportation. There is abundant evidence that early humans found it convenient to live in caves both for shelter and safety. The poor quality of the air is apparent from the residual soot coating the interior of caves used as dwellings. Indeed, pictographs of the interior of the caves provide documentation of aspects of the life of those early cave dwellers. As community life evolved, people continued to live and use fire for both cooking and heating in poorly ventilated dwellings.

Domestication of both plants and animals played a critical role in the development of agriculture-based societies and the growth of communities. The agricultural base influenced the size of communities and their proximity to one another. The ability to transport essential foodstuffs by ship or overland by horses, camels, and oxen allowed cities to emerge. With larger communities came increased air pollution and the impact of an individual family's pollution on their neighbors and vice versa.

Coal apparently was first used as a fuel in the Far East. The introduction of coal as an energy source in the Western world followed Marco Polo's return to the west from his trip to the more advanced societies of the Far East. As early as the thirteenth century, there was concern over coal smoke and odor in London, and the Queen of England reportedly moved from London to Nottingham because of the insufferable smoke. In 1661, John Evelyn published *Fumifugium: Or the Inconvenience of the Air and Smoke of London Dissipated*, which drew attention to the problem for air pollution.

The industrial revolution in the early years was dependent on wood as a fuel, and therefore, industry was located near forests. This restriction served as a throttle on industrial development. The development of effective steam engines in the eighteenth century provided a major impetus for the use of coal as a fuel. With coal, the pace of industrial activity increased, and factories developed near sources of coal and along the

waterways that served to efficiently transport the coal. The smoke and ash from coal-fired boilers in factories, power plants, and locomotives increasingly became of concern. Interestingly, this concern about air pollution was stimulated by impairment of visibility and soiling as well as effects on health. In addition, the damage to vegetation from emissions produced in the smelting of sulfide ores gave clear evidence of yet another effect of air pollution. Air pollution problems were recognized in many industrial countries in the late nineteenth century, but the problem was probably nowhere as apparent as in London. The high levels of pollutants combined with the notorious London fog created a serious problem and is reputed to have given rise to the term *smog*, a contraction of smoke and fog.

The development of steam engines soon led to their use in sea-going vessels that initially depended heavily on coal as a fuel. Later, coal would be replaced by oil as a fuel. Emissions from ships did not attract major attention until the late twentieth century when concern developed for air emissions when the ships were near land and especially when in harbor.

With the discovery of electricity a revolution occurred in the generation and use of energy. More appropriately, it is the conversion of energy from one form to another, for example, from coal to thermal energy to electric energy that could be easily transmitted. It was now possible to generate electricity with coal as an energy source at one location and transport it over long distances for use at multiple locations. Over the course of the twentieth century the generation of electricity from the combustion of fossil fuels in large power plants continuously grew, first in heavily industrialized countries and, ultimately, around the world.

In the 1900s, a series of incidents drew attention to air pollution as a serious and even acute health problem. In December 1930, static atmospheric conditions in the Meuse Valley of Belgium resulted in pollution that caused over 60 deaths and hundreds of illnesses. In December 1952, smog in London resulted in about 4,000 deaths, principally among the infirm, the old, and those with respiratory diseases. The effects were not restricted to humans. Acute respiratory symptoms were also reported in cattle at the Smithfield Club livestock show. The effects may have been most severe in the heavy-weight prize cattle, who were well cared for and had their litter and excreta promptly removed. Other cattle that were not as well cared for apparently fared better, perhaps because of some benefits of ammonia from the excreta neutralizing the effects of sulfur oxides and sulfuric acid. Another major smog episode in London during December 1962 resulted in 340 deaths.

In October 1948, a particularly calm and stable meteorology in Donora, Pennsylvania, about 30 km from Pittsburgh, PA, resulted in a 4-day buildup in levels of oxides and inorganic sulfates from the local steel and zinc smelters. More than 20 individuals died and 6,000 people developed respiratory problems. The official government report [57] on the Donora episode noted that the health effects were likely related to a combination of contaminants and identified sulfur dioxide as a chief culprit. The word smoke did not appear in the report. The attention previously focused on smoke was now broadening to include other airborne materials and, indeed, more broadly to air quality.

Despite early concerns about whether airborne materials could cause disease, relatively little research was conducted prior to World War I to improve our knowledge of the relationship between the air pollution and disease. The unfortunate use of poisonous gases in World War I provided a stimulus for developing a better understanding of how these specific agents produced disease. Unfortunately, the meager literature generated indicates that research in this area was not substantial or very long-lasting. In retrospect, the lack of research related to airborne toxicants is probably not surprising considering the generally low level of biomedical research activity in the first third of the twentieth century. The strong preventive medicine orientation that exists today toward diseases of both occupational and environmental origin had not yet developed.

Between World War I and World War II, concern for airborne materials impacting on human health centered primarily on occupational exposures. World War II brought with it renewed concern for purposeful exposures of people to toxic gases and biological agents. In both the United Kingdom and the United States, major research efforts were conducted to better understand the effects of these agents thereby providing improved approaches to defending against their use and effects. World War II also brought with it major

research efforts focusing on the potential toxic effects of uranium and newly discovered radionuclides such as plutonium and fission product related to the manufacture and use of nuclear weapons and, later, the development of nuclear reactors as energy sources to generate electrical power. These activities are noteworthy since many of the basic concepts of aerosol science and inhalation toxicology trace their roots to those research efforts.

The post-World War II era brought with it an increased awareness of air pollution arising from another source – motor vehicles. Perhaps nowhere was this more the case than in the Los Angeles basin with its marked increase in population, industry, and cars. As concern increased for the Los Angeles smog in the late 1940s and 1950s, the name "Bay of Smokers," which was coined in 1542 by Juan Rodrigues Cabrillo for San Pedro Bay, took on a contemporary tone. Haagen-Smit [25] of the California Institute of Technology reported the scientific basis for photochemical smog – reactions among oxides of nitrogen and hydrocarbons from vehicle exhaust in the presence of sunlight produced ozone and other photochemical oxidants that were the key components of Los Angeles smog. It is noteworthy that his early research was motivated by understanding the effects of smog on citrus fruit production. Haagen-Smith's findings were another key factor in broadening the concern for air quality from smoke to ozone and other air contaminants.

Post WWII then was a major and continuing increase in the use of airplanes both to transport people and goods. Indeed, transport of goods by aircraft is a central element of the global economy that emerged in the latter part of the twentieth century. As with ships, aircraft as sources of air pollution did not attract much attention in the late twentieth century when attention began to focus on air quality in the vicinity of major airports. In the case of some areas, such as the Los Angeles International Airport and a nearby harbor, concern has developed for the contribution of multiple sources: aircraft, cargo ships, locomotives, trucks, and passenger cars.

So far the discussion has centered on air pollution from combustion of hydrocarbons, from recently fixed carbon in wood and other plant materials to the fossil fuel energy sources, coal, oil, and natural gas, created in earlier geologic eras. With each of these fuel sources hydrocarbons are combusted releasing thermal energy, CO, CO_2, H_2O, variable amounts of Nitrogen Oxides, and traces of other elements.

There are non-hydrocarbon-based energy systems that do not depend on combustion of hydrocarbons that deserve mention. This includes wind, hydro, nuclear, and solar power. Some of these such as wind and water have been in use for centuries to provide power. Nuclear power had its advent post-WWII. Solar power with its current focus on photovoltaic conversion is relatively new. All of these systems have the advantage of not creating airborne emissions related to combustion. However, each of these energy sources has its own disadvantages related to potential impacts on human health and ecosystems.

It is important to recognize that there are a multitude of other industrial and personal activities beyond combustion of hydrocarbons that result in air emissions that may be harmful to human health and ecosystems. These range from mining and extraction of minerals to processes producing specialized products such as paper, fabric, silicon chips, and chemicals to the manufacture of vehicles and other commercial goods. Agricultural activities also have unique airborne emissions. Each of these activities require variable amounts of energy and, thus, contribute to the potential for local emissions of combustion products or emissions at a remote location such as a central facility producing electrical power. In addition, each of these activities has airborne emissions unique to the processes being used.

The focus of this entry is on the pollutants that arise from multiple sources and, thus, are found everywhere. These common air pollutants are identified as criteria pollutants in the Clean Air Act, the principal statute governing air quality in the United States [14]. Some of these same pollutants have been identified by the World Health Organization (WHO) as common air pollutants [94].

Air Quality Management Framework

Air quality guidelines and standards are a key element of air quality management as practiced around the world. Bachmann [7] provides an informative historical review of the evolution of air quality management in the United States with particular emphasis on the

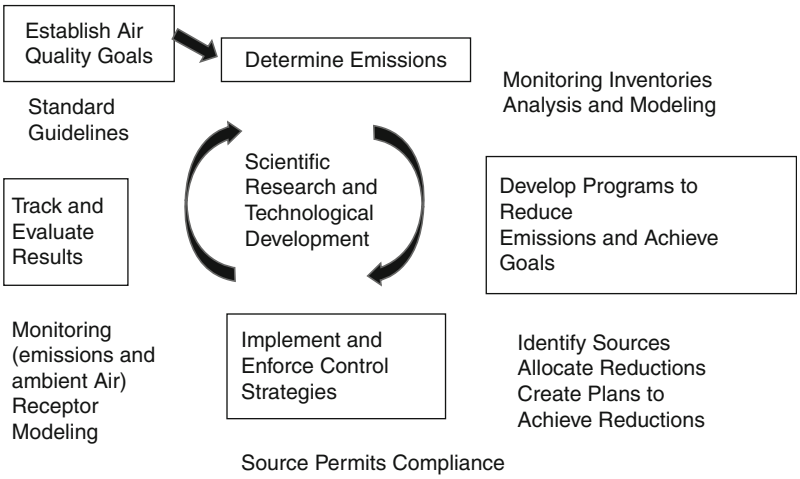

Air Quality Guidelines and Standards. Figure 1
Conceptual framework for air quality management

National Ambient Air Quality Standards (NAAQS). A conceptual framework for Air Quality Management is depicted in Fig. 1. Air quality goals, which may be expressed as air quality guidelines or standards, are the drivers for all the other elements of the framework. Emissions from various sources are considered within the context of the guidelines or standards. Are specific sources or kinds of sources significant contributors based on estimates of emissions? If so, what strategies can be used to reduce their emissions? Do source permits have a role in setting emission limits? Ambient monitoring can be used to provide an overall assessment of air.

Quality and, perhaps, over time monitoring can establish whether the intended improvements in air quality are being achieved. The total air quality management cycle shown should be viewed as an integrated system. The system is dynamic with new sources being introduced, old sources retrofitted with controls, and some sources removed. In addition, as I will discuss later, the guidelines and standards are periodically reviewed and the concentration levels reduced. As some would say, the goal posts are constantly being moved to lower concentrations making it more challenging to achieve success and declare victory. As will be discussed later, how low is low enough?

Another key concept embedded within the air quality management system is the linkage from sources to health responses illustrated in Fig. 2. The schematic rendering in the figure is a general concept not exclusively linked to air pollution. The goal of air quality management is to have a positive impact on human health responses, the endpoint at the right of the figure. As illustrated in Fig. 3, multiple factors, not just air quality, influence human health. Thus, in a specific sense, the goal is to minimize the health impacts of air pollution relative to all the other factors that influence human health while achieving an overall improvement in health. Implicit in the setting of air quality standards and guidelines is the treatment of specific concentrations of agents in ambient air as surrogates for human health. Air quality can be readily characterized with an appropriately designed monitoring scheme for multiple air pollutants. In contrast, it is challenging to attempt to determine the association between specific risk factors, such as air pollution, and the health response of an individual. This is especially the case for current ambient concentrations of air pollutants in industrialized countries, concentrations substantially reduced from those observed only a few decades ago. Even when the focus of research investigations shifts from individuals to large populations, it is a challenge to characterize an association between a specific air pollutant and increased probability of a specific kind of response compared to a baseline. It is rarely possible to establish a causal relationship.

The complexity of relationships between sources of air pollution and health responses can be readily

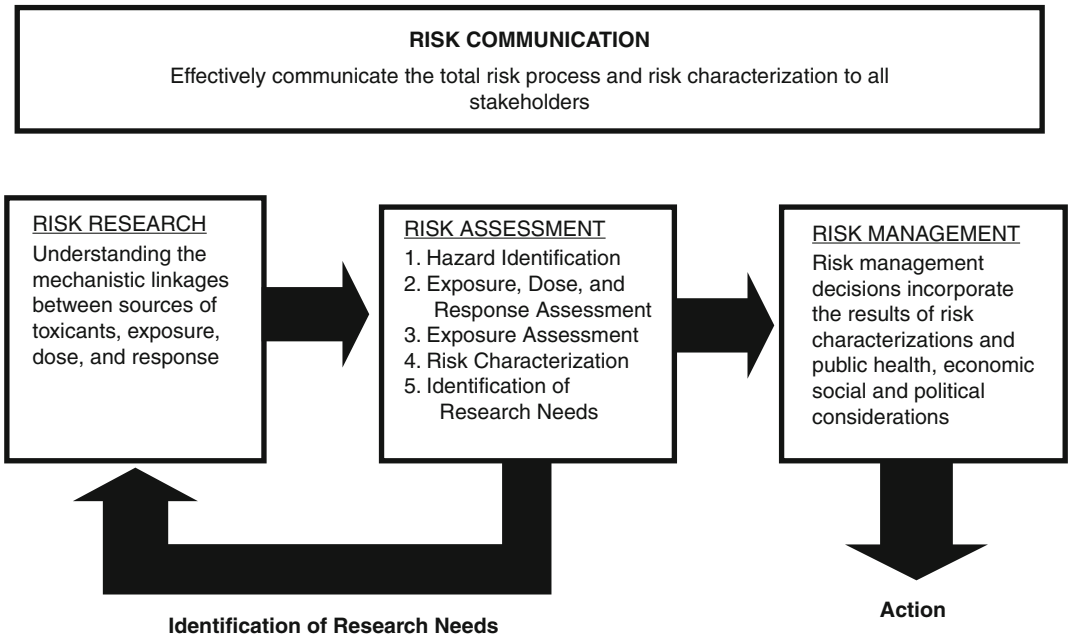

Air Quality Guidelines and Standards. Figure 2
The risk paradigm

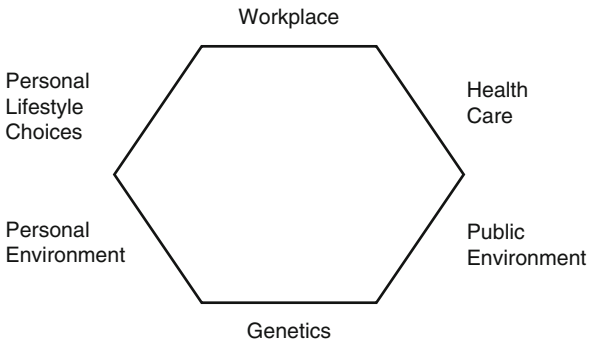

Air Quality Guidelines and Standards. Figure 3
Multiple factors influencing the health status of individuals and populations

grasped by considering Fig. 4. In this figure, the concept of outdoor versus indoor exposures is introduced. The situation with regard to indoor exposures is even more complicated than may initially appear. This is the case because most individuals, during the course of their daily lives, spend variable amounts of time in multiple indoor environments: home (their bedroom, kitchen, living room, etc.), workplace, school, automobile, etc. Each of these micro-environments may have a different mix of air pollutants, both as to kind and concentration, arising from multiple sources. Some variable portion of the indoor pollution may also arise from outdoors, the ambient environment.

The outdoor air pollution arises from multiple sources, some local, some regional, and some quite remote. Indeed, it is increasingly apparent that emissions arising in one continent such as Asia soon reach North America and then Europe. The air trajectory of emissions from coal-fired power plants in the Midwest extending to the Northeastern United States is well known. Dust originating from deserts in China regularly reaches the United States and Europe. Dust originating from the Sahara Desert also regularly circulates around the globe.

Context for Air Quality Impacts

Although the focus of this entry is on air quality and its influence on human health, it is important that context be provided for considering the role of air pollution on human health. The introductory chapter by Ayres et al. [5] in the textbook on *Environmental Medicine* [6] provides a useful review of the multiple factors influencing health. As noted earlier (Fig. 3) multiple factors influence the health of each individual and, in

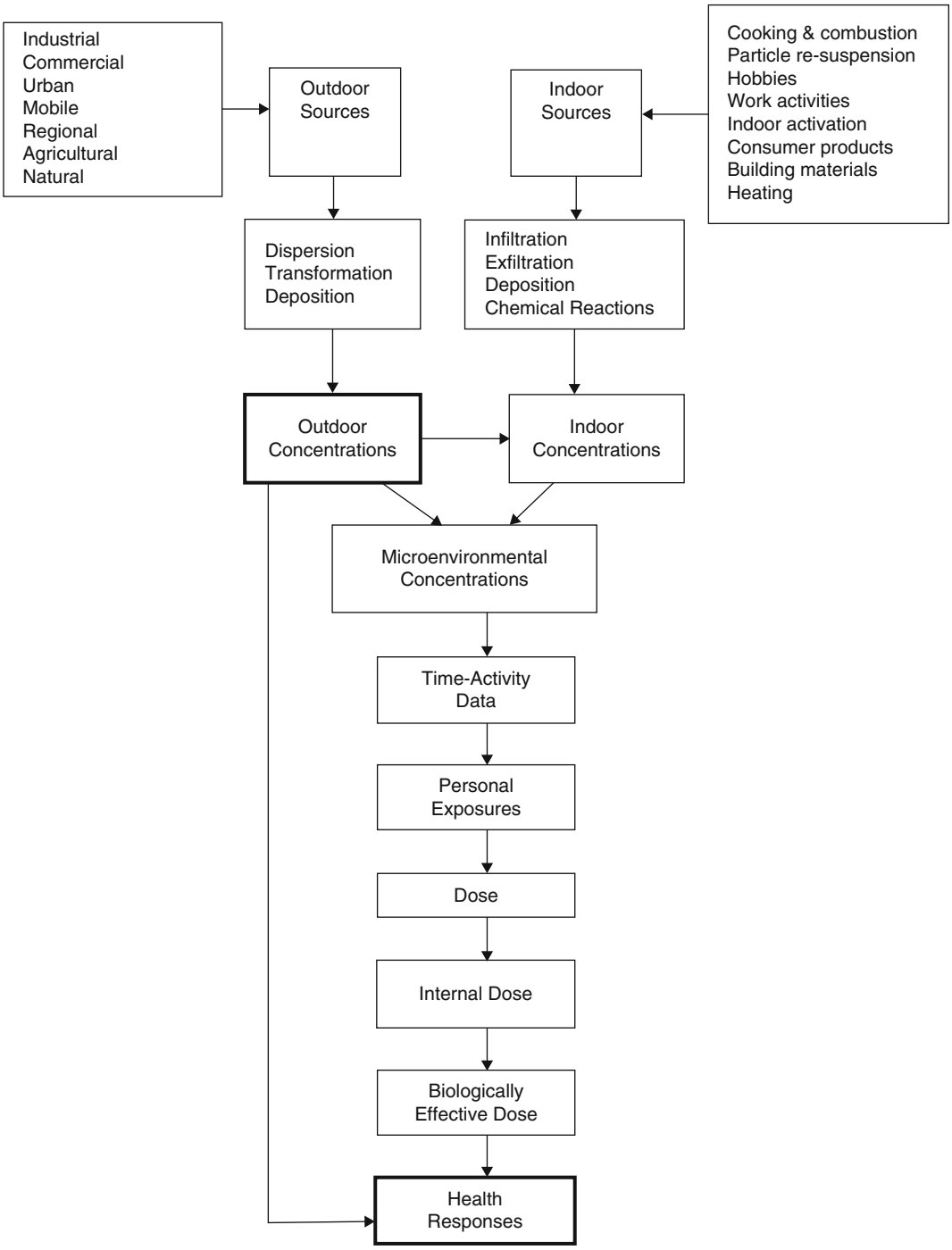

Air Quality Guidelines and Standards. Figure 4
Schematic rendering of the relationship between outdoor and indoor sources, personal exposure, biologically effective dose and health responses (Adapted from Özkaynak [50])

turn, the health of populations. Each individual has its own unique genetic background inherited from its parents. That genetic background can have a profound influence on the individual's potential health status throughout their life. Each of the other factors shown in the diagram can have a significant influence on the health status of an individual. Income and, more broadly, socioeconomic status are important factors influencing health.

The role of income and environmental factors are intertwined. This is readily apparent from considering Table 1 [31]. This table reports an analysis of the health impact of various risk factors in low- and middle-income countries versus high-income countries [31]. Urban air pollution and indoor smoke from household use of solid fuels are identified as risk factors. Taken together these two air pollution risk factors account for 5.2% of deaths in low- and middle-income countries versus 1.0% of deaths in high-income countries, the latter related exclusively to urban air pollution.

It is important to recognize that the role of socioeconomic status influencing health is a complex issue. Steenland et al. [59] have analyzed this issue for the US population and their findings are summarized in Table 2. Several points can be made using these findings. First, even for a country like the United States, typically identified as high-income, there are gradients in socioeconomic status and these have associated substantial gradients in health outcomes. Keep in mind the relative risks on the order of 2.0 when the relative risks of particulate matter and ozone are discussed. It is obvious that the national good will be served by improving the socioeconomic status of the total population. Second, a multitude of factors have a role in influencing the health status of the individuals in the lower quartile. Poor air quality to the extent it is experienced more by individuals in the lower quartile than in the upper quartile may be one of those factors. The substantial influence of socioeconomic status on health emphasizes the importance of attempting to control for it as a variable in epidemiological studies of air pollution and to report findings on it to provide perspective for the reported effects of air pollution.

Figure 5 provides a related perspective by contrasting environmental with non-environmental contributions to specific categories of disease using disability-adjusted life years as an endpoint [55]. The merits of monetizing risks and benefits as statistical life-years versus lives have been reviewed by Sunstein [61]. Of special note are four diseases: lower respiratory infections, chronic obstructive pulmonary disease (COPD), ischemic heart disease, and lung cancer. The first three of these conditions account for about 4% of the total global burden disease in disability-adjusted life years while lung cancer accounts for about 1%. Air pollution is generally viewed as a contributor to global disease burden. However, its contribution needs to be placed in perspective relative to other major contributors to ill health.

In this entry, there is a focus on the development of air quality standards in the United States since, to a large degree, these activities have served as a template for other countries. For comparative purposes, the World Health Organization's Air Quality Guidelines have also been summarized. Reference will be made at several junctures to the distinction between guidelines providing guidance for policymakers versus standards that are legally binding and, in turn, may mandate certain actions. The omission of detailed discussions of guidelines and standards as developed and used in other countries around the globe is not intended as a judgment of their quality or utility.

The US Legal Framework for Air Quality Standards

As concern mounted for the poor quality of air, citizens increasingly turned to the government to enact laws to restrict emissions and improve air quality [7, 60]. Bachmann's perspective is of special interest since as a US EPA employee for more than three decades, he had a central role in the setting of NAAQS. Readers interested in legal details of the Clean Air Act and NAAQS will find the summary of Martineau and Novello [33] useful. Initially, these air quality initiatives were focused at the local level in major cities around the world. In the United States, heavily industrialized cities, such as Pittsburgh, Chicago, Philadelphia, and Detroit, enacted legislation setting local standards. In most cases, these early standards focused on smoke.

By the mid-twentieth century in the United States, it had become apparent that local efforts on air

Air Quality Guidelines and Standards. Table 1 Deaths by cause: low- and middle-income countries, high-income countries, and world, 2001

	Low- and middle-income deaths	High-income deaths	World deaths
Total number (thousands)	**48,351**	**7,891**	**56,242**
Rate per 1,000 population	**9.3**	**8.5**	**9.1**
Age-standardized[a] rate per 1,000	**11.4**	**5.0**	**10.0**
Risk factor	*Number in thousands (percent)*		
Childhood and maternal undernutrition			
Childhood underweight	3,630 (7.5)	0 (0.0)	3,630 (6.5)
Iron-deficiency anemia	613 (1.3)	8 (0.1)	621 (1.1)
Vitamin A deficiency	800 (1.7)	0 (0.0)	800 (1.4)
Zinc deficiency	849 (1.8)	0 (0.0)	849 (1.5)
Other nutrition-related risk factors and Physical activity			
High blood pressure	6,223 (12.9)	1,392 (17.6)	7,615 (13.5)
High cholesterol	3,038 (6.3)	842 (10.7)	3,880 (6.9)
Overweight and obesity	1,747 (3.6)	614 (7.8)	2,361 (4.2)
Low fruit and vegetable intake	2,308 (4.8)	333 (4.2)	2,641 (4.7)
Physical inactivity	1,559 (3.2)	376 (4.8)	1,935 (3.4)
Addictive substances			
Smoking	3,340 (6.9)	1,462 (18.5)	4,802 (8.5)
Alcohol use	1,869 (3.9)	24 (0.3)	1,893 (3.4)
Illicit drug use	189 (0.4)	37 (0.5)	226 (0.4)
Sexual and reproductive health			
Unsafe sex	2,819 (5.8)	32 (0.4)	2,851 (5.1)
Nonuse and use of ineffective methods of contraception	162 (0.3)	0 (0.0)	62 (0.3)
Environmental risks			
Unsafe water, sanitation, and hygiene	1,563 (3.2)	4 (<0.1)	1,567 (2.8)
Urban air pollution	735 (1.5)	76 (1.0)	811 (1.4)
Indoor smoke from household use of solid fuels	1,791 (3.7)	0 (0.0)	1,791 (3.2)
Other selected risks			
Contaminated injections in health care setting	407 (0.8)	4 (<0.1)	412 (0.7)
Child sexual abuse	65 (0.1)	6 (<0.1)	71 (0.1)
All selected risk factors together	22,014 (45.6)	3,473 (44.0)	25,488 (45.3)

[a]Age-standardized using the WHO World Standard Population
Source: Adapted from [31]

Air Quality Guidelines and Standards. Table 2 The impact of socioeconomic status on mortality

Mortality rate ratio $= \frac{\text{lowest quartile}}{\text{highest quartile}}$ of socioeconomical status		
Mortality	Men	Women
All cause	2.02 (1.95–2.09)[a]	1.29 (1.25–1.32)
Heart disease	1.88 (1.83–1.93)	1.84 (1.76–1.93)
Stroke	2.25 (2.14–2.37)	1.53 (1.44–1.62)
Diabetes	2.19 (2.07–2.32)	1.85 (1.72–2.00)
COPD	3.59 (3.35–3.83)	2.09 (1.91–2.30)
Lung cancer	2.15 (2.07–2.23)	1.31 (1.25–1.39)
Breast cancer	–	0.76 (0.73–0.79)
Colorectal cancer	1.21 (1.16–1.27)	0.91 (0.86–0.96)
External causes	2.67 (2.58–2.78)	1.41 (1.35–1.48)

[a]95% confidence interval
Source: Steenland et al. [59]

pollution control were not sufficient, and complementary efforts were needed at the state or national level. At the national level in the United States post-WWII, the lead agency for air quality was the Division of Air Pollution of the Public Health Service within the Department of Health, Education and Welfare. The Air Pollution Control Act of 1955 [60] provided funding to the PHS for air pollution control research and to support the state's efforts. However, the impact of this Act on progress in managing air quality was limited.

In 1963, the Clean Air Act (CAA) was passed, which became the principal national statute in the United States concerned with air quality [14]. The original CAA [14] directed the then Department of Health, Education and Welfare (HEW) to "compile and publish criteria on the effects of air pollutants," hence the identification of "criteria pollutants" and "criteria documents" summarizing the scientific knowledge on certain air pollutants arising from multiple sources and found across the United States. The National Air Pollution Control Administration (NAPCA) within HEW was initially assigned responsibility of administering the CAA. The role of NAPCA was strengthened with the CAA Amendments of 1967. However, in the absence of a specific time schedule progress remained slow. A single document on SO_2 was developed [32]. When the US Environmental Protection Agency (EPA) was created in 1970 by consolidating numerous existing federal agencies, responsibility for administering the CAA was effectively transferred from NAPCA to the EPA.

In 1970, almost coincident with creation of the US Environmental Protection Agency, major amendments to the CAA were passed that opened a new era in managing air quality in the United States [15]. The Clean Air Act as amended is a very broad piece of legislation. The sections dealing with the establishment of National Ambient Air Quality Standards are a key part of the Act and are viewed by many individuals as the core of the Act. Other sections of the Act provide authority for implementing processes to achieve attainment of the NAAQS and otherwise in improving air quality. This includes a delegation of responsibility to the individual States for taking steps to attain the NAAQS. This includes the development of State Implementation Plans if the States have areas that are not in attainment with regard to any specific NAAQS as evaluated by the concentration and statistical form of the Standard.

Other sections of the Act address both Stationary and Mobile Sources and the control of their emissions. This includes specific emission standards for vehicles and provision for issuance of fuel efficiency goals that in the course of being achieved impact on air quality. The rigid "command and control" and

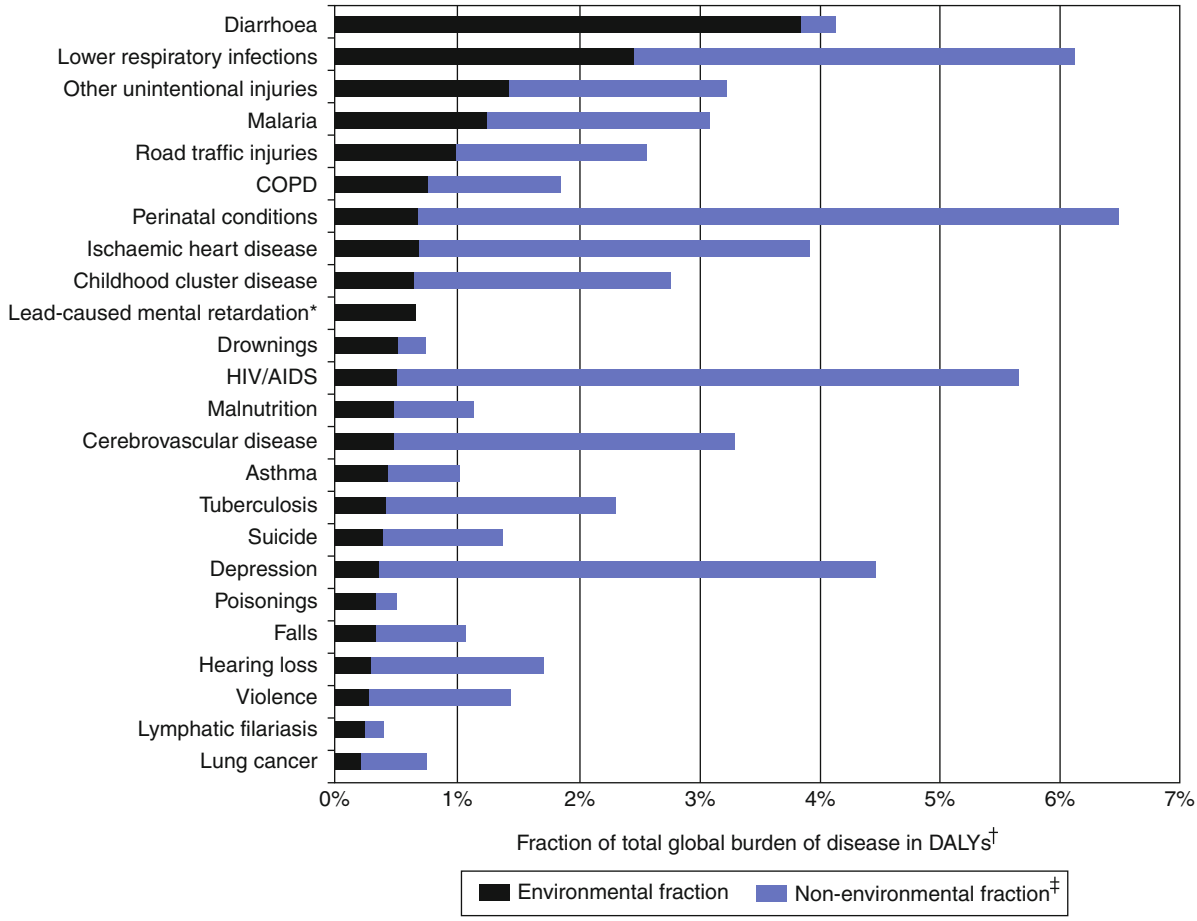

COPD, Chronic obstructive pulmonary disease.

* Lead-caused mental retardation is defined in the World Health Organization list of diseases for 2002, accessed at: www.who.int/evidence.

† DALYs represent a weighted measure of death, illness and disability.

‡ For each disease, the fraction attributable to environmental risks is shown in black, Grey plus black represents the total burden of disease.

Air Quality Guidelines and Standards. Figure 5

Diseases with the largest environmental contribution. *AIDS* acquired immune deficiency syndrome, *DALY* disability-adjusted life-year, *HIV* human immunodeficiency virus (Adapted from Pruss-Ustun and Corvalan, with permission)

standard-setting approach of the United States contrasts sharply with the guidance approach taken by the World Health Organization (WHO).

National Ambient Air Quality Standards

Section 108 of the amended CAA specifies the development of scientific criteria for certain air pollutants. It specifies that the Administrator publish a list for pollutants: (a) which have an adverse effect on public health or welfare, and (b) which are derived from numerous or diverse mobile or stationary sources. It explicitly states – "the criteria shall accurately reflect the latest scientific knowledge on the kind and extent of all identifiable effects on public health and welfare which may be expected from the presence of the pollutant in ambient air, in varying quantities" [15].

Section 109 of the CAA [15] directs the Administrator to propose and promulgate "primary" and "secondary" NAAQSs for criteria pollutants identified under Section 108. The primary Standards are to be set to protect public health; secondary Standards are to be set to protect the public welfare such as effects on soils, water, crops, visibility, and deterioration of property. In this entry, I focus on the setting of the primary Standards and on the specific NAAQS. However, the issues discussed are also broadly applicable to the setting of secondary Standards.

Section 109(b)(1) defines a primary NAAQS as one that "the attainment and maintenance of which in the judgment of the Administrator, based on the criteria and allowing an adequate margin of safety, is requisite to protect the public health." The margin of safety, as interpreted by the EPA, is intended to address uncertainties associated with inconclusive scientific and technical information at the time the Standard is set and to account for hazards that research has not yet identified.

The primary Standards are intended to protect against "adverse effects, not necessarily against all identifiable effects of changes produced by a pollutant." Although the US Congress did not rigorously define an adverse effect, it did provide general guidance in the legislative history of the debate on the CAA [30]. Congress was concerned with effects ranging from cancer, metabolic and respiratory disease, and impairment of mental processes to headaches, dizziness, and nausea.

Congress also noted concern for sensitive population groups in setting the NAAQSs. In particular, Congress noted that the Standards should protect "particularly sensitive citizens such as bronchial asthmatics and those with emphysema who in the normal course of daily activity are exposed to the ambient environment." This has been interpreted to exclude individuals who are not performing normal activities, such as individuals who are hospitalized. Further guidance was given noting that the Standard is statutorily sufficient whenever there is "an absence of adverse effect on the health of a statistically related sample of persons in sensitive groups from exposure to the ambient air."

The challenge of interpreting the "adequate margin of safety" language of the CAA was noted in an editorial by Donald Kennedy on *Risk versus Risk* published when he served as Editor-in-Chief of Science [27]. He wrote – "In the United States and some other industrial democracies, where people and their governments tend to be *risk averse*, legislatures, courts, and administrative entities usually create a presumption favoring more safety rather than less. The definitions of risk in law are often vague ('reasonable certainty of no harm' or 'adequate margin of safety') and are likely to encourage an *unrealistic belief* that risks can be minimized or even eliminated altogether." I think Kennedy has captured the conundrum posed by the language of the CAA, a conundrum that has been addressed by US Supreme Court Justice Stephen Breyer as I will relate later.

In 1977, several key amendments were made to the CAA [16]. Concern about slow action of the EPA in preparing criteria documents and reassessing NAAQSs prompted a legislated requirement that the NAAQSs be reevaluated not later than January 1, 1980, and at 5-year intervals thereafter. Reevaluation was not intended to automatically result in changes in the NAAQSs for a pollutant; rather, reevaluation was intended to ensure that the scientific database was reviewed and that the NAAQSs were consistent with current knowledge. To my knowledge, this requirement for mandatory review every 5 years is unique to the setting of the NAAQS in the United States. Indeed, I know of no other statute calling for an updating of the science and reconsideration of the Standard every 5 years.

Peer review of the earliest criteria documents prepared by the EPA was carried out by various committees of the agency's Science Advisory Board. The 1977 amendments to the CAA institutionalized the peer-review process for the NAAQS [16]. The amendment requires the EPA Administrator to appoint an independent scientific committee, composed of seven members, including at least one member of the National Academy of Sciences, one physician, and one person representing state air pollution control agencies to advise the Administrator on the science informing the policy judgments made in setting the NAAQS. The EPA has implemented this provision of the CAA by appointing a Committee, which designated itself as the Clean Air Scientific Advisory Committee (CASAC). The CASAC is directly responsible to the EPA Administrator, although it functions administratively as one of the standing committees of the

EPA Science Advisory Board. Traditionally, the requirement for one CASAC member to be a member of the National Academy of Sciences has been broadly interpreted to also include membership in either the National Academy of Engineering or the Institute of Medicine. To complement the expertise of regular members of the CASAC, a number of consultants, sometimes as many as a dozen, with specialized expertise usually have been added to the review panels for specific pollutants.

The CAA was amended again in 1990 [17]. Although major changes were made in the CAA with these amendments, especially with regard to the regulation of hazardous air pollutants, there were no changes in the fundamental approach to dealing with the setting of NAAQS for criteria pollutants. However, there were changes in the CAA that have had major impact on the regulation of emissions of PM and precursors especially from large power plants.

The pollutants originally designated as "criteria pollutants" because of their ubiquitous distribution and potential to endanger health were photochemical oxidants (later regulated as ozone), particulate matter (later regulated as Total Suspended Particulates, then PM_{10}, and $PM_{2.5}$), carbon monoxide, sulfur oxides (regulated as sulfur dioxide), nitrogen oxides (regulated as NO_2), and non-methane hydrocarbons (later dropped as a criteria pollutant). The EPA [64] established NAAQS for these pollutants soon after the Agency was created using existing scientific documentation, that is, criteria. The original NAAQS set in 1971 are shown in Table 3. As I will discuss below, the EPA later added Lead as a criteria pollutant with legal prodding from the National Resources Defense Council [49, 72].

US Process for Setting National Ambient Air Quality Standards

The process for developing and issuing NAAQS after the initial NAAQS were set is quite complex as discussed by Bachmann [7] and McClellan [36, 37, 39, 41]. Key elements of the process, as used until quite recently, include preparation and review of (a) criteria document, (b) staff paper, (c) more recently a risk assessment, and (d) a regulatory decision package leading to the Administrator's policy judgment decisions as to the proposed and final NAAQS which are

Air Quality Guidelines and Standards. Table 3 Primary and secondary National Ambient Air Quality Standards initially set by the US Environmental Protection Agency in 1971[a]

Pollutant (indicator)[b]	Level	Averaging time	Form[b]
PM (total suspended particulates)	75 μg/m^3	Annual	Geometric mean
	260 μg/m^3	24 h	Not to be exceeded more than once per year
TSP secondary standard	150 μg/m^3	24 h	Not to be exceeded more than once per year
SO_2	0.03 ppm	Annual	Arithmetic mean
	0.14 ppm	24 h	Not to be exceeded more than once per year
SO_2 secondary standards	60 μg/m^3 (0.02 ppm)	Annual	Arithmetic mean
	1,300 μg/m^3 (0.5 ppm)	3 h	Not to be exceeded more than once per year
CO	10 μg/m^3 (9 ppm)	8 h	Not to be exceeded more than once per year
	40 μg/m^3 (35 ppm)	1 h	Not to be exceeded more than once per year
Photochemical oxidants (as O_3)	200 μg/m^3 (0.08 ppm)	1 h	Not to be exceeded more than once per year
HC	160 μg/m^3 (0.24 ppm)	3 h, 6–9 a.m.	Not to be exceeded more than once per year
NO_2	100 μg/m^3 (0.053 ppm)	Annual	Arithmetic mean

[a]With the exception of PM and SO_2, secondary NAAQS set identical to the primary standards
[b]The terms "indicator" and "form" were not used in the 1971 notice

published in the Federal Register. Traditionally, CASAC focused its attention on reviewing the Criteria Documents and Staff Papers and, more recently, a formal Risk Assessment. As an aside, the process was changed at the end of 2006 [51] with an Integrated Science Assessment and Policy Assessment Document replacing the Criteria Document and Staff Paper. Time will tell if these changes really improve the overall process.

In addition to the documents noted above, the Agency now prepares a Regulatory Impact Analysis which is required under Executive Order 12866 issued by President Clinton [18] that applies to economically significant rules that have "an annual effect on the economy of $100 million or more or adversely effect in a material way the economy, a sector of the economy, productivity, competition, jobs, the environment, public health or safety or site, local, or tribal governments or communities." The results of the Regulatory Impact Analysis are not considered during the NAAQS rulemaking process given the prohibition of consideration of cost in the setting of the NAAQS [93].

It is important to recognize that the NAAQS process in the United States started as an informal rulemaking process [7, 41, 52]. The DC Court of Appeals found that the informal process was not sufficiently well documented with regard to the four key elements (indicator, averaging time, concentration, and statistical form) that the Court could perform a judicial review of the rules that were promulgated. This resulted in a judicial decision to overturn the secondary SO_2 NAAQS in 1973 [10]. This in turn led the US Environmental Protection Agency to develop more rigorous procedures including formal documentation [52].

Bachmann [7] summarized the adoption of these procedures in the late 1970s noting the following points: "(1) EPA was to make available to the public the information and technical methodologies it relied upon by the time of proposal; (2) the preambles to proposal and final rules were to provide a detailed explanation of EPA's decision; (3) EPA was required to respond to all "significant" comments on the proposal by the time it issues its final rule; and (4) all of the above documents, analyses, preambles, and responses constituted the record that the court would examine in reviewing the final standard decision. Objections not raised in the record could not be raised in court. The halcyon days of a speedy NAAQS process were over." I agree that the speed of the process was reduced, however, I would add that transparency of the process was also substantially improved. Congress apparently agreed and these provisions were substantially codified by the CAA Amendments of 1977 [16].

EPA's implementation of the CAA, especially its setting of NAAQS even with improved documentation, has been a matter of continuing controversy and litigation. Some persons might note that controversy and litigation were enhanced by improved documentation. Bachmann [7] summarizes many of the key legal cases in his review. In this entry, I will only highlight several key legal cases. The 1997 revisions of the Ozone NAAQS [65] and Particulate Matter NAAQS [66] proved to be very contentious including within CASAC. For example, the members of the CASAC PM Panel, chaired by George Wolff, had a range of views on the $PM_{2.5}$ standard that was being set for the first time replacing, in part, the PM_{10} standard. This range of views was clearly articulated in the CASAC Chair's letter [97] to the Administrator by including a Table showing the views of each individual member of the CASAC Panel. This approach stands in stark contrast to the approach of more recent CASAC Panels that have emphasized consensus advice.

The contentious nature of the debate over these revised NAAQS prompted Administrator Browner to involve President Clinton. Bachmann [7] recounts that Administrator Browner had a 1-h meeting on these standards with the President – "she reported that the President quickly accepted her decision and spent much of the time discussing how to reduce unnecessary burdens in the implementation process. This resulted in some of us writing the first draft of a letter that was later sent by President Clinton [19] to EPA directing implementation be carried out so as to "maximize common sense, flexibility, and cost effectiveness." Not surprisingly, President Clinton [46] had a role in announcing the tighter standards which included for the first time a separate $PM_{2.5}$ standard to complement the PM_{10} standard and a shift from a 1-h averaging time to an 8-h averaging time standard for Ozone.

The issuance of a revised PM NAAQS triggered the legal case of *American Trucking Associations* v. *EPA* [4]. The Court found "the growing empirical evidence demonstrating a relationship between fine particle

pollution and adverse health effects amply justifies establishment of new fine particulate standards." The Court went on to find "ample support" for EPA's decision to regulate coarse particulate pollution, but vacated the 1997 PM_{10} standards, concluding in part that PM_{10} is a "poorly matched indicator for coarse particulate pollution" because it includes fine particulates. Subsequently, EPA removed the vacated 1997 PM_{10} standard allowing the 1987 PM_{10} standard to remain in place along with the new $PM_{2.5}$ issued in 1997.

In addition, the three-judge panel held, two to one, that EPA's approach to setting the level of the PM and Ozone standards in 1997 effected "an unconstitutional delegation of legislative authority." The Panel found that "the factors EPA uses in determining the degree of public health concern associated with different levels of ozone and particulate matter are reasonable." However, it remanded the rule to EPA. The Judicial Panel stated that when the Agency considers these factors for potential non-threshold pollutants "what EPA lacks is any determinate criterion for drawing lines" to determine the level at which the standards should be set. The Panel also found that the Administrator, under the CAA, is not permitted to consider the cost of implementing these standards in setting them.

Not surprisingly, the nature of the Circuit Court opinion resulted in cross appeals being filed on the several issues and the involvement of the US Supreme Court. The Supreme Court in February 2001 issued a unanimous opinion upholding EPA's position on both the constitutional and cost issues [93]. On the constitutional issue, the Supreme Court held that the statutory requirement that the NAAQS be "requisite" to protect public health with an adequate margin of safety sufficiently guided EPA's discretion, affirming EPA's approach of setting standards that are neither more nor less stringent than necessary.

Supreme Court Justice Breyer, who participated in the *Whitman* v. *American Trucking Associations* case, is well known and highly regarded for his opinions and writings on risk assessment [11, 12]. Thus, it is not surprising that he took the opportunity in *Whitman* v. *American Trucking Associations* [93] to offer comments on the standard-setting process and, specifically, the identification of the level of the NAAQS and the associated level of health risk. While concurring that EPA cannot consider the costs of implementing the Standards, he went on to note – "this interpretation of §109 does not require the EPA to eliminate every health risk, however slight, at any economic cost, however great, to the point of "hurtling" industry over "the brink of ruin," or even forcing "deindustrialization." (Id. At 494) (Breyer, J., concurring in part and concurring in judgment) (citations omitted). Rather, as Justice Breyer explained:

- The statute, by its express terms, does not compel the elimination of all risk; and it grants the Administrator sufficient flexibility to avoid setting ambient air quality standards ruinous to industry.

  Section 109(b)(1) directs the Administrator to set standards that are "requisite to protect the public health" with "an adequate margin of safety." But these words do not describe a world that is free of all risk – an impossible and undesirable objective (citation omitted). Nor are the words "requisite" and "public health" to be understood independent of context. We consider football equipment "safe" even if its use entails a level of risk that would make drinking water "unsafe" for consumption. And what counts as "requisite" to protecting the public health will similarly vary with background circumstances, such as the public's ordinary tolerance of the particular health risk in the particular context at issue. The Administrator can consider such background circumstances when "deciding what risks are acceptable in the world in which we live." (Citation omitted).

  The statute also permits the Administrator to take account of comparative health risks. That is to say, she may consider whether a proposed rule promotes safety overall. A rule likely to cause more harm to health than it prevents is not a rule that is "requisite to protect the public health." For example, as the Court of Appeals held and the parties do not contest, the Administrator has the authority to determine to what extent possible health risks stemming from reductions in tropospheric ozone (which, it is claimed, helps prevent cataracts and skin cancer) should be taken into account in setting the ambient air quality standard for ozone. (Citation omitted).

  The statute ultimately specifies that the standard set must be "requisite to protect the public health" "in the judgment of the Administrator," §109(b)(1), 84 Stat. 1680 (emphasis added), a phrase that grants the Administrator considerable discretionary standard-setting authority.

> The statute's words, then, authorize the Administrator to consider the severity of a pollutant's potential adverse health effects, the number of those likely to be affected, the distribution of the adverse effects, and the uncertainties surrounding each estimate (citation omitted). They permit the Administrator to take account of comparative health consequences. They allow her to take account of context when determining the acceptability of small risks to health. And they give her considerable discretion when she does so.
>
> The discretion would seem sufficient to avoid the extreme results that some of the industry parties fear. After all, the EPA, in setting standards that "protect the public health" with "an adequate margin of safety," retains discretionary authority to avoid regulating risks that it reasonably concludes are trivial in context. Nor need regulation lead to deindustrialization. Preindustrial society was not a very healthy society; hence a standard demanding the return of the Stone Age would not prove "requisite to protect the public health."
>
> Although I rely more heavily than does the Court upon legislative history and alternative sources of statutory flexibility. I reach the same ultimate conclusion, Section 109 does not delegate to the EPA authority to base the National Ambient Air Quality Standards, in whole or in part, upon the economic costs of compliance.

The case of *Whitman* v. *American Trucking Associations* [93] is widely cited for the conclusion that EPA cannot consider the economic costs of compliance in the setting of NAAQS. Unfortunately, in my opinion, insufficient attention is given to the thoughtful guidance of Justice Breyer on exercising policy judgment informed by science in deciding on an acceptable level of health risk, a judgment that in turn determines the level and statistical form of each NAAQS. It is interesting that Justice Breyer's opinion appeared in Administrator Johnson's notice of the Ozone NAAQS [81], but did not appear in Administrator Jackson's "reconsideration" proposal for Ozone [85] that will be discussed later.

Paradigm Shift

At this juncture, it is appropriate to note that it is my view that a paradigm shift has taken place in the selection of the level of each NAAQS over the past four decades. In my opinion, the paradigm shift has been driven in part by the changing nature of the scientific evidence of pollution effects. In the 1970s, most scientists and regulations viewed the criteria pollutants as having a threshold in their ambient concentration-response relationship, sometimes referred to as a hockey stick function [36, 39]. In contrast cancer-causing agents have been assumed to have linear, non-threshold, concentration-response relationships.

In the late 1960s and early 1970s, the available data on each criteria pollutant were quite modest, with attention focusing on only a few epidemiological studies. For those few studies, attention often focused on whether a relative risk on the order of 2.0 was statistically significant or not. For a given pollutant there were few, if any, controlled human exposure studies. The data from laboratory animal studies with specific pollutants had frequently been acquired in studies with exposure concentrations much higher than ambient concentrations of the pollutants. The results of these studies raised questions about extrapolation both from laboratory animals to humans and high to low exposure concentrations. The general approach taken was to identify the lowest levels where effects were statistically significant and assume this was the inflection point in the concentration-response relationship. It could be argued that setting the Standard at a lower concentration satisfied the requirement for "an adequate margin of safety."

In contrast, the most recent reviews have involved thousands of papers with observations ranging from human population level to studies of intact laboratory animals to studies of effects of air pollutants on cells and molecules. Despite the huge number of published studies, attention has ultimately focused on the results of a few studies where attention turns to the critical issue of how they inform the setting of the level and statistical form of the standard. In the epidemiological studies, the debate often focuses on whether relative risks of less than 1.1 for excess morbidity and mortality are significant. Of course, the specific relative number is dependent on the denominator being used, for example, per 10 ppb of ozone (24-h average). For controlled exposure clinical studies, attention has focused on the lowest levels with statistically significant changes, which in turn, triggers debate over whether the changes are adverse.

A news report [63] in Science that I view as a classic report highlighted the issues involved in the search for subtle links between diet, lifestyle, or environmental factors and disease, especially using retrospective observational studies. I especially liked the quote at the end attributed to Sander Greenland, a well-known epidemiologist, in offering advice to his "most sensible, level-headed, estimatable colleagues." Remember, he says – "there is nothing sinful about going out and getting evidence, like asking people how much do you drink and checking breast cancer records. There's nothing sinful about seeing if that evidence correlates. There's nothing sinful about checking for confounding variables. The sin comes in believing a casual hypothesis is true because your study came up with a positive result, or believing the opposite because your study was negative."

It is interesting to note that CASAC discussions of criteria pollutant effects have frequently focused initially on the level of the standard sometimes devoid of any consideration of the statistical form of the level. This approach was in keeping with traditional practice in the setting of standards such as Threshold Limit Values for occupational exposures to chemicals based on scientific judgments [34–36, 40]. That approach has involved a review of the available human data on a toxic chemical to determine a no-observed effect level, or the lowest observed effect level, and then using safety factors to arrive at an acceptable exposure level set at a lower level. In the absence of adequate human data, laboratory animal data are used and an additional safety factor used to account for the potential that the animal observations might not adequately predict human effects. This approach was routinely used for a wide range of health responses that were assumed to have an exposure-response relationship that exhibited either a true or practical threshold, an excess of effects above some level and an absence of effects below that level. A review of the earliest Criteria Documents and, indeed, also the Staff Papers, documents that a similar line of reasoning was used in the setting of the NAAQS.

The implementation of standards set with this approach soon revealed that if the standard was to be rigorously enforced, that is, no exceedances of the specific level of the standard, the practical effect would be to cause average levels of the pollutant to be reduced to levels far below the standard so as to avoid the occasional high value exceeding the standard. Fortunately, common sense prevailed and the EPA, over time, moved to the practice of routinely linking the specific level of the standard with a statistical form such as the 98th percentile 24-h concentration averaged over 3 years or the fourth highest 8-h average concentration during a 3-year period. In my opinion, most of the attention of the CASAC in the NAAQS setting process has focused on the level of the standard with limited discussion of the statistical form of the Standard. In doing so, there has been a failure to recognize that the stringency of the standard and the degree of health protection provided depends on *both* the level and statistical form of the standard for a particular indicator and averaging time.

The challenges of selecting appropriate averaging times and statistical forms for the NAAQS are substantial. The original epidemiological and toxicological studies that provide the scientific information that should inform the setting of the NAAQS do not always report results with an averaging time that is the same as that ultimately selected for the Standard. Hence, the need to make extrapolations from results reported based on one metric, such as average daily exposure to a second metric such as an 8-h averaging time. The setting of standards at extreme values, the 98th percentile for NO_2 [86] or, even the 99th percentile form as done with the 1-h averaging time standard for SO_2 [87], results in extremely stringent standards that at best are only very loosely related to the underlying data. In my view, selection of the specific level and statistical form for a specific averaging time is clearly policy judgments beyond the dominion of the science. It is my opinion that decisions on the selection of specific averaging times are ultimately policy judgments reserved to the Administrator by the language of the CAA.

In the 1990s, concurrent with the increasingly widespread use of formal risk analysis procedures across society [35, 40], EPA moved to quantify the health benefits associated with setting the NAAQS at various levels, with an associated statistical form. I must admit to being an early advocate of formal quantification of health benefits. I viewed the approach then and I still do today, as providing useful guidance for making policy decisions. I did not envision that some enthusiastic

advocates of quantitative risk analysis would actually view the results of the analyses as being highly accurate projections of potential health benefits expressed to two or more significant figures, sometimes without any indication of uncertainty.

The quantification of health effects potentially associated with various levels and forms of the Standards requires several kinds of input. Examples are the risk assessments conducted by the USEPA for particulate matter [69], ozone [77, 78, 79] and sulfur dioxide [83]. Guidance has also been provided by the US National Research Council [48]. First and foremost, conduct of a risk assessment requires some knowledge of the nature of the ambient concentration-response relationships for various temporal metrics for the pollutant in question. Typically, the response term is expressed as excess risk per unit of increased concentration over some range of ambient concentrations. The question then becomes one of whether the relationship is linear and whether there is a threshold level below which the coefficient for excess risk holds or does not hold. The issue of whether there are or are not thresholds for non-cancer health endpoints from exposure to many agents is very contentious [56, 92]. It is well recognized that the use of linear no-threshold exposure-response relationships for cancer-causing agents is closely linked to experience with radiation [47]. An additional issue becomes the selection of suitable reference baseline statistics for the particular health effects to use along with a given ambient concentration-response coefficient. Yet another question becomes the appropriate population to be evaluated, a single city, multiple cities, or the population of the United States. It is obvious that there are substantial uncertainties associated with each component of the analysis of benefits of potential reductions in a given pollutant.

With the use of linear, no-threshold, ambient concentration-response models, the EPA has, on some occasions, calculated estimated excess morbidity and mortality effects attributable to the specific pollutant down to background concentrations. The Health Risk Assessment [77] and the Regulatory Impact Analysis [82] for the 2008 Ozone NAAQS [81] serve as examples. Further, dependent on the assumptions made with regard to how ambient concentrations of the pollutant would change in response to various levels and forms of the standard, substantial health effects avoided, that is, health benefits can be calculated. Expressing the benefits in monetary units raises some critical issues. Typically, mortality effects drive the monetized benefits calculations because of the substantial value placed on deaths avoided. Sunstein [61] has addressed this contentious issue and has argued that years of life loss is a more appropriate metric than is the use of lives lost as is the typical approach used by the USEPA.

A key consideration as to whether these benefits can be realized relates to whether the roll-back in air concentrations that is assumed in the analysis as a result of the new standard can actually be realized. In part, this relates to how realistic the assumptions have been with regard to background levels. The analysis of benefits of reducing a given pollutant, say Ozone, becomes even more convoluted when the analysis includes postulated reductions in a second pollutant, such as particulate matter, associated with achieving the Ozone Standard. A discussion of this issue for Ozone can be found in McClellan et al. [43]. Indeed, as the levels of the standards are ratchetted down toward background levels, there is increasing uncertainty as to whether there are any health effects attributable to single pollutants and even greater uncertainty as to the magnitude of the health benefits associated with any new lower standard. The use of single pollutant models for estimating benefits raises the issue of double-counting of benefits as the benefits of the individual pollutants are aggregated.

Hence, the paradigm shift. It is apparent that in setting the earliest NAAQS some individuals, including CASAC members, envisioned that the standards were being set at levels protective of public health with an adequate margin of safety based on threshold ambient concentration-response models. In short, if there were health effects at the level and form of the NAAQS, they were de minimis. It is useful to recall the Editorial by Kennedy [27]. In contrast, more recent NAAQS have been set at levels which both the CASAC and EPA characterize as having residual health effects even if the standard were to be attained. The central question remains – how low is low enough? I view the answer as a policy judgment informed by science that can only be made by the EPA Administrator [41].

WHO Process for Setting Air Quality Guidelines

The approach taken by the World Health Organization (WHO) contrasts with the USEPA approach. WHO was established in 1948 as a specialized Agency of the United Nations to be the directing and coordinating authority for international health matters and public health. WHO develops air quality guidelines (AQG) designed to offer guidance in reducing the health impacts of air pollution. The first AQG were produced in 1987 [94]. Updates were published in 2000 and 2005 [95, 96]. The AQG are intended to inform policymakers and to provide appropriate targets for a broad range of policy options for air quality management in different parts of the world, despite the more recent documents being titled AQG for Europe.

The WHO AQGs are developed by working groups of scientific experts [95, 96]. In addition to preparing AQG for the classical air pollutants (Particulate matter, Ozone, Nitrogen dioxide, and Sulfur dioxide) the WHO also developed AQG for (a) inorganic air pollutants, (b) certain indoor air pollutants, (c) polychlorinated biphenyls, dioxins, and furans, and (d) volatile organic compounds. The WHO AQG process does not include any opportunity for the involvement of interested parties such as the public, national governments, nongovernmental organizations, or industry. They represent expert judgment exercised by scientists knowledgeable of the subject material. This approach contrasts sharply with the more formal and complex approach followed by the US Environmental Protection Agency in developing NAAQS.

The primary aim [95] of the AQG is "to provide a uniform basis for the protection of public health and ecosystems from adverse effects of air pollution and to eliminate or reduce to a minimum exposure to those pollutants that are known or likely to be hazardous." "They have the character of recommendations, and it is not intended or recommended that they simply be adopted as standards." The WHO [95] report notes:

- In the process of moving from a "guideline" or a "guideline value" to a "standard," a number of factors beyond the exposure-response relationship need to be taken into account. These factors include current concentrations of pollutants and exposure levels of a population, the specific mixture of air pollutants, and the specific social, economic and cultural conditions encountered. In addition, the standard-setting procedure may be influenced by the likelihood of implementing the standard. These considerations may lead to a standard above or below the respective guideline value.

Assessing Hazards and Risks

The risk approach used around the world today (Fig. 2) developed within the USEPA in parallel with the process for setting NAAQS [35, 36, 38, 39]. The setting of air quality standards and guidelines may be viewed as a specialized use of the risk characterization paradigm illustrated in Fig. 2 [35]. In particular, the establishment of air quality standards and guidelines draws on the schematic rendering in the box labeled "risk assessment." An initial step in that process is to determine the hazard potential of the agent, in short, to determinewhether the specific agent has the potential for causing adverse health effects in humans. In the case of the criteria or common air pollutants discussed in this entry, there is sufficient evidence to establish that with exposure of sufficient duration and concentration the agent is capable of causing disease in people, based on epidemiological evidence. The key issue then becomes the nature of the relationship between ambient concentrations and duration of exposure and increased disease. The specific characteristics of that complex relationship are crucial to determining for a particular ambient concentration the estimated health impacts including the ambient concentration level. Moreover, the same information is required if one is to estimate the health benefits associated with a postulated improvement in air quality, that is, reductions in ambient concentrations.

Sources of Information for Setting Standards and Guidelines

The multiple sources of information for evaluating the potential health effects of any air pollutant are illustrated in Fig. 6 [35–39, 41]. In the case of all the criteria air pollutants, the dominant sources of information are those based on the study of humans, the left side arm of the figure. However, all of the common air pollutants have been viewed as being sufficiently innocuous, and

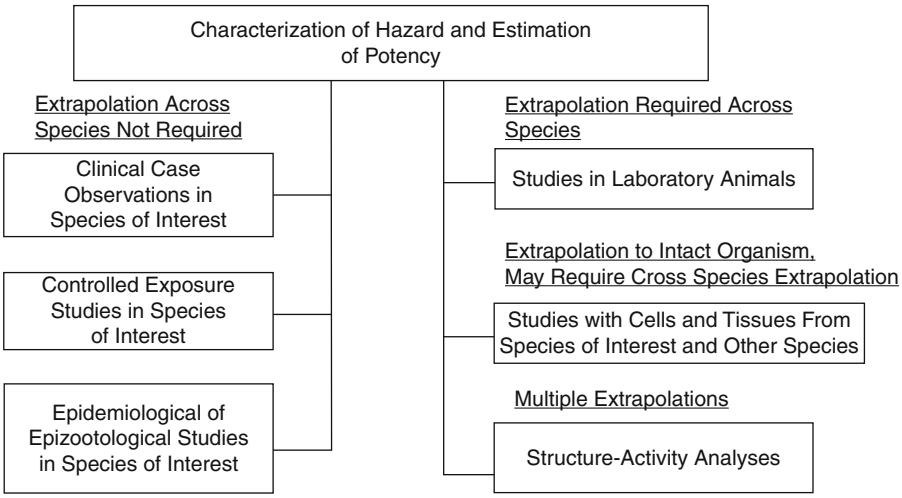

Air Quality Guidelines and Standards. Figure 6
Sources of information for evaluating potential health effects

with effects that are readily reversible when exposures are discontinued, that controlled human exposure studies can be conducted with the pollutant. Such studies have provided very useful information on short-term exposures, typically a few hours in duration as will be discussed later for ozone. A limitation of such studies is the appropriate requirement for the conduct of such studies only in healthy adults or individuals with modest preexisting disease. Controlled exposure studies in individuals with serious preexisting disease would not be ethical. The paramount advantage of controlled human exposure studies is that the exposures can be well characterized unlike the situation for field studies or epidemiological studies.

For some of the common air pollutants, valuable data on shorter-term exposures have been acquired from field studies of individuals exposed to ambient concentrations of pollutants. In these studies, the investigators can obviously only study air concentrations that are present and the extent they can be characterized and then relate the ambient concentrations to one or more health indices such as changes in lung function.

The predominant source of information on the health effects of the common air pollutants has been from epidemiological studies. It is beyond the scope of this entry to discuss the conduct and results of those studies in detail. The reader interested in more detail will find the textbook on Environmental Medicine edited by Ayres et al. [6] useful. Suffice it to note that most epidemiological studies of air pollution are a kind of cohort study or a time-series study. None of the studies are strict cohort studies in which a population is randomly assigned to one or more treatment groups. This is rarely possible in studying air pollution. Investigators are constrained to studying populations under natural conditions of ambient exposure and other risk factors associated with the natural course of life. The study that may come closest to the ideal cohort study is the Six-City Study [20, 23] which will be discussed later. In such a study, the investigators may use regulatory compliance monitoring data supplemented by research monitoring to characterize ambient air concentrations of the various pollutants. Health outcomes information may be obtained by contact with the enrollees supplemented by information acquired from Administrative databases such as records of deaths. Other studies such as those using the ACS populations, for example, Pope et al. [54] are totally dependent upon regulatory compliance modeling and administrative databases for health outcomes. As might be expected, the quality of these studies is dependent upon the quantity and quality of the monitoring data, the availability of data on other risk factors, the duration of follow-up, the quality of the health outcome data, and the rigor of the analyses.

A second type of study design is that used in the time-series studies as pioneered by the Johns Hopkins University investigators in the National Morbidity and Mortality Air Pollution Studies (NMMAPS). These studies utilize regulatory compliance monitoring data to characterize ambient concentrations of pollutants and administrative databases for morbidity and mortality. These studies seek to characterize the relationship between ambient concentrations on a given day or series of days and excess morbidity or mortality occurring concurrently or on subsequent days. An example is the study of Bell et al. [8, 9] and Smith et al. [58] that will be discussed later. An advantage is that it is assumed that many other risk factors that may be influencing the health of the population is not varying on a day-to-day basis, for example, socioeconomic status. Other factors such as temperature may vary along with pollution levels.

In the next section, information on the health effects of particulate matter and ozone will be briefly reviewed as examples of the kind of information used in setting NAAQS. In this section I draw heavily on a previous review of risk assessment/risk management [40].

Particulate Matter as an Example

The Particulate Matter (PM) NAAQS was initially set in 1971 using Total Suspended Particulate (TSP) Matter as an indicator [36, 37, 39, 42, 64]. Later, the standard was revised with the TSP indicator replaced by PM_{10}. PM_{10} is defined as the size fraction collected using a device that includes 50% of the particle with an aerodynamic diameter of 10 μm. A progressively smaller fraction of PM mass is collected as the particle size increases above 10 μm and a progressively larger fraction of PM mass is sampled as particle size decreases below 10 μm. Later, the standard was again changed with $PM_{2.5}$ introduced as an indicator to complement the PM_{10} indicator. $PM_{2.5}$, the fine particle fraction indicator is defined as for PM_{10} indicator with a 50% cut point at 2.5 μm aerodynamic diameter. To state the obvious, the $PM_{2.5}$ fraction is contained within the PM_{10} fraction which is contained within the TSP sample. In recent years, increased attention has been focused on the ultrafine particle number which is contained within the $PM_{2.5}$ size range. There has also been interest in characterizing health effects of the $PM_{10-2.5}$ fraction which has been called the course particle fraction. Consideration is given to regulating this fraction with a separate NAAQS.

A detailed review of the evidence for health effects of PM is beyond the scope of this entry. Suffice it to say, abundant data are available on the health effects of PM, characterized using different PM indicators, from epidemiological and laboratory animal studies using a range of indicators of morbidity and mortality [65, 68, 84]. In setting the PM standards, the greatest weight, appropriately, has been given to the epidemiological evidence and, specifically, to those studies which can provide quantitative exposure-response information.

Two large studies have yielded especially valuable information that has played a key role in the setting of the PM NAAQS using the PM_{10} and $PM_{2.5}$ indicators. The first of these is the Harvard Six Cities study designed by Ferris and colleagues [20, 23] to specifically evaluate the health effects of criteria air pollutants. In my opinion, this is one of the best studies ever conducted of the influence of air quality on health. It involves a 14–16-year follow-up of 8,000 subjects living in six communities in the United States selected to provide a gradient in several indices of air quality. Extensive efforts were made to characterize air quality. A second air quality study made opportunistic use of data from a population of 500,000 individuals who self-enrolled in 1982–1989 in an American Cancer Society Study [54]. A subgroup of 240,000 of these individuals lived in 50 metropolitan areas in which $PM_{2.5}$ measurements were made for regulatory compliance purposes.

The vast amount of information available from the Six Cities and ACS studies has been reviewed by the EPA [68, 70, 84]. Selected data will be presented here to illustrate some of the key results that have influenced the setting of the PM NAAQS. Figure 7 summarizes an impressive array of information from the ACS study on all-cause mortality, cardiopulmonary mortality, lung cancer mortality, and all other cause mortality [54]. With control for smoking, education, and national status, the controlled forward stepwise inclusion of additional covariants had little influence on the estimated associations between fine particulate ($PM_{2.5}$ indicator) air pollution on cardiopulmonary and lung cancer mortality. As may be noted, the inclusion of

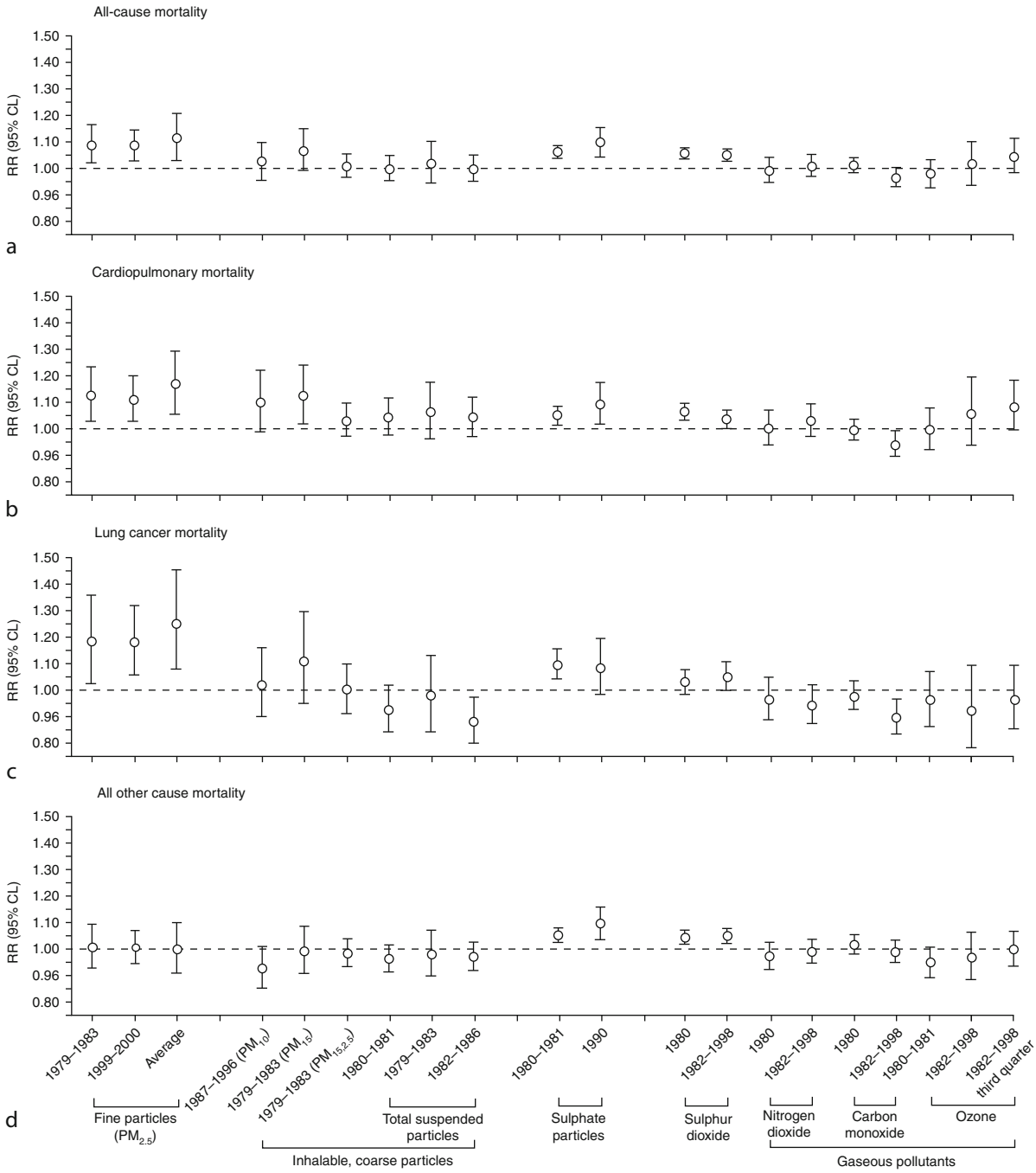

Air Quality Guidelines and Standards. Figure 7

Relative risk (RR) ratio for adjusted mortality evaluated at subject-weighted mean concentrations. *CI* confidence interval, $PM_{2.5}$ particles measuring less than 2.5 μm in diameter, PM_{10} particles measuring less than 10 μm in diameter, PM_{15} particles measuring less than 15 μm in diameter, $PM_{2.5-15}$ particles measuring between 2.5 and 15 μm in diameter (Adapted from Pope et al. with permission)

cigarette smoking attenuated the estimated relative risk of $PM_{2.5}$, which is not surprising. When this is done it is necessary to normalize the smoking history to pack-years, for example, 1 pack/day for 25 years or 2 packs/day for 12.5 years equals 25 pack-years. The relative risks for an average current smoker (men and women combined, 22 cigarettes per day for 33.5 years with smoking initiated before age 18 years) (equivalent to 37 pack-years) were equal to 2.58, 2.89, and 14.80 for all-cause, cardiopulmonary, and lung cancer mortality, respectively. The magnitude of these relative risks is substantially greater than that of $PM_{2.5}$ and emphasizes the critical importance of considering cigarette smoking in any study of air pollution. Moreover, it is important that investigators follow the lead of the ACS investigators and report the results of the analyses done for cigarette smoking at the same time they report relative risks for various air pollutants. These results on cigarette smoking provide valuable perspective for considering the results of analyses for the various air pollution indicators. A comparison of the relative risk estimates they obtain for smokers with those of other investigators serves as a "reality check" on their analyses.

The results from the Six Cities study and ACS-based studies are generally similar [28, 53]. Summary information from the two studies is given in Table 4 with a comparison made of the risk ratios for the most polluted versus least polluted cities. For comparison, results are also shown for typical smokers. Note that in this case the typical smoker has been defined as about a 25 pack-year smoker, about two thirds that of the current smoker discussed earlier for the ACS study. Interestingly, the relative risk, for example, for lung cancer mortality is about two thirds of the value cited earlier, 9.73 versus 14.80. The range of the confidence intervals for the association between $PM_{2.5}$ and cardiopulmonary mortality, even for these studies with thousands of subjects, emphasizes the challenges faced in teasing out small effects of air pollution in developed countries.

Laden et al. [29] extended the observations for the Six Cities Study Cohort by including deaths for 1990–1998 and compared those observations to the earlier time period (1974–1984) and for the entire period. The estimated city-specific average $PM_{2.5}$ levels were lower in the extended follow-up period in the 1990s than in 1974–1989 and the mortality risk ratios were lower.

A critical issue in interpreting the data shown in Fig. 8 is the nature of the exposure-response relationship. It must be noted that this is the ambient concentration for PM that is being evaluated for an association, not PM exposure. The PM exposure cannot be evaluated since the estimated indoor PM concentrations cannot even be estimated. Pope et al. [54], using the ACS cohort data, evaluated the nonparametric smoothed exposure-response relationships between cause-specific and average $PM_{2.5}$ (Fig. 8) [54]. They observed that the log-relative risk for all-cause, cardiopulmonary, and lung cancer mortality increased across the gradient of $PM_{2.5}$ concentrations. Goodness-of-fit tests indicated that the associations were not significantly different from linear associations. The mean concentration of $PM_{2.5}$ across the ACS cohort was 14 $\mu g/m^3$.

Air Quality Guidelines and Standards. Table 4 Comparison of mortality risk ratios (and 95% C.I.) for smoking and air pollution from the six cities and American Chemical Society (ACS) Prospective Cohort Studies

	Current smoker[a]		Particulate air pollution (most vs least polluted city)		
Cause of death	Six cities	ACS	Six cities ($PM_{2.5}$)	ACS ($PM_{2.5}$)	ACS (504)
All	2.00 (1.51–2.65)	2.07 (1.75–2.43)	1.25 (1.08–1.47)	1.17 (1.09–1.26)	1.15 (1.09–1.22)
Cardiopulmonary	2.30 (1.56–3.41)	2.28 (1.79–2.91)	1.37 (1.11–1.68)	1.31 (1.17–1.46)	1.26 (1.16–1.37)
Lung cancer	8.00 (2.97–21.6)	9.73 (5.96–15.9)	1.37 (0.81–2.31)	1.03 (0.80–1.33)	1.36 (1.11–1.66)
All others	1.46 (0.89–2.39)	1.54 (1.19–1.99)	1.01 (0.79–1.30)	1.07 (0.92–1.24)	1.01 (0.92–1.11)

[a]Risk ratios for current cigarette smokers with approximately 25 pack-years (about average at enrollment for both studies) compared with never smokers

Source: Adapted from Pope and Dockery [53]

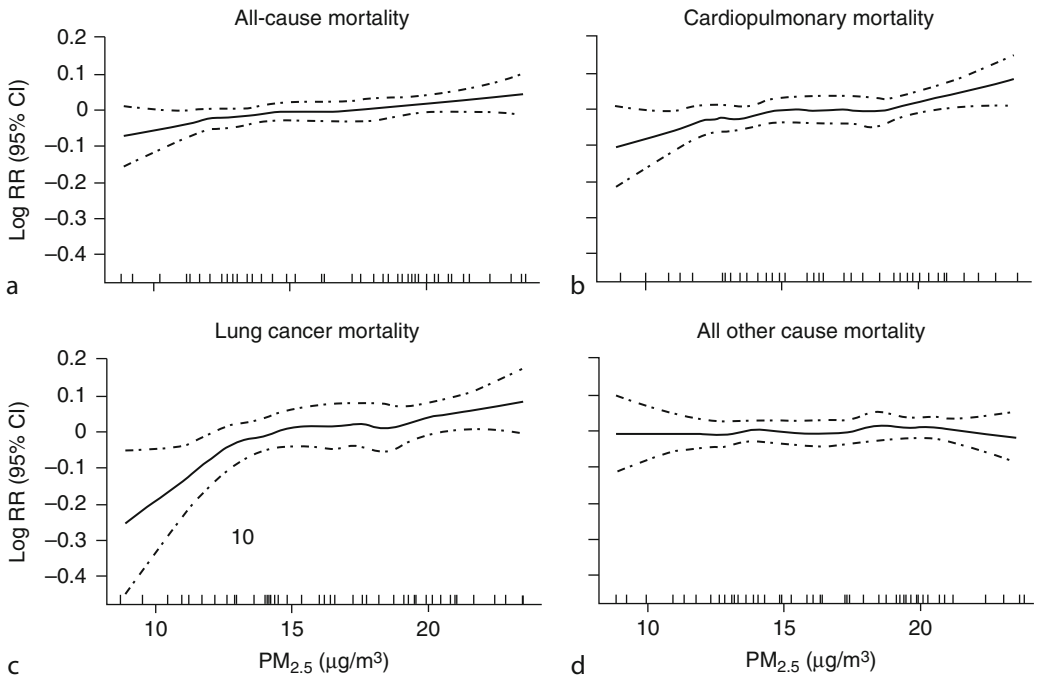

Air Quality Guidelines and Standards. Figure 8

Nonparametric smoothed exposure-response relationship. *Vertical lines* along the x-axes indicate a rug or frequency plot of mean fine particulate pollution. *CI* confidence interval, *$PM_{2.5}$*, fine particles measuring less than 2.5 μm in diameter, *RR* relative risk (Adapted from Pope et al. with permission)

Enstrom [22] evaluated the relationship between fine particulate air pollution and total mortality among nearly 50,000 elderly Californians for 1973–2002 using a subpopulation of the ACS enrollees. He concluded that the results did not support a current relationship between fine particulate pollution and total mortality, although he could not rule out a small effect, particularly before 1983. The 2006 EPA analysis used to revise the PM NAAQS interpreted the available epidemiological data as not clearly supporting or refuting the existence of a threshold. The EPA analysis did calculate added risks down to an assumed threshold of 7.5 μg/m^3; a level on the order of the ambient $PM_{2.5}$ concentrations found in many US cities.

While the estimated or excess risk for the various PM indicators are quite small, it is apparent that when used in company with standard baseline data for specific cities with populations measured in the millions, the calculated number of excess deaths appears large. The USEPA Administrator can consider such quantitative risk assessment results in making a "judgment call" in setting the standards. However, the Administrator is explicitly prohibited from considering cost when setting the standard. In separate regulatory impact analyses, the risk assessment results are monetized in economic analyses used to estimate the benefits associated with achieving a revised standard compared to maintaining an existing standard. The regulatory impact analysis prepared for ozone and particulate matter [67] and separately for particulate matter [76] and ozone [78] are examples.

Substantial controversy developed in the final stages of revision of the $PM_{2.5}$ standard announced in 2006. A majority of the EPA's Clean Air Scientific Advisory Committee's (CASAC) PM Panel recommended that the EPA Administrator reduce the $PM_{2.5}$ 24-h averaging time standard from the previous level of 65 μg/m^3 to a level in the range of 25–35 μg/m^3 and that for the $PM_{2.5}$ annual averaging time the standard be reduced from the previous level of 15 μg/m^3 to a level in the range of 12–14 μg/m^3. I was in the minority and argued that identifying a specific bright line, upper bound such

as 14 μg/m^3 was an issue that went beyond scientific interpretation of data and was a policy judgment as to acceptable risk. The Administrator, ultimately, revised the $PM_{2.5}$ NAAQS, 24-h averaging time standard, to 35 μg/m^3 and retained the annual standard at 15 μg/m^3 [74, 75]. Obviously, the majority of CASAC was not happy with the Administrator's policy judgment call.

Ozone

Ozone is an interesting air pollutant because it is not directly emitted from industrial sources except in rare circumstances. The majority of Ozone found in the ambient environment is formed from reactions of Volatile Organic Compounds (VOC) and Nitrogen Oxides (NO_x) in the presence of sunlight. The VOCs originate both from natural and industrial sources and the NO_x is largely from combustion of hydrocarbon fuels. Ozone concentrations typically have distinct diurnal cycles with the highest levels observed at mid-day and the lowest concentrations at night in the summer. Lower concentrations are typically observed in the winter than in the summer. This is the case because of the manner in which ozone is formed with sunlight driving the reactions between NO_x and VOCs.

To provide context for the discussion of the Ozone NAAQS it is important to understand the background levels of ambient ozone. A team of investigators at Harvard University led by Daniel Jacob have made major contributions to understanding tropospheric ambient ozone levels around the world using a global chemical transport model (GEOS-Chem). The Harvard team [90] reported the use of the GEOS-Chem model with 1° latitude by 1° longitude spatial resolution to quantify the effects of anthropogenic emissions from Canada, Mexico, and outside North America to estimate daily maximum 8-h average ozone concentrations in US surface air. Their simulations for summer 2001 estimated mean North American and US background contributions of 26 ± 8 ppb and 30 ± 8 ppb, as obtained by eliminating anthropogenic emissions in North America versus in the United States only. The background 8-h highest Ozone concentrations approached 60 ppb. The frequency distribution of the simulated daily 8-h-maximum surface Ozone concentrations are shown in Fig. 9. It is important to recognize that the statistical form of the Ozone NAAQS is directed at minimizing the occurrence of the highest ozone events, the right side tail of the distributions in the figure. The high levels of background Ozone will make it challenging to achieve any Ozone NAAQS set in the range of 60–80 ppb (8-h daily maximum).

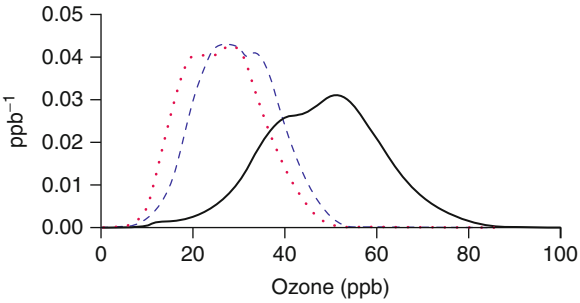

Air Quality Guidelines and Standards. Figure 9 Frequency distribution of the simulated daily 8-h-maximum surface ozone (*black solid line*). North American background (*red dotted line*) and US background (*blue dashed line*), for the contiguous United States during June–August 2001. The frequency distributions are constructed from the 1° × 1° daily model output (From [90])

The initial Ozone NAAQS in the United States was set in 1971 using photochemical oxidants as an indicator and with a 1-h averaging time [7, 64]. The standard was later revised with ozone as the indicator. Later the averaging time was changed from a 1-h maximum during a 24-h period to an 8-h rolling average maximum.

There is an abundant database on the health effects of ozone from epidemiological investigations and toxicity studies conducted in laboratory animals [38, 71, 80, 81]. In addition, there is a substantial amount of data acquired from studies conducted with human volunteers exposed to controlled levels of ozone for short periods of time. In the setting of the Ozone NAAQS, quantitative exposure-response data from human studies have been given the greatest weight. This is especially appropriate since there are well-established quantitative differences between laboratory animal species and humans in the disposition of inhaled ozone which minimize the utility of the data from laboratory animals for quantitatively estimating human risk of ozone exposures.

The effects of ozone on the respiratory tract are well known, thus it is not surprising that consideration of these effects has had a primary influence on the setting of the Ozone NAAQS. In the review culminating with a revised standard in March 2008, the information from pulmonary function evaluations conducted on young adult volunteers undergoing moderate exercise while exposed to various concentrations of ozone for 6.6 h played a prominent role. The key parameter evaluated, changes in the forced expiratory volume in 1 s (FEV_1), are shown in Fig. 10 [1–3, 13, 24, 26, 44, 45]. Data from individuals exposed to 0.08 ppm ozone and higher were considered in the previous review of the ozone standard. In the most recent review, data were available from the studies of Adams and colleagues [3] with 0.06 and 0.04 ppm exposures conducted to complement earlier studies conducted with 0.08 and 0.012 ppm, Adams [3] interpreted his studies as showing a statistically significant effect at 0.08 ppm, effectively reproducing the effects seen in earlier studies. However, he interpreted his studies at 0.06 and 0.04 ppm as not showing statistically significant changes compared to exposure to clean air. The USEPA reanalyzed the data of Adams and colleagues using different statistical procedures [13]. The USEPA reanalysis was included in the final compilation of information provided to the EPA Administrator to render a judgment on the revision of the Ozone NAAQS.

A key piece of information on the health effects of ozone came from the time-series study of Bell et al. [8, 9]. Their analysis used a 24-h averaging time and, thus, was not directly applicable to setting the Ozone NAAQS with an 8-h averaging time. Smith et al. [58] extended the analyses of Bell et al. [8] focusing on the development of city-specific ozone mortality estimates. The analyses of both Bell et al. [8] and Smith et al. [58] used the National Air Pollution Morbidity and Mortality air pollution database assembled at Johns Hopkins University. The results for the 8-h averaging time are shown in Fig. 11. The degree of intercity heterogeneity is noteworthy including recognition that only 5 cities of the 98 cities evaluated had statistically significant effects of ozone on acute mortality.

Smith et al. [58] called attention to this intercity heterogeneity across the United States (Fig. 12). The ozone effects are most striking in the Northeastern United States and absent in the Western United States including the Los Angeles Basin. It is not surprising that Smith et al. [58] caution against the use of national estimates of ozone concentration-response functions.

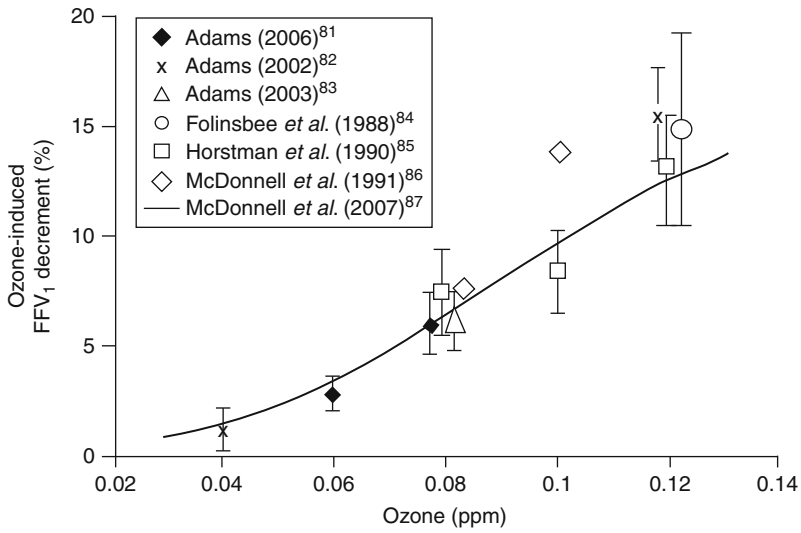

Air Quality Guidelines and Standards. Figure 10
Changes in the lung function of young health adults following a 6.6-h exposure to ozone. *FEV1* forced expiratory volume in 1 s, *ppm* parts per million (Adapted from Brown et al. with permission)

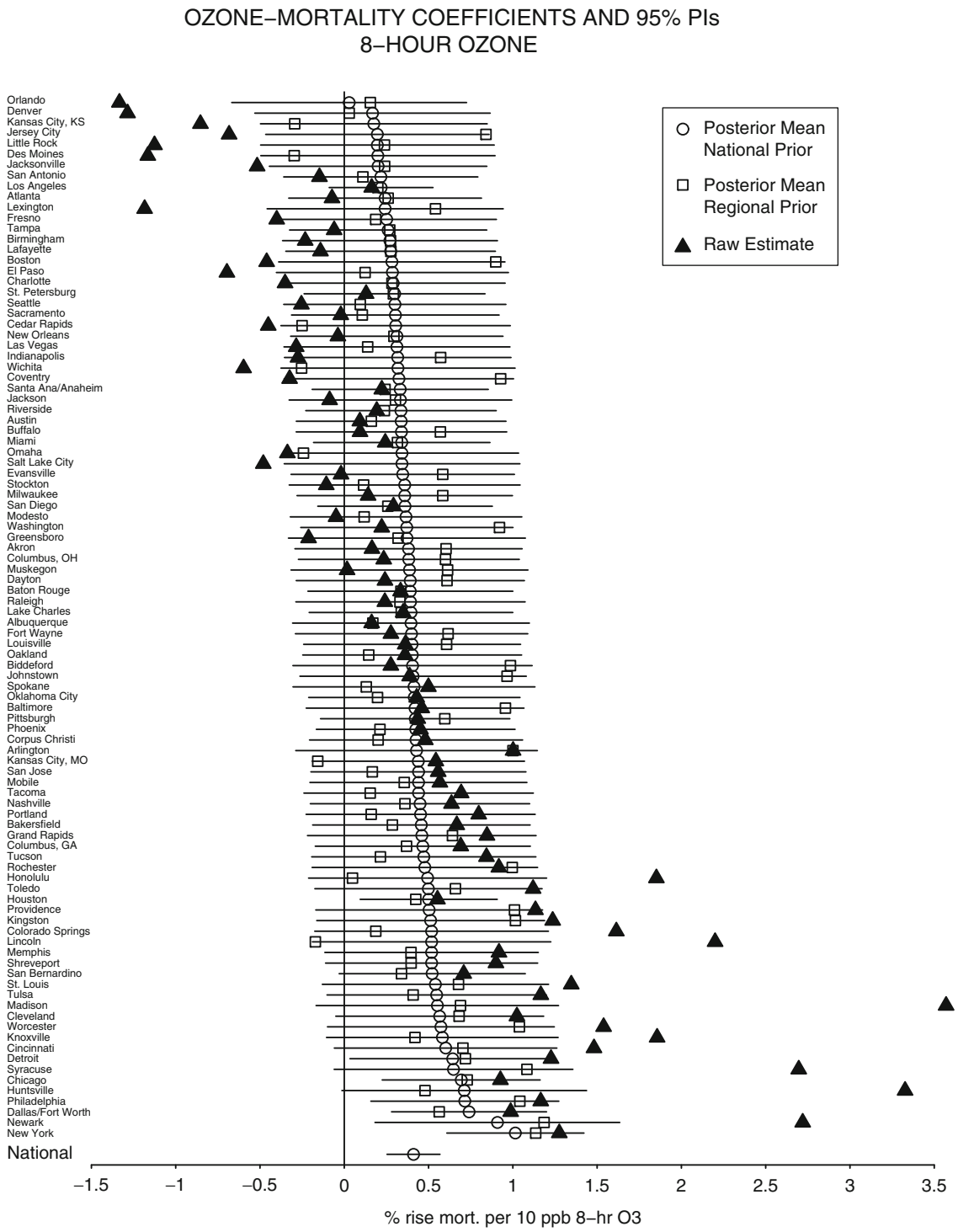

Air Quality Guidelines and Standards. Figure 11

Ninety-five percent posterior intervals for the ozone-mortality coefficients, based on 8-h ozone, all-year data. The Bayesian posterior estimates under the "national prior" (*circles*) are shown alongside those for the "regional prior" (*squares*) and the raw maximum likelihood estimates (*triangles*) (Adapted from [58])

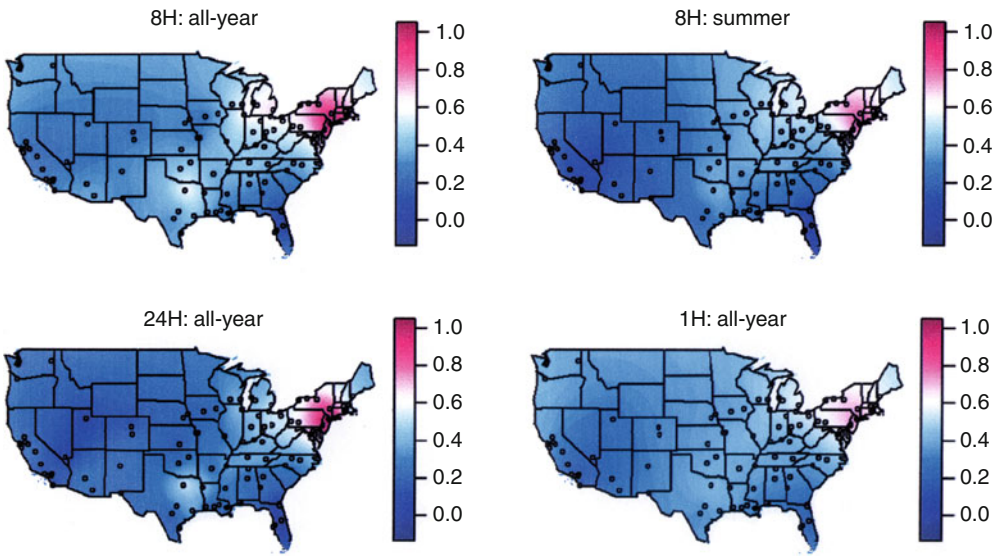

Air Quality Guidelines and Standards. Figure 12
Map of spatially dependent ozone-mortality coefficient for 8-h ozone (all-year data), 8-h ozone (summer data), 24-h ozone (all-year data), and 1-h ozone (all-year data) (Adapted from [58])

The EPA's CASAC recommended to the Administrator that he revise the Ozone NAAQS with an 8-h averaging time, from 0.08 ppm to a level within the range of 0.060–0.070 ppm. Ultimately, the Administrator exercised his judgment in revising the standard to 0.075 ppm. The CASAC Ozone Panel expressed its displeasure at the Administrator's setting the NAAQS at a level higher than they recommended. In my opinion, the science alone can never be sufficient for establishing a specific numerical standard. The setting of the standard also involves judgment as to acceptable risk, a judgment call I viewed as being delegated to the Administrator, not the Advisory Committee, by the Clean Air Act. After the revised standard was promulgated, the EPA's statistical reanalysis [13] was published with a conclusion that the Adams [3] data demonstrated a statistically significant, but small biological effect at 0.060 ppm. These published findings as well as any new data that may become available from studies conducted with human volunteers exposed to ozone at concentrations of less than 0.080 ppm will certainly be considered in the current review (post-2008) and potential revision of the Ozone NAAQS.

The setting of both the PM and Ozone NAAQS serves to illustrate the complex interplay between science and policy judgment in the setting of guidelines and standards [41]. In my opinion, the selection of any specific numerical standard for exposure to a chemical involves both science and a policy judgment as to an acceptable risk. The scientific information can identify for a particular level of exposure an associated level of risk (including an absence of excess risk) and the associated uncertainty in the estimate. However, the selection of a specific level for the standard goes beyond the science and represents a policy judgment or decision. The issue of the role of science and judgment in standard setting is drawn to the forefront by agents that do not have clear thresholds in their exposure-response relationships. In these cases, some level of excess risk may be calculated for exposures that extend down to ambient levels routinely observed in developed countries.

In March 2008, then EPA Administrator Stephen Johnson announced a revised Ozone NAAQS (8-h averaging time) of 75 ppb, a reduction from the previous level of 0.08 ppm (which by rounding convention was effectively 84 ppb) set in 1997 [81]. In setting the 75 ppb level, he explicitly noted that he was not explicitly following the advice of the CASAC which advised that he set the standard in the range of 60–70 ppb.

He noted that he viewed the CASAC advice as a blend of science and policy judgment which he was not compelled to follow. The previous statistical form for the standard was not changed.

The Administrator also elected to set the Secondary (Welfare) Standard equal to the Primary (Health) Standard. The 1997 Secondary Standards for Ozone [65] had been set equal to the Primary Standard based on the view that attainment of the Primary Standard would be protective of welfare impacts and effects on plants. The CASAC had recommended that the averaging time form of the Secondary Standard be changed to a more complex form that used a weighted average of the Ozone concentration over a growing season. Thus, it was not as easy to compare the Primary and Secondary Standards. As an aside, the revision of the Ozone NAAQS in March 2008 also set the dates for completing the next regularly scheduled 5-year review, March 2013.

The failure of the EPA Administrator to explicitly follow the advice of CASAC was greeted with outrage by the CASAC Ozone Panel. The Committee took the unusual step, post-final announcement of the new Ozone NAAQS, of holding a Panel meeting to discuss the new Standard and writing a letter to the Administrator reminding him of their previous advice and calling for the Administrator to follow their advice in future revisions of the standard [41].

In January 2009, President Barak Obama took office and Lisa Jackson was appointed EPA Administrator. Coincident with Obama taking office his Chief of Staff, Rahm Emanuel, took the customary step of reminding newly designated Senior Agency officials of the opportunity to review and, perhaps, revise any rules and regulations that originated with the prior Administration and not yet finalized [21]. Administrator Lisa Jackson took the bold step of announcing that she was going to reconsider the Ozone NAAQS set by Administrator Johnson in March 2008. In taking this action she was in essence saying – if I had been in office as EPA Administrator earlier I would have made a different policy decision. Administrator Jackson proceeded to publish a proposal to "reconsider" the Ozone NAAQS using the same science used as a basis of the March 2008 standard [81]. The proposal indicated Administrator Jackson intended to follow the advice of CASAC and set a primary standard (8-h averaging time) in the range of 60–70 ppb. The proposed date for release of a final standard was announced, a target date that was revised on multiple occasions. A Presidential Executive Order issued by President Clinton [18] requires that any proposed federal rule or action that will result in annual costs in excess of $100 million per year must be reviewed by the Office of Information and Regulatory Affairs in the Office of Management and Budget. On September 2, 2011, President Obama announced in a press release that he had advised EPA Administrator Jackson to not proceed with the "reconsideration" of the Ozone NAAQS [91]. At the same time, a brief summary of the conclusions of the OIRA review was released by the Director of that Office, Cass Sunstein [62]. It briefly noted that the EPA "reconsideration" proposal (a) was discretionary and not required by the CAA 5-year review schedule, (b) was not based on the best available science (the record was based on scientific literature that had been published in most cases before 2006), and (c) was not consistent with the President's desire for regulations that reduced uncertainty.

Environment groups greeted the President's announcement with dismay, while Business applauded it. A Forum (Forum.HSPH.org) held on September 21, 2011 at the Harvard School of Public Health entitled "Smog or Jobs: The Impact of Tighter Ozone Control" provides insight into the controversial nature of President Obama's decision informed by the views of his advisor, Sunstein. The current review of the Ozone NAAQS initiated in 2008 will now proceed. A key initial step in the review process occurred with release in March 2011 of new integrated science assessment for ozone [88]. A proposal for the Ozone Standard should be issued in 2012 for public comment and a final rule for continuing or revising the Ozone NAAQS should be issued in March 2013 if EPA adheres to the 5-year schedule specified in the Clean Air Act [16].

Current Air Quality Standards and Guidelines

As noted earlier, the National Ambient Air Quality Standards established by the US Environmental Protection Agency are constantly changing. Indeed, the Clean Air Act specifies that each NAAQS should be reviewed

Air Quality Guidelines and Standards. Table 5 Summary information on criteria air pollutants regulated as NAAQS[a] by the USEPA

Pollutant	Sources	Key effects of concern	Subpopulations of concern
Ozone	Photochemical oxidation of nitrogen oxides (primarily from combustion) and volatile organic compounds (from stationary and mobile sources)	Decreased pulmonary function, lung inflammation, increased respiratory hospital admissions	Children, people with preexisting lung disease outdoor-exercising health people
Nitrogen dioxide	Photochemical oxidation of nitric oxide (primarily from combustion of fossil fuels) and direct emissions (primarily from combustion of natural gas)	Respiratory illness, decreased pulmonary function	Children, people with preexisting lung disease
Sulfur dioxide	Primarily combustion of sulfur-containing fossil fuels; also smelters, refineries, and others	Respiratory injury or death, decreased pulmonary function	Children, people with preexisting lung disease (especially asthma)
Particulate matter	Direct emission of particles during combustion, industrial processes, gas reactions and condensation and coagulation natural sources	Injury and death	Children, people with preexisting heart and lung disease
Carbon monoxide	Combustion of fuels, especially by mobile sources	Shortening of time to onset angina and other heart effects	People with coronary artery disease
Lead	Leaded gasoline (prior to phase-out in gasoline); point sources such as Pb mines, smelters, and recycling operations	Developmental neurotoxicity	Children

[a]NAAQSs are specified by indicator concentration, averaging time, and statistical form. The latter used to determine compliance and is too complex for coverage here. However, suffice it to note that both the specific numerical level *and* the statistical form determine the stringency of the standard

every 5 years. Although this schedule has been rarely met, the reviews continue and changes in the NAAQS have occurred. There is no specified schedule for review of the WHO Air Quality Guidelines. However, it would be reasonable to assume that they will be periodically reviewed and possibly revised as new information is required.

The NAAQS as of September 18, 2011 are shown in Tables 5 and 6 in summary form. The reader interested in the details that support each of the NAAQS is referred to the US EPA's Website for criteria air pollutants where detailed documents can be found on each of the Criteria Pollutants. This includes information on previous reviews as well as reviews that are currently in progress.

The final rule for each of the primary (health) NAAQS published in the Federal Register are as follows: particulate matter [75], Lead [73], Ozone [82], Nitrogen dioxide [86], Sulfur dioxide [87], and Carbon monoxide [89]. Each of these final rules contains references to the Criteria Document (or Integrated Science Assessment), Risk and exposure assessment, and proposed rule that undergirds the final rule. In addition, the EPA Web site for criteria pollutants provides linkages to the Regulatory Impact Analyses (RIA) that has been conducted on the proposed final rule. The RIA contain information on the monetized benefits of the rule and the associated costs of achieving the NAAQS. In accordance with the US Supreme Court ruling in *American Trucking Associations* v. *EPA* [4] and *Whitman* v. *American Trucking Associations* [93], the costs of implementing the NAAQS may not be considered by the EPA Administrator in the setting of the NAAQS. However, these costs can be considered in developing a schedule for implementation of each NAAQS.

Air Quality Guidelines and Standards. Table 6 National Ambient Air Quality Standards for criteria pollutants

Pollutant	Primary standards		Secondary standards	
	Level	Averaging time	Level	Averaging time
Carbon monoxide	9 ppm (10 mg/m^3)	8-h[a]	None	
	35 ppm (40 mg/m^3)	1-h[a]		
Lead	0.15 μg/m^3 [b]	Rolling 3-month average	Same as primary	
Nitrogen dioxide	53 ppb[c]	Annual (arithmetic average)	Same as primary	
	100 ppb	1-h[d]	None[l]	
Particulate matter (PM_{10})	150 μg/m^3	24-h[e]	Same as primary	
Particulate matter ($PM_{2.5}$)	15.0 μg/m^3	Annual[f] (arithmetic average)	Same as primary	
	35 μg/m^3	24-h[g]		
Ozone	0.075 ppm (2008 std)	8-h[h]	Same as primary	
	0.08 ppm (1997 std)	8-h[i]		
	0.12 ppm	1-h[j]		
Sulfur dioxide	0.03 ppm	Annual (arithmetic average)	0.5 ppm	3-h[a]
	0.14 ppm	24-h[a]		
	75 ppb[k]	1-h	None[l]	

[a]Not to be exceeded more than once per year

[b]Final rule signed October 15, 2008. The 1978 lead standard (1.5 μg/m^3 as a quarterly average) remains in effect until 1 year after an area is designated for the 2008 standard, except that in areas designated nonattainment for the 1978 standard, the 1978 standard remains in effect until implementation plans to attain or maintain the 2008 standard are approved

[c]The official level of the annual NO_2 standard is 0.053 ppm, equal to 53 ppb, which is shown here for the purpose of clearer comparison to the 1-h standard

[d]To attain this standard, the 3-year average of the 98th percentile of the daily maximum 1-h average at each monitor within an area must not exceed 100 ppb (effective January 22, 2010)

[e]Not to be exceeded more than once per year on average over 3 years

[f]To attain this standard, the 3-year average of the weighted annual mean $PM_{2.5}$ concentrations from single or multiple community-oriented monitors must not exceed 15.0 μg/m^3

[g]To attain this standard, the 3-year average of the 98th percentile of 24-h concentrations at each population-oriented monitor within an area must not exceed 35 μg/m^3 (effective December 17, 2006)

[h]To attain this standard, the 3-year average of the fourth-highest daily maximum 8-h average ozone concentrations measured at each monitor within an area over each year must not exceed 0.075 ppm (effective May 27, 2008)

[i](a) To attain this standard, the 3-year average of the fourth-highest daily maximum 8-h average ozone concentrations measured at each monitor within an area over each year must not exceed 0.08 ppm.

(b) The 1997 standard – and the implementation rules for that standard – will remain in place for implementation purposes as EPA undertakes rule making to address the transition from the 1997 ozone standard to the 2008 ozone standard.

(c) EPA is in the process of reconsidering these standards (set in March 2008)

[j](a) EPA revoked the 1-h ozone standard in all areas, although some areas have continuing obligations under that standard ("anti-backsliding").

(b) The standard is attained when the expected number of days per calendar year with maximum hourly average concentrations above 0.12 ppm is ≤ 1

[k]Final rule signed June 2, 2010. To attain this standard, the 3-year average of the 99th percentile of the daily maximum 1-h average at each monitor within an area must not exceed 75 ppb

[l]On July 12, 2011, the EPA Administrator proposed to set Secondary NAAQS for NO_2 and SO_2 for a 1-h averaging time at concentrations equal to the Primary Standards, NO_2 – 100 ppb and SO_2 – 75 ppb (Note: This footnote was added by Roger O. McClellan)

Source: Taken from US EPA Website, July 26, 2011

Air Quality Guidelines and Standards. Table 7 WHO air quality guidelines and interim targets for particulate matter[a]

Annual mean concentration			
	PM_{10} ($\mu g/m^3$)	$PM_{2.5}$ ($\mu g/m^3$)	Basis for the selected level
Interim Target-1 (IT-1)	70	35	These levels are associated with about a 15% high long-term mortality risk relative to the AQG level
Interim Target-2 (IT-2)	50	25	In addition to other health benefits, these levels lower the risk of premature mortality by approximately 6% (2–11%) relative to the IT-1 level
Interim Target-3 (IT-3)	30	15	In addition to other health benefits, these levels reduce the mortality risk by approximately 6% (2–11%) relative to the IT-2 level
Air Quality Guideline (AQG)	20	10	These are the lowest levels at which total, cardiopulmonary and lung cancer mortality have been shown to increase with more than 95% confidence in response to long-term exposure to $PM_{2.5}$
24-h concentrations [99th percentile (3 days/year)]			
	PM_{10} ($\mu g/m^3$)	$PM_{2.5}$ ($\mu g/m^3$)	Basis for the selected level
Interim Target-1 (IT-1)	150	75	Based on published risk coefficient from multi-center studies and meta-analyses (about 5% increase of short-term mortality over the AQG value)
Interim Target-2 (IT-2)	100	50	Based on published risk coefficients from multiple-center studies and meta-analyses (about 2.5% increase of short-term mortality over the AQG value)
Interim Target-3 (IT-3)[a]	75	37.5	Based on published risk coefficients from multi-center studies and meta-analyses (about 1.2% increase in short-term mortality over the AQG value)
Air quality	50	25	Based on relationship between 24-h and annual PM levels been shown to increase with more than 95%

[a]The use of $PM_{2.5}$ guideline value is preferred
Source: WHO [96]

The current WHO air quality guidelines are summarized in Tables 7, 8, 9, and 10. The basis for these guidelines is contained in WHO documents [95, 96].

Future Directions

This entry has provided an overview of Air Quality Guidelines and Standards focusing on the standards developed by the US Environmental Protection Agency and the Guidelines developed by the World Health Organization. The latter Guidelines, although stated to provide guidance for use around the world, have focused on Europe. For Europe, the WHO Guidelines have provided valuable input to national and local authorities for developing legal binding air quality standards. The Standards developed by European nations and other nations round the world have not been reviewed in detail in this entry.

The section on "Air Quality Management Framework" emphasized that Air Quality Standards and Guidelines were a key element of the overall scheme; however, the Standards and Guidelines are just one element of an integrated air quality management scheme. It is noteworthy that substantial progress has been made in improving air quality in the United States and in western European countries. That progress has no doubt been facilitated by the Standards and Guidelines. However, setting up goal posts (Standards and Guidelines) does not necessarily mean the goals will be achieved. Specific emission reductions informed by the Standards and Guidelines are ultimately required to achieve the goals. In the United States, major regulations have mandated reductions in emissions of particulate matter, SO_2, and NO_2 from stationary sources such as power plants and from mobile sources such as passenger cars and on-road trucks and, more recently,

Air Quality Guidelines and Standards. Table 8 WHO air quality guideline and interim target for ozone: 8-h concentrations

	Daily maximum 8-h mean (μg/m^3)	Basis for selected level
High levels	240	Significant health effects; substantial proportion of vulnerable populations affected
Interim Target-1 (IT-1)	160	Important health effects; does not provide adequate protection of public health
		Exposure to this level of ozone is associated with: • Physiological and inflammatory lung effects in healthy exercising young adults exposed for periods of 6.6 h • Health effects in children (based on various summer camp studies in which children were exposed to ambient ozone levels) • An estimated 3–5% increase in daily mortality[a] (based on findings of daily time-studies)
Air Quality Guideline (AQG)	100	Provides adequate protection of public health, though some health effects may occur below this level. Exposure to this level of ozone is associated with: • An estimated 1–2% increase in daily mortality[a] (based on findings of daily time-series studies) • Extrapolation from chamber and field studies based on the likelihood that real-life exposure tends to be repetitive and chamber studies exclude highly sensitive or clinically compromised subjects, or children • Likelihood that ambient ozone is a marker for related oxidants

[a]Deaths attributable to ozone. Time-series studies indicate an increase in daily mortality in the range of 0.3–0.5% for every 10 μg/m^3 increment in 8-h ozone concentrations above an estimated baseline level of 70 μg/m^3

Air Quality Guidelines and Standards. Table 9 WHO air quality guidelines and interim targets for SO_x: 24-h and 10-min concentrations

	24-h average (μg/m^3)	10-min average (μg/m^3)	Basis for selected level
Interim Target-1 (IT-1)[a]	125	–	
Interim Target-2 (IT-2)			Intermediate goal based on controlling either motor vehicle emissions, industrial emissions, and/or emissions from power production. This would be a reasonable and feasible goal for some developing countries (it could be achieved within a few years) which would lead to significant health improvements that, in turn, would justify further improvements (such as aiming for the AQG value)
Air Quality Guideline (AQG)	20	500	

[a]Formerly the WHO Air Quality Guideline [95]

from off-road equipment, rail locomotives, and ships. These regulations have resulted in substantial reductions in the emissions of the criteria pollutants or their precursors while the economy also grew until recently. A stagnant economy in 2011 is raising questions as to the wisdom of further reductions in NAAQS

Air Quality Guidelines and Standards. Table 10 WHO (European) guideline values for carbon monoxide

100 mg/m^3 [a]	15 min
60 mg/m^3 [a]	30 min
30 mg/m^3 [a]	1 h
10 mg/m^3	8 h

[a]Exposure at these levels should be no longer than the indicated times and should not be repeated within 8 h
Source: WHO [95]

and aggressive regulatory actions to further reduce emissions.

Since the Clean Air Act Amendments of 1970 were passed in the United States there has been a steady increase in research on the health effects of air pollutants. The increase in research has been most notable since the mid-1990s when major controversies arose over the health effects of $PM_{2.5}$. Indeed, what has developed might be characterized as a "clean air enterprise" involving air quality regulators, the academic research community, and nongovernmental organization advocacy groups. Some individuals would quickly note that this enterprise is counterbalanced by corporations and industrial groups advocating for the status quo or "dirty air." This polarized approach has frequently resulted in the focus being on a single risk factor, air quality, rather than the overall well-being of the health of societies around the world.

The earlier section on "Context for Air Quality Impacts" noted the multitude of risk factors that impact on health. That section contrasted the burden of disease attributed to the various risk factors including urban air pollution and indoor smoke from household use of solid fuels. The contrast between the burden of disease for low- and middle-income countries versus high-income countries was striking. In the former, 3.7% of deaths were associated with indoor smoke and 1.5% from urban air pollutions. In contrast, in the high-income countries urban air pollution was estimated to be associated with 1.0% of the deaths and no deaths were estimated to be associated with indoor smoke. The health hazards associated with indoor smoke from use of solid fuels for cooking and heating has not been reviewed in this entry. It is sufficient to note here that the greatest hazards from indoor cooking are those related to burning of wood, agricultural residue, and coal in the same manner as was commonplace around the world centuries ago. It is clear that in the future a major challenge exists to improve the income of families in low- and middle-income countries so they can move away from uncontrolled combustion of solid fuels indoors. It is well recognized that improving the economy of a country or region inevitably requires increases in energy usage and the availability of clean water and adequate foodstuffs. A major challenge exists in providing adequate energy, in the form of distributed electricity and liquid fuels for transportation and also avoiding negative impacts on air quality. Major progress has been made in the highest income countries in the world in developing low-emission stationary sources for generating electrical power and low emission internal combustion [both spark ignition and compression ignition (diesel)] engines for on- and off-road use. The challenge is to facilitate the transfer of those low emission technologies to the rest of the world.

With the above as background, it is appropriate to return to the central focus of this entry – air quality standards and guidelines and their role in the future. The past 40 years have been a period of major activity in creating a science based on the health effects of air pollutants and the use of that science to inform the development of air quality standards and guidelines and to inform the development and implementation of strategies and technologies to improve air quality. The field is at an interesting juncture that may be framed with the question – "how low is low enough for air quality standards and guidance?"

Science should have an important role in addressing that question, however, scientific knowledge alone will not be sufficient to answer the question. Epidemiological studies with improved design and execution may give us some marginal improvement in estimates of the health risks associated with exposure to low ambient concentrations of various air constituents. It will be especially challenging to demonstrate the shape of the ambient concentration-response relationship at concentrations that include background levels. Rather than a singular focus on health effects attributable to air pollution as in the past, future epidemiological studies will better serve the needs of Society when

they consider more broadly the multiple factors that influence disease outcomes. A finding of relative risks of 1.1 or less for a specific air pollutant begs the question of what are the dominant risk factors driving the baseline health risks.

It has become commonplace for scientists using cellular and molecular approaches to argue for more research using their tools to investigate the mechanisms of action of various air pollutants. Based on the evidence that air pollution in the highest income countries of the world is not a major influence on the health of the population it is appropriate to ask whether a more detailed understanding of this specific risk factor, air pollutants, will be of value in guiding critical societal decisions. An alternative would be to focus on the broader range of risk factors that influence the baseline risk.

Irrespective of the specifics of the science available, it can be anticipated that increasing attention will focus on how science is used to decide on the level and statistical form of air quality standards and guidelines. The issue is relevant to both the setting of Standards and Guidelines, however, it is especially critical as it relates to standards which are legally binding. A review of all the existing Guidelines and Standards for criteria or common air pollutants suggests they have been based on judgment. In some cases, those judgments were made exclusively by scientists, that is, the WHO Air Quality Guidelines. In other cases, as in the setting of National Ambient Air Quality Standards by the US EPA, the decisions were made by appointed government officials and informed by the science reviewed by the Clean Air Scientific Advisory Committee. As best it can be determined none of the Guidelines or Standards were set at a specific defined level of risk. This is remarkable since each level (and its associated statistical form) for a Guideline or Standard reflects a level of acceptable risk: above this level and statistical form the health risks are *not* acceptable and below this level and statistical form the health risks of exposure are deemed acceptable. If scientists argue that there is a linear, no-threshold relationship between ambient concentrations of an air pollutant and associated health responses down to background concentrations, then no concentration is free of some level of calculated excess risk.

In this author's view, decisions on acceptable health risks for the public should be informed by the best science available. However, scientists alone are not in a position to make broad policy decisions on acceptable risk. Indeed, pronouncements by individual scientists or scientific committees need to be recognized as a statement of the individual preference for a particular policy outcome or the collective view of the Committee. The current worldwide economic crisis results in every major financial investment made by either public or private entities being considered in the context of the future return on the investment in terms of the public or private good that will result. The focus increasingly is on choices that must be made between alternative uses of funds, irrespective of whether the funding is from the public or private sector. Clean air is universally viewed as a right. The question increasingly for policy makers, as representatives of the public, is how clean is clean enough? This question cannot be addressed in isolation; it should be addressed in the context of all the risk factors influencing human health. The question for scientists is how to create the scientific knowledge on air pollutants and other risk factors that affect human health to inform these important societal decisions.

Bibliography

Primary Literature

1. Adams WC (2002) Comparison of chamber and face mask 6.6-hour exposure to 0.08 ppm ozone via square-wave and triangular profiles on pulmonary responses. Inhal Toxicol 15:265–281
2. Adams WC (2003) Relation of pulmonary responses induced by 6.6 h exposures to 0.08 ppm ozone and 2-h exposures to 0.30 ppm via chamber and face-mask inhalation. Inhal Toxicol 15:745–759
3. Adams WC (2006) Comparison of chamber 6.6 h exposures to 0.04-0.08 ppm ozone via square-wave and triangular profiles on pulmonary responses. Inhal Toxicol 18:127–136
4. *American Trucking Associations, Inc.* v. *U.S. Environmental Protection Agency* (1999) DC circuit, 19 May 1999
5. Ayres JG, Harrison RM, Maynard R, McClellan RO, Nicols GL (2010) Environmental medicine in context, chapter 1. In: Ayres JG, Harrison RM, Maynard R, Nichols GL (eds) Textbook of environmental medicine. Hodder Education, London, pp 3–21
6. Ayres JG, Harrison RM, Maynard R, McClellan RO, Nicols GL (eds) (2010) Textbook of environmental medicine. Hodder Education, London
7. Bachmann J (2007) Will the circle be unbroken: a history of the U.S. National Ambient Air Quality Standards. J Air Waste Manag Assoc 57:652–697

8. Bell ML, McDermott A, Zeger SL, Samet JM, Dominici F (2004) Ozone and short-term mortality in 95 US urban communities, 1987–2000. JAMA 292(19):2372–2378
9. Bell ML, Dominici F, Samet JM (2005) A meta-analysis of time-series studies of ozone and mortality with comparison to the national morbidity, mortality, and air pollution study. Epidemiology 16(4):436–445
10. Berry MA (1984) A method for examining policy implementation: a study of decision-making for the National Ambient Air Quality Standards, 1964–1984. U.S. Environmental Protection Agency, Research Triangle Park, NC
11. Breyer S (1982) Regulation and reform. Harvard University Press, Cambridge
12. Breyer S (1993) Breaking the vicious circle: toward effective risk regulation. Harvard University Press, Cambridge, MA (Based on 1992 Oliver Wendell Holmes lectures at Harvard Law School)
13. Brown JS, Bateson TF, McDonnell WF (2008) Effects of exposure to 0.06 ppm ozone in FEV_1 in humans: a secondary analysis of existing data. Environ Health Persp 116:1023–1026
14. CAA (1963) The Clean Air Act of 1963
15. CAA (1970) The Clean Air Act Amendments of 1970-P.L. 91–04 (December 31, 1970), Plus Technical Amendments Made by P.L. 92–157 (November 18, 1971)
16. CAA (1977) The Clean Air Act Amendments of 1977
17. CAA (1990) The Clean Air Act Amendments to 1990, Public Law No. 101–549; 104 STAT 2399, 1990
18. Clinton WJ, President (1993) Executive Order 12866 – regulatory planning and review. Fed Regis 58:51735
19. Clinton WJ, President (1997) Memorandum for the Administrator of the Environmental Protection Agency Implementation of Revised Air Quality Standards for Ozone and Particulate Matter
20. Dockery DW, Pope CA III, Xu X et al (1993) An association between air pollution and mortality in six U.S. cities. N Engl J Med 329:1753–1759
21. Emanuel R (2009) Assistant to the President and Chief of Staff, Memorandum to the Heads of Executive Departments and Agencies. Fed Regist 74(13):4435–4436
22. Enstrom JE (2005) Fine particulate pollution and total mortality among elderly Californians, 1973–2002. Inhal Toxicol 17(14):803–816
23. Ferris BG Jr, Speizer FE, Spengler JD et al (1979) Effects of sulfur oxides and respirable particles on human health: methodology and demography of populations in study. Am Res Respir Dis 120:767–779
24. Follinsbee LJ, McDonnell WF, Horstman DH (1988) Pulmonary function and symptom responses after 6-6-hour exposure to 0.12 ppm ozone with moderate exercise. JAPCA 38:28–35
25. Haagen-Smit AJ (1952) Chemistry and physiology of Los Angeles smog. Ind Eng Chem 44:1342–1346
26. Horstman DH, Follinsbee LJ, Ives PJ, Abdul-Salaam S, McDonnell WF (1990) Ozone concentration and pulmonary response relationships for 6.6-hour exposures with five hours of moderate exercise to 0.08, 0.10, and 0.12 ppm. Am Rev Respir Dis 142:1158–1163
27. Kennedy D (2005) Risk versus risk. Science 309:2137
28. Krewski D, Burnett RT, Goldberg, Hoover K, Siemiatycki J, Jerrett M, Abrahamowicz M, White WH (2000) Reanalysis of the Harvard Six Cities Study and the American Cancer Society Study of particulate air pollution and mortality. Special report, Health Effects Institute, Cambridge, MA
29. Laden F, Schwartz J, Speizer FE, Dockery DW (2006) Reduction in fine particulate air pollution and mortality: extended follow-up of the Harvard six cities study. Am J Respir Crit Care Med 173:667–672
30. Library of Congress (1974) A Legislative History of the Clean Air Amendments of 1970, vol 1; Serial Number 93–18: Environmental Policy Decision, Congressional Research Service, Library of Congress, Washington, DC
31. Lopez AD, Mathers CD, Ezzati M, Jamison DT, Murray CJL (eds) (2006) Global burden of disease and risk factors. Oxford University Press, New York
32. Martin R, Symington L (1968) A guide to the Air Quality Act of 1967. Law Contemp Probl 33:239–245
33. Martineau R, Novello D (2004) The clean air act handbook, 2nd edn. American Bar Association, Chicago, Illinois
34. McClellan RO (1997) Use of mechanistic data in assessing human risks of exposure to particles. Env Health Persp 105(5):1363–1372
35. McClellan RO (1999) Human health risk assessment: a historical overview and alternative paths forward. Inhal Toxicol 11:477–518
36. McClellan RO (1999) Ambient airborne particulate matter: toxicology and standards. In: Gardner DE, McClellan RO, Crapo JD (eds) Toxicology of the lung, 3rd edn. Taylor and Francis, Washington, DC, p 289
37. McClellan RO (1999) Developing risk assessments for airborne materials. In: Gardner DE, McClellan RO, Crapo JD (eds) Toxicology of the lung, 3rd edn. Taylor and Francis, Washington, DC, p 599
38. McClellan RO (1999) Health risk assessments and regulatory considerations for air pollutants. In: Swift DL, Foster WM (eds) Air pollutants and the respiratory tract. Marcel Dekker, New York, pp 89–338
39. McClellan RO (2002) Setting ambient air quality standards for particulate matter. Toxicology 181–182:329–347
40. McClellan RO (2010) Hazard and risk: assessment and management, chapter 4. In: Ayres JG, Harrison RM, Maynard R, Nichols GL (eds) Textbook of environmental medicine. Hodder Education, London, pp 59–88
41. McClellan RO (2011) Role of science and judgment in setting National Ambient Air Quality Standards: how low is low enough?" Air Qual Atmos Health J (Published on-line, June 1, 2011)
42. McClellan RO, Jackson TE (1999) Carcinogenic responses to air pollutants. In: Holgate ST, Samet JM, Koren HS, Maynard RL (eds) Air pollution and health. Academic, San Diego, pp 381–413

43. McClellan RO, Frampton MW, Koutrakis P, McDonnell WF, Moolgavkar S, North DW, Smith AE, Smith RL, Utell MJ (2009) Critical considerations in evaluating scientific evidence of health effects of ambient ozone: a conference report. Inhal Toxicol 21(Suppl 2):1–36
44. McDonnell WF, Kehri HR, Abdul-Salaam S et al (1991) Respiratory response of humans exposed to low levels of ozone for 6.6 hours. Arch Environ Health 46:145–150
45. McDonnell WF, Stewart PW, Smith MV (2007) The temporal dynamics of ozone-induced FEV_1, changes in humans: an exposure-response model. Inhal Toxicol 19:483–494
46. New York Times (1997) Clinton sharply tightens air pollution regulations despite concern over costs. NY Times, June 26, 1997
47. NRC (National Research Council) (2006) Health risks for exposure to low levels of ionizing radiation. BEIR VII – phase 2. Authored by Committee to Assess Health Risks from Exposure to Low Levels of Ionizing Radiation National Research Council
48. NRC (National Research Council) (2008) Estimating mortality risk reduction and economic benefits from controlling ozone air pollution. National Academies Press. http://books.nap.edu/catalog.php?record_id=12198&utm_medium=etmail&utm_source=National%20Academies%20Press&utm_campaign=New+from+NAP+4.29.08-May-7-2008&utm_content=Downloader&utm_term=. Accessed 2 Dec 2011
49. NRDC (1976) *Natural Resources Defense Council* v. *Train*, 411F. Suppl 864 (S.D.N.Y.) aff'd 545F. 2d 320 (2nd Cir., 1976)
50. Özkaynak H (1999) Exposure assessment. In: Halgate ST, Samet JM, Koren HS, Maynard RL (eds) Air pollution and health. Academic, London/San Diego, pp 149–162
51. Peacock M (2006) Memorandum from Marcus Peacock, Deputy Administrator to Dr. George Gray and Bill Wehrun. Process for reviewing the National Ambient Air Quality Standards. http://www.epa.gov/ttnnaaqs/pdfs/memo_process_for_reviewing_naaqs.pdf (accepted 2007). Accessed 7 Dec 2006
52. Pedersen WF (1975) Formal records and informal rulemaking. Yale Law J 38:38–88
53. Pope CA III, Dockery DW (1999) Epidemiology of particle effects. In: Holgate ST, Samet JM, Loren HS, Maynard RL (eds) Air pollution and health. Academic, London, pp 673–705
54. Pope CA III, Burnett RJ, Thun MJ, Calle EE, Krewski D, Ito K, Thurston CD (2002) Lung cancer, cardiopulmonary mortality, and long-term exposure to fine particulate air pollution. JAMA 287(9):1132–1141
55. Pruss-Ustun A, Corvalan C (2006) Towards estimation of the environmental burden of disease. World Health Organization, Copenhagen, Denmark
56. Rhomberg LR, Goodman JE, Haber LT, Dougson M, Andersen MT, Klaunig JE, Meek B, Price PS, McClellan CSM (2011) Linear low-dose extrapolation for non-cancer health effects is the exception, not the rule. Crit Rev Toxicol 41(1):1–19
57. Schrenk HH, Heimann H, Clayton GD, Gafafer WM, Wexler H (1948) Air pollution in Donora, PA. Epidemiology of the unusual smog episode of October 1948. Public Health Bull 306; U.S. Government Printing Office, Washignton, DC, 1949
58. Smith RL, Baowei X, Switzer P (2009) Reassessing the relationship between ozone and short-term mortality in U.S. urban communities. Inhal Toxicol 29(S2):37–61
59. Steenland K, Hu S, Walker J (2004) All-cause and cause-specific mortality by socioeconomic status among employed persons in 27 U.S. States, 1984–1997. Am J Public Health 94: 1037–1042
60. Stern AC (1982) History of air pollution legislation in the United States. J Air Poll Control Assoc 32:44–61
61. Sunstein CR (2004) Lives, life years, and willingness to pay. Columbia Law Rev 104(1):205–252
62. Sunstein CR (2011) Letter from Cass Sunstein, Administrator, Office of Information and Regulatory Affairs, Office of Management and Budget to Administrator Lisa Jackson, U.S. Environmental Protection Agency on "Reconsideration of the 2008 Ozone Primary and Secondary National Ambient Air Quality Standard" dated September 2, 2011
63. Taube G (1995) Epidemiology faces its limits. Science 269: 164–169
64. U.S. Environmental Protection Agency (1971) National primary and secondary Ambient Air Quality Standards. Fed Regist 36:8186
65. U.S. Environmental Protection Agency (1997) National Ambient Air Quality Standards for ozone. Fed Regist 62(138): 38856–38896
66. U.S. Environmental Protection Agency (1997) National Ambient Air Quality Standards for particulate matter: final rule. Fed Regist 82(138):38652–38760
67. U.S. Environmental Protection Agency (1997) EPA's Regulatory Impact Analyses (RIA) for the 1997 ozone and PM NAAQS and proposed regional haze rule. http://www.epa.gov/ttn/oarpg/naaqsfin/ria.html. Accessed 2 Dec 2011
68. U.S. Environmental Protection Agency (2004) Air quality criteria for particulate matter. Final report, Oct 2004. http://cfpub.epa.gov/ncea/cfm/recordisplay.cfm?deid=87903. Accessed 2 Dec 2011
69. U.S. Environmental Protection Agency (2005) Particulate matter health risk assessment for selected urban areas. U.S. Environmental Protection Agency, Research Triangle Park, NC, EPA 452/R-05-007A
70. U.S. Environmental Protection Agency (2005) Review of the National Ambient Air Quality Standards for particulate matter: policy assessment of scientific and technical information, OAQPS Staff Paper. U.S. Environmental Protection Agency, Research Triangle Park, NC, EPA-452/R-05-005a
71. U.S. Environmental Protection Agency (2006) Air quality criteria for ozone and related photochemical oxidants (2006 Final). EPA/600/R-05-004aF-cF. http://cfpub.epa.gov/ncea/cfm/recordisplay.cfm?deid=149923. Accessed 2 Dec 2011
72. U.S. Environmental Protection Agency (2006) Air quality criteria for lead. Final report. http://cfpub.epa.gov/ncea/cfm/recordisplay.cfm?deid=158823. Accessed 2 Dec 2011

73. U.S. Environmental Protection Agency (2006) National Ambient Air Quality Standards for lead: final rule. 40 CFR Parts 50, 51, 53 and 58. Fed Regis 73:66964–67062
74. U.S. Environmental Protection Agency (2006) National Ambient Air Quality Standards for particulate matter: proposed rule. Fed Regist 71:2620–2708
75. U.S. Environmental Protection Agency (2006) National Ambient Air Quality Standards for particulate matter: final rule. Fed Regist 71:61144–61233
76. U.S. Environmental Protection Agency (2006) Regulatory impact analysis for the National Ambient Air Quality Standard for particulate matter (Issues October 6, 2006). http://www.epa.gov/ttn/naaqs/standards/pm/s_pm_cr_fr.html. Accessed 2 Dec 2011
77. U.S. Environmental Protection Agency (2007) Ozone health risk assessment for selected urban areas. U.S. Environmental Protection Agency, Research Triangle Park, NC, EPA 452-R-07-009
78. U.S. Environmental Protection Agency (2007) Ozone population exposure analysis for selected urban areas. U.S. Environmental Protection Agency, Research Triangle Park, NC, EPA 452-R-07-010
79. U.S. Environmental Protection Agency (2007) Review of the National Ambient Air Quality Standards for ozone: policy assessment of scientific and technical information
80. U.S. Environmental Protection Agency (2007) National Ambient Air Quality Standards for ozone: proposed rule 40 CFR part 50. Fed Regist 72:37818–37919
81. U.S. Environmental Protection Agency (2008) National Ambient Air Quality Standards for ozone: final rule 40 CFR parts 50 and 58. Fed Regist 73:16436–16514
82. U.S. Environmental Protection Agency (2008) Final ozone NAAQS regulatory impact analysis, EPA-452/R-08-003. http://www.epa.gov/ttnecas1/regdata/RIAs/452_R_08_003.pdf. Accessed 2 Dec 2011
83. U.S. Environmental Protection Agency (2009) Risk and exposure assessment to support the review of the SO_2 primary National Ambient Air Quality Standards. U.S. Environmental Protection Agency, Research Triangle Park, NC, EPA/452/R-09-007
84. U.S. Environmental Protection Agency (2009) Integrated science assessment for particulate matter (Final report). http://cfpub.epa.gov/ncea/cfm/recordisplay.cfm?deid=216546. Accessed 2 Dec 2011
85. U.S. Environmental Protection Agency (2010) Proposed revisions to National Ambient Air Quality Standards for ozone: proposed release. Fed Regist 73:2938–3052
86. U.S. Environmental Protection Agency (2010) Primary National Ambient Air Quality Standards for nitrogen dioxides: final rule. Fed Regist 75:6474
87. U.S. Environmental Protection Agency (2010) Primary National Ambient Air Quality Standard for sulfur dioxide: final rule. Fed Regist 75:35520–35603
88. U.S. Environmental Protection Agency (2011) Integrated science assessment for ozone and related photochemical oxidants (first external review draft). U.S. Environmental Protection Agency, Washington, DC, EPA/600/R-10/076A
89. U.S. Environmental Protection Agency (2011) Review of National Ambient Air Quality Standards for carbon monoxide: final rule. Fed Regist 76:54204–54343
90. Wang H, Jacob DJ, Le Sager P, Streets DG, Park RJ, Gilliland AB, van Donkelaar A (2009) Surface ozone background in the US: Canadian and Mexican pollution influences. Atmos Environ 43:1310–1319
91. White House Press Release (2011) Statement by the President on the Ozone National Ambient Air Quality Standards
92. White RH, Cote I, Zeise L, Fox M, Dominici F, Burke TA, White PD, Hattis DB, Samet JM (2009) State-of-the-science workshop report: issues and approaches in low dose–response extrapolation for environmental health risk assessment. Environ Health Perspect 117(2). doi:10.1289/ehp.11502. http://www.ehponline.org/members/2008/1150211502.pdf
93. *Whitman* v. *American Trucking Associations* (2001) 531 U.S. 457, 121S. Ct. 903149L. Ed. 2d1
94. WHO (World Health Organization (1987) Air quality guidelines for Europe. World Health Organizaion Regional Office for Europe, Copenhagen (WHO Regional Publications, European Series No. 23). http://www.who.int/mediacentre/factsheets/fs313/en/index.html. Accessed 2 Dec 2011
95. WHO (World Health Organization (2000) Air quality guidelines for Europe, 2nd edn. WHO Regional Publications, European Series No. 91. http://www.euro.who.int/__data/assets/pdf_file/0005/74732/E71922.pdf. Accessed 2 Dec 2011
96. WHO (World Health Organization) (2005) WHO air quality guidelines for particulate matter, ozone, nitrogen dioxide and sulfur dioxide, global update 2005. Summary of risk assessment. http://www.who.int/phe/health_topics/outdoorair_aqg/en/. Accessed 2 Dec 2011
97. Wolff GT (1996) Letter to Carol M. Browner, U.S. Environmental Protection Agency Administrator. Closure on Draft Office of Air Quality Planning and Standards (OAPQS Staff Paper). Review of the National Ambient Air Quality Standards for particulate matter: policy assessment of science and technical information

Books and Reviews

Donaldson K, Borm P (eds) (2007) Particle toxicology. CRC Press/Taylor and Francis, New York

Finlayson-Pitts BJ, Pitts JN Jr (2000) Chemistry of the upper and lower atmosphere: theory, experiments, and applications. Academic, San Diego, California

Gardner DE (2005) Toxicology of the lung, 4th edn. CRC Press, Boca Raton, Florida

Gardner DE, Crapo JD, McClellan RO (eds) (1999) Toxicology of the lung, 3rd edn. Taylor and Francis, Washington, DC

Gehr P, Heyder J (eds) (2000) Particle-lung interactions. Marcel Dekker, New York

Godish T (2003) Air quality, 4th edn. Taylor and Francis, Philadelphia, PA

Harrison RM, Hester RE, Harrison RM (eds) (2009) Air quality in urban environments (Issues in environmental science and technology). Royal Society of Chemistry, London, UK
Hayward SF, Schwartz JM (eds) (2007) Air quality in America. AEI Press, Washington, DC
Hodgson E (2010) A textbook of modern toxicology. Wiley, Hoboken, New Jersey
Holgate ST, Samet JM, Koren HS, Maynard RL (eds) (1999) Air pollution and health. Academic, San Diego
Klaassen CD (ed) (2007) Casarete and Doull's toxicology, 7th edn. McGraw-Hill, New York, NY
Lippmann M (ed) (2009) Environmental toxicants, human exposures and their health effects, 3rd edn. Wiley, Hoboken
McClellan RO, Henderson RF (eds) (1995) Concepts in inhalation toxicology, 2nd edn. Taylor and Francis, Philadelphia, Pennsylvania
McMurry PH, Shepherd MF, Vickery JS (eds) (2004) Particulate matter science for policy makers – a NARSTO assessment. Cambridge University Press, Cambridge, MA
Morris JB, Shusterman DJ (eds) (2010) Toxicology of the nose and upper airways. Informa Health Care, London
Phalen RF (2002) The particulate air pollution controversy: a case study and lessons learned. Kluwer Academic, Boston, Massachusetts
Phalen RF, Phalen RN (2011) Introduction to air pollution science. Jones and Bartlett Learning, Burlington, MA
Preining O, Davis EJ (eds) (2000) History of aerosol science: proceedings of the symposium on the history of aerosol science, Vienna, 31 Aug–2 Sept 1999. Verlag Der Osterreichischen Akademie Der Wissenschaften, Wien
Ruzer LS, Haley NH (eds) (2005) Aerosols handbook: measurement, dosimetry and health effects. CRC Press, Boca Raton, Florida
Schäfer S, Marquardt H, Welsch F, McClellan R (1999) Toxicology. Academic, San Diego, California
Seinfeld JH, Pandis SN (2000) Atmospheric chemistry and physics: from air pollution to climate change, 2nd edn. Wiley, New York, NY

Air Quality, Surface Transportation Impacts on

Paul Boulter
PAEHolmes, Sydney, Australia

Article Outline

Glossary
Definition of the Subject
Introduction
Historical Trends
Air Pollution Pathways
Emission Processes
Modelling Transport Emissions
Pollutant Dispersion and Transformation
Modelling Air Pollution from Transport
Reducing Air Pollution from Transport
Future Directions
Bibliography

Glossary

DPF Diesel particulate filter, the preferred and most effective technology for removing particulate matter from diesel exhaust. DPFs can be broadly divided into two types: "full flow" and "partial flow." The latter are more permeable and are less effective, but need no maintenance. DPFs physically capture particles and can fill up rapidly. They must therefore be periodically "regenerated," and several passive and active systems have been developed for this purpose.

Emission standard A value that specifies the maximum amount of a pollutant that can be released into the environment per unit activity (e.g., g/km or g/kWh).

NO_2 Nitrogen dioxide, a gaseous air pollutant produced as a result of combustion. NO_2 is also a precursor for a number of harmful secondary air pollutants such as ozone, and plays a role in the formation of acid rain. Long-term exposure to high concentrations of NO_2 causes adverse health effects, and levels regularly exceed air quality standards.

O_3 Ground-level ozone, a secondary pollutant produced by reactions between NO_2, hydrocarbons, and sunlight. High levels of ozone are generally observed during hot, sunny weather, and concentrations tend to be higher in rural areas than in urban areas.

PM_{10} Mass concentration of particles with an aerodynamic diameter of less than 10 μm. Particles smaller than 10 μm (also known as "thoracic" particles) can settle in the bronchi and lungs.

$PM_{2.5}$ Mass concentration of particles with an aerodynamic diameter of less than 2.5 μm, sometimes referred to as "fine" or "respirable" particles. Particles in this size range can penetrate deep into the lungs.

Primary particles Particles emitted directly to the atmosphere, typically as a result of combustion or abrasion processes.

SCR Selective catalytic reduction, an exhaust aftertreatment method that is used to reduce emissions of nitrogen oxides. It will be the main technology for enabling compliance with future emission standards.

Secondary particles Particles formed within the atmosphere from gas-phase precursors. These include particles originating from atmospheric oxidation of sulfur and nitrogen oxides, and their reaction products with ammonia, and from the oxidation of organic compounds.

Ultrafine particles Particles with a diameter of less than 0.1 μm. These can pass through cell membranes and migrate from the lungs into other organs. There is evidence to indicate that they may be more damaging to the cardiovascular system than PM_{10} and $PM_{2.5}$.

Definition of the Subject

Until the middle of the twentieth century poor air quality in populated areas was usually associated with domestic and industrial combustion, with coal burning leading to high concentrations of smoke and sulfur dioxide. A recent retrospective analysis has indicated that the most famous example of this type of pollution – the great London smog of 1952 – was responsible for 12,000 deaths [1]. However, during the 1940s and 1950s an altogether different type of pollution was observed in the United States. Haagen-Smit identified a mechanism by which air pollutants reacted with the Los Angeles sunlight to produce a noxious photochemical smog [2], and it became clear that the pollution originated not from the use of coal but from road vehicles.

In the subsequent decades urban air pollution has become synonymous with road transport, the link being attributable primarily to the growth in the ownership and use of private cars. Photochemical smog has remained a problem in some of the largest cities in the world, and many people are exposed to pollutant concentrations which exceed health-based air quality standards. It has also become evident that some transport-derived pollutants can travel thousands of kilometers before deposition and damage occur and, in the case of greenhouse gases, can have a global effect over long timescales. If transport systems are to become environmentally sustainable, then the scale of such adverse effects will have to be greatly reduced.

The aim of this entry is to provide an overview of the impacts of surface transport (road, rail, and shipping) on emissions and air quality. Different regions of the world have different air pollution problems, and not all countries and issues can be covered here. The entry refers mainly, but not exclusively, to the European Union (EU), and the emphasis is on local air pollution in populated areas. Inevitably, the entry deals predominantly with road transport, but some consideration is also given to the other modes.

Introduction

Surface transport is an important, and in many respects, the most important source of air pollution. The pollutants released from road, rail, and waterborne traffic are implicated in a variety of direct and indirect detrimental impacts on amenity, health, ecosystems, and cultural heritage over different time periods and on different geographical scales. The effects of transport pollution can be very local and immediate, such as the nuisance caused by a plume of black smoke from the exhaust pipe of a car or a diesel train. More seriously, repeated exposure to exhaust gases and particles is linked to aggravated respiratory and cardiovascular disease, changes to lung tissue, changes in the function of the nervous system, and premature mortality [3, 4]. Threats to cultural heritage posed by atmospheric pollutants include the soiling of historical buildings – a common sight alongside busy urban roads – and indoor damage to works of art and museum exhibits. Transport emissions also contribute to the regional degradation of air quality, to eutrophication, and to acidification (see entry on ► Regional Air Quality). Moreover, stable pollutants, including the greenhouse gases carbon dioxide (CO_2), methane, and nitrous oxide can contribute to environmental problems on a global scale for decades and even centuries.

The pollutants that are currently causing the greatest concern in terms of air quality, primarily because of their impact on human health, are airborne particulate matter (PM), nitrogen dioxide (NO_2), and ground-level ozone (O_3). Surface transport is an important contributor to all three [5], but road

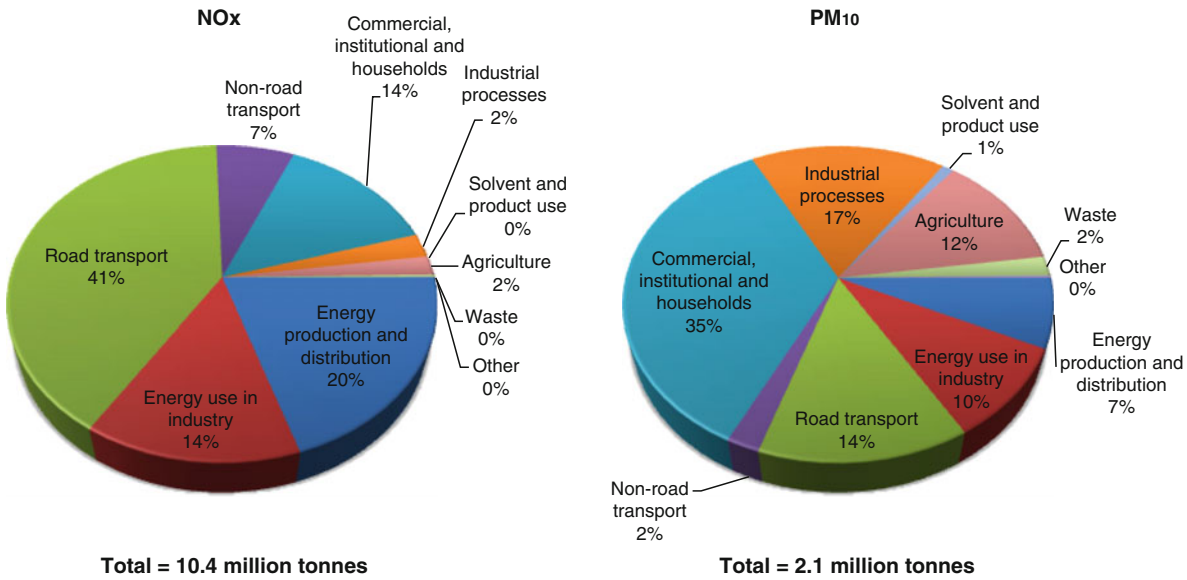

Air Quality, Surface Transportation Impacts on. Figure 1
NO_x and PM_{10} emissions in 2008 by sector, based on data submitted by EU-27 countries to CLRTAP [8]

transport is the main culprit, especially in population centers, and it presents some of the greatest challenges in terms of sustainability.

The importance of road transport as a source of pollution can be illustrated by reference to sectoral emissions in Europe. Figure 1 shows emission data for the EU-27 countries, based on submissions to the UNECE Convention on Long-range Transboundary Air Pollution (CLRTAP). In 2008, road transport was the largest contributor to NO_x emissions in Europe (41%), and was also a major contributor to PM_{10} emissions. By comparison, non-road transport was responsible for just 7% of total NO_x emissions and only 2% of total PM_{10} emissions. However, it is important to observe that the totals in Fig. 1 are based on national reporting, and do not include international aviation or international maritime shipping. The latter is an important source of NO_x and sulfur oxides (SO_x). Recent studies have indicated that around 15% of global NO_x emissions and 5–8% of global SO_x emissions are attributable to oceangoing ships [6, 7].

At the local level, the impacts of road transport are exacerbated by the proximity of vehicles (and their emissions) to the population, although the other surface transport modes can contribute significantly to poor air quality at specific sites such as busy railway stations, underground systems, and large ports.

Rail transport only contributes a small proportion to total emissions from the transport sector, but individual diesel locomotives have large engines, and exhaust aftertreatment equipment is not currently used on traction units. Elevated pollutant concentrations have therefore been observed where diesel locomotives are running with the engine at idle in enclosed stations [9]. Several studies have addressed the exposure of passengers to air pollution in underground rail systems, where pollutant concentrations appear to be considerably higher than those above ground. For example, consistently high concentrations of PM_{10} and $PM_{2.5}$ have been reported [10–12].

Many major ports are also major cities, and so emissions from seagoing ships in such ports can directly affect a large population [13]. Ships at berth are the main source of shipping emissions in ports; the time spent at berth is typically 1 or more days, whereas the time spent maneuvering is typically only a few hours [14]. Moreover, almost 70% of maritime ship emissions occur within 400 km of land, and ships therefore have the potential to contribute significantly to pollution in coastal communities [13].

On the global scale, PM emissions from marine shipping are thought to be responsible for around 60,000 deaths annually, with impacts concentrated in coastal regions on major trade routes. Most mortality effects are seen in Asia and Europe where high populations and high shipping-related PM concentrations coincide [13].

The literature on transport-related air pollution is very extensive, and it is not possible to cover every aspect in depth in this entry. The emphasis is therefore on key areas such as historical trends in transport activity and emissions, the processes of pollutant formation, and modelling approaches. Importantly, given the context of this encyclopedia, a substantial part of the entry is devoted to policies and measures which can be implemented to reduce the impacts of surface transport on air quality, and thus contribute to sustainability.

Historical Trends

The general trend in motorized transport has been one of unremitting growth, driven primarily by the association of personal mobility with quality of life [15] and its consequence in terms of passenger car ownership. In the United States the number of cars grew from 140,000 in 1907 to more than 20 million in 1927 [15]. A similar pattern occurred in Europe several decades later – Fig. 2 shows car ownership in some European countries since 1970 – and is being repeated again now in parts of Asia.

The recent evolution of transport activity in the EU-27 countries is shown in Fig. 3. The top graph shows passenger transport by mode in passenger-kilometers (pkm) (note the different scales), and the bottom graph shows freight transport in tonne-kilometers (tkm). Between 1995 and 2008, passenger transport by car increased by 21%. The growth in passenger transport was lower for buses/coaches (9%) and rail (17%), and there was a net reduction of 8% in passenger transport by sea. Although it is not of direct relevance to this entry, it should be recognized that during the same period passenger transport by air increased by 62% (see entry on ► Aviation and Atmosphere). Road freight in the EU-27 increased by almost 50% between 1995 and 2008, and there was also substantial growth in the transport of freight by rail (15%), inland waterways (19%) and shipping (30%).

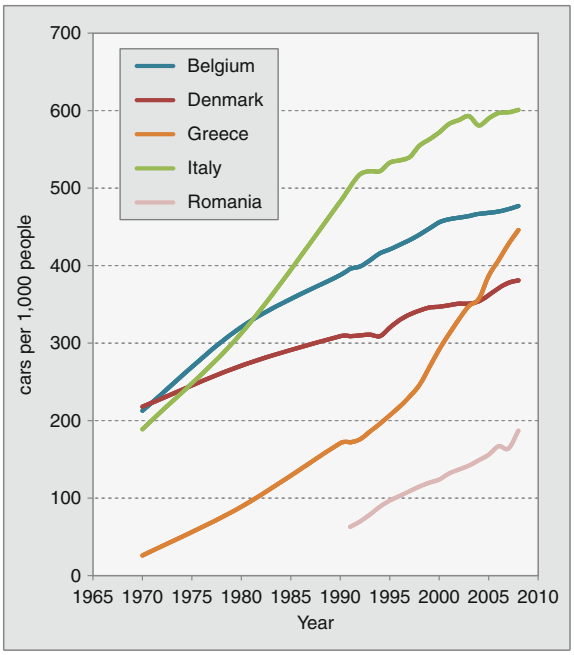

Air Quality, Surface Transportation Impacts on. Figure 2 Passenger car ownership in selected European countries (Adapted from [16, 17])

In response to similar trends in all industrialized countries and their implications for air quality, legislation and strategies have been put in place to combat transport-related emissions. Calculations have established that emissions from road transport in the EU peaked in the early 1990s [18] but have been reducing since then as controls on fuel and emissions have tightened (Fig. 4). Emissions of regulated pollutants are likely to continue to decrease in the future as new vehicles, locomotives, and vessels, which comply with more stringent emission limits, replace older ones, although the reductions will be offset to some extent by growth in transport activity.

There have been some notable successes. In spite of the continued growth in traffic in Europe, the emissions and atmospheric concentrations of some pollutants – such as lead, carbon monoxide and benzene – have decreased so dramatically that they are no longer considered to be a major threat to human health. However, in many urban areas the concentrations of NO_2 and PM_{10} still frequently exceed health-based limit values. According to the European Environment Agency, in 2004, more than 20% of the European

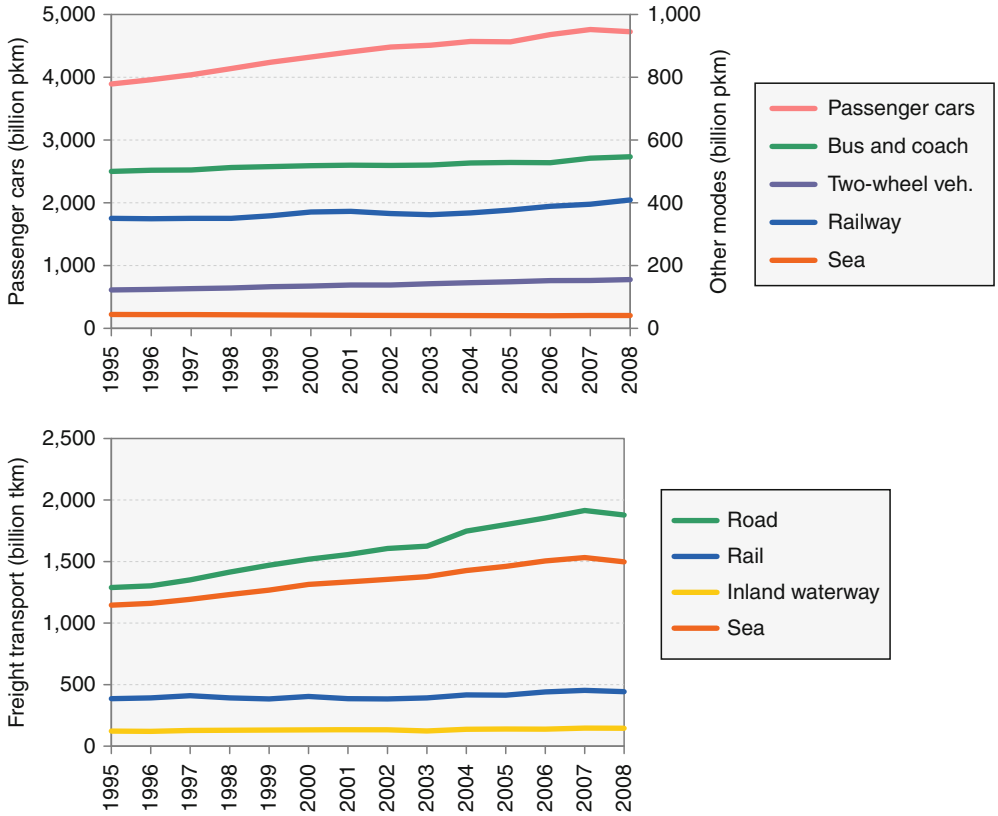

Air Quality, Surface Transportation Impacts on. Figure 3
Passenger and freight transport in the EU-27 countries by mode between 1995 and 2008 (Adapted from [17])

urban population were exposed to ambient NO_2 concentrations above the annual mean limit value (40 μg/m^3) [19]. Furthermore, NO_2 and PM_{10} concentrations at many roadside monitoring sites are not decreasing [19–21]. The problem is not confined to Europe; for example, a similar problem has been observed in Japan [22]. Some possible reasons for this are explored later in this entry. A further concern is that emissions of non-exhaust particles – especially those arising from road vehicle tire and brake wear – are not subject to legislation or control, and are currently increasing in line with traffic growth (bottom graph in Fig. 4).

Air Pollution Pathways

The links between transport, emissions, air pollution, and adverse impacts are not straightforward. To illustrate this, the complex pathway from emissions to one specific type of impact – the health outcomes of road transport pollution – is summarized in Fig. 5.

Many different pollutants are emitted by road traffic, and the strength of the source depends on the emission factors for the vehicles and the characteristics of the traffic (e.g., volume, speed and composition). The emitted (primary) pollutants are then dispersed in the ambient air according to the local topography and meteorology. The main direct impacts of primary pollutants are near to the point of emission; further away, concentration decreases rapidly as a result of dispersion and dilution. However, many of the primary pollutants react together, and with pollutants from other sources, to form secondary pollutants. Because of the time required for their formation, the concentrations of secondary pollutants are not always highest near the emission source.

The overall exposure of individuals to air pollutants is dependent upon the types of activity in which they

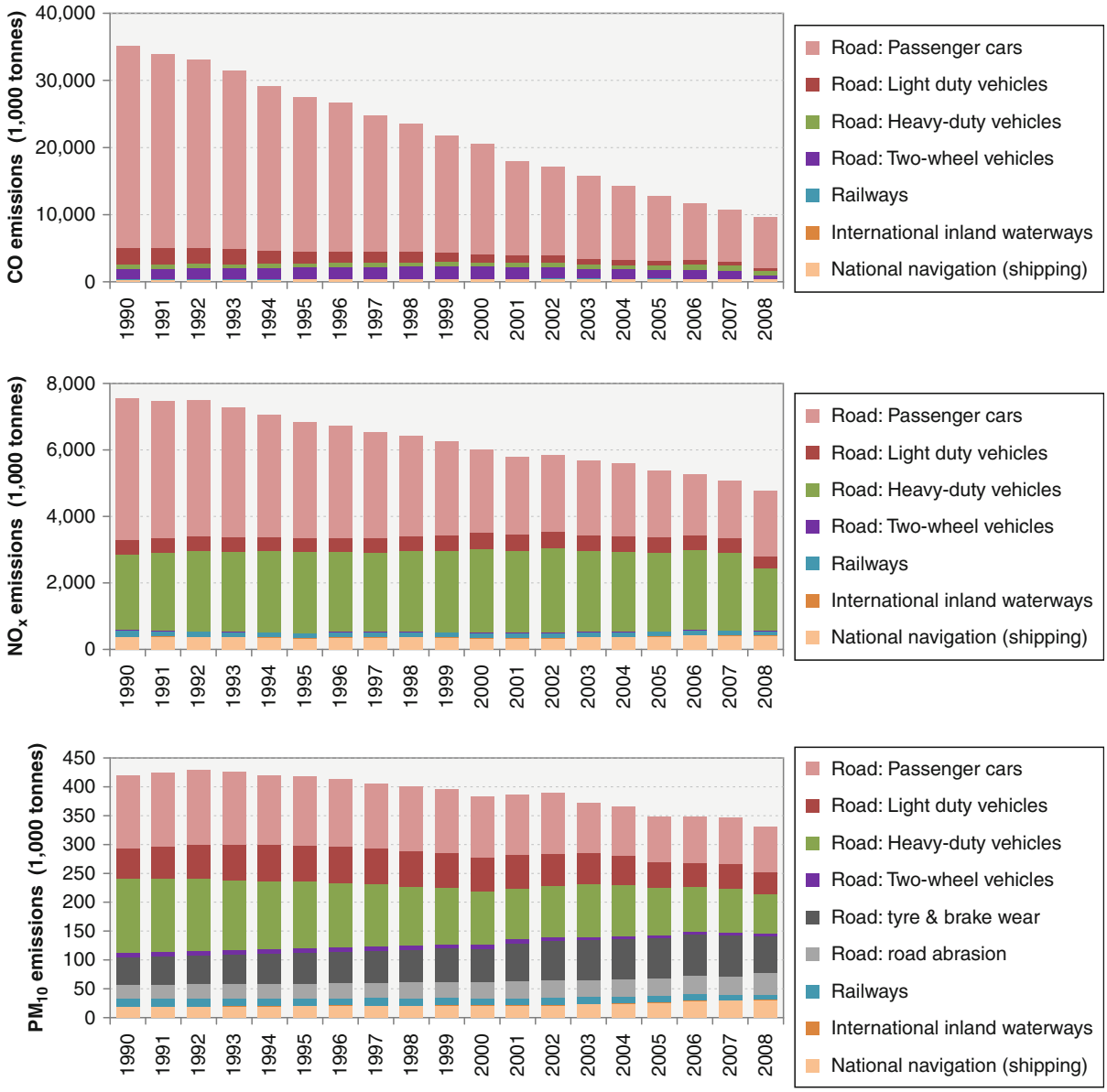

Air Quality, Surface Transportation Impacts on. Figure 4
CO, NO_x, and PM_{10} emissions by transport mode (excluding aviation) between 1990 and 2008, submitted by EU-27 countries to CLRTAP [8]

are engaged, the locations of those activities, and the pollutant concentrations in those locations. One way of determining "integrated" personal exposure is through the use of a "microenvironment" model [24]. The term microenvironment describes a location with a distinct level of pollution, such as outdoors in the street, indoors at home, in transit, at the workplace, etc. The fraction of time spent in each microenvironment allows the calculation of integrated exposure. However, the calculation of such an integral is often not possible because the pollutant concentrations in the different microenvironments are not known. The term "average exposure" is therefore commonly used, and this is normally taken to mean the pollutant concentration

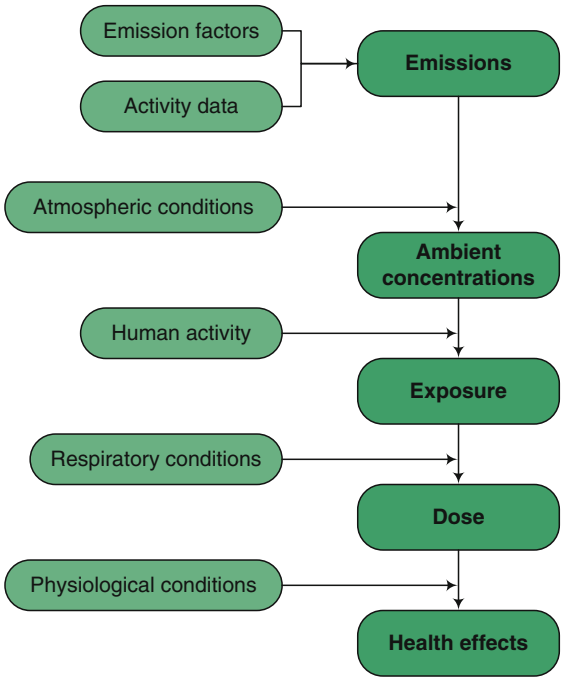

Air Quality, Surface Transportation Impacts on. Figure 5 Simplified pathway from transport emission to health effect (Adapted from [23])

over a specified period (e.g., annual mean) at an outdoor location which is broadly representative of where people are likely to spend time. This approach is used in the regulation of ambient air quality.

Once the pollutant has crossed a physical boundary (e.g., alveolar epithelial cells), the concept of "dose" is used [25]. The dose is the mass of material absorbed or deposited in the body during an interval of time, and depends on the respiratory activity of the individuals concerned. Responses to doses – the actual health effects – can also vary from person to person, depending on physiological conditions.

Emission Processes

Combustion

Most vehicles are powered by internal combustion engines (ICEs). Notable exceptions include vehicles powered by electricity drawn from an external grid (as in the case of rail locomotives), from on-board batteries (as in the case of road vehicles and waterborne vessels) or, more recently, from in situ generation involving fuel cells.

The principles of ICEs apply equally to road vehicles, rail locomotives, and waterborne vessels, the main differences being the size of the engine and the type of fuel used. In an ICE energy is derived from the burning of hydrocarbon fuel in air, with the main products being CO_2 and water vapor. Incomplete combustion results in the production of CO, PM (especially in the case of diesel engines), and many different organic compounds. In addition, at the high temperatures and pressures found in the combustion chamber, some of the nitrogen in the air is oxidized, forming mainly nitric oxide (NO) with some NO_2. By convention, the sum total of oxides of nitrogen (i.e., $NO + NO_2$) is termed NO_x.

NO formation proceeds via two main mechanisms: the "thermal" (Zel'dovich) and "prompt" mechanisms [26], with the former being responsible for more than 90% of emissions [27]. NO_2 is predominantly a secondary pollutant, its major source being the atmospheric oxidation of combustion-derived NO. The NO_2 emitted directly from vehicles is referred to as "primary NO_2," and its importance will be described later.

Particles in diesel exhaust cover a range of sizes, and the shape of the size distribution depends on whether the weighting is by number or mass (Fig. 6). There are three distinct size modes: the nucleation mode (sometimes referred to as nuclei or nanoparticles), the accumulation mode, and the coarse mode. The nucleation mode has traditionally been defined as particles with a diameter of less than 50 nm. Accumulation mode particles range in size from around 50 nm to around 1 μm, with particles smaller than 0.1 μm being referred to as ultrafine particles. When a nucleation mode is observed (this is not always the case in engine exhaust), it contains many more particles than the accumulation mode, although because each particle is so small the total mass will not increase substantially. The coarse mode consists of particles larger than around 1 μm.

The processes of particle formation during diesel combustion have been described in detail [26]. Carbonaceous spherules (soot) are initially created in the cylinder. A phase of particle growth then follows, involving the adsorption of gas-phase components, as well as coagulation and agglomeration. Almost all the particles found in the exhaust prior to dilution are

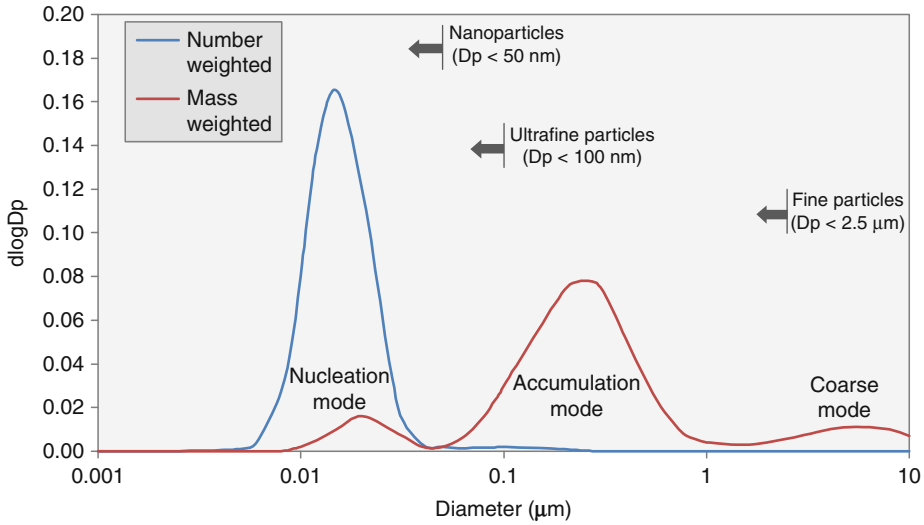

Air Quality, Surface Transportation Impacts on. Figure 6
Typical particle size distributions in vehicle exhaust. The *y*-axis is a normalized log scale (Adapted from [28])

present as these carbonaceous agglomerates (hence, accumulation mode), with a small amount of metallic ash. The processes leading to the presence of nucleation mode particles in the exhaust during measurement are quite complex. Most nucleation mode particles are thought to originate from the condensation of volatile material (hydrocarbons, hydrated sulfuric acid and salts) in the exhaust gas during dilution, rather than during combustion itself, and their formation is a function of measurement parameters such as temperature, dilution ratio, residence time, and humidity [28–30], as well as fuel sulfur content [31, 32]. Particles in the coarse mode are formed by re-entrainment of material previously deposited on engine cylinder and exhaust system surfaces. Some of the pollutants emitted by fuel combustion (sulfur oxides and nitrogen oxides) are also precursors of secondary particles in the atmosphere.

The main factors that govern exhaust emissions are the vehicle type, the fuel used, the vehicle technology, and the driving conditions. The term "vehicle technology" can be used to refer to either a specific type of engine or exhaust aftertreatment, or more generally compliance with a particular emission standard. Some examples of these effects are shown for road vehicles in Fig. 7. Other factors include vehicle weight, road gradient, vehicle load, and the use of auxiliary equipment such as air-conditioning. Another important consideration is the so-called dynamics of driving (see "Modelling transport emissions").

The thermal state of the engine and exhaust emission-control system also has a strong influence on emissions from road vehicles. Most emissions occur under what are known as thermally stable or "hot" engine and exhaust conditions. The temperature of engine coolant during normal operation is typically between around 70°C and 90°C, whereas the temperature of the exhaust system reaches several hundred degrees centigrade. During the warm-up period following an engine start, emissions and fuel consumption are elevated as a result of incomplete combustion, the low conversion rate of pollutants in the catalyst, and increased viscous friction due to the low lubricant temperature in the engine and transmission. These "cold-start" emissions can constitute a significant proportion of total road transport emissions, particularly in urban areas. Cold-start emissions and fuel consumption are higher for lower engine starting temperatures which will, in turn, depend upon factors such as the length of time the vehicle has been parked and the prevailing ambient temperature.

Rail locomotives are mainly powered by either diesel or electricity. The nature of the pollution emitted from rail transport is dependent upon the type of

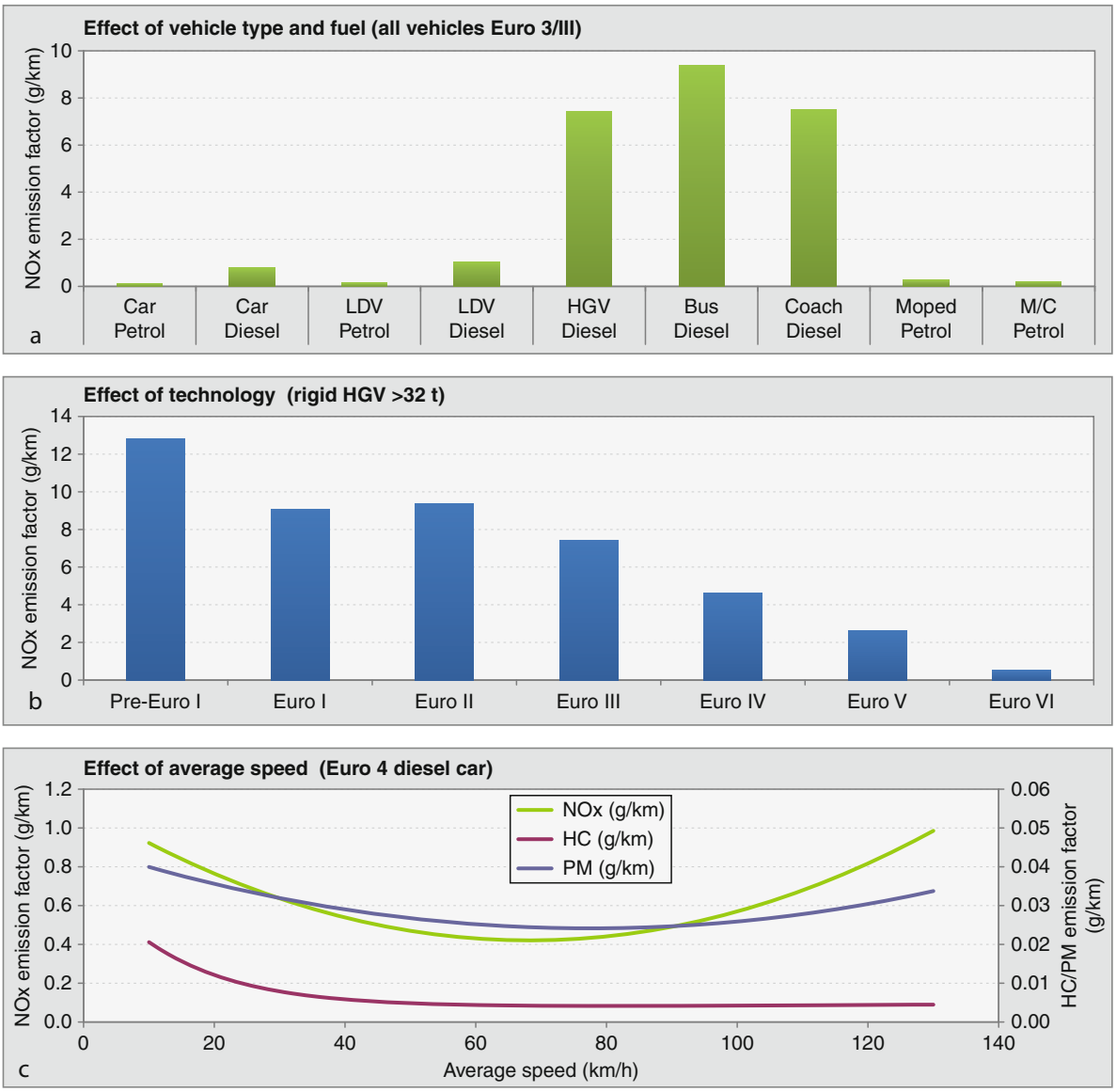

Air Quality, Surface Transportation Impacts on. Figure 7
Factors influencing emissions: (**a**) vehicle and fuel type, (**b**) technology, and (**c**) average speed (Adapted from [33])

traction. In the case of diesel locomotives, pollutants are emitted directly into the local environment as result of combustion, whereas for electric locomotives the emission is effectively transposed to the power stations which are responsible for producing the electricity. Emissions from electric trains are therefore normally allocated to the power generation sector. Compared with road vehicles, trains generally have low emissions per passenger-kilometer although this depends, of course, on the passenger load factors.

Shipping is responsible for a significant fraction of NO_x and primary PM emissions in some countries. Many ships have old engines or old technology, and compared with road transport few exhaust aftertreatment devices are in use. The quality of the fuel is also poor relative to that used for road vehicles. In particular, the

residual fuel oil used in ship engines contains very high levels of sulfur (up to 4.5% by mass), which leads to high PM emissions [34]. To put this in perspective, the PM emission factor for ship engines is typically around 1.25 g/kWh [35], compared with the legislative limit value of 0.02 g/kWh for a modern Euro V truck. There is little information on the size distribution of PM emissions from ships, although some recent data indicate that a large fraction of the emitted particles can be classified as $PM_{2.5}$ [34]. NO_x and sulfur dioxide (SO_2) emissions from shipping also contribute significantly to secondary particle formation.

Evaporation

Volatile organic compounds (VOCs) are emitted from the fuel systems of petrol vehicles as a result of evaporation. The compounds that are emitted are mainly of light hydrocarbons (C_4–C_6) [36]. Evaporative emissions from diesel-fuelled vehicles are considered to be negligible due to the low volatility of diesel fuel.

There are several different mechanisms of evaporation. "Diurnal losses" are due to the thermal expansion and emission of vapor, mainly in the fuel tank, as a result of changes in ambient temperature during the day. "Hot-soak losses" occur when a warm engine is turned off and heat is dissipated into the fuel system. Whilst a vehicle is being driven, the engine provides a continuous input of heat to the fuel system, resulting in "running losses." In addition, "refueling losses" occur while the tank is being filled and the saturated vapors are displaced and vented into the atmosphere, but these are usually attributed to the fuel handling chain.

Evaporative emissions are dependent upon four major factors: the vehicle design, the ambient temperature, the volatility of the petrol, and the driving conditions. Emissions have decreased significantly in recent years as a result of new cars being equipped with sealed fuel injection systems and activated carbon canisters in fuel tank vents [5].

Abrasion

As noted earlier, particles are also generated as a result of various unregulated abrasion processes, including tire wear, brake wear, and road surface wear. These sources are becoming increasingly important (Fig. 4), but the understanding of emissions of abrasion particles is relatively poor and their health effects are not well documented.

There is little information on the composition of tire wear particles. Components that have been suggested as environmental tracers of tire wear include styrene butadiene rubber [38], benzothiazole [39], and organic zinc [40]. Studies conducted in the 1970s revealed that wear particles had a bimodal distribution, with mass in the both the fine (<2.5 μm) and coarse (2.5–10 μm) modes [38, 41–43]. Several laboratory and field investigations have demonstrated that most particles are present in the coarse fraction [38, 44, 45], or are larger still [46], whereas others have indicated substantial mass in both the $PM_{2.5}$ and PM_1 fractions [40, 47, 48]. In one early study, it was observed that mean particle diameter decreases with increasing speed, and this may be one factor contributing to the differences in the reported findings [42].

Airborne brake particles are composed of metals (iron, copper, lead, etc.), organic material, and silicon compounds, which are used as binders in brake pads, but composition varies greatly [37]. Test track and wind tunnel measurements have revealed that typically 50% of the brake wear debris escapes the vehicle and enters the atmosphere, although the actual proportion depends on the severity of the braking and the design of the vehicle [49]. The remaining debris either falls on the road or is retained on the vehicle. It appears that most airborne brake wear particles can be classified as PM_{10}, although a substantial proportion has a diameter of less than 2.5 μm [49–52]. The highest proportions of $PM_{2.5}$ have been found under urban driving conditions [52].

Very little information is available on the size distribution of road surface wear particles. The data that are available suggest that airborne bitumen particles range in size between 0.35 μm and 2.8 μm [40].

Particle measurements conducted near a busy electrified railway line in Zurich showed that the main elements abraded by railway traffic were iron and manganese originating from the wheel–track interface, as well as copper from the overhead catenary system [53]. More than half of the iron and manganese particles resulting from wheel and track abrasion were in the

coarse range. The abrasion particles provided a small but measureable contribution to local PM_{10} concentrations [54]. However, the contribution of rail transport on lines with a larger diesel share of the traction could be much higher.

Resuspension

Another source of PM – the resuspension of material previously deposited on the road surface – occurs as a result of tire shear, vehicle-generated turbulence, and the action of the wind. Studies in the United States have indicated that resuspension is responsible for between 30% and 70% of total PM_{10} in urban areas [55–57]. Large contributions of resuspension have also been observed in Germany [44, 58, 59] and the UK [60], albeit with a large variation between locations.

Resuspension is a major concern in Scandinavian countries, especially in relation to the use of studded tires and "road sanding." Indeed, it can provide a much larger contribution to PM_{10} than exhaust emissions, and also form a significant fraction of $PM_{2.5}$ [61, 62]. An investigation in Sweden revealed that PM_{10} resuspension is highly dependent on vehicle speed [63].

Modelling Transport Emissions

Estimates of emissions from transport are required for various purposes. National inventories covering all sectors are part of the reporting obligations of CLRTAP, the United Nations Framework Convention on Climate Change and, in the European Union, Directive 2001/81/EC on National Emission Ceilings. At a more local level, emission estimates are required for assessing the impacts of policies and measures, and for input into air quality modelling studies. Separate modelling approaches have been developed for the different transport modes. Most emission models are empirical in nature, being based on data from laboratory or real-world tests. However, it is worth noting that such tests are not always designed to deliver emission factors for modelling, and simulate only a small fraction of all possible operational conditions [5].

Road Transport Models

Combustion In the simplest terms, the total emission of a given pollutant during a given time period is calculated as the sum product of specific emission factors and quantities of activity:

$$E_p = \sum_{v=1}^{v=n} e_{p,v} \times T_v \tag{1}$$

where

E_p = total emission (e.g., in grams) of pollutant p during the period
v = vehicle category (with n different categories)
$e_{p,v}$ = emission factor (e.g., in grams per kilometer or liter of fuel burnt) of pollutant p from vehicle category v
T_v = activity (e.g., in kilometers or liters of fuel) of vehicle category v

The definition of emission factors that represent different aspects of vehicles and their operation forms a substantial area of research. Emission models are generally classified in terms of how they take vehicle operation into account. Here, the term "vehicle operation" is used in a general sense, and refers to a wide range of parameters which describe the way in which a driver controls a vehicle (e.g., average speed, maximum speed, acceleration pattern, gear-change pattern), as well as the way in which the vehicle responds (e.g., engine speed, engine load). The main types of approach are aggregated emission factors, average-speed models, traffic situation models, multiple-regression models, modal models, and instantaneous models.

Aggregated emission factors operate on the simplest level, with a single emission factor representing a general type of driving; the traditional distinction is between urban roads, rural roads, and motorways. Vehicle operation is therefore only taken into account at a very rudimentary level. However, they are generally the only way of estimating emissions of unregulated pollutants, for which there is often insufficient information to define a more detailed relationship with vehicle operation.

Average-speed models are based upon the principle that the emission factor varies according to the average speed during a trip. The general process of model development is shown in Fig. 8. Firstly, vehicle operation in the real world is measured using on-board instruments, with the vehicles being driven under

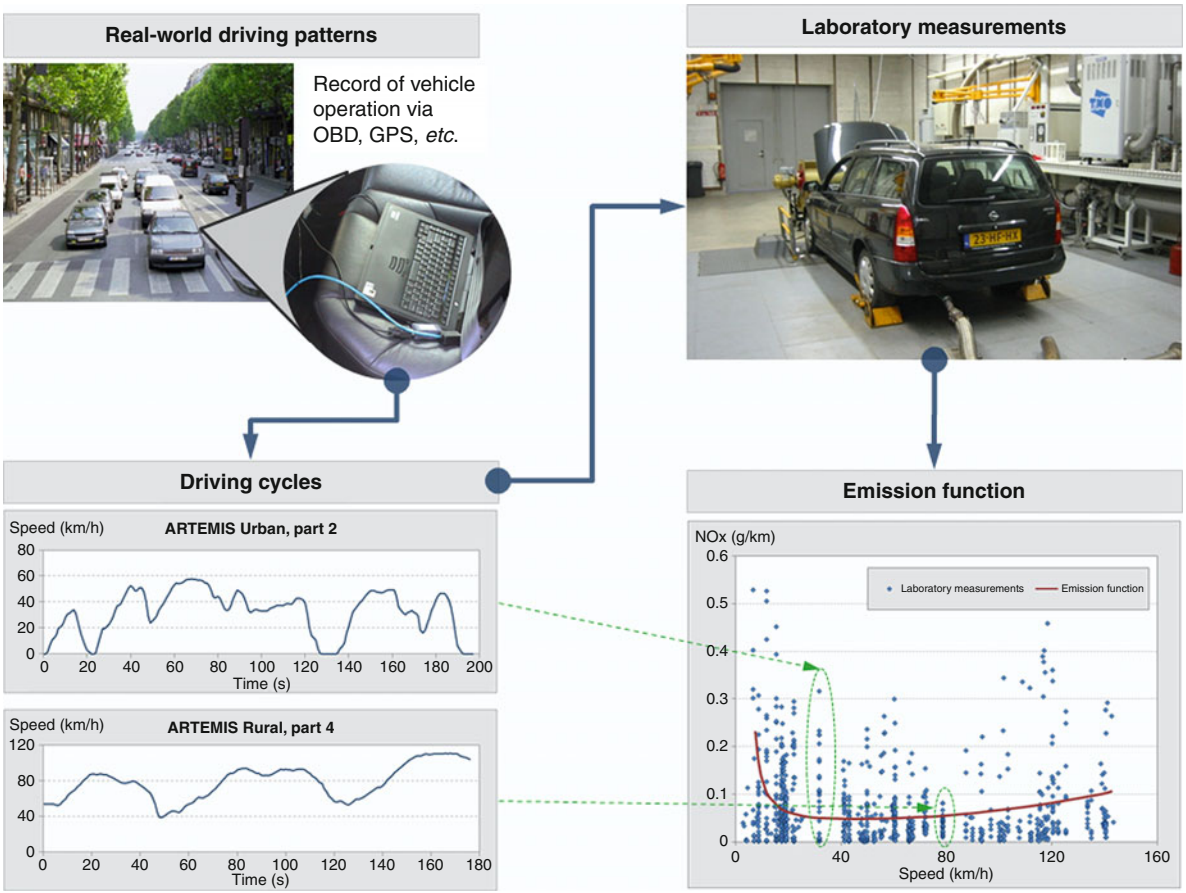

Air Quality, Surface Transportation Impacts on. Figure 8
Process of development for average-speed models (Photographs reproduced by kind permission of Alistair Smith, Tim Barlow of TRL in the UK, and TNO Automotive in the Netherlands)

a wide range of road and traffic conditions. The numerous resulting driving patterns are then condensed, using statistical methods, into a much smaller number of representative driving cycles which can be used to test vehicles in the laboratory. The results from the laboratory tests on vehicles in the same category (e.g., small petrol cars complying with the Euro 4 legislation) are then plotted as a function of average speed, and a regression curve is fitted to the date to give an emission function. Given that exhaust emissions are inherently variable, there is usually a considerable amount of scatter in the emission data.

Average-speed models are widely used in emission inventories and local air pollution models. In Europe, the most widely used example is COPERT [33]. A number of factors have contributed to their popularity. The modelling approach is one of the oldest, it is comparatively easy to use, several models are available free of charge, and there is a reasonably close correspondence between the required inputs and the data available to users. However, trips having very different vehicle operation (and different emission levels) can have the same average speed. Clearly, all the types of operation associated with a given average speed are not accounted for by the use of a single emission factor. This is a particular problem at low-medium average speeds, for which the range of possible operational conditions associated with a given average speed is great. In addition, for modern vehicles a large proportion of the total emission during a trip can be emitted as very short, sharp peaks, often occurring during gear changes and periods of high acceleration,

and this detail is lost when only average speed is considered. The concept of "driving dynamics" has therefore been developed to enable model developers to describe vehicle operation using additional parameters [64]. In qualitative terms, dynamics can, perhaps, be thought of as the "aggressiveness" of driving. Quantitatively, the term refers to the variation in various properties or statistical descriptors of a driving pattern. One of the more useful parameters appears to be relative positive acceleration (RPA) [65]. However, most model users have no straightforward means of quantifying such parameters.

In "traffic situation" models, emission factors are referenced to specific traffic situations that are known by the model user. A typical example is the Handbook of Emission Factors [66]. The traffic situations are characterized by the features of the sections of road concerned (e.g., "motorway with 120 km/h limit," "main road outside built-up area"). The driving dynamics are not quantified by the user, but are defined through a textual description (e.g., "free flow," "stop and go"). However, requiring the user to define the traffic situation using a textual description of dynamics may lead to inconsistencies in interpretation.

Multiple-regression models are another comparatively recent development, and the most prominent example is the Dutch VERSIT+ model [67]. The model contains test data for a large number of cars over a range of different driving cycles. Within the model, each driving cycle is characterized by various descriptive parameters (e.g., average speed, RPA, number of stops per km, etc.). A regression model is fitted to the average emission factors and cycle parameters for the various driving cycles, giving the descriptive variables which are the best predictors of emissions (the group of descriptors being different for each type of vehicle and each pollutant). The model requires a driving pattern (speed-time profile) as the input, from which it calculates the same range of descriptive variables and estimates emissions based on the regression results.

In modal models emission factors are allocated to the specific modes of vehicle operation encountered during a trip. In the simplest type, vehicle operation is defined in terms of a relatively small number of modes – typically idle, acceleration, deceleration, and cruise. For each of the modes the emission rate is fixed, and the total emission during a trip, or on a section of road, is calculated by weighting each modal emission rate by the time spent in the mode [68, 69]. This approach has usually been used to determine the impacts of traffic control measures and signal improvements [70].

Some more detailed modal models aim to give a precise description of vehicle emission behavior during a series of short time steps (often 1 s). These are commonly referred to as "instantaneous" models, although several alternative terms can be found in the literature, including "microscale," "continuous," and "online" [71]. In the simplest type of instantaneous model, emission rates are defined for different combinations of speed and acceleration, usually in the form of a matrix [72, 73]. Theoretically, the finer the resolution of the emission factor matrix the higher the model accuracy, but as the resolution improves the complexity of the calculations increases. Some models use the product of speed and acceleration instead of the acceleration alone [74]. A more flexible approach relies upon emission maps that relate to engine power [75, 76]. This allows all relevant factors to be taken into account, including rolling resistance, aerodynamic resistance, acceleration, gradient, transmission losses, and the use of auxiliaries.

Instantaneous models should have a number of advantages. Firstly, emissions can be calculated for any operational profile, and thus new emission factors can be generated without the need for further vehicle testing. Secondly, the models inherently take into account dynamics. Thirdly, emissions can be resolved spatially, and this ought to lead to improvements in the prediction of air pollution. However, detailed and precise data on vehicle operation and location are required, or any potential benefits may be lost. Such data are difficult to obtain for many model users. Moreover, it is extremely difficult to measure emissions on a continuous basis with a high degree of precision, and then it is not straightforward to allocate those emission values to the correct operating conditions. During measurement in the laboratory, an emission signal is dynamically delayed and smoothed, and this makes it difficult to align the emissions signal with the vehicle operating conditions [77]. Such distortions have not been fully taken into account in instantaneous models until relatively recently.

Once the basic modeling approach has been identified a number of other effects may need to be considered, depending on the type of model being used. These effects include potential future improvements to fuels and technologies, the deterioration of vehicle exhaust emissions with age, the presence and use of auxiliary devices (e.g., air conditioning, windscreen wipers, radios), road gradient, and vehicle load/occupancy. Such effects may be taken into account via separate models [78] or through adjustments to the basic emission factors, with assumptions concerning levels of uptake and effectiveness in future years.

Separate models also exist for the estimation of cold-start emissions. In some cases, the hot emission factor is multiplied by a ratio of cold-start to hot emissions for the fraction of kilometers driven with a cold engine [33]. In others, a reference cold-start excess emission value is adjusted to take account of, for example, the ambient temperature, the average speed, the parking duration, and the distance travelled (some trips are shorter than the distance needed to fully warm the engine) [79, 80]. Specific models have also been developed to determine the effects of different parking scenarios [81]. Cold-start emissions are usually included in regional and national emission inventories, but are often excluded from local air pollution studies. One of the main reasons for this is the difficulty associated with obtaining data on the temporal and spatial allocation of cold-start operation.

Evaporation The earliest studies of evaporative emissions were carried out in the United States in the 1960s [82], but the first European studies were only conducted 20 years later [36]. The models that were developed from the resulting data were not updated for many years. However, modelling improvements have recently been possible following a number of new investigations [83–85].

Abrasion and Resuspension One non-exhaust PM model in common use is that presented in the European Environment Agency's Air Pollutant Emissions Inventory Guidebook [33]. The method uses reference emission factors (in g/km) and incorporates corrections for both speed and, in the case of HDVs, vehicle load and number of axles. However, the use of average brake wear emission factors (in g/km) means that differences in the extent of braking for different traffic situations cannot be taken into account. Such emission factors are likely to overestimate brake emissions in areas of low brake use, and underestimate emissions in areas of high brake use.

The calculation method presented in the US Environmental Protection Agency's AP-42 document [86] is one of the more widely used for predicting resuspension on paved roads, although some shortcomings have been identified [87]. There is no widely accepted European method for calculating emissions due to resuspension.

Rail Transport Models

Emissions from electric trains occur at the power stations which are responsible for generating the electricity. The actual emissions will therefore be a simple function of power consumption and emission factors for power generation. However, power losses between the power station and the train, and within the train itself, also need to be taken into account where possible.

Emissions from diesel locomotives are typically estimated using fuel consumption data and fuel-specific emission factors. The types of train which are typically included in models include high-speed passenger trains, intercity passenger trains, regional passenger trains, urban passenger trains, and goods trains. Early models were based on empirical correlations between emissions, train type, operating speed, and other simple variables such as the distance between stops, and average emission factors for train types [88, 89]. More recent models allow the user to specify an operational matrix for a journey, from which energy consumption and emissions can be calculated [90, 91]. This approach is a broadly analogous to that used in modal models for road transport. As with road vehicles, passenger trains consume energy for loads other than propulsion. These include the heating and cooling loads, and electrical power to operate lights, instruments, and other electrical accessories. However, the energy consumption for auxiliary power is fairly low compared with that required for propulsion. The effects of regenerative braking on energy consumption may also be important.

Shipping Models

For shipping, both simple and detailed methods have been developed for calculating emissions [33, 92, 93]. The simple methods are essentially similar to that for road transport (see Eq. 1), and combine fuel use (in tonnes) with fuel-specific emission factors. Detailed calculation approaches firstly involve obtaining ship movement data, including sailing routes and distances between ports. Different ship operating modes may also be considered, such as cruising, in-port operation (hotelling, loading and unloading), and maneuvering. Each vessel also needs to be characterized. National and international shipping covers a wide range of vessels, from recreational craft to large oceangoing cargo ships that are driven primarily by large, low-, and medium-speed diesel engines. In addition, marine engines can be further classified according to their principal fuel: bunker fuel oil, marine diesel oil, or marine gas oil. Again, auxiliary engines are used to provide power and services when berthed [33]. In Europe, a widely used set of emission factors was determined in a study for the European Commission [92].

The fuel consumption and emissions of vessels operating on inland waterways were initially modelled by analogy to marine shipping. However, the operational characteristics of inland ships are rather different from those of their seagoing counterparts. Firstly, they sail at lower speeds and in restricted waterways. The lower speeds reduce energy consumption and emissions, whereas shallower depths increase sailing resistance and hence fuel consumption and emissions. In order to make the most of the limited space on inland waterways, vessels tend to be squarer in shape than seagoing ships. This also causes the sailing resistance to differ from that of seagoing ships [94]. Recent models are therefore more specific to inland vessels and their operating conditions. For example, in the ARTEMIS project, a model was developed and validated for nine types of vessel based on size and type of waterway [94]. The model calculates the energy consumption and emissions under different service conditions (speed, waterway dimensions, load, etc).

Activity Data

For all transport modes the accurate characterization of traffic activity (such as numbers vehicles, trip distances, and modes of operation) and the fleet composition is vital to the estimation of emissions. Although models and emission factors are continually improving, poor activity data remains one of the main sources of uncertainty in the calculation of emissions [95]. For many years, the direct measurement of road traffic has been the primary source of activity data. The collection of accurate information on important parameters such as traffic speed, road gradient, or vehicle load can often be difficult and time-consuming, rendering it impractical for large geographic areas. However, the quality and availability of activity data has increased substantially in recent years as a result of improved data collection technologies (e.g., tag-and-beacon systems, cameras, in-vehicle data collection, and satellite technology) and online dissemination. Furthermore, there have been significant advances in microsimulation traffic models, the outputs from which are well suited to integration with instantaneous emission data. Some workers have linked microscale traffic and emission models for practical applications [96].

In the case of passenger rail transport the activity data are available from timetables. Rail freight movements are more complicated, and data are generally more difficult to obtain. There are essentially three types of freight movement: long-term scheduled, short-term scheduled, and "on demand." Clearly, it would be difficult to incorporate on-demand movements in any emission calculations. Encouragingly, an increasing number of operators are adopting "black box" technologies, which can provide useful journey and fleet information. For example, in Germany, the rail company Deutsche Bahn has installed equipment to monitor the real-time location and energy consumption of its locomotives [97]. However, at the moment, it appears that access to the data from train event recorders is rather limited.

The primary source of information on ship movements is the database provided by Lloyd's Maritime Information Service. The database includes ship size, destination, approximate time of arrival and departure, engine type and number, but only for ships greater than 500 gross tons. Ferries, fishing vessels, and operations at smaller ports are not included. Port calling statistics are also available from national sources. In the future, the availability and accuracy of activity data and emissions data should improve further due to onboard GPS

technology, continuous emission monitoring systems (CEMS) and the development of a universal Automatic Identification System (AIS) [98]. For inland shipping there is currently a need for data that give a better description of the fleet, the traffic, and the waterways.

Pollutant Dispersion and Transformation

Once pollutants have been released into the atmosphere, they are subject to various processes of dispersion and physical or chemical transformation. Emissions from transport are also superimposed on emissions from other sources. Figure 9 shows a simplified representation of pollutant concentrations in and around an urban area with tall commercial buildings in the urban center and low residential buildings in the surrounding districts. The regional background pollution originates from a range of sources, extends over a wide area, and is relatively invariant outside the urban area. Within the built-up area there is an additional "urban background" component. This results from combined emission sources located within the urban area, including transport, power plant, industry, and domestic heating. Alongside heavily trafficked roads there is also likely to be a significant local contribution to the concentration.

Dispersion

The dispersion of pollutants is influenced to a large extent by the local weather conditions (see entry on ► Urban Air Quality: Meteorological Processes). In particular, the temperature inversions and low wind speeds associated with stable high-pressure systems can restrict dispersion and lead to high pollutant concentrations. Dispersion is also influenced by the local topography, and is reduced by the presence of local obstacles such as buildings. The effect is most pronounced in the case of so-called street canyons. Moreover, vehicle-induced turbulence needs to be taken into account.

Transformation

Some of the transformation processes that influence the concentrations of PM, NO_2 and ozone are summarized below. Meteorological factors, including solar radiation, precipitation, and humidity, also play important roles in these processes.

Particulate Matter The emission of primary particles from combustion sources was described earlier. Nucleation mode particles have a relatively short existence in the atmosphere since they readily transform into larger particles and deposit quite efficiently to surfaces because of their highly diffusive nature. Accumulation mode particles are too large to be subject to rapid diffusion and too small to settle from the air rapidly under gravity. Their further growth is inhibited because they do not coagulate quickly and there are diffusion barriers to their growth by condensation. Particles in

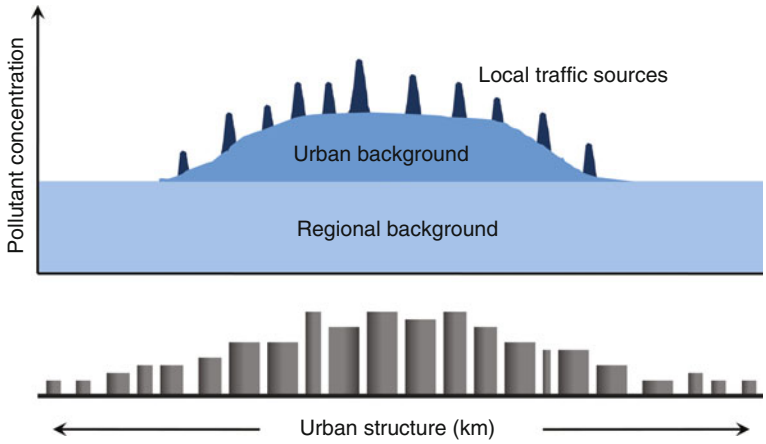

Air Quality, Surface Transportation Impacts on. Figure 9
Simplified representation of urban structure and pollution levels (Adapted from [18])

the accumulation mode can therefore have a long atmospheric lifetime (typically 7–30 days), although incorporation into rain can shorten it significantly. Within the coarse particle size range, gravitational settling velocities become appreciable and therefore atmospheric lifetimes are much shorter than for accumulation mode particles. Particles larger than ~100 μm in diameter rapidly settle out of the air and are of minor health significance because, although they can be inhaled, they do not generally penetrate beyond the nose and mouth [99].

A substantial fraction of the fine PM mass, especially at background locations, is secondary in nature [99–101]. Secondary particles are formed by atmospheric reactions involving both inorganic and organic gaseous precursors, several of which are emitted by transport. For example, particles can be produced by the oxidation of precursor gases such as SO_2 and NO_x to acids followed by neutralization with ammonia (NH_3), or by the partial oxidation of organic compounds. The formation of secondary particles is relatively slow. Their persistence in the atmosphere is therefore prolonged, and they are distributed more evenly throughout the air than primary particles. They can also travel large distances, resulting in the transport across national boundaries.

Nitrogen Dioxide The ambient concentration of NO_2 is dictated by various complex processes and factors. Under the majority of atmospheric conditions the following reaction is the dominant pathway by which NO is converted to NO_2:

$$NO + O_3 \rightarrow NO_2 + O_2 \tag{2}$$

At polluted locations comparatively close to sources of NO_x (such as road vehicles), NO is in large excess and the reaction proceeds quickly (seconds), with the availability of O_3 limiting the quantity of NO_2 that can be produced. Primary NO_2 emissions are therefore important at such locations. At unpolluted locations, when O_3 is present in excess, the timescale for conversion of NO to NO_2 is longer (minutes). When neither NO nor O_3 is in large excess, the reaction progressively depletes both reagents, and can become very slow [20].

Under normal ambient daytime conditions, the reverse process also occurs – the destruction of NO_2 by photolysis to form NO and ozone, as shown in reactions (3) and (4):

$$NO_2 + \text{sunlight} \rightarrow NO + O \tag{3}$$

$$O + O_2(+M) \rightarrow O_3(+M) \tag{4}$$

where M is a third body, most commonly nitrogen.

The mean daylight lifetime of NO_2 with respect to photolysis is around 3 min. In winter, it is typically a factor of 2 or 3 longer. Under conditions when photolysis is sufficiently rapid, NO, NO_2, and O_3 are potentially in chemical equilibrium, a condition usually referred to as the "photostationary state."

Other chemical processes that can convert NO to NO_2 involve the formation of free radicals, which can catalyze the oxidation of emitted hydrocarbons [20], but these reactions tend to be comparatively slow [102].

A third-order reaction, involving the oxidation of NO by oxygen, is of minor importance under normal atmospheric conditions:

$$2NO + O_2 \rightarrow 2NO_2 \tag{5}$$

However, this reaction is rapid at low temperatures and high NO concentrations, such that it is much more rapid at the elevated levels typical of those close to points of emission. Under wintertime pollution episode conditions, when a shallow inversion layer can lead to a combination of high NO_x levels and stagnant air for periods of a day or more, reaction (5) can potentially make a substantial contribution to NO_2 concentrations, as during an episode in London in December 1991 [20].

Given that model predictions show a decrease in NO_x emissions, the absence of a downward trend in NO_2 concentrations (see earlier section on "Historical trends") is not completely understood. Three contributing factors have often been cited:

1. The likelihood that the average proportion of NO_2 in NO_x (termed *f*-NO_2) in diesel exhaust is increasing. Analyses of NO_2 concentrations in urban areas have indicated that a significant proportion of NO_2 must be emitted directly from the exhaust, and that the *f*-NO_2 value has increased in recent years [104–108]. This has two causes:
   - The increasing market share for diesel vehicles in many European countries. For example, the

share of first registrations of diesel passenger cars in Finland increased from 17% in 2005 to 52% in 2008 [109]. Petrol cars emit less NO_x than diesel vehicles, and with a smaller proportion of NO_2.

- The increase in the use of specific aftertreatment technologies in modern diesel vehicles which involve in situ generation of NO_2, such as catalytically regenerative DPFs [106].

The changes in *f*-NO_2 for traffic emissions have not had a large impact on NO_2 concentrations away from the roadside, where the dominant contribution is from secondary NO_2.

2. The possibility that real-world NO_x emissions from road vehicles are not decreasing as rapidly as models are predicting [110].
3. Increasing background ozone concentrations [111]. As the O_3 concentration increases, the amount of NO converted to NO_2 increases.

Ozone Ground-level O_3 is implicated in summer smog, such as the one that affected large areas of Europe in the summer of 2003, and high concentrations lead to increases in the frequency of respiratory symptoms and in deaths [112]. It is not produced directly from emission sources but is created by photochemical reactions such as those described above. It can be transported over long distances, and is therefore regarded as a regional air pollution problem. High concentrations are typically observed downwind of large cities in the summer when photochemical formation is enhanced. Because road transport is a major source of ozone precursors (e.g., NO_x and hydrocarbons), it is an important contributor to ground-level concentrations. Globally, road transport is responsible for 5–15% of tropospheric O_3 [113, 114].

Modelling Air Pollution from Transport

Predictions from air quality models are used in a diverse range of applications. A common one is air quality management (AQM), which includes the identification of high-pollution areas ("hot spots"), the development of plans and programs for improving air quality, the checking of progress toward targets, and the provision of information to the public. Applications that are closely linked to AQM are transport planning and land-use planning. Air quality predictions are also an important element of environmental impact assessment (EIA).

Modelling methodologies can be categorized according to two general types: empirical/statistical models and deterministic models. Empirical models are based largely on correlations between pollutant concentrations and other variables, such as meteorological parameters. Although empirical models can be used for short-term predictions, they are most reliable for longer term averages. The assumptions that correlations represent cause and effect, and that regression parameters remain constant into the future, are their main weaknesses [20]. Deterministic models predict concentrations downwind of an emission source using mathematical formulae which describe the physical and chemical processes operating within the atmosphere [20]. They include Gaussian plume models, Eulerian grid models, Lagrangian trajectory models, and computational fluid dynamics (CFD) models. For transport sources, emissions are typically entered as a line source (such as a road or railway line), or as an area/volume source (such as a car park).

Models vary enormously in sophistication. The simplest and most common deterministic models are based on Gaussian dispersion theory. This assumes that a pollutant emission develops into a plume under the influence of the wind, and that the concentrations in the plume have Gaussian distributions in the horizontal and vertical directions. Two other types of model – Eulerian and Lagrangian – take as their basis the principle of conservation of mass of a pollutant as it spreads in the air. In Eulerian models, the calculations are undertaken simultaneously for all the grid points in the model domain, whereas in the Lagrangian approach the calculations relate to a parcel of air which follows a defined trajectory. Several thousand trajectories are usually required to generate statistically significant results. CFD models use numerical methods to predict air flows. They focus on the detailed modelling of complex structures on the local scale (e.g., street canyons), and are not appropriate for calculating area-wide concentrations [20].

The most commonly used street canyon model is the Operational Street Pollution Model (OSPM) [115]. The OSPM approach involves an idealized

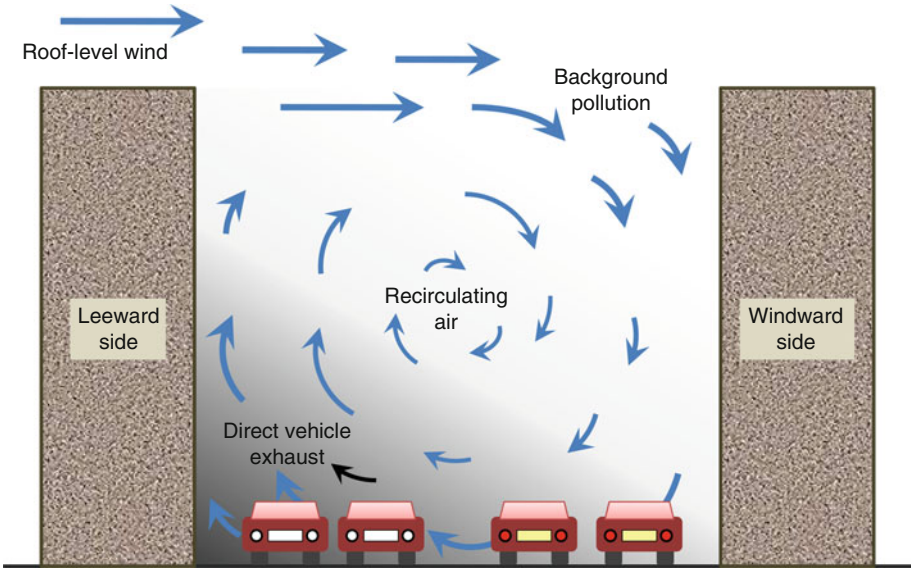

Air Quality, Surface Transportation Impacts on. Figure 10
Schematic illustration of street canyon modelling in OSPM (Adapted from [115])

representation of a street as a long road enclosed along its length on both sides by buildings of equal height (Fig. 10). The wind passing across the street induces a recirculation vortex in the street, and this leads to elevated pollutant concentrations on the leeward side of the canyon.

Some models include a preprocessor module for the input of meteorological data. Allowances can also be made for concentration changes produced by chemical reactions in the air. Again, the chemical reaction schemes vary greatly in sophistication.

Dispersion model outputs are often expressed as contour or surface maps in order to show the spatial variation in pollutant concentrations over a wide area. Such plots can enable spatial relationships between air pollution and other variables to be established, and sensitive locations to be identified. Appropriate pollution-reduction measures can then be developed. The example provided in Fig. 11 shows NO_2 concentrations in London. The area with high NO_2 concentrations to the west of London is Heathrow Airport.

Reducing Air Pollution from Transport

If transport systems are to become environmentally sustainable their impacts on air pollution will have to be greatly reduced, and it is therefore important to consider ways in which this might be achieved. The emphasis here is on road transport, but some measures for rail transport and shipping are also mentioned. It has been noted that if no aggressive emission-reduction strategies are introduced, global CO_2 and SO_2 emissions from ships could double from present-day values by 2050, and NO_x emissions could exceed the current value for road transport [117]. Shipping has therefore been recognized as a growing problem by policymakers and scientists.

This entry considers two philosophies: "prevention" and "mitigation." Of course, other distinctions are possible (e.g., "technical," "systematic," "behavioral," etc.), but in any case these tend to be artificial; interactions are often so strong that few strategies are based on a single measure of policy. In the context of the entry, prevention measures are designed to reduce or eliminate emissions at source, whereas mitigation measures are designed to remove pollutants which have already been emitted, or to convert them to more benign compounds.

An important tool is air quality legislation (see entry on ► Air Quality Guidelines and Standards), but it does not fall conveniently into the prevention or mitigation categories. Although air quality

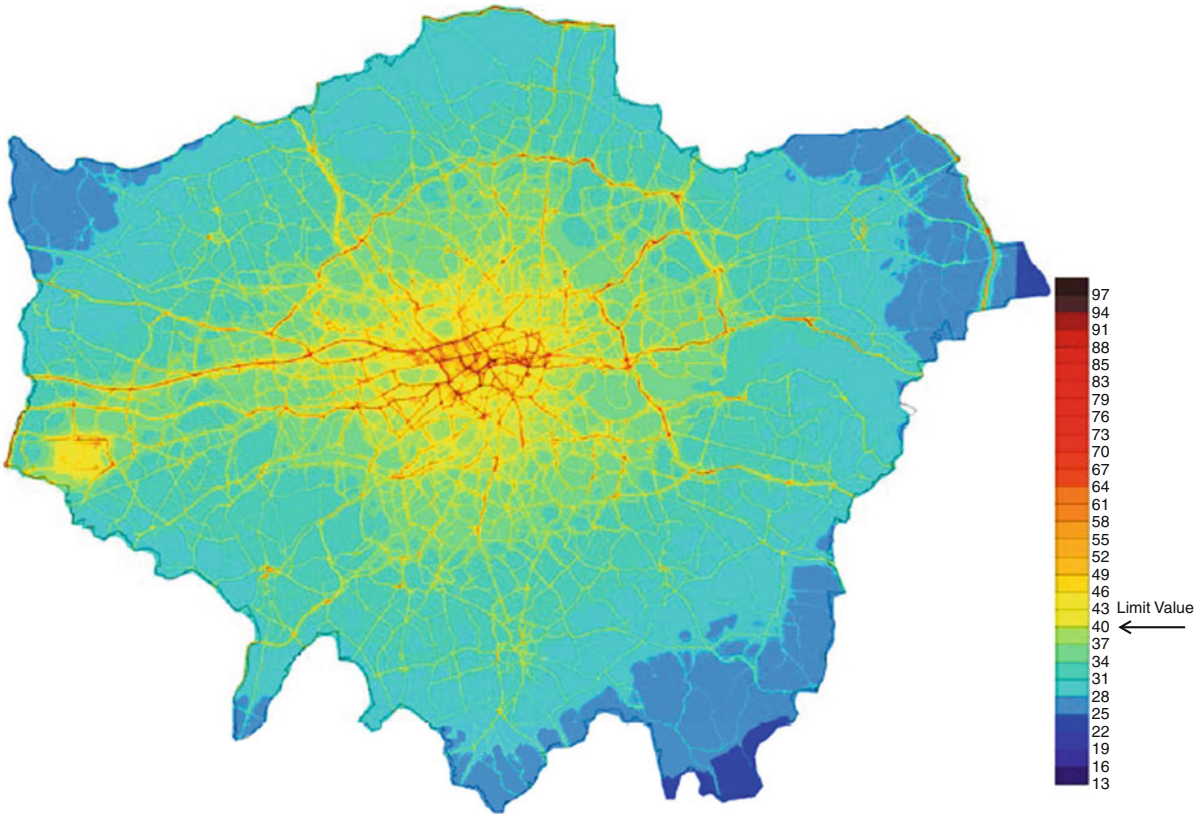

Air Quality, Surface Transportation Impacts on. Figure 11
Modelled annual mean NO_2 concentrations (μg/m^3) in London in 2008 [116] (Photograph reproduced by kind permission of Greater London Authority)

legislation acts as a driver for the development of pollution-reduction policies and technologies, and can thus be considered as "prevention," compliance with the legislation can only be determined from historical data, usually for the calendar year, such as the annual mean or the number of days on which pollutant concentrations were above a certain value. Neither does the legislation specifically target transport.

Compliance with air quality standards for PM_{10} requires control of both fine and coarse particles. As the two modes tend to have different sources and formation mechanisms, different types of control are required. The compounds that are precursors to secondary particles also need to be controlled. Primary fine particles from combustion sources are subject to regulation. The control of coarse particles is less straightforward [118], as such particles arise from diverse natural and anthropogenic disruption and attrition processes which are difficult to characterize (e.g., non-exhaust emissions, resuspension, dust from industrial processes, quarrying).

As a result of reaction (2), O_3 levels near to roads tend to be low. Thus, the limitation of local traffic emissions would tend to lead to increased O_3 concentrations at roadside locations. The control of O_3 depends ultimately on the control of emissions of NO_x and HC on a larger scale.

Prevention Measures

Some examples of prevention (i.e., emission-reduction) measures are listed in Table 1. The list is not comprehensive, but provides an indication of the types of action which are currently being considered. Two general approaches are noted here: reducing emissions per vehicle and reducing travel/transport activity, and

Air Quality, Surface Transportation Impacts on. Table 1 Prevention measures for surface transport

General approach	Type of measure	Measure	Applicability		
			Road	Rail	Shipping
Reducing emissions per vehicle, vessel or train	Emission legislation	Vehicle/engine type approval	✓	✓	✓
		In-service inspection	✓	–	–
		Roadside checks	✓	–	–
	Fuel legislation	Improved fuel quality	✓	✓	✓
	Exhaust aftertreatment	DPF	✓	✓	✓
		SCR	✓	✓	✓
		Scrubber	–	–	✓
	Alternative fuels	CNG/LPG	✓	✓	✓
		Biofuels (biodiesel, ethanol)	✓	✓	✓
	Vehicle/engine technology	Improved combustion	✓	✓	✓
		Improved aerodynamics	✓	✓	✓
		Hybrid	✓	✓	✓
		Fuel cell	✓	✓	✓
		Humid air motors	–	–	✓
	Eco-driving	Training	✓	✓	✓
		Engine switch-off	✓	✓	✓
	Cleaning	Road sweeping	✓	–	–
		Road washing	✓	–	–
		Vehicle cleaning	✓	–	–
	Dust suppressants	Chloride salts, CMA	✓	–	–
	Traffic management	Speed control	✓	–	–
Reducing travel/ transport activity	Traffic management	Access restrictions	✓	–	–
		Environmental zones	✓	–	–
		Parking restrictions	✓	–	–
	Economic measures	Congestion charges	✓	–	–
		Tolls	✓	–	–
		Road user charging	✓	–	–
		Incentives and taxes	✓	✓	✓

several specific measures are available in each case. The applicability of each measure to road transport, rail transport, and shipping is also shown. Several prevention measures are described in more detail in the following paragraphs.

Emission Legislation In Europe, emission tests are required at type approval for all new light-duty vehicle models and for the engines used in heavy-duty vehicles. Light-duty vehicles are tested using a power-absorbing chassis dynamometer, as shown in Fig. 8, whereas

heavy-duty engines are operated on a test bench. The sampling of exhaust emissions is then performed as the vehicle or engine progresses through a predefined driving cycle.

Limit values are usually defined for CO, HC, NO_x, and PM in exhaust, as well as evaporative emissions of VOCs. In the regulation of exhaust particles, practically all worldwide emission standards are expressed in terms of the mass of total particulate matter with no differentiation by particle size. Particle number emissions are included in the latest European legislation.

The most advanced regulations are to be found in the EU, the United States, and Japan. The specific differences between the legislation in different countries are too numerous to mention here, but the principles involved are broadly similar and there is a general move toward harmonization. Moreover, the technology being built into cars and trucks to comply with the European, US, and Japanese standards is very similar.

Over the course of several decades the limit values for the pollutants in vehicle exhaust have decreased (Fig. 12), and changes have been made to the test method to make it more realistic. As a result, manufacturers have been required to develop increasingly effective emission-control technologies (some effects of this were shown in Fig. 4b). For example, the latest EU emission standards for cars and heavy-duty vehicles require large reductions in PM and NO_x emissions, and these will be achieved through the use of DPFs and SCR.

Some examples of the progressive reduction in the exhaust emission limits in several countries (in terms of equivalence to the EU legislation) are illustrated in Fig. 13. Most developing countries lag behind the EU, although the gap is narrowing and in some places it has been possible to "leapfrog" standards. However, a prerequisite for the introduction of advanced engine and aftertreatment technologies is the availability of appropriate fuel, and in many developing countries this has presented something of a barrier.

Periodic in-service inspection and maintenance represents a further (and crucial) level of legislative

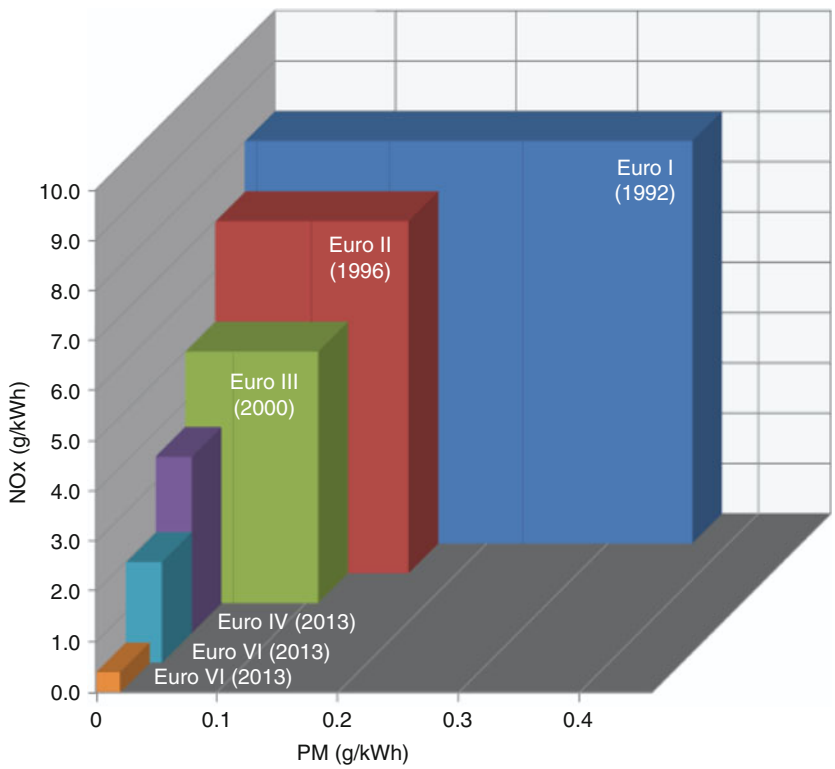

Air Quality, Surface Transportation Impacts on. Figure 12
Evolution of EU NO_x and PM emission limits for engines used in heavy-duty vehicles

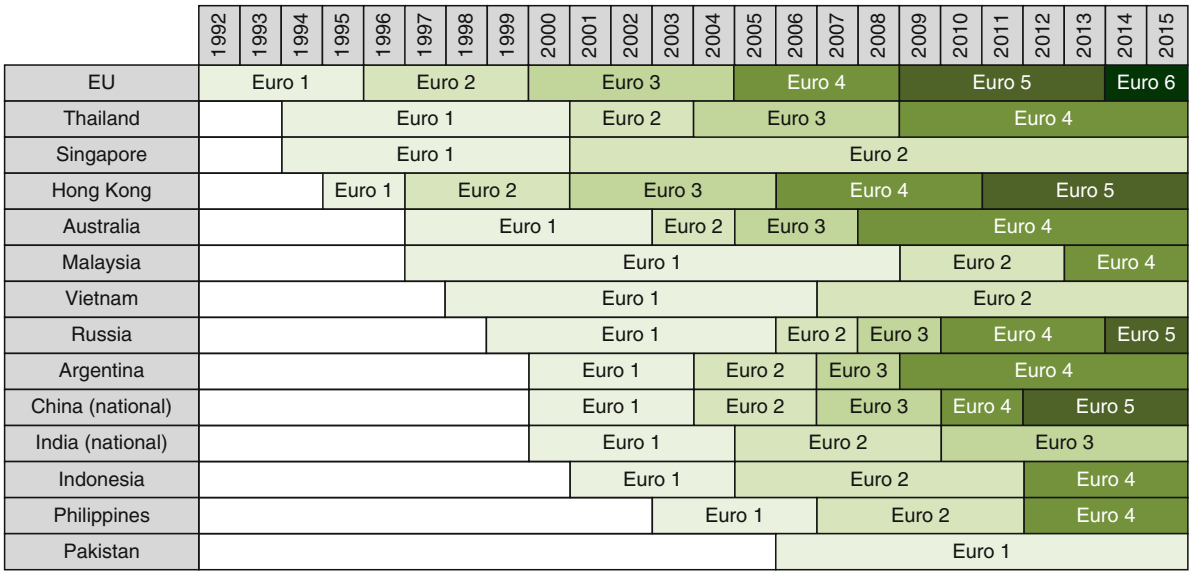

Air Quality, Surface Transportation Impacts on. Figure 13
Introduction dates for emission standards in different countries (Adapted from [119])

control, as it is designed to ensure that vehicles maintain low emission levels during real-world operation. However, whilst type approval checks are relatively detailed and involve the use of specialist and expensive laboratory equipment, in-service checks are based on shorter, simplified operations of the vehicle (usually in a repair center), and make use of equipment that is less precise and less expensive than that used in the laboratory. Moreover, the tests for petrol vehicles typically only involve the measurement of CO and HC whilst the vehicle's engine is running at idle or at fast-idle, and those for diesel vehicles tend to cover only smoke emissions. Therefore, the tests do not address the most important pollutants and operational conditions. In some countries, attempts have been made to address these issues. For example, in the United States, a loaded test (IM240) has been developed to simulate conditions under which high NO_x emissions may occur. Some authorities may also conduct random roadside checks, or use remote sensing devices to screen for high emitters. In addition, onboard diagnostics of emission-control systems are increasingly used to alert drivers to failures.

In Europe emissions from ships and railway locomotives are governed by the legislation for non-road mobile machinery (Stages III and IV of Directive 2004/26/EC). The Stage III standards are further divided into two substages: Stage III A and Stage III B. The Stage III B standards introduce PM limit of 0.025 g/kWh, representing a 90% emission reduction relative to Stage II. To meet this limit value it is anticipated that engines will have to be equipped with DPFs. Stage IV also introduces a stringent NO_x limit of 0.4 g/kWh, which is expected to require NO_x after treatment. Given the long working lives of the engines in question, these regulations will not have any considerable effect on emission levels for another couple of decades [94]. Again, a process of worldwide harmonization of regulations has begun.

Emission standards for diesel engines used in railway locomotives have also been established by the International Union of Railways (UIC), an association of European railway companies [120]. The standards apply to all new engines used in new vehicles or for repowering of existing locomotives, and are binding to UIC members.

Emission standards for marine engines are defined by the International Maritime Organization (IMO). The standards – for NO_x and SO_x – are contained in the International Convention on the Prevention of

Pollution from Ships, known as MARPOL 73/78 [121]. In addition, the first sulfur emission-control area (SECA, with a maximum fuel sulfur content of only 1.5% sulfur content) in the Baltic Sea entered into force in 2006, and further SECAs in the North Sea and English Channel entered into force in 2007.

Fuel Legislation Engine and vehicle technologies normally achieve their best emissions performance with high-quality fuels [122]. One property on which a great deal of attention has focused is the sulfur content, partly due to the need to reduce PM and SO_2 emissions and partly because fuel sulfur has an adverse effect on certain types of engine and exhaust aftertreatment technology [122]. In Europe, the controls on fuel sulfur content have been periodically tightened, and in the latest step Directive 2003/17/EC required a full transition to "sulfur-free" petrol and diesel (having less than 10 ppm of sulfur) by 2009. This should enable advanced technologies – such as lean-burn engines, particle traps, and regenerative NO_x storage systems – to meet stringent exhaust emission limits.

Because of the contribution of shipping to pollution at large ports, EU Directive 2005/33/EC limits the fuel sulfur content to 0.1% in marine fuels for harbor regions in 2010.

Improved Combustion and Exhaust Aftertreatment It is expected that petrol and diesel will power road transport for the foreseeable future, and considerable reductions in emissions might still be realized in the short term through improved engine design, fuel injection systems, electronic timing, etc. Developments in ship engine technology include direct water injection and humid air motors (in which water vapor is used to cool the charge air and reduce the NO_x formation during combustion) [96].

The main exhaust aftertreatment technologies that enable vehicle and engine manufacturers to comply with the exhaust emission legislation are three-way catalysts, oxidation catalysts, exhaust gas recirculation (EGR), DPFs, and SCR. Whilst such technologies are generally fitted during manufacture, retrofitting is a common pollution-reduction strategy. For example, DPFs have been fitted to all of London's 8,000 buses.

In EGR the recirculation of the exhaust air into the combustion chamber reduces the amount of oxygen available for NO_x formation. It has been fitted to light-duty diesel road vehicles in Europe for some years. For trains, EGR can give significant reduction in emissions but can be relatively expensive to retrofit. It may also not be possible to fit EGR to many classes of train due to space restrictions [123]. EGR is also applicable to ships but is not yet in regular use.

DPFs physically capture particles in the exhaust stream. They can be broadly divided into two types: "full flow" and "partial flow." The former lead to a reduction in PM emissions of more than 95%, whereas the latter are more permeable and less effective, but need no maintenance. In order to prevent the filter from blocking the particles captured by the filter must be periodically removed (a process referred to as "regeneration"). The regeneration may be induced using, for example, a heater, fuel burner, or a reactant (such as NO_2) generated in situ. DPF technologies are also suitable for use on rail and marine engines [124]. However, they can be very bulky and for rail locomotives there are questions concerning the feasibility of retrofitting. Moreover, they appear to be a less cost-effective measure than re-engining [123].

SCR will be the main technology for enabling compliance with future NO_x emission standards. The method works by injecting ammonia or urea into an exhaust stream to chemically reduce NO_x to nitrogen. Again, SCR systems are very bulky; the catalyst itself can be considerably larger than the engine. Space is also required for oxidation catalysts and the tank for storing urea or ammonia. This puts severe restrictions on its potential for use as a retrofit item to rail vehicles – where spare space and weight availability is limited – and again re-engining appears to be a more cost-effective option [123]. SCR is in use in a few ships and is still being developed. As well as being an effective NO_x-reduction measure, one study has also shown that SCR can reduce ship PM emissions by around 50% [35]. No limitations are thought to have been encountered regarding the fitting of SCR to different types of ship, and it can be integrated with other aftertreatment devices [96]. However, sufficiently high temperatures in the exhaust are required for the SCR process to function efficiently. Consequently, large NO_x reductions are mainly achieved at higher engine loads. Other drawbacks include the space and additional weight requirements, and the potential for "ammonia

slip." This occurs when excess urea or ammonia is injected into the exhaust stream, and any unused reagent is emitted from the exhaust. The risk of ammonia slip is higher for transient load changes (i.e., maneuvering) [96].

Another shipping technology is seawater scrubbing, in which the exhaust gas is passed through water. This is effective at reducing emissions of SO_2 and probably has benefits for other pollutants.

Alternative Fuel and Vehicle and Technologies The development of technology in the longer term will undoubtedly be driven more by the need to reduce CO_2 emissions than by the need to improve air quality. In many cases, a "win-win" outcome is possible, although there can be some conflicts. For example, some studies have indicated that NO_x emissions can increase as a result of biofuel use [125].

Alternative fuels include liquefied petroleum gas (LPG), compressed natural gas (CNG), and various biofuels (biomethane, ethanol, esterified vegetable oils, etc.). For road transport, limited supplies mean that LPG could never fully replace petrol or diesel, and the scale of uptake of CNG has been impaired by the cost of converting car engines [126]. The availability of suitable engines for rail applications is uncertain; available natural gas engines can also only cover the lower end of the power range needed for railway applications, and there appears to be no use of LPG [123]. Around 50 seagoing ships are currently powered by natural gas, with a reduction in emissions of PM and NO_x of at least 70% [127]. Biofuels can be used in low concentration blends (5–10%) with petrol or diesel without engine modification, and in high concentrations (85–100%) with specially adapted vehicles. The main benefit of biofuels is their contribution to the reduction of CO_2 emissions; its effects on NO_x and PM are less clear. Barriers to increased biofuel use include higher costs, compatibility with conventional fuels, and availability of technology for more advanced biofuels [15]. In addition, there have been warnings of hidden costs and adverse impacts on the environment and society, which could arise from the large-scale production of biofuels [128]. It has also been noted that the use of alternative fuels is context-specific; a fuel that is appropriate to one location may not be appropriate to another [23].

Automobile propulsion technologies that are currently under development include "mild" and "full" hybrid vehicles, "plug-in" hybrid vehicles, battery electric vehicles, hydrogen ICE vehicles, and fuel cell vehicles. Vehicle technologies are currently available that can reduce CO_2 emissions per car by 30%, but demand-side and supply-side barriers are delaying their deployment [126]. Cars that emit 50% less CO_2 per kilometer than the equivalent current models could be on the road by 2030, subject to advances in hybrid and battery technologies and industry overcoming cost barriers [126]. In the longer term, a 90% reduction in emissions is possible based on battery-electric propulsion systems [126].

In the rail sector, hybrid systems have been shown to result in reductions in exhaust NO_x and PM of up to 90% [123]. Hybrid propulsion has been used in shipping for many years, where the mechanical drive for the propellers has been replaced by electrical connections to electric motors, which in turn drive the propellers [129].

Electricity results in zero emissions at the point of use, giving it major local air quality benefits. Moreover, if it is produced from renewable energy it can have low or even effectively zero CO_2 emissions over its life cycle. The main drawbacks with electric road vehicles include a relatively low maximum speed, a short range, the lengthy recharging times and the cost [126]. However, there are continual improvements in the performance and marketability of electric vehicles.

In hydrogen vehicles the power is derived from either combustion or electrochemical conversion in a fuel cell. In hydrogen ICEs the combustion process is fundamentally the same as that in petrol ICEs. In a fuel cell the hydrogen reacts with oxygen to produce water and electricity, and the latter is used to power the vehicle. When hydrogen is used to generate power the only significant emission is water vapor (though a small amount of NO_x is produced by hydrogen ICEs). If the hydrogen is made from low-CO_2 energy sources, very low life-cycle emissions are possible. Some of the main obstacles to the wider use of hydrogen for transport are the lack of an adequate infrastructure for storage/distribution and the high cost of implementation [15].

Eco-Driving "Eco-driving" has been widely publicized as a means of reducing the fuel consumption

and emissions of road vehicles. It is aimed at both private motorists and fleet operators, and typically involves either a simple set of rules to be followed or a program of training. The advice or training varies considerably in terms of the level of detail, but it generally features a number of common actions, including keeping the tires at the correct pressure, reducing the vehicle weight, avoiding sharp acceleration and heavy braking, driving in the highest gear, and avoiding unnecessary engine idling. Average overall reductions in fuel consumption of around 5–10% are typically reported for eco-driving, and some specific examples are shown in Table 2. However, it should be noted that some adverse effects of eco-driving have been observed, such as an increase in NO_x emissions from diesel cars during urban driving [133].

It is possible that the principles associated with eco-driving on the road are transferable, with modification to the actual actions involved, to rail transport and shipping.

Leaving diesel engines in idle operation is a widespread practice at many rail termini. Reasons for this include keeping the engines warm and providing power brakes, heating/cooling, lights, catering facilities, and other auxiliaries. Whilst pollutant emissions per train at stations are relatively low compared with those during a trip, where several trains are running at idle and the station is enclosed there may be an issue regarding population exposure. There may therefore be significant potential to reduce emissions at stations simply through enforcing maximum idle running times [123].

When at berth, ships also need electrical power for emergency equipment, refrigeration, cooling, heating, lighting, loading/unloading equipment, etc. This power is normally provided by the auxiliary engines. However, such engines result in air pollutant emissions at the port, and these are often close to centers of population. An alternative approach is to obtain power from shore, a process known as "cold ironing." The port of Gothenburg in Sweden was the first in the world to provide a high-voltage onshore power supply for cargo vessels. Two local wind turbines are used to generate the electricity, and it is claimed that the system cuts emissions by 94–97% for ships at berth and has led to dramatic reductions in pollutant concentrations. Systems are also available for optimizing the energy efficiency of a vessel by advising the crew on the optimal speed for the prevailing water conditions [138].

Air Quality, Surface Transportation Impacts on. Table 2 Effects of eco-driving measures on fuel consumption

Action	Change in fuel consumption	References
Correction of low tire pressure	−2%	[130]
Removal of 100 kg load from a medium-size van	−7%	[130]
Removal of roof rack	−20%	[130]
Not driving with windows open	−10%	[131]
Not using air-conditioning	−18%	[131]
Eco-driving gear-change strategy	−18%	[132]
Use of a gear-change indicator	−1% to −11%	[133, 134]
Eco-driving training	+2% to −16%	[133, 135–137]

Road Sweeping and Washing Sweeping (or vacuuming) and washing have been applied in several countries as means of decreasing the silt loading of roads, the premise being that this will reduce PM resuspension. Purpose-built vehicles are usually employed, and the cleaning process can involve mechanical (broom) sweeping, vacuuming, spraying with water, or a combination of these. Some vehicles are specifically designed to reduce PM_{10} concentrations. A simpler approach is the spraying of water directly onto the road surface (Fig. 14) in an attempt to reduce resuspension on dry days.

Studies in the 1980s showed promising results in terms of the removal of particles from the road surface [139, 140]. However, the majority of later studies have indicated only limited effects on PM_{10} concentrations [141–145], and in some cases increases [146]. Where reductions in PM concentrations have been observed, these have generally been small and short-lived (a few hours) [147, 148]. Possible explanations for such limited effectiveness include the silt loading being rapidly

Air Quality, Surface Transportation Impacts on. Figure 14
Spraying the road with water in Nijmegen, the Netherlands (Photograph reproduced by kind permission of the Municipality of Nijmegen, the Netherlands)

replaced after sweeping, the frequency of sweeping/washing being too low, and the removal of only particles which are larger than PM_{10} [145]. The spatial distribution of material on roadways is also highly variable [149].

However, some investigations have indicated effects that are large enough to warrant the consideration of sweeping or washing for reducing roadside PM_{10} concentrations [150, 151], and if sweeping or washing can remove particles that could evolve into PM_{10}, then sweeping may have a delayed beneficial effect on air quality [144]. It should be technically undemanding, and relatively low cost. Clearly, both sweeping and washing programs would have to be conducted during periods when traffic flows are low, so that any disruption to the traffic is minimized.

Dust Suppressants Dust suppressants (or binders) appear to be an obvious choice for the reduction of resuspension due to road vehicles. Suppressants are chemicals applied to surfaces to maintain the moisture levels or to actually chemically bind the surface material to reduce fugitive dust emissions. The main suppressants in use are water (the oldest, and undoubtedly the cheapest) and solutions of salts such as calcium chloride ($CaCl_2$), magnesium chloride ($MgCl_2$) and calcium magnesium acetate (CMA). Little quantitative information exists on their effects on airborne particulate matter, although with the need to control PM_{10} the interest in suppressants is growing. There is reasonably convincing evidence from recent pilot studies in Scandinavia that the use of dust suppressants could make a significant difference to roadside PM concentrations on timescales of hours to days [144, 145, 152]. However, more information is needed on potential adverse effects of using dust suppressants on paved roads. A notable concern is road safety, as road surface friction is reduced when large amounts of suppressants are used.

Traffic Management Numerous forms of traffic management offer the possibility of reducing emissions from traffic. Local restrictions to the access and/or circulation of traffic have been introduced in many cities to reduce pollutant concentrations. Such restrictions can take a range of forms, including tolls, congestion charges, alternate number plate schemes, and weight restrictions. Cities that have implemented these types of schemes include London, Stockholm, Athens, Budapest, and Prague. Low emission zones (LEZs) are one of the more effective types of restriction. Entry to a LEZ is usually conditional on a vehicle

meeting specified standards. These standards can be set in various different ways, such as emission legislation, the use of specific exhaust aftertreatment (e.g., DPF), or vehicle age.

The potential beneficial effects of such measures can be illustrated by reference to a trial road charging scheme introduced in Stockholm City Centre in 2006. It was estimated that the scheme resulted in a 15% reduction in total road use within the charging zone. Emissions of NO_x and PM_{10} from road traffic in the zone fell by 8.5% and 13%, respectively. Air quality dispersion modelling was applied to assess the effects of the emission reductions on ambient concentrations. It was found that the annual average NO_x concentrations would decrease by up to 12% along the most densely trafficked streets and PM_{10} concentrations would decrease by up to 7% [153].

Other types of traffic management are designed to impose low-emission driving styles, including variable speed limits and synchronized traffic signals (so-called green waves).

Mitigation Measures

The possibilities for mitigation are less diverse than those for prevention. Mitigation measures typically involve the use of physical barriers, vegetation, or some form of air treatment.

Physical Barriers On open roads the emissions from traffic are subject to the normal processes of atmospheric dilution and dispersion. Barriers are common features alongside roads with high levels of traffic, particularly those which run through populated areas. These features are usually introduced to attenuate noise, but can also block pollutant dispersion, increase turbulence and initial mixing, or modify deposition. Any air flow perpendicular to the barrier can be deflected upward by the structure, and this can increase the apparent release height of the pollutant and increase vertical mixing due to the flow separation at the top of the barrier. A recirculation cavity forms in the lee of the structure, and this can also reduce pollutant concentrations relative to an open area with no barrier [155]. However, plume reattachment – and increased pollutant concentrations – can take place further downwind [155].

Inside a road tunnel the dilution and dispersion of pollution is restricted, and unless there is the injection of fresh air, the concentration of pollutants will increase from the entrance to the exit, and the emissions will be concentrated at the portals or ventilation points. Therefore, the road traffic source of pollution is effectively removed along the length of the tunnel and the exterior air quality ought to improve. However, pollutant concentrations can be particularly high in the vicinity of the exit portals. The air quality at the portals or ventilation points will depend upon the level of traffic and whether or not the polluted air is treated in some way before release. When considering the potential for tunnels for improving ambient concentrations, it should be borne in mind that vehicle occupants and tunnel workers may be exposed to increased concentrations, which could be detrimental in public health terms.

Vegetation The planting of vegetation can have a positive impact on air quality in the vicinity of roads [156–158]. A number of mechanisms are involved, but the main effects are dry deposition at the leaf surface and the modification of dispersion. The height, width, type, and porosity (leaf density) of the vegetation appear to be important, and greater deposition can occur on coniferous plants than on broadleaf plants due to the larger leaf surface area per unit ground area [159]. However, the results of trials have been mixed, and there are likely to be several practical difficulties associated with the use of vegetative barriers in built-up areas, including available space, soiling by traffic, and the general hostility of the roadside environment to plant life. In addition, analyses carried out for a busy arterial road show that very large vegetation areas (in excess of 10,000 m^2) would be needed to compensate for the local emissions from vehicles [160].

Air Treatment Various air treatment approaches have been devised with the aim of reducing air pollution. In recent years considerable efforts have been made to develop construction materials and coatings, which have the potential for reducing air pollution. These materials are often reliant upon photocatalysis, most commonly involving the compound titanium dioxide (TiO_2). Titanium dioxide acts as a catalyst to

oxidize NO and NO_2 into nitrate (NO_3^-) in the presence of oxygen and ultraviolet radiation. The nitrate is subsequently washed away by rainfall. The effectiveness of TiO_2 coatings has been successfully demonstrated in laboratory trials [161], but field trials have been less convincing. This is partly because it is difficult to distinguish the impact of chemical conversion on the catalyst surface from fluctuations in concentrations due to, for example, meteorology.

Several air treatment technologies have been developed for use in tunnels. For example, a number of denitrification systems are available; most work by either a chemical absorption or catalytic process. Tests in Norwegian and Japanese tunnels have indicated that removal rates for NO_2 of up to 90% are possible [162, 163]. The application of denitrification systems at open roadside locations does not appear to have been reported, and appears to be impractical at present. Electrostatic precipitators (ESPs) have been demonstrated as being effective in removing particles from tunnel air with varying efficiency. Some electrostatic systems have also been developed for exterior environments and tunnels [164], but further investigation into their effectiveness is required.

Future Directions

Outlook

The future global outlook for transport-related pollution currently looks rather bleak. In developing countries, the rise in car ownership and travel is predicted to be even more dramatic than it has been in industrialized nations. For example, the rate of car ownership in Brazil is predicted to overtake that in the country that has historically been the world leader – the United States – before the middle of the century. Car ownership in China has doubled in the last 5 years, and it already has the third highest car sales in the world [126].

However, at the time of writing there appear to be some signs of change, but probably not as a result of environmental pressures. Certain Member States of the EU reported rather large decreases in emissions from road transport between 2007 and 2008, reflecting at least in part the lower amount of freight transport by road in the second half of 2008 as a result of the economic recession [8]. In addition, the recession has had a significant effect on car sales. Several governments have introduced scrappage schemes to maintain or stimulate demand for new cars, but these schemes should also result in the replacement of older polluting vehicles with new and more efficient ones. Data sets from other regions also show the impact of the economic climate. In 2008, in the United States, the number of vehicles per 1,000 people decreased for the first time since 1997. Similarly, total vehicle-miles travelled decreased slightly from 2007 to 2008 – the first decline since 1980 [165].

Nevertheless, governments around the world are acknowledging that action is required to control the rate of traffic growth, to improve the environmental performance of vehicles, and to increase public awareness about the impacts of pollutant emissions from transport. As noted earlier, it is likely that the future shape of transport will be influenced more by the need to reduce greenhouse gas emissions than the need to improve local and regional air quality. The development of a sustainable transport system will involve a large number of interventions that are beyond the scope of this entry, but will probably include reducing dependence on cars, effective land-use planning to reduce journey distances, improving the quality of public transport, etc. Preventative measures will also need to be accompanied by mitigation measures which reduce human exposure to air pollution.

For the control of local air pollution, it is likely that emission legislation will still be the main instrument for governments in the future. However, the future of European emission legislation post-Euro 6/VI is somewhat uncertain. There is a drive toward the global harmonization of legislation, but given that the threat of climate change is increasing the pressure on manufacturers to develop low-carbon power sources as alternatives to fossil fuels (batteries, fuel cells, etc.), it is therefore unlikely that the current test procedures will remain relevant.

Shipping is currently one of the least regulated emission sources, with a high reduction potential through technological improvements, alternative fuels, and ship modifications. It has been observed that if the sulfur content of fuel oil remains at present-day levels, a doubling in the emissions of some pollutants from shipping can be expected by 2050. However, given the increasing concern about shipping-related air quality,

further reductions of NO_x and SO_2 emissions seem likely. Using aggressive NO_x emission reduction technologies, a decrease up to 85% in NO_x emissions could be reached through technological improvements by 2050, in spite of a growing fleet [166].

Research Needs

Emissions from transport, and the resulting ambient air pollution, have been studied intensively, although there are still a number of areas where the understanding is poor or incomplete. Some of these areas are summarized below.

Testing Methods for New Technologies In legislative terms, the emphasis at present is on the definition of appropriate procedures for the type approval of hybrid-electric, full-electric vehicles and hydrogen ICE vehicles. In some cases, certification will be problematic. For example, the current heavy-duty engine test procedure cannot be applied meaningfully to hybrid vehicles, as the instantaneous behavior of the engine is decoupled from the instantaneous road load. Vehicle-based tests may therefore become the norm in the future, although this in itself introduces certain challenges given the large number of possible vehicle configurations and differences in real-world operation. Such challenges might be overcome by the modelling of powertrains.

Understanding PM Emissions In recent years evidence has accumulated indicating that airborne particles exert a range of adverse health effects. These effects are diverse in scope, severity, and duration [4]. More work is needed in the future to accurately characterize particle emissions from surface transport modes and to uncover the mechanisms by which health impacts occur.

It has already been noted in this entry that a better understanding of non-exhaust PM is required, including characterization of the emitted particles, investigation of health impacts, and the development of methods of prevention and mitigation. The importance of brake wear may diminish in the future as regenerative braking systems in hybrid and electric vehicles partially or fully replace traditional mechanical ones. However, this is not currently taken into account in emission calculations and projections.

More detailed information on PM emissions from rail and shipping (especially inland shipping) is also required, including emission factors for different engines and fuel type combinations, in terms of size distribution, particle numbers, and chemical speciation [34]. Few studies have examined PM levels in the ambient air alongside railway lines. These often run very close to housing, and may contribute to local air quality problems, especially where large numbers of diesel trains are in use. PM concentrations could also be elevated near shunting yards and depots. In addition, there is little information on PM concentrations in stations where diesel trains are left running at idle and the dispersion of pollution is restricted.

Understanding NO_x Emissions In order to understand atmospheric NO_2 it is important to understand NO_x emissions, and it is possible that the latter are being underestimated by models. For example, there is evidence to suggest that NO_x emissions from Euro V heavy-duty vehicles are significantly higher than the limit at type approval [110]. Vehicles equipped with SCR have very low emission levels during rural and motorway driving, but not under the low engine loads associated with urban or driving. The reason for this is that the SCR system needs to attain a certain temperature for efficient NO_x reduction. The real-world performance of SCR should therefore be investigated. Furthermore, more extensive information on f-NO_2 values for a wider range of vehicles is required.

Improving Emission Models Accuracy, reliability, consistency, and credibility are prerequisites of emission estimates. However, comparisons between the results from different emission models have highlighted substantial differences. There is therefore a need for emission modelling approaches to be reevaluated, and for improvements to be made. This requires a better understanding of the circumstances under which emission models provide inaccurate predictions. For example, some modellers believe that the exhaust emission factors for road vehicles are unsuitable for certain road types and traffic conditions. Particular concerns have been expressed about the validity of the emission factors for so-called congested traffic. The term "congestion" also needs to be defined in a manner that is meaningful in terms of emissions.

Improving Activity Data While obtaining primary activity data for road transport by direct measurement remains the main approach for short-term modelling exercises, it tends to be a rather expensive activity, and would be unfeasible where an emission estimate is required for a large geographical area. Traffic assignment models and microsimulation tools are increasingly being used to provide the relevant data, and communications technology such as Intelligent Transport Systems and Advanced Transport Telematics enable transport networks to be monitored in real time. It could well be possible to adapt a number of models and new technologies to contribute appropriate information on fleets and traffic activity.

In shipping the use of data from AIS and CEMS has a great deal of potential, and even more so if it can also be extended to cover inland shipping. Data from AIS have already been incorporated into at least one model [167]. However, some work is required to validate emission estimates obtained using AIS data [34]. Research is also required on the movements of empty ships, as these are often excluded from emission estimates [34].

Model Validation Model validation is an important area for improvement. The literature on the validation of transport emission models is quite limited, and validation studies are often only partial in the sense that they address just one type of road, type of vehicle, or time period. The understanding of the uncertainties in emission models and the main factors affecting prediction errors is therefore poor [168]. Emission models should quantify prediction errors. The models in common use should also be compared for a wide range of traffic and fleet conditions and locations. This would allow for a better assessment of the relative performance of different model types.

Evaluation of Mitigation Measures The results of field trials on pollution mitigation methods have been rather mixed, and are probably confounded by site-specific factors. Consequently, much more work is required to determine which measures are likely to be most effective for a given set of circumstances.

Bibliography

Primary Literature

1. Bell ML, Davis DL, Fletcher T (2004) A retrospective assessment of mortality from the London smog episode of 1952: the role of influenza and pollution. Environ Health Perspect 112(1):6–8
2. Haagen-Smit AJ (1952) Chemistry and physiology of Los Angeles smog. Ind Eng Chem 44(6):1342–1346
3. COMEAP (2009) Long-term exposure to nitrogen dioxide: epidemiological evidence of effects on respiratory morbidity in children. Committee on the Medical Effects of Air Pollutants. Subgroup: Quantification of Air Pollution Risks II
4. Morawska L, Moore MR, Ristovski ZD (2004) Health impacts of ultrafine particles – desktop literature review and analysis. Australian Department of the Environment and Heritage, Canberra. ISBN 0642550557
5. Krasenbrink K, Martini G, Wass U, Jobson E, Borken J, Kuehne R, Ntziachristos L, Samaras Z, Keuken M (2005) Factors determining emissions in the WHO European Region. In: Krzyzanowski M et al (eds) Health effects of transport-related air pollution. Regional Office for Europe of the World Health Organization, Copenhagen. ISBN 92 890 1373 7
6. Corbett JJ, Wang C, Winebrake JJ, Green E (2007) Allocation and forecasting of global ship emissions. Submitted as a formal annex submission to the International Maritime Organization. Clean Air Task Force and Friends of the Earth International, Boston, 11 Jan 2007, pp 26
7. Eyring V, Köhler HW, van Aardenne J, Lauer A (2005) Emissions from international shipping: 1. The last 50 years. J Geophys Res 110(D17):D17305
8. EEA (2010) European Union emission inventory report 1990–2008 under the UNECE Convention on Long-range Transboundary Air Pollution (LRTAP). EEA Technical Report No 7/2010. European Environment Agency, Copenhagen
9. AIRPARIF (2001) Etude de la qualité de l'air dans le secteur de la gare de l'Est. Paris, AIRPARIF – Surveillance de la Qualité de l'Air en Ile-de-France, Laboratoire d'Hygiène de la Ville de Paris, Mairie de Paris, DASES, Laboratoire Central de la Préfecture de Police
10. Seaton A, Cherrie J, Dennekamp M, Donaldson K, Hurley JF, Tran CL (2005) The London underground: dust and hazards to health. Occup Environ Med 62(6):355–362
11. Branis M (2006) The contribution of ambient sources to particulate pollution in spaces and trains of the Prague underground transport system. Atmos Environ 40:348–356
12. Raut J-C, Chazette P, Fortain A (2009) Link between aerosol optical, microphysical and chemical measurements in an underground railway station in Paris. Atmos Environ 43:860–868
13. Corbett JJ, Winebrake JJ, Green EH, Kasibhatla P, Eyring V, Lauer A (2007) Mortality from ship emissions: a global assessment. Environ Sci Technol 41:8512–8518
14. Hulskotte JHJ, Denier van der Gon HAC (2010) Fuel consumption and associated emissions from seagoing ships at

berth derived from an on-board survey. Atmos Environ 44:1229–1236
15. Uherek E et al (2010) Transport impacts on atmosphere and climate: land transport. Atmos Environ 44(37):4772–4816
16. European Commission (2003) European Union energy and transport in figures – statistical pocketbook 2003. European Commission, Brussels
17. European Commission (2010) European Union energy and transport in figures – statistical pocketbook 2010. European Commission, Brussels
18. Keuken M, Sanderson E, van Aalst R, Borken J, Schneider J (2005) Contribution of traffic to levels of ambient air pollution in Europe. In: Krzyzanowski M et al (eds) Health effects of transport-related air pollution. Regional Office for Europe of the World Health Organization, Copenhagen. ISBN 92 890 1373 7
19. EEA (2007) Air pollution in Europe 1990–2004. EEA Report No 2/2007. European Environment Agency, Copenhagen
20. AQEG (2004) Nitrogen dioxide in the United Kingdom. Air Quality Expert Group. Published by the Department for Environment, Food and Rural Affairs. DEFRA Publications, London
21. Harrison RM, Stedman J, Derwent D (2008) Why are PM_{10} concentrations in Europe not falling? New directions, atmospheric science perspectives special series. Atmos Environ 42:603–606
22. Minoura H, Ito A (2010) Observation of the primary NO_2 and NO oxidation near the trunk road in Tokyo. Atmos Environ 44:23–29
23. Gorham R (2002) Air pollution from ground transportation an assessment of causes, strategies and tactics, and proposed actions for the international community. Department of Economic and Social Affairs, United Nations
24. Duan N (1982) Models for human exposure to air pollution. Environ Int 8:305–309
25. Ott WR (1982) Concepts of human exposure to air pollution. Environ Int 7:179–196
26. Heywood JB (1988) Internal combustion engine fundamentals. McGraw-Hill, London
27. Vestreng V, Ntziachristos L, Semb A, Reis S, Isaksen ISA, Tarrasón L (2009) Evolution of NOx emissions in Europe with focus on road transport control measures. Atmos Chem Phys 9:1503–1520
28. Kittelson DB (1998) Engines and nanoparticles: a review. J Aerosol Sci 29:575–588
29. Abdul-Khalek IS, Kittelson DB, Brear F (1999) The influence of dilution conditions on diesel exhaust particle size distribution measurements. SAE Technical Paper Series No. 1999-01-1142
30. Mathis U (2002) Influencing parameters of nanoparticle formation from diesel exhaust. In: Proceedings of the 6th international ETH conference on nanoparticle measurements, Zürich, 19–21 August 2002
31. Ntziachristos L, Samaras Z, Pistikopoulos P, Kyriakis N (2000) Statistical analysis of diesel fuel effects on particle number and mass emissions. Environ Sci Technol 34:5106–5114
32. Maricq MM, Chase RE, Podsiadlik DH (1999) Vehicle exhaust particle size distributions: a comparison of tailpipe and dilution tunnel measurements. SAE Technical Paper Series No. 1999-01-1461
33. EEA (2009) The EMEP/EEA air pollutant emission inventory guidebook – 2009. EEA Technical Report No 9/2009. European Environment Agency, Copenhagen
34. Denier van der Gon H, Hulskotte J (2009) Methodologies for estimating shipping emissions in the Netherlands – a documentation of currently used emission factors and related activity data. Report 500099012, Netherlands Environmental Assessment Agency, Bilthoven. ISSN: 1875-2322
35. Fridell E, Steen E, Peterson K (2008) Primary particles in ship emissions. Atmos Environ 42:1160–1168
36. CONCAWE (1987) An investigation into evaporative hydrocarbon emissions from European vehicles. Report No. 87/60. CONCAWE, The Hague
37. Thorpe A, Harriosn RM (2008) Sources and properties of non-exhaust particulate matter from road traffic: A review. Sci Total Environ 400:270–282
38. Pierson WR, Brachaczek WW (1974) Airborne particulate debris from rubber tyres. Rubber Chem Technol 47:1275–1299
39. Rogge WF, Hildemann LM, Mazurek MA, Cass GR (1993) Sources of fine organic aerosol. 3. Road dust, tire debris, and organometallic brake lining dust: roads as sources and sinks. Environ Sci Technol 27(9):1892–1904
40. Fauser P (1999) Particulate air pollution with emphasis on traffic generated aerosols. Riso-R-1053(EN), Riso National Laboratory, Roskilde
41. Cardina JA (1974) Particle size determination of tire tread rubber in atmospheric dusts. Rubber Chem Technol 47:1005–1010
42. Dannis ML (1974) Rubber dust from the normal wear of tyres. Rubber Chem Technol 47:1011–1037
43. Cadle SH, Williams RL (1978) Gas and particle emissions from automobile tires in laboratory and field studies. Rubber Chem Technol 52:146–158
44. Rauterberg-Wulff A (1998) Beitrag des Reifen- und Bremsenabriebs zur Russimmission an Strassen. Dissertation am Fachgebiet Luftreinhaltung der Technischen Universitat Berlin
45. Rauterberg-Wulff A (1999) Determination of emission factors for tyre wear particles up to 10 μm by tunnel measurements. In: Proceedings of 8th international symposium "Transport and Air Pollution", Graz, 31 May–2 June 1999. Technical University Graz. Institute for Internal Combustion Engines and Thermodynamics
46. Moosmüller H, Gillies J, Rogers F, DuBois D, Chow J, Watson J, Langston R (1998) Particulate emission rates for unpaved shoulders along a paved road. J Air Waste Manage Assoc 48:398–407
47. Dahl A, Gharibi A, Swietlicki E, Gudmundsson A, Bohgard M, Ljungman A, Blomqvist G, Gustafsson M (2006) Traffic-generated emissions of ultrafine particles from pavement-tire interface. Atmos Environ 40:1314–1323
48. Berdowski JJM, Mulder W, Veldt C, Visschedijk AJH, Zandveld PYJ (1997) Particulate matter emissions (PM_{10} – PM2.5 – PM0.1) in Europe in 1990 and 1993. TNO Report TNO_MEP – R 96/472.

TNO Institute of Environmental Sciences, Energy Research and Process Innovation, Apeldoorn
49. Sanders PG, Xu N, Dalka TM, Maricq MM (2003) Airborne brake wear debris: size distributions, composition, and a comparison of dynamometer and vehicle tests. Environ Sci Technol 37:4060–4069
50. Garg BD, Cadle SH, Mulawa PA, Groblicki PJ, Laroo C, Parr GA (2000) Brake wear particulate matter emissions. Environ Sci Technol 34(21):4463–4469
51. Abu-Allaban M, Gillies JA, Gertler AW, Clayton R, Proffitt D (2003) Tailpipe, resuspended road dust, and brake wear emission factors from on-road vehicles. Atmos Environ 37(1):5283–5293
52. Iijima A, Sato K, Yano K, Tago H, Kato M, Kimura H, Furuta N (2007) Particle size and composition distribution analysis of automotive brake abrasion dusts for the evaluation of antimony sources of airborne particulate matter. Atmos Environ 41:4908–4919
53. Bukowiecki N, Gehrig R, Hill M, Lienemann P, Zwicky CN, Buchmann B, Weingartner E, Baltensperger U (2007) Iron, manganese and copper emitted by cargo and passenger trains in Zurich (Switzerland): Size-segregated mass concentrations in ambient air. Atmos Environ 41:878–889
54. Gehrig R, Hill M, Lienemann P, Zwicky CN, Bukowiecki N, Weingartner E, Baltensperger U, Buchmann B (2007) Contribution of railway traffic to local PM_{10} concentrations in Switzerland. Atmos Environ 41:923–933
55. Kleeman MJ, Cass GR (1999) Effect of emissions control strategies on the size and composition distribution of urban particulate air pollution. Environ Sci Technol 33:177–189
56. Gaffney P, Bode R, Murchison L (1995) PM_{10} emission inventory improvement program for California. Air Resources Board, Sacramento
57. Zimmer RA, Reeser WK, Cummins P (1992) Evaluation of PM_{10} emission factors for paved streets. In: Chow JC, Ono DM (eds) PM_{10} standards and non-traditional particulate source controls., pp 311–323
58. Pregger T, Friedrich R (2002) Emission Sources of PM_{10} (coarse and fine fraction) in Germany, Universität Stuttgart, Stuttgart. Presentation at "Particles in the size of 2.5 to 10 microns in urban areas" workshop, in support of the Clean Air for Europe (CAFE) programme of DG ENV, Berlin, 4–6 Nov 2002
59. Düring I, Lohmeyer A (2003) Quantifizierung der PM_{10}-Emissionen durch Staubaufwirbelung und brieb von Straßen auf der Basis von vorhandenen Messdaten. http://www.lohmeyer.de
60. Thorpe AJ, Harrison RM, Boulter PG, McCrae IS (2007) Estimation of particle resuspension source strength on a major London Road. Atmos Environ 41:8007–8020
61. Johansson C (2002) Source contributions of PM in Sweden – implications for abatement strategies. Institute of Applied Environmental Research (ITM). Stockholm. Presentation at "Particles in the size of 2.5 to 10 microns in urban areas" workshop, in support of the Clean Air for Europe (CAFE) programme of DG ENV, Berlin, 4–6 Nov 2002
62. Areskoug H, Johansson C, Alesand T, Hedberg E, Ekengena T, Vesely V, Wideqvist U, Hansson H-C (2004) Concentrations and sources of PM_{10} and $PM_{2.5}$ in Sweden. ITM Report 110. Institute of Applied Environmental Research, Stockholm University. ISSN 1103-341X
63. Gustafsson M, Blomqvist G, Gudmundssson A, Dahl A, Johnsson P, Swietlicki E (2009) Factors influencing PM_{10} emissions from road pavement wear. Atmos Environ 43:4699–4702
64. Sturm PJ, Boulter P, de Haan P, Joumard R, Hausberger S, Hickman AJ, Keller M, Niederle W, Ntziachristos L, Reiter C, Samaras Z, Schinagl G, Schweizer T, Pischinger R (1998) Instantaneous emission data and their use in estimating passenger car emissions. Deliverable no. 6. Of the EC MEET Project. Technical University of Graz, Institute for Internal Combustion Engines and Thermodynamics, Austria
65. Van de Weijer C (1997) Heavy duty emission factors. Development of representative driving cycles and prediction of emissions in real life. Ph.D. thesis, Graz University of Technology, Oct 1997
66. INFRAS (2010) Handbook of emission factors for road transport, version 3.1. INFRAS, Zürich. http://www.hbefa.net/e/index.html
67. Smit R, Smokers R, Schoen E, Hensema A (2006) A new modelling approach for road traffic emissions: VERSIT+LD: background and methodology. Report 06.OR.PT.016.1/RS. TNO Science and Industry, Delft
68. Hassounah MI, Miller EJ (1995) Modelling air pollution from road traffic: a review. Traffic Eng Contr 35(9):510–514
69. Hung W-T, Tomg H-Y, Cheung C-S (2005) A modal approach to vehicular emissions and fuel consumption model development. J Air Waste Manage Assoc 55:1431–1440
70. Coelho MC, Fariasa TL, Rouphail NM (2005) A methodology for modelling and measuring traffic and emission performance of speed control traffic signals. Atmos Environ 39:2367–2376
71. De Haan P, Keller M (2000) Emission factors for passenger cars: application of instantaneous emission modelling. Atmos Environ 34:4629–4638
72. Sorenson SC, Schramm J (1992) Individual and public transportation-emissions and energy consumption models. Technical University of Denmark report, RE 91-5, Lyngby
73. Hansen JQ, Winter M, Sorenson SC (1995) The influence of driving patterns on petrol passenger car emissions. Sci Total Environ 169:129–139
74. Joumard R, Jost P, Hickman J (1995) Influence of instantaneous speed and acceleration on hot passenger car emissions and fuel consumption. SAE Paper 950928. Society of Automotive Engineers, Warrendale
75. Post K, Kent JH, Tomlin J, Carruthers N (1984) Fuel consumption and emission modelling by power demand and a comparison with other models. Transp Res 18A:191–213
76. Rexeis M, Hausberger S, Riemersma I, Tartakovsky L, Zvirin Y, Erwin C (2005) Heavy-duty vehicle emissions. Final report of WP 400 in ARTEMIS (Assessment and Reliability of Transport Emission Models and Inventory Systems); DGTREN Contract 1999-RD.10429; University of Technology, Graz, Report no.: I 02/2005/Hb 20/2000 I680

77. Atjay D, Weilenmann M (2004) Compensation of the exhaust gas transport dynamics for accurate instantaneous emission measurement. Environ Sci Technol 38(19):5141–5148
78. Roujol S, Joumard R (2009) Influence of passenger car auxiliaries on pollutant emission factors within the Artemis model. Atmos Environ 43(5):1008–1014
79. European Commission (1999) MEET – methodology for calculating transport emissions and energy consumption. Office for Official Publications of the European Communities, Luxembourg
80. André J-M, Joumard R (2005) Modelling of cold start excess emissions for passenger cars. INRETS Report LTE0509. Laboratoire Transports et Environnement, INRETS, Bron
81. Blaikley DCW, Smith AP, Feest EA, Reading AH (2001) UG219 TRAMAQ – cold-start emissions. Summary report, AEAT/ENV/R/0638 Issue 1, May 2001
82. Wade DT (1967) Factors influencing vehicle evaporative emissions. Esso Research and Engineering, Society of Automotive Engineers paper SAE 670126
83. Hausberger S, Wiesmayr J, Bukvarevic E, Tripold W, Brenner J (2005) Evaporative emissions of vehicles – final report. European Commission 5th Framework project ARTEMIS (Assessment and Reliability of Transport Emission Models and Inventory Systems) Technical University of Graz, Graz
84. Martini G et al (2007) Joint EUCAR/JRC/CONCAWE programme on effects of petrol vapour pressure and ethanol content onevaporative emissions from modern cars. Report number EUR 22715 EN. ISBN 978-1-4419-0851-3_554. Office for Official Publications of the European Communities, Luxembourg
85. Mellios G, Samaras Z (2007) An empirical model for estimating evaporative hydrocarbon emissions from canister-equipped vehicles. Fuel 86:2254–2261
86. USEPA (1995) Compilation of air pollutant emission factors AP-42, 5th edn. Stationary point and area sources, vol 1. Section 13.2.1: paved roads (updated November 2006). United States Environmental Protection Agency, Washington, DC
87. Venkatram A (2000) A critique of empirical emission factor models: a case study of the AP-42 model for estimating PM_{10} emissions from paved roads. Atmos Environ 32:1–11
88. Jørgensen MV, Sorenson SC (1996) Estimating emissions from railway traffic. Report for MEET, 4th framework project, (DG-VII contract no: ST-96-SC.204), as Report ET-EO-97-03, Department of Energy Engineering, Technical University of Denmark
89. Georgakaki A, Coffey R, Sorenson SC (2002) Development of a database system for the calculation of indicators of environmental pressure caused by railway transport. Transport and ENVIRONMENT DATABASE SYSTEM (TRENDS) project for EUROSTAT, Report MEK–ET–2002–03, Department of Energy Engineering, Technical University of Denmark
90. Lindgreen E, Sorenson SC (2005) Simulation of energy consumption and emissions from rail traffic. Report MEK-ET-2005-4, Department of Mechanical Engineering, Danish Technical University, February 2005. Deliverable 7a for ARTEMIS, DG-TREN contract 1999-RD.10429
91. Gijsen A, van den Brink RMM (2002) Energy use and emissions by rail transport; description and results of the model PRORIN (in Dutch). Report no. 773002021. RIVM, Bilthoven
92. Entec (2002) Quantification of emissions from ships associated with ship movements between ports in the European Community. Final Report to the European Commission, Entec UK Limited
93. Sjöbris A, Gustafsson J, Jivén K (2005) ARTEMIS: sea transport emission modelling. MariTerm AB, Gothenburg
94. Georgakaki A, Sorensen SC (2004) Report on collected data and resulting methodology for inland shipping. Workpackage 900: emission estimating methodology for ship transport of the European Commission fifth framework ARTEMIS project. Report No: MEK-ET-2004-2. ISBN 87-7475-314-2. Technical University of Denmark, Lyngby
95. André M, Rapone M, Adra N, Pollak I, Keller M, McCrae I (2006) Traffic characteristics for the estimation of pollutant emissions from road transport. Final Report of ARTEMIS Workpackage 1000. INRETS Report LTE0606. INRETS, Bron
96. Stathopoulos FG, Noland RB (2003) Induced travel and emissions from traffic flow improvement projects. TRR J Transp Res Board 1842:57–63
97. Schall V (2007) Energy-efficient driving. Presentation at the International Transport Forum workshop on eco-driving, Paris. 22 November 2007. Deutsche Bahn AG
98. Entec (2005) Ship emissions: assignment, abatement and market-based instruments – task 1: preliminary assignment of ship emissions to European countries. Report to the European Commission, Entec UK Limited
99. AQEG (2005) Particulate matter in the United Kingdom. Report of the Air Quality Expert Group, DEFRA, London
100. Matthijsen J, ten Brink HM (2007) $PM_{2.5}$ in the Netherlands – consequences of the new European air quality standards. MNP Report 500099001/2007. The Netherlands Environmental Assessment Agency (MNP), Bilthoven
101. Putaud J-P et al (2010) A European aerosol phenomenology – 3: physical and chemical characteristics of particulate matter from 60 rural, urban, and kerbside sites across Europe. Atmos Environ 44:1308–1320
102. Harrison RM, Shi JP, Grenfell JL (1998) Novel night-time free radical chemistry in severe nitrogen dioxide pollution episodes. Atmos Environ 32(16):2769–2774
103. AQEG (2007) Trends in primary nitrogen dioxide in the UK. The fourth report of the Air Quality Expert Group. Department for the Environment, Food and Rural Affairs, London, ISBN:978-0-85521-179-0
104. Jenkin ME (2004) Analysis of sources and partitioning of oxidant in the UK – part 2: contributions of nitrogen dioxide emissions and background ozone at a kerbside location in London. Atmos Environ 38(30): 5131–5138
105. Carslaw DC, Beevers SD (2004) Investigating the potential importance of primary NO_2 emissions in a street canyon. Atmos Environ 38:3585–3594

106. Carslaw DC (2005) Evidence of an increasing NO_2/NO_x emissions ratio from road traffic emissions. Atmos Environ 39:4793–4802
107. Hueglin C, Buchmann B, Weber RO (2006) Long-term observation of real-world road traffic emission factors on a motorway in Switzerland. Atmos Environ 40(20): 3696–3709
108. Grice S, Stedman J, Kent A, Hobson M, Norris J, Abbott J, Cooke S (2009) Recent trends and projections of primary NO_2 emissions in Europe. Atmos Environ 43:2154–2167
109. Lappi M, Laurikko J, Erkkilä K, Pellikka A-P, Koskentalo T (2008) Specific NO and NO_2 emissions from a wide range of current and future LD and HD vehicles in urban driving conditions. In: Proceedings of 16th international conference "Transport and Air Pollution" 2008, Graz
110. Rexeis R, Hausberger S (2009) Trend of vehicle emission levels until 2020 – prognosis based on current vehicle measurements and future emission legislation. Atmos Environ 43:4689–4698
111. Keuken M, Roemer M, van den Elshout S (2009) Trend analysis of urban NO_2 concentrations and the importance of direct NO_2 emissions versus ozone/NO_x equilibrium. Atmos Environ 43:4780–4783
112. WHO (2003) Health aspects of air pollution with particulate matter, ozone and nitrogen dioxide. Report on a WHO working group, Bonn, 13–15 Jan 2003. Document EUR/03/5042688. WHO Regional Office for Europe, Copenhagen
113. Granier C, Brasseur GP (2003) The impact of road traffic on global tropospheric ozone. Geophys Res Lett 30(2):1086. doi:10.1029/2002GL015972
114. Matthes S, Grewe V, Sausen R, Roelofs G-J (2007) Global impact of road traffic emissions on tropospheric ozone. Atmos Chem Phys 7:1707–1718, http://www.atmos-chem-phys.net/7/1707/2007/
115. Berkowicz R (2000) OSPM – a parameterised street pollution model. Environ Monit Assess 65(1/2):323–331
116. GLA (2010) Clearing the air: the mayor's draft air quality strategy for public consultation. Greater London Authority, London
117. Eyring V et al (2009) Transport impacts on atmosphere and climate: shipping. Atmos Environ 44(37):4735–4771
118. Harrison RM, Yin J, Mark D, Stedman J, Appleby RS, Booker J, Moorcroft S (2001) Studies of the coarse particle (2.5 – 10 μm) component in UK urban atmospheres. Atmos Environ 35:3667–3679
119. Delphi (2010) World-wide emission standards: passenger cars and light duty vehicles (2010/11). Delphi, Troy
120. UIC (2006) Exhaust emission tests for diesel traction engines, Leaflet 624, 3rd edn. Union Internationale des Chemins de Fer, Paris. ISBN 2-7461-1040-7
121. IMO (1998) Regulations for the prevention of air pollution from ships and NOx technical code, ANNEX VI of MARPOL 73/78. International Maritime Organization, London
122. ACEA, Alliance, EMA, JAMA (2006) Worldwide fuel charter, 4th edn. September 2006
123. Hill N et al (2005) Rail diesel study. Work package 2 final report: technical and operational measures to improve the emissions performance of diesel rail. Report ED05010/WP2/R02. AEA Technology, Didcot
124. MECA (2006) Case studies of the use of exhaust emission controls on locomotives and large marine diesel engines. Manufacturers of Emission Controls Association, Washington, DC
125. Karavalakis G, Stournas S, Bakeasb E (2009) Effects of diesel/biodiesel blends on regulated and unregulated pollutants from a passenger vehicle operated over the European and the Athens driving cycles. Atmos Environ 43(10):1745–1752
126. King J (2007) The King review of low-carbon cars. Part I: the potential for CO_2 reduction. HMSO, London
127. Bruckner-Menchelli N (2009) Scrubbers versus distillates. Bunkerworld, May/June 2009, p 24
128. Palmer MW, Pimentel D, Lal R, Kennedy D (2007) Biofuels and the environment. Science 317:897–898
129. Katsoulakos T, Morgan D (2009) Ship technologies. Deliverable D2.4.1 of the EC 7th framework programme coordination action SKEMA (Sustainable Knowledge Platform for the European Maritime and Logistics Industry)
130. SenterNovem (2005) Ecodriving – the smart driving style. Produced by SenterNovem, Utrecht for the EC TREATISE project, Sept 2005
131. Van Mieghem R, Gense R (2005) Extra brandstofverbruik door gebruik van accessoires in personenauto's. TNO report 05.OR.VM.066.1/RvM. TNO Science and Industry, Delft
132. Weilenmann M (2002) Emissions and fuel consumption with eco drive – English summary. Report number 201209e. EMPA, Dübendorf
133. Vermeulen RJ (2006) The effects of a range of measures to reduce the tail pipe emissions and/or the fuel consumption of modern passenger cars on petrol and diesel. TNO report IS-RPT-033-DTS-2006-01695. TNO Science and Industry, Delft
134. Fontaras G, Pistikopoulos P, Samaras Z (2008) Experimental evaluation of hybrid vehicle fuel economy and pollutant emissions over real-world simulation driving cycles. Atmos Environ 42:4023–4035
135. Johansson H, Gustafsson P, Henke M, Rosengren M (2003) Impact of EcoDriving on emissions. In: Transport and air pollution. Proceedings from the 12th symposium, Avignon, 16–18 June 2003
136. Parkes AM, Reed N (2005) Fuel efficiency training in a full-mission truck simulator. In: Behavioural research in road safety 2005: fifteenth seminar, London, pp 135–146
137. Zarkadoula M, Zoidis G, Tritopoulou E (2007) Training urban bus drivers to promote smart driving: a note on a Greek eco-driving pilot program. Transp Res D Transp Environ 12(6):449–451
138. Schweighofer J, Seiwerth P (2007) Environmental performance of inland navigation. European Inland waterway navigation conference, Visegrád, 27–29 June 2007
139. Duncan M, Jain R, Yung SC, Patterson R (1985) Performance evaluation of an improved street sweeper. US Environmental

Protection Agency (US EPA-600/7-85- 008), Government Printing Office, Research Triangle Park, NC
140. Cowherd C, Muleski GE, Kinsey JS (1988) Control of open fugitive dust sources. EPA-450/3-88-008, US Environmental Protection Agency, Research Triangle Park, NC
141. Chow JC, Watson JG, Egami RT, Frazier CA, Lu Z, Goodrich A, Bird A (1990) Evaluation of regenerative-air vacuum street sweeping on geological contributions to PM_{10}. J Air Waste Manage Assoc 40(8):1134–1142
142. Kuhns H, Etyemezian V, Green M, Hendrickson K, McGown M, Bartond K, Pitchford M (2003) Vehicle-based road dust emission measurement – part II: effect of precipitation, wintertime road sanding, and street sweepers on inferred PM10 emission potentials from paved and unpaved roads. Atmos Environ 37:4573–4582
143. Gustafsson M (2004) Nordic road and transport research, no.1. Road and street sweeping as a measure against high particle concentrations caused by road dust. http://www.vti.se/nordic/1-04mapp/annosv.htm
144. Norman M, Johansson C (2006) Studies of some measures to reduce road dust emissions from paved roads in Scandinavia. Atmos Environ 40(32):6154–6164
145. Aldrin M, Haff I, Rosland P (2007) The effect of salting with magnesium chloride on the concentration of particulate matter in a road tunnel. Norwegian Public Road Administration. Atmos Environ 43:4472–4480
146. Gertler A, Kuhns H, Abu-Allaban M, Damm C, Gillies J, Etyemezian V, Clayton R, Proffitt D (2006) A case study of the impact of winter road sand/salt and street sweeping on road dust re-entrainment. Atmos Environ 40(31):5976–5985
147. Chang Y-M, Chou C-M, Su K-T, Tseng C-H (2005) Effectiveness of street sweeping and washing for controlling ambient TSP. Atmos Environ 39:1891–1902
148. Chou C-M, Chang Y-M, Lin W-Y, Tseng C-H, Chen L (2007) Evaluation of street sweeping and washing to reduce ambient PM_{10}. Int J Environ Pollut 31(34):431–448
149. Kuhns H, Etyemezian V, Landwehr D, MacDougall C, Pitchford M, Green M (2001) Testing re-entrained aerosol kinetic emissions from roads (TRAKER): a new approach to infer silt loadings on roadways. Atmos Environ 35:2815–2825
150. John AC, Hugo A, Kaminski H, Brandt A, Kappert W, Falkenberg E, Kuhlbusch TAJ (2007) Effectiveness of street cleaning for reducing ambient PM_{10} concentrations. In: European aerosol conference 2007, Salzburg, Abstract T19A047
151. Amato F, Querol X, Alastuey A, Pandolfi M, Moreno T, Gracia J, Rodriguez P (2009) Evaluating urban PM_{10} pollution benefit induced by street cleaning activities. Atmos Environ 43:4472–4480
152. Berthelsen B-O (2003) The use of magnesium chloride as dust reducer at E6 through Trondheim (only in Norwegian). Report No. TM2003/2, Trondheim Municipality, Environment Division, Trondheim, ISBN:82-7727-087-9
153. Johansson C, Burman B, Forsberg B (2009) The effects of congestions tax on air quality and health. Atmos Environ 43:4843–4854
154. Bowker GE, Baldauf R, Isakov V, Khlystov E, Petersen W (2007) The effects of roadside structures on the transport and dispersion of ultrafine particles from highways. Atmos Environ 41:8128–8139
155. Baldauf R, Thoma E, Khlystov A, Isakov V, Bowker G, Long SR (2008) Impacts of noise barriers on near-road air quality. Atmos Environ 42:7502–7507
156. Morikawa H, Takahashi M, Hakata M, Sakamoto A (2003) Screening and genetic manipulation of plants for decontamination of pollutants from the environment. Biotechnol Adv 22:9–15
157. Beckett KP, Freer-Smith P, Taylor G (2000) Effective tree species for local air quality management. Journal of Arboriculture 26(1):12–19
158. Yang J, Yu Q, Gong P (2008) Quantifying air pollution removal by green roofs in Chicago. Atmos Environ 42:7266–7273
159. Cavanagh JE (2006) Potential of vegetation to mitigate road-generated air pollution. Part I – review of background information. Contractor Report LC0506/00xx. Landcare Research, Lincoln
160. Litschke T, Kuttler W (2008) On the reduction of urban particle concentration by vegetation – a review. Meteorol Z 17(3):229–240
161. Laufs S, Burgeth G, Duttlinger W, Kurtenbach R, Maban M, Thomas C, Wiesen P, Kleffmann J (2010) Conversion of nitrogen oxides on commercial photocatalytic dispersion paints. Atmos Environ 44:2341–2349
162. Child & Associates (2004) M5 East Freeway: A review of emission treatment technologies, systems and applications. Review undertaken by Child & Associates for the Roads and Traffic Authority of NSW. http://www.rta.nsw.gov.au/constructionmaintenance/downloads/2004_10_childrep-filtration.pdf
163. Willoughby P, Stricker J, Humphrey G (2004) Electrostatic precipitators and ventilation in road tunnels in Japan. Report of a visit by a delegation from the NSW Roads and Traffic Authority to Japan from 30 September – 10 October 2003. New South Wales Roads and Traffic Authority
164. TNO (2009) Conceptrapport IPL. Praktijkonderzoek "Elektrostatisch concept in Thomassentunnel". Report of the Dutch Air Quality Innovation Programme (IPL)
165. Davis SC, Diegel SW, Boundy RG (2010) Transportation energy data book: edition 29. Report ORNL-6985. Oak Ridge National Laboratory, Oak Ridge
166. Eyring V, Stevenson DS, Lauer A, Dentener FJ, Butler T, Collins WJ, Ellingsen K, Gauss M (2007) Multi-model simulations of the impact of international shipping on atmospheric chemistry and climate in 2000 and 2030. Atmos Chem Phys 7:757–780
167. Jalkanen JP, Brink A, Kalli J, Pettersson H, Kukkonen J, Stipa T (2009) A modelling system for the exhaust emissions of marine traffic and its application in the Baltic Sea area. Atmos Chem Phys 9:9209–9223
168. Smit R, Ntziachristos L, Boulter P (2010) Validation of road vehicle and traffic emission models – a review and meta-analysis. Atmos Environ 44:2943–2953

Books and Reviews

Boulter P, McCrae I (eds) (2009) ARTEMIS: assessment and reliability of transport emission models and inventory systems. Final Report. TRL Report PPR350. TRL Limited, Wokingham

Finlayson-Pitts BJ, Pitts JN (2000) Chemistry of the upper and lower atmosphere. Academic, New York. ISBN 0-12-257060-X

Sokhi RS (ed) (2008) World atlas of atmospheric pollution. Anthem Press, London. ISBN 9781843312895

USEPA (2009) Integrated science assessment for particulate matter. EPA/600/R-08/139F. United States Environmental Protection Agency. http://cfpub.epa.gov/ncea/cfm/recordisplay.cfm?deid=216546

Wayne RP (2000) Chemistry of atmospheres, 3rd edn. Oxford University Press, Oxford, UK. ISBN 0-19-850375-X

Airborne and Space-borne Remote Sensing of Cryosphere

Kenneth C. Jezek
Byrd Polar Research Center, School of Earth Sciences, The Ohio State University, Columbus, OH, USA

Article Outline

Glossary
Definition of the Subject: The Cryosphere
Introduction
Early History of Cryospheric Remote Sensing
Scientific Advances from Airborne and Space-borne Remote Sensing
Cooperative Efforts to Observe, Monitor, and Understand the Cryosphere
Future Directions
Bibliography

Glossary

Cryosphere Those components of the Earth system that contain water in its frozen form.

Radar Radio detection and ranging systems.

Lidar Light detection and ranging systems.

Radiometers Radio frequency receivers designed to detect emitted radiation from a surface and in accordance with Planck's law.

Synthetic aperture radar Radar system which increases along track resolution by using the motion of the platform to synthesize a large antenna.

Permafrost Persistently frozen ground.

Ice sheet Continental-scale, freshwater ice cover that deforms under its own weight.

Sea ice Saline ice formed when ocean water freezes.

Glaciers Long, channelized, slabs of freshwater ice thick enough to deform under their own weight.

Seasonal snow The annual snow that blankets land cover in the winter and melts by summer.

Definition of the Subject: The Cryosphere

The Cryosphere broadly constitutes all the components of the Earth system which contain water in a frozen state [1]. As such, glaciers, ice sheets, snow cover, lake and river ice, and permafrost make up the terrestrial elements of the Cryosphere. Sea ice in all of its forms, frozen sea bed and icebergs constitute the oceanic elements of the Cryosphere while ice particles in the upper atmosphere and icy precipitation near the surface are the representative members of the Cryosphere in atmospheric systems. This overarching definition of Earth's cryosphere immediately implies that substantial portions of Earth's land and ocean surfaces are directly subject in some fashion to cryospheric processes. Through globally interacting processes such as the inevitable transfer of heat from the warm equatorial oceans to the cold polar latitudes, it seems reasonable to argue that all regions of Earth are influenced by cryospheric processes and their integration into the modern climate of the planet. Observations of the cryosphere necessary to predict future variability in Earth's ice cover and its interaction with other Earth systems must be made on commensurate spatial and temporal scales. Consequently, airborne and space-borne remote sensing technologies with global reach play a key role in acquiring data necessary to understand the important physical processes and earth system interactions that govern the evolution of the Cryosphere (Fig. 1).

Introduction

The broad spatial and seasonally changing distribution of ice plays an important role in earth systems and human activities. At high latitudes, ice covered land and ocean surfaces are highly reflective thus redirecting incoming solar radiation back into space in the summer months. Indeed, reductions in the spatial area of snow and ice cover are believed to be an important

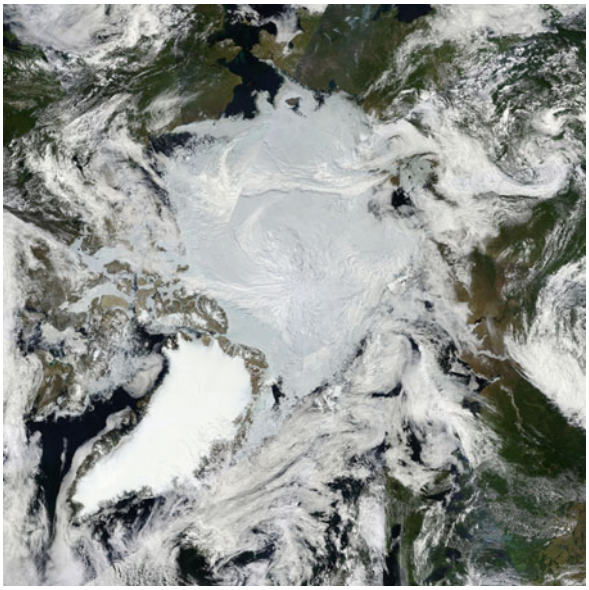

Airborne and Space-borne Remote Sensing of Cryosphere. Figure 1
NASA MODIS composite for July 7, 2010. Starting in the *lower left* quadrant and going clockwise, the Greenland sheet is almost cloud free as are the adjacent smaller ice caps on the Canadian Arctic Islands. Much of northern Canada and Alaska are cloud covered till the Bering Strait which is also almost sea ice free. Patches of sea ice cling to the Asian coast and there is a smattering of snow cover on the Putorana Mountains in western Siberia. The Gulf of Ob, Novaya Zemlya, the Franz Josef Land, and Spitsbergen Islands are barely visible through the cloud. The central Arctic basin is covered by sea ice. The image illustrates the scale of the cryosphere as well as some of the complications faced when trying to study it from space (Image prepared by NASA's MODIS Rapid Response team)

feedback mechanism that enhances warming at high latitudes [2, 3]. Essentially, reduced snow and ice cover exposes darker land and ocean surfaces that retain rather than reflect solar energy. This results in increased warming and hence a further decrease in the area of snow and ice covered surfaces. Sea ice is an important habitat for birds such as penguins and mammals such as seals and polar bears which thrive in this icy environment [4]. But the underside of sea ice is also an important refuge for some of the smallest creatures including the shrimp-like krill which graze upon algae that grows just beneath and within the ice canopy [5, 6]. Terrestrial permafrost and frozen sediments beneath the oceans support an important reservoir of organic carbon and gas hydrates [7]. As permafrost melts, methane can be released contributing to the increasing concentration of greenhouse gases in the atmosphere. Glaciers and ice sheets are vast reservoirs of Earth's freshwater. As the ice sheets thin, water flows from the ice sheets into the oceans raising global sea level [8]. In terms of our daily activities, seasonal snow and glaciers are important sources of spring runoff for irrigation and power generation, while ice jams on rivers constitute important obstacles to winter-time navigation and can cause low-land flooding [9]. Thawing permafrost causes the land near surface to become unstable which can result in catastrophic structural failures in buildings.

The global span of cryospheric processes and the strong daily to seasonal swing in the extent of snow and ice makes studying and monitoring the cryosphere an especially challenging scientific objective [10]. Moreover the variety of forms in which ice can be manifest in Earth systems means that no single observing system is capable of making adequate observations. Rather an ensemble of techniques is required to fully appreciate and eventually understand the complexities of the cryosphere and its interaction with other earth systems. Locally, observing tools may include direct, field measurements of snow pack thickness or physical temperature. Much different sets of tools are needed to characterize the cryosphere on a global and annual scale where the inhospitable climate and the physical remoteness of many sectors of the cryosphere represent obstacles to scientific investigation. Here, aircraft and spacecraft mounted instruments are required to infer geophysical properties from a remote distance (Fig. 2).

Compounded with these geographic challenges, observations of the icy surface often have to overcome cloud cover that frequently obscures the high latitudes, as well as continuing measurements during the long polar night. Consequently a range of instruments generally rely on distinguishing properties evident in the broad-spectral electrical characteristic of icy terrain. For example, even the cloudy atmosphere is largely transparent to microwave radiation. That fact combined with the very different microwave emission of open ocean and sea ice enables space-borne microwave observations of annual sea ice extent and concentration

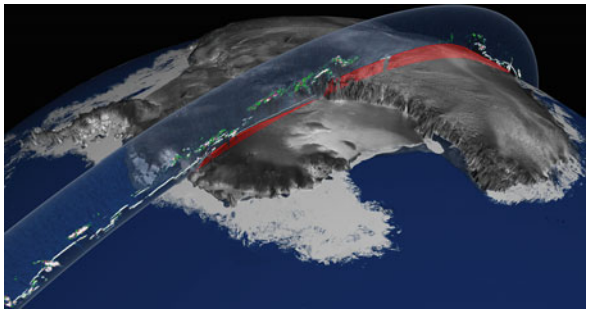

Airborne and Space-borne Remote Sensing of Cryosphere. Figure 2
Illustration of NASA's ICESat passing over the Antarctic. ICESat collected repeat elevation data over ice sheets and sea ice to study changing ice thicknesses. ICESat also sounded the atmosphere to study aerosols. NASA/Goddard Space Flight Center Scientific Visualization Studio, RADARSAT mosaic of Antarctica (Canadian Space Agency)

day and night and in all weather. Similarly the electrical contrast between rock and ice enables airborne radio frequency radar measurements of the thickness of polar ice sheets and glaciers. However some of the most recent advances in cryospheric science have been made by relying on one of the most basic properties of the icy cover, namely its mass. Space-borne measurements of the changing gravitational attraction of variably sized snow and ice bodies enables direct estimates of changing polar ice mass and the redistribution of melting ice into the liquid oceans. Indeed it can be argued that engineering and technological advances in airborne and remote sensing have had some of their greatest scientific impacts in the understanding the evolution of Earth's ice cover.

This article provides an overview of remote sensing of the cryosphere from both aircraft and spacecraft. A brief historical review of remote sensing of snow and ice is followed by a discussion of the physics of remote sensing of the cryosphere and how developments in remote sensing have led to a series of important scientific advances. These include the realization of the diminishing extent of Arctic sea ice and the thinning of glaciers, ice caps, and ice sheets worldwide. Both of these observations form critical, direct evidence of changing world climate. The article concludes with a discussion of developing international collaborations that are aimed at pooling technologically sophisticated and operationally expensive international assets so as to obtain an integrated system of continuing remote sensing observations necessary to predict future changes in Earth's ice and the consequent impacts on human activities.

Early History of Cryospheric Remote Sensing

The science and operational communities have always been quick to adopt new instruments and platforms for use in observing snow and ice in all of its forms. This section reviews early developments in cryospheric remote sensing – which were in part driven by science and in part by the basic desire to explore the most remote regions of Earth.

Airborne Photo-Reconnaissance

Aerial photography of ice covered terrain began during early twentieth century expeditions to the high atitudes and was used primarily to document the progress of the expedition. Survey quality aerial mapping was adopted using techniques primarily developed during World War I [11]. Mittelholzer and others [12] writing about the 1923 Junkers Expedition to Spitzbergen offer a very complete overview of the geographic and cartographic objectives for aerial photography in the North including a brief discussion of glacier formation as revealed by the aerial photographs. They also give an interesting technical discussion of the challenges faced when doing aerial photographic reconnaissance over highly reflective snow-covered terrain.

Wilkins documented ice cover in the Antarctic Peninsula during the first successful flight in Antarctica by using a hand-held, folding Kodak 3A camera [13, 14]. Richard E. Byrd devoted time and resources to aerial photography for quantitative surveying purposes during his first Antarctic Expedition of 1928–1930. In his book, "Little America," Byrd [15] writes that photographs from Ashley McKinley's laboratory provided "perhaps, the most important geographical information from the expedition." McKinley was third in command of the expedition and the aerial surveyor. McKinley operated his Fairchild K-3 mapping camera during Byrd's 1929 historic flight to the South Pole.

These early airborne photographic records were acquired with great skill and at considerable risk. The

quality of the photographs is often exceptional and the photos themselves represent an oft under-utilized resource for directly gauging century-scale changes in Earth's ice cover.

Satellite Photography

A mere 32 years after Byrd's aerial photographic surveying in Antarctica, space-borne cameras began capturing unique pictures of Earth. CORONA, ARGON, and LANYARD were the first three operational imaging satellite reconnaissance systems and they acquired data during the early 1960s for both detailed reconnaissance purposes and for regional mapping [16–18]. Early reconnaissance satellite photographs provide a unique view of our world as it appeared at the beginning of the space age. Researchers in the environmental science community are the most recent beneficiaries of these data after they were declassified and made publicly available in 1995 through the efforts of Vice President Al Gore along with several government agencies working together with civilian scientists as part of the MEDEA program [19]. Polar researchers in particular inherited a wealth of detailed photography covering both of the great polar ice sheets. After processing with sophisticated digitizing instruments and subsequent analysis with modern photogrammetric and image processing techniques, investigators have shown that these data can be used to characterize local fluctuations in glacier termini [20, 21], investigate large-scale flow features on ice sheets [22, 23] and to measure long-term average velocity by feature retracking techniques [24] (Fig. 3).

Development of Depth Sounding Radar

Early suggestions that glaciers were penetrated by radio signals are attributed to observations made at Little America during Byrd's 2nd Antarctic Expedition [25]. This observation, along with reports that pulsed radar altimeters were yielding faulty readings over glaciers, led to the first radar experiments to measure ice thickness in 1955. In 1960, Waite and Schmidt [25] made measurements over Greenland from aircraft at 110, 220, 440, and 4,300 MHz. These results initiated a revolution in glaciology because the ice thickness and internal structure of glaciers and ice sheets could be rapidly sounded from aircraft [26].

Although the sophistication of ice sounding radar systems has increased tremendously, the basic principle of the technique remains the same and continues to be a fundamental tool used by researchers (Fig. 4). Essentially, the one-way travel time of a radar pulse transmitted through the ice or snow is multiplied by the appropriate wave speed and the thickness so determined. More complex, two dimensional maps of the glacier bed topography can be assembled from multiple profiles that are combined using travel time migration techniques [27]. Several snow and ice sounding radars are part of the primary instrument suite presently

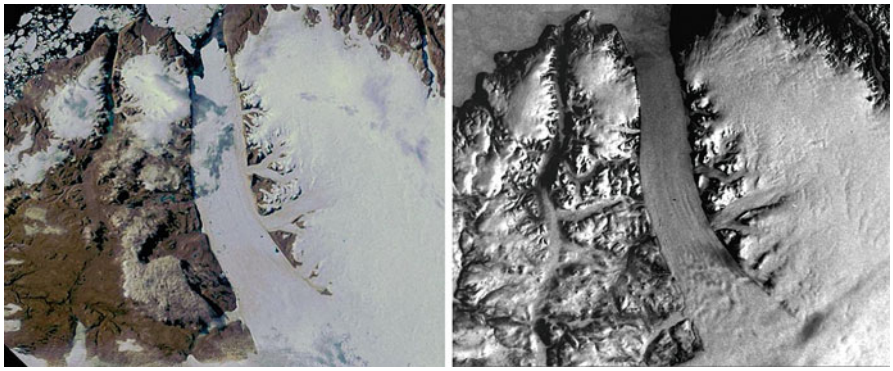

Airborne and Space-borne Remote Sensing of Cryosphere. Figure 3
European Space Agency MERIS image of Peterman Glacier, Greenland (*left*). The multispectral image was acquired in July, 2008 and before a large part of the floating ice tongue broke free. Argon panchromatic photograph acquired during the spring of 1962. The clarity of this early view from space is exceptional and provides a valuable gauge for assessing changes in glacier ice from the 1960s to the present

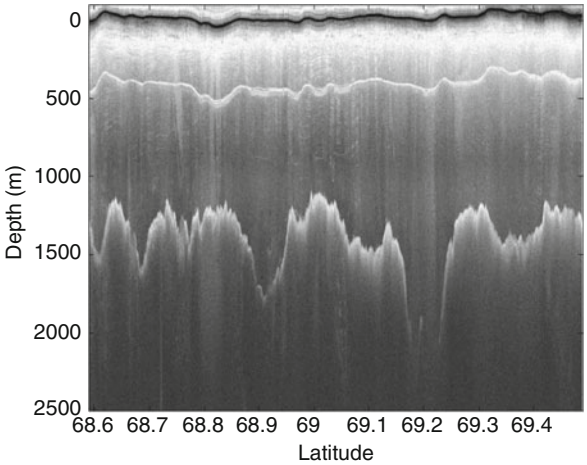

Airborne and Space-borne Remote Sensing of Cryosphere. Figure 4
North south airborne profile of ice thickness in west central Greenland. The *upper black line* is the radar reflection from the snow surface. The line at about 500 m depth is a multiple echo of the surface from the aircraft itself. The undulating line at an average depth of about 1,400 m is the reflection from the glacier bottom. The profile crosses the upstream segment of Jakobshavn Glacier at 69.2° N 48.1°W. There the 2,000 m thick ice has incised a deep channel into the bedrock. The data were acquired by the University of Kansas in 2008

carried aboard aircraft supporting NASA's IceBridge program [28].

Depth sounding radar remains one of the few techniques available to researchers interested in probing the volume of the terrestrial ice cover and the properties of the underlying bed. Airborne radars have been successfully used to study glacier, ice sheets, and to a more limited degree sea ice and permafrost. Seismic techniques yield important complementary information but can be carried out only in situ. Airborne gravity measurements provide important regional information but are generally less accurate than the radar technique for measurements on glaciers.

Scientific Advances from Airborne and Space-borne Remote Sensing

In most instances, airborne and space-borne platforms carry similar kinds of remote sensing instruments. Often times, space-borne instruments are first prototyped as part of initial airborne campaigns. However, advantages of instrument installations on multiple kinds of platforms go far beyond vetting the effectiveness of an instrument. For example, space-borne systems can provide global scale observations, with some imaging instruments yielding pole-to-pole observations on a daily basis. Manned and increasingly unmanned aircraft, with their ability to maneuver and loiter over an area, can provide much denser spatial and temporal coverage when profiling instruments, such as altimeters, are of interest. This section begins with a review of remote sensing physics and then summarizes key applications of remote sensing to several cold regions themes.

Basics of Remote Sensing of the Cryosphere

Airborne and space-borne sensors measure local changes in electromagnetic, gravitational, and magnetic force fields. Disturbances can arise from the passive, thermodynamically driven electromagnetic radiation emitted by the earth's distant surface, or the reflectance of incoming solar radiation from the Earth's surface, both of which change with the terrain type. Instruments and associated satellites of this type include the Electrically Scanning Microwave Radiometer (ESMR), Scanning Multichannel Microwave Radiometer (SMMR), Special Sensor Microwave Radiometer (SSMI), Advanced Very High Resolution Radiometer (AVHRR), Landsat, Moderate Resolution Imaging Spectrometer (MODIS), Medium Resolution Imaging Spectrometer (MERIS), Satellite Pour l'Observation de la Terre (SPOT). Disturbances can also arise from the active behavior of the sensor itself. Radars and lidars include the Airborne Topographic Mapper (ATM), Laser Vegetation Imaging Sensor (LVIS), synthetic aperture radar (SAR) and radar altimeters on the European Remote Sensing Satellite (ERS-1/2), RADARSAT 1/2, synthetic aperture radar and radar altimeter on Envisat, Phased Array L-band SAR, TerraSAR-X, GEOSAT, the Ice and Climate Experiment Satellite (ICESat) lidar, the Cryosat radar altimeter. These instruments illuminate the surface with electromagnetic signals, which upon reflection can be detected back at the sensor after an elapsed time. Local changes in the gravity field at airborne and space-borne elevations are indications of changes in the distribution of mass within the Earth. Such instruments include airborne

gravimeters on NASA's IceBridge, NASA's Gravity Recovery and Climate Experiment (GRACE) satellite, and ESA's Gravity field and Ocean Circulation Explorer (GOCE) satellite.

The task of the remote sensing scientist is to take measurements of these basic force fields and infer from them geophysical properties about the Earth [29]. For the cryosphere, examples include using changes in the gravitational field to estimate changes in the mass of glaciers and ice sheets as is done with the GRACE satellite. Other examples include using radars and lidars to measure the time of flight of signals reflected off the ice surface and use that information to measure elevation and elevation changes on sea ice and ice sheets. Finally, scattered solar radiation can be used to acquire hyper-spectral images for surface characterization and for traditional mapping of surface features.

Accomplishing this task requires technical information about the behavior of the instrument, knowledge about the physical relationships between the measured field and the surface under study, and the development of algorithms that correctly invert the measured signal into some desired property [30, 31]. In some cases this task can be relatively easy. Because glacier ice is nearly homogeneous and because it is almost transparent at radar frequencies from about 1 to 500 MHz [32], the propagation time of a radar echo through the ice sheet and back can be converted to ice thickness by simply knowing the average ice dielectric constant, which in turn is readily convertible into a propagation velocity. In other cases, the task is more challenging because of heterogeneities in the material. The physical and electrical properties of sea ice change substantially as the ice ages [33]. This leads to changes in the thermally driven, microwave emission from the surface. The amount of energy received, measured in terms of a brightness temperature, is related to the product of the physical temperature and the emissivity of the surface. For open water, the microwave brightness temperature is cool because little energy escapes from the ocean surface. For sea ice, the brightness temperature is warm because more energy is transmitted across the electrically less reflective snow surface at these frequencies. Consequently, brightness temperature can be used to measure sea ice concentration and extent with high accuracy (several percent). Figure 5 shows that just on the basis

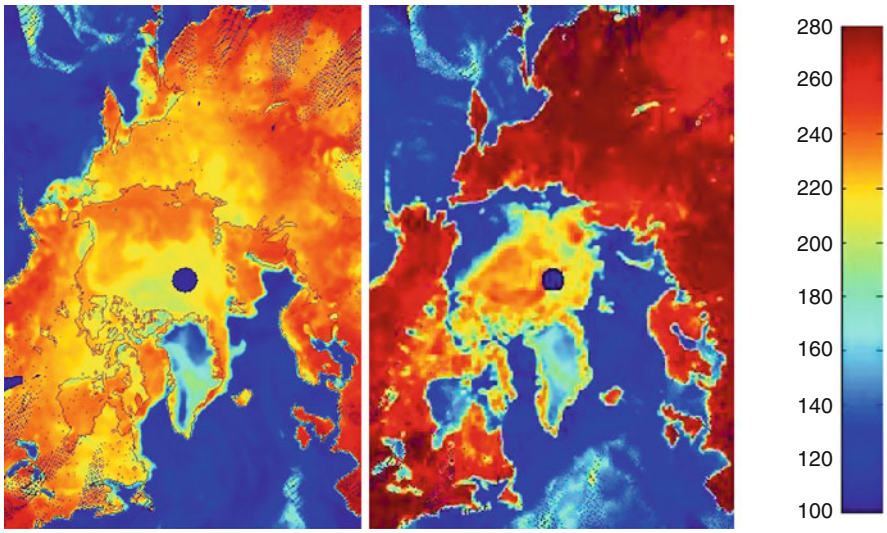

Airborne and Space-borne Remote Sensing of Cryosphere. Figure 5
19 GHz, horizontally polarized, special sensor microwave imager (SSM/I) brightness temperature data for the Arctic on February 15, 2004 (*left*) and August 25, 2004 (*right*). The brightness temperature scale (*far right*) is in degrees Kelvin. Differences between the emissivity of ocean, sea ice, land and ice sheets enable the relatively easy identification of the seasonal retreat in sea ice cover. Brightness temperature variations across the ice pack are caused by differences in ice type and age as well as in ice concentration

of brightness temperature maps alone it is easy to distinguish the annual cycle of sea ice growth and decay across the arctic.

Sea Ice Extent, Concentration, Motion, and Thickness

Sea ice modulates polar climate by restricting the flow of heat from the relatively warm polar ocean into the relatively cold polar atmosphere. Because freezing ice preferentially rejects impurities from the crystalline lattice, the growth of sea ice modulates ocean circulation by releasing dense, cold brine that sinks beneath the marginal ice zones and initiates oceanic convection. Sea ice represents a natural barrier to surface navigation and so changes in sea ice cover have important consequences for future development of the Arctic. While sea ice is usually distinguishable from open ocean at optical wavelengths, cloud cover and the long polar night dictate the use of all-weather, day/night passive microwave radiometers for monitoring sea ice extent and concentration. As noted above, these radiometers measure the radiant energy emitted from the surface that, on one hand, can help identify ice type and age but, on the other hand, leads to complexities in designing more sophisticated instruments capable of sorting out whether the observed changes are due to different ice types populating a scene or because of change in the fractions of sea ice and open water in the scene. Moreover, the dimensions of the area sampled on the surface are often quite large (Hollinger and others [34] quote a field of view of 37 × 28 km for the SSMI 37 GHz vertically polarized channel). Consequently, approaches for estimating the concentration within a single pixel are required. A simple algorithm relies on the fact that the total emitted energy or equivalently the brightness temperature must equal the brightness temperature of the components in the scene times their respective concentrations within the pixel [35]. The component brightness temperatures are selected by tie points (such as a tie point for the brightness temperature of open water or first-year sea ice) which allows for a solution. More sophisticated algorithms attempt to better characterize regions where ice concentrations are low and where the data may be contaminated by weather effects. The results of these analyses are detailed measurements of ice extent which document the dramatic decrease in Arctic sea ice cover (Fig. 6). Graphs such as these represent some of the most compelling and straightforward evidence for changing climate at high latitudes.

Images such as those in Fig. 5 can also be used to document the coarse motion of the sea ice by tracking common features in repeat images. Better results are obtained with increasing resolution ranging from the several kilometer resolution obtainable with AVHRR to the very fine resolutions (tens of meters or less) achievable with SAR. Combined with airborne (Airborne Topographic Mapper flown as part of IceBridge) and space-borne (ERS-1/2, ICESat, Cryosat-2) altimeter estimates of ice thickness, circulation driven changes in ice thickness about Antarctica [36] and the total ice flux across the Arctic and out into the marginal seas can be computed. Based on ICESat estimates of sea ice freeboard, Kwok and others [37] estimate a 0.6 m thinning in Arctic multiyear ice for the period from 2003 to 2008.

Regional Image Mapping of Glaciers and Ice Sheets

Airborne and space-borne image mapping of glaciers and ice sheets focuses on basic physical characteristics such as glacier termini, glacier snow lines, crevasse patterns, snow facies boundaries [38]. These properties have been successfully monitored with optical and microwave imaging instruments. As described in section "Early History of Cryospheric Remote Sensing," high latitude mapping began as early as 1962 with the launch of the Argon satellite. Shortly thereafter, the 1970s Landsat 1, 2, and 3 Multi-Spectral Scanner (MSS) images constitute an important glaciological resource [39, 40] and have been compiled into a series of beautiful folios edited by R. Williams Jr. and J. Ferrigno of the U.S. Geological Survey [see 41].

Compiling separate images into seamless, high-resolution digital maps of continental-scale areas is complicated by the data volume and the challenges in accurately estimating satellite orbits and instrument viewing geometries along orbit segments that might span from coast to coast. Initial successes in large-scale mapping were achieved through use of the moderate spatial resolution (1–2.5 km) and wide swath (2,400 km) Advanced Very High Resolution Radiometer (AVHRR) images [42] which helped reveal details

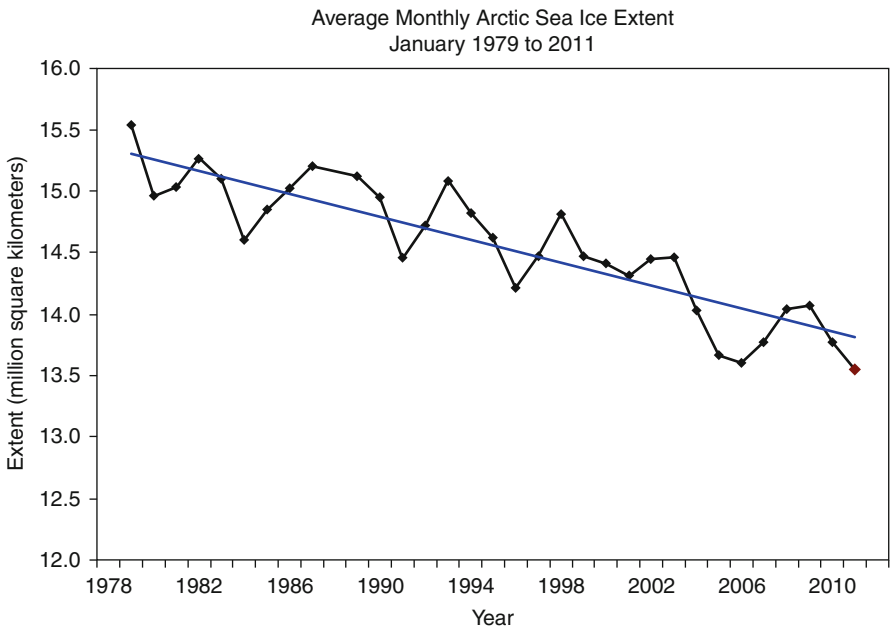

Airborne and Space-borne Remote Sensing of Cryosphere. Figure 6
Winter-time Arctic sea ice extent computed using passive microwave data. The decreasing trend illustrates the reduction in Arctic sea ice extent. There is a much more dramatic decline in ice extent during the summer months (Graph courtesy of the National Snow and Ice Data Center)

about ice stream flow in West Antarctica [43]. After the original AVHRR mosaic of Antarctica, the United State Geological Survey (USGS) made subsequent improvements to the mosaic by eliminating more cloud, separating the thermal band information to illustrate surface features more clearly, and correcting the coastline of the mosaic to include grounded ice while excluding thin, floating fast ice [44]. The European Earth Resources Satellite – 1 carried on board a synthetic aperture radar which allowed for large-scale regional mapping. Fahnestock and others [45] compiled a mosaic of Greenland which revealed the existence of a long ice stream in north east Greenland. In 1997, RADARSAT-1 synthetic aperture radar (SAR) data were successfully acquired over the entirety of Antarctica (Fig. 7). The coverage is complete and was used to create the first, high-resolution (25 m) radar image mosaic of Antarctica [46–48] The image was used to map the ice sheet margin [49] and to investigate patterns of ice flow across Antarctica resulting in the discovery of large ice streams that drain from Coates Land into the Filchner Ice Shelf. Other large-scale mapping has been completed with MODIS for both the Arctic and the Antarctic [50]. Most recently, Landsat imagery of Antarctica has been compiled into a single, easily accessible map-quality data set [51] and SPOT stereo imagery has been used to derive digital elevation models of ice sheets, ice caps, and glaciers [52].

InSAR Measurements of Glaciers and Ice Sheets Surface Velocity

Glaciers and ice sheets move under the load of their own weight. They spread and thin in a fashion dictated by their thickness, the material properties of ice, and the environmental conditions operative on the glacier surface, sides and bottom. The rate and direction of motion reveals important information about the forces acting on the glacier, provides knowledge about the rate at which ice is pouring into the coastal seas, and enables scientists to predict how the ice sheet might respond to changing global climate.

Since the International Geophysical Year of 1957–1958 and before, scientists have placed markers on the ice sheet and then, using a variety of navigation techniques from solar observations to GPS, have remeasured

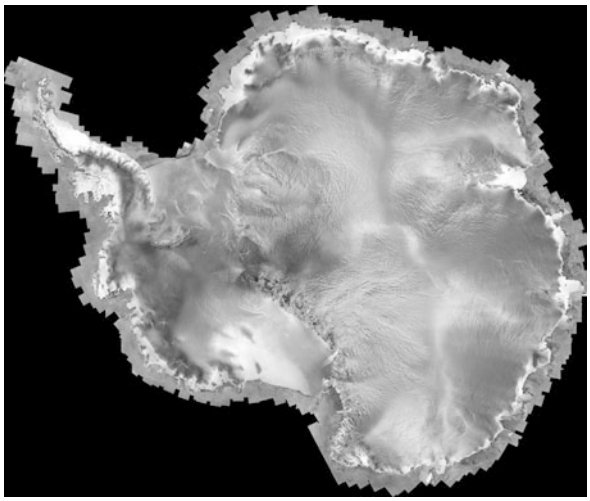

Airborne and Space-borne Remote Sensing of Cryosphere. Figure 7
Canadian RADARSAT-1 Antarctic Mapping Project synthetic aperture radar mosaic. The radar is sensitive to changes in the physical structure of the near surface snow. Bright coastal returns are scattered from subsurface ice lenses formed during fall freeze-up. Darker interior tones occur where snow accumulation is high. Other features such as ice streams and ice divides are visible (Map courtesy of K. Jezek. RADARSAT-1 data courtesy of the Canadian Space Agency)

their positions to calculate motion. More recently, scientists have used high-resolution satellite images to track the position of crevasses carried along with the glacier to compute surface motion. These approaches are time consuming and result in patchy estimates of the surface velocity field. During the early 1990s, researchers at the Jet Propulsion Laboratory showed that synthetic aperture radar (SAR) offered a revolutionary new technique for estimating the surface motion of glaciers [53]. Here, the SAR is operated as an interferometer. That is, the distance from the SAR to a point on the surface is computed by measuring the relative number of radar-wave cycles needed to span the distance between the radar and the surface. Later, another measurement is made from a slightly different position and the numbers of cycles is computed again. The difference in the number of cycles combined with control points is used to estimate relative displacement to about one quarter of a radar-wave cycle (just a few centimeters for RADARSAT-1). Given an estimate of surface topography, this enables measurement of even the slowest moving portions of glaciers [54, 55]. A related approach relies on the fact that images formed from coherent radar signals scattered off a rough surface will have a small-scale-speckly appearance. The speckle pattern is random over scene but it is stable from scene to scene over a short time. Tracking the speckle pattern over time enables another measurement of surface velocity and while less accurate than the interferometric phase approach, speckle retracking has the advantage of yielding estimates of two components of the velocity vector [56, 57]. Typically a mixture of phase interferometry and speckle retracking are used in glacier motion studies.

Surface topography can also be estimated using InSAR techniques in cases where the surface velocities are small, the period between repeat observations is short [58], when multiple interferometric pairs are available [59], or when multiple antennas enable acquisition of interferometric data in a single pass as was done with NASA's Shuttle Radar Topographic Mission [60]. Although the surface elevation accuracy of InSAR topography is typically on the order of a few meters, the results can be used to estimate local slopes and also in comparison with earlier data provide a rough estimate of mass change.

Surface elevation and velocity data are key to studies of glacier dynamics [61]. InSAR data have been used to investigate the relative importance of different resistive stresses acting on ice streams and to predict the future behavior of ice streams and glaciers currently in retreat [62, 63]. Measurements on mostly retreating glaciers in the Himalayas [64], Patagonia [65, 66], European Alps [67], and Alaska (Fig. 8) document changing surface elevation and internal dynamics, and, together with estimates of ice thickness and surface accumulation rate, can provide a direct estimate of glacier mass loss [68].

Glaciers and Ice Sheets Mass Loss

Glaciers and ice sheets are reservoirs of freshwater with over 90% of Earth's freshwater bound in the Antarctic Ice Sheet [69], which when depleted have local, regional and global impacts. Indirect approaches for identifying whether ice sheets are losing mass include using proxy indicators such as surface melt

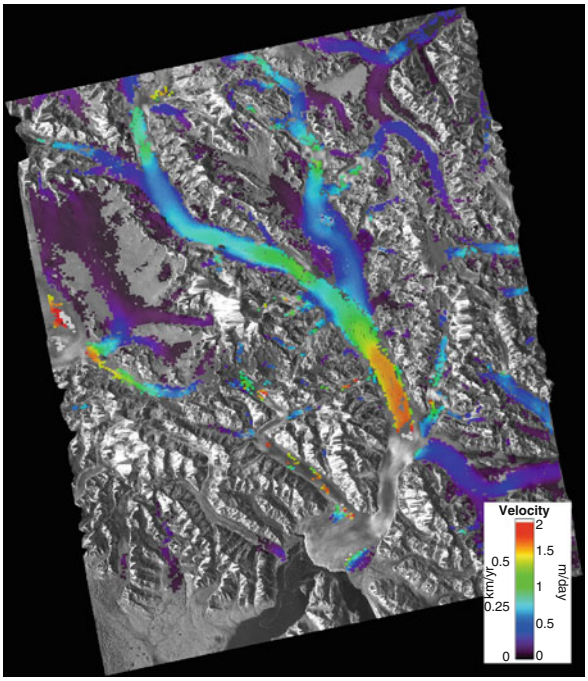

Airborne and Space-borne Remote Sensing of Cryosphere. Figure 8
Surface velocities on Hubbard Glacier Alaska measured using Japanese PALSAR L-band interferometric pairs. Hubbard Glacier is a tidewater glacier and ice from the advancing snout calves directly into Disenchantment Bay (*lower center*). Hubbard Glacier is one of the few in Alaska that is currently thickening and advancing (Image courtesy of E. W. Burgess and R. R. Forster, University of Utah)

area and duration – both measureable using passive microwave techniques [70, 71]. More directly, there are three primary remote sensing techniques currently used to assess the changing volume (or mass) of ice contained in glaciers [72]. The first involves an estimate of the difference between the annual net accumulation of mass on the surface of the glacier and the flux of ice lost from the terminus. The flux from the terminus is calculated using the measured ice thickness from airborne radar and the surface velocity, which is currently best estimated with InSAR [73]. The second approach is to measure surface elevation change. This has been accomplished with space-borne radar altimeters [74, 75] and airborne and space-borne lasers [76–78]. Finally, the changing glacial mass can be estimated directly by measuring changes in the gravity field as has been done with GRACE [79–81]. Figure 9 illustrates the estimated mass loss rate from Alaskan Glaciers as illustrated using GRACE data (Updated from [82]).

Recent analyses suggest these different techniques are yielding similar mass reductions for the Greenland Ice sheet [8, 83]. Thinning is primarily in the coastal regions where the rate of thinning has been increasing since the early 1990s and the current rates of mass loss estimated between 150 and 250 Gt/year. West Antarctica data indicate mass loss similar to Greenland, whereas East Antarctica retains a slightly positive (50 Gt/year) mass balance. Using surface mass balance estimates and GRACE gravity data, Rignot and others [84] report a combined ice sheet thinning rate of 475 ± 158 Gt/year. Cazenave and Llovel [8] conclude that for the period between 1993 and 2007 about 55% of total sea level rise can be attributed to melting of glaciers and ice sheets.

The Seasonal Snow Pack

Seasonal snow cover plays an important role in regional hydrology and water resource management. Rapid melting of the seasonal snow pack across the northern Great Plains in April 1997 resulted in catastrophic flooding of the Red River. From a climate perspective, the bright snow surface also serves as an effective mirror for returning incoming solar radiation back into space thus modulating the planetary heat budget.

The spectral reflectivity differences between snow, cloud, and other land cover types enables the seasonal snow cover to be routinely mapped globally using visible and infrared sensors such as NOAA's AVHRR, NASA's MODIS, and ESA's MERIS instruments. Snow may be mapped based on visual inspection of multispectral imagery. Automatic snow detection is accomplished by computing the normalized difference between, for example, the MODIS visible band (0.545–0.565 μm) and the near infrared band (1.628–1.652 μm). Snow is detected when the normalized difference exceeds a threshold value of 0.4 and when other criteria on land and cloud cover are met [85] (Fig. 10). Based on analysis of the NOAA 35 year data record, Dery and Brown [86] conclude that springtime snow extent across the northern hemisphere declined by some 1.28×10^6 km^2 over a 35 year period.

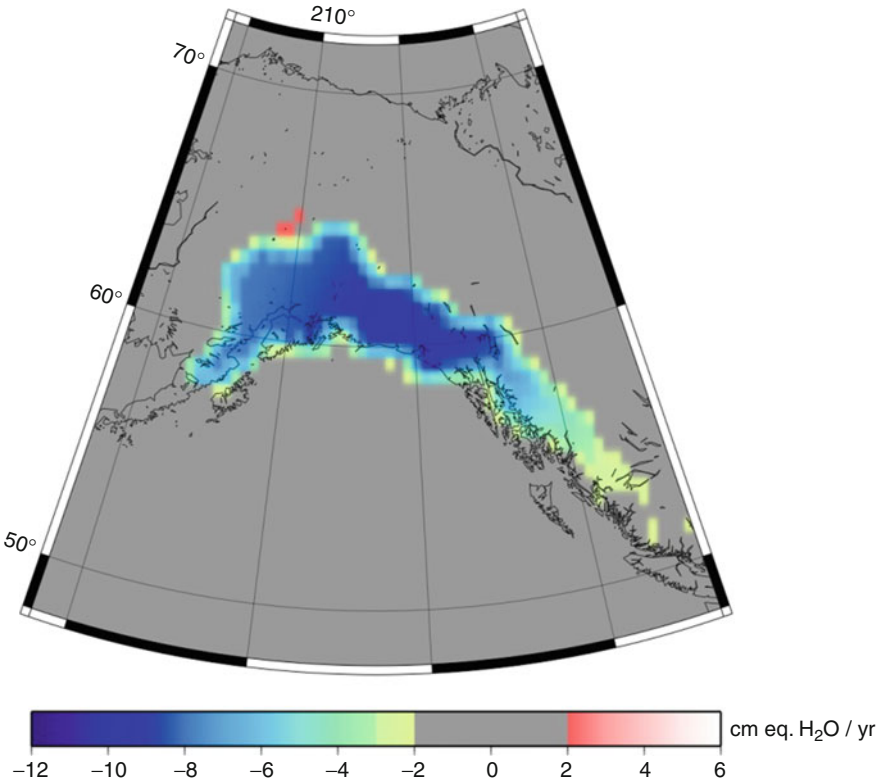

Airborne and Space-borne Remote Sensing of Cryosphere. Figure 9
Mass loss from Alaskan Glaciers in cm of water equivalent per year from GRACE (Image courtesy of S. Luthcke, NASA GSFC)

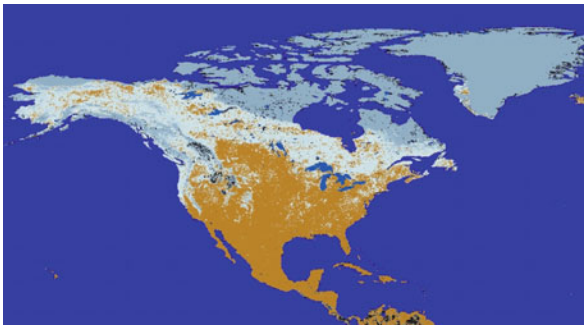

Airborne and Space-borne Remote Sensing of Cryosphere. Figure 10
Snow cover extent from NASA's MODIS. Increasing shades of *gray* indicate greater percentages of snow cover within each pixel. *Brown* denotes snow-free surface

Snow thickness and hence indirectly the mass of snow are key variables for estimating the volume of water available in a reservoir and potentially releasable as runoff. The most successful techniques to date have relied on passive-microwave-based algorithms. One approach for estimating snow thickness is to difference 19 and 37 GHz brightness temperature data that along with a proportionality constant yields an estimate of the snow thickness. The algorithm is based on the fact that 19 GHz radiation tends to minimize variations in ground temperature because it is less affected by the snow pack. The 37 GHz radiation is strongly scattered by the snow grains and brightness temperature at this frequency decreases rapidly with snow thickness/snow water equivalent. Factors which confuse this algorithm include topography and changes in ground cover [87].

Information about the seasonal onset of snowmelt can be obtained from microwave data. A few percent increase in the amount of free water in the snow pack causes the snow emissivity to approach unity resulting in a dramatic increase in passive microwave brightness temperature. This fact has been successfully used to track the annual melt extent on the ice sheets and also to track the springtime melt progression across the

arctic. Higher resolution estimates of melt extent can be obtained with scatterometer and SAR data. These data generally show an earlier spring time date for the beginning of melt onset and a later date for the fall freeze [88].

Lake and River Ice

Lake and river ice form seasonally at mid and high latitudes and elevations. River ice forms under the flow of turbulent water which governs its thickness. The combination of ice jams on rivers with increased water flow during springtime snowmelt can result in catastrophic floods. Lake ice forms under less dynamic conditions resulting in a smoother ice surface that acts as an insulator to the underlying water. Hence lacustrine biology is strongly influenced by the formation of the ice canopy. The start of ice formation and the start of springtime ice break up are proxy indicators for changes in local climate as well as impacts on the ability to navigate these waterways.

Streams, rivers, lakes of all sizes dot the landscape. Locally, ice cover observations can be made from aircraft. Regionally or globally, river and lake ice monitoring is challenging because physical dimensions (long but narrow rivers) often require high resolution instruments like medium- to high-resolution optical data (Fig. 11) or SAR to resolve details [89]. Moreover, since the exact date of key processes, such as the onset of ice formation or river-ice breakup are unknown, voluminous data sets are required to support large-scale studies.

Airborne and Space-borne Remote Sensing of Cryosphere. Figure 11
January 2010 NASA MODIS image of ice formed on the St. Lawrence River. Thin layers of new ice are distorted into swirls by the surface currents (*center left*). Thicker ice is held fast to the southern shore (Image courtesy of MODIS Rapid Response Team, NASA GSFC)

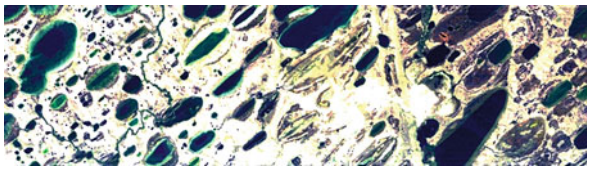

Airborne and Space-borne Remote Sensing of Cryosphere. Figure 12
EO-1 Hyperion satellite data acquired over the north coast of Alaska (70.5 N 156.5 W) and about 50 km inland from the coast, which is toward the *right* on this image. The image is 7.5 km wide (*top* to *bottom*). Color composite using channels 16 23 and 28

Permafrost

Permafrost presents one of the greatest challenges for regional remote sensing technologies [7, 90]. The near surface active layer, the shallow zone where seasonal temperature swings allow for annual freeze and thaw, is complicated by different soil types and vegetative cover. This combination tends to hide the underlying persistently frozen ground from the usual airborne and space-borne techniques mentioned above. Even in winter when the active layer is frozen, remote sensing of the permafrost at depth is extremely difficult because of the spatially variable electrical properties of the material. Thus far, the most successful airborne and space-borne remote sensing methods involve optical photography to identify surface morphologies as proxy indicators of the presence of permafrost. Patterned ground and pingos are examples of the types of features visible in optical imagery and that are diagnostic of underlying permafrost. SAR interferometry has been suggested as another tool that can be used to monitor terrain for slumping associated with thawing permafrost. Figure 12 shows E01 Hyperion satellite, visible-band data collected over the north slope of Alaska. Shallow, oval shaped lakes form in thermokarst, which develops

when ice rich permafrost thaws and forms a hummocky terrain. Lakes and depressions left by drained lakes are densely distributed across the tundra. The long axis of the lake is oriented perpendicular to the prevailing wind direction. SAR intensity images have been used to determine that most of these small lakes freeze completely to the bottom during the winter months [91].

Recent Developments in Airborne Radar Ice Sounding of Glaciers

Today, airborne radars operating between about 5 and 500 MHz are the primary tools used for measuring ice sheet thickness, basal topography, and inferring basal properties over large areas. These radars are typically operated as altimeters and acquire profile data only along nadir tracks that are often separated by 5 or more kilometers. The along track resolution is met by forming a synthetic aperture and the vertical resolution of the thickness is met by transmitting high bandwidth signal. Even though highly accurate thickness measurements can be achieved, information in the third cross-track dimension is absent.

While the surface properties of the ice sheets are becoming increasing well documented, the nature of the glacier bed remains obscured by its icy cover. Revealing basal properties, such as the topography and the presence or absence of subglacial water, is important if we are to better estimate the flux of ice from the interior ice sheet to the sea and to forecast anticipated changes of the size of the ice sheets. Recent experiments demonstrate how it is possible to go beyond airborne nadir sounding of glaciers and to produce three-dimensional images of the glacier bed. This development represents a major step forward in ice sheet glaciology by providing new information about the basal boundary conditions modulating the flow of the ice and revealing for the first time geomorphologic processes occurring at the bed of modern ice sheets. The approach relies on the application of radar tomography to UHF/VHF airborne radar data collected using multiple, independent antennas and receivers. Tomography utilizes phase and amplitude information from the independent receivers to isolate the direction of a natural target relative to the aircraft. Combined with the range to the target based on the echo travel time and position of the aircraft, tomographic methods yield swaths of reflectivity and topographic information on each side of the aircraft [92].

Cooperative Efforts to Observe, Monitor, and Understand the Cryosphere

Several cooperative, international scientific studies of the high latitudes have been organized. Beginning with the 1897 voyage of the Belgica to the Antarctic Peninsula and continuing to the 2007 International Polar Year, studies have relied on the most recent technologies to increase knowledge of the polar regions. To realize the benefit of the growing constellation of international satellites to the scientific objectives of the 2007 International Polar Year (IPY) (Fig. 13), the Global Interagency IPY Polar Snapshot Year (GIIPSY) project engaged the science community to develop consensus polar science requirements and objectives that could best and perhaps only be met using the international constellation of earth observing satellites [93]. Requirements focused on all aspects of the cryosphere and range from sea ice to permafrost to snow cover and ice sheets. Individual topics include development of high-resolution digital elevation models of outlet glaciers using stereo optical systems, measurements of ice surface velocity using interferometric synthetic aperture radar, and frequently repeated measurements of sea ice motion using medium resolution optical and microwave imaging instruments.

The IPY Space Task Group (STG), convened by the World Meteorological Organization (WMO), formed the functional link between the GIIPSY science community and the international space agencies. STG membership included representatives from the national space agencies of Italy, Germany, France, UK, US, Canada, Russia, China, Japan, and the European Space Agency (ESA), which in itself represents 19 nations. The STG determined how best to satisfy GIIPSY science requirements in a fashion that distributed the acquisition burden across the space agencies and recognized the operational mandates that guide the activities of each agency.

The STG adopted four primary data acquisition objectives for its contribution to the IPY. These are:

- Pole to coast multi-frequency InSAR measurements of ice-sheet surface velocity

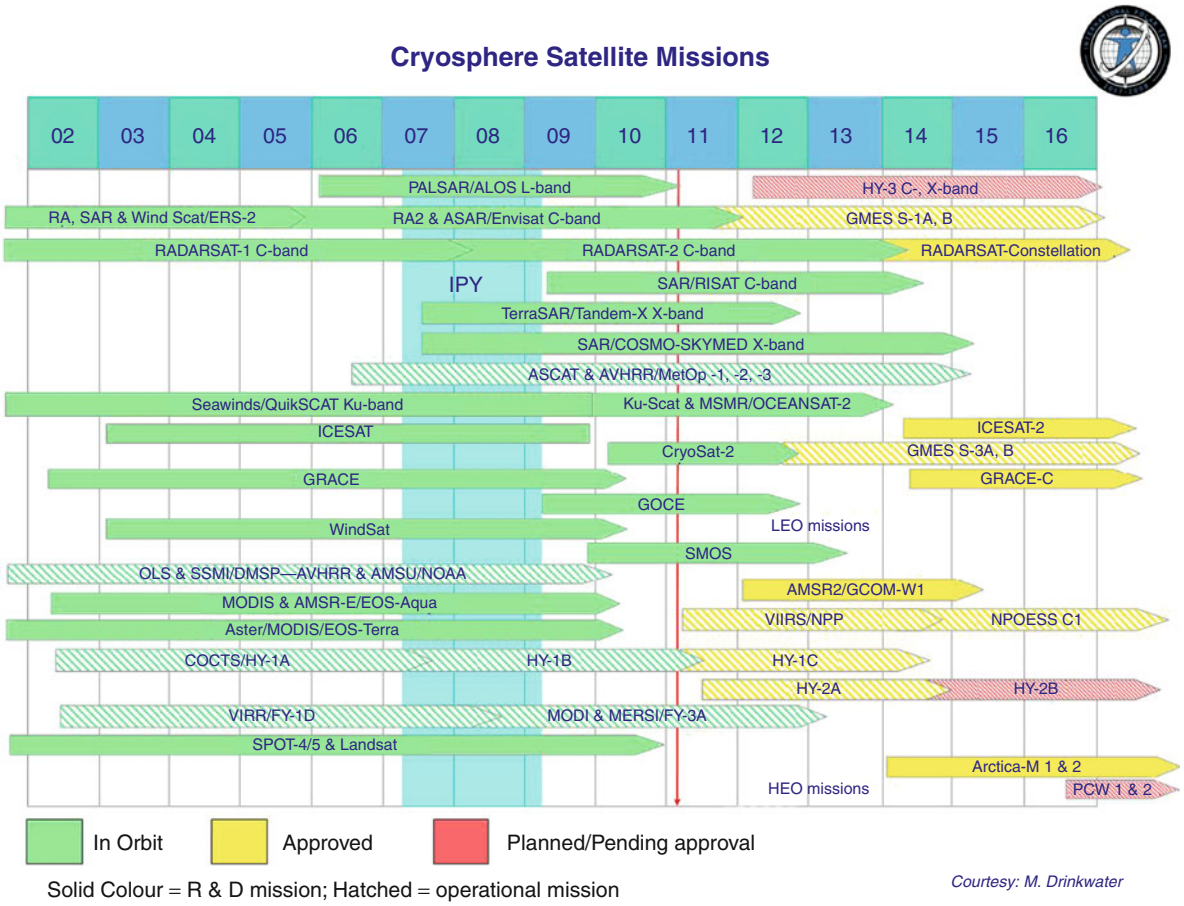

Airborne and Space-borne Remote Sensing of Cryosphere. Figure 13
Current, approved and planned satellites for studying and monitoring the Cryosphere (Figure courtesy of Mark Drinkwater, European Space Agency)

- Repeat fine-resolution SAR mapping of the entire Southern Ocean sea ice cover for sea ice motion
- One complete high resolution visible and thermal IR (Vis/IR) snapshot of circumpolar permafrost
- Pan-Arctic high and moderate resolution Vis/IR snapshots of freshwater (lake and river) freeze-up and breakup

The STG achieved most of these objectives including: acquiring Japanese, ALOS L-band, ESA Envisat and Canadian Radarsat C-band, and German TerraSAR-X (Fig. 14) and Italian COSMO_SKYMED X band SAR imagery over the polar ice sheets [94]; acquiring pole to coast InSAR data for ice sheet surface velocity; optically derived, high-resolution digital elevation models of the perimeter regions of ice caps and ice sheets; coordinated campaigns to fill gaps in Arctic and Antarctic sea ice cover; extensive acquisitions of optical imagery of permafrost terrain; observations of atmospheric chemistry using the Sciamachy instrument.

Future Directions

Emerging sensor and platform technologies hold great promise for future airborne and space-borne remote sensing of the cryosphere. Airborne programs are likely to continue to use large manned aircraft in a fashion similar to NASA's IceBridge program which integrates a sophisticated suite of instruments including lidars, radars, gravimeters, magnetometers, optical mapping systems, and GPS. But there will also be

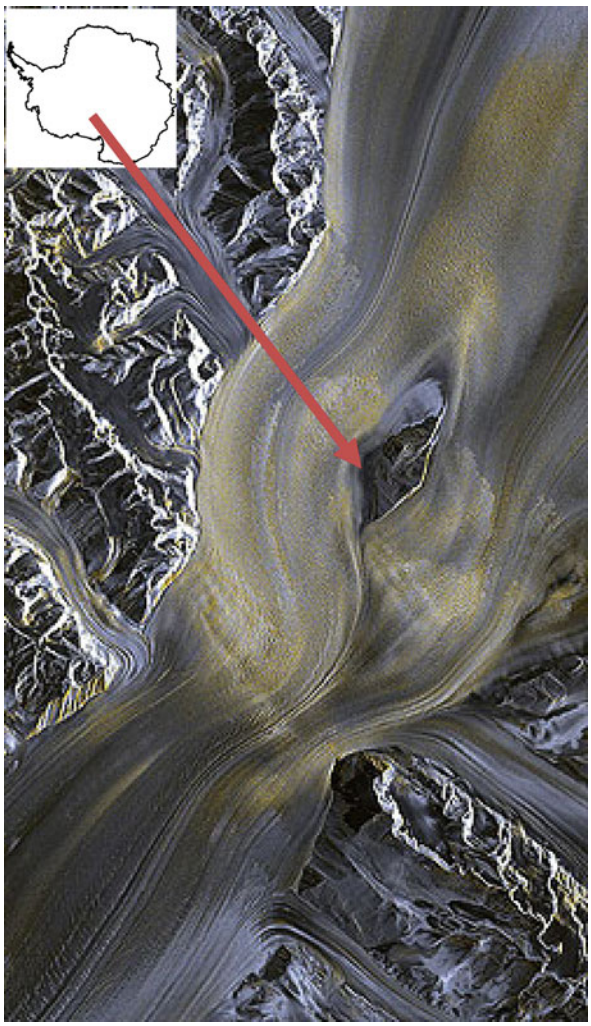

Airborne and Space-borne Remote Sensing of Cryosphere. Figure 14
German Aerospace Center TerraSAR-X observations of the Nimrod Glacier (inset map of Antarctica). Ice floes around a central nunatak and down toward the Ross Ice Shelf. Crevasses appear in conjunction with the interruption of flow by the nunatak. Cooperative use of Canadian, German, European Space Agency, Italian, and Japanese synthetic aperture radar (SAR) satellites along with ground segment and data processing capabilities provided by the United States yielded a rich and diverse SAR data set that will be a lasting legacy of the IPY (TerraSAR-X data courtesy of D. Floricioiu, German Aerospace Center. Inset coastline derived from RADARSAT-1 Antarctic Mapping Project map)

a steady shift toward smaller, more dedicated unmanned aerial vehicles capable of remaining on station for longer periods and fulfilling some of the temporal coverage requirements that are difficult to satisfy with larger aircraft requiring a substantial number of crewmen.

It is worth noting again that ice sounding radars are exclusively deployed on aircraft for terrestrial research. This is driven operationally by the challenges of ionospheric distortions and by governmental controls on frequency allocations available for remote sensing applications designed to limit interference with communications and other commercial uses of the frequency bands. Certainly the latter is not an issue for other planetary studies and in fact the Martian ice caps have been successfully sounded from the orbiting MARSIS and SHARAD radars [95]. These extraterrestrial successes motivate continuing interest in deploying similar instrument for observing Earth's ice cover in the future.

As indicated in Fig. 13, there will be an ongoing constellation of satellites capable of collecting valuable cryospheric data. Here, coordination amongst the different space faring nations will be key to realizing the greatest scientific benefit. Lessons about cooperation gleaned from the IPY can be profitably extended to the acquisition of data and the development of geophysical products beyond the polar regions to all sectors of the cryosphere. There could also be generally better integration of the atmospheric chemistry and polar meteorological communities, as well as incorporation of gravity and magnetic geopotential missions into the coordination discussions. It is also possible to envision discussion and collaboration on emerging technologies and capabilities such as the Russian Arktika Project [96] and advanced subsurface imaging radars. A primary objective of continued coordination of international efforts is securing collections of space-borne "snapshots" of the cryosphere through the further development of a virtual Polar Satellite Constellation [97]. A natural vehicle for adopting lessons learned from GIIPSY/STG into a more encompassing international effort could be the Global Cryosphere Watch [98] recently proposed by WMO to be in support of the cryospheric science goals specified for the Integrated Global Observing Strategy Cryosphere Theme [1].

Bibliography

Primary Literature

1. IGOS (2007) Integrated global observing strategy cryosphere theme report – for the monitoring of our environment from space and from Earth. WMO/TD-No. 1405. World Meteorological Organization, Geneva, 100p
2. Perovich D, Light B, Eicken H, Jones K, Runciman K, Nghiem S (2007) Increasing solar heating of the Arctic ocean and adjacent seas, 1979–2005: attribution and role in the ice-albedo feedback. Geophys Res Lett 34:L19505. doi:10.1029/2007GL031480
3. Perovich D, Richter-Menge J, Jones K, Light B (2008) Sunlight, water and ice: extreme arctic sea ice melt during the summer of 2007. Geophys Res Lett 35:L11501. doi:1029/2008GL034007
4. Ainley D, Tynan C, Stirling I (2003) Sea ice: a critical habitat for polar marine mammals. In: Thomas D, Dieckmann G (eds) Sea ice: an introduction to its physics, chemistry, biology and geology. Blackwell Science, Oxford, pp 240–266
5. Arrigo K (2003) Primary production in sea ice. In: Thomas D, Dieckmann G (eds) Sea ice: an introduction to its physics, chemistry, biology and geology. Blackwell Science, Oxford, pp 143–183
6. Lizotte M (2003) The microbiology of sea ice. In: Thomas D, Dieckmann G (eds) Sea ice: an introduction to its physics, chemistry, biology and geology. Blackwell Science, Oxford, pp 184–210
7. Grosse G, Romanovsky V, Jorgenson T, Water Anthony K, Brown J, Overduin P (2011) Vulnerability and feedbacks of permafrost to climate change. EOS 92(9):73–74
8. Cazenave A, Llovel W (2010) Contemporary sea level rise. Ann Rev Mar Sci 2:145–173
9. Prowse TD, Bonsal B, Duguay C, Hessen D, Vuglinsky V (2007) River and lake ice. In: Eamer J, Ahlenius H, Prestrud P, United Nations Environment Programme et al (eds) Global outlook for ice and snow. United Nations Environment Programme, Nairobi, pp 201–214. ISBN 978-92-807-2799-9
10. Kim Y, Kimball J, McDonald K, Glassy J (2011) Developing a global data record of daily landscape freeze/thaw status using satellite passive microwave remote sensing. IEEE Trans Geosci Remote Sens 49(3):949–960
11. McKinley AC (1929) Applied aerial photography. Wiley, New York, 341p
12. Mittelholzer W and others (1925) By airplane towards the north pole (trans: Paul E, Paul C). Hougton Mifflin, Boston, 176p
13. Wilkins H (1929) The Wilkins-Hearst Antarctic Expedition, 1928–1929. Geogr Rev 19(3):353–376
14. Wilkins H (1930) Further Antarctic explorations. Geogr Rev 20(3):357–388
15. Byrd RE (1930) Little America. G.P. Putman's Sons, New York, 422p
16. McDonald RA (1995) Corona: success for space reconnaissance, a look into the cold war and a revolution in intelligence. Photogramm Eng Remote Sens 61(6):689–720
17. Peebles C (1997) The Corona Project: America's First Spy Satellites. Naval Institute Press, Annapolis, 351p
18. Wheelon AD (1997) Corona: the first reconnaissance satellites. Phys Today 50(2):24–30
19. Richelson JT (1998) Scientists in black. Sci Am 278(2):48–55
20. Sohn HS, Jezek KC, van der Veen CJ (1998) Jakobshavn Glacier, West Greenland: 30 years of spaceborne observations. Geophys Res Lett 25(14):2699–2702
21. Zhou G, Jezek KC (2002) 1960s era satellite photograph mosaics of Greenland. Int J Remote Sens 23(6):1143–1160
22. Bindschadler RA, Vornberger P (1998) Changes in the West Antarctic ice sheet since 1963 from declassified satellite photography. Science 279:689–692
23. Kim K, Jezek KC, Sohn H (2001) Ice shelf advance and retreat rates along the coast of Queen Maud Land, Antarctica. J Geophys Res 106(C4):7097–7106
24. Kim K, Jezek K, Liu H (2007) Orthorectified image mosaic of the Antarctic coast compiled from 1963 Argon satellite photography. Int J Remote Sens 28(23–24):5357–5373
25. Waite AH, Schmidt SJ (1962) Gross errors in height indication from pulsed radar altimeters operating over thick ice or snow. Proc IRE 50(6):1515–1520
26. Bogorodsky VV, Bentley CR, Gudmandsen PE (1985) Radioglaciology. D. Reidel, Dordrecht, 254p
27. Fisher E, McMechan G, Gorman M, Cooper A, Aiken C, Ander M, Zumberge M (1989) Determination of bedrock topography beneath the Greenland ice sheet by three-dimensional imaging of radar sounding data. J Geophys Res 94(B3):2874–2882
28. Koenig L, Martin S, Studinger M (2010) Polar airborne observations fill gap in satellite data. EOS 91(38):333–334
29. Schanda E (1986) Physical fundamentals of remote sensing. Springer, Berlin, 187p
30. Hall D, Martinec J (1985) Remote sensing of ice and snow. Chapman and Hall, New York, 189p
31. Rees WG (2006) Remote sensing of snow and ice. Taylor and Francis Group, Boca Raton, 285p
32. Petrenko VF, Whitworth RW (1999) Physics of ice. Oxford University Press, Oxford, 373p
33. Carsey FD (ed) (1992) Microwave remote sensing of sea ice, A. G.U. geophysical monograph 68. American Geophysical Union, Washington, DC, 462p
34. Hollinger J, Peirce J, Poe G (1990) SSM/I instrument evaluation. IEEE Trans Geosci Remote Sens 28(5):781–790
35. Parkinson C, Gloersen P (1993) Global sea ice cover. In: Gurney R, Foster J, Parkinson C (eds) Atlas of satellite observations related to global change. Cambridge University Press, Cambridge, pp 371–383
36. Zwally HJ, Yi D, Kwok R, Zhao Y (2008) ICESat measurements of sea ice freeboard and estimates of sea ice thickness in the Weddell sea. J Geophys Res 113:C02S15. doi:10.1029/2007JC004284
37. Kwok R, Cunningham G, Wensnahan M, Rigor I, Zwally HJ, Yi D (2009) Thinning and volume loss of the Arctic ocean sea ice cover:2003–2008. J Geophys Res 114:C07005. doi:10.1029/2009JC005312

38. Williams R Jr, Hall D (1993) Glaciers. In: Gurney R, Foster J, Parkinson C (eds) Atlas of satellite observations related to global change. Cambridge University Press, Cambridge, pp 401–422
39. Swithinbank C (1973) Higher resolution satellite pictures. Polar Rec 16(104):739–751
40. Swithinbank C, Lucchitta BK (1986) Multispectral digital image mapping of Antarctic ice features. Ann Glaciol 8:159–163
41. U.S. Geological Survey (2010) Satellite image atlas of glaciers of the world. USGS Fact Sheet FS 2005-3056, 2p
42. Merson RH (1989) An AVHRR mosaic of Antarctica. Int J Remote Sens 10:669–674
43. Bindschadler R, Vornberger P (1990) AVHRR imagery reveals Antarctic ice dynamics. EOS 71:741–742
44. Ferrigno JG, Mullins JL, Stapleton JA, Chavez PS Jr, Velasco MG, Williams RS Jr (1996) Satellite image map of Antarctica, Miscellaneous investigations map series 1-2560. U.S Geological Survey, Reston
45. Fahnestock MR, Bindschadler RK, Jezek KC (1993) Greenland ice sheet surface properties and ice dynamics from ERS-1 SAR imagery. Science 262:1525–1530
46. Jezek KC (2008) The RADARSAT-1 Antarctic Mapping Project. BPRC Report No. 22. Byrd Polar Research Center, The Ohio State University, Columbus, 64p
47. Jezek KC (1999) Glaciologic properties of the Antarctic ice sheet from spaceborne synthetic aperture radar observations. Ann Glaciol 29:286–290
48. Jezek K (2003) Observing the Antarctic ice sheet using the RADARSAT-1 synthetic aperture radar. Polar Geogr 27(3): 197–209
49. Liu H, Jezek K (2004) A complete high-resolution coastline of Antarctica extracted from orthorectified Radarsat SAR imagery. Photogramm Eng Remote Sens 70(5):605–616
50. Scambos TA, Haran T, Fahnestock M, Painter T, Bohlander J (2007) MODIS-based mosaic of Antarctica (MOA) data sets: continent-wide surface morphology and snow grain size. Remote Sens Environ 111(2–3):242–257
51. Bindschadler R, Vornberger P, Fleming A, Fox A, Mullins J, Binnie D, Paulsen S, Granneman B, Gorodetzky D (2008) The Landsat image mosaic of Antarctica. Remote Sens Environ 112(12):4214–4226
52. Korona J, Berthier E, Bernarda M, Rémy F, Thouvenot E (2008) SPIRIT. SPOT 5 stereoscopic survey of Polar Ice: reference images and topographies during the fourth International Polar Year (2007–2009). ISPRS J Photogramm Remote Sens 64(2):204–212. doi:10.1016/j.isprsjprs.2008.10.005
53. Goldstein RM, Englehardt H, Kamb B, Frohlich R (1993) Satellite radar interferometry for monitoring ice sheet motion: application to an Antarctic ice stream. Science 262:1525–1530
54. Kwok R, Fahnestock M (1996) Ice sheet motion and topography from radar interferometry. IEEE Trans Geosci Remote Sens 34(1):189–199
55. Joughin I, Kwok R, Fahnestock M (1996) Estimation of ice-sheet motion using satellite radar interferometry: method and error analysis with application to Humboldt Glacier, Greenland. J Glaciol 42(142):564–575
56. Gray AL, Short N, Matter KE, Jezek KC (2001) Velocities and ice flux of the Filchner Ice Shelf and its tributaries determined from speckle tracking interferometry. Can J Remote Sens 27(3):193–206
57. Joughin I (2002) Ice-sheet velocity mapping: a combined interferometric and speckle-tracking approach. Ann Glaciol 34(1):195–201
58. Eldhuset P, Andersen S, Hauge EI, Weydahl D (2003) ERS tandem InSAR processing for DEM generation, glacier motion estimation and coherence analysis on Svalbard. Int J Remote Sens 24(7):1415–1437
59. Rignot E, Forster R, Isaaks B (1996) Mapping of glacial motion and surface topography of Hielo Patagonico Norte, Chile, using satellite SAR L-band interferometry data. Ann Glaciol 23:209–216
60. Surazakov A, Aizen V (2006) Estimating volume change of mountain glaciers using SRTM and map-based topographic data. IEEE Trans Geosc Remote Sens 44(10): 2991–2995
61. Joughin I, Gray L, Bindschadler R, Price S, Morse D, Hulba C, Mattar K, Werner C (1999) Tributaries of West Antarctic ice streams revealed by RADARSAT interferometer. Science 286:283–286
62. Stearns L, Jezek K, Van der Veen CJ (2005) Decadal scale variations in ice flow along Whillans ice stream and its tributaries, West Antarctica. J Glaciol 51(172): 147–157
63. Beem L, Jezek K, van der Veen CJ (2010) Basal melt rates beneath the Whillans ice stream, West Antarctica. J Glaciol 56(198):647–654
64. Luckman L, Quencyand D, Beven S (2007) The potential of satellite radar interferometry and feature tracking for monitoring flow rates of Himalayan glaciers. Remote Sens Environ 111:172–181
65. Floricioiu D, Eineder M, Rott H, Yague-Martinez N, Nagler T (2009) Surface velocity and variations of outlet glaciers of the Patagonia Icefields by means of TerraSAR-X. In: Geoscience and remote sensing symposium, IGARSS 2009, vol 2, Cape Town, 12–17 Jul 2009, pp 1028–1031
66. Forster R, Rignot E, Isacks B, Jezek K (1999) Interferometric radar observations of the Hielo Patagonico Sur, Chile. J Glaciol 45(150):325–337
67. Paul F, Haeberli W (2008) Spatial variability of glacier elevation changes in the Swiss Alps obtained from two digital elevation models. Geophys Res Lett 35:L21502. doi:10.1029/2008GL034718
68. Yu J, Liu H, Jezek K, Warner R, Wen J (2010) Analysis of velocity field, mass balance, and basal melt of the Lambert Glacier system by incorporating Radarsat SAR interferometry and ICESat laser altimeter measurements. J Geophys Res 115: B11102. doi:10.1029/2010JB007456
69. Thomas RH (1993) Ice sheets. In: Gurney R, Foster J, Parkinson C (eds) Atlas of satellite observations related to global change. Cambridge University Press, Cambridge, pp 385–400

70. Bhattacharya I, Jezek K, Wang L, Liu H (2009) Surface melt area variability of the Greenland ice sheet: 1979–2008. Geophys Res Lett 36:L20502. doi:10.1029/2009GL039798
71. Liu H, Wang L, Jezek K (2006) Spatio-temporal variations of snow melt zones in Antarctic ice sheet derived from satellite SMMR and SSM/I data (1978–2004). J Geophys Res 111: F01003. doi:1029/2005JF0000318
72. Rignot E, Thomas R (2002) Mass balance of the polar ice sheets. Science 297(5586):1502–1506
73. Rignot E, Kanagaratnam P (2006) Changes in the velocity structure of the Greenland ice sheet. Science 311(5673): 986–990
74. Zwally HJ, Giovinetto M, Li J, Cornejo H, Beckley M, Brenner A, Saba J, Yi D (2005) Mass changes of the Greenland and Antarctic ice sheets and shelves and contributions to sea-level rise: 1992–2002. J Glaciol 51(175):509–527
75. Wingham DJ, Shepherd A, Muir A, Marshall G (2006) Mass balance of the Antarctic ice sheet. Philos Trans R Soc A 364:1627–1635
76. Larsen CF, Motyka RJ, Arendt AA, Echelmeyer KA, Geissler PE (2007) Glacier changes in southeast Alaska and northwest British Columbia and contribution to sea level rise. J Geophys Res Earth 112:F01007
77. Thomas R, Frederick E, Krabill W, Manizade S, Martin C (2006) Progressive increase in ice loss from Greenland. Geophys Res Lett 33:L10503. doi:10.1029/2006GL026075
78. Herzfeld UC, McBride PJ, Zwally HJ, Dimarzio J (2008) Elevation change in Pine Island Glacier, Walgreen Coast Antarctica, based on GLAS (2003) and ERS-1(1995) altimeter data analyses and glaciological implications. Int J Remote Sens 29(19): 5533–5553. doi:10.1080/01431160802020510
79. Chen J, Wilson C, Blankenship D, Tapley B (2009) Accelerated Antarctic ice loss from satellite gravity measurements. Nat Geosci 2. doi:10.1038/NGEO694
80. Luthcke SB, Zwally HJ, Abdalati W, Rowlands D, Ray R, Nerem R, Lemoine F, McCarthy J, Chinn D (2006) Recent Greenland ice mass loss by drainage system from satellite gravity observations. Science 314(5803):1286–1289
81. Velicogna I (2009) Increasing rates of ice mass loss from the Greenland and Antarctic ice sheets revealed by GRACE. Geophys Res Lett 36:L19503. doi:10.1029/2009GL040222
82. Luthcke S, Arendt A, Rowlands D, McCarthy J, Larsen C (2008) Recent glacier mass changes in the Gulf of Alaska region from GRACE mascon solutions. J Glaciol 54(188):767–777
83. Thomas R, Davis C, Frederick E, Krabill W, Li Y, Manizade S, Martin C (2008) A comparison of Greenland ice-sheet volume changes derived from altimetry measurements. J Glaciol 54(185):203–212
84. Rignot E, Velicogna I, van den Broeke MR, Monaghan A, Lenaerts J (2011) Acceleration of the contribution of the Greenland and Antarctic ice sheets to sea level rise. Geophys Res Lett 38:L05503. doi:10.1029/2011GL046583
85. Hall D, Riggs G, Salomonson V, DiGirolamo N, Bayr K (2002) MODIS snow-cover products. Remote Sens Environ 83: 181–194
86. Dery S, Brown R (2007) Recent northern hemisphere snow cover extent trends and implications for the snow-albedo feedback. Geophys Res Lett 34:L22504. doi:10.1029/2007GL031474
87. Foster J, Chang A (1993) Snow cover. In: Gurney R, Foster J, Parkinson C (eds) Atlas of satellite observations related to global change. Cambridge University Press, Cambridge, pp 361–370
88. Forster R, Long D, Jezek K, Drobot S, Anderson M (2001) The onset of Arctic sea-ice snow melt as detected with passive and active microwave remote sensing. Ann Glaciol 33:85–93
89. Jeffries M, Morris K, Kozlenko N (2005) Ice characteristics and processes, and remote sensing of frozen rivers and lakes. In: Duguay C, Piertroniro A (eds) Remote sensing of northern hydrology, Geophysical monograph series 163. American Geophysical Union, Washington, DC, pp 63–90
90. Duguay C, Zhang T, Leverington D, Romanovsky V (2005) Satellite remote sensing of permafrost and seasonally frozen ground. In: Duguay C, Piertroniro A (eds) Remote sensing of northern hydrology, Geophysical monograph series 163. American Geophysical Union, Washington, DC, pp 91–142
91. Jeffries M, Morris K, Liston G (1996) Method to determine lake depth and water availability on the north slope of Alaska with spaceborne imaging radar and numberical ice growth modeling. Arctic 49(4):367–374
92. Jezek K, Wu X, Gogineni P, Rodriguez E, Freeman A, Fernando-Morales F, Clark C (2011) Radar images of the bed of the Greenland ice sheet. Geophys Res Lett 38:L01501. doi:10.1029/2010GL045519
93. Jezek K, Drinkwater M (2010) Satellite observations from the International Polar Year. EOS Trans AGU 91(14):125–126
94. Crevier Y, Rigby G, Werle D, Jezek K, Ball D (2010) A RADARSAT-2 snapshot of Antarctica during the 2007–08 IPY. Newsl Can Antarct Res Netw 28:1–5
95. Picardi G, Plaut JJ, Biccari D, Bombaci O, Calabrese D, Cartacci M, Cicchetti A, Clifford SM, Edenhofer P, Farrell WM, Federico C, Frigeri A, Gurnett DA, Hagfors T, Heggy E, Herique A, Huff RL, Ivanov AB, Johnson WTK, Jordan RL, Kirchner DL, Kofman W, Leuschen CJ, Nielsen E, Orosei R, Pettinelli E, Phillips RJ, Plettemeier D, Safaeinili A, Seu R, Stofan ER, Vannaroni G, Watters TR, Zampolini E (2005) Radar soundings of subsurface Mars. Science 310(5756):1925–1928. doi:10.1126/science.1122165
96. Asmus VV, Dyaduchenko VN, Nosenko YI, Polishchuk GM, Selin VA (2007) A highly elliptical orbit space system for hydrometeorological monitoring of the Arctic region. WMO Bull 56(4):293–296
97. Drinkwater MR, Jezek KC, Key J (2008) Coordinated satellite observations during the International Polar Year: towards achieving a Polar Constellation. Space Res Today 171:6–17
98. Goodison B, Brown J, Jezek K, Key J, Prowse T, Snorrason A, Worby T (2007) State and fate of the polar cryosphere, including variability in the Artic hydrologic cycle. WMO Bull 56(4): 284–292

Books and Reviews

Gloersen P, Campbell W, Cavalieri D, Comiso J, Parkinson C, Zwally H (1992) Arctic and Antarctic sea ice, 1978–1987: satellite passive microwave observations and analysis, NASA SP-511. NASA, Washington, DC, 290p

Parkinson C, Comiso J, Zwally H, Cavalieri D, Gloersen P, Campbell W (1987) Arctic sea ice, 1973–1976: satellite passive microwave observations, NASA SP-489. NASA, Washington, DC, 296p

Schnack-Schiel S (2003) The macrobiology of sea ice. In: Thomas D, Dieckmann G (eds) Sea ice: an introduction to its physics, chemistry, biology and geology. Blackwell Science, Oxford, pp 211–239

Weeks W, Hibler W (2010) On sea ice. University of Alaska Press, Fairbanks, 664p

Zwally H, Comiso J, Parkinson C, Campbell W, Carsey F, Gloersen P (1983) Antarctic sea ice, 1973–1976: satellite passive microwave observations, NASA SP-459. NASA, Washington, DC, 206p

Airborne Toxic Chemicals

April Hiscox[1], Mark Macauda[2]
[1]Department of Geography, The University of South Carolina, Columbia, SC, USA
[2]Health Promotion, Education, and Behavior, University of South Carolina, Columbia, SC, USA

Article Outline

Glossary
Definition of the Subject and Its Importance
Introduction
Toxics in the Air
Regulation and Monitoring
The Toxic Cycle: Specific Examples
Human Health
Future Directions
Bibliography

Glossary

Air toxic Substances that are known or suspected to cause cancer or other serious health effects. Also known as Hazardous Air Pollutants (HAPS).

Anthropogenic source A source of air toxics created by human beings.

Area source A single source of pollutant that emits less that 10 t per year of one air toxic, or less than 25 t per year of any combination of air toxics.

MACT (Maximum Achievable Control Technology) Standard that dictates emission limits of a source is set by the best performing 12% of similar sources, if more than 30 similar sources exist nationally. If less than 30 exist, the best five are used to set the standard.

Major source A single source of pollutant that emits 10 t per year or more of one air toxic, or 25 t per year or more of any combination of air toxics.

Mobile source A source of air toxics that moves (such as a car, truck, airplane, or boat).

Definition of the Subject and Its Importance

"Air toxics" is a term that is often used colloquially, but for the purposes of this article it will be used following the specific definition set forth by the US Environmental Protection Agency (EPA). Toxic (or Hazardous) air pollutants are those pollutants that are known or suspected of causing cancer or other serious health effects [1]. Air toxics are defined by the Clean Air Act, which explains what pollutants qualify, how different sources are categorized, and how they are to be regulated [2]. The Clean Air Act (CAA) is the most comprehensive modern legislation concerning air quality in the USA. The original 1970 Act defines "Hazardous Air Pollutants" (HAPS) or air toxics as those substances known or suspected of causing cancer, birth defects, or other adverse health problems. It charges the EPA to "Significantly reduce emissions of the most potent air pollutants" [2]. Initially, the Clean Air Act listed 189 chemicals as toxics; during the revision of 1990 caprolactam was eliminated based on new scientific evidence, leaving 188 [1].

Introduction

It can be said that air pollution is as old as civilization itself. With the discovery of fire, humans started emitting substances into the atmosphere. Ancient Rome had issues with pollution of land, water, and air, including emissions from copper and lead production that were greater than Europe during the nineteenth century [3]. In 1954, smog descended on London, primarily from coal burning, for 4 days and killed 4,000 people [4–6]. Air pollution has been known to affect evolution of species; the most famous example being the peppered moths of England, who evolved a darker color to match soot covered trees near industrial operations [7].

Despite its long history and fundamental importance to environmental health and quality of life, air quality is one of the harder aspects of environmental health to grasp, and even harder to control. Unlike water or soil, air cannot be picked up and held. How it travels from place to place is still the subject of intense scientific research. Human understanding of the air, how pollutants enter into it and travel, and how they ultimately affect human and animal health is still being actively investigated. This chapter will summarize the fundamentals of air toxics, a subset of air pollutants, from both an environmental and human health perspective. The following presents a synopsis of the current state of knowledge and discusses future directions for research in this area. The article will start off with a brief summary of air toxics, where they come from and where they go. Readers are encouraged to consult the numerous air pollution textbooks listed in the references for an in-depth treatment of these topics. Following this background material, three specific toxics, benzene, mercury, and perchloroethylene and their roles in modern living will be discussed. The article will finish with a discussion of future directions for better understanding of the role of air toxics from a sustainability standpoint.

Toxics in the Air

Where Do They Come From?

Any introductory textbook on the topic of air pollution starts with the fundamental knowledge that regulated pollutants are from both biogenic and anthropogenic sources. This information is typically presented in the context of the six major criteria pollutants, which constitute the EPA regulations for ambient air quality. Toxics, however, represent a different set of pollutants and by definition it is not necessarily their ambient concentration that is of main concern. It is important to recognize that while some toxics can be emitted from natural occurrences such as volcanic eruptions and forest fires, by and large, toxics come from anthropogenic sources.

Air toxics can be emitted into the atmosphere in several ways. Attrition occurs through the mechanical wearing of physical objects. Activities such as grinding, polishing, sanding, drilling, and spraying can lead to pollution by attrition. This can be found in activities such as drilling for oil [8], or in a local auto body shop that specializes in sanding and painting cars. Vaporization occurs when a liquid converts into its gaseous form. This can happen under temperature and pressure, or because the liquid is volatile (readily evaporates at normal temperatures). Gasoline is one such volatile liquid that readily evaporates [8]. One of the byproducts of gasoline evaporation is benzene, which is discussed in detail below. The third manner in which many toxics become airborne is through combustion. Combustion occurs when a substance is combined with oxygen in a chemical reaction that creates energy. If a fuel is perfectly combustible, meaning that all of it gets used in the combustion process, the two outputs are water vapor and carbon dioxide. Both of which, while not toxic to humans are greenhouse gasses that can contribute to global warming through the trapping of heat energy from the sun. Most fuels, however, are imperfectly combustible, meaning that they do not burn completely. This leaves byproducts such as benzene, toluene, and formaldehyde [8].

For a full understanding of the sources of air toxics and regulation, one must first be familiar with the source categories. The main concern for air toxics regulators are routine emissions: Those that are produced as a byproduct of a process, rather than accidental "one time" emissions [1]. Three major source categories exist. *Mobile sources* include any mechanical object that moves (cars, planes, trains, marine, farming equipment, etc.). Over 50% of air toxic released into the atmosphere come from mobile source emissions [9]. In addition to emitting greenhouse gasses, auto emissions also include several air toxics such as formaldehyde, acetaldehyde, 1,3-butadiene, and particulate matter from diesel engines. These are all considered possible carcinogens by the EPA. The EPA estimates that over half of all cancers caused by outdoor emissions are caused by motor vehicle emissions [9].

While motor vehicles contribute about half of hazardous air toxics, air toxics are also released by stationary sources, which are those sources that do not move. Stationary sources can fall into one of two categories: *Major sources* are a single (or point) source that emits 10 t per year of any one listed toxic air pollutant or 25 t of a mixture of any listed air toxic pollutants. *Area sources* are those single sources that emit less than 10 t of one, or 25 t of more than one air pollutant.

Area sources may not contribute a large portion of pollution on their own, but coupled with other small sources, such as one might find in a city, area sources can significantly impact air quality. As the population becomes denser, the impact of these small sources on overall air quality becomes greater; since there are more sources of toxics per unit area (such as combustion sources from cooking and heating). The urban poor are especially affected since they tend to live in more highly populated areas, as is the case in Hong Kong, where those more financially well off can live farther from the populous city center [10].

It should be noted that though sources that emit toxics into the atmosphere are of primary concern, a HAP may pollute an indoor area as well, such as coal burning for cooking or heating. Indoor sources present a concern as they can be contained in smaller spaces, and therefore expose those occupying that space (such as industry workers) to high concentrations of toxics. Indoor sources pose high levels of risk in developing areas like parts of China, where coal is used for home heating [11]. The full list of HAPs contains a wide array of compounds ranging from industrial chemicals to agricultural pesticides, which can be present in the air in particulate (solid), gaseous, or liquid (aerosol) form.

Where Do They Go?

Once a pollutant becomes airborne, it can have many potential pathways. It can remain in the air as is, become a component of a chemical reaction and transform, and/or it can be transported short or long distances and then follow another pathway. The complexities of each of these mechanisms depend on numerous factors ranging from the scale of long-term climates to the scale of short-term turbulence occurring within seconds of release. As long as the toxic is in the air, it can affect the global climate or an individual human in a single breath. The complexities of atmospheric interactions of chemicals can complicate efforts to reduce toxics; Each chemical that is emitted into the atmosphere can react differently with other chemicals, to the point that the reduction of one type of pollutant (such as NO_x) can actually increase the production of other pollutants (such as Ozone and aldehydes), depending on solar radiation, climate, and season [12].

The fate of pollutants can be affected by a number of complex physical transformations, including nucleation and coagulation (by which particles grow in size) or deposition through settling or precipitation. Toxics that leave the air and are deposited on the ground can continue to do environmental and health harm by contaminating land and water (including drinking water). Humans can then be exposed by drinking contaminated water, eating contaminated food, or by coming in contact with contaminated soils [8]. Toxics that have settled or precipitated out can also find their way into the food chain. As larger animals eat smaller animals that are contaminated, toxins can accumulate in biologic tissues, resulting in greater concentrations as one rises higher in the food chain. Human consumption of animals higher in the food chain can result in significant doses of toxin. The classic example of this is mercury contamination of tuna fish, which accumulate the toxin through feeding on smaller aquatic life forms [13].

The interactions between air toxics and the atmosphere is multilayered and dynamic, factors such as time of day, season, wind directions, and temperature can affect what happens to a toxic after it is released into the air. Concentrations of mercury, for example, increase in Korea during winter and at night because of increased coal burning. In contrast, in some areas of China, gaseous mercury concentrations increase in summer because high solar radiation transforms mercury trapped in soil into a gaseous form [11]. Some studies have shown that air toxics tend to have periods of low ambient concentrations that are followed by sharp spikes in output. Logue, Huff-Hartz et al. found that over 50% of the toxics measured by their high time resolved methods occurred during spikes in emissions of short duration; and that different areas (such high traffic areas, areas next to industrial sites, and general city buildings) can have very different release profiles, even if they are in close proximity (in this case 13 km) from one another [14]. Further examples of the importance of microclimates include Raymer et al. who showed that exposures to aldehydes (which are toxics formed from combustion engines, cigarette smoking, oil frying) have been shown to vary widely in different microenvironments, being higher in restaurants but lower in gas stations in the same city [15]. Similarly, areas of high automobile traffic have been shown to

equate with high levels of air toxics [16]. With timing and specific location being an important part of the exposure equation, individual human movement patterns are an important part of one's risk for exposure to air toxics [16]. Two individuals living in the same city, or even the same block, can have different exposures depending on when they are present in that block relative to the time of day that an exposure might be taking place.

Though two individuals living in the same city might be exposed to different levels of toxics, they are both likely to be exposed to worse air quality than their rural counterparts. Cities, where most anthropogenic sources are centered, present unique air quality challenges that go beyond the mere high concentration of toxic pollutants due to population. The physical layout of a city affects the air that moves within and around it. The buildings in large cities create a larger surface area to collect heat in the daytime, which they reradiate at night. Warm pollutant filled air concentrates in locations with high numbers of tall buildings (usually at a city's center). That air rises and spreads out over the city, cooling as it moves. As it reaches the city's edge it is drawn back in to fill the void left by the rising warm air in the center. The result is a convection current that circulates pollutants within the city [8]. Though particular microclimates within a city will have their own levels of air toxics based upon what is occurring locally [15], the overall air quality in a city can be worse than it is in less populated areas because of the properties of the physical landscape.

Regulation and Monitoring

As one might imagine, addressing the potential health implications of almost 200 different compounds, all with different sources, means of transport, fates and health effects presents a complex problem. During attempts to regulate air toxics, the EPA has tried several strategies. From 1970 to 1990, the EPA attempted to set standards and regulate each of the 189 toxic air chemicals based on the individual health risks that were posed by each one. The strategy was to identify all of the pollutants that could cause "serious and irreversible illness and death" and reduce the emissions of each to a point that provided a margin of safety to the public. Issues arose with this approach however, as the EPA attempted to create policy based on incomplete scientific evidence; pinpointing the level of reduction needed to avoid health effects proved to be easier said than done! How risk was to be assessed and the level of acceptable risk that should be incurred by the public for each of the pollutants created an inefficient and slow system that only saw regulation of seven pollutants in 20 years [1].

In 1990, with the revision of the Clean Air Act, congress charged the EPA to implement a new system of regulation using a technology-based approach called "Maximum Achievable Control Technology" or MACT. The MACT standard dictates that the emissions limits of a certain toxin be set by the average emissions of the best performing 12% of similar sources, if there are more than 30 sources nationally that are in the same category. If there are less than 30, the average emissions of the best five are used as a standard [1]. Since air toxics may still be harmful even at the emissions levels of the best emitters, the EPA is able to assess how well current technologies reduce risks and has the power to implement additional standards to deal with any remaining risk posed by generation of toxic pollutants. The EPA must explore the remaining health risks posed by a pollutant 8 years after issuing the MACT standard [1].

The 1990 amendments to the Clean Air Act also eliminated caprolactam as a HAP. This shows that the understanding of pollution and regulation is always changing and that the links between regulations, reductions of pollutants, and the health effects of pollutants are still being actively explored [17–20].

In order to evaluate toxic levels and create appropriate regulations, there must be an understanding of how much toxic is being emitted and how it behaves in the environment. Understanding how air toxics behave, the concentration level at any one time, and how and when an individual might be exposed is an evolving science. Both direct sampling of air quality and modeling of air toxics based upon preexisting data (or a combination of both) are used. The Environmental Protection Agency does not monitor the entire USA in order to gain an understanding of the concentration of air toxics; rather they receive reports from industries who account for their own emissions, which are compiled in the Toxic Release Inventory Report [21]. These emissions data are combined with data such as the rate

of toxic release, the location, the height of the release, the nature of the pollutants with respect to decay and longevity, wind speed, and wind direction. This information is then broken down by census track and used in models such as the Assessment System for Population Exposure Nationwide (ASPEN) in order to estimate the level of pollutants in a given area of USA [18, 20, 22]. The success and accuracy of a model depends upon the assumptions made and the inputs used, and different modeling techniques can produce different results for the same area [16].

Direct sampling of toxics can also take different forms. Some techniques, for example, collect an average concentration over a period of time, such as 24 h. Others are able to sample at more regular intervals, allowing a profile of different concentrations during different times of the day [14]. In addition, there may be several different sampling technologies for one pollutant, such as is the case with mercury [11]. *When* sampling occurs is also important: Concentrations can vary both by season, and by time of day. Sampling can help to test the validity of models, and help to determine what factors can make a model more accurate [18, 23].

The difficulties in monitoring and sampling air toxics have led to recent controversy. In 2009, USA Today and scientists from University of Maryland and Johns Hopkins tested the air outside 95 schools nationwide and found that seven schools had high enough levels of toxics such as benzene and chromium to elevate risks of cancer, and 57 schools had levels that were higher than their respective state guidelines. The article created a public outcry, and in response to the article, Louisiana and Pennsylvania conducted their own short-term monitoring and found that levels were not high enough to pose a health threat. This led to questions about how areas are monitored, the duration of monitoring, and whether the health threats existed or not [24, 25].

Monitoring and Regulation of hazardous materials is complex. The ways in which air toxics behave in the atmosphere are not always completely understood, and monitoring and modeling air toxic behavior is subject to several variables that can lead to different results. This can lead to controversy about the level of exposure (and thus risk) of the general public. In order to regulate such a complex issue, the EPA has taken a technological approach, based upon the level of control possible, which allows them to establish regulations despite incomplete knowledge about distribution and health effects.

The Toxic Cycle: Specific Examples

Mobile Sources: A Balancing Act

As mentioned above, mobile sources, most notably automobiles, represent a major contributor to air toxic emissions in the USA. Of high concern is benzene. Benzene is a colorless liquid with a sweet odor. It evaporates rapidly and is used in plastics, resins, and synthetic fibers. It also naturally occurs in crude oil and is present in gasoline when it is refined. The benzene that exists in gasoline can become airborne when gasoline evaporates or vaporizes. Most benzene, however, comes from incomplete combustion of other naturally occurring compounds in gasoline, namely, toluene and xylene [9]. Inhaling very high levels of benzene can cause death. At slightly lower levels, it can cause drowsiness, confusion, and increased heart rate. Most seriously, it has been linked to leukemia of the blood called AML, which is a byproduct of benzene's effect on blood cells and bone marrow [9, 26]. Children are of particular concern with respect to air toxics because their bodies are still growing, and air toxics can affect them developmentally [18, 20]. In a study by Whitworth et al., census tracks with the highest levels of air benzene based on ASPEN also had the highest levels of leukemia in children. Other studies have found that concentrations of benzene and 1,3-butadiene exceed EPA health benchmarks at hundreds of locations across the USA [18], making benzene a serious health threat.

In order to eliminate air toxics, including benzene, from gasoline, the 1990 revision of the Clean Air Act mandated that highly polluted cities use reformulated gasoline; which is required to be less likely to vaporize, and have lower levels of benzene and aromatics. In addition, in many states, gasoline pumps are required to have vapor recovery nozzles, in order to trap gasoline vapor that may evaporate during refueling [9]. Reformulation of gasoline to eliminate benzene has been successful. California saw reductions in benzene emissions of 54% in the mid-1990 s, corresponding with the introduction of reformulated gasoline [17].

Another requirement of reformulated gasoline is that it burns more efficiently. This last requirement is accomplished by adding compounds that oxygenate the gasoline, which allow gasoline to burn more completely and efficiently. Two such compounds are ethanol, and MTBE or methyl tertiary butyl ether. The goal of the increased efficiency is to reduce the production of carbon monoxide, a cause of smog and to conserve oil, which is a nonrenewable resource. Thus it serves several purposes [27].

Studies of the effectiveness and side effects of ethanol and MTBE gasoline have shown that the addition of these compounds does reduce CO emissions, but increases the concentrations of formaldehyde and ethyl-aldehyde [27]. Formaldehyde is one of the 188 EPA air toxics [28]. In addition, MTBE itself has been named as a health concern, causing irritation and nervous system effects [26]. Health concerns caused California to phase out MTBE in favor of ethanol as an oxygen booster [17]. The story of MTBE makes an important point about the efforts to lessen the impact of the industrial way of life on the environment, so that mankind sustains itself into the future. Interactions between chemicals and the atmosphere are complex, and adding something new to the equation can have unforeseen consequences, even if the original aim was to reduce the levels of a harmful substance. MTBE was introduced to help reduce smog, but it also increases levels of some air toxics, and has health concerns of its own.

The phase-in of reformulated gasoline highlights another issue in regulation; the economic, and by extension, political trade-offs inherent in regulating an industry: The phase-in of reformulated gasoline in California has led to higher gasoline prices for consumers, as well as disadvantaged smaller refiners who have had more trouble in meeting the regulations in relation to larger refiners [29]. Thus the regulation of air toxics can, and does, become a political and economic issue.

The most transformative solution to the problems of air toxics from gasoline is to simply greatly reduce or eliminate the use of gasoline altogether. In 2010, cars that run on both electric and gasoline power (i.e., hybrids) are gaining greater market share, and automotive manufacturers, both large and small, are designing and constructing vehicles that run exclusively on electric power. A complete transition from gasoline to electric power creates its own obstacles, however. Battery technology is one of them. Traditional lead acid batteries are inexpensive, but are heavy and cannot hold enough power for electric vehicles to be practical. Nickel-metal hydride batteries have more power but can become permanently damaged if over discharged. Lithium ion batteries, a newer technology, can store a good deal of power and are not affected by discharge, but some use cobalt, which is highly toxic [30]. Thus the ideal battery technology is yet to be developed, and existing technologies have inherent trade-offs between efficiency, cost, and environmental impact.

Technology development is not the only obstacle to changing the automotive landscape: The use of Electric cars could be a benefit to energy companies, allowing them to gain revenue as cars charge at night (when little electricity is being used elsewhere). The integration of electric vehicles, however, would necessitate a fundamental change in power infrastructure, which would take time and serious amounts of coordination between industries, such as the power generation industry and the automobile industry, two industries that have never worked together very closely [30]. This brings up a very important issue when talking about sustainability. The challenges and obstacles to sustainable practices are not just limited to developing technology, but are also problems of coordination, commitment and political will, and balancing the trade-offs inherent in changing from one system to another.

Perchloroethylene: Keeping Things Clean

A common site in cities (and suburbs) in the USA is a local, small neighborhood dry cleaner. In fact, there are about 27,000 free standing dry cleaners within the USA [31]. Many people, when entering a dry cleaners, will notice a particular odor; both in the establishment, and on their newly cleaned clothes. That odor is Perchloroethylene or PERC. It historically has been the most common chemical associated with dry cleaning. PERC has been linked to liver and kidney tumors in rats and is considered by the EPA to be a carcinogen. In high concentrations (such as that associated with occupational exposure) it is associated

with dizziness, confusion, nausea, difficulty in speaking, unconsciousness, and death [26]. Exposure to PERC can happen from inhaling the chemical directly or ingesting contaminated water. Once in the body, it can be stored in fat cells, and releases itself slowly into the blood stream [26].

The case of PERC provides a good example of how an air toxic is regulated, the different categories of emitters, and how technology provides the basis for guidelines. The 1990 revision of the Clean Air Act required regulation based upon available technology (MACT). The first rules for PERC dry cleaners were laid out in 1991, revised and finalized in 1993 and updated in 2005–2006 as technology improved and health effects were better understood. In regulating the industry, the EPA divided dry cleaners into three groups. The first were major sources (those that produce more than 10 t of PERC per year), the second were smaller area sources that were free standing or in shopping plazas, the third (which was a category that was not originally differentiated in the 1993 guidelines, but believed to cause a greater health threat) were dry cleaners that exist as part of residential buildings [31].

In 2005, the EPA estimated that nine million people lived within 6 miles of a major source of PERC [32]. The main strategy for the large cleaners (the major sources) is the requirement to use state-of-the-art recovery systems that do not permit PERC to be released into the air, but rather trap and filter it. They are also required to implement advanced leak detection practices to ensure that systems do not leak PERC into the atmosphere accidentally [31].

The guidelines for smaller area sources are based upon the standard of "Generally Available Control Technologies" or GACT. GACT is slightly less stringent than MACT and mandates that firms that emit HAPs use control technologies that are commercially available and the most appropriate considering the economic impact on regulated entities and the ability for entities to comply [33].

As per the GACT standard, new free-standing operations are required to build facilities with closed loop systems (that do not release PERC into the air) and implement advanced leak detection practices. Dry cleaners that already exist have to eliminate what are called transfer machines, those that require PERC soaked clothes to be moved to a second machine for drying, in favor of machines that wash and dry together [32].

Dry cleaning operations that are part of apartment buildings pose a greater risk to the public because people are living in close proximity to PERC emissions; thus more stringent regulations were proposed. According to the rule, all existing dry cleaners have to eliminate transfer machines, and are not able to replace PERC machines when the old ones wear out. PERC machines will have to be phased out completely by 2020 [31].

These regulations are not without costs. For example, implementation of these regulations has been estimated to cost the smaller dry cleaners 7.3 million dollars collectively. Though greater efficiency might save 2.7 million annually, these changes represent an overall net cost to the industry [32].

Dry cleaning of clothes is a service millions of Americans use without giving much thought to the health effects or environmental impacts of the service. Even though a small neighborhood dry cleaner might not cause a large environmental problem on its own; a densely populated area, such as a city, might have tens or hundreds of small establishments. Taken together, they can have a large environmental impact. The regulations are foremost to protect health, and those operations that cause a greater immediate threat (such as residential dry cleaners) are regulated more strictly. The regulations also attempt to take into account the ability of emitters to follow the regulations in a way that is not detrimental to their business, hence the GACT guidelines for smaller area emitters. Regulations are often a give and take.

Mercury: A Global Toxin

Air toxics are truly a global problem, and a good example of that is the harm posed by human exposure to mercury. Mercury is an element and is naturally occurring in the environment. It can be emitted through geothermal and volcanic activity. The main concern for human health, however, comes from human-made (or anthropogenic) sources of mercury emissions. In adults, mercury exposure can damage the brain, heart, kidneys, lungs, and the immune system. Brain effects can lead to personality changes, shyness, tremors, and hearing and sight problems. A bigger risk comes for children. Fetuses and young children exposed to mercury can develop neurological and developmental

disorders that can lead to mental retardation, blindness, seizures, inability to speak, and lack of coordination. It can also cause damage to kidney, liver, and digestive systems [34]. Mercury can be passed from mother to infant in breast milk or from mother to fetus directly during gestation.

Mercury poisoning goes far back into human history: Mercury poisoning can result from exposure during metalworking and gold extraction, and there is evidence of increased mercury concentrations globally during times of high levels of gold mining activity, including the ancient Roman and Incan empires [35]. Small-scale gold working is still a major source of mercury pollution in places such as Africa and Asia [36, 37]. Mining and metal working are not the only industries that historically exposed one to mercury: The term "Mad as a Hatter" comes from mercury poisoning among hatters, who used the element in the creation of hat felt from animal pelts and suffered cognitive effects [38].

Currently, humans introduce mercury into their environment through metal mining, waste incineration, refining, and manufacturing. The largest source of mercury comes from the combustion of coal for electricity generation and heating. In fact 60% of global mercury production in 2000 was due to coal burning [39]. Mercury can exist in several forms: Elemental mercury (Hg^0), divalent mercury (Hg^{2+}), and particulate mercury (Hg(p)). Elemental mercury is the most common form. It can exist in the atmosphere for extended periods of time, a year or more, which means that it can travel large distances, up to 1,000 km from its source. In fact, it has been argued that elemental mercury production in Asia contributes to mercury levels in North America [36]. Mercury occurs naturally in coal. The amount of mercury depends upon the type of coal and its origin. When coal is burned for fuel, elemental mercury, particulate mercury, and divalent mercury can be released. Elemental mercury can oxidize into Hg^{2+} and deposit in waterways and land. Hg^{2+} that is deposited in waterways can become transformed by certain bacteria into methyl mercury (CH_3Mg^+). Though these basics are understood, the details about how mercury cycles through the environment are still under investigation [40].

Methyl mercury is highly toxic to humans and animals, and can accumulate in animal tissue. Through this accumulation (called bioaccumulation) humans can receive large doses of mercury from ingesting several smaller animals that have been contaminated. Consumption of toxic fish is the primary risk of mercury globally. In the USA alone, 48 out of the 50 states had to advise residents to avoid consuming fish from certain bodies of water within their borders [39].

Mercury from coal-fired power plants is a particular problem since rapid development, and the associated need for power generation, has increased coal usage worldwide. Poland, for example, derives 93% of its power from coal and has no legal limitations on mercury emissions, making it the fourth highest emitter in Europe [41]. Asia, because of rapid development, is a source of mercury emissions from all sources, with a large portion coming from manufacturing [36] and coal burning [40].

The primary post-combustion technologies that reduce mercury emissions are not specifically for mercury control, but rather for controls of particulate matter, SO_2 and NO_x [40, 42]. Combinations of control technologies can be successful for mercury reduction. South Korea, for example, has seen a 68% reduction in mercury emissions by using a combination of technologies intended for control of SO_2 and NO_x [43]. Though reductions based on current technologies are possible, the lack of specific controls indicates that the science of mercury control is lacking. Even developed countries, such as the USA, do not have a clear direction in dealing with this hazard.

The path of regulation of mercury in the USA has taken a few interesting turns. In the USA, power plants are the largest emitters of mercury, and the Clean Air Act revisions of 1990 charged EPA to study coal burning in the USA. They found that about a third of the mercury found in coal was being removed by current filters (the ones primarily for SO_2 and NO_x), while the other two thirds were being released into the atmosphere. The EPA was in the process of developing new standards for mercury emissions under MACT until 2004, when they changed course and proposed a cap and trade system instead. In the cap and trade system, the mercury emissions would be limited nationally, and power plants would possess credits for each unit of mercury produced. Plants that produced *less* mercury than permitted could then sell their excess units to another power plant. That plant could then produce

more. The cap and trade system has come under fire, however, because though it would reduce emission of mercury nationally, it could create a situation where mercury emissions are high locally, affecting residents of an area disproportionately. It was ultimately struck down by the USA court of appeals, who ruled that the EPA did not follow the proper procedures for delisting mercury as an air toxic; therefore, it was still subject to the MACT standards as laid out in section 112 of the Clean Air Act. Currently the US government is likely to reinstate MACT standards for mercury, but until then, mercury control will be left to the states, many of whom adopted stricter standards than the federal ones [44].

Mercury is a highly toxic substance, and its toxic effects have affected humans for millennia. Mercury produced in one corner of the world can affect another, which can make mercury contamination a political issue. The case of the change in US regulations highlights issues of scale and social justice: The cap and trade system may reduce the levels of mercury nationally, but it may do so at the expense of some local populations. That raises questions of whom regulations benefit (such as more well-off people at the expense of poorer who may live near power generation). It also illustrates the importance of scale when thinking about pollution and regulation: Nationally the levels of mercury might look acceptable, but when the resolution is increased and examined locally some places may have unacceptably high levels. This ties back to the issue mentioned above about how an air toxic is measured, when and where; different levels of measurement can have different results, and the action taken based on those measurements can affect health and outcomes.

Human Health

Many of the health effects of different compounds that are considered air toxics are well established, and can be quite dramatic. In the early 1950s, residents of Minamata Bay, Japan began suffering from neurological illness. Adults began exhibiting symptoms such as blurred vision and difficulty in hearing, reduced ability to smell and taste, clumsiness, difficulty in walking, and mood changes. Children and newborns began suffering from impairments in chewing, swallowing, speech, and movement. All of these individuals were suffering from brain damage due to acute poisoning with methyl mercury. Contamination came from a local acetaldehyde plant (acetaldehyde is used in the making of plastics). The residents became ill from eating fish and shellfish that had stored mercury in their bodies through biomagnification. Estimates put the number affected since the 1950s at 200,000 and these acute cases of illness have been unequivocally linked to mercury [45].

The results of air toxics in lower doses (the type one might encounter living next to a dry cleaner, or living in a heavy traffic prone area) is much more difficult to understand and to illustrate. Knowing that chemicals like benzene and PERC have carcinogenic effects in laboratory animals and during heavy occupational exposures is not the same as claiming that the average residents of a city are at greater risk for cancer because they live in a high traffic area. The relationship between toxics and illness is not always clear-cut. Benzene is one of the best understood of the air toxic carcinogens, and the effects have been well explored in animal research as well as in humans who are exposed to benzene in occupational concentrations. Less is known, however, about the relationship between ambient concentrations and cancer, especially in children. Whitworth et al., for example, used EPA models of benzene levels and census track to show that census tracks that have the highest levels of benzene also have higher incidence of childhood leukemia [20]. On the other hand, Reynolds et al. found that traffic density (which is a predictor of benzene and butadiene levels) did not correlate with childhood leukemia rates [46]. Thus even though the health effects of benzene are well established, the effects of environmental concentrations on populations are more difficult to pinpoint. With respect to mercury, Lewandowski et al. note that correlations have been found between mercury levels and autism in 2002, for school districts in Texas, but that these correlations were not found for 2005 and 2006, calling into question the original correlations [47]. Understanding the health effects is an important issue since policy and regulation decisions are made, at least in part (remember the EPA can create stricter regulations based on health effects) upon the impacts on human health. Understanding how these effects unfold in real-world situations is crucial to assessing local impacts of

pollutants, the benefits of regulation, and the need for new cleaner technologies.

The health effects of air toxics cannot be completely decoupled from general problems of air pollution. Often, sources of pollution, such as power plants and automobiles, release more than one harmful substance. In addition, multiple sources will cluster in certain areas, such as cities (many cities have power plants, drycleaners, and cars!). In areas that are developing quickly and do not have strict environmental controls, such as parts of Africa, individuals may be exposed to mercury, lead, pesticides, contaminated water, and various air toxics simultaneously [48]. Air toxics and other forms of pollution are also part of larger issues of health and illness: Factors such as several environmental pollutants, nutrition, levels of stress, and poverty interact and can be considered to affect health synergistically, with each problem causing the others to become more dangerous and vice versa [49, 50]. The impacts of toxics are complex and intertwined with the fates of other pollutants and linked to other aspects of human health and well-being. While it is important to understand how a particular toxin reacts, and how it may affect health, it is important not to lose sight of the larger system and the interactions that play a role in determining who and what is ultimately impacted.

Future Directions

The regulation of air toxic chemicals is an evolving science. Not all aspects of transport and fate are completely understood (mercury is a good example of this). The activities that produce air toxics are part of the activities of daily life, and are difficult to terminate. People all around the world still need to get from place to place, and power must be generated. These needs have to be balanced with the impact from the consequences of these actions. The immediate strategy is to make current technologies (coal burning, gasoline automobiles, dry cleaning establishments) as clean as they can be. This presents challenges since the way in which toxics behave in the environment is not always completely understood (as is the case with mercury), regulations have costs to consumers and producers, and monitoring for toxics is still an underdeveloped science. In some cases, such as the push for cleaner burning fuels, attempting to solve one problem (higher efficiency) leads to another (higher levels of volatile aromatics such as benzene). Some toxic-generating activities may be supplanted with newer technologies in future. This presents challenges as well. Changing from gasoline to electric powered cars will necessitate a change in the infrastructure that supports the automobile, and will create the need for collaboration between very different industries. Alternative sources of power, such as nuclear, have their own drawbacks in risks and wastes generated. Even alternatives such as wind have opponents who are concerned about the space needed to house wind generation and the impact on the aesthetics and enjoyment of land [51]. There are political issues at play as well. Much of the reason for the increase in coal burning is that it is a relatively inexpensive means of power generation for countries that are expanding rapidly. Many in those countries argue that they cannot afford to implement stringent environmental control technologies at the expense of the development that they need. The picture becomes more complex with toxics such as mercury, which can travel half way across the globe, so that the energy choices made by one country may affect another.

The way forward is likely a mixture of better monitoring and regulation of current technologies, as well as implementation of newer technologies that have less environmental impact. Many of these will likely exist in tandem (as is seen today with gasoline cars and gasoline electric "hybrid" cars). In order to create a way forward that is sustainable, solutions must be found that can benefit most people. The concerns of developed countries, developing countries, industry, and citizens must be considered, with the overall health and well-being of humans everywhere being the foremost concern. Cooperation between corporations and governments, as well as long-term thinking will be key to meeting these challenges.

Bibliography

Primary Literature

1. US EPA (2000) Taking toxics out of the air. Brochure of the US EPA Office of Air Quality Planning and Standards, Research Triangle Park, NC. Accessed 11/223/2010, Available from: http://www.epa.gov/air/oaqps/takingtoxics/p1.html

2. EPA (2007) The Plain English Guide to the Clean Air Act. 2008, US EPA Office of Air Quality Planning and Standards, Research Triangle Park, NC. Publication No. EPA-456/K-07-001
3. Keys D (2003) How Rome polluted the world. Geogr Campion Interact Publishing 75(12):45–48
4. Bell ML, Davis DL (2001) Reassessment of the lethal London fog of 1952: novel indicators of acute and chronic consequences of acute exposure to air pollution. Environ Health Perspect Suppl 109:389
5. BeruBe K et al (2005) London smogs: why did they kill? Proc R Microsc Soc 40(3):171–183
6. Parris TM (2006) Smog Season. Environment 48(4):3–3
7. Aronson SM (2009) The ignoble fate of the peppered moth. In: Medicine & Health Rhode Island, pp 291–291
8. Corman R (1978) Air pollution primer. The American Lung Association, New York
9. US EPA (1994) Environmental fact sheet: air toxics from motor vehicles. In: Environmental Protection Agency (ed) Ann Arbor.
10. Stern RE (2003) Hong Kong Haze. Asian Surv 43(5):780–800
11. Fang G-C, Wu Y-S, Chang T-H (2009) Comparison of atmospheric mercury (Hg) among Korea, Japan, China and Taiwan during 2000–2008. J Hazard Mater 162(2/3):607–615
12. Luecken DJ, Cimorelli AJ (2008) Codependencies of Reactive Air Toxic and Criteria Pollutants on Emission Reductions. J Air Waste Manage Assoc 1995 58(5):693–701
13. McSwane D (2009) Food safety, in environmental health: from global to local. In: Frumpkin H (ed). Jossey-Bass, San Franscisco
14. Logue JM et al (2009) High time-resolved measurements of organic air toxics in different source regimes. Atmos Environ 43(39):6205–6217
15. Raymer JH et al (2009) Microenvironmental characteristics important for personal exposures to aldehydes in Sacramento, CA, and Milwaukee, WI. Atmos Environ 43(25):3910–3917
16. Oñzkaynak H et al (2008) Modeling population exposures to outdoor sources of hazardous air pollutants. J Expo Sci Environ Epidemiol 18(1):45–58
17. Harley RA et al (2006) Effects of Reformulated Gasoline and Motor Vehicle Fleet Turnover on Emissions and Ambient Concentrations of Benzene. Environ Sci Technol 40(16):5084–5088
18. McCarthy MC et al (2009) Characterization of the Chronic Risk and Hazard of Hazardous Air Pollutants in the United States Using Ambient Monitoring Data. Environ Health Perspect 117(5):790–796
19. Raun LH, Marks EM, Ensor KB (2009) Detecting improvement in ambient air toxics: An application to ambient benzene measurements in Houston, Texas. Atmos Environ 43(20): 3259–3266
20. Whitworth KW, Symanski E, Coker AL (2008) Childhood Lymphohematopoietic Cancer Incidence and Hazardous Air Pollutants in Southeast Texas, 1995–2004. Environ Health Perspect 116(11):1576–1580
21. US EPA (2009) Toxics Release Inventory (TRI) Program Fact Sheet. 2009 9/20/2009 [cited 2010 1/19]; Available from: http://www.epa.gov/triinter/triprogram/tri_program_fact_sheet.htm
22. US EPA (1996) The Aspen model. Technology Transfer Network 1996 National-Scale Air Toxics Assessment 2009 6/6/2007 [cited 2010 1/19]; Available from: http://www.epa.gov/ttn/uatw/nata/aspen.html
23. Venkatram A et al (2009) Modeling the impacts of traffic emissions on air toxics concentrations near roadways. Atmos Environ 43(20):3191–3199
24. Morrison B,Heath B (2009) States' tests of air questioned. *USA Today*
25. Heath B, Morrison B (2009) EPA study: 2.2 M live in areas where air poses cancer risk. *USA Today*
26. ATSDR (1997) American Toxic Substances and Disease Registry Toxfaqs: Tetrachloroethylene. US DHHS PHS ATSDR CAS#127-18-4
27. Graham LA, Belisle SL, Baas C-L (2008) Emissions from light duty gasoline vehicles operating on low blend ethanol gasoline and E85. Atmos Environ 42(19):4498–4516
28. US EPA (2006) Master list of compounds emitted by mobile sources. Environmental Protection Agency (ed) Washington, DC
29. Brown JL (2009) The Market Effects of Going Green: Evidence from California's Wholesale Reformulated Gasoline Market. Energy J 30(3):115–127
30. Tollefson J (2008) Car industry: Charging up the future. Nature 456(7221):436–440
31. EPA (2009) Fact sheet-final amendments to air standards for perchloroethylene dry cleaners. EPA, Editor
32. US EPA (2006) Proposed amendments to air toxics standards for perchloroethylene dry cleaners. Environmental Protection Agency, Editor
33. US EPA (1993) Air pollutants, hazardous; national emission standards: perchlorethylene emissions from dry cleaning facilities. Edited by Environmental Protection Agency, Research Triangle Park, NC, p 49354
34. Department of Health and Human Services (1999) Agency for toxic substances and disease registry, *Mercury*, Department of Health and Human Services, Atlanta
35. Sun L et al (2006) A 2000-year record of mercury and ancient civilizations in seal hairs from King George Island, West Antarctica. Sci Total Environ 368(1):236–247
36. Li P et al (2009) Mercury pollution in Asia: a review of the contaminated sites. J Hazard Mater 168(2–3):591–601
37. Tillett T (2009) The Price of Progress. Environ Health Perspect 117(6):A257–A257
38. Levin P (2007) From mad hatters to dental amalgams: heavy metals: toxicity and testing. MLO Med Lab Obs 39(12):20
39. Selin NE (2009) Global Biogeochemical Cycling of Mercury: A Review. Annu Rev Environ Resour 34:43–63
40. Streets DG, Zhang Q, Wu Y (2009) Projections of Global Mercury Emissions in 2050. Environ Sci Technol 43(8):2983–2988
41. Glodek A, Pacyna JM (2009) Mercury emission from coal-fired power plants in Poland. Atmos Environ 43(35):5668–5673
42. EPA (2002) National Risk Management Research Laboratory Research, Triangle Park, NC. Control of mercury emissions

from coal-fired elecric utililty boilers: interim report including errata dated 3-21-02
43. Pudasainee D, Kim JH, Seo YC (2009) Mercury emission trend influenced by stringent air pollutants regulation for coal-fired power plants in Korea. Atmos Environ 43(39): 6254–6259
44. Milford JB, Pienciak A (2009) After the Clean Air Mercury Rule: Prospects for Reducing Mercury Emissions from Coal-Fired Power Plants. Environ Sci Technol 43(8):2669–2673
45. Ekino S et al (2007) Minamata disease revisited: An update on the acute and chronic manifestations of methyl mercury poisoning. J Neurol Sci 262(1–2):131–144
46. Reynolds P et al (2002) Traffic patterns and childhood cancer incidence rates in California, United States. Cancer Causes Control 13(7):665–673
47. Lewandowski TA et al (2009) An Evaluation of Surrogate Chemical Exposure Measures and Autism Prevalence in Texas. J Toxicol Env Health A 72(24):1592–1603
48. Nweke OC, Sanders WH III (2009) Modern Environmental Health Hazards: A Public Health Issue of Increasing Significance in Africa. Environ Health Perspect 117(6):863–870
49. Singer M, Clair S (2003) Syndemics and Public Health: Reconceptualizing Disease in Bio-Social Context. Med Anthropol Quart 17(4):423–441
50. Goodman AH, Leatherman TL (eds) (1998) Building a new biocultural synthesis. University of Michigan Press, Ann Arbor, pp 3–42
51. Johansson M, Laike T (2007) Intention to respond to local wind turbines: the role of attitudes and visual perception. Wind Energy 10(5):435–451

Books and Reviews

Ganesan K et al (1996) Air toxics: problems and solutions. Gordon & Breach, Amsterdam, p 342

Griffin RD (2007) Principles of air quality management, 2nd edn. Taylor and Francis, London, 334 pp

Hanna SR et al (1982) Handbook on atmospheric diffusion. Office of Energy Research, US Department of Energy, 102 pp

Harrop O (2002) Air quality assessment and management: a practical guide. Taylor & Francis, London, 504 pp

Heinsohn RJ, Kabel RL (1999) Sources and control of air pollution. Pearson Education, Upper Saddle River, p 696

Jacobson MZ (2000) Atmospheric pollution: history, science and regulation. Cambridge University Press, New York, p 399

Spicer CW et al (2002) Hazardous air pollutant handbook: measurements, properties, and fate in ambient air. Lewis, Boca Raton, p 240

Turner DB (1994) Workbook of atmospheric dispersion estimates: an introduction to dispersion modeling. Lewis, Boca Raton

USEPA (2004) Air toxics risk assessment reference Library, edited by Office of Air Quality Planning and Standards, EPA, Research Triangle Park, NC

Vallero D (2008) Fundamentals of air pollution, 4th edn. Academic Press, San Diego, 942 p

Aircraft and Space Atmospheric Measurements Using Differential Absorption Lidar (DIAL)

Russell De Young
NASA Langley Research Center, Hampton, VA, USA

Article Outline

Glossary
Definition of the Subject and Its Importance
Introduction
Future Directions
Bibliography

Glossary

Absorption The process in which incident radiant energy is retained or absorbed by a gas.

Absorption coefficient The fraction of incident energy removed by absorption per unit length of travel of radiation through a gas.

Active remote sensing A remote sensing system that transmits its own energy source and measures atmospheric properties from the returned signal.

Aerosol A colloidal suspension of liquid or solid particles in air.

Aerosol extinction The reduction of optical energy passing through the atmosphere due to scattering and absorption of that energy.

Atmospheric boundary layer The bottom layer of the atmosphere that is in contact with the surface and is often turbulent with a capped stable layer of air or temperature inversion. The height is variable but is typically several kilometers during the day.

Depolarization ratio Defined as the ratio of the backscattered lidar power in the cross-polarization plane to the backscattered power in the polarization plane (transmitted laser beam) induced by the atmospheric constituents.

DIAL Differential absorption lidar is a lidar technique used to measure the atmospheric concentration of any gas as a function of altitude.

Extinction coefficient The fraction of incident radiant energy removed by extinction per unit of travel of radiation through the air.

In situ Methods for obtaining information about atmospheric properties through direct contact with the atmosphere as opposed to remote sensing.

Lidar Light Detection and Ranging is a technique for detecting and characterizing atmospheric properties using a pulsed laser.

Passive remote sensing A remote sensing technique that relies on the use of the Sun, Moon, or Earth surface as a radiation source to measure atmospheric gas species by absorption of that radiation as it passes through the atmosphere.

Polarization The property of light where the electric field vector is oriented in a single plane called plane polarization.

Primary trace atmospheric gas or particles Substances that are directly emitted into the atmosphere from the surface, vegetation, or natural or human activities such as fires, industrial processes, and car emissions.

Relative humidity The ratio of the vapor pressure of water to its saturation vapor pressure at the same temperature.

Scattering The process by which atmospheric gases are excited to radiate by an external source of light and the resultant light is usually detected in a direction not aligned with the light source.

Scattering coefficient The fraction of incident radiant energy removed by scattering per unit length of travel of radiation through the air.

Stratosphere The region of the atmosphere from the top of the troposphere to a height of 10–17 km (the base of the mesosphere).

Troposphere The region of the atmosphere from the Earth's surface to the tropopause at 10–20 km, depending on latitude and season, where most weather occurs.

Definition of the Subject and Its Importance

The study of the atmosphere has expanded greatly in the past decade due to concern about global climate change and air quality health effects. The natural atmospheric chemistry is complex but with anthropogenic emissions released into the atmosphere, the resulting complexity makes modeling very difficult. Chemical reactions generally increase with temperature and thus a warming climate may change the weather and climate in unpredictable ways. Also with increased regulations regarding air quality emissions, more attention is being directed toward atmospheric species measurements to assess the impact of specific emission regulations. As a result of these concerns, lidar has become a very valuable tool to directly measure the number density of specific atmospheric species as a function of altitude. This article will review the use of differential absorption lidar (DIAL) in current aircraft based missions and the potential for use of DIAL in orbiting spacecraft

A particular lidar technique called Differential Absorption Lidar (DIAL) has proven to be an especially powerful method to measure atmospheric species. It has been used both on the ground and in many aircraft to determine the concentration of gas species. There are presently no DIAL systems in space, but there are projections by NASA and other nations to place them in Earth orbit to measure critical gases over remote areas and for long periods of time. This article will discuss the DIAL technique, demonstrate its usefulness using airborne examples, and discuss the value of a space–based DIAL satellite system.

Introduction

The need for accurate atmospheric gas concentration measurements as a function of altitude has expanded as a result of predicted atmospheric changes associated with global climate change and the impact of air quality on human health. Both local natural and anthropogenic emissions can be transported around the Earth and thus have health impacts far from the emission sources. Lidar has proven to be a powerful technique for measuring the concentrations of many gas species related to health and climate change concern.

Differential Absorption Lidar (DIAL) from aircraft was first accomplished for ozone at NASA Langley Research Center in 1980 [1] and for water vapor in 1982 [2]. Currently DIAL systems are being flown by NOAA and European countries, but presently there are no DIAL systems deployed in space.

The DIAL system has the ability to address major questions concerning the atmosphere. DIAL systems can be deployed in fixed ground locations, in either piloted or unpiloted aircraft or in satellite platforms. Each has distinct advantages for addressing

atmospheric research questions. Some of these questions are:

- How does urban pollution transport out of the boundary layer into the free troposphere and then to continental scales?
- How do atmospheric species chemically transform with transport age and reaction with other species?
- What vertical and horizontal resolution measurements are needed to substantially improve chemical weather models?
- What atmospheric species need to be measured simultaneously to understand atmospheric chemical transformation?
- What are the temporal and spatial water vapor scales needed to improve hurricane intensification and path forecasting?
- To what resolution do we need to measure atmospheric water vapor to make future weather predictions for every square kilometer and for 1 month in the future for the entire globe?
- Can climate change impacts be measured for chemical weather?

Atmospheric Backscattering and the DIAL Equation

The ability to use laser remote sensing relies on the characteristic of electromagnetic radiation scattering from atmospheric aerosols and molecules. The atmosphere consists primarily of nitrogen and oxygen molecules as well as highly variable aerosols. Scattering from molecules or Rayleigh scattering can be calculated as [3]

$$\beta = (3/8\pi)\beta_s(P/P_s)(T_s/T) \quad (1)$$

where β_s is the volume scattering coefficient (km^{-1}) for the laser wavelength used, P_s is 1013.25 millibars, T_s is 288.15 K, and T and P are the standard pressures and temperatures at altitude. Equation 1 describes the backscatter coefficient that scatters some laser radiation back to the DIAL receiver system. Figure 1 shows the results of Eq. 1 for several common laser wavelengths. The wavelengths at 355, 532, and 1,064 nm are associated with the Nd:YAG laser system while 2,000 nm is commonly used for CO_2 DIAL measurements. Several important properties are noted from the figure. The backscatter coefficient decreases by three orders of magnitude from 355 to 2,000 nm making the use of DIAL more difficult in the infrared. The backscatter is much higher at lower altitudes due to the increased atmospheric density but this also has a disadvantage in that optical detectors are easily saturated by the near field atmospheric lidar return causing signal-induced noise. In contrast the backscatter at 10 km is much less, but this is an advantage for aircraft deployed systems in that the near field signal is substantially reduced, thus reducing signal-induced noise in optical detectors [4].

Scattering also occurs from atmospheric aerosols, but aerosols are highly variable in spatial and temporal

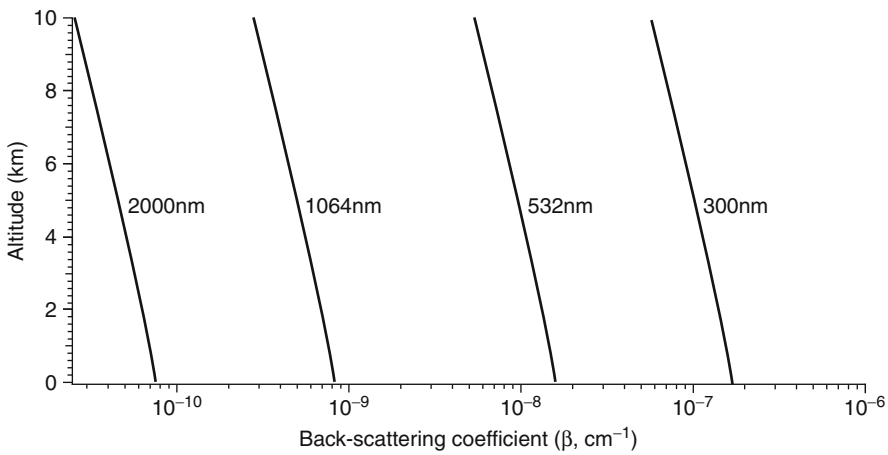

Aircraft and Space Atmospheric Measurements Using Differential Absorption Lidar (DIAL). Figure 1
Backscattering coefficient vs. altitude for different laser wavelengths and northern latitude standard atmosphere

extent. Nevertheless, both aerosols and molecules contribute to the lidar backscatter signal.

The DIAL equation, giving the atmospheric number density N of any gas species, is derived from the lidar equation which is discussed in detail in [5–7] and given as

$$\begin{aligned} N(R) = & 1/(2(R_2 - R_1)(\sigma_{on} - \sigma_{off})) \\ & * \ln(P_{on}(R_1)P_{off}(R_2)/P_{off}(R_1)P_{on}(R_2)) \\ & - 1/(2(R_2 - R_1)(\sigma_{on} - \sigma_{off})) \\ & * \ln(\beta_{on}(R_1)\beta_{off}(R_2)/\beta_{off}(R_1)\beta_{on}(R_2)) \\ & - 1/(\sigma_{on} - \sigma_{off}) * (\alpha_{on} - \alpha_{off}) \end{aligned} \tag{2}$$

where the third term is a correction for scattering and absorption of interfering gas species as well as the finite difference (due to the on- and off-line wavelength difference) in the average extinction coefficient, α. If care is taken on the choice of wavelengths to avoid interfering gases and the difference between on- and off-line wavelengths is small, then this term is negligible. The second term accounts for an inhomogeneous atmosphere where the backscatter coefficient, β, is different at ranges R_1 and R_2. Assuming a homogeneous atmosphere and a sufficiently small on- and off-line wavelength difference, then this term can be made negligible. The first term is the traditional DIAL equation. Here R_2–R_1 is the range cell defined by the digitization rate of the receiver digitizer. The differential absorption cross section, $\sigma_{on}-\sigma_{off}$, is the difference between the on- and off-line cross sections at the on- and off-line wavelengths. The "ln" term is the ratio of the on- and off-line powers received at either R_1 or R_2 ranges. Kuang [8] gives an example of a typical ozone DIAL analysis for a ground-based system with an aerosol correction procedure.

Figure 2 outlines the characteristics of the DIAL technique. A pulsed laser emits pulses at either the on- or off-line wavelength with a narrow divergence. The range of interest, R, is determined by ct/2 where c is the light velocity and t is the round trip time. At some point in the atmosphere, the laser divergence intersects the receiver field of view and due to atmospheric scattering, receives the power P(r). The range cell is usually set by the digitization rate, for example a rate of 5-MHz results in a 30-m range cell (R_2–R_1). The online

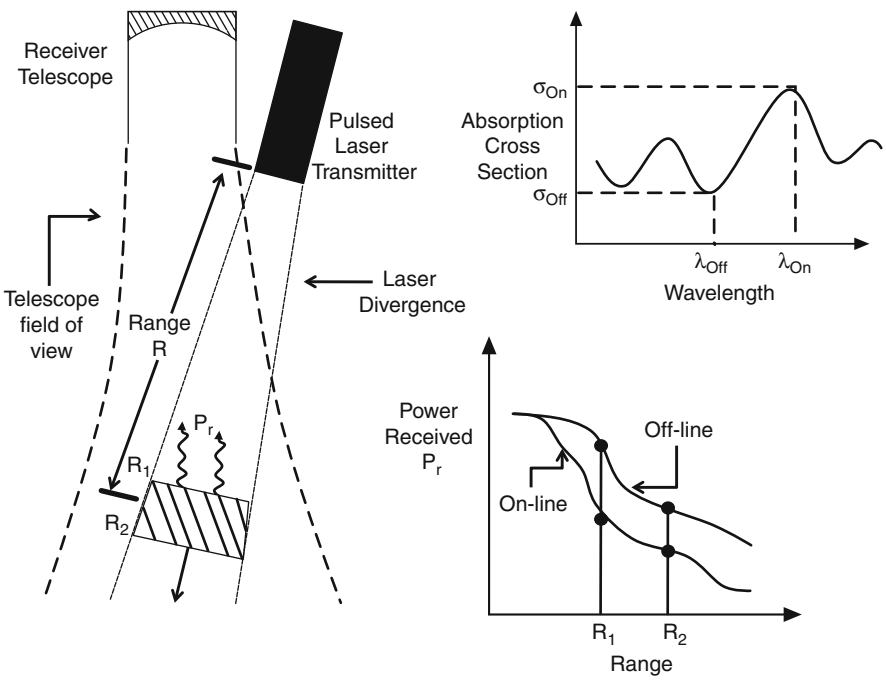

Aircraft and Space Atmospheric Measurements Using Differential Absorption Lidar (DIAL). Figure 2 Characteristics of the DIAL technique

wavelength corresponds to a well-known absorption feature of the particular gas species to be measured. Since the linewidth of the laser has some finite width, care is taken to determine the convolution of the laser linewidth with the absorption linewidth. The off-line is chosen near the online wavelength but in a region where there is no (little) absorption by the gas species of interest. Generally, the on- and off-line pulses are alternating at a repetition rate as high as possible to allow noise reduction by averaging without sacrificing horizontal resolution. The on- and off-line powers at each range cell R_2–R_1 are recorded at the receiver computer for postprocessing into curtain profiles of the particular gas species.

Several examples will now be described that illustrate the power of the DIAL technique to profile the atmosphere for different species from both aircraft and space platforms.

Airborne Ozone DIAL

NASA has a variety of aircraft that are regularly involved in atmospheric research. The most capable aircraft is the NASA DC-8 aircraft shown in Fig. 3, which has flown in research mission all over the world for the past 20 years. The DC-8 carries an ozone or water vapor DIAL system along with a dozen other instruments that probe the atmosphere resulting in a synergistic measurements platform.

Figure 4 shows a schematic of the NASA Langley ozone DIAL system on the DC-8 aircraft. There are two Nd:YAG lasers: one for the online (290 nm) and the other for the off-line (300 nm) wavelength. Each Nd:YAG laser pumps a corresponding dye laser which in turn is doubled into the ultraviolet spectral region at 300 or 290 nm with a pulse repetition rate of 40 Hz each and an on- and off-line separation of 350 μs. The on- and off-line laser pulse energy is split in two: One is transmitted in the zenith and the other in the nadir. As the aircraft flies, ozone profiles from the ground to the aircraft and from the aircraft to the stratosphere are simultaneously recorded. These two profiles can then be spliced together with the aircraft in situ ozone data, resulting in a complete ozone atmospheric profile. The ozone is usually presented in terms of mixing ratio or parts per billion by volume (ppbv). The vertical return signal is averaged to produce a resolution of 300 m and the horizontal resolution is 12 km.

The DIAL technique also has the advantage of retrieving data on clouds and aerosols. The residual dye laser energy at 599 nm (zenith) and at 583 nm (nadir) is vertically polarized and along with the residual 1,064-nm energy is transmitted with the UV ozone wavelengths. The visible wavelengths are received and

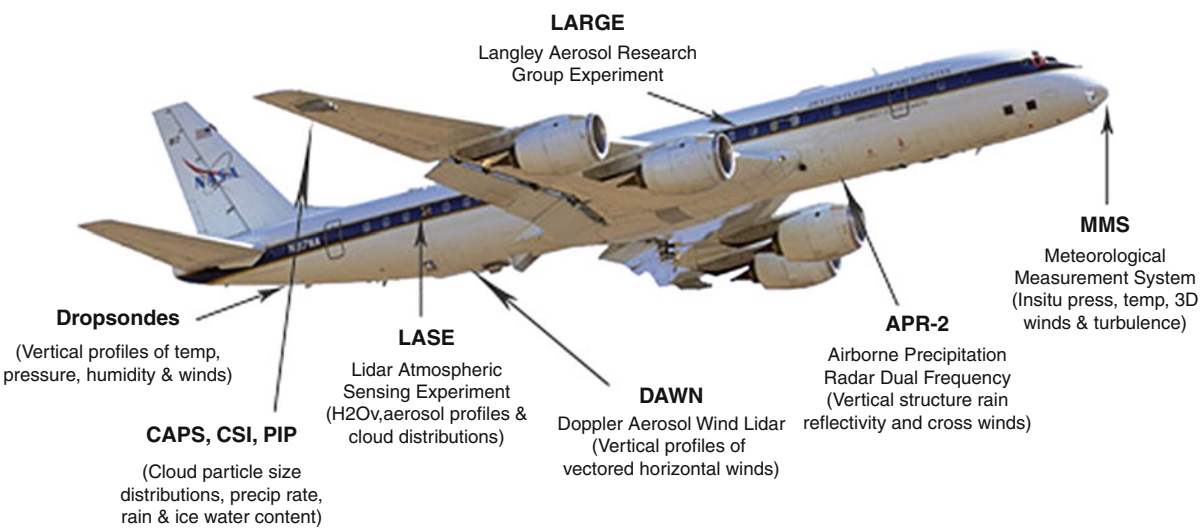

Aircraft and Space Atmospheric Measurements Using Differential Absorption Lidar (DIAL). Figure 3
The NASA DC-8 aircraft with several measurement systems listed including the water vapor DIAL system LASE

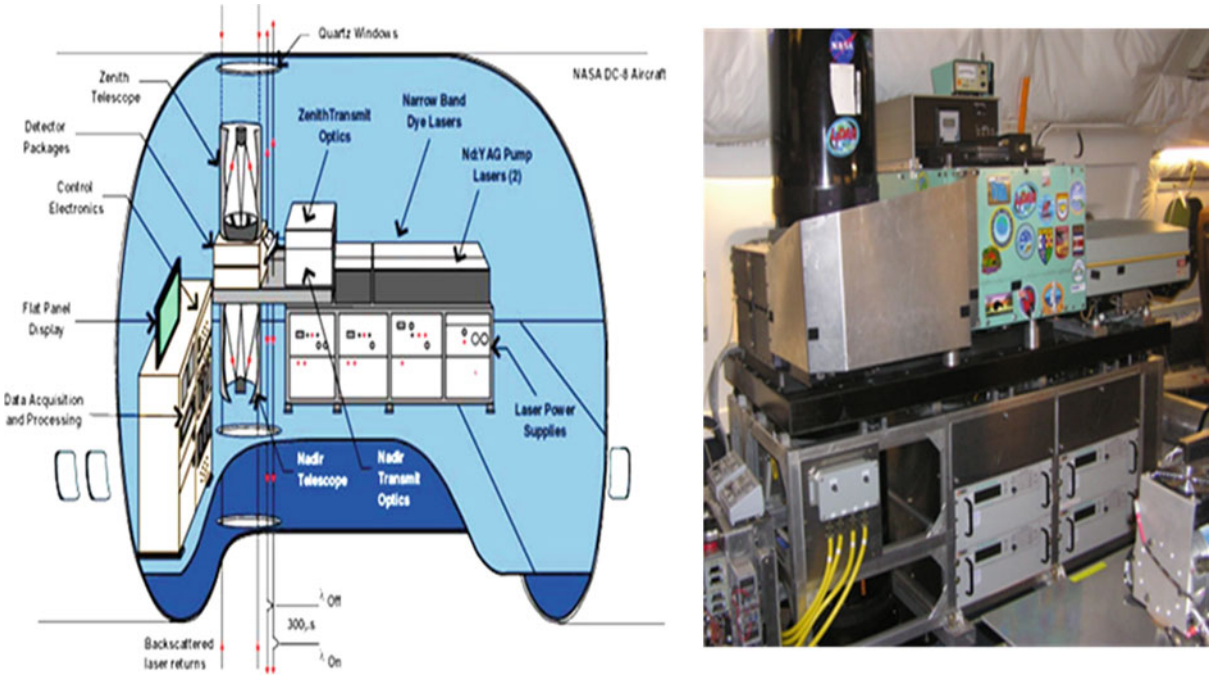

Aircraft and Space Atmospheric Measurements Using Differential Absorption Lidar (DIAL). Figure 4 Schematic and photo of the NASA Langley ozone DIAL system on the DC-8 aircraft

sent through a cross polarizer to determine the percentage of backscattered depolarization. The resolution of the aerosol channel is 60 m in the vertical and 400 m in the horizontal.

An example is given to demonstrate the science derived and the capability of the DIAL technique for measuring atmospheric ozone. This example is from the NASA **A**rctic **R**esearch of the **C**omposition of the **T**roposphere from **A**ircraft and **S**atellites (ARCTAS) mission [9] and presents a complete DIAL data set for flight 15 on June 24, 2008.

Figure 5 shows the 8-h DC-8 flight track around Los Angeles, CA. The corresponding ozone atmospheric profile is shown for the flight track. The ozone concentration, as a function of altitude, is colored and corresponds to an ozone mixing ratio of 0–125 ppbv. This profile is interesting as it shows both stratospheric and boundary layer ozone. In the stratosphere the ozone is typically greater than 2,500 ppbv, so the figure shows the lower edge of the stratospheric ozone layer that protects life from harmful UV exposure from the Sun. The dynamics of the stratospheric/tropospheric boundary cause ozone filaments to bleed into the troposphere at 12 km as shown in the figure. The ground profile is shown in kilometers above sea level and in the mountains north of Los Angeles high ozone concentrations are observed. At the flight time, there were numerous fires in the mountain region generating both aerosols and ozone. Ozone concentrations above 100 ppbv are measured and seen to transport out into the Pacific Ocean where the ozone decreases as the flight track moves northwest. While this ozone was generated in remote areas, the ozone generated in urban areas as a result of anthropogenic emissions can have severe health effects especially above background levels of 40 ppbv (U.S. EPA primary ozone standard is 75 ppb) and DIAL has the ability to measure the atmospheric distribution of this ozone. Likewise, stratospheric ozone has been measured especially with regard to stratoshperic depletion in Antarctica due to chlorofluorocarbon emissions.

The residual laser energy at 1,064 and 591 nm (average of the two dye laser wavelengths) is transmitted along with the DIAL UV wavelengths to probe the aerosol distribution above and below the aircraft. If the aerosol size parameter $2\pi r/\lambda < 1$, where r is the aerosol radius

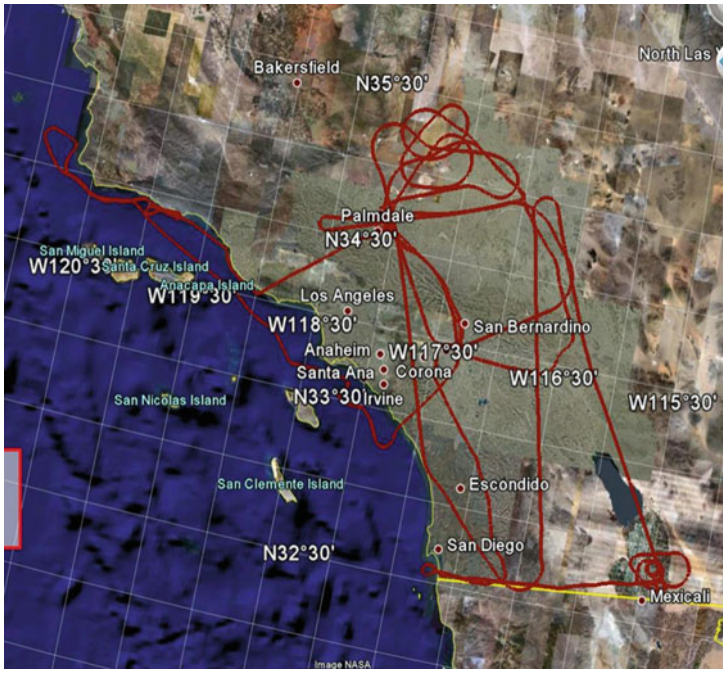

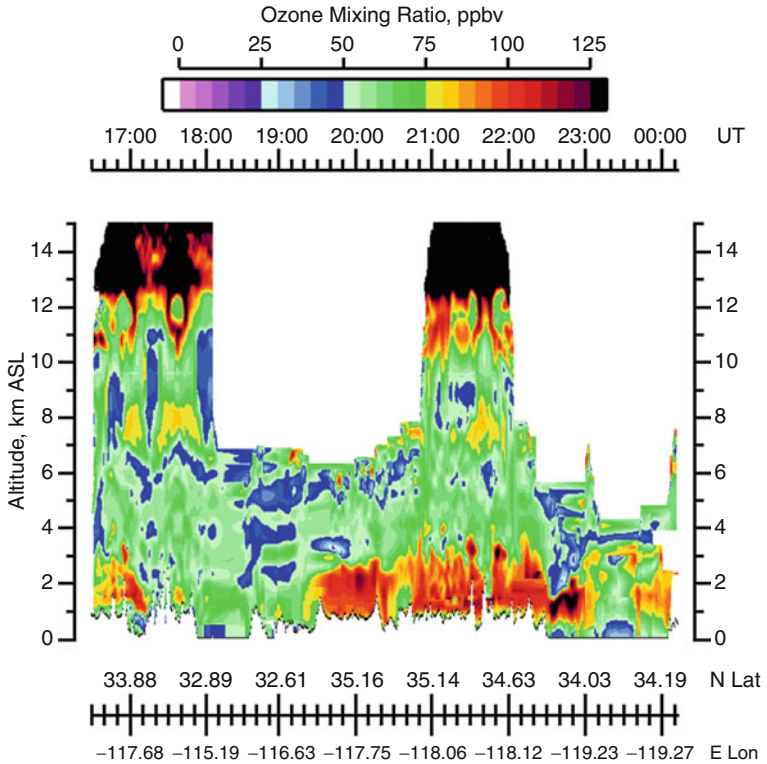

Aircraft and Space Atmospheric Measurements Using Differential Absorption Lidar (DIAL). Figure 5
The aircraft flight plan for ARCTAS campaign on June 24, 2008 and the corresponding DIAL ozone atmospheric profile in parts per billion by volume

and λ the lidar wavelength, then large backscattering occurs. The 1,064- and 591-nm wavelengths probe different aerosol size distributions. Figure 6 shows the aerosol backscattering ratio at both 1,064- and 591-nm wavelengths as a function of altitude. This ratio is the backscatter at either wavelength to the molecular atmospheric backscatter at the pressure altitude. If the ratio is zero, then there is no aerosol scattering, only

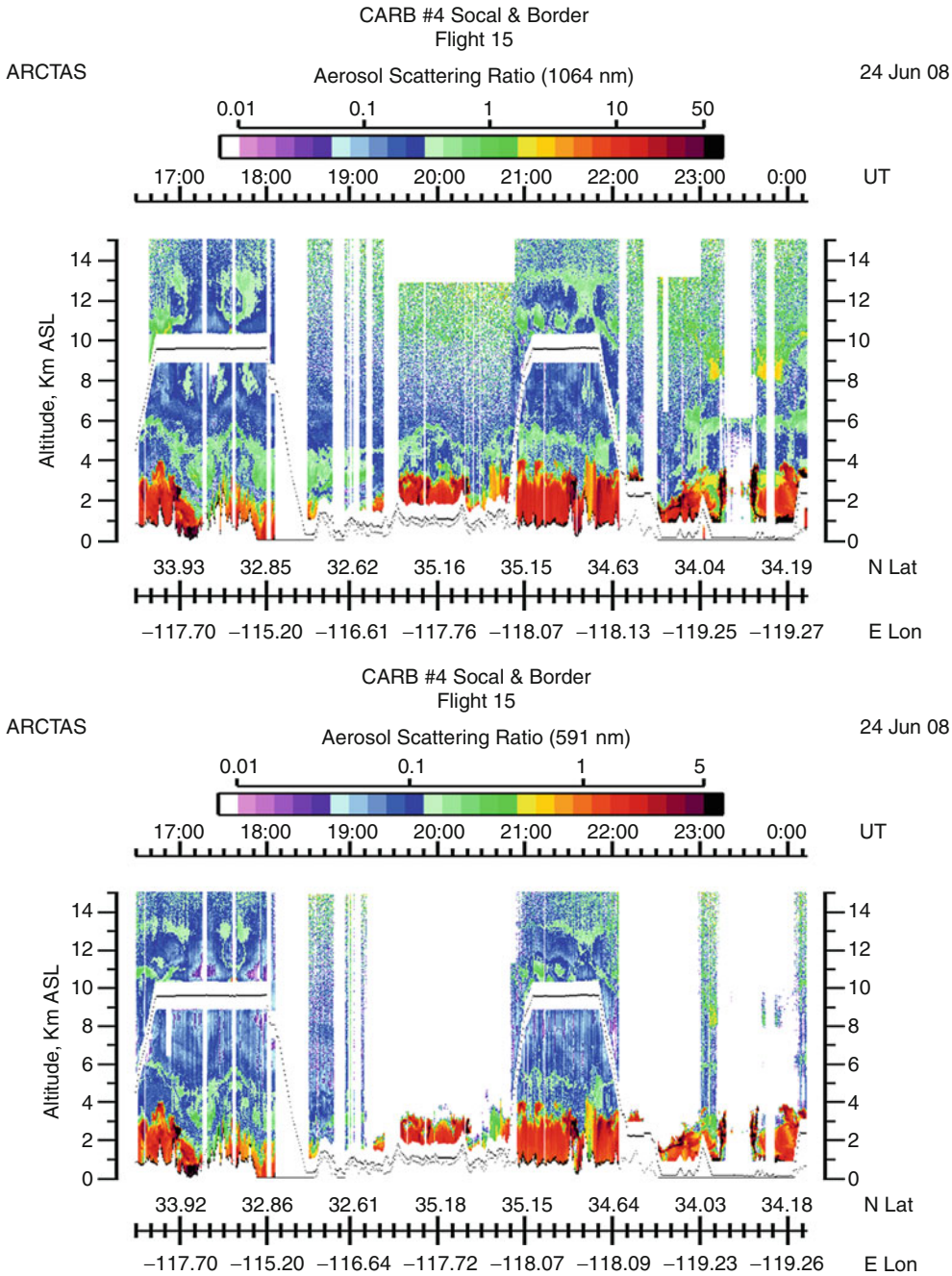

Aircraft and Space Atmospheric Measurements Using Differential Absorption Lidar (DIAL). Figure 6
The aerosol scattering ratio for 1,064 and 591 nm (average of the dye laser wavelengths) as a function of altitude. The ground profile above sea level is noted as well as the aircraft flight track

molecular scattering. Most of the aerosol backscattering occurs near the ground which is the atmospheric source of aerosols. In the figure, high aerosol scattering occurs near the fire sites in the mountains but aerosols are also transported out over the ocean (at times past 22.50 UT) where they are hydrated by moisture and thus grow in size producing greater backscatter. It is interesting to note that there are no clouds detected in the profile, yet nowhere in the atmosphere is there pure molecular scattering. This has implications for climate change as aerosols can either reflect or absorb incident energy, affecting the energy balance of the global atmosphere.

The aerosol wavelength dependence (color ratio) is shown in Fig. 7. The color ratio is the ratio of 1,064 to 591-nm backscattering and gives an indication of relative aerosol size with larger ratios indicating larger aerosols. As seen during the flight time of 21:00–22:00, finer particles are emitted by these fires but as they rise they grow in size, probably due to hydration. The aerosols also tend to grow in size as they transport over the ocean after time 22:30.

Figure 7 also shows the aerosol depolarization at 591 nm derived from the aerosol scattering ratio. The laser is linearly polarized as it is transmitted into the atmosphere and two receiver channels are used to detect the atmospheric return, one capturing the linear polarized return and the other the orthogonal or depolarized return signal. The ratio of the depolarized signal to the transmitted linear polarized signal is the aerosol depolarization. Spherical aerosols backscatter light with little polarization change, but nonspherical aerosols generally depolarize the backscatter signal depending on their shape [10]. Thus, the depolarization gives some information on the structure and shape of the atmospheric aerosols and can distinguish between liquid and solid phase aerosols. In the figure, the depolarization measured was generally between 3% and 9%. The fires at 17:00 UT appear to contain less dust (less depolarization) than fires at 21:00–22:00 UT, where the depolarization is higher, indicating the fires there lifted more dust into the fire plume.

This example of the DIAL technique for measuring ozone demonstrates the utility of DIAL. Here both the stratospheric and tropospheric ozone concentration can be determined simultaneously. Further the residual laser energy of the dye lasers is used to probe the aerosols at 591 and 1,064 nm, showing the importance of aerosols in the boundary layer as well as aerosol transport in the troposphere. This example shows the importance of measuring both ozone and aerosols simultaneously.

The ozone absorption cross section is broad in the ultraviolet spectral region (250–320 nm), allowing many different wavelength on- and off-line pairs to be used. Absorption cross section for ozone and a number of atmospheric gases of interest for atmospheric chemistry are shown by Schoulepnikoff [11]. For the stratosphere where ozone density is large, wavelength pairs near 320 are used in order to generate a significant return signal. Whereas in the troposphere where the ozone mixing ratio is lower, higher absorption is needed, thus wavelength pairs from 280 to 300 are used.

Airborne Water Vapor DIAL

Atmospheric water vapor is the most radiatively active gas in the atmosphere and as a result affects weather patterns, precipitation, clouds, and hurricanes. Water vapor and ozone affect the production of OH radicals which help determine tropospheric chemistry. At high relative humidities, aerosols grow hydroscopiclly and in turn reduce visibility. Water vapor has very high temporal and spatial variability in the atmosphere and radiosonde or space–based satellite passive instruments cannot fully characterize the global variability. Airborne and eventually space–based water vapor DIAL systems could characterize the water vapor distribution for climate change and real-time weather forecasting by providing high vertical and horizontal profiles of water vapor distributions for input into climate models. Like ozone DIAL, a water vapor DIAL system can also measure clouds and aerosols, which significantly improves our understanding of water vapor distribution dynamics. Clouds and aerosols are currently the largest source of uncertainty in global climate models and both play a major role in atmospheric chemistry.

Figure 8 shows a schematic and photo of the Laser Atmospheric Sensing Experiment (LASE) water vapor DIAL system on the NASA DC-8 aircraft. The LASE system uses a Ti:sapphire–based laser transmitter [12]. This laser is a 5-Hz double-pulsed (300-μs separation)

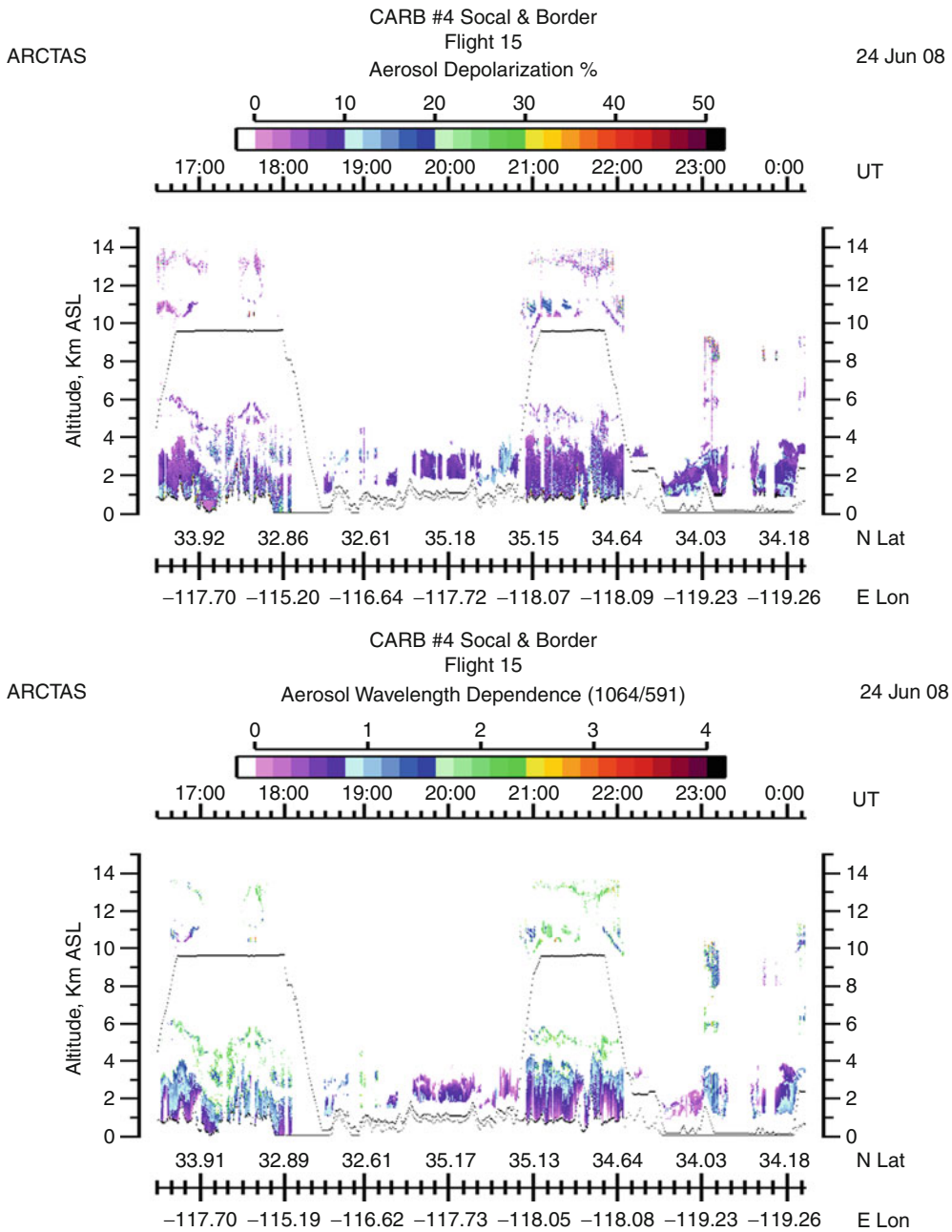

Aircraft and Space Atmospheric Measurements Using Differential Absorption Lidar (DIAL). Figure 7
The percent aerosol depolarization and the ratio of 1,064–591 nm backscatter is shown as a function of altitude

Ti:sapphire laser that operates on the 817.2213-nm (vac) absorption line of water vapor and is pumped by a frequency-doubled flashlamp-pumped Nd:YAG laser. The laser wavelength is varied along the water vapor absorption line to create an on- and off-line DIAL wavelength pair. LASE can operate over two or three water vapor concentration regions to cover a large altitude region (dynamic range) in the troposphere. This unique method of operation permits rapid and more flexible absorption cross-section selection

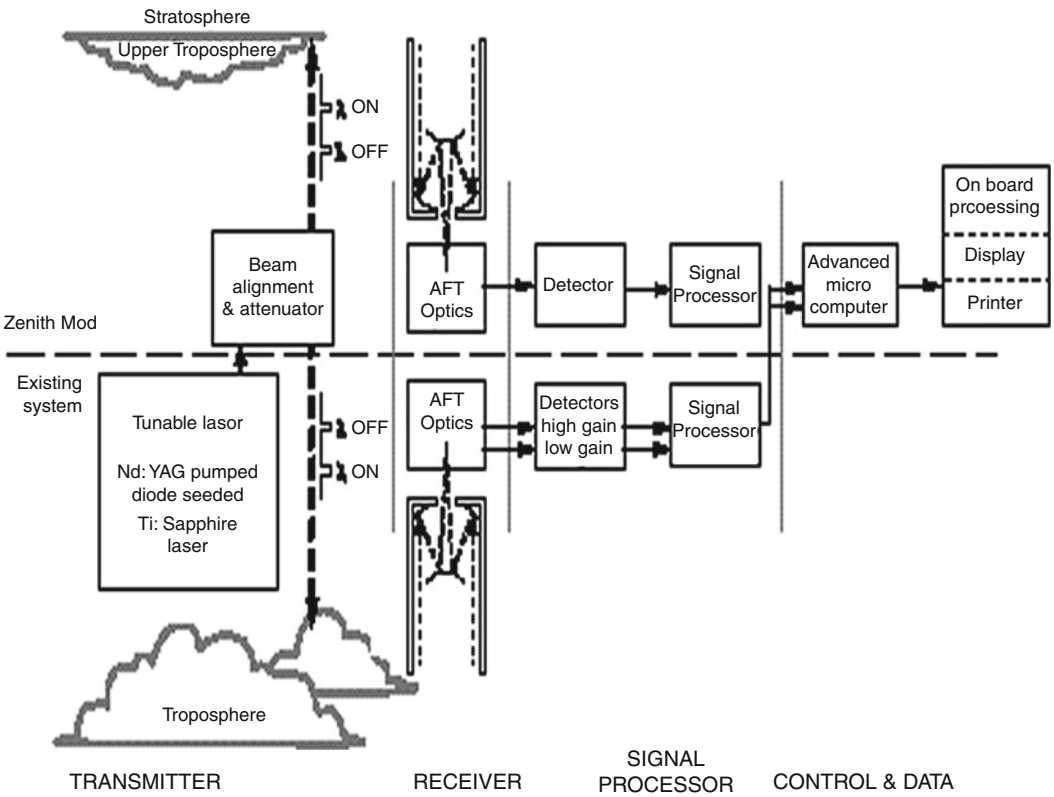

Aircraft and Space Atmospheric Measurements Using Differential Absorption Lidar (DIAL). Figure 8
The Laser Atmospheric Sensing Experiment (LASE) water vapor DIAL system schematic and photo of instrument on the NASA DC-8 aircraft

capability for water vapor measurements over the entire troposphere in a single pass. The off-line wavelength is used to measure the aerosol scattering ratio and is selected for minimum absorption by water vapor. The wavelength of the laser is controlled by diode laser injection seeding that is frequency locked to the water vapor line using a water vapor absorption cell. The laser linewidth is less than 0.25 pm and the line stability is approximately 0.35 pm, much less than the pressure broadened atmospheric water vapor linewidth. The pulse energy ranges from 75 to 100 mJ and approximately 60% of the energy is transmitted in the nadir direction and 40% in the zenith direction. The beam divergence is typically 1 mrad and the telescope field of view is 1.5 mrad. The detector system consists of two silicon avalanche photodiodes (Si:APD) and three digitizers to cover a large signal dynamic range (10^6). The data system on the DC-8 will enable real-time and postflight analyses onboard the aircraft.

Atmospheric water vapor profiles are taken during night or day with a vertical resolution of 330 m and horizontal resolution of from 14 to 42 km. The aerosol resolution is 30 m in the vertical and 200 m in the horizontal. The accuracy of the water vapor measurement is 6% or 0.01 g/kg whichever is greater. The atmospheric in situ water vapor aircraft data can be spliced into the LASE DIAL data to produce a complete water vapor profile throughout the troposphere.

Figure 9 is a profile example from the Genesis and Rapid Intensification Processes (GRIP) DC-8 aircraft campaign from August 15 to September 30, 2010 [13]. This flight segment took place east of Denver, CO over a relatively flat agriculture area. In the figure, the boundary layer is shown below 2 km containing significant amounts of water vapor. Above the boundary layer the air mass is quite dry. Back trajectories have determined that this air mass came from the California fires occurring at that time, thus there is enhanced backscattering from smoke particles at 5 km. The aerosol scattering ratio is increased at the top of the boundary layer due to absorption of water by the aerosols, increasing their size, thus producing this thin layer of enhanced backscattering.

Figure 10 outlines the analysis process by which the DIAL raw data is transformed into useful data products [14]. The atmospheric return signals are combined with ground elevation data and DC-8 navigation and in situ water vapor data to create a composite water vapor return. There are three wavelength on- and off-line pairs used for different atmospheric water absorption conditions as well as three amplifier gains to increase the measurement dynamic range. This data is used to create an initial DIAL calculation for water vapor and also relative aerosol backscatter. Temperature, pressure, and relative humidity data from radiosondes on the DC-8 are used to calculate the effect of temperature and pressure on water vapor line boarding as well as aerosol scattering. The nadir and zenith profiles are combined with in situ water vapor data to produce a complete water vapor profile of the troposphere. The aerosol scattering analysis is done in an iterative process to create the aerosol scattering ratio with water correction.

Space-Based DIAL

Currently there are no space deployed Earth orbiting DIAL systems. There are simpler backscatter Earth orbiting lidar systems to measure clouds and aerosols. The first of these was the Laser In-space Technology Experiment (LITE) which flew for 10 days on the Space Shuttle in 1994 [15]. This backscatter lidar used a flashlamp-pumped Nd:YAG laser with nonlinear conversion into 532 and 355 nm laser emission. Three beams were transmitted (1,064, 532, and 355 nm) and provided the first highly detailed global view of the vertical structure of clouds and aerosols from the surface through the middle stratosphere. The complexity of deploying a lidar in space is a daunting challenge and LITE performed extremely well demonstrating the utility of backscatter lidars in space even though its deployment was very short.

Another space-based lidar was the Ice Cloud and land Evaluation Satellite (ICESat) which was launched in 2003 and decommissioned in 2010 [16, 17]. The ICESat mission was designed to provide elevation data needed to determine ice sheet mass balance as well as cloud property information, especially for polar stratospheric clouds and aerosols. It provided topography and vegetation data around the globe, in addition to the polar-specific coverage over the Greenland and Antarctic ice sheets. It also provided planetary boundary layer heights which is an important parameter linking the surface to atmosphere dynamics, especially

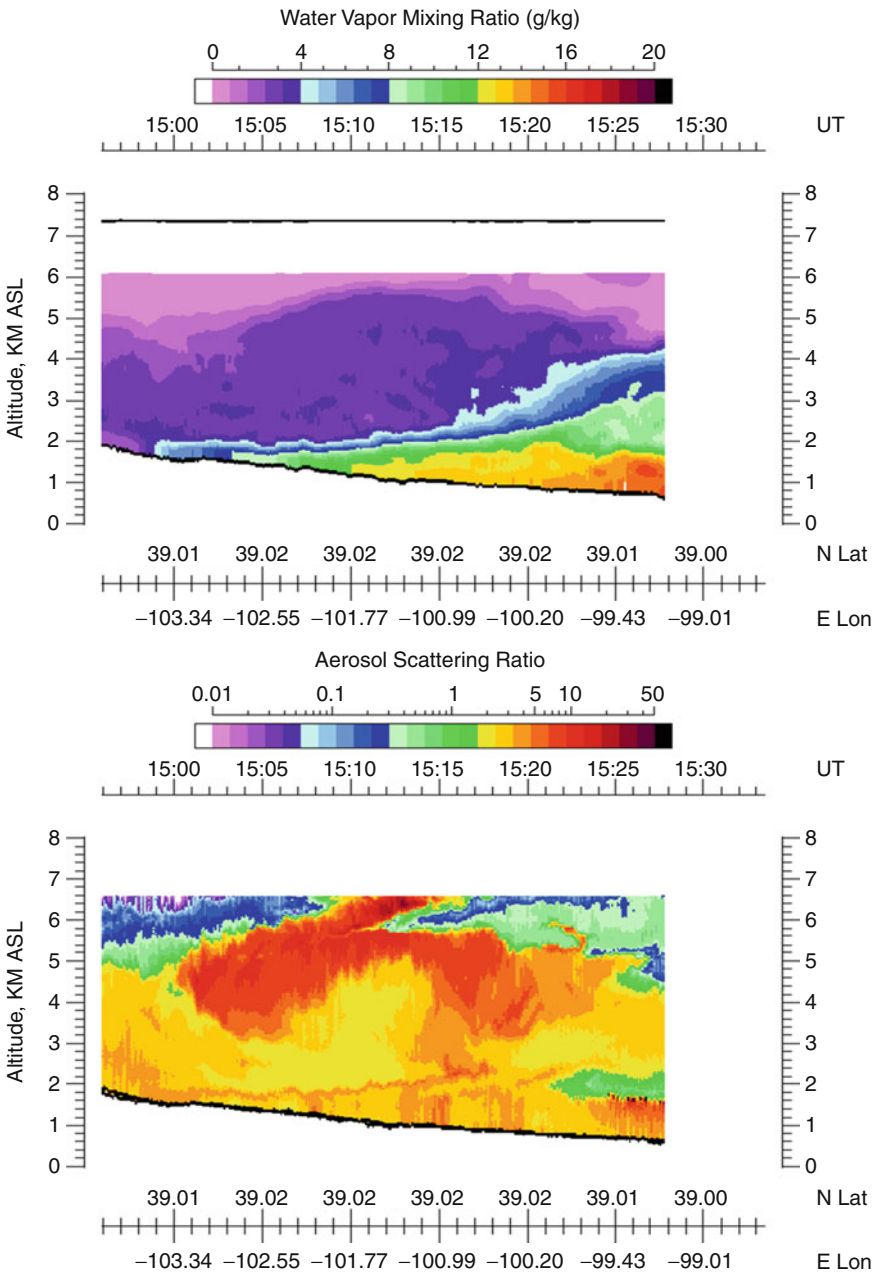

Aircraft and Space Atmospheric Measurements Using Differential Absorption Lidar (DIAL). Figure 9 Water vapor mixing ratio and the corresponding aerosol scattering ratio during the GRIP campaign [12]

over the world's oceans. The satellite combined a precision surface lidar with a sensitive dual-wavelength cloud and aerosol lidar. The lasers emitted infrared and visible laser pulses at 1,064 (75 mJ) and 532 (35 mJ) nm wavelengths using three identical diode-pumped Nd: YAG lasers (6-ns TEM00 spatial mode). The repetition rate was 40 Hz. There was a 1-m diameter beryllium telescope used in the receiver. As ICESat orbited, the laser produced a series of approximately 70-m diameter laser spots that are separated by nearly 170-m along the spacecraft's ground track. Aerosol data could also be retrieved.

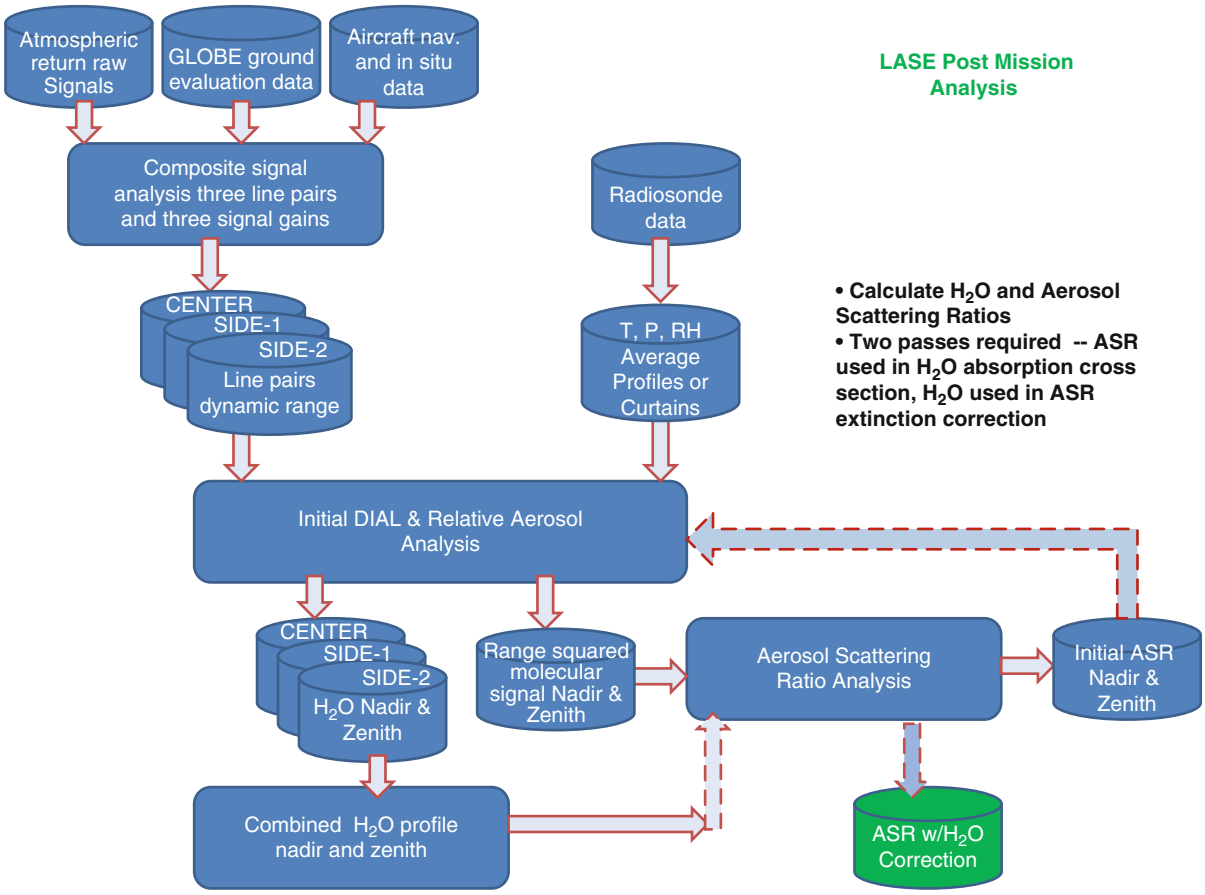

Aircraft and Space Atmospheric Measurements Using Differential Absorption Lidar (DIAL). Figure 10
The analysis by which the DIAL raw data is transformed into useful data products

ICESat was a major step forward for space-based lidars. It lasted for some 5 years and used diode laser pumping of the Nd:YAG laser transmitter. This is the only technique that can achieve the electrical-to-optical conversion to make space lasers practical. It was also low voltage technology minimizing corona discharge due to high voltage. It demonstrated the flexibility of taking multiple science measurements such as ice sheet height, cloud heights, atmospheric boundary layer height, and aerosol concentrations. It could be operated autonomously in the radiation and vacuum environment of space for many years until the pump diodes and other components eventually degraded. All this capability is directly related to future DIAL systems deployed in space.

The only current operational lidar satellite in orbit is the Cloud-Aerosol Lidar and Infrared Pathfinder Satellite Observations (CALIPSO) carrying a backscatter lidar instrument as shown in Fig. 11 [18]. The satellite was launched in 2006 to an orbit altitude of 705 km and after 5 years is still operational, gathering global data on clouds and aerosols.

The Nd:YAG laser transmitter has two wavelengths 1,064 and 532 nm each transmitting 110 mJ, 20-ns linearly polarized laser pulses. The 532-nm channel can measure depolarization with a polarization beam splitter resolving parallel and perpendicular return signal components. The repetition rate is 20.16 Hz. The beams form a footprint of 70-m diameter with 335-m spacing between footprints. The receiver telescope is 1-m diameter with a field of view of 90 m on the surface. Aerosol profiles can be retrieved from 40-km altitude to the surface with 60-m vertical and 5-km horizontal resolutions.

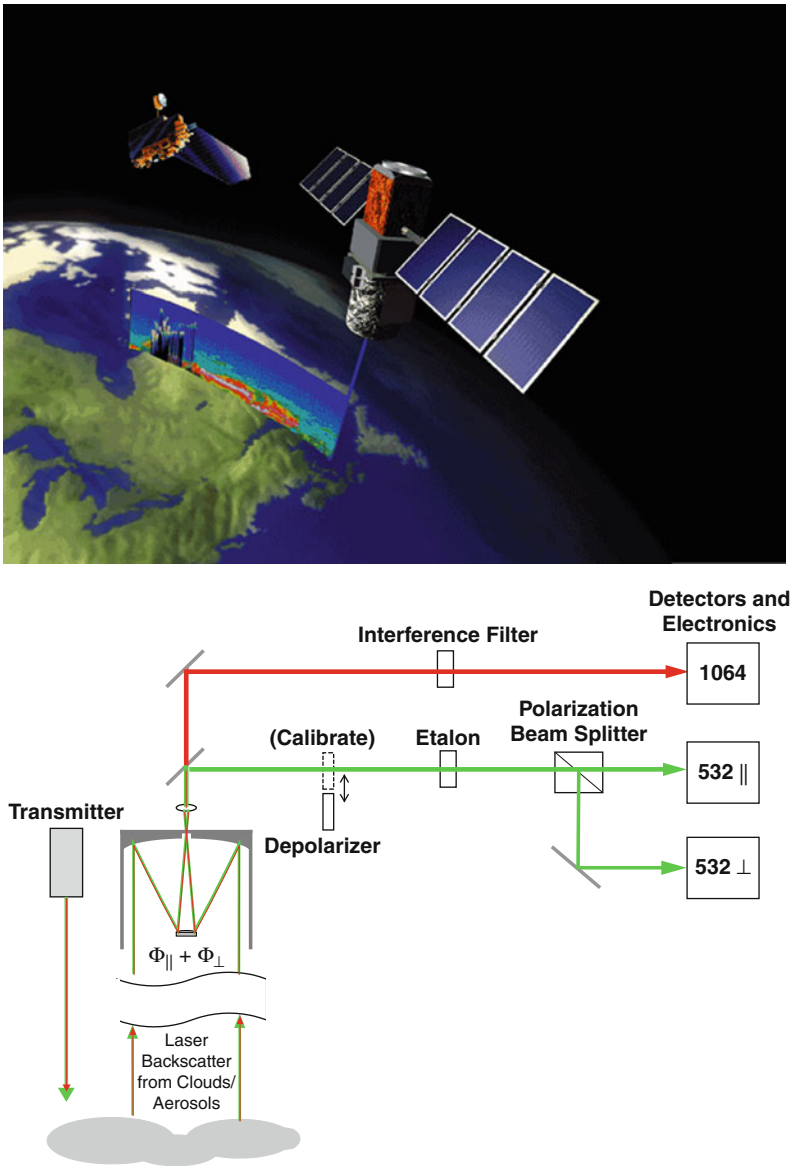

Aircraft and Space Atmospheric Measurements Using Differential Absorption Lidar (DIAL). Figure 11
The CALIPSO satellite showing a typical cloud and aerosol lidar retrieval. Also a schematic of the lidar optical system

CALIPSO is providing the first multiyear global dataset of lidar aerosol and cloud profiles. Figure 12 is an example of one flight track on July 16, 2009 over the African Continent. The insert shows the orbit track from north to south. The aerosol and cloud 532-nm profile moves from left to right. CALIPSO has the ability to identify broad groups of aerosol types. In the upper left are aerosols emitted from volcanoes and in the center dust plumes are seen. Near the coast of Africa, biomass burning is taking place and smoke plumes are noted near 3-km altitude. Over the ocean, clouds are forming at the top of the boundary layer. A space–based DIAL system would acquire aerosol and cloud data very similar to these CALIPSO results.

Two future lidar missions are planned by the European Space Agency the ADM-Aeolus [20] (launch 2013) and Earthcare [21] (launch 2016) satellites. The aim of the Atmospheric Dynamics Mission

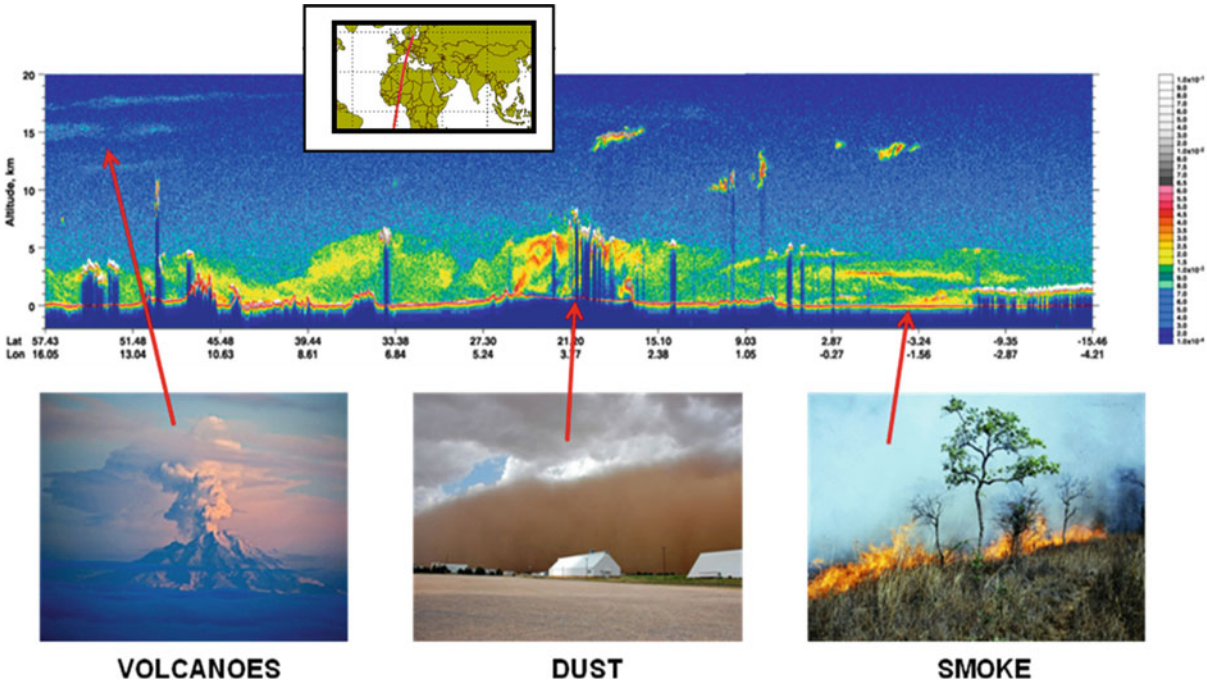

Aircraft and Space Atmospheric Measurements Using Differential Absorption Lidar (DIAL). Figure 12
CALIPSO image shows 532-nm attenuated backscatter profiles from 16 July 2009 (~01:35 UTC until ~01:55 UTC) [19]

(ADM-Aeolus) is to provide global observations of three-dimensional wind fields, which will improve current wind-profiling atmospheric modeling, operational weather forecasting, and climate research. ADM-Aeolus satellite (400-km sun synchronous) will gather data by the active doppler wind lidar (DWL) method, whereby laser (Aladin-Atmospheric LAser Doppler INstrument) pulses are transmitted in the atmosphere and then measure the backscattered Doppler shift of the received return signal, creating a wind profile showing the relative strength and direction of winds at different altitudes, as well as moisture and aerosol levels in the atmosphere. Wind speeds will be measured in the boundary layer (1-m/s resolution), in the free troposphere (2-m/s) with average wind velocities over 50-km tracks and 120 profiles per hour. The diode-pumped Nd:YAG laser is frequency tripled to 355 nm at 150-mJ pulse energy, 100-Hz pulse repetition rate, and 30-MHz laser linewidth (tunable over 10-MHz). The receiver has a Mie channel (aerosol and water droplets) with Fizeau spectrometer, and a Rayleigh channel (molecular scattering). The telescope is 1.5-m diameter.

The EarthCARE satellite (Earth Clouds, Aerosols, and Radiation Explorer) is a joint European-Japanese mission addressing the need for better understanding of the interactions between cloud, radiative and aerosol processes that play an important role in climate change by acquiring vertical profiles of clouds and aerosols, as well as the radiances at the top of the atmosphere. Cloud feedbacks are the main cause of uncertainty in predictions of future climate, and correct representation of clouds, aerosols, and radiation processes in models is needed. Current knowledge of the global profiles of aerosol and cloud properties is far too limited and the required profiles can only be provided by the high spectral resolution lidar. EarthCARE has been defined with the specific scientific objectives of quantifying aerosol-cloud-radiation interactions so they may be included correctly in climate and numerical weather forecasting models by providing:

- Vertical profiles of natural and anthropogenic aerosols on a global scale, their radiative properties and interaction with clouds.

- Vertical distribution of atmospheric liquid water and ice on a global scale, their transport by clouds and radiative impact.
- Cloud overlap in the vertical, cloud-precipitation interactions and the characteristics of vertical motion within clouds.
- The combination of the retrieved aerosols and cloud properties to derive the profile of atmospheric radiative heating and cooling.

The Atmospheric Lidar (ATLID) on the satellite is a high-spectral resolution with depolarization lidar system. The Nd:YAG laser produces 355-nm pulses at 30 mJ and a repetition rate of 74 Hz. High spectral purity demands a 50-MHz linewidth and stability of 50 MHz over a 1 month time in order to separate the Mie (100-m resolution) and Rayleigh (300 m) scattering atmospheric contributions by the high spectral resolution technique.

These backscatter lidar systems add to the technology base required by future space DIAL systems. The LITE system demonstrated that valuable aerosol and cloud data could be obtained from space. The ICESat mission used diode laser pumping, allowing efficient long-term lidar measurements from space. The CALIPSO mission is currently providing important long-term information on aerosols and clouds for climate models. In the future, ADM-Aeolus and ATLID EarthCARE missions will use large receiver telescopes and laser line narrowing techniques required to spectrally resolve atmospheric species by the DIAL technique for future missions.

While the DIAL technique is most often considered for measuring Earth's atmosphere, it could also be used for other planetary atmospheres such as Mars. A small lander could measure the water vapor concentration of the Mars atmosphere to help in the search for water-based life as life, as known on planet Earth, requires water. Although the atmospheric concentration of water vapor is very low, there is still sufficient vapor to form hazes, ground fog, frost, and clouds. An exchange of water vapor exists between the ice cap at the northern pole and the atmosphere. The DIAL technique could be utilized to measure the processes that determine the distribution of water vapor and thus indicate where sources and sinks of water vapor exist. This could then lead to sites where life on Mars might be found.

Figure 13 shows a Tm:germanate fiber laser, tunable around 1.9 μm, which when coupled to a low mass lidar receiver, can fulfill the requirements for a water vapor Mars DIAL system. Laser diodes are used to pump a Te:germanate fiber that lases on a water vapor absorption line near 1.9 μm. The DIAL system is very compact and low mass yet capable of measuring the water vapor profile up to about 6 km. Figure 14 shows the pulsed laser energy as a function of laser diode pumping current. The on- and off-line wavelengths are indicated where the online experiences more atmospheric absorption than the off-line wavelength. Such small systems could easily be packaged and deployed at multiple locations to profile the planetary water vapor distribution [22, 23].

Future Directions

Ground- and aircraft-based DIAL systems are now in regular use profiling many atmospheric species as well as clouds and aerosols [24]. The open question is when and how will the DIAL technique be deployed in space for global Earth and other solar system bodies atmospheric observations. The CALIPSO lidar system cost about $300 million (FY 06 dollars) including launch, thus a DIAL system deployed in space would cost over $1 billion due to its increased complexity when compared to a backscatter lidar such as CALIPSO.

A number of studies have been published describing concepts and characteristics of space deployed DIAL systems for ozone [25] and water vapor [26, 27]. A concept for a space–based ozone DIAL system called ORACLE would deploy a UV DIAL system at 400 km with a laser pulse energy of 500 mJ and on- and off-line wavelengths of 308 and 320 nm, respectively. The ORACLE system would measure a single species, ozone, as well as clouds and aerosols. The receiver would have a 4.5 m^2 telescope. For daytime operation, the ozone concentration error would be ~10% for altitudes between 5 and 45 km. Such studies demonstrated the utility as well as technology progress needed to deploy an ozone DIAL system in space.

With such a large investment in a space–based DIAL system, there would be a need to profile many different atmospheric species, some not recognized as important today for both air quality and global climate

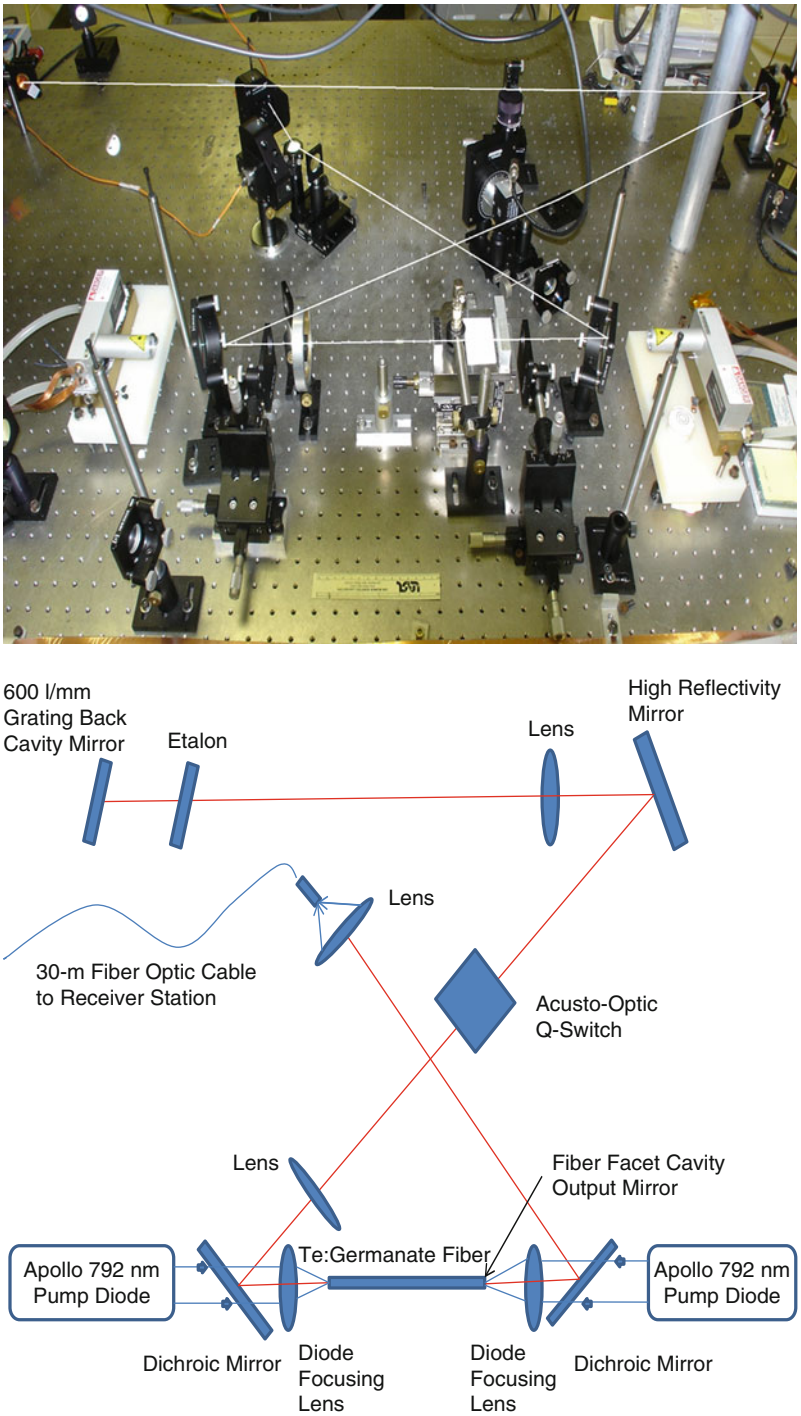

Aircraft and Space Atmospheric Measurements Using Differential Absorption Lidar (DIAL). Figure 13
Schematic and photo of the Tm:germanate fiber laser transmitter

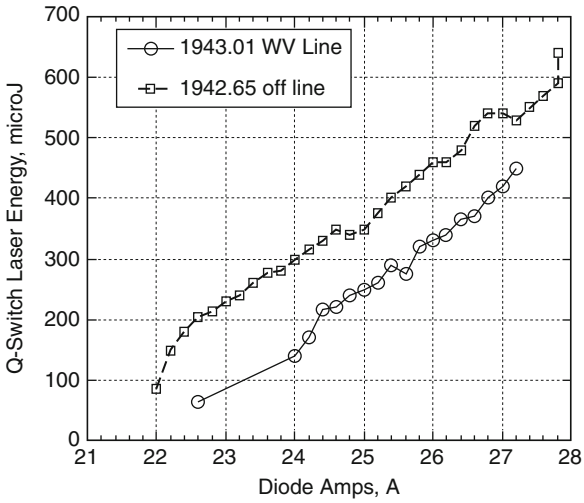

Aircraft and Space Atmospheric Measurements Using Differential Absorption Lidar (DIAL). Figure 14
Pulsed laser output vs. pump diode current

change applications. In this concept, the DIAL system would rapidly tune to several different online wavelengths corresponding to the species of interest in the present atmospheric campaign. Thus the species involved in the major atmospheric chemical reactions would be profiled and then would be used to initialize global chemical weather models. The off-line wavelength would be used, as it is presently, to profile clouds and aerosols. The laser transmitter would need to be reliably tuned to any online wavelength with narrow linewidth and broad tuning range to cover all molecular species of interest.

The DIAL laser transmitter would need to operate in the infrared spectral region from about 1 to 5 μm where there are many molecular absorption lines available for almost all atmospheric species of interest. The laser (orbit altitude 350–400 km) would need to generate 10-Hz pulse pairs at from 0.5 to 1.0-J energy per pulse. The receiver telescope would need to be about 5 m in diameter and the receiver optical system would need to be ~70% efficient [28]. Avalanche photo detectors (APDs) such as the HgCdTe are being developed which can photon count the return signal. Such a DIAL system could typically profile atmospheric ozone with horizontal resolution of 200 km, a vertical resolution of 2 km with 10% measurement accuracy. This would allow adequate profiling of regional and continental scale processes.

Future space–based DIAL systems will be driven by the science requirements that are related to the open questions with regard to climate change [29] and air quality [30, 31]. An example of how the above multiwavelength space–based DIAL system could impact an air quality global pollution field campaign can be demonstrated using the International Global Atmospheric Chemistry (IGAC) Lagrangian 2 K4 campaign [32]. In this field campaign, several aircraft were used to measure in situ concentrations of ozone, carbon monoxide, volatile organic compounds, NO_x ($NO + NO_2$), and NO_y (mainly in the form of PAN) created from Alaskan forest fires in 2004 and transported to Europe. These fires create polluted plumes that undergo chemical evolution and mixing with air masses of different origin such that their chemical composition can radically change. Ozone levels in such polluted plumes are of interest since it is a major health concern and also a major source of the OH radicals (most efficient cleansing agent in the atmosphere). Ozone is mainly produced by reactions involving oxidation of volatile organic compounds (VOCs), and carbon monoxide (CO) in the presence of nitrogen oxides ($NO_x = NO + NO_2$), and mainly destroyed by reactions involving water vapor and HO_x radicals. This long-range biomass burning plume was sampled in the troposphere over North America, the North Atlantic, and over Europe by three different aircraft. A photochemical trajectory model was used to examine the chemical processes responsible for the plume evolution. Six day modeled concentrations of O_3, CO, NO_y, NO, PAN, H_2O and temperature were compared to sparse in situ concentration measurements.

While campaigns such as the above are very costly and very infrequent, an orbiting IR tunable DIAL system could measure all the species giving a three-dimensional profile of the plume as it was transported toward Europe. The ability to accurately profile the chemical change as the plume aged demonstrates the unique and powerful ability to understand with high-resolution atmospheric chemical weather. Figure 15 shows the most important atmospheric molecular species to be profiled by DIAL and the corresponding need to measure these species [33–35].

Molecular Species	Measurement Need			
	Air quality	Oxidation efficiency	Climate	Stratosphere ozone depletion
O_3 (ozone)	■	■	■	■
CO (carbon monoxide)	■	■		
j (NO_2)	■	■		
j (O^1D)	■	■		
H_2O (water vapour)	■	■	■	■
HCHO (formaldehyde)	■	■		
VOCs (volatile organic compounds)	■	■		
Active nitrogen: NOx = NO + NO_2	■	■		■
Reservoir species: HNO_3	■	■	■	■
N_2O			■	
SO_2	■		■	
Active halogens: BrO, ClO, OClO				■
Reservoir species: HCl, $ClONO_2$				■
CO_2			■	
CH_4		■	■	■
OH	■			

Aircraft and Space Atmospheric Measurements Using Differential Absorption Lidar (DIAL). Figure 15 Important atmospheric molecular species that could be measured from space using DIAL and the corresponding measurement needed to profile these species

An IR tunable DIAL system could potentially measure all these species from space producing a three-dimensional profile of the chemical evolution and transport of these species with high spatial and temporal resolution.

As interest in transport of atmospheric pollution species and associated pollution species precursors increases, there may develop a need to monitor fluxes of these atmospheric species as they are transported across national boundaries. As noted above, the ADM-Aeolus satellite will have a lidar capable of measuring wind velocities as a function of altitude. This measurement can be combined with the IR DIAL space-based system resulting in the determination of molecular fluxes (#/cm^2-s) across national boundaries for regulatory and health monitoring purposes.

Differential absorption lidar systems have been deployed on the ground in aircraft and eventually in space. The essential components of a space–based DIAL system are now in place; efficient diode-pumped solid-state lasers, high pulse energy, narrow linewidth emission, large telescopes, autonomous operation, and radiation resistant long life operation. While more research needs to be invested in infrared tunable DIAL laser transmitters, nevertheless the ultimate utility of DIAL systems will be demonstrated in space deployed atmospheric measurement systems generating high spatial and temporal resolution atmospheric molecular profiles for chemical weather and health monitoring.

Bibliography

1. Browell EV, Carter AF, Shipley ST, Allen RJ, Butler CF, Mayo MN, Siviter JH, Hall WM (1983) NASA multipurpose airborne DIAL system and measurements of ozone and aerosol profiles. Appl Optics 22:522–534
2. Browell EV, Browell EV (1983) In: Killinger DK, Moorradian A, Killinger DK, Moorradian A (eds) Optical laser remote sensing. Springer, New York, pp 138–148

3. Bucholtz A (1995) Rayleigh scattering calculations for the terrestrial atmosphere. Appl Optics 34:2765–2773
4. Williamson CK, De Young RJ (2000) Method for the reduction of signal-induced noise in photomultiplier tubes. Appl Optics 39:1973–1979
5. Weitkamp C (2005) Lidar range resolved optical remote sensing of the atmosphere. Springer, New York
6. Kovalev VA, Eichinger WE (2004) Elastic lidar. Wiley, New Jersey
7. Browell EV (1989) Differential absorption lidar sensing of ozone. Proc IEEE 77:419–432
8. Kuang S, Burris JF, Newchurch MJ, Johnson S, Long S (2010) Differential absorption lidar to measure subhourley variation of tropospheric ozone profiles. IEEE Trans Geo Remote Sensing 49:557–571
9. http://www.espo.nasa.gov/arctas/
10. Flesia C, Mugnai A, Emery Y, Godin L, de Schoulepnikoff L, Mitev V (1994) Interpretation of lidar depolarization measurements of the Pinatubo stratospheric aerosol layer during EASOE. Geo Res Letts 21:1443–1446
11. Schoulepnikoff L, Van Den Bergh H, Calpini B (1998) Tropospheric air pollution monitoring LIDAR. In: Myers RA (ed) Encyclopedia of environmental analysis and remediation. Wiley, New York, pp 4873–4909
12. Ismail S, Browell EV (1994) Recent lidar technology developments and their influence on measurements of tropospheric water vapor. J Atmos Oceanic Tech 11:76–84
13. Ismail S (2011) GRIP Campaign data, private communication
14. Kooi S (2011) private communication
15. Winker DM, Couch RH, McCormick MP (1996) An overview of LITE: NASA lidar in-space technology experiment. Proc IEEE 84:164–179
16. Farrell SL, Laxon SW, McAdoo DC, Yi D, Zwally HJ (2009) Five years of arctic sea ice freeboard measurements from the ice, cloud and land elevation satellite. J Geophys Res 114:C04008. doi:10.1029/2008JC005074
17. Abdalati W, Zwally HJ, Bindschadler R, Csatho B, Farrell SL, Fricker HA, Harding D, Kwok R, Lefsky M, Markus T, Marshak A, Neumann T, Palm S, Schutz B, Smith B, Spinhirne J, Webb C (2010) The ICESat-2 laser altimetry mission. Proc IEEE 98:735–751
18. Winker DM, Pelon J, Coakley JA, Ackerman SA, Charlson RJ, Colarco PR, Flamant P, Fu Q, Hoff RH, Kittaka C, Kubar TL, Le Treut H, McCormick MP, Megie G, Poole L, Powell K, Trepte C, Vaughan MA, Wielicki BA (2010) The CALIPSO mission a 3D view of aerosols and clouds. Bull Am Met Soc. doi:10.1175/2010BAMS3009.1
19. Vaughan MA (2011) NASA Langley Research Center, private communication
20. Clissold P (ed) (2008) ADM-Aeolus, SP-1311, ESA Communication Production Office, The Netherlands, ISBN 978-92-9221-404-3
21. Le Hors L, Toulemont Y, Heliere A (2008) Design and development of the backscatter lidar ATLID for EARTHCARE. In: International Conference on Space Optics, Toulouse, 14–17 Oct 2008
22. Barnes NP, Walsh BM, Reichle D, De Young RJ (2009) Tm:fiber lasers for remote sensing. Opt Mat. doi:10.1016/j.optmat.2007.11.037, 31:1061-1064
23. De Young RJ, Barnes NP (2010) Profiling atmospheric water vapor using a fiber laser lidar system. Appl Optics 49:562–567
24. Browell EV (1995) Airborne lidar measurements. Rev Laser Eng 23:135–141
25. Ball DJ, Dudelzak AE, Rheault F, Browell EV, Ismail S, Stadler JH, Hoff RM, McElroy CT, Allan I, Carswell CTA, Hahn JF, Ulitsky A (1998) ORACLE (ozone research with advanced cooperative lidar experiment): joint NASA-CSA development of a space-base ozone DIAL. Proc SPIE 3494:223–226. doi:10.1117/12.332422
26. Ismail S, Browell EV (1989) Airborne and spaceborne lidar measurements of water vapor profiles: a sensitivity analysis. Appl Optics 28:3603–3615
27. Wulfmeyer V, Bauer H, Girolammo D, Serio C (2005) Comparison of active and passive water vapor remote sensing from space: an analysis based on the simulated performance of IASI and space borne differential absorption lidar. Remote Sens Environ 95:211–230
28. Ismail S, Peterson LD, Hinkle JD (2005) Applications of deployable telescopes for earth-observing lidar. In: Proceedings of the ESTO earth science technology conference, College Park, 27–28 June 2005
29. Chin M, Kahn RA, Schwartz SE (eds) (2009) CCSP 2009: atmospheric aerosol properties and climate impacts, Report by the U.S. Climate Change Science Program and the Subcommittee on Global Change Research, National Aeronautics and Space Administration, Washington, DC, 128 pp
30. Monks PS, Granier C, Fuzzi S, Stohl A, Williams ML, Akimoto H, Amanni M et al (2009) Atmospheric composition change – global and regional air quality. Atmos Environ 43:5268–5350
31. Browell EV, Ismail S, Grant WB (1989) Differential absorption lidar (DIAL) measurements from air and space. Appl Phys B 67:399–410
32. Real E, Law KS, Weinzierl B, Fiebig M, Petzold A, Wild O, Methven J, Arnold S, Stohl A, Huntrieser H, Roiger A, Schlager H, Stewart D, Avery M, Sachse G, Browell E, Ferrare R, Blake D (2007) Processes influencing ozone levels in Alaskan forest fire plumes during long-range transport over the North Atlantic. J Geo Res 112:D10S41. doi:10.1029/2006JD007576
33. Laj P, Klausen J, Bilde M, Pla-Duelmer C, Pappalardo G, Clerbaux C, Baltensperger U et al (2009) Measuring atmospheric composition change. Atmos Envir 43: 5351–5414
34. Ismail S, Gervin J, Wood HJ, Peri F (2004) Remote sensing of tropospheric chemistry using lidars from geostationary orbit. Proc SPIE 5659:146–154
35. World Meteorological Organization (2007) WMO global atmospheric watch strategic plan: 2008–2015. Report 172

Alaska Gas Hydrate Research and Field Studies

S. L. Patil, A. Y. Dandekar, S. Khataniar
Institute of Northern Engineering, University of Alaska Fairbanks, Fairbanks, AK, USA

Article Outline

Glossary
Definition of the Subject
Introduction
Global Distribution of Hydrate Resource
Gas Hydrate Resource Potential
Review of Global Gas Hydrate Projects
History of Gas Hydrate Exploration in Alaska
Alaska Gas Hydrate Production Potential
North Slope Borough Methane Hydrate Project Review
Future Directions
Conclusions
Disclaimer
Acknowledgment
Bibliography

Glossary

In-place The term used to estimate gas hydrate resources disregarding technical or economical recoverability. Generally these are the largest estimates [1].

Permafrost A layer of soil or bedrock that has been continuously frozen for at least 2 years.

Petrophysical Physical properties of the reservoir rock.

Resources Resources are those detected quantities of hydrocarbon that cannot be recovered profitably with the current technology but may be recoverable in the future. It also includes those quantities that geologically may be possible but have not been found yet [2].

Definition of the Subject

Gas Hydrates

Natural gas hydrates are solid, crystalline, ice-like materials made up of small molecules of gases, mainly methane confined inside cages of water molecules. These gas hydrates are solid solutions and are formed when water molecules linked by hydrogen bonding create cavities (host) that enclose a variety of molecules (guest). These molecules can be CH_4, C_2H_6, and CO_2 to name a few. It is interesting to note that there is no chemical bonding between the host water molecule and the caged molecule. Hydrates can form under high pressures or low temperatures, which are generally the conditions that exist in the Arctic or under deep ocean beds. Huge volumes of gas hydrates are expected to exist at various locations around the globe (Fig. 3). It is known that 1 m^3 of hydrates upon dissociation release about 180 std m^3 of gas, making them a huge potential as a future energy resource [3, 4].

History of Gas Hydrates

The discovery of hydrates dates way back in 1810 when Sir Humphry Davy conducted an experiment and discovered that an aqueous solution of chlorine can be converted into solid form when cooled below 9°C [5]. Faraday confirmed the existence of this solid compound and now it is known that there are more than 100 molecules that can form hydrates when combined with water. Few molecules that are very commonly found to form hydrates are CH_4, C_2H_6, C_3H_8, CO_2, and H_2S, with CH_4 being the most common molecule to form gas hydrates found in existence. It was as early as the 1950s when through x-ray diffraction methods the crystal structure of hydrates was known, and by late 1960 it was realized that the earth's crust is home to vast quantities of natural gas hydrates [5].

It was Powell, in 1948 at the University of Oxford, who was the first to describe clathrate structure and described clathrate compounds as those inclusion compounds *in which two or more components are associated without ordinary chemical union but through complete enclosure of one set of molecules in a suitable structure formed by another* [5]. The clathrate compounds are divided into two categories. One is aqueous clathrates in which water is the host species, commonly known as clathrate hydrates or gas hydrates, and the other category of hydrates where water is not the host molecule are known as nonaqueous clathrates [5]. It is known that water molecules are linked to each other through hydrogen bonding, which results in the

formation of cavities having dimensions of 780 and 920 pm [5]. The molecules that are smaller than the dimension of these small cavities and do not react with the hydrogen bonds of the water molecule form gas hydrates under appropriate conditions of temperature and pressure, thereby providing stability to the structure.

Introduction

Gas hydrates may become an important global source of clean burning natural gas. Scientists have considered the potential of gas hydrate as an energy resource for nearly four decades. However, until 2002, this knowledge has not been systematically applied to determine the economic practicality of gas hydrate resource development. The estimates of in-place unconventional gas hydrate volume are up to 100 Trillion Cubic Feet (TCF) within the existing oil development infrastructure of the Alaska North Slope (ANS) [6]. This region uniquely combines known gas hydrate presence, an undetermined volume of associated free gas accumulations, and existing production infrastructure (Fig. 1).

Initial research on Alaskan gas hydrates was focused on the Prudhoe Bay Unit (PBU), Kuparuk River Unit (KRU), and Milne Point Unit (MPU) infrastructure areas of the Alaska North Slope. These areas were being studied to determine gas hydrate reservoir extent, stratigraphy, structure, continuity, quality, variability, and geophysical and petrophysical property distribution. These initial studies characterized reservoirs and fluids, which led to in-place and recoverable resource estimates and commercial potential determination. Studies were conducted to determine best practices and procedures for gas hydrate drilling, data acquisition, completion, and production. This collaborative research provided practical input to reservoir and economic models, determined the technical feasibility of gas hydrate production, and influenced future exploration and field extension of this potential unconventional gas resource.

A successful drilling project to explore, confirm, and evaluate gas hydrates was conducted in February 2007 through a shallow seismic anomaly interpreted as hydrates. In this project, over 400 ft of sediments containing gas- and water-bearing core and well-developed gas hydrate zones (85% recovery) were cored. An extensive suite of electric logs were run to identify the gas hydrate zones, and gas hydrate saturations were computed. Open-hole pressure-transient analyses and fluid sampling tests were conducted using Schlumberger's Modular Formation Dynamics Tester (MDT™).

A second ANS gas hydrate research project was conducted for the Barrow Gas Field (BGF). Barrow, Alaska, is a remote and the northernmost city in the United States. The energy demands of the city and nearby localities are met by natural gas supply from the Barrow Gas Field consisting of three different gas pools: the East Barrow (EB) pool, the South Barrow (SB) pool, and the Walakpa (WAL) pool (Fig. 2).

Gas hydrate resource potential of the three BGF pools was analyzed by developing gas hydrate stability models. Material balance studies were performed on East Barrow (EB) gas pool to understand reservoir drive mechanisms and qualitatively estimate the hydrate resource. Field-scale dynamic reservoir simulation models were developed for the EB and WAL gas pools. Production history data were matched, reservoir drive mechanisms were confirmed, free gas and hydrate resources were quantified, hydrate dissociation patterns were examined, optimum locations for drilling infill wells were identified, and future production scenarios were simulated.

The vast amount of unconventional gas in-place combined with evaluation of conventional Alaska North Slope gas commercialization creates industry-government alignment to assess this potential future resource. This region uniquely combines known gas hydrate presence, an undetermined volume of associated free gas accumulations, and existing production infrastructure. However, many technical and economic challenges must be resolved before the gas hydrate becomes a viable commercial hydrocarbon resource.

Global Distribution of Hydrate Resource

Global volumes of gas hydrate estimated till now span several orders of magnitude and there is no certainty in methane hydrate resource estimates across the globe. This uncertainty in estimating the volume of gas hydrates present is majorly because of two factors: (1) The commonly used seismic methods and other geophysical methods that are used in estimating conventional hydrocarbon resources are not sensitive to the huge volumes of hydrates present in the seafloor

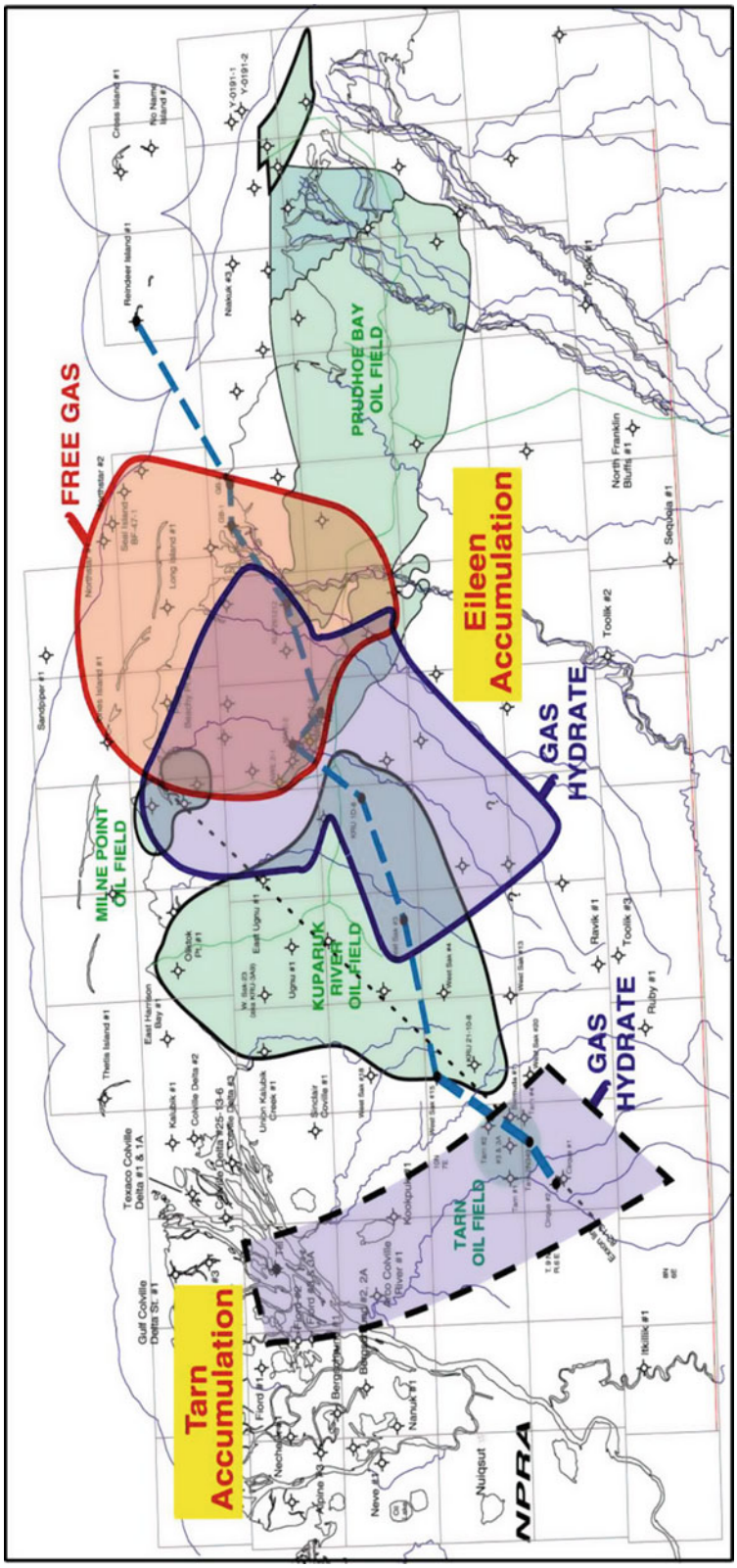

Alaska Gas Hydrate Research and Field Studies. Figure 1
Alaska North Slope oil field developments with Eileen and Tarn gas hydrate trends (Courtesy Collett [32])

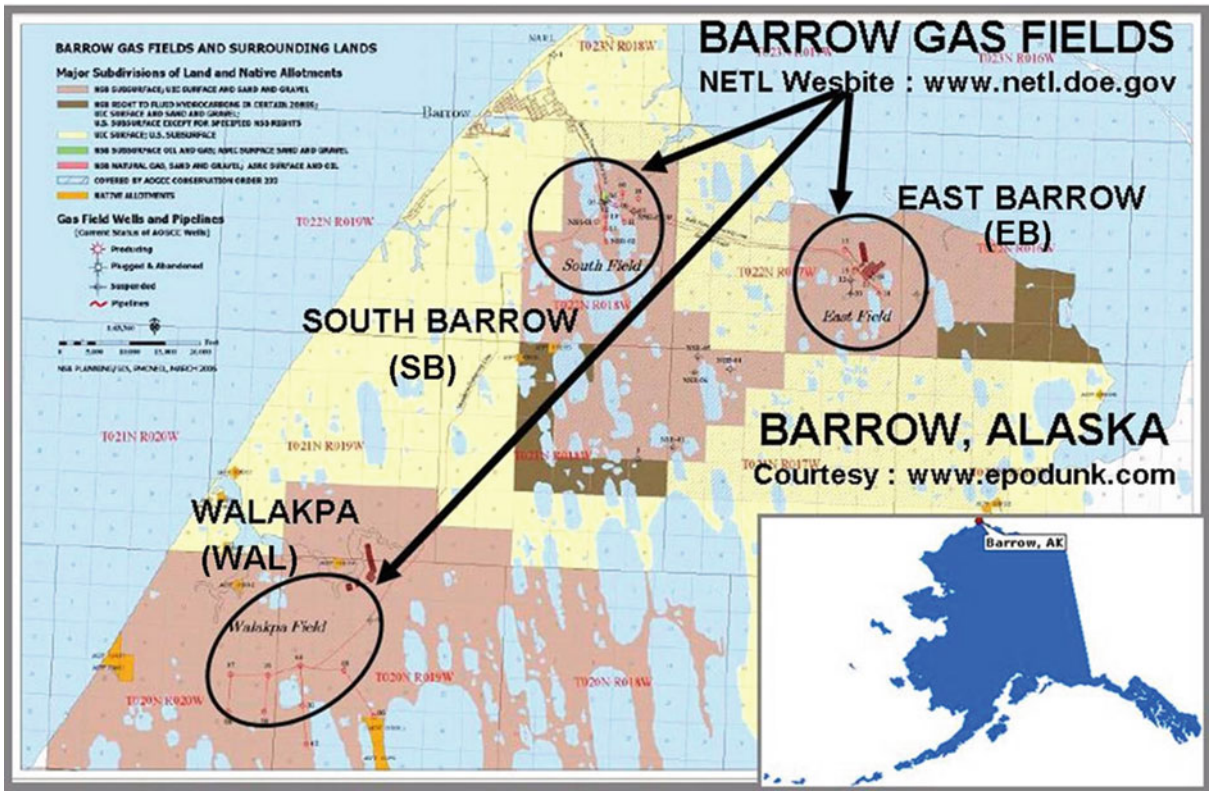

Alaska Gas Hydrate Research and Field Studies. Figure 2
Barrow gas fields, Alaska (Modified from NETL Website, www.netl.doe.gov)

section. (2) Drilling activities to directly confirm the presence of hydrates have a limited applicability due to limited spatial extent [7]. There is no direct evidence which can be used in estimating the occurrence of in-place gas hydrates. There are 23 locations where the presence of gas hydrates has been confirmed through the recovery of hydrate samples, 20 of them being in the oceanic and the rest 3 in the arctic environments [8, 9]. Since the discovery of gas hydrates, researchers have tried to estimate the amount of gas trapped in hydrates none being certain. Going by even the most conservative approximation of the estimation of the trapped gas, the amount of gas trapped in hydrates is enormous.

HEI (Hydrate Energy International) along with the International Institute for Applied Systems Analysis (IIASA) with funding from the World Bank, United Nations Organizations, and national governments has undertaken the task of assessing the global gas hydrate potential. For this study, data from every continental margin was studied and appropriate depositional models were utilized. The data was reported for 18 regions defined by the United Nations. For the Arctic Ocean, separate resource assessment was done without regard for national boundaries and for the southern ocean (from the coast of Antarctica north to 60° south latitude) [10]. The result of global hydrate resource estimate has been tabulated in Table 1 after Johnson [10]. Figure 4 depicts the hydrate resource pyramid after Boswell and Collett [11].

The production and commercialization of gas hydrate deposits rely heavily on two important factors: (1) the advancement in technology to prove and produce from these resources overcoming existing obstacles and (2) a natural gas supply market accelerating the need to progress and improve the gas hydrates resource potential [12]. Although various research activities are on way worldwide, gas hydrates are the most unlikely unconventional resource that will be tapped in the near future. But based on the demand for energy in the future, these research and exploration activities need

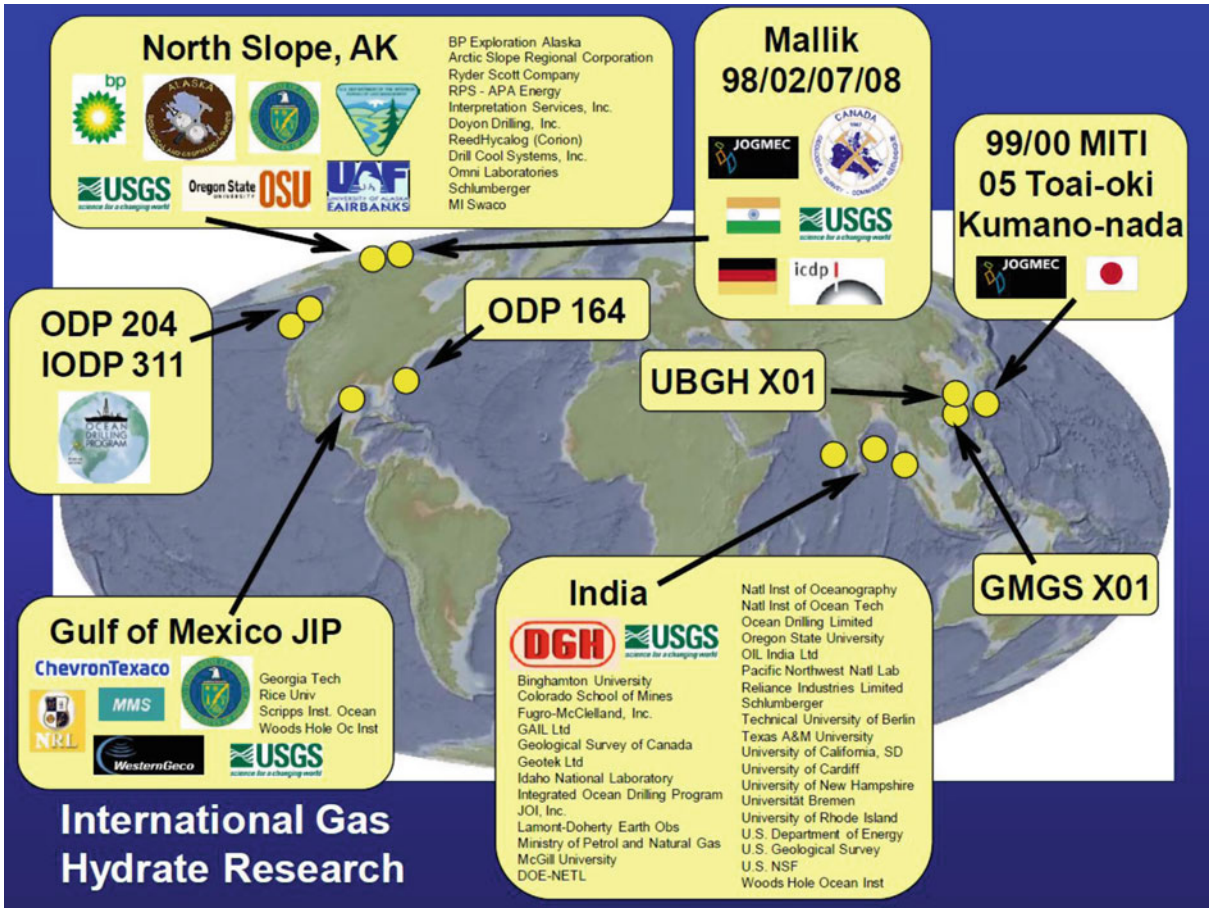

Alaska Gas Hydrate Research and Field Studies. Figure 3
World distribution of gas hydrates (Adapted from oral presentation at AAPG Annual Convention, San Antonio, Texas, April 20–23, 2008)

to go on and probably in a much more aggressive way to make these a viable energy source. Figure 5 depicts the time line for post 1990 global drilling efforts after Ruppel [12].

Gas Hydrate Resource Potential

Gas hydrates are naturally occurring ice-like substances composed of water and gas, in which a solid water-lattice accommodates gas molecules in a cage-like structure called a clathrate. This clathrate structure can store up to 180 unit volumes of methane gas per 1 unit volume clathrate. This large gas storage capacity makes methane hydrate a very attractive concentrated potential unconventional resource.

Gas hydrates accumulate within reservoirs located in permafrost regions and within subsea sediments of outer continental margins. While methane, propane, and other gases can be included in the hydrate structure, methane hydrates appear to be the most common in nature. The amount of methane sequestered in gas hydrates is probably enormous. However, the in-place and recoverable gas estimates are highly speculative and also dependent upon the conventional petroleum system components of source, charge, reservoir, trap, seal, and a highly uncertain recovery factor, as well as occurrence within the gas hydrate stability field (Fig. 6).

The successful production history of the Russian Messoyakha gas hydrate field [6] demonstrates that gas hydrates may provide an immediate source of natural

Alaska Gas Hydrate Research and Field Studies. Table 1
Gas in-place in hydrate-bearing sands (After Johnson [10])

Region (United Nations designation)	Gas in-place range (TCF)	Gas in-place median (TCF)
United States	1,500–15,434	7,013
Canada	533–8,979	2,228
Western Europe	36–14,858	1,425
Central and Eastern Europe	0–105	13
Former Soviet Union	1,524–10,235	3,829
North Africa	6–1,829	218
Eastern Africa	42–25,695	1,827
Western and Central Africa	79–26,672	3,181
Southern Africa	121–26,369	3,139
Middle East	31–3,848	573
China	10–1,788	177
Other East Asia	14–2,703	371
India	36–6,268	933
Other South Asia	20–3,497	557
Japan	71–471	212
Oceania	38–6,750	811
Other Pacific Asia	64–25,946	1,654
Latin America and the Caribbean	258–31,804	4,940
Southern Ocean	144–45,217	3,589
Arctic Ocean	178–55,524	6,621
Total	4,705–31,3992	43,311

gas that can be produced by conventional depressurization of an adjacent free gas. Gas hydrates also represent a significant drilling and production hazard. Russian, Canadian, and American researchers have described numerous problems associated with gas hydrates, including well control problems and casing failures.

Review of Global Gas Hydrate Projects

Several countries have active gas hydrate field programs (Fig. 3). The following gives an overview/status of these research activities.

Japan

The first remarkable gas hydrate research program in Japan was established in 1995 by the Government of Japan along with the Ministry of Economy, Trade, and Industry (METI). Since then the METI was very proactive in gas hydrate research field. It contributed to Canada's Mallik 2002 Gas Hydrate Production Research Well Program. In 2001, METI established Methane Hydrate R&D Program, which is currently in its Phase 2 (2009–2015). Within the Phase 2 production tests on the eastern Nankai Trough are planned for 2012 and 2014 respectively. Phase 2 also considers environmental impact assessment and development of optimal methane hydrate production approaches as its objectives [13].

China

Guangzhou Center for Gas Hydrate research was founded in 2004 to expand the research and to evaluate gas hydrate resource potential in offshore China. Guangzhou Marine Geological Survey (GMGS) conducted and expedition GMGS-1 in spring 2007 to perform offshore drilling in Shenhu area of the South China Sea. During the expedition eight holes were drilled. Wireline logging was performed on each site. Five wells were cored [14]. Future expeditions to the South China Sea are being considered. Besides, hydrate exploratory drilling takes place in Qinghai-Tibet Plateau.

South Korea

Gas Hydrate Research and Development Organization (GHDO-K), supported by the Ministry of Commerce, Industry, and Energy, is a South Korean gas hydrate program started in 2000. Its main objectives are to confirm gas hydrate resources in the East Sea and to commercially produce gas hydrates by 2015 [14]. It started with seismic data acquisition in the East Sea with shallow coring in the Ulleung Basin in order to define its gas hydrate potential. Ulleung Basin Gas Hydrate Expedition 1 (UBGH1) was the first exploration and drilling expedition launched on behalf of the Korean Institute of Geoscience and Mineral Resources in late 2007. During the expedition five wells were drilled with logging, and while drilling, some of them

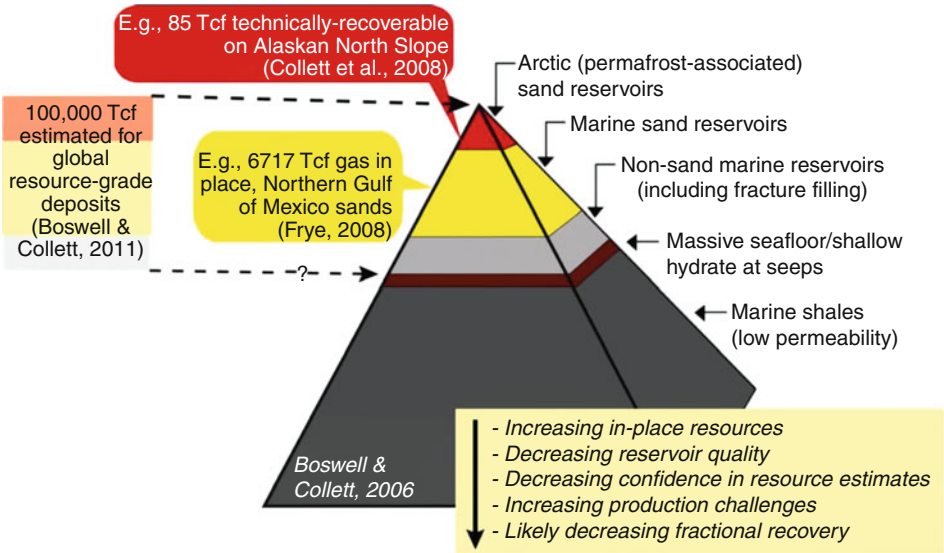

Alaska Gas Hydrate Research and Field Studies. Figure 4
The hydrate resource pyramid (Ruppel [12])

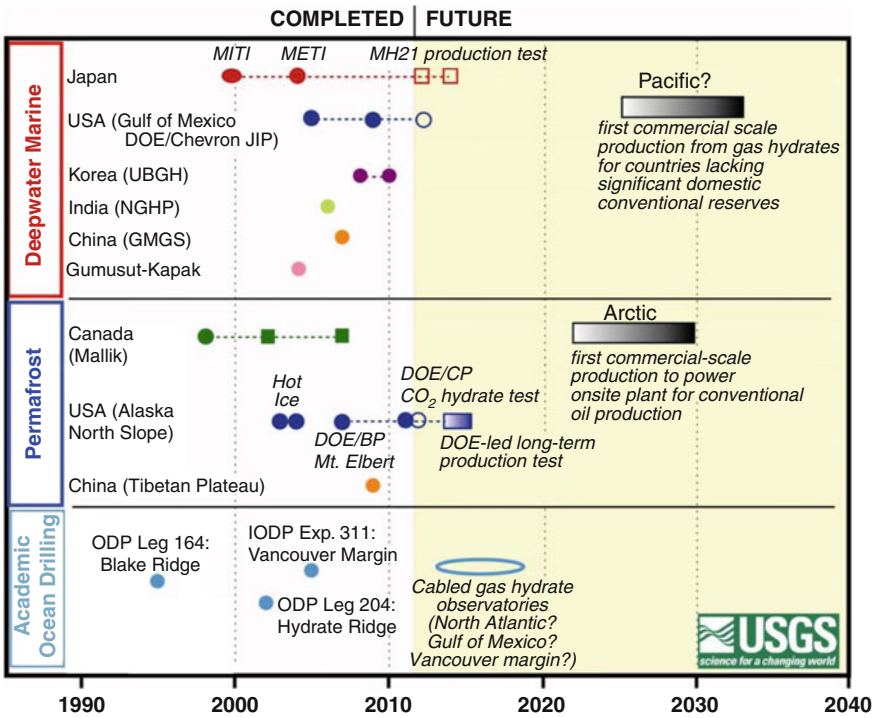

Alaska Gas Hydrate Research and Field Studies. Figure 5
Timeline of major post-1990 gas hydrate field programs and future activities. *Circles* correspond to logging and/or coring, while *squares/rectangles* denote activities that included/will include production testing. *Solid* symbols denote completed activities, and *open* symbols are potential or planned activities. *Rectangles* filled with *shaded pattern* refer to longer-term production activities that remain prospective (After Ruppel [12])

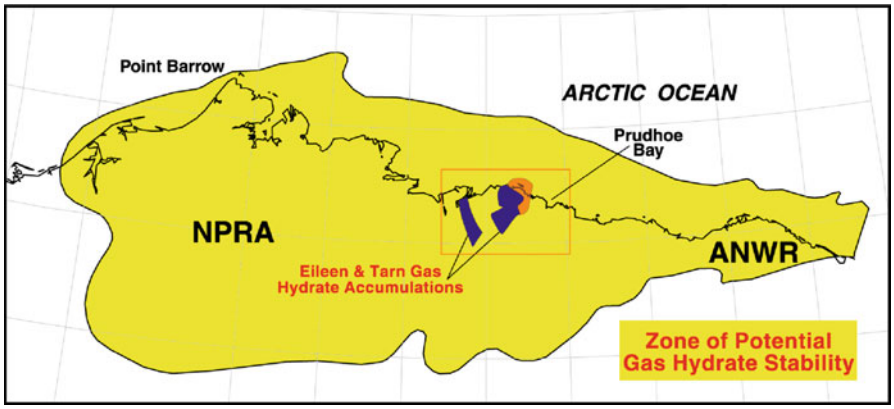

Alaska Gas Hydrate Research and Field Studies. Figure 6
Zone of potential gas hydrate stability, Alaska, North Slope (Courtesy Collett [32])

were cored as well [14]. In July 2010, the UBGH2 expedition was launched. It included vast amount of data acquired and lasted till early October. Subsequently, South Korea is planning field production tests (GHDO-K, 2010).

India

National Gas Hydrate Program (NGHP) of India was initiated in 1997. Its primary goals are performance of ocean drilling, coring, logging, and other activities in order to explore gas hydrate deposits and evaluation of the possibility of their economical production. The NGHP Expedition 1 was successfully conducted during mid-2006. During the expedition, 39 wells were drilled in various sites which are: Kerala–Konkan, Krishna–Godavari, Mahanadi, and Andaman. Special attention was paid to Krishna–Godavari gas hydrate site, where more than 10 wells were drilled [14]. Extensive coring and logging were performed in a number of wells and vast amounts of data were collected. NGHP Expedition 02 was also considered as a future possibility.

United States

In the United States, the Department of Energy (DOE) has been conducting extensive research on gas hydrates for the past several decades. Ocean Drilling Program (ODP) Leg 164 located on Blake Ridge, Atlantic shelf, was the first special attempt to identify gas hydrates [15]. It recovered hydrate cores and documented gas hydrate presence within the sediment [14]. ODP Leg 204 was another deep-sea expedition which discovered gas hydrates in the Hydrate Ridge, located on the Cascadia continental margin. Gulf of Mexico Gas-hydrate JIP consortium was formed in 2001 by industry participants and government agencies in partnership with DOE and led by Chevron. Its goals were studying hydrates both as drilling hazards and also as a potential methane resource. In 2005, it conducted scientific drilling and coring in the gulf [14]. On the North Slope of Alaska, gas hydrates encountered onshore are associated with permafrost. Despite an apparent likelihood of offshore gas hydrate existence in the Arctic Ocean, there is no proof so far. In 2002–2003 Anadarko Petroleum Corporation drilled the Hot Ice gas hydrate research well in Tarn gas hydrate accumulation on the North Slope of Alaska. However, no gas hydrates were encountered [14]. In 2007, the Mount Elbert Gas Hydrate Stratigraphic Test Well was drilled by BP Exploration (Alaska) on behalf of DOE. It was located on the Milne Point, Eileen gas hydrate accumulation. It revealed gas hydrates and even cores were recovered.

Canada

Canada does not have any official gas hydrate program. However, extensive study was performed in Canada of which the remarkable ones are Cascadia and Mallik. Both gas hydrate occurrences are associated with permafrost. ODP Leg 146 and IODP Expedition 311 to the offshore Vancouver Island discovered gas hydrate existence in Cascadia continental margin. Numerous

data including seismic, logs, and chloride concentration infer gas hydrate presence. Within IODP Expedition 311, hydrate-bearing cores were retrieved. Mallik-38 onshore well in the Mackenzie River Delta was believed to be drilled through 100 m of hydrate-bearing sandstone. Subsequently in 1998, Geological Survey of Canada on behalf of Japan Petroleum Exploration Company Ltd and Japan National Oil Corporation drilled Mallik 2L-38 gas hydrate research well. Coring and logging both revealed gas hydrates within the sandstone. As a next step, within Mallik 2002 program the partners drilled three more wells: Mallik 3L-38, Mallik 4L-38, and Mallik 5L-38 [14].

New Zealand

In 2010, Gas Hydrate Resources (GHR) program was funded for 2 years by the New Zealand Foundation for Research, Science, and Technology (FRST). It is mostly focused on Hikurangi margin located to the east of the islands. The program plans are: analysis of existing 2D and 3D seismic data acquisition, seafloor sampling in spring 2011, and production modeling [16].

History of Gas Hydrate Exploration in Alaska

The North Slope of Alaska contains two large gas hydrate accumulations within and near the Prudhoe Bay and the Tarn oil field developments (Fig. 1). This confirms the possibility that gas hydrates may represent an important future energy resource. The occurrence of gas hydrates on the North Slope of Alaska was confirmed in 1972 with data from the Northwest Eileen State-2 well, the first dedicated gas hydrate core and test well, located near the Prudhoe Bay Oil Field. Most of the gas hydrates near this Eileen trend discovery well occur in a series of laterally continuous sandstone reservoirs and are geographically restricted to the area overlying the western part of the Prudhoe Bay Oil Field and the eastern part of the Kuparuk River Oil Field. Three-dimensional seismic surveys in the Prudhoe Bay Oil Field indicate the presence of an undetermined amount of free gas trapped down deep below some of the gas-hydrate-bearing units. The volume of gas within the gas hydrates within the Eileen trend is estimated to be about 37–44 trillion cubic feet.

Recently, data from wells along the western margin of the Kuparuk River Field have shown presence of the large Tarn trend gas hydrate accumulation overlying the Tarn oil field. The Cirque-1 well, located about 4 miles southwest of the Tarn oil field, experienced severe well control problems in 1992 after drilling through what appeared to be a free gas interval possibly trapped below the gas hydrate stability zone. The gas-hydrate-bearing stratigraphic interval within the Tarn trend appears to be the up-dip equivalent of the West Sak sands. These sands are estimated to contain more than 20 billion barrels of in-place heavy oil and are the focus of recent development activity. Preliminary analyses of other recently completed wells along the western margin of the Kuparuk River oil field suggest that the volume of in-place gas hydrates within the Tarn trend may exceed that of the Eileen trend.

Alaska Gas Hydrate Production Potential

The production potential of the Eileen or Tarn gas hydrate accumulations has not been adequately tested. This area is a focus of the gas hydrate research programs by the industry, led by the US Department of Energy. In order to produce gas from gas hydrate, the in situ pressure-temperature regime must change to dissociate gas. Decreasing the reservoir pressure, increasing the reservoir temperature, and/or use of chemicals can allow gas to dissociate from the solid gas hydrate structure. Among the various techniques for production of natural gas from gas hydrates, the most economically promising method is considered to be depressurization of an adjacent free gas.

A growing body of evidence suggests that a huge volume of natural gas is stored as gas hydrates in northern Alaska and that production of natural gas from gas hydrates may be technically feasible. However, numerous technical and economic challenges must be resolved before this potential resource can be developed. Many wells have penetrated gas hydrate during oil production operations on the Alaska North Slope. During this time, gas hydrates were known primarily as a drilling hazard. Industry has considered the resource potential of conventional Alaska North Slope gas during industry and government efforts in working toward an Alaska North Slope gas pipeline. Consideration of the resource potential of this conventional Alaska North Slope gas created the industry–government alignment necessary to also consider the resource

potential of the potentially huge (40–100 TCF in-place) unconventional gas hydrate accumulations beneath existing production infrastructure. Two of the wells recently drilled as a part of the industry–government research programs to explore and evaluate gas hydrate production potential on the ANS were the Hot Ice #1 and the Mt. Elbert-01.

The Hot Ice No. 1

The Hot Ice No. 1 well was drilled on the Anadarko Petroleum leases, southwest of the main Kuparuk development, just outside the Kuparuk River Unit boundary. Drilling began in 2003 and ended in 2004. The well was drilled, cored, and logged to a depth of 2,300 ft (700 m), and ultimately abandoned as no hydrates were found [17]. However, the lessons learned from drilling this well were useful in designing future hydrate exploration wells such as the Mt. Elbert.

Hot Ice No.1 well also used water-based polymer drilling mud with KCl (salt) for freezing-point depression and a mud chiller for circulating chilled mud. This was problematic, with freeze-ups and mechanical problems impeding progress. This knowledge influenced decisions with regard to coring fluids and mud chilling on the Mt. Elbert-01 Gas Hydrate Stratigraphic Test Well.

The Mt. Elbert-01

The drilling, coring, and testing of Mt. Elbert-01 Gas Hydrate Stratigraphic Test Well was part of the DOE/NETL-funded "Alaska North Slope Gas Hydrate Reservoir Characterization Project," and was a cooperative effort between industry, academia, and government.

The Mt. Elbert-01 Hydrate Test well was located on a temporary ice pad in the Milne Point Unit on the ANS, south of the B-Pad and east of the E-Pad, with ice road access from the B-Pad. The location of the Mt. Elbert-01 relative to the Milne Point infrastructure is shown in Fig. 7. The location of the Mt. Elbert-01 Hydrate Well was chosen so as to drill in an area with "known" hydrate accumulations with isolation (stand-off) from the thermal effects of any adjacent wells. This would allow the best chance to find and test undisturbed hydrates.

Based on well log data from nearby offset wells, it was estimated that the Base of the Ice-Bearing Permafrost (BIBPF) was at approximately 1,850 ft TVDss and the Base of the Gas Hydrate Stability Zone (BGHSZ) was at about 2,950 ft TVDss. Coring operations were planned from three potential gas-hydrate-bearing zones (zones D, C, and B) within this depth range. A total of 23 coring runs were made using the wireline

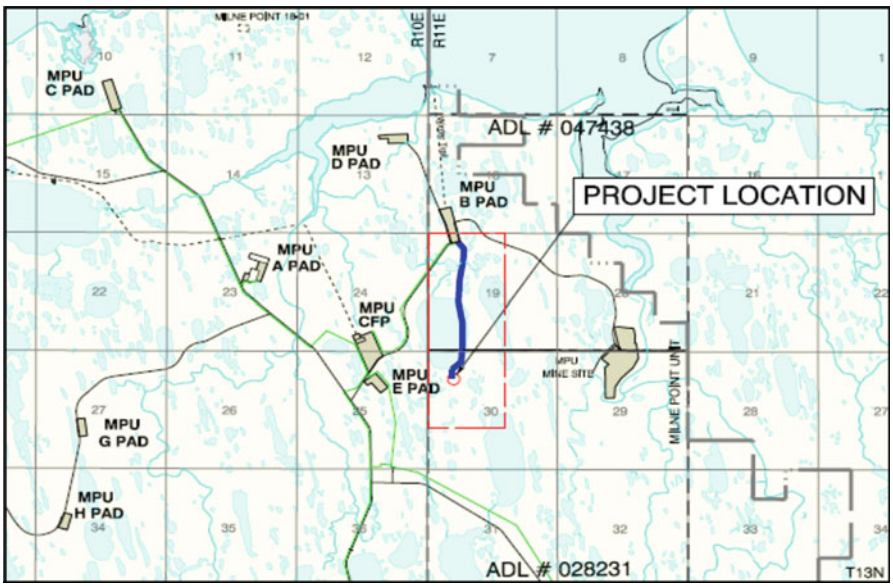

Alaska Gas Hydrate Research and Field Studies. Figure 7
Section Map – Mt. Elbert-01 location relative to Milne Point infrastructure (Courtesy Hanson [18])

retrievable coring method, which prevented the cored formations from being exposed to pipe tripping effects. This was the first application of wireline retrievable coring on the Alaska North Slope. Figure 8 shows a summary of the coring runs. The overall core recovery was 85%. The use of a chilled mineral-oil-based coring fluid and wireline retrievable coring method are believed to be mainly responsible for such high core recovery. The main advantage of a chilled oil-based coring fluid over a chilled water-based coring fluid is that the oil-based fluid would not freeze. Although additives were used, freezing of water-based coring fluids was a major problem in the previous hydrate wells Mallik and Hot Ice #1 [18]. Details of the drilling plan and coring operations for Mt. Elbert-01 are given by Hanson [18].

The logging suite for Mt. Elbert-01 consisted of three electrical resistivity tools and an extended MDT testing. Figure 9 shows a sample plot of the well logs, clearly delineating the upper D hydrate zone. Full analysis of Mt. Elbert-01 well logs showed no evidence of significant "contacts" between free gas sands and hydrate-bearing sediments [18]. Mt. Elbert-01 is the world's first successful application of the MDT™ tool in open-hole in gas hydrates.

North Slope Borough Methane Hydrate Project Review

Barrow, Alaska, is a remote and the northernmost city in the United States. The city serves both as the economic and administrative center of the North Slope Borough (NSB). The energy demands of the city and nearby localities are met by natural gas supply from the Barrow Gas Fields (BGF) consisting of three different gas pools: the East Barrow (EB) pool, the South Barrow (SB) pool, and the Walakpa (WAL) pool (Fig. 2). The Barrow Gas Fields have been producing natural gas for the last 25 years. It has been estimated that the proven gas reserves in these fields exceed over 250 billion standard cubic foot (BCF) [19, 20]. Based on the current demands for natural gas in the Barrow region and to enhance natural gas production and expand

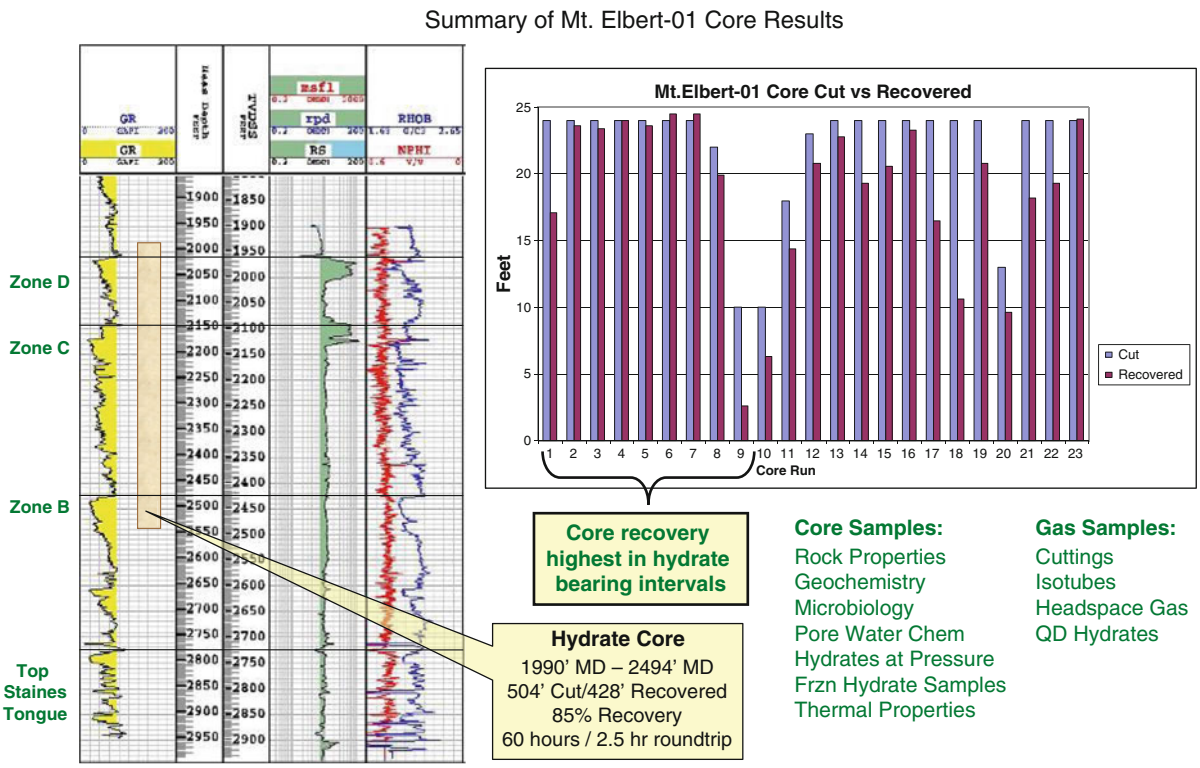

Alaska Gas Hydrate Research and Field Studies. Figure 8
Summary of core recovery by run relative to the log through the hydrate interval (Courtesy Hanson [18])

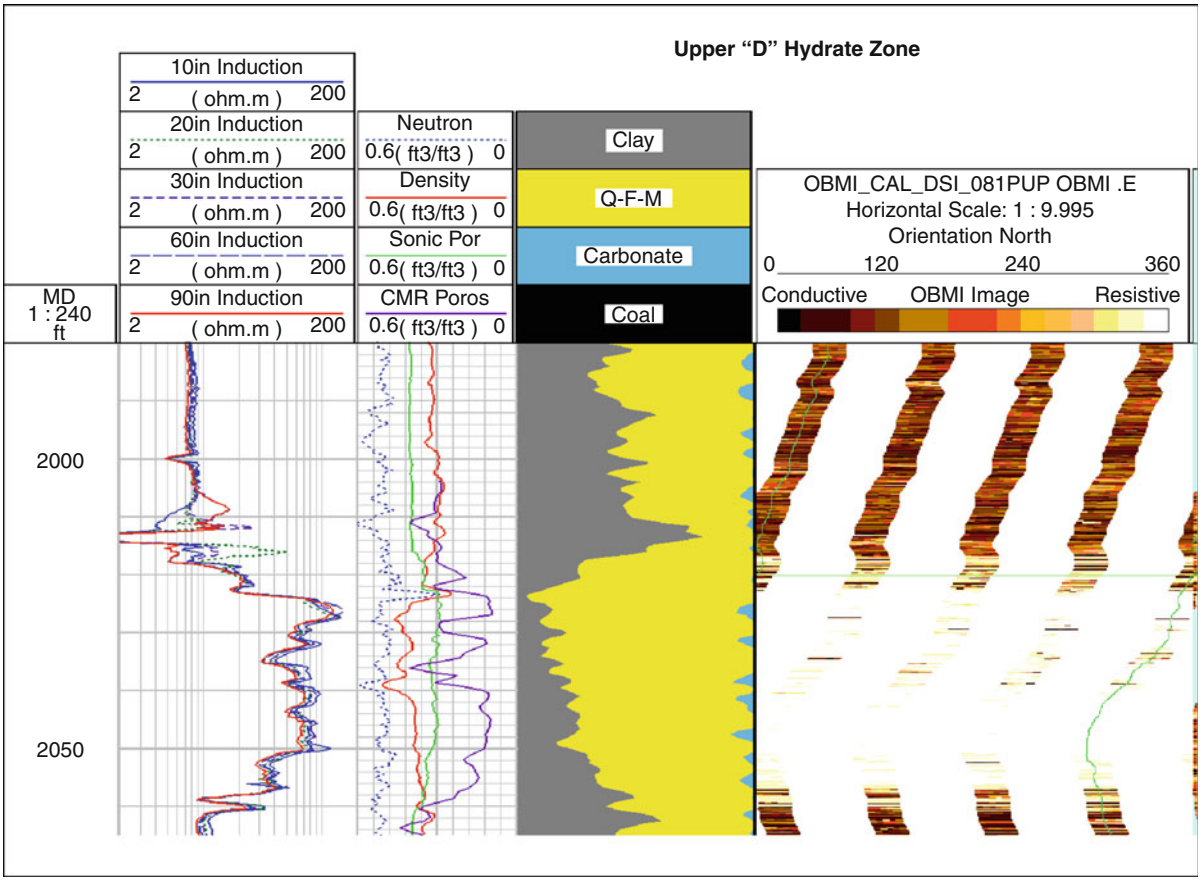

Alaska Gas Hydrate Research and Field Studies. Figure 9
Composite RT Scanner, Neutron, Density, Sonic, CMR and OBMI Log showing the upper "D" – Hydrate interval (Courtesy Hanson [18])

production facilities in order to provide cost effective and assured source of energy to Barrow and nearby areas, the Barrow gas hydrate project was proposed by the NSB to the US Department of Energy (DOE). In 2006, DOE and NSB jointly funded a research program to characterize and quantify methane hydrate resource potential associated with the BGF, with the ultimate goal of producing gas from the hydrate formations associated with individual gas pools of BGF.

Gas Hydrate Stability Modeling for BGF Pools

An engineering approach was first adopted to develop methane hydrate stability models for the three gas pools. This was performed on the basis of gas analysis, formation water salinity, and pressure and temperature gradient data available from various sources referenced in [21]. The studied literature indicated a gas composition of practically pure methane (99%) and water salinities in the range of 0–4% w/w. Details of the calculation procedures can be found in [21]. The hydrate stability models for EB and WAL gas pools are provided in Figs. 10 and 11. Results from the EB pool calculations indicate the existence of hydrate stability zones within the pay zone of 2,000–2,150 ft, which suggests that the in situ hydrates are possibly associated with free gas reservoir. Similar to EB, the hydrate stability model for WAL pool also showed promising results in that stable hydrate zones were not found within deeper zones of the WAL sand where existing gas wells were completed within the 2,000–2,600 ft interval but showed stable envelope existing in up-dip locations of the reservoir between 1,700 and 2,000 ft. To confirm these results, detailed geological and geophysical analysis of

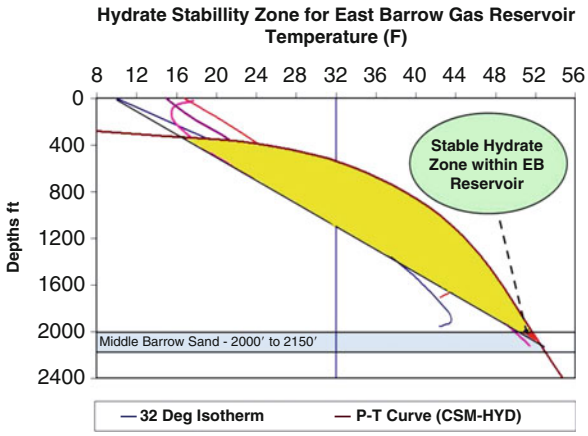

Alaska Gas Hydrate Research and Field Studies.
Figure 10
Hydrate stability model for EB pool

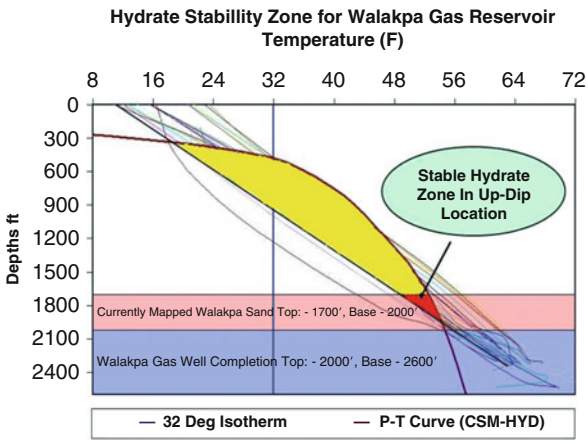

Alaska Gas Hydrate Research and Field Studies.
Figure 11
Hydrate stability model for WAL pool (Courtesy Singh [21])

unexplored regions of the pools are required to determine the association of gas hydrates with the prospective gas pools. Singh [21] conducted a material balance study to obtain additional confirmation of the presence of hydrates, especially associated with the EB pools.

The East Barrow Field Material Balance Study

The objective of the material balance study was to qualitatively understand the behavior of the EB pool under different drive mechanisms, and to confirm if hydrate dissociation was one of them. Stokes and Walsh [22] performed pressure buildup tests on two EB wells and later [23] compared the static reservoir pressure data with historical pressure data reported by Allen and Crouch [24]. Figure 12 represents the historical performance plot of the EB gas pool, which shows an initial drop in the static reservoir pressure with gas production, indicating a conventional response of a volumetric gas reservoir producing by gas expansion. However, long-term production data showed gradual pressure stabilization, which indicated the possibility of water influx from a communicating aquifer. But the possibility of a communicating aquifer was ruled out because (1) there was negligible water production (~1,600 bbls up to September 2007), (2) cumulative gas production of ~8 BSCF by 2007 was much higher than Allen and Crouch's [24] estimate of ~6 BSCF, and (3) none of the EB wells had watered out. Thus, the EB field performance data of Fig. 13 suggested possible contribution from an unknown drive mechanism, which could be gas recharge from dissociating gas hydrates, or water influx from a new aquifer.

In the EB material balance study, the overall performance of a tank type, static reservoir model representing the EB gas pool was compared against the available production data. The following drive mechanisms were studied with the tank model to see which drive mechanism would match actual production data: (1) volumetric gas tank, (2) water drive, (3) dissociating-hydrate drive, and (4) combination of water and hydrate drive. Reservoir and fluid properties and other details are found in Singh [21].

The study showed that the actual production data from the EB field could not be matched by assuming volumetric behavior, water drive, or dissociating-hydrate drive alone. However, a good match of modeled production response and actual production data, shown in Fig. 13 by red dotted circles, was obtained in the scenario where a free gas reservoir was in communication with a weak aquifer, but associated with a thick hydrate layer. Thus, a combination of aquifer support and hydrate dissociation is the most likely drive mechanism in the EB pool.

Field Scale Reservoir Simulation Study

Using the reservoir drive mechanism established through the material balance study on the EB pool,

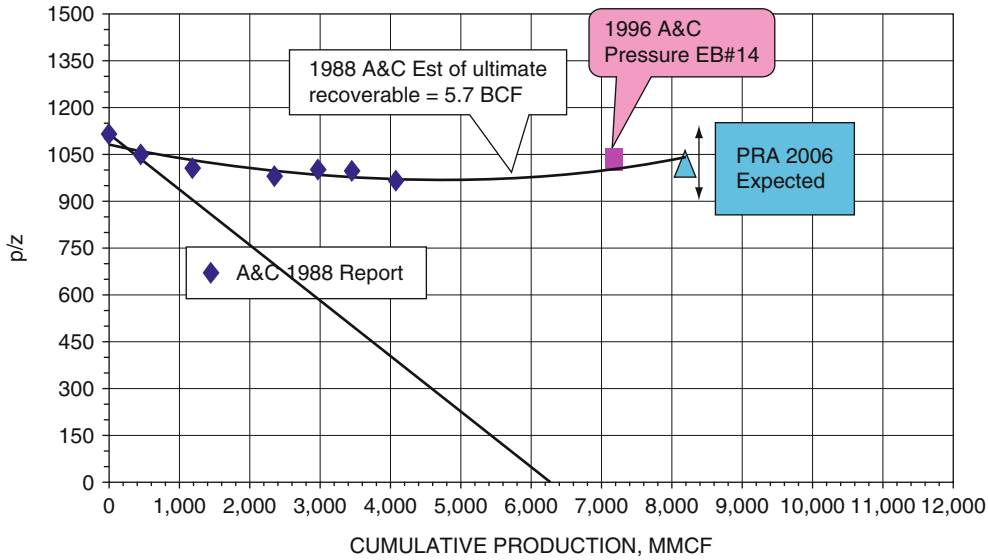

Alaska Gas Hydrate Research and Field Studies. Figure 12
EB gas pool performance (Stokes and Walsh [23])

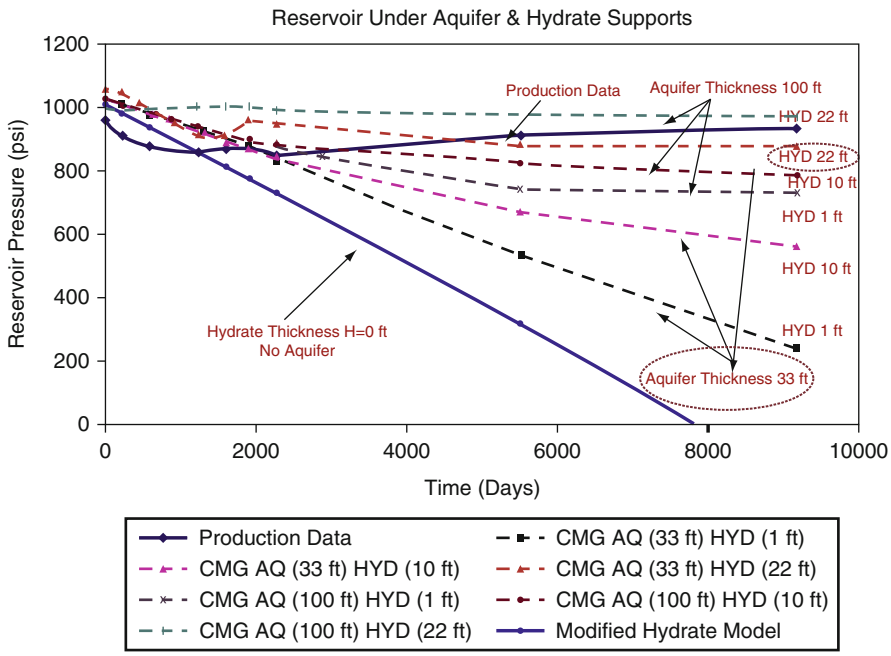

Alaska Gas Hydrate Research and Field Studies. Figure 13
Hydrate- and aquifer-supported gas reservoir performance prediction for EB pool (Courtesy Singh [21])

Singh [21] conducted numerical reservoir modeling studies using a full-scale, three-dimensional (3D) dynamic reservoir model. A commercial reservoir simulator (CMG-STARS) was used to perform the simulation studies. The static reservoir model of Panda and Morahan [25] was imported and built upon by adding reservoir properties and drive mechanisms. Other details can be found in Singh [21].

The simulation study predicted field-wide performance of the EB pool for a period of 30 years and investigated the impacts of well completion and orientation (vertical wells versus horizontal wells). History matching of the simulation results confirmed the previously estimated combination drive as the primary recovery mechanism for this reservoir. However, gas production by expansion dominates over hydrate dissociation mechanism after approximately 15–20 years of production. The simulation study also indicated that infill drilling using horizontal producing wells would offer the ideal combination of lower water production and higher gas recovery.

Future Directions

Various methods have been studied and have been proved to be successful in the extraction of gas from gas hydrate deposits. These are depressurization, thermal methods, and the use of inhibitors (e.g., methanol or glycols). Gas hydrate dissociation is an endothermic reaction and as the hydrate deposits dissociate, the surrounding temperatures decrease resulting in further hydrate reformation, thereby reducing the amount of gas that can be produced. Thus any method or a combination of methods used for hydrate dissociation has to not only consider the energy required to dissociate hydrates but also has to take in effect the energy that is required to counter the drop in temperature that takes place due to the endothermic nature of hydrate dissociation [26]. Yutaek and SeongPil [27] have shown how kinetic hydrate inhibitors (KHI) can be used to avoid hydrate reformation, the required concentration of these KHI being 0.5–5 wt%.

Recent experiments conducted by Shiang-Tai and Yen-Tien [28] illustrate how replacement of CO_2 with CH_4 in methane hydrates can help in the production of methane gas from methane hydrate deposits. When, liquid carbon dioxide is introduced into the methane hydrate system, rapid replacement of solid methane with carbon dioxide molecules takes place. This substitution of methane with carbon dioxide occurs spontaneously and large amounts of carbon dioxide are observed to penetrate methane hydrate molecules and expel methane especially near the hydrate melting point [28]. It has been shown how steam injection can be used effectively in producing gas from gas hydrate deposits [29], and the use of hot-brine injection for the production of gas from natural gas hydrates as well as how various factors like the temperature of the injected solvent, the injection rate, or the injection time impact the production of gas from such deposits has also been shown [30]. It is also proposed that a combination of thermal and depressurization technique can be used to produce from gas hydrates that will help in improving the economic efficiency, paving the way for the development of NGH reservoirs [30].

Weitemeyer and Constable [7] have shown how controlled source electromagnetics can be used to map gas hydrates. Further advancement of this technique has led to the creation of a fixed offset towed sensor that was able to image gas hydrates at MC118 with successful imaging of hydrates in the other three sites in the Gulf of Mexico [7]. Dai [31] has put forward a method to locate and quantify gas hydrate deposit using long-offset reflection seismic information, and since this method is not based on the AVO inversion method it stays away from the uncertainties that are a part of AVO-based seismic studies.

Conclusions

Significant improvements in the methods for drilling and evaluating potential gas hydrate zones in ANS have taken place in recent years. The drilling and formation evaluation of the Mt. Elbert-01 stratigraphic test well has successfully field-tested the modern geophysical prospecting methods used and has enabled the selection of target zones and field parameters for potential future production testing. The chilled, 100% mineral-oil-based coring fluid provided a significant improvement in wellbore quality as compared to the freezing-point-depressed water-based fluids used in the previous gas hydrate exploration projects. Core recovery, core quality, and electrical well log quality were significantly improved by using oil-based coring fluid, and operational downtime due to freeze-ups was eliminated.

The study of a producing gas field in the ANS has demonstrated the feasibility of producing natural gas from gas hydrates by depressurization to some extent. Diagnostic methodologies were developed to examine the production data from the Barrow gas fields to test the two fields for possible hydrate accumulations and to understand the gas recovery mechanisms. Engineering

approach was followed to construct hydrate stability models and material balance procedures for identifying the reservoir drive mechanisms. Based on these results, state-of-the-art dynamic reservoir simulation models were developed using an advanced commercial reservoir simulator to study hydrate reservoir development. Reservoir modeling confirmed the key findings of previous studies and projected the future performance of the reservoir under different scenarios. Finally, hydrate resource potential of EB and WAL pools appears to be promising, and both pools have considerable hydrate potential that can supply large volumes of gas for future years.

Disclaimer

This entry was prepared as an account of work sponsored by an agency of the US government. Neither the US government nor an agency thereof, nor any of their employees, makes any warranty, expressed or implied, or assumes any legal liability or responsibility for the accuracy, completeness, or usefulness of any information, apparatus, product, or process disclosed, or represents that its use would not infringe privately owned rights. References herein to any specific commercial product, process, or service by trade name, trademark, manufacture, or otherwise do not necessarily constitute or imply its endorsement, recommendation, or favoring by the US government or any agency thereof. The views and opinions of the author expressed herein do not necessarily state or reflect those of the US government or any agency thereof.

This entry is also based on research conducted by two petroleum engineering graduate students (Paul Hanson and Praveen Kumar) from the University of Alaska Fairbanks for their M.S. degree in petroleum engineering. The results of the two US Department of Energy–funded gas hydrate projects in Alaska (BP Alaska Gas Hydrate Project and the North Slope Borough Gas Hydrate Project) are also included. Several other companies, organizations associated, and individuals associated with these two projects have contributed to the work reported here.

Acknowledgment

The authors are grateful to the US Department of Energy (USDOE), BP Exploration (Alaska) Inc., North Slope Borough (NSB), Petrotechnical Resources of Alaska (PRA), and Petroleum Development Laboratory (PDL) at UAF for their financial support in accomplishing this work. The authors would also like to thank Dr. Tim Collet (USGS), Mr. Robert Hunter (ASRC Energy Services), Mr. Tom Walsh (Petrotechnical Resources Alaska, Inc.), and graduate students Praveen Singh, Andrew Johnson, Paul Hanson, and Vivek Peraser for their contribution, support, and help when needed.

Bibliography

1. Folger P (2010) Gas hydrates: resource and hazard. CRS report for congress, May 2010, CRS, Washington, DC
2. WEC (2007) Survey of Energy Resources, 2007. World Energy Council, London
3. Islam MR (1991) A new recovery technique for gas production from Alaskan Gas Hydrates. SPE 22924, Dallas, TX, USA
4. Garg R, Ogra K, Choudhary A, Menezes R. Chemical recovery of gas hydrates using fluorine gas and microwave technology. SPE 113556, TX, USA
5. Peter E (1993) Clathrate Hydrates. Ind Eng Chem Res 32:1251–1274
6. Collett TS (1992) Geologic comparison of the Prudhoe Bay-Kuparuk River (U.S.A.) and Messoyakha (U.S.S.R.) gas hydrate accumulations. SPE 24469, Texas, USA. pp 1–20
7. Weitemeyer K, Constable S (2011) Mapping gas hydrates with marine controlled source electromagnetics. In: Proceedings of the 7th international conference on gas hydrates (ICGH 2011), Edinburgh, UK
8. George MJ, Timothy CS, Boswell R, Kurihara M, Matthew RT, Koh C, Dendy SE (2008) Toward production from gas hydrates: current status, assessment of resources, and simulation based evaluation of technology and potential. SPE 114163, Texas, USA
9. Sloan ED, Koh C (2008) Clathrate hydrates of natural gases, 3rd edn. Taylor and Francis, Boca Raton, FL
10. Johnson Arthur H (2011) Global resource potential of gas hydrate – a new calculation. In: Proceedings of the 7th international conference on gas hydrates (ICGH 2011), Edinburgh, UK
11. Boswell R, Collett TS (2006) The gas hydrates resource pyramid. In: Fire in the ice, methane hydrate newsletter. US Department of Energy, Office of Fossil Energy, National Energy Technology Laboratory, Fall Issue, pp 5–7
12. Ruppel C (2011) Methane hydrates and the future of natural gas. In: MITEI Natural gas Report, MIT, MA (Supplementary paper on methane hydrates)
13. Nagakubo S, Arata N, Yabe I, Kobayashi H, Yamamoto K (2011) Environmental impact assessment study on Japan's methane hydrate R&D program. In: NETL, Methane Hydrate Newsletter, January 2011
14. Collett TS, Johnson AH, Knapp CC, Boswell R (2009) Natural gas hydrates. A review. AAPG Memoir 89:146–219
15. Paull CK, Matsumoto R (2000) Leg 164 Overview. In: Proceedings of the ocean drilling program, Scientific Results, vol 164. Ocean Drilling Program, TX, USA

16. Pecher IA, GHR Working Group (2011) Gas hydrates in New Zealand – a large resource for a small country? In: NETL, Methane Hydrate Newsletter, January 2011
17. Kadaster AG, Millheim KK, Thomson TW (2005) The planning and drilling of hot ice #1 – gas hydrate exploration well in the Alaskan Arctic. In: SPE 92764-MS presented at the SPE/IADC drilling conference, 23–25 February 2005, Amsterdam, Netherlands, pp 1–15
18. Hanson P (2007) The Mt. Elbert-01 Stratigraphic test well – lessons from drilling, coring and evaluating gas hydrates on the Alaska North Slope, MS project report, University of Alaska Fairbanks, Fairbanks, December 2007
19. Gruy HJ (1978) Reservoir engineering and geologic study of the East Barrow Field, National Petroleum Reserve in Alaska. Technical Report submitted to Husky Oil NPR Operations, Inc., Anchorage, Alaska, pp 1–62
20. Darkwah SA, Allen WW (1996) Engineering study of the South, East and Walakpa Fields, North Slope Borough, Alaska. Technical Report submitted to the North Slope Borough, Barrow, Alaska, pp 1–32
21. Singh PK (2008) An engineering study to investigate methane hydrate resource potential associated with barrow gas fields, Alaska. MS Thesis, University of Alaska Fairbanks, Fairbanks
22. Stokes PJ, Walsh TP (2006) South and East Barrow gas fields well improvements study. Technical Report submitted to the North Slope Borough, Barrow, Alaska, pp 1–70
23. Stokes PJ and Walsh TP (2007) South and East Barrow gas fields reserves study. Technical Report submitted to the North Slope Borough, Barrow, Alaska, pp 1–36
24. Allen WW, Crouch WJ (1988) Engineering study of South and East Barrow fields, North Slope Alaska, Alaska. Technical report prepared for North Slope Borough Gas Development Project, Barrow, Alaska, pp 1–56
25. Panda MN, Morahan GT (2008) An integrated reservoir model description for East Barrow and Walakpa gas fields. Topical Report prepared under DoE Project No. DE-FC26-06NT42962 submitted to the USDoE, Morgantown, WV, www.netl.doe.gov, pp 1–44
26. Sandilya P, Ganguly S (2011) Conceptual design of an experimental facility for extracting natural gas from natural gas hydrate. In: Proceedings of the 7th international conference on gas hydrates (ICGH 2011), Edinburgh, UK
27. Yutaek S, Seong-Pil K (2011) Dependence of drawdown pressure on the hydrate reformation during methane hydrate production and its inhibition with kinetic hydrate inhibitors. In: Proceedings of the 7th international conference on gas hydrates (ICGH 2011), Edinburgh, UK
28. Shiang-Tai L, Yen-Tien T (2011) Methane hydrate growth and its recovery with carbon dioxide via molecular dynamic simulations. In: Proceedings of the 7th international conference on gas hydrates (ICGH 2011), Edinburgh, UK
29. Lee Y, Shin C, Baek Y, Kim Y, Jang S, Lee J (2011) A study on the dissociation behavior of gas hydrate using the steam stimulation. In: Proceedings of the 7th international conference on gas hydrates (ICGH 2011), Edinburgh, UK
30. Shuxia L, Yueming C, Yongmao H (2011) Experimental study of influence factors of hot-brine stimulation for dissociation of NGH in porous medium. In: Proceedings of the 7th international conference on gas hydrates (ICGH 2011), Edinburgh, UK
31. Dai J (2011) A method to locate and quantify gas hydrate using long-offset seismic. In: Proceedings of the 7th international conference on gas hydrates (ICGH 2011), Edinburgh, UK
32. Collett TS (1993) Natural gas hydrates of the Prudhoe Bay and Kuparuk River area, North Slope, Alaska. AAPG Bull 77(5): 793–812

Algae, a New Biomass Resource

Cinzia Formighieri, Roberto Bassi
Dipartimento di Biotecnologie, Università di Verona, Verona, Italy

Article Outline

Glossary
Definition of the Subject
Introduction
Advantages of Algae as Biomass Producers
Present Algal Productivity in the Laboratory Versus Large Scale
Domestication
Light Use Efficiency
Non-Photochemical Energy Quenching at the Molecular Level
Interconversion and Storage of Photosynthetic Metabolic Products
Screening for State Transition as an Indirect Mean to Select Strains with Altered Redox Metabolism
Accumulation of Biomass as Neutral Lipids
Planning an Algal Refinery
Large-Scale Systems
Future Perspectives and Technological Developments
Bibliography

Glossary

Algae Oxygenic photosynthetic organisms, prokaryotic or eukaryotic, with organization ranging from unicellular to multicellular. Algae never have true stems, roots, and leaves, thus leading to their classification as "lower" plants.

Biofuel Renewable energy-rich compound derived from living organisms or from their metabolic by-products.

Biomass Organic raw material, stored as a result of the metabolism of a living organism, which can be used as a resource for energy and biofuels.

Photoautotrophy The ability of a living organism to use carbon dioxide as carbon source for biomass and light as source of energy.

Photosynthesis The overall process that converts light energy into chemical energy, finally used to fix inorganic carbon dioxide into organic compounds needed for growth. In oxygenic photosynthesis, light-induced redox reactions occurring in the photosynthetic electron transport chain are coupled to the extraction of electrons from water.

Photosystem A multipigment-protein complex composed of a light-harvesting antenna moiety energetically connected to a reaction center where the excitation energy is used for charge separation and production of a reduced product.

Light saturation constant The intensity of light at which photosynthetic oxygen evolution and specific biomass growth rate are half the maximum level. The energy absorbed in excess with respect to the photosynthesis saturation is dissipated as fluorescence or heat and not used for photochemistry.

Photoinhibition The light-induced inactivation of photosynthesis occurring when photooxidative damage of the photosynthetic machinery (particularly photosystem II) overcomes the capacity for repair.

Genetic improvement All procedures, including phenotypic selection, conventional breeding, mutagenesis, and genetic engineering, aimed at indirectly or directly influencing the genetic background of a wild strain, which was evolved following rules of natural selection. Genetic improvement is intended at improving existing characteristics or at introducing new traits to fit applications.

Genetic engineering All the techniques of recombinant DNA to directly manipulate genotypes.

Definition of the Subject

Algae are oxygenic photoautotrophs, offering a very high level of biodiversity and thus suitable for different practical applications. Today, they are mainly cultivated for human/animal food or to extract high-value chemicals and pharmaceuticals. However, their exploitation could be extended. Algae are attractive as high yield biomass producers, because of the short life cycle, the ability to grow up to very high cell densities, and the easy large-scale cultivation that does not compete with other demands such as those of conventional crops agriculture. Algae can be a resource of renewable, sustainable biofuels. In addition, they can be transformed into "cell factories" to produce recombinant proteins of interest for pharmaceutical companies.

Introduction

Algae are described as "lower" plants that never have true stems, roots, and leaves, and grow photoautotrophically by performing oxygenic photosynthesis [1]. They are mostly eukaryotic, although prokaryotic cyanobacteria are included in algae. More than 200,000 species are estimated and form a highly heterogeneous group, spread in all aquatic ecosystems but also in other habitats such as soil. A broad spectrum of phenotypes and specialized adaptation abilities exists within this group while members colonize diverse ecological habitats, from freshwater to marine and hyper-saline, at different temperatures, pH, and nutrient availabilities [1, 2]. Algae are classified as follows: cyanobacteria (Cyanophyceae), green algae (Chlorophyceae), diatoms (Bacillariophyceae), yellow-green algae (Xanthophyceae), golden algae (Chrysophyceae), red algae (Rhodophyceae), brown algae (Phaeophyceae), dinoflagellates (Dinophyceae), and "pico-plankton" (Prasinophyceae and Eustigmatophyceae). Algae are accountable for the net primary production of ~50% of the total organic carbon produced on earth each year [3], a reason for their massive biological importance. Long before the advent of biotechnology, algae were used as a human food source for centuries by indigenous populations [4, 5]. However, aside from some attempts to cultivate algae and to extract from them valuable products back to the seventeenth century [6], commercial large-scale production of algae began few decades ago [4, 7]. Currently, algae are mainly cultivated as human/animal food source and used in aquaculture, in agriculture, as fertilizers, and in order to produce high-value

chemicals, pharmaceuticals, and cosmetics, such as polyunsaturated ω3 fatty acids, proteins, biopolymers, and polysaccharides as agar, carrageenan, alginates, pigments, vitamins, and antioxidants [1, 4].

Recently, a new interest in algal biomass as renewable energy source is emerging. About 80% of world energy demands are met by the combustion of fossil fuels: coal, oil, and natural gas. However, fossil fuel reserves are limited and their exhaustion is estimated, assuming a stable consumption, to occur within few decades while their combustion has high impact on environment, due to releases of large amounts of carbon dioxide and other pollutants. This is considered a major problem for human society. Its becoming increasingly clear that finding alternative, renewable energy sources to sustain our lifestyle is striking and urgent. Such widespread and environmentally sustainable energy source will allow single countries to be more independent from the escalating prize of crude oil. The public conscience that search for energy sources alternative to fossil fuels is fundamental for future prospects is generally increasing and research is undertaken in many countries. Advances have been made recently on the exploitation of renewable energies such as sun and wind, which can be considered as "clean" and non exhaustible. Fuels derived from living organisms or from their metabolic by-product are defined as "biofuels." Photosynthetic organisms convert carbon dioxide into biomass, a form of stored chemical energy that can be used in substitution for fossil fuels. In some species of algae, 30% up to 80% of the biomass is accumulated as oil that can be extracted and converted to biodiesel [2, 8–11]. Some algae, mainly green, can photobiologically generate hydrogen [12–15], which is released from the culture with a purity up to 98% [16]. Spent algal biomass can be further valorized to produce biomethane from anaerobic digestion of the biomass itself [1, 5] and high-value ingredients for food and pharmaceuticals can be produced along with biofuels in order to reach cost-effectiveness and economic competitivity over conventional fuels.

Advantages of Algae as Biomass Producers

The use of algae for fuel production has notable advantages. First of all, algae are photoautotrophic organisms, thus able to produce biomass from solar energy, water, and carbon dioxide, all renewable and cheap components. Carbon dioxide removal, in addition, would contribute to reduce atmospheric levels of this pollutant which, instead, is stoichiometrically released in the atmosphere by conventional fuels. The use of fossil fuels currently releases about 6 billion tons of carbon dioxide per year, only partially compensated by re-assimilation by photosynthetic organisms in forests (about 1 billion ton year^{-1}) and oceans (2 billion tons year^{-1}) [17] leading to a 3-billion-ton year^{-1} increase in the global level of carbon dioxide in the atmosphere. This has been widely suggested to cause the so-called greenhouse effect, leading to world global warming [18]. To prevent undesired climate changes, carbon dioxide emissions need to be reduced in the near future [19]. Biofuels from algae are attractive because their combustion would not result in net carbon dioxide emissions since biofuels will only release the amount of carbon previously absorbed during growth of algae.

Advantages of algae over crop plants are many:

1. Photosynthesis increases with carbon dioxide concentration until saturation. Algae can grow with up to 18% of carbon dioxide, being more efficient carbon dioxide assimilators than land plants [20] and suitable for mitigation of carbon dioxide emissions when coupled to an industrial activity. *Chlorella vulgaris* was shown to respond well to elevated carbon dioxide levels (over 1,850 ppm CO_2) and to effectively remove up to 74% of the carbon dioxide in the airstream to ambient levels (330 ppm CO_2) with a 63.9 g m^{-3} h^{-1} bulk removal in the experimental photobioreactor of 2 L [21]. The carbon dioxide fixation rate by algal biomass is estimated ten times as large as that of the temperate forest [22].
2. Cultivation of algae does not compete with other demands such as food production because algae can grow in wastelands rather than in arable lands. Using the entire US soybean crop for biodiesel would replace only 10% of conventional diesel consumed and total world plant oil production would only satisfy 80% of US demand [23]. Exploiting algae rather than crops thus represents an essential, sustainable alternative to fulfill the energetic demands without affecting food supply.

3. Algae, differently from crops, do not require pesticides, which avoids contamination of water and soils and also fertilization is limited to the culture vessel without dispersion of nutrients in the environment and consequent eutrophysation of water bodies.
4. Algae can grow in seawater, brackish water, or wastewater making a substantial saving of freshwater that in contrast is required by conventional crops in high amounts. Extensive cultivation of algae would therefore be more environmentally sustainable than extensive cultivation of conventional crops.
5. Algae can utilize nutrients from a variety of wastewater sources (agricultural runoff, and industrial and municipal wastewaters), providing additional benefit of bioremediation.
6. The life cycle of algae is more rapid (hours to days) as compared to land plants (months to years), allowing for a faster turnover and a higher biomass yield. In more detail, crop plant life cycle has a long initial development phase using energy stored in seeds for building the organism, followed by a relatively short phase of full photosynthetic activity and then senescence, limiting the period of efficient light harvesting and utilization to a fraction of the year. In contrast, algae not only have a short life cycle but they remain productive throughout the year, allowing for a continuous biomass production when light is available and temperature allows.
7. Many algal species are competent for using organic carbon as energy source. This ability opens the possibility to allow for biomass production at night by supplying low-priced carbon substrates.
8. Algal biomass is fully photosynthetically active. In contrast, photosynthesis is localized exclusively in leafs of vascular plants, a fraction of the total plant body, while the rest is an energy sink, thus a disadvantage in terms of biomass productivity.

Present Algal Productivity in the Laboratory Versus Large Scale

Algae can convert solar energy into chemical energy through the process of photosynthesis. The whole process of oxygenic photosynthesis can be summarized by Eq. 1.

$$6H_2O + 6CO_2 \rightarrow C_6H_{12}O_6 + 6O_2 \quad (1)$$

Light energy is used to extract electrons from water (H_2O), thus generating oxygen (O_2). These electrons are transported through a linear electron transfer chain and finally reduce $NADP^+$ to NADPH. Photosynthetic electron transport is coupled to the generation of a transmembrane electrochemical gradient, whose stored energy is used to synthesize ATP. NADPH and ATP are then used to produce glyceraldehyde-3-phosphate from CO_2 in a metabolic pathway that is called the Calvin–Benson cycle [24]. Photosynthesis enables the cell to convert inorganic CO_2 into organic carbons and finally to accumulate biomass.

A theoretical estimation of algal biomass yield can be assessed considering the efficiency of photosynthesis. A minimum of 8 photons of light energy are absorbed per each oxygen molecule evolved, the actual average measurement is 9.5 photons per oxygen [25]. Per oxygen evolved, four electrons are channeled into the linear photosynthetic electron transport chain and in the process three molecules of ATP and two of NADPH are produced. In order to convert three carbon dioxide molecules into glyceraldehyde-3-phosphate, nine ATP and six NADPH are required. The ratio is 9.5 mol photons for the conversion of 1 mol CO_2 into biomass. The average insolation, that is the solar radiation energy on a surface area in a given time, is between 3 and 5 kWh m^{-2} day^{-1} (full solar spectrum) at temperate regions. However, only about 40% of solar radiation is photosynthetically active (PAR), because only photons with wavelengths between 400 and 700 nm (visible spectrum) can be absorbed by photosynthetic pigments, since these wavelengths carry an energy equal to the change in the energetic level between the ground state and the excited one.

A photon has an energy that is directly proportional to its frequency and inversely proportional to its wavelength, following Eq. 2.

$$E = h\nu = c/\lambda \quad (2)$$

(h, Planck constant, 6.626×10^{-34} Js; c, light speed, 3×10^8 m s^{-1}; ν, frequency; λ, wavelength)

For example, 1 mol photons (1 Einstein) at 440 nm has energy of 272 kJ, while 1 mol photons at 670 nm has

energy of 178 kJ. Out of the full solar radiation of 5 kWh m^{-2} day^{-1}, the photosynthetically active radiation (PAR) is about 35 mol photons m^{-2} day^{-1}. Considering the energy requirement of 9.5 mol photons per 1 mol CO_2, with such average available light radiation the cell could assimilate 3.68 mol CO_2 m^{-2} day^{-1}. Since biomass composition can be approximated to the formula CH_2O, the previous data would translate in the synthesis of about 110 g biomass m^{-2} day^{-1}. However, accumulation of organic carbons as biomass is lower, due to respiration and other metabolic activities and energy losses are accounted to 30%. The resulting expected maximum biomass productivity would be of 77 g biomass m^{-2} day^{-1} (280 t ha^{-1} $year^{-1}$), corresponding to a solar-to-biomass conversion efficiency of 8–10% [25]. This value is about 25 times higher than estimations for vascular plants, possibly due to algal biomass being fully photosynthetically active. Such estimation assumes that all available light energy is absorbed and utilized for photosynthesis. However, real algal biomass productivity achieved so far in the laboratory or small-scale systems does not exceed the 73–146 t dry weight ha^{-1} $year^{-1}$ (20–40 g dry weight m^{-2} day^{-1}) and 3% of solar-to-biomass conversion efficiency [25] in the best cases. Currently, commercial exploitation of algae mainly utilizes open ponds. They are usually raceway cultivators driven by paddle wheels or unstirred, operating at water depths of 15–20 cm, biomass concentration can be up to 1,000 mg L^{-1} and productivity between 60 and 100 mg L^{-1} day^{-1} (10–25 g m^{-2} day^{-1}) [26]. Commercial rates of production of *Chlorella* have been reported to be 60–75 t dry weight ha^{-1} $year^{-1}$ (17–20 g dry weight m^{-2} day^{-1}) [27]. Another example is *Dunaliella salina*, which is now being cultivated on a commercial scale and in pilot-scale projects to extract β-carotene and glycerol. Over short periods and in small-scale, productivity records 60 g dry weight m^{-2} day^{-1}. However, commercial production requires larger culture systems and is presently carried out in outdoor ponds (approximately 20 cm deep for 5 ha of surface, total ponds area of 50 ha), because of the still expensive constructing of closed photobioreactors. In these large-scale systems, the maximum productivity achievable is at present 30–40 g dry weight m^{-2} day^{-1} but more regularly is below 30 g dry weight m^{-2} day^{-1} [28]. Outdoor pond cultures of *Cyclotella* report a biomass productivity of 12 g m^{-2} day^{-1} [29]. With the present knowledge and with the available algal strains, real productivity is far below theoretical estimations, especially in large-scale and over long-lasting periods, and a major future goal would be to get rid of or reduce this gap.

As an alternative to open ponds, few relatively large-scale closed photobioreactors have been developed (refer to "Large-Scale Systems" section for a comparison between open ponds and photobioreactors in terms of advantages), displaying a productivity of 2.7 g L^{-1} day^{-1} in a small undular row tubular photobioreactor of 11 L, 1.9 g L^{-1} day^{-1} in a airlift tubular photobioreactor of 200 L and 0.05 g L^{-1} day^{-1} in a parallel tubular photobioreactor of 25,000 L [30]. Constructing of photobioreactors is still at the beginning and better productivities (up to ten times higher g L^{-1} day^{-1}) as compared to open ponds are obtained with pilot systems. It is likely that such interesting results would also be achieved at larger scale, by improving photobioreactor design and mechanics.

One major reason for the real lower biomass productivity with respect to the theoretical calculation is that photosynthesis light reactions have to fit downstream biochemical processes while excess absorbed energy is dissipated as heat. Photosynthesis displays a light saturation curve [25] (Fig. 1).

At low light intensities, light is the limiting factor for the photosynthesis rate, measured as photosynthetic oxygen evolution. At increasing light intensities, the limiting factor becomes carbon dioxide fixation. When light irradiance overcomes the rate of the downhill biochemical processes, excess absorbed energy is dissipated and photosynthetic oxygen evolution reaches a plateau. If light further increases, beyond the capacity of photoprotective mechanisms, photoinhibition leads to a decrease in photosynthesis rate. Therefore, all the absorbed light energy in excess with respect to the saturation level of photosynthetic electron transport does not contribute to biomass accumulation, but it is instead wasted as heat and/or leads to the formation of reactive oxygen species (ROS) that ultimately inhibit photosynthesis. Light saturation constant is defined as the intensity of light at which the specific biomass growth rate is half its maximum value [9]. For example, light saturation constants of microalgae *Phaeodactylum tricornutum* and *Porphyridium cruentum* are, respectively, 185 μmol photons m^{-2} s^{-1} [31] and 200 μmol

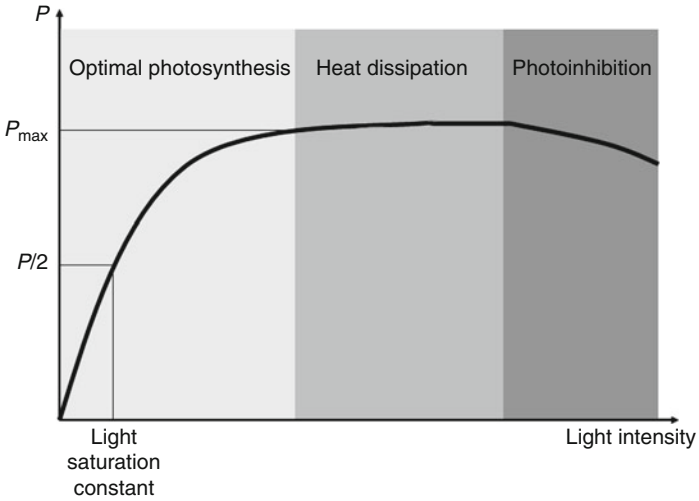

Algae, a New Biomass Resource. Figure 1
Light saturation curve. Photosynthetic oxygen evolution (*P*) increases with light intensity linearly until saturation. P_{max} is the maximum photosynthetic rate. *P*/2 is the photosynthetic oxygen evolution rate at half the maximum level. The light intensity at *P*/2 is defined as the light saturation constant. Upon saturation of photosynthesis, when downstream biochemical processes are limiting, excess absorbed energy is dissipated as heat and if light further increases beyond the capacity of photoprotective mechanisms, photosynthetic rate decreases because of photosystem II photoinhibition

photons m^{-2} s^{-1} [32], much lower than the maximum outdoor sunlight level that occurs at midday in equatorial regions, that is about 2,000 μmol photons m^{-2} s^{-1} [9]. In particular, considering a saturating light intensity of 400 μmol photons m^{-2} s^{-1}, photosynthesis would saturate at about 7 a.m. and remain saturated until 5 p.m. [25]. An average of 60% up to more than 80% of absorbed irradiance would be wasted and not converted into chemical energy during the course of a sunny day [25, 33]. These energy dissipation events have an important photoprotective role in the natural environment but reduce the potential growth rate in biomass culture conditions.

Domestication

Crop species currently widely cultivated are "domesticated" strains that evolved from wild ancestors [34]. A domesticated crop has been genetically altered and made into a resource for man through cycles of phenotypic selection, breeding, and mutagenesis. In this way, man can divert evolution of plants to fit agronomical, nutritional, and industrial applications. A fully domesticated crop cannot survive without the help of human mankind; meanwhile, farmers would not work with wild species because farming with wild-type (ancestral) genotypes would not be economically sustainable. Domestication began in Middle East around 10,500 years ago when humans applied selection to cereals and legumes, modifying morphological and nutritional traits. During history, all crop plants were domesticated in a process that took between decades and several centuries depending on the number of genes involved. For example, modern corn was domesticated from the wild *Teosinte* to improve productivity and the ability to grow at high density in cornfields. High plant densities in fields are not dissimilar to the high algal cell densities that are reached up in a photobioreactor. In the case of tomato, several mutations in genes involved, for example, in cell division, carotenoid biosynthesis, anthocyanin biosynthesis, and ethylene receptor altered fruit color, weight, shape, and ripening of the wild ancestor to finally obtain the now commercially cultivated tomato [35]. Indirect conventional approaches are now being supported by recombinant DNA techniques to directly manipulate genotypes and speed up the process.

The natural biodiversity of algae offers a wide spectrum of phenotypes and specialized adaptation abilities that can be exploited for commercial applications.

Relatively few algal strains have been examined to date, among all the species available in nature. Strains with very interesting features as accumulators of biomass, biofuels, or other high value products could be still unexplored and search for new strains is for sure a valuable strategy to pursue. However, similarly to crops, biofuel production with wild-type algal species collected from the environment, often proposed as a "green way" to energy supply, is unlikely to be economically sustainable, because wild-type algal strains evolved to better adapt to their natural habitats and some of their characteristics are far from optimal for growth in mass culture conditions. A domestication process needs to be applied to algal species preliminary to industrial applications are attempted. In particular, selection of strains with the desired properties combined with input of new alleles through mutagenesis and genetic engineering would help to generate strains with improved biomass yield, oil content, and fuel properties. For example, insertional mutagenesis can be used to generate random insertional libraries to be screened for selected phenotypes.

Algal biotechnology primarily utilizes unicellular species that can be propagated in the laboratory. For this reason, a great attention is focused on unicellular microalgae, more suitable for genetic manipulation and prospects of biofuels production [1]. Algae have several advantages over higher plants in genetic improvement:

1. A short life cycle enables to genetically manipulate them faster than crop plants.
2. Because of the usual absence of cell differentiation and haploid nature of most vegetative stages, microalgae allow faster phenotypic selection.
3. Microalgae are small and can be analyzed in large numbers in a Petri dish.
4. It is conceivable that substantial improvements in algae cultivation could be achieved in the future. In contrast, prospects of improvement in higher plants are less favorable, because current cultivated crops have already been genetically improved with respect to the wild ancestors and cultivation techniques are already well optimized. Algae have been less explored and exploited in the past and current biomass productivity is likely to be improved.
5. Algae are suitable for growth in photobioreactors, offering a confined environment for genetically modified organisms.

In the following sections, examples of targets for domestication are described.

Light Use Efficiency

A main process affecting solar-to-biomass conversion efficiency is light harvesting. The photosynthetic apparatus comprises two photosystems (photosystem II and photosystem I) operating in series. Each photosystem is composed of an essential core complex, decorated with an antenna system of variable size with functions in light harvesting and photoprotection. Chlorophyll molecules and other accessory pigments bound to photosystems act cooperatively in the absorption of incoming solar radiation. The ability to assemble large arrays of light-harvesting complexes has been positively selected during evolution since it represents a survival strategy and a competitive advantage in the wild, where light could be limiting [36]. Meanwhile, excess light conditions are mostly avoided by algal cells through changing their location in the water column. Up to 600 chlorophyll molecules can be found in association with photosystem II and photosystem I [25]. Light-harvesting complexes are however not a rigid apparatus and both short-term and long-term mechanisms to adjust the light-harvesting capacity to changing light conditions are present in photosynthetic organisms. These include heat dissipation of excess absorbed energy (non-photochemical quenching, NPQ) [37, 38] in the short term and regulation of photosynthetic gene expression during long-term acclimation [39–41]. Growth conditions in large-scale mass culture are very different with respect to those found in the natural environment. In photobioreactors, cellular concentration is many orders of magnitude higher than in water bodies, so as to increase production per volume. In these conditions, large-size light-harvesting antenna, an advantage in the wild, becomes detrimental for overall biomass productivity because high optical density of antenna pigments results in self-shading and light attenuation in deep layers of the culture. Incident light energy is mostly absorbed by cells at the surface, exceeding photosynthesis maximum rate and resulting in dissipation and loss of excess photons as

fluorescence or heat. Up to 80% of the absorbed photons could thus be wasted [33]. Moreover, these cells would be more subjected to photoinhibition, that is the light-induced inactivation of photosystem II due to photooxidative damage [42, 43], leading to losses in photosynthetic productivity [44]. Meanwhile, a suboptimal illumination would occur in the deepest layers, where energy consumption by respiration would reduce the overall yield [45, 46]. Only the intermediate layers are in conditions for optimal photosynthetic yield and thus determine the productivity of the mass culture. As a consequence of the light gradient formed across the photobioreactor diameter, the real solar radiation to biomass conversion efficiency decreases far below the calculated value of 8–10% [25], as also mentioned in the "Present Algal Productivity in the Laboratory Versus Large Scale" section. The unequal light distribution has another negative consequence: algal cells are stirred into the reactor where they can move from suboptimal illumination to strong light within few seconds, without having time to adjust the photosynthetic apparatus [47]. Intermittent light is highly stressful and contributes to the oxidative stress and photosystem II photoinhibition.

It was first postulated 60 years ago [48] that a truncated light-harvesting antenna size would optimize light utilization efficiency of microalgae in a mass culture. Such configuration would require a higher light intensity to reach photosynthesis saturation (refer to "Present Algal Productivity in the Laboratory Versus Large Scale" section for definition of light saturation constant) and would minimize wasteful dissipation of excess absorbed energy and photoinhibition. In particular, a better transmittance of light deeper into the culture would be allowed, enabling more cells to contribute to useful photosynthesis and culture productivity. It was estimated that a reduced optical density could improve solar radiation to biomass conversion efficiency up to three to four times [33]. Figure 2 schematically compares the behavior of the wild type to a truncated antenna strain, with respect to light distribution and growth inside a hypothetical tubular photobioreactor.

While algae with a truncated light-harvesting chlorophyll antenna size would be useful in controlled mass culture conditions, they are not competitive and do not survive in the wild, so are not encountered in nature. Although the advantages of strains with altered optical properties were recognized long ago, only recently, with molecular genetics coupled to biophysical phenotype screening methods, the problem of their construction can be addressed. Small antenna mutants can now be obtained through chemical/UV mutagenesis or insertion mutagenesis and tested for their light use efficiency. Small antenna strains described earlier carried mutations in pigment biosynthesis. Pigments are bound to photosystem protein subunits where they act cooperatively in light harvesting, meanwhile photosystem subunits require a specific set of bound pigments to be properly folded and assembled. Reduction of photosystem II antenna size was indeed observed as a consequence of mutations affecting the biosynthesis of chlorophyll *b* [49, 50] or the biosynthesis of xanthophylls [51], specifically coordinated by light-harvesting antenna subunits, in the model unicellular green alga *Chlamydomonas reinhardtii*. However, photosynthetic antenna components are devoted not only to light harvesting but also to photoprotection, meant as the ability to prevent reactive oxygen species in the light [52]. Moreover, carotenoids of the xanthophyll cycle have multiple roles in photoprotection [53–55]. Algal mechanisms of oxidative stress resistance are particularly important for growth in photobioreactors, especially the capacity to respond to fast alterations in light intensity that cells can face during stirring of the medium. Therefore, efforts at reducing the antenna must not compromise the photoprotection ability of the strain, otherwise the advantage obtained in terms of light distribution would be worthless. For example, pigments mutants of the diatom *Cyclotella*, without fucoxanthin, a xanthophyll synthesized in chlorophyll *a* and chlorophyll *c* containing algae, displayed a truncated antenna size and a higher light saturation, but no improvements in biomass productivities were observed in either laboratory cultures or outdoor ponds [29]. Every isolated antenna mutant must be tested for its growth performance and oxidative stress resistance before any application. Novel genes need to be found, whose deletion or mutation leads to phenotypes of selective downregulation of antenna components, retaining gene products with photoprotective function. Among available methods for the identification of these genes, random insertion mutagenesis is of choice (refer to "Future Perspectives and Technological Developments" section for further explanation).

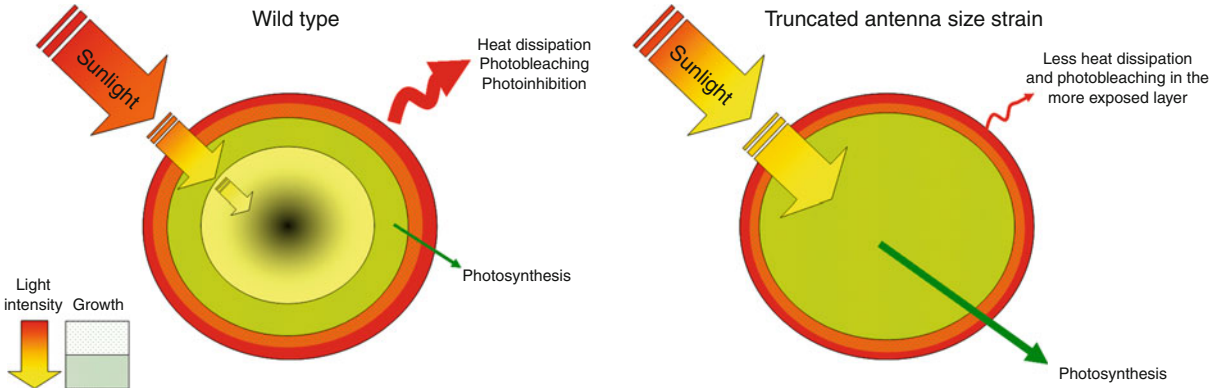

Algae, a New Biomass Resource. Figure 2
Schematic representation of a tubular photobioreactor transversal section. In wild type (*left*), most of light is absorbed by cells in surface layers. Excess light is transformed into heat by physiologic dissipation mechanisms. An algal strain with truncated antenna (*right*) is less efficient in absorbing light, thus allowing penetration of the irradiance deeper into the culture. As a consequence, a higher fraction of cells is photosynthetically active and accumulates biomass and a smaller fraction of the incident sunlight energy is dissipated into heat due to the lower number of photons intercepted by each photosystem. However, since antenna protein subunits, beside light harvesting, have important role in photoprotection preventing the formation of reactive oxygen species or scavenging them, it is essential that the reduction in the antenna system does not compromise photoprotection capacity of the strain in use

Once a mutant library has been generated by transformation with a cassette carrying a selectable marker gene, strains with the desired characteristics must be identified from the pool by high throughput methods. Truncated antenna size strains can be selected for a lower chlorophyll fluorescence yield and/or pale green appearance and/or lower accessory pigments versus chlorophyll *a* content with respect to wild type. The fluorescence screening is performed upon application of a saturating light pulse to dark-acclimated cells. Light excites chlorophylls connected to photosystem II which undergo a transition from an "open" state with low fluorescence to a "closed" state when all photosystem II primary acceptors are reduced and fluorescence level is maximal. The maximum fluorescence parameter depends on the number of chlorophylls bound to photosystem II and its value is therefore roughly indicative of photosystem II antenna size. Thus, mutants with reduced chlorophyll antenna are expected to show a phenotype with a lower yield of chlorophyll fluorescence with respect to the wild type [56]. At room temperature, chlorophyll florescence derives from photosystem II, since photosystem I fluorescence yield is negligible in this condition. Photosystem I is more efficient in quenching antenna excitation because of a faster turnover rate of the photochemistry reactions and its fluorescence is detectable only at low temperature (77 K). For this reason, room temperature fluorescence intensity is indicative of the sole photosystem II antenna. Meanwhile, since antenna subunits bind different pigments with respect to photosystem core complexes, namely chlorophyll *b* and xanthophylls, analysis of pigments by absorption spectra and/or HPLC can detect mutations in both photosystem I and photosystem II antenna systems. Since chlorophyll biosynthesis in the chloroplast is strictly coordinated with the expression of both nucleus and chloroplast-encoded chlorophyll-binding proteins, a "pale green" phenotype could arise from mutations affecting directly chlorophyll biosynthesis or from mutations impairing expression of chlorophyll-binding proteins, their import into the chloroplast or their assembly into photosystems. Mutations affecting these mechanisms are expected to yield strains with constitutively reduced antenna size, irrespective of the compensatory acclimative mechanisms which are involved in adapting the light-harvesting function to environmental conditions.

Factors controlling antenna proteins expression at the posttranscriptional level are attractive for genetic engineering manipulations [57] and a permanently active variant of NAB1, a novel cytosolic RNA binding protein, allowed to reduce photosystem II antenna size by 10–17% via translation repression, finally improving light-to-biomass conversion efficiency in high light. In particular, cell culture densities of the antenna mutant in the 200 mL bottles increased within 38 h from 5.97×10^5 to 1.2×10^7 cells mL^{-1}, whereas the parental strain reached only 5.72×10^6 cells mL^{-1} after the same time period [58].

Coordinated downregulation of the entire light-harvesting chlorophyll-binding *lhc* gene family was achieved by RNA interference technology, at last resulting in increased efficiency of cell cultivation under elevated light conditions of 1,000 μmol photons m^{-2} s^{-1}. Peak density of RNAi cultures was detected already after 26.5 h, at which parental strain cultures had only been able to grow to 54% of their maximal cell densities [59]. However, RNA interference-induced phenotypes can become unstable after some time. This technology would be useful to identify antenna components or modulators that can be depleted without compromising photoprotection ability. It should be noted, however, that strains for industrial use should be stable over time making deletion/insertional mutants preferable.

Through insertional mutagenesis of *C. reinhardtii*, an interesting mutant, called *tla1*, was isolated for a reduced yield of chlorophyll fluorescence. It displayed a residual chlorophyll content per cell of about 35–40% the wild-type level and a functional chlorophyll antenna size of both photosystem II and photosystem I reduced to 114 and 160 chlorophyll molecules, respectively [56]. This mutation allowed to identify a novel gene involved in the regulation of antenna proteins accumulation in algae. The *tla1* strain required a higher light intensity for the saturation of photosynthesis, about twofolds higher than wild type, and showed a higher photosynthetic productivity under mass culture conditions, reaching higher cell densities (10×10^6 cells mL^{-1} vs. 6.4×10^6 cells mL^{-1}) [56, 60]. Simultaneous reduction of photosystem II and photosystem I antenna systems is a desired advantage in terms of global optical density of the cell. In contrast, the sole reduction in photosystem II antenna, if not counterbalanced by an adjustment in photosystem II/photosystem I ratio, could decrease the photon use efficiency possibly because a portion of the light energy absorbed by photosystem I could not be efficiently utilized in the linear photosynthetic electron transport process [49]. The minimum number of chlorophyll molecules, needed for the assembly of the photosystem core complexes, has been estimated to be 37 for photosystem II and 95 for photosystem I [61]. This would be the minimum chlorophyll antenna size that would allow for assembly of the photosystems and that could be theoretically achieved through mutagenesis and genetic engineering [25]. Reduction in the antenna systems acquired so far is still above this estimated minimum chlorophyll antenna size and further improvements could be achieved in the future.

Although truncation of the antenna size of the photosystem unit can contribute to improve optical properties of the algal suspension, considering the important role of the antenna systems also in photoprotection, an alternative route to pursue could be to reduce the number of photosystems per cell and thus the pigment content per cell. In algae, acclimation to high light could rely more on the reduction of the photosystem density rather than on major adjustments in the antenna system to prevent overexcitation [62]. This natural light acclimation ability could be exploited in order to generate strains with a constitutive reduced optical density through the identification of involved regulatory factors and their genetic manipulation.

Non-Photochemical Energy Quenching at the Molecular Level

Oxygenic photosynthesis involves highly reactive intermediates, such as singlet excited state of chlorophylls that can decade into triplet excited state, and may lead to the formation of reactive oxygen species (ROS). These by-products can damage the photosynthetic apparatus and other chloroplast constituents. The potential for damage is exacerbated when the amount of absorbed light exceeds the capacity for light energy utilization in photosynthesis, a condition that can lead to decreases in photosynthetic efficiency. Non-photochemical quenching (NPQ) is the process of heat dissipation of excess absorbed energy, which is aimed at regulating light harvesting and preventing

overexcitation of reaction centers. The major component of NPQ, called qE, is the fastest established and more rapidly reversible quenching deriving from de-excitation of the singlet excited state of chlorophyll in the light-harvesting antenna of photosystem II in response to a change in thylakoid lumen pH. Excess light with respect to the capacity of CO_2 fixation promotes lumen acidification since ATP synthesis is limited by the low ADP + Pi concentration available. In addition to qE, a more slowly relaxing component of the NPQ process is known as qI, from photoinhibition, that is the light-induced inactivation of photosystem II reaction center. More recently, qI was shown to depend on the synthesis of zeaxanthin, promoted in excess light. Zeaxanthin binds to light-harvesting antenna proteins where it becomes a quencher for chlorophyll excited states. Its action relaxes when zeaxanthin is released and back-transformed into violaxanthin [63]. A third quenching component, relaxing within minutes, has been reported and called qT and proposed to depend on the phosphorylation of the outer antenna proteins that controls their partition between photosystem II and photosystem I during the process of state 1–2 transition [64].

Photosynthetic light harvesting in higher plants is mainly regulated through qE and requires PsbS, a photosystem II subunit [65], which is sensitive to pH through two lumen-exposed glutamate residues whose protonation is required for qE activation [66]. Since PsbS does not bind pigments, it cannot be a quenching site but rather a pH sensitive trigger [67] transducing a conformational change to antenna proteins binding chlorophylls and xanthophylls. Changes in the mutual distance/orientation of these chromophores reversibly promote energy-dissipation processes such as transient formation of carotenoid radical cations, which decay to the ground state dissipating energy as heat [68, 69]. Although light-dependent energy quenching is a property of all photosynthetic eukaryotes, strong differences in the underlying mechanisms are apparent. Although genes encoding PsbS are found throughout the green lineage, indicating that the protein was present before the separation between unicellular green algae and multicellular organisms, a PsbS protein is only accumulated in green macroalgae and land plants. Nevertheless, several algal species, such as *Chlorella zofingiensis* and *Scenedesmus communis*, exhibit strong light-dependent NPQ independent from light intensity during growth [70] or upon acclimation to high light as in *Chlamydomonas reinhardtii* [71], suggesting other gene products might be involved. The moss *Physcomitrella patens* and algal genomes, but not red algae and cyanobacteria, include LHCSR (stress-related members of the Lhc protein superfamily) genes that are essential for NPQ [72, 73]. Cyanobacteria and possibly red algae, which have phycobilisomes for light harvesting, perform excess energy dissipation by a mechanism distinct from qE, which depends on the *O*range *C*arotenoid *P*rotein (OCP) [74]. Understanding the mechanisms of NPQ and identification of the genes involved is valuable as a target for genetic improvement of algal productivity and domestication, since NPQ controls light stress resistance and energy losses in an algal mass culture.

Interconversion and Storage of Photosynthetic Metabolic Products

Aside from light harvesting, solar-to-biomass conversion efficiency strongly depends on downhill biochemical reactions influencing photosynthate production and utilization. Respiration and other metabolic activities are accounted for about 30% energy losses with respect to the light energy absorbed leading to an estimated solar-to-biomass conversion efficiency of 8–10% in algae [25]. Biomass accumulation ultimately depends on algal photosynthetic architecture and the intricate relationships between oxygenic photosynthesis, mitochondrial respiration, and catabolism of endogenous substrates. In order to improve solar-to-biomass conversion efficiency, it is essential to recognize bottlenecks in the processes interconnecting photosynthesis to other metabolic pathways to make them targets for engineering. Figure 3 is a schematic representation of the main anabolic and catabolic pathways influencing photosynthate production and biomass accumulation.

The primary reactions of photosynthesis in algae and plants occur in the chloroplast thylakoid membrane and are catalyzed by the multiprotein-pigment complexes photosystem II (PSII), cytochrome *b6f* (Cyt *b6f*), and photosystem I (PSI). The photosynthetic apparatus itself is a very flexible system, able to modify

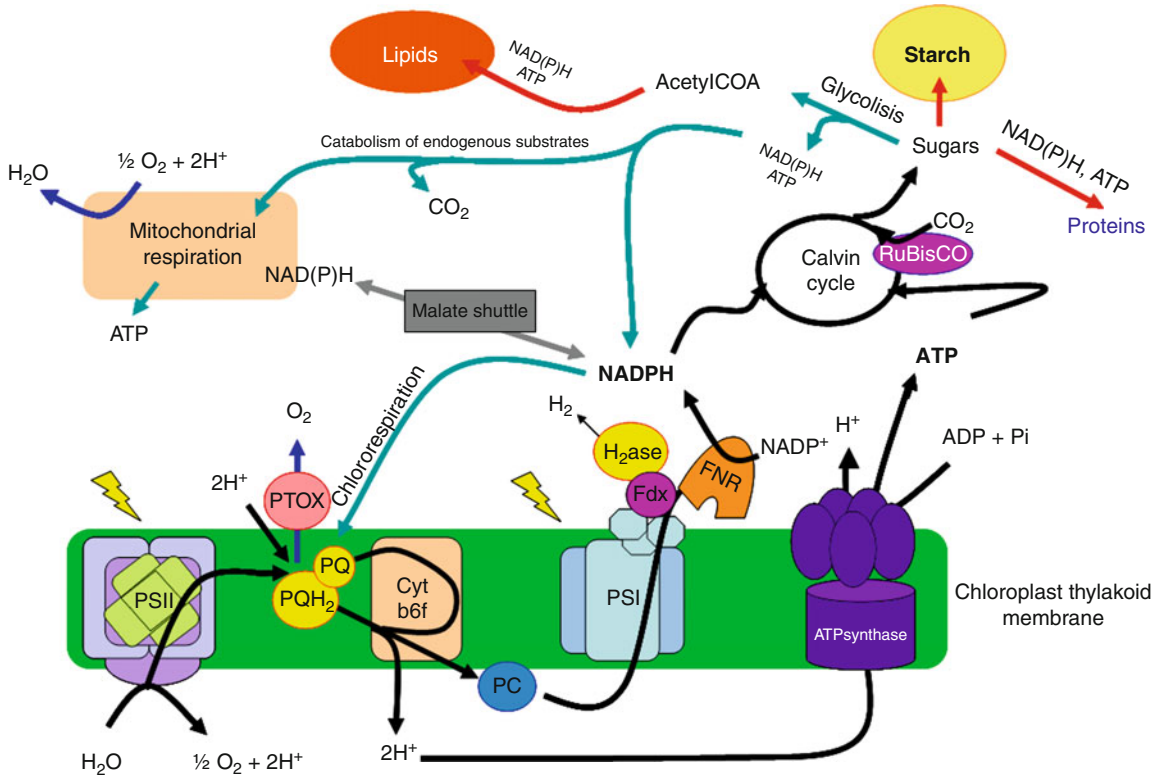

Algae, a New Biomass Resource. Figure 3
Metabolic overview. Components of the photosynthetic electron transport chain embedded in the chloroplast thylakoid membrane are depicted. *Black* lines mark biosynthetic reactions building up the main constituents of the cell, proteins, starch, and lipids. *Dark gray* lines mark catabolic reactions that consume endogenous substrates. *PSII* photosystem II, *PSI* photosystem I, *Cyt b6f* cytochrome b6f complex, *PQ* plastoquinone, *PQH2* plastoquinol, *PTOX* plastid terminal oxidase, *PC* plastocyanin, *Fdx* ferredoxin, *FNR* ferredoxin-NADP+ oxidoreductase, *H2ase* hydrogenase, *RuBisCO* ribulose-1,5-bisphosphate carboxylase/oxygenase

exciton fluxes within its antenna complexes as well as electron fluxes among its electron transfer components [75]. Photosystem II and photosystem I operate in series within the photosynthetic electron transport chain. However, alternative electron transport pathways could be engaged, as well as alternative electron sources or sinks that ultimately would affect availability of reducing power (NADPH) and ATP for carbon dioxide fixation. As a matter of fact, the net products of photochemistry, NADPH and ATP, that supply the Calvin–Benson cycle, are also used by other metabolic pathways such as nitrate assimilation, lipid, aminoacids, and pigments synthesis. These different sinks may significantly contribute to modify the ATP/NADPH ratio and, as a consequence, in vivo carbon fixation [76]. The photosynthetic process is divided into reactions that provide ATP and NADPH (photochemical light reactions) and reactions that consume both compounds (carbon assimilation through the Calvin–Benson cycle). The rate of these two phases may differ in several orders of magnitude, especially in high light when carbon assimilation is limiting the overall process, and alternative electron sinks may have an important photoprotective role to consume excess generated reductants. Respiration in mitochondria can serve as well as a sink for excess photosynthesis generated reducing power. Complex interactions between photosynthesis in the chloroplast and respiration in the mitochondria occur because both processes are linked by common key metabolites such as

ADP/ATP, NAD(P)H, triose-P, and hexose-P [75, 77, 78]. The chloroplast continuously communicates its metabolic state to the cell, for instance via the export of carbohydrates, which are synthesized during photosynthesis. The transport of carbohydrates across the chloroplast membrane directly allows to exchange reducing equivalents through "redox valves," such as the malate-oxaloacetate shuttle [79]. Different cellular compartments are thus strictly interconnected and photosynthesis is influenced by either the requirements of the chloroplast or the metabolic status of the whole cell. In particular, it was observed that efficient photosynthesis depends also on mitochondrial respiration in the light [16, 78, 80, 81].

Carbon fixation is influenced by alternative electron sinks as well as alternative electron sources. For example, reducing equivalents derived from catabolism of endogenous substrates can fuel the respiration chain in mitochondria but also the photosynthetic electron transport chain, thanks to a respiration pathway in the chloroplast. Respiration of the chloroplast, also called chlororespiration, was defined as a respiratory electron transport chain in interaction with the photosynthetic chain [82] and could have its origin in the cyanobacterial endosymbiotic ancestor of chloroplasts [82, 83]. This pathway was discovered about 30 years ago in algae and originally proposed to account for the changes in the redox state of plastoquinone, a photosynthetic electron carrier, in darkness [84]. Chlororespiration includes a NAD(P)H-dehydrogenase [85, 86] and a plastid terminal oxidase PTOX [87–91]. The NAD(P)H-dehydrogenase enzyme of chlororespiration is possibly involved also in recycling photosynthesis-generated NAD(P)H, establishing a cyclic electron transport around photosystem I [92–94]. This alternative electron transport could be engaged to balance the ATP/NADPH stoichiometry, since the net product is only ATP, in response to the requirements of the cell and is controlled by the redox state of the plastoquinone pool. The strong interplay between mitochondria and chloroplast metabolism is also evident from the characterization of *Chlamydomonas reinhardtii* mutants with defects in the mitochondrial electron transport chain: an enhanced glycolysis, to compensate for the absence of mitochondrial ATP input, is thought to increase plastoquinone reduction through chlororespiration and favor cyclic over linear electron transport in the chloroplast [80].

Cell fitness depends on the delicate equilibrium between biosynthetic and catabolic reactions, both essential. In order to use a photosynthetic organism as a biofuel or biomass producer, it is essential to control these intricate metabolic dynamics. Carbon assimilation rate may be a bottleneck, particularly in high light. *Dunaliella salina* was shown to upregulate key enzymes in the Calvin cycle at high salinity, possibly in order to enhance synthesis of glycerol as osmotic protector [95]. It is conceivable that improvements in carbon assimilation could be achieved in the future with the help of genetic engineering. Strategies to achieve this aim could be altering expression and/or activity of key enzymes or acting on ATP/NADPH availability.

Screening for State Transition as an Indirect Mean to Select Strains with Altered Redox Metabolism

The redox state of the plastoquinone pool is known to control a process called "state1–2 transition." Since the light-harvesting antennae of photosystem II and photosystem I have distinct absorption spectra, changes in the spectral composition of the incident light can lead to unequal excitation of the two photosystems and thus to a decreased photosynthetic yield. Plants and algae are able to balance the relative excitation of the photosystems through state transition, that is the reversible migration of a fraction of the light-harvesting antenna of photosystem II from photosystem II in state 1 to photosystem I in state 2, upon phosphorylation [96–98]. This process was discovered about 40 years ago in unicellular microalgae [99,100]. The state transition process has been widely studied in the unicellular green alga *C. reinhardtii*, where its amplitude is larger than in plants and appears to have a major role in balancing the ATP/NADPH stoichiometry by regulating the switch between linear and cyclic electron flow, in addition to the redistribution of the excitation energy between photosystems following changes in light conditions. Indeed, recycling of electrons around photosystem I was observed in state 2 [92–94]. The interplay between chloroplast and mitochondria metabolism is strong in algae. The mere inhibition of

state transition was shown to be insufficient to modify photosynthesis in the presence of active mitochondrial respiration, in contrast it is essential when respiration is compromised, revealing the physiological significance of state transition in the energetic contribution [81]. Up to 80% of the excitation energy absorbed by the photosystem II antenna can be redistributed from photosystem II to photosystem I in *C. reinhardtii* that is therefore well suitable for screening state transition mutants [96, 97, 101]. Large chlorophyll fluorescence changes occur during a transition from state 1 to state 2, due to the fact that most of the photosystem II antenna is displaced from photosystem II to photosystem I during this process and chlorophyll fluorescence at room temperature arises mostly from photosystem II. The difference in fluorescence between states 1 and 2 can be measured with a fluorescence video imaging system and used for screening mutants deficient in state transition. In the model plant *A. thaliana*, states 1 and 2 are induced by illuminating cells with light preferentially absorbed by photosystem I and photosystem II, respectively [102]. In *C. reinhardtii* cells, however, this procedure is not effective because in this alga the absorption spectra of photosystem II and photosystem I antennae overlap. Thus, states 1 and 2 are achieved in the dark by taking advantage of the ability of the chlororespiratory chain to change the redox state of the plastoquinone pool [96, 97]. State transition and cyclic electron transport around photosystem I are controlled by the redox state of the plastoquinone pool. This diffusible electron transport element is at the crossroad between linear electron transport from water to $NADP^+$ and the chlororespiration pathway dissipating excess redox power by reducing O_2 to H_2O. Thus, plastoquinone redox state is altered either by an imbalanced excitation of the photosystems or by changes in the rate of catabolic degradation of storage molecules and could therefore serve as a key sensor of both the incident photon flux and the cellular energetic status. Mutations in state transition can affect the non-photochemical reduction and oxidation of the plastoquinone, catabolism of endogenous substrates, and upstream reactions involved in feeding reducing equivalents into the stroma compartment of the chloroplast. Screening for state transition mutants is a useful strategy to isolate strains with an altered redox metabolism that could finally affect photosynthate generation/storage, growth rate, and biofuel production. It represents a mean of domestication alone or in combination with other characteristics.

Accumulation of Biomass as Neutral Lipids

Assimilated carbons can be stored in high energy value metabolites, such as starch, proteins, or lipids, as shown in Fig. 2. Some species of algae are particularly attractive because of their ability to produce high amounts (20–50% of dry cell weight) of neutral lipids that can serve as a source of biodiesel. Cellular lipid metabolism is altered toward the accumulation of neutral lipids, mainly triacylglycerols, under stressful conditions, such as nutrient starvation, salinity, nonoptimal growth medium pH, low temperature, high light, but also during aging of the culture [2]. These lipids do not have a structural role in membranes but serve as a storage form of carbon and energy, confined in lipid bodies in the cytoplasm. Lipid bodies also occur in the inter-thylakoid space of the chloroplast in certain green algae such as *Dunaliella bardawil* [103]. An attractive oleaginous green alga is *Botryococcus braunii* that produces up to 80% of dry weight of very-long-chain (C23–C40) hydrocarbons similar to those found in petroleum, under adverse environmental conditions [8, 104]. Neutral lipids can serve additional physiological roles. Fatty acids synthesis consumes twice the NADPH required for carbohydrate or protein synthesis and may thus provide an electron sink under photooxidative stress [2]. Moreover, coordination with carotenoid synthesis has been observed, in particular carotenoids are sequestered into cytosolic lipid bodies where they function as a sunscreen to reduce light striking the chloroplast [2, 105, 106].

Algae triacylglycerols can be exploited to produce biodiesel, via esterification of fatty acids. Biodiesel has a three to four times higher energy yield than ethanol; however, biodiesel still represents a small percentage of total diesel fuel consumption (1.6% in Europe and 0.21% in the USA, 2005–2007), while ethanol represents 5% of US gasoline consumption [23]. Currently, biodiesel is mainly produced from higher plants, such as palm and soybean [23]. But while extensive cultivation of crops to supply energetic demands is unsustainable, competing with food industry for arable

lands, oil production per hectare from algae, based on theoretical calculations, would be 100-fold higher than that of soybean and could meet 50% of present US transportation demand using less than 3% of available cropland [9]. Based on experimentally demonstrated biomass productivity, oil yield of microalgae could be 136 or 58 t ha^{-1} $year^{-1}$ considering 70% or 30% oil in biomass, respectively [9]. However, insufficient efforts for the establishment of algae-based biodiesel production plants have been made until now. The ability of algae to produce neutral lipids is species-specific rather than genus-specific [2]. Interesting species for biodiesel production include green algae, such as *Botryococcus braunii*, *Neochloris oleoabundans*, *Nannochloris* sp., *Chlorella* sp., and *Dunaliella primolecta*; diatoms, such as *Nitzschia*, *Phaeodactylum tricornutum*, and *Cylindrotheca* sp.; and members of other algal taxa, such as *Nannochloropsis* sp. and *Schizochytrium* sp. [9]. Relatively few algal strains have been examined to date, among the species available in nature. The possibility to isolate new oleaginous strains with the ability to accumulate high levels of oils with the best properties as fuel is likely to offer substantial improvements in lipid yield of industrial cultures while mutagenesis will further enhance the productivity of natural strains. Fatty acid composition can vary both quantitatively and qualitatively with the physiological status and culture conditions. Since oil accumulation is enhanced under stress, altering growth medium composition appears as a strategy to improve oil productivity. For example, high carbon dioxide concentrations (>5% v/v) in *Dunaliella salina* [107] or nutrient deficiency such as nitrogen deprivation in *Chlorella vulgaris* [108] can lead to a threefold increase in intracellular lipids.

Lipid metabolism has been poorly studied in algae. Nevertheless, available data suggest that the basic pathways are analogous to those experimentally detailed in higher plants. However, differences are distinguishable:

1. While in higher plants organic carbon is translocated from photosynthetically active tissues to sinks for lipid synthesis and storage, in microalgae triacylglycerols accumulation takes place within a single cell together with photosynthesis.
2. While neutral lipids synthesis is mainly associated to seed development in higher plants, it is triggered under stress conditions in algae [2].

A better knowledge of lipids synthesis pathways and regulation mechanisms is needed in order to implement genetic engineering strategies for oil production. Identification of metabolic differences between oleaginous strains and the species that do not accumulate substantial amounts of lipids is a possible research strategy to be realized using comparative transcriptomic, proteomic, and metabolomic profiles of different strains or the same strain under control versus stressful conditions. Microarray analysis of *Chlamydomonas reinhardtii* transcripts under anaerobic incubation has been performed [109], revealing fermentative pathways that produce acetyl CoA, the substrate for fatty acids synthesis. Genes encoding enzymes involved in these fermentative reactions represent putative candidates for increasing triacylglycerols accumulation [2].

The limiting step in fatty acids biosynthesis is the reaction catalyzed by the first enzyme of the pathway: acetyl CoA carboxylase (ACCase). The properties of this enzyme have been characterized in *Cyclotella cryptica* [110–113], but attempts to alter its expression level did not have effects on lipid production [113]. Some transformants showed two- to threefold higher ACCase expression and activity than wild-type cells; however, no detectable increase in lipid levels was observed. Overexpression of the endogenous enzyme may induce negative feedback so that increased activity of the ACCase enzyme could be compensated for by other pathways within the cell [113]. Indeed, feedback inhibition was reported in higher plants [114], where only a heterologous enzyme was successfully overexpressed really improving oil content [115, 116]. This approach could be proposed again and plants genes could be used for overexpression in algae.

Although activity and expression of single enzymes could be altered, a more powerful strategy might consist in the identification of transcription factors co-regulating all the genes of the pathway.

Lipids biosynthesis is strictly interconnected to other biosynthetic pathways in a unique global network. A *Chlamydomonas reinhardtii* starch-less mutant, defective in the ADP-glucose pyrophosphorylase, was shown to hyper-accumulate triacylglycerol by a factor of 10 [117]. A strategy to improve oil synthesis in order to produce biodiesel could be as well to act on the partitioning of carbon and energy between different pathways.

Finally, fatty acids composition of triacylglycerols influences diesel quality and must be considered for commercial application. Genetic engineering can additionally serve to alter the fatty acids profile thus improving fuel properties in engines [23]. Many algae can synthesize very long polyunsaturated fatty acids in large amounts (arachidonic C20:4, eicosapentaenoic C20:5, docosahexaenoic C22:6 acids), that are extracted as high added value products. Polyunsaturated fatty acids decrease in nutrient-limited medium and during heterotrophic growth, concomitantly with the increase of C16:0 and C18:1 fatty acids in triacylglycerols [118–120]. Monounsaturated fatty acids are indeed suitable for good diesel properties [23].

Research of new genes involved in lipid metabolism could be pursued by random mutagenesis. A mutant library represents a biological resource of novel strains that could include improved biodiesel producers. An easy and rapid strategy to screen for mutants with altered lipid content is by the use of Nile red [121]. Nile red is a hydrophobic molecule that emits a significant fluorescence signal when dissolved in lipids at 565–585 nm, in a spectral region where photosynthetic pigments fluorescence is negligible. Nile red fluorescence detection could be applied to screen and compare mutant colonies with respect to the wild type in a microtiter plate. Mutants displaying an altered Nile red fluorescence yield and thus altered lipid content with respect to the wild type can then be studied by molecular biology techniques to indentify the mutated gene and tested for oil productivity.

Planning an Algal Refinery

Algae convert solar energy into chemical energy and produce biomass through photosynthesis. The process requires light, carbon dioxide, water, and other essential nutrients and can be considered renewable. Minimal nutritional requirements can be estimated using the approximate molecular formula of the microalgal biomass, that is $CO_{0.48}$ $H_{1.83}$ $N_{0.11}$ $P_{0.01}$ [9, 122]. However, inorganic elements have to be added in excess because they form complexes in solution that are not bioavailable.

Algal biomass can be exploited in different ways, providing several products and biofuels. A scheme of the possible organization of an algal refinery is reported in Fig. 4.

Upon harvesting of the biomass, water and nutrients can be recycled, especially using closed photobioreactors. Then, biodiesel is obtained from

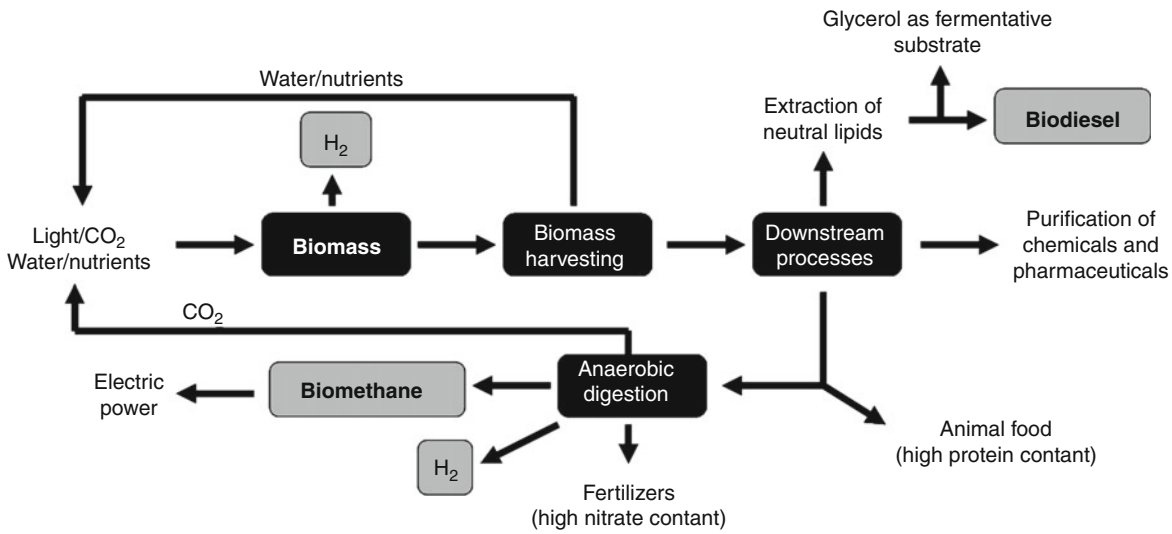

Algae, a New Biomass Resource. Figure 4
Scheme of the possible utilizations and products of an algal refinery

esterification of fatty acids contained in triacylglycerols or from other neutral hydrocarbons accumulated by oleaginous algae. A by-product from esterification of fatty acids to produce biodiesel is glycerol that can serve as fermentative substrate. For example, alga *Schizochytrium limacinum* produces docosahexaenoic acid, a polyunsaturated ω3 fatty acid with beneficial effects for human health, through fermentation on crude glycerol [123]. Currently, algae are already commercially used to extract chemicals and pharmaceuticals and this utilization can be combined with the need for biofuels. High added value products derived from algae include polyunsaturated fatty acids, proteins, biopolymers, polysaccharides, pigments, vitamins, and antioxidants [1, 4]. To date, commercialized algae are not transgenic, but this scenario could change in the near future. For instance, algae can be transformed in "cell factories" with the help of molecular biology techniques for manufacturing recombinant proteins with pharmaceutical or other applications, an approach also called "molecular farming." For example, expression of human antibodies and vaccines has already proven to be successful [124–128]. In general, algae are attractive as expression systems for the short life cycle, the cheap and easy large-scale cultivation, and the ability to grow up to high cell densities [129]. Algae have been shown free of human pathogens and toxins and thus considered safe.

After extraction of oils and other products, the spent biomass can serve as animal food or used as fermentative substrate for other microorganisms whose metabolic by-products include biomethane and biohydrogen. Effluents from the digestion can be used as fertilizers because of their high content in nitrate. Biomethane (or biogas) has a high energetic yield and is produced by anaerobic bacteria during fermentation of the biomass. The obtained gas contains methane (50–75%) but also carbon dioxide (25–50%). However, released carbon dioxide is equivalent to the carbon that algae have assimilated during growth, leading to zero net carbon dioxide emissions. Carbon dioxide released during the process can be immediately recycled for alga growth. Electric power produced from the biogas can sustain the energy demands of the photobioreactor plant itself [10]. Some algae have been evaluated for biomass conversion to methane, in particular the giant kelp *Macrocystis pyrifera* because of its high growth rate and ease of harvesting [5]. Alternatively, algal biomass can serve as fermentative substrate for heterotrophic or photosynthetic anoxygenic sulfur bacteria that use electrons coming from organic carbons to produce molecular hydrogen. In particular, photosynthetic anoxygenic sulfur bacteria use light energy to drive a fermentative reaction and organic acids are electron donors for molecular hydrogen evolution. Generated hydrogen is a high energetic fuel and clean since its combustion generates water [130].

In addition, algae have directly been evaluated for the production of biohydrogen. As a matter of fact, some algae are able to evolve hydrogen by a hydrogenase enzyme that catalyzes reduction of protons to molecular hydrogen. Hydrogen metabolism is primarily the domain of bacteria and microalgae. Microbial hydrogen formation is catalyzed by either nitrogenases or hydrogenases, enzymes that can only function under anaerobic conditions. Nitrogenases are used by certain cyanobacteria and photosynthetic bacteria, whereas green algae use hydrogenases [12]. In *Chlamydomonas reinhardtii*, the hydrogenase is expressed in anoxia together with the enzymes of the fermentative metabolism that is active in the dark [109]. However, algae are attractive for hydrogen production if photosynthetic electron transport can be directly exploited, since hydrogen would be generated from the most abundant of the natural resources, sunlight and water. Interestingly, after a period of anaerobic incubation in the dark, photosynthetic hydrogen evolution is detected transiently upon illumination [131]. The hydrogenase is transiently active during the dark-to-light transition, to consume reducing power in the time needed to fully activate the Calvin–Benson cycle, and receives electrons from ferredoxin reduced by photosystem I. This activity lasts until oxygen evolution by photosystem II restores aerobiosis and inhibits the hydrogenase enzyme. In order to photo-produce hydrogen on large scale, the major challenge to overcome is the inhibition by oxygen evolved by photosystem II during oxygenic photosynthesis. Up to now, encouraging hydrogen production rates have been obtained by a two-stage approach: the severe oxygen sensitivity of the hydrogenase is circumvented by temporally separating photosynthetic oxygen evolution and growth (stage 1) from hydrogen evolution (stage 2). A transition from stage 1 to stage 2 is performed upon sulfur

deprivation, which reversibly inactivates photosystem II and oxygen evolution. Under this condition, oxidative respiration by the cell in the light depletes oxygen and causes anaerobiosis in the culture, which is necessary and sufficient for the induction of the hydrogenase [13, 15]. Electrons for hydrogen production originate from the residual activity of photosystem II as well as from the consumption of endogenous substrates that generates extra electrons supplied to the photosynthetic chain through the chlororespiration pathway [16, 86]. Hydrogen production depends from available electrons sources and competitive sinks of reducing power and a strategy to improve its evolution would also be to increase electrons channeling toward the hydrogenase and to deplete competitive electron sinks. An improved hydrogen evolution under sulfur starvation was observed in a mutant affected in the mitochondrial respiratory chain and simultaneously impaired in the ability to activate state transition [16]. In this mutant, accumulation of starch in the chloroplast supplied the photosynthetic electron transport chain through chlororespiration, while downregulation of cyclic electron transport around photosystem I enabled a greater fraction of electrons to be used by the hydrogenase (see "Interconversion and Storage of Photosynthetic Metabolic Products" and "Screening for State Transition as an Indirect Mean to Select Strains with Altered Metabolism" sections for further explanations about state transition and cyclic electron transport). The hydrogen production rates of the mutant were 5–13 times higher than in wild-type strain, yielding about 540 mL of hydrogen per 1 L of culture over a 10–14-day period (up to 98% pure) [16]. However, sulfur deprivation is deleterious for the cell and this system is sustainable only for few days. Upon a recovery phase of sulfur repletion, and reconstitution of reserves as endogenous substrates, hydrogen production can be resumed. Nevertheless, continuous hydrogen production is not possible using this technology. An alternative two-stage approach to overcome the oxygen sensitivity of the hydrogenase, with respect to sulfur deprivation, involves the control of photosystem II expression [132]. The initial requirement for this application is a photosystem II-less mutant which would be complemented by an inducible cassette to switch on/off photosystem II activity and oxygen evolution. However, the most efficient method to obtain large-scale hydrogen production is believed to be the continuous production of hydrogen concomitantly to photosynthesis and growth. The limiting factor for such a technology is the finding of a hydrogenase enzyme with sufficient resistance to oxygen. Two different approaches are possible: to engineer existing hydrogenases by introducing mutations conferring resistance to oxygen or to find organisms that can synthesize hydrogen even in the presence of some oxygen, thus having hydrogenases less oxygen sensitive. Such hydrogenase could then be heterologously expressed in algae [130] to generate a hydrogen producing strain with increased yield of this biofuel.

Large-Scale Systems

Open ponds and closed photobioreactors have been evaluated for algae mass culture [9, 26, 30]. Currently, commercial exploitation of algae mainly utilizes open ponds, easier to construct and scale up, and less expensive. Open ponds can be categorized into natural waters (lakes, lagoons, ponds) and artificial ponds or containers. They are generally raceway cultivators driven by paddle wheels or unstirred. In contrast, closed systems like photobioreactors are more costly. Moreover, while many photobioreactors are operative at laboratory scale, their scaling up is more difficult and could be a limiting step. This is counterbalanced by several advantages over open ponds and some photobioreactors for large scale are in the process of being constructed. Closed systems are in the early stages of development but they are likely to become more attractive in the future.

1. Although photobioreactors could be artificially illuminated, to sustain growth during night, the use of natural sunlight is the major option for cost-effectiveness. Photobioreactors can be designed to improve the ratio between the illuminated surface and the total volume in order to minimize dark zones. From this point of view, flat-plate, horizontal and inclined tubular photobioreactors are promising [30]. A general tendency is to reduce the thickness, thus laminar layer plate or thin diameter tube configurations are becoming strongly favored, mimicking the leaves of land plants. For instance a 100-year-old, 10-m high lime tree shading an area of 100 m^2 has a leaf surface area of more than 2,500 m^2. Expressed as

a surface/volume ratio, this amounts to a value of 2.5 m^2 m^{-3} [26] and the design of large-scale photobioreactors should tend to this value.

2. Large-scale cultivation of algae requires first of all a good understanding of the physiology and ecology of the species, for example, with respect to nutrients requirements, optimum pH, and temperature. Close systems allow for a better control of growth conditions, with respect to pH, salts, CO_2 partial pressure, temperature, mixing, and light supply.
3. Photobioreactors allow for a shorter period until net productivity is reached, approximately 2–4 weeks over 6–8 weeks in open ponds [26].
4. The stability of the dominating algal species is easier to be maintained in photobioreactors because contamination by other organisms is lower. The growth process, thus, is more reproducible and standardized. Strict sterility and quality control allowed by closed systems are particularly required for the production of pharmaceuticals and food additives [133].
5. In closed systems, water and nutrients, such as salts, can be recycled for algal growth and loss of water due to evaporation and diffusion of CO_2 to the atmosphere would be minimized.
6. Efficient stirring mechanisms can be developed in photobioreactors ensuring homogeneity of the culture and finally influencing productivity in terms of growth. Flow is produced using either a mechanical pump or a gentler airlift pump. Mechanical pump could be more stressful and a strain with cell wall would be more suitable, because less sensitive to shear damage. Agitation is required to prevent cells sedimentation and to allow proper gas exchanges. As a consequence of the stirring and depending from the light gradient inside the culture due to the optical property of the strain, cells can suddenly be moved from suboptimal illumination to strong light at the surface without time to adjust the photosynthetic apparatus and finally leading to light stress. However, it was observed that light–dark cycling of above a certain frequency, such as 10 ms, can increase growth as compared with continuous illumination of the same intensity. It was proposed that a short dark period could allow the photosynthetic apparatus to recover from the excited state of the previous illumination pulse under light saturation conditions [9].
7. Harvesting of biomass is expensive since it requires energy. Biomass can be recovered from the broth by filtration or centrifugation [134]. Since concentration of biomass in photobioreactors is nearly 30 times higher than in open ponds (2–8 g L^{-1} vs. 0.1–0.2 g L^{-1}) [26], a much smaller volume of the photobioreactor broth needs to be processed to obtain a given quantity of biomass [9]. Once the biomass is harvested, processes to disrupt the cells and to extract desired products are being developed, for example, the high yield and scalable recovery of high purity fatty acids [135].

As a consequence of all aforementioned advantages of photobioreactors, productivity could be much higher than that of open systems and could balance the higher investment costs [9] (refer to "Present Algal Productivity in the Laboratory Versus Large Scale" section for biomass productivity data).

Future Perspectives and Technological Developments

Mutagenesis and genetic modification of algae for biofuel production has received so far little attention, despite molecular biology procedures appearing essential in order to remove limitations in the economic sustainability of the biofuel production process. In particular, a biotechnological approach is required to obtain domestication of algal strains for cultivation in mass culture in order to:

1. Improve light distribution into a photobioreactor by decreasing the optical density of the single cell
2. Increase the light intensity at which photosynthesis saturates, thus reducing light energy dissipation and photoinhibition
3. Increase resistance to photooxidative stress
4. Optimize light utilization and carbon assimilation, finally improving solar-to-biomass conversion efficiency
5. Channel the metabolism toward oil accumulation for biodiesel production and to adjust the fatty acid composition to fit required fuel quality
6. Produce high value products and recombinant proteins of interest for pharmaceutical and chemical companies

When considering the advancement that biotechnology can bring to algae cultivation, the algal system is extremely attractive for commercial utilization if transformation and thus genetic improvement are possible. Nevertheless, the basic requirements for genetic improvement are so far available for a low number of species which are not necessarily suitable for the many possible applications. The basis for domestication of algal species is a good general knowledge of the biology for the target alga, including ecological, physiological, biochemical, and genetic aspects. In addition, easiness of cultivation in the laboratory and availability of a protocol for breeding are of paramount importance. On this basis, further improvement requires development of transformation protocols to introduce a foreign DNA into the cell and identification of markers for selection of transformants. Currently, about 25 species are accessible to genetic transformation, mainly green and red algae [1]. However, many algal species, although of interest for commercial use, cannot be propagated in the laboratory and cannot be transformed. Overcoming this limitation will be a major target of research in the future.

Nuclear Genetic Transformation

Methods to introduce DNA into an algal cell exploited so far include vortexing in the presence of micro- or macroparticles such as glass beads, routinely used to transform *Chlamydomonas reinhardtii* [136] and successful for other green algae such as *Chlorella ellipsoidea* [137]; microparticle bombardment, used to transform species with a recalcitrant cell wall such as the diatoms *Phaeodactylum tricornutum* and *Cyclotella criptica* [138]; electroporation, effective in *Chlamydomonas reinhardtii* [139] and *Dunaliella salina* [124]. Cell wall-less mutants or protoplasts after cell wall digestion are more easily amenable to transformation. The limiting step is to allow survival of cells. Markers to select the transformants are classified as dominant, for example, conferring resistance to paromomycin [140] or zeomycin [136], or recessive. The latter require auxotrophic mutants and the corresponding endogenous intact gene for complementation. This strategy requires no exogenous gene expression [1]. As for genome sequence information, many genome sequencing projects, mainly for microalgae, are completed or in progress, including green algae *Chlamydomonas reinhardtii*, *Chlorella vulgaris*, *Volvox carteri*, *Dunaliella salina*, *Ostreococcus tauri*, and *Ostreococcus lucimarinus*; red algae *Cyanidioschyzon merolae*, *Porphyra yezoensis*, and *Porphyra purpurea*; and the diatoms *Thalassiosira pseudonana* and *Phaeodactylum tricornutum*. Additionally, there has been an increase in expressed sequence tags (ESTs) databases.

Besides the methods for introduction of DNA into the cell, genetic transformation with a recombinant cassette requires regulatory elements active in the target species to drive transgene expression and availability of such regulatory elements is often limiting. Promoters can be heterologous, such as the cauliflower mosaic virus promoter CaMV35s that proved functional in several algae [1]; however, heterologous sequences are often not recognized by the host cell. Alternatively, endogenous promoters can be exploited. Endogenous promoters can be either constitutive, such as the promoter of the small chain of the ribulose bisphosphate carboxylase, RBCS2 [136], the promoter of the PsaD subunit of the photosystem I core complex [141], or the promoter of the heat shock protein 70A [142] in *Chlamydomonas reinhardtii*, or inducible, such as the promoter of the cytochrome C6 by copper deprivation in *Chlamydomonas reinhardtii* [132] or the arylsulfatase promoter inducible by sulfur deprivation in *Volvox carteri* [143]. Important regulatory elements can be included within introns and their addition may be useful for improving expression levels [144]. Once the transgene is introduced in the host genome, transgene silencing often occurs due to positional effects and action of epigenetic mechanisms [145], particularly active in the case of sequences located in the nucleus. Improvement of transgene expression is required for genetic engineering and for exploiting algae as "cell factory." Inducible expression systems can be useful to partially overcome silencing of the recombinant gene.

Chloroplast Transformation

An alternative to nuclear genome transformation is chloroplast transformation that has potentially many advantages:

1. Transgene expression is more stable and uniform between different lines, because the mechanism of homologous recombination active in the

chloroplast generates uniform clones, while epigenetic control, positional effects, and gene silencing are not present. Thus, known variability of transgene expression only derives from plastid differentiation stages.
2. High level of expression is favored by high polyploidy.
3. Multiple transgenes expression upon a single transformation event is possible due to the organization of genes into operons.
4. The plastid genome shows uniparental inheritance in many species, offering a degree of transgene containment.
5. *Chlamydomonas reinhardtii* has a single chloroplast, which contains approximately 80 copies of its own genome. Obtaining homoplasmy, where all copies of the plastid genome are transformed, is the main obstacle to the application of this technology to many plant species. In contrast, this process is easier in *Chlamydomonas reinhardtii* because of its single chloroplast and is achieved by a sufficient number of cells division under high selective pressure, making *Chlamydomonas reinhardtii* chloroplast a suitable factory for recombinant proteins.

Nevertheless, the influence of nuclear factors controlling plastid gene expression at multiple levels may limit transgene expression level in the plastid [133, 146]. A better comprehension of these mechanisms and of nucleus-plastid signaling is currently a major subject of research.

Mutagenesis of the Nuclear Genome

Mutagenesis, besides its importance to investigate the physiological role of genes by analyzing phenotypic effects of their inactivation, is as well a powerful tool to generate strains with improved characteristics with respect to the wild type. Mutagenesis of the nuclear genome is the only way to obtain mutants for the majority of genes. Early work was performed using chemical or UV mutagenesis, a method that is of importance for species still not amenable to transformation. Chemical mutagenesis has evolved into a novel strategy of Targeted Induced Local Lesions in Genomes (TILLING) [147] where the chemical treatment is used to generate allelic series of point mutations. The target gene is then amplified by PCR and analyzed to verify if mutations have occurred. TILLING is therefore a technique to isolate point mutations within a target gene that overcomes the "null phenotype" limitations of insertional mutagenesis and generates stable mutants. This technique has been so far applied to crop plants but not yet to algae and could be used as an approach of reverse genetics, aimed to investigate the physiological role of a gene with a known sequence. In applied research, TILLING could be pursued to obtain a stable mutant for a target gene whose implications for applicative purposes have been recognized. This approach is of choice if transgenesis should be avoided. However, limitations to this strategy are due to the high number of induced mutations per cell in order to increase the probability of obtaining mutations in the target gene. Several backcross cycles are then needed to isolate the desired mutation from all the others that decrease cell fitness. This lengthy procedure has so far discouraged application of the technique to algae and in fact makes it impossible in species where sexual reproduction is not available as a breeding procedure.

When dealing with species in which transformation procedures are available, insertional mutagenesis is generally preferred. Transforming the cell with an exogenous DNA vector helps to select the transformants, thanks to a selectable marker and to localize the mutation by identifying the genomic regions flanking the known insertion cassette. Integration of the exogenous DNA in the nuclear genome of eukaryotic algae occurs randomly, by non homologous recombination. Insertion of the cassette could take place within an encoding sequence, interrupting the gene and leading to a knockout, or it could as well perturb the promoter or other regulative sequences. This strategy can thus be used to generate random insertional libraries. The number of insertions per cell can be controlled by adjusting the DNA/cell ratio. A haploid, mononucleated genome is preferred because effects of recessive mutations on the phenotype can be recognized without the need of homozygosis. Multiple mutations eventually present in the same cell can be sorted out if procedures for triggering mating under laboratory conditions are available. Beside, breeding offers the valuable opportunity to combine different mutations, contributing to the improvement of the strain for industrial purposes. Since insertion mutagenesis is not targeted, mutants

have to be screened for the desired characteristics. While large-scale screening strategies have been developed, a limiting step is the genetic characterization of insertion sites, that is, the identification of the mutated gene responsible for the observed phenotype. Large genome deletions can occur at the insertion site. The insertion cassette itself can be partially deleted or inserted as concatamer, so that the amplification of genomic regions flanking the insertion through PCR techniques [148] can be difficult. Protocol optimization and improved design of the insertion cassette can decrease these limitations; however, interesting mutants may well resist genetic characterization. Alternative strategies could be performed although time consuming, for instance the *tla1* mutation (see "Light Use Efficiency" section for further informations about *tla1* mutant) was identified via complementation of the mutant with a library of genomic restriction fragments [60]. In addition, recently developed high throughput sequencing technologies may prove to be effective in rapid re-sequencing of a mutant genome and in localizing the insertion mutation. This strategy is likely to provide future potential for high throughput identification of mutants and annotation of genomes in algae.

Concluding Remarks

Algae currently used in industry are wild-type strains and mainly cultivated for human/animal food or to extract high-value natural chemicals and pharmaceuticals. However, algae can be also exploited as biomass producers and a source for renewable, ecologically sustainable biofuels. In order to make algae suitable for cultivation in mass culture conditions and economically competitive, domestication of natural strains is required. Selection of the desired characteristics and introduction of new traits through mutagenesis and genetic engineering can substantially improve algae cultivation in the future and make it practicable. Moreover, algae can serve as a "cell factory" for the production of recombinant proteins with pharmaceutical applications. Concerns from public opinion and governments about biosafety can be satisfied and counterbalanced by the potential advantages of transgenic algae, also considering that algae offer the advantage to be grown in a confined environment. Therefore, the use of genetically modified algae for the production of renewable and sustainable biofuels and pharmaceuticals appears as a likely perspective. Genetic engineering is well useful to generate strains optimized for growth in photobioreactors but uncompetitive in the wild if released.

Bibliography

Primary Literature

1. Hallmann A (2007) Algal transgenics and biotechnology. Transgenic Plant J 1:81–98
2. Hu Q, Sommerfeld M, Jarvis E, Ghirardi M, Posewitz M, Seibert M, Darzins A (2008) Microalgal triacylglycerols as feedstocks for biofuel production: perspectives and advances. Plant J 54:621–639
3. Field CB, Behrenfeld MJ, Randerson JT, Falkowski P (1998) Primary production of the biosphere: integrating terrestrial and oceanic components. Science 281:237–240
4. Spolaore P, Joannis-Cassan C, Duran E, Isambert A (2006) Commercial applications of microalgae. J Biosci Bioeng 101:87–96
5. McHugh DJ (2003) A guide to the seaweed industry. FAO Fish Tech Pap 441:1–105
6. Pulz O, Gross W (2004) Valuable products from biotechnology of microalgae. Appl Microbiol Biotechnol 65:635–648
7. Borowitzka MA (1999) Commercial production of microalgae: ponds, tanks, tubes and fermenters. J Biotechnol 70:313–321
8. Banerjee A, Sharma R, Chisti Y, Banerjee UC (2002) *Botryococcus braunii*: a renewable source of hydrocarbons and other chemicals. Crit Rev Biotechnol 22:245–279
9. Chisti Y (2007) Biodiesel from microalgae. Biotechnol Adv 25:294–306
10. Chisti Y (2008) Biodiesel from microalgae beats bioethanol. Trends Biotechnol 26:126–131
11. Xu H, Miao XL, Wu QY (2006) High quality biodiesel production from a microalga *Chlorella protothecoides* by heterotrophic growth in fermenters. J Biotechnol 126:499–507
12. Ghirardi ML, Zhang L, Lee JW, Flynn T, Seibert M, Greenbaum E, Melis A (2000) Microalgae: a green source of renewable H2. TIBTECH 18:506–511
13. Melis A, Zhang LP, Forestier M, Ghirardi ML, Seibert M (2000) Sustained photobiological hydrogen gas production upon reversible inactivation of oxygen evolution in the green alga *Chlamydomonas reinhardtii*. Plant Physiol 122:127–135
14. Melis A, Happe T (2004) Trails of green alga hydrogen research - from Hans Gaffron to new frontiers. Photosynth Res 80:401–409
15. Zhang LP, Melis A (2002) Probing green algal hydrogen production. Philos Trans R Soc Lond B Biol Sci 357:1499–1507
16. Kruse O, Rupprecht J, Bader KP, Thomas-Hall S, Schenk PM, Finazzi G, Hankamer B (2005) Improved photobiological H-2 production in engineered green algal cells. J Biol Chem 280:34170–34177
17. Sabine CL, Feely RA, Gruber N, Key RM, Lee K, Bullister JL, Wanninkhof R, Wong CS, Wallace DWR, Tilbrook B, Millero FJ,

Peng TH, Kozyr A, Ono T, Rios AF (2004) The oceanic sink for anthropogenic CO_2. Science 305:367–371
18. Cox PM, Betts RA, Jones CD, Spall SA, Totterdell IJ (2000) Acceleration of global warming due to carbon-cycle feedbacks in a coupled climate model. Nature 408:184–187
19. Caldeira K, Jain AK, Hoffert MI (2003) Climate sensitivity uncertainty and the need for energy without CO_2 emission. Science 299:2052–2054
20. de Morais MG, Costa JAV (2007) Carbon dioxide fixation by *Chlorella kessleri*, *C. vulgaris*, *Scenedesmus obliquus* and *Spirulina* sp. cultivated in flasks and vertical tubular photobioreactors. Biotechnol Lett 29:1349–1352
21. Keffer JE, Kleinheinz GT (2002) Use of *Chlorella vulgaris* for $CO_{(2)}$ mitigation in a photobioreactor. J Ind Microbiol Biotechnol 29:275–280
22. Otsuki T (2001) A study for the biological CO_2 fixation and utilization system. Sci Total Environ 277:21–25
23. Durrett TP, Benning C, Ohlrogge J (2008) Plant triacylglycerols as feedstocks for the production of biofuels. Plant J 54:593–607
24. Benson AA, Calvin M (1950) Carbon dioxide fixation by green plants. Annu Rev Plant Physiol 1:25–42
25. Melis A (2009) Solar energy conversion efficiencies in photosynthesis: minimizing the chlorophyll antennae to maximize efficiency. Plant Sci 177:272–280
26. Pulz O (2001) Photobioreactors: production systems for phototrophic microorganisms. Appl Microbiol Biotechnol 57:287–293
27. Lee YK (1997) Commercial production of microalgae in the Asia-Pacific rim. J Appl Phycol 9:403–411
28. Borowitzka MA (2005) The mass culture of Dunaliella salina. http://www.fao.org/docrep/field/003/AB728E/AB728E06.htm
29. Huesemann MH, Hausmann TS, Bartha R, Aksoy M, Weissman JC, Benemann JR (2008) Biomass productivities in wild type and pigment mutant of *Cyclotella* sp. (Diatom). Appl Biochem Biotechnol. doi:10.1007/s12010-008-8298-9
30. Ugwu CU, Aoyagi H, Uchiyama H (2008) Photobioreactors for mass cultivation of algae. Bioresour Technol 99:4021–4028
31. Mann JE, Myers J (1968) On pigments, growth and photosynthesis of *Phaeodactylum tricornutum*. J Phycol 4:349–355
32. Grima EM, Fernández FGA, Camacho FG, Rubio FC, Chisti Y (2000) Scale-up of tubular photobioreactors. J Appl Phycol 12:355–368
33. Melis A, Neidhardt J, Benemann JR (1998) *Dunaliella salina* (Chlorophyta) with small chlorophyll antenna sizes exhibit higher photosynthetic productivities and photon use efficiencies than normally pigmented cells. J Appl Phycol 10:515–525
34. Doebley JF, Gaut BS, Smith BD (2006) The molecular genetics of crop domestication. Cell 127:1309–1321
35. Bai YL, Lindhout P (2007) Domestication and breeding of tomatoes: what have we gained and what can we gain in the future? Ann Bot 100:1085–1094
36. Kirk JTO (1994) Light and photosynthesis in aquatic ecosystems, 2nd edn. Cambridge University Press, Cambridge, UK
37. Holt NE, Fleming GR, Niyogi KK (2004) Toward an understanding of the mechanism of nonphotochemical quenching in green plants. Biochemistry 43:8281–8289
38. Niyogi KK (1999) Photoprotection revisited: genetic and molecular approaches. Annu Rev Plant Physiol Plant Mol Biol 50:333–359
39. Durnford DG, Price JA, Mckim SM, Sarchfield ML (2003) Light-harvesting complex gene expression is controlled by both transcriptional and post-transcriptional mechanisms during photoacclimation in *Chlamydomonas reinhardtii*. Physiol Plant 118:193–205
40. Teramoto H, Nakamori A, Minagawa J, Ono T (2002) Light-intensity-dependent expression of Lhc gene family encoding light-harvesting chlorophyll-a/b proteins of photosystem II in *Chlamydomonas reinhardtii*. Plant Physiol 130:325–333
41. Wobbe L, Schwarz C, Nickelsen J, Kruse O (2008) Translational control of photosynthetic gene expression in phototrophic eukaryotes. Physiol Plant 133:507–515
42. Powles S (1984) Photoinhibition of photosynthesis induced by visible light. Annu Rev Plant Physiol 35:15–44
43. Melis A (1999) Photosystem-II damage and repair cycle in chloroplasts: what modulates the rate of photodamage in vivo? Trends Plant Sci 4:130–135
44. Nakajima Y, Tsuzuki M, Ueda R (1998) Reduced photoinhibition of a phycocyanin deficient mutant of Synechocystis PCC 6714. J Appl Phycol 10:447–452
45. Naus J, Melis A (1991) Changes of photosystem stoichiometry during cell growth in *Dunaliella salina* cultures. Plant Cell Physiol 32:569–575
46. Neidhardt J, Benemann JR, Zhang L, Melis A (1998) Photosystem-II repair and chloroplast recovery from irradiance stress: relationship between chronic photoinhibition, light-harvesting chlorophyll antenna size and photosynthetic productivity in *Dunaliella salina* (green algae). Photosynth Res 56:175–184
47. Vener AV, Vankan PJM, Rich PR, Ohad I, Andersson B (1997) Plastoquinol at the quinol oxidation site of reduced cytochrome bf mediates signal transduction between light and protein phosphorylation: thylakoid protein kinase deactivation by a single-turnover flash. Proc Natl Acad Sci USA 94:1585–1590
48. Kok B (1953) Experiments on photosynthesis by *Chlorella* in flashing light. In: Burlew JS (ed) Algal culture: from laboratory to pilot plant. The Carnegie Institution, Washington, DC, pp 63–75
49. Polle JEW, Benemann JR, Tanaka A, Melis A (2000) Photosynthetic apparatus organization and function in the wild type and a chlorophyll b-less mutant of *Chlamydomonas reinhardtii*. Dependence on carbon source. Planta 211:335–344
50. Tanaka A, Ito H, Tanaka R, Tanaka NK, Yoshida K, Okada K (1998) Chlorophyll a oxygenase (CAO) is involved in chlorophyll b formation from chlorophyll a. Proc Natl Acad Sci USA 95:12719–12723
51. Polle JEW, Niyogi KK, Melis A (2001) Absence of lutein, violaxanthin and neoxanthin affects the functional chlorophyll

antenna size of photosystem-II but not that of photosystem-I in the green alga *Chlamydomonas reinhardtii*. Plant Cell Physiol 42:482–491

52. Elrad D, Niyogi KK, Grossman AR (2002) A major light-harvesting polypeptide of photosystem II functions in thermal dissipation. Plant Cell 14:1801–1816
53. Baroli I, Gutman BL, Ledford HK, Shin JW, Chin BL, Havaux M, Niyogi KK (2004) Photo-oxidative stress in a xanthophyll-deficient mutant of *Chlamydomonas*. J Biol Chem 279: 6337–6344
54. Dall'osto L, Cazzaniga S, Havaux M, Bassi R (2010) Enhanced photoprotection by protein-bound vs free xanthophyll pools: a comparative analysis of chlorophyll b and xanthophyll biosynthesis mutants. Mol Plant 3:576–593
55. Niyogi KK, Bjorkman O, Grossman AR (1997) The roles of specific xanthophylls in photoprotection. Proc Natl Acad Sci USA 94:14162–14167
56. Polle JEW, Kanakagiri SD, Melis A (2003) tla1, a DNA insertional transformant of the green alga *Chlamydomonas reinhardtii* with a truncated light-harvesting chlorophyll antenna size. Planta 217:49–59
57. Mussgnug JH, Wobbe L, Elles I, Claus C, Hamilton M, Fink A, Kahmann U, Kapazoglou A, Mullineaux CW, Hippler M, Nickelsen J, Nixon PJ, Kruse O (2005) NAB1 is an RNA binding protein involved in the light-regulated differential expression of the light-harvesting antenna of *Chlamydomonas reinhardtii*. Plant Cell 17:3409–3421
58. Beckmann J, Lehr F, Finazzi G, Hankamer B, Posten C, Wobbe L, Kruse O (2009) Improvement of light to biomass conversion by de-regulation of light-harvesting protein translation in *Chlamydomonas reinhardtii*. J Biotechnol 142: 70–77
59. Mussgnug JH, Thomas-Hall S, Rupprecht J, Foo A, Klassen V, McDowall A, Schenk PM, Kruse O, Hankamer B (2007) Engineering photosynthetic light capture: impacts on improved solar energy to biomass conversion. Plant Biotechnol J 5:802–814
60. Tetali SD, Mitra M, Melis A (2007) Development of the light-harvesting chlorophyll antenna in the green alga *Chlamydomonas reinhardtii* is regulated by the novel Tla1 gene. Planta 225:813–829
61. Glick RE, Melis A (1988) Minimum photosynthetic unit size in system-I and system-II of barley chloroplasts. Biochim Biophys Acta 934:151–155
62. Falkowski PG, Owens TG (1980) Light-shade adaptation - 2 strategies in marine-phytoplankton. Plant Physiol 66:592–595
63. Dall'osto L, Caffarri S, Bassi R (2005) A mechanism of nonphotochemical energy dissipation, independent from PsbS, revealed by a conformational change in the antenna protein CP26. Plant Cell 17:1217–1232
64. de Bianchi S, Ballottari M, Dall'osto L, Bassi R (2010) Regulation of plant light harvesting by thermal dissipation of excess energy. Biochem Soc Trans 38:651–660
65. Li XP, Bjorkman O, Shih C, Grossman AR, Rosenquist M, Jansson S, Niyogi KK (2000) A pigment-binding protein essential for regulation of photosynthetic light harvesting. Nature 403:391–395
66. Li XP, Gilmore AM, Caffarri S, Bassi R, Golan T, Kramer D, Niyogi KK (2004) Regulation of photosynthetic light harvesting involves intrathylakoid lumen pH sensing by the PsbS protein. J Biol Chem 279:22866–22874
67. Bonente G, Howes BD, Caffarri S, Smulevich G, Bassi R (2008) Interactions between the photosystem II subunit PsbS and xanthophylls studied in vivo and in vitro. J Biol Chem 283:8434–8445
68. Ahn TK, Avenson TJ, Ballottari M, Cheng YC, Niyogi KK, Bassi R, Fleming GR (2008) Architecture of a charge-transfer state regulating light harvesting in a plant antenna protein. Science 320:794–797
69. Holt NE, Zigmantas D, Valkunas L, Li XP, Niyogi KK, Fleming GR (2005) Carotenoid cation formation and the regulation of photosynthetic light harvesting. Science 307:433–436
70. Bonente G, Passarini F, Cazzaniga S, Mancone C, Buia MC, Tripodi M, Bassi R, Caffarri S (2008) The occurrence of the psbS gene product in *Chlamydomonas reinhardtii* and in other photosynthetic organisms and its correlation with energy quenching. Photochem Photobiol 84: 1359–1370
71. Niyogi KK, Bjorkman O, Grossman AR (1997) *Chlamydomonas* xanthophyll cycle mutants identified by video imaging of chlorophyll fluorescence quenching. Plant Cell 9:1369–1380
72. Alboresi A, Gerotto C, Giacometti GM, Bassi R, Morosinotto T (2010) *Physcomitrella patens* mutants affected on heat dissipation clarify the evolution of photoprotection mechanisms upon land colonization. Proc Natl Acad Sci USA 107: 11128–11133
73. Peers G, Truong TB, Ostendorf E, Busch A, Elrad D, Grossman AR, Hippler M, Niyogi KK (2009) An ancient light-harvesting protein is critical for the regulation of algal photosynthesis. Nature 462:518–U215
74. Wilson A, Ajlani G, Verbavatz JM, Vass I, Kerfeld CA, Kirilovsky D (2006) A soluble carotenoid protein involved in phycobilisome-related energy dissipation in cyanobacteria. Plant Cell 18:992–1007
75. Eberhard S, Finazzi G, Wollman FA (2008) The dynamics of photosynthesis. Annu Rev Genet 42:463–515
76. Kramer DM, Avenson TJ, Edwards GE (2004) Dynamic flexibility in the light reactions of photosynthesis governed by both electron and proton reactions. Trends Plant Sci 9:349–357
77. Hoefnagel MHN, Atkin OK, Wiskich JT (1998) Interdependence between chloroplasts and mitochondria in the light and the dark. Biochim Biophys Acta: Bioenerg 1366:235–255
78. Raghavendra AS, Padmasree K (2003) Beneficial interactions of mitochondrial metabolism with photosynthetic carbon assimilation. Trends Plant Sci 8:546–553
79. Scheibe R (1987) NADP-malate dehydrogenase in C3-plants: regulation and role of a light-activated enzyme. Physiol Plant 71:393–400

80. Cardol P, Gloire G, Havaux M, Remacle C, Matagne R, Franck F (2003) Photosynthesis and state transitions in mitochondrial mutants of *Chlamydomonas reinhardtii* affected in respiration. Plant Physiol 133:2010–2020
81. Cardol P, Alric J, Girard-Bascou J, Franck F, Wollman FA, Finazzi G (2009) Impaired respiration discloses the physiological significance of state transitions in *Chlamydomonas*. Proc Natl Acad Sci USA 106:15979–15984
82. Peltier G, Cournac L (2002) Chlororespiration. Annu Rev Plant Biol 53:523–550
83. Scherer S (1990) Do photosynthetic and respiratory electron-transport chains share redox proteins. Trends Biochem Sci 15:458–462
84. Bennoun P (1982) Evidence for a respiratory chain in the chloroplast. Proc Natl Acad Sci USA 79:4352–4356
85. Jans F, Mignolet E, Houyoux PA, Cardol P, Ghysels B, Cuine S, Cournac L, Peltier G, Remacle C, Franck F (2008) A type II NAD(P)H dehydrogenase mediates light-independent plastoquinone reduction in the chloroplast of *Chlamydomonas*. Proc Natl Acad Sci USA 105:20546–20551
86. Mus F, Cournac L, Cardettini W, Caruana A, Peltier G (2005) Inhibitor studies on non-photochemical plastoquinone reduction and H-2 photoproduction in *Chlamydomonas reinhardtii*. Biochim Biophys Acta: Bioenerg 1708:322–332
87. Bailey S, Melis A, Mackey KRM, Cardol P, Finazzi G, van Dijken G, Berg GM, Arrigo K, Shrager J, Grossman A (2008) Alternative photosynthetic electron flow to oxygen in marine *Synechococcus*. Biochim Biophys Acta: Bioenerg 1777:269–276
88. Cardol P, Bailleul B, Rappaport F, Derelle E, Beal D, Breyton C, Bailey S, Wollman FA, Grossman A, Moreau H, Finazzi G (2008) An original adaptation of photosynthesis in the marine green alga *Ostreococcus*. Proc Natl Acad Sci USA 105:7881–7886
89. Carol P, Stevenson D, Bisanz C, Breitenbach J, Sandmann G, Mache R, Coupland G, Kuntz M (1999) Mutations in the *Arabidopsis* gene immutans cause a variegated phenotype by inactivating a chloroplast terminal oxidase associated with phytoene desaturation. Plant Cell 11:57–68
90. Cournac L, Redding K, Ravenel J, Rumeau D, Josse EM, Kuntz M, Peltier G (2000) Electron flow between photosystem II and oxygen in chloroplasts of photosystem I-deficient algae is mediated by a quinol oxidase involved in chlororespiration. J Biol Chem 275:17256–17262
91. Wu DY, Wright DA, Wetzel C, Voytas DF, Rodermel S (1999) The immutans variegation locus of *Arabidopsis* defines a mitochondrial alternative oxidase homolog that functions during early chloroplast biogenesis. Plant Cell 11:43–55
92. Finazzi G, Furia A, Barbagallo RP, Forti G (1999) State transitions, cyclic and linear electron transport and photophosphorylation in *Chlamydomonas reinhardtii*. Biochim Biophys Acta: Bioenerg 1413:117–129
93. Finazzi G, Rappaport F, Furia A, Fleischmann M, Rochaix JD, Zito F, Forti G (2002) Involvement of state transitions in the switch between linear and cyclic electron flow in *Chlamydomonas reinhardtii*. EMBO Rep 3:280–285
94. Vallon O, Bulte L, Dainese P, Olive J, Bassi R, Wollman FA (1991) Lateral redistribution of cytochrome B6/F complexes along thylakoid membranes upon state transitions. Proc Natl Acad Sci USA 88:8262–8266
95. Liska AJ, Shevchenko A, Pick U, Katz A (2004) Enhanced photosynthesis and redox energy production contribute to salinity tolerance in *Dunaliella* as revealed by homology-based proteomics. Plant Physiol 136:2806–2817
96. Depege N, Bellafiore S, Rochaix JD (2003) Role of chloroplast protein kinase Stt7 in LHCII phosphorylation and state transition in *Chlamydomonas*. Science 299:1572–1575
97. Fleischmann MM, Ravanel S, Delosme R, Olive J, Zito F, Wollman FA, Rochaix JD (1999) Isolation and characterization of photoautotrophic mutants of *Chlamydomonas reinhardtii* deficient in state transition. J Biol Chem 274: 30987–30994
98. Rochaix JD (2007) Role of thylakoid protein kinases in photosynthetic acclimation. FEBS Lett 581:2768–2775
99. Bonaventura C, Myers J (1969) Fluorescence and oxygen evolution from *Chlorella pyrenoidosa*. Biochim Biophys Acta 189:366–383
100. Murata N (1969) Control of excitation transfer in photosynthesis. I. Light-induced change of chlorophyll a fluorescence in *Porphyridium cruentum*. Biochim Biophys Acta 172:242–251
101. Delosme R, Olive J, Wollman FA (1996) Changes in light energy distribution upon state transitions: an in vivo photoacoustic study of the wild type and photosynthesis mutants from *Chlamydomonas reinhardtii*. Biochim Biophys Acta: Bioenerg 1273:150–158
102. Bellafiore S, Bameche F, Peltier G, Rochaix JD (2005) State transitions and light adaptation require chloroplast thylakoid protein kinase STN7. Nature 433:892–895
103. Ben Amotz A, Shaish A, Avron M (1989) Mode of action of the massively accumulated beta-carotene of *Dunaliella bardawil* in protecting the alga against damage by excess irradiation. Plant Physiol 91:1040–1043
104. Metzger P, Largeau C (2005) *Botryococcus braunii*: a rich source for hydrocarbons and related ether lipids. Appl Microbiol Biotechnol 66:486–496
105. Rabbani S, Beyer P, Von Lintig J, Hugueney P, Kleinig H (1998) Induced beta-carotene synthesis driven by triacylglycerol deposition in the unicellular alga *Dunaliella bardawil*. Plant Physiol 116:1239–1248
106. Zhekisheva M, Boussiba S, Khozin-Goldberg I, Zarka A, Cohen Z (2002) Accumulation of oleic acid in *Haematococcus pluvialis* (Chlorophyceae) under nitrogen starvation or high light is correlated with that of astaxanthin esters. J Phycol 38: 325–331
107. Muradyan EA, Klyachko-Gurvich GL, Tsoglin LN, Sergeyenko TV, Pronina NA (2004) Changes in lipid metabolism during adaptation of the *Dunaliella salina* photosynthetic apparatus to high CO_2 concentration. Russ J Plant Physiol 51:53–62

108. Rodolfi L, Zittelli GC, Bassi N, Padovani G, Biondi N, Bonini G, Tredici MR (2009) Microalgae for oil: strain selection, induction of lipid synthesis and outdoor mass cultivation in a low-cost photobioreactor. Biotechnol Bioeng 102:100–112
109. Mus F, Dubini A, Seibert M, Posewitz MC, Grossman AR (2007) Anaerobic acclimation in *Chlamydomonas reinhardtii* - anoxic gene expression, hydrogenase induction, and metabolic pathways. J Biol Chem 282:25475–25486
110. Roessler PG (1990) Purification and characterization of acetyl-CoA carboxylase from the diatom *Cyclotella cryptica*. Plant Physiol 92:73–78
111. Roessler PG, Ohlrogge JB (1993) Cloning and characterization of the gene that encodes acetyl-Coenzyme-A carboxylase in the alga *Cyclotella cryptica*. J Biol Chem 268:19254–19259
112. Roessler PG, Bleibaum JL, Thompson GA, Ohlrogge JB (1994) Characteristics of the gene that encodes acetyl-CoA carboxylase in the diatom *Cyclotella cryptica*. Recombinant DNA Technol II 721:250–256
113. Sheehan J, Dunahay T, Benemann J, Roessler PG (1998) US Department of Energy's Office of Fuels Development. A look back at the US Department of Energy's Aquatic Species Program – Biodiesel from algae. Close out report TP-580-24190. National Renewable Energy Laboratory, Golden
114. Shintani DK, Ohlrogge JB (1995) Feedback inhibition of fatty-acid synthesis in tobacco suspension cells. Plant J 7:577–587
115. Klaus D, Ohlrogge JB, Neuhaus HE, Dormann P (2004) Increased fatty acid production in potato by engineering of acetyl-CoA carboxylase. Planta 219:389–396
116. Roesler K, Shintani D, Savage L, Boddupalli S, Ohlrogge J (1997) Targeting of the Arabidopsis homomeric acetyl-coenzyme A carboxylase to plastids of rapeseeds. Plant Physiol 113:75–81
117. Li Y, Han D, Hu G, Dauvillee D, Sommerfeld M, Ball S, Hu Q (2010) *Chlamydomonas* starchless mutant defective in ADP-glucose pyrophosphorylase hyper-accumulates triacylglycerol. Metab Eng 12(4):387–391
118. Arisz SA, van Himbergen JAJ, Musgrave A, van den Ende H, Munnik T (2000) Polar glycerolipids of *Chlamydomonas moewusii*. Phytochemistry 53:265–270
119. Guschina IA, Harwood JL (2006) Lipids and lipid metabolism in eukaryotic algae. Prog Lipid Res 45:160–186
120. Poerschmann J, Spijkerman E, Langer U (2004) Fatty acid patterns in *Chlamydomonas* sp. as a marker for nutritional regimes and temperature under extremely acidic conditions. Microb Ecol 48:78–89
121. Kimura K, Yamaoka M, Kamisaka Y (2004) Rapid estimation of lipids in oleaginous fungi and yeasts using Nile red fluorescence. J Microbiol Meth 56:331–338
122. Grobbelaar JU (2004) Algal nutrition. In: Richmond A (ed) Handbook of microalgal culture: biotechnology and applied phycology. Blackwell, Oxford, pp 97–115
123. Pyle DJ, Garcia RA, Wen ZY (2008) Producing docosahexaenoic acid (DHA)-rich algae from blodiesel-derived crude glycerol: effects of impurities on DHA production and algal biomass composition. J Agric Food Chem 56:3933–3939
124. Geng D, Wang Y, Wang P, Li W, Sun Y (2003) Stable expression of hepatitis B surface antigen gene in *Dunaliella salina* (Chlorophyta). J Appl Phycol 15:451–456
125. Mayfield SP, Franklin SE, Lerner RA (2003) Expression and assembly of a fully active antibody in algae. Proc Natl Acad Sci USA 100:438–442
126. Mayfield SP, Franklin SE (2005) Expression of human antibodies in eukaryotic micro-algae. Vaccine 23:1828–1832
127. Sayre RT, Wagner RE, Sirporanadulsil S, Farias C (2001) Transgenic algae for delivery antigens to animals. Int. Patent Number W.O.01/98335 A2
128. Sun M, Qian K, Su N, Chang H, Liu J, Shen G (2003) Foot-and-mouth disease virus VP1 protein fused with cholera toxin B subunit expressed in *Chlamydomonas reinhardtii* chloroplast. Biotechnol Lett 25:1087–1092
129. Walker TL, Purton S, Becker DK, Collet C (2005) Microalgae as bioreactors. Plant Cell Rep 24:629–641
130. Govoni C, Morosinotto T, Giuliano G, Bassi R (2007) Exploiting photosynthesis for biofuel production. In: Pavesi L, Fauchet (eds) Biophotonics. Springer-Verlag, Berlin Heidelberg, pp 15–28
131. Gaffron H, Rubin J (1942) Fermentative and photochemical production of hydrogen in algae. J Gen Physiol 26:219–240
132. Surzycki R, Cournac L, Peltiert G, Rochaix JD (2007) Potential for hydrogen production with inducible chloroplast gene expression in *Chlamydomonas*. Proc Natl Acad Sci USA 104:17548–17553
133. Purton S (2007) Tools and techniques for chloroplast transformation of *Chlamydomonas*. Adv Exp Med Biol 616:34–45
134. Molina GE, Belarbi EH, Acien Fernandez FG, Robles MA, Chisti Y (2003) Recovery of microalgal biomass and metabolites: process options and economics. Biotechnol Adv 20:491–515
135. Belarbi EH, Molina E, Chisti Y (2000) A process for high yield and scaleable recovery of high purity eicosapentaenoic acid esters from microalgae and fish oil. Enzyme Microb Technol 26:516–529
136. Stevens DR, Rochaix JD, Purton S (1996) The bacterial phleomycin resistance gene ble as a dominant selectable marker in *Chlamydomonas*. Mol Gen Genet 251:23–30
137. Dunahay TG, Jarvis EE, Zeiler KG, Roessler PG, Brown LM (1992) Genetic-engineering of microalgae for fuel production - scientific note. Appl Biochem Biotechnol 34–5:331–339
138. Falciatore A, Casotti R, Leblanc C, Abrescia C, Bowler C (1999) Transformation of nonselectable reporter genes in marine diatoms. Mar Biotechnol 1:239–251
139. Merendino L, Perron K, Rahire M, Howald I, Rochaix JD, Goldschmidt-Clermont M (2006) A novel multifunctional factor involved in trans-splicing of chloroplast introns in *Chlamydomonas*. Nucleic Acids Res 34:262–274
140. Sizova I, Fuhrmann M, Hegemann P (2001) A *Streptomyces rimosus* aphVIII gene coding for a new type phosphotransferase

provides stable antibiotic resistance to *Chlamydomonas reinhardtii*. Gene 277:221–229
141. Fischer N, Rochaix JD (2001) The flanking regions of PsaD drive efficient gene expression in the nucleus of the green alga *Chlamydomonas reinhardtii*. Mol Genet Genomics 265:888–894
142. Schroda M, Blocker D, Beck CF (2000) The HSP70A promoter as a tool for the improved expression of transgenes in *Chlamydomonas*. Plant J 21:121–131
143. Hallmann A, Sumper M (1994) An inducible arylsulfatase of *Volvox carteri* with properties suitable for a reporter-gene system - purification, characterization and molecular-cloning. Eur J Biochem 221:143–150
144. Lumbreras V, Stevens DR, Purton S (1998) Efficient foreign gene expression in *Chlamydomonas reinhardtii* mediated by an endogenous intron. Plant J 14:441–447
145. Cerutti H, Johnson AM, Gillham NW, Boynton JE (1997) Epigenetic silencing of a foreign gene in nuclear transformants of *Chlamydomonas*. Plant Cell 9:925–945
146. Mayfield SP, Manuell AL, Chen S, Wu J, Tran M, Siefker D, Muto M, Marin-Navarro J (2007) *Chlamydomonas reinhardtii* chloroplasts as protein factories. Curr Opin Biotechnol 18:126–133
147. McCallum CM, Comai L, Greene EA, Henikoff S (2000) Targeted screening for induced mutations. Nat Biotechnol 18:455–457
148. Dent RM, Haglund CM, Chin BL, Kobayashi MC, Niyogi KK (2005) Functional genomics of eukaryotic photosynthesis using insertional mutagenesis of *Chlamydomonas reinhardtii*. Plant Physiol 137:545–556

Books and Reviews

Beer LL, Boyd ES, Peters JW, Posewitz MC (2009) Engineering algae for biohydrogen and biofuel production. Curr Opin Biotechnol 20:264–271

Dolley TP, Moyle PR (2003) History and overview of the U.S. diatomite mining industry, with emphasis on the Western United States. Contrib Ind Min Res: US Geol Surv Bull 2209: E1–E8

Greenwell HC, Laurens LML, Shields RJ, Lovitt RW, Flynn KJ (2010) Placing microalgae on the biofuels priority list: a review of the technological challenges. J R Soc Interface 7:703–726

Rupprecht J (2009) From systems biology to fuel - *Chlamydomonas reinhardtii* as a model for a systems biology approach to improve biohydrogen production. J Biotechnol 142:10–20

Scott SA, Davey MP, Dennis JS, Horst I, Howe CJ, Lea-Smith DJ, Smith AG (2010) Biodiesel from algae: challenges and prospects. Curr Opin Biotechnol 21:277–286

Tredici MR (2003) Mass production of microalgae photobioreactors. In: Richmond A (ed) Handbook of microalgal culture. Blackwell Publishing, Malden, pp 178–214

Van den Hoek C, Mann DG, Jahns HM (1995) Algae: an introduction to phycology. Cambridge University Press, Cambridge, UK

Alkaline Membrane Fuel Cells

Robert C. T. Slade, Jamie P. Kizewski, Simon D. Poynton, Rong Zeng, John R. Varcoe
Department of Chemistry, University of Surrey, Guildford, UK

Article Outline

Glossary
Definition
Introduction
An Overview of Alkaline Anion-Exchange Membranes (AEMs)
Properties of AEMs
Synthetic Routes to AEMs
Development of Alkaline Ionomers
AMFCs with H_2 as Fuel
The Application of AEMs in Other Fuel Cell Types
A Brief Overview of the Patent Literature
Future Directions and Research Challenges
Acknowledgment
Bibliography

Glossary

AEM Alkaline (anion) exchange membrane.
AFC Alkaline fuel cell
AMFC Alkaline membrane fuel cell (also known as APEMFC)
DMFC Direct methanol fuel cell
MEA Membrane electrode assembly
OCV Open circuit voltage
PEM Proton-exchange membrane
PEMFC Proton-exchange membrane fuel cell
QA Quaternary ammonium
RG-AEM Radiation-grafted alkaline (anion) exchange membrane

Definition

The disruptive approach of applying alkaline anion-exchange membranes (AEMs) in alkaline membrane fuel cells (AMFCs) potentially meets several of the challenges facing other approaches to low temperature fuel cells, including the otherwise high catalyst and fuel costs. Thus, the move to alkaline conditions at the electrodes

opens the potential use of a range of low cost non-precious-metal catalysts, as opposed to the otherwise necessary use of platinum-group-metal (PGM) based catalysts. Further, it becomes possible to consider hydrogen fuels containing substantial amounts of impurities, whereas an acidic membrane approach (that in proton exchange membrane fuel cells, PEMFCs) requires high-purity gases and PGM catalysts.

Introduction

The first entry in the AMFC area was published in 2005 [1], since when activity and interest have continued to increase steeply internationally. Zeng and Varcoe have recently reviewed the developing patent literature [2]. Some researchers have recently termed these systems HEMFCs, hydroxide exchange membrane fuel cells; that terminology is not fully appropriate in view of the complex hydroxide/hydrogen carbonate/carbonate equilibria that are present (even after handling membranes in air), inevitable in the use of air (containing CO_2(g)) as source of oxidant and also produced in the oxidation of methanol in direct methanol fuel cells (DMFCs). Another acronym applied to these systems, APEMFCs, is also potentially confusing, the first three words of the full form then seemingly being "alkaline proton exchange" (following the very similar PEMFC acronym) but being readable alternatively as alkaline polymer electrolyte membrane fuel cells (possibly AEMFC would be clearer).

Alkaline fuel cells (AFCs, hydrogen-fuelled cells with an alkaline liquid electrolyte such as KOH(aq)) are the best performing of all known conventional hydrogen–oxygen fuel cells operable at temperatures below 200°C. This is due to the facile kinetics at the cathode and at the anode; cheaper non-noble metal catalysts can be used (such as nickel and silver [3, 4]), reducing cost. McLean et al. gave comprehensive review of alkaline fuel cell technology [5]. The associated fuel cell reactions both for a traditional AFC and also for an AMFC are:

$$\textit{Anode}:\ 2H_2 + 4OH^- \rightarrow 4H_2O + 4e^- \quad (E_a = 0.83\ \text{V vs. SHE at 1 bar, 298.15 K})$$

$$\textit{Cathode}:\ O_2 + 2H_2O + 4e^- \rightarrow 4OH^- \quad (E_c = 0.40\ \text{V vs. SHE at 1 bar, 298.15 K})$$

$$\textit{Overall}:\ 2H_2 + O_2 \rightarrow 2H_2O \quad (E_{cell} = 1.23\ \text{V at 1 bar, 298.15 K})$$

A major issue with traditional AFCs is that of electrolyte and electrode degradation caused by the formation of carbonate/bicarbonate (CO_3^{2-}/HCO_3^-) on reaction of OH^- ions with CO_2 contamination in the oxidant gas stream [5–7]:

$$\textit{Carbonate formation}:\ CO_2 + 2OH^- \rightarrow CO_3^{2-} + H_2O$$

$$\textit{Bicarbonate formation}:\ CO_2 + OH^- \rightarrow HCO_3^-$$

The major cause of the degrading performance of AFCs is the consequent precipitation of metal carbonate crystals (most commonly Na_2CO_3 or K_2CO_3, depending on the alkaline electrolyte used) in the electrolyte-filled pores of the electrodes, blocking pores and mechanically disrupting and destroying active layers.

The cost of fuel cells still retards commercialization in most markets. AFCs are promising on a cost basis mainly because cheap and relatively abundant non-platinum-group metals (non-PGM) are viable catalysts, but are hindered by degradation due to formation of precipitates as above. Catalyst electrokinetics (for fuel oxidation and oxygen reduction) are improved in alkaline, as opposed to acidic, conditions (the acid-stability criterion precludes the use of most non-PGM catalysts in PEMFCs). The replacement of the KOH (aq) electrolyte with an alkaline electrolyte membrane (AEM), to give AMFCs, retains the electrocatalytic advantages but introduces CO_2 tolerance (there being no mobile cations that could give carbonate/bicarbonate precipitates) with the additional advantage of being an all-solid-state fuel cell (as with PEMFCs – i.e., no seeping out of KOH(aq)). Additionally, thin (low electronic resistance) and easily stamped (cheap) metal mono/bipolar plates can be used, with reduced corrosion-derived problems at high pH (the cost of bipolar plates for PEMFCs can be as much as one third of the cost of the stacks themselves). A key and yet to be convincingly met requirement is, however, the development of a dispersible alkaline ionomer (sometimes termed an anionomer) to maximize ionic contact between the catalyst reaction sites and the ion-conductive membranes. As in the case of AFCs, water

is produced at anode and consumed at cathode in AMFCs (when fuelled with hydrogen and with four electron reduction of oxygen at the cathode), which is fundamentally different to what occurs in PEMFCs containing acidic electrolytes; this can cause high overpotentials at AMFC anodes, due to suspected flooding [8].

The use of an AEM as a solid electrolyte including no metal cations prevents precipitation of carbonate/bicarbonate salts. (The electrolyte containing the cationic groups is already a solid.) The carbonation process is quick even if the AEM has been exposed to the air for only a short time [9, 10]. The conductivities of the AEMs in OH^- form may have been underestimated because most studies to date have not disclosed vigorous CO_2 exclusion procedures during conductivity measurements. It has been hypothesized that OH^- ion conductivities in AEMs can be estimated by measuring the ionic conductivities of HCO_3^- from AEMs and multiplying by 3.8 [11]. This carbonation process may not to be a serious problem due to an in situ "self-purging mechanism" because OH^- anions are continuously generated at the cathode in AMFCs [12].

AEMs are solid polymer electrolyte membranes that contain positive ionic groups (typically quaternary ammonium (QA) functional groups such as poly-NMe_3^+) and mobile negatively charged anions. A widely quoted concern with AEMs is membrane stability, especially at elevated temperatures [13, 14]. The general issues are:

1. The diffusion coefficients and mobilities of OH^- anions are less than that of H^+ in most media, and QA ionic groups are less dissociated than the typical sulfonic acid groups (pK_a for sulfonic acid groups are typically -1 but for QA groups the related pK_b values are around +4); there were concerns that AEMs would not possess adequate intrinsic ionic conductivities for application in fuel cells.
2. The OH^- anions are effective nucleophiles which potentially cause degradation via (a) a direct nucleophilic displacement and/or (b) a Hofmann elimination reaction when a β-hydrogen is present; methyl ($-CH_3$) groups may also be displaced by OH^- ions forming tertiary amines and methanol [13, 14]. If the AEMs contain good leaving groups (e.g., QA $-NMe_3^+$ groups) then the chemical stability of the AEMs might have been inadequate for use in fuel cells, particularly at elevated temperatures.
3. Precursor anion-exchange membranes are generally submerged in aqueous NaOH/KOH solutions to exchange them to the OH^- form AEM; the AEM must have the chemical stability to withstand this process. Despite this, over a decade ago, the stabilities of various benzyltrimethylammonium-based AEMs were found to be stable at up 75°C in NaOH(aq) at concentrations up to 6 mol dm^{-3} for several days [15].

A major potential application of AMFCs is, however, as power sources for at or near room temperature (as for PEMFCs), which means such degradation can be minimal.

This entry considers the current understanding and application of AEMs in hydrogen-fuelled AMFCs and other fuel cell types employing AEMs. Figure 1 enables comparison between hydrogen- or methanol-fuelled PEMFCs and AMFCs; the electrode reactions in a hydrogen-fuelled AMFC are discussed above. In contrast to PEMFCs, operation of an AMFC requires the presence of water as a reagent at the cathode (oxygen reduction reaction, ORR – to form OH^-) and the product water is formed by the hydrogen oxidation reaction (HOR) at the anode (as opposed to being formed at the cathode in PEMFCs). The entry begins with consideration of the main classes of AEMs.

An Overview of Alkaline Anion-Exchange Membranes (AEMs)

AEMs and alkaline ionomers (anionomers) are key to the successful implementation of AMFCs. Anion-exchange membranes have, for a long time, been used as separation membranes for seawater desalination, the recovery of metal ions from wastewaters, electrodialysis and bio-separation processes, for example [16–26]. These membranes may, however, not be stable or conductive enough to be applied in AMFCs. AEMs used in early AMFC studies were reviewed in 2005 [1] and included polybenzimidazole (PBI) doped with KOH, epichlorohydrin polymer quaternized with 1,4–diazabicyclo[2,2,2]octane (DABCO) or quaternized with a 1:1 ratio of DABCO and triethylamine, and commercial membranes such as AHA (Tokuyama Co,

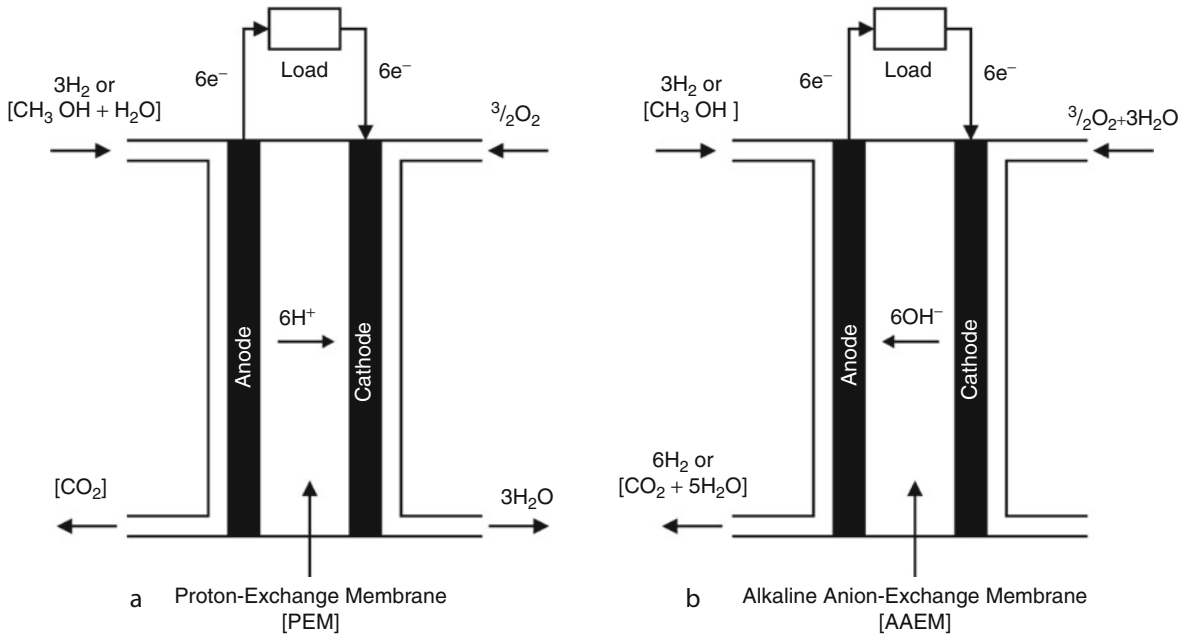

Alkaline Membrane Fuel Cells. Figure 1

A schematic presentation of (**a**) a proton-exchange membrane (PEMFC) and (**b**) an alkaline membrane fuel cell (AMFC), both fuelled either with H_2 gas or directly with methanol (DMFC mode). The stoichiometric ratios of reactants and products are shown in each case

Japan), Morgane ADP (Solvey S.A.), Tosflex® SF–17 (Tosoh) and 2259–60 (Pall RAI). Most of these fuel cells containing AEMs were, however, being operated in the presence of aqueous alkaline solutions (containing NaOH or KOH).

In the UK (at the University of Surrey), several kinds of QA-containing radiation-grafted AEMs (RG-AEMs) based on poly(vinylidene fluoride) PVDF [27–31], poly(tetrafluoroethylene–co– hexafluoropropylene) FEP [27, 28, 32] and poly(ethylene-co-tetrafluoroethylene) ETFE [32, 33], with good ion-exchange capacities (IEC) and ionic conductivities and with sufficient stabilities to test the proof of concept of using AEMs in fuel cells, have been developed. ETFE base films produce the best AEMs for testing in AMFCs. The radiation-grafted methodology (using gamma rays or electron beams for irradiation) allowed for the production of AEMs of different thicknesses, ion-exchange capacity, physical/mechanical properties, and chemistries that facilitated fundamental investigations. A water-insoluble alkaline ionomer that used *N, N,N',N'*–tetramethylhexane–1,6–diamine as the joint amination and cross-linking agent first enabled studies of the performance of metal-cation-free all-solid-state alkaline fuel cells with stable performance into the medium term at 50°C [33, 34]. Many other groups have now developed new conductive and chemically and thermally stable AEMs (and candidate alkaline ionomers), as discussed below. AEMs in the hydroxide form typically become brittle if allowed to dry; hydroxide forms are typically prepared just before use, from the chloride form analogue.

Properties of AEMs

The most common class of NaOH-/KOH-free AEMs being investigated for use in fuel cells is based on QA chemistry and has reasonable stability in alkaline environments (especially those AEMs containing benzyltrimethyl ammonium exchange sites). There are three main classes of chemical degradation reaction mechanisms by which nucleophilic OH^- anions can remove QA groups. The presence of β-hydrogens allows the Hofmann elimination reaction to occur (Scheme 1), often in parallel to the reactions discussed below, yielding alkene (vinyl) groups; this can give

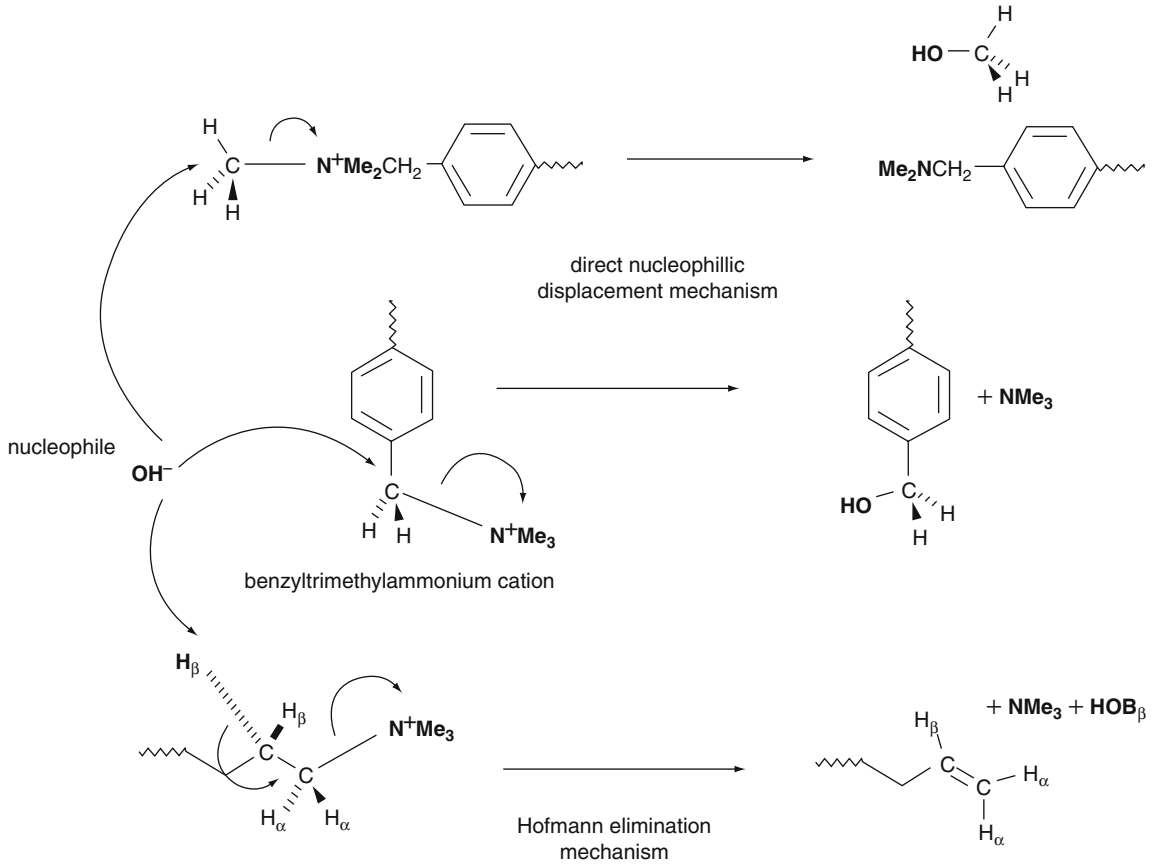

Alkaline Membrane Fuel Cells. Scheme 1
Alternative mechanisms for degradation of AEMs by displacement of the trimethylammonium groups by hydroxide anions at elevated temperatures

rise to QA–AEMs that have low thermal and chemical (to alkali) stabilities. If, as in RG-AEMs, no β-hydrogen atoms are present, direct nucleophilic substitution reactions were traditionally thought to take place yielding alcohol and tertiary amine groups. However, recent density functional theory (DFT) calculations and deuterium exchange experiments at Los Alamos National Laboratory (USA) on model small QA-containing compounds indicate that a mechanism involving an ylide intermediate(trimethyl ammonium methylide, also known as a 1,2-dipolar ylide compound) may predominate and be more severe when the AEMs are dehydrated [35].

AEMs from Tokuyama Co have good thermochemical stability. The thin (10 μm) Tokuyama "fuel cell grade" AEMs (A010, A201 – formerly A006 and A901) [9, 36–39] and their developmental dispersible alkaline ionomers (A3ver.2 and AS–4) have also been tested at up to 50°C by several research groups in direct alcohol fuel cells [40–42].

Quaternized pyridinium- or phosphonium-based AEMs were thought to have thermochemical stabilities that are not suitable for use in AEM fuel cells but there are reports of recent work on polysulfone-phosphonium-based AEMs and anionomers (see later).

Surrey's benzyltrimethylammonium-containing S80, S50, and S20 RG–AEMs (the number designating the fully hydrated thicknesses in micrometers) are chemically stable up to 80°C in aqueous KOH [32–34](aq, 1 moldm^{-3}) and can exhibit ionic conductivities > 0.03 S cm^{-1} at room temperature when fully

hydrated; the ex situ and in situ ionic conductivity of fully hydrated S80 is 0.06 S cm^{-1} at 60°C (cf. Nafion® acidic PEMs are typically > 0.1 S cm^{-1} at these temperatures). AEM conductivities are, however, considerably reduced at humidities RH/% < 100 and drop to values between 0.01 and 0.02 S cm^{-1} after only an hour when exposed to air (especially with very thin membranes) due to the reaction of OH^- anions with CO_2 forming CO_3^{2-} and HCO_3^- within the membrane. The lower dissociation constant for $-NMe_3OH$ groups (requiring a higher number of water molecules for complete dissociation), compared to $-SO_3H$ groups in PEMs, and a very low number of water molecules directly associated with the ionic groups lead to the poor performance at low RHs (at high humidities much of the water present in AEMs is located in aggregates not directly associated with the ionic groups) [32].

The developing published and patent literature in this area has recently been reviewed by Zeng and Varcoe [2]. Further classes of AEM for fuel cells have included membranes based on quaternized poly(epichlorohydrin), polysulfone, poly(phthalalazinone ether ketone), poly(2,6–dimethyl–1,4–phenylene oxide), and poly (vinyl alcohol) grafted with (2,3–epoxypropyl)trimethylammonium chloride. Common quaternizing agents include alkyliodides, trialkylamines, *N,N,N',N'*–tetramethylalkyl–1,*n*–diamines, polyethyleneimine, 1,4–diazabicyclo–[2.2.2]–octane (DABCO), and 1–azabicyclo–[2.2.2]–octane. The final two of these have been used extensively; they contain β–hydrogen but their structures do not permit molecular conformations favored in the Hofmann elimination mechanism. Metal-cation-containing AEMs based on doping polymer films (e.g., polybenzimidazole (PBI), poly (vinyl alcohol) and its composites, and biocompatible chitosan) with NaOH/KOH(aq) are also being investigated, but the presence of mobile cations may introduce problems associated with precipitation of carbonate salts.

Ionic conductivities of AEMs are generally lower than those of comparable PEMs. This is not surprising as the solution mobility of OH^- is one third to one half of that of a H^+ (depending on the environment and if there – $\mu_o \times 10^4/cm^2\ V^{-1}\ s^{-1} = 20.64$ for OH^-(aq) anions and 36.23 for H^+(aq) cations at 298 K) [1, 43]. One strategy for enhanced ionic conductivities is to increase the ion-exchange capacity (IEC) via synthetic methodology, but this often leads to a decrease in the mechanical strength due to excessive water uptakes. Another strategy is to synthesize tailored membranes that will exhibit hydrophilic(ionic)–hydrophobic(non-ionic) phase segregation and continuous ionic domains, which is hypothesized to increase ionic conductivities [44, 45].

Recent intensive studies have, however, been reported to lead to AEMs with high ionic conductivities, reportedly comparable to Nafion®. These promising AEMs [11, 45–51] are still to be evaluated in AMFCs. Most hydrocarbon AEMs are soluble in various solvents, which is potentially useful for the formulation of alkaline ionomers required for the preparation of high-performance membrane electrode assemblies (MEAs). If the conductive properties reported can be translated into high power outputs, then AMFC performances comparable to those of PEMFCs can be expected in the near future.

Synthetic Routes to AEMs

The preparation of applicable AEMs involves a compromise between the properties of the membrane, such as the chemical and thermal stability, ion-exchange capacity (IEC), ion conductivity, mechanical properties, water uptake, and dimensional stability. In general, alkaline anion-exchange polymer electrolytes can be polymerized directly from functionalized monomers, polymerized from monomers with subsequent functionalization or by functionalizing a commercially available polymer. The backbone of the polymer is usually selected for its good chemical and thermal stability and, therefore, typically includes aromatic rings and/or a degree of fluorination: typical polymer classes include polysulfones and polyetherketones, polyimides, poly(phenylene), poly(phthalazinone ether sulfone ketone), polyepichlorohydrin homopolymer, polybenzimidazole (PBI), poly(phenylene oxide), radiation-grafted copolymers, inorganic–organic hybrids, and even perfluoronated membranes such as Nafion. The active functional groups are commonly quaternary ammonium type ($-NR_3^+$) with a clear preference for trimethylammonium ($-N(CH_3)_3^+$) groups (pK_a (H_2O) = 9.8).

A suitable AEM will have a high ion-exchange capacity, high ionic conductivity, and thermochemical

stability, but will exhibit a low degree of swelling on hydration. There are several general synthetic methodologies for the preparation of AEMs [52, 53]. Fluorine-containing polymers generally show higher thermal stabilities than hydrocarbon polymers. AEMs based on a poly(arylene ether sulfone) containing fluorine atoms show high ionic conductivities (63 mS cm^{-1} in CO_3^{2-} form at 70°C) [53]; this is a key result as CO_3^{2-} anions have dilute solution mobilities that are less than 33% of that of OH^- anions. (It is rare to see CO_3^{2-} conductivities above 30 mS cm^{-1}.)

Irradiation of polymer films (and powders, etc.) using X-rays, γ-rays, or electron beams (as at Surrey, see previous section) is a flexible way to introduce various functional groups on the polymer backbones (Scheme 2). A wide range of chemically and thermal stable polymers, such as ETFE and FEP, can be chosen as the base films for the production of AEMs. Additionally, there is a wide choice of functional monomers available that can be used to introduce ion-exchange groups into the grafted polymeric chains.

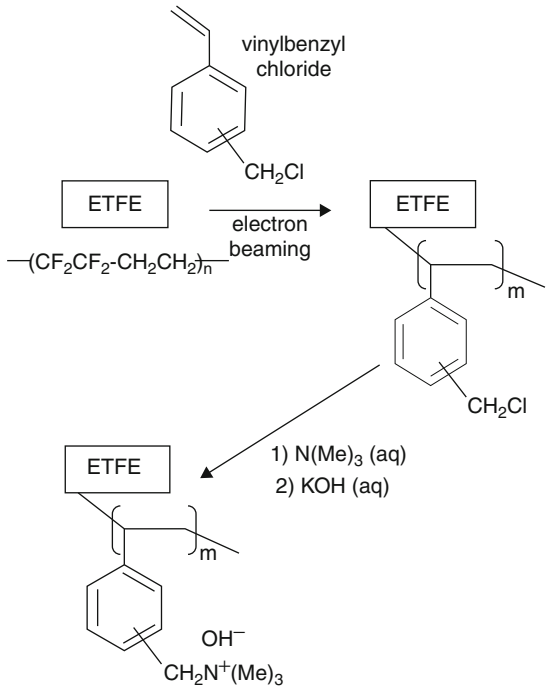

Alkaline Membrane Fuel Cells. Scheme 2
The radiation-grafting of vinylbenzyl chloride onto ETFE and subsequent amination and alkali-exchange, yielding alkaline anion-exchange membranes (RG-AEMs)

A common strategy in the synthesis of AEMs is to introduce halogen alkyl groups onto the backbone or side chains of the polymer via chloroalkylation, fluorination, bromination, or chlorination, followed by amination/quaternization and finally ion exchange. Highly carcinogenic chloromethylethers have traditionally been used as the chloroalkylation agent but safer strategies have been introduced, for example, the chloro methylation agent is generated in situ (e.g., [44, 55, 56]). An alternative strategy is the prior introduction of tertiary amine groups into the polymer, followed by quaternization.

The easiest synthetic route is to use inert polymers (as above) doped with concentrated KOH(aq) (as above): polybenzimidazole (PBI) [57–61], poly(vinyl alcohol) (PVA) [44], composite polymers such as PVA/hydroxyapatite (PVA/HAP) [62], quaternized–PVA/alumina (QPVA/Al_2O_3) [63], PVA/titanium oxide (PVA/TiO_2) [64, 65], chitosan and cross-linked chitosan [66–68], copolymers of epichlorohydrin and ethylene oxide [69], and cross-linked PVA/sulfosuccinic acid (10 wt.% SSA) [70] have all been doped with KOH and used as AEMs. Patent US5569559 [71] describes the use of polar polymers (most preferred being polyethylene oxide) doped with alkaline metal hydroxides (such as KOH), alkaline earth metal hydroxides or ammonium hydroxides such as tetrabutylammonium hydroxide; PBI doped with KOH showed the highest ionic conductivity, comparable to Nafion® (a standard acidic proton-exchange membrane, PEM). All of these materials could, however, lead to carbonate precipitates.

Anion-exchange polymers that contain methacrylate, ester, amide, or other carbonyl (C = O double bond) functional groups show low stabilities in alkali as these functional groups are highly reactive to nucleophiles such as OH^-.

Development of Alkaline Ionomers

Alkaline analogues to the oligomeric perfluorosulfonic acid dispersions used to produce optimized ionic contact between the catalyst reaction sites and the PEM in PEMFCs have yet to be convincingly developed and this has resulted in the use of nonideal strategies for the fabrication of alkaline MEAs: the use of Nafion dispersions (acidic, cation exchanging);concepts involving

adsorbed potassium hydroxide, and quaternized copolymers made from 4-vinylpyridine monomer at the electrode–AEM interface. Polysulfone-based alkaline ionomers that are compatible with polysulfone AEMs have been developed by various teams. On the commercial front, it has been reported that Fumatech have developed a ionomer concept for use with their commercial Fumasep®FAA AEMs, that uses two precursors that react to form a cross-linked polymer when mixed together, and Tokuyama's alkaline ionomers can be deposited from solution (designated A3 or AS-4) and are chemically compatible with Tokuyama's fuel cell AEMs.

Surrey developed an alkaline ionomer (SION1, Scheme 3) for MEA fabrication, with the objective of developing a system that would allow the testing of different AEMs and electrodes in AMFCs [72]; without this alkaline ionomer, the performances were too low for satisfactory testing. That alkaline ionomer also allowed for the operation of fuel cells in metal-cation-free mode, in contrast to the possible use of doped polymers containing alkali metal hydroxides. An alkaline MEA that was deliberately converted to the CO_3^{2-} form operated as well as an OH^- form MEA; even more interestingly, the CO_3^{2-} content of the carbonated MEA decreased during fuel cell operation with air (containing CO_2) at the cathode. The SION1 ionomer contains β–hydrogen atoms and, therefore, allows the Hofmann elimination degradation mechanism to operate, limiting the thermal stability to below ca. 60°C. Surrey is currently developing a next-generation β-hydrogen-free alkaline ionomers deposited from aqueous solutions (Patent GB 0814652.4).

Many researchers have reported that alkaline polymers with hydrocarbon backbones can be dissolved in solvents such as DMF, DMAc, and DMSO [47–49, 54, 73, 74], and this allows their use as the ionomer for the preparation of MEAs. Zhuang et al. [73, 75] used a quaternary ammonium polysulfone (QAPS) which can be dissolved in DMF and used as the ionomer; the QAPS polymer (in OH^- form: IEC = 1.08 mmol g^{-1}) was used to fabricate the membrane, while a QAPS film (OH^- form: IEC = 1.18 meq g^{-1}) was used as the ionomer.

The development of alkaline ionomers is one of the major challenges for the development of high-performance alkaline membrane containing fuel cells.

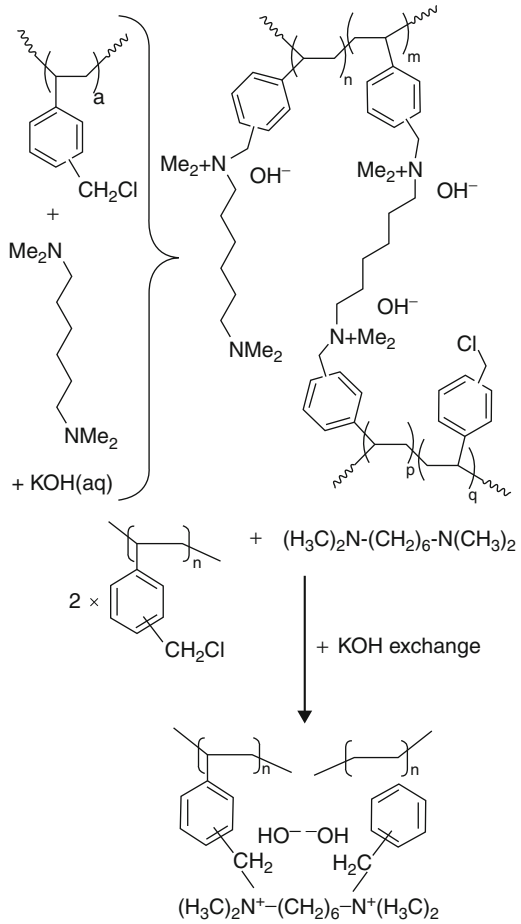

Alkaline Membrane Fuel Cells. Scheme 3
The formation of SION1 alkaline ionomer (anionomer) by cross-linkage of poly(vinylbenzyl chloride) with tetramethylhexanediamine (TMHDA)

In state-of-the-art AMFC technology, the role of the ionomer has not been fully investigated or understood; alkaline ionomer solutions/dispersions, comparable to the Nafion dispersions used in PEMFCS, remain highly sought after.

AMFCs with H_2 as Fuel

Fundamental studies at Surrey revealed the following [31–34]:

A major source of performance loss is the mass transport of H_2O to the ORR reaction sites. S80/S50/S20 radiation-grafted RG–AEMs, Solvay's Morgane®–ADP, and Tokuyama's A201 were evaluated in H_2/O_2

fuel cells at Surrey using both commercial (prefabricated) and in-house produced electrodes containing SION1 ionomer [72]. As discussed earlier, water is required as a stoichiometric reactant for the ORR at the cathode when using AEMs (unlike in PEMFCs).

The primary source of H_2O to the cathode appears to be the back transport of the H_2O electro-generated at the anode. Even with the use of fully hydrated gas supplies, evidence for this was that enhanced back transport of H_2O from the anode, and therefore superior performances, was observed with thinner AEMs: beginning-of-life peak geometric power densities, P_{peak}, of 54 → 94 → 130 mW cm^{-2} were recorded using 154 → 78 → 51 μm thick AEMs, respectively, under identical test conditions (less than 20 mW cm^{-2} was obtained with the 230 μm thick Tokuyama AHA AEM – not developed for use in fuel cells) (Fig. 2). The commercial Pt/C (20% mass – 0.5 mg_{Pt} cm^{-2} loading)-containing Type A carbon cloth prefabricated cathodes (E–Tek division of BASF) that were used contained PTFE binder (current commercially available fuel cell electrodes are optimized for use with PEMs and not for AEMs) and it was suspected that this restricted the transport of the H_2O supplied in the humidified oxygen supply to the reaction sites.

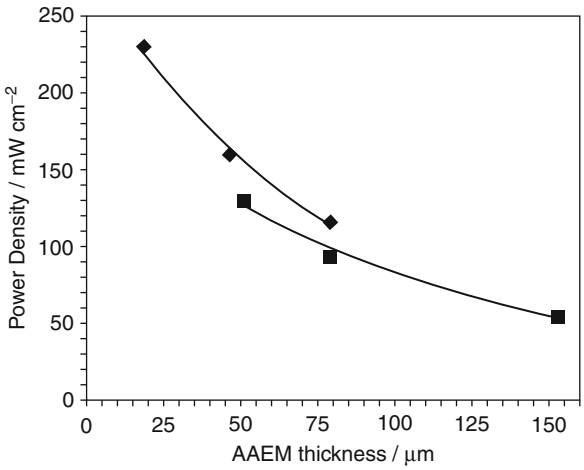

Alkaline Membrane Fuel Cells. Figure 2
Variation in power density for H_2/O_2 AMFCs as a function of fully hydrated RG-AEM thickness. The cells contained ETFE-derived RG-AEMs. All electrodes were treated with SION1 ionomer and utilized E-TekPt/C (20% mass) catalyst–loaded carbon cloth (*squares*) or carbon paper (*diamonds*) supports

Achieving an optimal MEA is still hindered by the available anionomers. Switching to the use of Toray carbon paper commercial electrodes (435 μm thick containing Pt/C (20% mass) catalyst at 0.5 mg_{Pt} cm^{-2} loading and containing PTFE binder – supplied by E–Tek division of BASF) at both the anode and cathode led to an increase in obtainable power densities (Fig. 2). P_{peak} = 230 mW cm^{-2} and a maximum i at full discharge of 1.3 A cm^{-2} was obtained in a H_2/O_2 fuel cell at 50°C with S20 (20 μm). A P_{peak} = 260 mW cm^{-2} was obtained at 50°C with Tokuyma A201 using SION1-treated electrodes. Fully satisfactory MEA lamination cannot, however, be achieved with SION1 alkaline ionomer and there are still considerable, variable, contact resistances.

Pt-free electrodes are viable in AMFCs (*more evidence is given below*). Ag/C (60% mass, 4 mg_{Ag} cm^{-2}) performed well when used as a cathode catalyst (Ag/C catalyst performed poorly in the cathode of a PEMFC). Open circuit voltages (V_{OC}) were normally in the range 1.0–1.1 V with Solvay ADP and Pt/C electrodes (ca. 100 mV higher than obtained with Nafion–115 PEMFCs); a drop of 100 mV in V_{OC} was observed when Pt was replaced with Ag at the cathode.

The activity of the carbon supports needs to be evaluated for each catalyst material to be tested. An important finding was that metal-free Vulcan XC–72R (i.e., carbon black only) cathodes produced significant currents (P_{peak} = 22 mW cm^{-2} and V_{OC} = 0.88 V with Solvay ADP at 50°C). Carbons reduce O_2 primarily through a $2e^-$ mechanism at high pH producing hydroperoxide anions (HO_2^-), which may form highly reactive hydroxyl radical species.

Other groups have been investigating nonradiation-grafted AEMs. A fully non-PGM-catalyst-containing metal-cation-free alkaline membrane fuel cell was first reported by the team at Wuhan University [73], for an AMFC containing a QA-polysulfone AEM and an MEA that did not contain any PGM catalysts; a P_{peak} = 52 mW cm^{-2}at 60°C (open circuit voltage, OCV, V_{OC} = 0.94 V) was obtained using Ni-based anode catalyst and a Ag cathode catalyst.

Polysulfone-based AEMs(see earlier) have been tested in H_2/air fuel cells at 60°C using a polysulfone alkaline ionomer (dew point of the gases was 55°C). A P_{peak} = 28 mW cm^{-2} at V_{cell} = 0.47 V was obtained

with Pt/C (40% mass, Johnson Matthey) with loadings of 0.5 mg_{Pt} cm^{-2}. P_{peak} = 30 mW cm^{-2} at V_{cell} = 0.42 V was obtained when the cathode contained a Ag/C catalyst (40% mass, E–Tek) at a loading of 2 mg_{Ag} cm^{-2}. OCVs were 100 mV lower with Ag compared to Pt, which correlates with the results above. A P_{peak} = 365 mW cm^{-2} at 0.4 V (V_{OC} = 1.04 V, r = 0.152 Ω cm^2) was reported at the 214th Meeting of the Electrochemical Society in 2008 by Wang's team at Penn State University, using Tokuyama's A901 (10 μm) AEM and AS-4 alkaline ionomer (IEC = 1.3 meq g^{-1}) at 50°C in a H_2/O_2 AMFC with 0.4 mg cm^{-2}Pt/C catalysts; these values dropped to 212 mW cm^{-2} (V_{OC} = 1.02 V, r = 0.19 Ω cm^2) when the O_2 at the cathode was replaced with purified air (<1 ppm CO_2) and the P_{peak} dropped to 113 mW cm^{-2} ($\underline{r}$ = 0.22 Ω cm^2). The higher value represents the highest H_2/O_2 AMFC performance publicly reported to date.

KOH-doped membranes (see earlier) represent metal-cation-containing AEMs. A H_2/O_2 fuel cell has been tested with a KOH-doped PBI membrane ($\underline{t}$ = 40 μm) at 50°C yielding an $\underline{i}$ = 620 mA cm^{-2} at V_{cell} = 0.60 V (P = 370 mW cm^{-2}) [60]. This performance was similar to that of the same apparatus with a Nafion–117 PEM and also, remarkably, with a PBI AEM doped with both KOH and K_2CO_3. The question of the long-term stability and leaching out of the KOH (if any) remains to be fully addressed for this class of AEM, as does the issue of potential for carbonate/bicarbonate precipitation.

Gu and Yan et al. [76] developed an ionomer, tris(2,4,6–trimethoxyphenyl) polysulfone–methylene quaternary phosphonium hydroxide (TPQPOH), which is soluble in low boiling point and water-soluble solvents such as methanol, ethanol, and *n*-propanol. The solubility of this kind of ionomer could be ideal for use in AMFC MEAs; 196 mW cm^{-2} was achieved at 80°C (H_2/O_2 gases supplied at 250 kPa back-pressure) using this phosphonium ionomer with a 70 μm thick FAA commercial membrane (Fumatech GmbH) as the AEM. A maximum power of more than 250 mW cm^{-2} was obtained in a H_2/O_2 fuel cell at 50°C with a 50 μm AEM and gas back-pressures of 250 kPa. The presence of methoxy ($-OCH_3$) groups on the aromatic rings that are connected to the phosphonium ion centers seems essential to adequate chemical stability.

The Application of AEMs in Other Fuel Cell Types

The utility of AEMs as potential electrolytes in fuel cells arises not only from the prospects for the use of non-Pt-group metal (non-PGM) catalysts and cheaper fuel cell components (less corrosive environment) but also from potential for use of alternative fuels.

Alcohols and diols, sodium borohydride ($NaBH_4$), and hydrazine (H_2NNH_2) have all been used directly as fuels in AMFCs. Patents [77, 78] introduced more fuels including hydrated hydrazine ($NH_2NH_2{\cdot}H_2O$), hydrazine carbonate ($(NH_2NH_2)_2CO_2$), hydrazine sulfate ($NH_2NH_2{\cdot}H_2SO_4$), monomethyl hydrazine (CH_3NHNH_2), ammonia (NH_3), heterocycles such as imidazole and 1,3,5–truazine and 3–amino–1,2,4–triazole, and hydroxylamines such as hydroxylamine (NH_2OH) and hydroxylamine sulfate ($NH_2OH{\cdot}H_2SO_4$); the catalysts were co-based for the fuel side (anode) and Ag/C, Pt/C and Ni/C for the oxygen reduction side (cathode). EP2133946 [79] disclosed the use of transition metals as catalysts in AMFCs. There are numerous reports on the use of non-Pt catalyst, such as MnO_2 [58], Ag/C [74, 75, 79], Au/C [80], FeTPP/BPC (Black Pearl Carbon) [81], CoPPyC [82], FeCo-CNF (Carbon Nanofiber) [83], CoFeN/C-HLH [84] in AMFC cathodes and Cr-decorated Ni/C [73], Fe-Co-Ni/C [85, 86] at anodes.

Zhuang et al. conducted a feasibility analysis of the use of AEMs in DMFCs [87]; this important study concentrated on the thermodynamic disadvantages versus kinetic advantages of such cells by considering the reactions taking place in aqueous solutions and the authors concluded that the thermodynamic voltage losses due to the pH difference across the AEM would be approximately canceled out by the kinetic voltage gains. Ogumi et al. studied direct alcohol fuel cells (methanol and ethylene glycol) with a commercial AEM (Tokoyama AHA, thickness ≈ 240 μm) [39]. Solutions of ethylene glycol and methanol were made to a concentration of 1 mol dm^{-3} dissolved in KOH (aq, 1 mol dm^{-3}), and so the system was not metal-cation-free (common with other AMFCs obtaining reasonable power levels with alcohols as fuels). Cell voltages were around 100 mV higher for ethylene glycol compared to methanol. This fuel cell is *not* quite an alkaline analogue of an acid membrane DMFC, as the authors used alkaline fuel solution. No indication was

given concerning completeness of oxidation of the ethylene glycol to CO_2 and H_2O. Yu and Scott also reported the operation of a direct methanol alkaline fuel cell, with platinized titanium mesh anodes (1.5 mg cm^{-2}Pt/Ti) and a commercial alkaline anion-exchange membrane (Morgane ADP membrane from Solvay SA) [88].

It has been proposed that ammonia would make a good energy vector/carrier [6] and an indirect fuel for a hydrogen fuel cell; ammonia is environmentally benign (it is already used as a fertilizer and neutralizes acid rain), already available cheaply, contains 50% more H per dm^3 than liquid hydrogen, and is a liquid at much lower pressures (8–9 bar); it also has the advantage of a strong smell, allowing the easier location of leaks. Cracking ammonia to form hydrogen free of traces of ammonia for use in traditional PEMFCs requires temperatures of above 900°C; PEMFCs cannot tolerate any NH_3 contamination. An advantage of AFCs is that they will tolerate low levels of NH_3, and so cracking can be undertaken at lower temperatures; this has yet to be explored using AMFC approaches.

A Brief Overview of the Patent Literature

Zeng and Varcoe have recently reviewed in depth the patent literature concerning AEMs [89]. A small number of patents of direct interest to application of AEMs in AMFCs are considered in this section.

In the area of novel AEMs:

- Patents relating to the application of radiation-grafted ion-exchange membranes in fuel cells have been granted to Scherer et al. [89] and to Stone and Steck [90, 91]. These patents mention the functionalization of base polymers with quaternary ammonium groups to yield alkaline polymers. The use of fluorine-substituted styrenic monomers is also claimed to improve membrane chemical stability when utilized in fuel cells (removal of undesired and reactive C–H bonds).
- Fauvarque was granted a patent on aqueous alkaline solid electrolyte based around polyether polymer matrices [92].
- Yao et al. were granted related patents on alkaline polymers containing alkyl quaternary ammonium salts, nitrogen containing heterocyclic quaternary ammonium salts, and metal hydroxide salts for potential applications in alkaline batteries and fuel cells [93–95].

In the area of device architecture:

- Jaouen patented a novel cathode structure for a solid polymer fuel cell [96]; that cathode structure consisted of a solid polymer anion-exchange membrane surrounding the catalysts particles (entirely within the cathode structure), which was in contact (surrounded) with a cation-conducting polymer membrane.
- Lu and Zhuang were granted a patent on alkaline-resin-containing fuel cells with direct fuelling with liquid organic fuels [97].
- Related patents from Divisek describe the invention of a methanol fuel cell utilizing an anion-exchange membrane [98, 99].

Future Directions and Research Challenges

There are a number of research challenges that must be overcome before AEMs can be successfully applied in pre-commercial AMFCs:

1. As a priority and to complement ex situ stability measurements, AEMs must be evaluated in H_2/O_2, H_2/air, and methanol/air fuel cells for several thousand hours to ensure adequate in situ membrane stability and assess the effect of and level of CO_2^{2-}/HCO_3^- formation. The effect of adding alkali to the methanol solution must also be thoroughly investigated over long timescales.
2. AEMs must be created with higher conductivities, to ensure good fuel cell performances at high current densities. It should be noted, however, that with application of an alkaline DMFC as a power source for portable devices, an overriding priority is maximizing the energy density of the fuel and fuel efficiency (cell voltage). These DMFCs will be operated at low-to-medium current densities (higher efficiencies), where electrode overpotentials are the dominant cause of voltage losses.
3. It is essential that a solubilized form of an alkaline anion-exchange polymer be developed to improve the interface between the electrodes and the AEM electrolyte. Success in this effort will decrease MEA resistances. A water-based soluble form which can

be rendered water insoluble when cast would be preferred, as there are safety concerns (primarily with industrial scale production) about using organic solvents near finely dispersed (pyrophoric) metal catalysts (unsupported or supported on carbon).

4. If AEMs are to be applied to fuel cells for other applications (such as automotive power etc.), more temperature stable AEMs must be developed. Operation of alkaline-membrane-based fuel cells at elevated temperature would reduce thermodynamic voltage losses due to pH differences across the AEM and would also improve the electrokinetics. Successful, stable over the long term, and being operational at elevated temperatures, all would allow application in fuel cells for the automotive mass market.
5. If AEMs are shown to be stable in fuel cells over thousands of hours, an in-depth investigation into effective and cheaper non-noble metal catalysts (e.g., Ni, Ag etc.) is indicated. There would also be a greater chance of finding methanol-tolerant catalysts for use in the cathodes than in related PEM-based DMFCs.
6. Finally, removal of fluorine from the polymer systems would be of interest to enhance the environmental credentials of the technology (facilitating easier disposal) and reduce costs. The substitution of fully fluorinated FEP with non-fluorinated LDPE is feasible. While oxidative radical degradation is a problem at the cathode and anode (via oxygen diffusion through the membrane) with non-fluorinated PEMs, it has been shown using electron paramagnetic resonance (EPR) studies that such degradation is prevented in highly alkaline (pH > 11.7) conditions pertinent to AEMs [100–102].

Acknowledgment

We thank the Engineering and Physical Sciences Research Council (EPSRC) of the United Kingdom for contracts with our team in the area of development of alkaline membrane technology for alkaline membrane fuel cells and associated electrical energy generation: GR/S60709/01, EP/F027524/1, EP/G009929/2 and EP/H025340/1.

Bibliography

Primary Literature

1. Varcoe JR, Slade RCT (2005) Prospects for alkaline anion-exchange membranes in low temperature fuel cells. Fuel Cells 5:189–200
2. Zeng R, Varcoe JR (2011) Alkaline anion exchange membranes for fuel cells – a patent review. Recent Pat Chem Eng 4:93–115
3. Schulze M, Gülzow E (2004) Degradation of nickel anodes in alkaline fuel cells. J Power Sources 127:252–263
4. Wagner N, Schulze M, Gülzow E (2004) Long term investigations of silver cathodes for alkaline fuel cells. J Power Sources 127:264–272
5. McLean GF, Niet T, Prince-Richard S, Djilali N (2002) An assessment of alkaline fuel cell technology. Int J Hydrogen Energy 27:507–526
6. Cifrain M, Kordesch KV (2004) Advances, aging mechanism and lifetime in AFCs with circulating electrolytes. J Power Sources 127:234–242
7. Gülzow E, Schulze M (2004) Long-term operation of AFC electrodes with CO_2 containing gases. J Power Sources 127:243–251
8. Zeng R, Poynton SD, Kizewski JP, Slade RCT, Varcoe JR (2010) A novel reference electrode for application in alkaline polymer electrolyte membrane fuel cells. Electrochem Commun 12:823–8355
9. Yanagi H, Fukuta K (2008) Anion exchange membrane and ionomer for alkaline membrane fuel cells (AMFCs). Electrochem Soc Trans 16:257–262
10. Kizewski JP, Mudri NH, Zeng R, Poynton SD, Slade RCT, Varcoe JR (2010) Alkaline electrolytes and reference electrodes for alkaline polymer electrolyte membrane fuel cells. Electrochem Soc Trans 33:27–35
11. Yan JL, Hickner MA (2010) Anion exchange membranes by bromination of benzylmethyl–containing poly(sulfone)s. Macromolecules 43:2349–2356
12. Adams LA, Poynton SD, Tamain C, Slade RCT, Varcoe JR (2008) A carbon dioxide tolerant aqueous–electrolyte–free anion–exchange membrane alkaline fuel cell. Chem Sus Chem 1:79–81
13. Zagorodni AA, Kotova DL, Selemenev VF (2002) Infrared spectroscopy of ion exchange resins: chemical deterioration of the resins. React Funct Polym 53:157–171
14. Neagu V, Bunia I, Plesca I (2000) Ionic polymers – VI. Chemical stability of strong base anion exchangers in aggressive media. Polym Degrad Stab 70:463–468
15. Sata T, Tsujimoto M, Yamaguchi T, Matsusaki K (1996) Change of anion exchange membranes in an aqueous sodium hydroxide solution at high temperature. J Membr Sci 112:161–170
16. Soda T, Kaisha K (1972) Anion exchange membranes and their production. GB Patent 1401997
17. Hansen RD, Wheaton RM (1966) Separation of acid from polymers by dialysis with anion exchange membrane. US Patent 3244620

18. Imoto R, Kosaka Y, Shimizu A (1966) Process for manufacturing anion-exchange membranes from a graft copoloymer of SBR and a vinylpyridine reacted with an epoxy resin. US Patent 3258435
19. Hansen RD, Wheaton RM (1966) Separation of acid by dialysis with anion-exchange membranes. US Patent 3272737
20. Süser A (1973) Preparation of anion exchange membranes from cellulose sheets. US Patent 3714010
21. Scott, Rosedale, Moulton, Taylor, Gough (1990) Anion exchange membranes. Patent EP0382439
22. Altmeier P (1995) Stark basische anionenaustauscher-membranen und verfahren zu deren herstellung. Patent WO9506083
23. Altmeier P (1998) Strongly alkaline anion exchange membranes and process for producing the same. US Patent 5746917
24. Ehrikhovich KJ, Viktorovna SN, Aleksandrovich FJ, Semenovich GS, Mikhajlovich AJ, Vladimirovna SI, Alekseevna JN, Fedorovich TS (1997) Method for production of anion-exchange membranes having high penetrability to chloride ion. Patent RU2074204
25. Jurevich TD (2007) Method for modifying anion-exchange membranes MA-40. Patent RU2303835
26. Aminabhavi T, Kulkarni PV, Kariduraganavar MY (2009) Ion exchange membranes, methods and processes for production thereof and uses in specific applications. US Patent 7544278
27. Danks TN, Slade RCT, Varcoe JR (2002) Comparison of PVDF– and FEP–based radiation–grafted alkaline anion–exchange membranes for use in low temperature portable DMFCs. J Mater Chem 12:3371–3373
28. Danks TN, Slade RCT, Varcoe JR (2003) Alkaline anion–exchange radiation–grafted membranes for possible electrochemical application in fuel cells. J Mater Chem 13:712–721
29. Herman H, Slade RCT, Varcoe JR (2003) The radiation–grafting of vinylbenzyl chloride onto poly(hexafluoropropylene–co–tetrafluoroethylene) films with subsequent conversion to alkaline anion–exchange membranes: optimisation of the experimental conditions and characterization. J Membr Sci 218:147–163
30. Tzanetakis N, Varcoe J, Slade RS, Scott K (2003) Salt splitting with radiation grafted PVDF anion–exchange membrane. Electrochem Commun 5:115–119
31. Tzanetakis N, Varcoe JR, Slade RCT, Scott K (2005) Radiation–grafted PVDF anion exchange membrane for salt splitting. Desalination 174:257–265
32. Slade RCT, Varcoe JR (2005) Investigations of conductivity in FEP–based radiation–grafted alkaline anion–exchange membranes. Solid State Ionics 176:585–597
33. Varcoe JR, Slade RCT (2006) An electron–beam–grafted ETFE alkaline anion–exchange membrane in metal–cation–free solid–state alkaline fuel cells. Electrochem Commun 8:839–843
34. Varcoe JR, Slade RCT, Yee ELH, Poynton SD, Driscoll DJ, Apperley DC (2007) Poly(ethylene–*co*–tetrafluoroethylene)–derived radiation–grafted anion–exchange membrane with properties specifically tailored for application in metal–cation–free alkaline polymer electrolyte fuel cells. Chem Mater 19:2686–2693
35. Chempath S, Einsla BR, Pratt LR, Macomber CS, Boncella JM, Rau JA, Pivovar BS (2008) Mechanism of tetra alkyl ammonium head group degradation in alkaline fuel cell membranes. J Phys Chem C 112:3179–3182
36. Piana M, Boccia M, Filpi A, Flammia E, Miller HA, Orsini M, Salusti F, Santiccioloi S, Ciardelli F, Pucci A (2010) H_2/air alkaline membrane fuel cell performance and durability, using novel ionomer and non–platinum group metal cathode catalyst. J Power Sources 195:5875–5881
37. Li YS, Zhao TS, Liang ZX (2009) Performance of alkaline electrolyte–membrane–based direct ethanol fuel cells. J Power Sources 187:387–392
38. Kim JH, Kim HK, Hwang KT, Lee JY (2010) Performance of air–breathing direct methanol fuel cell with anion–exchange membrane. Int J Hydrogen Energy 35:768–773
39. Matsuoka K, Iriyama Y, Abe T, Matsuoka M, Ogumi Z (2005) Alkaline direct alcohol fuel cells using an anion exchange membrane. J Power Sources 150:27–31
40. Li YS, Zhao TS, Liang ZX (2009) Effect of polymer binders in anode catalyst layer on performance of alkaline direct ethanol fuel cells. J Power Sources 190:223–229
41. Fujiwara N, Siroma Z, Yamazaki SI, Ioroi T, Senoh H, Yasuda K (2008) Direct ethanol fuel cells using an anion exchange membrane. J Power Sources 185:621–626
42. Bunazawa H, Yamazaki Y (2008) Influence of anion ionomer content and silver cathode catalyst on the performance of alkaline membrane electrode assemblies (MEAs) for direct methanol fuel cells (DMFCs). J Power Sources 182:48–51
43. Marx D, Chandra A, Tuckerman ME (2010) Aqueous basic solutions: hydroxide solvation, structural diffusion, and comparison to the hydrated proton. Chem Rev 110:2174–2216
44. Hibbs MR, Hickner MA, Alam TM, McIntyre SK, Fujimoto CH, Cornelius CJ (2008) Transport properties of hydroxide and proton conducting membranes. Chem Mater 20:2566–2573
45. Robertson NJ, Kostalik HA IV, Clark TJ, Mutolo PF, Abruna HD, Coates GW (2010) Tunable high performance cross–linked alkaline anion exchange membranes for fuel cell applications. J Am Chem Soc 132:3400–3404
46. Tanaka M, Koike M, Miyatake K, Watanabe M (2010) Anion conductive aromatic ionomers containing fluorenyl groups. Macromolecules 43:2657–2659
47. Wang JH, Li SH, Zhang SB (2010) Novel hydroxide–conducting polyelectrolyte composed of a poly(arylene ether sulfone) containing pendant quaternary guanidinium groups for alkaline fuel cell applications. Macromolecules 43:3890–3896
48. Guo ML, Fang J, Xu HK, Li W, Lu XH, Lan CH, Li KY (2010) Synthesis and characterization of novel anion exchange membranes based on imidazolium–type ionic liquid for alkaline fuel cells. J Membr Sci 362:97–104
49. Wang JH, Zhao Z, Gong FX, Li SH, Zhang SB (2009) Synthesis of soluble poly(arylene ether sulfone) ionomers with pendant quaternary ammonium groups for anion exchange membranes. Macromolecules 42:8711–8717

50. Tripathi BP, Kumar M, Shahi VK (2010) Organic–inorganic hybrid alkaline membranes by epoxide ring opening for direct methanol fuel cell applications. J Membr Sci 360:90–101
51. Clark TJ, Robertson NJ, Kostalik HA IV, Lobkovsky EB, Mutolo PF, Abruna HD, Coates GW (2009) A ring–opening metathesis polymerization route to alkaline anion exchange membranes: development of hydroxide–conducting thin films from an ammonium–functionalized monomer. J Am Chem Soc 131: 12888–12889
52. Shevchenko VV, Gumennaya MA (2010) Synthesis and properties of anion-exchange membranes for fuel cells. Theor Exp Chem 46:139–152
53. Varcoe JR, Poynton SD, Slade RCT (2009) In: Vielstich W, Gasteiger HA, Yokokawa H (eds) Handbook of fuel cells – fundamentals, technology and applications, vol 5, Advances in electocatalysis, materials, diagnostics and durability. Wiley, Chichester, pp 322–336
54. Zhou J, Unlu M, Vega J, Kohl P (2009) Anionic polysulfoneionomers and membranes containing fluorenyl groups for anionic fuel cells. J Power Sources 190:285–292
55. Fang J, Shen PK (2006) Quaternizedpoly(phthalazinon ether sulfone ketone) membrane for anion exchange membrane fuel cells. J Membr Sci 285:317–322
56. Zeng QH, Liu QL, Broadwell I, Zhu AM, Xiong Y, Tu XP (2010) Anion exchange membranes based onquaternized polystyrene–block–poly(ethylene–ran–butylene)–block–polystyrene for direct methanol alkaline fuel cells. J Membr Sci 349:237–243
57. Hou HY, Sun GQ, He RH, Wu ZM, Sun BY (2008) Alkali doped polybenzimidazole membrane for high performance alkaline direct ethanol fuel cell. J Power Sources 182:95–99
58. Hou HY, Sun GQ, He RH, Sun BY, Jin W, Liu H, Xin Q (2008) Alkali doped polybenzimidazole membrane for alkaline direct methanol fuel cell. Int J Hydrogen Energy 33:7172–7176
59. Modestov AD, Tarasevich MR, Leykin AY, Filimonov VY (2009) MEA for alkaline direct ethanol fuel cell with alkali doped PBI membrane and non–platinum electrodes. J Power Sources 188:502–506
60. Xing B, Savadogo O (2000) Hydrogen oxygen polymer electrolyte membrane fuel cells (PEMFCs) based on alkaline–doped polybenzimidazole (PBI). Electrochem Commun 2:697–702
61. Savadogo O (2004) Emerging membranes for electrochemical systems. Part II. High temperature composite membranes for polymer electrolyte fuel cell (PEFC) applications. J Power Sources 127:135–161
62. Yang CC, Lin CT, Chiu SJ (2008) Preparation of the PVA/HAP composite polymer membrane for alkaline DMFC application. Desalination 233:137–146
63. Yang CC, Chiu SJ, Chien WC, Chiu SS (2010) Quaternized poly(vinyl alcohol)/alumina composite polymer membranes for alkaline direct methanol fuel cells. J Power Sources 195:2212–2219
64. Yang CC, Chiu SJ, Lee KT, Chien WC, Lin CT, Huang CA (2008) Study of poly(vinyl alcohol)/titanium oxide composite polymer membranes and their application on alkaline direct alcohol fuel cell. J Power Sources 184:44–51
65. Yang CC (2007) Synthesis and characterization of the cross–linked PVA/TiO_2 composite polymer membrane for alkaline DMFC. J Membr Sci 288:51–60
66. Wan Y, Peppley B, Creber KAM, Bui VT, Halliop E (2006) Preliminary evaluation of an alkaline chitosan–based membrane fuel cell. J Power Sources 162:105–113
67. Wan Y, Creber KAM, Peppley B, Bui VT (2006) Chitosan–based electrolyte composite membranes II. Mechanical properties and ionic conductivity. J Membr Sci 284:331–338
68. Wan Y, Creber KAM, Peppley B, Bui VT (2006) Chitosan–based solid electrolyte composite membranes I. Preparation and characterization. J Membr Sci 280:666–674
69. Vassal N, Salmon E, Fauvarque JF (2000) Electrochemical properties of an alkaline solid polymer electrolyte based on P(ECH–co–EO). Electrochim Acta 45:1527–1532
70. Yang CC, Chiu SJ, Chien WC (2006) Development of alkaline direct methanol fuel cells based on cross–linked PVA polymer membranes. J Power Sources 162:21–29
71. Fauvarque JF (1996) Alkaline solid polymer electrolyte, electrode and electrochemical generator containing such as electrolyte. US Patent 5569559
72. Varcoe JR, Slade RCT, Lam How Yee E (2006) An alkaline polymer electrochemical interface: a breakthrough in application of alkaline anion–exchange membranes in fuel cells. Chem Commun :1428–29
73. Lu SF, Pan J, Huang AB, Zhuang L, Lu JT (2008) Alkaline polymer electrolyte fuel cells completely free from noble metal catalysts. Proc Natl Acad Sci 105:20611–20614
74. Park JS, Park SH, Yim SD, Yoon YG, Lee WY, Kim CS (2008) Performance of solid alkaline fuel cells employing anion–exchange membranes. J Power Sources 178:620–626
75. Tang DP, Pan J, Lu SF, Zhuang L, Lu JT (2010) Alkaline polymer electrolyte fuel cells: principle, challenges, and recent progress. Sci China Chem 53:357–364
76. Gu S, Cai R, Luo T, Chen ZW, Sun MW, Liu Y, He GH, Yan YS (2009) A soluble and highly conductive ionomer for high–performance hydroxide exchange membrane fuel cells. Angew Chem Int Ed 48:6499–6502
77. Asazawa K, Yamada K, Tanaka H (2007) Fuel cell. Patent EP1843416
78. Tanaka H, Yamada K, Asazawa K (2004) Fuel cell. Patent EP1460705
79. Asazawa K, Yamada K, Tanaka H (2009) Fuel cell. Patent EP2133946
80. Poynton SD, Kizewski JP, Slade RCT, Varcoe JR (2010) Novel electrolyte membranes and non–Pt catalysts for low temperature fuel cells. Solid State Ionics 181:219–222
81. Ramaswamy N, Mukerjee S (2010) Electrocatalysis of oxygen reduction on non-precious metallic centers at high pH environments. ECS Trans 33:1777–1785
82. Asazawa K, Yamamoto K, Yamada K, Tanaka H, Matsumura D, Tamura K, Nishihata Y, Atanassov P (2010) XAFS analysis of unpyrolyzedCoPPyC oxygen reduction catalyst for anion-exchange membrane fuel cells (AMFC). Electrochem Soc Trans 33:1751–1755

83. Jeong B, Uhm S, Lee J (2010) Iron-cobalt modified electrospun carbon nanofibers as oxygen reduction catalysts in alkaline fuel cells. Electrochem Soc Trans 33:1757–1767
84. Li XG, Popov BN, Kawahara T, Yanagi H (2010) Recent advances in non-precious metal catalysts for oxygen reduction reaction in fuel cells. Electrochem Soc Trans 33:1769–1776
85. Takeguchi T, Takahashi H, Yamanaka T, Nakamura A, Ueda W (2010) Development of direct-ethanol anion-conducting solid alkaline inorganic fuel cell. Electrochem Soc Trans 33:1847–1851
86. Nakamura A, Takahashi H, Takeguchi T, Yamanaka T, Wang Q, Uchimoto Y, Ueda W (2010) Effect of reduction temperature of Fe-Co-Ni/C catalyst on the solid alkaline fuel cell performance. Electrochem Soc Trans 33:1817–1821
87. Wang Y, Li L, Hu L, Zhuang L, Lu J, Xu B (2003) A feasibility analysis for alkaline membrane direct methanol fuel cell: thermodynamic disadvantages versus kinetic advantages. Electrochem Commun 5:662–666
88. Yu EH, Krewer U, Scott K (2010) Principles and materials aspects of direct alkaline alcohol fuel cells. Energies 3:1499–1528
89. Scherer GG, Büchi FN, Gupta G (Paul Scherrer Institut, Switzerland) (1997) US Patent 5656386
90. Stone C, Steck A (Ballard Power Systems Inc., Canada) (2002) US Patent 6359019
91. Stone C, Steck A (Ballard Power Systems Inc., Canada) (2000) PCT Patent 01/58576
92. Fauvarque J-F (CNAM Paris and Electricité de France) (1996) US Patent 5569559
93. Yao W, Tsai T, Chang Y-M, Chen M (Reveo Inc., USA) (2001) US Patent 6183914
94. Yao W, Tsai T, Chang Y-M, Chen M (Reveo Inc., USA) (2000) PCT Patent 00/16422
95. Yao W, Tsai T, Chang Y-M, Chen M (Reveo Inc., USA) (2000) Patent EP1116291
96. Jaouen F (ABB AB and Volvo, Sweden) (2002) PCT Patent 02/35633
97. Lu J, Zhuang L (Wuhan University) (2003) Patent CN1402370
98. Divisek J (Forschungszentrum Jülich, Germany) (2001) PCT Patent 01/61776
99. Divisek J (Forschungszentrum Jülich, Germany) (2001) Patent EP1256142
100. Yu J, Yi B, Xing D, Liu F, Shao Z, Fu Y, Zhang H (2003) Degradation mechanism of polystyrene sulfonic acid membrane and application of its composite membranes in fuel cells. Phys Chem Chem Phys 5:611–615
101. Hübner G, Roduner E (1999) EPR investigation of HQ• radical initiated degradation reactions of sulfonated aromatics as model compounds for fuel cell proton conducting membranes. J Mater Chem 9:409–418
102. Panchenko A, Dilger H, Möller E, Sixt T, Roduner E (2004) In situ EPR investigation of polymer electrolyte membrane degradation in fuel cell applications. J Power Sources 127:325–330

Animal Breeding and Genetics, Introduction

Ignacy Misztal
Department of Animal and Dairy Science Breeding and Genetics, University of Georgia, Athens, GA, USA

Informal animal breeding started thousands of years ago when hunter-gatherers started domesticating animals. Out of thousands of species available only few were domesticated as the requirements for domestication were numerous: plant diet, fast growth rate, ability to breed in captivity, good disposition, little tendency to panic, and ability to function well in groups [1]. An ancient farmer/herder took special care of well-behaving animals that provided good growth, or plenty of milk, or reliable draft, or lots of wool, etc., while eliminating the troublesome ones. The domestication greatly increased the nutritional output per unit of land although it also brought new problems, e.g., new diseases and wars. These problems were smaller than the benefits of the domestication as hunter-gatherers mostly disappeared. Some of the benefits could be due to a positive effect of animal products on IQ [2].

The natural selection maximizes survival under the natural conditions. Under domestication, the selection maximizes utility of a specie for a farmer while deemphasizing and thus reducing energy expenditure for characteristics less important or unimportant under domestication, e.g., fighting ability to select a mate or defend against predators, ability to cover long distances, etc. [3]. The degree of economically beneficial selection is environment dependent because some traits (e.g., resistance to harsh conditions) may be necessary in some environments while they are redundant in other environments. In the end, the improved animals have a smaller environmental imprint [4].

In ► Animal Breeding Methods and Sustainability, Agustin Blasco provides a historical perspective to animal breeding including the creation of breeds. Although the breeding has been practiced for many millennia, the science behind it is relatively recent. With new breeding tools, the genetic improvement accelerated resulting in much higher productivity per

animal with lower cost per unit of animal product. High productivity of a few improved breeds raises a question of survival and consequently conservation of less improved breeds. Also, highly improved breeds may not be optimal in more demanding environments.

In "► Animal Breeding, Foundations of," Guilherme Rosa focuses on theories that made modern animal breeding possible. These are population genetics, quantitative genetics, mixed models, and related issues. He examines the infinitesimal genetic model where it is assumed that a trait is controlled by a large number of independent loci, and he mentions models involving quantitative trait loci (QTL) or major genes. Selection can be for a single trait with possibly undesirable response for some of the remaining traits, or it can be multitrait, where weights on traits are economically derived for a more balanced breeding.

The selection in animal breeding depends on models and often sophisticated computing to estimate parameters of those models. In "► Animal Breeding, Modeling in," Lawrence Schaeffer presents mixed models that are commonly used to analyze many traits in small and large populations. In particular, an animal model considers all phenotypes and pedigrees to provide best unbiased linear predictions of animals' breeding values (EBV). While the basic animal model may be sufficient for fairly accurate predictions, sometimes additional features are necessary to better reflect the complexity of data. Large differences in variability within the environments require a model that accounts for heterogeneous variances per environment, categorical traits are best analyzed by a threshold model; special models are needed to analyze data censored, e.g., by time.

While most of the progress in animal breeding was based on the infinitesimal model, the availability of genetic markers raised hopes of finding major genes. Subsequently, marker-assisted selection (MAS) would allow determining EBV for young animals without waiting for phenotypes. In his entry "► Animal Molecular Genetics from major genes to genomics," Asko Mäki-Tanila describes theories for finding markers or QTL and applications of MAS. While several large QTLs have been found, in general, the estimated values for large QTL seem to be inflated while many QTLs are below the detection level. Thus, the total contribution of large QTLs seems to be small for most traits. Currently, individuals can be genotyped inexpensively for a large number of SNP markers. The use of these markers for breeding is called the genomic selection. The genomic selection is successful in populations with small effective population sizes where the genomic information provides more accurate relationships.

A selection is usually performed in a specific environment, which is defined as a combination of climate, nutrition, management, and stability. Animals excelling in one environment may perform poorly in another environment and vice versa, or show a genotype by environment interaction (GxE). In "► Animal Genetic in Environment Interaction," Erling Strandberg describes terms useful for quantification of GxE such as plasticity and homeostasis. GxE can be analyzed by reaction norms. We are interested in GxE only when genotypes rank differently in different environments.

The traditional selection is by selecting the "best" individuals. However, these individuals may indirectly be selected for poor group performance, e.g., aggression, and such animals may inhibit the growth of the other animals. In "► Socially affected traits, Inheritance and genetic improvement," Peter Bijma presents cases where the group performance is more important than the individual performance, proposes models that can be used to breed "socially adapted" animals, and describes results of experiments with such breeding. The social performance is most important for animals bred in cages such as poultry and pigs where the aggression can result in physical harm or even death. An intuitively obvious solution to aggression of allowing more space per animal in fact increases fighting and subsequently causes economic losses, as extra space allows for more fighting.

The next few entries are devoted to breeding for specific species.

In the entry ► Poultry Breeding, Yoav Eitan and Morris Soller document how, over the past 100 years, the chicken meat changed from being one of the most expensive to the least expensive. Such a progress required a good choice of initial breeds, intensive selection, and diligent research to discover sources of new problems and their mitigation, and constantly adapting management to address these problems. The success with chicken is possible only when the environment can be tightly controlled as highly adapted animals retain minimal flexibility to handle less than the optimal conditions. An important issue in chicken is

animal welfare. While some stresses are unavoidable, like in nature, reducing the avoidable distress can be good economics.

In the entry ► Pig breeding for increased sustainability, Pieter Knapp examines broader issues in breeding using pigs as an example. The first issue is diversity. Should different breeds be preserved or is it unimportant? What is the optimal size of the breeding population to sustain genetic variability and maximize the genetic progress over the long run? Pigs have been singled out as causing environment pollutions. Can breeding minimize the pollution? One way to minimize pollution and environmental damage is to breed efficient animals with good feed conversion ratio (FCR). Can one radically improve FCR? Is animal welfare a liability or an asset? The entry by Pieter Knapp contains extensive references.

Filippo Miglior, Sarah Locker, and Roger Shanks take a look into dairy breeding in their entry ► Dairy Cattle Breeding. An intensive selection for milk made Holsteins the highest producing and the most popular dairy breed in temperate countries. Most of the progress in Holsteins, and to a lesser intent, in other breeds, is through the extensive use of highly select sires through artificial insemination. The selection of sires is in fact global because national sire evaluation from some 30 countries are now pooled together by an international agency "Interbull," and semen of bulls ranked by this agency are available worldwide. Strong selection for production had an undesirable effect on fitness, including reduced fertility and survival. This side effect is remedied now by increased emphasis on fertility and survival in the selection index, and by crossbreeding. Lately, genomic selection greatly changed the breeding scheme in dairy.

Matthew Spangler describes beef breeding in the USA in his entry ► Breeding in Beef Cattle. As opposed to dairy, the beef population consists of many breeds, and most animals sold for beef are crossbreds. Beef is initially raised in ranches and later brought to feedlots for a short time for accelerated growth. Animals are genetically evaluated based on growth at a few age points, for carcass characteristics and for fertility. Important issues in beef evaluation are heterosis and recombination loss in crosses. FCR in beef is much lower than in poultry or pigs; however, beef can utilize land unsuitable for crops.

Thorvadur Árnason, in his entry ► Breeding in Horses, presents issues in breeding horses, predominantly for racing. Such breeding is successful as the trend for maximum speed is positive. As only selected individuals are run in races, breeding for speed requires accounting for censoring, i.e., lack of records for an important part of the population. This is done by treating as phenotype a categorical variable of "has" or "does not have" records. An issue specific for horses is increased inbreeding due to very intensive selection and small populations. Large increase in inbreeding has negative effects on many traits and also increases the chances of propagating a recessive gene.

SWP Cloete looks at aspects of ► breeding in developing countries and tropics. Increased production due to the animal breeding and limited population growth was successful in developing countries in creating surpluses of animal products. In developing countries, the animal breeding was less successful while the population exploded, resulting in shortages of animal products. The breeding was less successful because of specific challenges in developing countries and especially the tropics, and much smaller R&D. Traits especially important in the tropics are disease resistance (including tick and trypanosome), draft resistance, and ability to produce under periodic feed shortages. Subsequently, animals bred in the developed world may not survive in the tropics; however, their crosses sometimes do well. This entry contains a large number of references.

Even though the animal breeding is successful, there is a question whether the current pace of progress can be maintained. For example, FCR cannot be decreased below some 1.5 kg feed/1 kg of meat, unless the extra selection results in increased water content. Also, increased milk production at a cost of reduced fitness (less fertility, lower survival, more susceptibility to diseases) can at one point decrease overall profitability. Peer Berg ponders long-term challenges in animal breeding in his entry titled ► Animal Breeding, Long-term Challenges. Low effective population sizes make whole populations less biosecure. Too optimized genotypes may require huge facilities that could destroy the environment and rural life. Also, new requirements for welfare may require changing breeding goals. However, most long-term challenges are not well known.

Bibliography

1. Diamond J (2005) Guns, germs and steel. W.W. Norton, New York, 518 pp
2. Neumann CG, Murphy SP, Gewa C, Grillenberger M, Bwibo NO (2007) Meat supplementation improves growth, cognitive, and behavioral outcomes in Kenyan children. J Nutr 137(4):1119–1123
3. De Jong G, Van Noordwijk AJ (1992) Acquisition and allocation of resources: genetic (co)variances, selection, and life histories. Am Nat 139:749–770
4. Von Braun J (2010) The role of livestock production for a growing world population. http://www.lohmann-information.com/content/l_i_45_2010_10.pdf

Animal Breeding Methods and Sustainability

Agustin Blasco
Institute of Animal Science and Technology, Universidad Politécnica de Valencia, Valencia, Spain

Article Outline

Glossary
Definition of the Subject
Introduction
Animal Breeding and Sustainability
Animal Breeding Methods and Schemes
Future Directions
Bibliography

Glossary

Breed A population of animals with common morphological characteristics that is recognized as a breed by the administration, by a breeders association, or by other groups of people.

Best linear unbiased prediction (BLUP) It is the most common statistical method used in breeding evaluation.

Quantitative trait locus (QTL) A gene having influence in a quantitative trait.

Markers Fragments of the DNA molecule for which their position is known.

Response to selection Genetic progress.

Definition of the Subject

After domestication, animals were selected in different environments and for different traits leading to the modern breeds. Long before the appearance of the science called now as "Genetics," animal breeding had been practiced by humans following intuitive criteria, less efficient than the scientific ones, but criteria that had provided success along many generations of selection [1]. The lack of a theory explaining inheritance slowed down animal breeding for many years, but with the rediscovery of Mendel's rules at the beginning of the twentieth century and the development of quantitative genetics in the 1920s and 1930s animal breeding had the tools needed for its development. Animal breeding methods were developed in the 1930s and 1940s, and the first animal breeding companies and cooperatives started in using scientific methods for animal selection [2]. The development of artificial insemination in cattle in the 1940s and frozen semen in the 1950s led to the modern schemes of progeny test, in which bulls are proved with a high number of daughters, and semen of the best bulls is available worldwide. Large companies of animal breeding were created in the 1960s for poultry and pigs, and nowadays they dominate the market of reproducers, particularly in the avian case. In 1953 the structure of the DNA was published, leading to a quick development of all molecular genetics techniques. Today, DNA information is widely used as a complementary tool to the statistical methods based on data from records, to estimate the genetic values of the candidates to selection [3]. Although the commerce of genes is now extended worldwide, there is a recent interest in conserving breeds in danger of extinction due to this globalization. These breeds are a genes reserve for ensuring possible changes in the future market. Besides, some breeds can be helpful for developing sustainable systems in areas in which modern developed animals cannot be bred because of the lack of resources, climate, or other reasons [4].

Introduction

Long before the appearance of the science that is now called "Genetics," animal breeding had been practiced by humans following intuitive criteria, less efficient than the scientific ones, but criteria that had provided

success along many generations of selection. Darwin himself was impressed by the achievements of farmers, and artificial selection was a source of inspiration for his theory of evolution [5].

> ► We cannot suppose that all the breeds were suddenly produced as perfect and as useful as we see now them; indeed, in several cases, we know that this has not been their history. The key is man's power of accumulative selection: nature gives successive variations; man adds them up in certain directions useful to him. In this sense he may be said to make for himself useful breeds.
>
> C. DARWIN
> On the origin of species (1859, p. 30)

Animal breeding starts with domestication. Although there are several theories about the domestication process, it is generally admitted that selective breeding led to modern domestic animals, a hypothesis corroborated by the experiment of domestication of wild silver foxes started by Dimitri Belyaev in 1959 and still continued. After 40 years of selection for quiet temperament, silver foxes, which are aggressive to humans in the wild, became as friendly as dogs [6]. As a correlated response, some physical appearance also changed, and some bones of the skull were modified in the same direction as dogs when compared with wolves [7]. Modern molecular techniques permit to reconstruct the history of domestication [8]. After domestication, animals were selected in different environments and for different traits, leading to the modern breeds. References to animal breeding can be found in ancient Greek and Roman authors' works [9]; however, modern breeding practices start with the self-taught work of Robert Bakewell (1725–1795), who produced new breeds and had a high reputation as breeder [1]. He focused his work in the performances of his cattle and sheep, hiring rams, recording the offspring and keeping the sons of the best males. He fixed few and clear breeding objectives mating the best females with the best males. However, he disregarded the damaging effects of inbreeding and due to this, he had fertility troubles with his new breeds, but he is still considered as the first farmer practicing modern animal breeding.

The lack of a theory explaining inheritance slowed down animal breeding for many years. The theory of blending inheritance, sustaining that offspring was intermediate between parents, could not explain the persistence of genetic variability. Some hybrid breeders had noticed that crossing hybrids they can recover discrete traits that were present in the parental population [10], but Gregor Mendel (1822–1884) was the first in calculating the frequencies in which the observed traits were transmitted, allowing him to propose the first rules of genetic inheritance [11]. Although Mendel was conscious of the importance of his research, his work, published in a context of hybrid plant production, was largely ignored until it was rediscovered at the beginning of the twentieth century, and it was widely used to explain the inheritance of discrete observable traits. Mendel's rules worked well for discrete traits like yellow or green color, but many traits like milk production or body weight showed a continuous variation and seemed to follow different inheritance rules. The biometrician school, founded by Karl Pearson (1857–1936), was using and developing statistical methods, and rejected Mendel's rules, considering them as a special case of inheritance for some discrete characters [12]. Mendel was aware about the fact that the simple rules he discovered could not be applied to continuous variation, but he suggested that in these cases many inheritance factors might act simultaneously producing all intermediate indistinguishable classes. After some exam of this possibility, it was disregarded by the biometricians, and a bitter dispute about the mechanisms of inheritance started until Fisher (1890–1962), in a seminal paper [13], used statistical methods to reconcile Mendel's laws on inheritance with the continuous variation observed by biometricians. (For a history of early development of genetics and this dispute, see [12].)

The work of Fisher in this and subsequent papers started both modern statistics and modern quantitative genetics, but the methods of this new science had still to be applied to animal breeding. This task was accomplished by Lush (1896–1982), who harmonized breeding practices with the knowledge provided by the new discipline. Lush defined concepts like heritability, and proposed methods of selection including the information of relatives, weighed according to the genetic contribution predicted by Mendel's rules and quantitative genetics. The several editions of his book "Animal breeding plans" contributed to spread the new knowledge among scientists, technicians, and breeders [14]. Modern indexes of selection for several traits were

developed for plants by Fairfield Smith [15] closely following some indications given by Fisher, and Hazel [16] applied them to animal breeding allowing on one side to use family information and on the other side to weigh all traits of economic interest according to the predicted benefits that the offspring would give.

The development of artificial insemination permitted having offspring of the same sires in many farms (see [17] for a history of its development). As environmental effects were different depending on the farm circumstances, data had to be corrected in order to evaluate the animals properly. Corrections for environmental effects like parity, season, length of lactation, etc., had been made before, but then the problem was more complex. Several methods were developed to pre-correct the data before genetic analysis was made, but it was Henderson (1911–1989), who proposed a method for integrating the genetic values and the environmental ones in the same statistical model. This allowed the prediction of genetic values at the same time that corrections for environmental values were made [18]. The development of computers allowed using all relatives in the evaluation, and some computing difficulties derived from the use of all relatives were solved by Henderson himself [19]. Nowadays his method called best linear unbiased prediction (BLUP) is the standard method in animal breeding evaluation. BLUP needs the variance components (genetic and environmental) for predicting the genetic values. To estimate them is a difficult task, because data come from different farms and different environments and they should be corrected as before. Paterson and Thompson [20] showed how to correct for the environmental effects and how to estimate the genetic variance components at the same time. Their method is called REML (Residual or Restricted Maximum Likelihood) and it is a standard for variance component estimation.

Animal breeding was dominated by REML and BLUP – and they are still the most common methods – until the development of modern computers allowed the use of Bayesian methods. These methods use probabilities for inferences, which give them several advantages and permit to express the uncertainty about the unknowns in a natural way. For example, it is easier to understand that the probability of a breed having a higher growth rate than another is 93% than to understand that when estimating the difference in growth rate between breeds, in an infinite number of repetitions of the experiment, new samples will be higher than the actual sample in a 7% of the cases (which is the definition of a *P*-value of 7%). A review of Bayesian methods compared with classical statistical methods in animal breeding can be found in [21]. Bayesian methods were introduced by Daniel Gianola in the 1980s [22], but they lead to complicated integrals that could not be solved even by approximate methods. The rediscovery of a numerical method called Monte Carlo Markov Chains permitted to overcome this problem and to use Bayesian methods, leading to a high development and extension of them in animal breeding (see [23] for a detailed exposition of the methods).

With the arrival of DNA analysis techniques, a new field was open for research. Transgenesis looked as a promising area, but its real usefulness in animal breeding has been discussed [24]. Molecular markers, however, have been widely used in animal breeding as a complementary tool in genetic programs. They have been also used for capturing major genes; unfortunately, most traits are not controlled by major genes and molecular markers have had a limited success in this area [25]. Recently, simple molecular markers consisting in a single nucleotide substitution in the DNA chain (SNP) have been made easy and cheap to detect. This permits to use several thousand markers in each individual, thus all genes controlling a trait can potentially be associated to SNPs [26]. A main problem of this procedure is that these associations between SNPs and genes are lost after few generations of selection [27], but new associations can be reestimated. Nowadays genomics is being examined as a promising tool for many genetic programs, particularly in species like dairy cattle in which there is a continuous recording, the trait is expressed only in females, and generation intervals are large. In this case, genomics can be used for a better evaluation of young bulls that still have no offspring. Other uses of genomics will appear in the forthcoming years and it will be probably established as a useful complementary tool to current genetic programs.

Animal Breeding and Sustainability

Animal breeding consists essentially in selecting animals kept in close reproduction systems, often

accompanied with crosses between these groups of animals [2]. Historically, the groups of animals kept in close reproduction were breeds, although modern intensive meat production of prolific species is now based in selection of synthetic lines. These lines are called "synthetic" because they do not correspond to traditional breeds, but have been generated by crossing animals from different breeds or crossing commercial "hybrids" (which are not hybrids in a genetic sense, as it will be seen later). This procedure allows obtaining a large genetic variability available for selection on productive traits. The relevance of breeds for sustainability lies in that some breeds can be particularly well adapted to local conditions, although this does not mean that local breeds are always better for local conditions than foreign breeds. A foreign breed can be better adapted or can be economically more interesting than a local breed. This is common mainly in species like poultry, pigs, or rabbits, which are usually kept in better environmental conditions than beef, sheep, or goats, but it also happens in ruminants. For example, Nelore cattle, a foreign breed in Brazil, has had a high success and now it is extensively implanted there [28].

Definition of Breed

There is no consensus about the definition of what a breed is. Many definitions of breed have been compared [29–31], and the only common requirement to all of them is the genetic homogeneity, which applies essentially to external traits. It can be said that *a breed is a group of animals with some common external characteristics defined by some people who consider this group of animals to be a breed*. A breed requires some people who decide the external characteristics used to define the breed; often they also attribute some "average performances" to the breed. The problem with this definition is that it depends too much on external characteristics that may be very useful for dog or ornamental animals, but not necessarily for animals producing meat or milk in an efficient way. Some breeds were historically selected for improving some traits and they have been established as the most productive ones in intensive production systems; Leghorn hens for white eggs, Friesian cows for dairy cattle and Landrace and Large white in pig production are now widely established. However, the word "Leghorn" or "Landrace" only define the external appearance of the breeds; there are many types of Landrace in the world, depending on the traits for which they have been selected, and the few multinational companies that control the eggs market use specific highly productive Leghorn lines, therefore the concept of "breed" is often of little utility. Other words used in animal breeding that can lead to confusion are "pure breed" and "hybrid." In plants, a hybrid is the cross of two pure lines. A pure line is homozygous for all its genes, and all individuals have the same genotype, all hybrids have also the same genetic composition, and the cross of two plant hybrids produces very different plants due to the segregation of all the alleles (Fig. 1).

There are no "pure lines" in animals in the same sense as in plants. Pure lines in plants have been produced by self-fertilization or by fertilization of close relatives, something that is not possible in animals. Some attempts of creating highly inbred lines in pigs and poultry were done in the 1940s and 1950s, without positive results, because inbreeding produces infertility and abnormalities to a degree that prevents its use in animal breeding [2]. "Pure lines" in animals are only groups of animals in closed reproduction that will not be homozygous for all their genes, therefore animal "hybrids" will be crosses between lines or breeds with no genetic homogeneity. Moreover, it is a frequent practice in animal breeding to open the lines to some animals from other commercial lines in order to reduce inbreeding. This practice is also useful to capture genes that would be in lower frequency in the recipient line

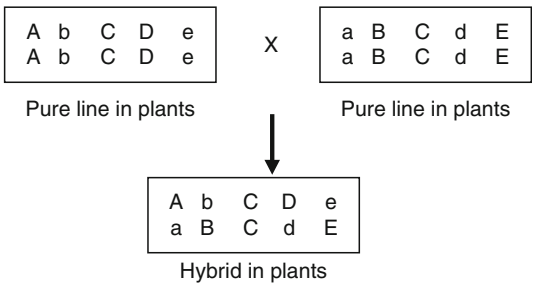

Animal Breeding Methods and Sustainability. Figure 1 Pure lines and hybrids in plants. Couples of letters indicate genes; capital letters indicate one allele of a gene and small letters another allele of the same gene

and that may be in higher frequency in the imported animals [32]. As "animal hybrids" are only crossed animals, they can be used to produce new "animal pure lines" with high genetic variability available for selection; for example, several rabbit breeds used for commercial purposes were originated by crossing commercial "hybrids" [33].

Breeds were created by humans after domestication by selecting traits they particularly liked. New breeds can be created nowadays. Apart from pets, many companies of pigs, rabbits, and poultry now use synthetic breeds without giving special importance to external characteristics, with the exception of the functional ones.

Breed Conservation

Some breeds, local or not, can perform better than some intensively selected lines in systems in which food is less rich in protein or energy, or less balanced than in intensive systems. Some breeds can also perform better in some areas in which climate or breeding conditions are very different from the ones of current intensive production systems. There are more reasons for conserving breeds [34]: keeping genes that may be useful in the future, supporting sustainable animal production systems for food security, maintaining genetic variability for further use, conserving cultural heritage, etc. However, when a breed is useful, it does not normally need special aids for conservation, since it produces some profit and then it is kept for obtaining benefits. Help is needed especially for breeds that are not profitable, but there are reasons for inferring that they have genes that may be useful in the future. A question then would be whether the object of conservation should be breeds or genes, that is, whether it can be created as synthetic breeds having the genes of interest instead of spending funds in several programs for conserving several breeds. Although focusing the problem in keeping genes seems to be simpler, this can produce some problems. A first problem is that creating synthetic breeds may lead to undesirable gene interactions, difficult to manage for both the survival of the breed and the transmission of the interesting genes. Another problem would be the difficulties in integrating new synthetic breeds in areas in which farmers would not be prepared or accustomed to manage [35].

One of the main objectives of breed conservation, keeping genes for the future, has been discussed [35]. This objective is too vague unless the concrete purpose for using these genes in the future is envisaged. When a breed is a tool for making meat, milk, or eggs, conservation should be focused on whether this tool works now or whether there are expectations for using this tool in the future. This is an important point, because the extinction of a breed is completely different from the extinction of species. Breeds extinction, which can be created, transformed, or recovered, should not be compared with losing unrecoverable species created by natural evolution and forming part of a peculiar ecosystem.

The more concrete objective of maintaining genetic variability can be attractive for two reasons. First, genetic variability is needed for selection. Second, genetic variability implies a gene reserve that may also be useful when a rapid change in selection objectives is needed, for example, the current fertility problem of Holstein, partially caused by the increasing levels of inbreeding, can be managed by crossing Holstein with more fertile breeds [36, 37]. We should, however, notice that the genes of interest in animal breeding control economically relevant traits, thus keeping genetic variability is not an objective if the trait is near its optimum (100% of survival, for example). Genetic variability can be divided in between breeds variability and variability within breeds. It is important to know how much of the total existing genetic variability can be found between and within breeds, because if most of the genetic variability is contained within breeds, there is no genetic reason for conserving many breeds. For example, measuring the number of SNPs per kb in chicken, the International Chicken Genome Sequencing Consortium [38] detected "surprisingly little difference in diversity in comparisons between red jungle fowl and domestic lines, between different domestic lines, and within domestic lines." For productive traits, it is generally admitted that about 50% of genetic variability is between breeds and 50% within breeds [39, 40]. Some methods of measuring genetic variability, like estimating genetic distances between breeds by molecular markers, have among other problems that they do not consider within breed genetic variability. The core of the argument for maintaining between breeds genetic variability is that

some breeds have genes that other breeds do not have or have in low frequency, and these genes may be useful in the future. It is a type of "insurance argument": insurance against changes in market or environmental conditions, and safeguard against potential emerging disasters as emergent diseases [4]. There is nothing wrong in keeping every breed in danger when having an unlimited amount of financial resources, but when resources are scarce, for example, in developing countries, a precise analysis of the foreseen benefits is needed.

Breeds and Sustainable Systems

By animal breeding sustainable systems, it is generally understood that farming systems are capable of maintaining their productivity indefinitely without damaging the environment [41]. This definition does not prevent having intensive systems with highly productive animals integrated in an industrial food chain, but sustainability is often associated to some kind of traditional farming at small scale in which waste is recycled, local breeds and local sources of food used and a rather high amount of hand labor is needed. Local breeds have a key role in this second type of sustainable systems, particularly when the environmental conditions are harsh or the food resources are not particularly good. This second type of sustainable systems is in general much less efficient for producing meat or animal products than intensive systems. There are, however, some reasons for establishing them:

1. *There are harsh environments in which no other systems will work properly.* A common example is cattle in swamp tropical areas. This applies essentially to cattle, sheep, and goats, and not necessarily to pigs, rabbits, or poultry, which have been kept in much better conditions traditionally.
2. *Using these systems in poor areas avoids land abandoning and migration of people to urban areas, avoiding desertification.* If life in these areas is hard for humans, this type of sustainable system should be considered as a temporary solution, because people living there deserve a better life.
3. *Sustainable systems are more environmentally friendly and produce a better animal welfare.* Although this reason is frequently invoked, this may or may not happen, and each case should be critically examined. Intensive industrial egg production can use enriched cages and manure process ensuring both welfare and sustainability. Moreover, animals in intensive systems arrive to commercial slaughter weight much earlier, thus they can produce less CO_2 and pollutants *per unit of product* than animals bred in extensive production systems, including pollution producing for transport, machinery, etc. A report ordered by the British government to the University of Cranfield [42] shows how this happens in poultry meat production, being organic chickens more contaminant *per kg of meat produced*, although results are more variable in pig production (for most pollutants, organic pigs contaminate less per kg of product). The same can be said about welfare: free-range hens are not necessarily happier than hens in enriched cages [43]. Looking for better animal welfare is not a particular task of industrial systems; it affects non-intensive systems as well.
4. *Some of these systems provide farmers an independence from big multinational companies.* This may be true, but is not necessarily good. Feeding people is a priority of poor countries, and the cheapest way may be to buy the genes to multinational companies. Genetics is very cheap; the genetic cost of 1 kg of pork, chicken, or rabbit meat is less than a 1% of the total cost of the meat as it will be seen in next section, and the same can be said about the genetics of 1 l of milk. Few companies provide the cheapest animal protein in the world (eggs and poultry meat and, up to a certain extent, pork meat), and genetics of dairy cattle is now managed in what is a world nucleus in practice. Poor countries need efficient genetic material for meat production even if this does not ensure genetic independence from multinational companies; this happens in industrial products and in other sectors (cars, industrial products, energy, etc.), and there is no reason for not accepting this in animal breeding.
5. *Some breeds are better adapted to local environment.* As said before, some breeds can be particularly well adapted to local conditions, although this does not mean that local breeds are better for local conditions than foreign breeds. There are spectacular examples of foreign breeds particularly well

adapted, as Nelore cattle in Brazil. Besides, adaptation is a bigger problem in some species than in others. Poultry, pigs, and rabbits have been raised in better environments than sheep or goats, thus intensive commercial breeds have less adaptation problems than in other species. Local food sources are often of lower quality than the usual food provided for highly productive breeds, and it has been said that local breeds can take a better profit of it. This is highly speculative, since the available information for these local breeds is normally scarce or null. Moreover, highly productive breeds of pigs, poultry, or rabbits can be bred with success in developing countries, even by small farmers [44]. Table 1 shows that small farms in rural conditions can obtain a similar profit as better farms using the same genetic material of a big multinational company (PIC). Local breeds of cattle, sheep, and goats may be better adapted in some harsh environments, although it is important to check whether this is true and when it is true.

6. *Local breeds produce better quality products.* The question is too general to give a simple answer. It is rather obvious that an Iberian pig (local breed) produces a much better cured ham than a Large White pig. Production of high quality products is one among several reasons for keeping breeds that are less efficient in producing meat or meat products. It is nevertheless convenient to check whether this better quality is detectable by the consumer. Some products like fresh cheese are not easy to differentiate, and local breeds sometime only show an external appearance of the animals different from the main breeds used for cheese production. It is also important, as St. Clair Taylor has stressed many times [45], that comparisons between breeds are performed at the same stage of maturity. As breeds have often different adult size and growth rate, if they are slaughtered at the same commercial weight, they can be compared at different stage of maturity, thus differences between them can be due to the fact that one breed is younger, in physiological terms, than the other. For example, a breed can have a better meat quality than another only because at the same commercial weight it is slaughtered at a more mature stage.

Animal Breeding Methods and Schemes

Breeding Companies: Organization and Diffusion of Genetic Progress

Animal breeding can be practiced at small scale by farmers or small farmers associations, but this affects only the local breeds and its efficiency is low [21]. Nowadays animal breeding is generally in the hands of multinational companies or large cooperatives, although there are still medium sized ones performing animal breeding at a smaller scale. There are two types of schemes, based on recording data on farm or concentrating on all animal improvement in a small nucleus and diffusing later the genetic progress. The first scheme applies mainly to dairy cattle, and the second one to pigs, poultry, and rabbits.

The standard example of the first scheme is dairy cattle. A 20% of the cows of a cooperative are inseminated with semen of young bulls that are going to be tested. The daughters are then inseminated with semen from other bulls in order to have lactation. Milk, protein, fat and cell count of the milk, and sometimes longevity, are recorded for each of the daughters, and these data are used to decide which 10% of the bulls being tested will pass to the catalogue of the cooperative (Fig. 2), to be used by the farmers to inseminate their cows in order to replace their stock. Each bull being tested provides semen for 1,000 cows in order to be sure that most of them will have at least 100 daughters, in order to achieve a high precision in the estimation of their breeding value [46].

Animal Breeding Methods and Sustainability. Table 1 Sow reproductive performance of PIC pigs in Philippines [44]

	Ave total born per litter	Ave born alive per litter	Ave weaned pigs per litter	Ave birth weight (kg)	Ave 30 day weight (kg)
Large farm sector	10.7	10.2	9.2	1.4	7.7
Small farm sector	11.9	11.4	11.1	1.5	8.8

Source: From Gibson et al. [44]

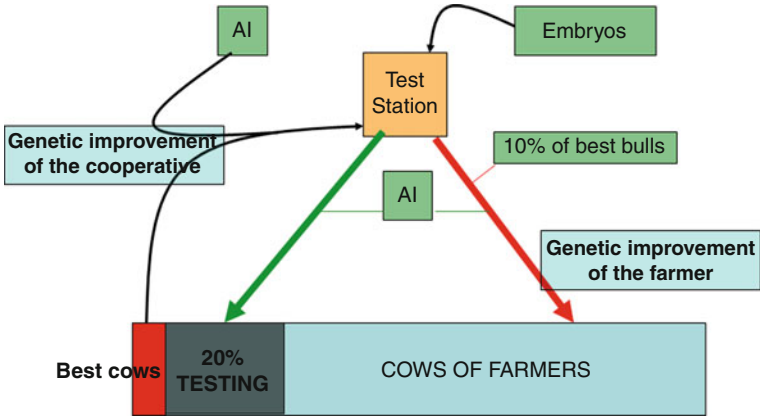

Animal Breeding Methods and Sustainability. Figure 2
Schemes of genetic evaluation and gene diffusion for dairy cattle

This implies that an association created for bulls testing should have at least 100,000 cows in order to include a couple of bulls per year in their catalogue. Nowadays there are many practices: big cooperatives test their bulls; some associations test few bulls that are available in their catalogue after having 60 or 70 daughters, and import semen and embryos making them available to the members; some companies test bulls and then commercialize the semen; etc. In a global society in which frozen semen can be bought worldwide and records are collected in different countries, a global genetic evaluation has been established by an association called Interbull that publish their world evaluation for all sires of different countries.

Selection is made from the records, but since a bull being tested will inseminate 1,000 cows, a previous strong selection is made when deciding which bulls will go to the test station to be proved. To do this, the best cows of the association are inseminated with the best semen available to produce the bulls to be proven. Nowadays it is also possible to buy embryos from the best cows evaluated in the world and the best semen available. Genomics is used here to help in the evaluation of these bulls that will arrive to the station. A particularity of the system is that individual farmers can make their own genetic improvement. Catalogues contain an accurate prediction of the genetic value of bulls for many traits, thus a farmer having particular problems with protein content of the milk, functional conformation, or other trait, can buy semen from bulls particularly well evaluated for these traits, improving the genetic level of his farm in the aspects he particularly needs.

The other scheme commonly used in animal breeding is the nucleus-multiplier scheme [47, 48]. Here all improvement is concentrated in a farm, from which it is spread to commercial farms through multiplication steps. This is the typical scheme for pigs, poultry, and rabbits (Fig. 3). Usually two lines are selected in closed reproduction, and males of one of the lines and females from the other are sent to farms called "multiplication units," in which both are crossed to produce the crossed female sent to the farmers. Typically, these lines are selected for prolificacy and they may be selected for other traits. A third line is selected to produce the males that the farmers will use (called "terminal sires"); in this case, the line is not selected for prolificacy because this is a trait attributed to the dam, in which males seem to have little influence. Commonly, there is only one nucleus of selection in each company, and multipliers are spread in several countries. Multipliers act usually under a contract with the company; they buy parental stock for multiplication and they are in charge of providing facilities for breeding and commercializing the product: This system has allowed a rapid development of the business. There are some variations of the scheme; terminal sires are sometimes the product of a cross between two lines C and D, and sometimes there is a multiplication step more, in which other multipliers receive females A × B to be crossed by a male from other line E to produce females (A × B) × E for the commercial farmers.

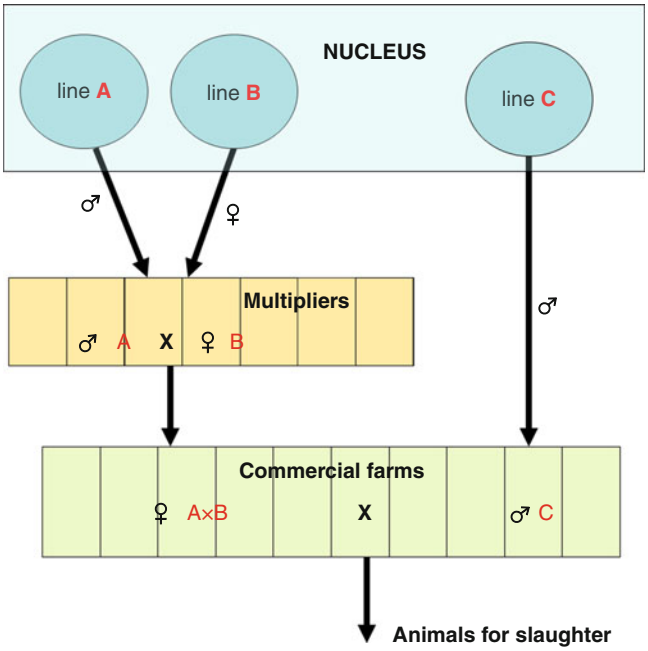

Animal Breeding Methods and Sustainability. Figure 3
Scheme of selection and gene diffusion in pigs, poultry, and rabbits

Multiplication permits to reduce the cost of selection, for example, in pigs, a female coming from one of the lines of the nucleus and entering a multiplier can cost 600 € from which 500 € is the cost of the genetics and the rest is the cost of producing a pig. This female will produce about 15 crossbred females for production farms during her life, the rest of them being culled for various reasons (leg problems, diseases, etc.). This means that the 500 € of the genetic cost should be divided by the 15 females, giving 33 € of genetic cost for the farmer. If each female produces an average of 50 pigs for slaughter during his life, the cost of genetics for slaughtered pig is about 67 cents per pig, less than 1 cent for kg. These figures are extreme in poultry production, in which each female of the nucleus can produce nearly 100 females for the multiplication step, and each female of a multiplier can provide about the same quantity for commercial farms.

Statistical Methods of Selection

Statistical methods used in animal breeding are essentially based in the infinitesimal model [49]. In this model, traits are determined by many genes independently distributed, having each one a small effect on the trait. A first consequence of the model is that genetically good animals can produce by chance some genetically poor sons, since by chance a son can inherit most of the alleles producing poor performances, whereas other sons can be genetically better than the parents if they get good versions of the alleles. As an average, all possible offspring of a parent will define how good this parent for breeding is. This is known as "breeding value" or additive value of the parent. The genetic value of an animal is not exactly this because genes can interact between them or among them producing better or worse individuals than the sum of their individual effects. These interactions are known as "dominance" when they appear between the two alleles of one gene or "epitasis" when they appear between alleles of different genes. Interactions can also occur between genotypes and environment, when the best genotypes in an environment (e.g., in the farm where the animals are selected) are not the best in other environments (e.g., in commercial farms). The development of artificial insemination in cattle and the prominent situation in the market of large

companies selling parent stock along the world has made the interactions between genotype and environment an important area of research in modern animal breeding [50].

Another consequence of the infinitesimal model is that it permits to invoke a theorem of statistics known as the *central limit theorem*, which permits considering the traits genetically distributed according to multivariate normal distributions. The multivariate normality has many advantages, for example, zero correlation implies independence between variables (which does not occur in other distributions), variables are determined by few parameters, and all relationships between variables are linear. Statistical methods in animal breeding are based thus in linear regression techniques. The most common models applied in animal breeding are called "mixed models" because they estimate simultaneously the breeding values, considered as random effects, and the environmental values, considered as fixed effects.

$$\mathbf{y} = \mathbf{Xb} + \mathbf{Zu} + \mathbf{e}$$

where $\mathbf{y}$ is a vector with the data, $\mathbf{b}$ is a vector containing the environmental effects (season, herd, parity, etc.), $\mathbf{u}$ is a vector with the breeding values, and $\mathbf{e}$ is a vector with the residuals. $\mathbf{X}$ and $\mathbf{Z}$ are known design matrixes containing 1s and 0s indicating the presence or absence of the effects. Fixed effects remain when repeating the experiment, and random effects change each repetition. Due to this, random effects are not usually estimated in classical statistical theory, but geneticists are interested in the value of these random effects, because they are the breeding values that, *as an average*, will be transmitted to the offspring; thus the best animals can be selected by taking offspring only from the ones with better predicted breeding values. The covariance structure of the breeding values is known due to our knowledge of Mendel's rules for gene transmission. For example, half brothers share *as an average* half of the genetic information of their father. This allows calculating the genetic covariance matrix between random effects $\mathbf{G}$ after knowing which part of the observed variance is due to the genes and which part to the environment. The most common method to estimate these variance components, correcting at the same time for the environmental effects, and using the same model as for estimating breeding values, is called REML (Restricted or residual Maximum Likelihood) [20].

The data need not be normally distributed; in these cases, the model gives the best linear solution. Directly solving this model for many individuals, for example, several thousands or millions of data in dairy cattle, would not be possible, but an equivalent system of equations allows finding the solutions easily [18]. This system is known as Mixed Model equations, and the solution is known as the best linear unbiased prediction (BLUP) of the random genetic values.

$$\begin{bmatrix} \mathbf{X'X} & \mathbf{X'Z} \\ \mathbf{Z'X} & \mathbf{Z'Z} + \mathbf{G}^{-1} \end{bmatrix} \begin{bmatrix} \hat{\mathbf{b}} \\ \hat{\mathbf{u}} \end{bmatrix} = \begin{bmatrix} \mathbf{X'y} \\ \mathbf{Z'y} \end{bmatrix}$$

There is a technical difficulty in solving the mixed model equations, because inverting a large matrix as $\mathbf{G}$ is difficult. However, there is an easy way for directly calculating $\mathbf{G}^{-1}$, allowing a general use of these equations in animal breeding programs [19]. The model can be complicated adding repeated data, effects corresponding to single genes, and many other possibilities. It can also be used for many traits simultaneously. When several traits are used, the random effects are correlated not only due to the relationships between individuals, but also due to the genetic correlations between traits, originated when some genes have influence not in one trait but in several ones. Multitrait genetic variances and covariances can be estimated by REML as before, but Bayesian techniques, using a numerical procedure known as Markov Chain Monte Carlo (MCMC), have been particularly useful in complex situations, for example, when some traits have repeated data and other traits not and consequently the design matrixes X, Z are not the same for both traits. Bayesian methods also permit to transform multivariate problems in series of unvaried estimations. Bayesian techniques with MCMC have been rapidly developed in the field of animal breeding, mainly for complex models, for example, when traits have different distributions, for censored data, for robust models, etc. (see [21] for a scope of their use and a comparison with classical methods and [23] for detailed description of Bayesian procedures).

In the case of using many traits, the objective is maximizing the economical benefit, which is obtained weighing each trait by economic weights. These weights can be calculated with more or less sophisticated

models [51, 52], but in essence they represent the amount of benefits, measured in economical units, obtained by improving one unity of the trait, for example, the number of euros of benefit for producing 1 kg of milk.

The Use of Molecular Genetics in Animal Breeding

Molecular genetics has influenced modern genetic programs. Two different aspects, will be commented here, transgenic animals and molecular markers, including in the late genomic selection. A critical review and discussion about the uses of transgenesis and cloning in animal breeding, with references to markers, can be found in [24]. Genomic selection is very recent and its possibilities and development are still under discussion.

Transgenesis The first transgenic mice growing twice than normal created an enormous expectation about what could be done with transgenic animals [53], particularly in the field of animal production. However, few transgenic animals are now available, and the economical advantage of transgenic animals is small [24]. Although apparently it is economically viable to produce transgenic products useful for human health, the application of transgenic animals in medicine will not be considered here.

To apply transgenesis in animal production, genes with major effects are needed, but unfortunately, most economically interesting traits are determined by many genes of small effects. Sometimes there are genes with major effects for some traits, for example, for fat deposition in pigs, but classical selection has fixed yet the favorable alleles in commercial populations, thus they are not particularly useful now. When a trait of an economic interest has a major gene segregating in the population of study, this gene can be easily captured by selection. This can be shown by computer simulation [54, 55] but a simple example can help in understanding this. In Fig. 4, it can be seen the phenotypical distribution of a trait is controlled by a single gene. When selecting the best 50% of the animals, copies of the allele "A" are selected with preference. Therefore, in few generations of selection the gene will be in high frequencies or will get fixed. If the frequency of the favorable allele is low, the process takes more

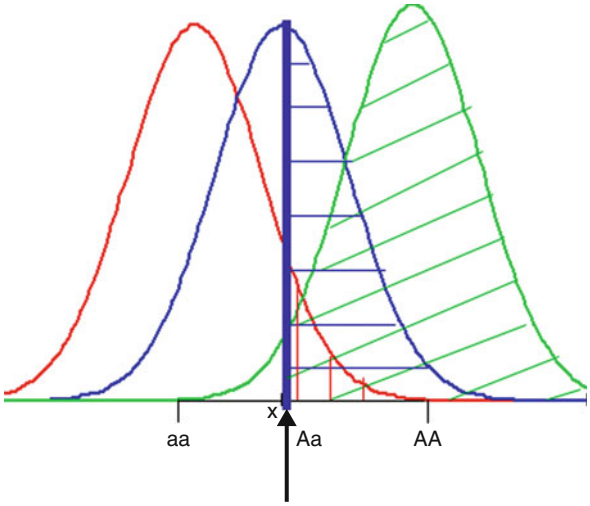

Animal Breeding Methods and Sustainability. Figure 4 Phenotypic distribution of a trait determined by a major gene with a high additive effect. Selection of the best 50% individuals

generations, but in general, it hardly will compensate to use transgenesis to capture it. Marker-assisted selection can be used for augmenting more rapidly the frequency of such genes of major effects, as it will be commented in next section.

Some major genes that are present in a breed or a line but not in other can be easily introduced by introgression without requiring transgenesis. The breed with the gene of interest G is crossed with the breed objective O, and then backcross is made by crossing O with the animals of the G × O cross that carry the gene of interest. After several backcrosses, the gene is introgressed. An example of gene introgression is often performed with the Boorola gene in sheep that augments litter size, due to the high prolificacy of the carriers that permit an easy identification. When the carriers do not clearly show the gene of interest, genetic markers can be used to help the introgression [56].

The process of transgenesis is extremely inefficient. Genes are placed at random, thus the gene can be inserted in an inappropriate tissue or it can happen that genes around the inserted gene modify the expression of it. Transgenes are not always expressed and they are not always transmitted to descents. Moreover, many animals are needed for obtaining a viable embryo expressing the genes transferred. For example,

36,500 embryos were needed to obtain 18 transgenic calves expressing the trait, and the cost of each transgenic cow was higher than 500,000 dollars [57]. Lentivirus vectors can produce transgenic animals more efficiently in some species and at a lower cost, but they still suffer the former problems [58].

Transgenic animals should be tested to prove that they are commercially viable [24]. They should be tested for the trait that is the object of transgenesis, because it should be proved that the transgene is expressed in the animal and in the offspring for several generations. They should be also tested for commercial traits, since a transgenic line might be good for a trait but might have a poor productivity for other economic traits. The overall productivity should be evaluated. Transgenic animals may have poor fitness, sensitivity to diseases for which non-transgenic animals are resistant and poor performances in other traits that might affect longevity; it is also frequent that transgenic animals have reproductive problems.

Once the major gene has been transferred in an animal, a whole population or line having this gene has to be constituted. In the nucleus-multiplier scheme, inbreeding depression will increase when creating the transgenic nucleus, since mating with relatives during several generations are needed to spread the gene [59]. The process of evaluation of transgenic animals, and the diffusion of the transgene in a line, increases the genetic lag between the transgenic line and the commercial lines, due to the genetic improvement made during this time by its competitors. Diffusion of a transgenic animal in dairy cattle, in which a world nucleus of selection is much higher than in prolific species, and generation interval is large due to progeny testing (6 years), has also been studied. It has been calculated that in a population of 10,000,000 cows, three generations later after the introduction of the transgenic founder (18 years later), the presence of the gene in the population would be between 1% and 4% [60]. The genetic lag produced, the fact that a transgenic animal may be genetically inferior for other traits not controlled by the gene transferred, the complications of the processes and the scarce number of gene candidates for being transferred, makes transgenesis little attractive, even if it would be a less expensive and more successful technique [24].

Genetic Markers and Genomic Selection Genetic markers are parts of the DNA molecule that can be identified in individuals. They may be close to a gene of interest, so they can be used to select the favorable version of a gene affecting a quantitative trait. Genes controlling a quantitative trait are called QTL (quantitative trait loci), and occasionally they can have a large effect and can be selected with the help of a marker. However, generally quantitative traits are controlled by many genes with small effects, thus the effectiveness of markers has been rather limited [25]. The situation has dramatically changed since it has been possible to obtain a large number of markers at low cost and since they can be associated to many of the genes controlling traits even having small effects. There are several types of markers; the simplest one is the Single Nucleotide Polymorphism (SNP), which marks a place in the genome in which there is variability in a single nucleotide. Nowadays there are microchips allowing detection of about 50,000 SNPs in a genome; the number of SNPs that can be easily detected is increasing to 500,000 and soon it will be possible to genotype the whole genome of livestock species at reasonable prices. Prediction equations can be fitted, in which a set of SNPs will be used for predicting breeding values. Taking data from 1,000 to 4,000 animals (calling this *training population*), the model to be fitted can be

$$y = b_0 + b_1x_1 + b_2x_2 + b_3x_3 + \cdots + b_{50,000}\, x_{50,000}$$

where $x_1, x_2, \ldots, x_{50,000}$ are the variables indicating the presence of one polymorphism (AA, Aa, aa) of each SNP (usually indicated by 1, 0, −1, or by 0, 1, 2), and $b_1, b_2, \ldots, b_{50,000}$ are the regression coefficients to be estimated. These equations cannot be solved by least squares given the high number of SNPS in relation to the data available for the prediction, and Bayesian techniques should be used. The use of prior information allows solving these big equation systems, and depending on how prior information is included, the Bayesian methods differ [61]. This method can also be used for several traits [27]. Many of these SNPs are noninformative, and there are some techniques to select only informative SNPs [61, 62]. There is now a promising research area for selecting informative SNPs for prediction, often using nonparametric statistics [62].

Genomic selection has been proposed for traits that are difficult or expensive to measure (e.g., adult weight [24], index of conversion [63], mortality [64]). It has also been proposed in dairy cattle, in which the traits of interest are expressed in dams but selection acts mainly in sires, and the generation interval is very long [65]. It may be useful for other traits like litter size, difficult to select due to their low heritability, but studies are needed to determine its usefulness in these cases, because very low heritabilities will give poor prediction equations since the records will then be determined mainly by the environment.

A main problem of genomics is that the association of SNPs with the genes responsible of the trait quickly disappears in few generations of selection, thus the prediction equations have to be reestimated and new training populations are needed. Figure 5 shows an example of the loss in accuracy of the prediction of genetic values. It can be observed that accuracy is practically halved in four generations of selection.

This limits the use of genomic selection in current programs, because in some species the generation interval is short (6–9 months in rabbits or hens, 1 year in pigs), and a continuous reestimation can be difficult or expensive. Finding when and how genomics can be included in current genetic programs is one of the most important research areas nowadays.

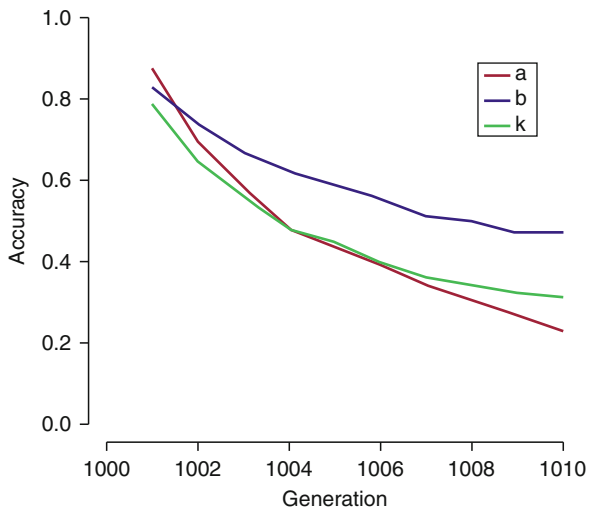

Animal Breeding Methods and Sustainability. Figure 5 Loss of accuracy of genomic selection on parameters a, b, and k of Gompertz growth curve. Selection acts on trait a, and the loss of accuracy of traits b and k are due to genetic correlations with trait a (From Blasco and Ibáñez-Escriche [27])

Future Directions

The Future Evolution of Methods and Schemes

Prediction of breeding values from records seems to be well established with the methods briefly exposed in section "Statistical Methods of Selection" and it does not seem that dramatic changes will occur in the future at short or medium term. The revolution in methods for estimating breeding values is in the area of genomics. The possibility of having information from several thousands of markers at a reasonable price, now from several hundred thousands and in the near future from the whole genome, has brought the problem of how to manage all these data, and prediction methods are examined from other areas of knowledge as artificial intelligence, using nonparametric or semi-parametric methods, Bayesian methods, etc.

Schemes of selection are also changing due to the globalization of the market of genes. Today the best cows of the world are not dedicated to produce milk but embryos that are sexed, frozen, and commercialized. Some of the deficiencies of current dairy cattle programs such as long generation intervals can be partially solved by using genomic selection and having a quicker and better evaluation of the bulls being tested. Larry Schaeffer suggested that genomic evaluation can substitute progeny test, dramatically shortening generation intervals [66], but it is doubtful that farmers will accept genomics evaluation as they accept now tests mainly based in offspring records [65]. It can also happen that private companies will compete with others or that breeders can organize brands in which semen is not identified, like in pigs, as Maurice Bichard suggests [67], but it looks unlikely, since farmers like to perform their own genetic improvement at farm level by buying semen from accurately tested sires. Poultry genetics is now in the hands of two large holdings, and the only change envisaged in their structure is related to possible troubles with laws about competence. Pig companies tend also to be bigger, but they will probably coexist with nucleuses of smaller companies well

established in local markets, and with large pig production companies producing parental stock for themselves. Both pigs and poultry companies will introduce genomics in their programs not only as a complementary tool for selection but also as a commercial strategy, using modern methodologies as an added value to their products. The interest in meat quality traits and quality of animal products will probably increase. Companies will also stress the sustainability of their productions and the good welfare of their animals, thus there will probably be an increasing interest in traits like robustness and disease resistance. The new emphasis in sustainability will give importance to breed conservation programs, which will receive more attention and will get substantial public funds. Nevertheless, no dramatic changes in objectives are envisaged in the near future. Changes in genetic objectives are slow and the product of the selection arrives with delay to the market, thus this prevents short-term selection policies.

The Limits to Genetic Progress

The theory of selection limits was developed by Alan Robertson (1920–1989) [68]. Classic quantitative genetics theory predicts the extinction of genetic variability by selection, and consequently the end of genetic progress. Frequencies of favorable genes increase with selection until they are close to 100%, and the genetic response is necessarily low, or genes are fixed by genetic drift, which occurs more likely when they are at high or low frequencies and when the selected population is small. Mutation can introduce new genetic variability, but useful mutations are rare and they were disregarded in the classical theory of limits of selection. A decline in genetic response is thus expected until genetic variability is exhausted, and some experiments arrived to a plateau after showing response to selection along 20 or 30 generations in drosophila [69] and mice [70]. However, there is little evidence of any loss of genetic variability in commercial populations [71, 72]. Heritability of milk production in dairy cattle is not decreasing with time but augmenting! [73] and this is not only due to a better control of environmental variance or methods of correction, but also to the continuously maintained response to selection in the last 50 years (Fig. 6).

Long-term genetic responses have been observed in both plants and animals, and there are several examples of continuous genetic progress in all livestock species. A part of the success of the phenotypic trends observed in animals is due to improvements in nutrition, but when comparing chicken broilers fed with food as prepared in 1957 and as prepared in 2001, most of the observed differences are due to genetic improvement [74]. Figure 7 shows carcasses of poultry from an unselected line and a selected line of the same company, fed with modern food.

Broilers show a continuous growth, egg mass production continuously increases, pigs' lean growth selection has dramatically decreased the amount of fat of the carcasses, and in general all selection programs

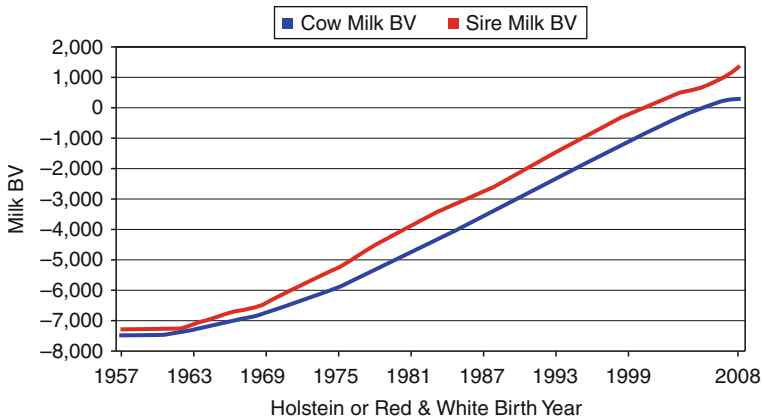

Animal Breeding Methods and Sustainability. Figure 6
Genetic values of sires and cows in USA in the last 50 years (From USDA http://aipl.arsusda.gov/eval/summary/trend.cfm)

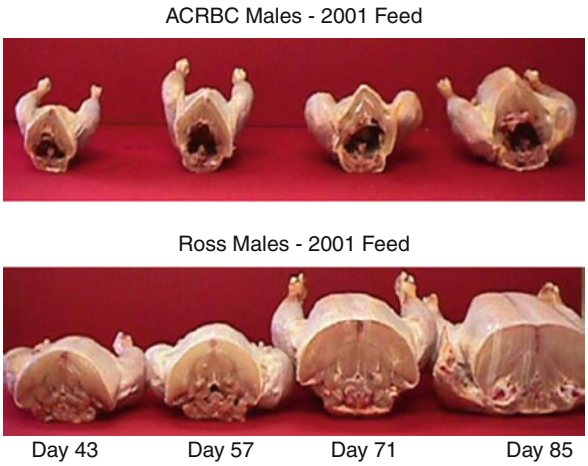

Animal Breeding Methods and Sustainability. Figure 7 Carcasses of 1957 and 2001 of an unselected and a selected line of poultry fed with the same food [75]

continue having success [72]. The reasons for this apparent non-limits to selection are selection pressure on genes produced by mutation (which has a heritability of about 0.1% [72, 76]) or epistatic interactions, but even when epistatic interactions are important, additive variance typically accounts for over half, and often close to 100%, of the total genetic variance [77]. Bill Hill moved further the classical theory of limits of selection showing how new mutations with selective advantage can increase genetic variability [78]. An experiment corroborating the theory showed how totally homozygous lines produced artificially in drosophila melanogaster could recover genetic variability by selection [79].

Are there limits to the genetic progress? Some traits have biological limits but still genetic progress can be obtained acting on related traits, for example, it is not possible to produce more than one egg per day, but it is possible to increase the laying period, and most of the new response to artificial selection in egg mass comes from this [72]. Highly productive animals can increase the incidence of pathological problems like ascites in broiler chicken or fertility in dairy cattle, but selection on these unfavorable traits [80] or crossbreeding [36] can be performed to continue the progress. Selection including traits different from strictly productive ones should be considered to avoid undesirable consequences of the continuous genetic progress [81]. Apart from some obvious limits (e.g., traits measured in percentage, like survival, cannot surpass 100%), it seems that genetic response can be directed to overcome the biological limits presented when selection acts only in one or few productive traits.

Bibliography

Primary Literature

1. Wood J, Orel V (2001) Genetic prehistory in selective breeding. Oxford University Press, Oxford
2. Johansson I, Rendel J (1972) Genetics and animal breedng. Oliver & Boyd, Edinburgh
3. Hayes BJ, Bowman PJ, Chamberlain AJ, Goddard ME (2009) Genomic selection in dairy cattle: progress and challenges. J Dairy Sci 92:433–443
4. Gandini G, Oldenbroek K (2007) Strategies for moving from conservation to utilisation. In: Oldenbroeck K (ed) Utilisation and conservation of farm animal genetic resources. Wageningen Academic Publishers, Wageningen, pp 55–74
5. Darwin C (1859, 1964) On the origin of species (a facsimile of the first edition). Harvard University Press, Cambridge, MA
6. Trut LN (1999) Early canid domestication: the farm-fox experiment. American Scientist 87:160–169
7. Trut LN, Plyusnina IZ, Oskina IN (2004) An experiment on fox domestication and debatable issues of evolution of the dog. Russ J Genet 40:644–655
8. Achilli A, Olivieri A, Pellecchia M, Uboldi C, Colli L, Al-Zahery N, Accetturo M, Pala M, Kashani BH, Perego UA, Battaglia V, Fornarino S, Kalamati J, Houshmand M, Negrini R, Semino O, Richards M, Macaulay V, Ferretti L, Bandelt HJ, Ajmone-Marsan P, Torroni A (2008) Mitochondrial genomes of extinct aurochs survive in domestic cattle. Curr Biol 18:R157–R158
9. Russell N (1986) Like enged'ring like. Cambridge University Press, Cambridge
10. Sageret A (1826) Considérations sur la production des hybrides des variantes et des variétés en général et sur celles de la famille des Cucurbitacées en particulier. Ann Sci Nat 8:294–314
11. Mendel JG (1866). Versuche über Plflanzenhybriden Verhandlungen des naturforschenden Vereines in Brünn, Bd. IV für das Jahr, 1865 Abhandlungen: 3–47. English translation at http://www.mendelweb.org/Mendel.html
12. Provine (2001) The origins of theoretical population genetics. The University of Chicago Press, Chicago
13. Fisher RA (1918) The correlations between relatives on the supposition of Mendelian inheritance. Trans R Soc Edinb 52:399–433
14. Lush JL (1937) Animal breeding plans. Collegiate Press, Ames
15. Smith F (1937) A discriminant function for plant selection. Ann Eugen 7:240–250
16. Hazel LN (1943) The genetic bases for constructing selection indexes. Genetics 28:476–490
17. Foote RH (2002) The history of artificial insemination: selected notes and notables. J Anim Sci 80:1–10

18. Henderson CR (1964) Selection index and expected genetic advance. In: Hanson WD, Robison HF (eds) Statistical genetics and plant breeding. NAS, NRC, Washington, pp 141–163
19. Henderson CR (1976) A rapid method for computing the inverse of a relationship matrix. J Dairy Sci 58:1727–1730
20. Patterson HD, Thompson R (1971) Recovery of interblock information when block sizes are unequal. Biometrika 58:545–554
21. Blasco A (2001) The Bayesian controversy in animal breeding. J Anim Sci 79:2023–2046
22. Gianola D, Fernando RL (1986) Bayesian methods in animal breeding theory. J Anim Sci 63:217–244
23. Sorensen D, Gianola D (2002) Likelihood Bayesian and MCMC methods in quantitative genetics. Springer, New York
24. Blasco A (2008) The role of genetic engineering in livestock production. Livest Sci 113:191–201
25. Dekkers JCM (2004) Commercial application of marker- and gene assisted selection in livestock: strategies and lessons. J Anim Sci 82:E313–E318, Suppl
26. Meuwissen THE, Hayes BH, Goddard ME (2001) Prediction of total genetic value using genome-wide dense marker maps. Genetics 157:1819–1829
27. Blasco A, Ibáñez-Escriche N (2010) Modifying growth curve parameters by multitrait genomic selection. 9th world congress on genetics applied to livestock production. Leipzig, 1–6 August 2010
28. Porter E (ed) (2002) Mason's world dictionary of livestock breeds, types and varieties. CABI Publ, Wallingford
29. Rodero E, Herrera M (2000) El concepto de raza. Un enfoque epistemológico. Arch Zootecnia 49:5–16
30. Hall SJG (2004) Livestock biodiversity. Blackwell, Oxford
31. Woolliams J, Toro MA (2007) What is genetic diversity? In: Oldenbroeck K (ed) Utilisation and conservation of farm animal genetic resources. Wageningen Academic Publishers, Wageningen, pp 55–74
32. Falconer D, Mackay TFC (1996) Introduction to quantitative genetics. Longman, Edinburgh
33. Baselga (2004) Genetic improvement of meat rabbits. Programmes and diffusion. In: Proceedings of the 8th world rabbit congress, Puebla, Mexico, pp 1–13, 7–10 September 2004. Available at http://world-rabbit-science.com/WRSA-Proceedings/Congress-2004-Puebla/Puebla-2004-a.htm#Genetics
34. Oldenbroeck K (ed) (2007) Utilisation and conservation of farm animal genetic resources. Wageningen Academic Publishers, Wageningen
35. Blasco A (2008) Breeds in danger of extinction and biodiversity. Rev Bras Zootecnia 37:101–109, Special Supp
36. Madalena FE (2008) How sustainable are the breeding programs of the global main stream dairy breeds? The Latin-American situation. Livest Res for Rural Develop 20, article19. Avalilabe at http://www.lrrd.org/lrrd20/2/mada20019.htm
37. Hansen LB (2006) Monitoring the worldwide genetic supply for dairy cattle with emphasis on managing crossbreeding and inbreeding. 8th world congress on genetics applied to livestock production, Belo Horizonte, Brasil, 13–18 August 2006. Avalilable at http://www.wcgalp8.org.br/wcgalp8/articles/paper/1_484-1695.pdf
38. International Chicken Polymorphism Map Consortium (2004) A genetic variation map for chicken with 2.8 million single-nucleotide polymorphisms. Nature 432:717–722
39. Hall SJG (2004) Livestock biodiversity. Blackwell, Oxford
40. Bennewitz J, Eding H, Ruane J, Simianer H (2007) Selection of breeds for conservation. In: Oldenbroeck K (ed) Utilisation and conservation of farm animal genetic resources. Wageningen Academic Publishers, Wageningen, pp 131–146
41. World Commission on Environment and Development (1987) Our common future. Oxford University Press, Oxford
42. Williams AG, Audsley E, Sandars DL (2006) Determining the environmental burdens and resource use in the production of agricultural and horticultural commodities. Main Report. Defra Research Project IS0205. Bedford: Cranfield University and Defra. Available at http://randd.defra.gov.uk/Document.aspx?Document=IS0205_3959_FRP.doc
43. Webster J (2005) Animal welfare: limping towards Eden. Blackwell, Oxford
44. Gibson JP, Steane DE, Plastow GS, Warkup C (2006) Meeting the needs of rich and poor: the needs, opportunities and trends in pig genetic improvement. 8th world congress on genetics applied to livestock production, Belo Horizonte, Brasil, 13–18 August 2006. Available at http://www.wcgalp8.org.br/wcgalp8/articles/paper/6_1040-2147.pdf
45. Taylor CSt (1985) Use of genetic size-scaling in evaluation of animal growth. J Anim Sci 61:118–143
46. Goddard ME, Wiggans GR (1999) The genetics of dairy cattle. In: Fries R, Ruvinsky A (eds) The genetics of cattle. CABI Publ, Wallingford
47. Bichard M (1977) Economic efficiency of pig breeding schemes: a breeding company view. Liv Prod Sci 4:245–254
48. Hunton P (1990) Industrial breeding and selection. In: Crawford RD (ed) Poultry breeding and genetics. Elsevier, Amsterdam
49. Bulmer G (1980) The mathematical theory of quantitative genetics. Oxford University Press, Oxford
50. Knap PW, Wang L (2006) Robustness in pigs and what we can learn from other species. 8th world congress on genetics applied to livestock production, Belo Horizonte, Brasil, 13–18 August 2006. Available at http://www.wcgalp8.org.br/wcgalp8/articles/paper/6_203-1825.pdf
51. Blasco (1995) Los pesos económicos en mejora genética animal. ITEA 91A:59–79
52. Weller I (1994) Economic aspect of animal breeding. Chapman & Hall, London
53. Palmiter RD, Brinster RL, Hammer RE, Trumbauer ME, Rosenfeld MG, Birnberg NC, Evans RM (1982) Dramatic growth of mice that develop from eggs microinjected with metallothionein-growth hormone fusion genes. Nature 300:611–615
54. Fournet F, Elsen JM, Barbieri ME, Manfredi E (1997) Effect of including major gene information in mass selection: a stochastic simulation in a small population. Genet Sel Evol 29:35–56

55. Villanueva B, Pong-Wong R, Grundy B, Wooliams JA (1999) Potential benefit from using an identified major gene in BLUP evaluation with truncation and optimal selection. Genet Sel Evol 31:115–133
56. Visscher PM, Haley CS (1995) Utilizing genetic markers in pig breeding programmes. Anim Breedg Abstr 63:1–8
57. Niemann H, Kues WA (2003) Application of transgenesis in livestock for agriculture and biomedicine. Anim Reprod Sci 79:291–317
58. Pfeifer A, Hofmann A, Kessler B, Wolf E (2004) Response to whitelaw: lentiviral transgenesis in livestock. Trends Biotechnol 22:159
59. Gama LT, Smith CS, Gibson JP (1992) Transgene effects, introgression strategies and testing schemes in pigs. Anim Prod 54:427–440
60. Hoeschele I (1990) Potential gain from insertion of major genes into dairy cattle. J Dairy Sci 73:2601–2618
61. Gianola D, De los Campos G, Hill WG, Manfredi E, Fernando R (2009) Additive genetic variability and the Bayesian alphabet. Genetics 183:347–363
62. Gianola D, De los Campos G (2008) Inferring genetic values for quantitative traits non-parametrically. Genet Res 90:525–540
63. González-Recio O, Gianola D, Rosa GJM, Weigel KA, Kranis A (2009) Genome-assisted prediction of a quantitative trait measured in parents and progeny: application to food conversion rate in chickens. Genet Sel Evol 41:3. Available at http://www.gsejournal.org/content/41/1/3
64. González-Recio O, Gianola D, Long N, Weigel KA, Rosa GJM, Avendaño S (2008) Nonparametric methods for incorporating genomic information into genetic evaluations: an application to mortality in broilers. Genetics 178:2305–2313
65. König S, Simianer H, Willam A (2009) Economic evaluation of genomic breeding programs. J Dairy Sci 92:382–391
66. Schaeffer LR (2006) Strategy for applying genome-wide selection in dairy cattle. J Anim Breed Genet 123:218–223
67. Bichard M (2002) Genetic improvement in dairy cattle – an outsider's perspective. Livest Prod Sci 75:1–10
68. Robertson A (1960) A theory of limits in artificial selection. Proc R Soc B 153:243–249
69. Robertson FW (1955) Selection response and the properties of genetic variation. Cold Spring Harb Sympos Quant Biol 20:166–177
70. Roberts RC (1966) The limits to artificial selection for body weight in the mouse. II The genetic nature of the limits. Genet Res 8:361–375
71. Hill WG (2008) Estimation, effectiveness and opportunities of long term genetic improvement in animals and maize. Lohmann Information 43:3–20. Available at http://www.lohmann-information.com/content/l_i_43_artikel1.pdf
72. Hill WG, Bünger L (2004) Inferences on the genetics of quantitative traits from long-term selection in laboratory and farm animals. Plant Breed Rev 24, part 2:169–210
73. Van Tassell CP, Wiggans GR, Norman HD (1999) Method R estimates of heritability for milk, fat, and protein yields of United States dairy cattle. J Dairy Sci 82:2231–2237
74. Havenstein GB, Ferket PR, Qureshi MA (2003) Carcass composition and yield of 1957 versus 2001 broilers when fed representative 1957 and 2001 broiler diets. Poult Sci 82:1509–1518
75. Havenstein GB (2006) Performance changes in poultry and livestock following 50 years of genetic selection. Lohmann Information 41:30–37. Available at http://www.lohmann-information.com/content/l_i_41_2006-12_artikel5.pdf
76. Hill WG (1982) Predictions of response to artificial selection from new mutations. Genet Res 40:255–278
77. Hill WG, Goddard ME, Visscher PM (2008) Data and theory point to mainly additive genetic variance for complex traits. PLoS Genet 4(2):e1000008. Available at http://www.plosgenetics.org/article/info:doi/10.1371/journal.pgen.1000008
78. Hill WG (1982) Rates of change in quantitative traits from fixation of new mutations. Proc Natl Acad Sci USA 79:142–145
79. López M, López-Fanjul C (1993) Spontaneous mutation for a quantitative trait in *Drosophila melanogaster*. 1. Response to artificial selection. Genet Res 61:107–116
80. Pavlidis HO, Balog JM, Stamps LK, Hughes JD, Huff WE, Anthony NB (2007) Divergent selection for ascites incidence in chickens. Poult Sci 86:2517–2529
81. Rauw WM, Kanis E, Noordhuizen-Stassen EN, Grommers FJ (1998) Undesirable side effects of selection for high production efficiency in farm animals: a review. Liv Prod Sci 56:15–33

Books and Reviews

Lynch M, Walsh B (1998) Genetics and analysis of quantitative traits. Sinauer Associates, Sunderland
Nicholas FR (2010) Introduction to veterinary genetics. Wiley-Blackwell, Oxford
Willis MB (1998) Dalton's introduction to practical animal breeding. Blackwell, Oxford

Animal Breeding, Long-Term Challenges

Peer Berg
Faculty of Agricultural Sciences, Aarhus University, Tjele, Denmark

Article Outline

Glossary
Definition of the Subject
Introduction
Sustainability
Sustainable Animal Breeding

Risks in Animal Breeding Schemes
Guidelines for Developing Sustainable Breeding Schemes
Future Directions
Bibliography

Glossary

Animal breeding Intentional breeding for certain traits, or combination of traits, by selecting animals for breeding with superior genotypes in growth rate, egg, meat, milk, or wool production, or in other desirable traits.

Animal genetic resources Genetic diversity, either characterized or as yet uncharacterized, that is found in economically important animals.

Animal welfare Animal welfare is the viewpoint that some or all animals, especially those under human care, should be treated in such a way that they do not suffer unnecessarily.

Effective population size Is the size of an idealized population that would behave the same as an actual population. The ideal population is one in which there is random mating and no selection. The effective size of a population is typically smaller than its actual size.

Genetic trends Changes in the mean breeding value of a population over time for one or more traits.

Stakeholders Any party that has an interest ("stake") in a project or activity, which in the context of this chapter is animal breeding.

Definition of the Subject

A major long-term challenge of animal breeding is to ensure that animal breeding is sustainable, in order to contribute to a stable long-term contribution of food for the globe. The need to address sustainability in animal breeding schemes has increased as the development in the last decades has been toward larger demands for food, fewer breeds contributing to the production of animal products, low effective population sizes despite the actual populations being large, and a decreasing number of breeding schemes providing the majority of the genetics underlying production of animal products.

The FAO report on *The State of the World's Animal Genetic Resources for Food and Agriculture* [1] indicates that the vast majority of developing countries have not been successful in sustaining genetic improvement in their livestock populations. Among the breeds considered to be in active use, 77% are located in developing countries. Animal genetic resources for food and agriculture (AnGR) provide the biological capital on which livestock production systems and food security are built. Planning for sustainable livestock development should, from the outset, take account of genetic differences among the species, the breeds, and the animals considered for use, along with their adaptive fitness to the production environments in which they will be kept. The different ways in which animals are used in different production systems and communities should also be recognized [2].

Introduction

Animal production has significantly increased its productivity during the last 50 years. This has been a combined effect of improvements in the environment provided to the animals, for example, improved feeding and management, as well as efficient breeding schemes resulting in significant and cumulating genetic progress. These improvements are synergistic, as genetic improvements and management and feeding improvements stimulate each other. Examples of drastic changes in productivity include

- Manyfold increases in milk production of dairy cattle
- Improvements of growth, leanness, and litter size in pigs
- Manyfold increases of growth and egg production in broiler and layer hens, respectively

This trend in productivity is expected to continue for several reasons. In a competitive market for food production, genetic improvements are an essential parameter to ensure a profitable production. However, the demand for food is also expected to increase, and thus stimulates a larger and more efficient production. The World Bank has estimated that it will be necessary to increase meat production by about 80% between 2000 and 2030.

However, the improvements in productivity have also contributed to a global concentration on fewer breeds for the largest part of animal production.

In dairy cattle, Holstein-Friesian is now the dominating breed of the world, with exchange of semen and embryos across countries resulting in a relatively low effective population size (∼40–70, [3, 4]). In poultry breeding, a few multinational companies now control the commercial genetic improvement and thus the genetics of the vast majority of eggs and poultry meat produced globally.

Recently, the effect of animal breeding has come under critical evaluations from an ethical point of view, reflecting public concerns on the effects of current and future animal breeding. Developments in biology, neuroscience, and genetics have resulted in changes in our perception of the world, and there is an increasing focus on the effects of animal breeding and the ethics of changing animals by selective breeding for our own good (e.g., [5, 6]). Ethical problems in animal production have historically focused on housing and husbandry, but more emphasis is now focused on the effect of animal breeding [7]. It is argued that the fact that selective breeding can introduce welfare problems places an ethical responsibility on the animal breeding industry [7].

The European animal breeders have realized that these powerful technologies to create genetic progress have generated public concern about the impact of animal breeding and the use of new technologies [8].

According to FAO [2]: *A strategic and logistical approach to sustainable livestock development is required. To appropriately address the use of available AnGR and the role of genetic improvement in sustainable development, from the outset, all policies, plans, and programs for the livestock sector must:*

- *Be based on soundly established and agreed livestock development objectives (LDOs) and well-integrated and realistic livestock development strategies (LDS) that are able to achieve the LDOs.*
- *Account for major environmental, structural, and socioeconomic differences among the production systems concerned.*
- *Ensure participation of the end users (the livestock keepers themselves). Both men and women should have access to relevant information, be involved in the formulation of policies and plans, and have ample opportunities to give their opinions.*
- *Be appropriately funded.*
- *Promote step-by-step development and the sustainability of the actions undertaken.*
- *Be based on well-documented approaches that are understood and agreed by all the stakeholders involved at each stage.*
- *Take fully into account the fundamental principles of genetic improvement and their technical implications.*

Thus, a major future challenge of animal breeding is to ensure a sustainable use of the animal genetic resources available and to implement sustainable breeding schemes in active populations.

The focus of this entry is the long-term challenges of animal breeding focusing on sustainability of animal breeding schemes. This is done by discussing the concept of sustainability in the context of animal breeding and then describing risk factors affecting sustainability. Then guidelines for developing sustainable and future directions to ensure sustainable are discussed.

Sustainability

Sustainability is a term that has a widespread use, and thus is often used in different meanings. It is often used in the sense of human sustainability on planet Earth and this has resulted in the most widely quoted definition of sustainability and sustainable development, that of the Brundtland Commission of the United Nations on March 20, 1987: "sustainable development is development that meets the needs of the present without compromising the ability of future generations to meet their own needs" [9]. This definition is also relevant to animal breeding; it is, however, not very operational.

In order to define and address sustainability in the context of animal breeding, it is first necessary to identify the stakeholders of animal breeding schemes. These stakeholders all have interests in animal breeding, and some of their interests might be conflicting. Understanding the diverse interest in animal breeding is a prerequisite for developing sustainable breeding schemes.

Obvious stakeholders are the animal breeders, breeding companies, and breeding associations, which have the major responsibility for defining and running the breeding scheme. Additional stakeholders include producers, veterinarians, manufacturers and retail enterprises, and consumers. For some aspects, the society as a whole may be considered a stakeholder in itself.

These stakeholders have different perceptions of the desired outcome of animal breeding schemes and thus sustainability, influenced by their role in production and utilization of animal products and their time horizon.

In the short term, objectives of different stakeholders can be very different. Animal breeders will typically focus on the factors limiting the profitability of the primary production. The interest of manufacturers and retail enterprises is on product quality, quantity, and possibilities of adding value to the primary product to ensure profitability of manufacturing and retail. Consumers will typically focus on product quality and price, product safety in addition to potentially cultural and political issues, such as environmental impact and animal welfare.

However, it can be expected that stakeholders will share many long-term interests in animal breeding schemes. Long-term interests of producers and manufacturers are likely to be more similar to the interests of consumers in the long-term, as they are the main actors determining quantity and quality demands. A thorough discussion of sustainability in the context of animal breeding is provided in [10], focusing on the need to address the interests of all stakeholders.

Interests of stakeholders include the following areas, which should be considered for defining sustainable animal breeding schemes for the future [11]:

- Food security, including
  - Quantity produced
  - Product quality
  - Food safety from both a biological and technical perspective
- Socioeconomic effects, including
  - Impacts of breeding schemes on rural economy, employment, and trade
  - Subsidies and their effects on objectives and methods used in animal breeding
  - Public (ethical) perception of the methods and technologies applied in animal breeding
- Environmental impact, including
  - The relationship between animal production and measures of environmental quality
  - Landscape management where animal production plays a major role
  - Interactions with biodiversity and ecosystems
- Health, welfare, and ethics including
  - Health management and biosecurity related to both the risk of zoonoses and contamination of products
  - Ethics of breeding and production

Sustainable Animal Breeding

Animal breeding is based on selecting animals with a superior genotype relative to the desired direction of selection, as reflected in the breeding objective. However, breeding values cannot be observed directly in animals, and they have to be predicted based on phenotypic records on the individuals themselves and their relatives and/or genetic markers. Thus, animal breeding is based on selecting the seemingly superior individuals given their predicted breeding values. Secondly, selected parents pass half of their genes to a given offspring, and each individual is thus a genetically unique individual. A direct result of this is that planning of animal breeding schemes is not an exact science. Genetic progress can be predicted but the realized response to selection can vary depending on a number of factors reflecting biological and economic uncertainty that influences the outcome of a breeding scheme. The breeding objective represents the desired direction of change of a population, most often expressed as the marginal economic value of changing a trait. The breeding objective should address all aspects of animal production and the characteristics of the product.

Ignoring the interests of some stakeholders when defining breeding objectives might negatively affect the success of a breeding scheme. This can be addressed by considering the interests of all stakeholders. The large potential of animal breeding is the contribution of additive improvements toward a long-term objective. However, there are factors that are not necessarily stable over time, factors that can potentially also change the interests of stakeholders. Examples of such factors include market structure, fluctuations in prices, regulations of production systems, disease outbreaks, and variation in the response to selection, both in the traits directly selected for and in traits indirectly affected as a correlated effect of selection. In addition to these factors, uncertainty on the assumptions underlying the design of a breeding scheme contributes to the

risk of this breeding scheme. The risk of a breeding scheme is related to the deviations of the realized effects of a breeding scheme relative to those planned. These factors have two effects: some contribute to a reduction of the realized outcomes of a breeding scheme (e.g., diseases) and others contribute to an increased variability of the outcome of a breeding scheme.

Thus, a sustainable animal breeding scheme should address the interests of all stakeholders and actively reduce the risks of the breeding scheme. This is in line with the SEFABAR project that produced a "Code of Good Practise for Farm Animal Breeding and Reproduction Organisations" [10, 12]. The code addresses issues of food safety and public health, product quality, genetic diversity, efficiency, environmental impact, animal health, animal welfare, and breeding and reproduction technologies. The code is based on the following six general statements:

- Breeding organizations must follow zootechnical, animal welfare, and animal health legislations and relevant regulations and practices.
- Breeding organizations must consult and collaborate with international, national, and regional authorities for the development and implementation of policies, practices, and regulations. These policies should assist the achievement of economic, environmental, and social sustainability of the animal breeding sector.
- Breeding organizations must use modern biosecurity methods to minimize disease transmission.
- Breeding organizations must ensure the health and welfare of the animals under their care.
- Breeding organizations must treat the animals under their care with respect.
- Breeding organizations must ensure that selection for production traits is balanced by appropriate attention to reproduction traits and health- and welfare-related traits.

The intention is that this should result in sustainable breeding programs by an economically viable balance of (a) food safety and public health, (b) product quality, (c) genetic diversity, (d) efficiency, (e) environmental impact, and (f) animal health and welfare.

Risks in Animal Breeding Schemes

The expected outcome of a breeding scheme might not be the same as the realized outcome for several reasons. These include

- Uncertainty on the genetic model assumed
- Uncertainty on the assumed genetic parameters (heritabilities, genetic correlations, etc.)
- Genetic drift resulting from finite population size
- Suboptimal decisions and implementation of the breeding scheme
- Breeding objectives that do not include all relevant costs and benefits of the production system targeted
- Changes in markets and consumer preferences

Some of these can contribute to both positive and negative deviations from the expected outcome, for example, deviations in genetic parameters from those assumed might either increase or decrease genetic gain relative to that expected.

However, most deviations are expected to result in a realized outcome of selection being lower than that expected, as the predictions assume that parameters are known and selection decisions are optimal. If the breeding objective does not reflect the true breeding objective, this will always result in selection decisions being suboptimal and response to selection being lower than expected. Likewise, changes in markets, consumer preferences, or political regulations of the industry will result in suboptimal goals being targeted by the breeding scheme, and thus the realized outcome being inferior to that expected.

Thus, two groups of factors contributing to the risk of animal breeding schemes can be identified.

The first group is risks intrinsic to the breeding scheme. The response of a breeding scheme might deviate from expectations due to variability of response to selection for the traits considered in the breeding objective and in the selection index. This can be due to uncertainties about genetic parameters used for predicting breeding values, uncertainties in the breeding values predicted from phenotypic records and/or genetic markers, and genetic drift.

Genetic drift can also increase the frequency of deleterious (recessive) alleles. Examples include BLAD [13] and CVM [14] in dairy cattle and the halothane sensitivity locus in pigs [15]. These alleles increased in

frequency either by directly having a positive impact on some of the traits selected for, or being linked to alleles with positive effects on the traits selected for. In general, all traits not directly selected for and not correlated with the traits in the selection criterion are most affected by genetic drift. In a closed population, genetic drift is highly related to the rate of inbreeding.

Unfavorable correlated responses to selection can appear if important traits are not included in the breeding objective and selection criterion. There is evidence of general negative effects of selection for increased production resulting in increased occurrence of behavioral, physiological, and immunological disorders [16]. A theory (resource allocation theory) has been proposed to explain the general negative correlated changes in fitness and health-related traits when selecting for production traits. The theory predicts that with limited resources available, selection for increased production results in less resources being allocated to, for example, health and reproductive traits [17]. In a mice model it was shown that a line selected for large litter size allocated more resources to lactation and mobilized body energy for a longer time period than a control line [18]. However, results suggest that not all aspects of immune response are decreased by selection for production. In a comparison of chicken lines from 1957 to 2001, it was concluded that the 2001 chickens selected for growth have a decreased adaptive immune response but a better cell-mediated immune response [19]. These examples highlight the need to consider the direct response to selection not only in the traits selected for, but also in other traits of relevance for production, animal health, and animal welfare.

Effective population size (which in a closed population is inversely proportional to rate of inbreeding) is the most important indicator of genetic risk in a breeding scheme, being inversely proportional to both genetic drift in a closed population and variation in selection response. Larger effective population size results in less genetic drift and less variability in the response to selection. Selection intensity, population size, and selection and mating criteria all influence the effective population size. It has been argued that the effective population size should be at least 50–100 individuals in order to avoid negative effects of genetic drift [20], but should be significantly larger in order to maintain mutations contributing to maintaining genetic variability.

The second group of risks is external to the breeding scheme. These include environmental risks due to changes in environmental factors unforeseen when planning the breeding scheme. Such risks are diseases, particularly epidemic diseases and diseases under national and international regulations (e.g., foot-and-mouth disease), and changed market and/or production regulations. These changes will most often result in the realized outcome of a breeding scheme being less than expected.

Guidelines for Developing Sustainable Breeding Schemes

Animal breeding schemes produce additive genetic improvement, and are thus most powerful when applied for a long-term improvement of a population. Thus, breeding objectives should reflect the future market for which production is aimed. The development of breeding objectives includes an assessment of the breed and its characteristics relative to the future market preferences. Traditionally, this includes an economic analysis aiming at estimating the marginal value of improving a trait. These marginal values are often the economic value of changing a trait given all other traits are constant. The breeding objective is then defined by the marginal values of the traits. However, this is not necessarily sufficient as a breeding objective should also consider the risk and uncertainty of aiming at a particular market, including status and trends in consumer preferences, social attitude, political and economic regulations, and infrastructure.

The breeding objective should reflect the most profitable improvement of the population, conditional on the current and future market conditions. The derivation should include traits beyond those currently recorded or included in a selection criterion.

The expected genetic trends should also be evaluated to ensure the breeding objective is sustainable. Ethical evaluations and public perception of animal welfare might alter the relative weights used in the breeding objective. Including a trait in the breeding objective does not guarantee that that particular trait is improved. Traits with low heritability, traits negatively correlated to important traits in the breeding objective, and traits measured late in life are at risk of not being improved despite being in the breeding objective. Traits that fulfill

all the above-mentioned criteria include health-related traits, such as mastitis and fertility in dairy cattle. It has been suggested that such traits should have a larger weight in the breeding objective, the larger weight reflecting a nonmarket value [21]. Such nonmarket values could reflect public concern on, for example, increased disease susceptibility resulting from the current breeding objective.

Ignoring important traits in deriving marginal (economic) values to be used in the breeding objective will bias the prediction of the economic outcome of the breeding scheme. For example, ignoring quality measures that are not considered in current market conditions but are important in distinguishing the product from other competing products might be harmful to the long-term competitive ability of the product.

Breeding objectives should not only be defined in terms of production, but should also include traits related to animal health and welfare resulting in robustness being part of the breeding objective [16].

Derivation of the marginal value of all important traits is crucial, in order to predict the effects of selection, not only on traits selected on, but also traits correlated to those traits. This is necessary to avoid unfavorable genetic changes in traits not selected for.

The expected outcome for a given breeding objective also depends on the recording scheme. Recording is often one of the most costly elements of a breeding scheme and should thus be an integral part of planning a breeding scheme. Generally, the objective of recording should be to allow for favorable genetic trends in the traits included in the breeding objective. This might be complicated by biological constraints of, for example, when a trait is realized and the number of individuals it can be recorded on. Examples are traits measured late in life (e.g., longevity), measured after slaughter (e.g., meat quality), or measured on one sex (e.g., female fertility), which poses challenges in defining efficient recording schemes. Modern technology allows for some remedies to this challenge. Genetic markers can be measured early in life, and in addition they can be used to predict the breeding value for traits not yet recorded [22].

In addition to the traits directly selected for, other important traits should also be recorded, in order to document the trend in these traits. Such traits include traits that are economically or ethically important, but they are not necessarily included in the breeding objective if they are at acceptable levels. However, correlated effects of selection might change these traits in undesired directions.

Two aspects of sensitivity to environmental factors should be considered. Chance events, such as disease epidemics have the potential to critically damage a breeding scheme, particularly if breeding animals are kept in a limited region or in a few herds. The foot-and-mouth disease outbreak is an example of a disease outbreak that has threatened breeding nuclei. Backup and safety procedures are necessary for safeguarding a breeding scheme. This can be done by implementation of techniques such as cryopreservation of embryos, eggs and semen, and segmentation of the breeding nucleus. This will naturally be very species specific, depending on the biological possibilities in the given species.

The second aspect of environmental sensitivity relates to environmental sensitivity, whether an individual's performance is sensitive to the environment in which it is kept. More specifically, this is an issue if genotypes and environment interact, such that an individual would be ranked differently in two environments relative to other individuals. A more realistic example is offspring from two bulls having different relative merits in two environments. The implications of an interaction are multiple. First, prediction of the performance in an environment that differs from the environment in which selection was performed might be impossible. Second, genetic improvement in one environment might not result in similar genetic changes in another environment. As an example, in some breeding schemes, candidates for selection are housed individually in order to allow for individual recording of the traits of interest, whereas animals in commercial production are housed in groups, providing a significantly different environment to that selected in. In such cases, where the environment of the breeding nucleus and the production herds differ, then genetic trend should be recorded in the production environment to ensure that selection is in the direction desired. If genotype–environment interaction exists, genetic evaluations should take this into account. Also the breeding objective should be specific

on which environment(s) genetic changes are optimized for. A specific type of genotype–environment interaction is the situation where environments describe a continuum of environmental effects, and thus cannot be grouped in classes of environmental effects. Reaction norm models describe such interactions, and a feature of these models is that they can model the sensitivity to the environment, and that this sensitivity is partly genetically determined. This has two implications. First, it is expected that environmental sensitivity will change as a correlated effect of selection on the mean, assuming nonzero correlations between mean performance and sensitivity. Second, it implies that environmental sensitivity can be selected for or against. The second implication also means that genetic changes will require changes in the environment to be fully expressed in all environments. This is an important outcome of a breeding scheme, and it has to be taken into consideration whether such environmental changes can be accommodated in commercial environments. There are many examples of highly improved breeds, selected in environments with a high level of management, that fail to express their genetic potential when transferred to environments characterized by lower management levels, for example, when highly selected breeds are transferred to tropical countries with lower input levels and other environmental characteristics. Thus, potential changes in environmental sensitivity have to be taken into account when predicting and evaluating the expected response to selection.

The optimum selection environment is not always equal to the environment in which the response is to be realized, but depends on the degree of genotype–environment interaction (determined by the ratio of variances in slope and level of a linear reaction norm), the correlation between level and slope, and the heritability of the trait [23].

In relation to breeding objectives, it was stressed that the market for which production is aiming should be defined. The reasoning is that this is a prerequisite to ensure that consumers will accept the product and its characteristics and that the product(s) addresses the preferences of the consumers. Consumer responses have been instrumental in changing egg production systems in European countries, and the use of gene transfer worldwide.

Measuring the success of a breeding scheme involves two components. First, expected response to selection should be predicted, as the measure against which to compare the operational and strategic outcome of the breeding scheme. To predict the expected response to selection estimates of genetic parameters, covariances between traits, generation intervals, recording scheme, and resulting accuracies of the predicted breeding values, selection intensities and the weights used in the breeding objective are required. Uncertainty about one or more of these should be taken into account when predicting response to selection. These predictions are based on a genetic model, on which there may also be uncertainty. Second, realized genetic trends should be compared to the predicted response to selection, both in order to evaluate the success of the breeding scheme, but also to modify it if required to better fulfill the overall objectives of the breeding scheme.

Most breeding schemes rely on genetic progress accumulating in a nucleus, representing the animals active in the breeding scheme. The genetic progress is then disseminated to production herds. This might involve several tiers, such as a breeding and multiplier level, in order to efficiently disseminate genetically superior individuals or semen to production herds. The time from genetic progress in the breeding nucleus to the dissemination of this progress in production herds is termed genetic lag, and is a major indicator of the efficiency of utilizing genetic progress in production.

The outcome of a breeding scheme is realized in the years following the selection decisions and the majority of the costs. An economic evaluation of a breeding scheme thus requires that costs and revenues are discounted back to a common base. This should take into account that returns more distant in time are more uncertain than those occurring in the near future. This involves defining the time horizon for which revenues are discounted, reflecting the uncertainties about the market and production conditions. This reflects an economic time horizon of the breeding scheme.

Expected and realized response to selection should be compared at regular interval as an integral part of controlling and optimizing the breeding scheme. This should be done at intervals shorter than the economic time horizon.

Future Directions

Following is a discussion including potential impacts on the development of certain areas of science.

Animal breeding is a competitive business, and producers pursue genetic material that best suits their needs. This naturally means purchasing animals that are economically optimal in the specific production. This potentially limits the focus on animal welfare–related traits not directly related to productivity.

However, since animal breeding decisions for most species are made centrally and, increasingly, internationally it has been argued that international agreements are needed [7] to ensure sustainable breeding schemes that address all relevant traits.

There is evidence that breeding companies are addressing these challenges. Survival in poultry has been improved by, among other initiatives, selective breeding and current focus is on selection against feather pecking, cannibalism, leg disorders, and heart/lung disorders [24]. And more generally, breeding objectives now contain more traits, also related to animal health and costs of production. In many cases, inclusion of health- and welfare-related traits results in more profitable breeding schemes than selection on production alone [25].

It should, however, also be acknowledged that despite the well-documented negative effects that selection for production traits has had on welfare-related traits, modern genetic technologies also give possibilities of understanding the biology underlying animal welfare and actively select for improved welfare [26]. Welfare-related traits are likely to show genetic variation, and it is thus also possible to select for increased animal welfare [27].

New technologies have the potential to affect animal welfare in both positive and negative directions [28]. Positive examples are the use of sexed semen in dairy cattle, which can decrease the number of unwanted male offspring that are killed after birth in some breeds and result in easier birth of female offspring. An overall positive effect is conditional on no adverse effects of the technology on the calves and/or the mothers.

Genomic selection [22] is currently under implementation in the large dairy, pig, and poultry breeding schemes. Genomic selection is fundamentally different to previous selection strategies, which relied on phenotypic records being recorded on the candidates for selection and/or their relatives. With genomic selection, this is replaced by a two-step procedure where the association being genome wide, markers and phenotypes are established in a part of the population where both phenotypic recording and genotyping are performed. Secondly, breeding values can be predicted for individuals based on their genotype. This allows for accurate breeding values being available earlier in life. This is particularly useful for traits recorded late in life, traits with low heritability, and traits recorded in one sex, which are largely the characteristics of many traits related to animal health and welfare. Genomic selection thus improves efficiency of selection for traits that are currently difficult to improve genetically, and thus has the potential to contribute to more sustainable animal breeding schemes [29].

Effective population size is a measure of the risk of a breeding scheme. Constraining the rate of inbreeding has the potential to reduce the variance of response to selection, reduce the loss of genetic variance, and reduce genetic drift. Quadratic selection indices jointly maximizing response to selection while constraining rate of inbreeding have been developed [30]. This quadratic index optimizes the genetic contributions of parents to the next generation, and the contribution of any parent depends on which other parents that are selected.

Acceptable rates of inbreeding are often described as being in the range of 0.5–1% per generation, equivalent to an effective population size of 50–100. More specifically, the acceptable level of inbreeding depends on the extent of inbreeding depression on fitness [20], and thus a sustainable breeding scheme ought to validate the acceptable level of inbreeding.

The implementation of sustainable breeding schemes requires, as described above, a thorough analysis based on an understanding of genetics, economics, and market characteristics. Training and education is a prerequisite for qualified personnel to contribute to the development and maintenance of sustainable breeding schemes.

Sustainability is a new measure in the context of animal breeding, but many elements contributing to sustainability are well known and have been taken into account previously. The aim of developing sustainable

animal breeding schemes puts these elements into a coherent context, highlighting the need to take interests of all stakeholders into account, as well as the risks and uncertainties of assumptions and outcomes.

Bibliography

Primary Literature

1. FAO (2007) The state of the world's animal genetic resources for food and agriculture. In: Rischkowsky B, Pilling D (eds) Rome (Available at www.fao.org/docrep/010/a1250e/a1250e00.htm)
2. FAO (2010) Breeding strategies for sustainable management of animal genetic resources: FAO animal production and health guidelines, vol 3. FAO, Rome, 160 pp
3. Kim ES, Kirkpatrick BW (2009) Linkage disequilibrium in the North American Holstein population. Anim Genet 40:279–288. doi:10.1111/j.1365-2052.2008.01831.x
4. Sørensen AC, Sørensen MK, Berg P (2005) Inbreeding in Danish dairy cattle breeds. J Dairy Sci 88:1865–1872
5. Hastedt H (2000) Beats, humans and the etics of animal breeding. Arch Tierz 43:218–225
6. Larrere R (2003) The issue of modern breeding a social request, consumer request or responsible inquiries? Prod Anim 16:329–332
7. Olsson IAS, Gamborg C, Sandoe P (2006) Taking ethics into account in farm animal breeding What can the breeding companies achieve? J Agric Environ Ethics 19:37–46
8. Neeteson-van Nieuwenhouven A, Merks J, Bagnato A, Liinamo A (2006) Sustainable transparent animal breeding and reproduction. Livest Prod Sci 103(3):282–291
9. United Nations General Assembly (1987) Report of the World Commission on Environment and Development: Our Common Future. Transmitted to the General Assembly as an Annex to document A/42/427 – Development and International Co-operation: Environment. Retrieved on: 2010-06-30
10. Gamborg C, Sandoe P (2005) Sustainability in farm animal breeding a review. Livest Prod Sci 92:221–231
11. Woolliams J, Berg P, Mäki-Tanila A, Meuwissen T, Fimland E (2005) Sustainable management of animal genetic ressources. Nordic Gene Bank Farm Animals, Nordisk Genbank Husdyr. ISBN 92-893-1089-8
12. CODE-EFABAR (2010). http://www.effab.org/CODEEFABAR.aspx. Assessed 30-6-2010
13. Shuster DE, Kehrli ME, Ackermann MR, Gilbert RO (1992) Identification and prevalence of a genetic defect that causes leukocyte adhesion deficiency in Holstein cattle. Proc Natl Acad Sci USA 89:9225–9229
14. Agerholm JS, Bendixen C, Andersen O, Arnbjerg J (2001) Complex vertebral malformation in Holstein calves. J Vet Diagn Invest 13:283–289
15. Carden AE, Hill WG, Webb AJ (1983) The inheritance of halothane susceptibility in pigs. Genet Sel Evol 15:65–82
16. Star L, Ellen E, Uitdehaag K, Brom FWA (2007) A plea to implement robustness into a breeding goal: poultry as an example. J Agric Environ Ethics 21:109–125
17. van der Waaij EH (2004) A resource allocation model describing consequences of artificial selection under metabolic stress. J Anim Sci 82:973–981
18. Rauw WM, Luiting P, Beilharz RG, Verstegen MWA, Vangen O (1999) Selection for litter size and its consequences for the allocation of feed ressources a concept and its implications illustarted by mice selection experiments. Livest Prod Sci 60:329–342
19. Cheema MA, Qureshi MA, Havenstein GB (2005) A comparison of the immune response of a 2001 commercial broiler with a 1957 randombred broiler strain when fed representative 1957 and 2001 broiler diets. Poult Sci 82:1519–1529
20. Bijma P (2000) Long-term genetic contributions. Prediction of rates of inbreeding and genetic gain in selected populations. PhD thesis. ISBN 90-5808-241-5
21. Olesen I, Groen AF, Gjerde B (2000) Definition of animal breeding goals for sustainable production systems. J Anim Sci 78:570–582
22. Meuwissen THE, Hayes BJ, Goddard ME (2001) Prediction of total genetic value using genome-wide dense marker maps. Genetics 157:1819–1829
23. Kolmodin R, Bijma P (2004) Response to mass selection when the genotype by environment interaction is modeled as a linear reaction norm. Genet Sel Evol 36:435–454
24. Flock DK, Laughlin KF, Bentley J (2005) Minimizing losses in poultry breeding and production: how breeding companies contribute to poultry welfare. Worlds Poult Sci J 61:227–237
25. Lawrence AB, Conington J, Simm G (2004) Breeding and animal welfare: practical and theoretical advantages of multi-trait selection. Anim Welfare 13:S191–S196
26. Jensen P, Buitenhuis B, Kjaer J, Zanella A, Mormede P, Pizzari T (2008) Genetics and genomics of animal behaviour and welfare – Challenges and possibilities. Appl Anim Behav Sci 113:383–403
27. Kanis E, van den Belt H, Groen AF, Schakel J, de Greef KH (2004) Breeding for improved welfare in pigs: a conceptual framework and it suse in practise. Anim Sci 78:315–329
28. Clark JAM, Potter M, Harding E (2006) The welfare implications of animal breeding and breeding technologies in commercial agriculture. Livest Sci 103:270–281
29. Mark T, Sandøe P (2010) Genomic dairy cattle breeding: risks and opportunities for cow welfare. Anim Welfare 19(1):113–121
30. Meuwissen THE (1997) Maximising the response of selection with a predefined rate of inbreeding. J Anim Sci 75: 934–940

Books and Reviews

FAO (2010) Breeding strategies for sustainable management of animal genetic resources: FAO animal production and health guidelines, vol 3. FAO, Rome, 160 pp

Animal Breeding, Foundations of

Guilherme J. M. Rosa
Departments of Animal Sciences, Biostatistics & Medical Informatics, Dairy Science, University of Wisconsin, Madison, WI, USA

Article Outline

Glossary
Definition of the Subject
Introduction
Principles of Selection
Mixed Model Methodology
Marker-Assisted Selection
Future Directions
Bibliography

Glossary

Bayesian inference Statistical inference approach based on the combination of prior information and evidence (i.e., observations) for estimation or hypothesis testing. In Bayesian analysis the prior information is updated with the experimental data to generate the posterior distribution of unknowns, such as model parameters. The name "Bayesian" comes from the use of the Bayes' theorem in the updating process.

Breeding value A measure of the genetic merit of an individual for breeding purposes.

Genetic correlation The correlation between traits that is caused by genetic as opposed to environmental factors. Genetic correlations can be caused by pleiotropy (genes that affect multiple traits simultaneously) or by linkage disequilibrium between genes affecting the different traits.

Genomic selection Genomic selection is a form of marker-assisted selection in which genetic markers covering the whole genome are used such that all quantitative trait loci (QTL) are in linkage disequilibrium with at least one marker.

Heritability (narrow sense) The fraction of the phenotypic variance that is due to additive genetic effects.

Infinitesimal genetic model A genetic model that assumes that a trait is influenced by a very large (effectively infinite) number of loci, each with infinitesimal effect.

Linkage disequilibrium Nonrandom association of alleles at two or more loci, leading to combinations of alleles (haplotypes) that are more or less frequent in a population than would be expected from a random formation of haplotypes from alleles based on their frequencies.

Mixed models A mixed-effects model (or simply mixed model) is a statistical model containing both fixed and random effects. Such models are useful in a wide variety of disciplines in the physical, biological, and social sciences, especially for the analysis of data with repeated measurements on each statistical unit or with measurements taken on clusters of related statistical units.

Population genetics The study of allele frequency distribution and change under the influence of the four main evolutionary processes: selection, genetic drift, mutation, and migration.

Quantitative genetics The study of complex traits (e.g., production and reproductive traits, disease resistance) and their underlying genetic mechanisms. It is effectively an extension of simple Mendelian inheritance in that the combined effect of the many underlying genes results in a continuous distribution of phenotypic values or of some underlying scale or liability thereof.

Definition of the Subject

The term *Animal Breeding* refers to the human-guided genetic improvement of phenotypic traits in domestic animals such as livestock and companion species [1]. Animal breeding is based on principles of *Quantitative Genetics* [2–4] and aims to increase the frequency of favorable alleles and allelic combinations in the population, which is achieved through selection of superior individuals and specific mating systems strategies. Selection methods and mating strategies are developed by combining principles of quantitative and population genetics with sophisticated statistical methods and computational algorithms for integrating phenotypic, pedigree, and genomic information, along with the utilization of reproductive technologies that allow for larger progeny cohorts from superior animals as well as shorter generation intervals.

Through selection and mating of superior animals the frequency of favorable alleles is increased, so the overall additive genetic merit of a population is increased through successive generations [5]. Selection can be regarded as the most important tool for the improvement of lines or breeds within a specific species in terms of additive genetic effects. Such lines or breeds can be then intermated such that nonadditive genetic effects such as dominance and epistasis can be exploited through specific inter- and intralocus allelic combinations [1–4].

The theoretical foundations of population and quantitative genetics can be traced back to the work of R. A. Fisher, J. B. S. Haldane, and S. Wright. The rational animal breeding has its origins in the work of J. L. Lush, who made substantial contributions to animal genetics and biometrics research and is generally referred to as the father of modern scientific animal breeding [1].

More recent theoretical developments in population and quantitative genetics have been fostered by researchers such as C. C. Cockerham, C. W. Cotterman, J. F. Crow, W. J. Ewens, W. G. Hill, M. Kimura, G. Malécot, T. Nagylaki, and B. S. Weir, among others. A landmark in the area of animal breeding and genetics is the development of mixed model methodology, first proposed by C. R. Henderson, which has been used extensively in many applications in the field, ranging from breeding value prediction under the infinitesimal assumption to gene mapping and segregation analysis. Most recently, Bayesian methods, Monte Carlo, and resampling techniques have been employed to fit and evaluate complex models in different contexts, including nonlinear systems, generalized models, survival analysis, and situations in which the number of parameters or covariates surpasses the number of observations, such as in association analysis and whole-genome marker-assisted selection using high density panels of single nucleotide polymorphism (SNP) markers.

Introduction

Since domestication, artificial selection has greatly changed the shape, size, and production and reproduction performance of livestock and companion animal species. For example, there is an incredible diversity of canine breeds – and between dogs and their wolf ancestors – from differences in overall appearance to behavior and their ability to perform specific tasks. Although to a lesser degree, the same can be observed in many other companion animal species, such as cats and horses. With livestock species, tremendous genetic changes have been accomplished as well, markedly in the last 50 years or so. For example, Fig. 1 depicts the average growth curves of broilers from selected and control populations. These results refer to a population of birds selected for over 40 years for increased growth rate and another population kept without artificial selection, with both groups derived from the same base population, starting in 1957 [6]. In the experiment presented in Fig. 1, the two groups of birds were fed diets typical of 1957 and 2001, such that the interaction between genetics and feed, as well as the genetic contribution to the phenotypic differences observed, could be assessed. It is seen that the 2001 genetics group presented an average body weight of about 4 kg at 56 days of age, while its 1957 counterpart weighed only 800 g or so. Moreover, it is shown that 85–90% of this fivefold improvement is accounted for by genetics with the remaining 10–15% to nutrition.

Similar levels of genetic improvement can also be observed in many other species, such as swine, beef and

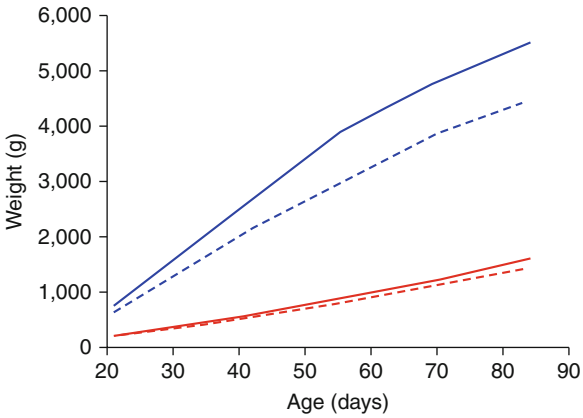

Animal Breeding, Foundations of. Figure 1
Average growth curves of commercial broilers. *Blue* and *red lines* represent birds with "2001" and "1957" genetics, respectively. *Solid* and *dashed lines* represent birds fed diets typical of 2001 or 1957, respectively (Adapted from [6])

dairy cattle, and some species of fish. For example, as illustrated in Fig. 2, the average breeding value for milk yield in the US Holstein, and Red and White populations has increased over 3,500 kg in the last 50 years.

Such genetic improvements have been accomplished mostly through the selection and breeding of superior animals, which can be chosen using specific statistical methods such as those discussed on the following sections. In this chapter, the discussion will focus on methods developed for normally distributed (Gaussian) traits, under the infinitesimal assumption, i.e., that traits are affected by a large (virtually infinite) number of genes of small effects [2–4], although this assumption is somewhat alleviated in marker- assisted selection, which is discussed later.

Principles of Selection

Basic Genetic Model for Quantitative Traits

The basic genetic model can be expressed as [2, 3, 7]:

$$y_i = \mu + g_i + e_i \tag{1}$$

where y_i is the phenotypic value of animal i (i.e., the animal's performance for a specific trait); μ is the population mean (average performance of the animals); g_i is the genotypic value of the animal, expressed as a deviation from the mean; and e_i is a term representing environmental factors affecting the animal's performance, also expressed as a deviation from the mean. Hence, it is assumed that $E[g_i] = 0$ and $E[e_i] = 0$, such that $E[y_i] = \mu$, where $E[.]$ represents the expectation function. Moreover, the variance of y_i is given by $\mathrm{Var}[y_i] = \sigma_y^2 = \sigma_g^2 + \sigma_e^2$, where $\sigma_g^2 = \mathrm{Var}[g_i]$ and $\sigma_e^2 = \mathrm{Var}[e_i]$ are the genetic and environmental variances, respectively. Normally distributed traits, i.e., phenotypic traits with a bell-shaped distribution, are generally represented as $y_i \sim N\left(\mu, \sigma_y^2\right)$. Such distribution has a probability density function that can be described as [2, 4]:

$$f(y_i) = \frac{1}{\sqrt{2\pi\sigma_y^2}} \exp\left\{-\frac{1}{2\sigma_y^2}(y_i - \mu)^2\right\},$$

for $-\infty < y_i < \infty$, $-\infty < \mu < \infty$, and $\sigma_y^2 > 0$, which can be represented as in Fig. 3. To simplify the notation used throughout the text, it is noted that either random variables or their realizations will be represented with lower case letters. However, the context should make it clear to the reader when a letter represents one or the other.

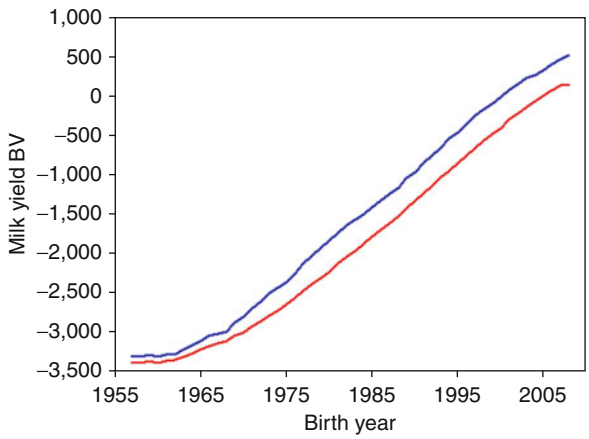

Animal Breeding, Foundations of. Figure 2
Genetic trend for milk yield in the US Holstein and Red and White populations. Males and females average breeding values are in *blue* and *red*, respectively; genetic base refers to cows born in year 2005 (*Source*: AIPL – USDA; http://www.aipl.arsusda.gov/)

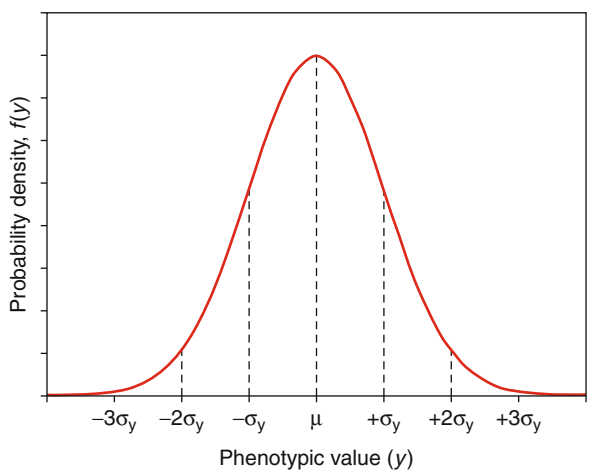

Animal Breeding, Foundations of. Figure 3
Probability density function of a normally distributed trait with mean $\mu = E[y_i]$ and variance $\sigma_y^2 = \mathrm{Var}[y_i]$, i.e., $y_i \sim N(\mu, \sigma_y^2)$

The genetic component g_i of Model (1) can be partitioned into additive (a_i) and nonadditive (c_i) genetic effects, i.e., $g_i = a_i + c_i$, where a_i is also called "breeding value," and c_i refers to the "gene combination value," which encompasses interaction effects between alleles within each locus (i.e., dominance effects) or between alleles in different loci (i.e., epistatic effects).

Hence, Model (1) can be expressed as:

$$y_i = \mu + a_i + c_i + e_i \tag{2}$$

where $a_i \sim N(0, \sigma_a^2)$, $c_i \sim N(0, \sigma_c^2)$, and $e_i \sim N(0, \sigma_e^2)$, with all these terms assumed independent from each other. The phenotypic variance can be then expressed as $\mathrm{Var}[y_i] = \sigma_y^2 = \sigma_a^2 + \sigma_c^2 + \sigma_e^2$, from which two important definitions are derived. The first one is called broad sense heritability, given by $\mathrm{H}^2 = \sigma_g^2/\sigma_y^2$, where $\sigma_g^2 = \sigma_a^2 + \sigma_c^2$, which gives the proportion of the phenotypic variance that is due to genetic effects. The second, called narrow sense heritability, refers to the specific contribution of additive genetic effects to the phenotypic variance, i.e., $h^2 = \sigma_a^2/\sigma_y^2$. These two quantities, particularly narrow sense heritability, will be further discussed and used in the next sections.

The breeding value of an individual (a_i) is equal to the sum of additive effects of individual alleles within and across loci, and it is sometimes called "additive genetic deviation" or "additive genetic effect." Because individual alleles, and therefore independent allele effects, are passed from parent to offspring, the breeding value of an individual is important for predicting its progeny's performance and so it is central to selection of superior animals [1, 3]. The gene combination value (c_i) is the difference between the genetic merit (g_i) of an animal and its breeding value, i.e., $c_i = g_i - a_i$, so it is often called "nonadditive genetic deviation." Because the component c_i involves interactions between alleles (both within and between loci), and only a single allele (as opposed to a pair of alleles) in each locus is transmitted from parents to offspring, nonadditive effects are not transmitted in a predictable manner. Hence, while average breeding value in a population can be changed through selection of superior animals, the gene combination value should be explored through specific mating systems. Here, the discussion will focus on selection approaches and the genetic improvement of a population in terms of additive genetic effects only. For a discussion on mating systems, such as inbreeding and outbreeding strategies, see for example, [1, 7, 8]. Additional discussion on inbreeding depression and heterosis (or hybrid vigor) can be found in [3, 4].

As discussed previously, the breeding value of an individual is equal to the sum of its independent allele effects. Because a parent passes a random sample of half of its alleles to its progeny, an animal's breeding value is twice what is often called "transmitting ability" or "expected progeny difference" [1, 5]. The expected breeding value of an offspring (a_o) is then equal to the average of its parents' breeding values (the same as the sum of its parents' transmitting abilities), i.e., $E[a_o|a_s, a_d] = \frac{a_s + a_d}{2}$, where a_s and a_d represent the (realized) breeding values of the offspring's sire and dam, respectively. However, there will be variability in terms of breeding values within a full-sib family because of the random sampling of parents' alleles that each offspring receives, the so-called Mendelian sampling [4].

The breeding value of an individual can be expressed as a function of its parents' breeding values as $a_o = 0.5a_s + 0.5a_d + \delta$, where δ refers to the Mendelian sampling component. It is interesting to notice that the variance of breeding values in a specific generation is equal to $\mathrm{Var}[a_o] = 0.25\mathrm{Var}[a_s] + 0.25\mathrm{Var}[a_d] + \mathrm{Var}[\delta]$. Assuming the same additive genetic variance across generations and for both sexes (i.e., $\mathrm{Var}[a_o] = \mathrm{Var}[a_s] = \mathrm{Var}[a_d] = \sigma_a^2$), it is shown that the Mendelian sampling variance is equal to half the additive genetic variance, i.e., $\mathrm{Var}[\delta] = \sigma_a^2/2$.

Phenotypic Selection

The most traditional approach of genetic improvement of livestock (and more generally any domestic animal or plant species) is based on selection of animals with the best performance, or "phenotypic selection" [1–4]. Accordingly, given a group of animals supposedly reared in similar environmental conditions, only those with the highest performance are allowed to breed to produce the next generation. As discussed previously (Model 2), the performance of each animal is a combination of its breeding value and all other nonadditive genetic effects and environmental factors, such that a superior performance does not always

represent superior breeding value. Nonetheless, whenever $\sigma_a^2 > 0$, there will be a positive correlation between performance and breeding value, and the effectiveness of phenotypic selection (i.e., selection response) will increase with such correlation.

To illustrate this concept consider Fig. 4, in which a scatter plot of breeding values and phenotypes (centered on zero, i.e., $y_i - \mu$) for a few fictitious animals is presented. As indicated before, in this chapter the discussion will be focused on selection approaches and the genetic improvement of a population in terms of additive genetic effects only, such that Model (2) can be conveniently reexpressed as:

$$y_i = \mu + a_i + \varepsilon_i \tag{3}$$

where $\varepsilon_i = c_i + e_i$ represents all nonadditive genetic and environmental effects affecting the phenotypic value y_i, assumed $\varepsilon_i \sim N(0, \sigma_\varepsilon^2)$.

Assuming that each effect in Model (3) is independent from each other, the covariance between phenotype and breeding value is given by:

$$\mathrm{Cov}[y_i, a_i] = \mathrm{Cov}[\mu + a_i + \varepsilon_i, a_i] = \mathrm{Var}[a_i] = \sigma_a^2,$$

such that the correlation between phenotype and breeding value is:

$$r_{y_i,a_i} = \frac{\mathrm{Cov}[y_i, a_i]}{\sqrt{\mathrm{Var}[y_i]\mathrm{Var}[a_i]}} = \frac{\sigma_a^2}{\sigma_y \sigma_a} = \frac{\sigma_a}{\sigma_y} = \sqrt{h^2},$$

i.e., the square root of the (narrow sense) heritability.

As the breeding values of animals are unknown in practice, what phenotypic selection does is to predict (or estimate) the animals' breeding values based on their own performance. The prediction is based on the regression of breeding values on phenotypes, and the regression coefficient (slope) is given by:

$$b_{a_i \bullet y_i} = \frac{\mathrm{Cov}[y_i, a_i]}{\mathrm{Var}[y_i]} = \frac{\sigma_a^2}{\sigma_y^2} = h^2.$$

This means that an animal's estimated breeding value (EBV) based solely on its performance (and with a single measurement only) can be expressed as:

$$\hat{a}_i = h^2(y_i - \mu).$$

The correlation between such EBV (which is a linear transformation of y_i) and the true breeding

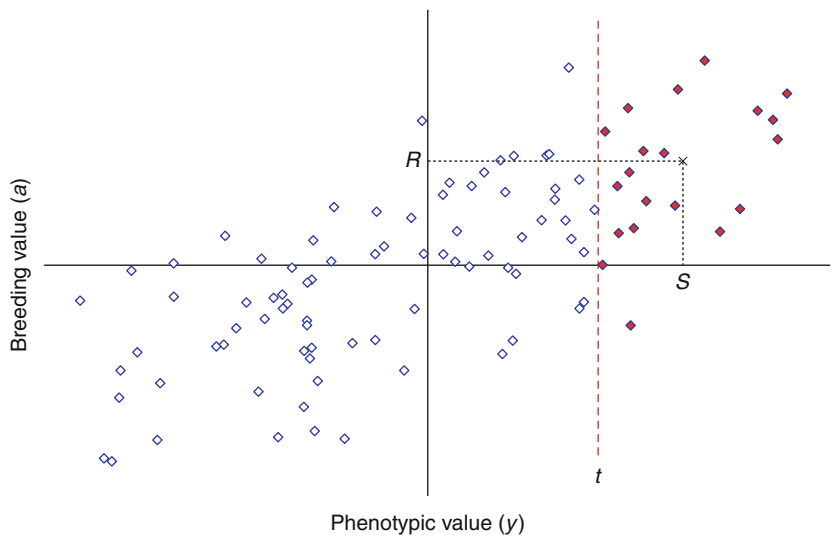

Animal Breeding, Foundations of. Figure 4
Scatter plot of breeding values versus phenotypic values. Each dot represents a specific animal and those colored in *red* are selected animals with performance (i.e., phenotypic value) above a specified threshold (*t*). *S* and *R* represent the average phenotypic and breeding values of the selected (*top*) animals, respectively

value (a_i) is $r_{\hat{a}_i,a_i} = \frac{\mathrm{Cov}[\hat{a}_i,a_i]}{\sqrt{\mathrm{Var}[\hat{a}_i]\mathrm{Var}[a_i]}} = \frac{h^2\sigma_a^2}{\sqrt{h^4\sigma_y^2\sigma_a^2}} = h$, which is generally referred to as "prediction accuracy" in the animal breeding literature [5]. The square of the accuracy in this case is equal to the heritability of the trait and is often called "prediction reliability." The prediction accuracy (and consequently the reliability) can be increased by using additional sources of information on an animal (such as repeated measurements of the trait or performance of progeny and other relatives) when estimating its breeding value. An example is with selection indexes and mixed model methodology, which will be discussed later in this chapter.

As indicated in Fig. 4, the selected animals (i.e., the best performing animals) will have an average phenotypic value equal to S and an average breeding value equal to R. The expected average breeding value (and also the expected phenotypic performance) of the progeny of the selected animals is also R, as illustrated in Fig. 5, and the ratio R/S is equal to the heritability (h^2) of the trait under selection. The genetic progress after one generation of selection is then given by:

$$R = h^2 S,$$

where $R = \mu_P - \mu$ and $S = \mu_S - \mu$, with μ_P, μ_S, and μ representing the average phenotypic performance of the progeny (generation 1), of the selected animals, and of the selection candidate (generation 0) populations, respectively.

The selection differential (S) can also be expressed as $S = i\sigma_y$, where $i = \frac{\mu_S - \mu}{\sigma_y}$ is called "selection intensity," and represents the selection differential in terms of phenotypic standard deviations. In addition, as R represents the genetic progress expected in a single generation of selection, the genetic improvement per unit of time is then given by $R^* = R/L$, where L is the generation interval. Hence, the expected genetic progress when phenotypic selection on a single trait is employed is [1, 3]:

$$R^* = \frac{h^2 i\sigma_y}{L},$$

which, given that $\sigma_y = \sigma_a/h$, can be expressed also as:

$$R^* = \frac{hi\sigma_a}{L}.$$

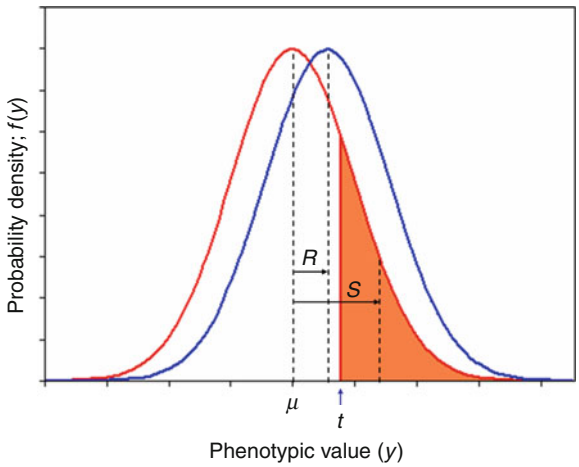

Animal Breeding, Foundations of. Figure 5
Probability density of the distribution of phenotypic values in the candidates-for-selection (*red*) and the progeny (*blue*) populations. The candidates-for-selection group represents the parental population (or generation 0), from which the top performing animals (above the threshold *t*) are selected and mated to produce the next generation, or progeny (generation 1). The difference between the phenotypic average of the selected animals and that of the generation 0 is called selection differential (represented by *S*), and the difference between the phenotypic mean of the progeny and that of the generation 0 is called genetic progress, or genetic response (represented by *R*)

This equation is a special form of the so-called "breeder's equation" (or "key equation"), for the case of phenotypic selection. In its general form, the breeder's equation is expressed as [5]:

$$R^* = \frac{\text{Accuracy} \times \text{Intensity} \times \text{Variation}}{\text{Generation interval}},$$

meaning that the genetic progress per unit of time is proportional to the accuracy of breeding values prediction, to the selection intensity, and to the genetic variation, and inversely proportional to the generation interval.

Hence, to increase the genetic progress in a population (e.g., breed or line) through selection, animal breeders (and similarly plant breeders) work to improve the four components of the equation above. As the genetic variability is a natural characteristic of a population and cannot be easily changed, genetic

progress is generally incremented by improving prediction accuracy (e.g., by using specific statistical techniques to combine different sources of information regarding the animals' genetic merit), by increasing the selection intensity, and by shortening the generation interval, which can be accomplished using molecular genetics techniques (e.g., the use of marker-assisted selection) and biotechnology approaches (e.g., artificial insemination).

It is important to mention that the breeder's equation discussed here can be extended for more complex scenarios, such as when males and females contribute differently for some components of the equation [5]. For example, prediction accuracies and selection intensity are generally higher for males if artificial insemination is used. Another important issue to mention here is that selection not only shifts the mean of the breeding values in a population but also changes the genetic variance (and heritability). A primary cause of the change in genetic variance is due to the fact that selected parents represent one tail of the phenotypic distribution, therefore their phenotypic variance is smaller than that of the whole candidates-for-selection population. This leads to a reduction in both the phenotypic and additive genetic variances in the progeny population, which is known as the "Bulmer effect" [2]. In addition, as selection modifies allele frequencies toward the fixation of favorable alleles, selection in one direction over many generations is also expected to reduce the genetic variation. Additional discussion on effects of selection on variance and other short-term and long-term consequences of artificial selection can be found, for example, in [2, 3].

In the remainder of this chapter specific statistical techniques (such as the selection index, BLUP, and genomic selection) for the improvement of accuracy, intensity, and generation interval, and consequently the increase of genetic progress from artificial selection, will be discussed.

Correlated Response and Indirect Selection

If two traits x and y are genetically correlated, direct selection on one of the traits (say y) will also cause a genetic change in the other trait (trait x), which is called "correlated response" [3]. Correlated response to selection ($R_{x\bullet y}$), that is, genetic change in trait x as a consequence of direct selection on trait y, can be predicted by:

$$R_{x\bullet y} = b_{x\bullet y} R_y,$$

where R_y is the genetic progress of trait y through direct selection on itself, and $b_{x\bullet y}$ is the genetic regression coefficient, given by:

$$b_{x\bullet y} = \frac{\mathrm{Cov}(a_x, a_y)}{\sigma^2_{a_y}},$$

where $\mathrm{Cov}(a_x, a_y)$ is the genetic covariance between traits x and y.

The genetic correlation between two traits x and y is given by:

$$\rho_{a_x,a_y} = \frac{\mathrm{Cov}(a_x, a_y)}{\sigma_{a_x}\sigma_{a_y}},$$

such that $\mathrm{Cov}(a_x, a_y) = \rho_{a_x,a_y}\sigma_{a_x}\sigma_{a_y}$ and the genetic regression can be expressed as:

$$b_{x\bullet y} = \frac{\rho_{a_x,a_y}\sigma_{a_x}\sigma_{a_y}}{\sigma^2_{a_y}} = \rho_{a_x,a_y}\frac{\sigma_{a_x}}{\sigma_{a_y}}.$$

Using this term, and recalling the selection response formula discussed before, given by $R_y = h_y i_y \sigma_{a_y}$, the correlated response can then be expressed as:

$$R_{x\bullet y} = \rho_{a_x,a_y}\frac{\sigma_{a_x}}{\sigma_{a_y}} h_y i_y \sigma_{a_y} = \rho_{a_x,a_y}\sigma_{a_x} h_y i_y,$$

or, given that $\sigma_{a_x} = h_x \sigma_{y_x}$, it can be finally written as:

$$R_{x\bullet y} = \rho_{a_x,a_y} h_x h_y i_y \sigma_{y_x}.$$

Such an equation can be used either to monitor potential genetic changes in correlated traits when performing direct selection on a specific trait of economic importance or, alternatively, to explore indirect selection strategies using indicator traits [5]. The latter use may be of interest when a trait of economic importance (e.g., trait x) is difficult or expensive to measure, or it is expressed later in an animal's life, so it may be advantageous to select on a correlated trait (e.g., trait y), which would be the indicator trait. To assess the effectiveness of indirect selection relative to direct selection, one may look at

the ratio of expected genetic progress per unit of time in each scenario, i.e.,

$$\frac{R_{x\bullet y}}{R_x} = \frac{\rho_{a_x,a_y}\sigma_{a_x}h_y i_y/L_y}{h_x i_x \sigma_{a_x}/L_x} = \frac{\rho_{a_x,a_y}h_y i_y L_x}{h_x i_x L_y}$$
$$= \rho_{a_x,a_y}\frac{h_y}{h_x}\frac{i_y}{i_x}\frac{L_x}{L_y}.$$

So, it can be seen that this ratio can be higher than 1 (meaning that the indirect selection is more effective than the direct selection) depending on the genetic correlation between the economic and the indicator traits, the ratios of their heritabilities, and their potential selection intensities and generation intervals.

Selection Index

In section "Phenotypic Selection," selection based on a single measurement on each animal was discussed. However, it is not always possible to observe the phenotype for all animals, such as traits that are expressed in only one sex or that require the sacrifice of animals to be measured, etc. In addition, even when it is possible to measure the phenotypic trait in each animal, information from relatives can be used to obtain earlier or more reliable predictions of breeding values. In this section, the prediction of breeding values using different sources of information (e.g., multiple measurements of the trait in each animal and progeny performance) will be discussed and a methodology (the selection index) that combines multiple sources of information into a single prediction for each animal will be presented.

When multiple measurements of the same trait are recorded (e.g., milk yield in multiple lactations), breeding values can be predicted using the average of observations ($\bar{y}_i$) from each animal as $\hat{a}_i = b_{a_i\bullet\bar{y}_i}(\bar{y}_i - \mu)$. However, to derive the genetic regression of breeding value on average phenotypic value, Model (3) must be expanded to include an additional term, which is discussed next.

It can be shown empirically that the covariance (or resemblance) between repeated measurements on the same animal is larger than σ_a^2, which is what would be expected under the assumptions of Model (3). This additional source of covariance between records for the same animal refers to environmental factors that affect all records similarly, the so-called "permanent environmental effects" [1, 4]. Under these circumstances, the Model (3) can be extended to:

$$y_{ij} = \mu + a_i + p_i + \varepsilon_{ij} \tag{4}$$

where y_{ij} represents the observation j ($j = 1, \ldots, n_i$) on animal i, with n_i being the total number of records on animal i; μ and $a_i \sim N(0, \sigma_a^2)$ are as defined previously; p_i refers to the permanent environmental effects affecting records on animal i, assumed $p_i \sim N(0, \sigma_p^2)$; and $\varepsilon_{ij} \sim N(0, \sigma_\varepsilon^2)$ represent residual effects (nonadditive genetic and temporary environmental effects) associated with observation y_{ij}. In addition, it is assumed that all random terms in Model (4) are independent from each other, i.e., $\mathrm{Cov}(a_i, p_i) = \mathrm{Cov}(a_i, \varepsilon_{ij}) = \mathrm{Cov}(p_i, \varepsilon_{ij}) = \mathrm{Cov}(\varepsilon_{ij}, \varepsilon_{ij'}) = 0$ for any i, j, and j' ($j \neq j'$).

Under these settings, the average phenotypic value of an animal is given by $\bar{y}_{ij} = \mu + a_i + p_i + \bar{\varepsilon}_{ij}$, where $\bar{\varepsilon}_i = \frac{1}{n_i}\sum_{j=1}^{n_i}\varepsilon_{ij}$, such that its variance is given by $\mathrm{Var}[\bar{y}_i] = \sigma_a^2 + \sigma_p^2 + \sigma_\varepsilon^2/n_i$, and the covariance between a_i and $\bar{y}_i$ is $\mathrm{Cov}(a_i, \bar{y}_i) = \sigma_a^2$. In this case, the regression of breeding values on phenotypic means is given by:

$$b_{a_i\bullet\bar{y}_i} = \frac{\mathrm{Cov}[a_i, \bar{y}_i]}{\mathrm{Var}[\bar{y}_i]} = \frac{\sigma_a^2}{\sigma_a^2 + \sigma_p^2 + \sigma_\varepsilon^2/n_i}.$$

An important definition related to repeated measurements refers to repeatability (r), which is given by the intraclass correlation, i.e., the ratio of the within-individual (or between repeated measurements) to the phenotypic variances [1, 4]:

$$r = \frac{\sigma_a^2 + \sigma_p^2}{\sigma_y^2} = \frac{\sigma_a^2 + \sigma_p^2}{\sigma_a^2 + \sigma_p^2 + \sigma_\varepsilon^2},$$

and measures the correlation between records on the same animal.

Noting that $r = 1 - \frac{\sigma_\varepsilon^2}{\sigma_a^2+\sigma_p^2+\sigma_\varepsilon^2}$, the variance of the average phenotypic value of an animal can be expressed as a function of the repeatability as $\mathrm{Var}[\bar{y}_i] = [r + (1-r)/n_i]\sigma_y^2$, such that the genetic regression becomes:

$$b_{a_i\bullet\bar{y}_i} = \frac{\sigma_a^2}{[r + (1-r)/n_i]\sigma_y^2} = \frac{n_i h^2}{1 + (n_i - 1)/r}.$$

The prediction accuracy in this case, i.e., the correlation between an animal's estimated breeding value

using repeated records and its true breeding value is given by:

$$r_{\hat{a}_i,a_i} = r_{\bar{y}_i,a_i} = \frac{\mathrm{Cov}(\bar{y}_i, a_i)}{\sqrt{\mathrm{Var}(\bar{y}_i)\mathrm{Var}(a_i)}} = \frac{\sigma_a^2}{\sqrt{r + (1-r)/n_i}\sigma_y\sigma_a} = h\sqrt{\frac{n_i}{1+(n_i-1)r}} = \sqrt{b_{a_i \bullet \bar{y}_i}}.$$

Hence, it can be seen that compared with single record phenotypic selection, there is a gain in accuracy when predictions are based on repeated records and that the gain will depend on the values of r and n_i; higher gain in accuracy is obtained when r is low and when n_i is high.

Another alternative to predict breeding values is to use progeny performance, which is often employed for predicting breeding values of males for traits where records can be obtained only on females, such as milk yield. For example, let $\bar{y}_i$ be the average of single records on n_i progeny of sire i, and assume that the sire was mated to a random sample of females not related to him. In this case, each progeny record can be expressed as:

$$y_{ij} = \mu + \frac{1}{2}a_i + \frac{1}{2}d_{ij} + \delta_{ij} + \varepsilon_{ij},$$

where a_i is the breeding value of a specific sire i; d_{ij} is the breeding value of dam j ($j = 1, \ldots, n_i$) mated with sire i; and δ_{ij} and ε_{ij} refer to the Mendelian sampling and residual (environmental) components associated with the observation y_{ij}. Using this notation, the following model can be used to describe the progeny average of sire i:

$$\bar{y}_i = \mu + \frac{1}{2}a_i + \frac{1}{2}\bar{d}_i + \bar{\delta}_i + \bar{\varepsilon}_i \tag{5}$$

where $\bar{y}_i = \frac{1}{n_i}\sum_{i=1}^{n_i} y_{ij}$, $\bar{d}_i = \frac{1}{n_i}\sum_{i=1}^{n_i} d_{ij}$, $\bar{\delta}_i = \frac{1}{n_i}\sum_{i=1}^{n_i} \delta_{ij}$, and $\bar{\varepsilon}_i = \frac{1}{n_i}\sum_{i=1}^{n_i} \varepsilon_{ij}$. Given that $E[\bar{d}_i] = 0$ and $E[\bar{\delta}_i] = 0$, the breeding value of sire i can be then predicted by $\hat{a}_i = b_{a_i \bullet \bar{y}_i}(\bar{y}_i - \mu)$, where $b_{a_i \bullet \bar{y}_i} = \mathrm{Cov}[a_i, \bar{y}_i]/\mathrm{Var}[\bar{y}_i]$. It is shown that:

$$\mathrm{Cov}(a_i, \bar{y}_i) = \mathrm{Cov}(a_i, a_i/2) = \sigma_a^2/2$$

and

$$\begin{aligned}\mathrm{Var}[\bar{y}_i] &= \mathrm{Var}\left[\frac{1}{2}a_i + \frac{1}{2}\bar{d}_i + \bar{\delta}_i + \bar{\varepsilon}_i\right] \\ &= \frac{1}{4}\sigma_a^2 + \frac{1}{4}\frac{\sigma_a^2}{n_i} + \frac{\sigma_a^2}{2n_i} + \frac{\sigma_\varepsilon^2}{n_i} \\ &= \frac{(n_i+3)\sigma_a^2 + 4\sigma_\varepsilon^2}{4n_i} \\ &= \frac{(n_i+3)h^2 + 4(1-h^2)}{4n_i}\sigma_y^2 \\ &= \left[k + \frac{1-k}{n_i}\right]\sigma_y^2,\end{aligned}$$

where $k = h^2/4$ is the intraclass correlation between half-sibs, such that the genetic regression coefficient is given by:

$$\begin{aligned}b_{a_i \bullet \bar{y}_i} &= \frac{\sigma_a^2/2}{[k + (1-k)/n_i]\sigma_y^2} \\ &= \frac{h^2\sigma_y^2/2}{[h^2/4 + (1-h^2/4)/n_i]\sigma_y^2} \\ &= \frac{2n_i h^2}{4 + (n_i - 1)h^2},\end{aligned}$$

and the prediction accuracy by:

$$\begin{aligned}r_{a_i,\bar{y}_i} &= \frac{\mathrm{Cov}[a_i, \bar{y}_i]}{\sqrt{\mathrm{Var}[a_i]\mathrm{Var}[\bar{y}_i]}} = \frac{h^2\sigma_y^2/2}{\sqrt{h^2\sigma_y^2[k + (1-k)/n_i]\sigma_y^2}} \\ &= \sqrt{\frac{n_i h^2/4}{1 + (n_i - 1)k}} \\ &= \sqrt{\frac{n_i h^2}{4 + (n_i - 1)h^2}} = \sqrt{b_{a_i \bullet \bar{y}_i}/2},\end{aligned}$$

which approaches unity (one) as the number of progeny records increases.

Up to this point, it has been discussed how breeding values can be predicted using different sources of information, such as an animal's own performance (either a single record or multiple measurements) or progeny performance. Other sources of information that could also be used are the performance of parents, sibling, or other kinds of relatives. However, what generally happens is that multiple sources of information are available simultaneously, so the question becomes how to best combine all the information in order to improve prediction accuracy. Here, a classical approach will be discussed, the "selection index," and later on in this

chapter a more general and modern alternative, based on mixed model methodology, will be presented.

Consider, for example, that there are three sources of information available on animal i (represented here as y_{i1}, y_{i2}, and y_{i3}, and expressed as deviations from their means), so the goal is to predict the animal's breeding value with a linear combination of such information, i.e.,

$$\hat{a}_i = b_{i1}y_{i1} + b_{i2}y_{i2} + b_{i3}y_{i3},$$

such that the prediction accuracy (i.e., correlation between predicted and true breeding value) is maximized.

Maximization of $r_{\hat{a}_i,a_i}$ is equivalent to the maximization of $\log(r_{\hat{a}_i,a_i})$, which is generally easier to accomplish. The log correlation can be expressed as (here, to simplify the notation, the index i indicating the animal is dropped):

$$\log(r_{\hat{a},a}) = \log\left[\frac{\sigma_{\hat{a},a}}{\sqrt{\sigma^2_{\hat{a}}\sigma^2_a}}\right] = \log(\sigma_{\hat{a},a}) - \frac{1}{2}\sigma^2_{\hat{a}} - \frac{1}{2}\sigma^2_a,$$

where the covariance between $\hat{a}$ and a, and the variance of $\hat{a}$ are given respectively by:

$$\sigma_{\hat{a},a} = b_1\sigma_{y_1,a} + b_2\sigma_{y_2,a} + b_3\sigma_{y_3,a}$$

and

$$\begin{aligned}\sigma^2_{\hat{a}} =& b_1^2\sigma^2_{y_1} + 2b_1b_2\sigma_{y_1,y_2} + 2b_1b_3\sigma_{y_1,y_3}\\ &+ b_2^2\sigma^2_{y_2} + 2b_2b_3\sigma_{y_2,y_3} + b_3^2\sigma^2_{y_3}.\end{aligned}$$

Substituting these expressions into $\log(r_{\hat{a},a})$, taking the partial derivatives of $\log(r_{\hat{a},a})$ with respect to each of the regression coefficients b_j $(j = 1, 2, 3)$, and setting them to zero, gives the following set of equations:

$$\begin{cases}\dfrac{\partial\log(r_{\hat{a},a})}{\partial b_1} = \dfrac{\sigma_{y_1,a}}{\sigma_{\hat{a},a}} - \dfrac{b_1\sigma^2_{y_1} + b_2\sigma_{y_1,y_2} + b_3\sigma_{y_1,y_3}}{\sigma^2_{\hat{a}}}\\ \dfrac{\partial\log(r_{\hat{a},a})}{\partial b_2} = \dfrac{\sigma_{y_2,a}}{\sigma_{\hat{a},a}} - \dfrac{b_1\sigma_{y_1,y_2} + b_2\sigma^2_{y_2} + b_3\sigma_{y_2,y_3}}{\sigma^2_{\hat{a}}}\\ \dfrac{\partial\log(r_{\hat{a},a})}{\partial b_3} = \dfrac{\sigma_{y_3,a}}{\sigma_{\hat{a},a}} - \dfrac{b_1\sigma_{y_1,y_3} + b_2\sigma_{y_2,y_3} + b_3\sigma^2_{y_3}}{\sigma^2_{\hat{a}}}\end{cases}$$

which can be rearranged as:

$$\begin{cases}b_1\sigma^2_{y_1} + b_2\sigma_{y_1,y_2} + b_3\sigma_{y_1,y_3} = k\sigma_{y_1,a}\\ b_1\sigma_{y_1,y_2} + b_2\sigma^2_{y_2} + b_3\sigma_{y_2,y_3} = k\sigma_{y_2,a}\\ b_1\sigma_{y_1,y_3} + b_2\sigma_{y_2,y_3} + b_3\sigma^2_{y_3} = k\sigma_{y_3,a}\end{cases}$$

where $k = \sigma^2_{\hat{a}}/\sigma_{\hat{a},a}$.

Extending the system for any number m of components (i.e., sources of information), these equations can be expressed in matrix notation as:

$$\mathbf{Pb} = \mathrm{k}\mathbf{c},$$

where $\mathbf{P} = \begin{bmatrix}\sigma^2_{y_1} & \sigma_{y_1,y_2} & \cdots & \sigma_{y_1,y_m}\\ \sigma_{y_1,y_2} & \sigma^2_{y_2} & \cdots & \sigma_{y_2,y_m}\\ \vdots & \vdots & \ddots & \vdots\\ \sigma_{y_1,y_m} & \sigma_{y_2,y_m} & \cdots & \sigma^2_{y_m}\end{bmatrix}$ is the covariance matrix of the vector $\mathbf{y} = [y_1, y_2, \ldots, y_m]'$, $\mathbf{b} = [b_1, b_2, \ldots, b_m]'$ is the vector of regression coefficients (weights) of each source of information, and $\mathbf{c} = [\sigma_{y_1,a}, \sigma_{y_2,a}, \ldots, \sigma_{y_m,a}]'$ is the vector of covariances between each piece of information and the breeding value of the animal, such that the weights $\mathbf{b}$ of the index $\hat{a} = \mathbf{b}'\mathbf{y}$ are given by $\mathbf{b} = k\mathbf{P}^{-1}\mathbf{c}$.

It should be noted that the constant k does not change the relative size of the regression coefficients $\mathbf{b}$ or the value of $r_{\hat{a},a}$, so it can be set to 1. In fact, if instead of maximizing $r_{\hat{a},a}$, the average square prediction error $E[\hat{a} - a]^2$ is minimized, then $\sigma^2_{\hat{a}} = \sigma_{\hat{a},a}$ and the system (usually called selection index equations) becomes:

$$\mathbf{b} = \mathbf{P}^{-1}\mathbf{c}.$$

The correlation between the index and the true breeding value is given by $r_{\hat{a},a} = \sigma_{\hat{a},a}/\sqrt{\sigma^2_{\hat{a}}\sigma^2_a} = \sqrt{\sigma_{\hat{a},a}/\sigma^2_a} = \sqrt{\frac{1}{\sigma^2_a}\sum_{j=1}^{m} b_j\sigma_{y_j,a}}$.

Multiple-Trait Selection

Usually more than one trait is considered in a selection program, as multiple traits may be economically important in a production system (e.g., [9]). There are many strategies for multi-trait selection, including the tandem approach (which selects rotationally one trait at a time) and the independent culling levels strategy (which sets minimum performance levels for each of the traits of interest), but they are generally suboptimal.

Here, the selection of a combination of multiple traits evaluated in economic terms will be discussed. Such a combination of traits is generally called "aggregate breeding value" or "breeding objective," and can be expressed as [3]:

$$T = \mathbf{w}'\mathbf{a} = w_1a_1 + w_2a_2 + \ldots + w_ka_k,$$

where $\mathbf{w} = (w_1, w_2, \ldots, w_k)'$ is the vector of economic weights (expressed as net economic value per unit of trait) for k traits of linear economic value, and $\mathbf{a} = (a_1, a_2, \ldots, a_k)'$ is a vector of breeding values relative to the k traits defining T. Here again, to simplify the notation, a subscript indexing the animal is suppressed.

Suppose records are available for m traits, which may or may not be included in the k traits describing the breeding objective. The goal then is to predict T based on the m traits observed, using the so-called economic selection index. The theory of selection index was introduced in the previous subsection as a means of combining multiple sources of information to predict breeding values for a specific trait. Here, similar methodology will be considered, but will be used to combine information from multiple traits to predict an overall economic merit for each animal, i.e.,

$$\hat{T} = I = \mathbf{v}'\mathbf{y} = v_1 y_1 + v_2 y_2 + \ldots + v_m y_m,$$

where $\hat{T}$ is the predicted overall economic merit of an animal, $\mathbf{v} = (v_1, v_2, \ldots, v_m)'$ is the vector of weighting factors, and $\mathbf{y} = (y_1, y_2, \ldots, y_m)'$ is the vector of phenotypic measurements.

An alternative for determining the weights $\mathbf{v} = (v_1, v_2, \ldots, v_m)'$ is to first predict separately the breeding values a_j, $j = 1, 2, \ldots, k$, for each trait involved in the breeding objective, using information from all the traits with measurements, $\mathbf{y} = (y_1, y_2, \ldots, y_m)'$. Afterward, such predictions are substituted for the true breeding values in the breeding objective equation, and then coefficients are grouped accordingly.

The breeding values a_j for each trait can be predicted by $\hat{a}_j = b_{j1} y_1 + b_{j2} y_2 + \ldots + b_{jm} y_m$, in which the weights are obtained as usual, to maximize $r_{\hat{a}_j, a_j}$ or minimize $E[\hat{a}_j - a_j]^2$. The equations which define the weights for the prediction of a_j are then given by:

$$\begin{cases} b_{j1}\sigma^2_{y_1} + b_{j2}\sigma_{y_1,y_2} + \ldots + b_{jm}\sigma_{y_1,y_m} = \sigma_{y_1,a_j} \\ b_{j1}\sigma_{y_1,y_2} + b_{j2}\sigma^2_{y_2} + \ldots + b_{jm}\sigma_{y_2,y_m} = \sigma_{y_2,a_j} \\ \vdots \qquad \vdots \qquad \vdots \qquad \vdots \\ b_{j1}\sigma_{y_1,y_m} + b_{j2}\sigma_{y_2,y_m} + \ldots + b_{jm}\sigma^2_{y_m} = \sigma_{y_m,a_j} \end{cases}$$

This procedure is repeated for all k traits in the breeding objective, and the predictions $\hat{\mathbf{a}} = (\hat{a}_1, \hat{a}_2, \ldots, \hat{a}_k)'$ are then substituted for the true values $\mathbf{a} = (a_1, a_2, \ldots, a_k)'$ in the aggregate breeding value, i.e.,

$$\hat{T} = w_1\hat{a}_1 + w_2\hat{a}_2 + \ldots + w_k\hat{a}_k.$$

This overall index estimating T can be rewritten as $I = v_1 y_1 + v_2 y_2 + \ldots + v_m y_m$, by using appropriate multiplications and grouping of coefficients. It is shown that each coefficient v_i is given by $v_i = w_1 b_{1i} + w_2 b_{2i} + \ldots + w_k b_{ki}$, with $i = 1, 2, \ldots, m$.

Another way of deriving the weights $\mathbf{v} = (v_1, v_2, \ldots, v_m)'$ defining the economic selection index $I = \mathbf{v}'\mathbf{y}$ is to maximize the correlation $r_{T,I}$, which will generate the following equations:

$$\begin{cases} v_1\sigma^2_{y_1} + v_2\sigma_{y_1,y_2} + \ldots + v_m\sigma_{y_1,y_m} = \sigma_{y_1,T} \\ v_1\sigma_{y_1,y_2} + v_2\sigma^2_{y_2} + \ldots + v_m\sigma_{y_2,y_m} = \sigma_{y_2,T} \\ \vdots \qquad \vdots \qquad \vdots \qquad \vdots \\ v_1\sigma_{y_1,y_m} + v_2\sigma_{y_2,y_m} + \ldots + v_m\sigma^2_{y_m} = \sigma_{y_m,T} \end{cases}$$

where $\sigma_{y_i,T}$ is the covariance between each measured trait i $(i = 1, 2, \ldots, m)$ and the linear function $T = \mathbf{w}'\mathbf{a}$, i.e., the aggregate breeding value. It can be shown that both approaches for determining the weights $\mathbf{v} = (v_1, v_2, \ldots, v_m)'$ are equivalent.

Mixed Model Methodology

Introduction

Many statistical methods for analysis of genetic data are specific (or more appropriate) for phenotypic measurements obtained from planned experimental designs with balanced data sets. While such situations may be possible within laboratory or greenhouse experimental settings, data from natural populations and agricultural species are generally highly unbalanced and fragmented by numerous kinds of relationships. Culling of data to accommodate conventional statistical techniques (such as those discussed to this point) may introduce bias and/or lead to a substantial loss of information. The mixed model methodology, on the other hand, allows efficient estimation of genetic parameters (such as variance components and heritability) and breeding values while accommodating extended pedigrees, unequal family sizes, overlapping generations, sex-limited traits, assortative mating, and natural or artificial selection.

The single trait prediction methods discussed in the previous section use only a single source of information or, when multiple sources of information are available, they require them to be split into independent subgroups, i.e., specific groups of relatives such as half-sibs, full-sibs, progeny, etc. However, in practice the data may be extremely complex due to the intricate pedigree structure commonly found in livestock species, e.g., beef and dairy cattle populations. Other drawbacks of the selection index include an inability to account for genetic trend over time and that the phenotypes must be pre-adjusted for environmental effects, which can be done, for example, using the average of contemporary groups of animals. However, contemporary group effects can be inferred only under the unrealistic assumption that they are genetically equal. Hence, a selection index can be reliably applied only to individual animals within same herd and born in same year.

In view of such limitations, linear mixed models (models including both fixed and random effects) and best linear unbiased predictions (BLUP) of breeding values were developed [10–12]. The BLUP methodology uses performance information from all known relatives to estimate breeding values, can be applied to whole herds or large populations using data from many years, and can also accommodate genetic differences between contemporary groups. Presently, mixed models are widely used in many fields of science as a flexible tool for the analysis of data where responses are clustered around some random effects, such that there is a natural dependence between observations in the same cluster. Examples of applications of mixed models in genetics and genomics include gene mapping and association analysis (e.g., [13, 14]), and gene expression assays using microarrays [15, 16] or RT-PCR [17], to name a few.

In some applications of mixed models the central objective is the estimation and hypothesis testing regarding fixed effects (e.g., treatment effects in an experimental study), in which case the random effects (e.g., block effects) are nuisance effects. In animal breeding, however, the main goal is the prediction of realized values of random effects (breeding values of animals), and the fixed effects are generally environmental factors that should be taken into account to adjust the observed phenotypic values. A third application or goal of mixed models is the estimation of variance components, such as genetic and environmental variances, or functions of them, such as heritability and repeatability.

In this section some basics regarding mixed models are briefly reviewed, with some emphasis toward the prediction of random effects, and subsequently some specific applications of the mixed model methodology in animal breeding and genetics are presented.

A linear mixed-effects model is defined as:

$$\mathbf{y} = \mathbf{X}\boldsymbol{\beta} + \mathbf{Z}\mathbf{u} + \boldsymbol{\varepsilon} \tag{6}$$

where $\mathbf{y}$ is the vector of responses (observations), $\boldsymbol{\beta}$ is a vector of fixed effects, $\mathbf{u}$ is a vector of random effects, $\mathbf{X}$ and $\mathbf{Z}$ are known incidence matrices relate $\mathbf{y}$ to the vectors $\boldsymbol{\beta}$ and $\mathbf{u}$, respectively, and ε is a vector of residual terms. Generally, it is assumed that $\mathbf{u}$ and ε are independent from each other and normally distributed with zero-mean vectors and variance–covariance matrices $\mathbf{G}$ and $\boldsymbol{\Sigma}$, respectively.

As mentioned before, in animal breeding a central goal refers to the prediction of random effects (breeding values). In linear (Gaussian) models as in (6) such predictions are given by the conditional expectation of $\mathbf{u}$ given the data, i.e., $E[\mathbf{u}|\mathbf{y}]$. Given the model specifications above, the joint distribution of $\mathbf{y}$ and $\mathbf{u}$ is:

$$\begin{bmatrix} \mathbf{y} \\ \mathbf{u} \end{bmatrix} \sim \mathrm{MVN}\left(\begin{bmatrix} \mathbf{X}\boldsymbol{\beta} \\ \mathbf{0} \end{bmatrix}, \begin{bmatrix} \mathbf{V} & \mathbf{ZG} \\ \mathbf{GZ}' & \mathbf{G} \end{bmatrix} \right),$$

where $\mathbf{V} = \mathbf{ZGZ}' + \boldsymbol{\Sigma}$.

From the properties of multivariate normal distributions, $E[\mathbf{u}|\mathbf{y}]$ is given by:

$$E[\mathbf{u}|\mathbf{y}] = E[\mathbf{u}] + \mathrm{Cov}[\mathbf{u}, \mathbf{y}']\mathrm{Var}^{-1}[\mathbf{y}](\mathbf{y} - E[\mathbf{y}]),$$

such that in this case:

$$\begin{aligned} E[\mathbf{u}|\mathbf{y}] &= \mathbf{GZ}'\mathbf{V}^{-1}(\mathbf{y} - \mathbf{X}\boldsymbol{\beta}) \\ &= \mathbf{GZ}'(\mathbf{ZGZ}' + \boldsymbol{\Sigma})^{-1}(\mathbf{y} - \mathbf{X}\boldsymbol{\beta}). \end{aligned}$$

This expression, however, depends on the fixed effects values $\boldsymbol{\beta}$, which also need to be inferred from the data. The fixed effects are then typically replaced by their estimates, such that predictions are made based on the following expression:

$$\hat{\mathbf{u}} = \mathbf{GZ}'\mathbf{V}^{-1}(\mathbf{y} - \mathbf{X}\hat{\boldsymbol{\beta}}).$$

To estimate the fixed effects $\boldsymbol{\beta}$, all random effects in Model (6) can be combined into a single vector,

$\boldsymbol{\xi} = \mathbf{Zu} + \boldsymbol{\varepsilon}$, such that the following fixed effects model is obtained: $\mathbf{y} = \mathbf{X}\boldsymbol{\beta} + \boldsymbol{\xi}$. It is shown that the expectation of the ξ term is $E[\boldsymbol{\xi}] = E[\mathbf{Zu} + \boldsymbol{\varepsilon}] = \mathbf{Z}E[\mathbf{u}] + E[\boldsymbol{\varepsilon}] = \mathbf{0}$, and that its variance is $\mathrm{Var}[\boldsymbol{\xi}] = \mathrm{Var}[\mathbf{Zu} + \boldsymbol{\varepsilon}] = \mathbf{Z}\mathrm{Var}[\mathbf{u}]\mathbf{Z}' + \mathrm{Var}[\boldsymbol{\varepsilon}] = \mathbf{ZGZ}' + \boldsymbol{\Sigma} = \mathbf{V}$. Under these settings, the distribution of $\mathbf{y}$ is multivariate normal with mean vector $\mathbf{X}\boldsymbol{\beta}$ and covariance matrix $\mathbf{V}$, i.e., $\mathbf{y} \sim MVN(\mathbf{X}\boldsymbol{\beta}, \mathbf{V})$, and the maximum likelihood estimator of β can be shown to be:

$$\hat{\boldsymbol{\beta}} = (\mathbf{X}'\mathbf{V}^{-1}\mathbf{X})^{-1}\mathbf{X}'\mathbf{V}^{-1}\mathbf{y},$$

which is distributed as $\hat{\boldsymbol{\beta}} \sim MVN(\boldsymbol{\beta}, (\mathbf{X}'\mathbf{V}^{-1}\mathbf{X})^{-1})$. If the design matrix $\mathbf{X}$ is not full column rank, a generalized inverse of $\mathbf{X}'\mathbf{V}^{-1}\mathbf{X}$ must be used to obtain a solution $\boldsymbol{\beta^0} = (\mathbf{X}'\mathbf{V}^{-1}\mathbf{X})^{-}\mathbf{X}'\mathbf{V}^{-1}\mathbf{y}$ of the system, from which estimable functions $\boldsymbol{\theta} = \mathbf{L}\boldsymbol{\beta}$ are estimated as $\hat{\boldsymbol{\theta}} = \mathbf{L}\boldsymbol{\beta^0}$.

The solutions $\hat{\boldsymbol{\beta}}$ and $\hat{\mathbf{u}}$ discussed before require $\mathbf{V}^{-1}$. As $\mathbf{V}$ can be of huge dimensions, especially in animal breeding applications, its inverse is generally computationally demanding if not unfeasible. However, Henderson [18] presented the mixed model equations (MME) to estimate $\boldsymbol{\beta}$ and $\mathbf{u}$ simultaneously, without the need for computing $\mathbf{V}^{-1}$. The MME were derived by maximizing (for $\boldsymbol{\beta}$ and $\mathbf{u}$) the joint density of $\mathbf{y}$ and $\mathbf{u}$, expressed as:

$$p(\mathbf{y}, \mathbf{u}) \propto |\boldsymbol{\Sigma}|^{-1/2}|\mathbf{G}|^{-1/2} \exp\left\{-\frac{1}{2}(\mathbf{y} - \mathbf{X}\boldsymbol{\beta} - \mathbf{Zu})' \boldsymbol{\Sigma}^{-1}(\mathbf{y} - \mathbf{X}\boldsymbol{\beta} - \mathbf{Zu}) - \frac{1}{2}\mathbf{u}'\mathbf{G}^{-1}\mathbf{u}\right\}.$$

The logarithm of this function is:

$$\begin{aligned}\ell &= \log[p(\mathbf{y}, \mathbf{u})] \propto |\boldsymbol{\Sigma}| + |\mathbf{G}| + (\mathbf{y} - \mathbf{X}\boldsymbol{\beta} - \mathbf{Zu})'\boldsymbol{\Sigma}^{-1} \\ &\quad (\mathbf{y} - \mathbf{X}\boldsymbol{\beta} - \mathbf{Zu}) + \mathbf{u}'\mathbf{G}^{-1}\mathbf{u} \\ &= |\boldsymbol{\Sigma}| + |\mathbf{G}| + \mathbf{y}'\boldsymbol{\Sigma}^{-1}\mathbf{y} - 2\mathbf{y}'\boldsymbol{\Sigma}^{-1}\mathbf{X}\boldsymbol{\beta} - 2\mathbf{y}'\boldsymbol{\Sigma}^{-1}\mathbf{Zu} \\ &\quad + \boldsymbol{\beta}'\mathbf{X}'\boldsymbol{\Sigma}^{-1}\mathbf{X}\boldsymbol{\beta} + 2\boldsymbol{\beta}'\mathbf{X}'\boldsymbol{\Sigma}^{-1}\mathbf{Zu} \\ &\quad + \mathbf{u}'\mathbf{Z}'\boldsymbol{\Sigma}^{-1}\mathbf{Zu} + \mathbf{u}'\mathbf{G}^{-1}\mathbf{u}.\end{aligned}$$

The derivatives regarding $\boldsymbol{\beta}$ and $\mathbf{u}$ are:

$$\begin{bmatrix} \dfrac{\partial \ell}{\partial \boldsymbol{\beta}} \\ \dfrac{\partial \ell}{\partial \mathbf{u}} \end{bmatrix} = \begin{bmatrix} \mathbf{X}'\boldsymbol{\Sigma}^{-1}\mathbf{y} - \mathbf{X}'\boldsymbol{\Sigma}^{-1}\mathbf{X}\hat{\boldsymbol{\beta}} - \mathbf{X}'\boldsymbol{\Sigma}^{-1}\mathbf{Z}\hat{\mathbf{u}} \\ \mathbf{Z}'\boldsymbol{\Sigma}^{-1}\mathbf{y} - \mathbf{Z}'\boldsymbol{\Sigma}^{-1}\mathbf{X}\hat{\boldsymbol{\beta}} - \mathbf{Z}'\boldsymbol{\Sigma}^{-1}\mathbf{Z}\hat{\mathbf{u}} - \mathbf{G}^{-1}\hat{\mathbf{u}} \end{bmatrix}.$$

Equating them to zero gives the following system:

$$\begin{bmatrix} \mathbf{X}'\boldsymbol{\Sigma}^{-1}\mathbf{X}\hat{\boldsymbol{\beta}} + \mathbf{X}'\boldsymbol{\Sigma}^{-1}\mathbf{Z}\hat{\mathbf{u}} \\ \mathbf{Z}'\boldsymbol{\Sigma}^{-1}\mathbf{X}\hat{\boldsymbol{\beta}} + \mathbf{Z}'\boldsymbol{\Sigma}^{-1}\mathbf{Z}\hat{\mathbf{u}} + \mathbf{G}^{-1}\hat{\mathbf{u}} \end{bmatrix} = \begin{bmatrix} \mathbf{X}'\boldsymbol{\Sigma}^{-1}\mathbf{y} \\ \mathbf{Z}'\boldsymbol{\Sigma}^{-1}\mathbf{y} \end{bmatrix},$$

which can be expressed as:

$$\begin{bmatrix} \mathbf{X}'\boldsymbol{\Sigma}^{-1}\mathbf{X} & \mathbf{X}'\boldsymbol{\Sigma}^{-1}\mathbf{Z} \\ \mathbf{Z}'\boldsymbol{\Sigma}^{-1}\mathbf{X} & \mathbf{Z}'\boldsymbol{\Sigma}^{-1}\mathbf{Z} + \mathbf{G}^{-1} \end{bmatrix} \begin{bmatrix} \hat{\boldsymbol{\beta}} \\ \hat{\mathbf{u}} \end{bmatrix} = \begin{bmatrix} \mathbf{X}'\boldsymbol{\Sigma}^{-1}\mathbf{y} \\ \mathbf{Z}'\boldsymbol{\Sigma}^{-1}\mathbf{y} \end{bmatrix},$$

known as the mixed model equations (MME).

Using the second part of the MME,

$$\mathbf{Z}'\boldsymbol{\Sigma}^{-1}\mathbf{X}\hat{\boldsymbol{\beta}} + (\mathbf{Z}'\boldsymbol{\Sigma}^{-1}\mathbf{Z} + \mathbf{G}^{-1})\hat{\mathbf{u}} = \mathbf{Z}'\boldsymbol{\Sigma}^{-1}\mathbf{y},$$

such that

$$\hat{\mathbf{u}} = (\mathbf{Z}'\boldsymbol{\Sigma}^{-1}\mathbf{Z} + \mathbf{G}^{-1})^{-1}\mathbf{Z}'\boldsymbol{\Sigma}^{-1}(\mathbf{y} - \mathbf{X}\hat{\boldsymbol{\beta}}).$$

It can be shown that this expression is equivalent to $\hat{\mathbf{u}} = \mathbf{GZ}'(\mathbf{ZGZ}' + \boldsymbol{\Sigma})^{-1}(\mathbf{y} - \mathbf{X}\hat{\boldsymbol{\beta}})$ and, more importantly, that $\hat{\mathbf{u}}$ is the best linear unbiased predictor (BLUP) of $\mathbf{u}$. Using this result into the first part of the MME,

$$\begin{aligned}&\mathbf{X}'\boldsymbol{\Sigma}^{-1}\mathbf{X}\hat{\boldsymbol{\beta}} + \mathbf{X}'\boldsymbol{\Sigma}^{-1}\mathbf{Z}\hat{\mathbf{u}} = \mathbf{X}'\boldsymbol{\Sigma}^{-1}\mathbf{y} \\ &\mathbf{X}'\boldsymbol{\Sigma}^{-1}\mathbf{X}\hat{\boldsymbol{\beta}} + \mathbf{X}'\boldsymbol{\Sigma}^{-1}\mathbf{Z}(\mathbf{Z}'\boldsymbol{\Sigma}^{-1}\mathbf{Z} + \mathbf{G}^{-1})^{-1} \\ &\qquad \mathbf{Z}'\boldsymbol{\Sigma}^{-1}(\mathbf{y} - \mathbf{X}\hat{\boldsymbol{\beta}}) = \mathbf{X}'\boldsymbol{\Sigma}^{-1}\mathbf{y}\end{aligned}$$

$$\begin{aligned}\hat{\boldsymbol{\beta}} = &\{\mathbf{X}'[\boldsymbol{\Sigma}^{-1} - \boldsymbol{\Sigma}^{-1}\mathbf{Z}(\mathbf{Z}'\boldsymbol{\Sigma}^{-1}\mathbf{Z} + \mathbf{G}^{-1})^{-1}\mathbf{Z}'\boldsymbol{\Sigma}^{-1}]\mathbf{X}\}^{-1} \\ &\mathbf{X}'[\boldsymbol{\Sigma}^{-1} - \boldsymbol{\Sigma}^{-1}\mathbf{Z}(\mathbf{Z}'\boldsymbol{\Sigma}^{-1}\mathbf{Z} + \mathbf{G}^{-1})^{-1}\mathbf{Z}'\boldsymbol{\Sigma}^{-1}]\mathbf{y}\end{aligned}.$$

Similarly, it is shown that this expression is equivalent to $\hat{\boldsymbol{\beta}} = (\mathbf{X}'\mathbf{V}^{-1}\mathbf{X})^{-1}\mathbf{X}'\mathbf{V}^{-1}\mathbf{y}$, which is the best linear unbiased estimator (BLUE) of $\boldsymbol{\beta}$.

It is important to note that $\hat{\boldsymbol{\beta}}$ and $\hat{\mathbf{u}}$ require knowledge of $\mathbf{G}$ and $\boldsymbol{\Sigma}$, or at least some function of them. As these matrices are rarely known, the practical approach is to replace $\mathbf{G}$ and $\boldsymbol{\Sigma}$ by some sort of point estimates $\hat{\mathbf{G}}$ and $\hat{\boldsymbol{\Sigma}}$ into the MME.

Many methods have been proposed to estimate variance components in mixed-effects models. The simplest is the analysis of variance (ANOVA) method, which works well for simple models (such as a one-way structure) or balanced data (such as data from designed experiments with no missing data), but they are not indicated for more complex models and data structures such as those generally found in the animal breeding context.

Alternative methods proposed for estimating variance components in more complex scenarios include

the expected mean squares approach of Henderson [19] and the minimum norm quadratic unbiased estimation [20]. However, maximum likelihood-based methods are currently the most popular (see, for example, [21]), especially the restricted (or residual) maximum likelihood (REML) approach [22], which attempts to correct for the well-known bias in the classical maximum likelihood (ML) estimation of variance components. Additional literature on variance component estimation and mixed model methodology can be found, for example, in [23–27].

The Animal Model

The advent of mixed-effects models has undoubtedly revolutionized the animal breeding field, and today they are widely used in the genetic improvement of many livestock and companion animal species. In this subsection some of the applications of mixed models for the genetic evaluation of populations using phenotypic and pedigree information will be presented. In the following section applications incorporating molecular marker information will be discussed as well.

As a first application of mixed models in animal breeding, the so-called "animal model" is considered here for the specific situation of a single trait and a single phenotypic observation (including missing values) per animal. The animal model can be described as:

$$\mathbf{y} = \mathbf{X}\boldsymbol{\beta} + \mathbf{Z}\mathbf{a} + \boldsymbol{\varepsilon},$$

where $\mathbf{y}$ is an $(n \times 1)$ vector of observations (phenotypic scores), $\boldsymbol{\beta}$ is a $(p \times 1)$ vector of fixed effects (e.g., herd-year-season effects in cattle evaluations), and $\boldsymbol{\varepsilon}$ represents residual effects, assumed $\boldsymbol{\varepsilon} \sim N(\mathbf{0}, \boldsymbol{\Sigma})$ as before. In most applications of animal models, however, residuals are assumed independent across animals, such that the residual covariance structure can be expressed as $\mathbf{R} = \mathbf{I}\sigma^2_{\boldsymbol{\varepsilon}}$, where $\mathbf{I}$ is an identity matrix of appropriate order, and $\sigma^2_{\boldsymbol{\varepsilon}}$ is the residual variance. In the case of animal models, the random effects $\mathbf{u}$ represent the breeding values, i.e., $\mathbf{u} = \mathbf{a}$, assumed to be $\mathbf{a} \sim N(\mathbf{0}, \mathbf{G})$. The vector $\mathbf{a}$, of dimension $(q \times 1)$, may include breeding values of all animals with record or in the pedigree file, such that q is generally bigger than n.

The matrix $\mathbf{G}$, which in this case describes the covariances among the breeding values, follows from standard results for the covariances between relatives. It is seen that the additive genetic covariance between two relatives i and i' is given by $2\theta_{ii'}\sigma^2_a$, where $\theta_{ii'}$ is the coefficient of coancestry between individuals i and i', and σ^2_a is the additive genetic variance in the base population [28]. Hence, under the animal model, $\mathbf{G} = \mathbf{A}\sigma^2_a$, where $\mathbf{A}$ is the "additive genetic (or numerator) relationship matrix," having elements given by $a_{ii'} = 2\theta_{ii'}$.

As mentioned earlier, in animal breeding the usual main interest is prediction of breeding values – for selection of superior individuals – and on estimation of variance components. The fixed effects are, in some sense, nuisance factors with no central interest in terms of inferences, but which need to be taken into account (i.e., they need to be corrected for when inferring breeding values).

Because under the animal model $\mathbf{G}^{-1} = \mathbf{A}^{-1}\sigma^{-2}_a$ and $\mathbf{R}^{-1} = \mathbf{I}\sigma^{-2}_{\boldsymbol{\varepsilon}}$, the mixed model equations reduce to:

$$\begin{bmatrix} \mathbf{X}'\mathbf{X} & \mathbf{X}'\mathbf{Z} \\ \mathbf{Z}'\mathbf{X} & \mathbf{Z}'\mathbf{Z} + \lambda\mathbf{A}^{-1} \end{bmatrix} \begin{bmatrix} \hat{\boldsymbol{\beta}} \\ \hat{\mathbf{a}} \end{bmatrix} = \begin{bmatrix} \mathbf{X}'\mathbf{y} \\ \mathbf{Z}'\mathbf{y} \end{bmatrix},$$

where $\lambda = \dfrac{\sigma^2_{\boldsymbol{\varepsilon}}}{\sigma^2_a} = \dfrac{1-h^2}{h^2}$, such that:

$$\begin{bmatrix} \hat{\boldsymbol{\beta}} \\ \hat{\mathbf{a}} \end{bmatrix} = \begin{bmatrix} \mathbf{X}'\mathbf{X} & \mathbf{X}'\mathbf{Z} \\ \mathbf{Z}'\mathbf{X} & \mathbf{Z}'\mathbf{Z} + \lambda\mathbf{A}^{-1} \end{bmatrix}^{-1} \begin{bmatrix} \mathbf{X}'\mathbf{y} \\ \mathbf{Z}'\mathbf{y} \end{bmatrix}.$$

It is worth mentioning that $\mathbf{A}^{-1}$ can be obtained directly from the pedigree, without setting up $\mathbf{A}$ [29, 30], which is computationally very convenient.

Conditional on the variance components ratio λ, the BLUP of the breeding values are given then by $\hat{\mathbf{a}} = (\mathbf{Z}'\mathbf{Z} + \lambda\mathbf{A}^{-1})^{-1}\mathbf{Z}'(\mathbf{y} - \mathbf{X}\hat{\boldsymbol{\beta}})$, which are the estimated breeding values (EBV). Alternatively, some breeders' associations express their results as predicted transmitting abilities (PTA) or expected progeny differences (EPD), which are equal to half the EBV, representing the portion of an animal's breeding values that is passed to its offspring.

The amount of information contained in an animal's genetic evaluation depends on the availability of its own record, and of phenotypic information from its relatives (including how many and how closely related to it). As a measure of amount of information in livestock genetic evaluations, EBV are typically reported with their associated accuracies, i.e. the correlation between true and estimated breeding values, $r_i = r_{\hat{a}_i, a_i}$. Instead of accuracy, some livestock species

genetic evaluations use reliability, which is the accuracy squared (r_i^2).

The calculation of r_i requires the diagonal elements of the inverse of the MME coefficient matrix, represented as:

$$\mathbf{C} = \begin{bmatrix} \mathbf{X}'\mathbf{X} & \mathbf{X}'\mathbf{Z} \\ \mathbf{Z}'\mathbf{X} & \mathbf{Z}'\mathbf{Z} + \lambda\mathbf{A}^{-1} \end{bmatrix}^{-1} = \begin{bmatrix} \mathbf{C}^{\boldsymbol{\beta}\boldsymbol{\beta}} & \mathbf{C}^{\boldsymbol{\beta}a} \\ \mathbf{C}^{a\boldsymbol{\beta}} & \mathbf{C}^{aa} \end{bmatrix}.$$

It is shown that the prediction error variance (PEV) of EBV $\hat{a}_i$ is given by:

$$\mathrm{PEV} = \mathrm{Var}(\hat{a}_i - a_i) = c_i^{aa}\sigma_\varepsilon^2,$$

where c_i^{aa} is the ith diagonal element of $\mathbf{C}^{aa}$, relative to animal i. The PEV can be interpreted as the fraction of additive genetic variance not accounted for by the prediction. Therefore, PEV can also be expressed as:

$$\mathrm{PEV} = (1 - r_i^2)\sigma_a^2,$$

such that $c_i^{aa}\sigma_\varepsilon^2 = (1 - r_i^2)\sigma_a^2$, from which the reliability is obtained as $r_i^2 = 1 - c_i^{aa}\sigma_\varepsilon^2/\sigma_a^2 = 1 - \lambda c_i^{aa}$.

Extensions and Variations of the Animal Model

The animal model discussed above can be extended also to multiple (correlated) traits [31, 32]. For instance, consider as an example the analysis of k traits, in which the model for each trait is expressed as:

$$\mathbf{y}_j = \mathbf{X}_j\boldsymbol{\beta}_j + \mathbf{Z}_j\mathbf{a}_j + \boldsymbol{\varepsilon}_j,$$

where $\mathbf{y}_j$, $\mathbf{X}_j$, $\boldsymbol{\beta}_j$, $\mathbf{Z}_j$, $\mathbf{a}_j$, and $\boldsymbol{\varepsilon}_j$ are defined as before, but here have an additional index to indicate the trait ($j = 1, 2, \ldots, k$).

For a joint analysis of the k traits, the single trait models can be combined as:

$$\mathbf{y} = \mathbf{X}\boldsymbol{\beta} + \mathbf{Z}\mathbf{a} + \boldsymbol{\varepsilon},$$

where $\mathbf{y} = [\mathbf{y}_1{}' \;\; \mathbf{y}_2{}' \;\; \ldots \;\; \mathbf{y}_k{}']'$, $\boldsymbol{\beta} = [\boldsymbol{\beta}_1{}' \;\; \boldsymbol{\beta}_2{}' \;\; \ldots \;\; \boldsymbol{\beta}_k{}']'$, $\mathbf{a} = [\mathbf{a}_1{}' \;\; \mathbf{a}_2{}' \;\; \ldots \;\; \mathbf{a}_k{}']'$, and $\boldsymbol{\varepsilon} = [\boldsymbol{\varepsilon}_1{}' \;\; \boldsymbol{\varepsilon}_2{}' \;\; \ldots \;\; \boldsymbol{\varepsilon}_k{}']'$, and the design matrices in this case are:

$$\mathbf{X} = \begin{bmatrix} \mathbf{X}_1 & \mathbf{0} & \cdots & \mathbf{0} \\ \mathbf{0} & \mathbf{X}_2 & \cdots & \mathbf{0} \\ \vdots & \vdots & \ddots & \vdots \\ \mathbf{0} & \mathbf{0} & \cdots & \mathbf{X}_k \end{bmatrix} \text{ and } \mathbf{Z} = \begin{bmatrix} \mathbf{Z}_1 & \mathbf{0} & \cdots & \mathbf{0} \\ \mathbf{0} & \mathbf{Z}_2 & \cdots & \mathbf{0} \\ \vdots & \vdots & \ddots & \vdots \\ \mathbf{0} & \mathbf{0} & \cdots & \mathbf{Z}_k \end{bmatrix}.$$

It is assumed that $\mathrm{Var}\begin{bmatrix} \mathbf{a} \\ \boldsymbol{\varepsilon} \end{bmatrix} = \begin{bmatrix} \mathbf{G} \otimes \mathbf{A} & \mathbf{0} \\ \mathbf{0} & \boldsymbol{\Sigma} \otimes \mathbf{I} \end{bmatrix}$, where $\mathbf{G} = \begin{bmatrix} \sigma_{a_1}^2 & \sigma_{a_1a_2} & \cdots & \sigma_{a_1a_k} \\ \sigma_{a_1a_2} & \sigma_{a_2}^2 & \cdots & \sigma_{a_2a_2} \\ \vdots & \vdots & \ddots & \vdots \\ \sigma_{a_1a_k} & \sigma_{a_2a_k} & \cdots & \sigma_{a_k}^2 \end{bmatrix}$ and $\boldsymbol{\Sigma} = \begin{bmatrix} \sigma_{\boldsymbol{\varepsilon}_1}^2 & \sigma_{\boldsymbol{\varepsilon}_1\boldsymbol{\varepsilon}_2} & \cdots & \sigma_{\boldsymbol{\varepsilon}_1\boldsymbol{\varepsilon}_k} \\ \sigma_{\boldsymbol{\varepsilon}_1\boldsymbol{\varepsilon}_2} & \sigma_{\boldsymbol{\varepsilon}_2}^2 & \cdots & \sigma_{\boldsymbol{\varepsilon}_2\boldsymbol{\varepsilon}_2} \\ \vdots & \vdots & \ddots & \vdots \\ \sigma_{\boldsymbol{\varepsilon}_1\boldsymbol{\varepsilon}_k} & \sigma_{\boldsymbol{\varepsilon}_2\boldsymbol{\varepsilon}_2} & \cdots & \sigma_{\boldsymbol{\varepsilon}_k}^2 \end{bmatrix}$ are the genetic and residual variance–covariance matrices, respectively, $\mathbf{A}$ and $\mathbf{I}$ are the numerator relationship matrix and an identity matrix, and $\otimes$ represents the direct (Kronecker) product.

The MME for multi-trait analyses are of the same form as before, i.e.,

$$\begin{bmatrix} \mathbf{X}'(\boldsymbol{\Sigma}^{-1} \otimes \mathbf{I})\mathbf{X} & \mathbf{X}'(\boldsymbol{\Sigma}^{-1} \otimes \mathbf{I})\mathbf{Z} \\ \mathbf{Z}'(\boldsymbol{\Sigma}^{-1} \otimes \mathbf{I})\mathbf{X} & \mathbf{Z}'(\boldsymbol{\Sigma}^{-1} \otimes \mathbf{I})\mathbf{Z} + \mathbf{G}^{-1} \otimes \mathbf{A}^{-1} \end{bmatrix} \begin{bmatrix} \hat{\boldsymbol{\beta}} \\ \hat{\mathbf{a}} \end{bmatrix} = \begin{bmatrix} \mathbf{X}'(\boldsymbol{\Sigma}^{-1} \otimes \mathbf{I})\mathbf{y} \\ \mathbf{Z}'(\boldsymbol{\Sigma}^{-1} \otimes \mathbf{I})\mathbf{y} \end{bmatrix},$$

from which the BLUEs and BLUPs of $\boldsymbol{\beta}$ and $\mathbf{a}$ can be obtained, respectively.

The dimensionality of such multi-trait MME, however, can become a hurdle for solving it when more than two or three traits are considered. An alternative for the analysis of multiple traits is to use a canonical transformation of the traits [33–35], which consists of transforming the vectors of correlated traits into a new vector of uncorrelated variables. In such case, each transformed variable can be analyzed independently using standard single trait models, and subsequently the estimated breeding values are transformed back to the original scale of measurement.

Some other interesting applications of mixed models in animal breeding involve multiple random effects, as in the cases of repeated measurements of the same trait or traits with maternal effects. For the analysis of repeated measurements, as discussed in section "Selection Index" (Model 4), environmental effects can be partitioned into permanent and temporary effects. In this case, the mixed model, usually called "repeatability model," can be written as:

$$\mathbf{y} = \mathbf{X}\boldsymbol{\beta} + \mathbf{Z}\mathbf{a} + \mathbf{W}\mathbf{p} + \boldsymbol{\varepsilon},$$

where all terms are as previously defined for a single trait animal model, and $\mathbf{p}$ is the vector of permanent

environmental effects, with each level pertaining to a common effect to all observations of each animal, and **W** is a known incidence matrix relating **y** to the vector **p**.

It is often assumed that $\mathbf{a} \sim N(\mathbf{0}, \mathbf{A}\sigma_a^2)$, $\mathbf{p} \sim N(\mathbf{0}, \mathbf{I}\sigma_p^2)$, and $\boldsymbol{\varepsilon} \sim N(\mathbf{0}, \mathbf{I}\sigma_{\boldsymbol{\varepsilon}}^2)$ are independent from each other. Under these assumptions, the MME becomes:

$$\begin{bmatrix} \mathbf{X'X} & \mathbf{X'Z} & \mathbf{X'W} \\ \mathbf{Z'X} & \mathbf{Z'Z}+\lambda_a\mathbf{A}^{-1} & \mathbf{Z'W} \\ \mathbf{W'X} & \mathbf{W'Z} & \mathbf{W'W}+\lambda_p\mathbf{I} \end{bmatrix} \begin{bmatrix} \hat{\boldsymbol{\beta}} \\ \hat{\mathbf{a}} \\ \hat{\mathbf{p}} \end{bmatrix} = \begin{bmatrix} \mathbf{X'y} \\ \mathbf{Z'y} \\ \mathbf{W'y} \end{bmatrix},$$

where $\lambda_a = \sigma_{\boldsymbol{\varepsilon}}^2/\sigma_a^2$ and $\lambda_p = \sigma_{\boldsymbol{\varepsilon}}^2/\sigma_p^2$.

There are some traits of interest in livestock, such as weaning weight in beef cattle, in which progeny performance is affected by the dam's ability to affect the calf's environment, such as in the form of nourishment through her milk production, the quantity and quality of which is in part genetically determined. In some cases, there can also be a paternally provided environmental component. In such cases, parents contribute to the performance of their progeny not only through the genes passed to the progeny (the "direct genetic effects") but also through their ability to provide a suitable environment (the "indirect genetic effects").

Here maternally influenced traits are considered, for which the mixed model can be written as [36]:

$$\mathbf{y} = \mathbf{X}\boldsymbol{\beta} + \mathbf{Za} + \mathbf{Km} + \mathbf{Wp} + \boldsymbol{\varepsilon},$$

where all terms are as before, except that the model now includes a vector **m** of random maternal genetic effects, and a vector **p** of random permanent environmental effects, with **K** and **W** as their respective incidence matrices. It is assumed that $\mathbf{a} \sim N(\mathbf{0}, \mathbf{A}\sigma_a^2)$, $\mathbf{m} \sim N(\mathbf{0}, \mathbf{A}\boldsymbol{\sigma}_{\boldsymbol{m}}^{\boldsymbol{2}})$, $\mathbf{p} \sim N(\mathbf{0}, \mathbf{I}\sigma_p^2)$, and $\boldsymbol{\varepsilon} \sim N(\mathbf{0}, \mathbf{I}\sigma_\varepsilon^2)$, and quite often a covariance structure between direct and maternal additive genetic effects is considered, assumed equal to $\mathbf{A}\sigma_{a,m}$.

Some other variations of the animal model, which are computationally convenient, include the "sire model" and the "reduced animal model" [37]. In the sire models, only sires are evaluated, using progeny records under the assumption of randomly selected mates. In the reduced animal model, instead of having equations set up for every animal (i.e., parents and progeny), it allows equations to be set up only for parents in the MME, making the dimensions of the system greatly reduced. The breeding values of the parents are estimated directly from the MME, and the progeny breeding values are then inferred by back solving from the predicted parental breeding values.

As a final note regarding the use of mixed models in animal breeding, it is important to mention that solving the MME does not necessary require the inversion of the coefficient matrix **C**. More computationally convenient alternatives for solving high dimensional systems of linear equations include methods based on iteration on the MME, such as the Jacobi or Gauss–Seidel iteration [38], and the "iteration on the data" strategy [39], which is a commonly used methodology in national genetic evaluations involving millions of records.

Marker-Assisted Selection

Introduction

The advent of molecular markers has created opportunities for a better understanding of genetic inheritance and for developing novel strategies for genetic improvement in agriculture. Molecular markers are used, for example, to study quantitative trait loci (QTL), which are defined as chromosomic regions contributing to variation in phenotypic traits. The location and effects of QTL can be inferred by combining information from marker genotypes and phenotypic scores of individuals and by exploring genetic linkage [40–43] and linkage disequilibrium [44, 45] information between marker loci and QTL, such as in experimental or mapping populations (e.g., backcross or F_2, or granddaughter designs) or in complex pedigrees in outbred populations. Information on markers associated with QTL can be used to enhance prediction of genetic merit of animals [46]. This is especially useful for low heritability traits, traits that are expensive or difficult to measure, or traits expressed in only one sex [47].

Classical Approaches with Few Markers

The application of molecular information for genetic improvement of animals and plants, or marker-assisted selection (MAS), requires that candidate-for-selection individuals are genotyped for specific markers. For MAS purposes, there are three types of genetic markers, and for each type there are specific statistical

approaches for incorporating their information into selection programs [47]. A first type of marker refers to situations in which the functional polymorphism itself can be genotyped. These markers are called "direct markers," as they indicate exactly the genotype an animal has at specific causative loci.

A second type of marker refers to those that are in population-wide linkage disequilibrium (LD) with the causative or functional mutations. In such cases, although the marker genotype of an animal does not unambiguously indicate the genotype at a specific functional locus, it still provide information regarding how likely an animal carries a specific allele or genotype at such a locus. Finally, a third kind of molecular marker refers to those loci that are in population linkage equilibrium with the functional mutations, which are often called "indirect markers." In such cases, although the marker information on a single animal in a population does not provide any information regarding the genetic merit of that animal, it still can be useful in exploring family (pedigree) structure when genotyped animals are related to each other.

While direct markers are the simplest and most efficient in MAS programs, their identification is much more difficult and generally involves a prescreening step using QTL mapping methods to identify promising chromosomic regions, followed by fine mapping (often using functional and positional candidate gene strategies), followed by validation (using some strategy such as a knock-out approach). On the other extreme, indirect markers are extensively available for most livestock species, but their use in MAS is more complex and the results are generally modest.

Statistical models to incorporate direct and/or LD markers in the genetic evaluations of animals are relatively straightforward. For example, a marker can be included into an animal model context with the following specification:

$$\mathbf{y} = \mathbf{X}\boldsymbol{\beta} + \mathbf{Z}\mathbf{a}^* + \mathbf{M}\mathbf{g} + \boldsymbol{\varepsilon},$$

where all terms are as defined before, except that $\mathbf{a}^* \sim N(\mathbf{0}, \mathbf{A}\sigma^2_{a^*})$ represents now the random additive (nonmarked) polygenic effects, and $\mathbf{g}$ and $\mathbf{M}$ are the (fixed) QTL effects and an incidence matrix, respectively. In the case of direct markers, the matrix $\mathbf{M}$ represents the marker genotypes and is obtained directly from the genotyping of animals. In the case of LD markers, the incidence matrix $\mathbf{M}$ will represent genotype probabilities at each QTL locus, which can be derived using segregation analysis. The overall genetic merits of the animals are then given by the sum of their $\mathbf{a}^*$ and $\mathbf{g}$ components. Other strategies for combining the infinitesimal and the QTL components to increase long-term genetic gain have also been proposed (e.g., [48–50]); a review of MAS strategies can be found, for example, in [47].

In the case of indirect markers, however, the within-family LD between QTL and linked markers must be explored. One approach is to determine the marker effects or the marker-QTL linkage phases separately for each family. Alternatively, more general MAS models have been proposed to incorporate marker data in genetic evaluations for complex pedigrees [13, 51], which can be represented as:

$$\mathbf{y} = \mathbf{X}\boldsymbol{\beta} + \mathbf{Z}\mathbf{a}^* + \mathbf{M}\mathbf{q} + \boldsymbol{\varepsilon},$$

where the terms are as before, but here the QTL effects $\mathbf{q}$ are assumed random and normally distributed, such that:

$$\begin{bmatrix} \mathbf{a}^* \\ \mathbf{q} \end{bmatrix} \sim \mathrm{N}\left(\mathbf{0}, \begin{bmatrix} \mathbf{A}\sigma^2_{a^*} & \mathbf{0} \\ \mathbf{0} & \mathbf{G}_\lambda\sigma^2_q \end{bmatrix}\right),$$

where $\mathbf{G}_\lambda$ is the gametic relationship matrix for the QTL, and σ^2_q is the additive variance of the QTL allelic effects. The gametic relationship matrix gives the probabilities of identity between each of the two alleles in each individual, and it can be derived based on the QTL position λ and the marker information.

Genomic Selection

As most quantitative traits are influenced by many genes, tracking a small number of them using molecular markers (as in the MAS approaches discussed above) will explain only a small fraction of the total genetic variance. Moreover, individual genes are likely to have small effects and so a large amount of data is needed to accurately estimate their effects [52]. Genome-wide Marker-Assisted Selection (GWMAS), or simply Genomic Selection (GS), on the other hand, makes use of a very dense set of markers covering the entire genome, which potentially explain all genetic variance. In addition, given the LD between the dense markers and the QTL, estimated marker effects pertain across the population [53].

Meuwissen et al. [54] were the first to propose GS and suggested a model that can be described as:

$$\mathbf{y} = \mathbf{1}\mu + \sum_{j=1}^{p} \mathbf{M}_j \mathbf{q}_j + \boldsymbol{\varepsilon},$$

where μ is the overall mean, $\mathbf{q}_j$ represents the genetic effects of marked genes (j=1, 2, . . ., p), and $\mathbf{M}_j$ represents the design matrices (genotypes) relative to a large number (p) of biallelic markers (e.g., SNP loci), which present different levels of LD with QTL affecting the phenotypic trait of interest ($\mathbf{y}$). Here it is assumed that the QTL affecting the trait act additively, and that $\mathbf{q}_j$ refers to per-allele effects; nonadditive effects as well as effects relative to nonmarked QTL are lumped together into the residual term of the model.

Fitting such GS model using standard regression approaches is not trivial, as the number p of markers (and so the number of genetic effects to be estimated) may easily exceed the number n of individuals available. The "large p small n paradigm" is central in many applications of genomic technologies, including expression profiling and association analysis, and various statistical strategies have been proposed in the literature to overcome this problem, such as dimension-reduction techniques, stepwise fitting procedures, ridge regression [55], and least absolute selection and shrinkage operator – LASSO [56].

Specifically in GS, hierarchical modeling has become the methodology of choice, due to its flexibility and good statistical properties. Within this approach, the genetic effects $\mathbf{q}_j$ are assumed random effects and distributed according to some prespecified distribution [54]. For example, $\mathbf{q}_j$ may be assumed normally distributed with mean 0 and variance σ_j^2, and the hierarchy can be extended by assuming a prior distribution for the variances σ_j^2 [54, 57–59]. Alternative distributions can be adopted for the $\mathbf{q}_j$, such as double exponential or mixture distributions including a mass point at zero. It is interesting to note the connection between the ridge regression approach and a Bayesian model with normal priors with common variances $\sigma_j^2 = \sigma_0^2$, as well as the LASSO methodology and a Bayesian model with double exponential priors for the genetic effects [60].

The potential of GS to accelerate genetic progress has been demonstrated through many simulation studies (e.g., [54, 61, 62]), and confirmed by some real data applications. The first use of GS using thousands of markers in livestock has been in dairy cattle [63, 64], followed by some breeds of beef cattle and more recently in poultry. Table 1 shows some encouraging results on dairy cattle obtained by the USDA.

Future Directions

As shown here, the mixed model methodology is extremely flexible and can be used in a wide variety of applications. Other extensions of the methods discussed here include models with nonadditive genetic effects (e.g., [65, 66]), mixed models for the analysis of non-Gaussian traits such as binary and categorical (e.g., [67, 68]) or counting data (e.g., [69]), robust models [70, 71], survival traits [72], nonlinear models to study, for example, growth curves (e.g., [73, 74]), among others. However, such models can get extremely complex and asymptotic statistical methods are generally required. Alternatively, Bayesian analysis employing Markov Chain Monte Carlo (MCMC) methods can be used, given their exceptional flexibility and the possibility of incorporating prior information regarding the model parameters [75].

Animal Breeding, Foundations of. Table 1 Comparison of April 2010 genomic and traditional evaluations for bulls with an AI status of active or foreign

Trait	Average reliability (%)		
	Genomic	Traditional	Difference
Net merit	87	81	+6
Milk yield	93	91	+2
Fat yield	93	91	+2
Protein yield	93	91	+2
Productive life	81	71	+9
Somatic cell score	88	83	+5
Daughter pregnancy rate	79	69	+10
Final score	89	85	+4
Sire calving ease	90	84	+6
Daughter calving ease	80	67	+13

Source: AIPL – USDA; http://www.aipl.arsusda.gov/

Bayesian analysis has been increasingly used in many applications of genetics and animal breeding, and for a review the reader can refer, for example, to [76–78]. A comprehensive treatment of Bayesian MCMC approaches in animal breeding is presented in [23].

Bayesian hierarchical modeling has also been extensively used in genomic selection [54, 79–81]. In addition, nonparametric and semiparametric methods, and machine learning techniques based on artificial intelligence have been proposed and used for the analysis of high density marker panels in the context of animal breeding, such as in [82–86]. Moreover, some other recent methods aim to combine all available phenotypic, pedigree, and genomic information for prediction of genetic merit of animals [87].

As indicated in the beginning of this chapter, the genetic improvement observed in many livestock and companion animal species is truly remarkable. Most of this genetic progress has been accomplished through selection, using the methods discussed here. Two technological and methodological developments however must be mentioned as turning points in the genetic trends observed in some species; these are the advent of artificial insemination and the mixed models. Seemingly, the development of high density SNP panels and, more recently, next generation sequencing technologies and their application in genomic selection strategies promise to be the next turning point. This new era for animal breeding and genetics will require a different profile of animal breeders, requiring not only knowledge of population and quantitative genetics, classical statistical and computational methods, but also some more modern statistical and computational methods based on hierarchical modeling [23, 88], non- and semiparametric methods, and machine learning techniques [60, 89]. It is indeed a very exciting time to work in animal breeding!

Bibliography

Primary Literature

1. Lush JL (1994) The genetics of populations. (Prepared for publication by Chapman AB, Shrode RR, with an addendum by Crow JF) Special report 94, College of Agriculture, Iowa State University, Ames
2. Bulmer MG (1985) The mathematical theory of quantitative genetics. Clarendon, Oxford
3. Falconer DS, Mackay TFC (1996) Introduction to quantitative genetics, 4th edn. Longmans Green, Harlow
4. Lynch M, Walsh B (1998) Genetic analysis of quantitative traits. Sinauer Associates, Sunderland
5. Hill WG (1969) On the theory of artificial selection in finite populations. Genet Res 13:143–163
6. Havenstein B, Ferket PR, Qureshi MA (2003) Growth, livability, and feed conversion of 1957 versus 2001 broilers when fed representative 1957 and 2001 broiler diets. Poult Sci 82:1509–1518
7. Bourdon RM (2000) Understanding animal breeding, 2nd edn. Prentice Hall, Upper Saddle River
8. Crow J, Kimura M (1970) An introduction to populations genetics theory. Haraper and Row, New York
9. Shook GE (2006) Major advances in determining appropriate selection goals. J Dairy Sci 89(4):1349–1361
10. Henderson CR (1949) Estimation of changes in herd environment. J Dairy Sci 32:709
11. Henderson CR (1975) Best linear unbiased estimation and prediction under a selection model. Biometrics 31:423–447
12. Henderson CR (1984) Applications of linear models in animal breeding. University of Guelph, Guelph
13. Fernando RL, Grossman M (1989) Marker-assisted selection using best linear unbiased prediction. Genet Sel Evol 21:467–477
14. Yu J et al (2006) A unified mixed-model method for association mapping that accounts for multiple levels of relatedness. Nat Genet 38:203–208
15. Wolfinger RD, Gibson G, Wolfinger ED, Bennett L, Hamadeh H, Bushel P, Afshari C, Paules RS (2001) Assessing gene significance from cDNA microarray expression data via mixed models. J Comput Biol 8:625–637
16. Rosa GJM, Steibel JP, Tempelman RJ (2005) Reassessing design and analysis of two-color microarray experiments using mixed effects models. Comp Funct Genomics 6:123–131
17. Steibel JP, Poletto R, Coussens PM, Rosa GJM (2009) A powerful and flexible linear mixed model framework for the analysis of relative quantification RT-PCR data. Genomics 94:146–152
18. Henderson CR (1950) Estimation of genetic parameters. Ann Math Stat 21:309
19. Henderson CR (1953) Estimation of variance and covariance components. Biometrics 9:226
20. Rao CR (1971) Estimation of variance and covariance components MINQUE theory. J Multivar Anal 1:257–275
21. Harville DA (1977) Maximum likelihood approaches to variance component estimation and to related problems. J Am Stat Assoc 72(358):320–338
22. Patterson HD, Thompson R (1971) Recovery of inter-block information when block sizes are unequal. Biometrika 58(3):545–554
23. Sorensen D, Gianola D (2002) Likelihood, Bayesian, and MCMC methods in quantitative genetics. Springer, New York
24. Littell RC, Miliken GA, Stroup WW, Wolfinger RD (2006) SAS system for mixed models, 2nd edn. SAS Institute, Cary

25. Pinheiro JC, Bates DM (2000) Mixed-effects models in S and S-Plus. Springer, New York
26. Searle SR, Casella G, McCulloch CE (1992) Variance components. Wiley, New York
27. Verbeke G, Molenberghs G (1997) Linear mixed models in practice: A SAS-oriented approach, Lecture Notes in Statistics 126. Springer, New York
28. Wright S (1921) Systems of mating I. The biometric relations between parents and offspring. Genetics 6:111–123
29. Henderson CR (1976) A simple method for computing the inverse of a numerator relationship matrix used in prediction of breeding values. Biometrics 32:69–83
30. Quaas RL (1976) Computing the diagonal elements of a large numerator relationship matrix. Biometrics 32:949–953
31. Henderson CR, Quaas RL (1976) Multiple trait evaluation using relatives' records. J Anim Sci 43:1188–1197
32. Schaeffer LR (1984) Sire and cow evaluation under multiple trait models. J Dairy Sci 67:1567–1580
33. Thompson R (1977) Estimation of quantitative genetic parameters. In: Pollak E, Kempthorne O, Bailey TB (eds) Proceedings of the international conference on quantitative genetics, Iowa State University Press, Ames, pp. 639–657
34. Meyer K (1985) Maximum-likelihood estimation of variance-components for a multivariate mixed model with equal design matrices. Biometrics 41:153
35. Ducrocq V, Besbes B (1993) Solution of multiple trait animal models with missing data on some traits. J Anim Breed Genet 110:81–92
36. Quaas RL, Pollak EJ (1981) Modified equations for sire models with groups. J Dairy Sci 64:1868–1872
37. Quaas RL, Pollak EJ (1980) Mixed model methodology for farm and ranch beef cattle testing programs. J Anim Sci 51:1277–1287
38. Misztal I, Gianola D (1988) Indirect solution of mixed model equations. J Dairy Sci 77(Suppl 2):99–106
39. Schaeffer LR, Kennedy BW (1986) Computing solutions to mixed model equations. In: 3rd World congress on genetic applied livestock production, Lincoln, Nebraska, 16–22 July 1986, vol XII. pp 382–393
40. Lander ES, Botstein D (1989) Mapping Mendelian factors underlying quantitative traits using RFLP linkage maps. Genetics 121:185–199
41. Haley CS, Knott SA (1992) A simple regression method to for mapping quantitative trait loci in line crosses using flanking markers. Heredity 69:315–324
42. Haley CS, Knott SA, Elsen J-M (1994) Mapping quantitative trait loci in crosses between outbred lines using least squares. Genetics 136:1195–1207
43. Pérez-Enciso M, Misztal I (2004) Qxpak: a versatile mixed model application for genetical genomics and QTL analyses. Bioinformatics 20(16):2792–2798
44. Meuwissen THE, Goddard ME (2000) Fine mapping of quantitative trait loci using linkage disequilibria with closely linked marker loci. Genetics 155:421–430
45. Pérez-Enciso M (2003) Fine mapping of complex trait genes combining pedigree and linkage disequilibrium information: a Bayesian unified framework. Genetics 163:1497–1510
46. Lande R, Thompson R (1990) Efficiency of marker-assisted selection in the improvement of quantitative traits. Genetics 124:743–756
47. Dekkers JCM, Hospital F (2002) The use of molecular genetics in the improvement of agricultural populations. Nat Rev Genet 3(1):22–32
48. Dekkers JCM, van Arendonk JAM (1998) Optimizing selection for quantitative traits with information on an identified locus in outbred populations. Genet Res 71(3):257–275
49. Manfredi E, Barbieri M, Fournet F, Elsen JM (1998) A dynamic deterministic model to evaluate breeding strategies under mixed inheritance. Genet Sel Evol 30:127–148
50. Chakraborty R, Moreau L, Dekkers JCM (2002) A method to optimize selection on multiple identified quantitative trait loci. Genet Sel Evol 34(2):145–170
51. Goddard ME (1992) A mixed model for analyses of data on multiple genetic-markers. Theor Appl Genet 83:878–886
52. Goddard ME, Hayes BJ (2007) Genomic selection. J Anim Breed Gen 124(6):323–330
53. Schaeffer LR (2006) Strategy for applying genome-wide selection in dairy cattle. J Anim Breed Genet 123:218–223
54. Meuwissen THE, Hayes BJ, Goddard ME (2001) Prediction of total genetic value using genome-wide dense marker maps. Genetics 157:1819–1829
55. Whittaker JC, Thompson R, Visscher PM (2000) Marker-assisted selection using ridge regression. Genet Res 75:249–252
56. Tibshirani R (1996) Regression shrinkage and selection via the Lasso. J R Stat Soc B 58:267–288
57. Gianola D, Perez-Enciso M, Toro MA (2003) On marker-assisted prediction of genetic value: beyond the ridge. Genetics 163:347–365
58. Xu S (2003) Estimating polygenic effects using markers of the entire genome. Genetics 163(2):789–801
59. ter Braak CJF, Boer MP, Bink MCAM (2005) Extending Xu's Bayesian model for estimating polygenic effects using markers of the entire genome. Genetics 170(3):1435–1438
60. Hastie T, Tibshirani R, Friedman JH (2001) The elements of statistical learning: data mining, inference, and predictions. Springer, New York
61. Calus MPL, Veerkamp RF (2007) Accuracy of breeding values when using and ignoring the polygenic effect in genomic breeding value estimation with a marker density of one SNP per cM. J Anim Breed Genet 124:362–368
62. Muir WM (2007) Comparison of genomic and traditional BLUP-estimated breeding value accuracy and selection response under alternative trait and genomic parameters. J Anim Breed Genet 124:342–355
63. VanRaden PM, Van Tassell CP, Wiggans GR, Sonstegard TS, Schnabel RD, Taylor J, Schenkel FS (2009) Reliability of genomic predictions for North American dairy bulls. J Dairy Sci 92:16–24

64. Weigel KA, de Los Campos G, González-Recio O, Naya H, Wu XL, Long N, Long N, Rosa GJM, Gianola D (2009) Predictive ability of direct genomic values for lifetime net merit of Holstein sires using selected subsets of single nucleotide polymorphism markers. J Dairy Sci 92:5248–5257
65. Henderson CR (1985) Best linear unbiased prediction of non-additive genetic merits in non-inbred populations. J Anim Sci 60:111–117
66. Hoeschele I, VanRaden PM (1991) Rapid inverse of dominance relationship matrices for noninbred populations by including sire and dam subclass effects. J Dairy Sci 74:557–569
67. Gianola D (1982) Theory and analysis of threshold characters. J Anim Sci 54:1079–1096
68. Gianola D, Foulley JL (1983) Sire evaluation for ordered categorical-data with a threshold-model. Genet Sel Evol 15(2): 201–223
69. Tempelman RJ, Gianola D (1996) A mixed effects model for overdispersed count data in animal breeding. Biometrics 52:265–279
70. Strandén I, Gianola D (1998) Attenuating effects of preferential treatment with student-t mixed linear models: a simulation study. Genet Sel Evol 31:25–42
71. Rosa GJM, Padovani CR, Gianola D (2003) Robust linear mixed models with normal/independent distributions and Bayesian MCMC implementation. Biom J 45(5):573–590
72. Ducrocq V, Casella G (1996) A Bayesian analysis of mixed survival models. Genet Sel Evol 28(6):505–529
73. Varona L (1997) Multiple trait genetic analysis of underlying biological variables of production functions. Livest Prod Sci 47:201–209
74. Forni S, Piles M, Blasco A et al (2009) Comparison of different nonlinear functions to describe Nelore cattle growth. J Anim Sci 87(2):496–506
75. Gianola D, Fernando RL (1986) Bayesian methods in animal breeding theory. J Anim Sci 63:217–244
76. Shoemaker JS, Painter IS, Weir BS (1999) Bayesian statistics in genetics - a guide for the uninitiated. Trends Genet 15:354–358
77. Blasco A (2001) The Bayesian controversy in animal breeding. J Anim Sci 79(8):2023–2046
78. Beaumont MA, Rannala B (2004) The Bayesian revolution in genetics. Nat Rev Genet 5:251–261
79. Yi N, Xu S (2008) Bayesian Lasso for quantitative trait loci mapping. Genetics 179:1045–1055
80. Gianola D, de Los Campos G, Hill WG et al (2009) Additive genetic variability and the Bayesian alphabet. Genetics 183(1):347–363
81. de Los Campos G, Naya H, Gianola D, Crossa J, Legarra A, Manfredi E, Weigel K, Cotes J (2009) Predicting quantitative traits with regression models for dense molecular markers and pedigrees. Genetics 182:375–385
82. Gianola D, Fernando RL, Stella A (2006) Genomic-assisted prediction of genetic value with semiparametric procedures. Genetics 173:1761–1776
83. Gianola D, van Kaam JBCHM (2008) Reproducing kernel Hilbert spaces regression methods for genomic assisted prediction of quantitative traits. Genetics 178:2289–2303
84. Long N, Gianola D, Rosa GJM, Weigel KA, Avendaño S (2007) Machine learning procedure for selecting SNPs in genomic selection: application to early mortality in broilers. J Anim Breed Genet 124(6):377–389
85. González-Recio O, Gianola D, Long N, Weigel KA, Rosa GJM, Avendano S (2008) Nonparametric methods for incorporating genomic information into genetic evaluations: an application to mortality in broilers. Genetics 178(4):2305–2313
86. Campos G, Gianola D, Rosa GJM (2009) The linear model of quantitative genetics is a reproducing kernel Hilbert spaces regression. J Anim Sci 87:1883–1887
87. Misztal I, Legarra A, Aguilar I (2009) Computing procedures for genetic evaluation including phenotypic, full pedigree, and genomic information. J Dairy Sci 92:4648–4655
88. Gelman A, Carlin JB, Stern HS, Rubin DB (2004) Bayesian data analysis, 2nd edn. Chapman and Hall, London
89. Bishop CM (2006) Pattern recognition and machine learning. Springer, New York

Books and Reviews

Chapman AB (1980) General and quantitative genetics. World animal science series. Elsevier, Amsterdam
Lange K (1997) Mathematical and statistical methods for genetic analysis. Springer, New York
Liu BH (1998) Statistical genomics. CRC Press, Boca Raton
Mrode R (2005) Linear models for the prediction of animal breeding values, 2nd edn. CAB International, New York
Ott J (1991) Analysis of Human Genetic Linkage. Johns Hopkins, Baltimore
Sham PC (1998) Statistics in human genetics. Arnold, London
Van Vleck LD (1993) Selection index and introduction to mixed model methods for genetic improvement of animals. CRC Press, Boca Raton

Animal Breeding, Modeling in

Lawrence R. Schaeffer
Department of Animal and Poultry Science, Centre for Genetic Improvement of Livestock, University of Guelph, Guelph, ON, Canada

Article Outline

Glossary
Definition of the Subject
Introduction

Animal Model
Genetic Relationships
Genetic Evaluation
Single Record per Animal
Repeated Records Animal Model
Maternal Effects Animal Model
Random Regression Animal Model
Multiple Trait Models
Models for Categorical Data
Models for Survival Data
Added Complexities
Future Directions
Bibliography

Glossary

Contemporary groups A group of animals of approximately the same age living in the same environment and being treated by the same management practices during the same interval of time.

Estimated breeding value An estimate of the total additive genetic merit of an individual, the effects that are directly passed to offspring.

Genotypes The particular set of alleles at all gene loci that influence the phenotypes.

Inbreeding coefficients The proportion of alleles at gene loci that are identical due to being inherited from a common ancestor.

Infinitesimal genetic model A genetic model that assumes there are an infinite number of gene loci affecting a trait each with a small and equal effect.

Mixed model equations Proposed by Henderson in 1949 for the estimation of breeding values and other nongenetic effects from phenotypes.

Phenotypes The observable characteristics of an animal that can be measured, scored, or recorded.

Definition of the Subject

Modeling in animal breeding involves describing the major factors that influence the performance ability or production level of animals in order to predict the genetic merit of future progeny for that ability. Successful modeling depends on good record collection systems, accurate pedigree records, and sophisticated statistical models. Models have evolved over time as computer technology has advanced. Genetic evaluation of dairy bulls began in the early 1930s using simple daughter averages for milk production in selection index procedures of Lush and his students [1]. Genetic evaluation systems spread to all livestock and to many countries due to Lush. Henderson [2] introduced best linear unbiased prediction (BLUP) around 1950, and this methodology is still widely used in animal breeding except that the models are more detailed and complex. Gianola and others [3, 4] taught animal breeders how to use Bayesian methods which are especially useful for non-normally distributed data.

All methods consider the total additive genetic merit of animals. Additive genetic effects are directly transmitted to progeny, assuming infinitely many gene loci, each with a small and equal effect on the trait of interest. Examples of traits are milk yields of dairy animals, growth rates of meat-producing animals, occurrence of health problems, ability to reproduce, and behavior.

Models to analyze traits differ depending on the nature of the traits being evaluated. Traits can be broadly grouped into production traits, growth traits, reproductive traits, health traits, and survival, and the models for each group are very specialized. In the 1930s, dairy bulls were selected almost solely for the ability of their daughters to produce milk. Over time, the success of that selection pressure for one trait caused negative correlated responses in reproduction potential and disease susceptibility. Genetic evaluation systems consider many traits simultaneously with a primary focus on efficiency of economic production and cost savings.

Introduction

Modeling in animal breeding began with the expression

$$\mathbf{p} = \mathbf{g} + \mathbf{e},$$

where $\mathbf{p}$ is the phenotype of an individual, $\mathbf{g}$ is the genetic source of variation or genotype in $\mathbf{p}$, and $\mathbf{e}$ is the environmental source of variation, presented by Wilhelm Ludwig Johannsen in 1909 [5]. A phenotype is a measurement of an animal's performance for an economically important trait, such as daily milk yield of a dairy cow, goat, or sheep; a growth record on a beef animal, pig, or rabbit; or wool production of a sheep or llama. Current models are extensions of this basic equation.

Genetic Component

The **g** term of the model is partitioned as

$$\mathbf{g} = \mathbf{g}_a + \mathbf{g}_d + \mathbf{g}_i,$$

where

$\mathbf{g}_a$ are additive genetic effects, the collective effects generated by individual alleles at every loci in the genome.

$\mathbf{g}_d$ are the dominance genetic effects, the collective effects generated by combinations of alleles at every locus in the genome.

$\mathbf{g}_i$ are the many interactions among loci throughout the genome, in a collective sense.

Animal breeders are primarily concerned with additive genetic effects because those effects are passed directly from parents to progeny. Dominance and interaction genetic effects occur depending on the combinations of alleles from the paternal and maternal sides of the pedigree, and cannot be predicted prior to making a mating of specific individuals.

Further, $\mathbf{g}_a$ is assumed to be the combined effects of an infinite number of loci, each with a small and equal effect, i.e.,

$$\mathbf{g}_a = \sum_{k=1}^{\infty} g_k.$$

The population is assumed to be very large and mating randomly. This is known as the *infinitesimal genetic model* upon which genetic evaluation systems are based. This is a reasonable model if you consider that there are roughly 30,000 loci (this estimate is continually changing), and if one assumes only two alleles at each locus, then there are three possible genotypes per locus, or $3^{30,000}$ possible genotype outcomes. This number is large enough to be nearly infinite for all practical purposes. The number of possible genotype outcomes is actually much bigger if you allow that there are more than two alleles for many loci.

Environmental Component

The **e** term can be split into identifiable factors that are known to have effects on the phenotypes. Some effects are shared with other animals in the same location at the same time, and some effects are specific to individuals.

Animal Model

The common model in animal breeding is called an *animal model*, based on the underlying infinitesimal genetic model, containing factors to account for time trends, contemporary groups, additive genetic effects, residual, and other factors, that depend on the species and trait of interest. Figure 1 depicts a typical animal model in a diagrammatic format. Each individual is affected by the additive genetic merits of its sire and dam, as well as year and month of birth or calving.

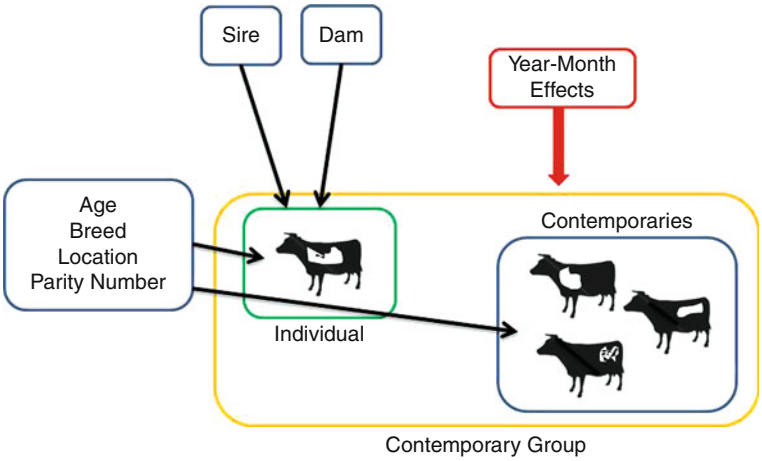

Animal Breeding, Modeling in. Figure 1
Diagram of genetic and environmental factors affecting dairy cow milk production

Contemporaries are animals that share the same year and month effects as the individual because they exist in the same space and time. These effects include weather, location, herd owner, and herd management practices of feeding, breeding, and health care. Individual production is affected by breed, age, and parity number, and these effects are common to all animals of the same breed, age, and parity number.

Depending on the species and trait, other factors could be included in the diagram.

Models in animal breeding are conveniently presented in matrix notation. Models consist of three parts which are the equation, the expectations and distributions of random variables, and finally a list of assumptions and limitations. The three parts are briefly described.

The Equation

A linear statistical model is written generally (in matrix notation) as

$$\mathbf{y} = \mathbf{Xb} + \mathbf{Zu} + \mathbf{e},$$

where

y is a vector of observations on the trait of interest from individual animals, either one or more per animal.

b is a vector of levels of factors that are known to affect the magnitude of the observations. These factors are fixed factors, in that they are constants and not random variables drawn from a particular distribution or population of effects. One factor that should always be included in an animal model is one that accounts for time, either year, or year-season. Seasons may be groups of months, individual months or weeks of the year. This time factor is meant to account for changes in average production over time due to changes in production technology, global warming, nutritional improvements, or financial impacts that affect the entire population. Other factors are effects of gender, breed, age of dam, and diet.

u is a vector of levels of random factors, which are random samples from a large population of levels of that effect. Animal additive genetic effects are one such random factor contained in **u**. Two random factors that should always be included in an animal model are the animal additive genetic effect, **a**, and the contemporary group effect, **c**, ($\mathbf{u}' = (\mathbf{a}' \;\; c')$). Contemporaries are animals that coexist in the same location and time space, and thus share the same management care and treatment during the time they are observed for a trait. Contemporary groups are commonly called herds, flocks, or tanks, and are nested within year or year-season effects. Contemporary groups are random because there are a large number of them, each contemporary group contains different individuals, and the effects during that one occurrence are random in nature.

e is a vector of random residual (environmental) effects specific to each observation, that cannot be accounted for by other factors in the model. The residual effects may be samples from different populations having different variances.

Expectations and Covariances

The model also describes the distributions of the random factors and indicates their expected values or means and covariance structures. That is,

$$\begin{aligned} \mathrm{Var}(\mathbf{u}) &= \mathbf{G} \\ \mathrm{Var}(\mathbf{e}) &= \mathbf{R}, \text{ and} \\ \mathrm{Cov}(\mathrm{u}, \mathbf{e}') &= 0, \end{aligned}$$

where Var() is a variance-covariance matrix, and Cov() is a covariance matrix.

Further, **G** can be partitioned into other matrices for each factor contained within **u**. Because **u** will contain animal additive genetic effects, **a**, and contemporary group effects, **c**, then both **a** and **c** are assumed to follow normal distributions with null means. The variance-covariance matrix of **a** is

$$Var(\mathbf{a}) = \mathbf{A}\sigma_{\mathrm{a}}^2,$$

where **A** is the numerator additive genetic relationship matrix of Wright (2), and σ_{a}^2 is the additive genetic variance of the trait of interest. More will be given on the additive relationship matrix shortly.

Similarly,

$$\mathrm{Var}(\mathbf{c}) = \mathbf{I}\sigma_c^2,$$

where σ_c^2 is the contemporary group variance (variance of all contemporary group effects), and **I** is an identity

matrix, which means the contemporary group effects are independent of each other. Finally,

$$\mathrm{Cov}(\mathbf{a}, \mathbf{c}') = 0,$$

additive genetic and contemporary group effects are independent.

The residual effects are assumed to be independent of all other random factors, meaning their covariances with other random factors are 0. If known, the ratios of residual variance to the additive genetic variance and to the contemporary group variance should be provided, or at least the values that are intended to be used.

Assumptions and Limitations

Limitations occur because of a lack of information in the data records. A factor that could be important is not included in the model because there is no information about that factor in the data files on animals. For example, an animal's record may or may not be affected by its health status. If the record was affected, then health status should be a factor in the linear model. However, health information may not be a part of the data files, and therefore, it cannot be included in the model. Consequently, an assumption is needed that animals were healthy when observations were taken. Depending on the trait and species, this assumption may or may not be critical.

A complete list of the explicit or implied assumptions should be a part of every model description, but often they are omitted. Readers of a scientific report may not be as familiar with the data files and production system as the authors, and may not be able to assess the assumptions that need to be made. The presence of this part of the model helps readers to judge the quality of an analysis.

Genetic Relationships

The animal model works best when pedigree information is complete and accurate. Preparing pedigree files can be tedious, depending on the species. Animals can be registered in different organizations with different identifications in each organization, both of which may be found in the data files. Efforts are needed to make sure that each animal has only one unique identification in both the data files and the pedigree file. Good identification systems include codes for breed of the animal and year of birth.

Next, pedigrees of animals need to be arranged in chronological order. Parents should appear in a list before (ahead of) their progeny. Ordering a pedigree is most easily accomplished by sorting animals by birthdate. Birthdates, however, can be incorrectly recorded, or for many individuals may not be available. One approach is to assume that all birthdates are incorrect. Assign all animals a generation number of 1. Then cycle through the pedigree file and modify the generation numbers so that the generation numbers of the sire and dam of an animal are at least one unit greater than the generation number of that animal. Iterate through the pedigree file as many times as needed until no further modifications are made to any generation numbers.

Inbreeding Coefficients

Genetic relationships among individuals were worked out by Wright [6] as correlation coefficients. Later, only the numerators of these correlation coefficients were needed in genetic evaluation, and were called Wright's numerator, additive genetic relationships. The dimensions of the additive genetic relationship matrix, **A**, equal the number of animals (N) in the pedigree. The pedigree file usually contains more individuals than are represented with records in the data file. If constructed, the **A** matrix would be 95% full (nonzero numbers). For one million animals, the storage of these numbers would be an overwhelming problem computationally. Fortunately, during genetic evaluation, only the inverse of this matrix is needed. The inverse is typically very sparse by comparison, and the elements in the matrix can be generated as needed and do not ever need to be stored. For this to work, the inbreeding coefficients of every animal need to be determined.

Henderson [7] showed that the additive relationship matrix could be written as

$$\mathbf{A} = \mathbf{TBT}',$$

where **T** is a lower triangular matrix and **B** is a diagonal matrix. The diagonals of **B**, say b_{ii}, were shown to equal

$$b_{ii} = (0.5 - 0.25(F_s + F_d)),$$

where F_s and F_d are the inbreeding coefficients of the sire and dam, respectively, of the ith individual. If one parent is unknown, then

$$b_{ii} = (0.75 - 0.25F_p),$$

where F_p is the inbreeding coefficient of the parent that is known. Lastly, if neither parent is known, then $b_{ii} = 1$. An inbreeding coefficient indicates the proportion of alleles that are in common within an individual due to being inherited from common ancestors some generations back in the pedigree. This happens when related animals are mated together.

The key discovery of Henderson [7] was that

$$\mathbf{A}^{-1} = \mathbf{T}'^{-1}\mathbf{B}^{-1}\mathbf{T}^{-1},$$

and that each row of $\mathbf{T}^{-1}$ had a one on the diagonal and two negative one-halves on the off-diagonals corresponding to the locations of the sire and dam of that individual. Only two nonzero numbers that are always equal to 1 or $-\frac{1}{2}$. The elements of $\mathbf{B}^{-1}$ are equal to b_{ii}^{-1}. Every animal could have a different b_{ii}, so these would need to be stored.

Meuwissen and Luo [8] developed a very efficient algorithm to compute inbreeding coefficients, and from these come b_{ii}. The algorithm requires animals to be chronologically ordered and processed, so that inbreeding coefficients of an animal's ancestors are known before that animal is processed. Once the inbreeding coefficients are known, then b_{ii} are easily obtained. Having b_{ii} for each individual, then elements of $\mathbf{A}^{-1}$ can be calculated readily, as needed. Consult Meuwissen and Luo [8] for details of their algorithm.

Missing Parents

Animals with unknown parents are assumed to be animals from a large randomly mating population of unrelated, unselected individuals. This group of animals is known as the *base population*. In dairy cattle, the base population might be animals that were born in the 1950s. However, even today, there are animals in the data files and pedigree files that have unknown parentage. Clearly, these animals are genetically different from animals born 60 years earlier, and they should belong to a population different from the base population. For this reason, unknown parents are assigned to genetic groups based on the year of birth of their progeny, and whether the progeny was male or female [9, 10]. Suppose an animal was born in 2009 and was a male. If the male parent of this animal was unknown, then it would be assigned to a Sire of Males group for 2009, and if the female parent was unknown assignment would be to a Dam of Males group for 2009. The assumption made for assignments is that the selection intensity of each pathway differs so that the genetic means of these groups would be different. The other two pathways are Sires of Females and Dams of Females. These groups may be further subdivided, based on breeds or countries of origin.

Computationally, genetic groups are treated as though they were a separate individual, which requires simple modifications in the computation of elements of $\mathbf{A}^{-1}$. Genetic groups are essential in the animal model in order to obtain unbiased estimates of genetic trends, and accurate evaluations of all animals. There are always animals with unknown parents resulting from movement of animals between countries, but also between herds or flocks within a country.

Genetic Evaluation

Best linear unbiased prediction (or BLUP) has been used since 1970 when Henderson applied the method to genetic evaluation of dairy bulls in the northeastern United States even though the theory had been available since 1950. BLUP requires setting up and solving a linear system of equations that is equal in size to the number of animals and number of levels of other effects that are in the model. The equations are known as the mixed model equations (MME). The solutions to these equations are usually obtained by iteration rather than through the direct inverse of the large coefficient matrix. Many various strategies have been devised to iterate solutions quickly.

Iteration is a technique where initial solutions begin at zero, and by going through one equation at a time, each solution is updated based on the values of the other solutions at that time. An updated solution causes all subsequent solutions to change during the updating process. Iterations continue until the changes are less than a certain value (like 1×10^{-9}), at which point the solutions have reached convergence.

Mixed Model Equations

The mixed model equations (MME) of Henderson [2] yield the BLUP predictors of the random effects of the linear model and generalized least squares estimators of the fixed effects. Following the notation for the linear model, the MME, generally, are written as

$$\begin{pmatrix} \mathbf{X}'\mathbf{R}^{-1}\mathbf{X} & \mathbf{X}'\mathbf{R}^{-1}\mathbf{Z} \\ \mathbf{Z}'^{-1}\mathbf{X} & \mathbf{Z}'\mathbf{R}^{-1}\mathbf{Z}+\mathbf{G}^{-1} \end{pmatrix} \begin{pmatrix} \hat{\mathbf{b}} \\ \hat{\mathbf{u}} \end{pmatrix} = \begin{pmatrix} \mathbf{X}'\mathbf{R}^{-1}\mathbf{y} \\ \mathbf{Z}'\mathbf{R}^{-1}\mathbf{y} \end{pmatrix}.$$

From one model to the next, **X**, **Z**, **R**, and **G** change in how they may be constructed, but the MME always have the same form. Computations also differ and may simplify in certain cases.

Estimation of Variances

Two methods of estimation of **G** and **R** are commonly used in animal breeding. First is Restricted (or Residual) Maximum Likelihood (REML) [11–13], of which there are four computational versions, and second is Bayesian Estimation using Gibbs Sampling as a tool to maximize the joint posterior distribution [14]. Both methods require major computing time, and consequently, smaller subsamples of the complete data file are chosen for estimating covariance matrices.

The main advantage of these two methods is that the estimated covariance matrices are positive definite matrices that can be used directly in MME. A covariance matrix must be positive definite like a variance must always be positive.

Another advantage of the methods is that the REML and Bayesian estimators are more accurate than other methods. The disadvantage is the increased computing demands necessitating the need to subsample the data into smaller sets.

Reliabilities

All estimates of breeding values of animals require information about the accuracy or reliability of that estimate. Theoretically, standard errors of prediction are derived from the inverse of the coefficient matrix of the MME. Given that solutions result from iteration techniques rather than inversion, the standard errors of prediction must be approximated. Standard errors of prediction are often converted into a percent reliability that goes from 0 to 100. There are many approximation methods in use.

Reliabilities depend on the number of progeny, the number of contemporaries of those progeny, the completeness of pedigree information, and the variance and covariance parameters. Depending on the reliability of an animal's Estimated Breeding Value, (EBV), the EBV may or may not be made officially public. Minimum standards are agreed upon by industry committees.

Genetic Trends

Genetic trends are estimated by averaging animal EBVs by year of birth, or by years in which they make records. In dairy cattle, for example, the EBVs of all cows that were born in a given year and which completed at least one lactation can be averaged. By plotting these averages by year of birth, the genetic trend in milk production can be quantified. Plotting the average EBVs of dairy bulls by their year of birth would give a different trend, reflecting how bulls were chosen to be in artificial insemination. The cow averages would reflect how those bulls were used in breeding programs, and would likely lag a couple of years behind the sire birth years. Graphs of genetic trends should have details of what the averages represent.

Single Record per Animal

The models presented in this and the following sections become progressively more complicated, due to the type of traits that are considered. First, a simple animal model is illustrated which covers traits that are observed only once in an animal's lifetime, such as age at first breeding. Next, the situation where animals can be observed more than once per lifetime, such as annual antler production in elk, wool production in sheep, or race results in horses. Then traits influenced by maternal effects, such as birth weights, weaning weights, and calving ease, are considered. Longitudinal data, traits observed over time, such as milk production or egg production, provide models that analyze the shapes of curves. Multiple trait models are applied to two or more traits at a time, and include genetic and environmental correlations among the traits. Threshold models for categorical data are described, and finally, a model for the analysis of survival data is presented.

Data

The case of a single record per animal is presented in some detail because this is the simplest model and illustrates the process of constructing mixed model equations, and what happens to the solutions to those equations. The models are presented in a generic fashion without reference to particular species.

Table 1 contains the pedigree information and data on 16 animals. The first four animals are base population animals without records and without known parents. The inbreeding coefficients are shown and the values of b_{ii} which come from the inbreeding coefficients. Records were made over 2 years, and there were two contemporary groups within each year. Assume that the residual variance is 600, the genetic variance is 300, and the variance of contemporary group effects is 100. Heritability (denoted as h^2) is defined as the genetic variance divided by the total phenotypic variance, which is the sum of the genetic, contemporary group, and residual variances. In this case, $h^2 = 0.3$.

Mixed Model Equations

The equation of the model is (in scalar form)

$$y_{ijk} = (YR)_i + (CG)_j + a_k + e_{ijk},$$

where

y_{ijk} are the observations on animal k, belonging to contemporary group, $(CG)_j$, born in year, $(YR)_i$,

$$\mathbf{y} = \{y_{ijk}\}.$$

$(YR)_i$ are the fixed, year effects,

$$\mathbf{b} = \{(YR)_i\}.$$

Animal Breeding, Modeling in. Table 1 Example data for simple animal model

Animal	Sire	Dam	F_i	b_{ii}	Year	CG	Record
1	0	0	0.00000	1.00000			
2	0	0	0.00000	1.00000			
3	0	0	0.00000	1.00000			
4	0	0	0.00000	1.00000			
5	1	2	0.00000	0.50000	1	1	78
6	3	4	0.00000	0.50000	1	1	26
7	3	2	0.00000	0.50000	1	1	111
8	1	4	0.00000	0.50000	1	1	122
9	5	6	0.00000	0.50000	1	1	98
10	7	8	0.00000	0.50000	1	2	48
11	5	8	0.12500	0.50000	1	2	109
12	7	6	0.12500	0.50000	1	2	94
13	1	6	0.00000	0.50000	1	2	103
14	3	8	0.00000	0.50000	2	3	78
15	5	4	0.00000	0.50000	2	3	69
16	7	8	0.00000	0.50000	2	3	44
17	9	6	0.25000	0.50000	2	3	12
18	11	10	0.18750	0.46875	2	4	54
19	11	12	0.06250	0.43750	2	4	89
20	9	8	0.12500	0.50000	2	4	82

$(CG)_j$ are the random, contemporary group effects,

$$\mathbf{c} = \{(CG)_j\}.$$

a_k are the random, additive genetic effects of individual animals,

$$\mathbf{a} = \{a_k\}$$

e_{ijk} are random, residual effects.

Also,

$$\mathbf{u} = \begin{pmatrix} \mathbf{c} \\ \mathbf{a} \end{pmatrix},$$

and

$$\mathrm{Var}\begin{pmatrix} \mathbf{c} \\ \mathbf{a} \end{pmatrix} = \begin{pmatrix} \mathbf{I}_4\sigma_c^2 & 0 \\ 0 & \mathbf{A}\sigma_a^2 \end{pmatrix} = \mathbf{G}.$$

Finally,

$$\mathbf{R} = \mathbf{I}_{16}\sigma_e^2,$$

and $\mathbf{Z}$ can be partitioned into one matrix for contemporary groups, and one for animal additive genetic values, i.e.,

$$\mathbf{Z} = \begin{pmatrix} \mathbf{Z}_{cg} & \mathbf{Z}_a \end{pmatrix}.$$

Inverse of Relationship Matrix

Notice that the MME contain $\mathbf{G}^{-1}$, which equals

$$\mathbf{G}^{-1} = \begin{pmatrix} \mathbf{I}\frac{1}{\sigma_{cg}^2} & 0 \\ 0 & \mathbf{A}^{-1}\frac{1}{\sigma_a^2} \end{pmatrix}.$$

Thus, the inverse of the relationship matrix is needed. This matrix can be constructed readily following simple rules that Henderson [7] provided. For each animal with both parents known, 9 numbers are added into the inverse matrix. For an animal with only one parent known, 4 numbers are added, and for an animal with both parents unknown, 1 number is added. Start with a matrix of order 20 that is completely null. Then process the pedigree file, one animal at a time until all animals are included.

Step 1: For animal i, let $\delta = b_{ii}^{-1}$. For animal 1, $\delta = 1$; for animal 6, $\delta = 2$, and for animal 19, $\delta = 2.2857$.

Step 2: Add δ to the diagonal element for that animal. For animal 19, add *delta* to element (19,19) of $\mathbf{A}^{-1}$.

Step 3: If the male parent is known, subtract -0.5δ from elements (i, s) and (s, i), where i is the animal's number and s is the sire's number. For example, for animal 19, $i = 19$ and $s = 11$. Also add 0.25δ to element (s, s).

Step 4: If the female parent (denoted by d) is known, subtract -0.5δ from elements (i, d) and (d, i), and add 0.25δ to element (d, d).

Step 5: If both parents are known add 0.25δ to elements (s, d) and (d, s).

Numbers are accumulative as the pedigrees are processed. Many of the elements will stay null values, especially for animals that do not have progeny.

Solutions to Equations

The resulting mixed model equations have 26 rows and columns with 26 unknowns to be estimated (2 year effects, 4 contemporary groups, and 20 animal effects). Even for this small example, to display the equations fully would take up too much space. The solutions to the MME were as follows:

Year 1	=	88.8
Year 2	=	61.6
CG 1	=	.015
CG 2	=	–.015
CG 3	=	–3.303
CG 4	=	3.303

Animal		EBV	Reliability
1	=	8.32	.13
2	=	1.06	.11
3	=	–5.68	.14
4	=	–3.69	.10
5	=	4.38	.23
6	=	–15.50	.25
7	=	–.95	.25
8	=	7.37	.23
9	=	–4.28	.20
10	=	–6.58	.18
11	=	9.49	.24
12	=	–3.79	.24
13	=	–.02	.17
14	=	4.61	.17
15	=	2.41	.18
16	=	–.30	.16
17	=	–17.17	.25
18	=	–.90	.21
19	=	6.66	.16
20	=	4.65	.18

The solutions for the animal additive genetic effects are known as *Estimated Breeding Values* or EBVs.

Progeny are expected to inherit an average of the EBVs of its parents, on average. EBVs are sorted from highest to lowest, or best animal to poorest animal. Every animal in the pedigree file obtains a solution due to genetic relationships to progeny and other individuals. The EBV of an animal consists of combined information from the animal's parents, its progeny, and its own performance record. The BLUP methodology combines the information in an optimal manner to maximize the correlation of the EBV with the animal's true genetic merit. The reliability is obtained from the inverse of the MME coefficient matrix, and expressed as a correlation coefficient. The greater is the reliability, the more certainty in the ranking of the animals. The highest reliability was 0.25, for animals 6, 7, and 17. Note that animal 6 had 4 progeny, plus a record on itself, and both parents were known. Animal 7 had 3 progeny. Animal 17 had no progeny, but was an offspring of animal 6 and was inbred the most. Reliability also reflects the number of contemporaries that each animal has, but the differences in this example were not great. The reliabilities of all animals in this example are very small, but there were only 16 observations in total. Dairy bulls, for example, can have hundreds or thousands of progeny giving them reliabilities above 0.99. A minimum reliability level is chosen before EBVs are released to the public.

The solutions for the year effects were 88.8 and 61.6, respectively. Thus, performances were lower in year 2 compared to year 1. There is likely a reason for this difference, such as year 2 being hotter, or a shortage of good feed, or feed prices may have caused many animals to be removed from farms. The difference between years is not genetic.

Contemporary group effects were random in the model, and the solutions have an average of zero as a consequence of how they were included in the model. The CG solutions average zero within the year effects, due to the fact they were a factor nested within year effects.

Genetic trends can be computed from the EBVs. Because animals have only one record each, the genetic averages for years 1 and 2 are the average EBVs of animals 5–13 for year 1, and animals 14–20 for year 2. These give −1.10 for year 1 and −0.01 for year 2. Thus, the animals in year 2 were slightly better than in year 1, genetically.

Repeated Records Animal Model

Animals are often observed more than once for some traits, such as

- Fleece weight of sheep in different years
- Calf records of a beef cow over time
- Test day records within a lactation for a dairy cow
- Litter size of sows over time
- Antler size of deer in different seasons
- Racing results of horses from several races

Animals are influenced by their environments, such as an athlete changes due to training and practice. These effects are called permanent environmental effects, and they accompany the animal every time the animal is observed for that trait as in Fig. 2. Permanent environmental effects are not genetic, in the sense that the animal does not transmit these effects to any of its offspring. The following figure illustrates a model to describe permanent environmental effects. Only with repeated records can the permanent environmental and genetic effects be separated and estimated.

Data

In the example data of Table 2, animals have either one, two, or three records made in different years.

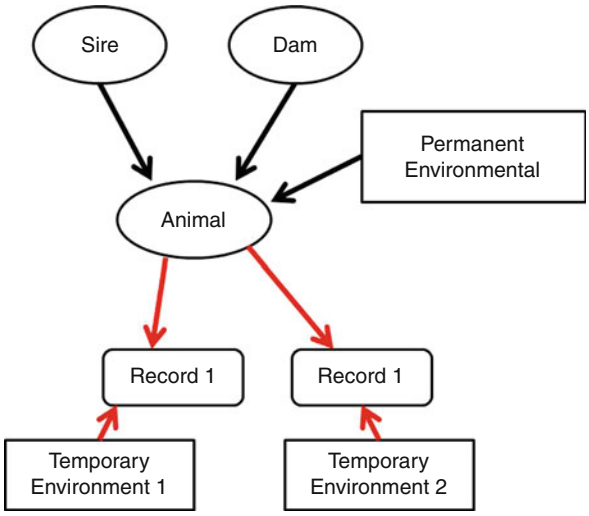

Animal Breeding, Modeling in. Figure 2
Diagram for an animal with repeated records including a permanent environmental effect

Animal Breeding, Modeling in. Table 2 Example data for repeated records animal model

Animal	Sire	Dam	Age	Year 1	Year 2	Year 3
			Yr 1			
1			3	22	35	
2			3	31	46	
3			3	44	24	
4			3	53		
5			2	61	57	42
6			2	32		39
7	1	2	2	39	51	62
8	3	4	1	48	72	
9	5	6	1	71		96
10	1	4	1	37	56	47
11	3	6	1	66		86
12	1	2	1		46	38

The contemporaries for each year differ, but are confounded with the year effect in this example. If the animals could be assigned to different herds or management groups, then contemporary groups and years would not be confounded.

Normally performance of animals either improves or declines with the age of the animal, so that ages of animals should be known. The age of the animal in year 1 is given in the table, and so ages range from 1 to 4 years.

Mixed Model Equations

The equation of the model is (in scalar form)

$$y_{ijkl} = (YR)_i + (\text{Age})_j + a_k + p_k + e_{ijkl},$$

where

y_{ijkl} is observation l on animal k, belonging to age group j, born in year i.
$(YR)_i$ are fixed, year effects.
$(\text{Age})_j$ are fixed, age group effects.
a_k are random, additive genetic effects of individual animals.
p_k are random, permanent environmental effects of individual animals.
e_{ijk} are random, residual effects.

The covariance matrices of the random variables (animals, permanent environmental, and residual effects, respectively) are

$$\text{Var}\begin{pmatrix}\mathbf{a}\\ \mathbf{p}\\ \mathbf{e}\end{pmatrix} = \begin{pmatrix}\mathbf{A}\sigma_a^2 & 0 & 0\\ 0 & \mathbf{I}\sigma_p^2 & 0\\ 0 & 0 & \mathbf{I}\sigma_e^2\end{pmatrix}.$$

The total variance is

$$\sigma_y^2 = \sigma_a^2 + \sigma_p^2 + \sigma_e^2,$$

and the heritability is

$$h^2 = \frac{\sigma_a^2}{\sigma_y^2}.$$

Repeatability is a measure of the average similarity of repeated records on animals across the population (part genetic and part environmental), and is defined as a ratio of variances as

$$r = \frac{\sigma_a^2 + \sigma_p^2}{\sigma_y^2},$$

which is always going to be greater than or equal to heritability.

Let

Xb represent the fixed factors of years and ages
Za represent the random animal additive genetic effects
Wp represent the random animal permanent environmental effects

then the mixed model equations may be written as

$$\begin{pmatrix}\mathbf{X}'\mathbf{X} & \mathbf{X}'\mathbf{Z} & \mathbf{X}'\mathbf{W}\\ \mathbf{Z}'\mathbf{X} & \mathbf{Z}'\mathbf{Z} + \mathbf{A}^{-1}k_a & \mathbf{Z}'\mathbf{W}\\ \mathbf{W}'\mathbf{X} & \mathbf{W}'\mathbf{Z} & \mathbf{W}'\mathbf{W} + \mathbf{I}k_p\end{pmatrix}\begin{pmatrix}\hat{\mathbf{b}}\\ \hat{\mathbf{a}}\\ \hat{\mathbf{p}}\end{pmatrix} = \begin{pmatrix}\mathbf{X}'\mathbf{y}\\ \mathbf{Z}'\mathbf{y}\\ \mathbf{W}'\mathbf{y}\end{pmatrix},$$

and let

$$k_a = \sigma_e^2/\sigma_a^2 = 1.33333, \quad \text{and} \quad k_p = \sigma_e^2\big/\sigma_p^2 = 3.$$

There are 26 observations in the example of Table 2, with 3 years and 4 age groups represented, plus 12 animal additive genetic effects and 12 permanent environmental effects giving a total of 31 equations.

The **A** matrix is simple to construct because none of the animals are inbred. The resulting solutions are given in Table 3.

There are two possible uses of these solutions. First is to rank the animals for their genetic ability in order to plan future matings using the Estimated Breeding Values. Secondly, there is the decision about which animals to keep to make another record. The criterion for making this decision is the Most Probable Producing Ability, [1] which is the sum of the genetic and permanent environmental solutions (shown in the last column of Table 3). Thus, Animal 9 would likely make the best future performance of those 12 animals and would also likely generate the best future progeny.

Comments

One could ask if permanent environmental effects are permanent. The answer is yes, but as an animal ages, it encounters new permanent environmental effects which accumulate with the previous effects. Hence, permanent environmental effects are cumulative over the life of an animal. This means permanent environmental effects are not constant throughout an animal's life. With the model as described in this section, the assumption is that permanent environmental effects are constant. Some of the cumulative parts, therefore, flow into the temporary environmental effects, and some are averaged with the previous permanent environmental effects.

Another assumption is that the genetic component of each record on an animal is the same. Genes are known to change in activity as an animal ages due to age, but also due to epigenetics (environmental effects that cause change to an animal's DNA). Thus, repeated records on one animal could have different genetic components. That means the genetic correlation between records is less than unity. A better model would be to assume that all records are genetically different (but correlated) traits. This would take into account both the different genetic effects associated with each record, and also the accumulation of permanent environmental effects with time.

Animal Breeding, Modeling in. Table 3 A set of solutions to the example data on repeated records model

Years		Ages		Animal			MPPA
				Genetic		Perm. Env.	
1	0.00	1	50.92	1	−8.37	−0.27	8.64
2	18.34	2	46.01	2	−1.50	0.98	−0.52
3	29.08	3	37.24	3	1.06	−1.84	−0.78
		4	19.50	4	3.14	3.16	6.30
				5	4.96	−0.84	4.12
				6	0.71	−5.00	−4.29
				7	−2.94	1.77	−1.17
				8	2.18	0.07	2.25
				9	9.68	6.08	15.76
				10	−6.66	−3.60	−10.26
				11	6.00	4.55	10.55
				12	−10.64	−5.07	−15.71

Maternal Effects Animal Model

In mammalian species of livestock, such as beef cattle, sheep, or swine, the female provides an environment for its offspring to survive and grow in terms of protection and nourishment. Figure 3 illustrates how maternal effects can affect offspring records. Females vary in their ability to provide a suitable environment for their offspring, and this variability has a genetic basis. Offspring directly inherit an ability to grow (or survive) from both parents, and environmentally do better or poorer depending on their dam's genetic

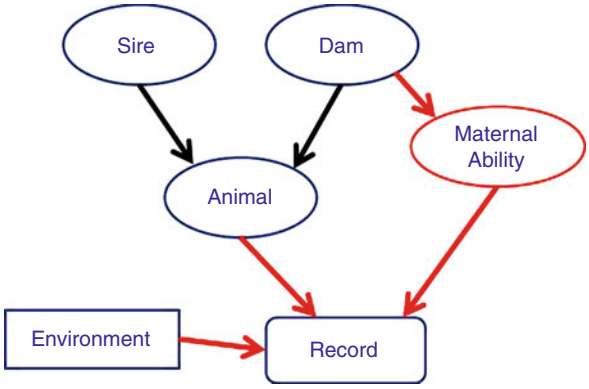

Animal Breeding, Modeling in. Figure 3 Diagram illustrating maternal genetic effects

maternal ability. Maternal ability is a genetic trait expressed by the dam in the offsprings' performance, and is transmitted, like all genetic traits, from both parents. Maternal ability is only expressed by females when they have offspring (i.e., much like milk yield in dairy cows) [15, 16].

Data

The example data of Table 4 are weights on animals at an early age.

A model to account for maternal ability is

$$\mathbf{y} = \mathbf{Xb} + \mathbf{Z}_1\mathbf{a} + \mathbf{Z}_2\mathbf{m} + \mathbf{Z}_3\mathbf{p} + \mathbf{e},$$

where $\mathbf{y}$ is the growth trait of a young animal, $\mathbf{b}$ is a vector of fixed factors influencing growth, in this case contemporary group effects, $\mathbf{a}$ is a vector of random animal additive genetic effects (i.e., direct genetic effects), $\mathbf{m}$ is a vector of random maternal genetic (dam) effects, and $\mathbf{p}$, in this model, is a vector of maternal permanent environmental effects (because dams may have more than one offspring in the data – repeated records).

The expectations of the random vectors, $\mathbf{a}$, $\mathbf{m}$, $\mathbf{p}$, and $\mathbf{e}$ are all null vectors in a model without selection, and the variance-covariance structure is

$$\mathrm{Var}\begin{pmatrix}\mathbf{a}\\ \mathbf{m}\\ \mathbf{p}\\ \mathbf{e}\end{pmatrix} = \begin{pmatrix}\mathbf{A}\sigma_a^2 & \mathbf{A}\sigma_{am} & 0 & 0\\ \mathbf{A}\sigma_{am} & \mathbf{A}\sigma_m^2 & 0 & 0\\ 0 & 0 & \mathbf{I}\sigma_p^2 & 0\\ 0 & 0 & 0 & \mathbf{I}\sigma_e^2\end{pmatrix},$$

where σ_a^2 is the additive genetic variance, σ_m^2 is the maternal genetic variance, σ_{am} is the covariance between additive and maternal genetic effects, and σ_p^2 is the maternal permanent environmental variance. Also,

$$\left(\begin{matrix}\mathbf{a}\\ \mathbf{m}\end{matrix}\middle|\ \mathbf{A},\ \mathbf{G}\right) \sim N\left(\begin{pmatrix}0\\ 0\end{pmatrix},\quad \mathbf{G}\otimes\mathbf{A}\right),$$

where

$$\mathbf{G} = \begin{pmatrix}\sigma_a^2 & \sigma_{am}\\ \sigma_{am} & \sigma_m^2\end{pmatrix},$$

and

$$\mathbf{p}|\mathbf{I}, \sigma_p^2 \sim N(0, \mathbf{I}\sigma_p^2),$$

and

$$\mathbf{e} \sim N(0, \mathbf{I}\sigma_e^2).$$

In this model, a female animal, i, could have its own growth record for estimating $\hat{a}_i$. The same female could later have offspring for estimating $\hat{m}_i$ and $\hat{p}_i$, and the offspring would also contribute toward $\hat{a}_i$. The maternal effects model can be more complicated if, for example, embryo transfer is practiced. Recipient dams would have maternal effects, but would not have direct genetic effects on that calf [17].

Animal Breeding, Modeling in. Table 4 Example data for maternal genetic effects model

Animal	Sire	Dam	CG	Weight
5	1	3	1	156
6	2	3	1	124
7	1	4	1	135
8	2	4	2	163
9	1	3	2	149
10	2	4	2	138

Mixed Model Equations

The MME are represented as

$$\begin{pmatrix}\mathbf{X}'\mathbf{X} & \mathbf{X}'\mathbf{Z}_1 & \mathbf{X}'\mathbf{Z}_2 & \mathbf{X}'\mathbf{Z}_3\\ \mathbf{Z}'_1\mathbf{X} & \mathbf{Z}'_1\mathbf{Z}_1 + \mathbf{A}^{-1}k_{11} & \mathbf{Z}'_1\mathbf{Z}_2 + \mathbf{A}^{-1}k_{12} & \mathbf{Z}'_1\mathbf{Z}_3\\ \mathbf{Z}'_2\mathbf{X} & \mathbf{Z}'_2\mathbf{Z}_1 + \mathbf{A}^{-1}k_{12} & \mathbf{Z}'_2\mathbf{Z}_2 + \mathbf{A}^{-1}k_{22} & \mathbf{Z}'_2\mathbf{Z}_3\\ \mathbf{Z}'_3\mathbf{X} & \mathbf{Z}'_{3'}\mathbf{Z}_1 & \mathbf{Z}'_3\mathbf{Z}_2 & \mathbf{Z}'_3\mathbf{Z}_3 + \mathbf{I}k_{33}\end{pmatrix}\begin{pmatrix}\hat{\mathbf{b}}\\ \hat{\mathbf{a}}\\ \hat{\mathbf{m}}\\ \hat{\mathbf{p}}\end{pmatrix} = \begin{pmatrix}\mathbf{X}'\mathbf{y}\\ \mathbf{Z}'_1\mathbf{y}\\ \mathbf{Z}'_2\mathbf{y}\\ \mathbf{Z}'_3\mathbf{y}\end{pmatrix},$$

where

$$\begin{aligned}\begin{pmatrix}k_{11} & k_{12}\\ k_{12} & k_{22}\end{pmatrix} &= \begin{pmatrix}\sigma_a^2 & \sigma_{am}\\ \sigma_{am} & \sigma_m^2\end{pmatrix}^{-1}\sigma_e^2,\\ &= \begin{pmatrix}49 & -7\\ -7 & 26\end{pmatrix}^{-1}(81),\\ &= \begin{pmatrix}1.7192 & 0.4628\\ 0.4628 & 3.2400\end{pmatrix}.\end{aligned}$$

The solutions to the MME are

$$\hat{\mathbf{b}} = \begin{pmatrix} 137.8469 \\ 150.4864 \end{pmatrix}, \quad \hat{\mathbf{p}} = \begin{pmatrix} 0.0658 \\ -0.0658 \end{pmatrix},$$

$$\hat{\mathbf{a}} = \begin{pmatrix} 2.3295 \\ -2.3295 \\ 0.1280 \\ -0.1280 \\ 5.1055 \\ -4.1143 \\ 0.2375 \\ 2.0161 \\ 0.5447 \\ -3.7896 \end{pmatrix}, \quad \text{and} \quad \hat{\mathbf{m}} = \begin{pmatrix} -0.3328 \\ 0.3328 \\ 0.1646 \\ -0.1646 \\ -0.6379 \\ 0.6792 \\ -0.1254 \\ -0.3795 \\ 0.0136 \\ 0.4499 \end{pmatrix}.$$

Comments

Maternal genetic models require a good data structure to be successful [18]. That means that there should be many females with weight records in the data who also have several progeny with weight records in the data. In this way direct genetic and maternal genetic effects can be efficiently separated during estimation. In the example data, the structure is not good because the females that were dams did not have any weight records on themselves. Hence the strong negative relationship between direct and maternal genetic estimates, which means the maternal genetic estimates are based mostly on the direct genetic estimates and the prior genetic correlation that was assumed, which was negative.

Sire structure is also important in that sires should have many daughters that have also had their own progeny. The maternal genetic ability of a sire's daughters cannot be accurately estimated without those daughters displaying their maternal ability on their own progeny. In many studies or application of maternal genetic effects models, the data structure is too poor from which to estimate variances and covariances of direct and maternal genetic effects.

Random Regression Animal Model

All biological creatures grow and perform over their lifetime. Traits that are measured at various times during that life are known as *longitudinal* data. Examples are body weights [19], body lengths, milk production [20], feed intake, fat deposition, and egg production [21]. On a biological basis, there could be different genes that turn on or turn off as an animal ages causing changes in physiology and performance. The time variable (or age) can be recorded in years, months, weeks, days, hours, minutes, or seconds, so that, in effect, there could be a continuum or continuous range of points in time when an animal could be observed for a trait. These traits have also been called *infinitely dimensional* traits.

If observations were plotted on a graph where the x-axis is time and the y-axis is the magnitude of the observations, then a *trajectory* is obtained for a group of animals. However, not every individual will follow the average trajectory, see Fig. 4. There are variations in the shape of their trajectory, and the breeder may wish to change the shape for animals in his(her) production system in order to be more profitable.

The average trajectory, in black, is given by the equation

$$f(t_i) = A + Bt_i + Ct_i^2 + Dt_i^3,$$

where $A = 2$, $B = 0.1$, $C = 0.03$, and $D = -0.001$. The red and blue trajectories are extremes for animals in the population. The assumption is that $f(t_i)$ is the average trajectory and every animal will have its own trajectory,

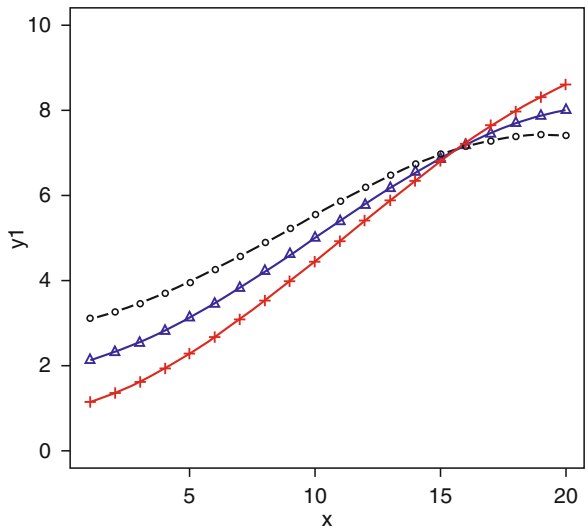

Animal Breeding, Modeling in. Figure 4
Trajectories of different animals for a trait measured over time

that means every animal will have different A, B, C, and D values. Because these parameters are regression coefficients, the model becomes the *random regression* model, and every animal will have four regression coefficients to be estimated, as deviations from the average trajectory regression coefficients.

Regression Functions

A problem in using time covariates to various powers is that the numbers can become very large, very quickly. For example, if the time variable, t, goes from 1 to 20, then t^3 would range from 1 to 8,000. In least squares like equations, the diagonal element for that variable would be $(8,000)^2$. Then there could be many thousands of observations. The large numbers can lead to serious rounding errors and may cause problems in solving the equations.

Another problem is that there will be high correlations among the time variables in the function, because they are all based on the same t value. This may also lead to near singularity and to problems in solving the equations. A solution for the above problems is to use Legendre polynomials which convert the time variable, t, into covariates that are firstly scaled to be between -1 and $+1$, and then converted to be independent of each other.

Scaling Time Variables Time variables have to be standardized to the interval between -1 and $+1$. The formula to standardize t_ℓ is

$$x_\ell = -1 + 2\left(\frac{t_\ell - t_{\min}}{t_{\max} - t_{\min}}\right).$$

Legendre Polynomials The first two Legendre polynomials are defined as

$$P_0(x) = 1, \quad \text{and}$$
$$P_1(x) = x,$$

then, in general, the $n+1$ polynomial is described by the following recursive equation:

$$P_{n+1}(x) = \frac{1}{n+1}\left((2n+1)xP_n(x) - nP_{n-1}(x)\right).$$

These quantities are "normalized" using

$$\phi_n(x) = \left(\frac{2n+1}{2}\right)^{0.5} P_n(x).$$

This gives the following series:

$$\phi_0(x) = \left(\frac{1}{2}\right)^{0.5} P_0(x) = 0.7071$$
$$\phi_1(x) = \left(\frac{3}{2}\right)^{0.5} P_1(x)$$
$$= 1.2247x$$
$$P_2(x) = \frac{1}{2}(3xP_1(x) - 1P_0(x))$$
$$\phi_2(x) = \left(\frac{5}{2}\right)^{0.5} (\frac{3}{2}x^2 - \frac{1}{2})$$
$$= -0.7906 + 2.3717x^2,$$

and so on. The first six can be put into a matrix, Λ, as

$$\Lambda' = \begin{pmatrix} 0.7071 & 0 & 0 & 0 & 0 & 0 \\ 0 & 1.2247 & 0 & 0 & 0 & 0 \\ -0.7906 & 0 & 2.3717 & 0 & 0 & 0 \\ 0 & -2.8062 & 0 & 4.6771 & 0 & 0 \\ 0.7955 & 0 & -7.9550 & 0 & 9.2808 & 0 \\ 0 & 4.3973 & 0 & -20.5206 & 0 & 18.4685 \end{pmatrix}.$$

Now define a vector, $\mathbf{m}$, containing the polynomials of standardized time values,

$$\mathbf{m}' = \begin{pmatrix} 1 & x & x^2 & x^3 & x^4 & x^5 \end{pmatrix}.$$

The covariates to use in the model are equal to

$$\Lambda'\mathbf{m}.$$

To illustrate, suppose time goes from 10 to 60 days over which animals are observed for their growth, $t_{\min} = 10$ and $t_{\max} = 60$. An animal is observed on day 43. The standardized time variable is

$$x = -1 + 2\frac{(43-10)}{(60-10)} = -0.32,$$

and

$$\mathbf{m}' = (1 \quad -0.32 \quad 0.1024 \quad -0.0328 \quad 0.01048 \quad -0.00336).$$

Finally,

$$\Lambda'\mathbf{m} = \begin{pmatrix} 0.7071 \\ -0.3919 \\ -0.5477 \\ 0.7446 \\ 0.0782 \\ -0.7961 \end{pmatrix}.$$

The order of Legendre polynomials is equal to the highest power of x. Research is needed to determine the best order of fit for any given situation.

Random Regression Model

Like other animal models, the random regression model (RRM) accounts for years, contemporary groups, and animal additive genetic effects, but in addition, it needs to account for the following:

- Curves for different groups of animals, such as age groups, month of calving groups, and breeds which could have different shapes of curves. These factors would be fixed effects in the model. The curves may be fit using Legendre polynomials, or other functions of time, or as classification variables with many levels.
- Curves for each individual animal, using Legendre polynomials, which are random factors in the model. Each animal has a number of regression coefficients to be estimated. For each animal, there are additive genetic parameters as well as permanent environmental parameters.
- The possibility of residual variances changing over the observable time period. For example, as animals grow, their mean weight increases and so does the variance of weights at a given age.

A simplified RRM for a single trait can be written as

$$y_{ijkn:t} = F_i + g(t)_j + r(a, x, m1)_k + r(pe, x, m2)_k + e_{ijkn:t},$$

where

$y_{ijkn:t}$ is the nth observation on the kth animal at time t belonging to the ith fixed factor and the jth group.

F_i is a fixed effect that is independent of the time scale for the observations, such as a cage effect, a location effect, or a herd-test date effect.

$g(t)_j$ is a function or functions that account for the phenotypic trajectory of the average observations across all animals belonging to the jth group.

$r(a, x, m1)_k = \sum_{\ell=0}^{m_1} a_{k\ell} x_{ijk:\ell}$ is the notation adopted for a random regression function. In this case, a denotes the additive genetic effects of the kth animal, x is the vector of time covariates, and $m1$ is the order of the regression function. So that $x_{ijk:\ell}$ are the covariables related to time t, and $a_{k\ell}$ are the animal additive genetic regression coefficients to be estimated.

$r(pe, x, m2)_k = \sum_{\ell=0}^{m_2} p_{k\ell} x_{ijk:\ell}$ is a similar random regression function for the permanent environmental (pe) effects of the kth animal.

$e_{ijkn:t}$ is a random residual effect with mean null and with possibly different variances for each t or functions of t.

The function, $g(t)_j$, can be either linear or nonlinear in t. Such a function is necessary in a RRM to account for the phenotypic relationship between y and the time covariables (or other types of covariables that could be used in a RRM). In a test day model, $g(t)_j$ accounts for different lactation curve shapes for groups of animals defined by years of birth, parity number, and age and season of calving within parities, for example. With growth data, $g(t)_j$ accounts for the growth curve of males or females of breed X or breed Y from young or old dams.

If the shape of the phenotypic relationship is not known or is nonlinear, then $g(t)_j$ could be a set of classification variables. Classification variables take up more degrees of freedom and require a large number of observations per level, but they do not force the user to explicitly define the shape of the trajectory. A mathematical function, on the other hand, does not use many degrees of freedom and gives a smooth trajectory over time regardless of the number of observations. The choice of classification variables or mathematical function is up to the researcher. If data are very numerous, and the mathematical function fits the data well, then either approach will generally lead to the same results. The phenotypic relationships, $g(t)_j$,

are important to a RRM analysis and deserve care and effort in their correct specification.

Mixed Model Equations In matrix notation, the RRM is

$$\mathbf{y} = \mathbf{Xb} + \mathbf{Z}_1\mathbf{a} + \mathbf{Z}_2\mathbf{p} + \mathbf{e},$$

where **b** contains F_i and $g(t)_j$ effects, **a** contains $m_1 + 1$ additive genetic regression coefficients for each animal, **p** contains $m_2 + 1$ permanent environmental regression coefficients for each animal with data, and **e** contains the temporary environmental effects. Also,

$$\mathrm{Var}\begin{pmatrix}\mathbf{a}\\ \mathbf{p}\\ \mathbf{e}\end{pmatrix} = \begin{pmatrix}\mathbf{A}\otimes\mathbf{G} & 0 & 0\\ 0 & \mathbf{I}\otimes\mathbf{P} & 0\\ 0 & 0 & \mathbf{R}\end{pmatrix},$$

where **G** is the variance-covariance matrix of the additive genetic random regression coefficients of order $m_1 + 1$; $\otimes$ if the direct product operator which multiplies every element of **A** by the matrix **G**; **P** is the variance-covariance matrix of the permanent environmental random regression coefficients of order $m_2 + 1$; and **R** is a diagonal matrix of temporary environmental variances which could vary depending on t, or **R** could be block diagonal with an autocorrelation structure for each animal's records. The mixed model equations (MME) are represented as

$$\begin{pmatrix}\mathbf{X}'\mathbf{R}^{-1}\mathbf{X} & \mathbf{X}'\mathbf{R}^{-1}\mathbf{Z}_1 & \mathbf{X}'\mathbf{R}^{-1}\mathbf{Z}_2\\ \mathbf{Z}_1'\mathbf{R}^{-1}\mathbf{X} & \mathbf{Z}_1'\mathbf{R}^{-1}\mathbf{Z}_1 + \mathbf{A}^{-1}\otimes\mathbf{G}^{-1} & \mathbf{Z}_1'\mathbf{R}^{-1}\mathbf{Z}_2\\ \mathbf{Z}_2'\mathbf{R}^{-1}\mathbf{X} & \mathbf{Z}_2'\mathbf{R}^{-1}\mathbf{Z}_1 & \mathbf{Z}_2'\mathbf{R}^{-1}\mathbf{Z}_2 + \mathbf{I}\otimes\mathbf{P}^{-1}\end{pmatrix}\begin{pmatrix}\hat{\mathbf{b}}\\ \hat{\mathbf{a}}\\ \hat{\mathbf{p}}\end{pmatrix} = \begin{pmatrix}\mathbf{X}'\mathbf{R}^{-1}\mathbf{y}\\ \mathbf{Z}_1'\mathbf{R}^{-1}\mathbf{y}\\ \mathbf{Z}_2'\mathbf{R}^{-1}\mathbf{y}\end{pmatrix}.$$

Example Data Analysis by RRM

A very simplified example is given below to illustrate the degree of complexity of RRM. Four animals were observed multiple times at different ages for a trait, as shown in Table 5.

The model equation might be

$$\begin{aligned} y_{jik:t} = {} & V_j + b_0 + b_1(A) + b_2(A)^2 \\ & + (a_{i0}z_0 + a_{i1}z_1 + a_{i2}z_2) \\ & + (p_{i0}z_0 + p_{i1}z_1 + p_{i2}z_2) + e_{jik:t} \end{aligned}$$

where

V_j is a random contemporary group (visit) effect which is assumed to follow a normal distribution with mean 0 and variance, $\sigma_c^2 = 4$.

b_0, b_1, and b_2 are fixed regression coefficients on $(A) =$ age and age squared which describes the general relationship between age and the observations.

a_{i0}, a_{i1}, and a_{i2} are random regression coefficients for animal i additive genetic effects, assumed to follow a multivariate normal distribution with mean vector null and variance-covariance matrix, **G**.

p_{i0}, p_{i1}, and p_{i2} are random regression coefficients for animal i permanent environmental effects, assumed to follow a multivariate normal distribution with mean vector null and variance-covariance matrix, **P**.

z_0, z_1, and z_2 are the Legendre polynomials based on standardized ages and derived as indicated earlier. The minimum age was set at 18 and the maximum age was set at 68 for calculating the Legendre polynomials.

and e_{jik} is a temporary residual error term assumed to follow a normal distribution with mean 0 and variance, $\sigma_e^2 = 9$. In this example, the residual variance is assumed to be constant across ages.

Animal Breeding, Modeling in. Table 5 Example data for random regression model

Cow	Sire	Dam	Visit 1		Visit 2		Visit 3		Visit 4	
			Age(m)	Obs.	Age(m)	Obs.	Age(m)	Obs.	Age(m)	Obs.
1	7	5	22	224	34	236	47	239		
2	7	6	30	244	42	247	55	241	66	244
3	8	5	28	224	40	242				
4	8	1			20	220	33	234	44	228

The model in matrix notation is

$$\mathbf{y} = \mathbf{Xb} + \mathbf{Wv} + \mathbf{Za} + \mathbf{Zp} + \mathbf{e},$$

where

$$\mathbf{X} = \begin{pmatrix} 1 & 22 & 484 \\ 1 & 30 & 900 \\ 1 & 28 & 784 \\ 1 & 34 & 1156 \\ 1 & 42 & 1764 \\ 1 & 40 & 1600 \\ 1 & 20 & 400 \\ 1 & 47 & 2209 \\ 1 & 55 & 3025 \\ 1 & 33 & 1089 \\ 1 & 66 & 4356 \\ 1 & 44 & 1936 \end{pmatrix}, \quad \mathbf{y} = \begin{pmatrix} 224 \\ 244 \\ 224 \\ 236 \\ 247 \\ 242 \\ 220 \\ 239 \\ 241 \\ 234 \\ 244 \\ 228 \end{pmatrix},$$

$$\mathbf{W} = \begin{pmatrix} 1 & 0 & 0 & 0 \\ 1 & 0 & 0 & 0 \\ 1 & 0 & 0 & 0 \\ 0 & 1 & 0 & 0 \\ 0 & 1 & 0 & 0 \\ 0 & 1 & 0 & 0 \\ 0 & 1 & 0 & 0 \\ 0 & 0 & 1 & 0 \\ 0 & 0 & 1 & 0 \\ 0 & 0 & 1 & 0 \\ 0 & 0 & 0 & 1 \\ 0 & 0 & 0 & 1 \end{pmatrix},$$

and for animal 1,

$$\mathbf{Z} = \begin{pmatrix} 0.7071 & -1.0288 & 0.8829 \\ 0 & 0 & 0 \\ 0 & 0 & 0 \\ 0.7071 & -0.4409 & -0.4832 \\ 0 & 0 & 0 \\ 0 & 0 & 0 \\ 0 & 0 & 0 \\ 0.7071 & 0.1960 & -0.7299 \\ 0 & 0 & 0 \\ 0 & 0 & 0 \\ 0 & 0 & 0 \\ 0 & 0 & 0 \end{pmatrix}$$

In order to reduce rounding errors, the covariates of age for the fixed regressions can be forced to have a mean of approximately zero by subtracting 38 from all ages and 1642 from all ages squared.

The entire MME cannot be presented, but parts of the MME are given below.

$$\mathbf{W'W} = \begin{pmatrix} 3 & 0 & 0 & 0 \\ 0 & 4 & 0 & 0 \\ 0 & 0 & 3 & 0 \\ 0 & 0 & 0 & 2 \end{pmatrix},$$

$$\mathbf{W'X} = \begin{pmatrix} 3 & -34 & -2,758 \\ 4 & -16 & -1,648 \\ 3 & 21 & 1,397 \\ 2 & 34 & 3,008 \end{pmatrix},$$

$$\mathbf{X'X} = \begin{pmatrix} 12 & 5 & -1 \\ 5 & 1,995 & 166,883 \\ -1 & 166,883 & 14,415,319 \end{pmatrix},$$

$\mathbf{Z'Z}$ is composed of the following four blocks of order 3, for the four animals with records;

$$\text{Animal1} \quad \begin{pmatrix} 1.5 & -0.9006 & -0.2335 \\ -0.9006 & 1.2912 & -0.8383 \\ -0.2335 & -0.8383 & 1.5457 \end{pmatrix},$$

$$\text{Animal2} \quad \begin{pmatrix} 2 & 0.7275 & 0.0259 \\ 0.7275 & 2.0233 & 1.3612 \\ 0.0259 & 1.3612 & 2.1815 \end{pmatrix},$$

$$\text{Animal3} \quad \begin{pmatrix} 1 & -0.6235 & -0.4902 \\ -0.6235 & 0.5615 & 0.0648 \\ -0.4902 & 0.0648 & 0.5761 \end{pmatrix},$$

$$\text{Animal4} \quad \begin{pmatrix} 1.5 & -1.1085 & 0.0134 \\ -1.1085 & 1.5121 & -1.2082 \\ 0.0134 & -1.2082 & 2.2687 \end{pmatrix}.$$

and $\mathbf{Z'X}$ for all animal is

$$\mathbf{Z'X} = \begin{pmatrix} 2.12 & -7.78 & -761.55 \\ -1.27 & 19.99 & 1516.76 \\ -.33 & -18.76 & -1201.42 \\ 2.83 & 28.99 & 2458.59 \\ 1.03 & 46.44 & 4337.80 \\ 0.04 & 27.97 & 2979.60 \\ 1.41 & -5.66 & -636.39 \\ -.88 & 7.05 & 636.63 \\ -.69 & -2.14 & -22.46 \\ 2.12 & -12.02 & -1061.36 \\ -1.57 & 23.03 & 1684.81 \\ .02 & -24.57 & -1515.25 \end{pmatrix}.$$

The right hand sides of the MME are

$$\mathbf{X}'\mathbf{y} = \begin{pmatrix} 2,823 \\ 2,070 \\ 68,064 \end{pmatrix},$$

$$\mathbf{W}'\mathbf{y} = \begin{pmatrix} 692 \\ 945 \\ 714 \\ 472 \end{pmatrix},$$

and

$$\mathbf{Z}'\mathbf{y} = \begin{pmatrix} 494.2629 \\ -287.6596 \\ -90.7117 \\ 690.1296 \\ 249.1165 \\ 7.3023 \\ 329.5086 \\ -200.1692 \\ -168.8920 \\ 482.2422 \\ -351.3606 \\ -7.8918 \end{pmatrix}.$$

The variance-covariance matrices of the additive and permanent environmental effects need to be known for BLUP. Normally, these are not well known and must be estimated simultaneously with the other effects of the model. Let

$$\mathbf{G} = \begin{pmatrix} 94.0000 & -3.8500 & 0.03098 \\ -3.8500 & 1.5000 & -0.0144 \\ 0.03098 & -0.0144 & 0.0014 \end{pmatrix},$$

and

$$\mathbf{P} = \begin{pmatrix} 63.0000 & -2.1263 & 0.0447 \\ -2.1263 & 0.5058 & -0.00486 \\ 0.0447 & -0.00486 & 0.0005 \end{pmatrix}.$$

The solutions to MME are

$$\hat{\mathbf{b}}' = (\,234.9797 \quad 1.4670 \quad -0.01399\,),$$

$$\hat{\mathbf{c}}' = \begin{pmatrix} -0.8630 \\ 1.2885 \\ 0.1443 \\ -0.5698 \end{pmatrix}.$$

Let the solutions for the animal additive genetic random regression coefficients be presented in tabular form as follows.

Animal	a_0	a_1	a_2
1	−2.021529	0.175532	−0.002696
2	5.751601	−2.139115	0.025848
3	−2.474456	2.554412	−0.029269
4	−5.376687	−0.370873	0.002174
5	−1.886714	1.464975	−0.016963
6	3.333268	−1.065525	0.013047
7	1.503398	−1.081654	0.012555
8	−2.948511	0.681643	−0.008633

Similarly, the solutions for the animal permanent environmental random regression coefficients can be given in tabular form.

Animal	p_0	p_1	p_2
1	−0.296786	0.246946	−0.002521
2	3.968256	−730659	0.009430
3	−0.834765	0.925329	−0.008164
4	−4.505439	−441805	0.001257

Ranking Animals The problem is to rank the animals for selection purposes. If animals are ranked on the basis of a_0, then animal 2 would be the highest (if that was desirable). If ranked on the basis of a_1, then animal 3 would be the highest, and if ranked on the basis of a_2, then animal 2 would be the highest. To properly rank the animals, an EBV at different ages could be calculated, and then these could be combined with appropriate economic weights. EBVs were calculated for 24, 36, and 48 mo of age, and economic weights of 2, 1, and 0.5, respectively, for the three EBVs were used to compute a Total Economic Value (TEV), as

$$2 * \mathrm{EBV}(24) + 1 * \mathrm{EBV}(36) + .5 * \mathrm{EBV}(48).$$

The Legendre polynomials for ages 24, 36, and 48 mo are given in the rows of the following matrix **L**,

$$\mathbf{L} = \begin{pmatrix} 0.7071 & -0.8328 & 0.3061 \\ 0.7071 & -0.3429 & -0.6046 \\ 0.7071 & 0.2449 & -0.6957 \end{pmatrix}.$$

The results are shown in the following table.

Animal	EBV(24)	EBV(36)	EBV(48)	TEV
1	−1.58	−1.49	−1.38	−5.33
2	5.86	4.78	3.53	18.26
3	−3.89	−2.61	−1.10	−10.93
4	−3.49	−3.68	−3.89	−12.61
5	−2.56	−1.83	−96	−7.43
6	3.25	2.71	2.09	10.25
7	1.97	1.43	.79	5.76
8	−2.66	−2.31	−1.91	−8.58

The animal with the highest TEV was animal 2. All animals ranked rather similarly at each age on their EBVs. Rankings of animals could change with age. Thus, the pattern of growth could be changed.

Plotting Curves The shapes of curves of individual animals could also be plotted from the solutions, and shown as deviations from the average curves. Figure 5 contains animals 1 (black), 2 (red), 4 (blue), and 6 (brown). Animal 2 had the highest TEV, but that ranking was achieved by Animal 2 having the highest initial deviation. However, the curve declines very rapidly after time 18. The curves of the other animals do not decline as rapidly, and the curve for Animal 1 actually increases slightly. Depending on the biology of the trait and the welfare of the animal, one may decide to select for animals with increasing curves rather than declining curves. The weights in the TEV could be adjusted accordingly.

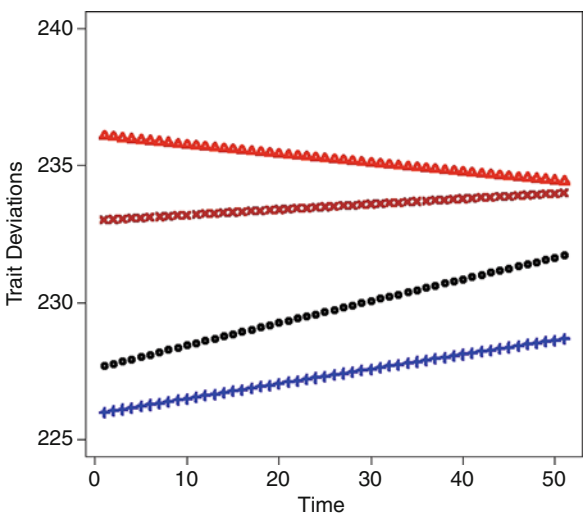

Animal Breeding, Modeling in. Figure 5
Curves for animals 1 (*black*), 2 (*red*), 4 (*blue*), and 6 (*brown*), in the example data

Comments

The orders of the Legendre polynomials do not need to be equal for both the animal additive genetic and animal permanent environmental effects. The order of the fixed regressions could also be different, and as seen in this example can be based on a different function of time covariates.

There are other kinds of orthogonal functions that could be used in place of Legendre polynomials, and some of these have been tried without much benefit to the analyses (Yazdi?). Another alternative has been spline (split polynomial) functions, [19, 22] in which a curve is broken down into sections. Within each section, a simple linear or quadratic function is sufficient to fit the data within that section. The sections are joined together by "knots," the locations of which need to be estimated. Spline functions have gained some popularity lately.

Because random regression models were new to animal breeding in 1994, [20] they were applied to many different types of research problems. RRM have been most successful in the analysis of dairy cattle test day production within lactations, and in growth of pigs, sheep, rainbow trout, and beef cattle. One limitation with growth data is that animals are not usually weighed more than three or four times in their life due to the amount of labor involved in collecting weights and the stress induced on the animals during the weighing process. The orders of the regression coefficients for growth traits are usually limited to 2 or 3.

Multiple Trait Models

Animals are observed for many traits relating to production, reproduction, conformation, longevity or

fitness, and health such that knowing the total economic merit of an animal helps to keep costs of production to a minimum. Most traits are genetically correlated to each other, meaning that some genes affect more than one trait. Because contemporary animals make their records in the same environment, environmental correlations due to management, feed, and temperature also exist to affect observations on all traits. Thus, a sensible approach is to analyze groups of traits using *multiple trait models* [23–26]. In this way, information from correlated traits can be used to improve the accuracy of all trait evaluations. A multiple trait (MT) model is one in which two or more traits are analyzed simultaneously in order to take advantage of genetic and environmental correlations between traits.

Low Heritability Traits: MT models are useful for traits where the differences between genetic and residual correlations are large (e.g., greater than 0.5 difference) or where one trait has a much higher heritability than the other traits. EBVs for traits with low heritability tend to gain more in accuracy than EBVs for traits with high heritability, although all traits benefit to some degree from the simultaneous analysis(24).

Culling: Another use of MT models is for traits that occur at different times in the life of the animal such that culling of animals results in fewer observations on animals for traits that occur later in life compared to those at the start. Consequently, animals which have observations later in life tend to have been selected based on their performance for earlier traits. Thus, analysis of later life traits by themselves could suffer from the effects of culling bias, and the resulting EBV could lead to errors in selecting future parents. MT analyses have been shown to partially account, to some degree, for the selection that has taken place [25, 26]. If the percentage of missing trait observations is high and the missing observations are not due to random chance, then biases could be very large in EBVs for that trait and maybe others.

The success of an MT analysis relies on the accuracy of the genetic and residual correlations that are assumed. Computations for MT models are more complicated than for single trait analyses. If m is the number of traits and N is the number of animals in the pedigree file, then there are at least mN equations to be solved rather than just N, and the same relative difference in memory space to hold solutions. However, computer hardware advances (with gigabytes of memory) have been very rapid in the last decade. Consequently, many genetic evaluation systems are now multiple trait systems.

Models and Traits

Usually, traits are grouped together for MT analyses because they are observed at approximately the same point in time. For example, milk, fat, and protein yields of dairy animals are observed on the same day, per animal. Thus, for a group of similar traits, the linear models associated with those traits include the same major factors like years, ages, contemporary groups, and animal additive genetic effects. Another grouping of traits would be those for reproductive traits, observed primarily on females, such as conception rate, litter size, birthing ease, and offspring losses at birth. The linear models used for production traits are quite different from those used for reproductive traits, or health traits.

Even within a group, the linear models for the traits within a group could be different from each other. Consider two traits with a single observation per trait on animals. Let the model equation for trait 1 be

$$y_{1ij} = B_{1i} + a_{1j} + e_{1ij},$$

where B_{1i} is a fixed effect with p_B levels, a_{1j} is a random, animal additive genetic effect for trait 1, and e_{1ij} is a random residual environmental effect for trait 1.

The model equation for trait 2 might be

$$y_{2ij} = C_{2i} + a_{2j} + e_{2ij},$$

where C_{2i} is a fixed effect (different from B_{1i} for trait 1) with p_C levels, a_{2j} is a random, animal additive genetic effect for trait 2, and e_{2ij} is a random residual environmental effect for trait 2.

For example, y_{1ij} could be birth weight, so that B_{1i} could identify animals born in the same season. Trait 2 could be yearling weights and C_{2i} could identify contemporary groups of animals of the same sex, same herd, and same rearing unit within herd.

Because the two traits will be analyzed simultaneously, variances and covariances need to be specified

for the traits together. For example, the additive genetic variance-covariance (VCV) matrix (between traits) could be written as

$$\mathbf{G} = \begin{pmatrix} g_{11} & g_{12} \\ g_{12} & g_{22} \end{pmatrix} = \begin{pmatrix} 1 & 2 \\ 2 & 15 \end{pmatrix},$$

and the residual environmental VCV matrix as

$$\mathbf{E} = \begin{pmatrix} e_{11} & e_{12} \\ e_{12} & e_{22} \end{pmatrix} = \begin{pmatrix} 10 & 5 \\ 5 & 100 \end{pmatrix}.$$

The genetic and residual correlations are, respectively,

$$\rho_g = 2/(15)^{0.5} = 0.516,$$
$$\rho_e = 5/(1000)^{0.5} = 0.158$$

with heritabilities specified as

$$h_1^2 = \frac{1}{11} = 0.0909,$$

and

$$h_2^2 = \frac{15}{115} = 0.1304.$$

For all data, using **A** as the additive numerator relationship matrix, then

$$\mathrm{Var}\begin{pmatrix} \mathbf{a}_1 \\ \mathbf{a}_2 \end{pmatrix} = \begin{pmatrix} \mathbf{A}g_{11} & \mathbf{A}g_{12} \\ \mathbf{A}g_{12} & \mathbf{A}g_{22} \end{pmatrix}.$$

Data Example

A two trait example with three factors is given in Table 6. Note that animals whose trait 1 observation was below 3.0 were not allowed to make a trait 2 observation. If the true variances and covariances are known, then this selection bias will be lessened through the multiple trait analysis, as long as the analysis includes the trait 1 records of animals with missing trait 2 observations.

There were two levels of factor B associated with trait 1, and 3 levels of factor C associated with trait 2. The models assumed are those given in the previous section including the covariance matrices that were given.

Animal Breeding, Modeling in. Table 6 Example data for multiple trait models

Animal	Sire	Dam	B-level	C-level	Trait 1	Trait 2
1	0	0	1	1	2.3	
2	0	0	1	2	2.6	
3	0	0	1	3	9.8	53
4	0	0	1	1	4.7	4
5	0	0	1	2	5.5	63
6	1	3	2	3	2.5	
7	1	4	2	2	8.4	35
8	1	5	2	3	8.2	41
9	2	3	2	1	9.0	27
10	2	4	2	1	7.8	32
11	2	5	2	2	2.8	
12	6	10	2	3	7.4	67

Mixed Model Equations

The models are written in matrix notation below.

$$\begin{pmatrix} \mathbf{y}_1 \\ \mathbf{y}_2 \end{pmatrix} = \begin{pmatrix} \mathbf{X}_1 & \mathbf{0} \\ \mathbf{0} & \mathbf{X}_2 \end{pmatrix}\begin{pmatrix} \mathbf{b}_1 \\ \mathbf{b}_2 \end{pmatrix} + \begin{pmatrix} \mathbf{Z}_1 & \mathbf{0} \\ \mathbf{0} & \mathbf{Z}_2 \end{pmatrix}\begin{pmatrix} \mathbf{a}_1 \\ \mathbf{a}_2 \end{pmatrix} + \begin{pmatrix} \mathbf{e}_1 \\ \mathbf{e}_2 \end{pmatrix}$$

Let **R** be the covariance matrix of residual effects. If observations are ordered by traits within animals, then **R** is the direct sum of submatrices, one for each animal. The submatrices depend on which traits are observed for a given animal. If an animal has been observed for both (all) traits, then the diagonal block is **E** as given earlier. If an animal has been observed only for trait 1, then the block is

$$\mathbf{E}_1 = \begin{pmatrix} e_{11} & 0 \\ 0 & 0 \end{pmatrix},$$

and if the animal has been observed only for trait 2, then

$$\mathbf{E}_2 = \begin{pmatrix} 0 & 0 \\ 0 & e_{22} \end{pmatrix}.$$

With more than two traits, the number of combinations of missing traits increases. The covariance

matrix of residual effects for the example data is a block diagonal matrix,

$$\mathbf{R} = diag(\mathbf{E}_1\ \mathbf{E}_1\ \mathbf{E}\ \mathbf{E}\ \mathbf{E}\ \mathbf{E}_1\ \mathbf{E}\ \mathbf{E}\ \mathbf{E}\ \mathbf{E}\ \mathbf{E}_1\ \mathbf{E}).$$

The inverse of **R** is needed for the mixed model equations, and this can be obtained by inverting the block diagonal matrices (ignoring the zero rows and columns when there are missing observations).

The resulting mixed model equations were of order 29 by 29. The solutions, for this example, were

$$B_{11} = 5.0209$$
$$B_{12} = 6.5592$$
$$C_{21} = 20.0882$$
$$C_{22} = 49.0575$$
$$C_{23} = 51.9553$$

Animal	Sire	Dam	Trait 1	Trait 2
1	0	0	−0.3573	−1.6772
2	0	0	−0.0730	1.0418
3	0	0	0.4105	1.1707
4	0	0	−0.0449	−1.4922
5	0	0	0.0646	0.9570
6	1	3	−0.1033	−1,410
7	1	4	−0.1975	−2.2983
8	1	5	−0.1410	−9,633
9	2	3	0.3079	1.6227
10	2	4	0.1426	1.1273
11	2	5	−0.1830	0.6418
12	6	10	0.1554	1.5089

Notice that every animal has an EBV for both traits, even though trait 2 was missing for some animals. The EBV for an animal with a missing trait observation is constructed based on the genetic and environmental correlations between traits, and based on their genetic relationships to other animals that were observed for both traits.

Economic Indexes

Many producers are so overwhelmed by the numerous EBV available for so many traits that they are unable to visualize the relative contributions of different traits to their overall productivity. Thus, economic indexes were developed where trait EBVs are scaled to unit variances, and then relative economic values are applied to the scaled EBVs. Sometimes different types of indexes are derived depending on the market objectives of the producers. A beef producer, for example, may be producing animals of high carcass merit, and would use an index that puts more weight on carcass traits of marbling score, tenderness, and dressing percentage. Another producer may be producing calves and may want more weight on the reproductive ability of cows and calf survival from birth to weaning. A particular breed may wish to be known as the "Have Everything" breed and would utilize a different set of economic weights where many traits are emphasized.

Economic weights are dynamic in that they change over time, and can often change very dramatically and quickly, usually more quickly than a breeding program can be changed due to the long generation intervals of the species involved. Producers must therefore continually reassess their goals and objectives.

Economic indexes based on multiple trait EBVs tend to be more stable over time compared to the same EBVs computed on each trait separately.

Models for Categorical Data

Categorical data arise in animal breeding in situations where a trait is subjectively scored by the producer or a trained individual. For example, calves can be born with absolutely no assistance of the producer or to the other extreme where the producer must ask for veterinarian assistance to perform a caesarian section to deliver the calf and save the cow. Between those two extremes are different levels of difficulty of calving. Recording programs provide four or five categories of difficulty, and the producer must decide to which category a calving belongs. The assumption is that one producer assigns all calvings based on the same criteria, but a different producer may have slightly different criteria.

The number of calvings falling into each category depends on the subjectivity of the producers. In most breeds, the category for unassisted or easy births is usually very high (from 50% to 90% of all calvings), while the other categories are often much smaller and

the category for caesarian births being the smallest. The categories are ordered from one extreme to the other.

In dairy cattle, cows are scored for 30 or more conformation traits (i.e., style points) by trained judges, and each trait has 9 or more categories. Judges are trained and updated annually, but judges can differ in their abilities to score traits, particularly when they are trained to score a cow in a few minutes.

Theory

Although a trait may be scored into one of a limited number of categories, an underlying non-observable, normally distributed trait could be hypothesized [27–29]. Then thresholds along the scale are where the categories of the observed scores are defined, as shown in Fig. 6.

Thus, when an animal's underlying scale trait exceeds a threshold value, then it belongs to the next higher category. The threshold model is ideal for analyzing categorical data. The analysis follows Bayesian concepts and is nonlinear in the solutions to this model.

Write a model for the underlying scale variable.

$$\ell_{ijkm} = t_i + b_j + a_k + e_{ijkm},$$

where ℓ_{ijkm} is an unobserved value on the underlying scale for the trait of interest; t_i is one of the threshold points; b_j is a fixed factor such as age of the dam, breed, year, or season; a_k is an animal additive genetic effect; and e_{ijkm} is a residual error effect. The model could be much more complex than that described here, depending on the trait and situation.

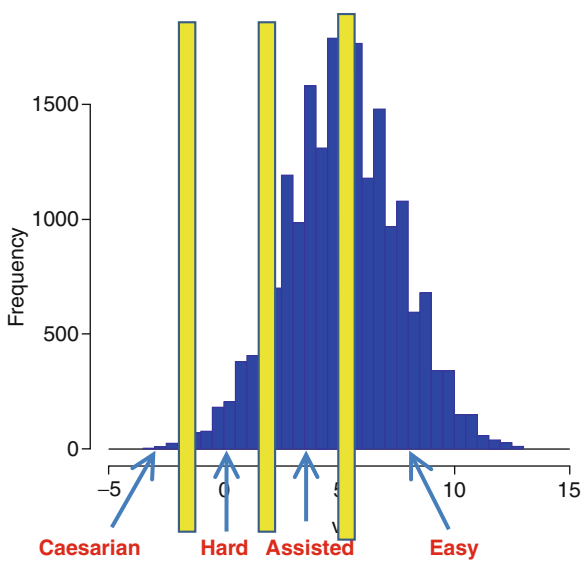

Animal Breeding, Modeling in. Figure 6
Normal distribution with thresholds for calving ease

Note that, instead of observations on the underlying scale, only the category to which an animal belongs is known. There are various quantities which need to be computed repeatedly in the analysis, and these are based on normal distribution functions.

1. $\Phi(x)$ is known as the cumulative distribution function of the normal distribution. This function gives the area under the normal curve up to the value of x, for x going from minus infinity to plus infinity (the range for the normal distribution). For example, if $x = 0.4568$, then $\Phi(x) = 0.6761$, or if $x = -0.4568$, then $\Phi(x) = 0.3239$. Note that if there are m categories and $k = m$, then $\Phi_k = 1$.
2. $\phi(x)$ is a function that gives the height of the normal curve at the value x, for a normal distribution with mean zero and variance 1. That is,

   $$\phi(x) = (2\pi)^{-0.5} \exp -0.5x^2.$$

   For example, if $x = 1.0929$, then $\phi(x) = 0.21955$.
3. $P(k)$ is the probability that x from a $N(0, 1)$ distribution is between two threshold points, or is in category k. That is,

   $$P(k) = \Phi_k - \Phi_{k-1}.$$

   If $k = 1$, then $\Phi_{k-1} = 0$.

Begin with phenotypic values for t_i based on a normal distribution. From the t_i, observations on the underlying scale can be "created." Each one would have a different weight in the analysis due to the frequency of a category being observed. Then new values of b_j and a_k are calculated. Finally, new values of t_i are determined, and the process is repeated. Eventually, the process converges until "solutions" for all variables do not change. This is an overly simplified explanation. For more details, see [30].

Solutions

Using the estimates from the nonlinear system of equations, the probability of a animal's offspring falling into each category can be calculated. Let $\hat{a}_k = 0.123$, and let

there be a 3 category trait. The solutions for the two thresholds were $\hat{t}_1 = 0.376$ and $\hat{t}_2 = 1.012$. Then the value on the underlying scale for the first category would be

$$\begin{aligned} x &= \hat{t}_1 + \hat{a}_k, \\ &= 0.376 + 0.123, \\ &= 0.499. \end{aligned}$$

Then

$$\Phi(x) = \Phi(0.499) = 0.691.$$

Similarly, the probability of the animal's offspring to be in categories 1 or 2 would be based on the second threshold,

$$x = 1.012 + 0.123 = 1.135,$$

or $\Phi(x) = 0.872$. Thus, the proportion of offspring that would fall in category 2 would be $0.872 - 0.691 = 0.181$. The proportion that would be in category 3 would be $1.0 - 0.872 = 0.128$.

Animals could be ranked on their $\hat{a}$, or the result could be expressed as a probability of being in a particular category. For a trait like calving ease, for example, one might want to maximize the probability of having an easy birth.

Comments

While a threshold model is a theoretically best approach to the analysis of categorical data, research has found small differences in accuracy of ranking animals from procedures that treat the category numbers as any continuously distributed trait [31]. As the number of categories increases, the differences between a threshold model analysis and simple linear model analysis become smaller.

Computational problems may arise with threshold models due to small numbers of observations in one or more categories. This often causes two categories to be merged into one to bypass the problem.

Categorical traits are often standardized to a normal scale, and then analyzed with a usual linear model [32]. If the threshold values on a normal scale were 0.376 and 1.012 for a three category trait, then all observations in category 1 would receive a score of $(0.376 - 0)/2 + 0 = 0.188$. Category 2 observations would be scored $(1.012 - 0.376)/2 + 0.376 = 0.694$, and category 3 would be scored $(3 - 1.012)/2 + 1.012 = 2.006$. Standardization is often conducted within years, or time periods in which the subjective scoring was applied consistently.

Because categorical traits are subjectively recorded, the subjectiveness can fluctuate over time. An animal that was assessed to be category 1 20 years ago, may now (if the animal were alive today at the same age) belong to category 2. The standards of the observer(s) have changed over those 20 years. The change is similar to the change in the value of the US dollar between now and 20 years ago. Today $1 does not buy as much as $1 back in 1990. The consequence of shifting standards (in animal breeding) is that genetic trends cannot be properly estimated. Comparing animals many years apart is not statistically accurate for categorical data. This is not a major problem because producers mainly want to compare animals that are alive today, and for this purpose, the assumption is that subjective standards change rather slowly and not by very much in a short time span of about 5 years.

Methods have also been developed for multiple trait models involving traits that are categorical and other traits that are continuous [33, 34]. These have primarily been cases of binomial traits, such as disease traits (yes or no situations). Binomial traits have only one threshold to be estimated, and binomial traits seem to benefit from a threshold model.

Models for Survival Data

In animal production systems, animals remain in the herd or flock as long as they are productive and generate more income than expenses. Eventually, animals leave the production unit due to natural death or injury, or due to lowered production levels or reproductive problems such that the animal is deemed unprofitable. The latter factors are determined by the owner, and owners differ widely in their management skills, accounting, and decision-making abilities. There seems to be a small amount of genetic variability among animals in survival rates that do not depend on productive abilities, and genetic evaluation systems for survivability or longevity have been developed. The heritability of survival is usually less than 0.02. Dairy sires, for example, need thousands of progeny in order to have an accurate Estimated Breeding Value for survival ability of their progeny.

Survival has been defined in many different ways. In a binary sense, alive is equal to 1, every day until the animal dies and thereafter becomes 0 for the remainder of the observable time period. For example, in dairy cattle, the observable period is from first calving until 100 months later (approximately 10 years of age) when the majority of cows have died. The time intervals in that range can be hours, days, weeks, months, or years. Define a survival vector for the ith cow as $\mathbf{s}_i$, in terms of months (from 1 to 100), such that the values of $\mathbf{s}_i$ are equal to 1 for every month the cow was alive, and equal to 0 for the month in which it dies and every month thereafter to the limit of 100 months after first calving.

A cow at 44 months after first calving today is still alive, and its future death time is unknown, then the values for months 45–100 need to be considered missing or not observed. For a cow that is still alive 100 months after first calving, then $\mathbf{s}_i$ contains all ones. If a cow has gone missing from the data, in the sense that it was sold to another owner and that owner is not on a milk recording program, then the cow has not died, but the exact time of its death is not known. In this case, $\mathbf{s}_i$ will contain 1s up until the time it was sold, and all remaining values in $\mathbf{s}$ are unknown (neither 1 nor 0).

Having defined $\mathbf{s}_i$ for cow i, then let $\mathbf{S}$ be the average of all $\mathbf{s}_i$ for cows that do not have any missing values. The elements of $\mathbf{S}$ are equal to the probabilities of being alive at each month after first calving, and can be plotted as shown in Fig. 7. The value at a given time (month) is a probability, p_t. The black points refer to the average $\mathbf{S}$ for all cows, while the blue and red lines indicate 2 standard deviations above and below the average, respectively. Note that the variation is less around p_1 and p_{100} than in the middle of the range.

Because a curve is involved, a random regression model could be applied [35, 36] such that a separate set of curve parameters could be estimated for each animal. The model would include the year-season of first calving (with separate curves for each year-season), random herd within year-season of first calving, a variable that indicates whether the herd was increasing, decreasing, or being stable in size at a particular instance of time, a regression on the genetic EBV of an animal for production, random animal additive genetic regression coefficients, and random animal permanent environmental regression coefficients. The model would also need to account for different residual

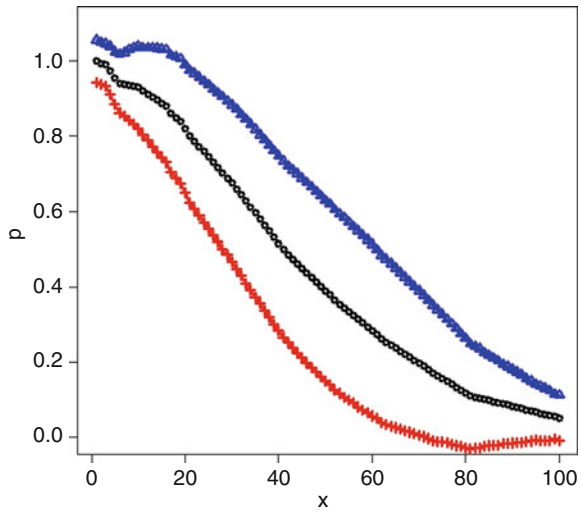

Animal Breeding, Modeling in. Figure 7
Survival curve for Jersey cattle after first calving, in months

variances for each month after first calving. Meuwissen et al. [36] have shown links between various models for survival analyses. Jamrozik et al. [37] did a comparison of the effectiveness of different models for survival.

Another model is the proportional hazard model (PHM) [38],

$$\lambda(t) = \lambda_{0,s}(t)\exp[\mathbf{x}'_m\beta + \mathbf{z}'_m u],$$

where $\lambda(t)$ is the probability of a cow being culled at time t given she was alive before time t; $\lambda_{0,s}(t)$ is the Weibull baseline hazard function; β contains time-dependent covariates affecting the hazard function with $\mathbf{x}'_m$ being the corresponding design vectors; $\mathbf{u}$ is a vector of random factors including herd, year-seasons, and animal additive genetic effects; and $\mathbf{z}'_m$ is the associated incidence vector. Thus, a nonlinear system of equations needs to be solved.

Lastly, survival could be defined as a discrete trait, such as the survival of an animal to the end of first, second, or third lactation. The three "traits" can be analyzed as a multiple trait system, in which cows need not be observed for all traits. This is similar to the random regression approach except the number of months after first calving is reduced to just 3 or 4 broader periods of time instead of monthly.

Because the heritability of survival is so low, and analyses are affected by the animals that are still alive at the time of analysis, perhaps a better indicator of

survivability would be a measure of profitability of the animal. The traits that are part of profitability would tend to have higher heritabilities, and would contribute toward an animal remaining in the herd. Further research on this area is needed.

Added Complexities

Heterogeneous Variances

In dairy cattle, the within contemporary group variation of records was deemed to differ between contemporary groups. That implied that the contemporary group effects were being sampled from different populations. Consequently, both the genetic and residual variation could be allowed to differ between contemporary groups. Bayesian methods were developed to simultaneously compute solutions to mixed model equations and to estimate the necessary contemporary group variances. Often, only the phenotypic variances within contemporary groups were assumed to differ such that the heritability was constant across contemporary groups.

Robust Estimation

Related to heterogeneous variances was the problem of outliers, records that were extreme values in the distribution of phenotypes. Sometimes the extremes were deliberately created by producers who thought they knew how to manipulate the data so that their good animals would receive high EBVs. Other times, the extremes were due to errors in recording, and occasionally were naturally extreme. Regardless of the reason for their existence, the result was a bias to EBVs of one animal or an entire group of animals. Robust estimation methods were introduced to pull the extreme records back toward the mean. Either the record itself or the estimated residual effect of the record could be modified toward the mean if it was beyond two and half standard deviations from the mean. Robust methods usually reduce the biases caused by extreme outliers, but the method requires nonlinear estimation.

Count Data

In swine and sheep breeding, interest is in litter size, which is not normally distributed and also not categorical, but is known as *count* data. Another trait is number of services to attain conception, or number of ovulations. Behavioral traits can also be count data, such as the number of times an animal takes water during the day. The appropriate distribution for count data is a Poisson distribution, and Bayesian methods for handling and modeling this distribution have been developed.

Hierarchical Models

Another Bayesian development was that of hierarchical models where a trait is modeled in the usual way, but then a component of that model has its own separate model. Thus, two models are solved in steps, until the solutions satisfy both models.

Model Comparisons

Methods have also been developed to compare different models, but even further to select from among a group of models for the better fitting model. Model comparisons are usually conducted using an "estimation" data set (with which to estimate variances and solutions to mixed model equations), and a second, sometimes smaller, "validation" data set to judge how well observations and rankings of animals can be predicted.

International Comparisons

Some species of livestock are traded among countries, depending on health restrictions, and this necessitates comparing the genetic abilities of animals between countries. Usually the genetic evaluation of animals within a country has enough complexities to it such that the models used in country A are very different and incompatible with the models in country B. Thus, EBVs from the different countries are collated and a multiple trait model (where each country is a different trait) is applied to the EBVs of male animals. Genetic correlations among countries are less than unity and rankings of animals may differ between countries. The Interbull organization in Uppsala, Sweden routinely computes evaluations for dairy bulls from 23 or more countries every year.

Future Directions

Molecular genetics will dominate animal breeding research in the next 20 years. The discovery of millions of single nucleotide polymorphisms as genetic markers has forced animal breeders to restudy their basic

quantitative genetics notes. The DNA genomes of animal species are being completely mapped, and someday soon all of the genes and their locations in the genome will be known. This is an exciting time for animal breeders and the opportunities for research will be huge.

Already DNA markers are being used to determine the relatedness of individuals to each other, to measure the amount of genetic diversity in a species, to identify genes with major effects on production traits, and to select future breeding animals more accurately than previously possible and as soon as an animal is born. Models for genetic evaluation of animals have been modified to include genetic marker information and are thus becoming more complicated, involving many thousands of markers such that computing issues are more demanding than for multiple trait models. The result is that animals are being selected more intensely at an early age, and the samples of progeny are no longer a random group of all possible progeny of a particular mating, but are highly selected. This lack of randomness of sampling progeny may cause biases in current genetic evaluation models. The possibility also exists that rates of inbreeding could be increased. Modeling of production systems and strategies for making continued genetic change will be utilized.

Bayesian methods will likely be utilized more heavily than the methods of Henderson [2] in order to deal with DNA modifications to statistical models. Structural equation models [39] will try to determine the cause and effects of multiple traits. Statistical models, linear and nonlinear, continue to be required background training for animal breeders. The complexity and usefulness of models will grow even with the emergence of genomics.

Bibliography

1. Lush JL (1945) Animal breeding plans. Iowa State University Press, Ames
2. Henderson CR (1984) Applications of linear models in animal breeding. University of Guelph, Ontario
3. Gianola D, Fernando RL (1986) Bayesian methods in animal breeding. J Anim Sci 63:217–244
4. Sorensen D, Gianola D (2002) *Likelihood,* Bayesian and MCMC methods in quantitative genetics. Springer, New York
5. Johannsen WJ (1909) Elemente der Exakten Erblichkeitslehre. Gustav Fischer, Jena
6. Wright SE (1933) Evolution and the genetics of populations, vol I. University of Chicago Press, Chicago
7. Henderson CR (1976) A simple method for computing the inverse of a numerator relationship matrix used for prediction of breeding values. Biometrics 32:69–79
8. Meuwissen THE, Luo Z (1992) Computing inbreeding coefficients in large populations. Genet Sel Evol 24:305–313
9. Quaas RL (1988) Additive genetic model with groups and relationships. J Dairy Sci 71:1338–1345
10. Robinson GK (1986) Group effects and computing strategies for models for estimating breeding values. J Dairy Sci 69:3106–3111
11. Patterson HD, Thompson R (1971) Recovery of interblock information when block sizes are unequal. Biometrika 58:545–554
12. Graser H-U, Smith SP, Tier B (1987) A derivative free approach for estimating variance components in animal models by restricted maximum likelihood. J Anim Sci 64:1362–1370
13. Meyer K, Smith SP (1996) Restricted maximum likelihood estimation for animal models using derivatives of the likelihood. Genet Sel Evol 28:23–49
14. Wang CS, Rutledge JJ, Gianola D (1993) Marginal inferences about variance components in a mixed linear model using Gibbs sampling. Genet Sel Evol 25:41–62
15. Bijma P (2006) Estimating maternal genetic effects in livestock. J Anim Sci 84:800–806
16. Thompson R (1976) The estimation of maternal genetic variances. Biometrics 32:903–918
17. Schaeffer LR, Kennedy BW (1989) Effects of embryo transfer in beef cattle on genetic evaluation methodology. J Anim Sci 67:2536–2543
18. Heydarpour M, Schaeffer LR, Yazdi MH (2008) Influence of population structure on estimates of direct and maternal parameters. J Anim Breed Genet 125:89–99
19. Meyer K (2005) Random regression analyses using B-splines to model growth of Australian Angus cattle. Genet Sel Evol 37:473–500
20. Schaeffer LR, Dekkers JCM (1994) Random regressions in animal models for test-day production in dairy cattle. In: Proceedings of the 5th world congress of genetics applied to livestock production, Guelph, 7–12 Aug 1994, vol 18 p 443
21. Schaeffer LR (2004) Application of random regression models in animal breeding. Livest Prod Sci 86:35–45
22. Misztal I (2006) Properties of random regression models using linear splines. J Anim Breed Genet 123:74–80
23. Henderson CR, Quaas RL (1976) Multiple trait evaluation using relatives' records. J Anim Sci 43:1188–1197
24. Pollak EJ, Quaas RL (1981) Monte Carlo study of within-herd multiple trait evaluation of beef cattle growth traits. J Anim Sci 52:248–256
25. Schaeffer LR (1984) Sire and cow evaluation under multiple trait models. J Dairy Sci 67:1567–1580
26. Pollak EJ, van der Werf J, Quaas RL (1984) Selection bias and multiple trait evaluation. J Dairy Sci 67:1590–1596
27. Gianola D (1982) Theory and analysis of threshold characters. J Anim Sci 54:1079–1096
28. Harville DA, Mee RW (1984) A mixed model procedure for analyzing ordered categorical data. Biometrics 40:393–408

29. Foulley JL, Gianola D (1984) Estimation of genetic merit from bivariate all or none responses. Genet Sel Evol 16:285–306
30. Gianola D, Foulley JL (1983) Sire evaluation for ordered categorical data with a threshold model. Genet Sel Evol 15:201–223
31. Meijering A, Gianola D (1985) Linear versus nonlinear methods of sire evaluation for categorical traits: a simulation study. Genet Sel Evol 17:115–132
32. Snell EJ (1964) A scaling procedure for ordered categorical data. Biometrics 20:592–607
33. Foulley JL, Gianola D (1986) Sire evaluation for multiple binary responses when information is missing on some traits. J Dairy Sci 69:2681–2695
34. Simianer H, Schaeffer LR (1989) Estimation of covariance components between one continuous and one binary trait. Genet Sel Evol 21:303–315
35. Veerkamp RF, Brotherstone S, Engel B, Meuwissen THE (2001) Analysis of censored survival data using random regression models. Anim Sci 72:1–10
36. Meuwissen THE, Veerkamp RF, Engel B, Brotherstone S (2002) Single and multitrait estimates of breeding values for survival using sire and animal models. Anim Sci 75:15–24
37. Jamrozik J, Fatehi J, Schaeffer LR (2008) Comparison of models for genetic evaluation of survival traits in dairy cattle: a simulation study. J Anim Breed Genet 125:75–83
38. Ducrocq VP, Solkner J (1994) "The survival kit", a FORTRAN package for the analysis of survival data. In: Proceedings of the fifth world congress on genetics applied to livestock production, Guelph, 7–12 Aug 1994, vol 22, pp 51–52
39. Wu XL, Heringstad B, Gianola D (2010) Bayesian structural equation models for inferring relationships between phenotypes: a review of methodology, identifiability, and applications. J Anim Breed Genet 127:3–15

Animal Genetic in Environment Interaction

Erling Strandberg
Department of Animal Breeding and Genetics, Swedish University of Agricultural Sciences, Uppsala, Sweden

Article Outline

Glossary
Definition of the Subject
Introduction
Plasticity, Environmental Sensitivity, Reaction Norms and Genotype by Environment Interaction
Models to Describe Genotype by Environment Interaction
Consequences for Breeding Programs
Future Directions
Bibliography

Glossary

Genotype by environment interaction It exists when the difference between the phenotypic values of two genotypes is not the same in two environments.

Plasticity The ability of an individual to respond to changes in the environment.

Reaction norms The phenotypic expression of a genotype as a function of the environment.

Definition of the Subject

The existence of genotype by environment interaction ($G\times E$) makes animal breeding more complicated. It means that the same genotype is not the best in all environments, and it implies that separate breeding programs might be needed to cater for these different environments. However, separate (and therefore, smaller) breeding programs might be less efficient than one large program. Small breeding programs might also encounter problems with inbreeding depression, but on the other hand, several populations with different breeding programs and breeding goals might increase the overall genetic diversity. Therefore, $G\times E$ is an important factor to consider when creating breeding programs for animals, especially in a global setting.

Introduction

The ability to respond to changes in the environment is a vital characteristic of all organisms. This ability is called *phenotypic plasticity* or sometimes, *environmental sensitivity*. Genetic variation in plasticity will lead to *genotype by environment interaction*. This paper starts by describing the phenomenon of plasticity, a term which is not well known in animal breeding. To describe it, several situations will be illustrated, with and without plasticity, by use of reaction norms. This will be followed by a description of various statistical models that can be used to study $G\times E$, including a brief description of genetic heterogeneity of residual variance. Finally, some consequences of $G\times E$ for breeding programs will be discussed.

Plasticity, Environmental Sensitivity, Reaction Norms, and Genotype by Environment Interaction

A *reaction norm* describes the phenotypic expression of a genotype as a function of the environment. One can say that the reaction norm translates the environmental values into phenotypic values. In Fig. 1, the reaction norm for a genotype is shown. The horizontal *x*-axis describes the environment, for simplicity let's assume a continuous scale, e.g., ambient temperature for a certain organism. The vertical *y*-axis gives the phenotypic value for this genotype for each environmental value. In this example, the reaction norm is linear, but it could have any form.

In Fig. 2a, genotypes that show no plasticity are depicted. Note that there is still variation in the level among genotypes, so there is genetic variation in the trait. In Fig. 2b, genotypes showing plasticity are presented. However, all genotypes react in the same way to an environmental change, i.e., there is no variation in plasticity.

In Fig. 2c, the genotypes are plastic, but some are more plastic than others. In other words, there is also variation in plasticity. Now, the genotype with the highest phenotypic value in the low environment also has the highest value in the highest environment. If high phenotypic value is desirable, which genotype to choose would be indisputable.

In Fig. 2d, there is also variation in plasticity; however, here the reaction norms also cross. Which genotype is the best, now depends on in which environment this genotype should be used.

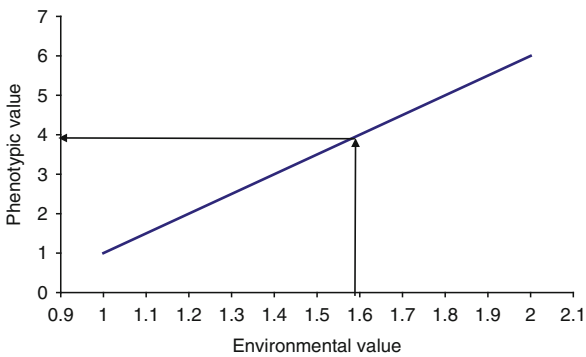

Animal Genetic in Environment Interaction. Figure 1 Schematic description of a reaction norm for a genotype

Thus, differences in phenotypic plasticity between genotypes result in *genotype by environment interaction*. Strictly speaking, $G \times E$ means that the difference between the phenotypic values of two genotypes is not the same in two environments. If the difference changes sign between environments, there is re-ranking of genotypes (Fig. 2d). If the difference changes in size only, there is a scaling effect (Fig. 2c). Note, however, that if the environmental scale had been drawn further to the left in Fig. 2c, there would have been re-ranking also here.

Comparison with the Usual Genetic Model

The most common quantitative genetic model is $P = G + E$ [1]. In this description, G is defined as the *genotypic value* and E as the *environmental deviation*. "We may think of the genotype conferring a certain value on the individual and the environment causing a deviation from this, in one direction or the other" [1]. This might already from the beginning give the impression that G is the central factor, whereas E is just a nuisance, the contribution of which should be decreased as much as possible.

This standpoint actually makes sense from a traditional animal production point of view. The intention is to give all animals as good and standardized treatment as possible in order for them to produce in the best possible way. Therefore, as little as possible should be out of human control (E). Then it can be considered that all animals have the same macroenvironment (same production system, same kind of feed, etc.) and are only affected by microenvironmental effects. To the microenvironmental effects, one might count the effect of the individual farmer (within the rather standardized system), season of production or parturition, etc. These factors can be adjusted for, if known. Thus the environmental or residual variation (σ_E^2) can be decreased. However, there are always some unknown microenvironmental effects (e.g., that the cow is standing close to a door with a cold draft during winter). This will end up in the residual. Therefore, given a certain phenotypic variance, the more that can be adjusted away, the higher the heritability of the trait, and the higher the expected selection response.

Expressed in a graphic way, this traditional model ($P = G + E$) is described in Fig. 2a, the genotypic value

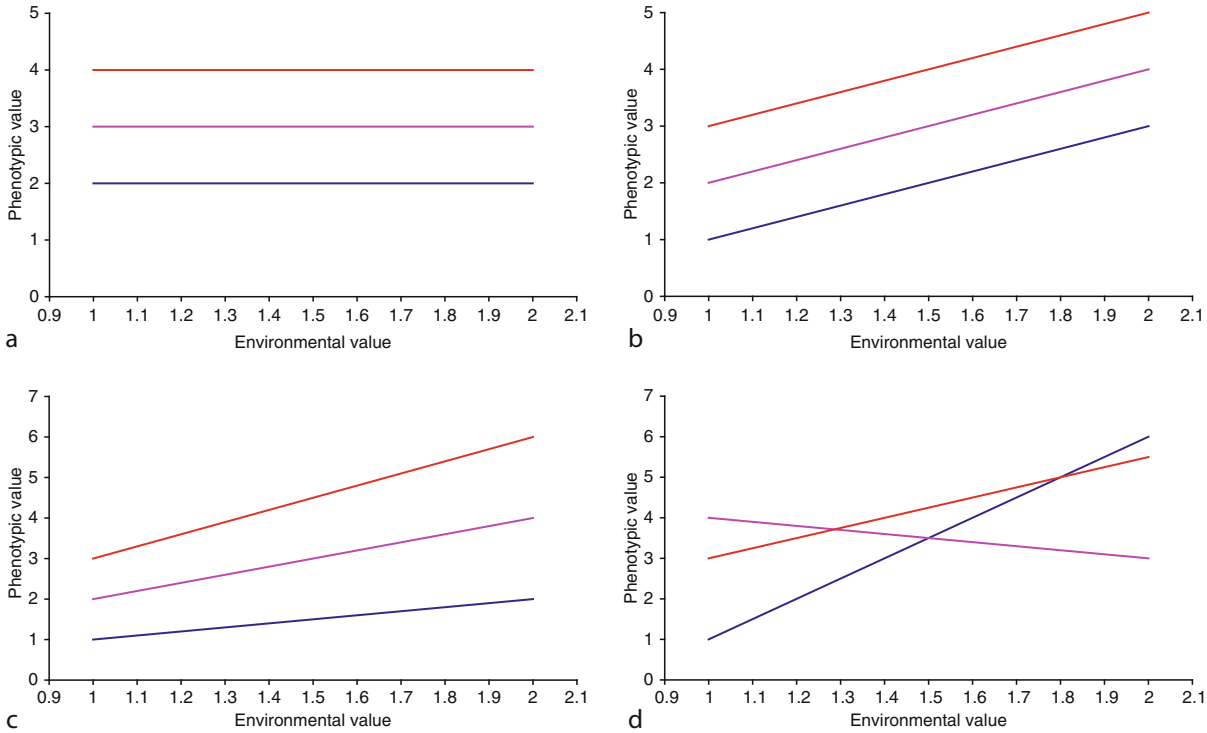

Animal Genetic in Environment Interaction. Figure 2
Description of the reaction norms for three genotypes. (**a**) No plasticity but genetic variation in level. (**b**) Plasticity but no variation in plasticity. (**c**) Variation in plasticity but no re-ranking of genotypes. (**d**) Variation in plasticity and re-ranking of genotypes

only gives a shift in the level of the curve. There may be environmental effects affecting the phenotypic value (as in Fig. 2b), but they affect all individuals in the same way. After adjusting for them (e.g., by a regression), Fig. 2a still applies.

If there are sufficiently different environments (e.g., Northern hemisphere vs. tropical environments), one would still be able to use the traditional model, or rather, two of the traditional models. One would assume that the trait expressed in the tropics is actually a different trait genetically from that in, say, Europe. However, within each environment i, the model $P_i = G_i + E_i$ would still apply.

The difference between this viewpoint and that embodied in the reaction norm and phenotypic plasticity approach is quite substantial, certainly in a conceptual way. In the reaction norm approach, *the environment and the genotype are on equal standing* – there is no way a phenotype can appear without an environment. Philosophically, this makes a lot of sense; a genotype without its environment is nothing, or at least not a phenotype. Certainly, the environment is not something to be "adjusted away" [2, 3].

Staying on the rather philosophical level, it might even be somewhat hard to define what "the environment" is. Obviously, the external environment will qualify (temperature, climate, amount and quality of food etc.). However, the internal environment within an organism is also an environment for the genome. If Richard Dawkins were asked, the whole organism (except the genome) could be considered as the environment (for the genes) [4]. In animal breeding, these fine distinctions are usually disregarded; it is difficult enough to define the external environment!

As stated earlier, the $P = G + E$ model can be said to make sense from an animal (and plant) breeding perspective, at least given certain conditions. It is clear why this model was developed within this setting.

The same applies to the reaction norm model and the developments related to phenotypic plasticity. These models were developed mainly within evolutionary biology and genetics, where the focus is on organisms living under natural conditions. Here, there is no way to standardize the environment – the environment is what it is and it is up to the organism to adapt (or die). Populations may adapt (to a changed or variable environment) by changing genetically, i.e., individuals with higher fitness give rise to more offspring that in turn survive better and so on. After some generations, the population has a different genetic constitution (gene frequencies have changed), which is better suited to this environment, and fitness is higher than before [2].

However, changing genetically is not an option for a given individual. So, what an organism really needs is plasticity! If it can change its phenotype – at least somewhat – it will have a better chance of surviving. Now, it is not necessarily so, that even though plasticity would be good for the individual, that it would occur: there has been a lot of discussing in evolutionary genetics literature about when plasticity is expected to develop in natural populations, but that will not be covered here [2, 5]. Students of natural populations and evolutionary genetics from very early on discovered that *there is phenotypic plasticity* in all organisms studied, at least for some traits. Therefore, it is a reality, and it should be modeled somehow.

Canalization, Homeostasis, and Plasticity

There are some terms that have been used in the evolutionary literature that need some explanation because they are sometimes referred to as the opposite of plasticity [2, 5].

Canalization means that a genotype can *buffer against small changes in the environment and in its own genotype* (mutations). The buffering means that even if small changes occur, the resulting phenotype is more or less the same. These terms are most commonly used for developmental traits, e.g., even if the environment is somewhat variable developmental plan is still followed and the resulting body, say, is still the same. It is, for instance, canalization that makes sure that cows have four legs whether they are born in Sweden or in Africa. In developmental genetics, if the environment has an effect on the phenotype, it is usually an either-or effect, i.e., one type or another, and not a gradual effect.

Homeostasis is the outcome of canalization. Homeostasis measures the degree of (in)variance in the phenotype when the individual is perturbed by changes either in the environment or in the genome (by mutation). A more canalized genotype has higher homeostasis (is changed less) and shows lower variance. In his definition of canalization, Waddington [6] defined it for *minor* variations in conditions, what might be called microenvironmental variation. As an example of canalization, he used the environmentally triggered metamorphosis of axolotls (salamanders)! They produce one of two distinct phenotypes; which one is defined by a large change in environment. Once the developmental pathway is chosen, however, small variations in environment do not affect the outcome, and within each phenotypic outcome, there is canalization.

Models to Describe Genotype by Environment Interaction

There are basically three different models to describe the extent of $G \times E$. For all methods, observations on the same or related individuals in two or more different environments are needed to study $G \times E$. In some organism (e.g., some plants), it is possible to use clones (i.e., numerous copies of the same genotype) and put them in different environments. With animals, that is generally not possible. However, the common use of artificial insemination in, e.g., dairy cattle makes it possible to compare the performance of daughters of the same sires in different environments [7].

In the following, the three methods will be described, not with the intent of understanding how to estimate $G \times E$ using these models (which is relatively straightforward), but more to understand the interpretation of these models, and the type of $G \times E$ that is detected.

Interaction Term Model

The traditional genetic model (e.g., as in [1]) is usually written as: $P = G + E$, where the phenotype P is made up of a genotypic value and an environmental deviation (a residual term) (The mean is either assumed to be included in G or that P is expressed as a deviation from the overall mean). This model corresponds to

Fig. 2a, where the effect of the genotype is just to shift the level by a certain amount, regardless of the environment. In this terminology, the genotype by interaction is often simply written as $P = G + E + G{\times}E$. This terminology is incorrect and confusing: it doesn't make sense to have an interaction with the residual.

The model can be rewritten slightly such that the phenotypic value of an individual is described as the sum of the genotypic value, an environmental value, and a residual:

$$P = G + E + e \tag{1}$$

The environmental value E could, e.g., be classification into herds, herd production classes, production systems or countries. When interaction between genotype and environment exists an interaction component, $G{\times}E$, is added to the equation:

$$P = G + E + G \times E + e \tag{2}$$

The phenotypic variance (σ_P^2) of the observed phenotypes (P) can be derived from Eq. 2 as:

$$\sigma_P^2 = \sigma_G^2 + \sigma_E^2 + \sigma_{GE}^2 + \sigma_e^2 \tag{3}$$

assuming all covariances being zero, and that all main effects are random (E might normally be considered as fixed, having only few levels).

If this model is compared to the graphs in Fig. 2, it is seen that in neither Fig. 2a nor 2b would this model detect any $G{\times}E$ (correctly so). The phenotype in Fig. 2b can be exactly described by the sum of the genotypic values and an environmental value, which is the same for all genotypes. However, in both Fig. 2c and 2d, a nonzero $G{\times}E$ term would show up, simply as a deviation from main effects model. Whether the $G{\times}E$ would give rise to re-ranking or not is not directly seen from the size of the $G{\times}E$ term (σ_{GE}^2), however. One would have to add $G + E + G{\times}E$ for each genotype and check whether there is much re-ranking for the environments chosen.

From this model, one could define the amount of $G{\times}E$ as a "heritability" of plasticity as σ_{GE}^2/σ_P^2. This measure is similar to a heritability in that it is a variance ratio; however, it is not useful to predict response to selection for plasticity in the same way as the "additive," narrow sense heritability [2, 8–10].

There is no specific limitation to the number of environments that can be defined in the term E in Eq. 2, e.g., this type of model has been used to estimate sire by herd interactions.

Multiple-Trait Model

The second method used to describe $G{\times}E$ is based on phenotypic values in different environments and genetic correlations (r_g) between these. The phenotypic expression in the two environments is seen as two separate traits and r_g can be studied to see whether $G{\times}E$ exists. When r_g between the phenotypic values of the same genotype expressed in different environments is high, the phenotypic expression is considered as the same trait in the different environments. In other words, if r_g between the phenotypic expressions of the trait in two different environments is close to 1, there is no $G{\times}E$. When r_g is low, the phenotypic expressions in the different environments are not the same trait and this is an indication of $G{\times}E$ [1, 11].

The genetic correlation (r_g) can be estimated using a multiple-trait analysis based on grouping herds with similar production environments to clusters and treating the observations from the different clusters as separate traits.

By just considering the genetic correlation between two environments, the $G{\times}E$ of interest is that type which gives rise to re-ranking (Fig. 2d). However, one could also use the estimates of genetic variances from the multiple-trait analysis to describe the kind of $G{\times}E$ that only gives rise to a scaling effect (Fig. 2c). The genetic correlation is not affected by scaling if the scaling is purely multiplicative.

This method can be used even if the environments cannot be ordered according to some meaningful scale. However, if there exists a continuous underlying scale and the environments chosen are just some representations of that scale (e.g., herd production levels: low, medium, and high), this approach can be modified to describe, by a covariance function, an infinite number of separate traits over a continuous gradient. The covariance function model was developed to model, e.g., growth trajectories, morphology, and reaction norms [12, 13]. Briefly, this method is based on applying a function to the estimated (co)variance components from a limited number of traits. Using this function, one can predict the variance for any environment (normally within the range studied in the data)

and also covariances between two environments. Further developments make it possible to estimate the covariance function directly without first using a MT approach (review in Gilmour and Thompson [14]).

Reaction Norm Model

When the production environment can be described as a continuous variable, a third method, called the reaction norm model, is possible to use [15]. The definition of the reaction norm (RN) has already been given: the phenotypic expression of a genotype as a function of the environment [16].

In population and evolutionary genetics, this model has often been statistically analyzed using a fixed regression approach as genotypes have been placed in the different environments. However, in animal breeding, predicting breeding values as random effects is a common practice, and therefore it is natural to estimate the parameters of the RNs for each genotype from a random regression approach [17]. A simple model based on ordinary polynomials with a fixed set of regression coefficients (an average RN) and a random set for each individual is:

$$y = \mu + \sum_{f=1}^{nf-1} \beta_f x^f + \sum_{i=0}^{ni-1} b_{im} x^i + e \qquad (4)$$

where x is the environmental value for the phenotypic value y, μ is the overall mean (fixed intercept), β_f are fixed regression coefficients, and b_{im} are random regression coefficients for animal (or sire), m: b_{0m} is the BV for level, b_{1m} is the BV for slope, etc. $G{\times}E$ is defined by variation in linear and higher terms.

If the (co)variance matrix for the random coefficients is defined as $\mathbf{G}$ (order $n_i \times n_i$), then the genetic covariance between environments x_j and x_k can be written as $\mathbf{x}'_j\mathbf{G}\mathbf{x}_k$, where $\mathbf{x}_j$ is a column vector with elements $\{x_j^i\}$ for $i = 0\ldots n_i\text{-}1$. For the linear RN, the vector $\mathbf{x}_j = [1\ x_j]'$. The genetic correlation between environments j and k is $\mathbf{x}'_j\mathbf{G}\mathbf{x}_k/\sqrt{\mathbf{x}'_j\mathbf{G}\mathbf{x}_j\ \mathbf{x}'_k\mathbf{G}\mathbf{x}_k}$ and the genetic variance in each environment is $\mathbf{x}'_j\mathbf{G}\mathbf{x}_j$. These can then be used to describe the re-ranking and scaling $G{\times}E$. The heritability in each environment can be estimated as $h^2 = \mathbf{x}'_j\mathbf{G}\mathbf{x}_j/(\mathbf{x}'_j\mathbf{G}\mathbf{x}_j + \sigma_e^2)$, where σ_e^2 is the residual variance from Eq. 4.

Using phenotypic average as environmental scale. In the ideal situation, the environmental scale is determined by the researcher, e.g., by subjecting the animal to various temperature, light, or nutrient conditions, and the trait measured is some phenotypic character. Although this situation may occur also in animal breeding situations, more often the environmental scale is directly related to the phenotypic values studied. The simplest example is probably the use of herd (or herd-year) average milk yield as the environmental scale when analyzing the phenotype milk yield [18, 19].

The herd average is most likely a combination of many factors, but it may give a good overall description of the type of environment the cow is exposed to, and the herd average is a practically useful description of the environment. However, the same trait occurs as both dependent and independent variable. To avoid a direct relation, the individual's own phenotypic value could be excluded from the herd average used for that individual. But a further problem is that the phenotypic herd average contains also the genetic component of those animals' phenotypes and is not only a measure of the environment. If the genetic material is not used randomly over herds, one would expect some bias to be introduced. One suggestion is to use an iterative procedure, either in a repeated REML [20] or a Gibbs sampling approach [21], in a model where the fixed regression in Eq. 4 is replaced with a herd effect. Simply expressed, this effect is estimated, used as the x-value, estimated again, and so on. It has been shown that this method gives more unbiased estimates of $\mathbf{G}$ than using the phenotypic herd averages. The latter approach results in more uncertainty in the x-values, which gives an underestimation of variance of the slopes of the reaction norms [21].

Group size. The group size used as basis for the calculation of the environmental values is also of importance. Naturally, a large group size is desirable to get as precise estimate of the environment as possible. Imprecise values for the x-values in a regression analysis is expected to lead to lower regression coefficients, which in this situation means lower variance of slopes and $G{\times}E$ may be underestimated [20]. However, increasing the group size (e.g., using herd average over several years rather than herd-year average) may also mean that the same environment is not measured anymore, leading to the same problem as above. These two factors must be balanced in a pragmatic way.

Improved environmental scales. There has been some work on defining environmental scales that are not directly dependent on the trait analyzed. Climate and weather conditions (temperature, humidity, rainfall), herd-year SD of production, replacement rate, persistency of lactation curves, calving patterns, and other measures of management practices have been studied [22–26]. This work should continue, and factor or principal component analysis might be of help in defining few but distinct environmental scales [e.g., 27]. Improved farm and animal data (e.g., management practices, feeding system, and intensity) would be of great value in this respect.

Heterogeneous residual variance. In model (4), it was assumed that the residual variance was constant over all environments. For many traits and environmental scales, this is not reasonable. For a sire model, it makes even less sense. By including the random regression, it is assumed that ¼ of the genetic variance is dependent on the environment, but the remaining ¾ (included in the residual) are not. A rough description of the residual variance structure can be found by saving the residuals from fitting model (4), dividing them into groups along the environmental scale, and calculate the residual variance within each group. If this indicates heterogeneous variance, it should be accounted for [e.g., 28].

Multiple environmental scales. A given phenotypic trait may be influenced by several environmental scales. One can accommodate this by extending model (4) to:

$$y = \mu + \sum_{i=1}^{ni-1} \beta_i x^i + \sum_{i=0}^{ni-1} b_{im} x^i + \sum_{j=1}^{nj-1} c_{jm} z^i + e \qquad (5)$$

In a linear reaction norm, there is one intercept, and one slope for each environmental scale, x and z. The genetic covariance and correlation between environments can now be depicted as a function of both environmental scales, i.e., as three-dimensional graph [18, 22].

Multiple-trait reaction norms. Reaction norm models, as other models, can be analyzed for more than one trait at a time. The **G**-matrix would then contain off-diagonal sub-matrices pertaining to the covariance between the traits, and the diagonal sub-matrices would have the meaning as before. As an example, in Fig. 3, the genetic correlation between the traits protein yield and fertility (days open) is shown [18]. It can be seen that the genetic correlation changes with the environment. Note that traits could share the same environmental scale but also have specific scales. That a certain trait shows $G \times E$ with respect to a certain environmental scale does not mean that all traits will do so.

Type of reaction norm function. In the example given, ordinary polynomials were used with the origin set to the average environment. It is also recommendable to standardize the environmental scale(s); this makes (co)variance parameters easier to interpret. Another common approach is to use Legendre polynomials. These often make convergence easier than ordinary polynomials. The resulting regression coefficients are only defined within a predetermined interval (usually from minimum to maximum environmental value, redefined from −1 to +1). This means that the level is defined in the middle of this interval, which is not necessarily the average environment. For other purposes, splines have been successfully used. Regardless of the approach used, it is vital to describe exactly what was done, otherwise parameter estimates may be difficult to interpret.

The shape of the reaction norm and the shape of the variance function are strongly connected. For a linear

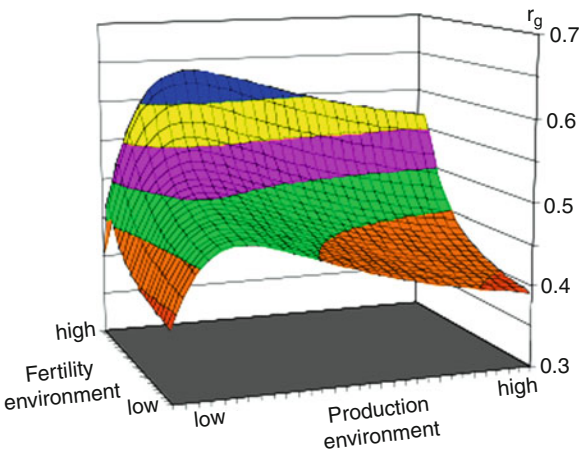

Animal Genetic in Environment Interaction. Figure 3 Genetic correlation between protein production and fertility (days open) in dairy cattle, in relation to environmental conditions (Data from Kolmodin et al. [22])

reaction norm, the variance function becomes $\sigma_a^2 + 2\sigma_{a,b1}x + \sigma_{b1}^2 x^2$. Because the term in front of the quadratic term is always positive, the variance curve will always be concave with an intermediate low point. In a certain data range, it may be increasing or decreasing as the minimum may be outside the range. However, it will never have a maximum intermediate point. This is a rather limiting feature of the linear reaction norm approach. With higher polynomial terms, the variance function becomes less constrained. The covariance function or character process approaches in a way work in the other direction and estimate the shape of the covariance function first. The shape of that function could be an indicator of what shape the reaction norms should be allowed to have. In most applications, only linear RNs have been found; however, there are exceptions where also higher-order RNs have been found [29–31].

Scaling can give re-ranking. It can be shown that even if there is only the scaling type of $G\times E$ for the traits, there can be re-ranking in the total merit index. A simple example is given in Fig. 4. Therefore, scaling $G\times E$ should not be considered irrelevant until the total evaluation has been done [32]; however, generally re-ranking $G\times E$ for traits is expected to be much more important.

The indication of $G\times E$ is that there is variation in the coefficients of the reaction norms. For linear reaction norms, this means that there is variation in the slopes. This definition would pick up plasticity of the kind shown in Fig. 2c–d. As for the interaction term model, this variation does not directly tell us how much re-ranking there is: in order to find out, one could calculate the predicted performance in various environments and get the correlation (or rank correlation) between these values.

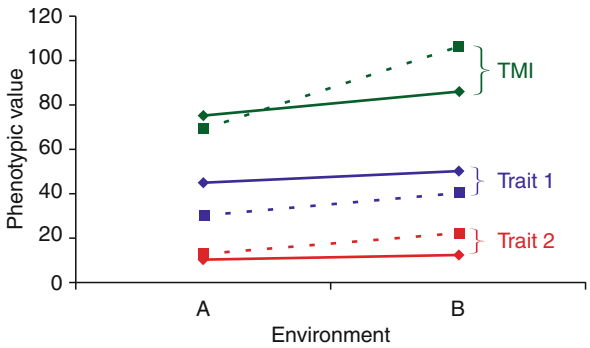

Animal Genetic in Environment Interaction. Figure 4 Breeding values for two individuals for two traits and total merit index (TMI) in two environments. There is scaling $G\times E$ for both traits, but re-ranking $G\times E$ for the total merit index (TMI = 1 × trait 1 + 3 × trait 2)

Genetic Heterogeneity of Residual Variation

The discussion so far has been related to macro-environmental sensitivity, i.e. the reaction of genotypes to large and known changes in the environment. However, as already mentioned, there is always unknown microenvironmental variation, variation that cannot be adjusted away or analyzed with any of the above methods, because it is not associated with any known factor. If there is genetic variation in how animals react to this variation, then there is genetic heterogeneity of residual variation (GHRV).

There are several different models possible to analyze GHRV, well summarized in Mulder [33]. The simplest additive model draws the residual not from a distribution with a constant variance but where it also depends on an additive breeding value, A_v. Thus, each individual has two breeding values, one (usual) breeding value for the mean (A_m) and one for the residual variance (A_v) [34]. One perhaps slight drawback with this model is that A_v is drawn from a normal distribution, and the sum of the average residual variance and A_v could become negative. The exponential model overcomes this problem: here the residual distribution is an exponential function of both the average residual variance and A_v, thus ensuring positive values [35]. Yet another option is to envision the microenvironmental sensitivity to be a special case of the reaction norm model, assuming an unknown environmental x-variable.

Selection for decreased heterogeneity is of interest for traits where large variation is undesirable. This might be true for, e.g., carcass traits where uniformity is favorable for the slaughtering process, but in general for traits with an intermediate optimum. When the mean performance is close to the optimum, more of the selection pressure will move toward reducing the residual variance [36]. Selecting for reduced residual variation might also be a way to select for more robust

animals, animals that can cope with unknown changes in the environment [33]. It would also be interesting to study the relationship between macro- and microenvironmental sensitivity.

Consequences for Breeding Programs

The first obvious consequence of re-ranking $G \times E$ (Fig. 2d) is of course that if you select individuals to become parents based on information from one environment and plan to use them in another environment, you have partially selected the wrong animals. One example of this could be a nucleus herd with very good environment but where the production animals are used under less optimal commercial conditions. The equally obvious solution is to include information from the production environment into the genetic evaluation. Mulder and Bijma [37] showed that the loss in genetic gain (compared with if there was no $G \times E$) was lowest when progenies of males were tested in the production environment, and that this system was better than testing of sibs in that environment, and both systems were superior to testing only in the selection environment.

Another question is whether two breeding programs should cooperate even if their breeding goals differ to a certain extent. This could apply to two countries or to different production systems, e.g., organic and conventional production. It has been shown that long-term cooperation was beneficial if the correlation between breeding goals were higher than 0.8–0.9. However, initial cooperation was beneficial even when the correlation was as low as 0.4–0.6, but after some generations, the two populations had diverged so much that selection was practiced only within population. Furthermore, small breeding programs benefited from long-term cooperation at values of genetic correlation also below 0.8 [38]. It was also shown that for dairy cattle breeding programs, the genetic correlation had to be lower than 0.6 before it was beneficial to run two separate breeding programs rather than progeny testing bulls in both environments. If the selection intensity was high, the genetic correlation increased to 0.7–0.8, below which separate programs were optimal. Again, for a small population (e.g., organic or niche production), the genetic correlation had to be even lower before two programs were optimal [39].

So, in summary, it seems that even if there is $G \times E$, it is beneficial to cooperate and use information from other environments, unless the $G \times E$ is extremely large. This is not the same as ignoring the existence of $G \times E$, rather it is to acknowledge its existence as something natural, and then adapting to that reality.

Future Directions

The trend toward globalization of breeding will emphasize the importance of $G \times E$. A breeding company that wants to be successful in a global setting must also take into account what environment the animal is going to encounter. This might be even more problematic with the advent of genomic selection because it requires reference populations with phenotypic observations from the appropriate environments, if $G \times E$ exists. And, in a global setting, there is no doubt that $G \times E$ exists to a large extent, e.g., between the industrialized production systems in Europe or USA and systems in tropical environments in Africa. Because an increase in production efficiency in developing countries is both a key factor in poverty alleviation and to decrease the ecological footprint, it is important that genetic improvement is aimed at the appropriate traits expressed in the appropriate environments.

Bibliography

Primary Literature

1. Falconer DS, Mackay TFC (1996) Introduction to quantitative genetics, 4th edn. Longman Group, Essex, UK
2. Pigliucci M (2001) Phenotypic plasticity: beyond nature and nurture. The Johns Hopkins University Press, Baltimore
3. Falconer DS (1952) The problem of environment and selection. Am Nat 86:293–298
4. Dawkins R (1982) The extended phenotype: the long reach of the gene. Oxford University Press, Oxford
5. Schlichting C, Pigliucci M (1998) Phenotypic evolution: a reaction norm perspective. Sinauer, Sunderland
6. Waddington CH (1942) Canalization of development and the inheritance of acquired characters. Nature 150:563–565
7. de Jong G, Bijma P (2002) Selection and phenotypic plasticity in evolutionary biology and animal breeding. Livest Prod Sci 78:195–214
8. Scheiner S (1993) Genetics and evolution of phenotypic plasticity. Annu Rev Ecol Syst 24:35–68
9. Scheiner SM, Lyman RF (1991) The genetics of phenotypic plasticity II. Response to selection. J Evol Biol 4:23–50
10. Scheiner SM, Lyman RF (1989) The genetics of phenotypic plasticity I. Heritability. J Evol Biol 2:95–107

11. Robertson A (1959) The sampling variance of the genetic correlation coefficient. Biometrics 15:469–485
12. Kirkpatrick M, Heckman N (1989) A quantitative genetic model for growth, shape, reaction norms, and other infinite-dimensional characters. J Math Biol 27:429–450
13. Kirkpatrick M, Lofsvold D (1989) The evolution of growth trajectories and other complex quantitative characters. Genome 31:778–783
14. Gilmour A, Thompson R (2006) Statistical models for multidimensional (longitudinal/spatial) data. In: Proceedings of the 8th World Congress on Genetics Applied to Livestock Production, Belo Horizonte, Brazil
15. de Jong G (1995) Phenotypic plasticity as a product of selection in a variable environment. Am Nat 145:493–512
16. Kolmodin R (2003) Reaction norms for the study of genotype by environment interaction in animal breeding. Swedish University of Agricultural Sciences, Uppsala
17. Strandberg E et al (2000) Genotype by environment interaction in Nordic dairy cattle studied by use of reaction norms. Interbull Bull 25:41–45
18. Kolmodin R et al (2002) Genotype by environment interaction in Nordic dairy cattle studied by use of reaction norms. Acta Agric Scand A Anim 52:11–24
19. Calus M, Groen AF, De Jong G (2002) Genotype × environment interaction for protein yield in Dutch dairy cattle as quantified by different models. J Dairy Sci 85:3115–3123
20. Calus M, Bijma P, Veerkamp RF (2004) Effects of data structure on the estimation of covariance functions to describe genotype by environment interaction in a reaction norm model. Genet Sel Evol 36:489–507
21. Su G et al (2006) Bayesian analysis of the linear reaction norm model with unknown covariates. J Anim Sci 84:1651–1657
22. Kolmodin R et al (2004) Reaction norms for protein yield and days open in Swedish Red and White dairy cattle in relation to various environmental variables. Acta Agric Scand A Anim 54:139–151
23. Fikse WF, Rekaya R, Weigel K (2003) Genotype by environment interaction for milk production in Guernsey cattle. J Dairy Sci 86:1821–1827
24. Zwald N et al (2003) Identification of factors that cause genotype by environment interaction between herds of Holstein cattle in seventeen countries. J Dairy Sci 86: 1009–1018
25. Raffrenato E et al (2003) Genotype by environment interaction for yield and somatic cell score with alternative environmental definitions. J Dairy Sci 86:2470–2479
26. Ravagnolo O, Misztal I (2000) Genetic component of heat stress in dairy cattle, parameter estimation. J Dairy Sci 83:2126–2130
27. Windig JJ, Calus M, Veerkamp RF (2006) Influence of herd environment on health and fertility and their relationship with milk production. J Dairy Sci 88:335–347
28. Meyer K (2001) Estimating genetic covariance functions assuming a parametric correlation structure for environmental effects. Genet Sel Evol 33:557–585
29. Calus M, Veerkamp RF (2003) Estimation of environmental sensitivity of genetic merit for milk production traits using a random regression model. J Dairy Sci 86: 3756–3764
30. Pollott GE, Greeff JC (2004) Genotype × environment interactions and genetic parameters for fecal egg count and production traits of Merino sheep. J Anim Sci 82: 2840–2851
31. Fikse WF, Rekaya R, Weigel K (2003) Assessment of environmental descriptors for studying genotype by environment interaction. Livest Prod Sci 82:223–231
32. Namkoong G (1985) The influence of composite traits on genotype by environment relations. Theor Appl Genet 70:315–317
33. Mulder HA (2007) Methods to optimize livestock breeding programs with genotype by environment interaction and genetic heterogeneity of environmental variance. In: Animal Breeding and Genetics Group, Wageningen University, Wageningen
34. Mulder HA, Bijma P, Hill W (2007) Prediction of breeding values and selection responses with genetic heterogeneity of environmental variance. Genetics 175:1895–1910
35. SanCristobal-Gaudy M et al (1998) Prediction of the response to a selection for canalisation of a continuous trait in animal breeding. Genet Sel Evol 30:423–451
36. Mulder HA, Bijma P, Hill W (2008) Selection for uniformity in livestock by exploiting genetic heterogeneity of residual variance. Genet Sel Evol 40:37–59
37. Mulder HA, Bijma P (2005) Effects of genotype by environment interaction on genetic gain in breeding programs. J Anim Sci 83:49–61
38. Mulder HA, Bijma P (2006) Benefits of cooperation between breeding programs in the presence of genotype by environment interaction. J Dairy Sci 89:1727–1739
39. Mulder HA et al (2006) Optimization of dairy cattle breeding programs for different environments with genotype by environment interaction. J Dairy Sci 89:1740–1752

Books and Reviews

Annicchiarico P (2002) Genotype × environment interaction: challenges and opportunities for plant breeding and cultivar recommendations. FAO Plant Production and Protection Paper (174). Food and Agriculture Organization of the United Nations, Rome

Hoffmann I (2010) Climate change and the characterization, breeding and conservation of animal genetic resources. Anim Genet 41:32–46

Pigliucci M (2001) Phenotypic plasticity: beyond nature and nurture. The Johns Hopkins University Press, Baltimore

Schlichting C, Pigliucci M (1998) Phenotypic evolution: a reaction norm perspective. Sinauer, Sunderland

Thiruvenkadan AK, Panneerselvam S, Prabakaran R (2010) Layer breeding strategies: an overview. Worlds Poult Sci J 66(3):477–501

Animal Molecular Genetics from Major Genes to Genomics

Asko Mäki-Tanila
Biotechnology and Food Research, MTT Agrifood Research Finland, Jokioinen, Finland

Article Outline

Glossary
Definition of the Subject
Introduction: From Infinitesimal Model to Major Genes
QTL Mapping
Genes Underlying QTL
Genomic Revolution
Future Directions
Acknowledgment
Bibliography

Glossary

Additive genetic variance is usually the largest part of genetic variation in the quantitative trait and is due to average effects of genes. The change in mean caused by selection is proportional to the additive genetic variance.

BLUP is a short name for Best Linear Unbiased Prediction. It is now a norm in estimating breeding values within populations. It uses information on all kind of relatives and corrects the data for differences in production environment.

Breeding value of an individual is the expected value of its progeny relative to the population mean.

Candidate gene is a possible mutation underlying the mapped QTL. A positional candidate is a gene located in the same region as a mapped QTL. A biological candidate for a QTL is a gene which has a function related to the quantitative trait.

Effective population size (N_e) is the number of individuals that with random mating result in the same rate of inbreeding as the population itself.

Genetic marker is a specific detectable sequence of DNA with a know location in the genome.

Heterosis Is the extent to which the performance of crossbred animals is better than the mean of two parental populations.

Infinitesimal model assumes the genetic variation of a quantitative trait is due to infinitely many unlinked genes each with an infinitesimally small additive effect, so that selection produces negligible changes in gene frequency and variance at each locus.

Linkage disequilibrium is a non-random association of alleles across loci. Recombination between loci will gradually reduce the associations, more slowly the closer the loci are to each other. Adjacent markers with correlated allele frequencies could be used for mapping and selection.

Marker-assisted selection is selection on a quantitative trait where also the information on associated markers is used as a selection criterion. Gene-assisted selection is a special case where the marker is at the major gene causing the variation.

Mixed model equations are providing a method to simultaneously solve the predicted breeding values (random effects) for animals and estimate the fixed effects due to differences in production environment.

Morgan is the unit for a map distance in the genome.

Quantitative trait locus (QTL) A short genomic region with a large effect on a quantitative trait.

Single nucleotide polymorphism (SNP) is variation caused by a mutation at a single nucleotide.

Definition of the Subject

Animal breeding is a major contributor to the vast improvements in animal production over decades. The main tool in breeding operations is selection; now, more and more attention is also paid to the amount and nature of genetic variation. It is on these topics that the chapter is built on. It starts from the fundamental methods in determining the genetic value of animals. The normal distribution and linear methods stemming from the concept of large number of loci with tiny effects causing variation are the base line. For quite some time, there have been observations on major loci causing deviation in linear prediction of genetic values. There is a part introducing methods to get around such cases and turning them advantageous by directly utilizing the variation mediated by major

loci. The longest section is on introducing molecular genetic tools to find areas in the genome harboring such major loci and to further characterize the actual underlying genes. The most recent development in DNA technology is the availability of high throughput analysis of individual genomes with tens of thousands of signposts or markers. Without knowing the causal factors, the extensive marker panels can dissect the variation for named markers and recompose the piecewise information for prediction and selection for individuals with respective marker information. Thus, with a sufficiently large number of genotyped and phenotyped animals, selection decisions can be made immediately after birth and very speedy genetic progress is achieved. The same marker panels could be used to have a detailed picture on the state of genetic variation in a population and genome areas causing heterosis in crosses between populations. The theory of animal breeding is thoroughly introduced and discussed in many books, for example those by Falconer and Mackay [1] and Lynch and Walsh [22]. The recent developments in the utilization of DNA markers in characterizing the variation is well covered in the textbook by Weller [2].

Introduction: From Infinitesimal Model to Major Genes

Animal breeding has been very successful in improving production efficiency through utilizing genetic variation between animals. Most of the economic traits are measurable and require own type of approach in analyzing the genetic variation, that is, quantitative genetics. Quantitative genetics theory provides a statistical description of the genetic and environmental variation affecting a particular measurement in a random breeding population as it is at the moment and allows some short-term predictions of the response to selection. In essence, the *additive genetic variance* and its related concept, heritability (h^2), give a coherent framework into which observations on individuals and population, such as the effect of selection or the similarity between relatives, can be fitted.

When there is additive gene action across loci and random mating, the contributions from different loci will be independent, so that their sum will become asymptotically normal as the number of loci increases (while each locus has an infinitesimally small effect). This is referred to as an *infinitesimal model*. Also, the joint distribution of parent and offspring – or of any related individuals – will be approximately normal when the number of loci is large. Therefore, linear methods could be used for prediction. Animal breeding data is typically influenced by many nongenetic factors. The Best Linear Unbiased Prediction (BLUP), due to Henderson [3], has been developed to simultaneously handle both fixed (environmental) and random (mainly genetic) effects in a mixed model. In symbols, denoting individual performance record by y, production environment effects by β and individual animal's genetic value by u, there is an equation for the genetic value of the ijth animal (with known sire and dam and n progeny of varying genetic value u_p with known mates)

$$\beta_i + (1 + 2k + {}^1\!/_2 kn)u_{ij} - k(u_{\text{sire}} + u_{\text{dam}}) + \sum_{\text{progeny}} \left({}^1\!/_2 u_{\text{mate}} - u_p\right)k = y_{ij} \tag{1}$$

where $k = (1 - h^2)/h^2$. The conventional *breeding value* estimation model for a large number of animals would contain the observation vector $\boldsymbol{y}$ explained by $\boldsymbol{u}$ of random additive genetic effects and $\boldsymbol{e}$ of random residual effects simultaneously correcting for the fixed environmental effects $\boldsymbol{\beta}$. The fixed effects and random genetic effects are connected to observations with the incidence matrices $\boldsymbol{X}$ and $\boldsymbol{Z}$, respectively, and $\boldsymbol{y} = \boldsymbol{X\beta} + \boldsymbol{Zu} + \boldsymbol{e}$. The genetic values are made of additive effects within and between loci, dominance deviations due to interaction within loci, and epistatic deviations due to interaction between loci. The covariance matrix of additive genetic effects can be expressed with the additive relationship matrix ($\boldsymbol{A}$) as $\boldsymbol{A}\sigma_a^2$. For solving the *mixed model equations*, one needs $\boldsymbol{A}^{-1}$ which is actually easier to form than the matrix itself [4]. From the inverse elements, one can extract equations like (1). Indeed, an approximate BLUP based on the consideration of a chosen set of close relatives gives satisfactory accuracy in comparing different selection schemes [5].

Matings between relatives cause inbreeding (increased probability for homozygosity) and inbreeding depression in loci with segregating recessive alleles with undesirable effects. In order to improve the genetic evaluation, the *mixed model equations* should also include dominance effects, although the inverse of

the joint covariance matrix of additive and dominance effects is very challenging under inbreeding [6]. It is indeed the inbred populations where the influence of dominance is more pronounced, or the crosses of inbred animals recovering from inbreeding depression or showing *heterosis*.

Selection at the Locus Level

All the concepts of quantitative variation can be expressed at the gene level [1], and therefore it is possible to describe how selection is altering allele frequencies of any locus causing variation in the quantitative trait. The genetic variance is made of contribution from individual loci. The change in mean or response to selection is proportional to the *additive genetic variance*. Hence, the contribution of any locus (or several loci) to the genetic progress under selection will be in proportion to its (their) contribution to the overall *additive genetic variance*. If a locus contributes 10% of the genetic variance, it will explain the same 10% of the total response to selection. Modifying the illustration in Alan Robertson's unpublished lecture notes at the University of Edinburgh, assume that in a dairy cattle population, there is an additively acting biallelic locus where the difference in average milk yield between two homozygotes is $2a$ = 400 kg. Further suppose that the two alleles have the same allele frequency of 0.5. If the selection lifts the mean milk yield by 500 kg, how much has the frequency (x) of the allele with increasing effect changed at the locus. Before selection, the locus contributes to the *additive genetic variance* by ½ x $(1 - x)$ $(2a)^2$ = 20,000. The total genetic variance is – say – 250,000, so that the current locus controls 8% of the total variance and will therefore be responsible for a selection change of 40 kg. This kind of change could be caused by a change 0.1 in allele frequency so that after selection the allele frequency in the progeny generation is 0.6.

The relationship between individual loci and selection response could be described yet another way. The population must respond to selection with an increase in the frequency of those alleles which increase the trait value. The population genetic theory says that the change in gene frequency caused by selection is ½ s x $(1 - x)$ where s is the selective advantage of one homozygote over the other. The aim is to find in the quantitative genetic context the selective advantage of the desirable homozygote compared to the other homozygote after imposing a certain selection intensity (i) for a measured trait. Or to know what is the relationship between a genetic effect on the quantitative trait and the consequent selective advantage caused by the selection on the trait. Falconer and Mackay [1] are showing that there is a linear relationship between the two so that $s = i\,2a/\sigma_p$ where σ_p is the phenotypic standard deviation, so the change in the population mean is equal to $2a$ times the change in allele frequency = $2\,i\,a^2 x\,(1 - x)/\sigma_p$. Since $2\,a^2 x\,(1 - x)$ is the *additive genetic variance* due to the locus, the response produced by a change in allele frequency at the locus is proportional to the *additive genetic variance* caused by the locus. Summing over all loci to compute the total response yields again the classical formula for the selection response $\Delta G = i\,\sigma_a^2/\sigma_p$.

Regarding the example and writing $\sigma_p = 1000$ (assuming h^2 = 0.25), if the selection response of 500 kg had taken place in just one generation, it would have to be caused by an intensity i = 2. The expected change of frequency at the studied locus then equals $^1/_2\ i\ 2ax\,(1 - x)/\sigma_p$= 0.1. The example has been on a simple additive locus. The same exercise could be done for dominance – or even for epistasis – considering the average effect of allele substitution on the mean of individuals within the population and the effect of small changes of allele frequency on the population mean.

Major Genes

Genes with smaller effects may have their gene frequencies altered less by selection. Highly selected populations might therefore be expected to be segregating for loci with smaller effects on a selected trait compared to those with no previous history of selection. For loci with a tiny effect on the characteristic, directional changes of gene frequency due to selection will be low and changes will occur mostly by chance, depending on the number of parents used each generation.

Loci with very large effects on the trait will have their frequencies changed much more by selection. Since their contribution to the genetic variance depends on the allele frequency, the genetic variance will also change. The immediate effect will depend on

the starting frequencies in the population. When the allele effects are large, it is necessary to include also second-order terms of a/σ_p for the allele frequency change (e.g., [7]) and the respective response would have a quadratic terms of phenotypic values (or selection intensity). These effects would be more pronounced when there are dominance effects between the alleles. In case of carrying selection in one sex only, for example, if the variance is due to a locus with complete dominance and $x = 0.9$ and $a/\sigma_p = .5$, the response upward is going to be overestimated with linear prediction by up to 31% and 21%, when the proportion selected is 10% and 20%, respectively [8]. Also the *mixed model equations* would work less efficiently when the variation is caused by a small number of loci [9].

Over the decades, there have been findings on major genes segregating in farm animal populations: the halothane gene mutation causing stress syndrome and leanness in pigs [10], dwarf affecting body size in chicken [11], double muscling in beef cattle [12], booroola lifting prolificacy in sheep [13]. There is clear evidence that the contributions from the loci affecting the quantitative variation are vastly unequal, there being a small number of major loci and a larger number of minor loci. Such an understanding has generated research on developing tools to utilize major genes and to detect them with new available mapping tools made available by molecular genetics.

Improvement Schemes Utilizing Major Genes

The previous discussion shows that segregating major genes may bias the linear prediction of response in selection. On the other hand, a direct selection on a gene with large effect should give higher overall gains in a selection scheme. If one is able to type the different genotypes at the major locus, it is possible to carry out gene-assisted selection. Until recently, this has not been possible and selection has been based on marker loci close to the actual gene, therefore the term "*marker-assisted selection*" (MAS). Earlier the markers were typed by utilizing protein variants, now the markers are solely based on DNA polymorphism.

While conventional selection is favoring desirable alleles in an indirect way, it should be beneficial to have a tool which can influence the allele frequencies in a much more direct way. The ordinary selection with intensity i would change the mean by $i\,h\,\sigma_a$. Denoting the variance due to the major locus with σ_M^2 and its size relative to the total *additive genetic variance* as R, it is possible to assess the advantages of exploiting the marker information in selection.

Lande and Thompson [14] used the selection index methodology in investigating the influence of gene or marker-assisted selection. The selection can be based both on phenotype (P) and marker genotype (M). First step is to compute the selection weights b_1 and b_2 in the index

$$b_1 \text{ phenotype} + b_2 \text{ marker genotype} = b_1 P + b_2 M$$

This could be used to generate equations for the covariance of the index with P and M (the genotypic value of the trait is denoted with G).

$$b_1 \operatorname{cov}(P,P) + b_2 \operatorname{cov}(M,P) = \operatorname{cov}(G,P)$$

$$b_1 \operatorname{cov}(P,M) + b_2 \operatorname{cov}(M,M) = \operatorname{cov}(G,M)$$

where $\operatorname{cov}(P,P) = \sigma_p^2, \operatorname{cov}(G,P) = \sigma_a^2$, $\operatorname{cov}(P,M) = \operatorname{cov}(G,M) = \operatorname{cov}(M,M) = \sigma_M^2$. The weights in the selection index are $b_1 = h^2(1-R)/(1-Rh^2)$ and $b_2 = (1-h^2)/(1-Rh^2)$. The correlation between the index and genotypic value is approximately $h\sqrt{1+R/h^2}$. In conclusion, the marker information would be useful, when R is high or when a major part of the variation is due the QTL and when the heritability of the trait is low (Fig. 1). Therefore, the selection of low heritability traits such as longevity traits (fertility or disease resistance) would benefit if useful genes or linked markers could be detected.

There are traits which are expressed only in one sex. The use of markers would be useful for such traits. Dairy cattle breeding is a good example: markers would allow pre-selection of bulls on milk traits which would mean savings in progeny testing. Selection could be carried out as early as the embryo stage, resulting even higher reductions in generation interval.

Genes or markers are also beneficial for traits that are difficult to improve under traditional selection. Good examples on such are carcass traits that require slaughtering before they can be measured. Meat pH, tenderness, and color are typical carcass traits. Traits that are available late in life, like longevity and lifetime fecundity, would benefit from MAS. The measurement

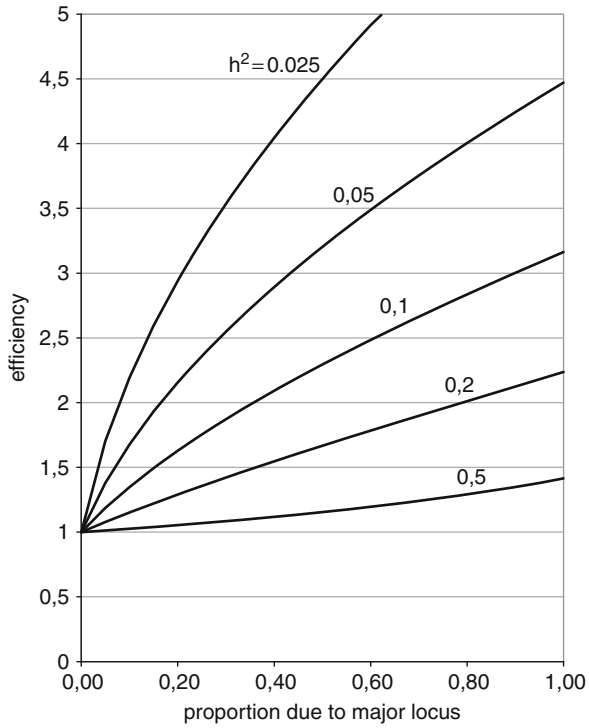

Animal Molecular Genetics from Major Genes to Genomics. Figure 1
Efficiency of marker-assisted selection relative to conventional phenotypic selection with the same selection intensity in large population with respect to the proportion of variance explained by a major gene, for different heritability values of the trait

and data collection of some traits, for example, disease resistance, is very expensive and therefore there is much interest in finding major genes for them.

In general, MAS has advantage over conventional selection for alleles that are initially rare and for alleles that are recessive. It is customary to think that the variation in a quantitative trait is caused by a large number of nongenetic factors. However, the marker genotype would be accurately known without environmental noise.

The consideration of gene or *marker-assisted selection* could therefore include the following points: difficulties of collecting performance records, heritability of the trait, proportion of variance explained by the major gene, and the availability of performance in the life cycle. Methods and applications of MAS are comprehensively reviewed by Dekkers [15].

The *marker-assisted selection* has also drawbacks. The direct selection on a gene would be efficient only for a short time. The desirable allele would quickly become common and new beneficial alleles should be found or new potential markers should be searched for useful segregation. If the selection is not directly on the gene, it is possible that the recombination between the used marker and QTL would gradually weaken the association. The use of markers would even be harmful if the association is not properly validated and efficiency of selection reduced compared to conventional selection.

There are also consequences for the overall genetic variation. The larger the effect of the QTL is, the faster it is fixed by selection and the more it will also reduce the variation in the surrounding genome area (e.g., [16]). An accelerated increase in the marker allele frequency may be accompanied by very unbalanced use of family lines. This is increasing the risks for the reduction of variance and enrichment of harmful recessives.

Introgression from Other Populations

Many local breeds carry interesting genetic variants that are considered beneficial to be introduced to a commercial main stream breed. The former is termed as a donor breed and the latter one as a recipient breed. The operation is usually done by an introgression program. It consists of forming an initial cross between the breeds followed by repeated backcrosses to the recipient one to recover the economically important genome. The target gene is maintained in the backcross generation through selection of donor gene carriers. After some generation of backcrossing the program will finish by a generation of intercrossing to make the population homozygous for the desired allele.

Genetic markers could be useful in introgression programs in two ways [17]. First, markers can be used to select individuals at each backcross generation which are heterozygous for the desired allele or homozygous in the last generation of intercross (foreground selection). Secondly, markers can be used to enhance the recovery of the recipient genome (background selection).

The introgression strategy is a popular genetic improvement method in plants, while there are still

very few applications in domestic animals. An example is the naked neck gene in chicken which reduces plumage in chicken and makes animals more tolerant to heat. It was introgressed from low body weight landrace chickens into a commercial meat-type Cornish chicken [18].

Most of the economic traits in farm animals are complex ones with polygenic variation. One of the most promising cases of introgressing exotic germplasm to commercial production populations has been the impact made on western pig production by the Taihu breeds of the Shanghai area (China). The background for the interest and the results have been reviewed by Knap and Neeteson [19]. Some of these pig breeds (Meishan and Jiaxing) were imported into France, the UK, and the USA in the 1980s. The interest is in reproductive traits: low age at puberty, high ovulation rate and embryo survival resulting in high litter size, and high teat numbers. The disadvantage is in high body fat levels and slow growth rates.

Several commercial breeding organizations in France, UK and Canada have invested in the introgression of Jiaxing and particularly Meishan pigs into their dam lines. This was accompanied by studies into the trade-off between improved fertility and reduced leanness (e.g., [20]). These suggested that the feasible way to commercially exploit these genotypes would be to have commercial sows with 12.5% Taihu genes [21].

While the fertility is improved, as a compromise, leanness is reduced in Taihu-based genotypes, which is a serious obstacle toward large-scale commercial exploitation, although persistent genetic improvement in the latter trait obviously would solve the problem. A complicating factor here is that a few years after the Taihu imports, large data bodies and improved statistical methods allowed for a faster genetic change of reproductive traits in pigs, while genetic improvement of leanness continued at the same rate as before.

Western commercialization of the Taihu breeds has been successful so that almost 100,000 Taihu-based parent gilts are currently sold per year in Europe and North America. It represents less than 1.5% of the total market volume. A good working example on successful introgression of exotic genotypes into advanced animal breeding program is still missing for a polygenic trait.

QTL Mapping

Markers and Linkage Maps

Better understanding and utilization of major genes would benefit from the location of genes or genome areas responsible for the variation in quantitative traits. The prerequisite for this is to have a reasonable skeleton of the genome sites to survey and locate the findings. The genome is made of chromosomes. There are two homologues of each chromosome in a typically diploid animal genome. One homologue is originating from sire (paternal chromosome) and the other one from dam (maternal chromosome). The alleles at the loci on the paternal (maternal) chromosome tend to be inherited together or they are said to be linked. The genome is full of variable sites which could be used as markers to construct a detailed map of locations for further work. The closer the markers are to each other, the more likely they are inherited together or the tighter is the linkage between them or the rarer are the recombinants between them. The distant markers are on the other hand showing independent segregation. Physically, recombination is seen as a crossing over of chromosome strands. The chromosomes could be termed as linkage groups.

The linkage is measured as recombination frequency (c) or the proportion of recombinant ones among all the gametes. If markers are very far from each other, they may be several crossing-overs between them. When the loci are freely combining, the number of recombinant and nonrecombinant gametes is equal and $c = 0.5$. The map distance is expressed in *Morgan*s (M) with its hundredth being cM (centimorgan). A low recombination frequency 1% corresponds to 1 cM. For longer distances, the possibility of several crossing-overs should be considered, as, for example, two crossing-overs between distant markers would often result in nonrecombinants of the marker pair itself.

The detection of linkage or computing map distances would require variable sites and use of heterozygotes. Ideal markers for mapping are the (codominant) loci with alleles not showing dominance (or recessivity). Linkage could be demonstrated with different mating options. For example, there can be double heterozygote $M_1 N_1/M_2 N_2$ mated with a double homozygote $M_1 N_1/M_1 N_1$, in which case

the offspring numbers in different genotype classes would give a straightforward measure for linkage. Inbred lines are homozygous for all loci and the first generation cross F_1 heterozygous, respectively. When F_1 animals are crossed with one of the parental lines, the resulting backcross animals would give direct estimates on recombination frequencies. Using inbred line terminology, the mating is called double backcross.

Although there are often heterozygotes available, only a limited number of cases are informative on possible recombinants and determining the amount of linkage. There are five different cases with respective information content.

$\frac{M_1\ N_1}{M_1\ N_1}$	$\otimes$	$\frac{M_1\ N_1}{M_1\ N_1}$	Not informative
$\frac{M_1\ N_1}{M_2\ N_1}$	$\otimes$	$\frac{M_1\ N_1}{M_1\ N_1}$	Not informative
$\frac{M_1\ N_1}{M_2\ N_2}$	$\otimes$	$\frac{M_1\ N_1}{M_1\ N_1}$	Informative (double backcross)
$\frac{M_1\ N_1}{M_2\ N_2}$	$\otimes$	$\frac{M_1\ N_1}{M_2\ N_1}$	Informative (single intercross)
$\frac{M_1\ N_1}{M_2\ N_2}$	$\otimes$	$\frac{M_1\ N_1}{M_2\ N_2}$	Informative (double intercross)

From the last mating type, there are nine different progeny classes with respective expected numbers according to the recombination frequency.

Before a marker is used, its suitability is assessed studying the allele frequencies (x_i). So far it is obvious that homozygous parents are of no use and among the progeny of heterozygous parents only the homozygotes (or for multiple alleles, the heterozygotes M_1/no M_2 or M_2/no M_1) would signal which allele of the parent has been transmitted to the progeny. So the quality of the marker is based on polymorphism information content (PIC), which is the probability of identifying which homologue of a given parent was transmitted to a given offspring, the other parent being genotyped as well, or in other words, probability that the parent is heterozygous × probability that the offspring is informative. Summing over alleles, the PIC for a multiallelic marker would be $1 - \sum x_i^2 - 2\sum\sum_{i<j} x_i^2 x_j^2$.

Mapping Function

In order to fill the linkage map with markers and genes, there is a need to have a good measure for the map distance. As there can be several crossing-overs between distant markers, recombination frequency as such is not an appropriate measure. If there are markers *M*, *N*, and *O* (with respective recombination frequencies c_{MN}, c_{MO} and c_{NO}) and crossing-overs in the adjacent genome regions would be independent, then the recombination frequency $c_{MO} = c_{MN} + c_{NO} - 2\,c_{MN}c_{NO}$. In other words, the recombination frequencies are additive only if they are small enough so that the product term could be ignored. A map distance is required that would give the total number of crossovers between even very distant markers. The measure should be additive so that the number of crossovers between *M* and *O* is the number of crossovers in the interval *M*–*N* plus those in the interval *N*–*O*.

The probability of no crossovers is $e^{-\lambda}$ (from the Poisson distribution) and the probability of at least one recombinant gamete is $c = ½(1 - e^{-\lambda})$. The latter is true, because for each crossover event only one-half of the gametes will be recombinant types there being only two of four strands involved in a crossover. The map distance is then $-½\ \ln(1 - 2c)$ in *Morgan*s for an observed recombination rate *c*. For short chromosome segments ($c < 10\%$), the map distance equals the recombination rate, while 50 cM corresponds to recombination rate 32%. The approach is called Haldane mapping function and is valid when the crossing-overs across the genome occur independently. If some degree of interference needs consideration, Kosambi mapping function should be applied. For more details, see Lynch and Walsh [22].

The number of chromosomes varies quite much over the animal species:

Cattle	Chicken	Pig	Sheep	Carp	Human	Mouse
30	39	17	27	52	23	32

When there are so many chromosomes in livestock species, the average recombination across the genome is very high. In comparison, the well-known lab organism Drosophila has only four chromosomes and no recombination in males.

The genome in mammals is about 3×10^9 b (base) and 3 M. The chicken genome is only about 1×10^9 b, while the linkage map is still around 3 M. The well-known lab organism Drosophila has only 275 cM and 0.13×10^9 b.

DNA Markers

Ideal markers for mapping purpose should be widely distributed over the genome. At the same time, it is important that there are several markers available within short genomic regions allowing high-resolution mapping. Good markers should have many alleles, and with frequencies as equal as possible. The alleles should be codominant to allow easy detection of heterozygotes. The allele typing should be straightforward with satisfactory repeatability across analyses. Alleles should also be stable from generation to generation with a low mutation rate. The cost of genotyping could be reduced if the genotyping could be done simultaneously for many loci and the analysis could be easily automatized to provide high throughput.

The most common markers are either microsatellites (based on loci which have a variable number of repeats of a same short sequence) or single nucleotide polymorphism (SNP, which is a nucleotide site in the genome sequence, predominantly biallelic, but possibly having four alleles with each of the four nucleotide bases appearing in the same location). Both these marker types are widely distributed and codominant. Microsatellites are now less popular because their repeatability is lower and there is a limited number of them for a high-resolution mapping in a chosen short region. SNPs have gained popularity and it is nowadays possible to have very large SNP panels typed moderately cheaply in a single analysis with a small microarray chip.

Microsatellites are still used when sufficient information is delivered by only few markers (e.g., as required for parentage testing), and in some applications, this will offset the relative disadvantage of throughput in comparison to SNP markers.

From Segregation Analysis to Use of Markers

Since the genes affecting quantitative genetic variation are behaving like genes with classical discrete genotypes, there have been attempts to characterize them. If in the population there is segregation at a major locus mediating quantitative trait variation, alleles with very large effect and extreme frequency could be causing a skewed phenotypic distribution. Even if allele classes are equally common, the distribution may have several peaks. The consequences due to major gene can be studied with segregation analysis (e.g., [23]). Segregation analysis is full of factors which are hard to be itemized and tested as the effect of several major genes, extreme allele frequencies and dominance gene action produce similar distribution patterns and are therefore hard to separate. Segregation analysis is historically important and would still be used for providing preliminary understanding about the inheritance pattern, especially for human familial diseases.

If one wants to demonstrate the existence of a major gene, it is better to anchor the analysis of distribution features to a known locus with visible genotype classes, and hope that the locus is a useful marker to demonstrate the existence of a linked major gene. Thereby, the analysis could be narrowed down to investigating one gene (or marker) at the time (Fig. 2). The statistical model could include the location of the gene, the effect size, dominance, and frequency of the alleles. Only the availability of marker loci supporting the localization was for a long time restricting the possibility for such a work.

It was half a decade ago when the blood group alleles became immunologically identifiable and possible signposts for analyzing quantitative genetic variation in farm animals. These markers were followed by electrophoretically (molecule size and electric charge) detected protein. The number of markers was still very low and even their rough location was not known. Enthusiastic researchers were facing frustrating results in hunting major genes, although the possibilities and optimum designs for analyzing quantitative traits were clearly envisaged by some groups (e.g., [24]).

The research chances improved a lot when molecular genetic techniques opened completely new kind of possibilities for mapping. With a lot of markers available all around the genome, it was soon rather rewarding to detect regions responsible for the variation. Also a new term, QTL or *quantitative trait locus*, for such genomic regions was coined.

QTL Mapping from Crosses of Inbred Lines

Inbred lines would be ideal resource populations for QTL mapping. They are homozygous for most of the genome, including, hopefully, the used marker locus and putative QTL, in which case the crossbred F_1 population would be heterozygous at both the loci. In other

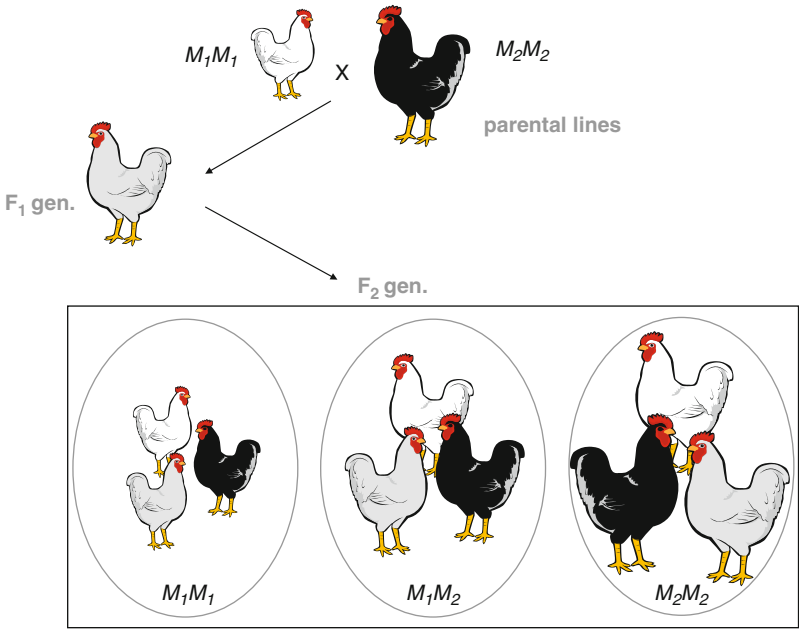

Animal Molecular Genetics from Major Genes to Genomics. Figure 2
Two chicken lines differing in body weight and plumage color are fixed for a marker allele (M_1 or M_2). The lines are crossed to follow the possible co-segregation of the traits and also of the marker locus in the F_2 animals where all possible combinations of phenotypic classes and marker alleles are appearing. The animals are grouped by the genotypes M_1M_1, M_1M_2, and M_2M_2. The M_1M_1 animals are the heaviest, while the M_2M_2 ones are the lightest with the M_1M_2 ones being intermediate. This would suggest that the marker is close to a QTL related to body weight. However, the plumage color which is also showing a simple pattern of inheritance, is segregating independently as the color types occur with equal frequencies in the different weight classes

words in the F_1 generation, there is a very high correlation of allele frequencies across the loci, or using population genetic terms, the *linkage disequilibrium* between the marker and possible QTL is maximized. *Linkage disequilibrium* is reduced over generations as recombination is gradually breaking the associations. However, very little of *linkage disequilibrium* will be lost within short map distances in producing backcross and F_2 generation. Starting from inbred lines, it is easy to follow the variation in the marker loci and the allele phases across marker and QTL would remain the same over further generations. While the use of line crosses is enhancing marker variation, it is also beneficial to choose lines that are phenotypically very divergent. Such a starting point would increase the chances of finding QTL.

Assume there are parent lines (P_1 and P_2) homozygous for marker locus (two alleles M_1 and M_2) and QTL (B and b). The crossed generations are mixtures of distributions with respect to the marker genotypes. The line differences could be associated with the marker classes using alternative crossing designs. Then the expected distribution and contrasts for the marker genotypes between the lines are

	Expected distribution among marker genotype classes			
	M_1M_1	M_1M_2	M_2M_2	Contrasted classes
Backcross with P_1	½	½		M_1M_1–M_1M_2
Backcross with P_2		½	½	M_1M_2–M_2M_2
F_2	¼	½	¼	M_1M_1–M_2M_2 M_1M_1–M_1M_2 M_1M_2–M_2M_2

The efficiency of associating the computed phenotypic differences with the marker variation depends on

how closely the analyzed single marker is to a gene affecting the variation. The F_2 generation (produced by intercrossing F_1 animals) is better than the backcrosses (crossing F_1 with one of the parent lines) as it is possible to estimate also the dominance effect via comparing the heterozygote class with the homozygote ones.

Random Breeding Populations

Typically, farm animals are forming a random breeding population. Such a population has many limitations for successful QTL mapping. The available phenotypes are within a relatively narrow range of variation and would generate much smaller class differences than in crosses from diverse inbred lines. The markers would also show less systematic polymorphism than crossbred populations, since in a large random breeding population the *linkage disequilibrium* is expected to be very low over moderate map distances. In that situation, the only chance to find QTL is to have a detectable marker at the gene itself or its immediate neighborhood. Still, some families or parent individuals may be useful for mapping studies as by chance they have marker and QTL variation phased in a useful manner. Although there is no *linkage disequilibrium* at the population level, there may be partial disequilibrium within families depending on the recombination rate. Such a *linkage disequilibrium* could be exploited in QTL screening. Assume sires that are heterozygous for the marker (M_1M_2) and have large progeny group of half-sibs with phenotype and marker genotype data. The data could be modeled for an analysis of variance around the average level μ as performance record = μ + marker genotype + residual.

Using the notation above, at the QTL locus the separation of two homozygotes is $2a$, the frequency of B allele in the population is x and the recombination rate between the marker and QTL is c. The analysis could be extended to include dominance by allowing the heterozygotes to deviate from the mean of the two homozygotes by da ($d = 1$ dominant, $d = 0$ additive, $d = -1$ recessive gene action with the intermediate values indicating partial dominance or recessivity).

Therefore the frequency of different progeny types would be across heterozygous sires with different QTL allele configuration as follows:

	QTL genotype in progeny		
	BB	*Bb*	*bb*
	0	$(1 + d)a$	$2a$
Sire genotype	M_1 allele from sire		
M_1B/M_2B	x	$1 - x$	0
M_1b/M_2b	0	x	$1 - x$
M_1B/M_2b	$(1 - c)x$	$(1 - c)(1 - x) + cx$	$c(1 - x)$
M_1b/M_2B	cx	$c(1 - x) + (1 - c)x$	$(1 - c)(1 - x)$
	M_2 allele from sire		
M_1B/M_2B	x	$1 - x$	0
M_1b/M_2b	0	x	$1 - x$
M_1B/M_2b	cx	$c(1 - x) + (1 - c)x$	$(1 - c)(1 - x)$
M_1b/M_2B	$(1 - c)x$	$(1 - c)(1 - x) + cx$	$c(1 - x)$

From these frequencies, one can compute for different progeny groups across the population:

Sire genotype	The expected phenotypic difference between M_1 and M_2 progeny
M_1B/M_2B	0
M_1b/M_2b	0
M_1B/M_2b	$(1 - 2c)[1 + (1 - 2x)d]a$
M_1b/M_2B	$-(1 - 2c)[1 + (1 - 2x)d]a$

Hence, the difference between subgroups disappears when recombination between the marker and QTL is 0.5 (or when the marker is very far from QTL). In general, it is not possible to separate the effect and location, for example, QTL which is 25 cM away from the marker would have an estimate like with the marker with half of the effect locating exactly at the QTL position. On the other hand, the frequency and dominance action will also affect the estimation and obviously the detection of rare recessives is very hard.

When at the population level there is no linkage disequilibrium, the occurrence of informative haplotypes in progeny depends on the allele frequencies at

the marker and QTL. The heterozygous sires M_1M_2 are investigated for the difference in performance between M_1/no-M_2 and M_2/no-M_1 progeny classes. In principle, the analysis should pool the results across sires to improve the power of the analysis. However, there are sires (like M_1 B/M_2 B, M_1 b/M_2 b) where the marker genotype contrast is zero. In some cases, the difference is positive (M_1 B/M_2 b) and in other cases negative (M_1 b/M_2 B). Therefore, the analysis is carried out within sires. Thereby, it is possible to include all the possible existing gametes (and alleles) with different combinations of marker and QTL alleles, and at the same time eliminate the spurious association caused by between sire variation [24, 25].

Interval Mapping

When the QTL screening is done marker by marker over the genome, the available information is utilized in a suboptimal way, and, for example, the effect and location of QTL cannot be separated. On the other hand, when there are many markers, some of them may by chance give a statistically significant result at the chosen risk level. If the significance threshold is 5%, then five out of hundred analyzed map positions may give a "significant" result. This could be taken into account by having a more stringent rejection criterion and have for testing each individual marker a statistical significance level of 1/(no. markers) times what it would be if only one hypothesis were tested (so called Bonferroni correction). When there are several (linked) markers available on the same chromosome, one should consider utilizing all the markers jointly and screen the whole chromosome interval by interval for existing of QTL.

Assume that the QTL is at the marker locus or in its immediate neighborhood. Therefore, it is possible to ignore how the recombination may reduce the estimate on the effect. When several linked markers are used, the localization part could be sharpened by the adjacent markers and subsequently, the estimation of QTL effect would receive better attention. Such an approach is called interval mapping. It was first developed for analyzing inbred lines [26].

Suppose there are now two markers M and N to test a case where B locus affecting the quantitative trait variation is assumed to be in the interval between them. Further, the alleles at B recombine with the alleles of M at the rate c_1 and with N with c_2. If the parental lines P_1 and P_2 are homozygous $M_1\ B\ N_1/M_1\ B\ N_1$ and $M_2\ b\ N_2/M_2\ b\ N_2$, respectively, then in the backcross to P_2 the expected progeny mean computed with respect to inheritance probabilities at the B locus is

$$\begin{aligned}&\text{prob}(B) \times \text{effect of } B \text{ allele} + \text{prob}(b)\\ &\times \text{effect of } b \text{ allele} = \text{effect of } b \text{ allele} + \text{prob}(B)\\ &\times (\text{effect of } B \text{ allele} - \text{effect of } b \text{ allele})\end{aligned}$$

In terms of different combinations of M and N alleles in the backcross progeny, the probability for them having B allele from F_1 parent is (recalling that the recombination rate c between M and N can be expressed as $c_1 + c_2 - 2\ c_1\ c_2$)

$$\begin{aligned}&M_1N_1 \quad 1 - c_1c_2/(1-c)\\ &M_1N_2 \quad (1-c_1)c_2/c\\ &M_2N_1 \quad 1-(1-c_1)c_2/c\\ &M_2N_2 \quad c_1c_2/(1-c)\end{aligned} \tag{2}$$

The prob (B) varies across the different positions between M and N. Different map positions could be converted to recombination rates in finding the map positions and allele effects that best explain the observations. The estimation could be done with computing the regression [27] at several positions between M and N with the model: performance record = intercept + regr coeff × prob (B) + residual. The regression coefficient is an estimate of the average effect of allele substitution at (biallelic) QTL. This is illustrated in Fig. 3. Like for any regression analysis, fitting the regression could be assessed with F test at different positions of the interval. If there are more markers along the studied chromosome, the analysis could be repeated over all the possible intervals.

When there is a reasonable coverage of the genome with interval mapping, the analysis is screening the whole genome for QTL. The same type of QTL analysis could be carried out for F_2 cross animals. In that case also the dominance deviations could be estimated for QTL.

In farm animals, the closest to an inbred line is a breed. The first major genome scan utilizing breed

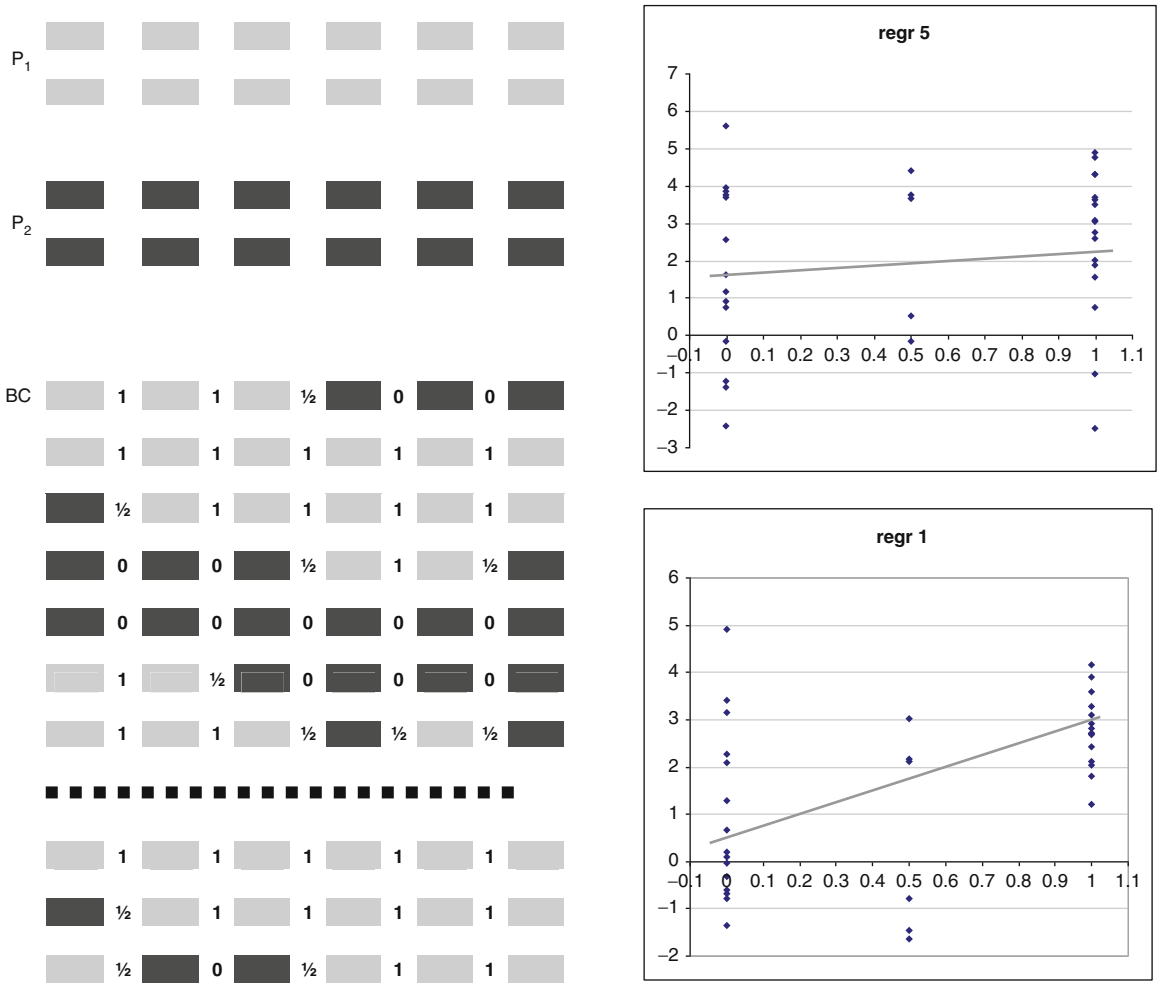

Animal Molecular Genetics from Major Genes to Genomics. Figure 3
QTL interval mapping via regression for backcross setting. The backcross (BC) population is produced by crossing phenotypically diverse "light" and "dark" parental lines (P_1 and P_2). The light line animals of P_1 have a higher phenotype. The BC population is genotyped with a marker panel covering the shown genomic region at regular intervals of 20 cM. Markers are represented by shaded bars. The BC population is formed by crossing F_1 animals with the P_2 animals. When all the transmitted P_2 markers are black, the BC animals are illustrated with the chromosomes from F_1 parents, with possible recombinants. Marker intervals are considered one by one for the presence of QTL. The probability that individual has received the "light" QTL allele from F_1 parent is computed (values in the brackets between the markers) and used as an explanatory variable to compute the regression of phenotypic value on it. The regression coefficient provides an estimate of the allele substitution effect. The QTL is in the first bracket and leads to higher regression coefficient than in the last (5th) bracket, far away from the QTL, both examples shown on the right. The illustration is modified from Georges [28]

differences was reported in the mid-1990s in pigs from a cross between the Large White breed and the wild boar [29]. Large QTL effects were found influencing both growth and fatness. After that study, several genome scans have been developed involving the commercial and exotic breeds.

In random bred populations, there is less regularity in many respects and the interval analysis should be preceded by the examination of allele phases across adjacent markers in heterozygous (say $M_1/M_2N_1/N_2$) sires. The phase determination would require a large genotyped half-sib family from the sire. The non-informative

heterozygous progeny M_1/M_2 cannot be automatically used for the analysis but the considered interval should be extended until an informative locus in the progeny is found. If the sire chromosome phases over the markers are M_1N_1/M_2N_2 and there is a progeny that has inherited the combination M_1N_1 (and assuming that the QTL allele B is on the same chromosome with M_1 and N_1), the progeny has B allele with probability $1 - c_1\, c_2/(1 - c)$. The other probabilities could be derived and would resemble the ones listed for the backcross case above at (2).

The interval analysis is again performed within a family. The power of the analysis could be improved (or residual variation reduced) by analyzing several families and pooling the results at the end. The statistical model for progeny mean is therefore average level + sire$_i$ + regr coeff$_i$ × prob (B) + residual. The sum of squares due to the regression is then obtained by pooling the sum of squares due to regression across sires as $\sum$ SS-regr$_i$/number of sires. The degrees of freedom in the F test for the residual variation are the total number of observations minus twice the number of sires. The analysis is repeated at several positions, say at cM intervals, between M and N and further across other intervals. The highest value for the test parameter is indicating the likely position for QTL with the regression coefficient itself giving the substitution effect. The first genome-wide screening for QTL was done in the outbred half-sib design for dairy cattle by Georges et al. [30].

Design of QTL Mapping Studies

It is important to understand what would be an optimal design and number of observations (n) for QTL mapping studies. First consider the regression with a single marker for a crossbred population (or single family). The explanatory variable (*prob*) is made of probabilities for the inherited QTL allele. For simplicity, there are so many observations (>50) that one can formulate the test for the regression coefficient as regr. coeff./its standard error = regr coeff/$\left(\sigma_e^2/SS_{\text{prob}}\right)^{1/2}$ = $\sqrt{n}\ \sigma_{\text{prob}}$ regr. coeff./σ_e In other words, the test parameter depends on the number of observations, variation range of explanatory variable, size of QTL effect and residual variation(σ_e).

Considering the type I error rate α and test power $1 - \beta$, then in terms of the respective standardized variates (z) of normal distribution, the number of observations required to detect a QTL with an effect a/σ can be deduced from $(z_{1-\alpha} + z_{1-\beta})^2/(\sigma_{\text{prob}}\ a/\sigma)^2$. For the 5% risk and power 90% with the effect sizes

0.1	0.4	0.7	1.0

the required number of animals (with observation and marker genotype) in a backcross is

4,202	262	85	42

Compared to backcross, the explanatory variable would double its variation in F_2 and therefore the F_2 cross would have twice the efficiency given the same number of genotyped individuals. So far it is assumed that in the single marker analysis, the marker is at QTL itself. When this is not so and the recombination between marker and QTL is c, then with the same criteria the number of genotyped individuals should be $1/(1 - 2\,c)^2$ times higher (for more details see [31]).

In conclusion, a cross between divergent lines is very powerful to detect QTL because the statistical power is high and a reasonable number (200–300) of animals is sufficient to detect a major gene. Experimental cross is also a useful approach for QTL screening as the production could be controlled in a small scale study and uncommon traits (disease resistance and quality traits) can be monitored. However, in farm animals, uniform lines are not common and rarely inbred enough to fully exploit the crossbreeding advantages. It is also very costly to maintain such lines or find facilities for generating and maintaining experimental crosses.

The random bred populations should be analyzed pooling within family results across families. When there are several groups in the analysis, the testing should follow the framework for the analysis of variance (F ratio). The test is improved with a large number of progeny. When there are s sires, the family size requirement could be computed from $F^2\sigma_e^2\, s/\Sigma\, SS_{prob}$. On the other hand, the more sires there are, the higher are the chances of finding a family with a segregating QTL.

With the half-sib design, the number of genotyped animals could be reduced by moving from daughter design to granddaughter design [32]. Instead of

genotyping daughters for markers, the progeny tested sons of the sires are now typed and their evaluation results are used in the analysis. Thereby the number of genotypings can be kept reasonable and the accurate genetic value of sons reduces the residual variation and thereby increases the power of analysis. The sons are genotyped for markers that are heterozygous in their sire. The analysis for a single marker is carried out within sires with the model: progeny test result value of son j from sire $i = \mu$ + sire$_i$ + son's genotype$_{ij}$ + residual.

With a given number of genotypings the test would be more powerful than the daughter design. When there are 200 daughters per sire versus 200 sons per sire and 100 daughters per son, one can compare the test power (risk 5%) with different effect sizes for daughter/granddaughter design.

Number of sires/paternal grandsires	No. genotypings	a/σ =.1	a/σ =.3
5	1,000	3/48	50/97
10	2,000	5/73	76/99
20	4,000	7/95	95/99

In order to reach the power of granddaughter design, the daughter design would need large progeny groups which – in terms of collecting DNA samples and carrying out genotypings – are workwise almost impossible.

For the interval mapping, both the variance of the explanatory variable and residual would be reduced while in general the aim should be to push down the residual variation as low as possible while keeping a wide range of alternatives for the explanatory variable. If only animals with extreme phenotypes are genotyped, the latter could be increased and the efficiency enhanced. Ultimately, genotyping only the very highest and lowest phenotypes, the variance of the explanatory variable is increased, and in the best situation the analysis would have only the extreme homozygotes for QTL. It is important to notice that the selective genotyping should be done within families to make sure that the selection is targeted on the QTL instead of the general genetic background. Selective genotyping has its drawbacks, as it would focus on a single trait at a time.

Genes Underlying QTL

In farm animals, the QTL mapping has been very popular since the microsatellites and later SNPs became available as mapping markers. Depending on the species, two designs have been used: crosses mainly in pigs and chicken and half-sib families in dairy cattle. The QTL investigations have been carried out with marker sets of 100–300 microsatellites covering the whole genome. This would correspond to a marker density of some 10–30 cM. QTL mapping in farm animals has been very prolific as it has been possible to have sufficiently large experiments or population samples to yield an adequate statistical power for QTL detection. Until today, thousands of QTL for numerous traits have been reported (see http://www.animalgenome.org/QTLdb/).

Year	Number of QTL (number of traits in brackets)		
	Cattle	Pigs	Chicken
2006	630 (89)	1,287 (246)	657 (112)
2011	4,682 (376)	6,344 (593)	2,451 (248)

Fine Mapping

A successful *marker-assisted selection* requires that the applied marker is at the QTL itself or very close to it. Otherwise there is a need to resort to linked markers which may differ across families, depending on how they are showing *linkage disequilibrium* with the targeted QTL. There are other reasons for the interest to find the underlying genes, as the general aim is to understand more about their function and utilize them in further studies and applications. It is hard to resist the temptation of trying to find the genes, the allelic variants within them, the allelic effects and frequencies, co-effects with the alleles of other loci, and effects on other traits. Moreover, the never-ending curiosity drives research to distinguish coding areas and regulatory elements (e.g., [33]). In a typical QTL study, it is possible to locate a QTL only within a fairly wide region of a chromosome. A region of 10–30 cM may still contain 100–300 genes which is making difficult to identify and characterize the responsible mutations [28].

There are several factors that affect fine mapping. An obvious criterion is high marker density. The design consideration showed how the sample size of animals contributes substantially to the mapping resolution. As high as 5,000 individuals are required to increase the resolution down to 5 cM in crossbreeding designs. Therefore, it is necessary to think about ways to produce new recombinants. It is easier with experimental laboratory strains serving as model organisms where with a short generation turnover it is possible to have intercross populations F_3, F_4, F_5, . . . In that context, by generation t the confidence interval for the QTL location is reduced to $1/t$ of the F_2 one given the same number of animals per generation [31]. In farm animals, such operations would be money and time consuming and practically unfeasible.

It is easy to produce a large number of markers for an interesting QTL area and find the markers with the best association with QTL alleles. Usually, combining individual marker variation over the area and assessing the association between haplotypes and QTL alleles may be more fruitful than analyzing single markers one by one [34]. In farm animals, the density of observable recombinants could be increased by exploiting historical recombination events in comparing the same genomic region within population or even across breeds (Fig. 4). Many breeds are originating from a small number of founders or have experienced bottlenecks alternating with periods of population growth. These events affect sampling of haplotypes and thereby cause *linkage disequilibrium* which can be used in fine mapping QTL regions. *Linkage disequilibrium* extends over longer genome stretches in young populations which hampers localizing causal mutations. In modern dairy breeds, *linkage disequilibrium* is seen as long haplotype blocks [35]. The older haplotypes shared by breeds can be exploited in high-resolution mapping.

In a QTL analysis one is following the transmittance of the variants over a chromosome section and computing probabilities for assumed QTL in the marker bracket. The more detailed variation within the chromosome interval is ignored and further it is assumed that the variants of the interval are unrelated. The intervals could be filled with more markers, especially

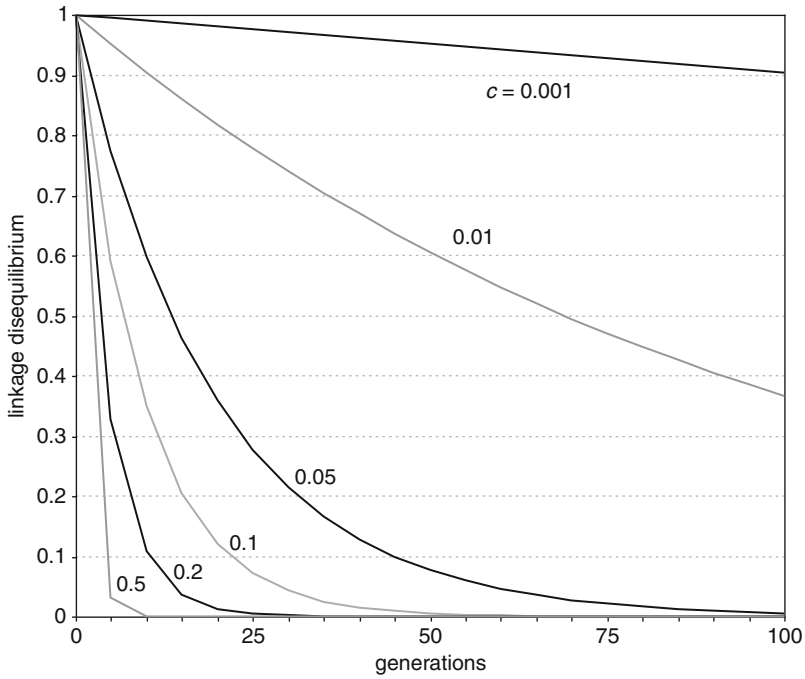

Animal Molecular Genetics from Major Genes to Genomics. Figure 4
The decay of linkage disequilibrium over generations for different values of recombination rate (c) between loci. It is noticeable that with a recombination rate 1% it takes some 80 generations to halve very high linkage disequilibrium

around the found QTL, to classify the relationships between the interval variants given the linkage disequilibrium. When there is evidence for a QTL from linkage analysis and from *linkage disequilibrium* around the putative QTL position, the linkage and *linkage disequilibrium* analysis could be combined [36]. The analysis would eliminate QTL effects from distant regions of the chromosome and other chromosomes because they do not appear as linked QTL. Therefore, the combined analysis would produce a clearer signal for the QTL position compared to the two separate analyses [37]. Such a combined linkage and *linkage disequilibrium* approach has been successfully exploited in cattle to map QTL within less than 1 cM [38].

The discussion above shows how important it is to eliminate the spurious associations due to linked genes or other genetic background. One approach is to use transmission disequilibrium test or TDT [39]. This compares the effect of the two alternative types of gametes from a common parent. For example, a sire heterozygous for a studied marker (or a putative gene) may have a large progeny group allowing a test to find how regular the difference is between progeny inheriting the alternative alleles. Such an analysis is extended over sires by treating them fixed.

Few Examples on Causal Mutations

The characterization of mutations underlying QTL is very hard in any species, and it is not too surprising that there are only few validated examples on such mutations in domestic animals. The work has usually started from a genome-wide screening for QTL and then proceeded to find genetic and functional support for possible causative mutations.

Many independent QTL mapping studies in dairy cattle have shown that there is QTL for milk traits on chromosome 14. After lots of effort and international collaboration it has been shown that the associations could be explained by the *DGAT1* gene that is coding acyl-coenzyme A: diacylglycerol acyltransferase. The enzyme is known to catalyze the last step in the triglyceride synthesis and a missense mutation (K232A) influences milk fat content in cattle (e.g., [40]). The fine mapping and gene identification took some 7 years.

The second example is from pigs. A single-nucleotide substitution of IGF2 (insulin-like growth factor 2) is a causal gene behind a major QTL for growth [41]. This is a regulatory mutation. It has been present in four different breeds selected for lean growth and a major reason for the successful detection is the finding of an ancestral haplotype that differs only by one nucleotide substitution from the mutant haplotype [42].

Another example is a single nucleotide substitution in the myostatin gene (*MSTN*) causing increased muscle mass in Texel sheep [43]. This mutation creates a new target site for two microRNAs expressed in muscle which leads to down regulation of MSTN transcripts.

The findings have a clear message: farm animal populations have a high haplotype diversity allowing successful genetics research to locate genes underlying QTL irrespective of the mode of action. The examples show that the molecular nature of a QTL can be as simple as a missense mutation in a coding sequence or a single nucleotide substitution in noncoding DNA. It is also impressive how in farm animals the genes behind the found QTL are regulatory mutations. The regulatory factors are much more challenging in showing the effect on gene function than mutation changing the protein sequence and structure.

There are others reported but in many cases more work is needed to demonstrate their effect in independent samples. The number of actual genes in the QTL seems very low so far but is comparable with the modest findings in man and mice where the work volume is more substantial. One obvious reason for a small number is the poor resolution in QTL mapping experiments. The confidence interval for a QTL is at best very wide and may contain hundreds of genes. Another reason is that many QTL will not have such a simple explanation as the examples described above. Some QTL will be due to several mutations present in one or many genes. Such QTL may break up into several linked loci for the fine mapping. Mutations in noncoding DNA make their detection and functional characterization also very difficult (see [28, 42] for more discussion).

Candidate Gene Approach

In the characterization of genetic factors, there are basically two types of approaches. The linkage studies

are aiming to locate genomic regions or QTL that are important sources of variation, or biological knowledge is used to deduce the genes most likely responsible for the variation. The examples above are indicating that studies to identify positional *candidate gene*s have a rather limited success. It is not therefore surprising that many researchers have restricted their studies to investigate the role of biologically deduced *candidate gene*s in explaining the variation in the available data. This approach is much more economical, on the other hand there is very little new knowledge to be discovered as the analysis only spotlights the chosen gene or genes. Sometimes, the studies have switched to candidate approach after the linkage approach has failed or included *candidate gene*s as a marginal part of wider analysis not originally designed to explore individual genes. The research angle is naturally highly subjective in choosing candidates from numerous promising ones.

The report on functional candidates should provide full details why the particular genes were chosen, where the genotyped group of animals is originating, what kind of marker set was used to eliminate the other associated effects in the genome, etc. For any gene, the combined data on its vicinity should be used to convince others about hitting the true gene in the face of too much interfering information from dozen other genes. A good design in such studies should be aiming at balanced genotype frequencies. If a gene is picked up because of ease of genotyping, the only hope is to have much luck to hold marker variants that are in *linkage disequilibrium* with the alleles causing a trait deviation. There is also the trick of having a "significant" result surface from the data by permuting several genes and traits (see [44, 45]).

It is a common problem that *candidate gene*s are not providing consistent evidence when exposed to validation in subsequent generations of the same population or more importantly, in other populations. The most beautiful investigations are finalized by functional mutation studies (knock-out or in) or complementation tests in a modeled mouse experiment, practically impossible in livestock species. One way to improve the analysis is to define a trait more explicitly. For example, calving interval could be itemized to several sub-traits, which in turn may prove to be more rewarding objects for QTL analysis. Likewise with the markers, instead of associating gene variants, it is now possibly to go a level deeper and excavate the respective gene expression patterns. The difficulties are not over when it comes to deciding which tissues and which developmental stage would provide appropriate samples for expression studies and how to plan a comparable and uniform production environment for such studies. The expression profiles are obviously an outcome influenced by several factors and their interactions are ever so hard to interpret (for more discussion, see [28]).

The complex traits in medical studies have experienced similar disappointing conclusion, and there are hardly any major genes manifesting the familial multifactor diseases. Researchers have voiced this by talking about missing explanations for the observed genetic variation or heritability [46]. In quantitative genetics, it is more and more obvious that the variation is simply caused by lots of genes with tiny effects and variants that are not appearing among the prior candidates [47]. With the rapid growth of high throughput marker typing and re-sequencing, there is now a possibility with very large population samples and concerted actions to detect reliable associations even for the small effects [48]. Different techniques, such as detailed mapping and functional studies, could be combined [49]. What remains is the requirement for large bodies of data, as has always been in analyzing genetic variation for animal breeding purposes.

Genomic Revolution

The very fast development of molecular genetic techniques has resulted in exploitation of the existing nucleotide diversity. The genome sequence is available for chicken [50] and cattle [51]. The sequences of the whole genome in pig and sheep are still on the way. The sequence information is indicating that a typical animal genome has almost endless amount of potential variable sites. Several descriptive measures are used to summarize polymorphisms of DNA sequences. Under a neutral model, the expected level of diversity can be deduced from the generation of new alleles by mutations and from the elimination of alleles by drift (which is inversely proportional to effective population size), that is, $4\ N_e \times$ mutation rate. For comparison, in a human population two randomly chosen individuals differ at ~1 in 1,000 nucleotides (1 SNP per kilo base).

The genetic diversity of mankind is low compared to other (older) species. In cattle and sheep the mean nucleotide diversity is 2–2.5 SNPs per kilo base [52], whilst for chicken the estimate is 4–5.5 [53]. With modern DNA chip technology up to hundreds of thousands of loci across the genome could be used to genotype animals with a reasonable cost. These possibilities have opened up completely new kind of possibilities to understand and utilize the genetic variation.

MAS with More Markers

When there are several markers available, the *mixed model equations* for *breeding value* estimation could be extended to accommodate several markers with a vector of QTL effects. Using the previously introduced notation (Fig. 5), the use of several markers is with matrix presentation $\boldsymbol{y} = \boldsymbol{X\beta} + \boldsymbol{Za} + \boldsymbol{Qq} + \boldsymbol{e}$, where $\boldsymbol{Q}$ is the incidence matrix for $\boldsymbol{q}$ [54]. Var $(\boldsymbol{q}) = \boldsymbol{G}\,\sigma_q^2$ where σ_q^2 is the variance due to QTL and $\boldsymbol{G}$ is the matrix of probabilities for QTL alleles being identical by descent. These probabilities can be computed from the pedigree, marker, and linkage map information. So far QTL mapping has produced fewer useful genes or markers for MAS than was anticipated when the QTL screening work started. The found QTL are contributing much less to the variation than would be satisfactory for a successful use of MAS, as its efficiency is affected by the proportion of variation due to a major locus [55]. Much caution should be also taken in MAS, as most of the found QTL have an overestimated effect (so-called Beavis effect). The availability of vast amounts of SNP markers should improve both these aspects: a dense marker panel covering the whole genome would be able to wrap all the genetic variation and avoid the problems of few overemphasized markers.

From MAS to Genomic Genetic Values

For the future practical application in estimating the genetic values, the most promising approach seems to be simultaneous utilization of a vast number of markers over the entire genome [56]. The map density is so high that the recombination between markers and QTL can be ignored. With a genome-wide set of markers, the estimate of individual's genetic value or genomic estimated *breeding value* is obtained by estimating effects associated with the markers from animals with both the phenotype and marker genotype information and summing the marker effects for recently genotyped animals available for selection. With genome-wide marker panel one can hopefully catch most of the genetic variation and produce a more attractive way to exploit markers.

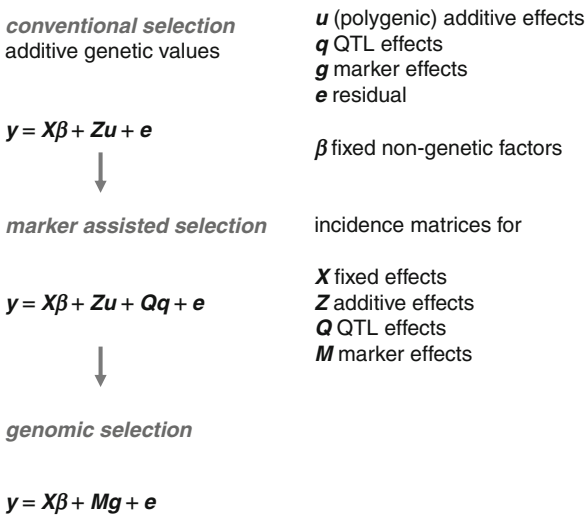

Animal Molecular Genetics from Major Genes to Genomics. Figure 5
The mixed model methodology is a flexible tool to accommodate the models ranging from simple breeding value prediction with polygenic model to QTL effects associated with known markers. The effects of genome-wide marker sets are computed through a straightforward summation over the genome. $\boldsymbol{X}$, $\boldsymbol{Z}$, $\boldsymbol{Q}$, and $\boldsymbol{M}$ are the incidence matrices linking the observations to respective effects

The process of predicting the *breeding value*s utilizing genomic information could be described in three steps:

1. Use a genome-wide marker panel to genotype animals. It is now a norm to use densely mapped SNPs as markers. The SNP variation is seen as two alleles (potentially with four). When the marker panel is very dense and genome-wide and each marker is wrapping the genetic variation for a measured trait in its neighborhood, the whole panel is covering all the genetic variation. With additive gene action the biallelic marker is assumed to have a substitution

effect. As the whole genome is covered with the dense map, the effects of the n SNP loci would sum the genetic value of the animal.

2. Estimate the effects of each marker locus. The model for the phenotype of animal i is $y_i = \sum_{j=1}^{n} m_{ij} g_j + e_i$ where m_{ij} (2, 1 and 0) is representing the marker genotypes in the ith animal, g_j is half of the substitution effect at the marker locus for the quantitative trait and e is the residual. The phenotype and genotype data could therefore be used to estimate the marker effects (ignoring all the nongenetic factors) with the model in matrix notation $\boldsymbol{y} = \boldsymbol{M}\,\boldsymbol{g} + \boldsymbol{e}$. The new method could be seen as part of the development in mixed model methodology (Fig. 5). The first two steps are carried out in a sufficiently large reference population with information on both marker genotypes and trait phenotypes.
3. The genomic *breeding value* could be computed for genotyped selection candidates by summing the estimated effects over the markers.

There are several options how the equations could be solved. Treating the marker effects as random, it is customary to assume that their variance is constant over the genome or that there are few loci with large effects with the majority having small effects. In addition, there are options for the distribution of the effects. The case of normally distributed effects with constant variance is interesting because the *breeding value* predictions would be equivalent with *BLUP* where the pedigree-based relationship matrix A is replaced by a relationship matrix estimated from the marker information [57]. The latter is also called genomic relationship matrix and is technically MM'. The genomic information has also been successfully used to incorporate the realized relationships into the A matrix used in *BLUP* [58].

It is the Bayesian methods that are able to cope with situations where an allowance for graduated effects of markers is made. This is beneficial as the QTL screening works is clearly showing that there are genomic regions having relatively large effects. Many distributions have been tried: a case where most markers have a small effect and very few a large effect, alternatively assuming 0 for several markers and nonzero for few markers. These were studied in the original paper [56] and the former approach is known as BayesA and the latter one as BayesB. Meuwissen and Goddard [36] also presented an alternative where the variances of marker effects are sampled from a mixture of two distributions allowing the variation in the effect size across markers. Simple methods are possibly favored so far, as pure Bayesian approaches would require more computing time. Related to this, the rapidly increasing number of markers – hundreds of thousands – and availability of sequence data and larger number of genotyped animals would also challenge the computing capacities.

The accuracy of genomic *breeding value*s depends of course on the number of records and proportion of genetic variation or heritability h^2. Small *effective population size* is generating linkage disequilibrium. Related to linkage disequilibrium, the genome contains regions of reduced haplotype diversity, termed haplotype blocks [59], separated by blocks of higher diversity. Within such blocks the frequencies of marker alleles may be highly correlated across loci. The genome blocking sets limits to the estimation even if the marker density is very high. The number of independent segments for a chromosome of length L (in *Morgan*s) is $2\,N_e\,L/\ln(4N_e\,L)$ [57]. So, a chromosome of $1M$ has some 33 independent segments and the whole genome of 30 such chromosomes would have 1,000 independent segments. If the *effective population size* is small, increasing more markers would not improve the accuracy or resolution in explaining the genetic variation and the best one can do in that situation, is increasing the number of animals in the analysis [57, 60]. In conclusion, the accuracy of genomic *breeding value*s would depend on the number of animals in the reference population, the heritability of the trait, the marker density, the number of independent genome segments (or effective population size) and the total length of the genome.

With best linear unbiased prediction and Bayesian method, the accuracy of predicting genetic values for offspring of the recorded animals has been shown to be of the order 0.7–0.8 [56], comparable to that of the progeny test. The genomic selection method was presented in 2001 and did not receive much attention, as at that time the required coverage of the whole genome with markers was not feasible, at least in terms of costs. When the high throughput genotyping

of SNPs with microarrays became available and Schaeffer [61] pointed out the remarkable returns and savings that the genomic selection could produce in dairy cattle breeding, the breeding companies rushed out to exploit the tool with unparalleled enthusiasm. He compared genomic selection with conventional progeny testing and assumed that there were marker effects available with accuracy 0.75 to select bulls and bull dams. As much less bulls would be kept after genomic "pre-selection," the cost of the marker-based improvement would be only 10% of the traditional one. Another radical feature of genomic selection, is the sufficiently reliable evaluation of young animals which would reduce the generation interval drastically, for example, in the bull–bull path from 6 years down to less than 2 years. When it takes 5–7 years to have the progeny test result for a dairy bull, the genomic genetic value is available at birth. Putting the slightly lower accuracy and shortened generation interval together, the annual genetic change is predicted to be doubled.

Much of the work on assessing the advantages of genomic selection has been done by simulation. The reliabilities of genomic *breeding value*s could be assessed by dividing the real data into two parts, usually over birth date and compare how the predictions based on older animals compare with the estimates obtained for the more recent ones with all the data. VanRaden et al. [62] concluded that the reliability is proportional to the size of the reference population while the increments in marker density had a smaller impact. They were implying that a reference population of few thousand progeny tested bulls is required to arrive at a satisfactory accuracy of genomic *breeding value*s. Only the Holstein breed has such numbers and even there the breeding companies would need collaborative efforts across countries for reaching a sufficient number of accurately known sires.

Breeds with smaller populations (and progeny tested bulls) could in principle resort to the marker effects estimated in a large population. If the marker density is very high, genomic *breeding value*s estimated in one breed may support the estimation in the other breed [63]. They may be some common *linkage disequilibrium* within a short distance across the breeds otherwise recombination has broken associations since the divergence. Selection and drift have also changed the genotype frequencies over time.

Management of Variation

Very intensively selected populations may suffer from losing variation or, in a more extreme case, from inbreeding depression and appearance of recessives defects. This is due to the reduced number of selected parents to generate the breeding bulls. The risk for inbreeding and drift is expressed with *effective population size* or rate of inbreeding ($\Delta F = 1/(2N_e)$). The safe areas for these would be over 50 and less than 1%, respectively (e.g., [64]). In dairy cattle, the awareness on rate of inbreeding was triggered by the breeding schemes utilizing multiple ovulation and embryo transfer (MOET). It was shown that the schemes could be optimized with respect to genetic progress and costs, by concentrating the MOET operation on cows in a nucleus of few hundred cows only. The apparent small number of parents and larger full-sib families accompanied by early selection would easily mean risks for higher rates of inbreeding. This kind of worries generated lots of research and now the better understanding about the related risks in selection programs has resulted in new tools. The most important aspect is to maximize the variation in selected groups of males and females while the formation of mating pairs is less relevant. Meuwissen [65] has developed so-called optimum contribution method which yields the guidance in choosing parents and their progeny numbers to maximize the genetic gain while minimizing the coancestry. The constraining on the coancestry is based on the relationship matrix and therefore the optimum contribution method could be easily integrated with the information needed for *BLUP* evaluation.

Genomic *breeding value*s are based on information on the individuals themselves and are therefore better than *BLUP breeding value*s which may more often lead to co-selection of sibs due to family information [66]. So the genomic selection has short-term advantages for the management of genetic variation. In the long-term an efficient genomic selection is automatically reducing variation. The genomic information is on the other hand giving an accurate estimate on the relationship between individuals. While the pedigree based matrix gives the expected relationships, the marker-based matrix yields the realized relationships. The earlier work (e.g., [67]) showed that tens or even hundreds

of markers (e.g., microsatellites), is of limited value in estimating the relationships and in controlling the rate of inbreeding. The use of genome-wide SNP panels has changed the situation and molecular similarities could be calculated very accurately and used like the genealogical information. Just like the relationship matrix in the *BLUP* context is improved by the genomic information, in the same way the genomic relationship matrix could enhance the management of variation. There are only preliminary results [68] which are indicating that high benefits could be anticipated from the use of genomic relationship matrix in promoting the sustainable use of genetic variation.

Genetic Correlation

It is a common observation that there is a negative genetic correlation between production traits and longevity, made of such traits as disease resistance and fertility. It is widely accepted that such a correlation is caused by pleiotropy so that the same genes would have opposite effects on the two sets of traits. This could be understood as a consequence of allocating limited metabolic resources to competing physiological compartments within an animal. If a genetic correlation between two traits is positive, it can be thought that the effects on the two traits are on average influencing to the same direction. On the other hand, if the majority of effects are of opposite "sign," a negative correlation would be seen. However, there should be some variation over the pleiotropic genes in the genome, there being also some with positive effect on both the traits. Therefore, selection could be differentiated over the genome to avoid undesirable effects in longevity traits while improving the production efficiency. This is something one is going to learn when multiple trait analysis are thoroughly investigated with the dense genome-wide marker information.

Extensions to a Pair of Populations

The introgression of multifactor traits from one population to another should enjoy the powerful genomic tools in making the procedure more precise and diminishing the compromises of receiving undesirable sections of the donor genome. Ødegård et al. [69] showed that genomic selection results in an efficient introgression of desirable QTL alleles from a donor line, as the genome of the donor apart from the QTL could be selected against. Lots of data is obviously needed for separating the beneficial and unattractive genome parts in a candidate exotic breed.

Heterosis or hybrid vigor in crosses has been long observed. Predicting which lines will give good crosses is a hit and miss affair. Simple dominance is sufficient to give crossbreds better performance than either parent provided that both parents are fixed for the dominant allele at some locus at which the other parent is fixed for the recessive one – that is with one parent being Bc/Bc and the other bC/bC, where B and C are the dominant alleles.

Several breeding procedures have been suggested and used in order to make best use of the *heterosis*, among them the reciprocal recurrent selection, proposed by Comstock et al. [70] makes the most use of quantitative genetic principles. The benefits from crossbreeding are highest with widely deviating allele frequencies between the breeds. There is a need for efficient methods with immediate returns to evaluate the most promising breed crosses jointly with the most potential mating pairs.

Starting from the results by Smith and Mäki-Tanila [6], theory and methods to compute genotypic means and covariances in a two-breed population under dominance inheritance have been presented by Lo et al. [71]. They showed that the genotypic mean is a linear function of 5 location parameters and that the genotypic covariance between relatives is a linear function of 25 dispersion parameters. These would include the additive (and the corresponding heritability) and dominance variance in both the purebred populations and the variation of contributions from the breeds to the F_1 individuals. Clearly simpler and more parsimonious methods are needed.

Genomic research has proven to be a powerful approach in quantifying the genetic distances between populations, in revealing history of animal populations, number and sites for domestication, population expansions and contractions, selection, origin, and mixing of maternal and paternal lineages (see [72]). Because *heterosis* is proportional to the differences in gene frequencies in the parental lines, it is possible to make marker-based prediction of hybrid performance based on genetic distances, despite having

only indirect estimates of allele frequencies for the interesting traits *via* the anonymous markers.

Xu [73] stimulated by the elegance of genomic selection has extended a Bayesian analysis to the F_2 population of inbred lines and has successfully also estimated the dominance deviations. However, the cases starting from random breeding populations – in subdivided population or in crossbred animals, typical in animal breeding – need research. Toro and Varona [74] have investigated the use of genomic information in predicting also dominance effects and the advantages of designing matings to have a full advantage of the extra component in the evaluation. First of all, the genomic approach was possible compared to the overcomplicated polygenic parameterization. Secondly, the prediction of additive effects had a higher accuracy. Finally, the immediate response was higher when dominance effects were estimated, although the subsequent progress stayed very much the same. If the cost of genotyping is reasonable, the estimation of dominance effects could be seen as a new tool in utilizing *heterosis* in chicken and pig production where crosses of different lines are a norm.

Research on Beneficial and Harmful Genes

Along the use of genome-wide marker sets in large reference populations, it is possible to map medium to large size QTL. This would yield genomic predictions that are stable across families and generations. If the genes underlying QTL are found, they may be further studied for the pleiotropic effects on other traits, dominance effects, interactions with other QTL (epistasis), or response to environmental changes. Information derived from such studies will lead to better models and better predictions and even management of phenotypes, which can be used for selection and production planning.

There are several Mendelian defects identified in farm animals. Recessive disorders are a problem in efficient improvement schemes, because healthy carriers can spread the disease allele quickly to a large number of progeny. A good example is BLAD (bovine leukocyte adhesion deficiency) causing a severe immunodeficiency. The mutation got widely distributed in the Holstein cattle due to a famous bull few decades ago. The missense mutation is now identified [75] and the eradication program has been successful. Charlier et al. [76] reported fine-scale mapping of five recessive disorders in cattle using large SNP panel. Between 25,000 and 50,000 SNPs were used in the discovery populations. Homozygosity mapping is used to detect mutations that cause disease when both copies are present (recessivity). Three disorders were mapped with a sufficient resolution so that the molecular basis could be characterized and effective eradication tools were established and used in mating planning. A prerequisite for finding recessive disorders is a well-organized recording of defects and diseases in the population. In general, molecular genetic techniques could be used to develop diagnostic tests. On the other hand the disorders are providing animal models to study human diseases.

Future Directions

The conventional prediction methods based on *infinitesimal model* have produced very impressive results in quantitative traits of animal production. There is, however, plenty of evidence on the existence of major genes mediation the variation in such measured traits. For some time now, it has been possible to map such genes in the genome using molecular genetic markers. The accurate localization is needed for estimating the gene effects and integrating their direct selection into methods predicting the polygenic effects. There has been extensive genome screenings for QTL carried out all the farm animal species, either with crossbreeding or half-sib design. The outcome is thousands of QTL while the high-resolution localization has yielded only very few causal mutations underlying the found QTL. Also the variation contributed by these QTL is far too low for efficient marker- or gene-assisted selection. The molecular genetic technology has in the mean time taken further leaps and now there are available microarray chips containing thousands or even hundreds of thousands of SNPs to allow genomic selection. Genomic selection is in principle genome-wide *marker-assisted selection.* As it covers all the genetic variation in the genome, the estimated of marker effects would give sufficiently reliable predictions of genetic values for young animals. Hence, the genetic improvements programs could be accelerated and high savings could be done in testing schemes. Genomic information could be further used for management of genetic

variation, mating planning utilizing non-additive variation, understanding genetic correlation architecture, etc. The animal breeding industry has quickly adopted the new technology and is now widely exploiting the latest SNP panels in the selection schemes. As a side product, the systematic genome-wide screening is picking up harmful and beneficial mutations for further research and applications. It is very tempting and certainly very challenging to try to model the variation via complicated pathways and interactions due to individual genes and regulatory factors. No doubt many would try. Luckily animal breeding research has a long and flourishing history of sophisticated mathematics and statistics. Hence, much research will be devoted to the area. The main test for a new method in animal breeding would consist of questions like: how it is going to help us in understanding variation, how would it help to improve prediction of breeding value, what gains are made in efficiency of selection programs, what kind of savings could be made in testing, etc. Finally, to have firm ground in analyses and decision making, there is a continuous need to have lots of information, both on the genomes and the measurable traits.

Acknowledgment

I am grateful to colleagues, especially Pekka Uimari, at MTT, for useful comments on the draft of the text, and to Ignacy Misztal for lots of encouragement.

Bibliography

Primary Literature

1. Falconer DS, Mackay TFC (1996) Introduction to quantitative genetics, 4th edn. Longman, Harlow, 464 p
2. Weller JI (2009) Quantitative trait loci analysis in animals, 2nd edn. CABI, Wallingford
3. Henderson CR (1984) Applications of linear models in animal breeding. University of Guelph, Guelph
4. Henderson CR (1976) A simple method for computing the inverse of a numerator relationship matrix used for prediction of breeding values. Biometrics 32:69–79
5. Wray NR, Hill WG (1989) Asymptotic rates of response from index selection. Anim Prod 49:217–227
6. Smith SP, Mäki-Tanila A (1990) Genotypic covariance matrices and their inverses for models allowing dominance and inbreeding. Genet Sel Evol 122:65–91
7. Silvela L (1980) Genetic changes with generations of artificial selection. Genetics 95:769–782
8. Mäki-Tanila A (1982) The validity of the heritability concept. Ph.D. thesis, University of Edinburgh, 120 p
9. Mäki-Tanila A, Kennedy BW (1986) Mixed model methodology under genetic models with a small number of additive and non-additive loci. In: Proceedings of 3rd world congress on genetics applied to livestock production 12, Lincoln, pp 443–448
10. Webb AJ, Carden AE, Smith C, Imlah P (1982) Porcine stress syndrome in pig breeding. In: Proceedings of 2nd world congress on genetics applied to livestock production 5, pp 588–608
11. Merat P, Ricard FH (1974) Etude d'un Gene de nanisme lié au sexe chez la poule: importance de l'état d'engraissement et gain de poids chez l'adulte. Ann Genet Sel Anim 6:211–217
12. Rollins WC, Tanaka M, Nott CFG, Theissen RB (1972) On the mode of inheritance of double muscled conformation in bovines. Hilgardia 41:433–456
13. Piper LR, Bindon BM (1982) The genetic segregation for fecundity in Booroola Merino sheep. In: Barton RA, Smith WC (eds) Proceedings of world congress on sheep and beef cattle breeding. Dunmore, Palmerston North, pp 315–331
14. Lande R, Thompson R (1990) Efficiency of marker-assisted selection in the improvement of quantitative traits. Genetics 124:743–756
15. Dekkers JCM (2004) Commercial application of marker- and gene-assisted selection in livestock: strategies and lessons. J Anim Sci 82:E313–E328
16. Pong-Wong R, Woolliams JA (1998) Response to mass selection when an identified major gene is segregating. Genet Sel Evol 30:313–337
17. Dekkers JCM, Hospital F (2002) The use of molecular genetics in the improvement of agricultural populations. Nat Rev Genet 3:22–32
18. Yancovich A, Levin I, Cahaner A, Hillel J (1996) Introgression of the avian naked neck gene assisted by DNA fingerprint. Anim Genet 27:149–155
19. Knap PW, Neeteson-Van Nieuwenhoven AMA (2005) Private and public roles in conservation. In: Proceedings of options and strategies for conservation of FAnGR., Montpellier, pp 62–67
20. Bidanel JP (1989) Etude de stratégies de valorisation en croisement de la race Meishan. 3 – evaluation comparée de différents systèmes de croisement. J Rech Porcine en France 21:361–366
21. Legault C (1998) Génétique et prolificité chez la truie: la voie hyperprolifique et la voie sino-européenne. INRA Prod Anim 11:214–218
22. Lynch M, Walsh B (1998) Genetics and analysis of quantitative traits. Sinauer, Sunderland
23. Elston RC, Stewart J (1973) The analysis of quantitative traits for simple genetic models from parental, F1 and backcross data. Genetics 73:695–711
24. Neimann-Sorensen A, Robertson A (1961) The association between blood groups and several production characteristics in three Danish cattle breeds. Acta Agric Scand 11:163–196

25. Soller M, Genizi A (1978) The efficiency of experimental designs for the detection of linkage between a marker locus and a locus affecting a quantitative trait in segregating populations. Biometrics 34:47–55
26. Lander ES, Botstein D (1989) Mapping Mendelian factors underlying quantitative traits using RFLP linkage maps. Genetics 121:185–199
27. Haley CS, Knott SA (1992) A simple regression method for mapping quantitative trait loci in line crosses using flanking markers. Heredity 69:315–324
28. Georges M (2007) Mapping, fine mapping, and molecular dissection of quantitative trait loci in domestic animals. Annu Rev Genomics Hum Genet 8:131–162
29. Andersson L, Haley CS, Ellegren H, Knott SA, Johansson M, Andersson K, Andersson-Eklund L, Edfors-Lilja I, Fredholm M, Hansson I et al (1994) Genetic mapping of quantitative trait loci for growth and fatness in pigs. Science 263:1771–1774
30. Georges M, Nielsen D, Mackinnon M, Mishra A, Okimoto R, Pasquino AT, Sargeant LS, Sorensen A, Steele MR, Zhao X, Womack JE, Hoeschele I (1995) Mapping quantitative trait loci controlling milk production in dairy cattle by exploiting progeny testing. Genetics 139:907–920
31. Darvasi A (1998) Experimental strategies for the genetic dissection of complex traits in animal models. Nat Genet 18:19–24
32. Weller J, Kashi Y, Soller M (1990) Power of daughter and granddaughter designs for determining linkage between marker loci and quantitative trait loci in dairy cattle. J Dairy Sci 73:2525–2537
33. Mackay TF (2009) The genetic architecture of complex behaviors: lessons from *Drosophila*. Genetica 136:295–302
34. Calus MP, Meuwissen TH, Windig JJ, Knol EF, Schrooten C, Vereijken AL, Veerkamp RF (2009) Effects of the number of markers per haplotype and clustering of haplotypes on the accuracy of QTL mapping and prediction of genomic breeding values. Genet Sel Evol 41:11
35. Farnir F, Coppieters W, Arranz JJ, Berzi P, Cambisano N, Grisart B, Karim L, Marcq F, Moreau L, Mni M, Nezer C, Simon P, Vanmanshoven P, Wagenaar D, Georges M (2000) Extensive genome-wide linkage disequilibrium in cattle. Genome Res 10:220–227
36. Meuwissen THE, Goddard ME (2004) Mapping multiple QTL using linkage disequilibrium and linkage analysis information and multitrait data. Genet Sel Evol 36:261–279
37. Goddard ME, Meuwissen TH (2005) The use of linkage disequilibrium to map quantitative trait loci. Aust J Exp Agric 45:837–845
38. Meuwissen THE, Karlsen A, Lien S, Olsaker I, Goddard ME (2002) Fine mapping of a quantitative trait locus for twinning rate using combined linkage and linkage disequilibrium mapping. Genetics 161:373–379
39. Spielman RS, McGinnis RE, Ewens WJ (1993) Transmission test for linkage disequilibrium: the sinsulin gene region and insulin dependent diabetes mellitus. Am J Hum Genet 52:506–516
40. Grisart B, Farnir F, Karim L, Cambisano N, Kim JJ, Kvasz A, Mni M, Simon P, Frère JM, Coppieters W, Georges M (2004) Genetic and functional confirmation of the causality of the DGAT1 K232A quantitative trait nucleotide in affecting milk yield and composition. Proc Natl Acad Sci USA 101:2398–2403
41. Van Laere AS, Nguyen M, Braunschweig M, Nezer C, Collette C, Moreau L, Archibald AL, Haley CS, Buys N, Tally M, Andersson G, Georges M, Andersson L (2003) A regulatory mutation in IGF2 causes a major QTL effect on muscle growth in the pig. Nature 425:832–836
42. Andersson L (2009) Genome-wide association analysis in domestic animals: a powerful approach for genetic dissection of trait loci. Genetica 136:341–349
43. Clop A, Marcq F, Takeda H, Pirottin D, Tordoir X, Bibé B, Bouix J, Caiment F, Elsen JM, Eychenne F, Larzul C, Laville E, Meish F, Milenkovic D, Tobin J, Charlier C, Georges M (2006) A mutation creating a potential illegitimate microRNA target site in the myostatin gene affects muscularity in sheep. Nat Genet 38:813–818
44. Tabor HK, Risch NJ, Myers RM (2002) Candidate-gene approaches for studying complex genetic traits: practical considerations. Nat Rev Genet 3:391–397
45. Zhu M, Zhao S (2007) Candidate gene identification approach: progress and challenges. Int J Biol Sci 3:420–427
46. Maher B (2008) Personal genomes: the case of the missing heritability. Nature 456:18–21
47. Hill WG (2010) Understanding and using quantitative genetic variation. Phil Trans R Soc B 365:73–85
48. Yang J, Benyamin B, McEvoy BP, Gordon S, Henders AK, Nyholt DR, Madden PA, Heath AC, Martin N, Montgomery GW, Goddard ME, Visscher PM (2010) Common SNPs explain a large proportion of the heritability for human height. Nat Genet 42:565–569
49. Karim L, Takeda H, Lin L, Druet T, Arias JA, Baurain D, Cambisano N, Davis SR, Farnir F, Grisart B, Harris BL, Keehan MD, Littlejohn MD, Spelman RJ, Georges M, Coppieters W (2011) Variants modulating the expression of a chromosome domain encompassing PLAG1 influence bovine stature. Nat Genet 43:405–413
50. Wallis JW, Aerts J, Groenen MAM, Crooijmans RPMA, Layman D, Graves TA, Scheer DE, Kremitzki C, Fedele MJ, Mudd NK, Cardenas M, Higginbotham J, Carter J, McGrane R, Gaige T, Mead K, Walker J, Albracht D, Davito J, Yang S-P, Leong S, Chinwalla A, Sekhon M, Wylie K, Dodgson J, Romanov MN, Cheng H, de Jong PJ, Osoegawa K, Nefedov M, Zhang H, McPherson JD, Krzywinski M, Schein J, Hillier L, Mardis ER, Wilson RK, Warren WC (2004) A physical map of the chicken genome. Nature 432:761–764
51. Bovine Genome Sequencing and Analysis Consortium (2009) The genome sequence of taurine cattle: a window to ruminant biology and evolution. Science 324:522–528
52. Meadows JRS, Hawken RJ, Kijas JW (2004) Nucleotide diversity on the ovine Y chromosome. Anim Genet 35:379–385
53. Hillier LW, Miller W, Birney E et al (2004) Sequence and comparative analysis of the chicken genome provide unique

perspectives on vertebrate evolution. Nature 432:695–716 (International Chicken Genome Sequencing Consortium)
54. Fernando RL, Grossman M (1989) Marker assisted selection using best linear unbiased prediction. Genet Sel Evol 21: 467–477
55. Meuwissen THE, Goddard ME (1996) The use of marker haplotypes in animal breeding schemes. Genet Sel Evol 28:161–176
56. Meuwissen THE, Hayes BJ, Goddard ME (2001) Prediction of total genetic value using genome-wide dense marker maps. Genetics 157:1819–1829
57. Goddard ME (2009) Genomic selection: prediction of accuracy and maximisation of long term response. Genetica 136:245–257
58. Legarra A, Aguilar I, Misztal I (2009) A relationship matrix including full pedigree and genomic information. J Dairy Sci 92:4656–4663
59. Wall JD, Pritchard JK (2003) Haplotype blocks and linkage disequilibrium in the human genome. Nat Rev Genet 4:587–597
60. Daetwyler HD, Villanueva B, Woolliams JA (2008) Accuracy of predicting the genetic risk of disease using a genome-wide approach. PLoS One 3:e3395
61. Schaeffer LR (2006) Strategy for applying genome-wide selection in dairy cattle. J Anim Breed Genet 123:218–223
62. VanRaden PM, VanTassell CP, Wiggans GR, Sonstegard TS, Schnabel RD, Taylor JF, Schenkel FS (2009) Invited review: reliability of genomic predictions for North American Holstein bulls. J Dairy Sci 74:2737–2746
63. De Roos APW, Schrooten C, Mullaart E, van der Beek S, de Jong G, Voskamp W (2009) Genomic selection at CRV. Interbull Bull 39:47–50
64. Woolliams J, Berg P, Mäki-Tanila A, Meuwissen T, Fimland E (2005) Sustainable management of animal genetic resources. NGH Nordisk Genbank Husdyr, Norway, 95 p
65. Meuwissen THE (1997) Maximizing the response of selection with a predefined rate of inbreeding. J Anim Sci 75:934–940
66. Daetwyler HD, Villanueva B, Bijma P, Woolliams JA (2007) Inbreeding in genome-wide selection. J Anim Breed Genet 124:369–376
67. Fernandez J, Villaneuva B, Pong-Wong R, Toro MA (2005) Efficiency of the use of pedigree and molecular marker information in conservation programmes. Genetics 170:1313–1321
68. Sonesson AK, Woolliams JA, Meuwissen THE (2010) Maximising genetic gain whilst controlling rates of genomic inbreeding using genomicoptimum contribution selection. In: Ninth world congress on genetics applied to livestock production, Leipzig
69. Ødegård J, Yazdi MH, Sonesson AK, Meuwissen TH (2009) Incorporating desirable genetic characteristics from an inferior into a superior population using genomic selection. Genetics 181:737–745
70. Comstock RE, Robinson HF, Harvey PH (1949) A breeding procedure designed to make maximum use of both general and specific combining ability. J Am Soc Agron 41:360–367
71. Lo LL, Fernando RL, Cantet RJC, Grossman M (1995) Theory for modelling means and covariances in a two-breed population with dominance inheritance. Theor Appl Genet 90:49–62
72. Toro MA, Mäki-Tanila A (2007) Genomics reveals domestication history and facilitates breed development. In: Oldenbroek K (ed) Utilisation and conservation of farm animal genetic resources. Wageningen Academic, The Netherlands, pp 75–102, 232 p
73. Xu S (2003) Estimating polygenic effects using markers of the entire genome. Genetics 163:789–801
74. Toro MA, Varona L (2010) A note on mate allocation for dominance handling in genomic selection. Genet Sel Evol 42:33. http://www.gsejournal.org/content/42/1/33
75. Shuster DE, Kehrli ME, Ackermann MR, Gilbert RO (1992) Identification and prevalence of a genetic defect that causes leukocyte adhesion deficiency in Holstein cattle. Proc Natl Acad Sci USA 89:9225–9229
76. Charlier C, Coppieters W, Rollin F, Desmecht D, Agerholm JS, Cambisano N, Carta E, Dardano S, Dive M, Fasquelle C, Frennet JC, Hanset R, Hubin X, Jorgensen C, Karim L, Kent M, Harvey K, Pearce BR, Simon P, Tama N, Nie H, Vandeputte S, Lien S, Longeri M, Fredholm M, Harvey RJ, Georges M (2008) Highly effective SNP-based association mapping and management of recessive defects in livestock. Nat Genet 40:449–454

Antibiotics for Emerging Pathogens

Vinayak Agarwal[1], Satish K. Nair[2]
[1]Center for Biophysics and Computational Biology, University of Illinois at Urbana-Champaign, Urbana, IL, USA
[2]Department of Biochemistry and Center for Biophysics and Computational Biology, University of Illinois at Urbana-Champaign, Urbana, IL, USA

Article Outline

Glossary
Definition of the Subject
Introduction
Emerging Targets of Antibiotic Molecules
Emerging Chemical Classes of Antibiotic Molecules
Future Directions
Acknowledgments
Bibliography

Glossary

Microorganism A microscopic or submicroscopic organism, too small to be seen by unaided human eye, comprising of bacteria, virus, yeast, protozoa and fungi.

Pathogen A disease-causing microorganism which may or may not be infectious.

Antibiotic A chemical substance, usually organic in nature, capable of destroying or inhibiting the growth of pathogenic microorganisms.

Antibiotic resistance The developed or acquired ability of antibiotic susceptible pathogenic microorganisms to grow and survive despite the inhibitory action of the antibiotic molecules.

Plasmid Small, linear or circular genetic elements which can replicate independently of the chromosomal DNA inside a cell.

Tuberculosis A highly contagious bacterial disease of humans and animals caused by various strains of *Mycobacterium*, which normally affects the lungs but can also spread to other organs of the body.

Malaria A highly contagious protozoal disease caused by various strains of mosquito-borne *Plasmodium*.

Peptide Short chains of amino acids connected by peptide bonds.

Polyketide Compounds characterized by more than two carbonyl groups connected by single intervening carbon atoms.

Definition of the Subject

Antibiotics are organic small molecules, many of which are from natural sources, which are used to treat human infections caused by pathogenic microorganisms. While most validated antibiotics are initially very useful clinically, the pathogenic microorganisms that these compounds target are able to evade the action of the antibiotic by development of resistance mechanisms, which eventually render these antibiotics ineffective. Moreover, these resistance mechanisms can be passed on among different types of bacteria in a very simplistic manner that further compromises the usefulness of antibiotics. As a consequence, many diseases that were thought to have been eradicated by antibiotics (such as tuberculosis) have reemerged within these antibiotic-resistant strains. Hence, there is a constant need for the development of new and better antibiotic molecules that can be used to target these drug-resistant microbial populations.

Traditionally, the discovery and development of new antibiotics and other drug molecules has relied on two parallel and complimentary approaches: the discovery of new molecules of clinical relevance from natural sources, and the use of synthetic chemistry methods to derive compounds, based on the scaffold of naturally occurring molecules, with enhanced favorable antimicrobial properties. More recent development includes the identification of molecules without any natural precedents, based on the use of high-throughput screening methods of potential antibiotic targets against a large number of synthetic compound libraries to identify new classes of antibiotic molecules. Continued developments in all of these approaches, by an amalgam of both academic and industrial efforts, are essential for the development of compounds aimed at treating the evolution of drug-resistant pathogenic microorganisms.

Introduction

The interaction of prokaryotic microorganisms with human beings is widespread and significant, and the number of bacterial cells within the human body far exceeds the number of the human eukaryotic cells. This interaction between humans and bacteria is designed to be mutually beneficial to both [1, 2]. However, a small number of these bacterial microorganisms are known to cause disease in human beings and are hence called pathogens. The mechanisms by which these pathogenic organisms cause disease are extremely diverse and affect nearly all types of tissues and organs. The advancement of medical science has resulted in the development of two frontline defense mechanisms to fight infections and diseases caused by microbes. The first line of defense is the vaccines that specifically elicit the human host's adaptive immune response to recognize and eliminate pathogenic and harmful microbes, while selectively preserving the beneficial microbe population. Vaccines are generally biological macromolecules, derived from the pathogenic microbes themselves, which provide the adaptive immune response with the information necessary to elicit an antibody or cellular immune response against future invasions by the pathogenic microbes. Vaccines have been developed against several pathogens and have led to very significant reductions of deadly diseases such as tuberculosis and tetanus. However, vaccinations are not currently available against all pathogens, and the

natural evolution of the pathogens themselves may render these vaccinations ineffective against future infections, as exemplified by the inherent difficulties in vaccine development against viral infections such as influenza and HIV/AIDS.

The second frontline defense against pathogenic infections is the discovery and development of small molecule antibiotics that are designed to target and kill the harmful microorganisms with minimal side effects against the human host. Antibiotics are naturally occurring molecules produced by a number of different bacterial species to give them a selective competitive advantage for nutrients or other growth necessities over other microorganisms with which they share their surroundings. Serendipitous discovery and exploitation of these molecules dates back to ancient history [3–5] with numerous early reports, such as the use of the bark from cinchona tree, which contains the antibiotic quinine, used to treat malaria. Antibiotics generally have well-defined mechanisms of action against microbes and target specific biological processes to either retard growth (bacteriostatic antibiotics) or kill the microbe (bacteriocidal antibiotics).

The first report of an isolated antibiotic molecule used to effectively treat infections was the development and use of penicillin from the fungus *Penicillium notatum* by Alexander Fleming in 1928. Penicillin was used to treat diseases such as syphilis and other infections caused by staphylococci and streptococci. The term "antibiotic" was coined by the microbiologist Selman Waksman in 1942 [6] and is derived from the Greek *antibiosis* ("against life"). Hailed as a wonder drug, the discovery of penicillin marked the beginning of the antibiotic age, during which time antibiotics were developed to treat almost all major human infectious diseases. During this era, thousands of antibiotic molecules were discovered and these compounds were applied to fight bacterial, fungal, protozoan, and yeast infections. Concurrently, synthetic organic chemistry was also applied for the production of derivatives of naturally occurring antibiotics, and these synthetic compounds exhibited more desirable properties, such as decreased incidences of allergic reactions in humans. The discovery and development of these molecules marked a decreased incidence of outbreaks of the most common infectious diseases and contributed to an increase in life expectancy around the world.

However, repeated challenge of the pathogenic microorganisms with these antibiotics, in combination with the natural evolution of their genetic information, has resulted in the development of antibiotic resistance in these pathogens [7–9]. This process has led to the development of microbial resistance against nearly all available antibiotic molecules and has precipitated to an immense medical and financial challenge. The arsenal available to fight infections is becoming increasingly limited, and the rate of development of new molecules has not kept pace with the emergence of antibiotic resistance.

Factors Contributing to Increased Antibiotic Resistance

1. Widespread and indiscriminate overuse of antibiotics in the clinical environment, which exposes pathogenic microorganisms to an ever increasing concentration of different antibiotic molecules, which in turn increases the selection pressure to develop resistance against these antibiotic molecules [10, 11].
2. Use of antibiotics in agriculture and livestock rearing also leads to increased exposure of pathogenic bacteria to antibiotic molecules. Many of the antibiotics in use in agriculture and livestock feeds are also used for treating humans, and hence, development of resistant bacterial strains can be transferred from one setting to the other very easily [12–14].
3. Genetic recombination and transfer of genes from an antibiotic-resistant microbe to a non-resistant microbe, which leads to spread of resistance among microbial species. Antibiotic resistance genes are usually borne on highly mobile genetic vehicles called plasmids, which can easily be transmitted among microbes [15]. Microorganisms are able to sequester multiple plasmids, resulting in the evolution of plasmids that contain more than one resistance determinant. For example, the *Shigella* epidemic that caused nearly a quarter million deaths in Guatemala in 1968 was caused by a pathogen that contained a plasmid with resistance against four of the most commonly used antibiotics [16–18].

Mechanisms by Which Microorganisms Develop Resistance to Antibiotics

1. Efflux pumps in the microbial cell walls and membranes which actively transport the antibiotic molecule out of the cell and hence decrease its concentration within the cell. Consequently, increasing doses of antibiotics are required to target such microbes [19–21]. This mechanism is typified by the resistance to the broad-spectrum antibiotic tetracycline, which is mediated by the genetically mobile *tet* genes that encode for active efflux pumps for tetracycline and its derivatives [22–24].
2. Chemical modification of the antibiotic molecule by specific enzymes within the target pathogenic microbe, which render the antibiotic ineffective [25]. This mechanism is of particular concern against β-lactam antibiotics, such as penicillin and its derivatives [26, 27].
3. Modulation of the antibiotic target within the target cell so that the antibiotic is no longer able to bind and engage the target. Random mutations within the antibiotic target genes may lead to the emergence and subsequent selection of microbe species with a desensitized antimicrobial target. This mechanism of resistance is operative for development of resistance against the macrolide antibiotic erythromycin, and resistance results from the modification of its target, the bacterial ribosome, such that the antibiotic is no longer able to find the target [28, 29]. Another example is resistance to the "drug of last resort" vancomycin, which results as a change in its target of the D-Ala- D-Ala dipeptide moiety of the bacterial cell wall to D-Ala- D-Lac or to D-Ala- D-Ser [30–32].
4. Alteration of the metabolic pathways that are targeted by the antibiotic molecule so that inhibition of these metabolic pathways is not inhibitory or lethal to the microbe. A primary example of this class of resistance is the alterations in the sterol biosynthesis pathway in fungi which confer resistance to azole antibiotics [33, 34].

In light of the above factors, there is an ever-growing need for academic laboratories as well as for the pharmaceutical industries to search for antibiotics that have new and as yet unexplored mode of actions. New chemical classes of drug molecules are needed to mitigate the effects of resistance against the current drug chemical entities.

Emerging Targets of Antibiotic Molecules

Several new classes of antimicrobial targets have been identified, and drug development based on these findings, though still in its infancy, have taken major leaps forward.

Microbial Fatty Acid Biosynthesis Inhibition

The microbial fatty acid biosynthesis pathway presents numerous targets for drug development, particularly against the causative agent of tuberculosis – *Mycobacterium tuberculosis*. The metabolic pathways and chemical mechanisms for the synthesis of fatty acids are shared between a majority of prokaryotes and eukaryotes, including humans. However, as a result of differences in protein sequence and different arrangement of the active sites, compounds that target the bacterial fatty acid synthesis pathway are not cross-reactive or toxic against humans. The most well-characterized class of fatty acid biosynthesis inhibitor molecules is the antituberculosis molecule isoniazid, which inhibits the biosynthesis of mycolic acid, an essential component of the mycobacterial cell wall. Triclosan, an extensively used molecule in consumer products, such as toothpastes and mouthwashes, is also a fatty acid biosynthesis inhibitor.

An example of an emerging molecule in this class of antimicrobials is platensimycin (Fig. 1), produced by the organism *Streptomyces platensis* [35], which inhibits the growth of several pathogenic Gram-positive bacteria such as *Staphylococcus aureus, Enterococcus faecalis, and Staphylococcus pneumonia* [36]. Platensimycin inhibits the 3-ketoacyl-ACP synthase (KAS) enzyme FabF. Continued high-throughput screening and host genetic engineering efforts led to the identification of a platensimycin analog, platencin [37–39], which, in addition to FabF, inhibits another KAS enzyme called FabH and displays enhanced pharmacodynamic properties as compared to platensimycin. Chemical structures of microbial fatty acid biosynthesis inhibitor molecules discussed in this section are illustrated in Fig. 1.

Other KAS inhibitor molecules include cerulenin and thiolactomycin [40, 41]. Cerulenin is a

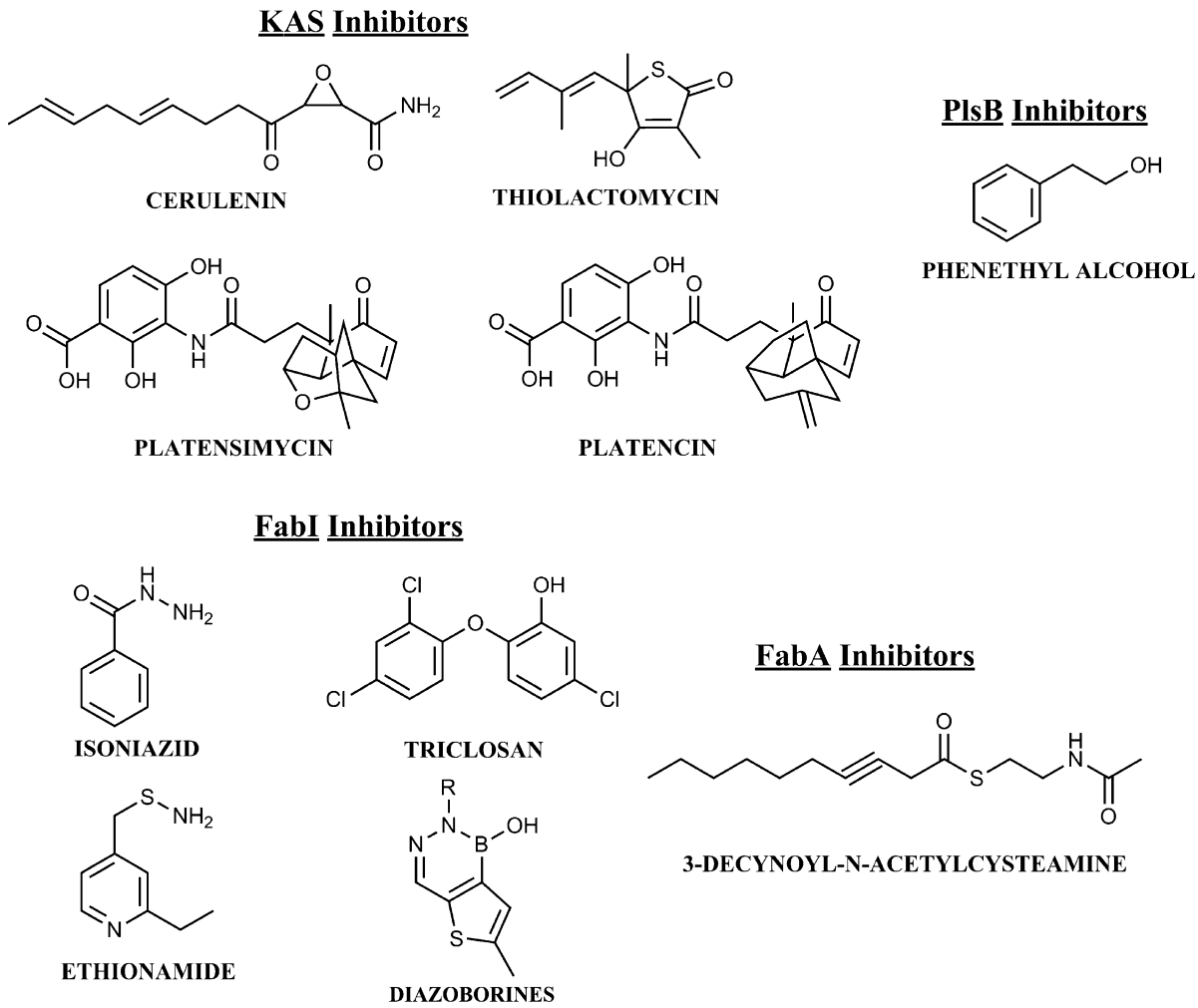

Antibiotics for Emerging Pathogens. Figure 1
Chemical structures of representative microbial fatty acid inhibitor molecules

broad-spectrum antifungal antibiotic produced by fungus *Caephalosporium caerulens* and preferentially inhibits the KAS enzymes FabB and FabF. Cerulenin forms a stable covalent adduct with the active site cysteine residue of these enzymes, and thus inhibits malonyl-group incorporation in the growing fatty acid chains [40, 42]. Thiolactomycin and related compounds have been isolated from various *Streptomycetes* and show potent inhibitory activity against fatty acid biosynthesis and mycolic acid biosynthesis in mycobacteria as well as against protozoan parasites such as malaria-causing *Plasmodium falciparum*. Thiolactomycin mimics the binding of malonyl coenzyme A molecule in the active site of KAS enzymes FabB, FabF, and FabH [41, 43]. Attempts for the preparation of semisynthetic derivatives of thiolactomycin are currently underway, and some of these derivatives are expected to improve upon its antimicrobial properties of thiolactomycin [44].

Molecules such as triclosan, isoniazid, diazaborines, and ethionamide target the enoyl-ACP reductase enzyme FabI of the fatty acid biosynthesis pathway. Each of these molecules binds in the active site of the enzyme and forms a tight complex with the nicotinamide adenine dinucleotide (NAD+) cofactor required for catalysis by FabI. However, pseudomonads and *S. pneumoniae* contain an additional enoyl-ACP reductase enzyme, FabK, which is not susceptible to

inhibition by these compounds, which allows these pathogens to overcome the antibacterial activities of these compounds.

The fatty acid biosynthesis pathways also present several other enzymes that can be targeted for drug development. The isomerase activity of the enzyme FabA can be inhibited by the drug candidate compound 3-decynoyl-*N*-acetylcysteamine. Metabolic interaction of the acetyl coenzyme A carboxylase enzyme with the fatty acid biosynthetic pathway also poses a potential target for inhibitor screening. Finally, compounds such as phenethyl alcohol, which inhibit the enzyme PlsB, responsible for the link between fatty acid biosynthesis and phospholipid biosynthesis, are also antimicrobial agents.

Isoprenoid Biosynthesis Inhibition

Isoprenoids are naturally occurring diverse organic compounds derived from the condensation of two or more isoprene monomeric units. They represent the largest class of small molecules on Earth. The isoprenoid pathways between prokaryotes and eukaryotes are very divergent: Humans synthesize isoprenoids by the mevalonate pathway, while microbes synthesize isoprenoids via the nonmevalonate pathways. Both pathways present numerous potential drug targets. One of the most widely used cholesterol-lowering drug, Lipitor, targets the mevalonate pathway in humans which is responsible for cholesterol biosynthesis. Antimicrobials such as terbinafine target the nonmevalonate pathways in fungi and yeast.

Several promising lead compounds that target the nonmevalonate pathway in the malaria parasite *Plasmodium falciparum* have been characterized. Principal among these are the phosphonate molecules fosmidomycin, first isolated from *Streptomyces lavendulae*, and its derivative FR900098, isolated from *Streptomyces rubellomurinus* [45, 46]. Fosmidomycin inhibits the enzyme 1-deoxy-D-xylulose 5-phosphate reductoisomerase (DXR) of the malaria parasite and has progressed to the stage of human phase II clinical trials for use in combination therapy with lincosamide antibiotic clindamycin [47–49]. However, the bioavailability of this molecule is low in bacterial models, with tuberculosis-causing bacterial pathogen essentially resistant to this molecule due to lack of uptake [50]. FR900098 is a structural analog of fosmidomycin and has been shown to demonstrate better efficacy in vivo than the parent compound. Synthetic and biosynthetic routes for the production and manipulation of this compound are currently being pursued [51, 52], as is the synthesis of several other structural analogs of fosmidomycin [53]. Fosmidomycin and FR900098 belong to the phosphonate class of antimicrobials, which are characterized by the presence of a stable carbon–phosphorous covalent linkage [54].

In addition to the DXR enzyme, a second potential drug target is the isoprenoid biosynthesis enzyme IspH, which is present in the vast majority of pathogenic bacteria and the malaria parasite but not in humans [55]. IspH is an attractive target for the development of inhibitors which could be potential drug and herbicide candidates. A series of diphosphate and bisphosphonate compounds have been synthesized, some of which inhibited the IspH enzyme at nanomolar concentrations [56, 57].

Other isoprenoid biosynthetic drug targets include the enzyme dehydrosqualene synthase CrtM, from the human pathogen *Staphylococcus aureus*, which can be inhibited by phosphonosulfonates and phosphonoacetamide compounds [58]. These compounds lead to inhibition of production of the *S. aureus* virulence factor staphyloxanthin, which makes these otherwise recalcitrant pathogenic cells susceptible to reactive oxygen species and subsequent clearance by the human immune system [59, 60]. Finally, the antiarrythmia drug amiodarone, which blocks various metal ion channels in the cell membrane [61], in conjunction with itraconazole, a fungal cytochrome P450 inhibitor [62], is also being reevaluated for the treatment of Chagas disease and cutaneous leismaniasis [63].

Cell Wall Biosynthesis Inhibition

Inhibition of cell wall biosynthesis has been one of the earliest validated targets for antibiotic development and still remains one of the most fruitful areas for the development of new drugs. However, drug development against cell wall biosynthesis is particularly challenging due to the presence of an additional lipopolysaccharide layer in Gram-negative bacteria and the fungal chitin cell wall in fungi, both of which are extremely rigid and impermeable to most small

molecule drugs. The following section focuses on some new nucleosidic antibiotic molecules that inhibit microbial cell wall biosynthesis and hold promise for future development. Chemical structures of microbial cell wall biosynthesis inhibitor molecules discussed in this section are illustrated in Fig. 2.

Nucleoside antifungal polyoxin molecules, such as nikkomycins, were isolated from several strains of Streptomyces [64] and have been shown to inhibit the biosynthesis of the fungal chitin cell wall. Nikkomycins display a wide spectrum of bioactivity while being nontoxic to animals and plants and have traditionally been used for controlling plant fungal diseases in agriculture. The parent nikkomycin compounds show relatively weak activity against opportunistic human pathogenic fungi, and semisynthetic derivatives are now being prepared which may display better pharmacological properties [65].

Capuramycin was first isolated from *Streptomyces griseus* in the 1980s and shows potent antibacterial properties against the human pathogens *Streptococcus pneumoniae and Mycobacterium smegmatis* [66]. Structure activity relationships have been explored by the synthesis of capuramycin derivatives [67, 68]. In in vivo studies against *Mycobacterium tuberculosis*, capuramycin demonstrated unique phenotypic changes in the pathogen which are not shown by any other currently available antibiotic and which may signify a mode of action distinct from those of known antibiotics [69].

Structurally related uridylpeptide molecules such as mureidomycins, pacidamycins, napsamycins, and sansanmycins have demonstrated activity against infections of the opportunistic human pathogen *Pseudomonas aeruginosa* in rodent models. Such infections are difficult to treat in immune-compromised patients as this pathogen can form a protective biofilm layer resulting in chronic infections [70–72]. These molecules do not show any cross-reactivity with mammalian cells.

Emerging Chemical Classes of Antibiotic Molecules

Peptidic Antibiotics

Peptidic antimicrobials are typically synthesized by the ribosome and consist of short polymers of the 20 naturally occurring amino acids linked together by

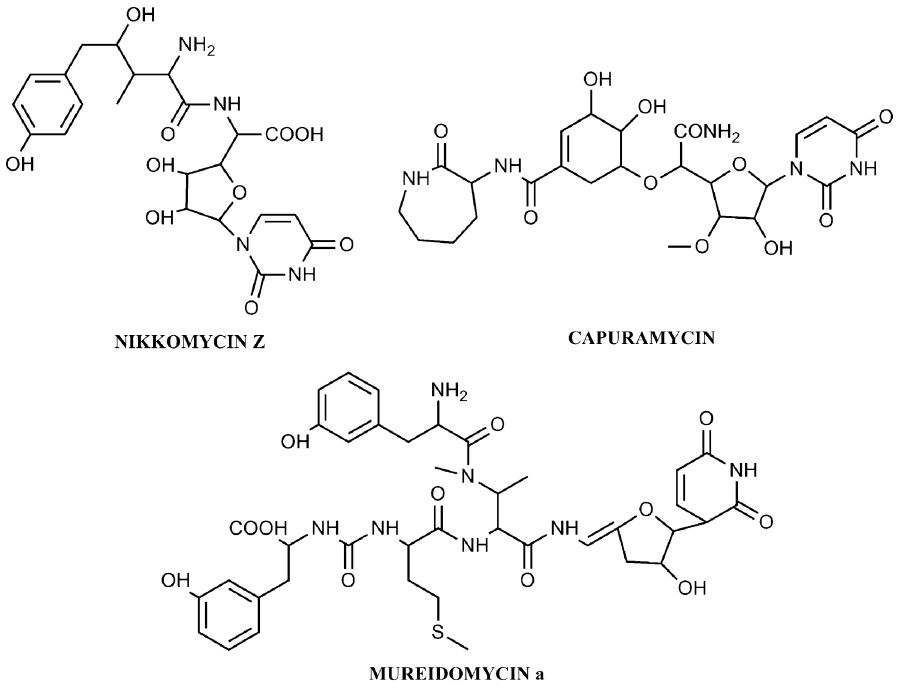

Antibiotics for Emerging Pathogens. Figure 2
Chemical structures of representative microbial cell wall biosynthesis inhibitor molecules

amide bonds. A second class of peptide antimicrobials are generated by a molecular assembly line, called nonribosomal peptide synthases (NRPS), which can incorporate nonnatural amino acids. The use of peptides to target pathogenic microbes is exemplified by the production of short cationic peptides by the human and plant immune systems, which either recruit the immune system for pathogen clearance or disrupt the outer cell and organelle cell membranes of microbes. A common conserved feature among all peptidic antimicrobials is posttranslational modifications conferred upon the peptide backbone, which are essential for their biological activities [73–75].

A well-known example of one class of ribosomally produced antimicrobial peptides is lantibiotics. Although these molecules are synthesized on the ribosome, they undergo posttranslational processing, resulting in the formation of several ring-like structures that add rigidity [76]. These compounds can be further modified on the amino and carboxy termini of these peptides as well, as shown in the structures of the lantibiotics epilancin [77] and microbisporicin [78]. Lantibiotics demonstrated multiple modes of action and exert their biological activities by binding to the lipid II cell wall moiety in bacteria [79], which leads to both inhibition of peptidoglycan biosynthesis as well as cell membrane permeabilization.

The most extensively used and well-characterized lantibiotic to date is Nisin (Fig. 3), initially identified as a by-product of milk fermentation, which contains seven lantibiotic rings, and has been used in the livestock industry for the treatment of bovine mastitis [80, 81]. Nisin, produced by the bacterium *Lactococcus lactis*, shows no adverse effects in humans and is being evaluated in human trials for the treatment of staphylococcal mastitis in lactating women [82].

Among the NRPS peptides, the most promising drug candidates are the lipopeptide antibiotic daptomycin and glycopeptides vancomycin and teicoplanin. Lipopeptide antibiotic such as daptomycin (Fig. 4) contains a long lipid chain attached to the peptide, which helps in targeting the bacterial cell wall. Daptomycin is produced by *Streptomyces roseosporus*, and genetic manipulations of the producer organism have led to the production of a combinatorial library of daptomycin derivatives [83–86]. Daptomycin shows potent antimicrobial activity against methicillin-resistant *Staphylococcus aureus* (MRSA) [87], infections by which are a rising global concern, and is already registered for the treatment of skin and soft tissue infections [88], bacteremia, and bacterial endocarditis [89].

The glycopeptide antibiotics are produced as cyclic aglycones (without sugars) and are then decorated by a number of different sugar molecules that are covalently attached by dedicated glycosyltransferase enzymes [90–92]. Among these, vancomycin (Fig. 5) [93], which prevents cell wall biosynthesis in Gram-positive bacteria, is clinically approved as the "drug of last resort" against MRSA infections [94]. Oritavancin (Fig. 5), a semisynthetic derivative of vancomycin, is potent against vancomycin-resistant enterococci (VRE) and is currently under human trials for the treatment of soft tissue infections by Gram-positive

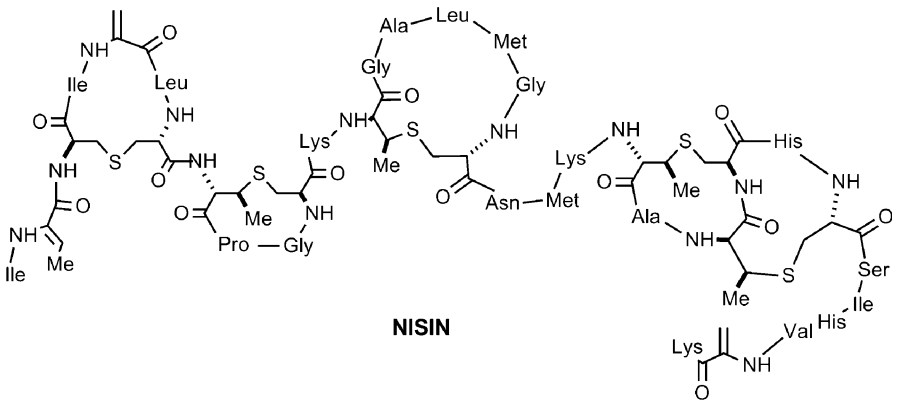

Antibiotics for Emerging Pathogens. Figure 3
Chemical structures of lantibiotic nisin. Some amino acids are abbreviated by their three-letter codes

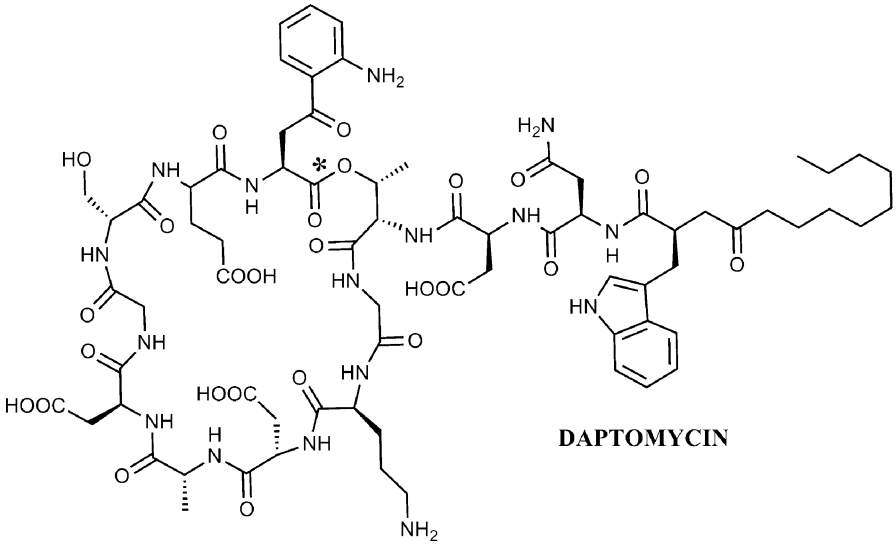

Antibiotics for Emerging Pathogens. Figure 4
Chemical structures of lipopeptide antibiotic daptomycin

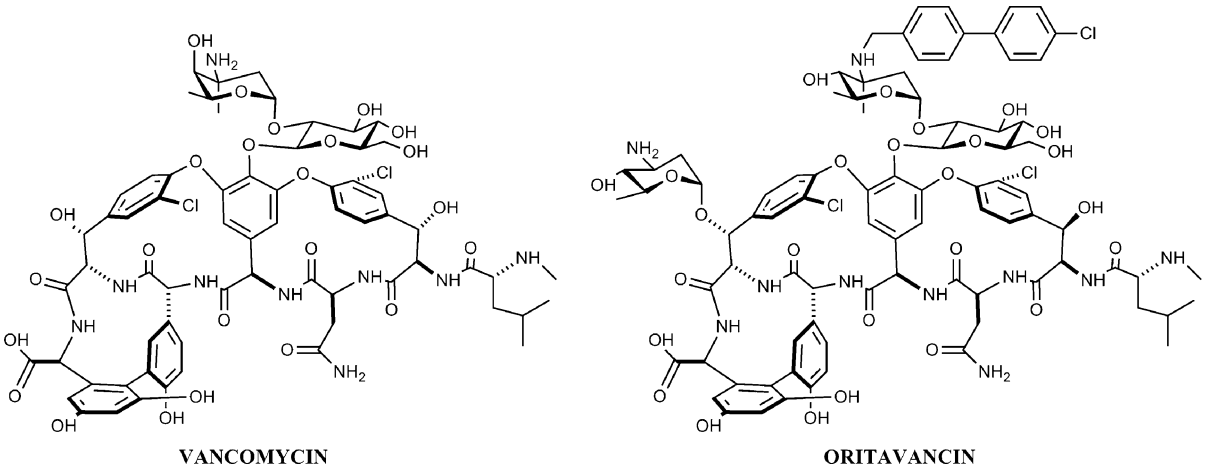

Antibiotics for Emerging Pathogens. Figure 5
Chemical structures of representative glycopeptides and lipoglycopeptide antibiotics vancomycin and oritavancin

bacteria [95]. Also of note are the cyclic lactone linkage–containing depsipeptides katanosins/plusbacins [96] and glycolipodepsipeptide ramoplanin [97], which are also active against MRSA.

Polyketide Antibiotics

Polyketide antibiotics are similar to nonribosomal peptide antibiotics as they are synthesized by multimodular polyketide synthases. These enzymes are analogous to the nonribosomal peptide synthases but typically catalyze the condensation of malonyl coenzyme A–derived monomeric units into cyclic lactone rings, onto which further modifications such as hydroxylations, glycosylations, and methylations are added. The most well-known polyketide antibiotic is erythromycin (Fig. 6), produced by *Streptomyces erythreus*, which has been in clinical use for more

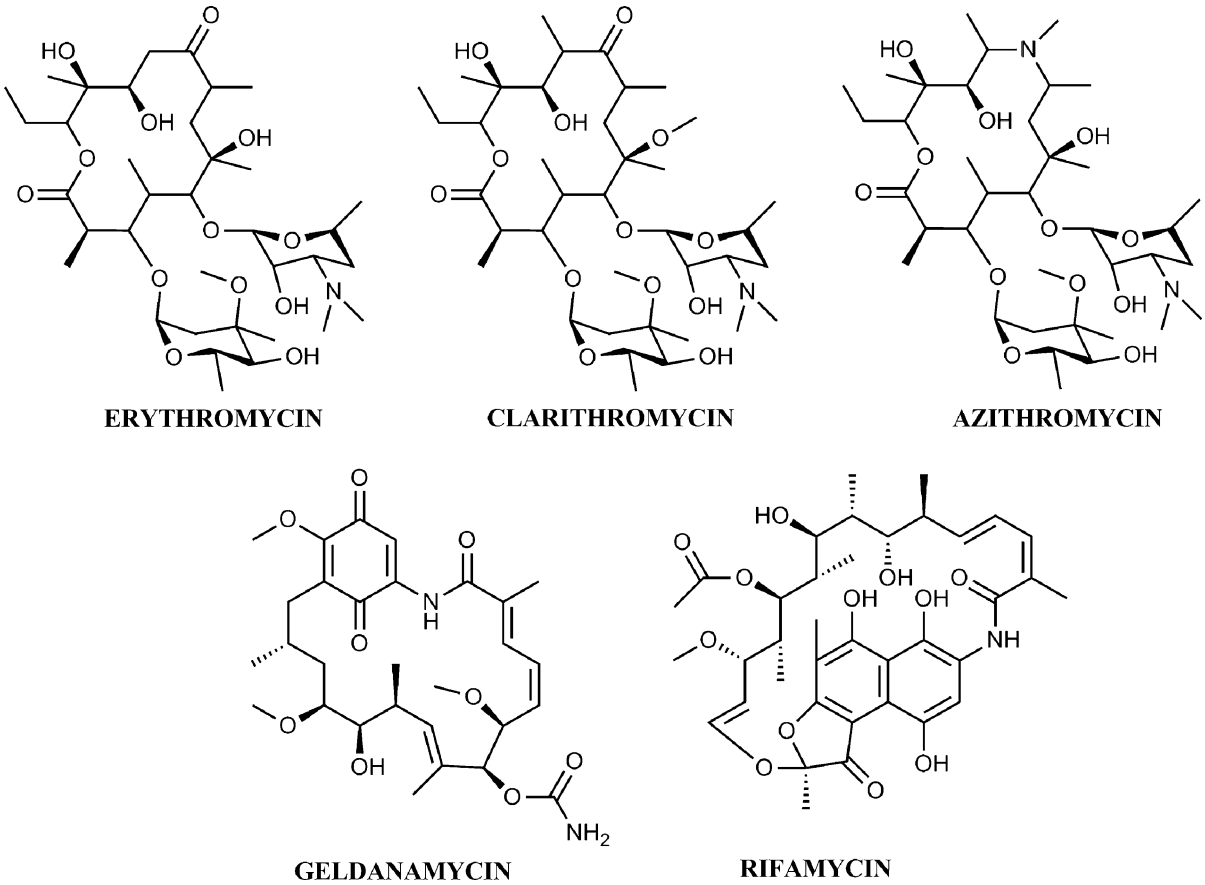

Antibiotics for Emerging Pathogens. Figure 6
Chemical structures of representative polyketide antibiotics

than 50 years. Several derivatives of erythromycin, such as clarithromycin and azithromycin (Fig. 6), have been developed for clinical use [98]. The mode of action of these compounds is inhibition of protein synthesis through binding to the various subunits of the bacterial ribosome [99].

Advancements in genetic technologies have opened up avenues for the manipulation and reprogramming of polyketide synthases for the production of new and novel molecules, which may yield drug candidates with enhanced pharmacological properties [100–102]. Of particular note are the ansamycin group of macrolide molecules, which differ from the molecules previously discussed in that the monomeric unit is 3-amino-5-hydroxybenzoic acid rather than a malonyl coenzyme A derivative. Various ansamycin molecules, such as rifamycin, geldanamycin, herbimycin, and ansamitocins, have been isolated, and their biosynthetic routes have been characterized. Of these, rifamycin, which inhibits bacterial RNA polymerase [103], is widely used in the treatment of tuberculosis. Geldanamycin, biosynthesized by *Streptomyces hygroscopicus*, and its analogs [104] inhibit heat shock protein 90 (Hsp90) [105] and are being evaluated in human clinical trials as antitumor agents [106].

Trojan Horse Antibiotics

A limiting factor for many antimicrobials and antibiotics is the lack of permeability across the microbial cell membranes. The outer membrane of the Gram-negative bacteria presents a formidable obstacle for drug entry [107]. Such Gram-negative bacteria employ a variety of active importer channels and pores to

internalize requisite nutrient material. Nature has ingeniously designed several antimicrobial compounds that utilize a "Trojan horse" strategy to overcome permeability barriers; specifically, these drug molecules are covalently attached to a carrier that facilitates recognition and import through the active transporters. Once inside the target cell, the carrier is removed to release the active drug, which then exerts its antimicrobial activities. This strategy for drug delivery has several advantages. First, active transport of the molecule inside susceptible cells alleviates the need for very high doses for the drug. Second, targeting of the molecule is highly specific only for those microbial cells that have the required transporter to internalize the molecules. Consequently, these "Trojan horse" are not taken up in humans and can be effective microbials even at very low doses.

Notable among this class of compounds are the sideromycins [108, 109], which are characterized by the attachment of the antibiotic molecule to ferric ion–binding chemical components called siderophores. The siderophore–iron complexes are specifically recognized and internalized by dedicated transport machinery in bacteria. Sideromycins consists of structurally diverse molecules including danomycins, salmycins, albomycins, ferrimycins, and microcins. Bioactivities for all these molecules have been established against several human pathogens [110]. Interestingly, as rapidly dividing cancerous cells also display siderophore uptake receptors on their cell surfaces, these molecules are also being evaluated as potential anticancer compounds [109]. Several synthetic conjugates of antibiotic molecules with siderophores have also been generated for evaluation of antimicrobial properties [111].

A different class of "Trojan horse" molecules consists of drugs that are attached to peptide carrier molecules. An example of one such drug is the compound (Z)-l-2-amino-5-phosphono-3-pentenoic acid (APPA), which is a potent inhibitor of the metabolic enzyme threonine synthase, and the "Trojan horse" version consists of APPA attached to a dipeptide. Depending on the amino acids in the dipeptide, the resultant conjugate can either be an antifungal (rhizocticins) or antibacterial (plumbemycin) [112]. Thus, a variety of activities can be encoded in the identical molecule by simply altering the nature of the conjugated peptide. A similar strategy for peptide attachment is utilized in the protein synthesis inhibitor microcin C7 [113].

Future Directions

Maintenance of global health in light of the reemergence of life-threatening infectious diseases requires a continuous influx of new and potent antibiotic molecules that are efficacious and safe for human and animal clinical use. Pathogenic organisms have displayed a remarkable resilience in both developing and propagating mechanisms for overcoming the activities of these antibiotic molecules. The development of new antibiotic molecules relies on two principal paradigms: the characterization of new microbial targets against which new drug molecules can be developed, and the identification of new chemical entities which can be used as antibiotics. Both routes have resulted in the production of very successful drug molecules, and future prospects for antibiotic development are reliant on further progress in these directions. Recent biotechnological advances in the area of microbial genome sequencing have led to a rapid increase in exploration of the microbial metabolome for both novel pathways to target in pathogens and new candidates for use as antibiotics. Semisynthetic chemical derivatization of naturally occurring antibiotics has further expanded upon the repertoire of candidate drugs, and combinatorial synthetic approaches have generated vast chemical libraries which may be screened for compounds with desired biological properties.

Future antibiotic development will require an amalgamation of various academic and industrial approaches such as (1) systems biology to explore metabolic connections and effects of antibiotic molecules on the human host and targeted pathogenic microbes, (2) synthetic biochemistry to generate and diversify arrays of compounds, (3) genomics and bioinformatics to identify and analyze antibiotic biosynthetic gene clusters, and (4) microbial ecological evaluations to better understand the role of naturally occurring antibiotic scaffolds in their native microbial niches. Another promising developing area is combinatorial therapy, in which multiple antibiotic molecules are administered together in order to overcome microbial resistance mechanisms and achieve better efficacy and pathogen clearance. This approach has

proven to be very successful in antiviral and oncological applications, and combination regimens have been used for the treatment of tuberculosis for several decades now. Another area of rapid progress in the future promises to be the development of narrow-spectrum antibiotics and better diagnostic tools which would aid in curtailing the indiscriminate use of broad-spectrum antibiotics, and thus reduce the incidence of microbial resistance against antibiotics.

Acknowledgments

Research in the Nair lab is supported by the NIGMS. We thank Neha Garg, Yue Hao, and Zhi Li for stimulating discussions.

Bibliography

1. Sears CL (2005) A dynamic partnership: celebrating our gut flora. Anaerobe 11(5):247–251
2. Backhed F et al (2005) Host-bacterial mutualism in the human intestine. Science 307(5717):1915–1920
3. Lindblad WJ (2008) Considerations for determining if a natural product is an effective wound-healing agent. Int J Low Extrem Wounds 7(2):75–81
4. Forrest RD (1982) Early history of wound treatment. J R Soc Med 75(3):198–205
5. Forrest RD (1982) Development of wound therapy from the dark ages to the present. J R Soc Med 75(4):268–273
6. Waksman SA (1947) What is an antibiotic or an antibiotic substance? Mycologia 39(5):565–569
7. Davies J, Davies D (2010) Origins and evolution of antibiotic resistance. Microbiol Mol Biol Rev 74(3):417–433
8. Allen HK et al (2010) Call of the wild: antibiotic resistance genes in natural environments. Nat Rev Microbiol 8(4):251–259
9. Moellering RC Jr (1998) Antibiotic resistance: lessons for the future. Clin Infect Dis 27(Suppl 1):S135–S140 discussion S141–2
10. Goossens H et al (2005) Outpatient antibiotic use in Europe and association with resistance: a cross-national database study. Lancet 365(9459):579–587
11. Tacconelli E et al (2008) Does antibiotic exposure increase the risk of methicillin-resistant *Staphylococcus aureus* (MRSA) isolation? A systematic review and meta-analysis. J Antimicrob Chemother 61(1):26–38
12. Mathew AG, Cissell R, Liamthong S (2007) Antibiotic resistance in bacteria associated with food animals: a United States perspective of livestock production. Foodborne Pathog Dis 4(2):115–133
13. Angulo FJ, Nargund VN, Chiller TC (2004) Evidence of an association between use of anti-microbial agents in food animals and anti-microbial resistance among bacteria isolated from humans and the human health consequences of such resistance. J Vet Med B Infect Dis Vet Public Health 51(8–9):374–379
14. Singer RS et al (2003) Antibiotic resistance–the interplay between antibiotic use in animals and human beings. Lancet Infect Dis 3(1):47–51
15. Koch AL (1981) Evolution of antibiotic resistance gene function. Microbiol Rev 45(2):355–378
16. Mendoza MC et al (1988) Plasmid typing of *Shigella sonnei* epidemic strains and molecular relationship of their R-plasmids. Eur J Epidemiol 4(2):158–163
17. Yagupsky P et al (1991) Use of multiple markers for investigation of an epidemic of *Shigella sonnei* infections in Monroe County, New York. J Clin Microbiol 29(12):2850–2855
18. Kariuki S et al (1996) Molecular typing of multi-drug resistant *Shigella dysenteriae* type 1 by plasmid analysis and pulsed-field gel electrophoresis. Trans R Soc Trop Med Hyg 90(6):712–714
19. Li XZ, Nikaido H (2009) Efflux-mediated drug resistance in bacteria: an update. Drugs 69(12):1555–1623
20. Lin L, Ling BD, Li XZ (2009) Distribution of the multidrug efflux pump genes, adeABC, adeDE and adeIJK, and class 1 integron genes in multiple-antimicrobial-resistant clinical isolates of *Acinetobacter baumannii-Acinetobacter calcoaceticus* complex. Int J Antimicrob Agents 33(1):27–32
21. Van Bambeke F, Balzi E, Tulkens PM (2000) Antibiotic efflux pumps. Biochem Pharmacol 60(4):457–470
22. Chopra I, Roberts M (2001) Tetracycline antibiotics: mode of action, applications, molecular biology, and epidemiology of bacterial resistance. Microbiol Mol Biol Rev 65(2):232–260, second page, table of contents
23. Rodrigues L et al (2009) The role of efflux pumps in macrolide resistance in *Mycobacterium avium* complex. Int J Antimicrob Agents 34(6):529–533
24. Pages JM, Amaral L (2009) Mechanisms of drug efflux and strategies to combat them: challenging the efflux pump of gram-negative bacteria. Biochim Biophys Acta 1794(5): 826–833
25. Wright GD (2005) Bacterial resistance to antibiotics: enzymatic degradation and modification. Adv Drug Deliv Rev 57(10): 1451–1470
26. Bradford PA (2001) Extended-spectrum beta-lactamases in the 21st century: characterization, epidemiology, and detection of this important resistance threat. Clin Microbiol Rev 14(4): 933–951
27. Jacoby GA, Sutton L (1985) Beta-Lactamases and beta-lactam resistance in *Escherichia coli*. Antimicrob Agents Chemother 28(5):703–705
28. Lovmar M et al (2009) Erythromycin resistance by L4/L22 mutations and resistance masking by drug efflux pump deficiency. EMBO J 28(6):736–744
29. Walsh C (2000) Molecular mechanisms that confer antibacterial drug resistance. Nature 406(6797):775–781
30. Bugg TD et al (1991) Molecular basis for vancomycin resistance in *Enterococcus faecium* BM4147: biosynthesis of a depsipeptide peptidoglycan precursor by vancomycin

resistance proteins VanH and VanA. Biochemistry 30(43):10408–10415
31. Bugg TD et al (1991) Identification of vancomycin resistance protein VanA as a D-alanine:D-alanine ligase of altered substrate specificity. Biochemistry 30(8):2017–2021
32. Walsh CT et al (1996) Bacterial resistance to vancomycin: five genes and one missing hydrogen bond tell the story. Chem Biol 3(1):21–28
33. Joseph-Horne T, Hollomon DW (1997) Molecular mechanisms of azole resistance in fungi. FEMS Microbiol Lett 149(2): 141–149
34. Lupetti A et al (2002) Molecular basis of resistance to azole antifungals. Trends Mol Med 8(2):76–81
35. Herath KB, Attygalle AB, Singh SB (2007) Biosynthetic studies of platensimycin. J Am Chem Soc 129(50):15422–15423
36. Wang J et al (2006) Platensimycin is a selective FabF inhibitor with potent antibiotic properties. Nature 441(7091): 358–361
37. Smanski MJ et al (2009) Engineered *Streptomyces platensis* strains that overproduce antibiotics platensimycin and platencin. Antimicrob Agents Chemother 53(4):1299–1304
38. Jayasuriya H et al (2007) Isolation and structure of platencin: a FabH and FabF dual inhibitor with potent broad-spectrum antibiotic activity. Angew Chem Int Ed Engl 46(25):4684–4688
39. Wang J et al (2007) Discovery of platencin, a dual FabF and FabH inhibitor with in vivo antibiotic properties. Proc Natl Acad Sci USA 104(18):7612–7616
40. Siggaard-Andersen M et al (1994) The fabJ-encoded beta-ketoacyl-[acyl carrier protein] synthase IV from *Escherichia coli* is sensitive to cerulenin and specific for short-chain substrates. Proc Natl Acad Sci USA 91(23):11027–11031
41. Machutta CA et al (2010) Slow onset inhibition of bacterial beta-ketoacyl-acyl carrier protein synthases by thiolactomycin. J Biol Chem 285(9):6161–6169
42. Johansson P et al (2008) Inhibition of the fungal fatty acid synthase type I multienzyme complex. Proc Natl Acad Sci USA 105(35):12803–12808
43. Nishida I, Kawaguchi A, Yamada M (1986) Effect of thiolactomycin on the individual enzymes of the fatty acid synthase system in *Escherichia coli*. J Biochem 99(5):1447–1454
44. McFadden JM et al (2005) Application of a flexible synthesis of (5R)-thiolactomycin to develop new inhibitors of type I fatty acid synthase. J Med Chem 48(4):946–961
45. Okuhara M et al (1980) Studies on new phosphonic acid antibiotics. III. Isolation and characterization of FR-31564, FR-32863 and FR-33289. J Antibiot (Tokyo) 33(1):24–28
46. Okuhara M et al (1980) Studies on new phosphonic acid antibiotics. I. FR-900098, isolation and characterization. J Antibiot (Tokyo) 33(1):13–17
47. Lell B et al (2003) Fosmidomycin, a novel chemotherapeutic agent for malaria. Antimicrob Agents Chemother 47(2):735–738
48. Missinou MA et al (2002) Fosmidomycin for malaria. Lancet 360(9349):1941–1942
49. Wiesner J, Jomaa H (2007) Isoprenoid biosynthesis of the apicoplast as drug target. Curr Drug Targets 8(1):3–13
50. Brown AC, Parish T (2008) Dxr is essential in *Mycobacterium tuberculosis* and fosmidomycin resistance is due to a lack of uptake. BMC Microbiol 8:78
51. Fokin AA et al (2007) Synthesis of the antimalarial drug FR900098 utilizing the nitroso-ene reaction. Org Lett 9(21): 4379–4382
52. Johannes TW et al (2010) Deciphering the late biosynthetic steps of antimalarial compound FR-900098. Chem Biol 17(1):57–64
53. Kurz T et al (2007) Conformationally restrained aromatic analogues of fosmidomycin and FR900098. Arch Pharm (Weinheim) 340(7):339–344
54. Metcalf WW, van der Donk WA (2009) Biosynthesis of phosphonic and phosphinic acid natural products. Annu Rev Biochem 78:65–94
55. Rohrich RC et al (2005) Reconstitution of an apicoplast-localised electron transfer pathway involved in the isoprenoid biosynthesis of *Plasmodium falciparum*. FEBS Lett 579(28):6433–6438
56. Wang K et al (2010) Inhibition of the Fe(4)S(4)-cluster-containing protein IspH (LytB): electron paramagnetic resonance, metallacycles, and mechanisms. J Am Chem Soc 132(19):6719–6727
57. Wang W et al (2010) Bioorganometallic mechanism of action, and inhibition, of IspH. Proc Natl Acad Sci USA 107(10): 4522–4527
58. Liu CI et al (2008) A cholesterol biosynthesis inhibitor blocks *Staphylococcus aureus* virulence. Science 319(5868): 1391–1394
59. Song Y et al (2009) Inhibition of staphyloxanthin virulence factor biosynthesis in *Staphylococcus aureus*: in vitro, in vivo, and crystallographic results. J Med Chem 52(13):3869–3880
60. Song Y et al (2009) Phosphonosulfonates are potent, selective inhibitors of dehydrosqualene synthase and staphyloxanthin biosynthesis in *Staphylococcus aureus*. J Med Chem 52(4):976–988
61. Kodama I, Kamiya K, Toyama J (1999) Amiodarone: ionic and cellular mechanisms of action of the most promising class III agent. Am J Cardiol 84(9A):20R–28R
62. Isoherranen N et al (2004) Role of itraconazole metabolites in CYP3A4 inhibition. Drug Metab Dispos 32(10):1121–1131
63. Paniz-Mondolfi AE et al (2009) Amiodarone and itraconazole: a rational therapeutic approach for the treatment of chronic Chagas' disease. Chemotherapy 55(4):228–233
64. Chen W, Zeng H, Tan H (2000) Cloning, sequencing, and function of sanF: A gene involved in nikkomycin biosynthesis of *Streptomyces ansochromogenes*. Curr Microbiol 41(5): 312–316
65. Stauffer CS et al (2007) Total synthesis and antifungal activity of a carbohydrate ring-expanded pyranosyl nucleoside analogue of nikkomycin B. J Org Chem 72(26):9991–9997
66. Yamaguchi H et al (1986) Capuramycin, a new nucleoside antibiotic. Taxonomy, fermentation, isolation and characterization. J Antibiot (Tokyo) 39(8):1047–1053
67. Hotoda H et al (2003) Synthesis and antimycobacterial activity of capuramycin analogues. Part 2: acylated derivatives of

capuramycin-related compounds. Bioorg Med Chem Lett 13(17):2833–2836
68. Hotoda H et al (2003) Synthesis and antimycobacterial activity of capuramycin analogues. Part 1: substitution of the azepan-2-one moiety of capuramycin. Bioorg Med Chem Lett 13(17):2829–2832
69. Reddy VM, Einck L, Nacy CA (2008) In vitro antimycobacterial activities of capuramycin analogues. Antimicrob Agents Chemother 52(2):719–721
70. Isono F et al (1989) Mureidomycins A-D, novel peptidylnucleoside antibiotics with spheroplast forming activity. III. Biological properties. J Antibiot (Tokyo) 42(5):674–679
71. Isono F et al (1989) Mureidomycins A-D, novel peptidylnucleoside antibiotics with spheroplast forming activity. II. Structural elucidation. J Antibiot (Tokyo) 42(5):667–673
72. Inukai M et al (1989) Mureidomycins A-D, novel peptidylnucleoside antibiotics with spheroplast forming activity I Taxonomy, fermentation, isolation and physico-chemical properties. J Antibiot (Tokyo) 42(5):662–666
73. Hancock RE, Sahl HG (2006) Antimicrobial and host-defense peptides as new anti-infective therapeutic strategies. Nat Biotechnol 24(12):1551–1557
74. Sahl HG (2006) Optimizing antimicrobial host defense peptides. Chem Biol 13(10):1015–1017
75. Peschel A, Sahl HG (2006) The co-evolution of host cationic antimicrobial peptides and microbial resistance. Nat Rev Microbiol 4(7):529–536
76. Willey JM, van der Donk WA (2007) Lantibiotics: peptides of diverse structure and function. Annu Rev Microbiol 61:477–501
77. Ekkelenkamp MB et al (2005) Isolation and structural characterization of epilancin 15X, a novel lantibiotic from a clinical strain of *Staphylococcus epidermidis*. FEBS Lett 579(9):1917–1922
78. Castiglione F et al (2008) Determining the structure and mode of action of microbisporicin, a potent lantibiotic active against multiresistant pathogens. Chem Biol 15(1):22–31
79. Bauer R, Dicks LM (2005) Mode of action of lipid II-targeting lantibiotics. Int J Food Microbiol 101(2):201–216
80. Cao LT et al (2007) Efficacy of nisin in treatment of clinical mastitis in lactating dairy cows. J Dairy Sci 90(8):3980–3985
81. Wu J, Hu S, Cao L (2007) Therapeutic effect of nisin Z on subclinical mastitis in lactating cows. Antimicrob Agents Chemother 51(9):3131–3135
82. Fernandez L et al (2008) The bacteriocin nisin, an effective agent for the treatment of staphylococcal mastitis during lactation. J Hum Lact 24(3):311–316
83. Nguyen KT et al (2006) Combinatorial biosynthesis of novel antibiotics related to daptomycin. Proc Natl Acad Sci USA 103(46):17462–17467
84. Penn J et al (2006) Heterologous production of daptomycin in *Streptomyces lividans*. J Ind Microbiol Biotechnol 33(2):121–128
85. Baltz RH, Miao V, Wrigley SK (2005) Natural products to drugs: daptomycin and related lipopeptide antibiotics. Nat Prod Rep 22(6):717–741
86. Miao V et al (2005) Daptomycin biosynthesis in *Streptomyces roseosporus*: cloning and analysis of the gene cluster and revision of peptide stereochemistry. Microbiology 151(Pt 5): 1507–1523
87. Tally FP, DeBruin MF (2000) Development of daptomycin for Gram-positive infections. J Antimicrob Chemother 46(4): 523–526
88. Henken S et al (2010) Efficacy profiles of daptomycin for treatment of invasive and noninvasive pulmonary infections with *Streptococcus pneumoniae*. Antimicrob Agents Chemother 54(2):707–717
89. Fowler VG Jr et al (2006) Daptomycin versus standard therapy for bacteremia and endocarditis caused by *Staphylococcus aureus*. N Engl J Med 355(7):653–665
90. Walsh C, Freel Meyers CL, Losey HC (2003) Antibiotic glycosyltransferases: antibiotic maturation and prospects for reproGramming. J Med Chem 46(16):3425–3436
91. Sussmuth RD, Wohlleben W (2004) The biosynthesis of glycopeptide antibiotics–a model for complex, non-ribosomally synthesized, peptidic secondary metabolites. Appl Microbiol Biotechnol 63(4):344–350
92. Donadio S et al (2005) Comparative analysis and insights into the evolution of gene clusters for glycopeptide antibiotic biosynthesis. Mol Genet Genomics 274(1):40–50
93. Levine DP (2006) Vancomycin: a history. Clin Infect Dis 42(Suppl 1):S5–S12
94. Gonzalez C et al (1999) Bacteremic pneumonia due to *Staphylococcus aureus:* A comparison of disease caused by methicillin-resistant and methicillin-susceptible organisms. Clin Infect Dis 29(5):1171–1177
95. Scheinfeld N (2007) A comparison of available and investigational antibiotics for complicated skin infections and treatment-resistant *Staphylococcus aureus* and enterococcus. J Drugs Dermatol 6(1):97–103
96. Maki H, Miura K, Yamano Y (2001) Katanosin B and plusbacin A(3), inhibitors of peptidoglycan synthesis in methicillin-resistant *Staphylococcus aureus*. Antimicrob Agents Chemother 45(6):1823–1827
97. Fulco P, Wenzel RP (2006) Ramoplanin: a topical lipoglycodepsipeptide antibacterial agent. Expert Rev Anti Infect Ther 4(6):939–945
98. Weissman KJ, Leadlay PF (2005) Combinatorial biosynthesis of reduced polyketides. Nat Rev Microbiol 3(12): 925–936
99. Menninger JR (1995) Mechanism of inhibition of protein synthesis by macrolide and lincosamide antibiotics. J Basic Clin Physiol Pharmacol 6(3–4):229–250
100. McDaniel R et al (1995) Rational design of aromatic polyketide natural products by recombinant assembly of enzymatic subunits. Nature 375(6532):549–554
101. Katz L (1997) Manipulation of modular polyketide synthases. Chem Rev 97(7):2557–2576
102. Ruan X et al (1997) Acyltransferase domain substitutions in erythromycin polyketide synthase yield novel erythromycin derivatives. J Bacteriol 179(20):6416–6425

103. Floss HG, Yu TW (2005) Rifamycin-mode of action, resistance, and biosynthesis. Chem Rev 105(2):621–632
104. Kim W et al (2009) Rational biosynthetic engineering for optimization of geldanamycin analogues. Chembiochem 10(7):1243–1251
105. Bedin M et al (2004) Geldanamycin, an inhibitor of the chaperone activity of HSP90, induces MAPK-independent cell cycle arrest. Int J Cancer 109(5):643–652
106. Neckers L, Schulte TW, Mimnaugh E (1999) Geldanamycin as a potential anti-cancer agent: its molecular target and biochemical activity. Invest New Drugs 17(4):361–373
107. Delcour AH (2009) Outer membrane permeability and antibiotic resistance. Biochim Biophys Acta 1794(5):808–816
108. Mollmann U et al (2009) Siderophores as drug delivery agents: application of the "Trojan Horse" strategy. Biometals 22(4):615–624
109. Braun V et al (2009) Sideromycins: tools and antibiotics. Biometals 22(1):3–13
110. Ballouche M, Cornelis P, Baysse C (2009) Iron metabolism: a promising target for antibacterial strategies. Recent Pat Antiinfect Drug Discov 4(3):190–205
111. Wencewicz TA et al (2009) Is drug release necessary for antimicrobial activity of siderophore-drug conjugates? Syntheses and biological studies of the naturally occurring salmycin "Trojan Horse" antibiotics and synthetic desferridanoxamine-antibiotic conjugates. Biometals 22(4): 633–648
112. Borisova SA et al (2010) Biosynthesis of rhizocticins, antifungal phosphonate oligopeptides produced by *Bacillus subtilis* ATCC6633. Chem Biol 17(1):28–37
113. Vondenhoff GH et al (2011) Characterization of peptide chain length and constituency requirements for YejABEF-mediated uptake of Microcin C analogues. J Bacteriol 193(14):3618–3623

Aquaculture and Renewable Energy Systems, Integration of

Bela H. Buck[1,2,3], Gesche Krause[4]
[1]Biological Sciences – Marine Aquaculture, Alfred Wegener Institute for Polar and Marine Research (AWI), Bremerhaven, Germany
[2]Marine Aquaculture for Sustainable Fisheries, Institute for Marine Resources (IMARE), Bremerhaven, Germany
[3]Maritime Technologies – Applied Marine Biology, University for Applied Sciences, Bremerhaven, Germany
[4]Leibniz Center for Tropical Marine Ecology (ZMT), Bremen, Germany

Article Outline

Glossary
Definition of the Subject
Introduction
Status Quo of Offshore Aquaculture Research Activities in Wind Farms
Future Directions
Bibliography

Glossary

Aquaculture Following the definition of the FAO [1, 2], *aquaculture* is the farming of aquatic organisms, including fish, molluscs, crustaceans, and aquatic plants with some sort of intervention in the rearing process to enhance production, such as regular stocking, feeding, and protection from predators. Specifically, *marine aquaculture*, also called *mariculture*, concentrates on aquatic organisms cultivated in brackish or marine environments.

Integrated Coastal Zone Management (ICZM) A process for the management of the coast using an integrated approach, regarding all aspects of the coastal zone, including geographical and political boundaries, in an attempt to achieve sustainability. The EU Commission [3] defines ICZM as a dynamic, multidisciplinary, and iterative process to promote sustainable management of coastal zones. It covers the full cycle of information collection, planning (in its broadest sense), decision making, management, and monitoring of implementation. ICZM uses the informed participation and cooperation of all stakeholders to assess the societal goals in a given coastal area, and to take actions towards meeting these objectives. ICZM seeks, over the long term, to balance environmental, economic, social, cultural, and recreational objectives, all within the limits set by the natural dynamics.

Mariculture See "aquaculture".

Offshore aquaculture A culture operation in a frequently hostile open ocean environment exposed to all kinds of sea states as well as being placed far off the coast.

Offshore co-management A dynamic partnership using the capacities and interests of different stakeholder groups for managing cross-sectoral activities

in cooperation with governmental authorities in the open sea.

Offshore wind farms A group of wind turbines in the same confined area used for production of electric power in the open ocean. Moving off the coast to the offshore, wind turbines are less obtrusive than turbines on land, as their apparent size and noise is mitigated by distance. Since water has less surface roughness than land (especially in deeper waters), the average wind speed is usually considerably higher over the open water. Therefore, the capacity factors are considerably higher than for onshore and nearshore locations [4].

Open ocean aquaculture See "Offshore aquaculture".

Definition of the Subject

"Fisheries have rarely been sustainable." This statement by Pauly et al. [5] was based on the recognition that this lack of sustainability was induced by a serial depletion of wild stocks worldwide. Causative for this trend is due to the improved fishing technology, geographical expansion, and exploitation of previously spurned species lower in the food web. In exchange, aquaculture was often either regarded to bridge the gap between supply and demand or, in contrast, even to exacerbate this scenario.

Since the 1970s, aquaculture production has grown quite rapidly and is by now one of the fastest growing aquatic food production sectors in the world [6]. Besides the rapid development of this sector, the wide-ranging decline in fisheries yields has been enhanced by an increase in public demand for aquatic products. With an annual share of more than 15% of total animal protein supplies, the production of captured fisheries and aquaculture plays a significant role in the global food security [6]. In 2007, approximately 160 million tons of aquatic organisms were produced worldwide (Fig. 1). From that, the share of global aquaculture production amounts to almost 47%, totaling about 60 million tons annually of aquatic organisms [7, 10]. A wide range of aquatic species is raised in various systems, onshore as well as in the ocean. According to the FAO [6], approximately 300 different species, ranging from fish to shellfish, crustaceans and algae are produced in aquaculture systems. Most of these aquaculture enterprises are concentrated in well-protected and therefore favorable inshore water areas [11].

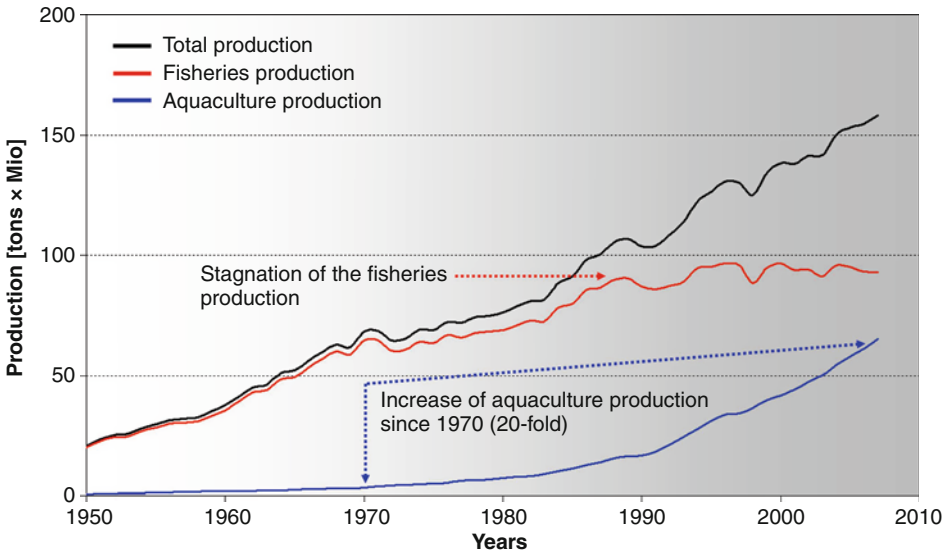

Aquaculture and Renewable Energy Systems, Integration of. Figure 1
Global production of aquatic organisms originating from fisheries and aquaculture within the last 55 years (Data source [7], modified after [8, 9])

Even probably though over-reporting its aquaculture production [12], the People's Republic of China has contributed approximately 70% to the world's aquaculture production in 2004. It is nevertheless debatable, whether this production can compensate for the global deficiency in aquatic food. In addition, the intensive traditional aquaculture of carnivorous species does not automatically relieve pressure on ocean fisheries [13]. Salmon farming, e.g., requires large inputs of wild fish as fish oil and fish meal for the production of fish feed for aquaculture. Hence, the farming of non-carnivorous species that is not dependent on fishmeal-based feeds is considered a sustainable way of producing food. However, the global increase in production originates from herbivorous species. Further, the balance between carnivorous and non-carnivorous species in aquaculture production is heavily skewed towards herbivorous species [14].

On top of this issue, an increasing limitation of favorable coastal sites for the development of modern aquaculture is evident in various countries, such as Germany, the Netherlands, Belgium, as well as others [15]. This spatial limitation is mainly caused by the lack of protected nearshore areas and by the fact that regulatory frameworks that assign specific areas for aquaculture operations are diverse and still emerging.

Further, the utilizations of coastal marine waters are manifold and quite competitive, such as shipping (trade or private), recreational activities, extraction or disposal of gravel, marine missions, fisheries, mariculture, offshore wind farms, cable and pipelines, establishment of nature reserves, and other marine and coastal protected areas. In addition, overlapping use of coastal habitats adds to the increasing pollution of coastal waters in various situations and gives rise to spatial conflicts, thus leaving little room for the expansion of modern coastal aquaculture systems.

This situation in most industrialized countries is often in contrast to the production progress in developing countries. Here, the installation of aquaculture systems benefits from the often weak enforcement of integrated coastal management schemes, which regulate equal access to the coastal resources [16, 17]. Thus, the rise of aquaculture production has specifically taken place in developing countries, especially in Asia, which holds approximately 91.4% of the global production share [10, 18, 19]. In contrast, the number of competing users within offshore regions is relatively low, thus favoring the offshore environment for further commercial development, such as offshore wind farming and open ocean aquaculture. So far, spatial regulations offshore are scarce and clean water can be expected [20]. Thus, there is an enormous economic potential for *extensive marine aquaculture* in offshore areas.

Introduction

Aquaculture has been increasing dramatically in most parts of the world and now accounts for more than 47% of the total global seafood supply [7]. Many people generally assess aquaculture positively as a potential alternative to global fishery resources, which are globally under stress as a result of overfishing. However, it also raises concerns over pollution, disease transmission, and other socio-economic impacts. Almost all efforts to develop marine aquaculture have focused on state jurisdictional waters of the coastal sea, which are generally situated within 3 nautical miles off the shore [21, 22]. With the convergence of environmental and aesthetic concerns, aquaculture, which is already competing for space with other more established and accepted uses, is having an increasingly difficult time expanding in nearshore waters [23]. Therefore, alternative approaches are needed in order to allow the expansion of the marine aquaculture sector to make a meaningful and sustainable contribution to the world's seafood supply.

The political recognition – on a national as well as on EU level – that the implementation of integrated coastal zone management (ICZM) is still fragmentary, acted as incentive to investigate in more detail how this could be overcome [e.g., 24]. This lack was recognized and led to the operation of a EU-Demonstration Programme on Integrated Coastal Zone Management from 1996 to 1999. This Programme was designed around a series of 35 demonstration projects and six thematic studies. In 2002, based on the experiences and outputs of the Demonstration Programme, the EU-Commission adopted a recommendation concerning the implementation of Integrated Coastal Zone Management in Europe (Recommendation of the European Parliament and of the Council, 2002/413/EC). In Germany, this generated a call of the Federal Ministry of Education and Research to the various federal states to

develop projects that address ICZM on a regional level. In 2004, the program *Coastal Futures* [25], which tied up various administrative and scientific bodies and the public along the west coast of the State of Schleswig-Holstein, was granted funding. This program focused primarily on two issues: [1] to develop the future of the coast as a living, working, and recreational space for the local population, and [2] to consider the potential contribution of coastal resources to the sustainable development on the national and EU/global level, i.e., by providing regenerative energy by wind power. In order to sustain sufficient open space for future development, the idea of combining offshore wind power generation with other uses, such as aquaculture operations, emerged [26]. Marine aquaculture is a growing enterprise in Germany as well as in the whole of Europe, strongly motivated by the decline of fisheries production and the search for alternative income options for rural peripheral coastal regions.

In order to stimulate multifunctional use of marine space, it was decided to develop a project on a showcase basis, which deals not only with different scientific fields but also with private–public partnerships and the relevant institutional bodies. In the following, an overview on the current state of research undertaken within this focus is provided. Offshore wind farms will hereby act as a case example for renewable energy systems in the open ocean.

Offshore Aquaculture – A New Addition to Marine Resource Use

Farming in the open ocean has been identified as one potential option for increasing seafood production and has been a focus of international attention for more than a decade. *Offshore aquaculture* or *open ocean aquaculture* are operations in a marine environment fully exposed to all kinds of oceanographic conditions [27] as well as located at least 8 nautical miles off the coast [15] to avoid the many stakeholder conflicts in nearer coastal areas [28]. The procedures and applied techniques for the cultivation of organisms mainly depend on the species; their life cycle determines the phases of cultivation and the location for the grow-out, where market size will be reached. First trials of cultivation were based on *extensive marine aquaculture*, which – in contrast to intensive aquaculture – is a line of production with little impact on the marine environment. These aquaculture operations are characterized by (1) a low degree of control (i.e., environmental control, nutrition, predators, competitors, and disease agents), (2) low initial costs, (3) low level technology, (4) low-production efficiency, and (5) high dependence on local climate and water quality (natural water bodies, such as bays, ponds, embayments) [29]. Mostly, they are regarded as a sustainable line of production.

Moving to the open ocean has been considered as a means for moving away from negative environmental impacts and negative public perception issues in the coastal zone. Favorable features for the transfer to open ocean waters include ample space for expansion and thus reduced conflicts with other user groups, lower exposure to human sources of pollution, the potential to reduce some of the negative environmental impacts of coastal fish farming, and optimal environmental conditions for various marine species through the larger carrying and assimilative capacities. However, this move should not be seen as an "out of sight, out of mind" attitude, as open ocean development will also come under scrutiny by the institutional bodies as well as by a more and more educated public. It is expected that, because of economies of scale, the open ocean farms of tomorrow will be larger than the present nearshore farms. Therefore, higher levels of waste can be generated. Even if greater residual effects occur, deeper waters and lower nutrient baselines are expected to reduce impacts from open ocean operations through wider dispersion plumes of nutrients, as compared to similarly sized nearshore operations. However, there will be a point when open ocean ecosystems will eventually reach their assimilative carrying capacities [30].

Offshore Wind Farms as a Case Example for Renewable Energy Systems

Wind energy continues to be the world's most dynamically growing energy source [31]. Drawing on the example of Germany, the first initiative toward an economy based on renewable energy resources was set by the governmental decision in the year 2000 to gradually reduce the use of nuclear energy and to respond to the gradually diminishing fossil- and nuclear-energy reserves. Simultaneously, the output of CO_2 to the

atmosphere would be reduced in accordance with the Kyoto protocol as well as the dependence on conventional fossil-energy resources is lowered.

As high and reasonably steady wind speeds are characteristic in Northern offshore areas, these areas are prime candidates for renewable energy production by wind-energy farms. For instance in the North Sea, a major political incentive exists currently to install large offshore wind farms [32, 33]. Thus, the emerging branch of offshore wind farms appears as a new stakeholder on the list of users [34, 35].

So far, this development has been successful to such an extent that around 7.2% of the total energy consumption in Germany is covered by this technology. At the end of 2007, Germany had an installed capacity of 22,247 MW, generated by 19,460 mainly land-based operating wind turbines [36]. Within Europe, as the leading market for wind energy with over 57 GW, Germany thus accounted for 39% in terms of the total installed capacity and still remains the world's leader. However, with the North American market currently experiencing a strong growth, it is expected that the US market will soon overtake Germany [37].

At present, 60 project applications for wind farms in the Exclusive Economic Zone (EEZ) of the German North Sea and in the Baltic Sea are in the planning process stage with the total number of wind turbines per farm ranging between 80 and 500 [26] (Fig. 2). In November 2001, the Federal Maritime and Hydrographic Agency (BSH) granted the first approval for the installation of a pilot offshore wind farm. Since then, a total of 23 wind farm development projects have been approved in German waters, most of them planned seaward of the 12 nautical miles zone [38]. Currently, a larger test farm of about 12 wind turbines (5 MW class) at the "Borkum West" site are in operation (Fig. 3) [39]. Experience gained in this project should give developers practical knowledge in the construction and operation of offshore wind farms at depths (down to 50 m) and at distances from the shore (up to 50 nautical miles and more) that are beyond comparison to those anywhere in the world [31, 33].

In contrast to neighboring European states, the prospect of moving wind energy developments offshore stagnated in Germany for years mainly due to a very complex licensing procedure and the high environmental constraints [33, 40]. A further obstacle roots in the spatial competition of offshore wind farms with other utilization of the marine waters in the German Bight [41, 42]. However, despite the number of competing users within offshore regions being lower compared to coastal areas [43], the quest for spatial efficiency remains to be a key incentive also for offshore developments in the future.

Moving Offshore: The Multiple-Use Concept

The plans for the massive expansion of wind farms in offshore areas of the North Sea triggered the idea of a combination of wind turbines with installations for extensive shellfish and macroalgae aquaculture [15, 26]. Offshore wind farms provide an appropriately sized area free of shipping traffic as most offshore wind farms are designed as restricted-access areas due to hazard mitigation concerns. Concurrently, the infrastructure for regular service support is readily available, and hence such sites provide an ideal opportunity for devising and implementing a multiple-use concept [42, 44]. However, in contrast to coastal inshore areas where beaches and their adjacent nearshore zones act as buffers to absorb wave energy, offshore regions are high-energy environments, fully exposed to waves, weather, and currents. Numerous studies have demonstrated that waves can reach remarkable heights (up to 10 m) in the offshore areas of the North Sea [e.g., 45, 46]. In this context, the solid foundation structure of wind turbines provides support for anchoring cultivation devices that can withstand the harsh oceanic conditions [47]. Furthermore, offshore structures are well known for their artificial reef function, thus supporting biodiversity in the ecosystem. The offshore water quality, which is a major issue in all kinds of aquaculture operations, is regarded to be excellent in comparison to inshore areas [48, 49]. Finally, the multifunctional use of offshore areas reduces conflicts between stakeholders if activities are concentrated and conjointly managed within so-called multiple-use marine areas. This, in turn, increases the amount of open ocean territory free of utilization by man. All of the above issues are considered as key incentives to move offshore with aquaculture operations.

In view of the many interests for the offshore move, different suggestions for technical structures for open

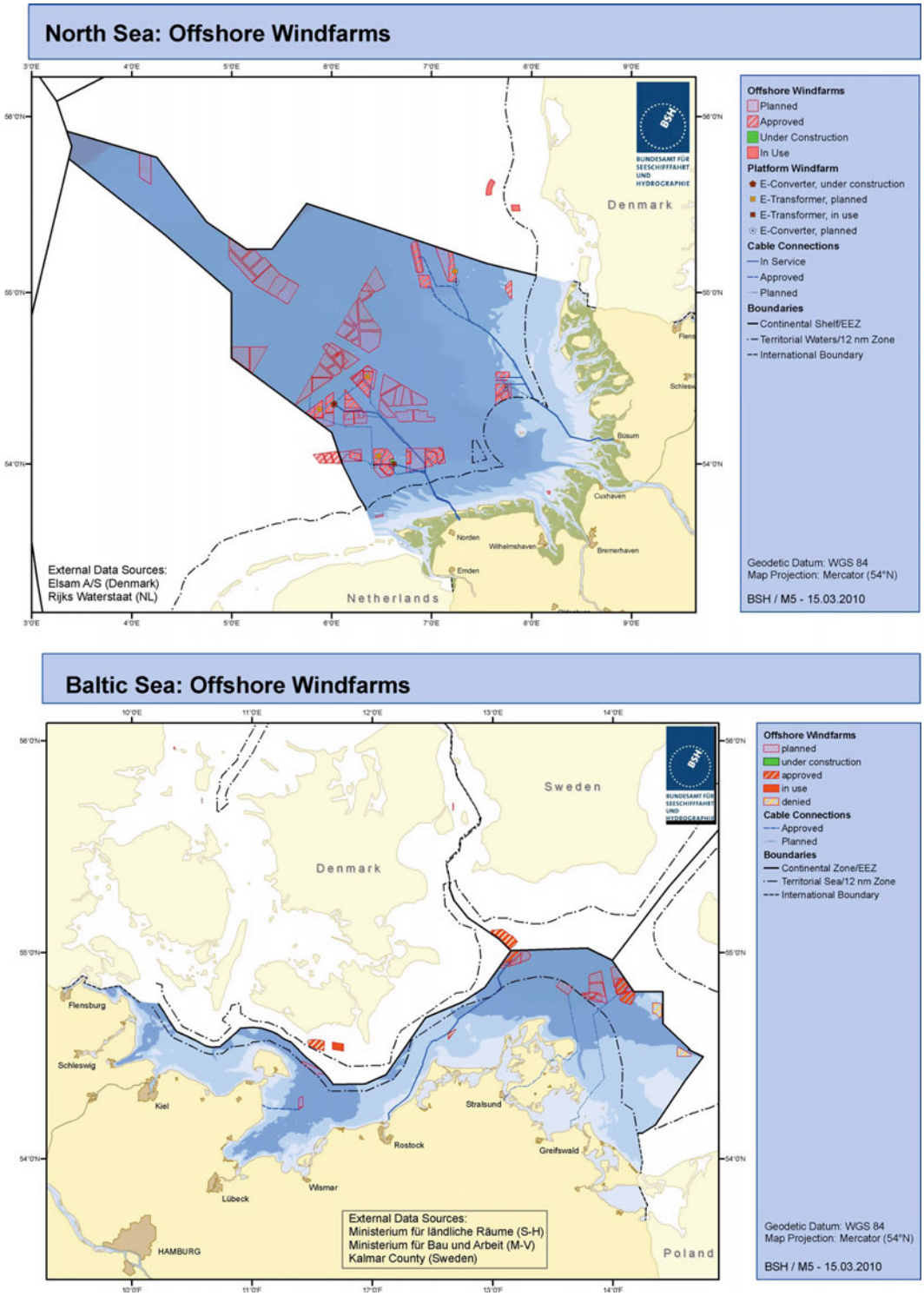

Aquaculture and Renewable Energy Systems, Integration of. Figure 2
Maps indicating all application sites for wind farm projects in Germany. At the top, the North Sea, below the Baltic Sea areas (Modified after [38])

a b

Aquaculture and Renewable Energy Systems, Integration of. Figure 3
Offshore wind farm Alpha Ventus. (**a**) Shows the transfer of the windmill tripods to the harbor of Wilhelmshaven and (**b**) displays the setup of an offshore windmill (REpower MI 068 [39])

ocean aquaculture were proposed (see proceedings of various OOA-Conferences [e.g. 50, 51]), which could cope with the harsh environmental conditions that place an enormous stress on the employed materials. It would be advantageous for the global offshore aquaculture development to plan for a combination of uses. While windmills use the wind above the surface to produce energy, their fixed pylons, commonly concrete fundaments (gravity foundation), metal jackets, tripods, or triples offer a possibility to connect systems used in aquaculture (Fig. 4). The combination of the respective two industries has to cope with the forces generated by the high-energy environment.

Since 2000, when the co-use of wind farms for off-bottom offshore cultivation [26] in the German Bight was proposed, several studies have been conducted to elucidate the potential as well as constraints of this offshore alternative for extensive aquaculture. Two pioneer studies, the project *Roter Sand* and *Offshore Aquaculture* were conducted between 2002 and 2004 by the Alfred Wegener Institute for Polar and Marine Research, Bremerhaven, Germany. These two projects followed a complex approach to obtain data about suitable indigenous candidates for the offshore cultivation [15], the technical requirements of longline systems for the cultivation of mussels or oysters [8, 9] and algal cultivation systems [53]. Insights into the feasibility of offshore seed and mussel production concerning larval, nutrient, and phytoplankton concentrations [8, 9, 54] were provided, and the existing legislation and regulations concerning marine aquaculture in Germany were listed [21]. In addition, all stakeholders potentially involved in a multifunctional use of offshore wind farms for aquaculture were identified [42]. This successful multifaceted approach helped to disperse many concerns and doubts on the offshore idea and initiated a sequence of and relations between various following projects, which are displayed in Fig. 5.

Candidates and Techniques for the Multi-Use Concept

In general, the cultivation process should consider only indigenous species for marine aquaculture operations to

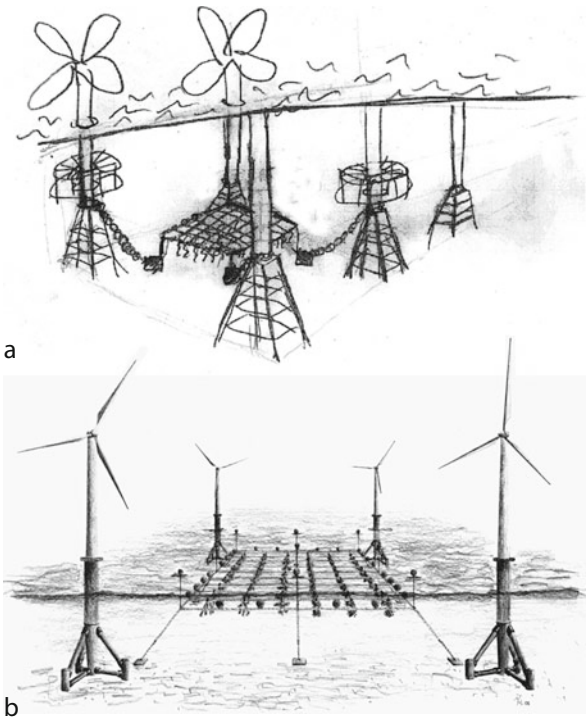

Aquaculture and Renewable Energy Systems, Integration of. Figure 4
Potential multifunctional use of fixed underwater structures of wind turbines for the operation of aquaculture facilities: 12 years ago and today (2010). (**a**) First drawing ever for the multi-use concept, including alternative solutions of oyster cages and mussel collectors attached to longlines in the inner section of the wind farm or offshore-rings (collar systems) attached directly to the pylon. The latter system can be submersed in case of wind-turbine maintenance. (**b**) Presents a design of a single mussel plot within a group of four wind turbines (not to scale) (Modified after [52], Buck personal drawing)

avoid the disruption with the local marine flora and fauna. This limits the economic opportunities of marine aquaculture enterprises since in certain sites only a few indigenous candidates are regarded as high-value species. Following a feasibility study by Buck [26], in Germany only culture species with modest service needs can be considered as favorable candidates for offshore aquaculture. In the offshore test trials in Germany, most suitable candidates suggested and tested were the sugar kelp (*Laminaria saccharina*), oarweed (*L. digitata*), dulse (*Palmaria palmata*), the blue mussel (*Mytilus edulis*), and two oyster species, the Pacific oyster (*Crassostrea gigas*) and the European flat oyster (*Ostrea edulis*). Mussels and seaweeds, for example, are cultured mainly in extensive systems throughout the world [8, 56, 57]; the latter occurs for historical and traditional reasons mostly in Asian countries.

According to Tseng [58], the cultivation procedure of brown seaweeds can be divided into two separate steps: In step (1), the seedling phase, spores are artificially released from mature sporophytes and seeded on a given substrate (ropes wrapped around plastic frames), where germination of gametophytes, the sexual maturation of male and female gametophytes, and finally, the development of zygotes into juvenile sporophytes takes place. In step (2), the grow-out phase, culture ropes with juvenile sporophytes are transferred to the open sea. In the grow-out phase, the macroalgal sporophytes grow on ropes for one season to a frond length of approximately 2 m.

When natural reproduction of mussels occurs, gametes are released into the water column where fertilization takes place [59]. The larvae undergo all trochophore and veliger stages when settling on a given substrate to start metamorphosis. According to Pulfrich [60] and Walter and Liebezeit [61], this process normally takes place at spring time (larval peak in May) in the German Bight. The cultivation of blue mussels can be divided into two steps: in step (1) the naturally occurring spat collection is achieved by deploying artificial substrates [62]. Usually, spat collectors are made out of unraveled polypropylene lines or sisal ropes, to offer the mussel's post larvae substrate for settlement [56]. After several months (step 2), collectors are retrieved and mussels thinned out and reseeded on ropes to provide space to improve growth and allow fattening [63, 64].

To operate culture phase (2) of both species, macroalgae and bivalves, an appropriate system design, such as suspended longlines or floating ring-structures, have to be deployed and securely moored in order to resist the stress forces of incoming waves and tidal currents, as well as swell. In addition, it was necessary to assess what kind of technical structure supports best the growth of the organisms (e.g., prevention from loss or mortality) while also assessing whether such systems provide reasonable production returns. Finally, potential combinations with offshore wind turbines had to be assessed.

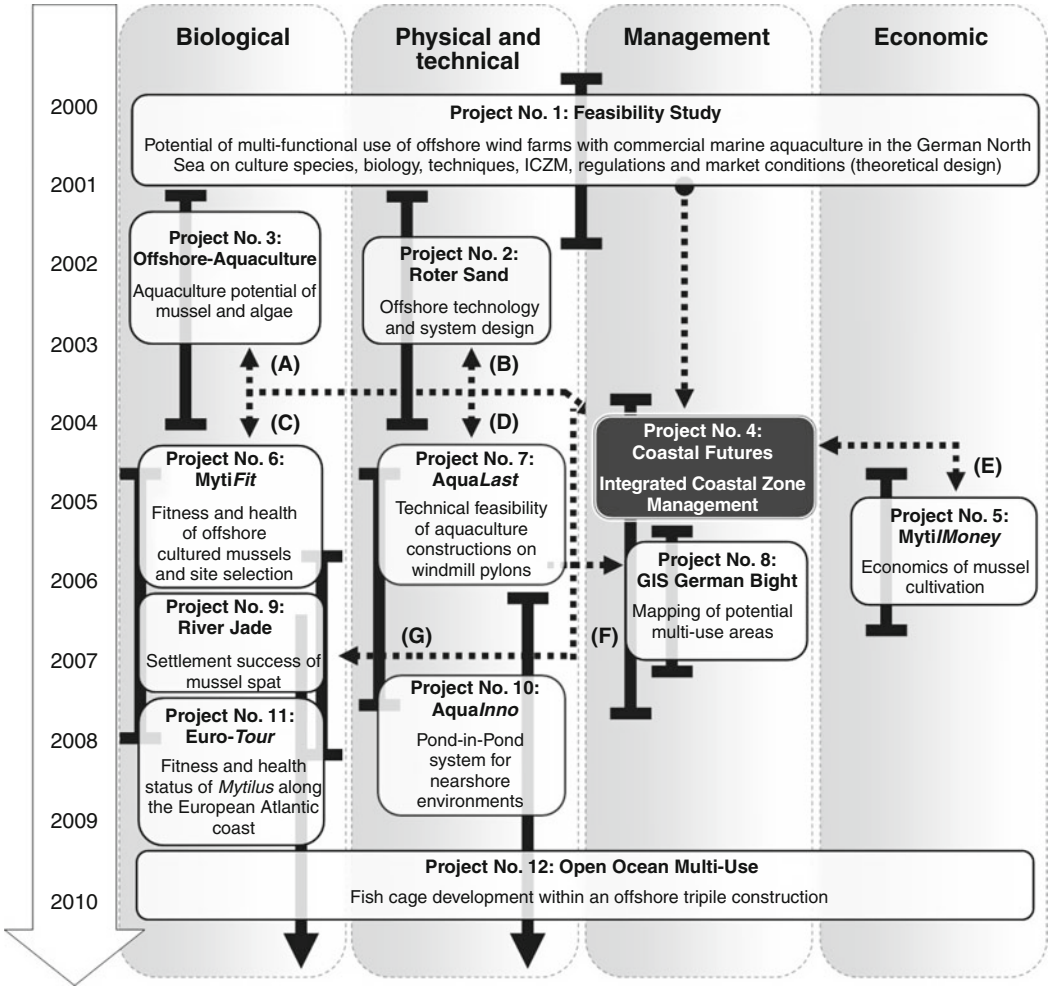

Aquaculture and Renewable Energy Systems, Integration of. Figure 5
Chronological order of conducted and ongoing research projects dealing with the combination of offshore wind farming and open ocean aquaculture. Project No. 1, the feasibility study, constituted the basis for all subsequent research. The *Coastal Futures Project* acts as a key node project to which the other projects either have contributed or by which they have been stimulated because of its transdisciplinary approach. It is visible that: (**a**) calls the wind farm developers' attention to offshore aquaculture; (**b**) and (**c**) include authorities and fishermen into the planning process for site-selection criteria of appropriate aquaculture sites; (**d**) involves offshore engineers and wind farm developers/operators into the technical part of an offshore aquaculture enterprise; (**e**) introduces (mussel) fishermen to the co-management idea and appraises the economics of mussel cultivation; (**f**) supplies authorities with maps and tools to limit regional stakeholder conflicts, (**g**) establishing an inshore reference station to support the data collected offshore, and (**h**) testing the first fish cage mounted within a tripile construction (Modified after [55])

However, currently even candidates requiring a semi-intensive as well as intensive cultivation process are in the testing phase. Salmon (*Salmo salar*), seabass (*Dicentrarchus labrax*), seabream (*Sparus aurata*), or some flatfish species are discussed for aquaculture in fish cages below windmill platforms at different offshore sites worldwide. Fish will firstly be reared in land-based facilities and will then be transferred as fingerlings to the offshore site and released into the submergible fish cages. After reaching market size, the

fish will be harvested and removed to the land and will undergo normal processing procedures.

Relocating cultivation systems offshore into high-energy environments requires the development of suitable culture techniques able to withstand the harsh conditions and minimize risk of economic loss [65].

Several techniques exist to cultivate mussels and seaweed either in co-culture or in single culture. Basically, both organisms are cultured in a suspended manner in the water column, floating or submerged. The use of rafts, longlines, and ring methods dominate. The latter two were the main cultivation techniques used in test trials offshore wind farm areas [8, 53, 56] (Fig. 6).

Major difficulties in the development of suitable techniques for open ocean aquaculture are – as mentioned above – the harsh environmental conditions which place an enormous stress on materials. Depending on the acting hydrodynamic forces, different technical setups can be distinguished. One of the interesting possible linkages of aquaculture is the combination with offshore wind farms as these would provide stable fixing structures for the cultivation systems. This is especially relevant from an economic point of view as so far the costly infrastructure for offshore aquaculture systems is one of the major drawbacks in the development.

Status Quo of Offshore Aquaculture Research Activities in Wind Farms

Only a few scientific studies dealing with the prospects of offshore aquaculture were available before 2000, and little was known about the biotechnological requirements, economic potential, or the socio-economic influence on the general feasibility of offshore aquaculture. Very few long-term experiments under harsh hydrodynamic conditions exist, e.g., Langan and Horton for offshore mussel cultivation [66]; Neushul and Harger [67]; Neushul et al. [68] for offshore seaweed cultivation. However, data on system and species performance are urgently needed to derive methodologies for the assessment of its environmental and economic viability. Therefore,

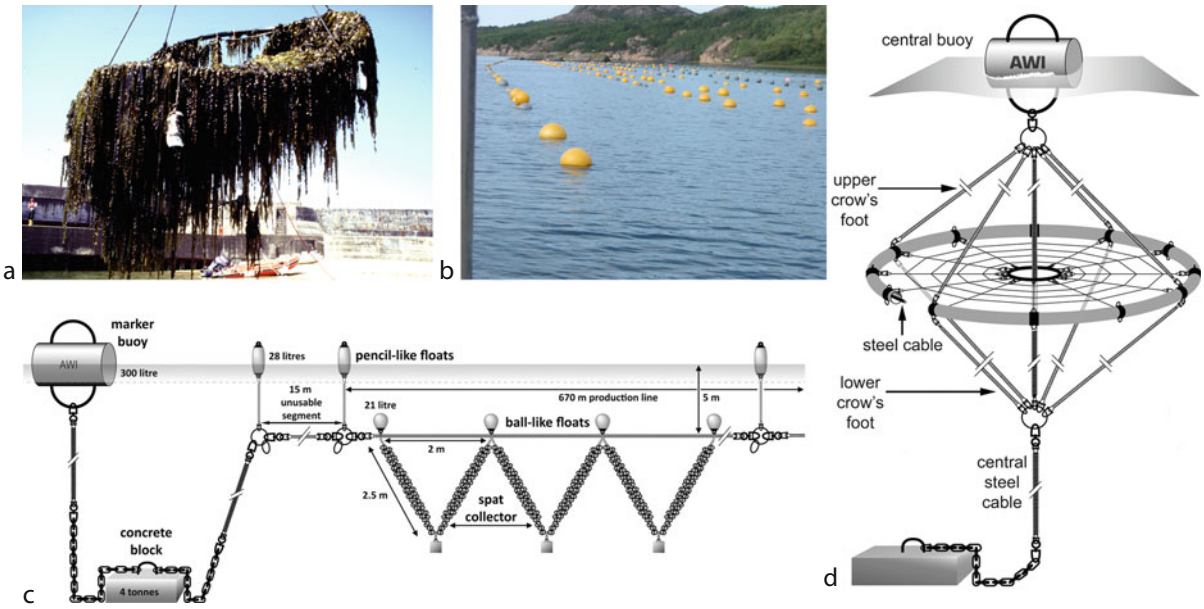

Aquaculture and Renewable Energy Systems, Integration of. Figure 6
Aquaculture constructions suitable for the cultivation in high-energy environments. (**a**) Offshore ring design for the cultivation of macroalgae (here: harvesting after grow-out in the harbor of Helgoland), (**b**) example of a nearshore, submerged longline design for mussels and oysters, (**c**) schematic drawing of a submerged longline suitable for exposed sites, and (**d**) a technical illustration of the ring design and its mooring system (Modified after [8, 9, 53])

the assessment of the potentials and constraints for sustainable aquaculture development in all marine habitats requires input from various scientific disciplines in order to direct this development towards a successful aquaculture undertaking. In particular, this holds true for offshore aquaculture, where little practical experience is available to date, although research in this area is evolving rapidly (e.g., Buck [15], Turner [69]; Pérez et al. [70]; Bridger and Costa-Pearce [51]; Dalton [71]; Naylor and Burke [72]).

The offshore wind farm and aquaculture investigations initiated an integrated assessment of theoretical and practical challenges of aquaculture operations in the North Sea. Several studies were carried out, all of which contributed to specific aspects of such a combined utilization of offshore space. These were:

(a) *Biological studies*, in which the focus was placed on cultivation and subsequent performance characteristics of indigenous bivalve, seaweed, and fish species exposed to extensive offshore aquaculture farming conditions. Further, the health status and infestation rates with parasites, bacteria, and viruses of candidates were determined to gain reliable predictions on where the highest growth rates and best product quality for consumers can be achieved. In nearshore intertidal areas, mussels and oysters are particularly exposed to high concentrations of pollutants, pesticides, near surface agents, estuarine run-offs, etc. that can pose a threat to consumer health. Buck [8, 9, 15] reported high growth rates for mussels cultivated in the German Bight. The scope of growth, i.e., the energy available for growth, is usually directly and positively correlated to a good overall health condition of the respective organism [73]. But organisms with high growth rates and a healthy appearance are no guarantee of a healthy food for human consumers. For instance, in coastal waters, eutrophicated by urban sewage, mussels show good growth performance. The microbial status of these mussels, however, mostly excludes them from consumption since they might carry various human pathogens. Even in developed countries with strict legislation for the treatment of wastewater, mussels can function as carriers of vector diseases. Whether this is also true for offshore cultivated mussels, where the environment is cleaner due to dilution of contaminants, remains open. Data for offshore-produced mussels, generated according to the analysis protocols of controlling authorities, are not readily available for all cultivation sites. However, new regulations are in the implementation process in all of the EU states and will fulfill the prerequisites for an official sampling design and assessment (i.e., sanitary survey).

To evaluate the significance and comparability of the employed parameters in a broader geographical context, the area of investigation was extended along the Atlantic coast from southern Portugal to northern Denmark. Further on, the closely related Mediterranean mussel *Mytilus galloprovincialis* was included in the analysis to test the effectiveness of all the parameters in different species.

Investigations on fish species for submerged cage-systems included aspects on growth, welfare, stress in exposed environments, and health.

(b) *Physical and technical studies* investigated the effects of the prevailing hydrodynamics on candidates and culture constructions at specific offshore sites. At the same time, the necessary technical requirements for farming structures in high-energy environments and their possible combination with offshore wind farms were assessed. New system designs for offshore farming were developed and prototypes (e.g., offshore ring, offshore collector) were tested. Technical details about the microstructure of artificial substrates were addressed to increase production per meter longline under offshore conditions. In addition to offshore seaweed and mussel cultivation, new technologies for submerged fish cages were investigated.

(c) *Management and institutional studies* focussed on the analysis of potential management approaches to implement a multi-use concept of offshore areas. Hereby, the various stakeholders and their respective views and knowledge systems were integrated. Against the background of the social and institutional dimensions, particular emphasis was given to the interrelationship between scientific findings on the one hand and effective implementation on the other. Key aspects included the social acceptance of combined use, as well as the possible management strategies that would govern it. This endorsed the examination of the prevailing case laws and regulative and management framework

conditions, as well as a suggestion of decisive offshore co-management strategies to support such activities. In this process, the continuous inclusion of the stakeholders in a participatory manner was a prerequisite. To address the respective technical, economic, social, and political challenges of mariculture and offshore wind farms, specific co-management strategies were elaborated that are either more results-oriented (e.g., for integrating technical knowledge of the two sectors) or more process-oriented (e.g., for establishing new linkages between different groups). Thus, in cooperation with governmental authorities, co-management in the offshore makes use of the capacities and interests of the respective stakeholder groups and employs these in managing cross-sectoral activities.

(d) *Economic studies* conducted an economic evaluation of such multi-use concepts in offshore locations that take into consideration market conditions as well as investment and operating costs.

All the above listed conceptual approaches relied on results of a theoretical feasibility study (Fig. 5) [26], which was carried out prior to practical research in the field. All of the results contribute to the *Coastal Futures* Program and support the quest to find innovative new approaches for sustainable use and alternative livelihoods of coastal populations.

Overview of Biological and Technical Investigations

Over the last decades, substantial insights have been gained on the terms and conditions active in the offshore environment. However, these data are only partly useful for the selection of offshore aquaculture sites because they have been gathered primarily for other user needs and thus lack the essential specificity to address the biological and cultivable potential of these sites. Prior to a multifunctional development comprising mariculture activities, it is therefore necessary to determine the appropriate biological, technological, and management requirements, as well as the performance characteristics that would allow the employment of favorable and cost-effective methodologies. To meet this end, special focus was placed on the combination of extensive offshore shellfish, seaweed, and fish farming at exposed sites within the proposed offshore wind farm boundaries.

Due to the wide spectrum of open questions, the outcomes are quite manifold. In the following, first results according to their contributions towards the main research topics involved are presented.

Biological Studies The theoretical *Feasibility Study* [13, 24] was aimed to ascertain the biological, technical, and economic feasibility of an offshore marine aquaculture structure with respect to the cultivation of marine organisms within wind farm sites in the German North Sea. One result was that to date, in terms of commercial marine aquaculture, Germany had little knowledge and background in offshore aquaculture compared to many other coastal countries throughout the world. Nevertheless, a synthesis of a selection of parameters (e.g., geophysical and biological parameters) allowed the identification of suitable candidates for commercial offshore aquaculture. These candidates include blue mussels (*Mytilus edulis*) and oysters (*Ostrea edulis*, *Crassostrea gigas*), which could be maintained extensively in the offshore region. Moreover, labor requirement for these candidates as well as for seaweeds, such as the sugar kelp (*Laminaria saccharina*) and dulse (*Palmaria palmata*), is supposed to be low.

Further, the biological feasibility of cultivating mussels, oysters, and kelp within offshore wind farm sites was assessed. The growth of these species is excellent in the rather eutrophicated offshore environments of the North Sea, but can differ depending on exposure sites, system designs, installation modes, and season.

For instance, settlement of young mussels on artificial collector substrates decreases with increasing distance from the shore [74]. However, this does not limit the economic potential if the thinning procedure will be omitted, following a “One-Step-Cultivation” concept [15]. In general it was found that mussels are free of parasites at offshore locations due to dilution effects and the interrupted reproduction cycles of some macroparasites [75]. Special focus was placed on the overall health status of mussels cultured under different conditions, and the impact on economic aspects was investigated [76]. Specific aims of the projects were the development of suitable offshore spat collecting techniques, detailed knowledge about parasites (macro and micro), bacteria and virus infestations at different sites, implementation of biodiagnostic techniques for the

health analysis of cultured mussels, and collection of all relevant data (e.g., shell stability and attachment strength of mussels), for the further processing of mussels as a product for human consumption.

Hydrodynamic forces support length increase of seaweed blades when transferring young sporophytes to sea. These algae will adapt to the occurring loads and develop strong holdfasts, preventing detachment of the entire plant [77].

Modified and improved techniques for offshore farming withstand high-energy environments, but will certainly cause higher investment costs. Therefore, site-selecting criteria for a culture area should be clearly identified to assess economic risks. Important for the cultivation success is the water quality. The analysis of the cultured organisms with biodiagnostic tools provides detailed insights into the water conditions the animals live in. By this approach, reliable predictions are possible as to which locations grant highest growth rates and best product quality for consumers. Preliminary results attest offshore areas satisfying settlement success and excellent growth rates [78], and low infestations with macroparasites [79], microparasites, bacteria, and toxins [76]. The results on consumption suitability show that water quality regarding the concentrations of pollutants in offshore areas of the German Bight is quite good. Lysosomal membrane stability is mostly relatively low at all tested nearshore and offshore sites. Interestingly, growth rates of the hanging cultivated mussels are not affected by this low fitness parameter [58].

First results on investigations along the Atlantic Coast show that mussels originating from offshore habitats have a better health status regarding the infestation with macroparasites and microparasites (Buck and Brenner, unpublished data). While macroparasites are still infesting mussels in nearshore areas in the Wadden Sea (the Netherlands, Germany, Denmark), microparasites are absent.

Physical and Technical Studies The results above allowed the identification of two offshore aquaculture systems that were best suited for offshore operations from a biological point of view. Depending on the acting hydrodynamic properties, different technical setups are regarded as favorable. The first one is a floating and submergible ring system for the cultivation of seaweed. It withstands rough weather conditions and allows easy handling [53]. The second system is a submerged longline design for blue-mussel culture [8]. The longline should ideally be installed 5 m below the water surface and should be connected to foundations of offshore windmills (Fig. 7) [47]. For the longline, polypropylene proved to be an appropriate material. The system design is made of various connected segments allowing an easy harvest and replacement of all parts of the construction. However, more technical engineering research is required to find the most cost-effective mode of construction and the best choice of materials (e.g., little corrosion, longevity in spite of mechanical stress) so that easy handling can be guaranteed under relatively harsh weather conditions (cf. construction, deployment, retrieval, service, repairs).

The experimental design also allowed work on such issues as the efficiency of the collecting devices themselves. Healthy mussels will reach market size in offshore conditions only if they are firmly attached to their artificial substrate. As mussels growing on suspended substrates need about 15 months [8, 9] on average to reach market size, they must survive one winter and withstand storm events producing wave heights up to several meters. Continuing investigations on the health and quality of market-sized mussels would be moot if mussels failed to stay attached to substrate gear.

To date, most available substrates are designed and deployed for nearshore use under calm water condition. However, it was found that improvement for construction of new collectors that are feasible for offshore cultivation is in mandate. Research showed that new substrates should have felt-like structures around the core of a collector for larval attraction and long appendices in high density to interweave the mussel conglomerates with the substrate [80]. Future investigations should focus further on the fabrication and testing of a prototype of this collector, concerning the results of this study. Besides providing optimal larval attraction and attachment for juvenile mussels even under winter conditions, any new substrate should proof its durability under conditions of a daily farming routine. This would include mechanical thinning, harvesting processes, and tests on the reusability of the material.

The technical realization and the implications of aquaculture technical requirements on design and construction of the grounding construction of offshore

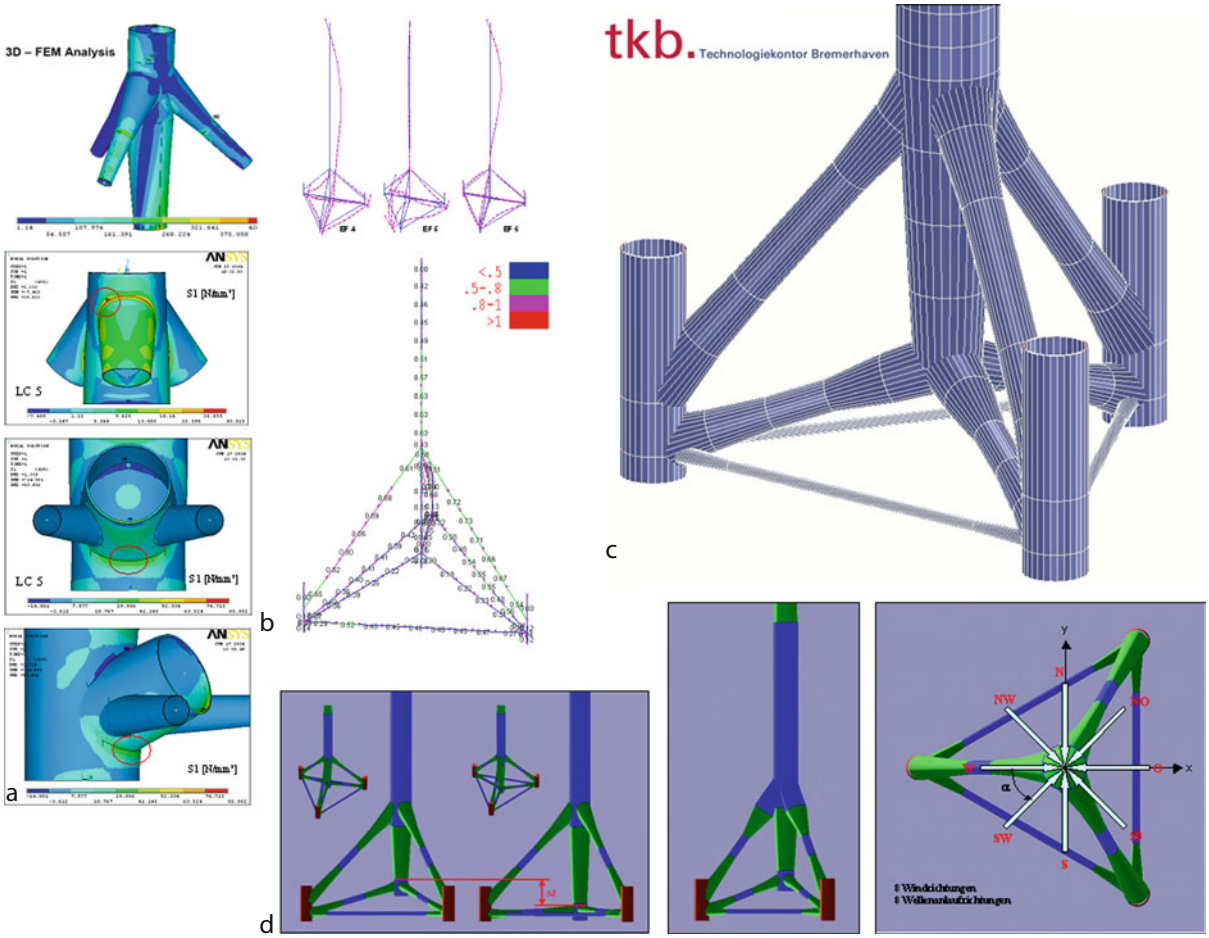

Aquaculture and Renewable Energy Systems, Integration of. Figure 7
Modeling of potential attachment points for the combination of longline connections to a tripod foundation. (**a**) Displays alternative connection points, (**b**) shows the generation of representative loads on the wind-energy installation, including vibrations, (**c**) shows the respective tripod foundation for offshore use in depths of about 20–50 m, and (**d**) shows the development of a static model (3–5 MW class) [47]

wind turbines were considered. So far, modeling and experimental validation of a submerged 50 m longline aquaculture construction mounted between two steel piles, 17 nautical miles off the coast, show significant forces of up to 90 kN (equivalent to 9 t) induced by waves of up to 1.8 m significant wave height and tidal currents of up to 1.0 m/s [81]. Given the high-energy environment in the North Sea and the non-linear relationship between water movement and its resulting forces, even higher mechanical loads are to be expected within the life cycle of such an arrangement. These must be taken into account when developing techniques for larger-scale offshore cultivation within wind farms.

Finally, a new cage design project has been initiated, where it will be investigated whether aquaculture of fish in between a tripile construction below a windmill has the potential to enlarge the diversity of candidates to be grown offshore (next to bivalve and seaweed) as well as widening the potential of offshore farming within wind farms. First insights are shown in Fig. 8 [82, 83].

Management and Institutional Considerations

From a spatial planning perspective, the ocean space in the Exclusive Economic Zones (EEZ) cannot be considered any more as "commons" in the sense of Ostrom

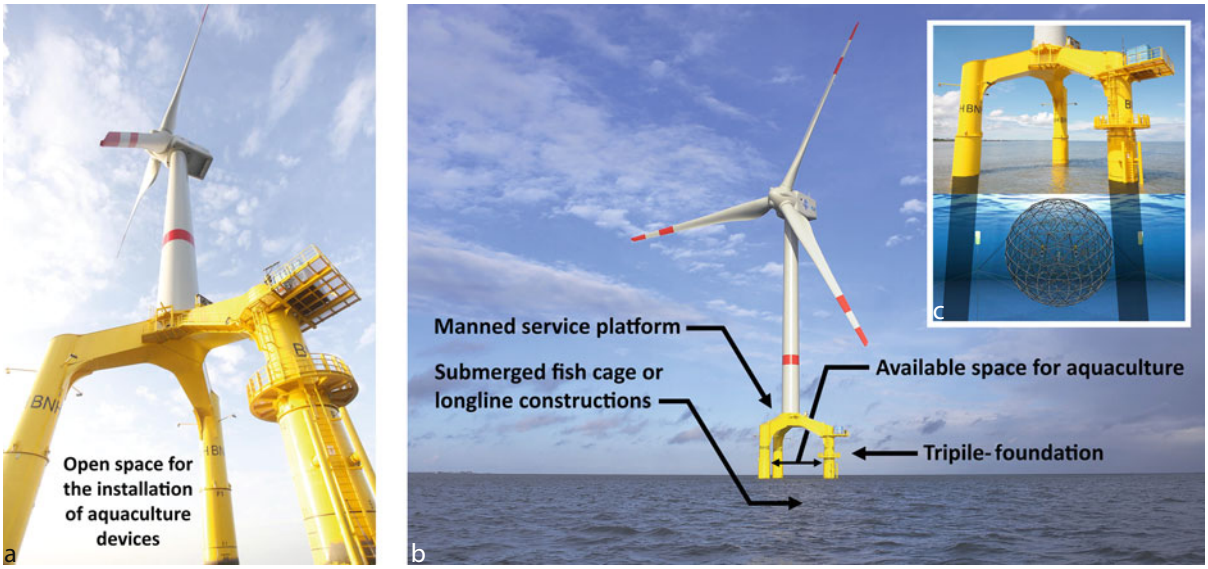

Aquaculture and Renewable Energy Systems, Integration of. Figure 8
Tripile construction for the secondary use for fish cages. (**a**) Shows the open space within a tripile foundation to be used for aquaculture purposes, (**b**) displays a lateral view of the Bard Windmill and the access to the fish cage, and (**c**) is a photo animation and gives an idea how a fish farm, such as an aquapod, could be moored below [82, 83]

et al. [84] wherein individuals or groups have the right to freely consume and return any kind of resources. As a matter of fact, the "tragedy of the commons" situation Hardin described in 1968 [85], has already been reached for most of the oceans today. Offshore waters are in a process of transition, revealing diverse and heterogenic interests in marine resources. For instance, the development of offshore renewable-energy systems is an international priority driven by the need to reduce the dependence on fossil fuels and decrease human impacts on the global climate regime. Simultaneously, the demand for high-quality seafood is accelerating globally. This leads to an increased complexity and thus to limitations in developing and managing the different and often spatially overlapping maritime activities independently of one another. The upcoming new utilization patterns of the German North Sea, such as wind farms, but also Marine Protected Areas (MPAs) reported to the EU commission in Brussels for the "European Natura 2000 network," reveal a trend toward the development of permanent constructs. Both are examples for new forms of use with a high spatial demand [86]. Not all uses are compatible with each other and user conflicts with existing activities, such as fisheries, maritime traffic, or military missions are preordained. The planned large-scale offshore wind farms as well as designated MPAs are prime examples for the development of lasting marine structures that take up a surface area of several square kilometers each [55].

At the same time, the increasing demand for high-quality foods worldwide accelerates the development of marine aquaculture. This potential newcomer can be expected to become an additional competitor in offshore waters [87], contributing to the increase in spatial competition and complexity in the ocean [20]. Conflicts among the respective user groups are inevitable. The growing competition for space represents a major challenge for further developing or even maintaining all forms of marine aquaculture, as well as freshwater fish farming. However, area choice is crucial and spatial planning has a key role to play in providing guidance and reliable data for the location of an economic activity, giving certainty to investors, avoiding conflicts, and finding synergies between activities and environments with the ultimate aim of sustainable development [88]. The inclusion of all

stakeholders in this process to find synergies in the open ocean is crucial.

Ongoing multidisciplinary social-science research in Europe shows that it is feasible to establish spatially efficient and effective wind farm–mariculture co-management regimes. A window-of-opportunity has opened as both groups have realized that they may benefit through the integration of operation and maintenance (O&M) activities vis á vis gaining support in collaborative action by the current impetus of the new EU Maritime Policy. The operation and maintenance of any offshore installation is a major challenge due to restricted logistics and accessibility, forming a large part of the overall costs. A five-to-ten time more expensive scale of operation and more difficult logistics for maintenance and/or harvesting compared to nearshore or onshore sites have to be taken into account [89–91]. Experiences with existing wind farms and mariculture sites off the coast show that work at the sea is not only significantly more cost-intensive, but also more time consuming than on land [92].

There are certain rights and duties involved if prospective spatial and organizational interaction of O&M activities of offshore wind turbines and mariculture installations are to be combined [20]. Different values, perspectives, and demands of the stakeholder groups need to be harmonized [93]. So far, disagreements on the distribution of entitlements to benefits and profits between the different stakeholder groups can be observed (Table 1). The two potential adopters of

Aquaculture and Renewable Energy Systems, Integration of. Table 1 Offers, needs, and constraints characteristics of mariculture operators and offshore wind farmers concerning O&M activities. Interrelated aspects between the two actor groups are indicated in bold (modified after [86])

Characteristics	Actor groups	
	Wind farmers	Mariculture operators
		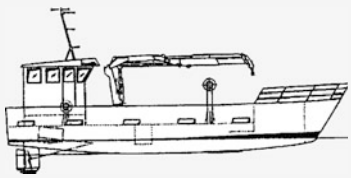
Offers	• Fixed offshore infrastructure • Logistic platform • Financial support (EEG amendment)	• Upgradeable sea-going vessels • Offshore mentality • Offshore skills and experience
Needs	• Specialization of equipment (construction vs hire; "marinization" of onshore equipment) • Specialization of personnel • Sea-going vessels • Service demands (man-hours) • Suitable O&M pattern (corrective vs preventive maintenance) • Suitable O&M pattern (opportunity vs periodic maintenance)	• Specialization of equipment (construction vs alteration of existing oil industry/fishery vessels) • Specialization of personnel • Fixed offshore infrastructure • Technical and logistic support • Service demands (man-hours) • Offshore skills and experience • Offshore mentality
Constraints	• Operation costs • Technical challenges • Distance to farm site • Available working days (estimated 100/year) • Difficult logistics for O&M • Reliability of offshore wind turbines	• Access to farm site (uncertain regulatory and permit requirements) • Distance to farm site • Available working days (estimated 30–100/year) • Difficult logistics for maintenance and harvesting • Reliability of culturing devices

such a multi-use scheme illuminate different sets of skills and capacities in terms of offers, needs, and constraints characteristics. These are vital resources, which provide the basis for forming any sustainable offshore co-management arrangements [85]. Hereby, a fair negotiation and bargaining process is the most essential component to effectively orchestrate co-management of offshore wind farmers and future mariculture operators, such as mussel harvesters. The latter already dispose vital skills and experiences for working in the open sea. Still, working methods have to be adjusted to the offshore culture production mode.

If such an offshore co-management is considered as a network activity between private actors, such as wind farmers or mariculture operators/fishermen and public authorities, one of its basic characteristics is the fact that a third party can coordinate the activities of formally separated parties [94]. Ways and means have to be developed that balance the respective interests of dominant and politically supported wind farming participants with small-scale entrepreneurial mariculturists. The key question is how institutional arrangements could act as "boundary organizations" [95] in an offshore co-management process. Such a process is more likely to develop and succeed if an interface management that acts as moderator, disclosing the interests of the actor groups and offering possibilities for concerted action, guides it. With respect to the decision-making arrangements at the three levels (operational level, organizational level, and legislative level), the interface management would thus help to determine the rules for interaction among the actor groups and state authorities at the organizational level. Besides, it would facilitate organizing and decision making of the day-to-day activities at the operational level. However, to authorize and legitimize new co-management arrangements for interacting offshore O&M activities, new policies must be developed or existing laws amended. Following a dynamic process of forming new institutional structures, the establishment of a communication arena may (a) support a common understanding of the entire co-management process, (b) provide the overall framing for an improved communication among the participating actor groups, (c) increase the level of trust among the actor groups, and (d) promote sustainability and efficiency in times of scarcity of spatial resources [85]. However, top–down induced management schemes by, e.g., the national government, hold a high potential for failure. Involving the relevant actors improves the social acceptability of innovative concepts and their applicability [96]. Consequently, it appears that for developing and implementing a wind farm–mariculture multiple-use concept, co-management, such as that described by Carlsson and Berkes [94], should ideally be carried out with the participation of different actors that typically try to find ways to learn from their actions and adapt the behavior to the consequences of their own and other's actions. This must be supported by the relevant authorities at all levels and must find its way into the legislative framework at the EU and national level.

On EU level, the issue of access to space for maritime activities, including aquaculture, has been recognized in several communications over the past years, e.g., in 2007 pertaining to the Integrated Maritime [97] Policy or in 2009 concerning a new impetus for sustainable aquaculture in Europe. In the latter, all Member States are asked to develop marine spatial planning systems, in which they fully recognize the strategic importance of aquaculture. This Strategy also aims at providing EU leadership and guidance to both stakeholders and administrations to ensure consistency and clarity in designing the necessary policies for the future sustainable development of European aquaculture. In this context, a partnership between public authorities and interested parties at EU, national, and local level play a crucial role.

Hence, European aquaculture should benefit from an improved framework for governance; however, it is stressed that the national authorities have a primary role in shaping aquaculture development in their territory. While in some countries aquaculture is defined and regulated under the agricultural laws, in other countries regulations are dispersed, and consequently the responsibilities are in the hand of several agencies with no clearly defined lead agency. So far, a number of important challenges that limit the development of European aquaculture directly depend on policies and actions taken at national or regional level. A bottom–up approach is therefore needed so that the public authorities can establish an appropriate framework for the vision of multiple-use of offshore areas to become operational. A participatory approach contributes to lifting bottlenecks in national legislation.

This framework needs to be transparent, consistent and cost-effective in order to allow the industry to realize its potential. Unless these and other regulative issues pertaining to multi-use offshore conditions remain unresolved, an establishment of offshore co-management arrangements may be very difficult. Still, the current lack of legislation in the EEZ holds the potential to implement concerted innovative concepts of offshore constructions and thereon-interacting activities.

However, several restrictions are still needed to be resolved. Questions pertaining to access rights within the wind farm area have to be deciphered. So far, approved offshore wind farm territories in, e.g., the German EEZ, are designated as restricted area, prohibiting any kind of public access [98, 99]. However, conveying access rights to a second party is inevitable if wind farm O&M is performed by a commissioned subcontractor and not by the licensee itself. In a wind farm–mariculture multiple-use arena, the same access and user rights have to be guaranteed to a mariculture operator who enters the territory for purposes not related to wind farming but for maintaining culturing devices and harvesting procedures. In this case, precise positioning of aquaculture installations within the wind farm territory as well as access lanes for both parties have to be specified.

In addition, the question of harmonizing the tenure or duration of a lease for offshore resources has to be tackled. If there is, i.e., significant discrepancy in the length of lease tenures between the two uses to be combined, the resource users may not be inclined to create long-term co-management arrangements. Furthermore, cooperative management structures also benefit if the leasing process was combined and/or effectively coordinated, since it facilitates, i.e., integrating O&M within a co-management scheme once the projects are operational.

Yet, in order to define the functional structure of such a co-management regime in detail, reliable outcomes on economic and technical integration prospects of a joint wind farm–mariculture venture have to be produced. The latter is a major research demand, which was voiced by most of the interview partners along the North Sea coast so far [93]. Cumulative impacts of different economic sectors, such as offshore wind farms and mariculture need to be addressed, which provides an opportunity to create synergies between different industrial sectors prior to their installation.

Outcome of Economic Studies

The *Feasibility Study* [13, 24] provided a general overview on market prices, market demands, classification of candidate species as high-value products, and the cost of some infrastructure. The study showed possible market value of offshore aquaculture products in comparison to the performance of existing conventionally operated farms in coastal waters.

Basic data for offshore mussel cultivation in close vicinity to a designated offshore wind farm in the open sea of the German Bight were compiled. It contained different case-scenario calculations to illustrate the impact of changing parameter values on overall profitability or non-profitability of this activity. Primary focus was placed on the production of consumer mussels, but seed mussel cultivation is also taken into consideration. This study concluded with providing some recommendations on how favorable terms or actions could further improve profitability of offshore mussel cultivation. Results intended to shed some light on business management topics that future offshore mariculture operators should follow in order to be efficient [100].

Nontheless, the economics of a joint offshore wind farm–mariculture utilization scheme still remain to be evaluated in more detail.

Future Directions

By setting higher value on an inclusion of stakeholder knowledge and opinions, the initiation of the *Coastal Futures Project* resulted in a stronger focus on the practicability of multifunctional use of offshore areas. It can be shown that such innovative new concepts are highly complex and interdependent. First, results indicate that secure technical and economic feasibility appears to be a basic prerequisite to assure that both offshore wind farm operators and aquaculturists will support the multi-use concept, especially as far as the management of joint activities is concerned.

This suggests that as soon as technical and economic aspects are evaluated in more detail, it is important to initialize a comprehensive communication program to provide information to the key public and private actor groups (stakeholders). Furthermore, effective and continuous participation of all

stakeholders on all levels from the very beginning of the multi-use approach must be ensured. This supports the orchestration of scientific and local user knowledge in an overall approach to combine different offshore uses. In addition, it contributes to adding a joint wind farm–mariculture venture to their future portfolio.

More detailed data are needed to calculate the economic potentials and risks of a co-used wind farm area for the production of seafood. Apart from the principal feasibility of an area as an aquaculture site, growth rates and product quality must be predictable. First, results on blue mussels from test areas show that highest product qualities can be expected from testing areas offshore. A proven product quality ensures higher market prizes, should compensate for higher investment costs for the culture systems, and help to install a functioning offshore aquaculture system in the German Bight.

Generall, science for open ocean aquaculture needs a transformative moment. It seems necessary to learn the skills to interact constructively with different scientific disciplines and different stakeholders. This will require a new science for managed marine seascapes [101]. Creating a system biology paradigm in ecosystem science and aquaculture will require a multidisciplinary input, with scientific interactions not just at the margins of each discipline, but focused collaboratively on the realization of a vision of multifunctional, spatially effective, and sustainable use of ocean space. This will require new kinds of scientists (with new kinds of career structures) who are trained to work in multidisciplinary teams. The need for such training is now widely recognized and is reflected in the emerging curricula's of many new MSc courses.

It is mandatory to discover what to do, at what scale, in what modality – engineering, farming, legislation, social organization, economic initiatives, etc. – and how to do it. Since the activities in the ocean realm are concerted in integration, future activities must also be integrated over all these modalities.

Bibliography

1. FAO/FIDI (1989) Aquaculture production (1984–1986) Food and Agriculture Organisation of the United Nations. Rome Fisheries Circular 815, 106
2. FAO (1997) Aquaculture development. Technical guidelines for responsible fisheries. Food and Agriculture Organisation of the United Nations, Rome, pp 5–40
3. EU Commission (2000) On integrated coastal zone management: a strategy for Europe. Communication from the Commission to the Council and the European Parliament, COM (2000) 547 final
4. Garvine R, Kempton W (2008) Assessing the wind field over the continental shelf as a resource for electric power. J Mar Res 66(6):751–773
5. Pauly D, Christensen V, Guénette S, Pitcher TJ, Sumaila RU, Walters CJ, Watson R, Zeller D (2002) Towards sustainability in world fisheries. Nature 418:689–695
6. FAO (2004) The state of world fisheries and aquaculture-2004 (SOFIA). Fisheries Department. Food and Agriculture Organisation of the United Nations, Rome, Italy
7. FAO (2009) The State of World Fisheries and Aquaculture (SOFIA) 2008, FAO Fisheries and Aquaculture Department. Food and Agriculture Organisation of the United Nations
8. Buck BH (2007a) Experimental trials on the feasibility of offshore seed production of the mussels *Mytilus edulis* in the German Bight: installation, technical requirements and environmental conditions. Helgol Mar Res 61:87–101
9. Buck BH (2007b) Marikultur als Co-Nutzung in Offshore-Windparks: Status Quo, Probleme und Perspektiven, Meeresumwelt-Symposium 2006: 16. Symposium, 13. bis 14. Juni 2006, CCH – Congress Center Hamburg/Bundesamt für Seeschifffahrt und Hydrographie in Zusammenarbeit mit dem Bundesumweltamt im Auftrag des Bundesministeriums für Umwelt, Naturschutz und Reaktorsicherheit, pp 167–179
10. FAO (2006) Fishery information, data and statistics unit. Aquaculture production: values 1984–2004. FISHSTAT Plus – universal software for fishery statistical time series. Food and Agriculture Organization of the United Nations, Rome, Italy
11. Burbridge P, Hendrick V, Roth E, Rosenthal H (2001) Social and economic policy issues relevant to marine aquaculture. J Appl Ichthyol 17:194–206
12. Rawski TG, Xiao W (2001) Roundtable on Chinese economic statistics: introduction. Chin Econ Rev 12:298–302
13. Naylor RL, Goldburg RJ, Primavera JH, Kautsky N, Beveridge MCM, Clay J, Folke C, Lubchenco J, Mooney H, Troell M (2000) Effect of aquaculture on world fish supplies. Nature 405:1017–1024
14. Roth E, Ackefors H, Asche F, Balnath C, Black E, Black K, Boghen A, Browdy C, Burbridge P, Castell JD, Chamberlain G, Dabrowski K, Davies I, Dosdat A, Eleftheriou A, Ervik A, Gordin H, Heinig CS, Hilge V, Karakassis I, Kuhlmann H, Landry T, von Lukowicz M, McGlade J, Price A, Rheault RB, Rosenthal H, Saint-Paul U, Sandifer PA, Saroglia M, Silvert W, SteVens W, Soto D, Varadi L, Verreth J, Verdegem M, Waller U (2002) An intellectual injustice to aquaculture development: a response to the review article on "Effect of aquaculture on world fish supplies", Report of the ICES working group on environmental interactions of mariculture, F:04 REF ACME, Annex 4, pp 83–89
15. Buck BH (2004) Farming in a high energy environment: potentials and constraints of sustainable offshore aquaculture in the

German Bight (North Sea). Dissertation. University of Bremen, Germany
16. Davis A, Bailey C (1996) Common in custom, uncommon in advantage: common property, local elites, and alternative approaches to fisheries management. Soc Nat Resources 9:251–265
17. Adger WN, Luttrell C (2000) Property rights and the utilisation of wetlands. Ecol Econ 35:75–89
18. Rana KJ (1997) Aquatic environments and use of species subgroups. In: Review of the state of world aquaculture. FAO Fisheries Circular FIRI/C886 (Rev. 1). Food and Agriculture Organisation (FAO), Rome, Italy, pp 7–16
19. Lee PG, Turk PE (1998) Overview of a modern, shore-based hatchery for offshore mariculture support. In: Stickney RR (ed) Joining forces with industry – open ocean aquaculture. Proceedings of the third annual international conference, May 10–15, Texas Sea Grant College Program, Corpus Christi, pp 87–102
20. Krause G, Buck BH, Rosenthal H (2003) Multifunctional use and environmental regulations: potentials in the offshore aquaculture development in Germany. Proceedings of the multidisciplinary scientific conference on sustainable coastal zone management "Rights and duties in the coastal zone", 12–14 June 2003. Stockholm, Sweden
21. Buck BH, Krause G, Rosenthal H, Smetacek V (2003) Aquaculture and environmental regulations: the German situation within the North Sea. In: Kirchner A (ed) International marine environmental law: institutions, implementation and innovation, vol. 64. International Environmental. Law and Policies Series of Kluwer Law International, The Hague, pp 211–229
22. Firestone J, Kempton W, Krueger A, Loper CE (2004) Regulating offshore wind power and aquaculture: messages from Land and sea. Cornell J Law Public Policy 14(1):71–111
23. Langan R (2009) Co-location of offshore energy and seafood production: potential synergies, compatibilities and conflicts. Conference paper, the ecology of marine wind farms: perspectives on impact mitigation, siting, and future uses, 8th annual Ronald C. Baird Sea Grant Science Symposium, November 2–4 2009, Newport, Rhode Island
24. BMU (2006) Integriertes Küstenzonenmanagement in Deutschland (IKZM). Nationale Strategie mit Bestandsaufnahme nach der EU-Empfehlung 2002/413/EG. Bundesregierung für Umwelt, Naturschutz und Reaktorsicherheit (Federal Ministry for the Environment, Nature Conservation and Nuclear Safety)
25. Kannen A (2004) Holistic systems analysis for ICZM: the Coastal Futures approach. In: Schernewski G, Dolch T (eds) Geographie der Meere und Küsten. Coastline reports, vol 1, pp 171–181
26. Buck BH (2002) Open Ocean Aquaculture und Offshore-Windparks: Eine Machbarkeitsstudie über die multifunktionale Nutzung von Offshore-Windparks und Offshore-Marikultur im Raum Nordsee. Reports on Polar and marine research. Alfred Wegener Institute for Polar and Marine Research, Bremerhaven, pp 412–252
27. Ryan J (2005) Offshore aquaculture – do we need it, and why is it taking so long? International Salmon Farmers Association (Ireland). Expert workshop on sustainable aquaculture, DG JRC European Commission, Institute for Prospective Technological Studies, 17–18 January 2005. Seville, Spain
28. Dahle LA, DePauw N, Joyce J (1991) Offshore aquaculture technology – possibilities and limitations. Aquacult Environ 14:83–84
29. Eleftheriou M (1997) Aqualex: a glossary of aquaculture terms. Wiley-Praxis series in aquaculture and fisheries, Aqualex Multimedia Consortium Ltd
30. Chopin T (2009) Let's not move just the fish to the open ocean... an integrated multi-trophic aquaculture approach should not be an afterthought for 2050. Conference paper, the ecology of marine wind farms: perspectives on impact mitigation, siting, and future uses, 8th annual Ronald C. Baird Sea Grant Science Symposium, November 2–4, 2009, Newport, Rhode Island
31. Dena (2007) Renewable energies: Germany's first test Weld for offshore wind energy. Dena fact sheet. German Energy Agency, Berlin
32. Tiedemann A (2003) Windenergieparke im Meer – Perspektiven für den umweltverträglichen Einstieg in eine neue Großtechnologie. In: Lozán J, Rachor E, Reise K, Sündermann J, Westernhagen HV (eds) Warnsignale aus Nordsee & Wattenmeer: Eine aktuelle Umweltbilanz. Wissenschaftliche Auswertungen, Hamburg, pp 142–148
33. BMU/SOW (2007) Offshore wind power deployment in Germany. In: Rehfeldt K, Paschedag U, Bömer J (eds) Federal Ministry for the Environment, Nature Conservation and Nuclear Safety (BMU) and Stiftung der Deutschen Wirtschaft zur Nutzung und Erforschung der Windenergie auf See/Offshore Wind Energy Foundation (SOW). Scholz-Druck GmbH, Dortmund, pp 31
34. Gierloff-Emden HGR (2002) Wandel der Umwelt der See-und Küstenlandschaft der Nordsee durch Nutzung von Windenergie. Mitteilungen der Österreichischen Geographischen Gesellschaft 144:219–226
35. Dahlke V (2002) Genehmigungsverfahren von Offshore-Windenergieanlagen nach der Seeanlagenverordnung. Natur und Recht 24:472–479
36. BWE (2008) Datenblatt 2007: Datenblatt Windenergie 2007. Bundesverband WindEnergie
37. GWEC (2007) Continuing boom in wind energy – 20 GW of new capacity in 2007. Press release 15/02 200. Global Wind Energy Council
38. BSH (2010) Wind farms. Bundesamt für Seeschifffahrt und Hydrographie. Federal Maritime and Hydrographic Agency, Hamburg/Rostock
39. Ventus A (2010) Der erste deutsche Offshore-Windpark (first german offshore wind farm). Deutsche Offshore-Testfeld und Infrastruktur. GmbH & Co. KG, Oldenburg
40. BWE (2007) Offshore Windenergie. BWE Hintergrundpapiere. Bundesverband WindEnergie

41. Wirtz KW, Tol RSJ, Hooss KG (2003) Mythos "Offene See": Nutzungskonflikte im Meeresraum. In: Lozan L et al (eds) Warnsignale aus Nordsee & Wattenmeer. Eine aktuelle Umweltbilanz. Wissenschaftliche Auswertungen, Hamburg, pp 157–160
42. Buck BH, Krause G, Rosenthal H (2004) Multifunctional use, environmental regulations and the prospect of offshore co-management: potential for and constraints to extensive open ocean aquaculture development within wind farms in Germany. Ocean Coast Manage 47:95–122
43. Jentoft S (2000) Co-managing the coastal zone: is the task too complex? Ocean Coast Manage 43:527–535
44. Michler-Cieluch T (2009) Co-Management processes in integrated coastal management: the case of integrating marine aquaculture in offshore wind farms. PhD thesis, University of Hamburg, Germany
45. Führböter A, Dette HH (1983) Wasserstände, Wind und Seegang im Seegebiet um Helgoland in den Jahren von 1969 bis 1983. Leichtweiß-Institut für Wasserbau der TU Braunschweig, Bericht Nr, 577
46. Becker G, Dick S, Dippner J (1992) Hydrography of the German Bight. Mar Ecol Prog Ser 91:9–18
47. Buck BH, Berg-Pollack A, Assheuer J, Zielinski O, Kassen D (2006) Technical realization of extensive aquaculture constructions in offshore wind farms: consideration of the mechanical loads. In: Proceedings of the 25th international conference on offshore mechanics and Arctic engineering, OMAE 2006: presented at the 25th International conference on offshore mechanics and Arctic engineering, 4–9 June 2006, Hamburg, Germany/American Society of Mechanical Engineers, pp 1–7
48. Takayanagi K (1998) Water quality guidelines for aquaculture: an example in Japan. In: Howell WH, Keller BJ, Park PK, McVey JP, Takayanagi K, Uekita Y (eds) Nutrition and technical development of aquaculture. Proceedings of the 26th US–Japan aquaculture symposium, Durham/New Hampshire/USA September 16–18, 1997. UJNR technical report No. 26, Durham, University of New Hampshire Sea Grant Program, pp 247–254
49. BSH (2006) MURSYS – marine environment reporting system information from the North Sea and Baltic Sea. Bundesamt für Seeschifffahrt und Hydrographie (BSH), Hamburg
50. Stickney RR (1998) Joining forces with industry – open ocean aquaculture. Proceedings of the 3rd annual international conference, May 10–15, Corpus Christi. TAMU-SG-99–103, Corpus Christi, Texas Sea Grant College Program
51. Bridger CJ, Costa-Pierce BA (2003) Open ocean aquaculture: from research to commercial reality. The World Aquaculture Society, Baton Rouge
52. Michler-Cieluch T, Kodeih S (2008) Mussel and seaweed cultivation in offshore wind farms: an opinion survey. Coast Manage 36(4):392–411
53. Buck BH, Buchholz CM (2004) The offshore-ring: a new system design for the open ocean aquaculture of macroalgae. J Appl Phycol 16:355–368
54. Buck BH, Walter U, Liebezeit G (2011) Larval occurrence and settlement in the German Bight: A trial to estimate potentials for *Mytilus edulis* culture in offshore areas, Helgoland Marine Research (in press)
55. BSH (2009) Bundesamt für Seeschifffahrt und Hydrographie – BSH (Federal Maritime and Hydrographic Agency), CONTIS-Geodata. Hamburg/Rostock
56. Hickman RW (1992) Mussel cultivation. In: Gosling E (ed) The mussel *Mytilus*: ecology, physiology, genetics and culture, vol 25, Development in aquaculture and fisheries science. Elsevier, Amsterdam, pp 465–510
57. Critchley AT, Ohno M, Largo DB (2006) World seaweed resources. An authoritative reference system. ETI BioInformatics. DVDROM
58. Tseng CK (1989) *Laminaria* mariculture in China. In: Doty MS, Caddy JF, Santelices B (eds) Case studies of seven commercial seaweed resources. FAO Fisheries Technical Paper – 281. Food and Agriculture Organization of the United Nations (FAO), Rome
59. Strathmann MF (1987) Reproduction and development of marine invertebrates of the northern Pacific Coast. University of Washington Press, Seattle, pp 670
60. Pulfrich A (1997) Seasonal variation in the occurrence of planktic bivalve larvae in the Schleswig-Holstein Wadden Sea. Helgol Wiss Meer 51:23–39
61. Walter U, Liebezeit G (2001) Abschlußbericht des Projektes: Nachhaltige Miesmuschel-Anzucht im niedersächsischen Wattenmeer durch die Besiedlung natürlicher und künstlicher Substrate. Forschungszentrum Terramare, pp 1–97
62. Walter U, Liebezeit G (2003) Efficiency of the blue mussel (*Mytilus edulis*) spat collectors in highly dynamic tidal environments of the Lower Saxonian coast (Southern North Sea). Biomol Eng 20:407–411
63. Scarratt D (1993) A handbook of northern mussel culture. Island Press, Montague, pp 167
64. Gosling E (2003) Bivalve molluscs: biology, ecology and culture. Blackwell Publishing/MPG Books, Bodmin/Cornwall, pp 443
65. Brenner M (2009) Site selection criteria and technical requirements for the offshore cultivation of blue mussels (*Mytilus edulis* L.). PhD thesis, School of Engineering and Science, Jacobs University, Bremen, pp 151
66. Langan R, Horton F (2003) Design, operation and economics of submerged longline mussel culture in the open ocean. Bull Aquacult Assoc Can 103:11–20
67. Neushul M, Harger BWW (1985) Studies of biomass yield from a near-shore macroalgal test farm. J Solar Energy Eng 107:93–96
68. Neushul M, Benson J, Harger BWW, Charters AC (1992) Macroalgal farming in the sea: water motion and nitrate uptake. J Appl Phycol 4:255–265
69. Turner R (2001) Offshore mariculture: site evaluation. In: Muir J, Basurco B (eds) Options méditerranéennes – Mediterranean offshore mariculture. Etudes et recherches, Serie B, Numéro 30, Zaragoza, CIHEAM, INO Reproducciones, pp 141–157

70. Pérez OM, Telfer TC, Ross LG (2003) On the calculation of wave climate for offshore cage culture site selection: a case study in Tenerife (Canary Islands). Aquacult Eng 29:1–21
71. Dalton R (2004) Fishing for trouble. Nature 431:502–504
72. Naylor R, Burke M (2005) Aquaculture and ocean resources: raising tigers of the sea. Annu Rev Environ Res 30:185–218
73. Allen JI, Moore MN (2004) Environmental prognostics: is the current use of biomarkers appropriate for environmental risk evaluation. Mar Environ Res 58:227–232
74. Buck BH, Walter U, Rosenthal H, Neudecker T (2006) The development of mollusc farming in Germany: past, present and future, World Aquaculture 37(2):6–11 & 66–69
75. Buck BH, Thieltges D, Walter U, Nehls G, Rosenthal H (2005) Inshore–offshore comparison of parasite infestation in *Mytilus edulis*: implications for open ocean aquaculture. J Appl Ichthyol 21:107–113
76. Brenner M, Buck BH, Koehler A (2007) New concept combines offshore wind farms, mussel cultivation. Global Aquacult Advocate 10:79–81
77. Buck BH, Buchholz CM (2005) Response of offshore cultivated *Laminaria saccharina* to hydrodynamic forcing in the North Sea. Aquaculture 250:674–691
78. Manefeld T (2006) Ansiedlungspotential von Miesmuschellarven (*Mytilus edulis*) an verschiedenen Substraten freihängender Brutkollektoren. Thesis, University of Applied Sciences Bremerhaven, Germany
79. Voss D (2006) Parasitierungsgrad der Miesmuschel (*Mytilus edulis*) in Abhängigkeit zur Tiefenzonierung und Entfernung zur Küste. Thesis, University of Applied Sciences Bremerhaven, Germany
80. Brenner M, Buck BH (2010) Attachment properties of blue mussel (*Mytilus edulis L.*) byssus threads on culture-based artificial collector substrates. Aquacult Eng 42:128–139
81. Zielinski O, Assheuer J, Berg-Pollack A, Buck BH, Geisen M, Henkel R, Kassen D (2006) Assessment of mechanical loads and environmental conditions for extensive aquaculture constructions within offshore wind farms: First results from the AquaLast study site. Proceedings of DEWEK 2006: presented at the DEWEK 2006, 22–23 November 2006, Bremen, Germany, pp 1–4
82. Bard (2010) Offshore wind farms. Bard Engineering GmbH. Emden, Germany
83. OFT (2010) *Aquapod* – a submergible fish cage. Ocean Farm Technologies, Searsmont
84. Ostrom E, Burger J, Field CB, Norgaard RB, Policansky D (1999) Revisiting the commons: local lessons, global challenges. Science 284(4512):278–282
85. Hardin G (1968) The tragedy of the commons. Science, 162. Reprinted in Dryzek JS, Schlosberg D (1999) Debating the Earth: the environmental politics reader. Oxford University Press, New York
86. Michler-Cieluch T, Krause G, Buck BH (2009) Reflections on integrating operation and maintenance activities of offshore wind farms and mariculture. Ocean Coast Manage 52(1):57–68
87. Buck BH, Krause G, Michler-Cieluch T, Brenner M, Buchholz CM, Busch JA, Fisch R, Geisen M, Zielinski O (2008) Meeting the quest for spatial efficiency: progress and prospects of extensive aquaculture within offshore wind farms. Helgol Mar Res 62:269–281
88. EU Commission (2009) Building a sustainable future for aquaculture. A new impetus for the Strategy for the Sustainable Development of European Aquaculture. The European Parliament and the Council, COM(2009) 162 final
89. McVey JP (1996) Overview of offshore aquaculture. In: Polk M (ed) Open ocean aquaculture. Proceedings of an international conference, May 8–10, Portland, Maine. New Hampshire/Maine Sea Grant College Program, pp 13–18
90. Braginton-Smith B, Messier RH (1997) Design concepts for integration of open ocean aquaculture and Osprey TM Technology. In: Howell WH, Keller BJ, Park PK, McVey JP, Takayanagi K, Uekita Y (eds) Proceedings of the twenty-sixth US–Japan aquaculture symposium, Durham, New Hampshire. UJNR Technical Report No. 26. University of New Hampshire Sea Grant Program, Durham, pp 239–245
91. Bussel van GJW, Zaaijer MB (2007) Reliability, availability and maintenance aspects of large-scale offshore wind farms, a concepts study. In: Proceedings of MAREC 2001. Delft University of Technology, The Netherlands, pp 119–126
92. Musial W, Butterfield S, Ram B (2006) Energy from offshore wind. In: Proceedings of the offshore technology conference (OTC), 1–4 May, Houston, 11 pp
93. Michler-Cieluch T, Krause G (2008) Perceived concerns and possible management strategies for governing 'wind farm–mariculture integration'. Marine Policy 32(6): 1013–1022
94. Carlsson L, Berkes F (2005) Co-management: concepts and methodological implications. J Environ Manage 75: 65–76
95. Cash DW, Moser SC (2000) Linking global and local scales: designing dynamic assessment and management processes. Global Environ Change 10:109–120
96. Heinelt H (2002) Achieving sustainable and innovative policies through participatory governance in a multi-level context. In: Heinelt H, Getimis P, Kafkalas G, Smith R, Swyngedouw E (eds) Participatory governance in multi-level context. Leske + Budrich, Opladen, pp 17–32
97. EU Commission (2007) An Integrated Maritime Policy for the European Union. Commission Staff Working Document, Accompanying document to the Communication from the Commission to the European Parliament, the Council, The European Economic and Social Committee and the Committee of the Regions, SEC (2007) 1278
98. Dietz T, Ostrom E, Stern PC (2003) The struggle to govern the commons. Science 302(5652):1907–1912
99. Steins NA, Edwards VM (1999) Synthesis: platforms for collective action in multiple-use common-pool resources. Agric Hum Values 16(3):309–315

100. Buck BH, Ebeling M, Michler-Cieluch T (2010) Mussel cultivation as a co-use in offshore wind farms: potential and economic feasibility. Aquacult Econ Manage 14(4): 1365–7305
101. Bradbury RH, Seymour RM (2009) Coral reef science and the new commons. Coral Reefs 28:831–837

Aquaculture, Ecological

Barry A. Costa-Pierce
Graduate School of Oceanography, Rhode Island Sea, Grant College Program, University of Rhode Island, URI Bay Campus, Narragansett, RI, USA

Article Outline

Glossary
Definition of Ecological Aquaculture
Introduction
Key Principles
The FAO Ecological Approach to Aquaculture (EAA)
Applying an Ecological Aquaculture Approach at Different Scales of Society
Social Ecology of Aquaculture
An Ecological Aquaculture Strategy for the "Triple Bottom Line"
Future Directions
Bibliography

Glossary

Biofloc A mixture of detritus, bacteria, and other microscopic organisms that aggregates in flocs, which are used for controlling water quality and enhancing the delivery of natural foods to omnivorous species in aquaculture.

Ecosystem An area of the natural environment in which the structure and functions of the physical (rocks, soil, etc.) and natural (all living organisms) environments are considered together in interacting food webs.

Escapees The unintended releases of cultured organisms from captivity into the wild.

Polyculture The practice of making compatible the culture of multiple species in the same physical space by stocking or planting organisms having different food, spatial, or temporal niches.

Resilience The ability of a natural or aquaculture system to absorb abrupt changes or disturbances without collapsing. A resilient aquaculture ecosystem can withstand physical and economic shocks and rebuild itself.

Stewardship An ethic that engages all affected stakeholders in the cooperative planning and management of the environmental quality to prevent degradation and facilitate recovery in the interest of long-term sustainability.

Watershed An area of land where all of the water that is under it or drains off of it goes into the same place.

Definition of Ecological Aquaculture

Ecological aquaculture is an alternative model of aquaculture development that uses ecological principles as the paradigm for the development of aquaculture [1, 2]. Ecological aquaculture plans, designs, develops, monitors, and evaluates aquatic farming ecosystems that preserve and enhance the form and functions of the natural and social environments in which they are situated. Ecological aquaculture farms are integrated "aquaculture ecosystems" designed to deliver both economic and social profit (Fig. 1).

Ecological aquaculture incorporates at the outset – and not as an afterthought – planning for not only the sustainable production of aquatic foods, but also for innovation [3], community development, and the wider social, economic, and environmental contexts of aquaculture at diverse scales, both large and small, and at the commercial, school, and homeowner scales [4, 5]. Ecological aquaculture also uses the "aquaculture toolbox" [6] to play vital roles in non-food, natural ecosystem rehabilitation, reclamation, and enhancement.

Introduction

The roots of ecological aquaculture are in Asia [7, 8]. In this century, however, Asia, especially China, during the period from 1980s to present has chosen the industrial model of aquaculture development, and has dismantled much of its rich ecological aquaculture heritage, and choosing instead to intensify and import vast quantities of feedstuffs. As a result of intensification and the use of imported feeds, freshwater

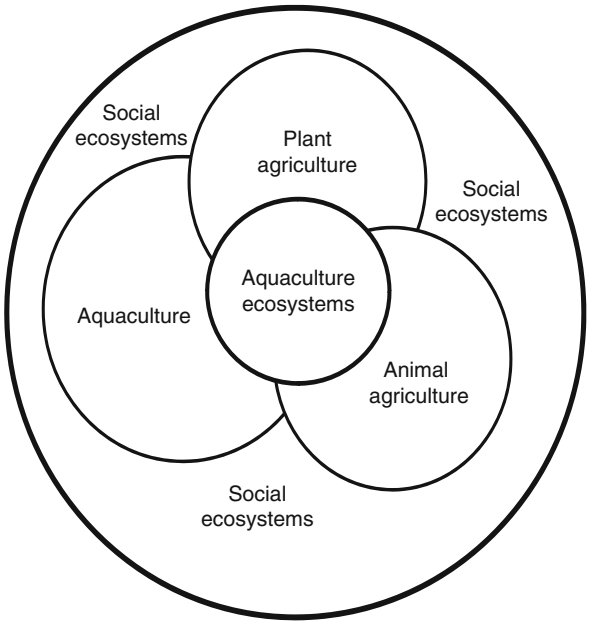

Aquaculture, Ecological. Figure 1
Aquaculture ecosystems mimic the form and functions of natural ecosystems, but are a sophisticated, knowledge-based designed farming ecosystem that are planned as combinations of land and water-based aquatic plant, agronomic, algal, and animal subunits, which are embedded into the larger context of human social systems

aquaculture yields from China have increased 10X in just 20 years, and comprise the world's largest aquaculture industries [9].

The FAO ecosystems approach to aquaculture [10] creates a new code for global aquaculture development, combining into one common framework the two most important social-ecological trajectories for global aquaculture – aquaculture for the world's rich, and aquaculture for the world's poor. Knowledge of the rich archeology and anthropology of aquaculture connects this FAO code to antiquity, creating a single development pathway for aquaculture throughout human history.

Key Principles

There are seven principles of ecological aquaculture:

1. **Ecological aquaculture systems are "aquaculture ecosystems" that mimic the form and functions of natural ecosystems.**

   Ecological aquaculture farms are designed, farming ecosystems. Sophisticated site planning occurs so that farms "fit with nature" and do not displace or disrupt invaluable natural aquatic ecosystems or conservation areas. If localized displacement or degradation does occur, active support of innovative, collaborative research and development programs for ecosystems redesign, relocation, rehabilitation, and enhancement efforts are initiated and supported by the ecological aquaculture farms throughout the life of their farming operations.

2. **Ecological aquaculture is integrated with communities to maximize not only local but also regional economic and social multiplier effects in order to provide maximal job creation and training, and create "aquaculture communities" that are an essential part of vibrant, working waterfronts.**

   Ecological aquaculture operations export to earn profits but also promote and market products locally to contribute to the development of society. Ecological aquaculture operations are committed to building the "culture" of aquaculture in order that "aquaculture communities" can develop and evolve as a source of innovation, education, and local pride. Aquaculture development as a means of community development can result in numerous, innovative economic and social multiplier effects such as aquaculture restaurants, marketing of "sustainable seafoods" that are branded as local and bioregional, and aquaculture tourism.

3. **Ecological aquaculture results in economic profit by practicing trophic efficiency to ensure that aquaculture is humanity's most efficient protein producer.**

   Non-fed, shellfish and algae culture are preferred choices for ecological aquaculture developments. In fed aquaculture, fish meals/oils are not used as either the major protein or energy sources, but are included in animal diets to solve issues of diet palatability only; and, if used, fish meals and oils originate from certified, sustainable fishmeal/oil fisheries only. Fed aquaculture ecosystems rely on protein and oil sources from agricultural sources and seafood processing wastes, and include science innovations such as the development of detrital

food webs ("bioflocs") to feed cultured, aquatic organisms.

4. **Ecological aquaculture results in social profit by integrating aquaculture developments into global fisheries, food, and poverty alleviation programs.**

   Ecological aquaculture is part of the global movement to eliminate extreme hunger and starvation (Millennium Development Goal #1) by being a part of comprehensive plans for sustainable fisheries for poverty alleviation. Ecological aquaculture uses alternative feeds to support programs to deliver more of the world's feed fisheries (sardines, anchovies, mackerels, etc.) away from aquaculture to the world's poor.

5. **Ecological aquaculture practices nutrient management by using ecosystems design, reuse, and recycling, and does not discharge any nutrient or chemical pollution causing irreversible damage to natural aquatic or terrestrial ecosystems.**

   No harmful metals, chemicals, or pharmaceuticals potentially harmful to long-term human or ecosystem health are used in the ecological aquaculture production processes. Ecological aquaculture farms have "sustainability strategic and implementation plans" in place to develop comprehensive, full cycle reuse, and recycling systems for all farming operations.

6. **Ecological aquaculture uses native species/strains, and does not contribute to "biological" pollution.**

   Escapees from aquaculture, especially aquarium operations, have severely impacted aquatic ecosystems worldwide. Exotics species/strains can be good choices only if long-term monitoring data and scientific research indicate that exotic species are unlikely to establish; if exotic species are widely established and provide economic and social profit without irreversible environmental harm; or, the use of native species puts at risk indigenous genetic diversity. Ecological aquaculture operations ensure that innovative engineering and complete escapement technologies are used; that control and recovery procedures are in place; that active research and development programs provide alternatives and new options; and that complete, transparent, public documentation and information are available.

7. **Ecological aquaculture is a global partner, producing information for the world, avoiding the proprietary.**

   Ecological aquaculture farms are aquaculture ecosystems that go beyond "meeting the regulations." They are sites of collaboration, leadership development, and innovation. They are outstanding community citizens and models of stewardship [4]. Successful leadership development triggers developments of innovation and more efficient aquaculture-related technology, and more ecologically appropriate legislation and regulations.

The FAO Ecological Approach to Aquaculture (EAA)

In 2006, the Fisheries and Aquaculture Department of Food and Agriculture Organization (FAO) recognized the need to develop an ecosystem-based management approach to aquaculture similar to the Code of Conduct for Responsible Fisheries. FAO [10] suggested that an ecological approach to aquaculture (EAA) would have three main objectives: human well-being, ecological well-being, and the ability to achieve both via effective governance, within a hierarchical framework that was scalable at the farm, regional, and global levels.

In 2008, FAO defined an EAA as: A strategy for the integration of the activity within the wider ecosystem such that it promotes sustainable development, equity, and resilience of interlinked social-ecological systems. An ecosystem approach to aquaculture, similar to other systems approaches to management, accounts for a complete range of stakeholders, spheres of influences, and other interlinked processes. Applying an ecosystem-based approach must plan for physical, ecological, social, and economic systems as a part of community development, taking into account stakeholders in the wider social, economic, and environmental contexts of aquaculture [10]. FAO developed three principles and key issues at different scales of society:

Principle 1: Aquaculture development and management should take account of the full range of ecosystem functions and services, and should not threaten the sustained delivery of these to society.

The key issue is to estimate ***resilience capacity***, or the limits to "acceptable environmental change."

A range of terms has been used to estimate the limits to environmental change, including "environmental carrying capacity," "environmental capacity," "limits to ecosystem function," "ecosystem health," "ecosystem integrity," "fully functioning ecosystems," all of which are subject to a specific social/cultural/political context [11]. Conventional environmental impact assessments touch on just some of these issues. Application of the precautionary approach is important but inadequate in aquaculture; use of aquaculture risk assessment is becoming widespread [12].

Principle 2: Aquaculture should improve human well-being and equity for all relevant stakeholders.

Aquaculture should provide equal opportunities for development, which requires its benefits to be more widely shared especially locally so that it does not bring detriment to any sector of society, especially the poor. Aquaculture should promote both food security and safety as key components of human well-being.

Principle 3: Aquaculture should be developed in the context of other sectors, policies, and goals.

Interactions between aquaculture and its influences on the surrounding natural and social environment must be recognized. Aquaculture often has a smaller impact than other human activities, e.g., agriculture and industry, but it does not take place in isolation. There are many opportunities to couple aquaculture activities with other primary producing sectors in order to promote materials and energy recycling, and the better use of resources in general.

Applying an Ecological Aquaculture Approach at Different Scales of Society

There are three physical scales important in the planning for and assessment progress toward an ecosystem approach to aquaculture: farm scale, watershed/aquaculture zone, and global. Each of these has important planning and assessment needs.

Farm Scale

Planning for aquaculture farms is easily defined physically and could be few meters beyond the boundaries of farming structures; however, the increasing size and intensity of some farms (e.g., large-scale shrimp farming or salmon farming) could affect an entire water body or watershed. Assessment of an EAA at the farm scale entails an evaluation of planning and implementation of "triple bottom line" programs – ecological, economic, and social programs – that in a comprehensive manner account for impacts to the wider ecosystem and social impacts of farm-level aquaculture developments, including use of better ("best") management practices, and use of restoration, remediation, and mitigation methods. Proper site selection, levels of production intensity, use of species (exotic vs. native), use of appropriate farming systems technologies, and knowledge of economic and social impacts at the farm level should be considered.

For fed aquaculture, there are many concerns as the current trajectory and growth of the large-scale aquaculture industries. Current aquaculture development models are being modified rapidly by advances that will affect the widespread adoption of ecological aquaculture, which, if projected to 2050, confirm that large-scale aquaculture may move fully toward ecological aquaculture approaches (Table 1). There are a growing number of well-documented success stories in ecological aquaculture (Table 2).

Watershed/Aquaculture Zone Scale

Planning for an EAA at watersheds/aquaculture scale is relevant to common ecosystem and social issues such as diseases, trade in seed and feeds, climatic and landscape conditions, urban/rural development, etc. Assessment of an EAA at this scale is a two-phase process and will include, at phase I, assessments of

1. Inclusion of aquaculture as a part of regional governance frameworks, e.g., the overall framework of integrated coastal zone management or integrated watershed, land-water resource management planning, and implementation. Assessments take into account existing scenarios, user competition, and conflicts for land and water uses, and comparisons of alternatives for human development.
2. Impacts of aquaculture on regional issues such as escapees, disease transmission, and sources of contamination to/from aquaculture.

Aquaculture, Ecological. Table 1 Major issues with fed aquaculture today (2010) and projections of these to 2050

Issues	Concerns	Modern developments (2010)	Trajectory of issues to 2050
Feeds/no net gain	Schroeder [28] documents pond can be a net consumer rather than a producer of animal protein. Fishing down and farming up marine food webs (Naylor et al. [29]; Pauly [30])	Food conversion rates improve to ~1:1; fish in/out (FIFO) ratios drop to ~1.7; domestication of farmed species turns carnivores into domesticated omnivores	FIFO ratios drop to 1 or less; aquaculture uses ~50% of world's fish meal and oil with balance met by agricultural meals/oils
Feeds/ocean sustainability	Integrity of marine ecosystems damaged by high removal rates of feed species	Aquaculture use dropping due to rapid cost increases in meals/oils; poverty/social concerns recognized	Ecosystem modeling parcels out science-based removal rates/allocations for aquaculture and ecosystems
Feeds/poverty	Massive poverty and hunger in fish meal/oil producing countries	New recognition in Peru; new international attention to role of meal/oil fisheries & fed aquaculture in poverty alleviation	Governments move to develop food products/prioritize human needs
Habitat destruction	Mangrove destruction and water diversions disrupt nearshore and riverine ecosystems (Macintosh and Phillips [31]; Pullin et al. [32]	Some nations (ex. Thailand) develop policies to prevent damage by proper siting and to rehabilitate damage of shrimp farms	Governments worldwide ban developments in sensitive conservation areas; widespread use of carrying capacity models (McKindsey et al. [33]) and ecological valuation for decision-making
Eutrophication	Intensive aquaculture operations are feedlots producing nutrient pollution loads comparable to human sewage (Folke et al. [21]; Costa-Pierce [34])	Complete feeds, automated feed delivery systems, and nutrition research deliver less pollution; wastes are primarily in the form of soluble nutrients and feces, not waste feeds	Development of land-based recirculating systems; widespread use of land-based integrated aquaculture and water-based IMTA systems
Energy	Intensive aquaculture operations are energy intensive comparable to industrial agriculture and fisheries (Weatherly and Cogger [35])	Scattered R&D in energy use, mostly Life Cycle Analyzes in aquaculture; little/no movement toward use of renewables	Renewable energy systems used

3. Social considerations such as comprehensive planning for all of the possible beneficial multiplier effects of aquaculture on jobs and the regional economy, and considerations of aquaculture's impacts on indigenous communities.

At phase II, progress toward a full implementation of an EAA at watersheds/aquaculture zone scale can be assessed by measuring the

1. Abilities of governments to implement new methods of coastal and water governance to include ecological aquaculture
2. Development of ecological aquaculture approaches that allow agencies responsible for permitting aquaculture to consider and manage activities impacting aquaculture and aquatic ecosystems (e.g., capture fisheries, coastal zone development, watershed management organizations, agriculture, forestry, and industrial developments) more holistically, such as new mechanisms to communicate, cooperate, and collaborate across sectors
3. Design of ecological aquaculture management zones and parks that encourage aquaculture education, research, and development innovations and

Aquaculture, Ecological. Table 2 Global success stories in ecological aquaculture

Region/countries	Aquaculture ecosystems	References
Asia (China, Vietnam, Indonesia)	Rice-fish culture benefits millions of rural people; rice-fish aquaculture ecosystems have been designated as a "Globally important Agricultural Heritage System" (GIAHS)	FAO [9]; Dela Cruz et al. [36]
Asia (China, Thailand, Cambodia, Vietnam, Indonesia)	Integrated aquaculture benefits millions of rural people	Edwards [8]
Asia (China)	Integrated Multi-trophic Aquaculture (IMTA) of fish, shellfish, and seaweeds bioremediates and increases total yields up to 50%	Zhou et al. [37]
Egypt	Integrated aquaculture produced over 650,000 tons of tilapia in 2008, ~60% of total fish production; provision of cheap source of fish at approx. same cost as poultry	McGrath [38]
Canada	IMTA has been adopted by Cooke Aquaculture, the largest salmon aquaculture company in eastern Canada	Chopin et al. [39]; Chopin [40]; Ridler et al. [41, 42]
Canada & USA	Shellfish aquaculture has become widely accepted as environmentally friendly and socially acceptable	National Academy [43, 44]
Tanzania	Seaweed and shellfish aquaculture	Seaweed grown by ~2,000 producers most women; new half-pearl industry growing

partnerships, and also emphasize streamlined permitting of integrated aquaculture, polyculture, or innovative, integrated aquaculture–fisheries businesses and initiatives

Global Scale

Planning for an EAA at a global scale considers aspects of transnational and multinational issues for global commodities (e.g., salmon and shrimp). Assessment of progress toward an EAA at the global level entails evaluation of issues such as: availabilities of fisheries and agriculture feedstocks for formulating aquaculture feeds and impacts on distant marine and social ecosystems, the economic and social impacts of aquaculture on fisheries and agriculture resources, impacts of aquaculture on markets, and impacts of globalization on social sustainability (social capital, goods, and social opportunities). Applications of tools such as lifecycle assessments of aquaculture commodities and the use of innovative social enterprise management guidelines and tools are useful to determine impacts at the global scale.

Social Ecology of Aquaculture

Many analysts are calling for more integrated, multidisciplinary ways of developing ecologically and socially responsible food, energy, water, and waste systems to meet society's needs [13]. Among the first was Lubchenco [14] who called for a new social contract for science and society. Industrial aquaculture in its current development phase does not have a social contract or social license to expand in many areas of the world, especially at the watershed/aquaculture zone and global scales.

Just as important are social investments in aquaculture at the individual level. Aquaculture has an urgent need for developing and engaging leaders who are well trained and experienced decision-makers who are

"honest brokers of policy alternatives" [15]. Keen et al. [16] believe transformation toward more sustainable practices will be much more likely if the individuals who make up society can accept change and modify their personal behaviors [17]. Changes in the behavior of individuals can "scope up" and result in larger changes at the community and societal scales by employing a combination of trust-building, favorable performance, accountability, flexibility and innovation, and the inclusion of stakeholders in strategic planning [18, 19].

Folke et al. [20] challenge our education system to continually adapt to the emergence of such new questions and changing social compacts as aquaculture. Any rapid progress toward an ecological approach to aquaculture will require development of education programs that promote broad awareness, recognition, and implications of new approaches to aquaculture, and the creation of new institutions. Bransford et al. [22] suggest that for such subfields of sustainability science as aquaculture more attention needs to be given to educating the next generation of leaders by teaching metacognitive skills such as practicing different ways of thinking in a variety of contexts, with less emphasis being placed on trying to fill students with a large volume of facts and knowledge.

An Ecological Aquaculture Strategy for the "Triple Bottom Line"

Aquaculture development plans will be incomplete unless both economic and social goals are articulated, and agreed upon, at the outset, in transparent, participatory processes. Only then can aquaculture can "evolve" as an integral part of – not separate from – farmers, fishermen, sustainable community development, and the future of "working waterfronts." Aquaculture's success cannot simply be defined as having successfully developed the hatchery, feed, and marketing components of a business plan – the old alignment of the "seed, feed, and the need." Rather, sustainable, ecological aquaculture nurtures "society's success" for the "triple bottom line" of economic, environmental, and social profit [23].

Adversarial social processes occur in jurisdictions where aquaculture is not being developed using a social-ecological "ecosystem approach." In these places, the blue revolution is being televised, tweeted, and blogged. Adversarial processes (conflicts) occur when stakeholders do not recognize each other's interests as legitimate. These processes increase conflict; thrive on uncertainty; have poor communication; are exclusive, divisive, opaque, and closed, and lack trust. Collaborative processes must be created that create trust through shared learning and ownership, creative problem solving, joint fact finding, and employ adaptive management. Robertson and Hull [24] call this a "public ecology" that has both process and content that emphasizes the participation of extended peer communities of research specialists, policy-makers, and concerned citizens. Dasgupta and Maler [25] have used tools developed by economists and ecologists to valuate choices in the midst of this complexity. In general, since aquaculture is such a dynamic, evolutionary field, managers, policy-makers, and community leaders need to participate to allow understanding of new and emerging problems and to stimulate multidisciplinary research; as analysts report that such work is the highest impact science being published today [26].

Clear, unambiguous linkages between aquaculture and the environment must be created and fostered, and the complementary roles of aquaculture in contributing to environmental sustainability, rehabilitation, and enhancement must be developed and clearly articulated to a highly concerned, increasingly educated, and involved public. New aquaculture operations must plan, at the outset, to:

1. Become an integral part of a community and a region.
2. Plan for community development by working with leaders to provide needed inputs and recycle wastes.
3. Create a diversity of unprocessed and value-added products, and provide local market access, since in rich societies, aquaculture products are high-value discretionary purchases that can easily be rejected by the public.
4. Plan for job creation and environmental enhancement on both local and regional scales.

It is well documented that most aquaculture jobs are not directly in production, rather in the affiliated service industries. In the USA, Dicks et al. [27] found

that aquaculture production accounted for just 8% of the income and ~16,500 jobs. Aquaculture goods and services accounted for 92% of the income and ~165,500 jobs (most jobs were in equipment, supplies, feeds, fertilizers, transport, storage, processing). However, most aquaculture development plans focus almost exclusively on production concerns and have little/no comprehensive plans for localization of seed, feed, markets, or other aquaculture service industries that produce the most benefits to local economies – to say nothing about employing local professionals (most industrial aquaculture operations import high paying professionals from the outside). In the vast majority of cases, feed and services are imported to sites, and local people cannot even buy the produce!

An ecological aquaculture development model will create new opportunities for a wider group of professionals to get involved in aquaculture since new advances will be needed not only in technology but also in information, community development, and facilitation. Ecological aquaculture as a "new" field, and one that is important for the future food security and environment of the planet, requires the much more comprehensive planning in order to evolve a new social contract with society.

Future Directions

By 2030, fed aquaculture will turn from the ocean to land-based agriculture to provide its feeds and oils. As such, more sophisticated, ecologically designed and integrated aquaculture systems will become more widespread because they better fit the social-ecological context of both rich and poor countries. Ecological aquaculture provides the basis for developing a new social contract for aquaculture that is inclusive of all stakeholders and decision-makers in fisheries, agriculture, ecosystems conservation, and restoration.

The wildly optimistic scenarios for aquaculture's expansion will not occur unless alternative ecological approaches and ecological intensification of aquaculture are widely adopted. Aquaculture needs to be better integrated into overall fishery societal plans for securing sustainable seafood supplies and restoring damaged, supporting fisheries ecosystems.

The overuse and degraded state of nearly all of the world's aquatic ecosystems, combined with public concerns about adding any "new" uses or sources of aquatic pollution to already overburdened natural and human systems, require aquaculture to develop ecosystems approaches; sustainable operating procedures; and to articulate a sustainable, ecological pedagogy. The fact that an ecological aquaculture approach can ensure aquaculture is a net gain to humanity; and it could be the key organizing paradigm to form a new social contract for aquaculture worldwide.

The massive globalization of seafood trade has meant less dependence on local natural and social ecosystems, and has resulted in some virulent opposition to aquaculture development, especially as industrial aquaculture has removed the local sources of production and markets, and jobs have been externalized. One major consequence of this globalization has been the increased dependence of industrial, "fed" aquaculture on the southeastern Pacific Ocean marine ecosystem for fish meals and oils. The global implications for the Humboldt ecosystem, for local poverty, and the scoping of this unsustainable situation to the entire global protein food infrastructure are profound, and are still largely unrealized.

Aquaculture sites are not only economic engines of primary production that meet the regulations of a society, but can be sites of innovation and pride if they can be well designed as community-based, aquaculture farming ecosystems. A review of the progress toward such an ecosystems approach to aquaculture is necessary to inspire planners and environmental decision-makers at many societal scales (national, regional, local) to make use of such innovative approaches. Sophisticated site planning of aquaculture can occur so that farms "fit with nature" and do not displace or disrupt invaluable natural, aquatic ecosystems, or conservation areas; but contribute to the local economy and society [5].

An ecological aquaculture approach to comprehensive planning for aquaculture at many different scales will integrate aquaculture into plans for not only environmental benefit and the restoration of coastal ecosystems, but also local market developments and the future of coastal communities. As such, ecological aquaculture can move aquaculture beyond endless user conflicts, and could stabilize the regulatory environment and ensure a more equitable process of eco-social design of aquaculture for the future.

Bibliography

Primary Literature

1. Costa-Pierce B (2002) Ecological aquaculture. Blackwell, Oxford
2. Costa-Pierce B (2003) Use of ecosystems science in ecological aquaculture. Bull Aquacul Assoc Canada 103(2):32–40
3. Culver K, Castle D (2008) Aquaculture, innovation and social transformation. Springer, New York
4. Costa-Pierce B (2008a) An ecosystem approach to marine aquaculture: a global review. In: Soto D (ed) Building an ecosystem approach to aquaculture, vol 14, FAO fisheries and aquaculture proceedings. FAO, Rome, pp 81–116
5. Costa-Pierce B (2008b) Epilogue. In: Culver K, Castle D (eds) Aquaculture, innovation and social transformation. Springer, New York, pp 315–325
6. Costa-Pierce B, Bridger C (2002) The role of marine aquaculture facilities as habitats and ecosystems. In: Stickney R, McVey J (eds) Responsible marine aquaculture. CABI, Wallingford, pp 105–144
7. Ruddle K, Zhong G (1988) Integrated agriculture-aquaculture in South China: the Dike-Pond system in Zhujiang Delta. Cambridge University Press, Cambridge
8. Edwards P (2009) Traditional Asian aquaculture: definition, status and trends. In: Burnell G, Allan G (eds) New technologies in aquaculture, improving production efficiency, quality and environmental management. Woodhead Publishing Ltd., Cambridge, UK, pp 1029–1063
9. FAO (Food and Agriculture Organization) (2009) The state of world fisheries and aquaculture 2008. Fisheries Department, Food and Agriculture Organization of the United Nations, Rome
10. Soto D et al (2008) Applying an ecosystem-based approach to aquaculture: principles, scales and some management measures. In: Soto D, Aguilar-Manjarrez J, Hishamunda N (eds) Building an ecosystem approach to aquaculture, vol 14, Rome: FAO fisheries and aquaculture proceedings. FAO, Rome
11. Hambrey J, Senior B (2007) Taking forward environmental carrying capacity and ecosystem services. Recommendations for CCW. CCW Policy Research Report No. 07/22
12. Black E (2006) A risk analysis approach to assessment of the potential genetic interactions of non-salmonid marine finfish escapes from aquaculture with local native wild stocks, pp 93–105. In: ICES WGEIM report on the environmental impacts of mariculture, 24–28 April 2006, Narragansett, Rhode Island, USA. ICES, Copenhagen, Denmark. (Available at www.ices.dk/reports/MCC/2006/WGEIM06.pdf)
13. Dees J, Backman E (1994) Social enterprise: private initiatives for the common good. Harvard Business School Publishing, Harvard University, Boston
14. Brown L (2009) Plan B 4.0: mobilizing to save civilization. W. Norton, New York
15. Lubchenco J (1998) Entering the century of the environment: a new social contract for science. Science 279:491–497
16. Pilke R (2007) The honest broker: making sense of science in policy and politics. Cambridge University Press, Cambridge
17. Keen M, Brown V, Dyball B (2005) Social learning in environmental management. Earthscan, London
18. Huckle J, Sterling S (1996) Education for sustainability. Earthscan, London
19. Brehm J, Rahn W (1997) Individual level evidence for the causes and consequences of social capital. Am J Pol Soc 41:999–1023
20. Knack S (2002) Social capital and the quality of government: evidence for the states. Am J Pol Sci 46:772–785
21. Folke C, Hahn T, Olsson P, Norberg J (2005) Adaptive governance of social-ecological systems. Ann Rev Environ Res 30:441–473
22. Bransford J, Brown A, Cocking R (2000) Hoe people learn: brain, mind, experience, and school. National Academy Press, Washington
23. Savitz A (2006) The triple bottom line: how today's best-run companies are achieving economic, social and environmental success – and how you can too. Jossey-Bass/Wiley, New York
24. Robertson D, Hull R (2003) Public ecology: an environmental science and policy for global society. Environ Sci Policy 6:399–410
25. Dasgupta P, Maler K (2004) The economics of non-convex ecosystems. Springer, New York
26. Jones B, Wuchty S, Uzzi B (2008) Multi-university research teams: shifting impact, geography, and stratification in science. Science 322:1259–1262
27. Dicks M, McHugh R, Webb B (1996) Economy-wide impacts of U.S. aquaculture. Oklahoma Agricultural Experiment Station, Norman, 946p
28. Schroeder G (1980) Fish farming in manure loaded ponds. In: Pullin R, Shehadeh Z (eds) Integrated agriculture-aquaculture farming systems. ICLARM, Manila, pp 73–86
29. Naylor R, Goldburg R, Primavera J, Kautsky N, Beveridge M, Clay J, Folke C, Lubchenco J, Mooney H, Troell M (2000) Effect of aquaculture on world fish supplies. Nature 405:1017–1024
30. Pauly D (2000) Global change, fisheries, and the integrity of marine ecosystems: the future has already begun. In: Pimental D, Westra L, Noss R (eds) Ecological integrity. Island Press, Washington, DC, pp 227–244
31. Macintosh D, Phillips M (1992) Environmental considerations in shrimp farming. Infofish Int 6:38–92
32. Pullin R (1993) Environment and aquaculture in developing countries. International Center for Living Aquatic Resources Management, Manila
33. McKinsey C, Thetmeyer H, Landry T, Silvert W (2006) Review of recent carrying capacity models for bivalve culture and recommendations for research and management. Aquaculture 261(2):451–462
34. Costa-Pierce B (1997) Environmental impacts of nutrients discharged from aquaculture: towards the evolution of sustainable, ecological aquaculture systems. In: Baird D, Beveridge M, Kelly L, Muir J (eds) Aquaculture and water resource management. Blackwell, Oxford, UK, pp 81–113

35. Weatherly A, Cogger B (1977) Fish culture: problems and prospects. Science 197:427–430
36. Dela Cruz C, Lightfoot C, Costa-Pierce B, Carangal V, Bimbao M (1992) Rice-fish research and development in Asia. ICLARM, Manila
37. Zhou Y, Yang H, Hu H, Liu Y, Mao Y, Zhou H, Xu X, Zhang F (2006) Bioredimation potential of the macroalga Gracilaria lemaneiformis (Rhodophyta) integrated into fed fish culture in coastal waters of north China. Aquaculture 252:264–276
38. McGrath C (2009) Egypt. A big catch feeds millions. Global geopolitics Net Sites/IPS http://globalgeopolitics.net/wordpress/2009/11/01/egypt-a-big-catch-feeds-millions
39. Chopin T, Buschmann A, Halling C, Troell M, Kautsky N, Neori A, Kraemer G, Zertuche-Gonzalez J, Yarish C, Neefus C (2001) Integrating seaweeds into marine aquaculture systems: a key toward sustainability. J Phycol 37:975–986
40. Chopin T (2006) Integrated multi-trophic aquaculture. What it is, and why you should care... and don't confuse it with polyculture. Northern Aquacult 12(4):4
41. Ridler N, Robinson B, Chopin T, Robinson S, Page F (2006) Development of integrated multi-trophic aquaculture in the Bay of Fundy, Canada: a socio-economic case study. World Aquacult 37(3):43–48
42. Ridler N, Wowchuk M, Robinson B, Barrington K, Chopin T, Robinson S, Page F, Reid G, Haya K (2007) Integrated multi-trophic aquaculture (IMTA): a potential strategic choice for farmers. Aquacul Econ Manag 11:99–110
43. National Research Council (2009) Shellfish mariculture in Drakes Estero, Point Reyes national seashore. National Academies Press, Washington, California
44. National Research Council (2010) Ecosystem concepts for sustainable bivalve mariculture. National Academies Press, Research Council, Washington

Books and Reviews

Alder J, Campbell B, Karpouzi V, Kaschner K, Pauly D (2008) Forage fish: from ecosystems to markets. Ann Rev Envir Res 33:71–714

Bell J, Waagbo R (2002) Safe and nutritious aquaculture produce: benefits and risks of alternative sustainable aquafeeds. In: Holmer M, Black K, Duarte C, Marba N, Karqakasis I (eds) Aquaculture in the ecosystem. Springer, New York, pp 185–226

Black K (2001) Sustainability of aquaculture. In: Black K (ed) Environmental impacts of aquaculture. Sheffield Academic Press, Sheffield, pp 199–212

Costa-Pierce B, Desbonnet A, Edwards P, Baker D (eds) (2005) Urban Aquaculture. CABI Publishing, Wallingford, UK

Duarte C, Holmer M, Olsen Y, Stot D, Maba N, Guiu J, Black K, Karakassis I (2009) Will the oceans help feed humanity? Bioscience 59:967–976

Gowen R, Bradbury N (1987) The ecological impact of salmonid farming in coastal waters: a review. Ocean Mar Biol Ann Rev 25:563–575

Stickney R, McVey J (2002) Responsible marine aquaculture. CABI, Wallingford

Tacon A, Hasan M, Subasinghe R (2006) Use of fishery resources as feed inputs for aquaculture development: trends and policy implications. FAO fisheries circular No. 1018. Food and Agriculture Organization of the United Nations, Rome

Tacon A, Metian M (2008) Global overview on the use of fish meal and fish oil in industrially compounded aquafeeds: trends and future prospects. Aquaculture 285:146–158

Turchini G, Bente E, Torstensen E, Ng W (2009) Fish oil replacement in finfish nutrition. Rev Aquacult 1:10–57

Aquaculture, Integrated Multi-trophic (IMTA)

Thierry Chopin
Canadian Integrated Multi-Trophic Aquaculture Network (CIMTAN), University of New Brunswick, Saint John, NB, Canada

Article Outline

Glossary
Definition of the Subject
Introduction: Aquaculture Is Needed But Some Practices Need to Evolve
IMTA: A Flexible and Functional Concept
The Need for Diversifying Responsible Aquaculture Systems and for an Ecosystem Approach
IMTA, While Not the Panacea to and for Everything, Is, Nevertheless, One of the Improvement Options
Recognizing and Valuing the Biomitigative Services Rendered by the Extractive Components of IMTA: Should a System of Nutrient and Carbon Trading Credits Be Developed?
What Will It Take to Increase the Acceptance and Adoption of IMTA as a Responsible Aquaculture Practice of the Future?
Future Directions: The Path Forward
Acknowledgments
Bibliography

Glossary

Biomitigative services provided by extractive aquaculture The environmental, economic, and societal services and benefits received by ecosystems – in their broad definition which includes humans who

depend on them – from the conditions and processes of cultivated species, such as seaweeds extracting inorganic nutrients and suspension- and deposit-feeders extracting organic particles recaptured from the activities of fed aquaculture (e.g., fish or shrimp aquaculture), to maintain their health. Biomitigative services can also be provided by natural populations of similar organisms.

Integrated multi-trophic aquaculture (IMTA) The farming, in proximity, of aquaculture species from different trophic levels, and with complementary ecosystem functions, in a way that allows one species' uneaten feed and wastes, nutrients, and by-products to be recaptured and converted into fertilizer, feed, and energy for the other crops, and to take advantage of synergistic interactions between species. Farmers combine fed aquaculture (e.g., finfish or shrimps) with extractive aquaculture, which utilizes the inorganic (e.g., seaweeds or other aquatic vegetation) and organic (e.g., suspension- and deposit-feeders) excess nutrients from fed aquaculture for their growth. The aim is to ecologically engineer balanced systems for environmental sustainability (biomitigative services for improved ecosystem health), economic stability (improved output, lower costs, product diversification, risk reduction, and job creation in disadvantaged communities) and societal acceptability (better management practices, improved regulatory governance, and appreciation of differentiated and safe products).

Definition of the Subject

Fulfilling aquaculture's growth potential requires responsible technologies and practices. Sustainable aquaculture should be ecologically efficient, environmentally benign, product-diversified, profitable, and societally beneficial. Integrated multi-trophic aquaculture (IMTA) has the potential to achieve these objectives by cultivating fed species (e.g., finfish or shrimps fed sustainable commercial diets) with extractive species, which utilize the inorganic (e.g., seaweeds or other aquatic vegetation) and organic (e.g., suspension- and deposit-feeders) excess nutrients from fed aquaculture for their growth. Thus, extractive aquaculture produces valuable biomass, while simultaneously rendering biomitigative services for the surrounding ecosystem and humans. Through IMTA, some of the uneaten feed and wastes, nutrients, and by-products, considered "lost" from the fed component, are recaptured and converted into harvestable and healthy seafood of commercial value, while biomitigation takes place (partial removal of nutrients and CO_2, and supplying of oxygen). In this way, some of the externalities of fed monoculture are internalized, hence increasing the overall sustainability, profitability, and resilience of aquaculture farms. A major rethinking is needed regarding the definition of an "aquaculture farm" (reinterpreting the notion of site-lease areas) and regarding how it works within an ecosystem, in the context of a broader framework of Integrated Coastal Zone Management (ICZM). The economic values of the environmental/societal services of extractive species should be recognized and accounted for in the evaluation of the true value of these IMTA components. This would create economic incentives to encourage aquaculturists to further develop and implement IMTA. Seaweeds and invertebrates produced in IMTA systems should be considered as candidates for nutrient/carbon trading credits (NTC and CTC) within the broader context of ecosystem goods and services. Long-term planning/zoning promoting biomitigative solutions, such as IMTA, should become an integral part of coastal regulatory and management frameworks.

Introduction: Aquaculture Is Needed But Some Practices Need to Evolve

The global seafood industry is at a crossroads: as capture fisheries stagnate in volume, they are falling increasingly short of a growing world demand for seafood. It is anticipated that by 2030, there will be a 50–80 million ton seafood deficit [1]. This gap will likely not be filled by capture fisheries but by aquaculture operations, which already supply almost 50% of the seafood consumed worldwide [1]. Consequently, it is imperative to design the ecosystem responsible aquaculture practices of tomorrow that maintain the integrity of ecosystems while ensuring the viability of this sector and its key role in food provision, safety, and security.

Without a clear recognition of the industry's large-scale dependency and impact on natural ecosystems and traditional societies, the aquaculture industry is

unlikely to either develop to its full potential, continue to supplement ocean fisheries, or obtain societal acceptance. The majority of aquaculture production still originates from relatively sustainable extensive and semi-intensive systems [2]; however, the rapid development, throughout the world, of intensive marine fed aquaculture (e.g., carnivorous finfish and shrimp) is associated with concerns about the environmental, economic, and social impacts that these, often monospecific, practices can have, especially where activities are highly geographically concentrated or located in suboptimal sites whose assimilative capacity is poorly understood and, consequently, prone to being exceeded. There are also some concerns with shellfish aquaculture, especially at high density, as shellfish occupy an intermediate trophic level and often play a dual role of organic filtering organisms and waste/nutrient generating organisms [3].

For many marine aquaculture operations, monoculture is, spatially and managerially, often the norm. Species are cultivated independently in different bays or regions. Consequently, the two different types of aquaculture (fed versus extractive) are often geographically separate, rarely balancing each other out at the local or regional scale, and, thus, any potential synergy between the two is lost. To avoid pronounced shifts in coastal processes, the solution to nutrification by fed aquaculture is not dilution, but extraction and conversion of the excess nutrients and energy into other commercial crops produced by extractive aquaculture.

To continue to grow, while developing better management practices, the aquaculture sector needs to develop more innovative, responsible, sustainable, and profitable technologies and practices, which should be ecologically efficient, environmentally benign, product-diversified, and societally beneficial. Maintaining sustainability, not only from an environmental, but also from economic, social, and technical perspectives, has become a key issue, increased by the enhanced awareness of more and more demanding consumers regarding quality, traceability, and production conditions. Integrated multi-trophic aquaculture (IMTA) has the potential to play a role in reaching these objectives by cultivating fed species (e.g., finfish or shrimps fed sustainable commercial diets) with extractive species, which utilize the inorganic (e.g., seaweeds or other aquatic vegetation) and organic (e.g., suspension- and deposit-feeders) excess nutrients from aquaculture for their growth (Fig. 1).

IMTA: A Flexible and Functional Concept

The IMTA concept is extremely flexible [4]. To use a musicology analogy, IMTA is the central/overarching theme on which many variations can be developed according to the environmental, biological, physical, chemical, societal, and economic conditions prevailing in parts of the world where the IMTA systems are operating. It can be applied to open-water or land-based systems, marine or freshwater systems (sometimes called "aquaponics"), and temperate or tropical systems. What is important is that the appropriate organisms are chosen at multiple trophic levels based on the complementary functions they have in the ecosystem, as well as for their economic value or potential. In fact, IMTA is doing nothing other than recreating a simplified, cultivated ecosystem in balance with its surrounding instead of introducing a biomass of a single type one thinks can be cultivated in isolation from everything else. Integration should be understood as cultivation in proximity, not considering absolute distances but connectivity in terms of ecosystemic functionalities.

It should be made clear that in the minds of those who created the acronym "IMTA," it was never conceived to be viewed with the minimalist perspective of only the cultivation of salmon (*Salmo salar*), kelps (*Saccharina latissima* and *Alaria esculenta*), and blue mussels (*Mytilus edulis*) within a few hundred meters: this is only one of the variations (Fig. 2) and the IMTA concept can be extended to very large ecosystems like the Yellow Sea (see below). This also means that IMTA variations include integrated agriculture aquaculture systems (IAAS), integrated sylviculture (mangrove) aquaculture systems (ISiAS), integrated green water aquaculture systems (IGWAS), integrated peri-urban aquaculture systems (IPUAS), integrated fisheries aquaculture systems (IFAS), sustainable ecological aquaculture systems (SEAS), integrated temporal aquaculture systems (ITAS), and integrated sequential aquaculture systems (ISAS, also called partitioned aquaculture systems, PAS, or fractionated aquaculture systems, FAS) [5–7]. There is no ultimate IMTA system to "feed the world." There is not one

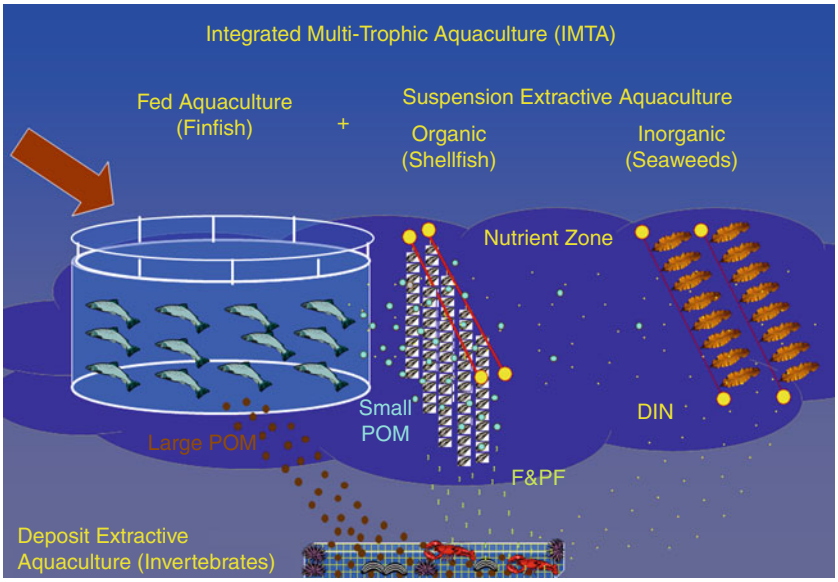

Aquaculture, Integrated Multi-trophic (IMTA). Figure 1
Conceptual diagram of an Integrated Multi-Trophic Aquaculture (IMTA) operation including the combination of fed aquaculture (e.g., finfish) with suspension organic extractive aquaculture (e.g., shellfish), taking advantage of the enrichment in small particulate organic matter (POM); inorganic extractive aquaculture (e.g., seaweeds), taking advantage of the enrichment in dissolved inorganic nutrients (DIN); and deposit organic extractive aquaculture (e.g., echinoids, holothuroids, and polychaetes), taking advantage of the enrichment in large particulate organic matter (POM) and feces and pseudo-feces (F&PF) from suspension-feeding organisms. The bioturbation on the bottom also regenerates some DIN, which becomes available to the seaweeds

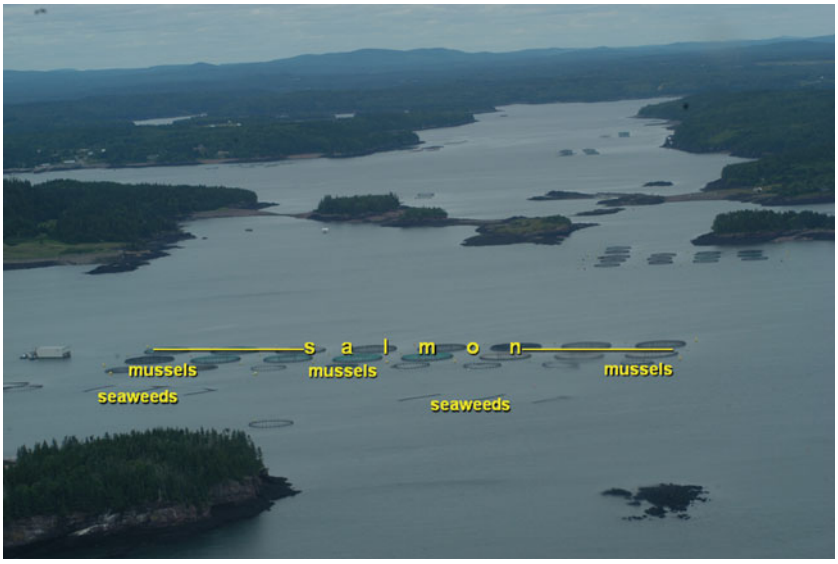

Aquaculture, Integrated Multi-trophic (IMTA). Figure 2
One of the Integrated Multi-Trophic Aquaculture (IMTA) sites in the Bay of Fundy, New Brunswick, Canada, operated by Cooke Aquaculture Inc.: two rows of salmon cages in the background, then a row of mussel rafts and two seaweed rafts in the foreground

world but climatic, environmental, biological, physical, chemical, economic, societal, and political conditions, each of which can lead to different choices of systems for feeding these microworlds.

The paradox is that IMTA is not a new concept. Asian countries, which provide more than two thirds of the world's aquaculture production, have been practicing IMTA (often described as a type of "polyculture") for centuries, through trial and error and experimentation. Why, then, is this common sense solution not more widely implemented? The reasons for this generally center around social customs and practices, and market-driven economic models not considering externalities that one is already familiar with, even if common sense tells one that one should modify them. Human society does not change quickly unless there are compelling reasons to do so. What to do when early large profit margins create short-term economic booms, followed within a few decades by dwindling meager profit margins? Often, the temptation is to throw more large volume cultivation operations and destructive methods into the mix, without proper regulations and business plans. Pollution, disease and economic busts generally ensue, major restructuring of the industry becomes necessary, and a few clairvoyant visionaries remain afloat and adapt to jump to the next curve to survive. This evolution is not exclusive to the aquaculture industry. Why do humans have such short and selective memories resulting in them repeating mistakes, regularly?

The fact that humans are currently at a crossroad should motivate them to improve current aquaculture practices, without further delay. Fishery management plans in most countries have been single-species approaches, completely neglecting the interactions between species, not understanding the synergies, or antagonisms, between them and how an ecosystem works based on the complementarities of the different functions of the different organisms inhabiting it. It seems that, despite the knowledge of the limitations of mono-agriculture and mono-fisheries, people are ready to develop similar plans for the management of mono-aquaculture. It should be recognized that there is still a chance for incorporating all the learning about the problems of terrestrial monocultures into the relatively new frontier of aquaculture. To better manage marine, brackish, or freshwater environments to the benefits of mankind and the ecosystem, one needs to develop a new science, marine agronomy, learning from the mistakes made in land agriculture over the centuries to do a better job with aquaculture. It is interesting to note that traditional agricultural practices, such as crop alternation and fallow, are now being transposed to aquaculture practices.

Why, then, is IMTA not more widely adopted, especially in the western world? Paul Greenberg, in his fascinating book "Four Fish" [8], mentioned a very interesting point. In Leviticus, the third book of the Hebrew bible in which, according to the Jewish tradition, God dictated commandments to Moses, one can read (19:19): "You must not sow your field with two different kinds of seed" (also translated as "two kinds of seed" or as "mixed seed"). One can wonder if this represents, in fact, one of the most ancient treatises recommending mono-agricultural practices and if it is not the reason why integrated culture techniques have been ignored for centuries in the Judeo-Christian civilization, while they have flourished in other civilizations, especially in Asia. Moreover, if Asian cultures are accustomed to the concept of considering wastes from farming practices as resources for other crops rather than pollutants, this attitude still has a long way to progress in the western world where aquaculture is a more recent development.

The Need for Diversifying Responsible Aquaculture Systems and for an Ecosystem Approach

The common old saying "Do not put all your eggs in one basket," which applies to agriculture and many other businesses, should also apply to aquaculture. Having excess production of a single species leaves a business vulnerable to sustainability issues because of fluctuating prices in what has become commodity markets and potential oversupply, and the possibility of catastrophic destruction of one's only crop (diseases, damaging weather conditions). Consequently, diversification of the aquaculture industry is advisable for reducing economic risk and maintaining sustainability and competitiveness.

From an ecological point of view, diversification also means cultivating more than one trophic level, i.e., not just raising several species of finfish (that

would be "polyculture"), but adding into the mix organisms of different and lower trophic levels (e.g., seaweeds, shellfish, crustaceans, echinoderms, worms, bacteria, etc.) to mimic the functioning of natural ecosystems. Staying at the same ecological trophic level will not address some of the environmental issues because the system will remain unbalanced due to nondiversified input and output needs. Evolving aquaculture practices will require a conceptual shift toward understanding the working of food production systems rather than focusing on technological solutions.

One of the innovative solutions promoted for environmental sustainability (biomitigative services for improved ecosystem health), economic stability (improved output, lower costs, product diversification, risk reduction, and job creation in disadvantaged communities), and societal acceptability (better management practices, improved regulatory governance, and appreciation of differentiated and safe products) is IMTA. The aim is to increase long-term sustainability and profitability per cultivation unit (not per species in isolation as is done in monoculture), as some of the uneaten feed and wastes, nutrients, and by-products of one crop (fed animals) are not lost but recaptured and converted into fertilizer, feed, and energy for the other crops (extractive plants and animals). These, in turn, can be harvested and marketed as healthy seafood, while feed costs are reduced because of their reuse in multiple niches and biomitigation is taking place (partial removal of nutrients and CO_2, and supply of oxygen). In this way, all the cultivation components have a commercial value, as well as key roles in recycling processes and rendering biomitigative services. Some of the externalities of fed monoculture are internalized, hence increasing the overall sustainability, long-term profitability, and resilience of aquaculture farms. The harvesting of the different types of crops participates in the capture and export of nutrients outside of the coastal ecosystem.

The biomass and functions of the fed and extractive species naturally present in the ecosystem in which aquaculture farms are operating must also be accounted for or this will lead to the development of erroneous carrying/assimilative capacity models. For example, the 158,811 t (fresh weight) of the intertidal seaweed, *Ascophyllum nodosum* (rockweed), in proximity to salmon aquaculture operations in southwest New Brunswick, Canada, are not neutral in the ecosystem and represent a significant coastal nutrient scrubber which should be taken into consideration to understand the functioning of that part of the Bay of Fundy.

IMTA, While Not the Panacea to and for Everything, Is, Nevertheless, One of the Improvement Options

IMTA has never been portrayed as the solution to and for everything! For example, IMTA does not address the issues of escapees from open-water fish farms. It is, of course, in the interest of everybody, especially the industry (to not lose money) to reduce the number of escapees. This is, however, a question of engineering of the rearing systems (cages, netting material, etc.) and the suitability of the environment to survival should escapes occur. To solve the escapee issue, it has been suggested that fish farms should be pulled from the open water and placed on land or in closed containment. Moving on land is, however, not a guarantee for zero escapees. There are well-known escapee cases from land-based operations, with serious consequences. For example, the bighead carp (*Hypophthalmichthys nobilis*) and the silver carp (*Hypophthalmichthys molitrix*) were brought from Asia to the southern USA in the 1970s to help control algal proliferation in channel catfish (*Ictalurus punctatus*) farms. There are reports of escapees into the lower Mississippi River system, especially associated with flood episodes in the early 1990s. Self-sustaining populations have been able to move northward to enter the Upper Mississippi River system and the Illinois River system. Presently, there are fears that these fish could enter the Great Lakes system through the Chicago Sanitary and Ship Canal and the Des Plaines River to finally reach Lake Michigan, after an escape of around 2,000 km in approximately 20–30 years. Electric fish barriers have been put in place, but their efficiency has been questioned. The use of rotenone, a biodegradable piscicide, was authorized but seemed to have killed more common carps (*Cyprinus carpio*; itself an introduced species from Europe in the 1830s) than bighead and silver carps. On April 26, 2010, the US Supreme Court decided not to get involved in a dispute over how to prevent these carps from making their way into the Great Lakes; it turned down a new

request by the State of Michigan to consider ordering permanent closing of the Chicago-area shipping locks. What the impacts on the ecosystems could be, should these fish get into the Great Lakes systems, is unknown, but they are well-known for their ability to consume large amounts of algae and zooplankton, eating as much as 40% of their body weight per day, and they are fierce competitors when it comes to securing their food needs. The silver carp is also a danger to recreational fishers, water skiers, and boaters because of its habit to jump out of the water when startled by boat motors or other noises, creating life-threatening aerial hazards with high speed impacts.

The number of escapees from land-based facilities is not as well documented as with cage-based aquaculture. Perhaps because land-based fish escapes are more likely to occur as a continuous "trickle" instead of a single major event such as a net tear that would lead to "large-scale" escapes. However, reports do surface from time to time in the media, particularly if there is some novelty in the story. A recent example is the report of the cultured salmonid brown trout, *Salmo trutta*, escaping from a pond farm in the UK. A wildlife photographer caught them in action, making large leaps out of the water straight into a metal feed pipe a meter above and connected to a tributary of a river (http://www.telegraph.co.uk/earth/earthnews/3318094/Photographer-captures-trouts-great-escape.html). Ideally, land-based recirculation systems would reduce the potential for escapes. However, most recirculation systems have at least partial water exchange [9] and where there is water exchange and discharge, there is a potential for escapees. These systems are still not widely used and to the authors knowledge there has not been any initiative taken to document escapees, or lack thereof, within these systems. It may, therefore, be premature to classify such systems as "escape proof." It is unlikely that any land-based aquaculture operations could ever be 100% "escapee-proof" and, consequently, they will also need to develop anti-escapee strategies (avoiding flood plains, electric fences, grids of the appropriate mesh, catchment basins, etc.).

Moving to land-based or closed-containment operations is one approach that may help address some sustainability issues but is not without its problems. Large amounts of energy, often diesel or electric power, are required to pump and aerate water. Nutrients are either pumped back into the water or settled somewhere and "trucked" offsite. All of these processes leave a "carbon footprint," and only partly solve the issue of excess nutrients. IMTA, or its variation called "aquaponics," will have to be added to closed-containment or land-based systems to treat the effluents. One "impact" may simply be traded for another. Ayer and Tyedmers [10], in their life cycle assessment of alternative aquaculture technologies, warned that one could be in a case of environmental problem shifting, not solving, where, while reducing local ecological impacts, the increase in material and energy demands may result in significant increased contributions to several environmental impacts of global concern, including global warming, nonrenewable resource depletion, and acidification.

Land-based or closed-containment operations have also been advocated as a way of controlling diseases and their transmission. However, the proponents very often equate diseases to the sole problem of sea lice, leaving the issues related to viral or bacterial pathogens unaddressed. Some concerns have been expressed that multiple species on the site might increase the risk for disease transmission. It must, however, be realized that sites in the ocean and on land will always have additional unintended species associated with the operation, ranging from microorganisms to marine mammals, depending on the situation. The question is not whether to have only one species on the site, but at what density do negative interactions occur with the unintended ones and whether there are any positive interactions associated with more diversified systems. In fact, two studies [11; Robinson, pers. comm.] have demonstrated in laboratory experiments that the blue mussel, *Mytilus edulis*, is capable of inactivating the infectious salmon anemia virus (ISAV), as well as the infectious pancreatic necrosis virus (IPNV). Mussels are, consequently, not a likely reservoir host or vector for ISAV and IPNV. Put in an IMTA perspective, this could mean that mussel rafts could be strategically placed to serve as a kind of sanitary/biosecurity cordon around salmon cages to combat certain diseases. Pang et al. [12, 13] also reported reduced total bacteria and *Vibrio* counts in a seaweed-abalone IMTA system.

In regard to parasites, two studies [14; Robinson, pers. comm.] indicate that blue mussels can consume copepodids, the planktonic and infectious stage of sea

lice, and several studies, in both Europe and New Zealand, have highlighted the fact that mussels can consume small zooplankton. Having a biofilter such as mussels at IMTA sites may decrease the frequency of exposure to pathogens and planktonic parasites. The hope is that having multiple species on a farm will result in some positive interactions between species allowing some biological control of the outbreaks of pathogens and parasites, hence reducing the number of costly chemical treatments required. If this is validated, filter feeders may have additional contributions to sustainability beyond reduction of the particle load. One of the 14 projects of the recently created Canadian Integrated Multi-Trophic Aquaculture Network (CIMTAN) is investigating the role of bivalves in potentially reducing sea lice populations. Most of the work has been conducted in the lab so far, but results are very positive and it has been demonstrated that mussels eat the larval forms. Ongoing work is developing a trap system that exploits various behaviors of sea lice to attract and filter them out of the system. Another CIMTAN project is looking into the possibility that mussels could reduce the horizontal transmission of *Loma salmonae*, responsible for microsporidial gill disease of salmon (MGDS), a serious endemic gill disorder in marine netpen reared, and wild, Chinook (and other Pacific) salmon. Trials will examine the proof of principle that blue mussels remove microsporidial spores from water and to what extent these spores retain short-term infectious potential as determined by branchial xenoma expression in test fish.

IMTA is not entering directly the debate regarding the inclusion of fishmeal and fish oil in commercial feeds (nor are land-based or closed-containment operations). IMTA could, however, provide a partial solution. Modern commercial salmon diets in Canada contain much less fishmeal (about 15–25%) and fish oil (about 15–20%) than they did less than 10 years ago (40–60%). By-products (trimmings, offal) of wild catch fisheries are now used to supply a major portion of the fishmeal ingredients. Finding replacements for marine ingredients is a priority and there are several large research projects worldwide addressing this issue. The feed company Skretting has now produced a salmon feed which includes no marine ingredients. Turning toward land plant proteins is not without its impacts. Extra farmland area (more deforestation) would be needed, which, moreover, would need to be irrigated and fertilized on a planet already suffering from water availability problems and with fertilizer prices soaring. The price of some staple food crops used in traditional agriculture (corn, soya bean, sugar cane, etc.) would rise considerably due to announced competition for their uses, as recently seen when they were potentially sought out as energy crops for the production of first-generation biofuels [15–17]. Reallocation of acreage for subsidized potential biofuel crops such as corn, sugar cane, oil palm, canola, switch grass, etc., has already had significant ecological and societal costs due to its impacts on ecosystem health, biodiversity, and food security [18–21]. Partial substitution with organisms already living in water and not needing extra fertilization in an IMTA setting, such as seaweeds, could, in fact, be a very interesting option, fitting well within the sustainability and management concept of IMTA, and representing a logical loop for companies developing an IMTA and diversification strategy. If cultivated in the water column in IMTA systems, there would, moreover, be no issue of raking natural beds of seaweeds attached to the bottom of the ocean (destruction of seafloor and impact on ecosystem functions such as nursery ground for animals).

Some environmental nongovernmental organizations arguing for fishmeal/fish oil replacement have also voiced concerns that, after all, marine fish should eat marine ingredients . . . obviously, one cannot have it both ways! There is also the paradoxical situation of farmed freshwater fish, which are being grown less and less on humans and animal wastes and naturally occurring algal blooms, but more and more on already competing staple foods such as corn and soy: they have lost their off-flavored or muddy taste to become tasteless or "unfishy"! So, what does one want to receive in one's kitchen? A flavor-neutral, versatile product easily adapted with numerous sauces, while one is lamenting that farmed salmon or bass are not what wild salmon or bass used to be? Quite an irony, even more so when people learn that these herbivorous whitefish are more and more being fed pellets containing fishmeal and fish oil because they grow faster! What is really important is a balanced diet using balanced sourcing of raw material.

Some will argue that "fish require nutrients, not ingredients." At the same time, there is also the

well-known saying "You are what you eat," and in this case, people have to realize and accept that humans are mostly corn, soya, and fishmeal, if they look at what the four mammals (cow, pig, sheep, and goat) and four poultry (chicken, turkey, duck, and goose) that they have selected as their meat choices are eating. Historically, most of the reduction fishery (small fish such as anchovies, herring, sardines, and menhaden) went into the production of pet feeds and farm animal feeds. Subsequently, this fishery supplied a significant part of the marine ingredients for fish feeds. The landing of the reduction fishery has been fairly stable (fluctuating between 15 and 30 million metric tons since the 1970s) and, in the absence of aquaculture, the fishery would likely return to supplying pet and farm animal feeds, and a current resurgence of interest directly by humans. This is not to justify relaxed vigilance for finding replacements for marine ingredients in fish feed, but simply to suggest that an absence of fish farming will not stop the use of this resource. How can one get out of this vicious circle? Cultivating several organisms, at different trophic levels, in proximity so that the food and wastes are utilized efficiently more than once through a cascade of recapturing and remetabolizing is one approach: that is IMTA. The other is to consider that if terrestrial food production systems are close to their limits, one does not have other options but to turn again to the sea, this time not for fish but to have seaweeds and invertebrates entering one's food habits, either directly or delivered through feed given to intermediates to what reach one's plate. The discrepancy between the marine and agricultural production systems has to be reduced: presently, especially in the western world, humans feed approximately two steps higher in the marine food web than in the agricultural food web.

People should continue to eat seafood (fish but also invertebrates and seaweeds), not according to seafood pocket guides which simplistically paint species with one stroke of green (best choice), orange (good alternative), or red (avoid), but according to the fishing and aquaculture practices used to grow, harvest, and process them: an admittedly more complex mosaic, but also much more realistic and attractive to look at than a traffic light!

Interestingly, what is referred to as the fifth tasting sense by Japanese (after sweet, sour, salty, and bitter) and called umami (= savoriness or good flavor) comes from seaweeds. The product responsible for umami was first identified in 1908 by Professor Kikunae Ikeda, of the Tokyo Imperial University, searching for the chemical reason of the strong flavor in seaweed broth (mostly of the kelp *Saccharina japonica*, formerly *Laminaria japonica*). It is due to the detection in our mouth of the carboxylate anion of the amino acid called glutamic acid and its salts, glutamates, in particular monosodium glutamate (MSG). Inosine monophosphate (IMP) and guanosine monophosphate (GMP), degradation products of the energy-storing molecule adenosine triphosphate (ATP) greatly enhance the perceived intensity of umami. This explains, chemistry displacing romantics, why a dead tuna (once full of energy) served with seaweeds is such a savory delicacy, the very essence of the success of the sushi bar fad gaining the western world.

We have never pretended that IMTA is the solution, the silver bullet, to and for everything. It is now up to us to develop the better aquaculture practices of tomorrow. IMTA is based on several common sense principles:

- The solution to nutrification is not dilution, but extraction and conversion through diversification.
- This is, in fact, a rewording of the first law of thermodynamics "Rien ne se perd, rien ne se crée, tout se transforme" ("Nothing is lost, nothing is created, everything is transformed") as summarized by Antoine Laurent de Lavoisier, the well-known French chemist and physicist (but also tax collector, which explains his premature death at age 51 in 1794 under the Terror period of the French Revolution).
- What is waste for some is gold for others.
- Do not put all your salmon eggs in the same basket.

A lot of common sense, but, unfortunately, common sense is not that common! IMTA is one of the promising options, but, certainly, it needs to be tailored to the location in the world where it is implemented. It should also be developed in association with other practices. Like for energy, not one solution will satisfy all the needs and it is a variety of solutions that will help one secure one's seafood procurement in a responsible manner. The solutions will be at the interfaces of these techniques and will be interdisciplinary. They will

embrace both scientific and technological advancements and traditional knowledge. IMTA is exactly at this interface, modernizing traditional practices: combining ecosystem complementary crops, bay management area, and fallowing are nothing new, but revisited and updated, based on what humans have learned from past experience (which includes a lot of mistakes over the centuries, but not assimilated by the characteristically short-term memory of humans!).

Recognizing and Valuing the Biomitigative Services Rendered by the Extractive Components of IMTA: Should a System of Nutrient and Carbon Trading Credits Be Developed?

A few economic analyses have indicated that the outlook for increased profitability through IMTA is promising [22, 23]. However, these analyses were based solely on the commercial values from the sale of biomass – being of fish, shellfish, or seaweeds – and used conservative price estimates for the cocultivated organisms based on known applications. One aspect not factored into these analyses is the fact that the extractive component of an IMTA system not only produces a valuable multipurpose biomass, but also simultaneously renders waste reduction services to society. It is particularly important to recognize that once nutrients have entered coastal ecosystems, there are not many removal options available: the use of extractive species is one of the few realistic and cost-effective options. The economic values of the environmental/societal services of extractive species should, therefore, be recognized and accounted for in the evaluation of the true value of the IMTA components. Further development of economic models is needed to help shed light on the economic (society) and commercial (industry) attractiveness of IMTA.

Ecosystem services have been ignored until recently [24]. To improve the sustainability of anthropogenic nutrient loading practices such as aquaculture, incentives such as Nutrient Trading Credits (NTC) should be established as a means to promote nutrient load reduction or nutrient recovery. During the last few years, there has been much talk and excitement about carbon credits. However, within coastal settings, the concerns have largely been with nitrogen, due to the fact that its typical role as the limiting nutrient is not any longer the case in some regions. Potential effects of carbon loading in the marine environment should also be considered: localized benthic anoxia and, consequently, hydrogen sulfide release may occur when solid waste deposition rate exceeds aerobic decomposition rate. Ocean acidification due to increased dissolved CO_2 levels has also prompted serious new concerns [25] and a Carbon Trading Credit (CTC) system should also be contemplated. With an appropriate composition of cocultured species, IMTA has the potential to reduce the amounts of dissolved (inorganic) and solid (organic) forms of nitrogen, carbon, phosphorus (more an issue in freshwater environments), etc., making extractive aquaculture a good candidate for a NTC and CTC, or other suitable approaches, to deal with the pressing issues of coastal nutrient loading.

Currently, there are few countries with laws or regulations that require aquaculture operations to responsibly internalize their environmental costs, such as nutrient discharges. There are some precedents, such as where land-based trout farmers in Denmark are allowed to increase their feed quota with documented evidence of reduced effluent discharge [26], but such incentives are not widely spread. In most jurisdictions, adjacent ecosystems are left to accommodate the nutrient load, and performance-based standards are used to determine if farms have exceeded their assimilative capacity.

The implementation of regulations resulting in internalization of environment costs by fish farms, without a direct economic compensatory response such as the Danish feed quota increase, could result in a significant reduction in profitability. In land-based systems, it is relatively easy to quantify nutrient load and concentration via comparison between farm inflows and outflows, thereby creating a benchmark for "economic compensation." Such values are practically impossible to empirically measure in an open-water system, "leaky" by definition, and, consequently, so is the practical implementation of such incentives. However, Troell et al. [27] and Chopin et al. [28] demonstrated that by integrating the seaweed, *Gracilaria*, in the dual role of nutrient scrubber and commercial crop (for agar production), with salmon farms in Chile, the environmental costs of waste discharges would be significantly reduced and profitability significantly increased.

Interestingly, the removal of nitrogen could be much more lucrative, by approximately a factor of 100, than that of carbon. The cost of removing nitrogen is not clearly defined, but there are several interesting studies that may help define a range of possible prices for economic evaluation of the NTC concept. The cost of removing 1 kg of nitrogen varies between US$3 and US$38 at sewage treatment facilities, depending on the technology used and the labor costs in different countries [28]. The municipality of Lysekil, in Sweden, is paying approximately US$10/kg removed by the filter-feeding mussel, *Mytilus edulis*, to the farm Nordic Shell Produktion AB [29, 30]. Ferreira et al. [31, 32], with the development of the Farm Aquaculture Resource Management (FARM) model, determined a net value of €18–26 billion/year of nutrient eutrophication reduction services provided by shellfish aquaculture in the coastal waters of the European Union. Gren et al. [33] calculated that the cleaning costs of nutrients by mussel farming can be considerably lower than other abatement measures and estimated that mussel farming should be credited between €0.1 and €1.1 billion/year in the Baltic Sea.

Using this information, and without presuming what the final design of IMTA sites will be in the future, preliminary calculations for the relatively small-scale IMTA project on the East coast of Canada indicate that the annual harvesting of kelps (Fig. 3) would equate to the removal of 35.75 t of nitrogen from the ecosystem, representing an NTC of between US$357,504 and US$1,072, 512. The same could be applied to another key nutrient, phosphorus. With an annual removal of 4.09 t and a value of US$4/kg removed [28], this would represent another contribution to the NTC of US$16,343, a much smaller amount but it could also be an important way of extracting phosphorus, at a time when some are predicting it to be the next element human society will be short of (in its natural or mined forms).

Carbon Trading Credits (CTC) could also be calculated. There may be some arguments about what is meant by trapping and sequestering carbon. Some may argue that it should be reserved to long/geological term storage (sink) and not to transient storage [34]. This is, in fact, a question of how long one allows the recycling clock to run. There is no permanent storage of carbon; it happened that a particular fossil biofuel, petroleum, has been sequestered over geological time to suddenly be reused at an accelerated rate over the last few centuries. But the first law of thermodynamics, as enunciated by Antoine Laurent de Lavoisier more than two centuries ago, still applies: "Rien ne se perd, rien ne

Aquaculture, Integrated Multi-trophic (IMTA). Figure 3
Harvesting of the kelp, *Saccharina latissima*, at an Integrated Multi-Trophic Aquaculture (IMTA) site in the Bay of Fundy, New Brunswick, Canada. Kelps remove dissolved nutrients from the ecosystem while providing commercial products

se crée, tout se transforme," i.e., "Nothing is lost, nothing is created, everything is transformed." If even temporary removal of carbon from the ocean by biomass harvesting until further transformation (and rerelease of carbon) can be credited for potentially increasing seawater pH and absorbing CO_2 from the atmosphere and/or the cultivated animals, then CTC should be calculated. Marine vegetation is getting more and more recognition as a sink for anthropogenic carbon emissions (the so-called blue carbon [35]). Marine primary producers contribute at least 50% of the world's carbon fixation and may account for as much as 71% of all carbon storage in oceanic sediments. Then, micro-algae, macro-algae, and marine plants, such as mangroves and seagrasses, have a role to play in CO_2 sequestration and removal, and carbon storage [36]. Marine photosynthesis accounts for 50% of the total primary productivity of the planet (54–59 PgC/year from a total of 111–117 PgC/year [37]). Of this, marine macrophytes (seaweeds and seagrasses) account for approximately 1 PgC/year concentrated in coastal regions where they can play a significant role in the sequestration of anthropogenic carbon emissions and the global carbon cycle. Brown marine macro-algae (such as *Macrocystis*, *Saccharina*, *Laminaria*, *Ecklonia*, *Sargassum*, *Ascophyllum*, and *Fucus*), red algae (such as *Porphyra*, *Palmaria*, *Eucheuma* and *Gracilaria*) and green algae (such as *Ulva*), are capable of very high rates of photosynthesis and productivity. These rates of productivity compare very favorably to those of terrestrial crops that have been recommended as possible sources of first-generation biofuels (corn, *Zea mays*) or second-generation biofuels (switch grass, *Panicum virgatus*; E-grass, *Miscanthus giganteus*) and position marine macro-algae very well for being part of the third-generation biofuels [36].

Coming back to the IMTA project on the East coast of Canada, using a value for carbon removal of around US$30/t [34], the annual harvesting of kelps would represent an annual removal of 306.43 t and a CTC of US$9,193: a larger amount of carbon, but for a much smaller value of trading credits, underlining the difficulty in removing dissolved nutrients from aquatic systems and the acute issue of their presence in coastal systems. Similar calculations could be applied to the organic extractive component of IMTA. In the case of shellfish, accumulation of nitrogen, phosphorus, and carbon should be considered both in meat and shells, which are especially rich in calcium carbonates.

At a much larger scale, the occurrence of large and recurrent "green tides" should also be brought into focus. Large proliferations of opportunistic green algae, especially of the genus *Ulva*, in response to large anthropogenic nutrient loading, have been in the news over the last few years in places around the world such as Northern Brittany in France, the southern regions of the UK, and Venice in Italy. The green tide in Qingdao, China, just before the sailing competitions of the 2008 Olympic Games, got a lot of attention (Fig. 4). The following question needs to be asked: Are these green tides a negative media photo opportunity, or are they reminders of the significant role seaweeds play in coastal processes and the services they render? Within 3 weeks, 1 million tons of *Ulva prolifera* were removed from the vicinity of Qingdao to allow the sailors and windsurfers to compete (but it is estimated that approximately 2 million tons of *U. prolifera* sank to the bottom of the Bay; another environmental problem shifting, but not a solution). The harvesting of 1 million tons equated to between 3,000 and 5,000 t of nitrogen removal for a NTC value between US$30 and US$150 millions! Additional NTC of US$1.6 million for the removal of 400 t of phosphorus, and CTC of US$900,000 for the removal of 30,000 t of carbon, should also be factored in.

A smaller green tide occurred in 2007. Large ones were also reported in 2009 and 2010 but they stayed offshore in the Yellow Sea [38, 39]. Out of sight should, however, not mean out of mind. If urgent measures are not taken, this will be a recurrent event for years to come. Is there a solution? Green tides are not the cause, but the unintentional consequence of coastal eutrophication. With the presence of sufficient nutrients and solar energy, these opportunistic species, with a well-adapted anatomy, morphology, and physiology, will proliferate. Obviously, it would be beneficial to reduce nutrient loading at the source, but this may not be possible in the present context of economic development along China's coastal zone. The problem is that *U. prolifera* is presently an unwanted and uncontrolled growing nuisance species of limited commercial value. To control its proliferation, the solution may be to create a competition for nutrients by intentionally

Aquaculture, Integrated Multi-trophic (IMTA). Figure 4
A green tide of *Ulva prolifera* in Qingdao, China, just before the 2008 Olympic Games, triggered a massive cleanup

cultivating algal species, which not only carry on the biomitigation, but also have a commercial value, where *U. prolifera* starts to enter the coastal environment (discharges from juvenile river crab land-based aquaculture ponds along Jiangsu province, south of Shandong province where Qingdao is located). This time, the IMTA concept has to be interpreted as an integrated land pond/coastal aquaculture system in a supra Integrated Coastal Zone Management (ICZM) effort, beyond provincial borders, to address issues at the Yellow Sea scale. It is understood that this "out of the box" approach to ICZM will, initially, raise eyebrows as the idea of growing more seaweeds (but of commercial value) to contain the proliferation of other seaweeds, presently considered nuisances, is not the most intuitive approach for a lot of people or decision makers! The question is simple: what are the best nutrient scrubbers once nutrients are in a dissolved state and have reached coastal waters? The answer is seaweeds, but can people, preferably, grow the ones they have applications for?

At the present time, there seems to be a stage of recognition, awareness, and communication of the concepts of ecosystem services and biomitigative services rendered by extractive aquaculture (the differences between the two not always being clearly identified and explained in some publications). Next will come the time to transform the concepts into biomitigative solutions and then their inclusion in regulatory and management frameworks. Establishing and implementing a structure for the payment schemes (credits or incentives) of these services will be a delicate matter. Will it be one agency, but with funds coming from where? Should it be a regional, national, or international agency(ies), trading at which scale(s)? Will an extractive aquaculture operation in existence for many years receive credits, or will only the new ones? Would a fed aquaculture operation also practicing extractive aquaculture be eligible for credits, or will it be the case for the extractive only aquaculture operations? What about the situation in which people run both types of farms. Moreover, due to complex hydrographic and current patterns, it is obvious that extractive species at a site are not limited to absorbing/sequestering the nutrients generated exclusively at that site. Consequently, is it possible to establish a clear spatial nutrient removal budget which would be associated with the corresponding credits/incentives? Will the sequestration have to be "permanent," or will a temporary removal/storage be acceptable and more realistic? A lot of regulatory details will have to be worked out before this complex scheme becomes a reality.

What Will It Take to Increase the Acceptance and Adoption of IMTA as a Responsible Aquaculture Practice of the Future?

Presently, the most advanced IMTA systems in open marine waters and land-based operations have three components (fish, suspension feeders or grazers such as shellfish, and seaweeds, in cages, rafts, or floating lines), but they are admittedly simplified systems [40]. More advanced systems will have several other components (e.g., crustaceans in mid-water reefs; deposit feeders such as sea cucumbers, sea urchins and polychaetes in bottom cages or suspended trays; and bottom-dwelling fish in bottom cages) to perform either different or similar functions, but for various size ranges of particles, or selected for their presence at different times of the year (e.g., different species of seaweeds). The most advanced IMTA systems, near or at commercial scale, can be found in Canada, Chile, South Africa, Israel, and China [41, 42]. Ongoing research projects related to the development of IMTA are taking place in the UK (mostly Scotland), Ireland, Spain, Portugal, France, Turkey, Norway, Japan, Korea, Thailand, the USA, and Mexico. It will also be interesting to observe how new seaweed cultivation initiatives in different parts of the world for biofuel production could be an additional driver to adopt IMTA practices.

For IMTA to develop to a commercial scale, appropriate regulatory and policy frameworks need to be put in place. Present aquaculture regulations and policies are often inherited from previous fishery frameworks and reasoning, which have shown their limitations. It is, therefore possible that some of the existing regulations and policies could impose unintentional constraints on the future growth of IMTA. To develop the aquaculture of tomorrow, current governance structures pertaining to aquaculture need to be revisited and reviewed with the aim of identifying changes in the regulatory/policy environment that are needed to facilitate the operation of IMTA farms. Adaptive regulations need to be developed by regulators with flexible and innovative minds, who are not afraid to put in place mechanisms that allow the testing of innovative practices at the R&D level, and, if deemed promising, mechanisms that will take these practices all the way to C (commercialization). As the IMTA concept continues to evolve, it is important that all sectors of the industry are aware of the implications of the changes involved, so that they can adapt in a timely and organized manner.

To move research from the "pilot" scale to the "scale up" stage, some current regulations and policies may need to be changed or they will be seen as impediments by industrial partners who will see no incentive in developing IMTA. For example, an earlier version of the Canadian Shellfish Sanitation Program (CSSP) prevented the development of IMTA because of a clause that specified that shellfish could not be grown closer than 125 m of finfish netpens. This paragraph was clearly not written with IMTA in mind, but it seriously impinged its development. After 4 years (2004–2008), it was amended so that IMTA practices could develop to commercial scale legally, based on recent, reliable, and relevant data and information provided by three government departments and the IMTA project on the east coast of Canada. While 4 years may seem long, it is a relatively short delay considering that regulations and legislations require thorough review with due governmental process involving several federal and provincial departments. This suggests that new aquaculture practices should be accompanied by timely regulatory review to avoid market delays for new products. As governments move to revise current regulatory regimes, it will be necessary to press the importance of accommodating and indeed encouraging new sustainable solutions such as IMTA. IMTA also requires approaching aquaculture development and management with a holistic approach and not one species, or group of species, at a time. It is known that this approach has led to many failures in the management of the fisheries; vigilance is required so that the same flaw is not repeated in the management of aquaculture.

Most current aquaculture business models do not consider or recognize the economic value of the biomitigative services provided by biofilters, as there is often no cost associated with aquaculture discharges/effluents in land-based or open-water systems. In order to ensure further development of IMTA systems worldwide, from the experimental concept to the full commercial scale, defining and implementing the appropriate regulatory and policy frameworks, and financial incentive tools such as NTC and CTC, may therefore be required to clearly recognize the benefits of the extractive components of IMTA systems. Better

estimates of the overall costs and benefits to nature and society of aquaculture waste and its mitigation would create powerful financial and regulatory incentives to governments and the industry to jointly invest in the IMTA approach, as the economic demonstration of its validity would be even more obvious. Moreover, by implementing better management practices, the aquaculture industry should increase its societal acceptability, a variable to which it is very difficult to give a monetary value, but an imperative condition for the development of its full potential. Reducing environmental and economic risk in the long term should also make financing easier to obtain from banking institutions [43].

The determination to develop IMTA systems will, however, only come about if there are some visionary changes in political, social, and economic reasoning. This will be accomplished by seeking sustainability, long-term profitability, and responsible management of coastal waters. There is still a large amount of education required to bring society into the mindset of incorporating IMTA into their suite of social values. Some of the attitudinal surveys conducted in Canada [23, 44] and the USA [45] indicate that the general public is in favor of practices based on the "recycling concept." Consumers' perceptions and attitudes may also have to change. Why is recycling and the concept of "what is waste for some is gold for others" well accepted in agricultural practices, but is not yet acquired when transposed to aquaculture practices? Will consumers come to accept eating products cultured in the marine environment in the same way they accept eating products from recycling and organic agricultural practices, for which they are willing to pay a higher price for the perceived higher quality or ethical premiums? After all, regulations require mushrooms to be specifically grown on farmyard manure and animal excrements to receive organic certification (European Community Regulations No 2008R0889 – Article 6). Will a greater appreciation of the sustainable ecological value of the IMTA concept, a willingness to support it tangibly with shopping money, and an increased pressure on elected representatives emerge? This will be the ultimate test. The degree to which researchers and extension people become creatively involved with this educational component will be vital to the success of IMTA practices. The differentiation of IMTA products through traceability and eco-labeling will also be key for their recognition and command of premium market prices.

Some have argued that the adoption of IMTA in the western world is slow. For example, on the east coast of Canada, there were obviously no IMTA sites in the Bay of Fundy in 2001 when IMTA research started. Nine years later, 8 of the 96 finfish sites in southwest New Brunswick have the combination salmon (or cod)/mussels/kelps and 8 other sites have been amended to develop IMTA. This is a respectable conversion of almost 16% in 9 years. Moreover, it would not be reasonable to anticipate an instant conversion, as the industry needs to develop markets to absorb the cocultured biomass: this also takes time and can only be progressive.

Future Directions: The Path Forward

Several IMTA projects, worldwide, have now accumulated enough data to support the proof of concept at the biological level. The next step is the scaling up of more experimental systems to commercial scale to further document the economic and social advantages of the concept, which will be key to offering IMTA to practitioners of monospecific aquaculture as a viable option to their current practices. Emerging responsible aquaculture approaches must generate net economic benefits for society if they are to be advocated. Working on appropriate food safety regulatory and policy frameworks in the respective countries will be essential for enabling the development of commercial scale IMTA operations in a more universal fashion.

It has taken decades to reach current finfish aquaculture production levels and learn new species husbandry. A major rethinking is, however, needed regarding the definition of an "aquaculture farm" by reinterpreting the notion of site-lease areas and regarding how it works within an ecosystem, in the context of a broader framework. Within Integrated Coastal Zone Management (ICZM), integration can range from the small scale (a leased site with its spatial limits) to a Bay Management Area (BMA) and to the larger scale of a region connected by the functionalities of the ecosystem. Amending regulations to allow a new type of aquaculture systems will not occur overnight. This should, however, not discourage the finfish aquaculture industry from practicing IMTA, as even small amounts

of cocultured species production are useful at the initial stage of development.

Selecting the right combination of species will be critical. They will have to be appropriate for the habitat, the available culture technologies and labor forces, and the environmental, climatic, and oceanographic conditions. They will have to be complementary in their ecosystem functions, growing to a significant biomass for efficient biomitigation, commanding an interesting price as raw material or presenting an interesting added value for their derived products. Their ecological interactions and synergies within an IMTA system will have to be identified and understood to take full advantage of them. Their commercialization should not generate insurmountable regulatory hurdles.

Optimal design will not only facilitate nutrient recovery, but should also promote augmented growth beyond what would be expected were these species cultured in isolation. In addition to the obvious economic return from increased growth rates from additional species, some less tangible benefits should also be factored in, such as the biomitigative services rendered by the extractive species. Economic analyses will have to recognize and account for the values of the environmental/societal services of extractive crops to estimate the true value of these IMTA components. Economic analyses will need to be part of the overall modelling of IMTA systems, as they get closer to commercial scale and their economic benefits and costs, as well as their impacts on coastal communities, are better understood. It will then be possible to add profitability, resilience, social/economic desirability, and economic impacts to the comparison between IMTA and monoculture settings. They will have to include the pricing and marketing potential and impact of organic and other eco-labellings, the value of biomitigative services for enhanced ecosystem resilience, the savings due to multi-trophic conversion of feed and energy which would otherwise be lost, and the reduction of risks through crop diversification and increased societal acceptability of aquaculture (including food safety, food security, and consumer attitudes toward buying sustainable seafood products). This would create economic incentives to encourage aquaculturists to further develop and implement sustainable marine agronomy practices such as IMTA, and would increase the societal acceptability of aquaculture by the general public. Seaweeds and invertebrates produced in IMTA systems should be considered as candidates for a variety of regulatory measures that internalize these benefits. For example, nutrient and carbon trading credits (NTC and CTC) could be used to promote nutrient removal, CO_2 sequestration, oxygen provision, and coastal eutrophication reduction within the broader context of ecosystem goods and services. Long-term planning/zoning promoting biomitigative solutions, such as IMTA, should become an integral part of coastal regulatory and management frameworks.

Nutrient extractive aquaculture appears to be a viable ecological engineering option for managing/internalizing some of the externalities generated by aquaculture operations. Effective government legislation/regulations and incentives to facilitate the development of IMTA practices and the commercialization of IMTA products will be necessary. The development and adoption of technology often depends in part on the level of legislative pressure from a nation's government, itself reacting to pressures from consumers, environmental nongovernmental organizations, and the public at large. If environmental legislation remains a low priority with government, then little progress toward the use of biofilters (as a means of effluent mitigation) will occur. The only motivator will be profits obtained from additional product growth and regulatory incentives. Therefore, if governments put legislative pressure on the proper management of wastewater effluent, openly support the use of biomitigation for effluent management, and put in place the appropriate corresponding financial tools (funding for IMTA Research & Development, outreach and technology transfer, and NTC and CTC incentives), then the development of IMTA will be encouraged.

Caution: Let's Not Promise the Moon and Let's Be Conscious of Societal Constraints, Particularly in the Western World

During the last few years, there has been a renewed interest in the mariculture of seaweeds and their uses, something that should make phycologists and ecologists rejoice, as this group of organisms, never clearly systematically circumscribed, has been misunderstood, unappreciated and under/misused over the centuries.

There is now an opportunity to explain what seaweeds are, and the many applications, benefits, and services they can provide. However, how can people do that appropriately and responsibly, without "promising the moon" that they will not necessarily attain, and risking another "purgatory period" in between each energy crisis?! Seaweeds (and algae in general) made the news in the 1970s–1980s; they are back in the news now (2000s–2010s). If people are not careful to distance themselves from charlatanistic claims, which abound in the media and even in certain scientific circles, they could be in a situation of not developing a sustained public interest and use of these organisms, but be in another phase of denial until the next fad cycle (2030s–2040s?), which is not productive for the acquisition of still much needed scientific knowledge, nor the teaching of our discipline or the placement of our in-between fashion students. While everyone wants the seaweed sector to develop, some biotechnological issues and societal constraints, particularly in the Western World, should be recognized and a responsible and gradual implementation strategy for the long term should be adopted.

The western marine biology community has been dominated by people who have received a mostly zoological training from kindergarten to high school, very often reinforced by a monospecific (or monogrouping) specialization at university, instead of receiving and developing an ecosystem approach to knowledge and issue solving, which are then sadly missing when concepts of ecosystem-based management, species cocultivation, and interdisciplinarity are mentioned. Not surprisingly, the knowledge of seaweeds and their functions and services in/to the ecosystem is reduced and remains at universities and research institutions that have been wise in keeping their diverse expertise, instead of succumbing to fad cycles, which, then, force them to periodically reinvent the wheel. The consequence is that every time one wants to raise the possibility of using seaweeds in research and development and commercialization (R&D&C), one has to go through a lonely period of "preaching in the desert" before facts and common sense start to prevail.

One key, common, and deeply rooted misunderstanding to shake from the minds of people is that there is more than fish in the ocean! Over the centuries humans have been quite minimalist in their meat choices: four mammals (cow, pig, sheep, and goat) and four poultry (chicken, turkey, duck, and goose), hence, Paul Greenberg's idea of four fish (salmon, sea bass, cod, and tuna) for the title of his book [8]. However, the ocean cannot function with only fish, and the seafood solutions cannot come from within only this group of organisms. Maybe the problem resides deeply among the English-speaking people with this overuse of "fish": fish is a noun, which can even encompass shellfish and seaweeds in its general use, and fish is a verb... if you go harvest seaweeds along the shore you could be paradoxically fishing seaweeds, which for a Cartesian French-speaking person does not make much sense! In French, there is "poisson" as a noun and "pêcher" as a verb, even if both come from "pisces" in Latin. So, when a French person "va à la pêche," it is not necessarily to get a fish, but also to go "à la pêche aux moules" (mussels), "aux oursins" (sea urchins), or "aux algues marines" (seaweeds, for which many languages also have a higher opinion, as marine algae, instead of weeds of the sea!). To function, IMTA requires, in fact, not four components but five: the fed organisms (e.g., fish or shrimps), the extractive inorganic component (e.g., seaweeds or other aquatic vegetation), the extractive small organic component (e.g., suspension feeders such as shellfish), the extractive large organic component (e.g., deposit feeders such as sea-urchins, sea cucumbers, or sea worms), and certainly a fifth component, the microbial component, of which presently not much is known. So, if people want aquaculture to work, they have to stop being obsessed with fish aquaculture! Paradoxically, it is interesting to know that fish aquaculture, of which so much is heard, represents, in fact, only 9% of the total mariculture (aquaculture in the marine environment). Shellfish aquaculture represents 43%. Seaweed aquaculture represents even more (46%), but 99.8% of it is carried out in Asia, hence the ignorance in the western world [46, 47].

It is also important to understand that sustained successful ventures rarely happen overnight and that more than a 3 year grant is generally necessary to successfully take a concept along the R&D&C continuum. For example, the IMTA program on the east coast of Canada is starting to collect the fruits of its tireless efforts as it enters its 15th year of activities, which so far could be divided into four periods: (1) the "preaching

in the desert" period from 1995 to 2000 [48], (2) the R&D proof of concept period from 2001 to 2006, (3) the R&D&C pilot scale period from 2006 to 2012, overlapping with (4) the R&D&C industrial-scale and networking period with the establishment of CIMTAN since 2009. People, consequently, have to stay away from claims of solving hunger in the world, converting everybody into frequent direct "seaweedivores," 100% biomitigation (which, in fact, is not necessarily the goal), renewing energy at unbelievable rates that defy the rules and equations governing photosynthesis, and all that within the next 5 years with the almighty, miraculous seaweeds and micro-algae!

If there is no shortage of interesting ideas that work at the small demonstration scale, the problems generally appear when scaling up is contemplated and people start to realize what the consequences will be and, especially, the realistic, or unrealistic, deployment footprints required to implement these experimental ideas to commercial-market scales, which should make sense from environmental, economic, and production perspectives and also have an acceptable societal impact.

People should also stay away from the cliché that around 71% of this planet is covered by oceans and that, consequently, there is a lot of space for aquaculture development. If aquaculture will most probably expand into more exposed and open ocean locations in the future, due to the reduced availability of new and appropriate sheltered nearshore sites, it is doubtful that one will see farms in the middle of the Atlantic, Pacific, and Indian Oceans, due to simple logistics and weather issues. Moreover, the present international law of the sea is not that comforting for privately owned equipment (farms in this case) found at sea. The vagueness of territorial jurisdictional competence in the Exclusive Economic Zone (EEZ) in different countries, and certainly in international waters, has been a major impediment to progress of the so-called offshore aquaculture. Moving to the open ocean has been considered a means for moving away from environmental and public perception issues in the coastal zone. However, this move should not encourage an "out of sight, out of mind" attitude, as open ocean development will also come under scrutiny by a more and more educated public. Even if greater residual currents, deeper waters, and lower nutrient baselines are expected to reduce impacts from open ocean operations through wider dispersion plumes of nutrients, as compared to similarly sized nearshore operations, there will be a point when reasonably accessible and manageable open ocean ecosystems will eventually reach their assimilative carrying capacities. Why should one think that open ocean aquaculture, the "last frontier," will be without its own border/limits? Despite the sea being so immense, one is now learning the hard way the concept of overfishing . . . Instead of taking the position that in open ocean environments the hydrodynamic conditions will be appropriate for dispersion (a way of exporting problems, not solving them) and reduced environmental impacts (but at a significant cost in lost food), the open ocean aquaculture sector will also have to capitalize on recapturing the by-products of fed aquaculture and, hopefully, engineer, right from the beginning, efficient open ocean IMTA systems with their built-in biomitigative functions. The solution to nutrification in the open ocean environment, like in the nearshore environment, should not be dilution, but extraction and conversion through diversification. Why repeat what was done with the development of nearshore aquaculture (fish aquaculture development in the 1970s and IMTA development in the 2000s) with open ocean aquaculture (moving the fish to the open ocean in the 2010s . . . oh, the extractive species should have also been moved in the 2050s!)? These open ocean systems will also require trophic diversification from an environmental and economic perspective, with "service species" from lower trophic levels (mainly seaweeds and invertebrates) performing ecosystem balancing functions while representing value-added crops [49, 50]. Open ocean IMTA should not be an afterthought for 2050.

For some, the ecological, engineering, economic, and social challenges remaining to be solved may be daunting. However, our goal is to develop modern IMTA systems, which are bound to play a major role worldwide in sustainable expansions of the aquaculture operations of tomorrow, within their balanced ecosystem, to respond to a worldwide increasing seafood demand with a new paradigm in the design of the most efficient food production systems. There are no simple solutions, but one thing is certain – the human population is increasing on this planet and as people get richer, and their standards of living increase, they want more meat and dairy products in their diet, the

temptation of the "western diet," while, ironically, Westerners aspire to change their diets! Will terrestrial agriculture be able to continue to supply most of this food? A balanced and responsible diet is required, and some of this food will have to come, increasingly, from aquatic food production systems, be them in seawater, brackish water, or freshwater. As was the case on land, where the acquisition of food by hunter/gatherer societies had to evolve toward agricultural practices, humans will have to accept an evolution in seafood procurement. It has to be understood, particularly in the western world, that "the modern global supermarket has a basic internal ecology" [8]. The average consumer is not a "foodie" and is not that interested in or cannot afford local, seasonal, less-than-100-miles food if not rich enough or not living within a region graced by a clement climate year long. The modern supermarket wants guaranteed supply on a 12 month basis, with limited variability in seasonality and quality. Most of the time, agricultural products can provide that comfort, barring the occurrence of an unexpected disease, contamination, drought, flood, economic protectionism, or political barrier. The seafood counter is a much more variable department to manage, at the present time, with a convoluted succession of many intermediates before seafood arrives on ice at a supermarket. It is interesting to note that the aquaculture industry's ability to provide 12 month availability of its products, moreover of consistent quality, is improving.

People are presently witnessing the emergence of a plethora of organizations developing their own standards and eco-label/certification schemes as they jockey for position in the global marketplace. The problem is that there are presently too many possible horses to ride and nobody really knows which one(s) will cross the finish line and, consequently, which one (s) to bet on as worth being associated with. One can only wonder what will happen when so many fisheries and aquaculture operations will be eco-certified. If everything is certified, nothing will be certified ... and certification will lose its aura the same way some argue organic labelling is losing its significance, after having been used and overused. All that, of course, to the great confusion of the consumers, who cannot follow this contradictory debate/competition among standard setters, and may decide to simply stay away from seafood all together when, in fact, seafood products are healthy [51]. One of the problems is that some of these standards are passing or failing grades, with no incentives for continuous improvement from a minimal baseline to be decided, followed by a tiered approach. Some argue that it would give accreditation to companies at a very low level. However, putting the bar so high is not a recipe for gradual improvement of everybody involved, to progress and gradually reach the ultimate goal, although admittedly not overnight. If 20% of the global farmed seafood producers are certified at the highest threshold, what happens to the remaining 80% and the chance of incentivizing them to improve their practices? What happens when, in a bay management area, several aquaculture companies have taken the appropriate measures to be certified, but a "black sheep" (should it be a black cod?!) makes the whole certification scheme crumble once the hydrodynamics of the bay are considered? By analogy, in which the vector this time is not water but wind, one sees the same dilemma in parallel agriculture situations where conventional and organic agriculture practices are separated by illusionary buffer zones. On one hand, one can understand the desire by suppliers and retailers to see a hard to meet certification scheme so as to differentiate themselves from the others (most probably amounting to the privilege of displaying a sticker or logo on the packaging); on the other hand, too high a certification carrot, or moving goalposts, may not be the best strategy if progress toward overall better and more responsible aquaculture practices is the goal. The market will ultimately decide who remains in the competition and which logo(s) will be trusted by the general public, but there still are several years of confusion ahead.

Agricultural development has been associated with significant changes in landscape and land use; one can expect that the evolution of sourcing one's seafood more and more through aquaculture will also trigger significant "seascape" and "sea use" modifications, all the way to one's deepest human social structures and governance. The transformation from hunters/gatherers to farmers happened many centuries ago on land. Humans are in the middle of this transformation at sea and that is maybe why they are so uncomfortable with this evolution they are part of, and not able to sit back and analyze without being emotional. It is up to them to be a link in the chain, which will hopefully lead

to fishing and aquaculture practices done right, enabling them to become herders and farmers of the sea. It should not be forgotten that they are still in the infancy of modern, intensive aquaculture and that some agricultural practices have taken centuries to develop into better, not necessarily yet best, management practices.

Beyond the market and marketing issues and the biological, environmental, economic, technological, engineering, and regulatory issues of aquaculture developments, the basic question will be that of societal acceptance. Are humans ready to evolve in their use of the "last frontier" of this planet and consider not only the challenges of the physical forces at sea (wave exposure, winds, currents, depth, etc.) but also those of shipping routes, fishing zones, offshore gas and mineral extraction areas, migration routes for marine mammals and birds, recreational uses, and then finally deal with the concept of zoning some portions of the oceans for large aquaculture parks, as sustainable food production systems for an ever-seafood-hungry human population? Despite all the campaigns, boycotts, documentaries, books, seafood pocket guides, scare tactics, sustainable/local/seasonal movements among affluent restaurant goers in weather clement regions and western world well offs, one can only admit that the global human population continues to grow and eat more seafood than ever per capita per year. So, where does that leave people? Paul Greenberg wrote that very often people consider fish as "a crop, harvested from the sea that magically grew itself back every year. A crop that never required planting" [8]. But are they investing in the principal, being in fisheries or in aquaculture, to only harvest the interests every year so as to not reduce/eat the capital for long-term sustainability? Are people ready to put some savings aside in the form of Marine Protected Areas (MPAs), not only for their natural beauty, but also for their functions in the ecosystem such as breeding grounds, nursery habitats, and food production areas? It seems that the concept of zoning the sea, or what is now called, in a softer terminology, "marine spatial planning" (MPS), is finally starting to be legislated in some countries, notably in the UK and the USA.

The same question of readiness for marine spatial planning could also be applied to emerging projects of wind farms and biofuel farms at sea. In fact, combining IMTA open-ocean farms with wind, underwater turbine, and/or biofuel farms into large multipurpose integrated food and renewable energy parks (IFREP) could be a means for reducing their cumulative footprint, while integrating green energy with food and fuel production and processing [52]. Our business models will have to change from "one species – one process – one product" to a streamed bioeconomic chain, or web, approach among different industry sectors for the production, on one hand, of a wide range of bio-based, high-valued food and feed products/ingredients/supplements, specialty fine and bulked chemicals, agrichemicals, biostimulants, pharmaceuticals, nutraceuticals, functional foods, cosmeceuticals, botanicals, pigments and, on the other hand, lower-valued commodity energy carrying molecules/biofuels, all of them produced within reduced footprint requirements. The synergies and the services rendered by cultivating organisms of different trophic levels in an integrated manner will have to be understood and valued. The physiological, biochemical, and production performances of the different organisms will have to be improved to make the systems even more efficient, profitable, and competitive. The aquaculturists and different multi-sector end users will need to become interdisciplinary in their approach and learn to collaborate and share/integrate the biomass cultivation and processing steps (production, harvesting, pretreatment and transportation, separation and fractionation, and sequential biomass processing), while aiming at the lowest resource and energy inputs. Culture diversification into species that might otherwise be inappropriate for food markets fits well within the sustainability and management concept of IMTA. Functionalities will have to be maintained, as much as possible, along the process for optimal use/valorization of the multipurpose biomass, and not necessarily the maximization of just one end product, as some coproducts will, in fact, reveal themselves as the real drivers of the emerging integrated sequential bio-refinery (ISBR) concept [53], extended to macro-algae instead of only considering micro-algae. Market volumes/values, biomitigative services, and public acceptance will have to be included and fit into the models.

If the "Not In My BackYard" (NIMBY) and the "Build Absolutely Nothing Anywhere Near Anything" (BANANA) attitudes continue to prevail, especially in

the western world, then humans will not be able to secure their food, chemicals, and energy in an intricately interconnected ecosystem responsible manner, despite all the rhetoric heard today regarding alternative technologies and solutions (the so-called "greenwash"). Self-sufficiency of humans will not be ensured but will become dependent on other food, chemicals, and energy "masters," who may no longer be in the Middle East but instead in the Far East (99.8% of the 15.8 million tons of cultivated seaweeds come from China, Indonesia, the Philippines, Korea, and Japan [46, 47]). It is time to walk the talk and recognize the implications – notably regarding marine spatial planning and our societal production and food habits – of the policies elaborated for the future.

The 1960s were the time of the "Green Revolution" on land, but some would question if it was really "green" (increased dependence on synthetic fertilizers and irrigation to increase crop yields per hectare at the expense of long-term soil health and yields per unit of input; increased dependence of indebted farmers on multinational producers of seeds, increasingly genetically modified, and which have not always delivered the touted benefits). It was thought that the sea was so immense that one needed not to worry about fishery limits, but now it is known that it is not always the case with many examples of overfishing of some populations. The 1980s were the time of the "Blue Revolution" of aquaculture development at sea, but it is also known that it is not always "green." It is, consequently, time to make the "Blue Revolution" greener; it is time for the "Turquoise Revolution" to move aquaculture to a new ERA of Ecosystem Responsible Aquaculture at sea and on land, in seawater and freshwater, and in temperate and tropical regions.

Acknowledgments

I greatly appreciate the support this work received from the Natural Sciences and Engineering Research Council of Canada (NSERC) strategic Canadian Integrated Multi-Trophic Aquaculture Network (CIMTAN) in collaboration with its partners, Fisheries and Oceans Canada, the University of New Brunswick, Cooke Aquaculture Inc., Kyuquot SEAfoods Ltd. and Marine Harvest Canada Ltd.

Bibliography

Primary Literature

1. FAO (2009) The State of World Fisheries and Aquaculture 2008. FAO of the United Nations, Rome, xvi+176 p
2. Tacon AGJ, Metian M, Turchini GM, De Silva SS (2010) Responsible aquaculture and trophic level implications to global fish supply. Rev Fish Sci 18(1):94–105
3. Troell M, Halling C, Neori A, Chopin T, Buschmann AH, Kautsky N, Yarish C (2003) Integrated mariculture: asking the right questions. Aquaculture 226:69–90
4. Chopin T (2006) Integrated multi-trophic aquaculture. What it is and why you should care . . . and don't confuse it with polyculture. North Aquacult 12(4):4
5. Edwards P (1993) Environmental issues in integrated agriculture-aquaculture and wastewater-fed fish culture systems. In: Pullin RSV, Rosenthal H, Maclean JL (eds) Environment and aquaculture in developing countries. ICLARM Conference Proceedings, vol 31, pp 139–170
6. Hambrey J, Edwards P, Belton B (2008) An ecosystem approach to freshwater aquaculture: a global review. In: Soto D, Aguilar-Manjarrez J, Hishamunda N (eds) Building an ecosystem approach to aquaculture. FAO/Universitat de les Iles Balears Experts Workshop. 7–11 May 2007, Palma de Mallorca Spain. FAO Fisheries and Aquaculture Proceedings 14. FAO, Rome, pp 117–221
7. Troell M (2009) Integrated marine and brackishwater aquaculture in tropical regions: research, implementation and prospects. In: Soto D (ed) Integrated mariculture: a global review. FAO Fisheries and Aquaculture Technical Paper 529. FAO, Rome, pp 47–131
8. Greenberg P (2010) Four fish – the future of the last wild food. Penguin Press, New York, 285 p
9. Timmons MB, Ebeling JM, Wheaton FW, Summerfelt ST, Vinci BJ (2002) Recirculating aquaculture systems (2nd edn). NRAC Publication No. 01-002. Cayuga Aqua Ventures, Ithaca, 769 p
10. Ayer NW, Tyedmers PH (2009) Assessing alternative aquaculture technologies: life cycle assessment of salmon culture systems in Canada. J Cleaner Prod 17:362–373
11. Skår CK, Mortensen S (2007) Fate of infectious salmon anaemia virus (ISAV) in experimentally challenged blue mussels *Mytilus edulis*. Dis Aquat Org 74:1–6
12. Pang SJ, Xiao T, Bao Y (2006) Dynamic changes of total bacteria and *Vibrio* in an integrated seaweed-abalone culture system. Aquaculture 252:289–297
13. Pang SJ, Xiao T, Shan TF, Wang ZF, Gao SQ (2006) Evidences of the intertidal red alga *Grateloupia turuturu* in turning *Vibrio parahaemolyticus* into non-culturable state in the presence of light. Aquaculture 260:369–374
14. Molloy SD, Pietrak MR, Bouchard DA, Bricknell I (2011) Ingestion of *Lepeophtheirus salmonis* by the blue mussel *Mytilus edulis*. Aquaculture 311:61–64

15. Johansson DJA, Azar CA (2007) A scenario based analysis of land competition between food and bioenergy production in the US. Clim Change 82:267–291
16. Naylor RL, Liska AJ, Burke MB, Falcon WP, Gaskell JC, Rozelle SD et al (2007) The ripple effect: biofuels, food scarcity and the environment. Environment 49:30–43
17. SOFA (2008) The state of food and agriculture. Biofuels prospects, risks and opportunities. FAO of the United Nations, Rome
18. Jordan N, Boody G, Broussard W, Glover JD, Keeney D, McCown BH, McIsaac G, Muller M, Murray H, Neal J, Pansing C, Turner RE, Warner K, Wyse D (2007) Sustainable development of the agricultural bio-economy. Science 316:1570–1571
19. Sawyer D (2008) Climate change, biofuels and eco-social impacts in the Brazilian Amazon and Cerrado. Phil Trans R Soc B 363:1747–1752
20. Koh LP (2007) Can palm oil plantations be made more hospitable for forest butterflies and birds? J Appl Ecol 44:703–713
21. Fargione J, Hill J, Tilman D, Polasky S, Hawthorne P (2008) Land clearing and the biofuel carbon debt. Science 319:1235–1238
22. Whitmarsh DJ, Cook EJ, Black KD (2006) Searching for sustainability in aquaculture: an investigation into the economic prospects for an integrated salmon-mussel production system. Mar Policy 30:293–298
23. Ridler N, Wowchuk M, Robinson B, Barrington K, Chopin T, Robinson S, Page F, Reid G, Szemerda M, Sewuster J, Boyne-Travis S (2007) Integrated multi-trophic aquaculture (IMTA): a potential strategic choice for farmers. Aquac Econ Manage 11:99–110
24. Costanza R, d'Arge R, de Groot R, Farber S, Grasso M, Hannon B, Limburg K, Naeem S, O'Neill RV, Paruelo J, Raskin RG, Sutton P, van den Belt M (1997) The value of the world's ecosystem services and natural capital. Nature 387:253–260
25. Feely RA, Sabine CL, Lee K, Berelson W, Kleypas J, Fabry VJ, Miller FJ (2004) Impact of anthropogenic CO_2 on the $CaCO_3$ system in the oceans. Science 305(5682):362–366
26. Thomsen B (2006) Freshwater aquaculture in Denmark: a new platform for sustainable growth. Proceeding of the Canadian Freshwater Aquaculture Symposium, Aquaculture Canada 2004. Aquaculture Association of Canada Special Publication vol 11, pp 26–30
27. Troell M, Halling C, Nilsson A, Buschmann AH, Kautsky N, Kautsky L (1997) Integrated marine cultivation of *Gracilaria chilensis* (Gracilariales, Rhodophyta) and salmon cages for reduced environmental impact and increased economic output. Aquaculture 156:45–61
28. Chopin T, Buschmann AH, Halling C, Troell M, Kautsky N, Neori A, Kraemer GP, Zertuche-Gonzalez JA, Yarish C, Neefus C (2001) Integrating seaweeds into marine aquaculture systems: a key towards sustainability. J Phycol 37:975–986
29. Lindhal O, Kolberg S (2009) Can the EU agri-environmental aid program be extended into the coastal zone to combat eutrophication? Hydrobiologia 629:59–64
30. Lindahl O, Hart R, Hernroth B, Kollberg S, Loo L-O, Olrog L, Rehnstam-Holm A-S, Svensson J, Svensson S, Syversen U (2005) Improving marine water quality by mussel farming: a profitable solution for Swedish society. Ambio 34:131–138
31. Ferreira JG, Hawkins AJS, Bricker SB (2007) Management of productivity, environmental effects and profitability of shellfish aquaculture – the Farm Aquaculture Resource Management (FARM) model. Aquaculture 264:160–174
32. Ferreira JG, Sequeira A, Hawkins AJS, Newton A, Nickell TD, Pastres R, Forte J, Bodoy A, Bricker SB (2009) Analysis of coastal and offshore aquaculture: application of the FARM model to multiple systems and shellfish species. Aquaculture 289:32–41
33. Gren IM, Lindhal O, Lindqvist M (2009) Values of mussel farming for combating eutrophication: an application to the Baltic Sea. Ecol Eng 35:935–945
34. Lackner KS (2003) A guide to CO_2 sequestration. Science 300:1677–1678
35. Nellemann C, Corcoran E, Duarte CM, Valdés L, De Young C, Fonseca L, Grimsditch G (2009) Blue carbon. A rapid response assessment. United Nations Environment Program, GRID-Arendal. www.grida.no
36. Chung IK, Beardall J, Mehta S, Sahoo D, Stojkovic S (2010) Using marine macroalgae for carbon sequestration: a critical appraisal. J Appl Phycol. doi:10.1007/s10811-010-9604-9
37. Beardall J, Raven JA (2004) The potential effects of global climate change on microalgal photosynthesis, growth and ecology. Phycologia 43:26–40
38. Liu F, Pang SJ, Chopin T, Xu N, Shan TF, Gao SQ, Sun S (2009) The dominant *Ulva* strain of the 2008 green algal bloom in the Yellow Sea was not detected in the coastal waters of Qingdao in the following winter. J Appl Phycol. doi:10.1007/s10811-009-9489-7
39. Pang SJ, Liu F, Shan TF, Xu N, Zhang ZH, Gao SQ, Chopin T, Sun S (2010) Tracking the algal origin of the *Ulva* bloom in the Yellow Sea by a combination of molecular, morphological and physiological analyses. Mar Env Res 69:207–215
40. Neori A, Chopin T, Troell M, Buschmann AH, Kraemer GP, Halling C, Shpigel M, Yarish C (2004) Integrated aquaculture: rationale, evolution and state of the art emphasizing seaweed biofiltration in modern mariculture. Aquaculture 231:361–391
41. Chopin T, Robinson SMC, Troell M, Neori A, Buschmann AH, Fang J (2008) Multitrophic integration for sustainable marine aquaculture. In: Jørgensen SE, Fath BD (eds) The encyclopedia of ecology, ecological engineering, vol 3. Elsevier, Oxford, pp 2463–2475
42. Barrington K, Chopin T, Robinson S (2009) Integrated multitrophic aquaculture (IMTA) in marine temperate waters. In: Soto D (ed) Integrated mariculture: a global review. FAO Fisheries and Aquaculture Technical Paper 529. FAO, Rome, pp 7–46
43. Brzeski V, Newkirk G (1997) Integrated coastal food production systems – a review of current literature. Ocean Coast Manage 34:55–71

44. Barrington K, Ridler N, Chopin T, Robinson S, Robinson B (2010) Social aspects of the sustainability of integrated multi-trophic aquaculture. Aquac Int 18:201–211
45. Shuve H, Caines E, Ridler N, Chopin T, Reid GK, Sawhney M, Lamontagne J, Szemerda M, Marvin R, Powell F, Robinson S, Boyne-Travis S (2009) Survey finds consumers support Integrated Multi-Trophic Aquaculture. Effective marketing concept key. Global Aquaculture Advocate 12(2):22–23
46. Chopin T, Sawhney M (2009) Seaweeds and their mariculture. In: Steele JH, Thorpe SA, Turekian KK (eds) The encyclopedia of ocean sciences. Elsevier, Oxford, pp 4477–4487
47. FAO (2010) The State of World Fisheries and Aquaculture 2010. FAO of the United Unions, Rome, xv + 197 p
48. Chopin T (1995) Mixed, integrated, poly-, or multi-level aquaculture – whatever you call it, it is time to put seaweeds around your cages! In: Proceedings of the Conference on cold water aquaculture to the Year 2000, St. Andrews, Canada, 6–8 September 1995. Aquaculture Association of Canada, Special Publication No. 2 (1997):110
49. Chopin T (2008) Integrated multi-trophic aquaculture (IMTA) will also have its place when aquaculture moves to the open ocean. Fish Farmer 31(2):40–41
50. Troell M, Joyce A, Chopin T, Neori A, Buschmann AH, Fang JG (2009) Ecological engineering in aquaculture – potential for integrated multi-trophic aquaculture (IMTA) in marine offshore systems. Aquaculture 297:1–9
51. Lee JH, O'Keefe JH, Lavie CJ, Harris WS (2009) Omega-3 fatty acids: cardiovascular benefits, sources and sustainability. Nat Rev Cardiol 6:753–758
52. Chopin T (2009) Let's not move just the fish to the open ocean. . . an integrated multi-trophic aquaculture approach should not be an afterthought for 2050. In: The ecology of marine wind farms: Perspectives on impact mitigation, siting, and future uses. 8th Annual Ronald C. Baird Sea Grant Science Symposium. 2–4 November 2009, Newport, USA. http://seagrant.gso.uri.edu/baird/2009_windfarms/abstracts/chopin.pdf
53. Subhadra B, Grinson G (2010) Algal biorefinery-based industry: an approach to address fuel and food insecurity for a carbon-smart world. J Sci Food Agric. doi:10.1002/jsfa.4207

Books, Reviews, and Websites

Costa-Pierce BA (2002) Ecological aquaculture: the evolution of the blue revolution. Blackwell Science, Oxford, 382 p

Soto D, Aguilar-Manjarrez J, Hishamunda N (2008) Building an ecosystem approach to aquaculture. FAO/Universitat de les Iles Balears Experts Workshop. 7-11 May 2007, Palma de Mallorca, Spain. FAO Fisheries and Aquaculture Proceedings 14. FAO, Rome, 221 p

Web site of Thierry Chopin: www.unbsj.ca/sase/biology/chopinlab/

Web site on IMTA on Wikipedia: http://en.wikipedia.org/wiki/Integrated_Multi-trophic_Aquaculture

Aquaculture, Sustainability Science in

Barry A. Costa-Pierce[1], Glenn G. Page[2]
[1]Graduate School of Oceanography, Rhode Island Sea, Grant College Program, University of Rhode Island, URI Bay Campus, Narragansett, RI, USA
[2]SustainaMetrix, LLC, Johns Hopkins University, Baltimore, MD, USA

Article Outline

Glossary
Definition
Introduction
Sustainability Strategic and Implementation Planning for Aquaculture
Improved Governance of Aquaculture Ecosystems
Social Ecology of Aquaculture
Future Directions: Sustainability Science Opportunities for Aquaculture
Determination of Sustainable Aquaculture for Retailers
Aquaculture and the Restoration of Ecosystems
Aquaculture and Agriculture Science
Aquaculture for the Poor
Bibliography

Glossary

Stewardship Ecosystem stewardship is an ethic practiced by aquaculture practitioners, organizations, communities, and societies who strive to sustain the qualities of healthy and resilient ecosystems and their associated human communities. Stewardship takes the long-term view and promotes activities that provide for the well-being of both the present and future generations.

Nested systems of governance Environmental and societal issues relating to sustainable aquaculture impact, and are influenced by, conditions and actions (at both higher and lower levels) in an ecosystem governance hierarchy. Some issues can be addressed more effectively at one level, and less effectively at another. The choice of the issue or set of issues to be addressed within a given site must

therefore be made in full knowledge of how responsibility and decision-making authority are distributed within a layered governance system. Planning and decision-making for aquaculture at one scale, for example, within a municipality or province, should not contradict or conflict with planning and management at another scale, for example, planning for large-scale aquaculture at the nation-state scale. The reality is that such contradictions and conflicts are common. A major challenge for the aquaculture practitioner is to recognize these differences and work to either change them or select goals and strategies that recognize that such contradictions must be accommodated or resolved. In practical terms, this means that a central feature of ecosystem-based aquaculture is that all planning and decision-making must recognize and analyze conditions, issues, and goals in respect to the next higher level in a governance system. Thus, ecosystem-based aquaculture at the municipal scale must – at a minimum – be placed within the context of governance at the scale of the province.

Participation One of the defining characteristics of the practice of the ecosystem approach to aquaculture is its emphasis on participation and its relevance to the people affected. The emphasis upon participation recognizes that if an aquaculture program is to be successful, those whose collaboration and support is needed must be involved in the processes of defining the issues that the program will address, and in selecting the means by which goals and objectives will be achieved. Both individuals and members of communities and institutions are more likely to comply with a management program when they feel that it is consistent with their values, responds to their needs, and to their beliefs of how human society should function. Voluntary compliance by a supportive population lies at the heart of the successful implementation of a program. A participatory approach helps stakeholders and the public to see the efforts of an aquaculture program as a whole.

Area of focus The area of focus (AoF) is the geographically defined area that an ecosystem-based aquaculture project or program has decided to address and that therefore is the focal point for a baseline. The term "area of focus" is a geographic limit set to model the choices available to the aquaculture practitioner and allows for a dialogue between stakeholders as to the influence of the production. The AoF is a simplification of the far more complex concept of an "action arena" put forward by Ostrom [1] to model the choices of individuals when studying the behavior of institutions.

Adaptive management A central feature of the practice of any form of ecosystem-based aquaculture is that it must respond positively to changing conditions within its AoF (and to its own experience). In other words, the practice of aquaculture must be grounded in a process of learning and adaptation (the "evolution of the blue revolution" [2]). Adaptive management is not reactive management, but proactive thinking and acting. This does mean that the aquaculture practitioner simply responds to the unexpected. Adaptive management in aquaculture is a conscious process of examining the course of events as these events are revealed by preselected indicators of changes in an aquaculture ecosystem (both its social and environmental components), and by events occurring at differing spatial scales.

Capacity building There is growing international recognition that the lack of human capacity to practice an ecosystem approach to aquaculture is a key factor in limiting forward progress in the conservation and sustainable use of aquatic systems [3, 4]. To date, however, no accepted performance standards have been developed for assessing the effectiveness and impacts of aquaculture projects and programs that have adopted the ecosystem approach. Conceptual frameworks and methods for assessing the maturity of aquaculture development and management initiatives, and gauging their impacts upon the condition of coastal ecosystems are offered herein. These are the core ingredients for an ecosystem's approach to aquaculture that builds the capacity of local populations and leaders to identify forces that shape the coastal ecosystems of which they are a part, and to select the actions that can maintain and enhance qualities that are critical to a desirable future.

Carrying capacity The carrying capacity is the number of organisms or farming operations that the

environment can sustain indefinitely without environmental harm, given the food, habitat, space, water, and other requirements from the environment.

Precautionary principle A principle that states that if an action or policy has a suspected risk of causing harm to the public or to the environment that in the absence of scientific consensus the burden of proof rests on those who advocate taking the action.

Sustainable development The management and conservation of the natural resource base and the orientation of technological and institutional change in such a manner as to ensure the attainment and continued satisfaction of human needs for present and future generations. Sustainable development conserves resources, is environmentally non-degrading, and is technically appropriate, economically viable, and socially acceptable [5].

Transdisciplinary A modern research strategy that crosses many disciplinary boundaries to create a holistic approach. Transdisciplinary research efforts are focused on problems that cross the boundaries of two or more disciplines, and develop new or reframe old concepts, methods, and findings that were originally developed by one discipline, but are now used by several others.

Definition

There is no one definition of "sustainability" as the concept applies to aquaculture. Most aquaculture scientists define sustainability as synonymous with "environmental sustainability." Sustainable aquaculture is however a concept broader than determinations of site-specific environmental impacts since it embodies a scientific knowledge of systematic impacts of aquaculture off-site, and impacts to combined human-environmental systems. Sustainable aquaculture incorporates the concepts of "stewardship," "design with nature," the "precautionary principle," "risk analysis," and "carrying capacity." Sustainability science in aquaculture is used to undertake more comprehensive planning for multiple impacts on multiple time and spatial scales to better understand and plan for the consequences of aquaculture development options.

Introduction

- "The changes taking place [on planet Earth] are, in fact, changes in the human-nature relationship. They are recent, they are profound, and many are accelerating. They are cascading through the Earth's environment in ways that are difficult to understand and often impossible to predict. Surprises abound" [6].

There are many definitions of "sustainability" as the concept applies to aquaculture. The most popular definition of sustainable development is to "meet present needs without compromising the ability of future generations to meet their needs" adopted at a United Nations conference in 1987. Most definitions of sustainability are synonymous with "environmental sustainability" of air, water, and land systems. Sustainability is however a concept broader than examining the site-specific environmental impacts of externalities in planning for site-specific developments; it also accounts for systematic impacts off site, and impacts to combined human-environmental systems for food, water, waste, energy, and shelter. The many definitions of sustainability all embody in common, the concepts of "stewardship," "design with nature," plus incorporate recent concepts of the "precautionary principle," and "carrying capacity." Sustainability science uses the wisdom from multiple disciplines in decision-making (e.g., it is "transdisciplinary"). In aquaculture, it is used to undertake more comprehensive planning for multiple impacts on multiple time and spatial scales to better understand and plan for the consequences of development options.

The emerging fields of ecological aquaculture [2,3] and agroecology [7, 8] recognize that the implementation of more sustainable food production systems require knowledge about how ecosystems are utilized and how conflicts among social groups are addressed. A baseline of response to social–ecological changes is the foundation for the implementation of more sustainable food systems, and the practice of adaptive management must be included as responses to changes in the condition of ecosystems in which new food production is conducted requires incorporation of an iterative learning process.

The use of sustainability science in aquaculture marks the path toward encouraging a long-term

perspective and an appreciation of the roles played not only by ecologists, but also by civil societies, markets, and governments in adapting to food systems and ecosystems changes. The use of sustainability science in aquaculture is an approach that is fundamentally a knowledge-based enterprise that incorporates baseline information on natural and human ecosystems, then develops, evaluates, encourages, and communicates imagination, ingenuity, and innovation at both the individual and institutional levels [9].

This information is designed for use by teams of aquaculture professionals working to apply the principles of ecosystem-based management. Information obtained is typically cross sectoral as interdisciplinary groups are needed that are educated in such diverse fields as the natural and social sciences, law, and business. Applying the notions of sustainability science in aquaculture is intended to inspire engagement of governmental agencies, businesses, nongovernmental groups, and academics to achieve the highest form of sustainable development in any known protein production food system by using the concepts of ecological design and through the many forms of stewardship. At present, there is a paucity of information targeted specifically for those engaged in aquaculture programs and projects in places where the ability of government to regulate and direct the processes of ecosystem change is weak or severely constrained.

Sustainability Strategic and Implementation Planning for Aquaculture

The concept of sustainability and the methods to measure the evolutionary progress toward more sustainable systems are limited, but have become a necessity. Wurts [10] stated that "Whether the word sustainability has become overused or not, it has catalyzed a forum for oversight of the growth and development of aquaculture on a global scale."

Sustainability is not a "black/white" phenomena; rather, it is many "shades of gray," an evolutionary process that is called the "sustainability trajectory" (Fig. 1). To measure and evaluate progress along

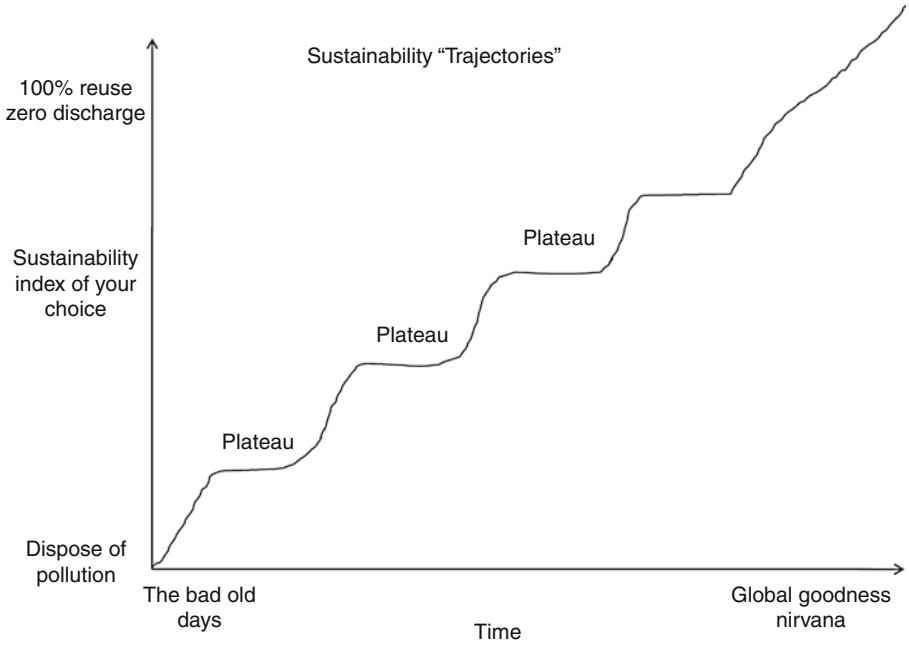

Aquaculture, Sustainability Science in. Figure 1
Sustainability is neither a "black or white," nor an "either or" concept. It is the evolution of practices and principles over time toward ameliorating environmental and social impacts, with plateaus along the way in changed states. In many cases, these "pauses" are done to ensure economic viability. In this diagram, one example indicator (water use, other important indicators have been proposed [17]) is plotted along such a "sustainability trajectory"

a trajectory requires establishment of baselines for the main issues of public concerns, then developing a diverse but targeted set of resource and social indicators. These indicators are then used to report progress on and analyze interactions between social, environmental, and economic impacts (both positive and negative ones). It is important to note that sustainability science as applied to aquaculture is driven as much by social as by environmental/ecological concerns; thus, sole involvement of technical experts in sustainability plans and assessments is insufficient.

Developing an operational framework for how the sustainability of aquaculture operations operates is the first step. Having such a blueprint is rare for aquaculture businesses and management entities, and is very much needed. There are numerous certification bodies that are vying for the opportunity to use their labels/logos to claim ownership of the sustainability rubric in aquaculture. An overall sustainability science approach is proposed, which can step above the cacophony of approaches and assist in developing a common language and can be used by international and national, non-advocacy organizations such as the FAO, ICES, or governments and industry.

The approach used here is based upon the development of a baseline that has two parts and then follows a sequence of five steps:

The *first part of a baseline* is an ecosystem audit of the AoF that defines the natural and social systems within which aquaculture is planned.

This involves the documentation and analysis of both natural and social systems, draws upon case studies of other aquaculture systems in the region and how the governance system in a specific place has responded – or failed to respond – to the trajectories of ecosystem change. It examines the long-term trends in both human well-being and the environmental conditions in the AoF and examines responses to the issues raised by past and current expressions of food production systems.

The *second part of the baseline* is an outline of the strategic approach to designing a new aquaculture program, or adapting an ongoing program, to address the ecosystem management issues of the place in terms of economic, environmental, and societal benefits. Together, these parts form the reference points against which future changes in the aquaculture ecosystem will be gauged. These methods encourage a long-term perspective, an appreciation of the roles played by civil society, markets, and government, and offer a holistic, ecosystem-based, approach to stewardship.

Baselines are not formulaic but are designed planning exercises with buy-in from key stakeholders such as the client, community, regulatory community, or identified group of people involved in the project. While not formulaic, baselines do comprise a set of common metrics to include

- Ecological aquaculture design (or redesign) of production practices (see Ecological Aquaculture chapter in this Encyclopedia)
- Health and quality control standards
- Social goals at both the individual and community levels for local food, job, and regional development (e.g., "green jobs," "local foods")
- Governance goals

The following five steps encompass some essential parts of any baselining process:

1. *Define the sustainability issues.* Aquaculture systems can use environmentally derived feeds, water, and energy, occupy land and water space, and generate wastes. There are at least eight issues of wide public and regulatory concerns regarding aquaculture development:
   - Destruction of habitats
   - No net gain to global seafood supplies
   - Environmental impacts of discharged wastes
   - Impacts of escapees
   - Diseases in farmed fish
   - Chemical use and discharge
   - Impacts on coastal marine mammals
   - Improper siting causes visual pollution

   Once issues are defined, a baseline can be further developed which can measure progress over time by
2. *Completing a sustainability assessment* of these issues by evaluating the status of current aquaculture practices that affect natural and social resource systems (Table 1), which also includes an assessment of governance systems (Tables 2 and 3) [11–13]
3. *Completing a detailed risk analysis* for all components of this comprehensive assessment [14]

Aquaculture, Sustainability Science in. Table 1 Important sustainability science tools used to assess and communicate the sustainability of aquaculture[1]

Social Sustainability	Environmental Sustainability	Economic Sustainability
Stakeholder analysis: analysis of attitudes of stakeholders at the initiation of and throughout a project. Allows tracking of how stakeholders change attitudes over time with educational processes [46–50]	**Life cycle analysis**: complete assessment of products from raw material production, manufacture, distribution, use and disposal, including all transportation; used to optimize environmental performance of a single product or a company. A similar analysis called a MET (Materials, Energy, and Toxicity) Matrix is also used [53–55]	**Cost-benefit analysis**: analysis of cost effectiveness of different uses to determine if benefits can outweigh costs [59]
ISO 26000 guidelines for corporate social responsibility [51]	**ISO 14000 certification:** norms to promote more effective and efficient environmental management and provide tools for gathering, interpreting, and communicating environmental information [56]	
ICLEI (International Council for Local Environmental Initiatives) provides software and tools to help local governments achieve sustainability goals [52]	**Environmental impact assessment**: the process of identifying, predicting, evaluating, mitigating biophysical, social, and other effects of development proposals prior to policy decisions [57, 58]	**Triple bottom line or "full cost" accounting:** costs considered for all environmental, economic, and social impacts; costs measured in terms of opportunity costs (the value of their best alternative use); guiding principle is to list all parties affected and place a monetary value on effects on welfare as valued by them [60, 61]
	Environmental indicators: the use of quantitative indicators of resource use, efficiency, and waste production in aquaculture [17]	

[1]This table does not contain a comprehensive list of all available tools; rather, tools selected here were chosen since they appear regularly in the modern sustainable aquaculture research, industry, and management literature. Gibson et al. [62] give a most complete analysis of all of the available tools for sustainability assessments.

4. *Completing a plan for ameliorating identified impacts* by incorporation of better (or best) practices [15–17], and/or enhancing reuse or recycling pathways, and
5. *Completing a plan for communicating* the evolution of operations toward greater stewardship and sustainability [14]

To be effective, sustainable aquaculture initiatives must: (a) be "profitable" over long periods of time – ideally many decades; (b) be capable of being adapted to changing conditions; and (c) provide the mechanisms to encourage both wise resource use and collaborative behaviors. Much of the challenge lies in achieving changes in the behavior of those who may be unaware of the benefits of sustainable aquaculture.

Sustainable aquaculture integrates the best available science with a transparent, equitable, and democratic approach to planning and decision-making. This ecosystem approach to management needs to be carried out in a strategic manner that tailors principles of good practice to the culture and the needs of a specific place. Successful, sustainable aquaculture operations advance through linked cycles of planning, implementation, and reassessment. These features of ecosystem management signal the transition from traditional sector-by-sector planning and decision-making to a more holistic

Aquaculture, Sustainability Science in. Table 2 Sustainability science assessments of aquaculture includes an assessment of governance systems, which examine the three processes of governance: the marketplace, the government, and civil society

Major Expressions of Governance
Government
Laws and regulations
Taxation and spending policies
Education and outreach
Marketplace
Profit seeking
Ecosystem service valuation
Cost-benefit analysis
Ecolabeling and Green Products
Civil Society: Organizations and Institutions
Product choices
Advocacy and lobbying
Vote casting
Comanagement
Stewardship activities

approach based on the interactions between sectors and within and among ecosystems.

Aquaculture that is constructed upon principles that encourages high-energy consumption and the profligate use of natural resources must give way to new locally derived values and new forms of practice. As suggested by Daly [18], qualitative development rather than quantitative growth is the path of future progress. If such ideas are to be made operational at the scale of an aquaculture operation, a trajectory can be established based on goals for profit as well as social and environmental benefit. Once the goals of an aquaculture program or project have been defined as expressions of the ecosystem approach, much of the day-to-day work is concerned with the well-known best practices of aquaculture management.

For example, there has been much debate about the impacts of shrimp pond mariculture on mangrove forests through the Topics. Mangrove ecosystems provide essential goods and services to humanity, harboring an extraordinarily large biodiversity for the small areas of the planet that these systems occupy, and provide a sustainable source of timber and charcoal to coastal communities while protecting fragile coastlines from erosion and storms. Establishment of proper scientific baselines to measure the true impacts of mariculture on coastal ecosystems is essential. Pullin [19] cautions that, "Analysis on depletion of mangrove cover in Asia point towards the fact that shrimp ponds have recently been and/or now being constructed either on former mangrove areas that were cleared long ago and considered degraded), or on more recently cleared areas for which the primary purpose of clearance was timber abstraction (logging, wood chip industries or charcoal production) or by adopting traditional trapping ponds. . . . Aquaculturists in Asia are therefore more often than not the end users of already degraded or destroyed mangroves rather an the primary culprits of mangrove destruction."

Good examples globally of an ecosystem approach to aquaculture at the watershed/aquaculture zone scale are found in both Israel and Australia. Both nations face severe land, water, and energy constraints. In Israel, highly efficient, landscape-sized integrations of reservoirs with aquaculture and agriculture have been developed [20, 21], as well as highly productive, land-based aquaculture ecosystems for marine species [22]. These aquaculture ecosystems are productive, semi-intensive enterprises that are water and land efficient, and are net energy and material gains to society. Aquaculture ecosystems are organized following well-established ecological principles similar to the fields of agroecology and agroecosystems [23].

In Australia, an Ecologically Sustainable Development (ESD) framework approach to aquaculture development was used [24]. This ESD framework identified important issues, developed comprehensive reports for each issue, and then prioritized each using risk assessments. The ESD process employed extensive community consultation that considered social and environmental values of all other marine users, and users' management plans for operations and administration as well as environmental administrative attributes, then proposed development and monitoring plans.

Aquaculture, Sustainability Science in. Table 3 Orders of governance outcomes [12, 13] applied to an ecosystem approach to aquaculture [2, 3]

Orders	Explanations	Indicators
First Order	Government at the national level commits to a plan of action designed to adopt an ecosystem approach to aquaculture (EAA) by issuing a formalized commitment to an EAA, thereby putting in place the "enabling conditions"	New laws, programs, and procedures are initiated that provide the legal, administrative, and management mechanisms to achieve the desired changes in behavior by:
		(i) Building constituencies that actively support EAA with the user groups that will be most affected; with government institutions involved; and with the general public
		(ii) Developing a formal government mandate for an EAA with the authority necessary to implement actions in the form of laws, decrees, or other high-level administrative decisions that create an EAA as a permanent feature of the governance structure of aquaculture; creation of commissions, working groups, user organizations, and nongovernmental organizations (NGOs) dedicated to the advancement of an EAA agenda; designating EAA zones
		(iii) Devoting resources, especially sustained annual funding, adequate to implement an EAA
		(iv) Developing an implementation plan of action for an EAA that is constructed around unambiguous goals
		(v) Creating the institutional capacity necessary to implement the new EAA plan of action
Second Order	Evidence of successful implementation of an EAA	1. Changes in the behavior of institutions and interest groups have occurred such as collaborative planning and decision-making through creation of task forces, commissions, civic associations, etc.
		2. Successful application of conflict mediation activities
		3. Evidence of functional changes such as establishment of new public–private partnerships, new collaborative actions undertaken by user groups, implementation of new school curricula that incorporates an EAA
		4. Changes in behaviors directly affecting ecosystem goods and services, such as the elimination of socially and environmentally destructive aquaculture practices
		5. Investments in infrastructure supportive of EAA policies and plans
Third Order	Evidence of sustained achievements in institutional and behavioral change due to an EAA as seen in the environment and indicators for the quality of life, incomes, or engagement in alternative livelihoods that have improved target communities	1. Improvements in ecosystem qualities, such as sustained conservation of desired ecosystems and habitats, halting or slowing undesired trends such as nutrient releases, feed wastage, diseases, damaged benthic ecosystems, etc.
		2. Improvements in society as evidenced by monitoring of social indicators such as increases in indices of quality of life, reduced poverty, greater life expectancy, better employment opportunities, greater equity in access to coastal resources, and the distribution of benefits from their use, greater order, transparency, and accountability in how planning and aquaculture development decision-making processes occur, greater food security, or greater confidence in the future

As a result of this ESD approach, nine marine aquaculture zones of 2,400 ha in Port Phillip Bay and Westernport, Victoria, Australia were permitted. The Australian ESD approach combined analytical and participatory methods and developed sustainability plans that considered both ecosystem and human well-being, then developed implementation strategies by designing and enhancing effective governance systems for the expansion of aquaculture.

The development of a sustainability baseline should be the responsibility of a lead aquaculture agency. Its full implementation may require alternative methods of governance and employ innovative management approaches. There may be a need to facilitate an operational definition of aquaculture ecosystem boundaries for assessment, or area of focus, to set geographical limits to assess parameters such as carrying capacity or water management needs, and to understand the governance regime within which the area of focus is nested in order to understand and clarify such things as administrative and legal jurisdictions.

Using such guidance and sustainability science frameworks, the possibilities for designing productive aquaculture ecosystems that better fit into the local social and ecological context are many, since aquaculture can encompass the wide availability of species, environments, and cultures.

Improved Governance of Aquaculture Ecosystems

To be effective, ecosystem-based aquaculture initiatives must (1) be sustainable over long periods of time – ideally over many decades, (2) be capable of being adaptable to changing conditions, and (3) provide the mechanisms to encourage or require specified forms of resource use and collaborative behaviors among institutions and user groups that are stakeholders of the aquaculture system. Much of the challenge lies in both understanding and achieving changes in the behavior of the stakeholder groups and institutions associated with the aquaculture production systems. Ecosystem-based aquaculture integrates the best available science with a transparent, equitable, and democratic approach to planning and decision-making. Management needs to be carried out in a strategic manner that tailors principles of good aquaculture practice to the culture and the needs of a specific place. Successful aquaculture programs advance and change through linked cycles of planning, implementation, and reassessment. These features of ecosystem management signal the transition from traditional food production sector planning and decision-making to a holistic approach based on the interactions between sectors and within and among ecosystems.

FAO Fisheries and Aquaculture Department [25] found that one of the key trends toward more sustainable forms of aquaculture development and management is enhanced regulation and better governance. Governance is defined as the formal and informal arrangements, institutions, and mores that structure and influence how resources or an environment are utilized, how problems and opportunities are evaluated and analyzed, what behavior is deemed acceptable or forbidden, and what rules and sanctions are applied to affect how natural resources are distributed and used.

As shown in Table 2, there are three mechanisms by which the processes of governance are expressed: the marketplace, the government, and the institutions and arrangements of civil society [11]. These mechanisms interact with one another through complex and dynamic interrelationships that are examined and contrasted and documented in a baseline. Each of the three governance mechanisms influence and can alter patterns of behavior through measures such as those identified in Fig. 2. For sustainable, ecosystems-based aquaculture, it is important to distinguish between management and governance. Management is the process by which human and material resources are harnessed to achieve a known goal within a known institutional structure. Aquaculture business management, park management, personnel management, or disaster management is therefore spoken about. In these instances, the goals and the mechanisms of administration are well known and widely accepted. Governance, in contrast, addresses the values, policies, laws, and institutions by which a set of issues are addressed. It probes the fundamental goals and the institutional processes and structures that are the basis for planning and decision-making. Governance sets the stage within which management occurs [12].

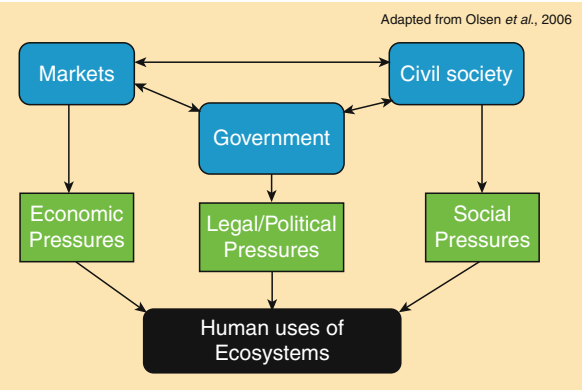

Aquaculture, Sustainability Science in. Figure 2 The three mechanisms by which the processes of governance are expressed interact with one another through complex and dynamic interrelationships that are vital parts of sustainability science assessments of aquaculture as each alter behaviors and decision-making that determine human uses of ecosystems [11–13]

The future of sustainable aquaculture is highly dependent on understanding the response by all three expressions of governance: markets, civil society, and government. For example, Kenya has fostered a participatory policy formulation for aquaculture, providing a legal and investment framework through government, establishing public–private partnerships to engage markets, providing basic infrastructure support, promoting self-regulation, providing a research platform for civil society to be engaged, undertaking zoning for aquaculture, and providing monitoring and evaluation support [25].

Adaptation of sustainability frameworks used to evaluate the needs and progress of governance on coastal management plans are essential to evaluate progress toward an ecosystem approach to aquaculture and build in adaptive learning and action into the strategic planning process. Governance frameworks recognize not only the importance of changes in practices such as changes over time in aquaculture farming ecosystems, but also recognize that for each change, there are correlated changes in the behavior of key partners and stakeholders within the sphere of influence of the management activity, and that these changes can be measured at local, regional, and national levels (Fig. 3, Table 3).

Sectoral agencies responsible for managing activities impacting aquatic ecosystems (e.g., capture fisheries, coastal zone development, watershed management organizations, agriculture, forestry, and industrial developments) will have to develop new ways of interacting to regularly communicate, cooperate, and collaborate. The need for innovative governance to implement an ecosystem-based approach to aquaculture can be seen as an obstacle but can also be seen as an opportunity to increase the social benefits that are likely to develop through synergies among food production sectors.

Social Ecology of Aquaculture

While there is much information on the natural ecology of food-producing ecosystems, there are few comprehensive frameworks for capturing the necessary social ecology of aquaculture.

Cadenasso et al. [26] have developed a "Human Ecosystem Framework" that could contribute to a baseline approach and assist in organizing multidisciplinary, social–ecological approaches to aquaculture development (Fig. 4). The most sustainable growth trajectories for aquaculture are to move toward more sustainable, social–ecological approaches to development; to shift patterns of production and consumption patterns from global to bioregional and local foods production and job creation; and to develop the indigenous human and institutional capacities that clearly demonstrate to society that "aquaculture is culture."

Future Directions: Sustainability Science Opportunities for Aquaculture

There are at least four major opportunities for sustainability science in the field of aquaculture in the

1. Determination of "sustainable aquaculture" for retail seafood companies
2. Growing fields of marine ecosystem and habitat restoration, conservation biology, and ecology
3. Accelerated use of agricultural meals and oils, and
4. Development of sustainable aquaculture for the poor

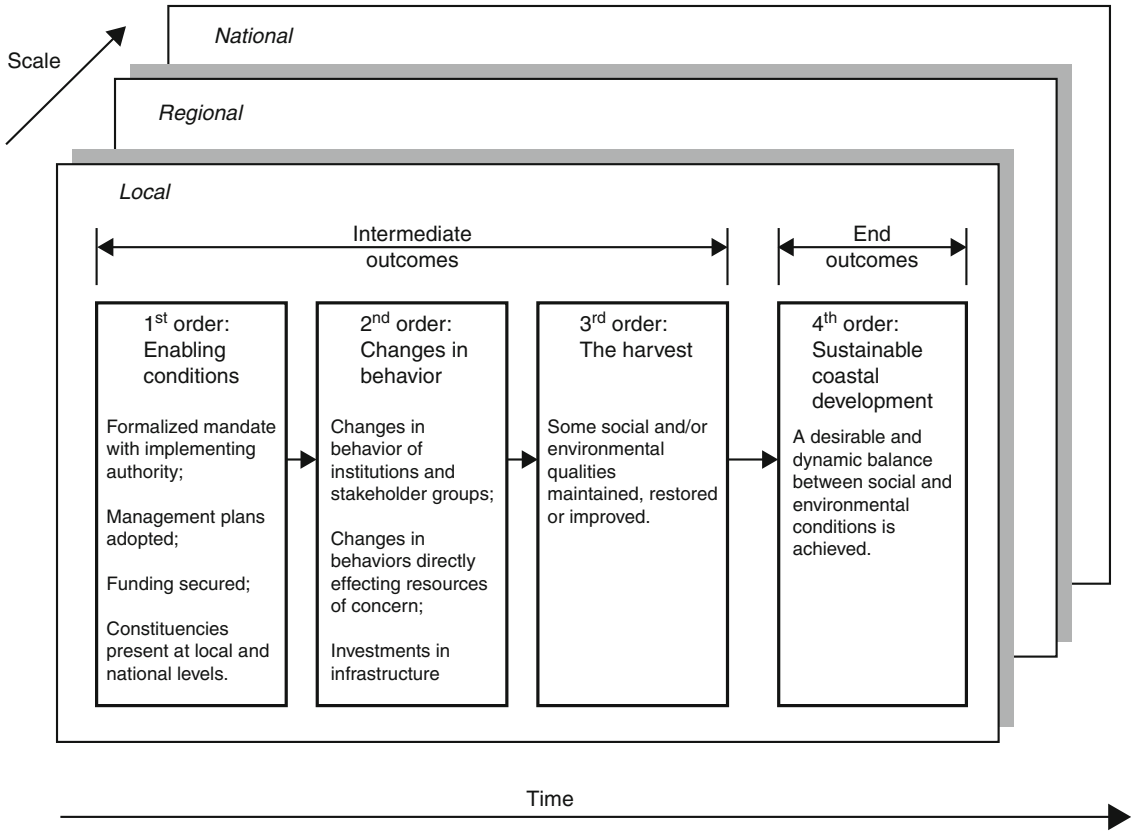

Aquaculture, Sustainability Science in. Figure 3
The four orders of coastal governance outcomes. This framework is used to develop governance baselines in environmental programs [12, 13]. An example of how progress toward better governance for sustainable aquaculture is shown in Table 3

Determination of Sustainable Aquaculture for Retailers

Sustainability science approaches to aquaculture can be used to better plan and develop aquaculture production networks for multiple species. Such planning approaches can be used to plan for the creation of highly diversified, segmented aquaculture networks, for maximal job creation at every unit step from "farm to plate" (e.g., seafood value chain planning), by creating numerous interconnections supplying inputs and outputs using local resources and recycled wastes and materials and expertise, and to close "leaky" loops of energy and materials that can potentially degrade natural ecosystems.

Behavioral changes will be required by industry. Social investments, strategic incentives/subsidies, and innovative market mechanisms can help facilitate change in behaviors. Self-regulation by the aquaculture industry has led to codes of practice and better management practices.

Sustainability assessments are predicated upon the fact that the modern aquaculture industry desires to be seen as a responsible steward. This means going beyond "meeting the regulations." There are a cacophony of certification bodies and seafood watch cards – there are an estimated 200 sustainable seafood guides available internationally – which has created a far too complex and sometimes conflicting recommendations to both consumers and retailers on what is "sustainable seafood" [27, 28]. Roheim [27] states that "Shrimp, in some form, appears as a green, yellow, red, and non-consensus list item" in the seafood "watch cards."

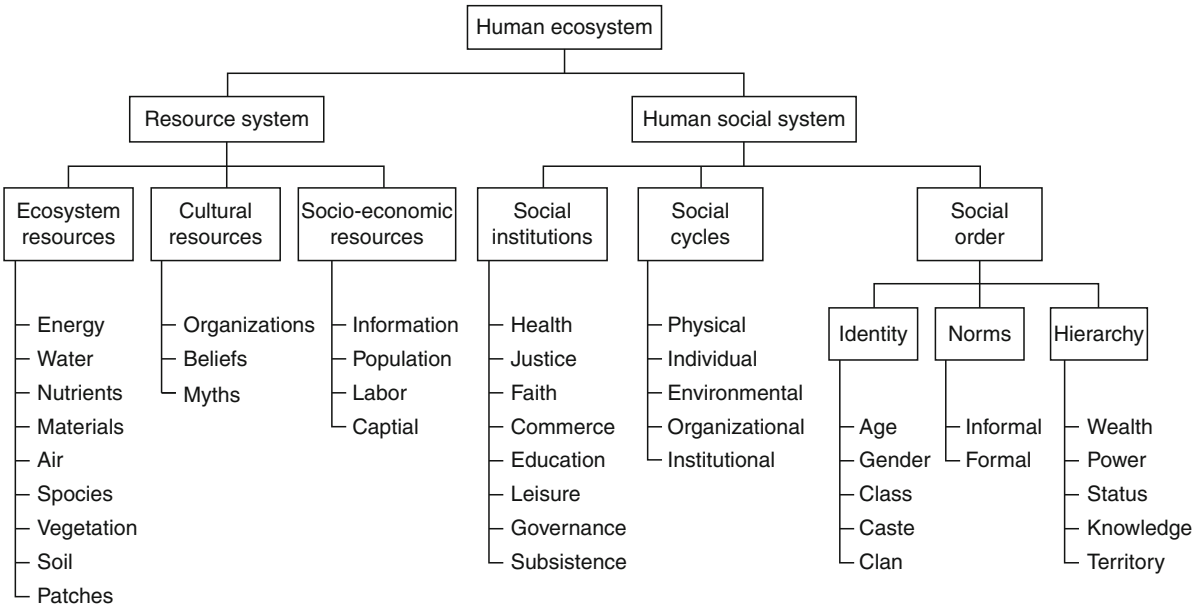

Aquaculture, Sustainability Science in. Figure 4
The Human Ecosystem Framework [26]. Assessment of new interventions such as aquaculture into societies requires knowledge of not only biophysical and natural resource systems but also social resources and human social systems

The logic behind consumer approaches is that informed consumers who care about sustainable seafood will demand aquaculture products that carry a label or fit into the "green" (buy) area of a watch card, as opposed to those products that do not have the label, sending a market signal back to aquaculture industries that only products from sustainable aquaculture farms are preferred. Many of the independent certification programs that have developed ecolabels and "seafood watch cards" to provide consumers with additional information come from nongovernmental organizations (NGOs) with specific advocacy agendas and not from neutral, scientific sources, or from regulatory bodies charged with protecting the environment and society. For example, many fisheries and aquaculture scientists are deeply concerned that consumer recommendations of NGOs are moving demand (and use) from farmed stocks to already overburdened wild fisheries. The Monterey Bay Aquarium's (MBA) Seafood Watch Program has produced millions of folding wallet cards featuring a "stop light" system of green (sustainable), yellow (chose with caution), and red (do not choose) recommendations. Farmed shrimp and salmon, two of the world's largest aquaculture industries are on the MBA red list. Roheim [27] mentions that the Compass Group a major food service company has used the MBA cards to decrease purchases of farmed shrimp and salmon, which, in effect, has created additional fishing pressure on wild shrimp and salmon stocks.

Most organizations believe that consumers' increasing awareness of environmental and food safety issues will lead them to accept a wide variety of standards and labels, most of which are specifically intended to allay consumers' concerns about negative environmental consequences.

However, Roheim [27–29] points out concerns over ecolabeling, especially the lack of transparency and opportunity for participation in the development of standards, and concerns of developing countries that ecolabeling schemes are an attempt at disguised protection of domestic industries to restrict market access and erode competitiveness. In addition, Wessels et al. [30] found that successful ecolabeling programs must accelerate consumer education programs so that consumers become more aware of differences in species, geographic regions, and certifying agencies.

Roheim [29] states that ecolabels require traceability. Traceability is the ability to follow the movement of a food through specified stages of production, processing, and distribution. Essentially, it is a record-keeping system that identifies and tracks products, transportation of products, and ingredients of products from origin to consumption, while providing the ability to quickly trace back products at any point along the supply chain. It is necessary for food safety purposes, in order to track backward in the food chain the source of food that made consumers ill, so that products could be removed from store shelves.

For consumers, Roheim [27] argues the need for ecolabels determined at the larger international levels, such as the Marine Stewardship Council (MSC), so that consumers "do not need to inquire about catch area or gear types, but only need to look for the label." The plethora of efforts has also confused and perplexed retailers who are the main "drivers" of certification at present, not consumers [27–29]. However, even though many buyers wish to purchase sustainable seafood, most seafood products are not certified, and they are very confused by the many NGO efforts. A purchasing policy determined by assessing which seafoods are "sustainable" by making an assessment of the plethora of NGOs, "opinions" seems confusing, risky, and costly. Rather, a simple, buying protocol (Fig. 5) that incorporates a sustainability assessment (where needed) as discussed here is recommended.

Aquaculture and the Restoration of Ecosystems

Aquaculture science can be viewed as a "toolbox" with great potential for restoring aquatic ecosystems. There is an unbalanced focus on marine animal husbandry (e.g., "fed" aquaculture) causing a lack of appreciation for the positive environmental attributes of nonfood aquaculture such as marine agronomy, endangered species aquaculture, and aquaculture for environmental enhancement and rehabilitation, all of which use modern marine hatchery and nursery aquaculture practices [31].

Aquaculture technologies (hatchery, nursery, grow-out) for marine plants are used for the restoration of mangroves, sea grasses, and coastal wetland plants such as *Spartina sp.* In addition, live rock and coral aquaculture facilities are active for not only the aquarium trade, but also for the environmental restoration of coral reefs (liveaquaria.com). In this regard, there is little difference between sustainable aquaculture and the emerging

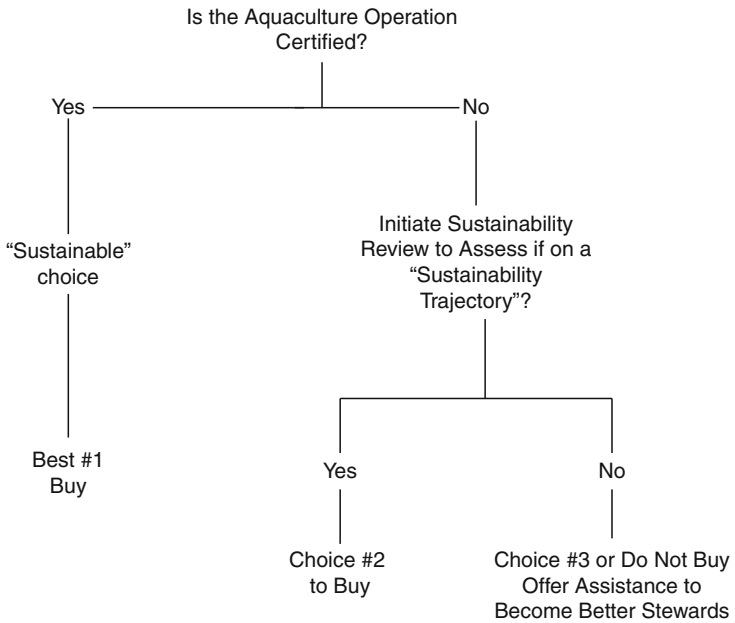

Aquaculture, Sustainability Science in. Figure 5
A simple decision tree for determinations of the sustainability of aquaculture products by retailers

fields of ecological engineering and industrial ecology. Indeed, tidal wetland, mangrove forest, coral, and sea grass restoration aquaculture – in addition to establishment and maintenance of oyster reefs – are important examples of aquaculture creating, enhancing, and maintaining productive marine ecosystems and habitats, and improving water quality.

Aquaculture and Agriculture Science

Here, science questions as to whether aquaculture contributes to the depletion of world fisheries. Fed aquaculture depends on both wild and farmed fish stocks and on intact aquatic habitats and excellent water quality, plus a growing quantity of agricultural resources. There is much ongoing policy, research, and management concerns on the interactions of marine food fish fisheries ("biomass fisheries") with aquaculture and human welfare. There is much less planning and research regarding the future impacts of fed aquaculture on agriculture.

Agricultural meals and oils as alternatives to marine sources are developing rapidly. Current projections forecast that fed aquaculture may use 50% or less of the world's fish meal [32], which would mean a large expansion of use of agricultural and other terrestrial sources of feed proteins and oils. Terrestrial proteins and oils from soybeans, sunflowers, and lupins are available at volumes larger than the available global quantities of fish meal. Soybeans have high protein content of ~28%, peas have ~22%, and these have good amino acid profiles. Other abundant agricultural cereals have lower protein contents of ~12–15%. Processing can create protein concentrates with protein levels of >50% [33]. Vegetable oils have very low EPA (eicosapentaenoic acid) and DHA (docosahexaenoic acid) levels. However, substitution of plant oils upward of 50% of added dietary oil has not resulted in growth reductions or increased mortalities in fish such as salmon and trout.

If agricultural sources of meals and oils are the future of fed aquaculture, there will be a need for a new sustainability planning and science on the impacts of fed aquaculture as a driver of agriculture production, especially so for soybeans. Increased aquaculture consumption of the world's grains and oils raises the concern over the spread of unsustainable agriculture practices. Brazil has been targeted as one of the world's major soybean suppliers. Costa et al. [34] have demonstrated that soybean farms are causing reduced rainfall in the Amazonian rainforest. About one seventh of the Brazilian rainforest has been cut for agriculture, about 15% of which is soybeans. Soybeans, which are light in color, reflect more solar radiation, heating the surface of the land less and reducing the amount of warm air convected from the ground. Fewer clouds form as a result, and less precipitation falls. In soybean areas, there was a 16% less rainfall compared to a 4% decrease in rainfall in land areas cleared for pasture.

Aquaculture for the Poor

Approximately 1.3 billion people live on less than a dollar a day, and half of the world's population lives on less than 2 dollars a day. FAO has stated that the world will need to produce 70% more food for an additional 2.3 billion people by 2050 [4]. Scarce natural resources will need to be used more efficiently, and there will be a need for proper socioeconomic frameworks to address imbalances and inequities to ensure that everyone in the world has access to the food they need. Food production will have to be carried out in a way that reduces poverty and takes account of natural resource limitations [4].

The world's population will rise from 6.8 to 9.1 billion in 2050, with nearly all population growth occurring in the economically developing countries. Without additional global food strategies, an estimated 370 million people will be hungry in 2050. The magnitude of the problem is most acute in Africa. In 10 African countries of an estimated 316 million persons where aquatic proteins are an important dietary component, 216 million live on US$2/day, 88 million are undernourished, and 16 million children under 5 are malnourished [35].

Small-scale coastal and inland freshwater fisheries provide more than 90% of the fish consumed in Africa. Over 2.5 million people are involved in fishing and 7.5 million in trading, marketing, and processing. The most important fisheries/aquaculture ecosystems are located on the coasts of west and southern Africa and the river basins of Senegal, Niger, Volta, Congo, Lake Chad, Nile, and Zambezi Rivers. But today, aquaculture provides less than 5% of Africa's fish, with most concentrated in Egypt and Nigeria [35].

Aquaculture is a global enterprise with local roots. There are strong concerns that aquaculture is evolving away from its global responsibility to provide net benefits (additional foods) for a protein-hungry planet [36–38]. Greater than 75% of global fisheries are traded. In 2000, more than 60% of fish meal was traded. Only 7% of meat is traded, 17% of wheat, and 5% of rice. To tackle this huge challenge, the FAO ecosystems approach to aquaculture [39] has created a new code for responsible global aquaculture development, and has combined this into one common development framework for a global implementation strategy for aquaculture that can be used to measure the trajectory of social responsibility for global aquaculture.

If aquaculture is designed, implemented, and evaluated as aquaculture ecosystems, a new social contract would have a close relationship between aquaculture professionals who not only develop an alternative model of aquaculture development but also interact closely with capture fisheries and agriculture but help deliver to the world's poor its needs for nutrient dense, protein-rich seafoods. Components of a global strategy could be to:

1. **Allocate more food fish and oils for poverty alleviation and human needs worldwide, and allocate less marine resources for feed fish for fed aquaculture so as to: (a) increase the ecosystem resilience of the Humboldt ecosystem, and (b) relieve the increasing overdependence of aquaculture countries such as Thailand (shrimp) and Norway (salmon) on this southeastern Pacific Ocean marine ecosystem.**

   Alder et al. [37] estimated that about 36% of the world's fisheries catch (30 million tons) are processed into fish meal and oil, mostly to feed farmed fish, chickens, and pigs. Daniel Pauly of the University of British Columbia has stated that "Globally, pigs and chickens alone consume six times the amount of seafood as US consumers and twice that of Japan." Jacquet et al. [28] reported that Peru exports about half of the world's fish meal from its catch of 5–10 MMT/year of anchovies while half of its population of 15 million live in poverty and 25% of its infants are malnourished. A campaign launched in 2006 combining scientists, chefs, and politicians to demonstrate that anchovies are more valuable to the Peruvian people and its economy as direct foods has resulted in a 46% increase in demand fresh and 85% increase in canned anchovies. One ton of fillets has sold for five times the price of 1 t of meal and requires half the fish (3 t for 1 t fillets vs. 6 t for 1 t meal). Peru has decided to dedicate 30% of its annual food security budget (approx. US$ 80 million) for programs to supply anchovies to its people. Higher prices for fish used as direct human foods for food security will limit processing of fish to meals for terrestrial animal and aquaculture feeds, thereby decreasing the supply of fish meals and oils for global aquaculture trade and development, but meeting the Millennium Development Goals of eliminating everywhere extreme hunger and starvation.

2. **Accelerate research into the elucidating functional feed ingredients in fish diets that are showing the potential to eliminate the needs for fish meal and oils in aquaculture.**

   Skretting Aquaculture Research Centre [40] reported a research on "functional ingredients" that are contained in fish meals and oils, which contribute to efficient feed conversions and high growth rates, fish health, and welfare. Initial research focused on beta-glucans that not only stimulate the immune system of fish and protect against the effects of bacterial furunculosis but also allow reductions in fish meal contents in diets to 25%. Additional research with phospholipids in meals, triglycerides in fish oil, and antioxidants in 2008 have resulted in excellent fish performances from feeds with almost no marine fish meal and oil. Current research is exploring the extraction of functional ingredients from other non-marine by-products.

3. **Develop alternative ecological aquaculture models that accelerate the movement toward use of agricultural, algal, bacterial, yeasts meals, and oils.**

   Aquaculture uses most of the world's fish meal (68%) and fish oil (88%); however, Tacon and Metian [32] predict that fish meal and oil use in aquaculture will decrease to become high priced,

specialty feed ingredients. Currently, about 40% of aquaculture depends on formulated feeds: 100% of salmon, 83% of shrimp, and 38% of carp. As stated previously, research on the use of agricultural meals and oils to replace use of ocean resources especially on the functional components of fish meals/oils needed for fish nutrition is a major subject of aquaculture research and development [41, 42]. Turchini et al. [43] reported that for all of the major aquaculture fish species that 60–75% of dietary fish oil can be substituted with alternative lipid sources without significantly affecting growth performance, feed efficiency, and feed intake. Naing et al. [44] found that palm oil could replace fish oil in rainbow trout diets, and reduce the dioxin contents in fish.

4. **Develop new governance systems that integrate aquaculture, agriculture, and fisheries using ecosystem-based management approaches, which combine production, distribution, and consumption networks that do not institutionalize poverty and hunger, but provide new alternative tools and education in multisectoral ecosystem approaches.**

   The massive environmental change being brought about by the accelerated growth of the world's population has caused profound change to the world's ecosystems. Crutzen and Stoermer [45] have called this new era the "Anthropocene." In this era, massive quantities of additional foodstuffs will be needed to sustain humanity; nutrient-dense, high-quality aquatic proteins will be especially important. The tools and training for creating the next generation of transdisciplinary, sustainability scientists will need to be further developed and well utilized; otherwise, it will result in serious consequences for the Earth's living systems.

Bibliography

Primary Literature

1. Ostrom E (1986) An agenda for the study of institutions. Public Choice 48(1):3–25
2. Costa-Pierce B (2002) Ecological aquaculture. Blackwell, Oxford
3. Costa-Pierce B (2008) An ecosystem approach to marine aquaculture: a global review. In: Soto D (ed) Building an ecosystem approach to aquaculture, pp 81–116. FAO Fisheries and Aquaculture Proceedings 14, FAO, Rome, 221p
4. FAO (Food and Agriculture Organization) (2009) The state of world fisheries and aquaculture 2008. Fisheries Department, Food and Agriculture Organization of the United Nations, Rome
5. FAO (1995) Code of conduct for responsible fisheries. FAO, Rome, 41 pp. Available at ftp://ftp.fao.org/docrep/fao/003/W4493e/W4493e00.pdf
6. Moore B III, Underdal A, Lemke P, Loreau M (2002) The Amsterdam declaration on global change. In: Steffen W, Jäger J, Carson DJ, Bradshaw C (eds) Challenges of a changing earth. Springer, Heidelberg
7. Gliessman S (1998) Agroecology: ecological processes in sustainable agriculture. Ann Arbor Press, Ann Arbor
8. Altieri M (2002) Agroecology: the science of natural resource management for poor farmers in marginal environments. Agr Ecosyst Environ 93:1–24
9. Kates R, Clark W, Corell R (2001) Sustainability science. Science 292:641–642
10. Wurts W (2000) Sustainable aquaculture in the twenty-first century. Rev Fish Sci 8:141–150
11. Olsen S, Sutinen J, Juda L, Hennessey T, Grigalunas T (2006) A handbook on governance and socioeconomics of large marine ecosystems. Coastal Resources Center, University of Rhode Island, Narragansett
12. Olsen S (2003) Frameworks and indicators for assessing progress in integrated coastal management initiatives. Ocean Coast Manage 46(3–4):347–361
13. Olsen S, Page G, Ochoa E (2009) The analysis of governance responses to ecosystem change: a handbook for assembling a baseline. LOICZ Reports & Studies No. 34. GKSS Research Center, Geesthacht, Germany
14. GESAMP (IMO/FAO/UNESCO-IOC/UNIDO/WMO/IAEA/UN/UNEP Joint Group of Experts on Scientific Aspects of Marine Environmental Protection) (2008) Assessment and communication of environmental risks in coastal aquaculture. FAO, Reports and Studies GESAMP No. 76, Rome, 198 pp
15. Tucker C, Hargreaves J (2008) Environmental best management practices for aquaculture. Wiley-Backwell, Ames, IA
16. National Research Council (2010) Ecosystem concepts for sustainable bivalve mariculture. National Academies Press, Research Council, Washington, DC
17. Boyd C, Tucker C, McNevin A, Bostick K, Clay J (2007) Indicators of resource use efficiency and environmental performance in fish and crustacean aquaculture. Rev Fish Sci 15:327–360
18. Daly HE (1996) Beyond growth: the economics of sustainable development. Beacon, Boston
19. Pullin R (1993) Discussion and recommendations on aquaculture and the environment in developing countries. In: Pullin R, Rosenthal H, Maclean J (eds) Environment and aquaculture in developing countries. ICLARM Conference Proceedings 31, pp 312–338

20. Hepher B (1985) Aquaculture intensification under land and water limitations. GeoJournal 10:253–259
21. Mires D (2009) Development of inland aquaculture in arid climates: water utilization strategies applied in Israel. Fisheries Manag Ecol 7:189–195
22. Neori A, Shpigel M, Ben-Ezra D (2000) A sustainable integrated system for culture of fish, seaweed and abalone. Aquaculture 186:279–291
23. Pimentel D, Pimentel M (2003) Sustainability of meat-based and plant-based diets and the environment. Am J Clin Nut 78(3):660–663
24. Fletcher W, Chesson J, Fisher M, Sainsbury K, Hundloe T (2004) National ESD reporting framework: the 'how to' guide for aquaculture. FRDC Project 2000/145.1, Canberra, 88 pp
25. FAO Fisheries and Aquaculture Department (2006) State of the world's fisheries and aquaculture. FAO Italy, Rome, 162 p. Available at http://www.fao.org/docrep/009/A0699e/A0699E00.htm#Contents
26. Cadenasso M, Pickett S, Grove M (2006) Integrative approaches to investigating human-natural systems: the Baltimore ecosystem study. Nat Sci Soc 14:4–14
27. Roheim C (2009) An evaluation of sustainable seafood guides: implications for environmental groups and the seafood industry. Mar Resour Econ 24:301–310
28. Jacquet J, Hocevar J, Lai S, Majluf P, Pelletier N, Pitcher T, Sala S, Sumaila R, Pauly D (2009) Conserving wild fish in a sea of market-based efforts. Oryx, The Int J Cons. doi:10.1017/S0030605309990470
29. Roheim C (2001) Product certification and ecolabelling for fisheries sustainability FAO Fisheries Technical Paper 422. FAO, Rome, Italy
30. Wessells C, Johnston R, Donath H (1999) Assessing consumer preferences for ecolabelled seafood: the influence of species, certifier, and household attributes. Am J Agr Econ 5: 1084–1089
31. Costa-Pierce B, Bridger C (2002) The role of marine aquaculture facilities as habitats and ecosystems. In: Stickney R, McVey J (eds) Responsible marine aquaculture. CABI, Wallingford, pp 105–144
32. Tacon A, Metian M (2008) Global overview on the use of fish meal and fish oil in industrially compounded aquafeeds: trends and future prospects. Aquaculture 285:146–158
33. Bell J, Waagbo R (2002) Safe and nutritious aquaculture produce: benefits and risks of alternative sustainable aquafeeds. In: Holmer M, Black K, Duarte C, Marba N, Karqakasis I (eds) Aquaculture in the ecosystem. Springer, New York, pp 185–226
34. Costa M, Yanagi S, Souza P, Ribeiro A, Rocha E (2007) Climate change in Amazonia caused by soybean cropland expansion, as compared to caused by pastureland expansion. Geophys Res Lett 34(L07706). doi:10.1029/2007GL029271
35. Allison E, Beveridge M, van Brakel (2009) Climate change, small-scale fisheries and smallholder aquaculture. In: Culberg M (ed) Fish, trade and development. Royal Swedish Academy of Agriculture and Forestry, Stockholm, pp 73–87
36. Goldburg R, Naylor R (2005) Future seascapes, fishing, and fish farming. Front Ecol Environ 3(1):21–28
37. Alder J, Campbell B, Karpouzi V, Kaschner K, Pauly D (2008) Forage fish: from ecosystems to markets. Ann Rev Environ Res 33:71–714
38. Naylor R, Hardy R, Bureau D, Chiu A, Elliott M, Farrell A, Forster I, Gatlin D, Goldburg R, Hua K, Nichols P (2009) Feeding aquaculture in an era of finite resources. Proc Nat Acad Sci 106(36): 15103–15110
39. Soto D, 21 co-authors (2008) Applying an ecosystem-based approach to aquaculture: principles, scales and some management measures. In: Soto D, Aguilar-Manjarrez J, Hishamunda N (eds) Building an ecosystem approach to aquaculture. Rome: FAO Fisheries and Aquaculture Proceedings 14. FAO, Rome, 221 pp
40. Skretting Aquaculture Research Centre (2009) Revealing the essential functions of vital feed ingredients. Accessed at http://www.skretting.com/Internet/SkrettingGlobal/webInternet.nsf/wPrId/D30B62DD93F65CFEC1257663004DA962!OpenDocument
41. Watanabe T (2002) Strategies for further development of aquatic feeds. Fish Sci 68:242–252
42. Opstvedt J, Aksnes A, Hope B, Pike I (2003) Efficiency of feed utilization in Atlantic salmon (Salmo salar L.) fed diets with increasing substitution of fish meal with vegetable proteins. Aquaculture 221:365–379
43. Turchini G, Bente E, Torstensen E, Ng W (2009) Fish oil replacement in finfish nutrition. Rev Aquacult 1(1):10–57
44. Naing A, Satoh S, Tsuchida N (2007) Effect of replacements of fishmeal and fish oil on growth and dioxin contents of rainbow trout. Fish Sci 73:750–759
45. Crutzen P, Stoermer E (2000) The "Anthropocene". Glob Change Newslett 41:17–18
46. Fletcher A (2003) Mapping stakeholder perceptions for a third sector organization. J Intell Cap 4(4):505–527
47. Savage G, Nix T, Whitehead B (1991) Strategies for assessing and managing orgnaizational stakeholders. Acad Manage Exec 5(2):61–75
48. Hemmati M, Dodds F, Enayti J, McHarry J (2002) Multistakeholder procesess on governance and sustainability. Earthscan, London
49. Dalton T (2005) Beyond biogeography: a framework for involving the public in planning of U.S. Marine Protected Areas. Conserv Biol 19:1392–1401
50. Dalton T (2006) Exploring participants' views of participatory coastal and marine resource management processes. Coast Manage 34:351–367
51. ISSD (International Institute for Sustainable Development) (2004) ISO social responsibility standardization. An outline of the issues. International Institute for Sustainable

Development, Winnipeg, Manitoba. http://www.iisd.org/pdf/2004/standards_iso_srs.pdf
52. http://www.iclei.org
53. American Center for Life Cycle Assessment. http://www.lcacenter.org
54. Bartley D, Brugère C, Soto D, Gerber P, Harvey B (2007) Comparative assessment of the environmental costs of aquaculture and other food production sectors: methods for meaningful comparisons. FAO/WFT Expert Workshop, 24–28 April 2006, Vancouver, Canada. FAO Fisheries Proceedings. No. 10. FAO, Rome, 241p
55. Ayer N, Tyedmers P (2009) Assessing alternative aquaculture technologies: life cycle assessment of salmonid culture systems in Canada. J Cleaner Prod 17:362–373
56. International Organization for Standardization (ISO). http://www.iso.org/iso/iso_14000_essentials
57. Environmental Impact Assessment Review. http://www.elsevier.com/wps/find/journaldescription.cws_home/505718/description#description
58. IAIA (International Association for Impact Assessment) (1999) Principles of environmental impact assessment best practices. IAIA, Fargo, ND, USA. http://www.iaia.org/publicdocuments/special-publications/Principles%20of%20IA_web.pdf
59. US Department of Transportation. http://www.fhwa.dot.gov/planning/toolbox/costbenefit_forecasting.htm
60. Savitz A (2006) The triple bottom line: how today's best-run companies are achieving economic, social and environmental success – and how you can too. Jossey-Bass/Wiley, New York
61. McCandless M, Venema H, Barg S, Oborne B (2008) Full cost accounting for agriculture – final report. Valuing public benefits accruing from agricultural beneficial management practices: an impact pathway analysis for Tobacco Creek, Manitoba. International Institute for Sustainable Development, Winnipeg, Manitoba, Canada. http://www.iisd.org/pdf/2008/measure_fca_2008.pdf
62. Gibson R, Hassan S, Holtz S, Tansey J, Whitelaw G (2005) Sustainability assessment: criteria and processes. Earthscan, London

Books and Reviews

Pullin R (1993) Environment and aquaculture in developing countries. International Center for Living Aquatic Resources Management, Manila

Smil V (2000) Feeding the world: a challenge for the twenty-first century. MIT Press, Cambridge MA

Tacon A, Hasan MR, Subasinghe RP (2006) Use of fishery resources as feed inputs for aquaculture development: trends and policy implications. FAO Fisheries Circular No. 1018. Food and Agriculture Organization of the United Nations, Rome

Aquapod Systems for Sustainable Ocean Aquaculture

Stephen H. Page
Ocean Farm Technologies, Inc., Morrill, ME, USA

Article Outline

Glossary
Definition of the Subject
Introduction
Aquapod Technology and Engineering Description
Aquapod Installations and Experience to Date
Future Directions
Bibliography

Glossary

Artisanal fisheries Traditional fisheries involving fishing households (as opposed to commercial companies), using relatively small amount of capital and energy, relatively small fishing vessels or canoes, often beach-based, making short fishing trips, close to shore, mainly for local consumption.

Biofouling The accumulation of living organisms on some surface by bacteria, fungi, protozoa, algae, and invertebrates.

Geodesic The shortest line between two points on a specific surface.

Open ocean aquaculture The culture of marine organisms in exposed ocean locations, not sheltered by islands or embayments.

Definition of the Subject

Open ocean aquaculture is not well defined by the industry, but in general refers to culture of marine fish, invertebrates, or algae in exposed ocean locations. Open ocean aquaculture is contrasted to near-shore marine aquaculture in that it occurs in areas removed spatially from land, typically by 1 km or more; deep water, generally deeper than 20 m; and exposure to wind, waves, and ocean currents without shelter from the mainland or islands. The subject of this entry is

principally the design and engineering of containment systems suited for open ocean aquaculture.

Introduction

Near-shore finfish aquaculture worldwide is challenged and constrained by resource user competition, environmental carrying capacity of near-shore environments, and, in most cold-water regions of the world essentially a monoculture of Atlantic salmon. Expansion of marine aquaculture in the next 20 years will happen substantially in offshore, exposed open ocean areas, with a diversification of species.

The patented Aquapod™ is a unique containment system for marine aquaculture, suited for rough open ocean conditions and a diversity of species. The Aquapod is constructed of individual triangular net panels fastened together in a spheroid shape (Fig. 1). The majority of the panels are simply structural members and netting. Some individual panels or groups of panels have other functions, such as access, feeding, fish transfer and grading, harvest, mooring, and mortality recovery. Other individual panels may have pneumatically controlled flotation devices which allow an almost infinite orientation of the Aquapod in the water. The Aquapod functions as a total containment system for finfish while submerged or partially surfaced.

Elements of the design have benefits for reduction in labor for routine husbandry tasks, reduction in maintenance costs, and reduction of stress on aquatic animals during handling operations such as transfer, treatment, and harvest. The "exoskeleton" design of the Aquapod containment system also allows for internal structures to provide for the cultivation of flatfish species such as halibut and flounder.

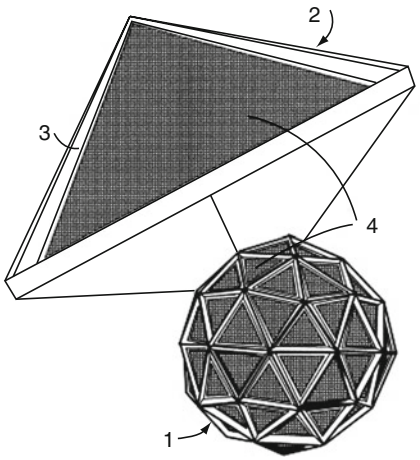

Aquapod Systems for Sustainable Ocean Aquaculture. Figure 1
The scale of contemporary net pens to date has become problematic especially in terms of net-handling activities, which are labor intensive, require significantly sized hydraulic equipment, and cannot be performed in rough ocean conditions. The modular nature of the Aquapod solves this problem by utilizing individual net panels which are interchangeable and scaled to be handled without difficulty in adverse conditions. These net panels are fastened together to form a secure enclosure, tailored to each customer's specific requirements

Features of the Aquapod Containment System

Submersibility: Submersion is the preferred, if not the only way to operate fish containment systems in the open ocean. Submergence is necessary to operate a fish pen below the destructive energy of surface waves. Submergence also allows fish to be kept at favorable temperatures below warm water thermoclines. The Aquapod can be operated partially surfaced (Fig. 2)

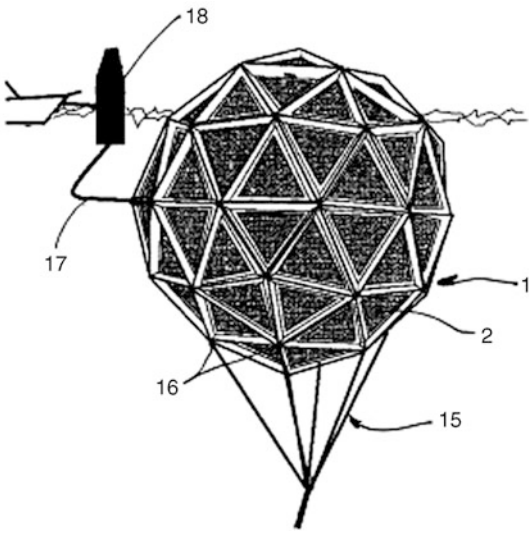

Aquapod Systems for Sustainable Ocean Aquaculture. Figure 2
The structure of the Aquapod net pen allows for many configurations of mooring attachment. Figure 2 shows an Aquapod net pen partially surfaced

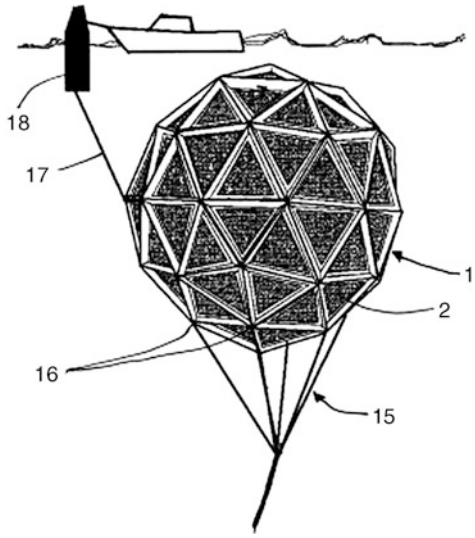

Aquapod Systems for Sustainable Ocean Aquaculture. Figure 3
An Aquapod net pen submerged

or fully submerged (Fig. 3). Although there are other pen designs which are designed to operate submerged, the spherical Aquapod design is well suited for species such as Atlantic salmon, which require periodic access to substantial surface area in order to gulp air.

Fixed volume: The Aquapod maintains its shape and volume in strong currents or undertow, reducing stress and physical damage to the fish contained within. Aquapod net pens can be constructed to any size to fit individual customer's needs, with a practical range of 8 m diameter (212 m^3) to 24 m diameter (7,000 m^3).

Containment: The structural exoskeleton of the Aquapod provides a high ratio of structural support to net area. Each triangular panel is comprised of an essentially rigid frame supporting tensioned netting. Frames can be constructed of marine grade aluminum, fiber-reinforced polymer, or even a combination of materials. The modular nature of the Aquapod containment system provides for easy inspection and inventory control as required by today's mandated containment management systems. Individual net panels are coded so they can be brought into a regular schedule of inspection, maintenance, repair, and replacement. While surfaced in suitable conditions, a single net panel or a group of net panels can be removed and replaced without compromising the integrity of the containment. No other system can offer this convenience.

Predator control and escapement: Tensioned netting has proven to be relatively predator proof in other engineered systems. The Aquapod goes one step further. Due to the modular structure and the relatively small triangular units, different types of wire mesh can be used in place of synthetic netting. This enhances predator control in areas where triggerfish, sharks, sea lions, and crocodiles have made fish farming impractical. Wire mesh also prevents escapement by chewing fish such as cod and sea bream, which readily chew through synthetic fiber netting.

Husbandry and fish health: Fish can be moved from one Aquapod containment to another without seining or pumping. Patent pending displacement technology is capable of transferring fish from one Aquapod containment pen to another without brailing or pumping, or from an Aquapod containment to a harvesting pump without seining or other stressful means of crowding the fish. While being transferred, fish can be graded and counted with automated technology. In competitive designs, these fish-handling operations are either impossible or very labor intensive and stressful on the fish.

Feeding: One or more panels in each Aquapod containment is modified to receive and distribute hydraulically supplied feed from a centralized feed barge or service boat. The semirigid and modular exoskeleton of the Aquapod allows easy attachment of any number of feeding ports. Multiple feed outlets provide better distribution of feed to the fish.

Safety: Worker safety is a paramount concern when operating fish farms in open ocean conditions. Since conception, the Aquapod containment system has been designed to maximize automation of routine husbandry tasks and reduce the amount of time divers are needed in the water. Although any containment system will need some diving, the ability of the Aquapod to rotate within its mooring grid, bringing any segment of the pen to the surface or near to the surface, reduces the amount of diving, and when diving is needed, the depth of the dives will be greatly reduced. One of the most dangerous jobs on a fish farm is net changing, and the Aquapod eliminates this chore by providing a means to clean nets at the surface.

Waste management: The spherical design of the structure causes mortalities to collect at the bottom of the pen where they can be brought to the surface with a conventional airlift pump, eliminating the routine and hazardous task of mortality collection by divers (Fig. 4).

Mooring. There are many options for mooring an Aquapod net pen. Each hub of the frame is a potential mooring point, which allows enormous flexibility in mooring placement and the ability to distribute loads over a large area for safety. Any specific net panel can be strengthened to facilitate predicted maximum mooring stresses, whether the Aquapod is attached to a single-point mooring or whether it is installed in a conventional submerged grid system (Fig. 5). Another mooring option available in suitable site is a two-point mooring (Fig. 6) that facilitates Aquapod rotation.

Cost: On a capital cost per cubic meter of containment basis, the Aquapod containment system is significantly more than conventional surface pens but significantly less than the cost of currently available submersible net pens. Furthermore, when submerged, the volume used to calculate containment is accurately figured, unlike surface pens which calculate the volume in the top part of the water column, although that space is not used by the fish. Operational costs are less than existing systems due to the efficiency of the proprietary fish transfer technology for routine husbandry tasks. Maintenance costs are reduced by the modular nature of the net panels and the ability to orient the Aquapod so that any part of the net pen is at or near the water surface, making it easy to inspect, remove, and replace individual net panels. When optional vinyl-coated wire mesh is used for netting, net replacement is reduced and net washing is greatly facilitated.

The true cost of any system is not only the initial capital cost, but the life cycle cost and the cost of operations, including risk. The Aquapod has been designed with these factors as principal drivers.

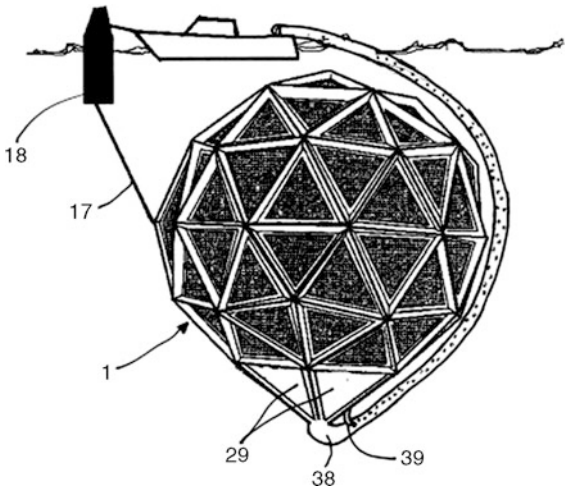

Aquapod Systems for Sustainable Ocean Aquaculture. Figure 4
A simple air lift suction pump can remove mortalities and waste from the bottom of the Aquapod net pen for removal and processing

Aquapod Technology and Engineering Description

Current State of Design and Materials

The engineering work to date on the Aquapod design has centered primarily on early 10 m (31 ft) diameter units, the larger 19 m (64 ft) diameter A3600 size, and more recent 8 m (27 ft) A212 Micropods. All these models have used recycled HDPE materials as the primary element for the struts, and plastic-coated welded wire mesh for the net fabric. Selective reinforcement around the mooring attachment points has addressed strength issues. So far these materials seem to work well and have been a basis for all Aquapod installations to date. The innovations by Ocean Farm Technologies

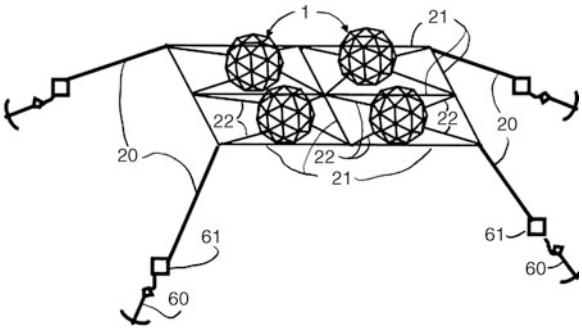

Aquapod Systems for Sustainable Ocean Aquaculture. Figure 5
Aquapod net pens can be moored in many different configurations of grids

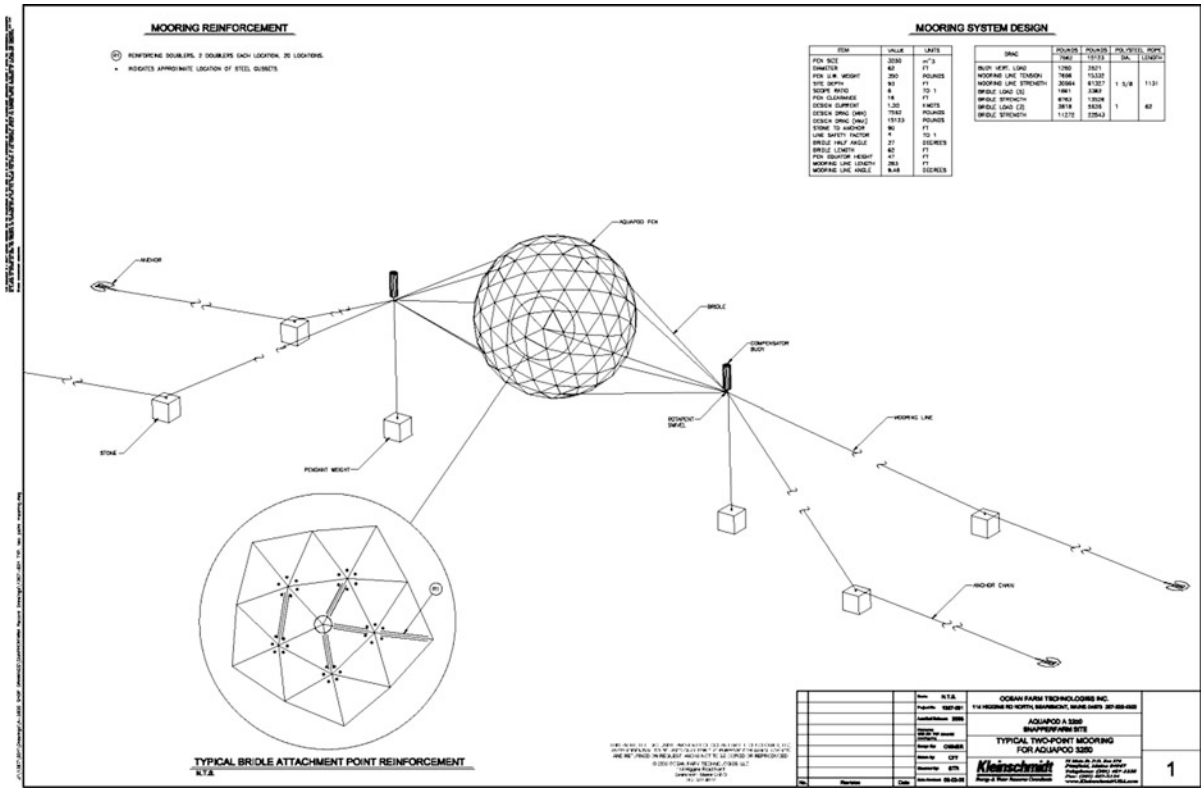

Aquapod Systems for Sustainable Ocean Aquaculture. Figure 6
Single Aquapod net pens can be moored individually in a two-point mooring. With swivels at the bridle attachment points, this allows for rotation of the net pen

(OFT) with testing and analysis have been steadily advancing the design, learning the relative cost and difficulty of various ideas, with the goal of refining the concept and improving the economy of the design, manufacture assembly, and installation procedures.

Mooring system components have been selected to create a two-point design allowing movement in the vertical direction and rotation, and single-point moorings. Buoyancy calculations have been done to confirm the near-neutral buoyancy of the system.

The main engineering goal is to design an economical pen that is strong enough, but not excessively heavy or expensive, by defining the real safety factor of the current design, and seeing where further structural design improvements might be made. With a large structure with so many repetitive elements, the changes in any one element are repeated hundreds of times, and thus has a real effect on cost and fabrication. Further work is also being done by OFT with more long-range improvements and concepts for different types of designs using different materials or assembly ideas.

Further data from the real size pens has been used to confirm drag forces. Loading of the pen has to date been based on a tow test performed by a University of New Hampshire boat on the 31-ft geodesic pen and has been scaled up for the 62-ft pen [1]. OFT plans to measure drag loads on existing pens as a function of current velocity and thus more accurately establish this relationship. The current drag forces used to date are on the conservative side, allowing for the effect of biofouling that increases drag.

The structural effect of wire mesh on the Aquapod is obvious but difficult to measure or model. The mesh contribution has not been credited in the analysis to date, except to provide buckling restraint for the compression member weak axes. As far as basic strength, the mesh can help reduce tension stresses, but will do nothing to reduce compressive stresses in the struts,

and since these are usually of about the same magnitude over the sphere, the overall effect may not be of much importance.

Results of University of Maine Engineering Study

The use of recycled HDPE [2] plastic extrusions in this type of structural engineering application is rare and, for the designer, the available data on materials and fasteners in the material is limited. For design of the Aquapod struts, it is necessary to check the capacity of the tension and compression members. Needed for compression members are values to use for modulus of elasticity, maximum allowable stresses for compression, based on buckling, yielding, and crushing, and creep rupture of the real life struts. For design of the tension members, the modulus of elasticity, maximum and allowable tensile stresses, and fastener strengths are needed. In addition, bolts and other fasteners are used in the Aquapod and data is needed regarding end and edge distances, strengths, and yield points. Testing of the full size members and hub assemblies has been desirable to confirm the actual strength of real life members, and thus provide an indication of the real safety factor provided in the pen.

The Hybrid Structures Testing Laboratory in the Mechanical Engineering Department, at the University of Maine, was engaged by OFT and performed initial testing (1) to determine engineering data for the plastic material that is used in the Aquapod net pen system and (2) to test sub-component details of the Aquapod system. The goal has been to have design guidance to use as the limits for the members, as calculated for the pen under the various load scenarios. Testing was performed under the direction of Vincent Caccese, Ph.D., P.E., Professor of Mechanical Engineering (Caccese).

The testing consisted of a total of 62 structural tests of components as follows:

1. Material Bolt Bearing, Tensile, and Shear-out Capacity (40 tests performed)
2. Column Compression Tests (20 tests performed)
3. Mesh Assembly Buckling (2 tests performed)

The bolt tests were done first and arrived early enough to size the bolts in the Aquapod 3250. These tests were primarily to determine the bolt capacities for the tension members in the Aquapod, and to determine how many, and what size bolts would provide the required tension transfer from component to component, principally in the steel-reinforced connections around the mooring attachment points. These tests also showed that the tensile capacity of the struts is a controlled by the holes, and tension members will fail first at the bolt holes.

The compression tests were primarily aimed at determining maximum compression loads that could be assigned to struts, which should be a safe percentage of the ultimate compression demonstrated by the full size tests, and should also be a safe amount below the maximum stress that induces the beginning of buckling.

While the sample sizes for the compression tests were small, the results indicate that the actual modulus of elasticity for design use is significantly higher than the published data provided by the plastic vendor for design of compression posts, but well under the value listed as an engineering property in their material property tables. The actual reinforcement of members with doublers could have been reduced somewhat and the current design is conservatively reinforced.

Assessment of Structural Stability of Aquapod Net Pens

The geodesic sphere that has been used for this pen is based on an icosahedron. The icosahedron is a geometric shape consisting of ten triangular faces that are further subdivided into triangular panels, in the process of creating the geodesic sphere. Each of the ten faces is subdivided into 16 triangular panels of 10 ft on a side. Each strut is a pair of extruded fiberglass-reinforced HDPE members. All panels are faced with $1'' \times 1'' \times 16''$ gage vinyl-coated galvanized steel wire mesh.

The geodesic sphere has been structurally analyzed using finite element computer modeling, for load cases due to various loading conditions that might be encountered in the life of a pen. Under each load case, an appropriate safety factor related to the likelihood of the case was used. The load cases are:

- Drag force from current at the site or when being towed. Using a total drag force that was extrapolated from the tow testing results, the total force is

distributed around the pen based on locating maximum forces on the leading and trailing faces, as oriented to the current.
- Dead load of a pen hanging from a crane on its five part bridle.
- Drag forces with the pen in a current but with one and two broken bridle lines.

There have been numerous numerical simulations made of mooring line arrangements to refine the mooring system arrangement, and this has been an iterative process of examining the forces in the pen from a given loading and mooring arrangement. Through examination and rejection of a number of possible mooring schemes, OFT was able to come up with the final bridle arrangement that minimizes and localizes the maximum loading in the struts. This arrangement features five tangent bridle lines attached at the intersections of the base icosahedron faces, which, in the pen, are seen as a five panel intersection. The five panels form a pentagon. The analysis has found that locating the mooring at this position and angle will reduce the maximum strut forces and provide a superior distribution of loads within the structure.

The hub reinforcement consists of bent steel gusset replacements for the plastic gussets in each corner of the panels framing into the pentagons, in effect creating a steel ring at each of these hubs. The central hub of each pentagon receives a steel fabrication that reinforces the hub and provides an attachment point for the mooring bridle. The design for the central hub was developed for the conservative a 2-knot current loading, and a lighter design was developed for the Beta pen where the current is less.

When the member strut forces from each load case were sorted by magnitude, they were compared to critical allowable loading, assigned to the compression or tension members. When mapped to the actual positions, in all cases, the maximum strut loads, both tension and compression, are relatively concentrated in the pentagons around the mooring forces, and a few panels around them. The geodesic sphere distributes loading very quickly away from these areas and the struts forces become very low. Thus, OFT developed the recommended reinforcement of the pentagons related to the mooring attachments. This consisted of selective triangle receiving steel gussets and some additional bolting.

In addition, OFT looked at the sphere under the same drag forces but with various broken tension or compression struts, and did not find much difference as compared to a broken bridle line. Critical strut failure, next to a mooring attachment, at most will relieve the mooring force of that line and redistribute load to the others. Failure of struts elsewhere in the sphere just redistributes around the broken strut area to adjacent struts, which have plenty of reserve. Thus, the structure appears to be very robust and redundant.

OFT has engineered on the conservative side with reinforcement requirements. The total test compressive load of 4,800 lbs on the unmeshed strut is more than the load previously calculated using the material properties provided by the vendor, and the load with the mesh included is even greater. The design has been using 3,800 lbs for the buckling strength of the short sides of the mooring panels, which is quite a bit less than either of the test results. The test data shows that the compressive buckling modulus of elasticity from the published value of the vendor is too low, since the test buckling strength is several times higher than the predicted strength. In the A3250, all members with compression loads greater than their buckling load calculated with E = 75,000 were reinforced. Since the tests show greater E, around 150,000, this reinforcement is quite conservative.

Feasibility of Scale-Up

OFT performed a preliminary analysis of a 28-m diameter pen using a scaled-up version of the A3250. This is an icosahedron but uses many additional panels of the same basic size of about 10 ft to a side, and encloses 11,000 m^3. The dead load case is the most severe. This is the load seen if the sphere were hung from a crane. The drag load with one broken mooring line appears to cause a similar magnitude axial loading in the worst struts. Since the dead load is 90,500 lbs., it will exceed the drag load determined using the drag calculation. The drag at 1 m/s current (2 knots) would be around 60,000 lbs.

The most-loaded members are all associated with the mooring line attachment points as before. The pentagon at each mooring line is highly loaded, more so than the previous A3250 aquapod, and will be

specifically reinforced as before. These loadings are relatively discrete areas and an inexpensive reinforcement will be devised for these pentagons, or they will be specially fabricated from a different material or configuration.

There are also high loads in the next members radiating from the pentagon on the downstream side. After the pentagon, most of the highest stressed members are in the hexagon of six panels just downstream of the pentagon. This hexagon will be treated like the pentagon and reinforced to handle the loads. The rest of the pen seems to have relatively lower loads. The extruded HDPE material with wire mesh is very capable of these loadings.

Aquapod Installations and Experience to Date

Ocean Farm Technologies has installed 26 Aquapod net pens prior to 2011. Initial prototypes were deployed in Maine and New Hampshire (Figs. 7–9). The first commercial-sized installation of a Beta model was in Culebra Puerto Rico at Snapperfarm Inc (Fig. 10). A commercial crop of cobia (*Rachycentron canadum*) was grown in this Aquapod. OFT proceeded to develop small net pens with installations in Panama (Figs. 11, 12 and 13) and Mexico 9 (Fig. 14). The first commercial sale, in 2008, was to a company in South Korea which was in transition from wild-catch fishery to farming (Figs. 15 and 16). Most recent sales have been to Mexico, where several sizes of Aquapods are deployed to grow shrimp (*p. vannemei*) (Figs. 17, 18, and 19).

Future Directions

Low-Volume High-Density Net Pen Culture for Open Ocean Aquaculture

The emergence of an open ocean aquaculture industry provides an opportunity to reexamine traditional practices, such as the preference for ever-larger net pens for fish containment. The industry's focus on maximizing

Aquapod Systems for Sustainable Ocean Aquaculture. Figure 8
Bucks Harbor, Maine 2005 prototype B A400

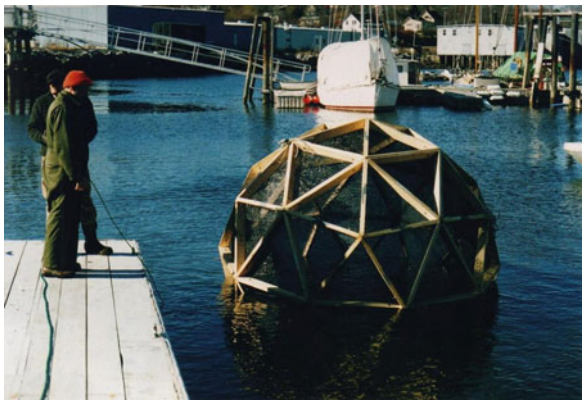

Aquapod Systems for Sustainable Ocean Aquaculture. Figure 7
Belfast, Maine, USA 2004 prototype A

Aquapod Systems for Sustainable Ocean Aquaculture. Figure 9
Portsmouth, New Hampshire, USA 2005 prototype C A400

net pen size is driven by the convention that large net pens provide more growing volume for a given investment. Because net pen costs can vary with the square of linear dimension while the volume varies by the cube, this assumption has merit. However, the assumption that larger net pens are more cost effective requires that stocking density remain unchanged throughout the size comparison. Stocking density in terms of kilograms per cubic meter is a useful fish-husbandry parameter in pond- and tank-based aquaculture where extensive research has been done and where water exchanges are predetermined. There is also a growing body of data regarding stocking density in salmon net pens; however, these studies have been done in near-shore, low-energy environments. Little or no research has been done in open ocean net pen culture comparing density optimization over a range of net pen volumes, especially small net pens.

The principle advantage of small pens is that ongrowing fish are closer to their source of clean

Aquapod Systems for Sustainable Ocean Aquaculture. Figure 10
Culebra, Puerto Rico 2006 Beta 1 A3250

Aquapod Systems for Sustainable Ocean Aquaculture. Figure 12
Woods Hole, Massachusetts, USA 2008 Aquadome

Aquapod Systems for Sustainable Ocean Aquaculture. Figure 11
Puerto Lindo, Panama 2008 Beta 2 Micropods

Aquapod Systems for Sustainable Ocean Aquaculture. Figure 13
South Korea, 2009 A3600

water. By similar logic, the small net pen, as a whole, because of its shorter stream-wide dimension experiences more water exchanges in a given current. From the perspective of an individual fish in an ocean net pen, water quality depends on how many other fish are metabolizing between it and its source of clean and oxygenated water from outside the containment. At constant kg/m^3, interior fish in a large net pen experience significantly degraded water quality compared to interior fish in a small net pen.

The potential advantage of low-volume, high-density (LVHD) net pen culture is not a new concept. Schmittou pioneered the concept of LVHD in 1968, and the approach has since been applied in a project sponsored by the American Soybean Association in China [4]. Growing densities of up to 200 kg/m^3 are recorded. McMaster et al. [5] suggests stocking density ranges for Florida pompano between 35 and 100 kg/m^3. Even at close to typical salmon stocking densities, the economics of small net pens become apparent. Table 1 shows a constant crop yield per capital investment in containment as density in the smaller net pens is increased.

Aquapod Systems for Sustainable Ocean Aquaculture. Figure 14
South Korea, 2009 3-A3600

Aquapod Systems for Sustainable Ocean Aquaculture. Figure 15
Panama, 2010 A132 copper mesh

Aquapod Systems for Sustainable Ocean Aquaculture. Figure 16
Mexico, 2009 A3600 under tow

Aquapod Systems for Sustainable Ocean Aquaculture. Figure 17
Sorrento, ME USA A400

Aquapod Systems for Sustainable Ocean Aquaculture. Figure 18
Mexico, 2010 2-A3600, 1-A212

In addition to this economic advantage, strong, secure small net pens will alleviate some of the economic barrier to entry for offshore fish farming. Small net pens require smaller vessels and support equipment; they are easily shipped, assembled, and deployed. In the near term, OFT sees a potential market for net pen hardware export to developing world economies that are transitioning from capture fisheries to fish farming, and who want to skip the near-shore environmental problems and user conflicts by moving directly offshore. This includes third world artisanal fishermen who in global aggregate contribute to marine fish resource depletion. Also, the mooring gear required for smaller net pens is lighter and more secure; scuba diving is reduced – especially deep diving; harvesting is easier; small pens are easier to tow; and risk is diversified.

Aquapod Systems for Sustainable Ocean Aquaculture. Figure 19
Mexico 2010 A212 under tow

Aquapod Systems for Sustainable Ocean Aquaculture. Table 1 The 212 m^3 net pen stocked at 51 kg/m^3 gives interior fish better access to clean water (less biomass between center of net pen and net) and an equal yield per capital cost of containment

Yield from various-sized Aquapod net pens							
Size of pen m^3	Radius (m)	Diameter (ft)	Approximate cost of aquapod (USD)	Final stocking density (kg/m^3)	Biomass of fish between center of pen and net	Yield per pen (kg)	Yield (kg) per capital cost of containment (kg/$)
7,000	11.87	77.8	$218,000	17	202	119,000	0.55
3,600	9.51	62.4	$140,000	21	200	75,600	0.54
212	4.04	26.7	$20,000	51	189	10,812	0.54

Use of Small Aquapods for Artisanal Fish Farming

According to the FAO, "Artisanal Fisheries" are traditional fisheries involving fishing households (as opposed to commercial companies), using relatively small amount of capital and energy, relatively small fishing vessels or canoes, often beach-based, making short fishing trips, close to shore, mainly for local consumption. Artisanal fisheries can be subsistence or commercial fisheries, providing for local consumption or even export. They are sometimes referred to as small-scale fisheries or day fisheries.

Numbers of artisanal fishermen are hard to obtain because the sector is informal, often outside the regulated fishery (some illegal) and part-time. In Ghana, for example, canoe fishermen go to sea for about 150 days a year. Half the catch is obtained in 2 months, so it is obviously a part-time endeavor. The FAO estimates that as much as 95% of the annual catch in Africa is from artisanal fisheries. In Mexico, the FAO estimates that 96.6% of the fishing fleet (108,205 boats) are *panga* (skiffs). Worldwide, the UN estimates there are 35-million people whose primary livelihood comes directly from fishing, and that artisanal fishermen outnumber large- and medium-scale fishermen by 4 or 5 to 1. This would put the number of artisanal fishermen in the range of 28 million to 30 million individuals worldwide (Table 2).

From NIOSH Second Conference on International Fishing Industry Safety and Health Overexploitation of coastal resources and decreasing catches has forced subsistence artisanal fishermen to go further offshore in search of fish in vessels designed for near-shore use. In a study done in 2000, the FAO reports an alarming increase in fishing-related fatalities as a result.

Small-scale marine aquaculture is one way to bring sustainability and consistency to this often-overlooked fishery sector. Turning artisanal fishermen into artisanal fish farmers will not be an easy task. However, small Aquapods have several advantages, beside

Aquapod Systems for Sustainable Ocean Aquaculture. Table 2 Estimates of the number of fishing vessels in Pacifica [3]

Location	Locally based vessels [3]	Motorized artisanal fishing vessels [6]	Nonmotorized artisanal fishing vessels [6]
Cook Islands	10 L/L	200	120
Fiji	96 L/L; 1 P/L	1,600	400
Fed. States Micro.	34 L/L; 8 P/S	2,000	600
Kiribati	2 L/L; 1 P/S	600	5,000
Marshall Islands	54 L/L; 5 P/S	500	250
Nauru	1 L/L	100	80
Niue	100 skiffs	60	240
Palua	71 L/L; 1 P/S	700	40
PNG	40 L/L; 24 P/S	8,000	10,000
Samoa	153 L/L	80	100
Solomon Islands	8 L/L; 2 P/S; 12 P/L	1,800	5,000
Tonga	26 L/L	800	200
Tuvalu	20 skiffs	200	500
Vanatu	10 skiffs	250	500
Total	495 L/L; 40 P/S; 14 P/L	16,890	24,530

P/L pole and line vessel, *P/S* purse seiner, *L/L* longliner

affordability, that makes them advantageous for artisanal aquaculture:

- Size of boats and equipment can be smaller
  - The 7–10-m diameter Aquapods can be serviced with existing artisan vessels, whether motorized or not. Equipment needs are minimized and may include a small air compressor or pump.
- Ease of assembly and deployment – lighter mooring gear
  - Small Aquapods are easy to assemble, and can be put together by several men using hand tools on a beach and rolled into the water (or rolled out of the water for harvest). The small sectional area means a relatively low drag resistance, so mooring gear can be much lighter than traditional net pens.
- Single-point moorings are simple and inexpensive
  - An attractive option from a cost and environmental standpoint for these small pens is a single-point mooring, allowing the net pen to swing in a watch circle just as a boat moored in a harbor. Low drag forces on the anchor make this feasible.
- Less deep diving, most diving can be done by hookah
  - A net pen less than 10 m in diameter, when brought to the surface for maintenance, will allow almost all underwater activity to be performed without scuba gear. The spherical shape of the pen and the ability to rotate it allows for all portions of the net to be surfaced.
- More available deployment areas due to shallower water depth
  - Conventionally sized submersible pens require water depths of more than 30 m. The small Aquapods can be deployed in water depths of 12–25 m. This means boat trips far offshore are not necessary.
- Easier harvest – selective harvest by netting or whole pen harvest is possible.
- Diversification of risk as opposed to "all eggs in one basket."
- Ease of towing – their small size and rigidity facilitate easy repositioning, or towing of a pen to market port.
- Predator proof
  - Sharks, seals, and sea lions are a huge risk to artisanal fisheries – in some places, sharks are one of the main targets of artisanal fishermen. According to the Chamber of Commerce in Somalia, sharks constitute 90% of the artisanal catch. Artisanal fish farmers cannot tolerate this risk to the crop and to human safety, and the shark proof Aquapod is the solution.
- Storm resistant
  - The Aquapod net pens are submersible, so they can be submerged below storm waves when a hurricane or typhoon approaches, eliminating a potentially devastating risk.

Economics of Artisanal Fish Farming with Aquapods

Catch estimates from artisanal fishermen are difficult to obtain – most are subsistence harvests, some excess is sold locally, and a little is exported. The sparse data that exists can only estimate the amount of fish that are consumed by the fisherman's family and community based on how much is sold. However, FAO estimates of annual catches range from 2.5 t per year per boat (Yemen) to 3.6 t per year per (Mexico). Considering that the smallest Aquapod ($212m^3$) could easily contain 5–10 t of fish at harvest, several of these small pens could probably produce more harvest than most artisanal fishermen ever see in a year.

Following is a spreadsheet analysis of what the economics of a small artisanal fish farm would look like. The assumptions include realistic and current pricing for commercial fish farm expenses, as low-volume pricing and sourcing of feed and fingerlings is unknown, and most likely would require some public sector support. As with all producing units, the sensitivity of market price trumps all other variables. Labor costs are assumed to be nil, as this is a family-scale operation.

The establishment of artisanal fish farms will likely be a private/public cooperative effort with governments and/or NGO's subsidizing some capital costs, providing low interest loans, organizing distribution of feed and fingerlings, and providing training to artisanal fishermen as incentives to evolve from dependence on shrinking capture fisheries to a sustainable farming economy.

Artisanal Aquapod Farm					
A212 Aquapod Net Pens (No. of Aquapod Net Pens: 4)					
Sales	$212,000		*Assumptions*		
Cost of goods sold			Biological FCR	1.7	
Feed	$124,879		Feed cost per kg	$1.65	
Fingerling	$34,980		Harvest size in kg	2.0	
Outside services	$1,000		Price of fingerlings	$1.50	ea.
Dive/Scuba expenses	$2,000		m^3 of growing vol.	848	
Workboat expenses	$3,000		Stocking final density	50	kg/m3
Fuel and oil expense	$1,500		Number of fish harvested	21,200	
Small tools	$250		Kg Harvested	42,400	
Concession	$500		Sale price	$5.00	Kg
Consumables	$750		Amortization period	7	years
Maintenance	$1,500		Aquapod A212 net pen cost	$19,000	ea.
Miscellaneous	$800		Mooring cost	$3,000	ea.
Fish health	$1,000		Total capital cost	$88,000	
Amortization of Aquapods	$12,571		Annual amortization expense	$12,571	
Cost of goods sold	$184,730				
Gross margin	$27,270				
Other overhead	$1,200				
Net Income	$26,070				

Bibliography

1. DeCew J, Page S, Turmelle CA, Irish J (2006) Interior current reduction of the Aquapod™ cage. In: OCEANS 2006, OCEANS'06MTS/IEEE, Boston
2. Caccese V (2006) Structural testing of various configurations for the aquapod net pen. Report No. C2004-018-001. Department of Mechanical Engineering, University of Maine, Maine, 38 pp
3. Gillett R (2003) Aspects of sea safety in the fisheries of pacific island countries. FAO, Rome, 12
4. Swick RA (2001) Feed based tilapia culture. Technical Bulletin AQ49-2001, American Soybean Association
5. McMaster MF, Kloth TC, Coburn JF (2003) Prospects for commercial pompano mariculture. Aquaculture America 2003
6. McCoy (1991) NIOSH Second Conference on International Fishing Industry Safety and Health 1991

Atmosphere-Water Exchange

Bernd Jähne
Institute for Environmental Physics and Heidelberg Collaboratory for Image Processing (HCI), University of Heidelberg, Heidelberg, Germany

Article Outline

Glossary
Definition of the Subject
Introduction
Mechanisms of Atmosphere–Water Exchange
Experimental Techniques and Results
Empiric Parametrization
Future Directions
Bibliography

Glossary

Bulk coefficients c_i relate the *transfer velocity* k for a species i to the *wind velocity* U_r in a reference height, typically at 10 m above the mean water level: $c_i = k_i/U_r$. From the bulk coefficient, the flux density j_i of a species can be computed as $j_i = c_i(C_r - C_0)U_r$, where C_r and C_0 are the corresponding concentrations at the reference height and right at the water surface, respectively. For momentum density (ρU) the bulk coefficients is also known as the *drag coefficient* c_D. It can also be expressed as $c_D = (u_*/U_r)^2$ with the momentum flux given by $j_m = \rho u_*^2$; u_* is the *friction velocity*.

Friction velocity u_* is a measure for the tangential force per area applied by the wind at the water surface, the shear stress $\tau = \rho u_*^2$, which is also equal to the vertical momentum flux density j_m.

Mass boundary layer Thickness of the layers at both sides of the water surface in which transport of mass by turbulence is smaller than by molecular diffusion.

Schmidt and Prandtl numbers, Sc and Pr The Schmidt and Prandtl numbers are the ratio of kinematic viscosity ν (molecular diffusion coefficient for momentum) and the molecular diffusion coefficients for the corresponding chemical species, D, and heat, D_h, respectively. Thus, these numbers express how much slower chemical species and heat, respectively, are transported by molecular processes than momentum. In air, these numbers are in the order of one; in water, the Prandtl number is about 10 and the Schmidt number about 1,000.

Transfer velocity k is the velocity by which a momentum, heat, and chemical are transported across the surface; because of the concentration discontinuity at the water surface, the transfer velocity on the air side is different from the transfer velocity on the water side.

Viscous boundary layer Thickness of the layers at both sides of the water surface in which transport of momentum by turbulent is smaller than by molecular friction, resulting in a linear velocity profile in this layer.

Definition of the Subject

Gaseous and volatile chemical species reside not only in the atmosphere. Because they dissolve in water, they are also distributed in the hydrosphere. The by far largest part of the hydrosphere is the ocean. Therefore, the exchange between atmosphere and oceans is the most important process for the fate of gaseous and volatile chemical species (Table 1).

For long-lived species, that is, life time by reaction larger than residence times in either the atmosphere or the ocean, two basic factors determine the fate of these species. For time scales longer than the turnover time of ocean mixing, which is much slower than the same process in the atmosphere, the solubility of the species determines where it ends up. On much shorter time scales, the speed by which the species are exchanged between atmosphere and ocean and the concentration difference determines the flux between these two compartments.

Atmosphere-Water Exchange. Table 1 Comparison of size (as depth in m over entire earth surface) and mass of atmosphere and global water storage

System	Depth (m)	Mass (10^{18} kg)
Oceans	2,624	1,382
Ice caps and glaciers	47	25
Total ground water	46	24
Lakes	0.35	0.18
Rivers	0.004	0.002
Atmosphere	8,000	5.3

While turbulent mixing is quite fast within the ocean and the atmosphere, it becomes more and more inefficient, the closer a species is transported to the surface. The final step toward the interface must be overcome by molecular diffusion, which is a slow process, especially in water. Therefore, very thin mass boundary layers at both sides of the water surface, in which turbulent transport is slower than molecular transport, are the bottleneck of the exchange between atmosphere and ocean.

In this way, tiny layers only about 20–200 μm thick in the water and 200–2,000 μm thick in the air control the exchange process. In consequence, the crucial question is which processes determine the thickness of these layers.

Introduction

Research in air–water gas exchange dates back more than a century. Bohr [1], for example, was one of the first to study the exchange of carbon dioxide in a stirred bottle. With the early observation of increasing carbon dioxide concentration in the atmosphere interest in air-sea gas exchange rose considerably, triggered by the question how much of the excess carbon dioxide would go into the ocean [2, 3]. Since then significant and continuous research work was devoted for a better understanding of air–water mass exchange, but the mechanisms of the exchange processes are still not fully understood even today.

This entry is divided into three major parts and partly based on previous reviews of the author on the same subject [4–6]. Section "Mechanisms of Atmosphere–Water Exchange" describes the basic

mechanisms of air–water exchange and the many parameters influencing it. Focusing on field data, section "Experimental Techniques and Results" summarizes the various experimental techniques and gives a synthesis of the available experimental data. Using the information collected in the previous two sections, section "Empiric Parametrization" tries to give the best possible empirical parametrization of the exchange rate and section "Future Directions" points to future directions of research.

Mechanisms of Atmosphere–Water Exchange

Turbulent and Molecular Transport

The transfer of gases and volatile chemical species between the atmosphere and oceans is driven by a concentration difference and the transport by molecular and turbulent motion. Both types of transport processes can be characterized by *diffusion coefficients*, denoted by D and K_c, respectively. The resulting flux area density $\boldsymbol{j}_c$ is proportional to the diffusion coefficient and the concentration gradient:

$$j_c = -(D+K_c(z))\nabla_c. \tag{1}$$

In a stationary homogeneous case and without sinks and sources by chemical reactions, the flux density $\boldsymbol{j}$ is in vertical direction and constant. Then integration of Eq. 1 yields vertical concentration profiles:

$$C(z_r) - C(0) = j_c \int_0^{z_r} \frac{1}{D + K_c(z)}\, dz. \tag{2}$$

The molecular diffusion coefficient is proportional to the velocity of the molecules and the free length between collisions. The same concept can be applied to turbulent diffusion coefficients. Far away from the interface, the free length (called *mixing length*) is set proportional to the distance from the interface and the turbulent diffusion coefficient K_c for mass transfer is:

$$K_c = \frac{k}{Sc_t} u_* z, \tag{3}$$

where $\kappa = 0.41$ is the *von Kármán constant*, u_*, the *friction velocity*, a measure for the velocity fluctuations in a turbulent flow, and $Sc_t = K_m/K_c$ the *turbulent Schmidt number*. Closer to the interface, the turbulent diffusion coefficients are decreasing even faster. Once a critical length scale l is reached, the Reynolds number $Re = u_* l/\nu$ (ν is the kinematic viscosity, the molecular diffusion coefficient for momentum) becomes small enough so that turbulent motion is attenuated by viscosity. The degree of attenuation depends on the properties of the interface. At a smooth solid wall, $K_c \propto z^3$, at a free water interface it could be in the range between $K_c \propto z^3$ and $K_c \propto z^2$ depending on surface conditions.

Viscous and Mass Boundary Layers

Boundary layers are formed on both sides of the interface (Fig. 1). When the turbulent diffusivity becomes equal to the kinematic viscosity, the edge of the *viscous boundary layer* is reached. As the name implies, this layer is dominated by viscous dissipation and the velocity profile becomes linear because of a constant diffusivity. The edge of the *mass boundary layer* is reached when the turbulent diffusivity becomes equal to the molecular diffusivity. The relative thickness of both boundary layers depends on the dimensionless ratio $Sc = \nu/D$ (*Schmidt number*).

The viscous and mass boundary layers are of about the same thickness in the air, because values of D for

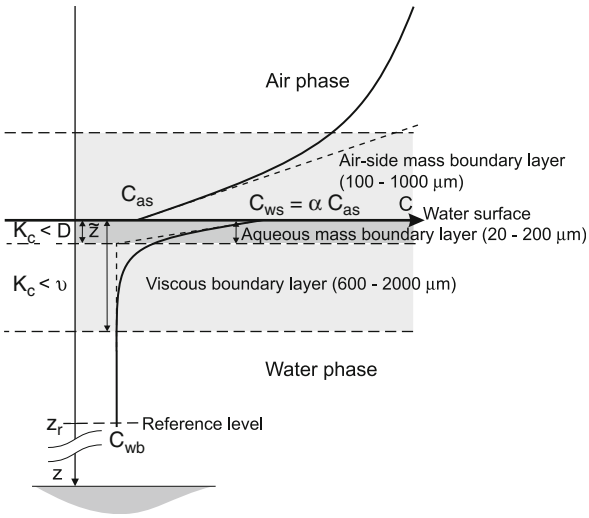

Atmosphere-Water Exchange. Figure 1
Schematic graph of the mass boundary layers at a gas–liquid interface for a tracer with a solubility $\alpha = 3$

various gaseous species and momentum are about the same (Sc_{air} is 0.56 for H_2O, 0.63 for heat, and 0.83 for CO_2). In the liquid phase, the situation is completely different. With Schmidt numbers in the range from 100 to 3,000 (Fig. 2, Table 3), molecular diffusion for a dissolved volatile chemical species is two to three orders of magnitude slower than diffusion of momentum (Table 2). Thus, the mass boundary layer is significantly thinner than the viscous boundary layer in the liquid phase. This means that the transfer of gases is much slower and almost entirely controlled by the tiny residual turbulence in the small top fraction of the viscous boundary layer. This basic fact makes it difficult to investigate the mechanism of air–water gas transfer both theoretically and experimentally. In addition, the transfer process depends strongly on the water temperature because the Schmidt number decreases by about a factor of 6 from 0°C to 35°C (Fig. 2, Table 3).

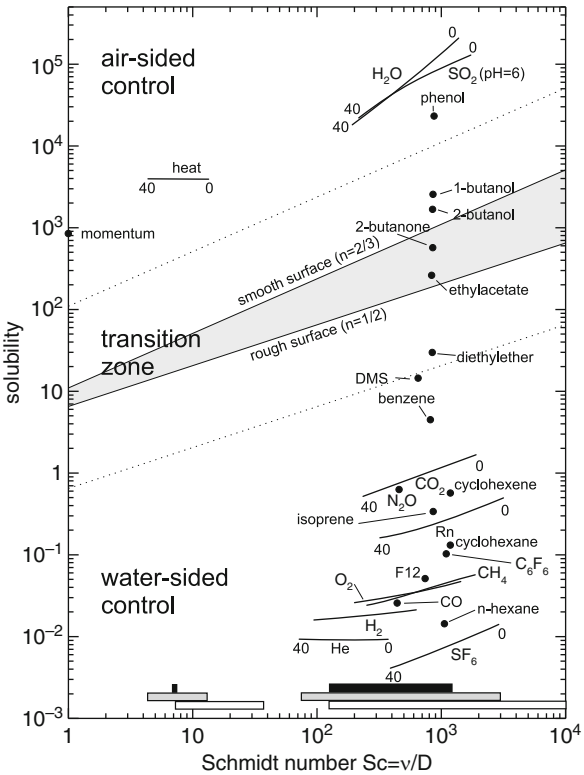

Atmosphere-Water Exchange. Figure 2
Schmidt number/solubility diagram including various volatile tracers, momentum, and heat for a temperature range (C) as indicated. *Filled circles* refer to only a temperature of 20°C. The regions for air-side, mixed, and water-side control of the transfer process between gas and liquid phase are marked. At the solid lines, the transfer resistance is equal in both phases. The following dimensional transfer resistances were used: $r_a = 31$, $r_w = 12Sc^{2/3}$ (smooth), $r_w = 6.5Sc^{1/2}$ (wavy surface) with $r_a = R_a u_{*a}$ and $r_w = R_w u_{*w}$ (Adapted from Jähne and Haußecker [6])

Description of Transport

The amount of species exchanged between the air and water across the interface can be described by a quantity with the units of a velocity. It represents the velocity with which a tracer is pushed by an imaginary piston across the surface. This quantity is known as the *transfer velocity* k (also known as the *piston velocity, gas exchange rate* or *transfer coefficient*). It is defined as the flux density divided by the concentration difference between the surface and the bulk at some reference level z_r:

$$k = \frac{j_c}{C_s - C_b}. \tag{4}$$

The inverse of the transfer velocity is known as the *transfer resistance* R:

$$R = \frac{C_s - C_b}{j_c}. \tag{5}$$

The indices s and b denote the surface and bulk. Both quantities can directly be related to vertical concentration profiles by introducing Eqs. 4 and 5 into Eq. 2:

$$R = \frac{1}{k} = \int_0^{z_r} \frac{1}{D + K_e(z)}\, dz. \tag{6}$$

Thus, the transfer resistances over several height intervals can be added in the same way as electrical resistances that are connected in series. Typical values of the transfer velocity across the water-side mass boundary layer are 10^{-6}–10^{-5} m/s (1–10 m/day). With respect to typical mixed layer depths in the ocean of about 100 m, gas transfer is a very slow process. It takes a time constant $\tau = h/k = 10$–100 days for the concentration of dissolved gases in the mixed layer to come into equilibrium with the atmosphere.

Atmosphere-Water Exchange. Table 2 Diffusion coefficients for various gases and volatile chemical species in deionized water and in some cases in sea water collected from Jähne et al. [18] and King et al. [20]. Die data for momentum (kinematic viscosity) are from Sündermann [22]. Column 3 and 4 contain the parameters for the fit of the diffusion coefficient: $D = A \exp[-E_a/(RT)]$, the last four columns the diffusion coefficients for 5°C, 15°C, 25°C, and 35°C

Species	Molecular mass	A (10^{-5} cm^2/s)	E_a (kJ/mole)	σ(Fit) %	Diffusion coefficient (10^{-5} cm^2/s)			
					5°C	15°C	25°C	35°C
Momentum	–				1,517	1,139	893.4	724.3
Momentum[a]	–				1,560	1,182	934.5	763.9
Heat	–	379.2	2.375		135.80	140.72	145.48	150.08
^{3}He[b,c]	3.02	941	11.70	2.1	5.97	7.12	8.39	9.77
^{4}He	4.00	818	11.70	2.1	5.10	6.30	7.22	8.48
^{4}He[a]		886	12.02	1.8	4.86	5.88	7.02	8.03
Ne	20.18	1,608	14.84	3.5	2.61	3.28	4.16	4.82
Kr	83.80	6,393	20.20	1.6	1.02	1.41	1.84	2.40
Xe	131.30	9,007	21.61	3.5	0.77	1.12	1.47	1.94
^{222}Rn[b]	222.00	15,877	23.26	11	0.68	0.96	1.34	1.81
H_2	2.02	3,338	16.06	1.6	3.17	4.10	5.13	6.23
H_2[a]		1,981	14.93	4.3	3.05	3.97	4.91	5.70
CH_4	16.04	3,047	18.36	2.7	1.12	1.48	1.84	2.43
CO_2	44.01	5,019	19.51	1.3	1.07	1.45	1.91	2.43
DMS[b]	62.13	2,000	18.10		0.80	1.05	1.35	1.71
CH_3Br[b]	94.94	3,800	19.10		0.98	1.31	1.71	2.20
F_{12}[b] (CCl_2F_2)	120.91	4,100	20.50		0.58	0.79	1.05	1.37
F_{11}[b](CCl_3F)	137.37	3,400	20.00		0.60	0.81	1.07	1.38
SF_6[b]	146.05	2,900	19.30		0.69	0.92	1.20	1.55

[a]In sea water
[b]Values of diffusion coefficients from fit, not measured values
[c]Set 15% higher than ^{4}He

Boundary Layer Thickness The *boundary layer thickness* $\tilde{z}$ is defined as the thickness of a fictional layer in which the flux is maintained only by molecular transport: $j = D(C_s - C_b)/\tilde{z}$. Then with Eq. 4 the boundary layer thickness is given by:

$$\tilde{z} = \frac{D}{k}. \tag{7}$$

Geometrically, $\tilde{z}$ is given as the intercept of the tangent to the concentration profile at the surface and the bulk (Fig. 1). With thicknesses between 20 and 200 µm, the mass boundary layer is extremely thin.

Boundary Layer Time Constant The *time constant* $\tilde{t}$ for the transport across the mass boundary layer is given by:

$$\tilde{t} = \frac{\tilde{z}}{k} = \frac{D}{k^2}. \tag{8}$$

Typical values for $\tilde{t}$ are 0.04–4 s. Any chemical reaction with a time constant larger than $\tilde{t}$ does not significantly affect the transfer process. Therefore, CO_2 can be regarded as an inert gas, but not fast hydrating acid gases such as SO_2.

Atmosphere-Water Exchange. Table 3 Schmidt numbers of various gases and volatile species in the temperature range from 0°C to 40°C

Species	Schmidt number								
	0°C	5°C	10°C	15°C	20°C	25°C	30°C	35°C	40°C
Heat	13.45	11.19	9.46	8.10	7.02	6.14	5.42	4.82	4.32
^{3}He	329	254	200	160	130	107	88	74	63
^{4}He	379	293	230	184	149	122	102	85	72
^{4}He[a]	411	319	252	201	164	135	112	94	79
Ne	768	579	445	347	276	221	180	148	122
Kr	2,045	1,478	1,090	819	625	483	379	301	241
Xe	2,701	1,930	1,409	1,047	791	606	471	370	294
^{222}Rn	3,168	2,235	1,611	1,182	883	669	514	400	314
H_2	633	473	360	278	219	174	140	114	94
H_2[a]	663	502	387	304	242	195	159	131	109
CH_4	1,908	1,400	1,047	797	616	483	383	308	250
CO_2	1,922	1,397	1,036	782	600	466	367	293	236
DMS	2,593	1,905	1,428	1,089	844	662	527	423	344
CH_3Br	2,120	1,545	1,150	870	669	522	412	329	266
F_{12} (CCl_2F_2)	3,639	2,624	1,931	1,447	1,102	851	666	527	422
F_{11}(CCl_3F)	3,521	2,549	1,883	1,416	1,082	839	658	523	420
SF_6	3,033	2,208	1,640	1,239	952	741	585	467	376

[a]In sea water

The definitions of the three parameters k, $\tilde{z}$, $\tilde{t}$ are generally valid and do not depend on any models of the boundary layer turbulence. According to Eqs. 7 and 8, they are coupled via the molecular diffusion coefficient. Therefore, only one of them needs to be measured to get knowledge of all three parameters provided the molecular diffusion coefficient of the species is known.

Partitioning of Transfer Between Air and Water

Because a mass boundary layer exists on both sides, it is important to determine which one controls the transfer, that is, exhibits the largest transfer resistance (or lowest transfer velocity). At the surface itself, the thermodynamic solubility equilibrium is assumed to be established between the tracer concentrations c_a in the gas phase and c_w in the liquid phase:

$$C_{ws} = \alpha C_{as}, \tag{9}$$

where α is the dimensionless solubility (partition coefficient). A solubility $\alpha \neq 1$ causes a concentration jump at the surface (Fig. 1). Thus, the resulting total transfer velocity k_t or transfer resistance R_t can either be viewed from the gas phase or the liquid phase. Adding them up, the factor α must be considered to conserve the continuity of the concentration profile:

$$\text{air side}: \frac{1}{k_{at}} = \frac{1}{k_a} + \frac{1}{\alpha k_w}, \quad R_{at} = R_a + R_w/\alpha, \tag{10}$$

$$\text{water side}: \frac{1}{k_{wt}} = \frac{\alpha}{k_a} + \frac{1}{k_w}, \quad R_{wt} = \alpha R_a + R_w.$$

The total transfer velocities in air and water differ by the factor α: $k_{at} = \alpha k_{wt}$. The ratio $\alpha k_w/k_a$ determines which boundary layer controls the transfer process. A high solubility shifts control of the transfer process

to the gas-phase boundary layer, and a low solubility to the aqueous layer. The solubility value for a transition from air-sided to water-sided control depends on the ratio of the transfer velocities. Typically k_w is about 100–1,000 times smaller than k_a. Thus, the transfer of even moderately soluble volatile chemical species with solubilities up to 30 is controlled by the water side. Some environmentally important species lie in a transition zone where it is required to consider both transport processes (Fig. 2). The transfer of highly soluble volatile and/or chemically reactive gas is controlled by the air-side transfer process and thus analogous to the transfer of water vapor. The following considerations concentrate on the water-side transfer process.

Gas Exchange at Smooth Water Surfaces

At smooth water surfaces, the theory of mass transfer is well established because it is equivalent to mass transfer to a smooth solid wall. The turbulent diffusivity can be described by the classic approach of Reichardt [7] with an initial z^3 increase that smoothly changes to a linear increase in the turbulent layer as in Eq. 3. Then integration of Eq. 6 yields the following approximation for Schmidt numbers higher than 100 [12, 16]:

$$k_w = u_{*w} \frac{1}{12.2} Sc^{-2/3} \quad Sc > 60. \tag{11}$$

This equation establishes the basic analogy between momentum transfer and gas exchange. The transfer coefficients are proportional to the friction velocity in water, which describes the shear stress (tangential force per unit area) $\tau = \rho_w u_{*w}^2$ applied by the wind field at the water surface. Assuming stress continuity at the water surface, the friction velocity in water is related to the friction velocity in air by:

$$u_{*w} = u_{*a} \left(\frac{\rho_a}{\rho_w} \right)^{1/2}. \tag{12}$$

The friction velocity in air, u_{*a}, can further be linked via the drag coefficient to the wind speed U_R at a reference height: $c_D = (u_{*a}/U_R)^2$. Depending on the roughness of the sea surface, the drag coefficient has values between 0.8 and $2.4 \cdot 10^{-3}$. In this way, the gas exchange rate is directly linked to the wind speed. The gas exchange further depends on the chemical species and the water temperature via the Schmidt number.

Influence of Waves

A free water surface is neither solid nor is it smooth as soon as short wind waves are generated. On a free water surface, velocity fluctuations are possible. Thus, there can be convergence or divergence zone at the surface; surface elements may be dilated or contracted. At a clean water surface, dilation or contraction of a surface element does not cause restoring forces, because surface tension only tries to minimize the total free surface area, which is not changed by this process. As a consequence of this hydrodynamic boundary condition, the turbulent diffusivity normal to the interface can now increase with the distance squared from the interface, $K_c \propto z^2$. Then:

$$k_w = u_{*w} \frac{1}{\beta} Sc^{-1/2}, \tag{13}$$

where β is a dimensionless constant.

In comparison to the smooth case in Eq. 11, the exponent n of the Schmidt number drops from $-2/3$ to $-1/2$. This increases the transfer velocity for a Schmidt number of 600 by about a factor of 3. The total enhancement depends on the value of the constant β.

Wind waves cannot be regarded as static roughness elements for the liquid flow because their characteristic particle velocity is of the same order of magnitude as the velocity in the shear layer at the surface. This fact causes a basic asymmetry between the turbulent processes on the air and on the water sides of the interface. Therefore, the wave effect on the turbulent transfer in the water is much stronger and of quite different character than in the air. This basic asymmetry can be seen if the transfer velocity for CO_2 is plotted against the transfer velocity for water vapor (Fig. 3, [15]). At a smooth water surface, the points fall well on the theoretical curve predicted by the theory for a smooth rigid wall. However, as soon as waves occur at the water surface, the transfer velocity of CO_2 increases significantly beyond the predictions.

Even at high wind speeds, the observed surface increase is well below 20% [24]. When waves are

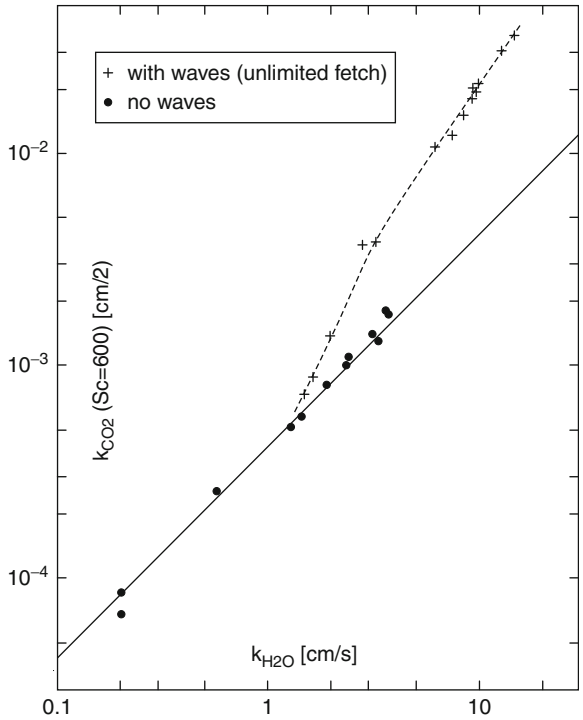

Atmosphere-Water Exchange. Figure 3
Transfer velocity of carbon dioxide plotted against the transfer velocity of water vapor. Measurements from a small annular wind/wave facility Jähne [15]

generated by wind, energy is not only transferred via shear stress into the water but a second energy cycle is established. The energy put by the turbulent wind into the wave field is transferred to other wave numbers by nonlinear wave–wave interaction and finally dissipated by wave breaking, viscous dissipation, and turbulence. The turbulent wave dissipation term is the least known term and of most importance for enhanced near-surface turbulence. Evidence for enhanced turbulence levels below wind waves has been reported from field and laboratory measurements. Experimental results also suggest that the gas transfer rate is better correlated with the *mean square slope* of the waves as an integral measure for the nonlinearity of the wind wave field than with the wind speed.

It is not yet clear, however, to what extent *microscale wave breaking* can account for the observed enhanced gas transfer rates. A gravity wave becomes instable and generates a steep train of capillary waves at its leeward face and has a turbulent wake. This phenomenon can be observed even at low wind speeds, as soon as wind waves are generated. At higher wind speeds, the frequency of microscale wave breaking increases.

At high wind speeds, wave breaking with the entrainment of bubbles may enhance gas transfer further. This phenomenon complicates the gas exchange between atmosphere and the oceans considerably [19, 26]. First, bubbles constitute an additional exchange surface. This surface is, however, only effective for gases with low solubility. For gases with high solubility, the gas bubbles quickly come into equilibrium so that a bubble takes place in the exchange only for a fraction of its life time. Thus bubble-mediated gas exchange depends – in contrast to the exchange at the free surface – on the solubility of the gas tracer. Second, bubble-mediated gas transfer shifts the equilibrium value to slight supersaturation due to the enhanced pressure in the bubbles by surface tension and hydrostatic pressure. Third, breaking waves also enhance near-surface turbulence during the breaking event and the resurfacing of submerged bubbles [17].

Experimental data are still too sparse for the size and depth distribution of bubbles and the flux of the bubbles through the interface under various sea states for a sufficiently accurate modeling of bubble-mediated air-sea gas transfer and thus a reliable estimate of the contribution of bubbles to the total gas transfer rate. Some experiments from wind/wave tunnels and the field suggest that significant enhancements can occur, other experiments could not observe a significant influence of bubbles.

Influence of Surface Films

A film on the water surface creates pressure that works against the contraction of surface elements. This is the point at which the physicochemical structure of the surface influences the structure of the near-surface turbulence as well as the generation of waves [13, 21]. As at a rigid wall, a strong film pressure at the surface maintains a two-dimensional continuity at the interface just as at a rigid wall. Therefore, Eq. 11 should be valid for a smooth film-covered water surface and has indeed been verified in wind/wave tunnel studies as the lower limit for the transfer velocity. As a consequence,

both Eqs. 11 and 13 can only be regarded as limiting cases. A more general approach is required that has not yet been established. One possibility is a generalization of Eqs. 11 and 13 to:

$$k_w = u_{*w} \frac{1}{\beta(s)} Sc^{-n(s)}, \tag{14}$$

where both β and n depend on dimensionless parameters describing the surface conditions s. Even films with low film pressure may easily decrease the gas transfer rate to half of its value at clean water surface conditions. But still too few measurements at sea are available to establish the influence of surfactants on gas transfer for oceanic conditions more quantitatively.

Experimental Techniques and Results

Laboratory Facilities

Laboratory facilities play an important role in the investigation of air-sea gas transfer. Only laboratory studies allow a systematic study of the mechanisms and are thus an indispensable complement to field experiments. Almost all basic knowledge about gas transfer has been gained by laboratory experiments in the past.

Geochemical Tracer Techniques

The first oceanic gas exchange measurements were performed using geochemical tracer methods such as the ^{14}C [2], $^{3}He/T$ [23], or $^{222}Rn/^{226}Ra$ [8, 9] methods. The volume and time-average flux density is given by mass balance of the tracer concentration in a volume of water V_w:

$$V_w \dot{c}_w = F_w j \quad or \quad j = h_w \dot{c}_w, \tag{15}$$

where F_w, and h_w are the surface area and the effective height V_w / F_w of a well-mixed water body, respectively. The time constant $\tau_w = h_w / k$ is in the order of days to weeks. It is evident that the transfer velocities obtained in this way provide only values integrated over a large horizontal length scales and time scales in the order of τ_w. Thus a parametrization of the transfer velocity is only possible under steady state conditions over extended periods. Moreover, the mass balance contains many other sources and sinks besides air-sea gas exchange and thus may cause severe systematic errors in the estimation of the transfer velocity. Consequently, mass balance methods are only poorly suited for the study of the mechanisms of air–water gas transfer.

Tracer Injection

The pioneering lake studies for tracer injection used sulfur hexafluoride (SF_6). However, the tracer concentration decreases not only by gas exchange across the interface but also by horizontal dispersion of the tracer. This problem can be overcome by the *dual tracer technique* [10] simultaneously releasing two tracers with different diffusivities (e.g., SF_6 and ^{3}He). When the ratio of the gas transfer velocities of the two tracers is known, the dilution effect by tracer dispersion can be corrected, making it possible to derive gas transfer velocities. But the basic problem of mass balance techniques, that is, their low temporal resolution, remains also with artificial tracer approaches.

Eddy Correlation Flux Measurements

Eddy correlation techniques are used on a routine basis in micrometeorology, that is, for tracers controlled by the boundary layer in air (momentum, heat, and water vapor fluxes). Direct measurements of the air-sea fluxes of gas tracers are very attractive because the flux densities are measured directly and have a much better temporal resolution than the mass balance based techniques. Unfortunately, large experimental difficulties arise when this technique is applied to gas tracers controlled by the aqueous boundary layer [Broecker 1986, 14]. The concentration difference in the air is only a small fraction of the concentration difference across the aqueous mass boundary layer. But after more than 20 years of research has this technique delivered useful results. Some successful measurements under favorable conditions have been reported and it appears that remaining problems can be overcome in the near future.

Passive and Active Thermography

The basic idea of this technique is to determine the concentration difference across the mass boundary layer when the flux density j of the tracer across the

interface is known. The local transfer velocity can be determined by simply measuring the concentration difference Δc across the aqueous boundary layer (cold surface skin temperature) according to Eq. 4 with a time constant $\tilde{t}$ for the transport across the boundary layer Eq. 8. This technique is known as the *controlled flux technique* (CFT).

Heat proves to be an ideal tracer for the CFT. The temperature at the water surface can then be measured with high spatial and temporal resolution using IR thermography. A known and controllable flux density can be applied by using infrared radiation. Infrared radiation is absorbed in the first few ten micrometers at the water surface. Thus a heat source is put right at top of the aqueous viscous boundary layer. Then the CFT directly measures the water-side heat transfer velocity.

A disadvantage of the CFT is that the transfer velocity of gases must be extrapolated from the transfer velocity of heat. The large difference in the Schmidt number (7 for heat, 600 for CO_2) casts some doubt whether the extrapolation to so much higher Schmidt numbers is valid.

Two variants of the technique proved to be successful. Active thermography uses a CO_2 laser to heat a spot of several centimeter in diameter on the water surface. The heat transfer rates are estimated from the temporal decay of the heated spot. Passive thermography uses the naturally occurring heat fluxes caused by latent heat flux j_l, sensible heat flux j_s and longwave emission of radiation j_r. The net heat flux $j_n = j_l + j_s + j_r$ results according to Eq. 4 in a temperature difference across the interface of $\Delta T = j_h/(\rho c_p k_h)$. Because of the turbulent nature of the exchange process any mean temperature difference is associated with surface temperature fluctuations which can be observed in thermal images. With this technique, the horizontal structure of the boundary layer turbulence can be observed. Surface renewal is directly observable in the IR image sequences, which show patches of fluid being drawn away from the surface.

With some knowledge about the statistics of the temperature fluctuations, the *temperature difference* ΔT across the interface as well as the time constant $\tilde{t}$ of heat transfer can be computed from the temperature distribution at the surface. Results obtained with this technique are shown in Fig. 4.

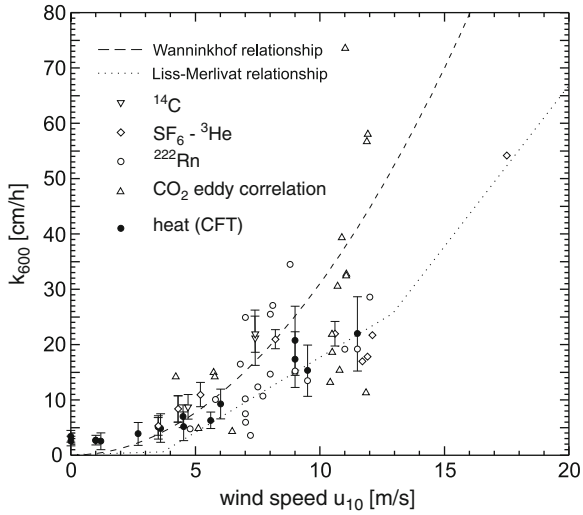

Atmosphere-Water Exchange. Figure 4
Summary of gas exchange field data normalized to a Schmidt number of 600 and plotted versus wind speed together with the empirical relationships of Liss and Merlivat [11] and ? (After Jähne and Haußecker [6])

Summary of Field Data

A collection of field data is shown in Fig. 3. Although the data show a clear increase of the transfer velocity with wind speed, there is substantial scatter in the data that can only partly be attributed to uncertainties and systematic errors in the measurements. Thus, in addition, the field measurements reflect the fact that the gas transfer velocity is not simply a function of the wind speed but depends significantly on other parameters influencing near-surface turbulence, such as the wind-wave field and the viscoelastic properties of the surface film.

Empiric Parametrization

Given the lack of knowledge, all theories about the enhancement of gas transfer by waves are rather speculative and are not yet useful for practical application. Thus, it is still state of the art to use semiempiric or empiric parameterizations of the gas exchange rate with the wind speed. Most widely used is the parametrization of Liss and Merlivat [11]. It identifies three physically well-defined regimes (smooth, wave-influenced, bubble-influenced) and proposes

a piece-wise linear relation between the wind speed U and the transfer velocity k:

$$k = 10^{-6} \begin{cases} 0.472U(Sc/600)^{-2/3} & U \leq 3.6\,\mathrm{m/s} \\ 7.971(U-3.39)(Sc/600)^{-1.2} & U > 3.6\,\mathrm{m/s}\text{ and } U \leq 13\,\mathrm{m/s} \\ 16.39(U-8.36)(Sc/600)^{-1/2} & U > 13\,\mathrm{m/s} \end{cases} \tag{16}$$

At the transition between the smooth and wavy regime, a sudden artificial jump in the Schmidt number exponent n from 2/3 to 1/2 occurs. This actually causes a discontinuity in the transfer rate for Schmidt number unequal to 600.

The empiric parametrization of Wanninkhof [25] simply assumes a quadratic increase of the gas transfer rate with the wind speed:

$$k = 0.861 \cdot 10^{-6}(s/m)U^2(Sc/600)^{-1/2}. \tag{17}$$

Thus, this model has a constant Schmidt number exponent $n = 1/2$. The two parameterizations differ significantly (see Fig. 3). The Wanninkhof parametrization predicts significantly higher values. The discrepancy between the two parameterizations and many others proposed (up to a factor of two) mirrors the current uncertainty in estimating the air-sea gas transfer rate.

Future Directions

In the past, progress toward a better understanding of the mechanisms of air–water gas exchange was hindered by inadequate measuring technology. However, new techniques have become available and will continue to become available that will give a direct insight into the mechanisms under both laboratory and field conditions. This progress will be achieved by interdisciplinary research integrating such different research areas as oceanography, micrometeorology, hydrodynamics, physical chemistry, applied optics, and image processing.

Optical and image processing techniques will play a key role because only imaging techniques give direct insight to the processes in the viscous, heat, and mass boundary layers on both sides of the air–water interface. Eventually, all key parameters including flow fields, concentration fields, and waves will be captured by imaging techniques with sufficient spatial and temporal resolution. The experimental data gained with such techniques will stimulate new theoretical and modeling approaches.

Bibliography

Primary Literature

1. Bohr C (1899) Definition und methode zur bestimmung der invasions- und evasionscoefficienten bei der auflösung von gasen in flüssigkeiten. Werthe der genannten constanten sowie der absorptionscoefficienten der kohlensäure bei auflösung in wasser und in chlornatriumlösungen. Ann Phys Chem 68:500–525
2. Bolin B (1960) On the exchange of carbon dioxide between the atmosphere and the sea. Tellus 12(3):274–281. ISSN 2153-3490
3. Revelle R, Suess HE (1957) Carbon dioxide exchange between atmosphere and ocean and the question of an increase of atmospheric CO_2 during the past decades. Tellus 9:18–27
4. Jähne B (1982) Dry deposition of gases over water surfaces (gas exchange). In: Flothmann D (ed) Exchange of air pollutants at the air-earth interface (dry deposition). Battelle Institute, Frankfurt
5. Jähne B (2009) Air-sea gas exchange. In: Steele JH, Turekian KK, Thorpe SA (eds) Encyclopedia ocean sciences. Elsevier, Boston, pp 3434–3444
6. Jähne B, Haußecker H (1998) Air-water gas exchange. Annu Rev Fluid Mech 30:443–468
7. Reichardt H (1951) Vollständige darstellung der turbulenten geschwindigkeitsverteilung in glatten leitungen. Z Angew Math Mech 31:208–219
8. Peng TH, Broecker WS, Mathieu GG, Li Y-H, Bainbridge A (1979) Radon evasion rates in the Atlantic and Pacific oceans as determined during the geosecs program. J Geophys Res 84(C5):2471–2487
9. Roether W, Kromer B (1984) Optimum application of the radon deficit method to obtain air–sea gas exchange rates. In: Brutsaert W, Jirka GH (eds) Gas transfer at water surfaces. Reidel, Hingham, pp 447–457
10. Watson AJ, Upstill-Goddard RC, Liss PS (1991) Air-sea exchange in rough and stormy seas measured by a dual tracer technique. Nature 349(6305):145–147
11. Liss PS, Merlivat L (1986) Air-sea gas exchange rates: introduction and synthesis. In: Buat-Menard P (ed) The role of air-sea exchange in geochemical cycling. Reidel, Boston, pp 113–129
12. Deacon EL (1977) Gas transfer to and across an air-water interface. Tellus 29:363–374
13. Frew NM (1997) The role of organic films in air-sea gas exchange. In: Liss PS, Duce RA (eds) The sea surface and global change. Cambridge University Press, Cambridge, pp 121–171
14. Jacobs C, Nightingale P, Upstill-Goddard R, Kjeld JF, Larsen S, Oost W (2002) Comparison of the deliberate tracer method

and eddy covariance measurements to determine the air/sea transfer velocity of CO_2. In: Saltzman E, Donelan M, Drennan W, Wanninkhof R (eds) Gas transfer at water surfaces. Geophysical Monograph, vol 127. American Geophysical Union

15. Jähne B (1980) Zur Parametrisierung des Gasaustauschs mit Hilfe von Laborexperimenten. Dissertation, Institut für Umweltphysik, Fakultät für Physik und Astronomie, Univ. Heidelberg, http://d-nb.info/810123614. IUP D-145
16. Jähne B (1987) Image sequence analysis of complex physical objects: nonlinear small scale water surface waves. In: Proceedings of 1st international conference on computer vision, London, pp 191–200
17. Jähne B (1991) New experimental results on the parameters influencing air-sea gas exchange. In: Wilhelms SC, Gulliver JS (eds) Air-water mass transfer, Selected papers from the 2nd international symposium on gas transfer at water surfaces, Minneapolis, 11–14 Sep 1990. ASCE, pp 582–592
18. Jähne B, Heinz G, Dietrich W (1987) Measurement of the diffusion coefficients of sparingly soluble gases in water. J Geophys Res 92(C10):10,767–10,776
19. Keeling RF (1993) On the role of large bubbles in air-sea gas exchange and supersaturation in the ocean. J Marine Res 51:237–271
20. King DB, Bryun WJD, Zheng M, Saltzman ES (1995) Uncertainties in the molecular diffusion coefficient of gases in water for use in the estimation of air-sea exchange. In: Jähne B, Monahan E (eds) Air-water gas transfer, Selected papers, 3rd international symposium on air-water gas transfer. AEON, Hanau, pp 13–22
21. McKenna SP, Bock EJ (2006) Physicochemical effects of the marine microlayer on air-sea gas transport. In Gade M, Hühnerfuss H, Korenowski GM (eds) Marine surface films: chemical characteristics, influence on air-sea interactions, and remote sensing. Springer, Berlin/Heidelberg, pp 77–91
22. Sündermann J (ed) (1986) Landolt-Börnstein, vol V 3c, Oceanography. Springer, Heidelberg
23. Torgersen T, Top Z, Clarke WB, Jenkins WJ (1977) A new method for physical limnology-tritium-helium-3 ages results for Lakes Erie, Huron, and Ontario. Limnol Oceanogr 22:181–193
24. Tschiersch J, Jähne B (1980) Gas Exchange trough a rough water surface in a circular windtunnel; Wave characteristics under limited and unlimited fetch. In: Broecker HC, Hasse L (eds) Berichte aus dem Sonderforschungsbereich 94 Meeresforschung – Symposium on capillary waves and gas exchange, Trier, 2–6 July 1979, number 17. Univ. Hamburg, pp 63–70
25. Wanninkhof R (1992) Relationship between wind speed and gas exchange over the ocean. J Geophys Res 97: 7373–7382
26. Woolf D, Leifer I, Nightingale P, Rhee T, Bowyer P, Caulliez G, de Leeuw G, Larsen S, Liddicoat M, Baker J, Andreae M (2007) Modelling of bubble-mediated gas transfer: fundamental principles and a laboratory test. J Marine Syst 66:71–91

Books and Reviews

Banner ML (ed) (1999) The wind-driven air-sea interface, electromagnetic and acoustic sensing, wave dynamics and turbulent fluxes, proceedings of the symposium Sydney, Australia, 11–15 January 1999. University of New South Wales, Sydney

Bengtsson LO, Hammer CU (eds) (2001) Geosphere-biosphere interactions and climate. Cambridge University Press, Cambridge

Borges AV, Wanninkhof R (2007) Fifth international symposium on gas transfer at water surfaces. J Mar Syst 66(1–4):1–308

Brasseur GP, Prinn RG, Pszenny AA (eds) (2003) Atmospheric chemistry in a changing world. An integration and synthesis of a decade of tropospheric chemistry research. Springer, Berlin

Brutsaert W, Jirka GH (eds) (1984) Gas transfer at water surfaces. Reidel, Dordrecht

Csanady GT (2001) Air-sea interaction, laws and mechanisms. Cambridge University Press, Cambridge

Cussler EL (2009) Diffusion – mass transfer in fluid systems, 3rd edn. Cambridge University Press, Cambridge

Danckwerts PV (1970) Gas-liquid reactions. MacGraw-Hill, New York

Davies JT (1972) Turbulence phenomena. An introduction to the eddy transfer of momentum, mass, and heat, particularly at interfaces. Academic, New York/London

Davies JT, Rideal EK (1963) Interfacial phenomena, 2nd edn. Acadamic, New York

Dobson F, Hasse L, Davis R (eds) (1980) Air-sea interaction: instruments and methods. Plenum, New York

Donelan MA, Hui WH, Plant WJ (eds) (1996) The air-sea interface, radio and acoustic sensing, turbulence and wave dynamics, proceedings of the symposium, Marseille, France, 24–30 June 1993. Rosenstiel School of Marine and Atmospheric Science, University of Miami, Miami, Florida

Donelan MA, Drennan WM, Saltzman ES, Wanninkhof R (eds) (2002) Gas transfer at water surfaces. American Geophysical Union, Washington, DC

Emerson SR, Hedges J (2008) Chemical oceanography and the marine carbon cycle. Cambridge University Press, Cambridge

Favre A, Hasselmann K (eds) (1978) Turbulent fluxes through the sea surface, wave dynamics, and prediction, proceedings of the symposium, Marseille, 1977. Plenum, New York

Fogg PGT, Sangster J (2003) Chemicals in the atmosphere: solubility, sources, and reactivity. Wiley, Chichester

Gade M, Hühnerfuss H, Korenowski GM (eds) (2005) Marine surface films: chemical characteristics, influence on air-sea interactions and remote sensing. Springer, Berlin

Garbe CS, Handler RA, Jähne B (eds) (2007) Transport at the air sea interface – measurements, models and parameterizations. Springer, Berlin

Gulliver JS (2007) Introduction to chemical transport in the environment. Cambridge University Press, Cambridge

Jähne B, Monahan EC (eds) (1995) Air-water gas transfer – selected papers from the third international symposium on air-water gas transfer. AEON Verlag & Studio Hanau. http://d-nb.info/946682526

Kantha LH, Clayson CA (2000) Small scale processes in geophysical fluid flows, vol 67, International geophysics series. Acadamic, San Diego

Komori S, McGillis W (eds) (2011) Gas transfer at water surfaces, selected papers from the 6th international symposium. Kyoto University Press, Kyoto

Kraus EB, Businger JA (1994) Atmosphere-ocean interaction, vol 27, 2nd edn, Oxford monographs on geology and geophysics. Oxford University Press, New York

Liss PS, Duce RA (eds) (2005) The sea surface and global change. Cambridge University Press, Cambridge

Robinson IS (2010) Discovering the ocean from space – the unique applications of satellite oceanography. Springer, Heidelberg

Sarmiento JL, Gruber N (2006) Ocean biogeochemical dynamics. Princeton University Press, Princeton

Soloviev A, Lukas R (2006) The near-surface layer of the ocean, vol 31, Atmospheric and oceanographic sciences library. Springer, Dordrecht

Wanninkhof R, Asher WE, Ho DT, Sweeney C, McGillis WR (2009) Advances in quantifying air-sea gas exchange and environmental forcing. Annu Rev Mar Sci 1:213–244

Wilhelms SC, Gulliver JS (eds) (1991) Air-water mass transfer – selected papers from the 2nd international symposium on gas transfer at water surfaces, Minneapolis Minnesota, September 11–14, 1990. American Society of Civil Engineers, New York

Zeebe RE, Wolf-Gladrow DA (2001) CO_2 in seawater: equilibrium, kinetics, isotopes, vol 65, Elsevier oceanography series. Elsevier, Amsterdam

Atmospheric Biogeochemistry

Natalie M. Mahowald
Department of Earth and Atmospheric Sciences, Atkinson Center for Sustainable Future, Cornell University, Ithaca, NY, USA

Article Outline

Glossary
Definition of the Subject and Its Importance
Introduction
Cycling in the Atmosphere
Atmospheric Modification to Other Biogeochemical Components
The Atmosphere as an Integrator
Future Directions
Acknowledgments
Bibliography

Glossary

Aerosol A solid or liquid suspended in the atmosphere. The definition usually does not include cloud droplets, although many aerosols have water vapor on their surfaces.

Dry deposition Removal process for gas and aerosol species in which the species are deposited onto the lower surface due to either turbulent fluxes (overturning air) forcing the constituent to hit and stick to the surface, or from gravitational settling of aerosols. Gravitational settling is the dominant mechanism for removal for larger aerosols.

Lifetime The atmospheric lifetime of a constituent describes how long the constituent will remain in the atmosphere. It is typically calculated by dividing the total amount of the constituent in the atmosphere by the total flux out of or into the atmosphere. The flux can be due to atmospheric chemical reactions, and/or exchanges between other reservoirs in the earth system (e.g., land or ocean). This lifetime is an e-folding lifetime; if one starts with an initial perturbation of the constituent, the amount of the perturbation remaining after a length of time equal to the lifetime is equal to 1/e of the original value of the perturbation.

Wet deposition Process by which an atmospheric constituent is removed by precipitation. This is especially important for water-soluble and aerosol species.

Definition of the Subject and Its Importance

Biogeochemistry represents the interaction of biology, chemistry, and geology in the Earth system. For many processes, an understanding of biological uptake and emission, chemical processing, and geological sequestration is necessary to resolve the sources and sinks of a particular constituent. For example, to discover the sources and sinks of atmospheric carbon dioxide, it is important to understand how biota take up carbon dioxide and chemically convert the carbon to organic carbon, and then how this organic carbon is used either to produce energy by biota or is deposited to the land

or ocean surface and can become sequestered in geological formations. Often when biogeochemistry is referred to, one refers to the nutrient cycling of important nutrients. Atmospheric biogeochemistry, as defined in its narrowest sense, is the flux of nutrients and pollutants important for biogeochemistry through the atmosphere. In its broadest sense, atmospheric biogeochemistry is the interaction of the atmosphere and atmospheric processes with the biogeochemistry of the earth system. This broader definition is used here. The hydrologic cycle is one of the most important biogeochemistry cycles, and is a worthy topic of its own. It is discussed in several other sections of this encyclopedia (e.g., Climate Change and Global Water Sustainability, Water Resource and Quality Management for Adaptation to Climate Change, Water Availability and Quality, Sustainable).

Introduction

Atmospheric biogeochemistry is increasingly relevant for today's society, as evidenced by the changing composition of the atmosphere. Atmospheric biogeochemistry views these changes in the composition as part of a collection of changes to the earth system occurring during the anthropocene. One very serious sustainability issue at the core of atmospheric biogeochemistry is the accumulation of carbon dioxide in the atmosphere. This is a result of human emissions of carbon dioxide both directly from fossil fuel burning, and from land use change, especially tropical deforestation [1]. Interestingly, only about ½ of the carbon dioxide emitted into the atmosphere remains there: The rest is taken up by the land and ocean. This important negative feedback on human emissions of carbon dioxide is a result of biogeochemical cycling of carbon in the system. As human emissions of carbon dioxide grow, it is not clear that the land and the ocean will be able to keep up, and thus more of the carbon dioxide is likely to stay in the atmosphere [2]. Some studies suggest that warming itself leads to less carbon dioxide being taken up by the land and ocean [2], although this also depends on the cycling of other nutrients such as nitrogen as well [3]. Thus understanding the biogeochemistry of carbon is required to understand how much carbon can be emitted in the future.

The atmospheric transport and subsequent deposition of trace gases and aerosols can provide an important mechanism for circulation of different constituents. Whether this deposition serves as a nutrient or a pollutant usually depends on the deposition level, as well as the ability of the biota to process these compounds. Some compounds can be nutrients at low levels, but pollutants at high levels. Thus, referring to the atmospheric transport of nutrients and pollutants as "atmospheric biogeochemistry" allows for these changes in impacts depending on amount. For transport from the land to ocean, many constituents can also be carried by rivers; in the sections below, the relative importance of atmospheric versus riverine inputs is discussed. The atmosphere tends to be able to transport species more quickly and farther distances; however the mass of the atmosphere is much less that of water, providing a constraint on the amount of constituent the atmosphere can transport. For the cases of constituent transport from the oceans to land, or upstream on land, atmospheric transport on short timescales is often the most important, as the only other mechanism would be geological changes in orography.

The final important aspect of atmospheric biogeochemistry is that it allows us to understand the composition of the atmosphere, and the fluctuation in this composition, in an earth system context. Thus understanding atmospheric biogeochemistry represents an integrative approach to understanding the atmosphere and its relationship with the land, ocean, and crysophere.

Cycling in the Atmosphere

Since most nutrients cycle through the atmosphere, the atmospheric portion of their biogeochemistry is important. The most important nutrients to sustain life are carbon, nitrogen, and phosphorus, but many other nutrients are required. Here some of the most important nutrient cycles for the earth system are discussed, and cycles that are being perturbed due to human activities have to be focused upon.

Carbon Cycle

The carbon cycle receives substantial interest today because of the anthropogenic perturbation of the carbon cycle and the documentation of global warming. The carbon cycle represents the most important of the

nutrient cycles, with the exception of water, for living organisms because living tissue is primarily composed of carbon. The dominant form of carbon in the atmosphere is carbon dioxide, a chemically inactive, but radiatively important species in the atmosphere. The riverine flux of carbon is 0.8 Tg/year, while the gross land and ocean fluxes with the atmosphere are closer to 120 and 70 Tg/year (the net fluxes are closer to zero). This suggests that changes in the land or ocean carbon balance will be communicated rapidly through the atmosphere.

Carbon dioxide is removed from the atmosphere, not through chemical reactions, but through huge fluxes into the land or oceans, with an atmospheric lifetime of several years (Fig. 1 from [4]). In reality, however, the land and ocean fluxes are reasonably well balanced and it is difficult for all the extra carbon to be taken up, suggesting that the lifetime of the additional carbon dioxide emitted by humans is on the order of a few hundred years [4, 5]. However, there will be some carbon (perhaps 20–35%) that stays in the atmosphere for 3–7 kyr, thus the lifetime for atmospheric carbon dioxide is ambiguous [5].

Carbon dioxide shifts between glacial and interglacial climates are one of the most robust signals from the ice core records [6], and carbon dioxide tends to be about 80–100 ppm smaller during glacial periods than during interglacial periods (like today). These changes in carbon dioxide have not yet been explained, but are likely to be caused by a combination of colder temperatures, changes in ocean circulation, and changes in ocean productivity [7]. Indeed these changes in carbon dioxide are important forcing agents for maintaining the cold temperatures in the glacial periods [8], and thus must be an integral part of explaining the glacial/interglacial cycles over the past several hundred thousand years.

Currently, carbon dioxide emissions are increasing, and while preindustrial values of carbon dioxide were about 280 ppm, current values are over 380 ppm [4]. The reason for these changes in carbon dioxide values are due to human emissions of carbon dioxide release from combustion of fossil fuels and deforestation or other land-use change process. Carbon dioxide emissions currently (2008) are estimated to be about 8.7 +/− 0.5 PgC/year from fossil fuels, and another 1.5 +/− 0.7 PgC/year from land-use change (e.g., deforestation) [1]. Recent studies suggest that about 43% of anthropogenic carbon dioxide, from fossil fuel burning

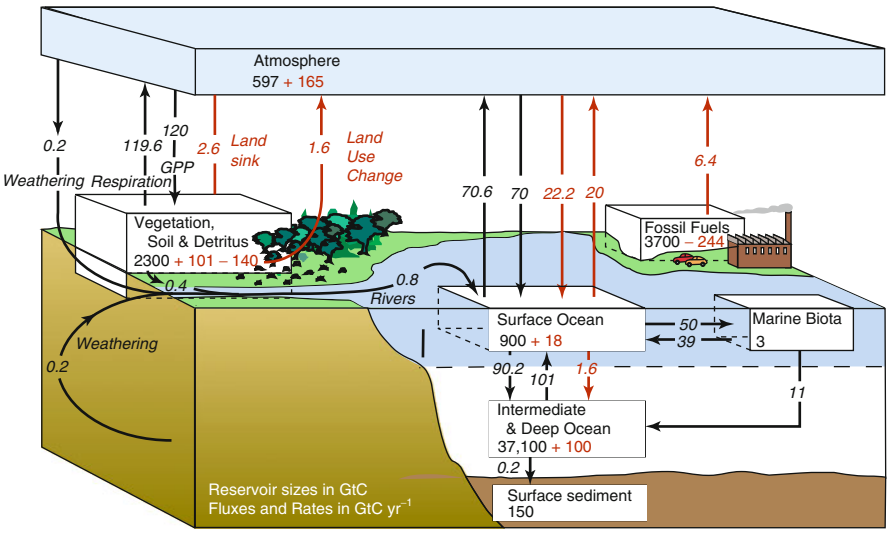

Atmospheric Biogeochemistry. Figure 1

The global carbon cycle for the 1990s, showing the main annual fluxes in PgC/year: preindustrial "natural" fluxes in black and "anthropogenic" fluxes in red. Gross fluxes generally have uncertainties of more than ±20% but fractional amounts have been retained to achieve overall balance when including estimates in fractions of PgC/year for riverine transport, weathering, deep ocean burial, etc. "GPP" is annual gross (terrestrial) primary production. Atmospheric carbon content and all cumulative fluxes since 1750 are as of end 1994 (Figure from [4])

or deforestation, remains in the atmosphere, while the remainder is taken up by the land or the ocean, with more than half going into the ocean [1]. In the future, it is likely that less of the carbon dioxide that is emitted will be taken up by the land and ocean, due to both a saturation of the sinks of carbon dioxide, as well as the impact of climate change on the carbon cycle [2].

This increasing carbon dioxide in the atmosphere may increase land productivity and change land biogeochemistry. Higher carbon dioxide levels may allow plants to better adapt to water stress and can enhance productivity, a process called the carbon dioxide fertilization effect [9]. It is unclear how strong this fertilization effect is on land, because of limitation by other nutrients or water [10, 11]; however, available ecosystem studies support the hypothesis that increased carbon dioxide will result in higher productivity [9].

Higher carbon dioxide levels will tend to cause the ocean to take up more carbon, since the atmosphere will be supersaturated with respect to the oceans, especially in colder regions. This additional carbon dioxide is likely to lead to lower pH values in the oceans, called ocean acidification [12], and reduce the ability of calcifying organisms to create skeletons [13, 14]. This has potentially huge repercussions on ocean biogeochemistry and biodiversity [13, 15].

Carbon also exists in the atmosphere in other forms. The next most important constituent in terms of atmospheric mass is methane. Methane is formed by the decay of reduced organic species under anerobic conditions, occurring in wetlands, in geologic formations, or in the intestines of animals. Methane sources are estimated to be about 580 Tg/year, with anthropogenic sources (such as fossil fuel extraction or agriculture) representing 55–70% of the total emissions [4]. Methane is oxidized in the atmosphere by the OH radical with a lifetime of about 9 years, as well as smaller sinks of removal at the surface and photolysis in the stratosphere [4]. Methane is even more radiatively important than carbon dioxide on a per molecule basis, and thus its accumulation in the atmosphere is of concern for global warming. Methane concentrations have increased from ~650–1,770 ppb over the past couple hundred years, largely due to human activity [16]. Methane oxidation converts the methane into carbon dioxide.

Other important carbon-containing gases include carbon monoxide and non-methane hydrocarbons. Carbon monoxide is a product of incomplete combustion, and after carbon dioxide is the largest form of emission of carbon into the atmosphere (1,800–2,700 Tg CO/year) [17]. Carbon monoxide chemically reacts with the OH radical in the atmosphere, and has a lifetime of about 2 months [17]. The oxidation of carbon monoxide to form carbon dioxide represents an important sink of oxidants in the atmosphere [17]. Non-methane hydrocarbons refer to a large collection of carbon-containing compounds that are important for tropospheric photochemistry and the generation of ozone and oxidizing compounds. Non-methane hydrocarbons undergo oxidation via many mechanisms. The complete oxidation results in one mole of carbon dioxide for each carbon atom in the original molecule [17]. The lifetime of non-methane hydrocarbons vary considerably, but are usually less than the lifetime of methane. They are important for air quality, since they are precursors to ozone, and may themselves be toxic, but are not sufficiently abundant to have radiative impacts [17].

Carbon is also a component of atmospheric aerosols, but at much lower concentrations than the gases described above. These aerosols can, however, be important for radiation and chemistry, because they exist as a solid in a gas phase. Sources of carbonaceous aerosols include by-products from combustion processes, compounds emitted from vegetation, and in situ product from the condensation of non-methane hydrocarbons.

Nitrogen Cycle

The dominant form of nitrogen in the atmosphere is molecular nitrogen (N_2), which represents over 70% of the air. However, this form is chemically inert and not biologically available. Thus, the nitrogen cycle usually refers to the cycle of reactive nitrogen compounds. The dominant form of reactive nitrogen in the atmosphere is nitrous oxide, a long-lived gas (>70 years), which is destroyed predominately in the stratosphere by photolysis. The sources of nitrous oxide are in the soils, as by-products of nitrogen fixation and denitrification processes, which convert molecular nitrogen to reactive nitrogen and back. Humans have increased nitrous

oxide from 270 to 319 ppb, largely due to an increase in nitrogen fertilizer application [4]. Emissions of nitrous oxide are estimated to be 11 Tg/year. Nitrous oxide is a potent green house, and represents the third largest radiative forcing gas (after carbon dioxide and methane) [4].

Potentially even more important than nitrous oxide are the nitrogen oxides (NO and NO_2), which currently have emissions of more than 140 Tg/year, while preindustrial emissions were thought to be closer to 30 Tg/year [18]. Nitrogen oxides are emitted during combustion process, with smaller contributions from soils and lightning. Nitrogen oxides have a short lifetime in the atmosphere (a few days), and are important for atmospheric photochemistry and air quality because of their role in producing ozone [17]. In addition, nitrogen oxides deposit onto the earth's surface as they are removed from the atmosphere, and thus move nitrogen from one region to another in large quantities (e.g., [19]).

Since preindustrial times, emissions and concentrations of ammonia have increased with current emissions of 52 Tg/year compared with an estimated 22 Tg/year in preindustrial times [18]. Ammonia is emitted predominately from natural soils and agriculture, with small contributions from oceans and energy use. Ammonia has a short lifetime in the atmosphere (a few days) and is removed through wet or dry deposition onto the surface.

Similar to carbon species, nitrogen is also contained in organic gas species and to a smaller extent in inorganic and organic aerosols. These species can act as reservoirs of reactive nitrogen (e.g., [17], and thus be important for atmospheric chemistry. The fraction of nitrogen species that are in aerosols is dependent on chemical equilibrium with other aerosols, especially the strong acid sulfate [20]. In the future, as sulfate emissions decrease, nitrogen aerosols may become more important in terms of the radiative forcing of the climate as the fraction of nitrogen in aerosol form increases [20].

Riverine inputs to oceans are thought to be 55–80 Tg/year [21], which is of the same magnitude as the fluxes of many nitrogen compounds discussed above, suggesting that the atmosphere plays an important role in the cycling of nitrogen between the land and ocean.

Because many terrestrial ecosystems are nitrogen limited, the impact of nitrogen deposition, especially from nitrogen oxides and ammonia, is thought to be large for land ecosystems [3, 22–25]. Nitrogen is also a limiting nutrient for ocean systems, and there have been large increases in nitrogen deposition to ocean systems [21]; however, because of the large reservoir of reactive nitrogen in the oceans, deposition to the oceans is not thought to substantially modify the ocean nitrogen budget [26].

Phosphorus Cycle

Unlike carbon or nitrogen, most of the phosphorus in the atmosphere is in the aerosol form, with little phosphorus in the gas phase (e.g., [27]. As phosphorus is approximately 700 ppm in crustal material, and mineral aerosols (soil particles suspended in the atmosphere) represent a major source of aerosols, most of the phosphorus in the atmosphere is in mineral aerosols [28] at about 1.15 TgP/year. The next largest source is thought to be primary biogenic particles (0.16 TgP/year), but these aerosols are very poorly understood [28]. Combustion sources from fossil fuels, biomass burning, and biofuels represent a small source (0.0.7 TgP/year), while volcanoes and sea salts are thought to provide small amounts as well [28]. Thus, continental regions, especially deserts are the dominant source of atmospheric phosphorus [28].

Aerosols deposited to ocean have a limited residence time in the ocean mixed layer, before they sink to the ocean floor and become incorporated into the sediment. Only the fraction of phosphorus which is soluble or bioavailable can contribute to the phosphorus cycle of the ocean [28, 29]. The bioavailable fraction is often considered phosphate or soluble-reactive phosphorus [28], and the fraction of phosphorus in aerosols that is soluble varies from 7% to 100% [28, 29]. Transects of the North Atlantic suggest that desert dust aerosols average about 10% solubility [30, 31]; however a gradient in solubility is observed as the particles move away from the desert dust source area, suggesting that atmospheric processing may make the phosphorus in aerosols more soluble [30]. Studies in Mediterranean suggest that acidification, partly due to anthropogenic emissions of sulfur and nitrogen species, can make the phosphorus in desert dust more soluble [32]. Non-dust

phosphorus is thought to be much more soluble (~50%), based on studies of European-derived aerosols in the Mediterranean [28, 33–36].

Phosphine gas (PH_3) has been measured in limited studies, with concentrations of between 0.39 and 2.45 ng/m^3 in remote regions and up to 178 ng/m^3 in urban locations or near paddy fields [37–39]. While traditionally, the gas phase transfer of phosphorus has been considered negligible [28, 40], some of the values listed here are similar in magnitude as those found for phosphorus in aerosols [28]. This suggests that phosphine could be an important mechanism for transferring phosphorus, yet is not well understood. Small amounts of phosphine could be generated in soils, agricultural and industrial processes, and lightning, but phosphine in the presence of sunlight is converted to phosphoric acid [37, 38].

Because phosphorus limitation is thought to be widespread in tropical forests and savannahs [41, 42], atmospheric deposition of desert dust may play a role in the long-term viability of tropical soils. For example, it has been suggested that the atmospheric deposition of desert dust from North Africa is responsible for the maintenance of the Amazon forest [43], and that deposition from Asia is important source of phosphorus to the tropical forests in Hawaii on long timescales [44]. The atmospheric deposition of phosphorus is likely to be important in many land ecosystems on geological timescales [45]. Forest and grassland ecosystems can also lose phosphorus through the atmosphere, as primary biogenic particles or biomass burning particles contain a large proportion of the phosphorus in tropical forests [46, 47].

The ocean tends to be a net sink of phosphorus from the atmosphere [28], and since productivity in the ocean is thought to be phosphorus limited on long timescales [48] and in some regions [49, 50], the atmospheric deposition of phosphorus could be an important source. Riverine inputs of phosphorus to the oceans are much larger than the atmospheric fluxes described here (11 Tg/year) [51]; however this phosphorus is input to the oceans in the coastal regions, and it is unclear how much of this phosphorus is advected into the open oceans [52]. However, on short timescales, large increases (25%) in phosphorus deposition to oceans which could be due to human activity [28] is not thought to substantially impact ocean biogeochemistry, because of the large reservoir of phosphorus already in the oceans [26].

Sulfur Cycle

Sulfur is an important trace compound in the earth system, used by some microorganisms for energy. It is commonly found in rocks with smaller quantities measured in the atmosphere [27]. The atmospheric portion of the sulfur cycle is important because of the climate interactions of the sulfur species, especially in the sulfate aerosol form. The sulfur compound with the longest lifetime (5 years) and most common by mass is carbonyl sulfide (OCS) [27]. The dominant sources (10 GgS/year) of carbonyl sulfide are the oceans and soils, with small contributions from combustion processes and the chemical oxidation of CS_2 [27]. Carbonyl sulfide is destroyed by oxidation in the atmosphere, as well as by stratospheric phytolysis and uptake by vegetation at the surface [27, 53]. Carbonyl sulfide is thought to contribute about half of the sulfur that forms the stratospheric aerosol layer, the other half coming from volcanic emissions [54].

Sulfur dioxide is a naturally occurring compound released from volcanoes and biomass burning (<10% total) as well as oxidation of the naturally emitted dimethyl sulfide (~20%), but the dominant source currently are human combustion activities with a total emission of about 91–125 TgS/year [16, 18]. Once released into the atmosphere, sulfur dioxide is oxidized within a few days to form sulfate aerosols. Because sulfate is highly hydrophilic, sulfate aerosols take up water and make a larger contribution to aerosol-radiation interactions than their mass would suggest [16]. In addition these aerosols readily interact with cloud droplets to modify cloud optical properties (aerosol indirect effect on clouds) [16]. Sulfur dioxide from human emissions is responsible for a large portion of the anthropogenic radiation forcing of aerosols [16].

Dimethyl sulfide is a natural source of sulfur gas to the atmosphere from the ocean, with a magnitude of about 15 TgS/year, which is readily oxidized to sulfur dioxide and then to sulfate aerosol (lifetime about 1.5 days). This is the dominant gas phase species of sulfur released from the ocean to the atmosphere. Because of sulfate aerosol interactions with clouds, it was hypothesized that biota could modulate their

temperature by modifying emissions of dimethyl sulfide [55]; however, recent studies suggest this mechanism is not a dominant mechanism, for example, under anthropogenic climate change [56].

Sea salts are 7.7% sulfate by weight [57], and represents the largest source of sulfur to the atmosphere. Approximately 10,000 Tg/year of sea salt aerosols [58] is emitted into the atmosphere, which translates to 770 Tg SO_4/year or 250 TgS/year. Sea salt aerosols reside in the atmosphere from hours to days, and tend to redeposit back onto oceans [58], and are important as cloud condensation nuclei [59].

Sulfur moves from the land to the ocean at a rate of approximately 130 TgS/year [27], which is similar in magnitude to many of the atmospheric fluxes, suggesting that atmospheric sulfur is an important part of the global biogeochemical cycle.

Iron Cycle

Iron is required in small quantities by almost all organisms (e.g., [48, 60]), and is often considered a micronutrient. Because some regions of the oceans are iron limited [61], atmospheric deposition of iron is important for providing new iron to ocean biota [62]. Riverine inputs of iron are large, but are largely removed in coastal regions [63]. There is some evidence that the nitrogen-fixing organisms have larger iron requirements

Similar to the phosphorus cycle, iron resides almost entirely in atmospheric aerosols, predominately in desert dust. Combustion and other sources of iron are estimated to be less than 5% of the total iron in aerosols [64, 65]. Crustal material is on average about 3.5% iron [66], with some minerals having substantially higher or lower concentrations [67, 68]. However, estimates and observations suggest that desert dust aerosols vary in their iron content by only a factor of 2, suggesting that the high heterogeneity in the soils is mixed in the atmosphere [65, 69]. There are also small sources of atmospheric iron from volcanoes [70, 71], cosmic dust [72], and combustion [64].

Because atmospherically deposited dust only resides in the mixed layer of the ocean for a short time, many researchers consider the soluble fraction of the iron the most relevant for ocean iota [73]. However, which fraction of the iron is really bioavailable is not well understood, but is likely to be a small fraction of the total iron in aerosols (1–80%) (see reviews in [65, 73]). Because the soluble fraction of iron in soils is much smaller than what is observed in the atmosphere, it is thought that atmospheric processing of iron is important [73, 74]. It is likely that the acidity and insolation play a role in processing of iron [73–75]. Some iron-containing minerals are more easily solubilized than others and iron in combustions is significantly more soluble than iron in mineral aerosols; these factors complicate our understanding of iron solubility [68, 76–78] (Fig. 2 from [65]).

Some regions of the ocean are iron deficient and additions of iron can result in phytoplankton blooms [79, 80]; however, there is limited evidence showing conclusively that a case of deposition of atmospheric iron results in a bloom [81, 82]. Additional atmospheric iron deposition could also lead to increases in ocean nitrogen, because of the potential for higher iron requirements for nitrogen-fixing organisms [48, 83]. There is some evidence for this effect [84–86], although some of these effects may be due to the isotopic signature of direct anthropogenic nitrogen deposition [87]. It is likely that human changes in iron deposition are more important than the large increase in direct nitrogen deposition to the ocean, in terms of both the nitrogen budget of the ocean, as well as carbon dioxide changes [26, 88].

Estimated changes in soluble iron due to increases in desert dust sources as well as the increase in atmospheric acidification (associated with more sulfate and nitrate aerosols) could be as large as a factor of 2–4 globally averaged [65, 89]. Model results suggest this would lead to an increase in the nitrogen fixation in the oceans, and a small sink of carbon dioxide [89, 90].

Oxygen Cycle

The atmospheric concentrations of oxygen are one of the clearest indications that life exists on this planet [27, 91]. The bulk of the atmospheric oxygen is in the gaseous state, in the form of molecular oxygen (O_2), which represents 21% of the atmosphere. Atmospheric oxygen is changing slightly due to human activity. For every molecule of CO_2 formed through combustion, one molecule of O_2 is lost from the atmosphere, and while small, these changes can be detected and provide important information about the carbon cycle [92, 93].

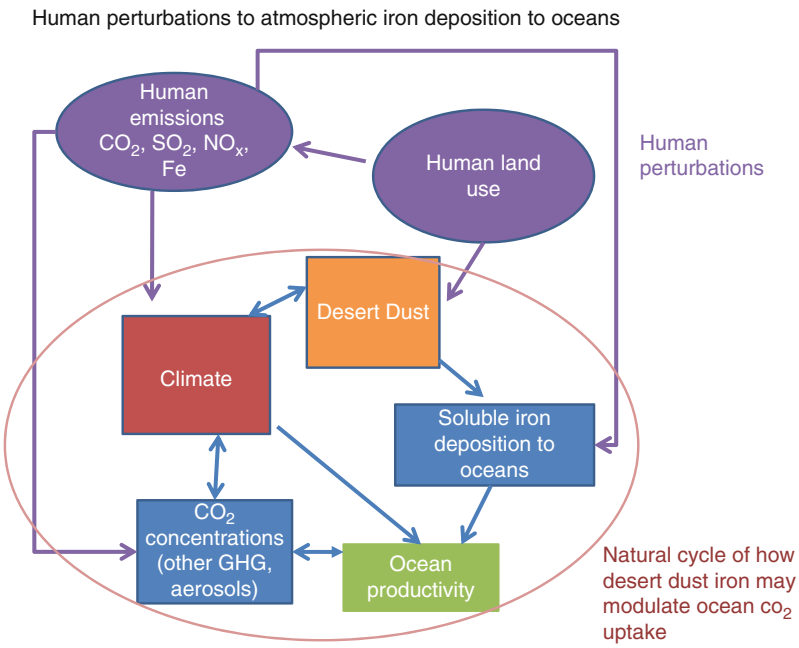

Atmospheric Biogeochemistry. Figure 2
Skematic representing feedbacks between natural ocean carbon cycle, carbon dioxide concentrations, and iron inputs also shows humans could be perturbing the iron deposition (Figure from [65])

This molecular oxygen is also important as it absorbs high-energy uv light from the sun [94].

The oxygen species that exist in very small quantities in the atmosphere are extremely important for atmospheric composition, and control the oxidation of reduced species such as methane or nitrogen oxides. Ozone is produced in the stratosphere in the presence of high-energy uv light, and this ozone, as well as the process which generates the ozone, protects life from uv light at very short wavelengths [17, 94]. This also changes the thermal structure of the atmosphere, contributing to the increasing temperatures in the stratosphere [94]. Stratospheric ozone has been impacted by the release of chlorofluorocarbons, which are inert enough to reach the upper atmosphere, where they are photolyzed [95]. The largest impact has been in the polar regions, where an "ozone hole" has appeared during the hemispheric spring, although midlatitude reductions in ozone have also been observed [96]. In the troposphere, human emissions of nitrogen oxides, carbon monoxide, and non-methane hydrocarbons have led to an increase in ozone [17]. While the bulk of the ozone remains in the stratosphere, ozone is a highly oxidizing substance, so that increases in tropospheric ozone impacts human health and materials [17]. Ozone acts as a greenhouse gas, and the observed changes in ozone, both in the troposphere and stratosphere, have impacted the radiative budget [16].

Oxidation of organic and reduced species in the troposphere is the sink for many important greenhouse gases (e.g., methane), and other important trace species in the atmosphere (e.g., sulfur dioxides, nitrogen oxides) [17]. Much of this oxidation does not occur directly by ozone, but rather by the hydroxyl radical, a by-product of ozone photochemistry in the troposphere [17]. Because this constituent reacts so quickly, it is difficult to determine its concentration directly, but it can be deduced from changes in concentrations in some of the compounds it reacts with [97]. It is unclear whether humans are increasing or decreasing the hydroxyl radical, and will continue to do so, because of the complex nonlinear chemistry [16].

Other Cycles

Most elements are cycled in the atmosphere, and because long-range transport is much faster in the atmosphere

than on land or oceans, this transport can be important for many elements. Here the focus is on a few critical elements for global biogeochemistry. However, some elements are important for their negative impacts, especially heavy metals. For example, mercury emissions from humans impacts human and ecosystem health [98]. Some studies have suggested that atmospheric deposition of heavy metals far from source areas can adversely impact ocean biogeochemistry [99]. In addition, atmospheric deposition of acid is thought to reduce the ability of some ecosystems to retain some nutrients and to negatively impact land and aquatic ecosystems [101–103], and to enhance ocean acidification [100].

Anthropogenic Modifications to Atmospheric Biogeochemical Cycles

Direct human emissions of carbon dioxide, sulfur dioxide, and nitrous oxides gases, as well carbonaceous aerosols, through the increase in combustion that humans use to generate energy, has substantially increased the sources and atmospheric concentrations of these compounds [16] (Fig. 3). In addition, changes in land use have increased carbon dioxide, methane, nitrous oxide, and ammonia emissions [16] (Fig. 3). These modifications are likely to continue into the future, with some decrease in emissions of combustion-sourced compounds estimated (Fig. 3) [101–107]. A combination of climate change and land-use change seems to have resulted in an increase in mineral aerosol over the past 100 years [89], which increases the flux of phosphorus and iron. In addition, bioavailable iron and phosphorus are likely to be even more susceptible to acidity and combustion sources; thus these compounds have changed more than simply from mineral aerosol changes over the past 100 years (Fig. 3). All of these factors have accelerated the atmospheric biogeochemical cycling of these compounds.

Atmospheric Modification to Other Biogeochemical Components

Atmospheric Biota

Atmospheric aerosols are likely to be composed in part by primary biogenic particles, or particles derived from the biota, for example, plant or insect bits, pollen, bacteria, or viruses [108]. Recent estimates suggest less than 5% of the aerosols are primary biogenic particles [109]. Some small fraction of these biogenic aerosols may contain viable living cells. While estimates of culturable bacteria are dependent on the methods used, estimates suggest that some bacteria do remain viable in the atmosphere, and can perhaps grow again if deposited onto the ground [110, 111]. Clearly, plants depend on pollen, and fungi on spores, to move genetic material from one place to another, and some fraction of this pollen and spores can be carried far from the source [112]. The amount of viable biota moving through the atmosphere and the importance of this process for global biogeochemical cycling is not well understood, but deserves future study.

Climate Modification of Biogeochemical Cycles

Changes in atmospheric biogeochemistry can modify climate, which in turn can also modify land and ocean biogeochemistry. This feedback has been used as a mechanism for understanding how carbon dioxide can be modulated on long timescales. For example, it is hypothesized that there are higher temperatures and more precipitation on land during higher carbon dioxide levels, thus increasing weathering [113]. This will reduce the atmospheric concentrations of carbon dioxide levels, acting as a feedback to prevent a runaway green house effect [113].

In the anthropocene, modeling studies have suggested that changes in anthropogenic aerosols and mineral aerosol particles can modify precipitation, incoming solar radiation, and temperature, and therefore modify land and ocean biogeochemistry enough to be seen at the global level [89, 90, 114, 115].

The Atmosphere as an Integrator

The atmosphere is the one part of the earth system that is transparent in many wavelengths of light, and thus can be readily observed using remote sensing methods. In addition, we live at the interface of the atmosphere and land surface, and thus have easy access to the lower layers of the atmosphere. This means that we have much better observations of the state of many biogeochemical cycles in the atmosphere, than in the land or ocean [16]. Thus understanding atmospheric biogeochemistry provides important information for understanding global biogeochemical cycles.

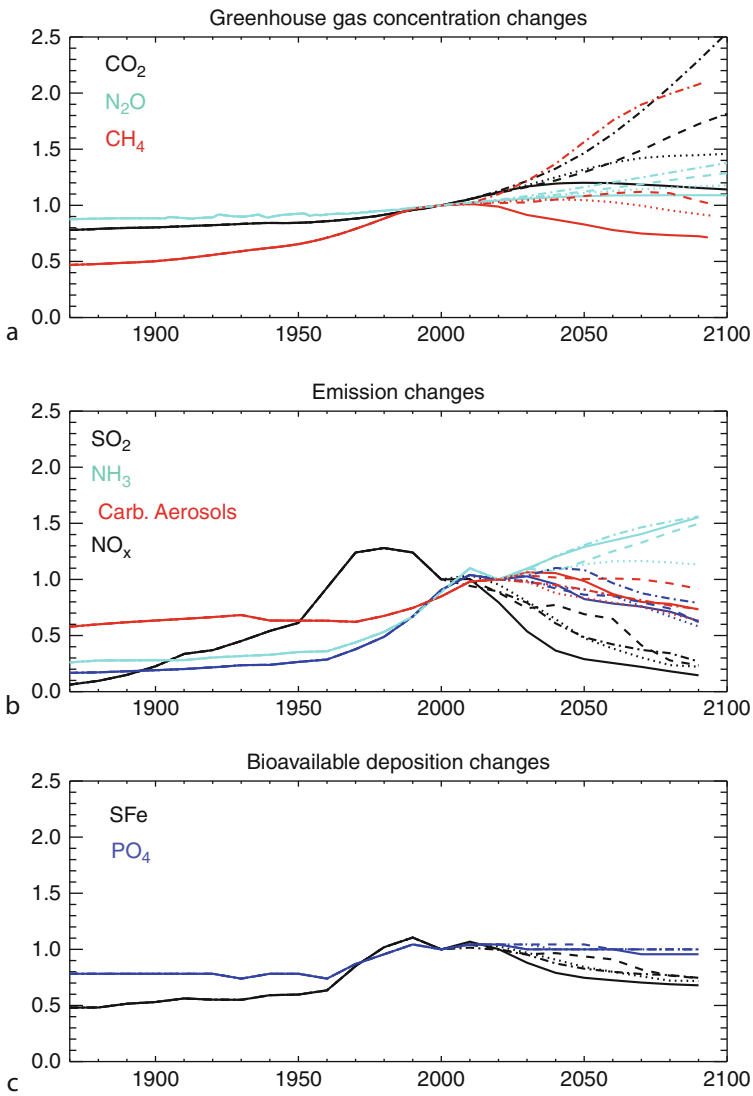

Atmospheric Biogeochemistry. Figure 3

Relative changes in green house gas concentrations (**a**), for carbon dioxide (*black*), nitrous oxide (*cyan*), and methane (*red*), relative to concentrations in 2000, based on atmospheric and ice core measurements for the past time period [127–130]. For the future, estimates are based on the representative concentration pathways estimates for four different scenarios [101–107], represented by the four lines into the future. Emission changes for important species, all normalized to 2000 values (**b**) for sulfur dioxide (*black*), ammonia (*cyan*), carbonaceous aerosols (*red*), and nitrogen oxides (*blue*) based on historical estimates [18], and for future estimates, the representative concentration pathways [101–107]. Deposition changes for bioavailable iron (*black*) and phosphorus (*blue*) are shown relatively to 2000 estimates (**c**), based on historical estimates and future estimates, using estimates of desert dust changes from [89], assuming in the future the model mean for no carbon dioxide fertilization changes in source area from [131], with iron solubility estimates from [64, 65], scaled by the sulfur dioxide emissions changes shown in (**b**), and for combustion soluble iron sources from [64] scaled by the black carbon emission changes included in (**b**). For soluble phosphorus (phosphates), desert dust estimate changes are the same as described for iron, and combustion sources of phosphorus come from [28], and are scaled by black carbon emissions, included in (**b**)

Transport in Atmosphere

The distance a chemical travels from its source region is highly dependent on its atmospheric lifetime. Many of the biogeochemically relevant gases discussed above are long-lived gases, which will reside in the atmosphere for several months to hundreds of years (e.g., CO_2, CH_4, N_2O). Other, reactive species (such as the hydroxyl radical OH), can have very short lifetimes (<1 day), and thus will not travel far from the sources. Aerosol species tend to have lifetimes between 1 day and a few weeks, and this lifetime is dependent on the size of the particle as well as whether precipitation has occurred, as this will remove particles.

For chemical species that have a relatively long lifetime (> a few days), long-range transport can occur. Once emitted into the atmosphere, constituents mix quickly into the atmospheric boundary layer (the lowest 1–3 km of the atmosphere, where mixing is strongest), and can be transported long distances. Air parcels stay on a constant buoyancy surface (called isentropes), unless they are heated or cooled [116]. These surfaces of constant buoyancy tilt upward between the tropics and the high latitudes, because the high latitudes are colder (Fig. 4a from [109]). An air parcel emitted in the tropical boundary layer can reach the stratosphere (>10 km high) in the high latitudes without being heated by moving along an isentropic surface. On average, most of the atmosphere is radiatively cooling slightly during non-stormy conditions, so, over time, parcels of air will become heavier and move downward. If the parcel encounters a storm system with clouds and precipitation, the parcel can

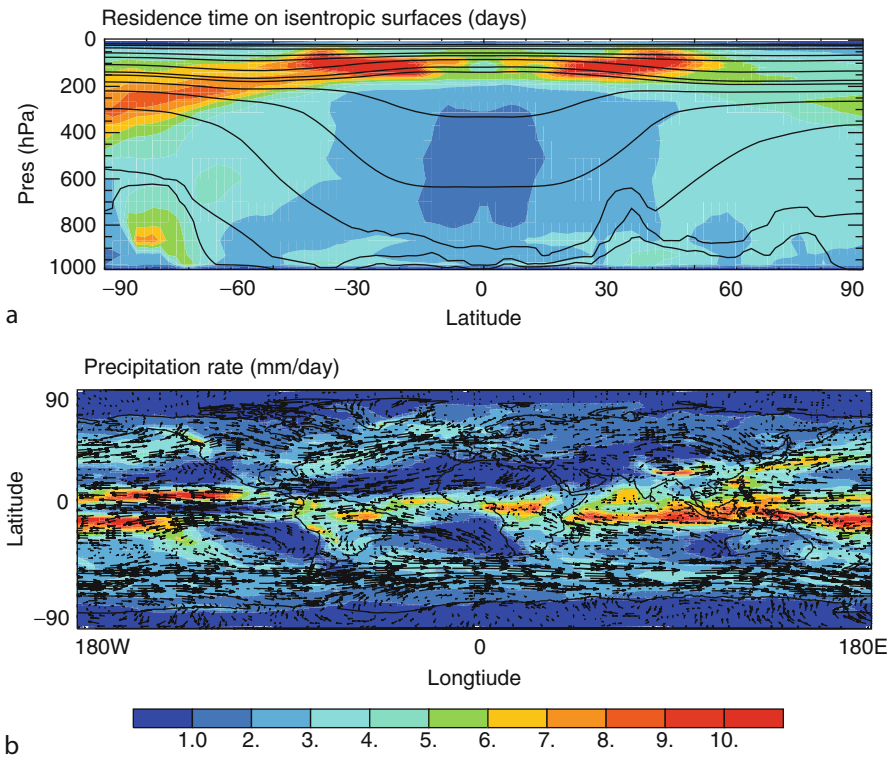

Atmospheric Biogeochemistry. Figure 4
Transport pathways of atmospheric constituents. Vertical distribution with latitude of the residence time of aerosols along a neutrally buoyant layer (isentrope), considering only vertical motion by heating in colors (**a**), with *black lines* marking surfaces of constant buoyancy (isentropes). These results are based on the 75% heating rates (warming or cooling) of the six hourly instantaneous results. Annually averaged precipitation rate (mm/day) in color, with annual mean wind vectors for 850 hPa (just above the boundary layer) (**b**) (Figure from [109])

experience large heating or cooling and move vertically very quickly, perhaps traveling from the boundary layer up to 10 km in less than 1 h [117]. At the same time, the precipitation within the storm system can cause wet deposition of soluble gases or aerosols. Based on atmospheric heating rates, the residence time for a parcel on a given isentropic surface varies between <1 day for the tropics to 3–6 days in midlatitudes (based on 75 percentile heating rates) (Fig. 4a). If a parcel moves away from the pole, the tilting of the neutral buoyant surfaces will direct the parcel downward vertically and vice versa.

Geographically, there tend to be particular regions in midlatitudes that have more storms (Fig. 4b), called the storm tracks. Winds in the midlatitudes (30–60°) tend to be from the west, while winds in the tropics and highlatitudes (>60°) are less uniform. Tropical aerosols are more likely to encounter storms, resulting in vertical mixing or quick removal (Fig. 4b). Transport across latitudes tends to occur less often than transport along a latitude [118]. Thus, in the midand high latitudes, one can think of a parcel containing a constituent moving along isentropes, following the local winds, slowly cooling, and moving to a lower isentropic surface until it encounters a storm system, at which time it can be quickly removed or vertically transported.

Inverse Modeling

Inverse modeling is the practice of using atmospheric concentrations to deduce the sources and sinks of various important compounds [119]. Because many biogeochemically relevant species have natural sources and sinks, they have sources of uncertain magnitude. Inverse modeling has become quite common for these constituents. The initial studies used simple models to best match available data [120, 121]. With time, studies focused on regional budgets but used higher temporal and spatially resolved datasets and models to resolve regional and time-varying sources as well as sophisticated statistical techniques [122–124]. These studies (called top-down studies, because they use atmospheric concentrations to constrain sources and sinks) provide important information about the sources and can provide alternative views from upscaling flux measurements or inventories (called bottom-up approaches) [125]. Current approaches often estimate parameters based on available data, instead of resolving budgets, allowing models to be tuned to best match observations at a site, before applying that model to other regions to extrapolate to regional and global budgets [126]. Thus understanding atmospheric biogeochemistry of important compounds can facilitate a better understanding of the land and ocean biogeochemistry, using inverse modeling approaches.

Future Directions

The study of atmospheric biogeochemistry as a field is just beginning, although some of the most important elements, such as the carbon cycle, have been studied for many years. Our knowledge, however, of even the carbon cycle is insufficient to understand how global carbon dioxide levels will respond in the future, even assuming that human emissions can be predicted [2]. Important nutrient cycles highlighted here include the carbon, nitrogen, phosphorus, sulfur, iron, and oxygen cycles. All of these cycles in some way are heavily impacted by human activities, and in addition, feedback onto our climate and environment in important ways. Many of the important innovations over the last few years have involved understanding how the different cycles interact. Thus atmospheric biogeochemistry remains an important field for continued research and innovations.

The atmosphere is unique with respect to the other components of the earth system in our ability to easily observe many layers using remote sensing. This means that the atmosphere provides a location where biogeochemistry as a whole can be better understood. Inverse methods and modeling, in addition to the many observations, may allow us to improve our understanding of not just atmospheric biogeochemical cycles, but land and ocean biogeochemical cycles.

Acknowledgments

The author would like to thank NSF (0932946, 0832782, 0758369) and NASA (NNG06G127G), as well as Rachel Scanza for assistance on the manuscript.

Bibliography

Primary Literature

1. LeQuere C, Raupach M, Canadell J, Marland G, Bopp L et al (2009) Trends in the sources and sinks of carbon dioxide. Nat Geosci 2:831–836. doi:10.1038/ngeo689

2. Friedlingstein P, Cox P, Betts R, Bopp L, Von Bloh W et al (2006) Climate-carbon cycle feedback analysis, results from the C4MIP Model intercomparison. J Clim 19:3337–3353
3. Thornton P, Doney S, Lindsay K, Moore JK, Mahowald N et al (2009) Carbon-nitrogen interactions regular climate-carbon cycle feedbacks: results from an atmosphere–ocean general circulation model. Biogeosciences Discussion 6:3303–3354
4. Denman KL, Brasseur G, Chidthaisong A, Ciais P, Cox PM et al (2007) Couplings between changes in the climate system and biogeochemistry. In: Solomon S, Qin D, Manning M, Chen Z, Marquis M, Averyt KB, Tignor M, Miller HL (eds) Climate change 2007: the physical science bases. Contribution of working group I to the fourth assessment report of the intergovernmental panel on climate change. Cambridge University Press, Cambridge, UK
5. Archer D, Eby M, Brovkin V, Ridgwell A, Cao L et al (2009) Atmospheric lifetime of fossil fuel carbon dioxide. Annu Rev Earth Pl Sc 37:117–134
6. Petit JR, Jouzel J, Raynaud D et al (1999) Climate and atmospheric history of the past 420,000 years from the Vostok Ice core, Antarctica. Nature 399:429–436
7. Sigman DM, Boyle EA (2000) Glacial/interglacial variations in atmospheric carbon dioxide. Nature 407:859–869
8. Hewitt C, Mitchell J (1997) Radiative forcing and response of a GCM to ice age boundary conditions: cloud feedback and climate sensitivity. Clim Dynam 13:821–834
9. Long SP, Ainsworth E, Rogers A, Ort D (2004) Rising atmospheric carbon dioxide: plants FACE the future. Annu Rev Plant Biol 55:591–628
10. Caspersen J, Pacala S, Jenkins J, Hurtt G, Moorcroft P, Birdsey R (2000) Contributions of land-use history to carbon accumulation in U.S. forests. Science 290:1148–1151
11. Joos F, Prentice IC, House JI (2002) Growth enhancement due to global atmospheric change as predicted by terrestrial ecosystem models: consistent with US forest inventory data. Global Change Biol 8:299–303
12. Caldeira K, Wickett M (2003) Anthropgenic carbon and ocean pH. Nature 425:365
13. Kleypas J, Buddemeier R, Archer D, Gattuso J-P, Langdon C, Opdyke B (1999) Geochemical consequences of increased atmospheric carbon dioxide on coral reefs. Science 284:118–120
14. Riebesell U, Zondervan I, Rost B, Tortell P, Zeebe R, Morel F (2000) Reduced calcification of marine plankton in respnse to increased atmospheric CO_2. Nature 407:364–367
15. Doney S, Fabry V, Feely R, Kleypas J (2009) Ocean acidification: the other CO_2 problem. Annu Rev Mar Sci 1:169–192
16. Forster P, Ramaswamy V, Artaxo P, Berntsen T, Betts R et al (2007) Changes in atmospheric constituents and in radiative forcing. In: Solomon S, Qin D, Manning M, Chen Z, Marquis M, Averyt KB, Tignor M, Miller HL (eds) Climate change 2007: the physical science basis. Contribution of working group I to the fourth assessment report of the intergovernmental panel on climate change. Cambridge University Press, Cambridge, UK/New York, pp 130–234
17. Jacob D (1999) Atmospheric chemistry. Princeton University Press, Princeton, p 266
18. Lamarque J-F, Bond T, Eyring V, Granier C, Heil A et al (2010) Historical (1850–200) gridded anthropogenic and biomass burning emissions of reactive gases and aerosols: methodology and application. Atmos Chem Phys 10:7017–7039
19. Galloway J, Townsend A, Erisman J, Bekunda M, Cai Z et al (2008) Transformation of the nitrogen cycle: recent trends, questions and potential solutions. Science 320:889–892
20. Adams P, Seinfeld J, Koch D (1999) Global concentrations of tropospheric sulfate, nitrate and ammonium aerosol simulated in a general circulation model. J Geophys Res 104:13791–13823
21. Duce RA et al (2008) Impacts of atmospheric anthropogenic nitrogen on the open ocean. Science 320. doi:10.1126/science.1150369
22. Holland E et al (1997) Variations in the predicted spatial distribution of atmospheric nitrogen deposition and their impact on carbon uptake by terrestrial ecosystems. J Geophys Res 102:15849–15866
23. Townsend A, Braswell BH, Holland E, Penner J (1996) Spatial and temporal patterns in potential carbon storage due to deposition of fossil fuel derived nitrogen. Ecol Appl 6. doi:10.2307/2269486
24. Sokolov AP, Kicklighter DW, Melillo JM, Felzer BS, Schlosser CA, Cronin T (2008) Consequences of considering carbon-nitrogen interactions on the feedbacks between climate and the terrestrial carbon cycle. J Clim 21:3776–3796
25. Zaehle S, Friedlingstein P, Friend AD (2010) Terrestrial nitrogen feedbacks may accelerate future climate change. Geophys Res Lett 37. doi:10.1029/2009GL041345
26. Krishnamurthy A, Moore JK, Mahowald N, Luo C, Zender CS (2010) The impacts of atmospheric nutrient inputs on marine biogeochemistry. J Geophys Res 115. doi:10.1029/2009JG001115
27. Schlesinger WH (1997) Biogeochemistry: an analysis of global change. Academic, San Diego, 588 pp
28. Mahowald N, Jickells TD, Baker AR, Artaxo P, Benitez-Nelson CR, Bergametti G, Bond TC, Chen Y, Cohen DD, Herut B, Kubilay N, Losno R, Luo C, Maenhaut W, McGee KA, Okin GS, Siefert RL, Tsukuda S (2008) The global distribution of atmospheric phosphorus deposition and anthropogenic impacts. Global Biogeochem Cycle 22. doi:10.1029/2008GB003240
29. Graham WF, Duce RA (1982) The atmospheric transport of phosphorus to the Western North Atlantic. Atmos Environ 16:1089–1097
30. Baker A, French M, Linge K (2006) Trends in aerosol nutrient solubility along a west–east transect of the Saharan dust plume. Geophys Res Lett 33. doi:10.1029/2005GL024764
31. Baker A, Jickells T, Biswas K, Weston K, French M (2006) Nutrients in atmospheric aerosol particles along the Atlantic Meridional Transect. Deep-Sea Res II 53:1706–1719
32. Nenes A, Krom M, Mihalopoulos N, VanCapellen P, Shin Z et al (2010) Atmospheric acidification of mineral aerosols: a source of bioavailable phosphorus to the oceans. Atmos Chem Phys Discuss 11:6163–6185

33. Bergametti G, Remoudaki E, Losno R, Stiner E, Chatenet B, Buat-Menard P (1992) Source, transport and deposition of atmospheric phosphorus over the Northwestern Mediterranean. J Atmos Chem 14:501–513
34. Herut B, Krom M, Pan G, Mortimer R (1999) Atmospheric input of nitrogen and phosphorus to the Southeast Mediterranean: sources, fluxes and possible impact. Limnol Oceanogr 44:1683–1692
35. Herut B, Collier R, Krom M (2002) The role of dust in supplying nitrogen and phosphorus to the Southeast Mediterranean. Limnol Oceanogr 47:870–878
36. Ridame C, Guieu C (2002) Saharan input of phosphate to the oligotrophic water of the open western Mediterranean Sea. Limnol Oceanogr 47:856–869
37. Glindemann D, Edwards M, Kuschk P (2003) Phosphine gas in the upper troposphere. Atmos Environ 37:2429–2433
38. Glindemann D, Edwards M, J-a L, Kuschk P (2005) Phosphine in soils, sludges, biogases and atmospheric implications–a review. Ecol Eng 24:457–463
39. Zhu R, Glindemann D, Kong D, Sun L, Geng J, Wang X (2007) Phosphine in the marine atmosphere along a hemisphere course from China to Antarctica. Atmos Env 41:1567–1573
40. Graham WF, Duce RA (1979) Atmospheric pathways of the phosphorus cycle. Geochimica et Cosmochimica Acta 43:1195–1208
41. Vitousek P (1984) Litterfall, nutrient cycling and nutrient limitations in tropical forests. Ecology 65:285–298
42. Okin GS, Mladenov N, Wang L, Cassel D, Caylor KK et al (2008) Spatial pattern of soil nutrients in two southern African savannas. J Geophys Res 111. doi:10.1029/2007JG000584
43. Swap R, Garstang M, Greco S, Talbot R, Kallberg P (1992) Saharan dust in the Amazon Basin. Tellus 44B:133–149
44. Chadwick OA, Derry LA, Vitousek PM, Huebert BJ, Hedin LO (1999) Changing sources of nutrients during four million years of ecosystem development. Nature 397:491–496
45. Okin G, Mahowald N, Chadwick O, Artaxo P (2004) The impact of desert dust on the biogeochemistry of phosphorus in terrestrial ecosystems. Global Biogeochem Cycle 18:GB2005. doi:10.1029/2003GB002145
46. Graham B, Guyon P, Maenhaut W, Taylor PE, Ebert M et al (2003) Composition and diurnal variability of the natural Amazonian aerosol. J Geophys Res 108:4765. doi:10.1029/2003JD004049
47. Mahowald N, Artaxo P, Baker A, Jickells T, Okin G et al (2005) Impact of biomass burning emissions and land use change on Amazonian atmospheric cycling and deposition of phosphorus. Global Biogeochem Cycle 19:GB4030. doi:10.1029/2005GB002541
48. Falkowski PG, Barber RT, Smetacek V (1998) Biogeochemical controls and feedbacks on ocean primary production. Science 281:200–206
49. Wu J, Sunda W, Boyle E, Karl D (2000) Phosphate depletion in the western North Atlantic Ocean. Science 289:759–762
50. Krishnamurthy A, Moore K, Zender C, Luo C (2007) Effects of atmospheric inorganic nitrogen deposition on ocean biogeochemistry. J Geophys Res 112. doi:10.1029/2006JG000334
51. Seitzinger S, Harrison J, Dumont E, Beusen A, Bouwman A (2005) Sources and delivery of carbon, nitrogen and phosphorus to the coastal zone: an overview of the Global Nutrient Export from Watersheds (NEWS) models and their application. Global Biogeochem Cycle 19. doi:10.1029/2005GB002606
52. Benitez-Nelson C (2000) The biogeochemical cycling of phosphorus in marine systems. Earh-Sci Rev 51:109–135
53. Crutzen PJ (1976) The possible importance of CSO for the sulfate layer of the stratosphere. Geophys Res Lett 3:73–76
54. Deshler T (2007) Stratospheric aerosol: measurements, importance, life cycle, anomalous aerosol. In: O'Dowd C, Wagner P (eds) Nucleation and atmospheric aerosols. Springer, Heidelberg, pp 613–624
55. Charlson RJ, Lovelock JE, Andreae M, Warren SG (1987) Oceanic phytoplankton, atmospheric sulfur, cloud albedo and climate. Nature 326:655–661
56. Kloster S, Feichter J, Maier-Reimer E, Roeckner E, Stier P et al (2007) Response of DMS in the ocean and atmosphere to global warming. J Geophys Res 142:G03005. doi:10.1029/2006JG000224
57. Seinfeld J, Pandis S (1998) Atmospheric chemistry and physics. Wiley, New York, p 1326
58. Gong SL, Barrie L, Lazare M (2002) Canadian aerosol model (CAM): a size-segregated simulation of atmospheric aerosol process for climate and air quality models 2. Global sea-salt aerosol and its budgets. J Geophys Res 107:4779. doi:10.209/2001JD002004
59. Carslaw KS, Boucher O, Spracklen D, Mann G, Rae JG et al (2010) A review of natural aerosol interactions and feedbacks within the earth system. Atmos Chem Phys 10:1701–1737
60. Morell F, Price N (2003) The biogeochemical cycles of trace metals in the oceans. Science 300:944–947
61. Martin J, Gordon RM, Fitzwater SE (1991) The case for iron. Limnol Oceanogr 36:1793–1802
62. Fung I, Meyn SK, Tegen I, Doney S, John J, Bishop J (2000) Iron supply and demand in the upper ocean. Global Biogeochem Cycle 14:281–295
63. Poulton S, Raiswell R (2002) The low-temperature geochemical cycle of iron: from continental fluxes to marine sediment deposition. Am J Sci 302:774–805
64. Luo C, Mahowald N, Bond T, Chuang PY, Artaxo P et al (2008) Combustion iron distribution and deposition. Global Biogeochem Cycle 22. doi:10.1029/2007GB002964
65. Mahowald N, Engelstaedter S, Luo C, Sealy A, Artaxo P et al (2009) Atmospheric iron deposition: global distribution, variability and human perturbations. Annu Rev Mar Sci 1:245–278. doi:10.1146/annurev/marine.010908.163727
66. Duce RA, Liss PS, Merrill JT, Atlas EL, Buat-Menard P et al (1991) The atmospheric input of trace species to the world ocean. Global Biogeochem Cycle 5:193–259
67. Claquin T, Schulz M, Balkanski Y (1999) Modeling the mineralogy of atmospheric dust sources. J Geophys Res 104:22243–22256

68. Journet E, Desbouefs K, Caqineau S, Colin J-L (2008) Mineralogy as a critical factor of dust iron solubility. Geophys Res Lett 35. doi:10.1029/2007GL031589
69. Hand J, Mahowald N, Chen Y, Siefert R, Luo C et al (2004) Estimates of soluble iron from observations and a global mineral aerosol model: biogeochemical implications. J Geophys Res 109:D17205. doi:10.1029/2004JD004574
70. Frogner P, Gislason SR, Oskarsson N (2001) Fertilizing potential of volcanic ash in ocean surface water. Geol Soc Am 29:487–490
71. Duggen S, Croot P, Schacht U, Hoffmann L (2007) Subduction zo006Ee volcanic ash can fertilize the surface ocean and stimulate phytoplankton growth: evidence from biogeochemical experiments and satellite data. Geophys Res Lett 34:L01612. doi:10.1029/2006GL027522
72. Johnson K (2001) Iron supply and demand in the upper ocean: is extraterrestrial dust a significant source of bioavailable iron? Global Biogeochem Cycle 15:61–63
73. Jickells T, Spokes L (2001) Atmospheric iron inputs to the oceans. In: Turner DR, Hunteger K (eds) Biogeochemistry of iron in seawater. Wiley, Chichester, pp 85–121
74. Zhu X, Prospero J, Millero F (1997) Diel variability of soluble Fe (II) and soluble total Fe in North Africa dust int he trade winds at Barbados. J Geophys Res 102:21297–21305
75. Meskhidze N, Chameides W, Nenes A (2005) Dust and pollution: a recipe for enhanced ocean fertilization? J Geophys Res 110. doi:10.1029/2004JD005082
76. Guieu C, Bonnet S, Wagener T, Loye-Pilot M-D (2005) Biomass burning as a source of dissolved iron to the open ocean? Geophys Res Lett 22:L19608. doi:10.1029/2005GL022962
77. Chuang P, Duvall R, Shafer M, Schauer J (2005) The origin of water soluble particulate iron in the Asian atmospheric outflow. Geophys Res Lett 32. doi:10.1029/2004GL021946
78. Sedwick P, Sholkovitz E, Church T (2007) Impact of anthropogenic combustion emissions on the fractional solubility of aerosol iron: evidence from the Sargasso Sea. Geochem Geophy Geosy 8. doi:10.1029/2007GC001586
79. Coale KH, Johnson KS, Fitzwater SE, Gordon RM, Tanner S et al (1996) A massive phytoplankton bloom induced by an ecosystem-scale iron fertilization experiment in the equatorial Pacific Ocean. Nature 383:495–501
80. Boyd PW, Law CS (2001) The southern ocean iron release experiment (SOIREE) introduction and summary. Deep-Sea Res II 48:2425–2438
81. Bishop J, Davis R, Sherman J (2002) Robotic observations of dust storm enhancement of carbon biomass in the north pacific. Science 298:817–821
82. Cassar N, Bender M, Barnett B, Fan S, Moxim WJ et al (2007) The southern ocean biological response to aeolian iron deposition. Science 317:1067–1070
83. Berman-Frank I, Cullen JT, Shaked Y, Sherrell RM, Falkowski P (2001) Iron availability, cellular iron quotas, and nitrogen fixation in *Trichodesmium*. Limnol Oceanogr 46:1249–1260
84. Michaels AF, Olson D, Sarmiento JL, Ammerman JW, Fanning K et al (1996) Inputs, losses and transformations of nitrogen and phosphorous in the pelagic North Atlantic Ocean. Biogeochemistry 35:181–226
85. Capone DG, Zehr JP, Paerl HW, Bergman B, Carpenter EJ (1997) Trichodesmium, a globally significant marine cyanobacterium. Science 276:1221–1229
86. Mahaffrey C, Williams R, Wolff G, Mahowald N, Anderson W (2003) Isotopic signals of nitrogen fixation over the eastern North Atlantic. Geophys Res Lett 40. doi:10.109/2002/GL016542
87. Knapp A, Hastings M, Sigman D, Lipschultz F, Galloway J (2010) The flux and isotopic composition of reduced and total nitrogen in Bermuda rain. Mar Chem 120:83–89
88. Okin G, Baker A, Tegen I, Mahowald N, Dentener F et al (2011) Impacts of atmospheric nutrient deposition on marine productivity: roles of nitrogen, phosphorus and iron. Global Biogeochem Cycle 25:GB2022
89. Mahowald N, Kloster S, Engelstaedter S, Moore JK, Mukhopadhyay S et al (2010) Observed 20th century desert dust variability: impact on climate and biogeochemistry. Atmos Chem Phys 10:10875–10893
90. Mahowald NM, Lindsay K, Rothenberg D, Doney SC, Moore JK et al (2011) Desert dust and anthropogenic aerosol interactions in the Community Climate System Model coupled-carbon-climate model. Biogeosciences 8:387–414. doi:10.5194/bg-8-387-2011
91. Lovelock J (1979) Gaia: a new look at life on earth. Oxford University Press, Oxford, UK
92. Keeling R, Shertz SR (1992) Seasonal and interannual variations in atmospheric oxygen and implications for the global carbon cycle. Nature 358:723–727
93. Bender M, Ho D, Hendricks M, Mika R, Battle M et al (2005) Atmospheric O_2/N_2 changes, 1993–2002: implications for the partitioning of fossil fuel CO_2 sequestration. Global Biogeochem Cycle 19. doi:10.1029/2004GB002410
94. Hartmann D (1994) Global physical climatology. Academic, San Diego
95. Solomon S (1999) Stratospheric ozone depletion: a review of concepts and history. Rev Geophys 37:275–316
96. Chipperfield MP, Randel WJ, Bodeker GE, Dameris M, Fioletov VE, AyitÈ-LÙ DLA, Ajavon N, MÈgie G, Watson RT et al (2003) Global ozone: past and future, chapter 4. In: Scientific assessment of ozone depletion: 2002. WMO, Geneva, p 498
97. Prinn RG, Weiss RG, Miller BR, Huang J, Alyea FN et al (1995) Atmospheric trends and lifetime of CH_3CCl_3 and global OH concentrations. Science 269:187–192
98. Selin N (2009) Global biogeochemical cycling of Mercury: a review. Annu Rev Env Resour 34:43–63
99. Paytan A, Mackey K, Chen Y, Lima I, Doney S et al (2009) Toxicity of atmospheric aerosols on marine phytoplankton. Proc Natl Acad Sci USA 106:4601–4605. doi:10.1073/pnas.0811486106

100. Doney S, Mahowald N, Lima I, Feeley R, Mackenzie F et al (2007) Impact of anthropogenic atmospheric nitrogen and sulfur depositionon ocean acidification and the inorganic carbon system. Proc Natl Acad Sci USA 104:14580–14585. doi:10.1073/pnas.07022181
101. vanVuuren D, den Elzen MG, Lucas P, Eickhout B, Strengers B et al (2007) Stabilizing greenhouse gas concentrations at low levels: an assessment of reduction strategies and costs. Clim Change 81:119–159. doi:10.1007/s10584-006-9172-9
102. Clarke L, Edmonds J, Jacoby H, Pitcher H, Reilly J, Richells R (2007) Scenarios of greenhouse gas emissions and atmospheric concentrations. Sub-report 2.1A of synthesis and assessment product 2.1 by the US climate change science program and the subcommittee on global change research. Department of Energy, Office of Biological and Environmental Research, Washington, DC
103. Smith SJ, Wigley T (2006) Multi-gas forcing stabilization with the MiniCAM. Energy J Special Issue #3:373–391
104. Wise M, Calvin KV, Thomson A, Clarke LE, Bond-Lamberty B et al (2009) Implications of limiting CO_2 concentrations for land use and energy. Science 324:1183–1186
105. Fujino J, Nair R, Kainuma M, Masui T, Matuoka Y (2006) Multi-gas mitigation analysis on stabilzation scenarios using AIM global model. Energy J Special Issue 3:343–354
106. Hijoka Y, Matuoka Y, Hisimoto H, Masui M, Kainuma M (2008) Global GHG emission scenarios under GHG concentration stabilization targets. Global Env Eng 13:97–108
107. Riahl K, Gruebler A, Nakicenovic N (2007) Scenarios of long-term socio-economic and environmental development under climate stabilization. Technol Forecast Soc 74:887–935
108. Jaenicke R (2005) Abundance of cellular material and proteins in the atmosphere. Science 308:73
109. Mahowald N, Ward D, Kloster S, Flanner M, Heald C et al (2011) Aerosol impacts on climate and biogeochemistry. Annu Rev Env Resour 36. doi:10.1146/annurev-environ-042009-094507
110. Lighthart B (2006) The ecology of bacteria in the alfresco atmosphere. FEMS Microbiol Ecol 23:263–274
111. Burrows SM, Elbert W, Lawrence MG, Poschl U (2009) Bacteria in the global atmosphere–Part 1: review and synthesis of literature for different ecosystems. Atmos Chem Phys 9:9263–9280
112. Heald C, Spracklen D (2009) Atmospheric budget of primary biological erosol particles from fungal sources. Geophys Res Lett 36. doi:10.1029/2009GL037493
113. Stanley S (1999) Earth system history. WH Freeman, New York, p 615
114. Jones C, Cox P, Essery R, Roberts D, Woodage M (2003) Strong carbon cycle feedbacks in a climate model with interactive CO_2 and sulphate aerosols. Geophys Res Lett 30:1479. doi:10.029/2003gl0166867
115. Mercado L, Bellouin N, Stich S, Boucher O, Huntingford C et al (2009) Impacts of changes in diffuse radiation on the global land carbon sink. Nature 458:1014–1018. doi:10.1038/nature07949
116. Holton JR (1989) Global transport processes in the atmosphere. In: Hutzinger O (ed) The handbook of environmental chemistry. Springer, New York, pp 97–144
117. Barth M, Stuart A, Skamarock W (2001) Numerical simulations of the July 10, 1996, stratospheric-tropospheric experiment: radiation, aerosols, and ozone (STERAO)-deep convection experiment storm: redistribution of soluble tracers. J Geophys Res 106:12381–12400
118. Bowman K, Carrie G (2002) The mean-meridional transport circulation of the troposphere in an idealized GCM. J Atmos Sci 59:1502–1514
119. Kasibhatla P, Heimann M, Rayner P, Mahowald N, Prinn R, Hartley D (eds) (2000) Inverse methods in global biogeochemical cycles. American Geophysical Union, Washington, DC, p 324
120. Bolin B, Keeling C (1963) Large-scale atmospheric mixing as deduced from teh seasonal and meridionial variations of carbon dioxide. J Geophys Res 68:3899–3920
121. Fung I, John J, Lerner J, Matthews E, Prather M et al (1991) Three-dimensional model syntehsis of the global methane cycle. J Geophys Res 96:13033–13065
122. Gurney KR, Law RM, Denning AS, Rayner PJ, Baker D et al (2002) Towards robust regional estimates of CO_2 sources and sinks using atmospheric transport models. Nature 415:626–630
123. Bousquet P, Peylin P, Ciais P, Quere CL, Friedlingstein P, Tans PP (2000) Regional changes in carbon dioxide fluxes of land and oceans since 1980. Science 290:1342–1347
124. Houweling S, Kaminski T, Dentener F, Lelieveld J, Heimann M (1999) Inverse modeling of methane sources and sinks using the adjoint of ta global transprot model. J Geophys Res 104:26137–26160
125. Kasibhatla P, Arellano A, Logan J, Palmer P (2002) Top-down estimate of a large source of atmospheric carbon monoxide associated with fuel combustion in Asia. Geophys Res Lett 29. doi:10.1029/2002GL015581
126. Braswell B, Sacks W, Linder E, Schimel D (2005) Estimating diurnal to annual ecosystem parameters by synthesis of carbon flux model with eddy covariance net ecosystem exchange observations. Glob Change Biol 11. doi:1111/j.365-2486.005.00897
127. Keeling RF, Piper SC, Bollenbacher AF, Walker JS (2009) Atmospheric CO_2 records from sites in the SIO air sampling network. In: Trends: a compendium of data on global change. Carbon Dioxide Information Analysis Center, Oak Ridge National Laboratory, U.S. Dept. of Energy, Oak Ridge
128. Etheridge DM, Steele LP, Langenfelds RL, Francey RJ, Barnola J-M, Morgan VI (1998) Historical CO_2 records from the law dome DE08, DE08-2, and DSS ice cores. In: Trends: a compendium of data on global change. Oak Ridge National Laboratory: Carbon Dioxide Information Analysis Center, Oak Ridge National Laboratory, U.S. Department of Energy, Oak Ridge

129. Etheridge DM, Steele LP, Francey RJ, Langenfelds RL (2002) Historical CH_4 records since about 1000 A.D. from ice core data. In: Trends: a compendium of data on global change. Carbon Dioxide Information Analysis Center, Oak Ridge National Laboratory, U.S. Department of Energy, Oak Ridge
130. Battle M, Bender M, Sowers T, Tans PP, Butler JH et al (1996) Atmospheric gas concentrations over the past century measured in air from firn at the South Pole. Nature 383:231–235
131. Mahowald N (2007) Anthropocence changes in desert area: sensitivity to climate model predictions. Geophys Res Lett 34. doi:10.1029/2007GL030472

Books and Reviews

Jacobson M, Charlson R, Rodhe H, Orians G (eds) (2000) Earth system science, vol 72. Academic, San Diego

Atmospheric General Circulation Modeling

Philip J. Rasch
Pacific Northwest National Laboratory, Richland, WA, USA

Article Outline

Glossary
Definition of the Subject
Introduction
Clouds and Aerosols in Climate Models
Climate Forcing and Response
Calibration (Tuning) and Evaluation of GCMs
Remaining Challenges in Modeling the Atmosphere
Acknowledgments
Bibliography

Glossary

Aerosols The small (solid and liquid) particles that are suspended in the atmosphere. Aerosols have both natural (e.g., sea-salt, dust, and some organic compounds released by vegetation) and anthropogenic origins (e.g., the pollution released by power plants, cars, trucks, agricultural burning, etc.).

Climate The statistical description of characteristics of our environment over long periods, including properties like the mean and extreme values of value of fields like temperature, winds, and moisture.

Climate sensitivity Usually used to mean the change in globally averaged surface temperature ΔT that would occur in a model if it were allowed to equilibrate to a forcing ΔF associated with a doubling of CO_2. It is sometimes used in a looser fashion to refer to the change in temperature resulting from a change in forcing.

Feedback A process in the climate system that can either amplify ("positive feedback") or diminish ("negative feedback") a change in climate forcing.

Lapse rate A term that refers to the vertical temperature decrease in the atmosphere. When that lapse rate exceeds certain thresholds, convective overturning can occur. Two threshold lapse rates are important. The dry adiabatic lapse rate identifies the rate at which an unsaturated parcel will cool if it is lifted adiabatically. If the environmental lapse rate is larger than the dry adiabatic lapse rate, a parcel lifted adiabatically will gain buoyancy and convective overturning can occur. When saturated air is lifted adiabatically, it will cool at a temperature-dependent rate as phase change occurs. At warm temperatures, the saturated adiabatic lapse rate is less than the dry adiabatic lapse rate. Since the atmosphere will produce overturning to reduce these instabilities associated with buoyant parcels, the lapse rate and water vapor amount play an important role in convection. The moist and dry adiabatic lapse rates explain much of the vertical temperature gradient to lowest order.

Parameterization The equations and computer code describing the representation of a particular physical process in a climate model, for example, the representation of convection.

Radiative forcing A change altering the energy budget of the climate system usually associated with changes in the atmospheric abundance of greenhouse gases and aerosols, or factors like solar variability and volcanic. These changes are expressed in terms of radiative forcing, which is used to compare how a range of human and natural factors drive warming or cooling influences on global climate.

Subgrid scale The behavior of a process at time and space scales that are smaller than the model can resolve.

Tropopause A permeable boundary separating two layers of the atmosphere: the stratosphere (a relatively stable region above) and the troposphere (a less stable region below where convective overturning often occurs). The tropopause varies quite smoothly in latitude. It is highest in the tropics (18 km) and decreases toward the poles (to 10 km or so).

Weather The short-term evolution of our environment.

Definition of the Subject

This entry provides a brief introduction to the computer models of the atmosphere used for climate studies. The concepts of atmospheric forcing and response are developed and used to highlight the importance of clouds and aerosols to the climate system and the many uncertainties associated with their representation. Many processes that are important to the accurate representation of clouds and aerosols for climate are subgrid scale, and present both physical and computational challenges in atmospheric modeling. Other factors contributing to uncertainties in models are discussed, and some remaining challenges in atmospheric models are introduced.

Introduction

This entry provides a brief description of models of the atmosphere used for climate studies. These models can be part of a coupled climate system model or ► Coupled Climate and Earth System Models, as described by Gent elesewhere in the section *Climate Change Modeling and Methodology*, but they can also be used separately with prescribed values for surface fields, or simpler treatments for surface processes.

The atmospheric component of climate models can vary enormously in complexity. Simple atmospheric models based on energy balance arguments can be run on a laptop to provide rapid estimates of global, annual averaged properties of the atmosphere (e.g., surface temperature, e.g., [22]). The simpler types of atmospheric models (Energy Balance Models and Models of Intermediate Complexity) are discussed in the entry ► Climate Change Projections: Characterizing Uncertainty Using Climate Models by Sanderson, and Knutti, and Edmonds et al.

Much more elaborate models typically used in Earth system models are capable of simulating the distributions (in space and time) of hundreds of atmospheric fields and processes, the interaction between those fields and processes, and their response to external forcing. In this entry, the focus is on the more complex form of atmospheric models. These models are frequently also called General Circulation Models (GCMs) or Atmospheric General Circulation Models (AGCMs). The term GCM will be used here. More detail is found in the textbooks by Washington and Parkinson [20], Jacobson [5], and McGuffie and Henderson-Sellers [9].

GCMs share a great many features with the weather prediction models described by Bacmeister in this section *Climate Change Modeling and Methodology*. Both use the "equations of motion" (simplified versions of the Navier–Stokes for fluid flow, coupled with thermodynamic and mass conservation equations) to describe the evolution of the atmosphere, and parameterizations, but the way the models are used, and the focus is different (discussed more below).

A nice history of climate science and the development of weather and climate models can be found in Weart [21]. The first incarnation of atmospheric models solved on computers can be traced back to the efforts of a small group of meteorologists and physicists initially lead by John von Neumann and later Jule Charney near Princeton, New Jersey, soon after World War II. That effort started with the solution of simplified versions of the equations of motion on the most powerful computers available at the time (less powerful than the laptops in use today).

The complexity of present-day models has increased enormously, and large communities have grown up around those models. There are perhaps a dozen comprehensive independent GCMs in use today around the world, and many more prototypes used for study and development. Those communities include scientists and computer staff engaged in the development of the basic model, including testing and evaluation, as well as scientists that use the model as a tool for investigating climate science.

An easy example of a community activity focused on a particular GCM is the Community Atmosphere Model (CAM; http://www.cesm.ucar.edu/working_groups/Atmosphere/) project, an activity started in the USA about 30 years ago. That model is part of the larger Community Earth System Modeling (CESM) Project (http://www.cesm.ucar.edu).

CAM is a computer code that is order 400,000 lines of FORTRAN90 code. It is capable of being run in a variety of configurations, each optimized for different purposes, for example:

- Configurations useful for paleoclimate problems. These simulations sometimes require different positions of the continents. Simulations might be performed over millennia to explore climate change in response to orbital changes, or the Sun's luminosity.
- Idealized model configurations that simplify the Earth system by assuming the underlying surface is an "aquaplanet" (a world entirely covered by water).
- Configurations able to simulate the reactive photochemistry important for understanding the evolution of ozone distributions in the middle atmosphere handling hundreds of trace constituents, and many chemical reactions between those constituents.
- Configurations useful for study the reasons for climate change arising from nature and mankind over the last two centuries, and useful for producing projections given various scenarios of change in the future.

There are many other model configurations, and this list is not inclusive.

Detailed technical notes and scientific papers describing these types of applications can be found on the web sites mentioned above. The model is "open source," and it can be downloaded and run by anyone (provided a sufficiently powerful computer is available to perform a desired calculation). Archives of previous simulations are also available for download and examination.

The CESM and CAM projects are perhaps the largest of the GCM modeling activities in existence today, and so it provides an easy example to discuss and describe, but perhaps a dozen other activities around the world have similar capabilities.

The rest of this entry discusses the "generic" characteristics of this kind of climate model.

Global GCMs are generally run at resolutions resolving horizontal features larger than hundreds of kilometers and vertical variations of a few hundred meters. These resolutions are somewhat lower than used by weather models, where more detail is often needed. GCMs frequently include representation of processes and variables that are neglected or treated more simply in weather models (e.g., weather models often neglect details of the evolution of aerosols, or the slow evolution of greenhouse gases that affect the Earth system over longer timescales than are important for weather). GCMs may also include external forcing terms (e.g., variations in solar fluxes, or a historic database of volcanic eruption information) that are neglected by weather models.

Weather prediction models have typically been optimized to provide information about local features of the atmosphere over shorter time periods at higher resolution. Because initial conditions for weather models are constantly being "reset" to observed values, less attention has been paid to processes that affect the simulation over longer timescales (months to years). Climate models, on the other hand, focus on a description of the subtle balances and feedbacks occurring between processes and tend to describe these relationships through statistics of their long-term behavior. For many applications, climate models ignore initial conditions (weather modelers have traditionally viewed their simulations as an initial value problem; climate modelers, as a boundary value problem). A focus on statistical properties necessarily requires "multiple samples" from a distribution, with less attention on initial conditions, and more attention on the processes that control the model equilibrium or produce a transition from one climate regime to another. These points of view are changing, as discussed below.

This divergence in focus between weather and climate has led to differences in model design and configuration. Climate scientists have developed models that allow simulations over centuries or millennia. Weather models provide much higher

resolution information, but those simulations are often for periods of only a few days or weeks.

GCMs being used around 2010 divide the atmosphere into columns of about a hundred kilometer on a side with 30–50 layers vertically (see Fig. 1). Most of the focus is on the atmosphere within the 40 km nearest the Earth's surface. Weather models may use columns as narrow as 10 km on a size with two to three times the number of vertical layers. Global weather models thus divide the atmosphere into volumes about 200 times smaller than climate models. Computational and accuracy constraints require that model time steps decrease in proportion to the size of the model volume. A reasonable first guess on model cost (the number of floating point operations required to complete a simulation of fixed length) is that it scales as the cube of the model resolution. Figure 1 shows a typical type of atmospheric model grid (in this case uniform in latitude and longitude), but other discretizations are possible (see Bacmeister, this volume).

This difference in horizontal and vertical resolution produces significant differences in the way some features important to weather and climate are represented in these models. An example is shown in Fig. 2, which displays the surface topography for North and South America at a 200-km horizontal resolution typical of climate models and a 20-km resolution typical of weather models. The very sharp, small-scale topographic features like the Andes have been significantly "smoothed out" at low resolution, differing in altitude by almost a factor of 2 and spread over a much broader horizontal extent, with measurable impacts on

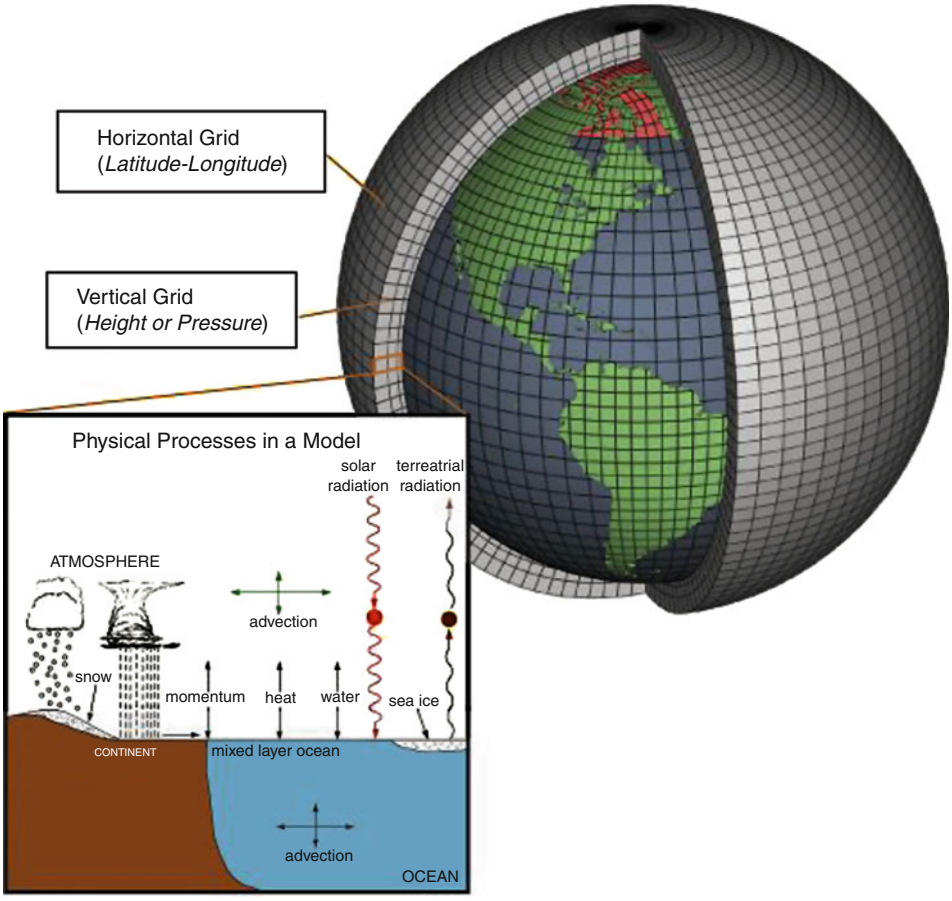

Atmospheric General Circulation Modeling. Figure 1
Typical discretization of a GCM or weather model (Figure from http://www.oar.noaa.gov/climate/t_modeling.html)

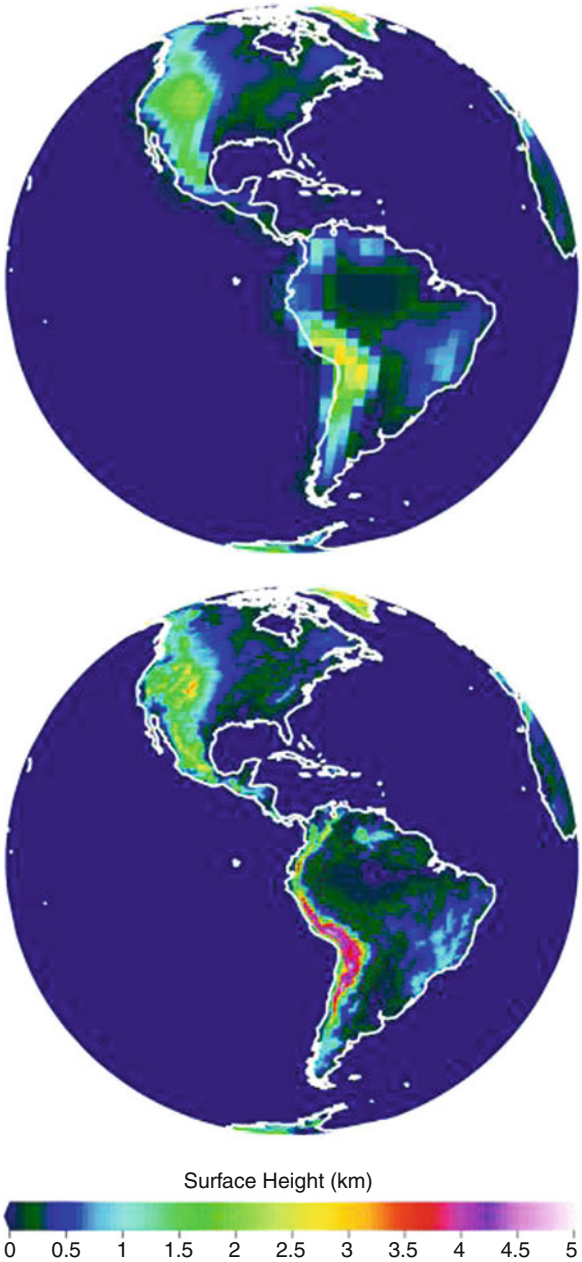

Atmospheric General Circulation Modeling. Figure 2 The topography used by a typical "low-resolution" global atmospheric model (approximately 2° horizontal resolution, *upper panel*) and the high-resolution topography more typical of weather models, and next-generation climate models (about 0.25° resolution). Note the factor of 2 difference in height of the Andes and similar differences over the Rockies of N. America

the role of the Andes as a barrier to winds, and their role in influencing precipitation patterns. The need to resolve some features important for climate at high resolution while minimizing computational cost is one of the motivations for the development of regional climate models (see ► Regional Climate Models by Leung), or models with variable resolution meshes to put the resolution where it is needed.

Figure 3 shows a typical layer structure for an atmospheric climate model. Most models in use today rewrite their equations to employ a vertical coordinate that follows the terrain near the surface, with a gradual transition to a fixed height or pressure coordinate at higher altitudes. Model layers are generally concentrated near the Earth's surface to deal with the complexity of processes taking place there due to boundary layer effects, terrain, interactions with surface models, and the fact that mankind lives in that region. Models typically use layers 10–100-m thick near the surface and gradually decrease that resolution to use 1–2-km-thick layers at higher altitudes. Other coordinate systems have also been considered for climate models. The equations of motion are expressed more simply with height- and pressure-based vertical coordinates, but treatment of boundary conditions is more complex. Some modeling groups have explored the use of vertical coordinates that approximately follow a material surface. These formulations result in more complex models with coordinate surfaces that can also intersect the surface of the Earth, introducing additional complexity in the treatment of boundary conditions, but the benefit is a model with much more accurate treatment of vertical transport.

Climate problems require descriptions of physical interactions at multiscale scales, leading to a very demanding challenge in physics and computational mathematics. Small-scale phenomena operating on the scale of molecules (e.g., chemistry, phase change of water, and radiative transfer) influence larger-scale features and eventually have global impacts. The physics and chemistry occurring at those small scales influence fluid motions through radiative heating and phase change to produce important phenomena like clouds with important features at scales of meters to kilometers, for example, updrafts and downdrafts. A brute force representation to treat fluid motions like up- and downdrafts would require a model

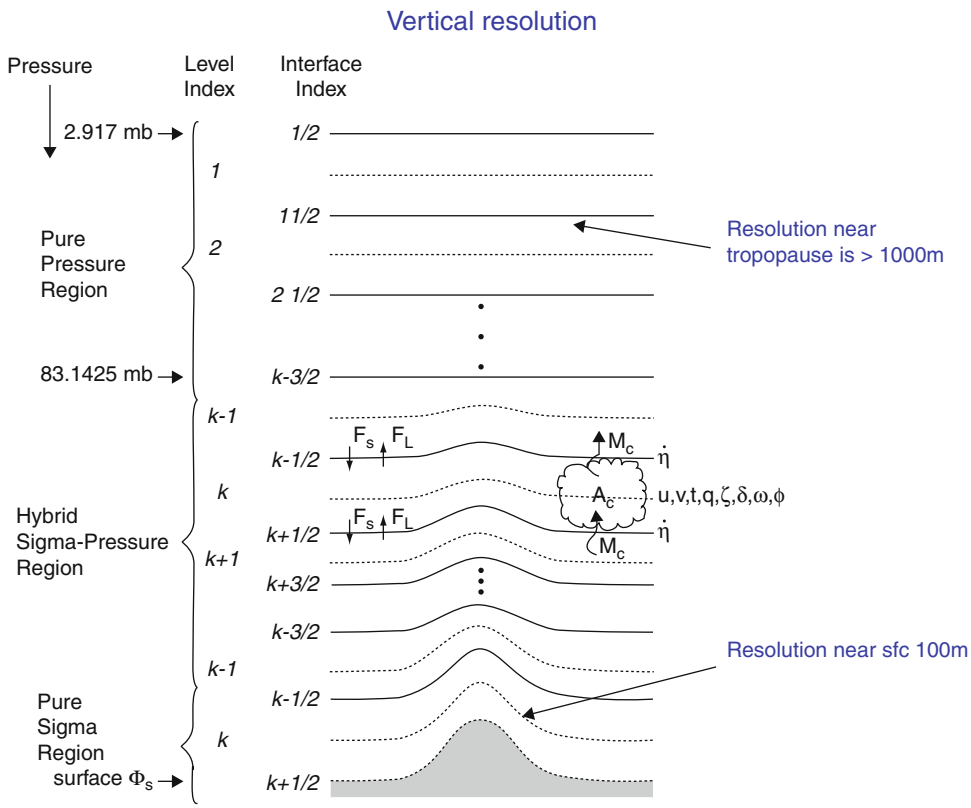

Atmospheric General Circulation Modeling. Figure 3
Typical distribution of layers in an atmospheric model. Top model layer will reach around 40 km for models with a focus on the troposphere and much higher for models interested in middle atmosphere problems (Figure from http://www.cesm.ucar.edu/models/atm-cam/docs/description/description.pdf)

that explicitly resolves those features, requiring discretizations with cells as small as a few meters on a side. It is not feasible to represent the whole globe at this resolution, and other methods are required. For this reason, many processes of climate relevance involve treatment of processes and features that are inevitably smaller than a GCM cell, or "subgrid." Figure 4 shows a satellite image of a cloud system in the equatorial eastern Atlantic with a typical GCM grid superimposed upon it in the right panel. The cloud features are clearly below the resolution of the model. A zoomed image of a small portion of a grid cell (outlined in red) is presented in the left panel, showing important cloud features at yet finer scales.

Parameterizations have been developed in order to represent processes that are important to the atmosphere, but occur at resolutions much below the scales the model is able to resolve (see Stensrud [16]). The equations describing the fundamental physics equations are sometimes abandoned, or simplified, through an "abstraction" to approximate that process. Sometimes those simplifications are based upon formal mathematical decompositions, like the turbulence parameterizations that depend upon "Reynolds averaging" of the equations of motion, along with appropriate choices for the constitutive equations, and "closure assumptions." In other parameterizations, the complete equations are simplified to speed the calculation: for example, the equations of radiative heating are often approximated by assuming plane-parallel radiative transfer, and integrated over wavelength intervals to capture the essential absorption and emission for the gases and condensed species present in the atmosphere.

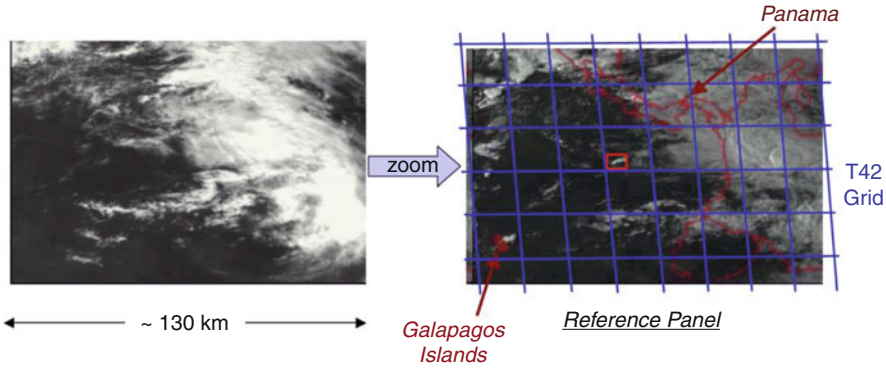

Atmospheric General Circulation Modeling. Figure 4
A satellite image (courtesy NASA) of the Eastern Central Pacific showing the cloud features in the context of a typical climate model resolution. The *blue lines* of the *right panel* show a superimposed grid typical of a low-resolution atmospheric model. A zoomed image of the small *red box* shown in the *right panel* appears on the left, showing even more detail

Other parameterizations are more explicitly "empirical," employing process representations which are based upon observed behavior of the atmosphere. For example, some parameterizations for convection [2, 8] attempt to represent the overturning that occurs in the atmosphere when less dense air resides below more dense air by simply adjusting the profiles of temperature and water vapor toward prescribed profiles that agree approximately with observations. Profiles can be defined for shallow (nonprecipitating) and deep precipitating convection based on both observational evidence and theoretical considerations. So, rather than identifying a mechanism through which convection operates to reduce instabilities in the atmosphere, the parameterization makes robust statements about the "end state" of an adjustment process, and introduces empirical tendencies in the evolution equations that adjust the profile to agree with the observed profiles. This type of parameterization is more frequently used in weather prediction than in climate modeling because these empirical parameterizations may not express enough of the physical underpinning to allow inferences to be made about how, why, and where that process is important, or allow extensions to handle additional model needs. Adjustment schemes, for example, would have difficulty handling convective transport of trace species, or adjusting to changes in the fundamental physics that might be occurring as the climate changes (e.g., the response of convective precipitation to pollution).

A third class of parameterizations resort to "process-based models." These parameterizations replace the basic physics with a conceptual model that is assumed to mimic the processes that occur in the real world. An example of a process-based model parameterization can be seen in the use of a "bulk plume model" to represent the role of convective clouds in a model column; this type of model is used in the majority of climate models in use in 2010 (see, e.g., [23]).

In a bulk plume model, the convective overturning occurring in the atmosphere in clouds, like those seen in the right panel of Fig. 5, is envisioned to take place through an ensemble of up- and downdrafts. The updrafts are assumed to begin at the "level of free convection" (the level where a parcel lifted from the surface will be both saturated and buoyant with respect to the ambient environment). The updraft is assumed to be driven by heat released during condensation taking place in parcels within the updrafts. The condensation produced in the updraft is assumed to produce rain. The rain falling into surrounding air is assumed to partially evaporate and initiate a saturated downdraft. These up- and downdrafts carry air from one level to another, entraining air from outside the cloud in the lower part of the cloud layers to dilute the updrafts, and detraining air to the environment aloft,

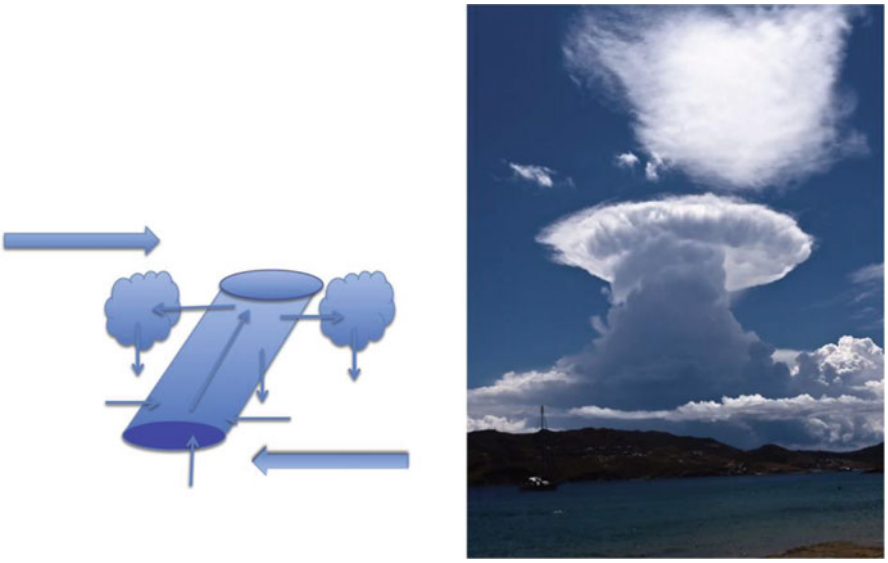

Atmospheric General Circulation Modeling. Figure 5
The conceptual model used to produce a parameterization of a convective cloud like that seen in the figure at right. See text for details

to moisten it and redistribute heat. The ensemble of updrafts is represented by a single "bulk" updraft plume that entrains and detrains at multiple levels and a single "bulk" downdraft driven by evaporating rain to produce a conceptual model of convection like that described in the left panel of Fig. 5. The details of the representative up- and downdrafts are in turn controlled by specifications of the rate of entrainment and detrainment, how condensation, conversion of condensate to precipitation, and evaporation occurs within those up- and downdrafts, and a "closure assumption" that describes how the buoyancy generation occurring outside of the clouds is reduced by the mass fluxes within the up- and downdrafts. These parameterizations are obviously gross simplifications of the way clouds behave in the real world. The parameterizations introduce many "uncertain parameters" that require tuning to mimic the behavior of clouds in the real world.

The reader will note that the citations chosen here describe convective parameterizations written in, or prior to, the 1990s. Progress has been slow in developing better formulations for convection. Most parameterizations of convection have made progress "around the edges" by incrementally improving some aspect of the parameterization, like "closure assumptions" (the assumptions that deter how buoyancy excesses are removed from a column) or the "microphysical formulations" (controlling the ways that condensation, conversion to precipitation, and evaporation operate within the up- and downdrafts). Cloud parameterizations are viewed by climate scientists as one of the least satisfactory components of a GCM [12]. Convective parameterizations based upon plume models have the advantage over the very simple formulations like the Betts-Miller scheme of providing a physical picture (albeit crude) of how convection works that permits the expression of conservation laws (conservation of energy, enthalpy, momentum, mass, etc.). Plume model parameterizations also allow extensions to represent interactions between aerosols and clouds, for example, or the transport of soluble and insoluble trace constituents through vigorous convection, but they still have many limitations. Recently, a new class of parameterizations has begun to be explored, in which a "nearly cloud-resolving model" is embedded within each column of a GCM (e.g., [6]). These "super-parameterizations" of clouds have their own strengths and weakness: they use equations which are very close to the original equations of motion, but those equations are solved at scales that do not really resolve cloud motions. The parameterizations also increase the cost

of the model by at least a factor of 100 over models using more traditional parameterizations so that their behavior for climate problems has not yet been thoroughly explored. Other new frameworks for cloud parameterization have also been suggested [1] that present an interesting approach to extending conventional parameterizations. There has not yet been time to evaluate the approach.

Clouds and Aerosols in Climate Models

The accurate representation of the effect of clouds and aerosols in the atmosphere is one of the most difficult and challenging tasks in climate models for scientists at the time this entry is written.

This task is important because clouds play many roles in the atmosphere: they scatter and absorb radiant energy in both the solar (shortwave) and infrared (longwave) part of the energy spectrum, reflecting sizable amounts of sunlight (shortwave energy) back to space and thus acting to cool the planet, but they also hinder the escape of heat/energy in the longwave, and thus can warm the Earth. Clouds are also reservoirs for heat and water acting to temporarily store energy and water in condensed phases, then return it to the atmosphere at other times and locations; they are sites for important in situ atmospheric chemistry and affect photolysis rates in both clear and cloudy regions of the atmosphere by changing the actinic flux; they are regions responsible for the rapid transport of atmospheric trace constituents from the lower to the upper atmosphere through vigorous convection; and they are also entities responsible for the removal of soluble species (gases and particles) through "wet deposition" processes. And, as discussed in the previous section, they are also incredibly difficult to represent accurately and comprehensively in GCMs.

But clouds are also strongly affected by "aerosols," the small (solid and liquid) particles with sizes less than about 10 um that are suspended in the atmosphere. Aerosols have both natural (e.g., sea-salt, dust, and some organic compounds released by vegetation) and anthropogenic origins (e.g., the pollution released by power plants, cars, trucks, agricultural burning, etc.). Like clouds, aerosols scatter and absorb radiant energy in both the solar and infrared part of the energy spectrum, and thus play a direct role in the energy budget of the planet. Aerosols also affect air quality and can affect ecosystems in a number of ways (e.g., the mobilization of dust particles from deserts, their subsequent transport by winds, followed by deposition; dust deposition is believed to be a source of iron as a nutrient to ocean biota). In addition, some aerosols act as sites that facilitate the phase change of water from vapor to liquid, or ice at far lower vapor pressures than would be needed for the phase change to occur in the absence of the particles. The aerosols that act as sites for water vapor condensation to form liquid cloud drops are known as Cloud Condensation Nuclei (CCN); those that are sites for formation of ice crystals are called Ice Nuclei (IN). Different types of aerosols are more and less effective as CCN and IN, and aerosols "compete" with each other and nearby cloud drops and ice crystals for water vapor, making their interactions extremely complex and hence difficult to model (see, e.g., Seinfeld and Pandis [14] and Lohmann and Feichter [7] for complementary discussions on some of these issues).

The aerosols that become part of cloud drops or ice crystals will eventually be removed from the atmosphere when those drops or crystals get large enough to precipitate out (this is termed nucleation scavenging). Aerosols are also removed as precipitation (raindrops, snow, hail, and graupel) falls and "collects" particles along the way (termed below cloud scavenging). The treatment of aerosols thus depends intimately on the treatment of clouds in GCMs.

Aerosols and clouds thus interact in many ways. It is easy to find examples of situations where aerosols can affect the cellular structure of clouds and their reflectivity. Figure 6 shows a dramatic example of the influence of pollution from ship emissions on the brightness of low clouds near the ocean surface. Climate scientists believe that anthropogenic emissions of many aerosol types, from pollution, biomass burning, agriculture, etc., affect both the reflectivity of low clouds with impact on how clouds cool the planet, and the partial opacity of the high ice clouds that hinder the escape of heat from the planet.

The subtle interactions between clouds and aerosols, and their interactions with other components of the climate system, produce some of the largest uncertainties in interpreting the signatures of climate change over the twentieth century and complicate modelers'

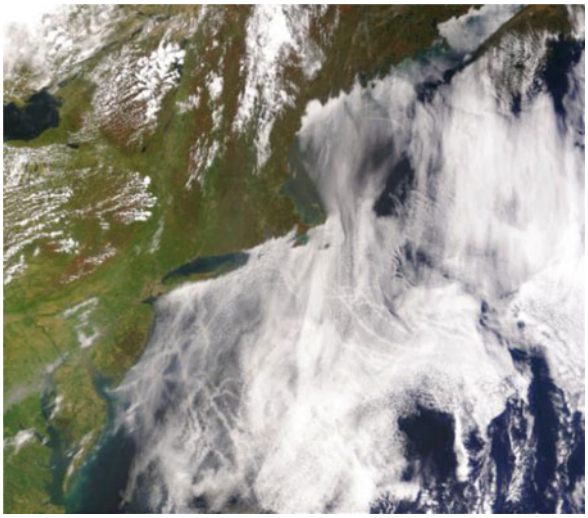

Atmospheric General Circulation Modeling. Figure 6 NASA image (http://eoimages.gsfc.nasa.gov/images/imagerecords/5000/5488/ShipTracks_TMO_2005131_lrg.jpg)

abilities to produce accurate projections of climate change in the future.

These issues are discussed in great detail in the fourth assessment of the Intergovernmental Panel on Climate Change (AR4, IPCC2007), and it is not possible to provide much detail here. The reader should consult AR4 and the references therein for more detail.

Figure 7 shows globally averaged radiative forcing estimates for various forcing agents from IPCC2007. Changes in the atmospheric abundance of greenhouse gases and aerosols, in solar radiation, and in land surface properties alter the energy balance of the climate system. These changes are expressed in terms of a "radiative forcing" (W/m^2), a term used to compare how a range of human and natural factors drive warming or cooling trends on global climate. The three estimates related to aerosols (surface albedo, direct effect, and cloud albedo effect) are particularly noteworthy when compared to other forcing agents.

Surface albedo changes through Black Carbon deposition on snow are estimated to have a relatively small warming effect (positive forcing) on the planet. The forcing is a result of the decrease in reflectivity of the snow that occurs when the dark material is deposited on the snow surface. Since sunlight is more easily absorbed by the darker surface in this situation, the snow melts more quickly, revealing other darker surfaces below (vegetation, dirt, sea-ice, etc.), which further increases the warming effect.

The "direct effect" of aerosols refers to the ability of aerosol to reflect or absorb sunlight as it enters the atmosphere. When the aerosols scatter sunlight back to space, the implied forcing is identified as negative (cooling) because less energy is absorbed by the planet. When aerosols absorb sunlight, they reduce the planetary albedo and warm the planet, producing a positive radiative forcing. The net radiative direct effect is estimated to be positive; models estimate that aerosols reflect more energy back to space than they absorb, but the uncertainty indicated by the horizontal whiskers is very large, and the level of scientific understanding (LOSU) is judged to be "low," as indicated in the figure.

The aerosol "indirect effect" refers to the role that aerosols play on clouds. Increasing aerosols (e.g., from pollution) can increase the number of particles available for cloud drops or ice particles to form on by acting as CCN or IN. Those "extra" cloud drops or ice particles introduced by the additional CCN and IN compete with the ambient aerosols for water vapor, and the result is that the cloud drops and ice crystals will be smaller than they would be in the absence of pollution. Smaller drops and particles scatter sunlight more efficiently (as demonstrated by simple physical arguments and the ship tracks seen in Fig. 6), and they frequently also precipitate less efficiently, affecting cloud lifetime and areal extent. Models estimate the indirect effect to produce a very large negative forcing, but the whiskers again indicate that the uncertainty is very large, and the LOSU very low. While the processes that produce cloud brightening in the presence of additional CCN and IN are well understood, there are numerous other factors that complicate the response of cloud reflectivity enormously, and scientists know that climate models treat these other factors very crudely, and inaccurately (see Stevens and Feingold [17]). For example, increasing the number of cloud drops and decreasing their size can also cause cloud drops to evaporate more readily, so the cloud reflectivity can actually decrease, and changing the reflectivity of particular regions of a cloud system can induce changes in the cloud dynamics (the intensity and extent of up- and

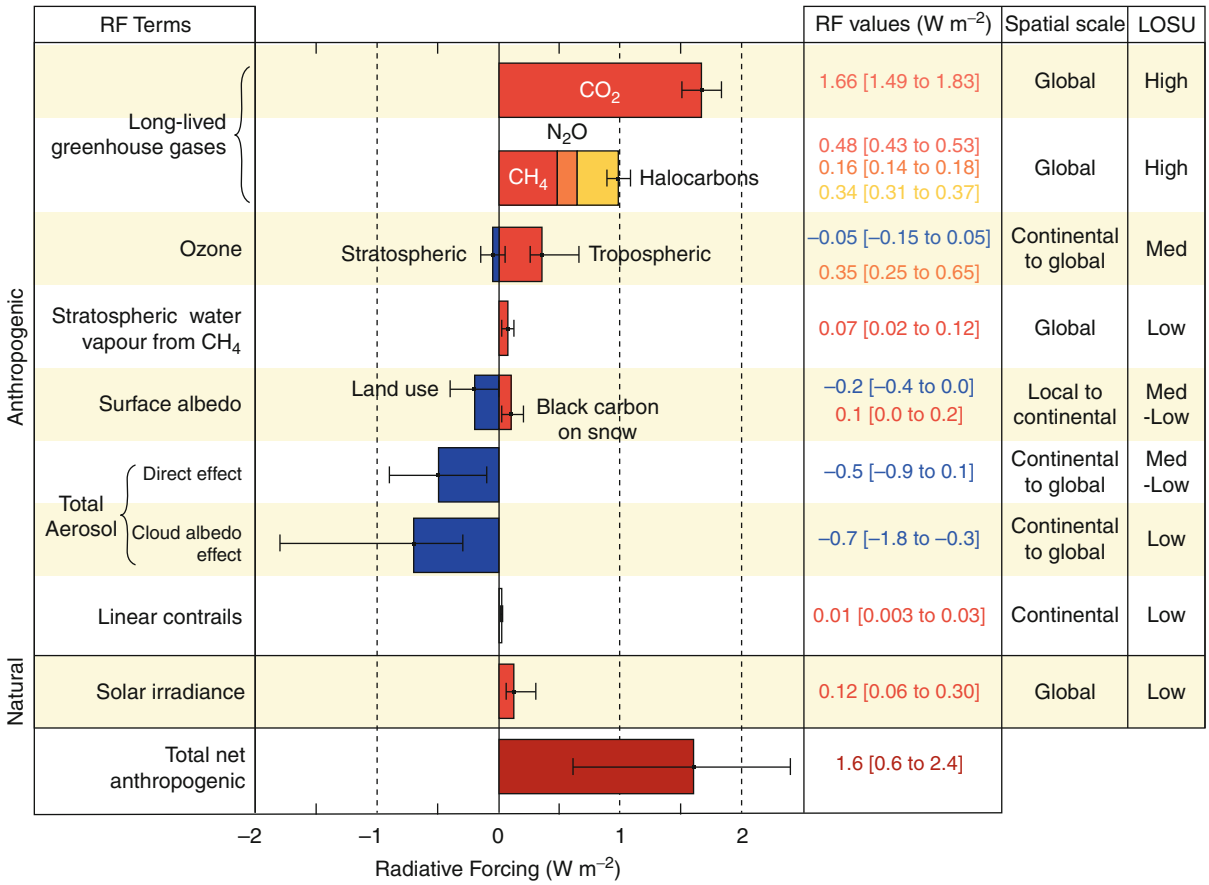

Atmospheric General Circulation Modeling. Figure 7

From the summary for policymakers, IPCC AR4 [4] showing the globally averaged radiative forcing estimates for various forcing agents along with uncertainty estimates and level of scientific understanding (LOSU)

downdrafts that control the precipitation and cloud areal extent; see, e.g., [19]), changing the cloud morphology and thus its radiative forcing.

The take-home message from the figure and discussion above is that aerosols of anthropogenic origin are currently estimated to have offset a substantial fraction of the positive forcing (heating) produced by increasing greenhouse gas concentrations over the twentieth century, but that result is very uncertain, and the level of understanding is low. These uncertainties in the estimates of the role of aerosols, clouds, and their interaction are strongly influenced by the deficiencies in the model representation of these processes, and by remaining deficiencies in our understanding of how these processes act.

Since it is not known how much of the twentieth century climate change (e.g., changes in surface temperature or precipitation) should be assigned to aerosol forcing and how much to the changes in greenhouse gas concentrations, it makes it much more difficult to interpret the system response to that forcing, and using understanding developed from simulations of past climate, provide accurate projections of how climate will change in the future.

Climate Forcing and Response

Climate change can be thought of as the response by the Earth system to the combination of externally imposed natural (e.g., solar variability and volcanic activity that changes the albedo of the planet) and

anthropogenic forcings (e.g., greenhouse gases and aerosols), modulated by the internal model processes that allow the system to adjust to the imposed forcing. The response is strongly influenced by internal feedbacks within the Earth system. Negative feedbacks will increase the rate of cooling in the presence of positive external forcing (warming). Positive feedbacks can amplify that warming (see the discussion in the entry ► Coupled Climate and Earth System Models by Gent). The relative importance of positive and negative feedbacks in the climate system controls the amplitude of climate change produced from a given amount of external forcing.

There are a variety of ways to characterize the ratio of forcing to response. One convenient measure is "climate sensitivity." Climate sensitivity is sometimes expressed in terms of a feedback parameter λ (expressed in W m^{-2} K^{-1}) or its inverse, $1/\lambda$. Oftentimes, the sensitivity is expressed as the change in globally averaged surface temperature ΔT that would occur in a model if it were allowed to equilibrate to a forcing ΔF associated with a doubling of CO_2:

$$\Delta T_{2\times CO_2} = \lambda^* \Delta F_{2\times CO_2}$$

It is generally assumed that λ can be expressed as the sum of a sequence of feedbacks λ_i where i indicates the process responsible for the feedback:

$$\lambda = \sum \lambda_i$$

The equilibrium change in surface temperature is a somewhat arbitrary measure of climate response, and other measurements have also been explored. The oceans have a very large heat capacity, and the rate of transport of heat into the deep oceans is very slow, which means that it would take a very long time (thousands of years) to reach an equilibrium. It is possible, with clever analytic methods, to estimate this equilibrium sensitivity, and other definitions are also used (e.g., the "transient climate sensitivity") to describe the ratio of forcing to response. The different ways are not critical for this discussion, and the equilibrium definition is followed here.

This value is estimated in IPCC2007 (*AR4*) as "*likely to be in the range 2–4.5°C with a best estimate of about 3°C, and is very unlikely to be less than 1.5°C. Values substantially higher than 4.5°C cannot be excluded, but agreement of models with observations is not as good for those values.*"

The first, largest, and perhaps easiest feedback to describe is the so-called Planck Feedback or Planck response, which describes the increase in emission that will occur as temperature increases due to a positive forcing. If one assumes from theory and detailed radiative calculations that the change in forcing F produced by a change in CO_2 from concentration C0 to C (e.g., Myhre [25]) can be written as

$$F = k^* \ln (C/C_0) \text{ where } k \sim 5 W m^{-2}$$

then a doubling of CO_2 will result in an increase in the forcing of roughly 4 W/m^2. That positive forcing will tend to increase surface temperature. If one then assumes that (1) the emission temperature of the planet is proportional to the surface temperature, (2) the planet radiates energy in proportion to the Stefan-Boltzman equation (σT^4), and (3) no other atmospheric properties (clouds, water vapor, etc.) change, then model calculations indicate that λ is about -3.2 ± 0.1 W m^{-2} K^{-1} where the sign is chosen negative to indicate that the feedback is negative. And it follows that an increase of 4 W m^{-2} in forcing will result in an approximate change of 1 K in surface temperature.

This feedback estimate is robust, with very little uncertainty, and it is much lower than AGCMs report. The higher values of climate sensitivity are a result of the amplification of the response by other positive feedbacks that exist in the climate system (see, e.g., [4, 15]).

The largest positive feedback is believed to be the water vapor feedback: observations and models indicate that relative humidity (the ratio of ambient water vapor to the saturation value at a given temperature) remains approximately constant as temperature changes, particularly at high altitude (5–20 km). Therefore, an increase in temperature (e.g., from CO_2) will produce an increase in water vapor, which is the strongest of greenhouse gases. That increase in water vapor hinders the escape of energy, and the warming is amplified. IPCC2007 estimated λ_{WV} to be about 1.8 W m^{-2} K^{-1}.

Another important feedback is the "lapse rate feedback" λ_{LR}. When estimating the Planck Feedback, it was assumed that temperature change was constant

(in latitude, longitude, and altitude). But it is known that the atmosphere will not produce a uniform change in the presence of a new forcing. The observed atmospheric lapse rate (vertical temperature gradient, see Glossary) roughly follows a "moist adiabatic lapse rate" in the tropics. It is temperature dependent and decreases more rapidly at cool temperatures than warm. So a temperature increase introduced near the surface in the tropics will produce adjustments that approximately follow a moist adiabatic lapse rate, and the perturbation will amplify with altitude. Since emission of infrared radiation varies with temperature, it will be more efficient as temperature increases, producing a negative *lapse rate feedback* that weakens the greenhouse effect. Model studies indicate that λ_{LR} has to be about –.84 W m^{-2} K^{-1}.

It is interesting to note that models suggest that the water vapor feedback and lapse rate feedback are strongly (negatively) correlated, and the agreement by models on the sum of these two feedbacks is much more robust than the individual components: $\lambda_{LR+WV} = 0.95 \pm 0.1$ W m^{-2} K^{-1}.

The surface albedo feedback occurs because an increase in surface temperature due to a positive forcing can melt surface snow and ice. A decrease in ice and snow reduces surface reflectivity, allowing more energy to be absorbed at the surface, producing further warming, and further reducing snow and ice. Soden and Held [15] and IPCC estimate the surface albedo feedback λ_{alb} to be 0.26 ± 0.08 W m^{-2} K^{-1}.

The last feedback to be discussed is the cloud feedback. A variety of observational, theoretical, and modeling studies suggest that low clouds tend to cool the planet by reflecting sunlight back to space. High ice clouds not only reflect sunlight back to space but also have a "greenhouse effect" and hinder the escape of longwave energy to space. Observational and modeling studies indicate that the net effect of high and low clouds is to cool the Earth (cloud reflection dominates the longwave trapping of energy). But it is by no means clear how cloud radiative forcing will change in the presence of external climate forcing. Clouds are so varied and complex that fewer clear general statements emerge to guide inferences about the sign and amplitude of their feedback processes. This is an area of very active research. Soden and Held found that all the GCMs used for AR4 had a positive cloud feedback (0.68 ± 0.37 W m^{-2} K^{-1}), even though half the models exhibited a reduction in net radiative forcing in response to a warmer climate. They concluded that change in cloud forcing itself is not a reliable measure of the sign or absolute magnitude of cloud feedback due to noncloud feedbacks on the cloud forcing. Note that the uncertainty in feedback amplitude from clouds is about three times larger than that found for the lapse rate + water vapor feedback, or the albedo feedback.

The combination of positive and negative climate feedbacks produces the likely warming range of 2–4.5°C for a CO_2 doubling cited in IPCC2007. Climate skeptics contend that the planet is unlikely to warm as much as GCMs predict by arguing that negative feedbacks are missing or underestimated or positive feedbacks overestimated in GCMs. These criticisms frequently appear in informal venues (blogs, the popular press, and elsewhere). When they are submitted to peer-reviewed refereed publications, they are taken seriously and scrutinized further. To date, the feedbacks described here have been found to be robust and dominant, and estimates of the range and distribution of climate quite robust.

Calibration (Tuning) and Evaluation of GCMs

There are still aspects of the atmosphere that are poorly characterized, and many processes remained crudely represented in GCMs. Even in situations where the correct physics is known, it is often too expensive to include the knowledge with brute force techniques, and approximations must be employed. Both lack of understanding and process approximation lead to uncertainties, and these uncertainties produce significant variations in model formulations adopted by groups around the world.

Multiple alternative parameterizations may also exist for a particular process (e.g., convection). Even in the event that a certain configuration of parameterizations is selected, there are many "uncertain" parameters within that configuration. The choices adopted for those uncertain parameters can have strong impacts on the behavior of the model.

So, substantial resources in the modeling community are invested in evaluating the behavior of the model in the presence of these uncertainties, and in selecting the parameterizations to be used in the model,

or the values of the uncertain parameters to be used in subsequent simulations. The process of choosing the parameter values is known as "calibration" or "tuning." Model tuning has historically been performed in a series of stages, and it is sort of an "Art" that requires a lot of insight by participating scientists, and perhaps multiple repetition of those stages.

One obvious method of tuning is to compare the behavior of a model, or a model component to observations that strongly constrain the process and adjust the parameters until the simulation agrees to some tolerance with observations. This tuning procedure can be considered an optimization problem, and it occurs frequently during model development.

For example, a parameterization of deep convection might first be tuned to make sure that it produces approximately the observed rate of precipitation, and observed tendencies of water vapor, and temperature, at a particular location and time period (the outputs) where deep convection occurs frequently, given a set of measurements of the atmospheric state (the inputs).

After this tuning, parameterization evaluation can begin by looking at its behavior at other locations and times not used for tuning. Some insight is gained during this process about reasonable values for parameter, and parameter sensitivity to variations of tunable parameters, and inputs. Sometimes "single-column model" versions of the GCM are used for this purpose. This is a version of the GCM in which a single-column model is isolated, and all lateral fluxes of information supplied from observations to identify the model behavior in strongly prescribed situations.

The model can also be tuned to optimize relationships after processes equilibrate with each other; the statistical characteristics of the model can be evaluated and compared with statistical properties of the atmosphere. For example, model top of atmosphere energy fluxes could be compared to observed energy fluxes. Small changes in tunable parameters may be performed to assure that the approximate global averages of top of atmosphere fluxes are similar to observed values without significantly degrading the agreement with observations at the process level.

The model can also be compared with observations for fields, processes, or situations that were not part of the calibration process. Figure 8 provides one example of this kind of evaluation showing differences between model annually averaged column-integrated water vapor in a long simulation of a climate model (top panel), compared to an estimate of the corresponding observed value (middle panel) and the difference. Column-integrated water is actually a pretty difficult field to observe and observational uncertainty quite high, but a variety of independent methods are available to provide estimates, and the signatures seen in the difference field are quite robust to choices of the observational dataset used. This particular model is quite moist in the tropics.

Another interesting evaluation and calibration method is the use of a climate model in "weather forecast" mode. The climate model is started from initial conditions from archives of meteorological conditions produced from a forecast center and run for a brief (few day) simulation. These kinds of simulations are often called "hindcasts." The evolution of differences between the short simulations and observed fields provides information about how and why errors develop in the model. Individual processes can be examined to help in identifying the role of each process in driving the error growth.

The strategy can also be extended to longer periods (months or seasons) as part of a strategy sometimes called "seamless prediction" [10]. Models are viewed as representing processes that operate over different timescales. Fast processes (e.g., clouds) respond and produce measurable signatures to forcing on timescales of a day or so, systematic changes to heating rates can perturb planetary-wave structures in the atmosphere on the timescale of 10 days, and ocean and land surface react to changes in wave structure on the timescale of 100 days. On timescales of a thousand days and longer, anomalies will produce modifications to the cryosphere and biosphere. Atmospheric models (without coupling to oceans, ice, and the biosphere) can thus react and produce meaningful information on forcing and response through processes like clouds and planetary waves. Longer timescale phenomena need to be evaluated with coupled models. Seamless prediction paradigms ask that models be evaluated and improved on each timescale to provide increasing confidence in the model.

Once an "optimized" or "calibrated" model configuration has been found, it can be compared with

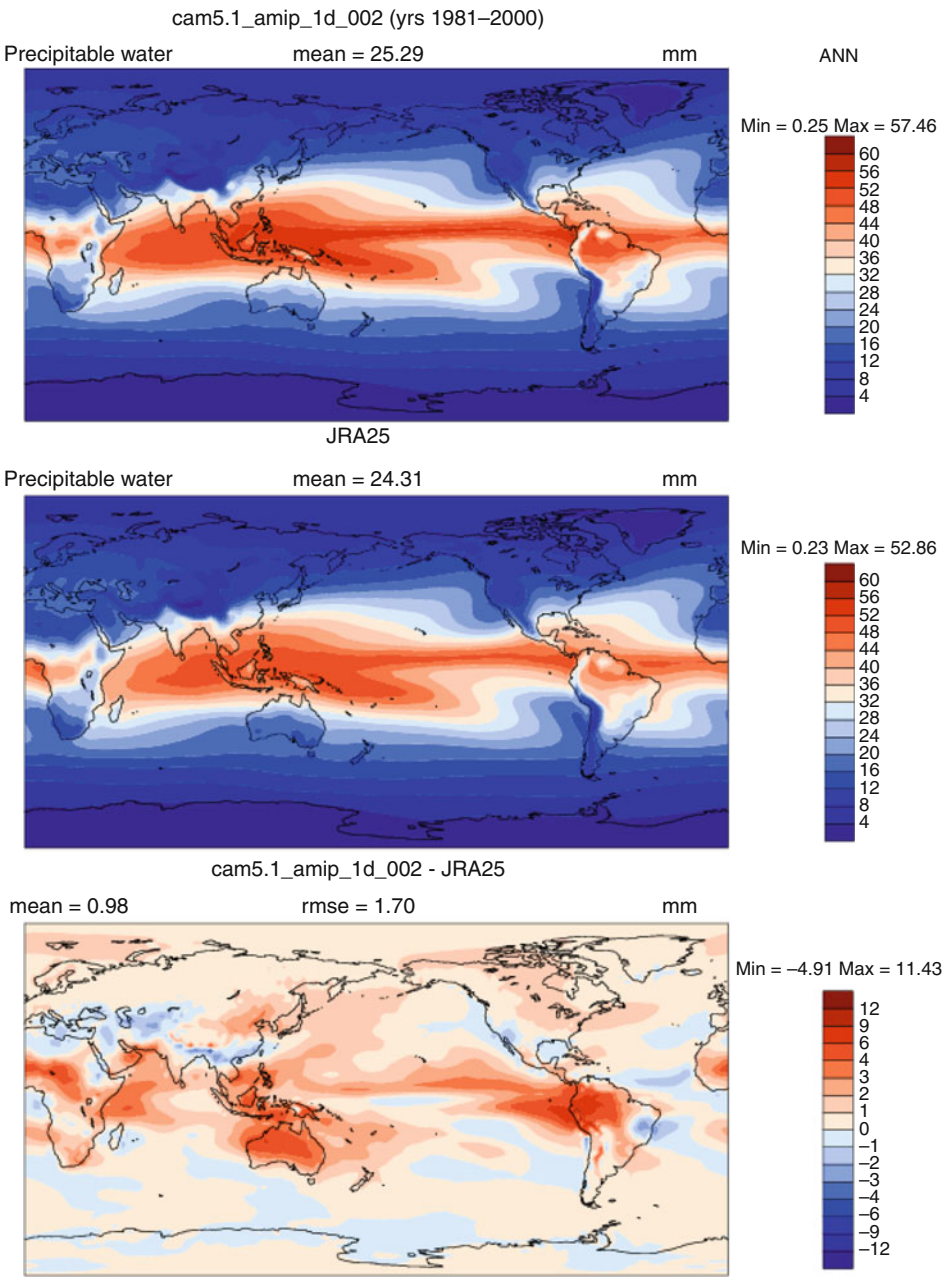

Atmospheric General Circulation Modeling. Figure 8
An example of the difference in the vertically integrated amount of water vapor simulated in a climate model run for 20 years with present-day forcing, compared with a reanalysis produce (an estimate produced from observations). The difference is shown in the *lower panel*

other models, or other configurations of the model to quantify its sensitivity to changes in forcing, to identify the reasons that it responds the way it does, and to put that sensitivity in context compared to the behavior of other models. This process is one component of an evolving field of climate change science called "Uncertainty Quantification."

Remaining Challenges in Modeling the Atmosphere

There are many situations where scientists understand the fundamental physics of a physical process much more thoroughly than they can afford to express in a climate model, and scientists know that it is important to represent those processes more accurately. These are, in a sense, "known unknowns" in the parlance of Donald Rumsfeld. Scientists know that the parameterizations of clouds and aerosols used in climate models today can be formulated more accurately, and they know (in principle) how to do it. The challenge is (1) representing fields and processes that are truly important for the relevant climate problem and (2) expressing knowledge about that process in a computationally tractable way. This requires both scientific study and computational work. Many of these improvements can be achieved by clever revisions to the computational representation of critical processes in models. Scientists are rewriting model components to make more efficient use of evolving computer architectures that are providing enormous increments in computational resources, and developing more accurate and efficient computation methods to represent those processes. It may be possible in a few years to "brute force" problems that in the past required clever but potentially inaccurate approximations.

While some efforts to create a global cloud-resolving model have been made, their computation cost is at least a million times higher than models run at current climate resolution (e.g., [13]). It is currently a challenge just to complete a single annual cycle with models at this resolution. Scientists are also rewriting models to support "variable resolution" to allow models to provide higher resolution in areas that require it. One of the immediate challenges in this situation is that many of the approximations currently employed in atmospheric parameterizations are "scale dependent," that is, the quantitative behavior of the parameterization changes behavior as the resolution changes. Current parameterizations are typically "retuned" for different resolutions, and any cloud parameterization that adapts to resolution changes is not yet known, although scale-aware parameterizations of subgrid-scale propagation of waves and wave breaking do exist. It is desirable that parameterizations become "scale aware" in the sense that they adapt to the resolution they are used at. Parameterizations of subgrid-scale processes should recognize that the definition of the phenomena they are being asked to resolve changes as the resolution changes [1]). Scale-aware parameterizations and the model equations that they are embedded in should reduce to "fundamental physics" as model resolution approaches the resolution of the process being represented. This is an area of active research.

There are also challenges for climate models in treating "unknown unknowns," or "missing physics." These are phenomena that scientists believe may be important to represent, but that they do not know about or are very unsure of. An example of this situation is the role of Organic Aerosols on climate. These aerosols are difficult to measure and model. They are semivolatile; the aerosols condense, evaporate, and evolve chemically with atmospheric dilution. Aerosol scientists now believe that these aerosols play a much larger role in the climate system than was originally recognized, but they only have hints as to the complex chain of events that produce these aerosols. Precursor emissions, chemical evolution, and interaction with other aerosols and atmospheric trace species are complex, and they are treated very simply in climate models today.

Finally, there are many ways that climate science can be advanced by improvements in methodology. Ensembles of model simulations can be used to characterize model uncertainty. Model intercomparison activities like AMIP [3] and CMIP5 [18] continue to improve and allow more robust evaluation of the strength and weaknesses of climate models and their ability to represent the real world and their performance as a tool for understanding climate change.

Acknowledgments

I would like to thank Sarah Fillmore for her editorial help and my colleagues at the Pacific Northwest National Laboratory and the National Center for Atmospheric Research for their willingness to share their expertise, knowledge, and model results with me over many years.

Bibliography

1. Arakawa A (2011) Toward unification of the multiscale modeling of the atmosphere. Atmos Chem Phys 11:3731–3742. doi:10.5194/acp-11-3731-2011, www.atmos-chem-phys.net/11/3731/2011/
2. Betts AK, Miller MJ (1993) The Betts–Miller scheme. In: Emanuel KA, Raymond DJ (eds) The representation of cumulus convection in numerical models of the atmosphere. American Meteorological Society, Boston
3. Gates WL et al (1999) An overview of the results of the atmospheric model intercomparison project (AMIP I). Bull Atmos Sci 80:29–55
4. IPCC (2007) Summary for policymakers. In: Solomon S, Qin D, Manning M, Chen Z, Marquis M, Averyt KB, Tignor M, Miller HL (eds) Climate change 2007: the physical science basis. contribution of working group I to the fourth assessment report of the intergovernmental panel on climate change. Cambridge University Press, Cambridge, UK/New York
5. Jacobson MZ (2005) Fundamentals of atmospheric modeling, 2nd edn. Cambridge University Press, New York, p 813
6. Khairoutdinov MF, Randall DA, DeMotte C (2005) Simulations of the atmospheric general circulation using a cloud-resolving model as a super-parameterization of physical processes. J Atmos Sci 62:2136–2154
7. Lohmann U, Feichter J (2005) Global indirect aerosol effects: a review. Atmos Chem Phys 5:715–737. doi:1680-7324/acp/2005-5-715, www.atmos-chem-phys.org/acp/5/715/
8. Manabe S, Smagorinsky J, Strickler RF (1965) Simulated climatology of a general circulation model with a hydrologic cycle. Mon Weather Rev 93:769–798
9. McGuffie K, Henderson-Sellers A (2005) A climate modeling primer. Wiley, New York
10. Palmer TN, Doblas-Reyes FJ, Weisheimer A, Rodwell MJ (2008) Towards seamless prediction: calibration of climate-change projections using seasonal forecasts. BAMS 89: 459–470
11. Philips TJ et al (2004) Evaluating parameterizations in general circulation models: climate simulation meets weather. Bull Am Meteorol Soc 85:1903–1915
12. Randall D, Khairoutdinov M, Arakawa A, Grabowski W (2003) Breaking the cloud parameterization deadlock. Bull Am Meteorol Soc 84:1547–1564
13. Satoh M, Matsuno T, Tomita H, Miura H, Nasuna T, Iga S (2008) Nonhydrostatic icosahedral atmospheric model (NICAM) for global cloud resolving simulations. J Comput Phys 227: 3486–3514
14. Seinfeld JH, Pandis SN (1997) Atmospheric chemistry and physics. Wiley, New York
15. Soden B, Held I (2006) An assessment of climate feedbacks in coupled ocean–atmosphere models. J Climate 19:3354–3360
16. Stensrud DJ (2007) Parameterization schemes: keys to understanding numerical weather prediction models. Cambridge University Press, Cambridge
17. Stevens B, Feingold G (2009) Untangling aerosol effects on clouds and precipitation in a buffered system. Nature 461:607–613
18. Taylor KE, Stouffer RJ, Meehl GA (2011) An overview of CMIP5 and the experiment design. Bull Am Meteorol Soc. doi:10.1175/BAMS-D-11-00094.1
19. Wang H, Rasch PJ, Feingold G (2011) Manipulating marine stratocumulus cloud amount and albedo: a process-modeling study of aerosol-cloud-precipitation interactions in response to injection of cloud condensation nuclei. Atmos Chem Phys Discuss 11:885–916. doi:10.5194/acpd-11-885-2011
20. Washington W, Parkinson CL (2005) An introduction to three dimensional climate modeling, 2nd edn. University Science, Sausalito, p 354
21. Weart SR (2010) The discovery of global warming. Harvard University Press, Cambridge, MA
22. Wigley TML, Raper SCB (2005) Extended scenarios for glacier melt due to anthropogenic forcing. Geophys Res Lett 32: L05704. doi:10.1029/2004GL021238
23. Zhang GJ, McFarlane NA (1995) Sensitivity of climate simulations to the parameterization of cumulus convection in the Canadian climate centre general circulation model. Atmos Ocean 33(3):407–446
24. Zhu P et al (2005) Intercomparison and interpretation of single-column model simulations of a nocturnal stratocumulus-topped marine boundary layer. Mon Weather Rev 133: 2741–2758
25. Myhre G, Highwood EJ, Shine KP, Stordal F (1998) New estimates of radiative forcing due to well mixed greenhouse gases. Geophysical Research Letters 25(14), pp. 2715–2718, doi:10.1029/98GL01908

Avian Specific Transgenesis

Michael J. McGrew
Avian Germ Cell Laboratory, Division of Developmental Biology, The Roslin Institute and Royal (Dick) School of Veterinary Studies, University of Edinburgh, Roslin, Midlothian, UK

Article Outline

Glossary
Definition of the Subject
Introduction
Methods of Avian Transgenesis
Improved Transgenesis by the Directed Targeting of the Germ Cell Lineage
Future Directions
Bibliography

Glossary

Founder bird (F_0) A bird into which a genetic vector was introduced. This vector may become incorporated into the chromosomes of some of the somatic and germ cells of the bird.

F_1 bird The offspring of the F_0 bird. Transgenic F_1 birds will contain the transgene incorporated into a chromosome in every cell of the animal.

Germ line chimera A genetically modified founder bird (F_0) in which the introduced biological material (i.e., DNA, virus, cells) has contributed to cells of the germ cell lineage of the host animal.

Primordial germ cells Cells in the developing embryo belonging to the germ cell lineage at a developmental stage before any sexual differentiation has occurred. These primitive germ cells may be located in the embryo in tissues other than the forming gonad.

Retrovirus A virus that carries its genome as an RNA molecule. After infecting a cell, the RNA is reverse transcribed into a DNA molecule that is inserted into the genome of the infected cell at which point it is referred to as a provirus. The provirus is passed to all daughter cells as part of the host cell's genome.

Recombinant proteins A protein produced using recombinant DNA technology. The DNA sequence encoding the protein of interest is artificially constructed using genetic engineering and the protein is produced by inserting the DNA along with DNA regulatory regions into a bacterium, a eukaryotic cell, or an animal.

Transgenic bird Any avian species in which part of its genetic component contains DNA deriving from an exogenous source, or that the genome of the bird has been altered by human intervention.

Transgenic bird lines A flock of birds deriving from a F_1 bird containing a transgenic modification at a defined genetic locus.

Definition of the Subject

Transgenesis is the process by which an *exogenous* DNA molecule is incorporated into the genome of an animal. This technology promises the possibility to investigate and manipulate the production traits of poultry, produce recombinant proteins in the eggs of genetically engineered layer lines, and directly intervene in the health and welfare of avian species. The complexity of the avian egg and the precocious development of the avian embryo in the female before oviposition (laying) have hindered endeavors in avian transgenesis. Three decades of effort have been carried out to achieve the genetic modification of the avian genome. The generation of novel methods for the modification of the avian genome has led to the current advances in the field of avian transgenesis. This entry will delineate the methods used for avian transgenesis, the current state of the art, and the potential future directions research in this field will take.

Introduction

Due to its use in meat and egg production and also as a model organism for developmental biology studies in laboratories, the chicken is the most widely used bird species for the development of transgenic technologies. There are three commonly cited incentives for the development of transgenesis in the chicken. These are the production of biopharmaceutical proteins in eggs, the generation of disease-resistant flocks along with an increase in understanding disease resistance in poultry, and the generation of useful transgenic lines for studies of developmental biology. With the recent development of novel avian transgenesis techniques, these goals are beginning to be achieved.

The principal rationale behind this emerging field is industry driven and is to produce a platform for the biosynthesis of biopharmaceutical proteins in chicken eggs. Animal-based bioreactors, a process sometimes referred to as animal "biopharming," were proposed as a non-cell-based method for the production of recombinant human proteins in the 1980s (reviewed in [1]). Animal-based bioreactors were inferred to be a lower cost, safe, and more efficient system in which to produce large quantities of bioactive recombinant proteins than cell-based production platforms. Efforts to produce recombinant proteins in larger animals have focused on the secretion of the target protein into the milk of the transgenic animal using the regulatory regions from a milk protein gene. Potential mammalian species commonly proposed and studied for recombinant protein production include cows, pigs, sheep, goats, lamas, and rabbits. After over two decades of investigations, the first biopharmaceutical protein produced in an animal's milk has been approved for use in

humans in Europe and the United States. This product is recombinant human antithrombin (ATryn-GTC Biotherapeutics) produced and isolated from goat's milk. Profitability in the marketplace along with consumer acceptance will be the key factor in determining the success of this and similar ventures using large animal delivery systems. In addition, the regulatory approval of this recombinant protein validates the use of animal bioreactors for protein production.

The chicken has also been proposed as a potential animal-based platform for the production of recombinant human proteins. In this case, the recombinant protein is produced in the oviduct of the hen and secreted in the forming egg as it passes down the oviduct. The target protein would be targeted to the egg white of the egg using the regulatory regions from one of several proteins expressed in the albumen of chicken eggs (reviewed in [2]). The chicken has several advantages over larger animal-based bioreactors. The chicken has a shorter generation time than a larger mammal (4 months for egg production vs. 14 months for first milk production in goats), which means a more rapid time from production of the transgenic animal until production of the recombinant protein (Fig. 1). This, in turn is reflected in the second advantage, which is the lower cost of protein production in chickens. One estimate predicts that the cost of recombinant proteins in chickens will be 1/5 of that of larger mammals [3]. This is due to the reduced costs of housing, feed, and quantity of recombinant protein produced per animal. In addition, the glycosylation pattern of secreted proteins in chickens is closer to the pattern seen on human proteins than those seen on proteins secreted in several large mammals [4].

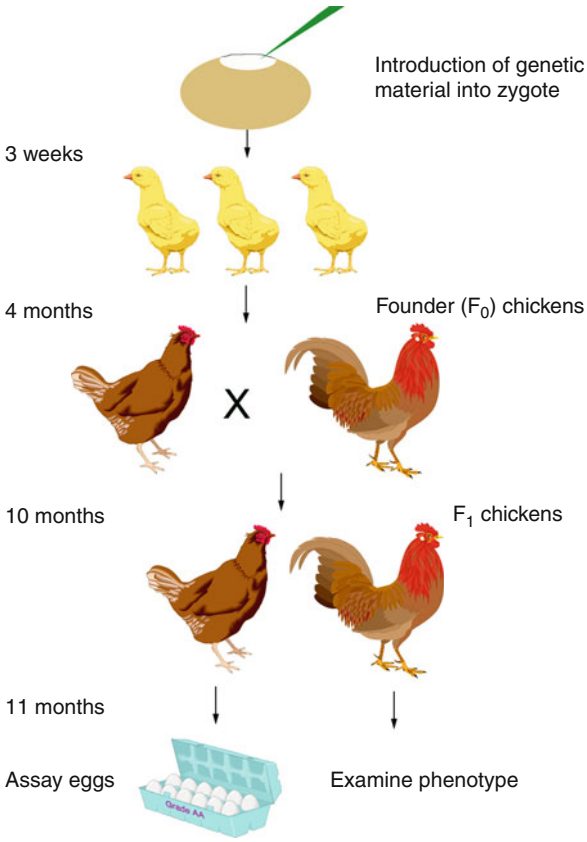

Avian Specific Transgenesis. Figure 1
Time line for production of transgenic chicken lines. The time line from the introduction of a transgenic construct into a fertilized chicken egg until the generation of F_1 offspring. The F_1 animals can be analyzed for gene expression or bred to transmit the transgene to the next generation

Several studies have reported the production of bioactive recombinant protein in chicken eggs [5–7]. The methods used to produce these transgenic animals will be discussed in the following sections. These initial reports demonstrated that bioactive recombinant human proteins can be produced in the eggs of transgenic chickens. To date, excluding the production in influenza vaccines, no proteins produced in chicken eggs have been approved for use in humans.

A second reason for the production of transgenic chickens is the development of transgenic models for the study of the biology of the chicken and developmental biology in general. The chicken has long been a model system for the study of developmental biology due to the accessibility of the chicken embryo in the developing egg [8]. The preeminence of the chicken as the model system for embryological studies is now taken by the mouse and the zebra fish due to the lower costs associated with maintaining colonies of these animals, quicker breeding times between generations, and most importantly, the ability to investigate gene function using transgenesis. New developments in avian transgenesis have led to the development of new avian models for developmental biology [9, 10]. The generation of transgenic lines containing the green fluorescent protein (GFP) in every cell of the

developing animal permits the fate mapping of living cells, the study of cells and their descendants during embryogenesis. This has facilitated the investigation of axial stem cell populations in the chicken embryo and the formation of a novel hypothesis for cellular sex identity in avian species [10, 11]. The development of more advanced methods of transgenesis will permit the generation of chickens containing genetically modified alleles, which will serve as models for investigations of early development, avian physiology, and production traits.

A third major reason for the generation of transgenic chickens is to use genetic modification for the increase of production traits that would lead to a decrease in environmental impact for poultry production. This could also be viewed as means of addressing the sustainability of the poultry industry with increasing demand on production and decreases in available resources. One manner in which this could be accomplished is by reducing waste production during rearing and increasing meat production for unit energy (reviewed in [12]). Several transgenic models have been developed in mammalian farm animals which exemplify the potential benefits of trait modification. A transgenic pig producing less organic phosphate waste products has been produced [13] and a similar strategy has been proposed for the chicken [14].

A comparable impact could be achieved on poultry production by reducing the losses attributable to disease. Avian transgenesis offers the potential to generate disease-resistant poultry and to investigate the genetic traits of disease resistance in poultry. It is estimated that during the avian influenza outbreak of 2004–2005, 100 million chickens were culled in Southeast Asia [15]. Using transgenic technology, the capability exists to generate a transgenic animal which will be resistant to several of the endemic diseases affecting poultry production (Avian influenza virus, Marek's disease, Newcastle disease, fowl cholera). While the production of these birds for use in meat and egg production is not currently accepted, transgenic chickens will be of use for investigating the pathogenesis of infection and the determination of viral targets of infection and pathogenesis. This in turn could generate targets for directed vaccine development. In addition, the validation of genetic traits for disease resistance also necessitates an analysis of the disease loci using transgenic technology in avian cells or the whole animal. Currently, no disease-resistant transgenic chicken models have been developed, but the production of transgenic cattle with resistance to mastitis suggests that this will be a profitable area of investigation [16]. With increasing demands on poultry production, an increase in methods of disease resistance will be needed.

Methods of Avian Transgenesis

The first efficient method developed for the introduction of exogenous DNA into mammals to create germ line chimeras was using pronuclear injection [17]. This technique entails the microinjection of DNA encoding the gene of interest (transgene) into the male pronucleus of the recently fertilized oocyte at a developmental stage previous to the first cell cleavage. Although pronuclear microinjection was primarily developed for transgenesis in the mouse, it has been exploited to generate transgenic animals in rats, sheep, cows, pigs, and rabbits [18–20]. Rates of transgenesis using pronuclear injection (transfer of the injected transgene to the genome of the offspring) in species other than mice are low. In general, only 1–5% of the offspring will have incorporated the transgene into their genome.

The use of pronuclear injection is even more problematic in the chicken. The laid chicken egg consists of a single epithelial layer of unpatterned cells termed the blastoderm consisting of 45,000–60,000 cells [21]. Injection of any biological material at this stage signifies that only a small proportion of the embryonic cells will be potentially exposed to and incorporate the transgene into their genome. The development of the chicken zygote in the hen before the egg is laid necessitates that pronuclear microinjection can only be carried out with surgical removal of the fertilized oocyte from the hen. This entails that the egg is subsequently surgical transferred to a surrogate host hen or cultured in vitro for 21 days until hatching [22]. The ovum of the avian egg is the large opaque yolk of the egg. The ovum contains a small pool of cytoplasm lying on the yolk material in which the pronuclei are located. Microinjection into the pronuclei is not possible because of the opacity of the yolk material underlying the nuclei; thus any injected biological material must be injected into the cytoplasm surrounding the pronuclei. For this reason, the rate of transgenesis for using

pronuclear injection chickens is much lower than in other vertebrates and the delivery of biological material is usually performed in the laid egg (Fig. 2).

Injection of DNA into Early Avian Oocytes

Microinjection of DNA transgenic constructs into the early chicken oocyte has proven to be a feasible procedure for the production of transgenic chickens. As described above, the DNA construct is injected into the cytoplasm of the fertilized oocyte at an early developmental stage (Fig. 2). The egg is subsequently cultured *ex ovo* in a host shell until normal hatching occurs. Love [23] introduced a β-galactosidase reporter construct into the fertilized chicken oocyte and cultured the embryos *ex ovo* until hatching. In this report, 50% of the injected embryos contained the transgene and 14% of the hatched founder birds transmitted the transgene to the next generation. This is a similar transmission rate to that observed in mammalian species using microinjection. A comparable result was observed in which founder transgenic chickens were obtained using microinjection and a modified *ex ovo* culture system [24]. In this example, no germ line transmission to the F_1 generation was observed. Although it is possible to produce a transgenic bird using microinjection, this avenue of research has not proven fruitful due to the cost and difficulty in obtaining and manipulating the early chicken oocyte. Instead, research has focused the use of retroviral vectors for the introduction of transgenes into the genome of the chicken at laid egg stages of development.

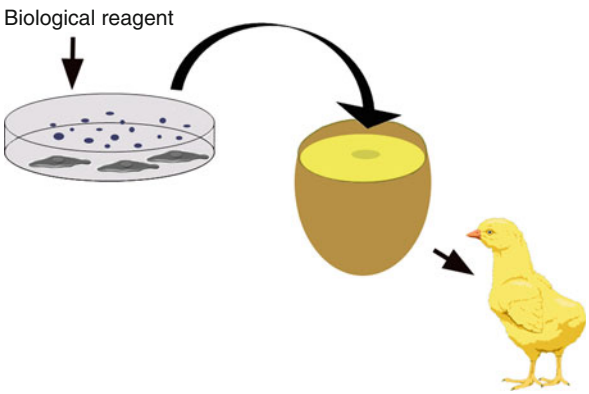

Avian Specific Transgenesis. Figure 2
Introduction of genetic material into the fertilized zygote. The genetic material to be introduced into the egg (DNA, viruses, transposons, purified proteins) is either first transfected into cells for packaging or directly introduced into the egg at an early stage of development (laid egg or fertilized oocyte). The embryo is subsequently incubated until hatching in its own shell or a host chicken shell. The hatchling will then be analyzed for the genetic modification

Replication-Competent Viral Vectors

A more efficient method to create genetically modified chickens is using retroviral vectors to introduce transgenes into the chicken genome. Retroviruses are RNA viruses that reverse transcribe the RNA genome into a DNA intermediary that is integrated into the genome of the infected cell. The integrated virus, or provirus, transcribes new copies of the viral genome that are packaged into new viral particles that bud from the infected cell and in turn infect neighboring cells. In this manner, most cells of the developing embryo will be infected along with the germ cells. Germ cells containing the integrated provirus in their genome will transmit this modification to all of the cells of the offspring deriving from that germ cell. Using recombinant DNA technology, it is possible to remove part of the viral genome and replace it with an inserted transgene. In this manner, a line of genetically modified chickens can be produced containing a transgene of interest.

The first use of retroviruses in chicken for transgenesis used viruses that were replication-competent (i.e., infective). In this case, the virus was injected at the laid egg stage and incubated until hatching. Though initially only a small portion of the blastoderm may be infected, because the viral infection spreads during development, many more cells will contain proviral inserts. The first demonstration of the genetic modification of the chicken germ line was accomplished using a replication-competent avian retrovirus. Salter [25] injected either reticuloendothelial virus or avian leukosis virus under the blastoderm of laid eggs. They demonstrated that the integrated provirus could be found in the offspring of the injected hosts [25]. As a further demonstration of this technology, using the ALV retrovirus, 24% of founder animals

contained the integrated provirus and this was transmitted to F_1 offspring with a transmission rate between 1% and 11% [26]. A replication-competent retrovirus was also used to introduce a transgene containing the bovine growth hormone under control of the mouse metallothionein promoter into founder (F_0) chicken [27]. Thus, replication-competent viruses offered an initial alternative to pronuclear injection for chicken transgenesis.

It must be noted that replication-competent viruses are limited in their usefulness in transgenesis for several reasons. First, since replicative virus can reintegrate into the genome, it is difficult to correlate a single integration site with the synthesis of recombinant protein from the integrated transgene. This is important as any regulatory approval procedure will require genetically defined transgenic animals containing a single defined transgenic insert which produces consistent levels of recombinant protein [28]. Second, insertion mutagenesis caused by the insertion of a retrovirus can disrupt an endogenous genetic locus and also lead to malignant cell growth in the host animal (reviewed in [29]). Third, and most important, a process called viral or transgene silencing is often observed in animals containing replication-competent proviral inserts. In transgene silencing, the transgene becomes silenced after it is introduced into early embryos, which is correlated with a high level of cytosine methylation throughout the proviral genome [30]. In the transgenic offspring of these founder animals, the transgene is not expressed or expression levels are severely reduced and the proviral genome is usually methylated in the long terminal repeat (LTR) region. It is believed that retroviral silencing occurs in the stem cell populations of the early embryo and leads to permanent silencing of transcription from the integrated provirus (reviewed in [31]). For these aforementioned reasons, replication-defective retroviruses have become the tool of choice for avian transgenesis.

Replication-Defective Viruses

Replication-defective retroviruses are modified retroviral vectors that are capable of infecting a host cell but lack key viral genes necessary to complete the viral life cycle and produce infective viral particles. In replication-defective retroviral vectors, a large portion of the viral genome has been removed from the virus and these genes are supplied in *trans* to allow for packaging of the defective viral particles. The envelope proteins of the viral vector can also be modified (viral pseudotyping) to permit infection of cell types and species normally outside of the retrovirus host range. The integrated provirus will contain a viral promoter in the LTR and few viral genes. It is also possible to incorporate a large transgene (8–9 kb) into the provirus in place of the truncated viral genome.

The first demonstration of germ line transgenesis in chicken used a replication-defective reticuloendothelial retroviral vector containing a neomycin reporter gene injected into the blastoderm of laid eggs [32]. Twenty-two percent of the F_0 hatchlings contained proviral integrations and the transmission rate to the F_1 generation was between 2–8%. Expression of the neomycin transgene in these birds was not demonstrated.

Since this first report, replication-defective retroviruses have been used extensively for chicken transgenesis. The most common retroviral vectors used are spleen necrosis virus, avian leukosis virus, reticuloendothelial virus mentioned previously, and Moloney murine leukemia virus (MMLV). All of these vectors have been used to generate several lines of transgenic chickens [33–36]. Transmission rates of the integrated provirus after blastodermal injection from F_0 cockerels to F_1 offspring have been reported to be as high as 8%.

A novel development of this technology is to induce expression of the recombinant protein at defined timepoints to avoid possible transgene toxicity during development. This was achieved by using a replication-defective MMLV containing a tetracyline-regulated promoter to drive expression of human-recombinant erythropoietin protein in chicken eggs only in the presence of the inducer, doxycycline [7]. More than 90% of the F_0 chickens contained proviral integrations, and these birds transmitted the transgene to between 0.7% and 1.8% of the F_1 generation. Recombinant erythropoietin was produced in eggs after doxycycline induction.

In some replication-defective retroviral vectors, there is ongoing transcription from viral regulatory LTRs in the proviral insert. This transcription is thought to lead to a partial silencing of the adjacent transgene. An example of transgene silencing in

birds was observed in transgenic quail containing a replication-defective MMLV using a LTR to drive expression of a GFP reporter construct [37]. Transgene expression was silenced in F_1 and F_2 birds. Other lines of transgenic chicken have displayed some suggestions of silencing between generations using the MMLV virus [38]. Researchers have attempted to circumvent this problem by using modified MMLV vectors containing internal promoters to drive transgene expression. This strategy appears to have worked in some transgenic birds that had no transgene silencing between generations [39]. Still, because of the perceived problems of silencing of these retroviral vectors, researchers have turned to a different class of retroviruses, the lentiviruses, for avian transgenesis.

Lentiviral Vectors

Lentiviral vectors have primarily been developed as potential viral agents for gene therapy in humans. Some of the advantages of lentiviral vectors are that the integrated provirus is preferentially incorporated into the open chromatin structure surrounding expressed genes, lentivectors will infect and integrate into the genome of post-mitotic cells, and the viral vector accepts a transgenic insert up to 9 kb in size. Moreover, there appears to be no transgene silencing upon transmission of the integrated transgene between generations [40, 41].

As an alternative to other retroviral vectors and to pronuclear microinjection, replication-defective retroviruses of the lentivirus class have proven to be very efficient for use in mammalian transgenesis [42, 43]. These vectors have been used successfully to generate transgenic cattle, pigs, rats, sheep, rabbits, and primates [44–48]. In these cases, the viral particles are injected into the perivitelline space surrounding the fertilized zygote. The zygote is reintroduced into surrogate hosts and the animals are bred and tested for germ line transmission.

The first demonstration of the use of lentiviral vectors for avian transgenesis used viral vectors containing transgenes encoding either GFP or β-galactosidase reporter genes [49]. Viral particles were injected into the blastoderm of laid eggs as described above. Efficiency of transmission of the integrated transgene from founders to the F_1 generation was between 4% and 45% and no transgene silencing was observed between generations. Since this report, lentiviral vectors have been used successfully to generate transgenic chickens containing a range of transgenes [6, 9, 10, 50, 51] and transgenic quail [52–54] and also transgenic zebra finch [55]. These vectors have also proven useful to generate biopharmaceutical proteins in eggs. Recombinant human β-interferon has been produced in the egg white of transgenic chicken [6], and recombinant human interleukin-1 receptor antagonist has also been produced in the eggs of quail [56].

While lentiviral vectors may now be the preferred method for generating transgenic birds, there will be public concerns with the use of transgenic birds containing retroviral transgenes, in particular, HIV-based lentiviral transgenes, for the production of biopharmaceutical recombinant proteins and the development of advanced production traits in avian species. It remains to be determined if consumer acceptance of these products will be forthcoming.

Transposons

Transposable elements were first identified by the seminal work by Barbara McClintock in maize [57]. Transposable elements are mobile genetic elements found in the genome of all organisms and are able to move (i.e., translocate) from one region of the genome to another. These are modules of selfish DNA that exist only to replicate their own DNA and are postulated as parasitic invaders of most genomes [58]. Transposable elements differ from viruses in that they do not spread by infection of neighboring cells; they are usually passed passively through cell division to daughter cells. Class II DNA transposons are a distinct type of transposable element that moves through the genome using a "cut and paste" method. The DNA transposon encodes an enzyme called a transposase which mediates the removal of the transposon from one chromosomal location and the insertion into a second chromosomal location. DNA transposons have been modified for the use in transgenesis in many vertebrates. This entails that the coding sequence for the transposase is deleted from the transposon and subsequently introduced into the cell with the transposon in *trans* [59]. The transposon will be incorporated into the genome of the cell but

cannot "jump" to a new genomic location because it lacks the transposase gene. This is similar in approach to the packaging of replication-defective retroviruses for transgene delivery. The truncated transposon can be engineered to contain additional DNA sequences which will be inserted into the genome of the cell upon transposon integration. The size of the transgene carried by the transposon can be up to 10 kb in size [60, 61].

Transposable elements have been shown to be efficient in the generation of transgenic chickens. The mariner transposon from Drosophila *maritiana* containing an internal transposase was used to generate transgenic chickens [62]. Mariner was microinjected into the fertilized zygote and chickens were hatched and bred to generate F_1 birds. One founder bird transmitted the mariner transposon to 29% of its offspring. This result demonstrates that transposable elements can be used to modify the genome of birds although no transgene cargo was introduced in this example. So far, no reports have been made to generating a transgenic chicken line using transposons containing a transgene. However, the Tol2 and piggyBac transposons have been shown to be functional in transient transgenesis in the chicken [63, 64] and other transposable elements have been used successfully for mammalian transgenesis [59].

Use of Chicken Embryonic Stem Cells

Whist the early embryonic development of the chicken is significantly different from that of a mammal, cells of the early chicken blastoderm do contribute to somatic and germ cell lineages when transferred to host chicken embryos [65]. This indicates that the early chicken blastoderm may have the developmental equivalence of the inner cell mass of the early mouse embryo, further suggesting that embryonic cell lines derived from the chicken blastoderm may be developmentally equivalent to mouse embryonic stem cells. In support of this hypothesis, several groups were able to derive cell lines from early chicken embryos that were putatively identified as chicken embryonic stem cells because of their ability to contribute to many tissues in chimeric birds [66, 67]. The isolation of embryonic cell lines that contribute to the forming avian embryo offers the opportunity to carry out gene targeting, whereby the introduced transgene can be targeted to a precise genetic locus. Gene targeting uses the process of homologous recombination. In this process, one genomic copy of a gene can be replaced by a second copy of this gene using normal DNA repair mechanisms. The replacement gene will display homology over most of its length but can be engineered to contain a foreign piece of DNA which could encode a recombinant protein or a selection marker. Using homologous recombination, researchers can disrupt a genetic locus, introduce a gene encoding a recombinant protein, or replace one genetic allele with a second allele. Homologous recombination has been carried out in chicken cells [68]. Genetic modification of chicken embryonic stem cells also has been achieved and chimeric animals have been produced which contain extensive contribution of these cells to all germ layers of the forming embryo [69].

An important caveat to this work is to note here that the germ cell lineage is segregated from the somatic cell lineage very early in development (see section "Methods of Avian Transgenesis"). It is believed that for this reason cESCs do not contribute to the germ lineage in chimeras after more than 7 days of in vitro culture [67, 69]. So, although cESCs may be useful for creating somatic chimeras, these cells will not be useful for generating lines of transgenic chickens.

Recent experimental evidence suggests that it may be possible to differentiate cESCs into germ cells in vitro. These cells could then be introduced into host birds and the cells could differentiate into gametes and be transmitted to the next generation [70]. If this is achievable, it will create the possibility to carry out gene targeting in the chicken and create transgenic chicken lines using homologous recombination in chicken embryonic stem cells.

Improved Transgenesis by the Directed Targeting of the Germ Cell Lineage

Most attempts to generate transgenic chickens have resulted in inefficient transmission of the integrated transgene from F_0 to F_1 animals. This inefficiency leads to an increase in cost for production of transgenic animals due to increase in both time and breeding numbers of F_0 founder birds (reviewed in [2]). Several methods have been developed to increase the rate of

transgenesis. These methods attempt to amplify the interaction of the exogenously introduced DNA or virus with the germ cell lineage of the avian embryo. The avian germ cell lineage comprises the only cells of the animal that will contribute genetic material to the next generation. Two methods developed to increase the interaction of DNA/virus with the avian germ cells are described in the next section. These methods are the purification of primordial germ cells from the developing embryo and the propagation of primordial germ cells for use as a cell-based method of transgenesis.

The germ cell lineage in birds is considered to be determined. The maternal determinants (protein, RNA) that specify the germ cell fate are thought to be deposited in the developing oocyte as it matures in the hen. During the initial segmentation of the zygote, these factors (maternal determinants) are segregated into a small number of cells of the forming embryo [71]. Descendants of these early germ cells will give rise to all cells of the germ cell lineage and are referred to as primitive or "primordial" germ cells. Moreover, since the germ cell lineage is segregated from the somatic cell lineage so precociously, chicken embryonic stem cells derived from the blastoderm will not contribute to the germ lineage when reintroduced into early embryos. The primordial germ cells are initially found in the center of the blastoderm of the laid egg [72] (Fig. 3). These cells actively migrate anteriorly in the embryo to an extraembryonic location near the future head, termed the germinal crescent. When the primitive circulatory system forms, the primordial germ cells enter the circulation and are carried to the lateral plate mesoderm adjoining the prospective gonad. During the next 2 days of development, the primordial germ cells migrate through the lateral plate mesoderm and enter the developing gonad. The germ cells subsequently differentiate into the gametes, sperm and eggs, in the maturing gonad. In the hens, the germ cells enter meiosis by day 16 of development. In the adult cockerel, a stem cell population of germ cells remain, the spermatiogonial stem cells, which generate spermatogonia during the life of the bird.

All methods of germ line transgenesis in all species are dependent on the integration of the introduced transgene into the genome of a germ cell, which will subsequently contribute its DNA to the next generation. Any interactions between the exogenously introduced DNA/virus and non-germ-line cells of the animal will lead to a reduction of transmission of the transgene to the F_1 birds. Thus, investigations in the chicken have concentrated on increasing the interaction of the transgenic vector with the germ cells of the founder animal to increase the rate of transgenesis. The next sections detail methods to isolate avian germ cells and increase this interaction.

Germ Cell Purification

The germ cell lineage of birds can be isolated and returned to a host embryo in which these donor germ

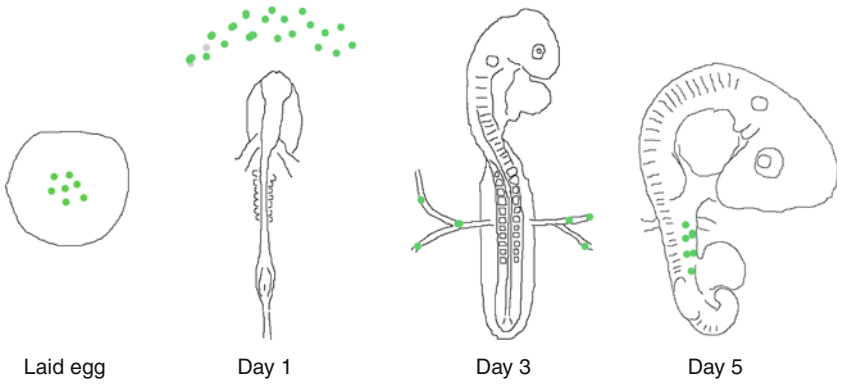

Avian Specific Transgenesis. Figure 3
Germ cell migration in the developing embryo. The primordial germ cells are initially found in the center of the developing blastoderm. From here the cells migrate anterior to the head region. The cells enter the circulation and congregate in the lateral plate adjoining the future gonad. The primordial germ cells subsequently migrate into the forming gonad

cells will migrate to the gonad and produce functional gametes [73, 74]. The intrinsic ability of donor germ cells to colonize the host germ cell lineage extends to germ cells from the germinal crescent, the circulatory blood, or post-migratory germ cells in the nascent gonad (Fig. 3). This provides the opportunity to genetically modify the donor germ cells before their introduction into host embryos. The first demonstration of this technique was carried out by Vick [75]. Primordial germ cells from the blood or the germinal crescent were incubated with replication-defective avian leukosis virus and subsequently returned to a host embryo. They observed that 3–23% of founder chickens were transgenic, and these birds transmitted the transgene to 2–4% of F_1 birds.

Several methods have been developed to purify PGCs from the developing embryo before which they are subsequently incubated with virus or transfected to introduce a transgenic vector before being reintroduced into host embryos. Primordial germ cells express the pluripotent stem cell marker, SSEA-1. Using an antibody to SSEA-1, these cells can be purified by either magnetic-activated cell sorting (MACS) or fluorescence-activated cell sorting (FACS). Both isolation techniques have been optimized for the isolation of thousands of germ cells from the blood or embryonic gonads of chicken embryos. After short periods of incubation, the isolated primordial germ cells still retain the ability to migrate to the gonad and contribute to the germ cell lineage [76]. Similarly, due to the large size of the PGC in comparison to other cells in the blood, it is possible to isolate these cells from the blood using density gradients. Density gradients have been used successfully for the purification of PGCs [77–80].

Kim [49] isolated PGCs from day 5 gonads using MACS. These cells were incubated with a lentivirus for 6 h and reinjected in host embryos. One (of 21) injected cockerels transmitted the transgene to F_1 offspring. A similar approach was used to generate transgenic quail. The rate of transmission from founder to F_1 birds was 1.9%, which was almost equivalent to what was found when the virus was injected under the blastoderm (1.6%) [54]. These results suggest that PGC isolation did not increase rates of transgenesis in comparison to blastoderm injection but further improvements on the interaction of the virus with the germ cells may augment rates of transmission.

Propagation of the Avian Germ Cell Lineage

The in vitro propagation of germ cells offers the prospect to carry out gene targeting in avian species. Both spermatogonial stem cells [81] and gonadal embryonic germ cells [82] have been cultured in vitro for shorter periods (5 and 30 days, respectively) and after culturing have contributed to the germ lineage. Moreover, the cultured gonadal embryonic germ cells generated F_1 offspring. These culture techniques, if extended, could offer the opportunity to carry out gene targeting in chickens. Recently, a breakthrough was described for the culture of primordial germ cells from the circulatory phase of development (Fig. 3). The culture of embryonic blood from day 3 chicken embryos using modified avian embryonic stem cells protocols led to the long-term expansion of primordial germ cells in vitro [83]. These cells contained telomerase activity suggesting that they may be immortal and the transmission of genetic material from both the male and female germ cells to subsequent generations was demonstrated after 110 days in culture (0.1–86% transmission). The authors genetically modified the cultured primordial germ cells using a transgene flanked by insulator sequences to prevent silencing. Founder birds containing the modified germ cells transmitted the transgene to 1–92% of F_1 birds which accurately expressed the GFP transgene. Important caveats for this procedure were that the derivation efficiency of primordial germ cell lines was low (12%), and this culture technique has not been repeated by other research groups. It was later shown that gene targeting using homologous recombination is also possible in cultured primordial germ cells [84]. This research presents the prospect of carrying out gene targeting in avian species for the production of pharmaceutical recombinant proteins and to investigate the function of genetic pathways that may be involved in production traits by directly modifying these pathways.

Future Directions

The field of avian transgenesis has progressed rapidly in the last 5 years. Useful transgenic chicken models for use in biological studies have been developed [9, 10, 51, 85]. In the near future, it can be expected that a plethora of new transgenic models for both

production traits and disease resistance to be generated. These transgenic models will generate impetus for trait selection breeding programs and rational vaccine development, first and foremost in the investigation of avian influenza.

Future uncertainties exist regarding the potential for commercialization of biopharmaceuticals proteins produced in chicken eggs and the acceptance of genetically modified chickens in general. To date, several recombinant human proteins have been produced in chicken eggs at levels up to 1 mg of protein per egg [5–7, 38, 56]. In addition, it remains to be seen if there will be consumer acceptance of genetically modified poultry products and if a functional transgenic chicken product will be brought to "market." The benefits of increased disease resistance and increased feed conversion will need to be weighed against consumer demand and acceptance. These opposing forces will have direct impact on the sustainability of the poultry industry as food demands continue to grow. The issuing of guidelines by the FDA for the regulation of genetically modified animals containing recombinant DNA should facilitate this process [28].

The development of new vectors, both viral and nonviral, for transgenesis should decrease the cost and accelerate the development of new avian transgenic models and the use of nonviral vectors may assuage public fears of transgenic modification of farm livestock. DNA transposons hold great promise as useful vectors for avian transgenesis. The next few years should bring new advances as some of the DNA transposable elements that are showing promise in mammalian transgenesis (Tol2, PiggyBac, Sleeping Beauty) are used for chicken transgenesis.

The greatest advance in avian transgenesis lies in the development of efficient gene targeting of specific genomic loci using homologous recombination. This objective may be accomplished using SSCs, gonadal embryonic germ cells, or primordial germ cells [80–83]. Gene targeting of primordial germ cells appears to be a viable technique [84] although it remains to be proven if this will be a viable method for avian transgenesis. The use of zinc finger nucleases which target specific loci in the vertebrate genome has proven to be useful for gene targeting in both zebra fish and rats [85, 86]. These proteins hold great promise for the potential manipulation of the avian genome. The generation of induced pluripotent cells (IPS cells) from somatic cells also needs to be investigated in avian species [70]. If this technique were further coupled with the conversion to germ cells, it would lay open new possibilities in avian cloning for species rescue.

Primordial germ cell culture also promises to be a viable technology for the preservation of avian germplasm (reviewed in [87]). Semen cryopreservation in avian species has proven problematic and for this reason an alternative method of germplasm cryopreservation is needed. An efficient method to preserve avian genetic resources is of importance for commercial breeders and also rare breed conservationists. The development of a robust method for avian cryopreservation would significantly enhance the biosecurity of the avian breeding industry and greatly reduce animal numbers bred for line maintenance. The use of PGCs could provide an alternative source of cellular material for cryopreservation efforts. At this stage, PGC cryopreservation offers only a slight advantage over semen cryopreservation for the preservation of single traits. Therefore, what is needed to extend this technology is to develop improved culture conditions for the efficient expansion and cryopreservation of both male and female PGCs from different breeds of chickens. This technology will need to be coupled with an efficient methodology to reconstitute the *complete genome* of avian lines from the cryopreserved cells.

Several recent reports have described transgenic offspring from quail [52, 54] and zebra finches [55] using the genetic techniques described above. To date, no transgenic modifications have been published for turkeys and duck. Since these are also important food production animals, it can be expected that advances in transgenesis will be made in these species in the near future. These potential models will be significant to the study of avian production traits but may also be pertinent to the investigation of avian influenza in which natural disease reservoirs reside in wild duck populations. It will be difficult to foresee if the transgenic technology being developed for the chicken will be easily transferred to other poultry species beyond the use of retroviral vectors. An illustration of foreseeable problems comes from investigations of embryonic stem cells. Derivation of ES cells from mammals

excluding the mouse has proven to be exceedingly difficult to achieve [88]. This may also hold true for avian transgenesis.

Bibliography

Primary Literature

1. Houdebine L-M (2009) Production of pharmaceutical proteins by transgenic animals. Comp Immunol Microbiol Infect Dis 32:2107–2121
2. Lillico SG, McGrew MJ, Sherman A, Sang HM (2005) Transgenic chickens as bioreactors for protein-based drugs. Drug Discov Today 10:3191–3196
3. Council for Agricultural Science and Technology (CAST) (2007) The role of transgenic livestock in the treatment of human disease. Issue Paper 35. CAST, Ames
4. Raju TS, Briggs JB, Borge SM, Jones AJS (2000) Species-specific variation in glycosylation of IgG: evidence for the species-specific sialyation and branch-specific galactosylation and importance for engineering recombinant glycoprotein therapeutics. Glycobiology 10:477–486
5. Rapp JC, Harvey AJ, Speksnijder GL, Hu W, Ivarie R (2003) Biologically active human interferon alpha-2b produced in the egg white of transgenic hens. Transgenic Res 12:569–575
6. Lillico SG, Sherman A, McGrew MJ, Robertson CD, Smith J, Haslam C, Barnard P, Radcliffe PA, Mitrophanous KA, Elliot EA, Sang HM (2007) Oviduct-specific expression of two therapeutic proteins in transgenic hens. Proc Natl Acad Sci USA 104:1771–1776
7. Koo BC, Kwon MS, Lee H, Kim M, Kim D, Roh JY, Park YY, Cui XS, Kim NH, Byun SJ, Kim T (2010) Tetracycline-dependent expression of the human erythropoietin gene in transgenic chickens. Transgenic Res 19(3):437–447
8. Stern CD (2005) The chick: a great model system becomes even greater. Dev Cell 8:9–17
9. Chapman SC, Lawson A, Macarthur WC, Wiese RJ, Loechel RH, Burgos-Trinidad M, Wakefield JK, Ramabhadran R, Mauch TJ, Schoenwolf GC (2005) Ubiquitous GFP expression in transgenic chickens using a lentiviral vector. Development 132:935–940
10. McGrew MJ, Sherman A, Lillico SG, Ellard FM, Radcliffe PA, Gilhooley HJ, Mitrophanous KA, Cambray N, Wilson V, Sang H (2008) Localised axial progenitor cell populations in the avian tail bud are not committed to a posterior Hox identity. Development 135:2289–2299
11. Zhao D, McBride D, Nandi S, McQueen HA, McGrew MJ, Hocking PM, Lewis PD, Sang HM, Clinton M (2010) Somatic sex identity is cell-autonomous in the chicken. Nature 464:237–242
12. Council for Agricultural Science and Technology (CAST) (2009) Animal productivity and genetic diversity: cloned and transgenic animals. Issue Paper 43. CAST, Ames
13. Golovan SP, Meidinger RG, Ajakaiye A, Cottrill M, Wiederkehr MZ, Barney DJ, Plante C, Pollard DW, Fan MZ, Hayes MA, Laursen J, Hjorth JP, Hacker RR, Phillips JP, Forsberg CW (2001) Pigs expressing salivary phytase produce low-phosphorus manure. Nat Biotechnol 19:741–745
14. Cho J, Choi K, Darden T, Reynolds PR, Petitte JN, Shears SB (2006) Avian multiple inositol polyphosphate phosphatase is an active phytase that can be engineered to help ameliorate the planet's "phosphate crisis". J Biotechnol 126:248–259
15. Tiensin T, Chaitaweesub P, Songserm T, Chaisingh A, Hoonsuwan W et al (2005) Highly pathogenic avian influenza H5N1, Thailand, 2004. Emerg Infect Dis 11:1664–1672
16. Wall RJ, Powell A, Paape MJ, Kerr DA, Bannermann SS, Pursel CG, Well KD, Talbot N, Hawk HW (2005) Genetically enhanced cows resist intramammary Staphylococcus aureus infection. Nat Biotechnol 23:445–451
17. Gordon JW, Scangos GA, Plotkin DJ, Barbosa JA, Ruddle FH (1980) Genetic transformation of mouse embryos by microinjection of purified DNA. Proc Natl Acad Sci USA 77:7380–7384
18. Hammer RE, Pursel VG, Rexroad CE, Wall RJ, Bolt DJ, Ebert KM, Palmiter RD, Brinster RL (1985) Production of transgenic rabbits, sheep and pigs by microinjection. Nature 315:680–683
19. Mullins JJ, Peters J, Ganten D (1990) Fulminant hypertension in transgenic rats harbouring the mouse Ren-2 gene. Nature 344:541–544
20. Krimpenfort P, Rademakers A, Eyestone W, van der Schans A, van den Broek S, Kooiman P, Kootwijk E, Platenburg G, Pieper F, Strijker R, de Boer H (1991) Generation of transgenic dairy cattle using 'in vitro' embryo production. Biotechnology (N Y) 9:844–847
21. Kochav S, Ginsburg M, Eyal-Giladi H (1980) From cleavage to primitive streak formation: a complementary normal table and a new look at the first stages of the development of the chick. II. Microscopic anatomy and cell population dynamics. Dev Biol 79:296–308
22. Perry MM (1988) A complete culture system for the chick embryo. Nature 331:70–72
23. Love J, Gribbin C, Mather C, Sang H (1994) Transgenic birds by DNA microinjection. Biotechnology 12:60–63
24. Naito M, Sasaki E, Ohtaki M, Sakurai M (1994) Introduction of exogenous DNA into somatic and germ cells of chickens by microinjection into the germinal disc of fertilized ova. Mol Reprod Dev 37:167–171
25. Salter DW, Smith EJ, Hughes SH, Wright SE, Fadly AM, Witter RL, Crittenden LB (1986) Gene insertion into the chicken germ line by retroviruses. Poult Sci 65:1445–1458
26. Salter DW, Smith EJ, Hughes SH, Wright SE, Crittenden LB (1987) Transgenic chickens: insertion of retroviral genes into the chicken germ line. Virology 157:236–240
27. Chen HY, Garber EA, Mills E, Smith J, Kopchick JJ, DiLella AG, Smith RG (1990) Vectors, promoters, and expression of genes in chick embryos. J Reprod Fertil Suppl 41:173–1782
28. U.S. Food and Drug Administration (2009) Guidance for industry #187: regulation of genetically engineered animals containing heritable recombinant DNA constructs. Final Guidance
29. Romano G, Marino IR, Pentimalli F, Adamo V, Giordano A (2009) Insertional mutagenesis and development of malignancies induced by integrating gene delivery

systems: implications for the design of safer gene-based interventions in patients. Drug News Perspect 22:185–196
30. Jahner D, Stuhlmann H, Stewart CL, Harbers K, Lohler J, Simon I, Jaenisch R (1982) De novo methylation and expression of retroviral genomes during mouse embryogenesis. Nature 298:623–628
31. Pannell D, Ellis J (2001) Silencing of gene expression: implications for design of retrovirus vectors. Rev Med Virol 11: 205–217
32. Bosselman RA, Hsu R-Y, Boggs T, Hu S, Bruszewski J, Ou S, Kozar L, Martin F, Green C, Jacobsen F, Nicolson M, Schultz JA, Semon KM, Rishell W, Stewart RG (1989) Germline transmission of exogenous genes in the chicken. Science 243:533–535
33. Thoraval P, Afanassieff M, Cosset FL, Lasserre F, Verdier G, Coudert F, Dambrine G (1995) Germline transmission of exogenous genes in chickens using helper-free ecotropic avian leukosis virus-based vectors. Transgenic Res 4:369–377
34. Harvey AJ, Speksnijder G, Baugh LR, Morris JA, Ivarie R (2002) Expression of exogenous protein in the egg white of transgenic chickens. Nat Biotechnol 20:396–399
35. Mozdziak PE, Borwornpinyo S, McCoy DW, Petitte JN (2003) Development of transgenic chickens expressing bacterial beta-galactosidase. Dev Dyn 226:439–445
36. Kwon MS, Koo BC, Choi BR, Park YY, Lee YM, Suh HS, Park YS, Lee HT, Kim JH, Roh JY, Kim NH, Kim T (2008) Generation of transgenic chickens that produce bioactive human granulocyte-colony stimulating factor. Mol Reprod Dev 75:1120–1126
37. Mizuarai S, Ono K, Yamaguchi K, Nishijima K, Kamihara M, Iijima S (2001) Production of transgenic quails with high frequency of germline transmission using VSV-G pseudotyped retroviral vector. Biochem Biophys Res Commun 286:456–463
38. Kamihira M, Ono K, Esaka K, Nishijima K, Kigaku R, Komatsu H, Yamashita T, Kyogoku K, Iijima S (2005) High-level expression of single-chain Fv-Fc fusion protein in serum and egg white of genetically manipulated chickens by using a retroviral vector. J Virol 79:10864–10874
39. Koo BC, Kwon MS, Choi BR, Kim JH, Cho SK, Sohn SH, Cho EJ, Lee HT, Chang W, Jeon I, Park JK, Park JB, Kim T (2006) Production of germline transgenic chickens expressing enhanced green fluorescent protein using a MoMLV-based retrovirus vector. FASEB J 20:2251–2260
40. Cockrell AS, Kafri T (2007) Gene delivery by lentivirus vectors. Mol Biotechnol 36:184–204
41. Wang Y, Song Y-T, Liu Q, Liu C, Wang L-L, Liu Y, Zhou X-Y, Wu J, Wei H (2010) Quantitative analysis of lentiviral transgene expression in mice over seven generations. Transgenic Res 19:775–784
42. Lois C, Hong EJ, Pease S, Brown EJ, Baltimore D (2002) Germline transmission and tissue-specific expression of transgenes delivered by lentiviral vectors. Science 295:868–872
43. Pfeifer A, Ikawa M, Dayn Y, Verma IM (2002) Transgenesis by lentiviral vectors: lack of gene silencing in mammalian embryonic stem cells and preimplantation embryos. Proc Natl Acad Sci USA 99:2140–2145
44. Hamra FK, Gatlin J, Chapman KM, Grellhesl DM, Garcia JV, Hammer RE, Garbers DL (2002) Production of transgenic rats by lentiviral transduction of male germ-line stem cells. Proc Natl Acad Sci USA 99:14931–14936
45. Hofmann A, Kessler B, Ewerling S, Weppert M, Vogg B, Ludwig H, Stojkovic M, Boelhauve M, Brem G, Wolf E, Pfeifer A (2003) Efficient transgenesis in farm animals by lentiviral vectors. EMBO Rep 4:1054–1060
46. Ritchie WA, King T, Neil C, Carlisle AJ, Lillico S, McLachlan G, Whitelaw CB (2009) Transgenic sheep designed for transplantation studies. Mol Reprod Dev 76:61–64
47. Hiripi L, Negre D, Cosset FL, Kvell K, Czömpöly T, Baranyi M, Gócza E, Hoffmann O, Bender B, Bősze Z (2010) Transgenic rabbit production with simian immunodeficiency virus-derived lentiviral vector. Transgenic Res Epub:Jan 13
48. Sasaki E, Suemizu H, Shimada A, Hanazawa K, Oiwa R, Kamioka M, Tomioka I, Sotomaru Y, Hirakawa R, Eto T, Shiozawa S, Maeda T, Ito M, Ito R, Kito C, Yagihashi C, Kawai K, Miyoshi H, Tanioka Y, Tamaoki N, Habu S, Okano H, Nomura T (2009) Generation of transgenic non-human primates with germline transmission. Nature 459:523–527
49. McGrew MJ, Sherman AS, Ellard FM, Lillico SG, Gilhooley HJ, Mitrophanous KA, Kingsman AJ, Sang H (2004) Efficient production of germline transgenic chickens using lentiviral vectors. EMBO Rep 5:728–733
50. Kim JN, Park TS, Park SH, Park KJ, Kim TM, Lee SK, Lim JM, Han JY (2010) Migration and proliferation of intact and genetically modified primordial germ cells and the generation of a transgenic chicken. Biol Reprod 82:257–262
51. McGrew MJ, Lillico SG, Sherman A, Taylor L, Sang H (2010) Functional conservation between rodents and chicken of regulatory sequences driving skeletal muscle gene expression in transgenic chickens. BMC Dev Biol 10:e26
52. Scott BB, Lois C (2005) Generation of tissue-specific transgenic birds with lentiviral vectors. Proc Natl Acad Sci USA 102:16443–16447
53. Poynter G, Lansford R (2008) Generating transgenic quail using lentiviruses. Methods Cell Biol 87:281–293
54. Shin SS, Kim TM, Kim SY, Kim TW, Seo HW, Lee SK, Kwon SC, Lee GS, Kim H, Lim JM, Han JY (2008) Generation of transgenic quail through germ cell-mediated germline transmission. FASEB J 22:2435–2444
55. Agate RJ, Scott BB, Haripal B, Lois C, Nottebohm F (2009) Transgenic songbirds offer an opportunity to develop a genetic model for vocal learning. Proc Natl Acad Sci USA 106:17963–17967
56. Kwon SC, Choi JW, Jang HJ, Shin SS, Lee SK, Park TS, Choi IY, Lee GS, Song G, Han JY (2010) Production of biofunctional recombinant human interleukin 1 receptor antagonist (rhIL1RN) from transgenic quail egg white. Biol Reprod 82:1057–1064
57. McClintock B (1953) Induction of instability at selected loci in maize. Genetics 38:579–599
58. Feschotte C, Pritham EJ (2007) DNA transposons and the evolution of eukaryotic genomes. Annu Rev Genet 41:331–368

59. Ivics Z, Li MA, Mátés L, Boeke JD, Nagy A, Bradley A, Zsuzsanna I (2009) Transposon-mediated genome manipulation in vertebrates. Nat Meth 6:415–422
60. Ding S, Wu X, Li G, Han M, Zhuang Y, Xu T (2005) Efficient transposition of the piggyBac (PB) transposon in mammalian cells and mice. Cell 122:473–483
61. Balciunas D, Wangensteen KJ, Wilber A, Bell J, Geurts A, Sivasubbu S, Wang X, Hackett PB, Largaespada DA, McIvor RS, Ekker SC (2006) Harnessing a high cargo-capacity transposon for genetic applications in vertebrates. PLoS Genet 2:e169
62. Sherman A, Dawson A, Mather C, Gilhooley H, Li Y, Mitchell R, Finnegan D, Sang H (1998) Transposition of the Drosophila element mariner into the chicken germ line. Nat Biotechnol 16:1050–1053
63. Sato Y, Kasai T, Nakagawa S, Tanabe K, Watanabe T, Kawakami K, Takahashi Y (2007) Stable integration and conditional expression of electroporated transgenes in chicken embryos. Dev Biol 305:616–624
64. Lu Y, Lin C, Wang X (2009) PiggyBac transgenic strategies in the developing chicken spinal cord. Nucleic Acids Res 37:e141
65. Petitte JN, Clark ME, Liu G, Verrinder-Gibbins AM, Etches RJ (1990) Production of somatic and germline chimeras in the chicken by transfer of early blastodermal cells. Development 108:185–189
66. Etches RJ, Clark ME, Toner A, Liu G, Gibbins AM (1996) Contributions to somatic and germline lineages of chicken blastodermal cells maintained in culture. Mol Reprod Dev 45:291–298
67. Pain B, Clark M, Nakazawa H, Sakurai M, Samarut J, Etches R (1996) Long-term in vitro culture and characterization of avian embryonic stem cells with multiple morphogenetic potentialities. Development 122:2339–2348
68. Bezzubova O, Silbergleit A, Yamaguchi-Iwai Y, Takeda S, Buerstedde JM (1997) X-ray resistance and homologous recombination frequencies in a RAD54-/- mutant of the chicken DT40 cell line. Cell 89:185–193
69. van de Lavoir MC, Mather-Love C, Leighton P, Diamond JH, Heyer BS, Roberts R, Zhu L, Winters-Digiacinto P, Kerchner A, Gessaro T, Swanberg S, Delany ME, Etches RJ (2005) High-grade transgenic somatic chimeras from chicken embryonic stem cells. Mech Dev 123:31–41
70. Lavial F, Acloque H, Bachelard E, Nieto MA, Samarut J, Pain B (2009) Ectopic expression of Cvh (Chicken Vasa homologue) mediates the reprogramming of chicken embryonic stem cells to a germ cell fate. Dev Biol 330:73–82
71. Tsunekawa N, Naito M, Sakai Y, Nishida T, Noce T (2000) Isolation of chicken vasa homolog gene and tracing the origin of primordial germ cells. Development 127:2741–2750
72. Eyal-Giladi H, Ginsburg M, Farbarov A (1981) Avian primordial germ cells are of epiblastic origin. J Embryol Exp Morphol 65:139–147
73. Simkiss K, Rowlett K, Bumstead N, Freeman BM (1989) Transfer of primordial germ cell DNA between embryos. Protoplasma 151:164–166
74. Chang IK, Jeong DK, Hong YH, Park TS, Moon YK, Ohno T, Han JY (1997) Production of germline chimeric chickens by transfer of cultured primordial germ cells. Cell Biol Int 21:495–499
75. Vick L, Li Y, Simkiss K (1993) Transgenic birds from transformed primordial germ cells. Proc Biol Sci 251:179–182
76. Mozdziak PE, Wysocki R, Angerman-Stewart J, Pardue SL, Petitte JN (2006) Production of chick germline chimeras from fluorescence-activated cell-sorted gonocytes. Poult Sci 85:1764–1768
77. Tajima A, Naito M, Yasuda Y, Kuwana T (1993) Production of germ line chimera by transfer of primordial germ cells in the domestic chicken (Gallus domesticus). Theriogenology 40:509–519
78. Ono T, Machida Y (1999) Immunomagnetic purification of viable primordial germ cells of Japanese quail (Coturnix japonica). Comp Biochem Physiol A Mol Integr Physiol 122:255–259
79. Zhao DF, Kuwana T (2003) Purification of avian circulating primordial germ cells by nycodenz density gradient centrifugation. Br Poult Sci 44:30–35
80. Park TS, Jeong DK, Kim JN, Song GW, Hong YH, Lim JM, Han JY (2003) Improved germline transmission in chicken chimeras produced by transplantation of gonadal primordial germ cells into recipient embryos. Biol Reprod 68:1657–1662
81. Kalina J, Senigl F, Micáková A, Mucksová J, Blazková J, Yan H, Poplstein M, Hejnar J, Trefil P (2007) Retrovirus-mediated in vitro gene transfer into chicken male germ line cells. Reproduction 134:445–453
82. Park TS, Hong YH, Kwon SC, Lim JM, Han JY (2003) Birth of germline chimeras by transfer of chicken embryonic germ (EG) cells into recipient embryos. Mol Reprod Dev 65:389–395
83. van de Lavoir MC, Diamond JH, Leighton PA, Mather-Love C, Heyer BS, Bradshaw R, Kerchner A, Hooi LT, Gessaro TM, Swanberg SE, Delany ME, Etches RJ (2006) Germline transmission of genetically modified primordial germ cells. Nature 441:766–769
84. Leighton PA, van de Lavoir MC, Diamond JH, Xia C, Etches RJ (2008) Genetic modification of primordial germ cells by gene trapping, gene targeting, and phiC31 integrase. Mol Reprod Dev 75:1163–1175
85. Doyon Y, McCammon JM, Miller JC, Faraji F, Ngo C, Katibah GE, Amora R, Hocking TD, Zhang L, Rebar EJ, Gregory PD, Urnov FD, Amacher SL (2008) Heritable targeted gene disruption in zebrafish using designed zinc-finger nucleases. Nat Biotechnol 26:702–708
86. Geurts AM, Cost GJ, Rémy S, Cui X, Tesson L, Usal C, Ménoret S, Jacob HJ, Anegon I, Buelow R (2010) Generation of gene-specific mutated rats using zinc-finger nucleases. Methods Mol Biol 597:211–225
87. Petitte JN (2006) Avian germplasm preservation: embryonic stem cells or primordial germ cells? Poult Sci 85:237–242
88. Muñoz M, Trigal B, Molina I, Díez C, Caamaño JN, Gómez E (2009) Constraints to progress in embryonic stem cells from domestic species. Stem Cell Rev 5:6–9

Books and Reviews

Nieuwkoop PD, Sutasurya LA (1979) Primordal germ cells in the chordates. Cambridge University Press, Cambridge

Petitte JD (2004) Isolation and maintenance of avian ES cells. In: Handbook of stem cells, vol 1, Embryonic stem cells. Elsevier, Amsterdam, pp 471–479, Chapter 44

Pfeifer A, Hofmann A (2009) Lentiviral transgenesis. Methods Mol Biol 530:391–405

Walsh G (2003) Biopharmeceuticals: biochemistry and biotechnology, 2nd edn. Wiley, Chichester

Aviation and Atmosphere

Hartmut Grassl
Max Planck Institute for Meteorology, Hamburg, Germany

Article Outline

Glossary
Definition of the Subject
Introduction
Emissions of Climatically Relevant Substances by Aviation
Aviation-Induced Cloudiness
Changes of Air Chemistry by Air Traffic
Transport Sector's Contribution to Future Climate Change
Why Did International Air Traffic So Far Escape from an Emission Reduction Policy?
The European Directive to Include Air Traffic into the Emission Trading Scheme
An Airline Emission Index
Conclusions and Outlook
Acknowledgment
Bibliography

Glossary

AIC Aviation-induced cloudiness is the sum of all changes in cloudiness associated with aviation operations hence, it combines contrails and so-called persistent contrail cover.

Airline emission index A measure to compare the performance of different airlines with respect to emissions relative to an ideal one.

Aviation Here: commercial air traffic.

Contrails Jet engine exhaust condensation trails of airplanes.

Emission trading A market-based approach used to control pollution by providing economic incentives for achieving reductions in the emissions of pollutants.

GWP The global warming potential is a relative measure of how much heat a greenhouse gas traps in the atmosphere. It compares the amount of heat trapped by a certain mass of the gas in question to the amount of heat trapped by the same mass of carbon dioxide.

GTP The GTP is defined as the ratio between the global mean surface temperature change at a given future time horizon following an emission (pulse or sustained) of a compound relative to a reference gas.

Radiative forcing When the balance between the radiative energy received from the sun and radiative energy leaving the Earth-atmosphere system is perturbed, e.g., by a concentration change of an absorbing gas, the resulting imbalance is termed radiative forcing that initiates climate change.

Definition of the Subject

Commercial air traffic's peculiarity, emissions into the atmosphere mainly at cruising altitude, leads to changed impacts on global climate in comparison to other modes of transport. This entry concentrates on these differences but also looks onto measures to reduce emissions, e.g., the emission trading scheme in the European Union, and presents an airline emission index comparing commercial airlines.

Introduction

The exhaust of commercial and also military aircraft needs – in comparison to the one from power plants, cars, trucks, heaters in buildings, railway, ships, and burners in industry – a special discussion, because of its main injection at cruising altitudes, i.e., into the upper troposphere or lower stratosphere from about 9 to 12 km height. This part of the Earth's atmosphere is nearly all the time colder than −40°C, often it is with about −70°C the coldest one in mid-latitudes in the lowest at least 60 km. Therefore, the water vapor

concentration in these layers must be lower by typically 3–4 orders of magnitude than at the Earth's surface in low- and mid-latitudes. Hence, several emissions of an aircraft besides carbon dioxide, for example unavoidable water vapor, in principle avoidable nitrogen oxides can lead to a considerable disturbance of the radiation budget of the planet. First, via the formation of rather persistent condensation trails, an ice cloud, during frequently favorable meteorological conditions, and second, via the formation of ozone around cruising altitudes because of the nitrogen oxide emissions.

In addition, the growth rate of commercial air traffic was on average above the one for the global gross economic product, leading to a growing relative contribution of air traffic to the changed composition of the atmosphere. Only very recently did the growth rate no longer surmount the growth rate of world economy as strong as before.

However, it was only in the late 1980s when first publications dealt with air traffic's potential influence on *climate*. Earlier, in the early 1970s, the planned supersonic aircraft fleet in the USA had led to an assessment of the impact of such aircraft on the stratospheric ozone layer. At this time the consequences of the emission of the trace gas nitrogen dioxide (NO_2) were the main reasons for the investigations, because it is strongly involved in stratospheric ozone chemistry leading to ozone depletion at altitudes above about 20 km but to ozone increases in the troposphere and lowest stratosphere.

In 1996, the steadily growing public and scientific discussions on air traffic and its potential effect on global climate have stimulated the International Civil Aviation Organization (ICAO), the UN specialized agency that has global responsibility for the establishment of standards, recommended practices, and guidance on various aspects of international civil aviation, including environmental protection, to ask the Intergovernmental Panel on Climate Change (IPCC) to assess in a special report [17] entitled "Aviation and the Global Atmosphere" the air traffic influence on global climate. In this report not only the effects of air traffic on atmospheric composition and on climate were assessed but also projected into the future using air traffic growth scenarios. These results and new findings have entered the third and fourth full IPCC assessments [19–21]; hence, the hitherto known facts have been presented to the political arena and have led to first hesitating measures to reduce emissions, like the European Union's decision in 2009 to include air traffic into the European emissions trading scheme, to become effective on January 1, 2012.

This entry will start with the greenhouse gas emission history of air traffic in section "Emissions of Climatically Relevant Substances by Aviation," influenced both by the above average growth rate of this economic sector but also by the strong increase in fuel use efficiency per passenger kilometer, which has been stronger than for road traffic and much stronger than for railways. This section will also include projections of future air traffic greenhouse gas emissions using estimates from scenarios of IPCC. It continues with the knowledge about long-lasting contrails and their dependence on favorable meteorological conditions in section "Aviation-Induced Cloudiness." This section will also include cirrus clouds formed or transformed because of air traffic, existing besides the easily detectable linear contrails. Section "Changes of Air Chemistry by Air Traffic" is then devoted to changes in air chemistry caused by air traffic emissions. Section "Transport Sector's Contribution to Future Climate Change" extrapolates into the 21st century with known scenarios of human behavior. It follows the section on "Why did International Air Traffic So Long Escape an Emissions Trading Scheme?" The first attempt of the European Union to include international air traffic into an emissions trading scheme will be described in section "The European Directive to Include Air Traffic into the Emission Trading Scheme." The second last section on "An Airline Emission Index" will present essentials of an airline index that includes a ranking concerning carbon dioxide and nitrogen oxides emissions, published very recently. The last section will provide the conclusions and also present avenues how to reduce or even to avoid air traffic emissions changing climate.

Emissions of Climatically Relevant Substances by Aviation

The estimates of climate effects of air traffic depend totally on a reliable time-dependent emission inventory on global scale for the past, the present, and the future. The major research project QUANTIFY of

the European Union's Sixth Framework Research Programme (finished very recently) has established such a consistent global three-dimensional air transport emission inventory for greenhouse gases, particles, and precursor gases of other greenhouse gases and for aerosol particles for the year 2000 (also for all other modes of transport), and has developed estimates of future emissions for the years 2020, 2050, and 2100. The example for air traffic is shown in Fig. 1 and Table 1, taken from [25].

Since different substances in the aircraft exhaust have very different concentrations and also very different radiative properties, a common scale must be created for a just assessment of the environmental burden caused by different aircraft and flight types. The next subsection will deal with it.

Creating a Common Scale for the Climate Effects of Air Traffic Emissions

The entire motorized transport sector (road traffic, shipping, rail, aviation) emits a wide variety of gases and aerosols into the atmosphere, with different characteristics, which either influence climate directly by their radiative properties or indirectly via chemical and physical processes influencing concentrations of other climatically relevant substances. We need metrics that allow these emissions to be placed on a common scale in terms of their impact on global climate. The applications of such metrics are manifold: First, they have served and will serve as basic information in negotiations for international agreements and emission trading schemes (see section "The European Directive to Include Air Traffic into the Emission Trading Scheme"); second, they allow the assessment of trade-offs between changes in emissions resulting from technological or operational developments; third, they serve for comparisons of different environmental impacts caused by the different transport sectors and thus help in traffic policy making. Usually, the CO_2 emission, common to all transport sectors, is used as a reference. Therefore, all other emissions have to be transformed into their "CO_2-equivalents." Ideally, the same equivalent CO_2 emissions should produce the same climate effect, regardless of their shares in the exhaust or after chemical transformation in the atmosphere. This is, however, only an approximation of reality, because most of the non-CO_2 emissions from the different transport sectors, and especially aviation, are short-lived substances with often rather regionalized concentrations. In addition, these short-lived substances are all not included in the Kyoto Protocol basket of solely long-lived greenhouse gases.

The challenges in developing generally accepted metrics are strongly magnified by the inclusion of short-lived species. One first difficulty concerns the choice of an appropriate structure for the metric. Should effects of an emission today be integrated over 10, 20, 50, 100, or even 200 years? Or should the impact, e.g., the global mean surface temperature increase after a certain time period, be used as a measure? The first approach is the most frequently used one, characterized by the global warming potential (GWP) and the one adopted in the Kyoto Protocol. The second one, called global temperature change potential (GTP), strongly reduces the influence of short-lived emissions if the same long time horizon is used as typically for GWP. In view of the lifetime (defined as the time for the decay of the concentration of an emitted pulse of a substance to 1/e) in the atmosphere of an anthropogenic addition of CO_2, which is well above 100 years, 100 years have been chosen for the Kyoto Protocol, although there was no specific argument put forward for this time horizon by IPCC. A further challenge is the quantification of input parameters for the metric, originating in the uncertainty of atmospheric processes. For example: How much of the nitrogen oxide emission remains available for the formation of ozone in the troposphere, a potent but short-lived greenhouse gas of the atmosphere? On top of these challenges we have to face the dependence of the effects on the location of the emissions for all short-lived substances, severest for air traffic, where for example the emission height is decisive for the formation of a long-lasting contrail. The QUANTIFY project has evaluated existing metrics and has introduced new concepts (for details see Fuglestvedt et al. 2009). All these metrics have been evaluated for emissions from the transport sector both in terms of integrated radiative forcing (When the balance between the radiative energy received from the sun and radiative energy leaving the Earth-atmosphere system is perturbed, e.g., by a concentration change of an absorbing gas, the

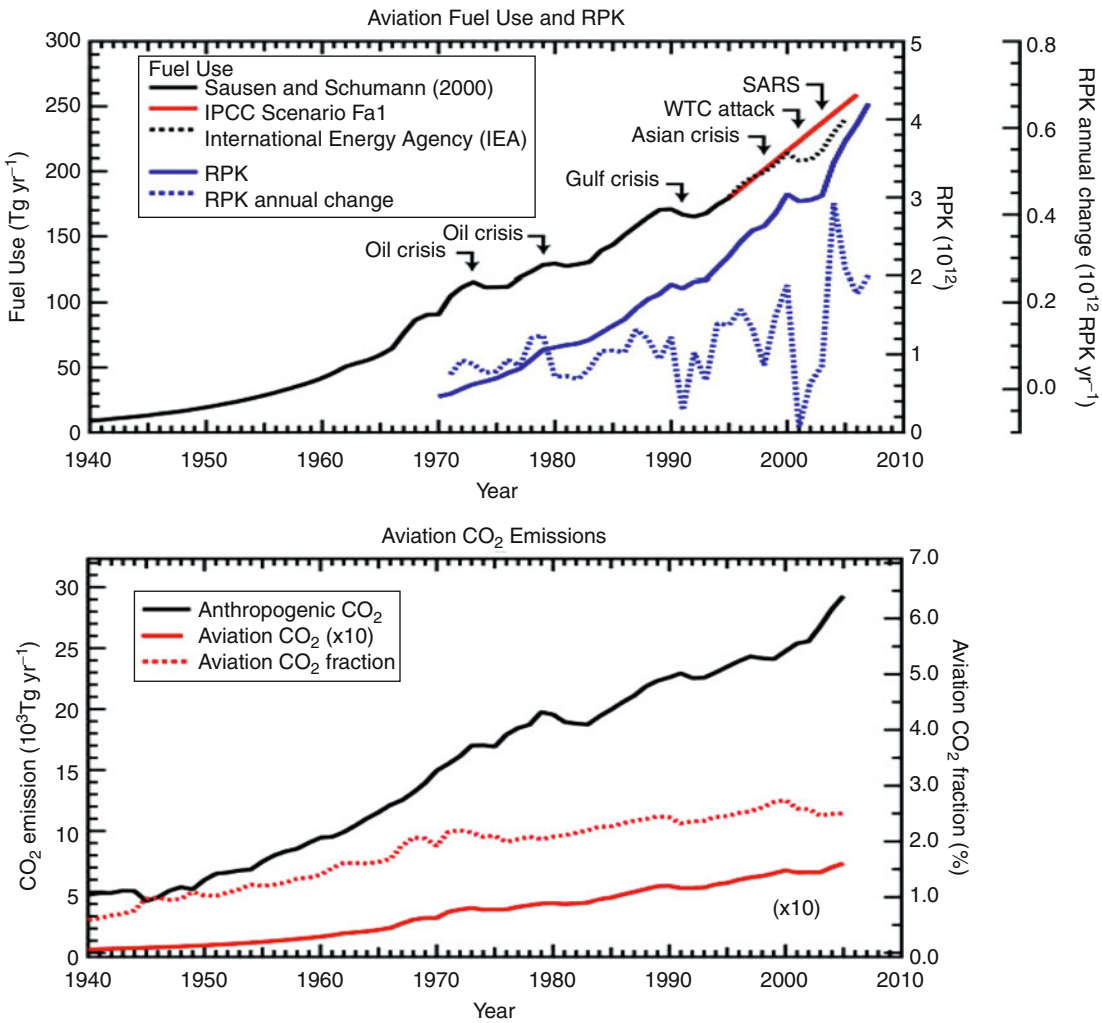

Aviation and Atmosphere. Figure 1

Upper Panel: Aviation fuel usage beginning in 1940 from Sausen and Schumann [32] and extended with data from IEA [16] and the IPCC Fa1 scenario of Henderson et al. [13]. The *arrows* indicate world events that shortly threatened global aviation use: the oil crises of the 1970s, the Gulf war crisis in the early 1990s, the Asian financial crisis in the late 1990s, the World Trade Center (WTO) attack in 2001, and the global health crisis brought about by the severe acute respiratory syndrome (SARS). Also shown is the growth in air passenger traffic from 1970 to 2007 in trillions of revenue passenger kilometers (RPK) (near right-hand axis) (Source: ICAO traffic statistics from http://www.airlines.org/economics/traffic/World/Airline/Traffic.htm. Accessed 19 Sept 2007) and the annual change in RPK (far right-hand axis [Note offset zero]). *Lower Panel*: Growth in CO_2 emissions in Tg CO_2/year for all anthropogenic activities and from aviation fuel burn (left-hand axis), and the fraction of total anthropogenic CO_2 emissions represented by aviation CO_2 emissions (%) (right-hand axis). Note scaling of aviation CO_2 emissions (Source: Lee et al. [24])

resulting imbalance is termed radiative forcing. It can be calculated by changing the concentration of the substance and keeping all other parameters fixed. In the real climate system, the imbalance stimulates climate change trying to restore the energy balance of the planet.) (GWP) and the net surface temperature change (GTP) of the various transport modes for several time horizons. For the series of tasks to be

Aviation and Atmosphere. Table 1 Estimations of historical and current emissions from inventory models, 1990–2005

Year	Inventory	Civil fuel Tg/a	Military fuel Tg/a	Total fuel Tg/a	Total CO_2 Tg/a	Distance (civil, 10^9 km)	NO_xTgNO$_2$/a	EINO_x g NO_x/kg fuel
1990	FAST	105	n.c.		331	15.7	1.42	
1992	NASA	114	25.5	139	359	n.c.	1.44	12.6(12.0)
1992	ANCAT/EC2	114	17.1	131	360	n.c.	1.60(1.81)	14.0(13.8)
1999	NASA	128 (134 inc. charter)	n.c.		404 (423 inc. charter)	25.8	1.69	13.2
2000	TRADEOFF	152	17.1[a]	169	480	25.1	1.95(2.15)	12.7(12.9)
2000	FAST	152	n.c.		480	26.9	2.03	13.4
2000	SAGE	181	n.c.		572	33.3	2.51	13.8
2001	SAGE	170	n.c.		536	31.9	2.35	13.8
2002	SAGE	171	n.c.		539	32.6	2.41	14.1
2002	AERO2K	156	19.5	176	492(553)	33.2	2.06(2.24)	13.2(12.7)
2003	SAGE	176	n.c.		557	34.5	2.49	14.1
2004	SAGE	188	n.c.		594	37.0	2.69	14.3
2005	SAGE	203	n.c.		641	40.7	2.90	14.2

References: "FAST," Lee et al. (2005); "NASA," (Baughcum et al. [3]) and (Sutkus et al. [33]); "ANCAT/EC2," Gardner et al. [12]; "TRADEOFF," Gauss et al. (2006); "SAGE," Kim et al. [22]; "AERO2K," Eyers et al. [10]

[a]Military emissions adopted from other study; *n.c.* not calculated, brackets include military emissions

performed starting from transport sector emissions and ending at climate impacts, see Fig. 2 [30].

For metrics, very different approaches are possible. One can look at the current radiative or temperature forcing relative to the preindustrial era or at the temporal development of the forcing over several decades for a pulse emitted today, or to the forcing for a sustained emission or a more elaborate emission scenario. Figure 3 shows the temperature change that will be caused by the emissions of the year 2000 for all transport modes for four chosen time horizons. In order to calculate surface air temperature changes ideally a coupled Atmosphere/Ocean/Land-Model has to be run. If this model gets as an input the three-dimensional emission distribution of air traffic, it must not lead to the same relation of different transport sectors as the radiative forcing calculation, because it adds the processes at the ocean air interface that are neglected in the chemical transport model used for the radiative transfer calculations because then sea surface temperature is fixed. Figure 4 clearly demonstrates that emissions from road transport in 2000 are dominating the traffic sector impact on surface temperature, with aviation as the second largest contributor to surface air temperature changes. For time horizons of 20 and 100 years, the net warming from road transport is seven and six times larger than the net warming from aviation. This is approximately the same ratio as the ratio between the CO_2 emissions from these sectors; thus, mainly CO_2 controls the climate response on timescales beyond 10 years for the GTP metric. The net temperature effect of shipping changes sign from negative for a time horizon of 20 years to positive for the longer time horizons. Both rail sectors' contributions seem small, but added together they reach 15–30% of the effect of aviation for time horizons between 20 and 100 years. The results in Fig. 3 show well how the relative importance of the different transport sectors changes depending on the time perspective.

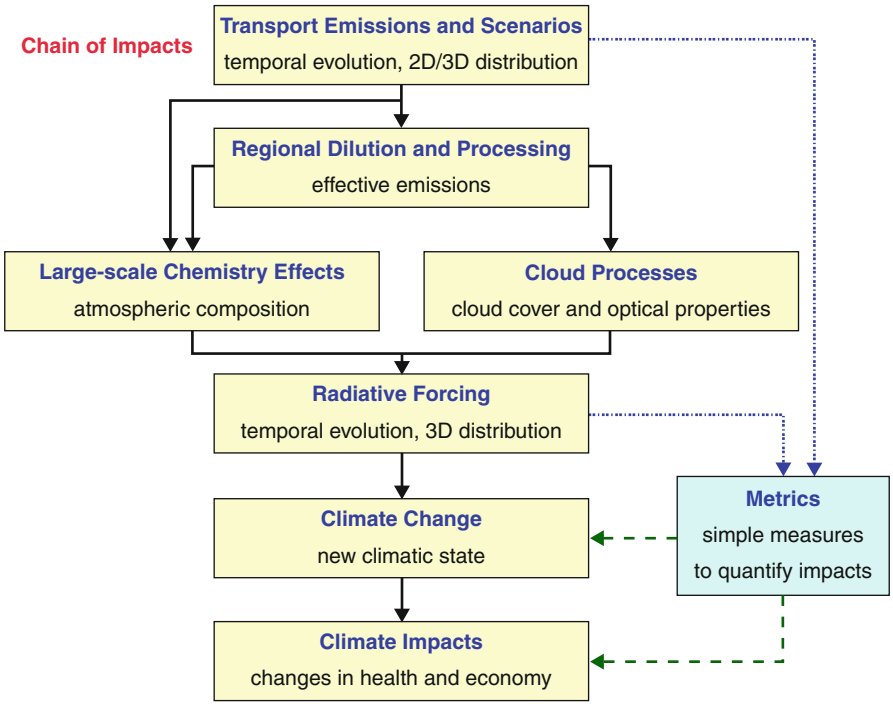

Aviation and Atmosphere. Figure 2

From emissions to climate change and climate impacts (a schematic). Only the main fluxes of information are indicated by *arrows*. QUANTIFY science tasks are printed in *blue*, output in *black* (Source: QUANTIFY [30])

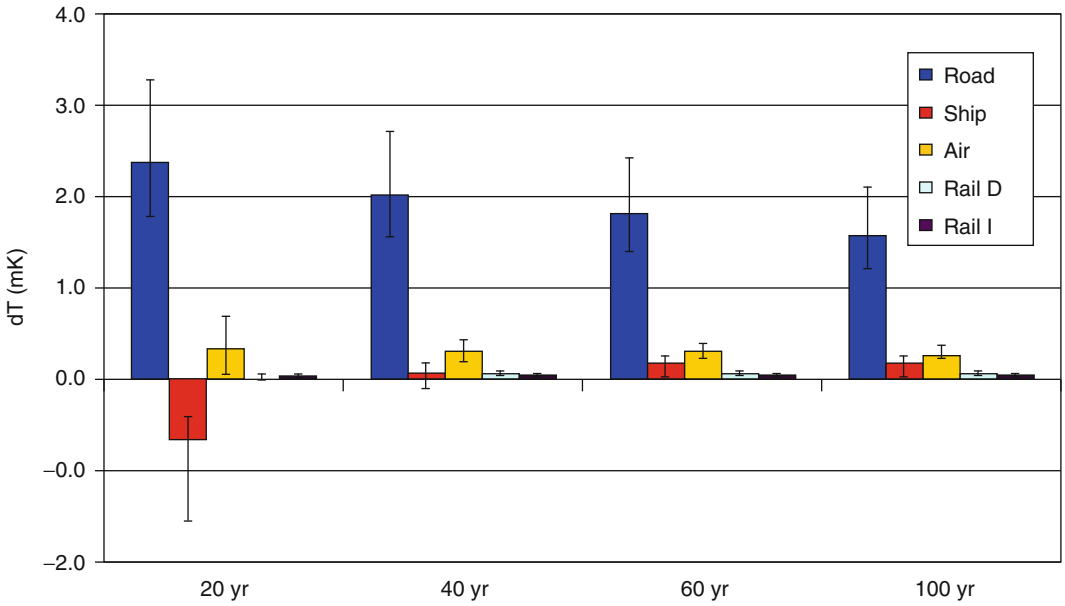

Aviation and Atmosphere. Figure 3

Contribution from a 1-year pulse of current (year 2000) emissions to net future temperature change (mK) for each transport mode for four time horizons (20, 40, 60, and 100 years), including the uncertainties, here given by the 1-sigma level (Source: Lee et al. [25])

Climate Change Contribution of Carbon Dioxide Emissions from Air Traffic

The entire transport sector contributes about one third of the total global anthropogenic CO_2 emissions. The annual growth rate of transport-related greenhouse gas emissions is larger than for other mature industrial sectors. In view of the United Nations Framework Convention on Climate Change (UNFCCC), its Kyoto Protocol, and possible follow-up protocols, this high rate of increase creates the severest problem for the aviation sector, when trying to achieve forthcoming emission reduction targets. Additionally, the impact of the transport sector on climate is at least as complex as for other sectors like heating of houses, because it also involves more strongly air chemistry and modification of cloudiness than the emissions from shipping, and in addition direct cloud formation (contrails) by air traffic. Thus an assessment of the full climate effects of the transport sector and especially aviation has to take into account more than just the list of gases in the Kyoto Protocol. The transport sector can impact on climate in the following ways:

- By direct emissions of greenhouse gases, mainly CO_2, but also by nitrous oxide (N_2O) and some halocarbons
- By emissions of precursors of ozone, such as nitrogen oxides (NOx), carbon monoxide (CO), and volatile organic compounds (VOCs)
- By emissions of aerosol particles or their precursor gases, in particular black carbon (soot) and sulfur dioxide (SO_2), which are directly and indirectly (via cloud formation and cloud modification) radiatively and chemically active
- By directly triggering additional clouds (e.g., contrails and contrail cirrus)

On the other hand, the global and economic system is largely dependent on an efficient transport system. This dependency has grown during recent decades not only because of an increasing world population but mainly because of globalization. Life style and the availability of cheaper transport (mainly because of lack of internalization of external costs) in developed and developing countries are also enhancing demand. Further very strong growth of the transport sector is expected in developing countries. In the long term, a sustainable transport system is needed that satisfies the demands of economy and population while following the constraints of climate change policy measures. In order to meet these constraints clear information on the climatic impact of different transport emissions is needed. Here we concentrate on aviation, a smaller part with respect to goods and passengers transported, but with many climatically relevant facets because of its already mentioned main emission height of about 10 km.

Each kilogram of aviation fuel, overwhelmingly kerosene, when burned in an engine, must lead to 3.16 kg carbon dioxide (CO_2) and 1.0 kg of water vapor (H_2O). These unavoidable emissions are two major reasons of an air traffic influence on the radiative transfer in the atmosphere, but not the only ones. The first one is nearly completely independent of the place where the emission occurs, because of the long lifetime of anthropogenic carbon dioxide being well above 100 years and thus resulting in a globally well-mixed anthropogenic carbon dioxide concentration addition. Aviation CO_2 will contribute to the entire CO_2 burden of the atmosphere like all other emissions into the atmosphere close to the surface of the Earth. For the second major emission, H_2O, the point where it is emitted is decisive: At the surface this addition is negligible in comparison to the natural fluxes of water, but not so at about 10 km height at a water vapor mixing ratio ranging from about 100 ppmv to as low as 5 ppmv. Flying by 1 km higher or lower in heights around the tropopause (the interface between the troposphere and the stratosphere; typically at 10 km height in mid-latitudes), however, can often avoid a long-lasting linear contrail (for more see section "Aviation Induced Cloudiness").

At present the global consumption of aviation fuel per year is equivalent to an emission of about 0.2 Gigatonnes of Carbon per year (GtC/a), which is about 2% of the entire anthropogenic carbon emissions, when emissions from land use change (deforestation being the main contribution to it) are included. If only counting the emissions originating from the burning of fossil fuels and cement production, the percentage of aviation emissions grows to about 2.4. Figure 4 presents an estimate of the time series of global CO_2 emissions by aviation since 1990 and extrapolation attempts by different groups as compiled

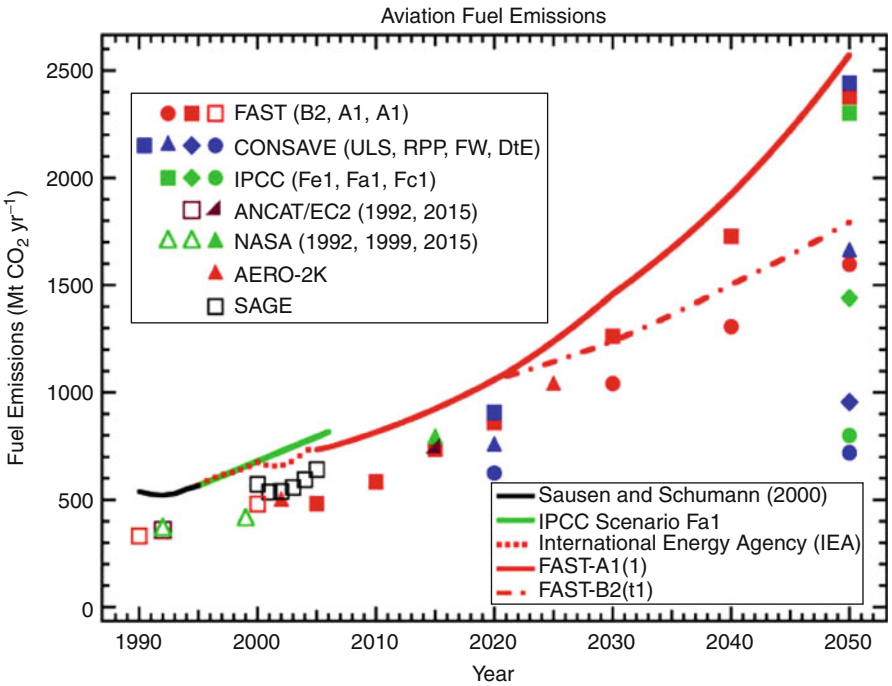

Aviation and Atmosphere. Figure 4

Historical and present-day inventories, and future projections of civil aviation CO_2 emissions from a variety of sources: AERO2K [10]; ANCAT/EC2 [12]; CONSAVE [5]; FAST (Owen and Lee 2006); IPCC [17]; NASA [3, 4, 33]; SAGE [22]. The *open symbols* indicate inventory analysis and the *closed symbols* indicate projections. Also shown are the CO_2 emissions implied by IEA fuel sales statistics [16]. The IEA data represent the total of civil and military usage because all kerosene sales are included. The Sausen and Schumann [32] data are also based on IEA. The solid (*dashed*) lines for FAST-A1 (B2) scenarios (evaluated with the t1 technology option) and the IPCC Fa1 scenario also account for all fuel sales in order to be consistent with the IEA values ending in 2005. In the figure legend, the FAST, CONSAVE, and IPCC symbols are shown in an order that matches the scenario labels in the parentheses in each case (Source: Lee et al. [24])

by Lee et al. [25]. Besides an overall growth of the emissions, it is evident that different scenarios of future economic development and technological progress lead to very different emission paths.

It is also interesting to compare the different modes of transport with respect to emissions per passenger and per tonne transported. Here again results from the recently finished major European Union's research project QUANTIFY [30], to which the author has contributed, are presented: Aviation is the strongest contributor to radiative forcing by CO_2 emissions per passenger kilometer in comparison to road traffic, shipping, and rail. As clearly visible from Fig. 6, this is not the case for freight transport, where road traffic contributes similarly to radiative forcing per tonne-kilometer (Fig. 5).

Aviation-Induced Cloudiness

There exist two types of impact on clouds caused by particle emissions from traffic. First, the particle emissions can cause the formation of clouds that would not form naturally. The most prominent example is jet exhaust condensation trails (contrails). This cloud circumvents the lack of so-called freezing nuclei in the rather clean and cold upper troposphere. The large emission of water vapor (1 kg/l of kerosene burned) in the hot exhaust plume together with the additional particles, also within the exhaust

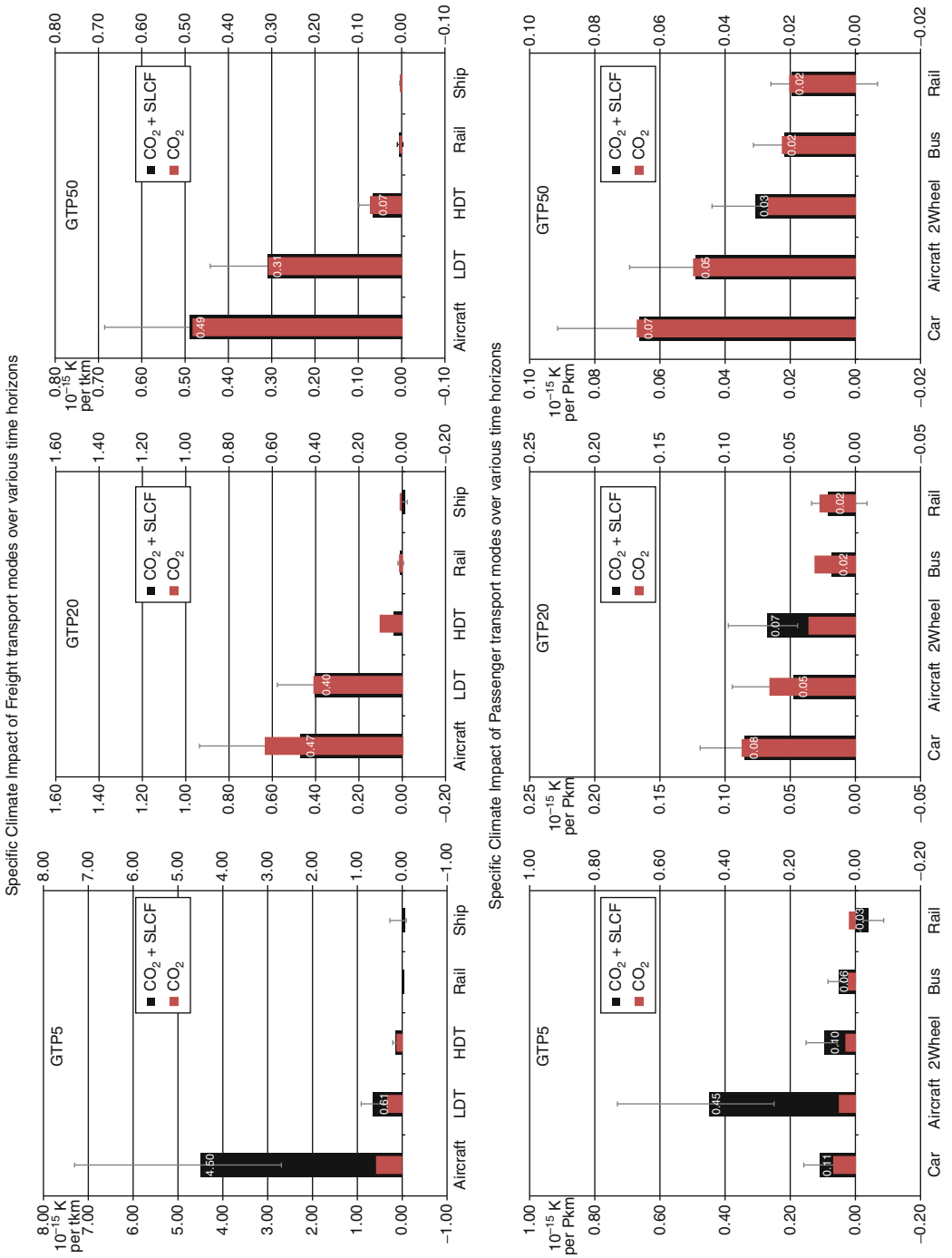

Aviation and Atmosphere. Figure 5
Temperature change caused by emissions in the year 2000 after 5, 20, and 50 years: For passenger transport modes (*upper panels*) per passenger kilometer, for freight transport modes (*lower panels*) per tonne-kilometer. The columns differentiate the impact when all short- and long-lived climate forcings (in *black*) are summed up and when only CO_2 (in *color*) is considered (Source: QUANTIFY [30])

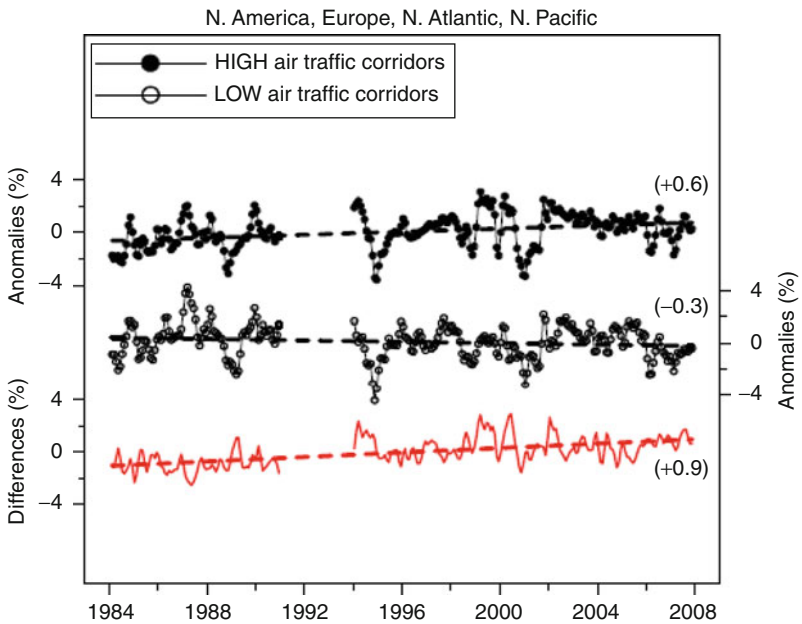

Aviation and Atmosphere. Figure 6

Averaged cirrus cloud trends over high and low air traffic regions in North America, Europe, North Atlantic, and North Pacific (Source: QUANTIFY [30])

plume, leads to cloud droplet formation, which rapidly freeze by mixing with the ambient air. If the flight corridor of an aircraft is supersaturated with respect to an ice surface, the contrail formed will survive and expand depositing all the supersaturated water vapor onto the contrail ice particles.

A second type of anthropogenic cirrus clouds, which is much more difficult to observe, are aerodynamic contrails involving a sequence of effects: The emitted particles first get mixed with the background aerosol particles and later – when the mix of anthropogenic and natural aerosol particles becomes involved into cloud formation processes – the particles emitted by air traffic will affect cloud formation, cloud evolution, cloud properties, and eventually precipitation. Also most so-called ship tracks belong to this category. A variant of this second aviation-induced cloud type, the hypothetical soot cirrus, is of interest here. It describes an ice cloud that is strongly affected by soot particles emitted by aircraft. To estimate the effect of aerosol particles emitted by air traffic (often soot) on ice clouds is difficult, because of the presence of various pathways to ice formation. In clean unpolluted air, ice clouds form via homogeneous nucleation, while in polluted air, like in air traffic corridors, heterogeneous nucleation might be dominant. Because there exist always very many other aerosol particles, which become solution droplets at higher relative humidity over a water surface (about 100/cm^3), an ice cloud forming homogeneously has a high number concentration of ice crystals. In contrast, heterogeneous ice cloud formation is a very selective process: Only about every millionth particle is an appropriate ice forming nucleus (IN). Thus, ice clouds forming predominantly by heterogeneous nucleation have a small number concentration of ice crystals. IN injection into a clean environment leads to heterogeneous ice crystal formation *before* homogeneous freezing can occur. Thus the ice cloud changed by air traffic has less but bigger crystals than a cloud that would have formed purely homogeneously. If heterogeneous ice formation is dominant as in a polluted air mass, the addition of IN can lead to more but smaller ice crystals. This simplified picture has to be modified: First, whether heterogeneous or homogeneous freezing dominates depends not only on the relative number of the respective

aerosol particle types but also on vertical wind speed (determining adiabatic cooling rates). Second, IN from various sources may have a spectrum of threshold supersaturations over an ice surface. These thresholds depend on temperature and on particle coating. Third, ice formation in supersaturated air with respect to an ice surface is difficult to be represented in large-scale models, because a supersaturated state is not uniquely related with a cloudiness state. Hence first model simulations like those by Penner et al. [29] have therefore rather the value of highlighting the problems than yielding firm results.

But also natural cirrus clouds can be affected by contrails formed within them or in their vicinity, in particular when these contrails spread and eventually form the so-called contrail cirrus, because these two ice cloud types compete for the same space and for the same supersaturated water vapor.

Aviation-Induced Cloudiness (AIC) has been defined as the sum of all changes in cloudiness associated with aviation operations [20]; hence, it combines jet exhaust condensation trails, often abbreviated as contrails, and so-called persistent contrail cover. The assessment of the latter is very difficult, because AIC may be indistinguishable from background cirrus cover. This was the reason for IPCC [20] not to give a best estimate of AIC amounts and its associated radiative forcing. The value given in IPCC [20] for emissions until 2005 and a time horizon of 100 years, namely 0.03 W/m, is above the radiative forcing of 0.025 W/m for CO_2 alone. Thus more than a factor of 2 would be needed, if the total air traffic influence on radiative forcing has to be accounted for, knowing only the fuel burned and excluding additions related to air chemistry. Have these values given by IPCC in 2007 changed during recent research? Yes, but earlier relations between the impacts by greenhouse gases and cloudiness changes (caused by contrails and contrail cirrus) have not been altered significantly [25]. There is, however, a discussion about a new potential influence of aviation on cloudiness, the so-called soot cirrus (as already discussed above), relating to effects of changed optical properties of ice clouds into which soot from aircraft exhaust is mixed and which may act after transformations in the atmosphere as ice nuclei. The related model estimates [26, 29] diverge so strongly (see also the values given for soot cirrus in Table 2) and they are not backed by observations that

Aviation and Atmosphere. Table 2 Year 2000 radiative forcing (in mWm^{-2}) for each transport sector and each forcing mechanism relative to pre-industrial times, together with uncertainties. SWV is stratospheric water vapor

	Road	Ship	Air	Rail
CO_2	131 ± 15	34 ± 6	20 ± 3	23 ± 7
Ozone	32 ± 9	24 ± 6	18 ± 3	2 ± 0.4
CH_4 lifetime	−7 ± 4	−19 ± 2	−5 ± 1	−1 ± 0.4
CH_4 – ozone	−3 ± 2	−8 ± 1	−2 ± 0.5	−0.3 ± 0.2
SWV methane	−1 ± 0.7	−3 ± 0.7	−1 ± 0.3	−0.1 ± 0.1
SWV direct			1 ± 0.2	
CFCs/HFCs	28 ± 3			
Stratospheric ozone	−2 ± 4			
Sulphate aerosol	−9 ± 4	−26 ± 11	−1 ± 0.4	−1 ± 0.3
Black carbon aerosol	44 ± 17	2 ± 1	0.3 ± 0.1	1 ± 0.3
Organic carbon aerosol	−2 ± 1	−1 ± 0.5		−0.5 ± 0.3
Indirect aerosol effect	6 ± 111	−49 ± 209	−127 ± 128	0.5 ± 10
Contrails			7 (−4, +6)	
Aviation induced cirrus			21 (−9, +17)	

much more research is needed before conclusions on a changed aviation policy could be drawn. In this context, it is too early to ask whether aviation's influence on radiative forcing might even change the sign.

Man-made changes in cirrus cloud cover can be detected by comparing cirrus trends over adjacent regions with dense and nearly no air traffic. Some exemplary long-term trends are shown in Fig. 6, taken from QUANTIFY [30]. It is evident that cirrus cloud coverage increases more or decreases less in regions with dense air traffic compared to regions with little air traffic. This could be considered a signature of increasing air traffic in the past 20 years. Such preliminary estimates from the differences in cirrus cloud cover, however, suggest an effect on radiative forcing of the order of only 6 mW/m for an assumed optical thickness of 0.4 for the cirrus clouds with air traffic influence.

Much better information on the statistics of optical thicknesses of single contrails, including the variation over their life cycle, can be obtained now from a contrail tracking algorithm that has been developed during QUANTIFY [34, 35]. The combination of such a tracking algorithm, based on satellite data from a polar orbiter (MODIS on NASA's Aqua and Terra satellites) and a geostationary one (MSG operated by EUMETSAT), with a numerical contrail plume model for which first developments have been made in the project allows to extend the observable fraction of a contrail life cycle in both directions, that is, from formation up to its end. There are, however, not yet trends available for a larger area with intense air traffic over Europe.

Changes of Air Chemistry by Air Traffic

The present and future impacts of emissions from aviation are typically evaluated using several global atmospheric chemistry models in order to obtain not only a quantification of the impact of a specific transport sector on global atmospheric composition but also an estimate of the associated model uncertainties. For the QUANTIFY project such an assessment included chemistry transport models and chemistry-climate models. For these simulations the global emission inventory EDGAR32FT2000 was used for anthropogenic emissions, with the transport sectors' emissions replaced by improved estimates for the present and for the IPCC A1 and B1 scenarios (2025, 2050) from the new QUANTIFY inventory. The A1 scenario represents a world of very rapid economic growth, especially in developing countries, and rapid introduction of new and more efficient technologies. The B1 scenario assumes rapid introduction of clean and resource-efficient technologies, and is considered to be far more optimistic with respect to environmental policy making than the A1 scenario. The results from the scenario calculations for the impact of shipping on ozone in the lower troposphere (surface to 800 hPa) point to a significantly increasing impact on ozone from the shipping sector, if emissions evolve according to the A1 scenario, while the B1 scenario leads to a much smaller increase. The results obtained for shipping are particularly interesting in the sense that the impacts on the hydroxyl radical (OH) and thus on methane (CH4) were larger than anticipated. The reduction of the global atmospheric lifetime of methane due to ship emissions was about a factor of 2–3 larger than that due to road emissions, and about a factor of 4 larger than that due to air traffic emissions [15]. This is a consequence of the more pristine chemical conditions over the oceans and the slightly different mix of emissions from ships. As a result, the net impact on radiative forcing of ozone and methane perturbations from shipping is negative, corresponding to a more or less globally uniform cooling. This adds up to the cooling via widespread cloud modifications caused by ship emissions of sulfate aerosols [27]. In contrast, the atmospheric chemistry influence on radiative forcing by aviation remains strongly positive.

The radiative forcing of aviation in the year 2000 in relation to all other transport sectors is given in Table 1 (QUANTIFY [30]. Peculiarities in comparison to other modes of transport emerge: First, the radiative forcing is nearly doubled by inclusion of the effect of ozone formation due to the emission of nitrogen oxides at cruising altitudes. Second, aviation-induced cloudiness in form of contrails and contrail cirrus adds substantially to the positive radiative forcing, however, is rather uncertain. Overall, aviation remains the sector with strongest additional effects besides the basic CO_2-related radiative forcing. The line named indirect aerosol effect in Table 2 needs a special remark. It is to a large extent due to model calculations using comparably crude parameterizations for the aerosol

influence on cloud droplet number and on absorption of solar radiation by soot. This research is still in its infancy as shown by the huge error bars, and one should not argue like very often lobbies would do that any climate policy measure concerning aviation has to be postponed until small error bars are reached for all entries. What is needed is a flexible reaction should major changes become evident.

Transport Sector's Contribution to Future Climate Change

Using a coupled atmosphere/ocean/land-model and the A1B scenario of IPCC as well as accounting for six different forcings (CO_2, CH_4, O_3, and aerosols for all sectors, CFCs and HCFCs for road traffic, and contrail formation for aircraft) Olivié et al. [28] found: In the year 2100, the warming from all transport sectors due to the CO_2 increase reaches about 0.5 K with the largest contribution from road traffic (0.3 K). The non-CO_2 impact from air traffic is larger than its CO_2 impact, the latter amounting to 0.15 K at 2100. It is caused by an enhanced O_3 production (compared to road and ship traffic) due to the altitude of the NOx emissions, and by the positive direct radiative forcing from linear contrails and contrail-induced cirrus. Because the total anthropogenic global temperature increase is about 3 K in 2100 with a contribution of about 0.65 K from the transport sector, with 0.5 K due to CO_2 impact and 0.15 K due to non-CO_2 impact dominated by aircraft traffic, the transport sector contributes slightly less than its share in total energy use. This reduced impact is caused by both the reduction in methane lifetime and comparably low N_2O and CH_4 emissions. The warming is in general more pronounced at high latitudes, but the signal there is strongly influenced by the timing of the Arctic sea-ice melting, which is quite uncertain.

It is clear from the above scientific findings that international air traffic cannot be excluded from climate policy making, although it managed to remain largely unaffected so far.

Why Did International Air Traffic So Far Escape from an Emission Reduction Policy?

When the Kyoto Protocol has been formulated in December 1997 the following sentence in its Article 2.2: "*Parties included in Annex 1 (these are the industrialized countries with emission reduction commitments under the Kyoto Protocol) shall pursue limitation or reduction of emissions of greenhouse gases not controlled by the Montreal Protocol from aviation and marine bunker fuels, working through the International Civil Aviation Organization (ICAO) and the International Maritime Organization (IMO), respectively*" started it. In other words: The reduction of emissions from international air traffic and international shipping has to be handled by two United Nations bodies often said to be closer to the respective industries than to the responsibility for entire society. Hence, about 6% of global emissions from the use of fossil fuels or up to 15% of all transport emissions factually escaped from any regulation by the UNFCCC and its Kyoto Protocol. Nineteen years after the signature under UNFCCC at the Earth Summit in Rio de Janeiro we are still without a global legal instrument for any mitigation measure to reduce aviation fuel's climate impact.

Why is it so? The following lines use a historical account given by EFTE [9]. At the first Conference of the Parties (COP 1) to UNFCCC in Berlin 1995 its Subsidiary Body on Scientific and Technical Advice (SBSTA) was requested to examine the allocation and control of emissions from international bunker fuels, the term used for shipping first and then also for aviation. COP 1 had identified eight options for SBSTA to be considered prior to COP 2. SBSTA rejected three options: first, allocation in proportion to national greenhouse gas emissions; second, allocation according to the country of origin of the passenger/cargo; and third, according to the actual location of the emission. No agreement could be reached for the remaining five. There was no progress at COP 2 in Geneva. At COP 3 in Kyoto at least the domestic part of aviation and shipping was integrated into national reduction targets, and for international flights the above mentioned responsibility of ICAO was decided. Although SBSTA continued to discuss methodologies to allocate emissions, it was without any agreement so far. ICAO often reported about progress in its deliberations, but never presented a real proposal to SBSTA that could have been tabled at the next COP. Already in 1996 ICAO had requested that IPCC should prepare

a report on the impact of aircraft engines on the atmosphere. In 1999, this first report on a specific industry sector named *Aviation and the Global Atmosphere* had been published [17] that clearly stated:

- Since 1960, aviation passenger traffic had grown rapidly by 9% per year and was estimated to grow by 5% per year between 1990 and 2015.
- Already in 1992, chosen as the base year for the report, aviation accounted for 2% of total anthropogenic CO_2 emissions.
- Including other effects of aviation on the atmosphere, e.g., contrails and contrail cirrus, about 3.5% of the total anthropogenic radiative forcing in the base year 1992 of the report were due to aviation.

Policy options were given as well including more stringent engine regulations, removal of subsidies, environmental levies, and emission trading schemes. IPCC also acknowledged that ICAO had already started to assess the need for aircraft emission standards at cruising altitude in addition to the already existing standards for nitrogen oxides. To make a long story short: At present, 12 years later, international air traffic is not included in any binding measure for climate protection policy, i.e., ICAO was unsuccessful to perform as requested by the international community.

The European Directive to Include Air Traffic into the Emission Trading Scheme

At least for the European Union the time for an escape of the international air traffic from an emissions trading scheme will end. The directive (Dir 2008/101/EC) to include aviation into the EU Emissions Trading Scheme (EU-ETS) was published on January 13, 2009 in the EU's Official Journal. It is valid for all flights to, from, and within the EU and starts on January 1, 2012. For 2012, an EU-wide cap on aviation emissions is set at 97% of the average annual emissions for the years 2004–2006. It will be lowered to 95% in 2013. All airlines will have to buy 15% of their allowance under the said cap through an auction. More allowances in order to cover growth of an airline have to be purchased. The revenues from selling, if emissions are below the cap, must not be put into the industry or climate protection measures. The inclusion of aviation into EU-ETS will be reviewed in 2014. There are exemptions for very small airlines, research, military, and rescue flights. The directive has been included into the one for EU-ETS (Dir 2003/87/EC).

An Airline Emission Index

As always in any economic sector there are large differences in behavior, here emissions, between different agents. In order to bring transparency into the aviation sector of global transport the German nongovernmental, nonprofit organization *atmosfair* has issued for the first time in spring of 2011 a global airline index, comparing nearly all airlines with respect to their environmental standards in the field of climatically relevant emissions. The *atmosfair* airline index (AAI) is a ranking of most airlines with respect to such climatically relevant emissions with the following characteristics [1]:

1. Inclusion of the 130 largest airlines in the world, arranged according to passenger kilometers as well as revenue, disregarding mere cargo flight companies.
2. Data from 2009 are used for the AAI 2011.
3. Airlines are subdivided into the following classes: net carrier, low cost carrier, charter, and regional carrier.
4. Solely climatically relevant emissions of a carrier are taken into account, disregarding noise pollution and further sustainability measures.
5. Restriction to carbon dioxide emissions, because other emissions causing for instance contrails are very similar for all airlines. There is only one exception: Nitrogen oxides (NOx) are included via an engine-related emission factor (needed to assess the radiative forcing by ozone and methane, both influenced due to chemical reactions of these oxides in the atmosphere, leading to higher ozone and lower methane concentrations).
6. Different business plans like those for net carriers and low cost carriers are not valued, despite the air traffic stimulation caused by the low cost carriers through subsidies often given to them by national governments or city councils.
7. All airlines are categorized into seven efficiency classes from A to G, in analogy to the European Union efficiency classes.

The AAI bases on a new *atmosfair* methodology, built upon the CO_2 emission calculations of ICAO. Its main data sources are the generally available data sets: ICAO TFS (Traffic Flight by Stage), IATA WATS, OAG, Piano-x, JP-Airline Fleet. This combination leads to 103 types of aircraft and 287 engines, constituting 87% of the global commercial air traffic with respect to number of flights. The parameters used are: aircraft type, engine, winglets, seating arrangement, cargo addition, and passenger number.

The comparison of airlines follows the following procedure:

1. Calculation of the CO_2 emission per kilometer for a flight between a city pair, taking into account the above parameters.
2. The CO_2 emission from step 1 for a city pair is compared with the best case (direct flight in best heights with least fuel consumption) and the worst case with three times higher emissions (chosen to fully embrace all airlines).
3. The airline reaching the best case for a city pair gets 100 points (it never happened), the one with higher emissions for the same city pair gets less points according to its reduced performance, reaching zero points if emitting three times as much.
4. All city pairs of an airline are combined by summing over all points reached for all pairs and dividing by the number of city pairs.
5. Categorization of all airlines into seven efficiency classes, in analogy to the color codes of EU for refrigerators, houses, etc. No single airline has reached class A or B.

This procedure allows the following comparisons:

- An airline with only a few city pairs can be compared to one servicing hundreds of city pairs.
- An airline with only short distance flights can be compared with one offering only long-distance flights.
- A low cost carrier can be compared with a net carrier.
- An airline offering only one city pair without competitors can be ranked.

The importance of the influencing factors age of an aircraft, number of seats, and percentage of seats occupied leads to an astonishing result: Charter airlines and low cost carriers have a lower climate impact than well-known carriers and no airline has reached category A or B. However, there needs to be a discussion on that: How should the stimulation of further air traffic by and the subsidies often given to low cost carriers be handled? The *atmosfair* group has decided not to include the low cost carriers in its first AAI although all the data are available. For the ranking of the airlines, excluding low cost carriers, see Fig. 7. There are only three factors nearly totally determining the higher ranking: high numbers of seats in a certain aircraft type, percentage of seats occupied, and age of the aircraft. Hence, an airline flying tourists to a destination with narrow seating and leased modern aircraft can reduce fuel consumption to about 3 l of kerosene per passenger and 100 km, while a net carrier with first and business class seats, some old aircraft and rather empty airplanes on certain dates for certain city pairs cannot reach higher ranks.

Conclusions and Outlook

Mobility has a growing share in changing climate in comparison to other human activities like industrial production and heating or cooling of houses. Fortunately, the European Union's major research project named QUANTIFY was able to compare all modes of transport and very recently quantified the different modes' contributions. Taking from their conclusions and focusing here on the contribution of aviation (see QUANTIFY [30] for all modes of transport) we find:

1. The impact of transport, in particular of aviation and shipping, on climate grows faster than the impact from other sectors of human activity. Hence, aviation has to excel concerning efficiency measures in comparison to all other human activities.
2. The effects of non-CO_2 emissions on climate caused by aviation and shipping (e.g., through nitrogen oxide emissions and induced changes in cloudiness) are particularly large in comparison to other modes of transport.
3. A NOx molecule from aviation is responsible for five times more ozone than a molecule from road transport.
4. A NOx molecule from shipping is four times more efficient in reducing methane concentration in the atmosphere than a NOx molecule from aviation.

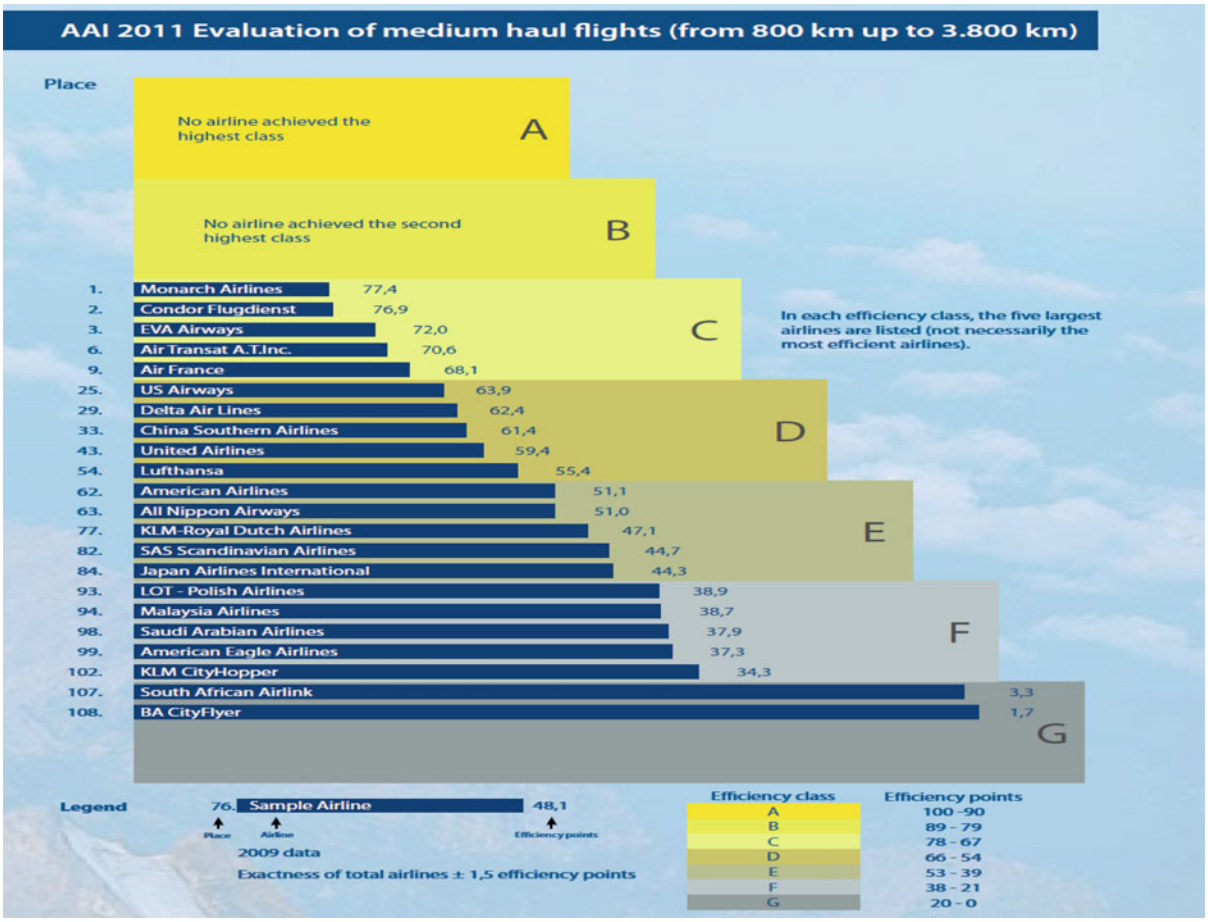

Aviation and Atmosphere. Figure 7

A sample from the AAI for medium distance flights. For all airlines, please see https://www.atmosfair.de/en/air-travel-climate/airline-index/

5. Aircraft-induced clouds warm the atmosphere. Their radiative forcing (RF) is of similar magnitude than RF from aviation CO_2. Hence, a multiplication factor of at least around 2 (including air chemistry effects) seems justified when dealing with climate effects of aviation.
6. The relative weights of the non-CO_2 effects of different modes of transport strongly depend on the metric chosen and on the time horizon.
7. A temperature-based climate metric leads to a very different result than one based on the radiative forcing and thus only on the greenhouse warming potential.
8. The per person and per kilometer climate impact of passenger transport is much lower for railways compared to road transport and aviation, and the per person per kilometer climate impact of passenger air travel approaches that of cars on time scale of decades. Despite all the progress achieved so far many open questions remain [30].

Most of the quantifications can only be given with partly substantial uncertainty, sometimes even effecting the sign of an effect. In particular, the climate impact of indirect aerosol effects on clouds is highly uncertain. We still do not know whether soot cirrus really exists. The net effect of NOx emission from air traffic might cause a net negative radiative forcing, if a recently proposed additional chemical reaction is confirmed. Therefore, it is presently difficult to include some non-CO_2 effects in climate policies related to

aviation or to develop suitable mitigation strategies for all non-CO_2 effects caused by the transport sector. Furthermore, many of the emitted species responsible for the non-CO_2 effects of air traffic emissions also impact air quality.

By applying a hierarchy of models (from process models, cloud resolving models to chemical transport models, global general atmospheric circulation models, and coupled atmosphere/ocean/land-models) and by analyzing measurements from satellites and dedicated field campaigns, the main uncertainties with respect to short-lived non-CO_2 effects on the atmospheric composition and on climate should be reduced:

1. The importance and magnitude of trade-offs in the NOx effect (short-term increase in ozone versus longer-term decrease in methane and the associated longer-term ozone decrease) should be explicitly simulated by comprehensive models covering the long response time of methane.
2. The climate impact of contrail cirrus should be simulated by climate models including parameterizations of contrail cirrus and evaluated by recently available tracking algorithms of these clouds in satellite data.
3. The climate impact of indirect effects on clouds (e.g., soot cirrus caused by air traffic) should be simulated by now available chemistry-climate models including aerosol-cloud interactions; the necessary parameters should be obtained by dedicated airborne measurement campaigns.
4. The regional response pattern in atmospheric composition and climate resulting from heterogeneous transport emissions need to be determined consistently in a multi-model approach.
5. The effects arising while replacing fossil fuel by biofuels should be considered. Finally, trade-offs between climate and air quality effects of emissions from different sectors should be examined for robust policy formulations.

Because the future will not only bring – with high probability – a global carbon emission trading scheme including all modes of transport but will also approach the metric "emissions per person per year" as the baseline of climate policy, the inclusion of aviation into the European Union emission trading scheme is just a first step on the way to a more just handling of the different modes of transport. This will give a push toward a much more efficient transport system, e.g., with a preference for high speed trains in comparison to short distance flights, and it will stimulate the search for new types of fuel for aircraft derived from renewable energy sources, be it methane or hydrogen or another fuel.

Acknowledgment

I am very thankful to Dietrich Brockhagen from *atmosfair* for many discussions over the years on attempts to integrate aviation into the emission reduction arena and especially on different metrics to account for the climate effects of air traffic besides those by CO_2.

Bibliography

1. atmosfair (2011) The atmosfair airline Index (AAI), atmosfair gGmbH, Berlin 2011. https://www.atmosfair.de/en/air-travel-climate/airline-index/
2. Balkanski Y, Myhre G, Gauss M, Rädel G, Highwood E, Shine KP (2010) Direct radiative effect of aerosols emitted by transport: from road, shipping and aviation. Atmos Chem Phys Discuss 10:1659–1691
3. Baughcum SL, Henderson SC, Tritz TG, Pickett DC (1996) Scheduled civil aircraft emission inventories for 1992: database development and analysis. NASA CR4700. NASA, Langley Research Center, Hampton
4. Baughcum SL, Sutkus DJ Jr, Henderson SC (1998) Year 2015 aircraft emission scenario for scheduled air traffic. NASA-CR-1998-207638. National Aeronautics and Space Administration, Langley Research Center, Hampton, 44 pp
5. Berghof R, Schmitt A, Eyers C, Haag K, Middel J, Hepting M, Grübler A, Hancox R (2005) CONSAVE 2050. Final technical report. DLR, Köln
6. Berntsen T, Fuglestvedt J (2008) Global temperature responses to current emissions from the transport sectors. Proc Natl Acad Sci (PNAS) 105:19154–19159
7. Borken-Kleefeld J, Fuglestvedt J, Berntsen T (2010) Specific climate impact of passenger and freight transport. Environ Sci Tech 44:5700–5706
8. Cariolle D, Caro D, Paoli R, Hauglustaine D, Cuenot B, Cozic A, Paugam R (2009) Parameterization of plume chemistry into large scale atmospheric models: application to aircraft NOx emissions. J Geophys Res 114:D19302
9. EFTE (European Federation for Transport and Environment) (2009) Bunker fuels and the Kyoto protocol: how ICAO and the IMO failed the climate change test, Brussels, June 2009, 19 pp
10. Eyers CJ, Addleton D, Atkinson K, Broomhead MJ, Christou R, Elliff T, Falk R, Gee I, Lee DS, Marizy C, Michot S, Middel J, Newton P, Norman P, Plohr M, Raper D, Stanciou R (2005)

AERO2K global aviation emissions inventories for 2002 and 2025. QINETIQ/04/0113, Farnborough
11. Fuglestvedt JS, Shine KP, Berntsen T, Cook J, Lee DS, Stenke A, Skeie RB, Velders GJM, Waitz IA (2010) Transport impacts on atmosphere and climate: metrics. Atmos Environ. doi:10.1016/j.atmosenv.2009.04.044
12. Gardner RM, Adams JK, Cook T, Larson LG, Falk RS, Fleuit E, Förtsch W, Lecht M, Lee DS, Leech MV, Lister DH, Massé B, Morris K, Newton PJ, Owen A, Parker E, Schmitt A, ten Have H, Vandenberghe C (1998) ANCAT/ EC2 aircraft emissions inventories for 1991/1992 and 2015. Final report. Produced by the ECAC/ANCAT and EC working group. European civil aviation conference
13. Henderson SC, Wickrama UK, Baughcum SL, Begin JJ, Franco F, Greene DL, Lee DS, McLaren ML, Mortlock AK, Newton PJ, Schmitt A, Sutkus DJ, Vedantham A, Wuebbles DJ (1999) Aircraft emissions: current inventories and future scenarios. In: Penner JE, Lister DH, Griggs DJ, Dokken DJ, McFarland M (eds) 'Aviation and the Global Atmosphere', intergovernmental panel on climate change. Cambridge University Press, UK
14. Hodnebrog Ø, Berntsen TK, Dessens O, Gauss M, Grewe V, Isaksen ISA, Koffi B, Myhre G, Olivie D, Prather M, Stordal F, Szopa S, Tang Q, van Velthoven P, Williams J, Ødemark K (2011) Future impact of nonland-based traffic emissions on atmospheric ozone and OH – an optimistic scenario and a possible mitigation strategy. Atmos Chem Phys Discuss 11:16801–16859
15. Hoor P, Borken-Kleefeld J, Caro D, Dessens O, Endresen O, Gauss M, Grewe V, Hauglustaine D, Isaksen ISA, Jöckel P, Lelieveld J, Myhre G, Meijer E, Olivie D, Prather M, Schnadt Poberaj C, Shine KP, Staehelin J, Tang Q, van Aardenne J, van Velthoven P, Sausen R (2009) The impact of traffic emissions on atmospheric ozone and OH: results from QUANTIFY. Atmos Chem Phys 9:3113–3136
16. IEA (2007) Oil Information 2006, Table 9, 749 pp. International Energy Agency, Paris
17. IPCC (1999) Aviation and the global atmosphere. In: Penner JE, Lister DH, Griggs DJ, Dokken DJ, McFarland M (eds) Intergovernmental panel on climate change. Cambridge University Press, Cambridge
18. IPCC (2000) In: Nakicenovic N, Swart R (eds) Emission scenarios. Cambridge University Press, Cambridge, pp 570
19. IPCC (2001) Climate change 2001: the scientific basis. Report of working group I. Cambridge University Press, Cambridge, UK
20. IPCC (2007a) In: Solomon S, Qin D, Manning M, Chen Z, Marquis M, Averyt KB, Tignor M, Miller HL (eds) Contribution of working group I to the fourth assessment report of the intergovernmental panel on climate change, 2007. Cambridge University Press, Cambridge/New York
21. IPCC (2007b) In: Parry ML, Canziani OF, Palutikof JP, van der Linden PJ, Hanson CE (eds) Contribution of working group II to the fourth assessment report of the intergovernmental panel on climate change, 2007. Cambridge University Press, Cambridge/New York
22. Kim BY, Fleming GG, Lee JJ, Waitz IA, Clarke JP, Balasubramanian S, Malwitz A, Klima K, Locke M, Holsclaw CA, Maurice LQ, Gupta ML (2007) System for assessing Aviation's Global Emissions (SAGE), Part 1: model description and inventory results. Trans Res D12:325–346
23. Koffi B, Szopa S, Cozic A, Hauglustaine D, van Velthoven P (2010) Present and future impact of aircraft, road traffic and shipping emissions on global tropospheric ozone. Atmos Chem Phys 10:11681–11705
24. Lee DS et al (2009) Aviation and global climate change in the 21st century. Atmos Environ. doi:10.1016/j.atmosenv.2009.04.024
25. Lee DS et al (2010) Transport impacts on atmosphere and climate: aviation. Atmos Environ 44:4678–4734
26. Liu X, Penner JE, Wang M (2009) Influence of anthropogenic sulphate and black carbon on upper tropospheric clouds in the NCAR CAM3 model coupled to the IMPACT global aerosol model. J Geophys Res 114:D03204. doi:10.1029/2008JD010492
27. Myhre G, Shine KP, Rädel G, Gauss M, Isaksen ISA, Tang Q, Prather M, Williams JE, van Velthoven P, Dessens O, Koffi B, Szopa S, Hoor P, Grewe V, Borken-Kleefeld J (2010) Radiative forcing due to changes in ozone and methane caused by the transport sector. Atmos Environ 45:387–394
28. Olivié DJL, Cariolle D, Teyssèdre H, Salas D, Voldoire A, Clark H, Saint-Martin D, Michou M, Karcher F, Balkanski Y, Gauss M, Dessens O, Koffi B, Shine KP, Sausen R (2010) Modeling the climate impact of road transport, maritime shipping and aviation over the period 1860–2100 with an AOGCM. Submitted to Atmos Chem Phys
29. Penner JE, Chen Y, Wang M, Liu X (2009) Possible influence of anthropogenic aerosols on cirrus clouds and anthropogenic forcing. Atmos Chem Phys 9(2009):879–896
30. QUANTIFY (2011) Quantifying the climate impact of global and European transport systems, integrated project, sixth framework programme, sub-priority 1.1.6.3: global change and ecosystems, final activity report, publishable summary
31. Sausen R (ed) (2010) Transport impacts on atmosphere and climate: the ATTICA assessment report. Atmos Env 44, 4645–4816 (special issue)
32. Sausen R, Schumann U (2000) Estimates of the climate response to aircraft CO_2 and NOx emissions scenarios. Clim Change 44:27–58
33. Sutkus DJ, Baughcum SL, DuBois DP (2001) Scheduled civil aircraft emission inventories for 1999: database development and analysis. National aeronautics and space administration, glenn research centre. NASA CR-2001/211216
34. Vazquez-Navarro M (2010) Life cycle of contrails from a time series of geostationary satellite images. DLR-Forschungsbericht 2010–19, 139 pp
35. Vazquez-Navarro M, Mannstein H, Mayer B (2010) An automatic contrail tracking algorithm; Atmos. Meas Tech 3:1089–1101

B

Batteries, Battery Management, and Battery Charging Technology

Robert S. Balog[1], Ali Davoudi[2]
[1]Department of Electrical and Computer Engineering, Texas A & M University, College Station, TX, USA
[2]University of Texas, Arlington, TX, USA

Article Outline

Glossary
Definition of the Subject
Introduction
Battery Chemistries
Lead Acid
Battery Charging Circuits
Battery Management
Future Direction
Bibliography

Glossary

Alternating current (AC) Usually in the form of a sine wave, the bidirectional current flow continually reverses. Typically, AC will have a zero mean (average) and a nonzero RMS value. In the USA, most "grid" electricity is generated and distributed in the form of 60 Hz sinusoidal waveform. In other areas of the world, 50 Hz is commonly used.

Amp-hour (Ah) A unit of electric charge, the amount of current delivered for 1 hour.

Battery A group of one or more cells electrically connected in series and/or parallel combinations to achieve higher voltage or current than what is capable from a single cell.

Battery management system (BMS) An electronic device or system that monitors and controls a rechargeable battery. Parameters measured may include cell temperature, voltage, and current. From this data, the BMS can compute the state of charge of the battery and estimate the state of health, remaining cycle lives, or remaining service life. Typically, a BMS system will include the ability to communicate with a host system and battery charger. The BMS may also contain sensors and circuitry for protection such as over-current, over-temperature, or over-voltage.

Battery pack A group of batteries or individual cells electrically connected in series and/or parallel combinations along with the required electrical interconnections, mechanical packaging, thermal management, and sensing circuitry. Because it is a self-contained assembly, a battery pack can be easily swapped in and out of the application.

Battery string Series-connected batteries used to produce a higher voltage. The same current passes through all the cells, but each cell voltage can vary. Charge balancing becomes a significant issue for a long string of 50 or more cells.

C-rate The rate at which a battery can deliver or accept current, stated in terms of the rated capacity of the cell in amp-hours. This may also be referred to as the hour rate, such as the 1-h rate.

Cell An individual electrochemical device that converts between chemical energy and electrical energy. The cell construction, open circuit voltage, energy, and power density, all depend on the chemistry of the cell (see section "Battery Chemistries").

Coulombic efficiency Ratio of charge delivered by a rechargeable battery during discharge cycle to the charge stored during charge cycle.

Depth of discharge (DoD) An alternate method to indicate the state of charge of the battery; it is the reciprocal of SoC.

Direct current (DC) Unidirectional current that continually flows only in one direction. Sources such as batteries, fuel cells, and solar cells produce electricity in the form of direct current.

Robert A. Meyers (ed.), *Encyclopedia of Sustainability Science and Technology*, DOI 10.1007/978-1-4419-0851-3,
© Springer Science+Business Media, LLC 2012

Memory effect An effect observed particularly in nickel cadmium batteries in which the cells gradually lose capacity when subject to repeated partial discharges followed by complete recharges cycles. This electrochemical effect is different than the loss of capacity due to aging and use. In some cases, a series of full discharge/recharge cycles can restore some or all of the lost capacity due to the memory effect but not due to cycle life or aging.

Proportional-integral (PI) controller A type of linear feedback control in which an error signal is calculated as the difference between a measured signal and the desired reference set point. The controller attempts to adjust the operation of the process using a weighted combination of the present error (proportional term) and accumulated past error (integral term).

Primary battery One-time-use batteries not capable of being recharged. They are discarded or preferably recycled once the stored energy has been depleted. These types of batteries will not be considered in this article.

Root mean square (RMS) A scalar quantity that is computed from the square root of the sum of the squares of a dataset and is commonly used to represent a voltage or current over one cyclical period. Average power is the product of the RMS current and RMS voltage.

Secondary battery Commonly referred to as rechargeable batteries, they can be repeatedly recharged electrically by passing current through them in the opposite direction to that of the discharge current. Secondary batteries are of significant interest for their ability to store and supply energy and are the focus of this article.

Self-discharge rate The rate at which a battery discharges, or looses stored energy, due to internal cell reactions.

SLI batteries Starting, lighting, and ignition (SLI) batteries are used in automobiles. These batteries are usually characterized by a high discharge rate.

State of charge (SoC) Defined as the capacity left in a battery expressed as a percentage of some reference. SoC of a battery is usually expressed as a percentage of the current battery capacity when it is fully charged.

State of health (SoH) A metric that reflects the general condition of a battery and its ability to deliver the specified performance compared with a fresh battery. It takes into account factors such as charge acceptance, internal resistance, voltage, and self-discharge. It is an estimate rather than a measurement.

Watt-hour (Wh) A unit of energy, the amount of power delivered for 1 h. It is equivalent to 3,600 Joules of energy.

Definition of the Subject

Batteries, both primary and rechargeable, are important energy storage devices ubiquitous in our daily, modern lives. Whether in our handheld portable electronics, conventional or hybrid/electric cars, or in the electrical "grid," battery technology will continue to evolve as technology improvements increase storage capacity and lifetime and reduce cost.

Introduction

Batteries are perhaps most synonymous with portable power such as flashlights and personal electronics like cell phones, music players, and laptops to name a few modern examples. We have become trained to monitor the battery "bars" to determine how much more we can talk, e-mail, or surf the "net." Batteries are far more prevalent, however, and they tend to be underappreciated, such as the ones in our automobiles which perform dutifully until suddenly, usually after years of neglect, they fail to start our car. An electrical power system is the ultimate in just-in-time manufacturing in that electricity generation and consumption must be perfectly balanced at all times. This imposes difficult operating constraints on the system when variability on both the load side and source side exists, such as with renewable energy sources like wind and solar. Therefore, energy storage is important to ensure that electricity can be generated and energy stored generated when the source is available, and the load can continue to be supplied when the variable, renewable energy source is insufficient. While there are many technologies for energy storage, batteries play an important role to improve the electric power system asset utilization, energy availability, reliability, and performance. Several large-scale, high-energy battery technologies hold

promise of providing economical energy storage for a wide range of these power system and energy management applications.

This chapter will discuss issues related to batteries, battery charging, and battery management. The first section will provide an overview of the different types of battery chemistries. The focus in this chapter is on rechargeable batteries which can accept, store, and then deliver energy at a future point in time. Subsequent sections will discuss circuits to charge and manage the batteries.

A detailed description of internal construction of the individual cell is beyond the scope of this chapter, but it is sufficient to consider that a battery is typically comprised of electrodes, electrolyte, and some form of case or enclosure as shown in Fig. 1. Various materials are commonly used, each with advantages and disadvantages. The voltage, current rating, and storage capacity are all functions of the material and construction.

Battery Failure

Some of the most common causes for battery failure are short circuiting of battery terminals, improper charge control while charging secondary batteries, improper polarity connections while charging a battery, and a long period of use. Internal failure modes include thermal runaway which is a major problem in lead-acid batteries, loss of electrolyte by gassing, mechanical damage, and warping of plates due to an excessively high rate of discharge.

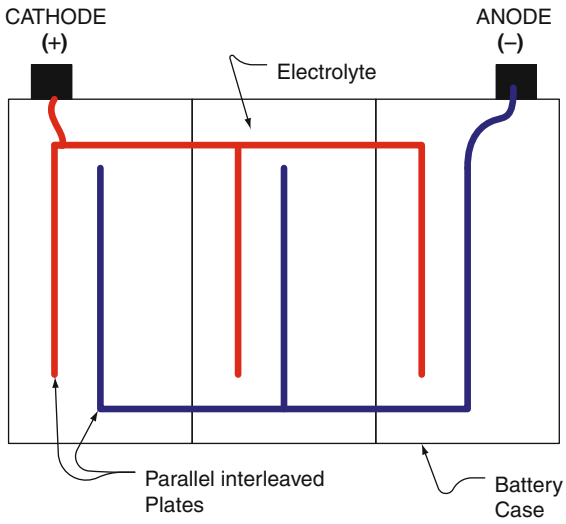

Batteries, Battery Management, and Battery Charging Technology. Figure 1
Conceptual illustration of a lead-acid battery with parallel, interleaved plate that comprises the anode and cathode. The electrolyte can be a liquid or a gel, and the enclosure can be vented or sealed

Methods of Charging

Float charge is most commonly used for non-sealed lead-acid batteries, which can tolerate sitting at an elevated voltage for prolonged periods of time. The original meaning of the term stems from the telecom industry's jar batteries in which the liquid electrolyte was exposed to the atmosphere and the batteries "sat on float" at a continuous elevated voltage to be sure they were fully charged when called upon to back up the telephone equipment. In this mode of operation, the charging current depends on the state of charge of the cells, and the current gradually declines to a minimum value as the cells become fully charged. Float charging could result in continuous out gassing which reduces the level of water in the electrolyte. Hence, float charging of lead-acid batteries often requires "watering" of the batteries to maintain the level of electrolyte.

Trickle charge is used to maintain a battery at a full state of charge by supplying a small current to offset the self-discharge characteristics of the battery. Some battery chemistries, like the lead-acid varieties, have relatively high self-discharge rates and can lose their ability to hold a charge when stored discharged for a long period of time due to sulfation, the crystallizing of the lead sulfate. A trickle charger, sometimes called a "battery tender" is often used in automobile, boats, motorcycles, RV and other seasonal equipment where the battery can sit for months without use.

Bulk charge involves restoring the majority of the energy storage capability of a battery. Hence, a bulk charge may be followed by an equalizing charge.

Equalization charge is the final stage of charging for a series-connected battery string in which the SoC of individual cells are forced to the same value. For lead-acid batteries, this can be as using a higher charging voltage. The cells with higher SoC begin to outgas while the weaker cells "catch up." Other battery chemistries

cannot tolerate overvoltage charging. Charge balancing techniques will be described in detail in the next section.

Rapid charge involves quickly recharging a battery at a high C-rate. Depending on the battery chemistry, this mode of charging may only replace a portion of the full capacity. It is usually imperative to monitor the cell temperature rise during rapid charging to avoid excessive outgassing or thermal runaway.

Regardless of the mode of charging, the charging types include constant-current charging and constant-current–constant-voltage charging (constant-current charge until current attains a flat profile, then constant-voltage charging takes over).

Battery Chemistries

A wide variety of battery electrochemistries are available today. While there is a clear evolution of technological progress, each technology has advantages and disadvantages that make them more or less suited for different applications. This section presents an overview of commonly available technologies and explores their general characteristics, advantages and disadvantages, and charging considerations.

Lead Acid

General Characteristics

Lead-acid batteries are by far the most common battery type and represent approximately 40–45% of the total global battery sales. Lead-acid batteries are available in large quantities and in a variety of sizes and designs. They are manufactured in sizes from smaller than 1 Ah to several thousand Ah. Design variations to electrode plates enable them to perform as batteries with high discharge rate and low-energy (automobile starting applications) and also for deep-cycle applications with moderate discharge rates.

The world's largest battery-based energy storage system is a 40-MWh battery located in Chino, California. It uses individual industrial-size lead-acid cells in series and parallel connection to make a 10-MW system capable of delivering energy into the utility grid at 2,000V and 8,000A for 4h.

Advantages and Disadvantages

Advantages include:

- One of the main reasons for the popularity of lead-acid batteries is that they can be manufactured on a local basis worldwide with high rates of production.
- Traditionally, they have been used as starting-lighting-ignition (SLI) batteries in automobiles, though now they are being slowly phased out by high-performing nickel cadmium and nickel metal hydride batteries.
- They have a high cell open-circuit voltage of 2.0 V which is one of the highest for aqueous electrolyte systems.
- SoC estimation is very easy in the case of lead-acid batteries. The specific density of electrolyte bears a direct relation to the SoC of the battery.
- It provides good charge retention for intermittent charge applications.
- Cell components can be easily recycled.
- They are very cheap compared to other secondary battery designs.
- They are also available in maintenance-free designs.

Disadvantages include:

- Lead-acid batteries require frequent maintenance. These batteries lose water while in operation, and the water level needs to be replenished.
- As they employ lead in their construction, they are usually heavy and not conducive for portability.
- Lead-acid batteries have a relatively low cycle life (50–500 cycles). However, up to 2,000 cycles have been achieved with cell design improvements, heavily derating the discharge capacity and using active charge equalization techniques (see section "Cell Charge Equalization").
- One of the major drawbacks is the thermal runaway problem. It can occur due to improper design of battery or charger.

Application Examples Lead-acid batteries are commonly installed in uninterruptible power supply (UPS) systems, in renewable and distributed power systems. Traditionally, they were used as SLI batteries in automobiles. Other applications include telephone systems, power tools, communication devices, emergency lighting systems, and as the power source for mining and material-handling equipment.

Charging Characteristics Lead-acid batteries do not exhibit memory effect. However, it is very vital to have the correct charge and float voltages to achieve a long life. Charging up to the rated voltage level is a must; any deviation from this voltage level leads to electrode corrosion or negative plate sulfation in the long run. Lead-acid batteries used for deep-cycle applications usually have a short life of about 300 discharge/charge cycles.

Lead-acid batteries are typically charged in three stages, which are constant-current bulk charge, equalization final charge, and float charge. The *constant-current charge* provides bulk of the charge and takes up about half of the required charge time. The *equalizing charge* continues charging at a lower charge current and ensures all cells are fully charged and the state-of-charges are similar. This may be done through active techniques or simply overcharging some cells to ensure the undercharged ones receive a full charge. The *float charge* compensates for the self-discharge loss when a battery sits unused for a period of time.

Valve-Regulated Lead Acid (VRLA)

General Characteristics The valve-regulated lead-acid (VRLA) battery is a completely sealed cell, which prevents electrolyte loss due to outgassing, and hence alleviates the need to water the cells. The VRLA battery incorporates the gas recombination principle which allows the oxygen generated at normal overcharge rates to be reduced at the negative plate, eliminating oxygen outgassing. If the rate of outgassing exceeds the rate of recombination, the partial pressure of hydrogen builds up and can cause the vent to open, which destroys the cell.

Advantages and Disadvantages

Advantages include:

- VRLA batteries do not require "watering" as is the case with other types of lead-acid batteries since the water level is maintained due to a regenerative cell reaction. Thus, VRLA batteries do not require the frequent maintenance for battery operation, which is an advantage over the conventional lead-acid battery.
- Battery cells can be packaged more tightly because of sealed construction and immobilized electrolyte, hence the footprint and weight of the battery are reduced.
- SoC is measured by measuring the voltage (The open-circuit voltage can therefore be used to approximate the state of charge). The measurement of the open-circuit voltage to determine the SoC is based on the relationship between the electromotive force and the concentration of the sulfuric acid in the battery.
- One of the major advantages with VRLA batteries is that they do not experience memory effect which is common with nickel cadmium batteries.

Disadvantages include:

- These batteries have a shorter life span than other types of lead-acid batteries. In UPS applications, a life span of 5–10 years is typical since their life reduces due to harsh operating conditions.
- They should not be stored in discharged condition.
- These batteries are sensitive to higher temperature environment. As with most batteries, the capacity is dependent on the discharge rate and temperature; the capacity decreasing with decreasing temperature and increasing discharge rate.
- Electrolytes act as heat sinks in batteries. However, VRLA batteries are "acid starved" as they use much less electrolyte, hence they do not have an effective heat-sink mechanism which makes them more prone to thermal runaway condition than compared to flooded lead-acid batteries.
- They have low cell resistance; hence immense short-circuit current is available.

Application Examples Because the VRLA batteries are sealed, they are ideal for many consumer applications. They are found in many uninterruptable power supply systems for computers, and as backup power for other electronics' light security systems, and emergency lighting. Because high discharge rates are possible, they are also advantageous for engine starting.

Charging Characteristics Constant-voltage charging is the most efficient and fastest method of charging the VRLA battery. To carry out fast charging of VRLA battery, the charger must be capable of charging the battery at the 2*C*-rate. Fast charging is usually possible with a full charge achieved within 4 hours, and some batteries that accommodate even higher C-rates can charge so that they are returned to full capacity within

1 h. When float charging is used, the charger maintains each cell at 2.3–2.4V in order to ensure a complete charge and maximum battery life.

Nickel Cadmium (Ni-Cd)

General Characteristics Nickel-cadmium battery is a very reliable, sturdy, long-life battery. Little maintenance is needed on nickel-cadmium batteries. These batteries have two major variants based on the intended application. Cells with thin sintered plates have low internal resistance and have a high power to volume ratio, while cells with thick electrode plates have a high energy storage capacity. Nickel-cadmium batteries are manufactured as unsealed open/semi-open batteries in which electrolyte/gas can escape through a vent (vented Ni-Cd batteries) and as fully sealed batteries which do not require topping up of the electrolyte with water. Nickel-cadmium batteries exhibit voltage suppression, also called as memory effect. The memory effect causes the battery to deliver only the capacity, which was used during the repeated charge/discharge cycles before. Because of this, the whole capacity of Ni-Cd batteries should be used for each discharge cycle to avoid a decrease of the maximum capacity. "Memory effect" makes this battery less suited for applications that don't allow a complete discharge.

Advantages and Disadvantages

Advantages include:

- They have a longer life than compared to lead-acid batteries.
- Extended operating temperature range compared to lead-acid batteries. This makes them more flexible in heavy duty applications in regard to temperature range.
- Extremely rugged batteries.
- Good charge retention. They can be stored for long periods without significant deterioration of SoC.
- These batteries require less maintenance.

Disadvantages include:

- Cadmium is an environmentally hazardous substance. Hence, disposal of Ni-Cd batteries is a major issue.
- They exhibit strong voltage depression (memory effect) phenomenon. This is a major drawback of Ni-Cd cells.

Application Examples Because of their favorable electrical properties, excellent reliability, low maintenance, rugged design, and long life, nickel-cadmium batteries are used in a large variety of applications. Unsealed Ni-Cd with higher capacity ranges are used in high-energy applications such as traction and large emergency power installations. Industrial nickel-cadmium batteries are used in train lighting and air conditioning for rail cars, emergency and standby systems such as emergency brakes and lighting in mass-transit and subway cars, diesel-engine cranking in locomotives and commuter cars, railroad signaling, communication along tracks, as well as standby power in rail stations and traffic control systems. The nickel-cadmium battery is also used in power-generating stations and power distribution. Sealed Ni-Cd batteries are usually of a low energy storage type (30 Ah). These are extensively used in consumer electronics, domestic markets, and low-energy applications.

Charging Characteristics Constant-voltage charging is the preferred method for unsealed nickel-cadmium batteries.

Nickel-Metal Hydride (Ni-MH)

General Characteristics Nickel-metal hydride (Ni-MH) cells share many of the same characteristics as nickel-cadmium cells and reduce some of the disadvantages. A major difference between nickel-metal hydride and nickel-cadmium cells is that cell reaction of nickel-metal hydride cells is exothermic, and hence, internal temperature of Ni-MH cell rises when it is in operation. On the other hand, nickel-cadmium cells have an endothermic cell reaction.

Advantages and Disadvantages

Advantages include:

- These batteries do not pose environmental hazards like Ni-Cd batteries.
- They possess higher specific energy and energy density than nickel-cadmium cells.
- Bipolar battery pack designs are popular as the energy storage in hybrid vehicles.

Disadvantages include:

- Overcharging leads to serious consequences for the battery; it leads to battery heating which in turn releases hydrogen gas and increases fire hazard. As a result, Ni-MH batteries require complex charging circuitry to ensure overcharging does not take place.
- Complex circuitry for charging implies Ni-MH cells cannot be charged on conventional battery chargers. This necessity contributes to an increased cost for Ni-MH battery.
- Limited service life of about 200–300 cycles if repeatedly discharged at high load currents.
- Higher self-discharge rate than Ni-Cd. Hence, the shelf-life of a fully-charged Ni-MH battery is much shorter. The shelf life is improved by adding chemical additives, which lowers the energy density.
- Memory effect is present but to a much lesser extent than Ni-Cd battery.

Application Examples The nickel-metal hydride battery used to be incorporated in computers, cellular phones, and other consumer electronic applications. In recent years, lithium-ion battery has replaced nickel-metal hydride batteries as it possesses a superior specific energy and energy density.

Charging Characteristics Repeated high load current discharging reduces the service life of nickel-metal hydride batteries to about 200–300 cycles. Ideal discharging of these batteries usually occurs at load currents of 0.2–0.5*C*. Ni-MH battery suffers from a high self-discharge rate. Self-discharge rates are reduced by adding chemical additives to the cell. However, this results in a trade-off, as chemical additives that slow down the self-discharge rate decrease the energy density of the cell. For a particular make of battery, it has been observed that it loses about 32% of charge if stored for about 80 h.

Lithium Ion (Li-Ion)

General Characteristics Lithium-ion cells are often specified for use in high-performance applications where small size and high performance are of paramount importance. They have higher specific energy and energy density than nickel-metal hydride cells. High energy density of Li-ion cell also makes it less stable. These cells pose a potential fire hazard if not managed properly.

Advantages and Disadvantages

Advantages include:

- Li-ion cells have a long cycle life (3,000 cycles at 80% depth of discharge). Hence, they are suited for applications which require a large number of charge-discharge cycles.
- They can operate over a wide temperature range.
- Low self-discharge rate leads to a long shelf life for these batteries.
- Rapid charge capability endears these batteries with consumer electronics applications.
- High energy efficiency. These cells can be up to 94% efficient in terms of energy over a cycle.
- No "memory effect."
- These batteries do not pose an environmental hazard as they are not made up of toxic materials.
- High energy density (300–400 kWh/m^3, 130 kWh/ton).
- One of the salient qualities of Li-ion cells is that they have a very high coulombic efficiency as compared to lead-acid cells. A new Li-ion cell exhibits up to 94% coulombic efficiency as against a lead-acid battery which has only 80% coulombic efficiency.

Disadvantages include:

- Li-ion cells have a moderately high initial cost.
- High energy density of Li-ion cells also gives rise to instability and fire hazard issues. This behavior of Li-ion cells makes it mandatory to have a complex protective circuitry. The battery management systems for Li-ion cell must be able to prevent overcharging of these cells. Overcharging in Li-ion cells leads to thermal runaway and subsequently a fire hazard.
- Venting and thermal runaway may take place when cells are crushed.
- Li-ion batteries composed of series strings of cells require charge equalization modules. Li-ion cells do not support low cost, easy to implement passive cell-balancing schemes.

Application Examples Li-ion batteries are employed in high-performance applications where size and energy are important. They are the preferred choice

for consumer electronics such as laptop computers, cellular telephones, and personal media player where long battery life is required. The suitability for use in military, aerospace, and automobile applications is also being explored.

Charging Characteristics Li-ion cells are fabricated in discharged state and thus must be charged before use. The cells are typically charged using either a constant current (CC) or a constant current-constant voltage (CCCV) with a taper charge regime. Exceeding the maximum voltage is a potential safety hazard and can result in irreversible damage to the battery. At the same time, charging to a lower voltage reduces the capacity of the battery. The construction of these batteries tends to make them susceptible to internal short circuits due to impurities. With the demand for higher energy density, an internal short can lead to catastrophic consequences including the risk of fire. Hence, internal temperature rise of the battery pack needs to be monitored as well as cell voltage. These considerations make it crucial to incorporate special control circuitry for lithium-ion batteries for management of charge and discharge. Although Li-ion cells have a flat voltage profile, it has been established in literature that cell open-circuit voltage provides a good estimate of the state of charge (SoC) ranging from 20% to 100%.

Sodium Sulfur (Na-S)

General Characteristics A sodium-sulfur battery is a type of molten metal battery constructed from sodium (Na) and sulfur (S). This battery has a high energy density, high efficiency of charge/discharge (89–92%), and long cycle life, and is fabricated from inexpensive materials. Sodium sulfur batteries usually have operating temperatures of 300–350°C. They are most prominently found in power grid operations, electric trains, and wind generation operations.

Advantages and Disadvantages

Advantages include:

- These batteries are constructed from inexpensive materials.
- Per unit volume, sodium sulfur batteries deliver three to five times more energy than lead-acid batteries. They have a high specific energy in the range of 160 kW/h.
- Designed to last 15 years through 2,500 full charge/discharge cycles.
- It has up to 89% cell DC efficiency with no self-discharge.
- Insensitive to ambient temperatures which make it suitable to be housed outdoors.
- Extremely fast charge cycling; it can transit from full charge to full discharge in milliseconds.
- Sodium sulfur battery facilitates remote operation and monitoring along with the added benefit of minimum maintenance.

Disadvantages include:

- These batteries require an elaborate thermal management system to ensure energy efficiency.
- Cells need to be hermetically sealed when operated in corrosive outdoor environments.

Application Examples Sodium-sulfur batteries have operating temperatures of 300–350°C and extensively employ sodium polysulfides which are highly corrosive. These considerations make Na-S batteries suitable for large-scale nonmobile applications such as grid energy storage. Sodium-sulfur batteries have many applications in power systems. They are used to provide additional power during voltage sags. They provide prompt spinning reserves for grid frequency control and reactive power support. Sodium-sulfur batteries also perform admirably in stabilization of wind energy fluctuations by providing the necessary additional power. Na-S batteries are a possible energy storage technology to support renewable energy generation, specifically wind farms and solar generation plants. They are also a better option as against pumped hydroelectric storage schemes. In Europe, motivation is toward implementing Na-S batteries for automotive traction applications.

Lithium-Iron Monosulfide

General Characteristics Practical energy densities of 100 Wh/kg are achieved by secondary lithium-iron monosulfide cells. Lithium-iron sulfide batteries require a thermal management system to maintain optimum operating temperatures. Precise voltage monitoring is needed from the charger. This battery

system requires a thermal management system to maintain the rated operating temperature for the battery and a specialized charger in which careful voltage control is maintained. This battery technology was under active research in the 1970s for electric vehicles. It is yet to be commercialized.

Nickel Zinc (Alkaline Rechargeable System)

General Characteristics The nickel-zinc (zinc/nickel-oxide) battery is an alkaline rechargeable system. Currently the nickel-zinc system is capable of delivering about 50–60 Wh/kg and 80–120 Wh/L depending on the specific design. Nickel-zinc batteries are suited for high discharge rate applications such as a camera flash.

Advantages and Disadvantages

Advantages include:

- Good capacity retention has made it a competitor of silver-zinc and silver-cadmium systems. Fully charged nickel-zinc batteries lose about 20% of their original capacity within a month when left on open-circuit at 25°C. Nickel-zinc batteries can be stored for up to 3 years.
- It has a wide range of temperature tolerance (−39°C to +81°C operating temperature).
- One of the major plus points is that it has a flat discharge voltage profile for a significant portion of the discharge.
- Ni-Zn battery possesses a fast recharge capability.
- It has a sealed maintenance-free design.

Disadvantages include:

- The main stumbling block for the success of Ni-Zn battery technology is that Ni-Zn battery possesses a poor cycle life (up to 150 cycles).
- It has a relatively low volumetric energy density.

Application Examples Nickel-zinc provides a very low-cost option for a long-cycle-life alkaline-rechargeable system. The nickel-zinc system is suited for mobile applications such as electric bicycles, electric scooters, electric and hybrid vehicles, or other deep-cycle applications. Deep-cycle applications for nickel-zinc batteries include trolling motors, electric bicycles and scooters, wheelchairs, golf carts, electric lawnmowers, electric vehicles, and similar uses. Nickel-zinc batteries have the required discharge-rate capability, high cycle life at deep depths-of-discharge, lightweight rugged construction, and are capable of being stored over the winter months without any maintenance charging.

Charging Characteristics The battery should be protected from excessive overcharge and over discharge. Extreme abuse may reduce battery performance and cycle life or cause a potential safety hazard.

Metal Air

General Characteristics The most popular metal-air battery is the zinc-air electrode battery. Zinc-air secondary batteries are being developed which can store three times as much as lithium-ion batteries but only cost half as much. The intended applications include cell phones, portable consumer electronic items, and electric vehicles. Lithium-air, calcium-air, and magnesium-air batteries have also been studied, but cost and problems such as anode polarization or instability, parasitic corrosion, nonuniform dissolution, safety, and practical handling have so far inhibited the development of commercial products.

Advantages and Disadvantages

Advantages include:

- Zinc-air battery has high energy density. Suitable for electric vehicle technologies.
- Zinc-air cells intake air with CO_2 removed. Earlier, this was seen as a disadvantage. However, deployment of this cell on electric vehicles with a CO_2 filter will lead to drastic reduction in CO_2 emissions. Hence, this cell is being proposed as a likely candidate for automotive applications.
- Zinc-air cells have a flat discharge voltage profile.
- These cells have a long shelf life (dry storage).
- Zinc-air battery has a safe battery chemistry which reduces fire hazards greatly.

Disadvantages include:

- Main difficulty in the development of rechargeable zinc-air battery is the deactivation in performance of air electrode after a few charge/discharge cycles.

- Internal short circuit is a major problem in Zn-Air secondary cells. Internal short circuit usually occurs after several charge/discharge cycles due to zinc dendrite growth through the separator.
- Depending on the discharge rate, the energy capacity of the cell drops drastically.
- Drying out of electrolyte limits shelf life once opened to air.
- Limited operating temperature range.

Application Examples Future applications for rechargeable zinc-air batteries include cell phones and electric vehicles. The high energy density, low-cost constituent materials, and relatively safe cell chemistry are some of the positive application advantages of this battery type. However, more efforts are required to increase the number of charge/discharge cycles of this battery before it becomes practical for commercial use.

Zinc-Bromine

General Characteristics The zinc-bromine battery is a high-energy-density battery. There are no toxic materials in this battery system. Zinc-bromine battery is constructed from low-cost materials; the battery cells are made up of plastic. It provides a viable energy storage option for a variety of generation sources and is ideally suited for applications requiring 2–10 h of energy storage. The energy density of this advanced battery makes it attractive for applications where traditional energy storage batteries, such as lead-acid batteries, are unacceptable due to size and weight restrictions. The zinc-bromine battery is a flow battery. Auxiliary systems are required for circulation and temperature control of the electrolyte. The zinc-bromine battery has a good shelf life. These batteries are more prominent in the high energy range: 10–500 kWh. These battery systems are custom built for specific applications.

Sodium-Beta

General Characteristics Sodium-beta batteries are high-temperature operating systems and hence have high energy density compared to ambient temperature systems.

Advantages and Disadvantages

Advantages include:

- Sodium-beta batteries are characterized by high energy density, lack of required maintenance, and performance independent of ambient temperature.
- They have a potential for low cost (relative to other advanced batteries) and are cheap as raw materials.

Disadvantages include:

- Thermal management is critical. Requires thermally insulated battery enclosure.
- These batteries operate in the region of 160–500°C. Hence, these batteries must not be affected by ambient temperatures.

Application Examples Sodium-beta battery technologies have been developed for use in relatively large-scale energy storage applications (10–1,000 kWh). Sodium-beta batteries can be used at generation facilities for load leveling, spinning reserve, and area regulation. They are also used for line stability and voltage-regulation purposes at distribution facilities. This technology is also suitable for peak demand reduction and power quality maintenance at a customer site. Sodium-beta batteries have also been investigated for their suitability in traction applications since, for a given physical envelope, sodium-beta batteries can provide significantly greater energy (range) at a reduced weight while meeting the vehicle power requirements compared with conventional battery technologies.

Battery Charging Circuits

Battery Charging Techniques

Proper battery charging techniques can significantly improve battery performance and life cycles. Thus, several factors such as fast charging, good quality of charging current, and avoiding under and over charging are considered. In particular, over charging can damage battery's physical components while under charging can reduce its energy capacity. Therefore, an appropriate control technique for charging process should be adopted. Different battery charging techniques are presented in this section. Operating principle of the battery charge controller is discussed for each technique, and the block diagram of the controller is depicted. Depending on the selected charging

technique, output voltage or current of the converter are fed back to the charge controller circuit. Each charging technique has a charging characteristic curve which is defined as the voltage-current trajectory of the battery during the charging period (v_{bat} versus i_{bat}).

Constant-Current Charging (CC) Constant-current charging is the most conventional battery charging technique. In the charging characteristic curve shown in Fig. 2a, the battery current is kept constant while battery voltage increases during charging until it reaches the maximum allowed value (i.e., rated voltage of the battery). Figure 2b shows the voltage and current profiles of the battery during the charging period. When the battery voltage has reached its final value, the charge controller circuit disconnects the battery from the converter to avoid overcharging and consequent battery failure. The voltage profile of the battery during the charging and discharging intervals is not necessarily linear, as shown in Fig. 2b, and depends on the type of the battery.

Figure 3 shows the associated control block diagram. The output current is compared with the reference current to produce the error current. The error current is fed to a proportional-integral (PI) controller to eliminate steady state error and generate the command signals for switching of the charger power electronic circuits.

The main advantage of this method is its simplicity. The converter circuit can be realized by an AC-DC or DC-DC converter based on the input type. Moreover, the output capacitor can be dropped as the output voltage regulation is not required, and regulating merely the output current is sufficient. Elimination of the output capacitor simplifies the converter circuit to a first-order current filter which can be analyzed simply and implemented inexpensively. Fast charging can be realized by large current pumping; however, this has the potential to degrade the internal chemical reactions in the battery. Alternatively, the low charging current prolongs the charging time. Therefore, proper choice of the charging current is crucial for enhancing the charging performance and increasing the lifetime of the battery charging system.

Constant-Voltage Charging (CV) Constant-voltage charging is another conventional battery charging technique. The charging characteristic curve of this technique is illustrated in Fig. 4a. In this method, the battery voltage remains constant while the battery current is decreasing and eventually becomes very low. The current and voltage profile during charging is shown in Fig. 4b. This initial high current (I_o) temporarily increases the battery temperature and can degrade the battery, depending on the chemistry. The battery charge controller disconnects the battery from the charger circuit when the current reaches a specific amount (I_{min}), as shown in Fig. 4b. The control block diagram is shown in Fig. 3, where the sensed and reference variable is the battery and reference voltage, respectively.

Similar to the CC methodology, the CV charging strategy is straightforward and easy to implement. As opposed to the CC charging strategy, a capacitive output is required to regulate the output voltage. This

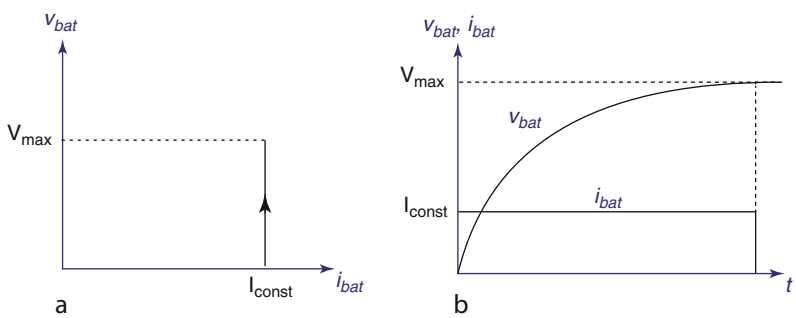

Batteries, Battery Management, and Battery Charging Technology. Figure 2
(**a**) Charging characteristic curve of the constant-current technique; (**b**) Current and voltage profiles of the battery during the charging process

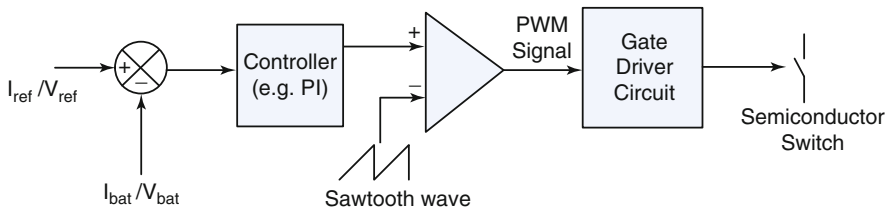

Batteries, Battery Management, and Battery Charging Technology. Figure 3
Block diagram of the controller circuit useful for constant-current or voltage charging

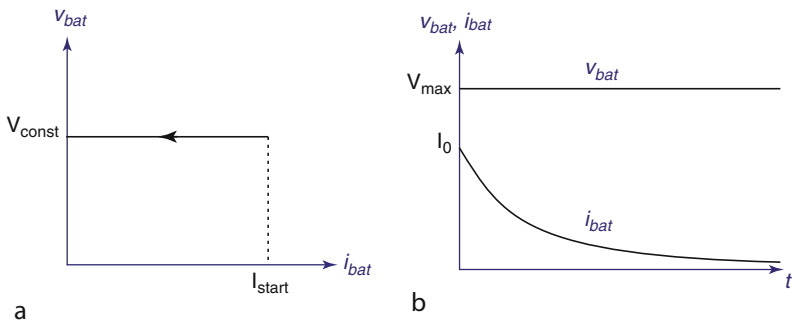

Batteries, Battery Management, and Battery Charging Technology. Figure 4
(**a**) Charging characteristic curve of the constant-voltage technique; (**b**) Current and voltage profiles of the battery during the charging process

output stage increases the model order, and therefore, the controller design process is slightly more complex than CC technique, yet simple enough for low-cost applications.

The main disadvantage of the CV charging methodology is the temperature rise of the battery during initial charging stages. While the internal voltage of the battery is very low, the applied voltage at the terminal of the battery is relatively high. Thus, considering the small internal resistance of the battery, a large current will flow which can damage the battery. Another drawback of CV charging is the long charge time due to very low currents at the final stages of the charging.

Mixed Constant-Current and Constant-Voltage Charging (CC-CV) The CC-CV charging technique utilizes both CC and CV charging. Figure 5a, b illustrates the charging characteristic curve and current-voltage profiles of this method, respectively. The charging is performed in three stages. First, the battery current is kept constant until the battery voltage reaches a predetermined value (V_{const}). Then, the battery voltage is kept constant while the battery current drops below a specific value (I_{min}). The final stage is the float charge stage where the battery voltage is reduced to compensate for the loss caused by self-discharge of the battery.

Since the current is kept constant at the first charging stage, the current rush disadvantage of CV charging technique is avoided. Also, since the voltage is kept constant at the second stage, the overcharging disadvantage of CC charging is avoided. Moreover, the float charging stage keeps the battery in full charge for a long time without degrading the battery. These advantages of CC-CV charging technique make it perfect for applications with high performance requirement. However, the design complexity makes this option more expensive compared to either CC or CV techniques.

Pulse Charging Pulse-charging technique is inherently a CC charging method that uses a pulsating charging current. This pulsating current causes the ions to distribute evenly throughout the battery and electrodes. Consequently, even distribution of ions

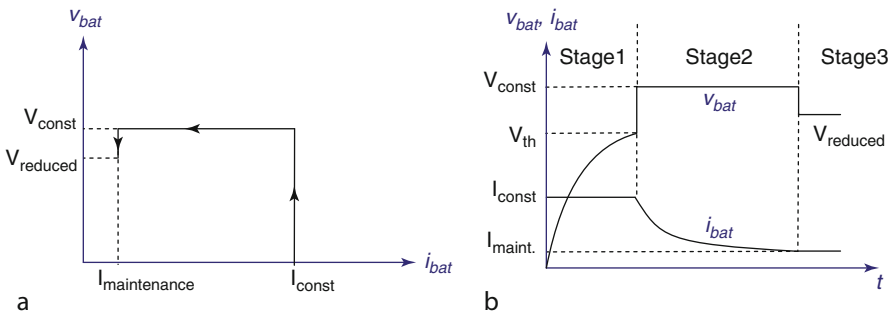

Batteries, Battery Management, and Battery Charging Technology. Figure 5
(**a**) Charging characteristic curve of the CC-CV technique; (**b**) Current and voltage profiles of the battery during the charging

prolongs the lifetime of the battery and enhances the charging performance. Figure 6 shows the current profile of the battery using pulse-charging technique. Due to the internal battery resistance, the battery voltage increases slightly during the charging subintervals. DC value of the charging current can be controlled by the duty cycle of applied current between zero and $I_{\max}$. The charging rate is controlled by the DC value of charging current; thus, charging time of the battery can be controlled by the duty cycle:

$$t_{\text{charge}} = f(I_{\text{DC}}) = f(DI_{\max}), \tag{1}$$

where D, I_{DC}, and $I_{\max}$ are the duty cycle, DC value, and the maximum of the battery current, respectively. Large duty cycles are applied during the initial stages of charging to ensure fast charging. After battery voltage is increased sufficiently, the duty cycle gradually decreases to prevent overcharging and consequent battery failure.

Pulse current charging needs an extra control loop to regulate the duty cycle of the reference current (I_{ref}) by the output voltage. As the output voltage decrease, this additional control loop decreases the duty cycle and consequently the DC value of the charging current. Following a pulsating reference current requires a fast control loop. The bandwidth of the control loop should be sufficiently higher than the switching frequency. This bandwidth is limited by the effective bandwidth of the current sensor. Thus, increasing the bandwidth of the controller requires high-bandwidth current sensors, which can be costly.

Taper Characteristic Charging In taper charging, neither battery current nor battery voltage is kept constant. Instead, a linear combination of battery voltage and current is kept constant:

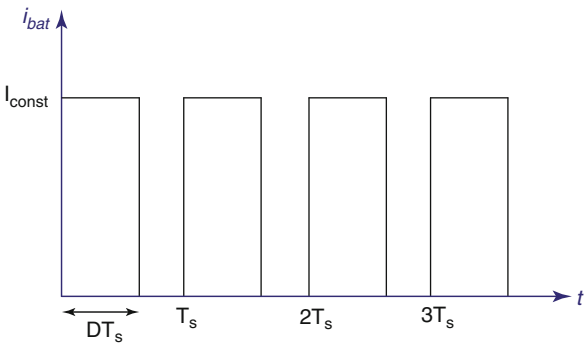

Batteries, Battery Management, and Battery Charging Technology. Figure 6
Current profile of the battery using pulse-charging technique

$$k_1 V_{\text{bat}} + k_2 I_{\text{bat}} = c = \text{constant}, \tag{2}$$

where k_1 and k_2 are constant coefficients which are determined by design requirements. CC and CV charging techniques are special cases of the taper characteristic charging in which $k_1 = 0$ or $k_2 = 0$, respectively. Figure 7a, b illustrates the charging characteristic curve and voltage-current profiles of the taper charging technique, respectively.

The block diagram of the charge controller using this technique is depicted in Fig. 8. Sensing of both battery voltage and current is required and is the main drawback of this strategy. Sensors are usually the most

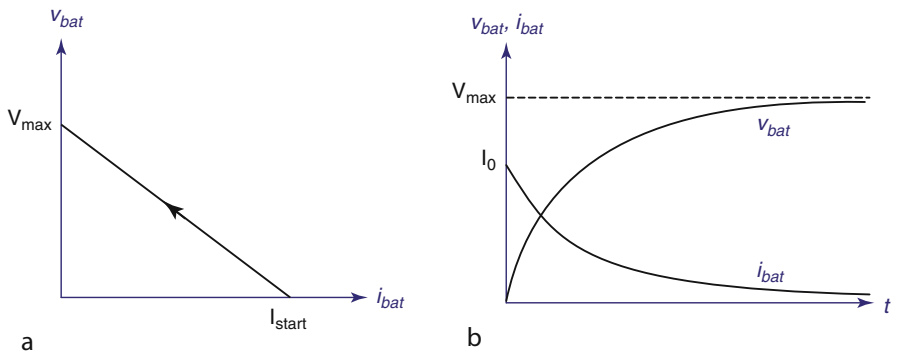

Batteries, Battery Management, and Battery Charging Technology. Figure 7
(**a**) Charging characteristic curve of the taper-characteristic-charging technique; (**b**) Current and voltage profiles of the battery during the charging

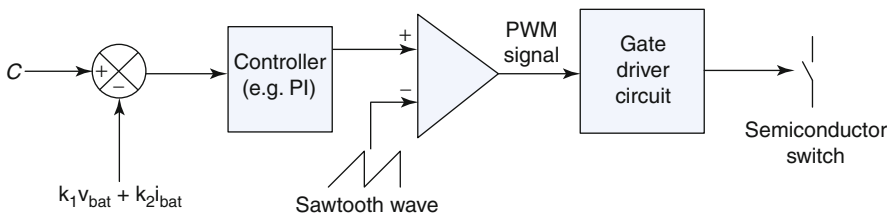

Batteries, Battery Management, and Battery Charging Technology. Figure 8
Block diagram of the controller for taper characteristic charging

expensive components of the converter circuits, and increasing the number sensor may drastically increase the total cost of the system.

Assembled Characteristic Charging Assembled or modified charging is a technique whose characteristic curve is a combination of CC, CV, or taper characteristic curves. In this technique, when a certain threshold is reached (e.g., certain voltage), the characteristic curve is changed from one technique to another. Two conventionally assembled characteristic charging methods are assembled constant-current charging and assembled taper characteristic charging.

Assembled Constant-Current Charging Figure 9a illustrates the charging characteristic curve of the assembled constant-current charging technique. As seen in Fig. 9a, battery is charged by a high constant current (I_1) until the output voltage reaches the threshold voltage (V_{th}), after which the CC charging will continue using a lower constant current (I_2). Then, charging with low current will continue until the output voltage reaches its maximum value (V_{max}), which is usually the rated voltage of the battery. The current and voltage profiles of the battery are shown in Fig. 9b.

As the high constant current reduces the charging time but increases the risk of overcharging, one may trade off between fast charging and overcharging protection. This drawback of CC charging has been overcome in assembled constant-current technique. Short charging time can be achieved by using high constant current (I_1) at the first stage ($v \leq V_{th}$), while overcharging can be avoided by using low constant current at the second stage ($v > V_{th}$).

Assembled Taper Characteristic Charging Assembled taper characteristic charging utilizes two different taper charging characteristic curves, as shown in Fig. 10a. The characteristic equation of this technique can be expressed as:

$$\begin{cases} k_1 V_{bat} + k_2 I_{bat} = c, & V_{bat} \leq V_{th} \\ k_1' V_{bat} + k_2' I_{bat} = c', & V_{bat} \geq V_{th} \end{cases} \quad (3)$$

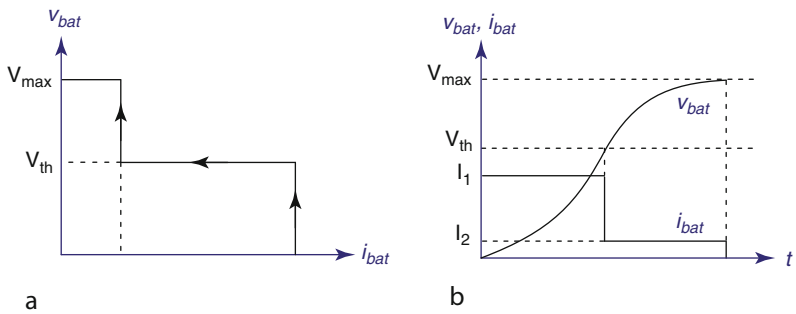

Batteries, Battery Management, and Battery Charging Technology. Figure 9
(**a**) Charging characteristic curve of the modified constant-current technique; (**b**) Current and voltage profiles of the battery during the charging process

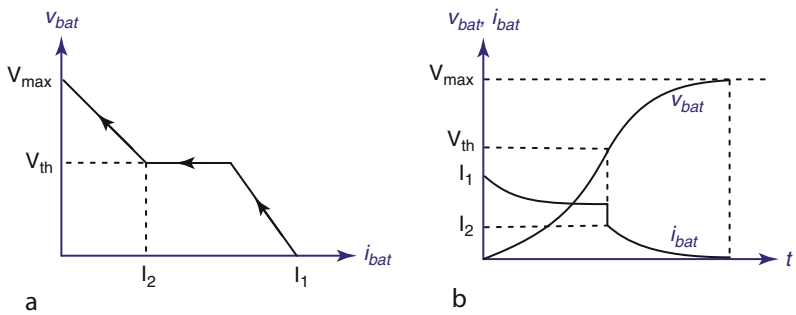

Batteries, Battery Management, and Battery Charging Technology. Figure 10
(**a**) Charging characteristic curve of the modified taper characteristic technique; (**b**) Current and voltage profiles of the battery during the charging

where $c > c'$. Figure 10b depicts current and voltage profiles of the battery during the charging time interval.

Enhanced charging performance and prolonged battery life can be achieved using this technique. The main disadvantages of this technique are implementation complexity and using two sensors (current and voltage sensors).

Qualitative Comparison Between Different Charging Techniques Table 1 summarizes different charging techniques and their main properties:

Battery Charging Circuits for Photovoltaic (PV) Systems

Energy storage components are an essential part of a stand-alone photovoltaic (PV) system as they store energy during the high radiation hours during the day and supply load during the low-radiation hours and nights. The battery is an effective energy storage technology for a PV systems. Lead-acid batteries are common due to their high energy density, prevalences and low cost. Different structures that can be used to connect the battery stack to the PV panel are presented in the next sections. In all of these structures, a series diode is connected between the PV panel and the battery to protect the battery against short circuit during the low-radiation conditions and nights.

Series Charge Regulators Figure 11 illustrates a typical charge regulator structure which can be used for both series and parallel charging. In series charging, switch S_2 is always open. Switch S_1 disconnects the PV panel from the battery when state of charge (SoC) of battery reaches 100% to protect the battery against overcharging. Switch S_3 disconnects the battery from

Batteries, Battery Management, and Battery Charging Technology. Table 1 Qualitative comparison between different charging techniques

Charging technique	Advantages	Disadvantages
Constant current (CC)	• Simplicity of implementation • First order open-loop transfer-function • Simplicity of the controller	• Overcharging risk if high charging current is used • Prolonged charging time if low current is used
Constant voltage (CV)	• Simplicity of implementation	• Battery temperature rise during the initial stages of charging • Prolonged charging time due to low current during the final charging stages • Second order open-loop transfer-function
Constant current – constant voltage (CC – CV)	• Protecting the battery against overcharging • No current rush at the beginning stage of charging • Enables float charging after the battery is fully charged • High performance	• Requires both voltage and current sensor for closed-loop control
Pulse current	• Even distribution of ions throughout the electrodes and inside the battery • Prolonged battery life due to maximizing chemical performance • Charging rate can be controlled by the duty cycle of the battery current	• Requires fast control-loop • Requires high bandwidth current-sensor • Expensive
Taper characteristic	• Gradual current decrease during the charging • Protection against overcharging	• Requires both voltage and current sensor for closed-loop control • Complexity of implementation
Assembled constant current	• Eliminates overcharging property of CC charging • Eliminates prolonged charge time property of CC charging • Takes other advantages of CC charging	• More complicated control scheme than CC charging
Assembled taper characteristic	• Different adjustment of characteristic curve is possible to satisfy different design requirements • Enhanced charging performance	• Requires both current and voltage sensors for closed-loop control • Most complex control scheme

the load when the battery SoC is less than a predefined value to avoid deep discharging mode, which can degrade the battery and shorten its life. All switches should have very low loss which means they should have very low forward voltage and on-time resistance. Thus, mechanical relays are preferred to fast power semiconductors such as IGBTs with high on-time voltage drops.

Shunt Charge Regulators In a typical shunt charge regulator, the switch S_1 in Fig. 11 is always closed, and switch S_3 operation is similar to series charge regulators to disconnect the load from the battery when battery SoC is less than a predefined value to prevent the battery from deep discharging. Switch S_2shorts the output of the PV panel during low-radiation conditions and nights. When the output of the PV panel is shorted, series diode protects the battery against short circuit condition.

Pulse-Width Modulation Charge Regulators Superior charging functionality can be achieved using

pulse-width modulation (PWM) charge regulators. PWM-type charge regulators are able to eliminate external disturbances and can be programmed to follow a specific charging technique that has been discussed in section "Battery Charging Techniques". Figure 12 shows a buck-boost-type PWM charge controller with voltage and current feedback. The charge controller also has the ability to control switch S_2 to disconnect the load under the condition in which battery SoC is less than a predefined value to protect the battery against deep discharging.

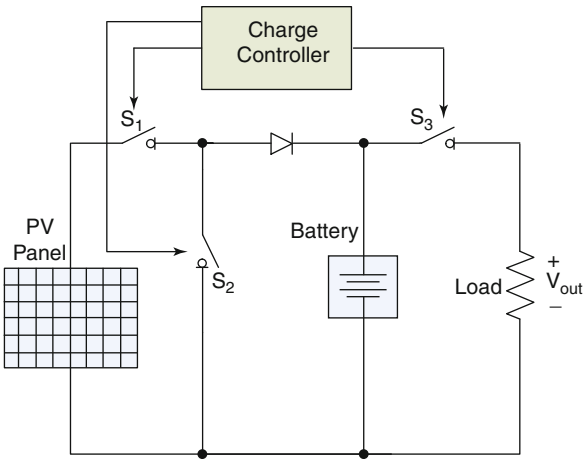

Batteries, Battery Management, and Battery Charging Technology. Figure 11
Circuit diagram of series and shunt PV charging system

Battery Charging Circuits with AC Sources

Several factors should be considered when designing a charging circuitry with AC input voltage, e.g., nominal output DC voltage, allowable ripple in output current, type of the input AC voltage source (single-phase or three-phase), AC voltage source ratings (voltage and frequency), charger efficiency and power factor, charger current limiting capability, and recharge duration time. In this section, the conventional battery charger's configurations with an AC input source are discussed.

Battery Charger Configurations Given the DC nature of batteries, a rectifier circuit is needed. In a conventional configuration, shown in Fig. 13, a phase-controlled rectifier is adopted. Another configuration is a rectifier bridge in series with a buck DC-DC converter as shown in Fig. 14. If an electrical isolation is required, a DC-DC converter with a high-frequency isolation transformer can be used as shown in Fig. 15.

Single-Phase, Phase-Controlled Rectifiers The circuit configuration of a single-phase thyristor-controlled rectifier is illustrated in Fig. 16. The battery is presented as a DC voltage source in series with

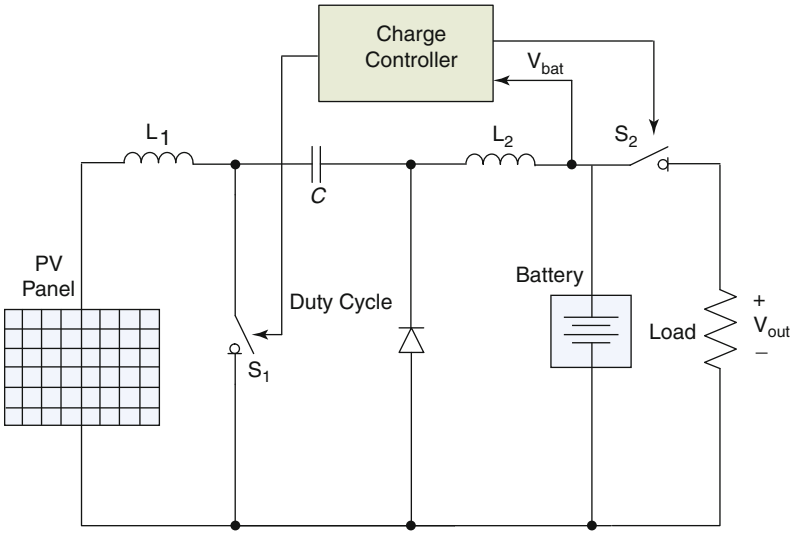

Batteries, Battery Management, and Battery Charging Technology. Figure 12
Circuit diagram of the PWM-PV charging system

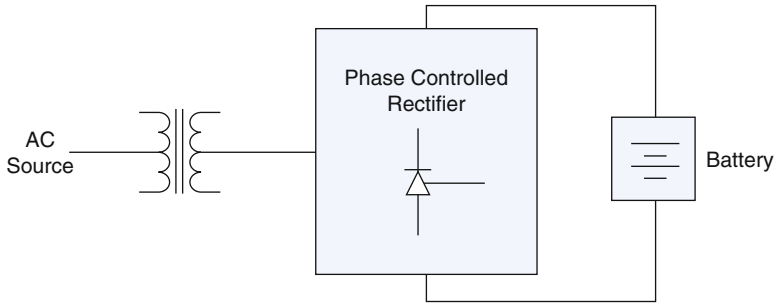

Batteries, Battery Management, and Battery Charging Technology. Figure 13
Phase-controlled rectifier

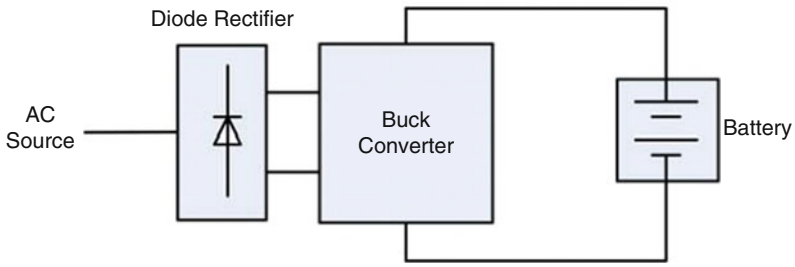

Batteries, Battery Management, and Battery Charging Technology. Figure 14
Rectifier bridge in cascade with a buck converter

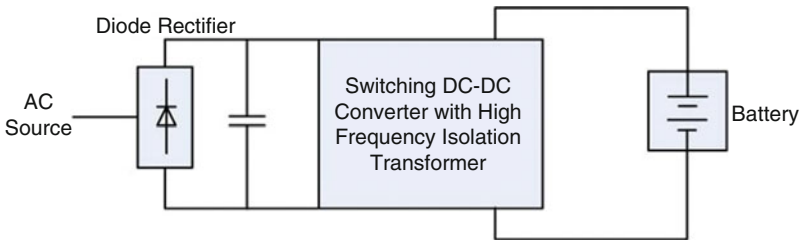

Batteries, Battery Management, and Battery Charging Technology. Figure 15
DC-DC converter with a high-frequency isolation transformer

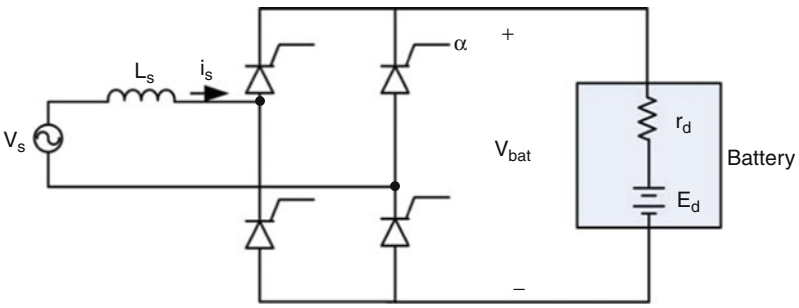

Batteries, Battery Management, and Battery Charging Technology. Figure 16
Single-phase thyristor rectifier

a resistor (r_d). Considering a continuous battery current, the voltage and current waveforms are illustrated in Fig. 17. Due to the presence of AC side inductance, there is a commutation interval, u. In the continuous mode of battery's current, the approximate average value of the battery voltage is:

$$V_{bat} \approx 0.9 V_S \cos\alpha - \frac{2}{\pi}\omega L_S I_{bat,min} \quad (4)$$

where $I_{bat,min}$ is the minimum value of battery current which occurs at $t = \frac{\omega}{\alpha}$.

The average value of battery current can be calculated using (5):

$$V_{bat} = r_d I_{bat} + E_d. \quad (5)$$

Figure 18 shows the input line current (i_s). Neglecting L_s, AC source current is a square wave current with only odd harmonics. These harmonics can be expressed as (6):

$$I_{sh} = \frac{I_{s1}}{h} \quad (6)$$

where I_{s1} is the RMS value of the fundamental frequency of I_s. The total harmonic distortion of input line current in a single-phase configuration is around 48.43%. The power factor of the single-phase configuration is expressed in (7):

$$PF = 0.9 \cos\alpha. \quad (7)$$

At low values of i_{bat}, the battery current waveform may become discontinuous as shown in Fig. 19. Through the appropriate choice of firing angle α, one can control the average value of battery voltage and thus battery current and, therefore, the power delivered. Figure 20 shows the variations of V_{bat} versus i_{bat} for different values of α. For a given value of α, if i_{bat} becomes less than a specific threshold, V_{bat} increases sharply. In such a case, α has to increase to keep V_{bat} constant.

Three-Phase, Phase-Controlled Rectifiers Figure 21 shows the circuit configuration of a three-phase phase-controlled rectifier connected to a battery. Similar to the single-phase configuration, the battery is presented as a DC voltage source in series with a resistor (r_d).

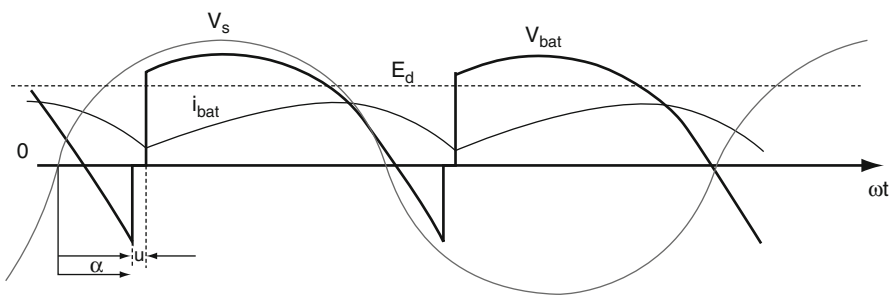

Batteries, Battery Management, and Battery Charging Technology. Figure 17
Battery's voltage and current waveforms

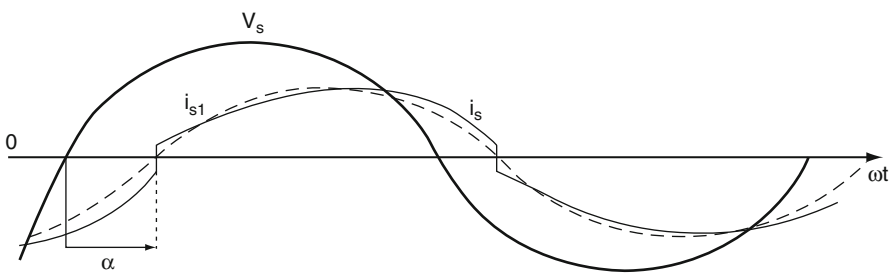

Batteries, Battery Management, and Battery Charging Technology. Figure 18
Input line current

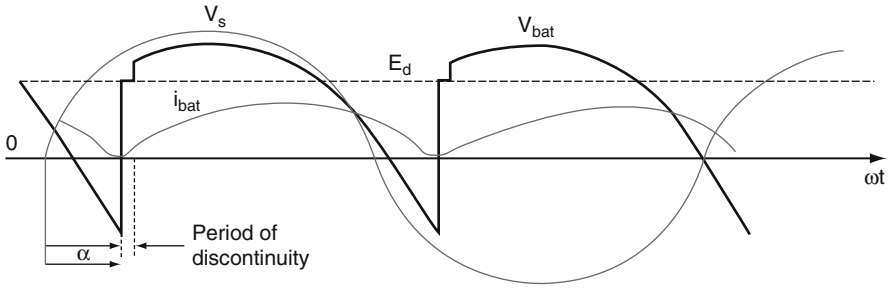

Batteries, Battery Management, and Battery Charging Technology. Figure 19
Battery voltage and current in discontinuous mode of operation

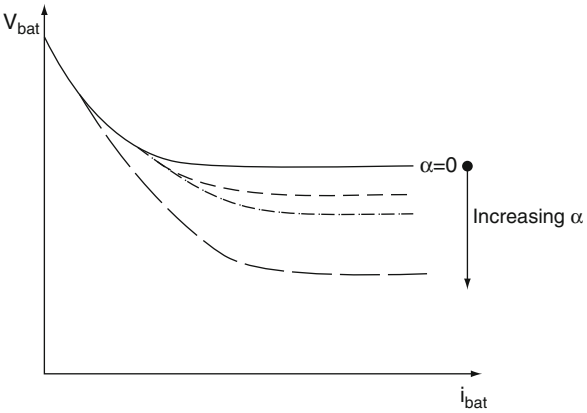

Batteries, Battery Management, and Battery Charging Technology. Figure 20
Rectifier output profile for different values of α

Assuming a continuous current for battery, battery's voltage waveform is illustrated in Fig. 22. In this figure, u and α present the commutation interval and delay angle, respectively. The average value of battery voltage can be expressed in terms of (8). Compared with the single-phase configuration, the ripple in the output voltage of three-phase rectifier is less:

$$V_{\text{bat}} \approx \frac{3\sqrt{2}}{\pi} V_{\text{LL}} \cos\alpha - \frac{3}{\pi}\omega L_{\text{S}} I_{\text{bat}} \tag{8}$$

where V_{LL} is the RMS value of the line voltage of AC source, and I_{bat} is the battery current.

Figure 23 shows the input line current of phase "a" (i_{S}). Neglecting L_{S}, AC source current harmonics can be expressed as (9):

$$I_{\text{sh}} = \frac{I_{\text{s1}}}{h} \quad \textit{where } h = 6n \pm 1 \tag{9}$$

The total harmonic distortion of input line current in three-phase configuration is around 31.08%, less than that of a single-phase configuration. The power factor of three-phase configuration is:

$$PF = \frac{3}{\pi}\cos\alpha. \tag{10}$$

Rectifier Bridge in Cascade with a Buck DC-DC Converter In this configuration a rectifier is in cascade with a buck DC-DC converter. In the buck converter, which is shown in Fig. 24, the average output voltage is lower than DC input voltage. Figure 25 shows the waveforms of V_{d}, V_{bat}, V_{L}, and i_{L} for a resistive load and continuous conduction of inductor. t_{on} denotes the time that the switch is on in a switching period. Because of the fact that the integral of the inductor voltage should be zero over a time period, the output voltage is:

$$\frac{V_{\text{bat}}}{V_{\text{in}}} = \frac{t_{\text{on}}}{T_{\text{s}}} = D. \tag{11}$$

Ignoring losses, the expression for output current is:

$$\frac{I_{\text{bat}}}{I_{\text{in}}} = \frac{V_{\text{in}}}{V_{\text{bat}}} = \frac{1}{D}. \tag{12}$$

DC-DC Converter with a High Frequency Isolation Transformer In this configuration using a diode rectifier, the input AC voltage is rectified into a primary DC voltage. Using high-frequency switching, the primary DC voltage is converted from one DC level to another. This task is done by using a high-frequency transformer. The output of this configuration is controlled by adopting a PWM feedback control. Figure 26 shows the simplified block diagram of this configuration with its control system. Flyback, forward,

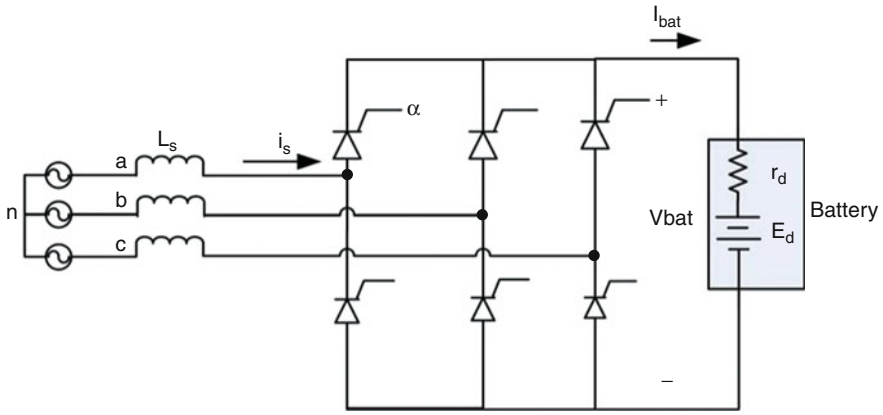

Batteries, Battery Management, and Battery Charging Technology. Figure 21
Three-phase phase-controlled rectifier

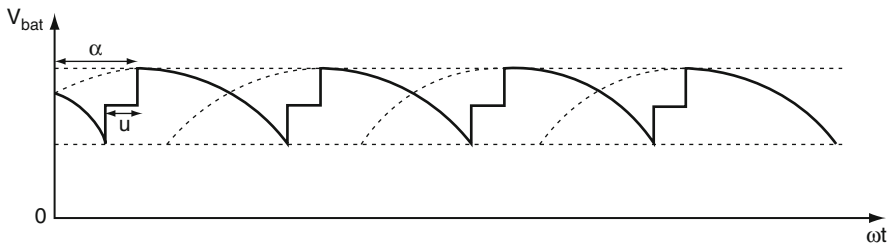

Batteries, Battery Management, and Battery Charging Technology. Figure 22
Battery's voltage waveform

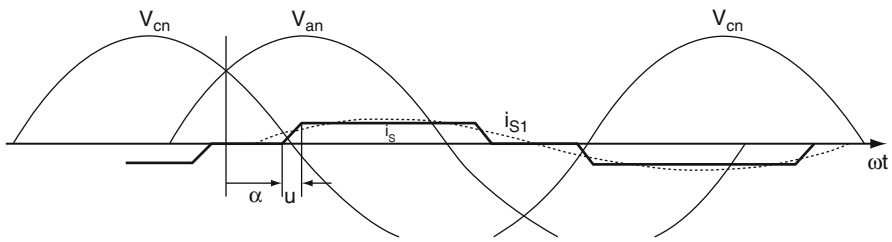

Batteries, Battery Management, and Battery Charging Technology. Figure 23
Input line current

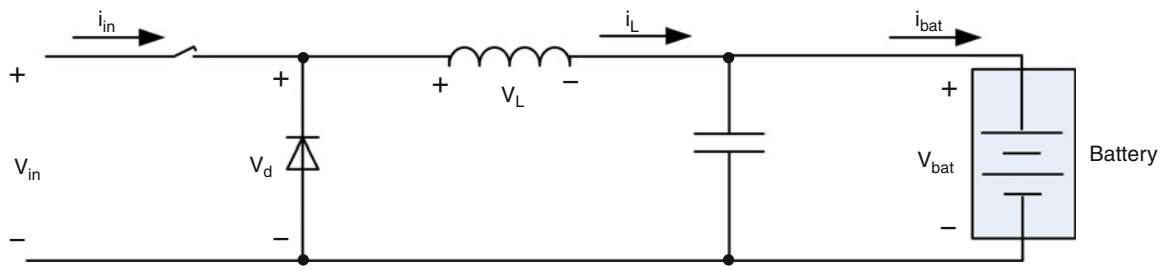

Batteries, Battery Management, and Battery Charging Technology. Figure 24
Buck converter

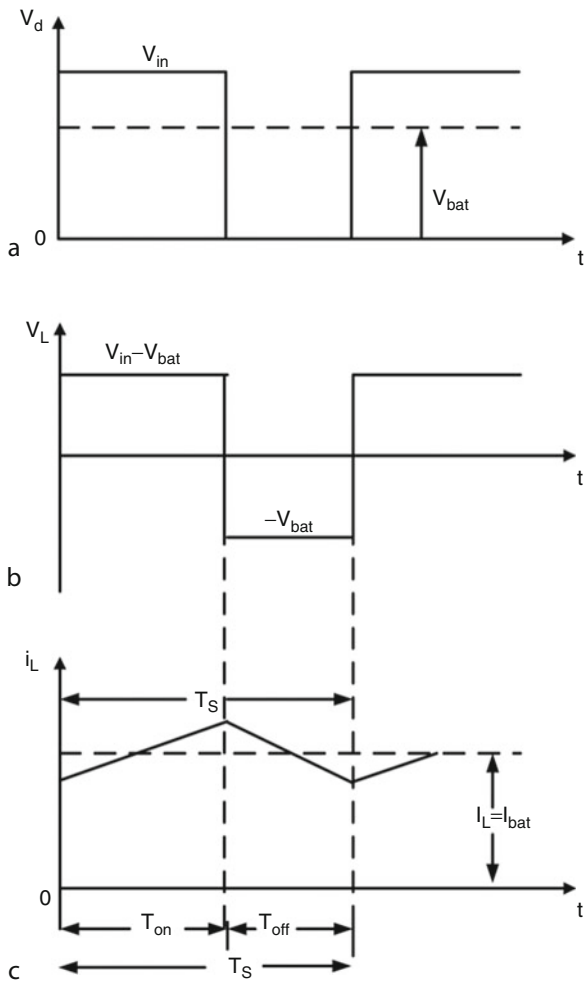

Batteries, Battery Management, and Battery Charging Technology. Figure 25
(**a**) Diode voltage; (**b**) Inductance voltage; (**c**) Inductance current

push-pull, half bridge, and full bridge are the main types of this battery configuration.

Flyback Converter Figure 27 shows the circuit topology of this converter. This converter is derived from buck-boost converter. Defining the switch duty ratio D as the ratio of the time the switch is on t_{on} to the total switching period T_s, $D = \frac{t_{on}}{T_s}$, the DC output voltage is:

$$\frac{V_{bat}}{V_{in}} = \frac{N_2}{N_1}\frac{D}{1-D}. \tag{13}$$

Forward Converter Figure 28 shows the circuit topology of this converter. This converter is derived from a step-down (buck) converter. The expression for the DC output voltage level is:

$$\frac{V_{bat}}{V_{in}} = \frac{N_2}{N_1}D. \tag{14}$$

Push-Pull Converter Similar to forward converters, push-pull converters also have the same operation as buck converters. Circuit configuration of these converters is shown in Fig. 29. The expression for the DC output voltage level is:

$$\frac{V_{bat}}{V_{in}} = 2\frac{N_2}{N_1}D\,, \quad 0 < D < 0.5. \tag{15}$$

In practice, in order to avoid simultaneous conduction of both switches, D should be less than 0.5.

Half-Bridge Converter Figure 30 shows the circuit configuration of this converter. This converter is also derived from step-down converters. The expression for the DC output voltage level is:

$$\frac{V_{bat}}{V_{in}} = \frac{N_2}{N_1}D\,, \quad 0 < D < 0.5. \tag{16}$$

Full-Bridge Converter Full-bridge converters also have the same operation as buck converters. Their circuit configuration is shown in Fig. 31. The expression for the DC output voltage level is:

$$\frac{V_{bat}}{V_{in}} = 2\frac{N_2}{N_1}D\,, \quad 0 < D < 0.5. \tag{17}$$

Bidirectional Configurations for Battery Charging with AC Sources

Bidirectional configurations for battery charging are used in multifunctional battery energy storage systems (BESS) and plug-in hybrid electric vehicles (PHEV). In the case of BESS, considering normal operation of the power system, the battery package can be charged and BESS can be controlled to shave the pick load. In the power failure condition, the battery pack is discharged and BESS provides an uninterruptible power for the utility grid. Figure 32 shows a three-phase configuration of a BESS system. Sophisticated control systems provide required commands for the switching system of the bidirectional converter which is a current-forced sinusoidal pulse-width modulated switching.

In the case of PHEVs, the battery pack should have this capability to store energy from an external power

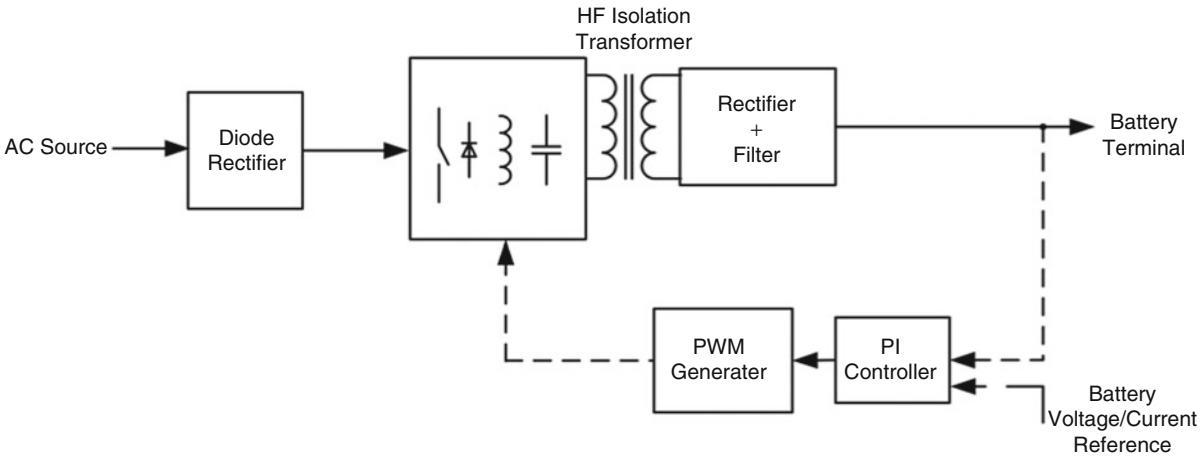

Batteries, Battery Management, and Battery Charging Technology. Figure 26
DC-DC converter with a high-frequency isolation transformer and its control system

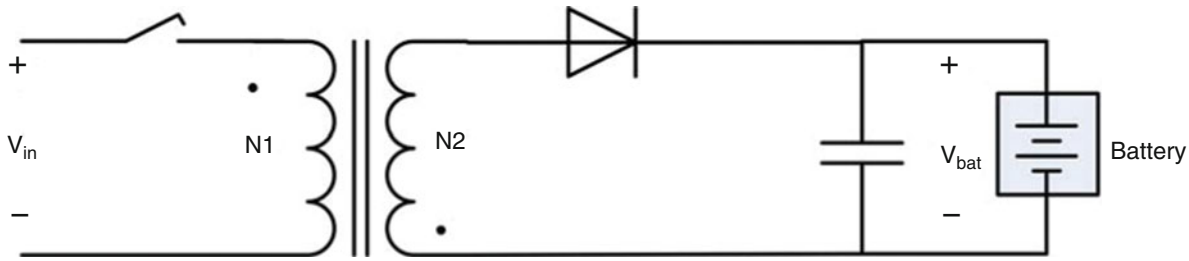

Batteries, Battery Management, and Battery Charging Technology. Figure 27
Flyback converter

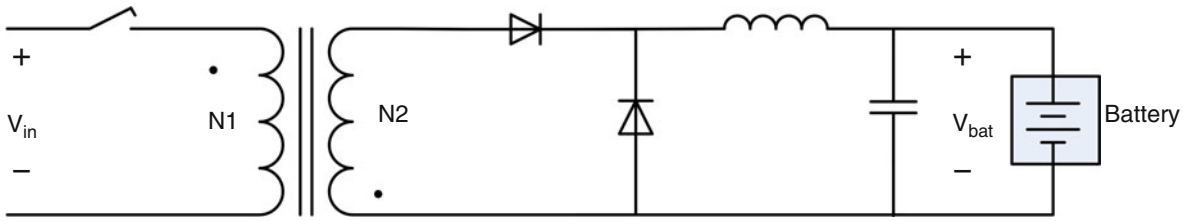

Batteries, Battery Management, and Battery Charging Technology. Figure 28
Forward converter

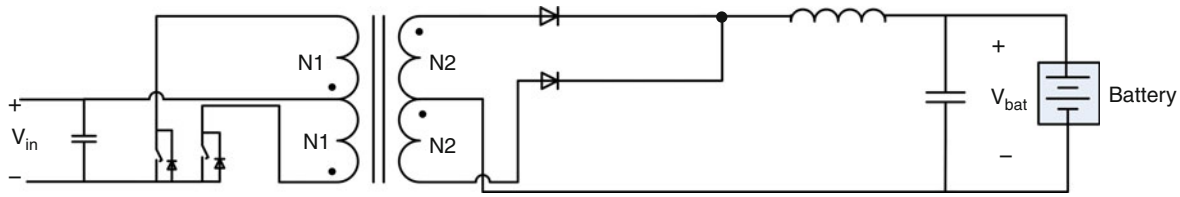

Batteries, Battery Management, and Battery Charging Technology. Figure 29
Push-pull converter

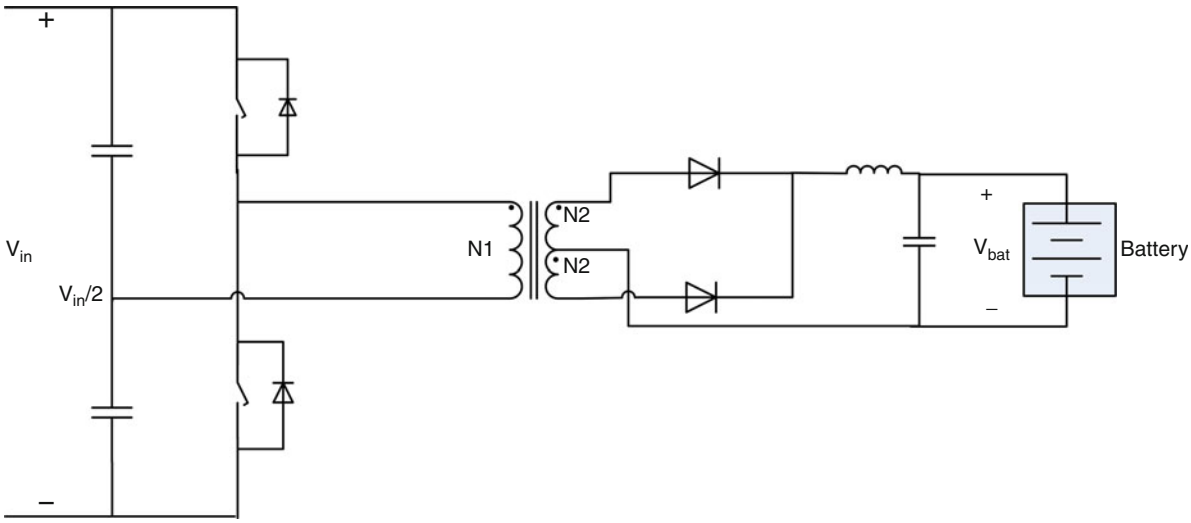

Batteries, Battery Management, and Battery Charging Technology. Figure 30
Half-bridge converter

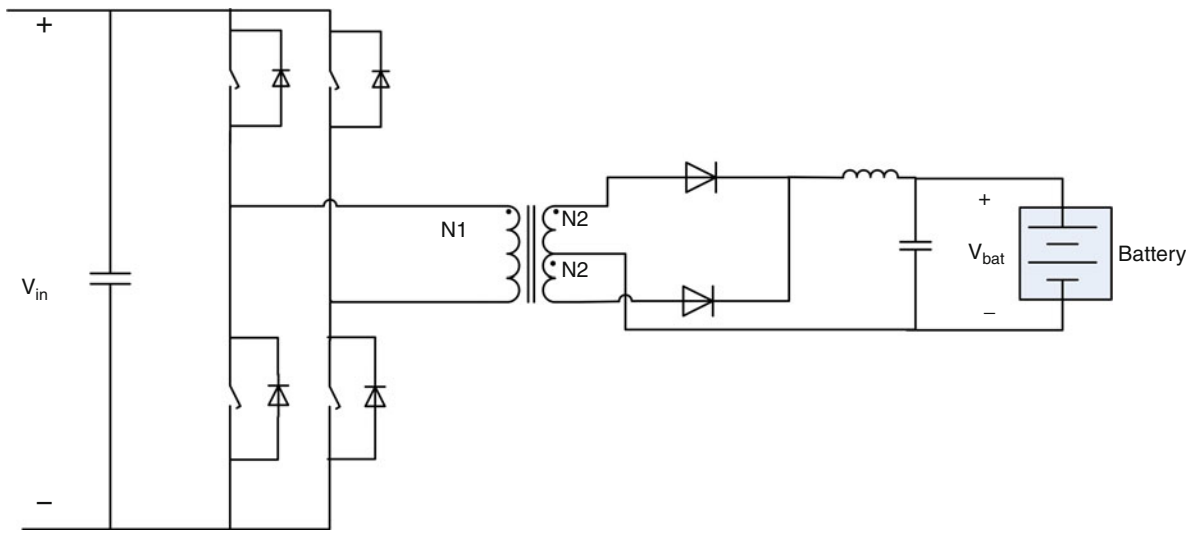

Batteries, Battery Management, and Battery Charging Technology. Figure 31
Full-bridge converter

source and regenerative braking as well as sending back the stored energy to the utility grid. Figure 33 shows the PHEV battery charger configuration. This battery charger consists of a bidirectional AC-DC converter in cascade with a bidirectional DC-DC converter.

Contactless Battery Charging

In recent years, a new approach for battery charging, named contactless battery charging, has emerged. This new charging scheme alleviates the wiring requirements and provides an easy charging process for cell phones, laptops, cameras, PHEVs, etc. Currently, there are two dominant technologies for contactless battery charging named inductive contactless battery charging and capacitive contactless battery charging.

Inductive Contactless Battery Charging The planar contactless battery charging platform is the

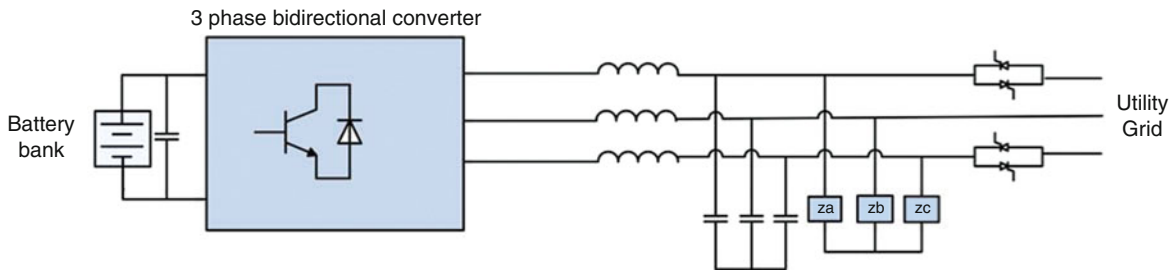

Batteries, Battery Management, and Battery Charging Technology. Figure 32
Bidirectional configuration for BESS

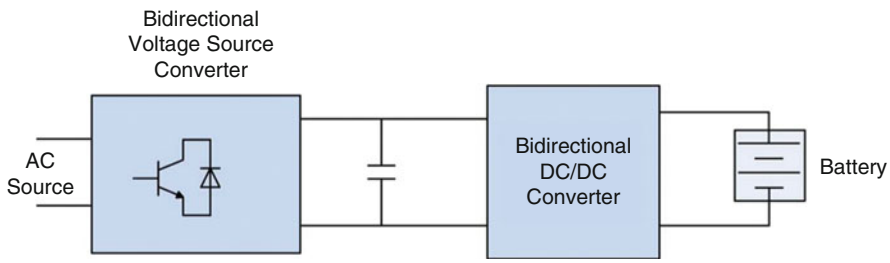

Batteries, Battery Management, and Battery Charging Technology. Figure 33
Bidirectional configuration for PHEV

predominant technology for contactless chargers. It uses inductive interface between energy transmitter and energy receiver and has the potential to unify all battery charging protocols related to portable electronic devices such as cell phones, music players, etc. Generally, there are two main schemes for implementing inductive contactless battery charging. The first scheme adopts horizontal flux in which magnetic flux moves horizontally onto the planar charging surface and flows on both sides of the planar. To achieve this requirement, a thick layer of soft magnetic material such as ferrite or amorphous alloy as the flux guide is used. Figure 34a shows the charging platform with horizontal magnetic flux trajectories. Figure 34b shows the secondary harvesting device which should pick up the fluxes from the surface of the charging platform. This energy-harvesting device consists of a magnetic core and a winding and is mounted into the portable electronic device. The cross-sectional area of this device should be large enough to collect enough flux and energy.

The second scheme adopts perpendicular flux in which magnetic flux has a perpendicular trajectory flow to the charging platform surface. The magnetic flux has uniform magnitude over the charging platform. This perpendicular flux trajectory allows a slim energy harvester device which is mounted into the portable electronic device. Figure 35 shows the

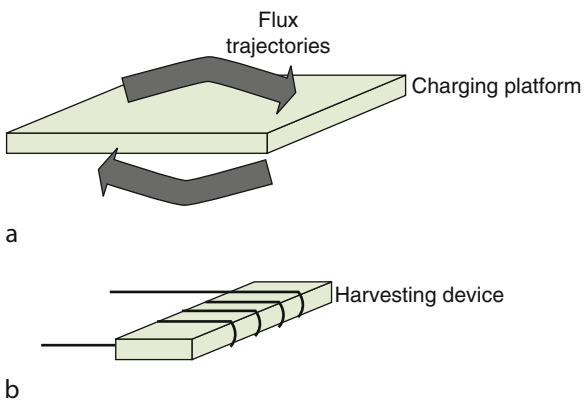

Batteries, Battery Management, and Battery Charging Technology. Figure 34
(**a**) Charging platform with horizontal magnetic flux trajectories; (**b**) Energy-harvesting device

charging platform with perpendicular magnetic flux trajectories.

Figure 36 shows the block diagram of an inductive contactless charger. The harvested energy is rectified, limited, and regulated to generate a DC voltage across the battery's terminals. Under and over discharge protection, setting of the battery voltage and current profiles, and implementing battery charging control techniques can be achieved by using an appropriate control system. Conventional configurations for battery charging circuits, explained before, can be used for the battery charger.

Capacitive Contactless Charger Thick electromagnetic flux guide is an important requirement in implementing efficient inductive contactless chargers. The confined electric field between conductive plates can alleviate this requirement in capacitive contactless chargers, as shown in Fig. 37. Figure 38 shows the circuit configuration of a capacitive contactless charger based on a series resonant architecture. Two coupling capacitors transfer power from V_{in} to battery. Considering a DC power supply, using an inverter, the input DC voltage is converted to an AC output voltage to enable current flow through the coupling capacitors. This inverter is not required if supplied from an AC source. Inductors are used to enable soft switching. At the final stage, a diode rectifier provides the required DC voltage for battery charging. The circuit parameters should be designed in such a way that a circuit with the least possible value of capacitor and the desired efficiency is achieved.

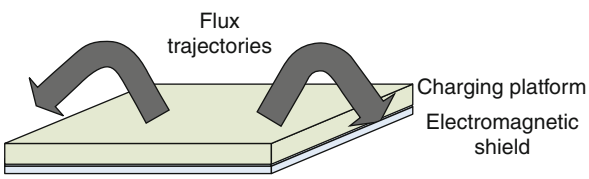

Batteries, Battery Management, and Battery Charging Technology. Figure 35
Charging platform with perpendicular magnetic flux trajectories

Electromagnetic Interference (EMI)

Electromagnetic interference (EMI) is defined as degradation in performance of an electronic system caused by electromagnetic disturbances. Electromagnetic compatibility (EMC) is the ability of that system to operate satisfactorily in an electromagnetic environment without introducing intolerable electromagnetic disturbances to other devices in that environment. Battery charging circuits are power electronic converters in nature. Therefore, EMC rules and regulations exist that apply to the battery charger circuits. Power electronic converters must emit electromagnetic disturbances below the maximum permitted amount (emission) and be able to operate properly when exposed to electromagnetic disturbances below the maximum permitted amount (susceptibility).

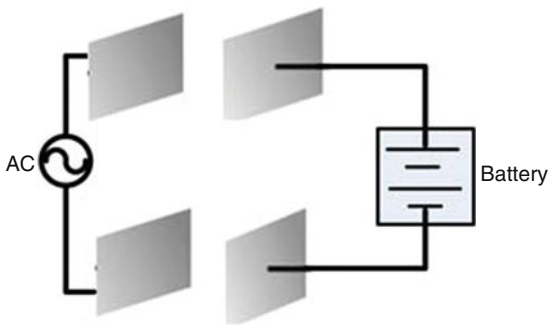

Batteries, Battery Management, and Battery Charging Technology. Figure 37
Capacitive contactless power transferring

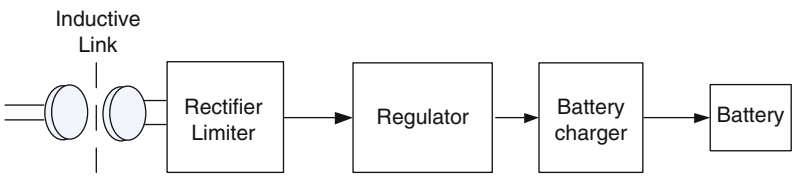

Batteries, Battery Management, and Battery Charging Technology. Figure 36
Inductive contactless charger scheme

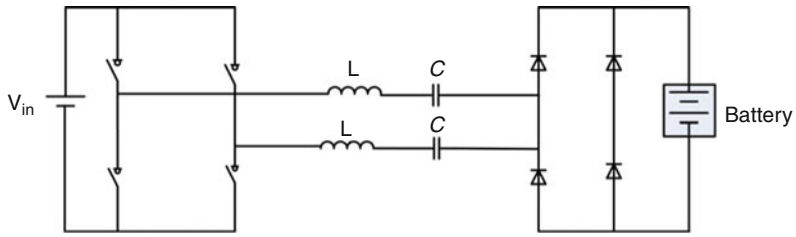

Batteries, Battery Management, and Battery Charging Technology. Figure 38
Capacitive contactless charger circuit configuration

There are four types of electromagnetic disturbances: conductive noise, inductive coupling, capacitive coupling, and radiation.

Conductive Noise Conductive noise addresses disturbances introduced by coupling of two or more circuits through interconnecting wires. For example, when a utility transformer supplies a rectifier, it is exposed to the same current as of the rectifier. Therefore, if the input current of the rectifier has harmonic content that is intolerable for the transformer, it can cause the transformer to malfunction.

Inductive Coupling Inductive coupling refers to disturbances that are caused by unwanted coupling of windings in different circuits. Leaking flux of an inductor inside a circuit may encircle a winding or a closed path in another circuit and results in inductive coupling. Figure 39 illustrates the modeling circuit of inductive coupling. Mutual inductance, M, indicates the degree to which two circuits are coupled. The winding voltage set is denoted in (18):

$$\begin{cases} v_1 = L_1 \dfrac{di_1}{dt} + M \dfrac{di_2}{dt} \\ v_2 = M \dfrac{di_1}{dt} + L_2 \dfrac{di_2}{dt} \end{cases} \tag{18}$$

The noise is represented as a mutual term using the mutual inductance

$$v_{\text{noise},12} = M \frac{di_2}{dt}. \tag{19}$$

Capacitive Coupling Figure 40 portrays the capacitive coupling circuit. Capacitive coupling happens when there is a small capacitance between different parts of different circuits, and the medium is electric field. The disturbance voltage caused by V_g can be expressed as:

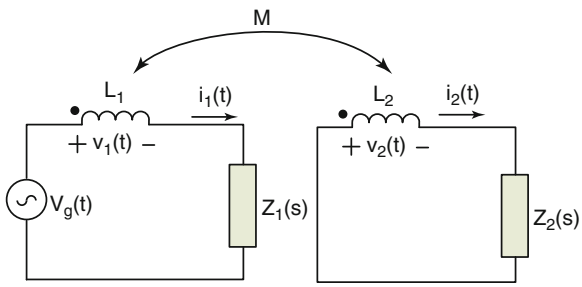

Batteries, Battery Management, and Battery Charging Technology. Figure 39
Modeling circuit of inductive coupling

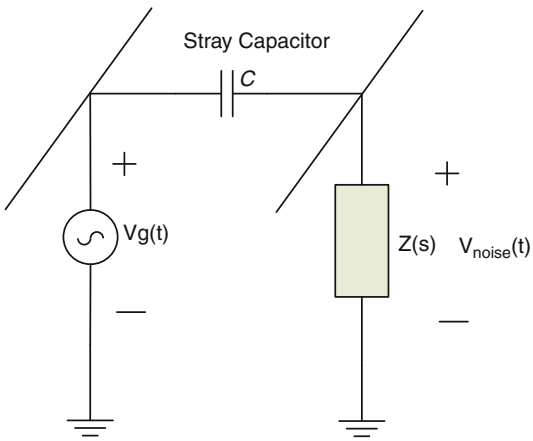

Batteries, Battery Management, and Battery Charging Technology. Figure 40
Modeling circuit of capacitive coupling

$$V_{\text{noise}}(s) = \frac{Z(s)Cs}{Z(s)Cs + 1} V_g(s). \tag{20}$$

Thus, decreasing C reduces the magnitude of induced noise voltage.

Radiation Radiation disturbance is caused by the absorption of electromagnetic waves where it is not intended. When the circuit dimensions are very small compared to one fourth of the wavelength of an electromagnetic wave, that electromagnetic wave cannot be fully absorbed by the circuit. Thus, radiation disturbance usually occurs in high-frequency waves with shorter wavelengths.

EMC in Battery Charging Circuits

Different guidelines should be followed in battery charging circuits to reduce electromagnetic susceptibility and emission of the converter circuit. Radiation disturbance is trivial in power electronic converters because switching frequency is relatively low, which means that the wavelength of the electromagnetic wave is much longer than the circuit dimensions. Susceptibility of the converter to capacitive and inductive noises can be diminished by shielding the converter. Air core inductors should be avoided in the converter circuit to meet electromagnetic interference (EMI) and electromagnetic compatibility (EMC) emission requirements. Using air core inductors causes long flux paths through the air that can encircle other windings and cause inductive coupling. On the other hand, using magnetic core inductors defines a specific path for flux through the core and prevents inductive coupling. The most challenging EMC issue of the power electronic converters is conductive noises. As discussed in the previous sections, battery charging circuits are mainly AC-DC or DC-DC circuits. In DC-DC battery charging circuits, pulsating input current should be prevented to meet EMC emission requirements. Thus, buck and buck-boost converters are not suitable candidates. As an alternative, Boost, Ćuk, and SEPIC converters can be used as they have built-in input current filters. The most suitable choice is a Ćuk converter as it has output current filter that makes it perfect for constant-current charging applications. There are two types of AC-DC battery charging circuits, namely phase-controlled rectifiers and PWM rectifiers. Phase-controlled rectifiers draw square shape input currents that have a very high harmonic content. Thus, the designed input current filter for phase-controlled rectifiers should have lower cutoff frequencies which requires larger and bulkier filter components. On the other hand, the input current of PWM rectifiers has less harmonic content that are located at higher frequencies. This characteristic of the PWM converters enables one to design input current filters by smaller inductors.

Regulations and Standards

Several standards have been developed by different institutes to regulate electromagnetic emission and susceptibility of electrical equipment, namely: MIL-STD 461; IEEE/ANSI SA-C63.14; IEEE 519, IEC 555-2, FCC, title 47, part 15; German VDE; and Japanese standards.

MIL-STD 461 establishes requirements for control of EMI emission and susceptibility of electronic and electromechanical equipment which are produced for use by agencies of the Department of Defense.

IEEE/ANSI SA-C63.14 provides the definitions for specific terms that are related to EMC, electromagnetic pulse (EMP), and electrostatic discharge (ESD).

IEEE-519 regulates the injection of harmonic currents to the power system due to nonlinear loads such as static power converters, arc discharge devices, saturated magnetic devices, and, to a lesser degree, rotating machines.

The IEC 555-2, IEC 1000-3-2, and IEC 1000-3-4 are emission standard related to operation of power electronic converter. These standards usually set an upper limit for harmonic content in each frequency.

Battery Management

Need for Battery Management

Two critical parameters for battery performance are battery voltage and operating temperature. A battery usually consists of a pack of cells connected in series. Manufacturing processes lead to imperfections in cells, as a result of which, all the cells in a pack are not identical. Electrical imbalances occur during charging and discharging of battery packs. Some cells in a battery will have different voltage levels for the same charging. This mismatch needs to be monitored to improve efficiency and safety of battery pack. Higher than rated temperatures in the batteries lead to undesirable chemical effects. Self-sustaining internal temperature buildup and gas pressure buildup are common. These conditions lead to safety hazards. It is vital to have a mechanism to monitor cell temperature and voltage and keep them within limits.

The main role of battery management systems (BMS) is to monitor cell voltage/current, state of charge/state of health, and the internal battery temperature and ambient temperature. The monitoring circuitry provides signals to the protection unit as well. Battery management systems differ on the basis of their primary functions, which depend upon the intended application. BMS for standby batteries in a power plant deal with monitoring of various battery parameters, maintaining readiness to deliver full power in the event of a system failure, and ensuring equal charging to increase battery life. On the other hand, a BMS in an electric vehicle must communicate with other controls in the automobile such as temperature controls, engine management, and safety systems.

There are three main objectives common to all battery management systems:

- Protect the cells or the battery from damage.
- Prolong battery life via smart control.
- Maintain battery in a state in which it can fulfill the functional requirements of the application for which it was specified.

State of Health Measurement

The state of health is a "measurement" that reflects the general condition of a battery and its ability to deliver the specified performance compared with a fresh battery. It takes into account such factors as charge acceptance, internal resistance, voltage, and self-discharge.

It is an estimate rather than a measurement. Battery manufacturers do not specify the SoH because they only supply new batteries. The SoH only applies to batteries after they have started their aging process either on the shelf or once they have entered service. The SoH definitions are therefore specified by test equipment manufacturers or by the user.

Any parameter which changes significantly with age, such as cell impedance or conductance, can be used as a basis for providing an indication of the SoH of the cell. Changes to these parameters will normally signify that other changes have occurred which may be of more importance to the user. These could be changes to the external battery performance such as the loss of rated capacity or increased temperature rise during operation, or internal changes such as corrosion.

Methods of Determining the State of Charge

State of charge (SoC) is defined as the capacity left in a battery expressed as a percentage of some reference. SoC of a battery is usually expressed as a percentage of the current battery capacity when it is fully charged. This definition may lead to an erroneous result when applied to a battery that has been in service for a long time. The maximum capacity of a battery reduces significantly with prolonged use. Considering this value to be the reference for state of charge measurement can lead to false results.

There are several techniques to determine SoC. A majority of them depend on measuring some convenient parameter which varies with the state of charge. Some are specific to particular cell chemistry. Some of the important ones are listed below:

Specific Gravity Measurement In lead-acid batteries, the electrolyte (sulfuric acid) is used up as the battery is subjected to a discharge cycle. As more and more electrolyte is used up, the specific density of sulfuric acid reduces. Thus, the specific gravity of the sulfuric acid is an indication of the state of charge for lead-acid batteries. This method is not feasible for VRLA batteries.

Voltage Measurement Cell voltage typically decreases for most cells during a discharge cycle. There is an almost linear relation between the state of charge and cell terminal voltage. Results may vary depending upon cell terminal voltage, temperature, discharge rate, and age of cell. A compensation factor needs to be included for SoC calculation by this method.

Li-ion cells have a flat voltage profile during a discharge cycle. The cell voltage drops abruptly when they are close to a complete discharge. As the cell voltage variation with SoC is not linear, cell voltage cannot be selected as a parameter to indicate SoC of Li-ion cells. In general, the voltage measurement technique fails for cells which have a flat voltage profile during a discharge cycle.

Current-Based SoC Estimation Charge in or out of the cell is calculated by integrating the current delivered by the cell for certain duration. This charge is

compared with the charge contained by a fully charged cell. This method provides a high accuracy for SoC measurement as it measures the charge directly. Three popular current sensing methods are used.

- Current shunt: The simplest method of determining discharge current is by measuring the voltage drop across a low ohmic value, high precision, series, sensing resistor. This resistor, connected between the battery and the load, is called a current shunt. This method of measuring current causes a slight power loss in the current path and also heats up the battery and is inaccurate for low currents.
- Hall-effect transducers: The Hall-effect transducers avoid the power loss problem, but they are more expensive. Unfortunately, they do not tolerate high currents and are susceptible to noise.
- Giant magneto resistance (GMR) sensors: These sensors are even more expensive than Hall-effect transducers, but they have higher sensitivity. They also have better high temperature stability than Hall-effect devices.

Kalman Filter Technique A Kalman filter is an algorithm to estimate the inner states of any dynamic system. The cell is represented by a mathematical state-space model, and SoC is considered as a state of the system. The Kalman filter accurately estimates the value of SoC and uncertainty. Armed with this information, the battery pack can be subjected to a more complete use, without fear of over- or under-charging cells. Nonlinear models of cells provide a highly accurate result.

The Kalman filter model for a rechargeable battery used in automobiles is initialized with a priori state estimate when the vehicle is turned on. The priori state estimate is provided on the basis of open-circuit voltage readings and a look-up table, self-discharge rate data from the cell model and the prior SoC when the vehicle was turned off. The algorithm then repeatedly updates the state estimate and state-uncertainty (error bound) estimate with each set of new measurements, as the system runs. Laboratory tests on real cells have shown that excellent SoC estimation with very tight error bounds are obtained whether or not the initial SoC estimate is accurate.

SoC Estimation from Internal Impedance Measurements During charge-discharge cycles, the composition of active chemicals changes in the battery, and this is reflected in the changes to internal impedance of the battery. Plots for variation of internal cell impedance with state of charge may be obtained for different cells. Thus, measuring internal impedance can indirectly provide information about SoC of the cell. However, on the flip side, cell internal impedance is also affected by temperature, which may lead to erroneous measurements.

Cell Balancing

When a battery pack is charged and discharged as a unit, individual cell temperature and internal chemistry characteristics can cause capacity imbalances in the form of voltage variations. Imbalances in cell voltages are caused by differences in cell capacities, internal resistances, chemical degradation, and inter-cell and ambient temperatures during charging and discharging. Any capacity imbalance between the modules can threaten the long-term reliability of the string as overall pack capacity is brought to the upper and lower limits of charge. Imbalances in cell voltages can cause cell overcharging and discharging, decreasing the total storage capacity and lifetime of the unit.

In a battery pack consisting of series connected cells, some cells have a diminished capacity owing to slight differences in manufacturing. When such a battery is subjected to charging cycle, the reduced capacity cells reach full charge earlier than the other cells in the battery, and there is a danger of overcharging these degraded cells. The capacity of the anomalous cells reduces even further with every successive charge/discharge cycle. The cumulative result is a temperature and pressure buildup which paves the way for an early failure of the cell.

Once a cell has failed, the entire battery must be replaced, and the consequences are extremely costly. Replacing individual failed cells does not solve the problem since the characteristics of a fresh cell would be quite different from the aged cells in the chain, and failure would soon occur once more. Some degree of refurbishment is possible by cannibalizing batteries of similar age and usage, but it can never achieve the level of cell matching and reliability that is possible with new cells.

Cell Charge Equalization

Battery management systems (BMS) for charge equalization monitor the state of charge of each cell. In low-cost applications, a circuit to monitor individual cell voltage may be employed. Switching circuits then control the charge applied to each individual cell in the series during the charging process to equalize the charge on all the cells in the pack.

A good charge/discharge equalization technique should ideally have the following features:

- High efficiency: Implementation of this technique should result in minimum power loss of the system.
- Small volume: Bulky volumes restrict portability and increase cost.
- Simple wiring schemes: Complex wiring schemes increase cost and decrease the reliability.
- In automobile applications, the cell must also be equipped to handle pulse charging from regenerative braking.

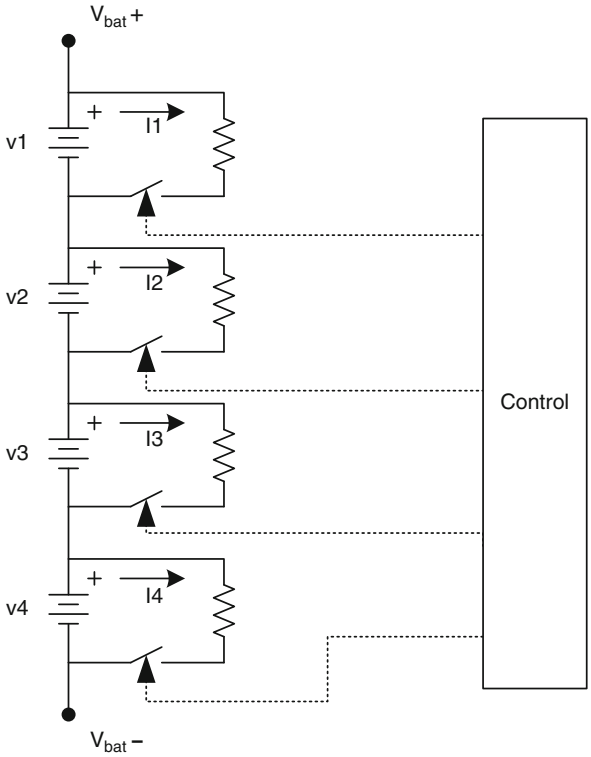

Batteries, Battery Management, and Battery Charging Technology. Figure 41
Passive charge balancing with a dissipative resistor

Passive Balancing Passive-charge balancing techniques involve bleeding off of charge from the cells with the highest voltage (hence, state of charge) in a battery pack (Fig. 41). A cell with a high charge is indicated by its higher cell voltage. Excess energy is removed through a bypass resistor until the voltage or charge matches the voltage on the weaker cells. Some passive balancing schemes stop charging the battery pack at the instant when any one of the cells in the pack reaches full charge. During discharge operation, they discharge the fully charged cells into a load until these cells reach the same charge level as the weaker cells. These schemes lead to underutilization of the battery pack.

Other schemes are designed to continue charging until all the cells are fully charged but to limit the voltage which can be applied to individual cells and to bypass the cells when this voltage has been reached. The shortcomings of this technique are that this method uses low bypass currents, and hence, equalization times are very long. Also, the battery pack performance is governed by the weakest cell. This process also causes power loss due to the bypass resistors which could drain the battery if operated continuously. It is however very easy to implement and is a low-cost option. Passive balancing is adequate for both lead-acid and nickel-based batteries, incorporating series string up to about six cells. Passive equalization cannot be employed for charge equalization in Li-ion-based battery strings.

Switched Capacitor The switched capacitor charge equalization method, also called a flying capacitor method, uses a capacitor to transfer charge between cells in a battery pack. Typically, these are adjacent cells in the series string as shown in Fig. 42. When the capacitor is connected to a cell with the higher voltage, the capacitor is charged. When the charged capacitor is connected to a cell with a lower voltage, the capacitor discharges and transfers charge into the new cell. When switched between two cells repeatedly, this movement of charge results in current from the cell with higher voltage to the cell with lower voltage. Finally, cell voltages of all cells in the string reach the same value and voltage equalization is achieved. High-frequency

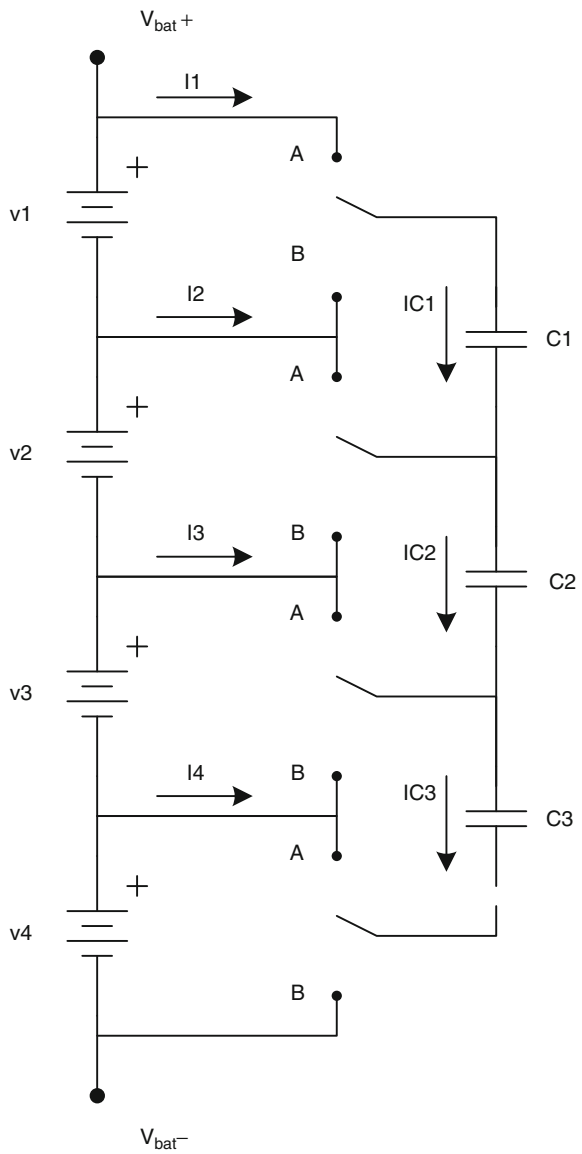

Batteries, Battery Management, and Battery Charging Technology. Figure 42
Schematic of a switched capacitor equalizer

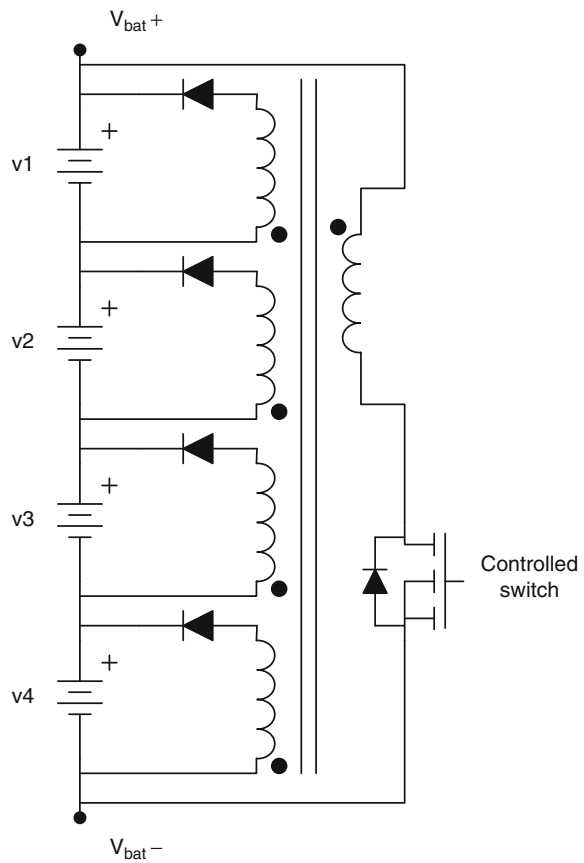

Batteries, Battery Management, and Battery Charging Technology. Figure 43
A schematic of a flyback-type inductive shuttle charge distribution

switching can be accomplished using a single-pole double-throw switch implemented using two sets of MOSFETs. The MOSFETs are switched with frequencies ranging in several kHz. An important feature in the switching scheme is that switches break before make to prevent momentary short circuits of the respective cells. Accordingly, the switch control signals incorporate a dead-band interval. This method is easy to implement and it results in reduced losses. A major drawback is that equalization process takes a long time if voltage differences between adjacent cells are small.

Multi-Output Transformer This method uses a transformer with its primary winding connected across the battery and one secondary winding which can be switched across individual cells. Both flyback and forward topologies are employed in practice. Figure 43 illustrates a flyback-based circuit to carry out charge balancing for a battery string. In the flyback structure, when the main switch is switched on, some energy is stored in the transformer magnetic field. When the switch is turned off, the energy is transferred to the secondary of the transformer, similar to the flyback concept. The bulk of the energy is taken up by

cells with lowest cell voltage. The main difference of this method over the switching capacitor scheme is that this method involves taking pulses of energy from the full battery, rather than small charge differences from a single cell, to top up remaining cells. Averaging of the charge level is similar to flying capacitor method, but it avoids the problem of small voltage differences in cell voltage and is consequently much faster. The transformer must have well-balanced secondary windings, otherwise voltage imbalances occur. Also, care must be taken to prevent transformer saturation.

DC-DC Converter Methods This technique involves using power electronics-based converters to transfer energy from higher charged cells to charge-efficient cells in a battery string. Different converter topologies such as the flyback, buck-boost, and Ćuk have been investigated to transfer energy between the batteries. Energy transfer may be unidirectional or bidirectional.

In unidirectional flyback mode, excess energy in the higher charged cell is transferred to the magnetized inductor of the transformer during turn-on operation of the converter. During the turn-off mode, this energy is returned to charge-deficient cells in the battery bank, and thus, charge leveling is achieved. Bidirectional converters are employed to facilitate local energy transfer between two neighboring cells independent of their respective cell voltage. The converters are operated in discontinuous mode to minimize switching losses. The disadvantage is that energy transmission efficiency is low when energy transfer occurs from the first cell to the last with many intermediate stages in a long string. To avoid power loss in intermediate stages, non-isolated buck-boost topologies have been explored in which energy is transferred from the first cell to all other cells in a bank without any intermediary.

Future Direction

Batteries and battery technologies are expected to become even more important in the future as consumers demand longer battery life from consumer electronics; variable energy sources, such as wind and solar, increase in prevalence in the electrical grid; and hybrid and all-electric vehicles become commonplace, to name a few applications currently driving technology development. The emphasis will be to develop batteries with low cost, high energy density, low weight/volume, completely safe, environmentally friendly, easily disposable, and made from abundant raw materials. Auxiliary battery management systems will become increasingly integrated into the battery pack to create a true "plug and power" energy storage module.

Lithium-based cells hold great promise for the future. Lithium-ion cells have nearly proliferated the consumer electronics market. These batteries are also expected to find a prominent role as ideal electrochemical storage systems in renewable energy plants, as well as power systems for sustainable vehicles, such as hybrid and electric vehicles. However, scaling up the lithium battery technology for these applications is still problematic since issues such as safety, costs, wide operational temperature, and materials availability are yet to be adequately resolved. Safety is an important issue with Li-ion technology, and hence, it forms one of the most important aspects of future research. Lithium-copper cells are seen as the future prospect for lithium-based batteries, although the technology is still in a nascent state. Traditionally, cathodes of Li-based cells have not been reusable and hence the motivation for Li-Cu system which makes provision for reusable electrodes.

Li-air batteries in which oxygen from the air serves as the cathode and lithium as the anode are also being explored and hold promise to increase energy density. Estimates indicated that the lithium-air battery could hold 5–10 times as much energy as a lithium-ion battery of the same weight and double the energy for the same volume. In theory, the energy density could be comparable to that of liquid fuels such as gasoline. However, rechargeable Li-air batteries are still some years away. Flow batteries hold promise for stationary, high-energy applications such as power stations to provide peak loads, backup energy in case of emergencies, and source leveling to mitigate variable production from renewable sources. Zn-Bromine, metal air, vanadium redox are some of the batteries which are being explored for UPS and grid storage applications as an alternative to VRLA batteries, which is currently the standard.

On the battery management side, mobile energy platforms are driving push toward wireless charging technologies and standards for contactless charging.

The Wireless Power Consortium has recently developed the standard for contactless charging called "Qi" for low-powered electronic devices (i.e., less than 5 watts). This standard is suitable for cellular phones and contains interface definition, performance requirements, and compliance testing. Further progress is expected for more powerful chargers for higher-power-consumption devices such as laptops. In the future, all compatible devices with the "Qi" standard will carry the "Qi" logo to show compatibility with "Qi" transmitters. The final goal is to have portable electronic devices charged with the stations with "Qi" logo in airports, railway stations, hotels, etc. Currently, the inductive contactless chargers can transmit power in short distance and with the same speed as wired chargers (e.g., cell phone applications). However, capacitive battery chargers can transmit higher levels of power in shorter time frame. Once the associated costs are alleviated, capacitive contactless charges can dominate the market. It has already started in applications such as a camera flash, where the ability to transfer high power over a short period of time is important. Inductive contactless chargers, however, will remain prime candidates for vehicular-charging applications.

Intermittency of renewable energy systems introduces some integration problems especially for high penetration levels of wind and solar energy systems. The battery energy storage systems are expected to play an important role in addressing intermittency. Appropriate control strategies are under development for charging systems to make wind and solar plant hourly dispatched based on forecasted conditions. Bidirectional converters are a key element here; the battery is charged by the grid during low-demand hours or by wind and solar plants during high-irradiance hours and windy periods. The battery is then discharged to the grid during shading of solar panels or lower wind speeds.

Charging circuitry is also used in stations for electric and plug-in hybrid vehicles (EVs and PHEVs). Three standardized charging levels are defined by the National Electric Code for EVs and PHEVs. Level one method uses 120 V, 15 A (12 A usable) power outlets which are common in residential and commercial units in the USA. However, they prolong the charging period due to limited maximum power (about 1.44 kW). Level two chargers use 240 V, single-phase, 40 A, outlets. They are known as the "primary" or "preferred" method of charging for PHEVs. There are two types of level two chargers, namely, inductive and conductive (wired). Although level two chargers enable faster charging, they require more safety restriction. Level three chargers use 480 V, 60–150 kW, three-phase power lines. They are intended to charge battery in about 10–15 min, also known as "fast charging" method. One may argue that PHEV batteries can be charged in 1–2 h using level two chargers, and thus, there are less incentives for higher power level three chargers in charging infrastructure for PHEVs.

Integrated battery chargers are an important aspect when considering system-on-chip devices. System-on-chip devices combine different parts of a system, which may conventionally require their own chip, into a single chip. For example, a typical system-on-chip sensor is designed to sense and transmit the data from an inaccessible location to the main controller. It is comprised of an integrated sensor, analog-to-digital converter, micro-controller, memory, and RF transmitter. Usually these system-on-chip sensors must be autonomous systems and thus generate their own power for an extended period of time. The required power for these micro-sensors can be supplied by solar cells or piezoelectric materials. Given the intermittency in the output of solar cell, micro-batteries are required to power the system during the low-light conditions. Therefore, integrated battery charging circuits are one of the essential components of system-on-chip sensors. Integrated battery chargers must meet specific criteria, namely, high efficiency, simple structure, and, most importantly, small size. Size is the prevalent factor in determining the total cost of the system in system-on-chip application. Therefore, in the applications that require extreme integration and low cost, battery is also integrated in the chip together with charger circuit.

Bibliography

1. Aditya JP, Ferdowsi M (2008) Comparison of NiMH and Li-Ion batteries in automotive applications. In: Proceedings, IEEE vehicle power and propulsion conference. IEEE, Piscataway
2. Available online: http://www.eetimes.com/electronics-news/4196006/Analyst-Super-capacitor-aided-wireless-charging-the-key-to-powering-mobiles
3. Available online: http://www.technology.am/wireless-charging-022522.html

4. Available online: http://www.wired.com/autopia/2010/11/ditch-the-cord-let-the-road-charge-your-ev/
5. Available online: http://www.wired.com/autopia/2011/03/google-installs-a-wireless-ev-charging-station/
6. Barnes FS, Levine JG (2011) Large energy storage systems handbook. CRC Press, Boca Raton
7. Beart P, Cheng L, Hay J (2006) Inductive energy transfer system having a horizontal magnetic field. UK Patent GB2,399,225
8. Bito A (2005) Overview of the sodium-sulfur battery for the IEEE stationary battery committee. In: Proceedings, IEEE power engineering society general meeting. IEEE, Piscataway, p 1232
9. Bullis K (2009) High-energy batteries coming to market: rechargeable zinc-air batteries can store three times the energy of a lithium-ion battery. http://www.technologyreview.com/business/23812/
10. Chia-Hsiang L, Chun-Yu H, Ke-Horng C (2010) A li-ion battery charger with smooth control circuit and built-in resistance compensator for achieving stable and fast charging. IEEE Trans Circuits Syst 57(2):506–517
11. Cong-Ling H, Jie W, Miao Z, Jin-Ming Y, Jin-Peng L (2004) Application of adaptive algorithm of solar cell battery charger. In: Proceedings of the 2004 IEEE international conference on electric utility deregulation, restructuring and power technologies (vol 2). IEEE, Piscataway, pp 810–813
12. Cope RC, Podrazhansky Y (1999) The art of battery charging. Battery conference on applications and advance, the fourteenth annual, California, pp 233–235
13. Crompton TR (1995) Battery reference book, 2nd edn. Butterworth-Heinemann Ltd, Oxford/Boston
14. Hua CC, Lin MY (2000) A study of charging control of lead-acid battery for electric vehicles. Industrial electronics ISIE, proceedings of the 2000 IEEE international symposium (vol 1), Puebla, pp 135–140
15. Hua CC, Lin MY (2000) A study of charging control of lead-acid battery of electric vehicles. IEEE proceedings. of ISIE (vol 1), Dallas, pp 135–140
16. Hui SYR (2006) Planar inductive battery charger. UK Patent GB238,972
17. IEEE Std 519 (2009) IEEE recommended practices and requirements for harmonic control in electrical power systems. IEEE, New York
18. Jaganathan SH (2009) Battery charging power electronics and control for plug-in hybrid electric vehicle. Thesis, Tennessee Technological University, pp 94–103
19. Kamibayashi M, Tanaka K (2001–2002) Recent sodium sulfur battery applications. In: IEEE transmission and distribution conference and exposition (vol 2). IEEE/PES, Atlanta, pp 1169–1173
20. Köhler U, Kümpers J, Ullrich M (2002) High performance nickel-metal hydride and lithium-ion batteries. J Power Sourc 105:139–144
21. Kiehne HA (2007) Battery technology handbook, 2nd edn. Chapter 12, Charging methods and techniques: general requirements and selection of chargers, Dekker
22. Kline M (2010) Capacitive power transfer. M.S. thesis, Department of Electrical Eng. and Computer Science, University of California, Berkeley
23. Kodali VP (1996) Engineering electromagnetic compatibility. IEEE Press, New York, pp 345–348
24. Koenig AA, Rasmussen JR (1990) Development of a high specific power sodium sulfur cell. In: Proceedings IEEE 34th international power sources symposium, Cherry Hill, pp 30–33
25. Krein PT, Balog RS (2002) Life extension through charge equalization of lead–acid batteries. In: Proceedings, IEEE international telecommunications energy conference (INTELEC). IEEE, Piscataway, pp 516–523
26. Kuhn BT, Pitel GE, Krein PT (2005) Electrical properties and equalization of lithium-ion cells in automotive applications. In: Proceedings, IEEE vehicle power and propulsion conference. IEEE, Piscataway, p 5
27. LeFevre BW (2003) Integrated microbattery charger for autonomous systems. Birgham Young University, Provo
28. Lex P, Jonshagen B (1999) The zinc/bromine battery system for utility and remote area applications. Power Eng J 13:3
29. Li P, Bashirullah R (2010) A wireless power interface for rechargeable battery operated medical implants. IEEE Trans Circuits Syst 54(10):912–916
30. Liawt CM, Chiangt SJ, Huang SC (1994) A three-phase multifunctional battery energy storage system. Proceedings of IECON 94 Conference. IEEE, New York, pp 458–463
31. Linden D, Reddy TB (2002) Handbook of batteries, 3rd edn. McGraw-Hill, New York
32. Liu X, Ron Hui SY (2007) Equivalent circuit modeling of a multilayer planar winding array structure for use in a universal contactless battery charging platform. IEEE Trans Power Electron 22(1):21–29
33. Marshman C (1992) Guide to the EMC directive. 89/336/EEC. IEEE Press, Piscataway
34. Mohan N, Undeland TM, Robbins WP (2003) Power electronics converters, applications and design, 3rd edn. Wiley, New York
35. Montrose MI (1996) Printed circuit design techniques for emc compliance. IEEE Press, New York
36. Moore SW, Schneider PJ (2001) A review of cell equalization methods for lithium ion and lithium polymer battery systems. SAE Technical Paper Series. pp 1–5
37. Morrow K, Karner D, Francfort J (2008) Plug in hybrid electric vehicle charging infrastructure review. US department of energy vehicle technologies program – advanced vehicle testing activity. Battelle Energy Alliance, The Idaho National Laboratory
38. Palanisamy T (1990) Charging techniques for a universal lead-acid battery charger. Proceedings of the 34th international power sources symposium. IEEE, New York, pp 72–76, 25–28
39. Plett G (2002) Kalman-Filter soc estimation for LipbHev cells. In: Proceedings of the 19th international battery, hybrid and fuel cell electric vehicle symposium & exhibition (EVS19). Busan, pp 19–23
40. Poon NK, Pong MH, Tse CK (2003) A constant-power battery charger with inherent soft switching and power factor correction. IEEE Trans Power Electron 18(6):1262–1269

41. Pop V, Bergveld H, Notten P, Regtien P (2005) State-of-the-art of battery state-of-charge determination. Meas Sci Technol 16(12):93–110
42. Rashid MH (2006) Power electronics handbook, 2nd edn. Academic, California
43. Redl R (1996) Power electronics and electromagnetic compatibility. Power electronics specialists conference, PESC '96 record. 27th annual IEEE (vol 1). IEEE, New York, pp 15–21, 1:23–27
44. Tamyurek B, Nichols DK, Demirci O (2003) The NAS battery: a multifunction energy storage system. In: Proceedings IEEE power engineering society general meeting (vol 4). IEEE, Piscataway, pp 1991–1996
45. Tamyurek B, Nichols DK, Vollkommer HT (2003) Sodium sulfur battery applications. In: Proceedings IEEE power engineering society general meeting (vol 4). IEEE, Piscataway, pp 2323–2324
46. Vrankovic Z, Abedini AZ, Nasiri A (2007) A novel battery charger for automotive applications. IEEE conference of PESC'07. IEEE, Piscataway, pp 1465–1470
47. Wiesener K, Ohms D, Benczúr-Ürmössy G et al (1999) High power metal hydride bipolar battery. J Power Sourc 84(2):248–258
48. Zhi-Guo K, Chun-Bo Z, Ren-Gui L, Shu-Kang C (2006) Comparison and evaluation of charge equalization technique for series connected batteries. In: Record, IEEE 37th IEEE power electronics specialists conference (PESC), Jeju, pp 1–6

Batteries, Introduction

Ralph J. Brodd
Broddarp of Nevada, Henderson, NV, USA

Batteries for storage of electricity from solar and wind generation farms are a key element in the success of sustainability. Electric vehicles are the second link in the chain powered by advanced battery systems. This section describes the various devices used in electrochemical energy storage including an overview of electrochemical processes and devices.

► Nanocarbons for supercapacitors describes electrochemical capacitors, sometimes called supercapacitors, and are energy storage devices similar to batteries but capable of delivering large amounts of energy in a very short time. These devices rely on the characteristics of the electrical double layer that forms on all conductors when immersed in an electrolyte. The electrical double layer has a high capacitance because the charges are separated on the order of atomic dimensions. Since there is no mass transfer involved in the delivery of current, response time to a change is 10^{-6} s or faster. As a result, electrochemical capacitors can deliver large amounts of energy in short periods of time. The double layer forms in less than 10^{-6} s and responds to changes in a similar time frame. This is about 1,000 times faster than the electrochemical reaction at a battery electrode that has a time constant in the range of 10^{-3} s. The devices find application wherever power is required to service an application.

► Electrochemical Supercapacitors and Hybrid Systems describes electrochemical energy storage devices having higher energy density than electrolytic capacitors and higher power density than batteries. These devices rely on the characteristics of the electrical double layer that forms on all polarized conductors when immersed in an electrolyte. The double layer forms in less than 10^{-6} s and responds to changes in a similar time frame. This is about 1,000 times faster than an electrochemical reaction at a battery electrode that has a time constant in the range of 10^{-3} s. As a result, these can deliver large amounts of energy in a very short time. These devices find application where high power delivery is required.

► Rechargeable Batteries, Separators for describes the characteristics of porous membranes that hold the electrolyte and physically separate the negative from the positive electrodes in battery systems. The separator is a key element in battery construction as it physically separates and prevents direct contact (shorting) between the positive and negative electrodes. The separator materials are insulators but have the capability to absorb conducting electrolyte solutions to provide electrical continuity between the anode (negative terminal) and cathode (positive terminal) of the battery system. Each new battery system places new requirements placed on the separator material. The recent growth in the battery industry with the introduction of several new battery systems has resulted in the need to create and optimize new separator materials to meet the market demands. Correspondingly, the demand for novelty in separator membranes, to match the newer battery chemistries and geometries, continues to grow.

► Lead Acid Battery Systems and Technology for Sustainable Energy describes the basis for the many different commercial lead acid battery designs and electrical requirements ranging from automotive and

stationary energy storage to sustainable energy storage and power system regulation. The lead acid batteries constitute the single largest battery market segment. The reliability, availability, and low cost are the key to the success of the lead acid system. It is among the greenest of battery systems because of its established recycling industry. The ability to adapt the system to new applications and to optimize their performance to meet the demands of new applications has been a successful international effort for 150 years and continues to generate improved battery designs and power systems for the future.

While graphite is the material of choice for the anode in present commercial lithium ion batteries, an active search to identify a new high-energy anode material has identified ► silicon-based anodes for Li-ion batteries as a promising replacement for the graphite anode material. The silicon-lithium alloy has promise to significantly increase the cell capacity up to ten times that of the present graphite lithium anode. The successful transition will require developing method to handle the volume change characteristic of the silicon materials without disintegration of the anode structure. Strategies are based on fundamental mechanistic research to better understand the electrochemical lithiation and delithiation processes of silicon materials during charge-discharge cycling in terms of crystal structure, phase transitions, morphological changes, and reaction kinetics. It is expected that a viable silicon nanostructure anode can be developed with three to five times the capacity of graphite.

► Nickel-based battery systems describes the progression of higher-energy nickel cathode battery systems starting with iron for electric vehicle applications; followed by cadmium, metal hydride, hydrogen, and zinc anodes and their high power and good cycle life; and ending with nickel-hydrogen batteries for long life in space applications. At the turn of the twentieth century, simultaneously, Edison in the USA and Junger in Sweden independently developed the nickel-iron rechargeable battery system. The system powered the first electric vehicles in the early 1900s and is still produced today for long-life energy storage applications.

► Lithium Ion Batteries, Electrochemical Reactions in details the various advanced experimental techniques that are used to define the characteristics of new high performance materials as well as improve the performance of existing materials for lithium ion batteries. X-ray, neutron and nuclear magnetic resonance techniques, etc. each provide essential complimentary information on solid materials on the crystal structure of new and potential cathode and anode materialsat an atom level leading to improved performance of existing materials as well as identifying potential high performance new materials.

► Medical Device Batteries describes wearable and implantable medical devices powered by batteries. Devices include those that are used for cardiac rhythm management (pacemakers, defibrillators, and heart failure devices), hearing loss, bone growth and fusion, drug delivery for therapy or pain relief, nerve stimulation for pain management, urinary incompetence and nervous system disorders, vision, diagnostic measurements and monitoring, and mechanical heart pumps.

► Lithium-Ion Battery Systems and Technology batteries have revolutionized battery powered electronic devices with its light weight, high energy storage capability, and long cycle life. Since its introduction in 1991, it has grown to a $4+ billion market in 2010 and dominated powering the modern portable electronic devices. It replaced nickel cadmium and nickel metal hydride batteries and is positioned to power the electric vehicle market in the near future. The prime reasons for its rapid success and proliferation in consumer electronic market are high unit cell voltage, high energy density, and long cycle and shelf life with no memory effect. The significant progress of Li-ion batteries is mainly due to numerous innovations and advancements in materials, designs, and safety. This entry is intended to provide an overview of Li-ion batteries on several aspects. Starting with a brief discussion on its history, commercial success, and working mechanism, all the critical components inside the cell have been discussed with adequate details. The later part of this entry will primarily focus on manufacturing process with detailed discussion on cell-level safety, followed by overview of recent advances and modern trends in Li-ion systems.

► Lithium-ion Batteries, safety provides an overview of the safety considerations for Li-ion cells. Presently, Li-ion cells have a record of field failures or safety incident of one incident every ten million cells. The 18650 cell used in portable electronic applications contains sufficient energy to self-heat the cell to over

600°C. This does not include oxidation of the electrolyte solvent by the cathode oxide materials. Adiabatically, including the electrolyte, the temperature is significantly higher. The causes of an incident include overcharge and heating from external sources. All cells have safety devices such as PTC, CID, vents, and safety circuitry. An internal short is the most common trigger for a safety incident.

► Lithium Battery Electrolyte Stability and Performance from Molecular Modeling and Simulations provide an example of the power of this experimental technique. Molecular orbital calculations have proven useful and have the capability to identify the details of lithium insertion into battery-related materials and to identify new cathode materials as well as improve the performance of existing materials. Crystallite size has tremendous effect to the thermodynamics and kinetics in intercalation compounds and impacts the diffusion/transport length, effective reaction surface area, surface energy, and interphase energy. Also, the experimental verification of one-dimensional lithium diffusion in Li_xFePO_4 was confirmed.

► Battery cathodes provides an overview of the current cathode materials available for use in Li-ion batteries and a discussion of the various battery systems. Li-ion batteries are dual intercalation systems, in which both the cathode and the anode have structures that allow reversible insertion and extraction of lithium cations. In principle, there are numerous materials that undergo reversible intercalation and can serve as electrode materials. Hence, unlike the lead acid battery which describes a specific chemistry, the chemistry of the Li-ion battery is not fixed but determined by the choice of anode and cathode materials.

► Olivine Phosphate Cathode Materials, Reactivity and Reaction Mechanisms provide a summary of the characteristics of the phosphate cathode materials. The interest in phosphates was triggered by the work of Goodenough in identifying lithium iron phosphate, $LiFePO_4$, as a promising cathode material for use in Li-ion battery systems. The nanosize crystal structure gives the material unique properties including high surface area, very long cycle life, and, just as important, a low-cost cathode material.

The ► Battery Components, Active Materials for reviews the role played by the pioneers Volta, Daniell, Davy, Galvani, Faraday, and Davie in providing the basis for batteries as they are known today. The key to identifying new battery materials is found in the fundamental properties of the materials and is the route to improve performance of present materials as well as the identification of new materials with long-life capability.

Battery Cathodes

Marca M. Doeff
Environmental Energy Technologies Division, Lawrence Berkeley National Laboratory, University of California, Berkeley, CA, USA

Article Outline

Glossary
Definition of the Subject and Its Importance
Introduction
Characteristics of Battery Cathode Materials
Future Directions
Acknowledgments
Bibliography

Glossary

Anode – (negative electrode) This electrode donates electrons during cell discharge.

Battery A device consisting of one or many electrochemical cells connected together, in which chemical energy is converted into power. These can be further categorized as primary (non-rechargeable) or secondary (rechargeable) systems.

Capacity The amount of charge that a battery contains, often expressed as mAh or Ah. This depends on the size of the battery and its chemistry. Rated capacity also depends on the current used.

Cathode – (positive electrode) This electrode accepts electrons during cell discharge.

Cell One unit of a battery, commonly consisting of an anode, a cathode, an electrolyte, a separator, and two current collectors.

Energy density or specific energy Energy per unit volume or weight of a material or a device, respectively, often expressed as Wh/L or Wh/kg. Energy is

a product of the cell voltage and capacity per unit volume or weight.

Intercalation compound (host material, insertion compound) Originally, this referred specifically to layered structures that can undergo insertion of ions or molecules between the van der Waals gaps, but is now commonly used for any structure that undergoes topotactic insertion reactions. For Li-ion battery materials, it refers specifically to compounds that undergo reductive insertion of lithium ions, such as graphite (used as an anode) or $LiCoO_2$ (used as a cathode).

Jahn–Teller effect The geometric distortion of nonlinear complexes of certain transition metal ions to remove degeneracy. For example, Mn(III) in octahedral coordination is expected to have an electronic configuration of $t_{2g}^3e_g^1$. Elongation along one axis of the octahedron, for example, decreases the symmetry and removes the degeneracy.

Power density and specific power Power per unit volume or weight, respectively, often expressed as W/L or W/kg. Power is the product of the current and the operating voltage. This is a function both of the materials used and the cell design.

Practical energy density or specific energy Based on the entire weight or volume of the device including inert components. It may be only 1/4–1/2 of the theoretical energy density. It may also refer only to the useable portion of the theoretical capacity of the anode or cathode material itself.

Ragone plot A plot showing the relationship between energy density and power density for any particular battery chemistry. This relationship is a function both of battery design and chemistry for Li-ion batteries.

Solid electrolyte interface (SEI) A very thin (nanometer scale) layer formed on a lithium or lithiated graphite anode, which develops upon reaction with certain kinds of electrolytic solutions. The SEI is a specific kind of reaction layer that is ionically conductive but electronically insulating. It passivates the electrode, preventing further reaction with the electrolytic solution, and allows reversible operation of the device.

Specific capacity The amount of charge per unit weight that a battery electrode material contains, often expressed as mAh/g. This is a fundamental characteristic of the material, and depends upon its redox chemistry and structure.

Theoretical energy density, specific energy, capacity Based on weight or volume of the electrode active materials only.

Topotactic transformation A transformation in a crystal lattice involving displacement or exchange of atoms, which maintains the basic structure.

Definition of the Subject and Its Importance

In a discharging battery, the cathode is the positive electrode, at which electrochemical reduction takes place. As current flows, electrons from the circuit and cations from the electrolytic solution in the device move toward the cathode. Although these processes are reversed during cell charge in secondary batteries, the positive electrode in these systems is still commonly, if somewhat inaccurately, referred to as the cathode, and the negative as the anode. Because this terminology is widespread throughout the Li-ion battery literature, this usage will be adopted for this article.

Li-ion batteries are dual intercalation systems, in which both the cathode and the anode have structures that allow reversible insertion and extraction of lithium cations. In principle, there are numerous materials that undergo reversible intercalation and can serve as electrode materials. Hence the chemistry of the Li-ion battery is not fixed, unlike the great majority of battery systems. The choice of cathode greatly affects the performance and cost of a Li-ion battery; for example, it is a major determinant of energy density, since it typically has a lower specific capacity than the most common anode material, graphite (372 mAh/g), to which it must be matched.

Introduction

The very high theoretical capacity of lithium (3,829 mAh/g) provided a compelling rationale from the 1970s onward for the development of rechargeable batteries employing the elemental metal as an anode. The realization that some transition metal compounds undergo reductive lithium intercalation reactions reversibly allowed the use of these materials as cathodes in these devices, most notably, TiS_2 [1–3]. Another intercalation compound, $LiCoO_2$, was described shortly thereafter [4, 5] but, because it was produced

in the discharged state, was not considered to be of interest by battery companies at the time.

Due to difficulties with the rechargeability of lithium and related safety concerns, however, alternative anodes were sought. The graphite intercalation compound (GIC) LiC_6 was considered an attractive candidate [6] but the high reactivity with commonly used electrolytic solutions containing organic solvents was recognized as a significant impediment to its use. The development of electrolytes that allowed the formation of a solid electrolyte interface (SEI) on surfaces of the carbon particles was a breakthrough that enabled commercialization of Li-ion batteries [7]. In 1990, Sony announced the first commercial batteries based on a dual Li-ion intercalation system [8]. These devices are assembled in the discharged state, so that it is convenient to employ a prelithiated cathode such as $LiCoO_2$ with the commonly used graphite anode. After charging, the batteries are ready to power devices.

The practical realization of high energy density Li-ion batteries revolutionized the portable electronics industry, as evidenced by the widespread market penetration of mobile phones, laptop computers, digital music players, and other lightweight devices, since the early 1990s. In 2009, worldwide sales of Li-ion batteries for these applications alone were US$7 billion [9]. Furthermore, their performance characteristics (Fig. 1) make them attractive for traction applications such as hybrid electric vehicles (HEVs), plug-in hybrid electric vehicles (PHEVs), and electric vehicles (EVs); a market predicted to be potentially ten times greater than that of consumer electronics. In fact, only Li-ion batteries can meet the requirements for PHEVs as set by the US Advanced Battery Consortium (USABC), although they still fall slightly short of EV goals.

In the case of Li-ion batteries, the trade-off between power and energy shown in Fig. 1 is a function both of device design and the electrode materials that are used. Thus, a high-power battery (e.g., one intended for an HEV) will not necessarily contain the same electrode materials as one designed for high energy (i.e., for an EV). As is shown in Fig. 1, power translates into acceleration, and energy into range, or miles traveled, for vehicular uses. Furthermore, performance, cost, and abuse-tolerance requirements for traction batteries [11] differ considerably from those for consumer electronics batteries. Vehicular applications are particularly sensitive to cost; currently, Li-ion batteries are priced at about US $1,000/kWh, whereas the USABC goal is US $150/kWh [12]. The three most

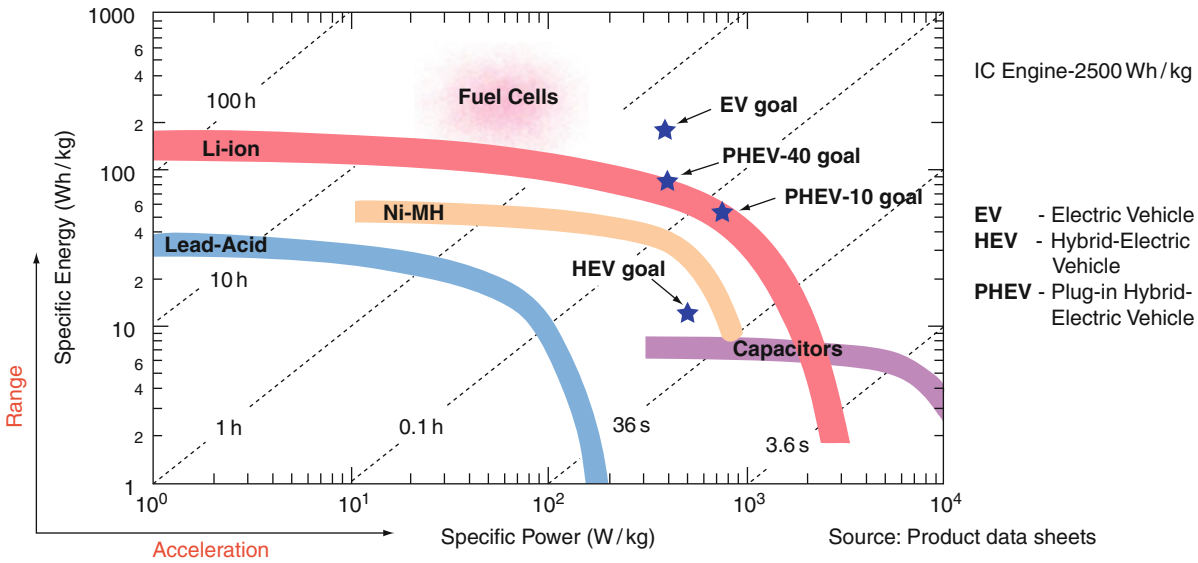

Battery Cathodes. Figure 1

A Ragone plot, showing the relationship between specific power and specific energy for several types of electrochemical devices. Goals set by FreedomCar for HEV, PHEVs, and EVs are also indicated (Used with permission from [10])

expensive components of a Li-ion battery, no matter what the configuration, are the cathode, the separator, and the electrolyte [13]. Reduction of cost has been one of the primary driving forces for the investigation of new cathode materials to replace expensive $LiCoO_2$, particularly for vehicular applications. Another extremely important factor is safety under abuse conditions such as overcharge. This is particularly relevant for the large battery packs intended for vehicular uses, which are designed with multiple cells wired in series arrays. Premature failure of one cell in a string may cause others to go into overcharge during the passage of current. These considerations have led to the development of several different types of cathode materials, as will be covered in the next section. Because there is not yet one ideal material that can meet requirements for all applications, research into cathodes for Li-ion batteries is, as of this writing, a very active field.

Characteristics of Battery Cathode Materials

Modern cathode materials for Li-ion batteries are generally prepared in the lithiated (discharged) state, so that they can be paired with delithiated anodes such as graphite. For ease of handling, it is desirable that the material be reasonably air-stable at room temperature. Furthermore, graphite anodes impose a penalty of approximately 0.1 V in average cell potential compared to Li metal. To compensate for this, and also to maximize energy density, cathodes intended for use in Li-ion batteries have higher average potentials versus Li/Li^+ than earlier materials such as TiS_2 and vanadates [14] developed for Li metal batteries. Furthermore, the requirement for high specific capacity generally restricts choices to compounds containing first-row transition metals (usually Mn, Fe, Co, and Ni). Environmental and toxicity concerns have precluded the development of most V or Cr-containing materials, although electroactive compounds containing these metals exist. Today's technologically important cathodes fall into two broad categories: metal oxides and polyanionic compounds.

Figure 2 shows representations of the crystal structures of the most commonly used cathode materials for Li-ion batteries, and Table 1 summarizes their general properties. Figure 3 shows typical discharge profiles of selected materials in Li half-cell configurations.

Layered Transition Metal Oxides

$LiCoO_2$ was the first of the layered transition metal oxides to be commercialized, and is still used today in batteries for consumer devices. It has the structure shown in Fig. 2a, where Co and Li, located in octahedral sites, occupy alternating layers along the 111 planes in a cubic close-packed (ccp) oxygen array, to form a structure with overall hexagonal symmetry (space group R-3m). This type of stacking arrangement is called O3 in layer notation, indicating that there are three transition metal layers per unit cell and the Li ions are octahedrally coordinated.

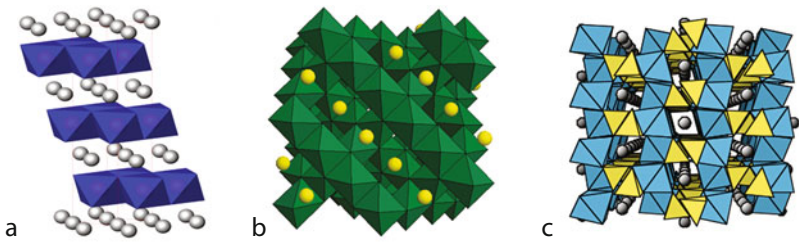

Battery Cathodes. Figure 2
Structures of common cathode materials: (**a**) The layered structure of $LiCoO_2$ with *c*-axis oriented vertically. The octahedrally coordinated Li ions in *3a* sites are represented as spheres and CoO_6 (Co in *3b* sites) as octahedra; (**b**) the cubic structure of $LiMn_2O_4$ spinel, with tetrahedrally coordinated Li ions (in *8a* sites) represented as spheres, and MnO_6 (Mn in *16d* sites) as octahedra; and (**c**) the olivine structure of $LiFePO_4$, looking down the *b*-axis. Octahedrally coordinated Li ions are represented as spheres, and FeO_6 and PO_4 as octahedra and tetrahedra, respectively

Battery Cathodes. Table 1 Characteristics of commercial Li-ion battery cathode materials

Material	Structure	Potential versus Li/Li^+, average V	Specific capacity, mAh/g	Specific energy, Wh/kg
$LiCoO_2$	Layered	3.9	140	546
$LiNi_{0.8}Co_{0.15}Al_{0.05}O_2$ (NCA)	Layered	3.8	180–200	680–760
$LiNi_{1/3}Co_{1/3}Mn_{1/3}O_2$ (NMC)	Layered	3.8	160–170	610–650
$LiMn_2O_4$ and variants (LMO)	Spinel	4.1	100–120	410–492
$LiFePO_4$ (LFP)	Olivine	3.45	150–170	518–587

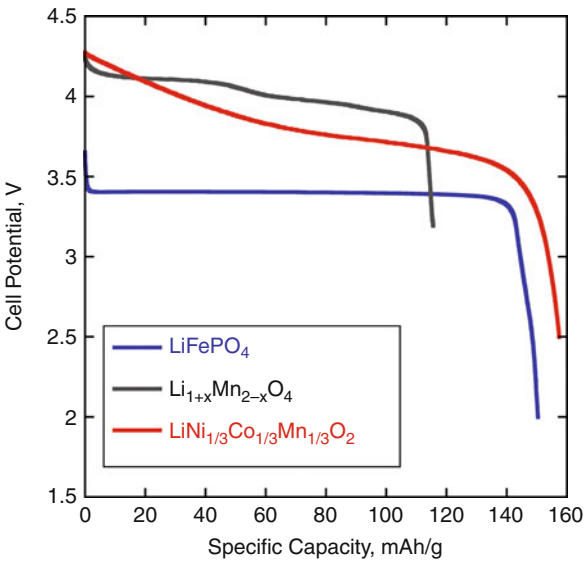

Battery Cathodes. Figure 3
Discharge profiles of lithium cells containing $LiFePO_4$, $Li_{1+x}Mn_{2-x}O_4$, or $LiNi_{1/3}Co_{1/3}Mn_{1/3}O_2$ electrodes

Delithiation proceeds topotactically [15, 16] and is reversible over the composition range $1 \geq x \geq \sim 0.5$ for x in Li_xCoO_2, giving a practical specific capacity of about 140 mAh/g below 4.2 V versus Li/Li^+. Extraction of lithium to values of $x < \sim 0.5$ results in higher practical capacities initially, but often increases cycling losses [17]. This has been attributed to side reactions involving particle surfaces, which increase cell impedance, and to structural instability associated with phase changes at very low values of x in Li_xCoO_2 [18–21]. Coating $LiCoO_2$ particles, or rigorous heat treatment to remove surface species [22–24], results in improved cycling below 4.5 V versus Li/Li^+, but full delithiation is still not possible without cycling losses.

A layered compound with the nominal composition of $LiNiO_2$ has also been extensively studied for battery applications [25–28]. Its lower cost compared to $LiCoO_2$, and the potential for higher energy density were driving forces for its development. Although the structure is similar to $LiCoO_2$, $LiNiO_2$ readily exhibits non-stoichiometry. During synthesis, there is a tendency toward loss of lithium and reduction of some Ni to the +2 oxidation state. The Ni^{2+} migrates to Li^+ *3a* sites, due to the similarities in size between the two types of ions. The actual composition can be written as $Li_{1-z}Ni_{1+z}O_2$ with $0 < z < 0.2$, or as $(Li_{1-z}Ni_z^{2+})_{3a}(Ni_z^{2+}Ni_{1-z}^{3+})_{3b}O_2$ [29]. The degree of disorder is influenced by the synthetic conditions, and the electrochemical properties (e.g., the first cycle reversibility) are affected by the degree of non-stoichiometry [30, 31]. The difficulty in synthesizing high-quality $LiNiO_2$ was one impediment to its widespread adoption as a cathode material in Li-ion batteries, although nearly ideal structures can be obtained if sufficient care is taken [29]. (However, perfectly stoichiometric $LiNiO_2$ materials probably do not exist). Partial substitution of Ni with Co [32] was later found to be effective at reducing the cationic disorder on *3a* sites, leading to compositions such as $LiNi_{0.8}Co_{0.2}O_2$. Cobalt also helps to reduce oxygen loss at high states-of-charge, improving safety.

The thermal instability of Li_xNiO_2 at high states-of-charge [33–36] also raised a great deal of concern about the safety of this material when used as a cathode. The properties of $LiNiO_2$ have been improved via coating and doping with Mg, leading to a very high-capacity electrode material [37] with better thermal properties. However, the most commonly

used electrode material related to $LiNiO_2$ is $LiNi_{0.8}Co_{0.15}Al_{0.05}O_2$ or NCA, which is now commercially produced (see Table 1 for general properties). The presence of Al in NCA improves both the thermal [33–36] and electrochemical properties [38, 39]. The high specific capacity and good power capability of this material make it attractive for vehicular applications although it is still not considered as inherently safe as other candidates such as LFP (see Table 2 and the discussion of olivines below).

Battery Cathodes. Table 2 Relative merits of selected commercial Li-ion battery cathodes

Advantages	Disadvantages
LMO ($LiMn_2O_4$ and variants)	
Low cost Excellent high rate performance High operating voltage No resource limitations Moderate safety (oxygen release)	Mn solubility issue, affecting cycle life Low capacity
LFP ($LiFePO_4$ and variants)	
Moderately low cost Excellent high rate performance No resource limitations Very slow reaction with electrolyte Excellent safety (no oxygen release)	Low operating voltage Low capacity, especially for substituted variants Controlling patents
NMC ($LiNi_{1/3}Co_{1/3}Mn_{1/3}O_2$) and variants	
High capacity High operating voltage Slow reaction with electrolytes Moderate safety (oxygen release)	High cost of Ni and Co Potential resource limitations Relatively new in performance Controlling patents
NCA ($LiNi_{0.8}Co_{0.15}Al_{0.05}O_2$)	
Performance is well established Slow reaction with electrolytes High capacity High voltage Excellent high rate performance	High cost of Ni and Co Potential resource limitations Controlling saft patents

Several ternary Li-Fe-O phases exist with differing arrangements of cations in cubic close-packed oxygen arrays [40]. However, $LiFeO_2$ with the R-3m structure is metastable and generally must be prepared via indirect methods such as ion exchange of $NaFeO_2$. The electrochemical properties of this material [41] and most other polymorphs [42, 43] are not, however, suitable for lithium-ion batteries due to low and highly sloping voltage profiles or poor cycling properties. Li_5FeO_4 with the anti-fluorite structure has a potential profile that may be compatible in a Li-ion battery configuration, but delithiation does not appear to proceed via simple oxidative deintercalation [44]. This material has been proposed for use as a lithium-ion source for lithium-ion batteries (i.e., to lithiate graphite anodes so that cathodes in the charged state may be used).

Ternary Li-Mn-O phases with Mn in the +3 or +4 oxidation state crystallize as spinels, the rock salt structure Li_2MnO_3, or as orthorhombic $LiMnO_2$ with a corrugated structure (o-$LiMnO_2$) but not as O3 layered structures. Lithium manganese oxide spinels (LMO) are technologically important cathodes and will be considered in a later section (*vide infra*). The Na-Mn-O system contains numerous polymorphs, including layered structures. $NaMnO_2$ has the same stacking arrangement as $LiCoO_2$, but is monoclinically distorted (space group C2/m), due to the abundance of Jahn–Teller distorted Mn^{3+} ions. Ion exchange of this compound yields a layered $LiMnO_2$ (designated O'3, with the prime indicating the monoclinic distortion) [45], but it rapidly converts to spinel upon electrochemical cycling, as does orthorhombic $LiMnO_2$ [46]. O'3-$LiMnO_2$, o-$LiMnO_2$, and spinel manganese oxide all have cubic close-packed oxygen arrays and differ only in the cation arrangement. Upon electrochemical delithiation of the first two materials, disproportion of Mn^{3+} into Mn^{2+} and Mn^{4+} ions occurs and Mn^{2+} ions subsequently migrate into vacant sites in the lithium layers via low-energy pathways, facilitating structural rearrangement to spinel [47].

Lithium-deficient layered Li_xMnO_{2+y} ($x \approx 0.7$, $y \geq 0.05$), which has an O2 rather than O3 stacking arrangement, does not convert to spinel upon cycling [48, 49], because the oxygen array is not ccp. In addition, non-stoichiometric lithium manganese oxides that are intergrowths of O2 and O3 phases show better

resistance to conversion than the pure O3 structure [50, 51]. The presence of transition metal vacancies in these compounds (which reduce the concentration of the Jahn–Teller Mn^{3+} ions) results in low rate capability, because the vacancies tend to trap nearby lithium ions, impeding their mobility [52].

Other lithium manganese oxides with tunnel structures [53–55] exhibit interesting electrochemical properties, particularly those based on the $Na_{0.44}MnO_2$ structure. This material has excellent cycling characteristics [56] and rate capability [57], and does not convert to spinel, although the practical capacity is limited by voltage considerations (the average potential at which lithium is extracted is the highest of any known manganese oxide [58]). All of these tunnel and O2 or O2/O3 layered materials, however, must be prepared via ion exchange of their sodium manganese oxide structural analogs, complicating their preparation. Furthermore, the lithium deficiency of the ion-exchanged materials limits the capacity in Li-ion battery configurations, as all of the cycleable lithium must originate from the cathode.

Li_2MnO_3 can be considered a layered structure similar to $LiCoO_2$, but with 111 planes alternately occupied by Li and $Li_{1/3}Mn_{2/3}$. Ordering of Li and Mn in the transition metal layer imposes a monoclinic superstructure, but the stacking arrangement is essentially identical to that of the R-3m structures discussed above. Mn in this compound is tetravalent and all lithium sites are occupied, precluding either oxidative deintercalation or reductive intercalation. Nevertheless, several researchers have observed electrochemical activity of Li_2MnO_3 when it is charged in lithium half-cells to high potentials [59]. Recent evidence [60] suggests that lithium deintercalation occurs with simultaneous oxygen loss during the initial charge, as well as H^+/Li^+ exchange. The converted material becomes electroactive and can subsequently be lithiated during cell discharge. Acid leaching of Li_2MnO_3 also yields an electroactive manganese oxide phase [61]. The reaction involves loss of Li_2O from the structure and ion exchange, to produce layered $H_{1-x}Li_x[Li_{0.33}Mn_{0.67}]O_2$ [62].

The compound $Li_{1.2}Mn_{0.4}Cr_{0.4}O_2$ [63] is essentially a solid solution of layered Li_2MnO_3 and $LiCrO_2$ with an O3 stacking arrangement [64]. Very high discharge capacities (~200 mAh/g) can be obtained based on $Cr^{3+}\leftrightarrow Cr^{6+}$ redox processes. Conversion to spinel phases does not occur because Mn remains in the +4 oxidation state throughout charge and discharge, nor does the electrode need chemical or electrochemical activation prior to use. Nevertheless, concerns over the environmental impact of hexavalent chromium have prevented further development of this material.

The search for improved layered oxide materials containing low-cost transition metals ultimately led to the discovery of $LiNi_{0.5}Mn_{0.5}O_2$ [65–67] as well as compounds with the general composition $Li[Ni_xLi_{(1/3-2x/3)}Mn_{(2/3-x/3)}]O_2$ [68]. Computational modeling [69] and spectroscopic investigations [70] show that the Ni and Mn in these materials are in the +2 and +4 oxidation states, respectively. During normal charge processes in an electrochemical cell, nickel is ultimately oxidized to the +4 oxidation state, and Mn remains tetravalent. $LiNi_{0.5}Mn_{0.5}O_2$ does not convert to spinel upon cycling, unlike the metastable O3-$LiMnO_2$, because no trivalent Mn is ever produced in the structure.

The defect chemistry of $LiNi_{0.5}Mn_{0.5}O_2$ also distinguishes it from $LiNiO_2$ (where nickel is primarily in the +3 oxidation state initially) discussed above. A feature of $LiNi_{0.5}Mn_{0.5}O_2$ is anti-site mixing [65–67, 71, 72] in which some Ni^{2+} ions are located on the Li *3a* sites, and some Li^+ ions on transition metal *3b* sites, that is, $(Li_{1-x}Ni_x)_{3a}(Li_xNi_{0.5-x}Mn_{0.5})_{3b}O_2$, $x\approx 0.08-0.12$. Mn ions in the transition metal layers preferentially surround the Li ions located in 3*a* sites to form Li_2MnO_3-like clusters, and Ni ions occupy sites adjacent to Mn, to form a "flower pattern" (Fig. 4). The anti-site mixing is thought to be a thermodynamically favored feature of the ion ordering and thus intrinsic to the structure. Unlike with $LiNiO_2$, simple manipulation of conditions during direct synthesis is therefore not likely to result in a near-ideal layered structure.

$Li[Ni_xLi_{(1/3-2x/3)}Mn_{(2/3-x/3)}]O_2$ compounds can be considered solid solutions of Li_2MnO_3 and $LiNi_{0.5}Mn_{0.5}O_2$. Although the discharge capacity between 4.4 and 3.0 V versus Li/Li^+ drops as the Ni content decreases, the opposite trend is observed after cell charge to 4.8 V and subsequent discharge to 2.0 V [73]. In addition, the Li_2MnO_3-rich materials exhibit a plateau at about 4.5 V during charge, the length of which is inversely proportional to *x*. This is thought to be deintercalation of Li ions with concomitant loss of

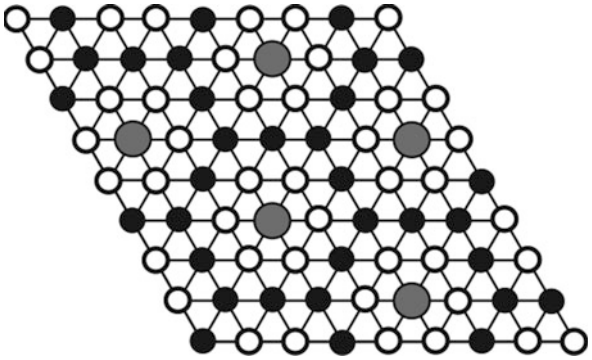

Battery Cathodes. Figure 4
A transition metal layer in $LiNi_{0.5}Mn_{0.5}O_2$ showing the flower pattern. Li is represented by the large gray circles, Mn by small white circles, and Ni by black circles (Used with permission from Ref. [71])

oxygen (for a net loss of Li_2O), similar to what happens when Li_2MnO_3 is charged in an electrochemical cell. This process can result in very high discharge capacities upon subsequent cycles (e.g., 230 mAh/g for $x = 1/3$). An advantage to these materials and related Li-rich materials (where excess lithium replaces some of the transition metal ions on *3b* sites, but the Mn content still equals that of the Ni content) is decreased cation mixing. This improves rate capability [74] as compared to $LiNi_{0.5}Mn_{0.5}O_2$.

The presence of a relatively large number of Ni ions in the Li *3a* sites of the $LiNi_{0.5}Mn_{0.5}O_2$ structure due to the anti-site mixing has a negative impact on the Li diffusivity, resulting in a low-rate cathode material. $LiNi_{0.5}Mn_{0.5}O_2$, prepared by low-temperature ion exchange of the nearly perfectly layered $NaNi_{0.5}Mn_{0.5}O_2$ analog, is capable of sustaining higher discharge currents than samples prepared by conventional methods [75]. However, the most successful method used to address this issue has been to incorporate some cobalt into the structure [76]. The best known of these compounds is $Li[Ni_{1/3}Co_{1/3}Mn_{1/3}]O_2$, sometimes referred to as NMC (Tables 1 and 2). This compound is gradually replacing $LiCoO_2$ in consumer batteries (in some cases, a mixture of the two are used as the cathode) and is under consideration for some vehicular applications. The voltage profile of NMC versus Li/Li^+ is gradually sloping (Fig. 3), as is typical of many layered compounds, and provides a somewhat higher capacity than $LiCoO_2$ below 4.3 V versus Li/Li^+ (typically about 160 mAh/g compared to 140). Capacities in excess of 200 mAh/g can be achieved when cells are charged to higher voltage limits, although this usually results in diminished cycle life.

The oxidation states of Ni, Co, and Mn in as-made $Li[Ni_{1/3}Co_{1/3}Mn_{1/3}]O_2$ are +2, +3, and +4, respectively [77]. First principle calculations suggest that Ni^{2+} is ultimately oxidized to Ni^{4+} during extraction of the first two-thirds of the lithium during electrochemical charging in lithium cells, and oxidation of Co^{3+} to Co^{4+} occurs only during removal of the last one-third [78] (i.e., at high cell potentials). As in $LiNi_{0.5}Mn_{0.5}O_2$, Mn remains inactive throughout normal operating cell voltages. The redox activity of Ni during the extraction of lithium from $Li[Ni_{1/3}Co_{1/3}Mn_{1/3}]O_2$ has been verified by in situ X-ray absorption spectroscopic (XAS) studies, although the details of the participation of Co in the electrochemistry are less clear [79–83]. Charge compensation associated with Co is currently thought to occur, at least partially, at oxygen sites, due to the covalency of the Co-O bonds.

The improved electrochemical properties and better structural, chemical, and thermal stability [84, 85] of $Li[Ni_{1/3}Co_{1/3}Mn_{1/3}]O_2$ compared to $LiCoO_2$ or NCA render it an attractive replacement cathode material for consumer batteries. Nevertheless, the presence of a significant amount of costly cobalt, albeit in reduced quantities compared to $LiCoO_2$, may still make it too expensive for most vehicular applications. Compounds having the general formula $Li[Ni_xCo_{1-2x}Mn_x]O_2$ with $x = 0.4$ or 0.45 have recently been developed by Whittingham and coworkers specifically to address the cost issue [86–89]. Although the amount of anti-site mixing increases with larger x, these materials exhibit very good electrochemical performances. The effect of increasing the Ni content of these materials on the thermal stability, especially at high states of charge, remains to be determined, however.

Another approach has been to partially substitute another metal such as aluminum for cobalt [89, 90]. Although the amount of substitution must be kept low to maintain the high specific capacities, both the thermal stability of the delithiated materials [91] and the electrochemical properties [92, 93] appear to be enhanced.

All of the NMCs discussed above contain equal amounts of Ni and Mn, which ensure that the oxidation states of the two metals are primarily +2 and +4, respectively. Recent attempts to increase Mn content in stoichiometric materials having the formula $Li[Ni_{0.45-x}Co_{0.1}Mn_{0.45+x}]O_2$ yielded phase mixtures for values of $x > 0.05$ [94] and a solid solution phase for $x = 0.05$. In this compound, $Li[Ni_{0.4}Co_{0.1}Mn_{0.5}]O_2$, the extra manganese is in the +3 oxidation state. Unfortunately, this material exhibits poorer capacity retention upon electrochemical cycling and lower rate capability than $Li[Ni_{0.45}Co_{0.1}Mn_{0.45}]O_2$. It is, however, possible to form solid solutions between $Li[Ni_{1/3}Co_{1/3}Mn_{1/3}]O_2$ and Li_2MnO_3 to make Li- and Mn-rich materials where the excess Mn is in the +4 oxidation state. As with the related $Li[Ni_xLi_{(1/3-2x/3)}Mn_{(2/3-x/3)}]O_2$ compounds, these materials can be electrochemically activated during charge to high potentials in lithium cells. The activation process (deintercalation of Li, concomitant loss of oxygen, and H^+/Li^+ ion exchange) yields electrodes with discharge capacities as high as 290 mAh/g [95, 96]. The very high capacities make these materials interesting for both consumer and automotive applications, and they are now being actively developed (e.g., by Envia Systems, Newark, CA).

Manganese Oxide Spinels

The marked tendency for many manganese oxide phases to convert to spinel structures during lithiation in electrochemical cells, or upon heating with a lithium source, attests to the stability of this structure in the Li-Mn-O system. The stoichiometric spinel, $LiMn_2O_4$, is easily synthesized in air from a variety of Li and Mn-containing precursors. Figure 2b shows its cubic structure (space group Fd-3m), where Li ions occupy tetrahedral *8a* sites and Mn is located in octahedral *16d* sites in a ccp array of oxygen anions. In addition, there are vacant tetrahedral and octahedral interstitial sites in the three-dimensional structure that provide pathways for lithium diffusion.

Early work [97] showed that it is possible to remove lithium from $LiMn_2O_4$ using a mild acid treatment. During this process, Mn is oxidized from an average +3.5 oxidation state to +4, and λ-MnO_2, which retains the spinel framework, is formed (Eq. 1). In addition, some dissolution of Mn occurs:

$$2LiMn_2O_4 + 4H^+(aq) \rightarrow 2Li^+(aq) + Mn^{2+}(aq) + 2H_2O + 3\lambda\text{-}MnO_2 \quad (1)$$

Oxidative extraction of lithium from the tetrahedral *8a* sites of $LiMn_2O_4$ to form λ-MnO_2 in a lithium cell [98, 99] was subsequently demonstrated to occur slightly above 4 V. It is also possible to insert lithium into the vacant octahedral sites of $LiMn_2O_4$ either chemically or electrochemically, with concomitant reduction of Mn. When carried out in a cell with a lithium anode, this process occurs below 3 V, and the discharge profile is flat, indicative of a two-phase reaction. The tetragonally distorted phase $Li_2Mn_2O_4$ (space group $I4_1/amd$) is formed due to the cooperative Jahn–Teller effect, which occurs when more than half the manganese is in the form of d^4 Jahn–Teller Mn^{3+} ions. The phase transition results in a 16% increase in the *c/a* ratio [100] ($a = c = 8.248$ Å in $LiMn_2O_4$; $a = 8.007$ Å, $c = 9.274$ Å in $Li_2Mn_2O_4$). In theory, lithium cells containing $LiMn_2O_4$ can either be charged or discharged initially, and then cycled over a composition range of $0 \leq x \leq 2$ in $Li_xMn_2O_4$ to give a total specific capacity of 285 mAh/g. Figure 5 shows the voltage profile of a Li/modified $LiMn_2O_4$ cell assembled in the author's laboratory, after discharging

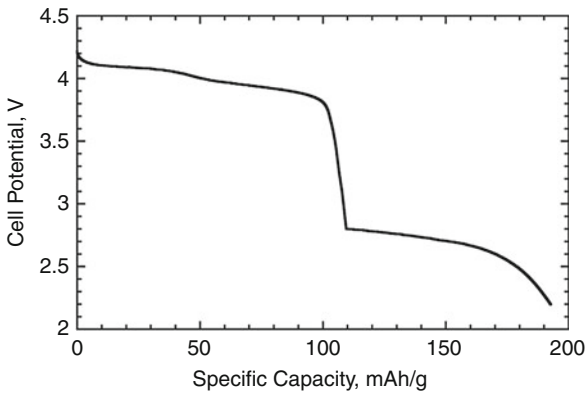

Battery Cathodes. Figure 5
Discharge profile of a Li/modified-$LiMn_2O_4$ cell at 0.1 mA/cm^2. Cell was initially discharged to 2 V and then charged to 4.3 V. This was the third discharge between 4.3 and 2.0 V

into the 3 V region and full recharge. Both 4 and 3 V plateaus are evident; although the overall capacity is somewhat lower than the theoretical value.

The large anisotropic volume change associated with formation of tetragonal $Li_2Mn_2O_4$ results in particle disintegration and loss of connection within the composite electrode. This causes such a rapid loss of capacity that, in practice, the cycle lives of cells containing $LiMn_2O_4$ discharged even a few times into the 3 V region are greatly compromised. In contrast, the extraction of lithium from $LiMn_2O_4$ above 4 V versus Li/Li^+ maintains the cubic structure and results in smaller volume changes. For this reason, discharge is typically limited to the 4 V plateau (Fig. 3), which exhibits much better reversibility. The theoretical capacity associated with this plateau is 148 mAh/g, although it is difficult to fully extract all the lithium, resulting in somewhat lower practical values.

From the early 1990s onward, intensive efforts were devoted to the development of $LiMn_2O_4$ for lithium-ion batteries, particularly at Bellcore Laboratories [101–103]. Although limiting discharges to the 4 V plateau resulted in much better cycling than when both the 3 and 4 V plateaus were utilized, gradual capacity fading was still observed [104]. This behavior was attributed to several factors, including irreversible side reactions with the electrolyte due to the high potential, loss of oxygen from the delithiated spinel, dissolution of Mn, and production of tetragonal $Li_2Mn_2O_4$ at particle surfaces, particularly at high discharge rates [100, 105].

Partial substitution of Mn to form $LiM_xMn_{2-x}O_4$ improves capacity retention [106–112]. Of particular interest are the lithium-substituted materials having the general formula $Li_{1+x}Mn_{2-x}O_4$. As lithium is substituted for manganese on the *16d* sites (x is increased), the average oxidation state of the latter rises. This effectively decreases the 4 V capacity in proportion to the amount of substitution but results in a higher average oxidation state of the Mn at the end-of-discharge. This ameliorates the tendency to form the tetragonally distorted phase under nonequilibrium conditions such as rapid discharging, because this occurs only when the Mn oxidation state falls below an average of 3.5. Because Mn is fully oxidized before all the lithium can be extracted from *8a* sites, side reactions are suppressed. Finally, dissolution of Mn decreases because this phenomenon is dependent on the concentration of trivalent ions.

Li substitution and the attendant increase in Mn oxidation state in the as-made $Li_{1+x}Mn_{2-x}O_4$ compounds decrease the lattice parameter, a (Fig. 6a and b). The magnitude of this value correlates closely with the amount of capacity loss upon cycling (Fig. 6c), so that it can be used to predict the cycling behavior of the spinel materials [113]. In particular, improvements are most marked when $a \leq 8.23$ Å. Because the cycling behavior is so much better than $LiMn_2O_4$, nearly all commercial manganese oxide spinel materials (LMOs) made today are lithium substituted. These have theoretical specific capacities of 100–120 mAh/g (Table 1), somewhat lower than that for $LiMn_2O_4$.

The maximum possible substitution in $Li_{1+x}Mn_{2-x}O_4$ corresponds to $x = 1/3$ (the compound $Li_{4/3}Mn_{5/3}O_4$ or $Li_4Mn_5O_{12}$), at which point all of the Mn is in the +4 oxidation state and there is no 4 V capacity, because oxidative extraction of lithium cannot occur. Nevertheless, it is possible to insert lithium reversibly into octahedral *16c* sites at about 2.9 V versus Li/Li^+ until a composition of $Li_7Mn_5O_{12}$ is reached, for a total of 156 mAh/g [114, 115]. The cubic symmetry is maintained until about $Li_{6.5}Mn_5O_{12}$, at which point Mn is reduced to an average oxidation state of 3.5 and the cooperative Jahn–Teller effect induces a tetragonal distortion. Because this process occurs only at the end-of-discharge, $Li_4Mn_5O_{12}$ exhibits much better cycling behavior on the 3 V plateau than does $LiMn_2O_4$. However, the low operating voltage and capacity, and the inability to extract lithium makes $Li_4Mn_5O_{12}$ impractical for Li-ion batteries.

It is also possible to prepare cation-deficient or defect spinels, $Li_{1-x}Mn_{2-2x}O_4$ [114]. The cation vacancies increase the average oxidation state of Mn and decrease the capacity above 4 V in favor of that below 3 V, proportionally with x. In the end-member compound $Li_2Mn_4O_9$ (corresponding to $x = 0.11$ in $Li_{1-x}Mn_{2-2x}O_4$), all Mn is tetravalent, and lithium cannot be extracted, so that there is no capacity at 4 V. Lithium can be inserted below 3 V versus Li/Li^+, to a maximum composition of $Li_5Mn_4O_9$. Although the theoretical capacity (213 mAh/g) is higher than that of $Li_4Mn_5O_{12}$, approximately 1/3 of it is associated with the formation of the Jahn–Teller distorted tetragonal phase.

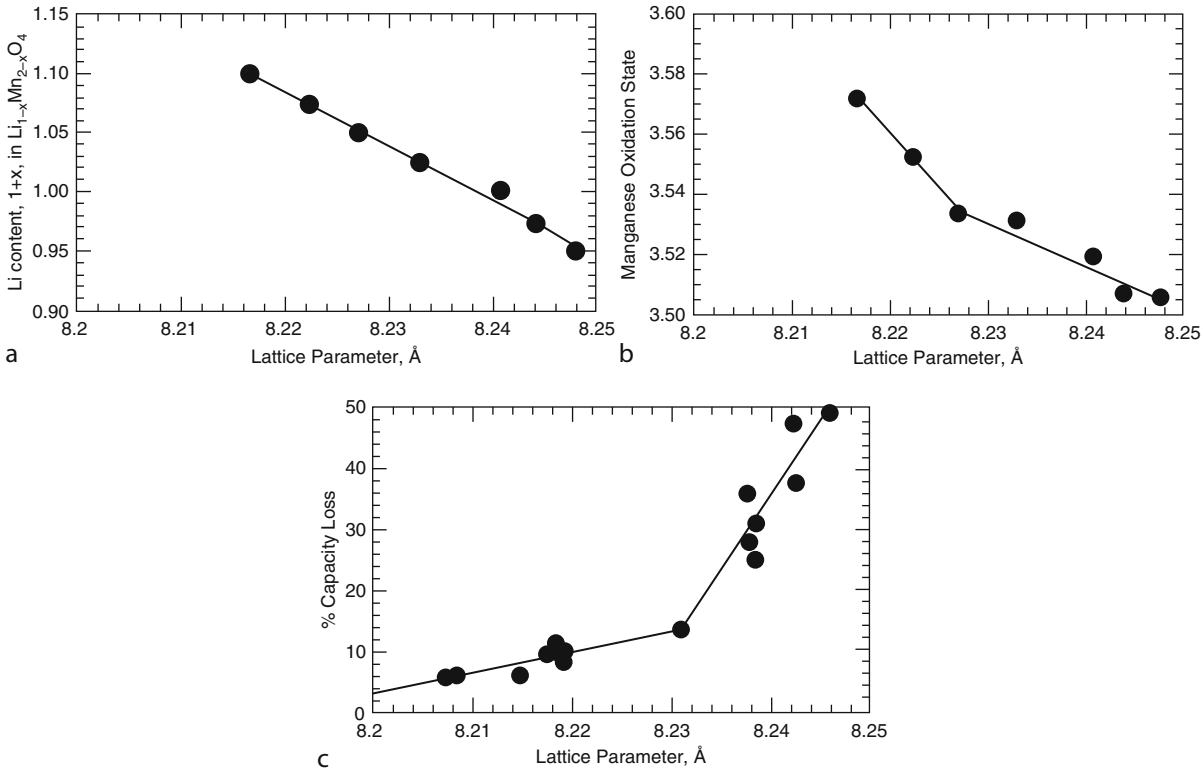

Battery Cathodes. Figure 6

(**a**) The variation of the lattice parameter, *a*, with the lithium content of $Li_{1+x}Mn_{2-x}O_4$; (**b**) the variation of lattice parameter with the average Mn oxidation state in $Li_{1+x}Mn_{2-x}O_4$; and (**c**) relationship between capacity loss after 120 cycles and the lattice parameter in $Li_{1+x}Mn_{2-x}O_4$ (Used with permission from Ref. [113])

In principle, defect spinels with values of $x < 0.11$ should cycle on the 4 V plateau better than $LiMn_2O_4$ for the same reasons as the lithium-rich stoichiometric spinels. In practice, it is difficult to control the degree of non-stoichiometry during synthesis, so these materials are not of interest commercially.

In spite of the improved performance exhibited by the lithium-substituted spinels, capacity fading upon cycling is still observed in electrochemical cells, particularly at elevated temperatures (55°C) [116–121]. This has negative implications particularly for vehicular applications, where batteries may be subjected to a wide variety of operating and storage conditions, including very warm environments. The dissolution is associated with Mn^{3+} disproportionation (Eq. 2) in the presence of acidic components of the $LiPF_6$/organic carbonate electrolyte solutions used in Li-ion batteries.

$$2Mn^{3+}(\text{solid}) \rightarrow Mn^{4+}(\text{solid}) + Mn^{2+}(\text{solution}) \quad (2)$$

Loss of manganese leads to the formation of a defect spinel structure with reduced or no 4 V capacity [104, 116–121]. Additionally, proton exchange [116–121], phase separation, film formation, and precipitation of MnO and MnF_2 may occur, increasing cell impedance and exacerbating the capacity fading. More significantly, dissolved Mn^{2+} can cross over to the anode, become reduced, and precipitate as the metal, increasing the charge-transfer resistance and disrupting the critical SEI layer [122, 123]. The graphite anode is

markedly more sensitive to this effect than lithium is. Thus, assessment of spinel cathodes to determine the effectiveness of an approach to improve resistance to dissolution should ultimately be carried out in a full cell configuration rather than in lithium half-cells.

Some methods designed to address the problem of spinel dissolution include coating of particles [124, 125] and the use of new non-fluorinated salts such as lithium bis(oxalato)borate (LiBOB) which do not generate HF in situ [126–128]. Interestingly, dissolution of manganese appears to be suppressed in electrodes where LMO is mixed with an NMC [129]. Although the cycling behavior of Li-ion cells with spinel electrodes is still inferior to that of devices containing alternative commercial cathode materials (Table 2), other aspects of performance such as rate capability and safety [33–36, 130], the wide availability of manganese precursors, and the potential for low cost make LMO attractive especially for vehicular applications. Thus, at least one battery manufacturer focused on vehicle technologies (e.g., Enerdel, Indianapolis, IN) is pursuing the development of Li-ion batteries with spinel cathodes and hard carbon anodes (which are less sensitive to the effects of manganese dissolution than graphite).

Several lithium-containing oxide spinels having transition metals other than Mn can also be synthesized. One example is $LiCo_2O_4$, which can be prepared from a low-temperature form of $LiCoO_2$ [131]. (The latter, known as LT-$LiCoO_2$, has a structure intermediate between that of a spinel and layered compound). Another is $LiNi_2O_4$ [25]. Unlike $LiMn_2O_4$, the electrochemical characteristics of most of these spinels are inferior to those of the layered analogs, so that they are not of technological interest as cathode materials. However, $Li_4Ti_5O_{12}$ (LTO), which, because of its voltage properties, functions as an anode material, demonstrates excellent cycling performance. Although the energy density is lower than that of graphite, it does not require the formation of an SEI. Thus, it is also an attractive match for LMO cathode materials. Batteries with LTO anodes and LMO or other high-voltage cathodes may find utility in HEVs, which do not require as high an energy density as pure EVs.

The intensive search for substituted lithium manganese spinels with better cycling performance led to the discovery of several materials having capacity near 5 V versus Li/Li^+. These include spinels substituted with Cr, Fe, Cu, Co, or Ni [132–136]. In most cases, these materials exhibit a plateau near 4 V as well as a second plateau near 5 V, with the magnitude of the latter increasing with larger x in $LiM_xMn_{2-x}O_4$ (where M = Cr, Fe, Cu, Co, or Ni). The 4 V capacity is associated with the usual Mn^{3+}/Mn^{4+} spinel redox couple, whereas the higher voltage plateau is associated with redox processes of the substituting metal. Interestingly, the compound $LiNi_{1/2}Mn_{3/2}O_4$ has very little 4 V capacity, unlike other $LiM_{1/2}Mn_{3/2}O_4$ spinels [137] (Fig. 7).

In the case of $LiNi_{1/2}Mn_{3/2}O_4$, nearly all of the Mn is tetravalent [136], so that further oxidation is not possible. The specific capacity of 147 mAh/g at 4.7 V is associated with Ni^{2+}/Ni^{4+} redox processes. The high energy density and high voltage makes this material attractive for vehicular applications, because fewer cells need to be connected in series to make the 300 V packs used in electric vehicles. This simplifies engineering, results in comparatively higher energy density on the system level because less hardware is required, and lowers costs. ETV Motors of Herzliya, Israel, is one company actively developing $LiNi_{1/2}Mn_{3/2}O_4$ batteries for this purpose.

The very high potential at which this cathode operates, however, presents considerable challenges for cycle life. Although conventional carbonate-based electrolytes used in Li-ion batteries have, in principle, excellent oxidative stability, the presence of impurities such as water may contribute to side reactions that decrease resistance to irreversible oxidation, resulting in shortened battery lifetimes. In addition, cell components such as carbon additives used to improve conductivity in composite cathodes, or surfactants that aid in wetting may oxidize irreversibly at high potentials, and current collectors may corrode. Thus, cycling is usually restricted to a voltage range below about 4.3 V versus Li/Li^+ (4.2 V in cells with graphite anodes). Stringent purification of electrolytes and the use of special protective additives are allowing gradual extension of this range. In addition, the development of new electrolytes containing ionic liquids or sulfolanes is expected to enable high-voltage cell operation, although the choice of anode may then be restricted

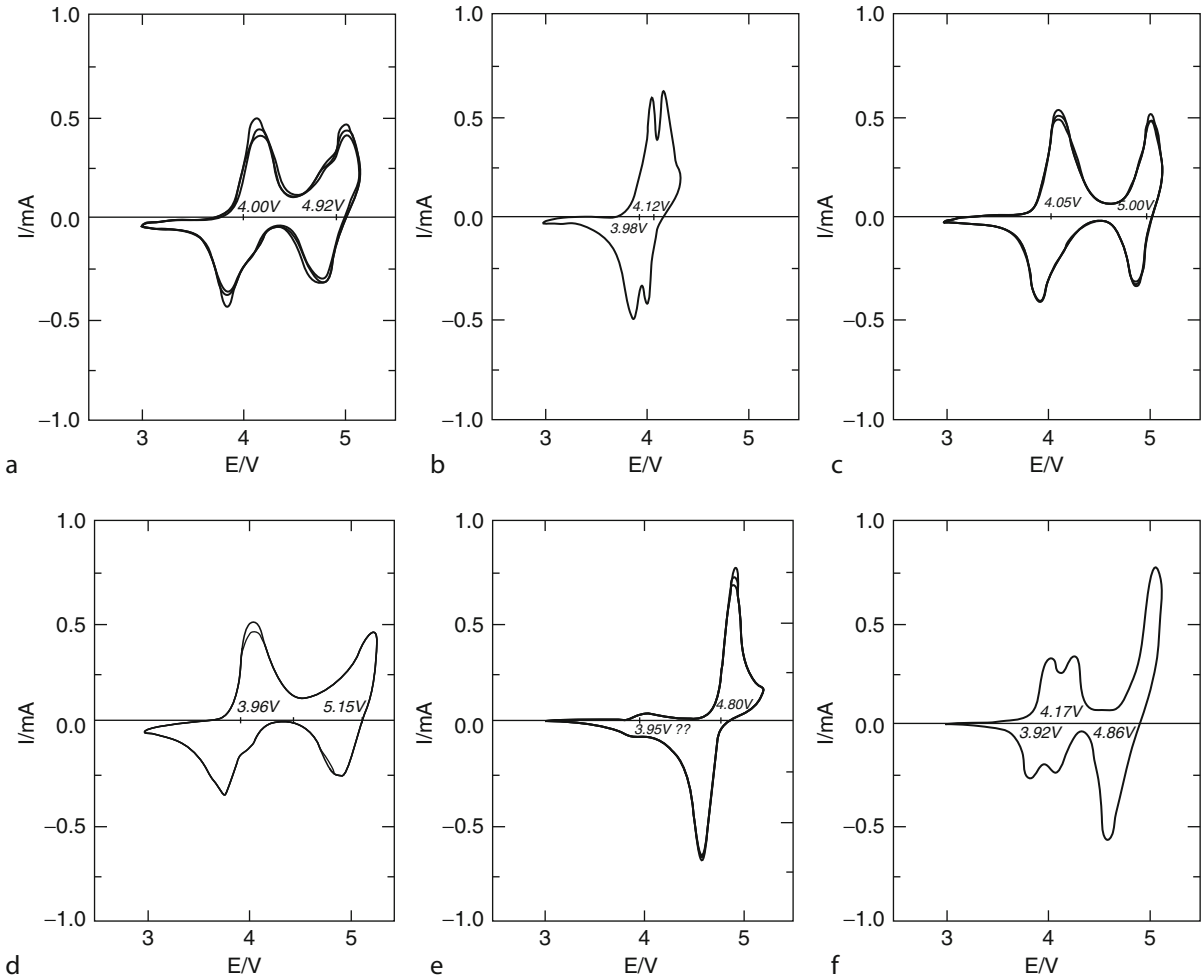

Battery Cathodes. Figure 7

Slow-scan voltammetry of Li/$LiM_{1/2}Mn_{3/2}O_4$ cells with M = (**a**) Cr, (**b**) Mn, (**c**) Fe, (**d**) Co, (**e**) Ni, and (**f**) Cu at a rate of 0.2 mV/s using 1 M $LiPF_6$ in 1:1 v/v EC/DEC electrolyte (Used with permission from Ref. [137])

to LTO or other materials that do not require SEI formation. Other strategies to prolong the cycle life of cells containing $LiNi_{1/2}Mn_{3/2}O_4$ include treating active material particles with protective coatings to minimize direct contact with electrolyte solutions [138–140], or partial substitution of Ni or Mn with other cations such as Ti, Mg, or Zn [141–143].

Synthesis of $LiNi_{1/2}Mn_{3/2}O_4$ is normally carried out at high temperatures to ensure good crystallinity and to lower the surface area and thus minimize reactivity with electrolyte solutions and other components. Under these conditions, oxygen loss may occur, leading to the formation of a non-stoichiometric material ($LiNi_{1/2}Mn_{3/2}O_{4-x}$) containing some Mn^{3+} in the structure. Additionally, a rock salt impurity, $Li_xNi_{1-x}O$, is also produced. Annealing at 700°C partially reverses the oxygen loss, but the telltale 4 V capacity indicative of the presence of electroactive Mn^{3+} can often be observed in cells made with these materials (e.g., in Fig. 7e). Substitution with other metals, as discussed in the papers listed in Refs. [141–143], often decreases the amount of Mn^{3+} in these compounds, which may play a role in the observed improvements in cycling.

If the sample is cooled slowly during synthesis, an ordered phase can be produced (space group $P4_332$ with Ni in *4b* sites and Mn in *12d* sites [144]). The

electrochemical properties (in particular, rate capability) of the ordered phase are inferior to those of the disordered non-stoichiometric phase [145, 146]. The mixed Mn valency in the disordered Fd-3m phase leads to an increase in the electronic conductivity of about 1.5 orders of magnitude compared to that of the ordered material. This is thought to be responsible for the increased rate capability of the former compared to the latter.

The presence of electroactive Mn in disordered $LiNi_{1/2}Mn_{3/2}O_4$ suggests that dissolution may be problematic, as it is with the $LiMn_2O_4$ variants. In spite of this and the high operating voltages, extremely stable cycling has been observed in full cell configurations, albeit with $Li_4Ti_5O_{12}$ anodes [147].

$LiFePO_4$ and Other Phospho-olivines

In 1997, Goodenough and coworkers reported on the electrochemical properties of a new class of cathode materials known as the phospho-olivines [148], which adopt the orthorhombic structure (space group Pnma) shown in Fig. 2c. In the case of $LiFePO_4$ (triphylite), Li^+ and Fe^{2+} occupy octahedral sites, and P is located in tetrahedral sites in a somewhat distorted hexagonal close-packed (hcp) oxygen array. The FeO_6 octahedra share corners and LiO_6 octahedra share edges along tunnels down the *b*-axis, through which the Li ions can diffuse. Extraction and reinsertion of Li from $LiFePO_4$ proceeds at about 3.45 V in a lithium cell with a theoretical specific capacity of 170 mAh/g. The potential is independent of the composition x in Li_xFePO_4 (i.e., the voltage profile is flat, Fig. 3) indicating that a two-phase reaction occurs. In situ X-ray diffraction and Mossbauer experiments on Li/$LiFePO_4$ cells [149] show that the two relevant phases are triphylite and $FePO_4$, also known as heterosite (Eq. 3).

$$LiFePO_4\ (\text{triphylite}) \leftrightarrow FePO_4\ (\text{heterosite}) + e^- + Li^+ \quad (3)$$

Initial reports on the electrochemical characteristics of $LiFePO_4$ emphasized its poor rate capability and the lower than expected utilization in lithium cells even when discharged at low current densities (e.g., only about 60% in Ref. [149]). This was attributed to the low electronic conductivities of both the triphylite and heterosite phases [150]. Coating particles with carbon ameliorates the low conductivity and result in better rate performance [151]. This is most conveniently achieved by including a carbon source during initial synthesis of the $LiFePO_4$ sample. The presence of carbon or carbon-containing precursors during calcination in an inert atmosphere has several additional beneficial effects; it retards grain growth, resulting in small particles that allow rapid extraction of Li ions, and prevents formation of Fe^{3+}-containing impurities. It also allows the use of easy-to-handle, low-cost, Fe^{3+}-containing starting materials such as iron nitrate, which are reduced during the heating process [152].

In practice, many lab-synthesized samples of $LiFePO_4$ contain carbon, due to the use of precursors such as iron oxalate [153]. Even small amounts of carbon can result in drastic sample color changes from the off-white of native $LiFePO_4$ (Fig. 8). The electrochemical performance is also greatly affected by the carbon content, although this also depends on the distribution of carbon over particle surfaces and details of its structure [154–157]. Carbons produced in situ during synthesis of $LiFePO_4$ are disordered due to the relatively low calcination temperatures (generally, 600–700°C). Disordered carbons are less conductive than graphite, and conductivity depends on the size and number of graphene domains. The use of graphitization catalysts (often containing iron) improves the conductivity of coatings by several orders of magnitude, and can also result in co-production of carbon nanotubes or fibers, which wire particles together [158, 159]. The result is that very small amounts of carbon, often less than 2 wt.%, are sufficient to produce high-rate $LiFePO_4$ samples. This is important because too much lightweight carbon adversely affects the tap densities of $LiFePO_4$ composites, further decreasing the already somewhat low energy density [160].

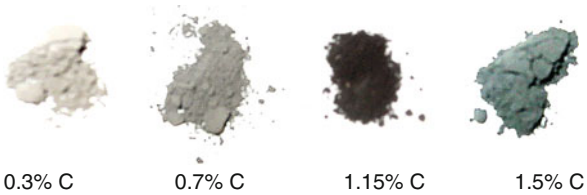

Battery Cathodes. Figure 8
Photographs of $LiFePO_4$ samples containing varying amounts of carbon (Used with permission from Ref. [153])

The changes in sample color, increases in bulk conductivities, and improved electrochemical performance induced by the presence of very small amounts of carbon (or other highly colored impurities) complicate the interpretation of results of doping experiments intended to increase the intrinsic conductivity of $LiFePO_4$. A color change from off-white to black or gray should not be regarded as proof-positive of successful doping and increased intrinsic electronic conductivity, for the reasons described above. Even when carbonaceous precursors are not used, the use of organic solvents or plastic containers during grinding or other processing steps may introduce carbon. Early claims of successful low-level aliovalent substitution [161] on the Li sites of $LiFePO_4$, resulting in greatly enhanced conductivities and electrochemical performance, may have been a fortuitous consequence of well-distributed electronically conductive impurities such as carbon and metal-rich phosphides [162–166]. Recent studies of the defect chemistry of $LiFePO_4$ show that substitution of multivalent ions on the Li site is very limited, and always accompanied by lithium vacancies, so that no mixed valency for iron occurs [167]. Earlier computational modeling of the defect, dopant, and Li transport properties of $LiFePO_4$ [168] indicates that substitution of multivalent ions on Li or Fe sites (other than divalent ions on the latter) is not energetically favored. It was predicted that the most likely type of defect is the Li-Fe anti-site pair, in which Li^+ ions are located on Fe^{2+} sites and are balanced by an equal number of Fe^{2+} ions on Li sites. Recent work, however, shows that there is a marked asymmetry between the number of Fe ions on Li sites and vice versa [169–171]. Very few lithium atoms can be accommodated on iron sites. More commonly, Fe ions on Li sites are accompanied by a small number of vacancies, to form $[Li_{1-2x}Fe_x]FePO_4$. The presence of relatively immobile multivalent ions on Li sites interferes with fast Li diffusion, since $LiFePO_4$ is essentially a one-dimensional ion conductor [172–174]. Likewise, a large number of anti-site defects are likely to impact electrochemical performance adversely [175, 176] as is seen in Refs. [169–171]. At any rate, it is apparent that near room temperature, only a relatively small concentration of vacancies or interstitial defects is possible.

Carbon coatings, although convenient for the reasons stated above, are not absolutely necessary to assure good electrochemical performance [177], as long as particle sizes are kept small and particle size distributions are narrow. Nanostructuring reduces diffusion distances and ameliorates the effects of low electronic conductivity, allowing full discharge at even moderate to high rates. Subtle changes in the discharge characteristics of $LiFePO_4$ samples occur as particle size is decreased, most notably, a stronger dependence of voltage upon composition (x in Li_xFePO_4) close to the end-of-charge and end-of-discharge, implying solid-solution behavior [178, 179]. Other researchers have observed XRD, neutron diffraction, and electrochemical evidence of a small degree of lithium non-stoichiometry in larger Li_xFePO_4 particles at both composition extremes [180, 181], as illustrated in Fig. 9.

The existence of a small degree of non-stoichiometry (and thus mixed valence states for iron) may explain why this system is electroactive, given that both end members have such poor electronic conductivity. It should be noted, however, that kinetic effects, surface impurities, and the presence of defects [179, 182–184] also influence the shape of the $Li/LiFePO_4$ discharge profile. This makes it hard to determine what the exact compositional ranges of solid-solution behavior are at room temperature from the electrochemical data alone. Complications from the effects of strain also make the interpretation of diffraction data difficult.

Experiments conducted on heated $LiFePO_4/FePO_4$ mixtures of varying concentrations [185, 186] show that solid solutions form from $0 \leq x \leq 1$ in Li_xFePO_4 at elevated temperatures, however. A representative phase diagram is shown in Fig. 10. The solubility limits of lithium in heterosite and vacancies in triphylite are approximated in the figure, because of the uncertainties outlined above. Additionally, due to slow kinetics, the exact temperature boundaries are not known, explaining the differences observed by various researchers. Depending upon the initial concentration, and details of the crystal sizes and morphologies, metastable lithium-deficient phases can persist for remarkably long times after cooling [187].

The mechanism of the $LiFePO_4/FePO_4$ electrochemical reaction has been described using a shrinking

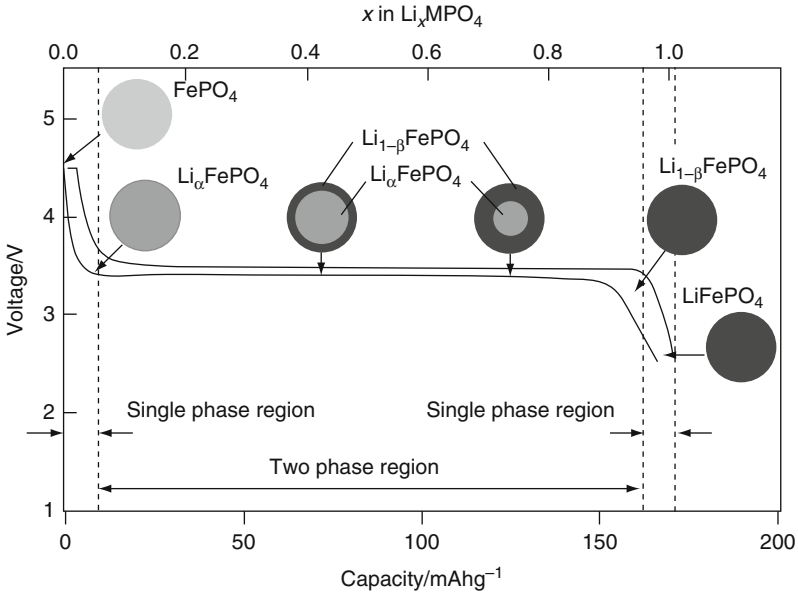

Battery Cathodes. Figure 9
Scheme of the discharge processes of Li_xFePO_4, showing solid-solution behavior close to $x = 0$ and $x = 1$ (Used with permission from Ref. [180])

core model [188], as depicted in Fig. 9. During discharge, lithium initially inserts into $FePO_4$ to form the solid-solution $Li_\alpha FePO_4$ phase, where α is close to 0. Upon further passage of current, a shell of a lithium-rich material ($Li_{1-\beta}FePO_4$) is produced on the surface, over a core of $Li_\alpha FePO_4$. As the reaction continues to progress, the shell grows at the expense of the core, and the interface between the two phases shrinks, until complete conversion to $Li_{1-\beta}FePO_4$ occurs. Further lithiation produces $LiFePO_4$ at the end-of-discharge. The entire process is reversed upon charge. The anisotropy of lithium diffusion in $LiFePO_4$ [172–174], however, complicates the interpretation of the shrinking core model. A transmission electron microscopy (TEM) study of partially delithiated large plate-like particles [189] show that ordered domains of $FePO_4$ and $LiFePO_4$ alternate in the *ac* plane, separated by narrow disordered (but not amorphous) regions, where lithium mobility is enhanced. The phase transformation proceeds in the direction of the *a*-axis at dislocation lines that run parallel to the *c*-axis, consistent with one-dimensional Li^+ diffusion in the *b*-direction (Fig. 11). This somewhat resembles an early "mosaic" model proposed by Andersson et al. as an alternative to the shrinking core model [190]. These observations also suggest that the best rate performance can be achieved with particles that are thin in the direction of Li diffusion (*b*-axis), but that nanostructuring in other directions may not be required.

In another recent study [191] using high-resolution electron energy loss spectroscopy (EELS) on a chemically prepared sample, a different distribution of the two phases in a partially delithiated particle was observed. In this case, $LiFePO_4$ was present only at the edges with $FePO_4$ located in the interior (but not on surfaces of the *ac* planes) of plate-like particles significantly smaller than those studied in Ref. [189]. This is consistent with a progressive emptying or filling of Li channels oriented along the *b*-axis, with the front between the two phases moving perpendicular to the *ac* plane. No disordered regions at the phase boundaries were detected, however. This lack of evidence for solid-solution behavior argues against a shrinking core mechanism, which requires that at least a small degree of non-stoichiometry exist in the system.

Variations in particle sizes and morphologies, as well as in the concentration of defects, may well

influence the progression of the delithiation reaction during chemical oxidation and explain these differing results. In electrochemical cells with composite electrodes, the reaction may nucleate preferentially at sites where contact with conductive carbon additives or coatings and the electrolyte solution is the closest, leading to a different pattern of phase distributions than is seen in the chemically delithiated samples, where nucleation can occur at numerous sites simultaneously. In partially delithiated Li_xFePO_4 samples recovered from electrochemical cells, no mixed-phase nanoparticles were observed, leading the researchers to surmise that the reaction front propagates much more rapidly than nucleation [192]. A recent kinetic study also indicates that the $LiFePO_4/FePO_4$ transformation is controlled by a phase-boundary reaction [193]. However, newly discovered evidence of intercrystallite ionic transport, leading to a redox reaction between delithiated and lithiated particles and subsequent equilibration [194] complicates the interpretation of these results. Moreover, areas of composite electrodes with poor electronic connectivity may be electrochemically inactive, leading to islands of unreacted $LiFePO_4$.

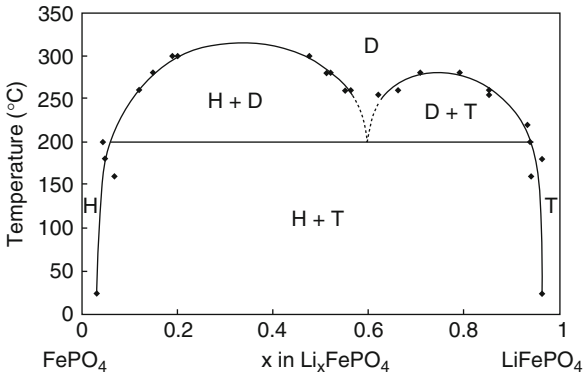

Battery Cathodes. Figure 10
Phase diagram of the Li_xPO_4 system, where T, H, and D denote triphylite, heterosite, and disordered (but not amorphous) phases, respectively (Used with permission from Ref. [186])

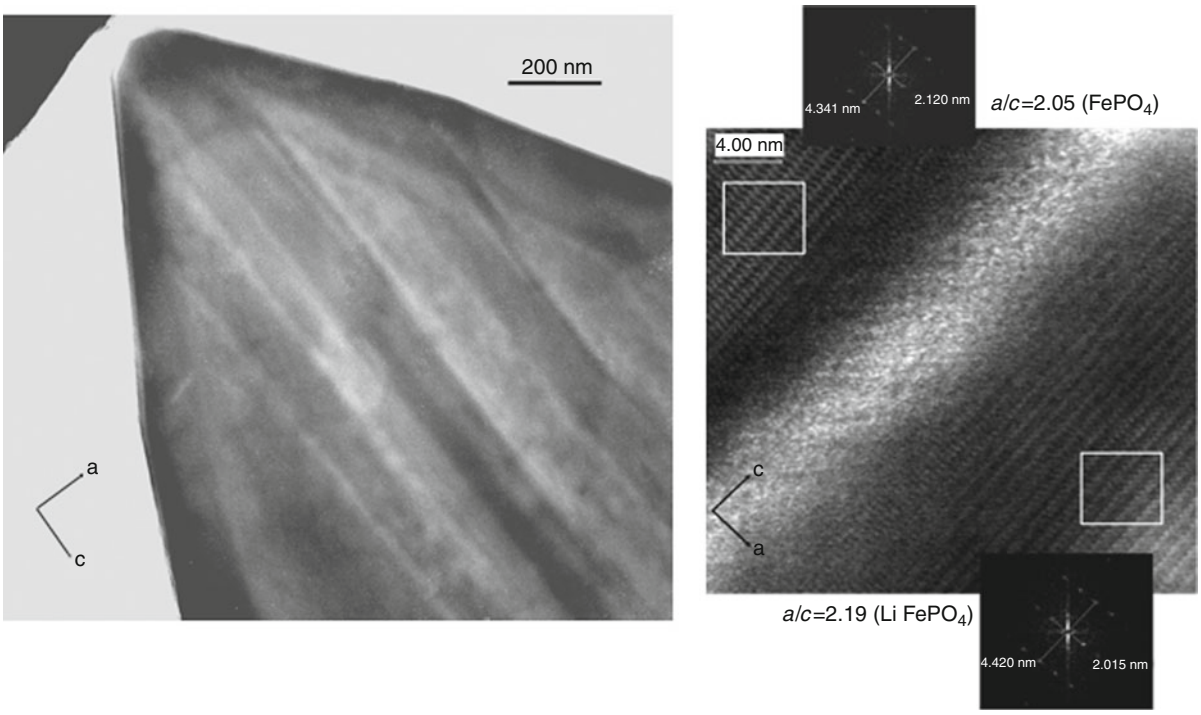

Battery Cathodes. Figure 11
Left: TEM image showing a partially delithiated crystal with the global composition $Li_{0.5}FePO_4$, showing domains of $LiFePO_4$ and $FePO_4$ aligned along the *c*-axis. *Right*: High-resolution TEM image with Fourier transforms of the boxed areas, identifying the two phases (Used with permission from Ref. [189])

In that case, all of the lithium will be extracted from $LiFePO_4$ in better connected areas, and mixtures of $FePO_4$ and $LiFePO_4$ will be observed, as in Ref. [192].

While the actual mechanism of the $LiFePO_4/FePO_4$ transformation remains a subject of debate, it seems clear that the shrinking core model does not apply to the primary particles themselves. The model may, however, still be applicable on a larger scale, for example, to the secondary particles comprised of agglomerates.

Over the past decade, better control of synthesis parameters, the use of conductive coatings, and nanostructuring have transformed $LiFePO_4$ from a poorly performing material to one of the most attractive cathodes for Li-ion batteries. $LiFePO_4$ appears to be particularly well suited to high-power applications including power tools and vehicle propulsion. A recent study shows that extraordinarily high charge and discharge currents can be sustained in cells designed so that a modified $LiFePO_4$ limits rate [195]. (While these devices are not practical for real-world use, they serve to demonstrate the intrinsic rate capability of $LiFePO_4$ without interference from mass transfer limitations in other cell components). There have been reports [196, 197] of iron dissolution in $LiPF_6$-containing electrolytes leading to capacity fading at elevated temperatures (analogous to the problems observed with manganese oxide spinels), although this may be due to the presence of iron-containing surface impurities such as Fe_2P rather than to the $LiFePO_4$ itself. The thermal properties of the $LiFePO_4/FePO_4$ system are a particularly attractive feature, leading to enhanced safety (LFP, Table 2). Upon heating, $FePO_4$ produced by charging $LiFePO_4$ transforms to the thermodynamically favored trigonal form (α-quartz structure). While this reaction is irreversible and leads to loss of capacity, it progresses without evolution of oxygen [198]. This is in contrast to transition metal oxides, all of which lose oxygen to some degree at high states-of-charge. This makes this cathode especially appealing for traction applications, where safety is paramount.

Because $LiFePO_4$ is less dense than the layered oxides or spinels (the crystallographic density is 3.6 g/cm^3 compared to about 5 g/cm^2 for the oxides), and the potential versus lithium is lower, the energy density is less than that of the oxides (Table 2). The specific energy, in contrast, is competitive with LMO (Table 1), but for many applications, the energy per unit volume matters more than per weight. The discharge potential of the isostructural $LiMnPO_4$ is about 0.5 V versus Li/Li^+ higher than that of $LiFePO_4$ [199], which increases the specific energy by about 15%. Unfortunately, this material is even less dense than $LiFePO_4$ (3.4 g/cm^3), and the conductivity appears to be several orders of magnitude lower [200, 201]. Synthetic procedures used to produce nanoparticulate $LiMnPO_4$ and variants include sol-gel, precipitation, combustion techniques, spray pyrolysis, and hydrothermal or solvothermal (polyol process) methods [176, 202–208]. For samples calcined in air for the sake of convenience, a fair amount of carbon is generally added after synthesis to offset the low conductivity. Coating can also be achieved via incorporation of carbonaceous precursors or elemental carbon during heat treatment under inert atmosphere, as with $LiFePO_4$. Electrochemical performance improves as the average primary particle size decreases [209]. Partial Mg substitution on the Mn site is also beneficial [208, 210–212]. This effect has been attributed to stabilization against strain associated with the Jahn–Teller distortion of Mn^{3+} ions in the delithiated phase, as well as decreased volume changes upon cycling. The best results reported so far have been for solvothermally prepared powders (polyol process) embedded in a carbon matrix [213]. Still, the rate capability of $LiMnPO_4$ is not as impressive as that of $LiFePO_4$, and many of the strategies employed to improve the electrochemistry (Mg substitution, addition of large amounts of carbon, nanostructuring) reduce the already fairly small energy density advantage. The disappointing performance has been variously attributed to poor transport properties in either the bulk $LiMnPO_4$ or $MnPO_4$ phases, the instability of the $MnPO_4$ phase itself, or surface effects [201, 214, 215]. While the voltage profile of $LiMnPO_4$ is flat during charge and discharge, indicating a two-phase process, evidence of solid-solution behavior near the $MnPO_4$ limit has been observed [216]. As with the $LiFePO_4/FePO_4$ system, the non stoichiometry may enable the electrochemical activity. However, no solid-solution behavior near the $LiMnPO_4$ end of the phase diagram has yet been detected.

Although the performance characteristics of the $LiMnPO_4/MnPO_4$ system may improve with further work, one troubling aspect of this electrode is its

thermal instability in the charged state. Unlike $LiFePO_4$, $MnPO_4$ evolves oxygen gas upon heating to 200°C and decomposes to form $Mn_2P_2O_7$ [217, 218]. The instability of $MnPO_4$ is probably related to the strong Jahn–Teller distortion of the Mn^{3+} ion. $LiMnPO_4$ is therefore less attractive than $LiFePO_4$ in terms of safety, and does not have better performance characteristics than the metal oxides. Charging is also somewhat problematic, because high over-potentials are required due to the kinetic limitations. Thus, it seems unlikely that this cathode material will prove useful for traction batteries in the near term, although other applications may be feasible.

Phospho-olivine compounds containing Co or Ni also exist. $LiCoPO_4$ exhibits electrochemical activity at about 4.8 V versus Li/Li^+ [219, 220]. $LiNiPO_4$ is predicted to discharge at about 5.1 V in a lithium cell, but appears to be nearly completely inactive [221]. Neither of these is likely to be used as cathodes for lithium-ion batteries in the near term in part because of the very high voltages needed to charge the materials, which present a number of practical problems.

Solid solutions containing a mixture of transition metals can be prepared over a wide composition range [176]. $Li[Mn_yFe_{1-y}]PO_4$ compounds exhibit two plateaus in the discharge profile at about 4.1 and 3.45 V versus Li/Li^+ with their relative magnitudes proportional to the amounts of Mn and Fe, respectively [148]. In general, for $y < 0.8$, the mixed metal phospho-olivines appear to undergo more facile electrochemical reactions than the pure end-member phase, $LiMnPO_4$ [215, 222]. A study of the delithiation reactions of these phases [223] suggested that the system is single phase when $x < 1-y$, but biphasic over the 4.1 V plateau (corresponding to the Mn^{2+}/Mn^{3+} redox couple). A later synchrotron diffraction study [224] showed two two-phase regions roughly coinciding with the two plateaus and a narrow solid-solution region between $x = 0.55$ and 0.67 for $Li_xMn_{0.6}Fe_{0.4}PO_4$, $_xMn_{0.6}Fe_{0.4}PO_4$, corresponding to the steeply sloping portion of the discharge profile between the plateaus.

Other mixed transition metal phospho-olivines have been prepared containing Ni and Co [220] and Fe, Mn, and Co [225–227]. In the case of the Li $[Ni_yCo_{1-y}]PO_4$, only one plateau was observed at 4.8 V, corresponding to the Co^{2+}/Co^{3+} redox couple. The only effect of the Ni substitution is to reduce the overall capacity, demonstrating the poor electroactivity of Ni in the phospho-olivine structure. In lithium cells containing $LiMn_{1/3}Fe_{1/3}Co_{1/3}PO_4$, on the other hand, three distinct electrochemical features are observed, corresponding to redox processes of the three types of transition metals (Fig. 12). Interestingly, the reaction appears to be single phase over the entire composition range, $0 \leq x \leq 1$ in $LiMn_{1/3}Fe_{1/3}Co_{1/3}PO_4$, and the redox potentials of the Fe^{2+}/Fe^{3+} and Co^{2+}/Co^{3+} couples are slightly shifted compared to the corresponding $LiMPO_4$ electrodes containing only one metal. The manganese redox processes appear to be more sluggish than those of iron and cobalt, and at higher discharge rates, the electrochemical feature at 4.1 V disappears. Tailoring of the voltage profile by incorporating multiple metals in the olivine structure may have practical use as a state-of-charge indicator for vehicular batteries (acting much like the gas gauge in conventional combustion engine automobiles).

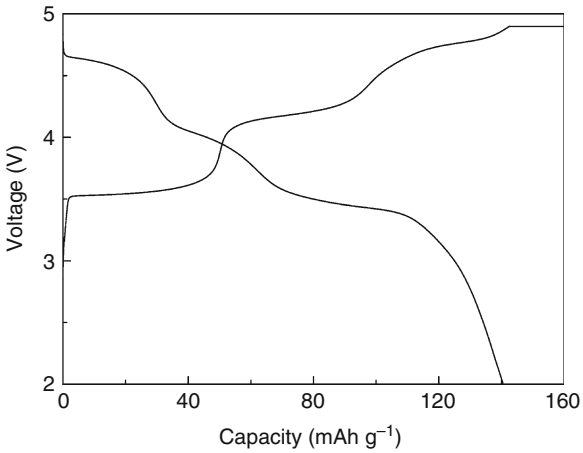

Battery Cathodes. Figure 12
Charge and discharge of a $Li/LiMn_{1/3}Fe_{1/3}Co_{1/3}PO_4$ cell, showing three distinct plateaus corresponding to the redox of Co (4.8 V), Mn (4.1 V), and Fe (3.45 V) (Used with permission from Refs. [225–227])

Other Phosphates and Poly-anionic Compounds

There are many other transition metal-containing poly-anionic compounds with structures amenable to lithium insertion processes. Among these are numerous materials with the Nasicon structure

(Nasicon stands for sodium superionic conductor and originally referred to $Na_{1+x}Zr_2P_{3-y}Si_yO_{12}$ compounds [228]). These have the general formula $A_xM_2(XO_4)_3$, where A is an alkali metal or alkaline earth, M is a transition metal or combination of transition metals, and X is P, As, Si, or S or a combination of these. M is octahedrally coordinated by oxygen, and X is tetrahedrally coordinated. All corners of the XO_4 tetrahedra are shared with MO_6 octahedra and vice versa; these link to form open channels in which the alkali or alkaline earth ions are located. There are also closely related three-dimensional framework structures with differing arrangements of corner-sharing polyhedra and distributions of alkali metal cations, such as the monoclinic $Li_3Fe_2(PO_4)_3$ shown in Fig. 13.

Transport of alkali metal ions through the tunnels in Nasicons can be extremely rapid, particularly at elevated temperatures, although the electronic conductivities are low. For these reasons, these materials were originally proposed for use as solid ionic conductors (e.g., to replace β″ alumina in high temperature Na/S batteries). In spite of their low electronic conductivities, researchers recognized that Nasicon structures with redox-active transition metals and related three-dimensional framework compounds could function as electrode materials as early as the late 1980s [229–231] and numerous materials were investigated [232, 233]. In many cases, the electrochemical properties are unsuitable for Li-ion batteries. For example, Li cannot be extracted from monoclinic $Li_3Fe_2(PO_4)_3$, only inserted, and the discharge occurs at a rather low voltage (2.8 V versus Li/Li^+). In contrast, up to two lithiums per formula unit can be extracted reversibly from monoclinic $Li_3V_2(PO_4)_3$, corresponding to a capacity of about 130 mAh/g at an average potential of 3.8 V [234–236]. Complex multiphasic behavior is exhibited upon redox, resulting in multiple plateaus in the discharge profile. In spite of significant volume changes upon lithium insertion and extraction, the material shows very good cycling behavior.

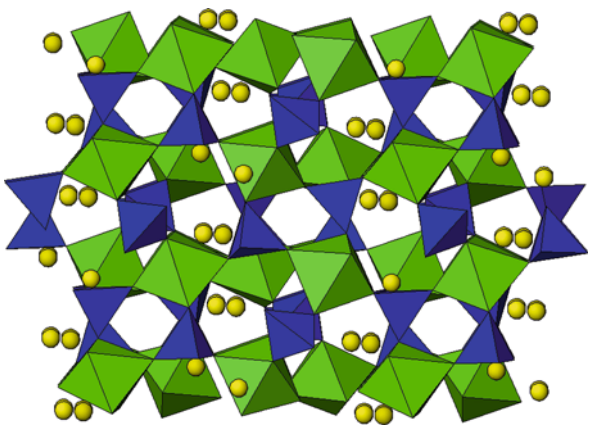

Battery Cathodes. Figure 13
The structure of monoclinic $Li_3Fe_2(PO_4)_3$ looking down the unique axis. P is located in the blue tetrahedra, and Fe in the *green* octahedra. Li ions are represented as spheres

Fluorophosphates are relatively rare, but have recently been studied for Li-ion applications. The lithium in $LiVPO_4F$ [237–239] can be extracted reversibly at a potential of about 4.2 V versus Li/Li^+. Interestingly, lithium can also be inserted at about 1.8 V. Thus, a graphite-free lithium-ion battery can be built, using $LiVPO_4F$ as both the anode and the cathode! $Na_3V_2(PO_4)_2F_3$ [240], Na_2FePO_4F [241], and $LiFePO_4F$ [242, 243] have also been investigated. The first two compounds were used as-is in electrochemical cells, and underwent ion exchange in situ. Although these cathodes eventually stabilize when used in lithium metal cell configurations and the cycling behavior is good, the presence of sodium in full cells with graphite anodes may disrupt the SEI layer and is therefore undesirable. Thus, these compounds will have to be ion-exchanged prior to use. In the case of $LiFePO_4F$, the investigators saw some evidence that a small amount of lithium could be extracted (with concomitant oxidation of Fe^{3+} to Fe^{4+}), but the main electrochemical reaction was insertion of lithium and reduction of Fe^{3+} to Fe^{2+}.

Other electroactive phosphorus-containing compounds include iron(III) hydroxyl phosphates with lipscombite or tavorite structures [244, 245], β- and ε-$VOPO_4$ [246–248], and $LiVP_2O_7$ [249]. Although the Nasicons, three-dimensional framework structures, and the aforementioned phosphates and diphosphates all have interesting electrochemical properties, most are not competitive with $LiFePO_4$ or the commercialized metal oxides for a variety of reasons. The iron-containing materials generally discharge at too low a voltage for use in Li-ion battery configurations and many have fairly low capacities. Some would need to be lithiated prior to use. The vanadium-containing

materials cycle well, and have sufficiently high voltages and capacities to ensure high energy density, but raise concerns about toxicity and environmental impact.

Interest has also recently been directed toward a family of silicates with the general composition Li_2MSiO_4, where M is a divalent cation such as Fe^{2+}, Mn^{2+}, and Co^{2+} or a combination of these [250–257]. The chemical formula implies that it may be possible to extract two Li ions per transition metal unit, giving a very high theoretical specific capacity of about 330 mAh/g. These materials adopt structures in which Li, Si, and the transition metal ions all occupy tetrahedral sites in a distorted close-packed oxygen array. The particular polymorph obtained depends upon the nature of the transition metal as well as the temperature and method of preparation. In the β-polymorphs (low-temperature forms), the tetrahedra share only corners, and all point in the same direction. In γ-polymorphs (high temperature forms), triads of tetrahedra are arranged so that the central one points in the opposite direction and shares edges with the two outer tetrahedra. Numerous tetrahedral structures exist, with different ordering of the ions and varying degrees of distortion. Several different views of an electroactive β-polymorph (space group $Pmn2_1$) are shown in Fig. 14, which illustrates its quasi-layered nature. Accurate structure determination of these phases is complicated by the presence of impurities in many preparations and variations in synthetic procedures, which may lead to subtle structural differences [256, 258].

About one Li^+ per formula unit can be extracted from Li_2FeSiO_4 in electrochemical cells at low current densities and at 60°C [250, 251]. The initial extraction takes place at about 3.1 V versus Li/Li^+, but subsequent discharges and charges occur at 2.8 V. This indicates that a structural change takes place, the exact nature of which is not entirely clear. After this initial change, however, relatively good cycling is observed, with an overall capacity of about 130 mAh/g (corresponding to somewhat less than 1 Li^+ per Li_2FeSiO_4). There is no experimental evidence that more than one Li^+ can be extracted, and first principle calculations indicate that it is not possible to do so at potentials compatible with conventional organic liquid electrolytes [259].

The differences between the potentials at which the first and second lithium ions can be extracted are much smaller when M=Mn, Co, or Ni in Li_2MSiO_4 than when it is Fe, however. As with the olivine system, the redox potentials for Li_2MnSiO_4 electrochemical processes (at least for extraction of the first lithium) are expected to be within the oxidative stability limits of organic electrolytes, while those of Li_2CoSiO_4 and Li_2NiSiO_4 are probably not. However the electrochemical behavior of Li_2MnSiO_4 appears to be much worse than that of Li_2FeSiO_4 [251, 254]. Belharaouk et al. [253] were able to achieve initial discharge capacities of about 135 mAh/g at room temperature, over a wide voltage range, by using carbon-coated submicron-sized particles, but this is still far less than predicted for complete extraction of all the lithium. Discharge capacities as high as about 250 mAh/g, however, can be obtained when

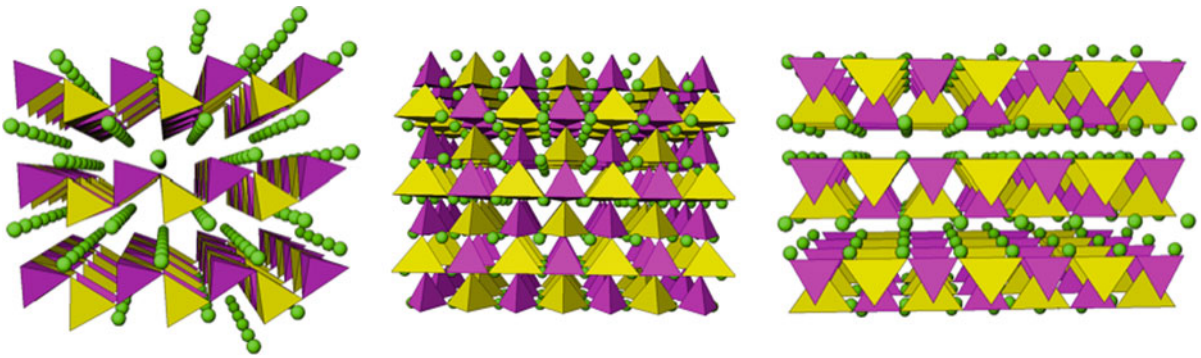

Battery Cathodes. Figure 14
Views of a β-polymorph of Li_2MSiO_4 looking down the *a*-axis (*left*), the *b*-axis (*middle*), and the *c*-axis (*right*). MO_4 (*yellow*) and SiO_4 (*pink*) tetrahedra alternate and connect to form layers through which lithium ions (*green spheres*) can diffuse

mixed metal compounds $Li_2Mn_xFe_{1-x}SiO_4$ [252, 256] are used as cathodes in lithium cells. Unfortunately, the quality of the energy obtained is poor because the voltage profiles are steeply sloping over a range of about 4.5–1.0 V versus Li/Li^+. At such low potentials, relatively little power can be obtained from the electrode. The extreme slope may be partly due to the severe kinetic and electronic limitations of the materials, leading to large over-potentials in lithium cells. If so, a combination of the carbon-coating and nanostructuring strategies used to improve the olivines may ameliorate the poor voltage characteristics and lead to new cathodes with nearly double the energy currently available.

Conversion Electrodes

A different class of electrode materials is based not upon insertion processes but on the displacement reactions of binary metal compounds [260, 261] (Eq. 4):

$$nLi^+ + ne^- + M^{n+}X_m \leftrightarrow M + nLiX_{m/n}(X = O, F, N, S) \quad (4)$$

Conversion electrodes have long been used in primary systems (e.g., Li/CF_x batteries), but have only been proposed for use in rechargeable devices recently, when it was recognized that the reactions could be made reversible for nanoparticulate materials. While the specific capacities can be enormous, the voltage characteristics make most of these electrodes more suitable for use as anodes rather than as cathodes. A notable exception seems to be that of metal fluorides, which are electroactive anywhere from 2 to 4 V versus Li/Li^+, depending on the identity of the metal, with specific capacities as high as 600 mAh/g. It is typical of conversion electrodes to exhibit significant hysteresis upon recharge, which may be intrinsic to the materials and processes. The mechanisms of conversion reactions are complex and involve bond breaking and considerable rearrangement, unlike that of insertion electrodes. The reassembly of the original phase upon recharge does not necessarily involve the same kinetic pathways and intermediates as the production of the elemental metal and LiF during discharge. Thus, it may not be possible to remove the hysteresis entirely either by engineering of devices or by improving the material properties to ensure faster rate capability. This property has an adverse effect on the round-trip efficiencies, and may make conversion electrodes unsuitable for Li-ion batteries unless a solution can be found to this problem.

Future Directions

Because none of the cathode materials discussed above are ideal for every application, the search for new insertion electrodes continues. Batteries are relatively simple devices, but the simultaneous requirements for high energy density, long cycle life, safety, and low cost impose stringent restrictions upon the choices available for cathode materials. The highly successful example of $LiFePO_4$ has directed researchers toward the exploration of other poly-anionic compounds that may share its excellent thermal stability at high states of charge. It is now evident that nanostructuring and/or conductive coatings can overcome kinetic and electronic limitations, allowing materials that would once have been thought of as unsuitable for electrodes to be considered. Changes in the phase behavior of nanoparticulate materials (in comparison to the conventionally sized powders) can render compounds electroactive that, in bulk form, appear to be unpromising due to their insulating nature. The shortened diffusion distances for lithium in nanoparticles may enable high rate capability in powders that appear to have severe rate limitations when micron-sized or larger. While this allows the menu of potential cathodes to be greatly expanded, the concept of "going nano" should be approached with caution. It is most successful when it is applied to materials that undergo redox well within the electrolyte stability range, such as with $LiFePO_4$. The increased surface area of nanoparticulate powders compared to conventionally sized materials exacerbates any tendency toward irreversible reaction with electrolytes. In addition to the very serious safety concerns this raises, the paradoxical result may be to lower rate capability due to the increased presence of resistive reaction layers on cathode particle surfaces [262]! Nano-sizing may also adversely impact practical specific energies because processing into electrodes becomes more difficult. It is often necessary, for example, to add more carbon to the composite cathode to ensure good electrical connectivity, but this contributes dead weight. High surface area particles also do not

pack well, leading to decreases in the tap densities and lower energy densities. Ensuring that nanoparticles are regularly shaped rather than irregularly can ameliorate these tendencies, however [263]. Another potentially useful approach is to synthesize mesoporous materials [264] in which the particles are micron-sized but contain pores of controlled sizes and distributions so as to maximize contact between the electrolyte and active material. This effectively shortens diffusion distances, while minimizing the tap density effects and maintaining the ease of electrode processing.

The use of nano metric or very thin coatings on cathode particle surfaces to improve the electronic conductivity of a material, to decrease dissolution, suppress oxygen loss, or to extend the operating voltage range is somewhat less problematic than simply nano-sizing cathode powders. In principle, this may allow using a wider variety of materials, including high-voltage/high-energy electrodes safely, without compromising cycle life or requiring the use of exotic electrolytes. Here the challenge is to identify and prepare coatings that prevent contact with electrolyte, yet allow the transport of lithium ions. They must also remain essentially defect-free over many cycles in which the cathode particles may undergo significant volume changes. A related concept is the preparation of "core-shell" or compositionally graded materials in which two or more compounds are combined in the same particle [265]. The core of the material can be a high-capacity material and the outer shell one that has lower energy but better thermal stability, for example. A difficulty is the tendency for the shell to become detached from the core if the volume changes upon cycling are not carefully matched. A compositionally graded material is less subject to these stresses, but more complex to prepare.

Researchers continue to look for materials that can deliver higher capacities and energies than those currently available. The layered-layered composite materials (i.e., the solid solutions between Li_2MnO_3 and $LiNi_{0.5}Mn_{0.5}O_2$ or $LiNi_xCo_{1-2x}Mn_xO_2$), which are very high capacity once they are activated in electrochemical cells, are a recent promising development. Cathodes that can undergo more than one oxidation state change per metal center reversibly could substantially increase the capacity of lithium-ion batteries. These include the Li_2MSiO_4 compounds and conversion electrodes discussed above, but these require much more work before they can be envisioned for use in lithium-ion batteries.

The challenges presented by these new materials illustrate the delicate balance of performance characteristics, cost, and safety that the battery electrode designer must be able to meet. There is now renewed interest among researchers in lithium metal batteries, because of the very high energy densities that might be achieved. However, now instead of intercalation electrodes, developers are reconsidering the use of sulfur and air (oxygen) cathodes for lithium metal batteries intended for vehicles. The extremely high theoretical capacities of these materials (e.g., over 1,600 mAh/g for sulfur) in lithium batteries are certainly tantalizing, but the difficulties associated with their use have proven daunting. In the case of sulfur, LiS_x intermediates dissolve in the electrolyte solutions, eventually migrating to the lithium anode and precipitating as Li_2S. The development of the protected lithium electrode (PLE) by PolyPlus Battery Company (Berkeley, CA) has extended the cycle life significantly, and Li/S batteries are now used for some military applications. In PLEs, the lithium anode is covered by a thin dense protective film (e.g., a lithium-ion conducting ceramic such as Lisicon, a ceramic with the Nasicon structure), which not only prevents contact with soluble intermediates but also with the electrolyte. An interlayer between the lithium and the protective layer is also needed to prevent reduction of the latter. Thus, in principle, it is possible to operate lithium cells with a wide variety of electrolytes, including aqueous ones. A lithium/water battery has even been developed for niche applications, although it is intended for use only as a primary, at present.

While in principle it should be possible to operate a lithium/air battery using a PLE to prevent contact of lithium with adventitious water and CO_2 in the atmosphere, rechargeable systems have so far eluded success. The reduction of oxygen itself is somewhat sluggish, necessitating the use of a catalyst. The Li_2O_2, which is the reaction product when nonaqueous electrolytes are used, precipitates out during discharge and eventually clogs the pores of the air electrode structure. While some researchers have claimed to have successfully recharged a lithium/air battery, the large hysteresis observed suggests that a side-reaction involving the

electrolyte is responsible for the charging behavior instead of reoxidation of Li_2O_2 to oxygen.

Ultimately, the success or failure of lithium/sulfur or air systems, however, hinges upon convincing demonstration of safe and reliable operation of the lithium anode over the many cycles required for applications requiring rechargeable devices.

Acknowledgments

This work was supported by the Assistant Secretary for Energy Efficiency and Renewable Energy, Office of Vehicle Technologies of the US Department of Energy under Contract No. DE-AC02-05CH11231. The author would like to thank Dr. Kinson Kam, Dr. Jordi Cabana, and Mr. Thomas Conry for helpful discussion.

Bibliography

Primary Literature

1. Whittingham MS, Gamble FR (1975) The lithium intercalates of the transition metal dichalcogenides. Mat Res Bull 10:363–372
2. Whittingham MS (1976) The role of ternary phases in cathode reactions. J Electrochem Soc 123:315–320
3. Whittingham MS (1978) Chemistry of intercalation compounds: metal guests in chalcogenide hosts. Prog Solid Stat Chem 12:41–99
4. Mizushima K, Jones PC, Wiseman PJ, Goodenough JB (1980) Li_xCoO_2 ($0 \leq x \leq 1$): a new cathode material for batteries of high energy density. Mat Res Bull 15:783–799
5. Goodenough JB (2007) Cathode materials: a personal perspective. J Power Sources 174:996–1000
6. Dresselhaus MS, Dresselhaus G (1981) Intercalation compounds of graphite. Adv Phys 30:139–326
7. Fong R, von Sacken U, Dahn JR (1990) Studies of lithium intercalation into carbons using nonaqueous electrochemical cells. J Electrochem Soc 137:2009–2013
8. Nagaura T, Tozawa K (1990) Lithium ion rechargeable battery. Prog Batteries Sol Cells 9:209–219
9. Akridge J, Brodd R (2010) Li-ion markets. In: Pacific power symposium, Waikoloa, HI
10. Srinivasan V (2008) Batteries for vehicular applications. In: AIP conference proceedings physics of sustainable energy, Berkeley, CA, vol 1044, pp 283–296
11. Karden E, Ploumen S, Fricke B, Miller T, Snyder K (2007) Energy storage devices for future hybrid electric vehicles. J Power Sources 168:2–11
12. Chalk SG, Miller JF (2006) Key challenges and recent progress in batteries, fuel cells, and hydrogen storage for clean energy systems. J Power Sources 159:73–80
13. Gaines L, Cuenca R (2000) Costs of lithium-ion batteries for vehicles. Report, Center for Transportation Research, Argonne National Laboratory, Argonne
14. Murphy DW, Christian PA (1979) Solid state electrodes for high energy batteries. Science 205:651–656
15. Ohzuku T, Ueda A (1994) Solid-state redox reactions of $LiCoO_2$ (R-3m) for 4 volt secondary lithium cells. J Electrochem Soc 141:2972–2977
16. Reimers JN, Dahn JR (1992) Electrochemical and in situ diffraction studies of lithium intercalation in Li_xCoO_2. J Electrochem Soc 139:2091–2097
17. Chen Z, Lu Z, Dahn JR (2002) Staging phase transitions in Li_xCoO_2. J Electrochem Soc 149:A1604–A1609
18. Aurbach D, Markovsky B, Rodkin A, Levi E, Cohen YS, Kim H-J, Schmidt M (2002) On the capacity fading of $LiCoO_2$ intercalation electrodes: the effect of cycling, storage, temperature, and surface film forming additives. Electrochim Acta 47:4291–4306
19. Amatucci GG, Tarascon JM, Klein LC (1996) CoO_2, The end member of the Li_xCoO_2 solid solution. J Electrochem Soc 143:1114–1123
20. Van der Ven A, Aydinol MK, Ceder G (1998) First-principles evidence for stage ordering in Li_xCoO_2. J Electrochem Soc 145:2149–2155
21. Xia H, Lu L, Meng YS, Ceder G (2007) Phase transitions and high voltage electrochemical behavior of $LiCoO_2$ thin films grown by pulsed laser deposition. J Electrochem Soc 154: A337–A342
22. Cho J, Kim G (1999) Enhancement of thermal stability of $LiCoO_2$ by $LiMn_2O_4$ coating. Electrochem Solid-State Lett 2:253–255
23. Kim B, Kim C, Kim T-G, Ahn D, Park B (2006) The effect of $AlPO_4$-coating layer on the electrochemical properties in $LiCoO_2$ thin films. J Electrochem Soc 153:A1773–A1777
24. Chen Z, Dahn JR (2004) Methods to obtain excellent capacity retention in $LiCoO_2$ cycled to 4.5V. Electrochim Acta 49:1079–1090
25. Thomas MGSR, David WIF, Goodenough JB (1985) Synthesis and structural characterization of the normal spinel $Li[Ni_2O_4]$. Mat Res Bull 20:1137–1146
26. Dahn JR, von Sacken U, Michal CA (1990) Structure and electrochemistry of $Li_{1\pm y}NiO_2$ and a new Li_2NiO_2 phase with the Ni $(OH)_2$ structure. Sol State Ionics 44:87–97
27. Broussely M, Perton F, Biensan P, Bodet JM, Labat J, Lecerf A, Delmas C, Rougier A, Pérès JP (1995) Li_xNiO_2, a promising cathode for rechargeable lithium batteries. J Power Sources 54:109–114
28. Dahn JR, von Sacken U, Juzkow MW, Al-Janaby H (1991) Rechargeable $LiNiO_2$/carbon cells. J Electrochem Soc 138: 2207–2211
29. Rougier A, Gravereau P, Delmas C (1996) Optimization of the composition of the $Li_{1-z}Ni_{1+z}O_2$ electrode materials: structural, magnetic, and electrochemical studies. J Electrochem Soc 143:1168–1175
30. Pérès JP, Delmas C, Rougier A, Broussely M, Perton F, Biensan P, Willman P (1996) The relationship between the composition of lithium nickel oxide and the loss of reversibility during the first cycle. J Phys Chem Solids 57:1057–1060

31. Delmas C, Pérès JP, Rougier A, Demourgues A, Weill F, Chadwick A, Broussely M, Perton F, Biensan P, Willman P (1997) On the behavior of the Li_xNiO_2 system: an electrochemical and structural overview. J Power Sources 68:120–125
32. Ohzuku T, Ueda A, Nagayama M, Iwakoshi Y, Komori H (1993) Comparative study of $LiCoO_2$, $LiNi_{1/2}Co_{1/2}O_2$ and $LiNiO_2$ for 4 volt secondary lithium cells. Electrochim Acta 38:1159–1167
33. Dahn JR, Fuller EW, Obrovac M, von Sacken U (1994) Thermal stability of Li_xCoO_2, Li_xNiO_2 and λ-MnO_2 and consequences for the safety of Li-ion cells. Sol State Ionics 69:265–270
34. Ohzuku T, Ueda A, Kouguchi M (1995) Synthesis and characterization of $LiAl_{1/4}Ni_{3/4}O_2$ (R-3m) for lithium-ion (Shuttlecock) batteries. J Electrochem Soc 142:4033–4439
35. Arai H, Sakurai Y (1999) Characteristics of Li_xNiO_2 obtained by chemical delithiation. J Power Sources 81–82:401–405
36. Albrecht S, Kümpers J, Kruft M, Malcus S, Vogler C, Wahl M, Wohlfahrt-Mehrens M (2003) Electrochemical and thermal behavior of aluminum- and magnesium-doped spherical lithium nickel cobalt mixed oxides $Li_{1-x}(Ni_{1-y-z}Co_yM_z)O_2$ (M=Al, Mg). J Power Sources 119–121:178–183
37. Onnerud PT, Shi JJ, Dalton SL, Lampe-Onnerud C (2008) Lithium metal oxide materials and methods of synthesis and use. US Patent 2008/0286460 A1
38. Chen CH, Liu J, Stoll ME, Henriksen G, Vissers DR, Amine K (2004) Aluminum-doped lithium nickel cobalt oxide electrodes for high-power lithium-ion batteries. J Power Sources 128:278–285
39. Kostecki R, Lei J, McLarnon F, Shim J, Striebel K (2006) Diagnostic evaluation of detrimental phenomena in high-power lithium-ion batteries. J Electrochem Soc 153:A669–A672
40. Tabuchi M, Tsutsui S, Masquelier C, Kanno R, Ado K, Matsubara I, Nasu S, Kageyama H (1998) Effect of cation arrangement on the magnetic properties of lithium ferrites ($LiFeO_2$ prepared by hydrothermal reaction and post-annealing method). J Solid State Chem 140:159–167
41. Ado K, Tabuchi M, Kobayashi H, Kageyama H, Nakamura O, Inaba Y, Kanno R (1997) Preparation of $LiFeO_2$ with alpha-$NaFeO_2$-type structure using a mixed-alkaline hydrothermal method. J Electrochem Soc 144:L177–L180
42. Kanno R, Shirane T, Kawamoto Y, Takeda Y, Takano M, Ohashi M, Yamaguchi Y (1996) Synthesis, structure, and electrochemical properties of a new lithium iron oxide, $LiFeO_2$, with a corrugated layer structure. J Electrochem Soc 143: 2435–2442
43. Morales J, Santos-Peña J (2007) Highly electroactive nanosized α-$LiFeO_2$. Electrochem Commun 9:2116–2120
44. Johnson CS, Kang S-H, Vaughey JT, Pol SV, Balasubramanian M, Thackeray MM (2010) Li_2O Removal from Li_5FeO_4: a cathode precursor for lithium-ion batteries. Chem Mater 22:1263–1270
45. Armstrong AR, Bruce PG (1996) Synthesis of layered $LiMnO_2$ as an electrode for rechargeable lithium batteries. Nature 381:499–500
46. Thackeray MM (1997) Manganese oxides for lithium batteries. Prog Solid State Chem 25:1–71
47. Reed J, Ceder G (2004) Role of electronic structure in the susceptibility of metastable transition-metal oxide structures to transformation. Chem Rev 104:4513–4534
48. Paulsen JM, Thomas CL, Dahn JR (1999) Layered Li-Mn-oxide with the O2 structure: a cathode material for Li-Ion cells which does not convert to spinel. J Electrochem Soc 146:3560–3565
49. Eriksson TA, Lee YJ, Hollingsworth J, Reimer JA, Cairns EJ, Zhang X-F, Doeff MM (2003) Influence of substitution on the structure and electrochemistry of layered manganese oxides. Chem Mater 15:4456–4463
50. Dollé M, Patoux S, Doeff MM (2005) Layered manganese oxide intergrowth electrodes for rechargeable lithium batteries. 1. substitution with Co or Ni. Chem Mater 17:1036–1043
51. Patoux S, Dollé M, Doeff MM (2005) Layered manganese oxide intergrowth electrodes for rechargeable lithium batteries. 2. substitution with Al. Chem Mater 17:1044–1054
52. Robertson AD, Armstrong AR, Bruce PG (2000) Influence of ion exchange conditions on the defect chemistry and performance of cobalt doped layered lithium manganese oxide based intercalation compounds. Chem Commun 20: 1997–1998
53. Doeff MM, Peng MY, Ma Y, De Jonghe LC (1994) Orthorhombic Na_xMnO_2 as a cathode material for secondary sodium and lithium polymer batteries. J Electrochem Soc 141:L145–L147
54. Doeff MM, Richardson TJ, Kepley L (1996) Lithium insertion processes of orthorhombic Na_xMnO_2-base electrode materials. J Electrochem Soc 143:2507–2516
55. Hu F, Doeff MM (2004) Electrochemical characterization of manganese oxide cathode materials based on $Na_{0.4}MnO_2$. J Power Sources 129:296–302
56. Armstrong AR, Huang H, Jennings RA, Bruce PG (1998) $Li_{0.44}MnO_2$: an intercalation electrode with a tunnel structure and excellent cyclability. J Mater Chem 8:255–259
57. Doeff MM, Anapolsky A, Edman L, Richardson TJ, De Jonghe LC (2001) A high-rate manganese oxide for rechargeable lithium battery applications. J Electrochem Soc 148: A230–A236
58. Akimoto J, Awaka J, Takahashi Y, Kijima N, Tabuchi M, Nakashima A, Sakaebe H, Tatsumi K (2005) Synthesis and electrochemical properties of $Li_{0.44}MnO_2$ as a novel 4 V cathode material. Electrochem Solid-State Lett 8:A554–A557
59. Kalyani P, Chitra S, Mohan T, Gopukumar S (1999) Lithium metal rechargeable cells using Li_2MnO_3 as the positive electrode. J Power Sources 80:103–106
60. Yu DYW, Yanagida K, Kato Y, Nakamura H (2009) Electrochemical activities in Li_2MnO_3. J Electrochem Soc 156:A417–A424
61. Rossouw MH, Thackeray MM (1991) Lithium manganese oxides from Li_2MnO_3 for rechargeable lithium battery applications. Mat Res Bull 26:463–473
62. Paik Y, Grey CP, Johnson CS, Kim J-S, Thackeray MM (2002) Lithium and deuterium NMR studies of acid-leached layered lithium manganese oxides. Chem Mater 14:5109–5115
63. Storey C, Kargina I, Grincourt Y, Davidson IJ, Yoo YC, Seung DY (2001) Electrochemical characterization of a new high capacity cathode. J Power Sources 97–98:541–544

64. Ammundsen B, Paulsen J, Davidson I, Liu R-S, Shen C-H, Chen J-M, Jang L-Y, Lee J-F (2002) Local structure and first cycle redox mechanism of layered $Li_{1.2}Cr_{0.4}Mn_{0.4}O_2$ cathode material. J Electrochem Soc 149:A431–A436
65. Ohzuku T, Makimura Y (2001) Layered lithium insertion material of $LiNi_{1/2}Mn_{1/2}O_2$: a possible alternative to $LiCoO_2$ for advanced lithium-ion batteries. Chem Lett 8: 744–745
66. Rossen E, Jones CDW, Dahn JR (1992) Structure and electrochemistry of $Li_xMn_yNi_{1-y}O_2$. Solid State Ionics 57:311–318
67. Makimura Y, Ohzuku T (2003) Lithium insertion material of $LiNi_{1/2}Mn_{1/2}O_2$ for advanced lithium-ion batteries. J Power Sources 119–121:156–160
68. Lu Z, MacNeil DD, Dahn JR (2001) Layered cathode materials $Li[Ni_xLi_{(1/3-2x/3)}Mn_{(2/3-x/3)}]O_2$ for lithium-ion batteries. Electrochem Solid State Lett 4:A191–A194
69. Reed J, Ceder G (2002) Charge, potential, and phase stability of layered $Li(Ni_{0.5}Mn_{0.5})O_2$. Electrochem Solid-State Lett 5: A145–A148
70. Yoon W-S, Grey CP, Balasubramanian M, Yang X-Q, McBreen J (2003) In situ x-ray absorption spectroscopic study on $LiNi_{0.5}Mn_{0.5}O_2$ cathode material during electrochemical cycling. Chem Mater 15:3161–3169
71. Van der Ven A, Ceder G (2004) Ordering in $Li_x(Ni_{0.5}Mn_{0.5})O_2$ and its relation to charge capacity and electrochemical behavior in rechargeable lithium batteries. Electrochem Commun 6:1045–1050
72. Yoon W-S, Paik Y, Yang X-Q, Balasubramanian M, McBreen J, Grey CP (2002) Investigation of the local structure of the $LiNi_{0.5}Mn_{0.5}O_2$ cathode material during electrochemical cycling by x-ray absorption and NMR spectroscopy. Electrochem Solid State Lett 5:A263–A266
73. Lu Z, Beaulieu LY, Donaberger RA, Thomas CL, Dahn JR (2002) Synthesis, structure, and electrochemical behavior of $Li[Ni_xLi_{1/3-2x/3}Mn_{2/3-x/3}]O_2$. J Electrochem Soc 149: A778–A791
74. Kang S-H, Park S-H, Johnson CS, Amine K (2007) Effects of Li content on structure and electrochemical properties of $Li_{1+x}(Ni_{0.5}Mn_{0.5})_{1-x}O_2$ ($0 \leq x \leq 0.15$) electrodes in lithium cells (1.0-4.8 V). J Electrochem Soc 154:A268–A274
75. Kang K, Meng YS, Bréger J, Grey CP, Ceder G (2006) Electrodes with high power and high capacity for rechargeable lithium batteries. Science 311:977–980
76. Yabuuchi N, Ohzuku T (2003) Novel lithium insertion material of $LiCo_{1/3}Ni_{1/3}Mn_{1/3}O_2$ for advanced lithium-ion batteries. J Power Sources 119–121:171–174
77. Koyama Y, Tanaka I, Adachi H, Makimura Y, Ohzuku T (2003) Crystal and electronic structures of superstructural $Li_{1-x}[Co_{1/3}Ni_{1/3}Mn_{1/3}]O_2$ ($0 \leq x \leq 1$). J Power Sources 119–121:644–648
78. Hwang BJ, Tsai YW, Carlier D, Ceder G (2003) A combined computational/experimental study on $LiNi_{1/3}Co_{1/3}Mn_{1/3}O_2$. Chem Mater 15:3676–3682
79. Kim J-M, Chung H-T (2003) The first cycle characteristics of Li $[Ni_{1/3}Co_{1/3}Mn_{1/3}]O_2$. Electrochim Acta 49:937–944
80. Kobayashi H, Arachi Y, Emura S, Kageyama H, Tatsumi K, Kamiyama T (2005) Investigation on lithium de-intercalation mechanism for $Li_{1-y}Ni_{1/3}Mn_{1/3}Co_{1/3}O_2$. J Power Sources 146:640–644
81. Tsai YW, Hwang BJ, Ceder G, Sheu HS, Liu DG, Lee JF (2005) In-situ x-ray absorption spectroscopic study on variation of electronic transitions and local structure of $LiNi_{1/3}Co_{1/3}Mn_{1/3}O_2$ cathode material during electrochemical cycling. Chem Mater 17:3193–3199
82. Kim MG, Shin HJ, Kim J-H, Park S-H, Sun Y-K (2005) XAS investigation of inhomogeneous metal-oxygen bond covalency in bulk and surface for charge compensation in Li-ion battery cathode $Li[Ni_{1/3}Co_{1/3}Mn_{1/3}]O_2$ material. J Electrochem Soc 152:A1320–A1328
83. Yoon W-S, Balasubramanian M, Chung KY, Yang X-Q, McBreen J, Grey CP, Fischer DA (2005) Electrochemical Li-ion deintercalated $Li_{1-x}Co_{1/3}Ni_{1/3}Mn_{1/3}O_2$ electrode system by combination of soft and hard x-ray absorption spectroscopy. J Am Chem Soc 127:17479–17487
84. Choi J, Manthiram A (2005) Role of chemical and structural stabilities on the electrochemical properties of layered $LiNi_{1/3}Mn_{1/3}Co_{1/3}O_2$ cathodes. J Electrochem Soc 152: A1714–A1718
85. Belharouak I, Lu W, Vissers D, Amine K (2006) Safety characteristics of $Li(Ni_{0.8}Co_{0.15}Al_{0.05})O_2$ and $Li(Ni_{1/3}Co_{1/3}Mn_{1/3})O_2$. Electrochem Commun 8:329–335
86. Ngala JK, Chernova NA, Ma M, Mamak M, Zavalij PY, Whittingham MS (2004) The synthesis, characterization and electrochemical behavior of the layered $LiNi_{0.4}Mn_{0.4}Co_{0.2}O_2$ compound. J Mater Chem 14:214–220
87. Xiao J, Chernova NA, Whittingham MS (2008) Layered mixed transition metal oxide cathodes with reduced cobalt content for lithium ion batteries. Chem Mater 20:7454–7464
88. Chernova NA, Ma M, Xiao J, Whittingham MS, Breger J, Grey CP (2007) Layered $Li_xNi_yMn_yCo_{1-2y}O_2$ cathodes for lithium ion batteries: understanding local structure via magnetic properties. Chem Mater 19:4682–4693
89. Liu D, Wang Z, Chen L (2006) Comparison of structure and electrochemistry of Al- and Fe-doped $LiNi_{1/3}Co_{1/3}Mn_{1/3}O_2$. Electrochim Acta 51:4199–4203
90. Hu S-K, Chou T-C, Hwang B-J, Ceder G (2006) Effect of Co content on performance of $LiAl_{1/3-x}Co_xNi_{1/3}Mn_{1/3}O_2$. J Power Sources 160:1287–1293
91. Zhou F, Zhao X, Lu Z, Jiang J, Dahn JR (2008) The effect of Al substitution on the reactivity of delithiated $LiNi_{1/3}Mn_{1/3}Co_{(1/3-z)}Al_zO_2$ with non-aqueous electrolyte. Electrochem Commun 10:1054–1057
92. Wilcox J, Patoux S, Doeff M (2009) Structure and electrochemistry of $LiNi_{1/3}Co_{1/3-y}M_yMn_{1/3}O_2$ (M = Ti, Al, Fe) positive electrode materials. J Electrochem Soc 156: A192–A198
93. Wilcox JD, Rodriguez EE, Doeff MM (2009) The impact of aluminum and iron substitution on the structure and electrochemistry of $Li(Ni_{0.4}Co_{0.2-y}M_yMn_{0.4})O_2$. J Electrochem Soc 156: A1011–A1018

94. Xiao J, Chernova NA, Whittingham MS (2010) Influence of manganese content on the performance of $LiNi_{0.9-y}Mn_yCo_{0.1}O_2$ ($0.45 \leq y \leq 0.60$) as a cathode material for li-ion batteries. Chem Mater 22:1180–1185
95. Thackeray MM, Kang S-H, Johnson CS, Vaughey JT, Benedek R, Hackney SA (2007) Li_2MnO_3-stabilized $LiMO_2$ (M=Mn, Ni, Co) electrodes for lithium-ion batteries. J Mater Chem 17:3112–3135
96. Johnson CS, Li N, Lifief C, Thackeray MM (2007) Anomalous capacity and cycling stability of $xLi_2MnO_3 \bullet (1-x)LiMO_2$ electrodes (M=Mn, Ni, Co) in lithium batteries at 50°C. Electrochem Commun 9:787–795
97. Hunter JC (1981) Preparation of a new crystal form of manganese dioxide: λ-MnO_2. J Sol State Chem 32:142–147
98. Thackeray MM, David WIF, Bruce PG, Goodenough JB (1983) Lithium insertion into manganese spinels. Mat Res Bull 18:461–472
99. Goodenough JB, Thackeray MM, David WIF, Bruce PG (1984) Lithium insertion/extraction reactions with manganese oxides. Rev Chim Miner 21:435–455
100. Thackeray MM (1999) Spinel electrodes for lithium batteries. J Am Ceram Soc 82:337–3354
101. Tarascon JM, Wang E, Shokoohi FK, McKinnon WR, Colson S (1991) The spinel phase of $LiMn_2O_4$ as a cathode in secondary lithium cells. J Electrochem Soc 138: 2859–2864
102. Tarascon JM, McKinnon WR, Coowar F, Bowmer TN, Amatucci G, Guyomard D (1994) Synthesis conditions and oxygen stoichiometry effects on Li insertion into the spinel $LiMn_2O_4$. J Electrochem Soc 141:1421–1431
103. Guyomard D, Tarascon JM (1994) The carbon/$Li_{1+x}Mn_2O_4$ system. Sol State Ionics 69:222–237
104. Xia Y, Zhou Y, Yoshio M (1997) Capacity fading on cycling of 4 V Li/$LiMn_2O_4$ cells. J Electrochem Soc 144:2593–2600
105. Amatucci G, Tarascon J-M (2002) Optimization of insertion compounds such as $LiMn_2O_4$ for li-ion batteries. J Electrochem Soc 149:K31–K46
106. Gummow RJ, de Kock A, Thackeray MM (1994) Improved capacity retention in rechargeable 4 V lithium/lithium manganese oxide (spinel) cells. Sol State Ionics 69:59–67
107. Shaju KM, Subba Rao GV, Chowdari BVR (2002) Spinel phases, $LiM_{1/6}Mn_{11/6}O_4$ (M=Co, CoAl, CoCr, CrAl), as cathodes for lithium-ion batteries. Sol State Ionics 148:343–350
108. Tucker MC, Reimer JA, Cairns EJ (2002) A 7Li NMR study of capacity fade in metal-substituted lithium manganese oxide spinels. J Electrochem Soc 149:A574–A585
109. Grush MM, Horne CR, Perera RCC, Ederer DL, Cramer SP, Cairns EJ, Callcott TA (2000) Correlating electronic structure with cycling performance of substituted $LiMn_2O_4$ electrode materials: a study using the techniques of soft x-ray absorption and emission. Chem Mater 12:659–664
110. Myung S-T, Komaba S, Kumagai N (2001) Enhanced structural stability and cyclability of Al-doped $LiMn_2O_4$ spinel synthesized by the emulsion drying method. J Electrochem Soc 148: A482–A489
111. Ariyoshi K, Iwata E, Kuniyoshi M, Wakabayashi H, Ohzuku T (2006) Lithium aluminum manganese oxide having spinel framework structure for long-life lithium-ion batteries. Electrochem Sol State Lett 9:A557–A560
112. Amatucci GG, Pereira N, Zheng T, Tarascon J-M (2001) Failure mechanism and improvement of the elevated temperature cycling of $LiMn_2O_4$ compounds through the use of the $LiAl_xMn_{2-x}O_{4-z}F_z$ solid solution. J Electrochem Soc 148: A171–A182
113. Whittingham MS (2004) Lithium batteries and cathode materials. Chem Rev 104:4271–4301
114. Thackeray MM, de Kock A, Rossouw MH, Liles D, Bittihn R, Hoge D (1992) Spinel electrodes from the Li-Mn-O system for rechargeable lithium battery applications. J Electrochem Soc 139:363–366
115. Kim J, Manthiram A (1998) Low temperature synthesis and electrode properties of $Li_4Mn_5O_{12}$. J Electrochem Soc 145: L53–L55
116. Pasquier Du, Blyr A, Courjal P, Larcher D, Amatucci G, Gérand B, Tarascon J-M (1999) Mechanism for limited 55°C storage performance of $Li_{1.05}Mn_{1.95}O_4$ electrodes. J Electrochem Soc 146:428–436
117. Wen SJ, Richardson TJ, Ma L, Striebel KA, Ross PN, Cairns EJ (1996) FTIR spectroscopy of metal oxide insertion electrodes. J Electrochem Soc 143:L136–L138
118. Eriksson T, Gustafsson T, Thomas JO (2002) Surface structure of $LiMn_2O_4$ electrodes. Electrochem Sol State Lett 5:A35–A38
119. Akimoto J, Takahashi Y, Kijima N (2005) Direct observation of the bulk degradation of $Li_{1.1}Mn_{1.9}O_4$ single crystals after high-temperature storage. Electrochem Sol State Lett 8:A361–A364
120. Kobayashi H, Sakaebe H, Komoto K, Kageyama H, Tabuchi M, Tatsumi K, Kohigashi T, Yonemura M, Kanno R, Kamiyama T (2003) Structure and physical property changes of delithiated spinels for $Li_{1.02-x}Mn_{1.98}O_4$ after high-temperature storage. Sol State Ionics 156:309–318
121. Quinlan FT, Sano K, Willey T, Vidu R, Tasaki K, Stroeve P (2001) Surface characterization of the spinel $Li_xMn_2O_4$ cathode before and after storage at elevated temperatures. Chem Mater 13:4207–4212
122. Tsunekawa H, Tanimoto S, Marubayashi R, Fujita M, Kifune K, Sano M (2002) Capacity fading of graphite electrodes due to the deposition of manganese ions on them in Li-ion batteries. J Electrochem Soc 149:A1326–A1331
123. Amine K, Liu J, Kang S, Belharouak I, Hyung Y, Vissers D, Henriksen G (2004) Improved lithium manganese oxide spinel/graphite Li-ion cells for high-power applications. J Power Sources 129:14–19
124. Cho J, Kim GB, Lim HS, Kim C-S, Yoo S-I (1999) Improvement of structural stability of $LiMn_2O_4$ cathode material on 55°C cycling by sol-gel coating of $LiCoO_2$. Electrochem Sol State Lett 2:607–609
125. Wang EI (1998) Method of treating lithium manganese oxide spinel. US Patent 5,783,328

126. Xu W, Angell CA (2001) LiBOB and its derivatives weakly coordinating anions, and the exceptional conductivity of their nonaqueous solutions. Electrochem Sol State Lett 4: E1–E4
127. Xu K, Zhang S, Jow TR, Xu W, Angell CA (2002) LiBOB as salt for lithium-ion batteries a possible solution for high temperature operation. Electrochem Solid State Lett 5(1):A26–A29
128. Chen Z, Amine K (2006) Capacity fade of $Li_{1+x}Mn_{2-x}O_4$-based lithium-ion cells. J Electrochem Soc 153:A316–A320
129. Kitao H, Fujihara T, Takeda K, Nakanishi N, Nohma T (2005) High-temperature storage performance of Li-ion batteries using a mixture of Li-Mn spinel and Li-Ni-Co-Mn oxide as a positive electrode material. Electrochem Sol State Lett 8:A87–A90
130. MacNeil DD, Dahn JR (2001) The reaction of charged cathodes with nonaqueous solvents and electrolytes II. $LiMn_2O_4$ charged to 4.2 V. J Electrochem Soc 148:A1211–A1215
131. Thackeray MM (1995) Structural considerations of layered and spinel lithiated oxides for lithium ion batteries. J Electrochem Soc 142:2558–2563
132. Sigala C, Guyomard D, Verbaere A, Piffard Y, Tournoux M (1995) Positive electrode materials with high operating voltage for lithium batteries: $LiCr_yMn_{2-y}O_4$ ($0 \leq y \leq 1$). Sol State Ionics 81:167–170
133. Kawai H, Nagata M, Tabuchi M, Tukamoto H, West AR (1998) Novel 5V spinel cathode $Li_2FeMn_3O_8$ for lithium ion batteries. Chem Mater 10:3266–3268
134. Ein-Eli Y, Howard WF (1997) $LiCu_x^{II}Cu_y^{III}Mn_{[2-(x+y)]}^{III,\ IV}O_4$: 5V cathode materials. J Electrochem Soc 144:L205–L207
135. Kawai H, Nagata M, Tukamoto H, West AR (1998) A novel cathode $Li_2CoMn_3O_8$ for lithium ion batteries operating over 5V. J Mater Chem 8:837–839
136. Zhong Q, Bonakdarpour A, Zhang M, Gao Y, Dahn JR (1997) Synthesis and electrochemistry of $LiNi_xMn_{2-x}O_4$. J Electrochem Soc 144:205–213
137. Ohzuku T, Takeda S, Iwanaga M (1999) Solid-state redox potentials for $Li[Me_{1/2}Mn_{3/2}]O_4$ (Me: 3d-transition metal) having spinel-framework structures: a series of 5 volt materials for advanced lithium-ion batteries. J Power Sources 81–82:90–94
138. Sun Y-K, Lee Y-S, Yoshio M, Amine K (2002) Synthesis and electrochemical properties of ZnO-coated $LiNi_{0.5}Mn_{1.5}O_4$ spinel as 5V cathode material for lithium secondary batteries. Electrochem Sol State Lett 5:A99–A102
139. Liu J, Manthiram A (2009) Kinetics study of the 5V spinel cathode $LiMn_{1.5}Ni_{0.5}O_4$ before and after surface modifications. J Electrochem Soc 156:A833–A838
140. Patoux S, Daniel L, Bourbon C, Lignier H, Pagano C, Le Cras F, Jouanneau S, Martinet S (2009) High voltage spinel oxides for Li-ion batteries: from the materials research to the application. J Power Sources 189:344–352
141. Kim J-H, Myung S-T, Yoon CS, Oh I-H, Sun Y-K (2004) Effect of Ti substitution of $LiNi_{0.5}Mn_{1.5-x}Ti_xO_4$ and their electrochemical properties as lithium insertion material. J Electrochem Soc 151:A1911–A1918
142. Arunkumar TA, Manthiram A (2005) Influence of lattice parameter differences on the electrochemical performance of the 5V spinel $LiMn_{1.5-y}Ni_{0.5-z}M_{y+z}O_4$ (M=Li, Mg, Fe, Co, and Zn). Electrochem Sol State Lett 8:A403–A405
143. Ooms FGB, Kelder EM, Schoonman J, Wagemaker M, Mulder FM (2002) High-voltage $LiMg_\delta Ni_{0.5-\delta}Mn_{1.5}O_4$ spinels for Li-ion batteries. Sol State Ionics 152–153:143–153
144. Gryffoy D, Vandenberghe RE, Legrand E (1991) A neutron diffraction study of some spinel compounds containing octahedral Ni and Mn at a 1:3 ratio. Mater Sci Forum 79–82:785–790
145. Takahashi K, Saitoh M, Sano M, Fujita M, Kifune K (2004) Electrochemical and structural properties of a 4.7V-class $LiNi_{0.5}Mn_{1.5}O_4$ positive electrode material prepared with a self-reaction method. J Electrochem Soc 151:A173–A177
146. Kunduraci M, Amatucci GG (2006) Synthesis and characterization of nanostructured 4.7V $Li_xMn_{1.5}Ni_{0.5}O_4$ spinels for high-power lithium-ion batteries. J Electrochem Soc 153: A1345–A1352
147. Wu HM, Belharouak I, Deng H, Abouimrane A, Sun Y-K, Amine K (2009) Development of $LiNi_{0.5}Mn_{1.5}O_4/Li_4Ti_5O_{12}$ system with long cycle life. J Electrochem Soc 156:A1047–A1050
148. Padhi AK, Nanjundaswamy KS, Goodenough JB (1997) Phospho-olivines as positive-electrode materials for rechargeable lithium batteries. J Electrochem Soc 144:1188–1194
149. Andersson AS, Kalska B, Häggstrom L, Thomas JO (2000) Lithium extraction/insertion in $LiFePO_4$: an x-ray diffraction and Mössbauer spectroscopy study. Sol State Ionics 130:41–52
150. Tarascon J-M, Armand M (2001) Issues and challenges facing rechargeable lithium batteries. Nature 414:359–376
151. Ravet N, Chouinard Y, Magnan JF, Besner S, Gauthier M, Armand M (2001) Electroactivity of natural and synthetic triphylite. J Power Sources 97–98:503–507
152. Barker J, Saidi MY, Swoyer JL (2003) A carbothermal reduction method for the preparation of electroactive materials for lithium ion applications. J Electrochem Soc 150:A684–A688
153. Doeff MM, Wilcox JD, Kostecki R, Lau G (2006) Optimization of carbon coatings on $LiFePO_4$. J Power Sources 163:180–184
154. Dominko R, Bele M, Gaberscek M, Remskar M, Hanzel D, Pejovnik S, Jamnik J (2005) Impact of the carbon coating thickness on the electrochemical performance of $LiFePO_4$/C composites. J Electrochem Soc 152:A607–A610
155. Huang H, Yin S-C, Nazar LF (2001) Approaching theoretical capacity of $LiFePO_4$ at room temperature at high rates. Electrochem Sol State Lett 4:A170–A172
156. Doeff MM, Hu Y, McLarnon F, Kostecki R (2003) Effect of surface carbon structure on the electrochemical performance of $LiFePO_4$. Electrochem Sol State Lett 6:A207–A209
157. Zaghib K, Shim J, Guerfi A, Charest P, Striebel KA (2005) Effect of carbon source as additives in $LiFePO_4$ as positive electrode for li-ion batteries. Electrochem Sol State Lett 8:A207–A210
158. Wilcox JD, Doeff MM, Marcinek M, Kostecki R (2007) Factors influencing the quality of carbon coatings on $LiFePO_4$. J Electrochem Soc 154:A389–A395

159. Doeff MM, Wilcox JD, Yu R, Aumentado A, Marcinek M, Kostecki R (2008) Impact of carbon structure and morphology on the electrochemical performance of $LiFePO_4$/C composites. J Sol State Electrochem 12:995–1001
160. Chen Z, Dahn JR (2002) Reducing carbon in $LiFePO_4$/C composite electrodes to maximize specific energy, volumetric energy, and tap density. J Electrochem Soc 149:A1184–A1189
161. Chung S-Y, Bloking JT, Chiang Y-M (2002) Electronically conductive phospho-olivines as lithium storage electrodes. Nat Mater 1:123–128
162. Thackeray MM (2002) An unexpected conductor. Nat Mater 1:81–82
163. Ravet N, Abouimrane A, Armand M (2003) From our readers. Nat Mater 2:702–703
164. Herle PS, Ellis B, Coombs N, Nazar LF (2004) Nano-network electronic conduction in iron and nickel olivine phosphates. Nat Mater 3:147–152
165. Delacourt C, Wurm C, Laffont L, Leriche J-B, Masquelier C (2006) Electrochemical and electrical properties of Nb- and/or C-containing $LiFePO_4$ composites. Sol State Ionics 177:333–341
166. Rho Y-H, Nazar LF, Perry L, Ryan D (2007) Surface chemistry of $LiFePO_4$ studied by Mössbauer and x-ray photoelectron spectroscopy and its effect on electrochemical properties. J Electrochem Soc 154:A283–A289
167. Wagemaker M, Ellis BL, Lützenkirchen-Hecht D, Mulder FM, Nazar LF (2008) Proof of supervalent doping in olivine $LiFePO_4$. Chem Mater 20:6313–6315
168. Islam MS, Driscoll DJ, Fisher CAJ, Slater PR (2005) Atomic-scale investigation of defects, dopants, and lithium transport in the $LiFePO_4$ olivine-type battery material. Chem Mater 17:5085–5092
169. Maier J, Amin R (2008) Defect chemistry of $LiFePO_4$. J Electrochem Soc 155:A339–A344
170. Axmann P, Stinner C, Wohlfahrt-Mehrens M, Mauger A, Gendron G, Julien CM (2009) Nonstoichiometric $LiFePO_4$: defects and related properties. Chem Mater 21:1636–1644
171. Amin R, Maier J (2008) Effect of annealing on transport properties of $LiFePO_4$: towards a defect chemical model. Sol State Ionics 178:1831–1836
172. Morgan D, Van der Ven A, Ceder G (2004) Li conductivity in Li_xMPO_4 (M=Mn, Fe, Co, Ni) olivine materials. Electrochem and Sol State Lett 7:A30–A32
173. Li J, Yao W, Martin S, Vaknin D (2008) Lithium ion conductivity in single crystal $LiFePO_4$. Sol State Ionics 179:2016–2019
174. Amin R, Maier J, Balaya P, Chen DP, Lin CT (2008) Ionic and electronic transport in single crystalline $LiFePO_4$ grown by optical floating zone technique. Sol State Ionics 179:1683–1687
175. Gardiner GR, Islam MS (2010) Anti-site defects and ion migration in the $LiFe_{0.5}Mn_{0.5}PO_4$ mixed-metal cathode material. Chem Mater 22:1242–1248
176. Chen J, Vacchio MJ, Wang S, Chernova N, Zavalij PY, Whittingham MS (2008) The hydrothermal synthesis and characterization of olivines and related compounds for electrochemical applications. Sol State Ionics 178:1676–1693
177. Delacourt C, Poizot P, Levasseur S, Masquelier C (2006) Size effects on carbon-free $LiFePO_4$ powders the key to superior energy density. Electrochem Sol State Lett 9:A352–A355
178. Meethong N, Huang H-YS, Carter WC, Chiang Y-M (2007) Size-dependent lithium miscibility gap in nanoscale $Li_{1-x}FePO_4$. Electrochem Sol State Lett 10:A134–A138
179. Gibot P, Casas-Cabanas M, Laffont L, Levasseur S, Carlach P, Hamelet S, Tarascon J-M, Masquelier C (2008) Room-temperature single-phase Li insertion/extraction in nanoscale Li_xFePO_4. Nat Mater 7:741–747
180. Yamada A, Koizumi H, Sonoyama N, Kanno R (2005) Phase change in Li_xFePO_4. Electrochem Sol State Lett 8: A409–A413
181. Yamada A, Koizumi H, Nishimura S-I, Sonoyama N, Kanno R, Yonemura M, Nakamura T, Kobayashi Y (2006) Room-temperature miscibility gap in Li_xFePO_4. Nat Mater 5:357–360
182. Hamelet S, Gibot P, Casas-Cabanas M, Bonnin D, Grey CP, Cabana J, Leriche J-B, Rodriguez-Carvajal CM, Levasseur S, Carlach P, Van Thournout M, Tarascon J-M, Masquelier C (2009) The effects of moderate thermal treatments under air on $LiFePO_4$-based nano powders. J Mater Chem 19:3979–3991
183. Yu DYW, Donoue K, Kadohata T, Murata T, Matsuta S, Fujitani S (2008) Impurities in $LiFePO_4$ and their influence on material characteristics. J Electrochem Soc 155:A526–A530
184. Dokko K, Shiraishi K, Kanamura K (2005) Identification of surface impurities on $LiFePO_4$ particles prepared by a hydrothermal process. J Electrochem Soc 152:A2199–A2202
185. Delacourt C, Poizot P, Tarascon J-M, Masquelier C (2005) The existence of a temperature-driven solid solution in Li_xFePO_4 for $0 \leq x \leq 1$. Nat Mater 4:254–260
186. Dodd JL, Yazami R, Fultz B (2006) Phase diagram of Li_xFePO_4. Electrochem Sol State Lett 9:A151–A155
187. Chen G, Song X, Richardson TJ (2007) Metastable solid-solution phases in the $LiFePO_4$/$FePO_4$ system. J Electrochem Soc 154:A627–A632
188. Srinivasan V, Newman J (2004) Discharge model for the lithium iron-phosphate electrode. J Electrochem Soc 151: A1517–A1529
189. Chen G, Song X, Richardson TJ (2006) Electron microscopy study of the $LiFePO_4$ to $FePO_4$ phase transition. Electrochem Sol State Lett 9:A295–A298
190. Andersson AS, Thomas JO (2001) The source of first cycle capacity loss in $LiFePO_4$. J Power Sources 97–98:498–502
191. Laffont L, Delacourt C, Gibot P, Wu MY, Kooyman P, Masquelier C, Tarascon JM (2006) Study of the $LiFePO_4$/$FePO_4$ two-phase system by high-resolution electron energy loss spectroscopy. Chem Mater 18:5520–5529
192. Delmas C, Maccario M, Croguennec L, Le Cras F, Weill F (2008) Lithium deintercalation in $LiFePO_4$ nanoparticles via a domino-cascade model. Nat Mater 7:665–671
193. Allen JL, Jow TR, Wolfenstine J (2007) Kinetic study of the electrochemical $FePO_4$ to $LiFePO_4$ phase transition. Chem Mater 19:2108–2111

194. Lee KT, Kan WH, Nazar LF (2009) Proof of intercrystallite ionic transport in $LiMPO_4$ electrodes (M=Fe, Mn). J Am Chem Soc 131:6044–6045
195. Kang B, Ceder G (2009) Battery materials for ultrafast charging and discharging. Nature 458:190–193
196. Amine K, Liu J, Belharouak I (2005) High-temperature storage and cycling of C-$LiFePO_4$/graphite Li-ion cells. Electrochem Commun 7:669–673
197. Koltypin M, Aurbach D, Nazar L, Ellis B (2007) On the stability of $LiFePO_4$ olivine cathodes under various conditions (electrolyte solutions, temperatures). Electrochem Solid-State Lett 10:A40–A44
198. Yang S, Song Y, Zavalij PY, Whittingham MS (2002) Reactivity, stability and electrochemical behavior of lithium iron phosphates. Electrochem Commun 4:239–244
199. Li G, Azuma H, Tohda M (2002) $LiMnPO_4$ as the cathode for lithium batteries. Electrochem Sol State Lett 5: A135–A137
200. Rissouli K, Benkhouja K, Ramos-Barrado JR, Julien C (2003) Electrochemical conductivity in lithium orthophosphates. Mater Sci Eng B 98:185–189
201. Delacourt C, Laffont L, Bouchet R, Wurm C, Leriche J-B, Morcrette M, Tarascon J-M, Masquelier C (2005) Toward understanding of electrical limitations (electronic, ionic) in $LiMPO_4$ (M=Fe, Mn) electrode materials. J Electrochem Soc 152:A913–A921
202. Delacourt C, Poizot P, Morcrette M, Tarascon J-M, Masquelier C (2004) One step low-temperature route for the preparation of electrochemically active $LiMnPO_4$ powders. Chem Mater 16:93–99
203. Yang J, Xu JJ (2006) Synthesis and characterization of carbon-coated lithium transition metal phosphates $LiMPO_4$ (M=Fe, Mn, Co, Ni) prepared via a nonaqueous sol-gel route. J Electrochem Soc 153:A716–A723
204. Kwon N-H, Drezen T, Exnar I, Teerlinck I, Isono M, Graetzel M (2006) Enhanced electrochemical performance of mesoparticulate $LiMnPO_4$ for lithium ion batteries. Electrochem and Solid State Lett 9:A277–A280
205. Kim TR, Kim DH, Ryu HW, Moon JH, Lee JH, Boo S, Kim J (2007) Synthesis of lithium manganese phosphate nanoparticle and its properties. J Phys Chem Sol 68: 1203–1206
206. Bakenov Z, Taniguchi I (2010) Electrochemical performance of nanocomposite $LiMnPO_4$/C cathode materials for lithium batteries. Electrochemistry Commun 12:75–78
207. Xiao J, Xu W, Choi D, Zhang J-G (2010) Synthesis and characterization of lithium manganese phosphate by a precipitation method. J Electrochem Soc 157:A142–A147
208. Doeff MM, Chen J, Conry TE, Wang R, Wilcox J, Aumentado A (2010) Combustion synthesis of nanoparticulate $LiMg_xMn_{1-x}PO_4$ (x = 0, 0.1, 0.2) carbon composites. J Mater Res 25:1460–1468
209. Drezen T, Kwon N-H, Bowen P, Terrlinck I, Isono M, Exnar I (2007) Effect of particle size on $LiMnPO_4$ cathodes. J Power Sources 174:949–953
210. Chen G, Wilcox JD, Richardson TJ (2008) Improving the performance of lithium manganese phosphate through divalent cation substitution. Electrochem Sol State Lett 11:A190–A194
211. Shiratsuchi T, Okada S, Doi T, Yamaki J-I (2009) Cathodic performance of $LiMn_{1-x}M_xPO_4$ (M = Ti, Mg, and Zr) annealed in an inert atmosphere. Electrochim Acta 54:3145–3151
212. Bakenov Z, Taniguchi I (2010) $LiMg_xMn_{1-x}PO_4$/C cathodes for lithium batteries prepared by a combination of spray pyrolysis with wet ballmilling. J Electrochem Soc 157: A430–A436
213. Martha SK, Markovsky B, Grinblat J, Gofer Y, Haik O, Zinigrad E, Aurbach D, Drezen T, Wang D, Deghenghi G, Exnar I (2009) $LiMnPO_4$ as an advanced cathode material for rechargeable lithium batteries. J Electrochem Soc 156: A541–A552
214. Yonemura M, Yamada A, Takei Y, Sonoyama N, Kanno R (2004) Comparative kinetic study of olivine Li_xMPO_4 (M=Fe, Mn). J Electrochem Soc 151:A1352–A1356
215. Yamada A, Chung S-C (2001) Crystal chemistry of the olivine-type $Li(Mn_yFe_{1-y})PO_4$ and $(Mn_yFe_{1-y})PO_4$ as possible 4 V cathode materials for lithium batteries. J Electrochem Soc 148:A960–A967
216. Chen G, Richardson TJ (2009) Solid solution phases in the olivine-type $LiMnPO_4$/$MnPO_4$ system. J Electrochem Soc 156: A756–A762
217. Kim S-W, Kim J, Gwon H, Kang K (2009) Phase stability study of $Li_{1-x}MnPO_4$ ($0 \leq x \leq 1$) cathode for Li rechargeable battery. J Electrochem Soc 156:A635–A638
218. Chen G, Richardson TJ (2010) Thermal instability of olivine-type $LiMnPO_4$ cathodes. J Power Sources 195:1221–1224
219. Okada S, Sawa S, Egashira M, Yamaki J-I, Tabuchi M, Kageyama H, Konishi T, Yoshino A (2001) Cathode properties of phospho-olivine $LiMPO_4$ for lithium secondary batteries. J Power Sources 97–98:430–432
220. Wolfenstine J, Allen J (2004) $LiNiPO_4$–$LiCoPO_4$ solid solutions as cathodes. J Power Sources 136:150–153
221. Deniard P, Dulac AM, Rocquefelte X, Grigorova V, Lebacq O, Pasturel A, Jobic S (2004) High potential positive materials for lithium-ion batteries: transition metal phosphates. J Phys Chem Sol 65:229–233
222. Chang X-Y, Wang Z-X, Li X-H, Zhang L, Guo H-J, Peng W-J (2005) Synthesis and performance of $LiMn_{0.7}Fe_{0.3}PO_4$ cathode material for lithium ion batteries. Mater Res Bull 40:1513–1520
223. Yamada A, Kudo Y, Liu K-Y (2001) Phase diagram of $Li_x(Mn_yFe_{1-y})PO_4$ ($0 \leq x, y \leq 1$). J Electrochem Soc 148: A1153–A1158
224. Bramnik NN, Bramnik KG, Nikolowski K, Hinterstein M, Baehtz C, Ehrenbert H (2005) Synchrotron diffraction study of lithium extraction from $LiMn_{0.6}Fe_{0.4}PO_4$. Electrochem Sol State Lett 8:A379–A381
225. Park Y-U, Kim J, Gwon H, Seo D-H, Kim S-W, Kang K (2010) Synthesis of multicomponent olivine by a novel mixed transition metal oxalate coprecipitation method and electrochemical characterization. Chem Mater 22:2573–2581

226. Gwon H, Seo D-H, Kim S-W, Kim J, Kang K (2009) Combined first-principle calculations and experimental study on multicomponent olivine cathode for lithium rechargeable batteries. Adv Funct Mater 19:1–8
227. Seo D-H, Gwon H, Kim S-W, Kim J, Kang K (2010) Multicomponent olivine cathode for lithium rechargeable batteries: a first-principles study. Chem Mater 22:518–523
228. Goodenough JB, Hong Y-P, Kafalas JA (1976) Fast Na^+-ion transport in skeleton structures. Mater Res Bull 11:203–220
229. Delmas C, Nadiri A (1988) The Nasicon-type titanium phosphates $ATi_2(PO_4)_3$ (A=Li, Na) as electrode materials. Sol State Ionics 28–30:419–423
230. Delmas C, Cherkaoui F, Nadiri A, Hagenmuller P (1987) A Nasicon-type phase as intercalation electrode: $NaTi_2(PO_4)_3$. Mat Res Bull 22:631–639
231. Manthiram A, Goodenough JB (1989) Lithium insertion into $Fe_2(SO_4)_3$ frameworks. J Power Sources 26:403–408
232. Nanjundaswamy KS, Padhi AK, Goodenough JB, Okada S, Ohtsuka H, Arai H, Yamaki J (1996) Synthesis, redox potential evaluation and electrochemical characteristics of NASICON-related-3D framework compounds. Sol State Ionics 92:1–10
233. Masquelier C, Padhi AK, Nanjundaswamy KS, Goodenough JB (1998) New cathode materials for rechargeable lithium batteries: the 3-D framework structures $Li_3Fe_2(XO_4)_3$ (X=P, As). J Sol State Chem 135:228–234
234. Saïdi MY, Barker J, Huang H, Swoyer JL, Adamson G (2002) Electrochemical properties of lithium vanadium phosphate as a cathode material for lithium-ion batteries. Electrochem Sol State Lett 5:A149–A151
235. Morcrette M, Leriche J-B, Patoux S, Wurm C, Masquelier C (2003) In situ x-ray diffraction during lithium extraction from rhombohedral and monoclinic $Li_3V_2(PO_4)_3$. Electrochem Sol State Lett 6:A80–A84
236. Yin S-C, Strobel PS, Grondey H, Nazar LF (2004) $Li_{2.5}V_2(PO_4)_3$: a room-temperature analogue to the fast-ion conducting high-temperature γ-phase of $Li_3V_2(PO_4)_3$. Chem Mater 16:1456–1465
237. Gover RKB, Burns P, Bryan A, Saidi MY, Swoyer JL, Barker J (2006) $LiVPO_4F$: A new active material for safe lithium-ion batteries. Sol State Ionics 177:2635–2638
238. Barker J, Gover RKB, Burns P, Bryan A, Saidi MY, Swoyer JL (2005) Structural and electrochemical properties of lithium vanadium fluorophosphate, $LiVPO_4F$. J Power Sources 146:516–520
239. Barker J, Gover RKB, Burns P, Bryan A (2005) A symmetrical lithium-ion cell based on lithium vanadium fluorophosphate, $LiVPO_4F$. Electrochem Sol State Lett 8:A285–A287
240. Gover RKB, Bryan A, Burns P, Barker J (2006) The electrochemical insertion properties of sodium vanadium fluorophosphate, $Na_3V_2(PO_4)_2F_3$. Sol State Ionics 177:1495–1500
241. Ellis BL, Makahnouk WRM, Makimura Y, Toghill K, Nazar LF (2007) A multifunctional 3.5 V iron-based phosphate cathode for rechargeable batteries. Nat Mater 6:749–753
242. Ramesh TN, Lee KT, Ellis BL, Nazar LF (2010) Tavorite lithium iron fluorophosphate cathode materials: phase transition and electrochemistry of $LiFePO_4F$–Li_2FePO_4F. Electrochem Sol State Lett 13:A43–A47
243. Recham N, Chotard J-N, Jumas J-C, Laffont L, Armand M, Tarascon J-M (2010) Ionothermal synthesis of Li-based fluorophosphates electrodes. Chem Mater 22:1142–1148
244. Song Y, Zavalij PY, Chernova NA, Whittingham MS (2005) Synthesis, crystal structure, and electrochemical and magnetic study of new iron (III) hydroxylphosphates, isostructural with lipscombite. Chem Mater 17:1139–1147
245. Marx N, Croguennec L, Carlier D, Bourgeois L, Kubiak P, Le Cras F, Delmas C (2010) Structural and electrochemical study of a new crystalline hydrated iron(III) phosphate $FePO_4{\cdot}H_2O$ obtained from $LiFePO_4(OH)$ by ion exchange. Chem Mater 22:1854–1861
246. Gaubicher J, Le Mercier T, Chabre Y, Angenault J, Quarton M (1999) Li/β-$VOPO_4$: a new 4V system for lithium batteries. J Electrochem Soc 146:4375–4379
247. Kerr TA, Gaubicher J, Nazar LF (2000) Highly reversible Li insertion at 4V in ε-$VOPO_4$/α-$LiVPO_4$ cathodes. Electrochem Sol State Lett 3:460–462
248. Song Y, Zavalij PY, Whittingham MS (2005) ε-$VOPO_4$: electrochemical synthesis and enhanced cathode behavior. J Electrochem Soc 152:A721–A727
249. Barker J, Gover RKB, Burns P, Bryan A (2005) $LiVP_2O_7$: a viable lithium-ion cathode material? Electrochem Sol State Lett 8:A446–A448
250. Nytén A, Abouimrane A, Armand M, Gustafsson T, Thomas JO (2005) Electrochemical performance of Li_2FeSiO_4 as a new Li-battery cathode material. Electrochem Commun 7: 156–160
251. Dominko R, Bele M, Gaberscek M, Meden A, Remskar M, Jamnik J (2006) Structure and electrochemical performance of Li_2MnSiO_4 and Li_2FeSiO_4 as potential Li-battery cathode materials. Electrochem Commun 8:217–222
252. Gong ZL, Li YX, Yang Y (2006) Synthesis and characterization of $Li_2Mn_xFe_{1-x}SiO_4$ as a cathode material for lithium ion batteries. Electrochem Sol State Lett 9:A542–A544
253. Belharouak I, Abouimrane A, Amine K (2009) Structural and electrochemical characterization of Li_2MnSiO_4 cathode material. J Phys Chem C 113:20733–20737
254. Lyness C, Delobel B, Armstrong AR, Bruce PG (2007) The lithium intercalation compound Li_2CoSiO_4 and its behaviour as a positive electrode for lithium batteries. J Chem Soc Chem Commun 46:4890–4892
255. Armstrong AR, Lyness C, Ménétrier M, Bruce PG (2010) Structural polymorphism in Li_2CoSiO_4 intercalation electrodes: a combined diffraction and NMR study. Chem Mater 22:1892–1900
256. Dominko R (2010) Silicates and titanates as high-energy cathode materials for Li-ion batteries. In: Proceedings of SPIE: energy harvesting and storage: materials, devices and applications II, Orlando

257. Zaghib K, Salah AA, Ravet N, Mauger A, Gendron F, Julien CM (2006) Structural, magnetic and electrochemical properties of lithium iron orthosilicate. J Power Sources 160:1381–1386
258. Nishimura S-I, Hayase S, Kanno R, Yashima M, Nakayama N, Yamada A (2008) Structure of Li_2FeSiO_4. J Am Chem Soc 130:13212–13213
259. Arroyo-de Dompablo ME, Armand M, Tarascon JM, Amador U (2006) On-demand design of polyoxianionic cathode materials based of electronegativity correlations: an exploration of the Li_2MSiO_4 system (M=Fe, Mn, Co, Ni). Electrochem Commun 8:1292–1298
260. Li H, Balaya P, Maier J (2004) Li-storage via heterogeneous reaction in selected binary metal fluorides and oxides. J Electrochem Soc 151:A1878–A1885
261. Bervas M, Mansour AN, Yoon W-S, Al-Sharab JF, Badway F, Cosandey F, Klein LC, Amatucci GG (2006) Investigation of the lithiation and delithiation conversion mechanisms of bismuth fluoride nanocomposites. J Electrochem Soc 153: A799–A808
262. Aurbach D (2000) Review of selected electrode-solution interactions which determine the performance of Li and Li ion batteries. J Power Sources 89:206–218
263. Jaiswal A, Horne CR, Chang O, Zhang W, Kong W, Wang E, Chern T, Doeff MM (2009) Nanoscale $LiFePO_4$ and $Li_4Ti_5O_{12}$ for high rate Li-ion batteries. J Electrochem Soc 156:A1041–A1046
264. Ren Y, Armstrong AR, Jiao F, Bruce PG (2010) Influence of size on the rate of mesoporous electrodes for lithium batteries. J Am Chem Soc 132:996–1004
265. Sun Y-K, Myung S-T, Park B-C, Prakash J, Belharouak I, Amine K (2009) High energy cathode material for long-life and safe lithium batteries. Nat Mater 8:320–324

Books and Reviews

Ammundsen B, Paulsen J (2001) Novel lithium-ion cathode materials based on layered manganese oxides. Adv Mater 13:943–956
Brodd RJ, Bullock KR, Leising RA, Middaugh RL, Miller JR, Takeuchi E (2004) Batteries, 1977 to 2002. J Electrochem Soc 151:K1–K11
Bruce PG (2008) Energy storage beyond the horizon: rechargeable lithium batteries. Solid State Ionics 179:752–760
Ellis BL, Lee KT, Nazar LF (2010) Positive electrode materials for Li-ion and Li batteries. Chem Mater 22:691–714
Fergus JW (2010) Recent developments in cathode materials for lithium ion batteries. J Power Sources 195:939–954
Goodenough JB, Kim Y (2010) Challenges for rechargeable Li batteries. Chem Mater 22:587–603
Huggins RA (2009) Advanced batteries, materials sciences aspects. Springer, New York
Nazri GA, Pistoia O (eds) (2003) Lithium batteries: science and technology. Kluwer, Norwell
Ohzuku T, Brodd RJ (2007) An overview of positive-electrode materials for advanced lithium-ion batteries. J Power Sources 174:449–456
Palacin MR (2009) Recent advances in rechargeable battery materials: a chemist's perspective. Chem Soc Rev 38: 2565–2575
Tarascon J-M (2010) Key challenges in future Li-battery research. Phil Trans R Soc Lond A 368:3227–3241
Yamada A, Hosoya M, Chung S-C, Kudo Y, Hinokuma K, Liu K-Y, Nishi Y (2003) Olivine-type cathodes achievements and problems. J Power Sources 119–121:232–238

Battery Components, Active Materials for

J. B. Goodenough
Texas Materials Institute, Mechanical Engineering, University of Texas, Austin, TX, USA

Article Outline

Glossary
Definition
Introduction
Batteries
Fundamental Constraints
Electrode Reactions
Primary Batteries
Secondary Batteries with Aqueous Electrolytes
Nonaqueous Electrolytes for Li-Ion Secondary Batteries
Insertion Compounds for Li-Ion Secondary Batteries
Secondary Batteries with Cathodes That Are Not Insertion Compounds
Future Directions
Bibliography

Glossary

Battery efficiency Output energy/input energy for storage of electrical energy as chemical energy.

Electrolyte window Separation of electrolyte LUMO and HOMO energies of a liquid electrolyte and of conduction and valence bands of a solid electrolyte.

Fermi energy Electrochemical potential of a solid.

HOMO Highest occupied molecular orbital.

Insertion compound A host solid into which a working ion (guest) can be inserted/extracted reversibly over a solid-solution range.

LUMO Lowest unoccupied molecular orbital.

Polarization, $\eta = V_{OC} - V(q, I)$ Loss of battery voltage at a state of charge q due to resistance to ion transfer inside battery cell where an electronic current I is flowing outside of battery.

Rate of charge/discharge, *nC* Time, (60/n) min, for complete discharge or charge of a battery or cell; it is also a measure of the current.

Redox couple Cation $M^{(m+1)}/M^{m+}$ mixed-valent energy applicable to localized-electron configurations.

SEI layer Solid/electrolyte interface (passivation) layer at an electrode having its Fermi energy outside the electrolyte window.

Separator A solid layer permeable to the working ion that separates anode from cathode to prevent electron transfer between them inside a battery cell.

Spin state Refers to spin of a redox couple, which may be reduced (low-spin state) from its free-ion value (high-spin state) by a ligand-field splitting of energies of atomic orbitals that is larger than the Hund intraatomic-exchange splitting of electron spins.

State of charge Amount of chemical energy in a battery or cell relative to the total energy available.

Tap density A measure of the volume density, which increases with compaction of the active electrode particles.

Working ion Ion carrying ionic current inside a battery cell.

Definition

The active materials of a battery are the chemically active components of the two electrodes of a cell and the electrolyte between them.

A battery consists of one or more electrochemical cells that convert into electrical energy the chemical energy stored in two separated electrodes, the anode and the cathode. Inside a cell, the two electrodes are kept apart by an inert separator that is permeable to a liquid electrolyte or by a solid electrolyte. The electrolyte allows transfer from the anode to the cathode of only the working cation, which carries the positive charge associated with the chemical reaction between the electrodes; the electrolyte and separator force the electrons of the reaction to flow outside the battery where they can be stopped (open circuit) or discharged from the anode to the cathode through a load where they do work. In a rechargeable battery, the chemical energy can be restored by the application of a reverse charging current. The active materials determine such parameters as the electric-power capability of a battery, its energy density, its calendar and cycle life, its cost, and its safety. Each battery application has a different set of requirements. Tailoring of the active materials to the demands of a particular application is an ongoing process. These applications range from the powering of heart pacemakers to portable electronic devices to electric vehicles to electrical-energy storage for the grid. The active materials used in batteries for some of these different applications are discussed.

Introduction

The conversion of chemical energy to electricity was first demonstrated in 1800 by Volta, who constructed a battery – the *voltaic pile* – from alternating plates of silver and zinc separated by a cloth soaked in a salt solution. In 1806, Davy used the electricity from a voltaic pile to convert electrical energy into chemical energy by separating electrochemically alkali metals from their hydroxides. The electrochemical cell was invented in 1836 by Daniell, who immersed Zn in an aqueous $ZnSO_4$ solution and copper in a $CuSO_4$ solution in separate tubes; the two tubes were joined by a salt bridge containing a porous glass frit. This cell was called a *galvanic cell* in memory of Galvani, who had discovered in the 1790s that two different metals and a salt solution could cause muscle contractions in a frog's leg. Galvanic cells were developed to supply electricity before electric generators were available. The gifted experimentalist, Michael Faraday, began his career as an apprentice in Davy's laboratory; he later went on to lay the foundations for the science of electrochemistry and the development of the modern battery. It was Faraday who was to refer to the two different metals of a voltaic pile and of a galvanic cell as electrodes; the reductant was called the anode and the oxidant the cathode. The salt solution connecting the two electrodes by an ionic current was the electrolyte. Negatively charged ions are referred to as anions and positively charged ions are referred to as cations because they are attracted, respectively, to the anode and the cathode when electrons flow from the anode to the cathode.

Batteries

A *battery* consists of one or more electrically connected *electrochemical cells* that store chemical energy in their two *electrodes*, the *anode* and the *cathode*; the battery converts the chemical energy into electrical energy on *discharge*. The electric output of a battery is a *discharge current* I at a voltage V to give an electric-power output $P = IV$. The power capability is expressed as *specific* or *gravimetric power* in watts per kilogram (W/kg) or *volumetric power density* in watts per liter (W/L). The *energy density* of a battery is the amount of *electrical energy* QV that is available from a fully charged battery per unit weight or volume; it is expressed as *specific* or *gravimetric* energy in watt-hours per kilogram (Wh/kg) or as volumetric energy density in watt-hours per liter (Wh/L). Q is the total charge transported by I over the time Δt of a complete discharge

$$Q = \int_0^{\Delta t} I dt = \int_0^{Q} (dq/dt)\, dt \qquad (1)$$

and Q/weight (Ah/kg or mAh/g) is the *capacity* of the battery. The voltage of a battery can be increased by connecting individual electrochemical cells in series; the current per cell for a given battery current can be decreased and therefore the time for a full discharge can be increased by connecting cells in parallel. The larger the voltage and capacity of an individual cell, the fewer the cells in the battery.

A *primary battery* is discarded after providing electrical power until its chemical energy is exhausted. A *secondary battery*, also called a *rechargeable battery* or an *accumulator*, can have its spent chemical energy restored by the application of a *charging current* in a direction opposite to that of the discharge current. The *cycle life* of a secondary battery is the number of discharge/charge cycles it can support before losing 20% of its capacity. The energy loss per cycle is the difference between the electric energy used to charge the battery and that gained on discharge; the electrical energy gained on discharge divided by the electrical energy spent on charge is the *efficiency* of a secondary battery for storage of electrical energy.

Figure 1 illustrates schematically the components of an individual electrochemical cell. The *anode* is a reductant and the cathode is an *oxidant*. Inside the cell, the two electrodes are kept apart by a physical barrier, a *separator*, that prevents any electron transfer between them inside the cell. However, the two electrodes are connected electrically inside the cell by an *electrolyte* that conducts a *working ion* and is an electronic insulator. A liquid electrolyte permeates a chemically inactive, porous separator; a solid electrolyte also acts as a separator. The working ion is normally a cation: H^+, Li^+, or Na^+. Chemical reaction between the two electrodes of a cell involves both electron and working-ion transfer between the electrodes. The electrolyte forces the electrons to flow outside the cell while allowing the working ion to be transported inside the cell. Therefore, a battery has a *negative terminal* that collects electrons via a *current collector* from all the cell anodes for delivery to an external circuit and a *positive terminal* that receives electrons from the external circuit and delivers them via a current collector to all the cell cathodes during a battery discharge.

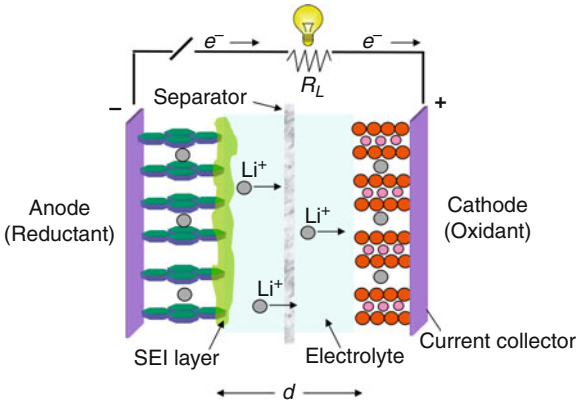

Battery Components, Active Materials for. Figure 1 Schematic showing components of $LiC_6/Li_{1-x}CoO_2$ cell. Internal Li^+-ion and external electronic (e^-) currents I_i and I are shown for discharge with switch closed. The SEI passivation layer is formed because the energy E_{FA} of the LiC_6 anode is higher than the LUMO of the carbonate electrolyte (see Fig. 3)

External connection of the battery terminals allows an electronic discharge current I to pass through an external load of resistance R_L, where it does work, to the cathode where it neutralizes the ionic current I_i inside the battery. Thus, on discharge the battery transforms its chemical energy into electrical energy at the load. The much higher electronic conductivity σ_e compared to the working-ion conductivity σ_i means that a cell is

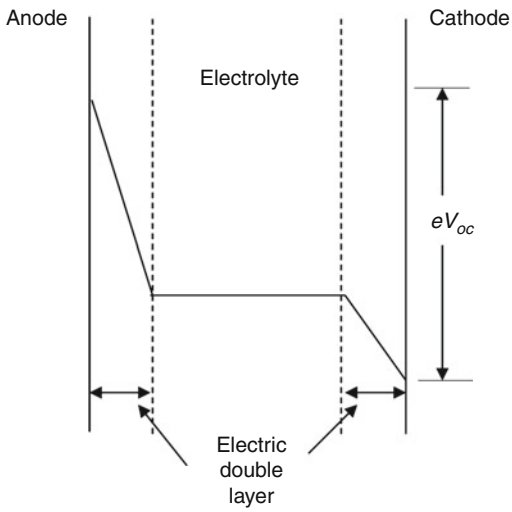

Battery Components, Active Materials for. Figure 2 Voltage levels in the various sections of a cell at open circuit. The double layers at the anode and the cathode have different structures and compositions

fabricated with a small thickness/area ratio. Disconnection of the two battery terminals stops not only the external discharge current, but also the internal ionic current since, without charge neutralization, an internal electric field between the cell electrodes is built up to stop further flow of the working ion. This electric field is expressed as a voltage between the terminals of a cell at open circuit, the *open-circuit voltage* V_{oc}, with a positive charge at the cathodic positive terminal and a negative charge at the anodic negative terminal. Mobile ions in the electrolyte form *electrical double layers* at the surfaces of the electrodes to neutralize the electrode charge, and the voltage drop inside the cell is across the double layers, Fig. 2.

This entry describes strategies used by the chemists to identify appropriate active materials, electrodes and electrolyte, for the individual electrochemical cells of a battery.

Fundamental Constraints

Maintaining Electrode–Electrolyte Contact

Ion transfer across the electrode/electrolyte interfaces requires retention of a good electrode–electrolyte contact during discharge and charge. Since ion and electron transfers between the electrodes change the volumes of the electrodes, it is advantageous to have a liquid or polymer electrolyte contacting solid crystalline electrodes; a solid electrolyte is needed to keep the electrodes apart if one or both of the electrodes is a liquid or a gas.

Electrolyte Window

The *window* of a liquid electrolyte is the energy gap E_g between its lowest unoccupied molecular orbital (LUMO) and its highest occupied molecular orbital (HOMO). The window of a solid electrolyte is the energy gap E_g between the bottom of the empty electronic conduction band, E_c, and the top of the filled electronic valence band, E_v. Figure 3 illustrates how the window of an electrolyte constrains the V_{oc} of a cell.

Figure 3a shows the case of solid electrodes having anode and cathode Fermi energies E_{FA} and E_{FC} in their electronically conductive state. An E_{FA} or E_{FC} may lie in a partially filled conduction band or in a mixed-valent redox couple. An E_{FA} above the electrolyte LUMO will reduce the electrolyte and an E_{FC} below the electrolyte HOMO will oxidize the electrolyte. Therefore, thermodynamic stability restricts the open-circuit voltage to

$$eV_{oc} = E_{FA} - E_{FC} \leq E_g \tag{2}$$

where e is the magnitude of the charge of an electron. However, charge transfer at an electrode/electrolyte interface may create a double layer and/or a passivation layer that blocks a subsequent ionic transfer at open circuit to stop any further electrolyte reduction or oxidation and therefore to give a *kinetic stability* for a limited $(eV_{oc} - E_g) > 0$. A passivation layer is referred to as a *solid-electrolyte interphase* (SEI); it should not block ion or electron transfer under closed-circuit conditions.

Solid electrolytes, Fig. 3b, are chosen to have a window $E_g > eV_{oc}$.

Ionic Conductivity

Kinetic limitations on the rate of working-ion transfer between electrodes cause the cell voltage V to drop relative to V_{oc}. The voltage drop

$$\eta(q, I) = V_{OC} - V \tag{3}$$

is called the *polarization* or the *overvoltage; q* is the state of charge. The polarization is due to the resistance to ionic motion inside the cell.

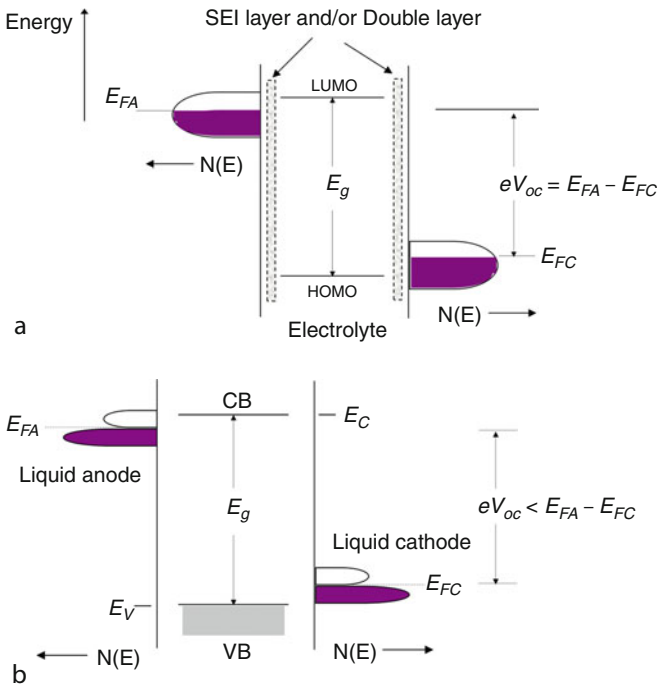

Battery Components, Active Materials for. Figure 3
Definition of the electrolyte window E_g for (**a**) liquid and (**b**) solid electrolytes. The E_{FA} and/or E_{FC} of solid electrolytes may lie in either a band of one-electron states as in (**a**) or a multielectron redox couple as in (**b**); for liquid electrodes, they lie in a mixed-valence redox couple

Ions move diffusively. Therefore, the ionic conductivity is given by

$$\sigma_i = (nq^2/kT)D_i \sim Nc(1-c)\exp(-\Delta H_m/kT) \quad (4)$$

where $n = cN$ is the density of carriers of charge q; $D_i = D_0 \exp(-\Delta G_m/kT)$ is the ionic diffusion coefficient containing a Gibbs free energy $\Delta G_m = \Delta H_m - T\Delta S_m$ for an ion to move from one position to another. The motional enthalpy ΔH_m is an activation energy for ion motion, and $(1-c)$ is the fraction of sites that are empty into which ions can move.

In a strong acidic or alkaline aqueous electrolyte, $n = cN$ is large and ΔH_m is small so long as the water molecules are free to rotate as in a liquid; the H^+ ions hop within hydrogen bonds, but molecular rotation is needed to subsequently reorient the hydrogen to a new bond direction (Grotthus motion). In a liquid aqueous electrolyte, the H^+-ion conductivities are generally $\sigma_H \approx 1$ S/cm at 20°C. However, the window of an aqueous electrolyte is only 1.23 eV, which has led to consideration of nonaqueous electrolytes. Since H^+ ions are not mobile in nonaqueous liquid electrolytes, the Li^+ ion is normally used in these electrolytes. Few organic solvents dissolve a sufficient concentration of lithium salts with good separation of the Li^+ ions from the anion of the salt. The Li^+-ion conductivities in the best nonaqueous liquid electrolytes are $10^{-3} < \sigma_{Li} < 10^{-2}$ S/cm at 20°C.

Solid cathodes of secondary-battery cells are *insertion compounds*. An insertion compound has a *host* crystalline structure into which a *guest* working ion can be inserted/extracted reversibly into/from its interstitial space while the ionic charge is being neutralized by reduction/oxidation of the host structure with electrons coming from/sent to the external circuit. These electrodes are mixed ionic/electronic conductors. During an insertion or extraction reaction, the essential architecture of the host structure remains intact throughout the process, but two types of insertion reaction need to be distinguished: (1) a single-phase solid-solution reaction between the guest and the host; (2) a two-phase reaction. A first-order transition

between two phases results in the coexistence of the two phases; a first-order transition may not be reversible, but where the host undergoes an ion-displacement transition that separates a phase rich in the working ion from one that is poor in the working ion, the two-phase reaction can be reversible. In a single-phase solid-solution reaction, the output voltage V of the cell decreases monotonically with its state of charge as is illustrated schematically in Fig. 4a. The *state of charge* of a cell refers to the fraction of the full-charge chemical energy existing in a partially charged cell. Where the host structure undergoes a first-order structural change during discharge, the output voltage V of the cell is independent of the state of charge over the two-phase region as is illustrated in Fig. 4b. This behavior follows from the Gibbs phase rule, which states that the number of thermodynamic parameters that are free to vary is

$$F = C - P + 2 \tag{5}$$

where P is the number of coexisting phases and C is the number of components, guest and host, taking part in the reaction. Where two phases coexist, $C = P$ and $F = 2$. Since temperature and pressure are specified, there is

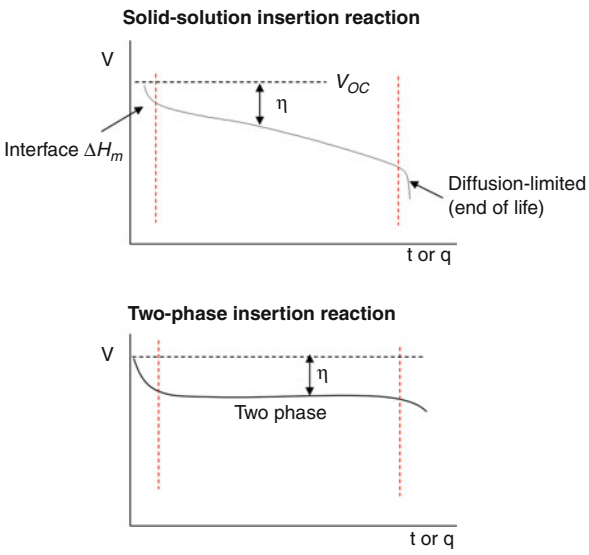

Battery Components, Active Materials for. Figure 4 Schematic profiles for (**a**) a solid-solution insertion reaction and (**b**) a two-phase insertion reaction showing the polarization $\eta = V_{OC} - V$. *Note*: Two-phase reactions retain the higher voltage found at the onset of the two-phase region

no degree of freedom left, so other parameters such as voltage have to be constants. In an insertion reaction, the host interstitial space into which the working ion can be inserted may be 1D, 2D, or 3D (D = dimensional) depending on the host structure.

In Fig. 4a, three ion-transfer processes are distinguishable: (1) an *activation polarization* due to the energy ΔH_m required to transfer ions across the electrode/electrolyte interfaces, (2) a change in $E_{FA} - E_{FC}$ and (3) an end-of-life *concentration polarization*. The slope in region (2) of a similar $V(q)$ vs. I curve gives the *ohmic polarization*. The activation polarization is manifest on the initiation of discharge; the ohmic polarization is manifest by the slope of the $V(I)$ profile in mid-discharge. At the end of life, either the concentration of working ions reaching the cathode is depleted and/or the concentration $(1-c)\,N$ of the cathode acceptor sites at the electrolyte/electrode interface is depleted to where the ionic diffusion current is no longer able to keep up with a fixed discharge current I. The increase in η causes a decrease in V at the end of life, and this decrease occurs at a larger state of charge the higher is I and, from Eq. 4, the lower is the temperature T. The end-of-life drop-off in V is also referred to as the *diffusion-limited* regime of the $V(t)$ profile. The loss of capacity at higher I and lower T is *reversible*; capacity is restored at lower discharge currents I and higher temperatures T where the working-ion profile across the electrolyte/electrode interface approaches more closely the equilibrium profile. Thus, the reversible Q of Eq. (1) decreases with increasing I; $Q = Q(I)$. Clearly, a fast diffusion of the working ion not only in the electrolyte, but also in any insertion-compound electrode is needed for a secondary power battery.

Energy Density

The specific energy QV/weight of a cell depends not only on the voltage V of the cell, but also on the total charge Q per kilogram that is transported between the electrodes. In order to achieve a high cell voltage, the E_{FA} of the anode and the E_{FC} of the cathode need to be matched to the LUMO and the HOMO, respectively, of an electrolyte with a large window E_g between its LUMO and HOMO. In a secondary battery, Q is the total charge that is transported reversibly between the electrodes. In a secondary battery in which the cells

are assembled in the discharged state, Q is limited to the number and charge of working ions that can be extracted reversibly from the cathode host. However, where the anode develops a non-blocking SEI layer, Li^+ ions are trapped irreversibly in the SEI layer during the initial charge, which reduces the capacity available from the cathode on subsequent charge/discharge cycles. To eliminate this loss of cathode capacity, it would be necessary to form the SEI layer on the anode before assembling the cells of a battery.

In addition to formation of an SEI layer on the anode, chemical reactions between the cathode and the electrolyte or within the cathode can deplete the amount of active cathode material. These reactions introduce an *irreversible* capacity loss that is expressed as a *capacity fading* with the number of charge/discharge cycles. The *cycle life* of a cell is the number of discharge/charge cycles a cell can undergo without too great an irreversible capacity loss to be useful; the *service life* of a cell is the length of time over which the cell retains more than 80% of its capacity. The service life depends on the cycle life, that is, the cell use as well as on the age of the cell.

Morphology

In order to minimize the reversible capacity loss at higher discharge/charge currents, solid electrodes are made porous so as to maximize the electrode/electrolyte interface area per unit planar area of the electrode. Solid porous electrodes are commonly a complex composite of the active material in the form of small particles coexisting with and contacting a current-passing additive such as carbon, metal particles, or a conductive polymer; the conductive additive percolates through the composite mass to connect electronically the active particles to one another and to the electrode current collector. This composite mass is commonly held together by a chemically inactive binder such as Teflon. Typically, such a composite electrode has about 30% porosity percolating through it so as to allow impregnation of the pores by a liquid electrolyte in order to have the electrolyte contact every active particle. The resulting electrode/electrolyte interface area is complex, and the ionic currents within the composite electrode are tortuous. Modeling the current flows within an electrode as well as the composite morphology has become an important tool in the design of a composite electrode and of the distribution of primary currents in the metallic current collectors.

Heat

The net useful energy released for a given chemical reaction between the electrodes is the enthalpy ΔH of the Gibbs free energy

$$\Delta G = \Delta H - T\Delta S \tag{6}$$

where $T\Delta S$ is the heat associated with the entropy change ΔS of the reaction at an absolute temperature T. For a fixed T, this heat is reversible, that is, it is exothermic on discharge and endothermic on charge or *vice versa*. In electrical terms,

$$\Delta S = nFdV/dT \tag{7}$$

where n is the number of electrons per mole of reactants participating in the discharge reaction and F is the Faraday constant, that is, the amount of charge transferred when one equivalent weight of mass reacts. From Eqs. 6 and 7, the reversible heat on discharge is $nFT(dV/dT)$, which may be positive or negative, exothermic or endothermic. In addition, the internal resistance R_b of a cell creates heat I^2R_b that must be dissipated. *Thermal runaway* occurs if the internal heat causes an electrode reaction with the electrolyte to become self-sustaining, the reaction entering an autocatalytic mode. This situation is responsible for fires associated with battery operations, and an internal electronic short circuit between the electrodes occasioned by dendrite growth from an anode across the electrolyte to the cathode with repeated cycling can trigger such an event where the electrolyte is flammable.

Cost

Cost as well as safety, capacity, and power capability are constraints on any commercial device. Lower cost requires not only low-cost, nontoxic materials, and simple battery-stack management, but also a long service life, ease of manufacture, and a minimization of the number of cells to achieve a specified voltage and discharge time. Safety of a secondary battery at an acceptable cost favors either a nonflammable electrolyte or a solid-electrolyte separator that blocks

short-circuiting from any dendrite formation on a solid anode where dendrite formation threatens short-circuiting of cells on repeated cycling. A long service life requires elimination of irreversible chemical reactions within the individual cells.

The cost and service life of secondary batteries for electric vehicles must compete against the cost and service life of the internal combustion engine. In their favor is elimination of the cost to the environment of distributed emissions of the greenhouse gas CO_2; and if charging of the battery of the electric vehicle can be done with wind or radiant solar energy, all CO_2 emissions associated with the vehicle can be eliminated.

Electrode Reactions

Primary batteries [1] having liquid electrolytes generally use a solution or a solution-precipitation reaction of an element at the anode and a displacement or insertion reaction at the cathode. Most secondary batteries use insertion reactions at a solid cathode and may also use insertion reactions at the anode.

Some common elemental solution or solution-precipitation reactions are:

$$\begin{aligned} &Li^0 - e^- = Li^+ \\ &Na^0 - e^- = Na^+ \\ &Zn^0 - 2e^- + HCl = ZnCl_2 + 2H^+ \\ &Zn^0 - 2e^- + 2H_2O = Zn(OH)_2 + 2H^+ \\ &Cd^0 - 2e^- + 2H_2O = Cd(OH)_2 + 2H^+ \\ &Pb^0 - 2e^- + H_2SO = PbSO_4 + 2H^+ \end{aligned} \tag{8}$$

The E_{FA} of Li^0 lies above the LUMO of a nonaqueous liquid-carbonate electrolyte containing a lithium salt. Although a non-blocking SEI passivation layer is created at the surface, lithium is not plated back uniformly during a charge; it forms a rough, mossy surface that, on repeated discharge/charge cycles, develops dendrites that can grow across the electrolyte to contact the cathode. Therefore, with a liquid electrolyte Li^0 is only used as an anode in a primary battery or in half-cells used to test the performance of candidate cathode materials for secondary batteries. However, it may be used in a secondary cell having a solid Li^+-ion electrolyte that blocks dendrite growth across it and is not reduced on contact with a dendrite.

The E_{FA} of Zn^0 lies 0.76 eV above the $2H^+/H_2$ LUMO of an aqueous electrolyte, which has previously prohibited its use in a secondary battery. However, it is used successfully as the anode of a primary cell having either an HCl acidic or KOH alkaline electrolyte. The Cd^{2+}/Cd^0 couple at 0.40 eV above the $2H^+/H_2$ couple is better matched to the aqueous LUMO, so Cd has been the preferred anode for a secondary alkaline battery with a KOH electrolyte. A lower electrochemical potential of an alkaline versus an acidic electrolyte allows the double layer in an alkaline electrolyte to lower the E_{FA} of Cd to below the $2H^+/H_2O$ LUMO. The Pb^{2+}/Pb^0 couple is only 0.13 eV above $2H^+/H_2$, so it provides a reversible anode reaction in a sulfuric-acid electrolyte. In all cases with aqueous electrolytes, the anode–electrolyte reaction releases mobile working H^+ ions to react with the cathode.

In a displacement reaction, the working ion displaces a cation of the electrode as is illustrated by the cathodic discharge reaction

$$2Li^+ + 2e^- + CuS = Li_2S + Cu^0 \tag{9}$$

Normally, such a first-order reaction is not easily reversed, and to date cathodes undergoing such a reaction are only found in primary batteries. However, they represent a Q corresponding to two electrons per electrode cation to give a large capacity. Although displacement reactions that leave a host framework intact may be reversible, for example,

$$2Li^+ + 2e^- + Fe_3O_4 = Li_2Fe_2O_4 + Fe^0 \tag{10}$$

the associated volume changes have made these reactions impractical unless they are buffered by an amorphous carbon matrix.

In a reversible insertion reaction, the working ion is inserted as a guest into a host structure forming either a solid solution in a single-phase reaction or two phases in a first-order reaction in which ionic displacements of the host segregate the electrode into guest-rich and guest-poor phases. For example, two anode reactions are the single-phase reaction of a metal hydride MH

$$MH - xe^- = MH_{1-x} + xH^+ \tag{11}$$

and the lithiated graphite two-phase reaction

$$LiC_6 - e^- = 6C + Li^+ \tag{12}$$

in which graphene sheets are shifted in stages relative to one another on Li insertion (Fig. 9). In anodes, the guest is inserted on charge and extracted on discharge. As a cathode, the guest is inserted on discharge and extracted on charge.

Primary Batteries

Zinc–Manganese Batteries

Zinc–manganese batteries [1] dominate the primary-battery market. These batteries are of two types depending on the pH of their aqueous electrolyte. Each uses a carbon-MnO_2 cathode; the carbon provides electronic conductivity. The MnO_2 is best prepared as αMnO_2 or γMnO_2, which have structures, Fig. 5, with 1D channels into which H^+ ions can be inserted. The Leclanché cell, $Zn/HCl/MnO_2$, is acidic, and the Zn anode undergoes a Zn-solution reaction; Zn^{2+} ions enter a $ZnCl_2 + NH_4Cl$ salt solution to displace $2H^+$ ions to the cathode. In the alkaline cell, $Zn/KOH/MnO_2$, the Zn anode reacts with the aqueous electrolyte to form $Zn(OH)_2 + 2H^+$; the $Zn(OH)_2$ subsequently transforms to $ZnO\downarrow + H_2O$. As shown in Fig. 6, the discharge voltage of a zinc–manganese battery exhibits two ranges, one corresponding to a single-phase solid-solution reaction

$$MnO_2 + H^+ + e^- = MnOOH \tag{13}$$

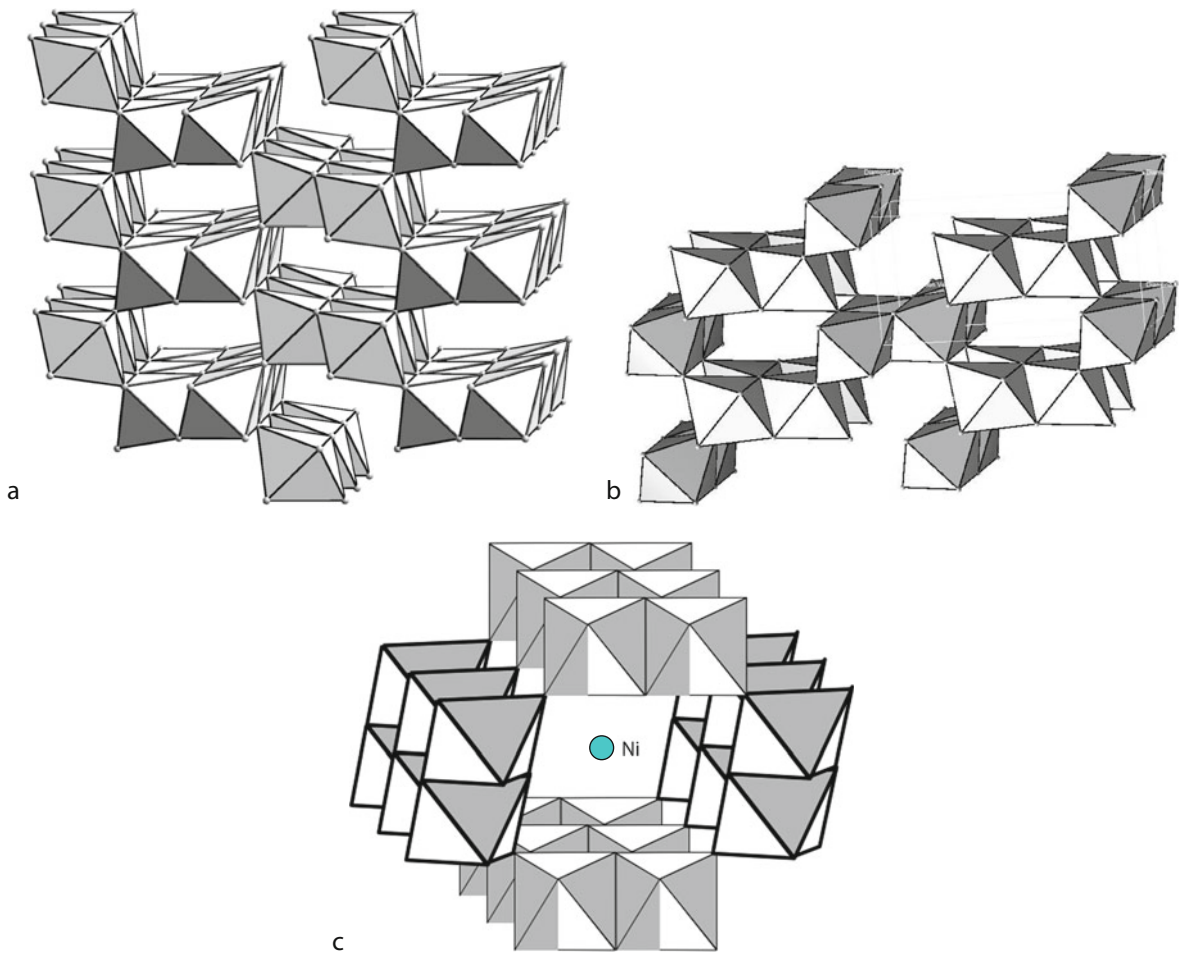

Battery Components, Active Materials for. Figure 5
Structures of (**a**) $\alpha - MnO_2$, (**b**) $\gamma - MnO_2$, (**c**) Ni-exchanged cryptomelane. Octahedral sites of MnO_2 share edges along the *c*-axis. H^+ ions are inserted into the 1×2 tunnels

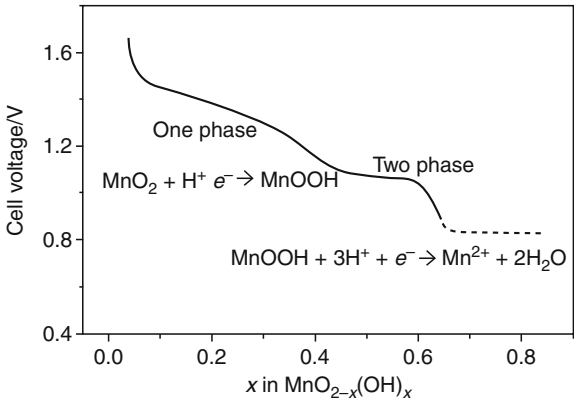

Battery Components, Active Materials for. Figure 6 Discharge voltage profile of the $MnO_{2-x}(OH)_x$ cathode of a Zn/MnO_2 primary battery showing solid-solution (one-phase) and two-phase compositional ranges

and the other to a two-phase reaction that is irreversible. An octahedral-site Mn(III) ion has a twofold orbital degeneracy, and at a sufficient concentration of Mn(III) ions, a cooperative site distortion to remove the degeneracy introduces a first-order displacive transition of the host structure. The Mn (III)-rich phase at the surface undergoes a disproportionation reaction: 2 Mn(III) = Mn(II) + Mn(IV) that is followed by an *irreversible* dissolution of Mn(II) into the electrolyte. The better match of the E_{FA} of Zn^0 to the $2H^+/H_2O$ LUMO of the KOH electrolyte makes the alkaline cell more reliable and gives it a better performance at higher discharge rates. However, in the discharge reaction, a mole of H_2O per two moles of MnO_2 is consumed, which increases the impedance of the cell where the amount of electrolyte has been minimized to maximize the cell capacity. Ni-exchanged cryptolmelane, Fig. 5c, alleviates this problem.

With 1D tunnels in the MnO_2 cathode, it is critical to remove impurities and structural stacking faults that would block a tunnel. Moreover, since the Zn^0/Zn^{2+} couple lies above the $2H^+/H_2$ LUMO of the electrolyte, the Zn anode of the alkaline cell consists of Zn particles of selected size bound with the KOH electrolyte in a stabilizing gelling agent to suppress H_2 evolution. The selection of the gelling agent and the size of the Zn particles are critical. The gelling agent creates a passivating SEI layer on the Zn to inhibit it from reducing the water at open circuit:

$$Zn + H_2O = ZnO + H_2 \uparrow \tag{14}$$

Zinc–Air and Silver–Zinc Batteries

The alkaline zinc–air battery has the highest energy density of all aqueous batteries since only the Zn-powder anode is contained in the cell; the other reactant, oxygen, is available from the surrounding air. The capacity of a cell is dictated by the amount of fine Zn powder that is available for discharge. Nevertheless, a light cathode structure is present; it consists of a porous carbon or nickel mesh containing both the liquid electrolyte to convey H^+ ions and MnO_2 or other particles as catalyst in the pores. Gaseous O_2 is given access to the porous carbon where it penetrates the pores to be reduced on the MnO_2 at a triple-phase boundary (TPB) by the reaction

$$O_2 + 4H^+ + 4e^- = 2H_2O \tag{15}$$

However, the oxygen–reduction reaction Eq. 15 forms an intermediate peroxide:

$$\begin{aligned} &O_2 + H_2O + 2e^- = O_2H^- + OH^- \\ &O_2H^- + H_2O + 2e^- = 3OH^- \\ &4H^+ + 4OH^- = 4H_2O \end{aligned} \tag{15a}$$

and breakdown of the peroxide H_2O_2 and/or its radical O_2H^- is rate-limiting. These cells are available in sizes small enough to fit into the ear to power a hearing aid.

The silver–zinc battery also uses a KOH alkaline electrolyte. In this battery, the cathode undergoes the displacement reaction

$$2H^+ + 2e^- + Ag_2O = 2Ag^0 + H_2O \tag{16}$$

This battery is primarily used in button cells for small portable devices such as watches.

Lithium Primary Batteries

Primary lithium cells use a lithium-metal anode and a nonaqueous electrolyte having a larger window than the 1.23 eV of an aqueous electrolyte. Both liquid and solid Li^+-ion electrolytes can be used.

Liquid Electrolytes. The carbonates dissolve a fair concentration of lithium salts, normally $LiClO_4$ or $LiSO_3CF_3$ in propylene carbonate-dimethyl ether in

primary cells. Since the Li^0/Li^+ couple lies about 1 eV above the LUMO of the carbonate, dimethyl ether is added to react with the Li^0 to form a passivating SEI layer. With a passivating layer on the Lithium anode and an electrolyte window $E_g \approx 3.5$ eV, cell voltages of 4.0 V or higher are possible. With a higher voltage V, the lithium primary batteries provide a larger energy density, but Li^+-ion transport across the SEI layer and a σ_{Li} in the nonaqueous electrolyte significantly lower than the σ_H in a strong acidic or alkaline aqueous electrolyte reduces the rate capability of a Lithium primary battery at 20°C. The solid-cathode insertion compounds CF_x and MnO_2 are thermodynamically stable and provide a long shelf life; Li/CF_x and Li/MnO_2 batteries have a $V = 3.0$ V and are designed for relatively low-rate applications.

The FeS_2 cathode of a Li/FeS_2 battery undergoes a two-step displacement reaction

$$4Li^+ + 4e^- + FeS_2 = 2Li_2S + Fe^0 \tag{17}$$

in which an amorphous Li_2FeS_2 is first formed by the breaking of the disulfide $(S_2)^{2-}$ ions of FeS_2. This battery only provides $V = 1.6$ V in the first step, but at higher temperatures it gives a high-rate performance superior to that of the alkaline Zn/MnO_2 cells.

The Li/I_2 cell is used preferably for implanted heart pacemakers; the di-iodine bond is broken at $V = 2.7$ V in the cathode reaction

$$2Li^+ + 2e^- + I_2 = 2LiI \tag{18}$$

Solid Electrolytes. A *protected Lithium anode* is under development for both primary and secondary batteries that promise much larger capacities. This strategy is illustrated by the Li/seawater primary battery in which a Lithium anode is immersed in a nonaqueous electrolyte, the *anolyte*, that is separated from seawater contacting a cathode current collector by a Li^+-ion solid-electrolyte separator. The seawater acts as a liquid cathode. Except for contact with a negative post, the Lithium anode and its anolyte are sealed in a compartment containing a Li^+-ion solid-electrolyte wall that interfaces the seawater. The anolyte is chemically stable to both the Lithium and the solid electrolyte; the solid electrolyte must not be reduced on contact with the Li^0 anode. Moreover, either the seal or the compartment must be compliant to allow for the change in volume of the Lithium on discharge. The seawater is not contained in an *open cell*; it is contained within a battery in a *closed cell*. The Li^+ ions from the anode react with water at the cathode current collector:

$$Li^+ + e^- + H_2O = LiOH + {}^1\!/_2H_2 \uparrow \tag{19}$$

to give a constant voltage $V = 2.7$ V. The efficiency of a Li/seawater secondary cell is not good, but other liquid cathodes, for example, $Fe(CN)_6^{3-}/Fe(CN)_6^{4-}$ in water, offer a more efficient electrical-energy storage than the seawater cathode and, with a solid electrolyte, permit a flow through of only the liquid cathode (see last section for flow-through rechargeable batteries).

Secondary Batteries with Aqueous Electrolytes

The *lead–acid battery* $Pb/H_2SO_4/PbO_2$ [1] provides a fast cell discharge at 2.0 V, it is relatively low-cost, and 98% of the batteries used in the USA are recycled. This battery has dominated the market for rechargeable batteries, but Pb is heavy and the practical energy density of the battery is only about 25% of its limited theoretical energy density (Wh/kg). Therefore, other secondary batteries are used for handheld devices and contend for the electric-vehicle market.

The Pb anode is matched to the $2H^+/H_2O$ LUMO of the aqueous H_2SO_4 electrolyte; during discharge, the Pb^{2+} ion forms $PbSO_4$ on entering the electrolyte to displace $2H^+$ to the PbO_2 cathode. On reduction of the PbO_2 by electrons from the anode, H^+ ions are inserted into the PbO_2 to form $PbO_{2-x}(OH)_x$. A kinetic stability impedes reaction of the reduced PbO_2 with the electrolyte, but electrons introduced into the Pb-6*s* band disproportionate into electron-rich $Pb(OH)_2$ regions within the PbO_2 matrix

$$PbO_{2-x}(OH)_x = {}^1\!/_2x Pb(OH)_2 + (1 - {}^1\!/_2x)PbO_2 \tag{20}$$

followed by a slow reaction

$$Pb(OH)_2 + H_2SO_4 = PbSO_4 + 2H_2O \tag{21}$$

At open circuit, electrode reactions that charge the electrodes lead to a slow oxidation of the electrolyte with H_2 evolution at the anode and O_2 evolution at the cathode. These reactions represent an irreversible *self-discharge*. Once the electrolyte is introduced, the battery has a poor shelf life. Under development

are acidic aqueous electrolytes in which Pb(II) is soluble rather than condensing into the solid $PbSO_4$. This development of the lead–acid cell promises a flow battery not requiring a separation membrane. The separation membrane of redox-flow batteries (see last section) remains a challenging problem for the aqueous redox-flow technology.

The *cadmium–nickel* cell, Cd/KOH/NiOOH, has its Cd anode and $NiO_{1-x}(OH)_{1+x}$, $0 \leq x \leq 1$, cathode well-matched to the LUMO and the HOMO of the alkaline KOH electrolyte; the small, sealed cell gives a fast discharge and charge at a discharge voltage of 1.2 V. Like the Pb anode of the lead–acid battery, the Cd anode undergoes a solution-precipitation reaction in which Cd^{2+} reacts with the water of the electrolyte, Eq. 4, to form reversibly solid $Cd(OH)_2$ and displace $2H^+$ ions to the cathode. The cathode is the layered, monoclinic β-NiOOH of Fig. 7; it converts to hexagonal β-$Ni(OH)_2$ in a two-phase reaction on insertion of H^+ to give a plateau in the V(x) discharge curve at 1.2 V versus Cd/$Cd(OH)_2$. In β-NiOOH, the oxygen stacking along the c-axis within a unit cell is ABCA, Fig. 7; the H^+ ions are located preferentially in the trigonal-prismatic sites between A-A stackings. Overcharging introduces water into the H-depleted galleries to give γ-NiOOH·yH_2O?. Best performance of the β-NiOOH-β-$Ni(OH)_2$ cathode is found with small particles having a large defect content. The gelatinous $Cd(OH)_2$ remains close to the anode; and during charge, the $Cd(OH)_2$ at the anode reverts to Cd + H_2O as the cathode releases $2H^+$ per Cd^{2+} ion to the electrolyte. At the end of charge, all the Cd^{2+} ions are reduced back to Cd and all the nickel is present as Ni(III). The Ni(IV)/Ni(III) couple cannot be accessed with a further increase in the charging voltage; instead, the electrolyte is oxidized:

$$2H_2O = 2H_2 + O_2 \tag{22}$$

This cell was the first rechargeable battery to be used in handheld devices.

With a suitable gelling agent to passivate carefully sized Zn particles, a Zn/KOH/NiOOH secondary battery may be marketed.

The metal hydride–nickel cell, MH_x/KOH/NiOOH, also makes use of the NiOOH cathode; it replaces the Cd anode with a metal hydride, MH_x, insertion alloy having its Fermi energy E_{FA}, like that of Cd, well-matched to the LUMO of the aqueous KOH electrolyte. However, the H^+-ion diffusivity in the hydride is slower than that in the gelatinous $Cd(OH)_2$, so it has a poorer rate capability at lower temperatures. On the other hand, it eliminates the heavy, toxic Cd to give a higher energy density (Wh/kg) and provides a safe power source for electric vehicles. However, a Zn/KOH/NiOOH cell of good cycle life may prove competitive.

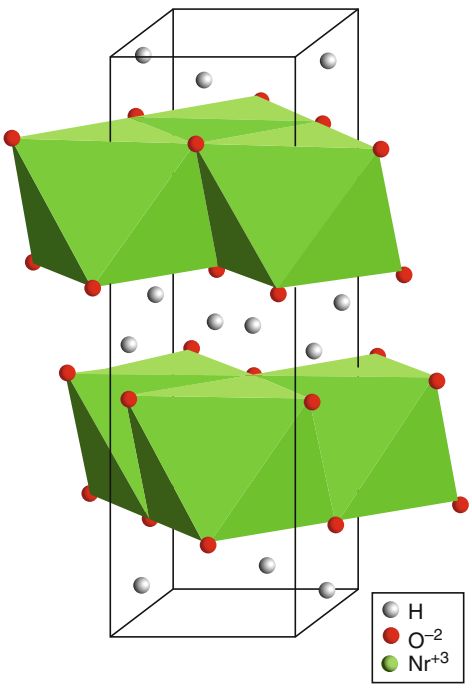

Battery Components, Active Materials for. Figure 7 Layered structure of monoclinic β − NiOOH

Nonaqueous Electrolytes for Li-Ion Secondary Batteries

The demand for a rechargeable battery with a greater specific energy requires a higher output voltage and therefore an electrolyte with a larger window E_g between its LUMO and HOMO than the 1.23 eV of an aqueous electrolyte. Since H^+ ions are not mobile over an appreciable temperature range above and below 20°C in the absence of water, the Li^+ and Na^+ ions are the next logical candidates for the working ion.

Early work with Na^+ ions concentrated on solid electrolytes. Although solid electrolytes have a large window, they do not retain a large-area interface with a solid electrode that changes its volume significantly with the state of charge of the battery. Although all solid-state microbatteries are made, a solid electrolyte preferably contacts a liquid, either a liquid electrode or a liquid electrolyte. The sodium–sulfur battery uses liquid electrodes and operates above 300°C [2]. On the other hand, a composite electrolyte having a solid-electrolyte separator and different liquid electrolytes either side, as in the Li/seawater primary battery, can provide a feasible room-temperature secondary battery [3]. For example, the Li^+-ion solid-electrolyte $Li_{1.3}Ti_{1.7}Al_{0.3}(PO_4)_3$ with the framework structure of hexagonal $Fe_2(SO_4)_3$, Fig. 8, can have interstitial Li giving $\sigma_{Li} > 10^{-4}$ S/cm at 20°C [4]. Rechargeable batteries based on this strategy are now being investigated. However, this commercially available inorganic solid electrolyte contains Ti(IV), which is too easily reduced. Another solid electrolyte with a $\sigma_{Li} > 10^{-4}$ S/cm needs to be identified.

A solid polymer electrolyte can retain contact over a large surface area of a solid electrode provided the changes in electrode volume with state of charge of a cell are modest. Polyethylene oxides (PEOs) containing a lithium salt are low-cost, nontoxic, Li^+-ion electrolytes with good chemical stability [5], but a $\sigma_{Li} < 10^{-5}$ S/cm at 20°C is too low for a power battery and the HOMO versus Lithium is below 4.0 V. The introduction of the oxide particles Al_2O_3, TiO_2, SiO_2, or ZrO_2 creates a more amorphous polymer matrix by inhibiting chain crystallization and attracting Li^+ from its salt; the result is an enhanced σ_{Li} and Li^+-ion transference number $t = \sigma_{Li}/\sigma$, where σ is the total anion plus Li^+-ion conductivity; but σ_{Li} is still not comparable to that of the best liquid electrolytes, [6]. Therefore, most attention has been given to Li^+-ion batteries containing liquid electrolytes.

The most widely used liquid electrolytes consist of Lithium salts dissolved in organic carbonates: propylene carbonate (PC), dimethyl or diethyl carbonate (DMC or DEC), ethyl methyl carbonate (EMC), and mixtures of DMC or DEC with ethylene carbonate (EC). The EC component provides a passivating SEI layer on a carbon anode where the E_{FA} of the anode lies above the LUMO of the carbonates, which is about 1.1 eV below the E_{FA} of Lithium. The carbonates are reasonably good solvents for Li salts and they have a relatively low viscosity, which results in a low activation energy for Li^+-ion diffusion to give a $\sigma_{Li} > 10^{-3}$ S/cm at 20°C and a ready penetration into a porous electrode. The HOMO is about 4.3 eV below the E_{FA} of Lithium, which gives an electrolyte

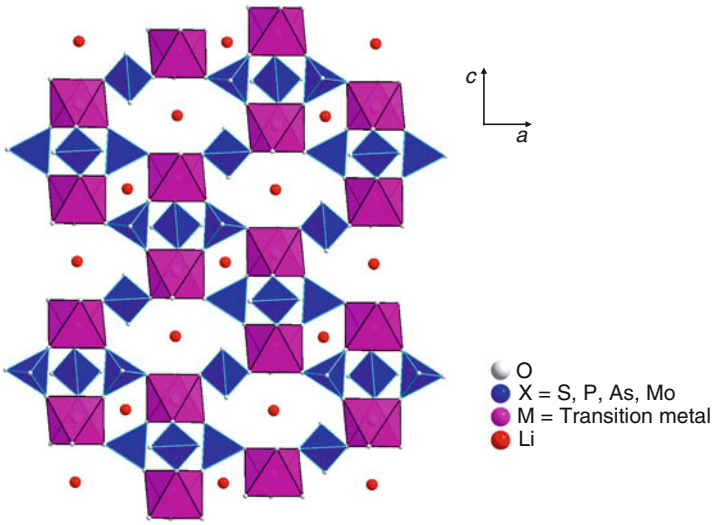

Battery Components, Active Materials for. Figure 8
NASICON (NA SuperIonic CONductor) framework structure, which is the same as that of hexagonal $Fe_2(SO_4)_3$

window $E_g \approx 3.7$ eV. A carbonate electrolyte decomposes at a voltage $V > 4.9$ V versus Lithium; an SEI layer can stabilize the Ni, Mn oxides with cathode voltages in the interval $4.3 < V < 4.9$ V, but at the expense of a larger activation energy for Li^+-ion transfer across it. However, this ΔH_m can be reduced either by doping to remove Ni from the surface or by coating the particles with a thin layer of a mixed Li^+-ion/electronic conductor that replaces the SEI layer and is not removed by the volume changes that accompany charge/discharge cycling. With this strategy, an effective electrolyte window $E_g^{\text{eff}} \approx 3.8$ eV can be created. However, organic electrolytes are flammable, which raises safety concerns where an SEI layer is formed on the anode. Ionic liquids are not flammable and have a larger window, but they are too viscous to be practical unless they are blended with a less viscous liquid. Carbonate-ionic liquid blends that are not flammable have been demonstrated, but they are more viscous than a pure liquid carbonate and the carbonate component determines the operative electrolyte window. The loss of rate capability must be weighed against the nonflammable property in any blend of a carbonate with an ionic liquid.

Alternatively, the salt $LiAlCl_4$ dissolved in the inorganic liquid SO_2 has been proposed [7]; this Li^+-ion electrolyte has a good room temperature $\sigma_{Li} = 7 \times 10^{-2}$ S/cm and is nonflammable; its electrolyte window may be too small to be competitive with the carbonates, but it deserves to be explored for Li batteries of lower voltage.

Insertion Compounds for Li-Ion Secondary Batteries

Anodes with Li^+-Ion Liquid Electrolytes

In a liquid-carbonate electrolyte, dendrites form on an elemental Lithium anode that can grow across the electrolyte to short-circuit a cell on repeated cycling. Therefore, carbon or an alloy buffered by carbon is used with a liquid electrolyte [8].

Graphite has the layered structure of Fig. 9a and Li can be inserted rapidly and reversibly between the layered sheets to create sites capped by six C atoms and form LiC_6, Fig. 9b, c. Similar reactions with graphitic sheets occur for the several different forms of carbon; but with a 2D insertion that shifts neighboring graphene sheets relative to one another, a more amorphous type of carbon is preferred over large crystallites of graphite. A carbon anode into which Li^+ ions from the cathode are inserted on an intial charge, Eq. 12, is commonly used in Li^+-ion rechargeable batteries. However, the E_{FA} of the reduced carbon in LiC_6 lies above the LUMO of a carbonate electrolyte, so on the initial charge it consumes irreversibly Li^+ ions from the cathode in the formation of a non-blocking SEI layer on the carbon unless the SEI layer is formed on the anode before battery assembly. Moreover, if a fast charge raises the charging voltage above Li^+/Li^0, Lithium is plated out on the SEI layer, which introduces the possibility of dendrite formation with a catastrophic short circuit within the cell after repeated cycling. This problem limits the rate of charge unless the E_{FA} is at least 0.5 eV below Li^+/Li^0. With a carbon anode at *ca.* 0.2 V vs Li^+/Li^0, this problem introduces complexity in the safety management of a Li^+-ion battery with a flammable electrolyte. To eliminate irreversible capacity loss due to SEI formation on the initial charge and to increase the rate of charge while simplifying safe battery management, it is necessary to introduce an insertion-compound anode giving a voltage versus Lithium greater than 1.0 V, but preferably less than 1.5 V. The spinel $Li_4Ti_5O_{12}$ gives a constant voltage versus Lithium of $V = 1.5$ V, but its capacity is disappointing. Preliminary studies have shown a layered niobate having a single-phase solid-solution Li insertion between 1.2 and 1.6 V versus Lithium has a higher capacity than that of $Li_4Ti_5O_{12}$, a good rate capability, and a promising cycle life; but Nb is more expensive than Ti and a fully satisfactory, safe anode material has yet to be accepted. The secondary Li^+-ion batteries using a liquid electrolyte are therefore identified by their insertion-compound cathode. The Li^+ ion is small enough to be inserted into the interstices of a close-packed anion array.

Cathodes with Li-Ion Liquid Electrolytes

Layered Sulfides [9]. The MS_2 (M = Ti, V, $V_{0.5}Cr_{0.5}$) sulfides have the layered structure of Fig. 10 in which strongly bonded sheets of edge-shared $MS_{6/3}$ octahedra are held together by weak Van der Waals bonds. In the late 1960s, it was reported that Li can be intercalated (inserted) reversibly between the TiS_2 layers to give the

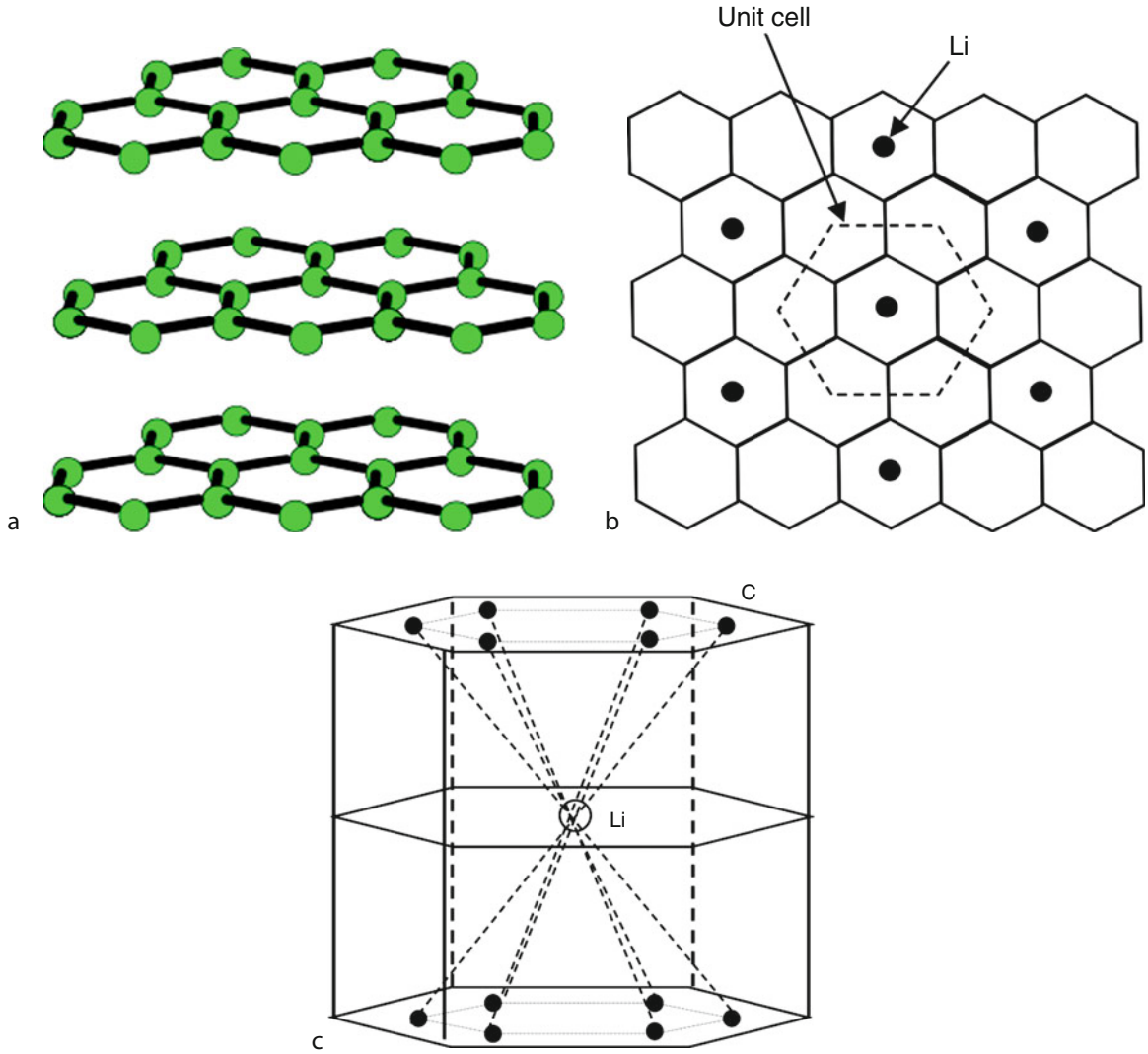

Battery Components, Active Materials for. Figure 9
Structure of (**a**) graphite, (**b**) graphene stacking in LiC_6, and (**c**) LiC_6

solid-solution reaction Li_xTiS_2 ($0 \leq x \leq 1$) with the voltage profile of Fig. 11 for a Li/$LiClO_4$ in PC/TiS_2 cell. However, catastrophic failures due to dendrite formation on the Lithium anode forced consideration of an anode that would lower the cell voltage to where the cell would not be competitive with secondary cells having an aqueous electrolyte. Nevertheless, this early report raised awareness that the designer of a cathode material for a Li^+-ion rechargeable battery should look to insertion compounds capable of providing a larger voltage versus Lithium than 2.5 V. However, the designer must not only identify a host structure into/from which Li can be inserted/extracted reversibly, but also consider the limiting E_{FC} of the host structure and whether its E_{FC} can be matched to the HOMO of the electrolyte. For this latter consideration, it is instructive to consider the limiting E_{FC} of a layered sulfide.

Figure 12a illustrates schematically the energy density of one-electron states of TiS_2 versus their energy ε relative to the E_{FA} of a Lithium anode. The outer *s* and *p* electrons of the Ti and S atoms are primarily involved in the strong Ti–S bonding. The ionic and covalent components of this bonding create a filled broad band of one-electron states that have a primarily S-3*p*

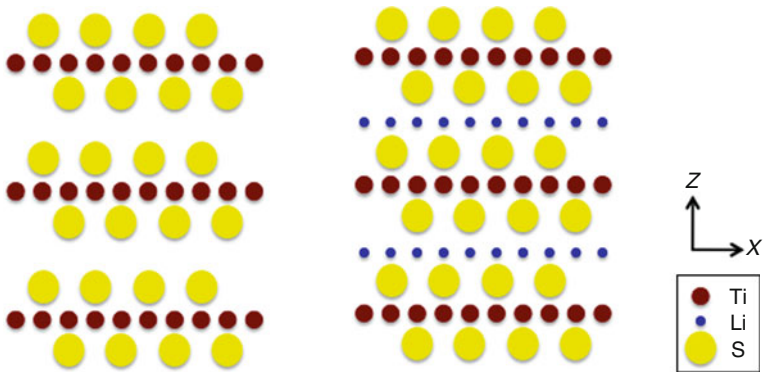

Battery Components, Active Materials for. Figure 10
Layered TiS_2 and $LiTiS_2$ structures

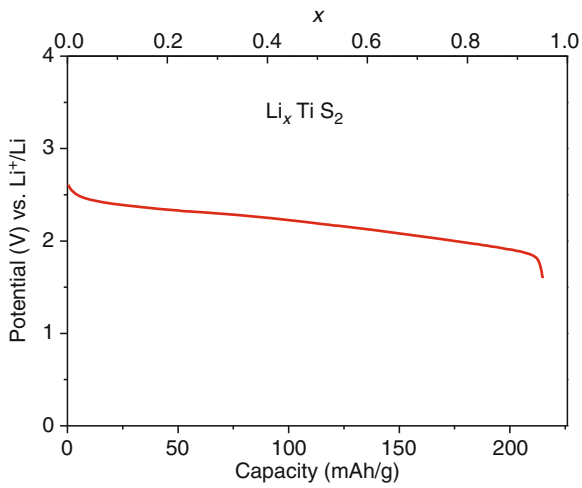

Battery Components, Active Materials for. Figure 11
V(x) versus Lithium profile for Li_xTiS_2 and $Li_{2x}[Ti_2]S_4$, $0 \leq x \leq 1$

character separated by an energy gap from an empty broad band of states that have a primarily Ti-4*s* character. These bands have similar energies in all the MS_2 layered compounds, but the bottom of the M-4*s* band falls progressively with increasing atomic number of the M atom. Empty Ti-3*d* states lie in the energy gap between these two bands. The cubic component of the site symmetry of a Ti(IV) cation splits the σ-bonding and π-bonding 3*d* orbitals by an energy Δ_c; the σ-bonding states, not shown, lie above the bottom of the Ti-4*s* band and the π-bonding states lie in the energy gap between the broad Ti-4*s* and S-3*p* bands. The trigonal component of the site symmetry splits the π-bonding 3*d* states into a lower, orbitally nondegenerate a_1 band and a higher, orbitally two-fold-degenerate e_π band. The Fermi energy of stoichimetric TiS_2 lies in a small energy gap between the bottom of the Ti-a_1 band and the top of the S-3*p* bands. Intercalation of Li^+ ions is neutralized by electrons entering the Ti-a_1 band; as E_{FC} rises with x in Li_xTiS_2, the voltage versus Lithium drops smoothly in this single-phase solid-solution reaction, Fig. 11. The Ti^{4+}/Ti^{3+} couple of Fig. 12a actually lies in an itinerant-electron a_1 band that is half-filled in $LiTiS_2$; however, displacement of Li to the tetrahedral sites of the Li layer in $Li_{1+x}TiS_2$ raises the Ti^{3+}/Ti^{2+} couple to just below the Ti-4*s* band.

As the atomic nuclear charge increases from Ti to V to Cr, the 3*d* electrons become more tightly bound to the nucleus, which lowers their energies. The E_{FC} of VS_2 is *pinned* at the top of the S-3*p* bands, Fig. 12b. Pinning of E_{FC} occurs because, as the cation-*d*-like states move from above to below the top of the bonding anion-*p* bands, the empty antibonding states remain above the anion-*p* bonding states; but the empty antibonding states change their character from primarily cation-*d* to primarily anion-*p* while retaining their *d*-orbital symmetry. On the other hand, if the cation-*d* states fall too far below the top of the anion-*p* bands, the holes in the antibonding states become trapped in purely anion-*p* antibonding states of a S–S bond to create the $(S_2)^{2-}$ ion. The Cr(IV) formal valence state cannot be accessed because a localized-electron Cr(IV)/Cr(III) redox couple lies too far below the top of the

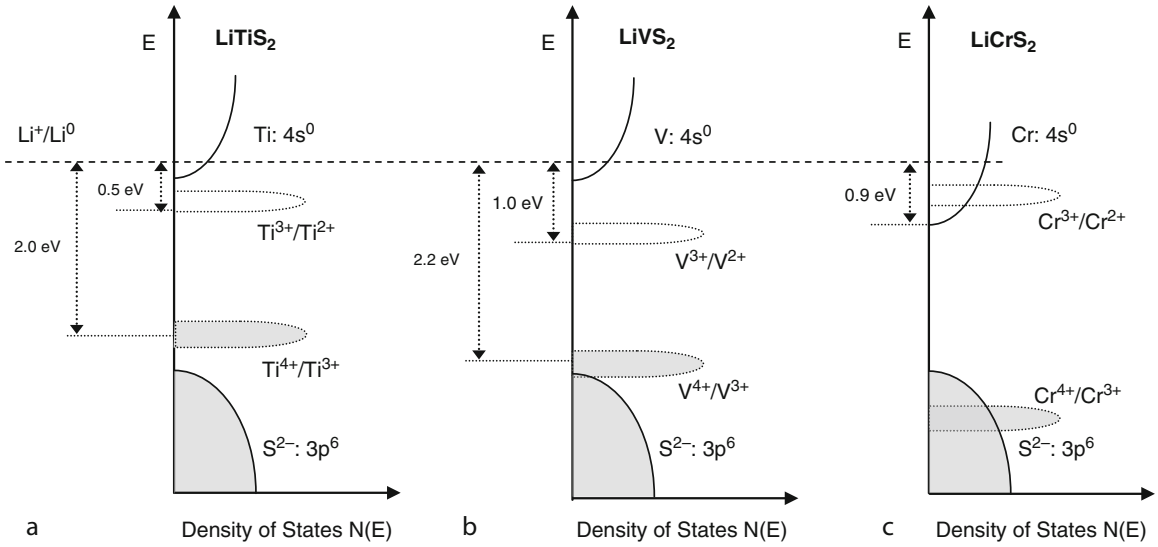

Battery Components, Active Materials for. Figure 12
Energies of the bottom of the 4*s* band, the top of the S-3*p* bands, and π-bonding d-electron energies relative to the E_{FA} of Lithium for TiS_2, VS_2, and $LiCrS_2$. In $Li_{1+x}MS_2$, all the Li occupy tetrahedral sites of the Li layer and the M(III)/M(II) levels are raised to give $V = 0.5$ V and 1.0 V, respectively, for $Li_{1+x}TiS_2$ and $Li_{1+x}VS_2$; the Cr(III)/Cr(II) level is raised above the bottom of the 4*s* band so that Li insertion into CrS_2 displaces Cr^0

S-3*p* bands. However, $V_{0.5}Cr_{0.5}S_2$ can be stabilized in the layered MS_2 structure, and reduction of this host by the intercalation of Li into $Li_xV_{0.5}Cr_{0.5}S_2$ accesses the V(V) to V(III) formal valences [10]. A flat $V \approx 2.7$ V for $x < 0.5$ in $Li_xV_{0.25}Cr_{0.75}S_2$ signals that the top of the S-3*p* bands is about 2.7 eV below the E_{FA} of Lithium. This limitation on the voltage in these sulfides motivated study of the extraction of Li from similarly layered oxides since the top of the O-2p bands would be below the top of the S-3*p* bands.

Layered Oxides. Most solid cathode hosts are transition-metal oxides in which E_{FC} lies in either a mixed-valent redox couple or a narrow band of *d*-electron states. The PbO_2 cathode of the lead–acid battery is an exception; its E_{FC} is located in a narrow Pb-6*s* band well-separated from the broad, empty Pb-6*p* band because Pb is heavy.

A layered transition-metal MO_2 oxide analogous to TiS_2 does not exist; the electrostatic repulsive forces between the oxygen layers are stronger than any Van der Waals bonding, which is much weaker in an oxide than in the chalcogenides. However, where the transition-metal M atom has no *d* electrons, or at most one *d* electron, and is too small to be stable in an octahedral site, it may undergo a ferroic M-atom displacement to form a short M = O bond with one oxygen of the octahedral site and a long $O \cdots M$ bond on the opposite side. These displacements create site dipoles that can stabilize a layered oxide as is illustrated by the structure of V_2O_5, Fig. 13a. On the other hand, several $LiMO_2$ oxides form rock-salt structures in which the Li^+ and M(III) ions occupy alternate layers of M(III) octahedral sites, Fig. 13c. The sheets of edge-shared $MO_{6/3}$ octahedra are analogous to those of TiS_2, but the stacking between sheets gives hexagonal-close-packed sulfide ions in TiS_2, cubic-close-packed oxide ions in $LiMO_2$. The layers can also be stacked to give trigonal-prismatic sites between the layers. Moreover, Li can be either extracted, $Li_{1-x}MO_2$, or inserted, $Li_{1+x}MO_2$. Insertion of more than one Li per formula unit displaces Li^+ ions from octahedral to tetrahedral sites in the Li layer to form Li_2MO_2 in a two-phase reaction. The two-phase insertion reaction $LiVS_2$-Li_2VS_2 gives a voltage of 1.0 V versus Lithium, and an SEI layer is formed on the electrode. The $Li_{1-x}MO_2$ oxides are of interest as cathodes.

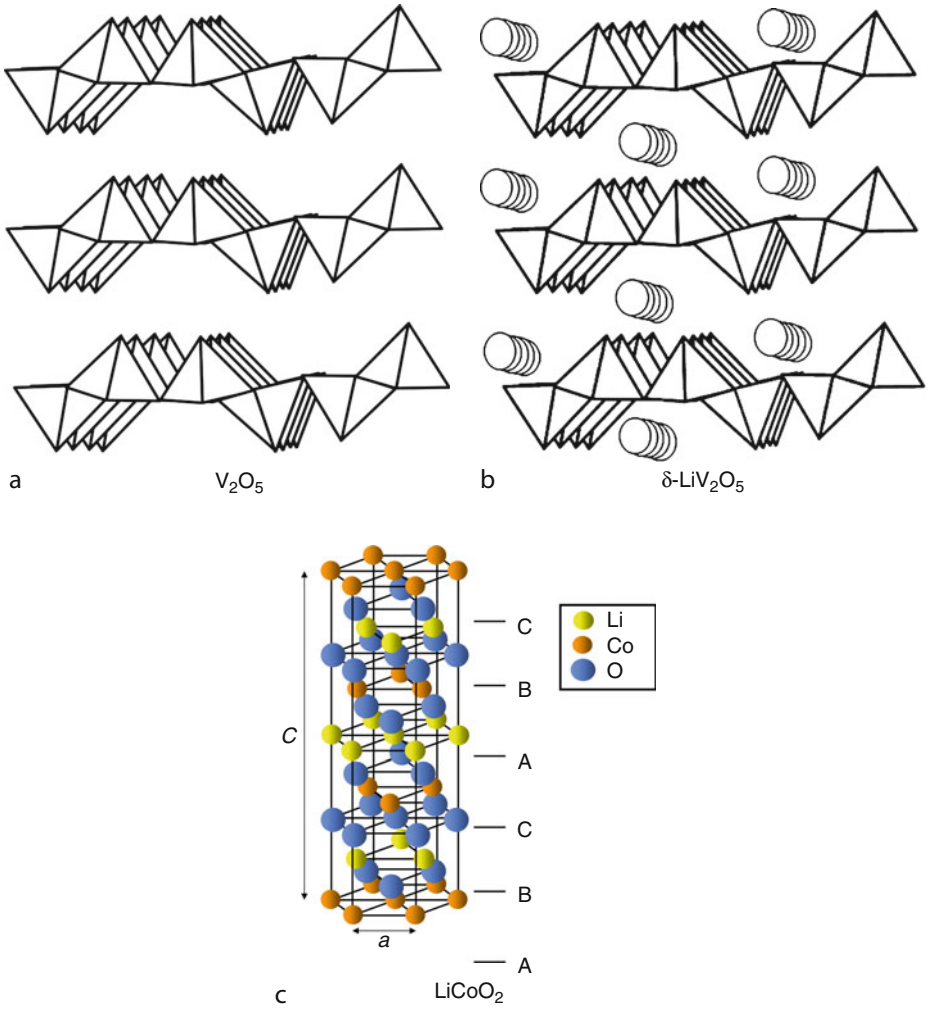

Battery Components, Active Materials for. Figure 13
The structures of (**a**) V_2O_5, (**b**) δ-LiV_2O_5, and (**c**) $LiMO_2$

Extraction of Li from $LiMO_2$ oxides creates M(IV)/M(III) mixed valence on the M atoms. Where the M atoms have a localized spin S associated with a cation configuration $3d^n$, the mobile electron of the mixed-valent system moves diffusively in a hopping transfer $d^{n+1} + d^n = d^n + d^{n+1}$ between like atoms on equivalent lattice sites. In this case, the d^n/d^{n+1} configuration of an M(IV)/M(III) mixed-valent system may be considered a redox couple because the time for a hop is long compared to the period of a lattice vibration that traps the mobile electron or hole at a single site. Where the empty d-electron states lie close to the top of an anion-p band, the electrons may occupy a narrow band of itinerant-electron states as in TiS_2 and VS_2. Electrons in a partially filled band of itinerant-electron states give a metallic conductivity, those in redox couples require an activation energy for a hop to a like neighbor.

The energies of successive redox couples, for example, M(IV)/M(III) to M(III)/M(II), are separated by an on-site electron–electron electrostatic repulsive energy. In the case of Cr(III) in Fig. 12c, the cubic crystal-field splitting is added to this electrostatic on-site energy to raise the Cr(III)/Cr(II) energy to above the bottom of the Cr-4s band while the Cr(IV)/Cr(III) couple lies below the top of the S-3p bands. Insertion of Li into

$LiCrS_2$ results in $Li_2S + Cr^0$; extraction of Li results in $(S_2)^{2-}$ formation. On the other hand, the electrons in the narrow V-a_1 band with E_{FC} pinned at the top of the S-3p bands allows access to both the V(V)/V(IV) and V(IV)/V(III) mixed-valence states without any energy gap between them [10].

The Co(III) ions in $LiCoO_2$ are in their low-spin $S = 0$ state, but the initial Co(IV) ions appearing on removal of Li in $Li_{1-x}CoO_2$ are in their high-spin $S = 5/2$ state [11]; the holes are trapped at a single Co(IV) site. However, in the range $0.05 \leq x \leq 0.45$, the voltage is flat at $V \cong 4.0$ V versus Lithium, which signals a two-phase reaction between a Li-rich phase containing high-spin Co(IV) and a Li-poor phase containing low-spin Co(IV/III) ions with holes in an itinerant-electron π^* band [12]. For $x \geq 0.55$, a new phase with different stacking of the CoO_2 sheets begins to appear as oxygen is evolved and/or H^+ ions from the organic electrolyte are inserted so as to retain the Co(IV)/Co ratio at about 0.45 [13]. The outgassing of oxygen shows that the holes in the π^* band have sufficient O-2p character, at least at a grain surface, to become trapped in peroxide ions $(O_2)^{2-}$ followed by $2(O_2)^{2-} = 2O^{2-} + O_2\uparrow$. Clearly, the $Li_{1-x}CoO_2$ electrode reaches its *intrinsic limit* at a ratio Co(IV)/Co ≈ 0.45; this limit is above the HOMO of the electrolyte, so the electrolyte is not being decomposed aside from loss of inserted H^+ ions. The intrinsic limit restricts the practical capacity of $Li_{1-x}CoO_2$ to only 50% of the theoretical capacity, that is, to a $Q = 140$ mAh/g.

A cell with a carbon anode forms an LiC_6 phase during an initial charge from the discharged cathode $LiCoO_2$, and formation of an SEI layer on the reduced carbon during the initial charge reduces further the available capacity of the cell unless the SEI layer on the anode is formed before the cell assembly. Moreover, by fabricating the cell with a discharged cathode, it is the capacity of the cathode that determines the capacity of the cell. Nevertheless, the E_{FA} of the carbon anode is only 0.2 eV below the E_{FA} of Lithium, so the cell has a high specific energy QV because of its $V \approx 3.8$ V. The cell also has a high volumetric energy density, which is why it captured the market for laptop computers, cell telephones, and other handheld devices. The *tap density* of an electrode refers to the density of active particles that can be packed into a given volume, and a high tap density of $LiCoO_2$ is responsible for the high volumetric energy density.

Cobalt is expensive and toxic, so it was natural to try substitution of Ni for Co. However, it proves difficult to prepare well-ordered $LiNiO_2$. The maximum Ni substitution for Co in a layered phase with well-ordered Li^+ ions is $LiCo_{0.15}Ni_{0.85}O_2$ [14]. Since the holes in $Li_{0.5}CoO_2$ occupy a π^* band whereas those on low-spin Ni(III) occupy a σ^* band of higher energy, the $LiCo_{0.15}Ni_{0.85}O_2$ system gives a loss of O_2 and/or H^+ insertion only for $(1-x) < 0.35$, which gives a $Q = 200$ mAh/g. Addition of a small amount of Al in $LiAl_{0.05}Co_{0.15}Ni_{0.8}O_2$ improves the ordering of the Li and optimizes the cyclability of this cathode.

The transfer of M atoms into vacant sites of the Li layer on Li extraction requires their transfer via a tetrahedral site of the interstitial space. The low-spin Co(IV/III) and Ni(IV/III) cations have a strong octahedral-site preference, so transfer to the vacancies in the Li layer is kinetically inhibited below 300°C. However, ions like Fe(III), Mn(II), and Cr(VI) have a strong tetrahedral-site preference and are easily displaced to the interstitial tetrahedral sites on Li removal. Therefore, $LiFeO_2$ does not retain its structure on Li extraction. The disproportionation reactions 2Mn(III) = Mn(II) + Mn(IV) and 3Cr(IV) = 2Cr(III) + Cr(VI) introduce Mn(II) and Cr(VI) ions into the interstitial space to block insertion of Li back into the structure. Therefore, in order to eliminate Co and to take advantage of the pinning of the Ni(IV)–Ni(II) valence states at the top of the O-2p bands, the $LiNi_{0.5}^{(II)}Mn_{0.5}^{(IV)}O_2$ structure was investigated [15]; the Mn(IV) ion has a strong octahedral-site preference and the Mn(V)/Mn(IV) redox couple lies well below the top of the O-2p bands where the disproportionation reaction 3Mn(IV) = 2Mn(III) + Mn(VI) is inhibited. However, the mean size of the Ni(II) and Mn(IV) ions is too large for good ordering of the Li^+ ions in $Li(Ni_{0.5}Mn_{0.5})O_2$ to be easily obtained. Therefore, considerable attention has been given to $Li(Ni_{0.5-x}Co_{2x}Mn_{0.5-x})O_2$ with $x \leq 1/6$ where the Ni (III)/Ni(II) and Ni(IV)/Ni(III) mixed valences are accessed without a step in the voltage profiles on passing from one to the other because of E_{FC} pinning. Moreover, solid solutions of these $LiMO_2$ oxides with $Li(Li_{1/3}Mn_{2/3})O_2$, commonly designated Li_2MnO_3, as a randomly intercalated second phase exhibit, after an

initial charge, a high reversible capacity of 250 mAh/g even though Li_2MnO_3 itself is not electrochemically active [16]. The voltage profiles of these solid solutions exhibit two distinct regions during the first charge, an initial sloping range corresponding to the oxidation of the Ni(II) to Ni(IV) and the Co(III) to Co(IV) followed by a plateau at V ≈ 5.5 V. The plateau at 4.5 V appears to signal oxidation of the electrolyte. The excess Li_2MnO_3 increases the Mn(IV) concentration, which lowers further the top of the O-2- bands and thus increases the intrinsic voltage limit of the layered oxide. The passivating SEI layer formed from the electrolyte at voltages $V > 4.3$ V inhibits Li^+-ion transfer across the electrode/electrolyte interface, but coating with an oxide layer that transports Li^+ ions suppresses formation of the electrolyte SEI layer to allow fast cycling. Nevertheless, these layered oxides must compete against spinel cathodes containing Ni(II) and Mn(IV).

Vanadium Oxides. Several intermediate phases appear between V_2O_3 and V_2O_5; Li insertions into V_2O_5 and V_6O_{13} were investigated in the 1970s, and an amorphous or low-crystallinity VO_x with a polyethylene oxide (PEO) electrolyte is used in a Li/PEO/VO_x secondary battery for stationary storage of electrical energy [17].

Figure 13a shows the structure of orthorhombic V_2O_5; corner-shared paired chains of distorted VO_6 octahedra parallel to the *c*-axis share edges to create *c*-axis zigzag chains. Ferroic *c*-axis displacements of V atoms in the paired chains create asymmetric *c*-axis bonds 0 . . . V = O, which places the V atoms in square-pyramidal sites. These chains share corners in the $a-b$ planes with antiferroelectric coupling across shared edges to create the $a-b$ layers of Fig. 13a. Li^+ ions can be inserted reversibly into the *b*-axis tunnels to form δ-LiV_2O_5 via an intermediate ε-$Li_xV_2O_5$ phase.

In the range $0 \leq x \leq 1$ of $Li_xV_2O_5$, reduction of the vanadium on Li^+-ion insertion only tilts the square-pyramidal sites of the $a - b$ planes, but three phases can be distinguished: α ($0 \leq x \leq 0.1$), ε ($0.35 \leq x \leq 0.7$), and δ ($0.9 \leq x \leq 1.0$). The reversible insertion of Li into V_2O_5 gives a voltage profile versus Lithium with two plateaus, one at 3.4 V for the $\alpha + \varepsilon$ range $0.1 \leq x \leq 0.35$ and the other at 3.2 V for the $\varepsilon + \delta$ range $0.7 \leq x \leq 0.9$. On further Li insertion, the voltage drops abruptly to 2.4 V followed by a monotonic decrease with x to about 1.5 V over the range $1 < x < 3$. Cycling through the first-order transition at $x = 1$ damages the crystallites and lowers the cyclability. However, insertion into amorphous or low-crystallinity V_2O_5 allows faster and better cyclability. Insertion of 1.5 Li per V atom gives a relatively large capacity.

The structure of V_6O_{13} shows how the particles of low-crystallinity or amorphous VO_x can accommodate Li^+-ion insertion into 1D tunnels. Figure 14 shows the structures of V_2O_5 and V_6O_{13} projected, respectively, onto its (001) and (010) plane, which illustrates how

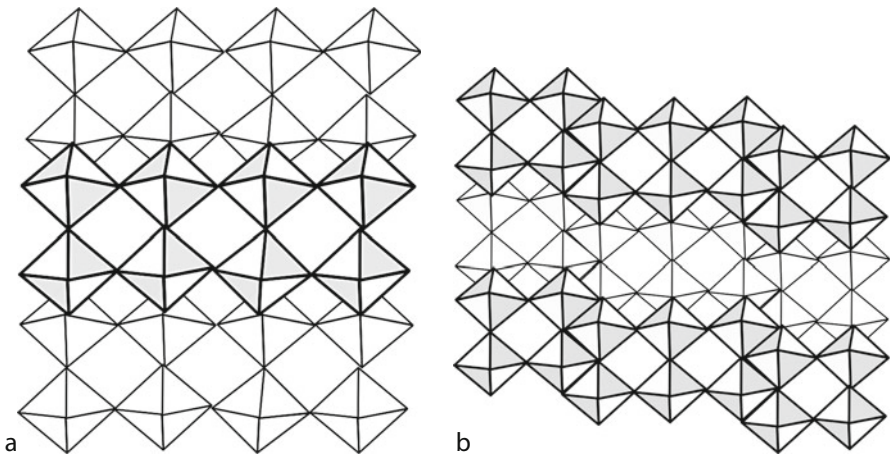

Battery Components, Active Materials for. Figure 14
Comparison of structures of V_2O_5 projected onto its (001) plane and V_6O_{13} onto its (010) plane

the V_6O_{13} structure can be derived from that of V_2O_5. Removal of oxygen from every third $a-c$ oxygen plane of V_2O_5 is followed by a shear, which leaves tunnels for Li^+-ion insertion as in V_2O_5. The shear planes need not be ordered as in V_6O_{13}.

These observations have led to the synthesis of a two-dimensional (2D) pseudocrystalline phase containing segments of three planes similar to those of V_2O_5 that are displaced from one another by a slip plane. This structure provides an insertion of up to two Li atoms per formula unit with a monotonic voltage decrease with x, except for a small step at $x = 1.5$, over the voltage range $2.5 < V < 3.4$ V versus Lithium. Nevertheless, there is a gradual capacity fade with cycle number.

The voltage profile of $Li_xV_6O_{13}$ shows small steps at $x = 1$, 2, and 3 as the voltage decreases from 2.8 to 2.4 V versus Lithium and a drop from 2.4 to 2.1 V in the interval $3 < x < 4$ that is followed by a gradual drop to 2.0 V as x approaches 6. The steps appear to correspond to Li^+-ion ordering with electrons entering $V - 3d$ bands rather than localized redox couples; the electronic states change character from $V - 3d$ with a large $O - 2p$ component to a dominant $V - 3d$ character with increasing x. Capacity fading on cycling makes this material not competitive as a cathode for a secondary battery.

Spinels. The $A[M_2]O_4$ spinels have a cubic-close-packed array of oxygen atoms with M-site cations in half of the octahedra, the 16*d* sites of space group $Fd\overline{3}m$ of Fig. 15. The $[M_2]O_4$ array represents a strongly bonded framework with A atoms in the interstitial tetrahedral sites 8*a*. The empty 16*c* octahedral sites share faces with the 8*a* sites to form, with the 8*a* sites, a 3D-interconnected interstitial space. On Li^+-ion insertion into an empty 16*c* site, the coulombic repulsive force between the Li^+-ion and the near-neighbor A-site cations pushes all the A-site cations in a cascade into the 16*c* sites [18].

In the case of magnetite, $Fe[Fe_2]O_4$, insertion of one Li per formula unit produces an ordered rock-salt array with Fe remaining on all the 16*d* sites and Li and Fe randomly distributed over the 16*c* sites. Further insertion of Li extrudes Fe reversibly from the 16*c* sites to form the ordered rock-salt structure $Li_2[Fe_2]O_4$ and amorphous Fe^0. From this observation, it was clear that Li insertion into the system $Li_{1+y}[Mn_2]O_4$ $(0 < y \leq 1)$ would place Li^+ ions in the octahedral 16*c* sites and Li extraction in the system $Li_{1-y}[Mn_2]O_4$ $(0 < y \leq 1)$ would leave the Li^+ ions in tetrahedral *8a* sites. Moreover, with only Li^+ ions in the 3D interstitial space, a fast Li^+-ion transport could be anticipated. The voltage profile of Fig. 16 for the system $Li_x[Mn_2]O_4$, $0 \leq x \leq 2$, shows a 1-V step at $x = 1$ where the Li^+ ions

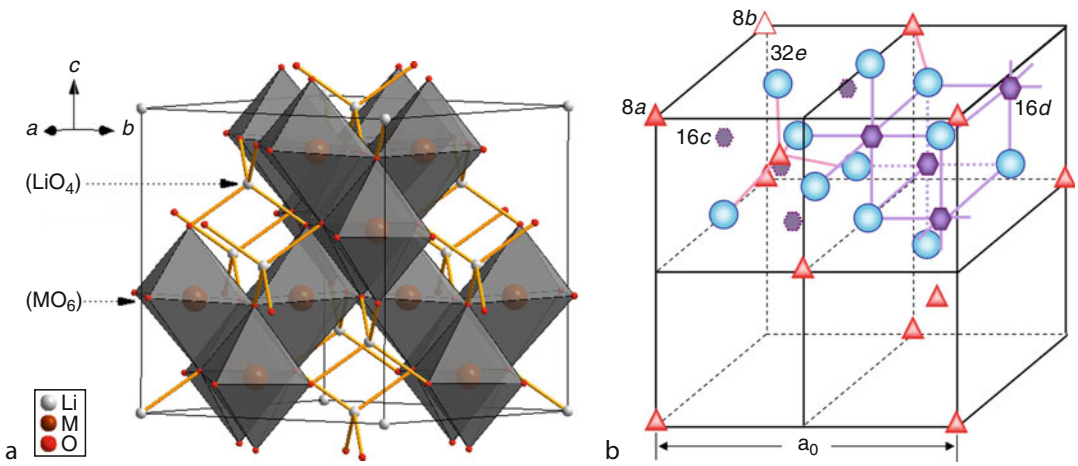

Battery Components, Active Materials for. Figure 15
(**a**) The structure of a cubic $A[M_2]O_4$ spinel showing quadrants of edge-shared $MO_{6/3}$ octahedra alternating with quadrants of tetrahedral-site A cations on traversing the <100 > axes. (**b**) Two quadrants of the cubic spinel structure showing the diamond array of the A-site sublattice *8a*; M cations are in *16d* and oxygen in *32e*

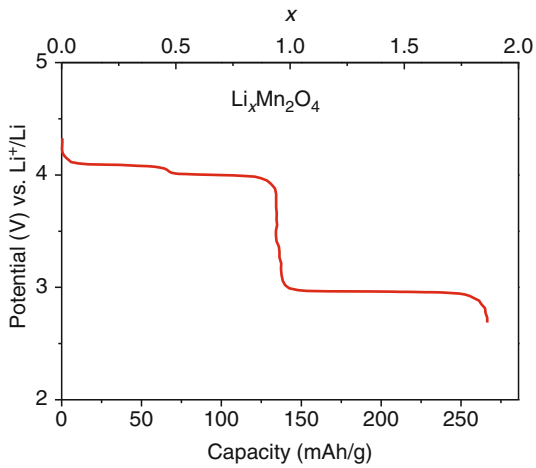

Battery Components, Active Materials for. Figure 16 The V(x) versus Lithium profile for $Li_x[Mn_2]O_4$ showing a 1 eV step in the M(IV)/M(III) redox couple at $x = 1$

shift from tetrahedral to octahedral sites. This remarkable 1-eV shift in the energy of the Mn(IV)/Mn(III) couple shows that the energy of an active redox couple is sensitive to the Madelung ionic electrostatic energy of the oxide.

In contrast, the voltage profile of Li insertion into the thiospinel framework $[Ti_2]S_4$ shows no step at $x = 1$ [19]; the profile of $Li_x[Ti_2]S_4$, $0 \leq x \leq 2$, is nearly identical to that for the layered system Li_xTiS_2, which shows that the Li^+ ions occupy only octahedral 16c sites for all x in $Li_x[Ti_2]S_4$. Preparation of the thiospinel Li $[Ti_2]S_4$ is not straightforward; the thiospinel framework $[Ti_2]S_4$ is prepared by chemical extraction of tetrahedral-site Cu^+ from the thiospinel $Cu[Ti_2]S_4$. In both the layered TiS_2 and the spinel framework $[Ti_2]S_4$, the octahedral $TiS_{6/3}$ sites share only edges, not corners, with neighboring $TiS_{6/3}$ sites; only the shape of the interstitial space has been changed from 2D to 3D. The 2D interstitial space of $LiTiS_2$ allows intercalation of other species than the Li^+ ions whereas the 3D interstitial space of the strongly bonded spinel framework does not.

The 1-V step in the voltage profile of $Li_x[Mn_2]O_4$ limits the capacity of this spinel to one Li^+ per two Mn atoms at either 3.0 V or 4.0 V versus Lithium. The flat 3.0 V plateau reflects a cubic to tetragonal transition of the $[Mn_2]O_4$ framework due to a cooperative Jahn–Teller site distortion where more than half of the 16d sites are occupied by Mn(III) ions. Octahedral-site, high-spin Mn(III) ions have a localized spin $S = 2$ with one electron occupying an orbitally twofold-degenerate pair of σ-bonding e_σ orbitals; a site distortion to tetragonal symmetry removes the degeneracy, stabilizing an occupied $(3z^2 - r^2)$ orbital at the expense of an empty $(x^2 - y^2)$ orbital of the e_σ pair. A cooperative site distortion minimizes the elastic energy per site that it costs to distort a site from cubic symmetry.

The 8a sites consist of two interpenetrating face-centered-cubic arrays to form the diamond lattice. The small step in the 4.0-V plateau of Fig. 16 reflects an ordered $Li_{0.5}[Mn_2]O_4$ phase in which the Li^+ ions occupy only one of the two interpenetrating face-centered-cubic 8a arrays; two-phase separations occur either side of $x = 0.5$. The two-phase separation due to Li^+-ion order enhances a surface disproportionation reaction 2Mn(III) = Mn(II) + Mn(IV) that is followed by Mn(II) dissolution into the electrolyte. The Mn(II) crosses over to the anode to poison Li^+-ion mobility across the anode SEI layer. As a result, operation on the 4.0-V plateau is plagued by a reduction in capacity that increases with cycling. The Mn(II) dissolution represents a chemical reaction of the electrode with the electrolyte that is to be distinguished from oxidation of the electrolyte by an E_{FC} below the electrolyte HOMO. The progressive increase with cycling in the irreversible loss of capacity is referred to as a capacity fade; it limits the cycle life of the cell. Substitution of Ni or Al and some Li for Mn suppresses any Jahn–Teller framework distortion near $x = 1$; it also disorders the Li^+ ions at $x = 0.5$ to reduce further the Mn(III)-ion concentration at the surface and hence the Mn(II) dissolution, but at the expense of the capacity of the cathode. Figure 17a shows charge/discharge curves for a $Li_{1-x}[Al_{0.1}Li_{0.1}Mn_{1.8}]O_4/Li_{1+x}[Li_{1/3}Ti_{5/3}]O_4$ cell that can undergo safely a fast recharge. At 55°C, this cell retains 80% of its rechargeable capacity after 3,600 cycles. Batteries of five cells connected in series deliver a nominal 12 V.

In the layered $Li_{1-x}Co_{0.15}Ni_{0.85}O_2$ system, pinning of E_{FC} at the top of the O-2p bands gave an intrinsic limit of 3.8 V versus Lithium for the Ni(IV)/Ni(III) couple. Removal of nearly all the Li from the layered oxide $LiNi_{0.5}Mn_{0.5}O_2$ containing Mn(IV) ions shows not only that Mn(IV) increases the voltage limit of the Ni(IV)/Ni(III) couple by lowering the top of the O-2p bands, but also that where E_{FC} is pinned, oxidation of

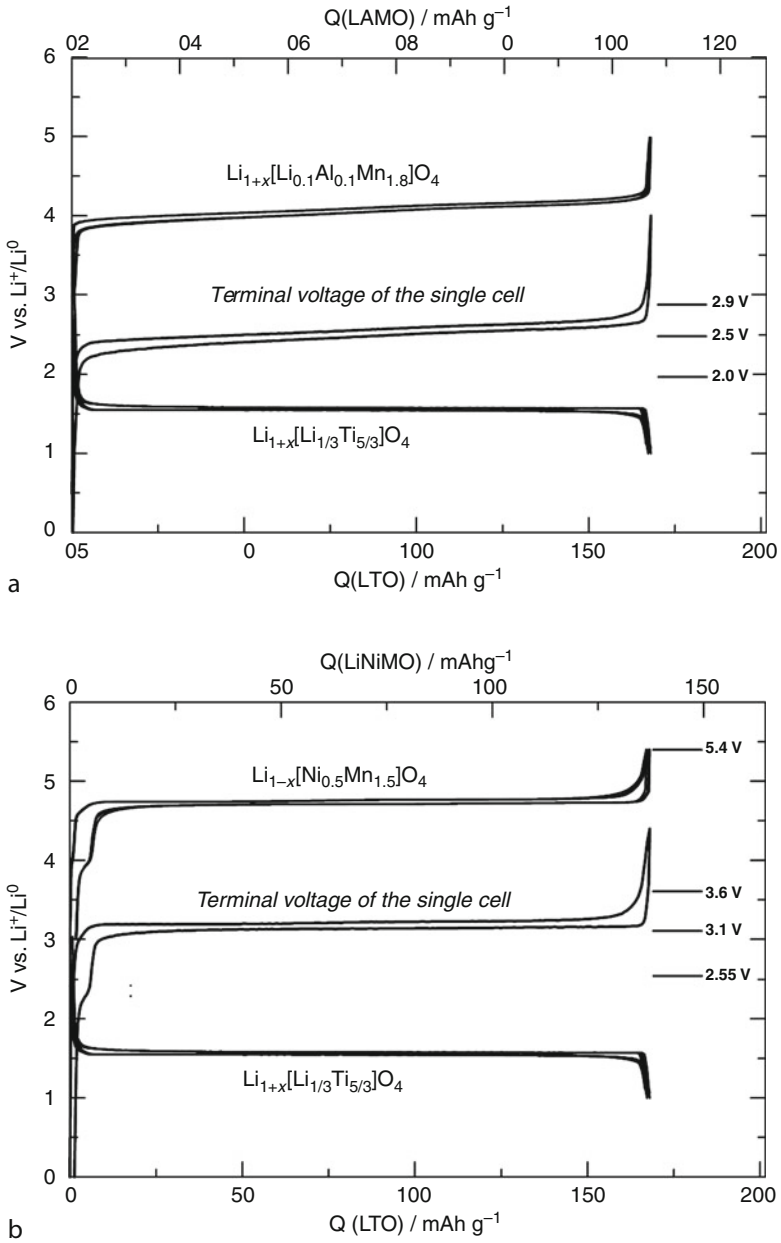

Battery Components, Active Materials for. Figure 17
Charge/discharge V(x) versus Li^+/Li^0 for (**a**) $Li_{1-x}[Al_{0.1}Li_{0.1}Mn_{1.8}]O_4$ and (**b**) $Li_{1-x}[Ni_{0.5}Mn_{1.5}]O_4$ with $Li_{1+x}[Li_{1/3}Ti_{5/3}]O_4$ to give terminal single-cell voltages (By courtesy of Prof. T. Ohzuku)

Ni(II) to Ni(IV) occurs without a step in the voltage profile. Moreover, pinning of E_{FC} gives the flat voltage profile of Fig. 17b; at room temperature, Li is removed over the range $0 < x < 1$ at $V \approx 4.7$ V, which is just below the carbonate-electrolyte decomposition voltage above 4.9 V versus Lithium. Batteries with only four $Li_{1-x}[Ni_{0.5}Mn_{1.5}]O_4/Li_{1+x}[Li_{1/3}Ti_{5/3}]O_4$ cells connected in series can deliver a nominal 12 V. Lowering the top of the O-2p bands in the spinel structure increases the intrinsic voltage limit of the oxide. In contrast, the Ti(IV) ion of $Li_{1-x}[Ni_{0.5}Ti_{1.5}]O_4$ prevents access to even the Ni(III) oxidation state. Unfortunately, although

the SEI layer on $Li[Ni_{0.5}Mn_{1.5}]O_4$ appears to stabilize the cathode at room temperature, raising the temperature to 60°C can introduce a capacity fade on cycling. Coating of the surface of the active oxide particles with another oxide permeable to Li^+ ions has been shown to reduce the activation energy for Li^+-ion transfer across the SEI layer as well as the capacity fade at 60°C. The spinel $Li_{0.5-x}[Ni_{0.5-x}Cr_{2x}Mn_{1.5-x}]O_4$ ($x \cong 0.05$) appears to stabilize the cathode at 60°C without sacrifice of the capacity since the Cr(IV)/Cr (III) couple is accessible and small Cr concentration inhibit the disproportionation of Cr(IV) into Cr(VI) and Cr(III) and are sufficient to remove Ni from the particle surface. The development of 12 V batteries based on spinel insertion compounds is targeted for plug-in hybrid vehicles and electrical-energy storage in solar-powered homes. The goal is a life in excess of 10 years and a driving range per charge in excess of 200 miles at an acceptable dollar and environmental cost.

NASICON Framework [20]. Use of a solid Na^+-ion electrolyte in the Na–S battery stimulated a search in the early 1970s for an improved Na^+-ion conductor. This search concentrated on open framework structures that were electronic insulators and hosts to mobile Na^+ ions. One of these framework structures was that of the system $Na_{1+3x}Zr_2(P_{1-x}Si_xO_4)_3$ with $0 \leq x \leq 1$ having the structure of hexagonal $Fe_2(SO_4)_3$ pictured in Fig. 8. This system with $x \approx 2/3$ was named NASICON to signify it is a NA SuperIonic CONductor, and the host framework is now referred to in the literature as the NASICON framework. Substitution of Na^+ ions by Li^+ ions and substitution of a smaller Ti(IV) for Zr(IV) gives LISICON having the same framework; up to 5 Li^+ ions per formula unit can be accommodated in this framework. Substitution of tetrahedral polyatom anions for oxygen opens up the interstitial space for fast Li^+-ion motion, and substitution for Zr of a smaller transition-metal atom having a lower-energy redox couple makes this framework a candidate host for the cathode of a Li^+-ion secondary battery. In this host, the octahedral-site cations share corners with the polyatom tetrahedral anions and *vice versa*, which isolates the transition-metal cations from one another. Therefore, the 3*d* configurations at the transition-metal ions are localized, so the successive redox couples are separated from one another by a finite energy gap. This gap may be large, as in the separation of the Cr(IV)/Cr(III) and Cr(III)/Cr(II) couples pictured in Fig. 12b or it may be small as between V(V)/V(IV) and V(IV)/V(III) couples in $Li_{3-x}V_2(PO_4)_3$, vide infra. Since this framework can accommodate up to 5 Li atoms without influencing significantly the redox energies on the octahedral-site cations, the framework lends itself to an examination not only of the influence on the redox energies of the counter cation within the polyatom anion, but also the relative energies of different redox couples for a fixed tetrahedral anion [21].

The Fe(III)/Fe(II) redox energy of $Fe_2(SO_4)_3$ is at 3.6 eV, those of isostructural $Fe_2(MoO_4)_3$ and $Fe_2(WO_4)_3$ are at 3.0 eV below the E_{FA} of Lithium. This finding demonstrates that the stronger the covalent bonding in the polyatom anion, the weaker is the bonding of the oxygen to the octahedral-site cation and therefore the more stable is the transition-metal redox energy. This electrochemical result provides a direct measure of the magnitude of this *inductive effect* [22]. It shows that a redox energy can be tuned not only by the position of the guest ion in the interstitial space of the spinel $Li_x[Mn_2]O_4$ or the redox energy of a near-neighbor cation coexisting in an equivalent lattice site as in $Li(Ni_{0.5}Mn_{0.5})O_2$ versus $Li(Ni_{0.8}Co_{0.2})O_2$, but also by the counter cation in a polyatom anion. Accordingly, the Fe(III)/Fe(II) redox couple in $Li_{3+x}Fe_2(PO_4)_3$ is 2.8 eV below the E_{FA} of Lithium. The 0.8 eV shift of the Fe(III)/Fe(II) redox couple on changing from $(SO_4)^2$ to $(PO_4)^{3-}$ is the same for all the redox energies of the NASICON framework.

As an illustration of how the structure lends itself to locating the relative positions of the available redox energies, Fig. 18a shows the voltage profile for $Li_{1+x}FeNb(PO_4)_3$ showing discrete steps on passing from the Fe(III)/Fe(II) to the Nb(V)/Nb(IV) couple to the Nb(IV)/Nb(III) couple at 2.8 eV, 2.3 eV, and 1.8 eV, respectively, below the E_{FA} of Lithium. The Ti(IV)/Ti(III) couple at 2.5 eV in $Li_xTiNb(PO_4)_3$ overlaps the Nb(V)/Nb(IV) couple at 2.5 eV to give the smooth voltage profile from 2.5 to 2.2 V shown in Fig. 18b. The relative energies of the redox couples with $(SO_4)^{2-}$ anions remain the same, but all are shifted by about 0.8 eV to lower energy. The voltage profile of a carbon-coated $Li_{3-x}V_2(PO_4)_3$ cathode versus Lithium shows a good cycle life over the interval $0 \leq x \leq 3$ with two-phase reactions at 3.59 V in the interval $0.5 \leq x \leq 1.0$

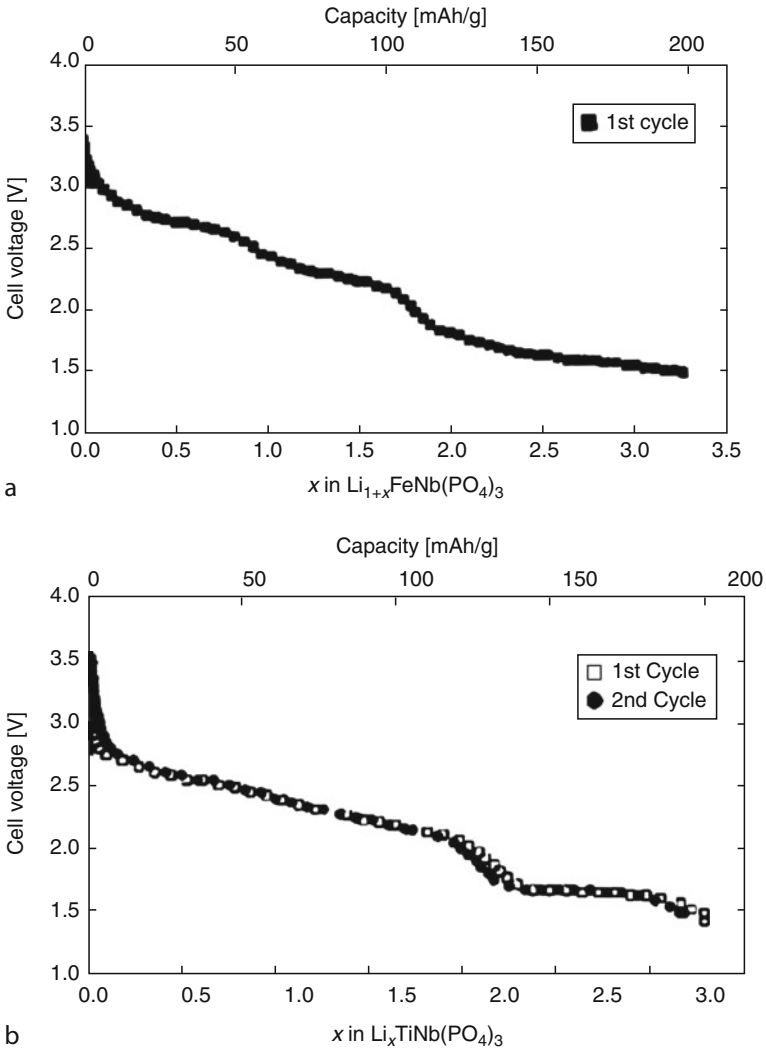

Battery Components, Active Materials for. Figure 18
Discharge V(x) versus Li^+/Li^0 for (**a**) $Li_{1+x}FeNb(PO_4)_3$ and (**b**) $Li_xTiNb(PO_4)_3$

and 3.67 in the interval $1.0 \leq x \leq 2.0$ corresponding to the V(IV)/V(III) couple and 4.06 V over $2.0 \leq x \leq 3.0$ of the V(V)/V(IV) couple. The 0.08 eV step for the V(IV)/V(III) couple is due to ordering of the Li^+ ions into the unique interstitial site per formula unit between M-atom sites of the framework; the larger 0.4 eV step at $x = 2.0$ is the separation of the V(IV)/V(III) and V(V)/V(IV) couples. Carbon coating of the particles is needed to facilitate these two-phase reactions; the large separation of the transition-metal ions makes any electron transport diffusive, which limits the power capability with this framework unless small, carbon-coated particles are used.

Ordered Olivines $LiMPO_4$. As in a spinel [23], in the olivine structure of Mg_2SiO_4, the cations occupy half of the octahedral and one-eighth of the tetrahedral sites of a slightly distorted, close-packed anion array, but the olivine anion array is close-packed-hexagonal rather than close-packed-cubic. Moreover, two types of occupied octahedral sites are distinguishable, which leads to an ordering of Li^+ and M(II) ions in the $LiMPO_4$ olivines whereas they are disordered in the spinel $V[LiM]O_4$. The ordered MPO_4 array forms a 3D strongly bonded framework in which octahedral-site M atoms share corners within $a-c$ planes of an orthorhombic unit cell, Fig. 19; these $a-c$ planes are

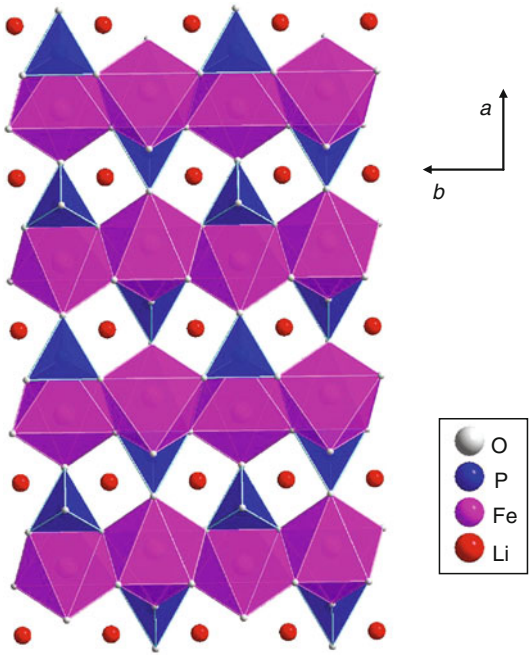

Battery Components, Active Materials for. Figure 19 Structure of the ordered olivine $LiFePO_4$

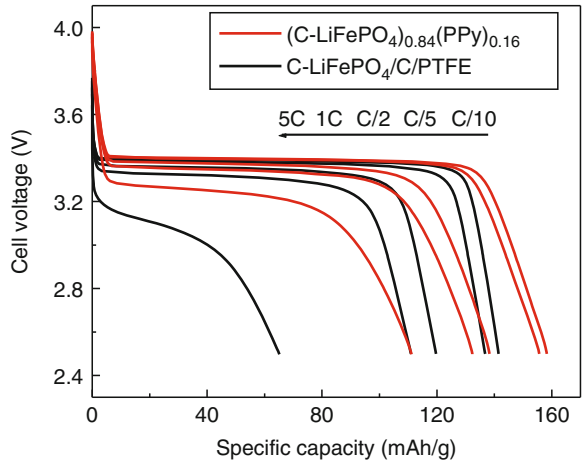

Battery Components, Active Materials for. Figure 20 Discharge V(*x*) versus Li^+/Li^0 for C-coated Li_xFePO_4 with/without PPy for different rates for full discharge from C/10 = 10 h to 5 C =12 min

bridged by the PO_4 tetrahedra and the guest Li^+ ions occupy 1D *a*-axis tunnels of edge-shared octahedra. Motion of the Li^+ ions to neighboring empty octahedral sites outside of the tunnels requires a larger activation energy than motion along the tunnels.

The M atoms of $LiMPO_4$ may be Mg, Mn, Fe, Co, Ni, or mixtures thereof. Of these possibilities, $LiFePO_4$ is the most promising cathode material; $Li_{1-x}FePO_4$ provides a flat $V = 3.45$ V versus Lithium. Removal of Li from $LiMnPO_4$ is difficult, but the Mn(III)/Mn(II) couple gives a more attractive $V = 4.1$ V. The Co(III)/Co(II) couple near 4.8 eV below the E_{FA} of Lithium is at the limit where a liquid-carbonate electrolyte becomes unstable.

It is not possible to substitute an aliovalent cation for Fe(II) in $LiFePO_4$. Synthesis of $LiFePO_4$ from nonstoichiometric starting mixtures results in the dissolution of a separate phase to the surface of stoichiometric $LiFePO_4$ particles. Electrochemical removal of Li results in the formation of $FePO_4$ as a separate phase. This situation means that the electronic conductivity remains low and the voltage profile of $Li_{1-x}FePO_4$ is flat. In order for Li^+ ions to move in or out of a particle rapidly with the electron of an Fe(III)/Fe(II) couple, it is necessary to have an electronically conducting coat on a small nanosize particle that also not only makes electronic contact with the current collector, but also is permeable to Li^+ ions. This coat may be a phase rich in Li that is dissolved from the $LiFePO_4$ particle or carbon; the coat makes electronic contact with the current collector either by added inert carbon or by contact to an electronically conducting polymer that also contacts the current collector and has an active redox energy that overlaps the energy of the Fe(III)/Fe(II) couple of $LiFePO_4$. Polypyrrole (PPy) and polyannaline (PANI) are two such polymers [24]. Figure 20 illustrates the voltage profile versus Lithium of carbon-coated $LiFePO_4$ with PPy for different charge/discharge rates. With a $V = 3.45$ V well below the 4.3 V limit imposed by the HOMO of the electrolyte, this cathode is safe; it also has an excellent cycle life. This cathode is used in secondary Li^+-ion power batteries and is an attractive contender for the battery of a plug-in hybrid vehicle despite a redox energy that is 1 eV higher than would appear to be optimal for a carbonate electrolyte.

It should be noted that $LiFePO_4$ nanoparticles embedded in a carbon matrix make a composite that shows promise for the cathode of an electrochemical capacitor of higher energy density than a purely carbon cathode.

Secondary Batteries with Cathodes That Are Not Insertion Compounds

The cell of a *sodium–sulfur* battery, illustrated schematically in Fig. 21, consists of two liquid electrodes, molten sodium and sulfur, separated by a ceramic Na^+-ion electrolyte; it operates in the 300–375°C range to maintain molten not only the sodium anode, but also both the sulfur cathode and the immiscible-in-sulfur sodium polysulfide (Na_2S_5 to Na_2S_3) products of the reaction of Na^+ ions from the electrolyte with the sulfur [2]. Because sulfur is an electronic insulator, the reaction of the Na^+ ions with the sulfur occurs at the surface of a carbon felt introduced into the sulfur to bring electrons to a large carbon–sulfur interface area. The negative post of the battery is attached directly to the molten sodium contained in a ceramic-electrolyte tube that is closed at one end and open to a molten-sodium reservoir at the other end; the reservoir keeps the Na^+-ion electrolyte covered with Na throughout a discharge. The sulfur with its carbon felt bathes the outside of the ceramic-electrolyte tube, the carbon felt contacting a metal container to which the positive post is attached. The critical component of the cell is the Na^+-ion ceramic electrolyte.

The Na^+-ion electrolyte for a Na–S battery needs to consist of a framework host with mobile Na^+ ions in the interstitial space, but it must also have the bottom of the conduction band of the host above the E_{FA} of elemental Sodium. These criteria are met in the Na-β and Na-β″ aluminas; but their frameworks have a 2D interstitial space and, therefore, an anisotropic thermal expansion. This anisotropic property is undesirable for a polycrystalline, thin ceramic membrane that is subject to repeated thermal cycling between room temperature and 350°C. Nevertheless, ceramic engineering of mixed β and β″ aluminas has resulted in a viable Na–S battery for stationary electrical-energy storage [25].

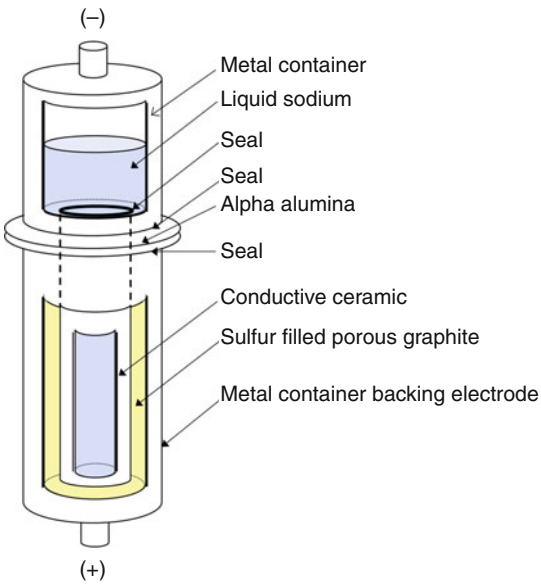

Battery Components, Active Materials for. Figure 21 Schematic of a sodium–sulfur cell

Stoichiometric Na-β alumina, $Na_2O \bullet 11Al_2O_3$, contains $Al_{11}O_{16}$ spinel slabs perpendicular to the [111] axis; the slabs are connected by oxygen bridges within intervening NaO planes containing intersecting 1D tunnels occupied by the Na^+ ions. In stoichiometric Na-β alumina, there are two inequivalent Na^+-ion sites in the NaO planes, one of which is occupied and the other empty. The inequivalence of the Na^+-ion sites raises the activation energy ΔH_m for Na^+-ion motion, but the introduction of excess Na^+ either in $(1 + x)$ $Na_2O \bullet 11Al_2O_3$ or by substituting some Li^+ or Mg^{2+} for Al^{3+} in the spinel blocks reduces ΔH_m in the β phase; in the β″ phase, the Li^+ or Mg^{2+} substitutions shift the spinel slabs relative to one another to make equivalent the Na^+-ion sites in the NaO layers, thereby reducing ΔH_m. A two-phase mixture of β and β″ phases with excess Na^+ ions gives a viable ceramic membrane.

The *ZEBRA cell*, which is under development by the General Electric Co., uses a molten-sodium anode and a solid β,β″-alumina solid electrolyte as in the sodium-sulfur cell, but the positive electrode is large-surface-area nickel rather than molten sulfur with a large-surface-area current collector. The electrolyte on the cathode side of the ZEBRA solid electrolyte is an aqueous $NaAlCl_4$ containing NaCl and NaI as well as a little FeS. The FeS and NaI are added to limit growth of the Ni particles and to aid the overall cathode reaction, which is

$$Ni^0 + 2Cl^- - 2e^- = NiCl_2$$

on charge and on discharge

$$NiCl_2 + 2e^- = Ni^0 + 2Cl^-$$

at a $V_{OC} = 2.58$ V. A *Lithium–Sulfur* battery also uses a sulfur cathode; its redox reaction is

$$S_8 + 16Li^+ + 16e^- = 8Li_2S \qquad (23)$$

in which the electrons from the anode on discharge are brought to the reaction by carbon [26]. The two-phase reaction proceeds in two steps, first to the polysulfides Li_2S_8, Li_2S_4, and Li_2S_2 at 2.4 V and then to Li_2S at 2.0 V. Best results to date have been obtained with a CMK-3 carbon impregnated by sulfur and electrolyte. The CMK-3 carbon consists of carbon nanorods kept apart by carbon bridges to give channels into which molten sulfur is introduced. On solidification, channels are opened for the impregnation of electrolyte to give Li^+ ions access to a large surface area of amorphous sulfur. The cathode reaction is relatively slow, and the efficiency of electrical-energy storage is not optimal. Nevertheless, the lower power density and the low voltage are compensated by a capacity of over 1,000 mAh/g. The low voltage requires use of a Li^0 anode. A protected Lithium anode (see Lithium/seawater battery) is a logical candidate for this battery, but a soluble Li_2S_n shuttle molecule may suppress build-up of the dendrites on the Li^0 anode. The jury is still out on whether this battery will be competitive for a low-power application.

Lithium–Metal Salt secondary batteries are analogous to the Lithium–seawater primary battery [3]. A Li^+-ion solid electrolyte separates a nonaqueous anolyte and an aqueous cathode. For example, a Lithium anode with a carbonate anolyte and an aqueous $Fe(CN)_6^{3-}/Fe(CN)_6^{4-}$ cathode has been shown to give a flat voltage $V \approx 3.4$ V with an efficiency that increases with the molar ratio of iron cyanide in the cathode solution [27]. This promising approach requires development of a Li-ion solid electrolyte having a $\sigma_{Li} > 10^{-4}$ S/cm at room temperature that is stable to an acidic cathode solution and is not reduced by contact with a Li^0 dendrite on the anode side.

Lithium-air batteries [28] may also use a solid separator that will block dendrite growth from the anode to the cathode but allows permeation of the Li^+ ion between an anolyte and a catholyte. The simplest such separator would be a solid Li^+-ion solid electrolyte, but a porous glass containing the liquid electrolyte has been used where the anolyte and the catholyte are identical. As in the Zn-air primary battery, a porous carbon containing an oxygen–reduction catalyst on the pore walls and the liquid electrolyte in the pores provides the structure needed to facilitate the catalytic reaction of Li^+ ions with the gaseous O_2 cathode. The cathodic reaction

$$2Li^+ + 2e^- + O_2 = Li_2O_2 \tag{24}$$

is reversible, but the voltage difference between charge and discharge currents is large even with the best catalyst, Pt–Au nanoparticles [29], which makes the battery inefficient for electrical-energy storage.

The *Redox-Flow Battery* [30] is a candidate for medium- and large-scale electrical-energy stationary storage. The cells of these batteries contain different redox energies in a liquid anode and a liquid cathode separated by either a solid electrolyte or a microporous polymer or glass separator. Reversible electrode processes take place at the surface of graphite-felt current collectors as in the sulfur cathode of a Na–S cell. The reactant redox couples flow across the carbon-felt conductors, entering the electrochemical cell from external reservoirs, Fig. 22. In theory, the capacity of a cell is determined by the volumes of the two electrolyte tanks. Under development is a cell containing vanadium ions in sulfuric-acid solution. The anode compartment contains V^{2+} ions, the cathode compartment VO_2^+; the cell reactions are

$$V^{2+} - e^- = V^{3+} \qquad \text{Anode}$$

$$VO_2^+ + 2H^+ + e^- = VO^{2+} + H_2O \qquad \text{Cathode}$$

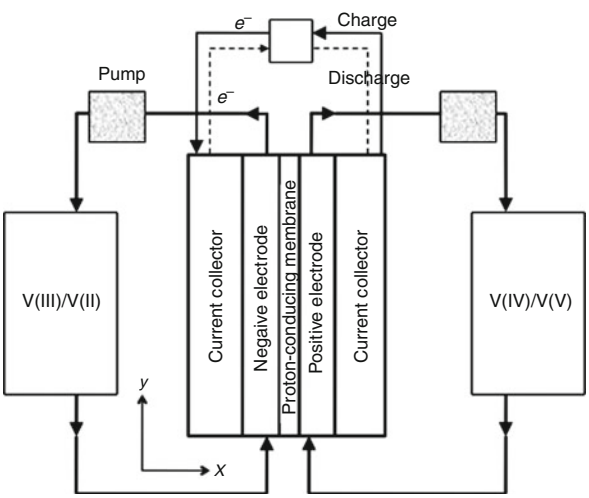

Battery Components, Active Materials for. Figure 22 Schematic of the all-vanadium flow-through battery

to take advantage of the 1.65 eV difference between the V(III)/V(II) and V(V)/V(IV) redox couples. Alternative couples include, for example, Fe^{3+}/Fe^{2+} and Cr^{3+}/Cr^{2+}. These cells can achieve 80–90% energy-storage efficiencies in large installations at a low cost per kWh. They promise a long cycle life, are relatively easy to maintain, and can be fully cycled without harm to the battery. However, in order to realize the commercial potential of these batteries, several challenges must be met, including development of electrodes resistant to oxidation in its electrolyte, membrane stability and prevention of redox crossover through the separator membrane while maintaining a fast H^+-ion transport across the membrane, easier flow across the current collectors, and scale-up optimization.

Future Directions

The Li-ion battery has already introduced the wireless revolution by powering the cell telephone and the laptop computer as well as their derivatives. Modest increases in anode capacity will improve the volume energy density for handheld electronic devices.

The Li-ion battery is also powering portable electric-power tools and small electric vehicles. However, its widespread application to the plug-in hybrid electric vehicle and the all-electric vehicle will depend on lowering the cost while increasing the driving range between recharges. To reach this target, it will be necessary to develop new cathode strategies. These strategies appear to depend on the development of a suitable solid electrolyte and sealants that can prevent crossover of different liquid electrolytes either side of the solid electrolyte.

Electrical-energy storage in batteries for the grid for increasing the efficiency of nuclear energy and for enabling the large-scale introduction of wind and solar energy will probably need the much larger capacities offered by flow-through batteries. In the interim, rebirth of the Na/S battery may provide some large-scale electrical-energy storage.

Realization of the great societal benefits to be derived from the new battery technologies has galvanized an extensive research activity that promises continued development.

Bibliography

Primary Literature

1. Winter M, Brodd RJ (2004) Chem Rev 104:4245–4269
2. Mennicke S (1992) In: Balkanski M, Takahashi T, Tuller HL (eds) Solid state ionics. North-Holland, Amsterdam, pp 3–15
3. Visco SJ, Nimon E, DeJonghe L, Katz B, Petrov A (2007) US Patent 2007/0037058
4. Aono H, Sugimoto E, Sadaoka Y, Imanaka N, Adachi G (1989) J Electrochem Soc 136:590–591
5. Armand MB (1986) Ann Rev Mater Sci 16:245–261
6. Croce F, Appetecci GB, Persi L, Scrosati B (1998) Nature 394:456–458
7. Zinck L, Borck M, Ripp C, Hambitzer G (2006) J Appl Electrochem 36:1291–1295
8. Dahn JR, VonSacken U, Juzkow MW, Al-Janaby H (1991) J Electrochem Soc 138:2207–2211
9. Whittingham MS, Jacobson AJ (eds) (1982) Intercalation chemistry. Academic Press, New York
10. Kim Y, Goodenough JB (2010) Chem Mater 22:587–603
11. Hert JT, Huang Q, McQueen T, Klimczuk T, Bos JWG, Viciu L, Cava RJ (2008) Phys Rev B 77:075119
12. Mizushima K, Jones PC, Wiseman PJ, Goodenough JB (1980) Mater Res Bull 15:783–799
13. Gupta R, Manthiram A (1996) J Solid State Chem 121: 483–491
14. Saadoune I, Delmas C (1992) Solid State Ionics 53:370–375
15. Ohzuka T, Makimura Y (2001) Layered lithium insertion material of LiNi1/2Mn1/2O_2: a possible alternative to $LiCoO_2$ for advanced lithium-ion batteries. Chem Lett 8:744–745
16. Thackeray MM, Kang SH, Johnson CS, Vaughey JT, Benedek R, Hackney SA (2007) J Mater Chem 17:3112–3125
17. Delmas C, Cognac-Auradon H, Cocciontelli JM, Ménétrier M, Doumerc JP (1994) Solid State Ionics 69:257–264
18. Thackeray MM, David WIF, Bruce PG, Goodenough JB (1983) Mater Res Bull 18:461–472
19. Sinha S, Murphy DW (1986) Solid State Ionics 20:81–84
20. Goodenough JB (1983) In: Wheat TA, Ahmad A, Kuriakose AK (eds) Progress in solid electrolytes. Energy, Mines and Resources, Canada, pp 53–76
21. Nanjundaswamy KS, Padhi AK, Goodenough JB, Okada S, Ohtsuka H, Arai H, Yamaki J (1996) Solid State Ionics 92:1–10
22. Manthiram A, Goodenough JB (1989) J Power Sources 26:403–408
23. Padhi AK, Nanjundaswamy KS, Goodenough JB (1997) J Electrochem Soc 144:1188–1194
24. Huang Y, Goodenough JB (2008) Chem Mater 20:7237–7241
25. van Gool W (ed) (1973) Fast ion transport in solids. North-Holland/American Elsevier, Amsterdam/New York, pp 559–590
26. Ji X, Lee KT, Nazar LF (2009) Nature Mater 8:500–506
27. Lu Y, Goodenough JB (2011) J Mater Chem. doi: 10.1039/c0jm04222f
28. Debart A, Paterson AJ, Bao J, Bruce PG (2008) Angew Chem Int Ed 47:4521–4524

29. Lu Y-C, Xu Z, Gasteiger HA, Chen S, Hamad-Schifferli K, Shao-Horn Y (2010) Platinum-gold nanoparticles: a highly active bifunctional electrocatalyst for rechargeable lithium-air batteries. J Am Chem Soc 132:12170–12171. doi:10.102/ja1036572
30. Rychick M, Skyllas-Kazacos M (1988) Characteristics of new all-vanadium redox flow battery. J Power Sources 22:59–67

Books and Reviews

Balbuena PB, Wang Y (eds) (2010) Lithium ion batteries: solid-electrolyte interphase. Imperial College Press/World Scientific, London/Singapore
Bockris JO'M, Reddy AKN (1970) Modern electrochemistry. Plenum, New York
Bruce PG (ed) (1995) Solid state electrochemistry. Cambridge University Press, Cambridge
Goodenough JB, Abruña HD, Buchanan MV (eds) (2007) Basic research needs for electrical energy storage. Office of BES, DOE, Washington http://www.sc.doe.gov/bes/reports/files/EES_rpt.pdf
Hagenmuller P, Van Gool W (eds) (1978) Solid electrolytes. Academic, New York
Huggins RA (2009) Advanced batteries. Springer, New York
Maier J (2004) Physical chemistry of ionic materials. Wiley, Chichester
Rieger PH (1994) Electrochemistry, vol 2. Chapman and Hall, New York
Wakihara M, Yamamoto O (eds) (1998) Lithium ion batteries. VCH, Weinheim
Zhang SS (ed) (2007) Advanced materials and methods for lithium-ion batteries. Transworld Research Network, Trivandrum

Battery Technologies

Ramakrishnan Mahadevan[1], Mohit Chhabra[2], Puneet Pasrich[3], Frank Barnes[3]
[1]Telecommunications, University of Colorado, Boulder, CO, USA
[2]Electrical Engineering, University of Colorado, Boulder, CO, USA
[3]Electrical, Computer, and Energy Engineering Department, University of Colorado, Boulder, CO, USA

Article Outline

Definition of the Subject
Introduction
Basic Characteristics of Batteries
Electrical Modeling for Batteries
Lead Acid Batteries
Nickel-Cadmium Battery
Nickel Metal Hydride Batteries
Lithium-Ion Batteries
Metal–Air Batteries
Zinc Bromine Battery
Supercapacitors
Recommendations for Future Work
Bibliography

Definition of the Subject

The demand for high performance and long life storage systems has lead to numerous research initiatives, aimed at the development of such systems. Developmental paths are aligned with the requirements of the applications of these systems. A detailed understanding of technical characteristics and cost considerations is provided in this paper for various battery chemistries: contemporary, vintage, and prospective. A clear understanding of battery characteristics is essential for guiding the selection of such batteries. Indeed, because of the critical functions fulfilled by batteries as well as the substantial costs of advanced batteries, a realistic appraisal of candidate battery performance and costs against requirements is key to judging the prospects of new applications such as EV, HEV, and plug-in hybrid electric vehicles (PHEV). Although electric vehicles (EVs) have been around since before 1900 the limitations of the batteries to drive them have not enabled them to compete in the general consumer's market with the internal combustion engine. Automotive parts are limited by space and weight. Therefore EVs and hybrid electric vehicles (HEVs) require a battery with high energy density. Specific energy is defined as the energy per kilogram of the battery while energy density is the energy per unit volume. Early designs (1990–1995) of lithium-ion batteries only had a specific energy of 0.2 kWh/kg. EVs also require a battery with high power output for large power draw, such as quick acceleration. The General Motors EV1 had a battery pack weighing almost 600 kg while the car weighed 1,350 kg. The battery would then account for more than 44% of the car's weight. A marked improvement in energy cell density of batteries was required for practical EVs.

Introduction

In this paper, the first section covers the relationship between the internal resistance of the cell, maximum power output, energy efficiency in charging and discharging, and reduction of cell heating. This is followed by a review of the characteristics of lead acid, nickel metal hydride, lithium-ion batteries, and supercapacitors.

Recent advances in power electronics provide competitive performance for electric cars so they provide the necessary acceleration for wide spread adoption [1]. However batteries still lack the energy density of gasoline or diesel fuels and thus cannot compete in terms of the overall range that can be driven between recharging. Additionally, recharging may be slow. However, ongoing research and improvements in manufacturing may reduce both energy density limitations and costs. Concerns about greenhouse gases and other air pollutants are the other driving factors for the renewed interest in EVs and HEVs, which may reduce or eliminate the emission of NO_x, CO_2, and hydrocarbon pollution from mobile vehicles depending on how the electricity used to charge the battery was generated. EVs and HEVs also reduce noise levels when running on electric mode. In 2009, 1.6 million HEVs were registered in the USA [2].

This section concentrates on a variety of battery technologies that have shown significant promise for long life and high performance. A brief, generic list of battery characteristics are provided in section "Electrical Modeling for Batteries". Section "Lead Acid Batteries" introduces various types of lead acid battery chemistries. Section "Nickel Metal Hydride Battery" introduces the nickel metal hydride chemistry, while lithium-ion is discussed in section "Lithium-Ion Batteries". The upcoming technology of supercapacitors is also introduced and a comparison to conventional electrochemical counterparts is provided.

This entry first gives a general overview of characteristics of batteries, followed by the electrical modeling used for batteries in EVs and concludes by presenting the different battery technologies used today.

Basic Characteristics of Batteries

An electrical battery is a power source composed of one or more electrochemical cells which convert stored chemical energy into electrical energy. In this section, rechargeable batteries which can be used multiple times is discussed. A battery is composed of one or more electrochemical cells, each consisting of two electrodes and one (or two) electrolyte-containing anions and cations.

Figure 1 depicts the typical electrochemical cell voltage behavior during charging (labeled "Charge curve V") and discharging (labeled "Discharge curve V"). Cell voltage drops and rises during discharging and charging respectively, in proportion to the cell's internal voltage. The difference between the terminal open-circuit voltage and the discharge and charge voltage is attributed to the cell's internal resistance. An ideal cell provides constant terminal voltage until empty. The internal resistance of real cells prevent ideal performance during discharge resulting in lower terminal voltage.

The essential characteristics of batteries are maximum power output, charging/discharging efficiency, and temperature effects. These are key factors to be considered when designing or choosing batteries for particular applications. These characteristics are further elaborated for each battery in the device specific sections of the paper. The basic definitions are shown below.

Maximum power output: A lower limit is set for each cell's voltage. The maximum dischargeable current value is determined such that the cell voltage does not fall to this limit. The maximum current is determined as

$$I_{max} = (\text{Open Circuit Voltage} - \text{Lower Limit Voltage})/\text{Internal Resistance}$$

Then, maximum power output of a cell can be calculated as $P_{max} = I_{max} \bullet$ (Open Circuit – Lower Limit Voltage). High power output requires low internal cell resistance.

Charging/discharging efficiency: Electrical energy transferred during a charging/discharging cycle can be computed as

$$E = \Delta Q \bullet V$$

where ΔQ is the transferred charge and V is the terminal voltage at that time.

In Fig. 1, the *area* between the charge curve and the horizontal axis is the total electrical energy transferred to the battery. Accordingly, the area between the discharge curve and horizontal curve is the total energy

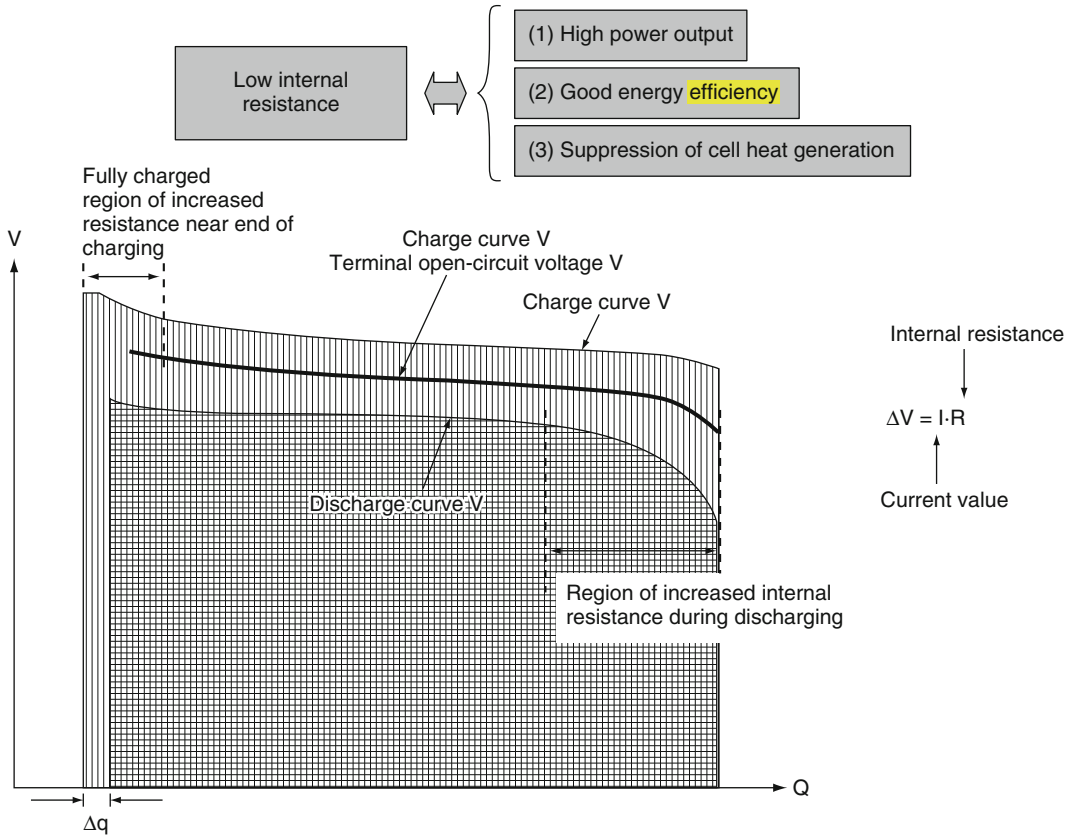

Battery Technologies. Figure 1
Cell voltage profile and internal resistance in charging and discharging operations with respect to cell charge Q [3]

drained from the battery. Battery efficiency is a ratio of discharge to charge energy values. It is imperative to reduce the difference between these two curves to improve battery efficiency.

Temperature effect: Charging and discharging cycles can cause a cell's temperature to rise. For lithium-ion cells, operating temperatures above 50°C can lead to cell degradation. Ozawa [4] attributes the difference in charging and discharging curves in Fig. 1 to heat lost due to different operating temperatures. To suppress this difference, the cell's internal resistance must be reduced.

Electrical Modeling for Batteries

A simple model of a battery can help alleviate issues of understanding of a battery's behavior. The simplest electrical equivalent model of a cell is a voltage source with a resistor in series, as shown in Fig. 2a. This is the internal resistance of the cell. Davide [5] provides corresponding voltage and current response curves for each proposed model.

A more complex model is described in Fig. 2b. This model emulates the behavior of a battery when instantaneously loaded. The initial voltage drop across battery terminals is small, due to R_1. The voltage then drops exponentially to the level of both resistances with a time constant $T = R_2 \bullet C_2$ (~1 min). This phenomenon is known as relaxation.

A variation on 2b is 2c, where the time constant $T = R_3 \bullet C_3$ is ~1 ms. This model correctly emulates AC impedances on the order of 1 kHz. This property can however be misleading to the user since such impedances are usually measured with no load by the manufacturer. The user may also misread this impedance as the cell's DC resistance. Figure 2(d) combines 2(b) and 2(c) and thus equally satisfies both the manufacturer and the user.

Internal resistance of a cell results from a series combination of resistances due to bulk metal, chemical processes, and terminals. Varying loads can have dynamic effects on these properties of a battery. Thus the battery's internal resistance (R_i) also has dynamic properties. Davide explains that internal resistance can vary with the following battery characteristics:

State of charge:	R_i is high for both high and low state of charge levels
Temperature:	R_i is higher at cold temperatures
Current:	R_i is higher at higher currents when charging (compared to the same current when discharging)
Usage:	R_i increases over time with cell usage

Figure 3 shows how the internal resistance of a lithium iron phosphate ($LiFePO_4$) battery varies versus the above four battery characteristics.

For preliminary research purposes, it is entirely possible to create a generic model and vary key parameters to simulate the performance of various battery chemistries. Table 1 provides a list of key parameters for three batteries chemistry as well as three types of supercapacitors.

Detailed reviews of various battery chemistry compositions are provided in the following sections. We consider not only relevant chemical reactions, but also applications, cost, and efficiency concerns associated with every chemistry type. The following section details lead acid batteries, their cell construction, and the electrochemistry, for several types of lead acid batteries used in EVs and their characteristics.

Lead Acid Batteries

Lead acid (PbA) batteries are inexpensive and have characteristics somewhat suitable for energy storage in EVs. Design is possible for short, high-rate discharges or for bulk energy storage. These batteries are commonly used to power the starter motor of conventional internal combustion engines.

Lead acid batteries are classified into two broad categories, traditional vented lead acid (VLA) batteries and valve-regulated lead acid (VRLA) batteries. The latter have dominated the stationary battery market over the past 20 years [1]. VRLA batteries have immobilized electrolyte and a means to recombine

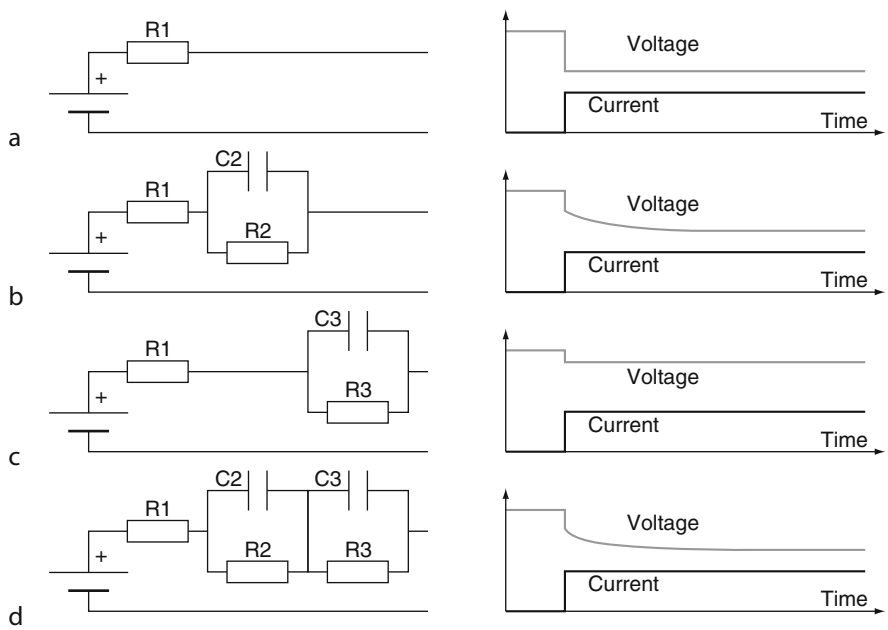

Battery Technologies. Figure 2
Electrical modeling schemes for a battery [5]

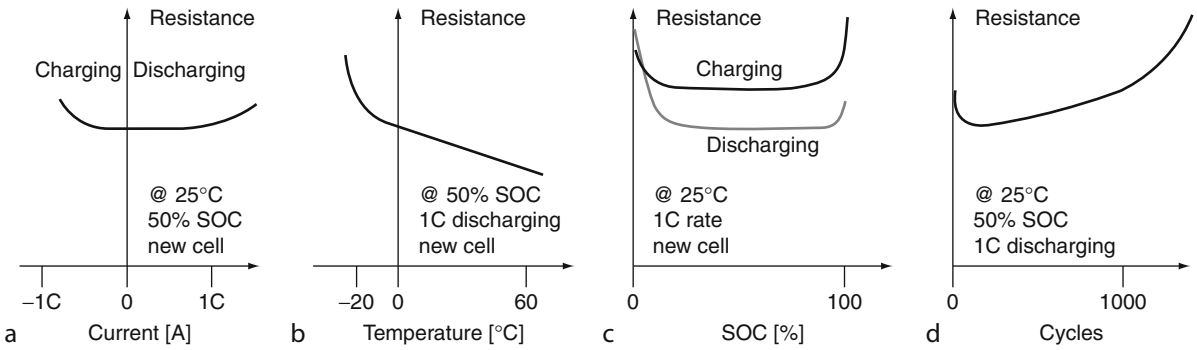

Battery Technologies. Figure 3
Internal resistance variation for a $LiFePO_4$ battery [5]

Battery Technologies. Table 1 Performance parameters

	Lead acid	Nickel metal hydride	Lithium-ion	Super capacitors		
Electrolyte	$H_2SO_4 + H_2O$	KOH	$LiPF_6$	Aqueous electrolyte	Organic electrolyte	Aqueous electrolyte
Anode	PbO_2	M (Metal)	Graphite	Carbon	Carbon	Metallic
Cathode	Pb	$Ni(OH)_2$	$LiMn_2O_4$	Carbon	Carbon	Metallic
Cell voltage (V)	2.4	1.2	4.0	1	3	1
Specific energy (Wh/kg)	35	50–80	250–400	0.2–1.3	3–6	1
Relaxation time constant (s)	5	2	1	N/A	N/A	N/A
AC impedance time constant (s)	10^{-1}–10^{-3}	10^{-1}–10^{-3}	10^{-3}	N/A	N/A	N/A
Recommended operating temperature (°C)	25	−20 to 50	50	−25 to 85	−40 to 85	−30 to 70

charged gas, thus conserving water in the cell. They are typically smaller than their vented counterparts and require less maintenance. Most of the VLA and VRLA batteries use pasted plate construction, in which a mixture of active materials is pasted onto lead alloy grids. The characteristics of the final battery are heavily influenced by the alloy composition. Tubular plate construction is also quite common, in which the active material is held in non-woven fibrous tubes with a center conductor of lead alloy.

Lead acid batteries have less energy density and specific energy as compared to the more recent lithium-ion and NiMH batteries but these batteries generally have high ampere rating. Since lead acid batteries do not have the deep cycling capability and energy density compared to other batteries used in EVs, they are being replaced by NiMH and Li-ion batteries for traction purposes. However earlier EVs used lead acid batteries like the GM EV1 (Generation 1). The Delphi 704 VRLA-Prismatic battery has an ampere rating of 53 Ah and a specific energy of 35.3 Wh/kg. These batteries have a good cycle life of 15,000–30,000 cycles. In the following section, the cell construction and electrochemistry of lead acid batteries are discussed [4].

Cell Construction and Electrochemistry

All lead acid designs share the same basic chemistry. The positive electrode (cathode) is formed of porous lead

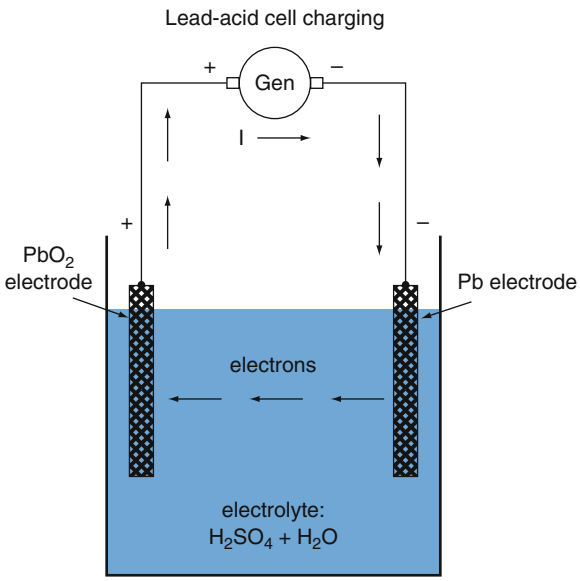

Battery Technologies. Figure 4
Charging lead acid cell schematic [3]

dioxide (PbO_2) while the negative electrode (anode) is composed of sponge lead (Pb). Sulfuric acid (H_2SO_4) in water serves as gelled electrolyte between the two electrodes. Lead dioxide at the cathode is supported by a thin lead grid. Figure 4 provides a cross-sectional view of a standard lead acid battery cell.

Pure lead is generally too soft to be used as a plate material and usually requires addition of an alloy. Alloy candidates vary and are responsible for positive plate subtypes such as lead-antimony, lead calcium, and pure lead. Lead-antimony cells are recommended for applications requiring very long life and discharging to depths greater than 20% of rated capacity. Pure lead cells are recommended for float and shallow cycling service where average discharge depth is less than 20%. Finally, pure lead alloy cell types are used when very low charged stand loss is a requirement in the application and occasional deep cycles are expected [6].

During charging, as the cell approaches full charge, a majority of the $PbSO_4$ is converted to Pb and PbO_2. Beyond this point and under high charging voltages, cell voltage becomes greater than the gassing voltage (about 2.39 V per cell) and the overcharge reactions begin. This results in the electrolysis of the water contained in the electrolyte, and the production of hydrogen and oxygen. In sealed lead acid cells, this reaction is controlled to minimize hydrogen evolution and loss of water by recombining evolved oxygen with the negative plate.

The discharge chemical reactions are as follows:

$$\text{Positive: } PbO_2 + 4H^+ + SO_4{}^{2-} + 2e^- \rightarrow PbSO_4 + 2H_2O$$

$$\text{Negative: } Pb + HSO_4{}^- \rightarrow PbSO_4 + H^+ + 2e^-$$

$$\text{Overall: } PbO_2 + Pb + 2H_2SO_4 \leftrightarrow 2PbSO_4 + 2H_2O$$

As the cell discharges, lead at the anode reacts with hydrogen sulfate ions to form lead sulfate, along with hydrogen ions and electrons. These electrons then travel through the external circuit. Note that sulfuric acid is a strong electrolyte and breaks down into hydrogen and hydrogen sulfate ions even before being placed in the battery. This breakdown is independent of the battery plates. At the cathode, lead dioxide is reduced by the two electrons released at the anode and the lead ion then reacts with sulfate to form lead sulfate along with water. Discharge continues until all of the sulfuric acid is converted to water. Discharging is an exothermic process and charging is an endothermic process.

As discharging progresses, the concentration of the sulfuric acid electrolyte falls. As a result, the no-load (open circuit) voltage of a lead acid cell varies during a cycle from approximately 2.1 V at the top of charge to approximately 2 V at the bottom of discharge. In addition, the decreasing concentration of electrolyte leads to an increasing internal resistance that reduces overall efficiency of the cell. All these factors come together to signify for a given current, the terminal voltage of a lead acid cell is lower at the end of discharge than at the beginning [3].

Lead is insoluble and stays at either plate during charging or discharging. This property allows recharging of the battery. In contrast, non-rechargeable batteries contain reaction products that either convert to an insoluble precipitate or are lost as gas.

Two side reactions can occur in lead acid cells, primarily at the top of charge: hydrogen production from the lead negative plates and oxygen generation from the lead dioxide positive plate. In flooded cells, these side reactions lead to a loss of water that must be made up periodically. The loss of water is particularly high during overcharge and equalization of batteries of

cells, which must be performed each full charge and once every 10 or 20 cycles, respectively. Overcharge and equalization both involve charging the lead acid cells somewhat beyond the ampere-hour capacity that has been discharged, so as to ensure that all the electrodes of all the cells of the battery are fully and equally recharged [3].

The next section gives a brief description of the different types of lead acid batteries.

Types of Lead Acid Batteries (by Electrode Material)

Lead Calcium Batteries Lead acid batteries with electrodes that are modified by the addition of calcium are more resistant to corrosion, overcharging, gassing, water usage, and self-discharge. All of these factors shorten the life of a battery. The increased resistance increases the battery life of lead calcium batteries. Additionally, they have a larger electrolyte reserve area above the plates, higher cold cranking ampere ratings, and require little maintenance [4].

Lead-Antimony Batteries Lead acid batteries with electrodes modified by the addition of antimony improve the mechanical strength of electrodes which is important for EV and deep discharge applications. Water loss and the internal heat are also minimized. They have a longer life than lead calcium batteries. These batteries are also easy to recharge when they are completely discharged and are comparatively less expensive compared to other types of lead acid batteries. However, lead-antimony batteries have a higher self-discharge rate typically 2–10% per week, whereas lead calcium batteries have a self-discharge rate of 1–5% per month [4].

Advanced Lead Acid Batteries In the early part of the decade, the lead acid battery community formed the Advanced Lead–Acid Battery Consortium (ALABC) in a concerted effort to make electric vehicles a reality by overcoming the shortcomings of the VRLA battery. Much has been achieved by the global research and development program of the ALABC [7].

The ALABC originally developed advanced lead acid batteries as a replacement for the more expensive NiMH batteries used in hybrid electric vehicles. These advanced lead acid batteries exhibit better performance as compared to VRLA batteries, in terms of stationary energy storage [8]. Some of the results of research in advanced lead acid batteries are discussed below.

Swelling of the positive active material in the direction normal to the plane of the plate remains a serious concern for VRLA batteries. The tendency for the positive active material to expand with repeated deep cycling is, however, beyond dispute. Experimental work at the University of Brno demonstrated a clear correlation between loss of capacity with cycling and increase of active-material resistance which is presumed to arise as a result of swelling [7].

An in-depth study of positive-grid alloys demonstrated that the introduction of tin brings additional benefits in the form of enhanced corrosion resistance and reduced electronic resistance. Positive grids that contain no antimony but have 1–1.5% by weight of tin do not suffer expansion in the plane of the plate and as a result of the lower corrosion rate, it is possible to contemplate a substantial reduction in grid thickness and weight in order to increase the specific energy [7].

Also, the ALABC development work discovered that adding a small amount of carbon (2–4% by weight) to the negative active material of the electrode minimized negative plate sulfation and enhanced VRLA battery cycling performance in partial-state-of-charge cycling. Battery developers/suppliers who are currently involved in research and development of advanced lead acid batteries include East Penn, North Star, Exide technologies, Axion Power, and Furukawa [8].

Types of Lead Acid Batteries (by Construction)

Flooded/Vented Lead Acid Batteries These batteries have electrodes or plates which are immersed in the electrolyte. The level of the electrolyte reduces as a result of charging and the gases formed which are vented to the atmosphere, so distilled water is added to bring the electrolyte back to its initial level. The most familiar example of a flooded lead acid cell is the 12 V automobile battery.

Valve Regulated Lead Acid (VRLA) Batteries VRLA batteries are also called sealed lead acid (SLA) batteries. They are designed to prevent electrolyte loss through evaporation, spillage, and gassing, which in turn prolongs the life of the battery and reduces maintenance cost. Instead of simple vent caps on the cells to let gas

escape, VRLA batteries have pressure valves that open only under extreme conditions. Hydrogen and oxygen are generated by galvanic action of the battery during charging. VRLA batteries need an electrolyte which reduces gassing by impeding the release of these gases to the atmosphere. A catalyst is usually involved that causes the hydrogen and oxygen to recombine into water. This system is called a recombinant system. Since acid electrolyte spillage is eliminated, these batteries are safer [4]. There are two categories of VRLA batteries.

Types of VRLA

AGM (Absorbed Glass Mat) Batteries AGM batteries are similar to VRLA batteries. A boron silicate fiberglass mat acts as a separator between the electrodes and absorbs the free electrolyte. The main purpose of this type of battery is to recombine the hydrogen and oxygen generated during the charging process. The fiberglass mat absorbs and immobilizes the electrolyte, but keeps it in a liquid rather than a gel form. In this way, the electrolyte is more readily available to the plates allowing faster reactions between the electrolyte and the plate material which gives higher charge/discharge rates as well as deep cycling capability. AGM batteries are very robust and can withstand severe shock and vibrations. Also, the self-discharge rate is low, typically 0.25–0.75% per month. They are also called "starved electrolyte" or "dry" batteries because the fiberglass mat is 95% saturated with the electrolyte and there is no excess liquid [4].

Gel Cell The gel cell is similar to the AGM battery, except that the electrolyte is gelled to immobilize it. The electrolyte is mixed with a silica compound to create the gelled solution. It uses an alternative recombinant technology to promote recombination of the gases produced during charging. It also reduces the possibility of spillage of the electrolyte. Charging rates are limited, because overcharging may cause excess of gases to be released causing damage. The gel cell cannot be fast charged on a conventional automotive charger since it can cause permanent damage [4].

Choosing a Battery

The ideal EV battery should have a constant output voltage at any value of current drawn over the entire state-of-charge (SOC) range and it should also accept high charge rates at the same voltage. No battery has such ideal characteristics but the suitability of a battery for EV use can be determined by the ratio of charging voltage to discharging voltage over the range of SOC and current [9].

Given below are the important factors to consider while choosing a battery for EV use.

Power Battery power performance is generally specified by manufacturers as W/kg at either 2/3 or 1/2 of the open circuit voltage. This ignores the ratio of the terminal voltage under load to that during charge or regenerative braking which is the relevant parameter for EV applications. A more useful figure of merit for comparing the power performance of EV batteries is the power density (W/kg) at 75% end-of-charge voltage (V_{eoc}). For example, if the battery voltage of an EV drops below 75% of V_{eoc} during acceleration, it means that the battery is operating at low cycle efficiency. Another consideration is the cost of the vehicle drive train which is proportional to the product of the maximum voltage rating and the current rating. A low power battery needs more expensive drive train components to achieve a given level of performance because it needs higher current to extract the same power at a lower voltage. A high power battery not only increases vehicle performance but it reduces the cost of the motor and electronics for equivalent performance.

Energy Energy capacity of an EV battery determines the vehicle range. The two parameters which are commonly used to specify energy capacity are specific energy and energy density. Reducing energy consumption is often a better way to increase EV range than increasing battery capacity. EV batteries cannot yet match the energy density of gasoline but provide power to exceed the acceleration of conventional vehicles. One of the unique features of EVs is the capability to provide high peak power and excellent acceleration without sacrificing operating efficiency [9]. The Tesla Roadster sports car demonstrates this by operating at 180 Wh/mile in normal driving and offering acceleration from 0 to 60 mph in 3.7 s, which is quicker than a gasoline-powered Mercedes-Benz SLR McLaren. The first-generation EV1 used Delphi's valve-regulated lead acid batteries, which is capable of operating at 164 Wh/mile. Nickel metal hydride batteries (NiMH)

batteries (See section "Nickel-Cadmium Battery") have twice the energy density and specific energy compared to lead acid batteries. An EV fitted with a NiMH battery which is of the same size and weight as a lead acid battery has twice the range. However, due to power considerations, it is not necessary that an EV could be built to match the range of a lead acid battery powered EV using a NiMH battery with half the size and weight [9].

Cost Although lead acid batteries have less energy density and specific energy and are bulkier compared to NiMH and lithium-ion batteries, they are typically inexpensive. Today, a lead acid battery pack for an EV costs $215/kWh, a NiMH battery costs $350/kWh, and a lithium-ion battery costs $400/kWh [9]. The lower cost of the lead acid battery makes it an affordable technology and also decreases the overall cost of EVs. Axion Power, a firm based in Pittsburgh, Pennsylvania, has come up with a new technology called lead-carbon battery which is derived from traditional lead acid battery technology. Axion Power has managed to convert a pickup truck to run on a pack of the lead-carbon battery for around $8,000 [10]. If further cost reductions are achieved in the production of batteries, then EV pricing can become competitive with conventional vehicles.

Temperature Effects on Batteries Batteries function because of electrochemical reactions (charging and discharging) taking place in the cell. These chemical reactions are dependent on temperature. Nominal battery performance is usually specified for working temperatures between 20°C and 30°C. However the actual performance can deviate substantially if the battery is operated at higher or lower temperatures. The operation of any battery generates heat due to the I^2R losses as current flows through the internal resistance of the battery whether it is being charged or discharged. This is also known as electrical heating or Joule heating. During discharge, since the total energy within the system is fixed, the temperature rise is limited by the available energy. Another factor which affects the performance of a battery is the ambient temperature. If the ambient temperature is higher than the temperature of the battery, the battery gains heat from the surrounding and if the ambient temperature is lower, the battery losses heat to the surrounding. The difference in the ambient and the optimal operating temperature of a battery reduces its performance. Overheating may also be caused in batteries because of highly exothermic reactions, which generate a lot of heat and may ultimately damage the batteries [4].

Lead acid batteries are exothermic during charging, which makes their temperature rise dramatically. If the temperature exceeds beyond a limit, the battery may be damaged. Also, being a galvanic cell, its internal resistance is temperature dependent. Internal temperature decreases as the temperature rises due to the increase in electron mobility. The cell is very inefficient at low temperatures but the efficiency improves at higher temperatures due to the lower internal impedance and also because of the increased rate of chemical reactions. However, the lower internal resistance also causes the self-discharge rate to increase. Additionally, the cycle life deteriorates at high temperatures. Some form of heating and cooling is therefore required to maintain the battery within a specific temperature range to achieve optimum performance [4].

Life Battery life represents an important parameter in battery performance that affects customer satisfaction and overall cost. Battery life depends mainly on the number of cycles. Technical factors such as temperature control, charging procedures, and exposure to abusive conditions also play an important role in determining the battery life. Lead acid batteries in EVs may last 15,000–30,000 cycles if used regularly. However, they start deteriorating after 2 years regardless of the kind of use. Lead acid batteries respond well to battery management systems that control temperature and maintain SOC equalization. A factor related to battery life is the battery residual value. Although virtually all EV batteries are recycled for economic and environmental reasons, EV batteries may retain value greater than their salvage value after their useful life as a traction battery is complete. AC Propulsion regularly sells spent traction modules as starter batteries with a 2-year warranty for $25 or about $50/kWh. These modules are retired because their capacity is diminished by 30% or more, but they serve well as starter batteries [9].

Table 2 below shows some typical specifications of VRLA batteries used in EVs.

Battery Technologies. Table 2 Specifications of VRLA batteries in EVs [11, 12]

Electric vehicle	1998 Ford Ranger EV	GM EV 1, first model
Manufacturer	Delphi	Delphi
Number of modules	39	26
Weight of module (kg)	19.3	18.8
Nominal module voltage (V)	8	12
Nominal system voltage (V)	312	312
Nominal capacity (Ah)	60 (100% capacity)	53 (50% capacity)
Specific energy (Wh/kg)	23.7–25.2	26.3–31.9
Efficiency (Wh/mile)	237–356	115–164

Lead Acid Battery Circuit Model

Consider Fig. 5 as a lead acid cell model. We construct this circuit using PSpice software. Consider the cell to provide 2 V nominal voltage, 10 Wh capacity, round-trip efficiency of 90%, and 70% initial state of charge. Here, available energy during operation is computed as

$$\mathrm{SOC(t)} = \mathrm{SOC_{initial}} + \frac{1}{\mathrm{Capacity(Wh)}}\int \frac{kV_1 I_{\mathrm{bat}}}{3600}\,\mathrm{dt}$$

where k is cell efficiency, V_1 is cell voltage, and I_{bat} is cell current. During discharge, current flows in the opposite direction when compared to charging, leading to a minus sign before the integral. Division by 3,600 is needed to ensure that cell capacity is in units of watt-hours, Wh. Alternate charging and discharging operation is conducted by applying AC current I_{AC} at 4 A, 100 Hz, as shown in Fig. 16. Resistor R_1 is chosen arbitrarily high to ensure there is no voltage drop at the cell's output terminals.

Figure 6 shows the state of charge (SOC) of the cell.

Note that the Y-axis provides state of charge as a percentage. Figure 7b provides cell voltage V_1, whereas I_{AC} is shown in 7a.

Note that in addition to the nominal 2 V, cell voltage is a function of state of charge of the cell. For example, a certain degree of overvoltage can occur with high state of charge. A 70% state of charge leads to a cell (over) voltage of 2.1 V in 7b.

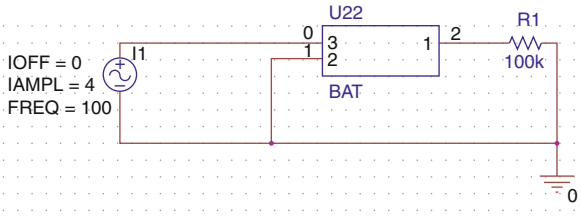

Battery Technologies. Figure 5 Lead acid cell model using PSpice

When I_{AC} is positive, current travels into the cell, simulating charging. This is evident in Fig 18b where V_1 drops while I_{AC} increases in the positive direction. Negative I_{AC} implies cell discharge, with V_1 above the nominal 2 V. An immediate advantage of lithium-ion batteries is their diversity in operation. Figure 19 shows only a few possible chemical combinations.

Nickel-Cadmium Battery

The nickel-cadmium battery commonly abbreviated as NiCd battery is a type of rechargeable battery which works by oxidizing nickelic hydroxide ($Ni(OH)_2$) into nickelous hydroxide (NiOOH) and has metallic cadmium as electrodes. The charge/discharge reaction can be given as follows:

$$2Ni(OH)_2 + Cd(OH)_2 \rightleftarrows 2NiOOH + Cd + H_2O$$

The features of this battery are that the electrolyte does not take part in any of the chemical reactions and the active materials are insoluble in the electrolyte. Nickel-cadmium batteries have a reputation for their robustness, reliability, and service life. They can also operate under severe weather conditions, with operating temperatures ranging from −40°C to +60°C (because the electrolyte has a very low freezing point), excellent cycling capability (up to 2,000 cycles at 80% depth of discharge), long storage life, and low or zero maintenance [10, 11].

NiCd batteries have been used extensively in consumer electronics and power tools. In the recent past, NiCd batteries have also been used in electric vehicles, an example being the Peugeot 106 electric, which used NiCd batteries manufactured by SAFT [12].

Nickel-cadmium cells have a nominal cell potential of 1.2 V. This is lower than the 1.5 V of many popular primary cells, and consequently they are not

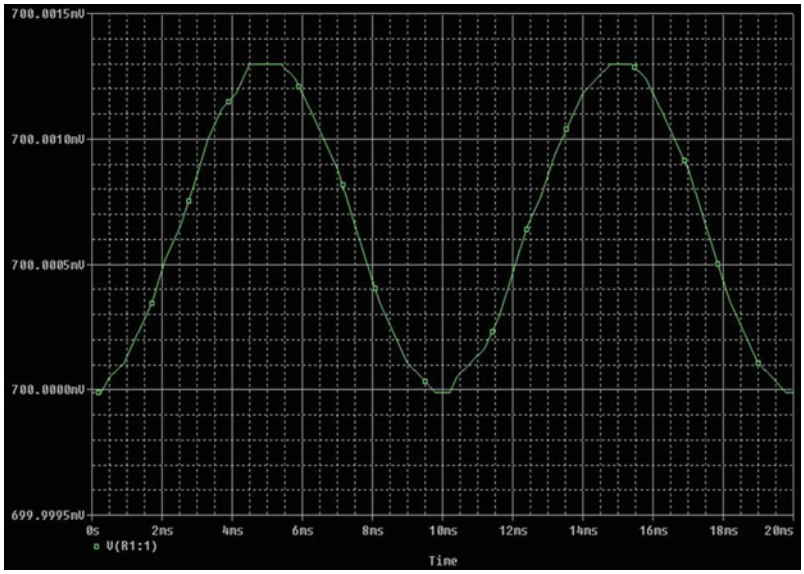

Battery Technologies. Figure 6
Cell state of charge

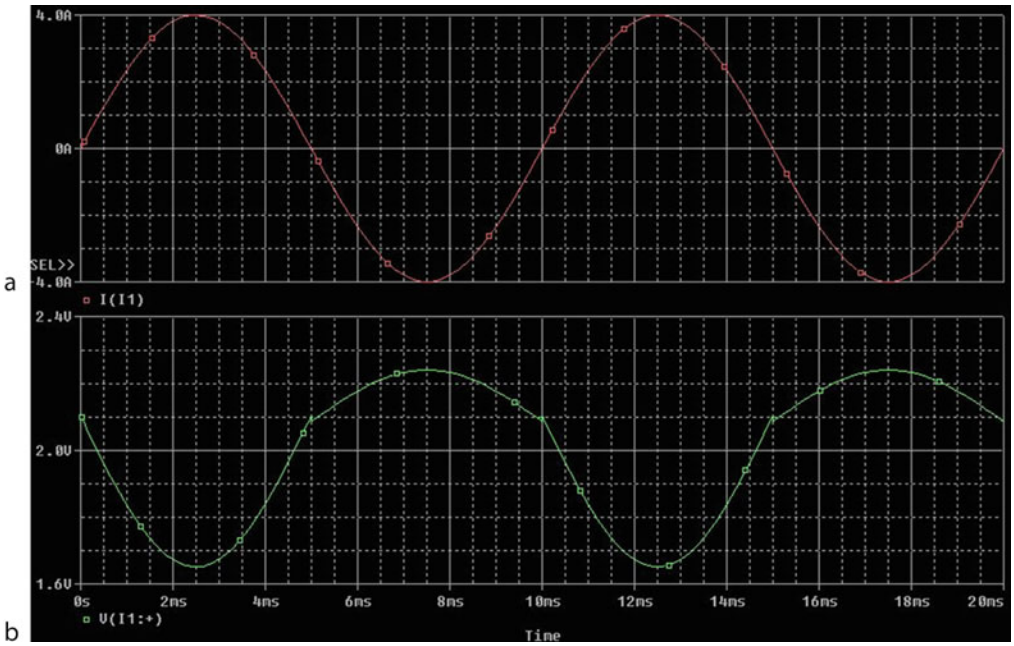

Battery Technologies. Figure 7
Applied AC current and cell voltage

appropriate as a replacement in all applications. NiCd batteries have an energy density of 40–60 Wh/kg, which is greater than that of lead acid batteries, but less when compared to NiMH and Li-ion batteries [14].

Advances in battery-manufacturing technologies throughout the second half of the twentieth century have made batteries increasingly cheaper to produce; about 1.5 billion NiCd batteries were produced

annually up until 2000. NiCd batteries never became widely used as a replacement for lead acid batteries in the areas where those batteries dominate, mainly because of the toxic nature of the battery and the reduction in its capacity as the battery ages. However, NiCd batteries had an overwhelming majority of the market share for rechargeable batteries in consumer electronics up until the mid-1990s [10].

Nickel Metal Hydride Batteries

Nickel metal hydride (NiMH) batteries were first developed in the late 1980s and ever since have been used in portable electronic devices like camcorders, power tools, and cell phones. NiMH batteries have high storage capacity and relatively high ramp rates. They have succeeded lead acid batteries owing to higher number of cycles and higher energy density [14]. A study by EPRI in 2004 showed that NiMH batteries are acceptable for full-function EVs, city EVs, and plug-in hybrid electric vehicles (PHEVs) [8].

Although the technology was largely driven by military and government research in its earlier days, recently, significant contributions have been made by EV manufacturers. Applications of NiMH EV batteries include all PHEVs manufactured by General Motors, Honda, Ford, Toyota, and the Vectrix scooter, among others. The town of Nice, France, now operates its low floor tram, manufactured by Alstom using NiMH batteries. Honda's humanoid prototype robot ASIMO is another application.

Nickel Metal Hydride Cell Construction and Chemistry

The basic representation of a NiMH cell is shown in Fig. 8. The positive electrode of a NiMH cell consists of a spongy mass of nickel hydroxide $Ni(OH)_2$. During charge, the positive electrode releases hydrogen into the electrolyte, which in turn combines with hydroxide (OH^-) ions. This reaction results in nickel oxyhydroxide (NiOOH) on the positive electrode and water (H_2O) in the electrolyte plus one free electron, e^-.

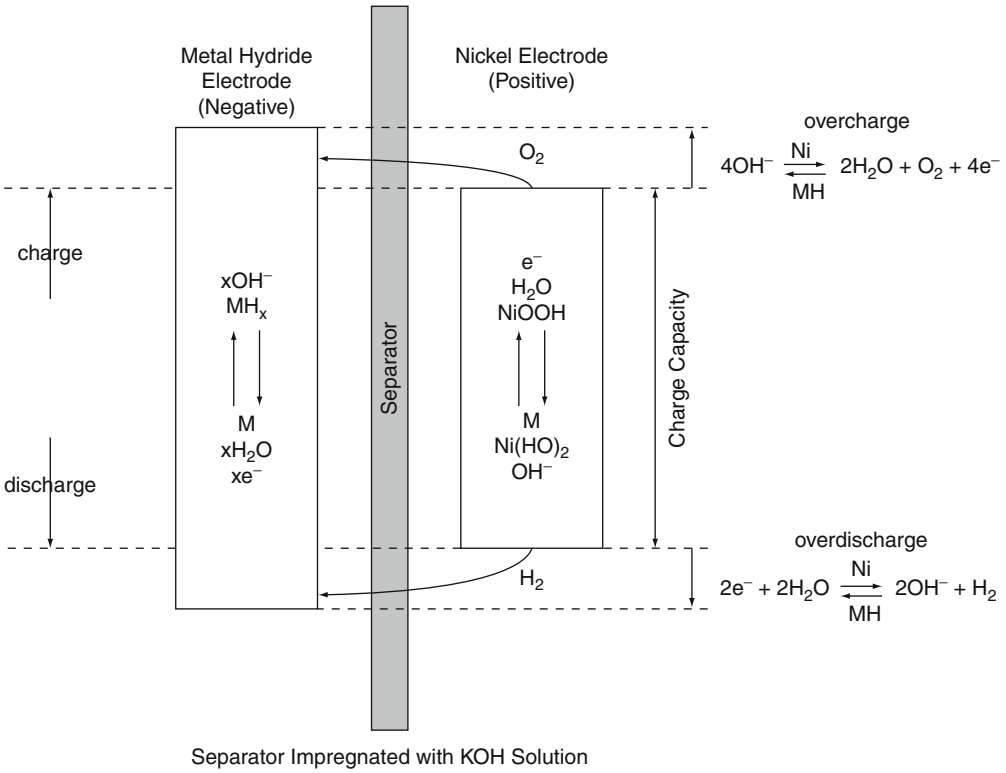

Battery Technologies. Figure 8
Schematic representation of a NiMH cell [7]

The equation for the positive electrode can be given by:

$$Ni(OH)_2 + OH^- \underset{\text{discharge}}{\overset{\text{Charge}}{\rightleftarrows}} NiOOH + H_2O + e^- \quad (1)$$

The negative electrode contains a metal alloy–hydride complex. In an exothermic reaction, the water (H_2O) from the electrolyte combines with the free electron to form metal hydride (MH) and hydroxide (OH^-). The metal alloy absorbs and desorbs the hydrogen, allowing the electrochemical reaction to occur without producing hydrogen gas. Equation 2 shows the net chemical reaction that occurs at the negative electrode during charge and discharge.

$$M + H_2O + e^- \underset{\text{discharge}}{\overset{\text{Charge}}{\rightleftarrows}} MH + OH^- \quad (2)$$

The most commonly used electrolyte is a solution of aqueous potassium hydroxide, KOH, in which the KOH concentration ranges from 25% to 40% by mass. The two equations show that there is no net change in electrolytic quantity. This result contrasts with other electrolyte systems like NiCd, where water is generated at both electrodes during charge and consumed at both electrodes during discharge. Although transient electrolyte concentration gradient occurs in NiMH batteries, its constant average concentration has good overall performance in gas recombination, kinetics, high and low temperature operation, and resistance to cycle life limitations caused by corrosion and swelling [7].

Overcharge and Over-discharge Reactions

The NiMH battery has overcharge and over-discharge reactions that allow the battery to handle abuse conditions of overcharge and over-discharge without adverse effects. The reaction that takes place at the two electrodes during overcharge is an oxygen recombination reaction. It can be shown as follows:

At the positive (Ni) electrode OH^- ions are oxidized generating oxygen:

$$4OH^- \leftrightarrow 2H_2O + O_2 + 4e^-$$

At the negative (MH) electrode the oxygen is reduced:

$$2H_2O + O_2 + 4e^- \leftrightarrow 4OH^-$$

The net result is generation of heat which is proportional to the energy input. This occurs at the expense of increasing the stored charge in the battery. If the rate of charge input exceeds the rate of recombination, the cell pressure increases, which may lead to cell damage.

During over-discharge, hydrogen is released at the positive electrode and recombined at the negative electrode. The reactions are as follows:

At the positive electrode, water is reduced and hydrogen gas is released:

$$2H_2O + 2e^- \leftrightarrow H_2 + 2OH^-$$

The hydrogen gas is then oxidized at the negative (MH) electrode:

$$H_2 + 2OH^- \leftrightarrow 2H_2O + 2e^-$$

The ability of the NiMH cell to tolerate over-discharge is very important for large series strings of batteries since capacity mismatches may cause some cells to over-discharge. To ensure that the overcharge and over-discharge reactions function properly and thus control the buildup of cell pressure, the NiMH battery is constructed with the Ni electrode as the capacity limiting electrode and the MH electrode with excess capacity to allow recombination reactions to take place during overcharge and over-discharge [7].

Types of NiMH Batteries

The earliest pioneering work on NiMH batteries was performed at the Battelle-Geneva Research Center starting after its invention in 1967. These batteries showed high specific energy up to 50 Wh/kg, power density up to 1,000 W/kg, and a reasonable deep cycle life of 500 cycles (depth of discharge: 100%). Due to the inherent deep cycling capability and the high specific energy, NiMH batteries have been used in EVs. The two major types of NiMH batteries used today are the cylindrical batteries and the prismatic batteries. The next section describes the cylindrical NiMH batteries in detail giving the battery structure and the battery characteristics. The later section describes prismatic NiMH batteries and gives the comparison between the two of them. Currently, there are over two million HEVs running worldwide, which use NiMH batteries [15].

Cylindrical NiMH Cell

Battery Structure The single cell shown in Fig. 9 is a sealed cylindrical battery of D-size with a diameter of 32 mm and a height of 60 mm. A sealing plate is equipped with a valve to prevent bursting with an increase in internal pressure. The battery case is made of steel and both positive and negative electrodes are coiled and separated by a separator. This battery optimizes the reaction area of the electrodes, reducing resistance for current collection and improving electrolyte composition to obtain high power characteristics. The nominal battery capacity is 6.5 Ah and the maximum output power is more than 100 W per cell. To reduce the internal resistance and shield against vibrations, disk plates are inserted for cell connection [13].

Battery Characteristics Table 3 gives the characteristics of a single cylindrical cell and battery consisting of six cells.

Discharge Power Characteristics Figure 10 shows the specific power characteristics of a battery module that consists of six cells at different state of charge (SOC). The module provides 800 W in 2 s and 650 W in 10 s. As seen in the graph, for a given range of charge capacity, the specific power is almost constant. Also, for the 50% SOC and 100% SOC, there is not much variation in specific power, giving 650 W/kg in 2 s and 600 W/kg for a 10 s duration. Relatively constant input and output power is highly desired by EV manufacturers. It can be clearly seen from the graph that NiMH prismatic batteries deliver an almost constant power for any SOC, which is highly desirable in batteries for EVs.

Charge Efficiency For practical use, high charge efficiency is required over a wide temperature range. Figure 11 shows the battery has a very high charge efficiency, which provides high regenerative acceptability over the SOC range, mostly used during normal vehicle operation. The ampere-hour charge efficiency is nearly 100%. Also because of the very small energy loss, heat generation of the battery is minimized.

Life Cycle Characteristics To preserve an active battery system, flow of power in and out of the battery needs to be maintained, even if minimal. The battery's

Battery Technologies. Table 3 Characteristics of a single cylindrical cell and battery consisting of six cells [13]

	Single cell	Battery module (six cells)
Output power	625 W/kg, 2,160 W/l	600 W/kg, 2,070 W/l
Input power	500 W/kg, 1,720 W/l	480 W/kg, 1,660 W/l
Energy density	45 Wh/kg, 172 Wh/l	43 Wh/kg, 161 Wh/l
Nominal voltage	1.2 V	7.2 V

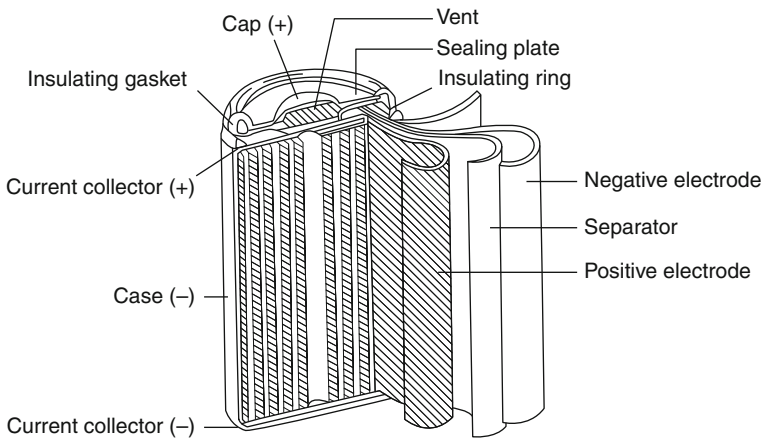

Battery Technologies. Figure 9
Structure of a cylindrical battery

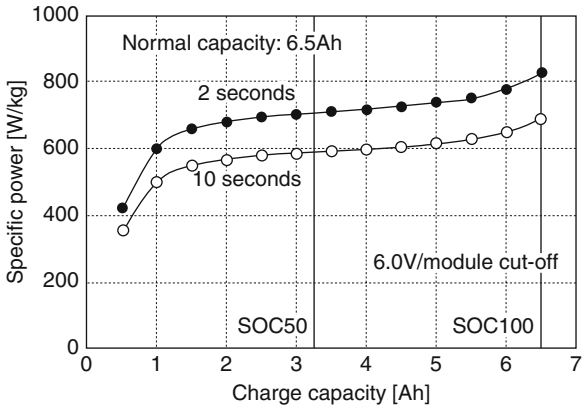

Battery Technologies. Figure 10
Specific power of a cylindrical battery at different state of charge levels [13]

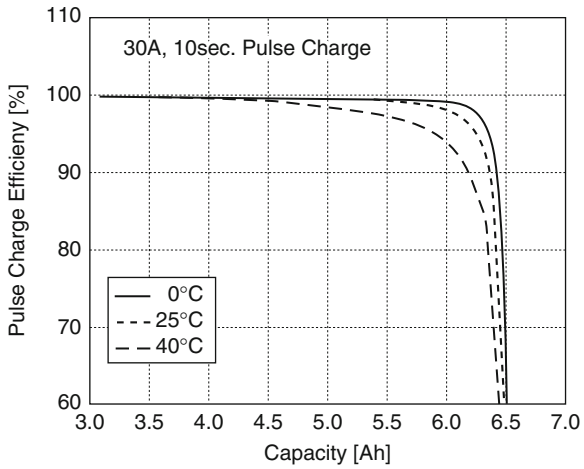

Battery Technologies. Figure 11
Pulse charge efficiency of cylindrical battery module at different temperatures [13]

controller needs to ensure that the battery is neither fully charged nor completely discharged. To test such operating conditions, a life test was conducted at Panasonic's test facility in Shizuoka, Japan. One example of the results is shown in Fig. 12 [13]. The test provides results in which the input and output power simulate real vehicle driving at 35°C. As a result, the durability was found to be equivalent to more than 100,000 km driving without deterioration of battery characteristics.

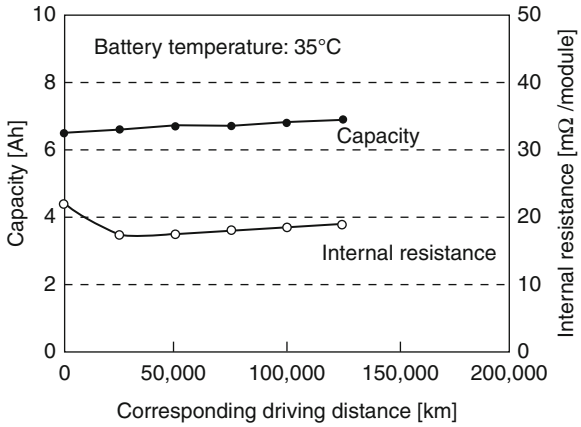

Battery Technologies. Figure 12
Life cycle characteristics of cylindrical battery module with simulated actual driving pattern [13]

Prismatic NiMH Battery

Structure To improve power, reduce the number of connected parts. Figure 13 shows the appearance of a prismatic module design consisting of six cells in series. The conventional cylindrical module has connecting plates to connect cells and plastic insulating rings to prevent external short circuits. The prismatic module adopts internal connection; therefore, connecting plates and plastic insulating rings are not required. As a result, a shorter current path is accomplished. The investigation of electrode dimensions and current collector design shows that the current flow path is shortened. By thinning the positive and negative electrodes, the number of electrodes are increased, which increases the reaction area and decreases the current density. Resin material is used to make the battery case, which provides increased safety and reliability. The resin material makes it easy to design bumps and ribs on the side of the battery case. The bumps and ribs provide cooling and also reduce the pack volume by 40%. The resin also reduces 20% of the prismatic battery's weight compared to a cylindrical battery pack. The six cells are internally connected to form one module. External connection parts like bus bars and connecting plates are also not required [13].

Figure 14 shows the improved power characteristics and reduced internal resistance of this battery, as compared to the cylindrical battery. The main source of the

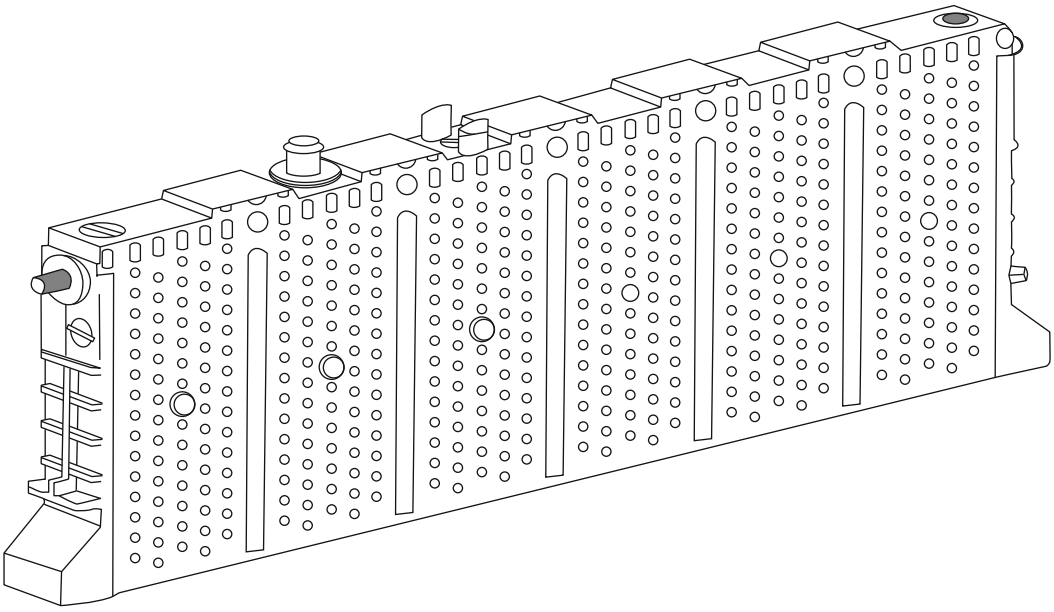

Battery Technologies. Figure 13
Prismatic NiMH battery [13]

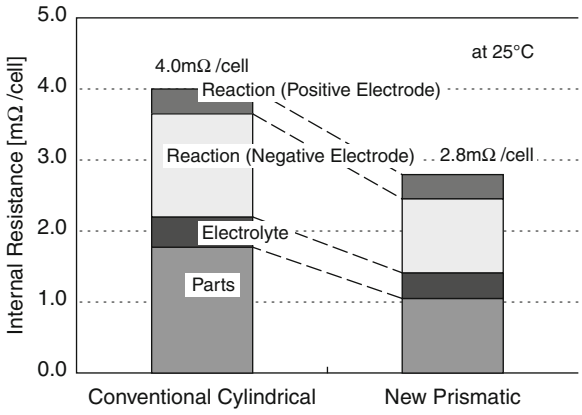

Battery Technologies. Figure 14
Internal resistance of prismatic and cylindrical battery cell before activation [13]

Battery Technologies. Table 4 Comparison between prismatic and cylindrical battery modules [13]

	Prismatic module	Cylindrical module
Dimensions (mm)	19.6 × 106 × 275 (width × height × length)	35 × 384 (diameter × length)
Nominal voltage (V)	7.2	7.2
Nominal capacity (Ah)	6.5	6.5
Specific power (W/kg)	1,000	600
Specific energy (Wh/kg)	46	43
Weight (g)	1,020	1,090

reduction in internal resistance is the components. A high specific power of 1,000 W/kg, which is higher than that of the conventional cylindrical battery, is also achieved.

Table 4 shows the module characteristics of both prismatic and cylindrical battery types. It is clear that the prismatic design is superior to the cylindrical design.

Discharge Power Characteristics Figure 15 shows the power characteristics of the prismatic module at different SOC. This battery provides 1,000 W of power per kilogram for 10 s and 1,150 W of power for 2 s with the SOC maintained in a range 40–60%. It also has high power density at low SOC; about 800 W/kg for 10 s and 1,000 W/kg for 2 s at 20% SOC.

Figure 16 shows the power characteristics at different temperatures for the cylindrical battery and

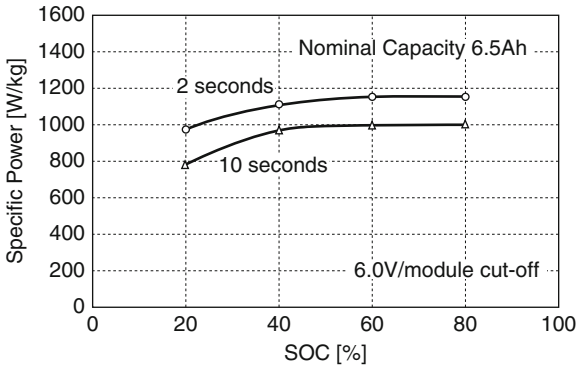

Battery Technologies. Figure 15
Specific power of prismatic battery at different SOC [13]

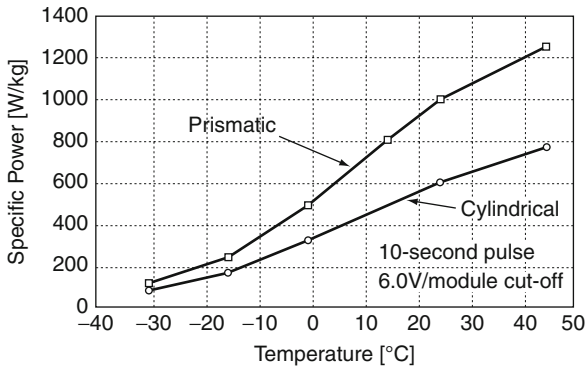

Battery Technologies. Figure 16
Specific power of prismatic and cylindrical battery module at different temperatures [13]

the prismatic battery. As seen, the characteristics of the prismatic battery are better (490 W/kg at 0°C and 120 W/kg at −30°C). Also the temperature where power discharge of 200 W/kg is possible is reduced by about 10°C as compared to the cylindrical battery.

Life Characteristics of Prismatic Batteries In Fig. 17, Pattern A represents a normal driving profile, with a maximum SOC deviation of 15% and pattern B represents a high load driving profile with a maximum SOC deviation of 30%. After tests corresponding to a driving distance of 300,000 km with pattern A at 35°C, there was no deterioration observed in battery performance. Also, with pattern B at 55°C, the battery was able to achieve a driving distance of 200,000 km [13].

Figure 18, above, shows the EV-95 (95 Ah) and EV-28 (28 Ah) units developed by Panasonic for EVs. EV-95 has long life characteristics of more than 1,000 cycles and 4 years of onboard driving [13].

The batteries shown above have the following characteristics:

1. Optimization of additives (Y_2O_3) for excellent charge efficiency of the positive electrodes
2. $MnNi_5$ system of hydrogen-absorbing alloy for the negative electrodes
3. High performance, hydrophilic-treated polypropylene separator

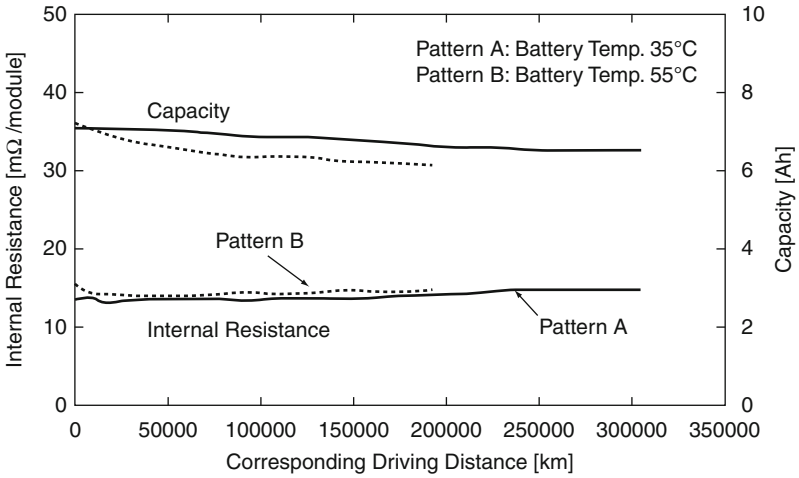

Battery Technologies. Figure 17
Life cycle characteristics of prismatic batteries [13]

Ev-95 Ev-28

Battery Technologies. Figure 18
EV-95 and EV-28 batteries by Panasonic

The electrode groups consist of alternately stacked positive electrodes and negative electrodes interleaved with separators. Inserting these electrode groups into a resin battery case and sealing with a cover equipped with a valve after filling with alkaline electrolyte forms the cell. A battery module consists of ten cells connected in series by metal plates and these are configured to permit airflow between the cells to ensure a uniform temperature distribution.

Table 5 gives the characteristics of the EV-28 and EV-95 batteries manufactured by Panasonic.

Below is Table 6, which gives characteristics of NiMH batteries, produced by Texaco Ovonic Battery Systems and VARTA.

The second-generation GM EV1 used NiMH batteries. Table 7 shows the specifications of that battery.

Battery Technologies. Table 5 Basic characteristics of the EV-28 and EV-95 batteries [13]

	EV-28	EV-95
Dimensions (width × height × length) mm × mm × mm	75 × 110 × 388	116 × 175 × 388
Nominal voltage (V)	12	12
Nominal capacity (Ah)	28	95
Weight (kg)	6	18.7
Specific energy (Wh/kg)	58	65
Specific power at 80% depth of discharge (W/kg)	300	200
Self discharge at 45°C, 1 month (%)	20	20
Cycle life at 25°C ambient temperature, 80% DOD (cycles)	>1,000	>1,000

Lithium-Ion Batteries

Lithium-Ion Battery Chemistry

Lithium is the least dense of all solid metals, has the greatest electrochemical potential, and provides the largest energy density by weight. For many years, lead acid had been the predominant battery for large-scale equipment. G. N. Lewis pioneered early work with lithium-ion battery technology but it was not until the early 1970s before it became commercially viable. Because of the inherent instability of lithium metal, early attempts at rechargeable batteries failed. Research then shifted to lithium-ion-based composites which, although less dense, are safer to use. Lithium-ion batteries emerged during the early 1990s. Today, lithium-ion is the fastest growing and most promising battery chemistry.

Battery Technologies. Table 6 Battery characteristics [8]

Manufacturer	Battery design	Cell size (Ah)	Specific energy (Wh/kg)	Specific power (W/kg)
Texaco Ovonic battery	High power	7.5	~40	650
	Medium power	28	48	~440
	Medium power	45	71	~390
VARTA	High power	10	30	630
	Medium power	45	50	220

Battery Technologies. Table 7 GM EV 1 (generation 2) battery specification [16]

Manufacturer	Ovonic energy products
Type	Nickel metal hydride
Number of modules	26
Weight of module	18.3 kg
Weight of pack(s)	481 kg
Nominal module voltage	13.2 V
Nominal system voltage	343 V
Nominal capacity (50% charge capacity)	85 Ah

As mentioned earlier in section "Basic Characteristics of Batteries," a battery functions as a combination of chemical reactions, oxidation at the anode (where electrons are generated in discharge mode), and reduction at the cathode (at which electrons enter the cell). Depending on the direction of the current (charge or discharge) each electrode is either the cathode or the anode. The electrolyte can serve as a reaction propellant or even as an integral part of the reaction. This combination of reactions is referred to as *redox*. Table 8 provides redox reaction potentials for eight elements.

Lithium and fluoride generate the highest potential during oxidation and reduction, respectively [7]. A significant advantage of lithium-ion batteries is their efficiency in charge retention and energy supply. The internal resistance of lithium-ion cells is comparatively low, which means they do not lose a considerable amount of energy as heat (I^2R loss) [8]. In general, the internal resistance of a cell is modeled as a resistor in series with an ideal voltage source. Maximum efficiency occurs with a low internal series resistance and a large load resistance. Maximum power can be extracted from a cell when load resistance is equal to the cell's internal resistance. Under this condition half the total power is expended as heat, while the other half is available for use. The availability of high power output is a useful property for lithium-ion cells, especially when instantaneous power is required. Consider the example of a race car looking to set a new quarter-mile speed record. This car would need high instantaneous power without regard to cell degradation due to overheating.

Battery Technologies. Table 8 Redox potential [7]

Electrode reaction	Potential (V)	Electrode reaction	Potential (V)
$Li^+ + e \leftrightarrow Li$	−3.01	$Cu^{2+} + 2e \leftrightarrow Cu$	0.34
$Na^+ + e \leftrightarrow Na$	−2.71	$Ag^+ + e \leftrightarrow Ag$	0.80
$Ni^{2+} + 2e \leftrightarrow Ni$	−0.23	$Cl_2 + 2e \leftrightarrow 2Cl^-$	1.36
$Pb^{2+} + 2e \leftrightarrow Pb$	−0.13	$F_2 + 2e \leftrightarrow 2F^-$	2.87

Operation

Numerous lithium-based alloys are available for use as anode. Lithium polymers are considered commercially safe, while metallic lithium is still at the developmental stage [17]. Charge flow for any of the combinations in Fig. 19 is typically the same, as shown in Fig. 20.

A common electrolyte is lithium hexafluorophosphate ($LiPF_6$). It was chosen for its high redox potential. Ehsani et al. [17] mentions that $LiPF_6$ is unstable under high heat and moisture. Hydrofluoric acid (HF) is produced as a by-product to the electrolyte's reaction with water. For this reason, there was significant opposition to its use in the early 1990s. Since then however, it has been revealed that a small amount of HF increases life cycle, because of the formation of a strong passive layer on the cathode.

The addition of HF prevents formation of lithium dendrite. (Most metals are combined with alloys for dexterity and strength. Due to the presence of alloys, the metal tends to exist in a nonuniform, snowflake-like distribution called *dendrite*.) $LiPF_6$ is also easily soluble in the solvent, making it a good solid interface on the surface of anode materials. Lithium-ion is considered to be the current generation technology for EV batteries, in part because of it high energy density. Also, lithium has the highest redox reaction potential of any metal. It is also necessary to consider the fact that key elements of lithium-ion batteries are facing exhaustion. Cobalt metal, used for cathode, has been in shortage for quite some time [17]. Most metals are combined with alloys for dexterity and strength. Due to the presence of alloys, the metal tends to exist in a, nonuniform, snowflake-like distribution called dendrite [17].

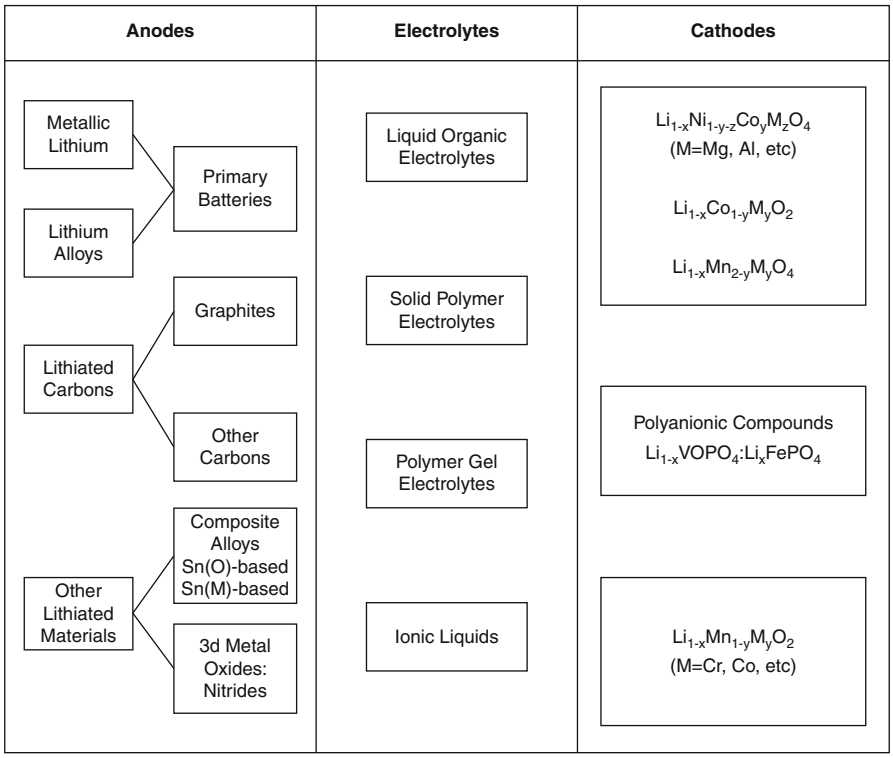

Battery Technologies. Figure 19
Numerous chemical combinations for lithium-ion batteries

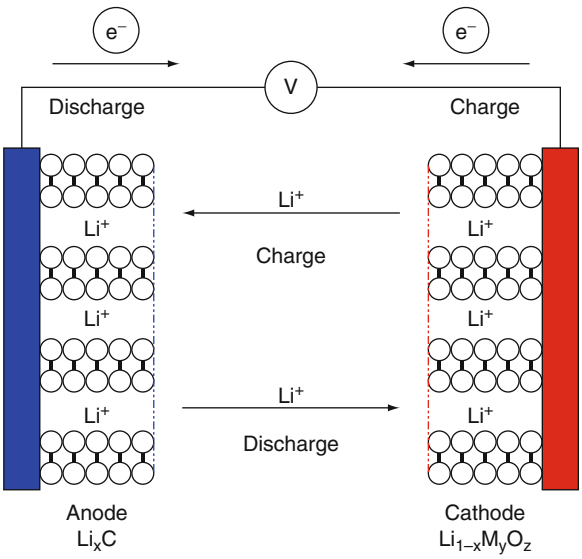

Battery Technologies. Figure 20
Charge flow for lithium-ion batteries [17]

Efficiency

Lithium-ion batteries are practically 100% charge efficient, according to Brodd et al. [5]. In essence, all the charge lost during discharging is recovered during charging. Note that there is a net loss in energy during each complete charging/discharging cycle. This is because the cell voltage is lower during discharging as compared to the charging cycle. Figure 21 provides discharge curves for voltage and current of a lithium-ion cell. Note that the voltage continues to drop during discharge before stagnating at a constant level toward the end of charge availability. This constant voltage can be attained by discharging at a lower current, as shown in the current curve of Fig. 21. As the current drops to zero, the total charge from the cell adds up to the same value regardless of the rate of discharge (whether the discharge was at a low current or at a high current) [5].

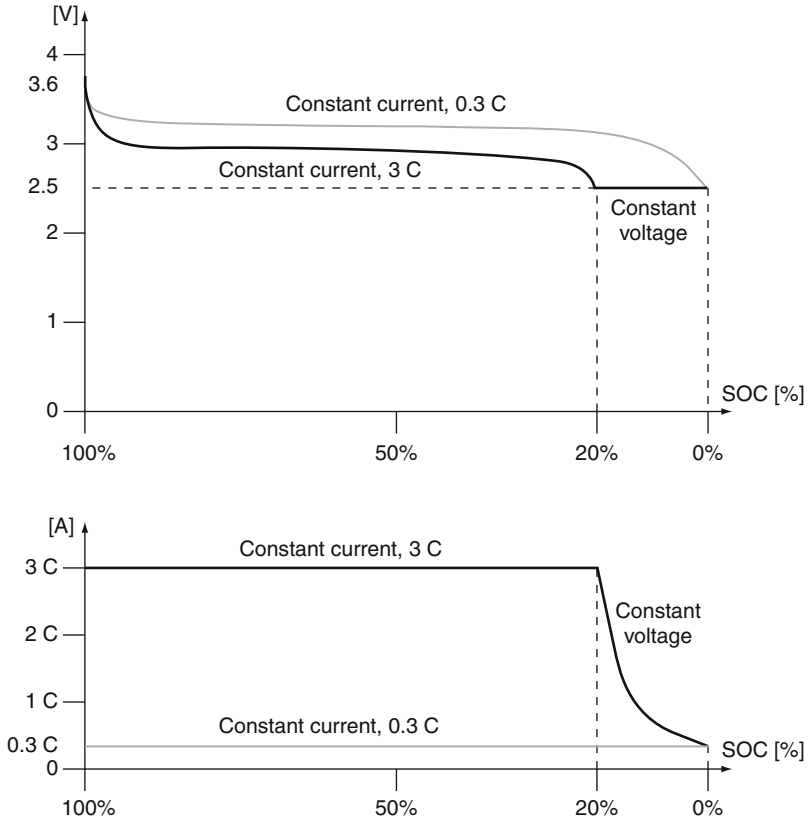

Battery Technologies. Figure 21
Voltage and current during discharge [18]

Applications that require constant current will be unable to extract the last bit of energy out the battery. Other applications, such as for EVs, have more flexibility. Some of today's EVs can operate at lower torque, which implies lower current, to allow the driver to reach a safe location before running out of battery power. Such applications can use the entire charge contained in a battery.

Although not obvious, both the graphs in Fig. 21 are related. As a cell ages, it appears to gradually lose capacity. Davide [18] explains that this capacity is actually unused, but not lost. Internal resistance of a cell increases with age, therefore the cell gets undercharged and under-discharged along the process. This issue can be resolved by allowed fixed cutoff voltages to vary internally. Due to fixed cutoff voltages, the cell charges/discharges less and less each time due to increasing internal resistance, resulting in an apparent loss of capacity. By raising the upper cutoff voltage during charge and lowering the lower cutoff voltage during discharge, we can recover some of this lost capacity. A battery management system that is able to measure a cell's internal resistance and compensate its cutoff voltage accordingly can make better use of the cell's capacity [18].

Reliability

To minimize operation and maintenance (O&M) costs for the customer, it is essential for a battery manufacturer to conduct rigorous stress tests on their battery systems. A common test adapted by manufacturers in the USA is known as the dynamic stress test (DST), developed by the United States Advanced Battery Consortium (USABC). Figure 22 shows an example of the battery charging and discharging power profiles that must be successfully followed to acquire DST conformation. The test can be performed at various temperatures to determine ideal operating conditions. The test

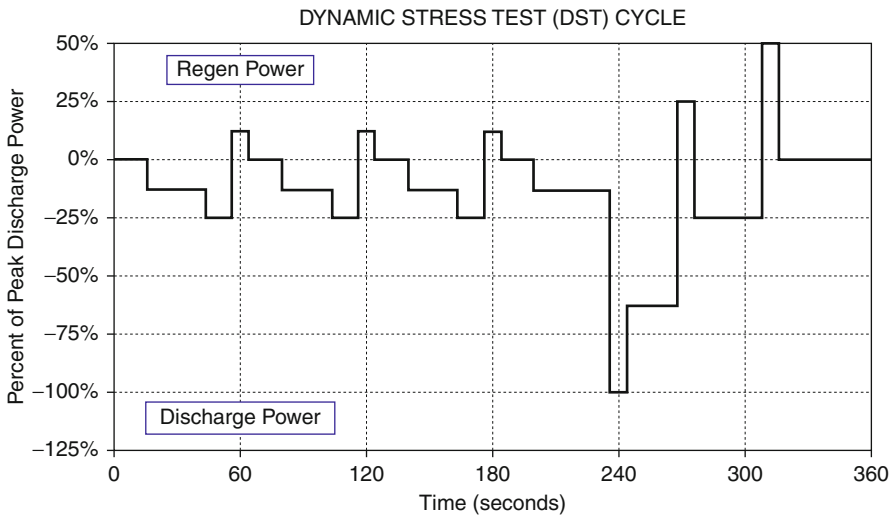

Battery Technologies. Figure 22
Dynamic stress test by USABC [19]

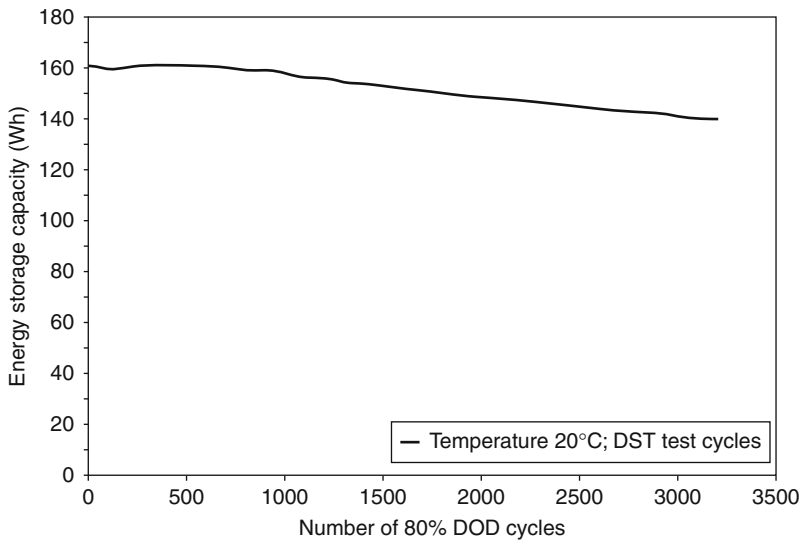

Battery Technologies. Figure 23
DST results for Saft's lithium-ion battery [20]

is designed to gauge battery performance characteristics such as partial discharge and hold, sustained climb, thermal performance, and fast charge response. One such battery was tested by the Electric Power Research Institute (EPRI). Figure 23 shows DST results of that battery, specifically energy storage capacity versus number of DST test cycles at 80% depth of discharge. As shown, a 12.5% drop in capacity is attained after 3,000 cycles. This is in contrast to a 37% drop in capacity for NiMH batteries subject to a similar test [20]. Longer life expectancy combined with larger power density make lithium-ion batteries an ideal candidate for EVs.

Twenty watt-hours of energy storage capacity is lost after 3,000 charge–discharge cycles, as seen in Fig. 23.

Thermal Runway

Thermal runaway (TR) is defined as a phenomenon where an increase in temperature creates conditions for further increases in temperature. Viable conditions for TR exist when a battery is producing more heat than it can dissipate. Thermal runaway can lead to leaks, venting of gas, and possibly a fire. According to Saft, temperature in a cell must be kept below 145°C to prevent conditions for TR from arising.

As battery temperature typically increases during operation, resistance of the ion-transferring electrolyte decreases. This leads to an increase in the current passing through the battery, raising the temperature of the battery even further. If the electrolyte becomes too hot, its resistance will become negligible and allow enough current to flow for chemical compounds on the cathode and anode to breakdown and short circuit.

Excessive ambient temperatures are another cause of TR, according to Saft. Computers, cell phones, and other portable devices are often subject to prolonged exposure to direct sunlight. Additionally, portable electronics could be operated in constricted spaces, with insufficient room for heat dissipation. High ambient temperatures can also harbor conditions for TR.

EPRI identifies overcharging as yet another source for TR [20]. Overcharging can lead to build up of lithium deposits that can penetrate the film separating the anode and the cathode, leading to a short circuit. All lithium-based batteries are equipped with protective circuitry to avoid overcharging. Failure of protective circuitry can lead to build up of lithium-ions on the graphite anode, forming lithium dendrite. (Most metals are combined with alloys for dexterity and strength. Due to the presence of alloys, the metal tends to exist in a nonuniform, snowflake-like distribution called *dendrite*.) With increasing formation of this dendrite, useful anode surface area diminishes, leading to reduced battery capacity. If charging continues even further, the dendrite will penetrate the separator and react with the cathode, creating a short circuit. Metallic lithium is still at the developmental stage because it is prone to dendrite formation. Figure 24 depicts EPRI's projection of effects of storage temperature on battery life.

Irrespective of the cause, TR is a dangerous prospect. Potential large-scale use will require development of adequate prevention of conditions leading to TR [20]. USABC and EPRI have proposed various solutions, albeit with negative impacts on power density and capacity.

Capacity Fading

Capacity fading (CF) refers to reduction in battery capacity after repeated charge or discharge cycles.

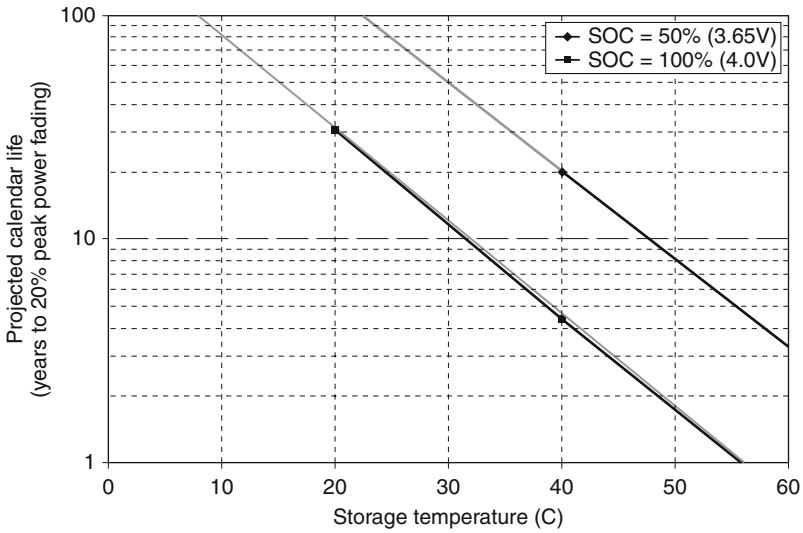

Battery Technologies. Figure 24
Projected calendar life as a function of storage temperature [20]

Yunjian et al. [21] uses a lithium-ion battery, with lithium manganese oxide ($LiMn_2O_4$) as cathode and graphite as anode to study capacity fading characteristics. Lithium hexafluorophospate ($LiPF_6$) is present as an electrolytic salt. The battery was charged to 4.2 V and then stored for a period of 96 h at 55°C. A notable reaction was the formulation of hydrofluoric acid (HF) and a consequent dissolution of manganese (Mn). The following reactions were noted:

$$LiPF_6 + 4H_2O \rightarrow PO_4^{3-} + LiF + 5HF$$

$$2LiMn_2O_4 + 4H^+ \rightarrow 3MnO_2 + Mn^{2+} + 2Li^+ + 2H_2O$$

Mn^{2+} enters the electrolyte and manganese dioxide (MnO_2) is deposited on the cathode. A reported 8 mAh/g of capacity was lost on the first day. Only 2 mAh/g of capacity was lost during each of following 3 days. MnO_2 formation on the cathode protected it from engaging in further dissolution of manganese (Mn), which explains the dwindling in CF. Charge retention of the battery was found to be 83.3%, 85.8%, 86.9%, and 88.6% for those 4 days.

Elevated temperatures can accelerate the rate at which CF occurs, as evident from work done by Xia et al. [22]. When operated above 65°C, the number of operational cycles is well below the EV requirement of 1,000–1,500. Degradation of electrode materials has been found to be the main reason for CF at high temperatures [22].

Cost

Lithium-based batteries are subject to aging even if not being used. Also, lithium batteries are dependent on protective circuits to maintain safe levels of voltage and current. These factors propagate into a 40% (average) higher manufacturing cost for lithium-based batteries compared to NiMH [20]. Figure 25 provides a breakdown of costs to manufacture an EV lithium-ion battery.

Several automotive manufacturers have announced plans to incorporate lithium-based batteries for use in HEVs, although NiMH batteries currently predominate. Lithium-ion batteries store more than twice as much energy per kilogram (250–400 Wh/kg) compared to the next-best battery technology, NiMH.

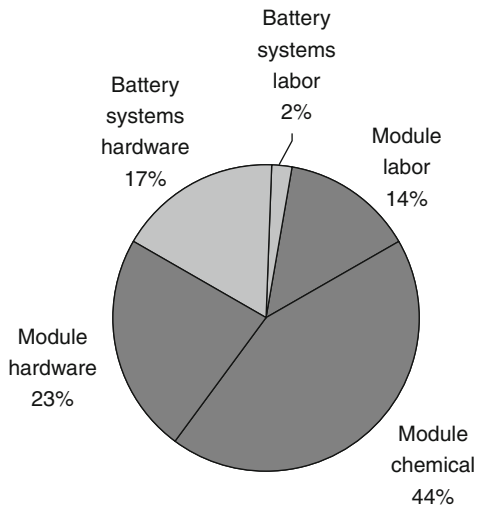

Battery Technologies. Figure 25
Component costs as percentage for Saft's EV lithium-ion battery [18]

After having purchased their EV, customers are now responsible for operating costs for as long as they own the vehicle. Operating costs can vary based on battery capacity, efficiency, environmental conditions, and usage. Nevertheless, once gas savings balance out the cost of the EV, long-term savings in operating costs become apparent. A lab experiment conducted by EPRI in 2010 [23] employed various EV types, each with a lithium-ion battery system. Operating costs (loosely termed "fueling costs") are shown in Fig. 26. Here, the following EV types were used: Fuel Cell Vehicle (FCV), Plug-in Fuel Cell Vehicle (PFCV), Range Extender Fuel Cell Vehicle (FCV), Battery Electric Vehicle (BEV), and Plug-in Hybrid Electric Vehicle (PHEV). A "20" (or "40") in the name indicates 20 (or 40) miles on a full charge.

In the near term, FCVs are more expensive due to the cost of hydrogen. The FCV fitted with a range extender module uses considerably lesser hydrogen, as consistent with the lower near term operating cost. As expected, predominant battery use in EVs results in lower near term costs. In the long term, the difference in cost of hydrogen versus electricity became smaller, as apparent in the near identical long-term costs for all vehicle types.

To make lithium-ion batteries practical for mass-produced electric-drive vehicles, new technologies

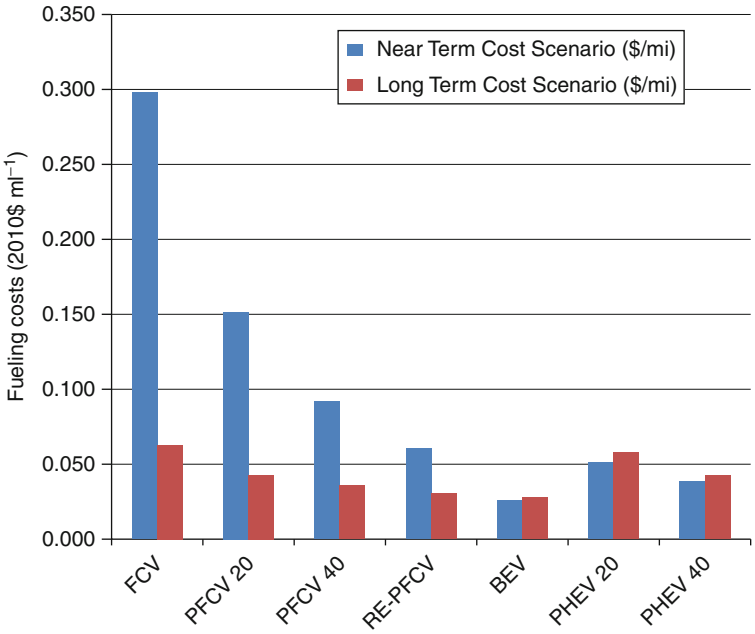

Battery Technologies. Figure 26
Operational costs per mile for various Li-ion EV configurations [23]

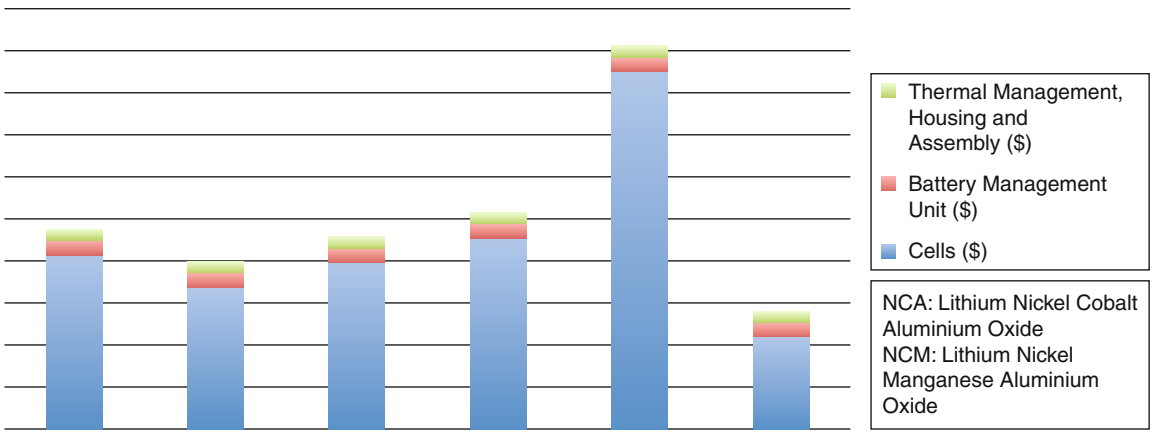

Battery Technologies. Figure 27
Cost breakdown for complete battery pack used for typical PHEV40

must increase the energy the batteries store and the speed with which they can discharge it. They must also lengthen cycle life to 15 years or 241,000 km (150,000 miles) – the average life of a vehicle [24].

Perhaps it would be appropriate to compare lithium ion to other chemistries in terms of cost of a battery pack for EVs. Figure 27 provides such a comparison for a PHEV-40, as per 2010 cost estimates made by EPRI's Duvall et al. [23] and the Electric Auto Association.

Notably, Pb-A and NiMH (best case) appear to carry the lowest and highest overall costs respectively. It is important to mention that a typical EV lead acid battery pack only has a life of approximately

14–16 months (assuming the vehicle is driven 20–40 miles daily). On the other hand, the NiMH pack has a life span of roughly 5.5 years.

Metal–Air Batteries

Metal–air batteries get their name from their reactants which undergo electrochemical reactions to release energy. They are one of the most compact and potentially the least expensive batteries available. They are also environmentally friendly. However, their main disadvantage so far has been that electrical recharging of these batteries is very difficult and inefficient. Although many manufacturers offer units that can be refueled, where the consumed metal is mechanically replaced and processed separately, there still have not been many developers who offer rechargeable batteries. Rechargeable metal air batteries that are under production have a life of only a few hundred cycles and an efficiency of about 50% [1, 6].

Current research in lithium–air batteries have shown that they can provide an energy density of 1,700 Wh/kg, which is more than the energy density of any other battery technology present today and is comparable to the practical energy density of gasoline [6] (Fig. 28).

Air electrodes and metal–air battery technologies have already been used in fuel cell systems. Earlier, zinc was the predominant metal used in metal–air batteries. Recently, lithium instead of zinc as the metal has started being used which has increased the energy output eightfold. As seen in the figure above, the lithium–air battery's porous carbon cathode (gray) is flooded with the electrolyte (blue). The Li^+ ions (small dots) react with oxygen molecules (pairs of dots) at catalyst sites (yellow) to form lithium oxides (orange). The oxygen electrode proceeding in tandem with lithium according to the reaction $2Li + O_2 \rightarrow Li_2O_2$ can deliver a capacity of 1,200 mAh/g. The first lithium–air cell was successfully assembled and discharged in 1996, but attractive rechargeability was demonstrated only recently [3].

It could be argued that such a system unites within the same device the two most prominent failures of battery and fuel-cell technologies, namely, the inability to master lithium and oxygen electrodes. These perceived issues have prevented the practical use of lithium–air batteries. Improving energy storage and preventing Li_2O_2 from clogging the electrode require a better understanding of the reaction mechanism of the oxygen electrode. Engineering and chemical advances are also required to prevent the ingress of either CO_2 or H_2O, which could react with either Li_2O_2 or lithium metal [3].

Zinc Bromine Battery

The zinc bromine battery is based on the chemical reactions between two commonly available materials, zinc and bromine. This battery was developed by Exxon in the early 1970s. It is a hybrid flow battery system since zinc is deposited on the negative electrode during the charge cycle. Unlike conventional flow batteries, the energy storage capacity of the zinc–bromine hybrid is constrained by the amount of surface area available for deposition [4, 9].

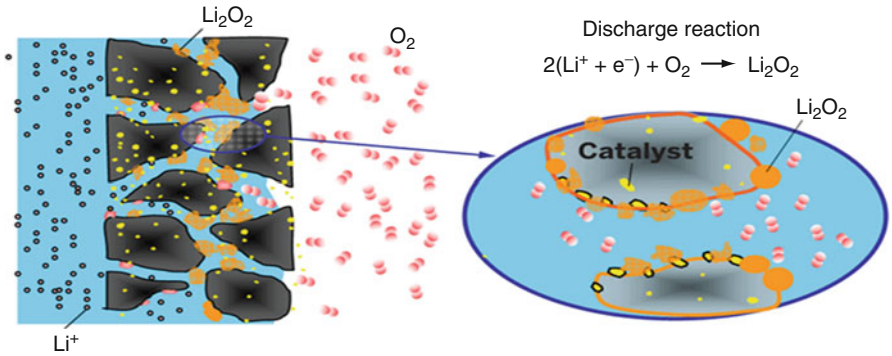

Battery Technologies. Figure 28
Li–air battery [6]

One of the main advantages of zinc–bromine batteries is that it can be fully discharged without any damage to the battery and has a life of at least 1,500 charge/discharge cycles. This battery is ideally suited in applications that require deep cycle and long cycle life energy storage. These batteries are made with low-cost, recyclable plastics and manufactured with techniques suitable for mass production and at low production costs [4].

As seen in the figure below, the battery consists of a zinc negative electrode and a bromine positive electrode separated by a microporous separator. An aqueous solution of zinc/bromide is circulated through the two compartments of the cell from two separate reservoirs. The electrolyte stream in contact with the positive electrode contains bromine which is maintained at the desired concentration by equilibrating with a bromine storage medium. The bromine storage medium is immiscible with an aqueous solution containing zinc bromide. All battery components are made from a bromine inert plastic [4] (Fig. 29).

During discharge, zinc is converted to zinc ion with the release of two electrons and bromine is converted to bromide, the zinc ion and bromine combine to form zinc bromide. The chemical process used to generate the electric current increases the zinc-ion and bromide-ion concentration in both electrolyte tanks. During charge, metallic zinc is deposited as a thin film on one side of the plastic electrode. Meanwhile, bromine is evolved as a dilute solution on the other side of the membrane, reacting with other compounds in solution (organic amines) to form viscous, dense bromine-adduct oil that sinks to the bottom of the tank. The bromine oil is allowed to mix with the rest of the electrolyte during discharge. The net efficiency of this battery is about 75% [9].

The zinc–bromine battery uses electrodes that do not take part in the reactions but merely serve as substrates for the reactions. Therefore, there is no loss of performance, as in most rechargeable batteries, from repeated cycling causing electrode material deterioration. When the zinc–bromine battery is completely discharged all the metal zinc plated on the negative electrodes is dissolved in the electrolyte and again produced the next time the battery is charged. In the fully discharged state the zinc/bromine battery can be left indefinitely [4].

The zinc–bromine battery has an energy density of 75–85 Wh/kg. The power characteristics of the battery can be modified for selected applications, making them extremely useful for multipurpose energy storage [4].

Supercapacitors

In the field of energy storage, two parameters are fundamental for storage devices: the energy density and

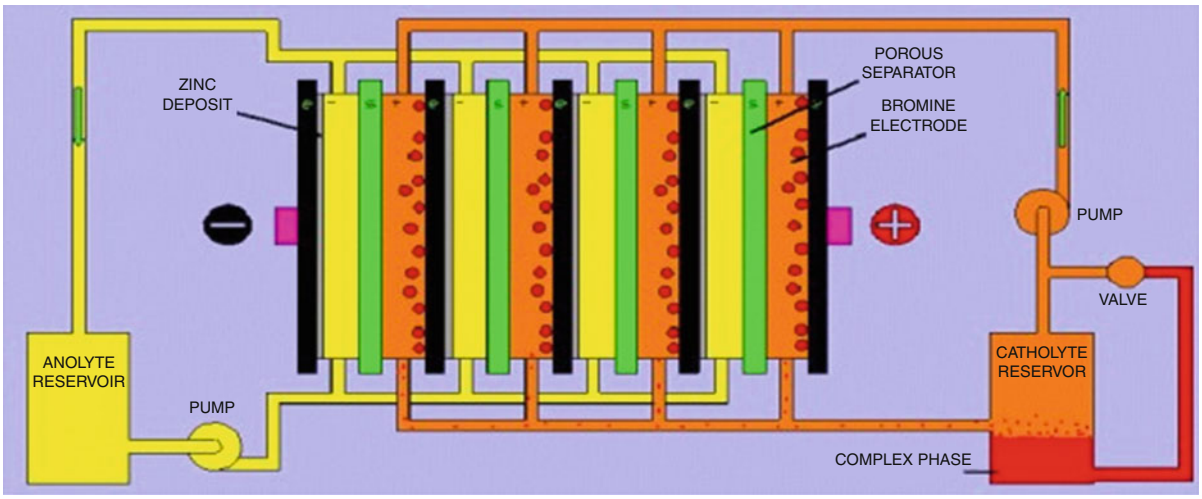

Battery Technologies. Figure 29
ZnBr battery [4]

the power charging and discharging rates. The first parameter defines the amount of energy that can be stored in a given volume. The lower the maximum charging and discharging rates, the more time that is required for loading and unloading the required amount of energy into the storage device. The ideal storage device should have both a high energy density together with high power charging and discharging rates. This is unfortunately not the case and compromises have to be made. Current battery technologies have relatively high energy densities but relatively poor power densities. Supercapacitors are a compromise between batteries and conventional capacitors. Their main characteristic is that they possess both a relatively high energy density and power density [25].

Integrating with an Onboard Energy Source for an EV

The integration of the onboard energy source for an electrically propelled vehicle with a supercapacitor bank (SB) as a peak power unit can lead to substantial benefits in terms of EV performances, battery life, and energy economy. An SB made up of single cells connected in series and in parallel, featuring appropriate parameters of energy density, power density, with high charging–discharging efficiency and affordable cost can be beneficial as a suitable device to support the energy source of an electric vehicle, thus providing optimized energy management [26].

The potential benefits of an integrated system SB-electrochemical energy source are the following:

- To improve the vehicle efficiency and energy economy over variable power driving conditions
- To assure high performance and good vehicle behavioral response independently from the status of the energy source (including age)
- To improve the endurance of the energy source to the extent of its dependence on the high rate power demand
- To extend the vehicle's range at full performance as a consequence of the combined effect of load leveling of the onboard energy source and of better efficiency of energy recovery

Second to the range of the EV, high acceleration performance is a highly desired feature to achieve integration with the majority of today's vehicles. The integration of an SB with a battery allows a system design optimized according to driving requirements, by making the specific power and specific energy parameters of the energy source independent of each other. As a consequence of this consideration, it will be possible to design the storage battery with respect to energy storage capability and life requirement without taking into account the power requirement [26].

Difference Between Capacitors and Supercapacitors

A supercapacitor differs from a conventional capacitor both in the physical phenomena and the materials from which it is made. In today's supercapacitors, the dielectric is an electrolyte interposed between two electrodes. When a voltage is applied, a double layer of charges is formed at the interface between the electrodes and the electrolyte. In the case of supercapacitors, the distance between the charges corresponds to the thickness of the double layer, that is, only a fraction of a nanometer. This accounts for the difference in terms of capacitance per square centimeter between a conventional capacitor in the (order of magnitude nF/cm^2) and a supercapacitor (order of magnitude 50,000 nF/cm^2) [26].

The way to increase the energy stored in a conventional capacitor is to operate at high voltages (up to 3,000 V) consistent with the dielectric breakdown voltage. In today's supercapacitors, the voltage to be applied must be limited by either the solvent or the organic electrolyte decomposition voltage (1.23 V and 3.5 V, respectively). In this case, the only way to increase the stored energy is to raise the capacitance value by adopting electrode materials with very high specific area. In particular, active carbon may reach, through suitable chemical processes, a specific area of 103 m^2/g, and a specific capacitance of 102 F/g. In addition, it is possible to reach very low values of the internal resistance that allows the device to provide high output power.

So far, only supercapacitors operating on the basis of charge separation phenomena due to the application of an external voltage between the electrodes have been considered. There is another type of supercapacitor, called pseudocapacitor, in which reduction and oxidation reactions occur during charge and discharge phases. The electrodes are made of metallic oxides

Battery Technologies. Table 9 Characteristics of supercapacitors based on the electrode and electrolyte material [26]

Electrode material	Carbon	Carbon	Metallic oxides
Electrolyte	Aqueous electrolyte	Organic electrolyte	Aqueous electrolyte
Maximum voltage (V)	1	3	1
Specific power (kW/kg)	0.8–2.6	1.5–5	0.5
Specific energy (Wh/kg)	0.2–1.3	3–6	1

(typically ruthenium or iridium) and electrolytes are liquid. The characteristics of supercapacitors are summarized as in Table 9 [26, 27].

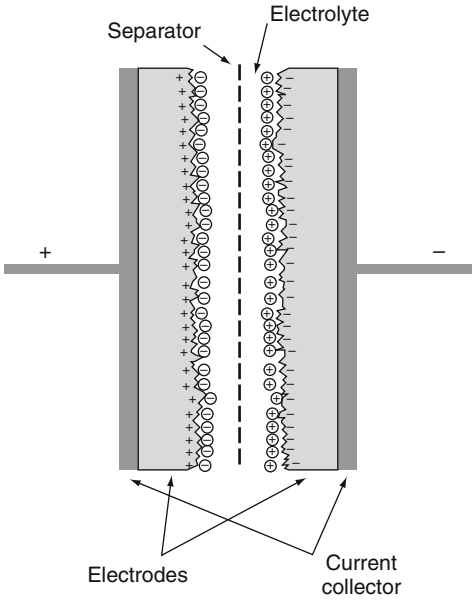

Battery Technologies. Figure 30 Principle of supercapacitors [25]

Working Principle of a Supercapacitor

Supercapacitors are electrochemical double layer capacitors (EDLC). Their technology is similar to that of batteries, but the main difference is that they involve only electrostatic phenomenon (non-faradic). This is the first difference between batteries and supercapacitors. Their power density is higher because there are no chemical reactions during charging and discharging. Also, for this reason, charge storage in EDLCs is highly reversible, which allows them to achieve very high cycling stabilities. EDLCs generally operate with stable performance characteristics for many charge–discharge cycles, sometimes as many as 10^6 cycles. On the other hand, electrochemical batteries are generally limited to only about 10^3 cycles. In double-layer capacitors, the energy is stored by charge transfer at the boundary between electrode and electrolyte. The amount of stored energy is a function of the available electrode surface, the size of the ions, and the level of the electrolyte decomposition voltage [25].

Supercapacitors contain two electrodes, a separator and an electrolyte, as shown in Fig. 30. The two electrodes provide a high surface area, defining the energy density of the component. On the electrodes, current collectors with a high conducting part assure the interface between the electrodes and the connections of the supercapacitor. The two electrodes are separated by a membrane, which allows the mobility of the charged ions and forbids electronic contact. The electrolyte supplies and conducts the ions from one electrode to the other. As the dissociation voltage of the electrolytes used is less than 3 V, this limits the maximum voltage that can be reached by the supercapacitor. Another disadvantage is lower ionic conductivity, which reduces the power capability [25].

The performance of an electrochemical double layer supercapacitor (EDLC) can be adjusted by changing the nature of its electrolyte. As mentioned earlier, an EDLC can utilize either an aqueous or organic electrolyte. Aqueous electrolytes generally have lower equivalent series resistance (ESR) compared to organic electrolytes. However, aqueous electrolytes also have lower breakdown voltages. Therefore, in choosing between an aqueous or organic electrolyte, one must consider the trade-offs between capacitance, ESR, and voltage. Because of these trade-offs, the choice of electrolyte often depends on the intended application of the supercapacitor [27].

While the nature of the electrolyte is of great importance in supercapacitor design, the subclasses of EDLCs are distinguished primarily by the form of carbon they use as an electrode material. Carbon electrode

materials generally have higher surface area, lower cost, and more established fabrication techniques than other materials such as conducting polymers and metal oxides.

Electrode Materials Used in EDLC

Activated Carbon Activated carbon is the most commonly used electrode material in EDLCs. It is less expensive and possesses a higher surface area than other carbon-based materials. Activated carbons utilize a complex porous structure composed of different sized micropores (<200 nm wide), mesopores (200–5,000 nm) and macropores (>5,000 nm) to achieve high surface areas. Although capacitance is directly proportional to surface area, evidence suggests that, for activated carbons, not all of the high surface area contributes to the capacitance of the device. This discrepancy is believed to be caused by electrolyte ions that are too large to diffuse into smaller micropores, thus preventing some pores from contributing to charge storage [27]. Research also suggests an empirical relationship between the distribution of pore sizes, energy density, and power density of the device. Larger pore sizes correlate with higher power densities and smaller pore sizes correlate with higher energy densities. As a result, the pore size distribution of activated carbon electrodes is a major area of research in EDLC design. In particular, research has been focused on determining the optimal pore size for a given ion size and upon improving the methods used to control the pore size distribution during fabrication [27].

Carbon Aerogels There is an increasing interest in using carbon aerogels as an electrode material for EDLCs. Carbon aerogels are formed from a continuous network of conductive carbon nanoparticles with interspersed mesopores. Due to their continuous structure and their ability to bond chemically to the current collector, carbon aerogels do not require the application of an additional adhesive binding agent. As a result of this, carbon aerogels have lower ESR than activated carbons. (The internal components of the capacitor (current collectors, electrodes, and electrolyte) contribute to a resistance, which is measured in aggregate by a quantity known as the equivalent series resistance (ESR). The voltage during discharge is determined by this resistance.) The reduced ESR yields higher power and this is the primary area of interest in supercapacitor research involving carbon aerogels [27].

Carbon Nanotubes Electrodes made from this material are grown as an entangled mat of carbon nanotubes with an open and accessible network of mesopores. Unlike other carbon-based electrodes, the mesopores in carbon nanotube electrodes are interconnected, allowing a continuous charge distribution that uses almost all of the available surface area. Thus, the surface area is utilized more efficiently to achieve capacitance comparable to those in activated-carbon-based supercapacitors, even though carbon nanotube electrodes have a smaller surface area compared to activated carbon electrodes [27]. As the electrolyte ions can easily diffuse into the mesoporous network, carbon nanotube electrodes also have a lower ESR than activated carbon. In addition, several fabrication techniques have been developed to reduce the ESR even further. Carbon nanotubes can be grown directly onto the current collectors, subjected to heat-treatment or cast into colloidal suspension thin films [27]. The efficiency of the entangled mat structure allows higher energy densities [27].

Pseudocapacitors

In contrast to conventional EDLCs, which store charge electrostatically, pseudocapacitors store charge faradically through the transfer of charge between electrode and electrolyte. This is accomplished through electrosorption, reduction–oxidation reactions, and intercalation processes. These faradic processes may allow pseudocapacitors to achieve greater capacitances and energy densities than EDLCs. There are two electrode materials that are used to store charge in pseudocapacitors, conducting polymers and metal oxides [27].

Electrode Materials Used in Pseudocapacitors

Conducting Polymers Conducting polymers have a relatively high capacitance and conductivity and a relatively low ESR and cost compared to carbon-based electrode materials [27]. In particular, the *n/p*-type polymer configuration, with one negatively

charged (*n*-doped) and one positively charged (*p*-doped) conducting polymer electrode, has the greatest potential energy and power densities. However, a lack of efficient *n*-doped conducting polymer materials has prevented these pseudocapacitors from reaching their potential. Additionally, it is believed that the mechanical stress on conducting polymers during reduction–oxidation reactions limits the stability of these pseudocapacitors through many charge–discharge cycles. This reduced cycling stability has hindered the development of conducting polymer pseudocapacitors [27].

Metal Oxides Metal oxides like ruthenium oxide have high conductivity, which makes them a good electrode material for supercapacitors [27]. The capacitance of ruthenium oxide is achieved through the insertion and removal of protons into its amorphous structure. In its hydrous form, the capacitance exceeds that of carbon-based and conducting polymer materials. Furthermore, the ESR of hydrous ruthenium oxide is lower than that of other electrode materials. As a result, ruthenium oxide supercapacitors may be able to achieve higher energy and power densities than similar carbon electrode supercapacitors. However, despite this potential, the success of ruthenium oxide has been limited by its prohibitive cost. Thus, a major area of research is the development of fabrication methods and composite materials to reduce the cost of ruthenium oxide, without reducing the performance [27].

Composite Electrode Capacitors Composite electrodes integrate carbon-based materials with either conducting polymer or metal oxide materials and incorporate both physical and chemical charge storage mechanisms together in a single electrode. The carbon-based materials facilitate a capacitive double layer of charge and also provide a high-surface-area backbone that increases the contact between the deposited pseudocapacitive materials and electrolyte. The pseudocapacitive materials further increase the capacitance of the composite electrode through faradic reactions [27]. Composite electrodes constructed from carbon nanotubes and polypyrrole, a conducting polymer, have been particularly successful. This electrode is able to achieve higher capacitances than either a pure carbon nanotube or pure polypyrrole polymer-based electrode [27]. This is attributed to the accessibility of the entangled mat structure, which allows a uniform coating of polypyrrole and a three-dimensional distribution of charge. Moreover, the structural integrity of the entangled mat limits the mechanical stress caused by the insertion and removal of ions in the deposited polypyrrole. Therefore, unlike conducting polymers, these composites have been able to achieve a cycling stability comparable to that of EDLCs having carbon-based electrodes [27].

Model for Supercapacitors

A conventional model describing the supercapacitor modeled as an equivalent electrical circuit is useful for developments of applications where supercapacitors can be used. Figure 31, below, shows such a model.

The first parameter is the capacitance of the component. It defines the capacitive behavior of the supercapacitor and the energy that can be stored. This capacitance is not constant. It is dependent on the voltage across and is the reason why the capacitance of the supercapacitor is modeled as a constant capacitor C_o, with a parallel capacitor C_v, which has a linear dependence on the voltage V [25].

$$C = C_o + C_v, \text{where } C_v = K \bullet V \tag{3}$$

This defines the capacitance C of the component.

Following this definition, the current capacitance can be derived from (3).

$$Q = CV$$

$$I_c = dQ/dt$$

Therefore,

$$I_c = (C_o + 2K \bullet V)dV/dt \tag{4}$$

$$\text{Currentcapacitance } C_i = C_o + 2K \bullet V$$

Similarly, energy capacitance can also be defined.

$$\text{Power } (P) = I_c \bullet V = (C_o + K \bullet V^2)dV/dt \tag{5}$$

$$\text{Energy } (W_w) = {}^1\!/_2(C_o + 4/3(K \bullet V))V^2 \tag{6}$$

$$\text{Energycapacitance } (C_w) = C_o + 4/3(K \bullet V) \tag{7}$$

The amount of energy that can be stored into a supercapacitor can be expressed as a function of the

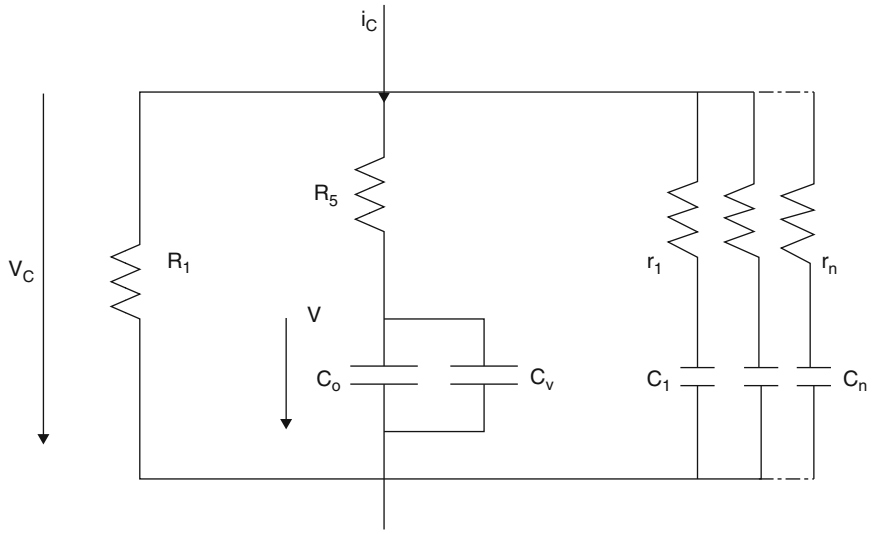

Battery Technologies. Figure 31
Equivalent circuit model for supercapacitors [25]

Battery Technologies. Table 10 Energy capability versus the capacitance [25]

Capacitance	C = 1,800 F	W = 5,625 J	
Current capacitance	C_i = 2,100 F	W_i = 6,562 J	+16.65% increase
Energy capacitance	C_w = 1,850 F	W_w = 5,781 J	+2.77% increase

capacitance that is considered. This is summarized for a 1,800 F/2.5 V supercapacitor, where measurements for C = 1,800 F and K = 150 F/V in Table 10.

The current capacitance C_i shows that it is possible to store 16.55% more energy than expected considering only the constant capacitance given by the manufacturer. Another consequence of this voltage-dependent capacitance is that the voltage will not increase linearly during the charge with a constant current. Two other parameters are conventional for a supercapacitor model. The first one is the series resistor R_s that induces voltage drops during charge and discharge. Its value influences the energy efficiency of the component and its power density. The second conventional parameter is the leakage resistor R_l that induces load losses when the component is in a standby mode. However, this resistor is not the only parameter that influences the voltage variation across a supercapacitor between a charge and discharge operation. This is illustrated in Fig. 32 [25].

The upper curve shows the typical voltage variation V_c across a 800 F/2.5 V supercapacitor during the end of its charge with a constant current. Once the charge is ended, the voltage decreases rapidly. This could be due to the leakage resistor but this is not strictly the case if the model in Fig. 31 is considered again. It makes n parallel RC circuits appear. This is illustrated in the lower part of Fig. 32 where the relaxation phenomena are presented as the charge of RC circuits with different constant times. The result is a decrease of the main voltage, not due to a dissipative component, but due to a homogenous arrangement of the loads and ions on the electrodes and in the electrolyte. Once all the voltages across all the equivalent capacitors are equal, then relaxation phenomena are supposed to be ended. The decrease of the main voltage is then linked to a leakage current. An ideal supercapacitor model should propose an infinite number of RC branches. For practical reasons linked to measurement, most of the models identify only two or three of these equivalent subcircuits [25].

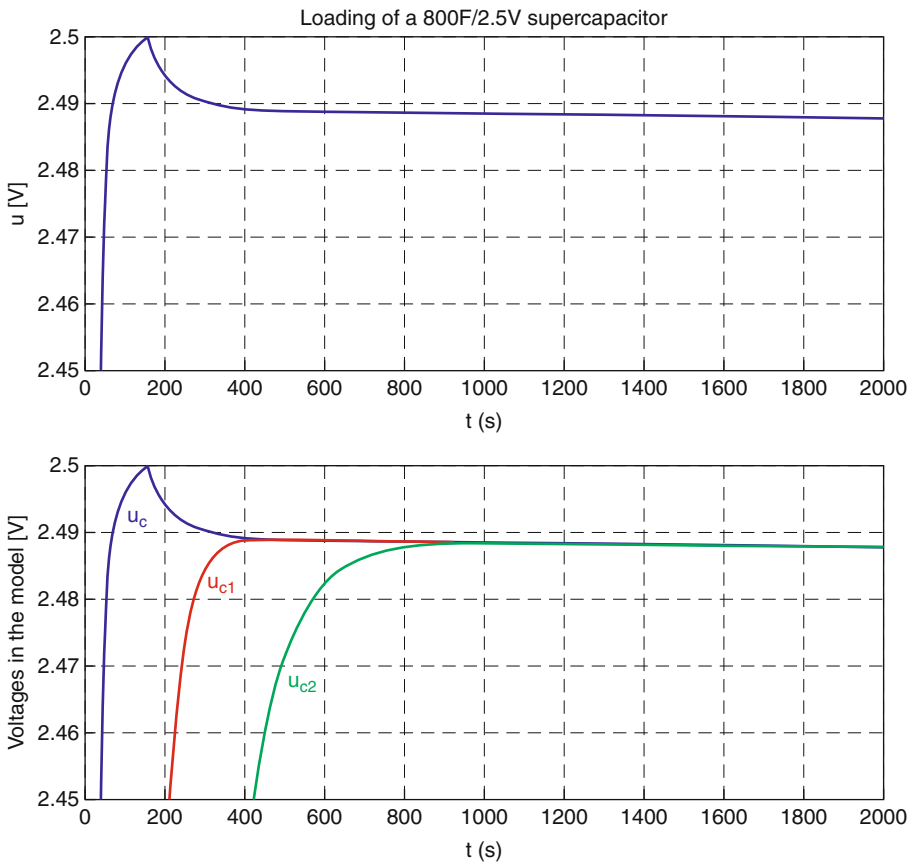

Battery Technologies. Figure 32
Relaxation phenomena [25]

Sizing Method of a Supercapacitive Tank

For a supercapacitor, the total amount of energy W_M that can be stored is expressed as a conventional capacitor:

$$W_M = \tfrac{1}{2}(C \bullet V_M{}^2) \tag{8}$$

where C is the capacitance of the component and V_M is the maximum voltage. The voltage across the component has to be decreased from its maximum allowed value to 0 V for the use of the total amount of stored energy. This is not possible because the current provided by the supercapacitor should be infinite. For this reason, the minimum voltage when discharging the component has to be limited and all the energy stored in the component is not used [25]. It is then necessary to define the parameter d, which is the ratio between the minimum allowed voltage V_m for the discharging, and the maximum voltage V_M that defines a full charging of the component. d is expressed in percent and is called the discharge voltage ratio:

$$d = (V_m/V_M) \bullet 100 \tag{9}$$

Under this condition, the usable energy W_v that a supercapacitor can provide is given by the equation:

$$W_v = W_M\left(1 - (d/100)^2\right)^2 \tag{10}$$

If d = 50%, the voltage is half of the maximum voltage at the end of the discharge, then the usable energy W_v will be 75% of the total stored energy W_M. For a given usable energy, the last two equations can be combined to identify the number of supercapacitors in the supercapacitor bank.

$$N_s = 2W_v/CV_M{}^2\left(1 - (d/100)^2\right) \tag{11}$$

Battery Technologies. Table 11 Sizing of a supercapacitor tank

N_s	d (%)	Volume (m^3)	Weight (kg)	E (kWh)
4,872	50	1.46	1,943	7.6
5,709	60	1.71	2,283	8.92
7,164	70	2.15	2,865	11.2

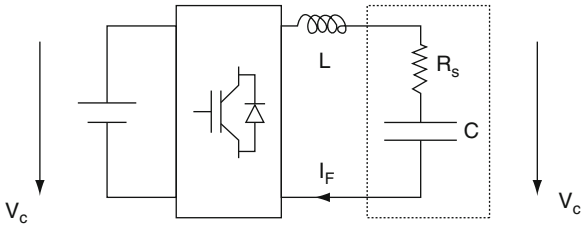

Battery Technologies. Figure 33 Interfaces for supercapacitors [25]

Let us take an example where the supercapacitor is 1,800 F/2.5 V and the usable energy $W_u = 0.55$ MJ = 5.7 kWh. The corresponding sizing of a supercapacitive tank is given for three different values of d according to (10) and this supercapacitor in Table 11 [25].

$$W_v = 0.55\text{MJ}, C = 1800, FU_M = 2.5, VI_M = 200\text{A}$$

The best choice should define a SB with d = 50% because of the reduced number of supercapacitors and because the usable energy W_v is 75% of the maximum stored energy W_M. On another hand, the choice of N_s = 7,164 (d = 70%) leads to a strong oversizing of the SB where the usable energy W_v is only 51% of the maximum stored energy. This offers an interesting versatility in the management of the energy that has to be provided. If that tank and its associated power converters are designed for d = 70%, it will be possible to vary the voltage more than that limit in case of stronger random power constraints [25].

Energy Efficiency and Power Availability

One of the main parameters of a supercapacitor is its series resistance. Independent of voltage falling during charge and discharge, internal losses are due to this element. Even if manufacturers succeed in reducing the value of the series resistor, its value induces an energy efficiency lower than unity with the consequence of a reduction of the power availability [25].

The energy efficiency of supercapacitors is taken into consideration while sizing a supercapacitive tank because the way supercapacitors are charged and discharged influence their performance. One of the only ways to control the charging/discharging process is to develop power electronics interfaces in order to control the current for loading/unloading the supercapacitors [25]. This is illustrated in Fig. 33. The charge of supercapacitors is realized with a constant current, as shown in Fig. 34, where supercapacitors are loaded from a dc voltage source. The charging/discharging current is adjusted to maintain the product of v_cI constant. The value of the charging/discharging current or power will define the energy efficiency of the supercapacitive tank together with the value of the equivalent series resistor. This is illustrated in Fig. 35 where the voltage discharge ratio d is 50%. In this case, 75% of the total used energy is loaded and unloaded for a 2,600 F/2.5 V/0.7 mΩ supercapacitor. The energy efficiency is presented versus the time, the current, or the power needed for loading/unloading the component [25].

The time for loading energy is chosen to be 10 s. Its energy efficiency is expected to be over 90%. This means a charging current limited to 320 A or a charging constant power limited to 700 W. The same can be applied to the current or the power during discharge. The constant power has to be kept lower than 420 W to obtain more than 90% energy efficiency. This has a consequence on the power density of the component which is 4,300 W/kg. Taking into account the energy efficiency, the power density will only be 806 W/kg if the energy efficiency is to be kept higher than 90%. This leads to an increased number of supercapacitors for the design of a storage tank. Therefore, the energy efficiency and the power availability both have to be taken into account for the design of a supercapacitor storage bank. The final parameter to be taken into account is the efficiency of the power converter needed for interfacing the supercapacitors with their load [25].

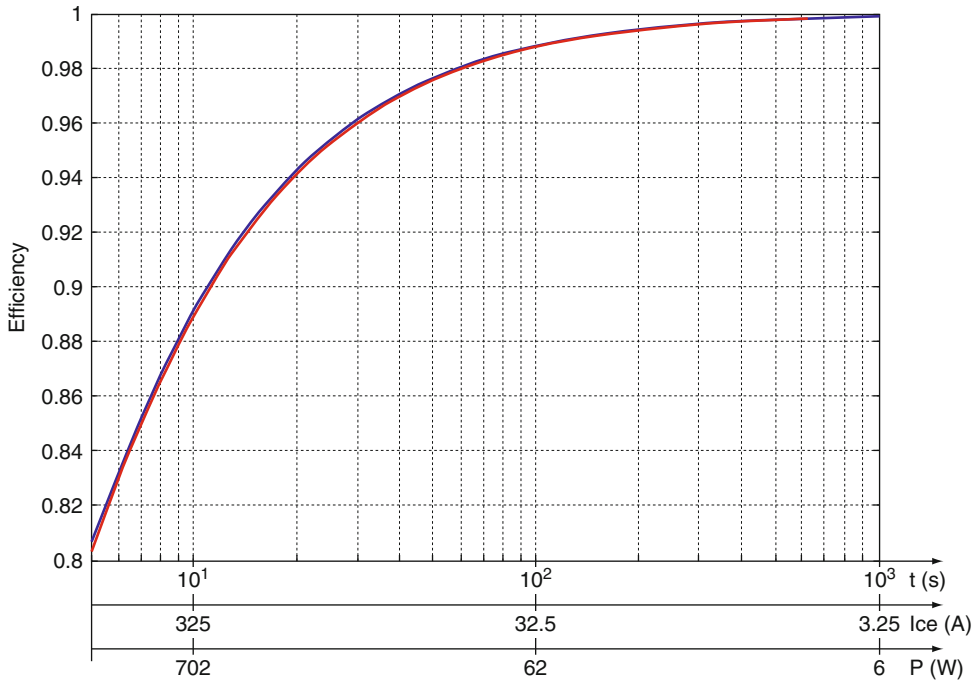

Battery Technologies. Figure 34
Charging characteristics [25]

Power Train System Architecture

Architecture conceived with the electronic interface between the SB and the traction battery are shown in Fig. 36 below.

The main characteristics of this architecture are:

- The DC-to-DC converter has to be dimensioned for the maximum power flow into and out of the SB [26].
- The SB voltage may be kept always lower than the minimum traction battery voltage. As a consequence, a simpler DC-to-DC converter design may be obtained. The DC-to-DC converter may operate only in step-up mode during the traction phase and only in step-down mode during the braking phase [26].
- A lower operating voltage implies a lower number of cells connected in series and a reduced complexity of the electronic module of the SB [26].
- The possibility to add an auxiliary generator (auxiliary power unit) configuration without modifying the existing structure [26].

Future Developments in Supercapacitors

Currently, there is work in progress on the development of supercapacitors using solid dielectrics.

The energy density stored in a capacitor is given by:

$$W = \frac{1}{2}\varepsilon_o \varepsilon_r E^2$$

ε_o is the dielectric constant of free space, ε_r is the relative dielectric constant, and E is the electric field strength. Relative dielectric constants of 200,000 have been measured for 500 nm particles of $BaTiO_3$ coated with 5 nm of SiO_2 [28]. If these particles can be fabricated into supercapacitors with breakdown electric field strengths of the order of the breakdown strength of SiO_2, around 6×10^6 V/cm, then energy densities of the order of

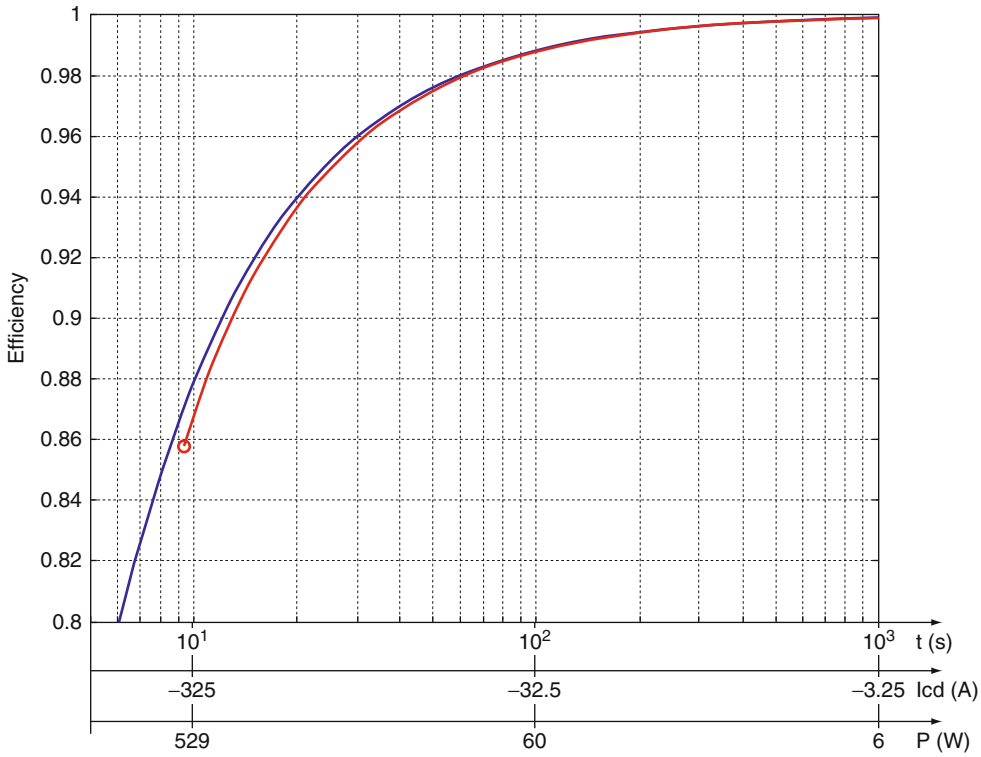

Battery Technologies. Figure 35
Discharging characteristics [25]

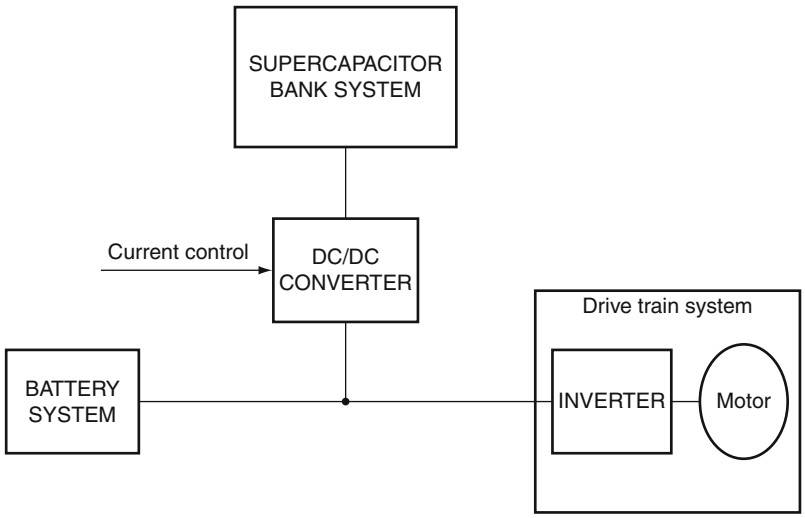

Battery Technologies. Figure 36
Powertrain architecture with DC/DC converter and series supercapacitor bank series connected [26]

Battery Technologies. Table 12 Recommendations for future work

Action	Short term	2011–2013	2012–2016	2015–2020
Develop value propositions for storage to enable more renewable integration	Conduct assessment of utility and private renewable integration	Simulation and cost-benefit analysis of renewable plants and private systems	Large-scale demonstrations	Value and risk of renewable integration verified by the utility and understood by the end user
Development and enforcement of regulations	Develop target for development of regulations to address issues and risks associated with storage systems	Persistent enforcement of regulations in all types of regions (high and low renewable concentration)	Monitor progress of regulations and provide feedback for improvement in methodologies of local utility	Identification and continued enforcement of key regulations
Scenario modeling	Develop models for accurate forecasting of resource accessibility, demand, dispatch capabilities, pricing, and reliability	Identify incremental (smart grid, nuclear) and detrimental (EV, storage) technologies, in terms of grid operational risk	Demonstration of effects of best- and worst-case scenarios on supply/demand, technological development, and capital costs	Identification of relevant scenarios that will help guide the future development of potential storage technologies
Contribution: utility and public	Development of customer and utility actions for propagation of the renewable agenda	Assessment and regulated enforcement of utility enforced actions (e.g., price incentive for customers, storage management)	Assessment of potential customer actions (e.g., use of energy efficient devices)	Identification of low-risk actions for the utility and the customer
Reliability assessment	Develop current, short- and long-term assessment roadmap for risks associated with storage integration	Identify key factors affecting reliability of storage systems (e.g., variability, ramping requirements, peak mismatch)	Develop plan to proportionally increase integration of low-risk storage systems, with increasing demand, to achieve higher base-load penetration	Studious development of reliability risks and solutions for potential storage technologies

100 KJ/cm^3 may be possible. If very high energy densities are achieved, these supercapacitors may replace batteries in EVs. There are a variety of materials with which very high dielectric constants can be obtained but there is a great deal of work to be done before these supercapacitors become available for EVs [28].

Recommendations for Future Work

Various applications and options discussed in this entry are still in the development phase and therefore are not "grid-ready." Current progress in the energy storage sector is limited to fulfillment of functional specifications only. Grid storage solutions are a long term goal for this sector. To develop these solutions, short-term goals need to include fundamental research, analysis, testing, evaluation of risk, and demonstration of technology. Table 12 is considered a starting point for the fulfillment of short- and long-term goals.

Bibliography

Primary Literature

1. Hatziargyriou N et al (2000) Cigre technical brochure on modeling new forms of generation and storage. TF 38.01.10 Nov 2000
2. HEV sales by models (2010) Alternative fuels and advanced vehicles data center. Retrieved Sept 2010 from http://www.afdc.energy.gov/afdc/data/vehicles.html
3. Lithium-Ion Technology Status Report (2005) EPRI
4. Lead acid batteries Woodbank Communications Ltd (2005) Retrieved 20 Nov 2010 from http://www.mpoweruk.com/leadacid.htm
5. Brodd RJ, Ozawa K, Yoshio M (2009) Lithium-ion rechargeable batteries, materials, technology and new applications. Wiley-VCH, Weinheim
6. Solar Energy Report (2005) Arizona Solar Center. Retrieved 12 Nov 2010
7. Kopera JJC (2005) Considerations for the utilization of NiMH battery technology in stationary applications. In: The Battcon 2005 proceedings, Albercorp, Florida, 2005
8. Duvall M (2004) Advanced batteries for electric-drive vehicles: a technology and cost-effectiveness assessment for battery electric vehicles, power assist hybrid electric vehicles, and plug-in hybrid electric vehicles. Final report 1009299. EPRI, Palo Alto, CA. Retrieved 30 Sept 2010
9. Gage TB (2000) Lead acid batteries: key to electric vehicle commercialization experience with design, manufacture, and use of EVs. Proceedings of the 5th Annual Battery Conference on Applications and Advances, 11–14 January 2000, pp 217–222
10. Lead Acid Batteries Recharged. The economist. http://www.economist.com/node/12924031?story_id=12924031
11. Ford Ranger EV Vehicle Specifications (1998) Electric transportation applications. http://avt.inel.gov/pdf/fsev/eva/ford_eva.pdf
12. General Motors EV1 Vehicle Specifications. Electric transportation applications. Retrieved 8 Oct 2010 from http://avt.inel.gov/pdf/fsev/eva/genmot.pdf
13. Taniguchi A, Fujioka N, Ikoma M, Ohta A (2001) Development of nickel/metal-hydride batteries for EVs and HEVs. J Power Sources 100(1–2):117–124, Elsevier Science
14. Notten PHL, Van Beek JRG (2000) Nickel-metal hydride batteries: from concept to characteristics. Chem Ind 54(3):102–115, CEON/CEES
15. Avicenne Conference, Nice 2008, M. A. Fetcenko/ECD
16. General Motors EV1 Vehicle Specifications with NiMH batteries. Electric transportation applications http://avt.inel.gov/pdf/fsev/eva/ev1_eva.pdf
17. Schalkwijk WAV, Scrosati B (2002) Advances in lithium-ion batteries. Plenum, New York
18. Davide A (2010) Battery management systems for large lithium battery packs. Artech House, Boston
19. General Outline for Advanced Battery Testing. USABC
20. Alexander M, Duvall M (2005) Batteries for electric drive vehicles – status 2005. EPRI
21. Huajun G, Qiyang H, Wenjie P, Xinhai L, Yong Y, Yunjian L (2009) Performance and capacity fading reason of $LiMn_2O_4$/graphite batteries after storing at high temperature. J Rare Met 28(4):322–327
22. Xia Y, Yoshio M, Zhou Y (1997) Capacity fading on cycling of 4 V Li/LiMnO cells. J Electrochem Soc 144:2593
23. Duvall M, Rogers A (2010) Plug-in fuel cell vehicle technology and value analysis. EPRI
24. Voelcker J (2007) Lithium batteries for hybrid cars. IEEE Spectrum. Retrieved from http://spectrum.ieee.org/green-tech/advanced-cars/lithium-batteries-for-hybrid-cars
25. Barrade P (2003) Energy storage and applications with supercapacitors. Laboratoire d'Electronique Industrielle (LEI), Ecole Polytechnique Fédérale de Lausanne (EPFL), Lausanne (Switzerland)
26. Faggioli E, Rena P, Danel V, Andrieu X, Mallant R, Kahlen H (1999) Supercapacitors for the energy management of electric vehicles. J Power Sources 84(2):261–269, Elsevier
27. Halper MS, Ellenbogen JC (2006) Supercapacitors: a brief overview. MITRE, Nanosystems Group, Virginia
28. Yang Cheng-Fu (1996) Improvement of the sintering and dielectric characteristics of surface barrier layer capacitors by CuO addition. Jpn J Appl Phys 35:1806–1813

Books and Reviews

Advanced Lead Acid batteries with Carbon enhanced electrodes. http://www.electricitystorage.org/ESA/technologies2/_advanced_lead-acid_batteries_with_caron-enhanced_electrodes_ala-cee_batter/. Accessed йил Sept 2010

Chan CC, Wong YS (November/December, 2004) Electric vehicles charge forward. IEEE Power Energ Mag 2(6):77–79

Everything about NiCd batteries. http://www.batterychronicle.com/2009/10/everything-about-nicd-batteries-2/. Accessed йил 26 Oct 2010

Jacoby M (2010) Rechargeable metal air battery. http://pubs.acs.org/cen/science/88/8847sci1.html. Accessed йил 22 Nov 2010

Metal-air batteries. http://www.electricitystorage.org/ESA/technologies/metal-air_batteries/. Accessed йил Sept 2010

Moseley PT (2000) Improving the valve-regulated lead-acid battery. J Power Sources 88(1):71–77, Elsevier, 10th October 1999

Putois F (1995) Market for nickel-cadmium batteries. J Power Sources 57(1–2):67–70, Elsevier

Riezenman MJ (1998) Engineering the EV future. IEEE Spectr 35(11):18–20

Tarascon JM, Armand M (2008) Building better batteries. http://www.nature.com/nature/journal/v451/n7179/full/451652a.html. Accessed йил 6 Feb 2008

Zinc-Bromine battery. http://energystoragedemo.epri.com/cec/zbb/tech_desc.asp

ZnBr batteries. http://www.electricitystorage.org/ESA/technologies2/_zinc_bromine_zn_br_batteries/. Accessed йил 2009 April

Bicycle Integration with Public Transport

John Pucher[1], Ralph Buehler[2]
[1]Bloustein School of Planning and Public Policy, Rutgers University, New Brunswick, NJ, USA
[2]School of Public and International Affairs, College of Architecture and Urban Studies Virginia Tech, Alexandria, VA, USA

Article Outline

Glossary
Definition of the Subject and Its Importance
Introduction
Trends in Bike-Transit Integration
Extent of Bike-and-Ride Facilities in North America
Case Studies of Bike-Transit Integration
Future Directions
Bibliography

Glossary

Bike lane A special road lane reserved for bikes only, usually about 4–6 ft wide, normally located on the right-hand side of the road.

Bike locker A box-like metal or plastic container for secure bike storage, often at rail stations, usually rented on a monthly basis.

Bike rack A device on which bikes can be mounted for transport (on buses) or attached for storage and security (on sidewalks).

Bike station Full-service, secure bike parking facility, usually providing repair and rental services, accessories, and touring advice.

Bus Motorized coach services providing communal transport on roads, usually in mixed traffic, but sometimes as part of special bus rapid transit (BRT) systems with separate rights of way.

Light rail Type of rail system similar to streetcars (trams) but often with separate right of way over at least part of its route, special boarding stations, and pre-paid fares.

Metro Urban rail system with separate rights of way, frequent service, and high carrying capacity, usually found only in large cities.

Public transport/transit General term for communal transport in cities, including buses, trams, trolleys, light rail, metros, suburban rail, ferries, and funiculars.

Suburban rail Short-distance passenger rail systems connecting large cities with their surrounding metropolitan areas, with longer distances between stops and less frequent service than metro systems.

Definition of the Subject and Its Importance

Coordinating bicycling with public transport is mutually beneficial, enhancing the benefits of both modes and encouraging more bicycling as well as more public transport use. Bicycling supports public transport by extending the catchment area of transit stops far beyond walking range and at much lower cost than neighborhood feeder buses and park-and-ride facilities for cars. Access to public transport helps cyclists make longer trips than possible by bike. Transit services can also provide convenient alternatives when cyclists encounter bad weather, difficult topography, gaps in the bikeway network, and mechanical failures.

Introduction

The overall importance of both bicycling and public transport in northern Europe has provided a strong rationale for coordinating these two modes of urban transport in recent decades [1]. European studies find that coordinating bicycling with public transport is mutually beneficial, enhancing the benefits of both modes and encouraging more bicycling as well as more public transport use [2–8]. In the Netherlands, 35% of all rail passengers reach their stations by bike – compared to 25% in Denmark and 9% in Sweden [1].

The main form of bike-transit integration in Europe is bike parking at suburban train and metro stations [1]. In the Netherlands, there are 350,000 bike parking spaces at train stations. German cities also have extensive bike parking at rail stations. The City of Berlin, for example, has over 32,000 bike parking spaces at its metro and suburban rail stations [9]. By comparison, no city in North America has more than 15,000 bike parking spaces of any kind, let alone at public transport stops.

The most impressive bike-and-ride facilities in Europe are state-of-the-art "bike stations," which

provide secure, sheltered parking as well as a wide range of services such as bike repairs, accessories, washing, rentals, and travel advice. In 2007, there were 67 bike stations in the Netherlands, 70 in Germany, and 20 in Switzerland, almost always located adjacent to train stations to facilitate bike-and-ride [1, 5, 10–12]. As noted later in this entry, there are only ten bike stations in all of North America, and they are much smaller than those in Europe.

North America obviously lags behind Europe in the integration of bicycling and public transport. In the past, bike-and-ride in North America was limited by low overall levels of cycling and public transport use in most cities, just the reverse of the situation in northern Europe [1, 5, 12, 13]. In recent years, however, both cycling levels and public transport use have risen sharply in the USA and Canada, and bike-and-ride trips have been increasing as well. Indeed, in some cities it has been so successful that the demand for bike-and-ride facilities exceeds the available supply [14, 15].

This entry describes the programs and policies currently being implemented in North America to integrate bicycling with public transport. It starts off with a brief overview of the various kinds of integration and the extent of their implementation. Most of the entry, however, is devoted to case studies of bike-transit integration in two large cities in Canada (Toronto and Vancouver) and six large cities in the USA (San Francisco, Portland, Minneapolis, Chicago, Washington, DC, and New York City). The case study analysis compares the type and extent of integration measures undertaken in the various cities, noting the strengths and weaknesses of each city's integration policies. The entry concludes by identifying the most innovative and successful policies in the eight cities and offers policy recommendations for future improvements.

Trends in Bike-Transit Integration

In recent years, levels of cycling and public transport use have reached record highs in both the USA and Canada. In 2008 public transport use in the USA was at its highest level since the early 1960s [16, 17]. Between 1995 and 2008, public transport trips rose by 38% in the USA and by 46% in Canada [17, 18]. Similarly, levels of cycling have increased considerably since 1990. In the USA the total number of bike trips to work increased by 32% from 1990 to 2005–2007 (averaged) [19, 20]. Over the shorter period 1996–2006, the number of bike trips to work in Canada rose by an even larger 42% [21].

While rising public transport use and increased cycling have provided the rationale for more bike-transit integration, federal funding in the USA has provided the necessary financing for a wide range of projects implemented in recent years at the state and local government levels [14, 15, 22, 23]. Indeed, the federal government finances some categories of bike-transit integration projects with an especially high 95% federal share. The integration of public transport with cycling has been endorsed by the Federal Transit Administration, the Federal Highway Administration, and the Transportation Research Board [14, 15, 24]. The Transport Association of Canada [25] and Transport Canada [26] have also endorsed bike-transit integration, but there is no federal funding for urban transport in Canada. There is no federal funding for urban transport in Canada, but provincial and local governments have provided large increases in funding for public transport and bicycling in recent years, including projects aimed at better integration [27, 28].

As documented in this entry, virtually every large city in the USA and Canada has been undertaking a range of measures to promote bike-and-ride. There are five main categories of measures to promote bike-transit integration:

(a) Provision of bike parking at rail stations and bus stops, with different degrees of shelter and security
(b) Multifunctional bike stations providing not only parking but also a range of services such as bike rentals, repairs, parts and accessories, bike washing, showers and lockers, and touring advice
(c) Bike racks on buses, usually exterior, but occasionally interior storage
(d) Bikes on board vehicles, usually rail vehicles, sometimes with special bike racks, hooks, or even bike cars on trains
(e) Bike paths, lanes, and on-street routes that lead to public transport stations and stops, thus facilitating the bike's role as feeders and collectors for public transport

Extent of Bike-and-Ride Facilities in North America

The only available national statistics on bike parking at public transport stops are from recent surveys of 272 American and Canadian transit systems by the American Public Transportation Association [29, 30]. In the USA, the supply of bike parking spaces in 2008 was 24,178 at rail stations, 9,005 at bus stops, and 176 at ferry terminals. For the same year, Canadian systems reported 2,892 bike parking spaces at rail stations and 481 at bus stops. Between 2006 and 2008, the supply of bike parking increased by 67% in Canada and 26% in the USA [29, 30]. That is impressive progress, but it is striking that in 2008, the total supply of bike parking at public transport systems in the entire USA was only slightly more than the 32,000 spaces in Berlin, Germany [9].

Not only is there much less bike parking in North America, but it is far less likely to be sheltered and/or guarded. Throughout northern Europe, there has been a trend toward sheltered, guarded bike parking, usually outdoors but increasingly in bike stations [1, 5, 9, 12, 31, 32]. By comparison, unattended bike lockers are the main form of secure bike parking at North American public transport stops. Of the 56 large American and Canadian transit systems surveyed by the Transportation Research Board [15], 14 systems provided bike lockers at some of their rail and bus stops, but the actual number of lockers was not reported. The same TRB survey reported eight staffed bike parking stations in 2005, mainly on the West Coast. A few more bike stations have opened since then [10].

By far the most important form of bike-transit integration in North America is bike racks on buses. Indeed, on this dimension, North America is far ahead of Europe, where very few buses come equipped with bike racks. That is not surprising since 60% of all public transport trips in the USA are by bus [18]. Bike racks are inexpensive to install, easy to operate, and do not take up space on the vehicles themselves [15]. The 2005 TRB survey found that systems throughout the USA and Canada provide bike racks on buses, and that most systems have eliminated fees they had previously charged for rack use. As shown in Fig. 1, the percentage of buses with bike racks almost tripled in the USA in only 8 years, from 27% in 2000 to 72% in 2009 [30, 33]. Since 60% of all public transport trips in the USA are by bus, it is understandable that the focus of bike-transit integration efforts in North America has been on bus-bike racks [18, 33]. They are inexpensive to install, easy

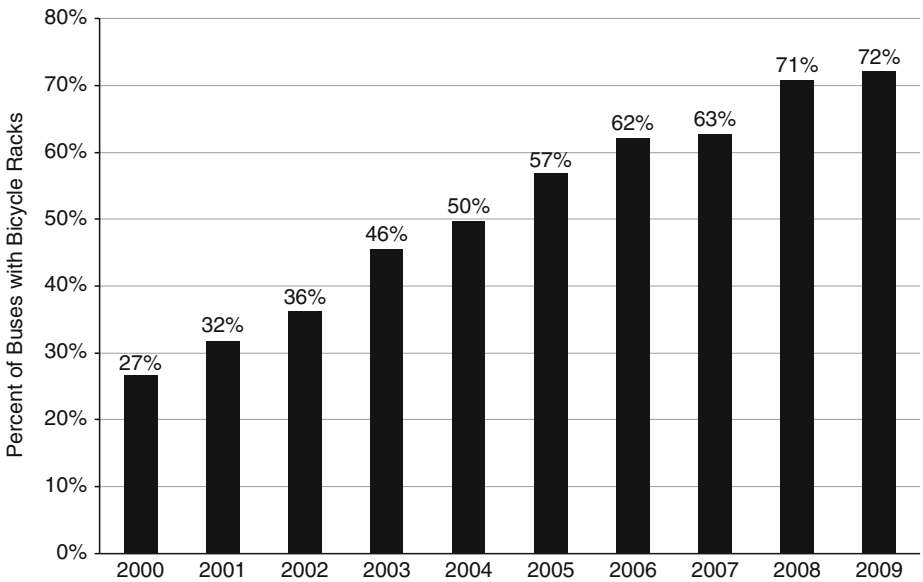

Bicycle Integration with Public Transport. Figure 1
Trend in percentage of buses with exterior bicycle racks in the USA, 2001–2009 [18]

to operate, and do not take up space on the vehicles themselves [15].

Another important form of bike-transit integration is the permission to take bikes on board public transport vehicles, since that enables cyclists to ride their bikes to and from public transport stops at both ends of their trips. Few public transport systems permit bikes to be taken on board buses unless they are compact, folding bikes. But most systems permit bikes on light rail, metro, and suburban rail trains, except during peak hour periods when crowding makes this infeasible [15]. Moreover, an increasing number of public transport systems are providing special accommodations for bikes on trains, such as bike racks, bike hooks, special bike holding areas near the doors, and even special bike cars – although rarely [15, 33].

The last aspect of bike-transit integration is the coordination of bike routes with public transport stops. There are no national statistics available on the extent of implementation, and it would be hard to quantify at any rate. Nevertheless, the eight case studies qualitatively assess this aspect of bike-transit integration in each of the cities.

Case Studies of Bike-Transit Integration

All eight of the case study cities are large, but they vary considerably in metropolitan area population, ranging from 2.2 million in Portland, Oregon, to 18.2 million in New York City. The cities also vary widely in their geographic locations, climate, and topography. Most important for this study, they vary greatly in the share of trips covered by bicycling and public transport, as shown in Figs. 2 and 3.

In 2006, public transport shares of work trips for central city residents ranged from only 13% in Portland to 55% in New York (Fig. 2). Public transport trip shares for metropolitan areas ranged from 5% in Minneapolis to 30% in New York. The Canadian cities of Vancouver and Toronto have relatively high public

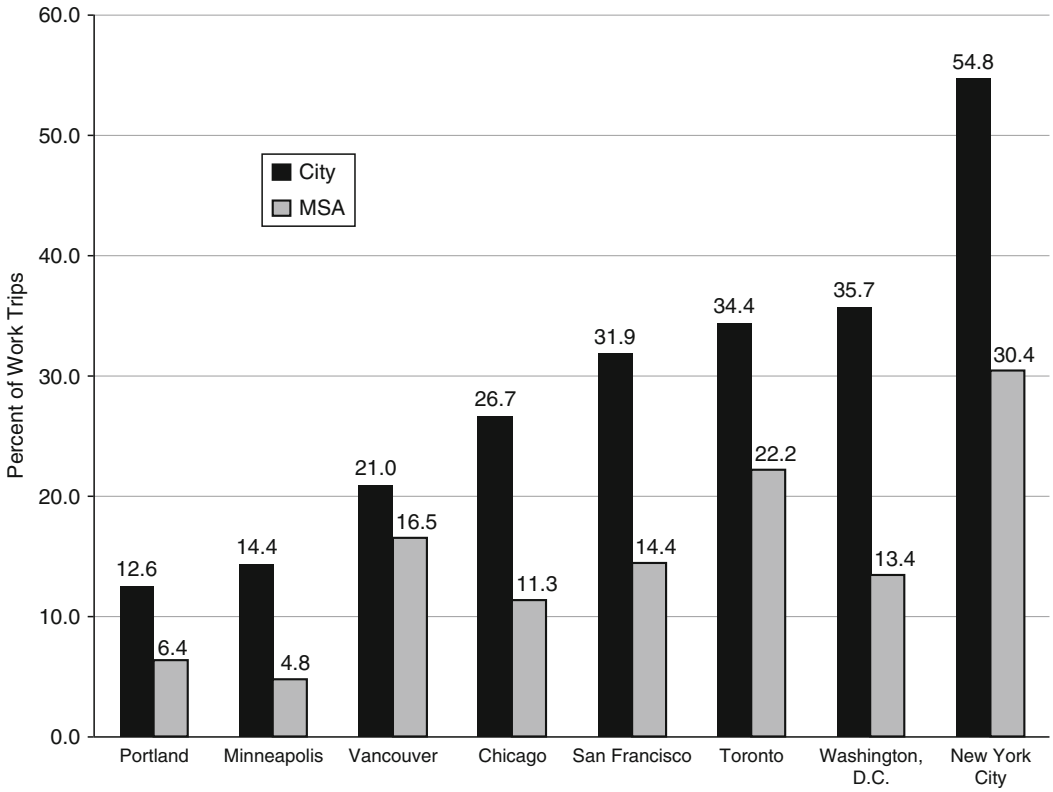

Bicycle Integration with Public Transport. Figure 2
Public transportation share of work trips in US and Canadian cities and metropolitan areas, 2006/2008 [20, 34]

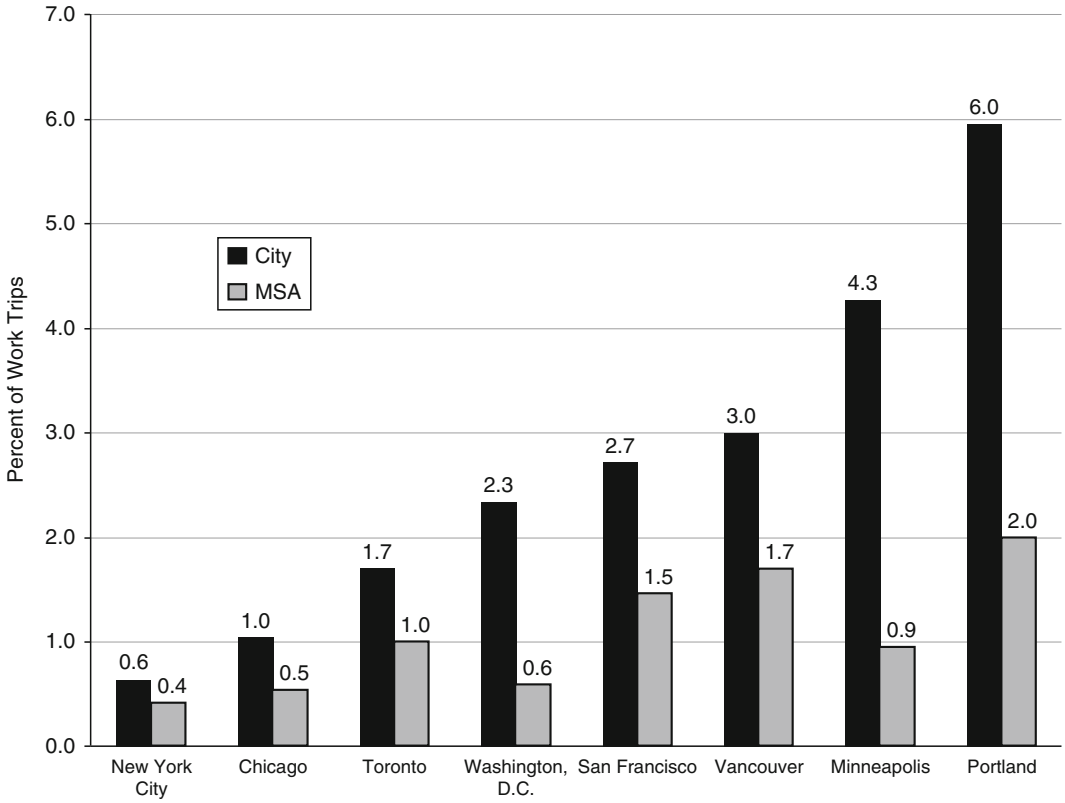

Bicycle Integration with Public Transport. Figure 3
Bicycling share of work trips in US and Canadian cities and metropolitan areas, 2006/2008 [20, 34]

transport use for their intermediate size. Indeed, their metropolitan areas have higher public transport mode shares than the Chicago area. Other studies confirm that, controlling for population size, Canadian cities have slightly more than twice as many public transport trips per capita as American cities [35, 36]. Without exception, public transport use is higher in all eight central cities than in their suburbs. The difference is far smaller in Toronto and Vancouver than for the American cities, because of the higher density of Canadian suburbs as well as the greater provision of public transport services there [35, 36].

Levels of cycling also vary greatly among the eight cities (Fig. 3). Portland (6.0%) and Minneapolis (4.3%) had the highest bike mode shares of work trips in 2006, but Vancouver (3.0%) and San Francisco (2.7%) were not far behind. By comparison, cycling to work in New York (0.6%) and Chicago (1.0%) is rare. Similar to levels of public transport use, bicycling is much higher in central cities than in the suburbs. The differences for Canadian cities, however, tend to be smaller than for American cities, and the reason, again, is the much higher density of Canadian suburbs vis-à-vis American suburbs [28].

There are no comparable statistics on levels of bike-and-ride in each of these cities, since the most recent American and Canadian national travel surveys only report the main mode of transport for the work trip. Figures 2 and 3 provide useful background, however, by portraying the overall levels of cycling and public transport in the eight cities and their corresponding metropolitan areas. On the basis of European experience, it would seem that the higher the levels of both cycling and public transport use, the greater the potential for bike-transit coordination. On the other hand, where there are large imbalances between the two modes, it might suggest that the modes substitute for each other rather than complement each other. For example, the

extremely low level of cycling in New York might be partly due to a high level of public transport use. Conversely, Portland and Minneapolis, the cities with the highest bike mode shares, have the lowest public transport mode shares, suggesting that some bike trips might substitute for public transport trips. There are many possible explanations for the different levels of cycling and public transport use, but a detailed analysis is beyond the scope of this entry, which is limited to the more modest goal of examining the nature and extent of bike-and-ride programs in these eight case-study cities [1, 4, 5, 7].

Efforts to integrate cycling with public transport vary greatly among the eight case studies. New York City, for example, has done little to promote bike-and-ride, while San Francisco, Vancouver, and Portland have implemented the entire gamut of integration measures. The following section highlights the most important aspects of bike-and-ride policies in each city, noting in particular the strengths and weaknesses of current policies.

Unless otherwise indicated, the information for these case studies was obtained by the authors directly from bicycling planners, public transport systems, metropolitan planning organizations, city transport departments, and nongovernmental cycling and sustainable transport organizations in each metropolitan area. The same panel of transit and cycling experts also reviewed the case studies of their cities at several stages to check for accuracy, consistency, and completeness.

San Francisco

The San Francisco Bay Area has been a leader in bike-transit integration efforts in North America. Its regional metro system Bay Area Rapid Transit (BART) provides bike parking at almost all 43 stations, with a total of 4,313 bike parking spaces in 2009, including 1,010 in secure bike lockers. In order to increase convenience and flexibility, BART has been introducing electronic bike lockers (294 as of 2009), which are available on a first-come, first-serve basis and do not require advance subscriptions. Caltrain, the suburban rail line from San Francisco south to Palo Alto and San Jose, provides bike parking at all 32 stations, with a total of 1,100 bike lockers and 400 bike racks.

The San Francisco Bay Area had five of the ten bike stations in the USA in 2009: 226 bike parking spaces at two Caltrain stations and 433 spaces at three BART stations. The BART and SF Caltrain Bike Stations provide free, attended bicycle parking, while the Palo Alto facility is an unattended, fee-based garage. Utilization rates of the bike stations vary widely, from over 100% at the Berkeley BART station to only 11% at the Palo Alto Caltrain station. BART will soon triple the size of the Berkeley bike station and move it above ground to increase accessibility.

Cyclists prefer to take bikes on board, however. A 2008 survey found that 72% of bike-and-ride passengers carried their bikes with them, compared to only 28% who parked them at BART stations. Bikes are allowed on BART trains except during peak hours in the peak direction. Although Caltrain has no time restrictions, cyclists are often denied boarding on rush hour trains because all bike spaces are already occupied. Neither BART nor Caltrain charge a fee for bringing bikes on board. Moreover, Caltrain's lead cars provide special accommodations for 16–32 bikes, depending on time of day and direction of travel. Most of the numerous ferry lines in the Bay Area also permit bikes on board with no extra fee. Folding bikes are allowed on BART and Caltrain at all times, but are not permitted on board San Francisco's MUNI buses, streetcars, cable cars, and light rail vehicles. Complementing bike access to BART and Caltrain services, virtually all buses of all public transport systems in the San Francisco Bay Area are equipped with bike racks, free of charge to cyclists.

There is limited coordination of bike routes with public transport routes. To avoid bus-bike conflicts, bike routes are not usually located on bus routes in San Francisco, but are on parallel streets. Due to the extensive and fine-grained network of bus and rail routes in San Francisco, bike routes often lead to public transport stops, even without any explicit coordination. The Regional Bicycle Plan as well as the Bike Plans of BART and Caltrain explicitly encourage coordination of bike routes and facilities with public transport. Outside of San Francisco, where public transport routes and stations are farther apart, many communities make an explicit effort to coordinate bike routes with key stops.

Overall, bike-transit integration efforts in the San Francisco Bay Area have been successful.

The percentage of public transport trips combined with cycling has more than tripled since 1990. Nevertheless, several problems remain. For example, it is difficult for cyclists to get across the San Francisco Bay during rush hours, since bikes are prohibited from BART trains in peak directions and not permitted on the Bay Bridge. Similarly, Caltrain has problems accommodating bikes on board in the peak hour and often denies boarding to cyclists. The exclusion of bikes from Muni's light rail lines is also a problem for cyclists. Overall, however, the available evidence suggests that bike-transit integration efforts have been successful.

Portland

As shown in Fig. 2, Portland has the highest bike share of work trips of any large American city (6.0%). Thus, one would expect a high degree of bike-transit coordination. Bike-and-ride in Portland, however, is quite different from that in San Francisco and mainly involves bikes on transit vehicles. TriMet, Portland's public transport system, estimates that ten times more bikes are taken on their LRT vehicles than parked at LRT stations (2,100 vs. 200 per weekday). There are no fees, no permit requirements, and no time of day or directional restrictions for taking bikes on LRT vehicles. Every train has a low-floor car especially designed to facilitate bike access, with waiting areas and four bike hooks located near the doors. But passengers without bikes have priority to board crowded trains. All buses in the Portland area have bike racks, another inducement for cyclists to ride with their bikes instead of parking them.

By comparison, Portland does not provide much bike parking at train and bus stops. In 2009, there were a total of 670 bike parking spaces at TriMet LRT stops and transit centers (major transfer hubs for several bus or LRT lines). Of those, almost half were bike lockers. In addition, there were city-owned bike lockers at 15 locations in downtown Portland, most of which are near bus or rail services. In sharp contrast to San Francisco, Portland does not have any bike stations, which is surprising given its high bike mode share and wide range of other pro-bike policies and programs. Bicycling planners and public transport officials in Portland plan to improve bike parking at transit stops by installing 196 bike lockers and 168 bike racks at LRT extensions.

Portland cyclists prefer taking their bikes on board transit vehicles. A survey by TriMet indicated that 76% of cyclists would not be willing to park their bikes at a transit stop even if there were sheltered and secure bike parking available. The advantage of taking bikes on buses or rail vehicles is that bikes can then be used at both ends of the transit trip. So the aversion to parking bikes at bus and rail stops may be due more to convenience than to concerns over theft or vandalism.

Portland carefully and explicitly coordinates its bikeway network with its public transport network. The city has set the goal of a seamless link between cycling and transit. Bike routes are designed to facilitate access to public transport stops. Most transit centers are served by multiple bikeways. Moreover, city planners give special consideration to enhancing bike access to transit stops in outlying areas too far away from the city center for most people to cover by bike alone. Nevertheless, as in most cities, there are some public transport stops that are difficult or dangerous to access by bike. As the largest of America's three platinum level Bicycling Friendly Communities, Portland has already made impressive progress at integrating cycling with public transport and seems sure to continue on that path.

Vancouver

Similar to San Francisco and Portland, Vancouver has vigorously promoted the integration of public transport and cycling. The unique advantage in Metro Vancouver is TransLink, the fully integrated, multimodal regional transportation authority. Unlike the other case studies, public transport, major roadways, and bicycling in Vancouver are all handled within the same agency. The coordination of cycling and public transport is obvious and natural in such a multimodal agency – as reflected in TransLink's plans, funding, construction projects, vehicle procurement, and operating procedures. Over the past 10 years, TransLink has spent over $12 million specifically on bike-transit integration.

As in the San Francisco and Portland areas, all buses in Metro Vancouver are equipped with bike racks. Similar to San Francisco's BART, bikes are allowed on Vancouver's SkyTrain except during peak hours in the peak direction due to problems of overcrowding. Until recently, there were no special accommodations for

bikes on SkyTrains, but all future vehicles will provide a special area for bikes in the rear of each car with a leaning rail and fold-up seats. Bikes are allowed at all times on West Coast Express trains for a $.50 charge. SeaBus ferries permit bikes on board at all times without charge. Almost all of TransLink's rail and ferry services are fully accessible – through elevators, ramps, or level boarding – thus facilitating bike-and-ride.

There are bike racks at all SkyTrain and West Coast Express rail stations as well as park-and-ride lots and transit nodes with interchanges of several bus or rail lines. In 2008, Vancouver had a total of 1,060 parking spaces at transit stops: 660 spaces in racks and 400 secure bike lockers. TransLink plans to increase the overall supply of bike parking at transit stops in the coming years, with a special focus on improving the quality of bike parking, especially secure short-term bike parking. Bike stations at the most important transit hubs are also being considered.

Thanks to its multimodal orientation, TransLink explicitly coordinates bike routes with public transport. For example, the construction of the Millennium, Expo, and Canada SkyTrain lines included traffic-protected, parallel bike routes to foster bicyclist access to public transport. Another aspect of TransLink's multimodalism is the focused promotion of cycling in central corridors where bus and rail vehicles are the most crowded, and where cycling has the potential to divert some of the overload and thus reduce crowding. That coordination of demand and supply between the two modes is rare and emphasizes the advantages of multi-modal agencies such as TransLink.

Minneapolis

Although Minneapolis is, by far, the coldest of the eight cities, it has the second highest bike share of work trips after Portland (4.3% vs. 6.0%). Public transport's share of work trips is slightly higher in Minneapolis than in Portland (13.4% vs. 11.2%), but much lower than in any of the other cities (Fig. 2).

Metro Transit had 497 bike parking spaces at its light rail and bus stops in 2007: 271 spaces in bike racks and 226 bike lockers. Minneapolis has a staffed bike station, the Midtown Bike Center, with 100 bike parking spaces, repairs, rentals, and a café. It is only a block from the Chicago and Lake Streets transit hub, which serves two of the city's busiest bus lines. Perhaps the city's most ingenious policy is the official designation of 35,000 traffic sign posts as bike parking with 70,000 bike parking spaces, assuming two bikes parked at each post. The city also considers that a form of bike-transit integration, since many traffic sign posts are near bus stops, including the bus stop post itself.

All Metro Transit and suburban transit buses are equipped with exterior bike racks, and the city has five stationary bike racks for first-time users to practice loading their bikes. Every light rail vehicle has interior vertical racks that accommodate four bikes. Bike-and-ride has become increasingly popular in Minneapolis. Metro Transit surveys in spring 2007 and fall 2008 found a doubling in the number of bicycles transported on bus racks and a 41% increase in bikes on light rail. On an average weekday in 2008 Metro Transit buses carried 870 bikes. Only 4% of cyclists had to wait for another bus due to racks being filled.

There is no explicit policy of coordinating bike routes and transit stops in Minneapolis, and city officials emphasize the need to improve cycling facilities feeding into public transport stops. Some bike routes already lead to transit stops or parallel transit lines. For example, the Hiawatha LRT line runs parallel to an off-street bike path for most of its length in Minneapolis, thus providing an alternative for cyclists on that route.

Chicago

With the second largest transit system in the USA, Chicago has made impressive efforts to integrate cycling with public transport. Its special distinction lies in the innovative provision of bike parking at rail stations, tailoring the design of parking facilities to each station's particular situation. With 6,420 parking spaces at its rail stations, Chicago has about the same amount of bike-and-ride parking as the San Francisco Bay Area, and far more than other cities in North America.

There are 2,153 bike parking spaces at 131 of the 143 CTA subway and elevated rail stations and 4,267 spaces at 50 of the 76 Metra suburban rail stations. Moreover, indoor or sheltered parking is available at 83 CTA stations, more than any other transit system in North America. The specific location of bike racks inside the stations provides both weather protection and greater

security, since they are usually placed within easy sight of station attendants and other passengers. Chicago is currently installing additional sheltered bike parking for 382 bikes at four CTA stations, and the city has funding to install bike shelters for 250 more bikes in 2010.

The largest bike station in the USA is located in Chicago's Millennium Park, immediately above the terminal station for two of Chicago's suburban rail lines. The bike station is easily accessible from downtown Chicago and the 18-mile Lakefront Trail. It provides secure, indoor parking for 300 bikes as well as convenient lockers, showers and towel service, bike rentals, bike repairs, and guided bicycling tours.

The CTA regularly monitors bike parking needs by conducting bi-annual bike rack inventories and measuring usage rates. It then works with Chicago DOT to install additional racks where needed.

As in most of the case study cities, all of Chicago's buses have bike racks – including CTA buses as well as PACE suburban buses. Bikes are permitted on CTA and Metra trains except during weekday rush hours. And just as most of the other cities, no fees or permits are required for the use of bike racks on buses or for bringing bikes on trains.

The biggest challenge to bike-transit integration in Chicago is the difficult access to train platforms. Because most of the rail lines are so old, only 54% of CTA stations and 68% of Metra stations are ADA accessible. Thus, cyclists are often forced to carry their bikes up long flights of stairs. Few stations have elevators, and cyclists are not permitted to use escalators.

Chicago DOT, transit agencies, and the cycling community are aware of these problems and have made improvements in bike-transit integration a top priority. Chicago's Bike Plan 2015 sets goals of further expanding and improving bike parking inside and outside of rail stations, remodeling stations to make them more accessible to bikes, providing more park-and-ride facilities, and establishing a second bike station with better transit connections.

Toronto

The combination of high rates of transit use and rising cycling levels has prompted a range of efforts to integrate the two modes in the Toronto metropolitan area. The main approach has been to provide ample bike parking. With over 15,000 post-and-ring bike racks throughout the city, Toronto has more bike parking than any other city in North America. That includes bike parking at almost all rail stations. In 2008, there were 1,192 short-term spaces in bike racks at Toronto Transit Commission (TTC) subway stations and 579 short-term spaces in racks at GO Transit suburban rail stations.

Yet there is a severe shortage of secure bike parking, with only 114 bike lockers in the entire transit network. Consequently, Toronto plans on greatly expanding the supply of secure parking in 2009 and 2010 through installation of more bike lockers and completion of a new bike station at Union Station, the main transit hub in downtown Toronto, providing bus, streetcar, subway, and suburban rail connections. The bike station will provide secure, sheltered parking for 200 bikes. Construction of an even larger bike station at City Hall is planned to begin in 2010. That facility will be close to several bus and streetcar lines. The GO Transit suburban rail system is improving its bike parking by expanding sheltered parking to all stations by the winter of 2009–2010.

As in most cities with high levels of rail transit use, bikes cannot be taken on TTC subways and streetcars during weekday peak hours. Even when permitted, there are no special provisions for bikes on TTC subway cars. Similarly, bikes are not allowed on any GO Transit trains headed toward Union Station in the morning peak (6:30–9:30) or departing Union Station in the evening peak (3:30–6:30). Folding bikes are permitted on all public transport vehicles at all times. Bike access to rail transit is limited by the lack of elevators in most subway stations. As in Chicago, cyclists in Toronto must carry their bikes up and down long flights of stairs to reach the train platforms. Only 41% of TTC subway stations are wheelchair accessible, while 75% of GO Transit stations are accessible, either through elevators or ramps.

Toronto is making rapid progress equipping its buses with bike racks, which can be used at any time, even during peak periods. In 2008 only 55% of TTC buses had bike racks, but all new buses have racks, and every month about 40 older buses are retrofitted with racks. By the end of 2010, all TTC and GO Transit buses will have bike racks, thus facilitating bike and ride throughout the region.

There is almost no explicit coordination of bike routes with transit routes and station stops. Instead, the guiding principle of bike route planning is to put every Torontonian within a 5-min bike ride of the bikeway network. The many transit stations and fine-grained street network in much of the central city facilitates bike access to TTC stations. In suburban areas, however, many streets are circuitous and do not connect across arterials, making it difficult for cyclists to avoid major arterials while en route to a transit station.

Although bike-transit integration in Toronto faces some serious challenges, much progress is being made, partly thanks to the Province of Ontario's Metrolinx BikeLinx Program, which helps finance bike parking at stations and bike racks on buses. With the two new bike stations, additional bike lockers, expansion of sheltered parking, and completion of bike rack installation on all buses by 2010, Toronto will have made great strides coordinating cycling and public transport.

Washington

Bike-transit integration in Washington is similar to the situation in the San Francisco Bay Area. Both metropolitan areas rely on regional metro systems started in the late 1960s and early 1970s: BART in San Francisco and Metrorail in Washington. There is bike parking at almost all of Washington's 86 Metrorail subway stations, with a total of 1,800 bike racks and 1,300 bike lockers. The parking facilities are popular, with usage rates at most stations ranging from 50% to 100%. In October 2009, a new bike station with spaces for 150 bikes will open next to Union Station, providing convenient connections to Metrorail as well as suburban trains leaving from Union Station. The bike station will also offer bike rentals, repairs, and accessories as well as storage lockers and changing rooms.

In 2008 a new bike sharing program began in Washington, similar in technology to the Velib system in Paris, but on a much smaller scale: only 120 bikes compared to over 20,000 bikes in Paris. It facilitates bike-and-ride because eight of the ten bike sharing docking stations are at Metrorail stops. The short-term rental bikes can be used to get to and from Metrorail stations, thus serving as feeders and distributors for transit.

Bikes are allowed on Metrorail trains except during morning and afternoon rush hours on weekdays: two bikes per car on weekdays, four bikes per car on weekends. Unlike the much older subway systems in New York and Chicago, all 86 Metrorail stations have elevators (271 in total) and are ADA accessible. That facilitates access to platforms for cyclists as well, who are, in fact, required to use the elevators and are not permitted on escalators. In contrast to the Metrorail, VRE and MARC suburban trains do not allow bikes on board at any time unless they are folding bikes. All 1,450 WMATA buses have bike racks, but some buses run by suburban agencies do not.

In theory, bike plans for the Washington area establish the goal of coordinating bike routes with transit routes, but in fact, nothing has really been accomplished in this area except by accident. Overall, however, bike-transit integration in the Washington area is successful. The biggest gap is the exclusion of bikes from the Metrorail system during peak hours. To some extent, this is unavoidable due to the overcrowding of metro cars, just as on the BART, Toronto, and Chicago subway systems. But it reinforces the need to expand bike parking at the many Metrorail stations where current capacity is insufficient.

New York/New Jersey

With 55% of all work trips by public transport, New York City has, by far, the highest transit mode share of any city in North America. Thus, one might expect substantial efforts to coordinate cycling with public transport. In fact, New York City's transit systems have done little to promote bike-transit integration, far less than any other city in this study. The Metropolitan Transportation Authority (MTA) does not provide bike parking of any kind at the city's 467 subway stations, so the only option for cyclists is to park on nearby sidewalks. The MTA's suburban railroads, the Long Island Railroad (LIRR) and Metro-North Railroad (MNR), offer bike parking at some of their stations – but MTA has no information on the total number of spaces (MTA, 2009).

Compounding the problem of insufficient bike parking along the many subway and suburban rail lines of the MTA, there is no secure bike parking at any public transport terminals in Manhattan. Train, bus, and ferry terminals do not even offer short-term

parking in bike racks. Thus, cyclists must seek out the occasional bike rack on sidewalks within a few blocks of the terminals or risk having their bikes confiscated if parked at traffic signposts, which is illegal in New York.

NYC subways are unique in permitting bikes on board trains at all times, but it is difficult to get bikes to the platforms. Only 16% of New York's subway stations are ADA accessible via elevators or ramps. At the remaining 84% of stations, cyclists must carry their bikes up and down long flights of stairs, as they are prohibited from using escalators in stations where they are available. Bikes are allowed on the MTA's two suburban railroads (MNR and LIRR) except during peak hours in the peak direction, but cyclists must register in advance and purchase $5 lifetime permits. Folding bikes are allowed at all times. In 2008, 18% of LIRR stations and 52% of MNR stations were not ADA accessible – considerably less than the 84% inaccessible MTA subway stations, but still a problem for cyclists having to carry their bikes up and down stairs.

Bike-bus integration is almost non-existent in New York City. Not a single bus in the MTA's fleet of 5,929 buses has a bike rack. That contrasts sharply with 100% of buses equipped with bike racks in most of the other case-study cities. Only since spring 2008 have folding bikes been allowed on most MTA buses.

There is no explicit effort to coordinate bike routes with transit routes in New York City. That is not a severe problem in most of the city because the transit network is so dense that most neighborhoods are served by a nearby subway or bus line. In the suburbs and the outermost portions of the city, however, the complete lack of bike-transit route integration is a serious shortcoming. Precisely in those lower density areas where cycling would provide an ideal feeder mode to more distant transit stops, bikeways are almost exclusively recreational paths that do not connect to practical destinations such as transit stations.

Not only does New York compare unfavorably in its bike-transit integration to the seven other case study cities, but it is surpassed by the New Jersey portion of the Greater New York metropolitan area. In 2008, New Jersey Transit (NJT) offered bike parking at 90% of its suburban rail stations and 80% of its light rail stations, with a total of 2,400 spaces, including 376 secure bike lockers. Unlike the MTA in New York, NJT provides bike racks at all three of its major terminals in Hoboken and Newark (Penn Station and Broad Street). Bikes are allowed on all suburban rail and light rail lines except during rush hours in the peak direction, and no permits or fees are required. Folding bikes are allowed on all NJT vehicles at all times. Roughly half of NJT's 2,000 buses are equipped with bike racks, and an additional 200 buses are outfitted with racks each year. By 2014, 95% of NJT's buses will have bike racks. The main problem in New Jersey is the almost complete lack of bike paths and lanes leading to NJT rail stations and bus stops.

Summary of Case Studies

Most of the case study cities have greatly improved the coordination of bicycling and public transport in recent years. They have increased bike parking at transit stops and better accommodated passengers wanting to take their bikes with them on buses and rail vehicles. Only a few transit systems have measured the actual extent of bike and ride, but the available evidence is encouraging. In Washington DC, for example, the number of bicyclists riding on Metrorail increased by 60% between 2002 and 2007. At some stations, cyclists accounted for up to 4% of all passenger boardings. In Minneapolis, Metro Transit carries over 250,000 bicycles annually and reports a doubling of bikes on buses between spring 2007 and fall 2008. Roughly 4% of Portland MAX light rail passengers carry their bikes onto the vehicles with them. In the San Francisco Bay Area, the share of passengers accessing BART stations by bike rose from 2.5% in 1998 to 3.5% in 2008, with an average of 10,920 bike-and-ride trips per day.

As shown in Table 1, there is considerable variation among the eight case studies. The San Francisco Bay Area, for example, provides the full gamut of bike-integration measures and has been at the vanguard of innovations to promote bike-and-ride. By comparison, New York's transit systems have made few provisions to accommodate cyclists, lagging behind the other case study cities in both the quantity and quality of bike-integration measures. All eight of the cities have plans to further improve bike-transit integration. Thus, it seems certain that the promising trends of recent years will continue.

Bicycle Integration with Public Transport. Table 1 Overview of bike-transit integration measures in eight large American and Canadian cities [37–54]

Bike parking at transit stops and stations	Bikes on transit		Bike routes and transit stops	Highlights: strengths and challenges
	Bike racks on buses	Bikes on trains		
San Francisco (population city: 0.8 m, metro: 4.2 m)				
BART provides 4,313 bike parking spaces, including 716 conventional and 294 electronic bike lockers	All buses have bike racks (usage rates vary from 17% to 43%)	BART allows bikes on all non-peak trains and during peak times in non-peak directions. BART expanded on-board space for bikes on select cars	Bike routes often parallel MUNI bus routes and intersect with transit stops. No explicit planning process coordinating transit and cycling routes in SF	Strengths: Racks on all buses; extra space for bikes on Caltrain cars; bike access to BART off-peak; extensive bike parking at BART and Caltrain stations; five bike stations
Caltrain's 32 suburban rail stations offer 400 bike racks and 1,100 bike lockers		Caltrain: special lead cars designated for bike use all day, space for 16–32 bikes	The Regional Bicycle Plan as well as the Bike Plans of BART and Caltrain encourage coordination of bike routes and facilities with public transport	Challenges: No bike access on MUNI light rail; need more dedicated space for bikes on Caltrain; no coordination of bike routes with MUNI routes; no rush hour access for bikes on BART
Five bike stations with 659 bike parking spaces at BART and Caltrain Stations				
Portland (population city: 0.5 m, metro: 2.1 m)				
Bike racks and/or lockers at almost all TriMet LRT stops and transit hubs providing 670 bike parking spaces; including 320 secured spaces	All buses have bike racks	MAX light rail: bikes permitted if space is available on cars, but non-cyclists passengers have priority	Explicit coordination of bike routes with transit stops with the goal of establishing a seamless link between the two modes	Strengths: Racks on all buses; dedicated space on LRT for hanging bikes near doors; free access for bikes 24/7; easy access to low-floor trains
15 downtown locations with bike lockers; usually close to light rail or bus stops				Challenges: Lack of good quality and quantity of parking at most train stations; poor design of access to stations by bike; cyclists are often denied boarding on LRT during peak
Vancouver (population city: 0.6 m, metro: 2.1 m)				
660 bike parking spaces in bike racks at SkyTrain stations and at transit transfer nodes	All buses have bike racks	SkyTrain: bikes allowed anytime except in peak periods in peak direction	Central Valley Greenway and BC Parkway facilitate access to and from transit stations	Strengths: Bike racks on all buses; bikes allowed on SkyTrain except during peak hours in peak direction; integration of bike network and transit stops; bike parking at all major transit stops; 24/7 no cost bike access on SeaBus
400 secure bike lockers at most Sky Train and all West Coast Express stations		SeaBus: bikes allowed at all times	Translink's $2.55 million annual cost sharing of cycling infrastructure favors projects that facilitate access to transit	Challenges: Need more and better bike parking; need more capacity on SkyTrain to accommodate cyclists

Bicycle Integration with Public Transport. Table 1 (Continued)

Bike parking at transit stops and stations	Bikes on transit		Bike routes and transit stops	Highlights: strengths and challenges
	Bike racks on buses	Bikes on trains		
Minneapolis (population city: 0.4 m, metro: 3.2 m)				
271 bike parking spaces and 226 bike lockers next to Metro Transit stops and at park-and-ride lots. Usage rate of 28% of bike parking spaces at Hiawatha LRT line	All buses have bike racks. Bike on bus demonstration racks in various locations	27 light rail vehicles with on-board interior vertical racks that accommodate 4 bikes per vehicle	No explicit coordination of bike routes and transit. But connection to transit lines is a prioritizing criterion for bike projects funded by the MPO	Strengths: Bike racks on buses and trains; bike racks and lockers at most train stations; marketing information on bike transit integration provided by Metro Transit
City bicycle ordinance encourages parking bikes at sign posts, which are within a block of most bus stops. Bike station 1/10 of a mile from the Chicago and Lake Street transit hub			The Hiawatha LRT line parallels an off-street bike path for most of its length in Minneapolis	Challenges: Bike racks needed at four more LRT stations; lack of bike paths and lanes leading to train stations and bus stops
Chicago (population city: 2.7 m, metro: 9.5 m)				
2,153 bike parking spaces at 131 of the 143 CTA stations and 4,267 bike parking spaces at 50 of the 76 METRA suburban rail stations. Most (83) CTA stations provide indoor or sheltered bike parking. Usage rates of 90% and 50% for indoor and outdoor racks	All CTA and PACE buses have bike racks	Bikes permitted on CTA and METRA trains during off-peak. Bikes not permitted on escalators in stations	The routing of on-street bikeways in Chicago takes the location of transit stations into account. CTA system maps show bike parking possibilities at stations	Strengths: Ample bike parking at 131 CTA stations, of which 83 provide indoor parking. State-of-the-art Millennium bike station at downtown terminus of suburban rail line; CTA regularly collects bike rack usage data to add parking where needed
Largest bike station in the USA with indoor parking for 300 bikes, right above the terminal station for two of Chicago's suburban rail lines				Challenges: The CTA subway is old with limited ADA facilities; flights of stairs make it difficult to bring bikes on board
Toronto (population city: 2.5 m, metro: 5.5 m)				
1,771 short-term bike parking spaces and 114 bike lockers at TCC subway and GO Transit stations	55% of TTC buses and all GO Transit buses have bike racks	Bikes permitted on TTC subways, RT trains, streetcars, and buses without bike racks except during peak hours	The guiding principle of bike facility planning is to put every resident with a 5 min bike ride of the bike network	Strengths: Extensive transit system with high mode share; bike racks on most buses; bikes allowed off-peak on streetcars, subways, and suburban rail; bike parking at most transit stops

Bicycle Integration with Public Transport. Table 1 (Continued)

Bike parking at transit stops and stations	Bikes on transit		Bike routes and transit stops	Highlights: strengths and challenges
	Bike racks on buses	Bikes on trains		
New bike station at Union Station (opening spring 2009) with secure, sheltered parking for 200 bikes. Second bike station planned	All TTC buses will be equipped with bike racks by end of 2010	Bikes permitted on GO Transit trains except on trains arriving and departing from Union Station in peak direction	The Waterfront Trail which spans the Greater Toronto Area parallels the busy GO Rail Lakeshore corridor and is in close proximity to many stations	Challenges: No bikes allowed on rail transit during peak hours; lack of elevators in many stations; more bike parking and secure lockers needed at stations; no coordination of bike routes with transit stops
Washington, DC (population city: 0.6 m, metro: 5.3 m)				
1,800 bike racks and 1,300 bike lockers at Metro stations. No bike parking at bus stops, except major transit hubs with rail stations	All WMATA buses have bike racks	Bikes allowed on Metro trains during off-peak. Cyclists must use elevators between the street and the station platforms	Drafting of DC bike plan took the location of metro stops into account, particularly for the bike route network and facility recommendations	Strengths: Bike racks on all buses; bikes on Metro except during peak; lockers and racks at all stations; SmartBike short-term rentals at 8 Metro stations
Bike station for 150 bikes to open in July 2009 at Union Station		Bikes not allowed on MARC trains. VRE allows bicycles on some trains		Challenges: Restricted bike access hours on Metro; bikes restricted on VRE and MARC suburban rail
New York City (population city: 8.2 m, metro: 18.8 m)				
No dedicated bike parking at rail stations or transit terminals. Some bike parking provided by NYCDOT on sidewalks, often near transit stops. No secure bike parking of any kind in NYC	No buses with bike racks in NYC; Roughly half of NJ Transit busses have bike racks in 2010 (planned increase to 95% by 2014)	Bikes permitted on the NYC subway at all times, but only 16% of stations ADA accessible, with elevators or ramps	No explicit coordination; but the transit network in the city is so dense that most of the bike network is close to transit	Strengths: 24/7 bike access and no fees or permits on NYC subway system, most extensive in North America; big increase in bike racks and bike parking on NJ Transit
Bike parking at a third of MTA suburban train stations in NYC; bike lockers at 18 LIRR and 6 MNR stations; bike parking at 90% of NJ Transit train stations and 80% of LRT stations (a total of 2,400 bike parking spaces, with 376 bike lockers)		All suburban trains allow bikes on board during off-peak hours, but limit of 2–4 bikes per car on weekdays; NJ Transit LRT allows bikes on trains during off-peak hours with a maximum of 4–6 bikes	No coordination of bike network with transit stations and routes in suburbs; most suburban cycling facilities are recreational and do not lead to transit stops	Challenges: No bike racks on MTA buses in NYC; limited parking at MTA suburban rail stations and no bike parking at two main train stations in Manhattan; no secure bike parking; difficult to access platforms: only 16% of subway stations with elevator access

Future Directions

North American cities have been making impressive progress integrating cycling with public transport. Since 2000, the percentage of buses with bike racks has almost tripled. Bike-rail integration has also advanced. Most light rail, metro, and suburban rail systems permit bikes on their rail vehicles except during peak hours, and they increasingly provide special accommodations for cyclists such as bike hooks, racks, and rails in special areas of rail cars. Complementing provisions for bikes on transit vehicles, bike parking at transit stops has been vastly expanded over the past 10 years, with large increases in the number of racks as well as improvements in the convenience, security, and shelter of bike parking.

While cycling and public transport have considerable synergies, there are some inevitable conflicts. Surveys in some cities indicated that cyclists prefer to take their bikes with them on rail vehicles so they can use them at both ends of the trip. That can cause problems during peak hours, however, when all available capacity is needed to accommodate passengers, and there is no extra room for bikes. Taking bikes on buses is much less of a problem since bike racks are external and do not reduce passenger-carrying capacity. But even bike racks can be filled to capacity during the peak, forcing cyclists to wait for later buses.

Paradoxically, bike-and-ride can become problematic where it is most successful. Capacity problems are most likely to arise in cities with well-used public transport and high levels of cycling. That is why the European approach to bike-and-ride has favored the provision of ample, sheltered, secure bike parking at transit stops instead of accommodating bikes on transit vehicles. Similarly, in North American cities with overcrowding of rail vehicles during rush hours, the focus should probably be on providing improved bike parking at rail stations. Not only is more parking needed, but it should be of higher quality, with more sheltered and secure spaces. Major transit terminals should include multi-service bike stations, such as those in northern Europe. Similar to the concept of "complete streets," an appropriate goal of transit systems in North America should be to provide "complete stations," which fully accommodate the needs of cyclists. That includes making rail platforms more accessible to cyclists, which would also improve accessibility for persons with disabilities.

Such bike-and-ride provisions cost money, but they are much cheaper than park-and-ride facilities for motorists [15]. Transit systems should shift their focus from park-and-ride to bike-and-ride, which is more cost-effective as well as more environmentally friendly. To encourage that shift, federal, state, and local government agencies should vastly expand funding for further improvements in bike-and-ride measures.

Bibliography

Primary Literature

1. Hegger R (2007) Public transport and cycling: living apart or together? Public Transp Int 2:38–41
2. Brons M, Givoni M, Rietvield P (2009) Access to railway stations and its potential in increasing rail use. Transp Res A 43: 136–149
3. Givoni M, Rietveld P (2007) The access journal to the railway station and its role in passengers' satisfaction with rail travel. Transp Policy 14:357–365
4. Martens K (2004) The bicycle as a feedering mode: Experiences from three European countries. Transp Res D 9:281–294
5. Martens K (2007) Promoting bike and ride: the Dutch experience. Transp Res A 41:326–338
6. McClintock H, Morris D (2003) Integration of cycling and light rail transit. World Transp Policy Pract 9(3):9–14
7. Rietveld P (2000) The accessibility of railway stations: the role of the bicycle in the Netherlands. Transp Res D 5:71–75
8. Tschopp J (1997) Integration of bicycles and public transport in Basel, Switzerland. In: Tolley R (ed) The greening of urban transport. Wiley, Chichester, pp 441–446
9. Pucher J, Buehler R (2007) At the frontiers of cycling: policy innovations in the Netherlands, Denmark, and Germany. World Transp Policy Pract 13(3):8–57
10. Litman T (2009) Bicycle parking, storage, and changing facilities. VTPI, Victoria
11. Pucher J, Dill J, Handy SL (2010) Infrastructure, programs and policies to increase bicycling: an international review. Preventive Medicine 50(S1):S106–S125
12. Pucher J, Buehler R (2008) Making cycling irresistible: lessons from the Netherlands, Denmark, and Germany. Transp Rev 28(1):495–528

13. Bassett D et al (2008) Walking, cycling, and obesity rates in Europe, North America and Australia. J Phys Activ Health 5(6):795–814
14. USDOT (1998) Bicycles and transit: a partnership that works. U.S. Department of Transportation, Federal Transit Administration, Washington
15. TRB (2005) Integration of bicycles and transit – TCRP Synthesis Report 62. Transportation Research Board, National Research Council, Washington, DC
16. APTA (2009) 2009 public transportation fact book appendix a: historical tables. American Public Transportation Association, Washington
17. APTA (2009) Transit statistics. American Public Transportation Association, Washington
18. APTA (2009) 2008 public transportation fact book. American Public Transportation Association, Washington
19. U.S. Census Bureau (2009) American fact finder: 1990 decennial census, journey to work. U.S. Department of Commerce, Washington
20. U.S. Census Bureau (2009) American fact finder: 2008 American Community Survey, Journey to Work. U.S. Department of Commerce, Washington
21. StatCan (2009) Place of work highlight tables: employed labor force by mode of transportation. Statistics Canada, Ottawa
22. Clarke A (2003) Green modes and US transport policy: TEA-21. In: Tolley R (ed) Sustainable transport: planning for walking and cycling in urban environments. Woodhead Publishing, Cambridge
23. Thunderhead Alliance (2007) Bicycling and walking in the U.S. – Benchmarking report 2007. Thunderhead Alliance, Prescott
24. USDOT (2004) National bicycling and walking study: A ten-year status report. U.S. Department of Transportation, Federal Highway Administration
25. TAC (1998) A new vision for urban transportation. Transportation Association of Canada, Ottawa
26. Transport Canada (2003) Sustainable development strategy 2004–2006. Transport Canada, Ottawa
27. CUTA (2008) Canadian urban transit fact book. Canadian Urban Transit Association, Toronto
28. Pucher J, Buehler R (2006) Why Canadians cycle more than Americans: a comparative analysis of bicycling trends and policies. Transp Policy 13(1):265–279
29. APTA (2006) Transit infrastructure database. American Public Transportation Association, Washington, DC
30. APTA (2008) 2008 Transit infrastructure database. American Public Transportation Association, Washington, DC
31. Dutch Bicycling Council (2006) Continuous and integral: the cycling policies of groningen and other European cities. Fietsberaad, Amsterdam
32. Buehler R, Pucher J (2010) Cycling to sustainability in Amsterdam. Sustain: J Environ Sustain Issues 21:36–40
33. APTA (2008) 2008 Public transportation vehicle database. American Public Transportation Association, Washington, DC
34. Statistics Canada (2009) Employed labour force by means of transportation. Statistics Canada, Ottawa
35. Pucher J, Lefèvre C (1996) The urban transport crisis in Europe and North America. Macmillan, Basingstoke
36. TRB (2001) Making transit work: insight from Western Europe, Canada and the United States. Transportation Research Board, National Research Council, National Academy Press, Washington, DC
37. Alliance for Biking and Walking (2010) Bicycling and walking in the United States: 2010 Benchmarking report. Alliance for Biking and Walking, Washington, DC
38. WMATA (2010) Bike and ride. Washington Metropolitan Area Transit Authority, Washington, DC
39. WABA (2010) Bikes on transit. Washington Area Bicyclist Association, Washington, DC
40. TransLink (2010) Cycling support services study: strategic plan. Third Wave Cycling Group. Via Architecture and Halcrow Consulting, Vancouver
41. SFMTA (2009) San Francisco bicycle plan. San Francisco Municipal Transport Authority, San Francisco
42. NYCDOT (2010) Bicycling. New York City Department of Transportation, New York City
43. NJTransit (2009) NJTransit – bike program. New Jersey Transit, Newark
44. MetroTransit (2010) Resources for bicycling. MetroTransit, Minneapolis
45. METRA (2009) Bikes on trains program. METRA, Chicago
46. DCDOT (2006) Bicycling master plan. Department of Transportation, Washington, DC
47. Bike Walk Twin Cities (2008) Snapshot Minneapolis: bicycling and walking. Bike Walk Twin Cities, St. Paul
48. City of Minneapolis (2010) Bicycles and transit. City of Minneapolis, Minneapolis
49. City of Chicago (2009) Bike 2015 plan-chapter 4. City of Chicago, Chicago
50. City of Portland (2010) Portland bicycle plan for 2030. Office of Transportation, Portland
51. DCDOT (2010) Bicycling in Washington, D.C. Department of Transportation, Washington, Washington, DC
52. City of Toronto (2001) Shifting gears: city of Toronto bike plan. City of Toronto, Toronto
53. CTA (2009) Bike and ride. CTA, Chicago
54. McDonald's Cycle Station (2006) History of the bike station. Chicago Bike Station, Chicago

Bioaccumulation/Biomagnifications in Food Chains

Paul K. Bienfang[1], Henry Trapido-Rosenthal[2], Edward A. Laws[3]
[1]Oceanography Department, School of Ocean and Earth Science and Technology (SOEST), University of Hawaii, Honolulu, HI, USA
[2]Center for Marine Microbial Ecology and Diversity, School of Ocean and Earth Science and Technology, University of Hawaii, Honolulu, HI, USA
[3]Louisiana State University, School of the Coast and Environment, Baton Rouge, LA, USA

Article Outline

Glossary
Definition of the Subject
Introduction
Ciguatera Fish Poisoning
Methylmercury
Future Directions
Bibliography

Glossary

Bioaccumulation An increase in the concentration of a substance obtained from the abiotic environment in one or more tissues of an organism. Bioaccumulation occurs within a given trophic level.

Bioconcentration An increase in the concentration of a substance from the abiotic and biotic environment in one or more tissues of an organism. Bioconcentration occurs within a given trophic level.

Biomagnification An increase in the concentration of a substance obtained from organisms at lower trophic levels by an organism at a higher trophic level.

Biosynthesis Many molecules that can be bioaccumulated or biomagnified by organisms at higher trophic levels enter the food web by being synthesized by organisms at lower trophic levels.

Food chain The simplest possible representation of producer–consumer relationships in an ecosystem.

Food web The representation of the network of producer–consumer–degrader relationships in an ecosystem.

Depuration The metabolic alteration and excretion of a substance, usually a xenobiotic molecule.

Trophic level The position in a food chain or food web occupied by a producer or consumer of food.

Definition of the Subject

In a meta-analytical review of biomagnification in marine ecosystems, Gray [1] noted that more than half of the papers purporting to study this topic were using the term incorrectly [1, p. 46]. He then went on to propose careful definitions of the ways in which xenobiotics can gain entry into organisms. As noted above in the glossary, bioaccumulation, bioconcentration, biomagnification, and biosynthesis of substances represent four different routes of entry. Bioaccumulation, bioconcentration, and biosynthesis typically account for the presence of toxic molecules in organisms at low trophic levels, with transfer of compounds from environment to organism via cell membranes in small organisms with high surface-to-volume ratios, and via gill membranes in many larger aquatic species. Accumulation of xenobiotics via biomagnification is more likely to be a phenomenon that occurs in larger animals at higher trophic levels. The suite of processes that leads to the accumulation of toxic compounds in organisms has been an important element of ecological research for decades and an issue of great practical concern relative to anthropogenic impacts on biological communities [2] as well as to the health and well-being of human populations [3].

Introduction

The Fundamental Ecological Context and Simple Food Chain Theory

A brief review of food chain theory will aid in understanding the processes that can lead to magnification of a non- or poorly metabolizable natural toxin or a non-biodegradable pollutant in a food chain. It is within this context of basic ecological principles that we can best view the movement, concentration, and/or transformation of such compounds that result in the degree of magnification that we find expressed in nature.

All animals need food to survive. Food may be burned (i.e., respired) to provide energy, incorporated into the animal's biomass as proteins, fats, and/or carbohydrates to provide essential structural or metabolic needs, or directed toward reproduction. Food used for these purposes takes the form of organic compounds that are collectively composed of (primarily) carbon, hydrogen, oxygen, nitrogen, phosphorus, and (secondarily) literally dozens of other elements. Organic compounds are produced from inorganic molecules such as carbon dioxide and water by a special category of organisms called autotrophs, or primary producers. Plants are the autotrophs with which most persons are familiar. They use the energy in sunlight to effect the transformation of inorganic compounds into organic matter and hence are called photoautotrophs. Less familiar to many people are the autotrophic bacteria that use chemical energy released from the mediation of oxidation–reduction reactions to synthesize organic matter from inorganic compounds. Such bacteria are referred to as chemoautotrophs. All living organisms that lack the ability to convert inorganic compounds into organic matter are called heterotrophs and depend either directly or indirectly on primary producers as a source of food.

The production of biomass by heterotrophs involves the conversion of one form of organic matter into another, a process called secondary production. Heterotrophs that eat plants are called herbivores. Heterotrophs that eat other heterotrophs are carnivores. Heterotrophs that eat herbivores are primary carnivores, and heterotrophs that eat primary carnivores are secondary carnivores. Not all heterotrophs are so easily classified. For example, some animals have rather cosmopolitan feeding habits and are called omnivores. Other heterotrophs feed primarily on nonliving organic matter (e.g., dead animals or the waste products of other heterotrophs) and are called detritivores. Regardless of whether the consumer is a herbivore, carnivore, omnivore, or detritivore, it is possible to make some broadly relevant generalizations about what happens to organic matter once it has been synthesized by autotrophs.

The successive transfers of food from prey to predator make up what is called a food chain. Each component of such a food chain is called a trophic level. Autotrophs are logically assigned to the first trophic level in such food chains, herbivores to the second trophic level, primary carnivores to the third trophic level, and so forth (Fig. 1).

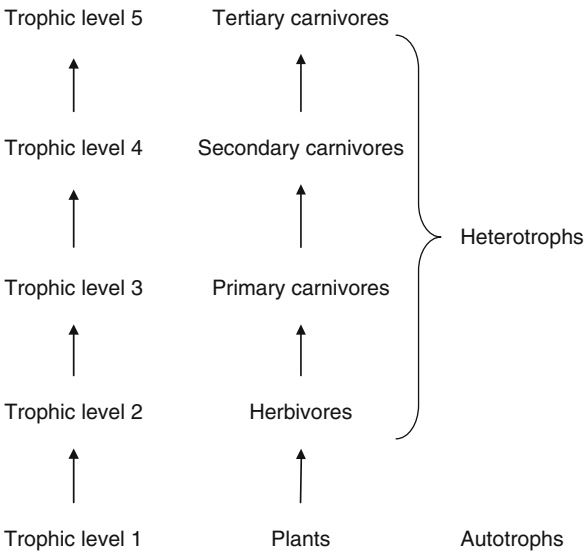

Bioaccumulation/Biomagnifications in Food Chains. Figure 1
Diagram of a simple grazing food chain with plants as the first trophic level. *Arrows* indicate transfers of biomass

In most natural systems only a small percentage of consumed food is passed along from one trophic level to the next highest trophic level. This percentage is referred to as an ecological efficiency and is typically no more than 20%. This means that the rate at which food is ingested by a trophic level is at least five times greater than the rate at which food is passed on to the next trophic level. Most of the consumed food is either respired or excreted. Because ecological efficiencies are low, the flux of food from one trophic level to the next steadily decreases as one moves up a food chain, and the steady decrease in the flux of food to higher and higher trophic levels usually results in decreases in the biomass of organisms at successively higher trophic levels. A caveat to this last generalization is associated with the fact that organisms at successively higher trophic level tend to become progressively larger, i.e., predators tend to be larger than their prey. There are exceptions to this generalization, mainly in the cases of predators that hunt in packs or groups, such as wolves or killer whales. Because large animals generally require less food per unit biomass to sustain themselves than

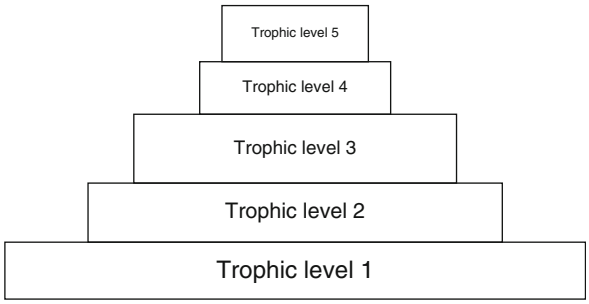

Bioaccumulation/Biomagnifications in Food Chains. Figure 2
An ecological pyramid. The decrease of biomass on successively higher trophic levels reflects the combined effects of low ecological efficiency and decreasing food requirements per unit biomass on higher trophic levels. Length of horizontal bars is proportional to biomass

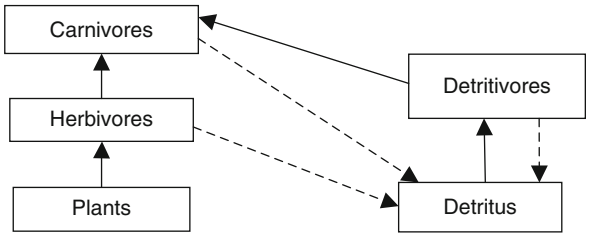

Bioaccumulation/Biomagnifications in Food Chains. Figure 3
Interactions between the grazing food chain (*left*) and detritus food chain (*right*). *Solid arrows* indicate grazing, i.e., consumption of prey (food) by a predator. *Dashed arrows* indicate excretion and/or death

small animals, the amount of biomass on successively higher trophic levels does not usually decline as much as one might expect based on the magnitude of ecological efficiencies, but in general one finds a decrease in total biomass at successively higher trophic levels. In other words, although the animals tend to be larger, there are a lot fewer of them. If the total biomass on successive trophic levels is represented by a series of horizontal bars, and if those bars are stacked on top of one another, the resultant figure has the appearance of a pyramid. That pyramid is called an ecological pyramid (Fig. 2).

The food chain consisting of plants, herbivores, and carnivores is often called the grazing food chain. Complementing the grazing food chain is another whose first trophic level consists of nonliving organic matter, i.e., dead remains of animals and plants and organic waste products excreted by heterotrophs. This nonliving organic matter is called detritus, and the associated food chain is called the detritus food chain. Simplistically, it consists of detritus, detritivores, and carnivores, and at the last step, the detritus food chain merges with the grazing food chain (Fig. 3). In a healthy ecosystem these two food chains work together to consume almost all the organic matter produced by the autotrophs. It is very important that the organic wastes produced by heterotrophs are consumed by detritivores, because such waste products are almost invariably toxic to the organisms that produce them. One food chain's waste is the other food chain's food, and of course, the carbon dioxide produced by the respiration of all heterotrophs is needed by all autotrophs for primary production. Thus the production and consumption of organic matter in a healthy community of autotrophs and heterotrophs is characterized by a great deal of recycling.

A variation on the concept of food chains is the depiction of feeding relationships as food webs (Fig. 4), in which the feeding relationships of (typically) individual species are represented in a two-dimensional diagram. Since a given predator may feed on more than one and perhaps many different prey species, such a diagram tends to have a very complex appearance and has the general characteristics of a web as opposed to a chain. However, careful examination of the feeding relationships depicted by a food web often reveals a pattern consistent with the food chain model. And the principles that govern the fate of consumed food apply regardless of whether feeding relationships are depicted by a food web or food chain. For purposes of this chapter, we will rely on the food chain model to rationalize/explain issues that arise from biomagnification, and we will use the interactions between the grazing and detritus food chains to illustrate how recycling can lead to results that are somewhat counterintuitive from the standpoint of simple food chain theory.

Food Chain Magnification Principles

Given the rather low ecological efficiencies that characterize most food chains, it is not hard to imagine how

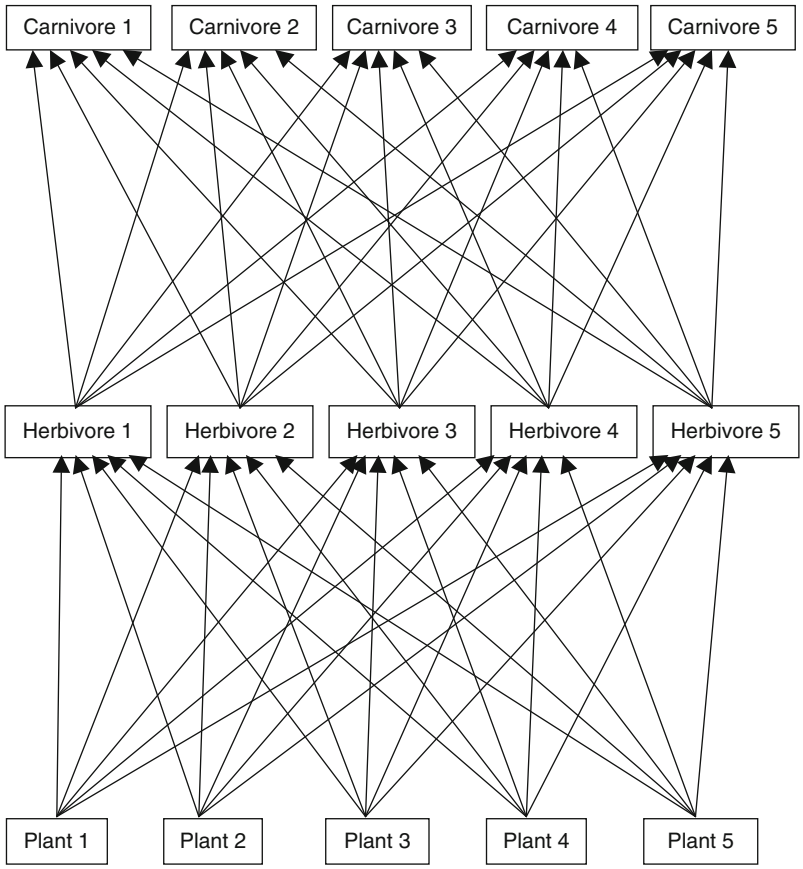

Bioaccumulation/Biomagnifications in Food Chains. Figure 4
Feeding relationships in a hypothetical food chain in which each of five plant species is grazed by each of five herbivore species, which in turn is grazed by each of five carnivore species. The arrows depicting the feeding relationships have the appearance of a web, and such diagrams are characterized as food webs. In this particular case, however, the flow of organic matter could be just as well represented by a simple food chain consisting of plants, herbivores, and carnivores, as on the left side of Fig. 3

the concentration of a relatively refractory substance might be magnified from one trophic level to the next. Assume for the sake of argument that xenobiotic substance X cannot be respired. This would be the case, for example, if X happened to be a metal such as lead or cadmium. Assume further that for whatever reason X is not effectively excreted. This happens to be the case for methylmercury. For humans, about 95% of ingested methylmercury is, at least initially, retained by the body. Assume as a worst case scenario that X is neither respired nor excreted and instead is retained with 100% efficiency in the body of the consumer organism. If the ecological efficiency in the food chain is 20%, then the concentration of X in the food consumed by one trophic level will be magnified by a factor of five in the food consumed by the next trophic level. In a grazing food chain consisting of five trophic levels, beginning with plants and ending with tertiary carnivores, the concentration of X in the tertiary carnivores should be $5^4 = 625$ times higher than the concentration of X in the plants. The fact that the concentrations of ostensibly refractory xenobiotics are sometimes found to be very high in the tissues of top-level carnivores has naturally led to speculation that exactly this sort of mechanism, i.e., biomagnification or food chain magnification, is responsible.

To illustrate this point, Table 1 shows concentrations of residues of the pesticide DDT in the water and

Bioaccumulation/Biomagnifications in Food Chains.

Table 1 DDT residues (DDT + DDD + DDE) in water and organisms taken from a Long Island Salt Marsh [2]

Organism	DDT residues (ppm)
Water	0.00005
Plankton	0.04
Silverside minnow	0.23
Sheephead minnow	0.94
Pickerel (predatory fish)	1.33
Needlefish (predatory fish)	2.07
Heron (feeds on small animals)	3.57
Tern (feeds on small animals)	3.91
Herring gull (scavenger)	6.00
Fish hawk (osprey) egg	13.8
Merganser (fish-eating duck)	22.8
Cormorant (feeds on larger fish)	26.4

in various organisms taken from a Long Island, New York, salt marsh [2]. The data illustrate how very low concentrations of toxic substances in the water and/or in organisms at low trophic levels may increase dramatically through the food chain. The residue concentrations increase steadily from the plankton to small fish, to larger and larger fish, and finally to fish-eating birds. The total concentration factor from plankton to fish-eating birds is about 600, which suggests that the concentration factor between successive trophic levels may be about a factor of 5 (see above).

Agreement between theory and observation does not, however, prove that the theory is correct. There are other processes that can affect the concentrations of xenobiotics in the tissues of animals. Fish, for example, must constantly pump water over their gills to breathe. It is certainly possible that direct transfers of xenobiotics from water to fish may occur through the gills. This exchange may lead to high concentrations in the tissues of the fish by a mechanism (bioaccumulation) that has nothing to do with food chains. In a classic study, Hamelink [4] demonstrated that the concentrations of DDT residues in the tissues of fish in experimental ecosystems were unaffected by whether the DDT residues entered the fish directly from the water or through a combination of entry via the water and food chain. The implication was that the food chain route was, at least in that case, insignificant compared to direct uptake from the water. And in contrast to the Woodwell et al. [2] results, Harvey et al. [5] found no evidence for biomagnifications of DDT residues in Atlantic Ocean food chains. In fact, the DDT residues were highest in the plankton and were ten times lower in flying fish, which feed largely on plankton. During the 1960s, when DDT was being used extensively in the United States and many other countries, sharks were found to contain high concentrations of DDT residues, but barracuda, which are also top-level carnivores, contained about 100 times lower concentrations than sharks [6]. The implication of these and other studies is that high concentrations of xenobiotics in top-level carnivores is not *prima facie* evidence of biomagnification, and among organisms occupying ostensibly similar positions in a food chain xenobiotic concentrations may vary widely as a result of differences in the extent to which organisms bioconcentrate xenobiotics directly from the environment.

An additional concern is the interaction between the grazing and detritus food chains, which is overlooked in the simple paradigm of food chain magnification. The consequences of this interaction are illustrated by a study of Isaacs [7, 8] that concerned concentrations of cesium (Cs) and potassium (K) in the muscle tissues of fish from the Salton Sea and Gulf of California. Briefly, the Cs/K ratio had been found to increase by a factor of three between successive trophic levels in the grazing food chain of the Salton Sea. However, the Cs/K ratios in similar fish from the Gulf of California were independent of the trophic level of the fish and about 16 times higher than the Cs/K ratios in the algae. Isaacs [7, 8] developed a mathematically complex unstructured food web to account for these differences. Laws [9] showed that the same results could be explained by taking into account the recycling that occurs between the grazing and detritus food chains (Fig. 3).

The conclusion is that a great many factors can influence the concentrations of xenobiotics in the tissues of plants and animals. Biomagnification, or food chain magnification, is one of those factors. But interactions between the grazing and detritus food chain can

lead to results that are not predicted when the detritus food chain is ignored, and bioaccumulation in at least some cases can be more important than biomagnification in determining xenobiotic concentrations within organisms. With this introduction, we consider in detail two human health issues potentially impacted by biomagnifications, ciguatera fish poisoning, and methylmercury intoxication.

Ciguatera Fish Poisoning

History

At the 14th Conference of the International Society for the Study of Harmful Algae, Fraga [10] described what is believed to have been the first reported case of ciguatera fish poisoning, an incident that occurred in 1525 in the Gulf of Guinea. An entry in an old manuscript described a case that happened in a Spanish fleet led by Andrés de Urdaneta. The fleet was en route to the Pacific through the Strait of Magellan. The journal entry translates as follows:

- On this island, a very beautiful fish called barracuda was caught by the flagship, and the Captain General invited some of the captains and officers of the King. All who ate the barracuda fell ill from diarrhea and were unconscious, so we thought they had died; however our Creator wanted everyone to be saved.

The fish responsible for this incident, a barracuda (top-level carnivore), is a fish not infrequently implicated in ciguatera fish poisoning. This case was subsequently reported by other early chroniclers, demonstrating how important the incident was.

Five years later, Peter Martyr, the early historian of the West Indies, wrote that when people eat certain fish, they "are attacked by divers strange maladies" [11]. Interestingly, Martyr ascribed this poisoning to movement of a toxin through what we would now call a food chain, from an origin in a plant, to fish, to humans.

In 1601, Pedro Fernandéz de Quirós, a Portuguese navigator in the service of Spain, reported that his entire crew was poisoned after eating "pargo," fish that may well have been snapper or grouper, that they caught while anchored off the island of Espiritu Santo in what is now Vanuatu [12]. The most descriptive of the early accounts of ciguatera, however, comes from the famous British explorer Captain James Cook. In his journal entry for Sunday the 24th of July, 1774 [13], Cook wrote:

- "The Night before we came out of Port two Red fish about the size of large Bream and not unlike them were caught with hook and line of which most of the officers and some of the petty officers dined the next day. In the evening everyone who had eat of these fish were seiz'd with violant pains in the head and Limbs, so as to be unable to stand, together with a kind of Scorching heat all over the Skin, there remained no doubt but that it was occasioned by the fish being of a Poisoness nature and communicated its bad effects to everyone who had the ill luck to eat of it even to the Dogs and Hogs, one of the latter died in about Sixteen hours after and a young dog soon after shared the same fate. These must be the same sort of fish as Quiros mentions under the name of *Pargos*, which Poisoned the Crews of his Ships, so that it was some time before they recovered. We had reason to be thankfull in not having caught more of them for if we had, we should have been in the Same Situation."

Another of Cook's officers identified the suspect fish as "Groopers"; it is likely that the fish Cook's men ate on the 23rd of July, 1774 were either snapper or grouper.

Nature and Extent of the Problem

Ciguatera fish poisoning (CFP) is a worldwide health problem that represents an example of biomagnification of a naturally produced marine toxin. CFP is a non-bacterial, food-borne disease associated with the consumption of seafood that originates from coral reef environments in tropical and subtropical regions of the world. Humans contract the disease by consuming reef fish that have accumulated ciguatoxins as a result of feeding in coral reef habitats. Public health institutions throughout the world rank CFP as the most common food-borne disease related to the consumption of marine finfish [14].

In the introduction to this entry, the distribution of concentrations of DDT residues in organisms representing various trophic levels in a Long Island salt marsh were shown to be positively correlated with trophic level. The biological world frequently does not present itself as being so orderly. The relationships

between concentrations of naturally occurring marine toxins and trophic levels are considerably more difficult to discern given the variability caused by the complexity of marine food web interactions [7–9]. The next few paragraphs will explore the scope of the CFP problem, including the organisms responsible for toxin synthesis, natural pathways of the toxin through food webs, and biological and clinical evidence related to ciguatera fish poisoning.

CFP represents an example of biomagnification of a marine toxin that is produced by natural processes and, while presenting substantial difficulties for quantification and study, affects humans like no other toxin from the marine realm. Early work by Randall [14], Banner et al. [15, 16], and Banner and Helfrich [17] indicated that ciguatoxin (CTX) was derived from food consumed by fish and showed that toxicity could be transferred to non-toxic fish via consumption of toxic fish. These contributions evolved into the food web concept for CFP that is the paradigm to this day.

CFP has affected coastal populations and travelers in tropical and subtropical regions throughout the world for centuries. From old ship logs noted above, through WWII chronicles when CFP was a serious problem for military troops stationed in Pacific island locales, to the present day, CFP has been a serious public health problem. Currently, there are at least 50,000 reported cases of CFP cases per year [18, 19], but due to the high degree of misdiagnosis and underreporting, it is estimated that the actual frequency of CFP cases is closer to 500,000 per year [20]. It is estimated that >50% of the populations of small islands in the Caribbean and South Pacific have suffered from CFP. Interested readers are directed to reviews by Lewis [21], Lange [22, 23], and Fleming et al. [24] for additional details on the degree of CFP incidence in populations inhabiting various locales.

Symptomology

CFP produces gastrointestinal, neurological, and cardiovascular symptoms. These normally develop within 12–24 h of eating contaminated fish. Gastrointestinal effects may disappear within 4 days. Normally gastrointestinal symptoms are followed by neurological symptoms. The gastrointestinal symptoms commonly include diarrhea, abdominal pain, nausea, and vomiting. The neurological symptoms that ensue may include numbness and tingling in the appendages (e.g., hands and feet), dizziness, altered hot/cold perception, muscle aches, low heart rates, and low blood pressure. The key pathognomonic symptom is the neurological malady of reversal of hot/cold sensation, i.e., hot feels cold and cold feels hot. Such conditions are caused by the disruption of the "vernacular" that neurons use to communicate with one another, i.e., the ion signals involving sodium and potassium. The suite of symptoms associated with CFP is caused by ciguatoxin's ability to increase Na^+ permeability through the Na^+ channels of excitable cells (e.g., neurons and muscle cells) that are open at normal resting membrane potentials. This enhanced excitability of the membrane in turn affects $Na^+ - Ca^{+2}$ exchange and mobilizes intracellular Ca^{+2}. The primary receptor site of the CTX action is the 5th domain of the Na^+ channel, where it causes increased sodium ion permeability and depolarization of the resting membrane. The prolonged depolarization of nerve cells is understood to cause the suite of sensory discomfort symptoms associated with CFP [25]. CFP symptoms may persist in some form for weeks, months, or even years [26]. Generally, the gastrointestinal symptoms and general weakness last about 1 week, but the neurosensory manifestations (e.g., muscle aches, tingling extremities, and thermal reversals) commonly represent the most prolonged discomfort. It is interesting that CFP intoxication does not confer any immunity in its victims; on the contrary, CFP intoxication results in a heightened sensitivity to ciguatoxin in the victim.

Fortunately, death from CFP is rare (i.e., <0.1%), and when it has occurred it was generally the result of respiratory failure due to cardiovascular shock induced by severe dehydration. Death is frequently associated with the consumption of internal organs of the fish (e.g., liver, brains, gonads, viscera, etc.) in addition to the muscle tissue that is usually consumed. Given the exceptional potency of ciguatoxin (CTX), the low death rate merits some discussion. The two most plausible explanations for the low frequency of fatalities associated with CFP are (a) the large size differential between the "average" human and the average serving of CTX-contaminated fish, and (b) the likelihood that ciguatoxin cannot biomagnify indefinitely in nature.

To understand the consumer meal size differential, consider a person weighing between 125 and 200 lbs who consumes an 8-oz portion of contaminated fish; that serving represents 0.25–0.4% of the biomass of the consumer. Since reef organisms do not attain a size of 125–200 lbs, the final "dilution" of the toxin at the point of the human is large with respect to the dilutions that are experienced at various junctures within the marine reef ecosystem. The second explanation is related to the effects that the CTX toxin has on the various animals within the marine reef ecosystem. The ingestion of the ciguatoxin via the consumption of a contaminated organism (lower on the trophic structure) has been shown to cause behavioral changes in animals [27]. If, as has been suggested, such impaired behaviors may make those infected animals more susceptible to death, it would present a natural truncation of the CTX magnification food chain. This, together with the roughly 300-fold dilution factor at the serving-human juncture, may be the reason that humans rarely ingest levels of CTX of sufficient magnitude to cause a fatality.

Environmental and Biological Controls

The distribution of ciguatoxic fish is frequently stated as being within the 35°N and 35°S latitudinal band. Patterns of CFP incidence are well known for the Pacific, Indian, and Atlantic oceans, as well as the Caribbean and Mediterranean Seas [28]. Nonetheless, recent scientific inquires have suggested an even more expansive geographic scale for ciguatera incidence [29]. It has also been suggested that the latitudinal range for CFP is expending as a consequence of warming sea surface temperatures associated with climate changes [30]. The relevance of the expanding latitudinal range lies in the fact that the inclusion of higher latitude regions will include some areas with high population densities, which suggests the potential for increased incidence rates. Several informative reviews on CFP may be found in Lehane and Lewis [31], Bienfang et al. [31], Dickey [26, 27], Dickey and Plakas [32], and references cited therein.

In contrast to the orderly increases of DDT residue concentrations in organisms at various trophic levels presented in the introduction to this entry, the biomagnification scenario for CTX is complex. The difference for CTX is nested in the fact that the concentrations and potency of this naturally produced marine toxin are modified through the complexity of marine food web interactions. Reasons for the apparent complexity of CTX biomagnification include the following:

1. Precursors of the CTX toxin, gambiertoxins, are produced by a variety of dinoflagellates belonging to the genus *Gambierdiscus*. These species vary significantly in terms of their tendency to produce toxins and the potency of the toxin they produce.
2. Metabolites of gambiertoxins, the CTX toxins themselves, appear in a variety of chemical forms (i.e., congeners). Additionally, the toxins are potent at very low dosages and are odorless, tasteless, and highly resistant to destruction/detoxification.
3. Spatial and temporal environmental variability appear to influence the production and flux of CTX into fish populations.
4. The complexity of the marine food web leading to the distribution of CTX among fishes harvested by man presents multiple vectors that may lead to human maladies in a given situation.
5. Humans display variable sensitivities to and symptomologies from CTX intoxication.

A genus of single-celled algae called *Gambierdiscus* (division Phyrrophyta, commonly known as dinoflagellates) produces the gambiertoxins that are the natural precursors of CTX. This genus of dinoflagellates does not form conspicuous blooms that color the water like some other dinoflagellates that are known to produce "red tide" aggregations. The *Gambierdiscus* species normally grow epiphytically on various macroalgae in coral reef ecosystems. The need of these sessile, benthic macroalgae for sufficient sunlight for photosynthesis accounts for the limitation of ciguatera to organisms that inhabit and derive most of their nutrition from the relatively shallow coral reef environments found in warm, tropical areas. *Gambierdiscus toxicus* was originally designated as a new genus and species by Adachi and Fukuyo [28]. Since then, at least ten new species have been added to this genus [33–36]. It has long been suspected that the various *Gambierdiscus* species differ significantly in their degrees of toxin production [33, 34, 37–41]. These dinoflagellates are consumed by herbivorous fish,

beginning the process of bioaccumulation and biomagnification through the reef food web. The herbivores are consumed by carnivores, which in turn are consumed by humans.

The Toxin

CTX is a polar, lipid-soluble, highly oxygenated polyether molecule; it consists of 13–14 rings that are fused by ether linkages into a ladder-like structure [42–48]. The seminal toxins that are produced by cells of *Gambierdiscus* are frequently designated as gambiertoxins. These are less polar than the ciguatoxins isolated from fish. These less polar precursors are considerably less potent than the CTX molecule found in high trophic level carnivores. Because the different *Gambierdiscus* species/strains often co-occur at various relative abundances and can vary with respect to their individual toxicities, the resulting variability of toxin flux into the food web has confounded monitoring efforts. Ciguatoxins are piscine metabolites of the gambiertoxins that are assimilated and metabolized through multiple trophic levels of the marine food web. Ciguatoxins in fish may comprise an assemblage of principal ciguatoxins and numerous closely related structural isomers and congeners. Toxins isolated from different regions and/or organisms have been shown to exist in a number of forms that have different molecular weights, chemical structures, and toxicities [42, 48–53]. The recognition of these congeners necessitated new nomenclature, and in the more recent literature an I, P, or C prefix refers to the ocean of origin (i.e., Indian, Pacific, or Caribbean), and a number following refers to a specific congener/form of CTX. Thus, P-CTX-1 would refer to CTX congener 1 isolated from the Pacific Ocean. There are currently understood to be 29 congeners of P-CTX, and 12 of C-CTX. More robust analytical methods have revealed important new details regarding the chemical structure of CTX and its congeners.

Ciguatoxin is one of the most potent natural toxins known; the intake of picogram (i.e., 10^{-12} g) amounts of toxin will cause clinical symptomologies in humans. Such potency at minuscule concentrations has presented imposing challenges to the analytical techniques that may be applied for measurement of CTX in fish tissues. The need for sophisticated chemistry presents exceptional challenges for the quantitative analysis of CTX at concentrations that produce clinical symptomologies in humans. The equipment required for analyses of complex organic compounds such as CTX is expensive to purchase and maintain, and requires highly talented analytical chemists to operate. This requirement for CTX detection has been addressed by a variety of approaches over the decades. Early work involved a number of non-ciguatera–specific bioassay procedures using mouse neuroblastoma cells and various invertebrates and vertebrates; these were followed by radioimmunoassay, enzyme immunoassay, and immunobead assays [54]. More recent analytical developments have focused on chromatographic methods involving high performance liquid chromatography (HPLC) combined with mass spectrometry (MS) [27, 55–57]. These robust analytical techniques are very expensive and require sophisticated infrastructural support. An important consequence of this range in analytical procedures used for CTX analyses has been a lack of uniformity, sensitivity, and specificity of analyses used by investigators working in various regions over the years.

Variability of Incidence

Within areas that are known to be prone to CFP incidence, the distribution of toxic fish can be highly variable on small scales both temporally and spatially. This is thought to be due to ecological factors that influence the degree of dietary intact of CTX by fishes, the degree of CTX biotransformation that may occur, the age/growth rates of the fish, and rates of CTX excretion (which are normally slow, and on the order of months). As a consequence, ciguatoxicity has been found to vary seasonally, from species to species, and from location to location within fairly proximate areas. A species of fish in one area may be relatively free of ciguatera but found in close proximity to an area where that same species is highly ciguatoxic. Such heterogeneous distributions of ciguatoxic fish have been described for numerous locations throughout the Caribbean Sea, Indian, and Pacific Oceans, and have been attributed variously to the combined forces of the territorial nature of carnivorous reef fish, differences in the abundance and/or

toxicity of *Gambierdiscus* spp., or variations in feeding patterns between locations.

An example was described by Lewis [58] for the mid-Pacific location of Kiribati, where southern (Tarawa) and western (Maraki) reefs were known for high CFP incidence, but not other reefs in the vicinity. Dierking [59] showed similar spatial heterogeneity in the distribution of ciguatoxic *Cephalopholis argus* throughout coastal areas on the islands of Oahu and Hawaii, Hawaii. The biomass of *C. argus*, introduced to Hawaii from French Polynesia in the 1950s, now surpasses the biomass of all other reef predators combined, and is one of the principal species associated with CFP in this area. Dierking's [59] findings showed substantial (8% versus 24%) differences in the prevalence of toxic *C. argus* between the islands of Oahu and Hawaii, large variations in toxicity within sites, no clear patterns between sites on either island, and very weak correlations of toxicity and fish size. Similar lack of correlation of either incidence or severity of ciguatoxicity with fish size, and high degrees of spatial heterogeneity in the incidence of ciguatoxicity in *C. argus* has been shown by Bienfang and DeFelice (unpublished data; www.fish4science.com).

The complexity of the marine food web leading to ciguatoxic fishes that are consumed by man has challenged marine scientists who have studied the ecosystem looking for vectors that contribute to this human malady. There is evidence that individual *Gambierdiscus* strains differ considerably in their inherent ciguatoxin production capabilities [34, 39, 56, 60]. Laboratory studies have suggested that individual *Gambierdiscus* strains are adapted to particular environmental regimes (e.g., different relationships between light intensity and growth rate, toxicity and light intensity, temperature, and/or salinity [60–63]. Changes in the dietary intake of ciguatoxins within food webs leading to fish have been described as being influenced by a variety of stochastic changes in predator–prey relationships within areas. Despite a low correlation between changes in ciguatera incidence rates and catastrophic events, it has also been repeatedly speculated that anthropogenic disruptions (e.g., shipwrecks, dredging) and/or natural environmental disturbances (e.g., hurricanes, cyclones, coastal inundations) may lead to the availability of new surfaces for colonization by macrophytic algae and/or the associated epiphytic *Gambierdiscus*.

The apparent differences in sensitivity of individuals to ciguatoxic fish and/or associated variability in the severity of symptomologies from CTX intoxication among afflicted victims, together with a high (e.g., 90%) degree of underreporting has also confounded elucidation of processes associated with ciguatera prevalence. Although symptomologies that are consistent with an interference with sodium channel activity are characteristically associated with CTX [27, 57], other biochemical aberrations have also been implicated [56, 64, 65]. Also, it is relatively infrequent that remains of a meal that apparently caused CFP in a human have been available for credible analysis of ciguatoxin. When possible, analyses have shown ciguatoxicity in humans at concentrations in fish ranging from 0.1 to greater than 1 part per billion P-CTX-1.

Evidence of Biomagnification

Despite all these vagaries in the databases associated with CFP, the role of biomagnifications is suggested by the fact that high-level carnivores are by far the fish most frequently associated with the presence of CTX. The data pertaining to CFP incidence in fishes comes from both clinical records and sampling studies that broadly examined various reef species for ciguatoxicity irrespective of associated incidence of reported symptomologies by humans. Not surprisingly, data from the clinical records have had considerably more influence on our perspective regarding the piscivorous vectors leading to CFP. This comes from the standpoints of both their numerical abundance and their role in initiating the broad-scale studies of ciguatoxicity across fish species inhabiting reef ecosystems in various geographic locations. CTX is capable of bioaccumulating through the food chain through herbivorous and carnivorous (i.e., predatory) reef fish.

The fish most commonly involved in CFP incidents within various geographic locations have been listed/prioritized in several summaries [54–56, 59, 66–71]. Such listings show that the fish species that are most commonly implicated with ciguatoxicosis are primarily carnivorous. The prominent carnivorous taxa include the barracudas (*Sphyraena* spp.), groupers (*Epinephelus*

spp.), jacks (*Caranx* spp.), snappers (*Lutjanus* spp.), mackerels (*Scomberomorus* spp., especially the Spanish mackerel), kingfish (*Seriola* spp.), and moray eels (e.g., *Gymnothorax* spp.).

Not all fish implicated in CFP are carnivores. Non-carnivorous taxa include the detritivorous/omnivorous surgeonfish (*Ctenochaetus* spp.), parrotfish (*Scarus* spp.), and wrasses (e.g., *Cheilinus* spp.). In the Pacific, the detritivorous grazer, *Ctenochaetus striatus* (a surgeonfish), is frequently ciguatoxic and is thought to be a key vector amplifying CTX up the food chain. High levels of CTX and other *Gambierdiscus*-associated toxins in biodetritus are believed to account for the frequency of ciguatoxicity in *C. striatus*, and occasionally, mullets (e.g., *Mugil* spp.) because both have detritivorous grazing behaviors [72]. The mouthparts of the *C. striatus* are especially well adapted for feeding on phytodetritus and certain filamentous macroalgae known to commonly be host to the epiphytic *Gambierdiscus* spp. Surgeonfish and parrotfish tend to be dominant families by weight on many coral reefs, and among the most common prey of larger piscivores. Interestingly, carnivorous species that are grown in tropical aquaculture settings have been shown not to display ciguatoxicity, despite the presence of *Gambierdiscus* spp. growing on the confining vessels used in the culture process [73]. This lack of ciguatoxicity due to bioaccumulation has been attributed to the fact that the majority of the nutrition of such cultured carnivores is provided through the provision of prepared feeds supplied to the culture systems, rather than (normal) grazing upon a heterogeneous suite of natural feedstuffs.

The perceived variety in CFP symptomologies between fishes from the Caribbean and Pacific has variously been attributed to differences in the gambiertoxins produced by different predominant *Gambierdiscus* species in these locales, and/or the portions of the fish traditionally consumed. Helfrich et al. [74] estimated that the relative toxicity of fish liver tissue was 50 times greater than that in the muscle tissue. Vernoux et al. [75] similarly showed that the relative toxicity of the liver and viscera tissues (e.g., brain, gonads, heart) was considerably higher than that of the muscle tissue. This has been attributed to the preferential sequestering of the lipid-soluble CTX molecule in the most lipid-rich portions of the fish. Such differences in the portions of a given fish species that are actually ingested by an assortment of populations from various geographic and/or ethnic backgrounds confound the analysis of the degree of trophic-level influence independent from other, potentially aliasing factors.

The high trophic level barracuda (*Sphyraena* spp.) has been shown to accumulate and retain CTX in its muscle tissue for extended periods of time, and toxicity was shown to be inducible. Banner et al. [16] and Helfrich and Banner [76] fed *Lutjanus sp.* ciguatoxic fish and showed the induction of toxicity within 6 months, and the subsequent retention of potency for 30 months following the cessation of feeding ciguatoxic fish. There exist chemistry results suggesting that CTX precursors from dinoflagellates may be oxidatively biotransformed to numerous congeners within herbivorous and carnivorous fish [53]. Biomagnification effects also appear to be evidenced in the human symptomologies caused by the consumption of herbivorous versus carnivorous fish. Bagnis and Legrand [77] and Kodama and Hokama [78] reported that the ingestion of ciguateric herbivorous fish caused mostly gastrological and mild neurological symptoms, while the consumption of carnivorous fish was associated with a broader and more severe suite of symptoms. This was attributed to differences in the ciguatoxin congeners produced by various (predominant) *Gambierdiscus* species in these locales, inevitably leading to an assortment of compounds present in fish representing a range of trophic positions.

There are many obstacles to a clearer definition of the prevalence of ciguatoxic fish and/or the distribution of ciguatoxic fish within a species or trophic structure. These impediments include vagary due to the temporally sporadic and spatially patchy distribution of both the causative agent (*Gambierdiscus* spp.) and the feeding patterns of the herbivorous and carnivorous fish species that lead to human CFP intoxications. The primary evidence for the biomagnification of CTX up the trophic structure is found in both the higher frequencies of CTX incidence in carnivores and the severity of symptomologies that have been observed in association with human consumption of carnivorous fish versus herbivorous fish.

Methylmercury

Hg: Sources and Cycling

Mercury (Hg) is a heavy metal. In nature, it exists in three chemical forms. These include the pure, elemental form (i.e., the form that in times past was used in thermometers), inorganic mercury compounds (i.e., mercury salts), and organic mercury (mercury incorporated into organic molecules). If you are old enough to remember gasoline at less than a dollar per gallon, you probably remember mercury as that strange, heavy, silver liquid that you rolled around on the counter top or in your hand. You are also likely to associate it with thermometers. If you are younger than that, you are most likely to think of mercury as a pollutant.

Methylmercury in the form of compounds such as methyl mercuric chloride, CH_3HgCl, and dimethyl mercury, $(CH_3)_2Hg$, is the most common form of mercury in the food people eat and is primarily responsible for the adverse human health effects attributed to mercury. Methylmercury is highly toxic and is readily bioaccumulated and biomagnified in freshwater invertebrates, marine invertebrates, freshwater fish, marine fish, marine mammals, and terrestrial mammals (including humans). The majority of methylmercury in freshwater and marine aquatic systems is derived from the conversion of other forms of mercury; rarely is methylmercury directly discharged into aquatic systems [79].

Mercury distribution within the environment (i.e., atmospheric, terrestrial, and aquatic) is controlled by complex biogeochemical cycles and ecological interactions. Sources of environmental mercury input may be divided into natural and anthropogenic categories: The relative magnitude of these categories is roughly equal [80, 81].

Natural contributions include such sources as volcanic eruptions, forest fires, weathering of mercury-bearing rocks/geological deposits, and aquatic volatilization [82]. Volcanic eruptions are enormous contributors on a per-event basis, but rare in terms of event frequency. Forest fires are intermediate contributors on a per-event basis but represent a higher frequency of event than volcanic eruptions. The weathering of geological deposits represents a slow but continuous contributory process. Volatilization, sometimes referred to as recycling, occurs when mercury is released back into the atmosphere as a gas from freshwater and marine aquatic systems. An example would be the breakdown of methyl mercury by sunlight [83].

The various natural inputs of mercury to the environmental enter primarily to the atmosphere. Once in the atmosphere, mercury can circulate for years, during which time it becomes widely distributed throughout the planet [84]. Mercury deposition from the atmosphere to the land or water can occur in either aqueous or dry forms. Aqueous forms include rain, snow, sleet, hail, and fog. Dry forms include gas or particulates. The principal atmospheric contributor is rain. Atmospheric deposition may enter aquatic systems directly as rainfall, or indirectly as a result of either surface runoff from terrestrial systems (i.e., in streams and/or rivers) or percolation followed by subsequent input from groundwater [83].

The anthropogenic sources of mercury are those inputs that result from the activities of humans. These anthropogenic inputs can be divided into four categories: (1) area sources, (2) combustion processes, (3) manufacturing activities associated with metals, alkali, and cement, and (4) other industrial processes. Landfills, dental preparations (e.g., mercury fillings), and laboratory operations are examples of area sources. Examples of combustion processes include coal-burning power plants and/or the burning of any other fossil fuel, medical waste incineration, and municipal waste combustion. Other industrial processes include such things as discharges from mining operations, hydroelectric plants, and pulp and paper production.

The primary anthropogenic contributors of mercury to the environment include coal combustion, chlor-alkali production (i.e., production of chlorine and sodium hydroxide), waste incineration, and metal processing. The relative proportions of mercury emissions to the atmosphere, exclusive of the burning of biomass, are illustrated by data from the year 2000 [80]. Relative proportions of mercury emissions to the atmosphere were 65% from stationary combustion, 11% from gold production [85], 6.8% from non-ferrous metal production, 6.4% from cement production, 3.0% from waste disposal (municipal and hazardous waste, crematoria and sewage sludge

incineration), 1.4% from pig iron and steel production, 1.1% from mercury production (mainly for batteries), and 2.0% from other sources.

Methylmercury is the most toxic form of mercury. It is formed by the methylation of inorganic mercury [79]; methylation means a single carbon methyl group (i.e., CH_3^-) is transferred from an organic compound and becomes bound to an inorganic mercury ion (i.e., Hg^{2+}) [86]. Methylation can occur by either biotic or abiotic means, with the former being the principal mechanism [83]. Examples of such biotic methylation include catalysis by microorganisms that live in freshwater systems (lakes, rivers, wetlands, sediments, soils) and/or the open ocean [87]. To a lesser extent, mercury methylation sometimes can occur via natural processes such as photochemical reactions; these are termed "abiotic processes" [83]. Methylmercury rather than inorganic mercury is bioconcentrated because organisms at various levels in the food chain retain it more efficiently. Inorganic mercury enters bacteria via a specialized transport protein that takes the mercury across the lipid membrane of the bacterial cell wall; this uptake is a key first step in both the methylation and bioaccumulation of mercury [83]. In contrast to other forms of mercury, which are not reactive and thus diffuse out of the cell as fast as they enter, methylmercury is reactive. This is the key to its accumulation in bacterioplankton and phytoplankton, which initiates the bioaccumulation process throughout the feedweb.

Bacteria that contain methylmercury may be passed to higher trophic levels when they are consumed by bacterivores or particle feeders. Alternatively, the bacteria may excrete the methylmercury into the water, where it can become adsorbed to planktonic particles and/or nonliving particulate material suspended in ocean systems. Similarly, methylmercury can be adsorbed by marsh grasses or other microscopic or macroscopic aquatic plants in freshwater systems. Through this mechanism mercury can enter the foodweb when these plants are subsequently consumed by herbivores or detritivores.

Methylmercury may be biomagnified in both marine and freshwater aquatic food webs, i.e., the methylmercury concentrations (i.e., grams mercury per gram biomass) increase at successive trophic levels. Methylmercury concentrations have been shown to generally increase as mercury is passed from invertebrates and/or herbivorous fish to piscivorous fish, and ultimately humans [88]. As was illustrated for DDT residues above, methylmercury concentrations in marine apex predators can reach a level orders of magnitude higher than the concentration present in the water. The extent of concentration at the highest trophic level is influenced by the number of trophic levels in the system [88]. Methylmercury has a half-life of approximately 2 years in aquatic organisms. Such a prolonged residence time results in its bioaccumulation within aquatic food chains [79]. By contrast, methylmercury has a half-life of about 50 days in human blood [89].

Mercury Poisoning: Human Symptomologies and Historical Examples

Mercury is a neurotoxin. Many adverse health effects are associated with its accumulation in the human body. These effects vary depending on the amount of mercury one is exposed to, time of exposure, the mode of entry to the human body, the chemical form of the mercury, and the age of the subject.

Methylmercury is easily absorbed through the gastrointestinal tract when ingested. Mercury readily binds to proteins and therefore is not easily eliminated. Unlike essential metals such as iron, copper, or zinc, the human body does not require mercury for any purpose. The toxicity of mercury is closely related to its tendency to bind to sulfur and selenium, and in particular to amino acids that contain these elements: cysteine and methionine in the case of sulfur, and selenocysteine, selenohomocysteine, and selenomethionine in the case of selenium. Methylmercury, for example, can form a complex with cysteine that resembles methionine. In this methionine-resembling complex, methylmercury may be transported freely throughout the body, including across the placenta and blood–brain barrier, as well as through breast milk.

The uptake of mercury by humans generally occurs via two modes. One is inhalation. Metallic mercury (Hg^0) may be present in ambient air, particularly downwind from coal-burning power plants. Alternatively, mercury may be released from dental amalgams, and as methylmercury (CH_3Hg^+) from the consumption of foods such as fish. The human body is better adapted for mitigating the potential toxic effects of

vaporous mercury, so health effects from this source are relatively rare and are generally limited to cases where the victim in question is in close and prolonged proximity to a source of elevated mercury in the atmosphere. Methylmercury, on the other hand, is the most biochemically active form of mercury. It affects the central nervous system and can cause irreversible damage to areas of the brain. Damage to the nervous system is the most prevalent of methylmercury effects on humans, but methylmercury exposure can also harm the lungs and kidneys [90] and has been linked to increased risk of cardiovascular disease [91–93]. The first symptom of methylmercury exposure in adults is generally paresthesia, a sensation of tingling on the skin. This usually manifests itself as numbness and tingling in the extremities, though paresthesia may also occur in other parts of the body as well. This is normally the first manifestation of damage to the central nervous system [94]. In cases where elevated, more extreme doses of methylmercury poisoning occur, the initial paresthesia symptoms may be followed by ataxia and generalized weakness. Ataxia refers to a wobbliness, unsteadiness, and general lack of coordination. It reflects dysfunctionality in the cerebellum and is manifested by the brain's failure to regulate body posture and/or direction of limb movements. Even higher doses may lead to dysarthria, i.e., the loss of vision, hearing, and finally severe tremors, coma, and/or death [95]. These severe symptoms have only been observed in people who repeatedly consumed fish that were contaminated directly by methylmercury from anthropogenic sources [94].

Because of the biochemical activity of methylmercury and thus its ability to cross the placenta, children exposed to methylmercury in utero display developmental impairments that reflect compromised brain function; these symptoms may include such things as lower IQ, decreased memory function, attention deficit, and/or impaired language skills. More serious physiological effects include motor difficulties, sensory problems, and mental retardation [96].

Physical and environmental parameters that influence methylmercury concentration in natural waters are water pH and dissolved organic carbon (DOC). Higher acidity and DOC increase methylation rates of mercury and enhance its mobility in the water, thus making it more likely to enter the food chain [97–99]. Additionally, algal blooms reduce the uptake of methylmercury in freshwater food webs [100].

Methylmercury released directly into aquatic systems can cause mass acute mercury poisoning in humans who consume contaminated fish and shellfish. Probably the most dramatic historical example of this occurred in Minimata, Japan. Minimata is considered to be one of the worst industrial disasters of all time. Between 1932 and 1968, a factory of the Chisso Corporation discharged roughly 27 tons of mercury into a waterway that fed directly into Minimata Bay. The factory was using mercury as a catalyst to produce acetaldehyde, a chemical employed in the manufacturing of plastics [101]. More than 3,000 people were "officially" recognized and reported by government officials as directly suffering from mercury intoxication. Later, however, estimates of the number of people from the contaminated area afflicted with health problems or left permanently disabled increased to two million [102]. The large difference between these two estimates of the number of Minamata Disease victims reflects the fact that a social stigma associated with the symptomologies caused denial and/or underreporting by the afflicted, the local populations, and the local/national governments.

The range and severity of the health effects from this incident of mercury poisoning were extreme. The afflictions included the various symptoms discussed above and extended to birth deformities and deaths. Public awareness of the incident became widespread at roughly the time of the birth of the environmental movement elsewhere in the world. The account of what happened was so highly publicized that mercury poisoning became known as "Minamata disease" [103, 104].

A similar event occurred in Niigata, Japan. Mercury waste from acetaldehyde production was released from the late 1950s to the early 1960s by the Shawa Denkó Corporation factory into the Agano River, 65 km upstream from Niigata. The quantity released remains unknown to this day [105]. The Minamata and Niigata examples illustrate instances where the use of inorganic mercury as a catalyst in an industrial process led to very serious impacts from methylmercury intoxication. Specifically, mercuric sulfate, $HgSO_4$, was used to convert acetylene into acetaldehyde, a precursor for, inter alia, acetic acid and acetone; and mercuric chloride, $HgCl_2$, was used to convert acetylene into vinyl

chloride, a precursor of polyvinyl chloride (PVC). Unfortunately in both cases a side reaction of the catalytic cycle led to the production of methymercury, by far the most toxic form of mercury, and the methylmercury was discharged with the wastewater from the factories, with tragic consequence for segments of the local population. Such examples clarified and galvanized societies' awareness of mercury as a pollutant with potentially direct and dire human impacts. It is important also to understand that the Minamata and Niigata cases represent examples where large, direct inputs of mercury were being made to water basins of relatively small volume, and very close to large human populations. In these cases, the delivery:dilution ratio was heavily skewed toward the delivery side, and there was a high probability of frequent human interaction with the introduced mercury through both direct and indirect pathways.

A somewhat different example of mercury pollution occurred at Dryden, Ontario in Canada. In this case, the Dryden Chemical Company repeatedly discharged inorganic mercury into the Wabigoon River between 1962 and 1970. Total discharges have been estimated at ~9 tons. The mercury was discharged with the wastewater from a chlor-alkali plant, where once again inorganic mercury was being used, in this case to convert sodium chloride (NaCl) into chlorine and sodium hydroxide. The inorganic mercury subsequently became methylated in the natural environment (i.e., not within the plant itself), resulting in serious methylmercury pollution in the downstream freshwater system and its various aquatic components [106]. This case again involved substantial inputs of mercury directly into aquatic systems of relatively small volume and close to large human populations.

Fish and shellfish have not been the only contaminated food source associated with methylmercury poisoning in humans. Other foods such as grain [107, 108] and meat [109] have caused mercury-related health effects, the most notable of these examples being the Basra grain disaster. In the 1960s and 1970s, seed grain containing ~8 μg/g mercury was shipped to Basra, Iraq. In Basra, it was coated with methylmercury as a preservative/fungicide. The seed grain was then distributed throughout Iraq with the expectation that it would be planted. However, people fed the grain to livestock destined for human consumption. The mercury was biomagnified through the food chain from grain to livestock to humans. People also consumed the grain directly by using it to make flour for bread and related food products. The decision of people to consume the seed grain instead of planting it resulted in mass mercury poisoning. Ten thousand people died and 100,000 were severely and permanently brain damaged [107].

Humans are not the only victims of environmental methylmercury contamination. Due to a commonality of certain biochemical processes across all animal groups, methylmercury has the potential to adversely affect many wild and domesticated animals. Such effects have been most notable proximate to areas of contamination and have been most evidenced as diminished reproductive success in fish, fish-eating birds, and mammals [88, 110].

Etiology of Mercury Intoxication

As noted above, mercury has a strong tendency to bind to sulfur and especially to selenium, which are essential elements. Because of this tendency, mercury can compromise the functionality of essential sulfur-containing amino acids (cysteine and methionine) and selenium-containing amino acids (selenocysteine, selenohomocysteine, and selenomethionine). The term "essential" in this context refers to compounds that humans cannot synthesize. Such compounds must be obtained from the food people eat. The distinction between essential and non-essential amino acids is somewhat unclear, as some amino acids can be produced from others. Methionine, for example, can be converted into homocysteine, which in turn can be converted into cysteine. Thus, given an adequate supply of methionine from food, humans can produce all the cysteine they need. But humans cannot synthesize methionine and cysteine de novo, and for this reason the sulfur-containing amino acids are often considered to be a pool of nutritionally equivalent essential amino acids. Similar logic applies to the selenium-containing amino acids.

One of the important functions of these two groups of amino acids is their role in determining the so-called tertiary structure of proteins. Simplistically, proteins are polymers of amino acids, and the sequence of

amino acids determines the primary structure of the protein. Hydrogen bonds between sequences of amino acids (peptides) determine the localized secondary structures of protein molecules. The tertiary structure is the overall three-dimensional structure of the protein and requires that certain parts of the molecule be locked into place by various mechanisms that include disulfide bonds, which is why cysteine and methionine are so important. Selenoproteins are analogs of ordinary proteins but contain one or more selenocysteines in place of cysteine. They are common in animals, and in humans ~25 selenoproteins have been identified. Health effects associated with an inadequate supply of selenium in the diet are believed to reflect the body's inability to synthesize sufficient amounts of these selenoproteins.

Exposure Limits

The unfortunate, industrially related incidents discussed above focused the attention of both health officials and the public on the perils associated with mercury. These were cases were mercury was discharged directly into bodies of water from which the local populace removed and consumed seafood containing up to 40,000 μg Hg/kg. Such industrial events are extreme, and the resultant concentrations of mercury in fish and shellfish were far above background levels. But the fact is that mercury occurs naturally in the environment, and through perfectly natural processes it finds its way into food that people eat. Incidents such as Minamata and Niigata contributed to public awareness of health issues associated with mercury bioaccumulation and biomagnifications in food chains leading to humans and led to the question, how much is too much. Studies began showing developmental effects in children, in particular among island/coastal populations that primarily consume seafood [111–113]. Federal and global organizations (e.g., US Food and Drug Agency (FDA), US Environmental Protection Agency (EPA), United National Food and Agriculture Organization (FAO), and the World Health Organization (WHO)) also took notice and began instituting guidelines for the consumption of fish and shellfish. Advisories, though intended for the general population, carried particular focus on pregnant woman, fetuses, and young children.

Currently the US EPA uses a Reference Dose of 0.1 μg methylmercury/kg body weight/day as an exposure limit without recognizably adverse effects. This limit carries a safety factor of 10 from the lowest observed adverse exposure level and corresponds to a blood mercury level of 5.8 μg/L or 5.8 parts per billion (ppb) mercury. Blood mercury levels below this value are considered to be without appreciable risk by the EPA [114]. The Joint FAO/WHO established a Provisional Tolerable Weekly Intake of Mercury (PTWI) of 1.6 μg of mercury/kg of body weight, somewhat higher than the EPA's recommendation. The WHO guideline of methylmercury intake is equivalent to a concentration in hair of 5 parts per million (ppm). Another study of mercury in hair conducted in the Seychelles Islands, where seafood consumption is significantly higher than average, found mercury levels in hair ranging from 7 to 26 ppm. The Seychelles study was supportive of the WHO guideline. Though the calculated FAO/WHO value for all adults was actually 3.3 μg Hg/kg of body weight, the published value of 1.6 μg of mercury/kg of body weight, which was weighted in favor of the most susceptible segment of the population (i.e., pregnant women, fetuses, young children) came to be commonly cited and used. Currently, the level of concern for mercury in fish is set by the FDA at 1.0 mg Hg/kg fish tissue.

Mercury in the Oceanic Ecosystem

Mercury from both natural and anthropogenic sources finds its way into the ocean, is taken up by plankton, and then transferred to small planktivorous fish. This begins a process of food chain magnification as the mercury is transferred to larger and larger predatory fish, ultimately finding its way into top-level carnivores like the tuna, swordfish, and sharks that people eat. Such large predatory fish tend to have the highest mercury concentrations (i.e., μg Hg/kg fish) and as such have attracted the most attention from the public, health officials, and scientists. The accumulation of methylmercury in high trophic level organisms results mainly from the ingestion of methylmercury-containing food (biomagnifications) rather than direct uptake of methylmercury from the water itself (bioaccumulation).

There are many factors that influence the concentrations of methylmercury in open ocean fish. These include size [115], age, trophic position [116, 117], physical and environmental parameters [100], and area of capture [118, 119]. There also remain large unexplained variations in the relationship of mercury concentration (i.e., μg Hg/kg fish tissue) versus fish size. In general, one would expect that, within a given species, larger fish are older fish and have consumed more prey to attain their size. A relationship between fish size and mercury content of the flesh is evident for some marine carnivorous species such as *Seriola rivoliana* (common name, bonita or jack), *Acanthocybium solandri* (common name, wahoo, ono), *Lutjanus syagris* (common name snapper), and *Epinephelis guttatus* (red hind, grouper) [120].

The age of the fish and preferred depth of feeding appear to explain more of the variance in mercury concentration than does size [117, 118, 121, 122]. Depth of habitat and foraging were found to be highly correlated with mercury concentrations [123]. This is because dissolved organic mercury concentrations increase with depth [123]. In addition, deeper waters (i.e., below the thermocline) tend to have lower oxygen, which leads to enhanced methylation rates [124–127]. This has led to the recent conclusion that the source of methylmercury in the open ocean is the deep water column [128, 129] and not coastal runoff [130] or the euphotic zone [131]. Many large oceanic predatory fish regularly dive to great depths to forage for prey from waters having lower oxygen concentration.

Mercury and Selenium

The confusion generated by the guidelines from the various agencies, along with repeated media attention to the presence of mercury in seafood has led to significant misunderstandings concerning the safety of seafood consumption and the role of seafood in a healthy diet. This has been to the detriment of both the commercial fishing industry and the consumers who have been confused and/or discouraged from regularly eating seafood.

What are some of the reasons that the perceived risk from eating seafood is overestimated? First, there has never been a confirmed case of mercury poisoning from the consumption of tuna or any other open ocean fish. The potential harmful effects of low levels of mercury from open ocean fish are undocumented and hypothetical. Mercury may be toxic at high levels, but not at the low levels typically found in oceanic fish. The joint advisory on seafood issued in 2004 by the FDA and EPA (www.cfsan.fda.gov/~dms/admehg3.html) was for pregnant women, nursing mothers, and young children. It directed pregnant women, nursing mothers, and young children to avoid eating swordfish, sharks, king mackerel, and tilefish, to limit consumption of other forms of fish to two meals per week, and to limit consumption of tuna to one meal per week. There has never been an advisory directed at the general consumer to limit seafood consumption.

Scientists are now realizing that earlier studies and resulting consumer guidelines were flawed. In fact, deliberately avoiding fish may increase the risk of adverse nutritionally related health effects. The benefits of fish oils (i.e., the omega-3 polyunsaturated fatty acids) on brain development are known and widely accepted. The basis of this realization began when adverse child brain development effects were not seen in multiple follow-up studies in populations consuming ocean fish [132–134]. Omega-3 polyunsaturated fatty acids (PUFAs) are critical to normal development of the human brain and nervous system. Pregnant women and nursing mothers who avoid foodstuffs rich in omega-3 PUFAs without replacement from another source risk adverse effects on their child's brain development. The excessive caution associated with fish consumption reflected knowledge that the fetal brain is very sensitive to maternal exposure to methylmercury. It is true that methylmercury can impair selenoenzyme activities in the brain.

Further exploration, however, revealed that selenium, an essential trace element, is simultaneously present with mercury in most oceanic fish. The ratios of selenium to mercury in these fish probably explain why consumption of ocean fish is not associated with mercury intoxication [135]. In almost all species of oceanic fish tested the amount of selenium exceeded that of mercury on a molar basis [136, 137]. Selenium was first considered to be a toxin, which it is when the dose is sufficiently high. Its essential antioxidant function was discovered in 1957. It is now considered an essential trace element, with a recommended daily allowance for adults of 55 μg/day. It is found in virtually

all commercial vitamin supplements. Selenium has been shown to protect against mercury toxicity in all animal species studied. Although historically the toxicity of mercury has been attributed to its great affinity to bond to sulfur-containing amino acids in protein, the binding affinity of mercury to selenium (to form inert mercury selenide) is a million times stronger than mercury's binding affinity to sulfur. In effect then, selenium can prevent mercury from causing health problems by sequestering mercury as mercury selenide. Alternatively, however, too much mercury in the diet can actually cause a selenium deficiency.

The conclusion then is that fish are unsafe to eat only when mercury concentrations in the fish are higher than the selenium concentrations [137]. In such cases the adverse health effects may reflect a combination of the directly toxic effects of the mercury and/or a selenium deficiency caused by the fact that selenium and mercury sequester one another. The only cases where mercury to selenium ratios exceed one is in some sharks and pilot whales. Selenium is necessary for cellular function in most animals. It is required for more than 25 enzymes with important functions [138, 139]. The ability of selenium to effectively detoxify metals such as mercury was first reported in 1967 [140]. The ability of selenium to decrease mercury toxicity has been established in all species examined to date [141, 142]. The high binding affinity between mercury and selenium [143] is very likely responsible for the ability of selenium to sequester and therefore detoxify mercury. As long as the ratio of selenium to mercury in the diet is sufficiently high, the selenium can sequester the mercury and effectively render the mercury harmless [136, 144]. Molar concentrations of selenium in fish are essential factors in evaluating risks associated with dietary mercury exposure. If the selenium level is higher in the fish than the mercury level, the fish is considered safe to eat [137]. The molar ratio of selenium to mercury is quite high in the muscle of most commercially important ocean fish [137, 145–148]. Pelagic oceanic fish are rich in selenium relative to mercury. Such fish appear more likely to prevent mercury toxicity than to cause it. The old thinking was that mercury was toxic by itself; the new thinking is that selenium and mercury sequester one another. Many of the symptomologies that were previously attributed to mercury toxicity are being reexamined as possible cases of selenium deficiency caused by mercury's role in sequestering selenium.

Future Directions

The prognoses for CFP and methylmercury are rather different. CFP is caused by a toxin that is naturally produced by certain species of marine dinoflagellates and passed up the food chain. Human activities appear to be largely unrelated to production of the gambiertoxins that are subsequently converted to various congeners of CTX. At the present time the best defense against CFP appears to be refraining from eating certain kinds of fish (e.g., barracuda) that have historically been associated with CFP. Based on extensive surveys in areas where CFP occurs, this policy would amount to erring on the side of safety but would apparently result in many harmless and nutritious fish being deleted from the menu. A preferable solution would be the development of a simple and inexpensive test to determine whether a fish contains CTX. Unfortunately, no such test currently exists, and because there are reported to be literally dozens of congeners of CTX, it is unclear that a single test could provide a reliable yes/no answer to the question. Ultimately an antibody-based assay may solve the problem, but at least at this point in time, development of such an assay is not imminent.

In the case of methylmercury, it is fair to say that very significant progress has been made since the discovery of Minamata Disease. Global production of mercury has declined by about 70% since 1970, a pattern that in no small part reflects recognition of the toxicity of mercury (especially methylmercury) and the efforts of government agencies to regulate mercury use and discharges and of industry to identify substitutes for mercury in many of its earlier applications and to reuse and recycle in cases where no substitutes exist. Probably the most important ongoing development is the controversy surrounding the health effects associated with consumption of fish and shellfish. With respect to this issue, public education is very important. The fact is that most fish and shellfish contain very little mercury. It is therefore straightforward to obtain the nutritional benefits of eating fish and shellfish without any risk from mercury intoxication.

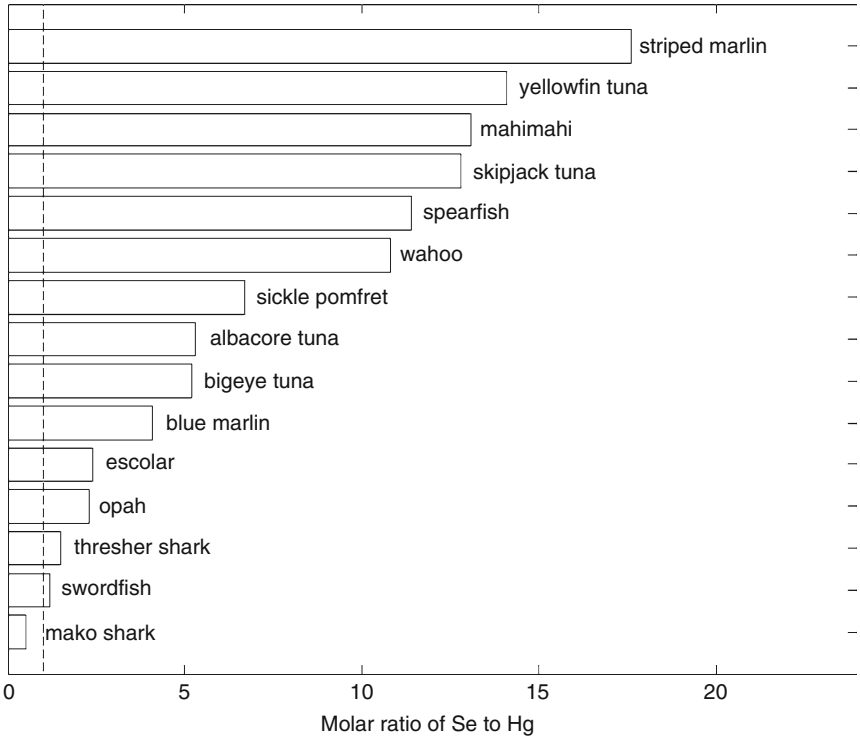

Bioaccumulation/Biomagnifications in Food Chains. Figure 5
Molar ratio of selenium to mercury in fish from the central North Pacific near Hawaii. Dashed line corresponds to a molar ratio of 1.0 (Data from Kaneko and Ralston [137])

Remarkably, almost all fish reported to contain more than trace amounts of mercury also contain substantially more selenium than mercury (Fig. 5), the result being that consumption of those fish may actually safeguard the consumer against mercury intoxication from other sources of exposure as opposed to being a threat to human health. The exceptions to this last statement include pilot whales and mako sharks, which are not in the creel of most fishermen, not on the menu at many restaurants, and not on the dinner table of most people.

Bibliography

Primary Literature

1. Gray JS (2002) Biomagnification in marine systems: the perspective of an ecologist. Mar Pollut Bull 45(1–12):46–52
2. Woodwell GM, Wurster CF, Isaacson PA (1967) DDT residues in an east coast estuary: a case of biological concentration of a persistent insecticide. Science 156:821–824
3. Bienfang PK et al (2011) Prominent human health impacts from several marine microbes: history, ecology, and public health implications. Int J Microbiol 2011:15, 152815
4. Hamelink JL, Waybrant RC, Ball RC (1971) Proposal – exchange equilibria control degree chlorinated hydrocarbons are biologically magnified in lentic environments. Trans Am Fish Soc 100(2):207–214
5. Harvey GR, Miklas HP, Bowen VT, Steinhauer WG (1974) Observations on distribution of chlorinated hydrocarbons in Atlantic Ocean organisms. J Mar Res 32(2):103–118
6. Giam CS, Hanks AR, Richards RL, Sackett WM, Wong MK (1972) DDT, DDE, and Polychlorinated Biphenyls in Biota from Gulf of Mexico and Caribbean Sea – 1971. Pestic Monit J 6(3):139–145
7. Isaacs JD (1973) Potential trophic biomasses and trace-substance concentrations in unstructured marine food webs. Mar Biol 22(2):97–104
8. Isaacs JD (1972) Unstructured marine food webs and pollutant-analogues. Fish Bull Natl Ocean Atmos Adm 70(3):1053–1059
9. Laws EA (1986) Unstructured food webs – a model for aquaculture. Aquacult Eng 5(2–4):161–170
10. Fraga S et al (2010) Ciguatera in macaronesia: an emerging problem. In Contribution to identification of gambierdiscus species. 14th conference of the international society for the study of harmful algae, Crete
11. Gudger EW (1930) Poisonous fishes and fish poisonings, with special reference to ciguatera in the West Indies. Am J Trop Med Hyg 10:43–55

12. Hessel DW, Halstead BW, Peckham NH (1960) Marine biotoxins. I. Ciguatera poison: some biological and chemical aspects. Ann NY Acad Sci 90:788–797
13. Beaglehole JC (1969) The journals of captain cook: the voyage of the resolution and adventure, vol 2. Cambridge University Press, Cambridge
14. Randall JE (1958) A review of ciguatera tropical fish poisoning with a tentative explanation of its cause. Bull Mar Sci Gulf Caribb 8:236–267
15. Banner AH, Scheuer P, Sasaki S, Helfrich P, Alender C (1960) Observations on ciguatera-type toxin in fish. Ann NY Acad Sci 90:770–787
16. Banner AH, Helfrich P, Piyakarn T (1966) Retention of ciguatera toxin by Red Snapper Lutjanus Bohar. Copeia 2:297–301
17. Banner AH, Helfrich P (1964) The distribution of ciguatera in the tropical Pacific. Hawaii Institute of Marine Biology, Honolulu, Hawaii
18. Pearn J (2001) Neurology of ciguatera. J Neurol Neurosurg Psychiatry 70(1):4–8
19. Arena P, Levin B, Fleming LE, Friedman MA, Blythe D (2004) A pilot study of the cognitive and psychological correlates of chronic ciguatera poisoning. Harmful Algae 3(1):51–60
20. Lewis RJ (1986) Disease and development: ciguatera fish poisoning. Soc Sci Med 23:983–993
21. Lange WR (1994) Ciguatera fish poisoning. Am Fam Physician 50(3):579–584
22. Fleming LE, Katz D, Bean JA, Hammond R (2001) Epidemiology of seafood poisoning. In: Hui YH, Kitts D, Standfield P (eds) Foodborne disease handbook. Marcel Dekker, New York, pp 287–310
23. Fleming LE, Baden DG, Bean JA, Weisman R, Blythe DG (1998) Seafood toxin diseases: issues in epidemiology and community outreach. In: Reguera B, Blanco J, Fernandez ML, Wyatt T (eds) Harmful algae. Zunta de Galicia and Intergovernmental Oceanographic Commission of UNESCO, Galicia, pp 245–248
24. Lehane L, Lewis RJ (2000) Ciguatera: recent advances but the risk remains. Int J Food Microbiol 61(2–3):91–125
25. Bienfang PK, Parsons ML, Bidigare RR, Laws EA, Moeller PDR (2008) Ciguatera fish poisoning: a synopsis from ecology to toxicity. In: Walsh PJ, Smith SL, Fleming LE, Solo-Gabriele HM, Gerwick WH (eds) Oceans and human health: risks and remedies from the sea. Elsevier, New York, pp 257–270
26. Dickey RW (2008) Ciguatera toxins: chemistry, toxicology and detection. In: Botana LM (ed) Seafood and freshwater toxins: pharmacology, physiology, and detection. CRC Press/Taylor & Francis, Boca Raton, pp 479–500
27. Dickey RW, Plakas SM (2010) Ciguatera: a public health perspective. Toxicon 56(2):123–136
28. Adachi R, Fukuyo Y (1979) Thecal structure of a marine toxic dinoflagellate Gambierdiscus-toxicus gen Et Sp-Nov collected in a ciguatera-endemic area. Bull Jpn Soc Sci Fish 45(1):67–71
29. Hokama Y, Yoshikawa-Ebesu JSM (2001) Ciguatera fish poisoning: a foodborne disease. J Toxicol Toxin Rev 20(2):85–139
30. Lewis RJ (2006) Ciguatera: Australian perspectives on a global problem. Toxicon 48(7):799–809
31. Dierking J (2007) Effects of the introduced predatory fish Cephalopholis argus on native reef fish populations in Hawaii. Dissertation Thesis, University of Hawaii, Honolulu, 125 pp
32. Steidinger KA, Baden DG (1985) Toxic marine dinoflagellates. In: Spector DL (ed) Dinoflagellates. Academic, Orlando, pp 210–261
33. Holmes MJ (1998) Gambierdiscus yasumotoi sp. nov. (Dinophyceae), a toxic benthic dinoflagellate from southeastern Asia. J Phycol 34:661–668
34. Chinain M, Feust MA, Pauillac S (1999) Morphology and molecular analysis of three toxic species of Gambierdiscus (dinophyceae): *G. pacificus* sp. Nov., *G. australes* sp. Nov. and *G. polynesiensis* sp. Nov. J Phycol 35:1282–1296
35. Richlen ML, Morton SL, Barber PH, Lobel PS (2008) Phylogeography, morphological variation and taxonomy of the toxic dinoflagellate *Gambierdiscus toxicus* (Dinophyceae). Harmful Algae 7:614–629
36. Litaker RW et al (2009) Taxonomy of Gambierdiscus including four new species, *Gambierdiscus caribaeus*, *Gambierdiscus carolineanus*, *Gambierdiscus carpenteri*, and *Gambierdiscus ruetzleri* (Gonyaulacales, Dinophyceae). Phycologia 48(5):344–390
37. Carlson RD (1984) Distribution, periodicity, and culture of benthic/epiphytic dinoflagellates in a ciguatera endemic region of the Caribbean. PhD thesis, Southern Illinois University, Carbondale
38. Bagnis R et al (1980) Origins of ciguatera fish poisoning: a new dinoflagellate, Gambierdiscus toxicus Adachi and Fukuyo, definitively involved as a causal agent. Toxicon 18:199–208
39. Holmes MJ, Lewis RJ, Gillespie NC (1991) Toxicity of Australian and French Polynesian strains of *Gambierdiscus toxicus* (Dinophyceae) grown in culture: characterization of a new type of maitotoxin. Toxicon 28:1159–1172
40. Faust MA (1995) Observation of sand-dwelling toxic dinoflagellates (Dinophyceae) from widely differing sites, including two new species. J Phycol 31:996–1003
41. Roeder K et al (2010) Characteristic profiles of Cigeatera toxins in different strains of *Gambierdiscus* spp. Toxicon 56(5): 731–738
42. Murata M, Legrand AM, Ishibashi Y, Fukui M, Yasumoto T (1990) Structures and configurations of ciguatoxin from the moray eel Gymnothorax javanicus and its likely precursor from the dinoflagellate *Gambierdiscus toxicus*. J Am Chem Soc 112:4380–4386
43. Lewis RJ et al (1991) Purification and characterization of ciguatoxins from moray eel (Lycodontis javanicus, Muraenidae). Toxicon 29:1115–1127
44. Satake M, Fukui M, Legrand AM, Cruchet P, Yasumoto T (1998) Isolation and structures of new ciguatoxin analogs, 2,3-dihydroxyCTX3C and 51-hydroxyCTX3C, accumulated in tropical reef fish. Tetrahedron Lett 39(10):1197–1198
45. Satake M et al (1997) The absolute configuration of ciguatoxin. J Am Chem Soc 119(46):11325–11326

46. Satake M, Ishibashi Y, Legrand AM, Yasumoto T (1996) Isolation and structure of ciguatoxin-4A, a new ciguatoxin precursor, from cultures of dinoflagellate Gambierdiscus toxicus and parrotfish Scarus gibbus. Biosci Biotechnol Biochem 60(12):2103–2105
47. Satake M, Murata M, Yasumoto T (1993) The structure of CTX3C, a ciguatoxin congener isolated from cultured Gambierdiscus-toxicus. Tetrahedron Lett 34(12): 1975–1978
48. Lewis RJ, Vernoux JP, Brereton IM (1998) Structure of Caribbean ciguatoxin isolated from Caranx latus. J Am Chem Soc 120:5914–5920
49. Scheuer PJ, Takahashi W, Tsutsumi J, Yoshida T (1967) Ciguatoxin isolation, and chemical nature. Science 155:1267–1268
50. Tachibana K, Nukina M, Joh YG, Scheuer PJ (1987) Recent developments in the molecular structure of ciguatoxin. Biol Bull 172:122–127
51. Yasumoto T, Nakajima I, Bagnis R, Adachi R (1977) Finding of a dinoflagellate as a likely culprit of ciguatera. Bull Jpn Soc Sci Fish 43:1021–1026
52. Murata M, Legrand AM, Ishibashi Y, Yasumoto T (1989) Structures of ciguatoxin and its congener. J Am Chem Soc 111:8929–8931
53. Legrand AM, Fukui M, Cruchet P, Ishibashi Y, Yasumoto T (1992) Characterization of ciguatoxins from different fish species and wild Gambierdiscus toxicus. In: Toteson TR (ed) Proceedings of the 3rd international conference on ciguatera fish poisoning, ciguatera fish poisoning. Polyscience Publications, Quebec, p 225
54. Hokama Y, Yoshikawa-Ebesu JSM (2001) Ciguatera fish poisoning: a foodborne disease. Toxin Rev 20(2):85–139
55. Lewis RJ, Jones A, Vernoux P-P (1999) HPLC/tandem electrospray mass spectrometry for the determination of sub-ppb levels of Pacific and Caribbean ciguatoxins in crude extracts of fish. Anal Chem 71:247–250
56. Lehane L, Lewis RJ (2000) Ciguatera: recent advances but the risk remains. Int J Food Microbiol 61:91–125
57. Dickey RW (2008) Ciguatera toxins: chemistry, toxicology and detection. In: Botana LM (ed) Seafood and freshwater toxins: pharmacology, physiology, and detection, 2nd edn. CRC Press/Taylor & Francis, Boca Raton, pp 479–500
58. Lewis RJ (2006) Ciguatera: Australian perspectives on a global problem. Toxicon 48:799–809
59. Dierking J (2007) Effects of the introduced predatory fish Cephalopholis argus on native reef fish populations in Hawaii. PhD thesis, University of Hawaii, 125 pp
60. Morton SL, Bomber JW, Tindall DR, Aikman KE (1993) Response of *Gambierdiscus toxicus* to light: cell physiology and toxicity. In: Smayda TJ, Shimizu Y (eds) Toxic phytoplankton blooms in the sea. Elsevier, Amsterdam, pp 541–546
61. Bomber JW, Tindall DR, Miller DM (1989) Genetic variability in toxin potencies among seventeen clones of *Gambiertoxicus toxicus* (Dinophyceae). J Phycol 25:617–625
62. Villareal TA, Morton SL (2002) Use of cell-specific PAM-fluorometry to characterize host shading in the epiphytic dinoflagellate *Gambierdiscus toxicus*. Mar Ecol 23:127–140
63. Parsons M, Settlemier C, Bienfang P (2010) A simple model capable of simulating the population dynamics of Gambierdiscus, the benthic dinoflagellate responsible for ciguatera fish poisoning. Harmful Algae 10(1):71–80
64. Cameron J, Capra MF (1993) The basis of the paradoxical disturbance of temperature perception in ciguatera poisoning. Clin Toxicol 31:571–579
65. Gordon CJ, Ramsdell JS (2005) Effects of marine algal toxins on thermoregulation in mice. Neurotoxicol Teratol 27:727–731
66. Anderson BS, Sims JK, Wiebenga NH, Sugi M (1983) The epidemiology of ciguatera in Hawaii, 1975–1981. Hawaii Med J 42(10):326–334
67. Tosteson TR, Ballantine DL, Winter A (1998) Sea surface temperature, benthic dinoflagellate toxicity and toxin transmission in the ciguatera food web in Reguera. In: Blanco BJ, Fernandez ML, Wyatt T (eds) Harmful algae. Xunta de Galicia and UNESCO, Paris, pp 48–49
68. Swift AEB, Swift TR (1993) Ciguatera. Clin Toxicol 31:1–29
69. Vernoux J-P, Lejeune J (1993) Ciguatera in the French West Indies. Mem Qld Mus 34:631–638
70. Friedman MA et al (2008) Ciguatera fish poisoning: treatment, prevention and management. Mar Drugs 6:456–479
71. Bienfang PK, Parson ML, Bidigare RR, Laws EA, Moeller PDR (2008) Ciguatera fish poisoning: a synopsis from ecology to toxicity. In: Walsh PJ, Smith SL, Fleming LE, Solo-Gabriele H, Gerwick WH (eds) Oceans and human health: risks and remedies from the sea. Elsevier Science, New York, pp 257–270
72. Steidinger KA, Baden DG (1985) Toxic marine dinoflagellates. In: Spector DL (ed) dinoflagellates. Academic, Orlando, pp 210–261
73. Campora CE, Hokama Y, Tamaru CS, Anderson B, Vincent D (2010) Evaluating the risk of ciguatera fish poisoning from reef fish grown at marine aquaculture facilities in Hawaii. J World Aquac Soc 41(1): 61–70
74. Helfrich P, Piyakarnchana T, Miles PW (1968) Occasional papers. Bernice P Bish Mus 23:305–369
75. Vernoux JP, Lahlou N, Elandaloussi SA, Riyeche N, Magras LP (1985) A study of the distribution of ciguatoxin in individual Caribbean Fish. Acta Trop 42(3):225–233
76. Helfrich P, Banner AH (1963) Experimental induction of ciguatera toxicity in fish through diet. Nature 197(487):1025–1026
77. Bagnis RA, Legrand A-M (1987) Clinical features on 12,980 cases of ciguatera (fish poisoning) in French polynesia. In: Gopalakrishnakone P, Tan CK (eds) Progress in venom and toxin research. Proceeding 1st Asia-Pacific congress on animal, plant and microbial toxins. National University of Singapore, Singapore, pp 372–384
78. Kodama AM, Hokama Y (1989) Variations in symptomatology of ciguatera poisoning. Toxicon 27(5):593–595
79. UNEP (2003) Global mercury assessment report: summary of the report. http://www.unep.org/gc/gc22/Document/UNEP-GC22-INF3.pdf85. Accessed 18 Apr 2011

80. Pacyna EG, Pacyna JM, Steenhuisen F, Wilson S (2006) Global anthropogenic mercury emission inventory for 2000. Atmos Environ 40(22):4048–4063
81. Solnit R (Sept/Oct 2006) Winged mercury and the golden calf. Orion Magazine
82. Tewalt SJ, Bragg LJ, Finkelman RB (2005) Mercury in U.S. coal – abundance, distribution, and modes of occurrence. U.S. Geological Survey Fact Sheet 095-01
83. Morel FMM, Kraepiel AML, Amyot M (1998) The chemical cycle and bioaccumulation of mercury. Annu Rev Ecol Syst 29:543–566
84. Keeler G, Glinsorn G, Pirrone N (1995) Particulate mercury in the atmosphere – its significance, transport, transformation and sources. Water Air Soil Pollut 80(1–4):159–168
85. Maprani AC et al (2005) Determination of mercury evasion in a contaminated headwater stream. Environ Sci Technol 39(6):1679–1687
86. March J, Smith MW (2001) March's advanced organic chemistry: reactions, mechanisms, and structure. Wiley, New York
87. Ullrich SM, Tanton TW, Abdrashitova SA (2001) Mercury in the aquatic environment: a review of factors affecting methylation. Crit Rev Environ Sci Technol 31(3):241–293
88. Wiener JG, Krabbenhoft DP, Heinz GH, Scheuhammer AM (2003) Ecotoxicology of mercury. In: Hoffman DJ, Rattner BA, Burton GA Jr, Cairns J Jr (eds) Handbook of ecotoxicology. CRC Press, Boca Raton, pp 409–463
89. Carrier G, Bouchard M, Brunet RC, Caza M (2001) A toxicokinetic model for predicting the tissue distribution and elimination of organic and inorganic mercury following exposure to methyl mercury in animals and humans. II. Application and validation of the model in humans. Toxicol Appl Pharmacol 171(1):50–60
90. Honda S, Hylander L, Sakamoto M (2006) Recent advances in evaluation of health effects on mercury with special reference to methylmercury: a minireview. Environ Health Prev Med 114(4):171–176
91. Salonen JT et al (1995) Intake of mercury from fish, lipid-peroxidation, and the risk of myocardial-infarction and coronary, cardiovascular, and any death in Eastern finnish men. Circulation 91(3):645–655
92. Guallar E et al (2002) Mercury, fish oils, and the risk of myocardial infarction. N Engl J Med 347(22):1747–1754
93. Choi AL et al (2009) Methylmercury exposure and adverse cardiovascular effects in Faroese whaling men. Environ Health Perspect 117(3):367–372
94. Clarkson TW, Magos L (2006) The toxicology of mercury and its chemical compounds. Crit Rev Toxicol 36(8):609–662
95. Shea KM, Perry KL, Shah M (2004) Health effects of methylmercury. Physicians for Social Responsibility, Washington, DC
96. Rice DC, Schoeny R, Mahaffey K (2003) Methods and rationale for derivation of a reference dose for methylmercury by the US EPA. Risk Anal 23(1):107–115
97. Miskimmin BM, Rudd JWM, Kelly CA (1992) Influence of dissolved organic-carbon, pH, and microbial respiration rates on mercury methylation and demethylation in lake water. Can J Fish Aquat Sci 49(1):17–22
98. Regnell O (1994) The effect of pH and dissolved-oxygen levels on methylation and partitioning of mercury in freshwater model systems. Environ Pollut 84(1):7–13
99. Xun L, Campbell NER, Rudd JWM (1987) Measurements of specific rates of net methyl mercury production in the water column and surface sediments of acidified and circumneutral lakes. Can J Fish Aquat Sci 44(4):750–757
100. Pickhardt PC, Folt CL, Chen CY, Klaue B, Blum JD (2002) Algal blooms reduce the uptake of toxic methylmercury in freshwater food webs. Proc Natl Acad Sci USA 99(7): 4419–4423
101. Nomura S (1968) Epidemiology of Minamata disease. Kumamoto Study Group of Minamata Disease, Kumamoto, Japan
102. McCurry J (2006) Japan remembers Minamata. Lancet 367(9505):99–100
103. Harada M (1995) Minamata disease – methylmercury poisoning in Japan caused by environmental-pollution. Crit Rev Toxicol 25(1):1–24
104. Anonymous (2002) Minamata disease the history and measures. http://www.env.go.jp/en/chemi/hs/minamata2002/. Accessed 18 Apr 2011
105. Myers GJ, Davidson PW, Weiss B (2004) Methyl mercury exposure and poisoning at Niigata, Japan. Seychelles Med Dent J 7:132–133
106. Fimreite N (1970) Mercury uses in Canada and their possible hazards as sources of mercury contamination. Environ Pollut 1:119–131
107. Bakir F et al (1973) Methylmercury poisoning in Iraq. Science 181(4096):230–241
108. Engleson G, Herner T (1952) Alkyl mercury poisoning. Acta Paediatr 41(MAY):289–294
109. Davis LE et al (1994) Methylmercury poisoning – long-term clinical, radiological, toxicological, and pathological-studies of an affected family. Ann Neurol 35(6):680–688
110. Scheuhammer AM, Meyer MW, Sandheinrich MB, Murray MW (2007) Effects of environmental methylmercury on the health of wild birds, mammals, and fish. Ambio 36(1):12–18
111. Grandjean P et al (1992) Impact of maternal seafood diet on fetal exposure to mercury, selenium, and lead. Arch Environ Health 47(3):185–195
112. Grandjean P et al (1997) Cognitive deficit in 7-year-old children with prenatal exposure to methylmercury. Neurotox Teratol 19(6):417–428
113. Grandjean P, Weihe P, White RF, Debes F (1998) Cognitive performance of children prenatally exposed to "safe" levels of methylmercury. Environ Res 77(2):165–172
114. WHO (1993) Evaluation of certain food additives and contaminants. Forty-first Report of the Joint FAO/WHO expert committee on food additives. Technical report series 837, World Health Organization, Geneva
115. Boush GM, Thieleke JR (1983) Total mercury content in Yellowfin and Bigeye Tuna. Bull Environ Contam Toxicol 30(3):291–297

116. Power M, Klein GM, Guiguer K, Kwan MKH (2002) Mercury accumulation in the fish community of a sub-Arctic lake in relation to trophic position and carbon sources. J Appl Ecol 39(5):819–830
117. Cai Y, Rooker JR, Gill GA, Turner JP (2007) Bioaccumulation of mercury in pelagic fishes from the northern Gulf of Mexico. Can J Fish Aquat Sci 64(3):458–469
118. Rivers JB, Pearson JE, Shultz CD (1972) Total and organic mercury in marine fish. Bull Environ Contam Toxicol 8(5):257–266
119. Colaco A, Bustamante P, Fouquet Y, Sarradin PM, Serrao-Santos R (2006) Bioaccumulation of Hg, Cu, and Zn in the Azores triple junction hydrotherinal vent fields food web. Chemosphere 65(11):2260–2267
120. Dewailly E, Rouja P (2008) Balancing the risks and the benefits of local fish consumption in Bermuda. Centre de Recherche Technical Report, Universite' Laval, Quebec, Canada
121. Yamashita Y, Omura Y, Okazaki E (2005) Total mercury and methylmercury levels in commercially important fishes in Japan. Fish Sci 71(5):1029–1035
122. Kojadinovic J, Potier M, Le Corre M, Cosson RP, Bustamante P (2006) Mercury content in commercial pelagic fish and its risk assessment in the Western Indian Ocean. Sci Total Environ 366(2–3):688–700
123. Choy CA, Popp BN, Kaneko JJ, Drazen JC (2009) The influence of depth on mercury levels in pelagic fishes and their prey. Proc Natl Acad Sci USA 106(33):13865–13869
124. Gill GA, Fitzgerald WF (1988) Vertical mercury distributions in the oceans. Geochim Et Cosmochim Acta 52(6): 1719–1728
125. Mason RP, Fitzgerald WF (1990) Alkylmercury species in the equatorial pacific. Nature 347(6292):457–459
126. Mason RP, Fitzgerald WF (1993) The distribution and biogeochemical cycling of mercury in the equatorial Pacific-Ocean. Deep Sea Res I 40(9):1897–1924
127. Mason RP, Fitzgerald WF (1991) Mercury speciation in open ocean waters. Water Air Soil Pollut 56:779–789
128. Sunderland EM, Krabbenhoft DP, Moreau JW, Strode SA, Landing WM (2009) Mercury sources, distribution, and bioavailability in the North Pacific Ocean: insights from data and models. Glob Biogeochem Cycles 23:1–14
129. Cossa D, Averty B, Pirrone N (2009) The origin of methylmercury in open Mediterranean waters. Limnol Oceanogr 54(3):837–844
130. Fitzgerald WF, Lamborg CH, Hammerschmidt CR (2007) Marine biogeochemical cycling of mercury. Chem Rev 107(2):641–662
131. Monperrus M et al (2007) Mercury methylation, demethylation and reduction rates in coastal and marine surface waters of the Mediterranean Sea. Mar Chem 107(1):49–63
132. Davidson PW et al (1998) Effects of prenatal and postnatal methylmercury exposure from fish consumption on neurodevelopment – outcomes at 66 months of age in the Seychelles child development study. Jama J Am Med Assoc 280(8):701–707
133. Hibbeln JR et al (2007) Maternal seafood consumption in pregnancy and neurodevelopmental outcomes in childhood (ALSPAC study): an observational cohort study. Lancet 369(9561):578–585
134. Myers GJ, Davidson PW (1998) Prenatal methylmercury exposure and children: Neurologic, developmental, and behavioral research. Environ Health Perspect 106:841–847
135. Ganther HE et al (1972) Selenium – relation to decreased toxicity of methylmercury added too diets containing tuna. Science 175(4026):1122–1124
136. Ralston NVC, Blackwell JL, Raymond LJ (2007) Importance of molar ratios in selenium-dependent protection against methylmercury toxicity. Biol Trace Elem Res 119(3):255–268
137. Kaneko JJ, Ralston NVC (2007) Selenium and mercury in pelagic fish in the central north pacific near Hawaii. Biol Trace Elem Res 119(3):242–254
138. Behne D, Pfeifer H, Rothlein D, Kyriakopoulos A (2000) Cellular and subcellular distribution of selenium and selenium-containing proteins in the rat. In: Roussel AM, Favier AE, Anderson RA (eds) Trace elements in man and animals. Kluwer, New York, pp 29–34
139. Rayman MP (2000) The importance of selenium to human health. Lancet 356(9225):233–241
140. Parizek J, Ostadalo I (1967) Protective effect of small amounts of selenite in sublimate intoxication. Experientia 23(2): 142–143
141. Cuvinaralar MLA, Furness RW (1991) Mercury and selenium interaction – a review. Ecotoxicol Env Saf 21(3):348–364
142. Ralston CR, Blackwell JL III, Ralston NVC (2006) Effects of dietary selenium and mercury on house crickets (*Acheta domesticus L.*): implications of environmental co-exposures: implications of environmental co-exposures. Environ Bioindic 1(1):98–109
143. Dyrssen D, Wedborg M (1991) The sulfur-mercury(Ii) system in natural-waters. Water Air Soil Pollut 56:507–519
144. Watanabe C, Yin K, Kasanuma Y, Satoh H (1999) In utero exposure to methylmercury and Se deficiency converge on the neurobehavioral outcome in mice. Neurotoxicol Teratol 21(1):83–88
145. Hall RA, Zook EG, Meaburn GM (1978) National marine fisheries service survey of trace elements in the fishery resource. US Dept of Commerce, National Oceanographic and Atmospheric Administration, National Marine Fisheries Service, Rockville, MD
146. Cabanero AI, Carvalho C, Madrid Y, Batoreu C, Camara C (2005) Quantification and speciation of mercury and selenium in fish samples of high consumption in Spain and Portugal. Biol Trace Elem Res 103(1):17–35
147. Robinson J, Shroff J (2004) Observations on the levels of total mercury (Hg) and selenium (Se) in species common to the artisanal fisheries of Seychelles. Seychelles Med Dent J 7(1):55–60
148. Plessi M, Bertelli D, Monzani A (2001) Mercury and selenium content in selected seafood. J Food Compos Anal 14(5): 461–467

Books and Reviews

Atwell L, Hobson KA, Welch HE (1998) Biomagnification and bioaccumulation of mercury in an arctic marine food web: insights from stable nitrogen isotope analysis. Can J Fish Aquat Sci 55(5):1114–1121

Cox PA, Banack SA, Murch SJ (2003) Biomagnification of cyanobacterial neurotoxins and neurodegenerative disease among the Chamorro people of Guam. Proc Natl Acad Sci USA 100(23):13380–13383

Gobas F et al (1999) Mechanism of biomagnification in fish under laboratory and field conditions. Environ Sci Technol 33(1):133–141

Gobas F, Zhang X, Wells R (1993) Gastrointestinal magnification – the mechanism of biomagnification and food-chain accumulation of organic-chemicals. Environ Sci Technol 27(13):2855–2863

Sijm D, Seinen W, Opperhulzen A (1992) Life-cycle biomagnification study in fish. Environ Sci Technol 26(11):2162–2174

Biochar, Tool for Climate Change Mitigation and Soil Management

Simon Shackley, Saran Sohi, Rodrigo Ibarrola, Jim Hammond, Ondřej Mašek, Peter Brownsort, Andrew Cross, Miranda Prendergast-Miller, Stuart Haszeldine
UK Biochar Research Centre (UKBRC), School of GeoSciences, Science and Engineering at The University of Edinburgh, Edinburgh, Scotland, UK

Article Outline

Glossary
Definition of the Subject
Introduction
What Is Biochar and How Can It Contribute to Carbon Mitigation
Biochar Production
Properties of Biochar
Carbon Mitigation Potential of Alternate Production Technologies
Evaluating Carbon Abatement from Biochar
What Are the Impacts of Biochar on Soil?
Conclusion: Evaluating the Sustainability of Pyrolysis-Biochar Systems
Future Directions for Research, Development, and Demonstration
Acknowledgments
Bibliography

Glossary

Biochar The porous carbonaceous solid produced by thermochemical conversion of organic materials in an oxygen-depleted atmosphere which has physiochemical properties suitable for the safe and long-term storage of carbon in the environment and, potentially, soil improvement.

Black carbon The continuum of solid combustion products ranging from slightly charred degradable biomass to highly condensed, refractory soot. All components of this continuum are high in carbon content, chemically heterogeneous, and dominated by aromatic structures.

Carbon (dioxide) equivalent Common measure of global warming potential constructed by converting the emissions of the six greenhouse gases under the Kyoto Protocol of the UNFCCC into the equivalent radiative forcing units of CO_2. CO_2, N_2O, and CH_4 are the relevant Kyoto gases to be considered in evaluating biochar.

Carbon abatement (CA) The net effect of changes in greenhouse gas fluxes that result from the production and application of biochar. This can include any or all of the following: carbon stored in biochar; CO_2 equivalent emissions released during pyrolysis; offset CO_2 equivalent emissions arising from avoided fossil fuel combustion; offset CO_2 equivalent emissions from reduced chemical inputs to agriculture; change in nitrous oxide and/or methane flux through biochar addition to soils; change in carbon in soil organic matter due to biochar addition; and offset CO_2 equivalent emissions from changed operations in the field. Which of these components is included will be specified in the text.

Carbon credit Any mechanism for allocating an economic value to a unit of carbon (dioxide) abatement. The most common units are EU Allowances (EUAs) (under the EU ETS), Emission Reduction Units (ERUs) (Joint Implementation, UNFCCC), Certified Emission Reductions (CERs) (Clean Development Mechanism, UNFCCC), and Verified Emission Reductions (VERs) (voluntary carbon market).

Carbon stability factor (CSF) The proportion of the total carbon in freshly produced biochar which remains fixed as recalcitrant carbon over a defined

time period (10, 100 years, etc., as defined). A CSF of 0.75 means that 75% of the carbon in the fresh biochar remains as recalcitrant carbon over the defined time horizon, and that 25% of the carbon has been converted into CO_2.

Charcoal The solid product of natural fire and traditional biomass conversion under partially pyrolytic conditions without yielding bioenergy coproducts.

Mean residence time (MRT) Inverse of decay rate, this is the average time for which carbon in new biochar remains present in a recalcitrant form.

Net primary productivity (NPP) A measure of plant growth and the additional CO_2 fixed and stored into plant biomass over a period of, for example, 1 year; technically, it is calculated as the balance between net photosynthesis and plant (dark) respiration.

Pyrolysis-biochar system (PBS) A combination of a specified pyrolysis technology, transport, distribution and storage infrastructure and application of biochar.

Recalcitrant carbon Aromatic carbon which is resistant to chemical or biological oxidation and subsequent conversion to CO_2.

Terra preta Literally "dark earth," these are localized soils, intensively studied, whose dark color appears to result from historic and prolonged management with charcoal, probably for the enhancement of agricultural productivity in and around the Amazon Basin.

Definition of the Subject

Biochar is the solid remains of any organic material that has been heated to at least 350°C in a zero-oxygen or oxygen-limited environment, which is intended to be mixed with soils. If the solid remains are not suitable for addition to soils, or will be burned as a fuel or used as an aggregate in construction, it is defined as char not biochar. There is a very wide range of potential biochar feedstocks, e.g., wood waste, timber, agricultural residues and wastes (straws, bagasse, manure, husks, shells, fibers, etc.), leaves, food wastes, paper and sewage sludge, green waste, distiller's grain, and many others. Pyrolysis is usually the technology of choice for producing biochar, though biomass gasification also produces smaller char yields. Syngas and pyrolytic bio-liquids, which have a potential use as energy carriers, are produced alongside biochar.

The strongest evidence for the beneficial effects of char additions to soils arises from the *terra preta* soils of the northern Amazon, where dark, highly fertile soils with very high levels of both stable (char) carbon and organic carbon were established and remain today [1]. Char was also added historically to soils in parts of northern Europe (including Netherlands, NW Germany, and Belgium) [2]. Chars have been, and are currently being used as soil amendments in Japan and West Africa.

The contemporary interest in biochar started in the early part of the twenty-first century and arises from the bringing together of the potential benefits for soils and agriculture with the carbon storage or sequestration opportunity afforded by recalcitrant, stabilized aromatic carbon. Biochar production and deployment has the potential to do one or more of the following:

- Reduce atmospheric greenhouse gas concentrations through CO_2 removal and avoided greenhouse gas emissions (perhaps on a gigaton carbon abatement scale)
- Improve the structure, properties, and "health" of soils
- Increase crop productivity
- Provide energy (e.g., electricity from syngas, heat from syngas, power from liquid fuels)
- Safely dispose of certain waste materials with potentially useful recovered by-products
- Absorb pollutants and contaminants and reduce nitrate leaching to water courses
- Suppress soil emissions of nitrous oxide and methane

Biochar is one of only a few strategies for actually removing CO_2 from the atmosphere (in addition to reducing atmospheric emissions where the use of fossil fuels is substituted for). While this feature may not currently be a top priority, it will become increasingly important in the decades to come, as it is almost inevitable that atmospheric CO_2 concentrations are now set to exceed what is commonly regarded as a safe level

(400–450 ppm). Biochar has consequently been termed ageo-engineering option, though it is a debatable point (See Box 1).

Introduction

Contemporary biochar research originates from several different sources: (a) research on *terra preta* soils from Amazonia dating back to the middle part of the twentieth century and earlier (e.g., the pioneering work of Sombroek) [3]; (b) research on the effects of charcoal on soils and plants, with initial contributions from the early- to mid-twentieth and more significant efforts in Japan in the 1970s and 1980s; (c) research on the properties and cycling of naturally occurring black carbon and charcoal; and (d) engineering RD&D on pyrolysis and gasification. The idea of the long-term storage of carbon in a stabilized form as found in charcoal (aromatic benzene-ring-type structures) was first proposed by Seifritz in 1993 [4], though his vision was storage in suitable land formations (such as valleys) rather than on agricultural land. This proposal was somewhat ahead of its time, and it was not until the first half-decade of the twenty-first century that the climate-change agenda provided a way of bringing the quite disparate areas of soil science, agronomy, environmental science, and engineering together under the banner of "biochar". Johannes Lehmann and Peter Read were important in making this conceptual linkage. A series of meetings took place in 2006 to 2008 which began to define and consolidate the emergent biochar community of researchers, practitioners, policy makers and entrepreneurs, including the first three meetings of the International Biochar Initiative (2007, Australia; 2008, UK; 2010, Brazil). In 2009, the first dedicated biochar book was published, edited by Lehmann and Joseph [5], and a series of national and regional meetings were held in 2009–2011, including in the USA, UK, Australia, China, Malaysia, and Brazil. Dedicated biochar research centers have now been established in the USA, Germany, New Zealand, and the UK, while existing departments, laboratories, or field stations in the disciplines of soil science, pyrolysis engineering and agronomy are increasingly turning their attention to biochar RD&D. Writing in 2010/2011, biochar has now become a distinct cross-disciplinary field of enquiry, a remarkable achievement given that the word was not even in circulation until the mid-2000s. Several comprehensive reviews of the biochar field were published in 2009 and 2010, and these can be read alongside the current chapter [2, 6, 7].

In this chapter, biochar is reviewed from the perspective of climate change, biomass and bioenergy resources, soils and agronomy. Biochar intersects all these issues and has to be evaluated against the dominant and emerging designs and options for solving problems and creating opportunities in those separate domains. As a multipurpose product and/or as an element of a multifunctional system, the different potential functions and purposes of biochar need to be dissected and analyzed. In section "What Is Biochar and How Can It Contribute To Carbon Mitigation?," biochar is defined, and the key arguments as to why it might be useful in carbon mitigation are presented. In section "Biochar Production," the main ways in which biochar can be produced are covered, briefly describing the key technological issues and challenges. Section "Properties of Biochar" covers some of the properties of biochar. Section "Carbon Mitigation Potential of Alternate Production Technologies" provides an account of the energy and carbon balance of the pyrolysis process that is at the core of biochar as a carbon abatement strategy. Section "Evaluating Carbon Abatement from Biochar" extends this to an analysis of carbon abatement across the biomass-bioenergy-biochar lifecycle and addresses three crucial questions.

- How much potential carbon abatement might arise from biochar globally?
- How efficient is carbon abatement through biochar compared to alternative use of the same organic matter across the life-cycle of the system?
- How cost efficient is carbon abatement through biochar?

Section "What Are the Impacts of Biochar on Soil" is a detailed analysis of the impacts of biochar in soils. In section "Conclusion: Evaluating the Sustainability of Pyrolysis-Biochar Systems," some preliminary conclusions regarding biochar and its wider sustainability are presented. Finally, in section "Future Directions for Research, Development and Demonstration," some key research needs and future directions are considered.

What Is Biochar and How Can It Contribute to Carbon Mitigation?

We define biochar as the porous carbonaceous solid produced by the thermochemical conversion of organic materials in an oxygen-depleted atmosphere and which has physiochemical properties suitable for the safe and long-term storage of carbon in the environment and, potentially, soil improvement. This definition is deliberately flexible and refers to both the production of biochar and its application.

Combustion of organic matter will take place if there is too much oxygen present during thermal conversion, and the resulting solid will be ash which typically contains just a few percent of carbon by mass, in addition to compounds and elements (phosphorus, potassium, other metals, etc.). With a low-level of introduced oxygen and thermal treatment of the organic matter, gasification may take place, during which volatile organic compounds are generated and released as vapor. This energy-rich synthesis gas ("syngas") can be cleaned and used for electricity-generation.

Pyrolysis occurs where the organic matter is subject to heat in the absence of any introduced oxygen and yields about a third of the feedstock as char (by weight), while gasification produces up to 10% char by weight. Charcoal is a type of char that has been produced (intentionally or otherwise) from wood for millennia, and much of our knowledge of biochar derives from the study of charcoal. Charcoal has also been used in soil-management practices for millennia and has well-documented benefits. While these are best observed in tropical environments – most famously in the *terra preta* soils of the Amazon – they have also been observed in temperate and semi-tropical regions.

It would be a mistake to equate biochar and charcoal however, since biochar represents a much wider group of materials which are likely to have far more variable properties than charcoal. Biochar comprises stabilized plant material in which carbon is stored mainly in a chemically recalcitrant form which will not significantly degrade through microbial activity or chemical reaction in the environment. It is this recalcitrance which is of interest from a carbon mitigation perspective since the carbon is thereby unavailable to microorganisms and does not return to the atmosphere as carbon dioxide (CO_2). But how long does carbon remain fixed in biochar? The mean residence time (MRT, the inverse of the decay rate) is the average time for which carbon in new biochar remains present in a stabilized aromatic form. The MRT of charcoal and analogous material is in the order of millennia [8]. Biochar may therefore provide an effective long-term store of carbon in soil and thus offer a potential abatement option for anthropogenic carbon emissions [9].

Stabilization of Plant-Captured Carbon

Annually, plants draw down 15–20 times the amount of CO_2 emitted from fossil fuels (7.5 Gt C year^{-1}), up to 20% of the entire atmospheric pool. About half of this is returned immediately to the atmosphere through plant respiration, but about 60 Gt C year^{-1} [10] is invested in new plant growth (about 45% of plant biomass is carbon) and contributes to net primary productivity (NPP). Since plant biomass is relatively constant globally, the magnitude of new plant growth must be approximately matched by harvest, litterfall, exudation by roots, etc. The annual CO_2 release from decomposition of these products by natural pathways and human cycling of plant-derived materials and products roughly equals NPP. The annual return of carbon to the atmosphere from the decomposition of all prior cohorts of plant material is thus approximately equal to NPP.

Intercepting and stabilizing plant-biomass production reduces the return of carbon to the atmosphere, with a relative reduction in atmospheric CO_2 (see Fig. 1). This reduction can be quite immediate if the default rate of decomposition is months to years, as it is for the dominant portion of biomass returned to soil in managed (agricultural and forest) ecosystems. Controlled charring (pyrolysis) can convert up to half of the carbon in plant biomass into chemical forms that are recalcitrant and, in principle, managed soils have a capacity to store pyrolyzed biomass at a rate significant in terms of emissions of carbon from fossil fuel.

The conversion of carbon in plant biomass to charcoal during natural fire is only about 1–5%, but the high level of stability established for such material in soil, which is generally a highly active biological medium, leads to expectation for similar stability in deliberately produced biochar. Biochar, deployed as a "carbon-negative" technology at the scale of 1 Gt C year^{-1}, would

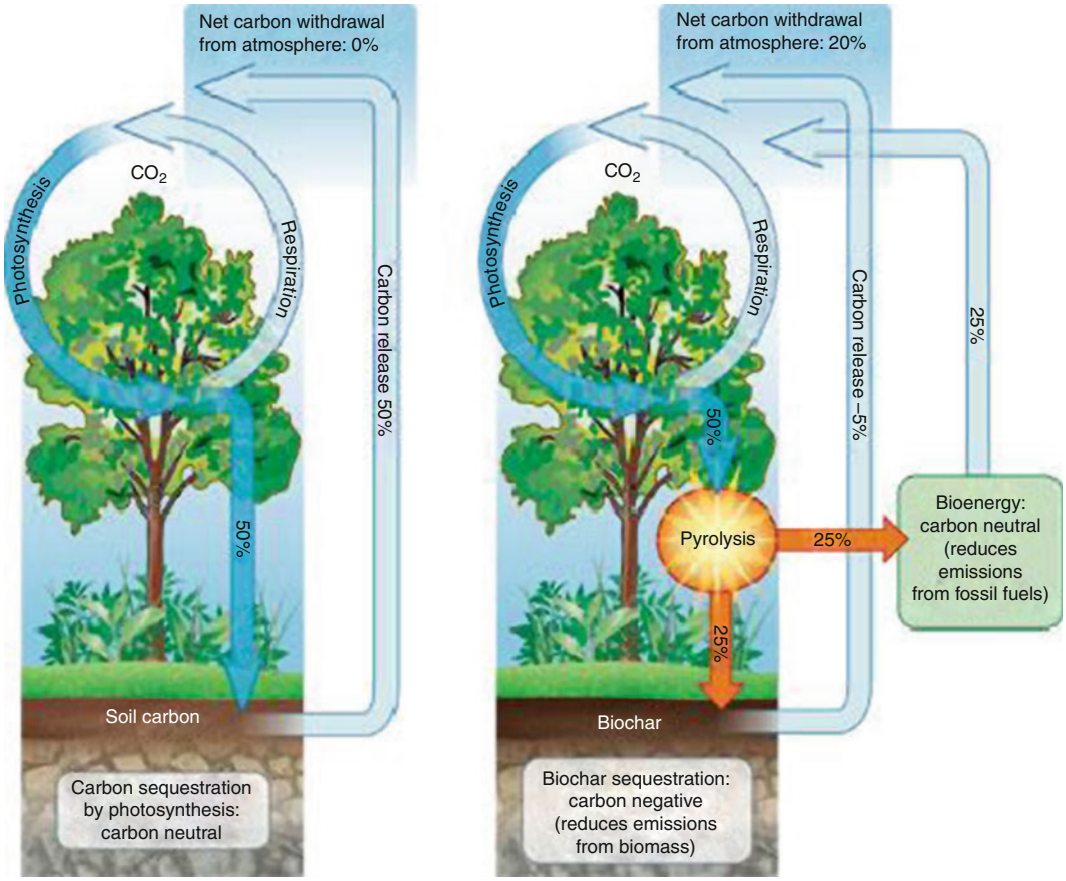

Biochar, Tool for Climate Change Mitigation and Soil Management. Figure 1
Schematic illustrating the pyrolysis-biochar concept [9] (With permission from Nature Publishing)

be equivalent to expanding the natural cycle of fire-derived charcoal storage in geographic terms and increasing its global magnitude by a factor of 4–20 [11].

Methane (CH_4) and nitrous oxide (N_2O) are the second- and third-largest contributors to radiative forcing of climate change after CO_2. Soil is a key source of both gases, which are emitted though natural microbial processes. The global significance of these processes has increased with agricultural expansion since higher CH_4 emission is associated with flooded soil conditions and with an enhanced nitrogen cycle (increased N_2O emissions) provided by the use of (synthetic) fertilizer, manures, and slurry. Since both CH_4 and N_2O are also associated in part with organic matter decomposition, stabilizing degradable organic matter could have a direct impact on soil-based emissions of these gases. Interventions in the nutrient or water balance of soil through changes in the dynamics of water in soil, or through the adsorption of nitrogen (as ammonium) may indirectly modify emissions of these gases from the soil.

To be a significant response to climate change, carbon abatement on a scale of millions of tons needs to occur, preferably hundreds of millions of tons. To intercept NPP and produce biochar at this scale presents a practical challenge, but still only involves a small fraction of total plant NPP (60 Gt C year^{-1}) of which 30% is already calculated to be "co-opted" by humans [12]. Increased efficiency of biomass recovery in managed ecosystems, diversion of biomass from current uses where it has a low value, and utilization of used biomass (organic waste) streams provide three ways in which it might be achieved. The fourth option is to sustainably harvest more biomass, which might be achieved by growing more productive plants, increasing the area of managed land, or adjusting harvesting

regimes. Clearly, demonstrable effects on NPP arising from the deployment of biochar could be factored into such strategies.

Indirect CO_2 Equivalent Impacts

Biochar can improve the pore-size distribution of soils, resulting in an improved retention of plant-available nitrogen in the soil, increasing plant N uptake and fertilizer-use efficiency. This implies lower fertilizer requirement and lower eutrophication risks. If the accumulation of biochar results in beneficial change in pore-size distribution, it would result in a more permanent change than can be achieved through the effects of degradable and thus transient organic matter that can be used to condition soil.

The release of nitrogen by soil microbes from decomposition of crop residues in the low-growth winter period (in temperate regions) is a key source of nitrogen loss to water and the atmosphere. Increasing the use-efficiency of nitrogen in recoverable crop residues is therefore of relevance to eutrophication through leaching, and N_2O emissions.

Changing the abundance or physical position of aerobic space in soil (with respect to loci of microbial activity) has the potential to mitigate CH_4 emission. The emission of N_2O from soil could be suppressed by adsorption of nitrogen in the form of ammonium (NH_4^+). Emissions of both CH_4 and N_2O are notoriously variable both temporally and spatially, and are also sensitive to soil pH. However, these mechanisms may be relevant in the suppression of CH_4 and N_2O by biochar observed at certain locations, or under certain controlled conditions [13].

The Haber–Bosch process used to fix atmospheric nitrogen into solid soluble (ammonium) form is an energy intensive process that accounts for about 40% GHG emissions associated with arable agriculture. Typical use-efficiency for fertilizer nitrogen globally is 30–50% [14] attributable to leaching, immobilization and gaseous loss, and leaching. Technologies that improve the management of these processes through the soil can therefore offer an indirect gain in agricultural carbon-equivalent balance.

Liming of agricultural soil also transfers carbon from the geological pool to the atmosphere through production (calcining of limestone) and subsequent neutralization in the soil [15, 16]. The alkalinity typical of biochar can potentially substitute for the use of lime in the management of soil pH without emission of CO_2 [13].

Reliable and secure storage for annual and large cumulative amounts of biochar would have to be available, and while simple burial (for example, in landfill or disused mines) has been considered [4], these possibilities would be limited, costly and potentially dangerous. The broader land surface, and in particular soils that are already actively managed, may therefore provide the required capacity for a large and enduring strategy for storing carbon in biochar [17]. The key assumptions are that the estimates for stability of charcoal made so far are typical and accurate, that biochar from modern pyrolysis technologies using more diverse feedstock exhibits broadly similar levels of stability as natural charcoal, and that appropriate feedstocks can be provided sustainably and without adverse environmental or sociopolitical impacts.

Box 1: Is Biochar Geoengineering?

Geoengineering has been defined as the "deliberate large-scale manipulation of the planetary environment to counteract anthropogenic climate change" [18]. Biochar is regarded as a form of geoengineering by the Royal Society of London, along with afforestation and associated removal of wood for long-term applications and a range of physiochemical methods, including direct air capture, ocean fertilization, ocean alkalinity enhancement, etc. This is because, at a large enough scale, biochar could have a noticeable influence upon the global carbon cycle. Yet, there are reasons why using the moniker geoengineering for biochar is misleading. Firstly, biochar might be a small-scale intervention. Secondly, biochar is not solely concerned with moderating global warming, and there will be instances where its main function is for agronomic purposes and soil improvement, water retention, leachate reduction, or treating contaminated land. Evaluating such projects as geoengineering could be misleading and result in unhelpful comparisons with very different technologies. In many cases, better comparisons can be made between the use of agricultural and organic residues and wastes for composting, incineration, gasification, second generation fermentation, anaerobic digestion, and biochar production.

Biochar Production

Processes

There are several processes which can be used to produce biochar, pyrolysis being the most common. Pyrolysis is a thermochemical decomposition process in which organic material is converted into a carbon-rich solid and volatile matter by heating in the absence of oxygen [19]. The solid product, char or biochar, is generally of high carbon content and may contain around half the total carbon of the original organic matter. The volatiles can be partly condensed to give a liquid fraction leaving a mixture of so-called "non-condensable" gases. Each of the three product streams from pyrolysis – solid, liquid, and gas – can have properties and uses that provide value from the process. There are two main classes of pyrolysis process as well as a number of other more or less related technologies that may be considered for biochar production.

Fast pyrolysis is characterized by high heating rates and short vapor residence times. This generally requires a feedstock prepared as small particle sizes, and a reactor design that removes the vapors quickly from the presence of the hot solids, typically at around 500°C, leading to high yields of liquid products with low char yields. There are a number of established commercial processes (as well as many R&D examples) where the target products are liquids – bio-oils – although biochar from such processes has also been studied [20]. The area of bio-oil from fast pyrolysis has been extensively reviewed [21, 22].

Of more interest for biochar production is slow pyrolysis, which can be divided into traditional charcoal making and more modern processes. It is characterized by slower heating rates, relatively long solid and vapor residence times and usually a lower temperature than fast pyrolysis, around typically 400°C. The target product is generally the char, but this will always be accompanied by liquid and gas products, although these are not always recovered.

Traditional processes using pits, mounds, or kilns, generally involve some direct combustion of the biomass, usually wood, as heat source in the kiln, which reduces the char yield. Liquid and gas products are often not collected but escape as smoke. As well as particulates and carbon dioxide, other greenhouse gases such as methane may be emitted, as well as other hydrocarbons, and amines, leading to a net positive radiative forcing effect even if the biochar product is used for carbon storage [24]. Hence, traditional charcoal-making techniques are not generally compatible with the objectives of pyrolysis-biochar systems (PBS) for carbon abatement.

Industrial-scale charcoal-making processes, using large retorts operated in batch or continuous modes, achieve higher char yields and avoid most of the issues of emissions by allowing recovery of organic liquid products and recirculation of combustible gases to provide process heat, either internally or externally [26]. Other developments have led to slow pyrolysis technologies which are of most interest for biochar production. These are generally based on a horizontal tubular kiln design, where the biomass is moved at a controlled rate through the kiln and include agitated drum kilns, rotary kilns, and screw pyrolyzers [27], as well as some gravity-driven designs. In several cases, these have been adapted for biomass pyrolysis from original uses such as the coking of coal with production of "town gas" or the extraction of hydrocarbons from oil shale. Although some of these technologies have well-established commercial applications, production of biochar is not yet one of them, and only limited reviews are available [27, 28]. Other technologies that may be considered for biochar production include flash pyrolysis (cf. fast pyrolysis but shorter residence times), intermediate pyrolysis (cf. slow pyrolysis with improved heat transfer, allowing faster throughput), flash carbonization (partial combustion in pressurized reactor), gasification (partial combustion in a gas flow), and hydrothermal carbonization (aqueous process at high temperature and pressure with catalysis) [28]. Typical values and reported ranges for key process variables and product yields of slow, intermediate, and fast pyrolysis processes are shown in Table 1 [28]).

Products

Composition of the three typical product streams from pyrolysis processes, solids, liquids, and gases, will vary with feedstock, process design, and conditions but can be generalized as follows. The solid product, char or biochar, has a varying carbon content, typically ranging from 60 to 90% [29]. In terms of proximate analysis, the char consists of four major components; fixed

Biochar, Tool for Climate Change Mitigation and Soil Management. Table 1 Scope of pyrolysis process control and yield ranges

Process	Slow pyrolysis	Intermediate pyrolysis	Fast pyrolysis
Temperature (in degrees centigrade)			
Range	250–750	320–500	400–750
Typical	350–400	350–450	450–550
Time			
Range	Min-days	1–15 min	ms-s
Typical	2–30 min	4 min	1–5 s
Yields (% oven dry weight)			
Char			
Range	2–60	19–73	0–50
Typical	25–35	30–40	10–25
Liquid			
Range	0–60	18–60	10–80
Typical	20–50	35–45	50–70
Gas			
Range	0–60	9–32	5–60
Typical	20–50	20–30	10–30

Based on review of over 30 literature sources [28]

carbon, volatile carbon, ash and moisture. Energy contents of biochar range typically 20–30 MJ kg^{-1} (Higher Heating Value (HHV), [28]).

Liquid products from biomass pyrolysis are frequently termed bio-oil. However, this is a somewhat confusing term as the organic liquid product is generally hydrophilic, containing many oxygenated compounds, and is present sometimes as a single aqueous phase and sometimes phase-separated, together with water produced in the pyrolysis reaction or remaining from the feedstock [19]. Energy contents of bio-oils range typically from 15 to 30 MJ kg^{-1} (HHV, [28]), but figures quoted may be given after a degree of purification. The gas product is termed synthesis gas, shortened to syngas. It is typically a mixture of carbon dioxide (9–55% by volume), carbon monoxide (16–51%), hydrogen (2–43%), methane (4–11%), and small amounts of higher hydrocarbons [28]. Literature values for syngas energy content ranges are sparse, partly due to varying composition during processing and the presence of inert gas, with available values ranging from 8 to 15 MJ kg^{-1} (HHV, [28]).

Effect of Feedstock and Process Variables

The nature and preparation of pyrolysis feedstocks as well as the process conditions used influence both the composition and distribution of products. The main effects are caused by feedstock properties, the gas environment, and temperature control; and are summarized here for slow pyrolysis [26].

High lignin biomass will tend to give higher char yields, with other components leading to more liquid and gas products. Minerals present in the ash can have a catalytic effect by increasing char yields in some cases. Moisture can have a positive or negative influence on char yields depending on conditions. Larger particle size can increase char yields by restricting vapor disengagement and increasing the scope for secondary, char-forming reactions.

Factors affecting the gas environment that lead to a longer contact time between hot solids (feedstock or char) and primary vapor products lead to increased char yields resulting from secondary char-forming reactions at the hot surface. These factors include particle size, heating rate, and gas flow rate; increased pressure has a similar effect.

Temperature control is one of the most important operational variable, particularly peak temperature. Higher peak temperatures lead to lower char yields and higher liquid yields. For instance, a typical biomass pyrolysis might yield 38% biochar by weight on a dry basis at 350°C, but only 27% when heated at 550°C [30]. Heating rates have a smaller and inconsistent effect on slow pyrolysis. Increasing residence time at peak temperature will lead to lower char yield, but again this is a smaller effect than temperature itself.

Temperature also influences the composition and structure of the biochar formed. Higher temperatures and longer residence times lead to chars with higher concentrations of carbon and fixed carbon (determined by proximate analysis), as more volatile matter is driven off; pore structure and surface area also develop with more severe conditions. Figure 2 shows some of these temperature effects, including the effect on elemental composition of char, in a series of

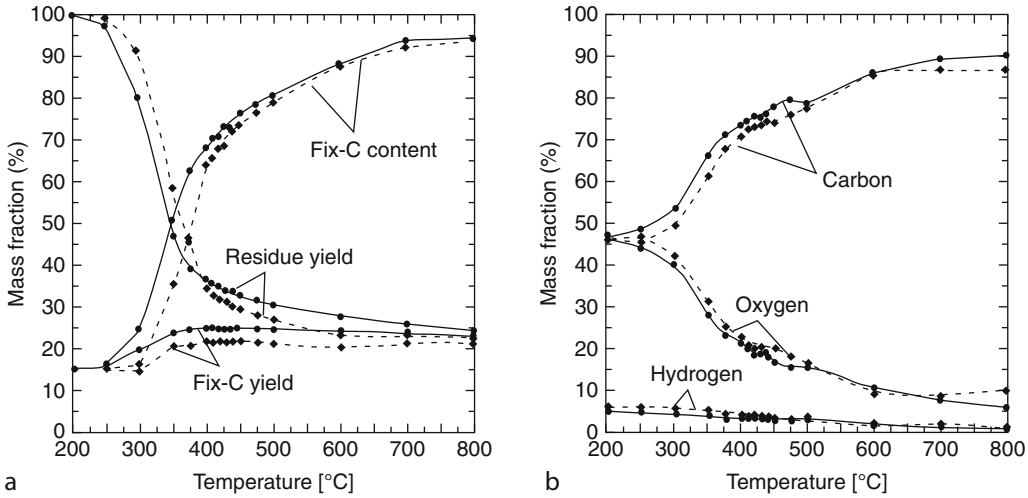

Biochar, Tool for Climate Change Mitigation and Soil Management. Figure 2
Effects of temperature and heating rate on (**a**) char yield, and (**b**) carbon, hydrogen, and oxygen content of beech chars. *Solid and dashed lines* are 2°C and 10°C min^{-1} heating, respectively [26] (Reproduced with permission from the American Chemical Society)

experiments with pyrolysed beech-wood [26]. Note that the complementary decrease in char (residue) yield and increase in fixed-carbon content at successively higher temperatures leads to a plateau in the fixed-carbon yield above about 400°C in this example. The relationship between fixed-carbon and soil-carbon stability is not yet clear [30].

Energy Balance

During pyrolysis, components of the biomass feedstock react by different pathways contributing to the complex products observed. Individual reactions may be endo- or exothermic and the combined process may also be endo- or exothermic depending on conditions of reaction [26]. Even when conditions favor exothermic reactions, initial heating to achieve onset temperature is required. Heat input may be provided by an external heat source, by partial oxidation of the feedstock, or by recycling and combustion of one of the product streams.

In conceptual designs for pyrolysis-biochar systems, the syngas, bio-oil, or combined gas/vapor stream are the preferred energy sources for the process. Data for process energy is not generally available in the literature but estimates suggest a requirement in the order of 10% of the energy value of the dry feedstock. In most cases, the product distributions will leave an excess of energy in the gas and/or liquid streams which can be used for electrical generation or exported heat, but note that the higher the biochar yield obtained, the lower this excess energy will be, a significant point for the economics of the process.

Properties of Biochar

Cation Exchange Capacity

Biochar has the capacity to exchange cations (e.g., ammonium, NH_4^+) with soil solution, and thereby store crop nutrients. The extent of this cation exchange capacity (CEC) is effectively absent at very low pH and increases at higher pH [32]. Experimental results show that the CEC of fresh biochar is typically low but increases with time as the biochar ages in the presence of oxygen and water [33–35].

Specific Surface Area

Biochar has a very high specific surface area (SSA) of several hundred $m^2\ g^{-1}$ to a thousand $m^2\ g^{-1}$ (Fig. 3). The main parameters influencing SSA are pyrolysis temperature, heating rate, residence time, and presence of active reagents (e.g., steam, CO_2, O_2, etc.). Figure 3a shows that the total surface area of biochar from most

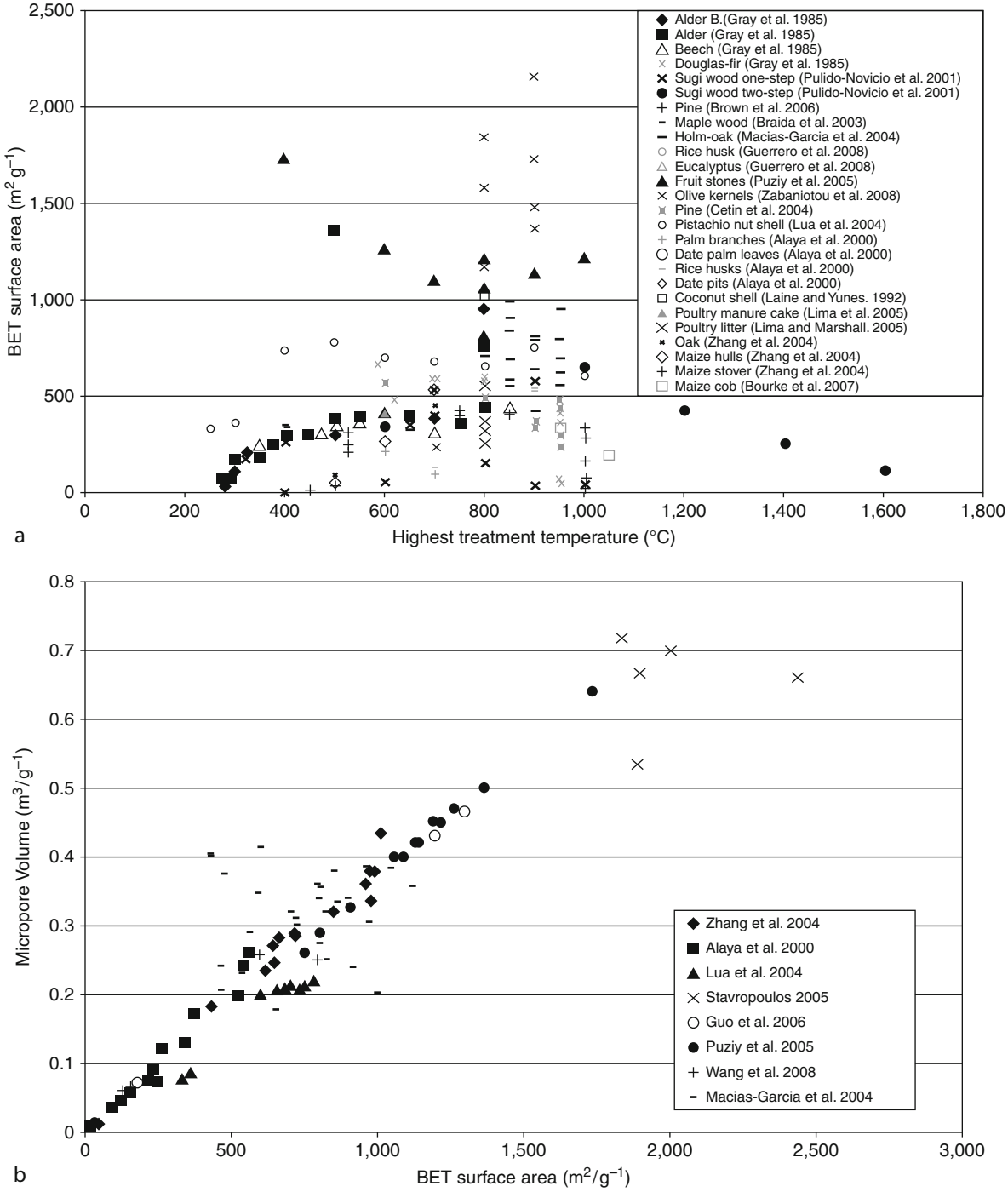

Biochar, Tool for Climate Change Mitigation and Soil Management. Figure 3

Biochar surface area (**a**) plotted against treatment temperature and (**b**) its apparent relationship with micropore volume [36] (Reproduced with permission from Earthscan Ltd.)

feedstocks tends to increase with increasing pyrolysis temperature. This is mainly due to the development of micropores that are responsible for most of the surface area, see Fig. 3b.

At present, it is not clear whether the additional surface area presented by micropores plays as important role in soils as macropores and, therefore, whether it is beneficial to produce a biochar with very high SSA. It may be possible to produce biochar with high SSA in the macropore range. However, the physical structure of biochar tends to be defined by the starting material, so fine milling or compaction of the feedstock before pyrolysis is necessary to achieve a well-defined macroporous product [37].

Contaminants

There are two main potential sources of contamination in biochar: feedstock and the conversion process. Depending on the origin and nature of the pyrolysis feedstock, biochar may contain contaminants such as heavy metals (potential toxic elements, PTEs) and organic compounds. Some of these compounds will undergo changes in the conversion process and might be destroyed (or converted to benign compounds), while others will remain unchanged or give rise to potentially harmful substances. In addition to the contaminants introduced in the feedstock, some contaminants can also be formed in the conversion (pyrolysis) process. These include polycyclic aromatic hydrocarbons (PAH) and potentially, in some cases, dioxins. Additionally, the physical form of pyrolysis products may present a direct health risk, and increase or decrease the risk posed by elements, compounds, or crystalline material both in feedstock or formed during pyrolysis.

Heavy Metals

Heavy metals present in the feedstock (e.g., MSW, sewage sludge, treated wood, etc.) are most likely to remain and concentrate in the biochar (with lower char yields, resulting in higher concentration of PTEs) [38–42]. Therefore, careful selection and analysis of feedstock is necessary to avoid contamination of biochar with increased levels of heavy metals. Heavy metals are stable materials and therefore retained (conserved) during volatilization of associated organic molecules. The majority of metals will therefore be present as ash within biochar (together with nutrient elements such as phosphorus and potassium). It may thus be possible to manipulate contaminant loadings through selective removal of ash [43]. Alternatively, it has been shown that high-temperature pyrolysis can release heavy metals from the solid product, thereby yielding char with lower loading of these contaminants [44].

Polycyclic Aromatic Hydrocarbons (PAHs)

PAHs can be formed from any carbonaceous feedstock. The major chemical pathways for (PAHs) formation in the pyrolysis process are the high-temperature secondary and tertiary pyrolysis reactions (homogeneous and heterogeneous), as shown in Figs. 4 and 5 [163]. The formation of these tertiary pyrolysis products increases with the pyrolysis severity (i.e., temperature and residence time) and becomes significant at temperatures around 750°C.

However, there exists also a second, less explored route for PAH formation. Evolution of PAHs from the solid substrate has been reported in the temperature range of 400–600°C [43, 45]. This pathway yields predominantly lower molecular-weight PAHs, although higher molecular-weight PAHs, such as benzo(a) pyrene, are also formed [45–47].

As the optimum temperature for biochar production is likely to lie in the region 450–550°C, in a well-controlled system (without hotspots), formation of PAH would proceed mainly by the evolution from solid substrates. PAH formation in the gas phase should be minimal due to the low pyrolysis temperature. Data on PAH content in pyrolysis char is scarce but indicate that the concentration and composition of PAHs in biochar are feedstock dependent [49]. Other data show that PAH concentrations in biochar produced from untreated biomass at temperatures of up to 600°C are considerably lower than those in urban soils in England, in the order of 10–100 mg kg^{-1} [50]. Biochar produced from chemically treated biomass is liable to contain considerably higher levels of PAHs than biochar from virgin feedstock due to the possibility of indigenous PAHs apparent in a study of biochar produced from railway sleepers previously treated with tar and creosote [49]. Available published data on the concentration of benzo(a)pyrene, one of the most toxic PAH compounds, is shown in Table 2.

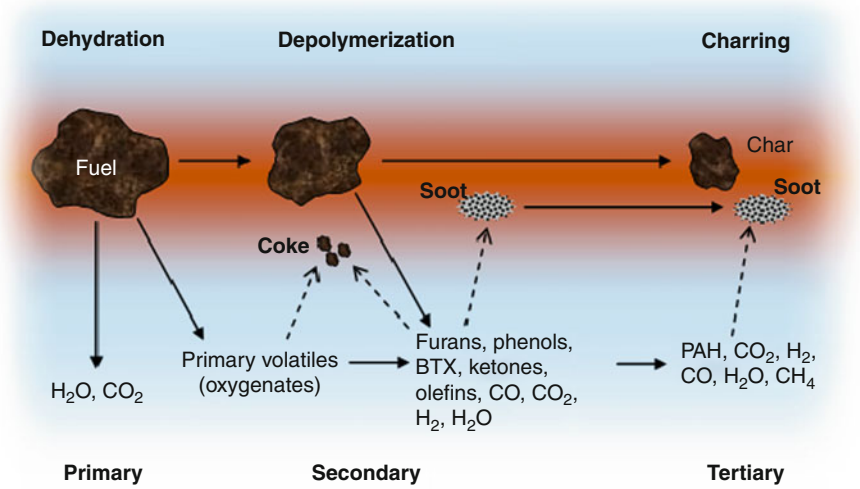

Biochar, Tool for Climate Change Mitigation and Soil Management. Figure 4
Progress of fuel particle pyrolysis [51]

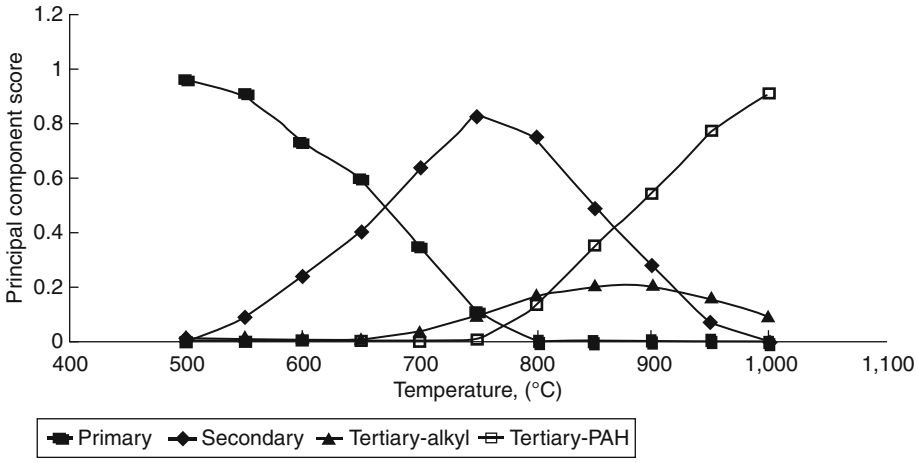

Biochar, Tool for Climate Change Mitigation and Soil Management. Figure 5
The distribution of the four "tar" component classes as a function of temperature with 0.3 s gas-phase residence time [48] (Reproduced with permission from NREL)

Biochar, Tool for Climate Change Mitigation and Soil Management. Table 2 Concentration of benzo(a)pyrene in biochar and UK soil [49, 50]

Benz[a]pyrene content ($\mu g\ kg^{-1}$)				
Birch char	Pine char	Pine sleeper char	Urban soil (England)	Rural soil (England)
310	570	4,040	714	67

Dioxins

Dioxins, unlike PAHs (which can be formed from any carbonaceous feedstock) require chlorine for their formation. Consequently, only biochar produced from feedstock containing significant amounts of chlorine (e.g. halogenated plastics) could be prone to generation of dioxins under certain conditions. The dioxin

formation process is heavily dependent on the temperature history of the pyrolysis products, and relatively high temperatures (around 750°C) are required for the formation of dioxin precursors (chlorinated benzenes and phenols). Therefore, it is unlikely that biochar produced by pyrolysis at temperatures between 450–550°C would contain dioxins in significant amounts even when produced from feedstock containing chlorine, despite the fact that dioxins can be formed from their precursors in this temperature range. The only exception would be biochar produced from feedstock already contaminated by dioxins or dioxin precursors.

Stability

The stability of biochar is one of its key properties as it determines its potential for long-term storage of carbon. However, despite its importance, there is no recognized way of determining stability of biochar. It is very difficult to predict stability of biochar over timescales relevant to carbon sequestration, i.e., centuries to millennia. This difficulty stems from the diversity of processes (biological, chemical, and physical) responsible for biochar degradation in the environment and the wide range of properties biochar from different sources pose. It seems that simple correlation of long-term biochar stability with any particular physical or chemical property of biochar is difficult, and new methods, such as accelerated aging, are being investigated. Preliminary results have shown that high levels of stability can be achieved in a wide range of production conditions [30].

Carbon Mitigation Potential of Alternate Production Technologies

The overall effect of pyrolysis-biochar production on carbon abatement, prior to soil incorporation, can be described as the sum of two main factors: the carbon stored in biochar (related to CO_2 removed from the atmosphere) and the CO_2 emissions avoided through substitution of fossil fuels by combustion of pyrolysis products for energy. In calculating avoided emissions, a baseline case needs to be established for comparison, selection of which can have a large impact on the results. There are three elements for selecting a baseline:

1. *Carbon intensity of displaced fossil fuel energy.* Avoided CO_2 emissions are calculated relative to the average CO_2 equivalent emissions (including contributions of CH_4 and N_2O) from generation of grid electricity (or that from a specific facility). The carbon dioxide emission factor (CEF) of the grid varies over time with the mix of fuels used. In the UK, it has decreased over recent decades with the trend away from coal toward use of natural gas. Expressed as kg CO_2eq kWheq^{-1} electricity, CEF has fallen from 0.78 in 1990 to 0.55 in 2007 [52]. Given this trend, the UK government recommends using a CEF of 0.43 kgCO_2eq kWheq^{-1} for comparisons when considering renewable electricity development [53]. The actual CEF value, e.g., 0.5 kgCO_2eq kWheq^{-1} in 2008, could also be used. The most appropriate CEF would be employed in a specific case-study context. It will be less for an energy system that is less reliant upon coal and other fossil fuels.
2. *Carbon neutrality or otherwise of biomass system.* Combustion of biomass for energy generation releases c. 99% of plant carbon as CO_2; it is conventionally assumed that the same quantity of biomass is replanted (without incurring any additional greenhouse gas emissions), hence the same quantity of CO_2 is taken up by the growing plants and the system is "carbon-neutral". Yet, if direct or indirect land-use change is entailed, carbon neutrality cannot be assumed: for instance, change from managed grassland (with c. 80 tC ha^{-1}) to energy-crop cultivation will involve immediate loss of CO_2 due to soil disturbance. Depending upon the energy crop, the equilibrium soil organic carbon content may decrease (e.g., to 45 tC ha^{-1} in a wheat for bioethanol context) or possibly increase (e.g., by up to 20 tC ha^{-1} over 20 years in the case of Miscanthus) [54]. It is therefore more accurate to include considerations of land-use change and the feedstock carbon cycle explicitly. Below we calculate the net carbon abatement from PBS assuming biomass replacement (carbon neutrality) and no replacement.
3. *Carbon Stability Factor (CSF) of biochar.* The CSF is defined as the proportion of the total carbon in freshly produced biochar which remains fixed as recalcitrant carbon over a defined time period (see Glossary). As yet, little information exists on the actual CSF of specific biochar samples due to

scientific uncertainties over biochar stability. A further uncertainty is the selection of the appropriate time period over which the stability is measured. Previous studies have used a range of values of the CSF from 0.68 over 100 years [55], 0.8 (time period undefined) [56], 1.0 (time period undefined) [57], 0.75 over 10 years [58], and 1.0 over 10 years [59]. As yet, there is no convention on the definition, measurement, and time horizon for reporting the CSF. To a certain extent, the selection of the time period is subjective and influenced by the decision-makers' preferences. In this review, we have adopted a time period of 100 years which is a compromise between the (multi-) millennial timescale of the climate system and the decadal (and frequently shorter) timescale of commercial and policy decision making. This also follows the convention of assessing Global Warming Potentials (GWP) to compare the radiative forcing of different GHGs over 100 years.

Equation 1 can be used to calculate the net carbon abatement arising from for combustion, PBS, or soil incorporation of biomass:

$$CO_{2na} = CO_{2av} + CO_{2fix} - CO_{2rel} \quad (1)$$

where:

CO_{2na} is net carbon eq. abatement
CO_{2av} is carbon eq. emissions avoided by replacement of fossil fuels
CO_{2fix} is carbon eq. fixed in the long-term (100 years)
CO_{2rel} is carbon eq. released by the biomass feedstock processing
(All expressed in $tCO_2eq.t^{-1}$ feedstock).

Meanwhile:

$$CO_{2fix(100)} = BM_{tot} \times BC_{yield} \times CO_{2tot} \times CSF \quad (2)$$

where:

$CO_{2fix(100)}$ is CO_2 eq. fixed over 100 years
BM_{tot} is biomass total dry weight
BC_{Yield} is biochar yield (ratio)
CO_{2tot} is total CO_2 eq. content of fresh biochar
CSF is carbon stability factor over 100 years
(All expressed in $tCO_2eq.t^{-1}$ feedstock).

Data for the example of 1 t of straw is given in Table 3. It can be seen that if combustion is used, 1.65 tCO_2 is released immediately, but there is an avoided emission of 0.66 tCO_2 arising from the substitution of fossil fuels (assuming a CEF of 0.5 $kgCO_2eq\ kWheq^{-1}$). The net CO_2 emission, assuming that there is no biomass replacement, is therefore c. 1 $tCO_2\ t^{-1}$ feedstock. If the same 1 t of straw is pyrolysed to produce biochar, the net CO_2 emission is lower at 0.45 $tCO_2\ t^{-1}$, assuming electricity generation from PBS is feasible. If no electricity cogeneration is possible, the net emission increases to 0.73 $tCO_2\ t^{-1}$, still lower than combustion (though obviously without the benefit of electricity generation). If full biomass replacement is assumed, biomass combustion and PBS both deliver net carbon abatement, though the biochar option more so.

If the alternative use of the straw is for incorporation into the soil however then the emission of CO_2 arising from decomposition would be slower. At day 1, 1.65 t of CO_2 remains in the biomass, and if we assume an exponential decay with a decay constant of 1.0, then after 4 years the vast majority of the straw has mineralized. Assuming that 5% of the straw biomass is stabilized as long-term soil carbon, then the direct incorporation abates more carbon from day 1 to 6 months. After that time, however, PBS with electricity generation and no biomass replacement abates more carbon, while after 1 year PBS without electricity generation and with no biomass replacement achieves higher carbon abatement than direct incorporation. The analysis is more complicated in the case of biomass replacement and is not attempted here. Clearly, this result is heavily dependent upon the decay function, and constant and slower rates of decomposition would give very different results under which direct incorporation would be more "competitive" in terms of carbon abatement relative to combustion and PBS.

In effect, pyrolysis has an associated "carbon debt" to pay-off due to release of CO_2 during pyrolytic conversion. The time period of this "carbon debt" is sensitive to the time horizon selected for measuring the CSF. If a shorter time horizon is chosen in measuring the CSF, then the carbon debt will appear to be smaller because the PBS CA will be larger, and vice versa. It is therefore important when evaluating options to be clear about what the PBS option is being compared

Biochar, Tool for Climate Change Mitigation and Soil Management. Table 3 Simple calculation of carbon stored and avoided CO_2 emissions arising from pyrolysis-biochar, combustion, and direct field incorporation for one oven dry ton of straw

Indicator	Combustion	Pyrolysis-biochar (with electricity generation)	Pyrolysis-biochar (no electricity generation)	Direct incorporation of straw into field[a]
Starting feedstock mass (t)	1	1	1	1
Carbon content at start (t)	0.45	0.45	0.45	0.45
Carbon content at end (stabilized) (t)[b]	0	0.25	0.25	0 year: 0.45 0.5 year: 0.27 1 year: 0.18 1.5 years: 0.11 2 years: 0.05
Expressed as CO_2 (t)	0	0.92	0.92	0 years: 1.65 0.5 year: 1.0 1 year: 0.66 1.5 years: 0.40 2 years: 0.18
Calorific value of straw: 13.5 GJ t^{-1}				
Efficiency of conversion	35%	15%	0%	0%
Delivered energy (GJ t^{-1})	4.725	2.025	0	0
Carbon emission factor: 0.5 kg CO_2 per kWh (2008 electricity mix)				
Delivered energy kWh	1,312.5	562.5	0	0
Avoided CO_2 emissions (t)	0.656	0.281	0	0
Total CO_2 abatement per ton feedstock (t) assuming carbon neutrality	0.656	1.2	0.92	
Total CO_2 abatement per ton feedstock assuming no biomass replacement (t)	−0.994	−0.449	−0.73	0 year: 0.18 0.5 year: −0.48 1 year: −0.81 1.5 years: −1.06 2 years: −1.28

[a]Assumes an exponential decay function with a decay constant of 1.0
[b]Assumes that 55% of the carbon in the feedstock is stabilized over 100 years

to, what the CSF and time period is, and to use these numbers to calculate the carbon debt of PBS.

A simplified model was developed to calculate net carbon abatement for slow, intermediate and fast pyrolysis [28]. The data required for the model (Table 4) were gathered in a comprehensive literature review complemented by direct communication with relevant experts [36, 58, 60–64]. Model outputs are all expressed on a feedstock dry weight basis. A default value of 33% for electrical conversion efficiency of the main model output data is assumed but with no use of spare process heat (beyond drying the feedstock). The CEF used is 0.43 $kgCO_2eq\ kWheq^{-1}$ and the results are shown in Table 5.

Results of the model show that fast pyrolysis may give the highest electrical energy product. This is due to the high liquid (oil) yields from the process, which can then be used for power generation. On the other hand, the electrical energy product is lowest for the slow pyrolysis process, where much of the energy value of

Biochar, Tool for Climate Change Mitigation and Soil Management. Table 4 Data required for the pyrolysis process model

Model inputs	Slow pyrolysis	Intermediate pyrolysis	Fast pyrolysis
Process input			
Biomass			
Carbon content (%)	46	43	50
Energy value (MJ kg^{-1})	17*	16	19
Pyrolysis process data			
Gas yield (% input mass)	45	32	13
Liquid yield (% input mass)	15*	35	72
Char yield (% input mass)	40	34	15
Energy loss (% input)	6*	0*	3
Process energy (% input)	10*	10*	10
Primary process output			
Gas			
Energy value (MJ kg^{-1})	13.1	11.0	11.5
Carbon content (%)	37.4	30.0*	36.0*
Liquid			
Energy value (MJ kg^{-1})	0.0*	12.0	17.9
Carbon content (%)	0.0*	30.0*	46.5
Char			
Energy value (MJ kg^{-1})	25.0*	24.7	27.0
Carbon content (%)	72.3	70.0*	78.0*

* = Estimated. See text for sources of other figures

the feedstock is stored in the biochar product. Abatement is greatest for slow pyrolysis, where most carbon is retained in biochar, and least for fast pyrolysis, where char yield is low. The values in Table 5 largely agree with those in Table 3, both in terms of energy product and net CO_2 abatement, with a 20% difference in calculated net carbon abatement for slow pyrolysis with associated energy generation.

"Carbon-Negative" Energy?

It has sometimes been claimed that PBS is a "carbon-negative" energy system, this being an extrapolation from "carbon-neutral" bioenergy systems. Using Eq. 2, and assuming that BM_{tot} is 1 t, BC_{Yield} is 0.4, CO_{2tot} is 0.85 and CSF is 0.75, then the $CO_{2fix(100)}$ is 0.935 $tCO_2eq.t^{-1}$ (assuming biomass used is then replaced). From Table 4, this is associated with 380 kWh electricity generation, hence, it can be argued that PBS is not only carbon neutral, but in fact a carbon-negative system. This is technically correct but only under the assumption of biomass replacement, namely that the same quantity of carbon in the biomass is taken up as CO_2 through subsequent photosynthesis, and no other land-use emissions are entailed. Furthermore, since PBS is currently an inefficient way of generating electricity, the moniker "carbon-negative energy" can be misleading and generate confusion. If the prime intention is to generate electricity, it is likely far better in most cases to utilize a more efficient conversion technology than pyrolysis.

Biochar, Tool for Climate Change Mitigation and Soil Management. Table 5 Pyrolysis process model results (assumes carbon neutral bioenergy)

Model outputs, carbon stability factor 0.75	Slow pyrolysis	Intermediate pyrolysis	Fast pyrolysis
Energy product (kWh eq kg^{-1} oven dry feedstock)	0.38	0.56	1.18
Net CO_2 abatement (kg CO_2 eq kg^{-1} oven dry feedstock) Pyrolysis	0.96	0.88	0.80
Combustion	0.67	0.63	0.75

Evaluating Carbon Abatement from Biochar

In order to determine the importance of a carbon abatement strategy from PBS (or variants thereof, such as Gasification-Biochar Systems, GBS), a number of questions need to be addressed, taking a systems-wide view, including techniques such as resource assessment, land-use modeling, Life-cycle Assessment and Techno-Economic Modeling.

- How much potential carbon abatement might arise from PBS globally?
- How efficient is carbon abatement through PBS compared to alternative use of the same organic matter across the life-cycle of the system?
- How cost efficient is carbon abatement through PBS in economic terms?

What Is the Potential Carbon Abatement Level?

Carbon abatement from biochar is a function of the amount of biochar produced which, in turn, is a function of the amount of biomass or other organic matter that is available. The resource pyramid approach [65] can be used to distinguish between "theoretical available resources" (i.e., the total amount which exists), "realistic available resources" (which applies a first level of pragmatic judgment to limit the supply), and "viable available resources" (which applies a second level of pragmatic judgment to further limit supply, taking particular account of likely or possible other demands in the market place). Even so, resource availability scenarios are likely to be necessary to account for irreducible uncertainties in future supply and demand (such as scenarios reflecting lower supply, higher supply, and very high supply of feedstocks available for pyrolysis, or scenarios which reflect low, medium, and high levels of competition for any available biomass for uses other than PBS).

Lehmann et al. [17] estimate that current global *potential* production of biochar is 0.6 ± 0.1 gigatons (Gt) per year (10^9 t or PgC $year^{-1}$). Lenton [66] argues that the present potential for biochar production from agricultural wastes, forestry fellings, and from shifting agriculture ("slash and char") is somewhat higher than in [17], increasing the potential carbon abatement through biochar to 0.77–0.87 Gt C (PgC) $year^{-1}$. Lehmann et al. [17] estimate that by 2100, production of biochar could reach between 5.5 and 9.5 Gt $year^{-1}$, assuming that biomass is grown specifically for the purpose of PBS. There are very large uncertainties attached to these numbers however, arising from competition for land-use, competition for use of biofuels, agricultural residues, and organic wastes, and a huge divergence (of nearly 1,000%) in different expert estimates of the potential future global supply of biomass for bioenergy purposes (see Box 2). Roberts et al. [56] arrive at a much smaller value for global CA (0.65 Gt CO_2 $year^{-1}$ or 0.18 Gt C $year^{-1}$) under the assumption that 50% of the 1.5 billion tons of currently unused crop residues globally is utilized for producing biochar. This might contribute 4% of the carbon reductions that are required globally by 2050 to limit climate change. However, after reviewing the literature on the potential production of biomass for bioenergy by 2100, Lenton [66] arrives at a carbon-abatement value from biochar that compares reasonably well with the larger Lehmann et al. value. He notes the potential constraint in carbon storage capacity in soil arising from biochar addition by about 2100, even assuming a high loading of 140 tC ha^{-1}.

Woolf et al. [68] have created and linked a global biomass feedstock availability model and a pyrolysis biochar production model, and calculate that between 1 and 1.8 Gt C $year^{-1}$ is feasible by about 2050 from the biochar mitigation option. The range is explained by the use of three different scenarios of biomass supply;

Box 2: Estimates of the Global Potential of Biofuels

A review by the OECD identifies four potential sources of bioenergy: additional land brought into production; crop residues; forest residues; and other organic waste (plant and animal) [70]. The OECD report suggests that, globally, 0.44 Gha is the upper limit on the land area that could be made available for dedicated bioenergy crop production by 2050. Models of land availability tend to underestimate the land that is already in use (by 10–20%), while overestimating the amount of land that could be brought into production. Limited water availability and competition for food and fiber production are frequently overlooked. The OECD estimate on new land available for bioenergy cultivation compares with the average of 0.59 Gha calculated from 11 studies reviewed [71].

The OECD report estimates that the total bioenergy available from the 0.44 Gha of new land is 100 EJ year^{-1}. The potential for marginal and degraded land is put at 29–39 EJ year^{-1}. As for crop residues, only 25–33% of residues are available for extraction because of competing uses and the need to return some to soil for nutrient replacement. Using yields from IIASA [72], bioenergy from crop residues is estimated at 35 EJ year^{-1} in 2050. The IIASA study estimates bioenergy from forestry residues to be 91 EJ year^{-1}, while other organic residues and wastes are expensive to collect, hence the potential is limited to 10 EJ year^{-1} by 2050 [73]. All in all, the OECD estimates that the primary energy available for heat, electricity, and motive power that could technically be made available globally is 245 EJ year^{-1}, which is at the lower end of the range reported by the IPCC in its Fourth Assessment Report (125–760 EJ year^{-1}) [74].

in each scenario, sustainability constraints have been met such that land upon which food is grown is not used for growing biomass for biochar production (i.e., only agri-residues and clean wastes are utilized) and indirect land-use change is not induced, incurring carbon-debt problems. Woolf et al. found that carbon abatement from use of biomass for biochar production was, on average, c. 20% higher than where the same biomass is used for bioelectricity generation through combustion. The comparison depends however on the fossil fuel offset. Where coal is offset, then biomass combustion and pyrolysis-biochar have similar carbon abatement. The higher bioelectricity generation from use of combustion avoids more carbon emissions due to the high carbon intensity of coal (compared, say, to gas, nuclear, renewables, etc.). Pyrolysis-biochar performs better in terms of carbon mitigation, where offsetting is against a fuel with a lower carbon intensity because the energy penalty of pyrolysis is therefore less important (from a carbon point of view) (a point also made by [69]). A further issue explored by Woolf et al. is the potential role of soil fertility in influencing the carbon mitigation potential of biochar; namely, in areas of low soil fertility, biochar is anticipated to have greater agronomic benefit, increasing yields with the use of fewer inputs (and their associated greenhouse gas emissions). This means that, according to this analysis and in terms of carbon mitigation, biochar is most effective, where it is incorporated into poorer quality soils in regions where less carbon-intensive fuels are being displaced.

The IEA's Energy Technology Perspectives project has suggested that a reduction of 13 Gt C year^{-1} is needed in 2050 relative to the "do-nothing" business-as-usual scenario [75]. If biochar could contribute 1 Gt C year^{-1} to "filling" this overall 13 Gt C year^{-1}, then its contribution would be roughly similar to the potential role of nuclear power expansion or enhanced power-generation efficiency and fuel switching.

The Carbon Abatement Efficiency of Pyrolysis-Biochar Systems

Carbon abatement efficiency (CAE) is defined as the net carbon abatement delivered for a given function unit (e.g., processing of a unit of feedstock, delivery of a kWh of electricity or heat, utilization of a given area of land, etc.). It is a way of comparing abatement efficiency between alternative uses of the same feedstock, land, or per unit of delivered energy. This is important in deciding how to use limited resources. The CAE is calculated from a life-cycle assessment (LCA) of the full PBS chain. An example of an LCA of a biochar system, including the impacts of biochar in the soil, is illustrated in Fig. 6.

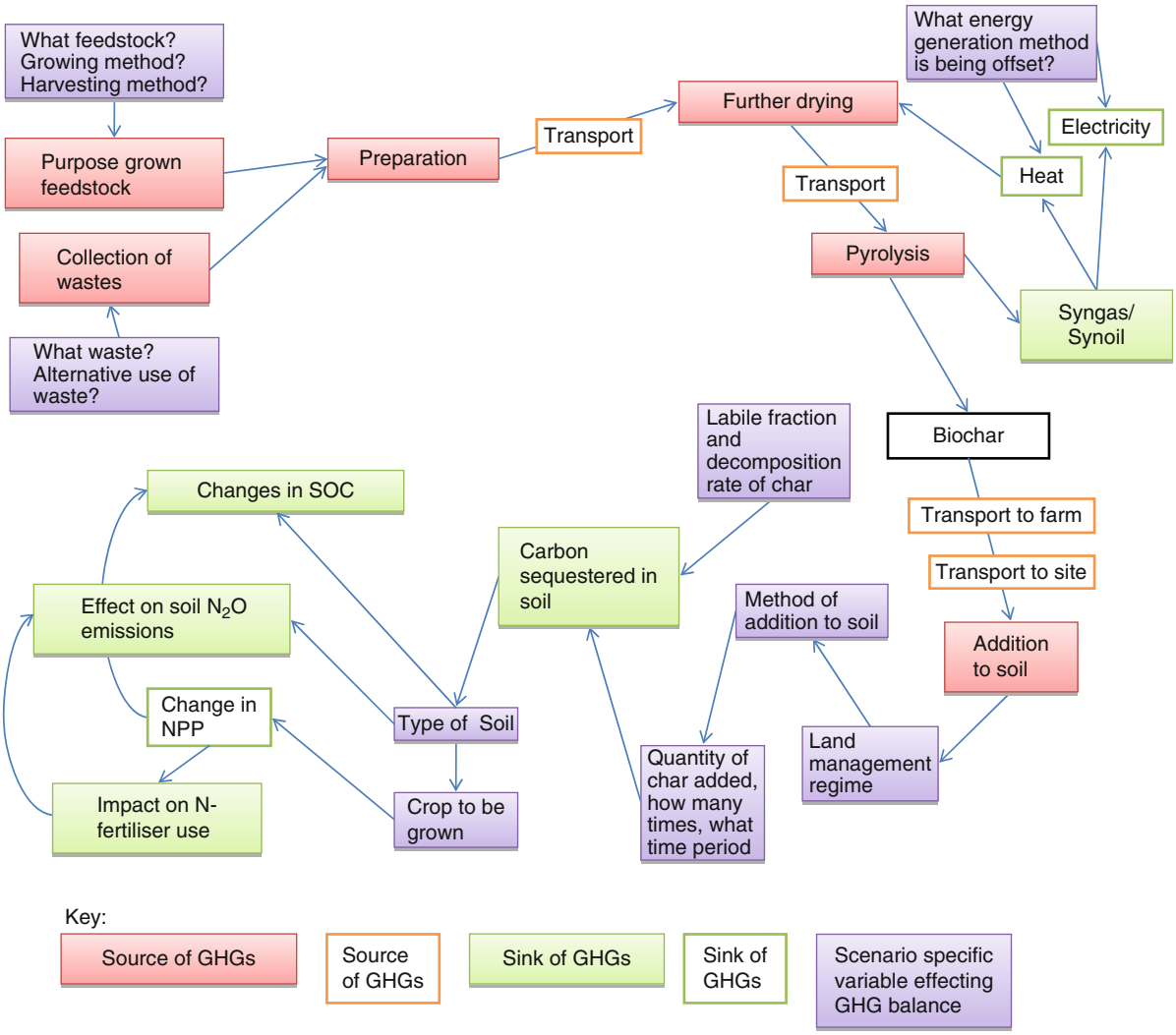

Biochar, Tool for Climate Change Mitigation and Soil Management. Figure 6
A life-cycle system model for pyrolysis-biochar systems [55]

A number of LCA studies of PBS have been conducted for a range of different feedstocks, technologies, and agricultural contexts. The results are summarized in Table 6.

Table 6 shows that some studies present significantly higher net carbon-abatement values than others. For instance, Gaunt et al. [59] present values for switchgrass that are several times larger than those of Roberts et al. [56]. Their respective values are closer for corn stover (30% different). At first glance, the net carbon abatement for Miscanthus from Gaunt [59] and Hammond et al. [55] appear to agree, but not when the results are compared with inclusion of the indirect effects of biochar in soil in the former study (in which case, the Gaunt et al. study has 60–100% greater net carbon abatement than the Hammond et al. study). While some results do appear to converge, the overall impression is of a wide range of different assumptions leading to a high degree of uncertainty. At present, it is not known which assumptions are most appropriate and in what context. For instance, the assumed CSF of studies in Table 6 varied from 0.68 to 1.0 (for a range of [not always specified] timescales). This difference alone can account for a 50% variation in net CA.

Biochar, Tool for Climate Change Mitigation and Soil Management. Table 6 Comparison of different life-cycle assessment studies of pyrolysis-biochar systems

Variable	Description	Gaunt and Lehmann [59]	Gaunt and Cowie [58]	McCarl et al. [76]	Roberts et al. [56]	Hammond et al. (2011) [55]	Ibarrola [57]
Feedstocks		Switchgrass, miscanthus, forage corn, wheat straw, corn straw	Green waste, cattle manure, wheat straw	Maize stover	Corn straw, yard waste, switchgrass	Wheat, barley, and oilseed rape straw, UK and Canadian forestry residues, short-rotation forestry, short-rotation coppice, miscanthus, sawmill residues, arboricultural arisings	Green and garden waste, sewage sludge, food waste, anaerobic digestate, construction and demolition wood waste
National context and applicability		USA	Undefined	USA (mid-West)	USA	UK	UK
Energy ratio	Energy outputs divided by energy inputs	Forage corn: 1.3 All others: 4.3 to 5.9	Not specified	Not specified	Corn stover: 2.8 Switchgrass: 3.1	Not specified	Not specified
Overall energy efficiency	Delivered energy (heat or power) divided by energy in feedstock + fossil fuel energy to operate process	38%	Green: 20% Cattle man.: 15% Wheat straw.: 25%		29% Heat	6–15% Electricity	20% Electricity
CO_{2av}	CO_2 avoided through fossil fuel substitution (% of total)	19–25%	10–18%	Not specified	26–40%	10–25%	20–30%
BC_{Yield}	Fresh biochar yield (as proportion of feedstock) (% DM)	8.5–8.7% (fast pyrolysis)	35–42%	35%	29%	33.5%	35%
CSF and time period	Carbon stability factor	1.0 over 10 years	0.75 over 10 years	1.0 time period not defined	0.8 (loss over small number of years then stable)	0.68 over 100 years	0.68 over 100 years

CO_{2tot}	Carbon content of fresh biochar			0.75	0.63–0.68	0.75	C&I wood: 0.72 Green: 0.50 Sewage sludge: 0.38 Food: 0.62
Proportion of the CA that is stabilized C in char (% of total)		58–63%	41–45%	Not specified	54–66%	40–50%	45–55%
Proportion of the CA that is indirect effects of char in soil (% of total)		17–19%	40–48%	Not specified	2–10%	25–40%	15–25%
Assumed size of pyrolysis unit (tons per annum)			16,000	70,000	10 t h^{-1} c. 50,000 tpa	Small: 2,000 Medium: 20,000 Large; 100,000	
CO_2na (tCO_2eq. t^{-1} oven dry)	Net carbon-equivalent abatement	Gaunt and Lehmann [59]	Gaunt and Cowie [58]	McCarl et al. [76]	Roberts et al. [56]	Hammond et al. [55]	Ibarrola [57]
	Corn stover			0.8–1.1	0.793–0.864		
	Switchgrass	1.307	1.16/1.82		0.442		
	Green waste/yard waste				0.885		0.855
	Miscanthus	1.328				1.14	
	Wheat straw		0.99/1.65			0.84	
	Cattle manure		1.085/1.745				
	Sawmill residues					1.17	
	Forestry residues					1.24	
	Short-rotation coppice					1.13	
	Sewage sludge						0.774
	Food waste						0.965
	Anaerobic digestate						0.785
	Construction and demolition waste						1.048

Biochar, Tool for Climate Change Mitigation and Soil Management. Table 6 (Continued)

Variable	Description	Gaunt and Lehmann [59]	Gaunt and Cowie [58]	McCarl et al. [76]	Roberts et al. [56]	Hammond et al. (2011) [55]	Ibarrola [57]
Notes		1	2	3	4	5	6
Reference		Gaunt et al. [59]	Gaunt et al. [58]	McCarl et al. [76]	Roberts et al. [56]	Hammond et al. [55]	Ibarrola [57]

1. The CEF assumes 50% coal and gas, hence it is the average of the two values in Table 3 in Gaunt and Lehmann [59] converted from per hectare to per ton basis using the yield figures provided in the paper. The yield for corn stover is not given, so the CO_2na cannot be calculated.
2. The CEF assumes 50% coal and gas, hence it is the average of the two values in Table 18.2a ([58]). The first value shown does not include the application of biochar to crops or indirect effects of biochar upon soil incorporation. The value of these effects can be inferred to be from 0.2 (low), 0.66 (medium) and 1.14 (high) $tCO_2eq.t^{-1}$. The second value shown uses the medium values of the indirect effects and adds this quantity to the pyrolysis + fossil fuel offsets value. If the lower estimate of the indirect effects is used instead, the overall effect is reduced by c. 0.4 $tCO_2eq.t^{-1}$. In calculating the proportional contribution to total CA from the avoided fossil fuel emissions, stabilized carbon in char and the indirect impacts of biochar in soils, the medium value of the indirect effects have been assumed.
3. Lower value for switchgrass refers to slow pyrolysis; the higher value refers to fast pyrolysis.
4. For corn stover, the lower value is early stover and the higher value is late stover. In the case of the switchgrass, this does not take account of indirect land-use change (ILUC) arising from use of bioenergy crops. If ILUC is included, then the net carbon abatement is -0.036 $tCO_2eq.t^{-1}$ (i.e., an emission).
5. The value for wheat straw is the same as for barley and oilseed rape straw. Where large quantities of forestry residues are imported into the UK from Canada, the CO_2na is 1.08 $tCO_2eq.t^{-1}$. The value for short rotation coppice (SRC) is similar to the values for small round wood (1.15 $tCO_2eq.t^{-1}$).
6. Results for green waste, sewage sludge, and food waste are relative to incorporation of material in landfill sites with UK-levels of methane recovery. Values are also provided for incorporation of material into fast pyrolysis (10% char yield).

Different assumptions about useable or delivered energy from pyrolysis are also important contributors to the uncertainty. Some studies assume a much higher energy conversion efficiency than others, e.g., Gaunt and Lehmann assume a value that is substantially higher than conventional biomass combustion, and even gasification, suggesting that useable heat is also being utilized. Roberts et al. also assume effective use of heat from pyrolysis, hence use a high overall energy efficiency. Hammond, on the other hand, uses a more conservative value for net energy efficiency, which is substantially lower than straight combustion. How energy is treated in the LCA is important in making comparisons with CA from straight combustion or gasification since it is frequently assumed that heat is not readily used from such technologies where the principal purpose is electricity generation. Comparing net CA from PBS with delivered power and heat with biomass combustion with only power generation is probably not a fair comparison to make.

Some element of "biochar proponent optimism" has likely entered into the existing studies, and a more critical approach will be needed for the future. In summary, there is a moderate to high level of uncertainty attached to all existing values, and one should not pay too much attention to the precise numbers as they are very likely to change in the future as more understanding and experience is gained. The lack of reliable engineering data on the slow pyrolysis process at a commercial scale is one of the critical uncertainties. Most of the existing studies have used data from a single technology (BEST Energies, now Pacific Pyrolysis Pty. Ltd.), yet the results from this process have not been published in the peer-reviewed literature. This creates a potential weakness in the current argument in favor of biochar that needs to be addressed by acquisition of much better engineering data on slow pyrolysis.

Energy-Output to Energy-Input Ratios

The energy-output to -input ratio (also known as the energy yield) is the quantity of delivered energy (i.e., useable power and/or heat) divided by the quantity of energy required to produce that energy. Bioenergy systems typically utilize as fuels widely distributed biomass resources which require energy – frequently supplied by energy dense fossil fuels – to cut, prepare, transport, store, process, and ignite feedstocks. Fossil fuel–derived energy is also required to manufacture, transport, and erect the equipment and infrastructure that is needed for the bioenergy system to function. In calculating the energy ratio, the energy content of the biomass itself is not included as an energy input since this is treated as "free energy," having been derived from the sun's energy through plant photosynthesis. The biochar energy system can be depicted as a set of inputs and outputs as in Fig. 7.

The energy ration in Fig. 7 is calculated as:

$$\text{Energy ratio} = \frac{\text{net energy output}}{\text{energy inputs}} = \frac{\text{E5}}{\text{E2} + \text{E3} + \text{E4}}$$

The use of highly dense energy sources (fossil fuels) to enable the utilization of very distributed bioenergy sources has to be carefully assessed to avoid the problems that have beset the production of bioethanol from maize in the USA. In that case, the energy output/energy input ratio (at between 0.7 and 2.2 MJ MJ^{-1}) is generally too low for the system as a whole to make energetic sense: what happens in effect is that the energy content of fossil fuels is being released to produce bioethanol with a similar energy content. The energy output/energy input ratio needs to be 2.0 or more for a bio-energy system to make energetic sense [77].

Several estimates of the energy-output/energy-input ratio of PBS are available, though due to the lack of reliable data on the pyrolysis process itself, especially at commercial scale, such estimates remain tentative. Gaunt et al. [59] provided a range of values that range from 2.3 to 7, depending upon the feedstock. However, Gaunt et al. use the gross energy output in calculating the energy yield, whereas the convention is to utilize the net energy output. The recalculated energy yield ranges in [59] from 1.3 (forage corn), 4.3 (switchgrass), 4.6 (miscanthus), to 5.9 (wheat straw and corn stover). The highest energy yields are associated with the use of crop residues (wheat straw and corn stover) since the energy inputs are lower for these feedstocks than for dedicated bioenergy crops (switchgrass and miscanthus). The study [59] assumes a biochar yield of c. 8.5–9%, with 38% of feedstock energy available as delivered energy. If a more modest net energy efficiency of 15% is assumed, however, then the energy yield is reduced to 1.1 (switchgrass), 1.2 (miscanthus), 0.1 (forage corn),

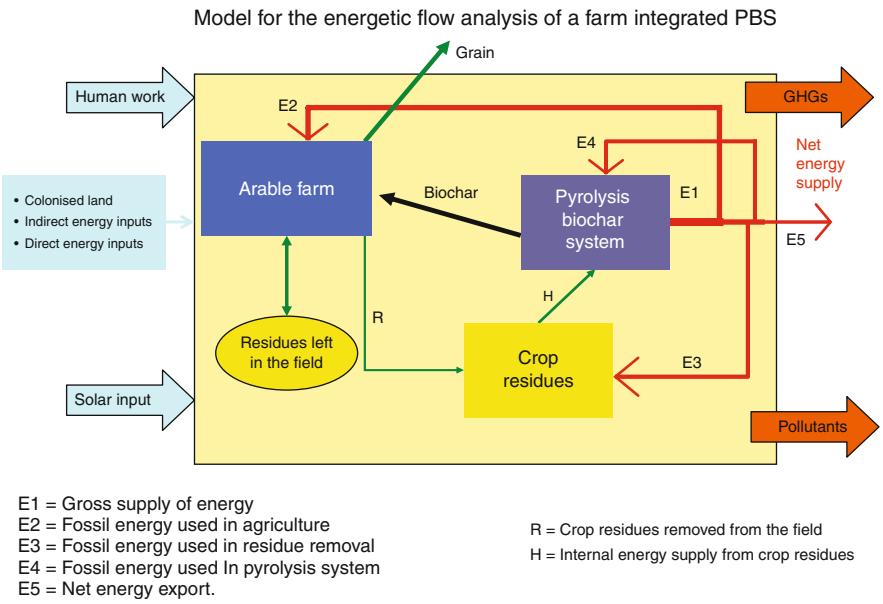

Biochar, Tool for Climate Change Mitigation and Soil Management. Figure 7
Pyrolysis-Biochar as an Energetic System (Jason Cook after Giampietro and Mayumi [77])

and 1.7 (wheat straw and corn stover). With a more conservative, and some would argue, more realistic assessment of the net energy efficiency, the energy yield falls below the critical value of 2 and is unlikely to make energetic sense.

Roberts et al. [56] provide values for the energy ratios of 2.8 for corn stover and 3.1 for switchgrass; however, as with Gaunt et al., this study makes highly optimistic assumptions regarding the net energy efficiency, using a value of 37%, requiring productive use of the heat from syngas combustion. Reliable and economic markets for heat from power plants are notoriously difficult to create, and much analysis avoids inclusion of heat in calculations of avoided fossil fuel emissions for this reason. It is therefore optimistic to assume effective markets for heat from pyrolysis plants, therefore. If the more conservative assumption is made that only electricity generation from pyrolysis at 15% efficiency will find an economically viable market, then the energy yields from Roberts et al. can be recalculated downward as follows: late stover from 5.5 to 1.65, early stover from 3 to 0.63, switchgrass from 5.5 to 1.65, and yard waste from 9.5 to 2.4. The energy yields turn out to be highly sensitive to the efficiency of the conversion process to delivered energy.

Assuming that Giampietro and Mayumi are correct in identifying 2 as a critical value for the energy yield for biofuels, below which the basic energetics of bioenergy systems cease to make sense, then it is apparent that pyrolysis-biochar systems need to be operating at net energy efficiencies of at least 20–30%, depending upon the individual feedstock and technology assumptions. Anything which increases the use of fossil fuels in the PBS (*ceteris paribus*) will also pose a challenge to the system energetics. Roberts et al. [56] report, for example, that an increase in transportation distance from the baseline (15 km) to 200 km reduces the net energy by 15%, while at 1,000 km, the net energy decreases by 79%. An 80% reduction implies an energy yield of 1 or below, but even a 15% reduction in net energy could bring the energy yield below 2.

More work on accurate calculation of energy yields is therefore urgently required. The most promising scenarios will be where forestry residues and other organic wastes are being utilized, i.e., where fossil fuel inputs to the provision of the feedstock are minimized (in the case of many wastes because some form of treatment is required in any case) and where long transportation distances are not required. The carbon-equivalent production emission for sawmill

residues in the UK is 4 $kgCO_2odt^{-1}$, while in the case of forestry residues, there is a negative emission of c. 50 $kgCO_2odt^{-1}$ as a consequence of avoided methane emissions from wood that otherwise decomposes [55]. UK arable straw entails a higher production emission of c. 200 $kgCO_2odt^{-1}$ (partly because c. 15% of the fossil fuels required for the arable crop production are allocated to the straw on economic grounds) [55]. This is actually greater than the production emissions of SRC and Miscanthus in UK conditions, where chemical fertilizers are not used (c. 20–40 $kgCO_2odt^{-1}$). Utilization of sewage sludge in SRC and Miscanthus results in higher N_2O emissions, though the sludge has to be disposed of in the baseline case so could arguably be ignored in LCA calculations.

It could be argued that if a key purpose of PBS is carbon abatement, critical values arising from energetic analysis are not necessarily relevant. This point may be valid, where the production of energy from the biomass is an ancillary benefit of a PBS development. For instance, the main purpose of a project may be the more effective disposal of an organic waste stream, and energy production a fortunate by-product and bonus: the waste would otherwise need to have been managed in some fashion. Yet, where the biomass has an alternative use as a fuel in co-firing, anaerobic digestion (AD), fermentation, dedicated biomass combustion or gasification, and where a market for such biomass and for bioenergy exists (e.g., whether with or without the aid of incentives), then an energetic analysis is appropriate to use. This is because a lower energy yield has to be compensated by increased energy production (or reduced demand) from some other part of the system.

Key Findings from Existing LCA Studies

Feedstock Suitability Hammond et al. [55] found that systems which utilize woody residue feedstocks tend to have the highest CAE, closely followed by purpose-grown woody feedstocks. Small-scale straw-based systems have a 15–30% lower CAE than wood residues, partly because of assumed scale-factors; the rest of the difference is explained by higher inputs for straw-based systems versus wood residues.

Roberts et al. [56] examined the impact of land-use change arising from the conversion of cropland from annual crops to perennial switchgrass (direct change) and the subsequent need to convert land to cropland to replace lost agricultural land (indirect change). They included two estimates of the size of these direct and indirect land-use changes (886 and 406.8 $kgCO_2\ t^{-1}$ dry switchgrass). If the larger land emission value is used, then the overall CA of the PBS is negative (i.e., a positive emission of 36 $kgCO_2\ t^{-1}$), but is positive if the lower land-use-change value is used (442 $kgCO_2\ t^{-1}$). Roberts et al. comment that PBS could conceivably *increase* net radiative forcing from GHG emissions if direct and indirect land-use-change emissions are associated with energy-crop establishment.

Ibarrola [57] found that biochar production from pyrolysis of wood waste (construction and demolition, plus commercial and industrial), garden and green waste, and food waste have greater CAE than sewage sludge or AD digestate (Fig. 8). This is because of the higher calorific value of the former, and the higher stabilized carbon content of their biochar product. Gaunt and Cowie [58] present a similar figure for CA

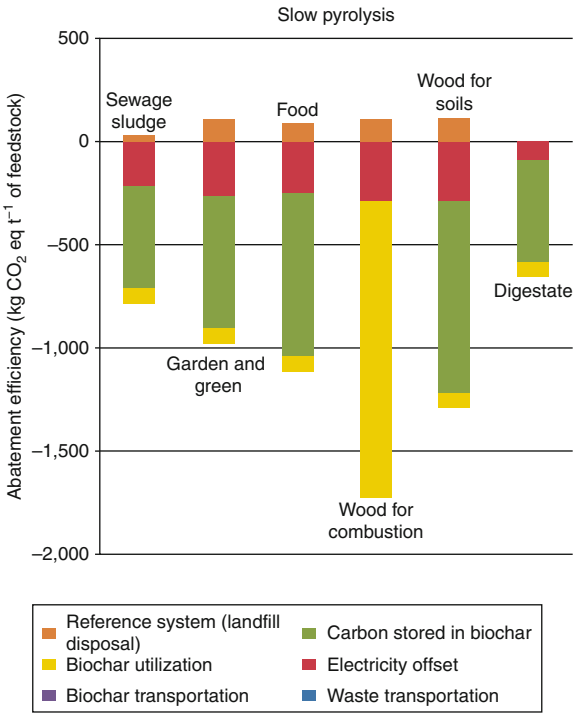

Biochar, Tool for Climate Change Mitigation and Soil Management. Figure 8
CA of PBS using different nonvirgin biomass feedstocks

of green waste compared to conventional landfill with CH_4 recovery (1.0–1.2 t CO_2eq.t^{-1} oven dry feedstock). Joseph et al. [79] have recently presented more results for a range of nonvirgin biomass feedstocks in Australia, including poultry litter, paper sludge and green waste: the CA is between 1.4 and just over 2.0 t CO_2eq.t^{-1} oven dry feedstock, the somewhat higher values being explained by the assumed waste-management baseline (which recovers less CH_4 emissions than is typical for many European countries).

Life-Cycle Stage Contributions to Carbon Abatement

Hammond et al. found that the largest contribution to CA is from stabilized carbon in biochar, accounting for approximately 40–50% of total CA. The next largest contribution is from the indirect impacts of biochar in the soil, all of which are currently uncertain: lower crop fertilizer requirement, lower soil N_2O emissions and increased SOC. These account for 25–40% of CA (the proportion changing with the size of other CA categories). The third major CA category in Hammond's et al. study is fossil fuel offsets from renewable electricity generation at 10–25% of total CA. Similar information is presented in Fig. 9 in which the life-cycle stages of the UK lower resource supply scenario are broken-down to illustrate CO_2 emitting and abating stages.

In the Roberts et al. study, the proportion from stabilized carbon in the biochar is larger at 54–66%. The proportion from avoided fossil fuel emissions is also larger at between 26% and 40% depending on feedstock.

The main difference between Hammond et al. and Roberts et al. is that the former study assumes a higher value for the indirect soil impacts of biochar, principally due to the assumed accumulation of soil organic carbon as a consequence of biochar addition. As a consequence, the proportional contribution of stabilized carbon and avoided fossil fuel emissions is lower than in Roberts et al., which makes more conservative assumptions about the indirect impacts of biochar in soil. Of the studies reported in Table 6, the indirect impacts of biochar in soils upon net carbon abatement tend to be smaller than assumed in Hammond et al., although Gaunt and Downie assume even higher values. Ibarrola's study presents a similar contribution breakdown as Roberts: the largest contribution to CA for both fast and slow pyrolysis in the case of wood, food, and green wastes is carbon stabilized in biochar (45–55%, excluding use of digestate case). The second largest contribution comes from offset GHG emissions from fossil fuel emissions (20–30%). Where the assumed indirect impacts are lower, then the contribution of stabilized carbon and avoided fossil fuel emissions are

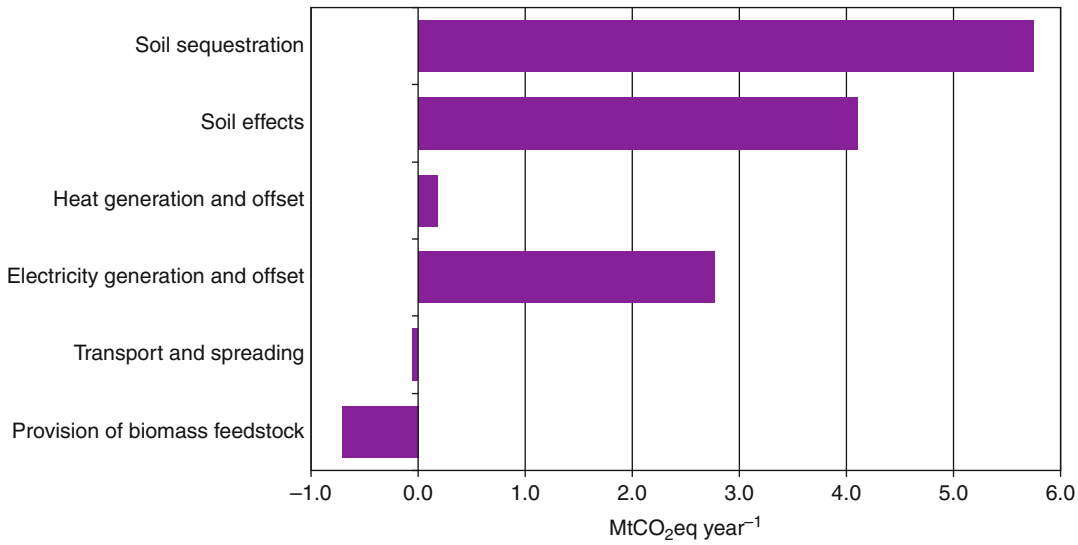

Biochar, Tool for Climate Change Mitigation and Soil Management. Figure 9
CO_2eq abatement by life-cycle stage for lower biomass supply scenario (UK conditions)

proportionally higher. The studies in Table 6 indicate that transport emissions are a relatively minor contribution to overall lifecycle emissions (several percent for biomass and biochar movement of c. 20 km each).

CO_2 Equivalent Emissions Per Unit Delivered Energy

Hammond et al. presents a carbon abatement for PBS of 1,500–2,000 kg CO_2eq MWh^{-1} (1.5–2.0 kg kWh^{-1}) for large systems, compared to a UK CEF of 0.56 $kgCO_2kWh^{-1}$ in 2006 [53]. For comparison, modern bioenergy systems (combustion with grate or fluidized bed, gasification) produce *emissions* from between 0.03 and 0.07 kg CO_2 kWh^{-1} [80], or from 0.05 to 0.30 kg CO_2 kWh^{-1} according to the Environment Agency [81]. While PBS appears to offer far better CA MWh^{-1} than conventional bioelectricity, this is a somewhat misleading finding. Much of the CA from PBS results from stabilized carbon in the biochar and from indirect soil effects (rather than from offset fossil fuel emissions), while the denominator – electricity generation per unit biomass – is lower than for conventional bioelectricity due to lower efficiency. Thus, the CA per unit electricity is high, but electrical efficiency is low.

CO_2 Equivalent Emissions Per Hectare

On an area basis in the UK, Hammond et al. found that CA ranges from seven to nearly 30 tCO_2eq ha^{-1} $year^{-1}$, depending on PBS feedstock (Fig. 9). Waste feedstocks such as arboricultural arisings are the most efficient in terms of land use as they do not require any additional land use change and do not interfere with crop-production systems; moreover, they are commonly disposed of as wastes and hence PBS incurs less emissions through additional transport, handling, and storage stages. Such numbers compare favorably with conventional bioenergy in the UK, which abate between 1 and 7 tCO_2eq ha^{-1} $year^{-1}$; the most productive biofuel system in the world – bioethanol from sugar cane in Brazil – abates c. 16 tCO_2eq ha^{-1} $year^{-1}$, so biochar performs well under this metric (Fig. 10).

Delivered Energy Generation from Pyrolysis-Biochar Systems Versus Combustion

Roberts et al. compared use of biochar for soil with use of biochar to replace coal and found that biochar to soil resulted in 29% more carbon

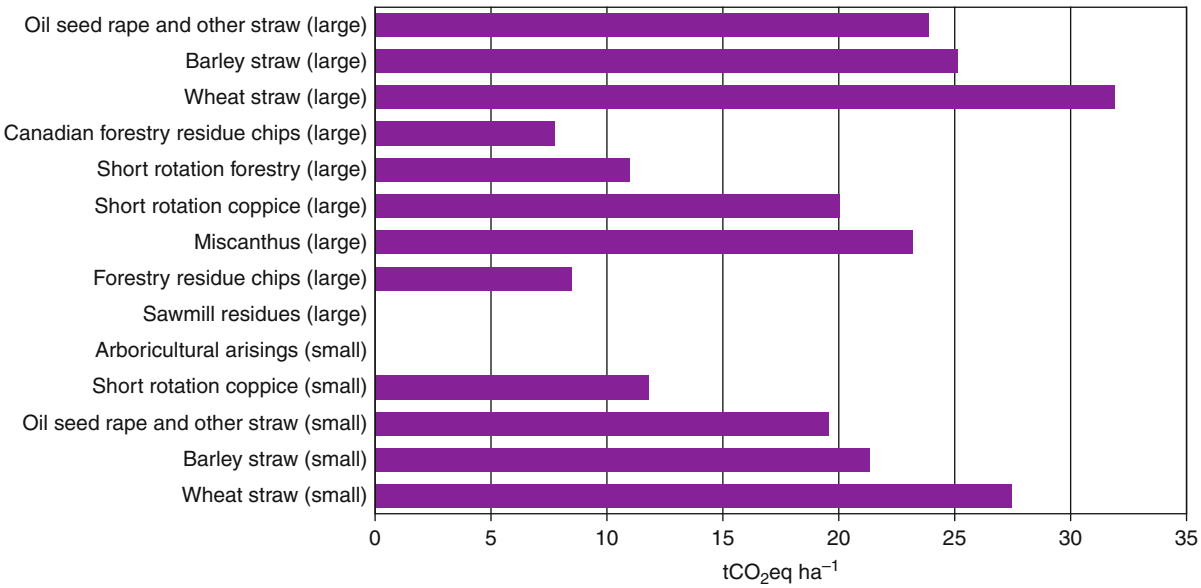

Biochar, Tool for Climate Change Mitigation and Soil Management. Figure 10
Annual CO_2eq abatement per hectare for UK conditions. No value is given for sawmill residues or arboricultural arisings since the plants are not grown specifically for pyrolyzable residues

abatement (627 vs 864 $kgCO_2eq\ t^{-1}$). A more realistic comparison is between PBS and direct biomass combustion and, in this case, Roberts et al. found that carbon abatement was actually less for PBS than for combustion (987 vs 864 $kgCO_2eq\ t^{-1}$) (using a CEF for natural gas). On the other hand, approximately half of the CA from PBS involves removal of CO_2 from atmosphere, compared to biomass combustion, where all the carbon abatement arises from avoided fossil fuel emissions.

In Hammond's et al. study, PBS performs somewhat better compared to combustion than in Roberts et al., partly reflecting somewhat higher CA per ton feedstock in the former than in the latter. The comparison depends upon the relative energy efficiencies of the two processes and upon the CEF used to calculate avoided fossil fuel emissions. For example, at an efficiency of 15% and with a CSF of 0.68, PBS appear to offer greater CA than combustion at 33% efficiency (using an average UK grid CEF) even without inclusion of indirect soil effects, but cannot compete with combustion (or gasification) at an efficiency over 40%. In systems co-firing biomass with coal, efficiency can be significantly higher in new plants (up to 42%). Hence, either the indirect benefits of biochar upon net GHG emission fluxes would need to be on the scale proposed in Hammond or else the efficiency of the PBS would need to increase (or some combination of the two). Where biomass co-firing is combined with CO_2 capture and geological storage (Bioenegy CCS, or BECCs), PBS is not able to compete in terms of carbon abatement (because the CCS process captures c. 90% of the carbon in the feedstock compared to c. 50% of feedstock carbon conserved during pyrolysis).

If grid average of 80 kg $CO_2eq\ MWh^{-1}$ is attained by 2030 (which is required in the UK context if the government's carbon-reduction targets of an 80% reduction by 2050 relative to 1990 levels are to be met) and assuming biomass is still available as a resource, biomass combustion offers almost no carbon abatement benefit [82]. PBS meanwhile still offers CA benefits, i.e., it has net negative $CO_2eq\ MWh^{-1}$ emissions. Yet, as noted above, at current net energy efficiencies, PBS is unlikely to be the technology of choice for generating electricity so it may have a rather limited role.

From the results of Roberts et al. and Hammond et al., it is evident that PBS is not necessarily more efficient in terms of CA than other bioenergy options: it will depend on the detailed analysis of each individual case. It is clear in general that conversion of the energy in feedstock into useful delivered energy (heat and power) will have to be reasonably efficient (20–30%) for PBS to compete on any scale with direct combustion. In the longer-term perspective, however, PBS may become more valuable (compared to combustion technology) due to its ability to actually remove carbon from the atmosphere. Exactly when this benefit would be realized is highly uncertain and context-dependent (e.g., reliant upon the outcome of other highly uncertain processes).

Sensitivity Analysis

Hammond et al. found that the following variables were all important in influencing the overall net carbon abatement: total handling losses, char yield, total electrical efficiency, use of heat, soil organic carbon accumulation, the allocation of GHG emissions to the production of the feedstock, fraction of labile carbon and – most importantly – the Mean Residence Time (MRT). If the MRT is below 500 years, there is a reduction in the CAE which begins to look concerning, although this partly depends on the time horizon over which an analysis is undertaken. Hammond found low sensitivity to the following variables: distance travelled (biomass and biochar) (up to 200 km), reduced nitrogen fertilizer application (0–50%), and reduced nitrous oxide emissions (0–100%).

In their LCA, Roberts et al. identified broadly similar sensitivities to Hammond et al. The results were sensitive to: emissions entailed in feedstock collection, stability of the carbon, biochar yield, and syngas yield. There was a lack of sensitivity to N_2O emission suppression and to distance travelled (except where this was 500 km +). Needless to say, the results of any such LCA are sensitive to the assumed CEF of the fossil fuel which is offset.

There are large uncertainties associated with the LCA work presented here. Biomass production systems vary in space and with time, making a calculation using a single number problematic. For the nonvirgin waste feedstocks, considerable uncertainties occur with

respect to the management of individual landfill sites (e.g., the biodegradable fraction, oxidation factors, CH_4 recovery, etc.), making comparison of PBS to existing options difficult.

How Cost-Effective Are Pyrolysis-Biochar Systems?

Gaunt and Lehmann [59] calculated that the cost of reducing a ton of CO_2 in the PBS they examined was between \$9 and \$16 compared to utilizing the same char as a fuel. Since they did not undertake a full economic costing, this figure does not allow comparison with other marginal abatement carbon costs (MACCs).

McCarl et al. [76] undertook a full economic costing and found that the net present value of the PBS examined (70 ktpa corn stover, mid-west USA conditions) was $-\$70\ t^{-1}$ feedstock for slow pyrolysis and $-\$45\ t^{-1}$ for fast pyrolysis, i.e., it is a loss-making venture under these assumptions. This assumed a carbon value of $\$4\ tCO_2{}^{-1}$ abatement and an agronomic value of $\$33t^{-1}$ biochar or $\$11.5\ t^{-1}$ feedstock. The biochar production cost (i.e., ignoring revenues from biochar as a form of carbon storage or arising from its agronomic value) is therefore approximately $\$85\ t^{-1}$ feedstock or c. $\$240\ t^{-1}$ biochar. The "energy penalty" cost of utilizing char as a soil amendment rather than as a fuel is $\$40\ tCO_2{}^{-1}$, considerably higher than Gaunt and Lehmann's estimate of $\$15\ tCO_2{}^{-1}$, though similar to other estimates (e.g., Lehmann [9]).

Roberts et al. [56] present data on net present value of their USA-based PBS (c. 50 ktpa) which appears to indicate some positive NPVs. This is as a consequence of a very high carbon-price assumption ($\$80\ tCO_2{}^{-1}$). Even their "low" carbon price ($\$20\ tCO_2{}^{-1}$) is actually higher than the 2008–2010 EU ETS market value of $\$10–20\ tCO_2{}^{-1}$. If we remove the carbon revenue from the calculation along with the small benefit in increased fertilizer efficiency (but retaining the value of the P and K nutrients in the char), the NPVs are all negative. The production costs, expressed per ton of biochar, are: $\$155\ t^{-1}$ for late stover, $\$124–142\ t^{-1}$ for switchgrass, and $\$13\ t^{-1}$ for yard waste. These costs are lower than McCarl et al. [76], but not much so (40% or so lower). The exception is for yard waste in which case the cost of production is much lower due to the revenue gained through tipping fees and the other avoided costs of organic waste management.

Shackley et al. [158] present economic data on the situation in the UK for a range of feedstocks, with three plant sizes (small: 2 ktpa; medium: 16 ktpa; large: 184 ktpa). They provide a range of values of the costs of biochar production from \$-220 to $\$580\ t^{-1}$. The negative values arise from waste feedstocks, where there is a revenue stream from tipping fees which can otherwise be large in the UK context. The production costs are typically lower for the large-scale pyrolysis units due to lower capital, operational, and maintenance costs per unit production. The costs also vary depending upon the assumed storage option. For the virgin feedstocks, production costs are closer to McCarl et al. than to the Roberts et al. estimate above.

Brown et al. [161] compared the internal rate of return (IRR) for slow and fast pyrolysis assuming an increasing carbon price to 2030, use of gas co-product for heating and bio-oil refined to gasoline (in the case of fast pyrolysis only). The projected IRR for slow pyrolysis is negative out to 2030 for feedstock costing \$83 per ton. A zero cost feedstock would deliver an IRR of between 8% and 17%, but this is not considered sufficiently profitable for investment in a new technology. Brown et al. [161] found that the profitability of both slow and fast pyrolysis depended primarily upon the value of the energy product(s). Yoder et al. [162] develop a product transformation curve using optimisation and econometric analysis of existing data for quantifying the trade-of in pyrolysis between bio-oil and biochar production.

As for the LCA, costs are typically context-specific, and there are some niche applications where the NPV will be more evidently favorable, e.g., where a type of biochar has a high agronomic or soil-related value. A further example is where the biochar is a "waste" product from an economically viable energy project (Box 3).

To summarize, the economic viability of biochar production and application are currently highly uncertain. Feedstocks – especially clean ones – are frequently expensive in developed countries and increasingly in demand by other users such as for Anaerobic Digestion, composting, combustion, gasification, and so on. Technology costs associated with pyrolysis are especially hard to predict at the present time, and most estimates in the literature are based upon one or a few designs. At present, the incentives structure in most

Box 3: Gasification of Rice Husks: Case Study from Cambodia

Rice husks are gasified in an Ankur gasifier to produce syngas that is fed into an engine that powers a rice mill. The system is economically viable (due to mill being off-grid, hence otherwise having to rely upon expensive diesel fuel for power generation). Carbonized rice husks (CRHs) are the waste product, which accumulate, and can become an environmental problem. The CRH yield is c. 30%, and the carbon content of the char is c. 35%. Therefore, for each ton of rice husk, 300 kg of CRHs are produced containing 105 kgC or 385 $kgCO_2$. The labile C content is <1% and the CSF is 0.92 hence the stabilized carbon content is c. 350 $kgCO_2t^{-1}$ biochar. The cost of application to agricultural fields in Cambodia is low – estimated at $1t^{-1}, while the agronomic value (based upon unpublished research) appears to be c. $2 to 8 t^{-1}. Since the CRHs are (currently) free, the value of the biochar is c. $1 to 7 t^{-1}; this is an important potential source of additional income in a subsistence farming system such as Cambodia.

If the rice husks were otherwise disposed of in irrigated paddy, there is also the value of avoided methane emissions from gasification. For every 1 t of applied rice husks, 40 kg of carbon is converted into 53 kg of methane, equivalent to 1,219 kg CO_2.

If the stabilized carbon can have a value, say at $5 t^{-1} CO_2, then the additional value of the CRHs is $1.6 t^{-1} biochar. Adding to the agronomic value, the overall value is between $3 and 8 t^{-1} biochar. And if the CA value of the avoided CH_4 emission is included, this would further rise to about $9–14 t^{-1} biochar. Clearly, if the CRHs do indeed have a demonstrable and predictable agronomic value, demand for its use may increase, and the producer may begin to sell the CRHs rather than give it away free as a waste product.

countries is focused upon renewable electricity generation, and there is no mechanism for rewarding stabilized carbon abatement in the soil. If carbon abatement is the primary policy driver, inclusion of stabilized carbon in biochar and its indirect impacts on soil GHG fluxes would need to be given some value alongside renewable electricity generation. One problem with carbon-based land crediting is that it raises the issue of how to establish a baseline, and many current land-owners and occupiers, e.g., farmers, are reluctant to begin to establish inventories of carbon-equivalent fluxes over their land (such as might be required to establish a baseline against which a biochar project could be assessed). Some countries, e.g., in Europe, have previously expressed their skepticism at including land-based carbon crediting as a major carbon-abatement strategy within the UNFCCC. Scientific uncertainties and technical challenges surrounding monitoring, verification, accounting, and reporting (MVAR) in relation to biochar additions will mean that developing a robust methodology for inclusion of biochar in carbon markets (voluntary or through the Clean Development Mechanism) will be challenging until scientific knowledge improves.

Where biochar is potentially more economically viable is where it is able to treat wastes that incur high tipping fees to landfills. In those situations, PBS may be a cheaper disposal route than landfill or incineration. Whether the char produced can be used in agricultural soils remains uncertain due to the risk of contamination. At present, there is a lack of a clear risk assessment and regulation pathway for such substances. A further situation where biochar might already be economically viable is the case of gasification char – which is a waste product of a financially solvent energy generation technology. If this char can be shown to be beneficial to soils and to avoid introducing contamination, then it could be financially viable to distribute such material to agricultural systems.

What Are the Impacts of Biochar on Soil?

In this section, we turn to the question of the impacts of biochar on soil. A summary of the published literature has been presented previously [6, 7]. Much of the evidence comes from the study of charcoal in the natural environment: this provides the only source of relevant direct evidence for long-term stability of biochar, having been used historically by humans or as a result of deposition after periodic fires in many natural ecosystems. Given the similar formation and chemical characteristics, charcoal in the natural environment provides a powerful tool to investigate the long-term stability of biochar. However, the short-term impacts of biochar may not be well represented in studies of old charcoal.

This is in part because the feedstock can be quite different, and partly because the more complex composition of biochar is overlooked. Also, any labile components associated with the charcoal will have been mineralized prior to sampling.

The more temporary beneficial impacts of biochar may be chemical and result from leachable ash and modification of soil pH, promotion of short-term microbial activity, including the effect of small labile fractions. Physical benefits may arise from modification of soil bulk density, water holding capacity, and promotion of soil aggregation (possibly in combination with soil biological effects). These effects may be temporary or long term. Thermal properties may change as well [83].

Other effects relate to the provision of cation exchange capacity (CEC) and specific surface area (SSA), biological associations (with micro-organisms, fungi, and with plant roots), and bio-physical benefits (mediating the connection of micro-organisms and microbial substrate, promotion of mesofaunal activity, including earthworms). The potential for detrimental effects on the soil would depend on the source of the biochar applied, and the rate and timing of its application. Negative impacts could include leaching of nutrients, addition of toxic elements (metals), or the introduction of organic contaminants. Where biochar has a high affinity for nitrogen, there may be negative short-term effects on crop nutrient supply, i.e., potentially reducing nitrogen availability to the plant in the period after application [84].

Scientific research of biochar is a relatively new topic, and therefore generality in site-specific observations is not yet apparent, while extrapolation from individual observations is not yet possible. At this point, a convergence in methodologies has not emerged and until recently, there have been no strategic research programs to provide a systematic evaluation. The nature of PBS also demands coordination and consolidation of research efforts with pyrolysis engineering in order to produce selected biochar that expresses particular and possibly multiple beneficial functions in soil.

Key Functions of Biochar

Provision of Labile Organic Carbon Rapid utilization of labile substrates in soil can build a store of nutrients in soil microbial biomass, which may become available for plant acquisition and growth over time. The potential benefits of labile carbon in soil can create a constraint to crop growth if substrate nitrogen is low, and if at the time of addition inorganic (i.e., available) nitrogen in the wider soil is limited. This is because nitrogen as well as carbon is required to build new biomass, and microbes will out-compete roots.

Nitrogen is progressively volatilized during pyrolysis so the ratio of carbon to nitrogen in biochar is generally much higher than in the feedstock. However, if biochar is entirely stable, it will not present the readily accessible carbon substrate necessary to create microbial demand for external nitrogen. Whether significant nitrogen immobilization of soil nitrogen occurs should therefore depend on the size of the biochar addition, the size of the labile fraction, and whether the ratio of nitrogen to carbon of the labile fraction reflects that of the bulk biochar sample.

Storage of Stable Carbon The stable portion of biochar is the fraction for which, in the future, a carbon credit might be claimed and, for the purpose of climate-change mitigation, may be the component that remains in the soil for at least 100 years [7]. There is, as yet, no robust methodology for establishing the MRT of a specific biochar product: this is one of the key scientific uncertainties and policy needs. The sum of stable and labile carbon should not reflect the total carbon content of biochar as fractions of intermediate stability are also likely to be present.

Supply of Plant Available Nutrients Aside from nitrogen, most potential nutrients in pyrolysis feedstock are largely conserved during pyrolysis (as also are potentially toxic elements). Progressive elimination of carbon, oxygen, and hydrogen during pyrolysis therefore increases the total concentration of minerals in the char residue, and in potentially extractable forms as ash. Biochar ash content increases in inverse proportion to retained carbon feedstock, analogous to that which arises during combustion but distributed within a complex physical matrix.

Solubilization of ash may result in minerals becoming available to plants on addition to soil, although since phosphorus (as phosphate) is rapidly complexed with minerals in soil, this may depend on scavenging

directly from char by roots or symbiotic mycorrhizal fungi. In general, introduction of readily available crop nutrients can promote mineralization of organic matter, especially in marginal environments.

However, porosity, and more specifically pore connectivity, may control the release of soluble nutrients from char, making release progressive rather than instantaneous as may be the case in the solubilization of combustion ash. This process could be associated with the mineralization of condensed tars and oils that appear to block biochar pores [85].

Modification of Soil pH The typically alkaline nature of biochar may increase microbial activity in acidic soils by increasing pH and with this, another potential source of "priming" for the decomposition of pre-existing organic matter, although modification of soil pH may also increase plant productivity and thus the amount of carbon substrate added to the soil through roots and residues. Mass for mass, the value of char in pH modification may be up to one third that of agricultural lime [86] and at experimental rates can increase soil pH by 1 unit.

Modification of Soil Physical Characteristics Depending on the distribution of particle size in the soil, the rate and nature of biochar applied and the time since application, soil pore–size distribution and water holding capacity may be affected. Porosity in char may occur at a range of scales, which affects the proportion of water that can be retained, and equally the accessibility of held water and solutes to plants which can exert sufficient tension to extract the contents of macropores (0.1–30 μm diam) that may not drain naturally. Structurally sound pores of this dimension are abundant in fresh wood-derived charcoal [87], and the connectivity of the relatively small number of larger pores has been investigated in three dimensions by tomography [88].

However, the fresh particle size of powdery charcoal created from grass feedstocks appears to be less than 50 μm [89], and weathered charcoal, while generally found in larger fragments, also resides in this size range [90]. In clayey soils, particles may be less than 5 μm [91]. During weathering, and particularly for char from woody substrate, the position of char fragments within the soil mineral matrix is likely to alter over time. The effect that this has on total porosity, accessible pores, and accessible surface areas has not been explicitly examined.

Nonetheless, while initially macroporous, it is established that the great majority of total porosity in wood-derived charcoal may reside in micropores of nanometer size [92]. Oils and tars could represent less stable components of biochar around which microbial activity could promote micro-aggregation, relevant to water infiltration and resistance to water erosion. An apparent role for charcoal in aggregation has been observed in field soils [90], although short-term incubation with activated charcoal did not cause aggregation under controlled conditions [93].

Cation Exchange Capacity and Sorption Progressive abiotic and biotic surface oxidation of charcoal results in surface proliferation of carboxyl groups and an increasing ability to sorb cations [33, 34], explaining high cation exchange in archaeological soils [35]. Negative charge provides the possibility for reversible storage of available nitrogen (ammonium, NH_4^+) relevant to soil-based N_2O emissions and nitrate leaching. A mechanism based on the dehydration of phosphate and charcoal has also been described for the adsorption of phosphorus [94], which may explain the apparent impact of biochar on crop phosphorus uptake, possibly aided by arbuscular mycorrhizal fungi [95].

Charcoal has the capacity to sorb polar compounds, including many environmental contaminants [96], particularly PAHs for which it may be the dominant sink in soils and sediments [97]. The significance of biochar addition in removing contaminants from the environment depends on its capacity to fulfill this function relative to charcoal, the affinity (security and reversibility) of stabilization, and the ultimate fate of both char and contaminants [164].

Microbial Activity The possibility that biochar catalyses breakdown of organic matter by providing microbial habitat alone is improbable since sustainable microbial proliferation depends on a renewable source of accessible carbon substrate as well as nutrients. Provided that the majority of biochar carbon is highly stable, after an initial flush of mineralization, microbes that inhabit biochar pores will depend primarily on the indirect effects of biochar to obtain an enhanced supply

of substrate. This could either be through the capture and retention of soluble organic matter otherwise lost to deeper horizons or watercourses, or through a change in loci of plant root activity. Increased plant productivity however should be reflected in increased exudation of carbon through roots, and the deposition of carbon from residues of above-ground growth. The complication that this adds to interpretation of field data has been highlighted by Major et al. [98].

Many plants can form symbiotic associations with mycorrhizal fungi, whose filamentous hyphae provide an extension to plant roots which can enhance acquisition of both nutrients and water, at the expense of some host plant carbon. Although potentially limited by inoculum, soil-chemical conditions and the abundance of exploitable nutrients are more likely to limit mycorrhizal proliferation in most circumstances. Reported promotion of mycorrhizal activity by biochar [99, 100] could reflect utilization of reversible stores of water and soluble nutrients, or exhaustible "mining" of nutrients embedded in ash. Warnock et al. [101] proposed a range of possible mechanisms.

Limitations of Existing Research Base Until recently, there have been no directed research programs to strategically evaluate biochar for its function in soil. Much of the current understanding of the function of biochar rests on published data for charcoal, often in the context of natural systems and wildfire. For reasons highlighted in sections "Biochar Production" and "Properties of Biochar," the function of biochar in soil is strongly influenced by feedstock and formation conditions, and charcoal may only provide an insight into some general principles of biochar function in soil. In addition to the problem of extrapolating from studies of charcoal, pilot- and commercial-scale pyrolysis may produce biochar that differs from the products of bench-scale pyrolysis systems operating under ostensibly the same conditions. There is no existing research to evaluate char from gasification, which is likely to provide a function between that of biochar and ash from straight combustion.

Categorization of Current Literature

- *Sediment or soil*: Early evidence for the stability of biochar arose from sediment studies, where charcoal is preserved under anoxic conditions in which decomposition proceeds inherently slowly [102, 103].
- *Static or dynamic*: Static studies provide snapshot comparisons for a response variable at locations where a relevant soil (or other) variable differs, e.g., presence or absence of vegetation burning history [104, 105]. In a dynamic experiment, a "treatment" is imposed, and change in response variables over a time period determined, or ideally its trajectory observed through intermediate measurement. Chronosequence studies are a variant of the latter that enable long-term dynamics to be studied using samples deemed comparable, aside from the point in history at which the (ideally singular) change or intervention occurred [106–108].
- *Biochar or charcoal*: Natural fire contains an anoxic zone, where biomass pyrolysis prevails over combustion. Natural fire yields low charcoal conversion rates in the range 0.1–5% [109]. Wildfire is typically brief and the peak temperature variable. With rapid heating rates, the conversion may be partial, superficial, or progressive and affected by vegetation moisture content. Wildfire and charcoal are significant considerations in the global carbon cycle, and now an established topic for research.
- Much work on the dynamics of charcoal has been undertaken in this context, and laboratory studies have aimed to mimic wildfire carbonization by exposing biomass to similarly brief, variable, but generally low (ca. 350°C) temperature and semi-oxic conditions, i.e., limited or partial restriction of air flow. Experiments with char produced with complete exclusion of oxygen are much more limited and recent. Published research using char from commercial pyrolysis reactors rather than material produced in a laboratory-scale batch process are very scarce. Only eight studies categorized in [7] used pyrolysis char.
- *Short term or long term*: The various functions of biochar (Fig. 11) may be manifest over different timescales and, crucially, the trajectory of these functions appears to be nonlinear and may not be entirely independent of other functions or the wider system. The average duration of the dynamic studies identified in one literature review [7],

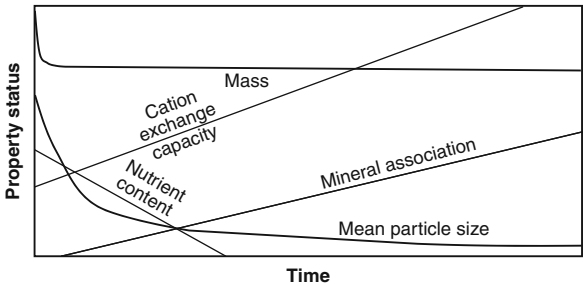

Biochar, Tool for Climate Change Mitigation and Soil Management. Figure 11
Schematic to illustrate the challenge of unraveling multiple functions of biochar whose possible trajectories strongly differ

including those undertaken in field plots (but excluding long-term chronosequences), was 11 months. Although the chronosequence approach has been employed to observe the development or demise of functions that change slowly over time (rather than emerge or decline rapidly at the start), few attempts have been made to short cut such change, other than by imposing favorable laboratory-imposed conditions.

- *Gasification or fast or slow pyrolysis*: After oven-drying, plant biomass usually contains about 45% carbon by mass, and a few per cent mineral ash. Ash is broadly conserved, but the proportion of carbon that is retained is specific to the process. Combustion leaves trace amounts of carbon, gasification less than 10%, and pyrolysis typically 30–40%. Ash includes key mineral nutrients such as phosphorus and potassium, other metals and a range of micronutrients concentrated by loss of total feedstock mass in the conversion process [110]. The nutrient value of the products differs markedly on a carbon-mass basis, but in terms of their value to crops will depend not only on rate of char application but on the physical accessibility of nutrients in the char to leaching, plant roots, and mycorrhizal fungi. The production process and feedstock mineral content will also modify the pH of the char by-products, which tend to be moderately to highly alkaline.
- *Feedstock*: Scanning electron microscopy of fresh charcoal and charcoal aged in the natural environment reveals a cellular structure resembling that of the woody feedstock from which it was derived, e.g., lignified cell walls of dead xylem cells. The structure of char from grass and nonwoody plant material is rarely reported and, similarly, nor is the structure of char produced from digested or composted materials.
- *Tropical or temperate*: Under otherwise equal conditions (moisture, nutrient, and substrate availability), biological activity increases with temperature. Consequently, soils in the tropics tend to be depleted in organic matter and associated biological activity relative to those from temperate regions. In addition, soils that are very old have usually been subjected to extensive weathering and leaching and display low-inherent fertility and are often acidic. Although all functions of biochar may be expressed at all locations, some will be more conspicuous in such soil. In field studies and controlled experiments, half of the research effort has been undertaken in regions with above 20°C mean annual air temperature, and only one fifth in temperate zones below 10°C.
- *Laboratory or field*: Laboratory conditions enable variables and functional attributes to be isolated or controlled, and the impact of climatic variation to be removed. Permutations of different factors are possible since the space and resource requirement may be relatively small and good replication is possible. The interactions between functional attributes of soil and biochar with the wider environment, such as fluctuations in rainfall and evaporation impacting leaching, soil structure, and microbial community composition, can only be assessed in the field. However, the rate at which processes proceed in the field is dictated by the ambient climate and cannot be manipulated. Spatial heterogeneity demands intensive sampling which can constrain experimental design.
- *Soil or soil with plants*: Plants provide a sink for soil nutrients, exert suction on soil pores, and secrete compounds and enzymes that mobilize nutrients and modify soil surfaces. The microbial activity that concentrates around plant roots may "prime" processes that would not otherwise occur, for example, the co-mineralization of recalcitrant biochar and labile glucose [111]. However, the complex soil environment does not comprise such discrete

components and plant-derived substrates are separated by the soil mineral matrix.

- *Empirical (descriptive) or mechanistic (predictive)*: Empirical studies identify statistical relationships between two or more test variables; mechanistic studies seek to understand the reason for such relationships. Mechanistic approaches should offer greater prospect for prediction of effects at other locations, being based on a fundamental understanding of the underlying process. Although technically more robust, mechanistic understanding may take time to acquire and still not be accurate; both approaches require considerable validation especially where multiple variables or processes are involved (Fig. 11).

Extrapolation from Studies of Environmental Charcoal

Given the basic similarity in formation and the relatively abundant literature, it is necessary to view biochar in the context of the existing understanding of charcoal, especially in terms of long-term stability. To date, however, studies that compare char produced under a range of conditions, e.g., varying levels of oxygen exclusion, in terms of agronomy, mineralization, or other parameters relevant to biochar deployment, are lacking. Until these studies have been completed, the congruence in the properties of these materials remains uncertain.

Does charcoal in soil constitute soil organic matter? In the discrimination of more and less recalcitrant forms of organic matter in soil generally, the ratio of oxygen to carbon broadly decreases with age with progressive removal of oxygen through biological or chemical "oxidation." Charcoal has a characteristically low O:C ratio, while graphitic black carbon (the most stable form derived in combustion) is essentially elemental carbon [112]. By comparison, charcoal and biochar are merely highly depleted in oxygen and hydrogen, containing groups that are strictly organic (most particularly aromatic forms), and part of the soil organic carbon pool.

Can charcoal be distinguished from other soil organic matter? Charcoal is particularly abundant in aromatic carbon that occupies a distinct position in the nuclear magnetic resonance spectrum for carbon (^{13}C NMR), displays a minor depletion in the abundance of the scarce carbon isotope (^{13}C) relative to other compounds, and is characterized by certain biomarkers (so far, benzene polycarboxylic acid and levoglucosan have been most extensively evaluated). Charcoal is partially resistant to some chemical oxidants typically used to quantify total soil carbon (potassium dichromate), and both chemical and photo-oxidation have therefore been used to quantify it. However, none of these signals have proven entirely exclusive, and the procedures for measurement are complex or slow. Because the functionally relevant level of stability is itself ill-defined or context specific, the analytical separation of charcoal and "ordinary" soil organic matter has yet to be perfected.

What is the historic significance of charcoal in the global carbon cycle? Models describing soil carbon in the agronomic or global change context consider a near-inert soil-carbon fraction to correctly simulate response to altered climate or organic matter inputs, which being site-specific generally reflect, at least in part, contrasting abundance of charcoal in regions where wildfire is more or less frequent. The rate, extent, and completeness of conversion of biomass to charcoal in wildfire is highly variable. Nonetheless, making assumptions about such factors based on available evidence leads to estimates for a mean residence exceeding 1,000 years [113]. Charcoal is thought to account for 1–20% of organic carbon in soils, and at least 150 GtC of the global soil pool comprises charcoal or its more condensed or graphitic relatives, soot and elemental black carbon [11]. This implies that up to 150 Mt of carbon has annually cycled through the biosphere in the formation and degradation of charcoal-derived carbon.

Are the impacts of biochar carbon analogous to those of soil organic matter? Some properties of biochar, and specifically its impacts on physical soil properties, are also associated with bulk soil organic matter. It is not, however, safe to assume that the mechanisms by which these are provided are identical, or that the impacts are equivalent in magnitude, direction, or duration – and thus that biochar can provide a direct substitute for higher levels of other organic matter in soil. This is of practical importance since biochar is carbonaceous and thus not readily distinguished from organic matter using current techniques. This is analogous to the challenge of discriminating chalk and limestone from organic carbon in soil.

Can impacts be predicted from ex situ properties? The ex situ characteristics of organic matter and biochar are unlikely to be additive with respect to a soil's properties. For example, certain soil minerals (clays) have a high cation exchange capacity; although organic matter has higher specific exchange capacity mass for mass, binding between organic and mineral fractions shields exchange sites at the molecular-scale and reduces the sum effect. At the moment, it is not completely clear whether interactions between char and mineral particles will occur significantly at this physical scale or primarily as discrete, disparate particles. Cation exchange capacity of biochar also appears to evolve over time, and it is likely that many other properties have a trajectory which is currently ill-defined.

Evidence to Address Key Questions around PBS

Biochar and Contaminants In terms of human health and the food chain, the irreversibility of biochar addition is a key consideration. Existing soil amendments contain immobile components, albeit in less visible form and biochar inherits the potential risk posed by the feedstock that might otherwise be directly applied (see section "Properties of Biochar"). However, the class of these compounds known to be formed in the charring process itself (polycyclic aromatic hydrocarbons, PAHs) is process dependent. Without extensive evaluation of pyrolysis char, it is difficult to assess the risk posed by PAHs in PBS specifically as most data available relates to charcoal.

Charcoal is generally produced at lower temperatures that might favor PAH formation, but vapors may combust rather than condense and could thus be eliminated. Levels of extractable PAHs in charcoal are variable, but reported concentrations [114–117] generally fall between those reported for urban and rural soil on a mass basis (see Table 2). These compounds are persistent but ultimately degradable in soil [50].

The effect of association with chars on rate of degradation of PAHs, and the balance between rates of accumulation and release has not been systematically addressed. Concentrations of PAHs in soils subjected to natural fire suggest, however, that degradation is in excess of sorption. The capacity of both activated and nonactivated charcoal, typically as charcoal from or mimicking natural fire to adsorb PAHs and other organic contaminants, has been relatively well assessed [118, 119].

Since metals are broadly conserved in pyrolysis, the total metal content of biochar will be determined largely by the feedstock content and the yield of char. The higher the carbon content of the char, the lower will be the mass concentrations of metals. On a biochar mass basis, the metal concentrations in products from gasification where char yield is small (a few to 10%) are likely to be up to tenfold higher than in slow pyrolysis. Data on the availability of metals from charcoal or biochar in soil is lacking. However, the potential for pyrolytic char to remediate land contaminated by metal cations has been demonstrated [120].

Stability of Biochar Carbon About 60% of the literature evaluated in [7] related to the stability of charcoal or to the quantification of char in soil (equally divided). Stability has been addressed both in real-time observation, where sensitivity can be enhanced through isotope tracers [121, 122], or extrapolation from measurements of soils from systems routinely experiencing natural fire [8, 106, 107]. In three cases, the effects of biological activity enhanced by substrate addition have been investigated [108, 111, 122]. Only in one case has pyrolysis char been evaluated [123] and, most often, the feedstock has been wood-derived.

Inference from measurements on soils in systems subject to natural fire suggests millennial stability, and in extrapolation from controlled incubations (elevated temperature and optimal moisture), the general acceleration of mineralization (decomposition) that occurs in such systems has been noted and accounted for [124].

Newly formed char appears to contain a small biologically labile fraction (see below), alkaline pH (mean pH = 8.5; ten studies), and nutrients available in ash from partial combustion embedded in the residual matrix. Only in one published study is this labile fraction deliberately extracted prior to evaluation [125]. Allowing for these characteristics that may lead to nonlinear carbon loss, other deficiencies in laboratory studies (simulation of natural char formation), and effects of induced changes in soil chemistry, the assumption of centennial to millennial stability does not appear unreasonable [122].

Experiments using newly formed charcoal have generally used particles <2 mm diameter (with no minimum particle size), but it has been noted that the physical fate of charcoal is predominantly in fine fractions, broadly <50 μm [90], and that its physical diminution appears relatively rapid, presumably through physical weathering and abrasion. There appears to be substantial evidence for intimate mineral–char interactions which, it has been hypothesized, might guard against degradation; however, discrete char particles have been found to persist within free organic fractions over a period of decades [126].

Three studies found no evidence for a role of tillage in the mineralization of wood-derived charcoal [122, 126, 127], and the single study that has explicitly examined the stability of pyrolytic char from wood and cereal straw suggested a slow and predominantly abiotic degradation which has been convincingly demonstrated for wood charcoal in a climosequence, which confirmed the sensitivity of absolute rates of degradation to temperature [33].

Oxidative measures are one of the key methods used to quantify char in soil, however they are used with the objective of retaining all charcoal in order to identify the wide continuum of char on soil (ranging from black carbon to soot), rather than identifying more or less stable subcomponents. However, the potential to develop artificial aging techniques (that simulate enzymatic oxidative degradation in soils) to rapidly compare and evaluate biochar stability (relative to charcoal) appears to have been rather overlooked and will be useful in seeking greater certainty on this critical matter [113, 112].

Labile Biochar Fractions Incubation of soil with manufactured or un-aged char typically results in higher CO_2 evolution than from the same soil without char. However, the degree of excess declines over time in a strongly nonlinear fashion in the short term [121, 123, 128–130]. This suggests a "priming" of decomposition of carbon, either of that already in the soil, or more likely of carbon in the added char. Priming of existing soil carbon could be a consequence of the modification of the soil-chemical environment (see below), while loss of carbon from biochar can result from the mineralization of a labile char fraction. These patterns also suggest that priming is complex and that extrapolation of stability using short-term decay rates will be unreliable; such rates are not consistent with the age of charcoal found in archaeological soils such as the *terra preta*. The parameters that govern the balance between labile and stable components are not yet fully understood.

Priming of Soil Carbon or Biochar Loss The potential for biochar, in the form of synthetic charcoal, to cause or accelerate the decomposition of preexisting soil organic matter (priming) has been reported in medium-term study of litter layers in the boreal zone [131]. The loss of litter carbon was measured over a period of 10 years, but almost all the loss occurred prior to the first annual sampling. The litter into which charcoal was introduced was likely to be acidic and nutrient constrained, in which case the decomposition response is expected.

In Canada, and with the benefit of a carbon isotope trace, information on priming in tilled arable soil was obtained on a 65-year timeframe. This indicated that the mean residence time for particulate organic matter in soil increased by a factor of 2.5 at sites where charcoal derived from historic natural fire was present [126]. Another study, also with a carbon isotope trace, suggested slower and less complete utilization (high stabilization) of organic material added to soils from a tropical environment containing aged charcoal [132].

A single laboratory study [111] showed an approximate doubling of charcoal degradation rates (charcoal priming) with the addition of glucose to soil, a compound often used as a simple analogue for the labile carbon exuded into soil by living plant roots. The initial rates of loss were still low (0.5% over 60 days, which is a smaller proportion of charcoal carbon that might reside in a labile charcoal component) – especially for higher temperature char created from wood and for an experiment conducted under optimal conditions in a sand matrix. Quantitative extrapolation of such laboratory studies to the priming that might be likely to occur in the field, particularly with contrasting levels of microbial and plant root activity, is difficult.

It has been noted that if priming of soil organic matter is a permanent function of charcoal, the amount of non-charcoal carbon present under equilibrium field conditions must be lower than in charcoal-free soils [133]. Available data do not support this, and the Amazonian *terra preta* are enriched in organic matter

relative to the surrounding soils, as well as containing large amounts of aged charcoal. Due to climatic influences, the Amazonian soils are rather low in organic matter naturally. The likelihood of an analogous accumulation in temperate soils amended with biochar is not certain, given higher background soil-carbon mineralization rates. Other studies have also suggested stabilization of soil organic carbon pools [134] and suppression of CO_2 production in biochar-amended soils [135].

Biochar and Soil Nutrient Dynamics Reported increases in crop yield with charcoal addition have precipitated a number of plot-scale field trials to evaluate impacts on soil fertility, mainly through crop grain or biomass yield, usually with some measure of nutrient uptake. Reviewing 19 relevant articles in the literature [7], none of the reported studies have been undertaken in temperate zones. As such, caution should be adopted in directly transferring knowledge gained from tropical environments to temperate regions. In the tropical environment, the impacts have generally been positive, though most often in combination with fertilizer nitrogen. Less than one third of these studies have used char application rates of less than 15 tC ha^{-1}, however, and only three used pyrolytic char.

Verheijen et al. [2] undertook a meta-analysis of the effects of biochar addition to soil on crop production using nine studies (all of which used replicates to measure variance), involving 86 separate "treatments". The results are reproduced in Fig. 12.

The sample means indicate a small, but positive, effect on crop productivity with a grand mean of c. 10%. While there is some apparent trend of increased biochar additions, resulting in higher yields, this is not

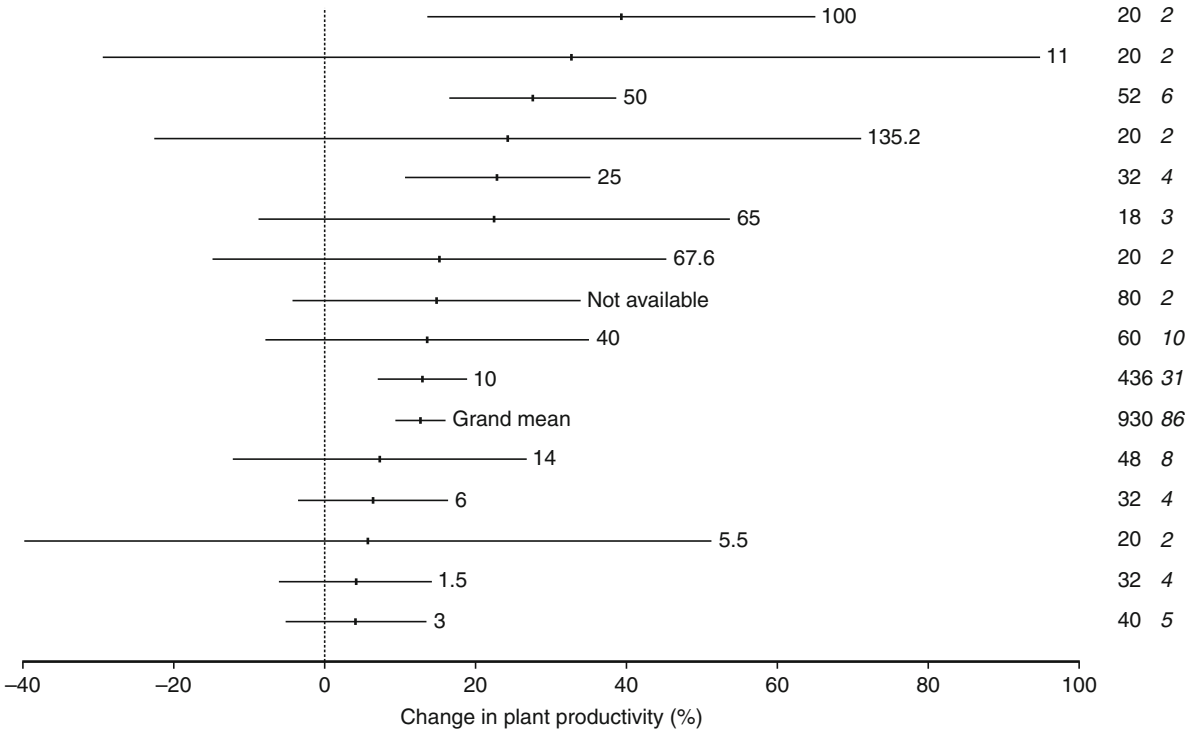

Biochar, Tool for Climate Change Mitigation and Soil Management. Figure 12
The percentage change in crop productivity upon application of biochar at different rates from a range of feedstocks along with varying fertilizer co-amendments. *Points* represent mean, and *bars* represent 95% confidence intervals. Numbers next to bars denote biochar application rates (t ha^{-1}). Numbers in the two columns on the right show number of total "replicates" upon which the statistical analysis is based (*bold*) and the number of "experimental treatments" which have been grouped for each analysis (*italics*) (Reproduced with permission from Verheijen et al. [2])

statistically significant at the P = 0.05 level as can be seen from the overlapping error bars at the 95% confidence interval. Biochar additions at rates of 10, 25, 50, and 100 t ha^{-1} led to statistically significant increases in crop yields compared to a control with no addition, though other studies using 40 and 65 t ha^{-1} did not show any statistically significant yield increase. Figure 12 illustrates that there is a wide variance in the response to biochar addition, e.g., at the 5.5, 11, and 135.2 t ha^{-1} application rates. Verheijen et al. speculate that the reasons for this are variability in the biochar, crop, and soil types. They also note that the means for each application rate are positive, and that no single biochar application rate had a statistically significant negative effect on crop productivity (though individual experiments have demonstrated negative effects, e.g., [84], [159]). On the other hand, the studies they examined do not cover a wide-range of latitudes and are heavily skewed toward (sub-) tropical conditions.

Substituting chemical fertilizer for the nutrients added into the soil as biochar has not resulted in the same increase of crop productivity as provided by biochar addition. In two cases where the effect of pH modification was controlled for by liming, the effect of char was still superior [7]. This suggests that char might impact crop growth through its impacts on soil physical properties and/or on mediation of nutrient exchange between soil and plant.

In classic studies of *terra preta* fourth-season maize yields were much higher in plots amended with char and fertilizer than the non-fertilized and non-char amended control [136], and similar results have been shown in experiments with maize carried out in Columbian savannah soil [137]. However, regarding the *terra preta* studies, it is strictly incorrect to say that the effect of the treatments was to increase yield, since the yields for all treatments displayed post-clearance decline, and the control yields were ultimately very low.

Limited evidence under tropical soil conditions suggest that the addition of fresh charcoal can reduce nitrogen leaching loss. Soils with higher and long-established charcoal content had enhanced nutrient status but leached extra added nitrogen [1]. There is a relatively large amount of consistent evidence for the partial surface oxidation of char by chemical and biological processes in soil and proliferation of carboxyl groups [138]. It appears that this is reflected in the cation exchange capacity of aged charcoal and charcoal-rich soils, but not shown in new char. Plot-scale experiments indicate that the uptake of other nutrients may be enhanced by charcoal, in particular phosphorus as ash in charcoal may be more available than phosphate in the soil.

Since biochar has a high carbon-to-nitrogen ratio, it is likely that rapid mineralization of a labile carbon fraction could – by immobilization – contribute to a draw on soil mineral nitrogen, in addition to an effect of ammonium sorption, and potentially reduce crop nitrogen supply. Evidence for this effect is relatively abundant and consistent in the literature, but the effect depends on the status of indigenous soil mineral nitrogen, and these studies have been undertaken exclusively in the tropics.

Immobilization tends to enhance soil nitrogen supply to the crop in the longer term since microbial proliferation builds a reservoir of mineralizable nitrogen. In field studies of charcoal or biochar extending beyond a single season, this effect may be observed, where second- or subsequent-season (but not first-season) are elevated relative to non-amended controls.

Biochar and Emission of Nitrous Oxide and Methane from Soil A single peer-reviewed study reports suppression of nitrous oxide emission from soil from charcoal [125]; however, in the light of the importance of N_2O emissions to total agricultural greenhouse gas emissions and emerging evidence reported in recent studies (e.g., [13, 139, 140, 141]) the effect warrants further attention. Results from planted fields in Columbia showing a large positive effect are unpublished [142] as are three studies showing conflicting outcomes in laboratory studies using soils from Australia [143, 144] and New Zealand [139]. Laboratory studies used high rates of application [125, 135], single soils [145], or single types of charcoal. Results from a laboratory study using biochar made from poultry manure and *Eucalyptus* wood showed N_2O emissions were reduced over a long-term (5-months with three wet-dry cycles) period [140].

Nitrous oxide is emitted mainly by specific groups of bacteria, which under anaerobic conditions reduce nitrate rather than oxygen (nitrate to N_2O via nitrite

and nitric oxide). Emission of N_2O at low rates may also occur under aerobic conditions from the activity of chemotrophic bacteria converting mineralized organic nitrogen (ammonium) to nitrate. Higher soil organic matter increases nitrification, but the application of nitrogen fertilizer has a greater immediate impact on soil nitrate concentrations and, hence, N_2O emission.

Proposed mechanisms for biochar suppression of N_2O revolve around modification of soil-water dynamics, e.g., drawing soil solution and dissolved nitrate into inaccessible pores (small pores saturating first) and maintaining aerobicity in inhabited soil-pore space; increase of soil pH which under anaerobic conditions favors completion of nitrate reduction to N_2 from N_2O; or the adsorption of ammonium and its protection from nitrification and denitrification [125, 145, 146]. Singh et al. [140] also propose the importance of time-induced changes ("aging") on biochar properties which were attributed to the reduction in ammonium leaching and N_2O emissions they observed.

The effect of water addition cannot be completely evaluated under constant conditions, but Yanai et al. [125] found suppression was reversed when water-filled pore space was increased from partial to near-complete saturation. In the same study, the addition of combustion ash to the soil, separately from charcoal, did not suppress emission. However, [140] and [147] have demonstrated reduced N_2O emissions after a sequence of wet-dry cycles. Therefore, there is the important influence of time which must be taken into consideration. Simultaneous monitoring of N_2 is also required to confirm N_2O reduction. It has also been shown that nitrate has also been reported to accumulate where N_2O is suppressed [147].

Mobility of Char Biochar and charcoal fines have a low bulk density of approximately 300 kg m^{-3} against a typical soil bulk density of 1,300 kg m^{-3}. Particles may be very fine in size and, in addition, surfaces may be hydrophobic [148]. Collectively, these characteristics indicate a higher potential for lateral transfer in water than for other soil components [149], and applied at a high rate in tropical environments subjected to frequent intense rainfall, erosion of charcoal off-site has been measured in proportions up to 25% in 2 years [150], and most of the 66% loss calculated by Nguyen et al. [106] in 30 years after surface deposition was attributed to erosion.

Negligible longer-term losses [106] and low rates of movement apparent for natural charcoal in a temperate environment [126] suggests a rapid decline in hydrophobicity, physical breakdown, and development of association with mineral particles [87, 151, 152]. The "anchoring" of particles within the soil matrix at depth may be critical in limiting erosion. The apparent combustion of fire-derived char in dry regions, where material remains at the surface between fires [153, 154], emphasizes the role of incorporation into deeper soil in ensuring longevity in the natural environment, and that in more biologically active soils, this must therefore occur. However, measured rates of transport into subsoil appear to be slow [150].

Meanwhile, studies of the global cycle of "black carbon" have established the existence of significant flux from land to ocean at a macroscale [102, 155]. Little literature has addressed the process of transport of char through the environment, although it has been noted that PAH is high in organic matter dissolved in alkali extracts after natural fire [156].

Char, Soil-Water Dynamics, and Irrigation In large quantities, wood-derived charcoal modifies soil physical properties. It has a low-inherent bulk density of 0.3–0.5 t m^{-3}, which is one third to one fifth that of typical NW European arable soil. Depending on particle-size distribution of the char relative to that of the soil and the extent to which added char may locate within existing pores, higher experimental rates of application could directly reduce soil bulk density and increase soil volume. This affects water-holding capacity and water-filled pore space, but declining hydrophobicity and the effects of weathering on particle size will determine the duration of this effect. In the experimental context, water-holding capacity is measurably increased by adding fresh charcoal and must be considered in the design of laboratory soil incubations [132]. Studies of amended soils can be adjusted for either equal gravimetric water content, or to equal tension (depending on the hypothesis). Water storage could be of critical value, yet the factors that determine the efficacy of char in this context have not been clarified.

Published evidence [88] for the effect of biochar on pore-size distribution, however, is remarkably scarce.

Some assessments have been made, and the problem appears to be in the level of replication required to demonstrate significant affects using methods best used in comparison of different soils. One study [157] has reported water-holding capacity of soils amended at low, medium, and high rates with pyrolytic char; one study has focused solely on pore-size characteristics of charcoal and pyrolytic char [88]; and one has measured the impact of charcoal residues on water-holding capacity at old kiln sites [83].

Summary

The evidence for the function of biochar in soil is based largely on evidence from studies of charcoal, and predominantly in the tropical environment. Triangulation of existing knowledge with systematic studies of biochar produced using technology and feedstocks relevant to viable temperate systems is needed, combined with techniques to rapidly assess long-term stability, and potential soil agronomic benefits.

Conclusion: Evaluating the Sustainability of Pyrolysis-Biochar Systems

A *sustainable biochar system* can be defined as one which: (a) produces and deploys biochar safely and without emitting non-CO_2 greenhouse gases; (b) reduces net radiative forcing; (c) does not increase inequality in access to and use of resources unduly, and (d) provides an adequate return on investment. Condition (a) is important to ensure that PBS technologies and practices do not pose undue risks to human health and safety and the environment (e.g., through inhalation of dust, biochar particles turning waterways or surrounding vegetation "black," adding N_2O, CH_4, or black carbon soot particles to atmosphere increasing net greenhouse forcing, etc.). Condition (b) is important to ensure that the net result of a PBS is indeed to reduce net radiative forcing relative to a baseline case. This is primarily due to reduction in atmospheric concentration of greenhouse gases through removal and avoided emissions. Condition (b) also takes account of direct and indirect land-use changes (I/LUC), which can result in one-off emission of hundreds of tons of carbon per hectare in the case of tropical and peatland rainforest. Clearing of Brazilian wooded *cerrado* incurs a carbon loss of c. 45 tC ha^{-1}, US grassland c. 30 tC ha^{-1}, and abandoned US crop land zero or only a few tons per hectare [160]. Clearly, there is no point in converting land that incurs a large loss of carbon to biomass production for energy if the main purpose (or a large part of the rationale) of a project is to abate carbon through biochar production.

Condition (c) is relevant because an increase in demand for biomass will have knock-on impacts upon other users or potential users of that biomass, or upon other biomass, demand for which increases due to substitution effects. This also relates to LUC and ILUC, which frequently encounters equity and justice problems and questions. Condition (d) refers to economic viability since in market economies investment will only follow favorable rates of return. Defining an "adequate rate of return" is fraught with difficulties and depends upon subjective considerations such as the discount rate selected.

Systems which meet all of the above criteria do not exist at demonstration or commercial scale at the current time, and do not include traditional charcoal production. This is not surprising, of course, because biochar has only been proposed as a carbon abatement and agronomic improvement technology since the early- to mid-2000s. The further development and eventual deployment of biochar will be driven by one or more of the following policy and economic drivers.

(a) *Agronomic value of the biochar*: This value could be quite large on depleted soils, but any value has to be offset against the costs of production, delivery, and application to soil. Where the biochar is a by-product of electricity (or heat) generation, it may have a zero production cost. Examples of zero-cost biochar are few and far between and unlikely to be the norm. The cost of biochar production will, in many cases, be hard to recoup from the value of the agronomic gain alone.

(b) *Carbon storage value of the biochar*: If biochar can be ascribed a carbon storage value, this could greatly accelerate its successful take-off. The difficulty in ascribing a carbon value to biochar relates to the scientific uncertainty over long-term stability and interactions with soil organic carbon, lack of agreement on (and difficulty relating to) inclusion of land-based carbon budgets in trading arrangements, and technical uncertainties around

Monitoring, Verification, Accounting, and Reporting (MVAR).

(c) *Waste management*: If pyrolysis-biochar systems are a cost-effective way of dealing with certain organic waste fractions (relative to other disposal/management options), this could drive the deployment of PBS through the value of the avoided tipping-fees to waste-management companies. The difficulty of this route is that waste biochar products are likely to pose more environmental and health and safety risks and will need to be carefully assessed and controlled. Such regulation is likely to drive-up the costs of biochar from wastes and to increase the regulatory barriers and hurdles, reducing interest from the industry. Furthermore, tipping fees are related to land-fill costs and taxation, which are subject to political change.

(d) *Renewable energy incentives*: To make pyrolysis-biochar add-up, it is likely that incentives will be required for the generation of renewable electricity and/or heat. Where the incentives are for electricity generation, however, other thermal conversion technologies such as combustion and gasification (with limited char production) will frequently have a competitive edge. Such incentives and subsidies are also vulnerable to political change.

(e) *Agri-environmental policies*: Another potential route to biochar deployment is through appropriate agri-environmental policies. If biochar addition can be demonstrated to have multiple benefits to agricultural land, agricultural support policies could be used to promote its adoption, for example, through inclusion in measures that are eligible for area-based and environmental stewardship payments.

One way forward in the short- to medium-term is to promote the use of biochar in particular niche applications, where its potential can be demonstrated and from there broader applications identified. This is broadly consistent with the innovation studies literature on socio-technical transitions: new technologies nearly always begin as niche applications that, if useful, find a wider role (3). The identity of the niche application will vary, depending on local, national, and regional context; policy; and socioeconomic drivers and incentives. In Europe, it may be sustainable biochar production from particular organic waste streams (paper or sewage sludge, for example), while in Asia, it may be carbonized rice husks from a gasifier as described in Box 2. In North America and Scandinavia, woody wastes from the timber industry may be ideal feedstocks, while in Africa, agricultural residues that would otherwise be burnt may offer-up opportunities.

Future Directions for Research, Development, and Demonstration

Biochar is a complex, multifunctional material that requires improved mechanistic knowledge and understanding – of its production, properties, impacts, interactions, costs, and benefits. Without this mechanistic process understanding, it is difficult if not impossible to predict and assess accurately the benefits of biochar for either greenhouse gas abatement or for addition to the soil even with evidence from individual field trials. We have identified the key research needs according to three broad headings below.

Pilot Production Research Facilities for Biochar and "Engineered" Biochar

What is the need? A strategic approach to producing, testing, and comparing biochar samples from different technologies, under specific reproducible conditions, would improve the evidence base. Facilities are needed to serve the research community, focusing current and future effort away from charcoal and toward biochar, produced from designated feedstocks under highly specified process conditions.

Why? The engineering and technological challenges are intimately related to the engineered biochar concept – namely engineering biochar with specific and controlled properties, designed for particular purposes (e.g., carbon abatement, short- and long-term agronomic gain, waste-management and pollution control, energy production, etc.) and contexts of application (soil types, agricultural systems, other land-uses, etc.).

When? The need is urgent if biochar is to have a role in tackling climate change in the next several decades and necessary for any future soil application of biochar.

Resource implications: The resources required are reasonably large, but not large compared to much technology-development since biochar can be

produced at small-scales using relatively straightforward equipment.

How well advanced is existing research? There is currently limited activity or capacity anywhere in the world for technological evaluation of biochar production.

Ability to address key questions: Once equipment is in place, it should be relatively straightforward to address the key questions which arise, though some issues will inevitably take time to answer.

Examples of key questions to address:

Recipes for producing engineered biochar with specific properties and functions – acquiring the technological know-how to produce biochar with defined properties based upon a process understanding of production conditions.

Better understanding of the carbon and energy balance of alternative biochar production technologies – as yet there is little consistent and high-quality data on pilot- and commercial-scale pyrolysis (especially slow and intermediate) without which any evaluation of biochar is impaired.

Better understanding of the superlabile, labile, and stabilized components of biochar – better knowledge of what influences the Carbon Stability Factor for biochar is required, along with the effects in soil and field of labile versus stable carbon.

The Predictability and Certainty of the Impacts of Biochar

What is the need? If biochar is to be a commercial proposition, it will be necessary for reliable predictive knowledge of its impacts in particular soil and agronomic contexts to be well established (just as is the case for chemical fertilizers or pesticides). There is also need for a practical and scalable method by which the stable component of biochar can be established experimentally through acceleration of initial degradation as well as for examining the change that occurs soon after incorporation in soil.

Why? Only if the user is confident of positive and cost-effective benefits of biochar, when applied at particular rates, will a biochar market emerge. If the purpose is solely carbon storage, then the key issue will be long-term stability of the biochar.

When? For the purposes of carbon storage, urgent knowledge of long-term stability will be necessary. Predictive knowledge of soil and plant impacts is necessary for development of a market for biochar addition to land.

Resource implications: the resources required are moderate, but progress is being held back by lack of samples and equipment.

How well advanced is existing research? Evidence for the stability of charcoal in agriculture and the wider environment has been inferred in detailed studies in the USA and Australia. Work on the definition and stability of biochar is ongoing by established research groups. Work on soil and plant effects is well established internationally (especially in the USA, Australia, Brazil and Japan). However, this research is still in its infancy with no systematic effort: the opportunity exists for a focused and deterministic approach.

Ability to address key questions: In principle, it should be possible to address the stability question relatively quickly. Addressing the soil and plant effects will be more complex and time-consuming because of variability and complexity.

Examples of key questions to address:

These questions/topics can be addressed/answered fairly quickly.

Short- and long-term effects – separating out the long-term and short-term effects of biochar by comparing the functions of fresh and artificially aged material

Available nutrients and contaminants – Agreement on a methodology to quantify "available" nutrients and contaminants in a biochar matrix.

Deployment equipment and appliances – Develop modifications of existing agricultural equipments and implements so as to develop effective and efficient ways of storing and deploying biochar in realistic farm-based scenarios.

Biochar in grassland systems – The potential to reduce methane emissions from cattle, biochar as a slurry additive for odor control, etc.

Methodologies for evaluating the migration of biochar by movement through the soil profile, wind-erosion, water-erosion, etc. – necessary for regulation and carbon accounting.

Low-cost monitoring of biochar – Investigation of field spectroscopy and remote sensing for the low-cost monitoring of biochar added to soil.

These questions/topics are more difficult, complex, and/or simply time-consuming, and will take longer to address or answer

Nitrous oxide suppression – Examination of the mechanism by which biochar, at least under certain conditions, can suppress nitrous oxide emission from soil.

Field experimentation and trials strategy – Field experiments and trials that encompass diverse rotations and systems (arable, horticulture, and grassland) and including feedstocks derived from (inter alia) agricultural residues.

The value of biochar-based soil management – Compare the likely value of biochar-based soil management against the return that has been established for active use of other organic resources in management of soil.

Biochar for the control of diffuse pollution – More research on the ability of biochar to reduce leaching from land (e.g., using buffer ditch experiments) or from other sources (e.g., waterways, road surfaces).

Wider Biochar Sustainability Issues

What is the need? What are the wider impacts of biochar as a system, potentially deployed at different scales and in different spatiotemporal and socioeconomic contexts? How can the biochar system be made sustainable?

Why? Pyrolysis biochar systems (PBS), or variants thereof, only make sense if they meet minimum sustainability requirements (standards) and avoid incurring adverse environmental, social, or economic impacts. Sustainability appraisal methods can be utilized to ensure that biochar at a system level "adds-up"

When? It is important to understand system level impacts as these help direct more basic research and development by identifying key sensitivities. It is necessary to evaluate system-level effects prior to real-deployment to understand knock-on effects and potential problems.

Resource implications: The resources required are small compared to the technological and basic scientific research and development required because equipment and experimental costs are typically lower.

Ability to address key questions: Rapid progress can be made once resource is available, though accuracy and precision is dependent upon the availability of new data from technological and natural scientific R&D.

Examples of key questions to address:

Better Life-Cycle Assessments of pyrolysis-biochar systems – improved data across the whole PBS supply chain (from feedstock to field) and alternative biochar-producing systems.

Better techno-economic cost modeling – using more accurate data and with an improved representation of the key processes and stages, including production, distribution, storage, and deployment.

Better comparative analyses of biochar versus *other resource-use options* – need for explicit and transparent comparisons using best-available data of the most effective way of using and managing limited biomass resources for, e.g., bioenergy generation, carbon/greenhouse gas abatement, sustainable soils and waste management, composting and sustainable agri-food systems.

Assessment of land-use implications of biochar deployment – how biochar might influence the competitive advantage of different crops and the knock-on impacts on land-use decisions, supply, and demand.

Acknowledgments

We would like to acknowledge financial support from the UK's Engineering and Physical Sciences Research Council (EPSRC), the UK Government, and the European Regional Development Fund (Interreg IVb) in supporting the UK Biochar Research Centre.

Bibliography

1. Lehmann J et al (2003) Nutrient availability and leaching in an archaeological anthrosol and a ferralsol of the Central Amazon basin: fertilizer, manure and charcoal amendments. Plant Soil 249:343–357
2. Verheijen F et al (2009) Biochar application to soils: a critical scientific review of effects on soil properties, processes and functions. Joint Research Centre, Institute for Environment and Sustainability, Ispra, Italy
3. Lehmann J et al (eds) (2003) Amazonian dark earths: origin, properties, management. Kluwer, Dordrecht

4. Seifritz W (1993) Should we store carbon in charcoal? Int J Hydrogen Energy 18:405–407
5. Lehmann J, Joseph S (eds) (2009) Biochar for environmental management: science and technology. Earthscan, London
6. Sohi S et al (2010) A review of biochar and its use and function in soil. Adv Agron 105:47–82
7. Shackley S, Sohi S (2010) An assessment of the benefits and issues associated with the application of biochar to soil. Department for Environment, Food and Rural Affairs, UK Government, London
8. Lehmann J et al (2008) Australian climate-carbon cycle feedback reduced by soil black carbon. Nat Geosci 1:832–835
9. Lehmann J (2007) A handful of carbon. Nature 447(7141):143–144
10. Prentice IC et al (2001) The carbon cycle and atmospheric carbon dioxide. In: Houghton JT et al (eds) Climate change 2001: the scientific basis. Contribution of Working Group I to the Third Assessment Report of the Intergovernmental Panel on Climate Change. Cambridge University Press, Cambridge/New York, 881pp
11. Kuhlbusch TAJ (1998) Black carbon and the carbon cycle. Science 280:1903–1904
12. Vitousek PM et al (1986) Human appropriation of the products of photosynthesis. Bioscience 36:368–373
13. Van Zwieten L et al (2009) Biochar and emissions of non-CO_2 greenhouse gases from soil. In: Lehmann J, Joseph S (eds) Biochar for environmental management science and technology. Earthscan, London, pp 227–250
14. Ladha JK et al (2005) Efficiency of fertiliser nitrogen in cereal production: retrospects and prospects. Adv Agron 87:85–156
15. Houghton JT et al (eds) (1997) Revised 1996 IPCC guidelines for national greenhouse gas inventories. Hadley Centre Meteorological Office, Bracknell
16. West TO, McBride AC (2005) The contribution of agricultural lime to carbon dioxide emissions in the United States: dissolution, transport, and net emissions. Agric Ecosyst Environ 108:145–154
17. Lehmann J, Gaunt J, Rondon M (2006) Bio-char sequestration in terrestrial ecosystems – a review. Mitig Adapt Strateg Glob Change 11:403–427
18. The Royal Society (2009) Geoengineering the climate: Science, governance and uncertainty. The Royal Society, London
19. Demirbas A, Arin G (2002) An overview of biomass pyrolysis. Energy Sources 24:471–482
20. Husk B, Major J (2010) Commercial scale agricultural biochar field trial in Quebec, Canada, over two years: effects of biochar on soil fertility, biology and crop productivity and quality. BlueLeaf, Quebec, p 35
21. Bridgwater AV, Meier D, Radlein D (1999) An overview of fast pyrolysis of biomass. Org Geochem 30:1479–1493
22. Bridgwater AV, Peacocke GVC (2000) Fast pyrolysis processes for biomass. Renewable Sustainable Energy Rev 4:1–73
23. Anderson-Teixeira K et al (2009) Changes in soil organic carbon under biofuel crops. GCB Bioenergy 1(1):75–96
24. Kammen DM, Lew DJ (2005) Review of technologies for the production and use of charcoal. National Renewable Energy Laboratory, Golden
25. Accardi-Dey AM, Gschwend PM (2002) Assessing the combined roles of natural organic matter and black carbon as sorbents in sediments. Environ Sci Technol 36(1):21–29
26. Antal MJ, Gronli M (2003) The art, science, and technology of charcoal production. Ind Eng Chem Res 42(8):1619–1640
27. Brown R (2009) Biochar production technology. In: Lehmann J, Joseph S (eds) Biochar for environmental management. Earthscan, London
28. Brownsort P (2009) Biomass pyrolysis processes: performance parameters and their influence on biochar system benefits. MSc dissertation, University of Edinburgh, p 84
29. Gaur S, Reed TB (1995) An atlas of thermal data for biomass and other fuels. NREL, Colorado, p 189
30. Masek O et al (2010) Pyrolysis systems for biochar production – influence of biochar production conditions on its structure, properties and environmental stability. Fuel. doi:10.1016/j.fuel.2011.08.044
31. Belanger N et al (2004) Forest regrowth as the controlling factor of soil nutrient availability 75 years after fire in a deciduous forest of Southern Quebec. Plant Soil 262(1–2):363–372
32. Lehmann J (2007) Bio-energy in the black. Front Ecol Environ 5(7):381–387
33. Cheng CH, Lehmann J, Engelhard MH (2008) Natural oxidation of black carbon in soils: changes in molecular form and surface charge along a climosequence. Geochim Cosmochim Acta 72(6):1598–1610
34. Cheng CH et al (2006) Oxidation of black carbon by biotic and abiotic processes. Org Geochem 37(11):1477–1488
35. Liang B et al (2006) Black carbon increases cation exchange capacity in soils. Soil Sci Soc Am J 70(5):1719–1730
36. Downie A (2009) Personal email communication with P. Brownsort concerning slow pyrolysis, July 2009
37. Kurosaki F et al (2007) Macroporous carbon prepared by flash heating of sawdust. Carbon 45(3):671–673
38. Helsen L et al (1997) Low-temperature pyrolysis of CCA-treated wood waste: chemical determination and statistical analysis of metal input and output; mass balances. Waste Manage 17(1):79–86
39. Lievens C et al (2009) Fast pyrolysis of heavy metal contaminated willow: influence of the plant part. Fuel 88(8):1417–1425
40. Ryu C, Sharifi VN, Swithenbank J (2007) Waste pyrolysis and generation of storable char. Int J Energy Res 31(2):177–191
41. Vassilev SV, Braekman-Danheux C (1999) Characterization of refuse-derived char from municipal solid waste: 2. Occurrence, abundance and source of trace elements. Fuel Process Technol 59(2–3):135–161
42. Vassilev SV, Braekman-Danheux C, Laurent P (1999) Characterization of refuse-derived char from municipal solid waste: 1. Phase mineral chemical composition. Fuel Process Technol 59(2–3):95–134
43. Hwang IH et al (2008) Improving the quality of waste-derived char by removing ash. Waste Manage 28(2):424–434
44. Miladinovic N, Bayer-Souchet F, Larsen HF (2009) Project neptune. In: End-User Workshop, Ghent

45. McGrath T, Sharma R, Hajaligol M (2001) An experimental investigation into the formation of polycyclic-aromatic hydrocarbons (PAH) from pyrolysis of biomass materials. Fuel 80(12):1787–1797
46. McGrath TE, Chan WG, Hajaligol MR (2003) Low temperature mechanism for the formation of polycyclic aromatic hydrocarbons from the pyrolysis of cellulose. J Anal Appl Pyrol 66(1–2): 51–70
47. McGrath TE et al (2007) Formation of polycyclic aromatic hydrocarbons from tobacco: The link between low temperature residual solid (char) and PAH formation. Food Chem Toxicol 45(6):1039–1050
48. Milne TA, Evans RJ, Abatzoglou N (1998) Biomass gasifier "tars": their nature, formation, and conversion. National Renewable Energy Laboratory, Golden, p 204
49. Zhurinsh A, Zandersons J, Dobele G (2005) Slow pyrolysis studies for utilization of impregnated waste timber materials. J Anal Appl Pyrol 74(1–2):439–444
50. Creaser CS et al (2007) UK soil and herbage pollutant survey: environmental concentrations of polycyclic aromatic hydrocarbons in UK soil and herbage. Environment Agency, Bristol
51. Mašek O (2007) Studies on pyrolytic gasification of low-rank solid fuels in the presence of steam. School of Engineering, Hokkaido University, Sapporo
52. Defra (2008) Guidelines to Defra's greenhouse gas conversion factors for company reporting. Defra, London
53. Defra (2009) Guidelines to Defra/DECC's GHG conversion factors for company reporting. Defra, London
54. Anderson-Teixeira K et al (2009) Changes in soil organic carbon under biofuel crops. GCB Bioenergy 1(1):75–96
55. Hammond J, Shackley S, Sohi S, Brownsort P (2011) Prospective life cycle carbon abatement for pyrolysis biochar systems in the UK. Energy Policy 39:2646–2655
56. Roberts KG et al (2010) Life cycle assessment of biochar systems: estimating the energetic, economic and climate change potential. Environ Sci Technol 44(2):827–833
57. Ibarrola R (2009) Pyrolysis for waste treatment: a life cycle assessment of biodegradable waste, bioenergy generation and biochar productionin Glasgow and Clyde Valley. Msc dissertaiton, School of GeoSciences, University of Edinburgh
58. Gaunt J, Cowie A (2009) Biochar, greenhouse gas accounting and emissions trading. In: Lehmann J, Joseph S (eds) Biochar for environmental management. Earthscan, London, pp 317–340
59. Gaunt JL, Lehmann J (2008) Energy balance and emissions associated with biochar sequestration and pyrolysis bioenergy production. Environ Sci Technol 42:4152–4158
60. Downie A, Klatt P, Munroe P (2007) Slow pyrolysis: Australian demonstration plant successful on multi-feedstocks. In: Bioenergy 2007 Conference, Finland
61. Dynamotive Energy Systems Corporation (1999) BioTherm™ – a system for continuous quality, fast pyrolysis biooil. In: Fourth Biomass Conference of the Americas, Oakland
62. Hornung A (2008) Fast, intermediate or slow pyrolysis for fuels production, power generation from various biomasses or as pre-conditioning unit for gasifiers. http://www3.imperial.ac.uk/pls/portallive/docs/1/44315696.pdf. Accessed 15 Aug 2009
63. Hornung A et al (2006) Thermo-chemical conversion of straw – Haloclean intermediate pyrolysis. In: 17th International Symposium on Analytical and Applied Pyrolysis, Budapest
64. Redlein D, Kingston A (2007) The portential role of agrichar in the commercialization of dynamotive's fast pyrolysis process. In: International Agrichar Initiative Conference, Terrigal
65. Bradshaw J et al (2007) CO_2 storage capacity estimation: issues and development of standards. Int J Greenhouse Gas Control 1:62–68
66. Lenton T (2010) The potential for land-based biological CO_2 removal to lower future atmospheric CO_2 concentration. Carbon Manag 1(1):16
67. Andreae MO, Gelencser A (2006) Black carbon or brown carbon? The nature of light-absorbing carbonaceous aerosols. Atmos Chem Phys 6:3131–3148
68. Woolf D, Amonette J, Street-Perrott A, Lehmann J, Joseph S (2010) Sustainable biochar to mitigate global climate change. Nat Commun 1:56
69. Fowles M (2007) Black carbon sequestration as an alternative to bioenergy. Biomass Bioenergy 31:426–432
70. Doornbosch R, Steenblik R (2007) Biofuels: is the cure worse than the disease? Organisation for Economic Cooperation and Development, Paris, p 57
71. Berndes G, Hoogwijk M, van den Broek R (2003) The contribution of biomass in the future global energy supply: a review of 17 studies. Biomass Bioenergy 25(1):1–28
72. Fischer G, Schrattenholzer L (2001) Global bioenergy potentials through 2050. Biomass Bioenergy 20(3):151–159
73. Hoogwijk M et al (2003) Exploration of the ranges of the global potential of biomass for energy. Biomass Bioenergy 25:119–133
74. IPCC (2007) Mitigation of climate change: contribution of the working group III to the fourth assessment report. Cambridge University Press, Cambridge
75. International Energy Agency (2008) Energy technology perspectives 2008. IEA/OECD, Paris
76. McCarl B et al (2009) Economics of biochar production, utilisation and emissions. In: Lehmann J, Joseph S (eds) Biochar for environmental management. Earthscan, London, pp 341–357
77. Giampietro M, Mayumi K (2009) The biofuel delusion: the fallacy of large-scale agro-biofuel production. Earthscan, London
78. Bapat HD, Manahan SE (1998) Chemchar gasification of hazardous wastes and mixed wastes on a biochar matrix. Abstr Pap Am Chem Soc 215:U571–U571
79. Joseph S et al (2009) Biochar for soil fertility and carbon sequestration: a review of current understanding. In: Australia and New Zealand Biochar Researchers Network, p 13
80. Thornley P (2009) Personal verbal communication with S. Shackley, Sept 2009
81. Agency E (2009) Minimising greenhouse gas emissions from biomass energy generation. Environment Agency, Bristol, p 43

82. Bates J, Edberg O, Nuttall C (2009) Minimising greenhouse gas emissions from biomass energy generation. Environment Agency, Bristol, p 43
83. Oguntunde PG et al (2008) Effects of charcoal production on soil physical properties in Ghana. J Plant Nutr Soil Sci 171:591–596
84. Asai H et al (2009) Biochar amendment techniques for upland rice production in northern Laos. Field Crops Res 111:81–84
85. Fernandes MB et al (2003) Characterization of carbonaceous combustion residues: I. Morphological, elemental and spectroscopic features. Chemosphere 51(8):785–795
86. Van Zwieten L et al (2010) Effects of biochar from slow pyrolysis of papermill waste on agronomic performance and soil fertility. Plant Soil, 327:235–246
87. Brodowski S et al (2005) Morphological and chemical properties of black carbon in physical soil fractions as revealed by scanning electron microscopy and energy-dispersive X-ray spectroscopy. Geoderma 128(1–2):116–129
88. Bird MI et al (2008) X-ray microtomographic imaging of charcoal. J Archaeol Sci 35:2698–2706
89. Janik LJ, Taylor JA, Skjemstad JO (1998) Non-living soil organic matter: what do we know about it? Aust J Exp Agric 38:667–680
90. Brodowski S et al (2006) Aggregate-occluded black carbon in soil. Eur J Soil Sci 57(4):539–546
91. Schmidt MWI, Noack AG (2000) Black carbon in soils and sediments: analysis, distribution, implications, and current challenges. Glob Biogeochem Cycles 14(3):777–793
92. Pignatello JJ, Kwon S, Lu Y (2006) Effect of natural organic substances on the surface and adsorptive properties of environmental black carbon (char): attenuation of surface activity by humic and fulvic Acids. Environ Sci Technol 40(24): 7757–7763
93. Watts CW et al (2005) Biological and physical processes that mediate micro-aggregation of clays. Soil Sci 170:573–583
94. Beaton JD, Peterson HB, Bauer N (1960) Some aspects of phosphate adsorption by charcoal. Soil Sci Soc Am Proc 24:340–346
95. Lehmann CJ, Rondon M (2006) Bio-char soil management on highly-weathered soils in the tropics. In: Uphoff NT (ed) Biological approaches to sustainable soil systems. CRC Press, Boca Raton, pp 517–530
96. Yu X-Y, Ying G-G, Kookana RS (2006) Sorption and desorption behaviors of diuron in soils amended with charcoal. J Agric Food Chem 54:8545–8550
97. Rhodes AH, Carlin A, Semple KT (2008) Impact of black carbon in the extraction and mineralization of phenanthrene in soil. Environ Sci Technol 42(3):740–745
98. Major J et al (2009) Fate of soil-applied black carbon: downward migration, leaching and soil respiration. Glob Change Biol. doi:10.1111/j.1365-2486.2009.02044.x
99. Yamato M et al (2006) Effects of the application of charred bark of Acacia mangium on the yield of maize, cowpea and peanut, and soil chemical properties in South Sumatra, Indonesia. Soil Sci Plant Nutr 52:489–495
100. Rondon MA et al (2007) Biological nitrogen fixation by common beans (Phaseolus vulgaris L.) increases with bio-char additions. Biol Fert Soils 43(6):699–708
101. Warnock DD et al (2007) Mycorrhizal responses to biochar in soil – concepts and mechanisms. Plant Soil 300:9–20
102. Masiello CA, Druffel ERM (1998) Black carbon deep sea sediments. Science 280:1911–1913
103. Masiello CA, Druffel ERM, Currie LA (2002) Radiocarbon measurements of black carbon in aerosols and ocean sediments. Geochim Cosmochim Acta 66(6):1025–1036
104. Oros DR et al (2002) Organic tracers from wild fire residues in soils and rain/river wash-out. Water Air Soil Pollut 137(1/4): 203–233
105. Dai X et al (2005) Black carbon in a temperate mixed-grass savanna. Soil Biol Biochem 37(10):1879–1881
106. Nguyen BT et al (2008) Long-term black carbon dynamics in cultivated soil. Biogeochemistry 89:295–308
107. Kimetu JM et al (2008) Reversibility of soil productivity decline with organic matter of differing quality along a degradation gradient. Ecosystems 11:726–739
108. Liang B et al (2009) Stability of biomass-derived black carbon in soils. Geochim Cosmochim Acta 72:6069–6078
109. Forbes MS, Raison RJ, Skjemstad JO (2006) Formation, transformation and transport of black carbon (charcoal) in terrestrial and aquatic ecosystems. Sci Total Environ 370: 190–206
110. Brewer CE et al (2009) Characterization of biochar from fast pyrolysis and gasification systems. Environ Prog Sustainable Energy 28(3):386–396
111. Hamer U et al (2004) Interactive priming of black carbon and glucose mineralisation. Org Geochem 35(7):823–830
112. Spokas KA (2010) Review of the stability of biochar in soils: predictability of O:C molar ratios. Carbon Manage 1(2): 289–303
113. Lehmann J et al (2009) Stability of biochar in soil. In: Lehmann J, Joseph S (eds) Biochar for environmental management. Earthscan, London, pp 317–340
114. Bucheli TD et al (2004) Polycyclic aromatic hydrocarbons, black carbon, and molecular markers in soils of Switzerland. Chemosphere 56(11):1061–1076
115. Rumpel C et al (2007) Composition and reactivity of morphologically distinct charred materials left after slash-and-burn practices in agricultural tropical soils. Org Geochem 38(6):911–920
116. Fernandes MB, Brooks P (2003) Characterization of carbonaceous combustion residues: II. Nonpolar organic compounds. Chemosphere 53(5):447–458
117. Brown RA et al (2006) Production and characterization of synthetic wood chars for use as surrogates for natural sorbents. Org Geochem 37(3):321–333
118. Cornelissen G et al (2005) Extensive sorption of organic compounds to black carbon, coal, and kerogen in sediments and soils: mechanisms and consequences for distribution, bioaccumulation, and biodegradation. Environ Sci Technol 39(18):6881–6895

119. Zimmerman JR et al (2004) Addition of carbon sorbents to reduce PCB and PAH bioavailability in marine sediments: physicochemical tests. Environ Sci Technol 38(20):5458–5464
120. Wingate JR, De Leij FAAM, Hutchings T (2009) Method of forming ion exchange charcoal. Patent No. GB2451509A, UK Intellectual Property Office, The Forestry Commission, p 51
121. Bruun S, Jensen ES, Jensen LS (2008) Microbial mineralization and assimilation of black carbon: Dependency on degree of thermal alteration. Org Geochem 39:839–845
122. Kuzyakov Y et al (2009) Black carbon decomposition and incorporation into soil microbial biomass estimated by 14C labeling. Soil Biol Biochem 41:210–219
123. Nguyen BT, Lehmann J (2009) Black carbon decomposition under varying water regimes. Org Geochem 40:846–853
124. Cheng CH et al (2008) Stability of black carbon in soils across a climatic gradient. J Geophys Res Biogeosci 113:2027
125. Yanai Y, Toyota K, Okazaki M (2007) Effects of charcoal addition on N_2O emissions from soil resulting from rewetting air-dried soil in short-term laboratory experiments. Soil Sci Plant Nutr 53:181–188
126. Murage EW, Voroney P, Beyaert RP (2007) Turnover of carbon in the free light fraction with and without charcoal as determined using the ^{13}C natural abundance method. Geoderma 138(1–2):133–143
127. Brodowski S et al (2007) Black carbon contribution to stable humus in German arable soils. Geoderma 139(1–2):220–228
128. Smith JL, Collins HP, Bailey VL (2010) The effect of young biochar on soil respiration. Soil Biol Biochem 42:2345–2347
129. Zimmerman AR (2010) Abiotic and microbial oxidation of laboratory-produced black carbon (biochar). Environ Sci Technol 44:1295–1301
130. Bruun EW et al (2011) Influence of fast pyrolysis temperature on biochar labile fraction and short-term carbon loss in a loamy soil. Biomass Bioenergy 35:1182–1189
131. Wardle DA, Nilsson M-C, Zackrisson O (2008) Fire-derived charcoal causes loss of forest humus. Science 320:629
132. Liang B et al (2010) Black carbon affects the cycling of non-black carbon in soil. Org Geochem 41:206–213
133. Woolf D (2009) Personal verbal communication with S. Sohi concerning recent meta-analysis of global soil carbon and soil black carbon data, Sept 2009
134. Kimetu JM, Lehmann J (2010) Stability and stabilisation of biochar and green manure in soil with different organic carbon contents. Aust J Soil Res 48:577–585
135. Spokas KA et al (2009) Impacts of woodchip biochar additions on greenhouse gas production and sorption/degradation of two herbicides in a Minnesota soil. Chemosphere 77:574–581
136. Steiner C et al (2007) Long term effects of manure, charcoal and mineral fertilization on crop production and fertility on a highly weathered Central Amazonian upland soil. Plant Soil 291(1–2):275–290
137. Major J et al (2010) Maize yield and nutrition during 4 years after biochar application to a Colombian savanna oxisol. Plant Soil
138. Lehmann J et al (2005) Near-edge X-ray absorption fine structure (NEXAFS) spectroscopy for mapping nano-scale distribution of organic carbon forms in soil: Application to black carbon particles. Global Biogeochemical Cycles 19(1): GB1013
139. Clough TJ et al (2010) Unweathered wood biochar impact on nitrous oxide emissions from a bovine-urine-amended pasture soil. Soil Biology and Biochemistry 74(3)
140. Singh BP, et al (2010) Influence of biochars on nitrous oxide emission and nitrogen leaching from two contrasting soils. Journal of Environmental Quality, 39. doi:10.2134/jeq2009.0138
141. Taghizadeh-Toosi A et al (2011) Biochar incorporation into pasture soil suppresses in situ nitrous oxide emissions from ruminant urine patches. J Environ Qual 40
142. Rondon M, Ramirez JA, Lehmann J (2005) Charcoal additions reduce net emissions of greenhouse gases to the atmosphere. In: Proceedings of the 3rd USDA Symposium on Greenhouse Gases and Carbon Sequestration, Baltimore, 21–24 Mar 2005
143. Rogovska N et al (2008) Greenhouse gas emissions from soils as affected by addition of biochar. In: The 2008 Joint Annual Meeting of ASA, CSSA and SSSA, Houston
144. Rogovska N et al (2009) Greenhouse gas emissions from soils as affected by addition of biochar. In: North American Biochar Conference, University of Colorado, Boulder, 9–12 Aug 2009
145. Condron L et al (2009) Biochar effects on nitrous oxide emissions from a pasture soil. In: Asia Pacific Biochar Conference, Gold Coast, 17–20 May 2009
146. Clough TJ et al (2008) Nitrous oxide – novel mitigation methodologies: objective 2 – biochar effects on urinary-N N_2O emissions. Report to the Ministry of Agriculture and Forestry (ed), p 15
147. van Zwieten L et al (2010) Influence of biochars on flux of N_2O and CO_2 from ferrosol. Aust J Soil Res 48:555–568
148. DeLuca TH, Aplet GH (2008) Charcoal and carbon storage in forest soils of the Rocky Mountain West. Front Ecol Environ 6:18–24
149. Rumpel C et al (2006) Black carbon contribution to soil organic matter composition in tropical sloping land under slash and burn agriculture. Geoderma 130(1–2):35–46
150. Major J et al (2010) Fate of soil-applied black carbon: downward migration, leaching and soil respiration. Glob Change Biol 16:1366–1379
151. Glaser B et al (2000) Black carbon in density fractions of anthropogenic soils of the Brazilian Amazon region. Org Geochem 31:669–678
152. Spycher G, Soilins P, Rose S (1983) Carbon and nitrogen in the light fraction of a forest soil: vertical distribution and seasonal patterns. Soil Sci 135:79–87
153. Czimczik CI, Schmidt MWI, Schulze ED (2005) Effects of increasing fire frequency on black carbon and organic matter in Podzols of Siberian Scots pine forests. Eur J Soil Sci 56(3): 417–428
154. Ohlson M et al (2009) The charcoal carbon pool in boreal forest soils. Nat Geosci 2:692–695

155. Seiler W, Crutzen PJ (1980) Estimates of gross and net fluxes of carbon between the biosphere and the atmosphere from biomass burning. Clim Change 2:207–247
156. Kaal J et al (2008) A detailed pyrolysis-GC/MS analysis of a black carbon-rich acidic colluvial soil (Atlantic ranker) from NW Spain. Appl Geochem 23:2395–2405
157. Gaskin JW et al (2007) Potential for pyrolysis char to affect soil moisture and nutrient status of loamy sand soil. In: Georgia Water Resources Conference, University of Georgia, Georgia
158. Shackley S, Hammond J, Gaunt J, Ibarrola R (2011) The feasibility and costs of biochar deployment in the UK. Carbon Manag 3(2):335–356
159. Deenik J, McClellan T, Uehara G, Antal M, Campbell S (2010) Charcoal volatile matter content influences plant growth and soil nitrogen transformations. Soil Sci Soc Am J 74:1259–1270
160. Fargione J, Hill J, Tilman D, Polasky S, Hawthorne P (2008) Land clearing and the biofuel carbon debt. Science 319:1235–1237
161. Brown T, Wright M, Brown R (2011) Estimating profitability of two biochar production scenarios: slow pyrolysis vs fast pyrolysis. Biofuels Bioprod Bioref 5:54–68
162. Yoder J, Galinato S, Granatstein D, Garcia-Perez M (2011) Economic tradeoff between biochar and bio-oil production via pyrolysis. Biomass Bioenergy 35:1851–1862
163. Garcia-Perez M (2008) The formation of polyaromatic hydrocarbons and dioxins during pyrolysis. Washington State University, 63pp
164. Beesley L, Moreno-Jimenez E, Gomez-Eyles J (2010) Effects of biochar and greenwaste compost amendments on mobility, bioavailability and toxicity of inorganic and organic contaminants in a multi-element polluted soil. Environ Pollut 158(1):155–160

Bioclimatic Design

Donald Watson
FAIA, Trumbull, CT, USA

Article Outline

Glossary
Definitions
Introduction
Strategies of Bioclimatic Design
Bioclimatic Analysis
Bioclimatic Design Practices
Bioclimatic Design of Atriums and Wintergardens
Large-Scale Applications
Future Directions: Bioclimatic Design at the Urban Scale
Summary
Acknowledgments
Bibliography

Glossary

Absolute humidity Absolute humidity is defined as the weight of water vapor contained in a unit volume of air. Typical units are pounds of water per pound of dry air or grains of water per cubic foot. Absolute humidity is also known as the water vapor density (D_v).

Celsius temperature (°C) Celsius temperature (°C) refers to temperatures measured on a scale devised in 1742 by Anders Celsius, a Swedish astronomer. The Celsius scale is graduated into 100 units between the freezing temperature of water (0°C) and its boiling point at normal atmospheric pressure (100°C) and is, consequently, commonly referred to as the *centigrade scale*.

Dew-point temperature (DPT) Dew-point temperature (DPT) is the temperature of a surface upon which water vapor contained in the air will condense into liquid water. Stated differently, it is the temperature at which a given quantity of air will become saturated (reach 100% relative humidity) if chilled at constant pressure. It is thus another indicator of the moisture content of the air. Dew-point temperature is not easily measured directly; it is conveniently found on a psychrometric chart if dry-bulb and wet-bulb temperatures are known.

Dry-bulb temperature (DBT) Dry-bulb temperature (DBT) is the temperature measured in air by an ordinary (dry bulb) thermometer and is independent of the moisture content of the air. It is also called "sensible temperature."

Fahrenheit temperature (F) Fahrenheit temperature (F) refers to temperature measured on a scale devised by G. D. Fahrenheit, the inventor of the alcohol and mercury thermometers, in the early eighteenth century. On the Fahrenheit scale, the freezing point of water is 32°F and its boiling point is 212°F at normal atmospheric pressure.

Humidity Humidity is a general term referring to the water vapor contained in the air. Like the word "temperature," however, the type of "humidity" must be defined.

Relative humidity (RH) Relative humidity (RH) is defined as the percent of moisture contained in the air under specified conditions compared to the amount of moisture contained in the air at total saturation at the same (dry-bulb) temperature. Relative humidity can be computed as the ratio of existing vapor pressure to vapor pressure at saturation, or the ratio of absolute humidity to absolute humidity at saturation existing at the same temperature and barometric pressure.

Water vapor pressure (P_v) Water vapor pressure (P_v) is that part of the atmospheric pressure exerted due to the amount of water vapor present in the air. It is expressed in terms of absolute pressure as inches of mercury (in. Hg) or pounds per square inch (psi).

Wet-bulb temperature (WBT) Wet-bulb temperature (WBT) is an indicator of the total heat content (or enthalpy) of the air, that is, of its combined sensible and latent heats. It is the temperature measured by a thermometer having a wetted sleeve over the bulb from which water can evaporate freely.

Definitions

Bioclimatic design – combining "biology" and "climate" – is an approach to the design of buildings and landscape that is based on local climate. The approach was promoted in a series of professional and popular publications in the 1950s [1, 2]. In using the term "bioclimatic," architectural design is linked to the physiological and psychological need for health and comfort. In adopting bioclimatic approaches, the designer endeavors to create comfort conditions in buildings by understanding the microclimate and resulting design strategies that include natural ventilation, daylighting, and passive heating and cooling. The premise of bioclimatic design is that buildings utilize natural heating, cooling, and daylighting in accordance with local climatic conditions.

Resilient design is an extension of bioclimatic design. It adds precautionary measures to provide health and safety to prepare for natural disasters, including extreme storms and flooding of inland watersheds and coastal areas. The concept of resiliency applies lessons from natural systems to design for extreme conditions using strategies found in natural systems, such as buffering, zone separation, redundancy, rapid feedback, and decentralization.

Introduction

Bioclimatic design had been part of practical knowledge of indigenous building throughout historical periods, including early modern architecture. When air-conditioning systems became widely available at the end of the 1950s, interest in bioclimatic design became less evident in professional and popular literature and in built work. The topic reemerged in response to energy shortages of the 1970s – when "passive solar design" became the popular term to describe the approach, at first emphasizing solar heating but soon broadened to passive cooling and daylighting.

With the emergence of global environmental concerns of the 1990s – recognizing that energy conservation has "cascading" effects and benefits in reducing pollution and in mitigating global warming – the scope of bioclimatic design was enlarged to include landscape, water, and waste nutrient recovery. *Sustainable design* of architecture and communities emerged as an approach to protect and improve the biological health of communities conceived as the ecology of building, site, and region.

Some bioclimatic design techniques – earth sheltering is an example – can contribute to comfort and reduce both heating and cooling loads year round. Other techniques are useful only part of the year. The effectiveness of passive solar heating, for example, is very specific to the need for heating and otherwise needs to be tempered by sun shading and thermal mass. Natural ventilation can provide comfort in all seasons, especially in summer when it can reduce or eliminate the need for air-conditioning in some climates.

All buildings experience interruptions of conventional energy availability, often coincident with weather extremes and natural disasters. A precautionary approach to the design of all buildings is to provide bioclimatic means to insure subsistence levels of heating, cooling, and daylighting for comfort, health, and safety in case all power sources are interrupted. For the longer term, in which conventional energy shortages and emergencies are unpredictable, buildings without natural heating, cooling, and lighting impose serious liabilities on occupants and owners.

Strategies of Bioclimatic Design

Bioclimatic design strategies are effective for "envelope-dominated" structures – such as homes

and one- or two-story facilities – to provide a large portion if not all of the energy required to maintain comfort conditions.

"Internal load dominated" buildings – such as hospitals, offices, commercial kitchens, and windowless stores – experience high internal gains imposed by the heat of occupancy, lights, and equipment. In such cases, the external climatic conditions may have less influence on achieving comfort and low energy utilization. However, as internal loads are reduced through energy-efficient design – such as low-wattage lighting, energy-efficient equipment, occupancy scheduling and zoning – the effects of climate become more obvious and immediate. All buildings can benefit from available daylighting, but large glazed areas require careful shading control, glazing selection, and possibly night insulation.

The "resources" of bioclimatic design are the natural flows of energy in and around a building – created by the interaction of sun, wind, precipitation, vegetation, temperature, and humidity in the air and in the ground. In some instances, this "ambient energy" is useful immediately or can be stored for later use. There are definable "pathways" by which heat is gained or lost between the interior and the external climate in terms of the classic definitions of heating energy transfer mechanics. From these, the resulting bioclimatic design strategies can be defined (Fig. 1 and Table 1).

- *Conduction* – from hotter objects to cooler objects by direct contact.
- *Convection* – by flow of air between warmer objects and cooler objects.
- *Radiation* – from hotter objects to cooler objects within the direct view of each other regardless of the temperature of air in between, including radiation from sun to earth.
- *Evaporation* – the change of phase from liquid to gaseous state: The sensible heat (dry-bulb temperature) in the air is lowered by the latent heat absorbed from air when moisture is evaporated.
- *Thermal storage* – from heat charge and discharge both diurnally and seasonally, as a function of its specific heat, mass, and conductivity. Although not usually listed alongside the four classic means of heat transport, this role of thermal storage is helpful in understanding the heat transfer physics of building climatology.

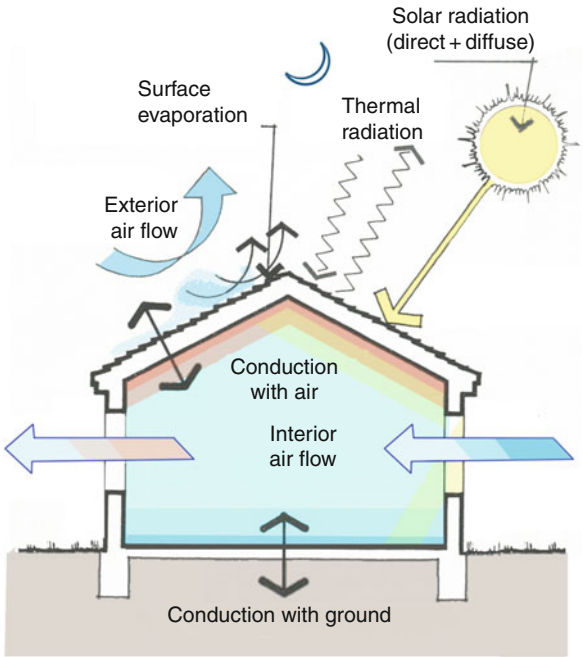

Bioclimatic Design. Figure 1
Paths of energy exchange at the building microclimate scale. Bioclimatic design is based upon understanding energy flows within and around buildings (Watson and Labs [13])

In winter (or underheated periods), the objectives of bioclimatic design are to resist loss of heat from the building envelope and to promote gain of solar heat. In summer (or overheated periods), these objectives are the reverse, to resist solar gain and to promote loss of heat from the building interior. The strategies can be set forth as:

- *Minimize conductive heat flow.* This strategy is achieved by using insulation. It is effective when the outdoor temperature is significantly different, either lower or higher, than the interior comfort range. In summer, this strategy should be considered whenever ambient temperatures are within or above the comfort range and where natural cooling strategies cannot be relied upon to achieve comfort (i.e., whenever mechanical air-conditioning is necessary).
- *Delay periodic heat flow.* While the insulation value of building materials is well understood, it is not as widely appreciated that building envelope materials also can delay heat flows that can be used to

Bioclimatic Design. Table 1 Strategies of bioclimatic design (Watson and Labs [13])

Bioclimatic design strategy	Predominant season[a]	Process of heat transfer			
		Conduction	Convection	Radiation	Evaporation
Minimize conductive heat flow	Winter and summer[b]	√			
Delay periodic heat flow	Winter and summer	√		√	
Minimize infiltration	Winter and summer[b]		√		
Provide thermal storage[c]	Winter and summer	√	√	√	
Promote solar gain	Winter			√	
Minimize solar gain	Summer			√	
Minimize external air flow	Winter		√		
Promote ventilation	Summer		√		
Promote radiant cooling	Summer			√	
Promote evaporative cooling	Summer				√

[a]Properly described as "underheated" and "overheated"
[b]In overheated periods where air-conditioning is required
[c]Thermal storage may utilize "phase change" materials and the latent heat capacities of chemicals such as eutectic salts

improve comfort and to lower energy costs. Time lag through masonry walls, for example, can delay the day's thermal impact until evening and is a particularly valuable technique in hot arid climates with wide day-night temperature variations. Techniques of earth sheltering and berming also exploit the long-lag effect of subsurface construction.

- *Minimize infiltration.* "Infiltration" refers to uncontrolled air leakage around doors and windows and through joints, cracks, and faulty seals in the building envelope. Infiltration (and the resulting "exfiltration" of heated or cooled air) is considered the largest and potentially the most intractable source of energy loss in a building, once other practical insulation measures have been taken.
- *Provide thermal storage.* Thermal mass inside of the insulated envelope is critical to dampening the swings in air temperature and in storing heat in winter and as a heat sink in summer.
- *Promote solar gain.* The sun can provide a substantial portion of winter heating energy through elements such as equatorial-facing windows and greenhouses that include other passive solar techniques which utilize spaces to collect, store, and transfer solar heat.
- *Minimize solar gain.* The best means for ensuring comfort from the heat of summer is to minimize the effects of the direct sun by shading windows from the sun, or otherwise to minimize the building surfaces exposed to the summer sun by use of radiant barrier and by insulation.
- *Minimize external air flow.* Winter winds increase the rate of heat loss from a building by "washing away" heat and thus accelerating the cooling of the exterior envelope surfaces by conduction, and also by increasing infiltration (or more properly, exfiltration) losses. Siting and shaping a building to minimize wind exposure or providing windbreaks can reduce the impact of such winds.
- *Promote ventilation.* Cooling by air flow through an interior may be propelled by two natural processes, cross-ventilation (wind driven) and stack-effect ventilation (driven by the buoyancy of heated air even in the absence of external wind pressure). A fan (using photovoltaic for fan power) can be an efficient way to augment natural ventilation cooling in the absence of sufficient wind or stack-pressure differential.

- *Promote radiant cooling.* A building can lose heat effectively if the mean radiant temperature of the materials at its outer surface is greater than that of its surroundings, principally the night sky. The mean radiant temperature of the building surface is determined by the intensity of solar irradiation, the material surface (film coefficient), and by the emissivity of its exterior surface (its ability to "emit" or reradiate heat). This contributes only marginally, if the building envelope is well insulated.
- *Promote evaporative cooling.* Sensible cooling of a building interior can be achieved by evaporating moisture into the incoming air stream (or, if an existing roof has little insulation, by evaporative cooling the exterior envelope such as by a roof spray). These are simple and traditional techniques and most useful in hot-dry climates if water is available for controlled usage. Mechanically assisted evaporative cooling is achieved with an economizer-cycle evaporative cooling system, instead of, or in conjunction with, refrigerant air-conditioning.

Bioclimatic Analysis

Analysis of climatic data is a first step in bioclimatic design. Preliminary design direction and rules of thumb can be determined by graphing bioclimatic data. While the method can be done by hand, computer-assisted methods allow this approach to be increasingly accurate.

Humans are comfortable within a relatively small range of temperature and humidity conditions, roughly between 68°F and 80°F (20–26.7°C) and 20–80% relative humidity (RH), referred to on psychrometric charts as the "comfort zone." These provide a partial description of conditions required for comfort. Other variables include environmental indices – radiant temperature and rate of airflow – as well as clothing and activity (metabolic rate). While such criteria describe relatively universal requirements in which all humans are "comfortable," there are significant differences in and varying tolerance for discomfort and conditions in which stress is felt, depending on age, sex, health, cultural conditioning, and expectations.

Givoni [3] and Milne and Givoni [4] proposed a design method using the building bioclimatic chart, modified by Arens [5] (Fig. 2). The chart adopts the psychometric format, overlaying it with parameters for the appropriate bioclimatic design techniques to create human comfort in a building interior. If local outdoor temperatures and humidity fall within specified zones, the designer is alerted to opportunities to use specific bioclimatic design strategies to create effective interior comfort.

Computer-based simulation and energy design tools make it possible to utilize site-specific hourly weather data to analyze data for bioclimatic design. This makes it possible to compare bioclimatic design strategies for a given climate, comparing a proposed design with a "base case," that is, the same building without a proposed design feature, such as south-facing glass, added insulation, shading, ventilation, and thermal mass.

Figure 3 depicts a simulated "representative winter week" (7 days) comparison of a "base case" house with a combined set of options, including solar-oriented windows (while decreasing windows on other orientations), increased insulation including nighttime curtains, and interior thermal mass. The "base case" house represented the US code-compliant national average construction, published by the National Association of Home Builders. Bioclimatic design strategies were added as achievable within a 5% increase in construction cost. The "representative winter week" represented a 30-year average winter week (November to January) in which 3 days of clouds were followed by 3 days of sunshine. Heat gains in Btu are indicated above the horizontal bars, and losses below it. The illustration indicates the benefit of the "solar pulse," that is, passive solar gain in the 3 sunny days at the end of the 7 days (lower right), compared to negligible solar benefit in the Base case during the same sunny period (upper right). In this particular week, the combined passive strategies accomplished a 38% in energy requirement.

The example in Fig. 3 was part of a research project that compared a variety of bioclimatic features, singly and together, in 20 US cities [6]. The results supported several conclusions. Firstly, the relative effectiveness of any particular bioclimatic design technique is more than additive, that is, when combined they supported larger efficiencies in performance than when used singly. Secondly, when compared in different climatic zones, the rank order of most effective strategies changed – perhaps obvious, but worthy as

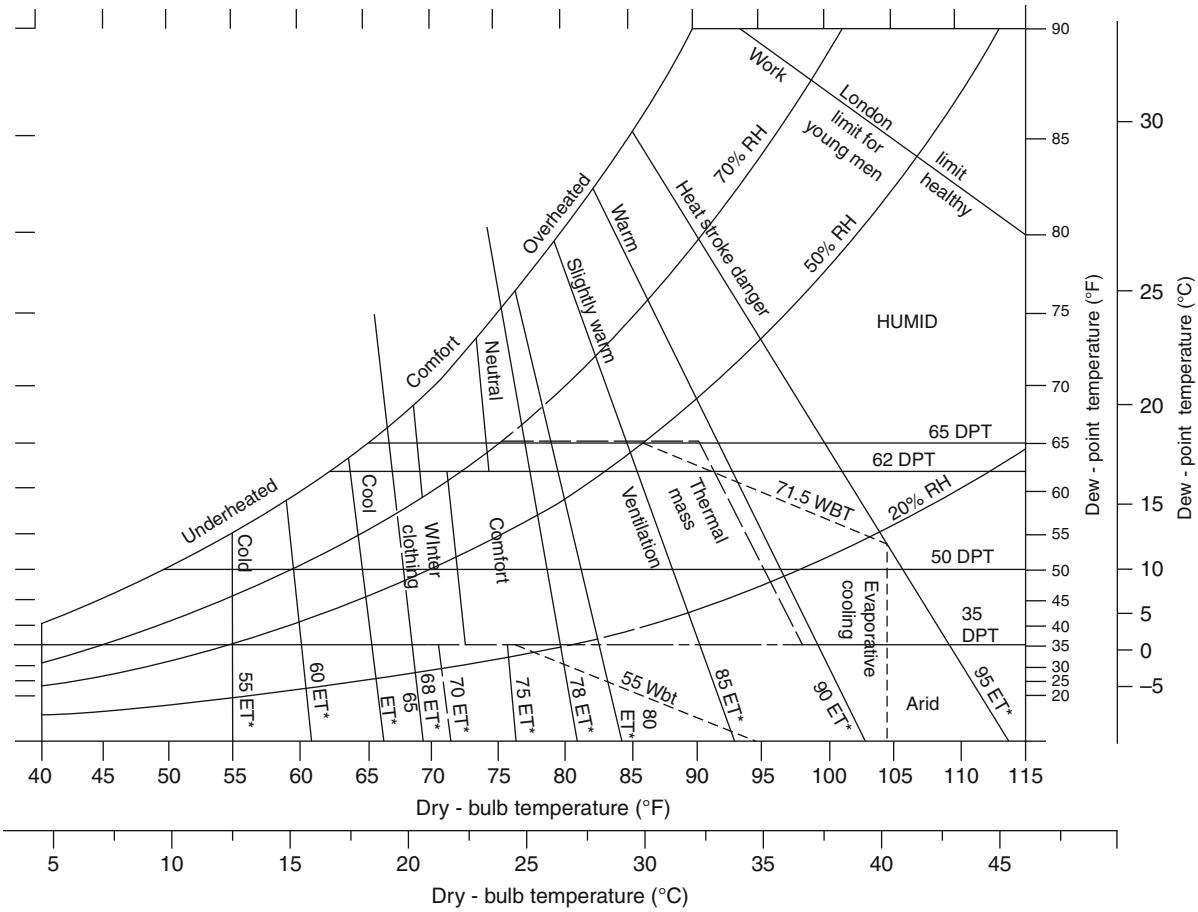

Bioclimatic Design. Figure 2

Building bioclimatic chart. The chart indicates parameters of local climatic conditions favorable for bioclimatic design strategies (Based on Givoni [3] and Arens [5])

confirmation that each climatic region has its own most appropriate design techniques. But finally, the difference between one top strategy and another was for the most part not so far ahead of others that there is any one answer. Designers have a choice, within a set of high performing strategies and techniques.

These findings are supported by a selective tabulation (Table 2), with results of the 20 city comparisons (simulated for a full year, compiling TMY data as available in 1984). For the four cities shown in Table 2, representatives of different US climates, the heating energy requirement is shown in blue and cooling in red. The "boxed" option indicates the most effective technique for combined heating and cooling energy for each location. In the case of Boston, the passive solar and super-insulation options are approximately equal and either one represents a 40% reduction of energy required compared to the base house. The same strategies achieved more that 46% reduction in Seattle, 62% in Los Angeles, whereas none of the solar options outperformed an 18% improvement achieved simply outside insulated block walls in New Orleans. While such results are "imagined," that is, the result of assumptions made in computation, they indicate the value of simulation to help understand the thermodynamics of climate, building design options, and resulting comfort and energy requirements.

Climatic data for computer simulation for locations worldwide are available on the Web. In regions of the world where extensive climatic data are not available

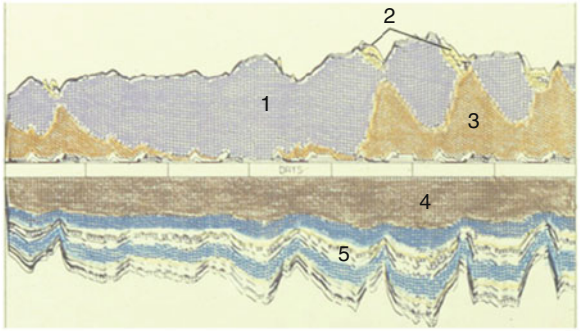

Base case house – Boston, MA

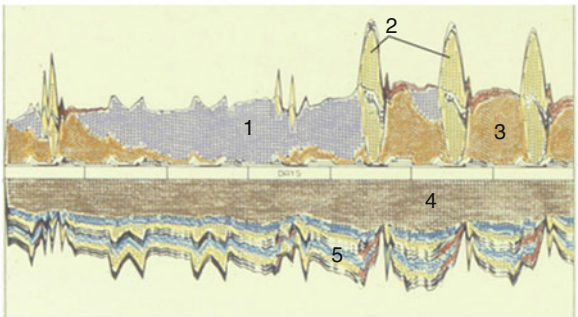

Base case w/ passive solar, insulation, shading

Bioclimatic Design. Figure 3
Simulation of bioclimatic design features. The simulation illustrates the energy performance of passive solar strategies compared to a base case in Boston, MA, climate (cool/temperate, partly sunny). (1) Heating energy required, (2) passive solar contribution, (3) thermal mass contribution, (4) roof heat loss, (5) heat loss various other surfaces (Watson and Harrington 1979. Unpublished manuscript)

and where, for example, data are limited only to monthly averages of temperature and humidity, the available data may not be coincident and must be interpreted with caution.

TMY summaries contain simultaneous climatic data for all 8,760 h in a "typical" year. Available for airport locations, mostly in the United States, each file contains one complete year of hourly data, including direct (beam) solar radiation, total horizontal solar radiation, dry-bulb temperature, dew-point humidity, wind speed, and cloud cover. Electronic files of climatic data for most US locations (major airports) are available through various sources on the Web from NREL [7]. Over 500 stations worldwide are available on the energy plus Web site [8].

Several papers by Arens [9, 10] describe techniques to interpolate multiple TMY3 data sets for locations "in between" airport locations to adjust them to match substation monthly means, or modify them further to account for the building-site surroundings.

Climate consultant is a computer-based program that can be downloaded at no cost from the Web [11]. Part of a career-long project of UCLA Professor Emeritus Murray Milne to develop public domain energy design tools [12], the software plots weather data, including temperatures, wind velocity, sky cover, percent sunshine, and beam and horizontal irradiation. It uses these data to create psychometric charts and plots hourly data in the above-mentioned zones that indicate timetables of bioclimatic needs, sun charts showing times of solar needs and shading requirements. It includes 3-D plots of temperature, wind speed, and related climatic data cross-referenced to bioclimatic design practices presented in Watson and Labs [13].

Figure 4 represents a typical bioclimatic chart generated by Climate Consultant. It displays an annual summary for Minneapolis and in the upper left, the percent (hours per year) that bioclimatic categories are effective.

Bioclimatic Design Practices

Each locale has its own bioclimatic profile, sometimes evident in indigenous and long-established building practices. Bioclimatic design techniques can be set forth as a set of design opportunities (adapted from Ref. [9]):

- *Wind breaks* (winter) – Two design techniques serve the function of minimizing winter wind exposure:
  - Use neighboring landforms, structures, or vegetation for winter wind protection.
  - Shape and orient the building shell to minimize winter wind turbulence (Fig. 5).
- *Thermal envelope* (winter) – Isolating the interior space from the hot summer and cold winter climate, such as:
  - Use attic space as buffer zone between interior and outside climate.
  - Use basement or crawl space as buffer zone between interior and grounds.
  - Use vestibule or exterior "wind-shield" at entryways.

Bioclimatic Design. Table 2 *Comparison of bioclimatic options in four US climates.* Requirements for heating (in blue) and cooling (in red) are compared for an identical "base case" house (code compliant). Different strategies are compared in representative US climates (Watson and Harrington [6])

	Base case[a]	Earth berms[b]	Trombe wall[c]	Block wall[d]	Passive solar[e]	Super insul.[f]
Boston	39.0[g] 5.2[h]	36.1 4.8	25.2 6.6	36.8 3.4	20.0 6.6	19 7.4
New orleans	4.4 15.9	3.9 15	.7 21.4	1.6 15.2	1.1 17.7	1.0 18.9
Los angeles	6.3 2.4	5.6 2.4	.3 3.0	1.8 2.0	.8 3.3	.7 3.6
Seattle	28.8 1.5	26.5 1.4	20.4 1.6	26.8 .5	16.4 1.7	11.5 2.3

All cases have shading and natural ventilation to reduce cooling load
[a]Base case R13 walls, R20 roof, 12% glazing
[b]Earthberms 4 ft. high on E, N, and W walls
[c]Trombe wall 12" concrete w/R5 nightshade unvented
[d]Block wall insulated on exterior
[e]Passive solar R20 walls, R3o ceiling, 24% glazing, R5 nightshade
[f]Super-insulation R40 walls, R50 roof, R5 nightshade
[g]Heating energy required in Btu
[h]Cooling energy required in Btu

- Locate low-use spaces, storage, utility, and garage areas to provide climatic buffers.
- Subdivide interior to create separate heating and cooling zones.
- Select insulating materials for resistance to heat flow through building envelope.
- Apply vapor barriers to the warm side of building envelope assemblies to control moisture migration.
- Develop construction details to minimize air infiltration and exfiltration.
- Provide insulating controls at glazing.
- Use heat-reflective (or radiant) barriers on (or below) surfaces oriented to the summer sun.
- Minimize the outside wall and roof area ratio of exterior surface to enclosed volume (Fig. 6).

- *Solar windows and walls* (winter) – Using the winter sun for heating a building through solar-oriented windows and walls is provided by a number of techniques:
  - Maximize reflectivity of ground and building surfaces outside windows facing the winter sun.
  - Shape and orient the building shell to maximize exposure to the winter sun.
  - Use high-capacitance thermal mass materials in the interior to store solar heat gain.
  - Use solar wall and roof collectors on equatorial-oriented faces.
  - Optimize the area of equatorial-facing glazing.
  - Use clerestory skylights for winter solar gain and natural illumination.
  - Provide solar-oriented interior zone for maximum solar heat gain, with solar control for shading in overheated periods (Fig. 7).
- *Indoor/outdoor rooms* (winter and summer) – Courtyards, covered patios, seasonally screened and glassed-in porches, greenhouses, atriums, and sun spaces can be located in the building plan for summer cooling and winter heating benefits:
  - Provide outdoor semi-protected areas for year-round climate moderation (Fig. 8).
- *Earth sheltering* (winter and summer) – Techniques such as banking earth against the walls of a building or covering the roof, or building a concrete floor on the ground, have a number of climatic advantages for thermal storage and damping temperature fluctuations (daily and seasonally), providing wind

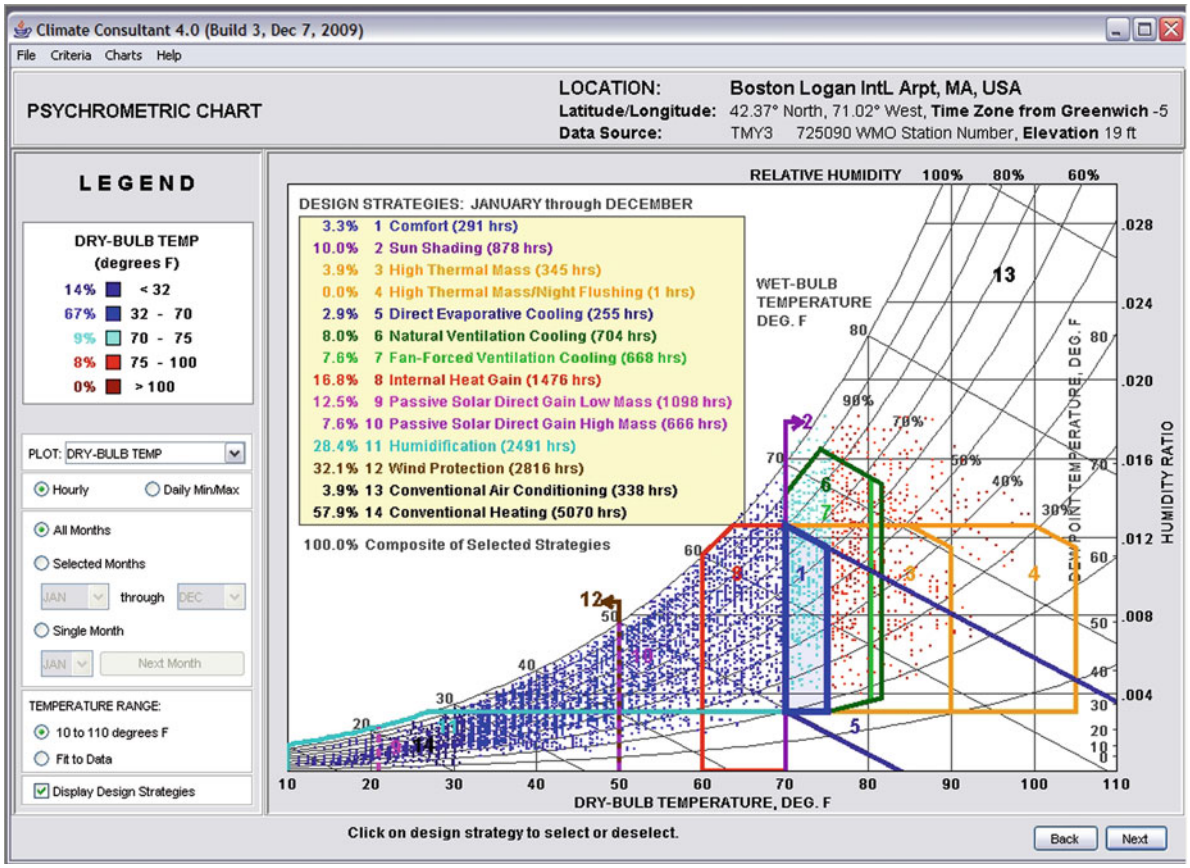

Bioclimatic Design. Figure 4

Climate consultant display of the building bioclimatic chart for Albany, NY. Climate Consultant provides visual displays of the Building Bioclimatic Chart, along with a wide range of other climatic data analyses (Milne and Li [12]) Climate Consultant Web link http://www.energy-design-tools.aud.ucla.edu/

protection and reducing envelope heat loss or gain (winter and summer). These techniques are often referred to as earth-contact or earth-sheltering design:

- Use slab-on-grade construction for ground temperature heat exchange and thermal storage.
- Use earth-covered or sod roofs.
- Recess structure below grade or raise existing grade for earth sheltering (Fig. 9).

- *Thermally massive construction* (summer and winter) – Particularly effective in hot arid zones, or in more temperate zones with cold clear winters. Thermally massive construction provides a "thermal fly wheel." Absorbing heat during the day from solar radiation and convection from indoor air can create comfort if it is cooled at night, if necessary through nighttime ventilative cooling (if air temperatures fall within the comfort zone):
  - Use high mass construction with outside insulation and nighttime ventilation techniques in summers.
  - For selected climates (hot dry), select high-capacitance materials to dampen heat flow through the building envelope (Fig. 10).
- *Sun shading* (summer) – Because midday solar altitude angles are much higher in summer than in winter, it is possible to shade windows from the sun during the overheated summer period while allowing it to reach the window surfaces and spaces

Bioclimatic Design. Figure 5
Sea Ranch, California. Landscape planting, roof slopes, and fencing designed for wind protection. Esherick, Homsey, Dodge, and Davis, Architects and Planners with Lawrence Halprin, Landscape Architect

in winter. Providing summer sun shading does not need to conflict with winter solar heat gain:
  - Minimize reflectivity of ground and building surfaces outside windows facing the summer sun.
  - Use neighboring landforms, structures, or vegetation for shading the summer sun.
  - Shape and orient the building shell to minimize exposure to the summer afternoon sun.
  - Provide seasonally operable shading, including deciduous trees.
- *Natural ventilation* (summer and seasonal)–Natural ventilation is a simple concept by which to cool a building:
  - Shape and orient the building shell to maximize exposure to summer breezes.
  - Use an "open plan" interior to promote airflow.
  - Provide vertical airshafts to promote "thermal chimney" or stack-effect airflow.
  - Use double roof construction for ventilation within the building shell.
  - Orient door and window openings to facilitate natural ventilation from prevailing summer breezes.
  - Use wing walls, overhangs, and louvers to direct summer wind flow into the interiors.
  - Use louvered wall openings for maximum ventilation control.
  - Use roof monitors for "stack-effect" ventilation (Fig. 11).
- *Plants and water* (summer) – Several techniques provide cooling by the use of plants and water near building surfaces for shading and evaporative cooling:
  - Use planting next to building skin (provided it does not interfere with ventilation).
  - Use roof spray or roof ponds for evaporative cooling.
  - Use ground cover and planting for site cooling.
  - Maximize on-site evaporative cooling (Fig. 12).

The Importance of Documenting Performance

Simulation is a design tool, most appropriately used during the early design phases when alternate design techniques are considered. Simulation is not necessarily a means to predict actual performance. Design knowledge requires post-occupancy evaluation after a building is built and occupied.

To compare performance with predesign-simulated expectations requires careful monitoring of on-site weather conditions. Variations of use, user behavior, and factors as simple as how operating temperature controls are adjusted will account for greater variation than climate alone.

A post-occupancy survey was undertaken to assess 84 solar homes built with the assistance of a Solar Grant Program in Connecticut [14]. A grant of $5,000 was offered to assist owners of existing homes to retrofit solar features, or, to incorporate into new construction. Solar features could include south-facing windows and skylights, thermal mass (Trombe wall), sunspace, and window insulation, as well as active solar domestic hot water systems. The survey asked what problems were notable after 1–5 years of occupancy, and of these what problems could be corrected and what could not (Table 3).

Bioclimatic Design of Atriums and Wintergardens

Atriums offer many energy design opportunities, depending upon climatic resources, to provide natural heating, cooling, lighting, and plants. It is necessary to establish clear design goals, defining the opportunities and liabilities of solar heating, natural cooling, and

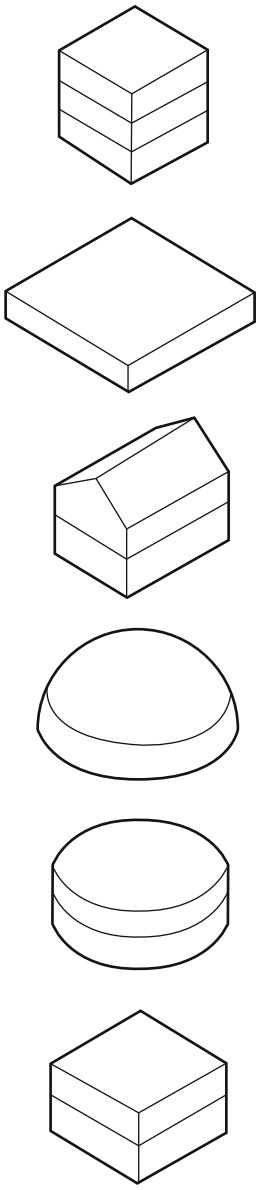

Total volume	=	32,000	
Surface area	=	5,039	SVR = 0.157
3rd Floor	=	1,007	
2ND Floor	=	1,007	
Base area	=	1,007	SFAR = 5.0
Combined area	=	3,021	SFAR = 1.67
Total volume	=	32,000	SVR = 0.17
Surface area	=	5,429	
Floor area	=	3,200	SFAR = 1.7
Total volume	=	32,000	
Surface area	=	4,754	SVR = 0.148
Upper floor	=	1,350	
Base area	=	1,350	
Combined area (includes attic)	=	2,700	SFAR = 1.76
Total volume	=	32,000	
Surface area	=	3,864	SVR = 0.12
Upper floor	=	1,618	
Base area	=	1,932	SFAR = 2.0
Combined area	=	3,550	SFAR = 1.09
Total volume	=	32,000	
Surface area	=	4,435	SVR = 0.138
Upper floor	=	1,600	
Base area	=	1,600	SFAR = 2.77
Combined area	=	3,200	SFAR = 1.38
Total volume	=	32,000	
Surface area	=	4,800	SVAR = 0.15
Upper floor	=	1,600	
Base area	=	1,600	SFAR = 3.0
Combined area	=	3,200	SFAR = 1.5

Bioclimatic Design. Figure 6

Analysis of building aspect ratio. Simplified building shapes are compared for ratio of exterior surface to enclosed volume (Watson and Labs [13])

daylighting choices. Provisions for healthy planting and indoor gardens can be combined with atrium design, which enlarges the design criteria to include healthy conditions for plants as well as people.

The atrium concept of climate control has been used throughout the history of architecture and in indigenous building in all climates of the globe. Suggested by its Latin meaning as "heart" or an open courtyard of a Roman house, the term "atrium" as used today is a protected courtyard or glazed winter garden placed within a building. Modern atrium design incorporates many architectural elements – wall enclosures, sun-oriented openings, shading and ventilation devices, and subtle means of modifying temperature

Bioclimatic Design. Figure 7
Solar windows walls. Keck + Keck, Architects developed solar design principles in the Chicago area in the 1930s. The solar home designs of Keck + Keck – in this example a prototype prefab homes for Green Ready-Built Homes – included large south-facing glass, exposed masonry floors with hypostyle (warm air radiant) heating, interior masonry walls, interior curtains, and exterior shading (Photo: William Keck, Architect)

Bioclimatic Design. Figure 8
Protected courtyard. Buli Khelam Ihakhang Monastery, Bhutan. In the Himalayan tradition of building, an enclosed courtyard with sun exposed adobe walls and windows creates a wind-protected microclimate, permitting a temperate planting regime to flourish within, in contrast to high mountain climatic conditions of its locale (Photo: Donald Watson)

and humidity – suggested by examples that derive from the courtyard designs of Roman, early Christian, and Islamic buildings, and the nineteenth-century greenhouses and glass-covered arcades of Great Britain and France.

Atriums offer many energy design opportunities: first, comfort is achieved by gradual transition from outside climate to building interior; second, designed properly, protected spaces and buffer zones create natural and free-flowing energy by reducing or by

a

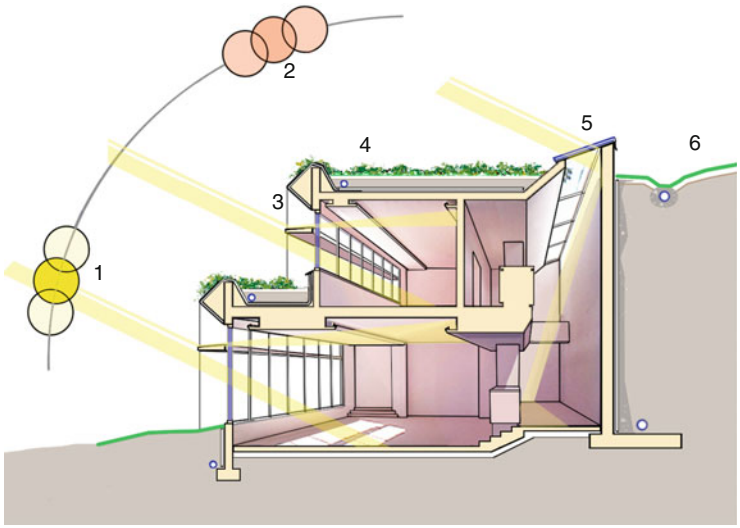

b 1 Winter solstice 3 Light shelf daylight reflector 5 Skylight
2 Summer solstice 4 Green roof 6 Earthsheltering

Bioclimatic Design. Figure 9
(**a**) *Earth-covered home*. New Canaan CT, USA. 1986. The design combines south-facing windows with light shelves to extend daylighting and provide summer shading, skylighting, and earth sheltering (Photo: Donald Watson, FAIA, Architect). (**b**) *Cross-section earth-covered home*. The cross-section of the earth-covered home was designed to provide balanced daylighting throughout the year, accomplished by light shelves and a clerestory light well

eliminating the need to otherwise heat, cool, or light building interiors. Depending on climatic resources and building use, the emphasis in atrium design has to be balanced between occupancy and comfort criteria and the relative need for heating, cooling, and/or lighting.

How the atrium can work as an energy-efficient modifier of climate is best seen by examining separately its potential for natural heating, cooling, and lighting. The first step is to establish a clear set of energy design goals appropriate to the specific atrium design. The resulting solution will depend upon its program

(whether for circulation only or for longer term and sedentary human comfort and/or for plant propagation and horticultural display) and the resulting environmental control requirements.

Bioclimatic Design. Figure 10
Thermal mass appropriate for hot-dry climate. Indigenous adobe block construction, with roof and window overhangs to shade and protect the walls. Tahono O'Odham Nation, Papago Indian Reservation, Arizona (Photo: Donald Watson)

Solar Heating

If heating efficiency alone is the primary energy design goal of the atrium, the following design principles should be paramount:

H1 – To maximize winter solar heat gain, orient the atrium aperture (openings and glazing) to the equator. If possible, the glazing should be vertical or sloped not lower than a tilt angle equal to the local latitude.

H2 – To store and distribute heat, place interior masonry directly in the path of the winter sun. This is most useful if the heated wall or floor surface will in turn directly radiate to building occupants.

H3 – To prevent excessive nighttime heat loss, consider an insulating system for the glazing, such as insulating curtains or high performance multilayered window systems.

H4 – To recover the heat that rises by natural convection to the top of the atrium, place a return air duct high in the space, possibly augmenting its temperature by placing it directly in the sun. Heat recovery can be accomplished if the warm air is redistributed

Bioclimatic Design. Figure 11
Shading and ventilation strategies. Built in an era well before air-conditioning, plantation manor houses such as the 1827 San Francisco Plantation House, New Orleans, combined a range of strategies for natural cooling in hot humid climates zones, including open understory and porches, cross-ventilation, and roofs designed to induce ventilation by thermal updraft (Photo: Robert Perron)

Bioclimatic Design. Figure 12
Evaporative cooling strategies: Public courtyard. Seville, Spain. The streets and passages of the city combine courtyards, gardens, and a landscape rich with planting and water fountains (Photo: Helen Kessler)

Bioclimatic Design. Table 3 Extract from consumer survey of 84 solar homes (Watson [14])

Perceived problems	% able to correct	% not able to correct
Glare	14	02
Excessive humidity	12	01
Condensation on windows	10	11
Keeping glass clean	26	07
Stagnant odors	10	00
Fading of furniture, walls, coverings	05	10
Lack of privacy	11	05
Drafts	07	04
Rooms cool down too fast	12	06
Not warm enough	07	02
Extreme temperature swings	10	06
Weather stripping or caulking maintenance	10	00
Covering sloped windows/ skylights	05	04
Assured solar access	00	01
Zoning restriction (solar panels)	00	01
Building code restrictions (retrofit)	01	01
Mechanical/electrical failures	02	00
Overall satisfaction with program	98	02

either to the lower area of the atrium (a ceiling fan) or redirected (and cleaned) to the mechanical system, or through a heat exchanger if the air must be exhausted for health and air-quality reasons.

Because a large air volume must be heated, an atrium is not an efficient solar collector per se. But the high volume helps to make an overheated space acceptable, especially if the warmest air rises to the top. If the atrium is surrounded by buildings on all sides, direct winter sun is difficult if not impossible to capture except at the top of the skylight enclosure. However, by facing a large skylight and/or window opening toward the equator, direct winter solar heating becomes entirely feasible.

In cool climates, an atrium used as a solar heat collector would require as much winter sunlight as possible. In overbright conditions, dark finishes on surfaces where the sun strikes will help reduce glare and also to store heat. On surfaces not in the direct sun, light finishes may be best to reflect light, especially welcomed under cloudy conditions. In most locations and uses, glass should be completely shaded from the summer sun. Although not practical for large atriums, in some applications greenhouse-type movable insulation might be considered to reduce nighttime heat loss.

Natural Cooling

Several guidelines related to the use of an atrium design as an intermediary or buffer zone apply to both heating and cooling. If an unconditioned atrium is located in a building interior, the heat loss is from the warmer surrounding spaces into the atrium. In buildings with large internal gains due to occupants, lighting, and machines, the atrium may require cooling throughout the year. If one were to design exclusively for cooling, the following principles would predominate:

C1 – To minimize solar gain, provide shade for the summer sun. According to the particular building use, the local climate and the resulting balance point (the outside temperature below which heating is required); the "overheated" season when sun shading is needed may extend well into the autumn months. While fixed shading devices suffice for much of the summer period, movable shading is the only exact means by which to match the seasonal shading requirements at all times. In buildings in warm climates, sun shading may be needed throughout the year.

C2 – To use the atrium as an exhaust air plenum in the mechanical system of the building. The great advantage is one of economy, but heat recovery options (discussed above) and ventilation become most effective when the natural airflow in the atrium is in the same direction and integrated with the mechanical system.

C3 – To facilitate natural ventilation, create a vertical "chimney" effect by placing ventilating outlets high (preferably in the free-flow air stream well above the roof) and by providing cool "replacement air" inlets at the atrium bottom, with attention that the air stream is clean, that is, free of car exhaust or other pollutants.

The inlet air steam can be cooled naturally, such as accessed from a shaded area. In hot, dry climates, passing the inlet air over water such as an aerated fountain or landscape area is particularly effective to create evaporative cooling. Allowing the atrium to cool by ventilation at night is effective in climates where summer nighttime temperatures are lower than daytime (greater than 15°F difference), in which case the cooling effect can be carried into the next day by materials such as masonry (although, as a rule, if the average daily temperature is above 78°F (25.5°C), thermally massive materials are disadvantageous in non-air-conditioned spaces because they do not cool as rapidly as a thermally light structure). The microclimatic dynamic is no different than that evident in the Indian tepee – when stack ventilation is possible through a roof aperture, the space will ventilate naturally even in the absence of outside breezes, by the driving force of heated air. If air-conditioning of the atrium is needed but can be restricted to the lower area of the space, it can be done reasonably; cold air, being heavier, will pool at the bottom.

While there is apparent conflict between the heating design principle to maximize solar gain and the cooling design principle to minimize it, the sun does cooperate by its change in its apparent solar position with respect to the building. There are, however, design choices to be balanced between the requirements for sun shading and those for daylighting. The ideal location for a sun shading screen is on the outside of the glazing, where it can be wind-cooled. When the outside air ranges about 80°F (26.7°C), glass areas – even if shaded – admit undesired heat gain by conduction. In truly warm climates, a minimum of glazed aperture should be used to prevent undesired heat gain, in which case the small amount of glazing should be placed where it is most effective for daylighting. Heat-absorbent or heat-reflective glass, the common solution to reduce solar heat gain, also reduces the illumination level and, if facing the equator, it also reduces desirable winter heat gain.

In temperate-to-cool climates, heat gain through a skylight can be tolerated if the space is high, so that heat builds up well above the occupancy zone and there is good ventilation. In hot climates, an atrium will perform better as an unconditioned space if it is a shaded but otherwise open courtyard.

Daylighting

In all climates, an atrium can be used for daylighting. Electric lighting cost savings can be achieved, but only if the daylighting system works, that is, if it replaces the use of artificial lighting. (Many daylit buildings end up

with the electric lights in full use regardless of lighting levels needed.) Atriums serve a particularly useful function in daylighting design for an entire building by balancing light levels – thus reducing brightness ratios – across the interior floors of a building. If, for example, an open office floor has a window wall on only one side, typically more electric lighting is required than would be required without natural lighting to reduce the brightness ratio. An atrium light court at the building interior could provide such balanced "two source" lighting. An atrium designed as a "lighting fixture" that reflects, directs, or diffuses sunlight can be one of the most pleasing means of controlling light.

The following principles apply to atrium design for daylighting:

L1 – To maximize daylight, an atrium cross-section should be stepped open to the entire sky-dome in predominantly cloudy areas. In predominantly sunny sites, atrium geometry can by based upon heating and/or cooling solar orientation principles.

L2 – To maximize light, window or skylight apertures should be designed for the predominant sky condition. If the predominant sky condition is cloudy and maximum daylight is required (as in a northern climate winter garden), consider clear glazing oriented to the entire sky-dome, with movable sun controls for sunny conditions. If the predominant sky condition is sunny, orient the glazing according to heating and/or cooling design requirements.

L3 – Provide sun-and-glare control by geometry of aperture, surface treatment, color, and adjustable shades or curtains. Designing for daylighting involves compromise to meet widely varying sky conditions. What works in bright sunny conditions will not be adequate for cloudy conditions. An opaque overhang or louver, for example, may create particularly somber shadowing on a cloudy day. Light is already made diffuse by a cloudy sky, falling nearly equally from all directions; the sides of the atrium thus cast gray shadows on all sides. For predominantly cloudy conditions, a clear skylight is the right choice. Bright haze will nonetheless cause intolerable glare at least to a view upward. Under sunny conditions, the same skylight is the least satisfactory choice because of overlighting and overheating. The designer's choice is to compromise. Unless the local climate is truly cloudy and the atrium requires high levels of illumination, partial skylighting can achieve a balance of natural lighting, heating, and cooling. Partial skylighting (i.e., a skylight design that occupies only a portion of the roof surface) offers the further advantage of controlling glare and sunlight by providing reflective and shady surfaces to the view, such as by the coffers of the skylights. Because it is reduced in light intensity and contrast, a surface illuminated by reflected light is far more acceptable to the human eye than a direct view of a bright window area. Movable shades for glare and sun control provide a further means of balancing for the variety of conditions. This can be provided simply by operable canvas or fiberglass shades.

The design principles for heating, cooling, and daylighting can be applied according to building type and local climate. In the northern climates, particularly for residential units or apartments that might be grouped around an atrium, the solar heating potential predominates, while the natural cooling potential predominates in the southern United States. In commercial and institutional structures, natural cooling and daylighting are both important. In this case, the local climate would determine the relative importance of openness achieved with large and clear skylighting (most appropriate for cloudy temperate-to-cool regions) or of closed and shaded skylighting (most appropriate for sunny warm regions). While no single recommendation fits any one climate, the relative importance of each of the design principles is keyed to different climatic regions in Fig. 13.

Garden Atriums

Plants have an important role in buffer zones. If the requirements of plants are understood, healthy greenery can be incorporated into atrium design and contribute to human comfort, amenity, and energy conservation. Plants, however, when uncomfortable, cannot move. Major planting losses have been reported in gardened atriums because the bioclimatic

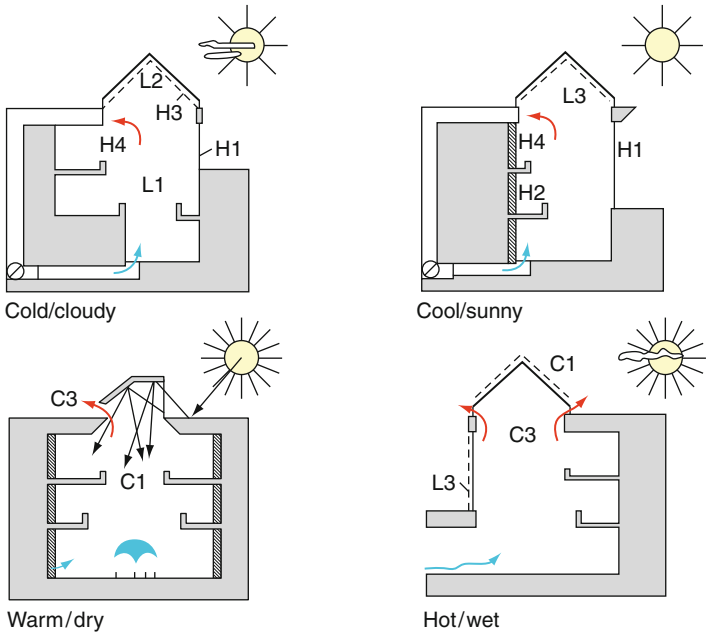

	Cold/cloudy Seatitle Chicago Minneapols	Cool/sunny Denver St. Louis Boston	Warm/dry LosAngeles Phoenix Midland TX	Hot/wet Houston New Orieans Miami
Heating				
H1 To maximize winter solar heat gain, orient the atrium aperture to the south.	●	■	▼	
H2 For radient heat storage and distribution, place interior masonry directly in the path of the winter sun.	▼	■	●	
H3 To prevent excessive nighttime heat loss, consider an insulating system for the glazing.	●	■		
H4 To recover heat, place a return air duct high in the space, directly in the sun	■	●	▼	
Cooling				
C1 To minimize solar gain, provide shade from the summer sun.		■	■	●
C2 Use the atrium as an air plenum in the mechanical system of the building.	■	■	■	■
C3 To faciliate natural ventilation, create a vertical "chimney" effect with high outlets and low inlets.	■	■	■	●
Lighting				
L1 To maximize daylight, use a stopped section (in predominantly cloudy areas).	■	▼		
L2 To maximize daylight, select skylight glazing for predominant sky condition (clear and horizontal in predominantly cloudy areas).	■	■	■	■
L3 Provide sun- and glare-control	■	■	●	■

Key: ● – Very important; ■ – positive benefit; ▼ – discretionary

Bioclimatic Design. Figure 13

Appropriateness of bioclimatic principles for atrium design. The diagrams provide guidelines for the design of atria and lightcourts in various climates. Watson [15]

a

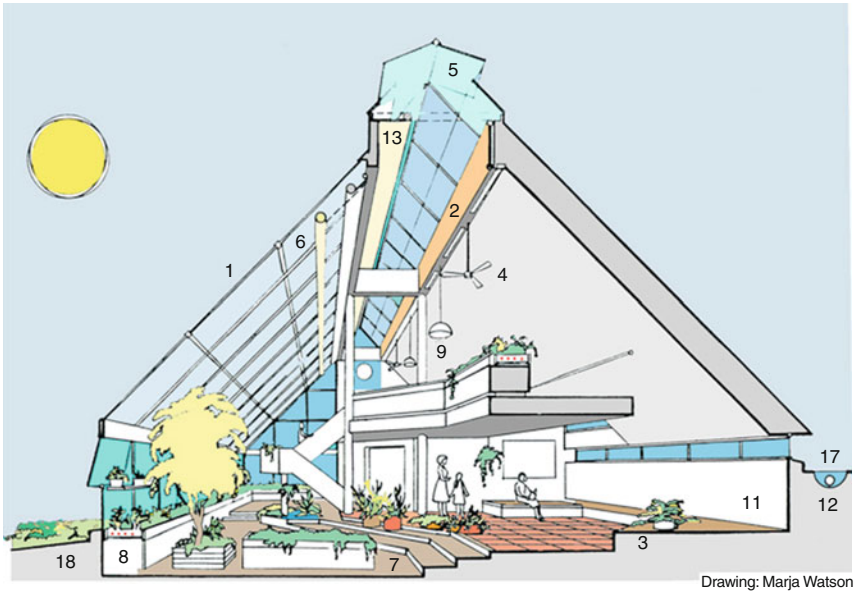

Drawing: Marja Watson

Design goals

Helps plants to grow
Uses solar heating (winter)
Uses natural cooling (summer)
Uses natural lighting
Saves non-renewable resources

b

Energy design techniques

1 South-facing greenhouse
2 Solar collectors
3 Thermal storage elements
4 Ceiling fans
5 Roof monitor
6 Operable sun-shade
7 Earth-contact floor
8 Root-bed heating
9 Grow-lights
10 Composting bins
11 Wood stove w/ heat recovery
12 Well-insulated structure
13 Operable insulating curtain
14 Automatic temperature controls
15 Energy-efficient lighting
16 Water-saving plumbing
17 Roof-water collection
18 Earth-berms

Bioclimatic Design. Figure 14
(**a**) Solar greenhouse and wintergarden. Nature Center, New Canaan, CT USA. Donald Watson, FAIA and Buchanan Associates, Architects. 1984 (Photo: Robert Perron). (**b**) *Cross-section New Canaan Nature Center Greenhouse.* A broad range of energy conserving and bioclimatic design features are integrated in the design (Illustration: Marja Watson)

requirements were not achieved. A greenhouse for year-round crop or plant production is intended to create spring-summer or the growing-period climate throughout the year. A winter garden replicates spring-summer conditions for plant growth in wintertime by maximizing winter daylight exposure and by solar heating. Plants need ample light but not excessive heat. Although it varies according to plant species, as

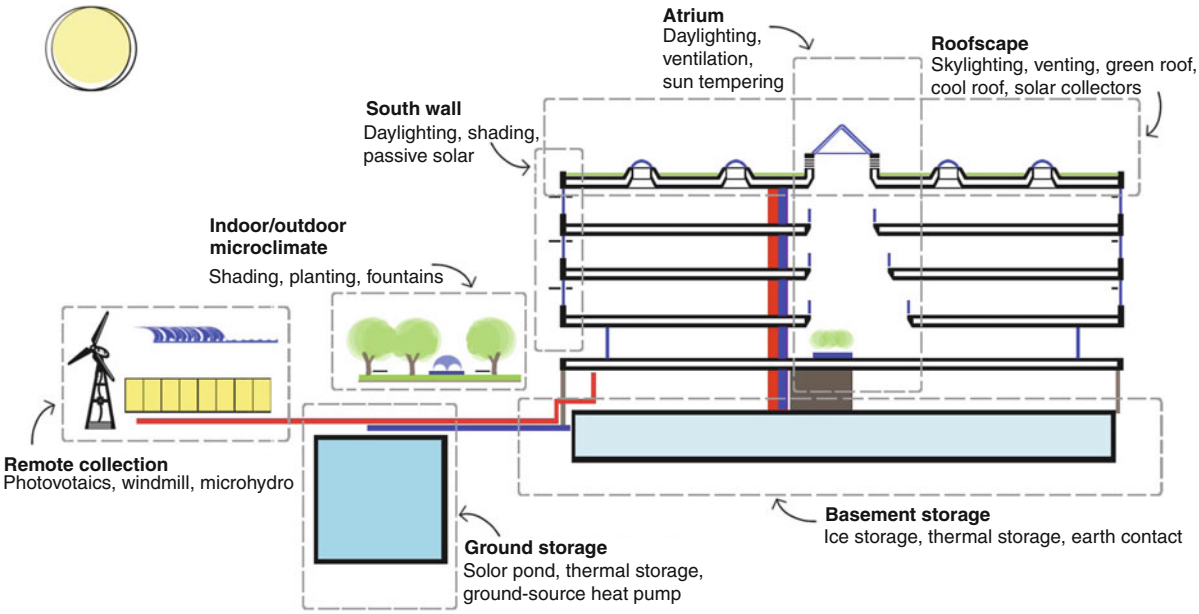

Bioclimatic Design. Figure 15

Large building opportunities for microclimatic design integration. Bioclimatic design extends to a larger scale and provides lower demand for integrated heating, cooling, and lighting systems (Watson [16])

a general rule planting areas require full overhead skylighting (essentially to simulate their indigenous growing condition). Most plants are overheated if their roots range above 65°F (18.3°C). Their growth slows when the root temperature drops below 45°F (7.2°C). As a result, a greenhouse has the general problem of overheating (as well as overlighting) during any sunny day and of underlighting (in intensity and duration) during any cloudy winter day.

If the function of the atrium includes plant propagation or horticultural exhibit (replicating the indigenous climate in which the display plants flower), then clear-glass skylighting is needed for the cloudy days and adjustable shading and overheating controls are needed for sunny days. If the plant beds are heated directly, by water piping, for example, then root temperatures can be maintained in the optimum range without heating the air. As a result, the air temperature in the atrium can be cool for people, in the 50°F (10°C) range, with the resulting advantage of providing a defense against superheating the space. People can be comfortable in lower air temperatures if exposed to the radiant warmth of the sun and/or if the radiant temperature of surrounding surfaces is correspondingly higher, that is, ranging above 80°F (26.7°C). Lower atrium temperature offers a further advantage to plants and energy-efficient space operation because evaporation from plants is slowed, saving water and energy (1,000 Btu are removed from the sensible heat of the space with each pound of water that evaporates). Air movement aids plant growth, if gentle and pervasive. Air circulation reduces excessive moisture buildup at the plant leaf and circulates CO_2, needed during the daytime growth cycle. The requirements for healthy planting and indoor gardening can thus be combined with energy-efficient atrium design for benefit of both plants and people (Fig. 14).

Large-Scale Applications

Bioclimatic design principles and practices are not limited to small-scale buildings alone. The physical basis of passive heating and cooling dynamics are somewhat constrained to near-envelope zones, subject to dimension of spaces in and around the building perimeter. However, these can and should be integrated with larger scale mechanical strategies of air movement, preheating, and ventilation.

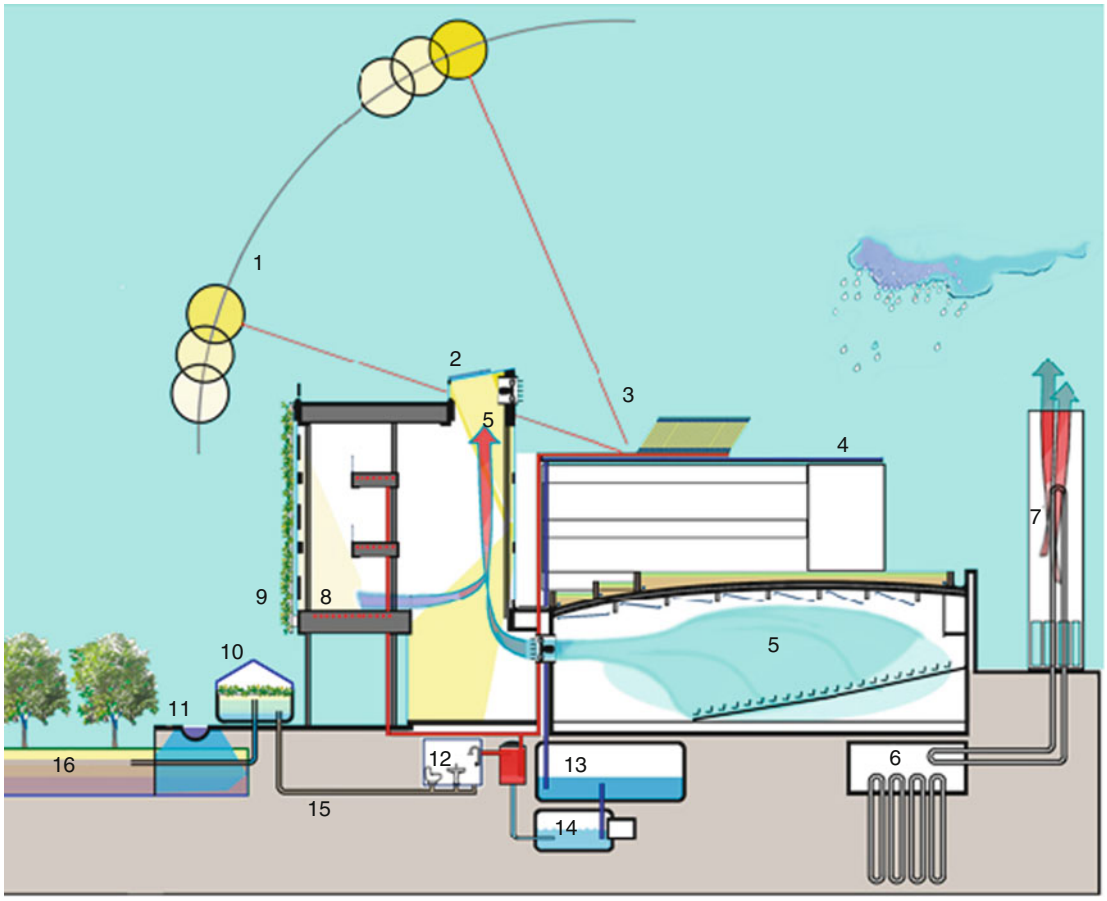

1 Daylighting and sun tempering
2 Photovoltaic collectors
3 Evacuated tube solar collectors
4 Rainwater harvesting
5 Displacement ventilation
6 Ground source heat pump
7 Heat recovery
8 Radiant heating
9 Deciduous living wall
10 Solar aquatic biofiltration
11 Stormwater to raingardens
12 Solar DHW
13 Rainwater cistem
14 Water purification
15 Grey and blackwater recovery
16 Greenscape irrigation

Bioclimatic Design. Figure 16
Center for interactive research on sustainability (CIRS) University of British Columbia, Vancouver, Canada. Designed as a "living laboratory" for study of building technologies (Busby Perkins+Will, Architects)

Daylighting techniques are scalable and can be applied to exterior envelope, skylighting, and atrium (light shaft) options. The history of buildings from the nineteenth century indicates possibilities, while improved glazing, shading, and insulation increase options for natural lighting that apply to large buildings.

Figure 15 diagrams the site and building opportunities for energy collection, storage, and distribution that may be integrated as combined passive and active means of bioclimatic design.

Several publications document 1980s' and 1990s' applications of passive solar, daylighting, and related bioclimatic elements in larger-scale buildings. Burt Hill Kosar Rittelmann/Min Kantrowitz Associates [17], provides a summary report, including several years of performance data, post-occupancy evaluation, and user surveys of 20 medium- to large-scale buildings

Passive measures	Active measures	Artic	Tundra	Upland	Continental	Temperate	Mediterranean	Subtropical	Tropical	Savannah	Steppe	Desert
Natural ventilation					4	2	2	1	1	1	1	1
	Mechanical ventilation	3	3				4	3	2	2	2	2
Nighttime ventilation						3	2	1	1	1	1	1
	Air conditioning							3	3	3	3	2
Evaporative cooling										3	2	1
Thermal mass			4	4	2	3	2				3	2
Light construction								3	3	2	4	4
	Mechanical heating	1	1	1	1	2	4				4	
Passive solar				2	2	1	2					
Heat of occupancy		2	2	2	3	3	4					
Insulation		1	1	1	1	2	3					4
Solar control shading					4	3	2	2	2	2	1	1
	Electric lighting	2	2	4	4	4						
Daylighting		2	2	2	2	2	2	3	3	3	4	4

Key
1 Highest value
2 High value
3 Good value
4 Some value

Bioclimatic Design. Figure 17
Summary of Bioclimatic/Energy-Efficient Design Measures. The relative value of bioclimatic design strategies depends upon on climatic zone variations (Adapted from Jones cited in UNEP 2007)

assisted by the US Department of Energy Passive Solar Commercial Demonstration Grants. The grant program provided design and research assistance for building owners who had projects underway, but no so far advanced that they could not incorporate significant innovative approaches to energy conservation.

William M.C. Lam [18], provides a detailed discussion of sunlighting large buildings, including performance documentation of case studies and lessons learned. Several related projects involved faculty and students of Schools of Architecture in courses that undertake post-occupancy evaluations of completed buildings, monitoring all building energy, including air quality and daylighting, providing an archive of critical building assessments [19].

A number of current building designs at a large scale provide exemplary applications of microclimatic design integration with heating, cooling, and lighting systems, with additional consideration of water and waste recycling. Such examples set standards for low energy and environmental impact, with relative value based upon building type and climate (Figs. 16 and 17).

Future Directions: Bioclimatic Design at the Urban Scale

Many studies address microclimatic impacts at the urban scale, described as "bioregional design" by the Olgyays [2]. Perennial topics have included solar access, evident in early twentieth-century studies related to daylighting and solar access for light and health, as well airflow and ventilation. Urban heat island effects have been addressed by studies of the effect of vegetation and "cool roofs." The prospect of climate change and extreme weather has, in recent

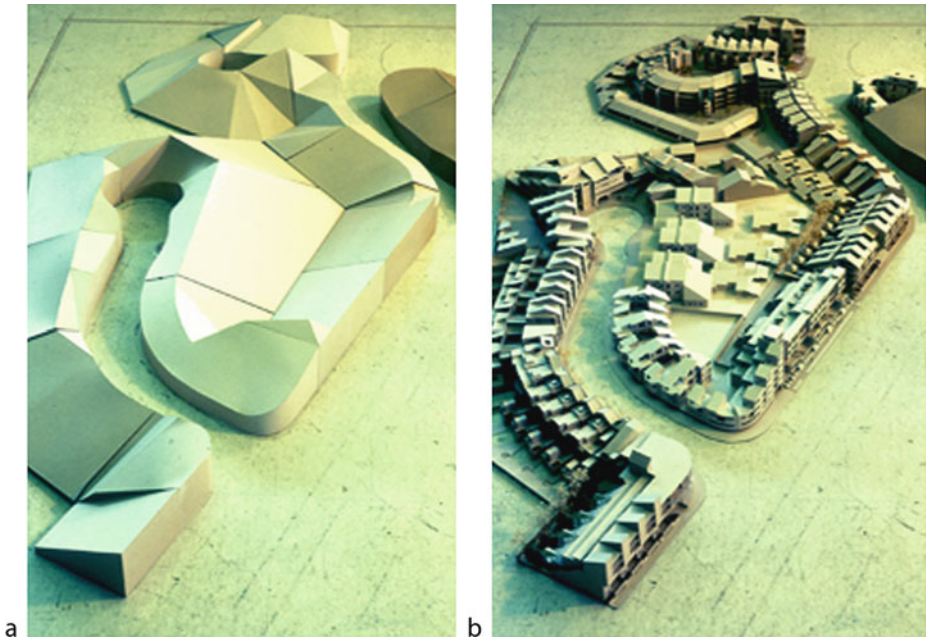

Bioclimatic Design. Figure 18
(**a**) Solar Envelope for a medium density neighborhood of Los Angeles. (**b**) A possible mixed-use community conforming to the solar envelope (Photos courtesy of Ralph L. Knowles)

Bioclimatic Design. Table 4 Average air and surface temperatures measured during a sequence of several clear days in summer (Givoni [21])

Location	Air temperature (°F)	Surface temperature (°F)	Air temperature (°C)	Surface temperature (°C)
Parking lot	79	122	26.1	50.0
Open plaza	78	107	25.6	41.7
Shaded walk	76	80	24.4	26.7
Grass lawn	75	88	23.9	31.1
Behind shrubs	74	73	23.3	22.8

years, added increased concern for design for resilience, mitigation, and adaptation to extreme weather, including flooding, drought, and increasing global warming. While full discussion of these topics is well beyond the scope of this entry, a few selected references indicate foundation studies and future directions.

Solar Access

Solar geometry. Studies by Ralph Knowles [20] undertaken over several decades with students at the University of Southern California have developed the notion of assuring solar access to buildings, for sun tempering, daylighting, and solar collection. His studies have demonstrated that solar access can be guaranteed in most urban areas while keeping within conventional medium to medium-high density floor to area ratios (FARs) (all but very high rise districts) (Fig. 18).

Bioclimatic Data at the Urban Scale

Baruch Givoni [21] compiles a broad survey of urban bioclimatic data and design applications, with emphasis on measured data, along with

Bioclimatic Design. Figure 19
Pocket Park, New York City. Paley Park creates a small area of respite, with a cooling microclimate created by evaporative cooling, shading, and wind protection, while water fountain sound helps neutralize urban clamor (Photo: Donald Watson)

discussions of challenges of data measurement at the urban scale.

Table 4 shows averages of air and surface temperatures measured at a height of 1 m (3.3 ft.) around noontime on the UCLA campus during a sequence of several clear days in summer. The lowest temperatures were in a space between a line of high shrubs and a wall of a building.

Givoni's research and overview points to opportunities for continued research at the urban scale, supporting an approach to urban planning based on bioclimatic analysis and design (Fig. 19).

Urban Air Quality

Studies of wind at the urban scale have considered force of winds for structural and exterior envelope design, as well as for wind tunnel (accelerating force of winds at constrained building openings), as well as aerodynamic shapes to induce natural ventilation. Models for such studies have included scaled wind tunnels, flow models, and full-scale mock-ups exposed to simulated wind forces (Fig. 20).

Bioclimatic Design. Figure 20
Wind tunnel. Smoke tracing helps to visualize wind effects of building form at the urban scale (Photo: Donald Watson)

Studies by Anne Whiston Spirn [22] have utilized research on urban wind effects to propose design strategies to reduce pollution in city streets and public ways, principally by opening building forms to less constrained airflow (Figs. 21 and 22).

Resilience to Natural Disaster

Climate change is evident in global warming, extreme weather and storm events, flooding, and drought. The line of influence that climate had upon design is in a sense reversed. Design now influences climate in the way that buildings, infrastructure, cities, along with agricultural and industrial practices have in fact been executed without regard for bioclimatic impacts.

The natural landscape that has evolved in response to climate and water regimes over millennia had adapted to long-evolving patterns of rainfall, aridity, heat, and cold. Historical flood conditions were accommodated within the watershed ecology and its

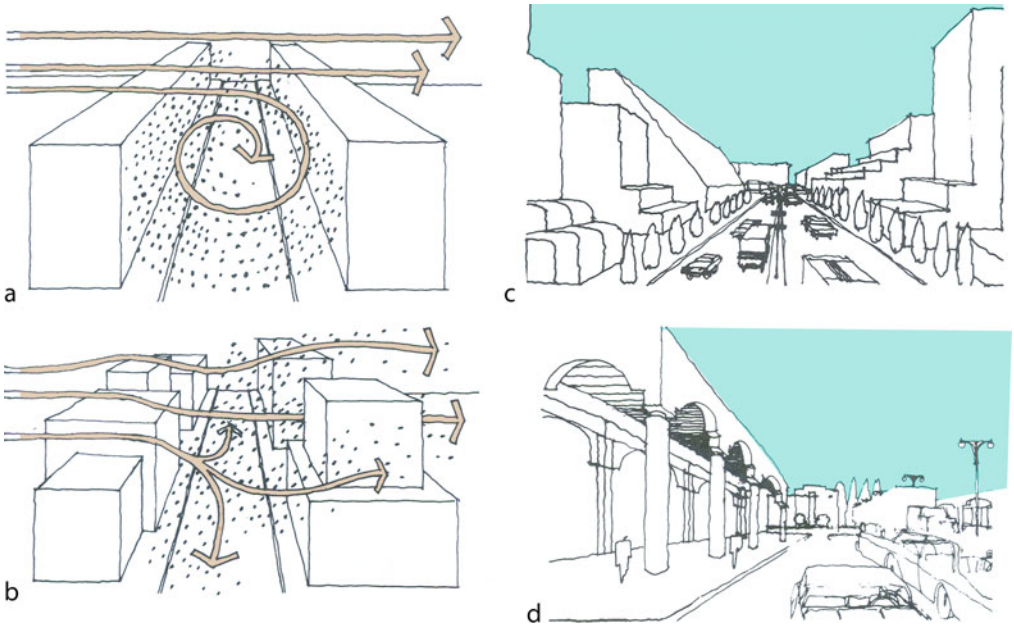

Bioclimatic Design. Figure 21
Air Quality. The urban designer has opportunity to utilize strategies to improve air quality at the urban microclimatic scale. Anne WS. [22]. (**a**) – Street canyons lined with buildings of a similar height, oriented perpendicular to the wind direction tend to have poor air circulation compared to (**b**). (**b**) – Street canyons lined with buildings of different heights and interspersed with open areas have better air circulation. (**c**) – To promote air circulation in street canyons, step buildings back from the street, increase openings, and vary building heights. (**d**) – To promote air circulation in street side arcades, design them with high canopies and airflow outlets

coevolving plants and animals. When those patterns are disrupted and the natural landscape is altered, flooding risks and disasters increase, as much a result of human actions as natural occurrence.

While the prospect of sea level rise is undefined as to extent and time, the recent incidence of historically unprecedented natural disasters has impelled some nations and regions to undertake programs of adaptation and mitigation. The Netherlands has undertaken a 100-year plan to address flooding by an integrated and phased set of improvements to dykes, removals, and elevations of buildings in increased flood plains, and abandoning the most exposed risk area to natural recovery. In Japan, where spring flooding from mountains has resulted in flash floods in densely populated urban areas that have built up in floodplain areas, the range of actions also include "super-levees," which essentially reconfigure land along river floodplain, while increasing floodable zones that can hold floodwaters during peak floods, while making them available for temporary use at other times, easily evacuated in case of emergency (Fig. 23).

Watson and Adams [23], propose an extension of bioclimatic design to include design for resilience, to adopt precautionary principles in design of buildings, communities, and cities. Resiliency describes the capacity to respond to stress and change of climatic conditions. Resiliency is evident in natural systems in strategies to adjust to variable and extreme conditions. Characteristics of resilient systems include buffering, storage, redundancy, self-reliance, decentralization, diversity, energy conservation, rapid adaptability, and replacement (Table 5).

Summary

Bioclimatic design is based on the analysis of the climate, including ambient energy of sun, wind, temperature, and humidity. Bioclimatic design utilizes passive

Bioclimatic Design. Figure 22
Comprehensive plan to improve air quality. Stuttgart, Federal Republic of Germany. Public gardens and open space atop the cities hills and hillside canyons are preserved as vegetated public stairways and watercourses. The hillside canyons funnel cool nighttime airflow to center city streets and downtown parks (Photo courtesy of Dr. Michael Trieb, Urban Planning Institute, University of Stuttgart)

and ambient energy sources to achieve human comfort through building design and construction, including heating, cooling, and daylighting techniques. Derived from regional and local conditions and opportunities, bioclimatic analysis and design provide both a knowledge base and an inspiration for architecture and sustainable design.

Bioclimatic design analysis is a foundation step in architectural design, essential in the beginning phases to set design guidelines and goals, which can then be compared with actual performance results. By tracking performance results, a designer can thus gain knowledge of the effectiveness of bioclimatic design strategies and techniques for a particular locale and regional microclimates.

A present day challenge is climate change, which portends to increase the severity and period of warming, or overheated, conditions. Climate and weather uncertainty and warming trends should be anticipated in building design to be adaptive by a balance of techniques for heating and for cooling. The challenge to reduce and eliminate where possible the use of fossil fuels for carbon reduction further supports the passive design strategies of bioclimatic design, for its combined advantages of comfort and health, environmental well-being, and resilience to extreme weather.

The enlargement of bioclimatic design to design for resilience is a necessary response to the increased severity of natural disaster. The science of building and urban climatology can fully inform steps to remediate flooding and other risks, so that the natural ecology of regions is returned to its role in moderating extremes and sustaining the diversity of species.

Acknowledgments

The author is indebted to Murray Milne, Baruch Givoni, and late Kenneth Labs, as well as those whose work is cited in the text and illustrations, all of whom contributed immeasurably to the development of the author's work described in this entry.

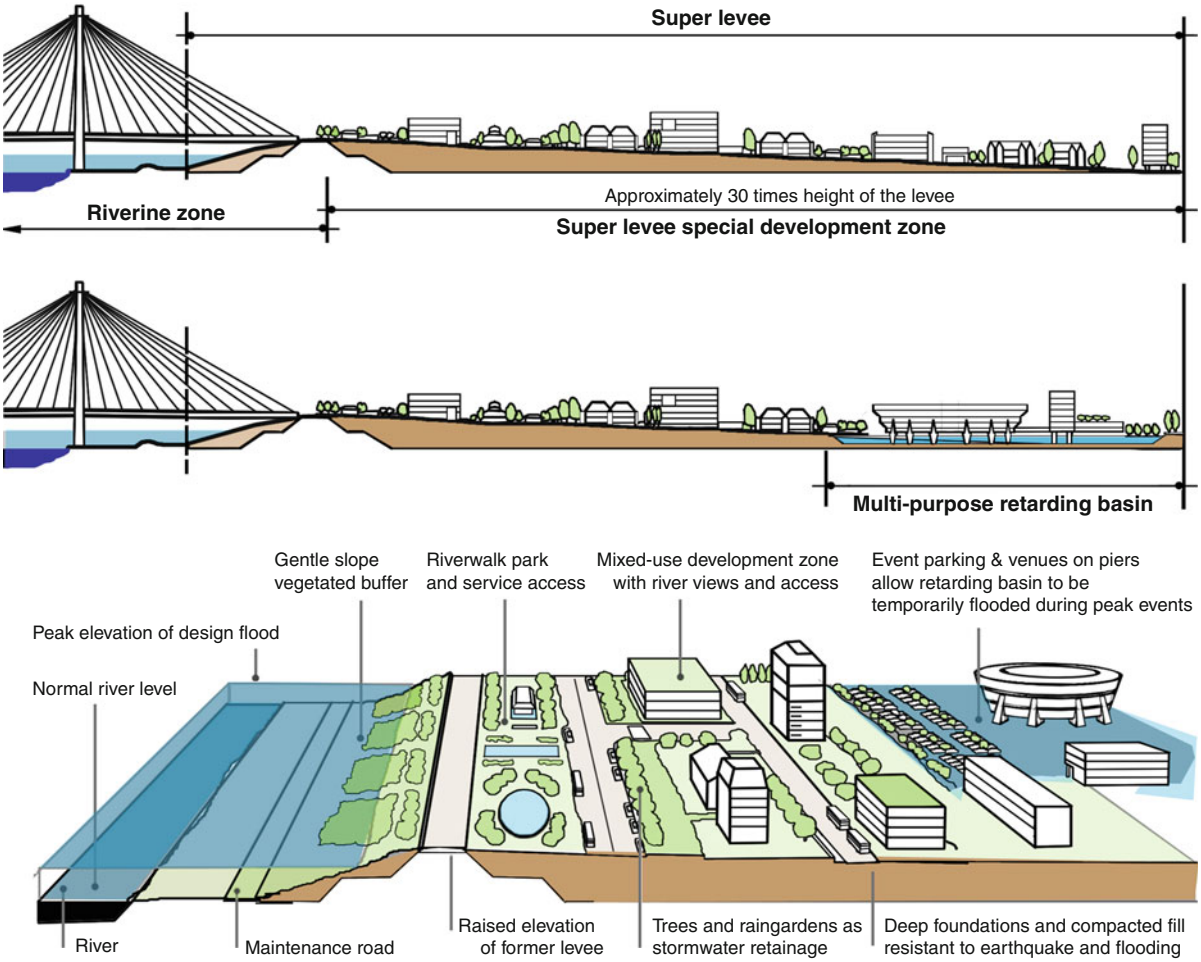

Bioclimatic Design. Figure 23
Super-levees (Japan). Designing infrastructure and buildings for resilience to flooding and extreme weather extends bioclimatic design to new needs and opportunities in regional and urban design (Watson and Adams [23])

Bioclimatic Design. Table 5 Mimicking lessons of nature for resilient design and construction

Principle from nature	Application to resilient design
Absorption	Watershed planning and design (reservoirs, retention ponds, green roofs)
Buffering	Breaks, riparian buffers, rain gardens
Core protection	Zoning, decentralization, self-reliant subsystems
Diffusion	Meanders, wetland and coastal zone landscape, open foundations
Storage capacity	Aquifers, wetlands, reservoirs, cisterns
Redundant circuits	Green infrastructure, wildlife corridors, and multiple service routes
Waste/nutrient recovery	Sustainable stormwater design and waste systems
Rapid response	Smart grid, early warning, emergency responsive systems

Bibliography

Primary Literature

1. Fitch JM, Siple P (eds) (1952) AIA/house beautiful regional climate study. Originally published in AIA bulletin 1949–1952. University Microfiche, Ann Arbor
2. Olgyay A, Olgyay V (1957) Design with climate. Princeton University Press, Princeton
3. Givoni B (1976) Man, climate and architecture, 2nd edn. Applied Science, London
4. Milne M, Givoni B (1979) Architectural design based on climate. In: Watson D (ed) Energy conservation through building design. ARB/McGraw Hill, New York
5. Arens E, Gonzales R, Berglund L (1986) Thermal comfort under an extended range of environmental conditions. ASHRAE Trans, vol 92, part 1. ASHRAE, Atlanta
6. Watson D, Harrington K (1979) Research on climatic design for home builders. In: Franta G (ed) Proceedings of the 4th national passive solar conference. ASES Publications, Boulder
7. NREL (n.d.) TMY-2 typical meteorological year climate data files. National Renewable Energy Laboratory. www.nrel.gov/docs/fy08osti/43156.pdf. Accessed 10 June 2011
8. Energy Plus website (2010). U.S. Department of Energy. www.eere.energy.gov/buildings/energyplus/weather.html. Accessed 1 Sept 2010
9. Arens EA et al (1980) Geographical extrapolation of typical hourly weather data for energy calculation in buildings. National Bureau of Standards Building Science Series 125. www.fire.nist.gov/bfrlpubs/build76/PDF/b76002.pdf. Accessed 10 June 2011
10. Arens EA et al (1985) SITECLIMATE: a program to create hourly site-specific weather data. Proceedings, ASHRAE/DOE/BTECC conference on thermal performance of the exterior envelopes of buildings III, Clearwater Beach, pp 91–108. http://escholarship.org/uc/item/3j62w3nm. Accessed 10 June 2011
11. Milne M (1997) Energy design tools. Department of Architecture and Urban Design. University of California Los Angeles (UCLA). http://www.aud.ucla.edu/energy-design-tools. Accessed 1 Sept 2010
12. Milne M, Li Y-H (1994) Climate consultant 2.0: a new design tool for visualizing climate. In: Proceedings of the 1994 ACSA architectural technology conference, Association of Collegiate Schools of Architecture Publications, Washington, DC
13. Watson D, Labs K (1983) Climatic building design. McGraw-Hill, New York (Revised 1993)
14. Watson D (1988) Solar mortgage subsidy program occupant survey. Energy Division, Office of Policy and Management, State of Connecticut
15. Watson D (1982) The energy within the space within. Progress Archit, July, pp 97–102
16. Watson D (1989) Bioclimatic design research. In: Boer KW (ed) Advances in solar energy: annual review of research and development, vol 5. American Solar Energy Society, Boulder
17. Burt Hill Kosar Rittelmann Associates/Min Kantrowitz Associates (1987) Commercial building design: integrating climate, comfort, and cost. Van Nostrand Reinhold, New York
18. Lam WMC (1986) Sunlighting as formgiver for architecture. Van Nostrand Reinhold, New York
19. Vital Signs. Prof. Chris Benton. www.arch.ced.berkeley.edu/vitalsigns; *Agents of Change*. Prof. Alison Kwok. http://aoc.uoregon.edu. Accessed 10 June 2011
20. Knowles RL (2006) Ritual houses: drawing on nature's rhythms for architecture and urban design. Island Press, Washington, DC. Also: Knowles RL (2003) The solar envelope. In: Watson D (ed) (2003) Time-saver standards for urban design. McGraw-Hill, New York
21. Hemiddi A (1991) Measurements of surface and air temperatures over sites with different land treatments. In: Proceedings PLEA 1991 Conference. Seville, Spain; Also: Givoni B (2003) Urban design and climate. In: D. Watson (ed) Time-saver standards for urban design. McGraw-Hill, New York
22. Spirn AW (2003) Better air quality at street level: strategies of urban design. Watson D (ed) Time-Saver standards for urban design. McGraw-Hill, New York; Also: Moudon AV (1987) Public streets for public use. Van Nostrand Reinhold, New York
23. Watson D, Adams M (2010) Design for flooding and resilience to climate change. Wiley, New York

Books and Reviews

Brown GZ, DeKay M (2001) Sun, wind & light: architectural design strategies. Wiley, New York

Fitch JM, Branch DP (1960) Primitive architecture and climate. Scientific American 219(3):190–202

Givoni B (1998) Climate considerations in building and urban design. Van Nostrand Reinhold, New York

Jones DL (1998) Architecture and the environment: contemporary green buildings. Laurence King, London

Koenigsberger OH, Ingersoll TG, Mayhew A, Szokolay SV (1974) Manual of tropical housing and building. Longman, New York

Kwok AG, Grondzik WT (2007) The green studio handbook: environmental strategies for schematic design. Elsevier, New York

Landsburg HE (1972) The assessment of human bioclimate. Technical note 123, World Meteorological Organization, Geneva, (UNIPUB) 36 pp

Loftness V (1977) Identifying climate design regions and assessing climatic impact on residential building design. Technical paper no. 1, AIA Research Corporation, Washington, DC, 25 pp

McDaniel CN, Magic T (2011) Creating a positive energy home. Sigel Press, Medina

Szokolay SV (2008) Introduction to architectural science: the basis of sustainable design. Elsevier, Amsterdam

United Nations Environmental Programme (UNEP) (2007) Buildings and climate change: status, challenges and opportunities. ISBN: 978-92-807-2795-1

Biodiesel

Martin Mittelbach
Institute of Chemistry, Karl-Franzens-University of Graz, Graz, Austria

Article Outline

Glossary
Definition of the Subject and Its Importance
Introduction
History of Biodiesel
Biodiesel Production and Utilization Worldwide
Feedstock for Biodiesel Production
Nonedible Oils as Feedstock for Biodiesel Production
Potential of Microalgae as Feedstock for Biodiesel
Biodiesel Production Technologies
Catalysts for Transesterification and Esterification Reactions
Biodiesel Quality and Specifications
Environmental Issues of Biodiesel
Future Directions
Bibliography

Glossary

Biodiesel Fatty acid methyl or ethyl esters made out of fatty acid material.

Catalyst Chemical compound that increases the reaction rate of a chemical reaction, either soluble (homogenous) or insoluble (heterogeneous).

BtL fuels Fuels made out of biomass by gasification and further synthesis with Fischer–Tropsch catalysts.

Esterification Chemical reaction of a carboxylic acid with an alcohol forming a carboxylic ester and water.

Feedstocks Any vegetable oil, animal fat, waste oils like used cooking oil, fatty acids.

Green house gas (GHG) savings Saving of the emissions of green house gases of a biofuel in the whole production chain in comparison to fossil fuel.

Life cycle analysis Assessment of the environmental impacts of a given product caused by its production and use.

Transesterification Chemical reaction of a carboxylic ester with an alcohol or a carboxylic acid in order to obtain another carboxylic ester.

Definition of the Subject and Its Importance

The transport sector is one the fastest growing segment using fossil-based products. Especially because of the economic development in countries like India and China, there is a need for high mobility and transport. Today's transport system is based on combustion engines using fossil fuels, leading to a sharp increase of emissions of green house gases (GHG) within the last decades. Furthermore, for most of the industrialized countries there is a strong dependency on oil-producing countries, which could cause political conflicts and even wars. Therefore, especially in times of a sharp increase in crude oil prices, the question of alternative fuels or transport systems is highly discussed. Moreover, the effects of global warming caused by the increased emissions of green house gases stimulate the call for alternative fuels. For kinds of energy like electricity and heating power, there are sufficient alternatives available like photovoltaics, wind energy, and biomass; in the transport sector, the alternatives are rare. Electric vehicles could be used in special segments of the transport sector like in urban areas, but due to the limited capacity of energy storage in batteries, these electrically powered cars could not substitute combustion engines in large extent within the next decades. For aviation fuels, there has not been any suitable alternative to kerosene. The use of alternatively produced hydrogen basically could power combustion engines as well as electric cars with fuel cells, but because of the high price and lack of infrastructure there would not be a market penetration within the next decade. So the only short-term alternative for the transport sector is the use of liquid biofuels, which are produced out of biomass and could be used in existing engines. Bio-ethanol is a well-established fuel for gasoline cars, starting with activities in Brazil in the 1970s, and biodiesel made out of fats and oils is an ideal alternative fuel for diesel engines, which are the only type of engine used in heavy-duty vehicles in the transport sector but also in large extent in passenger cars in Europe. Biofuels not only can substitute to a certain extent the high demand for fuels in the transport sector

and therefore lead to less dependency on fossil fuel imports, but also have an environmental effect in lowering local emissions of soot and particles and also global emissions of green house gases. Furthermore, the production of biofuels could also contribute to social welfare by increasing the employment in the agricultural and industrial sector. However, the sustainability of biofuels production and utilization has to be proven by life cycle assessment (LCA) and thorough evaluation of the social impacts.

Introduction

The main drivers for the fast development of biofuels in the last decade worldwide where on the one side the high dependence of most of the countries on imports of fossil fuels, and on the other side the need for reduction of green house gases.

Biodiesel today is the most popular biofuel besides bioethanol. Chemically, biodiesel is defined as fatty acid methyl or ethyl esters made out of vegetable oils or animal fats. Because of the limited availability of agricultural areas and because of the food versus fuel discussion in the last years, especially, waste oils like used frying oil or animal fat as well as microbial oils from microalgae are highly favored. But also other nonfood crops like *Jatropha curcas*, which could be also cultivated on marginal areas, are currently investigated. Other biofuels for diesel engines are pure vegetable oils or biomass to liquid fuels (BtL), made via gasification of biomass and Fischer–Tropsch synthesis. As most of the biodiesel today is used as blend with fossil fuel and the warranties of most of the engine manufacturers and fuel companies only are given up to a specific amount of conventional biodiesel in fossil fuel, also hydrogenation of vegetable oils to remove the oxygen leading to hydrocarbons, which could be mixed with biodiesel also in higher amounts, is a possible route. These fuels, which are called hydrogenated vegetable oils (HVO) or NExBtL fuels, will also come into the market within the next years.

In this entry, mainly conventional biodiesel, fatty acid methyl, and ethyl ester, will be covered in detail.

History of Biodiesel

The idea to use vegetable oils as fuels for diesel engines is more than 100 years old. As Knothe points out in a review on the historical development of biofuel production, Rudolf Diesel himself, the inventor of the diesel engine, conducted engine tests on plant oils [1]. So one prototype of his new engine presented at the World's Exhibition in Paris in 1900 ran on peanut oil and did so quite smoothly, so that hardly any visitor was aware of the fact. The idea for this test had apparently stemmed from the French government, which was searching for a means of domestic fuel production in their African colonies. Several other European countries took up the idea, which resulted in a number of articles on the use of tropical oils as diesel fuels by Belgian, French, Italian, British, and German authors. However, as petroleum-based fuels soon became available in large quantities at comparatively low cost, interest in plant oils diminished. Except for some attempts at utilizing renewable sources of energy during the Second World War, it was only in the 1970s that the worldwide oil crises and a growing environmental awareness led to the rediscovery of plant oils as possible alternatives to hydrocarbon-based fuels. The urge to fight agricultural overproduction served as an additional incentive to this development. As neat vegetable oils can only be used in modified diesel engines because of their high viscosity compared to fossil fuel, chemical transformation of the vegetable oils is the matter of choice to adapt the fuel to existing engines.

Transesterification of vegetable oils with lower alcohols has turned out to be an ideal modification, so that the term "biodiesel" is now only used to denote products obtained by this technology. The reaction between triglycerides and lower alcohols, yielding free glycerol and the fatty acid esters of the respective alcohol, was first described in 1852 [2]. The first reference to fatty acid alkyl ester fuels stems from 1937. A Belgian patent on the production of palm oil ethyl esters by acid-catalyzed transesterification describes the first use of a fuel, which would now be referred to as "biodiesel" [3]. Only a year later, in the summer of 1938, a bus fueled with palm oil ethyl esters ran between Brussels and Louvain [4]. However, these pioneering efforts in utilizing transesterified vegetable oils seem to have petered out soon afterward.

After a break in the study of fatty acid alkyl ester fuels of about 40 years, the idea was taken up again at the beginning of the 1980s. The topic was discussed in several international conferences and reappeared in

scientific publications. Rapeseed oil methyl esters (RME) was being produced and its feasibility as a diesel fuel was first being tested at Graz University [5]. Also other teams in South Africa (1981), Germany, and New Zealand (1982) soon directed their research efforts to the production of biodiesel. Already in 1987, a small pilot plant in Silberberg, Austria, started its production of rapeseed oil methyl esters, based on an innovative low-pressure, low-temperature technology, which had been developed by Mittelbach et al. 1986 [6]. The first industrial production plant for RME followed in 1991 (Aschach/Donau, Austria), and in 1995 two large-scale industrial plants in Rouen, France, and Leer, Germany, documented the rapid growth of the young biodiesel industry. The term "biodiesel" itself seems to have been coined in a Chinese article [7]. The next use of the expression in the scientific literature is documented in 1991 [8] after which the number of articles on the topic increased exponentially.

Biodiesel Production and Utilization Worldwide

Within the last decade, biodiesel production worldwide has been expanded enormously. Almost in every country worldwide, there are biodiesel activities, either in research, or in production in pilot or industrial scale. The main reasons for this rapid development are on one side the relatively easy process for transesterifcation of vegetable oils, which could be done without major investments, and on the other side the easy and well-established utilization of this biofuel either as pure fuel or as various blends with fossil diesel without any modifications of the engine.

As it can be seen in Fig. 1, the world production of biodiesel in 2008 was 12.2 million tons, out of which 65% have been produced in the EU-27. According to Table 1, the leading country is Germany with a long tradition in biodiesel, followed by the USA, which mostly produced biodiesel for the export to Europe; however, this export has been reduced significantly in 2009 due to new legislation in Europe. Outside Europe, the major biodiesel producers are the soybean-producing countries, namely, the USA, Argentina, and Brazil. Within Europe, there is a big gap between biodiesel production capacity and actual biodiesel production, as can be seen in Table 2. There are several reasons for that fact: First of all the dramatic increase in vegetable oil prices in 2008, which, however, stabilized in 2009, and the insecurity on the future of biofuels as long as the new European Energy Directive had not been finalized. Furthermore, especially in Germany the introduction of mineral oil tax for pure biodiesel almost totally shut down the use of pure biodiesel (B100).

Europe is still the biggest consumer of biodiesel, about 2 million tons of biodiesel are imported. Most of the biodiesel is used in blends with fossil diesel and regularly sold at filling stations as B5 or B7, which

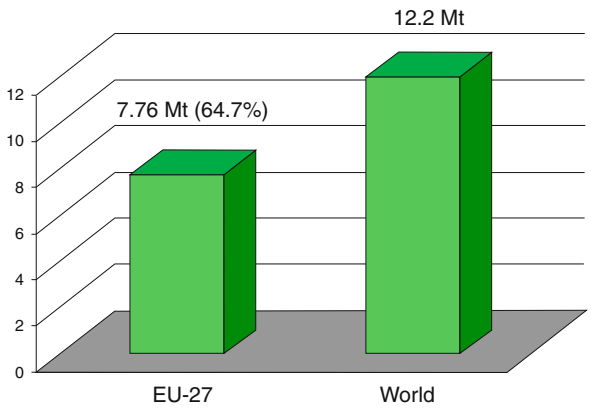

Biodiesel. Figure 1
Biodiesel production 2008 EU-27 and worldwide

Biodiesel. Table 1 Ranking of the biodiesel-producing countries worldwide (Source: Argentine Biofuels Chamber [9])

	Country	Biodiesel production million tons in 2008
1.	Germany	2,819
2.	USA	2,327
3.	France	1,815
4.	Brazil	1,027
5.	Argentina	960
6.	Italy	595
7.	Malaysia	420
8.	Belgium	277
9.	Poland	275
10.	Portugal	268

Biodiesel. Table 2 Biodiesel production and capacity in EU (European Biodiesel Board [10])

Country	Production 2008	Capacity 2009
Germany	2,819	5,200
France	1,815	2,505
Italy	595	1,910
Belgium	277	705
Poland	275	580
Portugal	268	468
Denmark/Sweden	231	352
Austria	213	707
Spain	207	3,656
UK	192	609
Slovakia	146	247
Greece	107	715
Hungary	105	186
Czech Rep.	104	325
The Netherlands	101	1,036
Finland	85	340
Others	215	1,360
Total	7,755	20,909

means 5% respectively 7%/volume blended with fossil diesel. Higher blends today have not been accepted by most of the engine manufacturers, so to reach the European goals of 10% biofuels (on an energy base) in 2020 either other biofuels have to be introduced (BtL or hydrogenated vegetable oils) or higher blends have to be used in special market segments like agriculture and captive fleets.

Feedstock for Biodiesel Production

The main feedstocks for biodiesel production are still the most common vegetable oils like rapeseed oil (Canola) or soybean oil. All major seed oils have similar fatty acid distribution, so the properties of the biodiesel produced is also quite similar except the cold temperature behavior, which depends on the sum of total saturated fatty acids. According to Fig. 2 in Europe the dominating source is rapeseed oil, which is also the main vegetable oil produced. Rapeseed oil gives

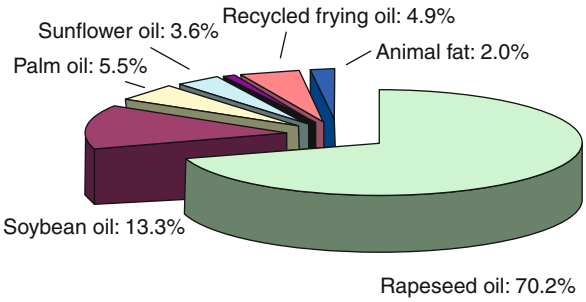

Biodiesel. Figure 2
Feedstocks for biodiesel production in Europe, estimation for 2009 (USDA [11])

a biodiesel, which meets the European specification for biodiesel, EN 14214, and has the best cold temperature behavior from all common feedstock. On the second place, there is soybean oil, which is mainly imported as biodiesel from the USA and Argentina. Biodiesel from 100% soybean oil does not meet the EN 14214 specification because of the higher Iodine Number due to the higher content of linoleic acid, however, it can be used as blend with other feedstock.

One of the most important factors for the economy of biodiesel production is the price of feedstock. Rapeseed oil is the most expensive vegetable oil for biodiesel production, so most of the biodiesel producers have to blend rapeseed oil with a certain amount of other oils, for example, used frying oil or waste animal fat. However, the amount of these products is limited and due to the high demand of these sources also the price increased significantly. One of the cheapest vegetable oil is palm oil, which is mainly produced in Malaysia and Indonesia, but the amount as blending feedstock is limited due to the poor cold temperature behavior.

The world production of vegetable oils and animal fats today is about 150 million tons, out of which already 12 million tons are used as feedstock for biodiesel. As most of the vegetable oil and animal fat production is used for food purposes, the maximum amount for biodiesel production is limited if there would not be any significant increase in oil and fat production. Twelve million tons of biodiesel together with about 40 million tons of bioethanol worldwide substitute fossil transport fuel with approximately 1.3%. As diesel fuel is the major fuel in transportation, it can be seen easily that vegetable oils and fats alone

cannot substitute diesel fuel in a significant share. So new feedstocks, which do not necessarily require common agricultural areas, have to be found in order to meet the high demand for biobased diesel fuel. High expectations were put into BtL (biomass to liquid fuels) production from lignocellulosic feedstock, so-called second-generation fuels, which however were not fulfilled until today because of high development and investment costs for such technology. Only one production plant in Freiberg, Germany (CHOREN), exists today, which until mid-2010 has not been put into standard operation. Other technologies like hydrogenated vegetable oils require the same feedstock as common biodiesel, so this route will not lead to higher amounts of biodiesel.

Promising feedstock in mid-term or long-term perspective are nonfood feedstock like *Jatropha curcas* L., which can be also grown on marginal areas or oils from microalgae that can be grown in open ponds or photobioreactors.

Nonedible Oils as Feedstock for Biodiesel Production

Out of the enormous potential of possible nonedible seeds, *J. curcas* as example will be described in detail to show the potential and risks of nonfood feedstock. *J. curcas* has shown to be the most promising nonedible crop for biofuel production. This can be seen on the one side on the number of international Jatropha conferences organized during the last decade, and on the other side on the increasing number of scientific publications, which are dealing with research on Jatropha as alternative feedstock (Fig. 3).

The first activities in the exploration of *J. curcas* as possible feedstock for biodiesel production has been carried out within the Biomass Project in Nicaragua between 1990 and 2000, financed by the Austrian government. Within that project, a total area of 1,000 ha of *J. curcas* had been planted, and also a biodiesel plant has been installed, which however, never went into operation. One highlight of the project was the organization of the first international conference on *J. curcas* in Managua in 1997. The proceedings of that conference covered the whole spectrum of *J. curcas* knowledge at that time [13]. However, the whole project was stopped according to an external evaluation coming to the conclusion: "The biofuel part, however, suffers from the development of fossil fuel prices, which makes the production of diesel from physic nut uneconomic at the moment."

The most influencing factor for the total economic evaluation of *J. curcas* utilization is the use of the side product oil cake, which would bring the most benefit if

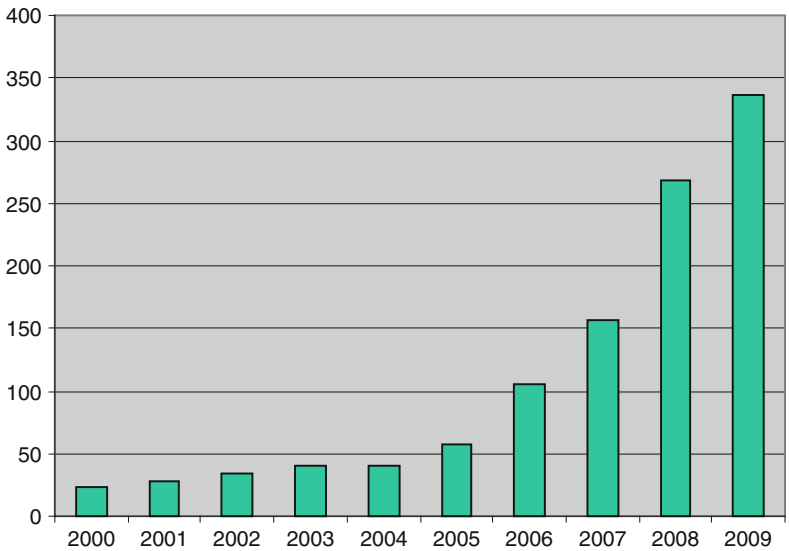

Biodiesel. Figure 3
Number of scientific publications on Jatropha according to SciFinder, CAS [12]

it could be used as animal feed. However, due to the remaining highly toxic phorbol esters in the oil cake the use as animal feed is not possible without any efficient detoxification. So today, the only possible utilization of oil cake would be the use as fertilizer, which, however, is far less profitable than the use as animal feed.

The main advantages of *J. curcas* over other food crops can be summarized in the following:

- Wide distribution in the tropics
- Good adaptation to marginal areas, poor soil
- Best adaptation to arid and semiarid conditions
- Easy agronomic handling
- No competition with food crops due to the content of toxic compounds
- High oil content in the seeds: up to 55% (dehulled)

On the other side, there are some drawbacks of *J. curcas* like the following:

- High yields need intensive agricultural production (water, fertilizer, pest control)
- Toxic seeds have to be processed in specified plants
- The use of side products like seed cake and glycerol is limited
- Harvesting is laborious, long harvesting period
- The actual yield of seeds per ha is lower than expected

One main disadvantage can be seen in the laborious harvesting, which today has to be done manually. On the one side, this fact is seen positively because the laborious harvesting could bring income to people living in rural areas, on the other side the total economy of *J. curcas* is mainly influenced by the costs of labor, which could increase rapidly. The advantage to use a nonedible crop could easily change into a disadvantage, if the utilization of side products like oil cake and glycerol is limited and less economic.

The main strategies to overcome these problems could be either the use of nontoxic varieties like some Mexican species or the detoxification of side products in order to get higher value-added products.

It can be seen that countries like China and India, where the use of food products for biofuel production is not accepted, have the greatest interest in nonedible plants like Jatropha. It is quite obvious that the utilization of Jatropha should not be focused on biofuels alone, but should include all other parts of the plants as well as the side products of biodiesel production. Especially in China, there is a big interest in the utilization of the biologically active components in the different parts of the plant. Also the extraction of phorbol esters out of the oil and further utilization of these products is of great importance. Especially high value-added minor components and side products could improve the overall economy of Jatropha production and could overcome the high costs of labor-intensive manual harvesting. The use of nontoxic varieties like some species from Mexico might be challenging and attractive, however, also the possible risks have to be considered. Within a global market for seeds and oil, the coexistence between nontoxic and toxic varieties might be a high risk, especially if nontoxic oil and oil cake are considered as potential food and feed. Special certification, labeling, and control systems have to be established in order to avoid serious accidents with dramatic consequences for the whole business.

In mid-term future, the use of toxic Jatropha varieties will be favored, especially because of already established large investments in classical Jatropha plantations in a series of areas like Africa, India, Indonesia, and China. However, research in nontoxic varieties has to be carried out in order to evaluate the potential of these varieties for food and feed production. The focus for the utilization of toxic varieties will be the detoxification of the oil in order to obtain additional high value-added products, and the detoxification of the oil cake in order to get a nontoxic animal feed.

Within the last years, a significant number on reviews on *J. curcas* have been published worldwide. In two recent reviews, the latest developments in agronomy, oil production, alkyl ester production, toxicity, plant breeding, and crop expansion of *J. curcas* are discussed [14, 15]. The seeds of the plant are not only a source of biodiesel but also contain several metabolites of pharmaceutical importance. Common exploitation for biopharmaceuticals and bioenergy production are some of the prospective future potential of this plant [16, 17].

A series of publications are dealing with the detoxification of either Jatropha oil and/or oil cake mainly focusing on the degradation of the highly toxic phorbol esters in order to use the oil cake as

animal feed [18, 19]. However, no technically feasible method has been developed so far to totally detoxify the seed cake for safe use as an animal feed.

Potential of Microalgae as Feedstock for Biodiesel

Because of the food versus fuel discussion within the last years, microalgae as potential feedstock for biofuel production has been discussed widely around the world. High expectations have been set into this kind of biomass, because no agricultural areas are necessary for cultivation and additionally green algae need CO_2 as carbon source, which could be taken out of flue gases from power stations and could help to reduce overall green house gases.

Almost 30 years ago, the US department of energy had launched a program studying the potential of microalgae as biofuel, but the program was stopped in 1996 due to the high production costs compared to the low fossil fuel prices.

Microalgae include a variety of photosynthetic microorganisms capable of fixing CO_2 from the atmosphere to produce biomass more efficiently and rapidly than terrestrial plants; algae require approximately 2 g of CO_2 for every g biomass generated [20]. The estimated productivity lie between 10 and 50 g/m^2 and day, the oil content lies between 15% and 50%, so a daily overall production of 15–250 kg oil/ha could be calculated. A dry biomass yield between 73 and 350 t/ha and year is estimated, depending on a photosynthetic conversion efficiency between 2.1% and 10% [21].

However, all these data are based on the assumption, that the extracted oil mainly consists of triglycerides, which easily could be converted into well-established biodiesel. However, it has been shown, that the content of triglycerides can vary widely, and a series of non-triglyceride material like hydrocarbons and terpenes can be found in the extractable oil mixture. Furthermore, there is a series of technical questions, which have to be solved and which make the production of algae for fuels today totally uneconomic. The choice of microalgae out of thousands of different species, the cultivation method like open ponds or photo-bioreactors, the harvesting, extraction of oil, and further processing are some of the challenges that have to be faced. Today the cultivation of algae only makes sense as integrated approach in a biorefinery, were valuable products like ω-3 fatty acids or carotenoids are produced and could be sold as nutraceuticals, proteins could be separated and used as animal feed, and the remaining biomass could be used for biofuel production.

So all in all microalgae could have a large potential for biofuel production in long-term perspectives, however, a lot of research is still necessary and the crude oil price must rise significantly in order to make the algae cultivation and processing for biofuels competitive.

Biodiesel Production Technologies

As it can be seen in Fig. 4, the number of publications and patents dealing with biodiesel has increased enormously within the last 10 years. Especially the number of patents on biodiesel production technology per year has reached over 500. A lot of new innovations regarding new types of catalysts, new purification and rafination steps, separation techniques, and new feedstock have been developed.

Chemically, biodiesel is equivalent to fatty acid methyl esters or ethyl esters, produced out of triacylglycerols via transesterification or out of fatty acids via esterification. In Fig. 5 the formula scheme for the production of fatty acid mono alkyl esters out of triacylglycerol is shown. Fatty acid methyl esters today are the most commonly used biodiesel species, whereas fatty acid ethyl esters (FAEE) so far have been only produced in laboratory or pilot scale.

As vegetable oils or animal fats mainly consist of triacylglycerol (triglycerides) the main reaction for the production of biodiesel is the transesterification or alcoholysis reaction (Fig. 5), whereas esterification is only necessary for feedstock with higher content of free fatty acids.

In a transesterification or alcoholysis reaction, 1 mole of triglyceride reacts with 3 moles of alcohol to form 1 mole of glycerol and 3 moles of the respective fatty acid alkyl ester. The process is a sequence of three reversible reactions, in which the triglyceride molecule is converted step by step into diglyceride, monoglyceride, and glycerol. In order to shift the equilibrium to the right, methanol is added in an excess over the stoichiometric amount in most commercial biodiesel

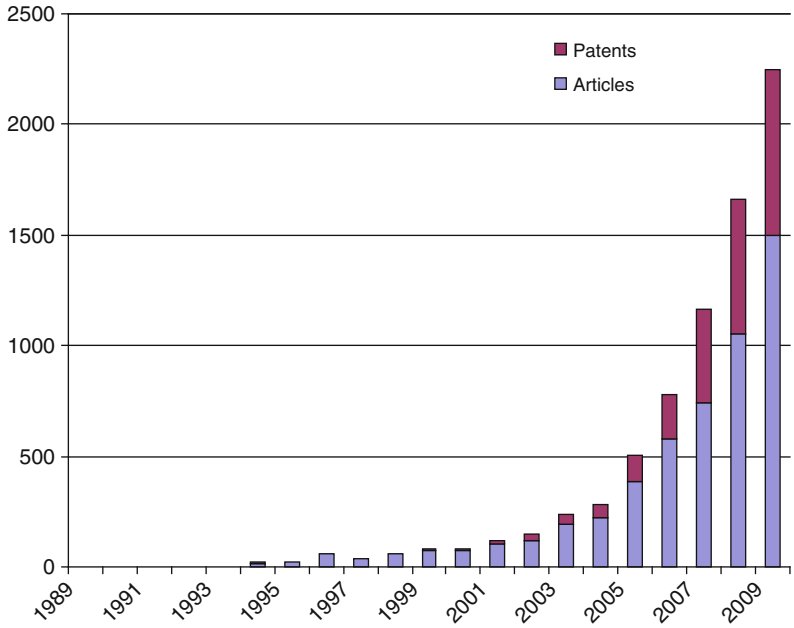

Biodiesel. Figure 4
Number of scientific publications on "Biodiesel" according to SciFinder, CAS [12]

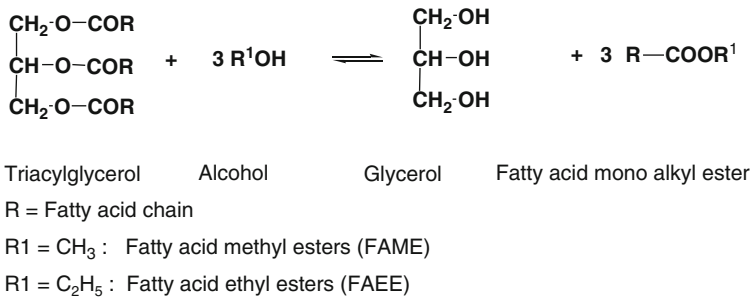

Biodiesel. Figure 5
Production of fatty acid mono alkyl esters via transesterification

production plants. A main advantage of methanolysis under alkaline catalysis is the fact that the two main products, glycerol and fatty acid methyl esters (FAME), are hardly miscible and thus form separate phases – an upper ester phase and a lower glycerol phase. This process removes glycerol from the reaction mixture and enables high conversion. Ester yields can even be increased – while at the same time minimizing the excess amount of methanol – by conducting methanolysis in two or three steps. Here, only a portion of the total alcohol volume required is added in each step, and the glycerol phase produced is separated after each process stage.

Catalysts for Transesterification and Esterification Reactions

Alkaline or basic compounds are by far the most commonly used catalysts for biodiesel production. The main advantage of this kind of catalysis over acid-catalyzed transesterifications is the high conversion

rate under mild conditions in comparatively short reaction times [22]. However, free fatty acids as minor components in unrefined oils, are converted into soaps and are separated together with the glycerine phase. So the maximum conversion rate depends on the quantity of glycerides in the feedstock. For oils with higher amounts of free fatty acids, a combination of an acidic esterification of free fatty acids and an alkaline transesterification lead to a conversion of almost 100% of fatty acid material. With oils up to 3% of free fatty acid content, the combination of an alkaline transesterification and a post-esterification of the fatty acids recovered out of the glycerol phase is an optimum solution [23]. Also a pre-esterification under acidic catalysis prior to an alkaline transesterification leads to high conversion rates. Concentrated sulfuric acid can be used as cheap catalyst, but this can lead to losses due to the formation of side products, so also heterogenous catalysts like ion exchange resins can be used [24].

As alkaline catalysts for transesterification mostly sodium or potassium hydroxide or alcoholates are used. In small-or medium-scale biodiesel production plants, the use of cheaper alkali hydroxides are preferred, however, there is the need of special equipment for dissolving the solid catalyst in methanol. As these homogenous catalysts can only be used once, they remain as salts in the glycerol phase. For the production of raw or pharmaceutical grade glycerol, the glycerol phase has to be neutralized with an acid, and the formed alkali salts either remain in the raw glycerol or can be filtered off. If sodium hydroxide is used as catalysts, these salts are special waste and have to be disposed, whereas in the case of potassium hydroxide these salts can be reused as fertilizer. For biodiesel production in huge industrial size production plants with a capacity of 100,000 t/year or more mostly refined vegetable oils are used, which at least have to be degummed and deacidified. In this case, the use of a solution of sodium methoxide in methanol is used as catalyst. Sodium methoxide is more expensive than hydroxides, but if refined oils are used as feedstock, less catalyst can be used and the formation of soaps as side products is minimized.

Whereas traditional homogeneous catalysis offers a series of advantages, the major drawback is the fact that homogenous catalysts cannot be reused. Moreover, catalyst residues have to be removed from the ester product, usually with several washing steps, which increases production costs. Thus, there have been various attempts at simplifying product purification by applying heterogeneous catalysts, which can be recovered by filtration or are alternatively used as fixed-bed in continuous operation. The most frequently cited heterogeneous alkaline catalysts are alkali metal- and alkaline earth metal carbonates and oxides [25].

The main disadvantage of heterogenous catalysis is the need for drastic reaction conditions like high temperature and pressure, which leads to higher investment costs and to higher operating compared to homogenous catalysis. Also higher reaction temperature facilitates the formation of side products. On the other side, most of the heterogeneous catalysts can be reused for a specific time and also most of these catalysts can be used simultaneously for esterification and transesterification [26, 27]. The first technology using heterogeneous catalysts like zinc oxides or zinc aluminates is used in several commercial biodiesel production plants in France and in the USA [28, 29]. The so-called Esterfip-H process was developed by the Institute Français du Pétrole (IFP) and is designed and commercialized by Axens. The main advantages of the process are described as the production of high-quality glycerol and no need for disposal of salts resulting from the catalyst. However, the overall economic advantages have to be proved in long-term running.

Within the last years, the use of enzymes as heterogenous catalysts for the production of biodiesel has been described widely in literature [29]. Lipases are enzymes that catalyze both the hydrolytic cleavage and the synthesis of ester bonds in glycerol esters. Their application in FAME production dates back to Choo and Ong [30], filing a patent application on lipase-catalyzed methanolysis in the presence of water, and to Mittelbach, reporting on the first water-free process for lipase-catalyzed biodiesel production [31]. As compared to other catalyst types, biocatalysts have several advantages. They enable conversion under mild temperature-, pressure-, and pH-conditions. Neither the ester product nor the glycerol phase has to be purified from basic catalyst residues or soaps. Moreover, both the transesterification of triglycerides and the esterification of free fatty acids occur in one process step. As a consequence, also highly acidic fatty materials, such as palm oil or waste oils, can be used without

pretreatment. Furthermore, enzymes could be perfectly used for the production of fatty acid ethyl esters using azeotropic technical ethanol. Though the use of enzymes seems to overcome most of the problems related to biodiesel production, the major drawback is still the price of enzymes for the production of bulk chemicals. Therefore, the enzymatic route for biodiesel production today is still too expensive for industrial application.

Basically, transesterification of triglycerides with lower alcohols also proceeds in the absence of a catalyst, provided reaction temperatures and pressures are high enough [32–34]. Above the critical temperature, a gas cannot be liquefied. The supercritical conditions show liquid as well as gaseous properties, so there have been a lot of applications for CO_2 extractions but also for carrying out chemical reactions. The advantages of not using a catalyst for transesterification are that high-purity esters and soap-free glycerol are produced. The high excess of methanol, which has to be used during supercritical transesterification, seems to make the process not economically feasible; however, a two-step process has been described, which in the first step hydrolyzes the glycerides into fatty acid with an excess of water, and in the second step esterification takes place, which requires lower amounts of methanol [35].

Though non-catalytical hydrolysis of vegetable oils today is common practice in industrial application of the production of fatty acids, the non-catalytical production of fatty acid methyl or ethyl esters has not yet been commercialized. The main reasons are the high investment costs for the high temperature and pressure procedure, and also the possibility of side reactions, which lead automatically to lower yields and higher purification costs.

A series of other approaches for biodiesel production have been reported including membrane technology for separating of methanol and glycerol from biodiesel [36], ultrasound-assisted esterification and transesterification [37], microwave-induced reactions [38], the use of different solvents for faster reaction rates [39] as well or the so-called in situ preparation of biodiesel directly from oil containing biomass have been described [40]. All these technologies seem to be very challenging and innovative, however, no practical industrial application has been reached so far mainly due to the higher investment or running costs compared to classical technology. However, all these approaches might be interested in the future in order to improve the whole life cycle assessment of the production of biodiesel in order to meet the high demands of international legislations for sustainable production.

Biodiesel Quality and Specifications

One prerequisite for marketing an alternative fuel is the existence of specifications, which of course are based on existing specifications for mineral-based products. Biodiesel has been commercially produced since almost 20 years starting with the first industrial scale production plants in Austria and Germany in 1991. As Austria was pioneer in biodiesel production and utilization, as early as in 1991 the first national specification for biodiesel worldwide was established. This standard was based on several years of experiments with biodiesel prepared from rapeseed oil. Three years later also in Germany, national standards were established, followed by Italy and France. Because of the rapid development of biodiesel utilization in Europe there was the need for a harmonized European Specification for biodiesel. After several years of intensive negotiations and discussions in CEN committees, the harmonized European specification for biodiesel used as 100% fuel or as blend component EN 14214 came effective in 2004 [41]. In 2001, also the US standardization body ASTM published the specifications ASTM D 6751 for pure biodiesel (B100) and for blending with fossil diesel in levels up to 20% by volume [42]. The different parameters can be divided into general parameters also valid for fossil fuel and biodiesel specific parameters, which have to be added because of the different chemical composition.

In Table 4, a comparison of general and biodiesel specific parameters and limits between the latest ASTM D 6751 and EN 14214 versions is given, based on the most recent developments.

As can be seen in Table 3, the different parameters and limits between CEN and ASTM standards for biodiesel are quite similar, however there are some differences, which can be seen as barrier for international biodiesel market. Especially the limitation for Iodine Number in the European Specifications excludes

Biodiesel. Table 3 Comparison of parameters and limits in European and US specifications

Parameter	Unit	EN 14214 [2008]	ASTM D 6751 09-a
Density	15°C [kg/m^3]	860–900	–
Viscosity	40°C [mm^2/s]	3.5–5	1.9–6
Flash point	[°C]	≥101	≥93
Sulfur	[mg/kg]	≤10	≤15
Sulfated ash	[% m/m]	≤0.02	≤0.02
Conradson carbon Residue	[% m/m]	≤0.30 (10% distil. residue)	≤0.05
Cetane number	–	≥51	≥47
Water	[mg/kg]	≤500	0.05 vol%
Total contamination	[mg/kg]	≤24	–
Copper corrosion	–	Class 1	–
Oxidation stability	[h]	≥6	≥3
Acid number	[mg KOH/g]	≤0.50	≤0.50
Distillation, T90	[°C]	–	≤360
Iodine number	[g Iodine/100 g]	≤120	–
Linolenic acid	[% m/m]	≤12	–
Polyunsaturated fatty acids (>4 double bonds)	[% m/m]	≤1	–
Methanol	[% m/m]	≤0.20	≤0.20
Monoglycerides	[% m/m]	≤0.80	–
Diglycerides	[% m/m]	≤0.20	–
Triglycerides	[% m/m]	≤0.20	–
Free glycerol	[% m/m]	≤0.02	≤0.020
Total glycerol	[% m/m]	≤0.25	≤0.250
Sum of Na, K	[mg/kg]	≤5	≤5
Sum of Ca, Mg	[mg/kg]	≤5	–
Phosphorus	[mg/kg]	≤4	≤10

biodiesel made from 100% soybean oil. However, it is allowed to blend different feedstock to reach the limits. Also there are some stricter European regulations for the oxidation stability and also for the limits of phosphorus as well as for calcium and magnesium.

The European as well as the US specifications have been the basis for a series of similar specifications in many countries around the world, so all in all there are quite similar regulations worldwide. However, these limits for different parameters are only technically based, in order to reach a sustainable biodiesel production. A lot of additional regulations have been discussed worldwide and are outlined within the next chapter.

Environmental Issues of Biodiesel

Engine Emissions

The diesel engine, also called compression ignition engine (CI), was patented by Rudolf Diesel in 1892.

Biodiesel. Table 4 Relative emissions from rapeseed oil biodiesel compared to fossil diesel (without catalytical converter) (From Mittelbach and Remschmidt, Biodiesel, the comprehensive handbook)

Reference	CO	HC	NO_x	PM
Mittelbach et al. [49]	−4%	−20%	+28%	−23%
Vellguth [50]	−8%	−20%	+7%	Soot number: −45%
Apfelbeck and Gessner [51]	−10%	−36%	+4%	−31%
Scharmer et al. [52]	±0%	−20 to −40%	–	Up to 40% lower
Krahl, Prieger et al. [53]	±0%	−10 to −20%	+10%	Up to 40% lower
Sharp [54]	−39%	−70%	+3%	−25%
May et al. [55]	−10%	−20%	+10%	−50%
Goerke [56]	−41%	−49%	+12%	−41%
Sams [57]	−16%	−33%	+4%	+11%
Krahl, Munack et al. [58]	−37%	−22%	+10%	−10%
	−39%[a]	−20%	+28%	+60%
Makareviciene and Janulis [59]	−6%	−74%	+10%	Smoke density: −68%

Unlike the spark-ignited gasoline engine, Diesel's invention works on self-ignition. Diesel engines offer a series of advantages over their gasoline-fueled counterparts. So they operate at higher compression ratios than Otto engines, which improve energy efficiency. Moreover, the fuel-to-air ratio varies with engine load and therefore with the quantity of fuel injected, resulting in lean fuel–air mixtures. This has positive effects on carbon monoxide (CO) and hydrocarbon (HC) emissions. Drawbacks of the diesel technology include a tendency for increased nitrogen oxide (NO_x) and particulate matter (PM) emissions. Moreover, diesel engines tend to be heavier than comparable gasoline engines.

With direct (DI) and indirect (IDI) injection engines, two types of combustion systems have been developed. In the first fuel is injected directly into the combustion chamber, whereas in the latter fuel is injected into a pre-chamber, from which partially oxidized gases and evaporated fuel are introduced into the main combustion chamber. Although characterized by a comparatively harsh combustion noise, DI engines are now commonly used for passenger cars due to their low fuel consumption [43, 44]. This is done at the expense of slightly increased NO_x emissions for DI engines [45]. However, modern, electronically controlled injection systems, such as the "common-rail-system," enable a compromise between conflicting interests [46].

The major part of combustion engine exhaust streams consists of the nontoxic components nitrogen, carbon dioxide, and water. However, about 1.4% of gasoline engine exhaust and 0.2% of diesel engine exhaust are composed of more or less harmful substances. The maximum amounts of certain pollutants in exhaust gases are regulated by national authorities in various countries throughout the world. In the European Union and the USA, these limited emissions are:

- Carbon monoxide, CO
- Hydrocarbons HC, resulting from unburnt or partially burnt fuel and lubricating oil compounds. Hydrocarbons are either regulated as total hydrocarbon emissions (THC) or as non-methane hydrocarbons (NMHC).
- Nitrogen oxides NO_x, including NO, which is produced in the engine, and NO_2, which results from NO through oxidation within the exhaust stream or later in the atmosphere. Other oxides, such as N_2O, which may also be present in the exhaust gas, are not regulated. Sometimes one

combined limit for HC and NO_x is used instead of two separate limits.

- Particulate matter, which is only regulated for diesel engines.

Carbon dioxide emissions today are not limited, but due to European regulations the overall average CO_2 emissions of a fleet from a car manufacturer should not exceed 130 g/km, starting from 2012 [47].

An enormous amount of data on measurements of legally limited exhaust components all over the world is available. In comparing these results, however, some points have to be kept in mind. First, exhaust emissions differ widely according to engine types, test cycles, and fuel grades used, so that a comparison of absolute pollutant concentrations derived from different sources hardly makes sense. Instead only relative emission changes between biodiesel from rapeseed oil and fossil diesel fuels are listed in Table 4. Second, emission values are greatly influenced by the application of an exhaust gas after treatment system. To demonstrate the effects of the fuels, only data without oxidation catalytic converters are listed. As it can be seen, literature data indicate an overall slight reduction of CO and a significant reduction of HC and particulate matter emissions, whereas NO_x emissions are slightly increased. The reason for the increase of NO_x emissions with biodiesel or biodiesel blends is not yet fully understood. Especially in newer types of heavy-duty engines, the increase of NO_x emissions is rather low. An assessment of North American heavy-duty engine emission test results for biodiesel from 49 experimental studies, including both engine dynamometer and vehicle test results, shows that the use of a common biodiesel blend (B20) consistently reduces emissions of particulate matter, hydrocarbons, and carbon monoxide by 10–20%. Especially for newer types of engines, there is no statistical evidence that the average NO_x emissions increase [48].

All these differences, however, will become irrelevant because of the future legislation for mandatory installation of efficient after treatment systems including particulate filters and SCR (selective catalytic reduction) technology.

Sustainability of Biodiesel

In the very first beginning of biodiesel development and utilization, no broad discussion has been taken place on the issue, that agricultural products are used for fuel production. Especially because of rising oil prices and overproduction of agricultural products in Europe, biodiesel produced out of vegetable oils was a well-accepted alternative supported by some governments. There have been plans that biodiesel should mainly be used for agricultural production, ensuring the food supply in times of crisis. Furthermore, biodiesel production should bring a secure and continuous income for farmers, leading to a higher job rate in rural areas. However, biodiesel production was more and more industrialized, and a huge number of industrial biodiesel plants have been installed within the last 10 years around the world. The main driver was the need for the reduction of the green house gas emissions in the transport sector, leading to a number of incentives and mandates especially in Europe for the use of biofuels. The European Directive on the promotion of the use of biofuels or other renewable fuels for transport from 2003, mandating a share of biofuels in the transport sector of 5.75% until 2010 [60], led to an enormous boom of biodiesel production installations. Since 2008, however, when there has been the enormous rise in crude oil and food prices as well as in all other commodities, the fuel versus food discussion became fully effective. The consequence of this debate was the development of sustainability criteria and the assessment of the full life cycle analysis for all different biofuels. A lot of these sustainability criteria were included in the new European directive on the promotion of the use of energy from renewable sources from 2008, mandating a 10% share of biofuels in all countries of the European Union until 2020 [61].

Basically, biodiesel as renewable biofuel is considered as environmentally friendly because of saving CO_2 emissions by absorbing CO_2 during the growth of biomass [62]. However, by considering the whole life cycle of biofuels or biodiesel from production of the biomass until the final end use as fuel there are not necessarily environmental advantages. All the energy used for the whole supply chain including cultivation, the use of fertilizers and pesticides, harvesting, processing, and transport has to be considered (Fig. 6). Also the side effects of cultivation, above all the use of fertilizers producing the highly active green house gas nitrous oxide N_2O (300 times more effective

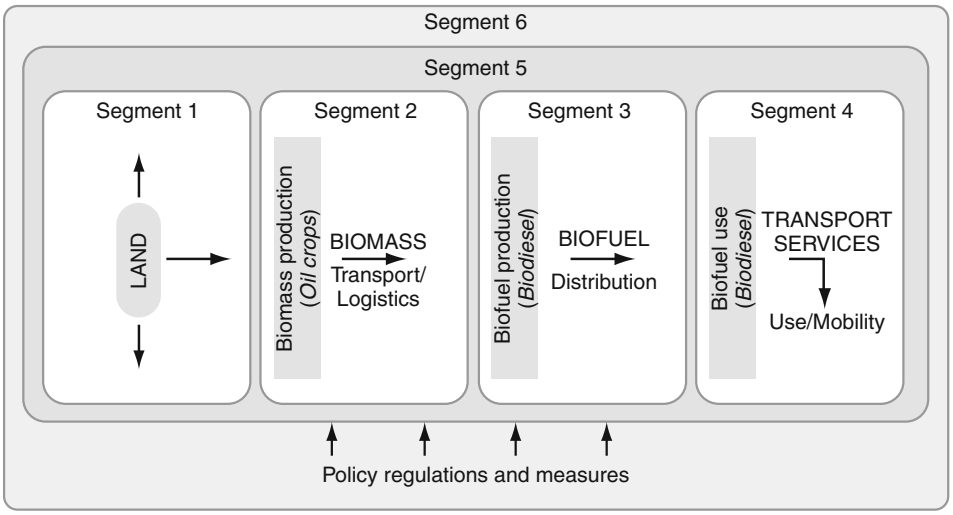

Biodiesel. Figure 6
Biodiesel supply chain (from well to wheel) [62]

than CO_2) have to be included. Furthermore, aspects of the use of ecological sensitive areas, as well as effects of direct and indirect land use change, have to be taken into consideration. Direct land use change (DLUC) concerns the case where production of energy crops for biofuels production leads to the conversion of land actually storing carbon-like grassland into cultivated land. This could lead to an overestimation of reduction of green house gases or in the case of degraded soil it could improve the soil carbon balance. Indirect land use change (ILUC) relates to the unintended consequence of releasing more carbon emissions due to land use changes around the world induced by the expansion of croplands for biofuel production. However, in most LCA studies ILUC is not considered, because more research is needed for harmonizing and improving the methodology.

Although there is a tool for the evaluation of the life cycle assessment existing in form of an ISO standard [63], it has been applied in literature in a variety of ways and thus often leads to diverging results. LCA is often limited to energy balance or to green house gas saving balance. Several LCA studies have been carried out under various frameworks, scopes, and consistency, making it difficult to compare the results [64]. One of the most important elements is to define the system boundaries, all individual processes of the complete life cycle have to be considered, and also all coproducts have to be taken into consideration, especially glycerol and protein as oil cake. In the so-called allocation procedure, the environmental implications of a product and its coproducts are split, whereas in the substitution procedure the desired product gets a credit, which corresponds to the environmental implications of an equivalent product [65]. The issue of allocation is one of the weaknesses of biofuels LCA.

A much simpler approach is the calculation of the energy balance, which means the ratio between the energy of biofuel produced in the engine and the total energy needed for the total production of the biofuel without considering the solar energy for the growing of the biomass. For the main feedstock rapeseed oil and soybean oil in all published data there is a positive energy balance, which means the total energy input is lower than the output. The corresponding factors for rapeseed oil lie between 1:2 and 1:3 (input:output) and for soybean oil between 1:3.2 and 1:3.5 (from *Biodiesel – The Comprehensive Handbook*). For palm biodiesel a ratio of 1:2.27–1:3.58 has been reported [66, 67].

In Fig. 7, the relative reduction of green house gas emissions of different biofuels compared to a gasoline-fueled car is outlined. It can be easily seen that the reduction varies enormously with the type of feedstock

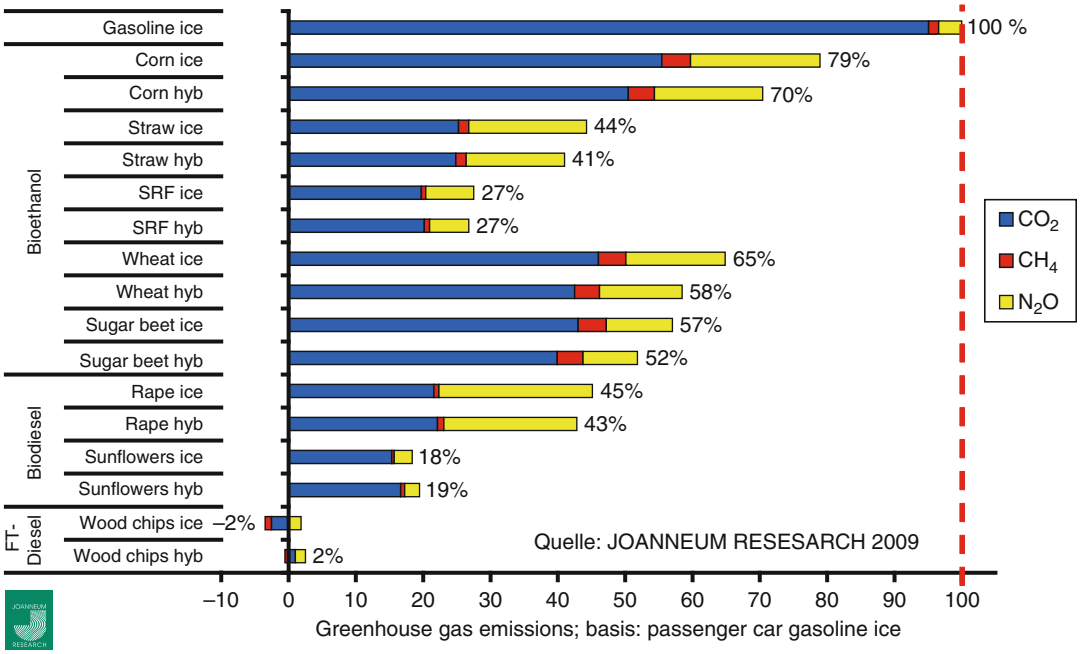

Biodiesel. Figure 7
Reduction of GHG emissions from different biofuels in relation to fossil gasoline-fueled passenger car [68] *Ice* internal combustion engine, *hyb* hybrid

and fuel. Overall a reduction of GHG emissions can be seen, the best values are obtained for biodiesel from sunflower oil and BtL Fischer–Tropsch diesel from wood chips. Bioethanol from corn and sugar beet does not show high reduction, however, bioethanol from sugar cane, which is not included in the figure, has the best values. Also biodiesel from palm oil or used frying oil or animal fat is not outlined but has a very good GHG saving potential.

According to the European Directive on the promotion of the use of energy from renewable sources [61] biofuels should reach at least 35% GHG reduction compared to fossil fuel. With effect from January 1, 2017, the greenhouse gas emission saving from the use of biofuels shall be at least 50% and from January 1, 2018, that greenhouse gas emission saving shall be at least 60% for biofuels produced in installations in which production started on or after January 1, 2017. It has to be mentioned that the data from the European Directive are based on the energy allocation method, whereas the figures presented in Fig. 7 are calculated according to the substitution method, which come closer to a real life cycle assessment.

Biofuels according to the new European Directive shall not be made from raw material obtained from land with high biodiversity value, like primary forest and other wooded land, namely forest and other wooded land of native species, highly biodiverse grassland, wetlands, and continuously forested areas.

Regarding the minimum values for GHG savings within the directive, there are typical and default values for the different biofuels produced from different sources. The default values could be used, if there are no own calculations for a specific type of biofuel, the typical values are mean values from literature data, which are always slightly higher. In Table 5, it can be seen that biodiesel from soybean oil would not meet the minimum value of 35%, so in that case it has to proved case by case by individual calculation, that the real value are over 35%. The minimum value has to be reached by each feedstock, so blending to reach the limit is not allowed. As the minimum value will be increased up to 50% in 2017 and up to 60% in 2018 only biodiesel from waste cooking oil or animal fat will be above the limit. This would be a high risk for biodiesel from vegetable oils, if there

Biodiesel. Table 5 Typical and default values for reduction of GHG according to the European directive 2009/28/EC [61]

Biodiesel type	Typical value	Default value
Biodiesel rapeseed oil	45%	38%
Biodiesel sunflower	58%	51%
Biodiesel soybean	40%	31%
Biodiesel palm (process not specified)	36%	19%
Biodiesel palm (process with methane capture at oil mill)	62%	56%
Biodiesel waste oil/animal fat	88%	83%

would not be any significant improvement of the whole life cycle assessment. However, within the next years there will be need for further adjustments and adaptations in order to guarantee sustainable biofuel production.

Future Directions

Within the next decades, there will be a constant rising demand for biofuels due to lack of alternatives in the transport sector and the need for lowering the emissions of green house gases. Due to national and international legislation especially so-called second-generation biofuels will be favorized, which are produced from nonfood biomass like lignocellulosic material. For heavy-duty vehicles mainly used for transporting goods diesel fuel is the main energy source. One possibility to produce second-generation biodiesel is gasification of biomass and further synthesis via Fischer–Tropsch reaction (biomass to liquid, BtL). This technology however is not yet commercialized industrially because of complicated and expensive installations. So fatty acid methyl or ethyl esters produced out of fatty acid material will be still the dominant biofuel in the diesel sector in mid-term perspective. However, the kind of feedstock will be more and more focused on nonfood crops like oil from *J. curcas* or microalgae. Also the use of waste material like used cooking oil or animal fats will become more interesting. The traditional sources for production of biodiesel like rapeseed oil, soybean oil, and palm oil will still be dominant, but it is also clear that this kind of feedstock could never substitute a significant amount of total demand of transport fuel. Theoretically microalgae, which could be grown on nonagricultural areas, could be produced in such amounts to substitute the total demand of fuels; however, a lot of research still has to be carried out in order to lower the total costs of cultivation and processing. Also all the different feedstock have to be evaluated and compared with life cycle assessments and the social impact of production and processing has to be considered carefully. So all in all biofuels will play an important role as alternative fuels in the transport sector as long as transport is based on combustion engines.

Bibliography

Primary Literature

1. Knothe G (2001) Historical perspectives on vegetable oil-based diesel fuels. Inform 12:1103–1107
2. Duffy P (1852) On the constitution of stearine. J Chem Soc 5:303
3. Bradshaw GB (1941) Preparation of detergents. US Patent 2 360 844 xc
4. Improvements in or relating to methods of alcoholysis of low grade fatty materials (1946). Patent GB 612,667
5. Mittelbach M, Wörgetter M, Pernkopf J, Junek H (1983) Diesel fuel derived from vegetable oils: preparation and use of rape oil methyl ester. Energ Agr 2:369–384
6. Mittelbach M, Andrae F, Junek H (1986) Verfahren und Vorrichtung zur Herstellung eines als Kraft-bzw. Brennstoffs geeigneten Fettsäureestergemisches. Austrian Patent AT 386 222 B
7. Wang R (1988) Development of biodiesel fuel. Taiyangneng Xuebao 9:434–436
8. Bailer J, de Hueber K (1991) Determination of saponifiable glycerol in "Bio-Diesel". Fresenius J Anal Chem 340:186
9. Argentine Renewable Energies Chamber (2009) State of the Argentine biodiesel industry, First Semester 2009
10. European Biodiesel Board (2010) http://www.ebb-eu.org/stats.php
11. USDA Foreign Agricultural Service (2009) EU-27 biofuels annual
12. Chemical Abstracts Service (CAS), SciFinder (2010) American chemical society
13. Gübitz G, Mittelbach M, Trabi M (1997) Biofuels and industrial products from *Jatropha curcas*. DbV-Verlag für die Technische Universität Graz, Graz
14. Carels N (2009) *Jatropha curcas*: a review. Adv Bot Res 50:39–86
15. King A, He W, Cuevas J, Freudenberger M, Ramiaramanana D, Graham I (2009) Potential of *Jatropha curcas* as a source of renewable oil and animal feed. J Exp Bot 60:2897–2905

16. Debnath M, Bisen P (2008) *Jatropha curcas* L., a multipurpose stress resistant plant with a potential for ethnomedicine and renewable energy. Curr Pharm Biotechnol 9:288–306
17. Achten W, Verchot L, Franken Y, Mathijs E, Singh V, Aerts R, Muys B (2008) Alternative uses of Jatropha oil cake. Biomass Bioenergy 32:1063–1084
18. Rakshit K, Darukeshwara J, Raj K, Narasimhamurthy K, Saibaba P, Bhagya S (2008) Toxicity studies of detoxified Jatropha meal (*Jatropha curcas*) in rats. Food Chem Toxicol 46:3621–3625
19. Devappa R, Swamylingappa B (2008) Biochemical and nutritional evaluation of Jatropha protein isolate prepared by steam injection heating for reduction of toxic and antinutritional factors. J Sci Food Agric 88:911–919
20. Pienkos P, Darzins A (2009) The promise and challenges of microalgal-derived biofuels. Biofuels Bioprod Bioref 3: 431–440
21. Stephens E, Ross I, King Z, Mussgnug J, Kruse O, Posten C, Borowitzka M, Hankamer B (2010) An economic and technical evaluation of microalgal biofuels. Nat Biotechnol 28:126–128
22. Freedman B, Kwolek W, Pryde H (1986) Quantitation in the analysis of transesterified soybean oil by capillary gas chromatography. J Am Oil Chem Soc 63:1370–1375
23. Mittelbach M, Koncar M (1994) Process for preparing fatty acid alkyl esters. European Patent EP 0 708 813 B1
24. Russbueldt B, Hoelderich W (2009) New sulfonic acid ion-exchange resins for the preesterification of different oils and fats with high content of free fatty acids. Appl Catal A 362: 47–55
25. Melero J, Iglesias J, Morales G (2009) Heterogeneous acid catalysts for biodiesel production: current status and future challenges. Green Chem 11:1285–130
26. Helwani Z, Othman M, Aziz N, Kim J, Fernando W (2009) Solid heterogeneous catalysts for transesterification of triglycerides with methanol. Appl Catal A 363:1–10
27. Stern R, Hillion G, Rouxel J (2000) IFP, US 6,147.196
28. http://www.ifp.fr/IFP/en/ifp/ab13_02.htm (2010)
29. Adamczak M, Bornscheuer U, Bednarski W (2009) The application of biotechnological methods for the synthesis of biodiesel. Eur J Lipid Sci Technol 111:800–813
30. Choo Y, Ong S (1986) Transesterification of fats and oils. British Patent GB 2 188 057
31. Mittelbach M (1990) Lipase catalyzed alcoholysis of sunflower oil. J Am Oil Chem Soc 67:168–170
32. Kusdiana D, Saka S (2001) Methyl esterification of free fatty acids of rapeseed oil as treated in supercritical methanol. J Chem Eng Jpn 34:383–387
33. Wen D, Jiang H, Zhang K (2009) Supercritical fluids technology for clean biofuel production. Prog Nat Sci 19:273–284
34. Demirbas A (2006) Biodiesel production via non-catalytic SCF method and biodiesel fuel characteristics. Energy Convers Manage 47:2271–2282
35. Kusdiana D, Saka S (2004) Effects of water on biodiesel fuel production by supercritical methanol treatment. Bioresour Technol 91:289–295
36. Cao P, Dube M, Tremblay A (2008) Methanol recycling in the production of biodiesel in a membrane reactor. Fuel 87: 825–833
37. Kalva A, Sivasankar T, Moholkar V (2009) Physical mechanism of ultrasound assisted synthesis of biodiesel. Ind Eng Chem Res 48:534–544
38. Geuens J, Kremsner J, Nebel B, Schober S, Dommisse R, Mittelbach M, Tavernier S, Kappe C, Maes B (2008) Microwave assisted catalyst free transesterfication of triglycerides with 1-butanol under supercritical conditions. Energy Fuels 22: 643–645
39. Mahajan S, Konar S, Boocock D (2006) Standard biodiesel from soybean oil by a single chemical reaction. J Am Oil Chem Soc 83:641–644
40. Haas M, Scott K, Foglia T, Marmer W (2007) The general applicability of in situ transesterification for the production of fatty acid esters from a variety of feedstocks. J Am Oil Chem Soc 84:963–970
41. EN 14214 (2008) Automotive fuels – fatty acid methyl esters (FAME) for diesel engines – requirements and test methods, CEN
42. ASTM D6751 (2009) Standard specification for biodiesel fuel blend stock (B100) for middle distillate fuels, ASTM
43. Fabri J, Dabelstein W, Reglitzky A (1990) Ullmann's encyclopedia of industrial chemistry, vol A 16, 5th edn. Weinheim, Basel/Cambridge/New York
44. Kroschwitz J, Howe-Grant M (1994) Kirk-Othmer encyclopedia of chemical technology, vol 12, 4th edn. Wiley, New York/Chichester/Brisbane/Toronto/Singapore
45. Guttmann H, Preuss A, Schädlich K, Schug K (1998) Breaking the link between NO_x and particulate emissions of diesel engines – potential of fuels and exhaust aftertreatment measures. Proceedings of the 15th World Petroleum Congress. Wiley, New York, pp 633–643
46. Tschöke H (1998) Ist eine spezielle Motorenentwicklung für Biodiesel notwendig? Landbauforschung Völkenrode. Sonderheft 190 (Biodiesel Optimierungspotentiale und Umwelteffekte) (1998), pp 81–87
47. Regulation (EC) No 443/2009 of the European parliament and of the council setting emission performance standards for new passenger cars as part of the community's integrated approach to reduce CO_2 emissions from light-duty vehicles
48. Yanowitz J, McCormick R (2009) Effect of biodiesel blends on North American heavy-duty diesel engine emissions. Eur J Lipid Sci Technol 111:763–772
49. Mittelbach M, Tritthart P, Junek H (1985) Diesel fuel derived from vegetable oils, II: emission tests using rape oil methyl ester. Energ Agr 4:207–215
50. Vellguth G (1988) Pflanzenöl als Dieselkraftstoff-Substitut. Sonderdruck aus Landbauforschung Völkenrode 1:12–16
51. Apfelbeck R, Gessner B (1992) Untersuchung der Abgaszusammensetzung von Dieselmotoren beim Betrieb mit Rapsöl und Rapsölmethylester sowie deren Mischungen mit Dieselkraftstoff. In Gelbes Heft No 40, TU München. Bayrische Landesanstalt für Landtechnik Freising-Weihenstephen

52. Scharmer K, Glüsing H, Krings L, Zimalla K (1995) Standardanforderungen an Rapsölmethylester als Motorkraftstoff. BMFT-Studie TV 91021
53. Krahl J, Prieger K, Munack A, Bünger J (1996) Übersicht über Emissionen von Rapsölkraftstoffen und deren Umweltauswirkungen. VDI-Berichte Nr. 1297. VDI-Verlag, Düsseldorf
54. Sharp C (1996) Emissions and lubricity evaluation of rapeseed derived biodiesel fuels. Final report from SWRI to Montana department of environmental quality
55. May H, Hattingen U, Klee P, Spitz M (1997) Vergleichende Emissionsuntersuchungen beim Betrieb verschiedener Dieselmotoren mit Dieselkraftstoff und Rapsmethylester. MTZ Motortechnische Zeitschrift 58
56. Goerke D (1998) Ansatzpunkte zur Verbesserung der Wettbewerbsfähigkeit von Pflanzenöl als Treibstoff gegenüber Dieselkraftstoff. Fortschritt-Bericht VDI. Reihe 12 Verkehrstechnik Nr. 368. VDI-Verlag, Düsseldorf
57. Sams T (1998) Exhaust components of biofuels under real world engine conditions. Plant oils as fuels. Present state of science and future developments. Proceedings of the symposium held in Potsdam, Germany. Springer Verlag, Berlin, 16–18 Feb 1997
58. Krahl J, Munack A, Schröder O, Stein H, Dutz M, Bünger J (2003) Comparison of biodiesel with different diesel fuels. Fuels 2003. Conference held at Technische Akademie Esslingen
59. Makareviciene V, Janulis P (2003) Environmental effect of rapeseed oil ethyl ester. Renewable Energy 28:2395–2403
60. Directive 2003/30/EC of the European parliament and of the council on the promotion of the use of biofuels or other renewable fuels for transport
61. Directive 2009/28/EC of the European parliament and of the council on the promotion of the use of energy from renewable sources
62. Majer S, Mueller-Langer F, Zeller V, Kaltschmitt M (2009) Implications of biodiesel production and utilisation on global climate – a literature review. Eur J Lipid Sci Technol 111:747–762
63. International Standardization Organization, ISO 14040–43. Environmental management life cycle assessment – principles and framework. Beuth Verlag, Berlin
64. Gnansounou E, Dauriat A, Villegas J, Panichelli L (2009) Life cycle assessment of biofuels: energy and greenhouse gas balances. Bioresour Technol 100:4919–4930
65. Gärtner S, Reinhardt G (2004) Environmental implications of biodiesel (Life-cycle assessment). In: Knothe G, Krahl J, van Gerpen J (eds) The biodiesel handbook. AOCS Press, Champaign
66. Lam M, Lee K, Mohamed A (2009) Life cycle assessment for the production of biodiesel: a case study in Malaysia for palm oil versus jatropha oil. Biofuels Bioprod Biorefin 3:601–612
67. Pleanjai S, Gheewala S (2009) Full chain energy analysis of biodiesel production from palm oil in Thailand. Appl Energy 86:209–S214
68. Jungmeier G, Spitzer J, Hofbauer H, Fürnsinn S, Wörgetter M, Bacovsky D, Lingitz A, Kaltenegger, Königshofer H (2009) F&E-Strategie für Biokraftstoffe

Books and Reviews

Balat M (2009) Biodiesel fuel from triglycerides via transesterification – a review. Energy Sources A 31:1300–1314

Demirbas M (2010) Micro-algae as a feedstock for biodiesel energy education science and technology, part A. Energ Sci Res 25:31–43

Fukuda H (2009) Enzymatic production of biodiesel. In: Soetaert W, Vandamme E (eds) Biofuels. Wiley, New York, pp 129–151

Knothe G, Krahl J, Van Gerpen J (eds) (2009) The biodiesel handbook, 2nd edn. American Oil Chemists' Society, ISBN 978-1-893997-62-2

Mittelbach M (2009) Process technologies for biodiesel production. In: Soetaert W, Vandamme E (eds) Biofuels (Wiley series in renewable resources). Wiley, New York

Mittelbach M, Remschmidt C (2006) In: Mittelbach M (ed) Biodiesel, the comprehensive handbook. Graz, ISBN: 3-200-00249-2

Moser B (2009) Biodiesel production, properties, and feedstocks. In vitro cellular & developmental biology. Plant J 45:229–266

Murugesan A, Umarani C, Chinnusamy T, Krishnan M, Subramanian R, Neduzchezhain N (2009) Production and analysis of bio-diesel from non-edible oils-a review. Renewable Sustainable Energy Rev 13:825–834

Ravasio N, Zaccheria F, Psaro R (2009) The use of catalysis in the production of high-quality biodiesel. In: Barbaro P, Bianchini C (eds) Catalysis for sustainable energy production., pp 323–344

Verhe R, Stevens C (2009) Production of biodiesel from waste lipids. In: Soetaert W, Vandamme E (eds) Biofuels. Wiley, New York, pp 153–170

Vyas A, Verma J, Subrahmanyam N (2009) A review on FAME production processes. Fuel 89:1–9

Biodiversity in Cities, Reconnecting Humans with Nature

Robbert P. H. Snep[1], Philippe Clergeau[2]
[1]Alterra, Wageningen University and Research Center, Wageningen, The Netherlands
[2]Department of Ecology and Biodiversity Management, National Museum of Natural History, Paris, France

Article Outline

Glossary
Definition of the Subject
Introduction
City Environments as Wildlife Habitat
Urban Wildlife Species and Communities

Opportunities to Connect City Actors with Urban Nature
Future Directions: Integrating Wildlife Conservation in Sustainable City Planning and Design
Bibliography

Glossary

Biodiversity The variability among living organisms from all sources, including, "inter alia," terrestrial, marine, and other aquatic ecosystems, and the ecological complexes of which they are part: This includes diversity within species, between species, and of ecosystems (United Nations – Convention on Biological Diversity).

Connectivity Landscape connectivity is the degree to which the landscape facilitates or impedes movement of plants and animals among habitat patches (cf. [70]).

Corridors and stepping stones Corridors are linear strips of habitat through the landscape of which the length, width, and design are depending on the species. Instead of continuous corridors, for some easy-migrating species (e.g., some bird species) also so-called stepping stones could support their dispersal through the city. A stepping stone connection consists of a subsequent series of small patches of habitat positioned between larger habitat structures [24, 25].

Dispersal Process of individuals leaving the place where they are resident (home) and looking for a new place to live. This behavior can occur both within and between habitat patches [33].

Fragmentation Describes the emergence of discontinuities (fragmentation) in an organism's preferred environment (habitat), causing populations to get isolated from each other, and increased disturbance of remaining habitat. Habitat fragmentation can be caused by geological processes that slowly alter the layout of the physical environment, or by human activity such as land conversion (e.g., natural area that gets "developed" into city area), which can alter the environment much faster and causes extinctions of many species (Wikipedia).

Habitat An ecological or environmental area that is inhabited by a particular species of animal, plant, or other type of organism. For wildlife in cities, this includes the total area used for foraging (e.g., gardens, parks), reproduction, and nesting (this may include buildings, e.g., for bats and some bird species), resting, hibernating, and migrating.

Habitat network An interconnected configuration of habitat patches and corridors.

Habitat patch A relatively homogeneous area that differs from its surroundings. Patches are the basic unit of the landscape that change and fluctuate, a process called patch dynamics. Patches have a definite shape and spatial configuration, and can be described compositionally by internal variables such as number of trees, number of tree species, height of trees, or other similar measurements [25].

Homogenization Biotic homogenization is the process by which the similarity of a biological variable increases across time and space. In the perspective of this chapter, the term "homogenization" is used to describe the increasing similarity of urban wildlife communities (especially "'bird species") in cities across the globe [44].

Landscape ecology The study of how the spatial structure of landscape elements (= different parts of the landscape) affects organism abundance at the landscape level, as well as the behavior and functioning of the landscape as a whole. This includes studying the influence of pattern, or the internal order of a landscape, on process, or the continuous operation of functions of organisms [71].

Metapopulation A metapopulation consists of a group of spatially separated populations of the same species which interact at some level. A metapopulation is generally considered to consist of several distinct populations together with areas of suitable habitat which are currently unoccupied (Wikipedia).

Urban wildlife This includes all non-domesticated animals, plants, and other organisms that live in city environments.

Definition of the Subject

Worldwide, the diversity of plant and animal life is diminishing at high speed. At the same moment, more and more humans become city dwellers, with both the proportion and absolute number of people living in cities increasing rapidly. An important link

between global biodiversity loss and fast urbanization is the enormous ecological foot print by urban dwellers, the huge demand for natural resources as required by the urban life style. Besides, a generally less well-known impact of the global urbanization of human society is the extinction of wildlife experience. People in cities lack frequent and intense human-nature interactions, as compared to our rural history. This leads to a decreased understanding of and support for plant and animal life. This not only negatively impacts biodiversity conservation efforts; it also restricts the long-term abilities of humans to benefit from nature. By promoting *urban* biodiversity, nature will be enhanced in the direct living and working environment of citizens, enabling humans to reconnect with nature.

This chapter addresses the opportunities to enhance urban biodiversity and its experience by citizens. First we illustrate how the city environment is perceived from a wildlife point of view, which is necessary to recognize opportunities to enhance urban biodiversity. Next, we discuss these opportunities one by one, illustrating with examples how to implement them in practice. We conclude with an exploration of future possibilities to integrate urban biodiversity conservation opportunities in the broader concept of sustainable city planning, design, and management.

Introduction

Why Attention for Urban biodiversity?

The latest global Living Planet Index [79] shows a decline of biodiversity about 30% between 1970 and 2007. This is based on trends in 7,953 populations of 2,544 mammal, bird, reptile, amphibian and fish species. We may therefore conclude that global biodiversity loss is currently happening on an immense scale and rate. This loss of biodiversity not only impacts ecosystem functioning, but also human well-being. The fact is that the world's ecosystems provide a wide range of services (so-called ecosystem services) that are of vital importance for the quality of human life. Degeneration of these services has huge direct or indirect negative consequences for human life: for example, (local) extinction of bees decreases pollination service and consequently food production linked to seed [2].

The urban growth of human society can be considered as one of the main causes of global biodiversity loss. According to the United Nations [73], the level of world urbanization crossed the 50% mark in 2009. In addition, between 2009 and 2050, the world population is expected to increase by 2.3 billion, passing from 6.8 billion to 9.1 billion [72]. At the same time, the population living in urban areas is projected to gain 2.9 billion, passing from 3.4 billion in 2009 to 6.3 billion 2050. Thus, the urban areas of the world are expected to absorb all the population growth expected over the next four decades while at the same time drawing in some of the rural population [73].

The impact of human lifestyle on the natural ecosystem, illustrated by a concept as the ecological footprint, is extremely high for humans living in cities [53]. As example, the city of Vancouver, Canada, requires 180 times more land to generate and process materials than the city actually occupies [52]. Already in the 1970s it was documented that modern cities consume 10–100 times more energy (per unit area) than natural systems [50]. All in all, the urban life style is an important cause of the worldwide decline of ecosystem functioning and biodiversity. It is therefore counterintuitive to think of urban areas as focal areas for biodiversity conservation, however there are several arguments to do so [45]:

1. *Source approach to diminish environmental impact*: As the majority of people is concentrated in urban areas, exploiting conservation efforts in cities (1) will reach many people and (2) any reduction in the huge city's environmental impact will be a positive step toward sustainability.
2. *To reconnect humans with nature*: Most people who live in urban areas are largely disconnected from nature. This means that a worldwide "extinction of (wildlife) experience" is currently taking place. To counteract, the places where people live and work should be designed so as to provide opportunities for meaningful interactions with the natural world. Doing so has the potential not only to engender support for protecting native species, but also to enhance human well-being [48]. Urban wildlife experience has psychological benefits for citizens [26] and may contribute to so-called socio-ecological systems, as such being an important

strategy to enhance the resilience of local citizens (see [23]).

3. *To recognize cities as (potential) biodiversity hotspots*: People, plants, and animals share the same preference for areas naturally rich of resources. Urbanization is occurring in numerous (former) biodiversity hotspots worldwide, and has been identified as a primary cause of declines in many threatened and endangered species [49]. Although urbanization processes often have diminished a large part of the original biodiversity richness, the remnant "green space" (according to its management) usually still contains a certain (potential) value for biodiversity conservation. For example, the UK city of Sheffield inhabits a high number of bird species (n = 77), with only three nonnative species [27].

A Different Scope: Approaching the City from a Wildlife Point of View

In natural situations, the appearance and change of landscapes and their attached biodiversity are products of abiotic and biotic processes. Human activities, such as agriculture, modify these relationships. In the urban landscape, the hierarchy of processes is absolutely different: Here, the biodiversity settlement is first depending on human appreciation and management, abiotic and biotic factors play a less important role. So, to better understand how plants and animals may survive in these man-made landscapes, a good understanding of the different actors in the urban environment and the "realities" they perceive is crucial.

Obviously, cities accommodate a range of human actors. Apart from humans as individuals inhabiting in the city (the "residents"), city dwellers employ various activities that makes that they can also be grouped as e.g., students, sportsmen, entrepreneurs, employees, patients, (allotment) gardeners, elderly people, or urban professionals (the latter term referring to those people who professionally deal with city planning, design, and management), etc. Depending on their age, societal status, and individual preferences, citizens may fit in only one or in a whole set of urban actor groups. Moreover, each of these urban actor groups, including residents, has its own favorite part of the city. They also have each their own demands concerning what the city should deliver: Residents like nice and safe residential neighborhoods; sportsmen and - women like good and sufficient sport accommodations; etc. This makes that city planning and design can be a complex process, as there usually are many urban stakeholders to be involved.

Some of the "actors" in cities are nonhuman, being plants and animals. Most species are considered as real "wildlife" because they survive in the city on their own; others are domesticated and (partly) depend on care by humans (pets and cultivated garden plants). For all of them, cities provide them with different needs, in essence similar as for humans, being "habitats" where they can live, eat, reproduce, move, and communicate with others. However, wildlife generally has specific habitat requirements that are generally different than those of humans. For example, most birds prefer trees and shrub as nesting place above buildings (although there are exceptions as swifts and house sparrows).

To understand what the city is like as wildlife habitat, humans should project themselves in the plants and animals that inhabit city environments. This is because wildlife often evaluate the reality of the city in a different way than people would do. Three different realities of the city can be perceived by human and nonhuman urban actors:

- *Biophysical reality*: The reality of what is physically there: buildings, roads, vegetation, bare soil, open water. Geographers use to describe the physical reality ("land cover"), these days more and more supported by satellite and aerial photo images. Urban actors (both human and wildlife) perceive the biophysical reality as (one of) the realities they have to deal with.
- *Functional reality*: The reality of how the city is actually *used* by different urban actors. In their use of the city, human actors thereby take the biophysical reality (what's there?), the functional reality (how the city is being used by themselves and others), and the planning and design reality (what is it meant to be?) in consideration. Wildlife only look to the biophysical and functional reality, the latter including the human and wildlife use. Obviously, wildlife does not take the planning and design reality into account, as they are unaware of city plans.

- *Planning and design reality*: This reality has to do what a specific part of the city officially is designated as, or what it meant to be for. The planning reality is predominantly shaped by urban professionals in planning and design (architects, landscape architects, urban planners, regional and landscape planners etc.), and subsequently assigned in municipal, regional, federal or national plans and documents, and as such taken in consideration by human actors.

Figure 1 presents an example that illustrates the differences between the realities, and why it is important to be aware of the differences among the realities and the way they are perceived by humans and wildlife in the city.

City Environments as Wildlife Habitat

Cities as Landscape

Although most people would only associate rural and natural environments with the term "landscape", city environments can also be considered as real landscapes (e.g., [12]). This is because due to their size (usually >100 km^2) they act on a landscape level, and because of their distinctive land use pattern they sharply contrast from their rural or natural surroundings. From a wildlife point of view the features of the urban landscape determine its habitat suitability and availability.

As the urban landscape largely consist of buildings and paved area, its stony and built-up character make that they resemble rocky and cliff landscapes. Sky scrapers thereby act as mountain cliffs, whereas the streets between high-rise buildings (e.g., in Manhattan, New York) act as canyons. For species as the Peregrine falcon (*Falco peregrinus*), these high-rise city environments have become a secondary habitat, next to their natural cliff habitat.

Cities also appear to be different in terms of climate, as compared with the often more vegetated surrounding landscapes such as forests, swamps, mountains, or agricultural land. Because of their stone surface (and lack of the evaporation possibilities that vegetation

Biodiversity in Cities, Reconnecting Humans with Nature. Figure 1
The Garden snail *Cornu/Helix aspersum* is a cosmopolitan species, originating from the south of Europe (Mediterranean). Buildings and surrounding green (*biophysical reality*) are considered by the snail as part of its urban habitat (*functional reality*), meanwhile humans designate these housing areas as living areas for themselves (*planning and design reality*). The coexistence of humans and these snails in residential areas leads to positive and negative interactions: the garden snail is seen as a pest for garden flowers, but also inspires people through its appearance and behavior, and acts as food for e.g., birds (which are preferred urban wildlife by residents). Photo: Robbert Snep

has), cities warm up faster, effectively retain the heat, and throw it out during the night. In addition, exhaustion gases (traffic and industry) and the heating of buildings add up to an increased temperature, especially during nights. The main reason for the nighttime warming, however, is that buildings prevent surface heat from radiating into the relatively cold night sky. As a result, city night temperatures surpass the average regional temperature with several degrees. During days there is also a, yet smaller, difference in temperature. This "being warmer than the rural surroundings" phenomenon is called the UHI (*urban heat island*) effect (e.g., [69]). The UHI effect causes health problems for humans during the summer (as it contributes to extreme heat, which causes high mortality rates), but also affects wildlife in different ways. For example, in temperate climates (sub)tropical plant and animal species are more likely to survive in city environments than in the natural or rural surroundings of the city. In Northwest Europe, plant species as Common Fig (*Ficus carica*) and Olive (Olea *europaea*) from the much warmer Mediterranean region can survive in sheltered spots within cities, but would die in the rural surroundings of these cities during winters. The same process is observed on small Mediterranean ferns in France [18] showing that cities therefore present an interesting preview on how global warming may support the invasion of thermophilic species into currently colder regions.

There are more features that distinguish urban landscapes from natural and rural environments. One of them is air quality. Because of traffic and industrial gasses, the quality of city air is often worse than in the rural surroundings. The air pollution directly limits the habitat suitability of cities for e.g., most lichen species but also impacts the survival rates of urban plants and animals in general [6].

Cities are places with an excess of noise. Car traffic is a main cause of city noise, thereby making it difficult for some animal species to communicate. For example, for territorial birds it is hard to make themselves heard through the traffic noise and as such to defend their territories [54]. Recent studies have shown that bird species may adapt to the noisy city environment. Urban Coal tits (*Parus major*) sing at a higher pitch than their rural congeners, to compensate for the city background noise [61]. From other birds it is known that urban individuals start to sing earlier in the morning than usual for these species, to avoid the noise of the city's rush hour.

Cities are constructed in a variety of places, neglecting whether the physical conditions of the original soil may support the construction of buildings. Some cities are developed in (coastal) wetland regions or in peat soil areas, locations that are not well-equipped for construction buildings. To compensate for this, urban developers make their development sites "construction ready" by removing the original upper soil layer and adding construction-supportive sand layers. In most cities this urban development process has been happening for ages, making that urban soils are highly heterogeneous, with many different soil compositions within a small area. In addition, pedogenesis (the formation of soils) is disturbed by the actual urban land use. As large parts of the city consists of buildings and roads, these parts are sealed and thus isolated from normal interaction with rain and surface water, plant life, sun heat, etc. Also, because of the weight of buildings and heavy car traffic, the soils are compressed, decreasing their permeability for water and soil organisms. On top of this, a portion of the pollution and eutrophication coming from industry and traffic will find its way to the urban soil. As an example, urban soils often appeared to contain much higher levels of heavy metals such as lead than its rural surroundings [19]. All in all, urban soils are quite different than rural and natural soils, more contaminated and eutrophicated, as soil profiles less developed (because of a disturbed pedogenesis), spatially more heterogeneous and – with all this – thereby in general impacting the habitat quality of cities for plant and animal life in a negative way. An exception would be that, because "to be" urban development sites are usually covered with sand, these young sandy soils provide a – often temporary – habitat for plant and animal species from early successional vegetation [64]. These pioneer habitats enrich the species composition of the city's biodiversity (Fig. 2).

The cycle of water (from clouds, precipitation, surface or groundwater back to clouds via evaporation) is essential for life on earth. On a landscape level, there are huge variations in the amount of water in each part of the cycle, as the cycle of water is taking place on a continental or even global level. In the vegetated

Biodiversity in Cities, Reconnecting Humans with Nature. Figure 2
The Natterjack toad (*Bufo calamita*) is a pioneer species of early successional habitats, including urban fringes. *Left*: tadpoles (black) of this toad species in a small temporary water body at a development location. *Right*: the male toad calling during mate season (Photo: Robbert Snep)

parts of the world, being the areas where most human activities occur, human land use has disturbed the water cycle process. In agricultural areas, the surface and ground water flows are highly manipulated to optimize crop yield. In urban areas, this manipulation of water has taken a much more far-reaching level. Surface water is largely canalized, with stony and steep embankments. Sewer systems catch most of the water that precipitates on buildings and streets. In cities with naturally high groundwater levels (like former wetlands), groundwater is sometimes drained or leveled in another way. The evaporation process in city areas is, due to the lack of vegetation, rather poor. In addition, urban water is contaminated by (former) industrial and household waste and by traffic, especially in cities where sewer systems do not function optimally. All in all, water is strongly manipulated in city environments. As water is a vital element for plant and animal life, the deviant quantity and quality of urban water restricts the habitat quality and availability for wildlife in cities.

Cities as Mosaic of Biotopes

Although city landscapes are quite different than rural and natural landscapes, they are all but homogeneous. City landscapes are in fact composed of a wide variety of urban land use types, ranging from residential areas, business districts, shopping malls, and (rail)road structures to urban parks, sport field complexes, allotment gardens, and cemeteries. Within each of these land use types, the actual land cover or soil occupation may also vary quite largely. The spatial heterogeneity is what makes the city that there is not such thing as "the urban biotope" (Fig. 3). Cities are mosaics of biotopes.

For long, ecologists have undervalued city environments in terms of species richness and composition. Most ecologists thought (and many of them still think) that cities would not accommodate a diversity of plant and animal life worth to study. A pioneer in the scientific field of urban ecology, Prof. Herbert Sükopp, provided the counterintuitive insight that cities are rich of species and numerous interesting ecological patterns and processes can be found here. In the 1960s, in the middle of the Cold War between the West and the Soviet Union, he was positioned at a university in West Berlin (Germany). By that time, West Berlin was governed by the West, but the surrounding area controlled by the Soviet Union. Normally, academic ecologists would leave the city and do their field work in rural and natural areas. This was not possible in the

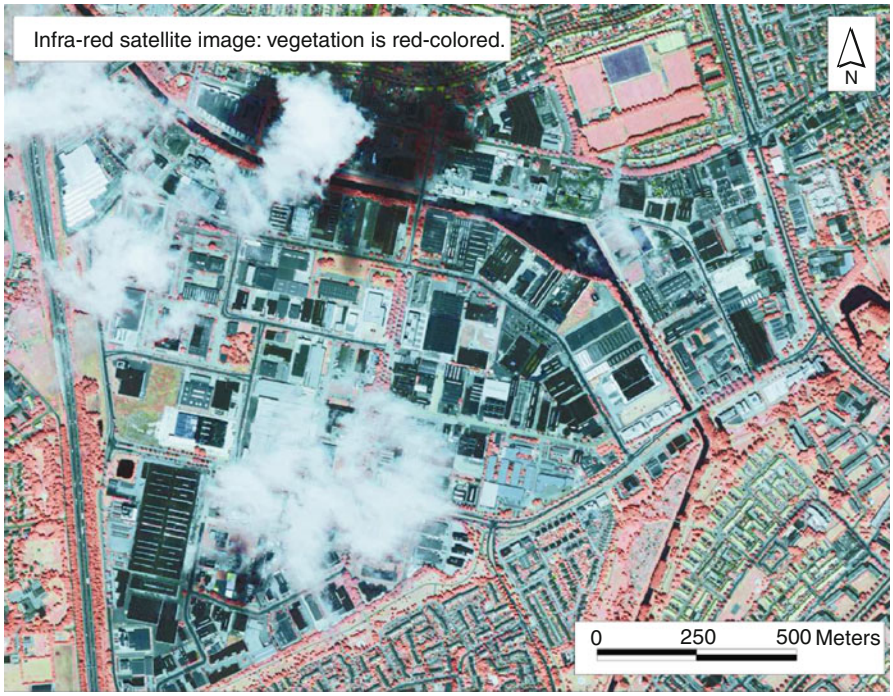

Biodiversity in Cities, Reconnecting Humans with Nature. Figure 3
Illustration of spatial distribution and portion of vegetation in different urban land use types: sporting fields (*right top*), residential areas (*right bottom*), infrastructure (*left*) and industrial sites (*center*). IKONOS satellite image (Photo: Robbert Snep)

case of West Berlin. Herbert Sükopp therefore decided to conduct his ecological field research within the urban area of West Berlin, a unique approach. By mapping the plant communities and biotopes of residential areas, shunting yards, and derelict industrial areas in the city in a systematic way, he discovered that urban environments have a much higher flora and plant community richness than expected. From further studies conducted in German cities, it was later also demonstrated that especially the transition zone from city to rural surroundings is species rich, and that the flora richness of cities can even be higher than the actual surrounding rural land [37]. This latter is due to two facts: (1) the heterogeneity and biotope richness of urban areas and (2) the low flora richness of the intensively managed agricultural regions in which many (German) cities are located. Modern operational management methods of farms focus on optimal yield for agricultural products, and include reshaping of the landscape (stripping off hedgerows, ponds etc.) for this purpose. Many of the species of traditional agricultural landscapes have disappeared in the modern agricultural "deserts" due to lack of habitat; some of them find a new habitat in the small-scaled structure of the city edge. As an example, Sálek et al. [55] described a case in which the Grey Partridge (*Perdix perdix*) has colonized derelict parcels in business districts and industrial land located at the city edge.

Urban biotopes can be classified in different ways. Based upon the three realities (biophysical, functional and planning and design reality, see section "A Different Scope: Approaching the City from a Wildlife Point of View"), each classification having its pros and cons. With the *biophysical or land cover* approach, good insights in the abiotic conditions are provided, enabling ecologists where potential habitat for wildlife could be found. For this purpose aerial or satellite images supply with basic information on where vegetation and other habitat characteristics are located (using e.g., infrared sensing techniques), but additional field work is required to detail the land cover of urban

Biodiversity in Cities, Reconnecting Humans with Nature. Figure 4
Bird monitoring in urban environments is not only conducted in backyards and urban parks, but also at industrial sites. At this photo ecologist Martin Melchers is observing urban gulls nesting at the roof of storage tanks in the Port of Amsterdam (NL) (Photo: Robbert Snep)

areas. With the *functional* approach, the actual use of the urban area by wildlife and humans is mapped. Wildlife can be monitored with a variety of techniques, of which bird counting techniques (e.g., by mapping territories) are probably most well known (Fig. 4). With these monitoring techniques, a good overview of the current habitat value of the urban area for wildlife species can be acquired. With additional inventories on the human use (recreation, traffic) of the urban area, possible causes for differences between apparently similar plots can be demonstrated. In Madrid (Spain) a study to the foraging behavior of Blackbirds (*Turdus merula*) in several urban parks showed that in parks frequently visited by people, the Blackbird behavior and density was different then in similar parks with a lower frequency of visitors [21]. Blackbirds in the more crowded parks spent more time being vigilant and moving away from people and less time searching for food (decreasing food intake). The number of pedestrians was positively correlated with Blackbird distance to pathways and negatively correlated with distance to protective cover. The number of active birds decreased with increase in the number of pedestrians during the day. Blackbird density was negatively related to the number of visitors per park. This study confirmed that human disturbance negatively affects Blackbird feeding strategies in urban parks, ultimately modifying spatial and temporal patterns of habitat selection and abundance [21]. This study also shows that land cover and land use destination alone (in this case "urban park") can be insufficient to determine the habitat value of urban biotopes for wildlife. The actual use of the biotope by others (humans, dogs) appears to have a – though rather invisible – impact. To implement urban ecological knowledge into the design, management, and use of the city (see "planning and design reality"), one should be able to link an urban biotope classification to the design and management jargon and concepts of the city's public space, residential areas, business districts, etc. As there is much variety in habitat quality and quantity within each of the official urban land use types (as assigned in zoning plans), the official land use legend of the city is often not well-equipped for mapping ecological knowledge, so translation between these two different classifications can be difficult.

Fragmentation and Connectivity of (Urban) Habitat

From the 1970s on, ecologists have linked the spatially explicit availability and connectivity of habitat at the landscape scale with the abundance of species at the

local scale. Ecological theories as the island biogeography [42] and the metapopulation theory [39, 51] explain how local plant and animal populations are depending of surrounding populations for their long-term persistence. The first publications about these theories mark the start of the scientific discipline of "landscape ecology."

The island biogeography originates from comparative studies on species richness of islands and mainland, thereby illustrating that islands with a larger size and a smaller distance to the mainland are more species rich than small islands that are located far from the mainland. The size of the island thereby is a good predictor of the probability of local population extinction. The smaller the island, the generally less habitat; the smaller the island population, the higher vulnerability for a disaster to impact the whole island population, the higher the extinction rate of the island population. After local extinction, the island may be inhabited again via colonizing individuals deriving from the mainland. The distance to the mainland thereby acts as a good predictor for the colonization probability: the smaller the distance, the larger the chance that the island will be re-colonized. The island biogeography theory can also be applied in situations where there is a very large "source population" (the mainland) and smaller local populations, all located in a larger area of non-habitat.

In the past, habitat used to be much more abundant and interconnected than in current landscapes. In today's human-dominated landscapes habitat is not only reduced in size and quality, but also fragmented by infrastructure and urban development. Here, the island biogeography with its mainland that acts as source area is not applicable, as there often is no enormous mainland habitat. The metapopulation theory is better equipped for these fragmented landscapes.

The metapopulation theory departs from the idea that in fragmented landscapes interconnected local populations may together make up a so-called metapopulation. The long-term persistence of such a metapopulation is achieved by the network setup: (1) local population extinction should be balanced with new colonization from neighboring local populations and (2) the total number of all individuals within the metapopulation should be sufficient. With an extra large local population (a so-called key-population), this total number can be lower than in case all local populations within the metapopulation are small. As the interlinkage between local populations is crucial for the mutual exchange, the habitat pattern at landscape scale determines whether local populations will together function as a metapopulation (Fig. 5).

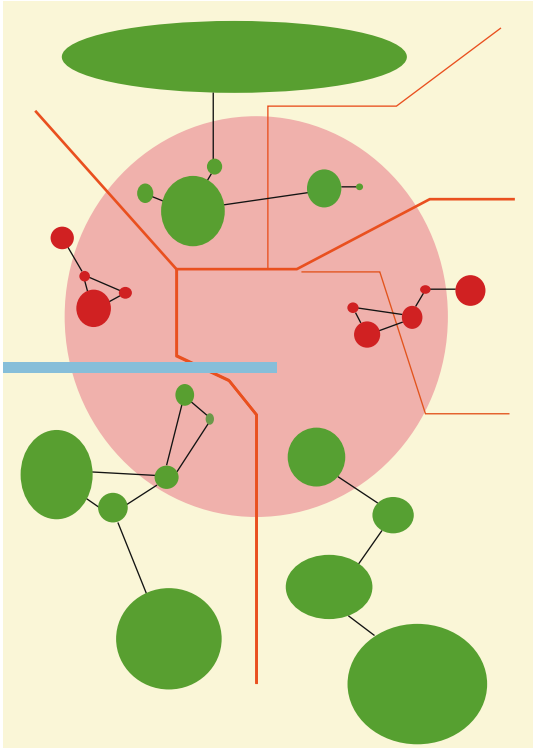

Biodiversity in Cities, Reconnecting Humans with Nature. Figure 5
Illustration of how networks of local populations (so-called metapopulations) of a ground-dwelling species are distributed in and around a city (*pink*). Road (*orange*) and water (*blue*) infrastructure act as barriers and makes that there are different metapopulations (that instead of one large network). As a result, some metapopulations have sufficient size to overcome environmental fluctuations, and are viable (*green*), others are too small and are nonviable (*red*) (Photo: Robbert Snep)

Several landscape parameters determine the probability that species may survive in the landscape:

- Habitat availability (the amount of habitat available for the species)
- Habitat quality (determines the carrying capacity per area of habitat)

- Habitat connectivity (extent to which habitat patches are mutually connected)
- Individual habitat patch size (determines whether there is a habitat patch in the landscape with sufficient space for a key population)
- Landscape permeability (extent to which the landscape pattern support the migration of species through the landscape, especially the size and character of the portion of nonhabitat is important in this case)
- Barriers (landscape structures that prevent the movement of species through the landscape (e.g., highways for ground-dwelling animals))

Also, some species-specific parameters determine how well the species would be equipped to survive in the landscape:

- Dispersal capacity (extent to which a species is able to migrate through the landscape, e.g., overcome barriers.)
- Dispersal distance (distance that individuals of a species are able to travel to colonize new habitat)
- Home-range size (the size of the area that an animal individual uses during everyday's activities)
- Disturbance sensitivity (level at which a species will be so much disturbed by traffic, recreation, noise, light, etc. in its habitat that this will impact its survival probability)
- Local population size (minimum amount of individuals required to function as local population)
- Key population size (minimum amount of individuals required to function as key population (and thus as an source for neighboring populations) [74])
- MVP size (minimum amount of individuals within the metapopulation necessary for a minimum viable population [59]; for metapopulations with a key population the minimum is lower than without a key population, [74]).

Each landscape is unique, each species is unique; however there are some general rules about how to deal with landscape planning and design, as seen from the viewpoint of biodiversity conservation:

1. Conserve (or re-develop) sufficient habitat area for conservation target species. "Sufficient" should meet habitat criteria for *viable* plant or animal populations [67].
2. Use the SLOSS (Single Large patch Or Several Small patches) principle while targeting (to be) habitat patches for conservation [1, 60]. This is as habitat networks should have sufficient size for a (meta) population size and sufficient connectivity (to support colonization of the patches).
3. To meet criteria for habitat connectivity, make sure that the habitat in the area is optimally interconnected, so species can migrate from one habitat patch to another [58]. In landscape and conservation planning, so-called ecological corridors are often assigned to support plant and animal dispersal [24]. These corridors are linear strips of habitat through the landscape of which the length, width, and design are depending on the species. Instead of continuous corridors, for some easy-migrating species (e.g., some bird species) also so-called stepping stones could support their dispersal through the city. A stepping stone connection consists of a subsequent series of small patches of habitat positioned between larger habitat structures.

Urban environments are highly fragmented landscapes, in which habitat availability and connectivity is generally insufficient to support the population viability norms of many species. So the application of the previous concept is not so easy. It appears today, after some urban studies on species dispersal and landscape availability to conserve populations, that complementary consideration has to be suggested in these highly fragmented urban landscapes. For example, the SLOSS rule is generally not possible and it seems interesting to promote also small green spaces and diverse kinds of green structures in dense city environments. The goal here is not to construct new large patches of biodiversity when it is not possible, but to permit, at least, both the dispersal of a maximum of species with "stepping stones" and to increase the interface between nature and citizens. After all, increasing the street plantation (street trees, road verges) in an ecological way would promote for several species the dispersal opportunities in towns: from park to park, and between areas of private gardens and business areas.

Another process that is generally forgotten is the impact of the city on the capacity of species dispersion at regional level. Under climatic change, wildlife

modifies their biogeographical area of distribution, moving to the north [32]. This adds a justification to the need of a good capacity of continuity in landscape at all the scales, including the urban areas. The town becoming megalopolis with continuous building land use acts as barriers to the species movement and especially to the dispersion to new area (to the north) for all the species that move with difficulty. Given transparency to the town, e.g., permitting the species movement is also a challenge of a sustainable city.

Urban Wildlife Species and Communities

On Eating and Being Eaten

The food resource and/or its quality are an important factor of the settlement of animal in town. The availability of grass for first consumers, insects or gastropods for first predators and small vertebrates for second predators are fundamental both to explain the presence of species in a habitat and to explain the stability of the biodiversity through the quality of the food chain. Obviously the urban areas do not present all the availability of food for each step of the food chain and some kinds of animals are favored. For example, the omnivorous and detritivorous animals, small (snails, flies...) as well as large (gulls, corvids, rats...) ones, are capable to use the rubbish dumps and all wastage from human activities. These species can become very numerous and create several problems of cohabitation (e.g., [10]). Other species take advantage of the feeding behavior of inhabitant that is important in private as well as public spaces. This typical urban source explains the success of pigeons [30] but also of some exotic species such as parakeets introduced in numerous towns [68]. However, the use of refuse is commonly reported for other species living in urbanized areas, for example, tits [14], blackbirds [57], gulls [7], or mammals such as raccoons [43] or foxes [56].

In general, urban areas appear clearly poor in food resources for specialist species. Wetlands are scarce, so water birds and aquatic fauna are also scares. The absence of old trees that permit settlement (shelter, food) of numerous insects and birds also explain the absence of several communities of animals. However, the town presents more and more vegetation and welcomes more animals today than some decades before. Insectivorous birds seems to decrease in numerous European town in 1970s [28], but today these birds appear to be more numerous with the reduction of car pollution and pesticide use. In the same time, the recent reduction of some garbage sources in numerous countries has also limited the proliferation of some problematic animals (rats, gulls,...).

For some generalist birds breeding in towns, a behavioral flexibility exists through diet plasticity, for example the Herring Gull [7], while for other generalists, such as the starling, it is less clear. Starlings can modify their diet composition in winter [20], but its diet variability in towns during the breeding period seems to be limited [46]. However, successful generalists compensate for feeding resource difficulties (poor quality of food, accessibility) linked to urbanization, and their behavioral flexibility allows to achieve similar breeding performances in rural and urban areas.

One of the characteristics of urban green spaces is the presence of a majority of exotic plants and trees. The consequence could be directly observed at the level of the community composition (e.g., more "coniferous" birds in town than in rural areas – [15]) as well as at the level of feeding behavior. For example, the bees give a more rich honey in town linked to the great diversity of exotic flowers. The quality of some urban food (richer, more fat) involves also some differences in individual morphology, and obesities can be observed in urban animals [35].

Wild predators are present in towns: foxes or stone martens are more common in suburbs but also sometimes in downtown [28]. Birds of prey such as falcons or sparrow hawks are today present in numerous European cities and some have adapted to the urban constraints changing their food items. The kestrel that eats small mammals in rural areas hunts particularly sparrows in towns. But the most important predator in town remains the domestic cat that eats numerous small birds (robins, house sparrows, ...), small mammals (shrew, vole, ...), and fragile lizards [22, 78].

Reproduction

In the same way than for food availability, the possibility to find nesting places explains the settlement or not of the species in the urban areas. For example, the study of breeding birds in town shows clearly the absence of

birds of open habitats, especially ground-nesting species such as larks [15], that need high grass and quiet places. Lancaster and Rees [38] found that cavity nesters were at an advantage in cities. However holes (in building or in trees) seem very dependent of the history of the building or of the park. The number of cavities in building appeared rapidly decreasing with the new architecture and the protection of all walls. In addition, linked to the hard urban disturbances, birds nest the higher possible and the installation of nest boxes (that are generally not sufficiently high) do not resolve always the problem of the lack of cavity. However, the management of parts of public parks in a more ecological way (especially increasing shrub plantation) favors the availability of the nesting places for numerous passerines. In the same time these sites become progressively more acceptable for a small fauna of soil, litter, grass, and shrub.

The reproduction success is highly variable according to the species. Urbanization profoundly affects the reproductive parameters of birds [9]. Mennechez and Clergeau [47] observed in starling that (1) although the rate at which parents feed their nestlings was higher in urban areas than in rural ones, the amount of food delivered to nestlings by parents in town was weak and (2) the body mass of nestlings reared in the urban sector was significantly lower. This supports the idea that urban nestlings received insufficient food loads or food of low quality (refuse food). Urban environment imposes severe constraints in terms of nutritional "conditions." So some generalist birds such as starling can have bad reproduction in town when generalist species such as the kestrel can have good urban breeding performance [36]. It seems difficult to generalize a relationship between habitat generalist and specialist, without integrating the capacity of adaptation of the different species.

Territorial Behavior

The behavior of wildlife in town is not well studied and today only some mammals have been seriously analyzed. For example, it is well known that cats change their social organization and their territorial behavior in town. In natural and in rural areas, wild cats or domestic cats each have a stable home range with only some spatial overlaps; the organization avoids all possibility of temporal contact. In town, the social organization is absolutely changed: Cats leave in group with one or two dominant males. The impact of punctual and abundant source of food (by human feeders) explains this structure [40].

The fox has been well studied and comparison between rural and urban are conducted in several countries (e.g., [31]). All the studies give the same results: The territory of urban foxes is smaller in town and changes regularly of place. The higher mobility of urban foxes is linked to the high mortality that involves change of individual and permanent reorganization of territories, but also to the shelter availability. In town the majority of fox holes do not exist and animals sleep during the day just in flower clumps, within pipeline, under bridge, etc.

Alien and Invasive Species

Numerous exotic animals and plants have settled into new geographical regions after voluntary or involuntary releases by humans. Although only 1% of alien plants have established populations and spread (Williamson 1996), this percentage can reach 15–50% for vertebrates [34]. When these alien populations increase in number, they often exert negative pressures on the native ecosystem, especially in terms of predation or competition with native species [75]. However, in numerous cases, the mechanisms underlying their success and the potential impacts of these aliens are not sufficiently well documented. The urban areas are the first source of introduced species [16] for plants with horticulture and garden plantation, and for animals with trade of pets. This process becomes an important point of biodiversity management also in town with the goal of urban corridors permitting the dispersion from and to the town (see after).

Consequently, a change in the work of landscape gardeners is awaited in order to limit the use of exotic species known as invasive in new garden and park management. This is especially important for site adjacent to rural and natural zones.

For animals too, the trade need to be examined but also the behavior of citizen that releases all kind of

exotic pets. One recurrent human behavior that seems to facilitate the establishment of exotic species in temperate regions and often in town is the supplemental provisioning of food. The provisioning behavior is observed for numerous exotic mammals (e.g., Coypu *Myocastor coypus*, Siberian chipmunk *Tamias Sibericus*, Grey squirrel *Sciurus carolinensis*), and birds (e.g., Mute swan *Cygnus olor*, Rock dove *Columba livia*, Rose-ringed Parakeet *Psittacula krameri*) and it could be one of the keys to the success of these species. Limiting the supplemental feeding of alien species could be an element of management for some invasive species and needs to be evaluated [13].

Urban Survival Strategies

Blair [4] working on birds and butterflies defined different kind of species according to their ability to colonize and settle in the town. He recognizes species that avoid the urban areas (the "avoiders" that are never present in this habitat) from species that exploit the town (the "exploiters"). These exploiters are generally "adapters" that modify their behavior to exploit better the town. Urban environment seems to impose so many constraints on birds (e.g., landscape fragmentation, isolation of habitat patches, noise, pollution, type and availability of food resources, human activities, vegetation quality in habitat patches. . .) that only species that have a (pre-) adapted way of life are able to tolerate them. Croci et al. [15] suggested that the urbanization filters bird species on the basis of their traits. That biological filter effect of urbanization seems to be a key determinant explaining which passerines can be found in town, urban adapters, and which cannot, urban avoiders. Studying bird avifauna at local and regional levels in France, Croci et al. [15] found 45 urban adapters that were mainly species that preferred forest (15 species) or meadow (14 species) habitats rather than open landscapes or aquatic habitats. The habitat availability in cities is a key determinant of the biological filter that urban constraints play on bird species from natural areas. Global abundance of species is not the main factor explaining their presence in cities. Indeed, urban adapters and avoiders were not associated with any of the modalities of the number of species pairs. Geographic distributions of urban adapters were especially wide and involved more diverse biogeographic areas than urban avoiders generally from temperate climates.

Most species with high nests are associated with tree availability and, therefore, forest habitats, whereas nesting at low or medium heights is often correlated to shrubby, aquatic, or open and appeared as gregarious species. Being with congeners landscapes, omnivorous species were at an advantage in town, whereas granivorous species were at a disadvantage. Eating a variety of food items permits an exploitation of new resources linked to the town, such as garbage. Croci et al. [15] observed also that at the contrary of urban avoiders, urban adapters did not especially present a plumage coloration dimorphism and that urban avoiders were associated with more than two clutches per year and less wingspan when compared to urban adapters. Urban adapters seemed to have larger life expectancy than urban avoiders and were more sedentary that may enhance opportunities to learn from others birds experience, for example, for food location or predation avoidance, and thus, be at advantages in new environments such urbanized areas. Urban adapters also molt once a year whereas urban avoiders molt two times. All these traits lead us to believe that during the breeding season, urban avoiders have not much resources as urban adapters to allocate for adaptation to urban areas.

Homogenization

Biotic homogenization is the process by which the similarity of a biological variable increases across time and space. According to the nature of the variable, homogenization is qualified of taxonomic when there is an increase of the similarity of species between biotopes, functional when there is an increase of the similarity of biological traits (e.g., biological characteristics), and genetics when there is an increase of the similarity of the gene pool.

Each eco-region presents its own pool of species; however, in town the species are often the same [5]. McKinney [44] suggests that the urbanization modifies the community of species, decreasing the specialist species (increasing the generalists) and increasing alien species. Consequently, the similarity between

community increases with urbanization and gives biotic homogenization. In USA the part of alien exotic species is high and can explain a large part of the homogenization; in Europe, alien species are not so numerous [11] and the homogenization is linked to the increase of similar generalists. The explanations could be obtained in the similarity of the urban variables through the world (light, buildings, laws, climate, etc.).

Opportunities to Connect City Actors with Urban Nature

City Planning

The overall shape of cities has a large impact on the extent to which wildlife can colonize city environments, and to which humans can experience these plants and animals. On the one hand, there are the circular-shaped cities, of which the urban fringe – the zone where city and rural nature may interact – is minimal. Besides, the distance from the rural habitats to the city center of such cities is large, and as a result wildlife has to overcome many barriers to colonize inner-city areas. On the other hand there are starfish-shaped cities, where in between built-up areas there are so-called green wedges that may penetrate all the way to the city center. These green wedges often are remnants of former natural stream habitats or other, linear-shaped natural structures that were conserved during the urbanization process. In these starfish-shaped cities, wildlife can much easier migrate through the city environment. Moreover, for citizens the proximity of green in these green-wedge cities is much higher than in circular-shaped cities.

At a next level, it is the design of the "green within the urban area" that has great influence on the abilities of citizens to interact with nature. Within the domain of green space planning, the city's internal major green structures are planned. The challenge is to find a balance between the portions and configuration of built-up area and those of urban green. From an estate development point of view, one could aim for a maximum portion of built-up area. Although this seems economically favorable at first sight, from a quality-of-life perspective a minimum amount of urban green is demanded to make that people like to live and work in such cities. Urban planners and landscape architects, therefore, plan for green structures as public gardens and parks in between new residential and business areas to provide recreational opportunities and support the visual qualities of the built-up areas.

From the wildlife point of view, the way in which green structures are planned is crucial. Not only the amount and size of green structures, but also their mutual cohesion and their connectivity with the rural hinterland determines the habitat suitability of city environments. If urban planners aim to optimize human-nature interactions in the city, they should consider that continuous green structures are best to support wildlife movements, and thus enable plants and animals to inhabit the areas where people live and work. Thereby, wildlife will not discriminate between public or private green (as long as the habitat quality is fine), so connecting public parks with private garden complexes would favor wildlife [29].

Another aspect to take into account is that different plant and animal species may use different parts of the urban green as their habitat. Forest species (like woodpeckers) perceive large open green areas (e.g., grassland or swamps) as nonhabitat and rely on forest and trees structures for their habitat and dispersal opportunities. Other species may prefer swamp vegetation of river banks (e.g., dragon flies), or the flower-rich vegetation of extensive grassland (e.g., butterflies). To support a rich diversity of plant and animal species in the city environment, interconnecting similar types of biotope (forest with forest etc.) is necessary.

To some extent, peri-urban areas may determine the richness of urban nature. Peri-urban areas are the rural areas that are located adjacent to the city. Snep et al. [65] illustrated for butterflies that such peri-urban areas could act as source areas to strengthen nature in the inner-city. With sufficient habitat (in quality and quantity), local butterfly populations may thrive. A surplus of these butterflies may disperse from the peri-urban areas into the city using the urban green structures as dispersal corridors. City planners could take advantage of the natural value of the peri-urban area by tuning the type and structure of the urban green with the peri-urban nature. By doing so, they may optimize the opportunities for peri-urban wildlife to colonize the city.

Different Opportunities for Different Parts of the City

The public green and water structure in cities can be considered as the basis for the city's ecological functioning, due to its size and connectivity. Public green areas with predominantly lawn and solitary trees have little habitat value for the urban wildlife and its experience by citizens. If the urban green is however designed and managed in a more ecological way, a whole array of plant and animal species can be accommodated. Especially the abundance of brush and shrub vegetation containing native plant species will contribute significantly to the habitat quality of the urban green. This is, as these vegetation layers act as reproduction habitat for birds, butterflies, dragon flies etc. Also, the banks of streams and other urban water bodies have a good potential for wildlife, if not "engineered" with concrete sheet piling.

For most citizens, urban parks and water bodies are the places where "urban nature" can be experienced. Although these public areas can make up an important contribution to the city's wildlife habitat, there are other, often private, areas that have good capacities to enhance the experience of urban nature by citizens. These areas are residential neighborhoods, school environments, and business districts.

Residential Neighborhoods A good way to (re)connect humans with nature is to enable citizens to experience nature in their own backyards. Many people like birdlife around their houses (especially songbirds), a conclusion that can be derived from the large portion of residential gardens with bird feeders and nesting boxes [17]. Abundant and diverse birdlife, however, is depending on more factors than only these specific bird features. To attract birds to residential areas, there should be enough habitat (being "urban green") in and around houses so birds have opportunities to eat, rest, reproduce, and gather. A high portion of urban green, as well as sufficient variety in plant species and vegetation structure, do not only enhance bird life, but also other animal groups as mammals (e.g., hedgehogs, bats) and insects (butterflies, (bumble)bees) (Fig. 6). Plants provide different habitat functions as food

Biodiversity in Cities, Reconnecting Humans with Nature. Figure 6
Urban green in the ecological housing area The Cherry Garden (NL), designed and maintained such that both biodiversity conservation as biodiversity experience is supported. The nectar plants and shrub provide habitat for butterflies, (bumble) bees, and song birds, the whole setting with the residential area is inviting for citizens to really experience the wildlife (Photo: Robbert Snep)

source (e.g., host and nectar plants for butterflies) and as reproduction or resting place (e.g., shrub and trees for bird nests). Native garden plants generally provide more habitat value for biodiversity than exotic garden plants, as the local animal life has coevolved with native plant species. Some exotic plant species are exceptions, like the cosmopolitan Butterfly bush (*Bhuddleja davidii*) that is a nectar source for butterflies in many parts of the world.

Incorporating small water bodies (garden ponds) in the gardens and neighborhood green structures adds extra habitat value to residential areas. Water habitats offer habitat for species with an entirely aquatic way of life (like fish and water plants), and also provide places to drink and forage for many terrestrial animal species. Additionally, they offer reproduction and nursery habitats for species with a partial aquatic way of life (e.g., amphibians, dragon flies).

On average, private gardens are too small to accommodate enough habitat, for example, a bird's territory. Animals therefore move between gardens to visit different resources. The urban design of the residential area as well as the vicinity of larger urban green areas have a great impact on the extent to which resources in a particular garden will be used by animals. If gardens are clustered, and fences between the individual gardens are permeable for wildlife, animal abundance will be more likely than in cases where gardens are walled and isolated from other green. Also, the presence of larger urban green areas in the vicinity of residential areas increase wildlife abundance, especially as there good opportunities for wildlife to exchange between urban green areas and residential neighborhood.

Finally, if wildlife is present in residential areas this does not automatically mean that citizens are aware of their presence, and as such are able to fully experience the diversity and phenomena of plant and animal life. On average, citizens often have low abilities to detect the presence of wildlife, as more and more citizens lack a history of growing up with wildlife [48]. There are two ways to increase wildlife experience opportunities:

1. To improve the visibility of wildlife for citizens, create habitat resources for wildlife in such way that wildlife will expose itself (to some extent) to citizens. Well-known examples are nesting boxes and feeders for birds, other examples are bee trap nests, nectar hot spots for butterflies (e.g., group of butterfly bush), and garden ponds. A more sophisticated way is installing webcams in bird and bat boxes, or infrared cameras for nocturnal wildlife.
2. To improve the wildlife detection ability of citizens. Educate citizens in detecting wildlife, using binoculars (birds) and netting (insects, aquatic life) and tracking (ground-dwelling mammals) techniques. Often, (local) conservation groups are best equipped to stimulate and educate people on wildlife monitoring, using citizen science for conservation purposes.

School Environments Richard Louv [41] wrote a well-known and inspiring book, entitled "Last Child in the Woods," addressing the rapidly decreasing experience of (urban) youth with nature. This book gives a plea for (re)connecting youth with plant and animal life. School areas are perfect places to do so, as children will spend a large part of their early years in these environments. School yards can be designed and managed such that wildlife experience is optimized. Replacing a part of the school yard tiles by urban green that has good habitat value for butterflies, birds, (bumble)bees will stimulate children to explore nature. By actually involving children in the realization and management of this "school nature," they will perceive it as "their own" nature (Fig. 7).

Not only at school yards but also at other places in the direct vicinity of schools there are opportunities to let children experience wildlife. In the Dutch city of Eindhoven, more than 20 primary and secondary schools participate in the "school pond project," a municipal project in which ponds and nearby schools are managed and monitored by youth, supervised by local wildlife experts and teachers. During classes the children visit the ponds, making sure they are well informed about the developments of the local nature. If necessary, additional conservation measures such as habitat improvement are executed to enhance populations of local plants and animals. Linking the outdoor school nature with the actual school lessons on environment and biology offer opportunities to

Biodiversity in Cities, Reconnecting Humans with Nature. Figure 7
Greening project at a primary school, together with the children. Plants with added value for biodiversity are planted (*left*), attracting small wildlife that can be experienced (*right*) (Photo: Soontiëns Stadsnatuur)

provide more background information about the local wildlife, and support children to understand the diversity of life and the working of the ecosystem.

Business Districts "Business districts" can be further classified as high-quality business sites, mixed business sites, logistic areas, heavy industrial areas, and seaport areas. Other names for these areas are business sites, business parks, industrial sites, industrial districts, or industrial estates. Opportunities for business sites to provide ecosystem services are now gradually being recognized. For example, recent studies have focused on how flat roofs, a typical feature of business site buildings, can be used (designed as green roofs) to reduce urban air pollution [80] or road traffic noise. Regarding biodiversity conservation at business sites, some initiatives are already under way in current practice. The US Wildlife Habitat Council (WHC) encourages corporations to voluntarily manage lands for wildlife and biodiversity protection, and certifies companies that substantially contribute to biodiversity conservation on their corporate lands [76]. Cardskadden and Lober [8] studied the benefits to corporations of participating in the WHC programme in terms of its influence on relationships with key corporate stakeholders including employees, host communities, environmental groups, and regulators. They report that at 164 sites, 95% of respondents indicated that wildlife habitat programs had led to improved employee morale; 72% indicated improved relationships with environmental groups; 60% noted a positive effect on community relations; and 49% of respondents reported improved relations with regulators. These benefits were in addition to the annual cost savings reported by 50% of the programs. Besides, relationships with the community, government, and environmental groups led to better wildlife programs due to increased expertise.

In another example, the UK British Trust for Ornithology (BTO) awards companies that take specific measures to conserve bird diversity on their lands. The Business Bird Challenge began in 1994 and is a partnership between businesses, the BTO, and local communities which encourages biodiversity on business and industrial sites. Sites range from working quarries, power stations, and oil refineries to research establishments, company headquarters, and restored nature reserves. The aim is to maximize the potential of business sites for birds and other wildlife whatever the business site size.

In the Netherlands, Dutch Landscape Management promotes the integration of landscape elements and species conservation measures into business site development. They aim to raise awareness among municipalities and the business community, but also among project developers and designers,

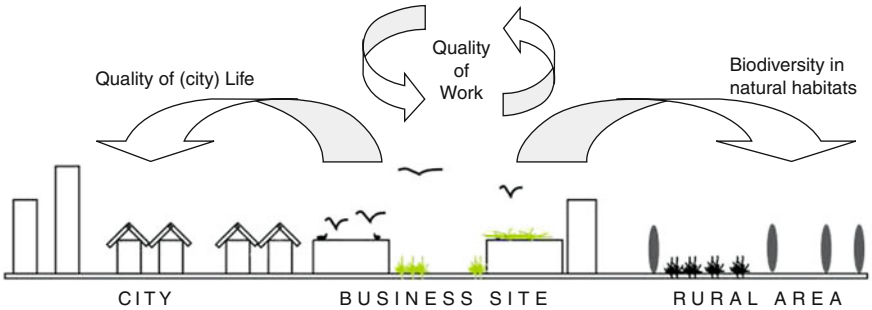

Biodiversity in Cities, Reconnecting Humans with Nature. Figure 8
Overview of how the greening of business sites with vegetation attractive for wildlife may improve both the business site as its urban and rural surroundings. The quality of life in adjacent residential areas can be enhanced by common wildlife originating from the business site [65]. The quality of work can be improved as the green enhances the aesthetic and recreation perception in the business environment [64]. The biodiversity in natural habitats near the business site can be enhanced as the business site may offer specific habitat for endangered butterflies and other species [66]

regarding opportunities and advantages that "green" business sites offer. They thereby focus on fitting business sites into their surrounding landscape, enhancing the ecological significance of business sites and increasing the accessibility of the sites for recreation purposes.

Business sites, often located at the city's edge, can offer habitats for rare species (e.g., pioneer butterflies and amphibians), which mainly occur in the surrounding rural landscape, and for common species that also occur in the city [63, 65, 66] (Fig. 8). This implies that if biodiversity conservation is incorporated in business site planning, design, and management, the effectiveness of investments in conservation measures will increase if the target species and type and amount of habitat are attuned with the regional context of ecological networks.

Biodiversity conservation at business sites can be shaped in different ways, each with its own (socio) economic and environmental characteristics. There are different options for biodiversity conservation at business sites: green roofs and walls, a more ecological management of the conventional business green, temporary early successional vegetation on vacant parcels, and the design of ecological corridors and stepping stones throughout the business site. Results from a stakeholder survey on this topic suggest that implementing measures to enhance biodiversity may be acceptable only if combined with other green functions (predominantly "recreation" and "health and well-being") and if suited to the functional appearance of the business site environment ("external appearance" and "tidiness") [64] (Fig. 9).

Future Directions: Integrating Wildlife Conservation in Sustainable City Planning and Design

Future directions in research, education, and practice on integrating wildlife conservation in sustainable city planning and design may focus on:

1. Climate-proof city green with ecological value
According to Pauleit et al. (see chapter "► Green Infrastructure and Climate Change") urban green may support the resilience of cities toward climate change, as vegetation is able to cool (evaporation, shade) city environments and storage storm water (pervious soil). This demand for additional, climate-proof, urban green opens an opportunity to enhance the ecological quality of the city, if executed in the right way. As example, green roofs have excellent capacities to deal with heat and storm water (see chapters "► Green Roofs, Ecological Functions" and "► Green Roof Infrastructures in Urban Areas"), however the *Sedum* monoculture roof type – that is currently applied at large scale – has less ecological value than green roof types with more diversity in plant species (preferably,

Biodiversity in Cities, Reconnecting Humans with Nature. Figure 9
Left: Illustration of how vegetation with ecological value (e.g., nectar plants) can be designed for a business site environment. *Right*: Actual urban green patch at a company with host plants for caterpillars of the Swallowtail (*Papilio machaon*) (Photos: Soontiëns Stadsnatuur)

Biodiversity in Cities, Reconnecting Humans with Nature. Figure 10
Green roof vegetation at an inner-city apartment block in Eindhoven (NL). A nice appearance of the green is combined with a plant choice and maintenance that supports wildlife (birds, butterflies) and its experience by the residents (Photo: Soontiëns Stadsnatuur)

native), soil type, and depth and other characteristics. A challenge for the future therefore is to design and manage the urban green meant for climate change mitigation purposes in an ecological way.

2. Urban agriculture with ecological value
Allotment gardens in city environments are an ancient phenomenon, subject to societal trends and thereby increasing and decreasing in popularity over time. A whole new global trend is the concept

of urban agriculture, beyond the traditional allotment garden. Urban farms produce food for the city, within the city itself. A well-known and quite extreme example are the urban farms at roof tops in New York City. Urban farms appeal to the current demand for "home-grown food."

Urban agriculture provides habitat opportunities for urban wildlife and wildlife experience, if the agricultural practices are based upon biological principles (e.g., no pesticides). Urban farmers as well as visitors of these farms will thereby experience how natural processes like pollination are essential for growing food. Though this used to be basic knowledge among people for ages, citizens often have lost this knowledge. Urban farms are therefore excellent places to teach citizens about vital ecosystem services such as pollination and biological control. A future challenge is to integrate the urban agriculture concept in the city planning and design, as such that this phenomenon contributes to the basic understanding of citizens about the natural world they live in.

3. Urban energy and commodity production with ecological value
With successive energy and commodity crises worldwide, urban regions start to explore possibilities to produce their own energy and commodities, thereby decreasing their dependence from energy and commodity producers outside their region. There are several ways to produce energy, using different techniques.

One way to generate electricity or commodity comes from biomass. Although urban regions in general have a low production of biomass (e.g., prunings of tree and shrub vegetation from urban green management), this method may enhance the citizens' awareness about energy ("burning") and commodity ("biorefining") production, and also provides an added value to the city green. If in the near future urban biomass targets are set, this may lead to more shrubs and trees in the city, meaning more habitat for wildlife. The biomass topic represents future benefits that urban green may provide and that are currently not taken into account by urban planners and landscape architects in city development (see also chapter ► Urban Forest Function, Design and Management).

Another way of producing energy in cities is by solar panels at roof tops. These solar energy systems work most efficiently if the outside temperature is not too high. At roof tops covered with bitumen, the temperature will increase too much for optimal functional of the solar panels. At green roofs the direct surrounding of the solar panels is cooled by the vegetation (evaporation) and thus there is more efficiency.

Snep and Opdam [62] and Beatley [3] have addressed the opportunities to integrate natural values in urban planning and design quite extensively, like in Fig. 10. These publications focus on the "nature" aspect of urban green. There is however a much larger, global trend of "green cities", in which "nature" is not mentioned explicitly. The term "green" here refers to "sustainable" ("green" being a modern alternative) or "vegetated" ("green cities" uses urban vegetation for its societal benefits). A challenge may be to connect these two worlds, to enable planners, (landscape) architects, project developers, and others to integrate wildlife conservation in the planning and design of sustainable cities. Future directions as mentioned above (climate-proof, urban agriculture, urban energy) can be seen as starting points to come to green, ecological cities with contain mutual benefits (both sustainable and natural).

Bibliography

Primary Literature

1. Abele LG, Connor EF (1979) Application of island biogeography theory to refuge design: making the right decision for the wrong reasons. In: Linn RM (ed) Proceedings of the first conference on scientific research in national parks, National Parks Service. U.S. Department of the Interior, New Orleans, pp 89–94
2. Allen-Wardell G, Bernhardt P, Bitner R, Burquez A, Buchmann S, Cane J, Cox PA, Dalton V, Feinsinger P, Inouye D, Ingram M, Jones CE, Kennedy K, Kevan P, Koopowitz H, Medellin R, Medellin-Morales S, Nabhan GP, Pavlik B, Tepedino V, Torchio P, Walker S (1998) The potential consequences of pollinator declines on the conservation of biodiversity and stability of food crop yields. Conserv Biol 12:8–17
3. Beatley T (2010) Biophilic cities: integrating nature into urban design and planning. Island Press, Chicago
4. Blair RB (1996) Land use and avian species diversity along an urban gradient. Ecol Appl 6:506–519

5. Blair RB (2001) Creating a homogeneous avifauna. In: Marzluff JM, Bowman R, Donnelly R (eds) Avian ecology and conservation in an urbanizing world. Kluwer, Norwell, Massachusetts, USA, pp 459–486
6. Bradley CA, Altizer S (2007) Urbanization and the ecology of wildlife diseases. Trends Ecol Evol 22:95–102
7. Brousseau P, Lebebvre J, Giroux JF (1996) Diet of ring-billed gull chicks in urban and non-urban colonies in Quebec. Colonial Waterbirds 19: 22–30. Clergeau P. coord. (1997) Oiseaux à risques en ville et en campagne; vers une gestion intégrée des populations. INRA Ed., 374 p
8. Cardskadden H, Lober DJ (1998) Environmental stakeholder management as business strategy: the case of the corporate wildlife habitat enhancement programme. J Environ Manage 52(2):183–202
9. Chamberlain DE, Cannon AR, Toms MP, Leech DI, Hatchwell BJ, Gaston KJ (2009) Avian productivity in urban landscapes: a review and meta-analysis. Ibis 151(1):1–18
10. Clergeau P, Burel F (1997) The role of spatio-temporal patch connectivity at the landscape level: an example in a bird distribution. Landsc and Urban Plann 38:37–43
11. Clergeau P, Croci S, Jokimaki J, Kaisanlahti-Jokimaki M-L, Dinetti M (2006) Avifauna homogenisation by urbanisation: analysis at different European latitudes. Biol Conserv 127(3):336–344
12. Clergeau P (2010) Aspects of urban landscape ecology both in cognitive ecology and spatial planning. Local Land Soil News 32(33):3–4
13. Clergeau P, Vergnes A (2011) Bird feeders may sustain feral Rose-ringed parakeets Psittacula krameri in temperate Europe. Wildl Biol 17Â:248–252
14. Cowie RJ, Hinsley SA (1988) Feeding ecology of great tits *Parus major* and blue tits *Parus caerulus* breeding in suburban gardens. J Anim Ecol 57:611–626
15. Croci S, Butet A, Clergeau P (2008) Does urbanisation filter birds on the basis of their biological traits? The Condor 110:223–240
16. DAISIE (2009) Handbook of alien species in Europe. Springer, Dordrecht
17. Davies ZG, Fuller RA, Loram A, Irvine KN, Sims V, Gaston KJ (2009) A national scale inventory of resource provision for biodiversity within domestic gardens. Biol Conser 142(4):761–771
18. Daniel H, Lecamp E (2004) Distribution of three indigenous fern species along a rural-urban gradient in the city of Angers, France. Urban For Urban Greening 3:19–27
19. DeKimpe CR, Morel JL (2000) Urban soil management: a growing concern. Soil Sci 165:31–40
20. Feare CJ (1984) The starling. Oxford University Press, Oxford
21. Fernández-Juricic E, Tellería JL (2000) Effects of human disturbance on spatial and temporal feeding patterns of Blackbird *Turdus merula* in urban parks in Madrid, Spain. Bird Study 47:13–21
22. Fitzgerald BM (1990) Is cat control needed to protect urban wildlife? Environ Conserv 17:168–169
23. Folke C (2006) Resilience: the emergence of a perspective for social–ecological systems analyses. Glob Environ Chang 16(3):253–267
24. Forman RTT (1983) Corridors in a landscape: their ecological structure and function. Ecology (CSSR) 2(4):375–387
25. Forman RTT (1995) Land mosaics: the ecology of landscapes and regions. Cambridge University Press, Cambridge, UK
26. Fuller RA, Irvine KN, Devine-Wright P, Warren PH, Gaston KJ (2007) Psychological benefits of greenspace increase with biodiversity. Biol Lett 3:390–394
27. Fuller RA, Tratalos J, Gaston KJ (2009) How many birds are there in a city of half a million people? Divers Distrib 15(2):328–337
28. Gilbert OL (1980) The ecology of urban habitats. Chapman & Hall, London
29. Goddard MA, Dougill AJ, Benton TG (2010) Scaling up from gardens: biodiversity conservation in urban environments. Trends Ecol Evol 25(2):90–98
30. Haag-Wackernagel D (1995) Regulation of the street pigeon in Basel. Wildlife Soc Bull 23(2):256–260
31. Harris S, Baker P (2001) Urban foxes. Whittet Books, Suffolk
32. Hickling R, Roy DB, Hill JK, Fox R, Thomas CD (2006) The distributions of a wide range of taxonomic groups are expanding polewards. Glob Chang Biol 12:450–455
33. Hilty J, Lidicker W, Merenlender A, Dobson AP (2006) Corridor ecology: the science and practice of linking landscapes for biodiversity conservation. Island Press, San Diego
34. Jeschke JM, Strayer DL (2005) Invasion success of vertebrates in Europe and North America. Proc Natl Acad Sci USA 102:7198–7202
35. Jones DN, Reynolds SJ (2008) Feeding birds in our towns and cities: a global research opportunity. J Avian Biol 39:265–271
36. Kubler S, Kupko S, Zeller U (2005) The kestrel *Falco tinnunculus* in Berlin: investigation of breeding biology and feeding ecology. J Ornithol 146:271–278
37. Kühn I, Brandl R, Klotz S (2004) The flora of German cities is naturally species rich. Evol Ecol Res 6:749–764
38. Lancaster RK, Rees WE (1979) Birds communities and the structure of urban habitats. Can J Zool-Revue Canadienne de Zoologie 57:2358–2368
39. Levins R (1968) Evolution in changing environments. Princeton University Press, Princeton
40. Liberg O, Sandell M, Pontier D, Natoli E (2000) Density, spatial organisation and reproductive tactics in the domestic cat and other felids. In: Turner DC, Bateson P (eds) The domestic cat, 2nd edn. Cambridge University Press, Cambridge, pp 119–147
41. Louv R (2005) Last child in the woods: saving our children from nature-deficit disorder. Algonquin Books, Chapel Hill
42. MacArthur NJRH, Wilson EO (1967) The theory of island biogeography. Princeton University Press, Princeton
43. Manski DA, Hadidian JM (1987) Racoon ecology in and adjacent to an urban national park. In: Adams LW, Leely DL (eds) Integrating man and nature in the metropolitan environment. National Institute for Urban Wildlife, Columbia, Maryland, p 237

44. McKinney ML (2006) Urbanization as a major cause of biotic homogenization. Biol Conserv 127(3):247–260
45. McKinney ML (2010) Urban future. In: Gaston K (ed) Urban ecology. Ecological reviews series. Cambridge university press, Cambridge
46. Mennechez G, Clergeau P (2001) Settlement of breeding European Starlings in urban areas: importance of lawns versus anthropogenic wastes. In: Marzluff JM, Bowman R, Donnelly R (eds) Avian ecology and conservation in an urbanizing world. Kluwer Academic, Boston, pp 275–287
47. Mennechez G, Clergeau P (2006) Effect of urbanisation on habitat generalists: starlings not so flexible? Acta Oecologica 30:182–191
48. Miller JR (2005) Biodiversity conservation and the extinction of experience. Trends Ecol Evol 20:430–434
49. Miller JR, Hobbs RJ (2002) Conservation where people live and work. Conserv Biol 16(2):330–337
50. Odum HT (1971) Environment, power, and society. Wiley-Interscience, New York
51. Opdam P (1991) Metapopulation theory and habitat fragmentation: a review of holarctic breeding bird studies. Landsc Ecol 5:93–106
52. Pickett STA, Cadenasso ML, Grove JM, Nilon CH, Pouyat RV, Zipperer WC, Costanza R (2001) Urban ecological systems: linking terrestrial ecological, physical, and socioeconomic components of metropolitan areas. Annu Rev Ecol Syst 32:127–157
53. Rees WE (1996) Revisiting carrying capacity: area-based indicators of sustainability. Popul Environ 17:195–215
54. Reijnen R, Foppen R, Meeuwsen H (1996) The effects of car traffic on the density of breeding birds in Dutch agricultural grasslands. Biol Conserv 75:255–260
55. Šálek M, Marhoul P, Pintír J, Kopecký T, Slabý L (2004) Importance of unmanaged wasteland patches for the grey partridge Perdix perdix in suburban habitats. Acta Oecologica 25:23–33
56. Saunders G, White PCL, Harris S, Rayner JMV (1993) Urban foxes (Vulpes vulpes): food acquisition, time and energy budgeting of a generalized predator. Symp Zool Soc Lond 65:215–234
57. Schnack S (1991) The breeding biology and nestling diet of the blackbird Turdus merula and the son thrush Turdus philomenos in Vienna and in adjacent wood. Acta Ornithologica 26:85–106
58. Schumaker NH (1996) Using landscape indices to predict habitat connectivity. Ecology 77:210–1225
59. Shaffer ML (1981) Minimum population sizes for species conservation. Bioscience 31:131–134
60. Simberloff D, Abele LG (1982) Refuge design and island biogeographic theory: effects of fragmentation. Am Nat 120:41–50
61. Slabbekoorn H, Peet M (2003) Birds sing at a higher pitch in urban noise – Great tits hit the high notes to ensure that their mating calls are heard above the city's din. Nature 424:267–267
62. Snep RPH, Opdam P (2010) Integrating nature values in urban planning and design. In: Gaston K (ed) Urban ecology. Cambridge University Press, Cambridge, pp 261–286
63. Snep RPH, Ottburg FGWA (2008) The "habitat backbone" as a nature conservation strategy for industrial areas: Lessons from the natterjack toad (*Bufo calamita*) in the Port of Antwerp (Belgium). Landsc Ecol 23:1277–1289
64. Snep RPH, Van Ierland EC, Opdam P (2009) Enhancing biodiversity at business sites: What are the options, and which of these do stakeholders prefer? Landsc Urban Plan 91:26–35
65. Snep RPH, Opdam P, Baveco JM, WallisDeVries MF, Timmermans W, Kwak RGM, Kuypers V (2006) How peri-urban areas can strengthen animal populations in cities: a modeling approach. Biol Conserv 127:345–355
66. Snep RPH, De Vries Wallis MF, Opdam P (2011) Conservation where people work: a role for business districts and industrial areas in enhancing endangered butterfly populations? Landsc Urban Plan 103:94–101
67. Soulé ME, Simberloff D (1986) What do genetics and ecology tell us about the design of nature reserve? Biol Conserv 35:19–40
68. Strubbe D, Matthysen E (2009) Establishment success of invasive ring-necked and monk parakeets in Europe. J Biogeogr 36:2264–2278
69. Sukopp H, Wurzel A (2000) Changing climate and the effects on vegetation in central European cities. Arboric J 24:257–281
70. Taylor PD, Fahrig L, Henein K, Merriam G (1993) Connectivity is a vital element of landscape structure. Oikos 68:571–573
71. Turner MG (1989) Landscape ecology: the effect of pattern on process. Annu Rev Ecol Syst 20:171–197
72. United Nations, Department (2009) World population prospects: the 2008 revision. United Nations, Department of Economic and Social Affairs, Population Division, New York
73. United Nations (2010) World urbanization prospects, the 2009 revision: highlights. United Nations, Department of Economic and Social Affairs, Population Division, New York
74. Verboom J, Foppen R, Chardon P, Opdam P, Luttikhuizen P (2001) Introducing the key patch approach for habitat networks with persistent populations: an example for marshland birds. Biol Conserv 100:89–101
75. Vila M, Basnou C, Pysek P et al (2010) How well do we understand the impacts of alien species on ecosystem services? A pan-European, cross-taxa assessment. Front Ecol Environ 8:135–144
76. WHC (2008) Wildlife habitat council, silver springs, Maryland. Available from http://www.wildlifehc.org. Accessed Oct 2008
77. Williamson M (1996) Biological invasions. Chapman and Hall, London
78. Woods M, McDonald RA, Harris S (2003) Predation of wildlife by domestic cats *Felis catus* in Great Britain. Mamm Rev 33:174–188
79. WWF (2010) Living planet report 2010 – biodiversity, biocapacity and development. WWF – world wide fund for nature (formerly world wildlife fund), Gland, Switzerland
80. Yang J, Yu Q, Gong P (2008) Quantifying air pollution removal by green roofs. Chicago Atmos Environ 42(31):7266–7273

Books and Reviews

Adams LW (2005) Urban wildlife ecology and conservation: a brief history of the discipline. Urban Ecosyst 8:139–156

Adams CE, Lindsey KS, Ash SJ (2006) Urban wildlife management. CRC Press, Boca Raton, p 331

Douglas I, Goode D, Houck M, Wang RS (eds) (2011) Routledge handbook of urban ecology. Routledge, London

Gaston K (ed) (2010) Urban ecology. Ecological reviews series. Cambridge University Press, Cambridge

ICLEI (2008) Cities and biodiversity – Bonn call for action. Available from http://www.iclei.org/. Accessed Oct 2008

Kaplan R, Kaplan S (1995) The experience of nature: a psychological perspective. Ulrich's Bookstore, Ann Arbor

Marzluff JM, Shulenberger E, Endlicher W, Alberti M, Bradley G, Ryan C, ZumBrunnen C, Simon U (eds) (2008) Urban ecology: an international perspective on the interaction between humans and nature. Springer, New York

McDonnell MJ, Hahs AK, Breuste JH (eds) (2009) Ecology of cities and towns – a comparative approach. Cambridge University Press, Cambridge

Müller N, Werner P, Kelcey JK (eds) (2010) Urban biodiversity and design. Wiley/Blackwell, Hoboken, p 626

Niemelä J (ed) (2011) Urban ecology: patterns, processes and applications. Oxford University Press, Oxford

Bioethanol from Celluloses

Mats Galbe, Guido Zacchi
Department of Chemical Engineering, Lund University, Lund, Sweden

Article Outline

Glossary
Definition of the Subject
Introduction
Basics
Process Options
Enzymatic Hydrolysis Route
Future Directions
Bibliography

Glossary

Bioethanol Ethanol produced by fermentation of sugars from plant materials, for example, sugar, starch, or cellulose.

Enzymatic hydrolysis A reaction where enzymes are used to catalyze splitting of molecules to smaller units by addition of water. Here, enzymatic hydrolysis refers to splitting of cellulose to glucose.

Ethanol fermentation The use of microorganism, in most cases yeast, for conversion of sugars to ethanol.

Flow-sheet design The use of computer programs for design and/or rating of complex production facilities, usually based on a conceptual drawing (flow sheet) of the process.

Lignocellulosic material A common name for plant biomass containing cellulose, hemicellulose, and lignin (e.g., hardwood, softwood, straw, bagasse).

Pentose fermentation Fermentation of sugars containing five carbon atoms, like xylose and arabinose, which are the main constituents in the hemicellulose fraction in agricultural residues and hardwoods.

Pretreatment Lignocellulosic material is by nature very recalcitrant to degradation. By pretreating the material, the structure is made more accessible for degradation by enzymes or microorganisms.

Process integration To design the unit operations involved in a process while considering the interaction between the units and to combine them in an optimal way. For instance, efficient use of heat and power is made possible by utilization of, for example, waste heat internally (in the plant), or externally (in a nearby plant), which can diminish requirement for expensive equipment, such as steam boilers.

Second-generation bioethanol Ethanol produced – in a sustainable way – from lignocellulosic materials (e.g., forest or agricultural materials).

Definition of the Subject

Bioethanol can be produced by fermentation of sugar present in the carbohydrate fractions (i.e., hemicelluloses and cellulose) available in all lignocellulosic materials. These could be agricultural residues (e.g., wheat straw, corn stover, sugarcane bagasse), forest residues (e.g., branches, tops, saw dust, thinning material), and energy crops (e.g., salix, hemp, Miscanthus, switchgrass).

To make ethanol from cellulosic materials is very similar to making ethanol from starch. First, the carbohydrates, hemicelluloses and cellulose, have to be hydrolyzed to monomer sugars and after that fermented to ethanol by a microorganism (e.g., yeast). There are, however, two major differences compared with starch ethanol:

- The structure of the lignocellulosic material is more difficult to break down due to stronger bonds between the sugar molecules in cellulose and the interaction between cellulose, hemicellulose, and lignin.
- While starch and cellulose are made up entirely of glucose, hemicelluloses comprise a variety of sugars, both pentoses (i.e., sugars with five carbons) and hexoses, which makes it difficult to find a single microorganism that can ferment all of these sugars.

This makes production of bioethanol from lignocellulosic materials much more complex than starch-based ethanol production. A third factor that differs is the presence of lignin, which protects the carbohydrates from degradation and makes enzymatic hydrolysis of the carbohydrates more difficult. However, having a lignin coproduct is also a possibility to improve the process economy as it can either be used as a valuable coproduct for chemical production or used for heat and power production as it has a higher heating value than the original biomass.

Introduction

Ethanol is currently the dominating renewable biofuel within the transport sector. It has been introduced on a large scale in Brazil, the USA, and some European countries and the production is expected to continue increasing during the years to come. The global production of ethanol in 2009 reached 73.9 billion liters [1]. Ethanol can easily be integrated in the existing land transportation infrastructure as a blend with gasoline, up to 20% ethanol, or as a neat alcohol in dedicated engines, taking advantage of the higher octane number and higher heat of vaporization. It is also an excellent fuel for future advanced flexi-fuel hybrid vehicles.

Ethanol can be produced through fermentation from a variety of sugar-containing crops such as sugar beet, sugarcane, sweet sorghum, and fruits; starch-containing crops such as corn, wheat, and potatoes; and so-called lignocellulosic material such as agricultural wastes, wood, and municipal waste. Ethanol produced in this way is sometimes referred to as bioethanol.

The production of ethanol from sugar and starch is a well-established technology, which has been used for many years mainly for production of alcoholic beverages, but also for fuel ethanol in the last few decades. Currently, ethanol for the fuel market is produced from cane sugar (Brazil) or corn starch (USA) at more or less competitive prices. However, this raw material base, which also has to be used for human needs and animal feed, will not be sufficient to meet the increasing demand for fuel ethanol, and the reduction of greenhouse gases resulting from use of sugar or starch-based ethanol is not as high as desirable [2].

It is, therefore, a general opinion that future expansion has to be based on bioethanol from lignocellulosic material, which is usually called second-generation bioethanol (2G). These raw materials are sufficiently abundant and also available worldwide. They generate very low net greenhouse gas emissions and thus helping to reduce environmental impacts. However, processes for the production of ethanol from lignocellulosic materials are much more complex and not yet fully developed although several pilot plants and some demo plants have been in operation during the last couple of years. The main by-product of the processes is a solid residue consisting mainly of lignin, which can be used as a fuel, where the market is basically unlimited, or to make products of higher value in order to improve the process economy.

A process for bioethanol from lignocellulosic material consists of the following main steps: Hydrolysis of the carbohydrates (i.e., cellulose and hemicelluloses), fermentation of all sugars to ethanol, separation and upgrading of the ethanol to water-free ethanol, wastewater treatment, and combustion of the solid residue for production of steam and electricity required for the process (Fig. 1). The various process steps can be performed in many different ways and also the overall process configuration can vary. Furthermore, the ethanol process can be integrated with other types of industrial processes. A selection of important possibilities is described below.

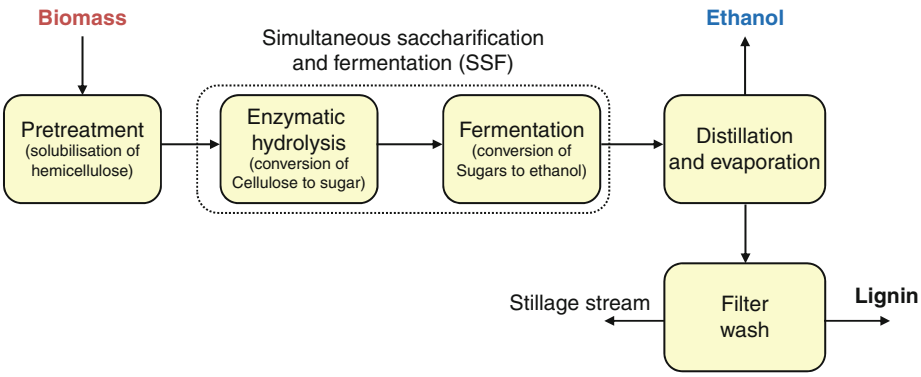

Bioethanol from Celluloses. Figure 1
Simplified process for production of ethanol from lignocellulosic materials

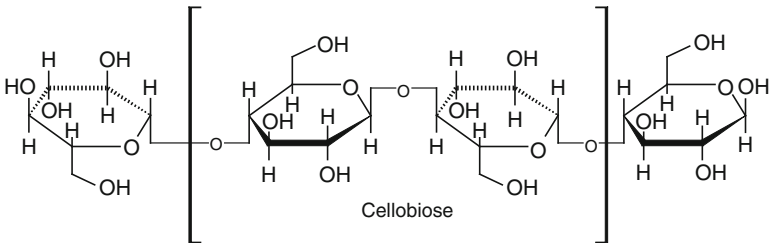

Bioethanol from Celluloses. Figure 2
Cellulose chain

Within the explanations given below, the principles for ethanol production from cellulosic materials, recent developments in the bioconversion processes, and future challenges are outlined. First, characteristics of biomass in general are presented together with typical material compositions for various lignocellulosic feedstock, followed by a summary of different process options for hydrolysis of biomass. This chapter focuses on one option – the enzymatic route – which is covered in more detail with some important methods for pretreatment of biomass. In a process, hydrolysis is followed by fermentation of sugars, which is an area with intense research. Full-scale plants are considered next and the necessity of process intensification and process integration are discussed in depth with a number of examples.

Basics

The composition of lignocellulosic materials differs from one species to another. However, the main constituents are of the same type: about 50–60% carbohydrates in the form of cellulose and hemicellulose, 20–35% lignin, and some other valuable components like extractives, fatty acids, and ash.

- *Cellulose* is the major component in the cell wall of plant cells consisting of linear chains of linked glucose units and it is the most abundant macromolecule on earth. The degree of polymerization (i.e., the number of glucose units) vary between 2,000 and 20,000. Every glucose unit is rotated 180° with respect to its neighbors and linked by β-1,4 glycosidic linkages, making the repeating unit the disaccharide cellobiose (Fig. 2). The linear chains associate strongly via intra- and interchain hydrogen bonding, which causes aggregation into so-called microfibrils with a largely crystalline structure combined with some amorphous regions. These microfibrils are highly stable and resistant to chemical attack, which makes cellulose insoluble in most common solvents, including water, and also very resistant to (enzymatic) hydrolysis.

- *Hemicellulose* consists of short, highly branched chains of heterogeneous polysaccharide sugars, comprising both five-carbon sugars, called pentoses (usually D-xylose and L-arabinose) and six-carbon sugars, called hexoses (D-galactose, D-glucose, and D-mannose) [3]. The branches also contain other groups (e.g., acetyl groups and glucoronic acid). The degree of polymerization is much lower than for cellulose, around 200. Hemicellulose is more hydrophilic and easier to hydrolyze than cellulose. The main carbohydrate in hemicelluloses from agricultural crops and hardwoods is xylose, while mannose is dominating in softwood (Fig. 3).
- *Lignin* is the major non-carbohydrate component in lignocellulosic materials comprising a highly complex, three-dimensional polyphenolic compound. It is closely attached to the cellulose and the hemicellulose and is responsible for the remarkable strength of plants, especially trees. The primary building units of softwood lignin are mainly guaiacyl, with minor amounts of syringyl and *p*-hydroxy-phenylpropane units, while hardwood contains more syringyl units (Fig. 4).

Cellulose can be hydrolyzed to glucose according to the following chemical formula:

$$[C_6H_{10}O_5]_n + n \cdot H_2O \rightarrow n \cdot C_6H_{12}O_6$$

that is, theoretically 1 kg of cellulose results in 1.111 kg of glucose.

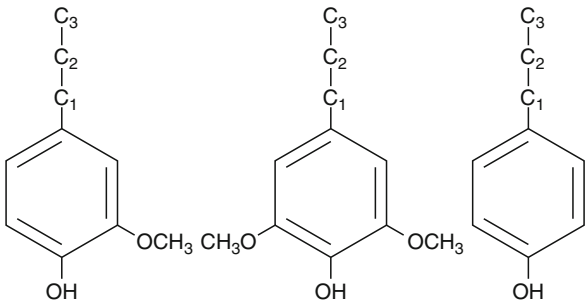

Bioethanol from Celluloses. Figure 4
The guaiacyl (*left*), syringyl (*middle*), and *p*-hydroxyphenyl (*right*) units in softwood lignin

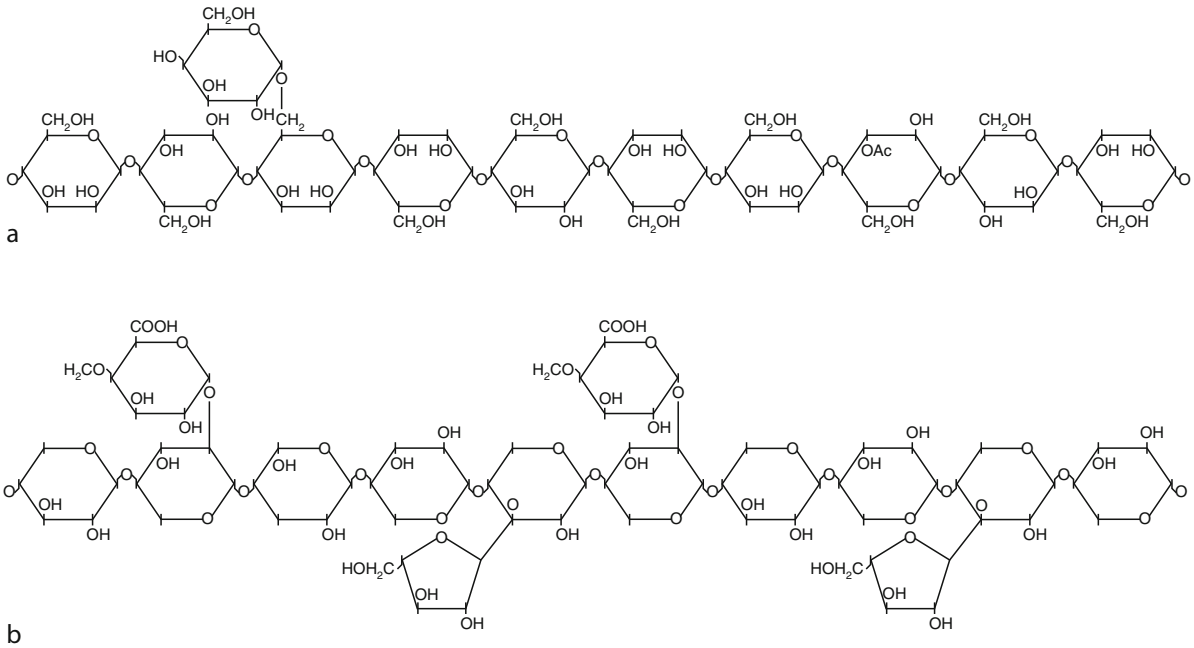

Bioethanol from Celluloses. Figure 3
Example of hemicellulose chains. (**a**): o-acetyl-galactoglucomannan; (**b**): arabino-4-o-methylglucoronoxylan

This is also valid for hydrolysis of the anhydrosugars in the hexose fraction in hemicelluloses, while the hydrolysis of the pentose fraction would be:

$$[C_5H_8O_4]_n + n \cdot H_2O \rightarrow n \cdot C_5H_{10}O_5$$

that is, theoretically 1 kg of xylan (or arabinan) may yield 1.136 kg of xylose (or arabinose).

The sugars can then be fermented to ethanol using some microorganism, like yeast or bacteria, which theoretically can result in 0.51 kg of ethanol and 0.49 kg of CO_2 from 1 kg of sugar (either hexose or pentose) according to:

$$C_6H_{12}O_6 \rightarrow 2C_2H_5OH + 2CO_2$$

$$3C_5H_{10}O_5 \rightarrow 5C_2H_5OH + 5CO_2$$

Table 1 shows typical compositions of some selected lignocellulosic materials. The composition may differ depending on where the biomass grows and at what time of the year it is harvested. For three of the materials, the standard deviation is given based on at least five different samples to show the extent of variations. The hemicellulose in agricultural crops and hardwood is primarily composed of pentose sugars, while softwood hemicellulose has a large fraction of the hexose mannan. This is reflected in the amount of ethanol that can theoretically be produced from 1 t of dry matter for the various biomasses according to the formulas given above (Table 1). It is quite clear that pentose fermentation is not so important for efficient utilization of softwood while it may constitute up to 40% of the potential ethanol production from agricultural crops like corn stover and wheat straw or from grass like switchgrass.

For spruce up to 50% of the energy can theoretically be obtained in the ethanol (if all the sugars are converted to ethanol) and another 35% is obtained in the coproduct lignin. In a real process, less than this theoretical yield will be obtained because of losses in the conversion and due to the needs for energy, heat, and power in the process.

In a longer perspective, lignin may be used for production of chemicals. Lignin is a very complex molecule, which contains numerous aromatic compounds of which some have interesting properties. In contrast to the coproduct from starch-based ethanol production (DDGS, which is used as animal feed), there is no real limitation for the use of the lignin-rich residue as a fuel. About the same ethanol yield could be expected from different crops, although agricultural residues in general contain less lignin; thus, the energy contribution from the lignin part will be lower.

Besides the carbohydrates and lignin, most lignocellulosic materials also contain other compounds like extractives and ash. The agricultural crops may also contain some residual fractions of starch, proteins, and pectin. The amounts of these compounds vary a lot between different types of lignocellulosic materials

Bioethanol from Celluloses. Table 1 Composition of various lignocellulosic materials in percentage dry basis (values in brackets are standard deviations from several studies)

	Glucan	Mannan	Galactan	Xylan	Arabinan	Lignin	Ethanol C6	Ethanol C5	Reference
Pine	43.6	10.8	2.2	6.6	1.6	26.8	411	28	[4]
Spruce	**48.7 ± *2.60***	**12.6 ± *0.55***	**2.4 ± *0.76***	**6 ± *2.11***	**1.5 ± *0.53***	**28 ± *0.47***	**463**	**29**	[5]
Aspen	50	2	1.5	18	4	18	389	164	[6]
Poplar [1]	43.8	3.9	1	14.9	0.6	29.1	354	115	[7]
Poplar [2]	45.1	1.7	1.5	17.8	0.5	21.4	351	136	[7]
Willow	43	3.2	2	14.9	1.2	26.6	350	120	[8]
Corn stover	**37.5 ± *2.2***	**0.6 ± *1.1***	**1.6 ± *1***	**21.7 ± *2.1***	**2.7 ± *1.6***	**18.9 ± *2.6***	**288**	**181**	[9]
Sugarcane bagasse	40.2	0.5	1.4	22.5	2	25.2	306	182	[10]
Wheat straw	32.6	0	0.8	20.1	3.3	26.5	243	174	[11]
Switchgrass	**34.2 ± *2.1***	**0.3 ± *0***	**1.4 ± *0.5***	**22.8 ± *1***	**3.1 ± *0.5***	**19.1 ± *1.7***	**261**	**192**	[9]

and are also affected by the geographical site of cultivation, the soil, and the season. These compounds are usually not discussed very much in research on ethanol production but must of course be considered in full-scale processes. They may both be an asset, in terms of coproduct value, and a problem due to influence on the biological conversion steps.

Process Options

There are several options for a lignocellulose-to-ethanol process but, regardless of which is chosen, the following challenges must be addressed [12]:

1. Efficient depolymerization of cellulose and hemicellulose to soluble sugars.
2. Efficient fermentation of a mixed-sugar hydrolysate containing six-carbon (hexoses) and five-carbon (pentoses) sugars as well as fermentation inhibitory compounds.
3. Advanced process integration to minimize process energy demand.
4. Integration with external processes for cost-efficient use of lignin and residual organic matter.

The first step in the conversion of biomass to ethanol is size reduction and hydrolysis of the carbohydrates. This can in principle be performed in three ways (Fig. 5):

(a) By use of concentrated acid hydrolysis
(b) By dilute-acid hydrolysis
(c) By enzymatic hydrolysis

Either way, the target is to access the cellulose and hemicellulose to generate individual sugar monomers for the fermentation process. In the following section, a summary of various methods is presented.

Concentrated Acid Hydrolysis

Concentrated acids (e.g., sulfuric, hydrochloric, hydrofluoric, and nitric acid) can be used to dissolve native cellulose at rather low temperatures. If the mixture is diluted with water and heated, the cellulose is

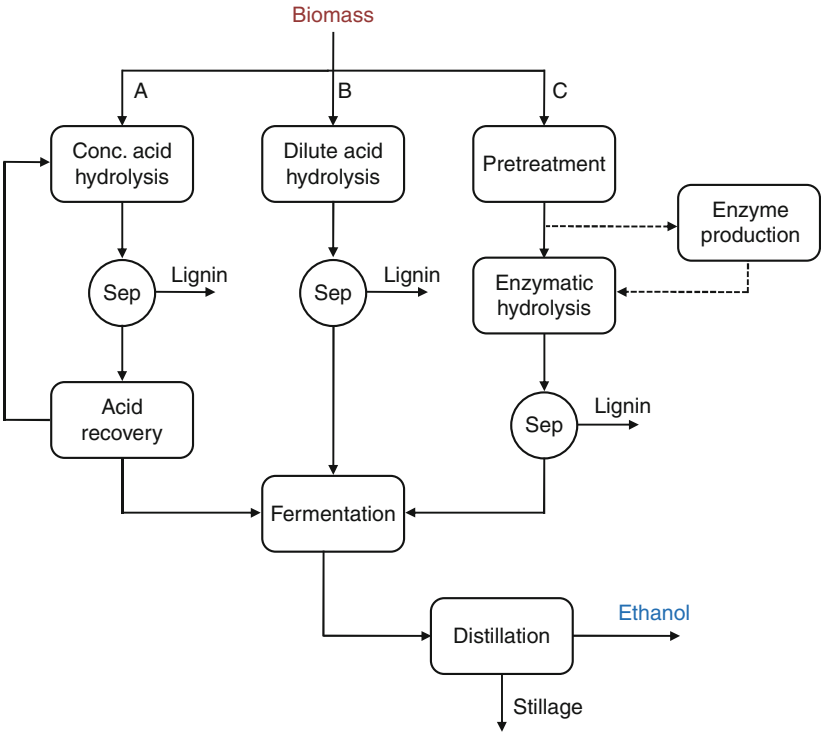

Bioethanol from Celluloses. Figure 5
Different routes for hydrolysis of lignocellulosic materials

hydrolyzed to monomer sugar. This has been known since the 1880s [13] and has been used in several full-scale processes during the twentieth century. For example, in Germany, several full-scale plants for hydrolysis of wood using concentrated hydrochloric acid (40% HCl) were operated during World War II. Several plants based on concentrated sulfuric acid were commercialized in the middle of the twentieth century in the former Soviet Union and in Japan [14]. However, these processes have only been run under times of national crisis and the products (e.g., chemicals, fuel, and feed) were not competitive on international markets.

The process results in rather high yields, but the large amount of acid used creates several problems such as corrosion and pollution. Furthermore, the dilution of the acid in the second hydrolysis step requires high amounts of energy for acid recovery. Nevertheless, the process using concentrated sulfuric acid has gained renewed interest due to the inventions of new methods to separate the acid from the sugar solution, based on ion exchange.

Dilute-Acid Hydrolysis

Dilute-acid hydrolysis of biomass is the oldest technology for conversion of cellulosic materials into sugars. The first commercial plant for production of ethanol from wood based on acid hydrolysis of sawdust, and using diluted sulfuric acid, was built already at the end of the nineteenth century. Since then, several plants have been operated in the USA, Japan, Germany, and the former Soviet Union [15]. There are still some plants operating in Russia. Most of the old plants were run with one-stage hydrolysis using some kind of percolation, where liquid is flushed through the reactor to remove the sugars formed. The main drawback was a moderate yield of sugars and also very dilute sugar solutions, which required a considerable input of energy in the distillation step for recovery of ethanol.

After 1973, several research programs were started around the world to improve the yield and increase the sugar concentration of this process. In the first step, hemicellulose is hydrolyzed under milder conditions (170–190°C), while in the second step the cellulose is hydrolyzed under more severe conditions (200–230°C). However, the high temperatures required for hydrolysis of the cellulose also result in sugar decomposition, which not only decreases the yield but also produces compounds that inhibit the microorganisms in the fermentation step. Also for a two-step acid hydrolysis, the overall sugar yield is usually lower than 60% [16].

Enzymatic Hydrolysis

One of the most promising process alternatives for production of sugar for fermentation from woody materials is the enzymatic process [17–19] because of its potential for high yields. Figure 5 provides a schematic view of the process. The enzymatic hydrolysis process comprises the following main steps: pretreatment of biomass, enzymatic hydrolysis, including enzyme production, fermentation of all sugars, ethanol upgrading, wastewater treatment, and heat and power production.

However, the hydrolysis of lignocellulose using enzymes can be hampered by the very low reaction rate. Lignocellulosic materials are by nature very recalcitrant and not very many microorganisms can degrade them in a fast and efficient way. The main reason is the requirement of a whole array of enzymes, each having more or less specific activity on a certain type of polymeric fragment, such as cellulases, xylanases, mannanases, and lignases.

It is, therefore, of vital importance to pretreat the material to alleviate the enzymatic attack on the structure. The complexity and interconnectivity of the polymers constituting lignocellulose materials makes it necessary to open up and/or partially hydrolyze the structure (Fig. 6). After pretreatment and enzymatic hydrolysis, the process steps are very similar to what is used in concentrated or dilute-acid hydrolysis processes (Fig. 5).

Enzymatic Hydrolysis Route

In general, enzymatic hydrolysis can be considered as more favorable to use than acid hydrolysis because of the milder conditions and higher potential yields of sugars. It does, however, require the pretreatment step, which can constitute a substantial fraction of the overall cost. Therefore, the enzymatic hydrolysis route is discussed below in more detail; however, the parts after pretreatment and enzymatic hydrolysis are to

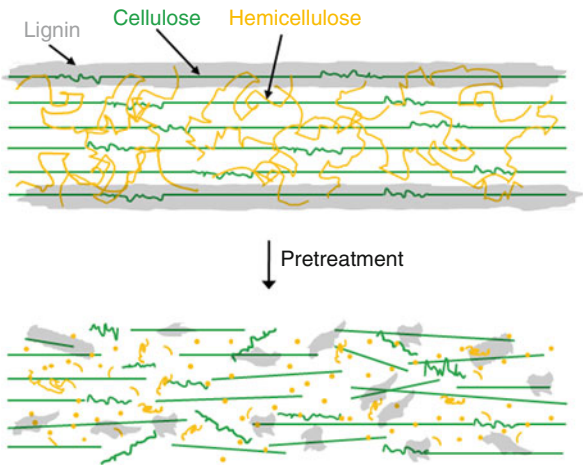

Bioethanol from Celluloses. Figure 6
Schematic view of the effect of pretreatment

a large extent valid also for the other two process alternatives (i.e., concentrated and dilute-acid hydrolysis).

The pretreatment step is perhaps the single most crucial step as it has a large impact on all the other steps in the process (e.g., enzymatic hydrolysis, fermentation, downstream processing, and wastewater handling in terms of digestibility of the cellulose, fermentation toxicity, stirring power, energy demand in the downstream processes, and wastewater treatment demands).

Pretreatment Methods

Pretreatment, to be effective, should have a number of features [20]. It has to:

- Result in high recovery of all carbohydrates.
- Result in high digestibility of the cellulose in the subsequent enzymatic hydrolysis.
- Produce no or very limited amounts of sugar and lignin-degradation products [21]. The pretreatment liquid should be possible to ferment without detoxification.
- Result in high solids concentration as well as high concentration of liberated sugars in the liquid fraction.
- Require a low energy demand or be performed in a way so that the energy can be reused in other process steps as secondary heat.
- Require low capital and operational cost.

During the last 2 decades, a number of alternatives have been proposed for pretreatment of various substrates. This can be achieved in various ways, using either physical (e.g., milling, grinding, or irradiation), or chemical (e.g., alkali, dilute acid, oxidizing agents, or organic solvents) methods, or (something in between) physicochemical (e.g., steam pretreatment/autohydrolysis, hydrothermolysis, or wet-oxidation) methods. This classification is rather vague since in some cases it is difficult to put a label on the chosen pretreatment type [21–26]. Some methods are more efficient than others when it comes to yield and recovery of the fractions. Also, some methods are better suited for hardwood or agricultural residues than for pretreatment of softwood, probably because of the different lignin structures in softwood as compared with that in hardwood or agricultural substrates. Below, a selection of important pretreatment methods is summarized.

Physical Methods Chipping, milling, and grinding are methods that aim at reducing particle size and thus increase the surface area exposed to enzymatic attack. The biomass is turned to a fine powder of some microns in size. To some extent decrystallization occurs, which also improves the hydrolysis rate. However, in order to achieve a high digestibility in the enzymatic hydrolysis step very small particles are required, which makes high power consumption unavoidable. Actually, it can be even higher than the theoretical energy content that is available in the biomass [27]. An interesting option could be physical treatment in an extruder combined with heating and addition of chemicals in which case the power requirements can be smaller [28].

Chemical Methods The most common chemical method is to use dilute-acid pretreatment, in which the material is impregnated by soaking (or by spraying) using a dilute strong acid. By heating the wetted material to temperatures in a range of about 140–200°C for a period of a few minutes to an hour, partial hydrolysis occurs resulting in monomeric sugars from the hemicellulose part of the substrate. Typically, sulfuric acid at concentrations less than 4% by weight has been added. The frequent use of H_2SO_4 is due to it being rather inexpensive and efficient. A drawback is the generation

of toxic compounds, if the pretreatment is too harsh, that may be detrimental to the fermenting organism [29–31]. Also, the sulfur may pose a problem if not taken care of properly. The residual lignin-rich fraction can be used for heat generation, but if the sulfur content is too high, it can only be used with careful desulfurization of the effluents. Too high sulfur content in the final ethanol can cause malfunctioning of the fuel-injection nozzles in some engines.

Pretreatment using alkaline conditions are commonly performed at lower temperatures and pressure than is acid pretreatment. When the material is soaked in an alkaline (e.g., hydroxides of sodium, potassium or ammonium), pore swelling results. As a consequence, the internal surface area increases, which makes the carbohydrates more accessible for the enzymes. Besides the area increase, breaking of the lignin–carbohydrate bonds takes place, which also allows for the enzymes to attack the cellulose and hemicellulose chains. Alkaline pretreatment has been shown to be more efficient for agricultural residues and herbaceous crops than for woody materials, as the former type of substrates contain less lignin. To reach similar results using woody materials, the cooking conditions must be much more severe, similar to the Kraft process for pulping.

Lime pretreatment is an alkaline method, which is useful when agricultural or hardwood residues are involved [32, 33]. Due to its relatively low cost, it has become an interesting alternative; also since it can be recovered as solid $CaCO_3$ when reacted with CO_2. The calcium carbonate can then be recovered and converted to lime again using a kiln. A disadvantage using calcium-containing salts is the risk for precipitations of, for instance, calcium oxalate, which is a well-known problem in the pulp industry. When process streams containing calcium salts are recirculated in the pulp plant, precipitation often takes place on heat-exchanger surfaces causing scaling.

Organic solvents such as methanol, ethanol, acetone, glycols, or phenol, with small amounts of an inorganic acid catalyst (e.g., HCl or H_2SO_4), comprise foundation for the organosolv method [34]. This option makes use of that lignin dissolves in the organic phase, where it can be recovered using various technologies. It is essential to recover the solvent both for economic and for environmental reasons, but also because the solvent itself may be inhibitory in the enzymatic hydrolysis and the fermentation steps. When ethanol is used as solvent the recovery is facilitated as this is part of the ethanol production plant.

Physicochemical Methods This category involves methods that combine a physical and a chemical effect (e.g., steam pretreatment with addition of a catalyst, hydrothermolysis, wet oxidation, and ammonia fiber explosion (AFEX)).

Steam pretreatment (sometimes called steam explosion) is commonly used for pretreatment of lignocellulosic materials. It is, in essence, a chemical method very similar to dilute-acid hydrolysis, but usually performed at higher dry-matter contents than is dilute-acid hydrolysis. The typical temperature range is between 160°C and 240°C, with a treatment time of 1–20 min, after which the pressure is rapidly released ("exploded") and the material transported to a flash-off vessel. It is well suited for most materials, also for softwood. In this case, a small amount of acid catalyst is added to improve hemicellulose hydrolysis; however, when treating agricultural residues or most hardwood species, the inherent acetic acid content is enough to initialize hemicellulose hydrolysis, so-called autohydrolysis. In this case, the final pH is usually around 3–4, while it is set to 2 or less when mineral acids are added. The steam pretreatment method has been tested in pilot- and demo scale.

Hydrothermolysis is similar to steam pretreatment but is performed using more water and usually at slightly lower temperatures and lower dry-matter content. The result of hydrothermolysis is a liquid containing solubilized material, of which much is in its oligo- or polymeric form [35, 36]. This is usually not a problem if the enzymes added during the subsequent hydrolysis are selected to break down the fragments to monomers. For example, autohydrolysis of straw in larger scale has been demonstrated [37]. A variation of hydrothermolysis is the wet-oxidation procedure [38], where air or oxygen is added. This method is suited for materials having low lignin content as the yield has been shown to decrease with increasing lignin content. A drawback is that the lignin is oxidized causing loss of valuable material.

Ammonia fiber explosion (AFEX) is an alkaline method, which operates at elevated pressures, similar to steam pretreatment. However, in the AFEX method,

instead of water, liquid ammonia is added and the substrate is treated for 10–60 min at around 100°C or less [39, 40]. The resulting material contains very much of the carbohydrates in their polymeric forms. If the material is to be fermented, hydrolysis must be performed. However, the material has interesting properties in terms of water-holding capacity and gel formation ability, which can lead to new biodegradable polymer materials (e.g., barrier films and capsules controlled release of drugs). Like other alkaline methods, AFEX performs best on agricultural waste [41, 42], while its efficiency toward wood is lower, probably because of the higher lignin content. The ammonia must be recycled in the process to make it feasible, from economic and environmental aspects.

Biological Methods Biological pretreatment can be performed using microorganisms or individual enzymes to degrade the biomass to polymers [43]. The actual degradation is usually performed using white-rot fungi or brown-rot fungi, which breaks down the lignin or the cellulose and the hemicellulose part, respectively. The method as such has not been attracting too much attention, mainly because some of material is lost in the breakdown process, but also since biological degradation is a slow process and, therefore, would require large treatment units. It would be possible to use the fungi as a first step, while the raw material is stored in piles prior to the main pretreatment step.

Ionic Liquids A rather new approach is to use ionic liquids [44] to fractionate the polymers of lignocellulosic materials. Ionic liquids (IL) are salts, typically consisting of a large organic cation (e.g., 1-butyl-3-methylimidazolium and a small inorganic anion moiety). They exist as liquids at room temperature and are chemically and thermally stable. They act by disrupting the bonds between cellulose, hemicellulose, and lignin thus dissolving the molecules, while forming very little degradation products. So far, it has been demonstrated using pure crystalline cellulose, but some work using straw has also been rather successful.

Before ionic liquids can be used commercially, a number of questions must be answered. It is still not clear how they influence fermenting organisms, although initial tests do not indicate any major problems. However, it is necessary to establish efficient methods to recover the dissolved macromolecules from the ionic liquid, or, put in other words: how can one recycle the ionic liquids? Currently, the cost for ionic liquids is very high, which makes them less suited for use in production of bulk chemicals, such as ethanol. If, however, value-added chemicals (from hemicellulose or lignin) can be produced in conjunction with ethanol production, and efficient means to recycle the ionic liquids are found, they constitute a very interesting option.

Evaluation Having an array of different pretreatment methods to choose from makes it necessary to have tools for evaluation of the optimal process in terms of economic and operational feasibility. Not only must the pretreatment result in a well-treated substrate, but also the yields of the fractions have to be high. More severe conditions during pretreatment will cause greater degradation of hemicellulose sugars [45–47]. It is also necessary to consider the by-products formed and the impact they may have on the enzymatic hydrolysis and the fermentation steps. It is presently difficult to say that one method is very much better compared to another option without taking into account, for example, the type of raw material that will be used in the process or what by-products can be expected. Also, it is of importance for the economics of the process to consider utilization of the energy content in lignin for internal heating purposes or for the production of lignin pellets for off-site markets.

Several pretreatment methods (e.g., dilute-acid hydrolysis, SO_2-catalyzed steam pretreatment, controlled pH, AFEX, ARP (ammonia recycled percolation), and lime pretreatment) have been compared using the same batch of raw material and exactly the same procedure and conditions for assessment of the pretreated material. This investigation has been carried out for two different batches of corn stover [48] and for poplar wood [7]. The assessment was performed by determining the recovery of glucose and xylose both as monomeric and oligomeric sugars in the liquid after pretreatment and in the liquid after enzymatic hydrolysis of washed solid material (from pretreatment). The enzymatic hydrolysis was performed using solid material at a concentration of 1% glucan (which is a low concentration) and an enzyme dosage of 15 FPU/g glucan of the untreated material. Table 2 summarizes

Bioethanol from Celluloses. Table 2 Summary of studies on corn stover. Yield of sugars[a], in percentage of theoretical available in the raw material, after pretreatment and after pretreatment + enzymatic hydrolysis [48]

Method	Catalyst	Time and temperature	Pretreatment		Pretreatment + enzymatic hydrolysis	
			Xylose	Glucose	Xylose	Glucose
Dilute-acid hydrolysis	H_2SO_4 0.49%	20 min, 160°C	85.1 (82.8)	6.3	93.6 (91.2)	91.7
Steam pretreatment[b]	SO_2 3%	5 min, 190°C	37.1	8.6	91.8	95
Controlled pH	None	15 min, 190°C	57.8 (2.4)	5.6 (0.3)	81.7 (26.3)	85.2
AFEX	Conc NH_3	5 min, 90°C	0	0	91.8 (77.7)	96
ARP	NH_3	10 min, 170°C	47.2	0	88.3 (41.1)	90
Lime	CaO 0.08 g/g biomass	4 weeks, 55°C	24.4 (0.8)	1.6 (0.5)	76.4 (52.8)	93.1 (92)

[a]Based on monomer and oligomer sugars obtained in the hydrolysate after pretreatment and in the enzymatic hydrolysis of pretreated material. Numbers in brackets are for monomer sugars only, when reported
[b]Performed for another batch of corn stover

Bioethanol from Celluloses. Table 3 Summary of studies on poplar. Yield of sugars[a], in percentage of theoretical available in the raw material, after pretreatment and after pretreatment + enzymatic hydrolysis [49]

Method	Catalyst	Time and temperature	Pretreatment		Pretreatment + enzymatic hydrolysis	
			Xylose	Glucose	Xylose	Glucose
Dilute-acid hydrolysis	H_2SO_4 2%	1.1 min, 190°C	62.4	23.9	71.7	86.7
Steam pretreatment	SO_2 3%	5 min, 190°C	74.4 (54.3)	3.1	83.7 (63.6)	100
Controlled pH		10 min, 200°C	58.1 (3.9)	2 (0.1)	95.7 (41.5)	55.9 (54)
AFEX	Conc NH_3	10 min, 180°C	0	0	51.9	53.1
ARP	NH_3 (39%)	27.5 min, 185°C	37.2 (0)	0.5 (0)	68.6 (31)	49.3 (48.9)
Lime	CaO 20%	120 min, 160°C	4.7 (0)	0.3 (0)	77.5 (65.1)	96 (90.6)

[a]Based on monomer and oligomer sugars obtained in the hydrolysate after pretreatment and in the enzymatic hydrolysis of pretreated material. Numbers in brackets are for monomer sugars only, when reported

the results for the second batch of corn stover, which are very similar to those for the first batch. The total yield of sugars obtained with the different pretreatment methods was more or less the same, around 90% or more. The main difference is that the low pH methods, like acid hydrolysis and SO_2-catalyzed steam pretreatment, result mainly in monomeric xylose, while the high pH methods (like AFEX) result in a large amount of oligomeric xylose, which requires also a whole range of hemicellulases in the enzymatic hydrolysis.

Table 3 shows the sugar yields from the poplar-wood study. The yield varies more for poplar than for corn stover. It is higher, especially regarding glucose, for the low pH methods with a glucose yield close to theoretical compared with the high pH methods with glucose yield as low as 50%. Also for poplar, the high pH methods result in more oligomeric xylose, with the

exception of lime. It should also be noticed that for poplar much more severe conditions, like a higher temperature, had to be used (Table 3) compared with the requirements for corn stover.

While many pretreatment methods have been investigated for agricultural waste and hardwood, the number of feasible pretreatment methods investigated for softwood is smaller. It appears that acid hydrolysis and steam pretreatment with acid catalyst are the most appropriate methods [20] to give high sugar yields from softwoods, which are much more recalcitrant than the other lignocellulosic materials. Acid hydrolysis and steam pretreatment with acid catalyst seem to be the methods that can be used for all types of raw materials and these are also the methods that have been most extensively used in pilot and demo plants. However, the drawbacks are the high equipment cost and the formation of inhibitors formed during pretreatment.

In most assessments of pretreated materials, a mixture of cellulases is used in the enzymatic hydrolysis step. Steam pretreatment of corn stover, with and without addition of SO_2, was assessed by enzymatic hydrolysis using ordinary cellulases supplemented with xylanases [49]. The additions of small amounts of xylanases had a major impact on the xylose yield and, surprisingly, even more on the glucose yield (Table 4).

The improvement of sugar yield in the enzymatic hydrolysis of corn stover by addition of xylanase was more pronounced for pretreatment methods that removed less xylose (e.g., AFEX) [50]. However, also for SO_2-catalyzed pretreatment, the increases in glucose and xylose yields in the enzymatic hydrolysis were about 15% and 34%, respectively. This was also shown for poplar wood [51]. This shows the importance of not using standard methods when assessing pretreatment, but to actually optimize the combination of pretreatment and enzymatic hydrolysis, and preferably also fermentation.

It is important, however, to keep in mind that the assessments described above are not performed under realistic process conditions as the substrate concentration in the enzymatic hydrolysis was very low and the influence of possible inhibitors present in the pretreated slurry was avoided. For a correct evaluation, the fully integrated process must be considered as the various pretreatment methods result in different types of materials. Hemicellulose sugars can be obtained either in the liquid as monomer or oligomer sugars, or in the solid material to various extents; lignin can be either in the liquid or remain in the solid; the composition and amount/concentration of possible inhibitory compounds also vary. This will affect how the enzymatic hydrolysis should be performed (e.g., with or without hemicellulases), how the lignin is recovered, and also the use of the lignin coproduct. This means that all process steps have to be optimized taking into account the special features of the pretreated material, and then comparing the production cost for the various alternatives.

Enzymatic Hydrolysis

Enzymatic hydrolysis of lignocellulosic materials requires a multitude of enzymes, which have activity

Bioethanol from Celluloses. Table 4 Overall sugar yields as percentage of theoretical based on content in raw material after enzymatic hydrolysis of steam-pretreated corn stover (with and without impregnation with SO2 [48])

Pretreatment conditions	Enzymatic hydrolysis using only cellulases[a]		Enzymatic hydrolysis using cellulases[a] with addition of xylanases[b]	
	Glucose	Xylose	Glucose	Xylose
170°C, 9 min + SO_2	62.2	67	70.7	70.6
190°C, 5 min + SO_2	83.2	70.5	96	73.9
190°C, 5 min, no catalyst	69.3	74.6	93.8	85.3

[a]Celluclast 1.5 L and Novozyme 188 (both from Novozymes A/SBagsaerd, Denmark)
[b]Multifect Xylanase (from Genencor) Int. Rochester, NY, USA)
Total amount of protein equal in all enzymatic hydrolysis

toward a variety of molecular groups. For example, to hydrolyze cellulose, at least three different types of enzymes must be present: endoglucanases, which disrupt amorphous areas of the molecule to create free ends; cellobiohydrolases that cleave cellobiose from both ends of the exposed chain to form cellobiose; and, finally, β-glucosidase that generates two glucose molecules from cellobiose. Most cellulases are end-product inhibited, that is, most cellulases are affected by cellobiose [52, 53], while β-glucosidase is particularly sensitive to glucose [54], resulting in an accumulation of these sugars, which slows down hydrolysis (or even stops it completely). Compounds that are generated in the pretreatment step can also have a negative impact on enzymatic hydrolysis. If the liquid fraction from the pretreatment step is replaced or if washed material is used for enzymatic hydrolysis, hydrolysis can be improved [55]. This improvement suggests that other inhibitory compounds than the sugars may play a vital role as inhibitor. Another important factor is the unproductive binding of the cellulase enzymes to lignin, causing the overall catalytic effect to be smaller.

There are many cellulase-producing species in nature, most of them various fungi. The maximum cellulase activity for most fungal-derived cellulases and β-glucosidase occurs at 50 ± 5°C and a pH of 4–5. During the last decade, much effort has been made to improve the overall activity of the enzymes and the yield of enzymes, but also production itself has been rendered more effective to decrease cost. Independently from ongoing cost-reduction efforts [56, 57], the production cost of enzymes is still rather high and requires further reduction. One way to achieve this is to use a fraction of the feedstock and/or the hydrolysate for on-site enzyme production by fungi or other microorganisms [58].

Some pretreatment methods leave the hemicellulose fraction more or less unaffected calling for additional hydrolysis using hemicellulases. The hemicellulose part of lignocellulosic materials requires other types of enzyme complexes for efficient hydrolysis. Since the raw material differs with regard to the composition of hemicellulose, ideally the enzyme cocktail should be prepared in a way that best meets the demand of the various materials. For example, agricultural residues require xylanases to be present, while it is preferable to have mannanases if the material is softwood. The hemicellulase system includes among others endo-1,4-*β*-D-xylanases, which hydrolyze internal bonds in the xylan chain; 1,4-*β*-D-xylosidases, which attack xylooligosaccharides from the nonreducing end to liberate xylose; endo-1,4-*β*-D-mannanases, which cleave internal bonds in mannan; and 1,4-*β*-D-mannosidases, which cleave mannooligosaccharides to mannose. The side groups are removed by a number of enzymes: α-D-galactosidases, α-L-arabinofuranosidases, α-glucuronidases, acetyl xylan esterases and feruloyl, and *p*-cumaric acid esterases [59–62].

Enzymatic hydrolysis of lignocellulosic materials has been studied on a number of substrates and under various conditions [55, 63, 64]. Separate hydrolysis and fermentation (SHF) is an attractive idea since it allows for different conditions during hydrolysis and fermentation, though the choice between SHF and simultaneous saccharification and fermentation (SSF, which is described in detail below) has to be made after economic optimization. It is possible to have a higher temperature during hydrolysis to benefit from the higher activity of the enzymes at elevated temperatures. However, it is important to note that the stability of the enzymes is affected by temperature. It has been shown that it can be favorable to operate at lower temperatures to reach higher yields of sugars. For spruce the optimal temperature was found to be dependent on both residence time and pH, and the maximum degree of cellulose conversion, 69.2%, was obtained at 38°C and pH 4.9 for a residence time of 144 h [65]. The decision regarding maximum reaction rate, optimal stability, and residence time has to be made based on economic considerations. It is also desirable to operate at high solids content to reach sugar concentrations that will result in ethanol concentrations around 4%. However, increasing solids concentrations create technical problems, since it can be difficult to mix the material efficiently, especially in the initial phase of hydrolysis, when the viscosity can be very high [66, 67, 110].

Fermentation of Sugars

Fermentation is performed using a microorganism, usually yeast, which converts sugar to ethanol. The yeast *Saccharomyces cerevisiae* (sometimes referred to as baker's yeast) is today the prime choice in industrial

ethanol production from starch and sugar. It is a very robust microorganism, which has a high ethanol tolerance and is also rather tolerant to inhibitors produced during pretreatment of biomass. It has also a high ethanol productivity (up to 1.3 g g^{-1} cell mass h^{-1}) and yield (higher than 0.45 g g^{-1} at optimal conditions) [68]. The main drawback is that it only ferments hexose sugars (i.e., glucose, mannose, and, under certain circumstances, galactose), but is not able to ferment the pentose sugars, xylose and arabinose, which are present in all hemicelluloses, especially in hardwood and agricultural residues (Table 4). There are naturally occurring yeasts (like *Pacchysolen tannophilus, Pichia stipitis, and Candida shehate*) and bacteria (like *Escherichia coli, Klebsiella, Erwina, Lactobacillus, Bacillus, and Clostridia*) able to utilize pentoses, but these have other drawbacks (e.g., less tolerance for ethanol and inhibitors, lower fermentation rate, and a need for rigorously controlled aeration), which make them less suitable for industrial applications [69, 70].

A lot of effort has been devoted to the development of efficient xylose-fermenting microorganisms [71, 72], as xylose is by far the most abundant pentose sugar, but there is also research going on to develop the arabinose fermentation [73, 74] as well as on genetically modified *S. cerevisiae* [12, 75, 76].

Genetic modification of *S. cerevisiae* has got a lot of attention due to the attractive properties of this yeast and its abundant use in industry. *S. cerevisiae* can naturally ferment xylulose; so in order to make it also ferment xylose, a pathway for conversion of xylose to xylulose has to be introduced. This can be done in two ways: either by introducing genes encoding for xylose isomerase (XI) from bacteria and fungi [77–79], which converts xylose to xylulose in one step, or by introducing genes encoding for xylose reductase (XR) and xylitol dehydrogenase (XDH) from fungi [80, 81], which first reduces xylose to xylitol and then xylitol is oxidized to xylulose.

Also, the endogenous XKS1 gene encoding xylulokinase (XK) has to be overexpressed to obtain significant xylose fermentation [81].

The uptake of xylose in *S. cerevisiae* is performed by glucose transporters, which have about two orders of magnitude lower affinity for xylose than for glucose [70] resulting in competitive inhibition of xylose uptake by glucose. A lot of research has been carried out on transport proteins and introduction of various sugar transporters to increase the uptake of xylose [82]. The presence of a small amount of glucose increases the xylose uptake [83]. This has also been shown in recent SSF studies, with co-fermentation of xylose and glucose, where a slow release of glucose, thus maintaining it at low concentration resulted in increased uptake and utilization of xylose [84–86].

Another challenge in fermentation of lignocellulosic hydrolysates is the presence of various compounds present in the hydrolysate that are inhibiting to the microorganism. These compounds comprise degradation products formed during pretreatment (like furfural, HMF, formic acid and levulinic acid, and phenolics) as well as compounds present in the biomass (like acetic acid and extractives) [87]. The concentrations of these and all other inhibitory substances in the fermentation step depend on the configuration of the preceding process steps.

The inhibitory effect can be overcome by detoxification of the hydrolysate before fermentation. There have been many chemical and physical methods proposed that reduce the concentration of inhibitors and improve the performance in the fermentation step.

Treatment with $Ca(OH)_2$ (so-called overliming), ion-exchange treatment, and steam stripping may increase the fermentability significantly but may also result in some sugar loss [88, 89]. This will also increase both the capital and running costs.

Another approach is to make the yeast more tolerant, by adaptation to the hydrolysate, and to design the fermentation procedure so that the concentrations of inhibitors are kept at a low level. Cultivation of *S. cerevisiae*, both natural strains and genetically modified strains capable of fermenting xylose, on hydrolysates of steam-pretreated spruce containing inhibitors have resulted in higher ethanol yield and productivity from the same hydrolysate than cultivation on pure sugars [90, 91]. The other approach is to run the fermentation in a fed-batch mode and feeding the hydrolysate at a rate that makes it possible for the yeast to detoxify the hydrolysate in situ [92]. Detoxification occurs when carbonyl compounds – like in furans and phenolics – are reduced to the corresponding alcohols, which are less inhibitory to yeast [93]. In such cases, the fermentation productivity

will be a function of the inhibitor concentration, the conversion capacity of the yeast, and the quality of the process control.

One inhibitor usually present in hydrolysates is acetic acid, formed from the acetyl groups present in most hemicelluloses. Acetic acid has a pK_a of 4.75, which is close to the pH of fermentation and therefore a significant amount is in undissociated form that can diffuse through the plasma membrane, and may dissociate inside the cell. This has an intense inhibitory effect on growth of *Saccharomyces cerevisiae*, but leads to an increased ethanol yield at low concentrations, up to 6 g/L [31, 94]. In order to avoid the drop in intracellular pH, the cell must pump out protons using the plasma membrane ATPase. To achieve this, the cells have to produce more ATP, which in anaerobic conditions is done by producing more ethanol and thus resulting in increased ethanol yield [30]. Increased ethanol yield has also been noted in the presence of furfural at low concentrations [95]. At higher concentrations of acetic acid (above 10 g/L), the ethanol yield is decreased while initial furfural concentrations below 5 g/L can be acceptable for fermentation; however, at higher concentrations severe inhibition may occur, which reduces the ethanol productivity [96].

Another option to run the fermentation is by continuous fermentation with several fermentors in cascade. In continuous fermentation, the yeast is retained in the fermentor either by running at a dilution rate below the growth rate of the yeast or by recycling the yeast. This would be beneficial as the yeast gets adapted to the inhibitors present in the hydrolysate. Furthermore, it results in reduced labor costs and reduced fermentor downtime for cleaning and filling, as well as in higher volumetric productivity (in case cells are recycled) compared with batch fermentation [97].

Process Intensification

One of the most crucial factors in process intensification of the ethanol production process is to run the process at as high dry-matter concentration as possible, which leads to decreased size of equipment as well as to reduced energy demands. This leads to less material being handled and less water to be removed in the downstream processing, which has a significant effect on capital and running cost [98, 99]. Figure 7 shows

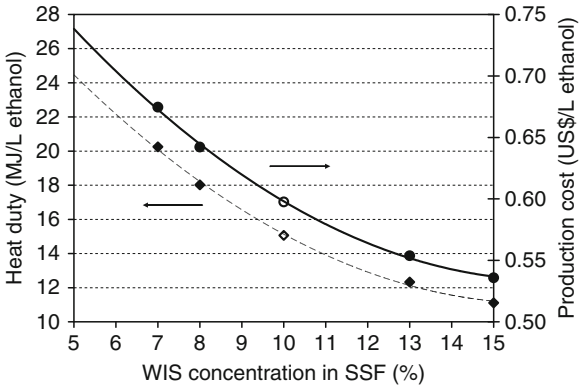

Bioethanol from Celluloses. Figure 7
Comparison of the overall energy demand and total production cost as function of the solid concentration

a comparison of the overall energy demand and total production cost as function of the solid concentration in the SSF for ethanol production from spruce [100] assuming that an increase in dry matter does not affect the conversion yield. Similar relationships were found for corn stover and salix [101, 102].

However, high dry matter leads to problems related to heat and mass transfer in the conversion steps (i.e., pretreatment, enzymatic hydrolysis, and fermentation (or SSF)) as well as higher concentration of inhibitors in the biological steps, as is outlined below. The concentrations of various inhibitors depend though on how the process is designed as can be seen in Fig. 8. In process configurations where the liquid after pretreatment is separated and used for other purposes, the effect of inhibitors on SHF or SSF of the solids diminishes (e.g., IBUS process [103]). The liquid could then be used for other applications (e.g., biogas production) where it may be diluted without negative effects as the product is recovered from a gas phase, where the product concentration is not affected by the substrate concentration in the liquid. Lower inhibitor concentrations can also be achieved by using pretreatment methods that do not create degradation products keeping in mind that several inhibitors, like acetic acid and extractives, are present in the lignocellulosic material and are difficult to avoid.

Another important way to reduce the energy demand in the process and reduce capital cost is by process integration, that is, by using as few process steps as possible. Simultaneous saccharification and

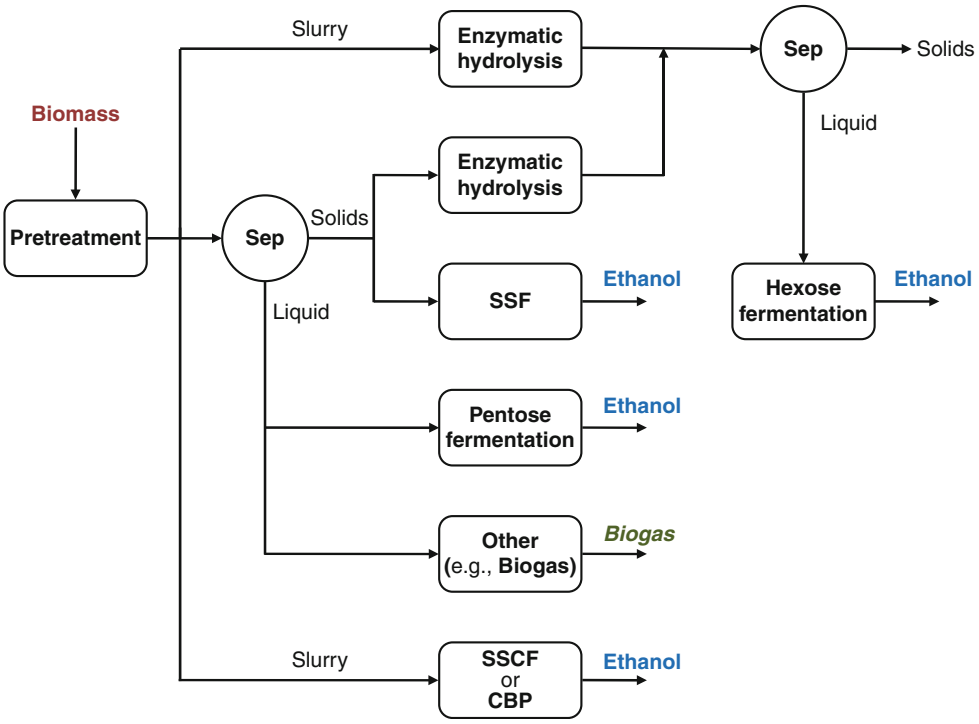

Bioethanol from Celluloses. Figure 8
Various process configurations and some potential products

fermentation (Fig. 8) can be seen as one type of integration that results in both lower energy demand and lower capital cost. SSF has been widely used also for industrial starch-based fuel-ethanol production. By performing the enzymatic hydrolysis and fermentation in the same reactor, the sugars formed by enzymatic hydrolysis are converted by the yeast as soon as they are released. This maintains a low concentration of sugars in the broth which alleviates the end-product inhibition of the cellulases and also diminishes the risk for infections. Another advantage is the capability of the yeast to partly detoxify the slurry [55]. These two effects result in an increased enzymatic hydrolysis productivity compared with enzymatic hydrolysis performed at higher temperatures. This results in higher overall ethanol productivity, which means a lower total reactor volume. It has also been shown in several studies that the ethanol yield is higher after SSF than after SHF both for softwood and agricultural residues [104, 105]. However, the development of new cellulases that are less end-product-inhibited may change this situation in the future.

Another advantage of SSF is that glucose does not need to be separated from the lignin fraction following a separate enzymatic hydrolysis step, thereby avoiding not only a potential loss of sugar but also excessive washing, which dilutes the sugar stream. After the SSF, the slurry is taken to a distillation step where ethanol is distilled off, with negligible loss of ethanol in the remaining stillage stream, and the lignin is then separated by filtration.

The main drawback with SSF is that the yeast after SSF is difficult to recover as it is mixed with the residual solid (i.e., mainly lignin) and also that the optimal temperature and pH for enzymatic hydrolysis and fermentation differ. In spite of this, SSF is in many studies considered as a better option than SHF for several raw materials investigated. The use of SSF is also cost effective, since it reduces the number of reactors [106].

Other studies on SSF have aimed at decreasing the enzyme and yeast concentrations and varying temperature and pH. The enzymes are either produced on-site, which results in less substrate available for ethanol production and thereby a lower overall ethanol yield, or

purchased and thereby add to the cost of chemicals. The yeast will most probably be cultivated using the hydrolysates after pretreatment, in order to adapt it to the hydrolysates. A higher yeast concentration will thus lead to a lower overall ethanol yield. As the rate of the enzymatic hydrolysis is rate-limiting in most SSF experiments, the yeast concentration can be lowered [8, 101, 107] but should not be too low to avoid a stuck fermentation.

When both pentoses and hexoses are fermented together in SSF, the process is referred to as SSCF (i.e., simultaneous saccharification and co-fermentation). In this case, the whole slurry from pretreatment is fed directly to SSF, which reduces the number of process steps compared to separate pentose fermentation and SSF. SSCF can also lead to better utilization of sugars. Studies [84, 85, 108] have shown that the utilization of xylose, using pentose-fermenting yeast, was improved when SSF was used for slow release of glucose, which facilitated the uptake of xylose, compared with when all glucose is available from the start, which is the case in traditional SHF. The slow release may be controlled either by the enzyme dosage, by the temperature during SSF, or by a combination of both [108]. However, it may be difficult to control the slow release of glucose in full scale, so it will be necessary to perform tests in pilot-plant size to evaluate the concept.

Still another option for an even more integrated process is to perform enzyme production, enzymatic hydrolysis, and fermentation in a single reactor, so-called consolidated bioprocessing (CBP) [109]. CBP has the potential for lower bioethanol production costs due to simpler feedstock processing, lower energy inputs, and lower capital cost than separate hydrolysis and fermentation processes. However, this requires a microorganism that produces all the required enzymes and ferments all sugars. This could either be done by engineering bacteria that naturally utilizes cellulose, like *Clostridium cellulolyticum* or *Clostridium thermocellum*, and improve the ethanol production in those or to genetically modify naturally good ethanol-fermenting microorganisms (like the yeast *S cerevisiae*) to express heterologous cellulase systems. Both approaches have been investigated but to date no microorganisms are available, which are sufficiently effective and the concept is subject to further research.

To avoid problems with mass transfer in enzymatic hydrolysis, SSF, SSCF, or CBP, a short prehydrolysis can be performed where the material is partly liquefied and the viscosity drops. This may be performed in specially designed reactors. One example [110] has been capable of liquefying pretreated wheat straw at solids concentrations up to 40% (w/w) by the use of enzymes. Another way of handling both the mass transfer and inhibitor problems in the biological conversion step, like SSF, is to run in a fed-batch mode.

In recent years, significant progress has been made in running SSF at higher solids loading both by using adaptation of yeast or fed-batch procedures to overcome the effect of inhibitors. Final ethanol yields higher than 70% of theoretical, based on total hexoses and pentoses, and final ethanol concentrations around 4% (wt/wt) can be expected [108].

In case the liquid after pretreatment is removed before the SSF step, that is, using only the cellulose for ethanol production, while the hydrolysate containing the hemicellulose sugars and the inhibitory compounds are used for other purposes (like biogas), the ethanol concentration in SSF can be even higher. An ethanol concentration higher than 6 wt-% has been demonstrated in a combined prehydrolysis and SSF of pretreated wheat straw although the running time was higher than 200 h [103].

The most obvious way to reduce energy demand is by heat integration of steam-requiring process steps. By running the various process steps at different pressures, it is possible to use the secondary steam obtained from the equipment run at high pressure to heat an equipment run at low pressure. This could include integration of the distillation step with the evaporation plant, increasing the amount of distillation columns, or increasing the number of units in the multiple-effect evaporation unit [111]. A somewhat different concept is to introduce mechanical vapor recompression in distillation and/or evaporation [111].

Another option is to replace energy-demanding process units with a less energy-demanding process step. One option that has been proposed to take care of the stillage stream is to evaporate it and concentrate the nonvolatiles to dry-matter content above 50–60 wt-% and then burn the residue in a boiler to produce heat for the ethanol process. Evaporation of the stillage is very energy demanding [100] and is performed mainly

as a wastewater treatment step. The energy obtained from combustion of the concentrated stillage stream is in the same order as the energy needed to perform the evaporation. One option could be to replace evaporation with anaerobic fermentation of the stillage stream for production of biogas. In this way, the energy demand for evaporation can be eliminated and also the capital cost. Both volatile and nonvolatile organic compounds are converted to biogas, which can then be used in the boiler for production of heat and power to the process. Alternatively, the biogas can be upgraded to pure methane to be used as transportation fuel. The amount of biogas that can be produced depends on the composition of the stillage stream and has to be verified experimentally for each specific stillage stream to assure that most of the organics are fermented. Also, the requirement of an aerobic treatment step for final wastewater handling needs to be evaluated. In a couple of studies where evaporation has been replaced by anaerobic digestion, it has been shown that the potential for reducing the energy demand and the ethanol production cost is substantial [112, 113].

External Process Integration

One approach to reduce the production cost for cellulosic ethanol production is to integrate it with another suitable plant (e.g., a combined heat and power plant, a starch-based ethanol plant, a sugar-based ethanol plant, or a pulp and paper mill). The type of plant to integrate with is very much dependent on the biomass that is to be used, the location, and also the process configuration. For instance, in case wood residues are used, it could be suitable to integrate with a CHP plant that is also using forest residues for heat and power production. Part of the solid residue can then be replaced by the lignin fraction available from the cellulosic ethanol plant and the CHP plant provides the ethanol plant with steam and electricity.

Another option is to integrate cellulosic ethanol production with starch-based ethanol production (e.g., from corn or wheat) to utilize the whole agricultural crop. One benefit is that the raw material is close to the factory and another is that the lignin from the cellulosic part of the material can provide heat and electricity for both processes, that is, both for the first-generation and the second-generation ethanol plant. Depending on how the integration is performed, it could also help to boost the ethanol concentration resulting from the lignocellulosic process, for example, if the same distillation unit is used for both plants. This will reduce the energy demands in the distillation and the evaporation steps. However, in case the residue from the first-generation plant is to be used as animal feed (DDGS), the integration approach must be carefully chosen to avoid affecting the value of the DDGS. In case the residue is used for biogas production, the integration is easier to implement.

A third option is integration with a sugar-based ethanol production plant (e.g., sugarcane-based ethanol production). The same benefits as for integration with starch-based ethanol production can be achieved.

The biorefinery concept, that is, to use the whole crop for production of a variety of chemicals and fuels using chemical and biological transformations, is also an interesting option. Figure 9 shows a variety of products that could be produced when ethanol is produced from either the cellulose fraction only or from both cellulose and hemicellulose. In this case, the income from other products improves the overall process economics.

Integration with Heat and Power Plant Integration of cellulose-based ethanol production with a combined heat and power plant (Fig. 10) has the possibility to reduce the production cost of ethanol. One of the benefits is that the syrup or lignin residue can be used for steam production without prior drying, which reduces the energy demand. This type of integration is even more interesting in case the plants are combined with district heating as the heat of condensation in the flue gases from the CHP can be utilized for district heating. Also the excess heat from the ethanol plant can be utilized for this purpose. Such integration has been shown to increase the energy efficiency and reduce the production cost by up to 20% for conditions prevailing in Sweden [114]. The study was based on ethanol production from 200,000 t of spruce per year. Various options for the utilization of the solid residue formed during ethanol production from spruce, such as the production of pellets, electricity, and heat for district heating, were compared. The overall energy efficiency ranged from 53% to 92% (based on the lower heating values, LHV) with the highest value for

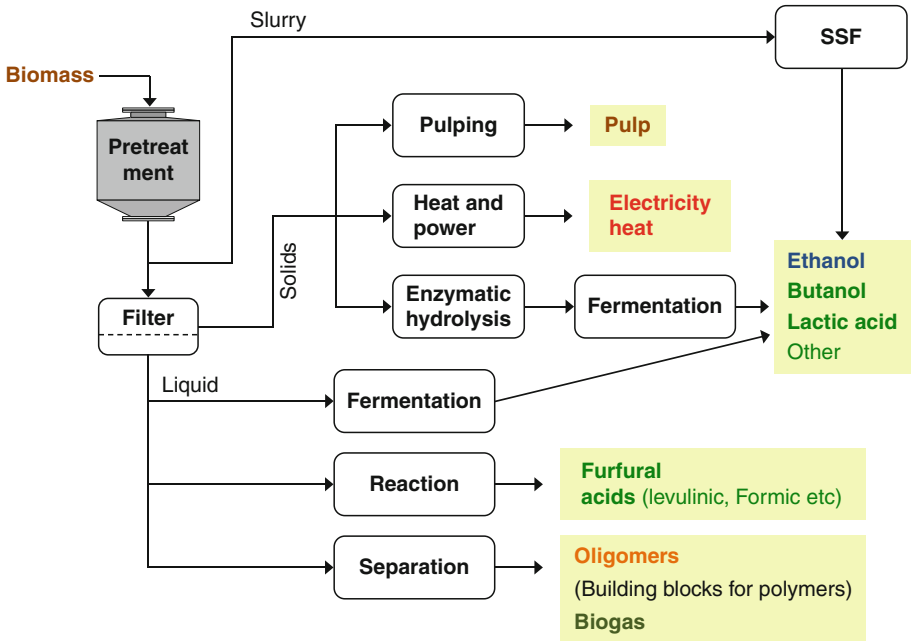

Bioethanol from Celluloses. Figure 9
A selected number of potential products from biomass

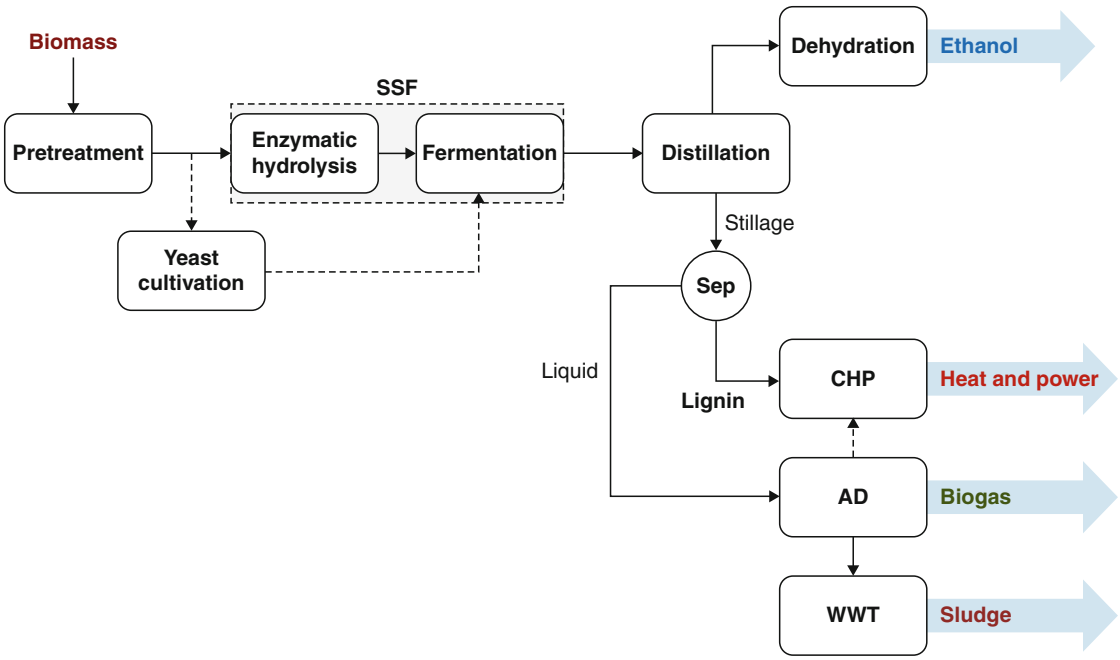

Bioethanol from Celluloses. Figure 10
Integration of a cellulose-based ethanol production with a combined heat and power plant

cases with district heating, where a large part of the low temperature waste heat from the process can be utilized. However, this option restricts the location to the vicinity of larger cities of the plant as there must be a demand for the surplus heat. Similar conclusions regarding utilization of waste heat were reached in a study on coproduction of ethanol and electricity from softwood, based on conditions in California [115].

In a recent study on ethanol from spruce [113] several configurations where evaporation of the liquid fraction of the stillage stream from distillation was replaced by anaerobic digestion (AD) followed by aerobic wastewater treatment were investigated. In the best case, the energy efficiency, based on LHV, for the combined production of ethanol and biogas was 59% and the overall efficiency, including the contributions from electricity and district heat, was 92%. This process configuration resulted also in the lowest ethanol production cost. The total ethanol production cost was diminished by 17–22% compared with the base case using evaporation of the stillage stream and burning of the concentrated syrup in the CHP.

Most of the existing pilot and demo scale plants for cellulosic ethanol production are integrated with production of power and steam, mostly using the lignin fraction.

Integration with First-Generation Ethanol Another option is to integrate second-generation cellulosic ethanol production with first-generation starch-based or sugar-based ethanol production to use the whole agricultural crop (Figs. 11 and 12, respectively). Suitable residues are corn stover, corn cobs, corn fiber, wheat straw, and sugarcane bagasse and leaves/trash. There are many possible ways to integrate the processes (Fig. 11) for the starch-based case, and the desired choice of integration is very much influenced by the choice of coproducts.

The absolute lowest degree of integration is to share the heat and power production plant where the lignin residue, and in some cases also biogas, from the second-generation plant is used to provide heat and electricity to both plants. This is perhaps the most obvious integration in corn-based ethanol plants in the USA where the corn is used to produce several different

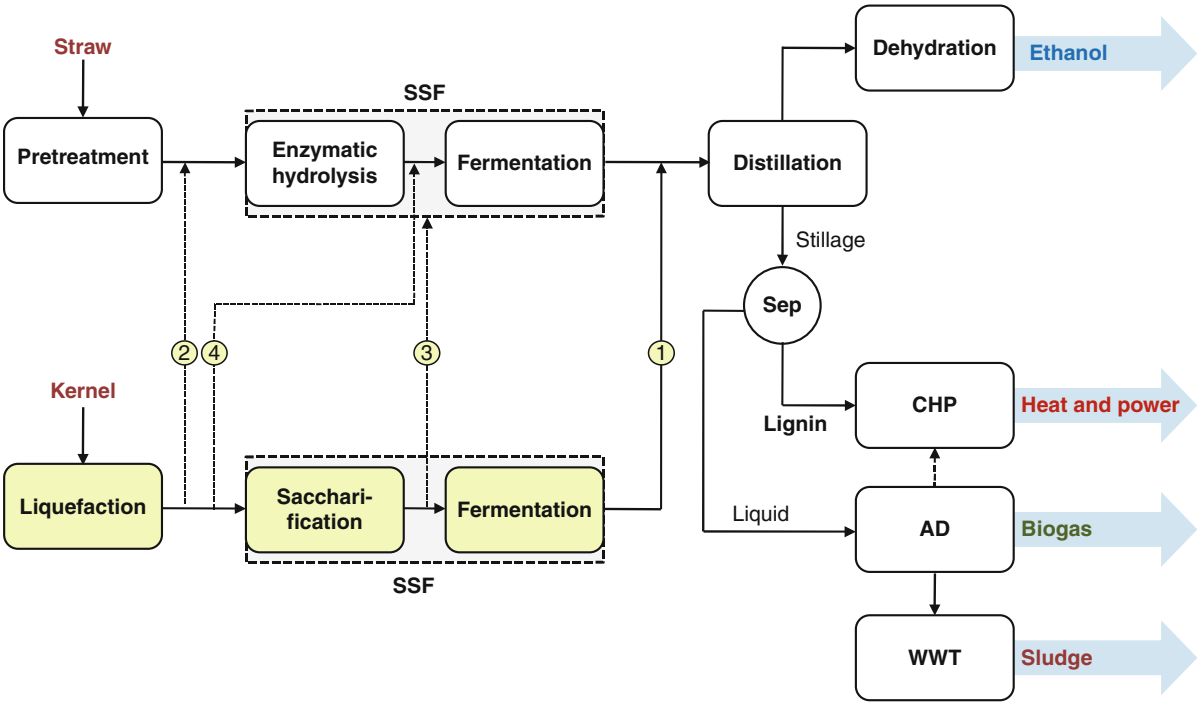

Bioethanol from Celluloses. Figure 11
Integration of starch-based and lignocellulose-based ethanol production

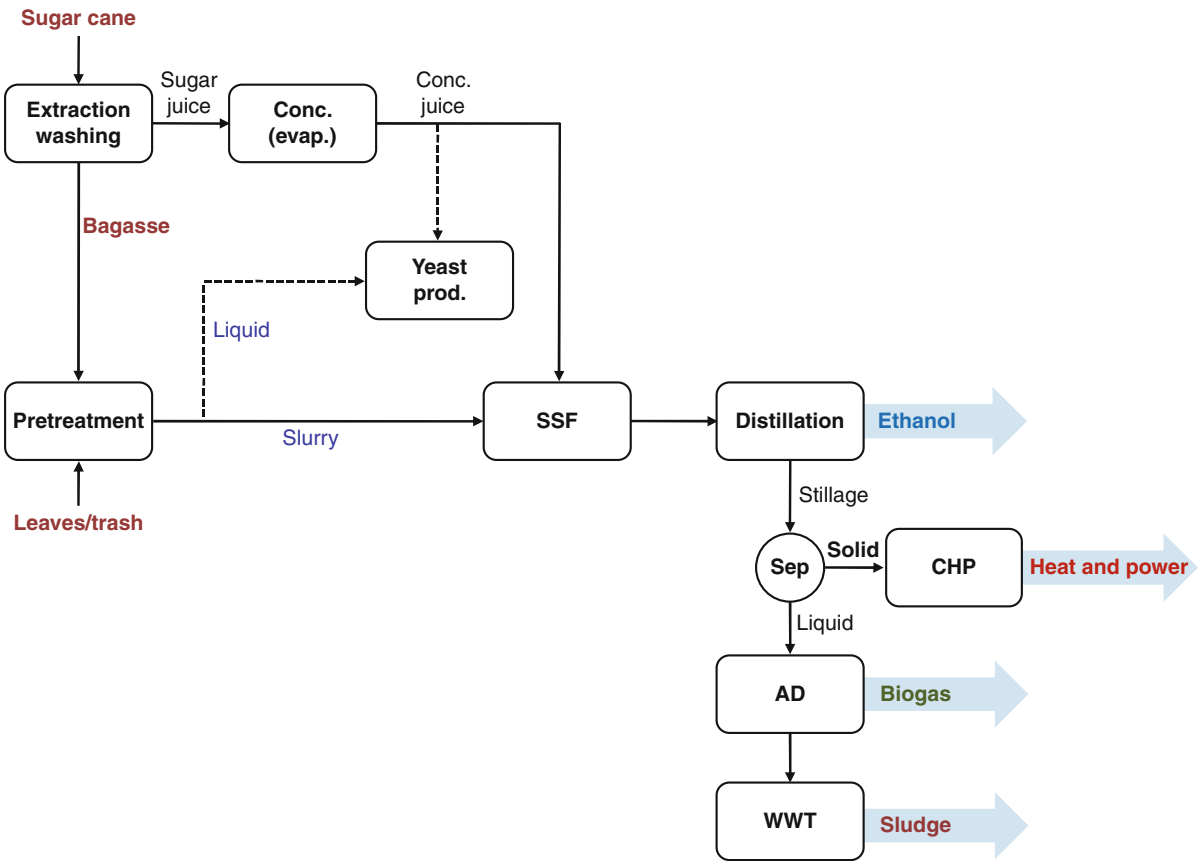

Bioethanol from Celluloses. Figure 12
Integration of sugarcane-based and lignocellulose-based ethanol production

coproducts, besides ethanol, and where most of the plants are using natural gas for heat and power production. In case this is replaced by heat and power from the cellulosic material, it will improve the sustainability of these plants. Another option, at a low integration level is to use a combined distillation plant (option 1 in Fig. 11). The two processes would have separate and dedicated equipment for pretreatment, hydrolysis and fermentation. As it is usually difficult to reach high sugar and ethanol concentrations in the second-generation ethanol production, while starch- or molasses-based ethanol production require dilution of the sugar, the latter could be used to boost the second-generation ethanol stream to reach ethanol concentrations well above 4–5 wt-%. This would result in a decrease of the critical energy demand in the combined distillation step compared with distillation in two units well below 4 wt-% ethanol (Fig. 13).

The possibility for integration in the upstream direction increases when both first- and second-generation plants are designed and erected simultaneously. Figure 11 shows some options [2–4] where material streams are combined further upstream. This could reduce not only the equipment cost but also the energy demand. Integration may also alleviate some of the inhibitory effects occurring from formation of toxic compounds in the pretreatment step. If the process streams are mixed prior to fermentation the lignocellulosic streams will be diluted by the starch- or sugar-based streams. The integration may in some cases also lead to higher ethanol yield from the first-generation plant. In a study where pretreated wheat straw was

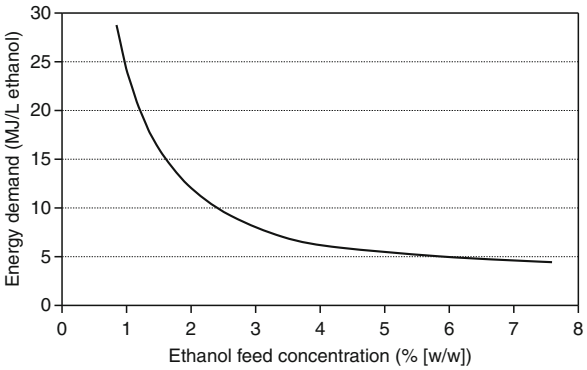

Bioethanol from Celluloses. Figure 13
Energy demand in the distillation step, where ethanol is concentrated to 94 wt-%, as a function of the ethanol feed concentration. The step was assumed to consist of two stripper columns (25 trays each) and a rectification column (35 trays) heat integrated by operating at different pressures. The inlet feed temperature was increased from 80°C to the boiling temperature before entering each stripper column

mixed with wheat starch, a higher ethanol yield as compared with using either only starch or only wheat straw was obtained using SSF [116]. This was probably due to the stress on *S. Cerevisiae* caused by weak organic acids present in the hydrolysate of steam-pretreated wheat straw. It is also easier to reach a high ethanol concentration using such a mixture than when using wheat straw only as a raw material. The use of the wheat starch, coming from wheat flour, is rather rich in nutrients, which could also contribute to decrease the amount of additional nutrients needed in SSF of wheat straw.

Figure 12 shows a fully integrated ethanol production process for utilization of the whole sugarcane plant. In this case, the sugarcane bagasse (i.e., the residue of the cane after extraction of sucrose) is already on site at the ethanol mill. In many sugarcane ethanol plants, the bagasse is used to provide steam for the process and to cogenerate electricity, but by using a part of it for ethanol production the value chain can be increased [117]. Another option is to also use the leaves of the sugarcane, which in many cases today are burnt on the field creating an air pollution problem. In Brazil, which is a large producer of sugarcane ethanol, the government is becoming more restrictive regarding burning of residue in the field [118]. The development of more efficient burners [119–121] will also allow more effective use of these resources.

To summarize, the integration of first- and second-generation bioethanol production results in higher ethanol yield, lower energy demand, and lower production cost than by using a stand-alone second-generation ethanol production. To define the most optimal way of integration requires detailed studies (e.g., by flow-sheeting calculations based on reliable experimental data).

Future Directions

Substantial progress has been achieved in the field of lignocellulosic fuel-ethanol production and several pilot and demo plants have been built the recent years [122]. However, there are still several challenges remaining before reaching a mature industrial technology. Some of the most important challenges are:

- To produce ethanol at a high concentration. The most obvious is to perform enzymatic hydrolysis or SSF at high dry-matter concentration. This requires improvement of enzymatic hydrolysis with efficient enzymes, reduced enzyme production cost, and novel technology for high solids handling. Another important factor is to utilize all the sugars available in the pretreated material, that is, either including pentose fermentation or to produce some other energy product like biogas. The former will lead both to a higher ethanol concentration and to a lower production cost, while the latter results in a facilitated ethanol production from hexoses.
- The increase in concentration of inhibitory compounds with increased dry matter may lead to a decreased ethanol yield. To cope with this, an option is to separate the solid and liquid fractions and only use the solid fraction (i.e., the cellulose) for ethanol production. The liquid could then be used for other applications (e.g., biogas production) where it may be diluted without negative effects in the product recovery as the biogas is obtained in the gas phase.
- Development of robust fermenting organisms, which are more tolerant to inhibitors and ferment both pentoses and hexoses in the raw material in concentrated hydrolysates with high yield, at high

productivity and with high ethanol concentration. The co-fermentation of pentoses and hexoses will lead both to a higher ethanol concentration and to a lower production cost.

- Extension of process integration to reduce the number of process steps and the energy demand and to reuse process streams to eliminate the use of freshwater and to reduce the amount of waste streams.
- Process integration with other types of industrial processes, for example, a combined heat and power plant or first-generation ethanol plant, which will reduce the production cost further. This may result in higher ethanol concentrations to the distillation step compared with a stand-alone second-generation plant.

One of the most important issues is to verify all process steps in an integrated way in pilot and/or demo scale. These plants should provide data for full-scale ethanol production and at the same time define new challenges for further research. The step from pilot- and demo-scale production of lignocellulosic ethanol to competitive full-scale production requires further reduction of the production cost. In pilot and demo scale, it is important to prove the whole process for longer periods of time with variation in raw material, which can be due to normal variations in crops due to where it is grown and the climate as well as by changes during storage. High accessibility and verification of yields and productivities obtained in lab and bench scale has also to be achieved, especially for critical process steps as pretreatment and SHF or SSF. Also more technical issues like separation of lignin and the influence of process integration and recycling of process streams on fouling. The qualities of products and coproducts as well as wastewater treatment are other important factors.

A conclusion to be drawn is that there is a significant potential of improvement and development. The production processes can be far more efficiently designed in the future as compared with prevailing concepts considering individual process steps, process configurations, and a huge number of combinations of process integration options.

This complexity and large number of design options could be considered both as positive and negative features when it comes to industrial implementation. The positive side is that the production process can be optimized for the specific local conditions, depending on available raw materials, heat sinks for use of district heating, demand for biogas as vehicle fuel, and other existing facilities to integrate with. The ethanol production system can then be designed to optimize the overall energy efficiency and profitability for the entire system. The negative side is that the high complexity requires a huge amount of knowledge for development of the most optimal production systems, which is not yet available.

To conclude, lignocellulosic ethanol has a promising role to play in the development of efficient and sustainable biofuel production systems in the future, but this requires improved knowledge and competence among all the different actors involved in this process. Furthermore, a more integrated work is needed between different research fields, such as process development and configuration and energy and environmental systems analysis (e.g., life cycle assessments) to optimize future production systems in a most efficient way regarding an economic, energy efficient and environmental sound perspective.

Bibliography

Primary Literature

1. Renewable fuels association, http//www.ethanolrfa.org
2. Farrell AE, Plevin RJ, Turner BT, Jones AD, O'Hare M, Kammen DM (2006) Ethanol can contribute to energy and environmental goals. Science 311:506–508
3. Lundqvist J, Teleman A, Junel L, Zacchi G, Dahlman O, Tjerneld F, Stalbrand H (2002) Characterization of galactoglucomannan extracted from spruce (Picea abies) by heat-fractionation at different conditions. Carbohydr Polym 48(1):29–39
4. Frederick WJ, Lien SJ, Courchene CE, DeMartini NA, Ragauskas AJ, Iisa K (2008) Co-production of ethanol and cellulose fiber from Southern Pine: a technical and economic assessment. Biomass Bioenergy 32:1293–1302
5. Söderström J (2004) Optimization of two-step steam pretreatment of softwood for bioethanol production. PhD thesis, LUTKDH/(TKKA-1002)/1-75/(2004). Lund University, Sweden
6. Grohmann K, Torget R, Himmel M (1986) Dilute acid pretreatment of biomass at high solids concentrations. Biotechnol Bioeng Symp 17:135–151
7. Wyman CE, Dale BE, Elander RT, Holtzapple M, Ladisch MR, Lee YY, Mitchinson C, Saddler JN (2009) Comparative sugar recovery and fermentation data following pretreatment of poplar wood by leading technologies. Biotechnol Prog 25(2):333–339

8. Sassner P, Galbe M, Zacchi G (2006) Bioethanol production based on simultaneoussaccharification and fermentation of steam-pretreated Salix at high drymatter content. Enzyme Microb Technol 39:756–762
9. Lee D, Owens VN, Boe A, Jerenyama P (2007) Composition of herbaceous biomass feedstocks. Report: North Central Sun Center. South Dakota State University, Brookings. http://agbiopubs.sdstate.edu/articles/SGINCI-07.pdf
10. Neureiter M, Danner H, Thomasser C, Saidi B, Braun R (2002) Dilute-acid hydrolysis of sugarcane bagasse at varying conditions. Appl Biochem Biotechnol 98–100:49–58
11. Linde M, Galbe M, Zacchi G (2006) Steam pretreatment of acid-sprayed and acid-soaked barley straw for production of ethanol. Appl Biochem Biotechnol 129–132:546–562
12. Hahn-Hägerdal B, Galbe M, Gorwa-Grauslund MF, Lidén G, Zacchi G (2006) Bio-ethanol? The fuel of tomorrow from the residues of today. Trends Biotechnol 24:549–556
13. Harris EE (1949) Wood saccharification. In: Advances in carbohydrate chemistry, vol 4. Academic, New York, pp 153–188
14. Wenzl HFJ (1970) The acid hydrolysis of wood. In: The chemical technology of wood. Academic, New York, pp 157–252, Chapter IV
15. Keller FA (1996) Integrated bioprocess development for bioethanol production. In: Wyman C (ed) Handbook on bioethanol: production and utilization. Taylor & Franics, Washington, pp 351–380
16. Nguyen QA, Tucker MP, Keller FA, Beaty DA, Connors KM, Eddy FP (1999) Dilute acid hydrolysis of softwoods. Appl Biochem Biotechnol 77–79:133–142
17. Ogier JC, Ballerini D, Leygue JP, Rigal L, Pourquie J (1999) Ethanol production from lignocellulosic biomass. Oil Gas Sci Technol 54:67–94
18. Yu ZS, Zhang HX (2004) Ethanol fermentation of acid-hydrolyzed cellulosic pyrolysate with Saccharomyces cerevisiae. Bioresour Technol 93:199–204
19. Sheehan J (2001) The road to bioethanol. A strategic perspective of the U.S Department of Energy's National Ethanol Program. In: Himmel ME, Baker JO, Saffler JN (eds) Glycosyl hydrolases for biomass conversion. American Chemical Society, Washington, DC, pp 2–25
20. Galbe M, Zacchi G (2007) Pretreatment of lignocellulosic materials for efficient bioethanol production. Adv Biochem Eng Biotechnol 108:41–65
21. Sun Y, Cheng J (2002) Hydrolysis of lignocellulosic materials for ethanol production: a review. Bioresour Technol 83(1):1–11
22. Sanchez O, Cardona AC (2008) Trends in biotechnological production of fuel ethanol from different feedstocks. Bioresour Technol 99:5270–5295
23. Hu G, Heitmann A, Rojas OJ (2008) Feedstock pretreatment strategies for producing ethanol from wood, bark and forest residues. Bioresources 3(1):270–294
24. Hendriks ATWM, Zeeman G (2009) Pretreatments to enhance the digestibility of lignocellulosic biomass. Bioresour Technol 100:10–18
25. Alvira P, Tomas-Pejo E, Ballesteros M, Negro MJ (2010) Pretreatment technologies for an efficient bioethanol production based on enzymatic hydrolysis: a review. Bioresour Technol 101:4851–4861
26. Chandra RP, Bura R, Mabee WE, Berlin A, Pan X, Saddler JN (2007) Substrate pretreatment: the key to effective enzymatic hydrolysis of lignocellulosics? Adv Biochem Eng Biotechnol 108:67–93. doi:10.1007/10_2007_064
27. Datta R (1981) Energy requirements for lignocellulose pretreatment processes. Proc Biochem 16(June/July):16–19
28. Litzen D, Dixon D, Gilcrease P, Winter R (2006) Pretreatment of biomass for ethanol production. US Patent 20060141584, June 2006
29. Palmqvist E, Hahn-Hägerdal B (2000) Fermentation of lignocellulosic hydrolysates, I: inhibition and detoxification. Bioresour Technol 74:17
30. Palmqvist E, Hahn-Hägerdal B (2000) Fermentation of lignocellulosic hydrolysates, II: inhibitors and mechanisms of inhibition. Bioresour Technol 74:25
31. Larsson S, Palmqvist E, Hahn-Hägerdal B (1999) The generation of fermentation inhibitors during dilute acid hydrolysis of softwood. Enzyme Microb Technol 24:151
32. Kim S, Holtzapple MT (2005) Lime pretreatment and enzymatic hydrolysis of corn stover. Bioresour Technol 96:1994
33. Chang VS, Kaar WE, Burr B, Holtzapple MT (2001) Simultaneous saccharification and fermentation of lime-treated biomass. Biotechnol Lett 23:1327–1333
34. Pan XJ, Arato C, Gilkes N, Gregg D, Mabee W, Pye K, Xiao ZZ, Zhang X, Saddler J (2005) Biorefining of softwoods using ethanol organosolv pulping: Preliminary evaluation of process streams for manufacture of fuel-grade ethanol and co-products. Biotechnol Bioeng 90:473–482
35. Bouchard J, Nguyen TS, Chornet E, Overend RP (1991) Analytical methodology for biomass pretreatment 2. Characterization of the filtrates and cumulative product distribution as a function of treatment severity. Bioresour Technol 36:121–131
36. Griebl A, Lange T, Weber H, Milacher W, Sixta H (2006) Xylo-oligosaccharide (XOS) formation through hydrothermolysis of xylan derived from viscose process. Macromol Symp 232:107–120
37. Inbicon A/S, http://www.inbicon.com/
38. Schmidt AS, Thomsen AB (1998) Optimization of wet oxidation pretreatment of wheat straw. Bioresour Technol 64:139–151
39. Dale BE, Moreira MJ (1982) A freeze-explosion technique for increasing cellulose hydrolysis. Biotechnol Bioeng Symp 12:31–43
40. Teymouri F, Laureano-Peres L, Alizadeh H, Dale BE (2005) Optimization of the ammonia fiber explosion (AFEX) treatment parameters for enzymatic hydrolysis of corn stover. Bioresour Technol 96:2014–2018
41. Hsu TA (1996) Pretreatment of biomass. In: Wyman CE (ed) Handbook on bioethanol production and utilization. Taylor & Francis, Washington, DC, pp 179–212, Chapter 10

42. Belkacemi K, Turtotte G, de Halleux D, Savoie P (1998) Ethanol production from AFEX-treated forages and agricultural residues. Appl Biochem Biotechnol 70–72:441–462
43. Lee J (1997) Biological conversion of lignocellulosic biomass to ethanol. J Biotechnol 56:1–24
44. Heinze T, Schwikal K, Barthel S (2005) Ionic liquids as reaction medium in cellulose functionalization. Macromol Biosci 5(6):520–525
45. Boussaid A, Robinson J, Cai Y, Gregg DJ, Saddler JN (1999) Fermentability of the hemicellulose-derived sugars from steam-exploded softwood (Douglas fir). Biotechnol Bioeng 64:284–289
46. Wu MM, Gregg CK, DJ BA, Beatson RP, Saddler JN (1999) Optimization of steam explosion to enhance hemicellulose recovery and enzymatic hydrolysis of cellulose in softwood. Appl Biochem Biotechnol 77–79:47–54
47. Nguyen QA, Tucker MP, Keller FA, Beaty DA, Connors KM, Eddy FP (1999) Dilute acid hydrolysis of softwoods. Appl Biochem Biotechnol 77–79:133–142
48. Elander RT, Dale BE, Holtzapple M, Ladisch MR, Lee YY, Mitchinson C, Saddler JN, Wyman CE (2009) Summary of findings from the biomas refining consortium for applied fundamentals and innovation (CAFI): corns stover pretreatment. Cellulose 16:649–659
49. Öhgren K, Bura R, Saddler J, Zacchi G (2007) Effect of hemicellulose and lignin removal on enzymatic hydrolysis of steam pretreated corn stover. Bioresour Technol 98(13): 2503–2510
50. Kumar R, Wyman CE (2009) Effect of xylanase supplementation of cellulase on digestion of corn stover solids prepared by leading pretreatment technologies. Bioresour Technol 100:4203–4213
51. Kumar R, Wyman CE (2009) Effects of cellulase and xylanase enzymes on the deconstruction of solids from pretreatment of poplar by leading technologies. Biotechnol Prog 25(2): 302–314
52. Mandels M, Reese ET (1963) Inhibition of cellulases and -glucosidases. In: Reese ET (ed) Advances in enzymic hydrolysis of cellulose and related materials. Pergamon, London, pp 115–157
53. Sternberg D, Vijayakumar P, Reese ET (1977) Beta-glucosidase – microbial-production and effect on enzymatic hydrolysis of cellulose. Can J Microbiol 23:139–147
54. Holtzapple M, Cognata M, Shu Y, Hendrickson C (1990) Inhibition of Trichorderma Reesei cellulase by sugars and solvents. Biotechnol Bioeng 36:275–287
55. Tengborg C, Galbe M, Zacchi G (2001) Reduced inhibition of enzymatic hydrolysis of steam-pretreated softwood. Enzyme Microb Technol 28(9–10):835–844
56. Genencor, USA. http://www.genencor.com/
57. Novozymes, Denmark. http://www.novozymes.com/
58. Szengyel Z, Zacchi G, Varga A, Reczey K (2000) Cellulase production of *Trichoderma reesei* Rut C 30 using steam-pretreated spruce – hydrolytic potential of cellulases on different substrates. Appl Biochem Biotechnol 84(6):679–691
59. Eriksson KEL, Blanchette RA, Ander P (1990) Microbial and enzymatic degradation of wood and wood components. In: Timell TE (ed) Springer series in wood science. Springer, Berlin, p 416
60. Biely P (2003) Xylanolytic enzymes. In: Whitaker RJ, Voragen AGJ, Wong DWS (eds) Handbook of food enzymology. Marcel Dekker, New York, pp 879–916
61. Beg QK, Kapoor M, Mahajan L, Hoondal GS (2001) Microbial xylanases and their industrial applications: a review. Appl Microbiol Biotechnol 56:326–338
62. Shallom D, Shoham Y (2003) Microbial hemicellulases. Curr Opin Microbiol 6:219–228
63. Jorgensen H, Kristensen JB, Felby C (2007) Enzymatic conversion of lignocellulose into fermentable sugars: challenges and opportunities. Biofuels, Bioprod Biorefin 1(2):119–134. doi:10.1002/bbb.4
64. Varga E, Klinke HB, Réczey K, Thomsen AB (2004) High solid simultaneous saccharification and fermentation of wet oxidized corn stover to ethanol. Biotechnol Bioeng 88:567–574
65. Tengborg C, Galbe M, Zacchi G (2001) Influence of enzyme loading and physical parameters on the enzymatic hydrolysis of steam-pretreated softwood. Biotechnol Prog 17(1):110–117
66. Mohagheghi A, Tucker M, Grohmann K, Wyman C (1992) High solids simultaneous saccharifi cation and fermentation of pretreated wheat straw to ethanol. Appl Biochem Biotechnol 33:67–81
67. Fan ZL, South C, Lyford K, Munsie J, van Walsum P, Lynd LR (2003) Conversion of paper sludge to ethanol in a semicontinuous solids-fed reactor. Bioprocess Biosyst Eng 26:93–101
68. Verduyn C, Postma E, Scheffers WA, van Dijken JP (1990) Physiology of Saccharomyces cerevisiae in anaerobic glucose-limited chemostat cultures. J Gen Microbiol 136:395–403
69. Saha BC (2003) Hemicellulose bioconversion. J Ind Microbiol Biotechnol 3:279–291
70. Hahn-Hägerdal B, Wahlbom CF, Gárdonyi M, van Zyl W, Otero R, Jönsson LJ (2001) Metabolic engineering of Saccharomyces cerevisiae for xylose utilisation. Adv Biochem Eng Biotechnol 73:53–84
71. Dien BS, Cotta MA, Jeffries TW (2003) Bacteria engineered for fuel ethanol production: current status. Appl Microbiol Biotechnol 63:258–266
72. Jeffries TW (2006) Engineering yeasts for xylose metabolism. Curr Opin Biotechnol 17:1–7
73. Becker J, Boles E (2003) A modified Saccharomyces cerevisiae strain that consumes L-arabinose and produces ethanol. Appl Environ Microbiol 69(7):4144–4150
74. Karhumaa K, Wiedemann B, Hahn-Hagerdal B, Boles E, Gorwa-Grauslund MF (2006) Co-utilization of L-arabinose and D-xylose by laboratory and industrial *Saccharomyces cerevisiae* strains. Microb Cell Fact 5:18. doi:10.1186/1475-2859-5-18
75. Hahn-Hägerdal B, Karhumaa K, Fonseca C, Spencer-Martins I, Gorwa-Grauslund MF (2007) Towards industrial pentose-fermenting yeast strains. Appl Microbiol Biotechnol 74: 937–953

76. van Maris AJA, Abbott DA, Bellissimi E, van den Brink J, Kuyper M, Luttik MAH, Wisselink HW, Scheffers WA, van Dijken JP, Pronk JT (2006) Alcoholic fermentation of carbon sources in biomass hydrolysates by Saccharomyces cerevisiae: current status. Antonie Leeuwenhoek 90(4):391–418, Int J Gen Molec Microbiol
77. Karhumaa K, Hahn-Hägerdal B, Gorwa-Grauslund MF (2005) Investigation of limiting metabolic steps in the utilization of xylose by recombinant Saccharomyces cerevisiae using metabolic engineering. Yeast 22:359–368
78. Kuyper M, Hartog MMP, Toirkens MJ, Almering MJH, Winkler AA, van Dijken JP, Pronk JT (2005) Metabolic engineering of a xylose-isomerase-expressing Saccharomyces cerevisiae strain for rapid anaerobic xylose fermentation. FEMS Yeast Res 5:399–409
79. Walfridsson M, Anderlund M, Bao X, Hahn-Hägerdal B (1997) Expression of different levels of enzymes from the Pichia stipitis XYL1 and XYL2 genes in Saccharomyces cerevisiae and its effects on product formation during xylose utilisation. Appl Microbiol Biotechnol 48:218–224
80. Kötter P, Amore R, Hollenberg CP, Ciriacy M (1990) Isolation and characterization of the Pichia stipitis xylitol dehydrogenase gene, XYL2, and construction of a xylose-utilizing Saccharomyces cerevisiae transformant. Curr Genet 18:493–500
81. Eliasson A, Christensson C, Wahlbom CF, Hahn-Hägerdal B (2000) Anaerobic xylose fermentation by recombinant Saccharomyces cerevisiae carrying XYL1, XYL2, and XKS1 in mineral medium chemostat cultures. Appl Environ Microbiol 66: 3381–3386
82. Hamacher T, Becker J, Gárdonyi M, Hahn-Hägerdal B, Boles E (2002) Characterization of the xylose-transporting properties of yeast hexose transporters and their influence on xylose utilization. Microbiology 148:2783–2788
83. Jeffries TW (1983) Utilization of xylose by bacteria, yeast, and fungi. Adv Biochem Eng Biotechnol 27:1–32
84. Öhgren K, Bengtsson O, Gorwa-Grauslund MF, Galbe M, Hahn-Hägerdal B, Zacchi G (2006) Simultaneous saccharification and co-fermentation of glucose and xylose in steam-pretreated corn stover at high fiber content with Saccharomyces cerevisiae TMB3400. J Biotechnol 126:488–498
85. Olofsson K, Rudolf A, Lidén G (2008) Designing simultaneous saccharification and fermentation for improved xylose conversion by a recombinant strain of Saccharomyces cerevisiae. J Biotechnol 134:112–120
86. Rudolf A, Baudel H, Zacchi G, Hahn-Hägerdal B, Liden G (2008) Simultaneous saccharification and fermentation of steam-pretreated bagasse using Saccharomyces cerevisiae TMB3400 and Pichia stipitis CBS6054. Biotechnol Bioeng 99(4):783–790
87. Palmqvist E, Hahn-Hagerdal B (2000) Fermentation of lignocellulosic hydrolysates. II: inhibitors and mechanisms of inhibition. Bioresour Technol 74:25–33
88. Larsson S, Reimann A, Nilvebrant N-O, Jönsson LJ (1999) Comparison of different methods for the detoxification of lignocelluloase hydrolyzates of spruce. Appl Biochem Biotechnol 77–79:91–103
89. Nilvebrant N-O, Persson P, Reimann A, de Sousa F, Gorton L, Jönsson LJ (2003) Limits for alkaline detoxification of dilute-acid lignocellulose hydrolysates. Appl Biochem Biotechnol 105:615–628
90. Alkasrawi M, Rudolf A, Liden G, Zacchi G (2006) Influence of strain and cultivation procedure on the performance of simultaneous saccharification and fermentation of steam pretreated spruce. Enzyme Microb Technol 38:279–286
91. Rudolf A, Alkasrawi M, Zacchi G, Liden G (2005) A comparison between batch and fed-batch simultaneous saccharification and fermentation of steam pretreated spruce. Enzyme Microb Technol 37:195–204
92. Taherzadeh MJ, Niklasson C, Liden G (2000) On-line control of fed-batch fermentation of dilute-acid hydrolyzates. Biotechnol Bioeng 69:330–33855
93. Taherzadeh MJ, Gustafsson L, Niklasson C, Liden G (2000) Inhibition effects of furfural on aerobic batch cultivation of Saccharomyces cerevisiae growing on ethanol and/or acetic acid. J Biosci Bioeng 90:374–380
94. Taherzadeh MJ, Niklasson C, Liden G (1997) Acetic acid – friend or foe in anaerobic batch conversion of glucose to ethanol by Saccharomyces cerevisiae? Chem Eng Sci 15:2653–2659
95. Palmqvist E, Hahn-Hägerdal B, Galbe M, Zacchi G (1996) The effect of water-soluble inhibitors from steam-pretreated willow on enzymatic hydrolysis and ethanol fermentation. Enzyme Microb Technol 6:470–476
96. Lu Y, Warner R, Sedlak M, Ho N, Mosier NS (2009) Comparison of glucose/xylose cofermentation of poplar hydrolysates processedby different pretreatment technologies. Biotechnol Prog 25(2):349–356
97. Brethauer S, Wyman EC (2010) Review – continuous hydrolysis and fermentation for cellulosic ethanol production. Bioresour Technol 101(13):4862–4874
98. Katzen R, Madson PW, Monceaux DA, Bevernitz K (1999) Lignocellulosic feedstocks for ethanol production: the ultimate renewable energy source. In: Jacquers KA, Lyons TP, Kelsall DR (eds) The alcohol textbook, 3rd edn. Nottingham University Press, Nottingham, pp 107–116
99. Wingren A, Galbe M, Zacchi G (2003) Techno-economic evaluation of producing ethanol from softwood: Comparison of SSF and SHF and identification of bottlenecks. Biotechnol Prog 19(4):1100–1117
100. Galbe M, Sassner P, Wingren A, Zacchi G (2007) Process engineering economics of bioethanol production. Adv Biochem Eng Biotechnol 108:303–327
101. Sassner P, Galbe M, Zacchi G (2008) Techno-economic evaluation of bioethanol production from three different lignocellulosic materials. Biomass Bioenergy 32:422–430
102. Sassner P (2007) Lignocellulosic ethanol production based on steam pretreatment and SSF. PhD thesis, LUTKDH/(TKKA-1006)/1-88/(2007). Lund University, Sweden
103. Larsen J, Petersen MO, Thirup L, Li HW, Krogh Iversen F (2008) The IBUS process – lignocellulosic bioethanol close to a commercial reality. Chem Eng Technol 31(5):765–772

104. Öhgren K, Bura R, Lesnicki G, Saddler J, Zacchi G (2007) A comparison between simultaneous saccharification and fermentation and separate hydrolysis and fermentation using steam-pretreated corn stover. Process Biochem 42:834–839
105. Söderström J, Galbe M, Zacchi G (2005) Separate versus simultaneous saccharification and fermentation of two-step steam pretreated softwood for ethanol production. J Wood Chem Technol 25(3):187–202
106. Wingren A, Galbe M, Zacchi G (2003) Techno-economic evaluation of producing ethanol from softwood: comparison of SSF and SHF and identification of bottlenecks. Biotechnol Prog 19(4):1109–1117
107. Rudolf A, Alkasrawi M, Zacchi G, Lidén G (2005) A comparison between batch and fed-batch simultaneous saccharification and fermentation of steam pretreated spruce. Enzyme Microb Technol 37:195–205
108. Olofsson K, Bertilsson M, Liden G (2008) A short review on SSF – an interesting process option for ethanol production from lignocellulosic feedstocks. Biotechnol Biofuels 1:7
109. Lynd LR, van Zyl WH, McBride JE, Laser M (2005) Consolidated bioprocessing of cellulosic biomass: an update. Curr Opin Biotechnol 16(5):577–583
110. Jørgensen H, Vibe-Pedersen J, Larsen J, Felby C (2007) Liquefaction of lignocellulose at high-solids concentrations. Biotechnol Bioeng 96(5):862–870
111. Sassner P, Galbe M, Zacchi G (2007) Techno-economic aspects of a wood-to-ethanol process – energy demand and possibilities for integration. Chem Eng Trans 12:447–452
112. Wingren A, Galbe M, Zacchi G (2008) Energy considerations for a SSF-based softwood ethanol plant. Bioresour Technol 99:2121–2131
113. Barta Zs, Reczey K, Zacchi G (2010) Techno-economic evaluation of stillage treatment with anaerobic digestion in a softwood-to-ethanol process. Biotechnol Biofuels 3:21. doi:10.1186/1754-6834-3-21
114. Sassner P, Zacchi G (2008) Integration options for high energy efficiency and improved economics in a wood-to-ethanol process. Biotechnol Biofuels 1:4. doi:10.1186/1754-6834-1-4
115. Kadam KL, Wooley R, Aden A, Nguyen QA, Yancey MA, Ferraro FM (2000) Softwood forest thinnings as a biomass source for ethanol production: a feasibility study for California. Biotechnol Prog 16:947–957
116. Erdei B, Barta Zs, Sipo B, Réczey K, Galbe M, Zacchi G (2010) Ethanol production from mixtures of wheat straw and wheat meal. Biotechnol Biofuels 3:16. doi:10.1186/1754-6834-3-16
117. Bon EPS, Ferrara MA (2007) Bioethanol production via enzymatic hydrolysis of cellulosic biomass. The role of agricultural biotechnologies for production of bioenergy in developing countries – FAO biotechnology and bioenergy seminar 2007. http://www.fao.org/biotech/seminaroct2007.htm
118. State of São Paulo Law no. 11.241, DE 19/09/2002, Brazil
119. Nogueira LAH (2008) Co-products of sugarcane bioethanol. In: Sugarcane-based bioethanol: energy for sustainable development. BNDES, Rio de Janeiro, pp 99–118
120. Lora ES, Andrade RV (2009) Biomass as energy source in Brazil. Renewable Sustainable Energy Rev 13:777–788
121. Goldemberg J (2008) The Brazilian biofuel industry. Biotechnol Biofuels 1:6. doi:10.1186/1754-6834-1-6
122. Bacovsky, Dallos, Wörgetter Status of 2nd generation biofuels demonstration facilities, T39-P1b, 27 July 2010. http://www.ascension-publishing.com/BIZ/IEATask39-0610.pdf

Books and Reviews

Barbosa Cortez LA (2010) Sugarcane bioethanol – R&D for productivity and sustainability (2010). Editora Edgard Blucher, São Paulo

Coombs J, Grassi G (1992) Cellulose hydrolysis and fermentation. CPL Press, Berkshire

Jacques KA, Lyons TP, Kelsall DR (2003) The alcohol textbook – a reference for the beverage, fuel and industrial alcohol industries, 4th edn. Nottingham University Press, Nottingham

Olsson LB (2007) Advances in biochemical engineering biotechnology, vol 108. Springer, Berlin

Saddler J (1993) Bioconversion of forest and agricultural residues. CAB International, Wallingford

Wyman CE (1996) Handbook on bioethanol: production and utilization. Taylor & Francis, Washington, DC

Bioethanol from Starch

Anton Friedl
Vienna University of Technology, Vienna, Austria

Article Outline

Glossary
Definition of the Subject and Its Importance
Introduction
State of the Art of the Production
Actual Status
Future Directions
Bibliography

Glossary

Alcohol Often used trivial name for ethanol, in chemistry it describes the class of alcohols including also methanol, butanol, etc.

Bioethanol Product of a fermentative process used mainly as a fuel from renewable substrates in comparison to the use of fossil fuels.

Ethanol Chemical name of an alcohol with the molecular formula CH_3–CH_2–OH and is the same chemical substance as bioethanol and has other synonyms like bioethanol, ethyl alcohol, pure alcohol, or drinking alcohol.

DDGS Animal feed called "distillers' dried grain with solubles."

Fermentation Process step which produces ethanol and CO_2 as product.

Liquefaction Enzymatic process step using amylases to cut the starch chains into oligosaccharides.

Saccharification Enzymatic process step using beta-amylases and glucoamylases to cut oligosaccharides into fermentable sugars.

Starch Starch is a very important part of the human food in sources like wheat, maize, rice, potatoes, and many other plants and is also a source of sugars for the fermentation.

Thin stillage Liquid stream received from the decanter containing dissolved nutrients and salts.

Yeast S*accharomyces cerevisiae* is the organism used in the ethanol production industry.

Wet cake Solid-rich stream received from the decanter containing nutrients like proteins.

Definition of the Subject and Its Importance

Ethanol is a very interesting chemical compound which can be used in different applications such as drinking alcohol in beverages as well as in chemicals, pharmaceuticals, and biofuels. Production of alcoholic beverages based on biomass containing sugar can be assumed as old as human civilization. The production of ethanol from starch using a fermentation process started most probably in beer-producing countries approximately in the twelfth century. The production of "pure" ethanol is also a very long known process. The development of more efficient distillation processes in the nineteenth century led to large increase in industrial trade of ethanol. The largest amount of the industrial ethanol was still used for alcoholic beverages. But also other applications like the use in the chemical industry, as lamp fuel and as a fuel have been exploited. The use of ethanol as a fuel started at the beginning of the twentieth century, the time the Ford Model T could run since 1908 on ethanol. With the fast development of the petroleum industry, the use of ethanol as a fuel was negligible till late twentieth century. Due to price increases of raw oil and also environmental concerns, ethanol showed a revival as a fuel based on renewable substrates like sugar and starch or even celluloses. For fuel applications, mainly the name bioethanol is used but the whole ethanol production chain including also the agricultural growth of the substrate has to be taken into account to prove that the produced ethanol really shows significant environmental benefits compared to fossil fuels.

This entry concentrates on bioethanol from starch only. Biothanol from other substrates like sugar and lignocellulosic material will be discussed in the respective entries. Bioethanol from starch reached 2009 a share of about 60% of the total worldwide production. Starch as a substrate is mainly used in the USA and Europe. Since the worldwide need for transportation fuels is steadily increasing, there is a need for a further increased production of sustainable produced biofuels like bioethanol. Since starchy substrates are also the basis for human nutrition and animal feeding, it is very important to balance the use of these very valuable materials. A large amount of the worldwide produced grain crops are used for animal feeding. Using these grain crops for bioethanol production, about the same amount of animal feed is produced as a very important second product. This allows a combination of animal feed production with bioethanol production and is already installed in many bioethanol-producing plants worldwide which use grain crops as substrate. Taking this fact into account, it will be possible to increase the bioethanol production based on grain crops further to a certain extent keeping the whole system of bioethanol production combined with human nutrition and animal feeding into account. Further significant increase in bioethanol production will be achieved if combinations of starch and lignocellosic substrates or lignocellosic substrates only are fully economically developed. Details on lignocellosic substrates for bioethanol production can be found in the respective entries.

Introduction

Production of bioethanol from starch is, in addition to the production from sugar, also a very well-known process. The technology and process steps needed for starchy materials differ compared to sugar-containing substrates in the substrate treatment section of the bioethanol plant and in the stillage treatment processes (Fig. 1). After milling of the starchy substrates two enzymatic process steps, the liquefaction and the saccharification, are needed to receive a fermentable sugar solution. The fermentation of this sugar stream can be done traditionally using yeast. The further downstream process steps are distillation and rectification of the liquid stream to increase the concentration of the bioethanol. The final product quality in terms of allowed water content in the bioethanol is reached normally by using an adsorption process. The stillage received from the distillation or beer column is further treated in a decanter to separate a wet cake stream and a thin stillage stream which can partly be recycled to mash preparation or concentrated in an evaporation process. After concentration, the thin stillage is mixed with the wet cake and together tried to produce an animal feed as a second product the so-called distillers' dried grain with solubles (DDGS).

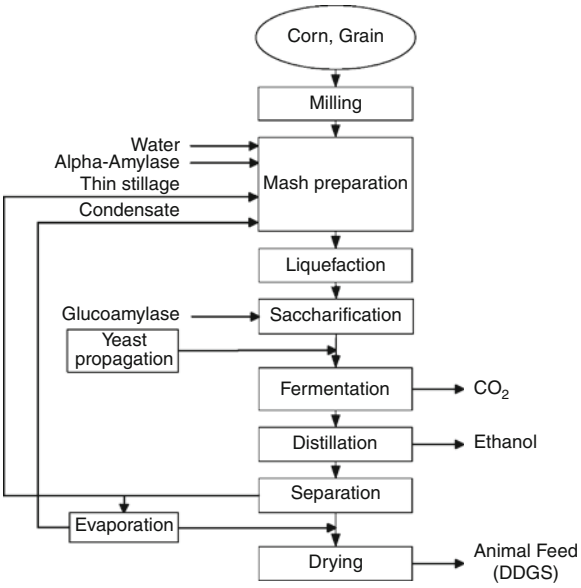

Bioethanol from Starch. Figure 1
Principle of dry-mill bioethanol process

Currently the world bioethanol production is based approximately to 40% of sugar crops and 60% of grain crops as feedstock. Sugar is mainly used as substrate in Brazil and other sugar-producing countries. Starch as main substrate for the bioethanol production is used in the USA and Europe and also in many other countries. In Europe, also sugar from sugar beet processing like molasses are used to some extend as co-substrate for bioethanol production depending on the price of the substrate.

State of the Art of the Production

Raw Materials Containing Starch

Starch is a polysaccharide consisting of a large number of D-glucose molecules which are linked by glycosidic bonds. Green plants can produce D-glucose from carbon dioxide (CO_2) from the atmosphere and water via photosynthesis using sunlight. D-glucose is used from the plant for growing. Access amount can be stored in the plant as starch in the form of granules. Within the stored polysaccharide glucose can be in the linear form via 1,4-alpha glycosidic bonds (amylose) as well as in the branched form via 1,6-alpha glycosidic bonds (amylopectin). In different plants, the starch content of amylose can vary between 20% and 25% and a respective content of amylopectin from 75% to 80% [1]. Within the bioethanol process, mainly the amylopectin content of the starch is responsible for the strong increase of viscosity during the treatment which has to be taken into account in designing the process.

For the bioethanol process, a broad variety of starch-containing plants are used. The choice of feedstock varies a lot in different regions of the world. Within the US Corn Belt, maize (or corn) is the main feedstock. In Europe, Canada, and many other regions wheat, corn, and other cereals like barley, rye, and triticale (a hybrid of wheat and rye) are used for bioethanol production.

Other interesting feedstocks are potatoes, cassava, and sorghum. Potatoes are grown in many countries. The main disadvantage is the high water content (Table 1) which results in high transportation costs

Bioethanol from Starch. Table 1 Feedstock composition

Component	Maize	Wheat	Barley	Rye	Sorghum	Potato	Cassava chips	Cassava roots
Water[a]	12–15	11–14	11–14	11–14	11–14	75	11–14	60–70
Starch[b]	65–72	62–70	52–64	52–65	72–75	60–75	65–82	40–85
Sugar[b]	2.2	–	–	–	–	0.3–5.5	0.25	0.75
Protein[b]	9–12	12–14	10–11	10–15	11–12	6–11	2.3	1.5–3.5
Fat[b]	4.5	3	2.5–3	2–3	3.6	0.5–1.1	0.8	0.2–0.4
Cell wall material[b]	9.6	11.4	14	–	–	–	–	0.6–1
Fiber[b]	–	–	–	–	–	–	4.6	1.6–2.9
Ash[b]	1.5	2	2.3	2	1.7	2.5–5.4	2–5	0.6–1.2

Adapted from [2, 3]
[a]% w/w (as-is basis)
[b]% w/w (dry basis)

Bioethanol from Starch. Table 2 Bioethanol and distillers' dried grain with solubles (DDGS) yield from various starchy feedstock

Yield (kg/t)	Maize	Wheat	Barley	Rye	Sorghum	Potato	Cassava chips
Ethanol (kg/t)	325	299	248	269	328	93	361
Ethanol (l/t)	411	379	314	340	415	117	457
DDGS (kg/t)	321	429	496	457	341	Wet cake	Wet cake

and losses during storing. Cassava with alternative names yucca, tapioca, or manioc is a tropical plant developing starch-containing roots. As a fresh root, it has high water content. Therefore, long-term storage without drying is barely possible. But drying needs separate handling and treatment. In Table 1, the composition of starchy feedstock is listed.

The bioethanol-producing potential from the listed feedstock is given in Table 2 [3]. An average bioethanol yield has been assumed and also the DDGS product yield is listed. For potato and cassava chips, usually the wet cake is further used and not dried.

From Table 2, it can be seen that the highest bioethanol yields from 1 t feedstock (as is basis) is achieved from cassava chips, sorghum, and maize followed by wheat. The yield of animal feed (DDGS) also varies with the substrate used. Substrates giving the lower ethanol yields give higher animal feed yields like barley, rye, wheat, sorghum followed by maize showing nearly the same yield for bioethanol and animal feed.

Processing of Starch-Containing Raw Materials

To achieve the highest bioethanol amount from the feedstock used, it is important that the optimal conditions are adjusted for the yeast. Hence, it is necessary that sugar and minerals are available in an ideal concentration. Additionally, the temperature and pH need to be kept in the optimal range for the microorganism.

In general, the design and mass balance of bioethanol plant based on corn and wheat is similar and both feedstocks can be used in the same plant if designed properly. Special attention need to be addressed to the fact that in wheat the content of

nonstarch polysaccharides is higher than in corn. Especially the pentosane and glucan are responsible for the increase of viscosity and fouling tendency in the process which leads to reduced heat transfer rates in the heat exchangers. To reduce or avoid problems in the process, special enzymes for reducing the chain length of these substances to make them soluble in the process stream need to be applied. Higher viscosity of the mash need to be controlled by solid concentration which might lead to lower ethanol concentration after the fermentation which results in a higher energy demand of the whole process. Also during processing of wheat the lower lipid concentration combined with higher raw protein content (approximately >13%) leads to an increased foaming tendency during fermentation which might need dosing of antifoaming agents [2]. In Fig. 2, a schematic layout of a dry-mill bioethanol process with DDGS production is shown.

In the following entries, the different process steps are discussed in detail.

Grinding Process The first step in the production of bioethanol from starch is the milling (grinding) of the feedstock. Two different processes are possible: the wet-mill or the dry-mill process.

- In the past, wet-mill processes were often used since several valuable products like corn oil, gluten meal, various starch qualities, and feed products can be derived besides bioethanol which is not the main product during this process [4]. Wet-mill plants are more complex and need approximately 40% more investment than a comparable dry-mill plant because the whole by-product separation equipment must also be installed [5].
- The dry-mill process [6] is optimized for the production of bioethanol and animal feed called distillers' dried grains with solubles (DDGS). The dry-mill process needs less energy per ton of bioethanol produced. Nowadays, most bioethanol for the use of fuel is coming from a dry-mill process. For this process, the corn or grain is ground into coarse flour which is further processed (Fig. 2).

In a standard dry-mill process, the grain is feed by gravity to the mill and grinded usually using a hammer mill. The particle size of the meal has an important influence on the enzyme effectiveness and also on the ethanol yield. The ground meal is mixed in the mashing tub with water (fresh or recycle streams) and alpha-amylase to prepare the mash as can be seen in Figs. 1 and 2.

Liquefaction Process For the nearly complete use of starch in a technical bioethanol production, an enzymatic process step using amylases is obligatory. Therefore, two different groups of starch-degrading enzymes are needed. Alpha-amylases are responsible for the fast break down of the viscosity of the starch solution by cutting the starch chains into oligosaccharides consisting of seven to ten glucose molecules. This is the so-called liquefaction step. Already in the mixing step during the mash preparation, the liquefying enzymes (alpha-amylase) need to be added to avoid problems due to gelatinization of the starch granules. The resulting mixture is heated and held at this temperature for a certain time. The pH also has to be adjusted according to the needs of the enzymes used.

The temperature ranges for the gelatinization of several cereals are well known (Ingeledew 2009). Depending on the type of cereal and the process strategy, the temperature can be held first below the gelatinization temperature which is usually in the range of 50–60°C for approximately 20 min and then heated up to the final liquefaction temperature which can be in the range of 80–85°C or even up to 105°C depending on the stability of the enzymes used. In another process strategy, the whole mash is heated up quickly to temperatures between 105°C and 120°C in a hydrotreater (jet cooker) unit. Here the temperature is held for approximately 5 min, then the whole mixture is fed to an atmospheric or vacuum flash vessel and from that to the liquefaction vessels where the enzymes are added. Within this process step, the temperature is held at around 80–90°C for about 30–60 min. The pH value can vary between 5.0 and 6.0 or 6.2 and 7.5 depending on the type of enzymes used [7].

If water is present during heating, the starch granules are dissolved which allows the enzymes to break the starch chains fast into smaller parts. This allows avoiding a very strong increase of viscosity and a blocking of the used equipment.

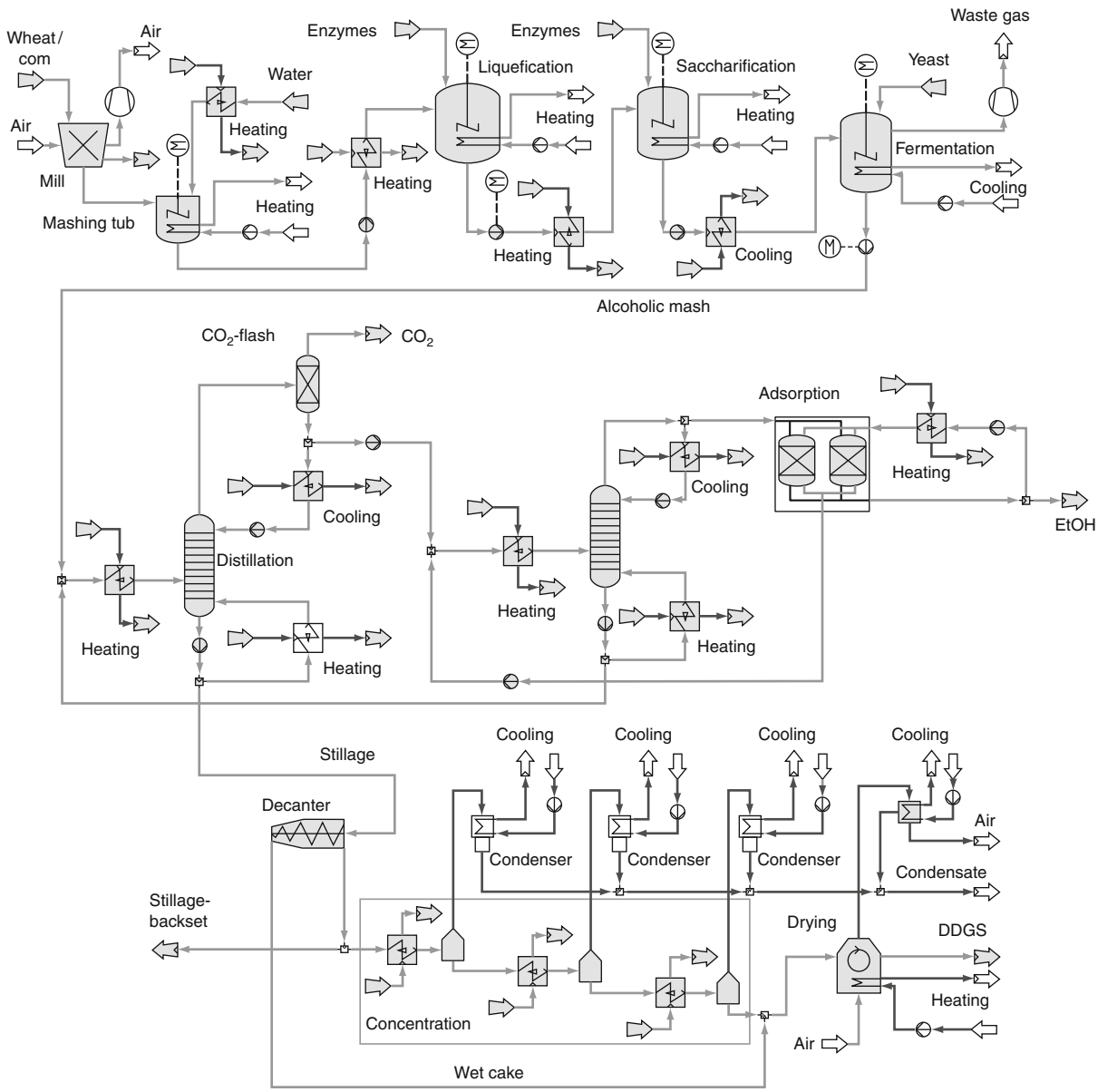

Bioethanol from Starch. Figure 2
Schematic layout of a dry-mill bioethanol process including distillers' dried grain with solubles (DDGS) production

After this liquefaction procedure, the whole mixture is cooled and the saccharification step is performed prior the start of the fermentation.

Saccharification Process As described above in the liquefaction step, the alpha-amylase can only break the 1,4-alpha glycosidic bonds of the starch. The second enzymatic process step is needed to break down the dextrins into single glucose molecules by beta-amylase and glucoamylase. The latter is an exoenzyme which attacks the oligomers in the solution from the chain ends. Glucoamylase can hydrolyze 1,4-alpha glycosidic bonds as well as 1,6-alpha glycosidic bonds. But the reaction rate is much slower. The result is

a fermentable sugar solution containing glucose and maltose. The glucoamylase used in technical processes has a temperature optimum of 60°C and a pH optimum of 3.4–5.0. This means that this enzyme is stable under fermentation conditions. Due to this fact, it is possible to perform the saccharification in two ways.

- The first option is a separate saccharification vessel where the optimal temperature of the enzyme of 60°C can be adjusted and the fastest enzyme reaction rate can be achieved as it is shown in Fig. 1. This process strategy is also called separate hydrolysis and fermentation (SHF).
- The second option is that the saccharification step is combined with the fermentation to a simultaneous saccharification and fermentation (SSF) procedure. In this case, the temperature is around 33–34°C and the pH is approximately 5.0 resulting in an enzyme activity that is not as high as at the optimum. But since the yeast activity is the time-limiting step, the slow release of sugars is not limiting the process. This approach evermore shows the advantage that the optimal release speed of fermentable sugars keeps the yeast at the best performance rate, optimal temperature and pH assumed, since glucose itself is limiting the yeast at higher concentrations. This is the reason that in modern technical bioethanol plants the SSF approach is mainly used.

Yeast Propagation Before the fermentation process itself takes place, it is necessary to produce the yeast needed. Very often the yeast is grown in the bioethanol plant itself in smaller yeast-growing fermenter to be provided for the ethanol production fermenter. Some yeast can be recycled after ethanol production depending on the substrates used. Additionally, the solid matter content is restricting the yeast recycling. Working with clear streams like during processing of sugar solutions, a high degree of yeast recycle is possible after treatment. With starch as feedstock, yeast recycling is restricted.

The dominant yeast strain used in the ethanol production industry is *Saccharomyces cerevisiae* because it is a very robust organism which also shows a relative high inhibitor tolerance and a very good production capacity. Using this yeast, many plants in the USA produce ethanol in the range of 20% (v/v) on volume basis which is equal to 16.5% (w/w) on weight basis [8].

Yeast shows the ability that only cell growth can be achieved in an aerobic environment in the presence of sufficient oxygen. Nearly no ethanol production occurs in this situation. This can be used for reproduction and increasing the cell mass as needed.

The commercial yeast production can start from active dry yeast supplied to ethanol production facility by specialized yeast-producing companies. Growing the yeast on site in a separate propagation vessel, it is possible to keep about 10% of concentrated yeast solution to start the next yeast production cycle. To continue this production cycle, it is very important that no bacterial infection occurs which has to be checked thoroughly. For the yeast propagation facility, sterile conditions are crucial. The same substrate as used for the ethanol production can be used for yeast propagation. In this case, the produced yeast is already adapted to the substrate. Only a dilution be a factor of 2 is used to keep the sugar concentration low and this also restricts the production of ethanol during yeast growth. The temperature is kept several degrees lower than during the ethanol fermentation and the propagation vessel is aerated to a sufficient amount avoiding the buildup of excessive foam.

The yeast propagation can be performed in a semicontinuous or in a continuous mode. The method chosen depends also on the performance mode of the ethanol fermentation itself.

Fermentation Process As the starch content in the feedstock cannot be directly converted by yeast cells to bioethanol, it needs to be broken down as described above into usable sugars before fermentation. These sugars can be the glucose itself or the maltose or maltotriose which consist of two or three glucose molecules. The different sugars which can be converted by the yeast *S. cerevisiae* are well known [2]. The resulting sugar solution is called mash. It can be used for fermentation which is started by adding the yeast inoculum.

During the fermentation, one glucose molecule is converted to two molecules of ethanol and two molecules of carbon dioxide. This means that in the ideal case from 1 kg Glucose, 0.511 kg ethanol and 0.489 kg

CO_2 are produced by yeast releasing 867 kJ heat [7]. The fermentation itself can be done in batch or continuous mode. Both systems have advantages and disadvantages.

- The batch fermentation mode is characterized by a discontinuous operation. First the fermentation vessel is cleaned and sterilized and then filled with the already liquefied mash after passing a heat exchanger to adjust it to the proper fermentation temperature below 35°C. Then the fermentation can be started by adding the already prepared yeast solution from the propagation vessel. The pH is adjusted to around 5.2 and kept constant by dosing a basic solution or allowed to decrease during the fermentation till a pH of 4.2. If the pH drops to a value lower than 4.0, most probably an infection with lactobacilli has occurred. During the fermentation period normally in the range of 50–60 h, the temperature has to be kept below 35°C by applying continuous cooling of the fermentation vessel. After finishing the fermentation, the alcoholic mash is pumped to a storage tank (called beer well). Then the cycle can be started again with cleaning and sterilization. Due to this procedure of emptying, cleaning, sterilization, and again filling of the fermentation vessel the effective time is reduced by around 20%. This means only 80% of the reactor volume is active. Therefore, a bigger reactor volume is needed. But since the whole plant requires a low degree on control equipment, low investment costs are resulting [2]. But high yields in the range of 90–95% of the theoretical yield combined with high ethanol concentration can be achieved. The size of the fermentation vessels are in the range of 800–1,500 m^3. In Brazil in new plants, the volume of the fermentation vessels is increased up to 3,000 m^3 [9].
- In the continuous fermentation mode, a constant stream of mash is fed to the first fermentation vessel. Depending on the feed volume stream and the vessel volume which is also in the range as mentioned above a certain resistance time of the mash combined with a defined specific dilution rate is applied. It is very important that the specific dilution rate is below the growth rate of the yeast to keep the microorganism in the fermentation vessel in the desired concentration range. Along the various fermentation vessels, the sugar is consumed by the yeast and ethanol and new yeast cells are produced during the fermentation. During this process the relevant parameters need to be measured and controlled properly. Additionally, a defined dosage of air is necessary to achieve a high specific production rate of ethanol of around 6 kg/m^3 h. This is about more than three times higher as in batch systems with approximately 2 kg/m^3 h. However, in the last fermentation vessels the yeast is already under stress due to high ethanol concentration so that cell recycling or fresh yeast addition might be required. In this case productivities of up to 30–50 kg/m^3 h are possible [2]. The increased ethanol productivity of the continuous fermentation leads to a smaller fermentation volume. And the continuous process needs less manpower. The ethanol yield is with 89–93% slightly lower than in batch fermentation. Further restrictions are the rather uniform raw material quality needs. Continuous sterilization of the medium is needed to avoid contamination. Nevertheless, the risk of contamination is higher than in batch fermentation due to long time performance.

In industry, both fermentation systems are in use for starch-based ethanol plants in Europe. For example, a continuous fermentation process is used in Zeitz in Germany and a batch fermentation process is implemented within a plant in Galicia in Spain. In Brazil, approximately 75% of all existing ethanol plants use the batch fermentation process. The main reasons for that are higher production stability and lower risk of contamination [9].

Distillation and Rectification The main target of the fermentation is to convert nearly all sugar into ethanol. The next step within the overall process is the recovery of ethanol from the fermentation mixture (beer). This is done by applying a combination of distillation and rectification columns. A simplified scheme with the two columns can be seen in Fig. 2.

To separate the ethanol from water the whole fermentation broth has to be heated up until the boiling point of this mixture is reached. The boiling point of pure water is 100°C compared to 78.33°C of pure

ethanol [10]. The actual boiling point of the mixture depends on ethanol concentration [7] and comes closer to the ethanol boiling point with increasing ethanol concentration.

The evaporation takes place according their vapor liquid equilibrium which leads to a higher concentration of ethanol in the vapor. Unfortunately, the ethanol–water mixture is not an ideal system and shows a so-called azeotrope with a minimum boiling temperature of 78.15°C. The azeotrope is a point where the concentration of the liquid phase is the same as the vapor phase. The ethanol water azeotrope is at around 96.5% (v/v) according to 95.57% (w/w). This concentration is the limit for the rectification process. Therefore, an additional separation process for dehydration of ethanol is needed (see entry "Dehydration of Ethanol").

Depending on the ethanol concentration in the fermentation mixture which is in the range of 12–20% (v/v) (corresponding to approximately 10–16.5% [w/w]) it can be seen in Fig. 3 that the energy needed to concentrate ethanol to 94% (w/w) is around 2–3 MJ/l. This energy demand is nearly constant for this concentration range. To reach these values, an optimization and energy integration of the whole downstream processes needs to be applied.

It is very important, especially in the stripping section of the first column where the whole fermentation broth is feed in, that precautions are made to avoid the blocking of the column internals with the solid matter of the mixture. Therefore, very open tray constructions are used which can cope with this kind of mixtures. Concentration of the derived vapor phase in the rectifying part of the following columns is like in any other ethanol processing plant and dominated by the vapor liquid behavior of the ethanol water mixture [7, 11].

Dehydration Around the globe, there is not a common standard for the fuel ethanol quality. The allowed maximum of the water content is 0.2–1.0% (v/v) and depends on the country in which the ethanol is sold [12]. For concentrating the ethanol from 94% (w/w) (nearly azeotropic mixture) to the required quality several options are possible. The first option is continuing with an azeoptropic rectification process which needs two additional columns and a third component added to the mixture to change the vapor liquid behavior [13–15]. Alternatively, an adsorption process can be applied [16, 17]. Also a membrane processes called pervaporation or vapor permeation can be used [18–20].

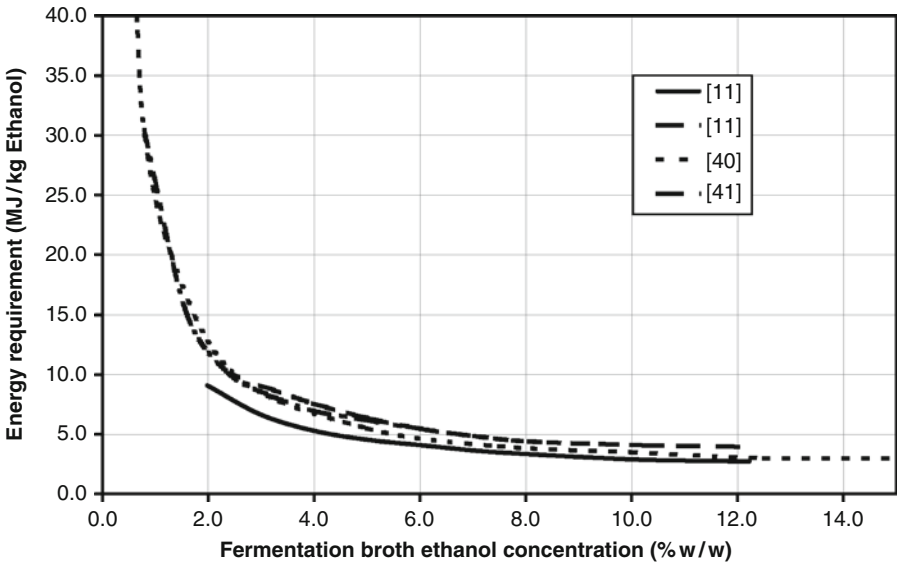

Bioethanol from Starch. Figure 3
Energy requirement for concentrating ethanol from fermentation broth concentration to a rectification column top product with 94% (w/w)

In Brazil, still many plants use an azeoptropic rectification process using monoethylene glycol for dehydration of ethanol. That technology has been developed more than 10 years ago especially for these plants in Brazil. Its advantages are lower investment costs and high robustness on the industrial scale [9]. In the USA and also in Europe, most of the ethanol plants apply the pressure swing adsorption process using molecular sieves for removing water from ethanol to reach the necessary fuel grade. The molecular sieve is a special designed hydrophilic zeolite with a pore diameter of about 0.3–0.4 nm. This allows only water with a molecular size of 0.28 nm to enter and ethanol with a molecular size of 0.44 nm is not able to enter the zeolite. For the technical process, at least two vessels filled with the zeolite are needed. One vessel is used for adsorbing the water from the ethanol vapor stream at around 1.7 bar [21]. The adsorption pressure applied depends on the design of the distillation and rectification system in which the column pressure is increased from the distillation to the rectification section due the energy optimization reasons. So that on the top of the rectifier column a vapor stream is received with respective pressure. In the second vessel at the same time the zeolite is regenerated applying vacuum and a small purge stream of already purified ethanol vapor. This purge stream removes the adsorbed water and after regeneration the cycle starts again. The purge stream with the increased water content from this desorption process is feed back to the rectification column (Fig. 2).

After the dehydration process, the ethanol stream is ready for use and stored in a tank. During the storage and handling one has to take care that due to the hygroscopic nature of the ethanol humidity is not allowed to come in contact with dehydrated ethanol.

Processing of Stillage The remaining liquid stream from the distillation column (beer column) after ethanol removal is called stillage. The maximum remaining ethanol concentration allowed is in the range of 0.02% (w/w). In some plants the untreated stillage is recycled up to around 25% to the liquefication vessel.

The remaining stillage coming from the beer column contains solids like the yeast cells and also dissolved matter like salts and other nutrients. Usually a solid liquid separation is applied using a centrifuge or a decanter. This treatment results in a thin stillage stream (with dissolved matter from the feedstock) and a wet cake (containing the solids with a dry matter of around 25–35%). Depending on the used feedstock, a high recycling rate of the thin stillage is possible. For example by using corn as feedstock, the possible recycling rate can be up to 75%. With wheat and triticale only 60% of recycling is possible [22].

The rest of the thin stillage is feed into a multistage evaporation system for further concentration. Using four or more integrated evaporation stages the steam requirement for evaporation can be reduced to 200 kg steam per ton of water evaporated. In the evaporation process a stream called syrup is produced. The evaporation condensate can be feed back to the mashing vessel to be used again and to reduce the fresh water consumption.

In the next step, the syrup is mixed with the wet cake and feed to the drying system. Here DDGS is produced. The drying procedure is, due to high heat of evaporation of water, very energy intensive. The mixture of syrup and wet cake is very viscose and very sticky. Therefore, it is rather difficult to treat. In addition, smell and dust emissions during processing have to be kept very low. As a drying technology, direct or indirect drying can be applied. The technical equipment is a rotary or drum dryer. For better handling the DDGS product is often pelletized (see [7, 23]).

The derived DDGS product is a protein-rich animal feed with a crude protein content of around 30% or more [24]. In Table 2, the estimated amount of DDGS produced for different feedstock can be found. Depending on the original used biomass some differences can be observed. In Table 3, an example is given for DDGS quality derived from ethanol fermentation with wheat and corn and a mixture of thereof as a feedstock [25].

DDGS as a product contributes to the economy of the process but also increases the energy needed for the ethanol and DDGS production approximately by a factor of 2. The results are higher energy costs needed for the process. This also has an effect on the environmental situation of the ethanol production itself.

Another possibility is to use DDGS as a source of energy within the ethanol plant. This could be of financial benefit if the costs for energy and the earning for DDGS do not match. Therefore, in many countries

Bioethanol from Starch. Table 3 Chemical characteristics of DDGS (% w/w DM) derived from corn, wheat/corn mixture, and wheat [25]

Value	Corn	Wheat/corn (4:1)	Wheat
Moisture	11.8	8.0	8.1
Crude protein	30.3	42.4	44.5
Nonprotein nitrogen	5.4	12.4	10.2
Crude fat	12.8	4.7	2.9
Ash	4.8	5.0	5.3
Acid detergent fiber	14.6	19.5	21.1
Neutral detergent fiber	31.2	30.6	30.3
Crude fiber	7.0	7.8	7.6

such projects are evaluated [26]. DDGS as a fuel could provide more energy than the ethanol plant itself needs since the energy content is rather high. This means that still some of the DDGS could be sold as animal food. The major drawback is that the very high nitrogen content leads to a very high NO_x concentration in the flue gas when the DDGS is used as a solid fuel. Additionally due to the high sodium and potassium concentration, the ash shows a rather low melting point. Therefore, the use of DDGS as a solid fuel is a less promising option.

Stillage can also be used as a feedstock for biogas plants [27]. The amount of stillage produced within an ethanol plant depends strongly on the size of the plant. Therefore, for large ethanol production facilities very huge biogas plants would be needed. Additionally, problems might occur concerning the direct usage of the digested residue in agriculture due to necessary transport or pumping cost. Further treatment using simple filtration or membrane filters would allow higher concentration and would lead to a reduced liquid volume for further handling.

The stillage contains different amount of organic dry matter depending on the feedstock used for ethanol production. Therefore, the possible biogas production might vary significantly. For example, it is possible to produce from corn stillage 0.347 m_N^3/kg oDM and 0.380 m_N^3/kg oDM from the wheat stillage [28]. A general layout of an ethanol biogas concept can be seen in Fig. 4.

The biogas produced can be used in many different ways. It is possible to use it directly in a gas-fired boiler for steam production to cover the energy requirement of the ethanol plant as well as for electricity production (if the biogas production facility is big enough). Or it can be used for electricity production in a biogas-fired engine within a CHP process. Such process combinations together with optimized process integration can lead to a significant decrease of the energy demand of ethanol production [29].

Actual Status

A large-scale ethanol production has been realized within the USA for more than 30 years. The main source of feedstock used is grain. In Europe, the large-scale ethanol production as a fuel started in 2003, initiated by the European Parliament and the Council with posting the directive 2003/30/EC on the promotion of the use of biofuels or other renewable fuels for transport [30]. Since than many new ethanol plants have been built within EC-Countries to meet the requirements of replacing at least 5.75% of fossil fuel by biofuels based on the energy content by 2010. Single European countries enacted individual laws to follow the EC directive and in several countries even a tighter time schedule has been applied. For example, in Austria in 2004 a change in the existing fuel legislation [31] posted for October 1, 2005, a value of 2.5%, October 1, 2007, a value of 4.3%, and already on October 1, 2008, a fulfillment of the EC legislation of 5.75% based on the energy content.

The strong efforts of the USA and the EU in contributing significantly with biofuel to cover the energy demand within the transportation sector led to the situation that the USA passed Brazil as the world's largest annual ethanol producer in the year 2005 where both countries produced around 16 million cubic meters of ethanol. The world production in this year was 46 million cubic meters of ethanol. Since then the annual production capacities increased steadily worldwide to 74 million cubic meters ethanol in 2009 with 41 and 25 million cubic meters ethanol in the USA and Brazil respectively [32].

Analyzing these figures it can be estimated that around the year 2000 the ethanol production was 60% from biomass containing sugar and 40% from

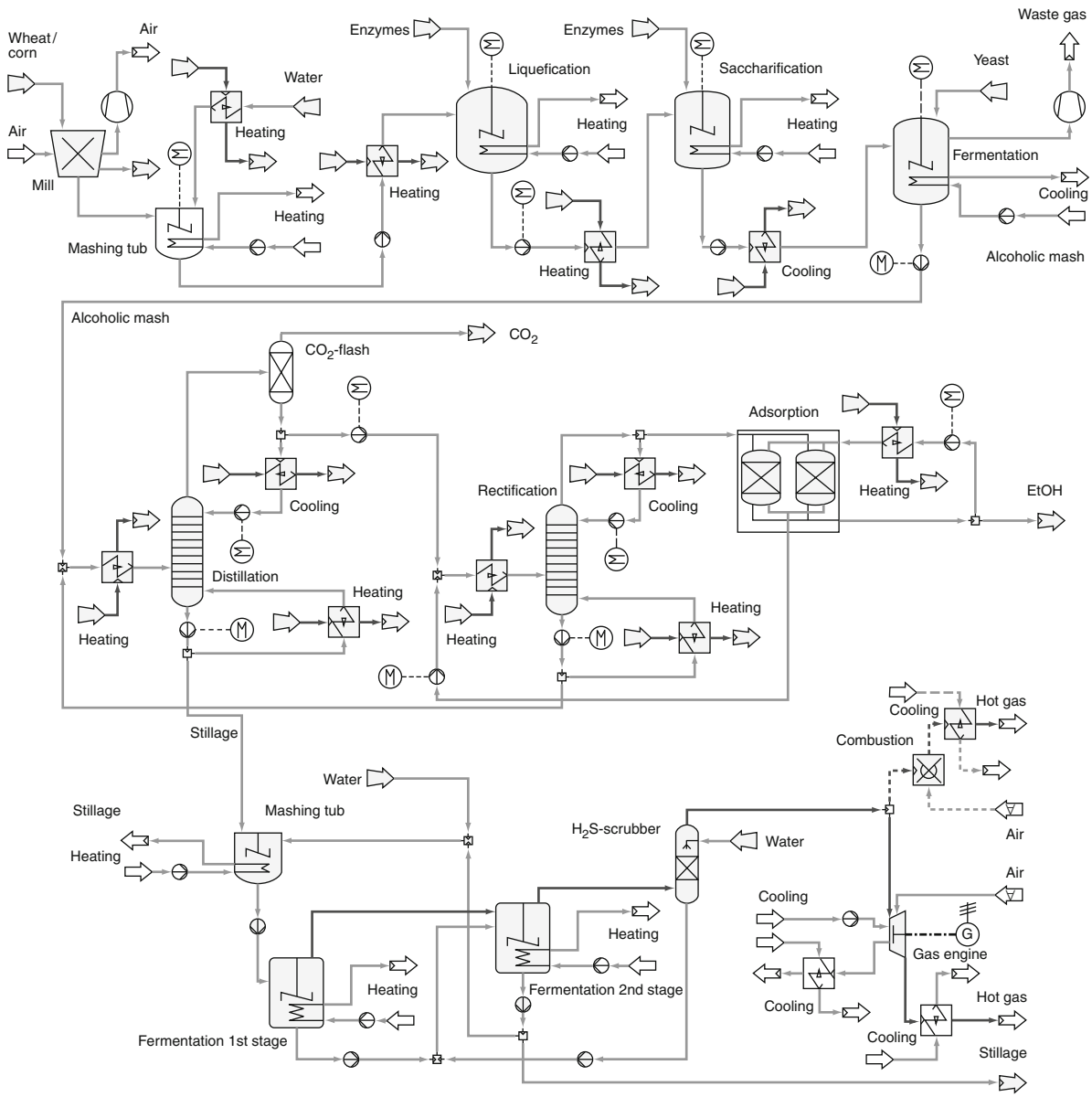

Bioethanol from Starch. Figure 4
Schematic layout of a dry-mill ethanol process including Biogas production

grain crops (i.e., starch). Between 2000 and 2009 the situation changed to a ratio of approximately 40% from sugar crops and 60% from grain crops.

Following the trend of increasing production figures of ethanol, increasing amounts of starch crops are needed as a feedstock. The world production of grain crops in the period 2008/2009 was 2,231 million tons (without rice). This was around 5.2% above the production of the year before 2007/2008 and has been the world's best production year ever. The prognoses for the year 2009/2010 are 2,196 million tons (without rice) which should be the second best production year ever. These record years in harvest are following after a deficit production in the year 2006/2007 which was followed by a very steep increase of price for the grain crops. A worldwide reaction was to

increase the land for grain crop production by 16 million hectares [33].

In the year 2008/2009, the worldwide harvest of corn was 791.9 million tons and that of wheat 682.8 million tons. In the European Community of 27 states (EC-27) the harvest of wheat was in the same year 315.2 million tons. For ethanol production, 5.0% of the wheat was used in the EC-27 in this period. Within the USA at the same period approximately 12% of the world corn production has been converted into ethanol [33].

Future Directions

After the rapid increase of large-quantity production of ethanol in a rather short time, it is important to continue on a settled basis to implement all experiences learned. This includes politics, environment, agriculture, and the ethanol process itself. The learning curve of the Brazilian and US ethanol industry over the last 30 years made it possible to reduce the production costs by more than 60% [34, 35]. This fact shows how important continuous process improvement is. For example, in the Brazilian ethanol industry it was possible to increase the fermentation yield from 75% to 92% based on the theoretical maximum during this time [9] which of course contributes significantly to the economics of the overall process. Actual production costs are estimated approximately with \$188/m^3 in Brazil and \$310/m^3 in the USA [35]. In Europe the estimated productions costs are around \$500/m^3. Due the fact that Europe started large-scale ethanol production for the use as a fuel in 2003 [30] it can be expected that due to significant improvements the production costs of ethanol in Europe can be reduced in the future.

Further developments are already initiated from the European directive 2009 [36]. This regulation demands that on January 1, 2017, a 50% GHG saving target and on January 1, 2018, a 60% GHG reduction target have to be meet. To reach these goals, the ethanol-producing industry is forced to improve the efficiency not only in the ethanol production process itself but also in the whole production chain to receive a better environmental performance.

This will influence the developments in all areas linked to the bioethanol production in industry and research. The latter is urgently needed along the overall process chain to identify and exploit the given GHG reduction possibilities. On the agricultural side, crop developments are necessary to maximize starch production and lower pentosan and glucan concentration (responsible for high viscosity in the broth) with lowest environmental impact. Additionally, the existing substrate basis has to be extended. The use of various sugar, starch, and lignocellulosic material streams, or even mixtures will be needed to accomplish the given demands.

For the ethanol process itself, the optimization of the enzymatic steps and the fermentation process with high solid content is needed to provide together with optimized ethanol-producing microorganism high ethanol concentration at the end [37]. One route for optimization of the fermentation could be the removal of the remaining rough grain after dextrinization during the dry corn milling process. This would lead to an approximate 11% volume reduction of the fermentation vessels. Energy savings along the fermentation and distillation processes are the result since energy for cooling of the insoluble particles and heating in the distillation column is avoided.

At the moment, most of the dry grind fuel ethanol plants using the SSF process. Wet milling technology leads to solid-free mashes, which makes the yeast separation possible and water as well as yeast recycling can be done to a higher extent. The distillation will receive a solid-free stream which makes this step easier. The question is how the fermentation conditions (e.g., temperature, feeding of the carbon source) need to be set? This should be a mid-term program of further research activities because the question of the optimal balance between the fermentation time, the final alcohol concentration and yeast cell viability will strongly influence the economic situation of ethanol plants in the future [9].

In the downstream part, the process intensification with the help of membrane processes needs to be investigated. A first step in this direction is a large-scale pervaporation plant for ethanol dehydration from about 93% (w/w) to a quality of 99.5% (w/w) [20]. Further optimization would be possible if the inlet concentration of the energy-effective pervaporation plant could be reduced to 70% (w/w). This would result to a significant energy saving in the rectification

column. An energy-saving potential of 30–50% could be achieved [38]. The next step of optimization would be the application of an alternative process combination like stripping and membranes to perform ethanol separation from the fermentation broth itself. If a concentration of 70% (w/w) can be reached in the first process step this would close the gap between the second membrane separation steps for dehydration. This would avoid the energy-intensive distillation and rectification totally [39].

Furthermore, alternative usages for the stillage will be needed due to the large increase of worldwide DDGS production. This increase already significantly influences the whole fodder market. Expected limits of DDGS demands would result in falling prices. Since the stillage contains proteins, betaine, lipids, and organic acids and within the yeast cell most nitrogen is fixed in vitamins it might be possible to recover products with high selective and cost-efficient separation processes. The use of the stillage itself for the biogas production is from the environmental point of view a very interesting option. But it might be restricted to small- or middle-scale ethanol plants without effective separation process to increase the solid load of the biogas fermenter and to reduce the water demand significantly. This is also an important task for research. The suspected high nitrogen content in the liquid has to be taken into account. A main advantage of the biogas option is that the nitrogen is kept in the liquid phase, and is not lost as it is in DDGS incineration. This nitrogen can be used as a fertilizer in the agriculture which again improves the environmental performance due to reduced need of mineral fertilizer.

After all optimizations, a remaining demand of energy will be needed to drive all the processes along the ethanol production chain. For this energy needed, the optimal application of renewable energy will be important.

Bibliography

Primary Literature

1. Brown WH, Poon T (2005) Introduction to organic chemistry, 3rd edn. Wiley, New York
2. Roehr M (2001) The biotechnology of ethanol. Wiley, Weinheim
3. Monceaux DA (2009) Alternative feedstocks for fuel ethanol production. In: Ingeledew WM (ed) The alcohol textbook, 5th edn. Nottingham University Press, Nottingham, pp 47–71
4. Bothast RJ, Schilcher MA (2005) Biotechnological processes for conversion of corn into ethanol. Appl Microbiol Biotechnol 76:19–25
5. Gallagher PW, Brubacker H, Shapouri H (2005) Plant size: capital cost relationships in the dry mill ethanol industry. Biomass Bioenergy 28:565–571
6. Kwiatkowski JR, McAloona AJ, Taylora F, Johnston DB (2006) Modeling the process and costs of fuel ethanol production by the corn dry-grind process. Ind Crops Prod 23:288–296
7. Senn T, Friedl A (2009) Ethanolerzeugung und –nutzung. In Kaltschmitt M (ed) Energie aus Biomasse, 2. Auflage, Springer, Berlin, pp 793–850
8. Bellissimi E, Richards C (2009) Yeast propagation. In: Ingeledew WM (ed) The alcohol textbook, 5th edn. Nottingham University Press, Nottingham, pp 145–159
9. Doerfler J, Amorim HV (2007) Applied bioethanol technology in Brazil. Zuckerindustrie 132:694–697
10. Gmehling J, Onken U, Arlt W, Grenzheuser P, Weidlich U, Kolbe B, Rarey J (1981) Dechema chemistry data series, vol 1, Part 1a. DECHEMA, Frankfurt/M
11. Madson PW (2009) Ethanol distillation: the fundamentals. In: Ingeledew WM (ed) The alcohol textbook, 5th edn. Nottingham University Press, Nottingham, pp 289–302
12. International Fuel Quality Center (2004) Setting a quality standard for fuel ethanol. Report to Department of the Environment and Heritage
13. Meirelles A, Weiss S, Herfurth H (1992) Ethanol dehydration by extractive distillation. J Chem Technol Biotechnol 53:181–188
14. Widagdo S, Seider WD (2004) Journal review. Azeotropic distillation. AIChE J 42:96–130
15. Udeye V, Mopoung S, Vorasingha A, Amornsakchai P (2009) Ethanol heterogeneous azeotropic distillation design and construction. Int J Phys Sci 4:101–106
16. Ruthven DM (1984) Principles of adsorption and adsorption processes. Wiley, New York
17. Ruthven DM, Farooq S, Knaebel KS (1994) Pressure swing adsorption. Wiley, New York
18. Kujawski W, Zielinsky L (2006) Bioethanol – one of the renewable energy sources. Environ Prot Eng 32:143–149
19. O'Brien DJ, Roth LH, McAloon J (2000) Ethanol production by continuous fermentation–pervaporation: a preliminary economic analysis. J Mem Sci 166:105–111
20. Morigami Y, Kondoa M, Abea J, Kitab H, Okamoto K (2001) The first large-scale pervaporation plant using tubular-type module with zeolite NaA membrane. Sep Purif Technol 25:251–260
21. Aden A, Ruth M, Ibsen K, Jechura J, Neeves K, Sheehan J, Wallace B, Montague L, Slayton A, Lukas J (2002) Technical Report NREL/TP-510-32438, NREL, Colorado
22. Stout BA (1990) Handbook of energy for world agriculture. Elsevier, London

23. Monceaux DA, Kuehner D (2009) Dryhouse technology and DDGS production. In: Ingeledew WM (ed) The alcohol textbook, 5th edn. Nottingham University Press, Nottingham, pp 303–322
24. Ortin WGN, Yu P (2009) Nutrient variation and availability of wheat DDGS, corn DDGS and blend DDGS from bioethanol plants. J Sci Food Agric 89:1754–1761
25. Widyaratne GP, Zijlstra RT (2007) Nutritional value of wheat and corn distiller's dried grain with solubles: digestibility and digestible contents of energy, amino acids and phosphorus, nutrient excretion and growth performance of grower-finisher pigs. Can J Anim Sci 79:103–114
26. Gorski M (2006) Alternatives to natural gas: more cost-efficient ways to generate steam. Ethanol Producer Magazine. http://www.ethanolproducer.com/articles/1834/. Accessed 27 July 2010
27. Wilkie AC, Riedesel KJ, Owens JM (2000) Stillage characterization and anaerobis treatment of ethanol stillage from conventional and cellulosic feedstocks. Biomass Bioenerg 19:63–102
28. Liebmann B, Pfeffer M, Wukovits W, Bauer A, Amon T, Gwehenberger G, Narodoslawsky M, Friedl A (2007) Modelling of small-scale bioethanol plants with renewable energy supply. Chem Eng Trans 12:309–314
29. Pfeffer M, Wukovits W, Beckmann G, Friedl A (2007) Analysis and decrease of the energy demand of bioethanol-production by process integration. Appl Therm Eng 27:2657–2664
30. Directive 2003/30/EC of the European Parliament and of the Council (2003) On the promotion of the use of biofuels or other renewable fuels for transport
31. Oesterreichische Biokraftstoff-Verordnung: 417 (2004) Aenderung der Kraftstoffverordnung 1999
32. http://en.wikipedia.org/wiki/Ethanol_fuel. Accessed 27 July 2010
33. Agrarmaerkte (2009) Jahresheft, 6. Jahrgang, Schriftenreihe der Bayrischen Landesanstalt für Landwirtschaft
34. Goldemberg J, Coelho ST, Nastari PM, Lucond O (2004) Ethanol learning curve – the Brazilian experience. Biomass Bioenergy 26:301–304
35. Hettinga WG, Junginger HM, Dekker SC, Hoogwijk M, McAloon AJ, Hicks KB (2009) Understanding the reductions in US corn ethanol production costs: an experience curve approach. Energy Policy 37:190–203
36. Directive 2009/28/EC of the European parliament and of the council (2009) On the promotion of the use of energy from renewable sources and amending and subsequently repealing Directives 2001/77/EC and 2003/30/EC
37. Lin Y, Tanaka S (2006) Ethanol fermentation from biomass: current state and prospects. Appl Microbiol Biotechnol 69:627–642
38. Górak A, Hoffmann A, Kreis P (2007) Prozessintensivierung: reaktive und membranunterstützte Rektifikation. Chem Ing Tech 79:1581–1600
39. Vane L (2005) A review of pervaporation for product recovery from biomass fermentation processes. J Chem Technol Biotechnol 80:603–629
40. Zacchi G, Axelsson A (1989) Economic evaluation of preconcentration in production of ethanol from dilute sugar solutions. Biotechnol Bioeng 34:223–233
41. Galbe M, Sassner P, Wingren A, Zacchi G (2007) Process engineering economics of bioethanol production. Adv Biochem Eng Biotechnol 108:303–327

Books and Reviews

Chaplin M, Bucke C (1990) Enzyme technology. Cambridge University Pres, Cambridge

Gwehenberger G, Narodoslawsky M, Liebmann N, Friedl A (2007) Ecology of scale versus economy of scale for bioethanol production. Biofuels Bioprod Bioref 1:264–269

Huang RYM (1991) Pervaporation membrane separation process. Elsevier, Amsterdam

Müller D, Marquardt W (1997) Experimental verification of multiple steady states in heterogeneous azeotropic distillation. Ind Eng Chem Res 36(12):5410–5418

Pereira CLF, Ortega E (2010) Sustainability assessment of large-scale ethanol production from sugarcane. J Clean Prod 18:77–82

Pereira NS, Peinemann KV (2006) Membrane technology in the chemical industry. Wiley, Weinheim

Schmitz N (2006) Bioethanol als Kraftstoff – Stand und Perspektiven. Technikfolgenabschätzung – Theorie und Praxis 1:16–26

Schulz M, Hebecker D (2005) Thermodynamische Analyse und Bewertung der Bioethanolherstellung, Chem Ing Tech 78:502–505

Wukovits W, Pfeffer M, Beckmann B, Friedl A (2007) Deckung des Energiebedarfs von Bioethanolanlagen durch erneuerbare Energieträger. Chem Ing Techn 79:617–620

Bioethanol from Sugar: The Brazilian Experience

Suani Teixeira Coelho, Regiane Gorren, Patricia Guardabassi, Renata Grisoli, José Goldemberg
CENBIO – The Brazilian Reference Center o Biomass, University of São Paulo, São Paulo, Brazil

Article Outline

Glossary
Definition and Importance of the Subject
Introduction
Ethanol from Sugarcane
Sustainability Aspects of Sugarcane Ethanol

The State of the Art on Sugarcane Ethanol
International Dimensions of the Ethanol Program
Future Directions
Bibliography

Glossary

Biofuel Biofuel is one type of bioenergy. In general, this term is used for liquid biofuels. The most known liquid biofuels are biodiesel and bioethanol.

Biofuel program In general, encompasses incentives to biofuels production and/or consumption through policies and regulatory frameworks.

Biomass Biomass is anything that has lived from vegetal or animal origin. The energy obtained from biomass (such as wood, straw, crops, etc.) to produce a fuel is known as bioenergy.

Energy balance Energy balance is the assessment of the energy content in a certain biofuel compared with the fossil fuel energy used to convert it.

Replication Repetition of an experiment utilizing key features. Following the Brazilian experience with ethanol, other countries have possibility to convert sugar plants into ethanol distilleries.

Sustainability Sustainability of biofuels production is related to environment protection, social welfare, and economic development.

Sustainable development Sustainable development is the utilization of the resources aiming to achieve better living conditions without disturbing the future generations' needs [1].

Tariff and non-tariff barriers Tariff barriers are duties imposed on tradable goods and services to be imported. Non-tariff barriers are a way to delimitate the trade by imposing conditions, quotas, and restrictions. Tariff and non-tariff barriers are barriers imposed mainly by developed countries against the import of products which may jeopardize local economy (or local farmers); they also occur in biofuels trade [2].

Definition and Importance of the Subject

The Brazilian ethanol program (Proalcohol) is the oldest of such programs and started in 1975, producing ethanol from sugarcane. A similar program using corn was initiated around the year 2000.

The 2009 world's ethanol production was 76 billion liters – of which 41 billion is in the United States (USA) and 26 billion comes from Brazil – equivalent to 34.8 million tons of oil equivalent or 1.5% of total world oil consumption. The rest of it comes from different countries, mainly Europe and China. Ethanol production is increasing in several regions of the world: Of the 24 producing countries, there are 14 countries in Europe and 5 countries in Asia and Pacific area.

Since transportation is almost entirely dependent on petroleum products, liquid biofuels represent an option to address this challenge in the transportation sector, where there is no other renewable energy commercially available. It should be emphasized that 14% of the world greenhouse gases emissions come from transportation sector.

The main increased importance of biofuels is closely related to the current energy challenges, which are energy security, global warming, and the increasing energy needs of developing countries. This entry presents an overview of the Brazilian experience, lessons learned, and current policies to guarantee the production of biofuels in a sustainable way, as well as, perspectives for replicating it in other developing countries.

Introduction

From a technical perspective, there is nothing new in the renewed interest in using biofuels in internal combustion engines. Late in the nineteenth century, Henry Ford already used ethanol to drive automobiles and Rudolf Diesel used biodiesel from peanuts to drive trucks.

In the beginning of the twentieth century, these fuels were replaced by gasoline and diesel oil distilled from petroleum due to their higher affordability and availability in the USA and a few other countries with easy access to oil, while biofuels, particularly ethanol (an alcoholic beverage), were expensive and produced in minor quantities when compared to the huge quantities needed for large vehicle fleets.

In case of Brazil, since 1920, technical studies have been conducted in Brazil on ethanol-run vehicles, including racing cars. The reason for that was the good performance of ethanol used for fuel purposes, which made it a good alternative to imported gasoline. The first Brazilian policy supporting bioenergy was launched in 1931. The Brazilian Decree No. 19,717

required that all imported gasoline had to be blended with 5% of bioethanol from sugarcane. Later on, in 1938, this blend was extended to the gasoline produced in the country through the Law No. 737. The blend remained around 5.5% from 1935 to 1945 [3]. Over the years, the blend remained almost constant and slowly reached 7.5%. Such blend did not require any changes in the engines.

By the early 1970s, Brazil imported most of gasoline and petroleum consumed in the country, at an annual cost of US$600 million. In 1973, with the first oil price shock, imports rose to more than US$4 billion annually, contributing greatly to the deficit in hard currency and badly damaging the economy.

This was indeed a turning point, where the ethanol was no longer deemed as a by-product of sugar. In November of 1975, The National Ethanol Program, which is known as Proalcohol, was established. This program was the Federal government reaction to the "oil shock" and was created by the Decree No. 76,593. The program also served to assist sugar sector that was facing problems due to the low sugar price in the international market [4]. The production targets were set for 3 billion liters of ethanol by 1980 and 10.7 billion liters in 1985.

There were two distinct phases in the program. The first phase occurred from 1975 to 1979, emphasizing the production of anhydrous ethanol for gasoline blending as an additive to substitute MTBE (methyl tertiary-butyl ether), which is an ether added to gasoline to increase the octane by given oxygen to the combustion reaction. Once ethanol was added to gasoline, MTBE was eliminated as an additive. Ethanol has higher octane number than gasoline and performs the same role as MTBE without the presence of the toxic lead.

Other support actions to increase the competitiveness of ethanol were low interest loans for the construction of distilleries, guaranteed purchase of ethanol by the state-owned petroleum company (Petrobras), and subsidies. In this phase, gasoline was blended with 20% of ethanol and it was adopted a fixed price system, where 44 l of ethanol corresponded to 60 kg of sugar.

The time frame of the second phase spanned from 1980 to 1985, when the focus was on the production of hydrous ethanol for engines designed to run this fuel. The supply side was stimulated by diminishing the parity of 60 kg of sugar to 38 l, and for the demand side, there were incentives among others over the fuel price and taxes reduction [5].

The background of the technological development of engines to run pure ethanol started in 1975 when the Federal Government learned about the research done by the Air Force Technological Center in São José dos Campos, São Paulo to develop ethanol-fueled cars using hydrated ethanol in a proportion of 95.5% pure ethanol to 4.5% water. Important changes in the engine were necessary in order to use that fuel.

One of those changes was the compression ratio that is 12:1 for ethanol fuel from sugarcane, while regular gasoline requires compression ratio of 8:1. Higher compression ratio signifies higher efficiency, which is partly compensated by the lower energy content in the ethanol. For the sake of the clarity, energy equivalence between the two fuels takes into account the final energy service provided. In this way, 199 l of pure (anhydrous) ethanol can replace one barrel of gasoline (159 l). The necessary changes in the engines to run ethanol meant a drastic change in automobile manufacturing, but under governmental pressure, local automobile manufacturers adjusted to that.

Sugar producers welcomed these changes that let them divert more sugarcane to ethanol production, and faced better oscillations in sugar prices in the international market. Another enthusiastic support came from nationalistic elements in the government, who saw ethanol as an instrument of national independence. One of the consequences was that driving Brazilian car with engine designed to run ethanol in neighboring countries (even some States of Brazil) was a problem because they did not have filling stations selling hydrated ethanol. The production of cars with pure ethanol engines began in 1978 with the participation of manufactures such as General Motors (Opel), Ford, Volkswagen and Fiat. Between 1979 and 1985, they accounted for 85% of all new car sales [6].

Over the same period, the percentage of ethanol in gasoline reached approximately 20%. The evolution of Brazilian ethanol production since beginning of the Proalcool is illustrated in the Fig. 1.

Therefore, two types of automotive vehicles were present in the country: some running on gasoline, using a blend of up to 20% anhydrous ethanol and 80% gasoline, and others running entirely on hydrated

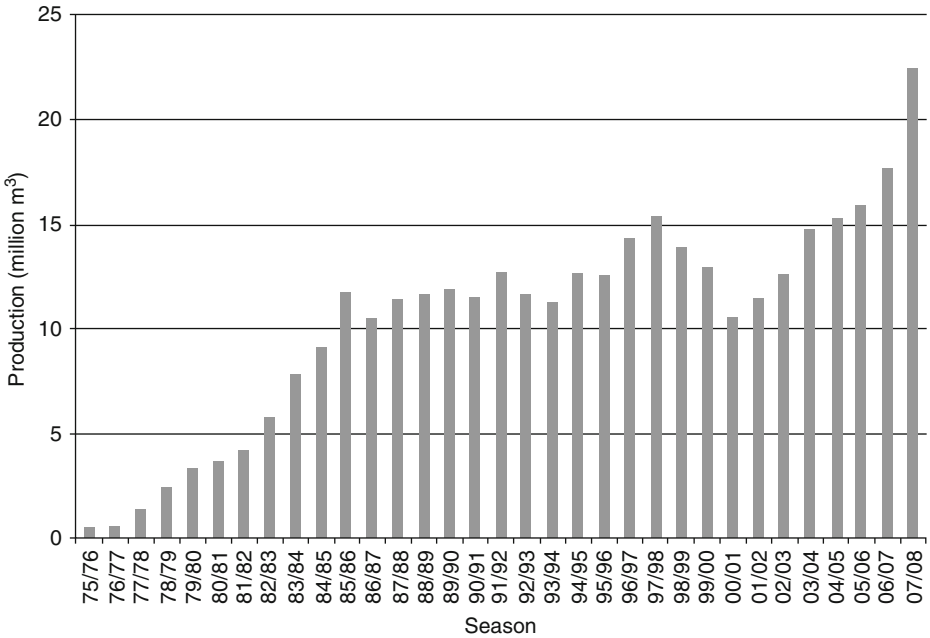

Bioethanol from Sugar: The Brazilian Experience. Figure 1
Evolution of ethanol production in Brazil [7]

ethanol. Nevertheless, it is important to mention that the targets were achieved through mandatory regulations, subsidies, and due to the unique characteristics of the country at that time, since Brazil was under an authoritarian government from 1964 to 1985.

In 1985, the scenario changed dramatically, as petroleum prices fell and sugar prices recovered on the international market. Subsidies were reduced and ethanol production could not keep up with demand. Therefore, by 1990, sales of cars running on pure ethanol dropped to 11.4% of the total [8].

The production of ethanol leveled off, but the total amount being used remained more or less the same because the decrease of hydrous ethanol cars was compensated by the increase on gasoline blending to 25% (Fig. 1). From 2003 onward, with the advent of flex fuel engines, ethanol consumption started to rise again. Since 2003, Brazilian automotive industry has introduced the so-called flex fuel vehicle, which means a vehicle running with any ethanol gasoline blend, from E-0 up to E-100. It must be noted that the Brazilian flex fuel vehicles are different from those produced in other countries (like USA), which can run with a maximum of 85% ethanol (E-85) only.

These cars are built to use pure ethanol with a high compression ratio (approximately 12:1); however, they can also run with any proportion of ethanol and gasoline, from zero to 100%. The increasing in the productivity of ethanol was reflected in costs (Fig. 2).

In 1980, ethanol cost roughly three times as much as gasoline in the international market (Fig. 2). And, since 2003, ethanol became fully competitive with gasoline without any subsidies. It is important to emphasize that this achievement is result of over 30 years of experience with technological gains, economies of scale, and political effort from policy makers and other stakeholders.

The expansion of ethanol production had important repercussions in the ownership and management of the sector, which in Brazil is entirely in the hands of private groups. Although Petrobras, the state-owned Brazilian oil company, is beginning to invest in this area, it is still a very small player [10].

Traditionally, sugar-producing units were family-owned enterprises such as Costa Pinho, São Martinho, and Santa Elisa, but new ones are owned by Brazilian companies including Votorantim, Vale, and Odebrecht. Also there are foreign companies entering the

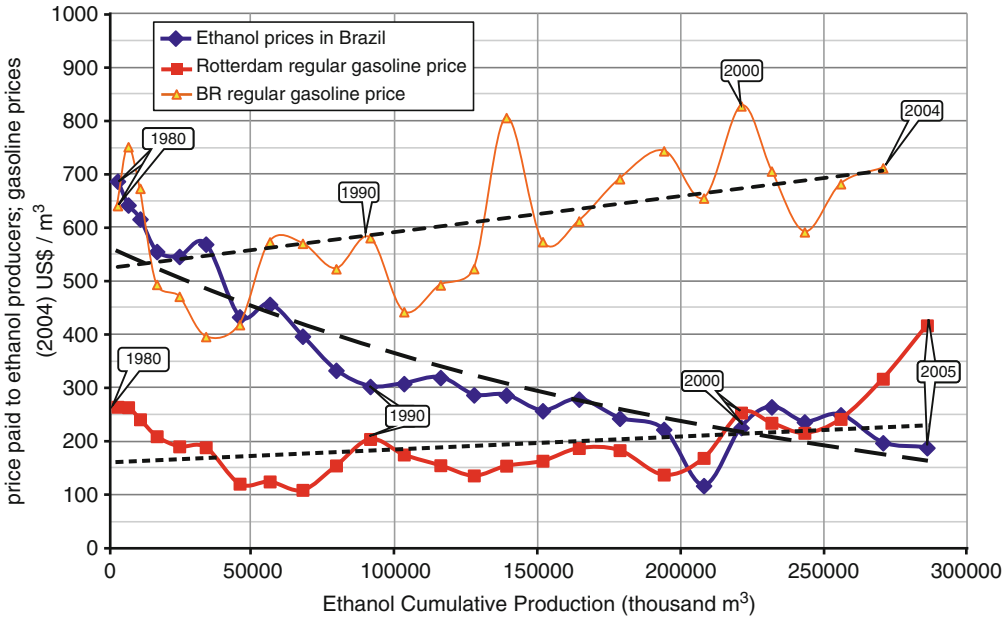

Bioethanol from Sugar: The Brazilian Experience. Figure 2
Brazilian ethanol learning curve [9]

sugarcane business, including French (Tereos, Louis Dreyfus), Spanish (Abengoa), British (BP) and Japanese (Mitsui, Marubeni) groups, among others.

The financial sector is also quite active in this area, including Merrill Lynch, Soros, and Goldman Sachs. The presence of foreign investors has given the sector a new dynamism and new concepts of management.

Ethanol from Sugarcane

Sugarcane

Brazilian ethanol is produced from sugarcane (*Saccarum officinarum*), which is not an indigenous plant from Brazil.

In 1532, sugarcane was brought to Brazil by the Portuguese during the colonization period. This plant is a type of grass that has fibrous stalks containing high concentration of sugar. In order to achieve a good development, sugarcane needs distinct climate seasons. One phase is dedicated to germination, in which adequate rainfall and higher temperatures are necessary. During the phase for sucrose accumulation, it can be colder and dryer. The cultivation requires a minimum rainfall of 1,200–1,300 mm a year, in order to avoid irrigation, and the ideal temperature ranges from 20°C to 24°C because this plant is not resistant to cold weather [10].

Brazil is a tropical country, and many of its regions have favorable climate characteristics for sugarcane cultivation without irrigation. Sugarcane is a semi-perennial crop, that is, after the planting phase, sugarcane can be harvested six to seven times without replanting; however, it is recommended one season of rotation with a different crop to rest the soil. This practice is common throughout the country.

Thus, in each harvesting season, 20% of the crop is replaced with crops that help to recover the soil such as beans, corn, or peanuts. The harvesting season follows the rainfall pattern of every region. As such, in the Center-South production region, it starts in April and finishes in December and in the North-East region, it spans from August to April. Depending on industrial process, sugarcane is transformed either in sugar or ethanol.

Sugarcane is the feedstock for alcohol (ethanol fuel, pharmacy or beverage), sugar, and electricity from bagasse as well. Vinasse (stillage), bagasse, filter cake, tops, and leaves (trash) are by-products from sugarcane that are also utilized in modern practices.

Bagasse (30% of the cane, 50% wet) is the remaining fibrous part of sugarcane after the crushing. It is rich in cellulose and contains more energy (560 Mcal/t of sugarcane) than ethanol itself (392 Mcal/t of sugarcane) [11]. This by-product is burned in boilers, providing heat and electricity.

Vinasse is generated from distillation. It consists of a liquid rich in organic matter and nutrients, such as potassium and calcium, but it is also a pollutant if not well managed. Vinasse production is around 10 l per liter of ethanol, but new technologies like vinasse concentration allows the reduction on the production of vinasse until 5 l for 1 l of ethanol (Magazoni LA, personal communication, magazoni@cerradinho.com.br). The use of vinasse in fertirrigation practice reduces the need for fertilizers and gives a no pollutant destination to this by-product. It must be noted that in the State of São Paulo, the use of vinasse for fertirrigation is controlled by the Environment Agency (CETESB) aiming to avoid contamination of underground water. This requirement will be probably followed by other States in Brazil.

Filter cake is also a by-product from juice filtration. It consists of rests of bagasse and sugar clarifier sludge, eliminating by 50% the need for phosphorus mineral fertilization. The production proportion for each ton of sugarcane milled varies from 30 to 40 kg of filter cake [11]. Tops and leaves (trash) represent 30% of the sugarcane. In many cases, they are the leftover of the harvesting and also left on the soil as preventive method avoiding erosion and nutrient depletion or utilized as cogeneration fuel.

From Field to Motor

Ethanol or ethyl alcohol is an organic compound that belongs to the first generation of biofuels (Box 1). Typically, ethanol is obtained through biological conversion involving fermentation process, which converts sugar into alcohol.

After the harvesting, sugarcane must be transported and processed in maximum of 72 h in order to avoid quality losses due to bacterial activity [12].

In the distillery, the grinding breaks the sugarcane fibers. Subsequently, acids or enzymes are added in

Box 1: Definitions of First- and Second-Generation Biofuels

First-Generation Biofuels The common forms of first-generation biofuels are those on the market in considerable quantities today. Typical first-generation biofuel is sugarcane ethanol, starch- or corn-based ethanol, biodiesel, biogas, and pure straight vegetable oil. The feedstock for producing first-generation biofuels are crops that produce sugars, starches, oils, or animal fats, most of them being food and feed, as well. It also can be obtained from residues. Other niche of biofuel is biogas, which results from an anaerobic treatment of manure, urban residues, and other biomass materials. Relatively small volumes of biogas are currently used for transportation. Today, the first-generation biofuels commercially produced is about 76 billion liters annually.

Second-Generation Biofuels Second-generation biofuels are those biofuels produced from cellulose, hemicellulose, or lignin. Examples of second-generation biofuels are cellulosic ethanol, Bio-SNG, and Fischer–Tropsch fuels. The latest technology synthesizes fuel from gases produced from the gasification of biomass. Both, first and second generation of biofuels can be blended with petroleum-based fuels, combusted in regular internal combustion engines, distributed through existing infrastructure. In addition, second generation may also be utilized in slightly adapted vehicles with internal combustion engines like vehicles designed to run Di-Methyl Ether (DME). According to Petrobras [17], the first bioethanol pilot plant has started activities utilizing enzymatic technology to convert waste into biofuels. Even though the second-generation biofuels are meant to be more sustainable, this technology needs technological breakthrough to reduce the production costs. Besides, second-generation biofuels are still in the development stage and production cost seems to be higher compared to first-generation ones.

Source: Reference [18].

order to precede the hydrolysis and obtain glucose. The glucose is then fermented to produce ethanol by the action of adequate yeasts.

Two important chemical characteristics of ethanol that should be emphasized are the boiling point (78.5°C) and the miscibility with water and organic components. There are two types of ethanol: The anhydrous form is used to blend gasoline and the hydrated one is used as fuel in engines specially designed for this type of fuel or flex fuel motor. The difference between the two types is the water content in the anhydrous and hydrated, which is 0.5% and 5%, respectively. Pure gasoline is called "gasoline A" and the gasoline blended with ethanol is "gasoline C" (gasohol). The percentage of ethanol blend in the "gasoline C" might range from 20% to 25%, according to the current legislation being regulated by The National Petroleum Agency (ANP). Among the ANP functions, supervision and control of the biofuel market is included.

Energy balance can be defined as the ratio of total fossil fuel energy required for the biofuel production process to the energy contained in the biofuel produced [13]. Energy balance of biofuel produced from a feedstock might be an indicator of the sustainability when taking into account greenhouse gas emissions avoided in a life cycle basis. A study on sugarcane ethanol energy balance shows significant differences between feedstock, where the energy balance of the ethanol produced from sugarcane is 8.9, from sugar beet 2, and from corn 1.3 (Fig. 3) [14]. The sugarcane ethanol presents less GHG emission compared to fossil fuels due to the nearly closed carbon cycle. In respect of land use, feedstocks with higher yields per hectare require less quantity of land.

The good performance of the ethanol produced from sugarcane is due to the use of sugarcane bagasse that provides the energy needs for the process, eliminating external sources of energy. Bagasse is the most important by-product from sugarcane, and it is burned in the boiler producing both mechanical and electrical energy (i.e., cogeneration, see Sect. "Cogeneration in Sugarcane Mills").

Another by-product that is increasingly growing in importance for energy generation to the process is the sugarcane leaves. This is happening due to the progressive decrease of the burning practice of sugarcane before harvesting and the progressive introduction of green cane harvesting.

Country Profile

Brazil is a large country and since the Proalcool program, it has always been an important player for ethanol production in the world. In order to give an idea of this country profile, the main social,

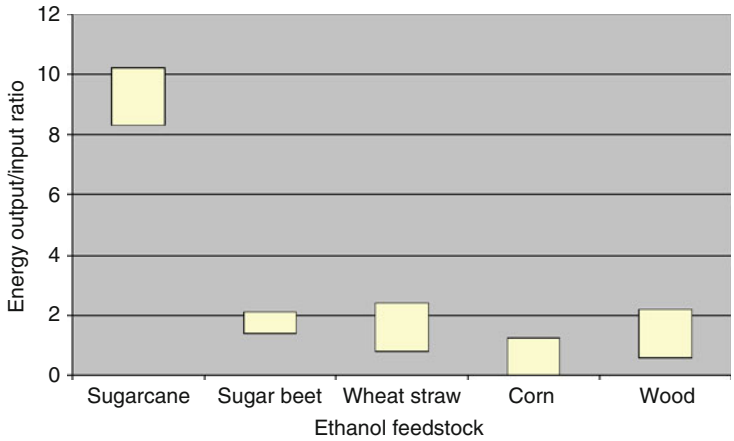

Bioethanol from Sugar: The Brazilian Experience. Figure 3
Energy balance from ethanol production from different feedstocks [14–16]

demographic, and economic indicators are summarized in the Box 2, as well as, relevant information regarding production and use of ethanol.

Box 2: Brazil in Figures

The Federal Republic of Brazil has a continental size, 8,514,876 km^2. In 2008, the total population was 194,228 million inhabitants [19], and in 2007, the population growth was 1.2% [20]. Regarding economy, the Gross Domestic Product (GDP) corresponded to 2.4% of the world's GDP [20]; with 10% participation of agricultural sector [21]. Regarding the wealth distribution, in 2008, the Gini index was 57 [22]. The Human Development Index (HDI), which is a more complete index encompassing educational level, longevity, and income dimension, was 0.807. Yet, concerning HDI, in 2008, the country was positioned at the 70th place [23] in the world. Brazil is the second largest producer of ethanol in the world with 26 billion liters in 2009 [24]. This amount accounted for 37% of the world's production. This country is the world's largest sugar producer, with 622 million tons (metric tons) in the 2008/09 harvesting season [25]. In Brazil, the mills can be either a sugar plant or alcohol distillery or sugar mill and alcohol distillery. Most of the 414 existing Brazilian mills (60%) are alcohol distilleries attached to a sugar plant. In the period of 2008/2009, 35 new distilleries were to start production and another 43 were in different stages of development. In order to process quickly the feedstock, the sugarcane distilleries need to be close to the sugarcane plantation. The Center-South region responds for nearly 80% of ethanol production in the country. There is a high concentration of distilleries in the Center-South production region, but with no pressure against the Amazon or other important biomes in the country. Today Brazilians are driving about 24 million automobiles. In 2000, there were 2.8 million pure ethanol engine cars. Most of the pure ethanol cars have been retired while seven million of flex fuel cars are on the road and their numbers are increasing rapidly [26]. The huge success of these flex fuel vehicles is due to the freedom of choice for the consumers, depending on the price of each fuel at the gas station.

Sustainability Aspects of Sugarcane Ethanol

What are the issues regarding environmental, economic, and social aspects of the sustainability? Several studies [36, 65, 79] explored these issues deeply in recent papers summarized in this section.

Environmental zoning is a crucial tool to guarantee the sustainable production of sugarcane ethanol. There are such zonings in São Paulo State [27], in Minas Gerais State, and from the Federal Government. A recent environmental zoning for sugarcane (2009) from the Federal Government defined areas available for the crops and protecting biodiversity of important biomes named "Sugarcane agroecological zoning" a jointly effort from the Ministry of Agriculture and the Ministry of Environment. Besides that, there are studies [28] indicating that there is no scientific evidence that sugarcane crops present pressure on Amazon (Indirect Land Use Change – ILUC).

Environmental Aspects

In the beginning of the program, economic and strategic factors were crucial in reducing Brazil's dependence on oil, but later on, environmental preservation became also a key issue.

Ethanol engines present lower emissions than gasoline ones, such as no sulfur oxides or particulates, which are the primary cause of poor air quality in large cities like Beijing, Mexico City, São Paulo, and Los Angeles. In São Paulo, the air quality has improved remarkably since gasoline was partially replaced by ethanol. Nowadays, it represents more than 50% of the fuel powering vehicles.

Acknowledging that the main contributor to global climate changing is CO_2 from fossil fuel energy, ethanol has lower CO_2 emissions than gasoline because of the lower amount of CO_2 from fossil fuel energy produced over the ethanol life cycle. An important result was the approval from United States Environmental Protection Agency (EPA) [29] of the use of sugarcane ethanol, accepting that overall carbon balance is highly positive [28].

Besides, many environmental problems associated with oil production (spills), transportation (leakages), and consumption (emission of greenhouse gases (CO_2,

CH_4, N_2O), SO_x, NO_x, H_2O vapor and acid gases like HCl) are not present when using ethanol.

Therefore, below a brief overview of environmental impacts is presented, together with existing legislation to control them.

Water in Sugarcane Ethanol Production One of the most important issues related to water pollution in sugarcane industry was the adequate disposal of vinasse. Vinasse is a black liquid derived from distillation and fermentation, as already mentioned; this by-product is rich in organic matter with an acidic pH [4, 5]. It is a potential pollutant to water and can therefore not be discharged directly on rivers.

In the beginning of the program, there was no control on vinasse disposal from the mills and, in most cases, it was disposed in rivers, being responsible for high pollutant impacts. The solution to dispose this by-product was found, and it started to be recycled and used for fertirrigation. For some time, it was used for fertirrigation without any control. Therefore, the impacts related to the contamination of underground waters became important.

In 2006, in São Paulo State, the Environmental Agency (CETESB) started to control the amount of vinasse disposed on soils, aiming to avoid the contamination of underground water [30]. Nowadays, other states are also introducing the same control for the licensing of the mills.

Also there are now some initiatives aiming to reduce the amount of vinasse produced using systems for concentrating it (Magazoni LA, personal communication). By introducing such systems, the amount of vinasse produced decreased to 5 l per liter of ethanol produced.

Additionally, local environmental agencies all over the country are controlling the maintenance of riparian forests nearby sugarcane crops and requiring the reforestation of such areas with native forests, according the Federal Forest Code. In fact, it must be noted that this Code only states that it is forbidden to jeopardize the growing (or re-growing) of riparian forests. However, environmental agencies are requiring more than that: They consider mandatory the conservation (and/or reforestation) of these riparian forest of the plantations. This is an important issue, since it protects the quality of water in rivers.

Water is used in two ways in producing sugarcane and ethanol. Firstly, large quantities of water are needed to grow the cane. The cane requires significant rainfall, in the range of 1,500–2,500 mm a year, ideally spread uniformly across the growing cycle. Most of the sugarcane production in Brazil relies on rainfall, rather than irrigation, including nearly the entire São Paulo State sugarcane-producing region. Secondly, also large amounts of water are also used to convert sugarcane into ethanol. In 1997, this amount was calculated as cubic meters per ton of cane, from which 87% was used in four processes inside the plant.

In general lines, there is one process for sugarcane washing and three other industrial processes for ethanol production. Water consumption has substantially decreased in recent years. Furthermore, sugarcane is 70% water, which should provide enough for all the steps needed in ethanol production. There are distilleries being developed to be self-sufficient regarding water consumption. Also, nowadays the dry cleaning of sugarcane is being introduced in several mills, reducing the water consumption in the process (Magazoni LA, personal communication).

Land Availability Concerns related to the conservation of native forests and other important biomes are always presented and some studies even consider that any bioenergy crop comes from deforestation [31–33]. Notwithstanding, these studies only consider the worst case, which is not currently occurring, since biofuel production is not expanding into pristine tropical forests. If that did happen, of course, it would release a large amount of CO_2, but extensive studies have been conducted on the CO_2 releases resulting from other agricultural practices that do not involve deforestation, and the results are much less alarming [34]. Nevertheless, other studies [35] show that this is not adequate and bioenergy crops are being expanded in pasturelands without any deforestation.

In 2007, the land availability for agriculture in Brazil was 355 million hectares, from which 21% had already been used for agricultural purposes and the area occupied by sugarcane ethanol accounted only for 1.5% [7].

Moreover, there were 30% available land and 49% was occupied by pastureland. In this land, there is the possibility of expansion of agricultural crops, like has already occurred in the state of São Paulo through the

replacement of pastures, which have become more intensive [36].

In 2001, in the State of São Paulo, the average number of heads of cattle per hectare was 1.28. As of 2008, it has been increased to 1.56 because of the expanding sugarcane plantations pressuring cattle grazing. In the country as a whole, the density is even lower, at closer to one head per hectare [37].

The Brazilian sugarcane crops expansion is concentrated in the Center-South production region that does not encompass important biomes like Amazon Rain Forest, the Atlantic Forest, and the Pantanal [38]. The deforestation in the Amazon basin is linked closely with the raising of cattle for meat, for both domestic consumption and export; it is not linked with ethanol production. Today, Brazil has approximately 200 million heads of cattle on 237 million hectares [39]. In fact, if this cattle could grow in a more intensive way, reaching 1.5 heads for hectare (which is not yet an intensive growth), the country could have around 60 million hectares available.

In addition, recent studies [28] have analyzed Indirect Land Use Changes (ILUC), showing that there is no concrete evidence that sugarcane expansion is producing deforestation.

Soil Quality Sugarcane culture has become more sustainable over the years as some practices have been introduced insuring the appropriate use of fertilizers and soil protection against erosion, soil compaction, and moisture loss. In Brazil, some soils have been producing sugarcane for more than 200 years, with no yield reduction. In fact, agricultural production has increased significantly. Sugarcane culture in Brazil is well known for its relatively small loss of soil to erosion, especially when compared to soybeans and corn.

Nowadays, with the introduction of the green harvesting of sugarcane, a significant discussion is on the way, related to the amount of residues that should be left in the field to protect the soil. Studies show the importance of the sugarcane residues left in the soil, since they protect the soil and allow the infiltration of water in the soil and reduce erosion, among other benefits.

Agrochemicals Many inorganic compounds are introduced during the production of ethanol, including chemicals that kill weeds, insects, mites, and fungi, along with defoliants and other chemicals that help the cane to mature more quickly. Concerning agrochemicals, fewer agrochemicals are used in sugarcane production than for some other crops. The pesticide consumption per hectare for sugarcane is lower than for citrus, corn, coffee, and soybeans. Nevertheless, sugarcane requires more herbicides per hectare than coffee.

Furthermore, comparing Brazil's major crops (those grown on areas larger than one million hectares), sugarcane uses smaller amounts of fertilizer than cotton, coffee, and oranges, and about the same amount as soybeans. Sugarcane also uses less fertilizer than sugarcane crops in other countries, for instance, compared to Australian sugarcane growers that use 48% more fertilizer than Brazilian ones [14].

One practice that helps here is using the vinasse as a fertilizer. This has led to a significant increase in productivity and in the potassium content of the soil [40]. Genetic research, especially the selection of resistant varieties, has made it possible to reduce the diseases affecting sugarcane, such as the mosaic virus, sugarcane smut and rust, and the sugarcane yellow leaf virus. With genetic modifications, plants are more resistant to herbicides, fungus, and the sugarcane beetle; some of these modifications are now being field tested.

Air Pollution Besides the advantages of sugarcane ethanol replacing gasoline in engines, with most of pollutant emissions being reduced, also emissions in sugarcane ethanol production must be addressed. In this area, there are two issues to be considered. Atmospheric emissions from sugarcane burning before harvesting and those from bagasse burned in boilers for cogeneration.

The sugarcane burning before harvesting practice was introduced in Brazilian sugarcane fields after the 1950s, aiming at higher productivity of the sugar cutter workers [40]. This practice eliminates the leaves of the sugar cane cleaning the way to proceed with the manual or mechanic harvesting. By doing this, up to 90% of undesirable vegetal matter can be removed from the harvesting feedstock [40]. Another reason for the burning is to avoid accidents with poisonous snakes and spiders.

However, there are serious drawbacks such as damaging the tissue of sugarcane and disturbing the soil structure enhancing the possibility of soil erosion [41]. Besides, there is an increase of pollutants such as particulate matter, carbon monoxide, and methane; locally it can increase the troposphere ozone concentration. Yet, there are several implications to the industrial phase like difficulties in the purification, need for faster utilization of the feedstock due to the shorter period for exteriorization [40].

It is important to emphasize that elimination of the burning practice raises the energy balance of the sugarcane, which means more energy is produced. Even though the burning is a controlled fire in a delimitated area with maximum duration of 10 min [12], it might represent risks to the grid cables, roads, and highway. On one hand, harvesting manually the green cane is possible, but the celluloid leaves can hurt if no protection equipment is used. On the other hand, sugarcane burning enhances the level of organic compounds, particulate matter, and methane.

Recently, environmental legislation enforces the phasing out of sugarcane burning in the State of São Paulo (State Law 11.241; see Fig. 4). Further on, the so-called Green Protocol was signed. This protocol is a voluntarily one, signed between the Government of São Paulo State, through its Environmental Secretariat and its Secretariat for the Agriculture, together with the Sugarcane Agroindustrial Sector of São Paulo State, reducing the timetable for the elimination of the burning process. The Green Protocol anticipated the timetable for elimination of sugarcane burning in the state from 2021 to 2014, as well as, increased the percentage of green cane harvesting from 50% to 70% in 2010, for soils with slope until 12%. In the case of slopes that are higher than 12%, the elimination of sugarcane burning was anticipated from 2031 to 2017 and it also intends to increase the harvesting of green cane from 10% to 30% in 2010. In many other states, the local environmental agencies are also requiring the harvesting of green cane as one of the exigencies for the environmental licensing.

Therefore, in the State of São Paulo, in the crop season of 2008/09, 49% of the cane was harvested mechanically [42] (Fig. 4). It is important to remind that 80% of the sugarcane produced in Brazil is from the Center-South producing region where the State of São Paulo is located.

Regarding the burning of bagasse in boilers for cogeneration, despite the advantages of this process for the industrial productivity of sugarcane ethanol, there are pollutant emissions to be controlled. Even considering that there is no sulfur in biomass (i.e., no SO_2-emissions), emissions of particulate matter and NO_x must be controlled. There is also an adequate environmental legislation in the country to do so. Therefore, there are now limits for emissions (particulate matter and NO_x) from such equipment [43].

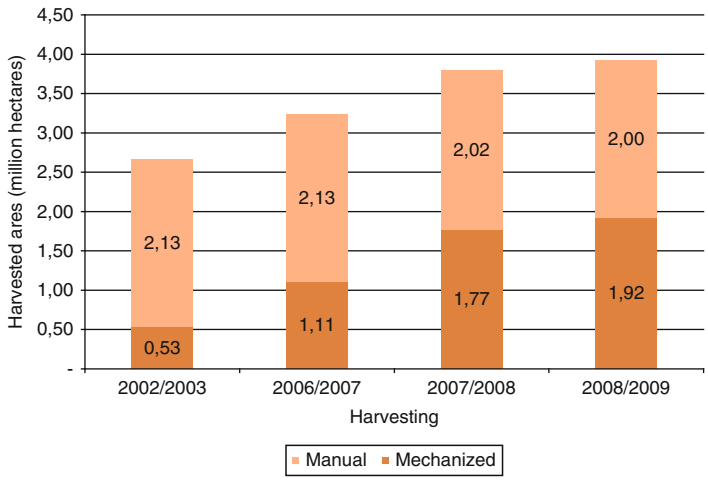

Bioethanol from Sugar: The Brazilian Experience. Figure 4
Evolution of mechanical harvesting in the state of São Paulo. (Law 11, 241/2002) [42]

Economic Aspects

In response to environment issues, marketing forces took place increasing the demand for biofuels. This is especially true when the oil price is high [44]. The producers as suppliers act in a market-oriented way following the demand and tending to seek for more productivity.

Sugarcane Ethanol Production Costs Analyzing the inputs that are part of the production costs of biofuels, it can be noted that fertilizers, feedstock, and energy consumption are important indicators. In the case of sugarcane ethanol, the feedstock (sugarcane) represents the highest share of the final production cost.

Considering the overall process, the ethanol price can be up to 70% of gasoline prices, ranging from US $0.18 to 0.25 per liter. This is the lowest production cost of biofuels in the world.

An analysis of the investment costs for plant with processing capacity of two million tons of sugarcane a year shows that it would be necessary an initial investment of around US$60 million, in 2005 prices [45]. Assuming the plant to be a regular mill, located in the Center-South of Brazil, the yield would be on average 79.39 l of anhydrous ethanol or 82.86 l of hydrous per ton of sugarcane. And one ton of sugarcane would cost US$11.4. Without computing the interest for a plant with a lifetime of 25 years would result in a cost of US $0.143 per liter of ethanol and an investment cost of about US$ 0.017 per liter of ethanol produced.

The learning curve showed in Fig. 2 illustrates the competitiveness of Brazilian ethanol with gasoline in the international market. Other sugarcane producer countries have potential to implement biofuel program following the production costs reduction achieved by Brazilian experience with biofuels.

It is important to note that nowadays there are no subsidies paid in the country, only special tariffs for ethanol when compared to gasoline.

Brazilian Taxes Associated to Ethanol By the end of the 1990s, ethanol subsidies have been removed by the government and, since then, there is no price control from the government [2]. The deregulation of the ethanol market began during the Real Plan, in 1994, with the reduction of tax discount on Federal Excise Tax on Industrialized Products (IPI) for new vehicles powered by ethanol and also reduction of price difference between gasoline and ethanol [46].

Nowadays, the only incentives in place are allocated in the acquisition of new vehicles on IPI and in the Tax on the Circulation of Goods (ICMS). Among the States, the lowest ICMS is in the State of São Paulo (12%) and highest is in the State of Pará (30%), the average being 24% [37]. Flex fuel vehicles or vehicles powered by ethanol have lower IPI (Federal Tax for Industrialized Products) than gasoline ones (Table 1).

Actually, a higher IPI levy on vehicles powered with fuels which have higher emissions of pollutants is a way

Bioethanol from Sugar: The Brazilian Experience.
Table 1 Taxes according to the fuel and vehicle type

Tax burden on new vehicles		
Type of vehicle	**Federal tax IPI [47, 48]***	
Gasohol vehicles (running on gasoline – anhydrous ethanol blends)	7–25%	
Ethanol vehicles	7–18%	
Flex fuel vehicles (running on any blend of gasoline/alcohol)	7–18%	
Tax burden on fuels		
	ICMS (range)**	**CIDE tax [12]****
Gasoline	25–31%	R$ 501.10/m^3
Diesel oil	12–17%	R$ 154.80/m^3
Natural gas	12%–	Zero
Hydrated ethanol	12–30%	R$ 22.54/m^3
Anhydrous ethanol (levy on gasohol)	–	–

*IPI – Federal tax where the levy varies according to the engine that ranges from 1,000 to 3,000 cm^3

**ICMS – State tax and is lower for ethanol. These taxes take into account the environmental benefits of alcohol. In the case of anhydrous ethanol (blended with gasoline), there is no state tax (ICMS); this tax is included in the final blend (gasohol). The tax varies according to the State

***CIDE (Contribution for Intervention in Economic Domain), a Federal tax established in 2002 for liquid/gaseous fuels. CIDE was created aiming to get funds for road conservation in the country and establishes differentiated values according to each fuel

of internalizing the costs of externalities caused by them. The structure of ethanol taxes burden can be described in a simplified way [12] as:

- At industry level, on the ethanol anhydrous and hydrated, the PIS/Cofins levy is 3.65%, on the revenue after the ethanol sales.
- Considering retailer, the so-called PIS/Cofins levy is 8.2% in the revenue from sales of ethanol hydrated by the retailer. In case of anhydrous ethanol, this fuel is blended with gasoline, thus the levy evenly to gasoline.
- In terms of State tax, the ICMS (Tax on the Circulation of Goods) is a state tax on industry and retailer and for ethanol, it ranges from 12% to 30%.

PIS and Cofins are concerned to social security, being PIS the acronym for Program for Social Integration contribution and Cofins the acronym for Contribution for the Financing of Social Security. Cofins is an additional contribution to finance social security based on the gross turnover of the company.

Social Aspects of Sugarcane Ethanol Production

Biofuels production generates significant social benefits for the developing countries, like economic growth and decrease of unemployment rate for people with low years of schooling in rural areas, through the creation of jobs in such areas.

Also the investment needed to create these jobs is much lower in biofuels sector than in others. In Brazil, one job position creation in ethanol agro industry costs about US$11,000 and for petrochemical industry the cost is 20 times more [49]. Figure 5 shows capital investment for job creation in different production areas and the quantity of job per unit of energy produced.

Another important aspect of social situation in sugarcane sector is related to the quality of jobs created. The evolution of the poor people income share of participation on GDP is shown in Table 2. There, not only an increase of this participation can be seen, but also an increase in the number of poor people.

The social inequality of rural areas in Brazil has not been improving significantly in the recent years. This fact is confirmed by the Gini index shown in the Table 3.

Normally, the agricultural sector presents many informal jobs, that is, the worker is not included in the national social security system. However, regions with sugarcane production in general present better social situation.

In 1992, the formal employment exhibited a rate of 53.6% that improved to 72.9% now. Taking into account the regional differences in the country, it can be seen that, in the State of São Paulo, formal employment rate in the sugarcane industry is 93.8%, whereas in the North/Northeast region, it is only 60.8%.

Regarding wages, in the Center-South production region, people working with sugarcane earn more than those working with coffee, citrus, and corn, but less

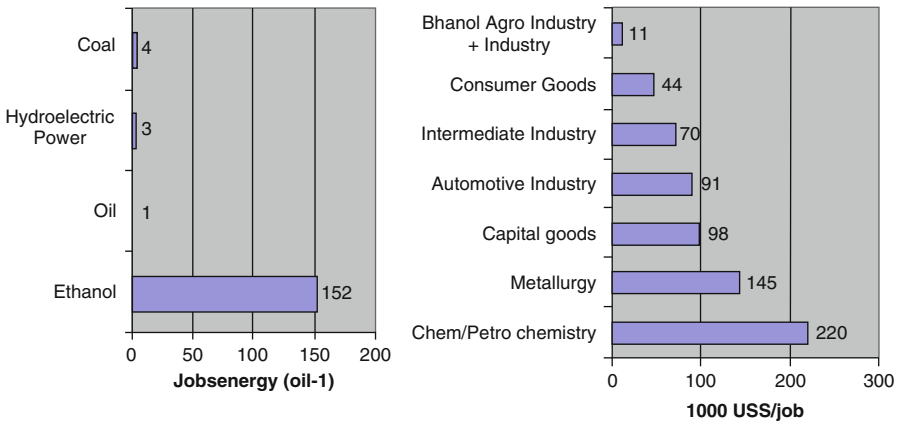

Bioethanol from Sugar: The Brazilian Experience. Figure 5
Jobs per energy and capital investment per job [49]

Bioethanol from Sugar: The Brazilian Experience. Table 2 Income share

	1999	2000	2001	2002	2003	2004
Share of income of the 50% Poorest*	12.69	–	12.58	12.98	13.36	3.85
Share of income of the 10% Poorest**	47.27	–	47.44	47.02	46.10	45.31
GDP per capita***	9,873	10,152	10,134	10,179	10,087	10,433
Number of poor people**** (million)	56.18	–	58.34	57.48	–	59.43

*This is the share of total income of the 50% poorest individuals, according to the per capita household income
**This is the share of total income of the 10% poorest individuals, according to the per capita household income
***2005 Reais
****Number of people in households with per capita income below the poverty line
Source: Reference [50].

Bioethanol from Sugar: The Brazilian Experience. Table 3 Gini indicator

Brazil	2003	2004	2005	2006	2007
Gini indicator for rural areas	0.5307	0.5166	0.5042	0.5003	0.5120

Source: Reference [50].

than those working with soybeans because this work is highly mechanized requiring more specialized workers. In the Northeast, people working in sugarcane crops earn more than those working in coffee, rice, banana, manioc (cassava), and corn crops, being their income approximately equivalent to the ones working in citrus, but lower than those ones working for soybeans. In fact, the enforcement of labor regulations in some regions of the country could indeed be improved, aiming to achieve the same situation already existing in several sugarcane regions.

Temporary migration of rural workers during the crop season occurs because the place where they come from does not offer many job opportunities. Usually, the profile of rural worker in the sugarcane crop is described as male, young (under 30 years old), with low level of education, and migrant from other region [51]. The labor journey of rural field workers according to the law is 8 h a day with a 1 h break for lunch. Considering rural workers in the sugarcane crop, in 2004, the number of workers was 493,162 and about 50% were seasonal workers [52]. Table 4 shows the educational level of several workers categories in the sugarcane production in the State of São Paulo. This table shows that the category holding the lowest educational level is the rural field workers (sugarcane cutters).

Manual Harvesting of Sugarcane Crops Manual harvesting of sugarcane is an old practice in every country producing sugarcane and the main problem is the working conditions. In order to facilitate the work and prevent accidents with poisonous spiders and snakes, it is a regular procedure to burn the leaves of sugarcane. Usually, sugarcane harvested manually occupies ten workers per hectare [53].

Considering the legislation related to work conditions, Brazilian Labor Law is strict with regulation, but there are exceptions. Thus, there is a need for more law enforcement, in order to reach welfare to all rural workers.

Regarding government social assistance to rural worker in Brazil, the latest social governmental program is "Fome Zero" (Zero Hunger) including initiatives like "Bolsa Família" (Family Allowance), an aid to rural family ensuring minimum price for their crop, taxes reduction on basic nutrition items. These are government tools of redistribution [54]; other instruments that can be associated to the rural worker are the minimum wage and the national social security system.

Mechanization of Sugarcane Harvesting Mechanization of the agriculture is a process that has been taking place all over the world. Similarly to the industrial revolution, in the mid 18th Century, man work

Bioethanol from Sugar: The Brazilian Experience. Table 4 Job distribution per educational level, State of São Paulo

Occupations (%)	Tractor driver and machine operators	Supervisors	Sugarcane cutters	Other agricultural occupations	Other non- agricultural occupations
Illiterate	0.1	0.7	3.7	2.5	0.5
Incomplete 4th grade education	8.5	16.3	31.7	34	7.2
Complete 4th grade education	19.4	19.7	26.7	25.4	15.8
Incomplete 8th grade education	22.1	19.6	20.2	14.7	16.4
Complete 8th grade education	21.3	15	10	18.2	15.6
Incomplete secondary education	8.1	5	3.3	2.2	7.9
Complete secondary education	20.1	21.4	4.2	2.9	31.6
Incomplete higher education	0.3	0.6	0.1	0.1	1.8
Complete higher education	0.2	1.8	0	0	3.3

Source: Reference [37].

was replaced by machines, and this trend is also observed in the agricultural sector in Brazil. The mechanization process is happening not only in sugarcane crops, but also in other agricultural cultures, as well as, in other countries [55].

Since the beginning, the mechanization process has not been uniformly developed in Brazil, exhibiting distinct levels of mechanization depending on the region and on the type of crop [56]. In this way, the mechanization process for some agricultural crops is deemed partial due to the fact that harvesting process continued to be manual; one example is sugarcane crops that require a number of workmen for harvesting tasks.

The mechanization of the planting phase process has already changed the work relation and contributed to deteriorate the rural work quality giving raise to seasonal job. After the introduction of the legislation for the mechanization of the sugarcane harvesting, the mills have been investing in capacity building for the rural workers aiming to develop more skilled people able to manage the mechanical harvesting machines, quite sophisticated equipment with computerized systems.

Seasonal Work Despite ethanol from sugarcane, rural field workers' condition is a subject of criticism, particularly the seasonal work. This sector holds the second highest seasonality in the country of 5.35 [57]. There is argumentation that seasonal job was a tendency of the agriculture [58].

Another reason pointed out was the agricultural modernization policy that was not favorable to small producers, who were not prepared either to production competition or work in the urban centers becoming seasonal workers [59]. Sometimes it is argued [60, 61] that the Federal Law N 4.214 from 1963, creating the Statute of the Rural Worker that extended to rural workers the same rights of the urban ones, has sped up the mechanization process.

In the State of São Paulo, the legislation goes beyond mechanizable areas with the recent legislation, Law N 11.241, of 2002. In order to follow the requirements of the legislation, the producers rapidly embrace mechanical power, but the level of mechanization depends upon availability of capital for investment.

As Brazil is a big country with regional differences, it is possible that part of the harvesting will continue to be manual, for some time, following the legislation schedule.

The alternative of harvesting with machines might cause unemployment of rural workers with low level of education that, possibly, will have difficulties to fit in the labor market. Regarding the sugar cutter unemployment, the legislation intends to tackle this problem including qualification of rural workers involving the partnership of unions. According to UNICA [62], with the effort of the associated companies, it is possible to improve the skills (qualification) of 7,000 workers a year.

The State of the Art on Sugarcane Ethanol

In the last 30 years, many technological improvements happened in ethanol field in agricultural and industrial production, in logistics and in the end users [63]. To do so, it was necessary to give subsidies at the initial stage, initiate negotiation among the sectors involved, and pass specific legislation [64] to open a window of opportunities and attract investments.

This topic will describe the state of the art of the fleet compatibility with ethanol, cogeneration process, technological development achieved, and logistic.

Compatibility of the Existing Fleet with Ethanol

This topic reports technological issues related to compatibility of the fleet with ethanol. Starting with the effect of ethanol on regular gasoline engine fleets, it then describes technological aspects of ethanol engine fleets and finally the new flex fuel engines.

Generally, the use of ethanol raises concerns about the compatibility of the regular existing fleet, as well as, the higher fuel consumption, since ethanol has lower energy content than gasoline.

The consumption drawback is partly compensated by the higher compression ratio that gives higher efficiency to the fuel. Regarding regular fleet compatibility, the concerns rely on drivability, cold start, and damages of components of the vehicle. The losses in drivability may arise due to different ratio air/fuel for the combustion while cold start difficulties are caused by the lower vapor pressure. Most of the worries are the chemical attack in plastic and rubber materials of vehicle and corrosion of metallic materials of vehicle. Notwithstanding, the occurrence of these events aforementioned depends upon the amount of ethanol blended with the gasoline, the vehicle age (reflecting its technological level), and the ethanol fuel specification and quality [45].

Furthermore, small blends of ethanol with gasoline up to 5% are acknowledged as inoffensive to the regular fleet. The World Wide Fuel Charter [65] establishes maximum oxygen content in gasoline of 2.7% m/m, that is, blends higher than 5% are allowed by this specification. Many countries have introduced low concentration of ethanol blended with gasoline (up to 10%) as regular fuel for vehicles developed for neat gasoline without significant performance loss. In case of vehicles with electronic fuel injection (EFI System), this device enables automatic correction of the engine air/fuel ratio. Ethanol blended with gasoline presents a relatively low consumption increase of less than 3%. Table 5 [66] displays the necessary adjustments in vehicles for the use of national sugarcane ethanol blends.

Cogeneration in Sugarcane Mills

Cogeneration process is the simultaneous electric/mechanical and thermal energy production from the same energy source. In the case of Brazilian sugar/ethanol mills, the source of energy is sugarcane bagasse.

Until the late 1990s, sugarcane bagasse was deemed an undesirable waste by the sector and was inefficiently burned or traded. Later on, the situation started to modify due to the need of changing the old boilers with 20 years in the edge of their life cycle. Some mills started to introduce more efficient boilers (higher-pressure boilers, up to 80 bar, instead of the old ones working with 21 bar) [4]. Step by step, other mills also became interested on this technology and the improvements started to happen.

Associated to this fact, another action that propelled the technological upgrade was the Program for

Bioethanol from Sugar: The Brazilian Experience. Table 5 Fleet adjustment to run ethanol

Ethanol content in the fuel	Carburetor	Fuel injection	Fuel pump	Fuel pressure	Fuel filter	Ignition system	Evaporative system	Fuel tank	Catalytic converter	Basic engine	Motor oil	Intake manifold	Exhaust system	Cold start system
≤5%	NN for any vehicle													
5–10%	PN	NN for relatively new fleets (10–15 years old)												
10–25%	PN, Brazilian application									NN				
25–85%	PN, US application													NN
≥85%	PN, Brazilian application													

Modifications: (not necessary – NN – and possibly necessary PN) in vehicles for different ethanol blends
Source: Reference [66].

Alternative Electric Generation Sources and Wind Energy (PROINFA) that was a political incentive to energy generated from renewable sources. In the case of biomass, where sugarcane bagasse cogeneration is included, the electricity surplus sold to the grid relies on several aspects, such as the type of cogeneration technology used, the quantity of steam consumed to produce sugar and/or ethanol, and the amount of bagasse available [64].

In 2007, the total electrical energy sold in the market was about 900 MW, and nowadays, it is 1,000 MW. The plants work in a complementary basis with the hydroelectric system, since the plants are operating at full power in the dry season in the Center-South. In fact, there are still several opportunities for enhancing the power generation if all the plants are modernized and the use of tops and leaves (trash) of the sugarcane is introduced with the mechanization of green cane.

PROINFA was created by the Law N 10438, 2002, that established that 3,000 MW would be purchased from renewable energy sources, specially wind, small hydro, and biomass. In the case of biomass, actually the price and long-term contracts (20 years), established for electricity purchase, were not considered attractive to make all the mills modernize to produce surplus of electricity. Therefore, the limit of 1,000 MW was not achieved by biomass and the share of power not bought from biomass was transferred to wind and small hydro sources of energy.

Actually, most mills prefer to send their electricity surplus to the utilities in short term contracts. Besides that, also the grid connection is still a barrier that needs to be overcome; by the time this entry was written, many mills were developing special agreements in order to allow the construction of transmission lines from the plant until the grid (see also [65]).

Technological Development

In Brazilian experience of producing ethanol, three technological phases can be identified [37]. In the first phase, from 1975 to 1985, the focus was on productivity to supply the growing demand. This phase was characterized by the search for higher milling capacity, improvements of distillation systems, fermentation productivity gains, and agricultural productivity increase.

Since the production was stabilized, as of 1980, the emphases shifted to better conversion efficiency such as higher efficiency of the extraction and fermentation phase. In the mid-1980s, there was more attention in technological tools for agro-industrial production management like optimization and renovation of sugarcane plantations in order to monitor the harvest, control the operational processes, and control simultaneously agriculture and industry. The development was not homogeneous, and the three phases can still be found. Comparing the maximum conversion efficiency to the average values, 10% difference could be found between the production units, but growing over the time indicating large internal technology transfer.

The most relevant information about the technological development is summarized in Box 3. According to this, the Brazilian technological level for ethanol fuel production is deemed the best in the world (as proven by the production costs and the conversion efficiencies). In the sugarcane research area, Brazil shows the largest number of technical publications [64].

Box 3: Technological Development

Period of 1980–1990: Large-scale introduction of sugarcane varieties developed in Brazil (mainly by CTC-Copersucar and Planalsucar programs); development of the full use of the sugarcane stillage in fertirrigation; biological controls in sugarcane production; development of the milling system with four cylinders; power production in the industry (self-sufficiency); end use; ethanol specifications; ethanol engines, ethanol transportation, blending and storage.

Period of 1990–2000: Optimization in sugarcane cutting, loading and conveyance; sugarcane genome mapping; genetic transformations, harvesting mechanization, achievement of electric power supply and their selling to the grid; advancements in industrial automatization; enhancement in technological management (both industrial and agricultural); introduction of flex fuel engines.

Source: Reference [63].

Logistics

The production of biofuels requires the existence or development of a support structure to collect the biomass, transport it to the industrial plant to be processed, and to distribute the biofuel. This is an important issue when the perspective of replication the Brazilian experience is being discussed, as is happening nowadays.

In addition to the requirements mentioned above, there is also the need for appropriate facilities for storage. The logistical structure of biofuels is complex and involves local, regional, and long distance transportation, delivering the product to other consumer centers or even to export. Depending on market destination of the ethanol (internal or exportation), the logistic must be handled separately.

If the final destination is the internal market, the production must be delivered to a fuel distribution base because of legal reasons; however, if the production is going to be exported, the commercialization can be developed directly from production plant or fuel distribution base [67]. Regarding the storage facilities, the storage might be done either by the producer storing the production surplus in tanks inside the industry or by the retailer in the terminals to guarantee the supply in short term [41].

Brazil has a logistic structure consolidated and well distributed for hydrated ethanol or anhydrous ethanol blended with gasoline, where both types of ethanol hydrous and anhydrous are transported via road, rail, and pipelines [68].

At long term, the infrastructure of storage capacity does not seem to be a limiting factor. In 2007, there were 273 retailer spread around all the states of the country with storage capacity of 3.75 million cubic meters [41]. Unlikely the storage, the infrastructure of ethanol transportation regarding the growing production seems to be a bottleneck for developing countries with a lack of local infrastructure.

International Dimensions of the Ethanol Program

Ethanol Programs in Other Countries

Several countries have already started biofuel programs. The most important one existing today (and also the largest one) is the US ethanol program, producing ethanol from corn. The current production of corn ethanol by the USA reaches 41 billion liters [69].

The 2007 US Energy Bill set a target of producing 15 billion gallons (56.8 billion liters) of ethanol a year from corn by 2015, using first-generation technologies, which will probably require an agricultural area of approximately 14 million hectares. Further expansion of production is planned, up to 21 billion gallons (79.5 billion liters) a year, using cellulosic materials and second-generation technologies that are still in experimental phase.

Another policy pointing in this direction is the European Union directive, which will require 3.9 billion gallons per year by 2020 in order to replace 10% of the gasoline for internal consumption. At the present, their production is two billion liters a year. Production of ethanol from corn, using first-generation technologies, will be at least 87.8 billion liters a year in 2015, up from 36.8 billion in 2006.

There is an important difference between the production of ethanol from sugarcane in Brazil or from corn in the USA, and from starch feedstock in Europe. The difference between them relies on industrial processes that require external sources of energy like oil or gas to supply electricity and heat.

In practical terms, in USA and European Union (E.U.), ethanol is obtained partly by burning coal (the main source of energy in the region) to produce the energy necessary to the processes inside the distilleries. Unlike USA and E.U., in Brazil, the use of sugarcane bagasse as feedstock makes far better energy usage avoiding fossil fuel consumption. This is possible due to energy content in the feedstock. The concept of energy balance used to evaluate the use of fossil fuels in preparing ethanol was already discussed in the Sect. "From Field to Motor".

Many studies have been conducted on this subject, and the results are sensitive to assumptions about the use of fertilizers, pesticides, and other energy inputs. According to one estimation compared to gasoline, ethanol from corn emits 30% less CO_2 and ethanol from sugarcane 82% less [70].

In the USA, efforts to expand ethanol production from corn face severe obstacles. The amount of corn directed to ethanol production is already 18% of the production, spread in a total area of 37 million

hectares. The increase in corn-planted area has been made at the expense of soybean-planted area. Production of ethanol from cellulosic materials, which could be a solution, is still facing technological problems that are not likely to be solved by 2015. Nevertheless, productivity increases including genetic modification might represent a significant reduction in the amount of additional land necessary.

This large demand for ethanol and the corresponding use of agricultural land to produce it have generated a number of objections to the use of biofuels. Some argue that the competition between land for fuel (ethanol) and land for food, in both the USA and Europe, is causing famine around the world and leading indirectly to deforestation in the Amazon and other tropical areas [31, 32]. The recent rise in the prices of agricultural products, after several decades of declining real prices, is often seen as a cause of famine, and led to the politically laden debate of fuel versus food. All together, the grain prices have more than doubled since January 2006, with over 60% of the rise happening since January 2008. It was closely following the price of petroleum that started to diminish when 2008 crop was harvested. In contrast, the point has been made that higher crop prices will not necessarily harm the poorest people because many of the world's 800 million undernourished people are farmers or farm labors, who could benefit from higher prices.

More recently, the price of agricultural products has decreased following the decline in petroleum prices. To keep the issue in perspective, it is important to remember several facts. First, around the world, 93 million hectares are currently being used to grow soybeans and 148 million hectares for corn, while the amount used in the USA to produce ethanol is approximately seven million hectares. Second, in general, the prices of food commodities have been decreasing since 1975, but fluctuations frequently occur in those prices, as well as, in the areas planted and the prices of crude oil. Those fluctuations, which have occurred for decades, result from many factors and events [64] and not due to biofuels expansion.

Worldwide, 1.5 billion hectares of the arable land is already being used for agriculture and another 440 million hectares is potentially available, including 250 million hectares in Latin America and 180 million in Africa. As such, the area currently being used for biofuels is only 0.55% of the land in use. This expansion has been extensively analyzed in many reports (e.g., [34]) which pointed out that several individual factors have driven up grain prices and in combination led to an upward price spiral. Among them are high energy and fertilizer prices, the continuing depreciation of the US dollar, drought in Australia, growing global demand for grains (particularly in China), changes in some nations' import–export policies, speculative activity on future commodities trading, and regional problems driven by subsidies of biofuel production in the USA and E.U.

One example is the land changes in the USA in the period 2006–2007, corn acreage grew 19% utilizing nearly 37 million hectares, an increase of 7 million hectares. Most of this expansion came at the expense of soybean acreage, which decreased by 17%, from 31 to 26 million hectares (i.e., 5 million hectares). This is approximately 6% of the world's area used for that crop, and that change is helping to drive up prices.

Because of this land changes, other countries had to expand their soybean production, possibly increasing deforestation in Amazon. Such speculations about a *domino effect* are not borne out by the facts since the area used for soybeans in Brazil (mainly in Amazon) has not increased from 2004 onward. The deforestation in the Amazon rain forest has been going on for a long time at a rate of approximately one million hectares per year [71], and recent increases are not due to soybean expansion but due to cattle and are inconsistently related to ethanol production [35].

Replicating the Brazilian Experience Elsewhere

Almost 100 countries are producing sugarcane over an area of 20 million hectares and the fifteen most important producers hold 86% of the sugarcane production. And the conversion of sugar plants into ethanol distilleries is relatively easy, and most of the existing plants in Brazil have these dual purposes. Taking advantage of the easy reversibility of the production units, the ethanol production in other countries could be significantly expanded following the Brazilian experience with ethanol, using a fraction of their sugarcane for ethanol.

The question that arises is: Why are other sugarcane-producing countries not using some of their raw material to produce ethanol? One, it could be export to the

Bioethanol from Sugar: The Brazilian Experience.
Table 6 Subsidies for biofuels in the USA and E.U., 2006

	Ethanol			Biodiesel		
	Total, in US$ billions	Billions of liters	US $/l	Total, in US$ billions	Billions of liters	US $/l
US	5.8	20.7	0.28	0.53	0.96	0.55
EU	1.6	1.6	1	3.1	4.43	0.70
Total	7.4	22.3	–	3.63	5.39	–

Source: Reference [72].

USA and E.U., where production costs are significantly higher. The main reason is the high import duties imposed on ethanol imports in the USA and E.U. to protect local industries, which are heavily subsidized. Table 6 displays an estimation of the subsidies in the USA and E.U., which totaled almost $12 billion in 2006.

Removing these subsidies is a topic of discussion in the Doha round of negotiations, but prospects for progress in this area are poor (Box 4). Several countries in Central America benefit from their privileged access to the US market. The members of the Caribbean Basin Initiative (CBI), the oldest group, up to 7% of the previous year's US ethanol demand is exempt from import tariffs [2, 73].

This agreement has been used mostly to allow these countries to import dehydrated Brazilian ethanol. In the past, European hydrous ethanol was also included. Dehydration plants are located in Costa Rica, the Dominican Republic, Trinidad and Tobago, El Salvador and Jamaica. The USA imported 482 million liters from these countries in 2006 and 877 million liters in 2007, considerably less than the 1.3 billion liters that the 7% limit represents on ethanol imported from Caribbean countries. The Central America Free Trade Agreement (CAFTA), signed in August 2004, immediately eliminated all tariffs and quantitative restrictions on 80% of manufactured goods in that market, including ethanol, with the remainder phased out over a few years. Nearly all of the 6 nations in CAFTA have already initiated plans to develop large-scale ethanol production. El Salvador is the most advanced, since it has already

Box 4: Biofuels and the World Trade Organization

Nowadays, the World Trade Organization (WTO) does not have a specific trade regime for biofuels. Therefore, international trade in biofuels falls under the rules of the General Agreement on Tariffs and Trade (GATT, 1994), which covers trade in all goods, as well as, other relevant WTO agreements such as those on agriculture, technical barriers to trade, the application of sanitary and phytosanitary measures, and subsidies and countervailing measures. Agricultural products are subject to GATT and to the general rules of the WTO, insofar the Agreement on Agriculture (AoA) does not contain derogating provisions. Key trade-related issues include the classification for tariff purposes of biofuel products as agriculture, industrial, or environmental goods; the role of subsidies in increasing production; and the degree of consistency among various domestic measures and WTO standards. The AoA covers products from Chaps. 1 to 24 of the Harmonized System, with the exception of fish and fish products and the addition of many specific products, including hides and skins, silk, wool, cotton, flax, and modified starches. The discipline of the AoA is based on three pillars: market access, domestic subsidies, and export subsidies. One of its main features is that it allows members to pay subsidies in derogation from the Agreement on Subsidies and Countervailing Measures. The Harmonized System classification affects the way products are characterized under specific WTO agreements. In this classification, ethanol is deemed as an agricultural product being subject to Annex 1 of the AoA, whereas biodiesel is classified as an industrial product and is therefore not subject to the disciplines of the AoA. The paragraph 3 (iii) of the Doha Development Agenda displays negotiations on "the reduction or, as appropriate, elimination of tariff and non-tariff barriers to environmental goods and services." Some WTO members have suggested that renewable energy products, including ethanol and biodiesel, should be classified as "environmental goods" and therefore subject to negotiations under the "Environmental Goods and Services" cluster.

Sources: References [76–78].

drafted legislation to continue developing a local ethanol market and is beginning to invest in ethanol production. An old distillery that can produce 60 million liters a year is being revamped to double its capacity and is already exporting all its production. Similar initiatives are underway in Guatemala and Costa Rica [74].

Across the Atlantic, two key elements of the E.U. General System of Preferences are the *Everything but Arms* (EBA) initiative and the *Special Incentive Arrangement for Sustainable Development and Good Governance* (GSP+). EBA provides special treatment for fifty least-developed countries, giving duty-free access to imports of all products except arms and ammunition, without any restrictions on quantity, with the exception of rice and sugar up to October 2009. At present, GSP+ benefits 16 countries, mostly in Latin America and the Caribbean. Any GSP+ beneficiary country must be both "vulnerable," according to a definition established in the regulation, and have ratified and effectively implemented 27 specified international conventions in the fields of human rights, core labor standards, sustainable development, and good governance. This program grants special duty-free access to the E.U. market for denatured or non-denatured alcohol [75]. In order to benefit from such advantages, a few countries in Latin America and Africa are starting to divert some of their sugarcane to ethanol production and others, especially Venezuela, are expanding their sugarcane plantations. Regarding these issues, some recent reports from UNCTAD discuss on only certification issues and the impact on developing countries, as well as, the perspectives for second-generation technologies in these countries [2]. Table 7 provides a list of projects underway around the world.

This development represents a modernization of the sector which traditionally was in the hands of prosperous family groups that benefited from special relationships with the E.U. that let them sell sugar at far more than the international price. Their price was based on the much higher price of locally produced sugar from sugar beets or sweet sorghum. This comfortable situation discouraged them from entering into the ethanol business, which required additional investments and know-how.

Bioethanol from Sugar: The Brazilian Experience.
Table 7 Projects under development

Country	Capacity (m^3 ethanol/day)	Status
Colombia	150 × 5	In operation
Venezuela	700 × 4	In construction
Angola	1,000	Firm proposal
Colombia	1,000	Firm proposal
Bolivia	500	Firm proposal
Paraguay	700	Firm proposal
Colombia	300 × 2	Firm proposal
Colombia	100	Firm proposal
Colombia	150	Firm proposal
Colombia	200	Firm proposal

Source: Olivério J, Vice President of Operations, Dedini Organization, personal communication.

Future Directions

If second-generation technologies do not materialize until 2022, most of the ethanol required in the USA will probably have to be imported from countries in the Southern Hemisphere, such as Brazil where the sustainable land expansion and good climate particularly favor its production from sugarcane.

In all likelihood, ethanol consumption, which represented 0.4 million barrels of oil equivalent per day in 2006 (1.2% of all gasoline in use in the world) will grow to 2.6 million barrels of oil equivalent per day in 2022, replacing 10% of all gasoline used in the world. Considering that current oil consumption is 85 million barrels a day and that it might grow to 100 million by 2012, ethanol would be contributing the equivalent of almost 3% of the world's consumption of oil. That is a significant amount and will help drive down the world price of petroleum.

Neither USA nor E.U. will be able to produce all the ethanol it needs; in all likelihood, they will have to import it from Brazil and other tropical sugarcane-producing countries. This could be a mutually beneficial solution, reducing the cost of fuel for consumers in the USA and E.U. and generating hundreds of thousands of jobs in the developing countries.

Bibliography

1. WCED (World Commission on Environment and Development) (1987) Resolutions adopted by the General Assembly 42/187. Report of the World Commission on Environment and Development. Brundtland Report. Available at: http://www.un-documents.net/a42r187.htm. Accessed June 2010
2. Coelho ST (2005) Biofuels: advantages and trade barriers, speech at the United Nations conference on trade and development. Geneva. Available at: http://www.unctad.org/en/docs/ditcted20051_en.pdf
3. Leite AD (2007) A Energia do Brasil. Elsevier, Rio de Janeiro, 2007. In cap. IV, "A era Vargas", p 89
4. Coelho ST (1999) Mecanismos para Implementação da Cogeração de Eletricidade a partir de Biomassa. Um Modelo para o Estado de São Paulo. Tese de doutorado apresentada no Programa Interunidades de Pós-Graduação em Energia da Universidade de São Paulo
5. Moraes MAFD, Rodrigues L (2006) Brazil Alcohol National Program. Relatório de pesquisa. Piracicaba, Junho 2006. Avaiable at: www.english.unica.com.br. Accessed May 2010
6. BNDES (Brazilian Development Bank) and CGEE (Center for Strategic Studies and Management Science, Technology and Innovation) (2008) Sugarcane-based bioethanol: energy for sustainable development. BNDES and CGEE, Rio de Janeiro. Available at: www.bioetanoldecana.org. Accessed May 2010
7. UNICA, Sugarcane Industry Association (2009) Statistical database from UNICA. Available at: http://english.unica.com.br/dadosCotacao/estatistica/
8. Scandiffio MIG (2005) Análise prospectiva do álcool combustível no Brasil – Cenários 2004–2024. PhD thesis, State University of Campinas, Faculty of Mechanical Engineering
9. Goldemberg J, Coelho ST, Lucon OS, Nastari PM (2003) Ethanol learning curve – the Brazilian experience. Biomass Bioenergy 26(3):301–304
10. Nogueira LAH, Lora EES (2003) Dendroenergia Fundamentos e Aplicações, 2a ed. Interciência, Rio de Janeiro, p 32
11. Piacente and Piacente (2003) *apud* Lucon (2006) Lucon O, Álvares OM Jr, Coelho ST (2006) Bioethanol: The way forward. In: International symposia on alcohol fuels, ISAF 15, California, Proceedings. Environmental Research Institute, University of California, California, pp 1–12
12. UNICA, Sugarcane Industry Association (2007) Produção e uso do Etanol combustível no Brasil. Respostas às questoes mais freqüentes (Fuel ethanol production and use in Brazil: answers to most frequent questions). São Paulo, May 2007. Available at: http://www.portalunica.com.br/portalunica/files/referencia_publicacoes_livros-3-Arquivo.pdf
13. CONCAWE (2002) Energy and Greenhouse Gas Balance of Biofuels for Europe – an update. Brussels. Available at: www.concawe.be. Accessed Jan 2010
14. Macedo IC (2005) Sugarcane's energy: sugar cane's energy: twelve studies on Brazilian sugar cane agribusiness and its sustainability. Berlendis & Vertecchia, UNICA – União da Agroindústria Canavieira do Estado de São Paulo, São Paulo
15. UK DTI (2003) Technology status review and carbon abatement potential of renewable transport fuels in the UK. Report B/U2/00785/REP, 2003. Available at: www.dti.gov.uk/renewables/publications/pdfs/b200785.pdf
16. USDA (United States Department of Agriculture) (1995) Estimating the net energy balance of corn ethanol. Report by Shapouri, H., Duffield, J.A., Graboski, M.S., US Department of Agriculture, Economic Research Service, Office of Energy, Agricultural Economic Report No. 721. Available at: http://www.ers.usda.gov/publications/aer721/AER721.PDF
17. Petrobras (2007) Social and environmental report. Available at: www.petrobras.com.br/en/environment-and-society/.../default.asp?pdf. Accessed May 2010
18. IEA Bioenergy Task 39. Available at: http://www.task39.org/About/Definitions/tabid/1761/languange/en_US/Default.aspx
19. UNSTATS (United Nations Statistics Division) (2008) Available at: http://unstats.un.org/unsd/demographic/products/socind/population.htm. Accessed Jan 2010
20. World Bank (2009) Available at: http://web.worldbank.org/WBSITE/EXTERNAL/DATASTATISTICS/0,contentMDK:20535285~menuPK:1192694~pagePK:64133150~piPK:64133175~theSitePK:239419,00.html. Accessed July 2009
21. FAO (Food and Agriculture Organization of the United Nations) (2004) ESSGA, November 2006. Available at: http://www.fao.com. Accessed May 2009
22. UNDP (United Nations Development Program) (2008) Available at: http://hdrstats.undp.org/indicators/147.html. Accessed Jan 2010
23. UNSTATS (United Nations Statistics Division) (2008) Available at: http://hdr.undp.org/en/statistics/data/. Accessed Jan 2010
24. MAPA (Ministério da Agricultura, Pecuária e Abastecimento) (Ministry of Agriculture, Cattle Breeding and Food Supply) (2009) Anuário estatístico da agroenergia. Available at: www.agricultura.gov.br. Accessed Jan 2010
25. CONAB (Compahia Nacional de Abastecimento) (National Supply Company) (2009) Available at: http://www.conab.gov.br/conabweb/download/safra/1cana_de_acucar.pdf. Accessed July 2009
26. DATAGRO (2009) Informativo Reservado Mensal sobre a Indústria Sucroalcooleira (Sugar/Ethanol Industry Reserved Monthly Newsletter), number 05P
27. Joly C et al (2010) Biodiversity conservation research, training, and policy in São Paulo. Science 328:1358–1359
28. Nassar A et al (2009) Impacts on land use and GHG emissions from a Shock on Brazilian Sugarcane Ethanol Exports to the United States using the Brazilian Land Use Model (BLUM). Report to the U.S. Environmental Protection Agency regarding the proposed changes to the renewable fuel standard program. Institute for International Trade Negotiations Report (ICONE)
29. EPA United States Environmental Protection Agency. Available at: http://www.epa.gov/oms/renewablefuels/420f09024.htm
30. Cetesb Technical Rule P4.231 (2005) www.cetesb.sp.gov.br

31. Fargione J, Hill J, Tilman D, Polasky S, Hawthorne P (2008) Land clearing and the biofuel carbon debt. Science 319:1235–1238
32. Searchinger T, Heimlich R, Houghton RH, Dong F, Elobeid A, Fabiosa J, Togkoz S, Hayes D, Yu T (2008) Use of U.S. croplands for biofuels increases greenhouse gases through emissions from land use change. Science 319:1238–1240
33. World Bank (2008) Double jeopardy: responding to high food and fuel prices. Available at: http://web.worldbank.org/WBSITE/EXTERNAL/NEWS/0,contentMDK:21827681~pagePK:64257043~piPK:437376~theSitePK:4607,00.html
34. Cerri CEP et al (2007) Predicted soil organic carbon stocks and changes in the Brazilian Amazon between 2000 and 2030. Agric Ecosyst Environ 122:58–72
35. Goldemberg J, Coelho ST, Guardabassi PM (2008) The sustainability of ethanol production from sugar cane. Energy Policy 36:2086–2097, doi:10.1016/j.enpol.2008.02.028, Elsevier
36. Lora BA, Monteiro MB, Assunção V, Frigerio R (2006) Levantamento Georreferenciado da Expansão da Cultura de Cana-de-Açúcar no Estado de São Paulo (Georeferenced Assessment of Sugarcane culture expansion in São Paulo state), São Paulo, December 2006
37. Goldemberg J, Nigro FEBN, Coelho ST (2008) Bioenergia no Estado de São Paulo: Situação Atual, Perspectivas, Barreiras e Propostas'. Imprensa Oficial do Estado de São Paulo, São Paulo
38. Smeets E, Junginger M, Faaij A, Walter A, Dolzan P (2006) Sustainability of Brazilian bio-ethanol. Report NWS-E-2006-110, Universiteit Utrecht Copernicus Institute, Department of Science, Technology and Society and University of Campinas, Brazil, p 35
39. IBGE (Brazilian Statistics Bureau) (2009) Sistema de Recuperação Automática – SIDRA. Availabe at: www.sidra.ibge.gov.br/bda/pecua/default.asp?t=2&z=t&o=22&u1=1&u2=1&u3=1&u4=1&u5=1&u
40. Ripoli TCC, Ripoli MLC (2005) Biomassa da cana-de-açúcar: colheita, energia e ambiente. ESALQ/USP, Piracicaba, pp 27, 38, 51
41. CENBIO, Brazilian Reference Center on Biomass (2006) Analysis of status and opportunities. Study prepared by the Brazilian Reference Center on Biomass to the BP
42. SMA, Sao Paulo State Secretary for the Environment (2010) Projeto Etanol Verde. Available at: http://www.ambiente.sp.gov.br/etanolverde/index.php#
43. CONAMA (2006) Federal Council for the Envirnment, Ministry of Environment. Resolution Number 382, 26 December 2006. Available at: http://www.ima.al.gov.br/legislacao/resolucoesconama/Resolucao%20nb0%20382.06.pdf
44. Tyner WE (2008) The US ethanol and biofuels boom: its origins, current status, and future prospects. Bioscience 58(7):646–653
45. Coelho ST, Guardabassi PM (2005) Brazilian biofuels experience. Iberoamerican Ministerial meeting. Montevideu, pp 4, 11, 14, 16
46. Barros AR (2005) Relatório setorial integrante do Projeto Economia de Pernambuco: Uma Contribuição para o Futuro. Governo do Estado, Secretaria de Planejamento, PROMATA
47. ANFAVEA, Brazilian Automotive Industry Association (2008/2009) Anuário Estatístico da Indústria Automobilística Brasileira. Available at: http://www.anfavea.com.br/. Accessed June 2009
48. MDIC (Ministério do Desenvolvimento, Indústria e Comércio Exterior) (Minister of Development, Industry and Foreign Trade) (2009) Available at: http://www.desenvolvimento.gov.br/sitio/interna/interna.php?area=2&menu=999. Accessed Sept 2009
49. Goldemberg J (2002) Brazilian energy initiative. World Summit on Sustainable Development, Johannesburg
50. IPEADATA (Instituto de Pesquisa Econômica Aplicada) (2006/2007) Available at: www.ipeadata.gov.br. Accessed July 2009
51. Moraes MAFD, Figueiredo MG (2008) Migração Espontânea de Trabalhadores no Setor Sucroalcooleiro. Relatório de Pesquisa, Grupo de Extensão em Mercado de Trabalho Piracicaba
52. Balsadi OV (2007) Mercado de trabalho assalariado na cultura da cana-de-açúcar no brasil no período 1992–2004. Informações Econômicas, São Paulo 37(2):40
53. Valor Econômico (2004) Hemeroteca do Instituto de Eletrotécnica e Energia, No: 77483, Valor Econômico, 16/02/2004. Available at: http://infoener.iee.usp.br/infoener/hemeroteca/imagens/77483.htm. Accessed May 2010
54. MDS (Ministry of Social Development) (2004) Available at: http://www.mds.gov.br/portalfederativo/fzero. Accessed Jan 2010
55. Gorren RCR (2009) Biocombustíveis – Aspectos sociais e econômicos: comparação entre Brasil, Estados Unidos e Alemanha. Dissertação de Mestrado apresentada no Programa de Pós-Graduação em Energia da Universidade de São Paulo
56. Kageyama A (2003) Os rurais e os agrícolas de São Paulo no Censo de 2000, Texto para discussão. IE/UNICAMP n. 112, p 3
57. IBGE (Brazilian Statistics Bureau) (2009) Available at: http://www.ibge.gov.br. Accessed May 2009
58. Aguirre BMB (1989) Reflexões sobre a Organização do Mercado de Trabalho Agrícola. Revista de Economia Política 9:31–46
59. Ribeiro DD, Mendonça MR, Hespanhol AN (2002) Relações de trabalho na agricultura mecanizada: A Monocultura Da Soja Em Goiás. Scripta Nova Revista Electrónica de Geografía y Ciencias Sociales Universidad de Barcelona. ISSN: 1138-9788. Depósito Legal: B. 21.741-98, vol VI, número 119(81)
60. Moraes MAFD (2007) Indicadores do mercado de trabalho do sistema agroindustrial da cana-de-açúcar do Brasil no período 1992–2005. Estudos Econômicos 37(4). São Paulo, doi: 10.1590/S0101-41612007000400007
61. Freitas EP (2008) Metamorfoses socioespaciais: os dilemas da modernização agrícola na região de Ribeirão Preto (SP), 1° SIMPGEO/SP, Rio Claro ISBN: 978-85-88454, p 8
62. UNICA, Sugarcane Industry Association (2008) Statistics of sugarcane – season 2006/2007. Available at: http://www.portalunica.com.br/portalunica/files/referencia_estatisticas_producaobrasil-9-Tabela.xls. Accessed Jan 2008

63. Macedo IC (2007) Situação atual e perspectivas do etanol. Estud. av 21(59):157–165. Available at: http://www.scielo.br/scielo.php?script=sci_arttext&pid=S010340142007000100012&lng=en&nrm=iso. ISSN 0103-4014. doi: 10.1590/S0103-40142007000100012 [cited 2010-08-26]
64. Goldemberg J (2009) The Brazilian experience with biofuels. Innovations Journal. Fall 4(4):91–107
65. Núcleo de Assuntos Estratégicos da Presidência da República (2005) Cadernos NAE/nº. 2–Biocombustíveis. Brasília. Available at: http://www.nae.gov.br/cadernosnae.htm
66. ANFAVEA, Brazilian Automotive Industry Association (2005) Ethanol Fuel Vehicular Application Technology. Presentation of Henry Joseph Jr. (Brazilian Automotive Industry Association´s Energy & Environment Commission anfavea@anfavea.com.br) at CEPAL/CENBIO/USP Seminar, São Paulo, 17 Aug 2005
67. FAPESP (Fundação de Amparo à Pesquisa do Estado de São Paulo) (2008) Relatório final projeto de pesquisa em políticas públicas (pppp) da cadeia cana-etanol. Workshop instrumentação e automação agrícola e agroindustrial na cadeia cana-etanol. Available at: http://www.apta.sp.gov.br/cana/anexos/RELATORIO_final_instrumentacao.pdf. Accessed May 2010
68. GTZ, German Technical Cooperation (2005) Liquid Biofuels for Transportation in Brazil. Potential and Agriculture for Sustainable Agriculture and Energy in the 21st Century
69. REN21 (Renewable Energy Policy Network for the 21st Century) (2010) Renewables 2010 global status report, REN21 Secretariat, Paris. Available at: http://www.ren21.net/globalstatusreport/REN21_GSR_2010_full.pdf. Accessed June 2010
70. Doornbosch R, Steenblik R (2007) Biofuels: is the cure worse than the disease? Presentation at OECD Roundtable on sustainable development, Paris, p 17. Available at: www.foeeurope.org/publications/2007/OECD_Biofuels_Cure_Worse_Than_Disease_Sept07.pdf
71. INPE, National Institute for Spatial Research (2008). Prodes Project: Satellite monitoring of Amazon forest, annual estimates 1988–2007. Avaiable at: www.obt.inpe.br/prodes/prodes_1988_2007.htm
72. Steenblik R (2007) Biofuels – at what cost? The Global Subsidies Initiative (GSI) of the International Institute for Sustainable Development (IISD), Geneva. Available at: www.globalsubsidies.org/files/assets/oecdbiofuels.pdf
73. HART Downstream Energy Services (HDES) (2004) Ethanol Market Fundamentals, document prepared for the New York Board of Trade
74. Nogueira LAH (2007) Biocombustíveis na América Latina: A situação atual e perspectivas. Biofuels in Latin America: Current situation and perspectives, vol 2, Série Cadernos da América Latina. Fundação Memorial da América Latina, São Paulo
75. EC (European Commission) (2008) Generalized system of preferences. Available at: http://ec.europa.eu/trade/issues/global/gsp/index_en.htm, http://eurlex.europa.eu/LexUriServ/LexUriServ.do?uri=OJ:L:2008:334:0090:0091:EN:PDF, http://trade.ec.europa.eu/doclib/docs/2008/july/tradoc_139962.pdf
76. FAO, Food and Agriculture Organization of the United Nations (2007) Recent trends in the law and policy of bioenergy production promotion and use. FAO Legislative Study No. 95. FAO, Rome
77. GBEP (2007) A review of the current state of bioenergy development in G8 +5 countries. GBEP, Rome
78. FAO, Food and Agriculture Organization of the United Nations (2008) Secretariat, FAO. The State of Food and Agriculture 2008. Biofuels: prospects, risks and opportunities. FAO, Rome. Available at: www.fao.org/docrep/010/a1348e/a1348e00.HTM
79. Goldemberg J, Guardabassi P (2009) Are biofuels a feasible option? Energy Policy 37:10–14

Biofuels and Sustainable Buildings

Frederik Betz
Affiliated Engineers, Inc, Madison, WI, USA

Article Outline

Glossary
Definition of the Subject and Its Importance
Introduction
Growth
Refining
Owner/Operator Concerns
Future Directions
Bibliography

Glossary

Alcohol A compound in which the –OH group is connected to an aliphatic carbon atom.

Biofuel General classification of a fuel refined from recently harvested organic matter.

Biomass The solid form of biofuel.

Biogas The gaseous form of biofuel.

Bioliquid The liquid form of biofuel, ethanol, and biodiesel.

Catalyst A substance that enables a chemical reaction to proceed at a usually faster rate or under different conditions (as at a lower temperature) than otherwise possible.

Cetane number A measure of the ignition quality of diesel fuel and influences combustion characteristics.

Feedstock The raw material that will be processed into a fuel.

Petrol-diesel Diesel fuel that is derived from petroleum.

Pour point The temperature at which a liquid stops behaving like a liquid.

Transesterification The process of converting one ester into another ester using an alcohol and oil.

Definition of the Subject and Its Importance

Biofuels come in many forms and from a variety of sources. The biofuels may be solid (biomass), gas (biogas), or in liquid form (biodiesel, ethanol, etc.). Biofuels may be derived from most plant material as well as some animal parts, typically animal fats. As plants grow over much of the world's landmass and their primary source of energy is the sun, biofuels are abundant and renewable. Furthermore, as biofuels absorb the sun's energy to grow, biofuels are nature's solar energy battery.

Biofuels have been used for thousands of years as a source of heat and light for civilization. However, as humanity's energy consumption has become more sophisticated, fossil fuels have gained a technological edge in refining and supply chain management. For the last decade, renewed interest in biofuels has increased the adoption of biofuels for making heat and electricity. The drivers for the interest in biofuels are many; including energy security, environmental concerns, and economic competitiveness.

To address all these interests, the entire life cycle of the biofuel and its use must be considered. Energy security or establishing an effective/reliable supply of biofuels is a must for any building operator considering biofuels as a primary fuel source. Pollution concerns may drive a building operator toward or away from biofuels. For example, soy-based biodiesel reduces particulate production in an engine generator; however, NO_X emissions may increase. Both particulates and NO_X are regulated emissions and a building operator will need to be aware of the implications of their fuel choices. Economic concerns are important for most building operators. A fuel source with a competitive/stable price is highly sought after. As recent history has shown, most fuels do not appear to be immune from macroeconomic price influences as was seen in gasoline and ethanol prices in the late 2000s.

Biofuels can be used to generate heat in boilers or both electricity and heat in engines, gas turbines, etc. Biomass in the form of wood pellets or chips are used with some frequency in residential and some commercial heating applications and a number of manufacturers of pellet and chip burning heating systems are on the market. Larger boilers may use biodiesel in place of fuel oil or biogas in place of natural gas to make larger quantities of heat.

Biofuels have also been used to make electricity and heat in power plants of a variety of sizes. Large amount of biomass such as sawdust are burned in boilers to make steam to drive a turbine, which in turn generates electricity. Smaller applications include using biodiesel, ethanol, and biogas in engine generators and gas turbines to provide backup power or primary power and heat. Similar to the wood chip and pellet burning, there are several manufacturers of engines and gas turbines that offer systems capable of using biofuels for building applications.

Introduction

Biofuels have been used for thousands of years to make heat and light; however, recent political, economic, environmental, and security concerns have refocused the world's attention on biofuels of all types.

The majority of attention is focused on biofuel for transportation purposes; however, as the U.S. Department of Energy has stated that, 40% of energy consumption and emissions come from building operations [1]. To alleviate the environmental impact of building operations, world governments, researchers, and building designers are looking for ways to reduce the carbon footprint of buildings as well as finding alternatives to dwindling supplies of fossil fuels required to operate modern buildings.

The building owner/operator should be aware of the entire life cycle of the selected biofuel to avoid any operational disruptions of embarrassment that may arise from a less efficient part of the biofuel delivery process. For example, high-quality palm oil may be very desirable for a boiler. However, if that palm oil comes from a plantation, where a rainforest once stood and was burned to the ground, the environmental benefit of that palm oil would be in doubt.

The life cycle of a biofuel is broken down into five parts, each of which has several considerations:

- Growth
  - How fast does the feedstock grow?
  - How much energy is derived per pound of plant material?
  - How much energy does it take to produce the plant material?
  - Where does the plant material grow?
  - What grew in this location before the biofuel crop?
- Harvest
  - What methods of harvesting the plant material are used?
  - Does the method of harvesting use more energy than the biofuel generates?
- Refining
  - Does the refining process generate large waste streams?
  - How much energy does the refinement process consume?
- Distribution
  - Does the shipping of the biofuel consume more energy than the biofuel generates?
- Use
  - How efficiently is the fuel being burned?
  - Is the fuel being burned cleanly to meet emissions standards?
  - Is the fuel being stored properly and safely?

The building owner/operator is most directly impacted by the "Distribution" and "Use" phases of the life cycle analysis, but as stated other parts of the life cycle may be significant to the user of the biofuels and undermine their broader sustainability goals.

Growth

Different sources of biofuels grow at varying rates, in varying conditions, with varying amounts of required resources. Needless to say, not all biofuels are created equally. For example, Fig. 1 shows the quantity of oil per unit area for many different types of crops. See reference for a more complete listing of plants.

While the actual input energy for growing an acre of crops varies depending on location and technology, it is clear that some crops are better than others for creating energy and the users of this energy should be aware of their impact. This same concept applies to biomass and biogas, where there can be great variability depending on the feedstock, which should be discussed with the fuel supplier.

Plant	Latin Name	kg Oil/hectare	lb Oil/acre
Corn	Zea Mays	145	129
Palm	Erythea Salvadorensis	189	168
Cotton	Gossypium Hirsutum	273	243
Soybean	Glycine Max	375	334
Pumpkin Seed	Cucurbita Pepo	449	400
Mustard	Brassica Alba	481	428
Sunflower	Helianthus Annuus	800	712
Peanut	Arachis Hypogaea	890	792
Opium Poppy	Papaver Somniferum	978	871
Rapeseed	Brassica Napus	1,000	890
Castor Bean	Ricinus Communis	1,188	1,058
Jatropha	Jatropha Curcas	1,590	1,416
Coconut	Cocos Nucifera	2,260	2,012
Buriti Palm	Mauritia Flexuosa	2,743	2,442
Macauba Palm	Acrocomia Aculeata	3,775	3,361
Oil Palm	Elaeis Guineensis	5,000	4,452

Biofuels and Sustainable Buildings. Figure 1
Average production rates of vegetable oils by plant type [2] (1 kg/ha ≈ 0.9 lb/acre)

Refining

Most of the processes to create biofuels are conceptually simple; however, the creation of high quality, certified biofuel typically requires specialized equipment and skilled personnel to carry out the process. The text below will outline the basic process for refining biofuels; however, the refinement steps required to make certified fuels are typically much more demanding.

Biomass

When using biomass as a primary energy source it is best to refine the fuel somewhat rather than just cutting down a tree and throwing it into a fire. Most biomass contains a significant amount of moisture, which reduces combustion efficiency and increases particulate and carbon monoxide pollution. As the moisture in the wood evaporates due to the heat from the fire, it displaces oxygen thus reducing the combustion efficiency, which is directly related to the amount of oxygen available. Therefore, wood is often dried prior to being supplied for use in commercial boilers.

In addition to drying the biomass, it is often pelletized or broken down into smaller pieces or chips. This simplifies distribution of the product and simplifies automatically feeding the biomass into boilers. Making smaller pieces of wood also aids the combustion process by making it easier for air to get to the fuel for burning cleanly.

There are many other types of biomass that have various refining methods, from sawdust at lumber mills to grass clippings and tree trimmings burned in an incinerator, but these are more customized systems. The wood chip or pellet burning boilers are the most common application of biomass fuel use in buildings.

Bioliquids

Bioliquids (biodiesel and ethanol) are more complex and require a basic knowledge of chemistry. Ethanol is made like any consumer alcohol through fermentation of sugars. Most commonly these sugars come from corn or sugar cane. The ethanol is then denatured to prevent the ethanol from being used in food products to avoid alcohol taxes which would significantly alter the price of ethanol.

Pure ethanol can be used directly in some engines; however, more commonly an 85% ethanol/15% gasoline mixture known as E85 is sold in the USA and can be used in vehicles with flex fuel engines. Flex fuel engines are defined as engines that can use multiple fuel types and grades. Currently, all modern vehicle engines sold in the USA can already accept up to 10% ethanol mixed in with the gasoline.

At this time there are no commercially available E85 boilers or generators; however, ethanol is the most common biofuel available in North America with its primary use for transportation.

Biodiesel is also mostly used for transportation purposes; however, more boiler and generator applications exist as it is more similar to standard Diesel fuel than E85 is to gasoline. Biodiesel is refined in a process known as transesterification. This process includes combining almost any vegetable oil or animal fat with an alcohol and a catalyst. The types of oils used are known as triglycerides, which are long-chain fatty acids joined by a glycerin backbone. Some of the most common alcohols used are ethanol, butanol, or methanol. The catalyst, typically sodium hydroxide or potassium hydroxide, speeds up the reaction which separates the esters. The chemical equation below depicts the basic transesterification process.

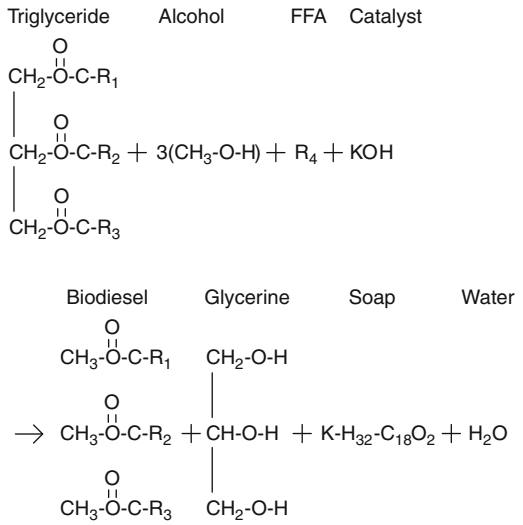

Equation 1: Basic transesterification process [3]

The two most important effects of the transesterification process are to reduce the freezing temperature of the ester and to reduce the viscosity of the ester so it can be used over a wider range of temperatures. Some older diesel engines have been observed running on heated, unaltered vegetable oil; however, newer high-precision engines require higher grade fuels, which the transesterification process provides.

Once the transesterification process is complete, a neutralizing acid is added to the system to cause the potassium or sodium to precipitate, which simplifies the processes of removing it from the biodiesel. Furthermore, the biodiesel is washed with water to remove excess alcohol from the biodiesel.

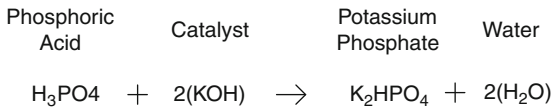

Equation 2: Neutralizing step for the transesterification process

There are dozens of proprietary processes used commercially that have reduced the refining time and improved the yields of the refining process; however, that is beyond the scope of this entry.

Biogas

Biogas can often be found on farms, landfills, and wastewater treatment plants. The process is complex but primarily involves capturing, cleaning, and dehumidifying the methane gas that is generated from decomposing organic matter.

As methane is the primary component in biogas as well as natural gas, it can be considered a direct alternative if the biogas has been sufficiently refined. A large portion of the biogas refining process is removing siloxanes and moisture from the gas, which can cause engines and boilers to fail prematurely.

There are many commercially available boilers, engines, and gas turbines that will run off less refined biogas; however, there is a cost premium due to more expensive materials. Therefore, a balance must be struck between refining and use.

Typically biogas refineries collect a significant amount of biomass such as municipal waste treatment facilities, landfills, and farms. It is difficult to justify the installation of such a system if little biomass is available. Working with the local gas company to find a supplier of biogas may be an alternative approach to supplying your building's systems with biogas. Figure 2 shows a system that is being constructed in 2011 to supply a university with biogas from a municipal landfill.

The system shown in Fig. 2 is being built in stages with the landfill flaring system being constructed first. The advantage of building the flaring system first is to determine how much gas is available before selecting

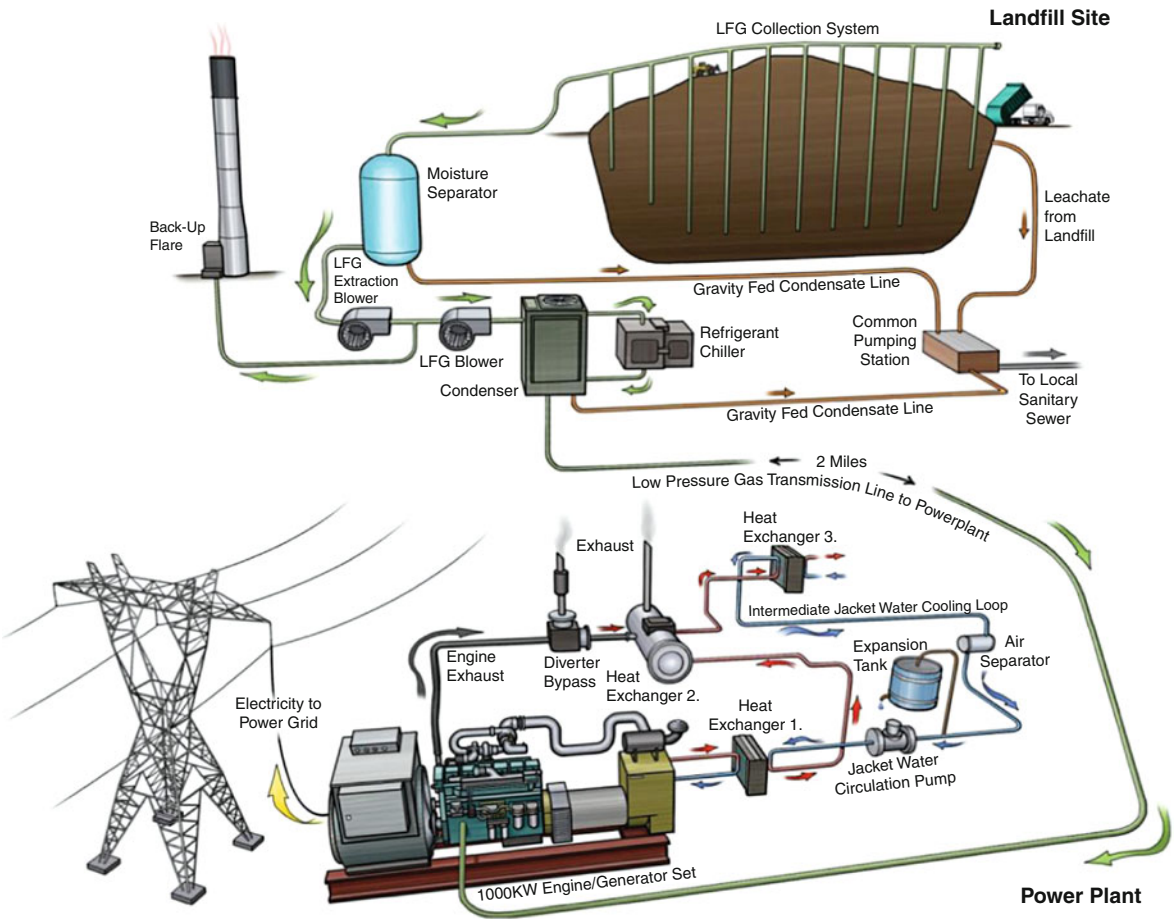

Biofuels and Sustainable Buildings. Figure 2
1 MWe landfill gas cogeneration system [4]

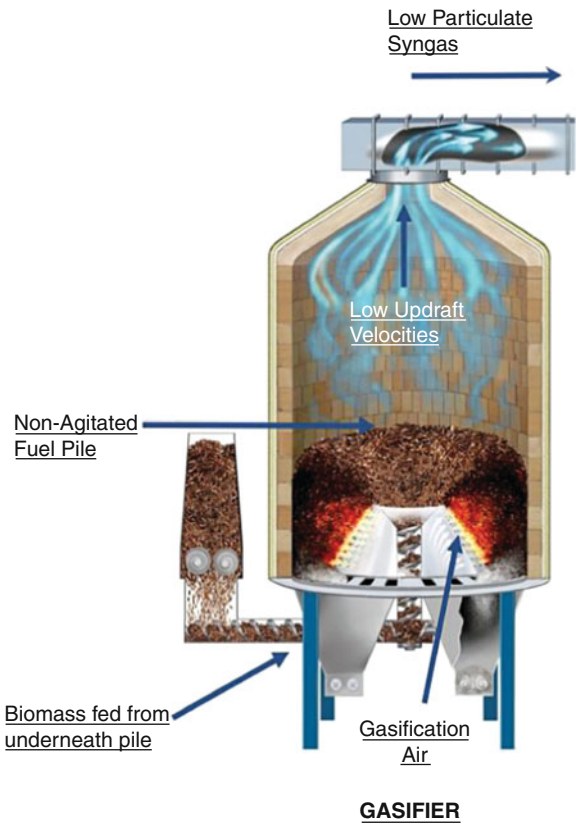

Biofuels and Sustainable Buildings. Figure 3
Biomass gasification system [5]

the pipeline and plant size. The quantity of gas production is very difficult to predict as the exact type of waste deposited in the landfill over the last 25 years is unknown.

An alternative system is a biomass gasification system that uses wood chips and process known as pyrolysis, which burns wood chips in an environment with little oxygen as shown in Fig. 3.

The balance of the biomass gasification system may use boilers or engines coupled with heat recovery, which will be addressed in later sections.

Owner/Operator Concerns

The day-to-day operations that effect building owners and operators include the supply, storage, use, emissions, and cost of the biofuel. As stated, the issues discussed in the background section should be of concern to the building owner in a holistic sense, the following sections will describe some of the challenges and considerations that directly impact the building owner and operators as well as the design team.

Supply Chain

Establishing a steady supply chain for biofuels is of vital importance to the successful operation of any system. Unlike fossil fuel distribution infrastructure, biofuel distribution infrastructure is limited and may be unreliable in certain areas for certain fuel types. There is a growing body of trade associations for commercial biofuels that can assist building owners in establishing a steady supply chain [6–8].

An alternative to commercial biofuel supply is to establish an independent biofuel infrastructure. Building designers and owners should be aware of nearby resources such as farms, waste treatment facilities, and/or cafeterias/restaurants that generate significant resources that could be converted into biofuels. While it is complex and expensive to setup independent refining facilities, it may be cost and environmentally beneficial in the long term. If it is financially feasible, a backup fossil fuel system may be desirable.

As stated in the refining section, certified fuel is often required for most biofuel burning equipment. It is important to verify that the fuel supplier is meeting the most recent fuel quality standards. The most recent standards can be obtained from the biofuel trade associations [7, 8]. These standards continue to be under development and receive frequent updates as the modern biofuel industry is not as mature as the fossil fuel industry. It is essential that fuel specifications are passed on to the boiler, engine, or turbine manufacturer to determine if the performance estimates are accurate as well as if the fuel will void the product warranty.

While getting biofuels to your site is a challenge, the U.S. Department of Energy's National Renewable Energy Lab (NREL) has assembled a map to assist biofuel users in determining where high concentrations of biofuels are likely to exist. Figure 4 below shows the approximate quantity of biofuel generated per year by location.

Fuel Delivery and Storage

Fuel storage is often a necessary part of biofuel systems, and there are a number of considerations to be

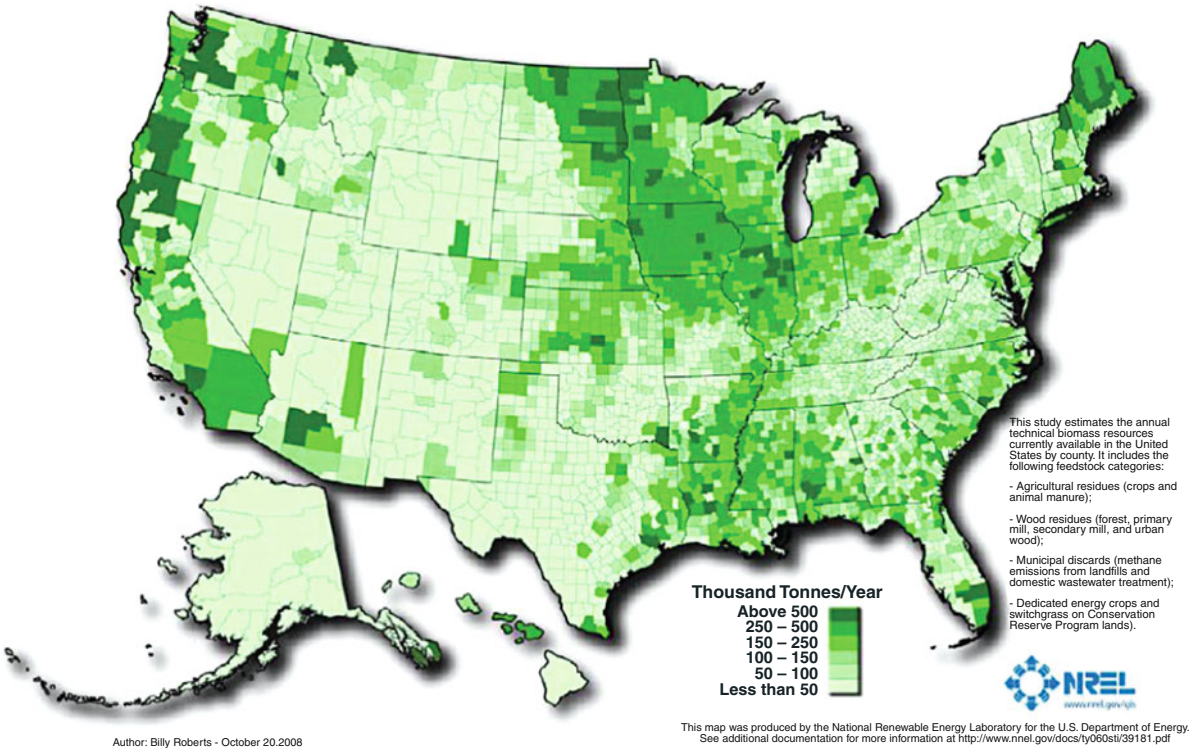

Biofuels and Sustainable Buildings. Figure 4
Biofuel potential by county for the USA [1]

investigated. First and foremost are fire code requirements, as biofuels, while often safer than fossil fuels, still pose a significant risk. The fire code is doubly important if fuel refining is done on-site as well. Local fire codes may not address biofuels and therefore fossil fuel requirements may be applied or a state fire code. Most biofuel trade associations will provide some assistance in the areas of fire safety.

The first step in storing fuel is getting the fuel from the delivery vehicle to the storage tank. For the biodiesel and ethanol, modified gasoline and diesel delivery vehicles are typically used, and are frequently available due to the large gasoline and diesel fuel infrastructure that exists. Again, local codes will designate safety features required to fill the storage tank. Independent biogas delivery is often done the same way as a standard natural gas line.

Wood pellets and chips vary in delivery methods. As such, the fuel transfer and storage system should be coordinated with the fuel supplier prior to design and construction. Some suppliers bring trucks that literally suck pellets out of the truck via hose and shoot them into the storage container using compressed air. Other methods include small dump trucks that pour the chips or pellets into a trough where an auger will transfer the chips or pellets into a storage tank.

Biogas is rarely stored on-site as the process of getting it to site is somewhat complicated and dangerous. First, the biogas is pressurized and bottled off-site by the biogas producer. The biogas bottles are then transported by truck to the building site and stored until needed. The biogas bottles require the necessary gas regulators and explosion proof equipment to distribute the biogas to the boiler or engine that it will fuel. Biogas systems like this are typically reserved for experimental systems.

Sizing the storage tank is a function of first cost, delivery cost, and rate of fuel consumption. It will be an iterative process to balance these criteria as delivery costs and the rate of fuel consumption will vary over time as it is a function of load, which is difficult to project accurately, and projections are very difficult to

make accurately. The larger a storage tank, the higher the first cost both in construction and physical space required.

Once the storage size is known, the tank materials must be selected. While no exotic or expensive materials are required to store most biofuels, some common materials can cause issues.

Wood pellet and chip storage should be in a dry, weather-protected location. However, the spaces do not need to be conditioned by mechanical systems.

Brass valves and some elastomers (rubber) used in seals may be problematic over time for ethanol and biodiesel. The U.S. Department of Energy, National Renewable Energy Laboratory has published material compatibility documents for both ethanol and biodiesel [9, 10].

Biofuel Use

The use phase of biofuels is often of greatest interest to the building owner/operator. Biofuels can be used in boilers and hot water heaters, reciprocating engines, gas turbines, and fuel cells. Most equipment manufacturers have standardized their products to work well with existing technology, making retrofits and new designs relatively simple.

Boilers/Water Heaters Boilers and water heaters are available to be used with almost any biofuel. The most common commercial products are wood pellet and chip boilers for residential use. However, larger commercial boilers are becoming more common as fuel availability, delivering, and automatic feed systems have become more refined. The smaller residential units are typically available as packaged systems and are relatively easy to install. The larger commercial units are more complicated to install as storage and delivery systems need to be tailored for each site.

Fuel oil and natural gas boilers and water heaters may also be available in biodiesel and biogas variants on a case-by-case basis. The performance of these systems will vary based on the manufacturer, but in general manufacturers of boilers and water heaters have gone to great lengths to achieve equivalent or better performance than conventional boilers regardless of fuel type.

The only noticeable change will likely be in the quantity of fuel burned to achieve the same output. For example, the energy density of pure biodiesel is approximately 5% less than that of standard fuel oil. As such, approximately 5% more biodiesel would need to be burned to achieve the same heat output. That said, all fuels, fossil and bio, have energy density tolerances and vary in quality over time depending on a variety of factors based on the recent inputs into the refining process.

The operators need to be aware that running a boiler in a not so cold month with a lower quality fuel may consume more gallons than a colder month with high-quality fuel. That said, prices should reflect the average value of the fuel delivered over the course of a year. Therefore, the cost per unit energy may be high one month and low the next; so it will balance out. The alternative is testing each batch of fuel to determine its energy density, which would be very costly.

Some issues exist with biomass boilers during low load conditions. Strict temperature controls should be put in place to properly regulate the burning of biomass. Low burning temperatures may cause the emissions to change, and create significant carbon monoxide and particulate issues. This will be revisited in the emissions section, but some manufacturers have addressed this issue in their product designs.

Ash removal is also a concern for biomass boiler operators. Like any fire, a small quantity of ash remains that must be disposed of. In facilities with significant land available, the operators may consider dumping the ash on-site as the plants may benefit from the increased nutrients. Any use of ash on-site should be coordinated with a personnel qualified to understand how the local plants will be effected by mixing ash into the soil. Some plants and soil will benefit, while others may be harmed. Urban users of biomass will need to coordinate waste removal with the local refuse company to verify if ash can be land filled or otherwise disposed of in a safe manner.

Reciprocating Engines, Gas Turbines, and Fuel Cells (Prime Movers) The alternative to burning biofuels to create heat is to use the fuel in an engine, turbine, or fuel cell to generate electricity and heat. The function of these systems is essentially unaltered; however, the performance and maintenance may change noticeably.

As of July 2009, NREL estimated that 10.5 GW of electricity was being generated with biofuels with a total potential of 78 GW [1].

Similar to the biofuel boilers and water heaters, manufacturers of prime movers (engines, gas turbines, fuel cells, etc.) have been addressing the compatibility of their products for use with biofuels. As stated in the boiler/water heater section, the energy density of the fuels may vary and the prime movers are no less affected by this difference. Often fuel pumps and capacities are oversized in many systems to account for peak demand operation. Some of this spare capacity is used to feed more biofuel into the prime mover to maintain the desired power level. For example, a Diesel engine fueled with 100% biodiesel operating at 30 kW (40 Hp) will consume fuel as if it were operating at approximately 32 kW using Diesel fuel.

Table 1 shows a selection of prime movers with some general comparisons.

The exhaust and reject heat streams of the prime mover perform nearly identically to fossil-fueled prime movers [11]. Therefore, converting a cogeneration plant from fossil fuel to biofuel may not require the balance of plant to be altered to maintain functionality.

Changes in maintenance cycles are often the cause of the greatest failures of biofuels. For example, a building operator may have been maintaining backup natural gas engine generators for years. However, if an owner has replaced the natural gas fuel supply with biogas, the previous maintenance cycles may be completely out of sync with the new reality. If the biogas is not the same quality as the natural gas, and is somewhat more corrosive, the engine seals could break down prematurely or the cylinders themselves could start to corrode. The operator must be vigilant about system performance and perform consistent maintenance checks. Additional equipment may be required to inspect the engine as compared to a conventional gas system. As there are relatively few long-term studies of biofueled systems, it is important for the building operator to coordinate and train with the prime mover manufacturers to avoid potential failures.

Cogeneration Prime movers are often paired with heat recovery systems to make combined heat and power (CHP) systems also known as cogeneration systems. The advantage of a cogeneration system versus grid power and standard boilers is that power plants waste approximately two-thirds of the fuel energy in the form of reject heat. Figure 5 shows the energy flow for the US power grid with approximately 68% of fuel energy being lost in conversion and transmission and distribution losses. With a cogeneration system, the majority of this energy can be recovered for useful purposes such as space heating and cooling.

The example shown in Fig. 6 shows a complete biomass gasification and cogeneration plant.

Biofuels and Sustainable Buildings. Table 1 Prime mover comparison by fuel, efficiency, and heat

Prime mover	Fuels	Electrical efficiency	% recoverable heat	CHP efficiency	Heat to power ratio
Boiler + steam turbine	Natural gas, coal, waste fuels, biomass	10–15%	45–65% low-quality steam	65–80%	4.3
Gas turbine	Natural gas, biogas	15–25%	45–55% 600°F exhaust	60–80%	2.8
IC engine					
-Diesel	Diesel, biodiesel	30–40%	15–20% 190°F coolant, 15–20% 900°F exhaust	60–80%	1.6
-Spark	Gasoline, E85, natural gas, biogas	20–42%	15–30% 190°F coolant, 15–20% 900°F exhaust	50–80%	2.0
Fuel cell					
-SOFC	Natural gas	35–45%	25–35% 500°F exhaust	60–80%	0.8
-PEM	Hydrogen	35–45%	25–35% 300°F exhaust	60–80%	0.8

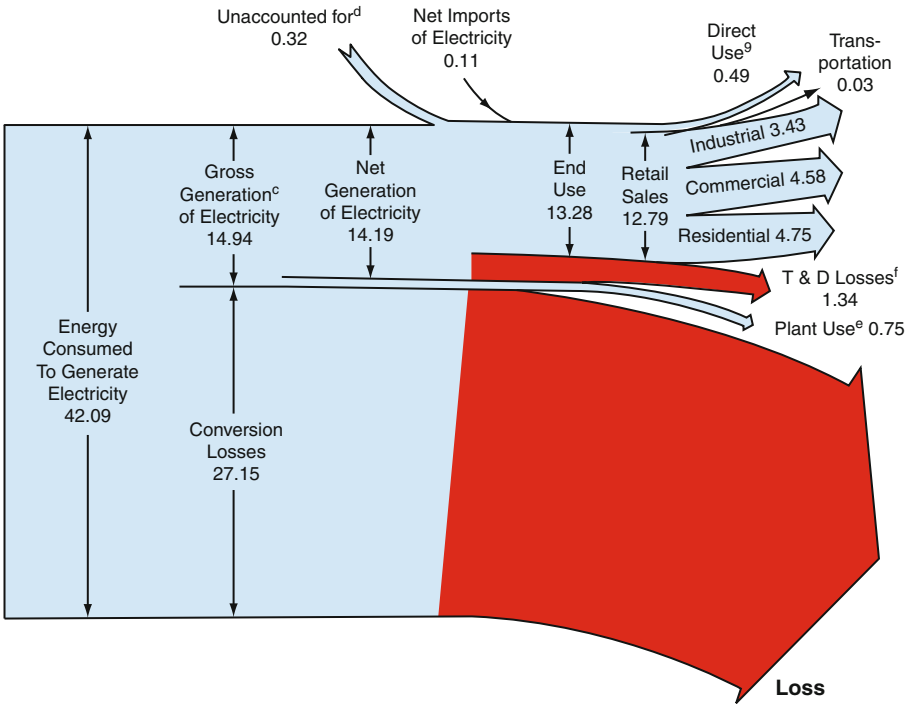

Biofuels and Sustainable Buildings. Figure 5
U.S. Electric grid energy flow [12]

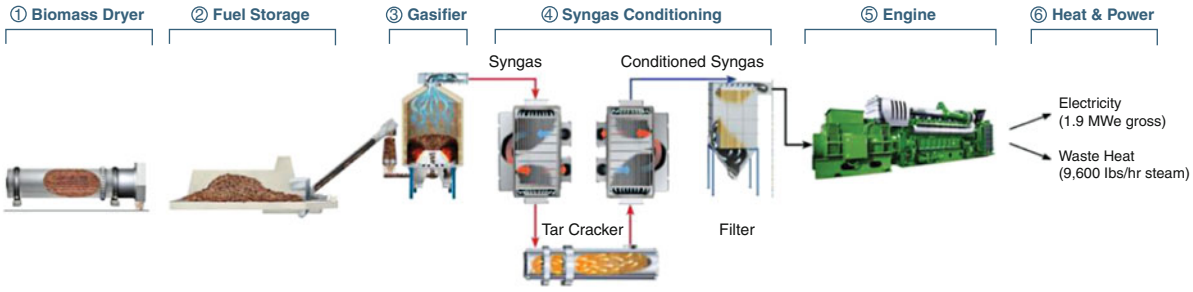

Biofuels and Sustainable Buildings. Figure 6
Cogeneration and biomass gasification plant [5]

This biomass plant includes a substantial amount of conditioning equipment for the synthetic gas (syn gas) created by the gasifier to clean it prior to use in the engine. Alternative systems that use boilers rather than engines may use less conditioning equipment.

Emissions

Emissions are of great concern to many biofuel operators as many emissions are regulated by the U.S. Environmental Protection Agency as well as state environmental agencies. Of particular concern are NO_X and particulates generated by combusting fuels. Unfortunately, characterization of emissions from biofuels is not a straightforward process. As stated, the quality and type of biofuels can vary and some equipment may not maintain optimal emissions in part load conditions. As such, emissions monitoring may be required for a period of time by local regulators to verify the installation meets local code. This is especially true in emissions non-attainment zones that provide additional focus on individual pollutants.

Biomass Emissions are of particular concern to regulatory bodies when the boilers are operating in part load conditions. As with any fuel, the temperature at which the fuel burns directly impacts the emissions characteristics. As the temperature decreases, carbon monoxide and particulates are formed. There are a number of ways to treat emissions, which include natural gas–fired afterburners to complete combustion and reduce particulate sizes.

Moisture content is also a large influencing factor in the emissions of biomass. Biomass moisture content below 50% is typically required by most boiler and water heat manufacturers [13, 14]. High moisture content will have the effect of boiling the water inside the fuel. As the water is turned to vapor, it will displace the oxygen in the combustion chamber and reduce the completeness of combustion leading to the creation of carbon monoxide. As a rule, the drier the fuel the better, but also the more expensive the fuel will be. Figure 7 shows a comparison of emissions for wood combustion.

Biodiesel Biodiesel can come from many sources including soybean oil and coconut oil. While the thermodynamic performance of these two biodiesel sources may be similar, their emissions characteristics are quite different. As a rule of thumb, soy-based biodiesel, which is the most common biodiesel source in North America, creates 5–10% more NO_X per kWh than diesel fuel. The emissions characteristics of the biodiesel are dependent on the molecular makeup of the original oil, especially polyunsaturated fat content. Soybean oil has a lot of polyunsaturated fat, as shown in Fig. 8, which indicates that the molecular structure has a lot of double bonds [15].

The consequence of double bonds is that the freezing point is low, which is good, but the cetane number is also low and somewhat unstable in an oxygen environment resulting in increased NO_X emissions [16–19]. Coconut oil on the other hand has very few polyunsaturated fats and a lot of saturated fats. Therefore, coconut oil–based biodiesel has a high freezing point, a high cetane number, is stable in oxygen environments, and has reduced NO_X emissions as shown in Figs. 9 and 10 [16–19].

As the emissions characteristics change per fuel type and content, and the status of pollutants changes per location; the design team must correlate local environmental regulations with available fuel supply to find the right match.

Carbon Neutrality of Biofuels Biofuels in and of themselves are carbon neutral because burning a certain mass of wood to generate heat will release

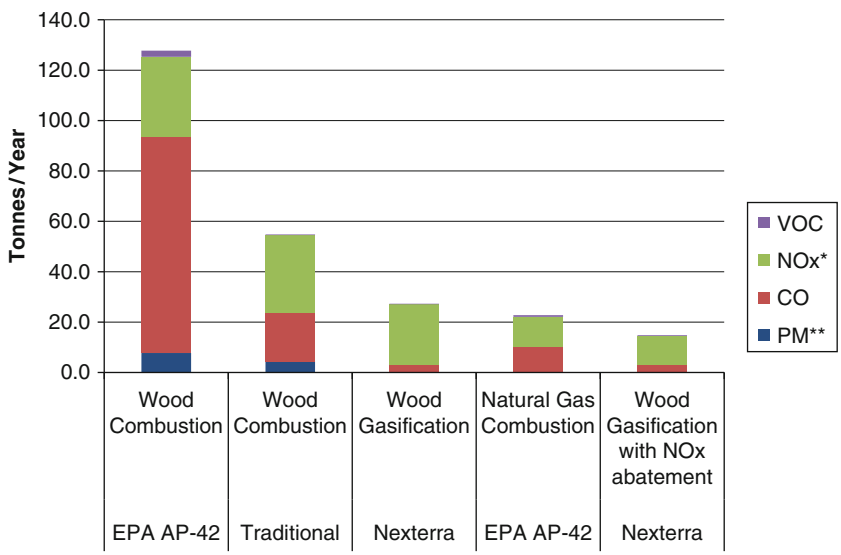

Biofuels and Sustainable Buildings. Figure 7
Comparison of wood combustion systems [5]

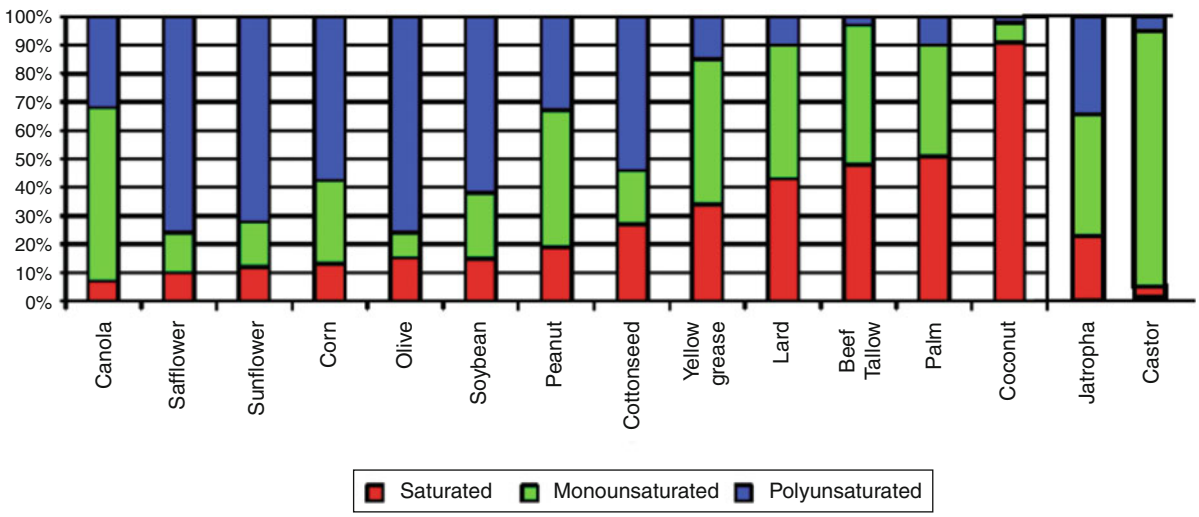

Biofuels and Sustainable Buildings. Figure 8
Average chemical makeup of oils [15]

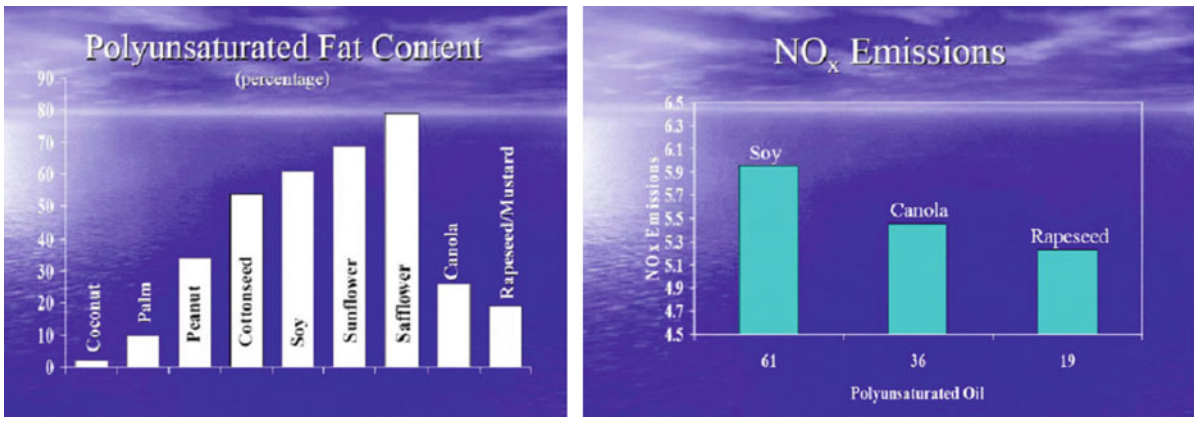

Biofuels and Sustainable Buildings. Figure 9
Polyunsaturated fat content of oils versus NO_X emissions [16]

Fuel Property	Saturated 0 double bonds	Monounsaturated 1 double bond	Polyunsaturated multiple double bonds
Freezing Point	High (–)	Medium	Low (+)
Cetane Number	High (+)	Medium	Low (–)
Oxidative Stability	High (+)	Medium	Low (–)
NOx Emissions	Reduction (+)	Medium Increase	Large Increase (–)

Biofuels and Sustainable Buildings. Figure 10
Fuel properties versus chemical makeup [17–19]

a certain mass of carbon dioxide into the air, which will then be absorbed by another tree to grow approximately the same mass of wood. This cycle is what is typically considered when calculating carbon neutrality and set in comparison to fossil fuels emissions.

However, these calculations often do not include the carbon emissions that are generated during farming, harvesting, refining, and distributing biofuels or fossil fuels. Completing a detailed life cycle analysis to determine precisely how much CO_2 is generated from a fuel can be challenging.

In general, the savings shown in Fig. 11 can be used to estimate savings of cogeneration and biofueled cogeneration versus standard heat and power generation.

Common sense can go a long way in determining the carbon impact of the harvesting, refining, and distribution of a biofuel for a building or campus. If wood pellets are made from waste wood from a nearby lumber mill, then the building owner can be reasonably certain that the CO_2 generated by collecting the waste wood, processing it into pellets, and shipping it the site are relatively small as compared to the boiler emissions.

However, if the biofuel must travel a large distance by truck, in an attempt to offset natural gas delivered via pipeline, then the owner may want to attempt a life cycle analysis. There are a number of sources that specify how much CO_2 is produced per mile traveled, or per unit energy consumed to assist in calculating a rough life cycle analysis [20–22].

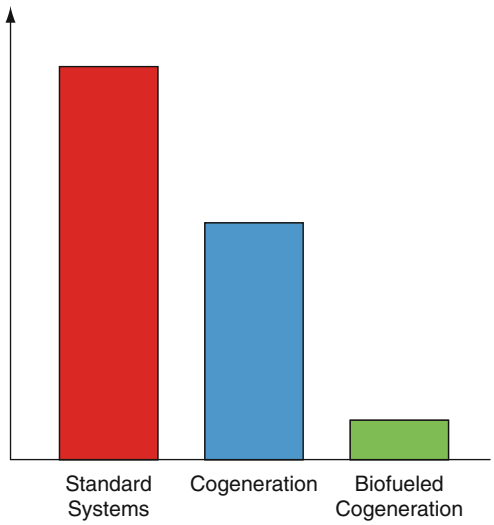

Biofuels and Sustainable Buildings. Figure 11
CO_2 generation of standard systems and cogeneration

Operating Costs

One of the largest pillars of sustainability is operational cost and operational performance. For owners and operators to be able to maintain effective operation of any system and their business, the following principles are good practices to avoid major cost fluctuations.

Buy Local First, pick the biofuel based on local availability. The distribution infrastructure for many biofuels is still weak, so most biofuels are shipped by truck. A closer supply chain is a great asset, and may give the owner some influence over regulation and pricing with the local government.

Quantify Supply Running out of the desired biofuel is a real concern in many parts of the USA, so it is important to identify multiple suppliers of the desired fuel. It is also important to understand the fuel supplier's supply chain and determine their vulnerabilities. Good things to look out for are large potential biomass sources such as lumber mills, nearby biofuel refineries, and landfills or wastewater treatment facilities. These fuel sources represent significant infrastructural investments and are unlikely to shut down rapidly.

Understand Competition The feedstock cost is the single largest influencing factor in the final cost of the refined biofuel. In 2008, the price of many food crops increased dramatically due to increased worldwide food demand and use of food crops for energy. Similarly, a demand for waste fryer oil changed the way restaurants and cafeterias view this waste stream. Several years ago restaurants had to pay to remove waste grease, then they were able to give it away to ambitious "do it yourself refiners," and now there is a commodity value to waste grease in some markets where refiners are purchasing the waste grease from restaurants. Identifying potential competition for the biofuel feedstock may alleviate future cost spikes.

Fuel Flexibility Fuel flexibility is the other option to reduce long-term fuel costs. The best example of this

concept is the flex fuel engines that run on E85. The E85 engine can run on any ratio of gasoline and ethanol below 85% ethanol. In other words, the fuel tank can be filled with E85 one day, and regular gasoline the next day as desired. Most gas turbines or engines that can run on biogas can also run on natural gas. The same is true for Diesel engines with respect to biodiesel and Diesel fuel. Some boilers can be co-fired natural gas and biomass, but this should be coordinated with the manufacturer.

Fuel flexibility is important in case there is a supply interruption, such as a reduced availability of biomass for the biogas digester, or a scheduled shutdown by lumber mill, or an equipment failure at the refinery. Suppliers may have contingencies in place to provide a supply during shutdowns. Also, building owners/operators may want to include a backup supply that could bridge the gap during outages. The size of the storage is a function of the load and how many days the supply needs to last.

Most fuels are regulated for quality by the American Society for Testing and Materials (ASTM) including ethanol and biodiesel [23–26]. Biogas must meet the local gas company's standards if it is to enter the natural gas network. Similarly, the biomass must meet the boiler manufacturer's standards in order to not void the warranty.

Future Directions

The technology to effectively employ biofuels into mainstream operation exists and has been effectively demonstrated throughout the USA and the world. Significant improvement needs to be made in the area of documentation and education of engineers, owners, operators, and code officials. Like any other industry, this will happen over time as owners request biofueled systems as an alternate to fossil-fueled systems. Owners and governments need to be willing to send their operators and code writers for training to assist in the adoption of these technologies. As owners increasingly demand biofueled systems, building designers, engineers, and the associated services will follow suit to meet demand.

The largest hurdle for the successful long-term operation of biofuels is understanding the minor differences between fossil fuel systems and biofuel systems. Often building operators will fail to see the subtle difference between the systems that can cause unnecessary problems or failures in long-term operation, and cast doubt on the biofuel industry or a particular technology. As the body of knowledge and experience grows, installers and operators will learn to benefit from the advantages of biofuels and avoid the potential pitfalls to make biofuels as common a part of building operations as fossil fuels are today.

Outside of building operations, continued improvement in supply chain management to keep costs under control will be the largest deciding factor for the long-term success of biofuels. A great deal of research is being conducted to replace the use of food crops as a biofuel feedstock with nonfood alternatives such as wood chips, grass clippings, algae, and other biomass residue as well as increasing the efficiency of refining biofuels.

Biofuels will solve some of the pollution problems faced by the building industry today as well as help diversify the energy portfolio to enhance price stability and energy security. Biofuels along with cogeneration systems will become increasingly attractive as fossil fuels become costlier and environmentally riskier to extract over time. However, biofuels are a commercial commodity and as such will be subject to market forces and the laws of supply and demand. The same price fluctuations that effect transportation fuels today are already starting to affect the biofuel market as demand increases. Owners and operators will need to be aware of where their biofuel comes from as the impacts may be felt more acutely by a local population as opposed to fuels that come from the other side of the world.

Bibliography

1. Arvizu D (director NREL) (2009) Frontiers of research in renewable energy, Key note speech ASME energy sustainability 2009, San Francisco, 20 July 2009
2. Tickell J (2000) From the fryer to the fuel tank. GreenTeach Publishing, Florida
3. Betz FJ (2005) A theoretical model of the processing and economics of a biodiesel refinery. Masters Thesis, Milwaukee School of Engineering, Milwaukee
4. Affiliated Engineers, Inc. www.aeieng.com
5. Nexterra Systems Corp. www.nexterra.com
6. Pellet Fuels Institute. Biomass Trade Association. http://pelletheat.org/

7. National Biodiesel Board, Biodiesel Trade Association. http://www.nbb.org/
8. Renewable Fuels Association, Ethanol Trade Association. http://www.ethanolrfa.org/
9. U.S. Department of Energy, National Renewable Energy Laboratory (2009) Biodiesel handling and use guide, 4th edn. http://www.nrel.gov/vehiclesandfuels/npbf/pdfs/43672.pdf. Dec 2009. Accessed 23 September 2010
10. U.S. Department of Energy, National Renewable Energy Laboratory (2002) Issues associated with the use of higher ethanol blends (E17-E24). http://www.nrel.gov/docs/fy03osti/32206.pdf. Oct 2002. Accessed 23 September 2010
11. Betz FJ (2009) Combined cooling, heating, power, and ventilation (CCHP/V) systems integration. Ph.D. Dissertation, Carnegie Mellon University, Pittsburgh
12. U.S. Department of Energy, Energy Information Agency. www.eia.doe.gov
13. Hurst Boiler & Welding Company, Inc (2010) Biomass boiler systems. http://www.hurstboiler.com/biomass_boiler_systems. Accessed 18 October 2010
14. Viessmann Werke GmbH & Co. KG. (2010) Heating with wood. http://www.viessmann.com/com/etc/medialib/internet-global/pdf_documents/com/brochures_englisch.Par.96358.File.File.tmp/pr-heating_with_wood.pdf. Accessed 18 October 2010
15. Environmental Protection Agency (2002) Draft technical report. A comprehensive analysis of biodiesel impacts on exhaust emissions. EPA420-P-02-001. www.epa.gov/OMS/models/biodsl.htm. Accessed 23 September 2010
16. Brown J (2006) Producing biodiesel from Brassica crops in the Pacific Northwest, National biodiesel conference, San Diego, 6 Feb 2006
17. U.S. Department of Energy, National Renewable Energy Laboratory (2004) Biomass oil analysis: research needs and recommendations. NREL/TP-510-34796, June 2004
18. Graboski et al. (2003) The effect of biodiesel composition on engine emissions from a DDC Series 60 Engine. NREL/SR-510-31461, Feb 2003
19. Kinast JA (2003) Production of biodiesel from multiple feedstocks and properties of biodiesel and biodiesel/diesel blends. NREL/SR-510-31460, Mar 2003
20. United States Environmental Protection Agency. eGridweb. http://cfpub.epa.gov/egridweb/ghg.cfm
21. U.S. Department of Transportation, Bureau of Transportation Statistics. National transportation statistics, Chapter 4. http://www.bts.gov/publications/national_transportation_statistics/#chapter_4
22. The Greenhouse Gas Protocol Initiative. Calculation tools. http://www.ghgprotocol.org/calculation-tools/all-tools
23. American Society of Testing and Materials (2010) ASTM D6751-09a, standard specification for biodiesel fuel blend stock (b100) for middle distillate fuels. www.astm.org
24. American Society of Testing and Materials (2010) ASTM D 4806, specification for denatured fuel ethanol for blending with gasolines for use as automotive spark-ignition engine fuel. www.astm.org
25. American Society of Testing and Materials (2010) ASTM D 4814, specification for automotive spark-ignition engine fuel. www.astm.org
26. American Society of Testing and Materials (2010) ASTM D 5798, specification for fuel ethanol (Ed75-Ed85) for automotive spark-ignition engines. www.astm.org

Biofuels: A Technical, Economic and Environmental Comparison

Franziska Muller-Langer[1], Stefan Majer[2], Anastasios Perimenis[2]
[1]German Biomass Research Centre gGmbH (DBFZ), Leipzig, Germany
[2]German Biomass Research Centre Non Profit Research Company (DBFZ), Leipzig, Germany

Article Outline

Glossary
Definition of the Subject
Introduction
Characteristics of Technologies
System-Technological Assessment
Economic Assessment
Environmental Assessment
Conclusions
Future Directions
Bibliography

Glossary

BtL Biomass to liquid
CH_4 Methane
CO Carbon monoxide
Co Cobalt
CO_2 Carbon dioxide
DDGS Distiller-dried grained solubles
DE Diesel engine
DE Diesel equivalent
DME Dimethylether
EJ Exajoule
eq Equivalent
EU European Union
EUR Euro
FAME Fatty acid methyl ester
FC Fuel cell
FE Fuel equivalent

FFA Free Fatty Acids
FFV Flexible fuel vehicle
FT Fischer–Tropsch
GHG Green House Gas Emissions
GWP Global warming potential
H_2 Hydrogen
HVO Hydrogenated vegetable oil
Hyb Hybrid engine
IEA International Energy Agency
km Kilometer
LCA Life cycle assessment
LCI Life cycle inventory analysis
LCIA Life cycle impact assessment
MeOH Methanol
MJ Megajoule
mn Million
Mo Molybdenum
Ni Nickel
OBR Onboard reformer
OE Otto engine
OECD Organisation for economic co-operation and development
R&D&D Research & development & demonstration
SNG Synthetic natural gas
SRC Short rotation coppice
TCI Total capital investment
th Thermal
US United States
VO Vegetable oil
WTW Well-to-wheel
ZnO Zinc oxide

Definition of the Subject

Biofuels are liquid, gaseous, and solid fuels derived from biomass based on a broad variety of conversion processes. Despite this definition that encompasses all physical states, the term "biofuels" has been linked throughout the years with the transport sector and considers only liquid and gaseous fuels as an alternative solution to fossil fuels that are used in transport. This entry will follow this trend and will consider under the term "biofuels" fuel options of biomass origin that are used (or intended to be used) within the transport sector. While fossil-based electricity and heat could be replaced from electricity and heat produced from different renewable sources (e.g., sun, wind), the only way, nowadays, to replace fossil fuels within the transport sector is biomass-based fuels; their importance is therefore undeniable, although their implementation is not free of concerns. The most important drivers for their implementation are the need for diversification of fuel sources, the fluctuations of fossil fuel prices and the associated need for security of fuel supply, and the need for mitigation of greenhouse gas emissions caused by the transport sector. Considering the variety of biomass conversion pathways, this entry provides a comprehensive analysis of current and most promising future biofuels options and highlights technical, economic, and environmental aspects along the entire production chain: from biomass production and transport, over biofuels production and distribution, to the final use of the biofuel (e.g., [1, 2]).

Introduction

Globally, many countries have been motivated to explore alternative energy sources due to increasing fossil fuel prices in average, energy supply security, and environmental consciousness (especially related to climate change). In developed and developing countries, fossil fuel price fluctuations and climate change are driven to the increasing interest in biofuels. Most developed countries are moving from voluntarily to obligatory legislations imposing market shares of biofuels in the transport sector [3]. With careful concepts and appropriate regulations, some biofuels might help to slow down global warming and to enhance energy security. Additionally, biofuels might provide countries opportunities to diversify agriculture production, to raise rural incomes, and to enhance access to commercial energy, especially for rural communities. However, media about the unintended side effects of bioethanol and biodiesel production has dominated the news about biofuels in the past. These headlines range from increasing world hunger and endangering forest reserves to increasing water pollution and wasting public funds [4].

Currently approx. 10% of the global primary energy demand (in 2007 approx. 516 EJ) is covered by biomass [5]. At present due to favorable policies and subsidy support in many countries, bioethanol based on sugar and starch crops (in 2009 approx. 58.4 million tons)

and biodiesel primarily based on vegetable oils (in 2009 approx. 14.4 million tons) are the most common biofuels representing approx. 2% of the total fuel consumption within the transport sector. Globally approx. 110 million tons of bioethanol and approx. 24 million tons of biodiesel are expected to be produced until 2020 which accounts for approx. 3.5% of the total global fuel consumption (Fig. 1).

All over the world, an increasing number of countries define declarations on bioenergy use with special regard to biofuels. Motivations for that are different (e.g., decarbonization strategy in Europe, increased security of supply in America, Asia, and Africa). In Fig. 1, the required biofuels demand according to these biofuel targets is compared to the projected biofuel production and the total transport energy demand according to the IEA reference scenario. Even if assuming that the biofuels targets will be reached fully only approx. 25% of the global additional energy consumption within the transport sector (based on 2005) could be covered by the year 2020. It is expected that in this time frame, biofuels of future generation will only play a minor role with regard to their current technology status and the expected business-as-usual development.

Against this background, this entry deals with the most important biofuel options for transportation purposes from a current point of view. Based on the characteristics of biomass as a multipurpose resource, technical profiles are shown for the different biofuel options. Furthermore, these technologies are considered concerning economic aspects (e.g., capital investment requirements, costs of production and use) as well as concerning environmental aspects (e.g., global warming effect).

Characteristics of Technologies

Advanced technologies are now under development to convert biomass into various forms of secondary energy including electricity, gaseous, and liquid biofuels. The purpose of biomass conversion is to provide fuels with clearly defined fuel characteristics that meet given fuel quality standards. In general, there are

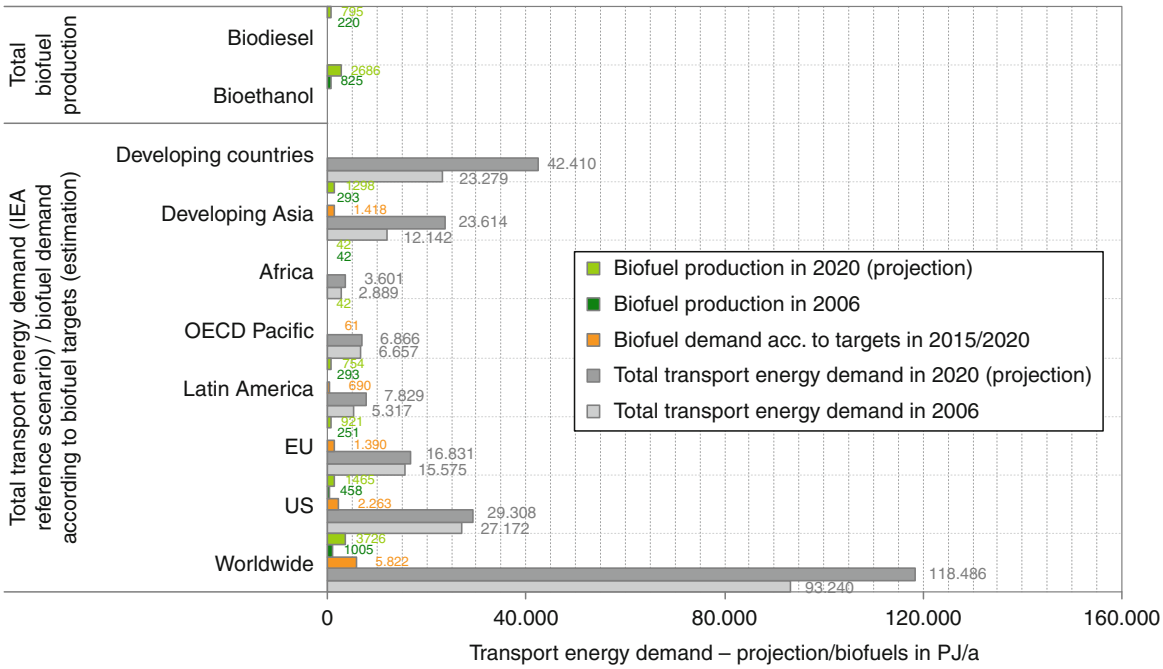

Biofuels: A Technical, Economic and Environmental Comparison. Figure 1
Comparison of global transport energy demand, biofuel targets, and projected biofuel production (based on [5, 6])

various options to produce alternative transportation fuels based on biomass. Depending on the conversion of biomass in principal, three main conversion pathways come into consideration: (1) the thermochemical pathway, (2) the physicochemical conversion pathway, and (3) the biochemical conversion pathway [7]. An overview is given in Fig. 2. For thermochemical and biochemical conversion, future lignocellulosic options might be promising. The use of lignocelluloses promises a larger non-food crop variety (e.g., woody and herbaceous residues and energy crops) with larger capacities and lower costs are expected at favorable environmental effects in future.

Current-generation biofuels are biofuels currently on the market in considerable amounts. The most important biofuels are bioethanol and ETBE and biodiesel using well-established processes for their production. For these types of fuels, only specific parts of the overall plant are used, such as the starch in corn kernels or grains, the sugar in canes or beet, or the oil in oilseeds. Residues from the production of these crops (e.g., straw) are currently used within the agricultural cycles (e.g., as fertilizer, for animal farming). Moreover, by-products accumulate during biofuel production and can be applied in the fodder and the chemical industry (e.g., press cake, glycerine, fertilizer when producing biodiesel, and vinasse or DDGS when producing bioethanol).

- Bioethanol is produced by fermenting sugars from starch and sugar biomass (e.g., cereal crops such as corn or wheat and sugarcane or beets). It is applied in pure form in specially adapted vehicles or blended with gasoline, provided that fuel specifications are met. Ethyl-tertiary-butyl-ether (ETBE) is synthesized from bioethanol and isobutylene. It is used as additive to gasoline.
- Biodiesel or fatty acid methyl ester (FAME) made from vegetable oils from the reaction with methanol in a catalyzed transesterification process. It is used in pure form in specially adapted vehicles or blended with diesel.

Different from that future biofuels can basically be produced (1) from an expanded range of feedstock as well as (2) from the whole plant (i.e., much more biomass per hectare land), including biomass waste streams that are rich in lignin and cellulose, such as straw, grass, or wood. It is expected that low-cost

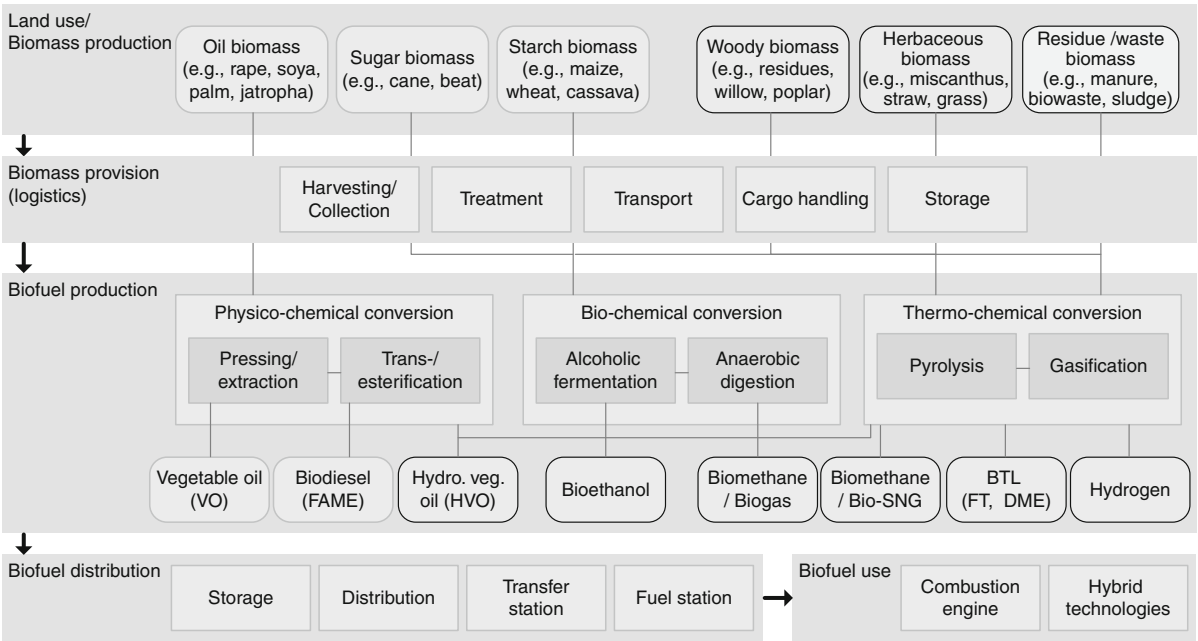

Biofuels: A Technical, Economic and Environmental Comparison. Figure 2
Simplified overview of biofuel pathways (future-generation feedstocks and biofuels marked in green)

residue and waste sources will be the primary feedstock for the next 10–15 years, followed by cellulosic perennial energy crops (e.g., willow, poplar, eucalyptus) with the potential to expand substantially after 2020 [8]. For the provision of these biomass sources, adapted logistic concepts (e.g., with regard to storage, transport, biomass handling) are required since logistic chain complexity increases with increasing biofuel plant size. In order to breakdown this biomass to produce biofuels with better fuel properties than, for example, vegetable oils and biodiesel, two main conversion pathways come into consideration:

- Firstly via biochemical processes that, for example, use special enzymes breaking down the lignocelluloses and releasing the sugars, which can then be fermented into bioethanol. Moreover, biogas that is produced from anaerobic treatment of biogas substrates and is then upgraded to biomethane, which can be fed into the natural grid and, for example, used in natural gas vehicles.
- Secondly via thermochemical processes based on gasification, where high temperatures are used to turn biomass into a raw gas that is treated and conditioned into a synthesis gas, consisting mainly of carbon monoxide and hydrogen. This gas can further be processed into different types of liquid and gaseous fuels via different types of fuel syntheses. Fuels from this route are then called "synthetic biofuels." Most promising liquid synfuel (also BtL, biomass-to-liquids) is, for example, Fischer–Tropsch fuel due to its favorable fuel properties. Gaseous synfuels are, for example, dimethylether (DME) and bio-SNG, which is also a form of biomethane and can be similarly used as a substitute for natural gas-like biomethane from biogas. Furthermore, available vegetable oils or animal fats can be treated by hydrogenation processes into so-called HVO, a biodiesel with comparably more favorable properties than conventional biodiesel.

Typically, future-generation biofuels production plants and the surrounding infrastructure are more complex than conventional biofuel options and thus more capital intensive (i.e., high capital risk). The technical measures shown with the future-generation concepts are possible in principle but have to be confirmed within future demonstration plants. Regardless of large differences of the different concepts under discussion, it also has to be pointed out that none of the concepts can be called "proven technology" that can be bought off the shelf as a turnkey plant. Some of the concepts show a promising maturity justifying the development of a first industrial demonstration project together with (industrial) monitoring. Except few demonstration plants under operation (e.g., for HVO, biomethane based on biogas and some bioethanol based on lignocelluloses, mostly integrated into existing conventional bioethanol plant), for all future-generation biofuels scale-up strategies are required. This includes the integration of the different process steps along the complete chain (biomass to transportation fuel) in order to demonstrate the effective process performances and reliability. Thereby the focus (also from an economic viewpoint) must be to achieve industrial reliability and technical performance (energy integration to achieve high efficiency/yields). According to this, it is attractive to build up HVO and BtL plants very close to crude oil refineries in order to use their infrastructure (e.g., with regard to hydrogen supply required for fuel upgrading). Moreover, existing biofuel concepts (e.g., for bioethanol) show the potentials to be a part of the so-called bottom-up approach for biorefinery plants that can function as multiproduct provider (e.g., biofuels, bulk chemicals, fertilizer, energy).

Therefore, enormous R&D&D efforts are required, including the demonstration of the overall chain under industrial conditions (including wastewater management, health and safety aspects, etc.) to prove (1) efficiency, (2) reliability, and (3) operability, also taking into account lessons learned from the implementation of conventional biofuels [6, 9, 10].

Biodiesel

Diesel based on biomass (i.e., biodiesel) can be produced by means of various production routes [1]:

- Via the physicochemical conversion by means of transesterification of vegetable and animal oils and fats; this is the most established pathway for biodiesel worldwide
- Via the thermo-chemical conversion by means of hydrogenation of bio-oils (e.g., palm oil) within

refinery processes that are established for the production of conventional diesel fuel from crude oil; this is still a niche option

Conventional Biodiesel Biodiesel production based on physicochemical conversion typically consists of the production of vegetable oil and fats via mechanical and/or solvent extraction (often within a combined process), followed by (trans)-esterification and the final treatment to biodiesel (Fig. 3). Today, resources for biodiesel are mainly vegetable oils produced from oil-containing crops (e.g., rape seeds, palm fruits, soy seeds, sunflower seeds). The oil crops (i.e., seeds and fruits) are characterized by a different specific total oil content, which are in the range of, for example, 17% for soy beans (with soy oil as by-product of soy meal production) to about 38% for rape seeds.

Chemically, transesterification (also called alcoholysis) means taking a triglyceride molecule (i.e., vegetable oil) removing the glycerine by substituting with an alcohol (e.g., methanol) and thus creating a so-called fatty acid methyl ester (FAME).

There are three basic steps in the biodiesel production from oils/fats: (trans)-esterification, ester processing, and glycerine purification. Therefore, oil is

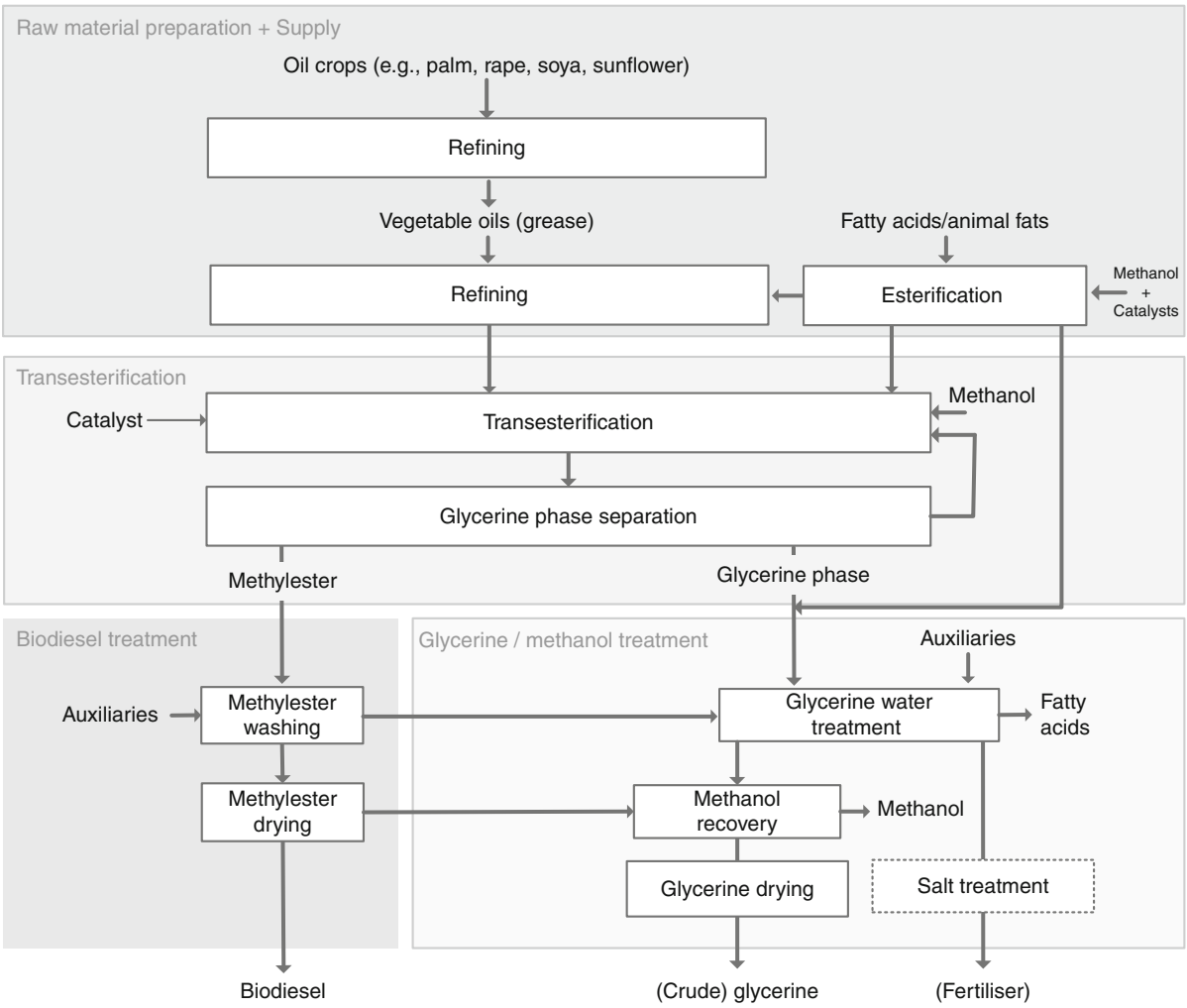

Biofuels: A Technical, Economic and Environmental Comparison. Figure 3
Principle of conventional biodiesel production

charged to the reactor and mixed with the alcohol (e.g., methanol) and the catalyst (typically hydroxides like NaOH or KOH or their methylates). A successful transesterification reaction produces two liquid phases: (1) methylester and (2) glycerine. Once separated from the glycerine, the ester is washed to remove any soap formed during the reaction as well as the residual free glycerol and alcohol. The ester is then dried to remove all water. In some cases, the esters are distilled under vacuum to achieve even higher purity in the fuel by removing sulfur and/or phosphorus. The washing step can be greatly affected by the free fatty acids (FFA) level of the feedstock, since all the FFA form soaps in the reaction.

To further refine the glycerine, it is neutralized with an acid to form salts and sent to storage as crude glycerine. Depending on the applied catalyst, surplus catalyst KOH and soaps can be split by producing, for example, potassium sulfate that can be applied as fertilizer. After the aqueous glycerine phase has been neutralized, the glycerine is processed further by evaporation. The glycerine is then typically 60–88 wt.% pure. The glycerine can again be further refined by drying it in a vacuum distillation unit and then cleaned in a continuous adsorption unit to receive technical or pharmaceutical-grade glycerine (up to 99.5 wt.%).

The excess methanol can be removed at different stages of the reaction – before or after the phase separation. In both cases, the methanol is recovered and reused using conventional equipment. Care must be taken to ensure that no water accumulates in the recovered methanol stream.

Depending on application schemes, biodiesel plants are designed in different capacity scales (e.g., from approx. 0.5 kt/a to several 100 kt/a) and performance types (e.g., batch and/or continuous biodiesel processes with or without oil mills as annex plants). The kind and quality of feedstock is the decisive factor for the technical design of a plant and the corresponding material and energy flows [1].

Advanced Biodiesel In order to produce a biodiesel with more favorable properties than biodiesel based on the (trans)-esterification of vegetable or animal oils and fats (i.e., conventional biodiesel production), conventional refinery processes can be also applied to convert the same feedstock into an advanced biodiesel. Properties that are similar to petroleum diesel can be achieved by blending vegetable oils with mineral oil previous to their upgrading to diesel in mineral refineries by using the existing refinery infrastructure including energy, blending facilities, logistics, and laboratories. One option, which is currently implemented at commercial level is the so-called NExBTL process [11]. The principle of this catalytic hydrotreating process is shown in Fig. 4. It is briefly explained below.

For the pretreatment of the feedstock (e.g., vegetable oils as crude oil, animal fats), conventional degumming technology known from vegetable oil processing or conventional biodiesel production is used to remove undesired impurities [11]. Firstly, the feedstock is filtered before reacting with hydrogen (demand approx. 0.09 $GJ_{H2}/GJ_{biodiesel}$ [12]) and passing through the catalyst beds at elevated temperatures and low space velocities. The hydrotreating process typically takes place in fixed-bed reactors at temperatures of approx. 350–450°C and at a partial hydrogen pressure of 48–152 bar. For that, standard catalysts are applied (such as CoMo and NiMo) [13]. During hydrotreating, oxygen is removed by adding hydrogen. Vegetable oil or animal fats (i.e., triglycerides) are converted into three separate branched chain paraffins. Oxygen in the triglyceride is removed as water and carbon dioxide. Side products of the process are fuel gas, which can be used for energy and a small amount of biogasoline. The main product NExBTL has similar

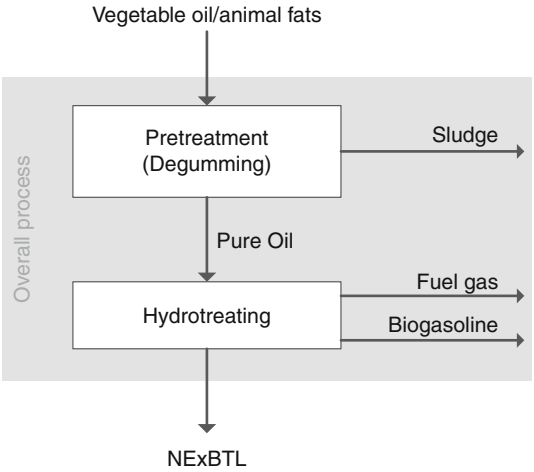

Biofuels: A Technical, Economic and Environmental Comparison. Figure 4
Principle advanced biodiesel production

chemistry and properties to the synthetic BtL fuels (e.g., Fischer–Tropsch diesel). The mass specific biomass conversion rate is – depending on the feedstock – approx. 1.23 $t_{feedstock}/t_{biodiesel}$ [11, 12].

Bioethanol

Bioethanol production is based on biochemical conversion processes (i.e., fermentation by microorganisms), which is also considered in the following (Fig. 5). Currently, worldwide conventional bioethanol is produced by using sugar crops (e.g., sugarcane in Brazil, sugar beet in the Europe) and cereals (e.g., corn in the US, wheat in Europe, cassava in Asia). The use of lignocelluloses offers several benefits regarding crop variety, feedstock costs and environmental impacts in the future. Technologies for conversion of lignocellulosic biomass to bioethanol are basically available. However, currently no commercial lignocellulosic bioethanol plant is being operated. The development of cellulosic ethanol concentrates on three main regions: the US, China, and Europe. Often, second-generation plants (biochemical) are planned as annex facilities to conventional plants. In addition to biochemically fermented ethanol, bioethanol can be produced as synthetic fuel by thermochemical conversion (Fig. 5).

Conventional Bioethanol When using cereals, the first step within the conversion plant is a milling station. Here, the flour is mixed with water and recycled thin stillage to form a mash. By adding enzymes and a thermal treatment at temperatures between 60°C and 90°C, the starch in the mash is broken down to glucose. The sugar solution, originating from the saccharification is cooled down and is transferred to the fermentation vessel. The alcoholic fermentation is realized at 35°C, which is the optimum temperature for the metabolism of the fermenting yeast. Within the fermentation step, glucose is metabolized by yeast to form ethanol, CO_2, and biomass. The CO_2 resulting

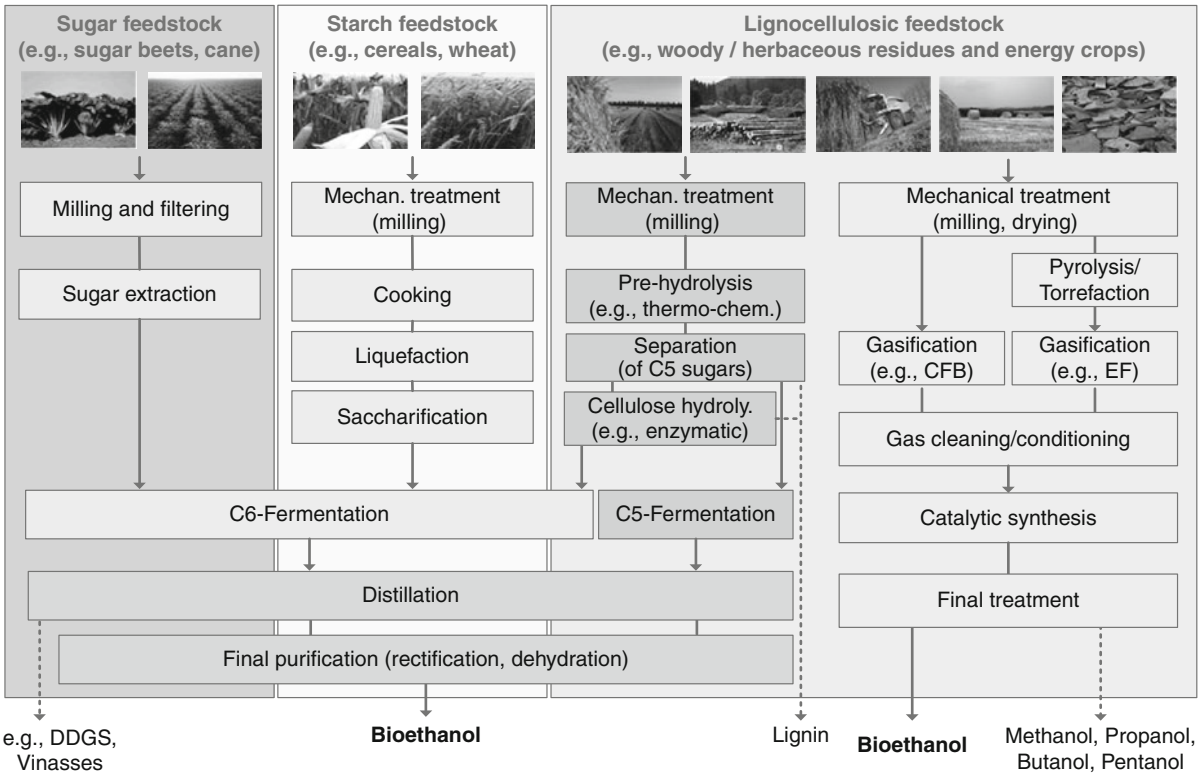

Biofuels: A Technical, Economic and Environmental Comparison. Figure 5
Principles of bioethanol production

from the fermentation process is discarded to the environment or can be used to carbonate soft drinks.

After fermentation, raw bioethanol needs to be treated by distillation and final purification (dehydration). In the process of distillation, the alcohol contained in the mash (concentration of up to 5 wt.% [14]) is separated based on a multistage distillation/rectification using steam. Beside water, several other substances are removed from the ethanol. Furthermore, the coproduct mash is gained as distillation residue. The main desired product of the distillation process is azeotrope ethanol with a maximum purity of 97 vol.%. The subsequent process of dehydration is used for further concentration of ethanol (to achieve an alcohol concentration of at least 99.8 vol.%). For that the method of the molecular sieves has detached the older membrane and entrainer distillation. The use of the molecular sieves also allows the dehydration of ethanol with a purity of down to 85 vol.%. Thereby it is possible to save energy in the process of thermal rectification [15–17].

Apart from concentration of the ethanol, the bottoms of the distillation column (stillage) have to be treated. The stillage is virtually free of ethanol, but contains soluble and insoluble organic and even some inorganic material. The first treatment step consists of a mechanical separation with a decanter, which yields the thin stillage and a decanter cake [18]. Half of the thin stillage can be recycled to the initial mashing process, whereas the rest is fed to a series of two evaporators, in order to further concentrate the soluble substances to syrup. Finally, syrup and decanter cake are blended and dried to reduce the water content. The product of this drying step is marketed as DDGS protein fodder (digesters dried grains with solubles).

Lignocellulosic Bioethanol For the following process stages, the lignocellulosic feedstock is pretreated and grinded to a small particle size of approx. 1–3 mm. Depending on the kind of hydrolysis used in the following procedure, a drying of the treated material to a humidity of less than 10 wt.% may be necessary [15].

To make the sugars available for the fermentation step, hydrolysis (i.e., saccharification) is carried out. The first step of hydrolysis contains the release of fermentable monosaccharides C_5 (i.e., xylose, arabinose) and C_6 (i.e., hexose, glucose) from cellulose and hemicellulose. The second step of hydrolysis is typically based on an enzymatic decomposition of the cellulose molecules. Alternatively, a single step process using concentrated hydrochloric and sulfuric acid could be used for cellulose extraction. Moreover, enzymatic procedures are still in the progress of development [14, 15].

In the next step, the sugars gained from hydrolysis are used as feed for the following process of fermentation. The remaining lignin could be used as a fuel for the production of process energy. Depending on the plant used, the process of fermentation takes between 2 and 5 days. Afterwards, the used mash contains 10–15 vol.% of ethanol. For process control, the used auxiliary materials are important (e.g., acids for the pH-value and ammonia for nutrient supply of yeast). These requirements in connection with an appropriate temperature are the basis of the yeast enzyme production and therewith of the glucose conversion to ethanol and carbon dioxide. For the fermentation of lignocellulose, the commonly used yeast is suitable only to a limited extent. From the contained sugar spectrum, only glucose, as a monomer component of the cellulose molecule, can be fermented to bioethanol. Based on biotechnological methods, new approaches for the fermentation of the whole sugar spectrum produced from lignocellulosic biomass have been developed over the last years [7, 14].

The additional steps for ethanol concentration are basically the same like for conventional bioethanol.

Synthetic Biofuels

The production of synthetic fuels (i.e., "designer fuels" with clearly defined properties) is characterized by three main steps to be performed after appropriate biomass pretreatment:

1. Gasification of lignocellulosic biomass to a raw gas
2. Cleaning and conditioning of raw gas to synthesis gas
3. Catalytic synthesis of this gas to synthetic biofuels (e.g., Fischer–Tropsch fuel, methanol (MeOH), dimethylether (DME), and synthetic natural gas (SNG))
4. Final product treatment

In the following, Fischer–Tropsch fuel (FT), biomethanol (MeOH), and dimethylether (DME) are briefly introduced. The principle is shown in Fig. 6.

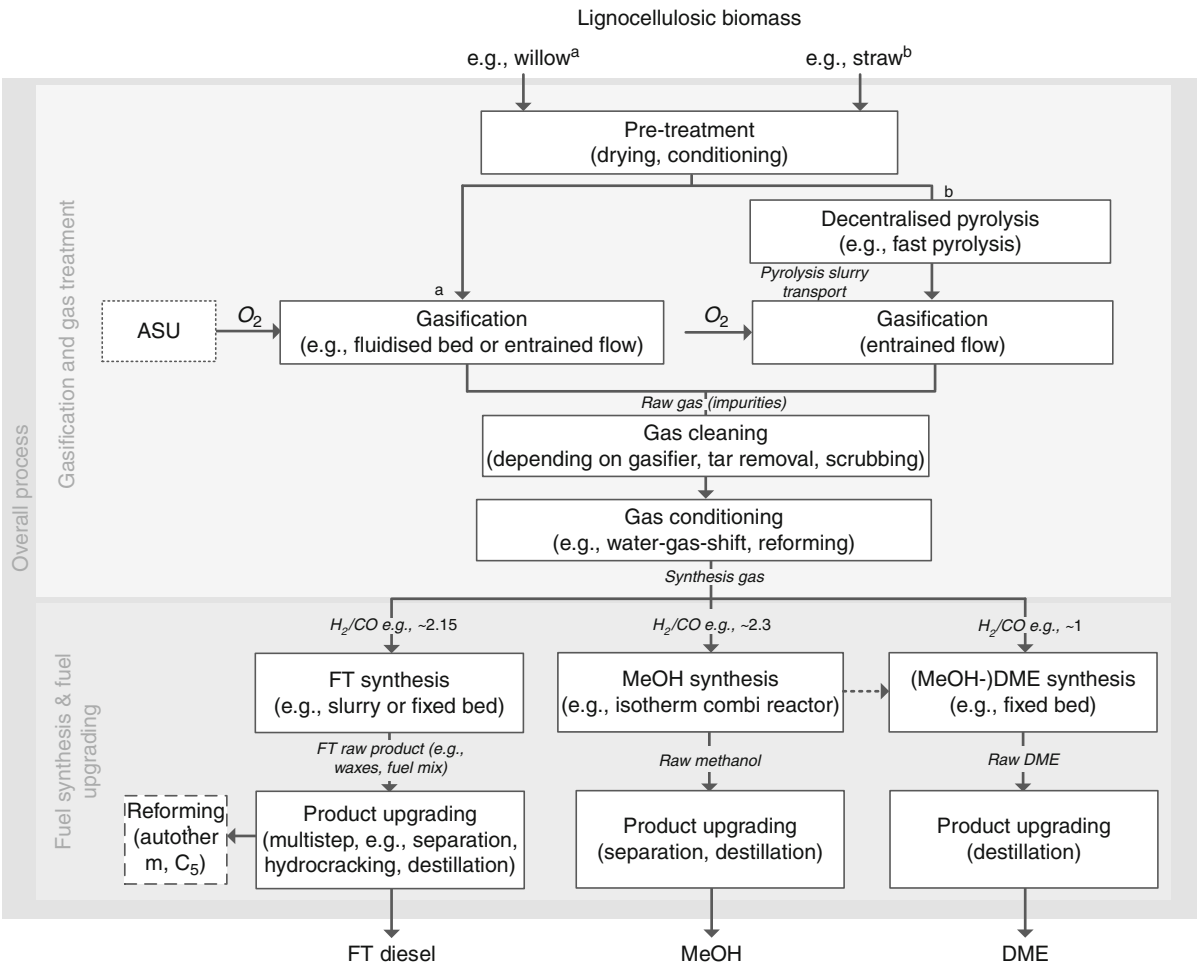

Biofuels: A Technical, Economic and Environmental Comparison. Figure 6
Principle thermochemical synthetic biofuel production

Despite of a long history of the development of a broad variety of system elements as well as system layouts for the provision of liquid and/or gaseous fuels via biomass gasification, no market breakthrough has been realized so far. One reason is, for example, difficulties in combining different system elements to an overall turnkey plant. Additionally, some system elements are still under development. For an efficient production of synthetic biofuels with regard to "economy of scale" within the conversion plant as well as the minimization of the biomass transportation costs, conversion concepts of a medium to large scale are required. Such a medium to large scale is necessary to provide sufficient amount of raw gas for gas cleaning/conditioning and fuel synthesis as well as to produce this gas via gasification at economically justifiable costs.

Regarding biomass pretreatment for gasification, mechanical-thermal biomass treatment (e.g., chipping and drying of solid biofuels) is mature. Processes to produce intermediate products that can be more easily transported and handled for gasification (i.e., pyrolysis and torrefaction) are still in a pilot/demo stage. Despite the scale of a gasifier, no gasification system is a priori appropriate for biomass. Among other criteria, chemical characteristics and physical and mechanical properties of the utilized biomass are of importance. However, all reactors for biomass gasification (e.g., fluidized bed reactors, entrained flow reactor) are still

in an R&D stage up to now. Furthermore, previous developments on gasification were mostly not focused on synthesis gas production but rather on the provision of a product gas intended to be used for heat and power generation.

Depending on fuel synthesis, specific qualities of synthesis gas at constant compositions and large amounts have to be provided (e.g., for the production of 100–1,000 m^3_{STP}/h of FT). Quality criteria are, for example, a certain degree of gas purity and a specific H_2/CO ratio. Because so far no gasification system meets these requirements, appropriate gas cleaning and conditioning system have to be applied. During gasification, besides the main components (CH_4, H_2, CO and CO_2) also impurities are generated such as tars, coarse and fine particles, sulfur compounds, alkalis, halogen and nitrogen compounds, as well as heavy metals. Their quantities vary depending on the gasification process as well as the type of biomass. For raw gas cleaning, either low temperature wet gas cleaning or, alternatively, hot gas cleaning can be applied. The effectiveness of wet gas cleaning (e.g., cyclone and filter, scrubbing based on chemical or physical absorption) has been well proven for large-scale coal gasification systems. Contrary to that, not all elements of hot gas cleaning (e.g., tar cracking, granular beds and filters, physical adsorption or chemical absorption, ZnO-bed, physical absorption) are of mature technology yet. Nevertheless, hot gas cleaning offers benefits for the overall energy balance and with regard to the avoidance of contaminated sewage. For gas conditioning, available system components can be applied: hydrocarbons in the product gas can be converted by means of an additional steam or autothermal reforming step resulting in a higher H_2/CO ratio. To achieve the required quality for fuel synthesis, the water–gas CO conversion is conducted as final step of synthesis gas production [19].

The production of synthesis biofuels primarily differ regarding a catalytic exothermic synthesis and product upgrading:

- *Fischer–Tropsch (FT) fuels.* FT synthesis is a polymerization process at low temperature (200–240°C) whereby synthesis gas is liquefied into hydrocarbon chains of different length. This synthesis is catalyzed either by iron- or cobalt-based catalysts. This conversion can be operated in a "full-conversion" or a "once-through" operation mode by using either tubular fixed bed or slurry bubble column reactor at an operating pressure range from 20 to 40 bars. The FT raw products consist of a wide spectrum of light hydrocarbons (C_1–C_4), naphtha (C_5–C_{10}), the main product FT diesel (C_{11}–C_{20}), and waxes (C_{21+}) that need to be separated afterwards. Naphtha is a gasoline fraction of minor value and is used as a resource for the petrochemical industry. It can be upgraded to motor applicable gasoline by isomerization. Wax upgrading is done by hydrocracking. Within this catalytic oil refinery process, long-chained hydrocarbons are split into the desired diesel and middle distillates in the presence of hydrogen [20, 21].
- *Methanol.* The operating pressure of methanol synthesis ranges from 45 to 100 bar and the temperature from 220°C to 280°C. Catalysts needed to steer the conversion process are based on copper, zinc, and aluminum oxide. Like within the FT synthesis, in the methanol synthesis two reactor types are commonly used: (1) fixed-bed reactors (e.g., ICI-quench reactor, isothermal reactor, Linde-isothermal reactor, multiple-bed reactor) or (2) slurry reactors (e.g., suspension/slurry reactor). Within the synthesis, several by-products (e.g., DME, alkalis, ethanol, propanol, butanol) are generated in addition to the methanol fraction, which appear gaseous together with unconverted syngas fractions. For separating higher hydrocarbons from the product gas stream, an oil separator is used. Afterwards the raw methanol is separated by condensing, stored and upgraded in a distillation column [22–24].
- *Dimethylether.* DME can be produced via direct synthesis or via indirect synthesis over the intermediate product methanol. For large-scale application, the fully integration of the two process steps, methanol and DME synthesis (i.e., direct synthesis), is very advantageous and the best choice for DME production in terms of efficiency; but this option is still within the R&D stage. Classically two methanol molecules react to produce DME and water, which is removed. The reaction takes place at temperatures of about 250–300°C. Commonly fixed-bed reactors without any special internal heat

exchangers are used. Stoichiometric efficiencies of about 86–88% referring to the raw methanol can be reached. Besides water and undissolved gases, the generated raw DME contains little amounts of ether compounds and alcohols. The gases can easily be removed by reducing the pressure. Subsequently follows the final product cleaning by distillation [20].

Biomethane (via Biogas and Bio-SNG)

The gaseous fuel biomethane can favorably be applied as a substitute for natural gas. This gas is produced either through the biochemical conversion of biomass with a subsequent gas upgrading or through the thermochemical conversion of solid biomass via gasification with subsequent gas cleaning, methanation, and product gas upgrading.

In the following (Fig. 7), these two processes are briefly described.

Biogas Biogas production is based on anaerobic fermentation, which requires a substrate pretreatment. On their way into the fermenter, the substrates undergo the following steps: (1) the delivery to the plant, (2) the

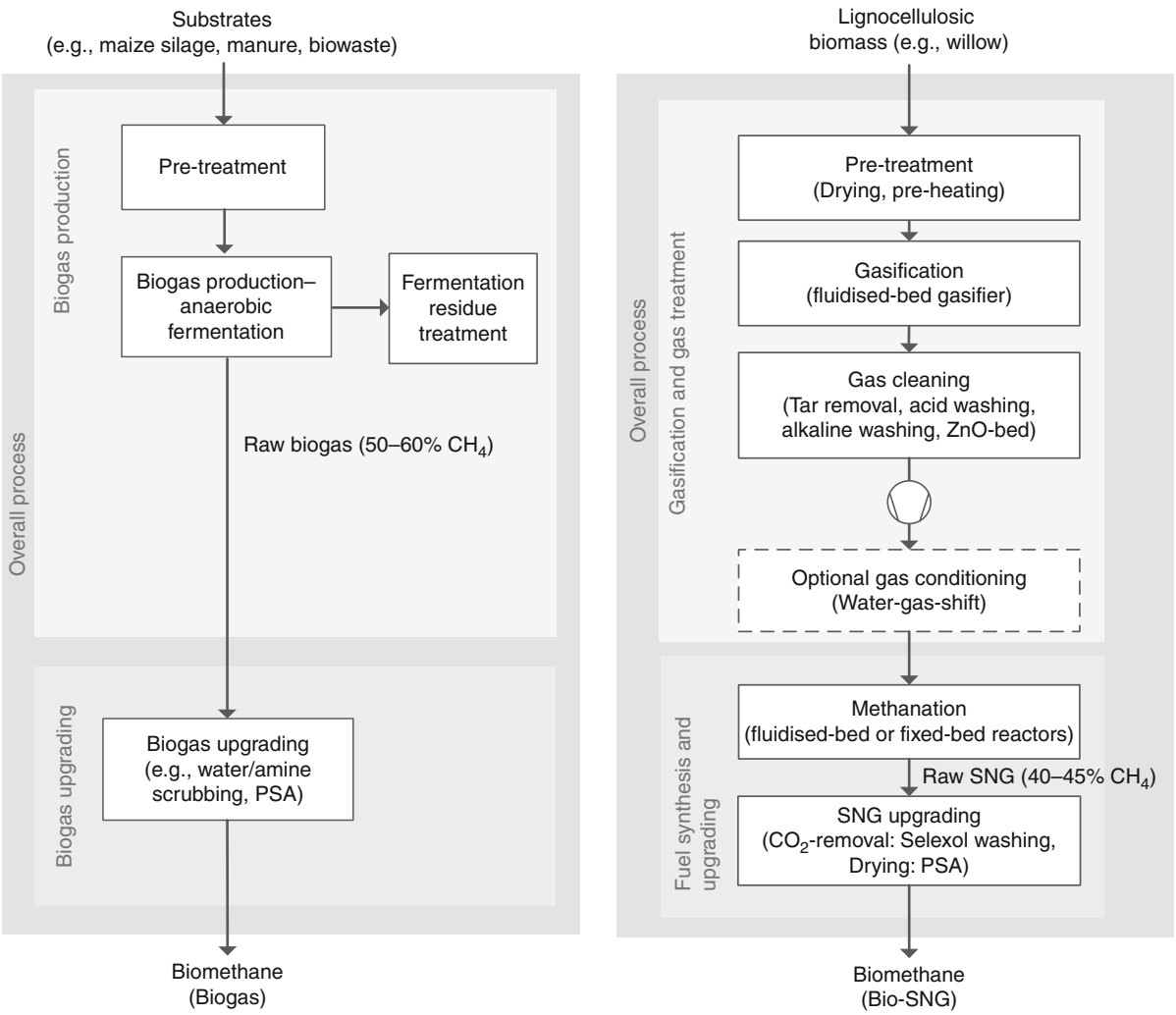

Biofuels: A Technical, Economic and Environmental Comparison. Figure 7
Principle of biochemical (*left*) and thermochemical (*right*) biomethane production

storage, (3) the upgrading (e.g., homogenization), and (4) the transportation from the storage to the fermenter [25, 26].

For the biogas production by anaerobic fermentation, a broad variety of different kinds of biomass can be used (e.g., liquid and pasty substrates such as manure, biowaste, maize silage, and wastewater). During this biochemical degradation process, organic material is decomposed in an oxygen-free atmosphere by several types of bacteria that produce a gas containing approximately 50–66% methane (CH_4) and 33–50% carbon dioxide (CO_2) plus some impurities (e.g., sulfur compounds like H_2S) of minor importance and water vapor. Digestion is a complex metabolism chain, whereby each step is characterized by the attendance of special bacteria.

In order to feed biogas into the gas grid, the raw biogas has to undergo cleaning and upgrading process steps that include biogas purification from trace components (primarily H_2O, H_2S, and NH_3). Moreover, the heating value, Wobbe index, and other parameters, which highly depend on the CH_4 content, need to be adjusted to pipeline specifications by removing CO_2. Some technologies enable the removal of H_2S and CO_2 in parallel. However, the relevance, feasibility, and sequence of the different cleaning and upgrading processes depend on the specific gas composition and pipeline specifications. Upgrading technologies for biogas result mainly from technological applications from the natural gas sector where partly comparable upgrading tasks have to be solved, but at a by far larger scale. Main technologies, where already experiences in practice exist, are, for example, water scrubbing, pressure swing adsorption, and chemical absorption (e.g., amine washing). Generally, it has to be stated that all processes available on the market pledge to reach a biomethane quality of more than 96% methane content and a methane loss with less than 3% [27].

Bio-SNG The SNG production is characterized by the possibility that relatively small conversion units with capacities in a range of 10 up to several 100 MW_{th} biomass input can be used. Thus, the conversion of locally available lignocellulosic biomass is possible to minimize the feedstock provision costs. The production of synthetic biofuel, electricity, and heat (so-called tri-generation) allows high overall efficiencies (e.g., high GHG mitigation potential) within the entire production process. Compared to the production of BtL-fuels (like Fischer–Tropsch fuels) the SNG production system is characterized by lower technical and financial risks due to a technology that is less complex (e.g., synthesis and fuel treatment) and basically smaller units can be used [28].

Regarding technology aspects, process steps such as biomass pretreatment, gasification, as well as gas treatment for synthesis are basically similar to that of the other discussed synthetic biofuel options. They have to be adjusted; especially the methanation requires high gas purity grades (nearly sulfur free gas) and a specific H_2/CO ratio.

At present, only the methanation of cleaned and conditioned gas out of coal is state of the art (e.g., SNG plant in US North Dakota with a capacity of 1.5 GW_{SNG} [29]). However, the methanation of gas generated out of biomass is under investigation in several test facilities and show up good results (e.g., energetic efficiencies of about 80%). For a fast and effective conversion, nickel- or copper-based catalysts are used for the exothermal methanation at a catalyst-specific temperature level of 200–450°C and pressures up to 50 bar. For managing the heat, currently several reactor concepts are in use or under investigation: (1) multiple fixed-bed reactors in one row with intermediate cooling or (2) fluidized-bed reactors with internal heat exchangers. Another heat management option is to recycle cold gas and to refeed it into the methanation [30]. The methane content after methanation is in a range of approx. 40–45 vol.%.

For bio-SNG upgrading to biomethane, basically the same is valid as shown for biogas upgrading. However, for CO_2 separation, typical large-scale technologies such as physical absorption processes (e.g., Selexol, Rectisol) and amine scrubber are applicable. Pressure swing adsorption can be used for final gas drying.

Biohydrogen

Hydrogen is basically used as raw material in chemical industries. Due to increasing environmental requirements and consumption of this industry (especially petrochemistry and refineries), the worldwide hydrogen demand is forecasted to increase annually with 5–7% [31]. While currently hydrogen is produced from fossil fuels, in the long run, renewable sources

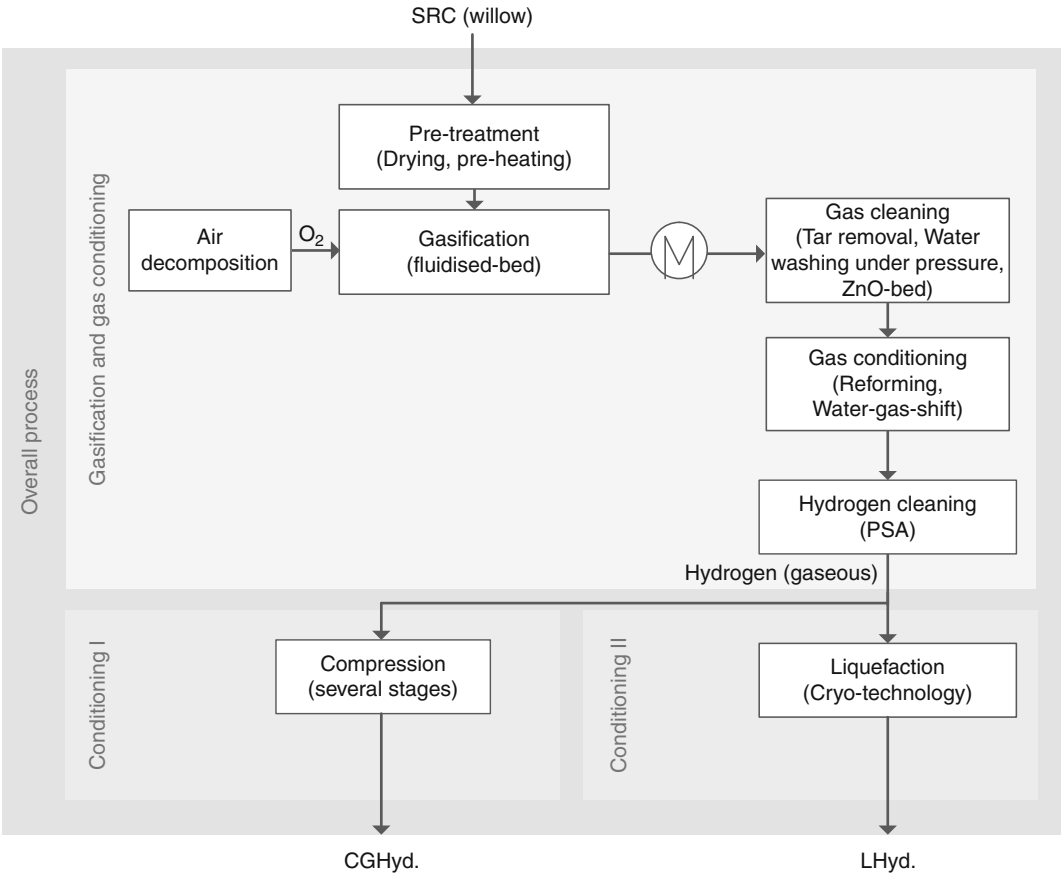

Biofuels: A Technical, Economic and Environmental Comparison. Figure 8
Principle of thermochemical biohydrogen production

need to be the fundament of hydrogen production. Thereby the hydrogen production via thermochemical biomass conversion (Fig. 8) seems to be one promising perspective. At present, this process is under investigation at the state of pilot plants [32].

Also for hydrogen production, the various process steps (such as biomass pretreatment, gasification, and gas cleaning) are similar to that described above. However, gasification and gas cleaning have to be adjusted to generate a hydrogen-rich gas.

Within the conversion of biomass into hydrogen, no synthesis step is needed. Thus, the gas conditioning to increase the hydrogen content of the producer gas is quite important. For this purpose, two process steps can be applied: (1) an optional reforming step (e.g., via an endothermic steam reforming or an autothermal reforming) and/or (2) a water–gas shift step. During water–gas shift reaction, part of the CO are converted into H_2 and CO_2 by addition of water-steam [33, 34].

In general, the first subsequent gas cleaning step is the water removal through condensation. In the following, the gas is cleaned by pressure swing adsorption (PSA). The PSA uses the different partial pressures of the gas components to adsorb undesired components. Remaining tail gas can be used for the process heat supply [35, 36].

For the final use of the produced hydrogen, the energy density has to be increased. For this purpose, there exist two common possibilities: (1) multistep hydrogen compression from about 13 to 30 bar to at least around 250 bar and (2) hydrogen liquefaction to

a higher density at final temperature of −253°C and a pressure of 1.2 bar by cryogenic procedures with an energy demand of 10 kWh/kg_{H2} [37].

System-Technological Assessment

Based on the technology characteristics, the biofuel options outlined above are compared based on criteria regarding biofuel production (i.e., stage of development, technical effort in terms of system complexity, expected plant capacity, and overall efficiency) and criteria regarding infrastructure and end use in vehicle fleets. With regard to European conditions, a summary is shown in Table 1.

According to Table 1, each biofuel option shows different benefits and bottlenecks along the overall production pathway. Conventional biofuel options are already established technologies and hold a certain market share. Most of the future options are in a pilot (i.e., bio-SNG) or demonstration (i.e., lignocellulosic ethanol) phase, with only advanced biodiesel and biogas being already commercially available. Future options are linked to upscaled plant capacities that would allow benefiting from economies of scale and thereby balance the increased capital investments; in return, however, such large facilities pose logistical complexities in terms of biomass supply, storage, and handling. Furthermore, all synthetic fuels are linked to increased technical complexity, due to the various steps for their production (i.e., gasification, gas cleaning, synthesis), a fact which also reflects to the final overall efficiency of the processes.

Considering infrastructure, lignocellulosic ethanol has the advantage of the same treatment steps following

Biofuels: A Technical, Economic and Environmental Comparison. Table 1 Comparison of biofuel-specific system technology aspects

Biofuel option	Biomass conversion to biofuel				Infrastructure and use of biofuels		
	Current state of technology	Technical effort[a]	Plant capacity[b]	Overall efficiency[c]	Availability distribution	Blend to fossil fuels	Availability vehicles
Conventional							
Biodiesel	+++++	++++	++++	+++	+++++	++++	++++(+)
Bioethanol	+++++	+++	+++	++(+)	+++	++++	++++(+)
Future							
Advanced biodiesel	++++	+++	++	+++(+)	+++++	+++++	+++++
Bioethanol (lignocelluloses)	+++	++	++(+)	++	+++	++++	+++(+)
Biomethane/ biogas	++++	+++(+)	++(+)	+++	+++	+++++	+++(+)
FT fuels	++	+	+	+(+)	+++++	+++++	+++++
Biomethanol	+(+)	++	++	++	++	++	++
Dimethylether	++	++	++	++	+	+	++
Biomethane/ bio-SNG	++	++	+++	+++	+++	+++++	+++(+)
Biohydrogen	+(+)	++	++	++	+	+	+

Legend: +++++ very promising, +++ promising, + unfavorable
[a]In terms of complexity of biofuel production (i.e., from biomass treatment to final product)
[b]In terms of biomass input and flexibility regarding capacity as indicator for suitable plant locations
[c](Concept-specific) energetic net efficiency (base current development stage, theoretical considerations)

fermentation like conventional bioethanol (i.e., distillation, purification); therefore, its production could be established adjacent to existing ethanol facilities. Advanced biodiesel and Fischer–Tropsch diesel show very good technical properties that allow them to be blended at any percentage with conventional diesel without the need for modifications. From that point of view, they are considered very promising in terms of infrastructure suitability. This applies also to the biomethane options since both a natural gas grid is already broadly in place and natural gas vehicles are continuously increasing their fleet. The least promising option as it appears from Table 1 is biohydrogen, which requires both high technical effort in terms of production and special vehicle infrastructure (i.e., fuel cells).

Economic Assessment

With regard to requirements for a successful market implementation of future biofuel options, the consideration of economic aspects include the investigation of capital investment requirements, biofuels production costs, and well-to-wheel costs (WTW) at European conditions. This is done for the different future biofuel options in comparison to costs for the conventional biofuels (i.e., biodiesel and bioethanol).

Basic Approach

Typically, economic assessment is aimed to compare different cost alternatives in order to identify relative advantages and determine important influencing factors. Especially with regard to assessing biofuel production costs, dynamic partial models (e.g., based on annuity) can be favorably applied since the accuracy is higher compared to static partial models due to a periodic accounting. The specific cost parameters relevant for biofuel production as well as the basic approach on the annuity model is presented in Fig. 9.

Capital Investment Requirements

Total capital investment (TCI) requirements of biofuels production plants are highly important with regard to financial risks on the one hand side and – as it is the case for more complex biofuel concepts – biofuel production costs on the other.

The determination of total capital investment costs is based on estimations (accuracy of approx. 20–30%) including the method of additional or overhead costs. According to this, plant equipment costs have been determined by up- or downscaling (typical scale factor of approx. 0.7) of existing costs data for similar devices. Moreover, component-specific installation factors

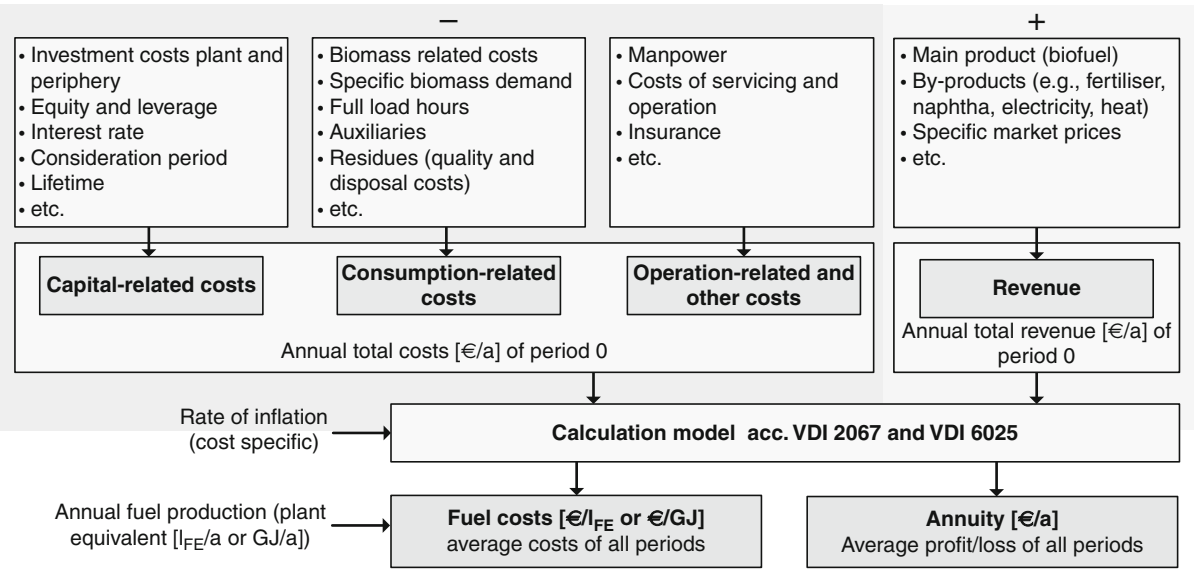

Biofuels: A Technical, Economic and Environmental Comparison. Figure 9
Model for cost calculation of biofuel production costs

(e.g., 1.54–1.66) have to be taken into account. For some components literature data are available; for some components (e.g., that are currently in pilot stage) only rough estimations of technology developers are available. The investment cost figures given were calculated with references from literature. An overview of rough estimations on total capital investment for future biofuel production plants is summarized in Table 2.

With regard to economy of scale, specific total capital investment typically decreases with increasing plant capacity. However, there is a continuous cost increase in the engineering and construction industries, which cannot be reflected at all. The price development of chemical plants and machinery (that also applies to biofuel production plants) is commonly indexed by means of the so-called Kölbel–Schulze methodology. According to this price index, the total capital investment for chemical plants has been increased by approx. 35% in the period from 2000 to 2007.

Biofuel Production Costs

Production costs of future biofuels have been analyzed for exemplary concepts at a database of the time horizon of 2005. The results are summarized in Fig. 10.

As the results of the economic analysis reveal, biofuel production costs show significant differences. Based on GJ fuel equivalent (FE), biomethane options (SNG and biogas) are the most favorable. The sensitivity analyses – carried out for the determination and optimization of cost components that influence the total biofuels production costs – show that feedstock costs (cf. Fig. 11), capital requirements, and the annual full load hours of the plant are strongly important.

Costs for conventional biofuels depend primarily on the prices of agricultural crops, which are relatively volatile and dependent on factors like climatic conditions, agricultural policies, intensification, and mechanization of production. On the other hand, future biofuel options may benefit from the use of residues but this advantage is partially outweighed from the increased supply costs and the more complex logistical aspects as well as the increased capital investments of large facilities. According to the fact that biomass supply depends largely on region-specific conditions, cost for the provision of biomass to the plants can be from 10% to 60% of total biomass supply (i.e., production and provision) costs depending on the favorable location of the plant and the infrastructure to reach it.

It is expected that biofuel production costs will moderately increase in the future due to rising energy prices with expected price effects (e.g., opportunity costs for feedstock providers in the multi-sectoral biomass market) during broad implementation of biofuel strategies. Crude oil and natural gas prices will largely determine the economic competitiveness of biofuels against fossil fuels and set "limits" for feedstock costs above which biofuels cannot compete with conventional gasoline and diesel.

Based on literature and study survey, the bandwidth of available production costs of biofuel options is shown in Fig. 12. Also other studies show that no significant cost reduction for future biofuels can be expected compared to biofuels of the current generation.

Well-to-Wheel Costs

However, for a market implementation not only biofuel production costs but also total driving costs relating to WTW are of importance for end users. Therefore, with regard to the WTW biofuel costs involving costs of fuel distribution (i.e., via pipeline or tank) and vehicles costs of new private cars (i.e., in combustion and hybrid engines, fuel cells, here estimated referring to [39]), the following results (Fig. 13) can be indicated per vehicle kilometer.

According to this, the differences in biofuel production costs will be lowered in terms of total driving costs as – except for fuel cell application – there is a similar cost range for all biofuels, primarily dominated by vehicle use costs. The costs for biofuel distribution play only a minor role. For a number of reasons (e.g., immature large-scale production), the biofuels of the future generation are significantly more expensive when compared to conventional oil-derived fuels such as diesel at total driving costs of approx. 0.33 €/km.

Environmental Assessment

The favorable political environment of the recent years has led to an increasing use of biofuels in the worldwide transportation sector. This development is mainly

Biofuels: A Technical, Economic and Environmental Comparison. Table 2 Overview of total capital investment for selected biofuel options (based on [6, 14, 16, 20, 38, 39])

Biofuel option	Basic plant equipment	Typical (expected) plant size ($MW_{biofuel}$)	Total capital investment (mn EUR)	Specific total capital investment ($EUR/kW_{biofuel}$)
Conventional options				
Biodiesel	Feedstock refinery, (trans)-esterification, biodiesel washing, by-product cleaning, and upgrading (e.g., glycerine, sulfates, methanol recovery), auxiliaries	4–190	0.9–65	190–340
Bioethanol	Feedstock pretreatment, hydrolysis/saccharification, fermentation, distillation/rectification, final upgrading, by-product treatment (e.g., DDGS, bagasse), auxiliaries	7–220	16–300	1,360–2,290
Future options				
Advanced biodiesel	Feedstock refinery, hydrogenation, product separation, auxiliaries	105–1,030	>100	390–470
Bioethanol	Feedstock pretreatment, hydrolysis/saccharification, fermentation, distillation/rectification, final upgrading, by-product treatment (e.g., lignin), auxiliaries	15–185	30–325	1,800–2,000
FT fuels	Feedstock pretreatment (e.g., mechanical, pyrolysis, torrefaction), gasification, gas cleaning and conditioning, FT synthesis, FT upgrading (e.g., hydrocracking), by-product treatment (e.g., naphtha), auxiliaries	>130–220	430–1,000	2,300–3,480
Biomethanol	Feedstock pretreatment, gasification, gas cleaning and conditioning, methanol synthesis, product upgrading (e.g., separation), auxiliaries	126–270	232–330	1,200–1,800
DME	Feedstock pretreatment, gasification, gas cleaning and conditioning, DME synthesis, product upgrading (e.g., destillation), auxiliaries	130–340	290–350	1,030–2,200
Bio-SNG	Feedstock pretreatment, gasification, gas cleaning and conditioning, methanation, final gas upgrading, auxiliaries	23–170	30–170	1,000–2,100
Biomethane/biogas	Feedstock pretreatment, digestion, final gas upgrading, auxiliaries	5–15	7.5–23	1,500–3,000
Biohydrogen	Feedstock pretreatment, gasification, gas cleaning and conditioning, final upgrading, auxiliaries	140–450	220–450	1,000–1,600

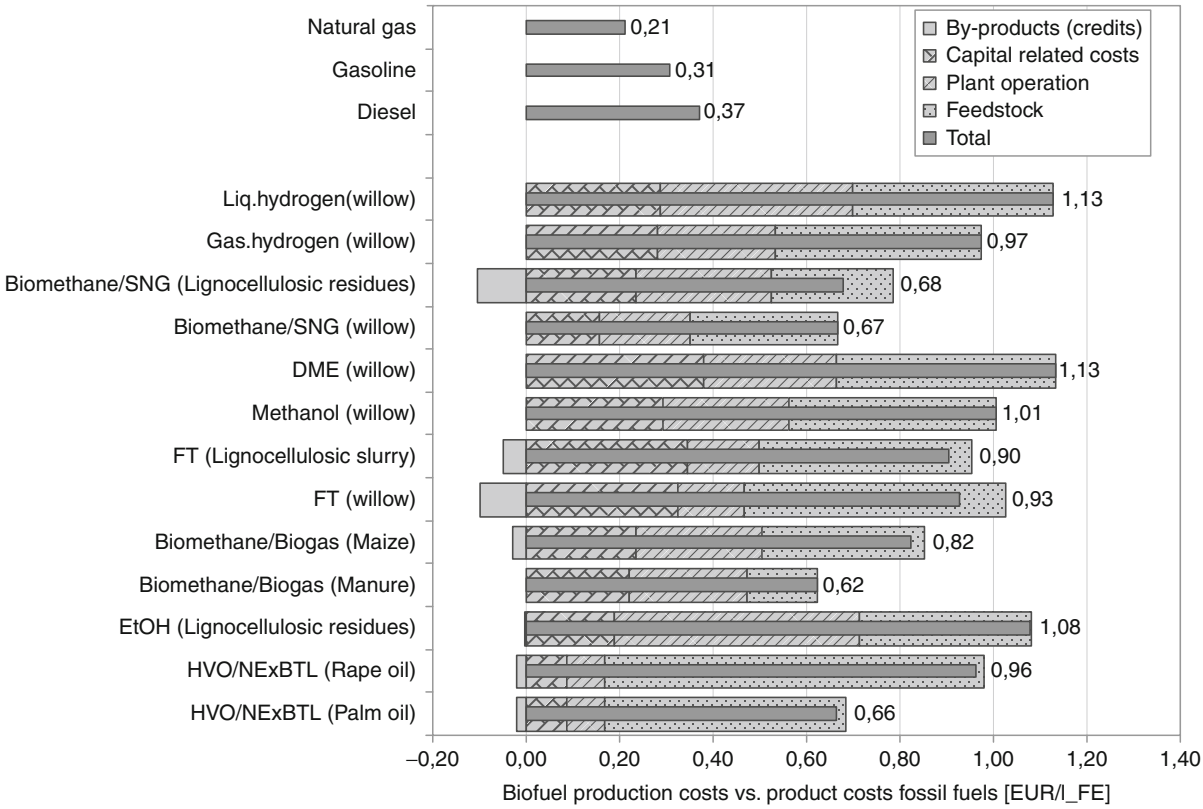

Biofuels: A Technical, Economic and Environmental Comparison. Figure 10
Exemplarily biofuel production costs vs. fossil fuels (refinery product costs)

driven by concerns about the security of energy supplies and the intention to mitigate anthropogenic greenhouse gases (GHG). However, recently, the sustainability of a broad biofuel production and use has been strongly questioned.

To secure especially the reduction of GHG emissions due to the use of biofuels in comparison to fossil fuels and a general sustainability of a broad biofuel production, an expanding biomass usage should also always follow certain sustainability criteria. Next to the environmental impacts related to the biofuel production and usage itself, these criteria should also cover aspects such as biodiversity, the conservation of ecosystems, or the protection of natural safeguards.

As an additional aspect, it is obvious that an increasing use of bioenergy together with a rising demand for food might result in an expanding pressure on limited land resources. A possible consequence of this development could be the displacement of food production caused by the use of arable land for bioenergy production or an expansion of agricultural production (due to the constant demand for food and feed) into areas not previously used for crop production. Such a development might have direct and indirect effects. While the so-called direct land use change emissions can be calculated and related to a certain biofuel, the quantification of indirect effects is even more complicated.

Within the international context, potential environmental impacts of products (e.g., biofuels) or services (e.g., driven kilometer) are often analyzed with the help of a so-called life cycle assessment (LCA).

Most of the available LCA studies for biofuels focus on the environmental impact categories global warming effect and the primary energy demand.

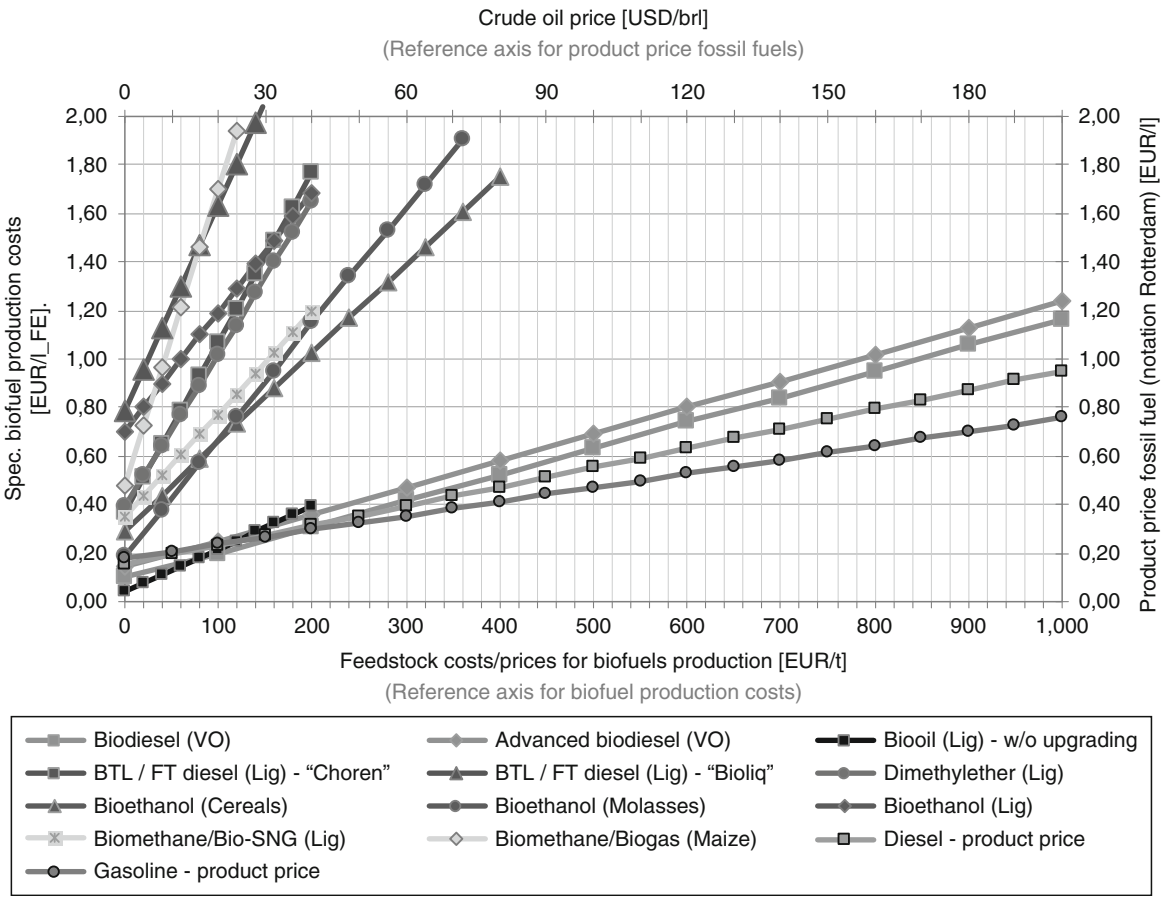

Biofuels: A Technical, Economic and Environmental Comparison. Figure 11
Exemplarily biofuel production costs depending on feedstock costs and in comparison to mineral oil fuel product costs (typical bandwidth approx. feedstock prices: vegetable oils 600–1,200 €/t, cereals 100–250 €/t, molasses 10–120 €/t, wood 50–150 €/t, straw 0–90 €/t, maize silage 25–30 €/t, based on [6, 40, 41])

Below a brief insight on the basics of the LCA methodology and some exemplary results of existing LCA studies for biofuels are provided.

Basic Approach

The environmental performance of biofuels is often described by the LCA methodology. The LCA method is defined within the international standards ISO 14040 [50] and ISO 14044 [51].

Since the methodology of LCA aims to quantify potential environmental impacts throughout the production, use, and disposal of products, the system boundaries of this investigation are very broadly defined. They generally comprise the overall product life cycle, starting with the extraction of raw materials ("from cradle") through to the utilization of the product and the disposal of all intermediate or waste products ("to grave"). The emissions linked to all production processes along the product life are considered. Most LCA studies that investigate potential environmental impacts of biofuel systems cover the whole supply chain of biofuels (Fig. 14).

According to the international standards ISO 14040 and ISO 14044, an LCA consists of four major iterative steps: (1) the goal and scope definition, (2) the life cycle inventory calculation, (3) the life cycle impact assessment, and (4) (result) interpretation.

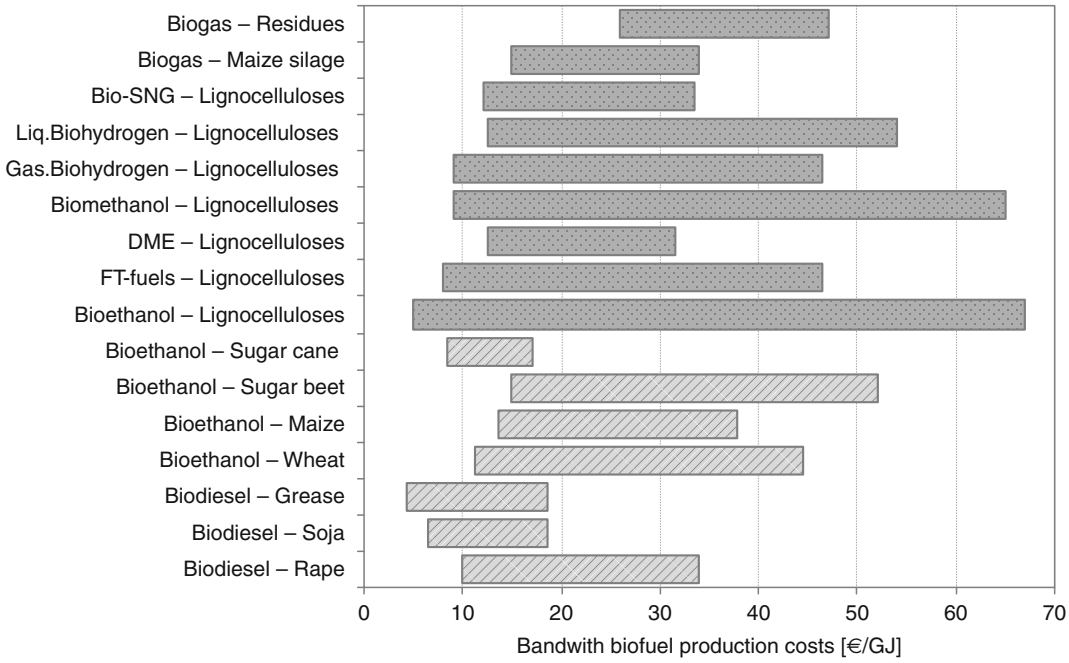

Biofuels: A Technical, Economic and Environmental Comparison. Figure 12
Results of studies on biofuel production costs [39, 42–49]

The goal and scope of definition describes, among others, the underlying questions of the case study and the considered system boundaries and defines the so-called functional unit (e.g., 1 km driven). Additionally, the calculation procedure for the consideration of possible by-products is defined (e.g., allocation or substitution method).

In the life cycle inventory analysis, the inputs of resources, materials, and energy as well as the outputs of products and emissions are investigated and listed for each intermediate step of the production chain. After calculation of all input and output streams, it is possible to identify the amount of emissions related to the overall process chain (including emissions from the production and use of inputs materials and energies).

Within the phase of the life cycle impact assessment, the results of the inventory analysis are associated to specific potential environmental impact categories (e.g., global warming potential) with the help of characterization factors (e.g., the conversion of the different green house gas emissions (GHG) into CO_2 equivalent values using Intergovernmental Panel on Climate Change (IPCC) characterization factors).

The last phase of the LCA is the so-called interpretation phase. Within this phase, the results of the life cycle impact assessment are discussed and conclusions are drawn [50, 51].

Comparison of Existing Results

Most of the available LCA case studies for biofuels focus on the environmental impact categories global warming effect and primary energy demand. Some results published within the available studies that evaluated greenhouse gas (GHG) emissions per driven kilometer (passenger cars) for conventional and future biofuel options are shown in Fig. 15.

Most of the shown results have been calculated based on the approach of the ISO 14040 and ISO 14044 standard. Since this standardized method is very flexible to allow the assessment of all different types of biofuels under various circumstances and changing conditions, this flexibility can lead to

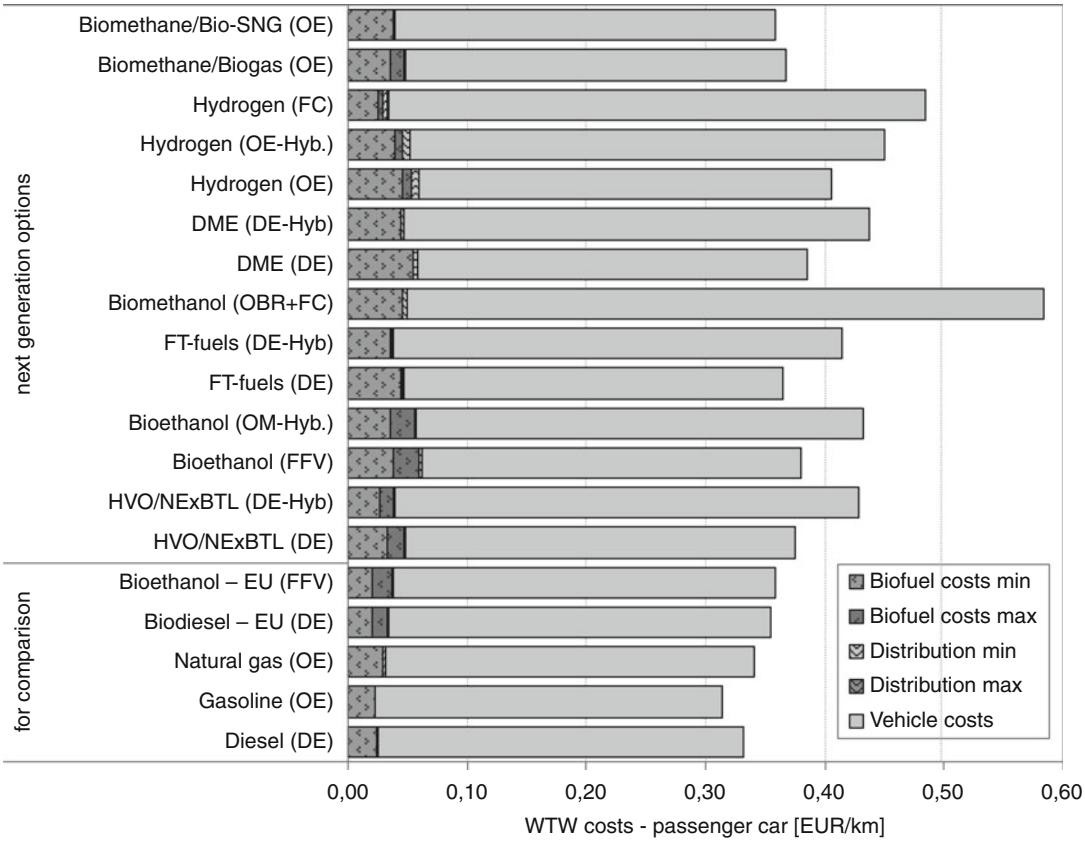

Biofuels: A Technical, Economic and Environmental Comparison. Figure 13
WTW costs (passenger cars) of different biofuel options

significantly varying results. As a consequence, the results from different LCA studies are in most cases very difficult to compare. This is also true for the results shown in Fig. 15.

As one can reveal there are partly large bandwidths of results for each of the different biofuel options. While current biofuel options show moderate GHG savings (in some cases the GHG emissions for biodiesel and bioethanol are even higher than for their fossil reference fuels), results for advanced and future biofuels show the tendency to increase the GHG mitigation potential. However, the results for the future biofuel options have been calculated for theoretical biofuel production concepts still to be demonstrated at commercial scale in most cases.

The main parameters influencing the total LCA result along the well-to-wheel chain are in most cases the production of biomass resources (especially for energy crops that, e.g., require mineral fertilization) as well as the biofuel production process (especially for concepts with a high demand for external process energy). Feedstock transport to the biofuel production plant as well as biofuel distribution and its use commonly show less negative impacts on the overall result.

Table 3 summarizes the main differences between current and future-generation biofuels with regard to the aspects of land use change and land use competition, feedstock cultivation, and nutrient cycle.

Up to now the majority of the available literature sources do not include effects and emissions from land

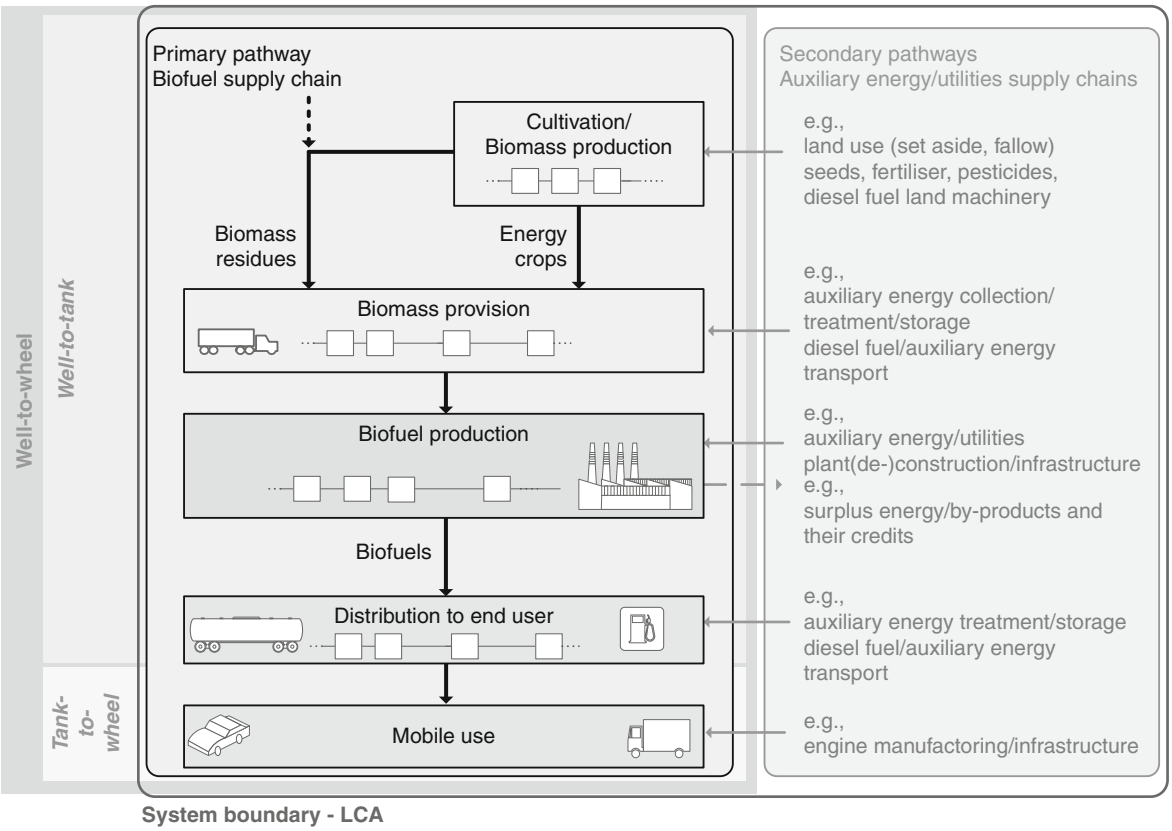

Biofuels: A Technical, Economic and Environmental Comparison. Figure 14
Example for an LCA system boundary to asses a biofuel production chain

use change. Land use change can have an effect on the increase or decrease of carbon stored in the vegetation and the soil of the considered area. Therefore, especially the conversion of areas with a high carbon inventory such as primary forests into agricultural areas can lead to significant CO_2 emissions. The consideration of these effects within a life cycle analysis typically will result in negative results and thus in decreasing potentials for GHG mitigation [57].

However, until now international support policies for transportation biofuels have made no or only minor differentiation according to how they have been produced (e.g., regarding environmental impacts). Thus, some governments partly support biofuels that have a higher negative environmental impact than the substituting fossil product. To ensure at least a minimum level of sustainability requirements for the production and use of biofuels, the European Union introduced different sustainability requirements and standards for biofuels defined within the recently published European Renewable Energy Directive (2009/28/EC). This directive includes standards for a sustainable production of the biomass needed for the biofuel production as well as requirements for a mandatory minimum GHG mitigation. According to this, GHG saving targets or at least a minimum GHG saving for different types of biofuels will be a mandatory requirement at a national and/or European level in the future.

Conclusions

Overall, current biofuels will only provide a niche market (mainly covered by bioethanol and biodiesel

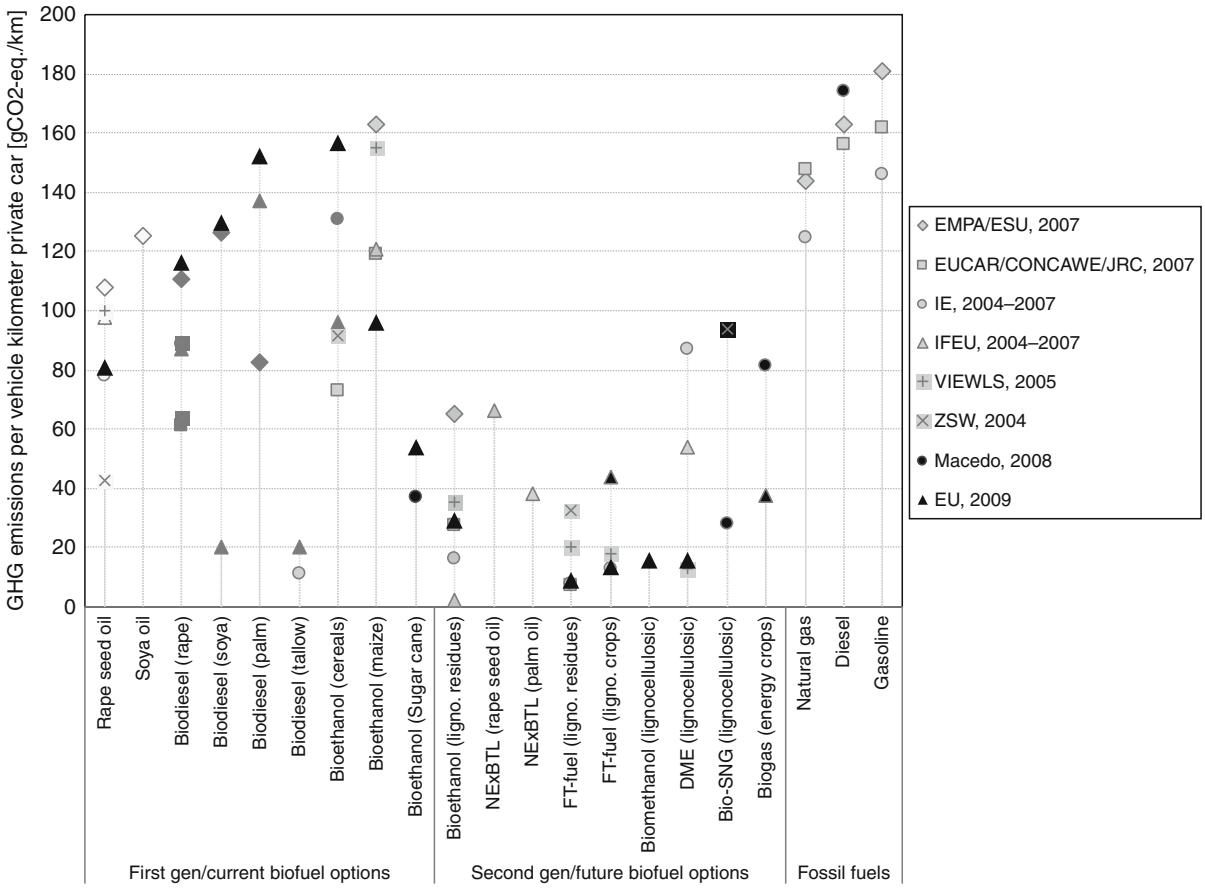

Biofuels: A Technical, Economic and Environmental Comparison. Figure 15
Literature results for GHG emissions (based on EMPA 2007 [52]; EUCAR, 2007 [39]; IE 2004–2007 [53]; IFEU 2004–2007 [12, 46]; Viewls [49]; ZSW 2004 [54]; Macedo 2008 [55]; EU 2009 [56])

until 2020). It is uncertain when next-generation biofuels will be a viable alternative and when significant production can be expected. It is certain that next-generation biofuels firstly will enter the market in the EU or the US before being introduced within developing countries. However, biofuels and bioenergy more generally have to increase in relevance in future in order to meet the energy and environment requirements in an efficient way. It is important to analyze and assess the real potentials of biofuels under consideration of region-specific frame conditions and sustainability criteria, since no biofuel option is suitable for all regions at all.

From a technical point of view, each biofuel option shows different benefits and drawbacks. Thus there is no silver bullet for biofuel; each of them needs to be considered with regard to available feedstock, surrounding available infrastructure, and demand of the market. Current options like bioethanol from sugar and starch as well as conventional biodiesel from oil crops and animal fats are market mature. Options like advanced biodiesel (HVO) and biomethane via biogas enter the market. And production concepts for biofuel option of the future generation are currently in laboratory (e.g., biohydrogen) to pilot and demonstration stage (e.g., bioethanol, Fischer–Tropsch fuel, dimethylether, and bio-SNG). Thus, further R&D&D is required with

Biofuels: A Technical, Economic and Environmental Comparison. Table 3 Main differences regarding environmental impacts of current and future biofuels

Issue	Current biofuels (first generation)	Future biofuels (second generation)
General database	Database on biofuel value chains are available based on practical experiences	Only limited database on biofuel value chains since they have not been demonstrated in practice at present, most of applied data background is based on theoretical concepts
Land use change/land use competition	Land use change has taken place	Potential of land use change, for example, from degraded land to arable land
	Feedstock cultivation on arable land that increase land use competition with food and fodder production	Potential feedstock cultivation (e.g., of perennials) on land which is not suitable for conventional agriculture; decrease of land use competition
		However, land is bounded for several years when applying perennial cropping
Cultivation	Intensification due to increased use of fertilizer and pesticides as well as increased use of water; thus, higher environmental implications	Potential decrease in cultivation due to decreased used of fertilizer, pesticides and water; thus, potential to lower environmental applications
Nutrient and humus cycles	By-products (e.g., straw, press cake, glycerine, fertilizer, DDGS) can be used for farming; thus, potential of closed nutrient and humus cycles	Use of the whole plant for biofuel production may lead to additional expenditures to achieve an well-balanced nutrient and humus cycle
		Usually no by-products that can be applied within the agricultural sector

regard to (1) further development and use of promising biofuel concepts in practice, (2) upscaling to medium- and large-scale plants, (3) the use of approved system components and demonstration of efficient interaction, and (4) plant operability and reliability. For a successful market implementation, existing techno-economic barriers have to be overcome and capital risks need to be minimized.

From an economic point of view, biofuels have so far required state support in order to be cost competitive with current fossil fuels. Feedstock production costs and their dependence on energy prices and climatic conditions are the factor that influences production costs of current biofuels the most (up to 70%). For future biofuels, these costs will play a smaller role, if residues and waste are used as feedstock but the supply and handling of large amounts to upscaled facilities will increase the complexity of logistics and balance this advantage. On the other hand, dedicated cultivation of lignocellulosic feedstock like short rotation forestry will again add up to the feedstock production and supply costs. Furthermore, the large capital investment associated with large plant sizes increase the risk of investment; therefore, economic viability will require the identification of an ideal location where a secure market for the product and a long-term continuous supply of feedstock can be guaranteed. In addition to that, complex conversion procedures (e.g., simultaneous C5 and C6 fermentation) increase the operating costs and subsequently total production costs. For all these reasons, future-generation biofuels are not expected to be cost competitive at least in the short term. However, ongoing research and development is expected to reduce the conversion costs and allow production in large commercial scale that would allow benefiting from economies of scale.

From the environmental point of view, all biofuels need to be analyzed and assessed regarding their environmental impacts. The political introduction of sustainability criteria for the production and use of biofuels, including minimum GHG mitigation threshold values could lead to a promotion of biofuels with favorable GHG footprints. Concerning these aspects, especially future biofuel options based on lignocellulosic feedstock or residues seem to be very promising. In general, it has to be noted that the current sustainability debate on biofuels is mainly focused on the impact category of global warming. However, an efficient and sustainable biofuel strategy should also consider other environmental aspects such as biodiversity and the protection of natural ecosystems.

Future Directions

An environmentally friendly transportation sector can only be realized by a combination of measures such as the development of new vehicle technologies, the provision of new infrastructure networks, and the application of alternative fuels. Nowadays, biofuels are the only way to substitute fossil fuels and contribute to the mitigation of greenhouse gas emissions within the transportation sector. For these reasons, their role is expected to increase, reckoning at the same time that fossil fuels will remain the dominant fuel option in the near future. Medium- and long-term research is focused nowadays to future-generation biofuels that use also residual feedstock and minimize problems associated with current generation biofuels. Some of these options are in a pilot or demonstration phase (e.g., lignocellulosic ethanol, biosynthetic fuels) and research funding in an international scale in areas like biomass gasification and gas cleaning, methanation, enzymatic hydrolysis of lignocellulose, simultaneous saccharification of C_5 and C_6 sugars will increase the potential for commercial application in the years to come. Other options like biohydrogen are closely linked to the development of vehicle infrastructure (e.g., fuel cells, batteries) and their implementation is interdependent. Similarly, electro-mobility that is surrounded with high hopes requires the development of both the vehicle fleet and the infrastructure network, a fact that places its implementation in the long term. Of great importance within this context is that electricity is produced from renewable sources, so that electromobility actually makes a difference in the transport sector.

On the biomass supply side, future research will focus on the sustainable use of all residue and waste sources for the production of future-generation biofuels. This will be complemented by the sustainable use of land for large-scale production of lignocellulosic crops, such as short rotation forestry or miscanthus; this combination should be able to secure the continuous supply of future-generation facilities that require large amounts of biomass.

Considering sustainability of production and the biomass use itself, the goal for the future is to use the largest possible amount of the initial feedstock, in other words maximize the biomass use efficiency. For that reason, the concept of biorefineries receives nowadays increasing attention and is expected to be the focus of research in the future. Following the example of conventional refineries, biorefineries use biomass as feedstock and produce an array of marketable products by integrating processes and processing all product streams. These products include biofuels, feed, food, heat, electricity, chemicals, polymers, and others. The term "biorefinery" as such is recently introduced but certain facilities that have used this principle are known for years (e.g., pulp and paper mills). Nowadays, the term is expanded and used in a wider sense and a different number of biorefinery concepts have been introduced. Within this context, future goal is to integrate existing processes with new technologies and thereby increase the opportunities for a more efficient biomass use.

Bibliography

1. Majer S, Mueller-Langer F, Zeller V, Kaltschmitt M (2009) Implications of biodiesel production and utilisation on global climate – a literature review. Eur J Lipid Sci Technol 111:747–762, WILEY-VCH Verlag GmbH & Co. KGaA, Weinheim
2. International Energy Agency (2010) Sustainable production of second generation biofuels potential and perspectives in major economies and developing countries. OECD/IEA
3. United Nations Industrial Development Organization (2007) Sustainable biofuels production and use – with focus

on Africa. Presentation, Eastern and Southern Africa regional workshop on biofuels – UNEP, Nairobi, June 2007
4. United Nations Conference on Trade and Development (2008) Making Certification Work for Sustainable Development: The Case of Biofuels. UNCTAD/DITC/TED/2008/1, United Nations, New York
5. International Energy Agency (2007) World energy outlook 2007. IEA, Paris. ISBN: 978-92-64-02730-5
6. German Biomass Research Centre (2010) Own calculations and data base available. Leipzig 2007 to 2010, Germany
7. Kaltschmitt M, Hartmann H, Hofbauer H (2009) Energie aus Biomasse – Grundlagen, Techniken und Verfahren. 2. neu bearbeitete und erweiterte Auflage. Springer, Berlin
8. Worldwatch Institute (2007) Biofuels for transport: Global potential and implications for sustainable energy and agriculture. Worldwatch Institute, Earthscan
9. IEA Bioenergy (2008) Gaps in the research of 2nd generation transportation biofuels. IEA Bioenergy, T41(2): 2008:01
10. European Biofuels Technology Platform (2008) Strategic research agenda and strategy deployment document. January 2008
11. Neste Oil Corporation (2005) NExBTL – Biodiesel fuel of the second generation. SAE Technical Paper Series No. 2005-01-3771
12. Reinhardt G (2006) An assessment of energy and greenhouse gases of NExBTL. Institute for Energy and Environmental Research GmbH by order of the Neste Oil Corporation, Porvoo/Heidelberg
13. Huber GW, Corma A (2007) Synergien zwischen Bio- und Ölraffinerien bei der Herstellung von Biomassetreibstoffen. Angew Chem 119:7320–7338, Wiley-VCH Verlag GmbH & Co KGaA, Weinheim, 2007
14. Hamelinck C (2004) Outlook for advanced biofuels. PhD thesis, UniversityUtrecht
15. Igelspacher R (2006) Methode zur integrierten Bewertung von Prozessketten am Beispiel der Ethanolerzeugung aus Biomasse. IfE Schriftenreihe, Heft 51, Lehrstuhl für Energiewirtschaft und Anwendungstechnik, Technische Universität München, ISBN 3-933283-43-4, München
16. Schmitz N (2003) Bioethanol in Deutschland – Verwendung von Ethanol und Methanol aus nachwachsenden Rohstoffen im chemisch-technischen und im Kraftstoffsektor unter besonderer Berücksichtigung von Agraralkohol. Studie im Auftrag des Bundesministeriums für Ernährung und Landwirtschaft und des Projektträgers Fachagentur Nachwachsende Rohstoffe (FNR), Schriftenreihe "Nachwachsende Rohstoffe", Band 21, Landwirtschaftsverlag GmbH, Münster
17. Schmitz N (2005) Innovationen bei der Bioethanolerzeugung und ihre Auswirkungen auf Energie- und Treibhausgasbilanzen. Studie im Auftrag des Bundesministeriums für Verbraucherschutz, Ernährung und Landwirtschaft sowie des Projektträgers Fachagentur Nachwachsende Rohstoffe (FNR), Schriftenreihe "Nachwachsende Rohstoffe", Band 26, Landwirtschaftsverlag GmbH, Münster
18. Roehr M (2001) The biotechnology of ethanol – Classical and future applications. Wiley-VCH Verlag GmbH, Weinheim
19. Mueller-Langer F, Vogel A, Kaltschmitt M, Thraen D (2007) Analysis and evaluation of the 2nd generation of transportation biofuels. In: 15th European biomass conference and exhibition – from research to market development, Berlin, May 2007
20. Ekbom T, Lindblom M, Berglin N, Ahlvik P (2003) Technical and commercial feasibility study of black liquor gasification with methanol/DME production as motor fuels for automotive uses – BLGMF. Nykomb Synergetics AB, Chemrec, Volvo, Ecotraffic, OKQ8, STFi; Methanex, Final Report, Altener Programme
21. Tijmensen M, Faaij A, Hamelinck C, Van Hardeveld M (2002) Exploration of the possibilities for production of Fischer-Tropsch liquids and power via biomass gasification. Biomass and Bioenergy 23:129–152
22. Saller G (1999) Technisch-wirtschaftliche Bewertung der Methanolerzeugung aus Biomasse mit Hilfe von Prozessmodellen. Siegen
23. Hoehlein B et al (2003) Methanol als Energieträger. Forschungszentrum Jülich GmbH, Institut für Werkstoffe und Verfahren der Energietechnik (IWV), Schriften des Forschungszentrums Jülich Reihe Energietechnik Band 28, ISBN 3-89336-338-6, Jülich
24. Cheng WH, Kung HH (1994) Methanol production and use. Marcel Decker, New York
25. Fachagentur Nachwachsende Rohstoffe e.V. (2004) Handreichung Biogasgewinnung und -nutzung. Institut für Energetik und Umwelt gGmbH in Kooperation mit der Bundesforschungsanstalt für Landwirtschaft und dem Kuratorium für Technik und Bauwesen in der Landwirtschaft e.V., Leipzig
26. Institut für Energetik und Umwelt (2005) Evaluierung der Möglichkeiten zur Einspeisung von Biogas ins Erdgasnetz. Endbericht, Leipzig
27. Scholwin F, Hofmann F, Plaettner A (2007) Biomethane from biogas: expectations from established vs. new technologies. In: Lechner P (ed) Waste matters. Integrating views; proceedings of 2nd BOKU waste conference 2007, Vienna, 17–19 April 2007, S.185–S.194. ISBN 978-3-7089-0060-5
28. Seiffert M, Vogel A, Hofbauer H, Kaltschmitt M, Stucki S (2007) Demonstration of the production and utilization of synthetic natural gas (SNG) from solid biofuels – presentation of the European project "Bio-SNG". In: 15th European biomass conference and exhibition – from research to market development, Berlin, May 2007
29. Perry M, Eliason D (2004) CO_2 recovery and sequestration at Dakota Gasification Company – a progress report. Gasification Technologies Council, Arlington
30. Technische Universität Wien (2005) Energiezentrale zur Umwandlung von biogenen Roh- und Reststoffen einer

Region in Wärme, Strom, Bio-SNG und flüssige Kraftstoffe. Institut für Verfahrenstechnik, Umwelttechnik und Technische Biowissenschaften, TU Wien, Endbericht, September 2005
31. Ranke H, Schoedel N (2004) Hydrogen production technology – status and new developments, OIL GAS European Magazine 01/04. Urban Verlag GmbH, Hamburg
32. Mueller-Langer F, Tzimas E, Kaltschmitt M, Peteves S (2007) Techno-economic assessment of hydrogen production processes for the hydrogen economy for the short and medium term. Int J Hydrogen Energy 32(16): 3797–3810
33. Contadini JF, Diniz CV, Sperling D, Moore RM (2000) Hydrogen Production Plants: Emissions and Thermal Efficiency Analysis. Institute of Transportation Studies, University of California
34. Lurgi (2003) Hydrogen. Brochure of Lurgi Oel Gas Chemie GmbH
35. Makihira A, Barreto L, Riahi K (2003) Assessment of alternative hydrogen pathways: natural gas and biomass. International Institute for Applied Systems Analysis, Austria
36. Molburg JC, Doctor RD (2003) Hydrogen from steam-methane reforming. In: Proceedings of the 20th annual international pittsburgh coal conference, Pittsburgh, 15–19 September 2003. Argonne National Laboratory
37. Altmann M, Stiller C (2001) Wasserstofferzeugung in offshore Windparks "Killer-Kriterien" – grobe Auslegung und Kostenabschätzung. Studie im Auftrag der Gesellschaft für Energie und Ökologie mbH, Ottobrunn
38. Ekbom T, Berglin N, Lögdberg S (2005) Black liquor gasification with motor fuel production – BLGMF II, A techno-economic feasibility study on catalytic Fischer-Tropsch synthesis for synthetic diesel production in comparison with methanol and DME as transport fuels. Nykomb Synergetics AB, STFi-Packforsk, KTH Royal Institute of Technology, Statoil, Structor Hulthén Stråth, Final report
39. EUCAR, CONCAWE, JRC/IES (2007) Well-to-wheels analysis of future automotive fuels and powertrains in the European context. European Commission, Version 2c
40. Food and Agricultural Policy Research Institute (FAPRI) (2008) Agricultural outlook 2007/2008. Ames (Iowa)
41. Organisation for Economic Co-Operation and Development, Food and Agriculture Organization of the United Nations (2008) OECD-FAO agricultural outlook 2008–2017, highlights. OECD, Paris
42. Doornbosch R, Steenblik R (2007) Biofuels: is the cure worse than the disease? Round table on sustainable development. Organisation for Economic Co-operation and Development, OECD, SG/SD/RT(2007)3, Paris
43. Gangl C (2004) Ethanolerzeugung aus stärkehaltigen Rohstoffen zur Treibstoffzwecke. Diplomarbeit, Universität für Bodenkultur, Wien
44. Hamelinck CH, Hooijdonk GV, Faaij APC (2003) Prospects for Ethanol from lignocellulosic Biomass: techno-economic performance as development progresses. University Utrecht, Utrecht
45. Kavalov B, Peteves SD (2005) Status and perspectives of biomass-to-liquid fuels in the European Commission. European Commission Directorate General Joint Research Centre (DG JRC) Institut for Energy, Petten
46. Quirin M, Gaertner SO, Pehnt M, Reinhardt GA (2004) CO_2-Studie – CO_2-neutrale Wege zukünftiger Mobilität durch Biokraftstoffe: Eine Bestandsaufnahme. Institut für Energie- und Umweltforschung Heidelberg GmbH (IFEU), Studie im Auftrag der Forschungsvereinigung Verbrennungskraftmaschinen (FVV), Heft 789, Frankfurt am Main
47. Schmitz N, Henke J, Keppler G (2006) Biokraftstoffe eine vergleichende Analyse. Fachagentur Nachwachsende Rohstoffe e. V. (Hrsg.) mit finanzieller Förderung des Bundesministeriums für Ernährung, Landwirtschaft und Verbraucherschutz, Gülzow
48. Thuijl EV, Roos CJ, Beurskens LWM (2003) An overview of biofuel technologies, markets and policies in Europe. Energy Research Centre of the Netherlands-ECN
49. Wakker A et al (2006) Biofuel and bioenergy implementation scenarios. Final report of VIEWLS WP5, modelling studies. Senter Novem, Petten
50. ISO (2006) DIN EN ISO 14040: environmental management – life cycle assessment – principles and framework
51. ISO (2006) DIN EN ISO 14044: environmental management – life cycle assessment – requirements and guidelines
52. Zah R, Boeni H, Gauch M, Hischier R, Lehmann M, Wäger P (2007) Ökobilanz von Energieprodukten: Ökologische Bewertung von Biotreibstoffen. Empa – Abteilung Technologie und Gesellschaft, Bern, Mai
53. Brauer S, Vogel A, Mueller-Langer F (2008) Cost and life-cycle analysis of biofuels. Long version. Institute for Energy and Environment gGmbH (IE) on behalf of Union for the Promotion of Oil and Protein Crops (UFOP), Leipzig
54. Specht M, Zuberbuehler U, Bandi A (2004) Kraftstoffe aus erneuerbaren Ressourcen – Potentiale, Herstellung, Perstpektiven. Nova Acta Liopoldina NF 91(339)
55. Macedo IC, Seabra JEA et al (2008) Green house gases emissions in the production and use of ethanol from sugarcane in Brazil: the 2005/2006 averages and a prediction for 2020. Biomass Bioenergy 32(7):582–595
56. Directive 2009/28/EC of the parliament and of the council on the promotion of the use of energy from renewable sources and amending and subsequently repealing Directives 2001/77/EC and 2003/30/EC, Brussels, 23 April 2009
57. Intergovernmental Panel on Climate Change (2003) Good practice guidance for land use, land-use change and forestry [Penman J, Gytarsky M, Hiraishi T, Krug T, Kruger D, Pipatti R, Buendia L, Miwa K, Ngara T, Tanabe K, Wagner F (eds)]. Institute for Global Environmental Strategies (IGES) for the IPCC, Kanagawa. ISBN 4-88788-003-0

Biofuels: Upgraded New Solids

Marco Klemm[1], Ralf Schmersahl[2,3], Claudia Kirsten[1], Nadja Weller[1]
[1]German Biomass Research Centre (DBFZ), Leipzig, Germany
[2]Deutsches BiomasseForschungsZentrum GmbH German Biomass Research Centre (DBFZ), Leipzig, Germany
[3]Institute of Agricultural Engineering Bornim e.V. (ATB), Potsdam, Germany

Article Outline

Glossary
Definition of the Subject and its Importance
Introduction
Pelletizing and Briquetting
Torrefaction
Hydrothermal Carbonization
Summary and Future Directions
Bibliography

Glossary

Upgraded solid biofuel is a solid fuel, which is produced in a technical process, using biomass as feedstock.

Pelletizing is the process of compressing material into the shape of a pellet.

Briquetting is a process of forming briquettes or compacts under pressure with bigger and other sizes than pellets.

Torrefaction is a mild pyrolysis process performed at temperatures between 200°C and 300°C within an inert atmosphere.

Hydrothermal carbonization is a process for the production of a solid fuel in hot pressurized water.

Biocoal is a solid fuel produced by hydrothermal carbonization

Definition of the Subject and its Importance

For the energetic use of biomass, a number of combustion and gasification processes exist. Especially high efficient processes, often developed for the use of coal, have very strict fuel requirements. In many cases, "classical" solid biofuels (like wood logs, wood chips) cannot fulfill the requirements of these conversion processes. The solution is the adaption of the fuel properties to meet the process requirement by a pretreatment step. The results are upgraded "new" solid biofuels suitable for highly sophisticated conversion processes.

A second driver for biomass pretreatment is the increased demand for biomass as a renewable energy carrier. Therefore it is necessary to utilize also organic mass streams with low quality, e.g., leaves, bark, straw, and hay. Biomass pretreatment alters the transport, storage, and handling characteristics of solid biofuels, as well as their combustion and gasification properties. In doing so, it enables enhanced utilization routes for lignocellulosic biomass resources. Whilst briquetting and pelletizing mainly adapt physical properties of the fuel, torrefaction and hydrothermal carbonization (HTC) also change chemical properties and produce a more coal-like solid biofuel.

Introduction

For the production of upgraded "new" solid biofuel, three main pathways are of major importance:

- Agglomeration as physical process including briquetting and pelletizing
- Torrefaction
- Hydrothermal carbonization as thermochemical processes

Although the products are comparable, the processes have completely different properties.

Briquetting is a well-known process where milled and often fine-particle biomass is compressed interfacially under high pressure. Pelletizing is a process with established technical equipment arising from the animal feed industry. By the end of the last decade, the process was adapted for the production of wood pellets. Today the pelletizing process is of great relevance for the development of alternative biomass pellets (i.e., agro-pellets).

Torrefaction is a mild pyrolysis process performed at temperatures between 200°C and 300°C within an inert atmosphere. Torrefied biomass contains typically 60–70% of the initial mass and 90% of the initial energy content (LHV). Benefits of torrefied biomass compared with green biomass are increased energy density and homogeneity, improved grindability, pronounced hydrophobic character, and enhanced reactivity.

The properties of torrefied biomass allow for the substitution of coal in existing gasification and combustion plants with low retrofitting requirements.

Hydrothermal carbonization is performed in pressurized hot water at 170–250°C using an acidic catalyst. The product is suspended in water resulting in additional efforts for separation and drying. Possible products of hydrothermal carbonization are either functional carbonaceous materials for a variety of applications or solid biofuels with properties similar to lignite.

The main historical keywords for the three pathways are:

- Agglomeration:
  - Briquettes are long-established upgraded solid fuels, especially based on coal.
  - 1970s: first small scale pellet heating units build in the USA.
  - Late 1970s: first pellet plants in Europe.
  - Middle/end of the 1990s: strongly increasing market importance.
  - Today: Wood pellets are a popular fuel for heating systems for households as well as for co-combustion in coal fired CHP-plants in various especially European countries.
- Torrefaction:
  - Last centuries: research on dry thermal upgrading of solid fuels based on charcoal and coke production.
  - Since the 1980s: scientific investigation of biomass torrefaction.
  - 1987: first commercial scale torrefaction plant by Le Bois Torrefie du Lot, a subsidiary of Pechiney (for economic reasons, the plant was decommissioned in the beginning 1990s).
  - Today: commercialization of first plants for pretreatment of biomass for co-firing, gasification, and pelletizing, as well as for better transportation and storage.
- Hydrothermal carbonization:
  - 1913: hydrothermal transformation of biomass into a coal-like product described by Bergius
  - In the 1920s, 1930s and 1960s: ongoing scientific investigation
  - Since 1995: development of a process for the hydrothermal use of waste biomass like sewage sludge by EnerTech (USA) and Mitsubishi (Japan)
  - 2008: first pilot-plant employing the SlurryCarb™-process in Rialto, USA
  - Today: investigation and commercialization of lower temperature hydrothermal carbonization especially in Germany

Pelletizing and Briquetting

Principles

Agglomeration is defined as a process that brings loose material (particles or fibers) together to agglomerated products with designated form and properties. Caused by the mechanical contact and the physical binding mechanisms a size enlargement compared to the original material is achieved whereas the free particle surface area is reduced. Usually, pressure agglomeration processes like briquetting and pelletizing are used to improve the mechanical and physical properties of solid biofuels. The main benefits of such a compressing are:

- Improvement of the flow, the dosing and conveying properties of the material
- Increase of the bulk density and for this reason reduction within the transport expenses
- Removal of the risk of solidification and bridging of fine bulk solids during transport and storage
- Decrease and removal of dust in the bulk good, reducing dust explosion risks
- Decrease of material loss and prevention of product losses, e.g., caused by oxidation and microbiological decomposition
- Stabilization and homogenization of heterogeneous mixtures of materials, e.g., for the development of blended pellets
- Improved thermal and combustion properties

Briquetting is a common process where milled and fine-particle biomass is compressed interfacially under high pressure. The friction between the material and the press mold releases heat, which activates the binding forces between the particles. The feasibility of briquetting depends on the plasticity of the biomass. The harder and more brittle the material is, the more binding agents are needed to form bridges between the particles. The addition of binding agents is mostly not required for biomass briquetting [1].

Pelletizing is another process for the agglomeration of biomass, where grinded biomass is compacted to pellets by pressure agglomeration. Similar to the briquetting process, the material needs to be plastic or deformable. Friction between the material and the friction channel leads to heat release responsible for the activation of binding forces. Additionally, the material needs an adequate moisture content, which in the easiest case can be achieved by adding water.

Depending on the feedstock and the agglomeration process different binding mechanisms and forces are relevant for the adhesiveness of individual particles (Fig. 1). The understanding of these binding mechanisms during pressure agglomeration is important since optimal particle and fiber bonds in agglomerates cause good physical and mechanical properties. Major binding mechanisms are [2–4]:

- Solid bridges caused by sintering, partial melting, chemical reaction, recrystallization of dissolved substances, hardening binders etc.
- Adhesion and cohesion forces by non-free-moving liquids, highly viscous binders, and adsorption layers (<3 nm thickness)
- Adhesion, surface tension, and capillary pressure by free-moving liquids in pendular, capillary, or funicular state

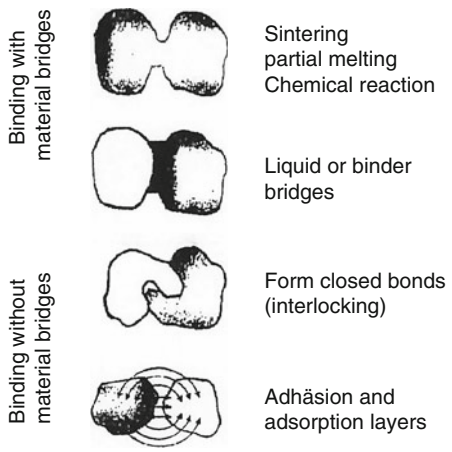

Biofuels: Upgraded New Solids. Figure 1
Illustration of selected binding mechanisms [4]

- Attraction forces between solids – molecular forces like van der Waals forces, free chemical bonds and associations
- Interlocking bonds

The agglomeration of fiber material like wood and herbaceous biomass is mostly based on interlocking bonds. Caused by pressure agglomeration the fibers twist, weave, and bend around each other forming a kind of mesh. Additionally, the formation of interlocking bonds is favored because of the high pore volume. Agglomerates like woody and herbaceous pellets, which mainly stick together by interlocking bonds and which are formed by pressure agglomeration, do not require the use of binding agents during the agglomeration process. However, binders reduce the abrasion of dies as well as the energy consumption. Therefore they are often used.

If the binding strengths achieved by the agglomeration process are too weak, the particle sizes are too large, or certain agglomerate characteristics have to be obtained, additives can be used. Additives are solid or liquid materials causing additional bindings through solid bridges or adhesion forces.

Low viscous liquids like water, which is the cheapest and most common additive, are motile and adsorb on the surface of the particles. If the proportion of the liquid is small, individual liquid bridges develop between the particles. The more fluid disperses between the particles, the higher the cohesion of the agglomerate becomes caused by the capillary pressure. Therefore, steam is used to produce liquid bridges forming solid bridges during the cooling process. Furthermore, steam preheats the material and increases the moisture content. This reduces the energy demand and provides higher stability [5, 6].

However, each process and material requires different moisture levels since too high liquid contents decrease the quality of the agglomerates. In contrast to these mechanisms, binding agents with a high viscosity (like molasses) inhibit the formation of capillary forces. Adhesion forces between the particles and the binding agent are formed instead. Since these forces are more intense, the agglomerates can be more strained. Additionally, binding agents can form solid bridges [4, 7]. Binding agents commonly used in wood pelletizing are wheat, maize starch, and thermally treated starch flour [1].

Pelletizing and Briquetting Processes

Agglomeration processes consist of individual process steps largely similar for the production of either briquettes or pellets. Figure 2 presents the entire process chains involving several biomass conditioning and post treatment steps.

The pressure agglomeration itself is achieved by applying external forces to particles in different shaped dies to form enlarged agglomerates. Table 1 provides an overview of established technologies.

Briquettes are fabricated either by punch-and-die presses or by extrusion presses. Pelletizing is usually done with roller presses. These roller presses can be subdivided in presses with one or two rollers. Double-roller presses have been originally developed for the agglomeration of coal and are often used for finely divided solids. Because of the low retention time and temperatures non-biomass briquettes can be produced with these presses. The industrial production of wood pellets mainly uses roller presses generally operating with tree rollers; they are called pellet mills or pellet machines.

Properties of Biomass Pellets and Briquettes

To utilize biomass as a fuel, the chemical properties and the properties like heating value and water and ash content need to be well known. Besides these mass-specific properties, the mechanical-physical properties, which can be influenced by the compaction process, are of importance (Table 2). Furthermore, these properties are used to evaluate the quality of a compaction process and of the produced pellets and briquettes.

Besides these properties, the physical properties of the raw material like the particle size distribution and the water content influence the quality of the compaction process. Therewith they influence the quality of the compressed fuels similarly to the compaction process.

Caused by their great relevance for combustion processes, the mechanical and physical properties of solid biofuels are standardized, like for wood pellets and briquettes in DIN 51731, DIN plus, or ÖNORM M 7135 (Table 3). Currently these values and standards are adapted on EU level in EN 14961 and its quality standards. Besides wood, the standard will also include values for nonwoody biomass pellets not regulated so far. Additional standardization activities have been carried out in some EU countries (like Austria) developing pre-standards like ÖNORM C 4000 for compressed Miscanthus and ÖNORM C 4002 for compressed straw (Table 4). These values are considered to evaluate the quality of briquettes and pellets produced out of other raw materials, like different straw types, hay, and rape press cake (Tables 5 and 6).

The required properties of the above-mentioned standards can be kept if the production process is

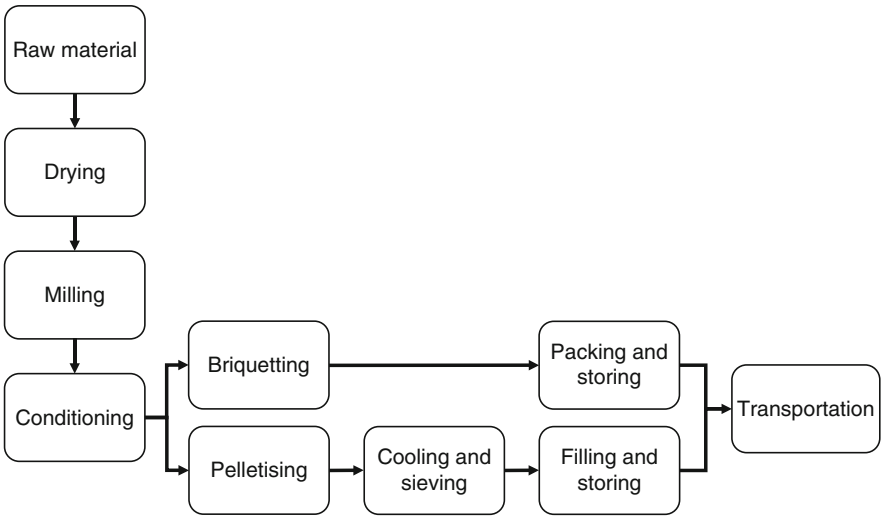

Biofuels: Upgraded New Solids. Figure 2
Production process of pellets and briquettes

Biofuels: Upgraded New Solids. Table 1 Classification of agglomeration processes according to their active principle

Punch-and-die press [8, 9]	
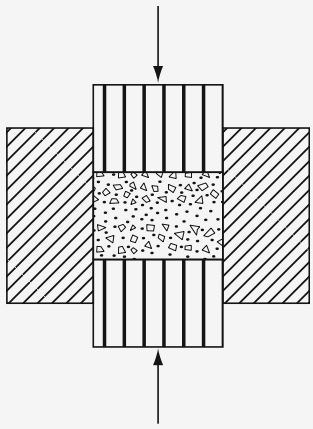	– Material is compressed with high pressure in closed and differently formed dies
	– One or two punches are possible, usually one punch from above with variable travel
	– Pressure induced hydraulically
	– Low friction, no cooling required
	– Briquettes often rectangular, stackable
Ram extrusion press [8–10]	
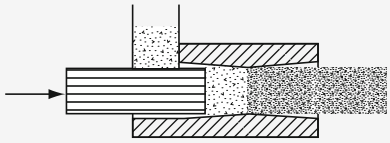	– Material pushed towards a cylinder by a ram
	– Loose material is punched against already initially compressed material
	– Compression and re-expansion leads to plastic deformation
	– Good adjustment of back pressure and friction
	– Briquettes round or of orthogonal profiles
	– suitable for elastic materials
Screw extrusion press [8, 11]	
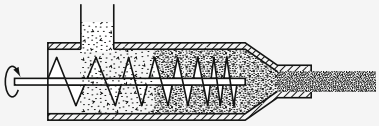	– Compression by single- or double-screw extruders where the pressure is generated by decreasing the screw thread
	– Allows high briquette qualities
	– High frictional resistance, higher energy consumption
	– Shape of the briquettes depends on extruder
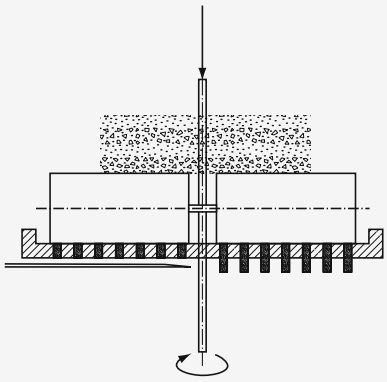	– common for animal feed pellets
	– Feed enters the press from above, falls down by gravity and is diverted evenly to the rollers and the track of the die
	– Even material densification, uniform extrusion
	– Pellets are homogeneous
	– Length adjustment by cutters underneath the die

Biofuels: Upgraded New Solids. Table 1 (Continued)

Pellet mill with ring die and press rollers [8, 13–15]	
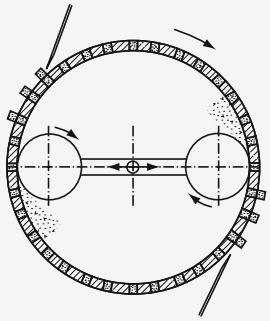	– Principle similar to pellet mills with flat dies
	– Ring die is driven
	– Material enters from the front side of the ring
	– Paddles or adjustable plows and three rollers are used to deal with uneven material
	– Internal rollers are moved by the continuous flow of feeding material inside the pellet mill.
	– State-of-the-art for wood pellets

Biofuels: Upgraded New Solids. Table 2 Mechanical and physical properties of compressed fuels with effects to combustion

Parameter	Role in compaction process	Influence on combustion system
Dimension	Regulated by the dimension of the pressing tools	Dimensioning of the feeding system of combustion plants
Gross density	Besides the durability an important measure to evaluate the quality of compacts	With higher particle densities the burnout rate might be increased
Bulk density	Dependent on the quality of the compaction process	Is increasing with increasing gross density; The higher the bulk density the higher the energy density of the biofuel
Amount of fines	Dependent on the quality of the compaction process	Fines cause problems in the combustion process and cause higher dust emissions during transport and handling
Durability	Typically used to evaluate the quality of produced pellets and briquettes (strength, amount of fines)	Risk of failures according to blocking and ash melting by fines

known. However, according to the raw material, the milling grade, and morphological characteristics, the compaction process can be difficult. Nevertheless, the mechanical and physical properties are not directly depended on the raw material. Crucial are the preprocessing of the raw material as well as the process parameters and control of the compaction.

Influencing Parameters for Biomass Pellets and Briquettes

The pellet quality is influenced by several parameters [9, 13, 19]. The raw material composition has the most severe influence on quality parameters like mechanical durability, bulk density or gross density, followed by the type of conditioning (e.g., preheating and addition of steam), and the milling technology (i.e., particle size and type of mill). The influence of the type of compaction is slightly smaller. Significantly lower is the influence of the cooling after the compaction process.

Raw Material and Raw Material Composition A wide variety of biomass can be used as raw material for the production of solid biofuels (e.g., energy crops like miscanthus, switchgrass and wood from short

Biofuels: Upgraded New Solids. Table 3 Values for mechanical and physical properties of the biofuels standard ÖNORM M 7135 "Compressed wood and compressed bark in natural state: Pellets and briquettes[a]"

Parameter	HP1 Wood pellets	HP2	HP3 Wood briquettes	RP1 Bark pellets	RP2	RP3 Bark briquettes
Diameter D (mm)	$4 \leq D < 10$	$10 \leq D < 40$	$40 \leq D < 120$	$4 \leq D < 10$	$10 \leq D < 40$	$40 \leq D < 120$
Length (mm)	$\leq 5 \times D$	$\leq 4 \times D$	≤ 400	$\leq 5 \times D$	$\leq 4 \times D$	≤ 400
Gross density (kg/dm^3)	≥ 1.12	≥ 1.10	≥ 1.10	≥ 1.12	≥ 1.10	≥ 1.10
Bulk density (kg/m^3)	–	–	–	–	–	–
Mechanical durability (wt.-%)	≥ 97.7	–	–	≥ 97.7	–	–
Fines < 3.15 mm (wt.-%)	–	–	–	–	–	–
Binders/lubricants (wt.-%)	≤ 2	≤ 2	≤ 2	≤ 2	≤ 2	≤ 2

[a]Wood and bark pressings are of various shapes and sizes. This includes the classes HP1 (wood pellets), RP1 (bark pellets) and HP3 (wood briquettes), RP3 (bark briquettes). HP2 and RP2 have sizes which are between pellets and briquettes: it depends on the type of agglomeration process.

Biofuels: Upgraded New Solids. Table 4 Values for mechanical and physical properties of the biofuels standards for compressed miscanthus and straw

Parameter	ÖNORM C 4000		ÖNORM C 4002	
	Compressed miscanthus		Compressed straw	
Fuel type	Pellets	Briquettes	Pellets	Briquettes
Diameter D (mm)	$6 \pm 1, 8 \pm 1, 10 \pm 1$	$\leq 60, \leq 100$	$6 \pm 1, 8 \pm 1, 10 \pm 1$	$\leq 60 \leq 100$
Length (mm)	$\leq 30 \leq 35 \leq 40$	$\leq 50 \leq 100 \leq 300$	$\leq 30 \leq 35 \leq 40$	$\leq 50 \leq 100 \leq 300$
Gross density (kg/dm^3)	–	–	–	–
Bulk density (kg/m^3)	≥ 580	≥ 480	≥ 600	≥ 480
Mechanical durability (wt.-%)	≥ 97.5	–	≥ 97.5	–
Fines < 3.15 mm (wt.-%)	≤ 1	≤ 10	≤ 1	≤ 10
Binders/lubricants (wt.-%)	Nature and level are indicated.		Nature and level are indicated.	

rotation coppice, biomass residues like straw, hay, and rape press cake). Several of these materials have been tested for the production of biofuels pellets [16, 20]. Additionally the pelletizing of wheat, barley, soy extraction goat, and alfalfa for animal food applications have been tested [21, 22]. They observed fluctuating mechanical and physical properties of the produced pellets for different raw materials. Additionally, the energy demand of the pelletizing process depends on the raw material [23]. In general, it is more challenging to produce high-quality pellets out of herbaceous biomass than out of raw materials with a high starch fraction.

Type of Compaction Most of the experiments to determine the influence of the die geometry as well as the compression force on the pelletizing process have been done with ring dies. Longer extrusion channels and smaller diameters result in a higher mechanical durability of the pellets but also cause higher energy demand. The flow rate has a linear relationship with the energy demand of the press [23]. Above a certain point,

the pellet press gets stuck and the material is carbonizes in the extrusion channel caused by too much friction and high temperatures. Generally, the densification ratio (i.e., the length to diameter ratio of the extrusion channels) needs to be higher for herbaceous biomass than for woody biomass, to achieve similar pellet qualities [13, 21, 22].

The compaction pressure in pellet mills is another important parameter influencing the pellet quality [22, 24, 25]. In general, the compaction pressure increases the bulk density of the pellets. The increased pellet durability has been traced back to the softening of lignin present in the pellet at 70°C acting as a binding agent. Consequently, pellets produced at 17 MPa and 75°C are more stable than pellets formed at 55 MPa and room temperature [26]. Thus, the effect of the compaction pressure on the pellet durability is not directly correlated and needs to be verified by further work.

Biofuels: Upgraded New Solids. Table 5 Mechanical and physical properties of different biomass pellets [16–18]

Raw material	Bulk density (kg/m^3)	Gross density (kg/dm^3)	Mechanical durability (wt.%)
Wheat straw	479–620	1.12–1.22	90.6–98.5
Rye straw	510–640	1.28–1.30	94.4–98.7
Hay	580	1.17–1.21	96.2–99.1
Miscanthus	480–649	1.11–1.33	91.1–97.5
Rape press cake	542–607	1.11–1.13	54.9–93.7

Conditioning The raw material for the pelletizing process can be conditioned by influencing the water content of the raw material, by adding binders and additives and by preheating and steam addition.

The optimum water content for the pelletizing process is different for each material. It needs to be verified and to be set by conditioning before the compaction. The optimum water content for wood pelletizing is about 12 wt.%. For herbaceous biomass, it is slightly higher. Experiments with alfalfa showed stable pellets using a raw material with 14 wt.% water content [27, 28]. Similar results have been achieved with reed canary grass where a water content of 14.9 wt.% has been optimal [29]. The water content is adjusted by adding water or steam. When steam is added to the raw material, a second positive effect is achieved; the material is preheated. The durability of blended pellets out of soy meal, ground yellow maize, and ground sorghum has been higher and the amount of fines decreased with higher temperatures at the conditioning process [6]. Additionally, the energy demand of the pelletizing process decreases with higher temperatures, but the overall energy demand of the process increased caused by the energy-intensive steam generation. For other raw materials, similar results were achieved [5, 22, 26, 29, 30].

The addition of binders (e.g., starchy residues like maize gravel, maize starch, rye flour, pea meal, lingosulfonate, or molasses) increases the stability of the pellets [22, 31–33]. Similarly, the addition of soy beans and pyrolysis oil showed positive binding effects and lowered the energy demand of the pellet mill [22]. Other additives (like lime, dolomite, kaolin, and talcum powder) are added during the pelletizing process to improve the combustion properties by

Biofuels: Upgraded New Solids. Table 6 Mechanical and physical properties of different biomass briquettes [13]

Raw material	Length (mm)	Diameter (mm)	Bulk density (kg/m^3)	Gross density (kg/dm^3)	Mechanical durability (wt.-%)
Bark briquettes	205–277	96	–	1.02–1.11	–
Wheat straw	–	15–25	440–493	0.90–0.95	95.2–99.4
Barley straw	–	15–25	318–416	0.80–0.85	97.5–99.0
Hay	–	15–25	412–438	0.95–1.10	90.2–95.0
Miscanthus	–	15	–	1.10–1.40	99.6

increasing the ash melting temperature of the pellets [34–36]. However, the addition of these substances mostly lowers the mechanical durability of the produced pellets. This can be countered by adding an additional binder [16, 35].

Milling Before pelletizing, the raw material needs to be grinded. The type of mill and the milling grade of the raw material are the most important parameters. Raw material such as wheat, barley, and soy extraction goat are grinded by using a hammer mill with a 1–4 mm sieve insert and a roller mill with a nip of 0.75 mm [21]. The grinding with a roller mill was found to be unsuitable for pelletizing. The energy consumption was lower than for the hammer mill but the mechanical durability of the produced pellets was significantly poorer. A higher reduction ratio of the raw material caused a high-energy consumption of the grinding process but a negligible higher durability and no energy saving for the pelletizing process. Similarly, more finely grounded alfalfa resulted in more stable pellets using a hammer mill with 2.0–3.2 mm sieves [22, 28]. In contrast, pellets produced with diameters of 10–25 mm from cut switchgrass and straw had better physicomechanical properties than the pellets produced out of shredded biomass (0–4 mm) [26]. On this basis, it can just be concluded that the required reduction grade needs to be tested for the respective biomass. Indeed, with increasing pellet diameter, a less fine grinding might be sufficient.

Torrefaction

Torrefaction is a mild pyrolysis process for the production of solid biofuels. It is performed at temperatures between 200°C and 300°C within an inert atmosphere. Under these conditions, lignocellulosic biomass is altered to an intermediate between wood and charcoal. After this treatment, the biomass contains typically 60–70% of the initial mass and 90% of the initial energy content referring to the lower heating value (LHV). The physicochemical properties of torrefied biomass are superior to those of the original biomass. Key benefits related to fuel storage, distribution, and utilization are:

- Energy densification
- Homogenization
- Improved grindability
- Pronounced hydrophobic character
- Enhanced reactivity

In the first half of the twentieth century, several patents established the denomination "torrefaction" for the underlying process without leading to commercial installations in that period. Not before the 1980s, growing interest in torrefied wood for applications in electrometallurgy and the domestic fuel market – namely, barbecue fuel – led to the construction of a first commercial plant in 1987 [37]. The continuous process involved chopping, drying, and roasting. Heat transfer has been realized indirectly via thermo-oil. The plant was in operation for a few years.

With the beginning of the twenty-first century, other applications renewed the interest in torrefied wood. Torrefied wood pellets have been identified as a favorable solid biofuel addressing the market of low-carbon fuels for decentralized biomass cogeneration, biomass gasification, and co-firing in coal-fired power plants [38].

Principles

Wood as well as herbaceous biomass is a complex material mainly composed of three sugar-based biopolymers: cellulose, hemicellulose, and lignin. Each of them shows a different behavior during a heating up. Therefore, it is important to distinguish between these fractions to understand the thermal decomposition of woody and herbaceous biomass.

Cellulose is the most common substance in living nature. It consists almost completely of D-glucoses forming an unbranched polysaccharide. On microscopic scale, wood cells are composed of bundles of cellulose, called microfibrils, forming a skeleton. Those bundles are coated with hemicellulose.

In contrast to cellulose, the term hemicellulose subsumes numerous distinct substances. Hemicellulose contains many different sugar monomers forming a branched polymer with an amorphous structure. Its function is manifold, reaching from reinforcing cell structure up to the provision of a reserve substance.

The third main green biomass component is lignin, a three-dimensional cross-linked aromatic biopolymer. Lignin subsumes different heterogeneous substances

that lack a defined primary structure. It acts as a binding agent for the microfibrils; it stabilizes and cements the plant structure.

The composition of hemicellulose and lignin as well as the proportion between cellulose, hemicellulose, and lignin fractions is different for every type of green biomass. Table 7 summarizes the lignocellulosic composition of different woody and herbaceous feedstocks. According to this, wood shows a higher lignin content than herbaceous biomass. Especially coniferous wood, often referred to as softwood, features a lignin content of about 30 wt.% on a dry basis.

The thermal decomposition of biomass is controlled by the chemical composition of its major components. Pyrolysis of these materials proceeds through a series of concurrent and consecutive reactions [39]. Each component reacts at different rates and by specific pathways. The rate and extent of degradation of each of these components depends mainly on temperature, particle size, and time of exposure.

Biofuels: Upgraded New Solids. Table 7 Composition of different biomass types [39–41, 43]

	Cellulose (wt.%)	Hemicellulose (wt.%)	Lignin (wt.%)
Woody biomass, dry basis			
Deciduous wood	40–44	15–35	18–25
Coniferous wood	40–44	20–32	25–35
Pine	42	22	30
Spruce	41	24	30
Beech	45	22	22
Willow	43	22	25
Poplar	48	18	22
Herbaceous biomass, dry basis			
Wheat straw	38	29	15
Miscanthus	43	24	19
Reed canary grass (ash free)	43	30	8
Tall fescue	25	25	14
Bagasse	38	39	20

According to Fig. 3 five temperature regimes for the pyrolytical decomposition of biomass in the low temperature range up to 300°C can be distinguished.

- Temperature regime A represents the physical drying of the biomass.
- Regime B is only valid for lignin and is defined as a temperature zone in which softening of this biomass constituent occurs.
- Regime C is characterized by depolymerization and condensation of the then shortened polymers.
- Temperature regime D leads to limited devolatilization and carbonization of the intact polymers and the solid structures formed before.
- Regime E leads to extensive devolatilization and carbonization of the polymers as well as of the solid products that were formed in regime D.

Figure 3 illustrates the different temperature regimes for each class of biopolymers. The blue line splits the torrefaction zone in a low and high temperature regime. Hemicellulose decomposition starts at lower temperatures and proceeds over a narrower temperature range as compared to cellulose and lignin. It is responsible for the main devolatilization in the torrefaction temperature regime of less than 250°C. Thereby, the reactivity of hemicellulose is depended on its specific composition. A significant difference between the decomposition of hemicellulose of coniferous and deciduous wood can be observed [42]. The latter consists predominantly of xylan-based hemicellulose, which is much more reactive and exhibits a higher degree of carbonization as compared to coniferous wood. Lignin and cellulose do not make a substantial contribution to mass loss so far, but their structure experiences chemical changes. Depolymerization reactions lead to a fragmentation and softening of the cell wall skeleton. The result is a better grindability of the torrefied biomass as compared to the raw material.

Above 250°C, both lignin and cellulose start to decompose while decomposition of hemicellulose gets extensive. A variety of permanent gases and condensable liquids is formed. The main gaseous species are carbon monoxide, carbon dioxide, water, and acetic acid. The reaction products remove part of both (i.e., the initial mass and the chemical energy represented by the organic part of the biomass). The decomposition

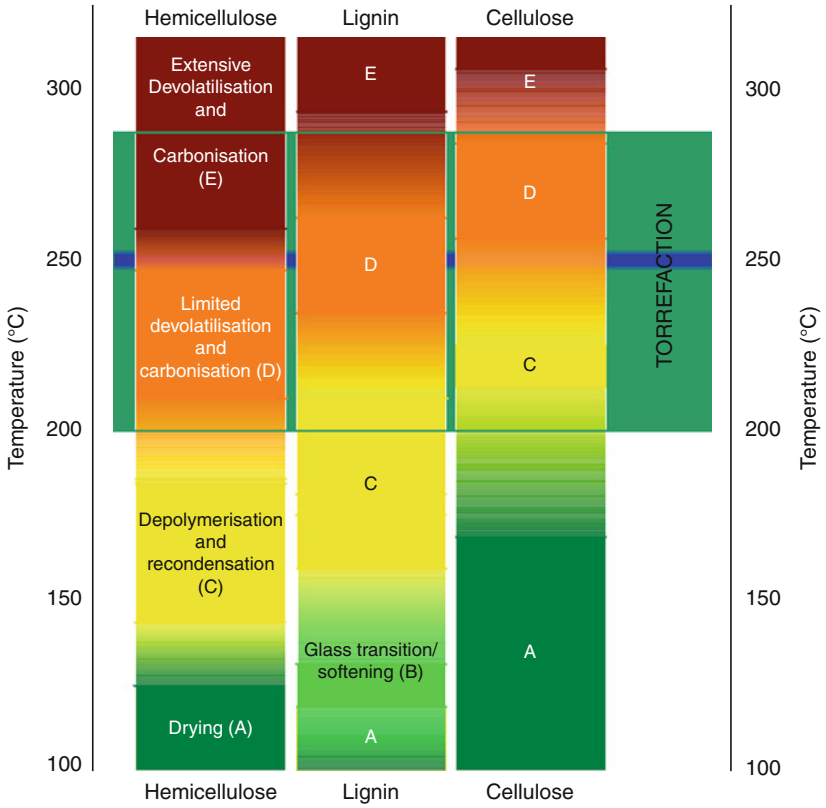

Biofuels: Upgraded New Solids. Figure 3

Temperature regimes for the low temperature pyrolytic decomposition of cellulose, hemicellulose and lignin (Taken from [42])

process is considerably faster at high temperatures. Decomposition is not completed within typical process residence times. Hence, higher temperatures as well as longer residence time cause lower mass yields but the remaining solids have different properties.

A main part of the available research work published so far concentrates on the influence of process parameters on the torrefaction of various biomass feedstocks under different conditions [1, 40, 43–48]. As the torrefaction characteristics in Fig. 4 indicate, reaction temperature and residence time are crucial for process design. Its choice faces a trade-off between: (1) high energy yields, required for good process efficiency; (2) substantial mass reduction, required for energy densification; and (3) high throughput, required for good process economics. The energy yields shown in Fig. 4 refer to the higher heating value (HHV) of the wood briquettes, neglecting the benefits from wood drying. Even so, the energy yield of torrefaction is always higher than the mass yield. Both higher reaction temperature and longer residence times cause a more pronounced biomass decomposition. Higher temperatures lead to greater differences between energy and mass yield as compared to longer residence times. With respect to process economics, it is advantageous to adjust the reaction temperature above 250°C, allowing for residence times of less than 30 min.

Particularly, the effect of the reaction temperature has been examined since it is the most influencing parameter on process yield and product properties. Figure 5 summarizes experimental results for different types of biomass. The acceleration of mass losses for reaction temperatures above 250°C is in good agreement with the temperature regime model.

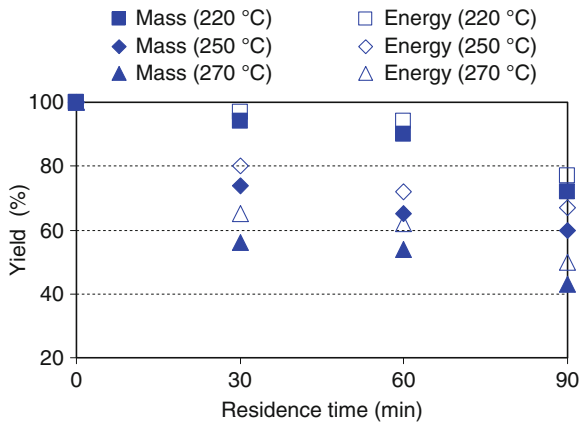

Biofuels: Upgraded New Solids. Figure 4
Mass and energy yields (HHV) from the torrefaction of wood briquettes. Values in brackets show reaction temperatures. Data taken from [44]

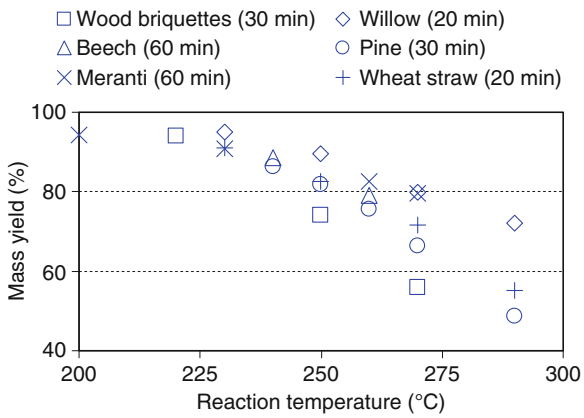

Biofuels: Upgraded New Solids. Figure 5
Influence of reaction temperature on the mass yield of torrefied biomass. Values in brackets show process residence times. Data taken from [1, 43–46]

Properties of Torrefied Biomass

Torrefied biomass can be classified as an intermediate product between raw biomass and charcoal [44]. By adjusting temperature and process time, it is possible to make the product more or less similar to charcoal.

The net calorific value (LHV) of torrefied biomass is in the range from 18 to 22 MJ/kg for herbaceous biomass and 20–24 MJ/kg for wood. Energy density is a factor of 1.2–1.3 higher compared to the raw biomass on a dry basis. Figure 6 shows that energy densification is related to an increase of the elemental carbon fraction, accompanied by a decrease of the molecular H/C and O/C ratios (Fig. 7), which is favorable for further utilization since less water vapor is formed, improving energy efficiency.

The equilibrium moisture of torrefied biomass is around 3% (i.e., roughly three times less than the equilibrium moisture of the raw materials). Two reasons for the low water uptake are proposed: (1) tar condensation inside the pores, obstructing the passage through the solid, and (2) the nonpolar character of condensed tar on the solid, also preventing the condensation of water vapor inside the pores [44]. Hence, transportation and storage of torrefied biomass are easier as compared to the raw material.

Usually, torrefied biomass is milled and pressed to form briquettes or pellets in order to enhance the handling properties. From the gasification point of view, a solid biofuel should be homogenous in chemical composition and size. Especially entrained-flow gasification asks for small particle sizes of less than 1 mm. Size reduction experiments have been performed with untreated and torrefied biomass in order to determine the power consumption of a cutting mill [40]. According to this, power consumption is greatly reduced when the biomass is torrefied. A reduction of maximal 85% has been measured (i.e., the electricity required for grinding torrefied biomass consumes only 1.5% of the biofuel energy content (assuming 40% power generation efficiency) as compared to 12–16% in case of untreated biomass). In these experiments, the mill capacity for torrefied wood was up to 6.5 times the capacity of untreated wood. Additionally, particle size distribution and shape is more uniform for torrefied wood.

The improvements of the grinding properties are caused equally by physical and chemical changes [40]. The chemical changes responsible for this behavior occur relatively fast and in the first stages of decomposition (temperature regimes C and D in Fig. 3). Hence, reaction temperatures above 250°C and residence times of >10 min hardly will bring further improvements.

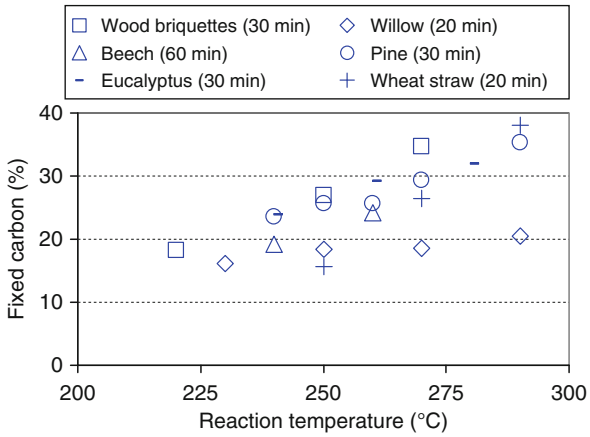

Biofuels: Upgraded New Solids. Figure 6
Fixed carbon of torrefied biomass. Values in brackets show process residence times. Data taken from [43–46, 49]

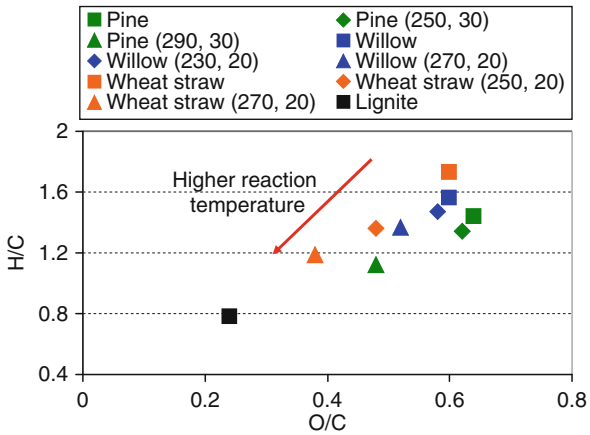

Biofuels: Upgraded New Solids. Figure 7
Van-Krevelen diagram of raw biomass, torrefied biomass and coal. Values in brackets show residence time and reaction temperature. Biomass data is taken from [43, 45], coal data from [50]

Torrefaction Plants

Torrefaction plants integrate several mechanical and thermal processes (i.e., chopping, drying, torrefaction, cooling, milling, and compaction). If the process aims to produce a commodity fuel as shown in Fig. 8. Compaction usually means pelletizing of the torrefied biomass since this kind of packing provides the best storage and transportation properties.

The first commercial-scale torrefaction plant was built in the frame of an EC Demonstration project in 1987 in France [37]. The plant has been operated with forestry wood. The capacity has been 12,000 t of torrefied wood per year. The product was mainly used as a coke substitute in electrometallurgy and some was sold as barbecue fuel. The plant has been decommissioned in the early 1990s for economic reasons [42].

This so-called Pechiney process [37] was based on an indirectly heated screw reactor. The process consisted of three main sections: chopping, drying, and torrefaction. Figure 9 gives an overview of the different basic process units and their interconnection.

Forestal wood with typically 40% moisture content was first chopped and screened. The wood fines were burned to supply heat to thermo oil circulating between the torrefaction reactor and the boiler. The remaining wood chips were dried to 10% moisture content before being fed into the torrefaction reactor. Hot air from the combustion of the torrefaction gas was used for this purpose.

The reactor was developed as a post-dryer for solids requiring homogeneous product moisture content. The size of that kind of reactor is typically determined by the heat duty, as the area for heat exchange is limiting. Higher feed moisture contents lower the reactor throughput capacity. Temperature control of the reactor is easy because of the limited heat transfer rates that are responsible for a limited capacity and long residence times of more than an hour. The result is a comparatively expensive process

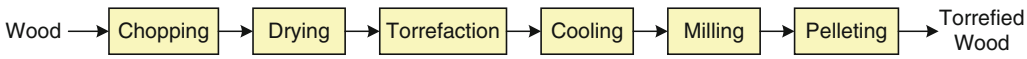

Biofuels: Upgraded New Solids. Figure 8
Process steps of a torrefaction plant

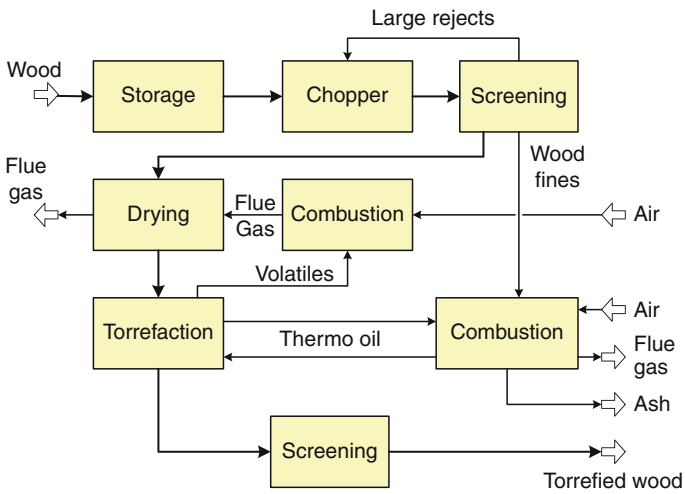

Biofuels: Upgraded New Solids. Figure 9
Flow sheet of the Pechiney torrefaction plant in France according to [42]

with production costs of roughly 100 €/t without feedstock costs [42].

The energy efficiency is in a range of 65–75% including feedstock and utility usage. Serious energy losses occur due to fines production during cutting and sieving of the biomass feedstock [42].

With the beginning of the twenty-first century other applications renewed the interest in torrefied wood. Worldwide, different companies announced plans for the construction of torrefaction plants on an industrial scale of some 10,000 t/a. They address the market of low-carbon fuels for decentralized cogeneration and co-firing in coal combustion and gasification plants. Most of the plants should not mainly supply a single recipient but produce a marketable biofuel suitable for different industrial applications.

Recently announced torrefaction plants rely on direct heat transfer. Most of the suppliers utilize rotating drums or circular trays which origin from drying technology. Others operate with a moving or fluid bed (Fig. 10). Direct heat transfer is usually realized by conducting the hot flue gas from the combustion of the torrefaction gases through the reactor, but some concepts operate with circulating inert gas reheated by heat exchanger. In that case, heat is generated by burning the torrefaction gases and some additional wood fuel.

Hydrothermal Carbonization

Although the scientific investigation of hydrothermal transformation of biomass is ongoing for decades, efforts of technical applications are quite young. Therefore a brief historic overview of hydrothermal carbonization is given.

In 1913, Bergius described the hydrothermal transformation of biomass into a coal-like product as one result of his investigations of the natural coal genesis [51]. In the 1920s and 1930s this investigations were continued and extended. These results have been confirmed in new test series in the 1960s. Around 1995 various companies started with the development of a process for the use of waste biomass (like sewage sludge) and for decontamination and disinfection. Based on this, the SlurryCarb™-process was developed as the first ever commercial process for the hydrothermal production of a coal-like product out of organic waste. Several laboratory and demonstration plants have been built and tested since 1997. In 2008, a first commercial pilot-plant started operation in Rialto, USA. It converts 900 t of biomass per day.

Besides solid biomass with limited water content usually converted thermochemically, there is a certain potential of wet biomass available (like manure, food industry wastes, digestates from biogas processes,

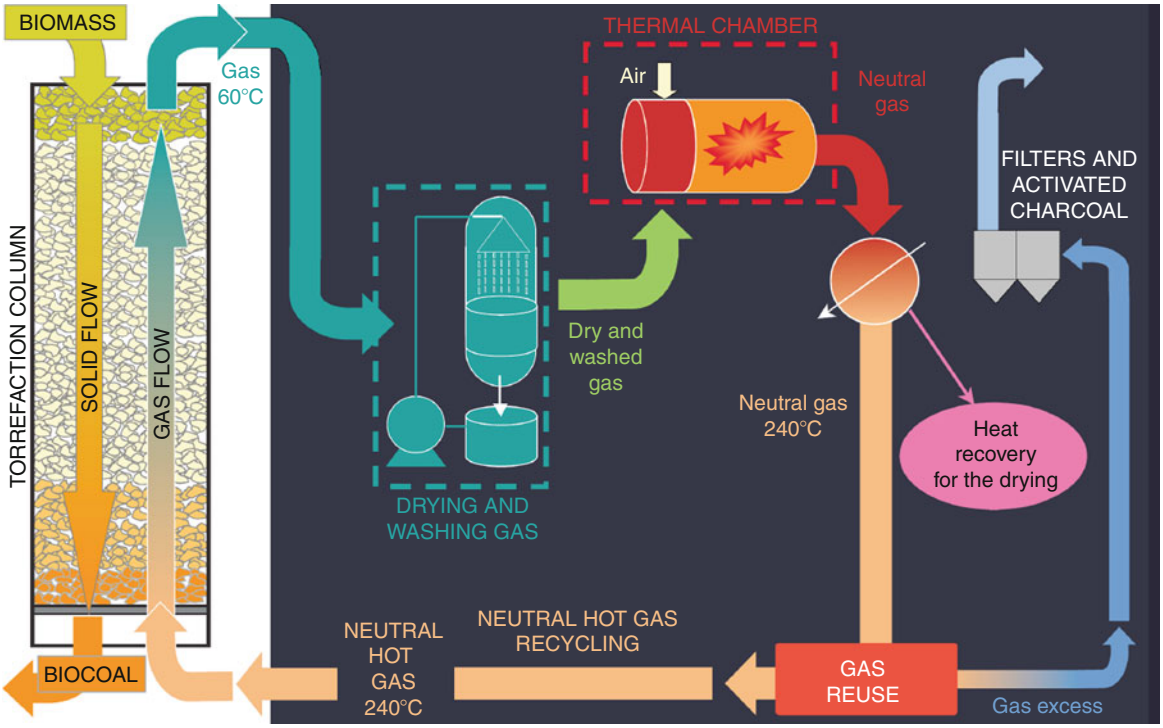

Biofuels: Upgraded New Solids. Figure 10
Torrefaction process using a moving bed reactor (Source: Thermya)

sewage sludge, and black liquor) [52]. The necessary drying obstructs the use of these kinds of feedstock in classical thermochemical processes. In case of wet biomass with 20–30% dry organic matter, the heat generated by the combustion of the organics has the same amount as the heat needed for the vaporization of the water. Therefore, wet biomass should be converted in processes without a need for preliminarily drying.

Mainly two processes fulfill this requirement for wet biomasses: biogas production and hydrothermal conversion. In the biogas process, wet biomass is biochemically converted into a methane-rich gas. However, mainly carbon hydrates are usable and the lignin remains unconverted due to biological constraints. This means, that the energy of the lignin cannot be used. Additionally, there are organic materials like straw, which can hardly be solubilized in the biogas process. In contrast, hydrothermal processes are able to convert all organic fractions.

Common hydrothermal processes are hydrothermal carbonization (HTC), hydrothermal gasification, and hydrothermal liquefaction also known as hydrothermal upgrading (HTU) [53–57]. Since the main product is a solid, only hydrothermal carbonization is tackled within the following explanations.

Principles

The properties of water at enhanced temperature and pressure may vary from those of cold water [57–59]. Above the critical point – characterized by 375°C and 221 bar – water is able to dissolve silicon dioxide and fat. At these conditions, basic properties of water change (e.g., the dielectric coefficient, the ion product) [60, 61].

During hydrothermal carbonization, the organic material is preheated. Due to this thermal energy, the macromolecules in the biomass are degraded and smaller molecules are formed out of them [62]. The pH-value mainly influences what kind of compounds is degraded. While carbohydrates can be decomposed under sour conditions, lignin degradation asks for a high pH-value. Favorably it will be converted into phenols while aldehydes and furfurals will be produced

from the decomposition of cellulose and hemicellulose [63–65]. Starting with these smaller molecules, new larger compounds are built. In these reactions, water is eliminated. Reaction mechanisms of hydrolysis, dehydration, decarboxylation, aromatization, and condensation polymerization are involved in the conversion of biomass into biocoal [66].

The new substances formed after the partial degradation of the macromolecules have properties like humic substance or lignite. For energy applications, the target has a lignite-like quality. In contrast to pyrolysis coke, which in principal consists of carbon, the product of the hydrothermal carbonization (so-called biocoal) is characterized by the elemental formula C_6H_2O.

Hydrothermal carbonization covers two different processes, the classical hydrothermal carbonization and the SlurryCarb™-process. The former uses mild reaction conditions of 170–250°C and 10–20 bar. A catalyst (e.g., citric acid, ferric sulfate) is necessary. Catalysts allowing to lower reaction temperature or residence time are a major target of fundamental research. At present, the operating conditions have to be applied for 3.5–16 h. This very long residence time is a weak point of the entire process.

The SlurryCarb™-process operates at 220–270°C and up to 220 bar. It needs only 10–60 min for the carbonization [67, 68]. However, high-pressure reactors are required. Additionally, above a reaction temperature of 240°C the phenol load of the wastewater increases strongly [69].

Energy Balance The hydrothermal carbonization is an exothermal process. Therewith, the process may proceed without an external heat supply. But the energy converted from chemical energy into heat is not contained as usable chemical energy in the product any more. This heat generation can amount of up to 30% of the energy contained originally within the feedstock. Thus, the energetic efficiency of the conversion process of biomass into biocoal is between 70% and 90% [67, 70].

For the operation of the hydrothermal carbonization, it is necessary that the biomass particles are surrounded by water. Otherwise, the reactions cannot occur regularly. Usually, HTC reactors require a pumpable or pasty feedstock. The minimum water content for such properties differs depending on the other characteristics of the biomass. Typically, a water-to-dry-mater ratio of 2:1 is necessary. In that case, one-half of the generated heat is needed for preheating the feedstock. Furthermore, the biocoal and the water do not separate themselves. After a mechanical water separation by filtering or centrifugation, an additional thermal drying is necessary to provide an energy carrier from the biocoal. For the efficiency of mechanical separation, first results are available [71]. As a result, after 2.5–5 min in action, water content in biocoal of 30–45% is reached. With centrifugation after SlurryCarb™-process, 50% water in the product is achievable [68].

Of course, the heat for feedstock preheating and drying is partially regenerable. But, considering the technical possibilities of heat transfer, characterized by the necessary temperature differences and the heat loses, hardly any heat for external use will remain.

All over, the energetic efficiency of the hydrothermal carbonization depends on the water-content of the raw material and how easy it can be dewatered mechanically.

Figure 11 compares brief process chains of biomass utilization, for example, combustion with and without hydrothermal carbonization.

Waste Water Until now, several questions of the hydrothermal carbonization are not clarified comprehensively. One of the most important open questions is the wastewater treatment. Different types of water pollutants have been identified (i.e., inorganic as well as organic substances). The water-soluble inorganic substances available in the feedstock will be dissolved. This affects both, the minerals typical for biomass (like ash components, nutrients) and the inorganic feedstock pollutants (like heavy metals). In this case, water pollution corresponds with a decontamination of the solid phase. The leaching of ash components can upgrade the combustion behavior.

Organic substances in wastewater can have two sources. The first source is water-soluble organic compounds preliminarily available in the feedstock. Those of these compounds not degradable under the conditions of hydrothermal carbonization could be dissolved in the process water. Additionally, substances formed in the hydrolysis process and not consumed during the new forming of large compounds can remain in process water. Typically, different kinds of

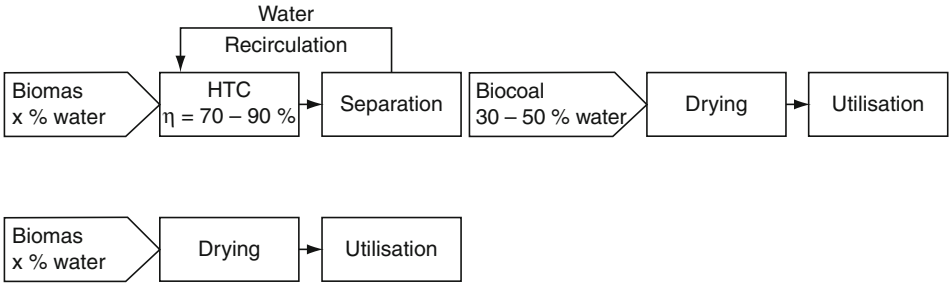

Biofuels: Upgraded New Solids. Figure 11
Process chains for the utilization of biomass with and without hydrothermal carbonization

Biofuels: Upgraded New Solids. Table 8 HTC waste water ingredients [71]

Parameter	Value
pH-value	3.7–7.2
Biochemical oxygen demand (BOD)	10,000–42,000 mg/L
Chemical oxygen demand (COD)	24,200–68,500 mg/L
Total organic carbon (TOC)	9,000–36,100 mg/L
Nitrate-nitrogen	2.9–58 mg/L
Ammonia-nitrogen	3.4–4.1 mg/L
Phosphate- phosphor	0.2–47 mg/L

phenol-like substances can be found in the wastewater. The chemical oxygen demand is correspondingly high. Typical amounts of wastewater ingredients are listed in Table 8.

Phthalates, pyrazines, phenols, other oxygen containing cyclic compounds, and aliphatic and aromatic hydrocarbons mainly represent the content of organic substances [71].

Apart from wastewater recycling, different water purification processes are possible. The content of organic pollutants, represented by chemical oxygen demand (COD), can be decreased by 90% within a biogas plant (i.e., anaerobic treatment). Downstream, a final cleaning can be done with activated carbon [71]. Often discussed is integration with a biogas plant in a manner that the HTC plant uses the digestates and the biogas plant uses wastewater from the HTC.

The flue gas of the HTC process contains less than 5% methane and more than 90% carbon dioxide with low amounts of hydrogen, oxygen, and hydrogen sulfide [72].

Hydrothermal Carbonization Processes

Currently, the transformation from laboratory scale to technical plants is ongoing. Therefore, the state of technology outlined below might change rapidly.

The reaction temperature and pressure of the hydrothermal carbonization are easy to handle with available process technology. The core question of the commercialization of the HTC process is the residence time. For example, for a resistant time of 12 h and a fuel output (dry matter) of 10 MW a reactor volume of 50–100 m^3 will be necessary to the discussed feedstock water contents. For the use of mechanical dewatered sewage sludge with the typical water content [73], the necessary reactor size for about 35 bar can increase up to 250 m^3. This is why the reduction of resistant time is crucial for the successful technical implementation. The SlurryCarb™-process with decreased residence times of minimum 10 min [74] is in this case is advantageous. But, because of the described problems with the wastewater quality, the resistant time reduction must be reached by advanced catalysts for the future.

The long residence time causes the use of several reactor types. Tube reactors and discontinuous reactors allow for the control of the residence time. Because of the necessary size of the reactors, uncommon designs (like sub-terrestrial pressure vessels) are discussed.

The SlurryCarb™-process is the only process realized in a larger pilot plant. This plant converts 900 t of

sewage sludge a day to 170 t of solid fuel [68]. For every other process, the construction of a demo plant or pilot plant is ongoing.

Biocoal Properties

The properties of biocoal depend on the reaction conditions. With increasing residence time, the product changes its manner from humus like to lignite like. Analysis values are listed in Table 9. General combustion properties are given in Table 10.

These chemical analysis values, especially the heating values and the contents of carbon, hydrogen, oxygen, nitrogen, and sulfur, show that biocoal can be used in energetic applications.

The biocoal is described to be a lignite substitute. Many chemical properties are in fact quite similar to lignite. But, it has to be seriously observed, that at least one of the main combustion properties, the content of volatile matter, differs completely. This parameter of HTC-biocoal is rather in a range typical for green biomasses. Because the ignitability and the properties of the flame are substantially determined by the content of volatile matter, the combustion of HTC-biocoal cannot be similar to lignite combustion. Instead of that, the combustion behavior will be between green biomass and lignite. Future research has to show which kind of combustion technology, either lignite technology or biomass technology, is able to utilize HTC-biocoal most efficiently.

The solid product has a macroscopic particulate shape or the shape of the feedstock particles remains. Only the physical and chemical properties change and the particles get a fissured and porous structure. Thus, the fibrous structure of the green biomass is destroyed. The biocoal is a highly functionalized carbonaceous material [77] microscopic composed of agglomerates of microspheres. This means that the biocoal is neither in the chemical surface properties nor in the microstructure, similar to pyrolysis coal with little functional groups at surface and also with a porous structure characterized by lots of micro-channels.

Biofuels: Upgraded New Solids. Table 9 Elementary analysis and heating value of biocoals from HTC compared with its biomass feedstock (dry matter) [75]

Feedstock	Condition	Elementary analysis					Heating value (LHV) (MJ/kg)
		C (%)	H (%)	N (%)	S (%)	Ash (%)	
bark mulch	green	45.5	6.1	0.6		5.8	18.7
	HTC-biocoal	55.7	5.8	0.6		6.8	22.1
leaves	green	45.3	6.8	1.1	0.02	11.1	18.1
	HTC-biocoal	56.4	6.1	1.1	0.01	11.7	24.2

Biofuels: Upgraded New Solids. Table 10 Combustion properties of biocoal from HTC compared with brown coal and biomass (dry matter) [1, 76]

	HTC-biocoal	Brown coal (Rhineland)	Brown coal (Lusatia)	Softwood (spruce)	Straw (wheat)
Water content (%)	8	11	10.5	15–20	10–20
Ash content (%)	1.5	4	6	0.6	5.7
Volatile matter (%)	74.5	46	45.5	82.9	77.0
Sulfur content (%)	0.2	0.4	0.8	0.02	0.08
Heating value (LHV) (MJ/kg)	20	22.2	21	18.8	17.2
Ash softening temperature (°C)	≈1,200	>1,100	>1,200	>1,400	<1,000

Other crucial properties for the applicability of the biocoal are the water content and in connection with this the consistency. Depending on the water content of the feedstock, the biocoal occurs as a suspension. Because of this, the water cannot be removed only with mechanical processes up to a content which make utilization in a classical thermochemical process (like combustion or gasification) possible. That is why an energetic reasonable application of the hydrothermal carbonization requires also an answer to the question of water removal.

In the contrary, the products of hydrothermal gasification and hydrothermal upgrading can be extracted from water by phase separation processes, which cause hardly any energy demand.

Biocoal Applications

The use of biocoal in lignite application processes is one option. Because of the analogy of some of the fuel properties, biocoal may substitute lignite in different fields of use. Such a substitution saves greenhouse gas emissions, which is important for the climate protection and governmentally funded in many countries.

Because the content of volatile matter of HTC-biocoal is similar to biomass and its heating value is high in comparison with biomass, pellets from biocoal (or with a percentage of biocoal) might be an important addition for the pellet markets of the future. Uses for coal sludge are currently in a research stage. They can avoid the energy demand for drying. Gasification and combustion of coal-slurries are state of the art, but in this case the energy demand is only removed into the gasifier or furnace.

In general, the solid fuel produced by hydrothermal carbonization requires a complex conversion process for solid fuels. In most cases, gaseous or liquid products will be easier to apply.

Apart from the energetic application, the use of biocoal from HTC for the fertilization of soil and carbon sequestration is intensively discussed. Here, biocoal is mixed into topsoil. But, the advantages (e.g., increase of fertileness and stability of the carbon disposal) to be achieved in practise are currently not clarified [78].

Biocoal has hardly any analogy with activated carbon or carbon black. That is why biocoal cannot be expected to be a substitution for these. Nevertheless, there are serious activities for the production of engineering carbon materials via hydrothermal carbonization [79].

Summary and Future Directions

Each of the discussed processes provides an important possibility for the production of high value solid biofuels. The main process characteristics are:

- Pelletizing and briquetting are physical processes; torrefaction and hydrothermal carbonization also influence the chemical structure and the chemical behavior of the fuel.
- Pelletizing, briquetting, and torrefaction occur in a gaseous atmosphere while hydrothermal carbonization runs in hot pressurized water
- Pelletizing, briquetting, and torrefaction require dry feedstock; hydrothermal carbonization has the greatest advantages for wet biomass.

Because of the different process characteristics, these processes have their own specific future directions and potential impacts on the development of certain areas of science.

For the further development of solid biofuels, produced by pelletizing and briquetting, the compaction process needs to be understood in depth to adjust the process parameters in an optimal way. Therefore, the interactions of the parameters influencing the process and their influence on the resulting properties of the compacts have to be figured out. Important questions are, for example, the influence of particle size distribution and the water content of the raw material on the mechanical durability of the compact or the optimal compaction pressure needed for a certain compact strength and the possibilities to influence it by conditioning or by adding binding agents. Besides the adjustment of optimal compact properties, the knowledge of these correlations allows the optimization of the process itself and of the energy efficiency which directly affects the costs of the biofuel production. Therewith the goal is the simulation of these processes for better understanding and for an optimal compaction of the raw materials.

The benefits of pelletizing and briquetting processes are (1) a higher durability because of reduced water

content and (2) a higher volumetric energy density. Furthermore, admixtures compensate variations. Nevertheless, there is no substantial change in the chemical composition during the pelletizing and briquetting processes [18, 80, 81, 83].

Torrefaction process technologies have reached a commercial scale. The process technologies are derived from drying technology. The major drawback is a comparatively long residence time of some 10 min resulting in large reactors with high investment costs. Process economics and the development of a sufficient market for torrefied biomass pellets is still an open question, but recent investment decisions indicate good market opportunities.

The torrefaction product is a highly reactive solid biofuel with good combustion properties. Torrefied biomass pellets are suitable for biomass combustion and gasification plants as well as for co-combustion and co-gasification plants.

The main question for the future of hydrothermal carbonization is for which feedstock and for which process chains an energetic, economic, and environmental benefit can be reached. Therefore, a lot of balancing and assessment work has to be done. Open questions in addition are: (a) decreasing of residence time and (b) equipment optimization for biocoal production (i.e., water recycling, removal of inorganic pollutants, search for high toxic organic components, removal for wastewater treatment, and combustion, as well as pelletizing behavior for energetic use).

In general, the possibility of thermochemical use of wet biomass is an important chance. But, the question not answered until today is whether hydrothermal carbonization is the best alternative compared with other hydrothermal processes and the biogas process. According to the fuel characteristics and the economic conditions, each of the three described technologies could find its special use for energy production in the future.

Bibliography

Primary Literature

1. Kaltschmitt M (2009) Energie aus Biomasse: Grundlagen, Techniken und Verfahren, vol 2, neu bearb. und erw. Aufl. Springer, Berlin, pp S. 264–S. 275
2. Rumpf H (1958) Grundlagen und Methoden des Granulierens. Chem Ing Tech 30(3):S. 144–S. 158
3. Rumpf H, Herrmann W (127) Eigenschaften, Bindungsmechanismen und Festigkeit von Agglomeraten. Aufbereitungstechnik 11(3):S. 117–S. 127
4. Pietsch W (2002) Agglomeration processes – Phenomena, technologies, Equipment. Wiley-VCH Verlag GmbH, Weinheim, pp S. 29–S. 138
5. Gilpin AS, Hermann TJ, Behnke KC, Fairschild FJ (2002) Feed moisture, retention time, and steam as quality and energy uitlization determinants in the pelleting process. Appl Eng Agric 18(3):S. 331–S. 338
6. Skoch ER, Behnke KC, Deyoe CW, Binder SF (1981) The effect of steamconditioning rate on the pelleting process. Anim Feed Sci Technol 6:S. 83–S. 90
7. Kaliyan N, Morey RV (2010) Natural binders and solid bridge type binding mechanisms in briquettes and pellets made from corn stover and switchgrass. Bioresour Technol 101(3):1082–1090
8. Pietsch W (2002) Agglomeration processes – Phenomena, technologies, Equipment. Wiley-VCH Verlag GmbH, Weinheim, pp S. 229–S. 383
9. Krug H, Naundorf W (1984) Braunkohlenbrikettierung – Grundlagen und Verfahrenstechnik, vol 1 + 2. VEB Deutscher Verlag für Grundstoffindustrie, Leipzig
10. Rieschel H (1963) Various types of briquetting presses and their applications. IBA Proc 8:S. 20–S. 34, In: Messman HC, Tibbetts TE: Elements of briquetting and agglomeration, Canada, 1977
11. Schubert H (2003) Handbuch der mechanischen Verfahrenstechnik: Partikeleigenschaften, Mikroprozesse, Makroprozesse, Zerteilen, Agglomerieren, Trennen, Mischen, Schüttgut, vol 1. Wiley-VCH, Weinheim, pp S. 433–S. 498
12. Ruttloff C et al (1981) Technologie Mischfuttermittel. VEB Fachbuchverlag, Leipzig, pp S. 286–S. 344
13. Obernberger I, Thek G (2009) Herstellung und energetische Nutzung von Pellets: Produktionsprozess, Eigenschaften, Feuerungstechnik, Ökologie und Wirtschaftlichkeit, 1st edn. BIOS Bioenergiesysteme, Graz
14. Thomas M, Zuilichem DJ, Poel AFBd (1997) Physical quality of pelleted animal feed 2. Contribution of processes and its conditions. Anim Feed Sci Technol 64:S. 173–S. 192
15. Robinson RA (1971) The pelleting of animal feeds. IBA Proc 12: S. 97–S. 112, In: Messman HC, Tibbetts TE Elements of briquetting and agglomeration, Canada, 1977
16. Kiesewalter S, Röhricht C (2006) Herstellung und Nutzung von Brennstoffpellets aus landwirtschaftlicher Biomasse, Poster, Version: 2006
17. Kiesewalter S, Röhricht C (2008) Nutzung von kontaminierten Böden, Schriftreihe der Sächsischen Landesanstalt für Landwirtschaft, Heft 30, 2008
18. Kirsten C, Weller N, Lenz V, Pilz B (2010) Miscanthuspellets – Chancen und Erfahrungen in Deutschland, European Pellet Conference 2010

19. Behnke KC (2008) Aufbereiten und Konditionieren für die Pelletherstellung: Weltweit ein Kernthema in der Mischfuttertechnologie. Mühle und Mischfutter 145(16):S. 523–S. 527
20. Samson R, Duxbury P (2000) Assessment of Pelletized Biofuels
21. Jansen HD, Friedrich W (1985) Einfluss der Aufbereitung auf Pressfähigkeit und Energiebedarf bei der Mischfutterproduktion. Mühle und Mischfuttertechnik 122(45)
22. Tabil LG (1996) Binding and pelleting characteristics of alfalfa: PhD Thesis. University of Saskatchewan, 1996
23. Friedrich W, Rohbohm KF (1979) Der Verdichtungsvorgang in der Futtermittelpresse: Einfluss der Betriebsbedingungen auf Energiebedarf und Pelletfestigkeit. Mühle und Mischfuttertechnik 116(39):S. 527–S. 530
24. Adapa PK, Singh AK, Schoenau J, Tabil LG (2006) Pelleting characteristics of fractionated alfalfa grinds: hardness models. Powder Handling and Processing 18(5):S. 294–S. 299
25. Mani S, Tabil LG, Sokhansanj S (2006) Effects of compressive force, particle size and moisture content on mechanical properties of biomass pellets from grasses. Biomass Bioenergy 30(7):S. 648–S. 654
26. Gilbert P, Ryu C, Sharifi V, Swithenbank J (2009) Effect of process parameters on pelletisation of herbaceous crops. Fuel 88(8):S. 1491–S. 1497
27. Adapa PK, Singh AK, SchoenauJ, Tabil LG (2006) Pelleting Characteristics of fractionated alfalfa grinds: hardness models. Powder Handling and Processing 18
28. Adapa PK, Tabil LG, Schoenau J, Sokhansanj S (2004) Pelleting characteristics of fractionated sun-cured and dehydrated alfalfa grinds. Appl Eng Agric 20(6):S. 813–S. 820
29. Larson SH, Thyrel M, Geladi P, Lestander TA (2008) High quality biofuel pellet production from pre-compacted low density raw materials. Bioresour Technol 99(15):S. 7176–S. 7182
30. Friedrich W (1983) Warum ist Dampfzugabe beim Pelletieren wirtschaftlicher als Wasser? Mühle und Mischfuttertechnik 120(14)
31. Kiesewalter S, Röhricht C (2004) Pelletierung von Stroh und Heu, European Pellets Conference 2004 – Proceedings, S. 283–S. 295
32. Löwe R (2004) Pelletierverhalten rohfaserreicher Futtermischungen. Mühle und Mischfutter 141(18): S. 577–S. 582
33. Kiesewalter, Röhricht C (2007) Untersuchungen zur energetischen Nutzung von Heupellets mit verschiedenen Zuschlagsstoffen in zwei unterschiedlichen Feuerungsanlagen. In: Nutzungsalternativen für Grünland, Schriftreihe der Sächsischen Landesanstalt für Landwirtschaft, Heft 2, 2007
34. Steenarie B-M, Lundberg A, Petersson H, Wilewska-Bien M, Andersson D (2009) Investigation of ash sintering during combustion of agricultural residiues and the effect of additives. Energy Fuels 23:5655–5662
35. Steenarie B-M, Lindqvist O (1998) High-Temperature reactions of straw ash and the anti-sintering additives Kaolin and Dolomite. Biomass Bioenergy 14:67–76
36. Fernández Llorente MJ, Díaz Arocas P, Gutiérrez Nebot L, Carrasco García JE (2008) The effect of the chemical materials on the sintering of biomass ash. Fuel 87:S.2651–S.2658
37. Girard P, Shah N (1989) Recent developments on torrefied wood, an alternative to charcoal for reducing deforestation. In: FAO/CNRE Workshop, Norway, 1989, pp 101–114
38. Bergman PC (2005) Combined torrefaction and pelletisation. ECN-C-05-073, Energy research Centre of the Netherlands (ECN). Petten, Netherlands, 2005
39. Shafizadeh F (1982) Introduction to pyrolysis of biomass. Name J Anal Appl Pyrol 3:283–305
40. Bergman PC, Boersma AR, Kiel J, Prins MJ, Ptasinski KJ, Janssen FJ et al (2005) Torrefaction for entrained-flow gasification of biomass. ECN-C-05-067, Energy research Centre of the Netherlands (ECN), Petten, Netherlands, 2005
41. Kaltschmitt M, Hartmann H, Hofbauer H (2009) Energie aus Biomasse. Grundlagen, Techniken und Verfahren. 2. neu bearbeitete und erweiterte Auflage. Media. Springer, Berlin Heidelberg, 2009
42. Bergman P, Boersma A, Kiel J, Zwart R (2005) Torrefaction for biomass co-firing in existing coal-fired power stations "BIOCOAL". ECN-C-05-013, Energy research Centre of the Netherlands (ECN), Petten, Netherlands, 2005
43. Bridgeman T, Jones J, Shield I, Williams P (2008) Torrefaction of reed canary grass, wheat straw and willow to enhance solid fuel qualities and combustion properties. Fuel 87:844–856
44. Felfli FF, Luengo CA, Suárez JA, Beatón PA (2005) Wood briquette torrefaction. Energy Sustain Dev IX:19–22
45. Bourgois J, Guyonnet R (1988) Characterization and analysis of torrefied wood. Wood Sci Technol 22:143–155
46. Couhert C, Commandre J, Salvador S (2009) Impact of torrefaction on syngas production from wood. Fuel 88:2286–2290
47. Prins MJ, Ptasinski KJ, Janssen FJ (2006) Torrefaction of wood Part 1. Weight loss kinetics J Anal Appl Pyrol 77:28–34
48. Deng J, Wang G, Kuang J, Zhang Y, Luo Y (2009) Pretreatment of agricultural residues for co-gasification via torrefaction. J Anal Appl Pyrol 86:331–337
49. Arias B et al (2008) Influence of torrefaction on the grindability and reactivity of woody biomass. Fuel Process Technol 89:169–175
50. Ullmann's encyclopedia of industrial chemistry (2002). Wiley-VCH.
51. Bergius F (1913) Die Anwendung hoher Drucke bei chemischen Vorgängen und eine Nachbildung des Entstehungsprozesses der Steinkohle. Knapp. Halle (Saale), 1913
52. Thrän D et al (2006) Sustainable strategies for biomass use in the european context. Analysis in the charged debate on national guidelines and the competition between solid, liquid and gaseous biofuels. IE-Report 1/2006. Leipzig, 2006
53. Guo Y et al (2010) Review of catalytic supercritical water gasification for hydrogen production from biomass. Renewable Sustainable Energy Rev 14:334–343

54. Berl E (1934) Origin of asphalts, oils, natural gas and bituminous coal. Science 80:227–228
55. Berl E (1944) Production of oil from plant material. Science 99:309–312
56. Goudriaan F et al (2001) Progress in thermochemical biomass conversion. Blackwell Science Ltd., Oxford, pp 1312–1325
57. Peterson A et al (2008) Thermochemical biofuel production in hydrothermal media: A review of sub- and supercritical water technologies. Energy Environ Sci 1:32–65
58. Matsumura Y (2002) Evaluation of supercritical water gasification and biomethanation for wet biomass utilization in Japan. Energy Convers Manage 43:1301–1310
59. Lu Y et al (2007) Thermodynamic modeling and analysis of biomass gasification for hydrogen production in supercritical water. Chem Eng J 131:233–244
60. Kruse A, Dinijus E (2007) Hot compressed water as reaction medium and reactant Properties and synthesis reactions. J Supercrit Fluids 39:362–380
61. Zhang L, Xu C, Champagne P (2010) Overview of recent advances in thermo-chemical conversion of biomass. Energy Convers Manage 51:969–982
62. Kruse A, Gawlik A, Henningsen T (2002) Reaktionen von Biomassen in heißem Hockdruckwasser: Schlüsselsubstanzen als Werkzeug zum Verständnis der Chemie bei Vergasung und Verflüssigung. DGMK-Fachbereichstagung "Energetische Nutzung von Biomassen." Velen, German, 22–24 April 2002
63. Karagöz S, Bhaskar T, Muto A et al (2005) Comparative studies of oil compositions produced from sawdust, rice husk, lignin and cellulose by hydrothermal treatment. Fuel 84:875–884
64. Sinag A, Gülbay S, Uskan B et al (2009) Comparative studies of intermediates produced from hydrothermal treatments of sawdust and cellulose. J Supercritical Fluid 50:121–127
65. Srokol Z, Bouche AG, van Estrik A et al (2004) Hydrothermal upgrading of biomass to biofuel; studies on some monosaccharide model compounds. Carbohydr Res 339:1717–1726
66. Funke A, Ziegler F (2010) Hydrothermal carbonization of biomass: A summary and discussion of chemical mechanisms for process engineering. Biofuels, Bioproducts & Biorefining, 2010
67. Titirici AM, Thomas A, Antonietti M (2007) Back in the black: hydrothermal carbonization of plant material as an efficient chemical process to treat the CO_2-problem. New J Chem 31:787–789
68. EnerTech Environmental Inc (2006) The SlurryCarb™-process
69. Wittmann T (2009) Energetische Nutzung von Kohle aus Biomasse. Fachgespräch der FNR "Hydrothermale Carbonisierung – Stand der Entwicklung." Berlin, 11/12 Feb 2009
70. BelusaT. et al (2010) Hydrothermale Karbonisierung und energetische Nutzung von Biomasse- Möglichkeiten und Grenzen. In: Hydrothermale Carbonisierung. Gülzower Fachgespräche, vol 33, FNR 2010
71. Ranke HG (2009) Wässrige Phase aus der HTC: Zusammensetzung und Abbaubarkeit. Fachveranstaltung „Energie und Rohstoffe aus landwirtschaftlichen Reststoffen – Hydrothermale Carbonisierung ein geeignetes Verfahren? des Johann Heinrich von Thünen-Instituts, Berlin
72. Altensen R, Richarts F (2008) Hydrothermal Carbonisierung (HTC) ein neues Verfahren zum Erzeugen von Kohle aus Pflanzen und Pflanzenresten. RENEXPO Augsburg 10. Oktober 2008
73. Griebe St, Krautz H-J, Paulick G Möglichkeiten der thermischen Verwertung von mechanisch entwässertem Klärschlamm und weiteren Reststoffen in einer mit Trockenbraunkohle betriebenen Zykloidfeuerung. www.kwt.tu-cottbus.de
74. Schuchardt F (2009) Organische Reststoffe aus Landwirtschaft, Agrarindustrie und Kommunen. Fachveranstaltung "Energie und Rohstoffe aus landwirtschaftlichen Reststoffen – Hydrothermale Carbonisierung ein geeignetes Verfahren?". des Johann Heinrich von Thünen-Instituts, Berlin 5
75. Richarts F (2009) Feste Bestandteile aus der HTC: Zusammensetzung und energetische Verwertung. Fachveranstaltung "Energie und Rohstoffe aus landwirtschaftlichen Reststoffen – Hydrothermale Carbonisierung ein geeignetes Verfahren?". des Johann Heinrich von Thünen-Instituts, Berlin
76. Wittmann T (2010) Veredlung von Biomasse zu SunCoal im CarboREN-Verfahren. Erdöl Erdgas Kohle 12(6):215
77. Sevilla M, Fuertes AB (2009) The production of carbon materials by hydrothermal carbonisation of cellulose. Carbon 47:2281ff
78. Kammann C (2010) Biokohle gegen den Klimawandel – Potentiale und Forschungsbedarf. Pyrolyse, HTC, Biochar Co., Hoechst, 17 März 2010
79. Hu B, Antonietti M et al (2010) Engineering carbon materials from the hydrothermal carbonization process of biomass. Adv Mater 22:813 ff
80. Nielsen NPK (2009) Taking analysis of raw material for wood – Pellets a step further. Bioenergie International 38(3):S. 17–S. 19
81. Nielsen NPK (2010) Production an R&D – Test facilities for biomass milling and pelletizing, Opening for test plant for bio-pelleting. Sdr. Stenderup, Denmark
82. Holm JK, Henriksen UB, Hustad JE, Sorensen LH (2006) Toward an understanding of controlling parameters in softwood and hardwood pellets production. Energy Fuels 20(6):2686–2694
83. Stelte W (2010) Predictive method for estimating the pelletizing properties of different types of biomass. European Pellet Conference, 2010
84. Gessner H (1985) Die pelletierung von Futtermitteln. Mühle und Mischfuttertechnik 122
85. Jannasch R, Quan Y, Samson R (2001) A process and energy analysis of pelletizing switchgrass: final report: prepared for: natural resources Canada. Alternative Energy Division, 2001

86. Yan W, Acharjee TC, Coronella CJ, Va VR (2009) Thermal pretreatment of lignocellulosic biomass. Environ Prog Sustainable Energy 28:435–440

Books and Reviews

Babu B (2008) Biomass pyrolysis: a state-of-the-art review. Biofuels Bioprod Bioref 2:393–414. doi:10.1002/bbb

Biogas for Electricity Generation, Hi-tech Applications

Frank Scholwin[1], Michael Nelles[2]
[1]University Rostock, Germany
[2]Department Waste Management, University of Rostock, Rostock, Germany

Article Outline

Glossary
Definition of the Subject
Introduction
History
Technology
Economics of Electricity from Biogas
Future Directions
Bibliography

Glossary

Biogas Biogas is a gas which is produced as waste product during anaerobic microbiological breakdown of organic substances. The main constituents are methane and carbon dioxide.

Biogas cleaning Biogas cleaning is a technical process which adapts the biogas quality to a defined gas quality defined by the subsequent usage. That includes mainly the reduction of trace gases (H_2S, NH_3, water vapor, and others). Biogas cleaning does not focus on the removal of carbon dioxide from the biogas.

CHP unit Combined Heat and Power unit which consists of a gas-burning engine driving a generator which produces electricity. The waste heat from electricity production can be used for further applications.

Landfill gas Landfill gas is a special type of biogas which is produced in landfills during the degradation of the organic constituents of wastes. It is characterized by many organic long-chain trace gases.

Sewage sludge gas Sewage sludge gas is a special type of biogas produced within wastewater treatment plants during the anaerobic treatment of sewage sludge. It is characterized by the content of siloxanes.

Definition of the Subject

This entry focuses on the development, its reasons, and the perspectives of the electricity supply based on biogas through anaerobic digestion. This sector is worldwide very important for decentralized energy supply from organic materials. Beneath this fact, electricity from biogas reduces the demand for fossil fuels and reduces greenhouse gas emissions connected with fossil-energy supply systems. Thus the development of this sector is analyzed. Based on this, the possibilities and the challenges of electricity supply from biogas and its contribution to reach national and international renewable electricity targets is discussed.

Introduction

Biogas can be produced from a very broad variety of organic substrates. Internationally, the main biomass sources are wastewater treatment sludge (to produce sewage sludge gas) and organic wastes from agriculture (e.g., excrements from animal farming, residues from processing of agricultural products). Additionally, high importance has to be paid to landfill gas production and utilization. In some countries as, e.g., Austria and Germany, the use of energy crops contributes additionally significantly to biogas production [10, 11].

Due to the fact that all these different kinds of biogases consist of roughly 50–70% of methane, the gas can be used easily as a fuel. In the past, very different engines have been developed to produce electricity from cleaned biogas. Parallel to these technologies, biogas can be used for cooking purposes, for heating, as well as a fuel for vehicles. But the latter is not a topic of this article.

History

The history of biogas production is already very long – especially for small-scale applications. Some very old experiences are recorded already from China and Persia. In industrial large scale, the first biogas plants were constructed for the purpose of wastewater cleaning. About 1897, at a hospital in Bombay, India, the first plant was constructed where the gas was used for lightening the streets, and from 1907 for the operation of a motor to run an electricity generator. After this beginning, more and more anaerobic wastewater treatment plants mainly in Europe were constructed and equipped partly with generators [1].

Due to the relatively high costs of electricity production from biogas, the gas was mainly used for heating and lightening, as well as a fuel for transportation purpose. But also, some enthusiastic farmers started between 1980 and 1990 with the construction of digesters and electricity generators with electrical capacities mainly below 20 kW based mainly on animal excrements. The electricity was produced to cover the own electricity demand within their farm.

With the implementation of feed-in laws for electricity into the national electricity grid, the technology got incentives, and a continuous growth of the use as well as the plant size began [2].

For example in Germany, based on the incentives introduced in 1999, the electricity production from biogas increased rapidly. Especially financial incentives for the production of electricity from energy crops–based biogas lead to the very strong development (Fig. 1) especially in this area.

Within Europe, about 3,000 MW electrical capacities based on biogas (including landfill gas and sewage sludge) have been installed in 2007. Only Germany contributes with about 50% to this number [4]. Compared to the international situation, Europe dominates the electricity production from biogas [5].

Looking into the future, it is estimated, for example, for Germany that in the year 2050 a total capacity of electricity production from biogas of about 11,000 MW can be reached. Worldwide, the capacity in 2050 is estimated to reach about 100,000 GW [5]. Thus a very rapid growth of this sector is expected worldwide.

Technology

After some cleaning processes, biogas shows very good combustion properties. This is also true for the use in

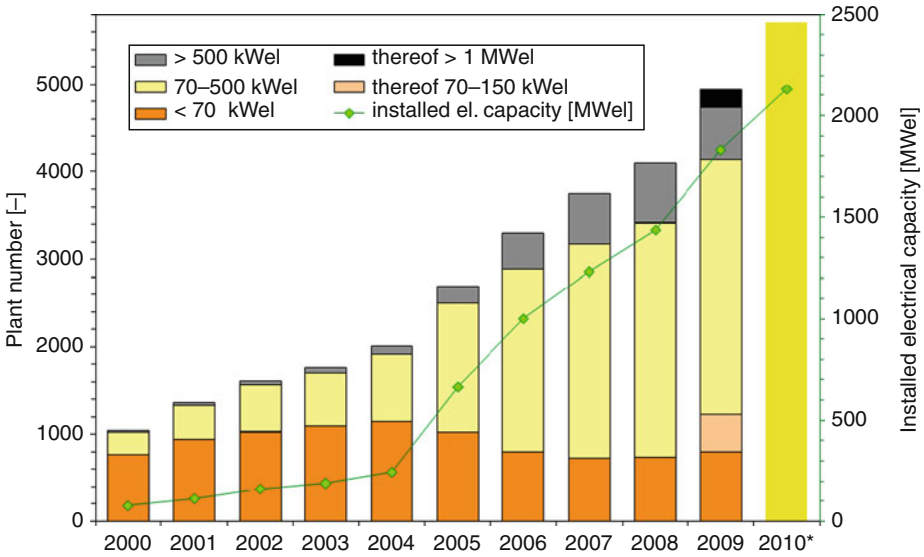

Biogas for Electricity Generation, Hi-tech Applications. Figure 1
Development of electricity production from biogas (without landfill gas and sewage sludge gas) exemplarily for Germany [3]

engines. For that reason the use of biogas for electricity supply has a long tradition. Thus, there are lots of experiences available and the obstacles for electricity supply from biogas under very different conditions are very well known. This is analyzed within the following chapters.

Biogas Production

Biogas is produced mainly from organic residues and wastes. Such organic matter can result from animal breeding (excrements), crop production (harvest residues), processing of agricultural products (residues from beer brewing, vegetables processing, beverage industry, and others), organic municipal or industrial wastes, organics in wastewater streams, wastewater cleaning processes, and many other sources. Energy crops are another (costly) biomass resource for biogas production which are actually only used in some countries. The question if a biomass source can be used for biogas production is answered by its anaerobic degradability.

Biogas production is a microbiological process taking place under anaerobic conditions (at total exclusion of oxygen). The microorganisms involved into this process are omnipresent but concentrated in anaerobic sources as, for example, the stomach of ruminants. For applications with the aim of biogas production, the ruminant's stomach has more or less to be emulated so that the process is mainly carried out in so-called fermenters which are gastight and mainly equipped with some stirring devices. Very simple household digesters which supply cooking gas, e.g., for families in rural areas of developing countries as well as industrial-scale solid substrate digesters (garage-type), are constructed without stirring devices. They show often comparably low gas yields. Therefore, most industrial applications realize some movement within the fermenter (Fig. 2).

The choice of the fermenter type depends mainly on the substrates. But also, the economic-frame conditions as well as the chosen installation company have a considerable influence. Therefore, a broad variety of technologies can be found on the market.

The dimension of the fermenter depends on the amount of biomass to be treated and the biological dimensioning to avoid an overload of the microbiological community. It also plays an important role if a one-staged or more-staged process is realized. So far, single fermenters with dimensions between 20 and 8,000 m^3 can be found on the market. Typical fermenters used, e.g., in Germany, for agricultural biogas plants are sized between 1,000 and 2,500 m^3. Biogas amounts of 2.5–500 m^3/h are produced which are equivalent with about 5–1,000 kW electrical capacity of a gas engine. For larger plants (the largest known is 10,000 m^3/h biogas production at one single place), two or more fermenters are connected or placed parallel.

Much attention has to be paid on the right temperature for the fermentation process. Active bacteria do not tolerate fast changes in temperature resulting in a reduced efficiency and in lower degradation rates within the fermenter. Thus, the temperature in the fermenter should be constant and changes should not exceed 2 K/week. For this reason, heating systems in industrial scale fermenters should be designed carefully.

Internal fermenter heating systems can be designed in various ways. One option is that stainless steel heat pipes are installed within the fermenter some centimeters away from the fermenter walls. Another possibility is that they are embedded within the concrete walls and the concrete bottom. The heat exchange rates are much higher when the pipes are not installed within the concrete, but the heat exchanger rate may be reduced due to dirt attachments at the pipes fixed within the fermenter. Additionally, technical stirrer faults can cause demolition of the pipes. Heat pipes at the fermenter bottom cannot be suggested because almost all biogas plants show sedimentation of material within the fermenter, reducing the heat exchange significantly.

External heating in heat exchangers is realized in cases where a continuous circulation of the fermenter content is technically necessary. If this is not the case, external heating requires additional electrical energy for a circulation pump. The advantage is that only external heating allows a regular cleaning of the heat exchanger surface.

All fermenters – except the garage-type fermenters – require movement of the substrate through any type of pipe.

Substrates with very high content of solids (20% and more) can be transported in screw surveyors.

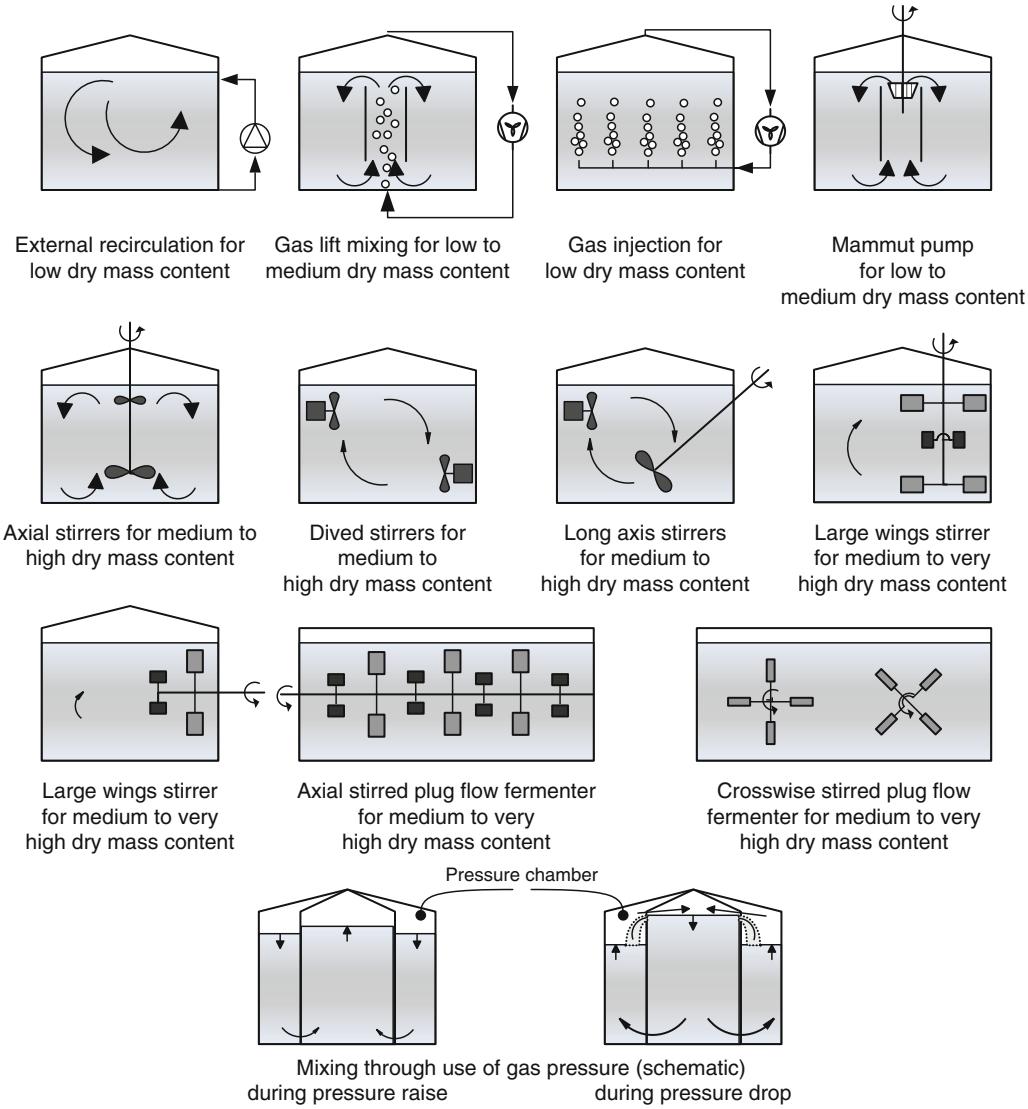

Biogas for Electricity Generation, Hi-tech Applications. Figure 2
Overview on the main types of industrial fermenters with stirring [6]

Due to high abrasion, screws and walls have to be constructed very robust preferably from stainless steel. Very positive effects on continuous operation and low maintenance show applications of walls which can be removed easily in two parts and which can be adjusted depending on the abrasion of the screw (the diameter will slightly decrease). Stones and solid parts have to be removed from the substrates before passing screw surveyors.

Substrates with a lower content of solids are transported in pipes mainly. They are moved by pumps. Special requirements on the pumps result from substrates with 5–20% solids content. In these cases, best experiences are reported from the use of rotating piston pumps and eccentric screw pumps, which can be found on almost every agricultural and industrial biogas plant nowadays. They are used for substrate supply to the fermenter as well as for transportation purposes between different fermenters and storage tanks. Only the removal of the digested slurry is not realized by a pump mostly. It is realized with an open siphon where the overflow from the fermenter

leaves due to gravity and due to processes of new substrates supply into the fermenter without additional energy demand. For this reason the fermenter will not be overfilled and maintain a constant filling level.

Operational experiences for the fermentation unit of a biogas plant are in most cases very good. Special attention has to be paid on the quality of the stirrers, the additional technical equipment, and the internal coating of the fermenters. The aggressive atmosphere within the fermenter (due to the formation of sulfuric acid) requires stainless steel or totally coated surfaces of steel and concrete, especially in the gas room under the roof of the fermenter. Fermenters are estimated with a technical lifetime of 20 years and more when they are constructed at high quality. But the technical equipment shows in most cases only technical lifetime of maximum 10 years [7].

Fermenters are able to produce biogas all year round. Practical experiences show that it has to be expected that due to biological or technical problems, the fermenter has to be opened about each 3 years. For example, a removal of a sand layer, the exchange of the stirring system, or some maintenance work has to be done. Then it has to be calculated that the fermenter is out of operation for 1–4 four weeks, and thereafter a new start of the plant is necessary which leads to a startup phase with a reduced biogas production rate. Annually (without a real opening of the fermenter), a fermenter is available with roughly 95%. Due to biological process problems, it is possible that 5% of the year in average, not enough biogas can be produced to run the CHP plant at full load.

Electricity Production from Biogas

So far basically only motor-CHP units are used for electricity production. Additionally to a minor extent micro-gas turbines (worldwide probably about 100) are used. Almost independent on the device, the biogas has to be cleaned from H_2S, water vapor, and – dependent on the substrate – siloxanes.

H_2S, which can form sulfuric acid and increase corrosion effects, must be removed to levels between 150 and 400 ppm depending on the requirements of the supplier of the CHP unit. It is always suggested to go for a very low H_2S level in the gas to minimize maintenance work at the CHP unit and to prolong the intervals for oil exchange; for example, levels of 100 ppm and below would result in notable reductions of maintenance cost which in many cases result finally in improved economic behavior of the overall biogas plant [7].

In many cases, with a low H_2S content, it could be sufficient to use the so-called internal biological sulfur-removal method. Here the H_2S content is reduced with sulfur-reducing bacteria (sulfobacter oxidants) living in the gas space of a fermenter. They convert H_2S into elementary sulfur which is then removed with the digested substrate. Such a sulfur-removal requires on the one hand sufficient area for settling of the bacteria (e.g., a layer of wood beams or nets) and, on the other hand, the continuous supply of some oxygen (about 3% to maximum 6% compared with the biogas production rate [8]).

For a higher H_2S content and/or improved reduction rates, additional equipment for external biological, physical, or chemical desulfurization is required. This can be [9]:

- External biological desulfurization, where within a washing column, a biological desulfurization as described above takes place under controlled conditions
- Biochemical washing, where the H_2S is bound in a first column chemically to, e.g., soda lye and is separated from that in a second column without bringing oxygen into the gas system
- Sulfide precipitation in the fermenter, where sulfide binding chemicals (Fe-III-chloride, Fe-II-chloride or Fe-II-sulfate) are given with the substrates into the fermenter
- Adsorption to activated charcoal, where in separate vessels, the raw gas is led through a packing of charcoal which allows the highest degree of gas cleaning

For water-vapor reduction in the gas phase, at least a condensation of water in the raw gas-pipe system has to be realized through piping the gas under the earth. For improved drying of the raw gas, the application of technical dryers is suggested. They have to be resistant against formation of sulfuric acid in the condensate. It has to be noted that the gas will be saturated with water at the temperature of fermentation, and notable condensate amounts have to be handled.

Siloxanes are relevant mainly for gases resulting from digestion of sewage sludge and municipal solid waste as well as from landfill gas. They can cause depositions of silicates in the engine. They could be the reason for massive technical problems. For reduction mainly, activated char coal filters can be used.

The different CHP-unit types do show differences in their technical performance and operational behavior. Mainly, it has to be distinguished between gas-otto-engine-driven CHP units, ignition-oil CHP units, and micro-gas turbines which are in practical and commercial use [9].

- Gas-otto-engines only use the biogas as fuel. They are operated with the otto-engine principle with air in excess and equipped with a turbocharger. The methane content in the biogas has to be above 45% (Table 1).
- Ignition-oil engines use the biogas, but always between 7% and 10% additional ignition oil (diesel, vegetable oil, biodiesel). The engines use the same principle as conventional diesel engines and are operated with air excess. In dependency of the gas quality and availability, the ignition oil share can be increased up to 100% so that not necessarily the engine has to be turned off during maintenance work at the biogas plant (Table 1).
- Micro-gas turbines only use biogas as fuel. They are fast-running gas turbines with a small electrical capacity (today max. 600 kW) with air preheating within a recuperator and a generator driven by the expanded gas after its combustion. The methane concentration in the fuel has to be above 35%, and the turbines tolerate higher H_2S concentrations than other CHP units. The high frequent noises can be quietened easily, and the waste heat can be delivered at a much higher level than from the other CHP units (Table 1).

From practical applications, it was measured that most plants do not run nonstop throughout the year due to maintenance but also due to faults and problems at the plant. For regular maintenance, about 150–200 h/year (less than 10 days) have to be calculated. Keeping that in mind and on condition that the fermenters continuously produce the full gas amount for full load of the CHP unit, it can be expected that the availability of the whole plant would be at 97%. Practically, gas production cannot run at exact 100% of the demand and should not waste gas what cannot be used in the CHP unit. Thus the gas production is mostly at about 95% or less in average compared with the capacity of the CHP unit. Therefore – as shown in Fig. 3 – in practice, most plants show a calculated standstill time

Biogas for Electricity Generation, Hi-tech Applications. Table 1 Comparison of the different types of CHP units; according to [7]

Parameter	Gas-otto engines	Ignition-oil engines	Micro-gas turbines
Capacities electrical	300 kW. . .3 MW	5 kW. . .500 kW	10 kW. . .600 kW
Electrical efficiency	35. . .43%	35. . .42%	21. . .33%
Thermal efficiency	40. . .44%	40. . .44%	50. . .60%
Heat-level water cooling/thermal oil	95/105 °C (50%)	95/105°C (50%)	Overheated steam
Heat-level waste gas	300–400°C	300–400°C	300–600°C (100%)
Lifetime	60,000 h	35,000 h	40,000 h
Emissions	NO_x and CO medium level	NO_x and CO at borders of legal limits	Very low
Special remarks	Engines designed for gas/biogas use	Highest electrical efficiency at low capacities; use of adapted standard diesel engines	Low noises

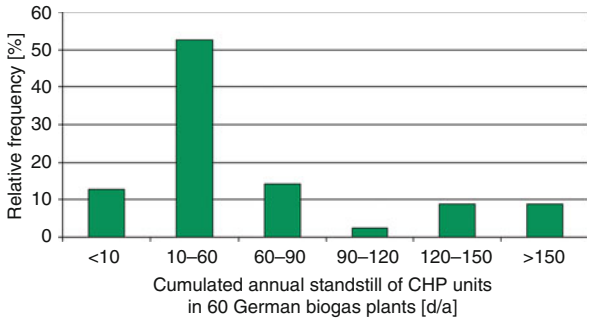

Biogas for Electricity Generation, Hi-tech Applications. Figure 3
Theoretical cumulated standstill time of CHP units in practical agricultural biogas plants; the frequency is calculated as the share of really produced electrical energy of theoretically possible electrical energy production [7]

less than 60 days. The plants with longer standstill times in Fig. 3 had during the period of analysis notable biological problems, they were not full time in operation or they had any technical fault so that they should be excluded from evaluation.

Expected Developments

Starting from the state of the art described above and keeping in mind the strong research and development activities ongoing currently on an international level, it is expected that during the next 20 years, substantial improvements will be done.

Biogas production is a biotechnological process. But research activities just start with modern biotechnological methods. Therefore, within the years to come, new knowledge about the microbiological processes will be available which will lead to technical improvements so that it is expected that around 10% increase in the biogas yields could be realized. Additionally, the biogas plants will be better adapted to the substrates as well as the microbiological requirements. Also complicated or challenging substrates (like grass or straw) can be used in a more efficient way.

Regarding the electricity production process, it is expected that electrical efficiencies will slightly raise with about 2% in common CHP units. Fuel cells can find their way from demonstration activities into practice, what leads to significant higher electrical efficiencies (45–60%). Other technologies are not expected to improve the overall behavior of decentralized electricity generation from biogas.

The overall plant behavior will show increased efficiencies in terms of reduced own heat and electricity demand, increased availabilities due to better knowledge on the processes, more applied measurement technologies, as well as more reliable technologies. Thus the expected full load hours are expected to rise to about 3–5%. At the same time, higher requirements regarding environmental impacts of biogas technology will lead to reduced direct and indirect emissions from today between 1% and 5% of the methane produced to a value lower than 1%.

Obstacles

There is no technology without obstacles. Technically it can be stated that biogas technology is well known, and biogas plants can be constructed and operated satisfactorily when suitable substrates are used. Obstacles result more from economic view interfering with the organizational/legal framework.

Thus the main question is the applicability of the electricity produced. For an economic successful operation, it is very important that the framework allows trading of heat and electricity to neighbors and feed in into national energy grids. Without these prerequisites, a biogas plant has to be designed for decentralized energy supply for a single company and then a balance between energy supply and energy demand has to be reached.

The second important question is if electricity production from biogas is economically viable. The production costs are often higher than local energy costs. This depends mainly on the costs for substrates and revenues for the products. The latter includes not only energy but also solid or liquid residues (i.e., digested slurry) which are a valuable fertilizer. Effects of reduction of greenhouse gas emissions and other environmental advantages should also be taken into account. Regarding the revenues for the electricity in many countries, very good experiences were gained with defined long-lasting guaranteed tariffs for each kWh fed in into an electricity grid.

Economics of Electricity from Biogas

The costs for electricity production from biogas depend on very many factors, mainly connected with substrate supply. Therefore only few examples are given from the German market of industrial biogas applications. Thus Table 2 shows the main cost positions for three different typical plant sizes and types.

Generally, the production costs of electricity from biogas are higher than 0.1 €/kWh, and so far higher than electricity production costs from fossil fuels in most cases (i.e., grid connected electricity generation in large-scale units). Only plant C shows lower costs, but this is caused by the very promising situation that the substrates are not connected with costs. If for some of the substrates paying would be necessary (and this is the case, e.g., for organic waste streams from food processing competing with fodder for animal breeding), the production cost would rise above 0.1 €/kWh. This would also be the case for plant A when the vegetable residues would have been paid.

Thus there is the question if some further revenues could reduce the production costs. This could be the case if heat could be supplied and sold for a typical price between 0.02 and 0.035 €/kWh_{th}. Additionally, it could be the case that a farmer who uses the fertilizer can be convinced about the worth of the organic fertilizer and pays something for it. Last but not least, it is possible to generate revenues from acceptance of residues and wastes (e.g., from slaughterhouses), where the producer of the waste has to pay for to get rid of the waste material. But all in all, it is to assume that the influence of these revenues will never be more important than maximum 0.03 €/kWh_{el} production-cost reduction.

Biogas for Electricity Generation, Hi-tech Applications. Table 2 Typical cost assumptions for different typical German biogas plants

Parameter	Unit	Plant A	Plant B	Plant C
Capacity electrical	kWel	190	600	1,200
Electrical efficiency	%	38%	39%	40%
Substrates used	–	50% Manure, 20% grass, 30% vegetable residues	35% Manure, 65% energy crops	20% manure, 30% food production wastes, 30% slaughterhouse wastes, 20% used fats
Full load hours	h/a	7,500	7,700	7,700
Electricity production	kWhel/a	1,425,000	4,620,000	9,240,000
Heat production	kWhel/a	1,650,000	5,212,308	10,164,000
Specific investment costs	€/kWel	4,500	3,500	3,000
Capital costs	€/a	98,325	241,500	414,000
Substrate costs	€/a	30,000	270,000	0
Maintenance costs	€/a	25,650	63,000	108,000
Operational costs	€/a	60,625	152,060	272,120
Residues transportation and use costs	€/a	18,000	36,000	60,000
Total annual costs	€/a	232,600	762,560	854,120
Specific electricity production costs	€/kWhel	0,163	0,165	0,092

Thus for making the biogas production and use for electricity generation economically viable from an investors' point of view, financial incentives are necessary. This is especially true if energy crops – offering the largest potential today – shall be used.

Future Directions

Today, electricity from biogas has in many countries settled as a promising renewable electricity supply technology.

Thus it is expected that worldwide the biogas production as well as the electricity production from biogas will continue to grow in the future. Considering the significant expectable improvements in overall efficiency and environmental behavior of biogas plants, the technology seems one of the most promising among the possibilities of sustainable energy supply.

In the future, with increasing fossil-fuel prices and optimized technologies for biogas production and use, the production costs will converge at the level of fossil-energy prices. So in 10 or 20 years, electricity from biogas might be able to compete at the market commercially.

Bibliography

1. Schulz H, Eder B (1996, 2001) Biogas-Praxis: Grundlagen, Planung, Anlagenbau, Beispiel, 2. überarbeitete Auflage, Ökobuch Verlag, Staufen bei Freiburg
2. Deutsches BiomasseForschungsZentrum gGmbH (2009) Monitoring zur Wirkung des Erneuerbare-Energien-Gesetzes (EEG) auf die Entwicklung der Stromerzeugung aus Biomasse. 1. Zwischenbericht, Leipzig
3. Deutsches BiomasseForschungsZentrum gGmbH (2010) Monitoring zur Wirkung des Erneuerbare-Energien-Gesetzes (EEG) auf die Entwicklung der Stromerzeugung aus Biomasse. 3. Zwischenbericht, Leipzig
4. Biogas Barometer 2008 (2009) EurObserver. Download from http://www.eurobserv-er.org/downloads.asp
5. Stinner W, Scholwin F, Mohrig V, Thrän D (2010) Biogasgewinnung und -nutzung. In: Wietschel M, Arens M, Dötsch C, Herkel S, Krewitt W, Markewitz P, Möst D, Scheufen M (eds) Energietechnologien 2050 – Schwerpunkte für Forschung und Entwicklung. Fraunhofer, ISI-Schriftenreihe Innovationspotenziale, Stuttgart
6. Scholwin F, Liebetrau J, Edelmann W (2009) Biogaserzeugung – Grundlagen und Verfahrenstechnik. In: Kaltschmitt M, Hartmann H, Hofbauer H (eds) Energie aus Biomasse – Grundlagen, Techniken und Verfahren. Springer, Heidelberg
7. Fachagentur für Nachwachsende Rohstoffe (ed) (2009) Biogas-Messprogramm II. 61 Biogasanlagen im Vergleich. Fachagentur für Nachwachsende Rohstoffe, Gülzow
8. Postel J, Schumacher B, Scholwin F, Gattermann H (2010) Gasaufbereitung und Verwertungsmöglichkeiten. In: Fachagentur Nachwachsende Rohstoffe e.V. (ed) Handreichung Biogasgewinnung und -nutzung. Gülzow
9. Scholwin F, Jung U, Postel J (2009) Stand der Technik beim Bau und Betrieb von Biogasanlagen – Bestandsaufnahme 2008. Studie des Deutschen BiomasseForschungsZentrums im Auftrag des Umweltbundesamtes, Leipzig
10. Scholwin F, Nelles M (2009) Biogastechnologie in Deutschland – Status und Optimierungspotenziale; Müll und Abfall; 5/2009; pp 228-232, ISSN 0027-2957, Rhombos Verlag Berlin
11. Nelles M, Scholwin F, Schüch A, Engler N (2010) Bioenergy as a sustainable technology for decentralized and centralized energy systems – basic parameters, current status in Germany and Outlook, Tech Monitor May–June 2010, pp 25–30, ISSN 0256-9957, New Delhi, India

Biogas Production and Energy Crops

Christoph Strauß[1], Armin Vetter[1], A. Von Felde[2]
[1]Plant Production and Agricultural Ecology, Thuringian State Institute for Agriculture, Dornburg, Germany
[2]Energy Plants, KWS SAAT AG, Einbeck, Germany

Article Outline

Glossary
Definition of the Subject
Introduction
Production and Provision of Energy Crops for Biogas Production
Sustainability Aspects
Future Directions
Bibliography

Glossary

Soil texture Describes the composition of the soil with regard to the proportion of the different grain size fractions of the mineral constituents. By adhesion forces in the varying pore sizes, the soil texture determines to a large extent the water storage capacity of soils as well as the capillary rise of water from deeper soil levels.

Effective root zone Soil depth, from which annual field crops can take up water by their rooting system. It is determined by soil texture as well as weather conditions.

Evapotranspiration coefficient (TC/ETC) The TC is a measure for the amount of water transpired by a plant stand for the production of a unit of plant matter (liters per kg DM), that is the reciprocal value of the water use efficiency (WUE). In addition to the transpiration, the water release of a plant stand is largely determined by the evaporation of the soil. Both processes are subsumed under the term "evapotranspiration," which can then accordingly be described by the evapotranspiration coefficient (ETC).

Field capacity The field capacity describes the amount of water in the pores of a water-saturated soil that can be held against gravity after a period of more than 3 days.

Vernalization Induction of stem elongation/development of main shoot and generative phase by the impact of cold temperatures. Vernalization need of plants, e.g., winter cereals, prevents their blooming before winter.

Water use efficiency (WUE) Measure for the amount of plant matter produced for a unit of water transpired. It is equal to the reciprocal value of the transpiration coefficient.

Crop rotation Temporal succession of crops on one site.

Second crop Crop that is grown after a winter intercrop.

Intercrop Crop grown between the cropping of two main crops. Differentiations can be made between summer intercrops (main mass production before winter) and winter intercrops (main mass production after winter dormancy).

DM/oDM – (organic) dry matter Dry matter refers to the harvested biomass after exclusion of the water, which is part of the fresh matter. For a specification of biogas yields, organic dry matter is given as a reference value, which makes a subtraction of inorganic ash fractions from dry matter values necessary.

Mycotoxin Toxins formed by mold fungi, which are toxic to humans and animals. Most important mycotoxins in wheat are deoxynivalenol (DON) and zearalenon (ZEA).

WC – Whole crop Crops are referred to as whole crops, when harvested before full ripeness as entire subsurface plant material mainly for silage preparation.

Definition of the Subject

Conversion processes in anaerobic digestion are realized by anaerobic prokaryotes that have been playing a major role in the transformation of chemical structures for a long period in evolution history. The product of such an anaerobic digestion process is a substance mixture. Its gaseous phase consists largely of methane and carbon dioxide and can be used for energetic purposes (Fig. 1).

The multitude of bacteria which are active within this anaerobic degradation process have the ability to digest a large spectrum of non-lignified biomass. Besides residual and waste biomass, the cropping of biomass (i.e., energy crops) is a possibility to supply larger amounts of biomass for anaerobic digestion processes.

Indisputable from a sustainability viewpoint is the fact that the land area for the production of agricultural goods is limited and that a conversion of land of high value for the storage of carbon or to sustain biodiversity should not take place. For this reason, the existing agricultural area should be used as efficient and

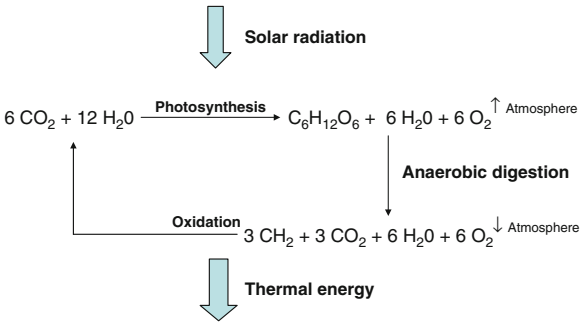

Biogas Production and Energy Crops. Figure 1 Schematic energy conversion process exemplarily demonstrated by the example of glucose without taking conversion losses into account

sustainable as possible also for energy provision. The cropping of energy plants can therefore be regarded as an important piece of a puzzle to complement existing production systems with its specific characteristics.

The agricultural production of substrates, which are the raw material for a sustainable substitution of fossil fuel energy, aims at designing systems that make a most efficient conversion of solar energy and a maximized substitution of fossil fuels possible. At the same time, all potentials should be utilized to ensure a long-term sustainability. Therefore, an intensive production and an environmentally sound production are to be harmonized. This article is going to concentrate on findings from Central Europe.

Introduction

Throughout the world, national legislations have introduced systems to promote an increased usage of biomass for energy production. Currently, in some countries incentive systems, which guaranteed fixed prices for electricity generated from renewable resources (feed-in-tariffs), are supporting this political goal [1, 2]. For example, by the amendment of the German Renewable Energy Act (Erneuerbare-Energien-Gesetz, EEG) in 2009, the German government put in place favorable conditions for biogas production. Tariffs set by this law guarantee degressive reimbursement for electricity from biogas for a period of 20 years. In addition to the basic reimbursement for each kWh dependent on capacity classes, additional premiums can be accessed. One of these premiums is a bonus payment for electricity from renewable raw material, which amounts to 0.07 €/kWh for plant sizes of up to 500 kW [3]. Similar incentives can also be found in other countries throughout Europe.

As shown in Fig. 2, the production of biogas from agricultural substrates contributes already noticeable to the overall Biogas production in Europe. The substrates currently used, for example, in Germany are dominated by animal excreta if the agricultural substrates are analyzed according to mass or volume. From an energy-related point of view, dedicated energy crops, which are again dominated by maize silage, make up the largest single share in Germany (Fig. 3).

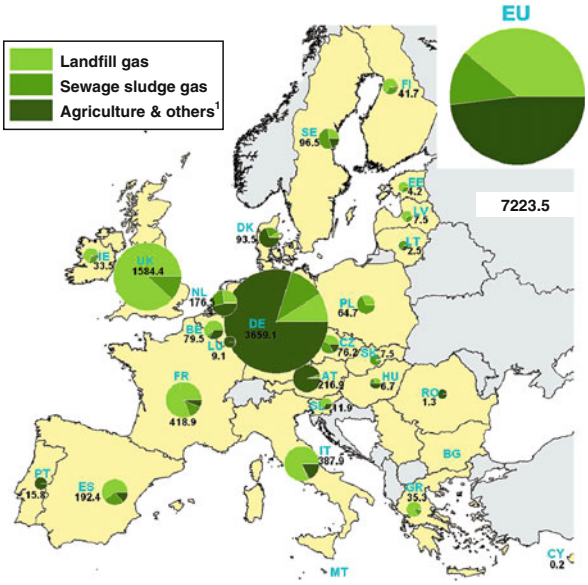

Biogas Production and Energy Crops. Figure 2
Primary energy production from Biogas in Europe in 2007 in kilotons of oil equivalent [ktoe] (Data from [4]). [1]"Others" are the communal digestion of solid waste as well as the centralized CHP-usage of biogas fed into the grid

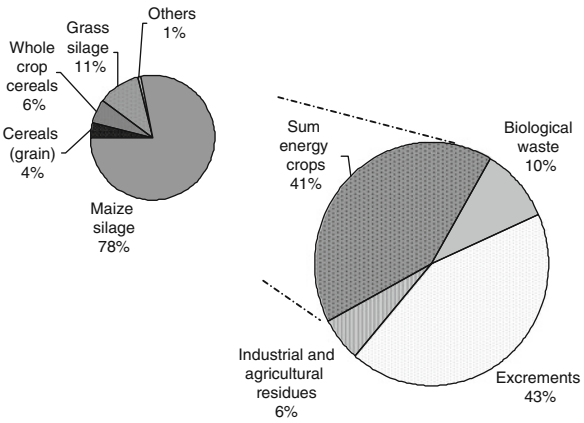

Biogas Production and Energy Crops. Figure 3
Substrate input in German biogas plants 2008/2009 – percentages of total fresh matter (*left*) (Adapted according to data from [5]) The shading is roughly indicating the energy yield of each substrate

The provision of energy crops is directly competing with food and fodder production. These two sectors are experiencing an advancing rate of specialization on a very narrow spectrum of crops in cultivation and

in a reduction in the number of crop types being rotated. The development of energy cropping as a new branch of production is therefore connected with the hope of providing possibilities for diversification in the context of a multifunctional agriculture [6]. High land productivity, maximum energy gain involving cost effectiveness and the optimization of non-commodities of cropping systems embedded in existing production regimes are major objectives of focus in public research.

Production and Provision of Energy Crops for Biogas Production

Biological and Agricultural Basis

The efficiency of the yield formation of agricultural crops is determined by an interaction of growth factors, that is, factors that are necessary for the metabolic processes of plants. These include solar radiation, temperature (progression), soil characteristics, and water availability as well as a controllable supply of macro- and micronutrients. For the choice of suitable crops and the design of cropping systems, the knowledge of these interactions is essential. The influence of the specificity of growth factors on yield can be roughly depicted by yield functions.

Efficiency of Photosynthesis The production of energy crops is, just as the entire plant production, based on the photosynthetic activity of higher plants. Ensuring a high efficiency of transforming solar radiation to simple organic carbon compounds, which are available for the formation of complex substances of content, is therefore a precondition for high energy yields.

The chain reaction involves the storage of solar radiation in energy-rich phosphate compounds. These are utilized to incorporate CO_2 into the acceptor molecule Ribulose-1,5-bisphosphate (RuBP) by means of the activity of the enzyme Ribulose-1,5-bisphosphate carboxylase oxygenase (RubisCO). As can be derived from the name, the enzyme also acts as an oxygenase. Hence, energy losses in the process of energy fixation are experienced. This part of the respiratory processes, which depends on the relation of O_2-to-CO_2 partial pressure, is called photorespiration.

Some plant species, which due to their differing physiology are called C_4 plants, possess an intra-leaf mechanism that enables them to retain CO_2 in their mesophyll cells. As this can result in CO_2 concentrations of up to 20 times as high as in most plants, C_4 plants have major advantages in efficiency. The fact that sufficient CO_2 is available for metabolic processes results in a minimized loss from photorespiration. Furthermore, with an increased photosynthetic activity, plants can respond to high light intensities, whereas insufficient concentrations of light are the limiting factor for most C_3 plants in solar radiation of more than 250 W/m^2. This explains why only C_3 plants can profit from an increase in CO_2 concentrations in the atmosphere (Fig. 5).

The efficiency of photosynthetic processes is theoretically determined by the amount of primarily generated carbohydrates in relation to the radiation provided. According to the basic processes of photosynthesis, theoretical values of more than 30% for assimilation in the chloroplasts can be calculated. In fact, efficiency values are limited by some inevitable losses.

Only a part of the solar radiation in the spectral range of 400–720 nm can be absorbed by pigments in the membranes of the chloroplasts. In relation to the overall radiation, this bandwidth covers only about half of the total energy reaching the earth's surface. Losses from absorption by photosynthetically inactive structures and from transmission and remission amount to at least 9%. Roughly, 8.5% of the primordial radiation is lost during absorption by pigments as thermal energy. This can be explained by the fact that the energy of the different photons within the bandwidth exceeds the energy needed for driving the separation of charges. The transportation of electrons and the secondary processes of carbon assimilation require 19–22%. Processes of photorespiration and dark respiration use another 6.2–7.3% in C_3-plants; dark respiration in C_4-plants accounts for 4.9–5.8% of the losses relating to primordial energy. The differences in these ranges confirm the advantage of C_4-plants in terms of efficiency. In a nutshell, different authors published an overall maximum efficiency level of 5.1% (C_3) and 6% (C_4) in chemically fixed energy in relation to the available radiation energy [7–14].

Efficiency levels that can be practically achieved are significantly lower. Maximum levels that could be measured in field experiments may reach a level of about 3.8% [15].

From the agronomists' point of view, it is vital that growing conditions are designed to allow for an approximation to the photosynthetically set limits of growth during the vegetation period. Harvesting and the reestablishment of a sufficient leaf-area index in the successive crop limit the time span for an optimized utilization of the progression of solar radiation in temperate climates (Fig. 4).

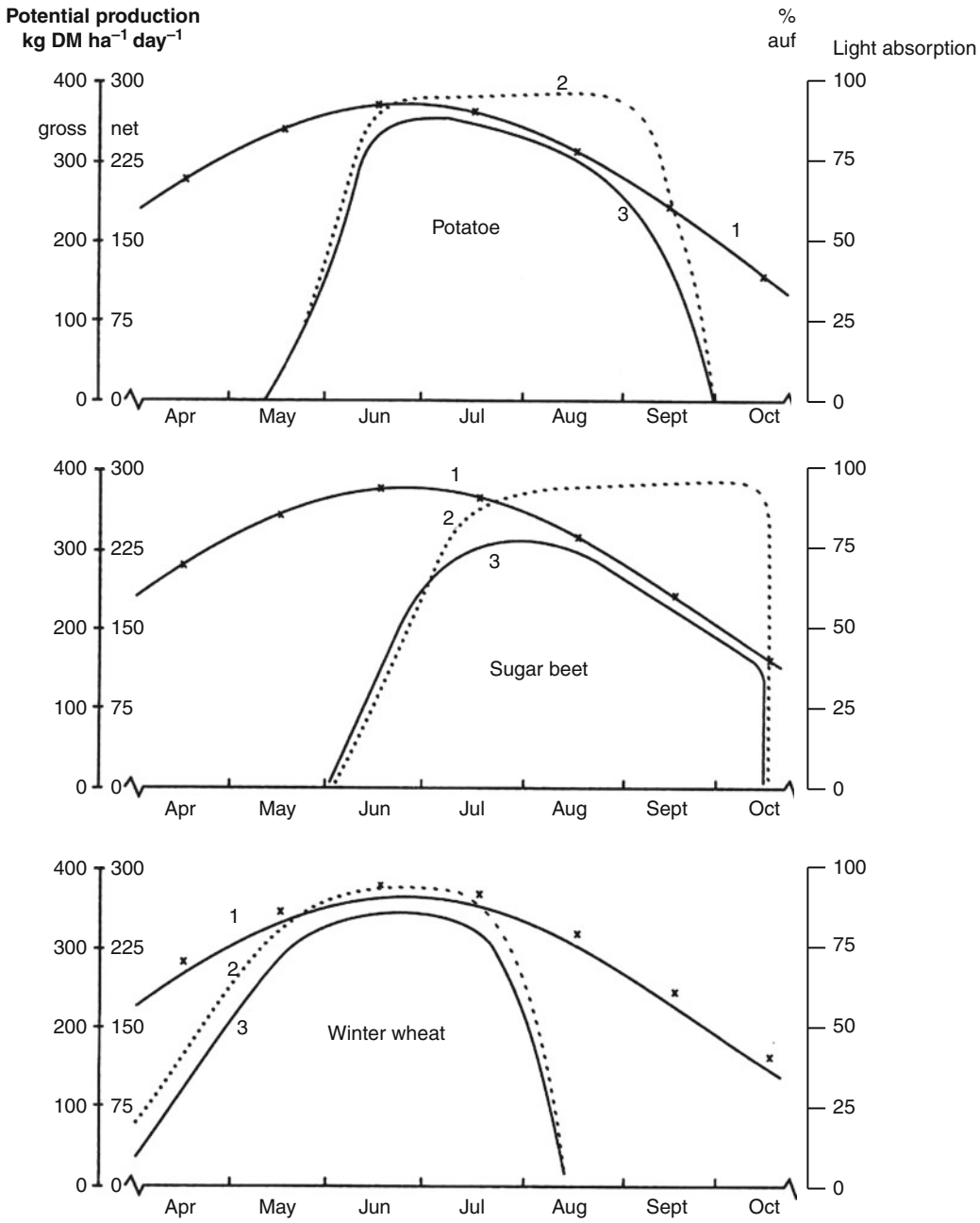

Biogas Production and Energy Crops. Figure 4
Potential of plant production derived from the radiation levels available (1); percentage of available radiation used by the crop stand (2); and calculation of daily increment (3) for potatoes, sugar beet, and winter wheat ([16] according to [17])

Temperature and Water Usage All processes determining plant growth are influenced by temperature. Depending on the species, a temperature range supplying optimum conditions for growth can be defined. C_4-plants show higher optimum levels (above 30°C) than C_3-plants (around 20°C). This can be explained by the relatively lower affinity of RubisCO for CO_2. Additionally, in warm conditions, CO_2 has a relatively lower solubility level in comparison to O_2. However, if temperatures are too low, the higher energy exertion for the refixation and transport of CO_2 by C_4-plants can be observed; this explains why the efficiency advantage of these plants can only be realized under conditions of adequate temperatures (Fig. 5).

Furthermore, temperature has an essential influence on the water balance of crop stands. This balance is decisively determined by the transpiration of leaf surfaces and the uptake of water by the roots. Due to the temperature-dependent differences in water potential between the atmosphere and the soil, water can move through the plant transporting nutrients and perform its essential functions in all the metabolic processes of the plant.

Of utmost importance is the evaporation through the stomata, by which gas is exchanged with the surrounding. The opening of the stomata is regulated, which accounts for the fact that water and gas exchange processes of plants are directly related to each other. This also explains why the available amount of water during the vegetative span, as well as the efficiency of its usage is crucial for crop yield and security.

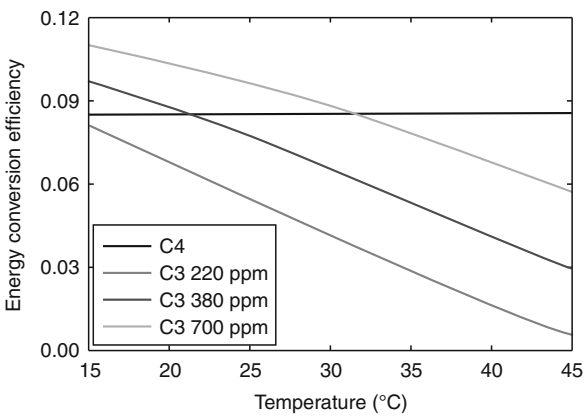

Biogas Production and Energy Crops. Figure 5 Theoretical energy conversion efficiencies of photosynthesis of C3- and C4- plants as a function of temperature and CO_2-concentrations of the surrounding environments [14]

During the growth period, values for the evapotranspiration coefficient (ETC) of about 350 l H_2O/kg DM for winter wheat, about 250 l H_2O/kg DM for winter rape and approximately 200 l H_2O/kg DM for maize could be identified. Due to different growth periods, ETCs of winter-annual crops are higher than those of summer-annual crops. By nature, low temperatures and low radiation intensities limit the growth of winter crops during long periods, so in relation to the available water, only little growth can take place. Hence, water consumption during the main growth periods should be regarded. In fully developed and healthy maize stands, this ranges roughly between 3.7 and 4.3 mm/day. Due to the described intra-leaf mechanism of CO_2-refixation, maize, just like other C_4-plants, exhibits higher water use efficiency (WUE). Still, necessary amounts of water cannot be provided by precipitation, which in the largest part of central Europe averages only between 1.6–2.5 mm/day. Therefore, with an increased optimization of other growth factors, also in temperate regions, water increasingly becomes the central limiting factor for plant yields.

In addition to the spatiotemporal distribution of precipitation, the soil functions of retention and storage of water from times in which water cannot be used for main growth periods is becoming increasingly important. Field capacity as well as the depth in which plants can potentially take up water by their roots is strongly determined by soil texture. In dry years, the effective root zone can vary between 50 (coarse sand) and 110 cm (loamy silt). By combining values of field capacities and effective root zone, the maximum amount of stored water available for plant growth varies between 30 and 220 l/m^3. From this quantity of water in combination with the amount of precipitation water added and the water use efficiency of plants, limits for the potential yield of crop stands under the given conditions can be estimated.

Soil and Nutrient Supply Soil development is based on the processes of physical and chemical weathering and the successive translocation of surface rock substratum. Besides minerals of varying size and composition, air, water, and organic mass are part of the layer called the pedosphere. The organic mass contains dead biomass as well as living organisms that are involved in matter-transforming processes.

Plants depend on absorbing all mineral nutrients (oxygen and carbon excluded) and trace elements from the soil. Therefore, physical and chemical properties of soils are essential for the attainment of yield potentials. Besides the thickness of the top soil layers, soil texture plays an important role. By structuring adhesion forces in the differently large pores, soil texture significantly determines the water storage capacity of soils (see above) and the capillary rise of water from deeper levels.

Products from the weathering and transformation of matter also determine the ability of soils to store nutrients. The enormous surface area of minerals, which are part of the clay fraction, can fix ions that are dissolved in water (e.g., nutrient salts) in the process of adsorption. This protects them from being eluted; due to the reversibility of the process, they are still available for plants.

Other than the composition of mineral constituents of the soil, organic matter, which is supplied to soils and subsequently underlying constant de-, trans-, and reformation processes, is relevant for storage functions. Input matter for dead organic material, called humus, is mainly made up of harvest residues, green manure, and organic fertilizers such as fermentation residues from biogas plants. The enormous plurality of forms in which organic matter in soils exists can be structured by its stability with regard to decomposition processes. Non-humic substances like polysaccharides, amino acids, and P-compounds show little resistance to decomposition. In the course of decomposition, plant nutrients such as nitrogen (N), sulfur (S), and phosphorus (P) compounds as well as potassium (K), sodium (Na), magnesium (Mg), and calcium (Ca) salts are released.

Parts of the organic matter, intensively altered with regard to morphology, show stabilization against further decomposition processes. These so-called humic substances form a large reservoir of nutrients due to their large exchange capacity. Furthermore, humic substances can occlude particulate organic matter within their structure and form compounds with clay minerals. This, in addition to its positive influence of transformation and storage functions, leads to a friable soil structure and the so-called mellowness of the soil [18].

For maintaining central soil functions and a constant flow of nutrients, a steady recirculation of organic substances is necessary. Since most forms of energy cropping aim at maximizing the energetic utilization of aboveground biomass, conflicts of interests can arise (see section Humus Balance).

From the perspective of plant production, planning the recirculation of residues is part of plant nutrition strategies. Central tasks in this planning are therefore to optimize the nutrition supply for the plants as well as to sustain and improve soil functions. The basic principle is that nutrients withdrawn from the soil should be returned. According to current knowledge, at least 14 elements are necessary for the normal development of plants. Quantities needed vary between the development stages, though.

The strongest influence on yield is to be seen in the variation of nitrogen supply. The reason can be found in the fact that nitrogen (N) is largely relevant to mass development and that its prevalence in most soils, relative to other nutrients, is yield-limiting. The uptake from soils mostly happens in the form of Nitrate (NO_3^-) or Ammonium (NH_4^+) ions. Besides organic fertilizers, the fixation of atmospheric elementary nitrogen in the course of cultivating legumes as well as the atmospheric deposition (caused, for example, by nitrogen emissions from combustion processes), the most important nitrogen source is mineral fertilizer. In contrast to nitrogen drawn from processes of the decomposition of organic matter, mineral fertilizer allows for a more pinpoint application.

Apart from nitrogen, fertilizer application of phosphorus (P) and calcium (Ca), as well as, depending on geological origin of the soil, of potassium (K) and Magnesium (Mg) has to be undertaken regularly. Phosphorus (P) is taken up by plants mainly in an

inorganic form ($H_2PO_4^-$ und HPO_4^{2-}). It has a key function in energy-related processes and is a component of organic compounds that are crucial for a plant's life. Potassium, Magnesium, and calcium are taken up as cations (K^+, Mg^{++}, and Ca^{++}) from the soil. Potassium is used for osmoregulation and influences numerous enzymatic reactions, which are important for the formation of macromolecules. Transportation of assimilates, winter hardiness, and drought resistance are raised by a good supply with potassium. Likewise, Magnesium is a nutrient for constructional and functional purposes. It is used in oxidation processes of the chlorophyll during radiation impact and is employed in energy-related metabolism as well as for the activation of enzymes. Calcium is an important component of the plants' matrix structure but also accounts for the bulking state of plants and the activation of various enzymes. The application of calcium is mostly aimed at regulating pH-levels for the optimization of nutrient availability for plant nutrition. Furthermore it stabilizes soil texture due to its bond-building function, which prevents puddling, erosion, and oxygen shortage. Other nutrients are available in sufficient quantities in most central European agricultural soils.

The amount of nitrogen fertilizer given should be oriented at the withdrawal of the plant stand. One of the central challenges is to plan optimum quantities before knowing the realizable yield. From an economic point of view, the optimum amount is characterized by the fact that the cost of the last unit of nitrogen given should be covered by the net revenue of the additionally attained amount of yield (marginal revenue). By approaching and exceeding the maximum attainable yield, the latter decreases (Fig. 6).

An optimized application of fertilizer, which avoids sumptuary consumption, can contribute to minimizing negative effects on the environment. Such negative effects are, for example, the leaching of nutrients into deeper soil layers, groundwater or receiving streams, nitrous gas emissions or the loss of nutrients into ecosystems by means of erosion processes. Risks of nitrate leaching are particularly high. Therefore, within Europe various regulations exist regarding fertilizer application.

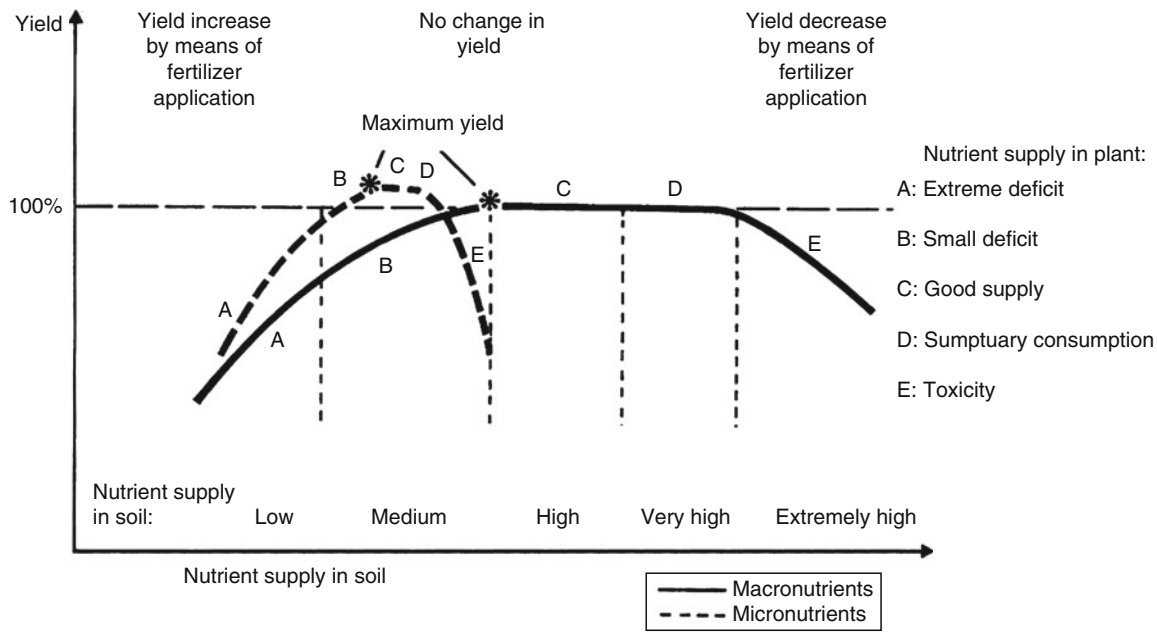

Biogas Production and Energy Crops. Figure 6
Relation between nutrient supply in the soil and in the plant respectively and the yield [19]

Organic Substance Groups as Raw Material for Anaerobic Digestion

The different substances incorporated in plant matter show, depending on their specific composition, a differentiated suitability for decomposition in anaerobic processes. Therefore, they can contribute in a differentiated manner to biogas and methane formation respectively which means, that the composition of plant matter plays a decisive role for the usability of chemical energy fixed in the substrate.

Organic Substance Groups The primary substances formed in the process of photosynthesis and the higher-molecular carbohydrates, lipids, and proteins formed in the following metabolic processes serve for the formation of the matter of plant cells, which are largely composed of macromolecules. The structure of these macromolecules follows universal laws; largely, they are formed according to the principle of replication from smaller units that are similar or congeneric.

For an assessment of the transformation of differently composed material, long-term experiences in the field of ruminant nutrition can be referred to. The analysis of plant material and its description can be conducted by the *Weende Analysis Standard* and its extension by van Soest [20]. This standard does not produce exactly defined chemical substances as parts of the cell wall or cell interior, but it can deliver statements on the energy value and the usability for digestion processes.

Internal Cell Substances In the field of ruminant nutrition, those parts of the cell substance that are soluble in a neutral detergent are called internal cell substances. A further subdivision can be done by classifying the different substances as part of different nonstructural carbohydrates, crude protein, crude fat, crude ash, or as part of the residual fraction.

Crude ash is the inorganic part of the assay, which remains after incineration. Still, the minerals remaining are mostly not isolated constituents of plant matter but are mostly part of organic compounds. Crude protein includes the actual protein fractions as well as the nonprotein nitrogen compounds. Being the nitrogen-consisting fraction, crude protein is being calculated from the nitrogen content of the assay and the average nitrogen content of proteins.

All substances that can be extracted using ether are called crude fat. Apart from actual fats (Triglycerides), this fraction also includes fat-like substances (lipoids). Nonstructural carbohydrates can be subdivided into water-soluble carbohydrates; that is, sugars and fructanes that consist of a buildup of laevulose components as well as starch, which functions as the most important reserve carbohydrate build up of sugar components. All other substances soluble in a neutral detergent are called organic residues and mostly consist of organic acids.

Cell Wall Substances (Skeletal Substance) Those parts of plant matter that are not soluble in a neutral detergent are called cell wall substances or NDF (neutral detergent fiber). A further subdivision can be made by classifying the different substances as part of the fraction of structural carbohydrates (pectins, hemicelluloses, and cellulose) or lignin.

Cellulose forms the skeletal substance of the non-lignified cell walls and is relevant for the tensile strength of the plant. The buildup is formed by the connection of monosaccharides (D-Glucose) by hydrogen bonds. The collective term hemicellulose includes a variety of other polysaccharides. Unlike cellulose, these consist of a variety of different monomers and a branching buildup. In combination with pectins and most of all, lignin, hemicellulose forms the cell wall matrix in which cellulose fibers are embedded. In the course of plant development and aging, the share of the different components in the cell wall changes. From primary to secondary cell wall structures, the share of pectin and hemicellulose falls while the share of lignin rises.

Analytically the combination of cellulose and lignin can be found as insoluble substances in acid detergent (ADF: Acid detergent fiber). Approximately, this fraction is comparable to the former crude fiber content of the *Weende Analysis Standard*, which comprises a lesser detailed subdivision of substance groups.

Figure 7 shows the development of different substance groups during the generative phase from the example of a maize plant. The change of cob mass in relation to the mass of the rest of the plant due to an increased storage of starch becomes very obvious.

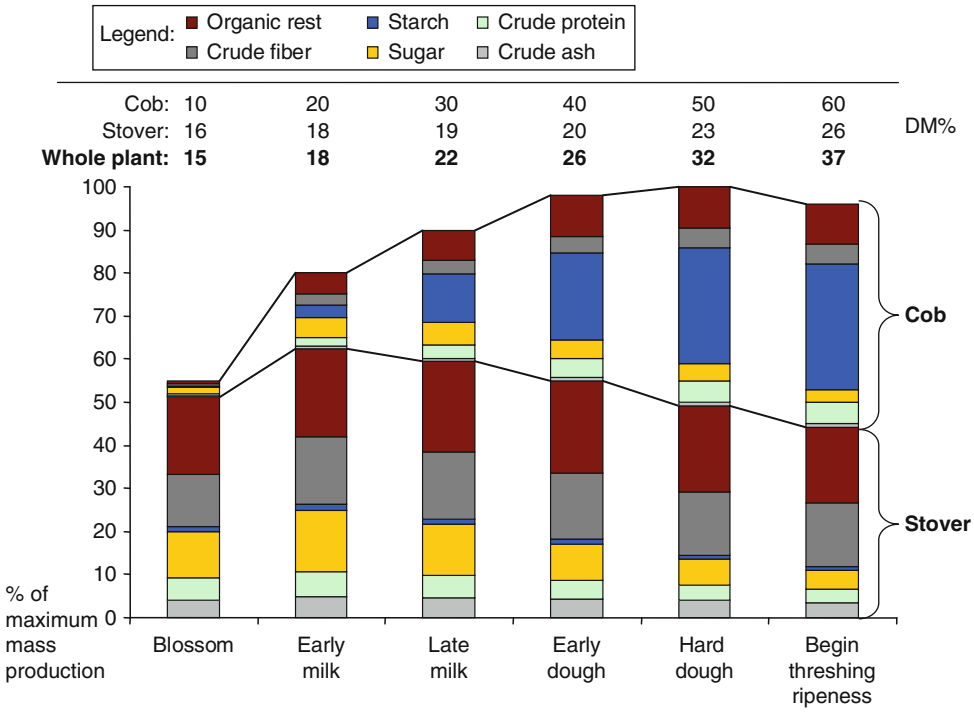

Biogas Production and Energy Crops. Figure 7
Development of the dry matter content (DM%) and substance composition of a maize plant from flowering to threshing ripeness (subdivided into cob and stover) ([21], complemented and altered)

Biogas Production and Energy Crops. Table 1 Substance composition of different energy plants for potential use in anaerobic digestion (Data from EVA – project [22, 23])

Crops	Crude Ash	ADL	Cellulose	Hemicellulose	Organic Rest	Crude Protein	Crude Fat	Starch	Sugar
Maize (early dough/dough)	4.3	3.4	23.1	22.8	9.5	8.0	2.5	15.6	10.8
Sugar beet, clean	16.6	0.2	21.0	21.6	0.6	15.9	2.1	0.0	22.0
Winter triticale WC (medium milk – early dough)	4.8	4.8	27.8	22.7	8.0	8.4	1.8	7.4	14.4
Clover grass first cut	9.8	2.8	28.2	11.8	17.4	13.7	3.0	1.6	11.7
Clover grass third cut	12.1	5.6	27.5	8.0	18.0	16.6	3.3	3.7	5.2
Cup plant	9.7				8.3	19.8	1.8		
Sorghum (*Bicolor* × *sudanense*) (up to early dough)	5.4	5.9	30.9	25.5	7.4	8.5	1.7	3.5	11.1

WC whole crop

At the same time, due to the transport and transformation of sugars as well as the lignification of the cell wall (characterized as crude fiber) and the digestibility of the stover sinks considerably.

Accordingly, Table 1 shows characterization of potential energy plant substrates for silage preparation. Values are given for "optimum" harvest dates for ensiling processes and anaerobic digestion.

Substrate Requirements and Biogas Yields Simple carbohydrates, fats, and proteins are the most accessible nutrients for bacteria involved in the process of anaerobic digestion. Thus, substrates containing high percentages of sugar and starch can be used to react quickly to low supply situations of the bacteria. Lignin, on the other hand, can be characterized as inert inside the fermenter and has no value for biogas production. Cellulose and hemicellulose form an interim position (Fig. 8). Also the digestibility of these groups can be limited by their being included in lignin–cellulose–hemicellulose complexes. In addition to the share of lignin, a mass of approximately 1.4 times this amount cannot be digested by the bacteria involved [24].

Planning of fermenter volume and the retention time or volume load is therefore also linked to the characteristics of substrates. The larger the share of slowly digestible substance groups, the larger the size of the fermenter to be constructed, in order to allow for an extensive digestion of organic matter (e.g., [25]).

Additionally, in planning other parts of the biogas plant, the feedstock plays a major role. Feeding, stirring, and pumping/discharging technology should be chosen according to the characteristics of substrates, for example, regarding the tendency to form deposition or floating layers [27].

While these characteristics influence the investment cost, the direct revenue of feedstocks is largely depending on their specific biogas formation potential. An approach to the derivation of the biogas formation potential is to be seen in stoichiometric calculations (e.g., [28–31]). According to these sources, the elementary composition of plant material (C, H, and O) allows for an approximate estimation of the gas formation potential (see, e.g., Table 2).

Due to the fact that values are calculated for a complete digestion of substances for the derivation of practically achievable yields, it is necessary to involve the actually digestible share of each substance group. One frequently used approach is to be seen in the utilization of digestibility coefficients known from feeding experiments, which are multiplied with potential methane yields (e.g., [32] based on [22, 30]). Despite various formulas that have been suggested (e.g., [33–35]), the usability for a wide range of plant and substrate types is limited in its validity, due to a so far non-sufficient parameterization for different plants and harvest stages.

Another possibility is the identification of gas yields using laboratory methods, for example, the utilization of batch tests (e.g., [36]). Methane yields for different energy crop substrates are shown in Fig. 9. Based on findings from different plant species a correlation between methane yield and the lignin content (R^2 = 0.78) or the sum of lignin and cellulose (R^2 = 0.60) can be seen [37]. Low methane yields of the Asteraceae sunflower and Jerusalem artichoke as well as *Miscanthus* go along with high lignin shares in plant matter.

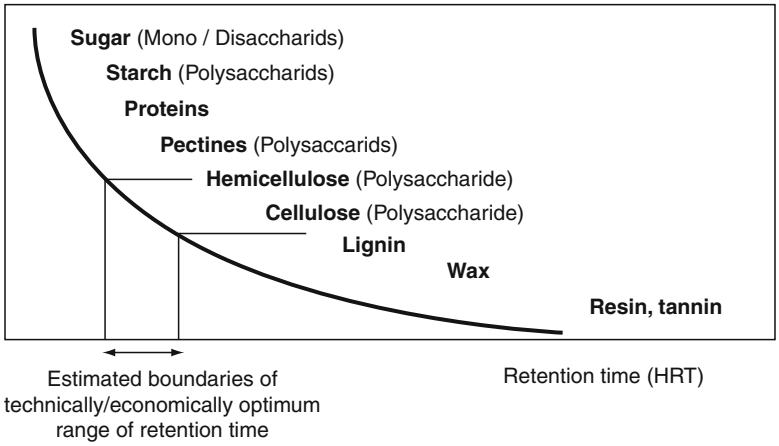

Biogas Production and Energy Crops. Figure 8
Digestion time of different substances [26]

Biogas Production and Energy Crops. Table 2 Potential and composition of biogas from different substance groups [31]

Substance group	Molar weight (g/mol)	Molar share of CO_2 and CH_4 in biogas (mol)	Molar volume of biogas (g/mol)	Potential biogas yield (l/g)
Carbohydrates $C_6H_{12}O_6$ or $(CH_2O)_n$	180	3 CO_2 + 3 CH_4	6·22.4 = 134.4	134.4/180 = 0.746
Fats, e.g., Palmitin $C_{16}H_{32}O_2$	256	4.5 CO_2 + 11.5 CH_4	16·22.4 = 358.4	358.4/256 = 1.39
Proteins incorp. 21 amino acids $C_{13}H_{25}O_7(N_3S)$	367	5.125 CO_2 + 7.857 CH_4	13·22.4 = 291	291/367 = 0.79
Plant biomass $C_{38}H_{60}O_{26}$	932	18 CO_2 + 20 CH_4	38·22.4 = 851	851/932 = 0.91

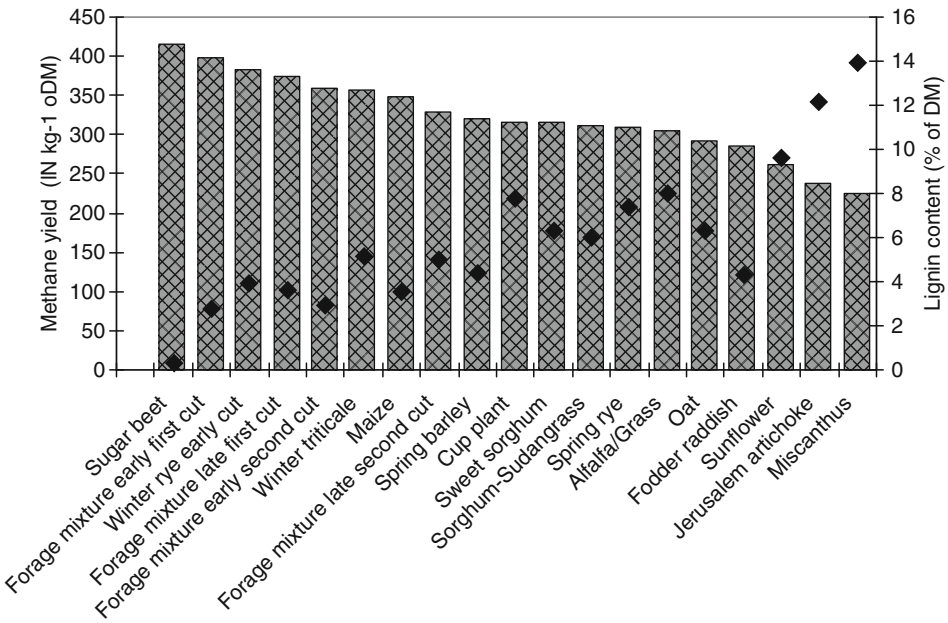

Biogas Production and Energy Crops. Figure 9
Methane yields and lignin content of silages from different plant material. Values shown are identified according to VDI 4360 and do not include ensiling losses. ([37]; sugar beet according to [38]; cup plant calculated value according to [39])

Since minerals (ash) do not hold a proper methane formation potential, gas yields are given as the potential per unit of organic dry matter (unit: liters under standard conditions for temperature and pressure per kg of organic dry matter l_N/kg DM). For the metabolic processes of bacteria, which are involved in the process of digestion, a variety of minerals are required. Roughly a relation of 600:15:5:1 of C:N:P:K is regarded as optimal [27]. A lack of availability of elements such as nitrogen

(C:N > 40) can limit the growth of bacteria. The same applies for potassium, sodium, calcium, and a variety of other trace elements (e.g., Co, Ni, Mo, Se, Fe). Optimum concentrations are commonly approximated at between 1 and 10 mg/l for iron, 0.005–0.5 mg/l for Nickel, 0.003–0.06 mg/l for cobalt, and 0.005–0.05 mg/l for Molybdenum. For co-digesting manure, a sufficient supply of bacteria is, in most cases, provided. With very high concentrations of nutrients, risks of inhibition of digestion processes rise.

Accordingly, nitrogen can lead to toxic reactions and the inhibition of bacterial activity by the formation of ammonia (C:N < 15:1). High sulfur values can lead to the formation of hydrogen sulfide, which – in sparsely adapted conditions in the fermenter – can lead to inhibitions at concentrations of 50 mg/l and above. Furthermore, its corrosive impact on copper and copper-compounds should be mentioned. Table 3 shows data on critical concentrations. It should be noted though, that vast interactions between inhibitors limit the force of expression of single values. Additionally, bacteria involved are able to adapt to and, in some parts, even decompose some inhibiting compounds [40].

Biogas Production and Energy Crops. Table 3 Critical concentrations of different inhibitors in biogas reactors. Shown in brackets are values for adapted bacteria populations [40]

Inhibitor	Critical concentration
Sodium	6–30 g/l (60 g/l)
Potassium	3 g/l
Calcium	2.8 g/l $CaCl_2$
Magnesium	2.4 g/l $MgCl_2$
Ammonium/ ammonia	2.7–10 g/l (30 g/l)/ 0.15 g/l
Sulfur	50 mg/l H_2S; 100 mg/l S_2-160 mg/l Na_2S (1,000 mg/l H_2S; 600 mg/l Na_2S)
Nickel	10 mg/l
Copper	40 mg/l; carbonate 170 mg/l
Chrome	130 mg/l; carbonate 530 mg/l
Plumbum	340 mg/l
Zinc	400 mg/l; carbonate 160 mg/l
Iron	Carbonate 1,750 mg/l

Apart from the crop used, substrate characteristics can also be influenced by the date of harvesting, the choice of which should aim at optimum yield and conservation properties (Fig. 7). Choice of crops can influence soil input into the fermenter, which can lead to deposition layers such as in the case of sugar beet (below). Furthermore, chopping size, which influences the surface area prone to microbiological attack as well as the tendency of a substrate to form floating layers, are factors influencing the fermentation process.

Production Systems for Different Energy Crops

Intensive breeding work and optimized production systems were able to contribute to a major increase in the yield of agricultural crops during the last decades. Therefore, many of the crops used for biogas purposes are crops known from food or feed production, which are harvested at the time of maximum biomass yields for silage preparation.

Besides crops from the family of *Poaceae* (true grasses such as maize, sorghum, and other cereals), leaf fruits like sugar beet can also be used. Currently, perennial types of the family of *Asteraceae* (aster family), *Malvaceae* (mallow family), *and Polygonaceae* (knotweed family) are also in discussion. *Brassica* (mustard family) types are not suitable due to high sulfur contents in the plant material.

Maize

Distribution and relevance Worldwide, maize (*Zea mays*) is one of the major agricultural crops. It belongs to the family of true grasses (*Poaceae*) and is a C_4-plant. Globally, it is dominantly cultivated for food production as grain maize. The cropping of maize in temperate climates could be extended largely by the development of adapted breeds that were developed during the last decades. In temperate climates, silage maize (SM) for fodder production (harvesting and ensiling at dough stage, Fig. 7) is of highest relevance. Regionally, the cropping area of maize has been increased by an increased biogas

production (Fig. 2). To some extent, new breeds sold especially for biogas production are grown (see section "Breeding").

Demands on site and climate Maize requires 200 mm of precipitation during its vegetation span, whereas the main demand is set during the flowering period. The crop is less demanding with regard to soil type; however, more importance is given to soil structure. A good supply of nutrients and water is only guaranteed if the soil is well penetrable for rooting. For germination, a soil temperature of between 8°C and 10°C is needed.

Temperature remains largely the limiting factor in temperate climates. Even precocious breeds demand minimum mean air temperatures of more than 13°C during summer months (May to September) [41]. Temperature sums can therefore provide information for choosing a breed adapted to the site-specific growing period. They are also used for harvest date prognosis models.

An international classification of maize breeds, albeit not specified by utilization purposes, is given by the three-digit FAO number. The first and second digits refer to ripeness classification and subclassification respectively. Under central European conditions, a difference of 10 units roughly describes a difference in ripening of 1–2 days [42]. Breeding approaches aiming at the provision of breeds for the specialized purpose of biogas production use breeding material with higher FAO classifications. Yield increases could be noted on comparatively warm sites. The difference in FAO numbers should not exceed 30–40 due to the danger of not reaching sufficient dry matter values of >30%.

Distinctive aspects of cropping system Commonly, sowing is done with single-seed sowing techniques with row distances of 75 cm. A low coverage level during early summer (around June) leads to a comparably high exposure to the increasingly erosive precipitation. Accordingly, on sites with a slope of more than 5%, erosion risks have to be taken into account. These risks can be encountered by using lower row width, under-sown crops, or non-tillage systems. Non-tillage systems can be well used after the harvest of a winter (first or inter-)crop for the establishment of maize. To avoid yield risks, slow development in early growth stages also makes weed control necessary.

Some investigations point out an influence of the harvest date on the specific methane yield of maize, while other results show no significant changes within the possible harvest time [43, 44]. Despite the possibility of higher methane yields (l_N/kg oDM) at early stages, investigations have shown that dry matter increment during the ripeness phase makes higher overall methane yields per hectare possible [35, 43], so most probably, substrate quality issues for ensiling (maximum 35% DM) determine optimum harvest date.

Apart from the high efficiency in using available water resources, the nutrient efficiency of maize is also very high. Per ton of dry matter, a withdrawal of 11–13 kg N, 2.1–2.6 kg P, 12–13.5 kg K, 2.5–3 kg Ca, and 1.8 kg Mg is a common range for analysis and for the estimation of the required amount of fertilizer.

Sorghum

Distribution and relevance Sorghum, just like maize, is part of the true grasses (*poaceae*) family and a C_4-plant. Cropping of sorghum is most relevant on the African continent, where it is mostly grown for grain utilization for food purposes. In the USA, sorghum is also highly relevant for silage preparation especially in the regions of the Great Plains where other fodder crops risk high yield losses due to summer drought. *Sorghum bicolor* and *Sorghum sudanense* as well as hybrid breeds of *Sorghum bicolor* and *Sorgum sudanense* are currently discussed and tested as substrates for biogas production.

Demands on site and climate The different sorghum types have a much higher demand regarding temperature conditions in comparison to maize. For germination, minimum soil temperatures of 14°C are needed [45]. Temperature sum from May to October should at least add up to 2,000°C (>5°C) [46]. Sorghum is frost-susceptible: Below temperatures of 4°C, it can suffer cold injuries.

To develop its characteristic rooting, sorghum breeds require deep soils without compactions. Despite slower root development, the subsequent deep rooting makes it possible to adequately utilize soil water and hence leads to good drought resistance properties and very fast growth during summer months. Compared to

maize, this is one of the decisive advantages of sorghum breeds (e.g., [47, 48]).

Experiments in Central Europe show a high yield potential for sorghum breeds. In many cases, the duration of the vegetation span was not sufficient for the development of sufficient dry matter values [49].

Distinctive aspects of the cropping system Sowing can be done with standard drill sowing techniques at a depth of about 2–3 cm. After a rather slow development in early development stages (especially in low temperature conditions), sorghum breeds show a rapid growth. In contrast to maize, sorghum tillers with 2–3 (bicolor – breeds) or 4–6 (*sudanense/sudanense* × *bicolor* – breeds) shoots respectively. *Sudanense* and *sudanense* × *bicolor* types can potentially be harvested more than once a year. Advantages in yield are not to be expected under Central European conditions and dry matter contents will not be reached in any of the cuts.

The height of sorghum breeds can exceed 4 m; however, it should be mentioned that tall-growing breeds often lack a sufficient stability. Sorghum shows a good appropriation of nutrients and can accordingly, similar to maize, make use of organic fertilizers. Withdrawal of nutrients for silage sorghum equals approximately 11 kg N, 4 kg P, 12.5 kg K, 1.5 kg Ca, and 1.2 kg of Mg per ton of dry matter.

The high sugar content of more than 20% for many *bicolor*-breeds (which are also specified as *Sorghum bicolor* ssp. *Saccharatum*) [50] lead to comparatively good ensiling properties. On the other hand, the lignin/crude fiber content is comparatively high, which leads to methane yields per mass unit that are around 10% lower than those of maize. In some breeds, there are high values in hydrocyanic acid, which are problematic for utilization as fodder but however do not inhibit anaerobic digestion properties [51].

Whole-Crop Cereals

Distribution and relevance Whole-crop cereals are cereals yielded from the early milk stage for silage preparation by the utilization of the entire plant matter. Generally, all cereals that are productive in market cereal production are suitable for this utilization purpose. In Central Europe, this encompasses predominantly wheat, rye, triticale, and barley. Due to their higher yield expectancy, winter forms are preferred for substrate production. Grain-straw ratios in earlier literature suggested a high yield potential of the summer-annual oat; though, this could not be confirmed in testing newer breeds [49].

Demands on site and climate Winter forms of cereals are sown in autumn and demand the impact of cold temperatures during early growth (vernalization) to be able to proceed to the generative phase. This period of cold temperatures is shorter in winter barley (20–40 days) than in winter rye and winter triticale (30–60 days) and winter wheat (40–70 days). Spring forms of cereals do not demand vernalization and are sown as early as possible in spring (Central Europe: March). The gradation in genotype disposition, in terms of temperature demand and photoperiodic reaction, therefore play a major role for the question of suitability.

Germination of cereals starts at low temperatures. Rye has the lowest demand with temperatures of 1–3°C. Minimum temperatures for the net primary production of most cereals are around 3–5°C, and for oats between 4 and 6°C. Winter hardiness differs between the different types of cereals. While winter rye can sustain snowless frost periods with temperatures of up to −25°C, temperature values of around −20°C for winter triticale and winter wheat and of around −15°C for winter barley can be sustained. After field emergence in spring, oat can also sustain frosts of −6°C.

Winter wheat has the highest water and soil requirements and – when provided – shows high productivity. On lighter soils, rye can produce yields similar to those of winter wheat. Barley also has fairly low requirements concerning soil quality. Triticale, as a cross of wheat and rye, was supposed to combine the relatively low requirements of rye with the high yield potentials of wheat. High whole-crop yield potentials on sites providing good soil characteristics can be confirmed. Since the crop ratio of comparatively high-yielding wheat is already high on accordant sites, winter triticale is being recommended because in addition to its high-yielding potential, its cultivation provides possibilities to extend crop rotations (see section "Cropping Systems"). On low-yielding sites, winter rye has the best suitability in whole-crop cereal production as

well. Rye shows higher self-compatibility than wheat, which lowers the necessity for alternatives.

Winter cereals, just as other C_3-plants, commonly have lower water use efficiency than C_4-plants such as maize or sorghum. The decisive advantage of winter annuality is that in temperate climates, during tillering and stem elongation stages, these plants can convert winter precipitation stored in soils much better into biomass.

Distinctive aspects of cropping system In general, cropping systems for cereals aimed at substrate production are to be oriented at market cereal production. From an agronomic point of view, during the last years, various options to reduce factor intensity have been discussed. These discussions were based on the changed quality requirements and the shorter growing periods of whole-crop cereals (see section "Factor Intensity").

Biomass yield of cereals can increase until the stage of yellow ripeness. From then respiration of assimilates and loss of leafs lead to a net yield reduction [52]. For the choice of harvest time, considerations on intended silage quality and the establishment of a subsequent crop play a major role. For instance, during yellow ripeness, dry matter contents exceed the optimum range in many cases. Accordingly, simultaneous optimization of yield and ensiling properties, brings about short time frames for harvesting in most years at the end of milky stage. Since the correlation between dry matter content and the development stage is low, tentative testing of plant material before harvest is advisable. From the viewpoint of crop rotation design, harvest time can also be influenced by the choice of cereal. Winter barley reaches an optimum harvest time much earlier than winter wheat (Fig. 10).

Depending on the type of cereal and the harvest stage, withdrawal of nutrients from the early milk stage amount to 11–15 kg N, 2–2.5 kg P, 14–17.5 kg K, 0.9–1.2 t Mg, 2–3.2 kg Ca per ton of dry matter.

Cropping systems for whole-crop cereals should not be mistaken for intercropping systems. Green-cutting of rye, for which special breeds are sold, starts from the visibility of the first awns. Yield quantity can be approximated at around half of the yield of whole-crop yields. Due to low dry matter contents, swathing and pre-wilting is required in many cases.

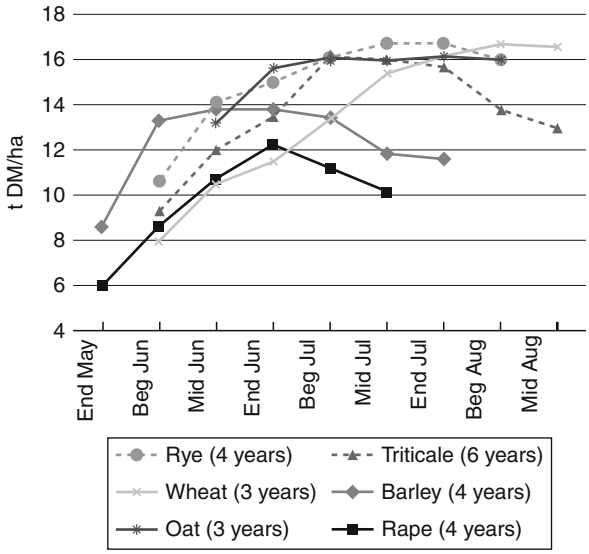

Biogas Production and Energy Crops. Figure 10 Development of dry matter for winter rape, barley, rye, wheat, triticale, and oat on central German sites [52]

Yields of winter cereals vary, depending on site characteristics, according to grain production largely. On loess-influenced sites, yields of up to 20 t DM can be achieved. On sandy soils, yield expectations are approximately half of this value. Despite these major differences between the different sites, intertemporal yield variations on the specific sites are lower than those of maize.

Sugar Beet

Distribution and relevance Sugar beet (*Beta vulgaris* ssp. *maritima*) is mainly grown in Central Europe. As the beet may take advantage of large parts of the available vegetation period of temperate climates, it is one of the most yielding crops in those regions. Due to the reform of the Common Market Organization for sugar in 2006, sugar beet cropping for sugar production has sensibly gone down. As expertise and machinery still exist, there is growing interest for the utilization of sugar beet for other purposes. Therefore, technical equipment and machinery must be adapted correspondingly.

Other than sugar beet, fodder beet is of less importance. As they have low dry matter contents and the existing varieties lack resistance against Rhizomania,

leaf spot, or nematodes, it is at present not of interest to grow fodder beet for biogas production.

Demands on site and climate Sugar beet cropping is done best on deep, medium-heavy soils that allow good rooting. Therefore, chernozem and brown earth with loess with a stable soil structure and a high, usable field capacity are particularly well suited. From the point of view of substrate production, keeping troublesome substances away from the digester is an issue of decisive importance. Beets from sandy soils have less soil tare, while loam, clay, or silt adheres more easily to the beets. However, practical experience has shown that such particles stay in suspension due to agitating and pumping in the digester; they stick to organic matter and thus leave the digester with the residues. Sand, however, tends to sediment and form a layer. Another problem, which is much more dangerous, arises from stones, as they might damage the feeding system and the agitators. Therefore, cost-saving technologies to remove hazardous material before it gets into the digesters will be of decisive importance in the future. At present, mobile units to clean the beet are being developed.

Distinctive aspects of cropping system The sugar beet is drilled in rows with a special precision drill as soon as the soil is well settled and dry, and night frosts are not any more to be expected. It is better to drill later instead of disturbing and hindering the sugar beets' growth by soil compaction as a consequence of the wrong soil management.

In conventional sugar beet cropping, the extraction rate per ton of dry matter is around 8 kg N, 1.8 kg P, 9 kg K, 2.2 kg Mg (the root) and/or 22 kg N, 2.8 kg P, 27 kg K, and 3.3 kg Mg (leaves). The quality parameters of sugar production do not apply to sugar beet cropping for biogas production; fertilization programs may thus be modified. More nitrogen fertilization leads to disproportionate increase of leaf growth compared to root growth. Nitrogen fertilization should not be increased by more than 20% with regard to the level applied for sugar beet for sugar production. It may be that boron could be necessary at canopy closure to prevent from heart and root rot, especially if the beets are supposed to be stored in field clamps for a longer period.

Other than for sugar production, the grown biomass of beets should be used completely. When defoliating the beets, they are not topped but only stripped of their leaves, and the crown is harvested together with the root. This allows a surplus yield of 5–10% [53]. However, when using this method, sugar beets should be fed into the digesters before too long, as the leaves may start to regrow. Sugar beet leaves are to be considered an additional yield factor, as the leaves mean an additional fresh matter yield of around 3.5–4.0 t of dry matter/ha, the equivalent of up to 15% more methane yield per hectare. But as leaves contain less energy than the roots, in general only short transport distances are profitable.

As sugar beets have a low dry matter content and are therefore less suitable for silage, bridging the time between the moment the beet is mature and the moment it is fed into the digester constitutes a certain challenge.

Storing the fresh beets in clamps and feeding them into the biogas production plant is possible between the months of September through mid-February under Central European conditions. However, clamps should be covered by mid-November. When clamps thaw after long periods of frost, the beets should be processed as soon as possible. At present, it is checked whether the beets may remain in the soil during winter and be harvested before bolting. Compared to storage in clamps, relatively mild winters thus allowed gaining yield surpluses of 10% [54]. With less favorable conditions and strong ground frosts, however, it is necessary to harvest and process the beets as quickly as possible.

When beets are to be stored for a longer term, they must be ensiled. The latest findings open up the following possibilities:

1. Ensiling in plastic tunnels: Up to now, good experiences have been made with ensiling whole beets. Chopped beets in foil tunnels would run the risk of causing the tunnel to burst due to the resulting seepage.
2. Ensiling entire beets in bunker silos: The density of the sugar beets changes in the course of the ensiling process. The piles slump down to almost half the height during ensiling. Sampling of such beets has shown pH-values of 3.5. In any case, it is important to collect the seepage.

3. Ensiling as mixed silage with maize: Good experiences have been made during the past years with mixed silage (maize/sugar beets in layers with a ratio of up to 50/50) in bunker silos. The main challenge consists of finding an optimal harvest date for sugar beets and maize, and coordinating two harvesting processes for different crops at a time. For example, in large parts of Germany, maize is harvested during mid-September until the end of the month – a time, where sugar beets have not yet reached their maximum yield. Therefore, a late maize variety should be chosen (see section "Breeding"). Another possibility is ensiling beets together with dryer substances, for example, ground ear maize (GEM). In such cases, even a ratio of up to 70% of sugar beets would be possible.
4. Ensiling in existing tower silos: If tower silos already exist, they are useful. Main stress should be put on producing beet pulp which is as homogeneous as possible, to avoid sedimentation in the silo.

Depending on the storage method, it is necessary to provide for adequate chopping technique before and/or after storage. Practical experience has shown that when whole beets are stored, it is sufficient for fermentation needs to chop the beets to a size of 3–4 to 1 cm, to take advantage of the specific properties offered by sugar beets for biogas production.

These favorable properties are quick fermentation (Fig. 8), high methane yields (Fig. 9), easy pumpability, and a process-stabilizing influence compared to the specific acid values prevailing in biogas plants despite quick acidification in the digester when sugar beets are fed in [55].

Perennial Forage Grasses and Forage Mixtures

Distribution and relevance Multi-cut forage crops consist of annual and perennial grasses, small-seed legumes or mixtures including various types. In Europe, these were traditionally grown to provide protein-rich fodder for dairy cows. Due to the expansion of maize cropping, the crop ratio of perennial fodder plants decreased largely [42]. In Europe, grasses cultivated include mostly species from the *Poaceae* subfamily of *Pooideae*, mainly ryegrass (*Lolium*), Festuce (*Festuca*) and hybrid crossings (*Festulolium*) accordingly as well as Timothy grass (*Phleum*) breeds and cocksfoot (*Dactylis glomerata*).

During the last years, perennial warm-season grasses of the *Poaceae* subfamily of *Panicoideae* such as Miscanthus (*Miscanthus Gigantheus*), Andropogon (*Andropogon gerardii*), or Switchgrass (*Panicum virgatum*) were also tested for energy cropping in temperate climates. According to current knowledge, good yields can be achieved with warm-season grasses. For the utilization as a biogas substrate an extensive lignification (Miscanthus, Fig. 9), a lack of persistence or a high damage from early cuts proved to be disadvantageous [56]. As such, other conversion routes are more reasonable (see other article, e.g., on combustion).

Demands on site and climate Production of grasses and forage mixtures can be set on all arable sites. Mostly, it is advantageous on sites that are too cold for the cropping of maize or sorghum or where late frosts in spring or early frosts in autumn are to be expected. For the cropping of red clover (and grass mixtures), continental sites with average precipitation levels of 650 mm are most suited. Ryegrasses show suitability on fresh to moist sites with precipitation of more than 650 mm. Alfalfa (and grass mixtures) are advantageous on anhydromorph calcareous soils and weathered loess soils. Alfalfa and cocksfoot are also advantageous on drier sites.

Distinctive aspects of cropping system For an optimum choice, apart from site characteristics, the planned utilization period is of major importance. Generally, the cropping of mixtures is preferable due to weather and utilization conditions, risk minimization, and their higher adaptation potential to the specific site. Furthermore, the nitrogen fixation of mixtures, including legumes, as well as the positive impact of perennial grasses and mixtures on the humus balance should be included into the evaluation.

The choice of cutting frequency influences the specific methane yield as well as the yield of perennial forage cropping. In later and hence reduced cutting during the vegetation span, substrates may on the one hand become less digestible. On the other hand, yield increases. According to current knowledge, reduced cutting frequency, which means 3–4 cuts instead of 4–5 cuts can be advantageous and lead to a 10% increase in overall methane yields per hectare [57–59].

Due to the low dry matter content of the cuts of grasses and forage mixtures, fresh material shows low suitability for ensiling. Commonly, swathing and pre-wilting to a dry matter content of 30% is done before the work step of picking up under the precondition of sufficiently warm conditions.

Overall, during the main utilization years, yields of ryegrass mixtures on maritime influenced sites can exceed 20 t DM/ha, on better but in summer dryer continental sites, yield of 16 t DM/ha can be achieved. Multi-cut systems including production steps for swathing demand higher production costs per hectare. Due to low income of fodder production from permanent grassland, the utilization of these sites for energetic purposes might increase as well [60, 61].

Additional "New" Energy Crops Given the specific substrate requirements of the utilization pathway of anaerobic digestion, during the last years, the cropping of a range of other energy crops that have no or only little share in current cropping systems of temperate agricultural regions has been discussed. Whereas knowledge on the cropping of some of these plants as the cup plant (*Silphium perfoliatum*) or the Jerusalem artichoke (*Helianthus tuberosus L.*) exists, for other options, very little experience is reported.

Cup Plant (Silphium perfoliatum) The cup plant is a perennial plant of the aster family (*asteracea*) that originates from the temperate regions of North America. While little experience in agricultural cultivation has been made there, the plant was tested in the 1970s and 1980s in Japan, Russia, and Eastern Germany among others concerning its properties as a fodder plant [62]. Due to lack of seed production, cultivation could not be implemented practically.

Demands of the cup plant with regard to soil texture is not high; it can also be cultivated on sandy soils at fairly low annual precipitation levels of 350–440 mm. Water-logged soils are not suitable; best growth can be expected on humus sites with good water supply. For germination, seeds require a longer phase of cool or changing temperatures.

For the establishment of practically applicable cropping systems, current works focus on the pretreatment of seed and single-seed sowing techniques – currently establishment has to be done, using seedlings. During the year of establishment, plant development is slow and no linear growth takes place. Weed control is necessary. Planting should be finished at the beginning of June, to tap the full yield potential from the second year on. As a utilization period, a 15-year period is currently being focused on. Nutrient withdrawal amounts to 10 kg N, 1.9 kg P, 16–17 kg K, and 4 kg Mg per t DM.

Harvesting starts from the flowering period at dry matter contents of 28–30%. Ensiling properties are good and deliver methane yields that are slightly lower than those of maize at 300 l_N/kg DM (Fig. 9). Yields of 17–20 t DM/ha from the second year on better soils [39] and 12 t DM/on weaker soils [63] can lead to the appraisal that the cup plant might in future be a new crop for energy production in temperate climates.

Jerusalem Artichoke (Helianthus tuberosus L.) Jerusalem artichoke is, like the cup plant, part of the aster family (*Asteraceae*). Instead of starch, the plant uses Inulin, a fructose-polysaccharide, as a reserve carbohydrate. This is stored in irregularly shaped tubers measuring up to 10 cm in diameter from which several pith-filled stems of up to 3 m in length are formed.

Jerusalem artichoke also grows on sandy soils and shallow alteration soils. High yields require a good water supply during summer months. For the utilization of the tubers, the same restrictions apply as for the utilization of sugar beet. This means, that sites should be avoided, that entail an intensive input of soil, especially sand and stones into the fermenter.

Since plants do not reach seed ripeness in temperate climates, reproduction is done vegetatively using potato planters for the deposition of tuber. Choice of breeds and planting density depend on the utilization aim. For the utilization of aboveground biomass, the planting density is lower (about 40,000 tubers/ha) than for the utilization of tuber biomass itself (45,000–50,000 tubers/ha). Nutrient withdrawal ranges at approximately 10–12 kg N, 2–3 kg P, 23–25 kg K, and 2 kg Mg per t DM of tuber and 7.5 kg N, 0.8 kg P, 20–21 kg per ton DM of the aboveground biomass respectively.

By leaving the tuber in the soil, the utilization of the aboveground biomass can be done for several years. Haulm biomass ranges between 10 and 16 t DM/ha. From the second year onward, stands have to be thinned to prevent yields from decreasing. Yielding of

tuber can be done with potato harvesting technology. At the optimum stage, yields of the tuber range between 6 and 8 t DM/ha. If tuber and haulm is to be harvested, a compromise between maximizing tuber yield and the earlier maximization of haulm yield has to be found. Concerning the tuber, just as for sugar beet ensiling can be a challenge. From a cropping perspective, regrowth even from small tuber parts remaining in the soil may cause problems in the successive crop. While methane yields of haulm biomass is relatively low due to lignification (Fig. 9), the tuber can reach methane yields of up to 400 l_N/kg DM [64].

White sweet clover (Meliotus albus) The cropping of the biennial White Sweet Clover is currently being discussed on sites that fall below the suitability for Alfalfa or Red Clover. According to current knowledge, under Central European conditions, it can reach yields of up to 7 t DM/ha on these sites, which is around 30% lower than the comparable yield of maize. On better sites, yields of 10.1 t DM/ha were stated [65]. Additionally, an extensive fixation of nitrogen (90–150 kg/ha) and intensive and deep rooting (Root biomass of 12–18 t DM/ha) have to be included into the evaluation. On the other hand, the methane yield of below 275 l_N/kg DM is comparatively low. White sweet clover (*Melilotus albus*), which originates from Eurasia, is assessed as invasive and problematic in many parts of North America.

Rumex Originating from Ukraine, the cross of *Rumex patencia* und *R. tianschanius* can be cultivated using standard drill technology. Utilization of cultivation material from the second cropping year can be carried out for 15–20 years in two cuts per year. Sufficient dry matter contents at the harvesting stage should be aimed at. Current results show yields of 9 t DM with low dry matter contents and hence no explicit suitability as biogas substrate [66].

Virginia Fanpetals Virginia Fanpetals (*Sida hermaphrodita*) is a perennial crop, which has little demands concerning site condition and shows strong winter hardiness [67]. On a sandy loam yields of the second and third year of cropping equaled 11 t DM/ha (Ibid.). On Eastern German loess sites, yields of the second cropping year were between 5 and 9 t DM [66] and 12 t DM [68].

Polygonum Cropping experience of the species originating from Northeast Asia is limited. Up to 25 t DM for *P. sacchalinense* can be achieved [56]. The large leaf biomass (LAI 18–25) makes stands vulnerable to hail damage. Lower yield, which is on average slightly lower than for maize, were recorded for *P. weyrichii* [69].

It should be noted that *P. sacchalinense* is closely related to *P. japonicum*. In North America and Europe, *P. japonicum* is one of the most problematic invasive species (www.issg.org). Due to the fact that *P. sacchalinense*, similar to *P. japonicum*, has an invasive root system and thus proves to be hard to control, and more so since it can hybridize with *P. japonicum*, cropping is not advisable.

Breeding (*Author A. Von Felde*)

In the past efforts in breeding of agricultural crops had been concentrated exclusively on progress in foodstuffs and animal feed production, mainly for the production of starch, sugar, and oil. Maximizing the production of energy with environmentally sound and resource-friendly cropping methods constitutes a new breeding goal, which expectedly will be honored by impressive results and successes within a short time. Energy maize (EM) breeding can serve as one example (Fig. 11).

Biogas Production and Energy Crops. Figure 11 Biomass yield potential of maize: Three German, one Italian, and one Peruvian maize variety (left to right) in an energy maize performance test near Wesel in 2004

The example of maize allows illustrating the enormous increase possible in biomass and therefore energy production within a short time period due to breeding efforts, if breeders do not think any more in categories typical for grain and silage use. Freed from those restrictions, new ways may be opened. Such new approaches will make it possible to increase the total dry matter (TDM) yield of maize from today's 15–18 t/ha to more than 25 t/ha. This equates to a methane output of more than 8,000 m^3/ha, or a petrol equivalent of 8,000 l/ha. Figure 11 gives an impression of the biomass yield potential of maize, potential to be exploited in breeding and plant production.

The following breeding approaches may be used to increase biomass production and subsequently energy production of maize:

1. Prolongation of the phase of vegetative growth
2. Combination of late maturity and cold tolerance through breeding
3. Integration of short-day genes from exotic populations

These methods are completed by further long-term breeding goals, for example, improvement of drought tolerance, adaptation of maize to a C_3/C_4 energy crop rotation, and adaptation of energy maize to the conditions of organic farming (by striving for robustness and competitiveness in mixed and underseed cropping).

Prolongation of the Vegetative Growth The simplified graph in Fig. 12 illustrates the reasons for which the approach of prolonging the phase of vegetative growth promises to increase the biomass potential and therefore the energy potential. The black curve (Fig. 12) depicts the course of total dry matter production of a maize variety which has been breed for silage use (SM = silage maize). The red curve shows the development of a maize variety which has been optimized for energy production through breeding (EM = energy maize).

As starch and cellulose offer the same specific methane yield, an increased vegetative growth phase of stem and leaves as such is not necessarily disadvantageous (reduced starch content).

Until the flowering of the silage maize variety, both growth curves show an identical shape. The vegetative total dry matter of both varieties increases exponentially.

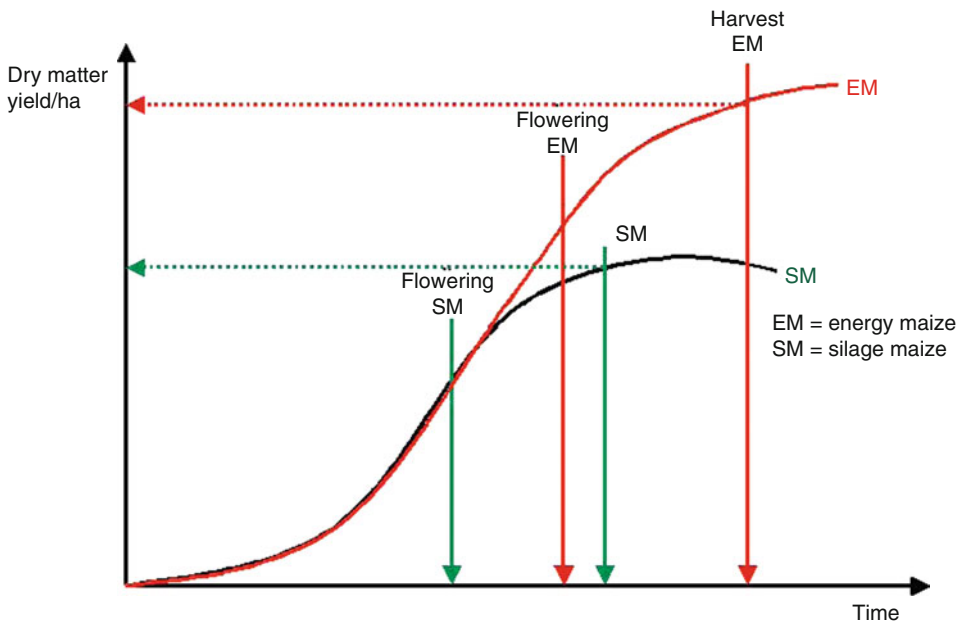

Biogas Production and Energy Crops. Figure 12
Formation of total dry matter (TDM-yield) in a silage maize (SM) variety and an energy maize (EM) variety

After the flowering of the silage maize variety, however, both growth curves increasingly diverge. The silage maize's curve has a linear growth and soon flattens, while the energy maize's growth curve continues with its exponential growth. This further growth is due to the simple physiological fact that the energy maize variety continues to invest its assimilation performance in supplementary vegetative leaf mass instead of investing it in ear production, which is what happens with the silage maize variety. These supplementary leaves contribute to assimilation in the energy maize variety, while the carbohydrates stored in the silage maize variety's ears do not. This explains the superiority of the energy maize variety's yield compared to the silage maize variety's yield. The later the energy maize variety is harvested, the more pronounced its superiority compared to silage maize.

This relatively simple physiological trick of prolonging the phase of exponential growth of the plants by postponing the flowering time helps to achieve enormous increases in yield not only for maize, but as well for most of the crops.

Late Maturity and Cold Tolerance Basically, it is easy to postpone the flowering time of maize varieties.

For example, the only thing to do is to change the maturity groups cropped in Southern France, Hungary, or Italy and one immediately has breeding material at hand that flowers sufficiently late, which is what is needed for energy maize cropping in Germany.

Unfortunately, there is a big drawback regarding the breeding material groups used in such regions: They are not adapted to the cold climate and therefore do not show enough development during the early stages. All the recent hybrids from Southern European breeding programs have been tested most intensively under German as well as Dutch cropping conditions to find out whether they are suitable for energy maize hybrids. In 3 out of 4 test years, some of the Southern European varieties (and some of them even clearly) outmatched the best conventional German silage maize varieties. The only exception was the year 2004, which was extremely cold. Due to the very cold spring, practically all the Southern European varieties fell strongly behind (Fig. 13) as they had a bad initial development compared to the German silage maize varieties. In general, this backwardness was so important that they were not able to compensate during the warmer summer months.

Biogas Production and Energy Crops. Figure 13 The cold-tolerant German standard variety GAVOTT (on the right side) surrounded by numerous cold-sensitive Italian hybrids, photographed in July 2004 in an energy maize performance test in Wesel

Therefore, breeding is called to unite late maturity and cold tolerance in energy maize hybrids. One of the obvious ways suggesting themselves is to start selecting for cold tolerance where full genetic variance is still available, which is not the level of varieties, but the level of breeding lines, which is one level earlier. At that stage, the material is not yet limited as it has not yet been checked about its ability to be combined. Figure 14 illustrates the performance of experimental crossings of 90 South European lines, which had been selected sharply. They were tested in one out of three ten times ten-lattices together with ten standards regarding their combinability with a German flint tester of a conventional silage maize breeding program. This test was carried out at Bernburg and Wesel, both German places, and also at two Dutch places. Three elite lines were tested twice together with those lines: the early German line 5G355, the medium-early French line 5F279, and the medium-late German line 5G393. The results show that it is possible to reach new yield performances of 27 t/ha with Southern European DH-lines, which have been selected for cold tolerance. This is a level that is not even reached by the presently best-performing German silage maize breeding

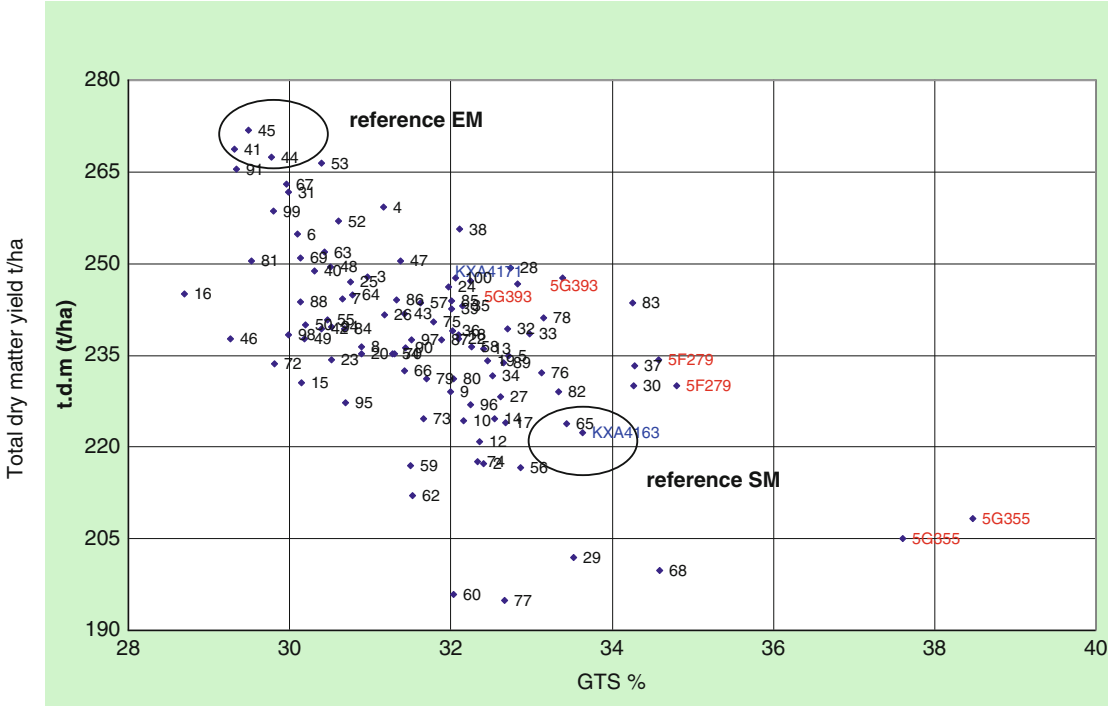

Biogas Production and Energy Crops. Figure 14
Dry matter yield (DM in dt/ha) as a function of the maturity of the entire plant (DM in%) of 90 new energy maize hybrids (and 10 standards) from late, Southern European lines which had been selected for cold tolerance and crossed with a German flint tester. Reference SM - Silage maize for fodder production; Reference EM - Potentiale "Energy Maize" - Breeds showing higher yield potential

material, which is represented by the three elite lines in the diagram. The late hybrids' dry matter content amounting to 30% guarantees safe ensiling without seepage and simultaneously offers good methane output. When trying to assess these results, it should be taken into account that the progress in breeding was achieved by improving just the female side of the experimental crossings, as the pollinizer used (= father) had been a line from conventional European silage maize breeding programs.

The results shown in Fig. 14 are representative for the further about 180 Southern European lines tested in the two further ten times ten-lattices with a German flint tester. They confirm the results of both previous years, where Southern European lines had been evaluated the same way, and with the same results [70, 71].

An obvious possibility is to cross Southern European lines, which had been selected previously for their cold tolerance, among themselves in order to maybe achieve energy maize hybrids that are even more yielding. Therefore, the best Southern European lines, which had been identified in energy maize trials, were used to produce and test around 250 factorial crossings. The best performances of these hybrids reached 28 and 29 t/ha. They achieved a level of performance, which was about 7 t/ha higher than for instance the yield potential of the hybrid KXA 4163 (Fig. 15).

Integration of Short-Day Genes from Exotic Populations There is another, and quite different, way of increasing biomass and therefore energetic performance of maize. If South American or Central American maize populations adapted to tropical short days are cropped in Central European long-day climates, those populations react with increased vegetative growth. Some of these exotic maize breeds reach heights of 4–5 m (Fig. 11). But not only the length of the stem is increased, but as well its diameter (Fig. 16).

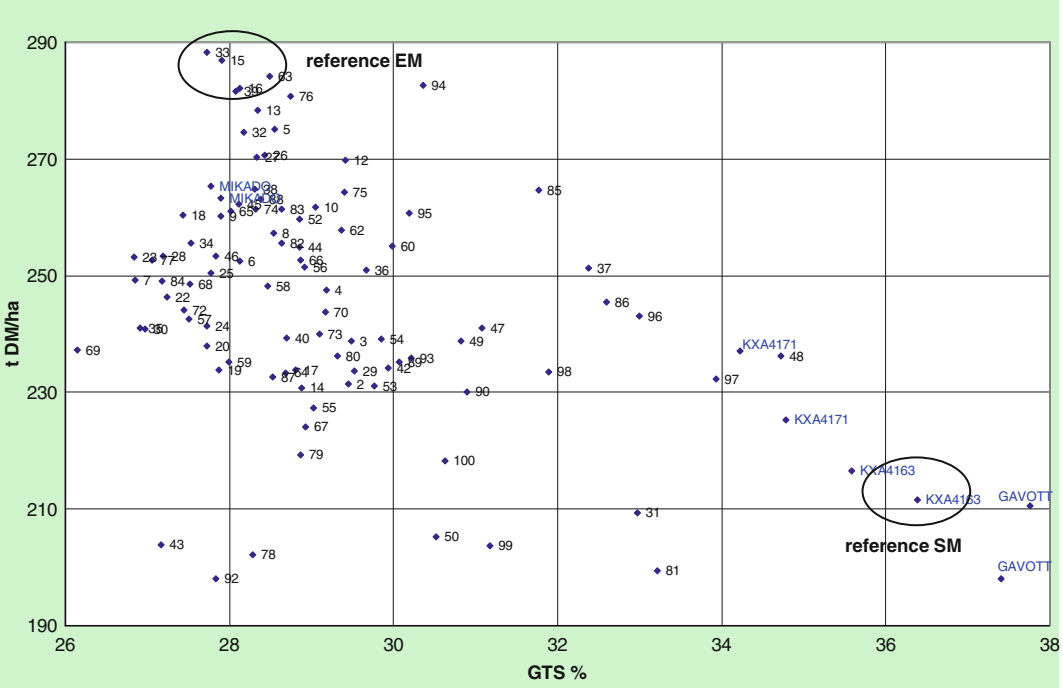

Biogas Production and Energy Crops. Figure 15
Dry matter yield (DM in t/ha) as a function of the maturity of the entire plant (DM%) of 90 new energy maize hybrids (and 10 standards) from a factorial of late, Southern European DH-lines which had been selected for cold tolerance. Reference SM - Silage maize for fodder production; Reference EM - Potentiale "Energy Maize" - Breeds showing higher yield potential

Biogas Production and Energy Crops. Figure 16
Comparison of stems from a German, Italian, and Peruvian breed [72]

Therefore, it seems reasonable to check the effect of such genetically steered growth regulation mechanisms in an energy maize breeding program. If photoperiodic sensitivity (short-day reaction) is fixed on the female side as well as the pollinizer side of energy maize hybrids, their vegetative mass performance may be improved considerably. Integrating such short-day genes proceeding from Mexican sources for the female side, and from Peruvian sources on the pollinizer side, guarantee, that heterosis between female and male gene pools is conserved.

In Fig. 17, the yields of 90 energy maize hybrids are shown. They contain new German–Mexican inbred lines on the female side, and a conventional flint tester from the silage maize breeding program on the pollinizer side. All of the German–Mexican inbreeds consist 75% of the German dent elite line 5G355 and 25% of gene material of Mexican origin. The superiority of the new German–Mexican inbreeds compared to the recurrent parent 5G355 is visible; they are yielding up to 10 t/ha more. This is superiority to an unexpected extent and surprising at first sight. As soon as the individual performance of the lines is checked, this increase becomes comprehensible: By selecting very sharply over several steps, it was possible to fix lines, which proved to be much more productive (Fig. 18).

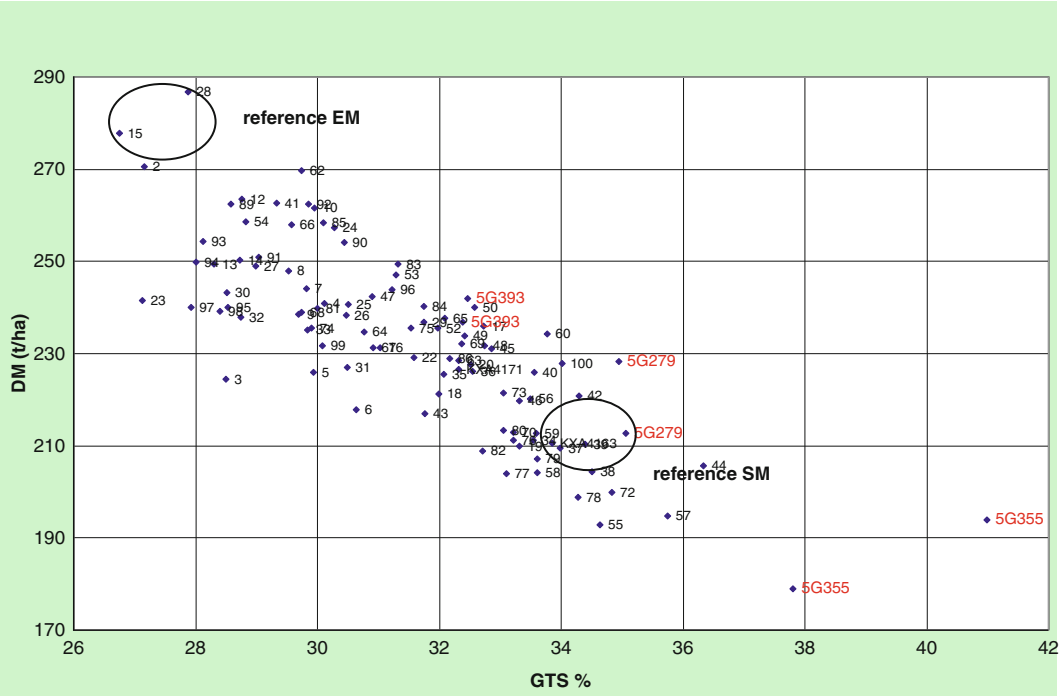

Biogas Production and Energy Crops. Figure 17
Dry matter yield (DM in t/ha) as a function of the maturity of the entire plant (DM% of 90 new energy maize hybrids (and 10 standards) from German–Mexican energy maize inbred lines, crossed with a German flint single. Reference SM - Silage maize for fodder production; Reference EM - Potentiale "Energy Maize" - Breeds showing higher yeild potential

Biogas Production and Energy Crops. Figure 18
New German–Mexican energy maize inbred lines (in each picture on the left side) next to conventional silage maize lines

It should be taken into account that this enormous increase in yield was achieved by improving just the genetics of the female parents of the experimental crossings. Therefore, those short-day genes should be used on the pollinizer side as well to increase the biomass potential of energy maize hybrids even more.

Outlook The outlined results demonstrate that different breeding strategies with very varied breeding material groups allow to realize enormous progresses in biomass performance and therefore in energy output of maize as an example crop. The results achieved up to now are considerably higher than expected.

The next goal of the energy maize breeding program is already defined: The considerable progresses in breeding, which could be generated up to now in the different breeding material groups, have to be united in the basic populations on which reciprocal recurrent selection is based, as well as in the hybrids. The breeding goal mentioned first (i.e., improving the total dry matter yield of maize in Central European temperate climate and stabilize it above 35 t/ha) will be reached within a short term.

The other energy plant species like sorghum, sunflower, or sugar beet have their specific breeding programs to combine most diverse genetic material to improve mass production. Energy plant breeding programs thus significantly differ from already existing standard breeding programs, as they focus on other breeding goals like energy efficiency and energy yield per hectare.

Cropping Systems

The decision on how to design cropping systems, and especially on which crop to choose, is based on the farmers' expectation of the economic gain from a specific production alternative. Apart from the natural yield capacity of a site and the revenues that can be achieved, this is determined by the crops' integration into agro-technology systems and the work organization. Importantly, the cropping structure is influenced by the existence of value-adding production capacities. These also include the biogas production.

Crop Rotation Design Rotation of crops is a basic element of crop production. The term rotation refers to the temporal follow-up of crops on one site. At the same time, the spatial juxtaposition of crops in a specific region is of special interest. Both aspects have a major influence on biodiversity, erosion by wind and water, and the appraisal of landscape characteristics; additionally, they directly influence aspects relevant to production. Extended or wide crop rotations, meaning crop rotations including a spectrum of different crops, for example, have the advantage of an increased utilization of water and nutrition reserves as well as the diminishment of weeds and pest biota.

A significant improvement of regulation possibilities, meaning the availability of plant protection products and mineral fertilizers, has led to a reduced economic importance of crop rotation design during the last century. Presently, control of nutrient supply by mineral fertilizers allows for the stabilization of yields. Yield breakdown caused by weed or pest biota can be prevented by plant protection measures. This, in combination with the tendency for specialization on a farm-scale as well as regional level has led to a narrowing of crop rotations. Presently, in Central Europe crop rotations including a high share of leaf fruits (i.e., potato, sugar beet) of 25–33% are only left common in the vicinity of starch or sugar plants.

On better production sites, cropping concentrates on winter wheat, winter rape, grain maize, and barley. In areas with best conditions for cereal production, the share of wheat can take up to 70% of the arable land, which implies a frequent self-succession of this crop. On less favorable sites, cropping concentrates on barley and rye. In regions with a concentration of livestock production, cropping concentrates on maize and barley; this – in the case of maize – can lead to a monoculture on some sites.

Energy plants can intensify this trend, for example, by extending the cropping of silage maize in livestock production areas. On the other hand, the cropping of plants that have little or no share in regional cropping systems can lead to an extension of rotations. Under present conditions, this can still imply free bonus effects, for example, cost reduction possibilities (e.g., plant protection or mineral fertilizers) or yield effects. Concerning winter wheat, depending on the fertilizing regime, the plant protection intensity and preceding

crop, yield increases of 10–50% can be achieved in comparison to a self-procession [73]. Providing for shares of sugar beet in the crop rotation can accordingly account for yield effects of 17% [74].

Furthermore, possibilities are given to productively use crops in the biogas plant, originally included into crop rotations for other reasons. Examples are the utilization of clover grass, which is primarily grown for nitrogen fixation on biological farms, or the combination of protective erosion measures by means of intercrops for their energetic use. As an overview and extension of the possible crops mentioned above, Fig. 19 shows possible options for energy cropping for anaerobic digestion and their rotational position.

Systems, which are based on the cropping of annual single main crops, either summer or winter crops, are of highest relevance in temperate climates. For energetic purposes, the cropping of a main crop is currently also tested in mixtures of species or breeds.

By adding intercrops, the vegetation time not used by the main crop can be utilized, for example, to increase annual yields for substrate production. Figure 20a and b show schematically the yield development process of winter and summer main crops with regard to solar radiation. Included into the Figure is the combination with intercrops.

Based on the approach of changing the cultivation span of the crops by shifting harvesting and sowing dates the so-called double-cropping system, including two equally productive crops, was proposed [75]. During the last years it was discussed if and on which sites a yield increase can be achieved. At the same time granting ecological advance, is one of the aims pusued by the system set-up (Fig. 20c).

As shown in Fig. 21, various combinations exist to combine winter and summer crops. The possible time span for the change between winter and summer crop is flexible, depending on the choice of crop and the harvest stage. All in all, the time span for two crops providing similar yield amounts as shown in Fig. 20c covers a transition period of approximately 30 days. If winter intercrop and second crop (Fig. 20b) are also taken into account, the time span covers approximately 60 days.

Criteria for the possibility of yield increase by using these systems are the availability of water and the duration of the vegetation span. On soils with low field capacity, winter crops use the water reserve of the soil in spring, so without sufficient precipitation in the following period, risks for the establishment of the second crop rise. Still, even in the case of establishment success, lower water availability might reduce the yield of the summer crop, so combined yield might not be higher than the use of a single crop. On sites that

Single main crop		Double – cropping system/ Winter intercrop + second crop (including mixtures)		Perennial crops	
One crop	mixed cropping				
	Mixed cropping of species	Winter (inter-)crop	Second crop	< 4 years	≥ 4 years
Sugar beet	Maize + Sunflower	Winter rye	Maize	Clover/Grass	Cup plant
Cereal (grain)	Whole plant cereals	Winter rye + w. vetch	Sweet sorghum	Alfalfa/Grass	Sida hermaphrodita
Maize	Maize+ White sweet clover	Hairy vetch	Sorghum-Sudangrass	Grass mixture	Rumex
Whole plant cereal	Maize + Sorghum	+ crimson clover	Summer rape	Jer. Artichoke	Polygonum
Sweet Sorghum	Whole plant cereal + winter pea	+ ann.Ryegrass	Sunflower		(Switchgrass)
Sorghum-sudangrass		Grass mixture	Mustard		(Miscanthus)
		Clover/Grass mixture	Ryegrass/Grass mixture		
	Mixed croppingof breeds:	Winter pea			
	Whole plant cereals				
	Sorghum				

Green = traditional
Orange = tested
Red = new

Biogas Production and Energy Crops. Figure 19
Optional positions of energy plants for anaerobic digestion in the cropping system

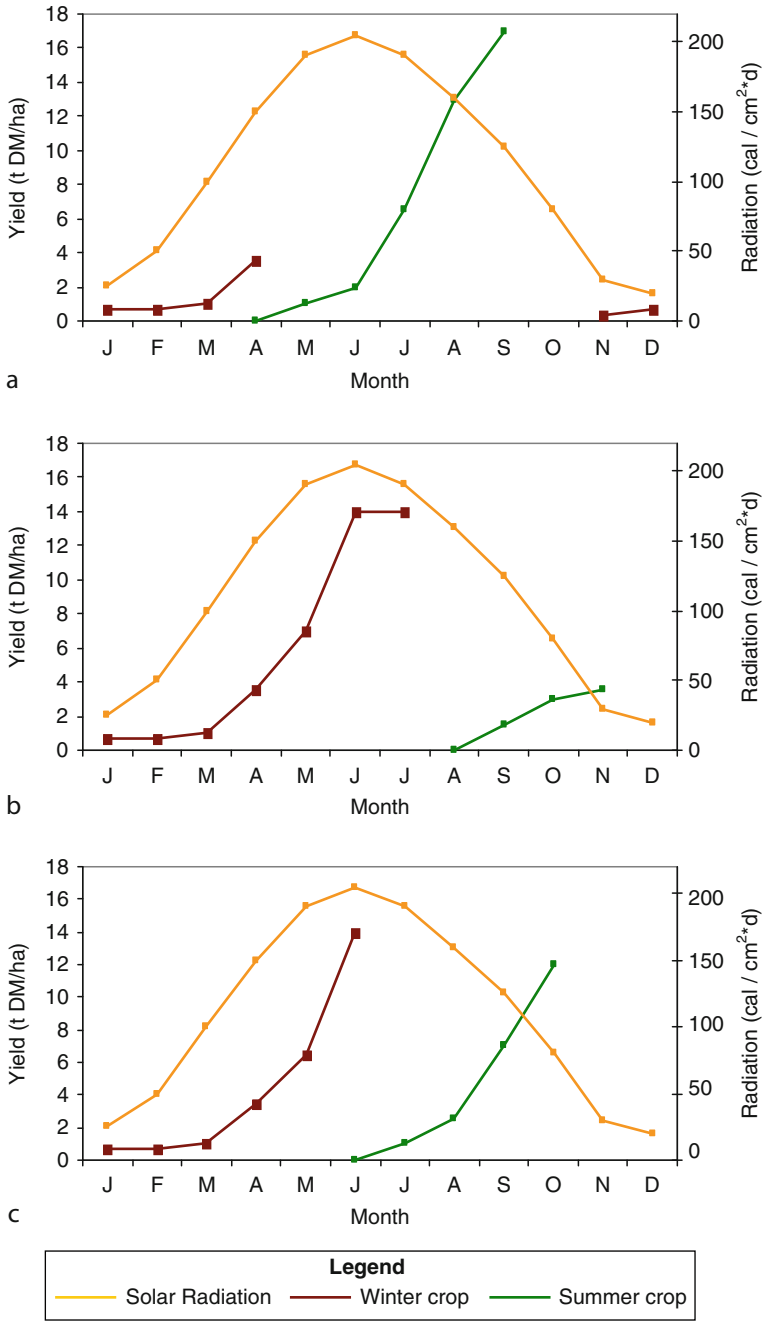

Biogas Production and Energy Crops. Figure 20
(**a, b**) Schematic yield development of winter and summer crop in combination with winter intercrop (*above*) and summer intercrop (*below*) (According to [75]). (**c**) Schematic yield development in the double-cropping system

show good water storage capacities (Quality wheat region, discussed later in the chapter) or sites with sandy soils but good precipitation amounts, by growing maize in combination with winter rye green cut, a significant yield increase compared to maize as a sole crop can be achieved.

Also systems using late transition between winter and summer crop could provide surplus yields. In a 3-year

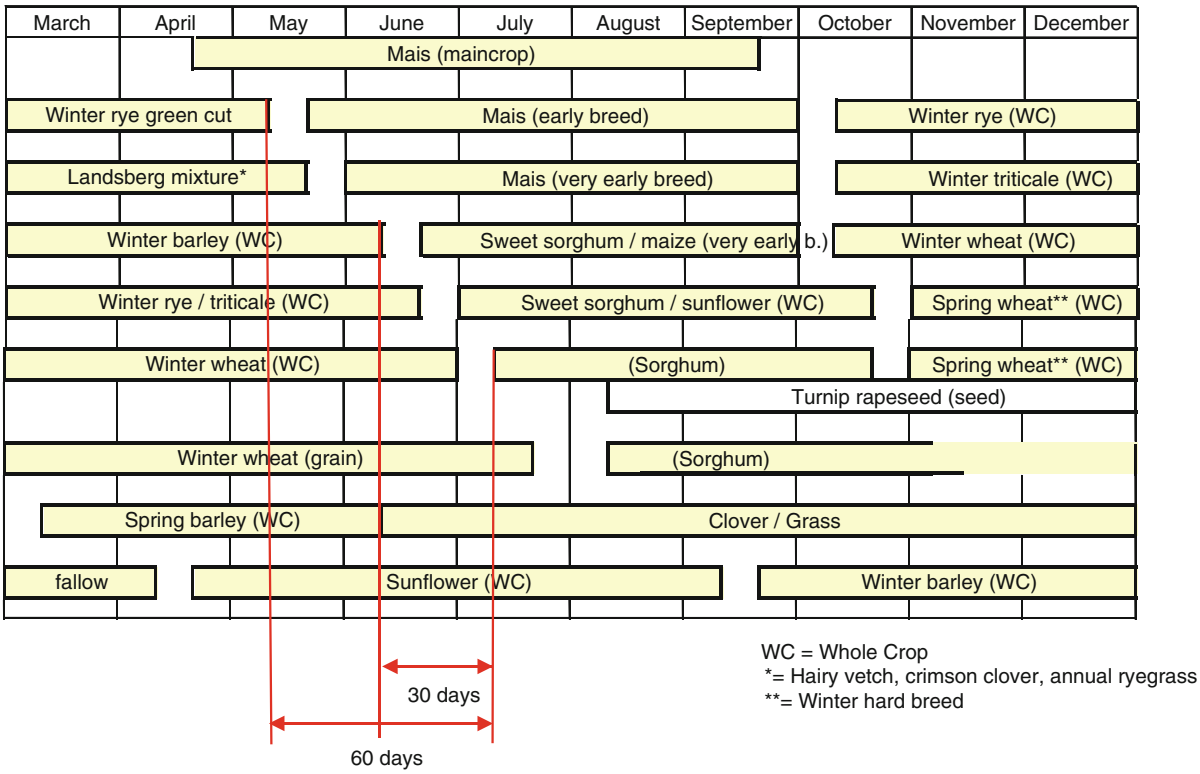

Biogas Production and Energy Crops. Figure 21
Options for the utilization of two crops in one vegetation period

trial, a yield increase could be demonstrated for a range of different sites [76]. For the combination winter rye whole crop – maize, the comparative increase was 3.9 t DM/ha, whereas the variation in sites showed a variety of yield surplus of on average 1.9–5.8 t DM/(ha a) for a 3-year period. Under present conditions, the higher production cost for these systems in most cases exceeds benefits. For an evaluation, all free bonuses, starting from improved nutrient utilization due to all-year coverage of the soil, equalization of peak times, as well as improved ecological features should be taken into account. One of the central focus points to be set is the reaching of a sufficient dry matter yield for ensiling (see the section "Harvest, Transport and Storage") by the second crop. An adapted choice of breeds can provide some leeway.

Regional Examples for Adapted Crop Rotations

Quality Wheat Region The quality wheat region (Fig. 22) is characterized by fairly low temperatures (mostly 500–600 mm) and loess soils with high field capacity. Conditions are good to produce medium to high yields of quality wheat with high protein content. Within the region, livestock production is low and the share of wheat in cropping systems is very high. As a typical crop rotation, winter wheat – winter wheat – winter or spring barley – winter turnip rape can be pointed out.

Starting from this, winter cereal whole crops, for example, winter triticale can be included. Although shares of this crop are low, the yield expectations characterized are high. Exemplarily, the combination winter wheat – winter triticale WC – winter turnip rape is suitable for regional conditions. In addition, it is a cropping alternative, from an economic point of view, to the relatively unattractive winter barley. The yielding of whole-crop cereals or green-cut cereals in regions with extensive cereal cropping can also be regarded as an option to cut weeds with the crop

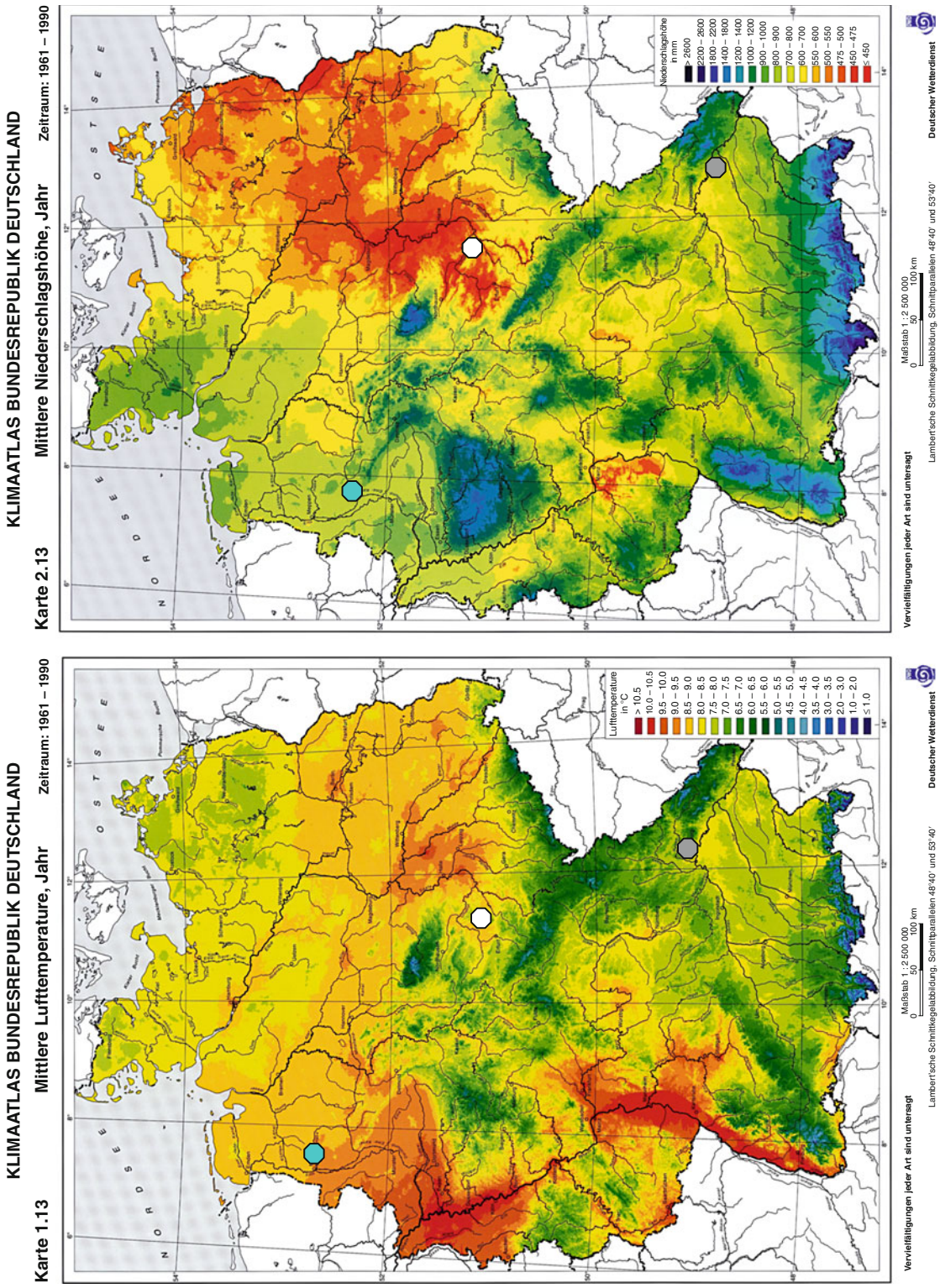

Biogas Production and Energy Crops. Figure 22
Annual precipitation (*left*) and annual temperature (*right*) in Germany as long-term mean (1961–1990) [77]

before the seed ripens and spreads. In this context, a significant decrease in focal weeds of plant protection has been shown [78]. A further possibility of crop rotation design for sites with a good availability of water in spring can be seen in:

winter wheat – winter rye green cut – maize – winter wheat – sugar beet – maize

Instead of maize, for diversification and risk reduction, the cropping of sorghum is possible, too. Another option is the exchange of winter rye green cut for winter barley as a whole crop. Risks in the late establishment of maize have to be considered though. Additionally, the ripening of the summer crop as well as the trafficability of the field for the sowing of wheat should be considered.

Forage Cropping: Livestock Production Region This region of northwestern Germany (Fig. 23) is characterized by sandy soils. The maritime influence and the evenly distributed precipitation of an annual mean of more than 700 mm make good yields possible. The region is characterized by intensive livestock production and respective fodder production. The utilization of large amounts of manure for anaerobic digestion is advantageous; the problem of nutrient surplus will not be solved by anaerobic digestion though.

Due to a further increasing maize cultivation area for the purpose of biogas production in addition to fodder cropping, there is a further increased availability of nutrients; approaches focus on the increased combination of maize with intercrops. The breaking up of maize-based crop rotation, for example, by

Winter barley WC – maize – winter rye green cut – maize

can offer possibilities for increasing yields and serve further purposes such as nutrient leakage reduction and erosion mitigation due to a prolonged utilization period. Nutrient surplus in phosphorous balances in many cases limit possibilities for the utilization of fermentation residues. Therefore, approaches for the separation of fermentation residues are currently being discussed. A much higher dry matter and phosphorous content in the solid phase allows for comparably good transportability, which makes export to sites with phosphorous demand possible. From a sustainability point of view, the decreased humus reproduction of the lacking solid phase has to be considered. From this perspective, ryegrass (mixtures) is mentioned as an alternative for the prevention of humus balance deficits and proves to be productive.

Forage grasslands – winter barley – region of German foothills and uplands

Large parts of Germany may be characterized as foothills and upland area. The conditions are, depending on altitude, relatively cool and moist. Soils are shallower and the relief is sloped. Lower temperatures make the cultivation of crops with high temperature demand or less winter hardiness more difficult. Winter turnip, rape, and sugar beet are not suitable for higher regions. Maize has some importance on the more favorable foothill sites of Southern Germany. Of all the cereals, winter barley is the most important. One possibility for crop rotation design can be seen in:

Winter barley (grain) – winter triticale whole crop – spring barley + underseed clover grass – clover grass 2nd year – clover grass 3rd year

On farms with livestock production or possibilities for the sale of fodder, utilization of clover grass for both biogas and cattle fodder is a possible option. Hence, systems can be based on the fact that due to differing substrate demands, a (relatively observed) higher usability of the late cuts in the biogas plant can be pointed out. This is based on the higher risk of the higher contents of acetic acid, which does not, in comparison to cattle fodder production, pose a quality issue in biogas substrates.

For the design of varied crop rotations with high shares of energy plants, different crop rotations were tested in plot experiments on seven sites in various agricultural regions in Germany as part of a large cooperative project since 2005. The aim of the project is to

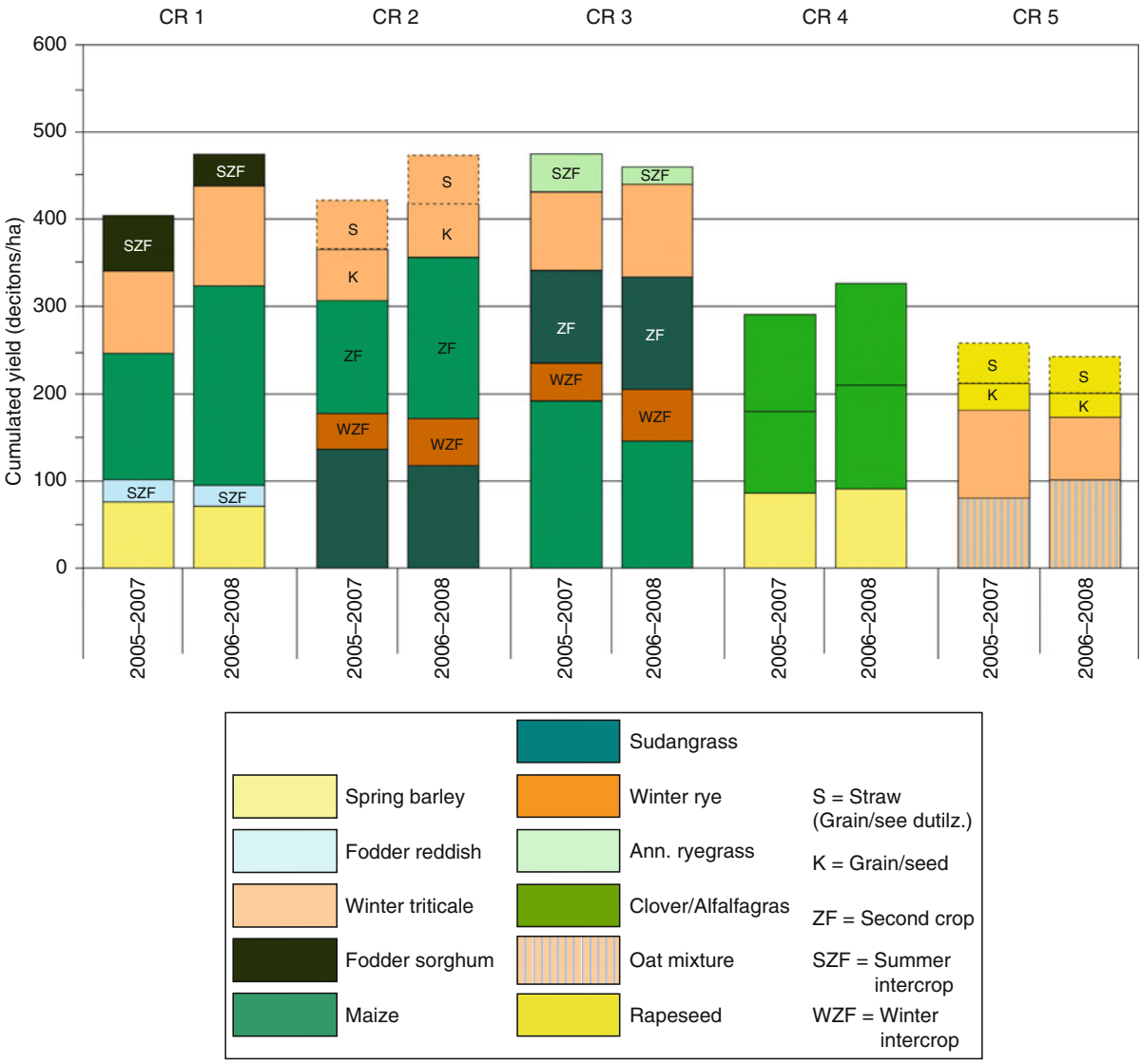

Biogas Production and Energy Crops. Figure 23
Cumulated yields of the uniformly tested crop rotations as a mean of all sites for the first (2005–2008) and second (2006–2009) plot set (CR = Crop rotation) [79]

evaluate which crop rotations are preferable from an economic, ecological, and plant-production point of view. On the different sites, five uniform and three to four regionally specific crop rotations were tested from 2005 to 2008 and shifted by 1 year from 2006 to 2009. Figure 23 exhibits a general overview of the mean yields on all sites of the five uniform crop rotations.

Crop rotation number 3 (maize – winter rye (green cut) – Sudan grass – whole crop winter triticale – annual ryegrass) was the most productive crop rotations on many of the sites, despite yield variations ranging from 33.6 to 56.7 t DM/ha. Sites in the regions described above could in general provide very good results. On the site of the quality wheat region, the cropping of Jerusalem artichoke and crop rotation

number 2 (Sudan grass – winter rye (green cut) – maize – winter triticale (grain usage)) could produce the highest yields, which were higher than those of a maize-monoculture. On the site representative to the forage grasslands – winter barley – region of German foothills in Ascha, relatively high yields could be provided, using a crop rotation consisting of maize – winter rye green cut – maize – winter rye/w. vetch mixture – Sorghum – Sudan grass. An explanatory approach for the high yield of this crop rotation, which is rather untypical of elevated sites, is in comparison, the higher long-term mean temperature during the experimental years with a sufficient water supply. On the site of the *forage cropping livestock production region* (Werlte), a 3-year combination of winter rye green cut and maize had a significant advantage compared to other options.

In total, the advantage of maize as a biogas substrate under a large spectrum of conditions in Central Europe could be confirmed. By also confirming the high yields of other substrates such as whole-crop cereals, sorghum, legume-grass, or grass mixtures (which can be taken into consideration in crop rotation design), complementarities could be pointed out [49].

Excursus: Factor Intensity with a Focus on Plant Protection Aspects With regard to the design of cropping systems for energy plants, altering the cropping intensity to contribute to an optimization of production systems has been discussed. On the one hand, this was related to the reduction in intensity of cropping systems by maintaining yield levels. On the other hand, questions dealt with a significant increase in yields by increasing the cropping intensity and at the same time considering sustainability issues.

Besides the above-mentioned considerations on double-cropping systems, one example for the latter is the irrigation of energy crops. In a 3-year trial, it has been pointed out that irrigation is suitable for securing a high yield level [80]. At the same time, a prognosticated climate change toward dry/hot summers and moist/mild winters in Central Europe could lead to a higher need for irrigation during summer months. Apart from the yield increase and the level of product price and the cost of irrigation, risk considerations are to be taken into account when deciding if, where and to what extent irrigation should be implemented.

Examples for a reduction of intensity levels which can be mentioned include a reduction in cutting frequency within cultivation systems of multi-cut perennial forage mixtures, reduced tillage intensity [49], or the design of cropping systems with regard to aspects concerning factor input reduction (plant protection or fertilizer management).

In the production of whole-crop cereals, different quality requirements compared to the production of baking cereals make quality-oriented nitrogen applications for increased protein contents dispensable. A reduction in fertilizer levels below withdrawal values is noticeable much quicker than in maize though. On sites with a sufficient supply of organic nitrogen stock, maize can show better results as times of high mineralization concur with times of high nitrogen demand. In a mid-term view, a yield reduction in any crop cannot be avoided if fertilizer application is reduced below withdrawal values.

Likewise, minimal reduction possibilities can be pointed out for the reduction of plant protection measures in maize cropping in comparison to existing cropping systems. Weed control for example, is indispensable due to slow youth development of the plant. However, given the very high cropping share of maize in crop rotations and regional cropping structures the risk of problematic weeds increases (such as Crane's Bill (*Geranium L.*)). Additionally, the risk of an increased appearance of the European corn borer (*Ostrinia nubilalis*), and in some regions the Western corn rootworm (*Diabrotica virgifera*), has to be mentioned as this can lead to an increased necessity for plant protection measures.

Whole-crop cereals differ from cereals harvested for grain purpose with regard to the cropping span. Risks of ear infection, pest biota, and weed problems are therefore comparatively lower. Depending on the type of cereal, breed and site characteristics, and yield expectancy accordingly, plant stability may be sufficient to dispense with growth regulators. This is the case primarily on dry and low-yielding sites and for winter triticale and winter barley. On productive sites, growth regulators should not be dispensed with. Turning down fungicides can result in a decrease in yield. Under the

conditions of the quality wheat region, in most cases, reduced benefits are lower than the economic cost for treatment [81]. On sites with low weed pressure, the comparatively high competitive strength of whole plant cereals can provide possibilities for the reduction of herbicide measures.

In a broader perspective on entire farming systems, anaerobic digestion may also provide possibilities to utilize lots for conventional grain/seed production with heavy pest or weed infestation in biogas plants. Importantly, it was questionable if pest biota or weed seeds can outlast the biogas process and lead to higher infection/weed pressures when recirculating fermentation residues to the field.

According to [82], preliminary results are available for 14 phytopathogens involving relevant quarantine diseases of potato. Following these results, most pathogens cannot persist in digesters working in mesophillic conditions under common retention times. Only *Clavibacter michiganensis* subsp. *sepedonicus* shows a viability of more than 100 days. When supplying entire potato tubers, *Ralstonia solanacearum* could persist for 30 days in a batch experiment. According to this, a retention time span from practical biogas plants could be sufficient to provide the required sanitizing environment. *Xantomonas tranlucensis* pv. *graminis* survived the process for 26 days. After 6 days however, infectiousness stopped. Additionally, it should be pointed out that ensiling might already kill pathogens before anaerobic digestion.

Of high relevance for intensive cereal cropping regions is the statement that the decomposition of *Fusarium graminearum* could be observed after 1 day [82]. This confirms results from [83], which, in addition, point out the disintegration of mykotoxins.

Survival of the seeds of some weed species is possible and continues to be the focus of research activities. One of the key parameters appears to be the temperature level of the biogas plant. In thermophilic conditions, seeds of blackgrass (*Alopecurus myosuroides*), goosefoot (*Chenopodium album*), stinkweed (*Thlaspi arvense*), broad-leaved dock (*Rumex obtusifolius*), and wild mustard (*Sinapis arvensis*) lose their ability to germinate after a retention time of 24 h. In mesophillic conditions, this only applies to blackgrass and wild mustard. Goosefoot had a germination ability of 75%. The durability of the testa against microorganisms could play a major role. Seeds of goosefoot, black-bindweed (*Polygonum convolvulvus*), and cockspur (*Echinochloa crus-galli*), which proved to be unable to germinate on agar, were still found to be viable in a Tetrazolium test [84]. Further results on the topic are awaited.

Harvest, Transport, and Storage

The bridging of the spatiotemporal difference between yielding of the crop at the optimum time on the field and the feedstock requirements in the digester make an optimized planning of harvesting procedure, transport, and storage of a specific substrate necessary. The specific challenges of supplying sugar beet are described in the section "Production Systems of Sugar Beet".

Harvest and Transport Harvest date of the chosen crop type and breed is primarily oriented according to the maximum yield and substrate quality, but also according to the inclusion into crop rotations and work organization of the farming company. With regard to these factors, time frames for harvesting are determined for the different crops.

Most crops can reach the dry matter contents necessary for ensiling (see below), so harvest procedure can be single-stepped. For Grasses and green-cut cereals with low dry matter contents, the cutting can be done as a separate step, after which a phase of wilting is followed up, needing a period of 1–2 days of suitable weather conditions. When reaching optimum dry matter contents, swathed material is picked up by a chopper. Compared to sufficiently dry substrates, which are directly harvested, additional losses have to be calculated with.

Standard operation system for harvest and transport is the chopping chain. A central element is the utilization of a self-propelled forage harvester; to some extent is also that of tractor-mounted choppers. Capacities of forage harvesters sold on the market are in the range of up to 1,000 HP effective output. Depending on the substrate to be harvested/picked up, harvesters can be fitted with different harvesting units. One of the most important parameters for an economic operation is the throughput rate (Harvested Mass times Working Speed). In the forage harvesters currently available, depending on the installed engine

power, this can be equal to up to 300 t of fresh matter per hour.

For an optimized anaerobic digestion, chopping size is an important parameter. In batch tests, maize, which was chopped to an average size of 4.7–5.4 mm showed 8% higher methane yields per t DM than maize with average chopping sizes of 7.9–9.9 mm [85]. With increased lignification, finer chopping, which can be characterized as mechanical pretreatment, makes an even higher percentage of methane yield increase probable [85–87]. Short chopping sizes lead to a loss of efficiency and higher diesel demand during chopping operation – therefore an economic optimum is to be aimed for. For an efficient design of operation procedures, a continuous transport from the field is to be vouched for. Most commonly, a parallel operation procedure is used in which changing transport units (consisting of tractor and transport hanger) move besides the harvesting unit and transport the feedstock to the silo. The loading mass is influenced by the bulk density of the substrate. Even with an optimized design of the operation procedure, cost is significantly increasing with transport distance. The cost increases disproportionately (Fig. 24) [88, 89]. Low dry matter contents also have an effect on transport cost per dry matter (and energy yielded).

Storage To ensure continuous feeding of the plant with seasonally harvested material, the process of ensiling is used. For this, the substrate is compacted, with the goal of appropriately excluding air to ensure that the lactic acid fermentation process is optimized. In this type of fermentation, carbohydrates from plant material are converted into acids, which have a conserving influence. The conversion processes of ensiling involve an unavoidable loss of energy and matter. The overall losses, which might also involve noxious fermentation, seepage sap losses, and aerobic deterioration during storage and withdrawal, can be minimized, though [90]. The specific challenges in conserving root and tuber substrates which show little ensiling quality is dealt with exemplarily in the section "Sugar Beet". A high share of usable carbohydrates and a sufficient number of suitable microorganisms on the plant material has a positive influence on the process. A high share of proteins and minerals (buffer) leads to the bonding of acids, which reduces the ability to lower pH-values. The deciding criterion for the design of cropping systems is the achievement of dry matter contents favorable for ensiling processes. Depending on the substrate type, values of at least 28% should be aimed at. Substrates significantly lower in dry matter content have a lower

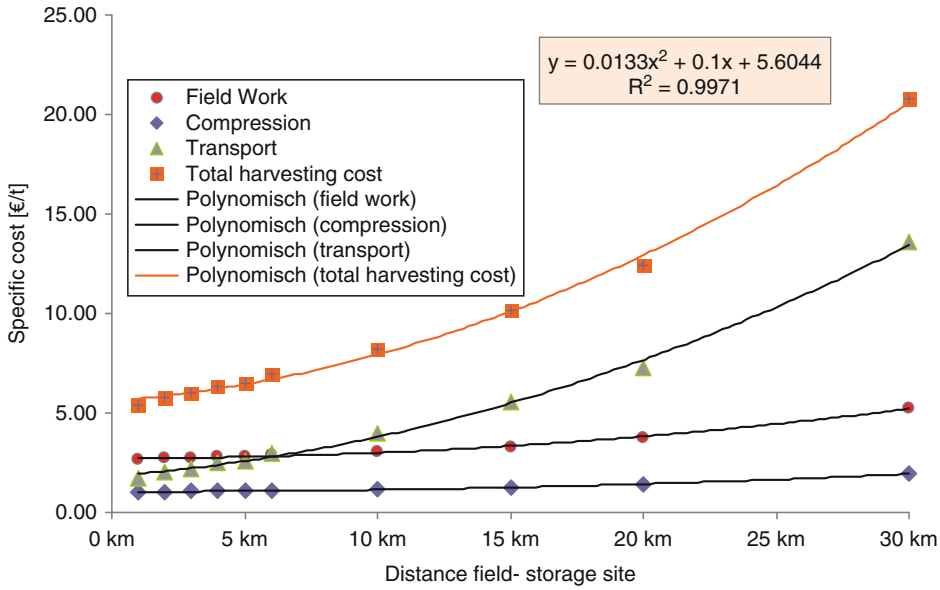

Biogas Production and Energy Crops. Figure 24
Specific harvesting cost of maize from a 5 ha-plot as a function of transport distance [88, 89]

suitability for ensiling and depending on the height of the substrate in the silo, big quantities of seepage sap can leak from the silo. These quantities are to be used in the biogas plant. Dry material (>35% dry matter content) is much harder to be compacted, so risks for large losses from aerobic deterioration are increasing. With regard to overall losses in this step of the process due to insufficient ensiling qualities, up to 31% decreased methane yield in comparison to laboratory-scale ensiling has been found [91].

Losses that occur in form of carbon dioxide, hydrogen, nitrogen oxides, or ammonia are unavoidable though. The inevitable losses by final respiration processes and the activity of fermentation organisms are at least 5% of the net energy in the plant material [21]. In addition, losses occur by incomplete exclusion of air in boundary areas and aerobic conditions at times of withdrawing the substrate. Additional losses of at least 3% of the net energy can be expected. Biological or chemical silage additives can be added to the substrate to avoid large silage losses. It should be noted that by using biological silage additives, which are based on homo- and heterofermentative lactic acid bacteria, an increased amount of acetic acid might be formed [92]. While this is a negative aspect for the quality assessment of silages used for fodder, in the process of biogas formation, acetic acid has no negative influence.

Considering the requirements for a loss-minimizing ensiling process, the silages can be stored for a longer period of time [93]. Despite the higher cost for storage space, this gives leeway for substrate provision. In laboratory-scale experiments, losses of silages stored for 365 days were increased by 1.2–6.4% compared to silages with a short storage period. The tendency of increased gas formation potential of the longer stored silages could compensate for the losses though.

Utilization of Fermentation Residues

Production systems for anaerobic digestion are specifically characterized by the fact that fermentation residues can be recirculated as organic fertilizer. After the digestion process in the plant as shown in Fig. 8, barely digestible substances are still in their original structure. Substance groups with good digestibility are largely mineralized to soluble inorganic compounds.

Due to the fact that only little substance losses occur (e.g., in the process of ensiling, see above), and that nutrients in the residues are – in comparison to those in feedstock before digestion – by far more available to plant uptake, biogas systems are suitable to design largely closed nutrient cycles.

A factor in the evaluation of nutrient cycles, which also has to be taken into account, is that only few biogas plants only use plant material for digestion. In fact, anaerobic digestion is very suitable to utilize excreta from animal production. Mass flows, which in many cases include nutrient input by imported fodder, also have to be taken into account.

Analysis of the fermentation of different biogas plants fed with dedicated energy crops and carried out at different times show the large variety of nutrient levels (dependent on substrate input, pretreatment, and digestion rates) in fermentation residues (Table 4).

Biogas Production and Energy Crops. Table 4 Dry matter and nutrient contents as well as pH values of fermentation residues exemplarily in central (Thuringia) and south-western Germany (Baden-Württemberg) [93, 94]

		TM%	pH	N_{ges}	NH_4-N	P_2O_5	K_2O	MgO	CaO	S
Baden-Württemberg *N* = 102	Mean	7.0	8.3	4.7	2.7	1.8	5.0	0.84	2.1	0.33
	80%-qrtl.	5.0	7.9	3.9	2.1	1.2	3.8	0.47	1.5	0.26
	20% qrtl.	8.5	8.6	5.5	3.3	2.1	5.5	1.04	2.6	0.41
Thüringen *N* = 60	Mean	5.8	7.7	4.2	3.1	1.8	3.4	n.v.	n.v.	0.04

Compared to animal manure, the relatively close relation of C/N in fermentation residues is to be mentioned. This leads to a decreased immobilization of the nitrogen included in the fermentation residues [95]. Due to the comparably high contents of ammonium, nitrogen is also present in a form well available for plant growth. Depending on the crop type, recommendations are to calculate 60–80% of the total nitrogen in the fermentation residues as equivalent to mineral fertilizer [94, 97]. In summer crops, in comparison to winter crops, higher percentages can be taken into account. Values for mineral fertilizer equivalents of 77% for maize and 86% for spring wheat have been shown [96]. Phosphorous and potassium can almost completely be recycled [97].

The release of calcium in anaerobic digestion leads to higher pH-values compared to animal manure, which is not utilized in biogas processes. Whether higher values for ammonia emissions occur, is in discussion. Fermentation residues have a relatively low viscosity, which leads to better handling (homogenization, pumpability, etc.) and soil-infiltration properties. This leads to the fact that the higher emission risk due to increased pH-values can be compensated for [96]. In any case, loss-minimizing technologies as well an immediate incorporation into the soil are means of avoiding ammonia losses. These can be minimized, but not completely eliminated.

The usability of a relatively good fertilizer and a saving of mineral fertilizers (in comparison to grain/seed production systems) have to be considered when evaluating biogas systems. It should also be noted that in regions with high nutrient input by fodder imports and an increased cycling of nutrients, nutrient balances, for example, of phosphorous, can be limiting due to maxima set by legislation. Solutions, such as the separation of liquid and solid parts of the residue are currently under discussion. Different technical approaches to the separation have in common that both phases have a different nutrient content. The liquid phase is higher in NH_4-content related to total N-content, but has a smaller phosphorous content. The solid phase can include up to 70% of total phosphorous. It is more transportable and can be exported into regions with a phosphorous demand [98].

From an economic and an ecological point of view, the utilization of nutrients in the fermentation residues should be in the most efficient manner. Rules of "good agricultural practice" as well as binding legal regulations are to be followed. These include:

- Limiting the fertilization span on times in which nutrients can be used by crops
- Knowledge of plant demand and nutrient contents of the fertilizer
- Limiting the quantities and area balances accordingly
- Specification on the storage of residues
- Specification of the loss-minimizing deployment technique
- Extended requirements in the utilization of waste material, for example, contagion hygiene requirements

Already during the planning phase of biogas plants, the management of fermentation residues should be involved. Especially in large plants, the low transportability of the fermentation residues should be considered. Optimized fertilizing strategies require efficient deployment logistics, especially in times where deployment makes a maximum uptake of nutrients by plant growth possible.

Sustainability Aspects

For a long time, sustainable management has been a basic principle of agricultural production. As part of this production, the cultivation of dedicated energy crops is therefore underlying the rules and guiding principles of "good agricultural practice" in addition to Cross Compliance requirements and further regulatory and prohibitive instruments. The increased production of dedicated energy crops and the associated support programs were linked to public institutions formulating further goals that aim at an increased contribution of energy cropping toward a sustainable design of energy and land use systems. Central aims are to contribute to greenhouse gas mitigation and environmental protection, as well as saving fossil fuels and decreasing the cost of energy supply also with regard to external costs and technology development [3]. Furthermore political aims are targeted at safeguarding the energy supply, preserving

biodiversity and soil fertility, and contributing to employment and value creation especially in rural areas [99].

Depending on the weighting of the different target values, differing assertions and deductions toward the design of agricultural systems can be drawn. Additionally aggravating is the fact, that quantitative and comparable evaluation categories can sometimes be barely defined and controlled for a number of targets. Accordingly, for the quantitative approach of life cycle assessment, in addition to the definition of a reasonable "balance scope," for the evaluation of target values, a subjective value system has to be referred to [100].

Green House Gas Balance

Based on the fixation of carbon dioxide by photosynthetic processes and the utilization of the fixed carbon to substitute fossil fuels, agricultural production can contribute to climate gas mitigation. Furthermore, the anaerobic digestion of excrements can also contribute to the reduction of emissions caused by other fields of agricultural production. To estimate to what extent the utilization of dedicated energy crops can contribute to a mitigation of climate gas emissions, the net climate gas reduction is to be calculated. Basically, this is determined by the balance of reduced emissions due to substituted fossil energy sources and the sum of emissions in the production system.

Emissions in the production system are not only determined by the factor input (fuel and fertilizer production) for cultivation steps, but also by climate gases emitted in substance cycles such as methane and nitrous oxide. Influence on the emission of methane is provided by mitigation potentials during the utilization of excrements. Otherwise, risks of methane emissions during the process of anaerobic digestion and utlization of the gas have to be mentioned. The largest emissions that are relevant to climate warming from soils are those of nitrogen compounds, which are linked to the utilization of mineral and organic nitrogen fertilizers.

For the evaluation of climate gas mitigation in the cultivation of renewable raw materials, a range of values can be looked at. Apart from the overall emissions that are avoided by the substitution of fossil fuels by biogas, these are mainly evaluation values for a specified area (kg CO_{2-eq}/ha) or product quantity (kg CO_2/GJ) as well as the associated cost. Furthermore, when looking at evaluation values, the subdivision into avoidable and unavoidable emissions is helpful.

Output and Substitution Values Decisive values for energy and climate gas balances are the methane yields of the different crops and crop rotations per unit of area. High hectare yields provide the possibility to substitute high amounts of fossil fuels. Relative indices, which give (energy) input in relation to output, often have the weakness of not considering the area as the scarcest factor.

Extensive production can lead to a reduction of energy-related factor usage and emissions. However, a thorough risk evaluation should be done, when assessing minimization strategies as well. An extreme example can be seen in the waiving of plant protection measures in the cropping of maize – yield loss and the respectively lowered energy gain will overcompensate the reduction in energy input by several times [101].

For a further evaluation of greenhouse gas savings potential, the reference base for example, the emissions of the substituted energy also plays a major role. Highest greenhouse gas reduction potentials can to be seen in the substitution of electricity produced from coal (e.g., lignite). Against this assumption, assuming a flexible electricity production with biogas substituting natural gas-driven peak load power stations leads to lower greenhouse gas savings.

Primary and Secondary Emission Values Primarily relevant to greenhouse gas emissions are factor inputs for the working processes that are necessary for the establishment, fostering, and harvest of a crop. These are most importantly not only fuels, but also fertilizer and plant protection products. Energy- and material-related emission values for provision of machinery and maintenance should be accounted for as well.

Of high importance is the kind of tillage system used. Minimum-tillage-systems waiving the usage of plowing measures have an advantage because of less fuel demand. Furthermore, the distance of the field from the biogas plant is relevant, since large parts of the energy have to be used for transporting processes. Values for conventional

plowing systems and a transport distance of 6 km have been calculated. For a Thuringian site, for example, these add up to between 58.9 l/ha (sorghum) and 82.9 l/ha (maize) [102].

Fertilizing can be regarded as the quantitatively most relevant part of emissions. Firstly, this is due to the energy-intensive production of mineral fertilizers. Because of the possibility to efficiently recirculate nutrients in biogas production systems, in comparison to market crops bonuses (when used in other crops) or reduced mineral fertilizer input have to be taken into account, though.

Secondly, secondary emissions from production-related nutrient cycles have to be considered. Of high relevance are the emissions of nitrogen compounds (most importantly nitrous oxide) emitted in the course of nitrification and denitrification processes. The emissions of this gas are relatively small quantitatively; though with a high radiative forcing, they make up a large part of climate gas emissions of intensive cropping systems.

Figure 25 shows the resulting climate gas emissions for the production of one kWh of methane that can be attributed to energy cropping systems on different sites in Germany.

Shown as white columns are the balances of emissions and bonuses which have been taken into account by the recirculation of residues (green). The relatively low values for maize can be explained by the good yield (and energy gain accordingly) in relation to the input and according emissions. The combination green-cut rye and sorghum on the dry and sandy site Güterfelde leads to the highest emissions, which can be explained by the relatively low yields at this site. With regard to the high share of emissions in the field of fertilizing, the nitrogen efficiency, and therefore, the nitrogen input per unit of product (in this case methane) is of outstanding importance. In this context, it should be

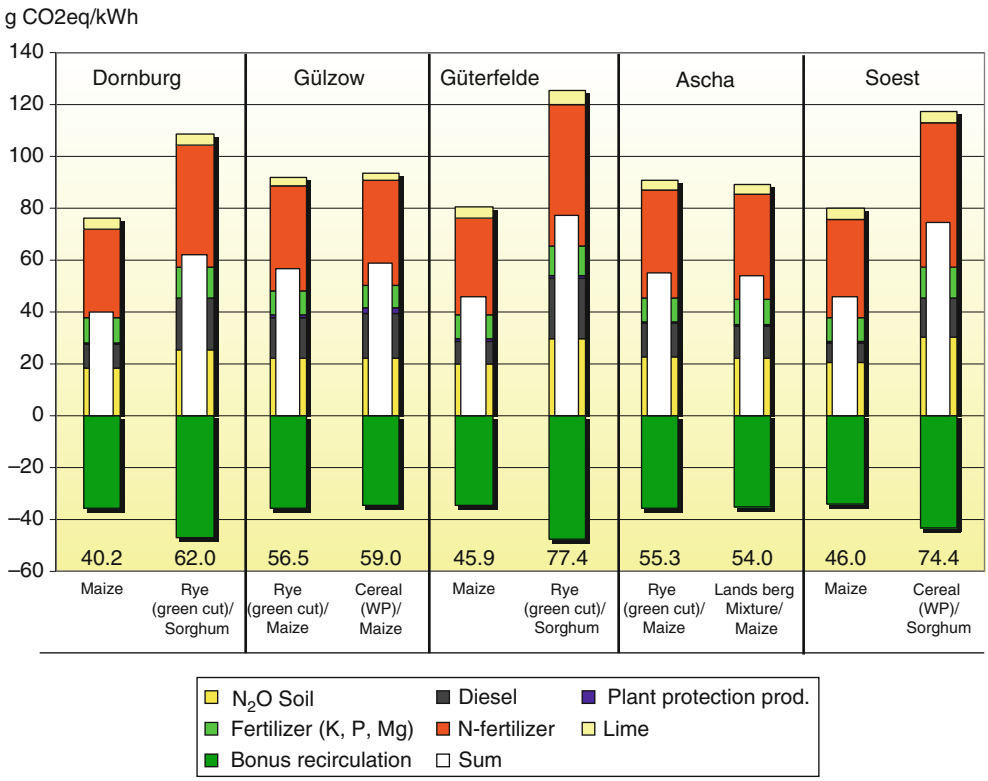

Biogas Production and Energy Crops. Figure 25

Resulting climate gas balances for different options of cropping of energy plants on different sites in Germany [102]

mentioned that the values used in Fig. 17 are calculated on the base of standard values proposed by IPCC, who recommend a calculation involving the emission of 1% of fertilized nitrogen as nitrous oxide.

For the specification of this simplified quantitative interrelation, as well as for the closer characterization of the "new" fertilizer fermentation residues, several research projects are currently ongoing. One thing that can already be stated is that the processes of nitrification and denitrification, which are the base of nitrous oxide emissions, are based on the insufficient utilization of nitrogen rather than the total amount of fertilized nitrogen [103]. Additionally, the availability of oxygen during the alteration processes of nitrogen compounds is of high relevance. On soils with high contents of clay and a nitrogen utilization of less than 30%, the emission of nitrous oxide is increasing disproportionally [104]; nitrous oxide emission also increases considerably on water-saturated soils emissions after organic fertilizing [105]. Furthermore, the frost–thaw cycles during winter seasons in temperate climates lead to large quantities of nitrous oxide emissions. These emissions are unavoidable, but can be minimized by an optimized fertilizer application in spring and an optimized plant uptake before winter takes place. Influence on emissions of nitrous oxide and ammonia also can be taken by an optimized fertilizer application technology (Fig. 26).

From a technological point of view, the splash plate is obsolescent. Injector technology is largely avoiding ammonia emissions, but this leads to the highest emissions of nitrous oxide [107]. Ultimately, a target conflict between minimizing emissions of ammonia and nitrous oxide can be pointed out.

Clearly, nitrogen fertilizing should always aim at an optimized utilization within the entire system. An optimized adaptation of crop rotations under consideration of intercrops, in addition to the efficient inclusion of maize into market cereal crop rotations, can promote a more efficient usage of nitrogen within the farming system. As an example, for an extension of the crop rotation of a cereal-oriented farm by producing biogas and selling straw a clear reduction of overall nitrogen surplus is achieved [107]. This example also points out that not only is the reference system of substituted energy form, but the reference system of alternatively

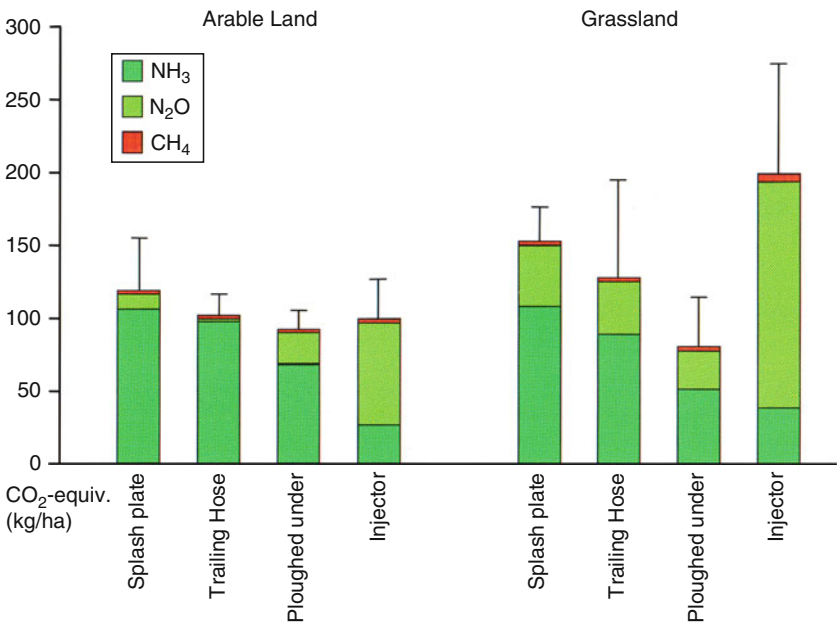

Biogas Production and Energy Crops. Figure 26
Influence of spreading technique for fermentation residues on resulting emissions (Shown in CO_2-equivalents) [106]

stated usage of the arable land is of major importance for evaluation of ecological impacts.

In conclusion, on the field of optimized organic fertilizing with fermentation residues, there is still a demand for further research. From a practical agriculture standpoint, research should point out possibilities to optimize the utilization of nutrients in the fermentation residues; from a sustainability point of view, on the other side of that same coin, the minimization of nitrogen losses should be strived for.

Humus Balance and Preservation of Soil Fertility

As mentioned in the section "Soil and Nutrient Supply", organic substances in agricultural soils play a major role for nutrient storage and transformation processes. Furthermore, on a global scale, organic substances in soil serve as an important carbon sink. Contents of carbon and humus are not identical, though. In most cases, the carbon content (C_t) multiplied by the factor 1.706 equals the humus content. In soils containing carbonate, the share of inorganic carbon has to additionally be taken into account.

The dynamic character of trans- and deformation processes of organic substances in soils makes it necessary to perpetually supply soils with organic matter, in the appropriate amount of the microbial disintegration to mineral substances, in order to sustain the level of soil organic matter content. Therefore disintegration rates are of interest. These are influenced by climate, nutrient supply, soil structure as well as the tillage system used.

Major sources of supply for organic substances are roots and harvest residues. Crops can accordingly be differentiated into humus-diminishing crops (e.g., sugar beet) or humus-increasing crops (e.g., perennial grasses). Furthermore, the supply of additional aboveground biomass such as straw and the recirculation of organic fertilizers are important sources for soil organic carbon.

In energy plant production, which aims at a utilization of total aboveground biomass, only little harvest residues are left on the field in comparison to, for example, the production of cereals for grain usage. By recirculating fermentation residues, large quantities of carbon-rich substances, which could not be disintegrated in the process of anaerobic digestion, are resupplied to the soil, though.

Distinct changes in the humus content of soils can only be observed within longer periods of time. In this context, it should be noticed that depending on site characteristics and the chosen management system, only in the long-term specific humus content is materializing. To be able to evaluate these processes quantitatively, several models exist that provide reference values for humus formation and decomposition derived from long-term tests.

Such models are the VDLUFA-Method, the Repro-Method and the Site-adapted Balancing Method [108]. All methods differentiate between the cultivated crops. Exemplarily, the VDLUFA-Method exhibits an annual humus decomposition for maize of between 560 Humus-C ha^{-1} (on soils showing a good state of cultivation with optimum mineral fertilizing) and 800 kg Humus-C ha^{-1} (on soils which have been poorly supplied with humus for a longer time and soils under ecological management practices) (Table 5).

A calculation of humus balances of cropping systems for rotations including a high share of energy plants shows that except for the rotation which includes a perennial forage mixture, a cropping without recirculation of residues would lead to a decreasing humus content in soils and hence a decreasing soil fertility on Central European sites (for a description of the crop rotations see Fig. 24). This should be considered, for example, in concepts for fuel production (Biomass to Liquid, BtL) which, in contrast to biogas production, do not allow for a recirculation of residues which contribute to a supply of organic matter.

As can be seen on the right part of Fig. 27 a recirculation can lead to a much better supply of humus in the tested crop rotations, when considering the recirculation of residues. In crop rotations with a high share of perennial forage mixtures (CR 4), the recirculation of organic matter causes balances which bring about the risk of high and uncontrollable mineralization. For the calculation, a humus reproduction rate of 0.3 for the fermentation residues was estimated. The reproduction rate describes the

Biogas Production and Energy Crops. Table 5 Change of Humus-Carbon dependent on specific cropping in various energy crops ([109] according to data from the EVA-project)

Crop	DM-yield (tha^{-1})	Specific change of Humus-C	
		Dynamic HE-method [110, 111] (kgha^{-1})	VDLUFA [112] Lower value to Upper value (kg ha^{-1})
Whole-crop cereal	8.1	−595	−280 to −400
Silage maize	17.6	−969	−560 to −800
Sorghum (bicolor × sudanense)	12.3	−609	
Sorghum (bicolor × bicolor)	9.0	−592	
Rye (green-cut intercrop)	4.8	87	120 to 160
Annual ryegrass (summer intercrop)	3.7	81	100 to 150
Clover/Alfalfa grass (Main utilization year)	10.9	829	600 to 800

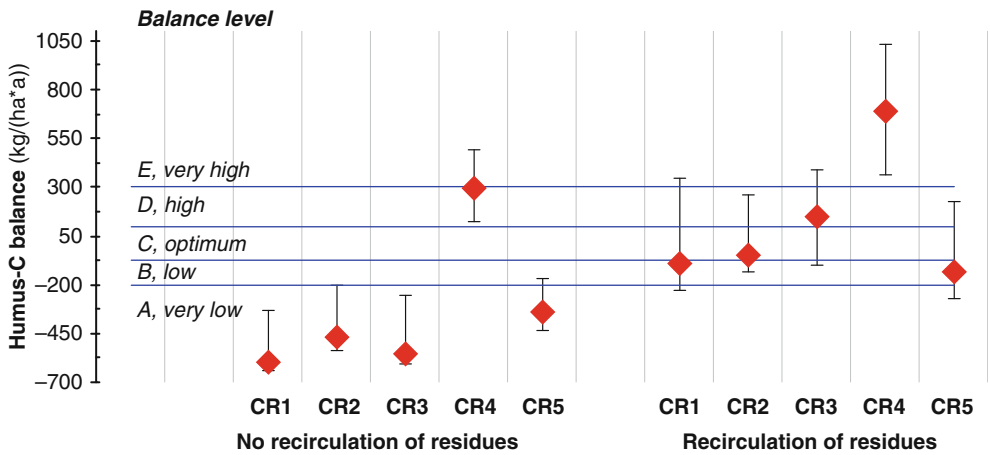

Biogas Production and Energy Crops. Figure 27
Resulting humus balances of crop rotations with high shares of energy plants without including humus reproduction by recirculated residues (*left*) and with the inclusion of reproductive values (*right*) according to the REPRO-method. The *dots* indicate the median; *error bars* indicate the span of tested sites [109]

amount of carbon in the residues that can be regarded as effective for humus formation. The scientific discourse on the definition of scientifically secured values is not terminated yet [110, 113–115].

Biodiversity

The increased cropping of energy crops is falling into a time in which a preceding reduction of biodiversity in Europe has been observed (e.g., [116]). Model-based evaluations, which attribute negative impacts for energy plant production (e.g., [117, 118]), often have the weakness that they do not allow for a differentiated analysis of cropping techniques. Other approaches focusing on this aspect could – in the analysis of different cropping systems – point out that the different energy plants that can be used can provide habitat for a variety of wild-living species.

To answer the question on what impact can be expected from an extended energy plant production,

not only the chosen energy plant species has to be regarded. More importantly, each plant in its spatial context has to be analyzed. This means that besides the habitat conditions during the course of management and the development of the crop stand itself, the neighboring structures have to be taken into account.

The most important finding is that, in a cultural landscape, each crop can contribute to biodiversity, depending on the grade of differentiation from the other crops under cultivation regarding its characteristics such as cropping time span, horizontal and vertical vegetation structure or flowering. The more diverse a regional cropping structure, the higher the probability that wild-living species can find suitable habitat conditions. This effect is demonstrated for plant species and fauna (ground beetles, spiders, and apidae/syphidae) (Fig. 28) [78].

The Figure shows the number of species occurring, depending on the number of crops in the crop rotation. The number of individuals of the different species or the level of coverage of weed species/side flora is not increasing parallel to the number of species. It can rather be quantified by the mean of the individuals that can be observed in the single crops. If the number of crops in a rotation is reduced down to monocultures, the species number is reduced, too. The danger of the prevalence of single organism types is increasing significantly [78].

Positive impacts on the species number of most organism groups can be expected by an increased cropping of perennial crops. As an example, the cropping of perennial forage crops provides habitats for species that can only seldom be found in other crops. Examples of such species include species whose occurrence is dependent on a period of resting soil for several years such as grasses in general, rhizomatic species and hemikryptophytes and when regarding fauna, species that are active throughout the whole year, such as some spiders and some apidae/syphidae are notable examples. Perennial forage crops also provide hibernation possibilities which other crops lack [119].

Multi-cut perennial forage crops might also become a trap for some species, since high cutting frequencies and especially the first cuts in spring times might lead to a destruction of the clutches of ground-nesting birds [120]. The same applies to whole-crop cereals that are harvested earlier than cereals produced for grain use.

On the other hand, the combination of whole-crop cereals harvested comparably early with second crops, as described above (double-cropping system, Fig. 20c), can lead to a prolonged habitat utilization period for

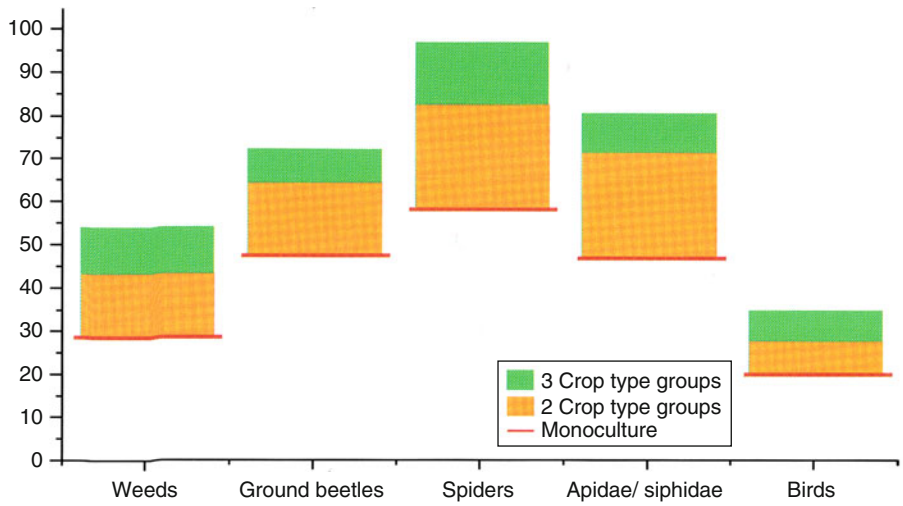

Biogas Production and Energy Crops. Figure 28

Species number of different organism groups in crop rotations containing high shares of energy plants depending on the number of crops included into rotation systems. Base EVA-Project (Data from Thuringia, Bavaria, Mecklenburg-Pommerania for 2005–2007.) Values for birds are based on a consultation of experts and are inflated by a factor of 10 [78]

the different organism groups. Another example, for land use change leading to a multitude of effects that are positive and negative for biodiversity, is the fact that early cuts might lead to a decreased spreading of weeds. For example, 35% of flowering plants occurring in winter cereal stands and 25% of flowering plants in spring cereals do not reach seed ripeness in the case of whole plant harvest [78]. From the viewpoint of the farmer, this might be an option for weed regulation and the minimization of herbicide treatments, especially when taking the multiresistance of some weed species into account.

A differentiated view on the impact of different crops can be observed in the occurrence of flower-visiting animals. While winter wheat provides good conditions for the occurrence of solitary bees, bumblebees and hover flies are rather to be found in maize. Depending on the importance set on the occurrence of organisms, the evaluation of different energy crops is therefore variable. In the end, the evaluation of the impacts of feedstock production for anaerobic digestion on biodiversity amounts to the question, if the energy plant production with its various options results in an extended variety in cropping structures or if in a mid-term perspective, no such extension will be the case. For an evaluation of the different options, regional cropping structures should be taken into account. The fact that an extended cropping of silage maize is not necessarily leading to a reduction, can be shown at the cropping structure of the "Saale-Holzland-Kreis" as part of the "Quality wheat region" mentioned above. The cropping for silage maize in 2007 was less than a quarter of the area for winter cereals. An extension of the maize cropping area would therefore be linked to an increased biodiversity in organisms, whose population development takes place in late summer, for example, summer-flowering plants, as part of the flora, or ground beetles larvally hibernating as well as summer-active spiders and syrphidae.

Future Directions

The utilization of energy plants for biogas production provides chances for a sustainable provision of quantities of substrate which are not available from other sources. Solar radiation that is saved in the substance groups of biomass can, in the following utilization chain, be stored and, after anaerobic fermentation processes, be used in the form of methane. The utilization chain allows for a steady-going electrification or the upgrading of biogas for the feeding in of methane into the gas grid.

The particularity of biomass production for energy purposes is the fact that it is always part of the existing agrarian (eco-)systems and can therefore complement these. Chances therefore exist that biomass production can be seen as a structuring element, which can provide chances for farming income diversification, extension of crop rotations, risk diversification, and the equaling out of work peaks as well as for sustainability targets such as biodiversity and climate gas mitigation.

As for future directions, it becomes obvious that the extension of biomass production is not leading to the achievement of the variety of the different goals per se. In fact, the application of sustainable farming options for biomass production and the achievement of societal goals are also linked to the question, to what extent the application of these systems is interesting from the economic point of view of farming practice. Since in most cases energy farming is dependent on public subsidies, the challenging task is resulting to design mechanisms that in the context of volatile markets for agricultural goods can keep planning security and the long-term character of targets in focus and avoid bringing forward systems that are based on the pursuance of one-sided and short-term goals.

Bibliography

Primary Literature

1. Couture T, Gagnon Y (2010) An analysis of feed-in tariff remuneration models: implications for renewable energy investment. Energy Policy 38:955–965
2. Mendoca M, Jacobs D (2009) Feed-in tariffs go global: Policy in practice. Renew Energy World Mag 12(4):106–113
3. EEG (2008) Gesetz für den Vorrang Erneuerbarer Energien (Erneuerbare- Energien-Gesetz – EEG). 25 Oktober 2008. In: Bundesgesetzblatt I: 2074
4. Observ'ER (2009) Etat des energies renouvables en Europe. The state of renewable energies in Europe. 9th Eurobserv'ER report, Paris
5. Thrän D, Witt J, Henning C, Daniel-Gromke J, Rensberg N, Schwenker A, Scheftelowitz M, Wirkner R, Vetter A, Graf T, Reinhold G (2009) Mointoring zur Wirkung des

Erneuerbare-Energien-Gesetzes (EEG) auf die Entwicklung der Stromerzeugung aus Biomasse. Zwischenbericht. FKZ: 03MAP138, Leipzig
6. Maier L, Shobayashi M (2001) Multifunctionality: towards an analytical framework. OECD Organisation for Economic Co-operation and Development (ed). OECD Publications, Paris
7. Monteith JL (1973) Principles of environmental physics. Arnold, London
8. Monteith JL (1977) Climate and the efficiency of crop production in Britain. Phil Trans R Soc Lond 281:277–294
9. Bolton JR, Hall DO (1978) Photochemical conversion and storage of solar energy. Ann Rev Energy 4:353–401
10. Bolton JR, Hall DO (1991) The maximum efficiency of photosynthesis. Photochem Rhotobiol 53:545–548
11. Beadle CL, Long SP (1985) Photosynthesis – is it Limiting to Biomass Production. Biomass 8:119–168
12. Long SP, Naidu ZhuXG, SL ODR (2006) Can improvement in photosynthesis increase crop yields? Plant Cell Environ 29:315–330
13. Lewandowski I (2009) Primärproduktion/Standortfaktoren. In: Kaltschmitt M, Hartmann H, Hofbauer H (eds) Energie aus Biomasse. Grundlagen, Techniken und Verfahren, 2nd edn. Springer, Heidelberg, pp 41–61
14. Zhu XG, Long SP, Ort DR (2008) What is the maximum efficiency with which photosynthesis can convert solar energy into biomass? Curr Opin Biotechnol 19:153–159
15. Morison JI, Piedale MT, Muller E, Junk LSP, WJ JMB (2000) Very high productivity of the C4 aquatic grass Echinochloa polystachya in the amazon floodplain confirmed by net ecosystem CO2 flux measurements. Oecologia 125:400–411
16. Diepenbrock W, Fischbeck G, Heyland KU, Knauer N (1999) Spezieller Pflanzenbau, 3rd edn. Verlag Ulmer, Stuttgart
17. Simba L (1977) Maximization of arable crop yields in the Netherlands. Neth J Agric Sci 25:278–287
18. Scheffer F, Schachtschabel P (2010) Lehrbuch der Bodenkunde, 16th edn. Revised and extended by Blume H-P, Brümmer GW, Horn R, Kandeler E, Kögel-Knabner I. Spektrum Verlag, Heidelberg
19. Oehmichen J (1983) Pflanzenproduktion, Band 1: Grundlagen. Parey, Berlin, Hamburg
20. Van Soest PJ, Robertson JB, Lewis BA (1991) Methods for Dietary Fibre, Neutral Detergent Fibre, and Nonstarch Polysachharides in Relation to Animal Nutrition. J Dairy Sci 74(10):3583–3597
21. Jeroch H, Flachowsky G, Weißbach F (eds) (1993) Futtermittelkunde. G. Fischer, Jena, Stuttgart
22. Universität Hohenheim (ed) (1997) DLG Futterwerttabellen. Wiederkäuer, 7th extended and revised edition. DLG Verlag. Frankfurt/Main
23. Neumerkel W, Märtin B (1982) Die Durchwachsene Silphie (Silphium perfoliatum L.) – eine neue Futterpflanze. In: Arch. Acker Pflanzenbau Bodenk 26:261–271
24. Chandler JA, Jewell WJ, Gossett JM, Van Soest PJ, Robertson JB (1980) Predicting methane fermentation biodegradability. Biotechnol Bioeng Symp 10:93–107
25. Demirel B, Ergun S, Neumann L, Scherer P (2009) Performance and behaviour of the microbial community of an anaerobic biogas digester using sugar beet silage as mono-substrate. Biosyst Eng 102:444–452
26. Vollmer GR (1982) Abbaugeschwindigkeit unterschiedlicher Stoffgruppen. Cited in Schulz H, Eder B (2006) Biogas-Praxis. Grundlagen – Planung – Anlagenbau – Beispiele – Wirtschaftlichkeit 2007. Ökobuch Verlag, Staufen/Freiburg
27. Weiland P (2010) Biogas production: current state and perspectives. Appl Microbiol Biotechnol 85:849–860
28. Buswell AM, Müller HF (1952) Mechanism of Methane Fermentation. Ind Eng Chem 44(03):550–552
29. Boyle WC (1977) Energy recovery from sanitary landfills. In: Schlegel AG, Barnea J (eds) Microbial energy conversion. Unitar. Pergamon, Oxford, pp 119–138
30. Baserga U (1998) Landwirtschaftliche Co-Vergärungs-Biogasanlagen. FAT-Berichte No. 512. Eidgenössische Forschungsanstalt für Agrarwirtschaft und Landtechnik (FAT) (eds), Ettenhausen
31. Linke B, Heiermann M, Grundmann P, Hertwig F (2003) Grundlagen, Verfahren und Potenzial der Biogasgewinnung im Land Brandenburg. In: Biogas in der Landwirtschaft – Leitfaden für Landwirte und Investoren im Land Brandenburg, 2. überarb. Aufl., Ministerium für Landwirtschaft, Umweltschutz und Raumordnung des Landes Brandenburg, Herausbeber, Potsdam, pp 10–23
32. Schattauer A, Weiland P (2006) Grundlagen der anaeroben Fermentation. In: FNR (Hrsg.) Handreichung Biogasgewinnung und –nutzung. Fachagentur Nachwachsende Rohstoffe, Gülzow, pp 25–35
33. Kaiser FL (2007) Einfluss der stofflichen Zusammensetzung auf die Verdaulichkeit nachwachsender Rohstoffe beim anaeroben Abbau in Biogasreaktoren. Dissertation, Munich University of Technology, p 176
34. Weißbach F (2008) Zur Bewertung des Gasbildungspotenzials von nachwachsenden Rohstoffen. Landtechnik 63(06):356–358
35. Amon A, Amon B, Kryvoruchko V, Machmüller A, Hopfner-Sixt K, Bodiroza V, Hrbek R, Friedel J, Pötsch E, Wagentristl H, Schnreiner M, Zollitsch W (2007) Methane production through anaerobic digestion of various energy crops grown in sustainable crop rotations. Bioresour Technol 98:3204–3212
36. Helffrich D, Oechsner D (2003) Hohenheimer Biogasertragstest – Vergleich verschiedener Laborverfahren zur Vergärung von Biomasse. In: Agrartechn. Forsch. 9/3:27–30
37. Herrmann C, Heiermann M, Idler C, Scholz V (2009) Einfluss der Silierung auf die Biogasbildung – Aktuelle Forschungsergebnisse. In: 18. Jahrestagung des Fachverbandes Biogas e.V. Tagungsband, Hannover
38. Linke B (2008) Gärbiologische Prozesse von Energierüben und Substratmischungen. Fachtagung Energierüben 16.7.2008. Fachhochschule Südwestfalen und Zentrum für Nachwachsende Rohstoffe
39. Conrad M, Vetter A (2010) Optimierung des Anbauverfahrens für Durchwachsene Silphie (Silphium perfoliatum) als Kofermentpflanze in Biogasanlagen sowie Überführung in

die landwirtschaftliche Praxis. Abschlussbericht. Gefördert von der Fachagentur Nachwachsende Rohstoffe (FNR). FKZ: 22004307 (in press)
40. Scholwin F, Liebetrau J, Edelmann W (2009) Biogaserzeugung und -nutzung. In: Kaltschmitt M, Hartmann H, Hofbauer H (eds) Energie aus Biomasse. Grundlagen, Techniken und Verfahren, 2nd edn. Springer, Heidelberg, pp 851–932
41. Peyker W (2006) Luft nach oben – Ertragspotenzial des Maises ist noch lange nicht ausgeschöpft. In: Neue Landwirtschaft. Landwirtschaftsverlag GmbH, Berlin, pp 52–54
42. Lütke-Entrup N, Oehmichen J (2000) Lehrbuch des Pflanzenbaus. Band 2: Kulturpflanzen. Verlag Th. Mann., Gelsenkirchen
43. Amon T, Amon B, Kryvoruchko V, Zollitsch W, Mayer K, Gruber L (2007) Biogas production from maize and dairy cattle manure – influence of biomass composition on the methane yield. Agric Ecosyst Environ 118:173–182
44. Eder B, Eder J, Papst C, Darnhofer B, Mukengele M, Heuwinkel H, Oechsner H (2009) Welcher Maissortentyp zur Biogaserzeugung? In: Proceedings of Internationale Wissenschaftstagung Biogas Science 2009. 2–4 December 2009 Erding/Germany. Oral presentations, vol 02. Bayerische Landesanstalt für Landwirtschaft (ed), Freising
45. Zacharias A (2007) Entwicklung von Energie-Sorghum. Aktueller Stand und Forschungsschwerpunkte. In: Proceedings of KWS Energiepflanzen-Kolloquium, 5–6 November 2007. http://www.kws.de/global/show_document.asp?id=aaaaaaaaaaejrvl&download=1. Accessed 20 March 2011
46. Leible L, Kahnt G (2008) Untersuchungen zum Einfluss von Standort, Saatstärke, N-Düngung, Sorte und Erntezeitpunkt auf den Ertrag und die Inhaltsstoffe von Zuckerhirse. J Agron Crop Sci 1(166):8–18
47. Cabelguenne M, Debaeke P (1998) Experimental determination and modelling of the soil water extraction capacities of crops of maize, sunflower, soya bean, sorghum and wheat. Plant soil 202:175–192
48. Klodpeng T, Sukasame S, Nimmalungkul C (1985) Rooting depth and rooting density of corn and sorghum under rainfed condition. In: Proceedings of the 16th conference on Thailand national corn and sorghum, 22–26 April 1985, Phuket, Thailand
49. Nehring A, Vetter A (2009) Entwicklung und Optimierung von standortangepassten Anbausystemen für Energiepflanzen im Fruchtfolgeregime. Abschlussbericht 2009 Teilprojekt 1. Verbundvorhaben. Gefördert von der Fachagentur Nachwachsende Rohstoffe (FNR). FKZ: 22002305
50. Roller A (2007) Sorghumarten – Sorten und Herkünftevergleich. In: FNR (ed) Schriftereihe Nachwachsende Rohstoffe. Bd. 31. Proceedings of symposium Energiepflanzen 2007, 24–25 October 2007, Berlin, pp 141–148
51. Biertümpfel A, Conrad M, Gödeke K (2009) Rinderfütterung: Zu hohe Blausäuregehalte in Hirsearten. Pflanzenbau Aktuell. Bauernzeitung 50(17):9
52. Karpenstein-Machan M (2005) Energiepflanzenbau für Biogasanlagenbetreiber. DLG-Verlags-GmbH, Frankfurt
53. Beer W, Michiels-Corsten F (2009) Rüben nicht mehr köpfen? Auswirkungen entblätterter Rüben auf die Verarbeitung. Zuckerrüben J. 1(2009):18–19
54. Hesse F (2008) Nordzucker, Personal communication
55. Ernst D (2010) Algermissen, KWS-Expertenrunde, Personal communication
56. Vetter A (2009) Biogassubstrate: Welche Exoten haben Potenzial für die Zukunft? In: Gülzower Fachgespräche. Bd. 32:289–298. Biogas in der Landwirtschaft – Stand und Perspektiven. Weimar 15–16 September 2009, Tagungsband
57. Gödeke K, Benke M (2008) Standortangepasste Mischungen und Schnittregime für Ackerfutter und Grünland. Vortrag zum Forum Energiepflanzen 07./08.10.2008. Jena. http://www.tll.de/ainfo/pdf/epfl/epf07_08.pdf. Accessed 28 Feb 2011
58. Geber U (2002) Cutting frequency and stubble height of reed canary grass (*Phalaris arundinacea* L.): influence on quality and quantity of biomass for biogas production. Grass Forage Sci 57(4):398–394
59. Rieckmann C, Benke M (2009) Teilprojekt Ackerfuttermischungen: Eignung von Ackerfuttermischungen für die energetische Nutzung. In: Nehring A, Vetter A (eds) Entwicklung und Optimierung von standortangepassten Anbausystemen für Energiepflanzen im Fruchtfolgeregime. Abschlussbericht 2009 Teilprojekt 1. Verbundvorhaben. Gefördert von der Fachagentur Nachwachsende Rohstoffe (FNR). FKZ: 22002305
60. Smyth B, Murphy J, O'Brien C (2009) What is the energy balance of grass biomethane in Ireland and other temperate northern European climates? Renew Sustain Energy Rev 13:2349–2360
61. Gödeke K (2009) Grünlandnutzung und Biogas, Vortrag im Workshop 5, Nachhaltiger Anbau von Nachwachsenden Rohstoffen"der 18. Jahrestagung des Fachverbandes Biogas e.V, 3–5 February 2009, Messe Hannover
62. Standford G (1990) *Silphium perfoliatium* (Cup-Plant) as a new forage. In: Proceedings of the 12th North American Prairie Conference, University of Northern Iowa, Cedar Falls, pp 33–37
63. Filatov VI, Bakalov BV, Lavrov BV, Komyagin NA (1986) Productivity of *Silphium perfoliatum* as a function of agricultural technology practices on ameliorated soils. Biological Abstracts 82(6):50072. CAB International Abstracts. OG056-02413
64. Hengelhaupt F, Nehring A, Gödeke K (2008) Biogas-und Methanerträge alternativer Fruchtarten. Posterpräsentation. 120. VDLUFA-Kongress. 16–19 September 2008, Jena
65. Lütke-Entrup N, Gröblinghoff F (2005) Erzeugung von Biomasse vom Grünland und im Ackerbau. In: Proceedings of Biogastagung im Landwirtschaftszentrum Haus Düsse, 15 April 2005
66. Biertümpfel A, Graf T, Vetter A (2010) Feldversuchsbericht 2008/2009. Ölfrüchte und Nachwachsende Rohstoffe. TMLFUN (Hrsg.)
67. Borkowska H, Molas R, Kupczyk A (2009) Virginia Fanpetals (*Sida hermaphrodita* Rusby) Cultivated on Light Soil, Height of Yield and Biomass Productivity. Pol J Environ Studies 18(4):563–568

68. Rumpler J, Reichardt I (2009) Neue Kulturen für die Bioenergie. Thermoenergetische Nutzung von Stroh und Strohähnlicher Biomasse. In: Proceedings 20th Bernburger Winterseminar für Arznei- und Gewürzpflanzen. 23–24 February 2010, Strenzfeld, Bernburg
69. Märtin B, Linke G (1983) Bedeutung und Anbau von Weyrichknöterich (Polygonumweyrichii F. Schmidt) als Futterpflanze. Wiss. Z. Uni Halle XXXII'83 M, H. 1:89–97
70. Schmidt W (2004) Energiemais für die Praxis – Welchen Beitrag kann die Züchtung leisten? Vortrag bei der Tagung des DMK in Bad Sassendorf, 18 November 2004
71. Schmidt W (2005) Die faszinierenden Möglichkeiten der Energiepflanzenzüchtung – Chance für mehr Ökologie und Ökonomie in der Landwirtschaft Vortrag bei der Biogas-Fachtagung in Kaisersesch, 01 June 2005
72. Schmidt W (2003) Hybridmaiszüchtung bei der KWS SAAT AG. Vortrag bei der Tagung der Saatzuchtleiter in Gumpenstein, 25 November 2005
73. Christen O (1999) Untersuchungen zur Anbautechnik von Winterweizen nach unterschiedlichen Vorfruchtkombinationen. In: Schriftenreihe des Instituts für Pflanzenbau und Pflanzenzüchtung. Bd. 7. Kiel
74. Claupein W, Zosche M (1987) Einfluß langjähriger Winterweizen-Monokultur auf Ertragsbildung, Krankheitsbefall und Nematodenbesatz im Vergleich zum Winterweizenanbau in der Fruchtfolge. In: Zeitschrift für Acker- und Pflanzenbau. 158:227–235
75. Scheffer K, Stülpnagel R (1993) Wege und Chancen bei der Bereitstellung des CO2-neutralen Energieträgers Biomasse - Grundgedanken zu einem Forschungskonzept. Tropenlandwirt Suppl 49:147–161
76. Stülpnagel R, von Buttlar C, Heuser F (2008) Teilprojekt 6 (FKZ 220022805). Systemversuch zum Zweikulturnutzungssystem auf sechs Standorten im Bundesgebiet. Schlussbericht. Universität Kassel/Witzenhausen
77. DWD (ed) (1999) Klimaatlas Deutschland. Teil 1. Lufttemperatur, Niederschlagshöhe, Sonnenscheindauer. Offenbach am Main
78. Glemnitz M, Platen R (2009) II – Biotische Folgewirkungen. In: Willms M, Glemnitz M, Hufnagel J, Ökologische Folgewirkungen des Energiepflanzenanbaus. Schlussbericht. FKZ 22002405
79. Strauss C, Vetter A, Nehring A (2009) Development and comparison of optimised cropping systems for the production of energy plants under the variety of regional conditions in Germany ("EVA"). In: Proceedings of the 17th European biomass conference. ETA-Florence Renewable Energies, Florence, pp 218–221
80. Schittenhelm S, Kruse S, Hufnagel J (2009) Einfluss von Zusatzbewässerung auf den Biogasertrag von Energiepflanzen. Endbericht. FKZ: 2002705
81. Schreiber E, Jentsch U, Guddat C (2010) Sortenversuche in Thüringen. Wintergerste, Wintertriticale, Winterroggen und Hafer. Ganzpflanzengetreide zur Biogasgewinnung. Endbericht. TLL (eds) (in press)
82. Friedrich R, Kaemmerer D, Büttner P, Seigner L (2009) Evaluierung des Hygienisierungspotenzials des Biogasprozesses im Hinblick auf phytopathogene Schaderreger. In: Proceedings of Internationale Wissenschaftstagung Biogas Science 2009. 2–4 December 2009 Erding/Germany. Oral presentations, vol 02. Bayerische Landesanstalt für Landwirtschaft (ed.), Freising
83. Frauz B, Oechsner H (2008) Untersuchung zur Inaktivierung von Fusariensporen und zur Reduzierung von Deoxynivalenol in Weizen bei dessen Vergärung in landwirtschaftlichen Flüssig- und Trockenfermentierungsanlagen : Abschlussbericht, Berichtszeitraum 1 April 2006 to 31 October 2007. FKZ: 22015903
84. Westermann PR, Monserrat PX, Struck C, Gerowitt B (2009) Experiments with weed seeds in the silage and fermentation process for biogas. In: Proceedings of Internationale Wissenschaftstagung Biogas Science, 2–4 December 2009, Erding/Germany. Posters, vol 03. Bayerische Landesanstalt für Landwirtschaft (ed), Freising
85. Herrmann C, Heiermann M, Idler C, Hertwig F (2009) Effect of dry matter content, chopping length and ensiling proces on biogas yield of maize. In: Landbauforschung. vTI (eds). Special Issue 331:87–105
86. Palmowski L (2000) Zerkleinerungs- und Abbauverhalten organischer Materialien, Dissertation, Göttingen, 144 S
87. Badger DM, Bogue MJ, Stewart DJ (1979) Biogas production from crops and organic wastes. NZ J Sci 22:11–20
88. Toews T (2009) Ökonomie. In: Vetter A, Heiermann M, Toews T Anbausysteme für Energiepflanzen. Optimierte Fruchtfolgen + Effiziente Lösungen. DLG Verlags-GmbH, Frankfurt/Main
89. KTBL (2009) Feldarbeitsrechner. http://daten.ktbl.de/feldarbeit/entry.html. Accessed 28 Feb 2011
90. Heiermann M, Idler C, Herrmann C, Scholz V (2009) Ermittlung des Einflusses der Pflanzenart und der Silierung auf Substratqualität und Biogasausbeute in Labor und in der Praxis. Abschlussbericht des Teilprojektes 4. FKZ 22002605
91. Herrmann C, Heiermann M, Idler C (2009) Qualitätssilage für die Biogasproduktion. In: Gülzower Fachgespräche. Bd. 32: Biogas in der Landwirtschaft – Stand und Perspektiven. Weimar 15–16 September 2009. Tagungsband:314–323
92. Heiermann M, Herrmann C, Idler C (2009) Silierung von Energiepflanzen. In: Vetter A, Heiermann M, Toews T Anbausysteme für Energiepflanzen. Optimierte Fruchtfolgen + Effiziente Lösungen. DLG Verlags-GmbH. Frankfurt/Main
93. Kluge R, Wagner W, Mokry M, Dederer M, Messner J (2008) Inhaltsstoffe von Gärprodukten und Möglichkeiten zu ihrer geordneten Verwertung. Projektbericht 2008. Landwirtschaftliches Technologiezentrum Augustenberg (ed)
94. Reinhold G (2009) Einfluss der Biogaserzeugung auf das Restgaspotenzial und Eigenschaften der Gärreste sowie Anforderungen an das Gärrestlager. Internationale Bio- und Deponiegas-Fachtagung "Synergien nutzen und voneinander lernen III." 28/29.04. Weimar, pp 179–197

95. Döhler H, Grebe S, Häußermann U (2009) Düngewirkung von Gärresten. In: Gülzower Fachgespräche. Bd. 32: Biogas in der Landwirtschaft – Stand und Perspektiven. Weimar 15–16 September 2009. Tagungsband pp 223–235
96. Sensel K, Wragge V (2008) Pflanzenbauliche Verwertung von Gärrückständen aus Biogasanlagen unter besonderer Berücksichtigung des Inputsubstrats Energiepflanzen. Schlussbericht. Verein zur Förderung agrar- und stadtökologischer Projekte e. V. (A.S.P) FKZ 22012105
97. Möller K, Schulz R, Müller T (2009) Mit Gärresten richtig Düngen. Universität Hohenheim, Institut für Pflanzenernährung, p 56
98. Wulf S, Döhler H (2009) Verfahren und Kosten der Gärrestaufbereitung. In: Gülzower Fachgespräche. Bd. 32: Biogas in der Landwirtschaft – Stand und Perspektiven. Weimar, 15–16 September 2009. Tagungsband, pp 180–209
99. Bundesministerium für Umwelt, Naturschutz und Reaktorsicherheit, Bundes-ministerium für Ernährung, Landwirtschaft und Verbraucherschutz [BMU & BMELV] (2009) National Biomass action plan for Germany. Biomass and Sustainable Energy Supply. BMELV, Berlin
100. Reinhard G, Köppen S (2008) Ökobilanzen zu Bioenergiesystemen, Vorgehen, Beispiele, Aussagekraft. In: Ökologische und ökonomische Bewertung nachwachsender Energieträger. KTBL-Tagung 08/09.09. Aschaffenburg, pp 78–89
101. Deiglmayr K, Heimler F, Fritz M, Willms M (2009) Veränderte Energiebilanzen bei reduziertem Produktionsmitteleinsatz im Energiepflanzenanbau. In: Gülzower Fachgespräche. Bd. 32: Biogas in der Landwirtschaft – Stand und Perspektiven. Weimar 15–16 September 2009. Tagungsband, pp 412–413
102. Arnold K, Vetter A (2010) Klima- und Umwelteffekte von Biomethan: Anlagentechnik und Substratauswahl. Wuppertal Papers 182. Wuppertal Institut (ed)
103. Van Groenigen JW, Kasper GJ, Velthof GL, van der Pol-van DA, Kuikman PJ (2004) Nitrous oxide emissions from silage maize under different mineral nitrogen fertilizer and slurry applications. Plant Soil 263:101–111
104. Ruser R (2008) Klimawirkung der Düngung. Wie wirken sich N-Düngung und Beweitschaftung auf N20-Emissionen auf Böden aus? In: Klimawandel und Bioenergie – Pflanzenproduktion im Spannungsfeld zwischen politischen Vorgaben und ökonomischen Rahmenbedingungen, pp 113–124
105. Senbayram M, von Mühlhausen AC, Mühling KH, Dittert K (2008) Lachgasemissionen aus Böden nach Düngung mit Biogasabfällen, Rinder-, Schweinegülle oder Mineral-N-Düngung – erste Ergebnisse. Posterbeitrag. 01.02. Hochschultagung der CAU Kiel
106. Wulf S (2003) Untersuchung der Emission direkt und indirekt klimawirksamer Spurengase (NH3, N2O und CH4) während der Lagerung und nach der Ausbringung von Kofermentationsrückständen sowie Entwicklung von Verminderungsstrategien (DBU-AZ 08912) Abschlussbericht. Verein zur Förderung der Agrikulturchemie c/o Inst. für Pflanzenernährung (ed), Bonn
107. Breitschuh T, Eckert H, Maier U, Gernand U, Müller A (2009) Folgenabschätzung einer zunehmenden Bereitstellung von Bioenergieträgern auf die Nachhaltigkeit landwirtschaftlicher Unternehmen, bewertet mit dem Kriteriensystem KSNL. Abschlussbericht. UBAFBNr 001267
108. Kolbe H (2009) Das Ziel bestimmt den Weg Humusbilanzierung: Methoden nach Anwendungsziel aussuchen. Neue Landwirtschaft 6:54–57
109. Wilms M, Deumlich D, Wenkel KO (2009) Abiotische Folgewirkungen. In: Willms M, Glemnitz M, Hufnagel J, Ökologische Folgewirkungen des Energiepflanzenanbaus. Schlussbericht. FKZ 2200240
110. Hülsbergen KJ, Schmidt H (2008) Humusbilanzen und C-Kreisläufe in Betriebssystemen mit Bioenergieerzeugung. In: Ökologische und Ökonomische Bewertung nachwachsender Energieträger. KTBL-Tagung vom 8. bis 9. September 2008, Aschaffenburg, KTBL-Schrift 468, p 230
111. Hülsbergen KJ (2003) Entwicklung und Anwendung eines Bilanzierungsmodells zur Bewertung der Nachhaltigkeit landwirtschaftlicher Systeme, Habil., Shaker, p 257
112. Körschens M, Rogasik J, Schulz E (2004) VDLUFA Standpunkt Humusbilanzierung, Methode zur Beurteilung und Bemessung der Humusversorgung von Ackerland: 12 P, Bonn. www.vdlufa.de
113. Dominik P, Jäger N, Sänger A, Flessa H (2009) Wie wirken NaWaRo-Gärreste auf den organsichen Bondenkohlenstoff? In: Gülzower Fachgespräche. Bd. 32: Biogas in der Landwirtschaft – Stand und Perspektiven. Weimar 15–16 September 2009. Tagungsband, 210–222
114. Vetter A, Reinhold G (2009) Gärresteanfall und Verwertung. In: Vetter A, Heiermann M, Toews T (eds) Anbausysteme für Energiepflanzen. DLG-Verlags-GmbH, Frankfurt, pp 193–205
115. Leithold G (2010) Bedeutung von Gärsubstraten aus der landwirtschaftlichen Biogaserzeugung für die Humusbilanz. http://geb.uni-giessen.de/geb/volltexte/2010/7412/pdf/LeitholdGuenter_2010_01_21.pdf. Accessed 28 Feb 2011
116. Donald PF, Green RE, Heath MF (2001) Agricultural intensification and the collapse of Europe's farmland bird populations. Proc R Soc Lond B 268:25–29
117. European Environment Agency (EEA) (2006) How much bioenergy can Europe produce without harming the environment? – EEA-Report No 7, Office for Official Publications of the European Communities, Luxembourg, p 72
118. Sachverständigenrat für Umweltfragen (eds) (2007) Sondergutachten: Klimaschutz durch Biomasse Erich Schmidt Verlag GmbH & Co., Berlin, p 125
119. Bürki HM, Haumann A (1993) Überwinterung von Arthropoden im Boden und an Ackerkräutern künstlich angelegter Ackerkrautstreifen. Verlag Paul Haupt, Bern
120. Dziewaty K, Bernardy P (2007) Auswirkungen zunehmender Biomassenutzung (EEG) auf die Artenvielfalt – Erarbeitung von Handlungsempfehlungen für den Schutz der Vögel der Agrarlandschaft – Endbericht – Studie im Auftrag des Ministeriums für Umwelt, Naturschutz und Reaktorsicherheit. Eigenverlag, p 128

Books and Reviews

Karpenstein-Machan M (2005) Energiepflanzenbau für Biogasanlagenbetreiber. DLG-Verlags-GmbH, Frankfurt

KTBL (eds) (2009) Faustzahlen biogas, 2nd edn. KTBL Verlag, Darmstadt, p 240

Vetter A, Heiermann M, Toews T (eds) (2009) Anbausysteme für Energiepflanzen. DLG-Verlags-GmbH, Frankfurt

Biogas Production, Developing Countries

Heinz-Peter Mang[1], Zifu Li[2], Martina de Mantopi Porres Lebofa[3], Elisabeth-Maria Huba[3], Dishna Schwarz[4], Roland Schnell[5], Nguyen Gia Luong[6], Christopher Kellner[7], Johannes Selke[8]

[1]German Society for sustainable Biogas and Bioenergy Utilization, Freudenberg-Boxtal, Baden-Wuerttemberg, Germany

[2]Centre for Sustainable Environmental Sanitation, University of Science and Technology, Beijing, China

[3]Technologies for Economic Development, Maseru, Lesotho

[4]Deutsche Gesellschaft für Internationale Zusammenarbeit GmbH, Eschborn, Germany

[5]Graskraft Ltd, Berlin, Germany

[6]Biogas Technology Centre (BTC) of the Vietnam Union of Science and Technology Association (VUSTA), Hanoi, Vietnam

[7]Water and Sanitation Association of Zambia, Lusaka, Zambia

[8]International Biogas & Bioenergy Centre of Expertise (IBBK GmbH), Stuttgart, Germany

Article Outline

Glossary
Definition of the Subject
Introduction and Development History
Basics of the Biogas Process
Biogas Systems and Their Importance
Selected Low-Tech Biogas Design and Post-Treatment Units Descriptions
Development of Biogas Use in Various Countries
Challenges, Success, and Failures
Future Directions
Bibliography

Glossary

ABR Anaerobic baffled reactor
ADB Asian Development Bank
AF Anaerobic filter
BOD Biological oxygen demand
BORDA Bremen Overseas Research and Development Association
CAMARTEC Centre for Agricultural Mechanization and Rural Technology
COD Chemical oxygen demand
CSES Centre for Sustainable Environmental Sanitation
DEWATS Decentralized wastewater treatment systems
DM Dry matter
EGSB Expanded granular sludge bed
FB Fluidized bed
GATE German Appropriate Technology Exchange Centre
GIZ Gesellschaft für Internationale Zusammenarbeit - German International Cooperation
HIV Human immunodeficiency virus
HRT Hydraulic retention time
IADB Inter-American Development Bank
IC Integrated circulation
IFAD International Fund for Agricultural Development
KfW Kreditanstalt fuer Wiederaufbau – German Development Bank
NGO Nongovernmental organization
ODM Organic dry matter
PVC Polyvinylchloride
R&D Research and development
SEI Stockholm Environmental Institute
SIDO Small Industries Development Organisation
SNV Netherlands Development Organisation
SRT Solid or sludge retention time
TED Technologies for Economic Development
UASB Up-flow anaerobic sludge blanket
USTB University of Science & Technology Beijing
WASAZA Water and Sanitation Association of Zambia

Definition of the Subject

Energy is essential for human development. Without an adequate basic energy supply, people cannot cook their food, light their homes, or keep food and drinks chilled for storage. Alongside the introduction of efficient and clean thermal use of waste biomass for

cooking, the provision of electricity from renewable energy sources can provide basic energy services for lighting and communication and promote local economic growth.

Biogas-producing (anaerobic) treatment units as part of an integrated waste-to-energy treatment system are an alternative to use waste biomass as feedstock due to their energy and soil conditioner production capacity, low-tech components, and adaptability. It is also an excellent technology for treatment and reuse of manure and straw, organic sludge treatment collected from septic tanks, holding tanks, dry toilets, or for organically loaded wastewater pretreatment.

Decentralized low-tech biogas system solution provides a unique possibility for promoting appropriate household and community scale solutions to social and environmental problems; it is apparent that worldwide still many people are seeking friendly, small scale solutions for themselves and their communities, including biogas systems with lower specific performance efficiency, but out-balanced with lower degree of system mechanization and larger construction volumes.

Several research institutions and international agencies rate biomass as one of the cheapest available renewable energy sources for heat and power generation. Furthermore, conversion from biomass to useable energy is a low-carbon process as the resulting CO_2 is captured by plant regrowth. In contrast to other renewable energies, biomass energy conversion technology can generate heat and power on demand at flexible time, as long as a sufficient supply of feedstock is assured. Many municipal, agricultural, and livestock residues can provide feedstock for bioenergy conversion without increasing land requirements.

The main advantages of the anaerobic treatment process compared to the aerobic treatment process are the generation of biogas and significantly less sludge production. The fact that the plant nutrients phosphorus and potassium are not removed in the treatment process can also be an advantage for the application of the effluent in agriculture to replace chemical fertilizer, but the final effluent should never be discharged directly into water bodies without further treatment, unless the carrying capacity of the receiving water body is not exceeded.

Often industrialized countries neither have sufficient experience nor appropriate technologies to build on in developing countries. Transferable experience in low-tech biogas systems was identified in 1978 first in India and China and transmitted initially by a South-North-South transfer during 1980–1993 by international development cooperations. In the first decade, biogas technology focused on small-scale farmers. At a later stage, also larger farms as well as waste treatment issues increasingly became the additional focus of biogas technology. The term "appropriate technology" seemed justified by the fact that low-tech biogas systems are still adapted to the respective local conditions during a "learning-with-developing-countries" process.

Introduction and Development History

The topic "biogas" is relevant to all areas of rural development. Often overlooked, biomass is the most important renewable energy source in developing countries. Nearly one third of the world population cooks on open fires or traditional stoves with biomass (like wood, dung, straw, and agricultural waste). When cooking on biomass in huts, without chimney, flue gas causes significant respiratory and eye disorders. Therefore, the use of chimney-connected wood-saving stoves and biogas as clean cooking fuel is indispensable for improving health of women and children.

Inadequate sanitation in developing countries is a big issue. Moreover, manure, slaughterhouse waste, and untreated sewage pose major problems to health and environment. To use the energy potential of wastewater and waste, these organic substances can be treated in anaerobic (biogas) plants. The biogas produced can be used for cooking, lighting, heating, and cooling, and – if sufficient – to run engines. As a by-product, a valuable organic fertilizer is produced. Biogas plants therefore provide not only advantages for environment and sanitation, often, the most important aspect is the localized energy production and supply with biogas.

Due to the increasing awareness on climate change impacts, eco-friendly renewable energies are nowadays more in demand than ever. In relation to

these changing conditions and technical developments, biogas as a greenhouse gas neutral source of energy is an often-discussed topic in developing countries.

There are different expressions used for the same technology: anaerobic digestion, biogas plants, anaerobic fermentation, and biogas-sanitation system. The technology has been used for excreta treatment now for more than 100 years; thus, biogas is for sure the oldest "modern" renewable energy. Anecdotal evidence indicates that combustible natural gas (obviously natural gas, or marsh gas from swamps) was used for heating bath water in Assyria during the tenth century BC and in Persia during the sixteenth century BC. The science of anaerobic digestion is as old as scientific research can be and includes the names of world's most famous researchers.

The word methane comes from the Greek "Μεθάνιον αέριον" *(Methanion Aerion-swamp or foul air/gas)* and thus shows that the Greeks already centuries ago knew about the flammable gas. In Asia Minor, in places where ignited natural gas (methane) sources have been well known, is a volcanic area in which such gases occurred and this gas was named *Methana*. The alchemists in the Middle Ages knew methane as a swamp gas under the name *marsh gas*.

One of the earliest scientific "methane" gas discoverers was the Belgian Jan Baptista van Helmont (1579–1644) in 1630; his knowledge is documented in a communication about an inflammable gas "*gas pingue*" emanating from decaying organic matter. In 1667, the British Thomas Shirley (1638–1678) described "coal bed methane gas" more precisely in a brief report entitled "*A Well and Earth in Lancashire taking Fire at a Candle*" in the "Transactions of the Royal Society," about his observations in February 1659. The Italian Alessandro Giuseppe Antonio Anastasio Volta (1745–1827) wrote a letter on November 14, 1776, about a combustible gas "*Aria inflammabile nativa delle Paludi*" evolved when the bottom sediments of ponds near the town of Como, northern Italy, and in the Lake Maggiore, were stirred. He experienced that the gas exploded when mixed with air and ignited; he even determined the gas-to-air ratio that resulted in the loudest explosion. It was in 1804 when the British John Dalton (1766–1844) established the chemical constitution of methane. The gas attracted the attention of famous scientists of those days. The British William Henry (1775–1836) deduced the probable identity of the synthetic illuminating gas as methane. In 1806, he showed that Volta's gas was identical with methane gas.

The first allusion to animal manure came from the British Sir Humphrey Davy (1778–1829), who reported the presence of combustible biogas in fermenting farmyard manure, in 1808. Therefore, he can be considered as the first real discoverer of biogas as a mixture of methane and carbon dioxide.

By that time the physical scientists (physicists and chemists) had advanced knowledge about biogas as far as their knowledge allowed, and from thereon the microbiologists took over the scientific investigation on biogas. In 1868, the French microbiologist Mme. Antoine Bechamp (1816–1908) identified the microorganism responsible for methane production. She showed as well that different fermentation products are formed during the digestion process, depending on the type of substrate. The Russian Leo Popoff from Petersburg published 1875 in Strasbourg, Elsass, that fermentation of cellulose could form *swamp gas* at temperatures still as low as 6°C. His experimental studies brought out the optimum temperature for their action and the effect of antiseptics, with some knowledge of the gaseous decomposition products.

The first attempts in using biogas in France were undertaken when the French Ulysses Gayon (1845–1929) produced biogas energy from animal manure. In 1875, he became director of an agricultural research institute in Bordeaux. His trials to produce biogas from manure and to use this gas for lighting and heating were published in the *Comptes Rendus of the Séances de l'Académie des Sciences*, tome 90, 1884. Dr. P. Duvernay reported about this event on March 5, 1884, in the daily newspaper "Le Figaro" under the title "*Une Drôle d'Eclairage*."

Already earlier, in 1881, the French journal Cosmos cited the first full-scale anaerobic treatment of domestic wastewater as "*Mouras Automatic Scavenger*." Louis Mouras of Vesoul, France, obtained

a septic tank patent in 1881 and was credited with this invention. Baffles, which regulate the flow and increase sanitization, were added in 1905 in order to make the septic tank more efficient. It is reported that this kind of septic tank without biogas recovery was introduced in the USA in 1883, in England in 1895, and in South Africa in 1898. Anaerobic digestion is therefore the oldest technology applied for domestic wastewater treatment. Since 1850 until this date, open constructed rectangular settling tanks (cesspools) were operated intermittently, meaning that the sewage inflow had to be stopped regularly for sludge removal.

In 1895, Donald Cameron, City Surveyor of Exeter, England, constructed in this town a line of six "*Mouras*" septic tank, covered to avoid smell, as the tanks were placed near dwellings. From 1911 onward, under the guidance of Mr. T. Moulding, the collected biogas was used in sewer gas destructor lamps, a type of street gas lighting.

Combustible biogas that could be obtained from human excreta was also demonstrated in India, where in 1897 a biogas-generating plant treating toilet wastewater was constructed in Matunga, more specifically in the Homeless Lepers' Asylum, known as the Acworth Leprosy Hospital in Wadals, founded 1890. The biogas was used for lighting. This may be the first application worldwide of the so-called biogas-sanitation.

The roots of technical applicability of microbiological digestion probably lie with methane-producing bacteria "*Methanobacillus omelianskii*" discovered by the Ukrainian Vasilii L. Omelianskii (1867–1928). From 1893 to 1928, he worked in the department of general microbiology of the Institute of Experimental Medicine. His classic studies on methane fermentation bacteria were reported during 1903/1904. He isolated organisms that produced hydrogen, and acetic and butyric acids. He also reported the formation of methane from hydrogen and carbon dioxide. The development of microbiology as a science led to more research by the American team A.M. Bushwell, G.E. Symons, C.S. Borruf, and W.C. Boyle; they published in 1936 a scientific formula describing the composition of biogas based on the chemical composition of the substrates undergoing an anaerobic digestion process.

William Owen Travis sought to improve the contact bed procedure for municipal wastewater treatment. As local health officer in charge of a contact filter at Hampton, England, Dr. Travis was quite familiar with the problem of bed clogging. His solution, introduced in 1904 as the *Travis Hydrolytic Tank*, was essentially configured as a multistage septic tank. Successively divided into detritus, hydrolytic, and finishing tanks, the latter two zones contained wooden baffles or laths placed in a parallel array. These baffles were intended to retain fine particles for subsequent degradation. Based on this development, Karl Imhoff (1876–1965) shifted the focus from anaerobic wastewater treatment to anaerobic sludge treatment with his *Imhoff tank* (1905/1906). An upper section of this tank is designed for sedimentation; the solids fall from it through a slot into a lower section for digestion. Experiments on a similar unit, called Biolytic tank, were carried out in the USA between 1909 and 1912. With the installation of the first sludge heating system, separate digestion of sludge was reported at the Essen-Rellinghausen wastewater treatment plant in Germany in 1927. The separated sludge digestion became increasingly popular in larger German towns and cities, and the importance of methane gas generation was widely recognized. Methane gas was used for digester heating; it was collected and delivered to municipal gas systems, and it was used for power generation for operating biological wastewater treatment systems, and as transport fuel. The sale of sewage gas was, in addition to the sale of sewage sludge as fertilizer, one of the few ways from which the sewage treatment plant could generate revenue to reduce wastewater treatment costs. In the USA at Belleville Water Works, Maryland, Illinois, the first *Clarigester* was installed in 1938 to separate the sludge from the wastewater stream, and to treat the sludge anaerobically, recovering sewage biogas.

In China in 1927, Luo Guorui developed in Shantou city, Guangdong province a small-scale agricultural biogas plant, using the gas for lighting; the design was based on existing urban household septic tanks. This may be considered as the worldwide first agricultural biogas digester.

Inspired by the research work of the Rothamsted agricultural experimental station in England in

1929, the British Lord Iveagh was the first builder of a European agricultural biogas reactor on his property in Pyrford Court, Surrey. He had a 300 m^3 volume biogas tank and used straw as feedstock, which was inoculated twice a year with fresh manure. For 20 years, the daily gas production was recorded, which indicated daily 12–120 m^3. The gas was used on the farm even for cooking and lighting. It was used until 1960, before it ceased operations.

G. Ducellier and M. Isman developed the design and prototypes of another dry-fermentation biogas digester since 1937 at the Institute of Agriculture in Algeria. Since 1946, the technology had been transmitted to France and Mr. Renandat was one of the first farmers at Levroux, Indre, who constructed a biogas plant which consisted of a battery of four tanks (100 m^3 volume), gasholder and compressor, pressure storage tank, and a biogas-fueled tractor. It was estimated that such an installation would pay for itself within ten years of construction by the production of gas and savings in fertilizer costs. Since then, French farmers constructed perhaps 1,000 low-tech plants along the lines of the *Ducellier-Isman* design.

In India, in 1946, a social worker within the Khadi and Village Industry Commission (KVIC), Mr Jashbhai Patel, started to work on developing a liquid manure biogas digester design placing the digestion chamber below ground.

Imhoff drafted in 1944 an agricultural biogas plant for the farm Zitzstaudenhof in Olching, Germany. Although this plant was never built, the draft, published several times by the designer, gave the model for the first agricultural biogas plant called "*Darmstaedter Gaerkanal - gas factory on a farm*" in 1947/1949 on the farm Bertaloth in Rohrbach; improvements were guided by Prof. F. Reinhold, State Laboratory of Road and Urban Engineering at the Technical University Darmstadt, and built by the Casting and Valve Works Kaiserslautern, Germany.

Nowadays, such low-tech anaerobic reactors are widely adopted for the stabilization of municipal sludge, human excreta, and animal manure, aiming at the generation of renewable energy in the form of methane and the generation of bioslurry.

The National Institute for Water Research of the South African Council for Scientific and Industrial Research published in 1950 research results from G.J. Stander, which recognized the importance of solid retention time (SRT) for a successful anaerobic treatment of different wastewaters. This has been the basis for the worldwide development of the so-called high-rate anaerobic biogas reactors, in which SRT and hydraulic retention time (HRT) are uncoupled, but both fractions are undergoing anaerobic treatments in one constructed tank. Further development led to a wider application of anaerobic biotechnology, particularly for industrial wastewater treatment combined with biogas recovery. Some of the present widely used high-rate anaerobic treatment processes for industrial wastewater treatment are anaerobic filter (AF), up-flow anaerobic sludge blanket (UASB) reactor, expanded granular sludge bed (EGSB), fluidized bed, internal circulation (IC) reactor, and hybrid systems.

Basics of the Biogas Process

Anaerobic digestion is a complex biological process that takes place in the absence of oxygen. The decomposition process is possible under anoxic (presence of nitrate) and anaerobic conditions: Bacteria split organic substances into their components, and these components are "re-arranged"; other bacteria originate from biochemical degradation.

The digestion is a multistage process consisting of hydrolysis, acido- and acetogenesis, and methanation performed by different bacteria and microorganisms. In low-tech biogas systems, the different degrading reactions take place in one or two digester(s) or digestion chambers. The digestion process starts with hydrolysis of the input material caused by exoenzymes of facultative and obligatorily anaerobic bacteria in order to break down insoluble organic polymers such as cellulose, proteins, and fats. Acidogenic bacteria then convert sugars and amino acids into carbon dioxide, hydrogen, ammonia, and organic acids, followed by acetogenic bacteria converting the resulting organic acids into acetic acid, along with additional ammonia, hydrogen, and carbon dioxide. At the end of the process, methanogens convert these products into methane and carbon dioxide.

To summarize, the anaerobic digestion process consists of the following steps:

1. Hydrolysis: (a) The organic matter is hydrolyzed by extracellular enzymes. (b) Bacteria decompose the long chains of complex to simpler substances, for example, polysaccharides to monosaccharides.
2. Acidification: (a) Acid-producing bacteria convert intermediate fermentation products into acetic acid, H_2, and CO_2. (b) Acid-producing bacteria create anaerobic conditions for CH_4 (methane)-producing bacteria.
3. Methanization: Methanogens, that is, methane-producing bacteria, acetic acid, and/or hydrogen are used to form methane. Sulfate reduction leads to the formation of hydrogen sulfide.

Higher concentrations of, for example, ammonia, heavy metals, light metal cations, oxygen, short chain organic acids, other organic acids, and sulfides could inhibit the anaerobic process. Short-term biogas productivity tests are available to investigate this.

One result of such an anaerobic digestion is biogas. The term "biogas" refers to a gas produced by anaerobic digestion or fermentation of organic matter including manure, sewage sludge, municipal solid waste, biodegradable waste, or any other biodegradable feedstock under anaerobic conditions. Biogas is comprised primarily of methane and carbon dioxide. In conventional septic tanks, biogas from Imhoff tanks (combined settler and sludge treatment units) and anaerobic lagoons vented out, creating climate critical emissions due to its methane content. The rate of methane production depends on the rate of removed COD, BOD, and the temperature. It is also common to relate the biogas production to the dry matter (DM) or organic dry matter (ODM) of the input material.

Practically most anaerobic bioprocesses stabilize organic wastes that are formed from mixtures of fats, proteins, and simple carbohydrates, and this typically results in biogas composition illustrated below:

- Methane (CH_4): 50–70 vol%
- Carbon dioxide (CO_2): 28–48 vol%
- Other gases: up to 2 vol% including trace components such as hydrogen, nitrogen, oxygen, ammonia, argon, carbon monoxide, hydrogen sulfide, non-methane volatile organic carbons, halocarbons

Biogas-producing systems are used as environmentally friendly technology for waste and wastewater treatment, and for renewable energy generation in many countries. The average calorific value of biogas is about 6 kWh/m^3; this corresponds to about half a liter of diesel oil. The net calorific value depends on the efficiency of the burners or appliances. Methane is the valuable component under the aspect of using biogas as a fuel.

Biogas can be used for (in order of simplicity, with simplest option first): cooking with gas stoves, lighting, heating, electricity generation, simultaneous generation of both electricity and useful heat (with combined heat and power (CHP) units), cooling, or as transport fuel. Some options are only feasible for larger biogas systems, but the smallest combustion engine–based "mini" biogas GENSETs – commercially offered – is 4 kVA.

As common figures for methane production 0.25 m^3CH_4/kg COD (chemical oxygen demand) removed or 1 kg BOD (biological oxygen demand) removed results in practice in about 0.6 kg methane at 273 K (energy content of methane 35.8 MJ/m^3).

Sulfur content in biogas in form of hydrogen sulfide (H_2S) has to be taken into account and possibly filtered out or eliminated chemically. H_2S is a colorless gas presenting a strong odor of rotten eggs; it fatigues the sense of smell, which cannot be counted on to warn of the continued presence of the gas. While biogas is used for cooking, the presence of H_2S in the biogas results in smell disturbance and faster corrosion of the cast iron burner parts, which are in direct contact with biogas.

Additionally, a part of H_2S might be converted through the incomplete combustion of biogas into sulfur dioxide (SO_2), which could result in headache and breathing problems. Even it is known that H_2S needs a lower (260°C) combustion temperature than methane (CH_4) at 560°C, temperatures over 850°C throughout the flame are necessary to prevent the formation of carbon monoxide (CO), partially oxidized hydrocarbons, dioxins and furans, and polycyclic aromatic hydrocarbons (PAHs).

Stoichiometrically, 9.6 volumes of air per volume of methane are required to achieve complete oxidation by burning. For the typical biogas composition given above, this ratio reduces to 5.7:1. Similarly, the energy released by pure methane is 36 MJ/m^3 (gross calorific value) and is reduced to 21 MJ/m^3 for biogas.

Organic material degrades more rapidly at higher temperatures because all biological processes operate faster at higher temperatures up to the limit of sterilization. The three ranges of temperatures in which methanogens could work are called psychrophile (8–25°C, with an optimum at 17°C), mesophile (30–42°C, with an optimum at 40°C), and thermophile (53–65°C, with an optimum at 55°C).

Low-tech, non-heated, and poorly insulated biogas systems are often applied in countries where the ambient average annual temperature ranges above 12–25°C. In ambient temperatures below 8°C, digestion capability is very much reduced without active and passive heating and insulation of the digester. The methane formation process is also sensitive to daily temperature variations of more than 3°C; therefore, day-night variations or temperature shock loads have to be kept in a limited range to ensure a steady biogas production. The higher the process temperature the more sensitive is the process (bacteria).

To improve low-tech biogas systems, the application of improved insulation (above and below ground), keeping the plant environment dry (drainage layer and plant area roofing), active and/or passive heating of plant, and filling substrate should be considered (preheating, solar heating), depending on available design, funds, and micro-environment.

Biogas Systems and Their Importance

Biogas systems are defined here as "engineered systems designed and constructed to utilize biological processes which break down solids and soluble organics in the liquid by anaerobic bacteria action under exclusion of free oxygen in treating organically loaded sludge."

A process design differentiation between highly diluted (low dry matter content) wastewater and solids or sludge (high dry matter content) treatment has to be made. For the first one, bacteria have to be accumulated and kept in the system, while in the second one, organic biodegradable solids are hydrolyzed and then converted into biogas. Anaerobic wastewater treatment, biogas sanitation, bio-waste fermentation, and manure treatment are using the same biological process, but the goal of anaerobic wastewater treatment is to purify wastewater. The goal of animal manure treatment in biogas plants is to generate energy, avoid methane emissions, and to produce an improved soil conditioner. The goal of biogas sanitation is to prepare "*humanure*" for safe reuse and to produce biogas. The goal of bio-waste fermentation is to reduce volume of waste for post-treatment and to produce carbon emission free energy, rather than to prepare manure for fertilizing reuse and to produce biogas.

Biogas systems may treat a wide range of waste and wastewater; here a focus is put on biogas production in developing countries (low-tech applications) for small-scale heat and cooking gas provision, by treating animal manure, organic waste from industries and settlements, black water or brown water, excreta, fecal sludge, wastewater from low or no flush toilets, and kitchen waste.

Anaerobic treatment units are often an alternative or a pre-treatment to aerobic treatment systems due to their energy and soil conditioner production capacity, low-tech components, and adaptability. It is also a technology for organic sludge treatment. The main advantages of the anaerobic treatment process compared to the aerobic treatment process are the generation of biogas and significantly less excess sludge production as well as smaller reactors. The fact that the plant nutrients phosphorus and potassium are not removed in the treatment process can also be an advantage for the application of the effluent in agriculture to replace mineral fertilizer. However, the effluent should never be discharged directly into water bodies without further treatment, unless the carrying capacity of the receiving water body is not exceeded. Anaerobic technology has advantages in terms of nutrient recycling, energy balance, and CO_2 emission reduction compared to conventional aerobic treatment systems.

Toilet wastewater alone could not produce enough biogas to cover completely the energy demand for cooking or lighting of a household, at least the excreta of five persons are needed to cover the daily cooking energy demand of one person. Feeding easy biodegradable organic kitchen waste or animal dung into the biogas-sanitation digester could increase the biogas yield. An organic garbage disposal unit in the kitchen sink (grinder) is useful in this respect.

In decentralized or semi-centralized wastewater treatment systems, biogas-sanitation units are often designed as primary treatment of wastewater to remove large particles and some organic matter by settling and digestion.

Besides the feedstock material, local circumstances must be taken into consideration before designing a biogas plant, such as the dilution of the influent with (gray) water or urine; addition of organic waste; the settle-able solids content in the influent; the climate and soil temperatures; available space; and the intended reuse or disposal pathway.

Methane (CH_4) is a greenhouse gas that remains in the atmosphere for approximately 9–15 years. Methane is 21 times more effective in trapping heat in the atmosphere than carbon dioxide (CO_2) over a 100-year period. It is emitted from a variety of natural and human-influenced sources. Human-influenced sources include landfills, natural gas and petroleum systems, and agricultural activities; coal mining; stationary and mobile combustion; wastewater treatment; and some industrial processes. Methane is also a primary constituent of natural gas and an important energy source. As a result, efforts to prevent methane emissions or utilize methane can provide significant energetic, economic, and environmental benefits.

Biogas systems can be classified according to various parameters; the three most important design criteria are (1) hydraulic retention time (HRT in days), (2) organic load rate (OLR in kg COD/m^3 or kg ODM/m^3 active fermenter volume), and (3) settled sludge retention time (SRT in days or years).

The required hydraulic retention time (HRT) of the substrate in the digester depends on the process temperature and the type and concentration of the substrate itself. This will then determine the volume of the digester. Digesters are generally designed for an optimum economic balance between highest biogas yield and smallest volume (HRT). Therefore, the retention time is chosen as the total time required, producing a certain amount of the total biogas (to size the digester to obtain all possibly generated biogas is often not economically viable). A low-tech energy-optimized biogas system should have a minimum of 20 days of hydraulic retention time due to bacterial reproduction time, but from a health point of view, the hydraulic retention time in a biogas-sanitation system should be extended to more than 60 days, if no adequate post-treatment of effluent is foreseen.

For animal manure undergoing low-tech fermentation process in the upper psychrophilic and lower mesophilic temperature range (17–33°C), the following approximate hydraulic retention time values are usually applied:

- Cow or cattle manure: at least 30 days
- Pig manure: at least 25 days
- Poultry manure: at least 40 days
- Animal manure mixed with easy biodegradable plant material: about 80 days
- Fecal material: at least 60 days

A sludge retention time (SRT) of at least 10 days is necessary to promote methanogenesis in the anaerobic treatment of primary sludge at a process temperature of 25°C while a sludge retention time of 15 days is necessary for sufficient hydrolysis and acidification of lipids. For temperatures as low as 15°C, a sludge retention time of at least 75 days has to be considered to achieve methanogenic conditions. The longer the sludge retention time, the better the degradation and stabilization of the sludge will be and less sludge will remain. This is of special importance for biogas-sanitation units; the handling of not-sufficient treated sludge can be also a problem in densely populated areas.

Parameters for monitoring anaerobic processes are: organic dry matter content, pH value, carbon-to-nitrogen ratio (C/N ratio), redox potential, volatile fatty acids, moisture content of the biogas, temperature stability, and substrate composition. Biogas amount and quality should be used for monitoring the plant performance – related to the applied feedstock biogas potential; the total solids content in the reactor influent and effluent is an important parameter, too.

It is always important to maintain by weight a carbon-to-nitrogen (C/N) ratio between 8 and 30:1 for achieving an optimum rate of digestion. Combining materials low in carbon with those that are high in nitrogen can manipulate the C/N ratio. If the C/N ratio is very high, nitrogen limitation could cause low gas production, since nutrients for the growth of anaerobic bacteria are lacking. If the C/N ratio is very low, the pH value may increase, and will have a toxic effect on bacteria, and also result in lower biogas production.

Different types of biogas digesters could be combined (so-called combined systems, multistep systems, or decentralized wastewater treatment systems) in order to benefit from the specific advantages of the different systems. The quality of the final effluent

from the systems improves with the multiple steps of the treatment facility. Design and engineering information for the worldwide used fixed dome, baffle reactors, anaerobic filter, covered lagoon, stirred systems, up-flow systems, or composite plant design variations are available through many websites, literature, and expert consultations.

Local design adaptations to different local human diets, livestock keeping habits and manure types (influencing organic load and biogas potential), sanitization needs, and effluent reuse options (for energy crops, tree nursery, grassland, vegetable, grains) are always necessary.

Selected Low-Tech Biogas Design and Post-Treatment Units Descriptions

Below some selected low-tech biogas designs are described. The key to the optimal operation of a reactor selection and design is to understand the bacteria: how much, how active, how good in resisting shock loads.

Fixed Dome Digesters. Chinese model biogas plant with manhole (also called drum-less digester) consists of an underground compartment (fermentation chamber) with a dome on the top for gas storage. In this design, the fermentation chamber and gasholder are combined as one unit. The construction details of a biogas plant (with or without baffle(s), size of integrated gasholder) depend on the further treatment step chosen and on the expected biogas use pattern. In a special design, the so-called biogas settler (BS), to achieve that the sludge retention time (SRT) is longer than the hydraulic retention time (HRT), baffle or separation walls should be added when it is operated as stand-alone sanitation system. The accumulated settled sludge must be removed from the base of the biogas settler (BS) periodically.

Floating Drum Digesters. In the digester chamber, a floating drum (bell) is placed on top of the digester to collect the biogas produced from the digester. Thus, there are two separate structures for gas production and collection. The construction details of a biogas plant (with or without baffle) depend on the further treatment step.

Covered Lagoon Digester. A sealed pond or lagoon operated for the stabilization of manures, anaerobically and fitted with an impermeable cover (polyvinyl chloride (PVC), ethylene propylene diene monomer rubber (EPDM), or high density polyethylene (HDPE)) to capture the biogas generated as the product of waste stabilization. Disadvantages are the land area needed for anaerobic lagoons and sludge sedimentation problems, if digester is un-stirred.

Plug-Flow Biogas Digester. Plug flow is a simple model of the velocity profile of a fluid flowing in a pipe. In plug flow, the velocity of the fluid is assumed to be constant across any cross section of the channel perpendicular to the axis of the channel. Essentially no back mixing is assumed with "plugs" of fluid passing through the reactor. Many different forms of construction are known, for example, fixed-dome tunnel plants, floating gas holder tunnel plant, PVC or PE-plastic bag "sausage" tubular digester, composite tank plant, covered sedimentation channel lagoons. The digester is a long, rectangular container or tank or channel (1/5: about 1 times large related to 5 times long), with gastight cover. New material added to the tank at one end pushes older material to the opposite end.

Anaerobic Baffled Reactor. The anaerobic baffled reactor (ABR) has a series of up-flow and down-flow baffles which are used to direct the flow of wastewater in an up-flow mode through a series of sludge blanket reactors. This configuration provides a more intimate contact between anaerobic biomass and liquid, thus improving the treatment's performance. It could be used as primary treatment as well, especially where influents are highly diluted with flush water (from pig stable or toilet buildings). Separation of the sludge retention time (SRT) from the hydraulic retention time (HRT) is the key to the successful operation of an anaerobic baffled reactor. Due to this fact, a baffled reactor is considered as the best alternative to aerobic treatment and posterior to primary settlement in a biogas digester. The treatment efficiency achievable is usually superior to that of a conventional septic tank.

Anaerobic Filter. The anaerobic filter (AF) is suitable for effluents with a low content of suspended solids and a narrow COD/BOD ratio, for instance, from biogas settlers or biogas septic tanks or anaerobic baffled reactor as initial treatment unit. The bacteria in the filter are immobile and generally fix themselves to solid particles (carrier material) or to the reactor walls. Filter materials like rocks, cinder, plastic, or gravel provide additional surface area for bacteria to settle. The larger

surface area for the bacterial growth helps in the quick digestion of the wastes. A good filter material provides a surface area of 90–300 m^2/m^3 reactor volume. Anaerobic filters are reactors consisting of supporting material layer. On the surface of these material layers or bed fixation of microorganism the development of biofilm takes place. In the case of concentrated feedstock, the risk of blockage of the filter material increases with the concentration of suspended solids. Therefore, it is best suited for posttreatment.

Up-flow Anaerobic Sludge Blanket Reactor. The up-flow anaerobic sludge blanket reactor (UASB) is a tank filled with anaerobic granular or flocculants sludge with good settling properties. (The bacteria spontaneously agglomerate to form granules.) Influent wastewater is distributed at the bottom of the UASB reactor and travels in an up-flow mode through the sludge blanket. The anaerobic degradation of organic substrates occurs in this sludge blanket, where biogas is produced and serves to mix the contents of the reactor as they rise to the surface. The UASB reactor has the potential to produce higher quality effluent than biogas septic tanks, and can do so in a smaller reactor volume. The design of an UASB reactor must provide an adequate sludge zone since most of the biomass is retained there. The granulated sludge zone is completely mixed because the wastewater is fed into the reactor through a number of regularly spaced inlet ports. The UASB is also characterized by a much longer SRT in comparison with the HRT.

Development of Biogas Use in Various Countries

In the following some developing country programs and developments in the biogas sector are briefly described; the list is however incomplete as about all countries have nowadays their own biogas history.

Asia

Bangladesh The Institute for Fuel Research and Development (IFRD) of Bangladesh Council of Scientific and Industrial Research (BCSIR) has been the main actor for the dissemination of domestic biogas plants in Bangladesh till date. Other organizations being involved at different stages have been Bangladesh Rural Advancement Committee (BRAC), Local Government Engineering Department (LGED), Department of Environment (DoE), Grameen Shakti (GS), Bangladesh Agricultural University (BAU), Bangladesh Small & Cottage Industries Corporation (BSCIC), Danish International Development Agency (DANIDA), and Department of Livestock Services (DLS).

In 1972, BAU set up a first floating-drum plant in the University campus to study the characteristics of gas production, followed later by a plant that provided gas for cooking and lighting for a family of six members. In the campus of BCSIR, another plant was constructed by IFRD in 1976, followed by a plant at the KBM College in Dinajpur in 1980. Seventy-two plants were constructed for farmers with technical assistance by IFRD. In 1981, DoE started its program through which about 150 floating-drum and 110 fixed-dome plants were installed by contractors free of cost. Other efforts were undertaken by BSCIC (a number of plants), DANIDA and LGED (more than 200 trench and bag type digester), and DLS (about 70 plants). Also the Grameen Bank installed 17 polyethylene plastic bag digesters. Under the "Fuel Saving Project" implemented from 1989 to 1991, IFRD trained local youths who constructed in total 146 plants in the premises of well-to-do farmers. The gasholder was supplied free of cost. In 1994, LGED supported the establishment of an ecological village (Amgram in Madaripur district) among others by converting 95 open latrines into family biogas-sanitation plants.

An important dissemination push was delivered by the "Biogas Pilot Plant (1st phase) Project" implemented by BCSIR in the period July 1995 to June 2000. In total, 4,664 fixed-dome plants were constructed throughout the country. BCSIR employed and trained 128 diploma civil engineers who were assigned responsibilities for motivation, installation, and after-sales service throughout the country. In addition, 898 youths were trained to support the project. The biogas farmers received an investment subsidy of Taka 5,000 (US$ 64) under the project. Memorandum of Understanding (MoU) were signed between BCSIR and several other institutes like BRAC, LGED, and DLS for research, training, and dissemination of the biogas technology. The cooperation with BRAC was the most successful as this organization managed to motivate about 1,200 farmers. An interim evaluation report in 1999 reported 99% of the plants installed under the

project were in operation, while 91% of the owners could meet their household fuel demand through biogas. Bioslurry from the biogas plants was used in horticulture, pisciculture, and agriculture. The average saving per plant amounted to Taka (US$ 10) per month.

As the first phase was successfully completed and the potential for biogas in Bangladesh considered huge, BCSIR implemented the second phase of the Biogas Pilot Plant in the period July 2000 to June 2004. The target for this phase was to put on 20,000 biogas plants, out of which 17,194 plants were finally realized. The investment subsidy for the owner was increased to Taka (US$ 96) per plant. In addition to the diploma civil engineers employed and paid on a monthly basis by BCSIR, an agency system was introduced on incentive basis. About 50 agencies were recognized in defined areas (mostly districts) and received a lump-sum fee of Taka (US$ 64) per plant as service charge. About 1,000 masons and youths were trained under the project as well.

In the period from October 1998 to June 2003, the LGED implemented a parallel biogas project aiming to install 1,900 domestic plants. As the investment subsidy for this project amounted to Taka (US$ 64) only, it proved to be rather difficult to motivate farmers during the implementation of the second phase of the Biogas Pilot Plant Project when BCSIR was providing a subsidy of Taka 7,500 to farmers. Therefore, the LGED project was terminated prematurely, after having constructed about 1,120 biogas plants. Under the Secondary Town Infrastructure Development Project-II, another 20 domestic biogas plants were installed using human excreta only.

Of more recent date is the initiative of GS aiming to construct not less than 200,000 biogas plants within a period of five years. This initiative is still in the preparatory phase; at the time of the mission a total of 10 plants were installed or under construction. Agency holders also continued to construct plants without any subsidy in very limited numbers after the termination of the second phase of the BCSIR pilot project in June 2004. By the end of 2008, about 40,000 family-sized low-tech biogas plants of different designs had been installed throughout Bangladesh.

Since 2006, Netherlands Development Organisation (SNV) is implementing the "National Domestic Biogas and Manure Programme" (NDBMP) in Bangladesh involving the "Infrastructure Development Company" (IDCOL), and other national and local partner organizations. The overall objective of the NDBMP is to further develop and disseminate domestic biogas plants in rural areas with the ultimate goal to establish a sustainable and commercial biogas sector in Bangladesh. This program will help to attain Millennium Development Goals (MDG) set by Government of Bangladesh as well. The overall objective of the National Domestic Biogas and Manure Programme (NDBMP) is to develop and disseminate domestic biogas plants in rural areas with the ultimate goal to establish a sustainable and commercial biogas sector in Bangladesh. The National Strategy for Economic Growth, Poverty Reduction and Social Development prepared by the Ministry of Finance and Planning also puts emphasis on "creating a policy environment that is capable of providing right incentives to adopt new technologies." It also emphasizes the integration of environmental conservation strategy into national poverty alleviation strategies. NDBMP further contributes to achieve millennium development goals set by the Government. Contribution of biogas in this regard will help poverty reduction through (1) savings on energy expenditure, (2) increased agriculture production by maximum utilization of bioslurry as fertilizer, (3) gender equality through empowering women in decision making and maximization of their participation in the program, (4) improved health through provision of clean cooking energy, (5) improving sanitation by toilet construction connection to the biodigester, and (6) creation of opportunities for local employment.

Until April 2009, about 35,000 plants were already newly installed in Bangladesh. Considering only smaller sized household biogas plants the total technical potential from the available raw material reaches up to about a potential of three million biogas plants. Under the on-going program a total of 37,269 plants are aimed to be constructed in the period 2006–2012. Several activities are implemented to achieve this target: promotion and subsidy administration to provide Taka 9,000 (US$ 115) per household as investment subsidy. To ensure proper functioning of the plant, guarantee on plants for 5 years and maintenance services are provided for 3 years, and training on

operation and maintenance will be provided to each biogas plant owner family. Trainings will be developed and imparted to the staff of the partner organizations to strengthen their capabilities. Proper management and utilization of bioslurry is given high emphasis. IDCOL plays a role of refinancing whereas another program implementing organization will be engaged for program activities of the (technical) implementation. This program is subsidized by the Government of Bangladesh, the Netherland development cooperation, local Micro Finance Institutions, and supported with development cooperation loans by the German Bank for Reconstruction and Development (KfW). In addition to these budgetary sources, there is an opportunity of generating carbon finance through trading carbon emission reduction from well-performing biogas plants.

China In 1927, Luo Guorui developed in Shantou city, Guangdong province, a small-scale agricultural biogas plant, based on existing urban household septic tanks. As a standard, the toilet and the pigsty were connected to an underground 8 m^3 digester. The *Shantou Guorui Natural Methane Gas Lamp Company* has commercially promoted the system. In the *Shantou* newspaper in 1930, he advertised the benefits of natural methane lamps. The inventor moved in 1931 to Shanghai and founded the *Chinese Guorui General Natural Methane Company* with many branches along the Yangtze River and in the southern provinces. In April 1935, Chinese lecture notes about *Guorui methane digesters* were published as the first scientific presentation about low-tech household-based agricultural biogas technology in the world; this publication initiated the first wave of biogas application in China.

Since 1957 biogas research and technology were developed at high speed, and the Chinese government promoted farm biogas technology vigorously. At the Beijing Agricultural University, 1958, the first "international" training course on low-tech biogas technology was held with Soviet Union invitees. The technology was found to be appropriate to both the livelihood systems of rural farmers and the political intention of the communist party to become independent of fertilizer imports. Up to seven million biogas units have been constructed in China between the years 1968 and 1978. The main feedstock was pig manure, and the main emphasis of the Chinese program was to provide an efficient and economic fertilizer, rather than household energy aspects of biogas technology. One of the lessons learned from this Chinese biogas program is that technology dissemination to a very large number of households is possible if it is supported by a strong political will.

The today worldwide known Chinese round shaped fixed-dome biogas plant was developed in 1973, and in 1980 – after 7 years of experience and adaptations – it was standardized nationwide. In 1980, the China Biogas Association was founded to coordinate the biogas development inside the country and internationally.

In 1978, the Zhangzhou College of Education developed a small-scale three-chamber biogas-sanitation digester for anaerobic treatment of excreta from household toilets, which was added to the agricultural standards. In 2000, the composite fiberglass household biogas plants entered the commercial market with volumes between 6 and 10 m^3. This prefabricated biogas digester offers some significant improvements: improved gas tightness, long life span, lower maintenance costs, and shorter construction period from at least 10 days with brickwork and concrete to half a day. Since then, other prefabricated models, mainly based on high-density polyethylene (HDPE) material, have been developed and entered the market as well.

In 2003, the national biogas development plan for China 2003 till 2010 suggested to increase the use of biogas until the year 2005 from 11 million households to 20 million households, promoting biogas use in one of ten agricultural households. In 2010, the number of biogas-using households reached 40 million, with an operational rate of at least 60%, as estimated by Chinese evaluations. Since 2003, the government subsidizes each low-tech biogas plant with an average of 1,000 CNY (about 110 €).

India In 1946, a social worker within the Khadi and Village Industry Commission (KVIC), Mr Jashbhai Patel, started to work on developing a biogas design placing the digestion chamber below ground. Whereas in the former Indian model, reactor and gasholder have been separated, the new feature integrated gasholder and reactor into one unit, saving both space and material. Further innovations of this design were the

continuous flow system and automatic overflow when overloading. It was also equipped with a device that should prevent scum to enter the gas pipes. The first unit of this type was installed in 1950 at Osmania University, Hyderabad. The design was called Gramalakshmi; Grama meaning "rural" in Hindi, and Lakshmi is the Goddess of wealth and prosperity in the Hindu religion. There is also a notion of the word Grama toward the Gandhian movement of rural development.

The work of Mr. Patel continued during the 1950s; other institutions such as the Rama Krishna Mission in Calcutta and Khadi Pratisthan Sodepur in West Bengal did also develop new designs. A number of pilot units were constructed especially in the regions of Maharashtra and in the vicinity of Delhi. KVIC included dissemination of biogas technology in its rural development program since 1961, as a result of the earlier field trials. The Planning Research and Action Division (PRAD) of Uttar Pradesh took further national initiatives by establishing a research station in Ajitmal. This research station later became known as the Gobar Gas Research Station, and one of the influential persons was Mr. Ram Bux Singh. Until 1974, about 6,000 biogas units were set up in India.

In 1975, the years following the worldwide energy crisis, it was considered that a well-tested low-tech biogas technology existed, and the required infrastructure for carrying out a nationwide dissemination program was planned, with the aim to install 1.5 million biogas units by 2001. Many organizations and institutions were involved, but the main responsibility for the implementation of the program was held by KVIC. The biogas program was in many respects in line with the development goals defined by Indira Gandhi and the government. The technology was indigenously Indian; it was expected to develop the rural areas and to improve the livelihoods of rural population. It was also a response to the increased oil import expenditures India had experienced some years ago. Identifying the fuel wood crisis, biogas technology was considered, among many planners and policy makers, to be a real solution to the problem. International organizations and donors were beginning to show interest in the technology. Rural development and appropriate technology were attractive for any development program. Small-scale technologies were given attention as possible solutions to the limits of finite resources. It was considered that the dissemination of biogas technology was a potential way to improving the situation for rural people with limited budgets. In 1978, the Gobar Gas Research Station in Ajitmal, Uttar Pradesh, came up with a prototype of a new design called Janata biogas plant, meaning "public" or "people" in Hindi. The Janata design was similar in several ways to the Chinese fixed-dome design, but with one notable difference: The Janata design was not equipped with a manhole on the top of the digester, which was a common feature of Chinese designs. The (Chinese) manhole or the floating gas drum on the top made it possible to use other feedstock than manure, as feedstock that floated on top of the slurry could be taken out. Floating biomass can cause blockage of gas pipes as well as the digester volume is not used efficiently with reduced gas production as a result. Therefore, the main advantage of the Janata type over the KVIC design was the reduced cost for construction. By 1980, approximately 90,000 low-tech rural biogas units had been installed in India of which only a small number were of the Janata type.

The Government of India launched in the years 1981/1982 an extension and development program called National Programme for Biogas Development (NPBD). The Ministry of Agriculture was only to implement the program. NPBD still exists and the goal, as it is presented today, is: . . .*providing clean and cheap source of energy in rural areas, producing enriched organic manure for supplementing the use of chemical fertilizers, improving sanitation and hygiene and removing drudgery of women (MNES 1996).*

In 1984, the NGO Action for Food Production (AFPRO) introduced their new biogas design called *Deenbandhu* biogas plant meaning "friend of the poor" in Hindi. This design was approved for inclusion in the NPBD in July 1986. The Deenbandhu design was claimed to further cut the cost of biogas installations. Actually it was not a really new design, but rather a further development of the Janata type. The cost reduction was due to the use of some standardized pipes and a different construction technique. The design soon became the most popular design within the NPBD.

In 1996, there were a total of seven biogas plant designs approved by the Ministry of Non-conventional

Energy Sources (MNES). Besides the Khadi and Village Industries Commission (KVIC), Janata, and Deenbandhu, there were the Pragrati design, KVIC design with reinforced plastic dome (composite), KVIC design with ferro-cement dome, and the FLEXI-design (rubber based).

Since 2002, national dissemination speed achieved about 1.2 million biogas plants per year, rising from 100,000 units yearly before. Today basically one design, the Deenbandhu, is disseminated throughout the whole country, thus following a "one design fits all" approach.

Nepal Biogas in Nepal can look back on a long, eventful history. The Belgian Reverend Saubolle first introduced it on an experimental basis in 1955. Subsequently, several organizations became involved in promoting the technology. His Majesty's Government of Nepal launched the first official biogas program in 1974. Under this program, the Agricultural Development Bank of Nepal offered construction loans to potential customers. In 1977, the Government established the Biogas and Agricultural Equipment Pvt. Ltd. popularly known as Gobar Gas Company (GGC). This state-owned entity was in charge of the development and promotion of large-scale dissemination of biogas technology in Nepal.

Started in the 1980s as a technological research project with a limited number of test models, it was expanded during the 1990s by the Biogas Support Program into a successful market development program with the active involvement of the private sector and business community. Over the last 20 years, more than 200,000 biogas installations have been built and the sector now comprises more than 70 local companies and employs about 11,000 people.

Pakistan The history of biogas technology in Pakistan started 1974. Around 6,000 mainly small 6 m^3 scale digesters have been installed across the country till the end of 2006 – against the technical potential of about five million digesters based on its suitable climate and availability of cattle dung as feedstock.

The Government of Pakistan started a comprehensive biogas scheme in 1974, and commissioned 4,137 household biogas units by 1987 throughout the country. These were metal floating-drum biogas plants with a capacity varying from 5 to 15 m^3 biogas productions per day. This program was implemented in three phases. During the first phase, 100 demonstration units were installed under grant by the government. During the second phase, the cost of biogas plants was shared between the beneficiaries and the government. In the third phase, the government withdrew financial support for the biogas plants, although technical support continued to be provided free of cost. Unfortunately, after the withdrawal of the government financial support, the project did not progress any further.

The Pakistan Centre for Renewable Energy Technologies (PCRET) started the fourth biogas phase in early 1997 with the installation of 4,000 household plants in several major cities of the country, having a digester volume between 5 and 15 m^3 biogas productions per day. PCRET disseminated small-scale biogas technology and has supported installation of around 1,600 biogas plants in 2006. In addition, PCRET had plans to install 2,500 plants by 2008 for which the Government of Pakistan had approved financial support. Three community size biogas plants have been installed in rural areas of Islamabad, which are meeting domestic fuel needs of 20 houses.

The NGO Initiative for Rural and Sustainable Development (IRSD) has installed around 150 biogas plants with support from the United Nations Development Programme (UNDP) Small Grants Program. Some Regional Support Programs and NGOs have also included biogas among their projects: "Koshis" in Sialkot, Punjab, helped villagers to build over 200 biogas plants; "Green Circle Organization" is building community-based plants with funding from the Pakistan Poverty Alleviation Fund. Most NGOs received technical assistance from PCRET in the design of their plants. With some exceptions most plants are still installed on a pilot basis and have not been promoted commercially to any large scale. During the years 2005/2006, the Alternate Energy Development Board (AEDB) installed 1,200 family-size biogas plants to cover fuel needs of 1,200 households in the rural area of the Punjab province.

Most of the biogas plants installed in recent years were smaller household designs with 3–5 m^3 gas production per day, compared to the larger plants constructed in the 1970s and 1980s. The biogas technology most commonly used in Pakistan is the

floating-drum design. The Chinese fixed-dome design was installed on a pilot basis but was reported not to be successful. Obviously due to poor construction quality, the Chinese dome design pilot biogas plants showed persistent leakage and seepage problems, and therefore, the gas pressure was reported to be low. Twelve fixed-dome "Nepalese design" biogas plants of Model GGC 2047 of 6 m^3 were installed in the "*tehsil*" (sub-division) Pasrur of Sialkot District in partnership with the Punjab Rural Support Program (PRSP) and four plants of the same design were installed in different sizes of 8 m^3 (2 units), 20 m^3, and 35 m^3 in Dera Ismail Khan in partnership with the Foundation for Integrated Development Action (FIDA) by the Rural Support Program-Network (RSPN) in June of 2007. FIDA was reported to have plans to continue supports to install biogas plants in its working areas. In 2006 SNV started to support a new nationwide biogas dissemination program for low-tech household biogas digester systems.

During 2002, a more efficient and cheaper "Thailand model" of a household biogas plant was installed at the Green Circle Organization (GCO) working model site to compare efficiency and cost-effectiveness of two models, the Thai and the formerly applied one. Transfer of the new Thai biogas technology and dissemination of information started in the Village Shirin Muaafe, *tehsil* Depalpur of Okara District. The results are that due to the proper dissemination of information, GCO have facilitated the farmers to install 80 biogas plants in the vicinity of the project area.

A governmental supported project on White Revolution "Dhoodh Darya" started in 2009 with 10 components with main thrust on development of milk pockets and establishment of milk pasteurization plants, infrastructure development of military dairy farms, bulk vending of milk, training and extension of Pakistan Dairy Development Company's (PDDC) breeding program, and promotion of biogas units. It has already developed 48 community farms, trained a large number of farmers, and installed 825 medium-sized biogas units. The work started in the year 2009 for the establishment of community farms, biogas plants, large and small pasteurization plants, and bulk vending units, and training of master trainers will be continued up to the end of 2011.

Philippines Dr. Felix C. Maramba, an agricultural engineer by profession of the then Araneta University Foundation, introduced biogas technology in 1965. The today De La Salle Araneta University (DLSAU) was formerly known as the Gregorio Araneta University Foundation, which was established in 1946 as the Araneta Institute of Agriculture. The university specializes in Veterinary Medicine and Agricultural Sciences. He is the founder of the Maya Farm Biogas Model. In the early 1970s, the Maya Farm, a commercial piggery farm located 40 km east of Manila, has been the pioneer in the development of biogas technology. In order to obtain the necessary experience and to assess the suitability of different types of plants, demonstration models of Indian, Chinese, and European types were set up. The models were later modified and used as pilot plants. Biogas produced at the farm supplies 40% of the total power requirement of the farm and is used for home applications, cooking vats in the canning plant, fuelling of burners for heating and gasoline engines, running a feed mill, operating a 60 kVA electric generator and running farm vehicles. The organizations engaged in extension of biogas technology are the National Housing Authority, the Engineering Battalion of the Military, and the Department of Community Development. The Development Bank of the Philippine granted loans to farmers at low interest rates for the biogas project.

The Philippine NGO Rural Life Centre (PRLC) promoted a culvert-type biogas system in the early 1980s. The PRLC trains people from the government as well as from the private sector in the field of animal production and biogas technology. Many units of the model were copied and installed in selected villages but the continuity ceased because the PRLC project was terminated in the late 1980s.

The Philippine National Biogas Technology Extension Program in Key Livestock Areas was established in 1996 in cooperation with the Department of Energy and the Department of Agriculture where Cavite State University was designated as the National Biogas Centre. Since then, a number of local, regional, and national seminars, trainings, and workshops were conducted to promote the technology. Participants came from various sectors of the society: private individuals, companies, NGOs, agro-industry, and government agencies.

The Philippine Agricultural Engineering Standard PAES 413:2001 about Agricultural Structures–Biogas Plant was initiated by the Agricultural Machinery Testing and Evaluation Centre (AMTEC) under the project entitled "Enhancing the Implementation of Improved Agricultural Engineering Standards" which was funded by the Bureau of Agricultural Research (BAR) of the Department of Agriculture (DA).

Thailand Thailand was introduced to the biogas technology in 1950 by Kasetsart University (KU), which continues to be a cooperating agency even today. In 1960, due to poor hygiene and the need to improve health conditions in rural areas, the Department of Health (DoH) within the Ministry of Health (Sanitation Division) became involved, promoting biogas tanks as a sanitation technology.

The need to conserve energy dominated during the first and second oil crises between 1970 and 1980. It was then that the National Energy Administration (NEA) and the Department of Agricultural Extension (DoAE) started to introduce biogas programs for rural energy on small farms. By 1988, about 5,500 biogas plants were constructed, those being mainly 4 and 6 m^3. In order to overcome the numerous technical and managerial uncertainties, an improved Biogas Programme in Thailand was implemented in September 1988. Responsibilities for carrying out its activities were with the Chiang Mai University (CMU) and with the Department of Agricultural Extension (DoAE) within the Ministry of Agriculture and Cooperatives. The German Development cooperation supported the program from September 1988 until December 1994 (Thai-German Biogas Programme). Several systems of all sizes have been constructed in the northern and western regions of Thailand, partly supported through loans from the Bank of Agriculture and Agricultural Cooperatives (BAAC) in Thailand.

Biogas Advisory Unit (BAU) at Chiang Mai University, with a grant supported by the government under The National Energy Policy Office (NEPO), launched the National Biogas Dissemination Program for the medium and large-scale livestock farms in October 1995. A target of 50,000 m^3 biogas system within 6 years, starting from 3,000 and 7,000 m^3 in the first and the second year, with another 10,000 m^3 annually in the following years, is the goal of the program. The program concept consists of two major parts: (1) the dissemination of small household biogas digesters (8, 12, 16, 30, and 50 m^3 volume) under the responsibility of the Department of Agricultural Extension (DoAE) within the Ministry of Agriculture and Cooperatives and (2) applied research and development at CMU, including the provision of consultancy services for anaerobic wastewater treatment to specialized pig farms.

From 1995 until 2000, 70,000 m^3 volumes of digesters had been built with support through the Energy Conservation Fund under the National Energy Policy Office (NEPO) in Thailand. The Energy Conservation Fund (through the Renewable Energy Programme) aims to provide financial incentives, as well as awareness campaigns, in order to promote the generation of methane gas from agricultural wastes. Only a few provinces with a high potential for biogas utilization (i.e., high concentration of suitable animal farms) will be selected for this program. Since 2001 the implementation was fully transferred to the responsibility of private contractors, as a regular business sphere in the field of environment protection ("commercialization" of the technology).

Vietnam Biogas technology has been introduced and developed in Vietnam since 1960. The history of biogas technology began in the South; the Department of Animal Husbandry conducted research on collecting methane gas from animal manure.

In the northern part of the country, biogas technology was introduced in 1964, when the Ministry of Industry started the first "Methane power station" in Bac Thai province. Between 1965 and 1975, Ha Noi, Ha Nam Ninh, and Hai Hung provinces also built biogas plants. These plants stopped functioning after a short time due to a lack of access to technology and management experience.

After the country's reunification in 1975, it was one of the top priorities of the state research program on new and renewable energy until 1990. Within the framework of this program, there were many research projects focusing on biogas technology. The institutions participating in the program were the Institute of Energy, Technology University of Hanoi, Technology University of Ho Chi Minh city, Technology University of Da Nang, Can Tho University, and provincial

departments of Science, Technology and Environment. In 1976, the Vietnam Institute of Energy began researching "Fermentation for methane gas production." From 1981 to 1990, there was renewed interest in biogas technology with the introduction of the National Research Program on New Energy Sources within the Institute of Electricity Science and Technology and international support from the Soviet Union, OXFAM UK, UNICEF, Sweden, and others. Institutes, research centers, colleges, army units, and individuals collaborated on biogas projects.

By 1990, about 2,000 small biogas units had been build in Vietnam with size ranging from 3 to 10 m^3. Some of the most common types of biogas plants used in Vietnam include floating gas holding units, biogas units with plastic bags; fixed-dome brick biogas plants some with composite cover, spherical form digesters, Energy Institute type NL.6 digesters, and household models KT1, KT2, and KT2B. In general, while all biogas technologies have advantages and disadvantages, biogas is the most suitable technology for livestock waste treatment. The first national workshop on biogas was organized within the frame of the National Program on New Energy Source. This workshop helped build momentum to advance research and development of methane gas and biogas technology in Vietnam. From 1991 to 2001, biogas technology developed rapidly with continued support from the Vietnamese government and international partners.

Since 1992, within the framework of the projects of the Ministry of Agriculture and Rural Development of Vietnam (MARD), polyethylene plastic bag digesters have been developed. Owing to low cost and simplicity of installation, this technology has been rapidly adopted and disseminated by the network of Agricultural and Forestry Extension, Association of Vietnam Gardeners (VACVINA), and some local private actors. It is estimated that up to one million of such simple very low-tech plastic bag digesters may exist today.

By the end of the 1990s, the Centre for Rural Communities Research and Development (CCRD) further developed the original model and has successfully designed and introduced a new advanced biogas model, named "Hybrid Technology Bio-digester with Automatic Scum Control" or VACVINA Bio-digester, in order to help farmers to apply biogas technology, generate biogas for cooking, reduce workload for women, actively treat waste from livestock, protect the environment, and reduce pressure on forests. In 2000, the Toyota Foundation provided support to enhance capacity building of VACVINA's staff and to disseminate the VACVINA biogas model nationwide. More than 300 technicians had been trained on all necessary skills on building VACVINA bio-digesters and more than 750 biogas demonstration models have been built in the 61 provinces of the country. In conjunction with CCRD, from 2006 to 2009, ETC Foundation (Netherlands) and Research Centre for Energy and Environment (RCEE) started a development strategy for Enabling Access to Sustainable Energy, including the VACVINA biogas model in a market orientation approach in Thanh Hoa province. In 2011, there are more than 11,000 VACVINA biogas plants constructed by farmers themselves with technical assistance of trained technicians. MARD in Decision Nr.4414/QĐD-BNN-KHCN of October 18, 2002 recognized this initiative and allowed its application nationwide.

Also in 2002, MARD issued standards for small-scale biogas systems (10TCN 492÷499-2002 and 10TCN 97÷102-2006). In 2003, the "Support Project to the Biogas Program for the Animal Husbandry Sector in Some Provinces of Vietnam" has been initiated. The goal of this project was to develop a commercially viable and market-oriented biogas industry and contribute to avoiding the use of fossil fuels and biomass resource depletion. The Department of Livestock Production, MARD, and the Netherlands Development Organisation (SNV) are the primary implementing agencies for the project. By the end of 2008, the program provided training for 500 provincial and district technicians, 700 biogas mason teams, and organized thousands of promotion workshops and trainings for biogas users. By the end of 2009, the project has supported construction of over 78,480 biogas plants and received recognition for its efforts by winning the Ashden Energy Award. The project aims to develop around 167,000 low-tech biogas projects in 63 provinces throughout Vietnam by end 2012.

Under the World Bank funded and MARD implemented Livestock Competitiveness and Food Safety Project (LIFSAP) there is also a small household biogas component, running from 2010 to 2014. The project supports up to 12 provinces which will meet the eligible criteria established by MARD,

including: (1) the density of livestock farms and livestock populations, (2) livestock market share, (3) the availability of livestock support infrastructure, and (4) a viable policy to support the development of livestock production. The total grant amount per biogas plant is US$ 200 to support both the construction of the biogas plant and for additional bio-security measures. Without taking into account program costs the funding will be enough to support the construction of a maximum of 20,600 biogas plants.

In addition, the Asian Development Bank loan financed "Quality and Safety Enhancement of Agricultural Products and Biogas Development Project" (QSEAP) commenced in 2010 and will end in June 2015 and covers 16 provinces in the country. The project's purpose is to build 40,000 biogas plants with the provision of subsidy to at least 20,000 households, and credit to households and farms raising animals. Up to now, the project team received initial results: training 276 technicians, 359 skill masons, and constructing 6,953 biogas plants of small scale of model KT1 and KT2 in 16 provinces.

Parallel to the agricultural-dominated biogas activities, the National Rural Clean Water Supply and Environmental Sanitation Program is targeting to promote the construction of 1,000,000 household biogas-sanitation plants or at least toilet connection to existing agricultural biogas plants in the period 2000–2020.

Africa

The first aid-driven approach for biogas extension in Africa dates back to the early 1970s, when politicians and decision makers from different African countries visited India and were fascinated by the biogas technology. The Indian Government, and later also the Chinese Government, showcased their specific biogas technologies in different African countries in such a way that a foreign expert team built a few institutional biogas digesters and trained numerous people in design and construction only. As no funds have been made available for long-term commitment and dissemination programs, these approaches led to failures in operation, management, and even construction copies, which are scattered all over the continent, particularly in agricultural institutions. At this time, the main actors in potential biogas dissemination programs were identified in the governmental agricultural or energy research institutions of the respective countries. But a deeper rooted operational and managerial know-how or commitment could not be developed or conserved.

In the late 1970s, triggered by Ernst Friedrich Schumacher's (1911–1977) "Small is Beautiful" (first published in 1973) appropriate, simple technologies entered the arena of development work in the South. Not northern high-tech, but innovative, affordable, simple, and traditional technologies were believed to be the remedy for the development and technology gap between industrialized and developing countries. This resulted in a cross-sectorial scheme of many development cooperation institutions accompanying and supporting the development and dissemination of biogas technology in Latin America, Asia, and Africa. Industrialized countries neither had sufficient experience nor appropriate technologies to build on in developing countries. Rather, this experience was identified in India and China and became an issue for a South-North-South transfer.

In 1980, the German Federal Ministry for Economic Cooperation (BMZ) instituted a "Biogas Extension Programme" (1980–1993) as part of the German development aid. It was prompted by the realization, and by analyzing the results of the first German development supported biogas projects in Cameroon in 1978, and short-term consulting work done between 1977 and 1980 in India and China, that biogas extension requires an integrated approach. After understanding the reasons for the failures in the past, it was realized that compromises in technology quality could not be accepted. Only proven designs with good building material were used. Piping was changed to galvanized steel or HDPE pipes only, instead of garden hoses and gate valves, which both leak after a short time.

Prepared in October 2005 in Beijing as a Chinese-Netherland-German effort, and based on the success in some Asian countries, in May 2007, representatives from 27 African countries met in Nairobi, Kenya, to formally launch the "Biogas for Better Life Initiative." Since then, a number of country biogas program prefeasibility and feasibility studies have been completed by the Netherlands Development Organization (SNV) and the German International Cooperation (GIZ), and programs are already being launched in Rwanda,

Uganda, Burkina Faso, Senegal, South Africa and Ethiopia. The group discussed important aspects of developing and implementing national biogas programs including sanitation, gender integration, technology, costs, program structure and management, financing and subsidy structure, carbon financing, and marketing and communications.

A Foundation "Biogas for Better Life: An African Initiative" has been established on February 28, 2008, in the Netherlands to provide this initiative with a legal basis. This allows the initiative to sign agreements with sponsors to support the initiative financially; to enter into agreements for the implementation of national biogas programs, such as the one for Rwanda; to support research and development and knowledge management in biogas; and support all the components of the Initiative Business Plan 2006 till 2020. Until recently, this was done on an individual and ad-hoc basis with individual sponsors such as Shell Foundation, International Humanist Institute for Cooperation with Developing Countries (HIVOS), German International Cooperation (GIZ), the Netherlands Development Organization (SNV), Dutch Ministry of Foreign Affairs (DGIS), Practical Action, German Bank for Reconstruction and Development (KfW), and many others.

Today, "Biogas for Better Life" is an African initiative that aims to improve the health and living conditions of men, women and children; to reduce the use of firewood and charcoal for cooking; to improve soil fertility and agricultural production; to reduce greenhouse gas emissions; and to create new jobs through the development of a robust biogas-related business sector throughout the African continent.

The initiative will identify "pockets of opportunity," and initially focus on programs in African countries with the strongest market potential. The initiative aims to install two million household-level biogas plants in 10 years. The ultimate objective is to develop a sustainable, commercial biogas sector, which will in turn improve the lives and livelihoods of families in Africa. The initiative will foster partnerships and knowledge exchange, provide leadership and experience to developing and implementing national programs, stimulate further technology and market-based research, and help identify and develop financial resources for the biogas programs. Further extension is planned soon to Kenya, Mali, Zambia, Niger, Ghana, Malawi, Lesotho – where biogas technology is already successfully disseminated since 2003, namely, Swaziland, Sudan, and the West African countries.

Algeria French researchers in North Africa, between the years 1940 and 1951, are reported to have made extensive efforts to develop so-called dry-fermentation methane digesters based on straw and manure. There is ample literature on their work in French journals. G. Ducellier and M. Isman developed the design and prototypes in the then French North Africa already as early as 1937. The technique of Ducellier and Isman, at the Institute of Agriculture in Algeria, was the first ever batch-fermentation system with pre-aerating (pre-composting) of the waste mass (straw-manure-organic waste) for 20 hours in order to raise the temperature to 70–80°C. The wastes were then flooded with water and liquid manure, and the anaerobic process commenced. A floating gasholder covered the tank and straw had been packed to a thickness of 40 cm out around the walls to serve as insulation. In unmixed tanks of several 10 of m^3 of size the biogas production was 70–90 m^3/t wastes capacity, averaging 0.4 m^3 per tank volumes/day for the duration of the fermentation.

Burundi The first national biogas program, started in 1984, was supported by German Development Cooperation (GIZ) and established in cooperation with a Belgium research project and a Chinese training program for biogas constructors, using livestock manure, toilet wastewater, and human excreta as feedstock. A countrywide biogas school sanitation project with World Bank support was carried out from 1985 to 1989 led by the Ministry for Energy and Mining. Several projects were initiated by the GIZ Biogas Dissemination Programme, which started in 1984 in the eastern region of Cankuzo. In 1988, this project was integrated into the "Special Energy Programme" and was stopped due to civil war in 1992.

After first experiences with family-sized biogas plants, the project team started in 1987 to build medium-scale biogas-sanitation systems (100–250 m^3) to treat human excreta and gray water of boarding schools. Private contractors were responsible for the plants. The training of craftsmen, the establishment of a service system, and the setup of material credit funds

were to provide the basis for a self-reliant dissemination concept. By 1992, 206 small-scale biogas plants, and 84 institutional medium-scale biogas-sanitation plants (tunnel and fixed-dome plants) had been constructed. Six out of ten households examined under the Biogas Survey in 1992 used liquid slurry as fertilizer. Learning from Burundi, biogas units were also constructed in Bukavu/Congo.

Ethiopia Biogas technology was introduced to Ethiopia in 1977 through the German NGO Bremen Overseas Research and Development Association (BORDA) with German development cooperation support. In the years 1986 to 1988 in 21 counties (Woredas) west of the Amhara State, Indian design floating-drum plants with a volume of up to 8 m^3 have been financed and built by the Rural Technology Promotion Centre Bahir Dar. In a bilateral project, German development cooperation supported the construction of 120 biogas plants between 1999 and 2002 by informal private firms and the local NGOs.

Since 2008, the Netherlands Development Organisation (SNV) supported a pilot phase of a National Biogas Program Ethiopia (NBPE) aiming to build within 5 years up to 14,000 low-tech fixed-dome biogas plants in four regional states. It is expected to develop a private and competition-based biogas industry. The NBPE promotes only plants of 4, 6, 8, or 10 m^3, thus limiting subsidies to farms with a maximum of 100-kg manure per day, corresponding to approximately 20 local cattle.

Kenya First attempts to use biogas technology to obtain energy from coffee pulp go back to the mid-1950s. In the following 25 years, the private entrepreneur Hutchinson sold more than 100 plants of various types mainly to large-scale farmers. In 1983/1984, Germany supported the training of craftsmen in the construction of biogas plants; as a result, 40 biogas plants were built in the Meru region. Until 1988, extension of dissemination efforts into other regions led to about 250 floating-drum plants in various regions, mainly for energy supply. Following the philosophy that an extensive project apparatus with a solid financial background has time limitations, emphasis was placed from the very beginning on private entrepreneurs for the construction of the plants and the provision of biogas accessories. Only demonstration plants in new project areas were subsidized by the project; in other cases, biogas customer pays the market price for his plant.

From 2006 until June 2011 with funding from the European Union dissemination measures for resource-friendly technologies succeeded in the installation of more than 200 low-tech biogas plants. Since 2003, and jointly coordinated in one program, Germany and the Netherlands are supporting the integrated biogas development in the agricultural sector. A national biogas technology standard is under preparation since 2011.

Lesotho Since 2003, after Food and Agriculture Organization of the United Nations (FAO) and China supported pilot experiences during the 1980s, a digester design that has undergone various adaptations in African countries under the umbrella of the German Development Cooperation (GIZ) has been implemented in Lesotho by a newly launched NGO, Technologies for Economic Development (TED). Since then, it is widely proven that biogas technology can work successfully in the Mountain Kingdom.

TED was created as a successor of the *Lesotho Biogas Technicians Self Help Group*. With the TED design, incorporating household wastewater into the feeding material for anaerobic digestion, a solution for the most pressing problems especially for urban households was identified: lack of water for irrigation, expenses for construction, and maintenance of septic tanks.

In cooperation with TED, more than 300 digesters of varying sizes were built and most of them are still in operation. The TED bio-digester works well on household, institutional and settlement level as well as for an industrial abattoir with its special feedstock. Today, biogas in Lesotho is a technological package where wastewater and other organic matter are treated in a bio-digester producing gas as an energy source and water is further purified as fertilizer or sludge as soil conditioner or fertilizer. The technology follows the concept of DEWATS (Decentralised Wastewater Treatment Systems) as developed by BORDA (Bremen Overseas Research and Development Association), however, with special focus on energy generation that substitutes up to 20% of a household's cooking fuel demand.

The system is found appropriate not only for the capital Maseru and the district towns as many households and institutions have serious problems, and high cost burden with the disposal of their sewage; the TED system does not cater only for water-borne sanitation but also for dry systems. Peri-urban farms start nowadays to be interested in the system, too. TED provides 12 months after-sales service free of charge, a paid life-long after-sales service, and trains owners on how to care for the system. Currently, about 25 units are constructed per year, totally financed by the individual clients.

Morocco The dissemination of biogas technology focused on the Souss-Massa region. Initially three fixed-dome plants were rehabilitated, and three 12 m^3 plants, five 20 m^3 plants, and two 85 m^3 plants were constructed with the main purpose of electricity generation. By 1998, 80 digesters have been installed (10–100 m^3) with a total volume of 2,000 m^3.

In 1995, a biogas plant was constructed at the wastewater treatment plant in Ben Sergao to use sewage sludge for biogas production. Since 2008, German Development Cooperation (GIZ) started to support low-tech biogas installations for wastewater and manure treatment.

Tanzania The history of biogas dissemination in Tanzania dates back to 1975 when the Small Industries Development Organisation (SIDO) built 120 floating-drum biogas installations up to 1984. In 1982, the newly created Centre for Agricultural Mechanization and Rural Technology (CAMARTEC) took over the promotion of biogas in the Arusha area. In 1983, German Development Cooperation (GIZ) introduced a biogas extension service and disseminated biogas plants mainly in this region where favorable agricultural and socioeconomic conditions let expect a high dissemination for biogas plants. The project worked with a standardized plant design, clearly defined administrative procedures, and offered a warranty of 2 years and technical advice to the users in the villages. In 1984/1985, household biogas plants were offered with digester volumes of 8, 12, and 16 m^3, and in 1990, the program included standardized plants of 12, 16, 30, and 50 m^3 for households and institutions as well as a special "toilet biogas plant" for institutions.

Request which could not be covered by the standardized range of plants and services and which required additional research and development work had to be financed completely by the customer. The program introduced the *biogas unit concept* defining the *unit* as (1) an appropriate stable with solid floor, (2) a pressure tested piping system, (3) gas use appliances, and (4) a slurry utilization system adequate to the individual farm. The costs for a biogas unit increased from around TSh 300,000 in 1989 to TSh 400,000 to 7,000,000 in the beginning of the 1990s. Despite this, the number of units constructed until 1992 increased to about 400. Between 1990 and 1993 CAMARTEC conducted four international training courses with national and international participants and trainers, leading to the popularization of the CAMARTEC design in Ethiopia, Kenya, Uganda, and Thailand.

The dissemination strategy and project structures underwent decisive changes around 1990 as a result of transfer of the project to the counterpart organization. German experts also studied large-scale application of industrial biogas units for sisal industry; the first unit in Tanzania was constructed in 2007 by a Chinese-German consortium supported by the United Nation Industrial Development Organization. Since 2008 Tanzania established a nationwide new biogas dissemination program with SNV support.

Tunisia Biogas was introduced in the Sejenane region in 1982 as an 11 m floating-drum plant. In 1986, the first fixed-dome plant (6 m^3) was built. With German Development Cooperation (GIZ) support, in 1989, non-functioning plants in the region were rehabilitated and 10 new plants built. The first technicians received training in Burundi and Germany. A biogas laboratory was installed at the Technical University Tunis in the framework of German Development Cooperation (GIZ). The activities focused on the modification of the technical aspects (mainly gas appliances), training measures, and slurry experiments under local conditions. Between 1990 and 1992, 16 more biogas plants were constructed. The first solar-heated low-tech fixed dome digester was reported to be operated by the Technical University Tunis. Then China took over the activities, supporting Tunisia until 2003 with the training of biogas technicians and supporting some more

biogas plant construction. Since 2011, World Bank is strongly supporting the new biogas development for large dairy farms in Tunisia.

Rwanda In Rwanda, biogas technology is quickly catching up through the efforts of Kigali Institute of Science Technology and Management (KIST), where several former counterparts of the Germany supported Project in Tanzania (with CAMARTEC) are working. KIST has designed and built a 150 m^3 fixed-dome digester in Cyangugu prison that is fed with waste generated by 1,500 prisoners. This digester produces methane gas that caters for 50% of the cooking needs for the 6,000 inmates. KIST has also solved the sewerage and hygiene problem at the school "Lysee de Kigali" by providing a 25 m^3 fixed-dome digester connected to six bio-latrines. The biogas produced is used as cooking fuel for 400 students and for operating Bunsen burners in the school laboratories. KIST was also supported for many years by Chinese experts to introduce biogas digester design–based decentralized wastewater treatment systems (DEWATS). Since 2007, Rwanda established a SNV-supported National Biogas Program with the target of 14,000 plants in 5 years. China is once more engaged in the Rwandan biogas sector since 2009, and has promoted since then at least 100 prefabricated composite biogas plants, which had been delivered from China.

Central and South America

In Central and South America, biogas plays a role within the renewable energy sector, too, although many countries are still missing in the list of advanced renewable energy technologies and dissemination.

Belize The first project in biogas technology started in 1988. It evolved from a Caribbean biogas dissemination program carried out by the Caribbean Development Bank. German and local biogas consultants and biogas technicians have been active in the region constructing three floating-drum plants following the BORDA model within the Caribbean Technology Consultancy Services (CTCS). As neither the market forces could take up biogas technology nor could independent dissemination structures grow, the program continued in 1989 along the lines of experience gained during biogas activities in the Caribbean and Nicaragua – to anchor biogas-specific, national know-how in a local and regional dissemination structure. With this background experience and the financial, personnel, and material support of the Caribbean Biogas Dissemination Program, a German integrated expert under local project contract and a Belizean expert have been employed to build up such a structure in cooperation with the state Central Farm and to demonstrate the high performance and efficiency of biogas technology. In 1991 the CAMARTEC model from Tanzania was introduced. In comparison to the high input of material and work in plants used previously (reinforced steel vault and fundament), a cost reduction of approximately 15–20% was achieved. Since 1993, at least 20 plants have been built (of these, five are constructed at institutions, 13 at household, and two are medium-sized farm biogas plants). The target group for the household biogas plants so far consisted of farmers involved in commercial pig production. Low-tech household biogas system users in Belize mostly own 5–40 pigs.

Nowadays, with support of the European Community and through the partnership with the Ministry of Agriculture and Fisheries (MAF), the Inter-American Institute for Cooperation on Agriculture (IICA) and the Belize Audubon Society (BAS), small- and medium-sized farms are benefitting from biogas installations as a low-cost alternative and renewable energy source.

The first phase of biogas digester implementation was initiated by a "training the trainer" course conducted by the EARTH University in Costa Rica. This training received a follow-up by means of the installation of biogas digesters at Central Farm and Yo Creek Agricultural Stations, San Antonio and San Marcos in the Cayo district, Maskall and Crooked Tree in the Belize district, and San Antonio in the Orange Walk district. The promoted low-tech biogas digester (called "the worm") is a tubular structure made of polyethylene plastic which is placed in a pre-dug pit. The system serves for anaerobic fermentation of organic materials such as manure from pigs, cattle, sheep, and other organic wastes, thus reducing the risk of pollutants and contaminants in the environment. Farmers understand the opportunity to obtain alternative fuel and organic fertilizers, reducing the need for chemical

fertilizers and significantly reducing the cost of production.

The construction of this type of biogas digester is quite simple; it is made of a tubular plastic bag and other basic parts could be found in local hardware and mechanic shops. These basic parts include a few feet of PVC pipes, a few elbows and connections, used bicycle tubes and recycled buckets.

Bolivia In 1986, the GIZ started as project in cooperation with the Universidad Mayor de San Simon (UMSS) in Cochabamba to disseminate biogas technology. Until 1989 these activities were part of the supra-regional GIZ Biogas Dissemination Programme. From January 1990 to the end of 1992, the biogas activities were continued as a component of the Bolivia Special Energy Program. By consolidating biogas technology into the Cochabamba Department and into the general background of national energy and landscape planning by means of the National Biogas Network, the aim was to integrate "biogas technology into the agricultural production process" so that the "destruction of agricultural ecosystems" could be curbed and "energy and organic fertilizer" could be produced in a decentralized manner. A total of 27 plants, nine of them in the Cochabamba area, have been constructed by different organizations already before the German support started.

In 1988, the German Development Cooperation (GIZ) purpose was defined as "the creation of fundaments on which Bolivian institutions will be enabled to disseminate biogas technology extensively through training and construction of demonstration plants." Loans, training, and the improvement of project management were to allow a high-performance dissemination structure. Emphasis was given to the integration of the technology into local, regional, and national socioeconomic structures and on the dissemination of "Integrated Farming Systems." The biogas plants were mainly understood as "fertilizer-producing plants" making a significant contribution to the strengthening of intensive animal husbandry and agricultural production.

After constructing the first four solar-heated biogas plants in the 1980s in the Bolivian highlands at 4,000 m altitude, the project regions of higher altitude were declared unsuitable for low cost, but not for low-tech biogas plant dissemination. Therefore the biogas office concentrated more and more on the migration regions in the tropics with an inferior infrastructure. In these regions about 35 plants were built between 1989 and 1992. A survey carried out by the biogas office has identified potential, particularly in the area of Santa Cruz de la Sierra, in the field of industrial and communal sanitation. After having built a UASB (up-flow anaerobic sludge blanket) digester at the Palmasola prison, knowledge about anaerobic wastewater treatment technology was established in local NGOs, supported by integrated experts from Germany.

As Bolivian NGOs continued with successful biogas extension of 250 PVC-plastic plants from 2002 to 2005 in high altitudes, in a second attempt by German and Netherland development support, a new program was launched in September 2005 with the goal to supply 575,000 people, corresponding to 6% of the Bolivian population, with modern renewable energy. Donors like the World Bank, International Fund for Agricultural Development (IFAD), and the Inter-American Development Bank (IADB) evinced interest to participate in this program. With the approach of process consulting and human presence on the ground, the German Development Cooperation (GIZ) took an important role as adviser of the national biogas program.

Since 2007 about 250 low-tech and low-cost PVC-plastic bag sausage-shaped biogas plants of 8 m^3 have been disseminated in Alti-Plano villages at 4,000 m and in the temperate area of Cochabamba. Packed in earth wall bricks and covered with straw roofs for insulation, they produce enough biogas to provide cooking fuel for 4–5 hours per day. This design receives attention also in the tropical areas and is now promoted as low-tech and low-cost biogas plant.

Columbia In May 1985, the Special Energy Program Columbia located in Barranquilla started. The project concept focused on "investigation of the possibilities of producing and using biogas" in Valle de Cauca. Corporación Autónoma Regional del Cauca (CVC) was the executing organization. A German long-term expert has been integrated into the project from November 1985 to 1992. During the first project phase, the central problem was the pollution of water resources, which should be reduced by the

dissemination of biogas technology. Project activities were characterized by research and development; investigations were carried out on the use of slurry generated in biogas plants. In 1989 the project goal switched to a clear contribution to the improvement of the rural energy situation and the conservation of water resources by the use of biogas plants. This phase was then characterized by rehabilitation of non-functioning biogas plants and the setup of a dissemination structure. The construction of demonstration plants on selected farms aimed at introducing biogas technology in the rural region. Further involvement in the agro-industrial sector was suspended due to the sector's complexity although initial investigations on anaerobic digestion of agro-industrial wastewater had been carried out. Between 1985 and 1992, a total of 25 biogas plants were built, including a floating-drum plant (BORDA type), a tunnel plant, various fixed-dome plants, a balloon plant, and a UASB (up-flow anaerobic sludge blanket) plant.

When the international support came to an end in 1992, standards of biogas plants existed for four fixed-dome plants of 14–48 m^3 and three fixed-dome plants of 67–115 m^3 with a separate gasholder. In line with the heterogeneity of biogas users' agricultural household and farm systems, the integration of biogas technology into agricultural and farm systems required to be highly flexible. The plants were mainly built for medium-sized and large-scale pig and cattle farms with 20 and 2,000 animals. The heterogeneity of the farms was also reflected in the pattern of utilization and the condition of the plants.

Since 1986, with Belgium and Netherland support, industrial size biogas technology was developed as treatment and reuse system for agro-waste in the tropical regions. During the first years (1986–1989), biogas digesters have been classified as farming intensification technologies. These reactors transformed liquid manure into organic fertilizer; the generated biogas was just a sub-product. This intensification was also applied to the flower agro-business where flower wastes were fed into biogas digesters. Since 1989 anaerobic systems for agro-industries and municipal sewage (UASB technology/anaerobic filter/contact bio-digester/covered anaerobic lagoons) have been built. The biggest municipal wastewater anaerobic treatment plant was installed in Bucaramanga for 100,000 people equivalent (PE). Since 2005, due to rise of crude oil prices and the implementation of the Kyoto Protocol, activities have shifted toward biogas capture and use.

The low-tech biogas digester technology exists in the country only on small scale, although with a trend to expansion, particularly in suburban areas. Local craftsmen in partnership with NGO have constructed many of these biogas digesters.

Cuba Supported by India, Cuba started its national biogas program in the 1970s; in a second attempt at 1990, biogas was rediscovered with German and Chinese support. Having created a national biogas expert group in Santa Clara in 1994, the current national biogas expert association was formed under the Ministry of Agriculture. Since 1992 international biogas advisers from Germany, Canada, and China have worked with Cuban counterparts supported by Germany, EU, UN-agencies, international NGOs from Canada and the Netherlands, or as part of the Chinese development cooperation with the Ministry of Sugar, the Ministry of Agriculture, and the Ecumenical Council of Cuban Churches. Industrial-sized biogas plants were installed at distilleries, and for sisal and sugar processing wastewater, and for dairy farms and pig breeding farms of about 20,000 animals (e.g., Soroa Farm). In addition to other donors, supported by German, Canadian, and Spanish NGOs, small-scale low-tech biogas digesters, such as fixed-dome plants, floating gasholder plants, tubular PVC and PE bag biogas plant designs, and prefabricated glass-fiber (composite) biogas plants, were jointly developed and locally adapted.

Today (2010) about 1,000 biogas plants are operating throughout the country, mainly low-tech PVC-plastic tubular "sausage" plants and fixed-dome plants; target groups for these plant types are suburban and rural households with pigs, vegetable production, and decentralized small- and medium-scale dairy farms. Biogas is used only for cooking, due to commonly experienced energy shortages. Local institutions nationwide, with an umbrella of a National Biogas Association, are planning to construct yearly about 400 low-tech biogas plants.

Jamaica A document on the Biodigester Septic Tank (BST) was prepared in 2000 by the Scientific Research

Council of Jamaica (Ministry of Land and Environment, 2002) and presented to the Ministry of Commerce and Technology, the Ministry of Health, and the Ministry of Land and Environment/Ministry of Water and Housing for approval to be used as the system for future on-site sewage treatment for housing developments. In the following years a wide range of requests were received from housing developers to utilize the biogas technology which has been developed with German support for the on-site treatment of domestic sewage for urban, suburban, and rural housing, thus replacing septic tanks and soak-away pits.

Nicaragua After a pilot Biogas Dissemination Program supported by the German Development Cooperation (GIZ) in the early 1980s, Stichting Nederlandse Vrijwilligers – Netherlands Development Organization (SNV) restarted pilot activities to prepare a national biogas program in Nicaragua and Honduras in 2010.

Challenges, Success and Failures

Challenges, success and failures of any technology are always linked to a number of factors and influences of quite a variety of characteristics. In the case of "biogas technology," given that applications occur worldwide under a range of frame conditions that cannot be easily compared, the influencing factors for success and failures are shaped by researchers, housewives, farmers, engineers and technicians, economists and politicians, bankers, energy suppliers, donors, hardware dealers, masons, and plumbers – just to name a few.

Therefore, the following chapter picked one example – the case of a pure market-oriented dissemination approach performed by a non-profit non-governmental organization in Lesotho, southern Africa. The challenges, success, and failures are analyzed against the overall dominating issues of sustainability.

Social and Cultural Sustainability

In order to achieve social and cultural sustainability of the promoted wastewater treatment technology in general and the installed Biogas/DEWATS systems in each specific case, TED, the Lesotho based Non-Governmental Organization "Technologies for Economic Development" applies social marketing principles adapted to sanitation requirements. The strategy is based on three pillars: (1) stimulating demand, (2) private sector involvement in the supply chain, (3) social status. Following the guideline "Social marketing works to help people change their behaviors positively," TED engages also in hygiene education, sanitation awareness raising, and sanitation marketing at all levels in Lesotho and abroad.

The creation of a sustainable sanitation market involves five "P"s: (1) product, (2) price, (3) place, (4) promotion, and (5) people, whose quality of life is directly influenced by the improvement of sanitation and hygiene.

Up to now, TED's Biogas/DEWATS product has several "unique selling points," as the NGO is still the only national organization to offer a real alternative to a conventional septic tank. Price comparison between the conventional on-site wastewater treatment system and Biogas/DEWATS results currently in lower investment costs for the conventional system, but in significantly lower operational costs for Biogas/DEWATS. Given the specific geophysical context of Maseru and its growth rate into peri-urban hilly areas, the connection to centralized sewer lines and wastewater treatment plants is for most of TED's clients just not possible.

The sustainable social and cultural integration of TED's biogas-sanitation system is also enhanced by the strong involvement of the future system owner in the decision on where to place the treatment system for the household's waste water and the technology choice on reuse options. Also, wherever possible, already existing septic tanks and VIP latrines are integrated into the new design of the treatment system. Due to these close and personal relations with its clients, TED's promotion strategy relies on "word of mouth" and clients' testimonies to interested households.

In cases where communities (villages, schools, orphanages) ask for upgraded sanitation systems, TED informs the communities about different options, including urine diversion dry toilets. Urine diversion technologies and Biogas/DEWATS could be successfully combined.

Working closely with local partners at all levels TED spreads the message about the importance of sanitation, hygiene, and water for human well-being to different groups applying appropriate information and

education material. Local authorities, civil society organizations, and media form already part of the still informal sanitation network that TED intends to set up in Lesotho.

Economic and Financial Sustainability

The level of sanitation infrastructure in Lesotho is generally very low; a decentralized approach to sanitation services is a must. Biogas/DEWATS is one alternative to septic tanks in Lesotho. Wastewater naturally produces biogas and purified water that still contains plant nutrients for reuse in the garden. Owners save money because they do not have to call (and pay) a truck to empty the septic tank every year or even in a very much shorter period; they can use the biogas for cooking, and they can use the water for irrigation, thus reducing the fresh water bill. The money saved within a reasonable time (some owners calculate a maximum of 3 years as period of internal return rate) can be used for further investments to develop the local economy.

The costs for a biogas digester and related wastewater posttreatment steps are divided into production costs, running costs, and capital costs:

- Production costs include all expenses necessary for the erection of the plant (e.g., land, excavation work, construction of the Biogas/DEWATS, piping, and gas utilization system). The construction costs comprise wages and material. They depend on size and dimensioning of the biogas unit, amount and prices of material, and the labor.
- Running costs occur in some cases more often and in some cases rarely; they could include feeding and operating of the plant; supervision, maintenance and repair of the plant; storage and disposal of the slurry; gas distribution and utilization, and administration. The running costs of a biogas plant with a professional management are just as important as the construction costs, for example, for operation, maintenance, expenses for painting, service, and repair.
- Capital costs consist of redemption and interest for the capital taken up to finance the construction costs. It has to be mentioned that many customers provide themselves with, e.g., building material to cut their costs; therefore, just a few have to borrow money. In calculating the depreciation, the economic life span of plants can be taken as 15–20 years, provided maintenance and repair are carried out regularly. The money, which is saved by using "waste" as energy source and irrigation water, needs to be calculated for each specific case.

TED's clients have various problems and therefore various reasons why they want to have a Biogas/DEWATS. That is why the "real" investment costs can be higher than the "real" outcome costs. But the problem, for instance a septic tank, which is always overflowing, is solved. Additionally, it is true that one saves a lot of money by having this technology. There is just the question if the client can furnish the start capital to invest in this technology.

Environmental Sustainability

The following analysis refers to international experiences:

- Wastewater and manure are naturally treated by bacteria, which upgrade wastewater and stabilize sewage sludge. The system improves the fertilizer quality of human and animal waste.
- It reduces the greenhouse gas emissions by using the produced biogas.
- Protected areas or the ecosystem are not affected because the construction is realized close to villages. As the system is mostly underground, the landscape is not damaged or negatively influenced.
- The treated water – still containing plant nutrients – should be (and is) reused for irrigation.
- Where biogas is an alternative to fossil-based fuels, it is, on a national level, considered to improve the balance of payments since less oil products have to be imported.
- On the individual level, system owners save valuable fresh water resources by using treated wastewater for irrigation; in addition, they do not need mineral fertilizer because the irrigation water still contains valuable plant nutrients.

Technical Sustainability

Low-tech biogas plants are related to low-volume efficiency; therefore, simple design and low-cost construction materials are required to compensate this disadvantage with larger digestion volumes, multiple

step treatment system, and even posttreatment steps – if sanitization requires. Therefore, creative solutions have to be developed by the designers to integrate these required volumes in the given space, often solved by underground constructions, cylinder designs or round shape design, which allows also construction material economy combined with optimal strength. Local service structure must be established for maintenance, spare parts, and repairing. In order to assure technical sustainability and continuous updating of technical staff, TED Lesotho applies the following approaches:

1. To be integrated into worldwide networks and close cooperation with technology and research partners like Bremen Overseas Research & Development Association (BORDA), University of Science & Technology Beijing–Centre for Sustainable Environmental Sanitation (USTB-CSES), and Water and Sanitation Association of Zambia (WASAZA).
2. To offer – in collaboration and consultation with cooperation partners – service packages to integrate the technology into an environmental sanitation concept. This includes, e.g., school sanitation, community-based sanitation, and sanitation systems for hospitals, hotels and tourism resorts, military camps, and for agricultural enterprises.
3. To include Research & Development into implementation in order to achieve safe upscaling of implementation; R&D includes the following topics (list not exhaustive): (a) sanitation & renewable energies; (b) sustainable environmental sanitation, and (c) agriculture & livestock. Regular monitoring of the system performance and external evaluation of the results by academic cooperation partner support these R&D activities. TED thus offers researcher opportunities to gain experience in reuse-oriented wastewater treatment systems under Lesotho-specific conditions.
4. To train system owners and operators and to offer after-sales services: Well-informed system owners and operators ask only in very critical situations for special maintenance activities to be provided by TED staff. Experience shows that owners, understanding that Biogas/DEWATS functions due to a well-maintained biology of microorganisms, are operating their wastewater treatment system throughout the years without any problem, and without requiring additional maintenance support. During the first 12 months after construction, TED provides training and accompaniment to the owners and operators (in the case of community, school, or enterprise connected systems) in order to familiarize the responsible person with all relevant details to maintain a successful wastewater treatment process for biogas production and irrigation water reuse.

Lessons Learned

TED's experience and "success story" shows that there are acceptable, affordable, and environmentally safe sanitation technologies based on anaerobic digestion, already successfully installed in urban settlements in Lesotho. Given the fact that TED is implementing Biogas/DEWATS without any subsidies but fully paid by the customers, it is clear that a sanitation market is viable. Sanitizing wastewater on the compound, making it fit for irrigation, saving valuable drinking water, and encouraging home gardening especially in an HIV & AIDS suffering country clearly helps to improve the living conditions of the population. Turning organic waste (solid and liquid) into biogas for cooking is an important measure for climate protection, climate change mitigation, and resilience.

Challenges encountered and relevant for the way forward are craftsmanship's quality, expertise in Biogas/DEWATS construction, ownership, and how to cope with the increasing demand. TED's way of dealing with these challenges is and was always developed in a very pragmatic manner due to its characteristics as a nonprofit-making NGO in a country with an endless number of constraints and limitations. The following overview should be read as an outline for "lessons learned" on how to upscale implementation of "biogas for sanitation" purposes:

- Craftsmanship's Quality: TED engages in continuous quality control of its construction staff. In cooperation with international partners, quality parameters have been established, in-house training is carried out, and a quality management system related to Biogas/DEWATS construction is in place.
- Expertise in Biogas/DEWATS construction: Considering the limited labor market for specialized

technical professionals in Lesotho, TED encounters difficulties in identifying and hiring qualified civil engineers. International cooperation partners currently provide engineering expertise in Biogas & DEWATS construction, but contacts with national sector institutions are sustained and enforced to achieve knowledge transfer on a long term.

– Ownership: When a Biogas/DEWAT system has been sponsored by a third party and not – at least in a significant part – been financed by the system owner himself/herself, lack of responsibility and ownership often leads to system performance problems. This could also be observed in cases of community-based systems. TED therefore developed a user training principle that includes not only the technically responsible person but also the person who will benefit most from a well-functioning Biogas/DEWATS – like the cook in a school or orphanage.
– Increasing demand: Increasing demand could only be answered by an increasing number of Biogas/DEWATS constructions; therefore, TED applied for funds from a private donor foundation to train masons, who became part of the TED construction team after an intensive on-the-job training.

Future Directions

Nowadays the highest degree of market maturity of low-tech biogas technology can be found in the area of housing wastewater in decentralized wastewater treatment systems (biogas sanitation or DEWATS), organic sludge treatment, agro-industrial wastewater pretreatment, and treatment of livestock manure. The use of the biogas technology in housing (municipal) wastewater treatment is currently experiencing a rapid increase in Chinese and Indian suburban development. Household biogas plants in developing countries are today usually promoted on a large scale in connection with rural cooking energy supply and environmental issues, and are installed particularly where water pollution through liquid manure from land area unbalanced livestock activities – small, medium, and large – is most severe.

The increasing emission of greenhouse gases, increasing water pollution, declining soil fertility, unsatisfactory waste management, and the promotion of sustainable renewable energy supply must be seen as parts of the driving factors for biogas technology as one of the important hardware components in a chain of measures to counteract the mentioned challenges.

Due to the fact that often trained constructors leave to search non-rural income in cities and processing industries, the development of prefabricated (composite or membrane) low-tech biogas plant elements will dominate the future constructions. Maintenance issues and responsibilities will be settled by rural plumbers as water and gas supply infrastructure accompanies rural housing development processes. Highly efficient end-energy use appliances for biogas, developed and produced from specialized industries, as already could be learned from China, are contributing to farmers' kitchen hygiene as well as social status upgrading of rural households. Centralized biogas plants will dominate the technology development in densely populated areas as waste-to-energy treatment plants. They could deliver cooking gas for surrounding households, provide electricity and heat for living areas, and cold for dairy farms milk cooling chains.

Bibliography

1. Cheng L, Yao-fu L (1991) A study of purifying domestic sewage biogas tank. BORDA Biogas Forum 3(46):7–10, http://www.borda-net.org/modules/wfdownloads/visit.php?cid=5&lid=19
2. Eckenfelder WW, Patozka JB, Pulliam GW (1998) Anaerobic versus aerobic treatment in the USA. In: Proceedings of the 5th international symposium of anaerobic digestion. IWA Publishing, London, pp 105–114. http://www.patoczka.net/Jurek%20Pages/Papers/Anaerobic%20vs%20Aerobic%20Treatment.pdf. Accessed 3 Dec 2011
3. Eggeling G, Mackensen G, Sasse L (1985) Production and utilization of biogas in rural areas of industrialized and developing countries. GTZ, Germany, http://openlibrary.org/b/OL20817984M/Production_and_utilization_of_biogas_in_rural_areas_of_industrialized_and_developing_countries
4. Gasparikova E, Kapusta S, Bodík I, Derco J, Kratochvil K (2005) Evaluation of anaerobic-aerobic wastewater treatment plant operations. Pol J Environ Stud 14(1):29–32, http://direct.bl.uk/research/37/48/RN163712281.html
5. GATE-GTZ (2000) Basic sanitation and human excreta disposal in latrines, Naturgerechte Technologien, Bau- und Wirtschaftsberatung (TBW) GmbH, Frankfurt, Germany, Dec 2000
6. GATE-GTZ (2001a) Anaerobic methods of municipal wastewater treatment, Naturgerechte Technologien, Bau- und Wirtschaftsberatung TBW GmbH, Frankfurt, Mar 2001

7. GATE-GTZ (2001b) Anaerobic treatment of municipal wastewater in UASB-reactors, Naturgerechte Technologien, Bau- und Wirtschaftsberatung TBW GmbH, Frankfurt, Mar 2001
8. GATE-GTZ (2001c) Decentralized wastewater treatment methods for developing countries, Naturgerechte Technologien, Bau- und Wirtschaftsberatung TBW GmbH, Frankfurt, Mar 2001
9. Guo-Qiang C (1992) Overview on bio digester development in China. BORDA Biogas Forum 1(48):7–20, http://www.borda-net.org/modules/wfdownloads/visit.php?cid=5amp;lid=19
10. Helmig S, Schroth S, Pluschke P, Hulshof P, Grohganz D, Kraemer P, Euler H (1998) Anaerobic processes for the treatment of municipal and industrial waste and wastewater – an overview. GTZ-Department Environmental Management, Water, Energy, Transport, Viña del Mar
11. House D (2006) Biogas handbook. Alternative House Information, Aurora, USA. http://www.completebiogas.com/toc.html
12. Kellner C (2002) Biodigester Septic Tank and Biolatrine, LUPO (Land Use Planning and Resource Management, Oromia), supported by GTZ (German Technical Cooperation) and the DED (German Development Service LUPO Project, Ethiopia (not published: GTZ-DED internal Project document)
13. Kossmann W, Pönitz U, Habermehl S, Hoerz T, Krämer P, Klingler B, Kellner C, Wittur T, von Klopotek F, Krieg A, Euler H (1996) Biogas digest volume I–IV, Biogas – Country Reports, GTZ, Germany, Volume I, http://www2.gtz.de/Dokumente/oe44/ecosan/en-biogas-digest-volume-1-1999.pdf, http://www2.gtz.de/Dokumente/oe44/ecosan/en-biogas-digest-volume-2-1999.pdf, http://www2.gtz.de/Dokumente/oe44/ecosan/en-biogas-digest-volume-3-1999.pdf, http://www2.gtz.de/Dokumente/oe44/ecosan/en-biogas-digest-volume-4-1999.pdf. Accessed 3 Dec 2011
14. Liu DHF, Liptak BG (eds) (1999) Wastewater treatment – environmental engineers' handbook. CRC Press LLC, Boca Raton, http://www.scribd.com/doc/8063671/Fm
15. Lohri C (2009) Evaluation of biogas sanitation systems in Nepalese prisons. ICRC & EAWAG. http://www.eawag.ch/organisation/abteilungen/sandec/publikationen/publications_swm/downloads_swm/icrc_biogas_pres.pdf. Accessed 3 Dec 2011
16. Müller C (2007) Anaerobic digestion of biodegradable solid waste in low- and middle-income countries. EAWAG/SANDEC, Dübendorf, http://www.eawag.ch/organisation/abteilungen/sandec/publikationen/publications_swm/downloads_swm/Anaerobic_Digestion_high_resolution.pdf
17. Paulwell P (2006) Sectoral presentation 2006 by the Hon. Phillip Paulwell, M.P. minister of industry, technology, energy and commerce of Jamaica. www.jis.gov.jm/PaulwellSpeech.pdf. Accessed 3 Dec 2011
18. Sasse L (1988) Biogas plants. A publication of the Deutsches Zentrum für Entwicklungstechnologien - GATE in: Deutsche Gesellschaft für Technische Zusammenarbeit (GTZ) GmbH. http://www.borda-net.org/uploads/sasse-borda_carmatec_1991_improved_biogas_plants.pdf. Accessed 3 Dec 2011
19. Sasse L (1998) DEWATS – Decentralized wastewater treatment systems in developing countries. BORDA, Bremen, http://www.indiawaterportal.org/sites/indiawaterportal.org/files/DecentralisedWastewaterTreatmentinDevelopingCountries_Handbook_LudwigSasse_BORDA_1998.pdf
20. Sasse L, Kellner C, Kimaro A (1991) Improved biogas unit for developing countries. A publication of the Deutsches Zentrum für Entwicklungstechnologien - GATE in: Deutsche Gesellschaft für Technische Zusammenarbeit (GTZ) GmbH. http://www.borda-net.org/uploads/sasse-borda_carmatec_1991_improved_biogas_plants.pdf. Accessed 3 Dec 2011
21. SuSanA, Technical drawings collected on the website of SuSanA. http://www.susana.org/lang-en/cap-dev/technical-drawings/biogasplant. Accessed 3 Dec 2011
22. Ulrich A, Reuter S, Gutterer B, Sasse L, Panzerbieter T, Reckerzugl T (2010) Decentralized wastewater treatment systems and sanitation in developing countries (DEWATS): a practical guide, Bremen Overseas Research and Development Association (BORDA), ISBN 9781843801283, WEDC: Loughborough University, http://www.wedc-knowledge.org/wedcopac/opacreq.dll/fullnf?Search_link=AAAA:2660:68760624. Accessed 3 Dec 2011
23. Van Buren A (1979) A Chinese biogas manual. Intermediate Technology Publications, London, http://www.fastonline.org/CD3WD_40/JF/432/24-572.pdf
24. Werner U, Stöhr U, Hees N (1989) Biogas plants in animal husbandry. A publication of the Deutsches Zentrum für Entwicklungstechnologien – GATE, a Division of the Deutsche Gesellschaft für Technische Zusammenarbeit (GTZ) GmbH, http://www.cd3wd.com/cd3wd_40/JF/JF_OTHER/BIG/GTZ-%20Biogas%20Plants%20-%201989.PDF. Accessed 3 Dec 2011
25. Williams P (2004) Dispose of your waste water and save money doing it! Jamaica observer, 2 May 2004. http://www.jamaicaobserver.com/news/59286_Dispose-of-your-waste-water-and-save-money-doing-it-. Accessed 3 Dec 2011
26. Renwick M, Subedi SP, Hutton G (2007) Biogas for better life: an african initiative - a cost-benefit analysis of national and regional integrated biogas and sanitation programs in Sub-Saharan Africa. Winrock International. http://www.susana.org/lang-en/library?showby=default&vbls=8-7&vbl_7=27&vbl_8=39
27. Songful Y, Ibo Q, Yunnan G, Hue Z, Yuan sheng X, Changing X, Gueydan F, Joaquin X, Taming Z (1992) The biogas technology in China. Agricultural Publishing House, Beijing. ISBN 7-109-01777-X
28. Zeeman G, Sanders W (2001) Potential of anaerobic digestion of complex waste (water). Water Sci Technol 44(8):115–122, http://www.ncbi.nlm.nih.gov/pubmed/11730126
29. Zeeman G, Konawa K, Mels A, Meulman B, Kwant F (2006) Full scale demonstration of vacuum collection, transport & treatment of black water; WaterForum online, 1 June 2006. http://www.wur.nl/NR/rdonlyres/F44C9DCC-F10F-4287-8B5F-06102EC52668/64546/Sneekdemonstration.pdf. Accessed 3 Dec 2011

Biogas Substrates from Municipalities and Industries

Ulrike Seyfert[1], Daniela Thrän[2,3]
[1]German Biomass Research Centre, Leipzig, Germany
[2]German Biomass Research Centre (DBFZ), Leipzig, Germany
[3]Helmholtz–Centre for Environmental Research (UFZ), Leipzig, Germany

Article Outline

Glossary
Definition of the Subject
Introduction
Biogas Substrates from Municipalities
Biogas Substrates from Industries
Future Directions
Bibliography

Glossary

Bioenergy Energy from Biomass [1].

Biogas Gas originating from fermentation [2].

Biogas substrate Biomass that can be used for fermentation processes and which mainly are wet energy crops or residues.

Biomass Material from biological origin excluding material embedded in geological formations and transformed to fossil [1].

Biomethane Upgraded biogas generated through the removal of carbon dioxide.

Biomass residues Biomass originating from side-streams from agricultural, forestry, and industrial operations [1].

Black liquor Liquor obtained from wood during the process of pulp production, the energy content is mainly originating from the content of lignin removed from the wood in the pulping process [1].

Chemical oxygen demand (COD) Amount of oxygen needed for the complete oxidation of the compounds included in the water [4].

Contamination Impurities resulting from exposure to or addition of a poisonous or polluting substance to a fuel [1].

Economic biomass potential Fraction of the technical potential that can be used economically in the context of the economic framework [4].

Energy crops Woody or herbaceous crops grown specifically for their fuel value [1].

Fruit biomass Biomass from the parts of a plant which holds seeds [1].

Fuel Energy carrier intended for energy conversion that can be solid, liquid, or gaseous [1].

Herbaceous biomass Biomass from plants that has no woody stem and which dies back at the end of the growing season [1].

Horticultural residues Biomass residues originating from production, harvesting, and processing in horticulture, including greenhouses [1].

Landscape management residues Residues of woody, herbaceous, and fruit biomass originating from landscape, park, and cemetery management [1].

Realizable biomass potential Expected use of biomass for energy purposes that mainly is part of the economic potential, but can as well be greater is, the option of using bioenergy is subsidized [4].

Segregated biomass Landscape management residues.

Sludge Sludge formed in the aeration basin during biological waste water treatment or biological treatment process and separated by sedimentation or flotation [1].

Technical biomass potential Part of the theoretical biomass potential which can be used for energy purposes given technical as well as structural and environmental restrictions, including priority for food and fodder production and material uses of biomass [4].

Theoretical biomass potential Theoretical limit of the available energy supply from biomass in a defined area [4].

Definition of the Subject

The production of biomethane can be done following two pathways as shown in Fig. 1. The established one is the anaerobic digestion of wet biomass and the adjacent upgrade of the resulting gas. The second one is based on the thermochemical treatment of solid (dry) biomass as wood. This article focuses on the anaerobic fermentation using residues from municipalities and industrial processes. This process in general includes the degradation of organic matter to acetic acid and other short-chain hydrocarbons as well as the conversion to CH_4, CO_2, and H_2O in an anaerobic milieu.

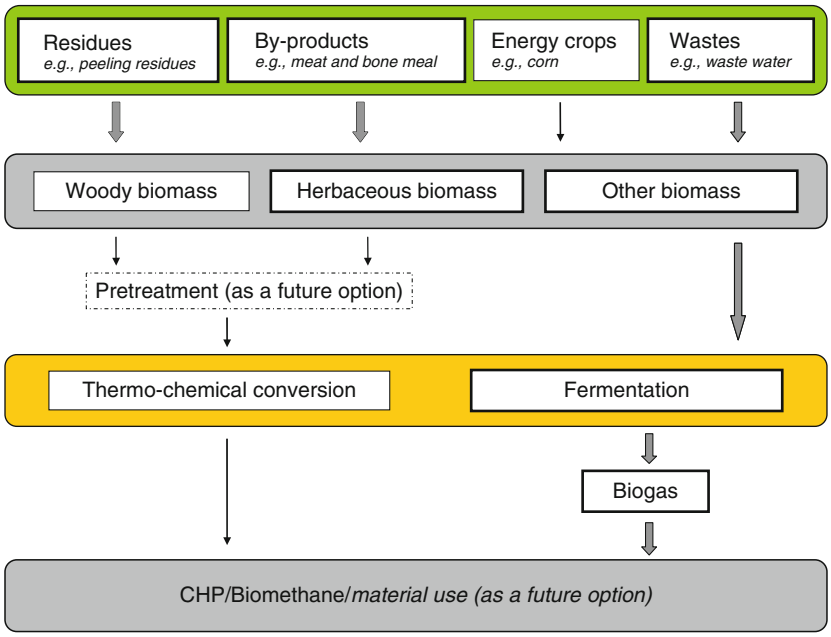

Biogas Substrates from Municipalities and Industries. Figure 1
Different categories of biomass and possible energetic uses

Suitable substrates have to show the following characteristics:

- Fermentative degradability
- Availability in aqueous milieu

The generation of biogas using anaerobic processes is possible for the conversion of wet organic biomass with little lignin content and organically polluted waste waters [4].

The term potential can be categorized as follows:

- The theoretical potential refers to a theoretical limit of the available energy supply from biomass meaning all phytomass and zoomass. Due to technical, economic, environmental, structural, and administrative restrictions, only a small part of the theoretical potential is available for energy uses.
- The technical potential describes the part of the theoretical potential that can be used given current technical possibilities. The calculation of the technical potential considers available utilization technologies and their efficiency as well as structural, environmental (such as nature conservation areas), and other nontechnical restrictions.
- The economic potential refers to the fraction of the technical potential that can be used economically in the context of the given economic framework. The economic potential is affected, for example, by the development of conventional energy systems and prices of energy sources.
- The realizable potential depicts the expected current use of bioenergy. Usually, it is lower than the economic potential, but can also be greater if, for example, the option of using bioenergy is subsidized in the framework of a market introduction programme [4].

The explanations of biomass potentials for the different categories of residues within this paper refer to the technical potential. Furthermore, the focus is put on biomass fractions which are currently available.

Introduction

Residues, by-products, and wastes are organic materials (biomass) which are generated next to the production of other goods and are suitable for an energy use. These biomass fractions could result from agriculture,

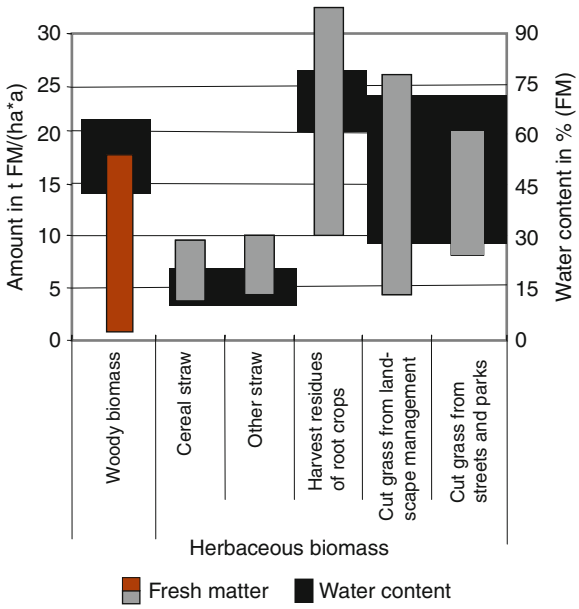

Biogas Substrates from Municipalities and Industries. Figure 2
Bandwidth of area-specific amounts of selected residues, by-products, and wastes in Germany

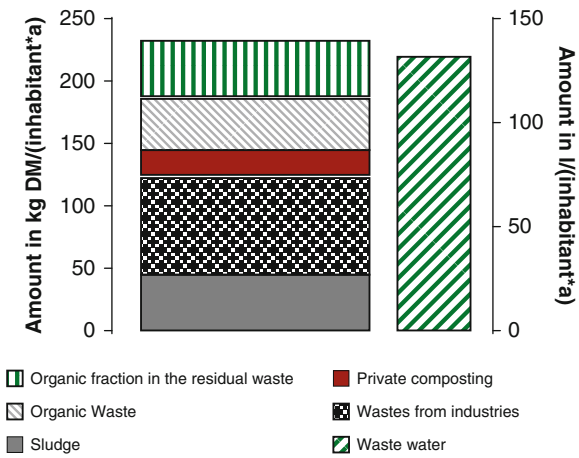

Biogas Substrates from Municipalities and Industries. Figure 3
Average specific amount of selected organic residues, by-products, and wastes from households and industry, exemplarily for Germany (2003); the amount can differ regionally; the amounts of manure and organically polluted waste water are not included

forestry, as well as industry. Furthermore wastes from municipalities with high contents of organic matter are included [2]. This kind of biomass can arise generally during the whole provision chain from supply, production, and use up to the disposal of the organic material.

Residues generally arise depending on area or population, as well as production capacities. Therefore the generated amounts are very heterogeneous based on different factors as climate, type of cultivation, gross national product, and wastes. Especially the amount and composition of industrial wastes vary to a great extent since manufacturing processes have a huge influence regarding the residues and wastes.

Figure 2 shows area-specific amounts of some residues, by-products, and wastes typical for Germany to illustrate the diversity and partially considerable differences of such mass flows. Additionally, Fig. 3 shows examples of generated amounts of significant organic mass flows depending on the population which could be used energetically. According to that especially organic wastes, particularly from industrial processes, provide a substantial population-specific potential.

Regarding this background, the intention of the following explanations is the presentation of different organic by-products, wastes, and residues from municipalities and industrial processes.

Biogas Substrates from Municipalities

Organic biomass resulting from municipalities can be herbaceous biomass from landscape management measures as well as waste and sludge from households. Some of these materials can be used for the production of biogas. Below these residues and wastes are characterized and their worldwide potential determined.

Landscape Management Residues

Segregated herbaceous biomass results from management measures in gardens, parks, cemeteries, and roads. They accumulate in varying amounts. The herbaceous biomass can be used as biogas substrate.

Herbaceous biomass can result from management measures beside roads. But some of the material stays next to the road because the collection is intensive in labor and costs and thus not realized. In Germany, for example, a collection rate of around 50% can be assumed. The collected material can be composted or

used for energy purposes, for example, as combustion fuel or biogas substrate. But considering the problems regarding the material collection, it does not seem very probable that herbaceous biomass from roadsides will be used for energy generation and especially as biogas substrate in a significant amount. Furthermore, in some countries, there are some limitations resulting from contaminant loads in the biomass.

Herbaceous biomass also arises in parks and cemeteries. The varying area-related amount of the biomass results from different management concepts (e.g., mowing once or more times per annum), and therefore clear and general statements about the available biomass are difficult to make. As an average value 20 t/ha of fresh biomass per annum can be assumed. Furthermore, the composition of this material is quite inhomogeneous and alternates in a huge range. In cemeteries, the amount of flowers, branches, etc., has to be added which cannot be quantified generally. The accumulated biomass often shows a high water content and isn't adapted to an energetic use. Also, some of the material stays on the area which helps closing the nutrition cycle. The rest of the biomass is collected and in most cases still composted although a use for energy purposes is possible. The fresh material can be used as biogas substrate or as solid fuel if it is dried in advance. But both applications are still an exception. Only in waste incineration plants a thermal utilization of the material is realized at the moment to certain extend.

Municipal Waste

Regarding the definition of the Intergovernmental Panel on Climate Change (IPPC) municipal waste includes all wastes collected in municipalities and/or other local authorities. Typically, it comprises household waste, commercial/institutional waste, as well as garden and park waste, and therefore organic compounds and used wood [1]. Below the potential and characteristics of the organic part of the municipal waste will be discussed since this can be used in biogas plants.

Because of its low dry mass content of around 40%, organic waste is particularly suitable as biogas substrate and not as a fuel for a thermochemical conversion [1]. Therefore anaerobic fermentation is used especially in Central Europe, but develops as well in other regions. But this is also a promising option for rural areas in Asia [3]. Competing uses of the organic waste as material uses don't arise because the digested residue can be used as fertilizer following an aerobic treatment (composting) [4].

The amount of the municipal waste depends more or less directly on the population. The huge amounts of organic waste accumulate in countries with a huge population as China and the USA. In the USA, the generation rate of municipal solid waste is around 1.14 t/cap/year and therefore the highest rate worldwide (Fig. 4). In China, this generation rate is only around 0.27 t/cap/year. Approximately 40% of the waste materials are of organic origin. Also the state of the industrialization is an important factor. The more advanced the industrialization process the more municipal waste is produced.

At present, the organic waste is not separated from the rest of the municipal waste in most cases. This is a huge obstacle regarding the energetic use as a biogas substrate. A separation is common only in Central Europe, but here as well some impurities as plastics cannot be avoided [2].

With regard to the access to the substrates, a general collection rate of 75% can be reached in the medium term if the efforts are intensified accordingly.

This leads to a technical potential of 1,160 PJ from organic waste in 134 countries which correspond to around 94% of the world population. The highest potential offers Asia with more than 500 PJ (Fig. 5).

Sludge/Organically Polluted Waste Water from Municipalities

Sludge and organically polluted waste water result from domestic and industrial waste water treatment processes [1]. Aerobic and anaerobic processes can be used for the treatment of these waters. The aerobic treatment is much more common and has a long tradition. However, a huge disadvantage is the high amount of energy needed during the process as well as the great deal of sludge resulting of the treatment. Anaerobic processes on the other hand need more strongly defined conditions and are advantageous especially with a huge part of organic compounds.

Waste waters from municipalities result from households, municipal facilities (schools, hospitalities), and small companies (laundries, restaurants).

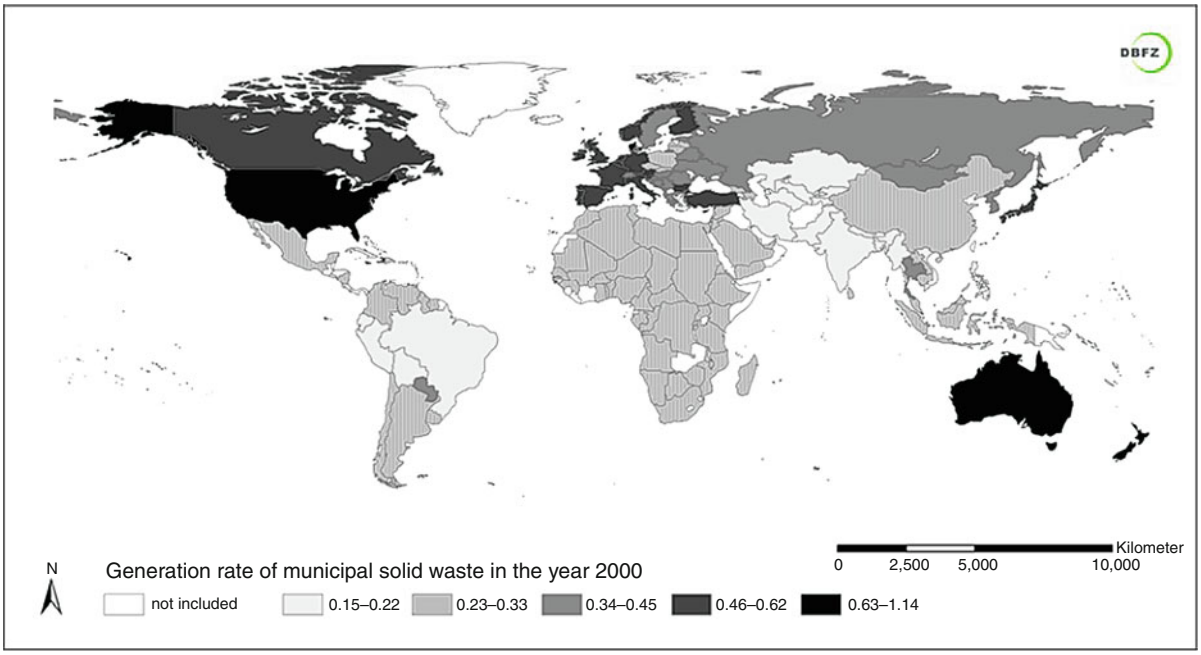

Biogas Substrates from Municipalities and Industries. Figure 4
Specific waste production rate in different regions and countries

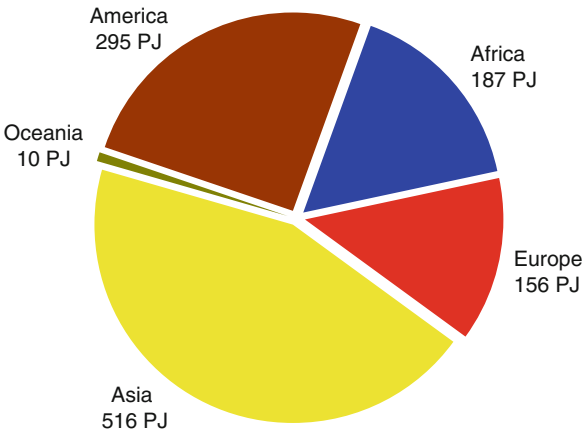

Biogas Substrates from Municipalities and Industries. Figure 5
Technical potential of municipal waste in different regions in the world

Table 1 shows typical amounts of wastes in the waters exemplarily for Germany. Sewage from municipalities is characterized by variable amounts of pollutants. Roughly one half of these pollutants are of mineral origin (e.g., sand, ash) and organic compounds (e.g., excrements, food residues). The waste water is characterized by variations regarding the arising amounts, the composition and the degree of pollution during the seasons and the day. A minimum of the waste water amount is typical in the morning and in winter and a maximum at noon.

Municipal waste water treatment plants separate organic material using a preceding mechanical treatment. Thereafter the waste water is cleaned with aerobic microorganisms which results in a surplus sludge consisting of these microorganisms. Together with the organic sludge from the mechanical treatment, it is fermented in an anaerobic process within a digester. During this process, sewage gas develops which can be used for energy purposes. At first, not the generation of energy but the stabilization of the sludge has been the priority of this specific treatment. But until now, the digesters are also connected to a combined heat and power plant (CHP) to use the energy content of the sewage gas and to contribute to the energy supply of the waste water treatment plant. The quantity of sewage gas averages adds up to around 0.52 m^3/kg organic dry substance in the sludge. The composition of the sewage gas is very similar to biogas. In the past, a huge part of

the sludge was used in agriculture and horticulture. Due to more strict limits for selected trace elements more and more sewage sludge is co-fired together with coal in coal fired power plants [2].

Biogas Substrates from Municipalities and Industries. Table 1 Average pollution of municipal waste water exemplarily for Germany [2]

	Mineral compounds	Organic compounds	Sum
	in g/(inhabitant*day) or in g/m^3 (in parentheses)		
Sediments	20 (100)	30 (150)	50 (250)
Suspended compounds	5 (25)	10 (50)	15 (75)
Dissolved compounds	75 (375)	50 (250)	125 (625)
Sum	100 (500)	90 (450)	190 (950)

Biogas Substrates from Industries

Industrial wastes are those products of a production process that are not reused or recycled and arise next to the production of the primary product. Furthermore, by-products can accumulate during the production. Rather than being waste, these biomass can be reprocessed and used for various material and energy purposes. The residues which amount to significant quantities all over the world can be, for example, residues from the food production industry and from the pulp production or waste paper treatment. Table 2 shows the most important categories of potential biogas substrates generated in the industrial production processes, including characteristic values [2].

The organic residues from industrial processes are often characterized by high water contents and huge loads of nutrients. Therefore a large part of the residues is used for animal feeding and is not (or only in restricted amounts) available for energy purposes. In the course of the industrial processes, a lot of waste water accumulates which could be used for energy generation through anaerobic fermentation [2].

Biogas Substrates from Municipalities and Industries. Table 2 Residues resulting from collected industry segments [2]

Industry segment	Substrate	Typical production specific amounts of waste	Typical organic dry matter content
Cereal manufacturing	Bran, husks, pastry residues	0.2–0.3 kg/kg cereals	85–97%
Manufacturing of fruits, vegetables, and potatoes	Peeling and cleaning residues	0.1–0.35 kg/kg feedstock	20–60%
Sugar production	Chips, molasses	0.7 kg/kg sugar	35–85%
Vegetable oil production	Press cake	1–3 kg/l vegetable oil	80–85%
Beer production	Draff, barm	0.25 kg/l beer	12–25%
Wine production	Marc	0.2–0.3 kg/l wine	30–55%
Alcohol production (distilleries)	Mash	1–3 kg/l ethanol	5–9%
Milk treatment	Whey, mixed with washing water	1–2 kg/l cow milk	5–7%
Meat processing/butchery	Rumen content, meat and bone meal, animal fat	15–60 kg/animal	8–98%
Pulp production	Black liquor	2–3 kg/kg pulp	35–50%
Waste paper treatment	Sludge	0.1–0.3 kg/kg waste paper	40–55%

The specific industrial residues listed in Table 2 will be outlined in the following. Additionally, organic wastes result as well, for example, from the processing of tea and coffee, the production of natural fiber and textiles, the manufacturing of leather, and some further industry sectors [2].

The following numbers given in the text below are valid mostly only for industrialized countries. Furthermore, they can vary significantly in particular cases.

Residues from Cereal Processing

Before cereals can be processed in the baking industry, they have to be ground in mills. There, residues as bran and hulks accumulate which amounts to around 20% of the delivered cereals. Ninety percent of the residues are bran which is used as fodder today. The husks that accumulate additionally during the process can be used as biogas substrate or combustion fuel but could also be composted. Additionally to these residues a certain amount of cereals can be used energetically because of an infection with mycotoxins caused by the weather. These infected cereals cannot be used for the food production any more. These organic residues have to be incinerated.

During the processing of the meal in the baking industry, pastry residues accumulate amounting to 10% of the produced pastries. These residues can be used in biogas plants. All residues from the cereal production show a huge amount of dry matter. Waste waters arise to a small degree regarding to washing and peeling processes [5]. The highest amounts of residues from cereal production can be expected in Asia where most cereals are produced (Table 3).

Biogas Substrates from Municipalities and Industries.
Table 3 Total cereal production in different regions worldwide [6]

	Total cereal production (t)
Asia	1,188,100,000
Africa	151,370,000
Oceania	34,560,000
Europe	504,365,000
America	646,710,000

Residues from the Manufacturing of Fruits, Vegetables, and Potatoes

This group of residues contains quite a lot of producers and products (e.g., fruit juice, vinegar, dry fruits). The fruits, vegetables, and potatoes are mostly of agricultural origin and are processed in bigger companies of the food industry. Different organic residues and wastes as peeling residues, washing waters of fruits, and pressed out fruits can accumulate during the treatment. Further possible residues are filtration residues, draff, and marc from the distillation of fermented fruits, potato peels, concentrates, returned goods, and more. Depending on the production process, different amounts of residues (10–30% of the fruits, vegetables, and potatoes) can arise. These materials can be fermented, composted, burned, or used in other ways as the production of alcohol, soups, pectin, aroma, and cosmetics. Furthermore, organic polluted waste waters can accumulate amounting to 1–3 m^3/t of the product which could be used in the farm animal keeping [2].

Residues from fruit originate from the production from fruit juices and derived products. Due to an increasing popularity of these products, the amounts of the residues rise as well. The most important fruits are citrus fruits, apples, and grapes. Around 27 mn t of the citrus production are processed to juice, essential oils, and other products which leaves around 50% of the fresh fruit weight as a by-product. The world apple production comprises approximately 54.2 mn t of apples whereof China alone produces 25 mn t. Apples which are not suitable for consumption generate large amounts of residues which can be processed. In total, around 14 mn t of apples are processed for the production of juice, pulp, and jelly (Table 4). Apple pomace results from the fruit pressing and represents up to 30% of the fresh fruit. Grapes can be processed to wine, juice, jams, and raisins. In total, 58 mn t are produced annually especially in Italy (16%), France (12%), the USA (11%), and Spain (10%). Eighty percent of these fruits are used for wine making, and as a by-product from the production, grape pomace results in an estimated amount of 13% of the original fruit.

Biogas Substrates from Municipalities and Industries.
Table 4 Amounts of processed citrus, apples, and grapes worldwide per annum and resulting by-products, respectively, residues

	Processed amount (mn t/a)	By-products/ residues (%)	By-products/ residues (mn t/a)
Citrus	27	50	13.5
Apples	14	30	4.2
Grapes	46.4 wine	13	6

Biogas Substrates from Municipalities and Industries.
Table 5 Residues from the production of 100 l of beer

	Residue per 100 l of produced beer
Spent grains	2,000 g
Spent hop	100–300 g
Surplus yeast	?

Residues from Sugar Production

Sugar can be produced from sugar-beet or from sugarcane. The production of sugar based on sugar-beet generates crystal sugar amounting to around 17% of the original weight of the beet. The residues are wastes from sugar-beet (around 1.5 kg/kg of sugar), pulp, and molasses (0.24 kg/kg sugar). Currently, these mass streams are used for the production of syrup and yeast and as fodder. Additionally, huge amounts of organically polluted waste waters result, for example, from the washing of the sugar-beet and the chemical extraction of crude sugar. These waters however are recycled and used in the process water cycle.

Residues from Vegetable Oil Production

Additionally huge amounts of residues, wastes, and by-products result from the production of vegetable oils. The production of 1 l rapeseed oil, for example, leads to 1.4 kg rapeseed cake or rapeseed meal. These by-products are often used as fodder for animal breeding. If the rising demand for oil as fuel leads to higher amounts of residues, the additional rapeseed cakes and rapeseed meals could be used for energy purposes. Especially the use as combustion fuel seems promising. Furthermore, the glycerine from the process of transesterification could be an interesting residue.

Residues from Beer Production

The manufacture of beer involves the generation of some typical by-products and residues which are spent grains, hops, and surplus yeast. These result from the processing of the raw materials and are available in huge amounts because the use is still limited. Therefore the residues represent large potentials for various uses which would also be a solution to environmental problems which arise with the disposal and land filling of the material.

The by-products from the beer production can accumulate as a residue from the malting at the end of the process and comprise the husks of the malt which are rich of cellulose. Furthermore, it consists of nitrogen and vegetable fats and is therefore used as fodder, for example, in the dairy farming. Other possible uses are in biotechnological processes as fermentation, as substrate for the cultivation of microorganisms, or as raw material for the extraction of proteins, sugars, and acids [7].

Additionally, 2.5–6 l waste water arises from the production of 1 l beer which can be treated in biogas plants together with the other residues [2]. Furthermore, 200 t of spent grains (70–80% water content) are generated with the production of 10 mn l of beer. They are basically composed by barley grain husks. The material is rich in cellulose, hemicellulose, and lignin and has high protein content. The hop is used for the brewing and is rich in components which supply the bitter and aroma components to the beer. However, 85% of the raw material ends up as residues [7]. For the production of 100 l of beer, 100–300 g of hop is needed, and therefore 85–255 g are left as residue (Table 5). The third residue of the brewing process is the surplus yeast. However, it is not easy to state how much of the yeast is left for other uses because it can be used for the next brewing process.

In 2008, the global beer consumption reached 146.2 billion litres which would cause around 365.5–877.2 billion liters of waste waters [6].

Residues from Wine Production

The production of wine is a very important industry in many countries all over the world and generates huge amounts of organic residues such as sugars and cellulose. One of the residues is distilled grape marc which is a complex lignocellulosic material [7]. It is produced after pressing the grapes in white wine processing or after the fermentation and maceration in the red wine production. The production of 100 l of wine generates 25 kg of marc and 200–300 l of waste waters as residues. These are used especially in distilleries or in agriculture as fertilizer or animal feed. As an alternative the fermentation in biogas plants is possible as well [2].

In 2008, the wine production reached around 27,270 million liters [6]. Therefore the amount of residues generated worldwide was about 6,818 million kilogram of marc and 54,540–82,810 million liters of waste waters.

Residues in Distilleries

The fermentative conversion of sugar (e.g., from fruits) and starch (e.g., from cereals) to ethyl alcohol is made in distilleries. This processes of fermentation and distillation generates residues (draff, stillage) which can be used energetically by an anaerobic fermentation. The production of 1 l ethanol from cereals produces around 10–14 l of wet stillage (2–8% of dry substance) which can be concentrated to 0.75 kg of dried distillers grains with soluble (DDGS). The draff can be used as fertilizer on agricultural areas or as animal feed. Thus, distilleries are predominantly in peripheral areas and a use could only be reasonable if the generated energy can be used locally [2].

Residues from Milk Production

Whey is the characteristic by-product of the processing of milk to cheese, curd, and cream cheese. It can be distinguished between sweet whey and acid whey which is generated using lactic acid producing bacteria. Furthermore, waste water accumulates amounting to about 2 m^3 per liter milk. With a total milk production of 690 mn l in 2008 [6], this would generate about 1,380 mn l of waste water. Generally these waters are mixed with other solid and fluid residues and reprocessed to whey powder and drinks or used as fodder for pigs, etc. In some cases, the residues can be fermented in biogas plants [2].

Residues from Meat Processing

Every year, around 50,000 head of cattle, 500,000 pigs, and 28,000 sheep, goats, and horses are slaughtered per one million inhabitants, for example, in Germany. The residues from the slaughtering amount to 30 kg per inhabitant in a year. These can be used for material as well as for energy purposes. Especially since the emergence of BSE meat and bone meals are applied in the chemical industry and for the production of fertilizer. Furthermore, few plants for the generation of methyl ester from animal fats to be used as fuel exist, for example, in Germany. Prospectively, the recycling of phosphate from meat and bone meal could gain in importance [2]. Nevertheless, there is indeed a potential of such residues to be used as a feed for biogas plants.

Residues from Pulp and Paper Production

In the pulp and paper industry, two processes have to be distinguished: the generation of cellulosic pulp and the production of paper and cardboard. The production of cellulose leads to the generation of black liquor. It contains the lignin part of the wood which cannot be utilized for the paper production. Black liquor is already used in most paper plants as a fuel to meet the internal energy demand. Another residue of the pulp and paper production is industrial sludge contaminated with fiber which could account up to 30% of the raw material. These sludge can be dried and combusted as a solid fuel. They can as well be used for material purposes such as amelioration in the agriculture and for the production of bricks. Furthermore, huge amounts of waste waters accumulate during the paper production process – around 10 m^3/t paper produced [2]. This waste water can be treated under anaerobic conditions.

Sludge/Organically Polluted Waste Water from Industries

Organically polluted waste waters from industries are characterized by huge variations in the available

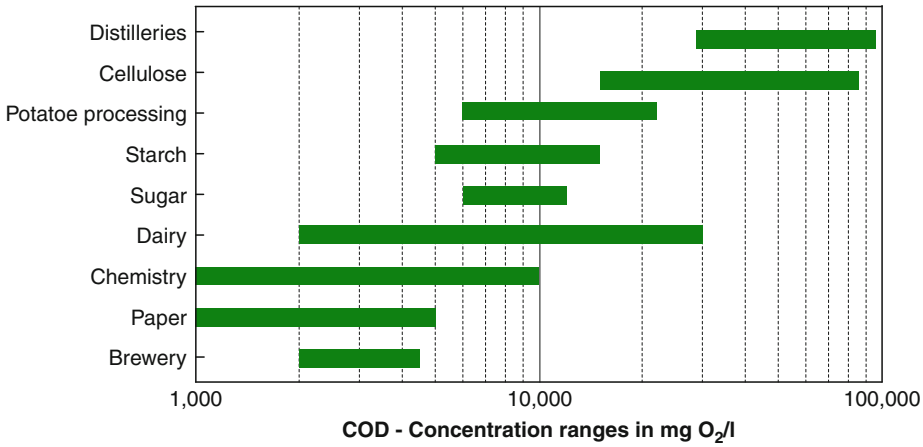

Biogas Substrates from Municipalities and Industries. Figure 6
COD – Concentration ranges of waste water from different industrial sectors [4]

amount throughout the course of a day or a year. Variations can as well be observed regarding the degree of contamination which varies especially in sugar refineries, vegetable processing, and distilleries and depending on technical aspects. Internal water circulation, for example, leads to considerable reductions of waste water amounts. On average, 2–3 m^3 of industrial waste water accumulate per inhabitant and year in Germany. Typical contaminations are around 1,000 and 100,000 g COD/l (COD describes the amount of oxygen needed to oxidize all ingredients completely; Fig. 6). Industrial sludge account to up to 10 kg_{DM} per inhabitant and year, for example, in Germany, and is used for energy purposes almost completely [2].

Future Directions

Residues from industrial processes and municipalities are diverse and offer various possibilities for material and energy. Furthermore, residues offer huge potentials for the production of biogas, although it is difficult to quantify the potentials of all residues and by-products worldwide since statistical data are not available in many cases. Additionally, a part of the biomass is already in use. They can be used for material purposes or for feed and fodder such as rapeseed cakes. Other materials are already in use for energy purposes such as black liquor which covers parts of the internal energy demand of paper production plants.

The future trends regarding the amount and availability of municipal and industrial residues and by-products for the biogas production depend on the development of the population, the progress of the industrialization process, and development of the specific industries. Furthermore, competitive uses have to be considered.

Bibliography

1. Eggleston HS, Buendia L, Miwa K, Ngara T, Tanabe K (eds) (2006) Intergovernmental Penal on Climate Change (IPCC). 2006 IPCC guidelines for national greenhouse gas inventories, vol 5 Waste. Prepared by the National Greenhouse Gas Inventories Programme, IGES, Japan
2. European Committee for Standardization (CEN) (2010) Solid biofuels – Terminology, definitions and descriptions. Final draft of the norm 14588, CEN, Brussels
3. Fachagentur für Nachwachsende Rohstoffe. http://www.nachwachsenderohstoffe.de/ (23.08.2010)
4. http://faostat.fao.org/ (08.04.2010)
5. International Energy Agency (IEA) (HRSG): world energy outlook 2006. Paris, Frankreich. http://www.iea.org/textbase/nppdf/free/2006/weo2006.pdf
6. Kaltschmtt M, Hartmann H, Hofbauer H (2009) Energie aus Biomasse – Grundlagen, Techniken und Verfahren, 2nd edn. Springer, Berlin
7. Öko-Institut & Partner (2004) Stoffstromanalyse zur nachhaltigen energetischen Nutzung von Biomasse,

Endbericht F&E-Vorhaben i. A. des BMU. Freiburg/Darmstadt/Berlin
8. Scholwin F, Witt J (2005) Potenziale der Biogaserzeugung aus industriellen Rückständen, Nebenprodukten und Abfällen. Institut für Energetik und Umwelt, unveröffentlichter Bericht, Leipzig
9. Singh nee'Nigam et al (2009) Biotechnology for agro-industrial residues utilisation. Utilisation of Agro-Residues

Biomarkers and Metabolomics, Evidence of Stress

Young Soo Keum[1], Jeong-Han Kim[2], Qing X. Li[3]
[1]Division of Applied Life Sciences, Konkuk University, College of Life and Environmental Science, Seoul, South Korea
[2]Department of Agricultural Biotechnology, Seoul National University, Seoul, South Korea
[3]Department of Molecular Biosciences and Bioengineering, University of Hawaii, Honolulu, HI, USA

Article Outline

Glossary
Definition of the Subject
Introduction
Applications of Metabolomics
Future Directions
Acknowledgments
Bibliography

Glossary

Stress Any change(s) in physiology and biochemical process that causes deviation from a normal state of an organism and requires an adjustment to return to the normal state.

Stressor An agent, condition, or other stimulus that causes stress.

Biomarker A biological chemical or macromolecule used as an indicator of a biological state that is often reflected by changes in its concentration.

Toxicity Degree of poisoning or damage caused by a substance to an exposed organism.

Metabolome The whole set of metabolites, forming an extensive network of metabolic reactions, in a biological system (e.g., an organism, organ, or cell).

Metabolomics Comprehensive study of a metabolome or a set of metabolites in which one metabolite from a specific pathway affects one or more biochemical reactions, or a comprehensive and quantitative analysis of all metabolites.

Omics Comprehensive study of a biological system. Omics fields include genomics, proteomics, metabolomics, and transcriptomics.

Definition of the Subject

To evaluate the biological effect(s) of a stress, it is necessary to identify and characterize the stressor (s). In general, stressors can be classified as toxicants, pathogens, and physical stimulants. Although the reactions and the degree of response may vary, stressors frequently induce extensive metabolic changes in a living organism. Comparative research on a large set of metabolites at different stress states can provide detailed insights into specific biochemical reactions and metabolic networks. Such information can be used for diagnosis of a disease or toxic effect, development of therapeutic remedies to relieve the stress or its detrimental effect, etc.

The rapid accumulation of genomic and proteomic information of various organisms and rapid advancement in analytical capability make new disciplines of omics possible. In comparison with conventional approaches that usually focus on specific biochemical pathways, a major interest of omics is to gain system-wide information about the target organism and biochemical events. The main goal of metabolomics is qualitative and quantitative differentiation of an entire set of metabolites and the biological networks in the target organism [1, 2]. Metabolite profiles, fingerprints, and related concepts have been applied in various biochemical and toxicological studies since the 1980s [3, 4]. Metabolomics is an emerging discipline and has been shown to be a powerful tool for biomarker discovery and stress research. A related term, metabonomics has also been widely used in the

literature. In this chapter, both metabolomics and metabonomics are regarded as having the same meaning. This chapter discusses the metabolomics of animals, plants, and microorganisms relevant to environmental toxicology.

Introduction

Biomarkers provide direct evidence of stress or potential stress. There are different types of biomarkers. Some biomarkers indicate different stages of disease: early threat (i.e., risk indicator or predictive biomarkers), existence (i.e., diagnostic biomarker), and disease development (i.e., prognostic biomarker). Some biomarkers give an indication of chemical toxicity, while others indicate physical stresses. It is widely known that cholesterol values are a biomarker indicating coronary and vascular disease risks. Molecular biomarkers need to be naturally stable for chemical analysis, to be reliably quantified, and to be effective for diagnosis, prognosis, and risk assessment. In environmental toxicology, biomarkers play a major role in environmental risk assessment, exposure, and management. Biomarker-based biological monitoring aids in early risk diagnosis, risk prevention and minimization, action target identification, toxic response, bioremediation, etc. The analytical method for a biomarker must be accurate, simple, reproducible, and cost-effective. Many genomics, metabolomics, and proteomics techniques are available for biomarker discovery. It is noteworthy that discovery of a biomarker typically requires a large amount of research effort. Biomarkers can be difficult to validate and may require different levels of validation.

Metabolomics has been largely employed to analyze all metabolites (i.e., global analysis) in a biological sample. Metabolomics experiments typically involve sampling, sample preparation, extraction, fractionation, detection, measurement, and data mining and management. Although metabolomics concerns the entirety of metabolites as analytical targets, it is practically impossible to cover all with a single analytical method. A large portion of metabolites are water-soluble, whereas steroids and respiratory quinones, for example, are practically water insoluble. It is well recognized that metabolomic responses are more rapid than other omics targets upon a stimulus. Hence, cautious and rapid handling of samples is very important to preserve the integrity of the metabolome. Common sample preparation protocols include proper labeling and storage of biological specimens, homogenization, extraction, cleanup, and concentration (Fig. 1). Additional procedures are often used to enhance the data quality and instrument performance, including enzymatic treatment to remove proteins and excess metabolites. In a metabolomics study targeting a specific set of metabolites, specialized enrichment techniques are often utilized [5, 6].

Instrumental analyses are an integral step in metabolomics research. Metabolomics methodologies can be divided into chemical separations and measurements. Instrumentation commonly used in metabolomics includes nuclear magnetic resonance

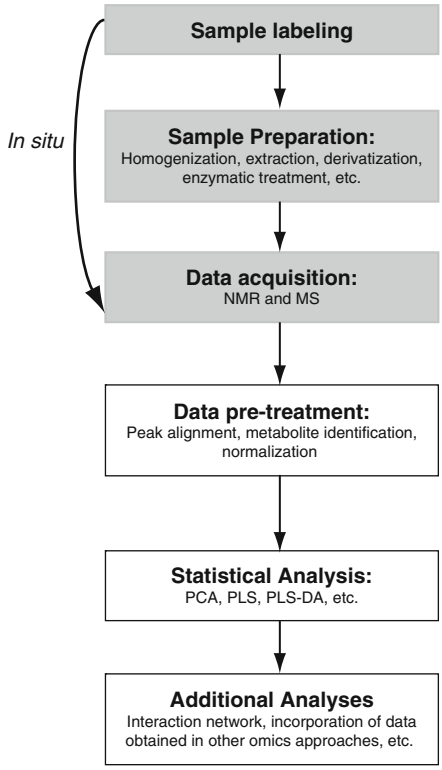

Biomarkers and Metabolomics, Evidence of Stress. Figure 1
A common metabolomics workflow. PCA, principal component analysis; PLS, partial least squares; DA, discriminant analysis

spectroscopy (NMR) and mass spectrometry (MS). MS is widely used in metabolomics because it can provide rapid and sensitive qualitative and quantitative analyses of metabolites [7, 8]. High selectivity and sensitivity can be achieved by using tandem mass spectrometer systems where a mass spectrometer is hyphenated with another mass spectrometer and/or coupled with a separation technique. Some mass spectrometers such as Fourier Transform-ion cyclotron resonance MS (FT-ICR MS) have enough resolution power, eliminating chromatographic or electrophoretic separation requirements [9–11]. NMR has been applied in metabolomics since the 1980s [4]. Its strengths include rapid data acquisition with minimal sample preparation time, high reproducibility, and rich structural information. These factors make NMR among the most popular tools for high throughput applications. Disadvantages in comparison with gas chromatography-MS (GC-MS) include low sensitivity and less comprehensive spectral libraries. Data from instrumental analysis require comprehensive interpretation, often accompanied by pretreatment of data (e.g., spectral deconvolution, peak alignment, and structural identification of specific metabolites).

A single metabolomics experiment can generate huge amounts of data leading to a comprehensive understanding of metabolic networks, whereas conventional approaches deal with a limited number of biochemical reactions. Complementary information from proteomics and genomics is often incorporated into a metabolomics data set to further interpretation of the biological events. Sophisticated statistical procedures are often necessary to uncover data of biological significance. Several data reduction methods, including principal component analysis (PCA), discriminant analysis (DA), partial least squares (PLS), and other newly introduced methods (e.g., Support Vector Machine and Neural Network) are used [12–15].

Integrated omics approaches are increasingly being used to verify and visualize metabolic differentiations. For example, Okuda et al. [16] reported the potential utility of the KEGG (Kyoto Encyclopedia of Genes and Genomes) atlas for global analysis of metabolic pathways and metabolomics. Many excellent reviews of metabolomics are available [17–22].

Applications of Metabolomics

Metabolomics in Animal Sciences

Metabolomics is considered to be the most promising omics tool for system-wide evaluation of stressors because primary metabolites are well conserved throughout the phylogenetic kingdoms [23, 24]. Chemical, physical, and biological stimuli have been studied. Much of the current research deals with mammals challenged by diseases, toxicants, and pathogens. Applications in this field are centered on the discovery of biomarkers for specific stressors, as exemplified in Table 1. Furthermore, metabolomics can provide insights into mechanisms of stress response, which can assist in the development of proper treatment methods [25, 26].

Mammalian metabolomes are more complex than those of plants and microorganisms. The concentrations of different metabolites in the same sample vary dramatically. In addition, both the concentrations and chemical identities of metabolites vary largely among different organs, sexes, ages, physiological stages, and numerous other factors. One of the most noticeable recent advancements was the construction of a metabolite database [27]. The human metabolome database (HMDB) is a comprehensive data resource of metabolites found in the human body (http://www.hmdb.ca). Many toxicological studies via metabolomics are approached with metabolic fingerprinting and pattern recognition where knowing the exact identities of metabolites is not a prerequisite. Such applications of metabolomics have been used in clinical diagnostics. Biofluids such as blood and urine are commonly used samples. Figure 2 shows several common marker metabolites regardless of the stressor types (i.e., non-stress-specific biomarkers) [28–30]. In environmental toxicology, this type of biomarker can be used for the first tier of monitoring. The use of organic acids and creatine as biomarkers is often criticized due to their lack of stress specificity. It is noteworthy that the data from metabolomics should be interpreted on the basis of pattern changes rather than simple concentration changes of a few metabolites. The simple fingerprints along with structural identification can give comprehensive and detailed information of cellular status. Metabolomic profiles and structural analyses, for

Biomarkers and Metabolomics, Evidence of Stress. Table 1 Examples of metabolomics studies of stressed animals

Type of study	Animal	Stressor	Description	Reference
Biomarker discovery	Rat	Drug (acetaminophen)	Depletion of antioxidants as marker	[37]
	Rat	Heavy metal (As, Hg)	Accumulation of creatine, lactate, and decrease of some amino acids	[46, 47]
	Human	Food (chocolate)	Decrease of stressor hormone (cortisol) by chocolate consumption	[55]
	Rat	Physical stress (shaking)	Accumulation of glucose, lipid and repression of acetate, amino acid	[56]
	Various	Environmental stress	Review of stress-metabolomics of non-model organism in ecosystem	[17]
Mode of action	Rat	Cancer and drug	Mode of action of anticancer drug	[33]
	Rat	Triazole fungicide	Unexpected toxicity of triazole fungicides	[43, 44]
Database	Human	Nontargeted	Identification of metabolites in the metabolome of healthy adults	[27]
	Human	Miscellaneous	Construction of metabolite database (http://www.hmdb.ca)	[115]

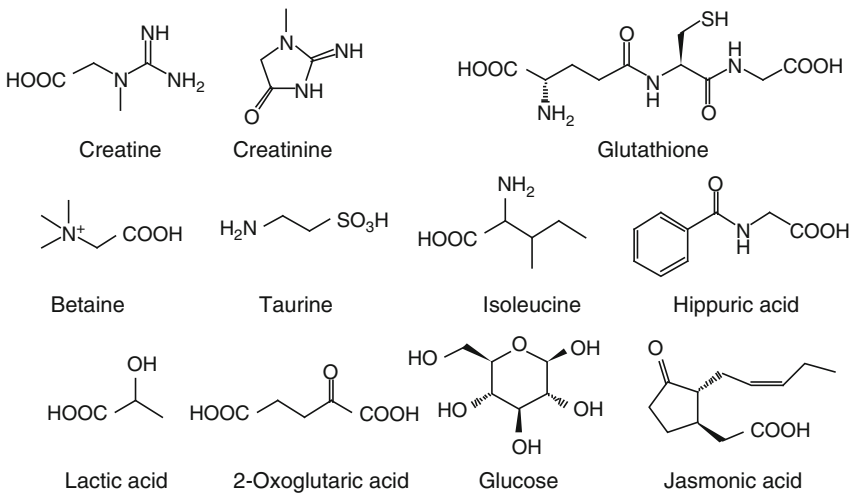

Biomarkers and Metabolomics, Evidence of Stress. Figure 2
Structures of selected biomarkers in stressed animals, plants, or microorganisms

example, delineated a potential role for sarcosine in prostate cancer progression [31].

In drug discovery, many steps of evaluation are required, including screening for intended bioactivity (potency), adverse effects (toxicity), dose–response (efficacy), and metabolism (detoxification). Metabolic modulation of xenobiotics (drugs and pesticides) can trigger complicated problems because the extensive structural modification of xenobiotics through metabolism can alter the

potency or toxicological profiles of the parent compounds. Holistic approaches, like metabolomics, may be a useful solution for drug discovery [32]. Metabolomic investigation of mode of action has been used to identify the exact targets and metabolic pathways of preclinical drugs. Watson et al. [33] identified the mode of action of an anticancer drug through global metabolic profiling. The mode of action of complex molecules (e.g., peptides and proteins) has been assessed with metabolomics. Angiotensin II (a well-known hormone) induces mitochondrial dysfunction. Mervaala et al. [34] used metabolomic methods to study the influence of angiotensin II on the metabolic profile and determine the mode of action of angiotensin II. They found that distinct patterns of cardiac substrate use in angiotensin II-induced cardiac hypertrophy are associated with mitochondrial dysfunction. In addition to natural primary metabolites, drug metabolites are profiled to obtain comprehensive data. The recent studies with naphthoquinone derivatives revealed that the toxicity of these chemicals is due to redox impairment, which causes strong oxidative stress [35]. It was found that oxidative stresses in response to acetaminophen in rats include depletion of antioxidants (e.g., ferulic acid), trigonelline, *S*-adenosyl-L-methionine, and energy-related metabolites [36, 37].

Pesticides are the cornerstones of pest management, food security, and public health. There are, however, public concerns about potential adverse effects of pesticides. Metabolomic evaluations of pesticide toxicity are much fewer than those of human drugs and diseases [38]. Similarly, a limited number of publications are available concerning metabolomics with organic pollutants. However, related research has gained some attention from scientific communities and regulatory organizations. Earlier studies of in vivo pesticide evaluation have indicated the complexity of the issue, particularly in higher animals. A specific pesticide can yield many metabolites with different toxicities [39–41]. In general, recently registered pesticides have much improved performance, including higher target selectivity, shorter half-lives, and fewer side effects (e.g., toxicity to nontarget organisms). In spite of these improvements, side effects are inevitable. Acetylcholine esterase is the target enzyme of organophosphorus insecticides (OPs). Some OPs are potent inhibitors of cytochrome P450 (CYP), a key enzyme of xenobiotic detoxification [42]. Azole fungicides target the fungal sterol 14[α]-demethylase used in ergosterol biosynthesis, but some of them can also inhibit mammalian sterol 14[α]-demethylase. Ekman et al. [43] analyzed metabolomic differences between normal and triazole fungicide-treated rats. The differential accumulation and depletion of some marker metabolites (creatine, choline, some osmolytes, and branched amino acids) in a dose-dependent manner were observed. Distinguishable metabolomic patterns indicated chemical-specific stresses of these fungicides [43, 44].

Mammalian metabolomics in response to heavy metals are frequently reported. Several heavy metals such as arsenic, cadmium, and mercury are commonly known environmental contaminants, especially in mining areas. Mally et al. [45] reported that 4-hydroxy-2(E)-nonenal is a potential biomarker of toxic mineral exposure, and its accumulation possibly indicates heavy metal-induced renal failure. Metabolomic analyses in the sera of cinnabar (mercury sulfide)-treated rats showed elevated concentrations of ketone bodies (3-D-hydroxybutyrate and acetoacetate), branched amino acids, choline, and creatine and decreased concentrations of glucose, lipids, and lipoproteins [46]. Similar metabolic profiles were also found in rats in response to realgar (arsenic sulfide) [47]. Accumulation of creatine, betaine, and some nitrogen-containing metabolites was the common, characteristic response to arsenic and mercury. The levels of glutathione and *N*-acyl amino acids, however, varied depending upon heavy metals and tissues [46, 47]. Toxicities of nano-materials are an emerging issue. Nano copper particles induced extensive changes of rat metabolomes [48]. An increase in triglycerides in the serum, liver, and kidney tissues could serve as a potentially sensitive biomarker for nano copper-induced lipidosis.

Target analytes in most metabolomics are naturally produced metabolites. However, recent studies of drug metabolism in conjunction with profiling natural metabolites suggested and confirmed novel toxicity biomarkers and toxicity mechanisms [49–52]. These studies produced extensive metabolic profiles of specific chemical stressors (e.g., drugs, pesticides, or environmental contaminants). Because the potency or toxicity of metabolites may differ from the parent

chemicals, comprehensive profiling of metabolites can offer valuable information to evaluate chemical toxicity. Chen et al. [51] profiled both natural and drug metabolites and identified conjugates of acetaminophen metabolites as promising biomarkers of acetaminophen-induced toxicity. In addition, the oxidative stress elicited by CYP2E1-mediated acetaminophen metabolism might significantly contribute to its toxicity.

Recent studies have indicated several interesting aspects of nutritional metabolomics. Synergistic effects of co-application of anticancer drugs and methionine deprivation are well known for treatment of some cancers. However, the exact mechanism was not well understood. Guenin et al. [53] found that methionine deprivation affects several metabolite pools, including phospholipid and S-adenosylmethionine. Changes of these metabolites are accompanied with abnormal expression of some proteins and other key metabolites involved in tumor proliferation. Colon cancer is associated with diet, including higher intake of dietary sugar. Hansen et al. [54] applied metabolomics to investigate the relationships between the incidence of colon cancer and sucrose, glucose, and fructose. These sugars increased mutation rates in the colon and bulky adduct levels in the colon and liver to a similar extent. The metabolomics studies indicated disturbed amino acid metabolism and a decrease in plasma and urinary acetate to be a common feature for all dietary sugars and confirmed triglyceridemic effects of fructose. Accumulation of DNA-adducts was usually accompanied with a decrease of antioxidants, especially methionine. Increased colon cancer with associated changes of metabolic profiles indicated that a high sugar diet may affect the biochemical environment and may increase the probability of cancer development. In comparison with other stress-related metabolomic research, effects of food are often difficult to study, since food is a very complex mixture of chemicals. Routes of absorption, distribution, metabolism, and excretion (ADME) of specific constituents in the tested food can influence metabolic responses. A recent study on human consumption of chocolate has illustrated interesting metabolomic effects and a strong correlation with psychological activity [55]. Decreased excretion (or levels) of cortisol (stress hormone) was the most apparent effect of chocolate in reducing anxiety. This exemplifies the power of metabolomics to evaluate the effect of complex mixtures.

Animals are frequently exposed to physical stress (temperature, wound, etc.). Teague et al. [56] studied metabolomic responses of rats under physical stresses – namely, shaking the cage occasionally. They found several different marker metabolites, depending upon the shaking duration. As acute response, the accumulation of glucose and ketone bodies was accompanied with the repression of acetate and branched amino acids. Prolonged shaking induced additional metabolomic changes (e.g., increase of choline). A recent study with rats indicated that extensive metabolomic changes can occur during restraint stress [57]. Notable responses included differential levels of metabolites in glycolysis, the tricarboxylic acid (TCA) cycle, fatty acid oxidation, and urea cycles.

Environmental metabolomics, particularly targeting non-model animals, is more difficult because the needed information such as gene sequences and protein databases is limited, and the organisms are usually exposed to multiple stressors [17]. The recent social interests in environmental issues have accelerated such research needs. Metabolomes of various organisms were recently assessed, and fish were the most common model organisms. These species include Chinook salmon (*Onchorhynchuss tshawytscha*), flatfish (*Limanda limanda*), fathead minnow (*Pimephales promelas*), and Japanese medaka (*Oryzias latipes*) [43, 58–62]. Although multiple stressors are common in the environment, metabolomic studies with these animals often focus on a specific stimulus (disease or chemical stress). Ekman et al. [58] reported that metabolomic responses to the fungicide vinclozolin in fathead minnows included changes in the concentrations of several metabolites including creatine and betaine. Viant et al. [61] reported that several metabolites, most notably of energy-related intermediates (e.g., ATP), amino acids, and creatine, accumulated in Chinook salmon exposed to the pesticides dinoseb, diazinon, and esfenvalerate. Japanese medaka also gave a similar response to dinoseb [62]. In general, hydrophilic metabolites are more common metabolomics target molecules. Steroidal lipids were also proven to be good marker metabolites in rainbow trout (*Oncorhynchus mykiss*) in response to environmental estrogens [59].

Recent metabolomics studies revealed the effects of pesticides on several invertebrate species such as earthworms (*Eisenia* spp. and *Lumbricus rubellus*) [63–68]. In a multi-platform analysis of earthworm metabolomes, McKelvie et al. [68] found that DDT and endosulfan affected the levels of sugars and amino acids. The comparative analyses suggested the ratio of alanine to glycine as a potential biomarker of pesticide exposure. Rochfort et al. [69] observed a clear indication of different metabolomic patterns in earthworms being relevant to soil health.

Mollusks such as abalones and mussels are usually considered to be relevant marker species of chemical stress in the marine environment. Tuffnail et al. [70] investigated metabolomic responses of blue mussels (*Mytilus edulis*) under various physical and chemical stressors. In this case, alanine and some osmolytes were the important factors to discriminate different stress types. Research with red abalone (*Haliotis rufescens*) also indicated several osmolytes, amino acids, and storage carbohydrates (e.g., glycogen) to be the common indicators of environmental stresses [71]. Metabolomics studies with either freshwater or marine-dwelling crustaceans are quite limited. Recent examples with *Daphnia* and *Diporeia* concerned the metabolomic evaluation of atrazine and heavy metals [11, 72]. Several amino acids and amines were characterized as useful biomarkers through the analysis of metabolomes. However, detailed connections between this information and other biochemical observations are still missing.

Birds are important parts of ecosystems and food resources. However, metabolomic research has been very limited in this subject. Approximately 300 research articles have been published in other omics areas for chickens, but only one metabolomic publication was found as of April, 2010. Huber et al. [73] studied the effects of organically and conventionally produced feeds on a chicken model. Small but noticeable differences of metabolic profiles were observed, which may be correlated with animal productivity. Research is needed to fill in the knowledge gaps of metabolomic responses to stressors in birds.

Metabolomic research has also been very limited in insects, which are important parts of ecosystems. Recent studies with *Drosophila melanogaster* indicated that several metabolites (e.g., glutamate and choline) give differential responses against hypoxia and heat [74, 75]. Future metabolomics studies with insects are of great significance, particularly for ecosystems, agriculture, and food security.

Applications in Plant Sciences

Plants are fundamental to our life. Much research has been published on practically every aspect of plants. Most applications of metabolomics in plant sciences are phenotyping or simple mapping of metabolites. Many publications of plant metabolomics under various types of stresses have been published [76–79] although fewer than those concerning animals. Table 2 shows common physical, chemical, and biological stressors.

Temporal dynamics of metabolomes in heat and cold-stressed *Arabidopsis thaliana* have been monitored [80]. In general, cold shock influences metabolism far more profoundly than heat shock. However, a large portion of heat- and cold-shock responses overlaps. Those include accumulation of amino acids derived from pyruvate and oxaloacetate, polyamine precursors, and compatible solutes [80]. Rudell et al. [81] studied metabolomic changes of apples in response to cold and suggested that a wide array of metabolomes were changed under the specified conditions. Studies indicated that some antioxidants or plant growth regulators may alleviate the damage of cold stress. Although there were several unique responses, depending on the nature of stressors, physical stimuli usually induced accumulation of oxylipins [82]. Several jasmonate derivatives were identified as useful biomarkers of wound-induced response in *A. thaliana* [83] (Fig. 2).

Heavy metals are common stressors to plants. They are commonly used as toxicant models in metabolomics and other omics research. Plants that are highly tolerable to heavy metals usually produce a large amount of small peptides, called phytochelatins. Metabolic profiling of cadmium-treated *A. thaliana* has shown an accumulation of several phytochelatins [84]. Phytochelatins are oligomers of glutathione containing cysteine, glutamate, and glycine. Metabolomic differentiation in sulfur-containing amino acids is a commonly observed phenomenon in heavy metal-stressed plants, signifying an adaptive response to heavy metals. Other common metabolites indicating

Biomarkers and Metabolomics, Evidence of Stress. Table 2 Examples of plant metabolomic studies under various stressors

Type of study	Plant	Stressor	Description	Reference
Biomarker discovery	*Arabidopsis thaliana*	Physical (heat, cold)	Accumulation of amino acid and osmolytes	[80]
	A. thaliana	Physical (wound)	Accumulation of oxylipins and jasmonates	[82, 83]
	A. thaliana	Heavy metal (Cd)	Accumulation of phytochelatins and precursors	[84]
	Hordeum vulgare (barley)	Salt stress	Accumulation of proline, sucrose, and glucose	[91]
	A. thaliana	Nutritional stress	Repression of many metabolites with reduced metabolic rates	[93]
Mode of action	*Zea mays* (corn)	Pesticides	Mode of action specific metabolomic response to 24 herbicides	[94]
	Lemna minor	Pesticides	Mode of action-dependent changes of amino acids and precursors	[96]
Toxicity	*Oryza sativa* (rice)	Ozone	Integrative approaches with metabolomics, transcriptomics, and proteomics	[103]
Biological stress	*Brassica rapa* (Chinese cabbage)	Insects	Differential accumulation of alanine, threonine, glucose, sucrose, feruloyl malate, sinapoyl malate, and gluconapin	[99]

adaptive changes include sugars and sugar alcohols. Plants can also modulate secondary metabolism in response to heavy metals such as copper and mercury. Jahangir et al. [85] observed an increase in the secondary metabolism and differentiation of amino acid and sugar levels in Chinese cabbage (*Brassica rapa*) when it was treated with copper, iron, and manganese. Rapid accumulation of glucosinolates (a secondary metabolite) was observed in *A. thaliana* under nutritional stresses [86]. These findings indicate that there may be a common feature of stress from exposure to heavy metal and nutrient deficiency.

High soil salinity significantly impacts plant growth and decreases crop yields. Salinity-related stresses are frequently accompanied with low water supplies in agricultural practices. The metabolic impact of salt stress was assessed on several crops and plant models (e.g., *A. thaliana*, barley, grape, rice, and tomato) [78, 87–91]. Accumulations of proline, sucrose/glucose, and inositol are the most frequently observed response in salt-stressed plants. Another common response includes up-regulation of proteins involved in polyamine and γ-aminobutyric acid metabolism and associated metabolites. The levels of organic acids in the TCA cycle usually decrease under salt stress, which may indicate reduced cellular activity. A general conclusion from metabolomics studies of salt-stressed plants includes changes in organic acid, amino acid and sugar metabolism.

Metabolomic profiles of plants under water stress share a common feature with those under salt stress, including increased sugar content [92]. Plants are primary sources of human foods. Therefore, plant metabolism under different nutritional conditions (i.e., fertilization) is of tremendous importance. However, only a limited number of papers have been published. *A. thaliana* is the most commonly used plant model. Hirai et al. [93] studied metabolite profiles and transcriptomes of *A. thaliana* under sulfur or nitrogen limitation. Several genes and metabolites were

commonly expressed under both sulfur and nitrogen deficiencies. For example, nitrate reductase, a key enzyme of nitrogen assimilation, was down-regulated under both conditions. Reduction of this enzyme and the associated metabolites indicated that reduced metabolic rates may be a common response to nutrient deprivation. However, some metabolites such as glucosinolates were differently accumulated between nitrogen- and sulfur-deficient conditions. Metabolic consequences of sulfur-limitation in plants were further investigated by Nikiforova et al. [86]. Limited supplementation of sulfate leads to a decrease in sulfur metabolite pools (e.g., cysteine and methionine). Because these metabolites are an integral part of plant metabolism, sulfur deficiency induces a number of adaptive responses. Decreases in biomass, levels of proteins, chlorophylls, and total RNA suggest a general reduction of metabolic activity. These responses are compensated by a systemic adjustment of the major metabolic pathways. Representative responses include re-partitioning of sulfur, carbon, and nitrogen through the accumulation of metabolites.

Metabolomic investigations of pesticide effects on plants are limited. Ott et al. [94] studied metabolomic responses in corn (*Zea mays*) treated with 24 different herbicides. They successfully discriminated chemicals having different modes of action. Comparative metabolomic studies with pyrenophorol indicated that this fungal toxin may have different modes of action from the commercial herbicides used on the oat *Avena sterilis* [95]. Recently, the metabolic response of the aquatic weed *Lemna minor* was investigated in relation to herbicidal activities of glyphosate, atrazines, and other chemicals [96]. GC-MS based metabolomics of *A. thaliana* indicated that herbicides having different modes of action result in notably different metabolomes [97]. For example, sulfonylurea herbicides induced large differences in metabolite profiles, specifically those involved in glycolysis, the TCA cycle, and nitrogen assimilation. Applications of novel statistical tools in conjunction with LC-MS analysis indicated that the insecticide carbofuran can induce large changes of endogenous metabolomes in tomato fruits [98].

Interactions among plants, pest insects, and pathogens are another interesting subject of metabolomics. For example, *B. rapa* leaves, attacked by the diamondback moth (*Plutella xylostella*) or beet armyworm (*Spodoptera exigua*), differentially accumulated alanine, threonine, glucose, sucrose, feruloyl malate, sinapoyl malate, and gluconapin, depending upon the insect species and the developmental stages [99].

Metabolomics with aquatic plants or algae are scarce, although their environmental significance is as important as their terrestrial counterparts. Representative examples include metabolomic evaluations of the green algae *Chlamydomonas reinhardtii* under nutritional stress [100, 101]. This microalga is known to produce hydrogen under anaerobic conditions. Recent studies indicated that a large portion of metabolites are differentially expressed, depending upon the deprived nutrients. Time-resolved assays suggested that the kinetic responses also differ among nutrients. For example, the response to phosphorus deprivation was slower than to sulfur or nitrogen [100]. Matthew et al. [101] found that hydrogen overproduction in *C. reinhardtii* is induced by sulfur-deprivation through metabolic re-programming or a build-up of the toxic fermentative products formate and ethanol. An excellent review has been published about metabolomic studies of marine macroalgae [102].

The most notable trend in recent plant metabolomics is integrated omics. By integrating transcriptomics, proteomics, and metabolomics, characteristic differentiation of metabolomes was identified as a defensive response in rice seedling (*Oryza sativa*) [103]. These findings provided insights into metabolic responses against stresses.

Another interesting advance in metabolomics is the development of novel data-mining technologies. Sato et al. [104] investigated rice foliage metabolomes through correlative approaches between metabolites and regulatory networks. In general, most metabolomic research gives numerical data with no correlative information among metabolites. Correlations among metabolites, genes, and proteins will give more comprehensive understanding of stress response.

Metabolomics in Microbiology

There have been a limited number of publications on metabolomics of microorganisms, particularly under stressed conditions. Microorganisms are more prone to metabolic changes than higher organisms because they

are directly exposed to the stimuli. Tweeddale et al. [105] reported that *Escherichia coli* underwent interesting metabolic changes under oxidative stress. Paraquat, a well-known respiratory inhibitor, can induce the up-regulation of several oxidative stress-related proteins and an increase of branched amino acid and sulfur-containing metabolite pools (e.g., valine and glutathione) [105].

Elucidation of mode of action is a very important subject in pesticide and drug discoveries. However, this can be a laborious and time-consuming task because a biological system contains a wide array of metabolites, proteins, and genes. Metabolomics is a high throughput, comprehensive analytical option for this purpose. The first example can be found in metabolic phenotyping of the yeast *Saccharomyces cerevisiae* mutants [9]. Metabolic patterns of *S. cerevisiae* treated with 10 commercial fungicides were differentiated via metabolomics, where two large clusters were derived according to the inhibitory activities [106]. Such a study was extended to non-model diatoms under iron starvation [107].

Heavy metals are stressors to microorganisms [107–109]. Heavy metals can induce metabolic changes in glutathione and osmolytes (e.g., glycine and betaine) as well as other metabolites. Among these metabolites, glutathione and betaine are commonly found in stressed plants, animals, and microorganisms. Recent studies with the anaerobic bacteria *Shewanella oneidensis* indicated that the overall metabolisms are highly stable even under extremely stressed conditions. Only part of the metabolic pathways (e.g., sulfur amino acid metabolism) gave rapid responses to the external toxicants [110].

Bacterial metabolomics with environmental relevance were recently reported [111, 112]. For example, the bacterium *Sinorhizobium*, upon exposure to environmental contaminants, has shown a characteristic shift to a more hydrophobic fatty acid profile. In addition, the amount of storage metabolites such as polyhydroxyalkanoates decreased under stressed conditions. A large portion of the metabolites decreased, while trehalose, branched amino acids and sulfur-containing acids accumulated. The results indicated that oxidative stresses and metabolic confinement are a response to nutritional deficiency [112].

A recent trend in microbial metabolomics is integrative omics. Intracellular metabolism of benzoic acid in the white-rot basidiomycete *Phanerochaete chrysosporium* was investigated at the proteome and metabolome levels. Up-regulation of aryl-alcohol dehydrogenase, arylaldehyde dehydrogenase, and cytochrome P450s suggested that these enzymes play key roles in benzoic acid metabolism. Intracellular metabolic shifts to the TCA cycle indicated activation of heme biosynthesis and the production of NAD(P)H. Both metabolites are the most important components of oxidative enzymes. The analyses also indicated the role of trehalose as a storage disaccharide and the presence of an alternative energy-producing pathway [113]. The bacterium *Streptomyces tenjimariensis* can produce istamycins, displaying a high potency against many Gram-negative and Gram-positive bacteria. Denery et al. [114] used metabolic profiling and polymerase chain reaction (PCR) techniques as a means of studying the growth of *S. tenjimariensis*. The study showed metabolite profiles that are unique to growth phase and signify how they can be used for further applications in the understanding of microbial metabolism, antibiotic production, and physiology.

Future Directions

Metabolomics is an emerging field. It has started to play an important role in biological sciences, particularly in systems biology and biomarker studies. However, its applications are still limited by many challenges in methodologies and applications. A noteworthy example is "lipidomics," a branch of metabolomics focusing on lipids. A tremendous amount of research has been done with hydrophilic metabolites, whereas applications of lipidomics are very limited. It is no doubt that lipidomics will become an important tool in lipid research, particularly concerning the physiological significance and function of lipids. The metabolome is the down-stream product of genes and proteins. Metabolomics alone can give the final outcome of specific stresses, but does not provide direct information on the up-stream changes such in genes and proteins. This is both the strength and weakness of metabolomics and, therefore, integrated omics approaches seem to be inevitable. Many examples of integrated omics have recently been published, and this

approach will become more popular in the future. Such a trend will improve both the quality and quantity of metabolomic data, especially in environmental toxicology. Technological challenges include data mining, analysis, and synthesis (i.e., data dimensionality and processing). Comprehensive networks of metabolites, proteins, and genes provide an overview and in-depth understanding of biological events and processes. Metabolomics tells what is happening at the metabolic level, provides direct evidences of stress, and will therefore contribute significantly to environmental toxicology.

Acknowledgments

This work was supported in part by grants from the US Fish and Wildlife Service and Hawaii Energy and Environmental Technologies Initiative Award No. N00014-09-1-0709. We thank Adam Baker and Margaret R. Ruzicka for comprehensive review of this chapter.

Bibliography

Primary Literature

1. Fiehn O (2001) Combining genomics, metabolome analysis, and biochemical modeling to understand metabolic networks. Comp Funct Genom 2:155–168
2. Oliver SG, Winson MK, Kell DB, Baganz F (1998) Systematic functional analysis of the yeast genome. Trends Biotechnol 16(9):373–378
3. Blanchard J, Sawers SJ, Jonkman JH, Tang-Liu DD (1985) Comparison of the urinary metabolite profile of caffeine in young and elderly males. Br J Clin Pharmacol 19:225–232
4. Nicholson JK, Timbrell JA, Bales JR, Sadler PJ (1985) A high resolution proton nuclear magnetic resonance approach to the study of hepatocyte and drug metabolism. Application to acetaminophen. Mol Pharmacol 27:634–643
5. Carlson EE, Cravatt BF (2007) Chemoselective probes for metabolite enrichment and profiling. Nat Methods 4:429–435
6. Carlson EE, Cravatt BF (2007) Enrichment tags for enhanced-resolution profiling of the polar metabolome. J Am Chem Soc 129:15780–15782
7. Dunn WB, Ellis DI (2005) Metabolomics: Current analytical platforms and methodologies. Trend Anal Chem 24:285–294
8. Ramautar R, Somsen GW, de Jong GJ (2009) CE-MS in metabolomics. Electrophoresis 30:276–291
9. Allen J, Davey HM, Broadhurst D, Heald JK, Rowland JJ, Oliver SG, Kell DB (2003) High-throughput classification of yeast mutants for functional genomics using metabolic footprinting. Nat Biotechnol 21:692–696
10. Brown SC, Kruppa G, Dasseux J-L (2003) Metabolomics application of FR-ICR mass spectrometry. Mass Spectrom Rev 24:223–231
11. Taylor NS, Weber RJM, Southam AD, Payne TG, Hrydziuszko O, Arvanitis TN, Viant MR (2009) A new approach to toxicity testing in *Daphnia magna*: application of high throughput FT-ICR mass spectrometry metabolomics. Metabolomics 5:44–58
12. Beckonert O, Bollard ME, Ebbels TMD, Keun HC, Antti H, Holmes E, Lindon JC, Nicholson JK (2003) NMR-based metabonomic toxicity classification: hierarchical cluster analysis and k-nearest-neighbour approaches. Anal Chim Acta 490:3–15
13. Goodacre R, Vaidyanathan S, Dunn WB, Harrigan GG, Kell DB (2004) Metabolomics by numbers: acquiring and understanding global metabolite data. Trends Biotechnol 22:245–251
14. Qiu Y, Rajagopalan D, Connor SC, Damian D, Zhu L, Handzel A, Hu G, Amanullah A, Bao S, Woody N, MacLean D, Lee K, Vanderwall D, Ryan T (2008) Multivariate classification analysis of metabolomic data for candidate biomarker discovery in type 2 diabetes mellitus. Metabolomics 4:337–346
15. Wang Y, Bollard ME, Keun H, Antti H, Beckonert O, Ebbels TM, Lindon JC, Holmes E, Tang H, Nicholson JK (2003) Spectral editing and pattern recognition methods applied to high-resolution magic-angle spinning ^{1}H nuclear magnetic resonance spectroscopy of liver tissues. Anal Biochem 323:26–32
16. Okuda S, Yamada T, Hamajima M, Itoh M, Katayama T, Bork P, Goto S, Kanehisa M (2008) KEGG Atlas mapping for global analysis of metabolic pathways. Nucleic Acids Res 36(Web Server):W423–W426
17. Bundy JG, Davey MP, Viant MR (2009) Environmental metabolomics: a critical review and future perspectives. Metabolomics 5:3–21
18. Simpson MJ, McKelvie JR (2009) Environmental metabolomics: new insights into earthworm ecotoxicity and contaminant bioavailability in soil. Anal Bioanal Chem 394:137–149
19. Viant MR (2008) Recent developments in environmental metabolomics. Mol Biosyst 4:980–986
20. Viant MR (2009) Applications of metabolomics to the environmental sciences. Metabolomics 5(1):1–2
21. Weckwerth W (2003) Metabolomics in system biology. Annu Rev Plant Biol 54:669–689
22. Villas-Boas SG, Mas S, Akesson M, Smedsgaard J, Nielsen J (2005) Mass spectrometry in metabolome analysis. Mass Spectrom Rev 24:613–646
23. Griffin JL, Shockcor JP (2004) Metabolic profiles of cancer cells. Nat Rev Cancer 4:551–561
24. Miller MG (2007) Environmental metabolomics: a SWOT analysis (strengths, weaknesses, opportunities, and threats). J Proteome Res 6:540–545
25. Dix DJ, Gallagher K, Benson WH, Groskinsky BL, McClintock JT, Dearfield KL, Farland WH (2006) A framework for the use of genomics data at the EPA. Nat Biotechnol 24:1108–1111

26. Mench M, Schwitzguebel J-P, Schroeder P, Bert V, Gawronski S, Gupta S (2009) Assessment of successful experiments and limitations of phytotechnologies: contaminant uptake, detoxification and sequestration, and consequences for food safety. Environ Sci Pollut Res 16:876–900
27. Lawton KA, Berger A, Mitchell M, Milgram KE, Evans AM, Guo L, Hanson RW, Kalhan SC, Ryals JA, Milburn MV (2008) Analysis of the adult human plasma metabolome. Pharmacogenomics 9:383–397
28. Kleno TG, Kiehr B, Baunsgaard D, Sidelmann UG (2004) Combination of "omics" data to investigate the mechanism(s) of hydrazine-induced hepatotoxicity in rats and to identify potential biomarkers. Biomarkers 9:116–138
29. Masuo Y, Imai T, Shibato J, Hirano M, Jones OAH, Maguire ML, Satoh K, Kikuchi S, Rakwal R (2009) Omic analyses unravels global molecular changes in the brain and liver of a rat model for chronic Sake (Japanese alcoholic beverage) intake. Electrophoresis 30:1259–1275
30. Robertson DG (2005) Metabonomics in toxicology: a review. Toxicol Sci 85:809–822
31. Sreekumar A, Poisson LM, Rajendiran TM, Khan AP, Cao Q, Yu J, Laxman B, Mehra R, Lonigro RJ, Li Y, Nyati MK, Ahsan A, Kalyana-Sundaram S, Han B, Cao X, Byun J, Omenn GS, Ghosh D, Pennathur S, Alexander DC, Berger A, Shuster JR, Wei JT, Varambally S, Beecher C, Chinnaiyan AM (2009) Metabolomic profiles delineate potential role for sarcosine in prostate cancer progression. Nature 457:910–914
32. Nicholson JK, Connelly J, Lindon JC, Holmes E (2002) Metabonomics: a platform for studying drug toxicity and gene function. Nat Rev Drug Discov 1:153–161
33. Watson M, Roulston A, Bélec L, Billot X, Marcellus R, Bédard D, Bernier C, Branchaud S, Chan H, Dairi K, Gilbert K, Goulet D, Gratton M-O, Isakau H, Jang A, Khadir A, Koch E, Lavoie M, Lawless M, Nguyen M, Paquette D, Turcotte E, Berger A, Mitchell M, Shore GC, Beauparlant P (2009) The small molecule GMX1778 is a potent inhibitor of NAD biosynthesis: strategy for enhanced therapy in nicotinic acid phosphoribosyltransferase 1-deficient tumors. Mol Cell Biol 29:5872–5888
34. Mervaala E, Biala A, Merasto S, Lempiainen J, Mattila I, Martonen E, Eriksson O, Louhelainen M, Finckenberg P, Kaheinen P, Muller DN, Luft FC, Lapatto R, Oresic M (2010) Metabolomics in angiotensin II-induced cardiac hypertrophy. Hypertension 55:508–515
35. Parry JD, Pointon AV, Lutz U, Teichert F, Charlwood JK, Chan P, Athersuch TJ, Taylor EL, Singh R, Luo JL, Phillips KM, Vetillard A, Lyon JJ, Keun HC, Lutz WK, Gant TW (2009) Pivotal role for two electron reduction in 2, 3-dimethoxy-1, 4-naphthoquinone and 2-methyl-1, 4-naphthoquinone metabolism and kinetics in vivo that prevents liver redox stress. Chem Res Toxicol 22:717–725
36. Coen M, Lenz EM, Nicholson JK, Wilson ID, Pognan F, Lindon JC (2003) An integrated metabonomic investigation of acetaminophen toxicity in the mouse using NMR spectroscopy. Chem Res Toxicol 16:295–303
37. Sun J, Schnackenberg LK, Holland RD, Schmitt TC, Cantor GH, Dragan YP, Beger RD (2008) Metabonomics evaluation of urine from rats given acute and chronic doses of acetaminophen using NMR and UPLC/MS. J Chromatogr B 871:328–340
38. Keum YS, Kim J-H, Li QX (2010) Metabolomics in pesticide toxicology. In: Krieger R (ed) Hayes' handbook of pesticide toxicology, 3rd edn. Academic, New York, pp 627–643
39. Coleman S, Linderman R, Hodgson E, Rose RL (2000) Comparative metabolism of chloroacetamide herbicides and selected metabolites in human and rat liver microsomes. Environ Health Persp 108:1151–1157
40. Hodgson E (2001) In vitro human phase I metabolism of xenobiotics I: pesticides and related chemicals used in agriculture and public health. J Biochem Mol Toxicol 15:296–299
41. Hodgson E, Levi PE (2010) Metabolism of pesticides. In: Krieger R (ed) Hayes' handbook of pesticide toxicology, 3rd edn. Academic, New York, pp 893–921
42. Abass K, Turpeinen M, Pelkonen O (2009) An evaluation of the cytochrome P450 inhibition potential of selected pesticides in human hepatic microsomes. J Environ Sci Health B 44:553–563
43. Ekman DR, Keun HC, Eads CD, Furnish CM, Murrell RN, Rockett JC, Dix DJ (2006) Metabolomic evaluation of rat liver and testis to characterize the toxicity of triazole fungicides. Metabolomics 2:63–73
44. Cherney DP, Ekman DR, Dix DJ, Collette TW (2007) Raman spectroscopy-based metabolomics for differentiating exposures to triazole fungicides using rat urine. Anal Chem 79:7324–7332
45. Mally A, Amberg A, Hard GC, Dekant W (2007) Are 4-hydroxy-2(E)-nonenal derived mercapturic acids and ^{1}H NMR metabonomics potential biomarkers of chemically induced oxidative stress in the kidney? Toxicology 230:244–255
46. Wei L, Liao P, Wu H, Li X, Pei F, Li W, Wu Y (2008) Toxicological effects of cinnabar in rats by NMR-based metabolic profiling of urine and serum. Toxicol Appl Pharmacol 227:417–429
47. Wei L, Liao P, Wu H, Li X, Pei F, Li W, Wu Y (2009) Metabolic profiling studies on the toxicological effects of realgar in rats by ^{1}H NMR spectroscopy. Toxicol Appl Pharmacol 234:314–325
48. Lei R, Wu C, Yang B, Ma H, Shi C, Wang Q, Wang Q, Yuan Y, Liao M (2008) Integrated metabolomic analysis of the nano-sized copper particle-induced hepatotoxicity and nephrotoxicity in rats: a rapid in vivo screening method for nanotoxicity. Toxicol Appl Pharmacol 232:292–301
49. Aubert S, Pallett KE (2000) Combined use of ^{13}C- and ^{19}F-NMR to analyze the mode of action and the metabolism of the herbicide isoxaflutole. Plant Physiol Biochem 38:517–523
50. Chen C, Gonzalez FJ, Idle JR (2007) LC-MS-based metabolomics in drug metabolism. Drug Metab Rev 39:581–597
51. Chen C, Krausz KW, Idle JR, Gonzalez FJ (2008) Identification of novel toxicity-associated metabolites by metabolomics and mass isotopomer analysis of acetaminophen metabolism in wild-type and Cyp2e1-null mice. J Biol Chem 283:4543–4559

52. Patterson AD, Gonzalez FJ, Idle JR (2010) Xenobiotic metabolism: a view through the metabolometer. Chem Res Toxicol 23:851–860
53. Guenin S, Morvan D, Thivat E, Stepien G, Demidem A (2009) Combined methionine deprivation and chloroethylnitrosourea have time-dependent therapeutic synergy on melanoma tumors that NMR spectroscopy-based metabolomics explains by methionine and phospholipid metabolism reprogramming. Nutr Cancer 61:518–529
54. Hansen M, Baunsgaard D, Autrup H, Vogel UB, Moller P, Lindecrona R, Wallin H, Poulsen HE, Loft S, Dragsted LO (2008) Sucrose, glucose and fructose have similar genotoxicity in the rat colon and affect the metabolome. Food Chem Toxicol 46:752–760
55. Martin F-PJ, Rezzi S, Pere-Trepat E, Kamlage B, Collino S, Leibold E, Kastler J, Rein D, Fay LB, Kochhar S (2009) Metabolic effects of dark chocolate consumption on energy, gut microbiota, and stress-related metabolism in free-living subjects. J Proteome Res 8:5568–5579
56. Teague CR, Dhabhar FS, Barton RH, Beckwith-Hall B, Powell J, Cobain M, Singer B, McEwen BS, Lindon JC, Nicholson JK, Holmes E (2007) Metabonomic studies on the physiological effects of acute and chronic psychological stress in Sprague-Dawley rats. J Proteome Res 6:2080–2093
57. Chen M, Wang Y, Zhao Y, Wang L, Gong J, Wu L, Gao X, Yang Z, Qian L (2009) Dynamic proteomic and metabonomic analysis reveal dysfunction and subclinical injury in rat liver during restraint stress. Biochim Biophys Acta 1794:1751–1765
58. Ekman DR, Teng Q, Jensen KM, Martinovic D, Villeneuve DL, Ankley GT, Collette TW (2007) NMR analysis of male fathead minnow urinary metabolites: a potential approach for studying impacts of chemical exposures. Aquat Toxicol 85:104–112
59. Samuelsson LM, Forlin L, Karlsson G, Adolfsson-Erici M, Larsson DGJ (2006) Using NMR metabolomics to identify responses of an environmental estrogen in blood plasma of fish. Aquat Toxicol 78:341–349
60. Stentiford GD, Viant MR, Ward DG, Johnson PJ, Martin A, Wei W, Cooper HJ, Lyons BP, Feist SW (2005) Liver tumours in wild flatfish: a histopathological, proteomic and metabolomic study. OMICS-J Integr Biol 9:281–299
61. Viant VR, Pincetich CA, Hinton DE, Tjeerdema RS (2006) Toxic actions of dinoseb in medaka (*Oryzias latipes*) embryos as determined by in vivo ^{31}P NMR, HPLC-UV and ^{1}H NMR metabolomics. Aquat Toxicol 76:329–342
62. Viant VR, Pincetich CA, Tjeerdema RS (2006) Metabolic effects of dinoseb, diazinon and esfenvalerate in eyed eggs and alevins of Chinook salmon (*Oncorhynchus tshawytscha*) determined by ^{1}H NMR metabolomics. Aquat Toxicol 77:359–371
63. Bundy JG, Osborn D, Weeks JM, Lindon JC, Nicholson JK (2001) An NMR-based metabonomic approach to the investigation of coelomic fluid biochemistry in earthworms under toxic stress. FEBS Lett 500:31–35
64. Bundy JG, Lenz EM, Bailey NJ, Gavaghan CL, Svendsen C, Spurgeon D, Hankard PK, Osborn D, Weeks JM, Trauger SA (2002) Metabonomic assessment of toxicity of 4-fluoroaniline, 3, 5-difluoroaniline and 2-fluoro-4-methylaniline to the earthworm Eisenia veneta (Rosa): Identification of new endogenous biomarkers. Environ Toxicol Chem 21:1966–1972
65. Bundy JG, Lenz EM, Osborn D, Weeks JM, Lindon JC, Nicholson JK (2002) Metabolism of 4-fluoroaniline and 4-fluorobiphenyl in the earthworm *Eisenia veneta* characterized by high-resolution NMR spectroscopy with directly coupled HPLC-NMR and HPLC-MS. Xenobiotica 32:479–490
66. Bundy JG, Sidhu JK, Rana F, Spurgeon DJ, Svendsen C, Wren JF, Stürzenbaum SR, Morgan AJ, Kille P (2008) "Systems toxicology" approach identifies coordinated metabolic responses to copper in a terrestrial non-model invertebrate, the earthworm *Lumbricus rubellus*. BMC Biol 6:25
67. Guo Q, Sidhu JK, Ebbels TMD, Rana F, Spurgeon DJ, Svendsen C, Sturzenbaum SR, Kille P, Morgan AJ, Bundy JG (2009) Validation of metabolomics for toxic mechanism of action screening with the earthworm *Lumbricus rubellus*. Metabolomics 5:72–83
68. McKelvie JR, Yuk J, Xu Y, Simpson AJ, Simpson MJ (2009) ^{1}H NMR and GC/MS metabolomics of earthworm responses to sub-lethal DDT and endosulfan exposure. Metabolomics 5:84–94
69. Rochfort SJ, Ezernieks V, Yen AL (2009) NMR-based metabolomics using earthworms as potential indicators for soil health. Metabolomics 5:95–107
70. Tuffnail W, Mills GA, Cary P, Greenwood R (2009) An environmental ^{1}H NMR metabolomic study of the exposure of the marine mussel *Mytilus edulis* to atrazine, lindane, hypoxia and starvation. Metabolomics 5:33–43
71. Rosenblum ES, Tjeerdema RS, Viant MR (2006) Effects of temperature on host-pathogen-drug interactions in red abalone, *Haliotis rufescens*, determined by ^{1}H NMR metabolomics. Environ Sci Technol 40:7077–7084
72. Ralston-Hooper K, Hopf A, Oh C, Zhang X, Adamec J, Sepulveda MS (2008) Development of GCxGC/TOF-MS metabolomics for use in ecotoxicological studies with invertebrates. Aquat Toxicol 88:48–52
73. Huber M, van de Vijver LPL, Parmentier H, Savelkoul H, Coulier L, Wopereis S, Verheij E, van der Greef J, Nierop D, Hoogenboom RAP (2010) Effects of organically and conventionally produced feed on biomarkers of health in a chicken model. Br J Nutr 103:663–676
74. Feala JD, Coquin L, McCulloch AD, Paternostro G (2007) Flexibility in energy metabolism supports hypoxia tolerance in *Drosophila* flight muscle: metabolomic and computational systems analysis. Mol Syst Biol 3:99
75. Malmendal A, Overgaard J, Bundy JG, Sørensen JG, Nielsen NC, Loeschcke V, Holmstrup M (2006) Metabolomic profiling of heat stress: hardening and recovery of homeostasis in *Drosophila*. Am J Physiol Regul Integr Comp Physiol 291:205–212
76. Guy C, Kaplan F, Kopka J, Selbig J, Hinch DK (2008) Metabolomics of temperature stress. Physiol Plant 132:220–235

77. Hoefgen R, Nikiforova VJ (2008) Metabolomics integrated with transcriptomics: assessing systems response to sulfur-deficiency stress. Physiol Plant 132:190–198
78. Sanchez DH, Siahpoosh MR, Roessner U, Udvardi M, Kopka J (2008) Plant metabolomics reveals conserved and divergent metabolic responses to salinity. Physiol Plant 132:209–219
79. Shulaev V, Cortes D, Miller G, Mittler R (2008) Metabolomics for plant stress response. Physiol Plant 132:199–208
80. Kaplan F, Kopka J, Haskell DW, Zhao W, Schiller KC, Gatzke N, Sung DY, Guy CL (2004) Exploring the temperature-stress metabolome of *Arabidopsis*. Plant Physiol 136:4159–4168
81. Rudell DR, Mattheis JP, Hertog MLATM (2009) Metabolomic change precedes apple superficial scald symptoms. J Agric Food Chem 57:8459–8466
82. Thiocone A, Farmer EE, Wolfender J-L (2008) Screening for wound-induced oxylipins in *Arabidopsis thaliana* by differential HPLC-APCI/MS profiling of crude leaf extracts and subsequent characterisation by capillary-scale NMR. Phytochem Anal 19:198–205
83. Glauser G, Guillarme D, Grata E, Boccard J, Thiocone A, Carrupt P-A, Veuthey J-L, Rudaz S, Wolfender J-L (2008) Optimized liquid chromatography-mass spectrometry approach for the isolation of minor stress biomarkers in plant extracts and their identification by capillary nuclear magnetic resonance. J Chromatogr A 1180:90–98
84. Sarry J-E, Kuhn L, Ducruix C, Lafaye A, Junot C, Hugouvieux V, Jourdain A, Bastien O, Fievet JB, Vailhen D, Amekraz B, Moulin C, Ezan E, Garin J, Bourguignon J (2006) The early responses of *Arabidopsis thaliana* cells to cadmium exposure explored by protein and metabolite profiling analyses. Proteomics 6:2180–2198
85. Jahangir M, Abdel-Farid IB, Choi YH, Verpoorte R (2008) Metal ion-inducing metabolite accumulation in *Brassica rapa*. J Plant Physiol 165:1429–1437
86. Nikiforova VJ, Kopka J, Tolstikov V, Fiehn O, Hopkins L, Hawkesford MJ, Hesse H, Hoefgen R (2005) Systems rebalancing of metabolism in response to sulfur deprivation, as revealed by metabolome analysis of *Arabidopsis* plants. Plant Physiol 138:304–318
87. Cramer GR, Ergul A, Grimplet J, Tillett RL, Tattersall EAR, Bohlman MC, Vincent D, Sonderegger J, Evans J, Osborne C, Quilici D, Schlauch KA, Schooley DA, Cushman JC (2007) Water and salinity stress in grapevines: early and late changes in transcript and metabolite profiles. Funct Integr Genomics 7:111–134
88. Kim JK, Bamba T, Harada K, Fukusaki E, Kovayashi A (2007) Time-course metabolic profiling in *Arabidopsis thaliana* cell cultures after salt stress treatment. J Exp Bot 58:415–424
89. Sanchez DH, Lippold F, Redestig H, Hannah MA, Erban A, Kraemer U, Kopka J, Udvardi MK (2008) Integrative functional genomics of salt acclimatization in the model legume *Lotus japonicus*. Plant J 53:973–987
90. Smith AR, Johnson HE, Hall M (2003) Metabolic fingerprinting of salt-stressed tomatoes. Bulgarian J. Plant Physiol 29:153–163
91. Widodo PJH, Newbigin E, Tester M, Bacic A, Roessner U (2009) Metabolic responses to salt stress of barley (*Hordeum vulgare* L.) cultivars, Sahara and Clipper, which differ in salinity tolerance. J Exp Bot 60:4089–4103
92. Foito A, Byrne SL, Shepherd T, Stewart D, Barth S (2009) Transcriptional and metabolic profiles of *Lolium perenne* L. genotypes in response to a PEG-induced water stress. Plant Biotechnol J 7:719–732
93. Hirai MY, Yano M, Goodenowe DB, Kanaya S, Kimura T, Awazuhara M, Arita M, Fujiwara T, Saito K (2004) Integration of transcriptomics and metabolomics for understanding of global responses to nutritional stresses in *Arabidopsis thaliana*. Proc Natl Acad Sci USA 101:10205–10210
94. Ott KH, Aranı´bar N, Singh B, Stockton GW (2003) Metabonomics classifies pathways affected by bioactive compounds. Artificial neural network classification of NMR spectra of plant extracts. Phytochemistry 62:971–985
95. Aliferis KA, Chrysayi-Tokousbalides M (2005) Metabonomic strategy for the investigation of the mode of action of the phytotoxin (5 S, 8R, 13 S, 16R)-(-)-pyrenophorol using H nuclear magnetic resonance fingerprinting. J Agric Food Chem 54:1687–1692
96. Aliferis KA, Materzok S, Paziotou GN, Chrysayi-Tokousbalides M (2009) *Lemna minor* L. as a model organism for ecotoxicological studies performing 1 H NMR fingerprinting. Chemosphere 76:967–973
97. Trenkamp S, Eckes P, Busch M, Fernie AR (2009) Temporally resolved GC-MS-based metabolic profiling of herbicide treated plants treated reveals that changes in polar primary metabolites alone can distinguish herbicides of differing mode of action. Metabolomics 5:277–291
98. Perez IS, Culzoni MJ, Siano GG, Garcia MDG, Goicoechea HC, Galera MM (2009) Detection of unintended stress effects based on a metabonomic study in tomato fruits after treatment with carbofuran pesticide. Capabilities of MCR-ALS applied to LC-MS three-way data arrays. Anal Chem 81:8335–8346
99. Widarto HT, Meijden E, Lefeber AWM, Erkelens C, Kim HK, Choi YH, Verpoorte R (2006) Metabolomic differentiation of *Brassica rapa* following herbivory by different insect instars using two-dimensional nuclear magnetic resonance spectroscopy. J Chem Ecol 32:2417–2428
100. Bölling C, Fiehn O (2005) Metabolite profiling of *Chlamydomonas reinhardtii* under nutrient deprivation. Plant Physiol 139:1995–2005
101. Matthew T, Zhou W, Rupprecht J, Lim L, Thomas-Hall SR, Doebbe A, Kruse O, Hankamer B, Marx UC, Smith SM, Schenk PM (2009) The metabolome of *Chlamydomonas reinhardtii* following induction of anaerobic H_2 production by sulfur depletion. J Biol Chem 284:23415–23425
102. La Barre SL, Weinberger F, Kervarec N, Potin P (2004) Monitoring defensive responses in macroalgae – limitations and perspectives. Phytochem Rev 3:371–379

103. Cho K, Shibato J, Agrawal GK, Jung Y-H, Kubo A, Jwa N-S, Tamogami S, Satoh K, Kikuchi S, Higashi T, Kimura S, Saji H, Tanaka Y, Iwahashi H, Masuo Y, Rakwal R (2008) Integrated transcriptomics, proteomics, and metabolomics analyses to survey ozone responses in the leaves of rice seedling. J Proteome Res 7:2980–2998
104. Sato S, Arita M, Soga T, Nishioka T, Tomita M (2008) Time-resolved metabolomics reveals metabolic modulation in rice foliage. BMC Sys Biol 2:51
105. Tweeddale H, Notley-McRobb L, Ferenci T (1999) Assessing the effect of reactive oxygen species on *Escherichia coli* using a metabolome approach. Redox Rep 4:237–241
106. Allen J, Davey HM, Broadhurst D, Rowland JJ, Oliver SG, Kell DB (2004) Discrimination of modes of action of antifungal substances by use of metabolic footprinting. Appl Environ Microbiol 70:6157–6165
107. Allen AE, Laroche J, Maheswari U, Lommer M, Schauer N, Lopez PJ, Finazzi G, Fernie AR, Bowler C (2008) Whole-cell response of the pennate diatom *Phaeodactylum tricornutum* to iron starvation. Proc Natl Acad Sci USA 105:10438–10443
108. Tanaka Y, Higashi T, Rakwal R, Wakida S-I, Iwahashi H (2007) Quantitative analysis of sulfur-related metabolites during cadmium stress response in yeast by capillary electrophoresis-mass spectrometry. J Pharm Biomed Anal 44:608–613
109. Tremaroli V, Workentine ML, Weljie AM, Vogel HJ, Ceri H, Viti C, Tatti E, Zhang P, Hynes AP, Turner RJ, Zannoni D (2009) Metabolomic investigation of the bacterial response to a metal challenge. Appl Environ Microbiol 75:719–728
110. Tang YJ, Martin HG, Deutschbauer A, Feng X, Huang R, Llora X, Arkin A, Keasling JD (2009) Invariability of central metabolic flux distribution in *Shewanella oneidensis* MR-1 under environmental or genetic perturbations. Biotechnol Progr 25:1254–1259
111. Barsch A, Patschkowski T, Niehaus K (2004) Comprehensive metabolite profiling of *Sinorhizobium meliloti* using gas chromatography–mass spectrometry. Funct Integr Genomics 4:219–230
112. Keum YS, Seo JS, Li QX, Kim JH (2008) Comparative metabolomic analysis of *Sinorhizobium* sp. C4 during the degradation of phenanthrene. Appl Microbiol Biotechnol 80:863–872
113. Matsuzaki F, Shimizu M, Wariishi H (2008) Proteomic and metabolomic analyses of the white-rot fungus *Phanerochaete chrysosporium* exposed to exogenous benzoic acid. J Proteome Res 7:2342–2350
114. Denery J, Cooney M, Li QX (2010) Diauxic and antimicrobial growth phases of *Streptomyces tenjimariensis*: metabolite profiling and gene expression. J Biomed Biotechnol (submitted)
115. Wishart DS, Knox C, Guo AC, Eisner R, Young N, Gautam B, Hau DD, Psychogios N, Dong E, Bouatra S, Mandal R, Sinelnikov I, Xia J, Jia L, Cruz JA, Lim E, Sobsey CA, Shrivastava S, Huang P, Liu P, Fang L, Peng J, Fradette R, Cheng D, Tzur D, Clements M, Lewis A, De Souza A, Zuniga A, Dawe M, Xiong Y, Clive D, Greiner R, Nazyrova A, Shaykhutdinov R, Li L, Vogel HJ, Forsythe I (2009) HMDB: a knowledgebase for the human metabolome. Nucleic Acids Res 37(Database issue): D603–D610

Books and Reviews

Fiehn O (2001) Combining genomics, metabolome analysis, and biochemical modeling to understand metabolic networks. Comp Func Genom 2:155–168

Hodgson E, Levi PE (2010) Metabolism of pesticides. In: Krieger R (ed) Hayes' handbook of pesticide toxicology, 3rd edn. Academic, New York, pp 893–921

Biomass as Renewable Source of Energy, Possible Conversion Routes

Martin Kaltschmitt
German Biomass Research Centre, Leipzig, Germany
Institute of Environmental Technology and Energy Economics, Hamburg University of Technology, Hamburg, Germany

Article Outline

Glossary
Definition of the Subject
Introduction
Biomass Sources
Conversion Routes
Thermochemical Conversion
Physicochemical Conversion
Biochemical Conversion
Future Directions
Bibliography

Glossary

Biochemical conversion Conversion of biomass based on biological processes into energy carriers and/or energy.

Bioenergy Bioenergy is defined as energy from biomass.

Biofuel Biofuel is a fuel produced directly or indirectly from biomass.

Biomass From a scientific and technical point of view, biomass is defined as material of biological origin excluding material embedded in geological formations and/or transformed to fossil.

Conversion route A conversion route is defined as the overall processes of production, provision, handling, and processing biomass to the point of delivery of the useful energy.

Physicochemical conversion Conversion of biomass based on physical and/or chemical processes into energy carriers and/or energy.

Thermochemical conversion Heat induced conversion of biofuels into energy carriers and/or energy.

Definition of the Subject

Biomass, a renewable source of energy, has been used since the beginning of human culture. Until the introduction of coal, crude oil, and natural gas, wood and other forms of biomass were the most important sources of energy available to humans. Today, biomass accounts for roughly 10–12% of the global primary energy consumption and, at a time of politically forced and environmentally needed greenhouse gas mitigation and an expected shortage in fossil fuel energy resources, this energy carrier is becoming more and more important. The goal of this chapter is to give an overview of the technical possibilities and challenges of energy provision from biomass. First, the various biomass sources available are discussed briefly. Next, available conversion routes are presented, showing the broad variety of possible options to provide heat, electricity, and/or transportation fuels. Based on these fundamentals, the thermochemical, physicochemical, and biochemical conversion possibilities are discussed. For these three options, in addition to the basics, the technical possibilities are briefly presented to indicate the current status of technology. Finally, future directions are discussed.

Introduction

Biomass currently provides 10–12% of global primary energy. Due to geographical, economic, ethical, and climatic differences, as well as different frame conditions within the energy system, the share of bioenergy in relation to the total energy consumption differs widely between different countries, ranging from less than a few percent in some industrialized countries like the United Kingdom to significantly more than 50% in some developing countries in Africa and Asia. Nevertheless, biomass is by far the most important renewable energy source in most countries, being significantly larger in use than the second largest source, hydropower. The energy from these sources – the oldest fuels utilized by humans – is even larger in absolute terms than the energy from one of the newest – nuclear fuels.

Solid biofuels dominate the global biomass picture. It is safe to say that significant shares of the world's population still rely on solid biofuels for most of their energy. This situation has not changed since the mastery of fire some hundred thousand years ago. This is due to the relatively low cost of and easy access to solid biofuels such as wood, dried dung, and crop residues (like straw) in rural areas of developing countries where more than one third of humanity lives. In addition, other bioenergy carriers such as wood pellets, bioethanol, and biogas play an increasingly important role in some regions in developing as well as in industrialized countries, where their costs and access compare favorably with fossil fuel–based energy in the context of the frame conditions defined by the respective governments. Additionally, the potential of the biomass resources available to humans is significant on a worldwide scale. Sustainably produced solid, liquid, and/or gaseous biofuels also have the advantage of being climatically neutral and environmentally sound compared with other sources of fossil fuel energy, which has led to a resurgence in interest in biomass throughout the world.

Compared with other renewable sources of energy, biomass has the advantage that it can be used for heat provision, electricity production, and the provision of liquid and gaseous fuels for transportation purpose. And within all of these markets, biomass already plays a certain and increasing role within the global energy system. This development will accelerate in the years to come, with an increasing energy price level.

Heat from biomass is used for cooking and/or space heating. While cooking with (solid) biofuel is rare today in industrialized countries (with the exception of outdoor barbecue), this is still the "classical" bioenergy application in most developing and threshold countries. It is likely that this market will continue to grow in the years to come due to a significant increase in population, especially in these countries. Heat provision from biomass for domestic and industrial applications is realized in all countries worldwide,

but generally more in rural areas of countries during the cold season. This heating market is also likely to grow in the future, especially if crude oil prices continue to stay relatively high or increase further. Additionally, due to the political goal to reduce greenhouse gas emissions and the development of highly efficient and more comfortable combustion technologies, heat provision from solid biofuels is undergoing a renaissance in some industrialized countries.

Demand for electricity has increased greatly in recent years in all countries. Even though the use of electricity is widely accepted, the provision of electrical energy can be controversial in some countries with a strong environmental movement. The debate about the pros and cons of nuclear power and the discussion about the contribution of electricity from hard coal and lignite to the global greenhouse effect are only two examples. Therefore, the generation of electricity from biomass is seen in some countries as a promising alternative, contributing in parallel a more indigenous and safer electricity provision, as well as increasing prosperity in rural areas. For this reason, it can be expected that the production and provision of electricity from biomass will significantly increase in the years to come. Within combined heat and power (CHP) plants, electricity generation can be combined in an ideal way with heat provision by maximizing the overall energetic efficiency. With limited available biomass resources, this option is gaining more importance, especially in countries with a high heat demand due to cold winters. For this reason, a considerable and growing share of the increasing electricity production from biomass is realized in CHP plants, depending on the frame conditions set by the respective government.

Production of transportation fuels from biomass is also increasing. The need for mobility is dramatically growing on a worldwide scale, particularly in some of the emerging economies in Asia. Therefore, finding ways to provide cheap, technically mature, climatically sound, and environmentally benign fuels based on renewable energy in general and biomass in particular is an extremely active endeavor. Therefore, the research and development (R&D) activities in this field have increased significantly in recent years in most of the Organization for Economic Co-operation and Development (OECD) countries, as well as in selected developing countries and emerging economies; the main challenge is to produce more liquid and/or gaseous transportation fuel from the limited available biomass. This challenge is the same worldwide, but, so far, only Brazil and the United States produce liquid biofuels (ethanol) for transportation purposes on a large scale with a measurable impact within the energy system.

In the following sections, the available biomass resources are discussed, and the various conversion routes of biomass – thermochemical, physicochemical, and biochemical – into useful energy will be described.

Biomass Sources

Biomass consists primarily of the elements carbon (C), hydrogen (H), and oxygen (O) (Table 1). Additionally, significant amounts of trace elements can be found in some types of biomass. For example, straw may contain fairly high amounts of chlorine (Cl) and/or silicon (Si) and rapeseed contains a relatively high amount of nitrogen (N). These trace elements can sometimes cause problems during the conversion into an energy carrier and/or useful energy. For example, during combustion chlorine might cause high temperature corrosion in boilers, silicon can lead to boiler slagging, and nitrogen can be responsible for high NO_x emissions, which are limited in most countries.

In most practical applications, the energy content of biofuel is best described by the net calorific value. Besides the chemical composition of the organic material, net calorific value is influenced by the water content of the biomass. Due to the fact that the chemical composition of most solid biomass fractions does not vary significantly (Table 1), the net calorific value related to the dry matter is similar for most of the biomass streams used (e.g., wood, straw) for the provision of solid biofuels. This might be different for liquid or gaseous fuels provided by a more or less complex conversion process based on heat-induced (i.e., thermochemical conversion) and/or biological processes (i.e., biochemical conversion).

Figure 1 shows that the net calorific value of wood decreases from approximately 18.5 MJ/kg dry matter with increasing water content. The net calorific value is zero at water content of approximately 88%. Normally, the water content of air-dried wood is between 12%

Biomass as Renewable Source of Energy, Possible Conversion Routes. Table 1 Energy content and concentrations of some elements in untreated biomass (various sources, e.g., [1])

Type of biomass	Net calorific value in MJ/kg	Ash content in %	Volatile compounds in %	C	H	O	N	K	Ca	Mg	P	S	Cl
				in % of dry substance									
Spruce wood (with bark)	18.8	0.6	82.9	49.8	6.3	43.2	0.13	0.13	0.70	0.08	0.03	0.015	0.005
Beech wood (with bark)	18.4	0.5	84.0	47.9	6.2	45.2	0.22	0.15	0.29	0.04	0.04	0.015	0.006
Poplar wood (Short rotation)	18.5	1.8	81.2	47.5	6.2	44.1	0.42	0.35	0.51	0.05	0.10	0.031	0.004
Willow wood (Short rotation)	18.4	2.0	80.3	47.1	6.1	44.3	0.54	0.26	0.68	0.05	0.09	0.045	0.004
Bark (softwood)	19.2	3.8	77.2	51.4	5.7	38.7	0.48	0.24	1.27	0.14	0.05	0.085	0.019
Rye straw	17.4	4.8	76.4	46.6	6.0	42.1	0.55	1.68	0.36	0.06	0.15	0.085	0.40
Wheat straw	17.2	5.7	77.0	45.6	5.8	42.4	0.48	1.01	0.31	0.10	0.10	0.082	0.19
Triticale straw	17.1	5.9	75.2	43.9	5.9	43.8	0.42	1.05	0.31	0.05	0.08	0.056	0.27
Barley straw	17.5	4.8	77.3	47.5	5.8	41.4	0.46	1.38	0.49	0.07	0.21	0.089	0.40
Rape straw	17.1	6.2	75.8	47.1	5.9	40.0	0.84	0.79	1.70	0.22	0.13	0.27	0.47
Corn straw	17.7	6.7	76.8	45.7	5.3	41.7	0.65					0.12	0.35
Sunflower straw	15.8	12.2	72.7	42.5	5.1	39.1	1.11	5.00	1.90	0.21	0.20	0.15	0.81
Hemp straw	17.0	4.8	81.4	46.1	5.9	42.5	0.74	1.54	1.34	0.20	0.25	0.10	0.20
Rice straw	12.0	4.4											
Husk	14.0	19.0											
Rye whole crop	17.7	4.2	79.1	48.0	5.8	40.9	1.14	1.11		0.07	0.28	0.11	0.34
Wheat whole crop	17.1	4.1	77.6	45.2	6.4	42.9	1.41	0.71	0.21	0.12	0.24	0.12	0.09
Triticale whole crop	17.0	4.4	78.2	44.0	6.0	44.6	1.08	0.90	0.19	0.09	0.22	0.18	0.14
Rye grain	17.1	2.0	80.9	45.7	6.4	44.0	1.91	0.66		0.17	0.49	0.11	0.16
Wheat grain	17.0	2.7	80.0	43.6	6.5	44.9	2.28	0.46	0.05	0.13	0.39	0.12	0.04
Triticale grain	16.9	2.1	81.0	43.5	6.4	46.4	1.68	0.62	0.06	0.10	0.35	0.11	0.07
Rape grain	26.5	4.6	85.2	60.5	7.2	23.8	3.94					0.10	
Miscanthus	17.6	3.9	77.6	47.5	6.2	41.7	0.73	0.72	0.16	0.06	0.07	0.15	0.22
Switchgrass													
Sugar cane stalk (bagasse)	8.0	4.0	80	45	6.0	35	0.0					0.0	
Hay from various sources	17.4	5.7	75.4	45.5	6.1	41.5	1.14	1.49	0.50	0.16	0.19	0.16	0.31
Roadside greenery	14.1	23.1	61.7	37.1	5.1	33.2	1.49	1.30	2.38	0.63	0.19	0.19	0.88

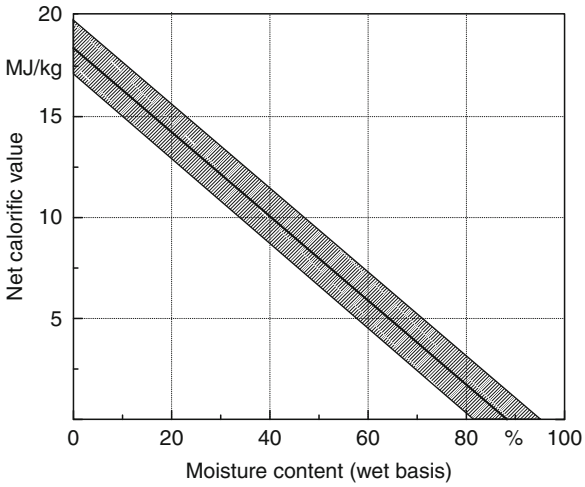

Biomass as Renewable Source of Energy, Possible Conversion Routes. Figure 1
Net calorific value of wood depending on the moisture content [1]

and 20%, yielding a calorific value between 13 and 16 MJ/kg. Freshly harvested wood is characterized by a water content of about 50% or more. A significantly lower net calorific value is the result. This is the reason why wood is usually dried with solar energy.

Independent of the fact that the heating value is more or less similar for organic matter used for the provision of solid biofuels, there is a huge variety of different biomass material streams available to be used as a source of energy. The properties of these biomass fractions define the conversion routes that are technically possible and economically feasible. The most important biomass fractions are discussed below.

Woody Biomass

Wood is the "classical" solid biofuel, used for thousands of years (basically since the mastery of fire by humans). This is especially true for wood from forests. In most countries fire wood as an energy carrier is a product from forestry management like timber for the use as a raw material (e.g., for construction purpose). In addition to forest wood, woody biomass to be used as a source of energy can also be grown on agricultural land. To maximize the average yield and thus minimize the land needs, tree plantations are harvested after a couple of years (i.e., short rotation coppice). Beside this, wood fuel can be derived from production and consumption of wood and wood products as a residue, a by-product, and/or a waste material all along the supply chain of wood as a raw material as well as pulp and paper products (Fig. 2). For example, thinning wood and forest residues are produced as a by-product during the production of stem wood as a raw material for case goods and furniture production. Industrial residual wood, bark, and wood dust are by-products and/or waste materials resulting from the production of timber and the manufacturing of wood structures or wood products. At the end of the product lifetime and after recycling of some wood fractions (such as old furniture or roof timbering, chipboards), partly contaminated woody material and waste wood remain, which can be used as fuel.

Herbaceous Biomass

The available organic material flow from herbaceous biomass can be subdivided into herbaceous energy crops grown specifically as biomass fuels (like whole crop cereal, rape or sunflower seed, *Miscanthus*, switchgrass, sugar cane, maize silage) and by-products of the production of non-energy products (like straw produced during the production of cereals). The latter arise primarily from the production processes for the provision of food, fiber, and fodder (e.g., the production of grain is necessarily connected with the production of straw). The same is true for the production of crops with special substances (e.g., specific oily substances, specific scents) to be used as a raw material (e.g., in the chemical industry, for the production of pharmaceutics). Additionally herbaceous biomass is also produced, for example, in conservation areas, parks, cemeteries, gardens, and on roadside areas.

Other Biomass

Various other organic materials usable as a source of energy are available within the overall economy, including by-products and waste materials from agriculture (e.g., animal manure), industrial food and fodder processing processes (e.g., slaughterhouse residues, vegetable waste, olive and fruit pits), food

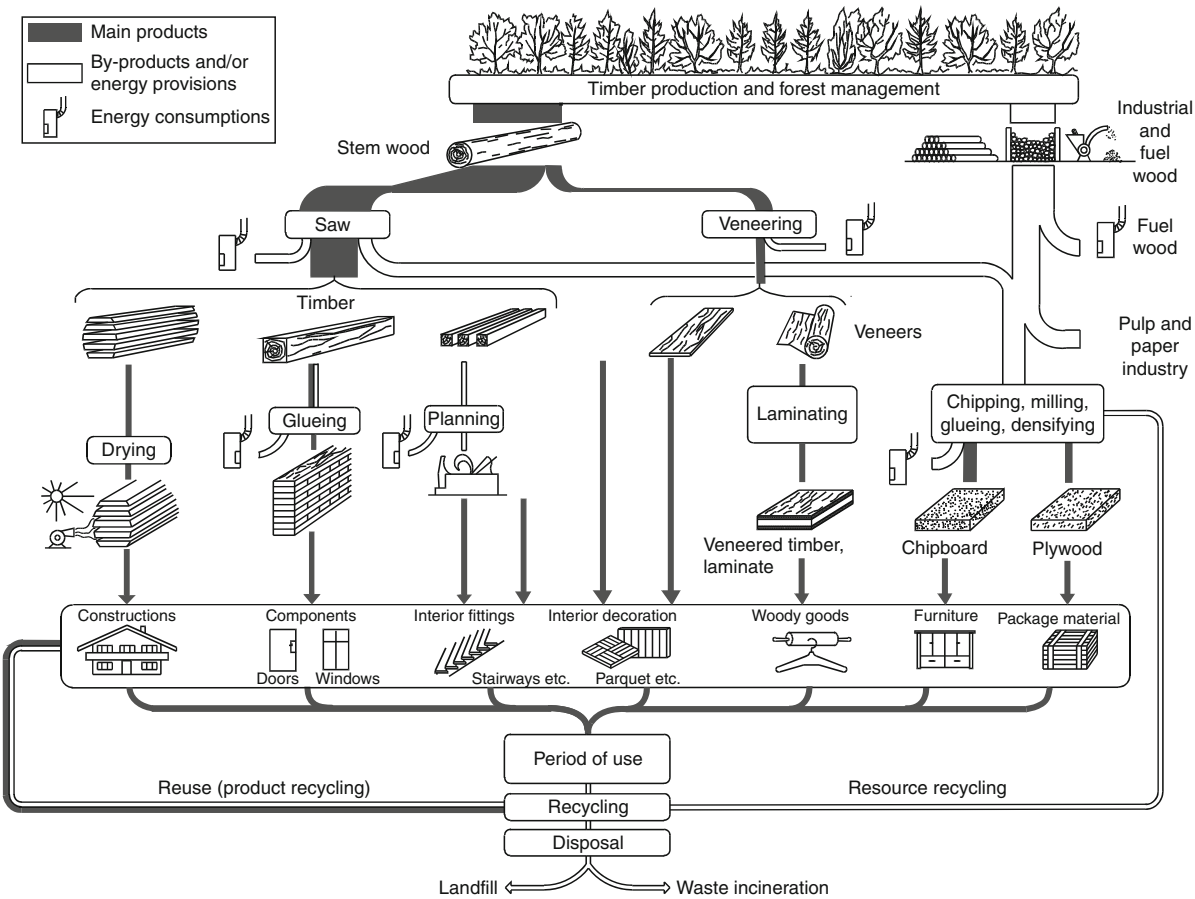

Biomass as Renewable Source of Energy, Possible Conversion Routes. Figure 2
Material flow of wood within the overall economy [1]

and fodder trading (e.g., spoiled food and fodder, contaminated fruits), households (e.g., the organic fraction of municipal solid waste (MSW)), as well as from wastewater processing (i.e., sewage sludge). Such biomass material flows might contain a high share of water, could include a high proportion of (unwanted) trace elements (like nitrogen, potassium, chlorine), and can be characterized by strong variations in their composition.

Conversion Routes

Bioenergy is generated in a multistage supply chain that starts with the collection of residues, by-products, or waste, or the cultivation of energy crops. This biomass then undergoes a variety of mechanical processing, storage, and transportation steps – depending on the local conditions – and perhaps industrial conversion processes to produce secondary solid, liquid, and/or gaseous energy carriers or biofuels. These fuels can be used to meet the given demand for different forms of useful energy (i.e., mostly power and heat, but also liquid or gaseous transportation fuels) (Fig. 3).

The different possibilities to provide secondary energy carrier with more promising fuel characteristics compared with mechanically treated biomass (like wood chips, wood logs, pellets, silage, organic waste) can be subdivided in options based on heat induced processes (i.e., thermochemical conversion), on biological processes (i.e., biochemical conversion), and on physicochemical processes (physicochemical conversion). These

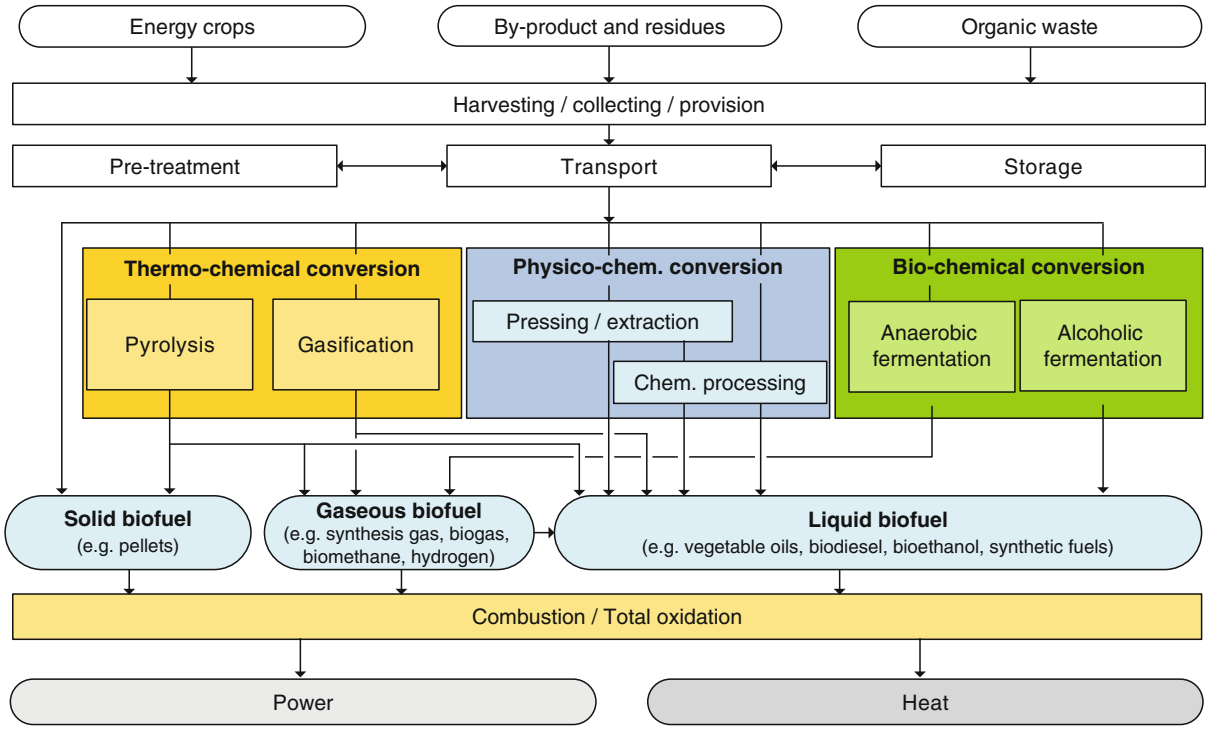

Biomass as Renewable Source of Energy, Possible Conversion Routes. Figure 3
Possibilities to provide heat and/or power from biomass (Based on [1])

different options are discussed briefly below. But before that the provision of biomass free conversion plant is analyzed.

Design of Typical Conversion Routes

In general, the conversion route describes the pathway from the production of the energy crops, the provision of residues, by-products, and/or wastes at the place of origin until the provision of the biomass in a predefined form at the gate of the conversion plant, the provision of secondary energy carrier (e.g., solid, liquid, or gaseous fuel, district heat), the provision of final energy (e.g., heat, electricity), or the provision of useful energy (e.g., heat, power). Thus, such a conversion route describes the overall life cycle from the production respectively the come up of the organic matter (i.e., the primary energy) up to the provision of the secondary, useful, or final energy.

The overall goal of such a conversion route is to meet a varying demand of final or useful energy with a predefined security of supply. To reach this goal, appropriate conversion plant(s) with a reliable technical performance are needed as well as the necessary amount of biomass of a predefined quality.

Each conversion route consists of the life cycle steps of biomass production, and each of these steps is composed of various single technical processes. For example, biomass production requires preparation of the seed bed, distribution of fertilizer as well as plant protecting agents, and selected cultivation measures.

Because the different life cycle stages of a biomass conversion route normally do not take place at the same location, the distances have to be travelled by various means (e.g., trucks, pipelines, conveyor belts). The choice of transportation is – beside technical aspects – mostly based on economic considerations.

A specific conversion route is thus very much defined by the frame conditions fixed by the available biomass

(supply side) on the one hand and the requested provision of the final and/or useful energy (demand side). Additionally, technical, economic, and environmental (as well as administrative and/or legal (and emotional)) aspects significantly influence the realization of such a conversion route. For example, the choice for a specific conversion technology is influenced by the desired final or useful energy carrier (e.g., thermal energy, mechanical energy, electrical energy) and the (cheap) locally available biomass. The environmental standards defined by governments (e.g., emission limits, noise limits, odor regulations, waste disposal directives) and the economic frame conditions pertaining to the specific circumstances define the design and practical realization of such a biomass conversion route. Additionally, the disposal of waste produced by different processes within the overall route (e.g., digested animal manure leaving the biogas plant, ash remaining after the combustion of wood pellets) might influence the layout of such a route dramatically. Based on the consequences resulting from the thus necessary (expensive) waste disposal, a certain demand could be formulated to the quality of the biomass (e.g., water content, dimensions, impurities) used within such an overall conversion route. To achieve the desired effects, the quality of the used biomass has to be guaranteed within the overall route, with the consequence that there might be the need to include additional processing steps in the provision chain.

Biomass availability can vary throughout the different seasons of the year, which has to be taken into consideration as energy demand changes over time. This means that certain storage options (e.g., wood chip storage, heat storage) have to be included within the overall chain to ensure a predefined degree of security of supply.

Additionally, the developed conversion route matching all these demands has to be economically viable under the frame conditions defined by the investor, the local frame conditions, and the government, have the opportunity to receive the required legal authorization (if applicable), and – last but not least – be socially and emotionally acceptable to the people living close to the conversion plant. And – which makes the design, successful operation, and ongoing optimization of such a conversion route even more challenging – different players with different backgrounds and understanding (like farmers, power plant operators, investors) have to communicate and interact successfully with each other as well as with the representatives of the (local) regulatory authority. Thus a biomass conversion route is defined by technical as well as various nontechnical aspects. This makes the set-up of new chains exiting and demanding.

Conversion Options to Provide Secondary Energy Carriers

The conversion of biomass (i.e., organic material of very different origin) into solid, liquid, and/or gaseous secondary energy carriers can be realized via heat-induced processes (i.e., thermochemical conversion), via transformation by bacteria (i.e., biochemical conversion), and/or via physicochemical processes. These conversion processes are, in most cases, the "heart" of such a conversion route. Below, an overview is given to explain the most important possibilities as well as the main differences.

Thermochemical conversion. Biomass can be converted into useful energy or into secondary energy carriers using conversion processes based on heat.

During the "classical" combustion of biomass for the provision of heat and/or electricity, the biomass is fully oxidized, basically with oxygen from the surrounding air, by releasing heat. Various chemical processes are realized during this oxidization. These processes take place in parallel at the same place. Due to the frame conditions defined by the involved combustion technology and its defining control parameters, the chemical reactions can be influenced to a certain degree to minimize the creation of unwanted substances harmful to the environment.

Alternatively, the thermochemical conversion can be split up and realized at different places. Within such conversion processes, solid biomass is mixed under defined conditions (pressure, temperature, etc.) and high temperatures with an oxidizing agent (e.g., air, water) clearly below the stoichiometric concentration. This enables them to be converted into solid, liquid, and/or gaseous secondary biofuels to be used somewhere else. The chemical processes underlying the respective conversion routes are based on the same fundamental reactions. But the composition of the resulting secondary energy carrier varies depending on, for example, the involved technology, the selected

process parameters, the catalyst involved (if applicable), and the type of biomass used.

In gasification, the solid biofuels are converted as completely as possible into an energy-rich producer gas or synthesis gas and thus into a gaseous secondary energy carrier. After expensive cleaning processes, the gas can be used directly without any further chemical transformation, for example, in an engine, a turbine, or even a fuel cell to provide heat and/or electricity. Alternatively, the gas can undergo a subsequent synthesis process to be converted into a liquid or gaseous biofuel with clearly defined properties (e.g., Fischer-Tropsch diesel, synthetic natural gas (biomethane), hydrogen) for easy use within the transportation sector, for example.

In pyrolysis, solid biomass is converted solely by the (short- or long-duration) application of heat into solids (charcoal), liquids (bio-crude oil), and gases (e.g., CO, H_2, CO_2).

- The aim of fast pyrolysis or intermediate pyrolysis processes is to obtain a maximum yield of liquids (i.e., bio-crude oil). The by-products – e.g., combustible gases and charcoal – can be used to provide the energy needed for the conversion process and/or as a raw material (e.g., active coal as a filter medium). The produced pyrolysis oil or bio-crude oil has to be refined and can then be utilized either as feedstock for the chemical industry and/or as liquid fuel for engines and/or turbines.
- The goal of slow pyrolysis processes is it to convert solid biomass into a solid energy carrier with clearly defined characteristics (i.e., charcoal) and thus improved combustion characteristics compared to the feedstock. This solid carbon can then either be used as a more pleasant source of energy (e.g., for daily cooking in developing countries and for leisure activities (barbecue) in industrialized countries) or as a raw material, for example, in the chemical industry (e.g., as a filter material).

Thus, based on such a thermochemical conversion – besides the provision of heat and electricity – the direct and/or indirect production of solid, liquids and/or gaseous secondary energy carriers is also possible.

Physicochemical conversion. This conversion pathway is used to produce liquid biofuels from organic matter containing oils and fats (e.g., rapeseed, oil palm fruits, sunflower seeds). The oil is separated from the seed, for example, by pressing and/or extraction based on existing process technology well known for centuries. Afterwards the oil is cleaned with existing technical processes to meet the given predefined product standards. The clean vegetable oil can be used as an energy source in its straight form (if the engine is able to burn such a relatively inhomogeneous fuel characterized by considerable differences from conventional diesel fuel) or after a chemical treatment conversion (e.g., transesterification with methanol to fatty acid methyl ester [FAME]). Alternatively, the vegetable oil can be treated with hydrogen (i.e., hydrogenation to hydrogenated vegetable oil [HVO]) or processed together with crude oil in existing oil refineries to provide a fuel with clearly defined characteristics meeting the requirements for the existing transportation fuels (e.g., diesel fuel specification, kerosine specification).

Biochemical conversion. In this group of conversion processes using microorganisms, organic material is split into fragments that could be used to provide new chemical compounds. Hence, this conversion is based on biological processes.

- During alcoholic fermentation, the sugar, starch, and cellulose contained in some types of biomass is transformed into ethanol, which, after distillation and dehydration, can be used as pure alcohol or blended with conventional gasoline to fuel engines and/or turbines.
- In anaerobic fermentation, organic matter is converted into biogas (slightly more than 50% methane; the rest is mainly carbon dioxide). This gas can be used in CHP generating stations to produce electricity and heat or, alternatively, after further processing, upgrading, and where necessary distribution through the existing natural gas grid, used to fuel vehicles designed to use of natural gas.
- Other biochemical conversion options currently under discussion include the production of, for example, hydrogen from some specific types of organism living in an aqueous environment.

Thermochemical Conversion

Thermochemical conversion describes the conversion of preferably solid biofuels into secondary energy

carriers, into final energy, and/or into useful energy based on heat-induced processes. For this conversion option, the chemical basics are discussed below. Then, the solid biofuels usually used within such conversion units are briefly described. The technologies for direct combustion, pyrolysis, and gasification are then presented.

Basics

During the complete thermochemical conversion, solid biofuels are oxidized primarily to carbon dioxide and water by releasing heat. Equation 1 shows the approximate process for wood, which can be described chemically as $C_nH_mO_p$.

$$C_nH_mO_p + \left(n + \frac{m}{4} - \frac{p}{2}\right) O_2 \rightarrow n\,CO_2 + \frac{m}{2}\,H_2O + \text{heat} \quad (1)$$

The complete thermochemical conversion of solid biofuels consists of the following steps: heating and drying, pyrolytic decomposition, gasification, and oxidation (Fig. 4). Within a "classical" biomass combustion unit for heat provision, these four different thermochemical conversion steps are realized at the same place and at the same time. Equation 1 is performed – via different intermediate steps as discussed below in detail – completely (i.e., full oxidation).

Alternatively to overall oxidation (Eq. 1) can be split and performed at different points of time and in various locations. For example, such an interruption can be realized after the steps of heating and drying as well as pyrolytic decomposition; gasification and oxidation take place within another device (i.e., in a different place) and at a different point in time. Another possibility is it to split the process after three intermediate conversion steps (i.e., heating and drying, pyrolytic decomposition, and gasification).

These different steps of the thermochemical conversion are explained below.

Heating and drying. Before any chemical reaction of the organic material (e.g., wood, straw, rice husks) can take place, the biomass has to be heated up. During this endothermic process, water is evaporated at temperatures up to approx. 200°C. Below roughly 100°C free water, and above this temperature, water bound to the molecule structure of the solid biomass, is released as vapor. The water may leave the organic material and thus the reaction zone. Alternatively and/or additionally, this water vapor may act as an oxidizing agent within the processes taking place within subsequent

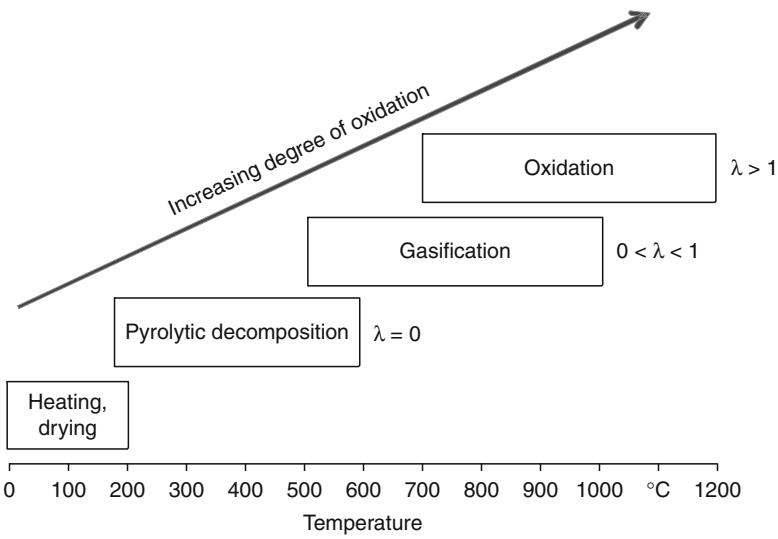

Biomass as Renewable Source of Energy, Possible Conversion Routes. Figure 4
Processes realizing the thermochemical conversion of solid biofuels [1]

conversion steps (e.g., gasification). This process of heating and drying requires energy (i.e., the process is endothermic).

Pyrolytic decomposition. Organic material consists of large macromolecules. If they are sufficiently exposed to thermal energy they are thermally decomposed in smaller chemical molecules (i.e., chemical compounds with only few elements). The products of this pyrolytic decomposition of the solid biomass (i.e., the so-called volatile compounds) are driven out of the organic material. This process is endothermic (i.e., energy is needed) and requires no oxygen.

For example, for wood the pyrolytic decomposition starts at about 200°C with the decomposition of hemicellulose, which is a part of wood material. The decomposition of cellulose (another component of wood) takes place at temperatures of 300°C and higher. Finally the decomposition of lignin (another component of wood) takes place at even higher temperatures. The yield and composition of the volatiles vary depending on the temperature and velocity at which the pyrolytic decomposition is realized. Additionally, the composition of the solid organic material (e.g., wood, straw, leaves) might have an influence overlaid by possible catalytic effects. In general, however, the result of the pyrolytic decomposition is very much the same for different types of solid biomass under comparable process conditions.

During this process, the macromolecules that biomass consists of are fragmented due to the influence of the heat by a similar set of complex decomposition reactions. As a result of such decomposition processes at relative high temperatures, the following components are formed:

- Volatile compounds, such as hydrogen (H_2), carbon monoxide (CO), methane (CH_4), carbon dioxide (CO_2), nitrogen (N_2) and steam (H_2O)
- Carbon rich solid fraction (char)
- Low molecular weight organic compounds and high molecular weight (condensable) compounds (i.e., liquid products)

Gasification. In order to convert the solid carbon remaining after the pyrolytic decomposition into a gas, an oxygen containing gasification agent such as air, pure oxygen, or water is required. Based on this, at temperatures between 700°C to 1,500°C, the solid carbon as well as gaseous products (CO, H_2, CH_4) are oxidized as follows (Eqs. 2–6):

Partial oxidation of solid carbon:

$$\begin{aligned} &C + \tfrac{1}{2}O_2 \rightarrow CO \\ &\Delta H = -111\,\mathrm{kJ/mol} \end{aligned} \tag{2}$$

Complete oxidation of solid carbon:

$$\begin{aligned} &C + O_2 \rightarrow CO_2 \\ &\Delta H = -197\,\mathrm{kJ/mol} \end{aligned} \tag{3}$$

Oxidation of carbon monoxide:

$$\begin{aligned} &CO + \tfrac{1}{2}O_2 \rightarrow CO_2 \\ &\Delta H = -283\,\mathrm{kJ/mol} \end{aligned} \tag{4}$$

Oxidation of hydrogen:

$$\begin{aligned} &H_2 + \tfrac{1}{2}O_2 \rightarrow H_2O \\ &\Delta H = -242\,\mathrm{kJ/mol} \end{aligned} \tag{5}$$

Oxidation of methane:

$$\begin{aligned} &CH_4 + 2O_2 \rightarrow CO_2 + 2H_2O \\ &\Delta H = -802\,\mathrm{kJ/mol} \end{aligned} \tag{6}$$

Additionally, balance reactions take place. The most important are the reduction of CO_2 to CO (Boudouard reaction) and of H_2O to H_2 (heterogeneous water gas reaction). Also, carbon can be transformed to CH_4 (Eqs. 7–9).

Boudouard reaction:

$$\begin{aligned} &C + CO_2 \rightarrow 2CO \\ &\Delta H = 173\,\mathrm{kJ/mol} \end{aligned} \tag{7}$$

Heterogeneous water gas reaction:

$$\begin{aligned} &C + H_2O \rightarrow CO + H_2 \\ &\Delta H = 131\,\mathrm{kJ/mol} \end{aligned} \tag{8}$$

Heterogeneous methane production:

$$\begin{aligned} &C + 2H_2 \rightarrow CH_4 \\ &\Delta H = -87\,\mathrm{kJ/mol} \end{aligned} \tag{9}$$

These and other reactions take place during this gasification conversion step. Depending on the given conditions within the reaction zone (i.e., temperature level, pressure, gasification agent, catalyst (if applicable),

gasification technology), different chemical reactions might contribute in a varying share to the overall gasification. The consequence is that the composition of the gas might be different. Therefore, the gas composition can be influenced to a certain degree by setting the frame conditions within the reactor where these reactions are taking place. For these reasons, during gasification, sometimes energy is needed and sometimes energy is released.

Additionally, some of these reactions can also take place during the pyrolytic decomposition at higher temperatures because the biomass itself contains oxygen. Therefore, the borderline between these two conversion steps can not always clearly defined.

Oxidation. Within this last step of the thermochemical conversion, the gaseous products produced during the previous steps are fully oxidized to carbon dioxide and water. In this chemical reaction, energy is released (i.e., they are exothermic). After the performance of this step, Eq. 1 showing the overall reaction equation is fully realized. At this point the biomass is fully oxydized. Under these conditions, the excess air ratio is 1.0 or above (the excess air ratio is defined as the ratio between the amount of oxidizing agent fed to the conversion process and the amount of oxidizing agent needed to fully oxidize all reaction products; per definition the excess ratio is 1.0 if the conversion process is realized exactly stoichiometrical as shown in Eq. 1).

Solid Biofuels

For thermochemical conversion processes, usually solid biomass is available on the local, regional, and/or global markets. To allow for a highly efficient and an environmentally sound conversion, they should match easily and reliably the needs of the conversion units (and vice versa).

Based on this precondition for sustainable biomass use, two approaches are possible: (a) solid biofuels with very narrowly defined and preferably standardized fuel characteristics and (b) solid biofuels with very low respectively no requests on the fuel characteristics (i.e., no standardized fuel characteristics). The former option has the consequence that a high technical and thus resulting economic effort is needed to provide such clearly defined solid biofuels (as is the case for wood pellets). The advantage is that the fuel characteristics can be adapted accurately to the specification of a specific type of conversion units (and vice versa). For the latter possibility, it is exactly the other way around. Here, the effort to produce the fuel is in general relatively low (e.g., manually produced wood logs, shredded demolition wood). Thus, the technical effort within the conversion plant is significantly higher because it is technologically more demanding to convert fuels with strongly varying fuel characteristics efficiently, securely, economically, and environmentally sound into useful energy compared with the former option.

The choice of which combination will be realized on the market is influenced by the user group, the installed capacity, the environmental demands defined by the responsible legal body, the economic frame conditions, the required comfort level, and the competing energy carrier as well as manifold other reasons.

For the reasons outlined above, currently the following different types of solid biofuels can be found on the local, regional, and global biofuel market.

- *Wood logs.* Wood logs are the "classical" fuel for small-scale heat application in rural areas. The fuel characteristics vary in a relatively wide area and thus the combustion unit has to be designed to ensure that nevertheless a highly efficient combustion is possible meeting local environmental standards. This fuel is mostly traded locally or on a regional basis. Often the fuel is produced by the user itself with a high amount of manual labor.
- *Wood chips.* Wood chips are a bulk fuel characterized by a higher uniformity of the fuel properties compared to wood logs. The consequence is that the production and provision is more technologically demanding. On the other hand – also in opposite to wood logs – a fully automatic production and provision from the forest to the gate of the combustion device is possible. This is also true for use within a conversion unit allowing for a fully automatic operation with a high overall efficiency meeting high environmental standards. Generally, wood chips are used in large-scale units and are traded as an energy carrier mainly on a regional basis.
- *Wood pellets.* Pelletized wood as a bulk material shows very sharply defined and uniform fuel characteristics. To achieve such standardized fuel

properties, a comparably high technical effort (compared to wood chips and especially to wood logs) is needed. This makes the production technologically demanding and the fuel relatively expensive. But such a pelletizing of wood allows for a completely mechanized fuel provision throughout the overall provision chain and a fully automatic fuel provision and use within the conversion plant. And the conversion unit can be adapted in an optimal way to the fuel characteristics. Therefore, this fuel is used in small-scale units for heating purpose as well as in very large units together with coal (i.e., co-combustion). The fuel is traded internationally.

- *Other solid biomass fuels.* In addition to the three groups of wood fuels covering an important part of the globally used solid biofuels, other biomass-based solid fuels are used in some niche markets. This is true, for example, for demolition wood, straw, coconut shells, dried dung, road side green, and dried sewage sludge processed to specific fuels (like straw bales, crushed demolition wood, sewage sludge pellets). These types of solid biofuels can only be used environmentally if the provision chain and especially the conversion unit is fully adapted to the fuel characteristics. Therefore, such special fuels are mostly used on a regional basis, partly under very specific circumstances and/or frame conditions (e.g., dried dung as a solid fuel in India because of a lack of wood fuel, sewage sludge in co-combustion with lignite in large-scale power plants to get rid of this material for environmental reasons, demolition wood in Sweden for greenhouse gas reduction reasons).

Direct Combustion

The thermochemical conversion of solid biofuels produced from biomass into heat is called combustion (i.e., the simultaneous performance of the conversion steps of heating and drying, pyrolytic decomposition, gasification, and oxidation). The heat released during the fully oxidation of the organic material can be used directly at the conversion plant (e.g., for cooking, space heating) or can be transported by means of a heat carrier (i.e., hot water, steam) to the place of consumption (e.g., district heating systems, heat distribution system within a dwelling house). The thermal energy can also be converted via a steam turbine or by co-generation (also known as combined heat and power (CHP) process) into electricity and low temperature heat. Because of economic limits, only relatively low conversion rates of biomass fuel energy into electrical energy (maximum of 30–35%) are possible at present in typically realized biomass plants due to economic constraints. Therefore, biomass co-firing in modern, large-scale coal power plants with efficiencies up to 45% is regarded as a cost-effective option for the use of solid biofuels if the goal is only the provision of electrical energy. In addition, the use of CHP could increase the overall conversion efficiency significantly to roughly 80% and even more by lowering the electricity generation efficiency slightly. The obstacle preventing an increased use of such highly efficient CHP systems based on solid biofuels is the often missing heat sink characterized by a high demand throughout the overall year (i.e., 8,000 full load hours) and/or the nonexisting (expensive) heat distribution infrastructure.

The conversion technology required to realize a full combustion of the solid biofuel depends on the installed capacity, the fuel consistency, water content within the solid fuel, the ash melting behavior, trace elements contaminants, and many other factors. Where these conditions vary unexpectedly (the conversion plants are designed for a specific fuel with clearly defined characteristics), for example, with changeable mixtures of biomass species in the feed, performance of the conversion plant will inevitably suffer.

Modern combustion devices are designed to realize a spatial separation between the thermochemical conversion process heating and drying, pyrolytic decomposition, and gasification as well as the full oxidation of the released gases into CO_2 and H_2O. The former is realized by primary air feed into the glowing fire and the latter through secondary air feed preheated into the burning gas released by the glow, preferably in a relatively hot after-burning chamber. To achieve low unwanted airborne emissions, especially of volatile organic compounds (VOC; i.e., the typical smell of combusted wood), good mixing of air and combustible gas at high temperatures as well as a sufficient residence time of the gases within the hot zone to allow them to be fully oxidized are necessary. Additional design features assist in reducing particulate matter emissions, including those for keeping flue gas velocities low in

some specific places within the combustion unit so that ash particles can settle down and thus are not entrained.

Table 2 gives an overview of combustion technologies primarily used in industrialized countries. The characteristics of a few major systems are discussed in more detail below.

Wood pellet stove. One example of such combustion technologies are automatically feed wood pellet stoves. These combustion devices have been developed throughout the last decades for standardized pellets. On the back side of the device for the provision of heat (e.g., for a living room; Fig. 5), a container is located to store the solid fuel for automatic operation over a certain period of time. The pellets are transported from this storage facility via a screw to a pipe from where the wood pellets fall into a special designed combustion chamber. Primary air is fed by nozzles through the bottom of this combustion bowl. Preheated secondary air is blown above the burning fuel via ring-shaped nozzles to ensure the complete oxidation of the gaseous fuel components released by the glow into CO_2 and H_2O. Additional air is feed into the system via the fall pipe to prevent fire flashback into the fuel container. This design allows achieving very low airborne emissions. It fulfills even the very strict emission regulations valid in some European countries. The ash produced during the combustion of the wood pellets is collected within an ash container to be removed and drained off manually. During ordinary operation the combustion residues (i.e., ashes) contain less than 1% carbon and can thus be used as a fertilizer or taken to a landfill depending on the legal regulation.

The thermal efficiency of such systems can reach 95% or more. Emissions are considerably lower compared to "classical" stoves fired with wood logs because the design of the combustion device is optimal adjusted to the standardized and well-defined characteristics of the pellets. Additionally, the fully automatic control system allows for a plant operation within the most efficient point of operation. This ensures that the conversion efficiencies are maximized. Also, a continuous, fully automatic operation is possible and in most cases realized; the operational comfort is basically comparable with a boiler operated with light heating oil or even natural gas. Such heating ovens can be operated over a wide range of power demands, that is, between approx. 30% and 100% of the rated capacity.

Biomass as Renewable Source of Energy, Possible Conversion Routes. Table 2 Typical combustion technologies and their characteristics

	Combustion technology	Typical thermal capacity	Biofuels
Manually fed systems	Open/closed chimney	2 to 15 kW	Wood logs, wood briquette
	Single stove	3 to 12 kW	
	Tiled stove	2 to 15 kW	
	Pellet stove	3 to 10 kW	Pellets
	Wood log stove	10 to 500 kW	Wood logs, wood briquette
Automatic fed systems	Gasification firing system	20 kW to 2 MW	Wood chips
	Under feed system	20 kW to 2 MW	Wood chips, wood shavings and filings
	Grate firing system for wood	150 kW to 15 MW	Wood, bark
	Fluidized bed system	From 10 MW	Wood, bark, sewage sludge, black liqueur
	Grate firing system for herbaceous biomass	50 kW to 20 MW	Bales, chipped herbaceous biomass
	Blow in firing system	200 kW to 50 MW	Dust, shavings and filings

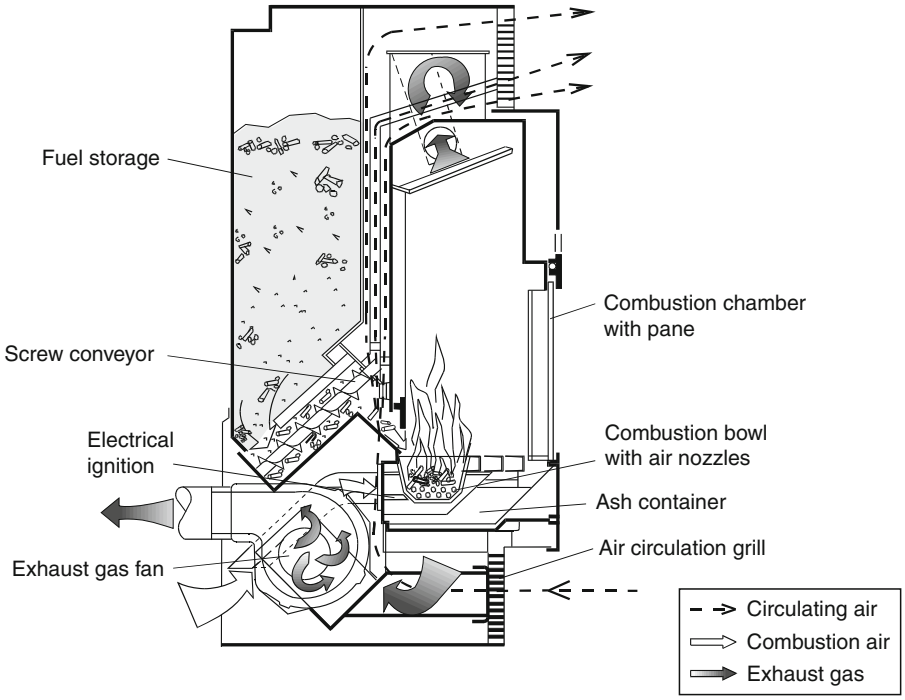

Biomass as Renewable Source of Energy, Possible Conversion Routes. Figure 5
Combustion device fired with wood pellets [1]

Wood chips combustion unit. A typical example for a heating device for wood chips is equipped with a throw-charging system where wood chips are transported from fuel storage with a stoker scroll and thrown with the help of a centrifugal wheel into a combustion chamber designed with a stiff grate. Such a fully automatic feeding system allows the smaller fuel particles to be combusted during the flight to the grate while more coarse fuel particles are burned on the grate. The system also has the advantage that the fuel is fed gently on the fire, thus reducing airborne emissions of particulate matter.

The primary air is blown with an automatic ventilator through holes in the grate into the glowing fire. The preheated secondary air is blown into the combustion chamber on the top of the burning fuel. The air feeding system adjusts itself automatically according to information from a sensor fixed in the flue gas outlet, minimizing unburned flue gas components and thus meeting the given emission limits. Such devices are characterized by relatively low emissions and the ash can be used as a fertilizer or put on a landfill site depending on the legal frame conditions.

The heat is extracted from the flue gas via a heat exchanger located on top of the combustion device. Within the heat exchanger, the flue gas is cooled down and water is heated up – depending on the heat utilization system – either close to the boiling point (to be used in hot water systems) or to steam, for example, for electricity generation.

Such combustion systems are characterized by a fully automatic operation. They are available on the market in the range of thermal capacities of 300 KW up to approximately 3,500 kW and can be used either for the heat provision for single- or multi-family houses or for industrial process heat. Also, a CHP operation is basically possible for such systems in the upper capacity range if an ORC (Organic Rankine cycle) process is integrated; but the electrical efficiency of such CHP-units are relatively low.

Pyrolysis

In this technical conversion process, solid biofuels are heated up within a nearly oxygen-free environment

(i.e., no oxygen from outside is added, but within the biomass some oxygen is present that might influence the conversion process). At temperatures up to about 200°C, the biomass is first dried and water is evaporated. With increasing temperatures up to roughly 500°C, the organic matter is almost decomposed (i.e., the macromolecules originally within the biomass are split into smaller molecules). During this decomposition process, solid, liquid, and gaseous products are provided from the solid biomass. The share and composition of the different products or product groups depends, for example, on the temperature range the pyrolytic decomposition is realized at, the presence of catalysts, the heating up rate of the biomass, the speed of cooling down the provided products, and the composition of the used solid biofuels. At the moment, two main applications of such a pyrolytic decomposition can be found on the market: processes designed for the production of charcoal and for the provision of bio-oil.

Charcoal from wood or from herbaceous biomass can be produced with a broad variety of different technologies. In developing countries, for example, basic traditional charcoal kilns are usually made from earth or brick, although low-end metal kilns are sometimes found. The overall conversion efficiency between the energy content of the wood and the energy content of the charcoal of such basic devices is rather low (sometimes less than 25%) in general and the airborne emissions of, for example, volatile organic compounds and odorous substances are relatively high. Additionally, considerable amounts of a mixture of toxic liquids (like alcohols and tars) are produced depending on the conversion technology and their operation management.

In industrialized countries, charcoal is produced in large, fully automatic industrial devices. In general, a differentiation is made between retort and flush gas processes.

- Within the retort processes the charcoal is produced in a batch mode within a closed container (i.e., retort). Here, the conversion from wood or other solid organic matter to charcoal takes place. The thermal energy necessary to run this process is obtained from the combustion of the gaseous and even liquid products released from the biomass feedstock during this charcoal production. If there is a market the liquid products might be sold.
- Within continuous charcoal production systems (like flush gas processes), the wood (or other solid biomass) is moving continuously through a reactor. This reactor is characterized by different zones with various settings of reaction conditions (e.g., temperature) to ensure that the charcoal is produced continuously and efficiently during the migration of the biogenic material through the reactor. Here, too, the gases and maybe even liquids produced as by-products are used as a source of energy to keep the coalification process going. Depending on the market conditions, the liquid by-products can be sold, for example, to the chemical industry.

With basically similar processes – but different process conditions – the solid biomass can be converted to maximize the yield of liquid products (i.e., bio-oil); the process conditions where the pyrolysis takes place are set to ensure that the main products of the thermochemical conversion process is liquid rather than solid or even gaseous. Due to extensive research activities carried out during the last decades, a broad variety of different technologies are available in various technical development stages attempting to provide pyrolysis oil (i.e., bio-oil), which can easily be used as an liquid energy carrier to be used, for example, in diesel engines. Besides the use as a liquid fuel, bio-oils are also used as a raw material, for example, as a flavor substance for meat products.

With current knowledge, such a conversion of solid organic matter to a liquid can most promisingly be realized with so-called flash pyrolysis. Here the biomass particles are heated up very rapidly (more than 1,000°C/s) and remain in the hot zone for a very short retention time (in general less than 1 s). After this very short time period, the volatile compounds produced by decomposing the organic macromolecules of the solid biomass (i.e., lignin, celluloses) and released from the organic matter are removed quickly from the hot reaction zone. Then they are cooled down rapidly to avoid a further decomposition into gases. To date, various technological approaches for such flash pyrolysis reactors have reached laboratory and pilot stage development level. The first semi-commercial plants are even available. There is also a commercially viable niche application with a very similar technology producing flavor substances.

One example for the technical realization of this principle is a reactor with ablative impact design. Here,

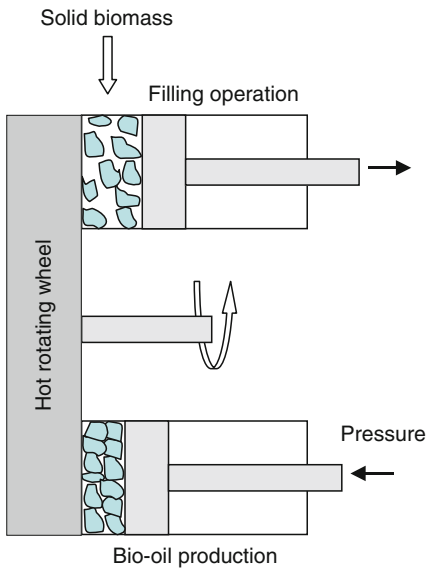

Biomass as Renewable Source of Energy, Possible Conversion Routes. Figure 6
Pyrolysis system based on a hot rotating wheel [1]

the organic raw material is decomposed into liquid and gaseous components on the surface of a hot rotating wheel (Fig. 6). To avoid further decomposition of the components released from the solid biomass, these products are removed immediately from the hot zone. After that they are quickly cooled down to produce the desired liquid energy carrier. Gaseous and solid components are also produced, which are used to heat the wheel and/or to provide additional products (e.g., charcoal).

The produced pyrolysis oil is a mixture of different hydrocarbons (many of which are partly oxygenated and some of which might be toxic) along with solid carbon (i.e., charcoal particles), ash particles, and water. The actual composition strongly depends among other influencing parameters on the pyrolysis process as well as the specific process conditions, the availability of catalysts, and/or the type of biomass. This is especially true for the composition and structure of the produced hydrocarbons (e.g., chain length, degree of double bonding). This bio-oil is in most cases not stable in air because the double bounds are oxidized. The average heating value of pyrolysis oil is approximately 40% that of petroleum-based fuels. Also, the conversion efficiency between the energy content of the solid biomass and the produced bio-oil of the fast pyrolysis processes available so far is relatively low.

The overall development goal of such processes is the provision of a liquid energy carrier that can be used directly in engines, for example, for the provision of heat and electricity (CHP) and/or within the transportation sector. Thus far, the pyrolysis oil produced in the available plants cannot be used directly in existing engines. Therefore, the produced oil needs to be upgraded within an expensive process. For example, charcoal and ash particles have to be removed to ensure a clean fuel, and, to increase stability, double bonds need to be broken by adding hydrogen. Additionally, other measures have to be taken to ensure that the viscosity and combustion behavior required by the respective engine is fulfilled. This upgrading process lowers the overall efficiency even further and makes the overall process even more expensive.

Gasification

Gasification describes the conversion of solid biomass at high temperatures into a gaseous fuel. The main objective of this thermochemical conversion is to transfer the maximum possible share of the chemical energy within the biogenic feedstock into a gas useable, for example, as a source of energy. To realize this for physical and chemical reasons, small amounts of oxidizing agents need to be added to this process; this is the difference with pyrolysis, where basically no additional oxygen is added to the conversion process.

This so-called "producer gas" can be used, on one hand, as a fuel for the provision of heat through direct combustion or for the provision of heat and electricity (CHP) in engines, turbines, or even fuel cells. On the other hand, the producer gas can act as a feedstock for the production of liquid and/or gaseous biofuels (like Fischer-Tropsch diesel, biomethane, methanol, hydrogen) as well as for the provision of bulk chemicals and other raw materials.

Biomass gasification consists of the following, more or less spatially distributed, conversion steps: heating and drying, pyrolytic decomposition (i.e., extracting the volatile components by heat), and gasification (i.e., partial oxidation of the products of the pyrolytic decomposition, partial reduction of the oxidation products [CO_2 and H_2O to CO and H_2], and

simultaneous transformation of solid carbon [i.e., charcoal] to CO).

This conversion of solid biomass into an energy rich gas is carried out within a broad variety of different technical concepts developed during the last decades. Each of them offers certain advantages and disadvantages concerning, for example, required feedstock characteristics, installed thermal capacity, technical efforts, and gas quality.

These gasification techniques can be subdivided related to different criteria such as, for example, reactor type (fixed bed or fluidized bed), gasifying agent (air, oxygen, or steam), heat supply into the reactor (directly or indirectly heated) and reactor pressure (atmospheric or pressurized). Here a distinction is made according to the reactor type.

- In fixed-bed reactors (Fig. 7), the feedstock is exposed to the gasifying agent in a packed bed that slowly moves from the top of the gasifier to the bottom, where the ash is discharged. Fixed-bed gasifiers are dense-phase gasifiers. They are characterized by a relatively large amount of fuel exposed to a limited amount of reactive gas. In fixed-bed reactors, the solid feedstock occupies most of the reactor volume. Depending on the way of the gas flow through the reactor relative to the fuel flow, two types of fixed-bed gasifiers are distinguished: the updraft and the downdraft type. The former is characterized by a relatively cold producer gas with a high amount of condensables (i.e., tars) compared to the latter (i.e., hot producer gas, low tar content). Fixed-bed reactors are used mostly only for small-scale applications.
- Fluidized-bed gasification reactors are lean-phase gasifiers having a low ratio of solids to reactor volume. Typically, the solid feedstock is occupying only a small fraction of the total reactor volume. Such fluidized-bed gasifiers are classified, depending on the intensity of fluidization, as bubbling fluidized-bed gasifiers, or circulating fluidized-bed gasifiers. Basically, fluidized bed gasifiers are a large-scale technology. So far, they are used for CHP applications. In the years to come, the provision of a producer gas to be used for the synthesis of liquid or gaseous biofuels might gain more importance.

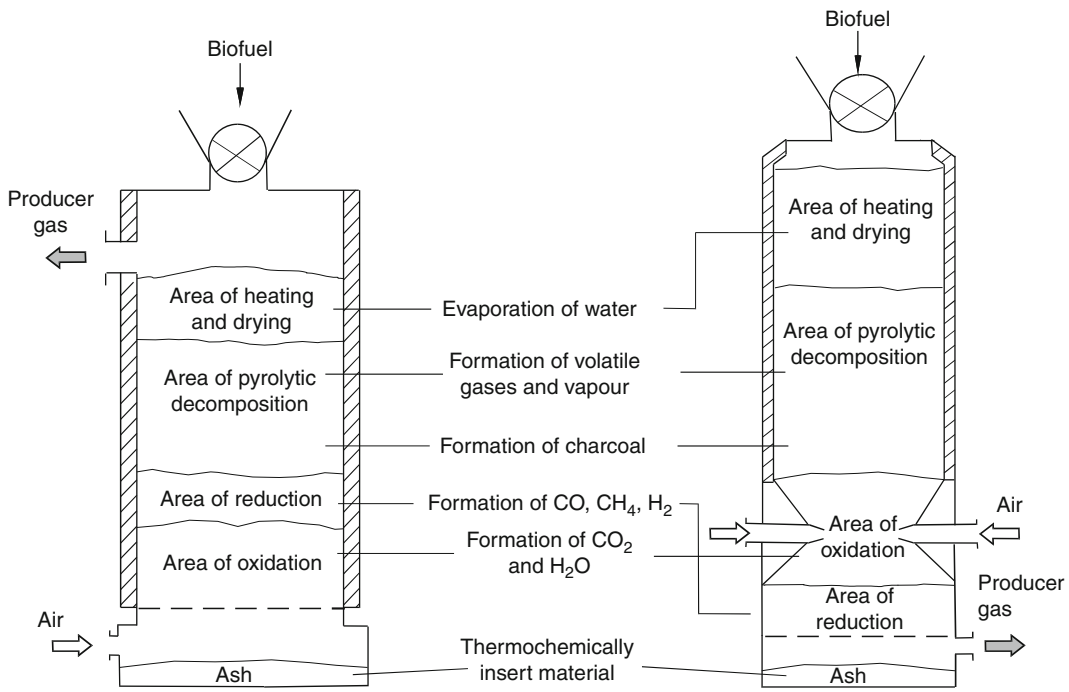

Biomass as Renewable Source of Energy, Possible Conversion Routes. Figure 7
Principle of an updraft gasifier (*left*) and a downdraft gasifier (*right*) [1]

Thus, this option is often seen as a key technology also for such applications.

- Within entrained flow gasifier the gasification of the biomass particles takes place within a few seconds during pneumatic transport through the reactor. This requires very small biomass particle diameters and high temperatures to complete the gasification reactions within this short time. The fuel is typically feed in from the top together with the gasification agent (steam/oxygen). In the upper part of the reactor gasification is carried out and in the lower part the producer gas is quenched and separated from the ash. The latter is withdrawn in granulated form. Producer gas leaves the reactor at the lower part.
- Gasifiers have also been developed that cannot easily be classified as belonging to one of the former groups but might have features of both.

Commonly, the overall goal of such a thermochemical gasification is not to provide the gaseous fuel itself but to provide an easy-to-handle and environmentally sound intermediate energy carrier with clearly defined fuel characteristics that can be converted easily into another, more valuable, energy carrier (e.g., electricity, biomethane). Alternatively or additively, the producer gas can also be used as a feedstock for the production of raw materials (e.g., bioplastics, lubricants, bulk chemicals, pharmaceutics). To reach that goal, an extensive cleaning of the producer gas to fulfill clearly predefined threshold values and even a conditioning is usually necessary to ensure a long lifetime of the downstream conversion with its respective processing device. The reason for this is that the gas produced within the gasifier does usually not match the fuel requirements in terms of condensable organic compounds and/or particles. Additionally, the producer gas might contain some trace elements (like sulfur) that could poison the catalysts used during the downstream processing. If this is the case, additional expensive gas cleaning steps are necessary.

For the provision of a gas to be used as a fuel, for example, for CHP-systems (e.g., engines, turbines) a raw gas cleaning operation – either low temperature wet gas cleaning or, alternatively, hot gas cleaning – can be applied. The technical maturity and effectiveness of wet gas cleaning (e.g., cyclone and filter, scrubbing based on chemical and/or physical absorption) has been well proven for large-scale coal gasification systems. However, not all elements of hot gas cleaning (e.g., tar cracking, granular beds and filters, physical adsorption or chemical absorption, physical absorption) are market mature. Nevertheless, hot gas cleaning offers benefits for the overall energy balance and avoids the production of contaminated waste.

The cleaned producer gas can be used for the provision of electricity within engines or gas turbines. The former has been demonstrated already for years within the gasification plant in Güssing/Austria, where wood chips are gasified and the producer gas is then used within an engine-based CHP-plant for the simultaneous provision of heat and electricity. Similar systems are in operation and under construction or planning in other countries. The next development step will be biomass-based integrated gasification combined cycles (IGCC). Such plants allow providing a significantly higher share of (valuable) electricity and a smaller share of heat. But the technical realization is still quite challenging.

According to the ongoing discussion in energy industry and energy politics, biomass gasification is currently more in discussion as the key process step for the production of synthesized biofuels (Fig. 8) (so-called biofuels of the next generation). Such a synthesis of a secondary energy carrier based on carbon monoxide and hydrogen consists mostly of catalytic induced chemical synthesis processes. And these catalysts used for the realization of such chemical processes are sensitive with respect to some trace elements (e.g., sulfur). If such trace elements are present within the process, the catalyst could be poisoned on the shorter or longer term. This lowers the technical lifetime significantly and makes the process much more expensive. For this reason the producer gas has to be characterized – depending on the demand defined by the involved catalyst – by very low content of impurities that are potentially harmful to the downstream processing steps.

For the provision of a synthesis gas basically the same gas cleaning processes and technologies are used as for gas cleaning for the provision a producer gas, for example, for electricity provision. But due to the much more demanding requests and demands on the quality of the producer gas (e.g., the amount of unwanted impurities) these cleaning technologies are used more intensively within combined processes.

In addition to extensive gas cleaning, the ratio between carbon or carbon monoxide and hydrogen,

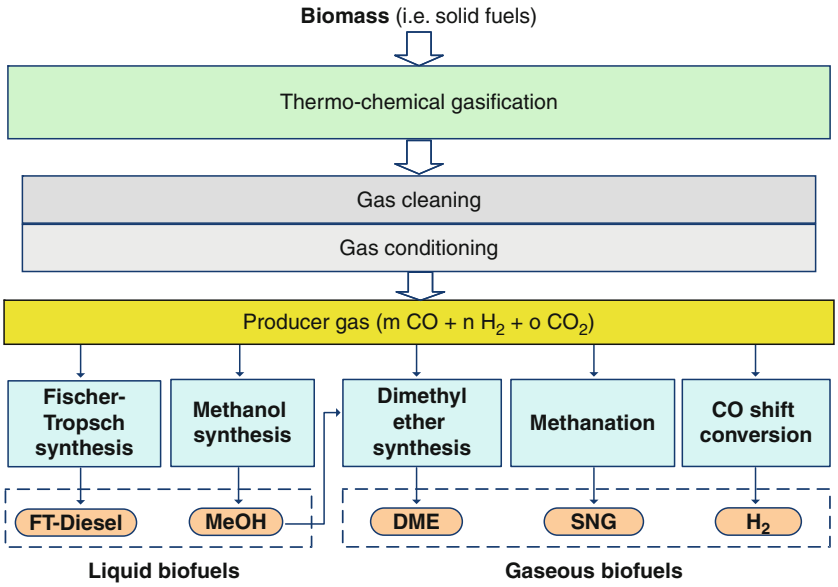

Biomass as Renewable Source of Energy, Possible Conversion Routes. Figure 8
Possibilities to produce liquid and/or gaseous fuels from producer gas respectively from biomass

for example, within the cleaned producer gas and the desired product (i.e., DME, SNG) has to be adjusted (i.e., the producer gas has to be conditioned). For example, the C to H ratio within the solid biofuel (e.g., wood, straw) is in most cases significantly lower compared to this ratio in methane or Fischer-Tropsch diesel. This makes it necessary in most cases to add hydrogen to the overall process (or to remove carbon, which is the less promising option).

Such a necessary adjustment of the gas quality can be realized, for example, by a steam reforming step. Additionally or even alternatively, the gasification can be realized with a gasifying agent rich in hydrogen (e.g., water) instead of air or oxygen to add hydrogen already at this early stage to the overall process.

The cleaned and conditioned gas can then be used for the synthesis of liquid and/or gaseous fuels. Currently, the following four conversion routes for the provision of a liquid or gaseous fuel for transportation purpose are under investigation and partly under development.

- Fischer-Tropsch Synthesis:
  $CO + 2\ H_2 \rightarrow (-\ CH_2\ -)n + H_2O$
- Methanol Synthesis:
  $5\ H_2 + CO + CO_2 \rightarrow 2\ CH_3OH + H_2O$
- Dimethylether (DME) Synthesis:
  $3\ CO + 3\ H_2 \rightarrow CH_3OCH_3 + CO_2$; $CO + CO_2 + 5\ H_2 \rightarrow CH_3OCH_3 + 2\ H_2O$
- Methanation:
  $CO + 3\ H_2 \rightarrow CH_4 + H_2O$; $CO_2 + 4\ H_2 \rightarrow CH_4 + 2\ H_2O$

The synthesis of Fischer-Tropsch diesel, methanol, and methane is market mature and in large-scale operation for decades using fossil fuels (e.g., coal). For biomass feedstock, however, this technology is still under development. So far, none of these synthesis processes are realized on a commercial basis. But due to the successful demonstration of the technological maturity for fossil fuel energy, it can expected that these processes can also be realized successfully for biomass feedstock.

Physicochemical Conversion

Some biomass components contain fatty and/or oily components (e.g., rape and sunflower seeds, coconuts, peanuts, corn, palm fruits). The content of the vegetable oil or fat within the biomass varies quite significantly. In some cases, the oil seed may contain 40–45% vegetable oil; in other cases the oil content is only within the one digit percent range.

Based on physicochemical processes, the vegetable oil or fat can be removed from the organic material in its pure form and can then be used as a source of energy. Compared to solid biofuels, vegetable oil or fat has some outstanding advantages. It is easy to store, has a high energy content, can easily be handled, and can be used as an energy carrier, for example, in existing oil burner for the provision of heat and/or in some (older) engines for the provision of heat and electricity (CHP). However, just like crude oil, pure vegetable oil cannot always be used easily in its raw or unprocessed form because the fuel characteristics do not necessarily match the fuel standards the conversion device (e.g., engine) is designed for. Thus, this organic material needs to be additionally processed to fulfill the fuel standards valid for the specific application aimed for. Such a processing of the crude vegetable oil or fat can be realized within a crude oil refinery together with crude oil to yield kerosene or diesel fuel (i.e., co-rafination). Alternatively, vegetable fats and oils can be hydrogenated and/or chemically treated to meet the fuel characteristics of conventional diesel fuel.

Next, the process technology for the provision of vegetable oil or fats from oil seeds and the provision of a fuel meeting current fuel standards are described.

Oil Production

Depending on the vegetable oil content, the oil characteristic, and the properties of the oil seed, different technical approaches have been developed throughout recent centuries to produce the oil or fat in a cost-effective way. Basically, these approaches consist of one or a combination of the two technical processes, pressing and extraction.

During pressing, the "classical" process for vegetable oil production used by humans since ancient time, the oil is squeezed out of the oil seeds (and therewith out of the organic material) based on a one- or two-stage pressing process. To achieve a maximum oil yield, the organic matter is preheated to lower the viscosity of the oil. Two products are obtained as a result of such a treatment: the liquid vegetable oil and the solid oil cake. The latter still contains 4–10% oil. Sometimes this oil cake is used as cattle feed where the remaining oil contributes to the nutrition value of this product. Even today such processes are still in large-scale operation (e.g., traditional olive oil production).

Alternatively and/or additionally, the vegetable oil can be removed from the organic material by means of extraction. Such an extraction is realized with the help of a solvent (e.g., hexane) applied in a countermovement to the biomass containing the oil. This technology has been widely employed and optimized for many decades worldwide. It is used on a large scale with in all existing large industrial oil mills. Within such a technical process, two different material streams are produced: the solvent saturated with vegetable oil and the oil-free extraction residue saturated with solvent. Therefore, the solvent must be removed from both material streams. This is usually realized by introducing heat. The solvent is evaporated and leaves the material as vapor. The solvent vapor is collected, condensed, stored, and reused. Compared to pressing, a much higher share of the oil originally contained within the biomass (e.g., oil seed) can be removed. After extraction the meal contains significantly less than 1% oil. In most cases, this basically oil-free residue is used as cattle feed. Alternatively, this biomass can also be used as a substrate for biogas plants or as a fertilizer.

For oil seeds with high oil content, like rape seed, pressing followed by extraction will allow minimizing the costs by maximized oil yields and minimized losses. But also from a technological point of view the combination is more promising for such types of biomass. Therefore, the decisions about using pressing or extraction is mainly determined by economic constraints.

The produced vegetable oil contains about 0.5–6% oil-free solid residues originating from the seed. The amount of such solids within the oil mainly depends on the condition of the pressing aggregate, the realized flow-rate, the kind and status of pressed seed, and the water content in the oil seeds. These solid impurities have to be separated from the vegetable oil by filtration and/or sedimentation to prevent possible problems during the further downstream processing of the vegetable oil. But even after this cleaning step, the vegetable oil is not qualified for direct utilization as an energy carrier because in most cases it still contains unwanted substances (fatty acids, ketones, waxes, pigments, heavy metals, pesticides), reducing shelf life and complicating subsequent processing and use. For this reason, a further refining is needed. This leads typically to a loss of 4–8% of the usable

vegetable oil mass through de-acidification, de-coloring, and steaming. These processes are also needed for the production of vegetable oil as food and fodder as well as for the provision of oil as a raw material (e.g., for the production of cosmetics or chemicals).

Pure vegetable oil can be used in some (mostly older) existing engines, either for mobile (e.g., in cars or especially trucks) or stationary applications (i.e., in engine-based CHP systems). In most cases, vegetable oil in its natural form lowers engine lifetime and increases maintenance requirements because the standards for fossil fuels (like diesel) are only partly fulfilled by crude vegetable oil. Therefore, only under very specific frame conditions the use of crude vegetable oil is a promising option for the transportation sector or to provide power (or power and heat (CHP), if required). Only for heat provision crude vegetable oil can be used in most cases. But due to economic constraints, these applications are only very scarce.

Conversion to a Standardized Fuel

Due to problems with the use of crude vegetable oil in existing diesel engines outlined above, in most cases the oil is converted into a liquid fuel fulfilling characteristic parameters defined within valid fuels standards. Different approaches are possible and realized on the market to achieve this goal.

The most widely realized option to convert refined vegetable oil into a standardized fuel is the conversion of the oil into fatty acid methyl ester (FAME) (Fig. 9). During this process the glycerin is removed from the triglyceride, which is the common chemical structure of vegetable oil (Fig. 9). To saturate the ester bindings instead of the glycerin, methanol or even ethanol is added to the remnant. This reaction is realized at a certain temperature level and triggered by a catalyst.

This transesterification process can be transformed in various ways into process technology. One example for the technological realization is shown in Fig. 10. According to this, a mixture of vegetable oil together with a catalyst and methanol in surplus (to force the reaction into the right direction) is pumped with a low velocity through a vertical pipe. The low-flow velocity of the liquid ensures that the glycerin produced during the transesterification process taking place can settle down within the reactor and can then be removed from the process. The glycerin can then be cleaned and used as a raw material (e.g., within the pharmaceutical industry) or as a source of energy (e.g., as an additional feedstock for biogas plants). After the removal of the methanol not used during the transesterification process from the remaining mixture, the liquid is cleaned by a multi-stage washing process to fulfill the standardized fuel characteristics. The produced FAME now shows characterizing parameters close to those of conventional diesel fuel. This can be used as a fuel either within most of the existing diesel-driven power trains for cars and trucks or in engine-based CHP-systems without any further problems. Additionally, a mixture

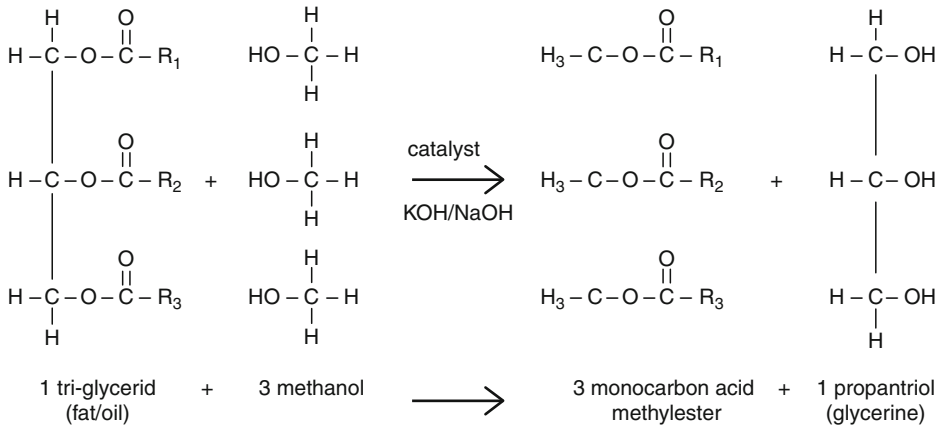

Biomass as Renewable Source of Energy, Possible Conversion Routes. Figure 9
Transesterification of vegetable oil to fatty acid methyl ester [1]

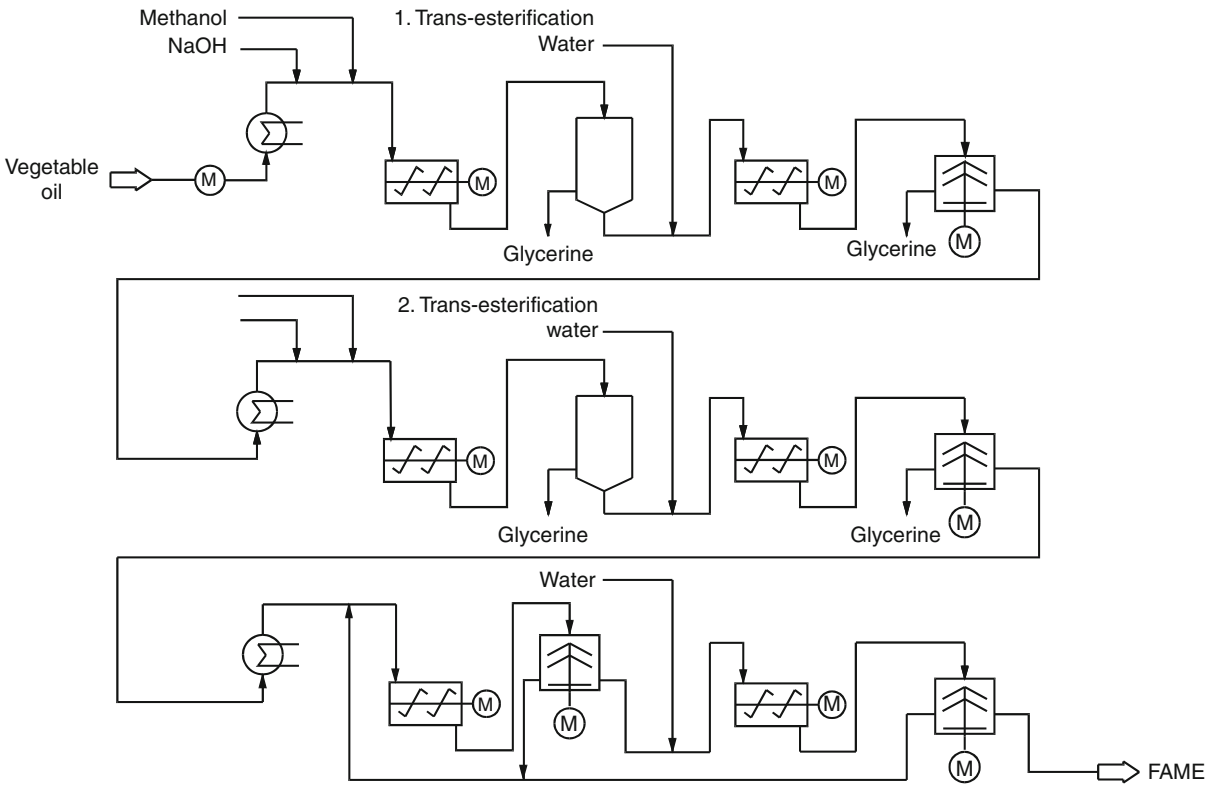

Biomass as Renewable Source of Energy, Possible Conversion Routes. Figure 10
Example for a continuously working transesterification process for FAME manufacturing [1]

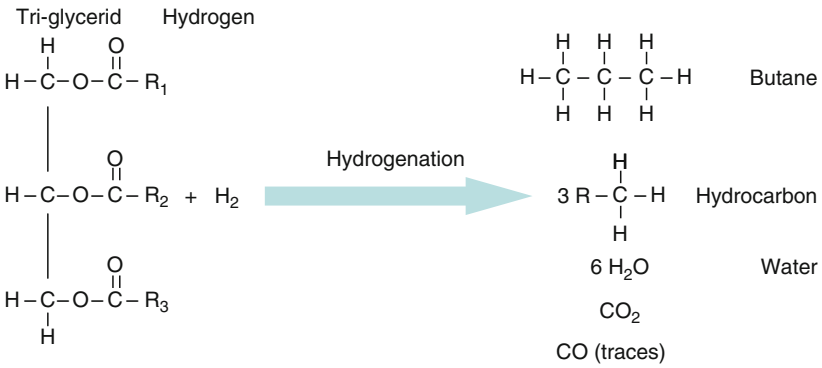

Biomass as Renewable Source of Energy, Possible Conversion Routes. Figure 11
Hydrogenation of vegetable oil [2]

between 0% and 100% with conventional fossil diesel is easily possible. This makes the logistics much easier.

Alternatively to the conversion into FAME, vegetable oil can be treated with hydrogen under presence of a catalyst using the hydrotreating technology usually employed in conventional crude oil refineries. The product is called hydrogenated vegetable oil (HVO). By doing this the partly existing double bonds of the vegetable oil are saturated with hydrogen and only fully saturated hydrocarbons remain (Fig. 11). Additionally,

the oxygen that is naturally part of the crude vegetable oil molecule is removed from the oil and converted into water. This produced water can then be easily removed from the process. Also, the glycerin linking the three hydrocarbon chains within the oil molecule (i.e., triglyceride) is hydrogenated. During this process (bio-) butane is produced. Thus, fully saturated hydrocarbons (i.e., alkane chains), water and butane are produced. All of these chemicals are desirable within such a hydrogenation process. Not desired (but unavoidable) is the production of carbon dioxide or even carbon monoxide. The former might cause problems within the process technology and the latter could poison the catalyst needed within the process. Therefore, based on technical measures, such a production has to be avoided as much as possible.

Such a hydrogenation is realized within a hydrotreater, which is also a part of a conventional crude oil refinery. Within such a reactor, the chemical reactions mentioned above take place. They are supported by catalysts to ensure that hydrocarbon chains are produced that fulfill the given fuel specifications. This production pathway is market mature and it can be expected that it will be used more widely in the years to come.

Basically the same process can also be realized within a conventional crude oil refinery. Here, the crude vegetable oil and the crude fossil oil can be treated together (so-called co-refining). The vegetable oil is mixed with the crude oil fraction coming from the atmospheric distillation before it is pumped into the hydrofiner. Within the hydrofiner, the hydrogenation of the vegetable oil is realized. In parallel, the sulfur originating from the crude fossil oil is converted into H_2S, which is the main task of this system element within a conventional refinery to fulfill the ambitious sulfur limits set by the government in recent years within the refinery products. The gaseous H_2S can then easily be removed from the liquids and converted within a Claus process into elementary sulfur. It has been shown that co-processing of vegetable oil with the diesel or kerosene crude oil fraction within a hydrofiner usually available in existing crude oil refineries can be realized successfully without major technical problems.

Basically, all three ways to treat vegetable oil are technically feasible and allow the production of a fuel fulfilling the existing diesel standards.

Use

FAME, HVO, or co-processed vegetable oil can be used directly as a substitute for diesel fuel in conventional compression ignition engines or in CHP-systems with installed capacities from some tens of kW up to several tens of MW. Prerequisite for that is that the treated vegetable oil fulfils the existing standards (Table 3). Normally, this is easily possible with co-refined vegetable oil and HVO. But also with FAME based on rape oil this is usually the case. It might be difficult, however, using other types of vegetable oil for the production of FAME (like palm oil).

Biomass as Renewable Source of Energy, Possible Conversion Routes. Table 3 Selected properties of diesel fuel, FAME and rape oil (various sources)

	Diesel fuel/light heating oil	FAME	Rape oil
Density (15°C) in kg/m^3	820–845	875–900	900–930
Viscosity (40°C) in mm^2/s	2.0–8.0	3.08	78.7
Flash point in °C	>55	130	Min. 220
CFPP-value in °C (summer/winter)	Max. 0 Max. −20	Max. 0 Max. −20	
Sulfur content in mg/kg	Max. 350	Max. 100	Max. 20
Cetan-value	Min. 51	55	
Calorific value in MJ/kg	42.7	37.9	Min. 35

Biochemical Conversion

All existing organic matter can be decomposed naturally through biological processes. But some of these biological degradation processes can be harnessed to produce fuels useable in technical processes.

- Composting occurs if oxygen is available. During this aerobic biological process biomass is degraded by bacteria mainly to carbon dioxide (CO_2) and water (H_2O) while releasing low-temperature heat. This thermal energy can, in principle, be used via a heat pump for heat provision. But, for the time being, this option is only of theoretical importance. Nevertheless large volumes of biomass are composted and the released thermal energy is wasted.
- Under anaerobic (oxygen free) or nearly anaerobic conditions, a huge variety of partly very different degrading processes are employed by microorganisms. Only very few of them are deeply understood and used by humans so far. Currently, most relevant to energy are ethanol production via alcoholic fermentation and biogas (methane) production via anaerobic digestion. Nevertheless other biochemical conversion processes under anaerobic conditions for the provision of energy carrier and chemicals are under investigation and/or development.

Alcoholic Fermentation

Under anaerobic conditions, sugar ($C_6H_{12}O_6$) can be converted to ethanol (C_2H_5OH), carbon dioxide (CO_2), and low temperature heat by yeast (and thus by biological processes). Because starch and even celluloses can be transformed more or less easily into sugar, biomass fractions containing these components are also a potential resource for the production of ethanol in addition to naturally sugar-containing crops like sugar cane and sugar beet. For fuel, ethanol is needed in its pure form and therefore further processing and upgrading steps are needed after fermentation has taken place.

Basics Sugar ($C_6H_{12}O_6$) is converted to ethanol (C_2H_5OH), carbon dioxide (CO_2), and low-temperature heat by yeast under anaerobic conditions according to Eq. 10.

$$C_6H_{12}O_6 \rightarrow 2C_2H_5OH + 2CO_2 + 88\,\mathrm{kJ/mol} \tag{10}$$

According to this equation, 100 kg of sugar is converted into 51.14 kg of ethanol and 48.86 kg of carbon dioxide and 400 kJ of heat. This thermal energy is needed to support the growth of the microorganisms realizing the bio-chemical conversion. To reach a quick and complete transformation of the available sugar into ethanol, additional growth supporter and mineral nutrients, as well as an optimal environment (i.e., temperature level, pH-value) are needed. Most bioethanol processes are realized at a temperature level between 25°C and 40°C. This process and the influencing parameters are well known because of humanity's long and extensive production of alcoholic beverages.

Because starch and even celluloses can be converted into sugar, such biomass fractions are also a potential resource for the production of ethanol in addition to naturally sugar-containing crops.

Substrate Production For fermentation, sugar needs to be available in a water solution. The technological processes to provide such a sugar solution depend on the used feedstock.

- *Biomass containing sugar.* Typically sugar is produced from sugar cane and sugar beet.
  - Sugar cane is a grass growing mainly under tropical conditions containing a sweet liquid that can easily be removed by pressing from the organic matter. It accounts for about 30% of the weight of fresh cane. The fiber remaining after pressing (bagasse) is often used as a solid biofuel for the provision of the energy needed to run a sugar mill and/or an alcohol production factory. After several preparation and processing steps this liquid can be used as a feedstock for alcoholic fermentation.
  - Sugar beet, which grows in temperate climates, is first chipped into small pieces from which the sugar is extracted by means of water applied in countercurrent to the flow direction of the chips. The remaining products are the nearly sugar-free extracted beet chips, which can

be used, for example, as a cattle feed or a substrate for biogas plants and the water with the sugar. After several cleaning steps this mixture of water and sugar can be used for the alcoholic fermentation.

- *Biomass containing starch.* Beside other chemical substances cereal, corn, potatoes, topinambur, maniok, and other similar crops contain also starch. Starch is a polysaccharide consisting of long chains of different glucose molecules. To produce sugar from starch, this polysaccharide has to be decomposed in single saccharide rings by means of, for example, biological processes based on enzymes. Due to the broad variety of starch-containing biomass crops, no typical conversion process is available on the market. Therefore, for each raw material used so far, a conversion process has been developed and optimized in the past. In most cases, however, water is added to the chipped or milled organic material. The consequence is a swelling of the mixture because the water is attached to the starch. Due to this process the starch becomes a paste. To this paste the respective enzyme adapted to each type of biomass feedstock is added. Under the right process conditions (e.g., temperature, pH-value), starch is then converted into sugar. And this sugar can then be used as a feedstock for the alcoholic fermentation.
- *Biomass containing celluloses.* Basically, all organic matter contains cellulose as this is one of the most important elements of plant material. This is especially true for lignocellulosic biomass (like wood) that cannot be used for food or fodder (and thus there is no competition between food and fuel). Like starch, cellulose is composed during the plant growth from different sugar components. Therefore, cellulose can be split again into sugar molecules. This can be realized through biological and nonbiological processes. The former are based on special enzymes still under development and optimization. But the conversion rate of such biological conversion routes is still relatively slow and the biocatalysts are comparable expensive; therefore, commercialization has not taken place so far. The latter are realized with an acid-based hydrolysis partly supported by a catalyst and thus in a "classical" chemical way. Such a hydrolysis process is technologically very demanding and characterized by a low overall efficiency. Therefore, this pathway is not realized on a commercial basis for the time being. To minimize the drawbacks of both options, R&D activities are focusing on a combination of a chemical and a biological conversion. For these reasons so far, alcoholic fermentation based on sugar from celluloses has no market importance, but numerous R&D and market introduction activities are ongoing in this field.

Fermentation For alcoholic fermentation, the sugar and water mixture is inoculated with yeast catalyzing the conversion process. From a technological point of view, this can be accomplished in two different ways. Discontinuous (batch) operation is usually done for small-scale production of high-quality spirits as beverages; continuous operations are used in large-scale systems for production of ethanol as a raw material for the chemical industry as well as for fuel. Within such a continuous operation the temperature as well as the pH-value has to be controlled. Additionally, it might be necessary to add some nutrients to allow a fast and efficient conversion. After fermentation, the yeast is removed from the slurry and recycled.

Production of Pure Alcohol After fermentation has taken place, the resulting material contains only 8–10% alcohol. The rest is primarily water and among others residues from the sugar- or starch-containing organic material. To remove the alcohol from this mixture distillation and/or rectification are done using a crude alcohol column.

Due to physical reasons, the result of such a distillation is an alcohol-water-mixture with a high share of alcohol (more than 80%) and a slurry without significant alcohol content (i.e., stillage). The latter is a by-product and can be used in its dried form as an animal fodder and/or fertilizer. It is also suitable for biogas production. This technology is in large-scale operation worldwide.

For physical reasons, at best, distillation and rectification will only achieve 95–96% pure ethanol because at this concentration water and ethanol forms an azeotropic mixture. A mixture of those two substances cannot be subdivided based on physical processes (like distillation) any more. But bioethanol used as an

engine fuel must be 99.9% pure. For this reason, an additional cleaning step called purification is integrated within the overall process. One (older) possibility for that is to add a third chemical (expedient) to the alcohol-water-mixture producing a mixture of alcohol-chemical plus water-chemical. Afterwards, the chemical is removed from both mixtures and re-used. Another nowadays more widely used possibility is the use of molecular sieves.

Use In engines, ethanol can be used fully or partly as a substitute for gasoline although the lower heating value (LHV) of ethanol is lower compared to that of gasoline (Table 4). The combustion of ethanol, however, requires a lower air volume. Therefore, the heating value of the mixture pressed into the cylinder is more or less the same for ethanol and gasoline. This is the reason why an engine powered by ethanol produces the same power as an engine driven by gasoline.

Nevertheless, internal combustion engines must be specially adapted to the use of pure ethanol, because ethanol shows a different combustion behavior compared to gasoline. Therefore, adaptation kits have been developed for several types of engines and been successfully used in several countries (e.g., in Brazil). Thus pure ethanol is an (expensive) alternative for the substitution of fossil gasoline under specific frame conditions to be defined by the respective government. One challenge of the use of pure ethanol is that the existing distribution networks need to be adjusted and persistent problems (like water retention during storage) have to be solved. For this reason, in most countries bioethanol is not used in its pure form to avoid these challenges. Therefore, a low share of ethanol is mixed with a high share of gasoline (a maximum of 10% ethanol to gasoline). With such a relatively low fraction of bioethanol within the usually used gasoline, the resulting mixture can be used without any known problems in basically all existing gasoline driven engines and within the available distribution infrastructure. Such a solution is also supported by the fact that ethanol contributes still and will contribute in the foreseeable future only to a minor extent to cover the demand for transportation fuels. Another benefit of such a strategy is that the supply is fully secured even if the availability of bioethanol is interrupted.

Alternatively, ethanol can be converted into ETBE to be used as a pollution-reducing gasoline additive. Bioethanol is also being considered for powering fuel cells in future design and applications.

Biomass as Renewable Source of Energy, Possible Conversion Routes. Table 4 Selected properties of fuels

	Ethanol	Gasoline
Carbon-share in %	52	86
Hydrogen-share in %	13	14
Oxygen-share in %	35	0
Net calorific value in MJ/kg	26.8	42.7
Net calorific value in MJ/l	21.3	ca. 32.0
Density (15°C) in kg/l	0.794	0.72–0.78
Viscosity (20°C) in mm^2/s	1.5	0.6
Boiling point in °C	78	25 – 215
Flame point in °C	12.8	−42.8
Ignition temperature in °C	420	ca. 300
Evaporation heat in kJ/kg	904	380–500
Minimum air volume in kg/kg	9	14.8
Octane-value	107	93

Anaerobic Digestion

During anaerobic digestion, organic material is decomposed in an oxygen-free atmosphere by bacteria releasing an energy rich gas, called biogas or, depending on where it is produced, landfill gas (LFG) or sewage gas. This gas usually contains slightly more than 50% methane (CH_4), which is the only energy providing component. The rest is carbon dioxide (CO_2) and some impurities of minor importance. Such biologically driven decomposition of biomass occurs in nature, for example, at the bottom of lakes within the oxygen-free parts of sediments containing crushed organic material, and takes place in oxygen-free parts of landfills and dumps where the organic fraction of the waste material is converted into landfill gas.

Basics Degradable organic material and freedom from oxygen, nutrients for the bacteria and absence of harmful, pathologic. and inhibiting substances are needed for a successful biogas production. The organic

material should also be easily accessible to bacteria. Therefore, a slurry of biomass with high water content is most promising.

Well-suited for such an anaerobic digestion are material streams where the biomass occurs already within an aqueous solution. Typical examples are agricultural residues (e.g., liquid manure, leaves from sugar beet), residues from the food processing industry (e.g., slurry of fruit and potato processing, some types of slaughterhouse residues), and some other waste streams (e.g., sewage sludge, organic waste fraction from municipalities). Additionally, energy crops like maize silage or silage based on a corn-cob-mix can be used as a substrate. Only biomass containing high shares of lignin like wood cannot be degraded by anaerobic bacteria due to biological reasons.

During the anaerobic digestion process, organic matter is degraded by three different kinds of bacteria: fermentative, acetogenic, and methanogenic. The first two bacteria families degrade the complex organic compounds biomass consists of into simpler intermediates (Fig. 12). These intermediate products are then converted to methane and carbon dioxide by the methanogenic bacteria.

Anaerobic digestion relies on a dynamic equilibrium among the three bacterial groups, which is influenced, for example, by temperature. Most digesters operate in the mesophilic temperature regime, which is characterized by temperatures of around 35°C. Others operate in the thermophilic regime, around 55°C. Up to the temperature of peak microbial activity, which depends on the type of the involved bacteria groups, higher operating temperatures produce greater metabolic activity within either regime. Additionally to that, the pH-value as well as the composition of the biomass in relation to easily degradable compounds of the organic material affects the performance of the bacteria also. For optimal fermentation, pH-values between 6.8 and 7.2 are often maintained by use of buffers. Additionally, the availability or absence of nutrients and/or trace elements needed for the growth of the bacteria could influence the anaerobic degradation significantly.

The composition of the produced biogas is typically about one half to maximum two thirds methane and one third to one half carbon dioxide. Additionally, the biogas may contain trace substances such as H_2S. The mixture of the biogas depends on the composition of the biomass, the process conditions, and various other parameters. The lower heating value (LHV) of biogas, which depends basically only on the methane content, ranges from 14 to 29 MJ/m^3.

Expected biogas yields for different substrates are given in Table 5. Already within the animal stomach digested substrates like animal manure and droppings show in general considerable smaller yields than fresh material (e.g., road side green, sugar beet leaves).

The bacteria mixture realizing the anaerobic decomposition of the organic material use relatively little of the energy contained within the biomass for their own survival; this is one of the reasons why the growth rate of these bacteria is relatively slow. Additionally, they produce only very few (waste) heat; this is why the substrate used within biogas plants have to be

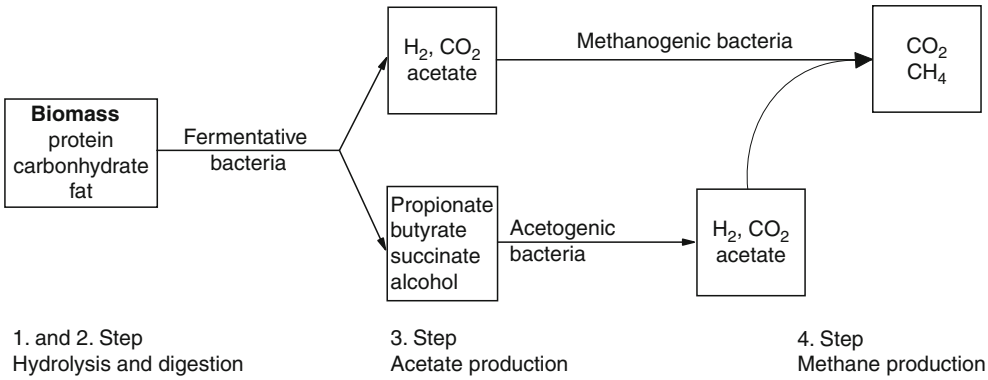

Biomass as Renewable Source of Energy, Possible Conversion Routes. Figure 12
Anaerobic digestion process scheme [1]

Biomass as Renewable Source of Energy, Possible Conversion Routes. Table 5 Average biogas yields for different substrates (various sources)

Material	Yield of biogas in m^3/t organic dry matter	Material	Yield of biogas in m^3/t organic dry matter
Liquid manure from beef	250	Paunch content	420–520
Liquid manure from pork	480	Rey straw	300–350
Droppings from chicken	450	Potato herbs	560
Sewage sludge	400	Sugar beet leaves	550
Organic waste from households	170–220	Food residues	80–120
Waste fat	1,040	Waste water from brewing industries	500
Roadside green	550	Waste water from sugar industries	650

heated. These two facts make this conversion process of organic material into an energy rich gas fairly efficient compared to, for example, the aerobic conversion processes.

Slurries of organic matter with more than roughly 66% water ensure optimal process conditions with a good access of the bacteria to the organic material. Under these circumstances, the gas yield is maximized. To stabilize and optimize the overall production rates, the slurry should be kept stable at a certain temperature level corresponding to the temperature optimum defined by the used bacterial species. Nevertheless, biogas production will also occur at lower temperatures, but essentially stops below 10°C. But due to very low conversion rates the biogas production on such low temperatures has no importance for technical processes optimized to maximize the space time yield.

Process Technology The biological degradation process can be transformed into process technology, taking the substrate characteristics as well as the demands of the bacteria into consideration. Due to very different substrates as well as changing bacteria groups a broad variety of different concepts for an optimized biogas production have been developed. And this development is still ongoing with the overall goal to increase the space time yield.

A biogas plant as shown in Fig. 13 is a typical example for a small scale plant using agricultural substrates available within industrialized countries. Within such a plant, preparation of the feedstock is needed that might include short-time storage, sedimentation of mineral contaminants (like sand, stones), crushing the organic material into small pieces (if necessary), mixing of different types of feedstock to maximize the gas yield and to harmonize the substrate composition, and heating to the temperature level the biogas plant operates. After this preparation, the feedstock is pumped into the biogas reactor where the anaerobic fermentation takes place. For successful operation and a maximized gas yield, the bacteria must always be well-mixed with the organic material to be decomposed; therefore, a respective system element is conclusively needed. It is also important to realize a good temperature distribution within the reactor. Within the example shown in Fig. 13, this is realized by a heater that is integrated within the reactor together with the mixer. The biogas is removed from the top of the plant and, after removal of impurities like water and particles, stored before use as a source of energy is realized. Depending on the substrate, sulfur has to be removed from the biogas for environmental reasons and to extend the technical lifetime of the plant (i.e., H_2S forms with water an acid responsible for an increased corrosion). Especially in agricultural biogas plants, this is realized by a biological process where the H_2S occurring within the biogas is reduced to elementary sulfur by specific bacteria groups.

The digested material is removed from the reactor and stored in a tank where a small amount of additional biogas is produced. Therefore, this storage facility should be covered gas tight to avoid the release of

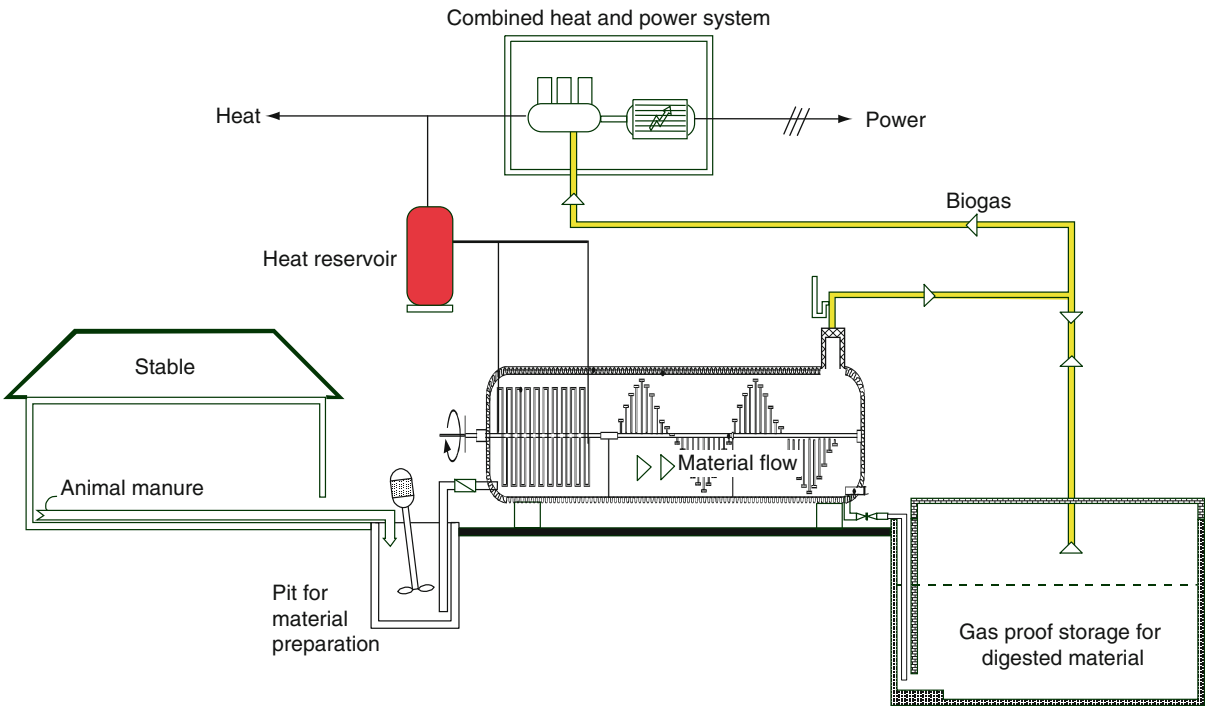

Biomass as Renewable Source of Energy, Possible Conversion Routes. Figure 13
Small scale biogas plant using animal manure as feedstock and commonly used in countries like Denmark, Germany, and Austria [3]

the produced gas into the atmosphere because methane as the most important component within the biogas is harmful to global climate. This digested slurry can be used as a fertilizer, because it contains the nitrogen as well as all the other trace elements originally part of the feedstock and needed to allow plants to grow. Thus, biogas technology could help to close the nutrient cycle. This is of increasing importance for the environmentally sound management of organic material.

Biogas as a Fuel So far biogas is used mainly in a boiler, stove, or engine for the provision of heat, mechanical power, and/or electricity. From a systems point of view, the use within a CHP unit is most promising related to the overall energetic and exergetic efficiency. Part of the heat and electricity produced within such a coupled process is often partly used for heating up the feedstock and running the electrically driven system elements of the plant. Such a system layout is most widely used in industrialized countries.

Alternatively or additionally, biogas can also be feed into the natural gas system. This requires an upgrading of the biogas to fulfill the gas standards valid for the gas distribution system. Such a feed-in of the biogas upgraded to biomethane is realized in an increasing manner in Switzerland, Germany, and Sweden, for example. Based on that feed-in into the gas grid, the biomethane can be used highly efficient within the heat market (with condensing-boiler technology), the electricity market (with IGCC plants), and/or the transportation market (within CNG vehicles). The use as a transportation fuel seems to be an especially promising option due to the very high hectare-specific conversion efficiency.

Future Directions

Biomass as an energy carrier will continue to be an important source of energy within the global energy system. Political efforts to reduce greenhouse gas emissions will continue to grow in the years to come and thus support the use of biomass as an energy carrier. This development will additionally be supported as prices for fossil fuel energy move upwards and as

awareness grows of the unwanted effects on global climate of the use of fossil fuel energy.

But, the limited biomass resources are also needed to meet the demand for food and fodder as well as for raw material. To meet the growing demand for bioenergy against this background biomass conversion technologies are forced to convert the biomass highly efficient into heat, electricity, and/or power not only due to the resulting economic constraints. The biomass conversion technologies must be technologically reliable, environmentally sound, socially acceptable, and economically feasible. Due to the long history of the energetic biomass use and the successful R&D activities in recent years, especially within the European Union, already today a wide range of conversion technologies fulfilling these criteria are available for the provision of useful energy and/or secondary energy carrier from the various biomass fractions available on the market. These conversion plants are designed mostly to be used in industrialized countries. Nevertheless, the development of further improved systems for industrialized as well as for developing countries will remain on the R&D agenda for academia and industry with highest priority in the years to come. This is especially true due to the fact that heat provision from solid biomass in developing countries (which is globally the biggest single energy market for biomass) is still realized in a very inefficient and environmentally harmful manner.

The foreseeable shortage in biomass available to be used as an energy carrier and the resulting price increase makes it necessary in the future to further optimize the overall provision chain. Improved and new biomass conversion technologies can only be operated with a maximum technical, economic, and environmental benefit if they are embedded within an overall provision chain where the different single processes covering the life cycle from biomass to bioenergy (i.e., from cradle to grave) are interlinked in an optimal way. Therefore, another important task for the years to come is it to develop procedures and tools for the assessment and optimization of overall provision chains. This is especially true for the optimal definition of the interface between different processes composing an overall provision chain.

Besides better conversion systems embedded in improved provision chains, the biomass available for energy purposes must be expanded. Increasing demand for biomass by a globally fast growing population of humans has to be taken into consideration. Therefore, this goal can only be achieved if better agricultural and forestry management schemes are developed and implemented based on existing and "new" cash crops with significantly higher yields in average. Such measures are probably not sufficient to cover the increasing demand for biomass from the food and fodder markets, and the markets for biomass as a raw material and the energy markets. For this reason, the limited biomass resources must be used more efficiently – and this is true for all markets.

Based on such measures, it can be expected that biomass for energy can contribute increasingly to help meeting some of the global energy demand in a technical feasible, environmentally promising, and economic sound way.

Bibliography

Primary Literature

1. Kaltschmitt M, Hartmann H, Hofbauer H (eds) (2009) Energie aus Biomasse, 2nd edn. Springer, Berlin (in German)
2. Kaltschmitt M, Andrée U, Majer S (2010) Koraffination von Pflanzenöl in Mineralölraffinerien – Möglichkeiten und Grenzen. Erdöl – Erdgas – Kohle 126(5):203–210 (in German)
3. Kaltschmitt M (2009/2010) Lessons at Hamburg University of Technology. Winterterm

Books and Reviews

Abatzoglou N (1998) Biomass gasifier tars: their nature, formation, and conversion. NREL/TP-570-25357 Report, Golden, Colorado

Aivasidis A, Diamantis VI (2005) Biochemical reaction engineering and process development; in: anaerobic wastewater treatment. Adv Biochem Eng Biotechnol 92:49–76

Allen MR, Braithwaite A, Hills CC (1997) Trace organic compounds in landfill gas at seven U.K. waste disposal sites. Environ Sci Technol 31:S1054–S1061

Amen-Chen C, Riedl B, Wang XM, Roy C (2002) Softwood bark pyrolysis oil-PF resols – Part 1. Resin synthesis and OSB mechanical properties. Holzforschung 56:167

Amen-Chen C, Riedl B, Wang XM, Roy C (2002) Softwood bark pyrolysis oil-PF resols – Part 3. Use of propylene carbonate as resin cure accelerator. Holzforschung 56:281

Andersson G (1995) Transport of forest energy wood in Sweden. In: Hudson B, Kofman D (eds) Harvesting, storage and road transportation of logging residues. Proceedings of a workshop of IEA-BA-Task XII, Glasgow, Scotland, pp 17–21

Antal MJJ, Varhegyi G (1995) Cellulose pyrolysis kinetics: the current state of knowledge. Ind Eng Chem Res 34:703–717

Antal MJ, Allen SG, Dai X, Shimizu B, Tam MS, Gronli M (2000) Attainment of the theoretical yield of carbon from biomass. Ind Eng Chem Res 39:4024

Antal MJ, Mochidzuki K, Paredes LS (2003) Flash carbonisation of biomass. Ind Eng Chem Res 42:3690–3699

Baadsgaard-Jensen J (1988) Storage and energy economy of chunk and chip piles. Report No. 2, EU-Project: Exploitation of marginal forest resources for fuel (CEC Nr. EN-3B-069-DK). Danish Institute of Forest Technology (Hrsg.), Frederiksberg

Ballesteros I, Negro J, Oliva JM, Cabañas A, Manzanares P, Ballesteros M (2006) Ethanol production from steam-explosion pretreated wheat straw. Appl Biochem Biotechnol 129–132:496–508

Baltensperger U (1997) Analysis of aerosol. Chimia 51(10):686–689

Baxter L (2005) Biomass-coal co-combustion: opportunity for affordable renewable en-ergy. Fuel 84(10):1295–1302

Baxter LL, Jenkins BM, Miles TR et al (1994) Alkalis in alternative biofuels. FACT, vol 18, Combustion Modeling, Scaling and Air Toxins, ASME

Bemtgen JM, Hein KRG, Minchener A (1998) Combined combustion of biomass/sewage sludge and coals. Volume II: Final Reports, APAS Clean Coal Technology Programme, EC, Brüssel

Bergman PCA, Boersma AR, Kiel JHA, Prins MJ, Ptasinski KJ, Janssen FGGJ (2005) Torrefied biomass for entrained-flow gasification of biomass. Report ECN-C-05-026, ECN, Petten

Berndes GM, Hoogwijk M, van den Broek R (2003) The contribution of biomass in the future global energy system: a review of 17 studies. Biomass Bioenergy 25(1):1–28

Bolhar-Nordenkampf M, Kaiser S, Pröll T, Hofbauer H (2008) Operating experiences from two new biomass fired FBC plants. In: 9th International Conference on Circulating Fluidized Beds, Hamburg, Mai

Bridgwater T (2006) Biomass for energy. J Sci Food Agric 86:1755

Brouwers J (1996) Rotational particle separator: a new method for separating fine particles and mists from gases. Chem Eng Technol 19:1–10

Brunner T (2006) Aerosol and coarse fly ashes in fixed-bed biomass combustion. Dissertation an der Eindhoven University of Technology (Faculty of Mechanical Engineering), The Netherlands, Eigenverlag T. Brunner

Caballero MA, Corella J, Aznar MP, Gil J (2000) Biomass gasification with air in fluidized bed. Hot gas cleanup with selected commercial and full-size nickel-based catalysts. Ind Eng Chem Res 39:1143–1154

Cheng WH, Kung HH (1994) Methanol production and use. Marcel Decker, New York

Christensen KA (1995) The formation of submicron particles from the combustion of straw. Ph.D. Thesis, Department of Chemical Engineering, Technical University of Denmark, Lyngby, Denmark

Cralle HT, Vietor DM (1989) Solar energy and biomass. In: Kitani O, Hall CW (eds) Biomass handbook. Gordon and Breach Saina, New York

Cuchet E, Roux P, Spinelli R (2004) Performance of a logging residue bundler in the temperate forests of France. Biomass Bioenergy 27:31–39

Czernik S, Bridgwater AV (2004) Overview of applications of biomass fast pyrolysis oil. Energy Fuels 18:590

Daugbjerg Jensen P, Hartmann H, Böhm T, Temmerman M, Rabier F, Morsing M (2006) Moisture content determination in solid biofuels by dielectric and NIR reflection methods. Biomass Bioenergy 30(2006):935–943

Deurwarder EP, Boeringter H, Mozaffarian H, Rabou LPLM, van der Drift P (2005) Methanation of milena product gas for production of BioSNG. In: 14th European Biomass Conference, Paris

Devi L (2003) A review of the primary measures for tar elimination in biomass gasification processes. Biomass Bioenergy 24:125–140

DiBlasi C (2008) Modelling gasification/combustion of wood and char particles, ThermalNet Deliverable 2 F-2

DiBlasi C, Galgano A (2009) Literature review about fundamental aspects of thermal and chemical conversion of biomass. ThermalNet Endbericht, WP2F: Science and Modelling

Dry ME (2002) The Fischer-Tropsch process: 1950–2000. Catalysis Today 71(3–4):227–241

Edgerton S et al (1986) Source emission characterization of residential wood-burning stoves and fireplaces. Environ Sci Technol 20:803–807

Emilsson S (2006) International handbook – from extraction of forest fuels to ash recycling. Swedish Forest Agency, Stockholm

Emrich W (1978) Handbook of charcoal making – the traditional and industrial methods; solar energy R & D in the European Community, Series E, vol 7, Energy from biomass. D. Reidel Publishing Company, Dordrecht/Boston/Lancaster

Fernando R (2007) Cofiring of coal with waste fuels, CCC/126. IEA Clean Coal Centre, London

Gates D (1965) Energy, plants and ecology. Ecology 46:1–14

Gerpen J van (2004) Biodiesel management for biodiesel producers. NREL/SR-510-36242, National Renewable Energy Laboratory

Gil J, Corella J, Aznar MP, Caballero MA (1999) Biomass gasification in atmospheric and bubbling fluidized bed: effect of the type of gasifying agent an the product distribution. Biomass Bioenergy 16:1–15

Gustafsson G (1981) Artificial drying of wood chips for energy purposes. In: Fazzolare RA, Smith CB (eds) Beyond the energy crisis – opportunity and challenge. Third international conference on energy use management, Berlin, pp A151–A171

Hamelinck CN, Faaij A (2002) Future prospects for production of methanol and hydrogen from biomass. J Power Sources 111:1–22

Hamelinck CN (2004) Outlook for advanced biofuels. Dissertation, Universität Utrecht

Hartmann H, Höldrich A (2007) Bereitstellung von Festbrennstoffen. In: Hartmann H (Hrsg.) Handbuch Bioenergie-Kleinanlagen (2. vollst. überarbeitete Auflage). Sonderpublikation des Bundesministeriums für Verbraucherschutz, Ernährung und Landwirtschaft (BMVEL) und der Fachagentur Nachwachsende Rohstoffe (FNR), Gülzow, pp 18–55

Hartmann H, Thuneke K (1997) Ernteverfahren für Kurzumtriebsplantagen – Maschinenerprobung und Modellbetrachtungen. Landtechnik Bericht, Heft 29, Selbstverlag Landtechnik Weihenstephan (Hrsg.), Freising

Hartmann H, Böhm T, Daugbjerg Jensen P, Temmerman M, Rabier F, Jirjis R, Hersener J-L, Rathbauer J (2004) Methods for bulk density determination of solid bio-fuels. In: Van Swaaij WPM, Fjällström T, Helm P, Grassi A (eds) 2nd World Conference and Technology Exhibition on Biomass for Energy, Industry and Climate Protection, Rome, 10–14 May 2004, pp 662–665

Hartmann H, Roßmann P, Link H, Marks A, Müller R, Amann E (2004) Secondary flue gas condensation for domestic wood chip boilers. In: Van Swaaij WPM, Fjällström T, Helm P, Grassi A (eds) 2nd World Conference and Technology Exhibition on Biomass for Energy, Industry and Climate Protection, Rome, 10–14 May 2004, pp 1334–1337

Hartmann H, Turowski P, Roßmann P, Ellner-Schuberth F, Hopf N (2007) Grain and straw combustion in domestic furnaces – influences of fuel types and fuel pretreatment. In: Maniatis K, Grimm H-P, Helm P, Grassi A (eds) Proceedings 15th European Biomass Conference & Exhibition, 7–11 May 2007, Berlin, Germany, ETA Renewable Energies, Florence, Italy, pp 1564–1569

Hasler P, Nusbaumer T, Bürli J (2001) Herstellung von Holzpellets – Einfluss von Presshilfsmitteln auf Produktion, Qualität, Lagerung, Verbrennung sowie Energie- und Ökobilanz von Holzpellets. Schweizerisches Bundesamt für Energie (Hrsg.), Bern, Eigenverlag

Houck JE (1993) Atmospheric emissions of carbon dioxide, carbon monoxide, methane, non-methane hydrocarbons, and submicron elemental carbon particles from residential wood combustion; Air Ampersand Waste Management Association; 86th Annual Meeting Ampersand Exhibition, Pittsburgh, USA, pp 245–246

Hüglin C (1996) New applications of aerosol photoemission: characterisation of wood combustion particles and time resolved thermal desorption studies. Dissertation ETH Zürich

Jacques K, Lyons TP, Kelsall, DR (Hrsg.) (1999) The alcohol textbook, 3 Auflage. Nottingham University Press, Nottingham

Jørgensen H, Kristensen JB, Felby C (2007) Enzymatic conversion of lignocellulose into fermentable sugars: challenges and opportunities. Biofuels, Bioprod Biorefin 1:119–134

Kinast JA (2003) Production of biodiesels from multiple feedstocks and properties of biodiesels and biodiesel/diesel blends. Final Report, Report 1 in a series of 6, Gas Technology Institute, National Renewable Energy Laboratory, NREL/SR-510-31460

Knoef H (2005) Handbook of biomass gasification. BTS Biomass Technology, Enschede

Knothe G, Krahl J, van Gerpen J (Hrsg.) (2005) The biodiesel handbook. AOCS Press, Urbana, Il

Kujawski W, Zielinski L (2006) Bioethanol – one of the renewable energy sources. Environ Prot Eng 32(1):143–149

Laitila J, Asikainen A, Liiri H, (2006) Cost calculators for the procurement of small sized thinning wood, delimbed energy wood and stumps for energy. In: Proceedings World Bioenergy 2006, Jönköping, Sweden, Swedish Bioenergy Association, pp 326–330

Ledin S, Willebrand E (eds) (1996) Handbook on how to grow short rotation forests, 2nd edn. Swedish University of Agricultural Sciences, Uppsala, Sweden

Lee J (1997) Biological conversion of lignocellulosic biomass to ethanol. J Biotechnol 56:1–24

Lee D, Owens VN, Boe A, Jeranyama P (2007) Composition of herbaceous biomass feedstocks. North Central Sun Grant Center (Hrsg.), South Dakota State University, Brookings, Selbstverlag

McCrillis RC, Randall RW, Warren SH (1992) Effects of operating variables on PAH emissions and mutagenicity of emissions from woodstoves. J Air Waste Manage Assoc 42:691–694

Meier D, Faix O (1999) State of the art of applied fast pyrolysis of lignocellulosic materials – a review. Bioresour Technol 68:71

Mitchell CP (1997) Development of harvesting and storage technologies essential for the establishment of short rotation forestry as an economic source of fuel in Europe. Final technical report for the European Comission (AAIR3), Project No. CT 941102. Aberdeen University (Hrsg.), UK, Selbstverlag

Mitchell CP (1997) Development of harvesting and storage technologies essential for the establishment of short rotation forestry as an economic source of fuel in Europe. Technical report for the European Commission (AAIR3), Project No. CT 941102. Aberdeen University, Aberdeen

Oasmaa A, Czernik S (1999) Fuel oil quality of biomass pyrolysis oils. In: Overend RP, Chornet E (eds) Biomass – a growth opportunity in green energy and value-added products, Proceedings of the 4th Biomass Conference of the Americas, Pergamon Elsevier, Oxford, pp 1247–1252

Ogawa T, Inoue N, Shikada T, Ohno Y (2003) Direct dimethyl ether synthesis. J Nat Gas Chem 12:219–227

Pröll T, Bolhàr-Nordenkampf M, Strauss T, Hofbauer H (2006) Description of local heat release in an industrial scale bubbling bed waste incinerator. In: Proceedings of the 19th International Conference on Fluidized Bed Combustion, Vienna, 23–25 May 2006

Prins MJ (2005) Thermodynamic analysis of biomass gasification and torrefaction. Dissertation, Technische Universität Eindhoven

Rehm HJ, Reed G (eds) (1996) Biotechnology. Weinheim, VCH

Ribbing C (2007) Environmentally friendly use of non-coal ashes in Sweden. Waste Manag 27:1428–1435

Samuelsson R, Burvall J, Jirjis R (2006) Comparison of different methods for the determination of moisture content in biomass. Biomass Bioenergy 30:929–934

Sander B (2004) Full scale experience on co-firing of straw. In: 2nd World Biomass Conference, Workshop 4: Co-firing, Rome

Schneider C, Hartmann H (2006) Maize as energy crop for combustion. Agricultural optimisation of fuel supply. Berichte aus dem TFZ, Nr. 9. Straubing: Technologie- und Förderzentrum im Kompetenzzentrum für Nachwachsende Rohstoffe; Download unter: www.tfz.bayern.de

Smeets E, Faaij A, Lewandowski I, Turkenburg T (2007) A bottom-up assessment and review of global bio-energy potentials to 2050. Prog Energy Combust Sci 33:56–106

Stevens DJ (2001) Hot gas conditioning: recent progress with large-scale biomass gasification systems, update and summary of recent progress, National Renewable Energy Laboratory, Golden, Colorado

Strauss K (1998) Kraftwerkstechnik zur Nutzung fossiler, regenerativer und nuklearer Energiequellen. Springer, Berlin, p 4, Auflage

Strauss T, Pröll T, Hofbauer H (2006) Start up and operation optimization of a 39 MWth bubbling fluidized bed incinerator for domestic waste and sewage sludge. In: Proceedings of the 19th International Conference on Fluidized Bed Combustion, 23–25 May 2006, Vienna

Stucki S, Biollaz S, Schildhauer T, Vogel F (2007) New approaches to SNG production from biomass. In: Energy Delta Conference 2007, Green Gas Session Groningen, 20–21 November 2007

Sun Y, Cheng J (2002) Hydrolysis of lignocellulosic material for ethanol production: a review. Bioresour Technol 83:1–11

TEKES: Stumps – an unutilised reserve. Wood energy technology programme – Newsletter on Results 4/2004. TEKES, Helsinki, Finland

Thörnqvist T (1988) Wood fuel storage in large piles - mechanisms and risks of self-ignition. In: Danielsson BO, Gislerud O (eds) Production, storage and utilization of wood fuels; Proceedings of IEA/BE Conference, Task III/Activity 6 and 7, Uppsala, Sweden, pp 193–197

Thrän D u. a. (2006) Sustainable strategies for biomass use in the european context. Analysis in the charged debate on national guidelines and the competition between solid, liquid and gaseous biofuels. IE-Report 1/2006, Leipzig

Travis C et al (1985) Health risks of residential wood heat. Environ Manag 9(3):209–216

Wayman M, Parekh SR (1990) Biotechnology of biomass conversion. Open University Press, Milton Keynes

Wieck-Hansen K, Sander B (2003) 10 years experience with co-firing straw and coal as main fuels with different types of biomasses in A CFB boiler in Grena, Denmark. VGB PowerTech 83(10):64–67

Wingelhofer F (2007) Directly wood particle fired gas turbine plants: concept, experimental results and potential applications for combined heat and power generation with moderate output. In: 15th European Biomass Conference and Exhibition, Berlin, Germany, 7–11 May 2007

Wischnewski R, Werther J, Heidenhof N (2006) Synergy effects of the co-combustion of biomass and sewage sludge with coal in the CFB combustor of Stadtwerke Duisburg AG. VGB PowerTech 12:63–70

Worley JW, Cundiff JS (1991) System analysis of sweet sorghum harvest for ethanol production in the Piedmont. Trans ASAE 34(2):539–547

Wyman C (ed) (1996) Handbook on bioethanol. Taylor and Francis, Washington

Zheng Y, Jensen PA et al (2007) Ash transformation during co-firing coal and straw. Fuel 86(7–8):1008–1020

Biomass Combustion for Electricity Generation

Andreas Wiese
Energy Division, Lahmeyer International GmbH, Bad Vilbel, Germany

Article Outline

Glossary
Subject Importance and Definition
Introduction
Biomass as Energy Carrier
Energy Conversion Technology
Environmental Impacts
Cost Analysis
Future Perspectives
Bibliography

Glossary

Biomass Includes all kinds of material that were directly or indirectly derived not too long ago from contemporary photosynthesis reactions, such as vegetal matter and its derivatives.

Biogas A mixture of mainly methane and carbon dioxide produced by bacterial degradation of organic matter and used as a fuel.

Biofuel Fuel derived from organic matter (obtained directly from plants, or indirectly from agricultural, commercial, domestic, and/or industrial wastes) instead of from fossil products.

Renewable energy Energy, which is energy generated from natural resources such as sunlight, wind, rain, tides, and geothermal heat, which are renewable (naturally replenished).

Combustion A chemical reaction that occurs between a fuel and an oxidizing agent that produces energy, usually in the form of heat and light.

Gasification Any chemical or heat process used to convert a substance to a gas.

Environment Most commonly used describing "natural" environment and means the sum of all living and nonliving things that surround an organism, or group of organisms.

Electricity generation The process of creating electricity from other forms of energy.

Combined heat and power The use of a heat engine or a power station to simultaneously generate both electricity and useful heat.

Subject Importance and Definition

Biomass contributes worldwide around with more than 10% to the overall primary energy consumption. Whereas the majority of this is the traditional utilization of biomass (firewood) in developing countries, a substantial portion is also used for electricity generation. In 2009, biomass contributed almost 10% to the overall renewable energy electricity generation worldwide [10, 18].

Subject of this article is therefore the description of the state-of-the-art technologies, environmental impacts including greenhouse gas emission balances, as well as financial aspects of using biomass for electricity generation by means of combustion.

Biomass can be converted by various types of technologies to a solid, liquid, and/or gaseous fuel. Solid biomass can be burned in boilers to run, e.g., steam turbines or steam engines. Biogas can be combusted in engines; this is also true for liquid biofuels like biodiesel or bioethanol. The latter two options can of course also be burned in a boiler to produce steam and then electricity. As it can be seen from this, the general term "biomass combustion to electricity generation" includes a very wide spectrum of different technologies.

However, within the modern electricity sector the widest application by far is to burn solid biofuels. With the resulting thermal energy a water-steam cycle is operated to produce electricity through a steam turbine and an electric generator. Therefore the focus of this article is related to this way of energy conversion.

Introduction

Biomass is the oldest way of satisfying the energy demand of humankind. Historically, using firewood was for a long time the only way of satisfying the energy needs of human beings.

When the electricity sector started to develop in the late nineteenth century, the main energy sources used for the conversion into electricity have been for a long time coal and oil. Then in the 1950s and 1960s the introduction of nuclear energy followed. Nowadays, additionally, natural gas and all types of renewable energies are used for electricity generation. It was only in the last 3 decades, starting with first biomass and biogas plants in the 1970s, that biomass was also regarded as a possible energy source for the grid-connected electricity generation. First applications came along mostly in Western Europe, here mainly in Scandinavia, and in the USA. For example, in the early 1980s about 850 MW of biomass power plant capacity had already been operated grid-connected in California [1].

The term "biomass combustion to electricity generation" is defined broadly and covers a wide spectrum of possible conversion technologies. For this reason, the focus of this paper is put on the combustion of solid biomass and the use of a water-steam cycle. For this so defined subject, this article provides a comprehensive overview of technology, environmental and financial aspects, whereby the major focus is put on technology. Within this part, the article tries to follow the energy conversion path from biomass (and briefly extending this energy chain before the biomass formation to solar energy) to electricity.

Therefore, after a general overview of the energy conversion path from solar energy to electricity (section "Biomass Chains for Electricity Generation"), the technical description starts with the discussion of the origination of biomass which can be used for combustion together with some key features of biomass (section "Key Properties of Biomass"). This is followed by the description of the energy conversion pathway from the solid biofuel to the electricity to be feed into the grid (section "Energy Conversion Technology"). This part starts with an overall presentation of the energy chain from biomass to electricity. After a description of preprocessing, transportation, and storage of biomass, the different conversion steps of biomass are presented – (1) from chemical to thermal energy, (2) from thermal energy to mechanical energy, and (3) from mechanical energy to electrical energy (sections "Conversion of Chemical into Thermal Energy" to "Electric Energy Transformation"). Of the various conversion steps, combustion and gasification are explained. Additional plant components are discussed to round up the technical picture given (sections "Other Plant Components" and "Ash").

After analyzing the environmental impacts (section "Environmental Impacts"), including carbon footprinting and an excursus on biomass co-firing as a very important side-topic within the biomass to electricity subject (section "Excursus: Co-firing Concepts") an overview of the actual cost situation is given, together with an example for a financial calculation (section "Cost Analysis").

Finally an overview of the actual market status is given followed by a discussion on the future perspectives of biomass in the electricity sector (section "Future Perspectives").

Biomass as Energy Carrier

The energy on earth origins from three different primary energy sources: solar radiation, geothermal heat, as well as gravitation and motion of planets. Out of this, solar radiation has by far the largest share [16].

From these three natural sources a broad variety of different further energy streams or carriers are resulting on earth. This can be seen in Fig. 1. From all the different energy sources provided indirectly by solar energy (like wind, hydro, wave) biomass is one of these energy carriers representing stored solar energy.

Additionally, Fig. 1 shows in green the principle path of biomass combustion to electricity generation and its utilization, which is the subject of this article. According to this, the conversion pathway under consideration here is from solar energy over biomass to any kind of energy conversion within a thermal power plant, in which, beside boilers and other plant components, the key component is the facility, in which thermal energy is converted into mechanical energy, which

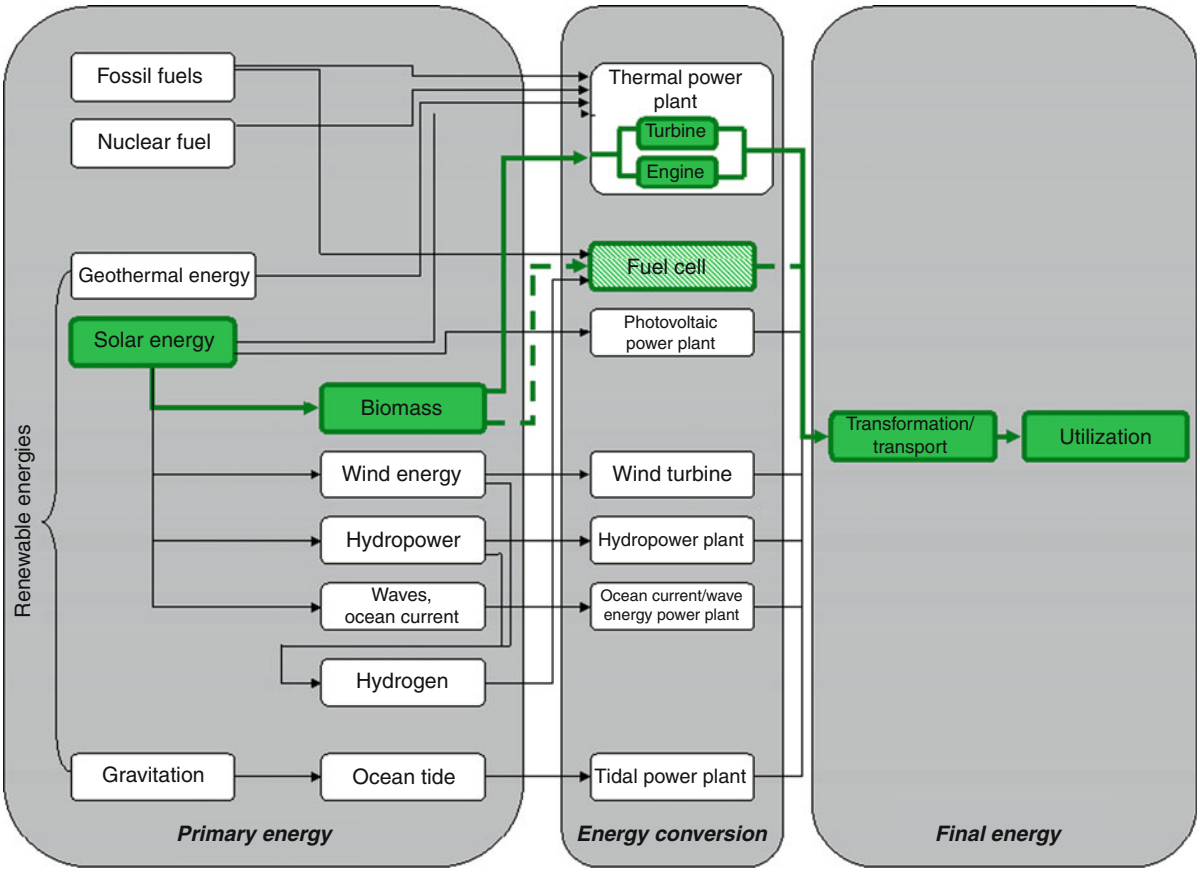

Biomass Combustion for Electricity Generation. Figure 1
Energy sources on earth; solar-biomass-heat-electricity path in green (According to [6], with own adjustments)

can either be a turbine or an engine. Beside this major path, biomass also can be converted into electricity by means of using fuel cells. However, this application is actually only of minor importance due to its high cost and therefore not further analyzed below.

Within a photosynthetic process, solar radiation is converted into organic material. Animal biomass results from this type of biomass via the food chain. Based on this, a definition of biomass can be derived: biomass includes all kinds of materials that were directly or indirectly derived not too long ago from contemporary photosynthetic reactions, such as vegetal matter and its derivatives: wood fuel, wood derived fuel, fuel crops, agricultural and agro-industrial by-products, and animal by-products [12].

The term biomass does not include all materials based on organic molecules (hydrocarbons), e.g., plastics. Additionally most of the definitions, like the above, does not include fossil organic material like peat and (petroleum based) oil.

Biomass therefore includes vegetal and animal mass (plants and animals), the resulting residues (e.g., animal excrements), dead (but not fossil) plant material (e.g., straw) and animal mass, as well as material resulting from technical conversion and/or a material utilization processes (e.g., paper, vegetable oil, alcohol) [6].

Biomass Chains for Electricity Generation

For the conversion of biomass to electricity, a number of processing and energy conversion steps are needed. The variety of the respective process and supply chains for biomass-to-energy and how herein the pathway to electricity is embedded is shown in Fig. 2. When talking about biomass combustion to electricity, usually any kind of solid biomass is used. This is very often true for residues, mostly from plant material to be harvested or collected. Then the biomass is transported from its location of origin either directly to the location of the combustion plant or any kind of pretreatment facility. The biomass is then feed as a solid fuel into the boiler.

Biomass is then converted into heat within the combustion process. Afterward this heat is transferred first into mechanical energy via any kind of turbine or engine and afterward into electricity via a generator.

An efficient use of biomass through the combustion process usually involves a combination of using electricity and heat in parallel as final energy, thus speaking about combined heat and power plants (CHP).

In the following descriptions, the focus is on systems based on combustion as well as on heat and power generation facilities. This facility is in most cases associated with a number of side facilities needed for a proper functioning of the whole plant. Among them are biomass pretreatment facilities and storage facilities.

Key Properties of Biomass

The whole process of biomass utilization to electricity generation is influenced by the physical characteristics as well as the chemical composition of the solid biofuel. Some of these characteristics most important with regard to biomass combustion are discussed below.

The heating value (H_i, also called net calorific value, NCV) is the amount of heat released in case of 100% oxidation without considering the condensation enthalpy of the water contained in the flue gas in form of water steam. The gross calorific value (GCV) is defined as the net calorific value (NCV) plus the condensation enthalpy of the water steam (i.e., water formed during combustion and water already contained in the fuel). The gross calorific value (GCV) of biomass of lignocelluloses biomass varies in a small bandwidth around 18.5 MJ/kg only. Some examples are shown in Table 1.

The water (or moisture) content varies greatly within one and between different types of biomass, the season of the year, and the time between harvesting and energetic utilization. The water content is often related to the amount of fresh biomass and therefore describes the amount of water, which is inside the wet biomass. Another term to express the amount of water in biomass is the moisture (or moisture content). Mostly the biomass moisture is related to dry basis: the weight of water contained within the lignocellulosic biomass expressed as a percentage of the weight of the oven dry biomass. Usually the water content of biomass varies between 10% and 50%; some examples are given in Table 1.

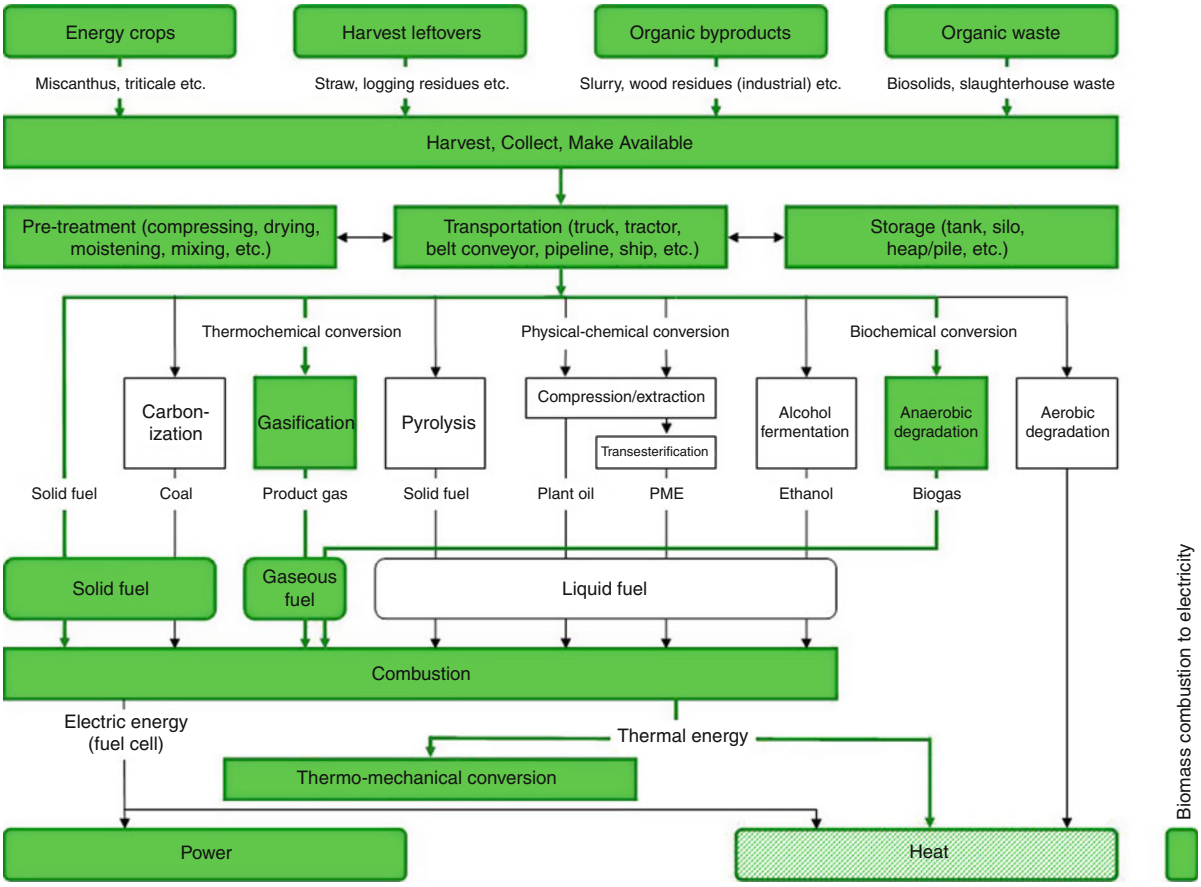

Biomass Combustion for Electricity Generation. Figure 2
Schematic of the typical process and supply chains of providing end use out of biomass (in *green*: process chains, which are the most common ones with regard to electricity generation through combustion of biomass [6]

Water content and heating value are closely related and this relation is linear within some areas. Whereas water free biomass has a gross calorific value of 18.5 MJ/kg, biomass with a water content of 40% has a gross calorific value of only 10 MJ/kg. Usually for air-dry wood or straw, the water content varies between 12% and 20% and therefore the gross calorific value are in a range from 13 to 16 MJ/kg. Wood coming fresh from the forest has a water content of sometimes around 50% and in such cases the heating values is around 8 MJ/kg.

Solid dry lignocellulosic biomass consists mainly of carbon, hydrogen, and oxygen. Carbon is the most important one. For example, wood has a carbon content of almost 50%. Oxygen counts for little more than 40%. The hydrogen content is usually less than 10%. Other components are nitrogen (N), and trace elements like potassium (K), phosphorous (P), sodium (Na), calcium (Ca), magnesium (Mg), sulfur (S), and chlorine (Cl). Other trace elements like, e.g., silicon (Si) or iron (Fe) are also included in the biomass, but are of less significance.

The ash content of biomass fuel varies within a broad range from approx. 0.5% for, e.g., clean wood without bark up to more than 10% for some straw and cereal assortments. It can go even higher if the fuel is contaminated with impurities (like demolition wood). The ash content of the biomass influences the technology of de-ashing and the combustion technology. Transport and storage of the ash produced also depends on the ash

Biomass Combustion for Electricity Generation. Table 1 Water content, gross calorific value, net calorific value, bulk density, and energy density of biomass fuels [6]

	Water content (wt% w.b.)	GCV (MJ/kg d.b.)	NCV (MJ/kg w.b.)	Bulk density (kg w.b./m^3)	Energy density (MJ/m^3)
Wood pellets	10	19.8	16.4	600	9,840
Woodchips – hardwood – pre-dried	30	19.8	12.2	320	3,900
Woodchips – hardwood	50	19.8	8	450	3,600
Woodchips – softwood – pre-dried	30	19.8	12.2	250	3,050
Woodchips – softwood	50	19.8	8	350	2,800
Grass – high-pressure bales	18	18.4	13.7	200	2,740
Bark	50	20.2	8.2	320	2,620
Triticale (cereals) – high-pressure bales	15	18.7	14.5	175	2,540
Sawdust	50	19.8	8	240	1,920
Straw (winter wheat) – high-pressure bales	15	18.7	14.5	120	1,740
Olive residues (from 2-phase production)	63	21.5	6.1	1,130	6,890
Olive residues (from 3-phase production)	53	22.6	8.5	650	5,530

GCV gross calorific value, *NCV* net calorific value, *d.b.* dry basis, *w.b.* wet basis

content of the fuel. Fuels with low ash content are better suited for thermal utilization than fuels with high ash content, as lower amounts of ash simplify de-ashing, ash transport and storage, as well as utilization and ash disposal. Higher ash content in the fuel usually leads to higher dust emissions and has an influence on the heat exchanger design, the heat exchanger cleaning system, and the dust precipitation technology.

The ash melting temperature is very important for the combustion processes. High process temperatures initiate ash melting, forming solid deposits, which might result in loss of efficiency, plant breakdown and high maintenance. Low ash melting temperatures are characteristic for most of the herbaceous biomass (e.g., straw, rice husk), while woody biomass does normally not cause problems related to ash melting (see Chapter 5.9).

Energy Conversion Technology

In a typical facility "Biomass Combustion for Electricity Generation" the following energy conversion steps are taking place:

1. Conversion from chemical energy into thermal energy (heat)
2. Conversion from thermal energy into mechanical energy (usually rotational energy)
3. Conversion from mechanical energy into electrical energy

The biomass enters into this energy conversion chain in an already pre-processed form. At the end of the energy conversion chain, the electricity is feed into the grid to be transported to the end-users. An additional interface might be a district heating system or a single major heat user (e.g., an industrial company

with a high low temperature heat demand). In this case the system is designed as a combined heat and power station.

Figure 3 shows the general flow diagram and the interfaces of such a biomass to electricity generation facility. According to this there are other interfaces – or better to say – input/outputs into the energy conversion chain: ash, gaseous emissions, energy losses, air and, in most cases, water for cooling purposes.

In order to operate the energy conversion chain described above, different devices are needed. Theses major plant components are:

- Biomass preprocessing plant (if needed, sometimes not located at the combustion site)
- Biomass storage (open or closed)
- Firing unit
- Steam generator (i.e., boiler)
- Water-steam cycle including feed water pump
- Steam turbine (or steam engine, stirling engine, etc.)
- Generator
- Transformer
- Flue gas treatment facility
- Back cooling facility for the condenser
- Ash disposal
- Other plant components
  - Pumps and auxiliary motors
  - Pipes
  - Fresh water supply
  - Feed water preparation system

Additionally other units are of great importance for the plant as well, e.g., instrumentation and control system (I&C). But they do not have any direct influence on the energy conversion chain. They are therefore not discussed in further detail here.

Below the major processes and their main components of this energy conversion chain are described in detail.

Biomass Preprocessing

The biomass fuel is usually pre-processed already before it arrives at the combustion site. It is then either burned directly in the form of arrival, or another preprocessing step is taking place at site.

Fuel pretreatment includes all steps necessary to produce an upgraded biofuel from a lignocelluosic biomass resource or from various kinds of organic waste materials (e.g., waste wood, demolition wood). The reasons for such a pretreatment step can be manifold: (1) homogenization for better handling

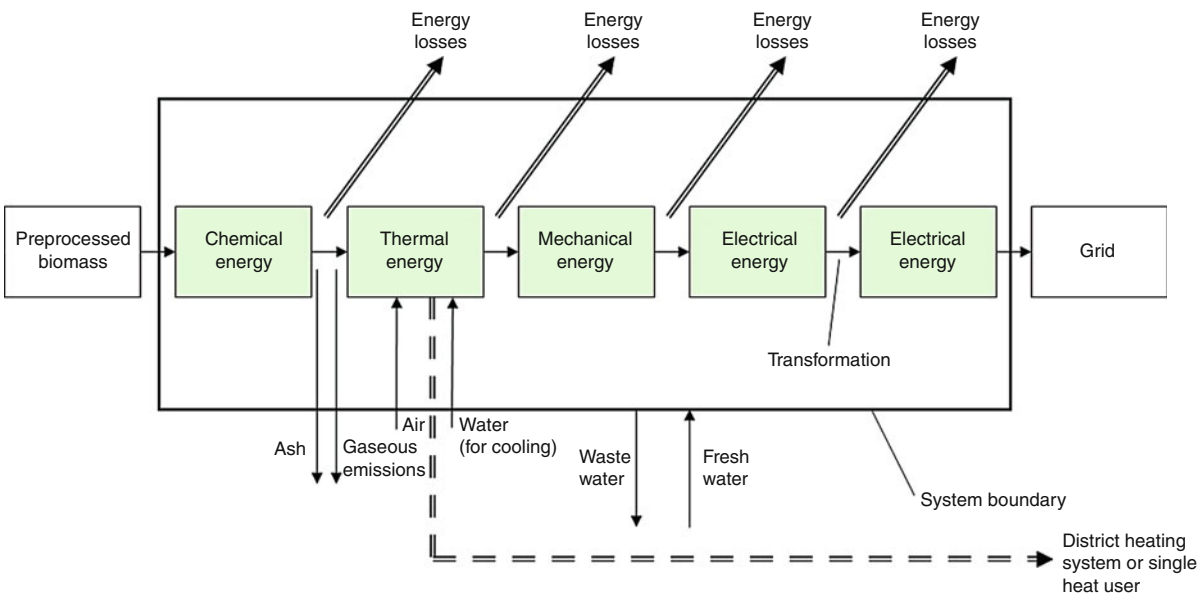

Biomass Combustion for Electricity Generation. Figure 3
Energy chain of biomass combustion for electricity generation

during storage and feeding into the combustion chamber as well for better combustion and (2) reduction of impurities to improve the fuel resp. the combustion quality. All this finally aims to increase the efficiency, to increase the technical availability, to lower the environmental impacts (emissions, ash volume), and to reduce the investment cost as well as the operation and maintenance cost at the power plant.

For the purpose of large biomass combustion plants, usually the following preprocessing possibilities are of importance:

- Wood fuel (e.g., shrubs, bushes, forest residues, stems or bark up to a diameter of around 50 cm, sawmill residues, demolition wood) is usually chipped in wood chippers. The main purpose of this is to reduce the particle size. Common types of wood chippers are disk chippers and drum chippers.
- Mostly wood is chipped decentralized directly at the harvest site. However, under specific frame conditions also a large-scale centralized chipping can be an economic viable solution.
- Additionally also mills are used to further decrease the particle size of already pre-chipped wood. These could be hammer mills or grinding mills.
- Beside particle size reduction, other pretreatment processes are grading, drying, conditioning, and cooling.
- Pelleting is a combination of several of these processes. The production of pellets might make sense economically under certain frame conditions.

At the end of the various preprocessing steps, the biomass fuel must fulfill the specification required by the combustion device. This specification itself depends on the technology and the individual design. For a typical grate firing device designed for burning woody biomass the specification is given exemplarily in Table 2.

Biomass Storage

The main purpose of a storage facility at a conversion plant is to bridge the time span between the provision of the biofuel free plant gate and its energetic utilization within the plant.

Biological Processes During Storage Biological processes take place during the period where the biomass is stored within the storage facility. The most important process is an aerobic degradation of organic matter (composting). One effect of such degradation is self-heating, which can even result in self-ignition. This may take place if the storage facility is not controlled and maintained properly. The velocity of such self-heating might vary significantly. It depends on the water content, material structure, material density, amount and volume of material, type of storage facility, type of biomass, impurities, storage and ambient temperature, oxygen concentration in the storage facility, and finally the initial amount of bacteria and fungi within the biomass. Another important effect of such biological processes during biomass storage is the appearance of bacteria and fungi itself.

This storing biomass is connected with several risks:

- Loss of matter
- Self-ignition
- Growth of bacteria and fungi, which can be a health risk (e.g., allergic reaction)
- Smelling
- Increase of the water content
- Agglomeration due to freezing
- Decomposition and fine abrasion
- Discharging water, respectively, leakage water

Storage Facilities Biofuels can be stored within ground storage facilities (i.e., open-air) and in buildings. Both types can be found at biomass-to-electricity-generation plants.

Wood, wood chips, etc., are very often stored directly on the ground. Since at the site the biomass is stored only a few hours up to a couple of days, usually no rain or snow protection device is used.

The advantage of storing biofuels in buildings is the better protection against rain or snow. Storage containers can be either simple halls or silos. But always an adequate air ventilation system has to be installed to avoid (1) an unwanted self-heating and (2) condense water generation and the resulting damages to the building.

The storage is charged and discharged either with wheel-mounted front loaders or – in case of larger

Biomass Combustion for Electricity Generation. Table 2 Fuel specification of a typical 5 MW biomass power plant, located in Germany, burning solid residual wood

Size of wood chips						
Class	Mass fraction of relevant particle size area				Extremum 1% outliers	
	Max. 20% (mm)	60–100% (mm)	Max. 20% (mm)	Max. 4% (mm)	Cross-section (cm^2)	Length (cm)
G 100 coarse	>63	63–11.2	11.2–1	<1	10	25
	<150					

Heating values of fuels			
Description	Fraction (v%)	Heating value (kWh/kg)	Heating value (MJ/kg)
Woody landscape conservation crop	0–60	1.9	7.2
Forest clearance wood	0–30	2.9	10.5
Forest residues	0–100	2.8	10.4
Filter spill	0–20	1.8	6.5
Av. values		*2.6*	*9.36*

Ash content		
Class	Ash content (dry)	Description
A5	<10%	Normal ash content
A6	>10%, <15%	Increased ash content

Bulk density of wood chips		
Class	Limiting value (bulk density in kg dm/m^3)	Description
S 160	<160	Low bulk density (spruce, fir, poplar, willow)
S 200	160–200	Medium bulk density (pine, larch, birch, alder, maple, elm, Douglas fir)
S 250	>200	High bulk density (oak, robinia, ash, beech)

Chemical analysis of dry fuel mixture			
		Design	Variation
Carbon (C)	Mass-%	50	50.6–54.5
Hydrogen (H)	Mass-%	5.5	4.7–6.8
Nitrogen (N)	Mass-%	0.6	0.1–1
Sulfur (S)	Mass-%	0.1	<0.1
Chlorine (Cl)	Mass-%	0.1	<0.1
Ash content (dry)	Mass-%	10	1.5–15
Sand content	Mass-%	<2	
Other limitations			
Energy density	MJ/m^3	2,160–3,000	
	MWh/m^3	0.60–0.83	
	MWh/m^3/40 min	0.05	
Ash sintering point	°C	>1,000	

facilities – the lorries are directly unloading the biomass onto an automatic feeding system, which can be push floors, different types of screws or crane facilities.

Conversion of Chemical into Thermal Energy

In most of the existing biomass-to-electricity plants, the conversion from chemical energy within the biofuel into thermal energy is realized by combustion. The device in which this takes place is in most cases a boiler – which is a combination of combustion device and steam generator.

However, solid biomass can also be converted into a liquid or gaseous secondary energy carrier. Such energy carriers can be burnt in a boiler as well. However, in most cases they are burnt in other devices. These are either of the following:

- Internal combustion engines (piston motor engines)
- Combustion chambers of gas turbines
- Other forms of devices (not common)

Combustion Ideally combustion can be defined as the complete oxidation of any kind of fuel. Overall, it is an exothermic chemical reaction between a fuel and an oxidant releasing heat. The release of heat can result in the production of light in the form of either glowing or a flame [6, 9, 12].

This chemical reaction can be described by means of a sum formula, wherein the biomass, consisting mainly of carbon (C), oxygen (O), and hydrogen (H), reacts with oxygen (O_2) to form the products carbon dioxide (CO_2) and water (H_2O) (Eq. 1):

$$C_nH_mO_p + \left(n + \frac{m}{4} - \frac{p}{2}\right)O_2 \rightarrow nCO_2 + \frac{m}{2}H_2O \tag{1}$$

This total combustion process can be divided into the following processes: drying, pyrolytic decomposition, gasification, and (complete) oxidation. For the individual particle it is a sequence of these processes; however, all takes place in parallel in the firing device.

During the drying phase, the water within the biofuel is evaporated at temperatures below 150°C. During this phase the biomass is not destroyed. Vaporization requires energy released from the combustions process. Therefore it lowers the temperature within the combustion chamber by slowing down the combustion process. With regard to biomass, this means that if the water content exceeds a certain percentage (e.g., 60%), the combustion process cannot be maintained: the wet biomass requires too much energy to evaporate the moisture and subsequently to heat the water vapor that the temperatures within the combustion device are reduced below the minimum temperature required to sustain combustion.

Pyrolytic decomposition is defined as thermal degradation at temperatures between 150 and 500°C in the absence of an externally supplied oxidizing agent. The excess air coefficient is zero. A number of variables influence the amount and the properties of the products formed during this endothermic process. These influencing parameters are mainly fuel type, temperature, pressure, heating rate, and reaction time. Fast heating rates favors the formation of products liquid under standard conditions. Slow heating rates provide mainly tar and charcoal as well as low molecular weight gases. Among them, CO and CO_2 are formed in considerable quantities.

Gasification is defined as the conversion of a solid (e.g., charcoal remaining after the pyrolytic decomposition has been taken place) into a gaseous fuel within an endothermic process in the presence of an externally supplied oxidizing agent. The excess air coefficient is between 0 and 1, resulting in a partial oxidation. Gasification takes place within a temperature range starting from approx. 400°C up to more than 1,000°C. The products of the gasification step are combustible product gases, which contain as major components carbon monoxide (CO), carbon dioxide (CO_2), hydrogen (H_2), methane (CH_4), and water (steam) (H_2O). In case air is used for oxidation, also nitrogen (N_2) and nitrogen compounds like nitrogen oxides are included within the product gas. In addition, usually small portions of undesired by-products (like tar, ammonia, hydrogen sulfide, ash) are within the product gas.

Oxidation is the last step and (ideally) means the complete oxidation of the products resulting from the pyrolytic decomposition and the gasification at high temperatures (1,000°C and more) under heat release (i.e., exothermic process). The results are mainly water (H_2O) and carbon dioxide (CO_2). The excess air

coefficient is higher than one. To allow for a full oxidation, the gases to be oxidized and the air have to be mixed quite well.

The efficiency of the overall combustion process – chemical process only – could be described by the combustion efficiency. This efficiency is defined as the ratio of the heat energy generated during combustion and the heating value of the fuel. The (chemical) losses are due to incomplete oxidation with the result that energy is still contained in some un-oxidized components (e.g., char, tar, unburned gases). Today combustion processes in power plants or CHPs achieve combustion efficiencies of significantly more than 95% (95–98%). However, the performance of the combustion process is usually not expressed in terms of efficiency. It is controlled by analysis of the ash – stating the unburned matter – and the flue gas (i.e., the un-oxidized organic compounds).

All other losses, in form of heat – e.g., with the flue gas, with the ash, from the boiler or the gas turbine casing – are not considered here since they are related to the technical devices.

Thermal Cycles The combustion of the solid, liquid, or gaseous fuel for electricity generation is usually part of a thermal cycle, in which a media is undergoing phase changes between the liquid and the gas phase and where energy is added and released in certain parts of the cycle. Such cycles are divided into open and closed thermal processes.

Open cycles are commonly applied for gaseous and liquid fuels since they have fewer impurities than solid biomass. They are realized in internal combustion engines and gas turbines. The fuel is either burned directly inside an internal combustion engine, which is operated cyclically (like a four stroke or two stroke engine), or it is burned continuously in an external combustion chamber and then led through a gas turbine for expansion. The working fluid does not circulate through the system; therefore it is not a true cycle. The direct use of solid biomass fuels in internal combustion engines is technically not feasible and their application in open cycle gas turbines is regarded as complex.

In closed thermal cycles the combustion process and the power generation cycle are physically separated by a heat transfer device between the combustion and the process medium used within the secondary cycle. Due to the separation between fuel and power generation equipment, the latter is solely in contact with a clean process medium and thus undesired elements like fuel, ash, tar, and flue gas are not harming. Hence, closed cycles are well suited for solid fuels and widely applied for power production from biomass or waste.

The cycle mostly applied for electricity generation from solid biofuels is the Clausius Rankine Process [11] (Fig. 4). Water at low pressure is transferred with a feed pump to a higher pressure level. The pressurized water is then heated up to the evaporation temperature in the boiler, then evaporated to saturated steam, and finally superheated in the superheater section to dry steam. This steam is then expanded to the back pressure in the turbine, which provides kinetic energy to the generator. The back-pressure steam is led to the condenser, where the remaining condensation enthalpy needs to be transferred to the cooling medium. Finally water at low pressure leaves the condenser and is transported to the feed pump to start the cycle again.

Basically, thermal efficiency of the thermal cycle depends on the temperature difference of the hot steam and the "cold" water (Carnot law). As an example, using Carnot's law, for a typical rankine cycle with steam temperature of 543°C (816 K) and a temperature of the condensed water of 23°C (296 K), the maximum theoretical efficiency can be calculated as with 64%. However, typical thermal efficiencies of realized Clausius Rankine processes in biomass power plants are in the range of 30 to a maximum of 40% (i.e., with own consumption and without any mechanical losses). This is lower as in modern state-of-the-art large-scale coal-fired thermal power plants. Here the Clausius Rankine cycle can reach efficiencies up to 50% or more. This is mostly because the temperature differences between the upper and the lower side of the thermal cycle can be increased due to the utilization of more sophisticated material.

Another closed cycle sometimes used in biomass combustion facilities is the Organic Rankine Cycle (ORC). This cycle is similar to the Rankine Cycle. However, instead of water an organic fluid with a lower boiling temperature is used as a process medium. This enables operation with heat sources of relatively low temperatures (e.g., 90–150°C); this is the

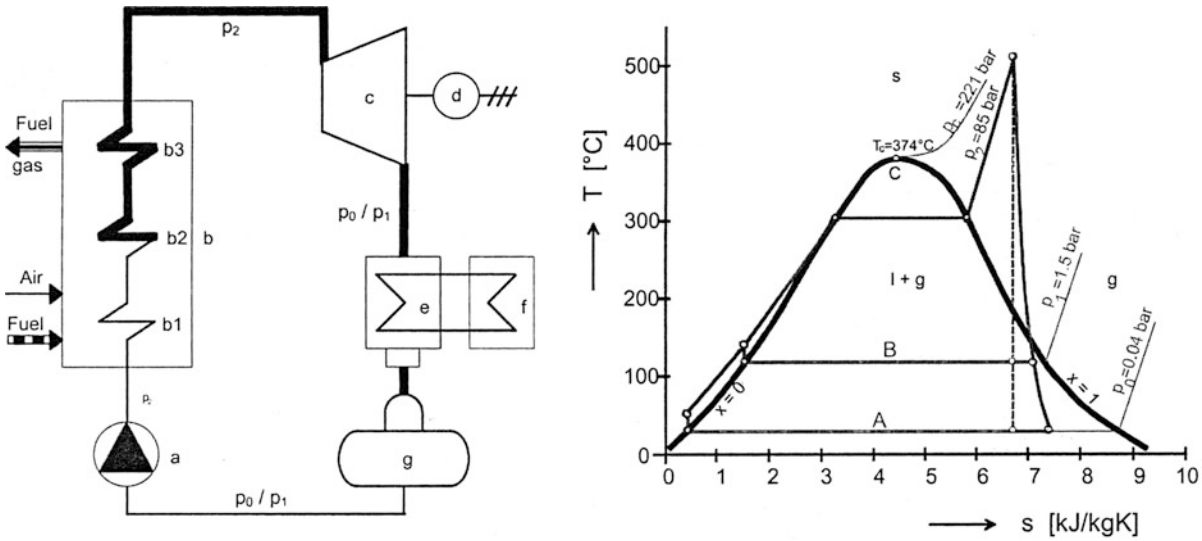

Biomass Combustion for Electricity Generation. Figure 4
Flow and T/s diagrams of back-pressure plants based on the Rankine cycle [12]. *Left*: Principle of a power plant based on a *Rankine cycle with steam superheating*. *Right*: In the T/s-diagram (temperature versus entropy). *Case A* describes a *condensing plant* with component f in the flow diagram being an air cooler or a cooling tower for heat transfer to the ambient. *Case B* describes a *back-pressure* plant with utilization, of the heat at a higher temperature level, hence component f corresponds to a heat exchanger used for heating purposes or process heat. In a back-pressure plant, the condensation temperature $T_6 = T_1$ is increased to enable heat utilization, thus reducing the electrical efficiency. For small turbines, the back-pressure steam needs to be saturated, as droplets are not allowed. Hence point 6 in the *T/s*-diagram needs to be on the condensation line, thus resulting in a reduced efficiency. Components in the flow diagram: a = feed water pump, b = boiler with b1 = water preheater, b2 = evaporator, and b3 = superheater, c = steam turbine, d = generator, e = condenser, f = heat exchanger to transfer condensation enthalpy in a secondary circuit to the ambient (case A corresponding to a condensing plant) or to a heat consumer (case B corresponding to a back-pressure plant), g = feed water tank. Abbreviations in the T/s-diagram: s = entropy, t = temperature, 1 = liquid, g = gas (vapor), s = supercritical, c = critical point, p = pressure, p_2 = high pressure of the live steam, p_0 = back pressure for a condensing plant A, p_1 = back pressure for back-pressure plant B. 1–2 Adiabatic pressure increase of the water in the feed pump. 2–3 Heating of the water to evaporation temperature in the water preheater. 3–4 Evaporation of the water in the evaporator in the boiler. 4–5 Superheating of the steam in the superheater. 5–6 Isentropic expansion of the steam (ideally). 6–7 Polytropic expansion of the steam in the turbine (real process). 6–1 Condensation of the steam, with either heat transfer in a secondary circuit either to ambient (condensing plant) or heat utilization (back pressure plant)

reason why this cycle is often used for electricity generation from geothermal energy. ORC processes within the biomass sector are sometimes added after a "classical" Rankine Cycle to make use of the residual heat in the flue gas at low temperature and use it for electricity generation.

Thermal efficiency of the ORC process is significantly lower compared to the Clausius Rankine process, being in the range between 12% and 17% (process only, excluding own consumption and mechanical losses of the turbine). This is due to the lower temperature of the driving heat source and therefore the lower temperature differences used hereunder.

Technical Devices Combustion of solid biofuels in biomass-to-electricity generation facilities usually takes place in boilers. The differentiation is made by the technology of the firing system into:

- Fixed bed combustion (usually on a grate)
- Fluidized bed combustion
- Pulverized fuel combustion

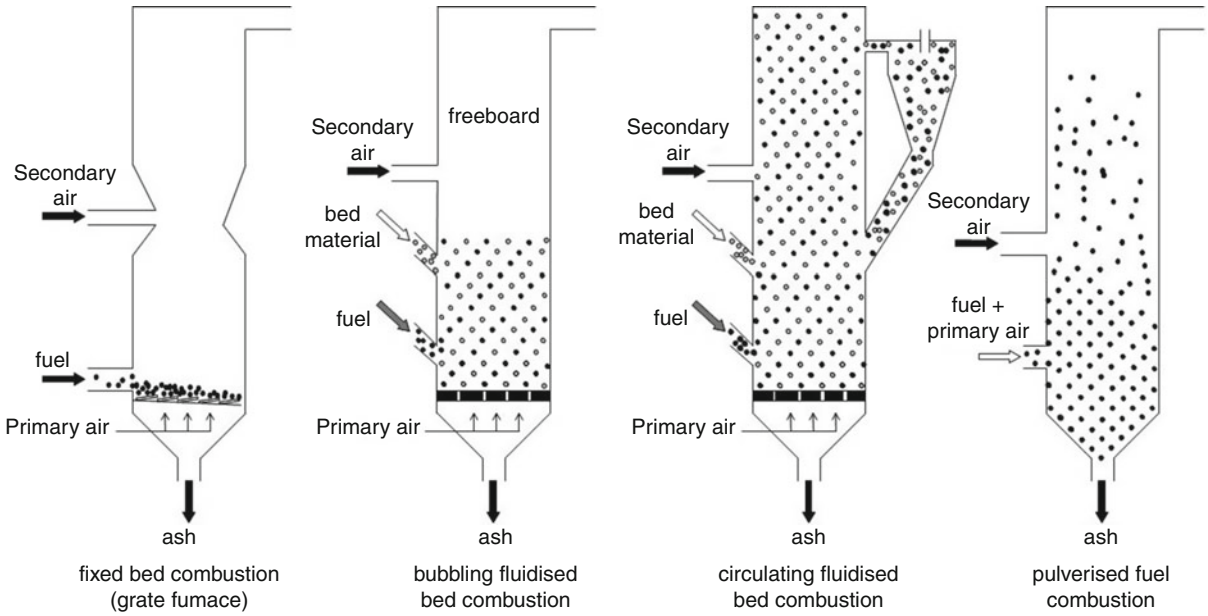

Biomass Combustion for Electricity Generation. Figure 5 Principal combustion technologies for biomass [12]

Figure 5 shows the main principles.

All of the boiler types have in common that the biomass is burned and then the thermal energy is used to heat water running through pipes – mostly inside the boiler. After preheating (economizer), the water is heated up to the point of evaporation, evaporated, and then superheated. The relevant tubes are located in different parts of the boiler.

The energy losses within such a boiler are of different type and dependent on the boiler type, size, and material, and the fuel type mainly.

- Dry flue gas loss is the sensible heat loss that is due to the temperature difference between flue gas and the inlet air temperature (the flue gas carries heat up the stack). It is a function of excess air as well as the flue gas temperature and combustion air temperature.
- Latent heat loss is due to the water vapor in the flue gas leaving the boiler without being condensed (not used condensation enthalpy). It comes from (a) the combustion of hydrogen (respectively hydrocarbons) in the fuel and (b) water contained in the fuel ("Moisture-in-fuel loss") and (c) water in the combustion air. Significant levels of water are found naturally in biomass.
- Casing losses are the radiant and convective heat losses from the boiler casing.
- Losses due to incomplete combustion (unburned matter in ash and flue gas).
- Other losses are caused by air or flue gas leaks, and by heat in the ash.

Boiler efficiency (including the firing system) is the ratio of heat absorbed in steam to the heat supplied in the fuel. Modern biomass boilers (from 20 MW_{th} upwards) can achieve energy efficiencies of 90–95%. As for all solid fuel combustion systems, the boiler efficiency is mostly related to the net calorific value.

Below the most important types of boilers are discussed in detail.

Fixed Bed Combustion Systems Fixed bed combustion systems in biomass power plants are usually realized in form of a grate firing system. Smaller furnaces and boilers (a few MW_{th}) can be realized as well with underfeed firing. Primary air passes through a fixed bed, in which drying, pyrolytic decomposition, and gasification take place. The combustible gases are burned after secondary air has been added usually in a combustion zone separate from the fuel bed.

Such kind of combustion usually takes place on grates, of which various types are available: fixed grates, moving grates, traveling grates, rotating grates, and vibrating grates. The grates can be horizontal or inclined. The correct selection of the grate depends on the fuel properties and the size of the plant.

As a standard rule, grate firing is appropriate for fuels with a water content up to 60%, varying (but not smaller than approximately 2 mm) particle sizes, and high ash content. Thus, mixtures of wood and other type of biomass can be used.

Of great importance is always to allow a homogenous distribution of the fuel to keep the bed of embers at the intended location of the grate surface – over the full width, but only in a well-defined zone in the moving direction. A homogenous fuel layer is important to guarantee an equal primary air supply over the various grate areas. Inhomogeneous air supply may cause slugging, higher fly-ash amounts, and may increase the excess oxygen needed for a complete combustion resulting in boiler heat losses. Furthermore, the transport of the fuel over the grate has to be as smooth and homogenous as possible in order to keep the bed of embers calm and homogenous, to avoid the formation of holes, and to avoid the release of fly ash and unburned particles as much as possible.

Fluidized Bed Combustion Systems In fluidized bed combustion, the solid biofuels are suspended during the combustion process within a moving gas and particle stream, called the bed. The result is a turbulent mixing of gas and solids, which provides very effective chemical reactions and heat transfer.

The core of this technology is the fluidized bed reactor. A fluid (gas or liquid) is passed through a granular solid material at high enough velocities to suspend the solid. The reactor is usually a cylindrical vessel with a perforated bottom plate filled with a suspension bed of hot, inert, and granular material. Common bed materials for combustion are, e.g., sand.

Through the air distribution plate, primary combustion air enters the reactor from below. When the slackening velocity (minimum velocity to de-lock the bed) is reached, the bed expands and the gas/solids mixture behaves like a fluid. This process is known as fluidization. With further increasing gas flow the bed will change its fluid dynamic behavior: gas bubbles form in the bed, they will agglomerate to larger ones, the bed begins to slug, finally when one bubble reaches the diameter of the reactor, it moves up the bed, showing a piston-like behavior, an extreme form of a slugging bed. Depending on the fluid dynamic regime during operation, the reactor is called a bubbling fluidized bed, etc.

Intense heat transfer and mixing provides good conditions for complete combustion with low excess air demand. Between 650°C and 900°C, the combustion temperature is usually low in order to prevent ash sintering in the bed. Keeping the temperature in such lower ranges can be achieved by, e.g., (1) heat exchanger surfaces or (2) flue gas circulation.

Fluidized bed combustion plants are in widespread use, since the fluidized bed can deal flexibly with various fuel types, including very high water content, as a result of the good mixing achieved. Different kinds of solid fuels like woody biomass, coal, and special kind of waste (e.g., RDF) can be burned. Fluidized beds are as well the standard technology for burning sludges (e.g., sewage sludge from waste water treatment). However, the fluidized bed performance is sensitive toward particle size and inert impurities in the fuel. Therefore, usually an appropriate fuel pretreatment system for particle size reduction and separation of metal parts and stones is necessary. Particle sizes between 40 and 80 mm are common for woody biomass. Further considerations are, e.g., regarding high alkali biomass fuels (e.g., straw), due to possible ash agglomeration.

During start-up time of fluidized beds, which can take longer period of times (8 till 15 h), oil or gas burners are used. Due to higher specific investment of the overall plant, fluidized bed combustion is more common in larger applications (usually nominal thermal boiler capacity above 20 MW_{th}). With regard to emissions, low NO_x emissions can be achieved due to good air staging, good mixing, and low requirement of excess air. Low excess air quantities reduce the overall flue gas flow and increase the overall combustion efficiency. Usually the flue gas leaves the reactor with high dust loads. Therefore efficient dust precipitators and boiler cleaning is necessary. Bed material is also lost with the ash, making it necessary to periodically add new material to the plant, even though part of the bed material inside the ash can be separated from the fine particles and sand in air classifiers.

Different types of fluidized bed combustions are distinguished: (1) stationary fluidized bed combustion and (2) circulating fluidized bed combustion.

Stationary fluidized bed combustion has the main principle that the flow velocity of the gas in the vessel is between the slackening velocity (minimum velocity to enable fluidization) and the floating velocity of a single particle of the bed material. Usually the flow velocity of the gas is between 5 and 15 times the slackening velocities. In such cases a clearly defined fluidized bed usually with a thickness between 1 and 2 m is created.

In circulating fluidized beds the gas velocity is significantly above the floating velocity of the individual particles. Due to this there is no clearly defined bed surface: the fluidized bed expanded in the whole vessel. Due to the high gas velocity bed material is entrained out of the vessel and has therefore to be recirculated back to the vessel, after it has been separated in one or several cyclones from the gas flow.

Pulverized Fuel Combustion Systems In pulverized fuel combustion, fuels such as saw dust and fine shavings are pneumatically injected into the combustion room. The transportation air is used as primary air.

When starting a pulverized fuel combustion reactor, usually an auxiliary burner is used for preheating. After the temperature in the boiler has achieved a certain level, biomass is injected through a burner.

Fuel quality has to be quite constant. Particle size is usually limited between 10 and 20 mm. Fuel moisture content should not exceed 20%. Due to the explosion-like combustion of the fine biomass particles, the fuel feeding needs to be controlled very carefully.

Fuel/air mixtures are usually injected tangentially into the combustion room to establish a rotational flow. The rotational flow can be supported by flue gas recirculation in the combustion chamber.

Excursus: Co-firing Concepts

Co-firing means that biomass and fossil fuels are being used jointly in a plant to produce electricity and/or heat.

Such co-firing can provide a reasonable attractive option for the utilization of biomass for the generation of power and in some cases heat. Co-firing makes use of the extensive infrastructure associated with an existing power plant system based on fossil fuel energy, and requires only relatively modest additional capital investment.

The principal driver for the increasing amount of co-fired biomass materials in new and existing coal boiler plants is that co-firing is regarded as representing a very attractive option for biomass utilization, and therefore of the delivery of electric energy out of renewable energy, in terms of the capital cost requirement, security of supply, power generation efficiency, and generation cost.

The great majority of biomass co-firing worldwide is carried out in large pulverized coal power boilers, and the focus in this section is very much on this type of plant. The basic co-firing options can be categorized according to Fig. 6.

- Concept 1: direct co-firing. Under this concept, biomass and fossil fuel is being burned in the same conversion unit; usually it means that the biomass is fed directly to the coal firing system of the boiler. This co-firing approach can be implemented in a number of ways. The first option involves the mixing of the biofuel with the coal upstream of the coal feeders, and generally within the coal conveying system. The mixed fuel is then processed through the installed coal milling and firing system. This is the simplest option and involves the lowest capital cost. This approach has been applied widely for co-firing biomass in granular, pelletized, and dust forms, generally at relatively low co-firing ratios. The second option involves separate handling, metering, and comminuting of the biofuel and injection into the pulverized fuel pipe work upstream of the burners or at the burners. This option can permit co-firing at elevated levels. The third option involves the separate handling and comminuting of the biofuel with combustion through a number of dedicated burners. This approach involves significant modification of the combustion equipment and the boiler, and represents the highest capital cost direct co-firing option. It is, in principle, possible to inject the pre-milled biomass into the upper part of the combustion room as a reburn fuel for NO_x emission control; however, this option needs significant further development prior to full scale implementation. Some test work has been carried out in small-scale test facilities.

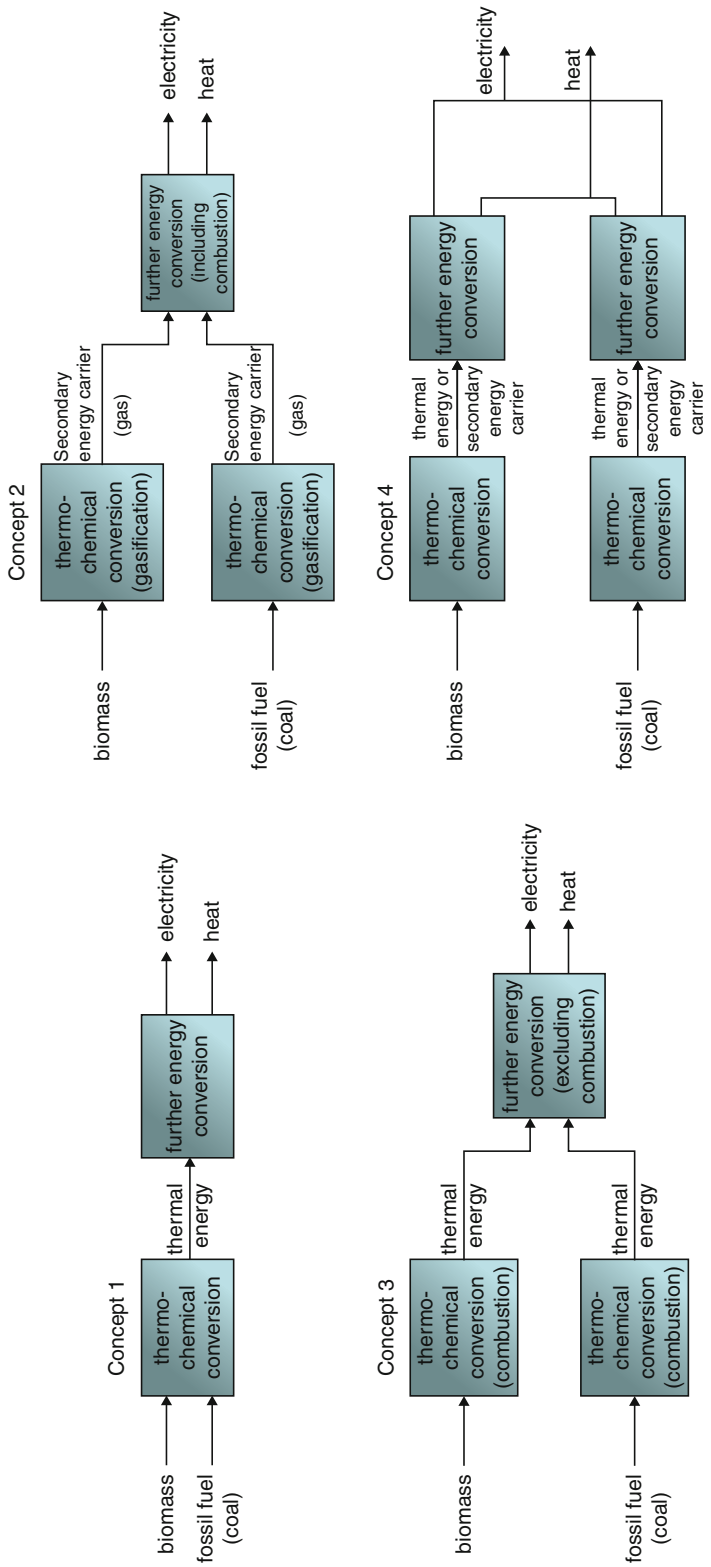

Biomass Combustion for Electricity Generation. Figure 6
Biomass co-firing concepts

- Concept 2: indirect co-firing. This concept involves the conversion of the biomass and the fossil fuel each in a separate unit into a secondary energy carrier. Usually this is a gasifier. Then these two secondary energy carriers are fed into one combustion system and then to go on with the further energy conversion steps. The usual system hereunder is the gasification of the biomass and the combustion of the product fuel gas in the boiler or gas turbine.
- Concept 3: parallel combustion. In this case, biomass and fossil fuel are first being converted thermochemically separately. The result of these two separate conversions is thermal energy (heat). This heat is then converted in further conversion steps to electricity and heat. Usually this process is called parallel combustion. Parallel firing involves the installation of a separate combustor for the biomass to produce steam, which, in turn, is used in the coal-fired power plant steam circuit. Although parallel firing installations involve significantly higher capital investment than direct co-combustion systems, they may have advantages such as the possibility to use relatively difficult fuels with high alkali metal and chlorine contents and the production of separate coal and biomass ash streams.
- Concept 4: separate combustion and conversion. Under this concept, the biomass and the fossil fuel are utilized for electricity/heat generation in two separate units, but at the same power plant site. Therefore, only several BoP (balance of plant) parts of the power plant site are used jointly like, e.g., grid connection, road infrastructure, and water supply. A separate combustion and separate further conversion of the secondary energy or heat into electricity and heat means that only the final energy carriers (electricity and heat) are flowing together. This is usual praxis in a number of biomass combustion plants. The advantage is that the infrastructure on site can be used by both plants as well as several selected BoP components.

Conversion from Thermal to Mechanical Energy

The conversion from thermal energy into mechanical energy is performed in devices, which can generally be divided into those of turbine type and those of engine type:

- Steam turbines
- Engines
  - Steam engines
  - Stirling engines

These different types of conversion devices are discussed below.

Steam Turbines Mostly applied in biomass to electricity generation systems is the steam turbine. Steam turbines are by definition fluid flow engines, in which the energy of a flowing working fluid (e.g., steam) is converted into kinetic energy and then in mechanical energy of the turbine shaft. Usually the turbine shaft is connected to a generator, in which the rotational mechanical energy is converted into electrical energy.

Steam turbines are available within a large range of different capacities, from few 100 kW (mechanical energy), commonly several 10s to several 100s of MW, up to the largest one with roughly 1,600 MW, currently under construction for the Olkiluoto III nuclear power plant in Finland. Within the biomass sector steam turbines in the range of several MW up to some 50–100 MW are most common.

A typical steam turbine consists of shaft, rotating shuffle wheel(s), fixed shuffle wheel(s), and the turbine casing. Fixed and rotating shuffle wheel are together forming one turbine step, whereby usually – apart of very small turbines – a turbine consists of several steps.

The working fluid flows usually in axial direction and only sometimes in radial direction between the annular gap between chamber and shaft, where the shuffle wheels are located.

Different types of steam turbine exist:

- Back-pressure steam turbines, in which the total waste heat from the condensation of the steam is utilized; the back pressure corresponds to the temperature needed for heat utilization (i.e., close to or greater than 1 bar).
- Condensing turbines are used in power plants without heat utilization; the back pressure and the corresponding temperature are as low as possible to achieve maximum efficiency, and hence the temperature is close to ambient temperature while the back pressure is significantly below 0.1 bar.

- Extraction turbines allow a power plant with variable heat output. Such a turbine enables a variable extraction of steam at an intermediate pressure and temperature level for heat utilization, with the remaining steam being utilized to drive an additional low-pressure section of the turbine in condensing mode.

Energy losses of the steam turbine are (1) heat losses through the casing, (2) steam leakages, and (3) energy loses with the steam flow leaving the turbine, due to non-ideal fluid dynamics while converting the energy of the steam to mechanical energy. In modern state-of-the-art steam power plants in the range of several 100 MW such losses total to less than 8%. For typical power plants in the range of several MW up to several tens of MW (this is the most common range of biomass power plants), such losses sum up to usually between 15% and 22%. Thus, the overall efficiency of the steam turbine in such typical biomass power plant defined as the ratio between mechanical energy at the turbine shaft and the difference of the thermal energy at the inlet and outlet point of the turbine (enthalpy difference) is between 78% and 85%.

Engines Steam piston engines have a similar working principle as other engines. They are available with an installed power between 25 kW up to 1.5 MW per unit. Very often the plant size is larger and in such a case several units are simply added in series. Typical mechanical efficiencies are in the range of 6–10% for single stage pistons and 12–20% for multistage engines. For this reason such devices are only used in CHP mode.

Stirling engines are indirectly fired gas engines with air, helium, or hydrogen as a process medium used within a closed cycle. External heat is transferred to the gas, followed by forced cooling of the gas. Expansion and compression of the medium inside the chamber are allowed over a piston. A Stirling engine is the thermodynamic ideal process for transforming heat into mechanical energy. It has thus the same theoretical efficiency as the Carnot process. In addition, in contrast to the Carnot process, it can actually be realized. However, in practical application the theoretical high efficiency is reduced by friction, limited heat transfer and heat recuperation, pressure losses, and other influences. Thus the actual efficiency for power production is only in the range of 15–25%. Additionally such devices are only limitedly available in the market.

Conversion from Mechanical to Electrical Energy

The conversion from mechanical into electrical energy takes place within the generator. The basic energy conversion principle is electromagnetic induction [3]. Such principle means that if an electric conductor, like a copper wire, moves through a magnetic field, an electric current is induced within the conductor. Thus the mechanical energy of the moving wire is converted into the electric energy of the current that flows in the wire. The main elements of the generator are the rotor and the stator. The stator is the fixed part and is winded with wires through which alternate electrical current is flowing, in which an alternate voltage is induced. The stator is usually connected directly or indirectly to the grid and therefore also the frequency of the electrical current in the stator is either the grid frequency or in any defined relation to it.

The rotating magnetic field induces an AC voltage in the stator windings. The rotor is also with wire, and this wire is rotating in the magnetic field inducing electric current in the stator. The rotor is connected usually mechanically via a gearbox with the rotating axes of the engine or turbine. The gearbox allows that the rotational speed of the rotor fits to the frequency of the stator.

Although different types of generators are used for different applications, in biomass to electricity generation as in other thermal power plant synchronous single-fed generators are applied in general. Other types are, e.g., asynchronous or induction single-fed generators, doubly fed generator, or brushless wound-rotor doubly-fed generator.

Independently from the type of generator, the electric power at the output of the generator has a fixed voltage level, which can be chosen among the typical standard voltage classes. Typical voltage levels for biomass combustion plants up to 20 MW_{el} are 400 V, 6.3 kV, and 11 kV.

Energy conversion efficiencies in the electrical generator are usually quite high. Losses mainly occur in form of heat, due to the wire resistance, and mechanical losses in the bearings of the rotor. The efficiency of modern synchronous generators is usually in the range between 96% (1,500 kVA at biogas plants, cos phi = 0.8) and 98% in large power plants.

Electric Energy Transformation

Usually the generator generates electricity at a typical voltage level. But the voltage level of the (local, regional, or supra-regional) grid is different in most cases. The electricity generated is therefore feed into the grid via a transformer station, whose main purpose is to transform the voltage coming from the generator into the voltage of the grid. Losses in the transformer are usually low and in the range of 1–3% of the input electricity. The losses can be divided into copper losses and iron losses. They are resulting out of (1) winding resistance, (2) hysteresis, (3) eddy currents, (4) magnetostriction, (5) mechanical losses, and (6) stray losses [4].

Other Plant Components

Within this chapter, additional system elements needed within an electricity generation plant operating based on biomass are discussed in detail.

Cooling Facility After the steam has flown through the steam turbine, it has to be cooled down. Thus, cooling water circulates around the tubes of the condenser and by this means the low-pressure steam after the turbine is cooled down and condensed.

The heat absorbed by the circulating cooling water in the condenser tubes must also be removed to maintain the ability of the water to cool as it circulates. The easiest option is getting the cooling water from a river or the sea and pumping the warm water back to the river or the sea. However, since sea water is not available at most power plant sites, and environmental restrictions limit temperature increase of rivers, waste heat is in most cases transferred to the atmosphere based on a cooling tower, or a combination of river and cooling tower cooling is realized. The warm water is pumped from the condenser through the cooling tower. A wet (or open) cooling tower reduces the temperature of the water in direct contact to the air, mainly by evaporation of a part of the water.

There are natural (air) draft and mechanical draft towers. The latter uses power driven fan engines to force or draw air through the tower. Within this type it can be differed between (1) induced draft, wherein a mechanical draft tower with a fan at the discharge pulls air through tower, and (2) forced draft, which has a blower type fan at the intake.

A dry (or closed) tower is a water–air heat exchanger, with a fan to increase air circulation. If the availability of water is not an issue at the location, usually a wet cooling tower is used, since lower temperatures are achieved. At other sites, where water availability is critical, or the formation of clouds has to be avoided, dry cooling towers are applied, which usually drops down the efficiency of the plant.

Flue Gas Treatment After the combustion, the flue gas is treated usually in different ways before it is emitted into the atmosphere due to legal obligations. All equipment and measures to treat the flue gas between the boiler outlet and the atmosphere is named together flue-gas-treatment-facility. The core objective of this facility is to reduce the emissions to a level that the power plant facility at the location has to fulfill.

To achieve the desired emission level, different measures are applied. They are subdivided in primary (i.e., directly influencing the combustion process itself) and secondary measures. Primary measures can be found under section "Gaseous Emissions". Secondary emissions reduction measures are part of the flue-gas-treatment-facility.

Flue gas treatment measures in biomass power plants derive from coal power plants. In a standard coal combustion plant, the flue-gas-treatment-facility consists of (in this sequence, with regard to the flow direction of the flue gas):

- A particle control and reduction facility
- NO_x control and reduction facility
- SO_2 reduction facility

Whether all of the above components or only some of them are part of the flue-gas-treatment-facility of a biomass combustion plant and which specific type of emission reduction technology has to be selected depend

on the biomass characteristics (chemical composition, particle size, etc.), the combustion technology, and the environmental regulations to be applied. In most cases, the flue-gas-treatment-facility of a biomass combustion plant is much simpler:

- For power plants burning only clean (natural) wood an electrostatic precipitator is sufficient to meet the emission limits for particulate matter.
- Larger power plants, burning contaminated wood as well, often apply dry sorption by spraying, e.g., calcium hydroxide into the flue gases and filtering them within a bag filter.

The principles of flue-gas-treatment-facilities are explained below.

Particle Control Systems For meeting the limits for particulate matter emissions the following reduction technologies are used commonly: cyclones, multicyclones, electrostatic precipitators, and bag house filters. They are discussed below.

Within a cyclone for particle separation, the flue gas and the solid particles are exposed to centrifugal forces. Due to these forces, the particles hit the wall of the cyclone and slide down into a container. The cleaned gas leaves the cyclone on the upper side.

In multicyclones, several cyclones are used in parallel. This is because the efficiency of a cyclone can be improved by increasing the centrifugal forces through a reduction of the cyclone diameter. However, this has the disadvantage that the throughput through one cyclone is reduced. To compensate this drawback some small cyclones are installed in parallel. The consequence are, obviously, higher cost due to the larger number of cyclones – even though each individual one is smaller – and a higher energy consumption due to the higher pressure drop in a smaller compared to a larger cyclone. Nevertheless often multicyclones are state-of-the-art technology and used frequently.

The principle of operation of an electrostatic precipitator is that the particles are first electrically charged and second exposed to an electric field in which they are attracted to an electrode. This electrode is cleaned periodically by means of vibration with the consequence that the dust falls off the electrode into a collection unit. Electrostatic precipitators are state-of-the-art technology and used commonly in large-scale units.

Bag house filters consist of a filter or cloth, tightly woven from special fibers and hung up in a closed construction through which the flue gas passes. Usually the separation efficiency of bag house filters is quite high, even with flue gas at low flow rates and high particle content. Because the particles settle on the cloth and form a particle layer (i.e., filter cake), the pressure drop between the two sides of the cloth increases during operation and therefore the cloth has to be cleaned periodically. One possibility is to use pressurized air passed through the cloth in reverse direction, removing the particle layer falling down to the bottom of the filter casing. This flue gas treatment technology is state-of-the-art technology and commonly used in medium scale units [6, 12].

NO_x Control Systems Secondary NO_x-emission control and reduction measures in biomass combustion facilities are mostly selective catalytic reduction (SCR) or selective non-catalytic reduction (SNCR). Both types have in common that a reducing agent is injected (e.g., ammonia (NH_3) or urea) to reduce NO_x to N_2, with or without a catalyst.

In case of using ammonia, the stoichiometric equations are as follows [6]:

$$4NO + 4NH_3 + O_2 \rightarrow 4N_2 + 6H_2O \quad (2)$$

$$2NO_2 + 4NH_3 + O_2 \rightarrow 2N_2 + 6H_2O \quad (3)$$

$$4NH_3 + 3O_2 \rightarrow 2N_2 + 6H_2O \quad (4)$$

$$4NH_3 + 4O_2 \rightarrow 2N_2O + 6H_2O \quad (5)$$

$$4NH_3 + 5O_2 \rightarrow 4NO + 6H_2O \quad (6)$$

Of the reactions listed above, the first two are the desired ones and the last three are undesired reactions.

Equations 2 and 3 take place within a temperature range of 220–270°C. If urea is used, the temperature level has to be increased to 400–450°C. The reason to realize a non-catalytic instead of catalytic reduction is mainly the amount of catalyst needed and the associated cost. For such a non-catalytic reduction, the reactions above described are taking place at temperatures between 850°C and 950°C, whereby for wood a temperature range between 840°C and 920°C has

proved most appropriate. Just due to the high temperature, there is no need for a catalyst.

Both types of reduction facilities have reduction efficiencies – defined as the amount of NO_x separated out of the flue gas related to the total amount of NO_x contained in the flue gas before entering the flue gas treatment facility – between 60% and up to 95% in biomass combustion applications. The efficiency depends very much on the quality of control and regulating the temperature. If the temperature is too high, ammonia is oxidized to NO; if the temperature is too low, ammonia does not react at all and is emitted together with NO_2.

SO_2 Control Systems SO_x emissions from biomass combustion facilities are usually at a very low level and sulfur is emitted basically as SO_2. Due to the low content of sulfur in wood, the combustion of wood usually results in little SO_2 emissions making secondary measures for flue gas treatment unnecessary. However, there are certain biomass types (e.g., straw, grass, Miscanthus) for which the SO_2 emissions can be significantly and in such a case SO_2 reduction measures must be applied.

The typical secondary measure for SO_2 reduction is scrubbing the flue gas with water containing finely grounded limestone (i.e., limestone wet scrubber). The flue gas, from which the solid fly-ash particles have already been removed, passes through a tower where the scrubbing slurry containing water and limestone particles is pumped through countercurrent. The scrubber vessel can be realized as a spray tower with multiple sprays and a mist eliminator. Other approaches are characterized by a packing with a very high opening integrated within the tower or a specialized bubbler designs.

Other Emission Control Systems Depending on the type of biomass fuels, other secondary control and reduction measures might have to be applied:

- Straw, for example, has a high content of chlorine (Cl), which one finds later in the flue gas as hydrogen chloride (HCl). In case primary measures and, e.g., binding the chlorine into the ash is not sufficient to reach the required emission limits for HCl, combined fine dust separation with dry sorption or with a wet washing can be applied.
- Sometimes it might be necessary to include secondary reduction measures to reduce dioxins and furans. Quite frequently this is combined with the SCR facility with a catalytic oxidation of particle-binding and filter-passing dioxins. Other possibilities for particle-binding dioxins are special dioxin filters.
- By condensing the water within the flue gas, the overall efficiency of the power plant can be improved since the latent energy of the water is used. In addition, this allows reducing or avoiding vapor clouds in the air, usually regarded as a negative visual impact especially in touristic areas. Furthermore, within such a flue gas condensing unit a cleaning effect is realized (e.g., particulate matter). The operating principle is that the flue gas is cooled below the dew-point, by which a part of the water steam is condensed. The energy set free during this condensing process can be used as usable heat. The efficiency of the condensing unit depends on the amount of excess air, the water content of the biomass fuel, the flue gas temperature, and the lower temperature level of the usable heat.

Chimney The cleaned flue gas is finally emitted to the atmosphere via a chimney or smoke-stack. Chimneys are typically vertical structures to ensure that the gases flow smoothly. Additionally they draw air into the combustion what is known as the stack or chimney effect. This effects uses the density difference between the hot flue gas inside the chimney (hotter means lower density) and the colder air outside the chimney (i.e., air with a higher density). Due to this density difference, the flue gas is flowing upward within the chimney. Thus the reason for the height of the chimney is not only to emit the flue gas to higher air levels so that it is dispersed better, but also to create sufficient pressure difference between hot flue gas and the outside air.

For biomass power plants with 5 and 20 MW_{el}, chimneys have heights of 30–50 m. Usually they are constructed in the outer part out of concrete. Inside this supporting structure, a jacket pipe per boiler is installed in which the flue gas is flowing. It is built out of flue gas resistant material.

Ash

Burning of solid biomass is inevitably related to the generation of ash as a by-product. Ash, produced in large-scale biomass combustion plants, can usually be separated in three different fractions [15]:

- Grate ash. Usually this fraction consists of the mineral residual of the biomass feedstock produced on the grate or within the circulating fluidized bed. In addition, inert material (i.e., mainly soil) which has been within the biomass fuel can be found herein. Beside this sintered ash particles and slack stones – particularly in the case of straw and bark – might be found. The share of the grate ash related to the total amount of ash is usually in the range of 60–90%.
- Cyclone ash. Cyclone ashes are fine particles entrained with the flue gas stream. Usually this ash fraction originates from inorganic matter like, e.g., salts and silicates being a part of the organic structure of plants. This ash fraction can be found as dust in turnaround chambers and in the heat transfer area of the boiler, as well as in the cyclones after the boiler. This ash accounts generally for around 10–35% of the total amount of ash.
- Fly ash. This ash fraction is generated within a bag house filter and/or an electrostatic precipitator. Additionally or alternatively, fly ash can be produced as condensate sludge in flue gas condensation units. In case of combustion plants without such kind of flue gas cleaning, this ash fraction is emitted as residual dust via the chimney into the atmosphere. Usually the fly ash is the smallest portion of the total amount of ash and totals to 2–10% of the total ash amount.

Ash Characteristics In very general terms, the inorganic materials within most solid fuels, including biomass, can be divided into two broad categories:

(a) The inherent inorganic material exists as part of the organic structure of the fuel. It is most commonly associated with oxygen-, sulfur-, and nitrogen-containing functional groups. These fundamental groups can provide suitable sites for the inorganic species to be associated chemically in the form of cations or chelates. Biomass materials tend to be relatively rich in oxygen-containing sites. Thus a significant fraction of the inorganic material in most biomass fuels is in this form. For some inorganic species, it is also possible to be present in very fine particulate form within the organic structure of the fuels, and to behave essentially as an inherent component of the fuel.

(b) Extraneous inorganic materials have been added to the fuel through geological processes or during harvesting, handling, and processing. Biomass fuels, for instance, are commonly contaminated with soil and other materials, which have become mixed with the fuel during collection, handling, and storage.

A listing of the major inorganic species found in the higher plants, and hence in the inherent inorganic material in most biomass materials, is given in Table 3. These data provide a rough quantitative overview of the major element speciation in biomass, divided into different categories.

The table makes it obvious that much of the inherent inorganic material in biomass is in the form of simple inorganic salts, and principally as the oxides and hydroxides of silicon, and the nitrates, sulfates, chlorides, phosphates, and oxalates of the alkali and alkaline earth metals. Table 3 shows further that a significant fraction of the inorganic material, in particular of the alkali metals, occurs in a water-soluble form.

The extraneous inorganic material can be in many forms. In most cases, however, it takes the form of contamination with sand, soil, or other mineral materials, tramp metal components, etc.

Ash Behavior There are inorganic constituents of biomass materials that are volatile at combustion temperatures, particularly some of the alkali metal (K and Na) compounds, the phosphates, and some of the heavy-metals species. These species might be released into the flue gases in the form of fume or as condensable vapor. Other inorganic species, principally the compounds of calcium and silicon, can be released from the burning fuel particle as very finely divided, submicron particles.

The balance of the inorganic fraction of the biomass will undergo a number of chemical and physical transformations, depending on the chemical composition, combustion temperature, and residence time, to form the larger residual ash particles.

Biomass Combustion for Electricity Generation. Table 3 Speciation of inorganic materials in higher plants, according to the classes "water soluble," "organically associated," and "precipitated" [12]

Element	Compound	Formula	Share of total element
Class 1 – water soluble (free ionic form)			
Na	Sodium nitrate, chloride	$NaNO_3$, NaCl	>90%
K	Potassium nitrate, chloride	KNO_3, KCl	>90%
Ca	Calcium nitrate, chloride, phosphate	$Ca(NO_3)_2$, $CaCl_2$, $Ca_3(PO)_4$	20–60%
Mg	Magnesium nitrate, chloride, phosphate	$Mg(NO_3)_2$, $MgCl_2$, $Mg_3(PO_4)_2$	60–90%
Si	Silicon hydroxide	$Si(OH)_4$	<5%
S	Sulfate ion	SO_4^{2-}	>90%*
P	Phosphate ion	PO_4^{3-}	>80%*
Cl	Chloride ion	Cl^-	>90%*
Class 2 – organically associated (covalent)			
Ca	Calcium pectate	Macromolecule	0.8–2.6%
Mg	Chlorophyll, magnesium pectate	$C_{55}H_{72}MgN_4O_5$, macromolecule-	8–35%
Mn	Various organic structures	Mn^{2+}, Mn^{3+},Mn^{4+}	>80%*
Fe	Organic complex, organic sulfates	Fe^{3+}, Fe^{2+}	>90%*
S	Sulfolipids, amino acids, proteins	SO_4^{2-}, S	–
P	Nucleic acids	PO_4^{3-}	–
Class 3 – precipitated (pure compound, amorphous, or crystalline)			
Ca	Calcium oxalate	$CaC_2O_4.nH_2O$	30–85%
Fe	Phytoferritin	$(FeO.OH)_8.(FeO.OPO_3H_2)$	Up to 50% in leaf tissue
P	Phytates	Ca-Mg(-K)-salt of $C_6H_6[OPO(OH)_2]_6$	Up to 50–86% in seeds
Si	Phytolyte	$SiO_2.nH_2O$	

For items marked * no quantities have been reported. The value quoted indicates that the speciation is dominant one for that element

The key mineral transformations and chemical reactions that may occur at elevated temperature include:

- The fusion or partial fusion of quartz and silica particles and, at high temperatures, chemical interactions with other ash components, principally to form alkali and alkaline earth metal silicates
- The fusion or partial fusion of alumina-silicates
- The decomposition of carbonates, oxalates, chlorides, etc., and other inorganic salts
- The volatilization of alkali metals and some heavy metals
- Particle fragmentation by thermal shock and the rapid release of gaseous species from particles
- The coalescence of intra-particle mineral particles

The specific details of the release mechanism and residual ash formation processes depend largely on the type of combustor, i.e., on the flame temperature and the residence times at elevated temperatures.

Of relevance to the ash behavior at elevated temperatures is particularly the type of combustion technology, since the combustion conditions tend to be significantly different. For the three main different types (grate firing, fluidized bed combustors, and

pulverized fuel combustion systems) this is described below.

Grate-Fired Combustors In grate-fired systems, the fuel particles are distributed over a moving or static grate to form a fuel bed, with some of the combustion air being supplied from underneath. The normal intention is to retain the majority of the ash on the grate to be removed either manually or mechanically to an ash pit. Nevertheless a significant quantity of the ash will be released from the bed as fly-ash particles entrained in the combustion gases or in the form of vapors and fine fumes.

The maximum fuel bed temperatures in grate combustion of biomass materials are generally between 1,000°C and 2,000°C. The overall residence times on the grate are relatively long; they are commonly in the range of several minutes.

Depending on the chemical composition of the ash and the local bed temperature, a degree of sintering or fusion of the bed particles may occur. If the degree of fusion is excessive, relatively large ash agglomerates may be formed. This can interfere with the distribution of air through the fuel, and may affect the burnout of the char. The bed ash composition is usually fairly similar to that of the laboratory-prepared fuel ash, although it can sometimes be depleted in the more volatile inorganic species, principally potassium.

The coarse fly-ash particles are small particles of ash of up to an aerodynamic diameter of some 200–500 μm. They are entrained with the upward flow of under-grate air and the combustion gases, and are carried upward through the combustion room and the steam generator (i.e., heat exchanger). The chemical composition of the coarse fly ash is normally similar to that of the bed ash. There is commonly condensation of volatile inorganic species, particularly alkali metal sulfates, and some heavy-metal compounds, on the surface of the coarse fly-ash particles.

The fine aerosols generally within the submicron area are generated by condensation of the volatile inorganic species from the vapor phase (i.e., the alkali metal and some heavy-metal compounds) mostly as chlorides and sulfates. This happens as the flue gas cools down by passing through the boiler.

With regard to fly ash and aerosol generation from the grate combustion of woody biomass the following needs to be considered:

- The particle size distributions of the fly ashes are commonly bimodal. The main coarse fly-ash peak is in the range larger than 1 μm with a maximum particle size up to 500 μm and with the aerosol peak in the submicron range.
- The total fly-ash concentration in the flue gas is dominated by the generation of the coarse fly ashes by bed ash particle entrainment in the combustion gases. The quantity of fly ash is influenced by the ash content of the fuel and the grate operating parameters.
- The aerosol concentration in the flue gas and the composition of the aerosol material are influenced mainly by the chemical composition of the fuel (i.e., by the levels of volatile species (alkali metals, lead, and zinc) and of the very fine calcium-rich particulate material contained in the fuel).

Fluidized Bed Combustors In fluidized bed combustion systems, the fuel particles are suspended in a fluidizing air stream, along with a relatively coarse-grained bed material. The great majority of the ash leaves the fluidized bed combustors in the form of fly ash particles, generally of up to around 50–100 μm in diameter. This material also contains fine particles of elutriated bed material, which is commonly quartz, or unreacted limestone, with lime and calcium sulfate/sulfite.

The combustion temperatures that apply in fluidized beds are somewhat lower than those that apply in fixed beds. The bed and freeboard temperatures when burning biomass materials tend to be less than 900°C, and the ash particles tend, in a number of ways, to resemble the ash produced by combustion of the fuel in a laboratory furnace at similar temperatures.

In most fluidized bed combustion systems, the fuel ash and bed material particles tend to sinter and form agglomerates. The avoidance of this is an important combustor design and operational issue. Excessive agglomeration of the bed particles can lead to poor air distribution and eventually defluidization of the bed. In extreme cases, it may be necessary for the

operator to bring the combustor off line to remove and replace the bed material.

The bed ash sintering process involves the formation of particle-to-particle bonds, commonly by a viscous flow sintering mechanism, involving the low melting temperature ash components, initially in the form of necks between the particles. The key processes responsible for the formation of bonds between the bed particles in biomass-fired fluidized bed combustion systems are:

- Partial melting of the low melting point ash components to form a liquid phase of low viscosity, which, in turn, forms the necks between the bed particle.
- In some cases, the solid ash and bed particles, and particularly silicates and alumina-silicates species may be partially soluble in the liquid phase at the sintering temperature, and this can contribute to the strength of the particle–particle bonding. At higher bed temperatures, it is possible for a silicate melt of high viscosity to form on the surfaces of the bed material. The viscous liquid phase can also flow to form necks between the ash and bed particle.
- It is also possible for chemical reactions to occur at the surfaces of the bed particles, which can increase the strength of inter-particle bonds. The fact that lime on the surface of the bed particles reacts with SO_2 to form calcium sulfate is considered responsible for the sintering of bed particles in fluidized bed combustors firing high calcium biomass material [6].

Pulverized Fuel Combustors In pulverized fuel combustors, wherein biomass is usually fired together with coal since these are usually large-scale systems, the peak flame temperatures are very high compared to those of most other combustion systems. They are commonly around 1,600°C. The residence times at these temperatures are relatively short; they are in the order of a few seconds. The basic concerns in this case are with the behavior of the inorganic materials associated with the biomass when exposed to these very high temperatures and the conditions that apply in suspension flames. Another concern is the impact of the co-firing of the biomass on the behavior of the resulting ash (i.e., the mixed biomass-cal ash).

In general, the products of combustion of biomass materials when co-fired with coal in large-scale power plants show a higher level of submicron fume and vapor. Additionally the fly-ash particles tend to be significantly smaller than those formed by the combustion of pulverized coal.

The key ash-related impacts of the co-firing of biomass with coal are potentially on the slugging and fouling deposit formation potential of the mixed biomass-coal ash, and on the efficiency of the installed particulate collection equipment. Even biomass materials tend to have a relatively low ash content compared to most coals, the biomass ash materials tend to be relatively rich in alkali and alkaline earth metals, and these are effective fluxes for the alumina-silicate coal ashes. Therefore, the co-firing of biomass with coal will tend to increase both the slugging and fouling propensity of the mixed fuel, depending on the chemistry of the coal and biomass ashes and the co-firing ratio. At low co-firing ratios (i.e., less than about 10% on a mass basis) plant experience has indicated that these effects tend to be modest.

Ash Utilization For utilization and disposal of ash, the following possibilities are available:

- Industrial utilization (e.g., as additional component or raw material for cement, as chemical raw material, as additive in the metallurgical industry)
- Utilization in road construction
- Application as secondary feedstock with fertilizing and soil improving impact in the agriculture and forestry industry
- Dumping

Below different possibilities are discussed.

Industrial Utilization An industrial utilization of ash from biomass power plants may only be applied if a reasonable amount of ash with equal quality over time is available. In most cases, wood firing systems have only small throughput capacity and therefore produce not a sufficient amount of ash. For this reason an industrial utilization of ash from biomass is for the time being of academic interest only.

Utilization in Road Construction Slacking grate ash may be utilized in road construction, e.g., as replacement for gravel. This is only possible if

biomass fuel is used, which has not been chemically treated. Then the latent-hydraulically characteristics of wood ash is of advantage, since they contribute to a good setting of the humid material in the ground. In case of burning bark, e.g., the crude fraction of the grate ash is sieved and used in road construction. The fine fraction of the grate ash as well as the fine fly ash are usually not recommended to be used for that due to their high content of heavy metal and the higher amount of water-soluble components.

Utilization as Fertilizer and Soil Improving Material The following considerations can be made with regard to using ash as a fertilizer and soil improving material in agriculture and forestry:

- A mixture of crude ash and cyclone ash in plant-specific amount relations should be brought back to the area the biomass comes from in order to close the mineral and nutrient cycle as much as possible.
- The fine fly ash, being the smallest ash fraction, but shows the richest part of heavy metal, has to be dumped. This is valid also for ashes from the cleaning of heat exchangers of boilers and chimneys of small plants.
- The separation between multi cyclone and fly-ash stripper is the most efficient. However, this means that the biomass combustion plant has to have a fly-ash separation unit and this has to be located behind the multi cyclone. Otherwise a separation of this fraction is not possible.
- Ashes from plants firing waste wood usually cannot be brought to agricultural or forestry areas without prior treatment, since they are usually contaminated with heavy metals.
- Ashes from industrial residual wood combustion plants have an intermediate position between ashes from waste wood and ashes from natural wood with regard to their composition and amount of heavy metals. It depends to which extent the industrial wood has been contaminated in order to decide which measures and utilization options can be chosen.

In order to allow an unproblematic utilization, the ash has to be provided to the farmer in a suitable form:

- The ash fractions crude ash and cyclone ash have to be mixed according to the relation they are produced. By this means a so called ash mixture after the ash formation is being created. The fly ash has to be collected separately and to be dumped according in accordance with the legal framework.
- The ash has to be provided in a condition that it can be strewed. This means it has to be free from slacking and stony parts with corn sizes above 1.5–2 cm.
- Iron parts, which are eventually in the ash (wires, nails, etc.), have to be removed as well. This can be done by means of permanent magnets.
- In a biomass power plant an automatic ash removal is recommended and usually standard. In case the bark portion inside the biomass fuel is more than 30%, an additional ash treatment (sieving or grinding) is required, since the slacking portion inside the ash is higher due to the mineral contamination in the bark (e.g., sand, soil, stones). Also for straw and cereal firing slacking is more common due to lower ash melting point and therefore such ash need to be treated similarly.

Biomass ash can be spread on land in a direct and an indirect way.

- Suitable for a direct spreading of ashes on agricultural areas and meadows are fertilizer caster with dust skirting. They allow a low cost, time saving, consistent, and mainly dust free distribution of the ash. For bringing the ash into the forest blowing machines are most suitable. They blow the ash from forest roads into the woods up to a distance of around 50 m.
- Alternatively the ash can also be used as additive in the agricultural composting. The advantage is that such an ash utilization can be performed almost dust free and that during the composting process also slacking and stone parts inside the ash do not negatively affect as they can be crushed inside the compost or sorted out during the resetting of the compost.

To avoid ecological negative impacts caused by ash spreading on soil, the following aspects should be considered.

- Only ash of chemically non treated biomass should be spread.
- Cyclone and fly ash must be collected separately and the fly ash should be dumped orderly.

- The usable part of the ash must be analyzed prior to the first spreading with regard to its nutrient and heavy metal content; such analysis must be repeated regularly according to the legal rules.
- For the usable portion from bark, wood chips, and shaving ash, the maximum amounts which should be spread on agricultural land shall be not more than 1,000 kg/(ha a), for grass land not more than 750 kg/(ha a) and not less than 3,000 kg/ha one time in 50 years [8]. In case the heavy metal fraction inside the ash is lower as the legally approved limits, the amounts given above can be increased.
- For the usable portion of the straw and cereal ash the amount of spreading has to be adjusted according to the nutrient needs of the respective plant culture.

Overall Energy Conversion Chain: Losses

Each energy conversion step is associated with losses and a certain "conversion step efficiency." As a result, only a fraction of the energy fed as biomass into the biomass combustion to electricity generation facility can finally be fed into the grid as end energy (electricity) or used as heat.

A typical facility often used in Europe burns solid woody biomass on a grate or in a fluidized bed and generates electricity out of this. Very often they are realized within an electrical power range between 5 and 20 MW_{el}. For such kind of standard application, Fig. 7 shows the energy flow and the average range of losses for each major conversion step. According to this out of 1,000 kWh (3,600 MJ) of biomass fuel such a standard plant can finally generate in the average around 251 kWh (903 MJ) of electricity. The biggest losses are within the water-steam cycle with 60–70% and within the turbine with 15–22%. Thus, the overall efficiency of such plant configuration ranges around 25%.

Environmental Impacts

Although biomass-to-electricity is a form of renewable energy generation, it is characterized by a number of environmental impacts. Most substantially are hereby the gaseous emissions, which are emitted via the chimney into the atmosphere.

Gaseous Emissions

There are a great number of different types of gaseous emissions from biomass power plants. They and their potential impact on environment, climate, and health are described in Table 4.

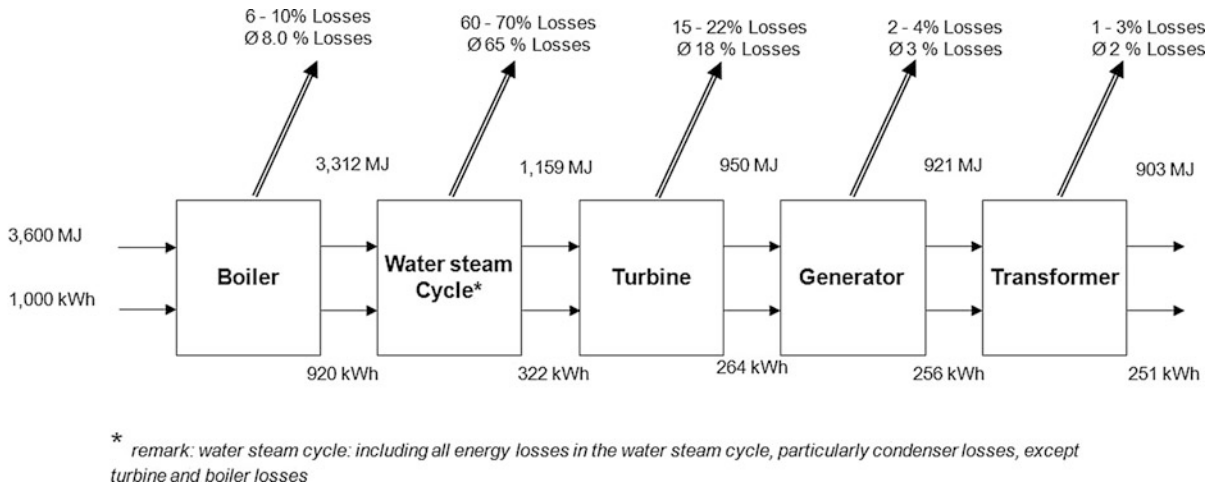

Biomass Combustion for Electricity Generation. Figure 7
Energy conversion chain of a typical biomass combustion facility for electricity generation in the range of 5–20 MW electricity (MJ and kWh values are calculated with the average loss figures)

Biomass Combustion for Electricity Generation. Table 4 Pollutants from biomass combustion and their impacts on climate, environment, and health [14]

Component	Biomass sources	Climate, environmental, and health impacts
Carbon dioxide (CO_2)	Major combustion product from all biomass fuels	*Climate*: Direct greenhouse gas. However, CO_2 emissions from biomass combustion are regarded as being CO_2-neutral with respect to the greenhouse gas effect[a] since biomass is a renewable fuel (if sustainably cultivated). (see also section "The Greenhouse Gas Balance")
Carbon monoxide (CO)	Incomplete combustion of all biomass fuels	*Climate*: Indirect greenhouse gas through O_3 formation
		Health: Reduced oxygen uptake especially influences people with asthma, and embryos. Suffocation in extreme cases
Methane (CH_4)	Incomplete combustion of all biomass fuels	*Climate*: Direct greenhouse gas. Indirect greenhouse gas through O_3 formation
Non Methane Volatile Organic Components (NMVOC)	Incomplete combustion of all biomass fuels	*Climate*: Indirect greenhouse gas through O_3 formation
		Health: Negative effect on the human respiratory system
Polycyclic Aromatic Hydrocarbons (PAH)	Incomplete combustion of all biomass fuels	*Environment*: Smog formation
		Health: Carcinogenic effects
Particles	Soot, char and condensed heavy hydrocarbons (tar) from incomplete combustion of all biomass fuels. Fly ash and salts	*Climate and environment*: Reversed greenhouse effect through aerosol formation. Indirect effects of heavy-metal concentrations in deposited particles
		Health: Negative effect on the human respiratory system. Carcinogenic effects
Nitrogen oxides (NO_x, (NO, NO_2))	Minor combustion product from all biomass fuels containing nitrogen. Additional NO_x may be formed from nitrogen in the air under certain conditions	*Climate and environment*: Indirect greenhouse gas through O_3 formation. Reversed greenhouse effect through aerosol formation. Acid precipitation. Vegetation damage. Smog formation. Corrosion and material damage
		Health: Negative effect on the human respiratory system. NO_2 is toxic
Nitrous oxide (N_2O)	Minor combustion product from all biomass fuels containing nitrogen	*Climate*: Direct greenhouse gas
		Health: Indirect effect through O_3 depletion in the stratosphere[b]
Ammonia (NH_3)	Small amounts may be emitted as a result of incomplete conversion of NH_3, formed from pyrolysis/ gasification, to oxidized nitrogen-containing components. Secondary NO_x reduction measures by NH_3 injection (SNCR, SCR)	*Environment*: Acid precipitation. Vegetation damage. Corrosion and material damage
		Health: Negative effect on the human respiratory system
Sulfur oxides (SO_x (SO_2, SO_3))	Minor combustion product from all biomass fuels containing Sulfur	*Climate and environment*: Reversed greenhouse gas effect through aerosol formation. Acid precipitation.[c] Vegetation damage. Smog formation. Corrosion and material damage
		Health: Negative effect on the human respiratory system, asthmatic effect

Biomass Combustion for Electricity Generation. Table 4 (Continued)

Component	Biomass sources	Climate, environmental, and health impacts
Heavy metals	All biomass fuels contain heavy metals to some degree, which will remain in the ash or evaporate	*Health*: Accumulate in the food chain. Some are toxic and some have carcinogenic effects
(Ground level) Ozone (O_3)	Secondary combustion product formed from atmospheric reactions including CO, CH_4, NMVOC and NO_x	*Climate and environment*: Direct greenhouse gas. Vegetation damage. Smog formation. Material damage
		Health: Indirect effect through O_3 depletion in the stratosphere.[b] Negative effect on the human respiratory system, asthmatic effect
Hydrogen chloride (HCl)	Minor combustion product from all biomass fuels containing chlorine	*Environment*: Acid precipitation. Vegetation damage. Corrosion and material damage
		Health: Negative effect on the human respiratory system. Toxic
Dioxins and furans (PCDD/PCDF)	Small amounts may be emitted as a result of reactions including carbon, chlorine, and oxygen in the presence of catalysts (Cu)	*Health*: Highly toxic. Liver damage. Central nervous system damage. Reduced immunity defense. Accumulate in the food chain

[a]*The greenhouse gas effect*: The natural greenhouse gas effect keeps the Earth's mean temperature at about 15°C. Without the greenhouse gas effect, the Earth's mean temperature would be −18°C. Anthropogenic sources of greenhouse gases are generally believed to contribute to an increasing greenhouse gas effect, causing the Earth's mean temperature slowly to increase. From 1750 to 1994, the concentration of the three most important greenhouse gases – CO_2, CH_4, and N_2O – increased by 30%, 145%, and 15%, respectively (contributing to an increasing greenhouse gas effect). However, particles, SO_2 and NO_x contribute, to some degree, to a reversed greenhouse gas effect caused by aerosol formation

[b]*Depletion of the ozone layer*: The atmospheric ozone layer is found in the stratosphere, 10–40 km above ground level. Ozone absorbs ultraviolet radiation from the sun and prevents damaging radiation from reaching the Earth's surface. Ozone in the stratosphere may be reduced by reactions with NO, where NO may be formed from N_2O in a first reaction step. Ground level ozone, however, is a pollutant and a greenhouse gas

[c]*Acid precipitation*: Emissions of NO_x, SO_x, and HCl result in acid precipitation through the formation of acids

The amount of emissions is usually given in mg/MJ fuel and these are dependent from a huge number of items. A very important one is certainly the type of technology used for combustion. The typical amount of emissions for different important combustion technologies are shown in Table 5.

These emissions can be reduced by primary measures and secondary measures. Secondary measures belong to the flue gas treatment facility and have already been described in section "Flue Gas Treatment". The main primary emission control and reduction measures are described below.

Generally it can be stated that all emissions which are avoided by primary emission control and reduction measures do not need to be targeted by any secondary emission control measure. Thus the usual way is to use as much as possible the primary emission control and reduction measures to limit the effort (investment and operating cost) for secondary emission reduction measures.

Primary emission reduction measures aim to prevent or reduce the formation of emissions and/or a reduction of emissions within the combustion chamber. Several possible measures exist. The most important with regard to the combustion of solid biomass are described below:

- Modification of the fuel composition. The concentration of K, Na, S, Cl, Zn, and Pb in the fuel determines the mass of aerosol emissions as well

Biomass Combustion for Electricity Generation. Table 5 Arithmetic average emission values from wood combustion applications [12]

	NO_x as NO_2 (mg/MJ)	Particles (mg/MJ)	Tar (mg/MJ)	CO (mg/MJ)	UHC as CH_4 (mg/MJ)	VOC (mg/MJ)	PAH (μg/MJ)
Fluidized bed boilers	170	2	n.m.	0	1	n.m.	4
Pulverized fuel burners	69	86	n.m.	164	8	n.m.	22
Grate plants	111	122	n.m.	1,846	67	n.m.	4,040

Data were collected from investigations in various IEA countries (Norway, Switzerland, Finland, the UK, and Denmark)
n.m. not measured, *UHC* unburned hydrocarbons

as their chemical composition. These elements can be removed from the fuel to a certain extent. A possible measure is fuel washing. For example, straw can be washed by leaving it on the field for some time after harvesting, exposing it to rain. Another possibility is a controlled washing. However, this may go along also with energy losses which might be counterbalanced by the positive effect on reduced emission control measures (and even a longer lifetime of the boiler).

- Modification of the moisture content of the fuel. High moisture content in the biomass fuel makes it difficult to achieve a sufficiently high temperature in the combustion chamber. However, high temperatures (above 850°C) are necessary to ensure a sufficiently low level of CO within the flue gas. Thus, due to incomplete combustion high emissions may be the result. Drying the fuel helps to solve this problem. Drying can be done naturally or artificial. Natural means, e.g., that the biomass is left at the atmosphere protected by rain and simply is getting dryer by time. With artificial drying, the water content can be reduced much further. However, if no waste heat without additional cost is available, artificial drying of biomass is much too costly. Therefore, mostly the biofuel is dried with solar energy.
- Modification of the particle size of the fuel. The size of the particles is important for the emissions to be produced for two reasons: The particle size defines very much the combustion technology selection. Technology selection has an impact on the amount of emissions produced. For a given or selected technology, the size of particle can still vary and insufficient precise sizing may result in incomplete combustion. The consequences are a lower efficiency and higher emission.
- Selection of the type of combustion technology and the type of equipment. There are various reasons for choosing a certain combustion technology. Based on this decision the design of the other components is realized. One of the results of this technology selection is the amount of emissions produced during the combustion process. Substantial emission reduction can be achieved by selecting the best possible combustion technology for a given fuel and by optimizing the combustion process including primary reduction measures.
- Improved construction of the combustion application. In order to obtain a full combustion by minimizing emissions, (1) sufficiently high combustion temperatures, (2) sufficiently long residence time, and (3) optimal mixing of the fuel gas and air have to be ensured. These items are partly determined by the combustion technology and the design of the boiler and partly by the combustion process operation.
- Combustion process control optimization. A combustion control system aims to govern selected process parameters according to a predefined scheme. Whereas usually the primary goal of a process control device in a biomass combustion facility is to adjust the heat production in the boiler according to what is required (e.g., by the steam turbine), the process control unit can be also programmed for simultaneous optimization of the combustion

process with respect to minimize emissions and maximize thermal efficiency. An adequate combustion control system can substantially lower the emissions in the flue gas. Typical process parameters to be used as process control parameters are the concentration of CO, C_xH_y, and O_2 in the flue gas, the combustion chamber temperature, and the boiler temperature. Process variables directly adjusted to achieve the targets for the aforementioned process parameters are typically the amount of fuel fed into the boiler.

- Staged-air combustion. Staged-air combustion makes it possible to reduce simultaneously emissions from incomplete combustion and NO_x through a separation of devolatilization and gas phase combustion. This results in improved mixing of fuel gas and combustion air. In the first stage, primary air is added for devolatilization of the volatile fraction of the fuel, resulting in a flue gas consisting mainly of CO, H_2, C_xH_y, H_2O, CO_2, and N_2. For NO_x-emission reduction, the fuel gas content of NH_3, HCN, and NO is also of particular interest. In the second stage, sufficient secondary air is supplied to ensure a good burnout and low emission levels from incomplete combustion. An improved mixing of fuel gas and secondary air reduces the amount of secondary air needed. This results in higher flame temperatures and a lower overall excess air ratio. Hence, emissions from incomplete combustion are reduced by a temperature increase, which speeds up the elementary reaction rates, and by improved mixing, which reduces the residence time needed for mixing the fuel gas and the secondary combustion air. However, this does not mean that the NO_x-emission level is reduced automatically as well. An efficient reduction of emissions from incomplete combustion and NO_x emissions can only be achieved by optimization of the primary excess air ratio.
- Staged fuel combustion and re-burning. Staged fuel combustion and re-burning are other possibilities for NO_x reduction in biomass combustion applications. The primary fuel is combusted with an excess air ratio above 1, and no significant NO_x reduction occurs. Then a secondary fuel is injected into the flue gas after the primary combustion zone, without additional air supply. Based on this a substoichiometric reducing atmosphere is created in which NO_x formed in the primary zone may be reduced, by reacting with NH_3 and HCN formed from the secondary fuel (if the secondary fuel contains nitrogen) in a similar manner as for staged-air combustion. Additionally, NO is converted back to HCN by reactions with HCCO and CH_i radicals (i = 0–3) formed from the secondary fuel. This process is called re-burning. Under typical conditions, HCCO appears to be the most effective radical for removing NO. Finally, a sufficient amount of air is added after the reducing zone to achieve a good burnout with an overall excess air ratio above 1. Staged fuel combustion requires automatic feeding of the primary and secondary fuel, and the secondary fuel must be easily adjustable. This limits the use of stage fuel combustion to large-scale biomass combustion applications, since a suitable combustion process design with two fuel-feeding systems as well as an accurate combustion process control is necessary. Natural gas, fuel oil, pyrolysis gas, biomass powder, sawdust, or similar fuels can be used as secondary fuels.
- Catalytic converters. A catalytic converter consists of a durable, heat-resistant ceramic composition extruded into cellular or honeycomb configuration. After extrusion, this ceramic monolith is fired and then covered with a noble-metal catalyst (usually platinum, rhodium or palladium, or combinations of these) or metal oxides. It is of paramount importance that the catalyst has a high thermal stability and a good poison resistance to avoid its deactivation. Such catalytic converters are utilized to some degree in small-scale biomass combustion applications (e.g., wood-stoves) but rather seldom in biomass-to-electricity applications.

The Greenhouse Gas Balance

Special attention has to be given to the carbon emissions of biomass power plants. As every thermal power plant using carbon-based fuel (e.g., coal, gas, oil), a biomass power plant emits CO_2 into the atmosphere. It is therefore not CO_2 neutral. And due to the fact that typical biomass-to-electricity power plants have – mainly due to smaller electrical capacities – lower

average efficiencies as, e.g., large-scale modern coal power plants, gas combined cycles or other types of fossil thermal power plants operated with fossil fuel energy, the direct emissions of a biomass power plant per unit of generated electricity are usually higher.

However, in order to assess the impact on the climate, and this is the main issue of the discussions about the pros and cons of CO_2 emissions, the entire life cycle of the biomass has to be considered. Assuming a sustainable biomass production, the same amount of CO_2, which is being emitted during combustion into the atmosphere, has been absorbed out of the atmosphere during the growing phase of the plants on the fields or in the forests. Thus, the assumption can be made that electricity generation from sustainable produced biomass is climate neutral.

Nevertheless, this is not the full truth. In fact, to allow that the biomass can be converted to electricity, there are a number of energy conversion steps necessary, which either need additional auxiliary energy or where energy is getting lost (see section "Overall Energy Conversion Chain: Losses"). These losses respectively needs for auxiliary energy result all in climate gas emissions.

Figure 8 shows exemplarily for a biomass plant for electricity generation the conversion chain and the resulting portion of emissions in CO_2-equ./kWh_{el}. Overall the carbon footprint results in 35–36

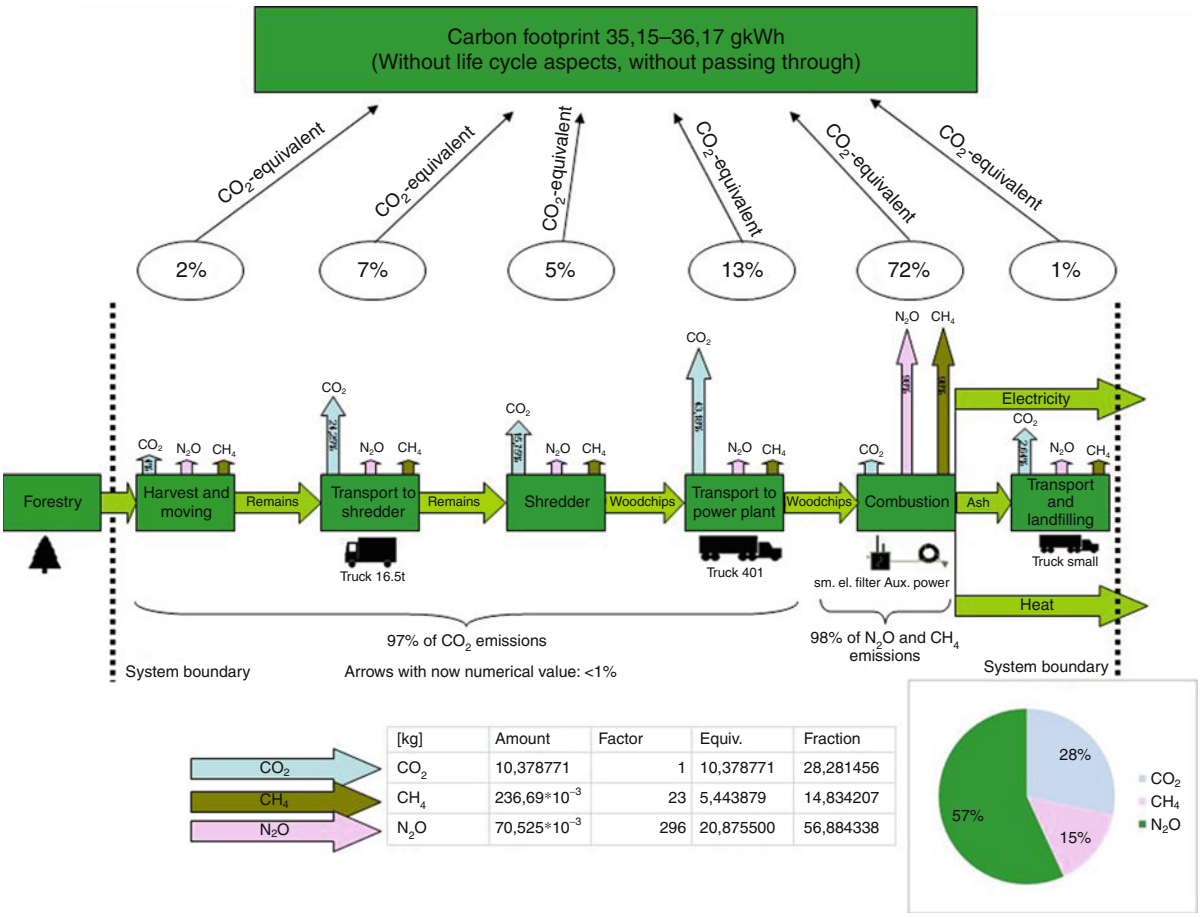

[kg]	Amount	Factor	Equiv.	Fraction
CO_2	10,378771	1	10,378771	28,281456
CH_4	$236,69*10^{-3}$	23	5,443879	14,834207
N_2O	$70,525*10^{-3}$	296	20,875500	56,884338

Biomass Combustion for Electricity Generation. Figure 8

Carbon emissions at the example of a medium size biomass power plant (5 MW_{el}), 20% efficiency fired with residual forest wood [16]

CO_2-equ./kWh$_{el}$, whereby the carbon footprint is defined as the total set of greenhouse gases (GHG) emissions caused by a product during its lifetime [17]. For climate relevant gases other than CO_2 (e.g., methane, see also Table 4) their impact on climate is calculated relative to 1 ton of CO_2. This bandwidth does not include the CO_2 emissions due to combustion, which have been absorbed before by the photosynthesis from the atmosphere. Most of the carbon footprint in Fig. 8 is contributed during the combustion due to the emissions of CH_4 and N_2O [13, 16].

The greenhouse gas balance of biomass has to be compared with other forms of producing electricity in order to arrive at an overall judgment of the balance. Figure 9 therefore shows the average bandwidth of CO_2equ.-emissions of different electricity generation options. According to this biomass is characterized by very low greenhouse gas emissions, being in the range of 35 to almost 100 gCO_2-equ./kWh$_{el}$. For example, for lignite the values are more than 10–20 times as high as for biomass. Still for natural gas, which has a much less carbon content as coal and can be converted into electricity with a much higher efficiency, there is a factor of between 6 and 10 between these two technologies.

In case the electricity generation is combined with heat utilization (combined heat and power) and subject to the methodology, how the carbon emissions are distributed between the final end products electricity and heat, the greenhouse gas balance, or so to say the carbon footprint can become even negative. This can be seen in Fig. 10, wherein once again several technologies are compared based on special designed technology layouts and differentiated between pure electricity generation and combined heat and power. According to this, biomass- and biogas-combined heat and power options are the only technologies showing a negative carbon footprint, in case the emissions saved due to the replacement of heat from other conventional sources and their resulting CO_2 emissions are being subtracted from the carbon footprint of biomass or biogas.

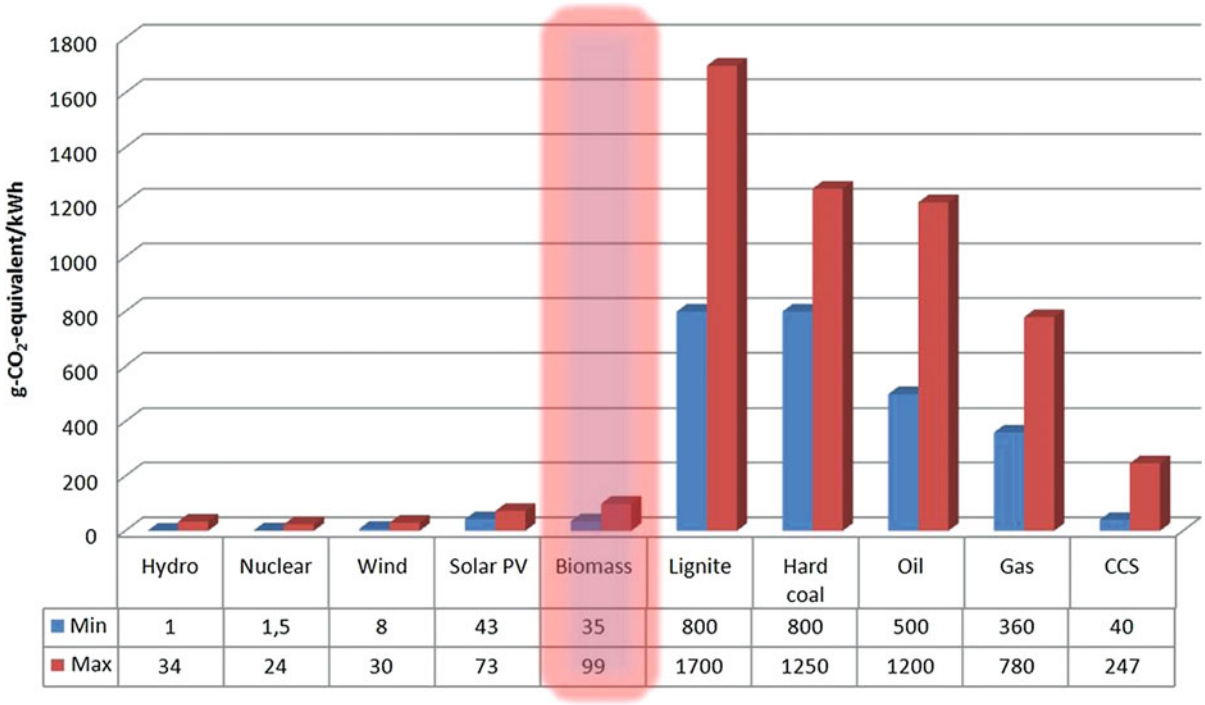

Biomass Combustion for Electricity Generation. Figure 9
Life cycle emissions of selected electricity generation technologies [16]

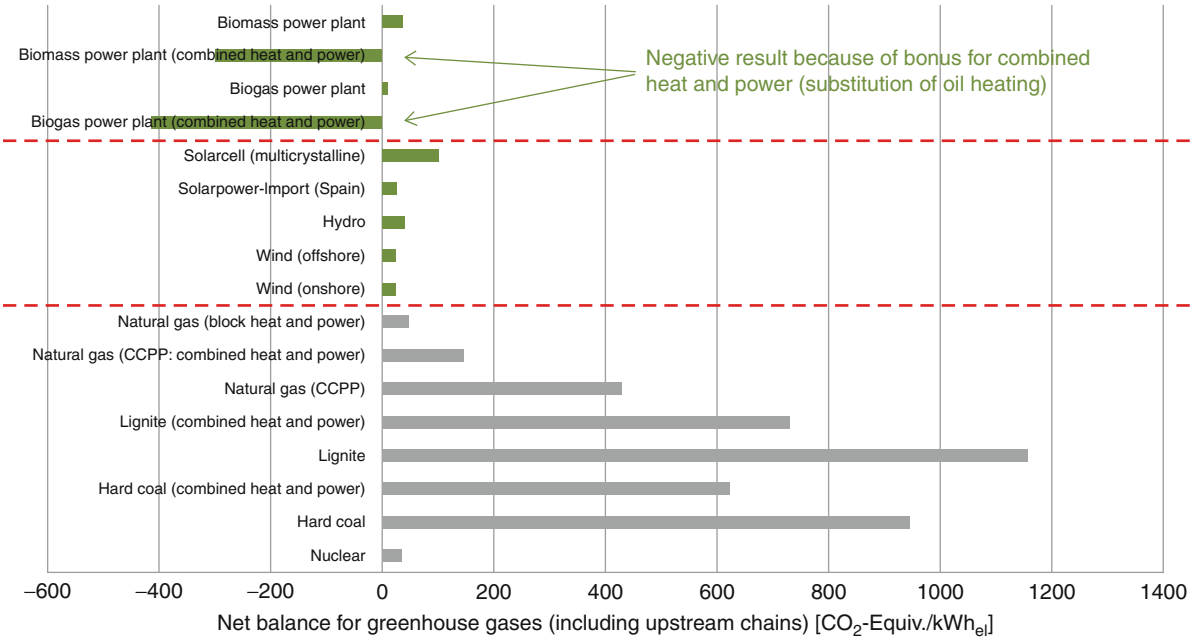

Biomass Combustion for Electricity Generation. Figure 10
Net balances of carbon equivalent emissions of different power generation technologies with and without combined heat and power generation [16]

Other Environmental Impacts

Other environmental impacts that may occur with biomass-to-electricity-generation can be (1) emissions in liquid form into the ground, (2) smelling, (3) noise emissions, and (4) visual impacts. Smell usually is a result of any gaseous emissions and occur sometimes, e.g., from the fuel storage. The others (point (1), (3), and (4)) are usually at a low level, if the plant is well planned and designed and fulfills the respective local requirements.

Cost Analysis

As with all energy conversion technologies, it is differed generally also in biomass-to-electricity facilities between investment and O&M cost. The overall cost varies widely. Some of the most important dependency factors are:

- The type and quality of the fuel
- The combustion technology as well as the whole concept and design of the plant
- The capacity of the plant
- The country
- The location of the power plant (country, and the specific location inside the country)
- The available infrastructure at the site
- The available know-how to design, build, and operate the power plant

Investment Cost

Investment cost covers the cost for all equipment and services necessary prior to the commercial operation of the power plant: biomass preparation facility, biomass storage and handling facilities, the power plant itself, emission reduction devices, cooling devices, grid connection, water supply, waste water system, all other balance of plant components, concept and detailed engineering, all consultancy fees and financing cost.

The following Table 6 provides with an overview of typical ranges of specific investment cost for different but quite common types of biomass to electricity generation plants. As can be seen therein, the most

Biomass Combustion for Electricity Generation. Table 6 Overview of investment of biomass to electricity combustion facilities

	Biomass steam power plants	IGCCs with biomass	CHP engines	Biogas plant + engine	Steam engines	Stirling engines
Usual type of biomass fuel	Solid biomass	Biogas, wood gas	Biofuel, biogas, wood gas	Biogas	Solid biomass	Solid biomass
Typical plant size range	5–20 MW	10–50 MW	500 kW to several MW	100 kW to several MW	100 kW to several MW	<100 kW to 1 MW
Investment cost range in €/kW	3,000–5,000	4,000–7,000	1,000–2,000	3,000–5,000	4,000–6,000	up to 10,000

common type biomass steam power plants have investment cost usually in the range between 3,000 and 5,000 €/MW.

O&M Cost

O&M cost are the annual cost of the power plant and are differentiated between:

- Fuel cost, which are usually the most important cost component
- Cost for waste disposal (ash, waste from emission cleaning devices)
- Regular and irregular maintenance
- Auxiliary media (water, electricity, lubricants)
- Operation personnel cost (administration staff and monitoring personnel)
- Spare parts
- Insurances
- Land lease

The above mentioned cost can be divided into two main classes: those which are fixed (i.e., independent from the amount of electricity produced annually) and those which are variable (i.e., depend on the annual electricity generation). Fuel costs as well as cost for auxiliary media are typical variable costs, whereas cost for land lease, insurances, and part of the operation personnel costs are usual fixed costs.

The typical relation between the overall investment cost and the overall O&M cost during the life time of a project depends on the cost impact of each cost component, but mostly it is influenced by the fuel cost. An example the typical fuel cost of a waste wood burning biomass power plant in Germany are in the range of 30–50 €/t. Taking 50 €/t as example and average energy efficiencies for a 20 MW-plant (i.e., base load plant) with 8,000 h/y of nominal load hours into account, the overall fuel cost over a 20 year life cycle of the plant is around 180 Mio. € (assuming additionally a calorific value of the biomass fuel of 16 MJ/kg). This is then double the amount of investment cost being between 80 and 100 Mio €. This example shows how important the fuel price, but also any measure to reduce the fuel consumption is (i.e., to increase conversion efficiency).

All other O&M cost are together substantially less than the fuel cost. For biomass power plants they are roughly in a range of around 4% of the total investment.

Example: Cost Analysis

A first indication of the financial feasibility of a biomass power plant can be derived by calculating the levelized electricity generation cost (LEC). They are calculated based on the annuity of the investment cost over the technical lifetime of the plant, adding to this the average annual O&M cost and dividing this through the average annual electricity generation. In case of combined heat and power production, the investment and O&M cost need to be divided to these two products, whereby different methods for such division exists.

For a standard example based on German frame conditions for purely electricity generation (i.e., no combined heat and power supply) and based on the technical and financial frame conditions as given in Table 7, the levelized electricity generation cost are calculated hereunder. The results are given in the

Biomass Combustion for Electricity Generation. Table 7 Example calculation of the levelized electricity generation cost of biomass and biogas power plants in Germany, 2009 figures

		Case 1	Case 2
Installed capacity	MW	5	20
Full load hours	h/year	8,000	8,000
Annual electricity sales	MWh/year	40,000	160,000
Technical lifetime	Year	25	25
Total average efficiency	%	24	30
Total amount of fuel needed (in form of wood or biogas)	MWh/year	167,000	533,000
Specific investment	€/kW	3,000	2,600
Total investment cost	€	15,000,000	52,000,000
Specific O&M cost without fuel	€/kW year	300	113
Fuel cost incl. logistics	€/t	20	25
Fuel cost	€/kWh fuel	0.008	0.006
Fuel cost	€/year	1,340,000	3,000,000
Total O&M cost incl. fuel cost	€/year	2.840,000	5,250,000
Equity	%	20	20
Loan	%	80	80
Required RoE	%	12	12
Interest on loan	%	5	5
Average interest	%	6.4	6.4
Annuity	€/year	1,218,000	4,224,000
Total annual cost	€/year	4,058,000	9,474,000
Levellized Electr. Gen. Cost (LEC)	€/kWh	0.10	0.06

table below. Under these assumptions the levelized electricity generation cost are between 0.06 and 0.10 €/kWh for biomass power plants.

Future Perspectives

Due to high energy price levels and promising policy conditions electricity generation from biomass is increasing on a worldwide scale. This is especially true for industrialized countries. Table 8 summarizes the worldwide use of biomass for electricity generation as per status end of 2008. As one can see, in total an amount of 256–386 TWh/year of electricity has been generated globally in 2008 from biomass including also the biomass fraction of waste-to-energy plants. Around 90 TWh/year has been generated in the Europe. Compared to the overall electricity generation from renewable energies, this is a share between 7% and almost 10%. Compared to the overall electricity generation worldwide in total (in 2008 estimated to be around 21,000 TWh/year), biomass contributes roughly around 1–2%.

With regard to the various submarkets, differentiated with regard to the fuel type/origin, the market consideration are as follows:

- *Solid fuel.* Currently, as end of 2008, at least 46 GW of solid biomass is utilized to produce electricity via mono- and co-combustion worldwide. The electrical power is installed equally in developing and industrial countries. With this installed capacity at an average of 4,000–7,000 of full load hours per year

Biomass Combustion for Electricity Generation.

Table 8 Electricity generation from biomass worldwide and in the EU-countries (status end of 2008) [9]

	Installed capacity in GW[a]		Electricity generation in TWh/a[a]	
	World	EU 27	World	EU 27
Solid Biomass	46	10	(190–320)	50
Municipal solid waste[b]	n.a	n.a	29	15
Biogas	>6	6	37[c]	25[c]
Total Biomass	52	16	256–386	90

[a]As far as statistical data available, values in brackets are estimated
[b]Only OECD countries
[c]Including the use of liquid biofuels

between 180 and 320 TWh of electricity can be produced. About 40% of the total electricity generated by solid biomass in the OECD countries has been realized within the European Union. There, the main producers are the three densely wooded countries Finland, Germany, and Sweden, producing more than half of the electricity generated by solid biomass in the EU. In many countries the energy recovery of municipal solid waste is counted to solid biomass. In the OECD about 29 TWh of electricity is estimated for 2008 assuming a similar increase as in 2007. Considering the measures taken to protect the world's climate a further growth of the power production from solid biomass is to be expected in the years to come. The growth will be very much influenced by the price level of the biomass materials which itself is strongly influenced by the fossil fuel price levels.

- *Biogas.* The electricity generation from biogas mainly takes place in industrialized nations. Considering the around 29 TWh of electricity from biogas, which has been generated in OECD countries in 2007, a total of roughly 32 TWh can be estimated for 2008. The main contribution comes from the EU. Global players on the biogas market are Germany (9–10 TWh) and the United Kingdom (5–6 TWh). Nearly half of the biogas in the EU is generated by landfills, of which almost half is produced in the United Kingdom. The remaining biogas is produced by agricultural biogas power plants, using mainly liquid and solid manure and maize, and by sewage gas power plants.
- *Liquid fuels.* Only a small part of liquid fuels is used for electricity generation globally. However, this use is statistically recorded in very few industrial nations only. Compared with the prior years, the use of liquid fuels for electricity generation in combined heat and power plants has stagnated or decreased in selected countries in 2008.

The worldwide electricity generation from biomass is characterized by a large spectrum of available technologies. The technologies used in developing countries show on average very low efficiencies and rather high emissions. In contrast, in industrialized countries more innovative technologies with significantly higher efficiencies and rather lower airborne emissions are applied. The longest history and best knowledge exists with the use of woody biomass. Due to its favorable fuel properties large quantities can be easily stored. Moreover, the used combustion and power generation techniques are upgraded technologies of the coal firing industry. Other technology trends are a further increase of the efficiency, e.g., by minimizing heat losses and utilizing heat recovery from exhaust gases, by increasing the conversion rates (on a lower temperature level), and the development of interim storage capacities for a more flexible energy supply. Such technologies are in place next to the generally known steam turbines and Stirling engines as well as complex concepts like the Organic-Rankine-Cycle (ORC) and Kalina-Cycle process. Furthermore, due to the strongly varying price level of fossil fuels and the growing competition on reasonably priced biofuels, the use of a wide range of solid biomass residues from industry, forestry, and agriculture as well as the use of energy crops becomes more prominent. Thus, R&D moves toward the development of new and more specialized technologies able to accept unfavorable fuel properties like high concentrations of nitrogen, potassium, or sulfur. Furthermore, fuel and logistic concepts based on the use of compacted biofuels with high energy densities (like briquettes and pellets including pellets from torrefied biomass) will be more and more interesting in the future and can improve the total efficiency and economy of energy supply concepts.

Abbreviations

BoP Balance of plant
CHP Combined heat and power plant
GCV Gross calorific value
GHG Greenhouse gases
LEC Levelized electricity generation costs
NCV Net calorific value
ORC Organic Rankine Cycle
SCR Selective catalytic reduction
SNCR Selective non-catalytic reduction

Bibliography

1. Canadian Centre for Energy Information (2010) Biomass timeline. Calgary. Website access 2010
2. Fachagentur Nachwachsende Rohstoffe e.V. (FNR) (2005) Leitfaden Bioenergie: Planung, Betrieb und Wirtschaftlichkeit von Bioenergieanlagen. FNR, Gülzow
3. Griffiths DJ (1998) Introduction to electrodynamics. Prentice Hall, Englewood Cliffs
4. Heathcote M (1998) J&P transformer handbook. Elsevier, Oxford
5. Kaltschmitt M, Bridgwater AV (Hrsg.) (1997) Biomass gasification and pyrolysis – state of the art and future prospects. CPL Scientific, Newbury
6. Kaltschmitt M, Hartmann H (2001) Energie aus Biomasse: Grundlagen, Techniken und Verfahren. Springer, Berlin/Heidelberg/New York
7. Kaltschmitt M, Rösch C, Dinkelbach L (Hrsg.) (1998) Biomass gasification in Europe. European Commission, DG XII, Brussels
8. Kaltschmitt M, Streicher W, Wiese A (2007) Renewable energies – technology, economics, environment. Springer, Berlin/Heidelberg/New York
9. Lackner M, Winter F, Avinash K (2010) Handbook of combustion. Wiley, Chichester
10. Lahmeyer International GmbH (2010) Data bank on World Wide renewable energies for electricity generation. Lahmeyer International GmbH, Bad Vilbel
11. Langeheinecke, P Jany, Sapper E (2004) Thermodynamik für Ingenieure. Vieweg Verlag, Wiesbaden
12. von Loo S, Koppejan J (2008) The handbook of biomass combustion and cofiring. Earthscan, London
13. Nertinger S (2009) Methoden des Carbon Footprinting zur Beurteilung der Nachhaltigkeit – an den Fallstudien Betapharm und Prolignis. Wirtschaftswissenschaftliche Fakultät der Universität Augsburg, Augsburg
14. Obernberger I (1997) Nutzung fester Biomasse in Verbrennungsanlagen unter besonderer Berücksichtigung des Verhaltens aschebildender Elemente. In: Thermal Biomass Utilization Series, vol I. dbv-Verlag, Graz
15. Obernberger I (1998) Decentralised biomass combustion – state-of-the-art and future development, keynote lecture at the 9th European biomass conference in Copenhagen. Biomass Bioenergy 14(1):33–56
16. Wagner B (2010) Methoden des Carbon Footprinting zur Beurteilung der Nachhaltigkeit – Fallstudie Prolignis. Presentation for the Prolignis Steering Committee Prolignis, Ingolstadt
17. Wiedmann T, Minx J (2008) The definition of carbon footprint. In: Perstova CC (ed) Ecological economics research trends, chapter 1. Nova Science, New York, pp 1–11
18. Wiese A, Kleineidam P, Schallenberg K, Ulrich AJ, Kaltschmitt M (2010) Power generation from renewable energies – world market status report 2009. In: Renewable Energy Focus, July/August 2010. Elsevier, Oxford

Biomass Crops for Biofuels and Bio-based Products

Elizabeth E. Hood[1], Keat (Thomas) Teoh[2], Shivakumar P. Devaiah[2], Deborah Vicuna Requesens[2]
[1]College of Agriculture and Technology, Arkansas State University, AR Biosciences Institute, Jonesboro, AR, USA
[2]Arkansas Biosciences Institute, Arkansas State University, Jonesboro, AR, USA

Article Outline

Glossary
Definition of the Subject and Its Importance
Introduction
Agricultural Residues for Bioenergy
Perennial and Annual Herbaceous Biomass Crops
Woody Biomass Crops
Conclusions and Future Directions
Bibliography

Glossary

Agriculturally marginal land Land that is not arable without compromising soil stability and increasing salinity. It requires large number of inputs.

Bio-based products Products derived from biological sources as opposed to oil.

Bioenergy Energy derived from biological, renewable sources – not from petroleum.

Biofuel Fuels derived from biological sources.

Biomass Materials derived from plant or animal origin, i.e., dedicated agriculture, agricultural residues, municipal waste, and forestry.

Corn stover The remaining stalks and leaves of the corn plant after the grain has been removed.

Dedicated energy crops Crops grown only for use in the biofuels industry, e.g., switchgrass and *Miscanthus*, poplar and *Eucaly*ptus.

Herbaceous Plant materials that have green, nonwoody above-ground parts rather than lignified stems and those parts generally die at the end of the growing season.

Lignocellulose Cell wall materials from plants that contain cellulose, hemicellulose, and lignin.

Megagram (Mg) A unit of mass equal to 1,000,000 g. Also referred to as a metric ton (US)

Perennial Plants that persist for multiple years and often have woody stems.

Renewable resources Materials and products derived from plants that are generated through growth using energy from sunlight and nutrients from soil.

Sustainable Materials that can be maintained through inputs that are equal or less than harvested output.

Water use efficiency The amount of biomass produced from photosynthesis compared to the amount of water taken up by the plant. C4 plants are more efficient in photosynthetic sugar production per CO_2 taken in, thus lowering the amount of water required to obtain the CO_2 and thus the sugars.

Definition of the Subject and Its Importance

Humans currently consume at least 25% more raw materials every year than are replaced through biological growth [150]. In order to sustain quality of life and have adequate environmental resources, those resources must be balanced and renewable. Pressure on those resources has never been greater with the world population nearing seven billion people, and estimated to plateau at 10.5 billion by 2050. That number represents 35–40% more people than currently inhabit the earth.

Sustainable, renewable resources are those derived from biological sources, primarily plant biomass. The underlying principal is that the materials can be reproduced with minimal inputs using energy from the sun. Biomass is thus derived directly or indirectly from original sources that grow and reproduce biologically.

Biomass for biofuels and bio-based products can include many sources of material. In general, biomass includes any biological materials whether of plant or animal origin: agricultural harvests such as grains, agricultural residues such as stalks and leaves, perennial crops such as hay and trees, animal manures, building waste wood, municipal solid waste such as paper, and various food industry wastes.

Introduction

The heavy reliance of the western economies on fossil fuels has given rise to energy security concerns. These concerns taken together with the sustainability issue, negative environmental impacts, and the rising cost of petroleum fuel have prompted the development of viable alternatives that are sustainable, cleaner, and environmentally neutral. Biofuels, which have emerged as one of the alternatives to address these concerns, are obtained from renewable biomass which represents a key long-term component of a sustainable biofuels industry. Ethanol from corn is the first-generation biofuel produced in USA and Europe. However, corn ethanol alone will not be sufficient to address the nation's energy needs. Cellulosic ethanol from renewable resources such as forest and agricultural biomass must also be considered. The "Billion Ton Study" supported by the US Department of Energy (DOE) and US Department of Agriculture (USDA) estimated that renewable resources are available from forest and agricultural lands to produce enough cellulosic ethanol to displace 30% or more of transportation fuel needs annually [1]. This will significantly reduce the country's dependence on imported oil.

This review deals only with plant-based crops that are used as biomass sources. Crop categories discussed include agricultural residues, dedicated woody crops – poplar and *Eucalyptus*, perennial herbaceous grasses – *Miscanthus* and switchgrass, and grass species that produce soluble sugar streams – sweet sorghum and sugarcane. Although many other crop sources are generally considered as potential sources of biomass, these are the front line crops that are considered to be "near term" candidates.

Agricultural Residues for Bioenergy

Availability of Feedstock

The Billion Ton Study on biomass estimated that 388 megagrams (Mg) of agricultural postharvest residues per year could be available from agriculture for conversion to energy resources in the USA within the next 20 years [1]. The estimated crop residues were primarily from corn stover, wheat straw, rice straw, and hulls as well as other crops with lesser individual contributions. The estimated amount of ethanol that can be derived from crop residues totals 138 billion liters assuming 356 L Mg^{-1} (85 gal t^{-1}). Additionally, the study made the assumptions to support three different scenarios for productivity. The first scenario was to maintain the status quo for all resources available today, and those would be available at the same level in the future. The second scenario focused on technology changes being applied to current crops to generate higher yields. The third and most lucrative scenario assumed that the technology changes would be applied to current crops as well as new perennial crops, combined with significant land use changes. The 388 Mg estimate is based on the third scenario.

One of the major contributors to crop residue potential in the USA is corn stover, whether under current production or assuming increased crop yields [1]. Stover can be used for many bio-based products, and the use of corn stover for those products would remove it from its contribution to liquid transportation fuels. Some of these current and potential uses include pulp and paper, animal feed, composite products such as boards, and chemicals, such as furfural [2].

Impact on soil fertility: Crop residues contribute an interesting array of benefits to the soil from which grain is harvested. These benefits include lowering soil erosion, increasing moisture content, and increasing soil organic matter and total carbon. When removing crop residues from agricultural land, the loss of these benefits must be managed [3].

However, in some situations removal of residues is recommended because they cover too much of the surface and prevent warming of the soil in the spring, delaying seed germination and thus lowering yields (Table 1; [4, 5]). Moreover, too much organic matter on the surface of the soil also can increase moisture and the threat of increased fungal growth, contributing to diseases. Clearly, the issues vary with location and crop. Each situation will have a unique solution.

Biomass Crops for Biofuels and Bio-based Products.
Table 1 Potential effects of corn stover harvest [4]

Factor	Benefits of removal	Cost of removal
Economic	Stover sale revenues ($35/t);	Yield decreases in dry years due to lower soil moisture
	Greater seed germination in colder climates	Yield decreases with increased soil loss; Poorer germination but no yield effect
Fossil fuel use	Increased EtOH production	More field passes required; Fossil fuel needed for conversion to biofuel
Micro-climate	Warmer spring temperatures	Increased evaporation, lower soil moisture
Pests and disease	Increased control for some	Decreased control of others
Carbon and nutrients	Decreased but moderated by tillage and N rate	Nutrient loss predicted greatest in Midwest
Erosion	Moderated by amount of harvest and tillage type	Increased soil loss and water run-off

The most important practice that will need to be adopted for residues to be sustainably removed from crop land is no-till agriculture. Currently, only 20% of corn acreage and 15% of wheat acreage are cultivated with no-till practices [5]. Tillage increases the rate at which organic matter is decomposed and increases nitrogen losses due to microbial activity. No-till cultivation allows more of the remaining residue to be removed for alternative uses.

Farmer involvement: One of the major concerns with agricultural residues being used for a reliable supply of biomass is compliance of the farmer for collection and delivery of the residues. Because the residues vary by year and region, management of the residues

requires consideration of many factors including maintenance of soil fertility, weather, crop yields, and economics.

The average age of US farmers is 62. This is both an advantage and a disadvantage. The collective experience of farmers is tremendous – management practices are based on their extensive knowledge. In contrast, their retirement is eminent and their replacement uncertain. Their motivation to try new crops is often high though their approach is conservative. Although most farmers may be willing to try new crops, they will approach the change cautiously, planting only a few hectares in the beginning until yield and economics are understood [5]. If the results are economically favorable, in that inputs are lower than harvested material profits, the farmers are often willing to change their practices and participate in the new system. In directed dialogs conducted in 2000–2002, farmers generally agreed that US$20 ha^{-1} pre-tax margin would generate their interest in harvesting residues, as long as grain harvesting is not hindered [5]. The value of the residues is not near to the value of the grain, thus logistics and income must make it worth the farmer's time and investment to participate in the residue harvest. The industry estimate for biomass that is delivered to biorefineries is US$30–$50 Mg^{-1} in order to produce commodity ethanol at target prices. However, in order for the farmer to reap a benefit considering the equipment, time, and field issues, the price would have to approach US$70–$100 Mg^{-1}. Clearly, policy and logistics research must address this discrepancy.

Logistics and economic issues: Small grains, mostly wheat, produce straw that can be baled and stored. However, the amount available from nonirrigated wheat is minimal after leaving USDA recommended amounts of residue on the ground to improve fertility. If the average dry land wheat straw yield is 2.7 Mg ha^{-1}, and 1.34 Mg ha^{-1} must be left on the surface to avoid erosion, then less than 2.5 Mg ha^{-1} of straw would be available for harvest [5]. Because corn stover yields about 11 Mg ha^{-1}, leaving 2.24 Mg ha^{-1} on the soil surface for organic matter and erosion control, leaves 8.8 Mg ha^{-1} for harvest. However, in each case if a cover crop is employed, the residues are not required for erosion control and can be harvested in larger amounts.

Because wheat is harvested early in the summer, the straw has low moisture content and can be immediately baled. In contrast, collecting residues as feedstocks from corn fields in particular requires altering harvesting practices. Corn is harvested in the fall and the stover moisture content is usually 30–50%, and must be left in the field to dry, although often fall rains prevent this from happening in a timely manner. In addition, if stover is harvested separately after grain harvest, field machinery must be deployed a second time and this compacts the soil more. The stover that is raked and baled also contains rocks and soil particles which have a negative impact on biorefinery machinery. These issues suggest that one-pass harvesting is an alternative that must be considered.

A detailed description of grain and stover harvesting logistics was recently published [5]. The additional requirements for trucks, combines, and potentially one-pass harvesters, baling equipment, and additional personnel are enormous. The personnel needs are transient in that the harvest window is usually 30–50 days. However, the investment in additional equipment, whether purchased or leased is significant. Harvesting stover while harvesting corn grain requires three times the number of trucks and personnel if using a one-pass harvester. Although this equipment is not yet commercially available, several agricultural machinery manufacturers are designing these harvesters. Because most of the stover currently is either left in the field, tilled under, or used for bedding, or local markets (e.g., corn cobs), baling equipment is not adequate in most farm operations to handle a large increase in biomass harvest. One possible solution could be transporting the field materials to a collection station, possibly associated with a grain elevator operation, and the stover separated from the grain at these off-field locations. The stover then could be stored either as stacked bales or as a wet pile. Bales require protection from the elements, they are dry when baled and must remain dry, at less than 20% moisture, to keep them from deteriorating. In addition, the height of the stacks is limited by the weight and heat that is generated, thus requiring large amounts of field space. However, if the biomass is in compacted, anaerobic, wet piles at greater than 60% moisture, fungal growth is

inhibited and the biomass is very stable [5]. The pile size is only limited by the height of a pump head that continuously recycles the water from a base collection reservoir. This configuration has the added advantage of washing contaminants out of the biomass that were collected from the field. These "haystacks" are large and much higher than bale stacks and thus have far less of a footprint on the ground, minimizing field requirements. Wet storage is a proven industry logistic in that the nonwood fiber pulpers moved to this method of feedstock storage several decades ago.

Recommendations: The production of ethanol from corn stover as opposed to grain has significantly more greenhouse gas reduction potential, 79% versus 25%, when burning E85 (85% ethanol with 15% gasoline) on a per km basis [4, 6]. This fact alone motivates development of logistics and infrastructure solutions to develop the industry for all concerned. Nevertheless, county by county plans will be required to sustainably harvest agricultural residues from any crop, based on climate, tillage, and residue type. Farmer networks should be included as part of the value chain to encourage participation (Fig. 1). Small biomass facilities, including portable facilities, could be a positive development for on-farm production of ethanol from excess residues without investment in large biorefinery infrastructure.

Perennial and Annual Herbaceous Biomass Crops

Sugar Crops

Introduction Sugar cane and sweet sorghum which produce sugary syrup in their stems are members of the Panicoid subfamily of the *Poaceae* family [7]. They share the physiologically distinctive and highly productive C4 photosynthetic pathway. The C4 pathway is fundamentally more efficient than the C3 classic Calvin cycle alone and C4 plants are able to convert up to 2% of incident solar energy into biomass [8]. Compared to C3 plants, C4 plants lose less water as they can photosynthesize with stomata nearly closed, thus reducing water loss to the environment and increasing water use efficiency. In addition, plants using the C4 photosynthetic pathway are better equipped to handle high temperatures, drought, and nitrogen limitations than closely related C3 plants [9, 10].

Sugar from sugar-producing plants can be used for direct fermentation into ethanol. Among three major sugar-producing plants, sugar cane and sweet sorghum are adapted to warm temperate to tropical areas, whereas sugar beet is grown only in temperate areas. Sugar cane is the major crop in the Brazilian national ethanol program which produces 15.9 billion liters of ethanol a year [11]. Sweet sorghum is considered to be one of the promising feed stocks for the production of first-generation ethanol. Studies are being conducted to produce ethanol from sweet sorghum sugary syrup

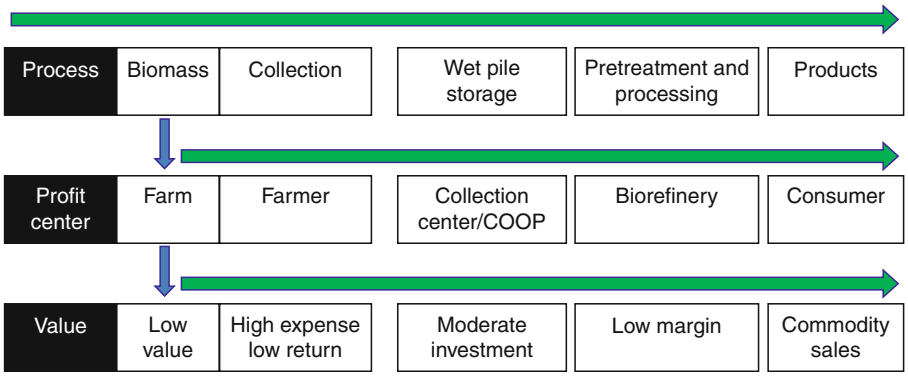

Biomass Crops for Biofuels and Bio-based Products. Figure 1
Agricultural residue value chain. Residue collection and processing must yield value to each link in the chain for the process to be instituted. One solution to this is to have the farmer involved in the collection and storage of the residues to be sold to the biorefinery during the production year

in the USA, India, and China [12–14]. Most ethanol production using sugar beet takes place in Europe; however, using sugar beet to produce ethanol could potentially increase soil erosion and lower net energy balance [15]. All the three sugar-producing plants are a good source for first-generation ethanol production. Compared to sugar beet, both sugar cane and sweet sorghum produce higher biomass and additionally are a good source of lignocellulosic biomass which can also be used for second-generation ethanol production.

Sugar Cane Crystallized sugar from sugar cane was reported in India 5,000 years ago [16]. Sugar cane is a tall perennial grass of the genus *Saccharum*, native to warm temperate to tropical regions of Asia. The plant grows in clumps, and has solid, jointed, fibrous stalks that are rich in sugar. Sword-shaped leaves, similar to those of the corn plant, fold in a sheath around the stem. Mature canes may be 3–6 m tall and 2.5–7.5 cm in diameter (Fig. 2a). All sugar cane species interbreed, and the major commercial cultivars are complex hybrids. Different species likely originated in different locations with *S. barberi* originating in India and *S. edule* and *S. officinarum* coming from New Guinea. Sugar cane is grown in over 110 countries with an estimated total production of 1,627 million Mg in 2009, (FAOSTAT, http://faostat.fao.org/site/339/default.aspx) more than six times the output of sugar beet. Brazil is the world's largest producer of sugar cane, producing about one-third of the world's crop, followed by India (FAOSTAT).

Cultivation: Sugar cane cultivation requires a tropical or temperate climate, with a minimum of 60 cm of annual moisture. In prime growing regions of India, Peru, Brazil, Bolivia, Colombia, Australia, Ecuador, Cuba, Philippines, El Salvador, and Hawaii, sugar cane can produce 20 kg m^{-2} biomass exposed to the sun. Although sugar cane species produce seeds, sugar

Biomass Crops for Biofuels and Bio-based Products. Figure 2
(**a**) Sugar cane. (**b**) Sweet Sorghum

cane propagation is through stem cuttings of immature canes 8–12 months old, called "setts." The setts are best if taken from the upper third of the cane because the buds are younger and less likely to dry out. Each sett must contain at least one bud. The setts can be planted at a 45° angle or laid horizontally in a furrow. It takes 12,500–20,000 setts to plant 1 ha. The setts are lightly covered with soil until they sprout (10–14 days) and then the sides of the furrow are turned inward [17, 18]. In the USA and Australia, billet planting is common. Billets harvested from a mechanical harvester are planted by a machine which opens and recloses the ground.

Sugar cane is a perennial crop which usually produces harvests for about 3–6 years before being replanted. The first crop is called the "plant crop" and takes 9–24 months to mature, depending on location [18, 19]. The cane is cut close to the ground because the lower stem has the highest sugar content and low cuts aid in ratooning, the emergence of new crops from the stems and trash (leaves and tops) left behind. Ratoon crops take about 1 year to mature. As many as four or more ratoon crops may be produced before replanting is necessary, mostly due to the slow decline in yields.

The complete sugar cane crop cycle is variable, depending on local climate, varieties, and cultural practices. In Brazil, usually it is a 6-year cycle, in which five cuts, four ratoon cultivation treatments, and one field reforming are performed. Generally, the first harvest is made 12 or 18 months after planting. The following ratoon cane harvests are made once a year, during 4 consecutive years [20].

Sugar cane is harvested by hand and mechanically. Hand harvesting accounts for more than half of the production, and is dominant in the developing world. Mechanical harvesting uses a sugar cane combine, a harvesting machine that can harvest 100 Mg each hour, but machine-harvested cane must rapidly arrive at the processing facility. Once cut, sugar cane begins to lose its sugar content, and damage to the cane during mechanical harvesting accelerates this decline. Some sugar cane varieties are known to be capable of fixing atmospheric nitrogen in association with a bacterium, *Acetobacter diazotrophicus*. Unlike legumes and other nitrogen fixing plants which form root nodules in the soil in association with bacteria, *A. diazotrophicus* lives within the intercellular spaces of the sugar cane's stem [21].

Breeding: The goal of cane breeding is to produce an economic yield of sugar that can be sustained over several ratoons. Breeding and selection of cane are not simple processes since viable seeds are seldom produced. Sugar canes are highly polyploid, wind-pollinated outbreeders. They are clonally propagated, highly heterozygous, and intolerant to inbreeding. New varieties are sought from the first-generation progeny of crosses between clones. Five species are of interest to cane breeders. *S. officinarum* ($2n = 80$) has good sugar quality and low fiber, although it is susceptible to most of the main diseases, except gumming disease and smut. *S. spontaneum* ($2n = 40$–128) is a source of resistance to many diseases, including "Sereh," mosaic, gumming, red rot, and downy mildew. *S. barberi* ($2n = 82$–124) are considered the most important breeding canes and are immune to gumming and mosaic and resistant to downy mildew, but susceptible to smut and red rot. *S. sinense* ($2n = 82$–124) is difficult to breed, but has given rise to some useful breeding lines. *S. robustum* ($2n = 60$–194) has been used to some extent in breeding lines [22].

Yields: The annual global production of dry cut sugar cane (sugar content: 55% dry basis) is about 328 million Mg. Asia is the primary production region, which produces 44% of the total. South America stands second with a total production of 110 Tg of sugar cane (34%). The annual yield of dry sugar cane ranges from 14 to 22 Mg ha^{-1} with an average of 17 Mg ha^{-1}. Brazil is the largest single producer of sugar cane with about 27% of global production and a yield of 18 Mg ha^{-1}. The highest yield occurs in Peru, which produces more than 32 Mg ha^{-1} of dry sugar cane [23].

Diseases and pests: Many diseases and pests affect sugar cane. Bacterial diseases include gumming disease caused by *Xanthomonas vasculorum* (Cobb) Dows. Yellowish stripes occur at the leaf tips, leaf blisters occur, and the vascular bundles exude a yellowish gum when cut. *X. albilineans* (Ashby) Dows causes yellow stripes to occur on the leaf blade, many side-shoots are produced, and the vascular bundles of the stalk are red [24]. Fungal diseases such as red rot (*Colletotrichum falcatum* Went), root rot (*Pythium graminicolum* Subr.), pineapple disease (*Thielaviopsis parodoxa* (de Seynes) C. Moreau), downy mildew

(*Sclerospora sacchari* Miy), and smut (*Ustilago scitaminea* Syd.) can also cause damage. Red rot causes the setts to be seriously damaged at low temperatures. Root rot was responsible for the failure of "Otaheite" (a noble cane) in Mauritius in 1846. Downy mildew is currently only found in the western Pacific and was responsible for severe losses in Queensland until rigorous controls were initiated. Smut causes black whiplike organs to emerge from the center of the leaf-roll and affects crops in southeastern Asia and South Africa [18]. Mosaic is a viral disease, whose vectors include *Aphis maidis* Fitch. It was first documented in Java in 1892 and causes severe stunting in some cases. Other viral diseases include ratoon stunting, chlorotic streak, Fiji disease, and Sereh disease. The most destructive insects of sugar cane are stem-borers, the larval stage of several genera of moths. The larvae burrow into the stem and on emergence cause weakened stems and loss of sucrose. Biological control and use of transgenic *Bt* sugarcane are the most efficient control for these insects [18].

Commercial and industrial use: Sugar cane has many industrial uses and is one of the most widely used and cheapest sources of domestic products, including table sugar, molasses, and ethanol. Cane juice contains 10–20% sucrose and about 1 Mg ha^{-1} of raw sugar can be extracted from 8 to 9 Mg ha^{-1} of cane. Molasses is a by-product of the manufacturing of cane sugar. It is residual syrup from which no more crystalline sucrose can be obtained by simple techniques. Approximately 2.7% of cane can be extracted as molasses, which can be used as an animal feed as it has high carbohydrate contents. Molasses along with cane juice and other by-products can be fermented to produce an alcoholic distillate, rum, or similar liquors. Ethanol is also produced from molasses, which can be used in vinegar, cosmetics and pharmaceuticals, cleaning preparations and solvents, and coatings [16]. One of the important uses of ethanol is as a transportation fuel (see below). Still other products from molasses are butanol (a solvent), lactic acid (a solvent), citric acid (mostly for foods and beverages), glycerol, and yeast media [25].

Sugarcane as a bioenergy crop: Sugar cane being a C4 plant is one of the most efficient photosynthesizers in the plant kingdom [26]. Sugar cane's high concentration of sugar, which is readily available to microorganisms, makes it uniquely suitable for ethanol production. As a producer of sugar for fermentation bio-products, sugar cane is found to have advantages in relation to fossil-energy input, emissions of greenhouse gases, and possibly acidification, when compared with corn and sugar beet [15]. Another useful by-product of sugar production is bagasse, the fibrous residue left after the juices are extracted from the cane. It is the main source of fuel in sugar factories. It can also be used in paper, cardboard, fiber board, and wall board [27]. It is quite possible that further uses of sugar cane will be developed in the future, but even now it can be seen that sugar cane is a very important and useful plant crop worldwide. Uses of sugar cane in different parts of the world are shown in Table 2. The resulting energy and greenhouse gas benefits of sugar-cane-derived products have been shown previously [28]. For sugar cane, the main co-product is surplus energy

Biomass Crops for Biofuels and Bio-based Products. Table 2 Uses of sugar cane [23]

	Feed (%)	Seed (%)	Waste (%)	Food manufacture (%)	Food (%)	Other uses (%)
Africa	0.14	2.02	2.12	89.43	4.44	1.85
Asia	3.14	4.68	1.13	86.19	4.57	0.30
Europe	0.18	0.00	0.00	87.90	0.00	11.92
North America	0.00	5.37	0.00	94.62	0.00	0.00
Central America	1.80	0.25	1.06	95.40	0.05	1.45
Oceania	0.00	0.00	0.00	99.99	0.01	0.00
South America	0.98	0.00	0.68	97.83	0.27	0.24
World	1.91	2.35	0.97	91.88	2.40	0.48

from bagasse. The most successful story of using sugar cane as a bioenergy feed stock is in Brazil. Brazil is considered to have the world's first sustainable biofuels economy and is the biofuels industry leader. Its sugar cane ethanol program is considered a model for other countries and is the most successful alternative fuel program to date. Brazil's 40-year-old ethanol fuel program is based on the most efficient agricultural technology for sugar cane cultivation in the world. It uses modern equipment and cheap sugar cane as feedstock. The residual cane-waste (bagasse) is used to produce heat and power, which results in a very competitive price and a high-energy balance (output energy/input energy). This energy balance varies from 8.3 for average conditions to 10.2 for best practice production. Brazil is recognized as the world's second-largest producer of ethanol (DOE-EIA, 2007, http://www.eia.doe.gov/emeu/cabs/Brazil/full.html). Brazil and the USA lead the world in global ethanol production, accounting for nearly 70% of the world's production. Brazil produces approximately 37% of the world's total ethanol and 48% of the world's ethanol uses as fuel. They began promoting the production of crops for ethanol in the mid-1970s after the first global energy crisis. In 2008, 454,000 barrels per day (bbl/day) of ethanol were produced, up from 365,000 in 2007. Because ethanol production continues to grow faster than domestic demand, Brazil has sought to increase ethanol exports, becoming the largest ethanol exporter in the world, holding over 90% of the global export market. According to industry sources, Brazil's ethanol exports reached 86,000 bbl/day in 2008, with 13,000 bbl/day going to the USA (DOE-EIA, 2007).

Sugar cane bagasse is the residue obtained after crushing of sugar cane during sugar production and consists of cellulose 43.6%, hemicellulose 33.8%, lignin 18.1%, ash 2.3%, and wax 0.8% on a dry weight basis [29]. About 180–280 kg ha^{-1} of sugar cane bagasse could be produced after squeezing [30]. The second-generation process revolves around accessing the large amounts of cellulosic material blocked within the lignin-based shell and creating ethanol from it [31]. Currently the leftover bagasse is burned to co-generate power. In the future, the process should be similar, but instead of burning all of the bagasse, the material will be sorted so that the cellulose and hemicellulose are processed further into cellulosic ethanol with only the remaining high-lignin content materials being used as an alternative energy source. The move toward utilizing sugar cane bagasse for the production of ethanol instead of power generation is a question of economics. The current process of burning the bagasse for energy is not as energy efficient as using it to produce ethanol. Theoretically, 1 Mg of sugar cane bagasse can produce up to 300 L of ethanol. In reality the yield depends on a number of parameters including efficiency of the process. Currently, 6,000–7,000 L of ethanol is produced from 1 ha of sugar cane-not including the bagasse. When bagasse can be utilized for ethanol production, the output could double to 12,000–15,000 L ha^{-1} [31].

Sweet Sorghum Sweet sorghum is a C4 crop in the grass family belonging to the genus *Sorghum,* which also includes grain and fiber sorghum and is characterized by high photosynthetic efficiency. Sweet sorghum is of interest as a dedicated agricultural energy crop because of its drought tolerance, relatively low input requirements and ability to produce high yields under a wide range of environmental conditions [12, 32]. These traits make sweet sorghum a potentially important feedstock for bioenergy production, mainly in regions where conditions are not favorable for growing starch-rich crops such as maize. The great advantage of sweet sorghum is that it can become dormant under adverse conditions and can resume growth after relatively severe drought which has implications for crop management. Sweet sorghum is typically an annual, but some cultivars are perennial. Like other sorghum types, sweet sorghum probably originated from East Africa and spread to other African regions, Southern Asia, Europe, Australia, and the USA. Plants grow in clumps and height of stalks ranges from 0.8 to 4 m (Fig. 2b). The thickness of stalks also varies, ranging between 1.25 cm and 3.75 cm. Prop roots regularly grow from the lower nodes. Seeds are produced by self-pollination from a panicle that emerges at the top of the plant and contains both the male and female inflorescences. Seeds are small, round, and may be white, yellow, brown, or red in color. Each panicle can produce up to 4,000 starch-containing grains. Although native to the tropics, sweet sorghum is well adapted to temperate climates. Like its close relative sugar cane (*Saccharum* spp.), sweet sorghum has been selected to accumulate high levels of edible sugars in

the stem. Sweet sorghums are tall and produce high biomass in addition to sugar. In all varieties, the primary carbohydrate is sucrose, with variable amounts of reducing sugars and starch [33].

Cultivation: Sweet sorghum is very drought resistant and shows good adaptability to poor soil types including saline soils. It has a very short vegetation period and thus is ideal for double cropping, either three crops of sweet sorghum or with an alternative crop [13]. Propagation is accomplished through seeds. It is easily grown in areas that are too dry for maize. Seeds are typically sown in widely spaced rows (75–100 cm) manually or using a corn planter in spring after the rainy season and as soon as the soil temperature remains above 15–18°C. The ideal seeding rate for most sweet sorghum varieties is 3–4 seeds per foot of row with a final stand of 2–3 plants per foot of row. If plant populations are too high, the canes will be spindly and contain less juice than an equal tonnage of larger diameter canes. Seed germination takes place within 24 h in warm and moist soils, and the time to maturity lies between 90 and 120 days. The plant grows to a height of from about 1.2 to above 4 m, depending on the varieties and growing conditions. Even though sweet sorghum is predominately self-pollinating, hybrids and crosses can be produced using male-sterile maternal parents. Sugar content in the juice increases with maturity, and is low prior to seed development. Controlling nitrogen fertilizer and its application time promotes sucrose content and growth rate in sweet sorghum. Application of adequate amounts of K fertilizer increases yield responses more than high levels of nitrogen fertilizer alone [34]. Currently, the only commercially viable harvest method for sweet sorghum is removing the entire crop with a forage harvester and transporting it to a mill/pretreatment/ethanol facility. Bennett and Anex [12] indicate that fermentable carbohydrates can be produced at less expense from sweet sorghum than from corn grain. Further results on costs associated with off-farm transportation, storage, or capital costs associated with milling and energy recovery equipment reevaluates sweet sorghum as a biocommodity feedstock [12].

Breeding: Roughly 4,000 cultivars of sweet sorghum are distributed throughout the world [35] providing a diverse genetic base from which to develop regionally specific, highly productive cultivars. In addition to producing large amounts of sugar-rich biomass, hybrids can be developed from crosses between grain-type seed parents and sweet-type pollen parents [36]. The product of these crosses typically increases biomass yields and sugar content when compared to the original grain-type seed parents. Such hybrids can co-produce grain at levels approaching the yields of the grain-type seed parent [37]. The co-produced, protein-rich grain can be consumed as food, animal feed, or converted to bioproducts like ethanol [13, 36]. Proper variety selection will play a large role in the success of sweet sorghum production for ethanol. The ideal variety for a particular location should produce high yields with minimal inputs, have a high percentage of high quality and easily extractable juice, be disease and insect tolerant, and tolerate both drought and wet conditions.

Yields: Sweet sorghum yields vary considerably depending on the varieties/hybrids that are used, the location (soil, water, climate, pests and diseases), inputs, and production practices. The annual global production of dry sorghum is about 53 Tg with the an average yield of 1.2 Mg ha^{-1}. The USA is the largest producer of sweet sorghum (23%) at a yield of 3.7 Mg ha^{-1}. The highest yield occurs in Israel and Jordan, which produce more than 10 Mg of dry sorghum per hectare [23]. When considering sweet sorghum for ethanol production, the most important yield components are biomass yield, juice yield, and sugar production per hectare. The concentration of soluble sugars in sorghum ranges widely depending upon variety. Biomass yields of sweet sorghums are also variable ranging from 20 to 120 Mg ha^{-1} and juice content from 65% to 80% of biomass. The combined sugar content of the juice varies between 9% and 15%. Sugar yields vary from 4 to 17 Mg ha^{-1}. The bagasse (crushed stalks) and leaves make up the remainder of the wet biomass. The bagasse represents approximately two-thirds of the dry matter and leaves represent the remaining portion. Fermentation of the sugar in the juice yields 600–900 L ha^{-1} of ethanol [38].

Diseases and pests: Disease and insect problems may also limit yield potential, suggesting that further research in this area is essential. Leaf diseases are the most troublesome for forage producers. These are anthracnose caused by *Colletotrichum graminicola* (which can be overcome by using resistant varieties) and leaf blight caused by *Helminthosporium turcicum*.

Charcoal rot (*Macrophomina phaseoli*) causes plants to lodge badly. Grain may be affected by covered smut (*Sphacelotheca sorghi*) in which the seed is replaced by a sac of spores; fungicidal seed treatment before planting prevents this latter malady (FAO, 2009, http://www.fao.org/ag/agp/agpc/doc/gbase/data/pf000319.htm). From a forage point of view, grasshoppers appear to be the worst pest, and feral pigs can damage the crop in some locations. Grain pests include the sorghum midge, *Contarinia sorghicola*, whose larvae feed on the developing seeds. Bird damage is also important with the weaver bird, *Quelea quelea*, causing major losses in Africa. Damage can be prevented by using awned varieties of sorghum, giving some hope of reducing losses. The high tannin content of sweet sorghum seed is another deterrent, and early harvesting for silage avoids the major problems.

Commercial and industrial use: Worldwide, the major uses of sweet sorghum are animal feed (49%) and human food (40%; Table 3). In Africa and Asia, over 60% of sweet sorghum is used for human food. In the other regions, most sorghum is used for animal feed. There is no use of sorghum for human food in Europe and South America. Although the juice, grain, and bagasse from sorghum provide many opportunities, most applications around the world are for syrup and forage. An average yield of 1,900 L ha^{-1} of syrup can be achieved, although yields of 800–1,200 L ha^{-1} can result if weather conditions are poor. In forage applications, chickens can be fed with seed heads and ruminant livestock can use the grains, leaves, and stalks. The organic by-product from sweet sorghum syrup processing is often fed to livestock, left on the field, or composted. Sweet sorghum bagasse is used currently to manufacture chemical pulp. The quality of the pulp obtained is excellent for the paper industry. Sweet sorghum can be considered as a major raw material for the paper industry [39].

Sweet sorghum as a bioenergy crop: Sweet sorghum is attractive for bioethanol production because of its high fermentable sugar content and very high yield of green biomass (20–30 dry Mg ha^{-1}), its low requirement for fertilizer, high water use efficiency, and short growth period; and, it is well adapted to varied climate and soil conditions. These advantageous agricultural characteristics make sweet sorghum a promising substitute feedstock for fuel ethanol production in the southern USA [32]. Based on a recent economic analysis, sweet sorghum is considered to be one of the most drought-resistant crops and has higher biomass yield and lower production costs than many other plants [40]. Sweet sorghum can produce fermentable sugars (sucrose, glucose, and fructose) in its juice, starch in its grain, and lignocellulose, which can be used in both current starch-based ethanol plants and future cellulosic ethanol plants. Of the 20–30 dry Mg ha^{-1} of biomass, approximately 40–45% is fermentable sugars and starch, equivalent to more than 500 bushels ha^{-1} of corn yield. If all fermentable sugars in sweet sorghum are converted to ethanol, potential ethanol yield could be 5,500–6,100 L ha^{-1}. However, normal pressing can recover only ≈50% of the total sugars in the sorghum stalk [41]. Increasing the juice yield or making proper use of remaining sugars in the bagasse is crucial for

Biomass Crops for Biofuels and Bio-based Products. Table 3 Uses of sweet sorghum [23]

	Feed (%)	Seed (%)	Waste (%)	Food manufacture (%)	Food (%)	Other uses (%)
Africa	6.90	2.01	13.02	5.21	72.76	0.11
Asia	32.29	2.21	4.94	0.00	60.52	0.04
Europe	98.76	0.53	0.71	0.00	0.00	0.00
North America	86.80	0.30	0.00	0.00	3.03	0.00
Central America	94.85	0.38	2.19	0.00	2.58	0.00
Oceania	97.71	0.39	0.04	0.11	1.75	0.00
South America	95.09	0.69	4.21	0.00	0.00	0.00
World	49.10	1.39	6.11	3.20	40.15	0.05

realizing the high ethanol yield of sweet sorghum and is of important economical value.

Similar to sugar cane bagasse, sweet sorghum bagasse is the residue obtained after crushing of sweet sorghum cane for sugar production and consists on average of cellulose 34%, hemicelluloses 25%, lignin 18%, and ash 4% on a dry weight basis [42]. Sweet sorghum bagasse was found to be a remarkable raw material for the paper industry, yielding high-quality pulp [39]. The most promising future utilization of bagasse is cellulose-based ethanol production, while the residual solids (mainly lignin) can be burned to provide heat and power. Hydrolysis of the cellulose and hemicellulose fractions can be catalyzed by acids or cellulolytic enzymes. Enzymatic processing needs a pretreatment step to increase the susceptibility of the cellulose, which can be degraded by cellulolytic enzymes to glucose.

Miscanthus and Switchgrass – Dedicated Perennial Energy Crops

Introduction *Miscanthus* and switchgrass are two perennial herbaceous crops with attributes generally considered as ideal for biomass crops, making them well suited as dedicated energy crops for biofuel production (Table 4). They are members of the grass family, *Graminae* (*Poaceae*). The perennial herbaceous crops have long-lived roots that may establish beneficial interactions with root symbionts, facilitating acquisition of mineral nutrients from the soil which may result in lesser amounts of fertilizer needed [44]. This can translate into cost saving on fertilizer and minimizing water pollution from leachates and runoff. A very important physiological characteristic of the perennial herbaceous crops is the recycling of nutrients within the plants. Nutrients are moved from roots to growing shoots at the beginning of each growing season and from the senescing shoots to the roots at the end of the growing season [45]. This recycling characteristic gives the perennial herbaceous crops many advantages over other plants and at the same time reduces the amount of fertilizer needed. In spring, when mineral nutrients are translocated from the roots to the shoots, the perennial grasses get a rapid start in forming a photosynthetically active canopy leading to biomass accumulation when many annuals are still seedlings.

Biomass Crops for Biofuels and Bio-based Products.
Table 4 Attributes of an "ideal" biomass crop [43]

The "ideal" biomass crop?	Corn	Short-rotation coppice[a]	Perennial grass
C4 photosynthesis	⋆		⋆
Long canopy duration		⋆	⋆
Recycles nutrients to roots			⋆
Clean burning			⋆
Low input		⋆	⋆
Sterile (noninvasive)	N/A	⋆	*M. giganteus*
Winter standing		⋆	⋆
Easily removed	⋆		⋆
High water use efficiency			⋆
No known pests or disease			*M. giganteus*
Uses existing farm equipment	⋆		⋆

[a]Coppice is a grove of densely growing small trees pruned to encourage growth

Conversely, in fall, mineral nutrients from the senescing shoots are transferred to the roots where they are stored over the winter. This has the positive effect of lowering the ash content of the shoots, improving their overall energy content and quality for biofuel production and at the same time improving the viability of the roots during the cold winter. Another advantage of the perennial grasses is the low input cost in establishing the crops. Once the perennial grasses are established, they can be harvested annually without replanting and no tillage is needed for the next 15–20 years. This leads to a substantial saving in labor cost and at the same time reduces soil erosion and nutrient loss. *Miscanthus* and switchgrass are C4 plants [46]. A higher solar energy conversion rate should lead to a higher total biomass yield per unit of land area. Perennial grasses are also known to exhibit increased soil-carbon levels by sequestering portions of atmospheric carbon in the soil in root biomass and in root

turnover creating soil organic matter. The perennial herbaceous crops therefore, represent significant soil carbon sinks [47]. The perennial grasses are also known to be better adapted than conventional crops to different types of soils which means they can also be grown on marginal land not used for food crops.

Miscanthus *Origin and distribution*: *Miscanthus* is native in many parts of Asia such as China, Japan, and the Pacific Islands, and can grow up to 4 m tall. *Miscanthus* was first introduced into Denmark from Japan in 1935 as an ornamental plant and is now cultivated throughout Europe and North America primarily for energy production with other end uses being explored. It is estimated that there are about 14 species of *Miscanthus* [48] and the most common species investigated as a biofuel in Europe and North America is *Miscanthus* × *giganteus*, a naturally occurring sterile triploid hybrid that has its origin in Japan [49]. The genetic origin of *M.* × *giganteus* is uncertain but some evidence suggests that this hybrid is a result of a cross between *M. sinensis* (diploid) and *M. sacchariflorus* (tetraploid) [50]. In general, *M. sinensis* types are well adapted for cooler climates, whereas *M. sacchariflorus* can provide genetic resources for warmer regions [51].

Growing conditions: Extensive studies and evaluation of *Miscanthus* as a biomass resource for biofuel and bio-based products have been going on in Europe for the last 2 decades under the umbrella of the *Miscanthus* Productivity Network [52]. These studies have provided much of the currently available information on *Miscanthus* as a renewable feedstock for bioenergy. In recent years, similar studies have also been conducted in the Midwest of North America but on a smaller scale. The studies in Europe were conducted in 15 cities from southern Italy (37° N latitude) to Denmark (56° N latitude) [53]. Although *Miscanthus* prefers the mild temperatures and high water availability of its natural habitats in the tropics and subtropics, the successful establishment of *M.* × *giganteus* in Europe and North America suggests that it is relatively tolerant of temperate temperatures and low water availability. In North America, *M.* × *giganteus* has been established successfully in the Midwest from latitude 38° N to 48° N covering Ohio, Michigan, Indiana, and Illinois, and expanding into other areas in the south like Georgia and Florida and as far north as Quebec, Canada. *M.* × *giganteus* has been demonstrated to be more tolerant of low temperatures than most C4 perennials [54, 55]. Nevertheless, low temperature still limits the growth of *Miscanthus*. It is estimated that *Miscanthus* requires a minimum of 500 mm of annual rainfall and where the annual rainfall is typically below that amount, irrigation is necessary for substantial growth and biomass yields [53]. *M.* × *giganteus* can adapt to a wide range of soil, from sands to high organic matter soils. It is also tolerant to a wide range of pH, the optimum being between pH 5.5 and 7.5 [56]. Generally, areas with higher rainfall and soils with high water-holding capacity will favor production of *Miscanthus*. Limited soil water availability during the growing season will decrease production.

M. × *giganteus* being a sterile hybrid is established from rhizomes. The rhizome pieces, approximately 200 mm in length, are planted directly into the soil at a depth of 200 mm [56]. Fresh rhizomes are generally used because rhizomes stored for a period of time are likely to dry out and exhibit less vigor. Planting takes place after the risk of the latest spring frost is over, typically between March and May. The annual fertilizer requirement is very low. Results from field trials in Europe and from reviews of literature showed that nitrogen has only a modest influence on the yields of *M.* × *giganteus* [43]. It is estimated that the annual requirement of nitrogen is 50–70 kg ha^{-1}, phosphorus is 5–10 kg ha^{-1} and potassium is 70–100 kg ha^{-1} [56, 57].

Harvesting is carried out after the crop has senesced with moisture content preferably at its lowest and with nutrients translocated into the rhizomes. Harvesting is timed to achieve a balance between attaining lowest moisture content and minimizing biomass losses caused by adverse winter conditions. Crops grown in cooler climates are typically harvested in early spring when moisture content is lowest. Crops grown in warmer climates reach their maturity earlier and can be harvested in late autumn or delayed until early spring. However, delaying harvest until early spring will result in yield reduction by as much as 30–50% due to winter losses of dead and decaying leaves and upper stem parts. But such loses are tolerated because the lower moisture content (20%) improves the fuel quality, permits ease of handling, and requires little drying.

Yield: Miscanthus takes about 2–3 years to establish and so the first-year crop does not yield sufficient biomass to merit harvesting. The crop is normally harvested from the second year onwards but yields will continue to improve after year two until they level off. Ceiling yields can be reached in 2 years under good growing conditions but may take up to 5 years at some locations. The ceiling yields are attained more quickly in warmer climates and those total yields are higher than in cooler climates. The winter yields reported for Europe following the third growing season varied with location and ranged between 6.4 and 23.6 Mg ha^{-1} from northern to southern Europe [53]. Data on *Miscanthus* productivity in North America are still lacking but mathematical productivity modeling [58] based on the European studies projected yields of *Miscanthus* in the Midwest to far exceed those of switchgrass [43]. A recent report comparing productivity of *Miscanthus* and a locally adapted switchgrass cultivar (Cave-in-Rock) grown side by side in field trials in Illinois seems to support the projection [59]. The reported average winter yields of dry matter for the 3 years following the third growing season were 19, 30.3, and 31.4 Mg ha^{-1} in the northern, central, and southern plains, respectively [59]. The average yield per year across the three sites is approximately 27.2 Mg ha^{-1}. This yield is significantly higher than the yields reported in Europe and almost three times higher than for switchgrass cv. Cave-in-Rock, grown side-by-side with *Miscanthus* in the same field trials (Table 5). A yield of 27.2 Mg ha^{-1} would achieve the projected target of 342 million Mg on 12.6 million hectares, half the area estimated in the billion-ton-study projections [1]. No disease has been reported to date for *Miscanthus* but the crop has been known to be susceptible to *Fusarium* blight and Barley Yellow Dwarf Luteovirus [52]. Weed control is essential during the long establishment phase. Fields are typically sprayed with herbicide before planting followed by at least two sprayings a year for the first 2–3 years.

Uses: Miscanthus is grown primarily to be used in the bioenergy industry. It is being tested in Europe as solid fuel for combustion in farm-heating plants as well as for co-combustion with coal, straw, and wood to generate power [53]. Its potential lies in the abundance of raw cellulose biomass that can be converted to cellulosic ethanol. Nonenergy applications for *Miscanthus* include material for thatching [60], paper pulp production [61], and as a bio-composite in construction/building materials such as panel board and building block [62] and as a substitute for the plastics or light metals in the core of light natural sandwich material (LNS). LNS materials are light building materials used for plane and molded structural parts with high form stability at low weight, used for a broad range of applications. Such substitutions are used in carrying cases for

Biomass Crops for Biofuels and Bio-based Products. Table 5 Comparison of mean harvestable dry matter, Mg ha^{-1} ($\pm$ 1 SE), at the time of peak biomass production (Hmax), and after complete plant senescence (H1) from *Miscanthus* (M) and switchgrass (S) grown at three locations in the Midwest USA during 2004–2006 (n = 4) [59]

Year	Harvest time	North		Central		South		State average	
		M	S	M	S	M	S	M	S
2004	Hmax	38.1 (5.7)	*	60.8 (3.9)	26.0 (3.1)	48.5 (1.8)	*	48.3 (3.5)	26.0 (3.1)
	H1	13.7 (1.6)	*	25.1 (2.5)	12.8 (1.2)	37.3 (3.0)	*	25.4 (3.2)	12.8 (1.2)
2005	Hmax	25.6 (1.1)	7.8 (0.6)	40.7 (2.3)	11.5 (1.8)	40.4 (4.1)	7.8 (0.6)	33.3 (2.6)	7.9 (0.8)
	H1	13.7 (1.6)	7.8 (0.6)	31.1 (3.2)	10.6 (1.3)	27.3 (5.7)	7.8 (0.6)	25.8 (3.8)	7.9 (0.8)
2006	Hmax	29.9 (3.3)	8.4 (0.9)	44.1 (2.6)	22.0 (5.2)	51.3 (2.6)	9.6 (2.9)	39.0 (4.6)	15.6 (2.6)
	H1	29.9 (3.3)	7.7 (1.0)	44.1 (2.6)	15.6 (2.6)	39.2 (2.9)	9.1 (2.6)	377 (2.4)	15.6 (2.6)
3-year	Hmax	31.2 (3.7)	8.1 (0.5)	45.5 (3.9)	19.8 (2.6)	42.3 (3.6)	8.7 (1.8)	**38.2 (2.3)**	**12.5 (1.8)**
average	H1	20.9 (2.4)	7.8 (0.6)	33.4 (2.8)	13.0 (1.1)	34.6 (2.6)	6.7 (1.1)	**29.6 (1.8)**	**29.6 (1.8)**

*Data is not available for these points. Bold values highlight geographic and temporal averages of both parameters in both species

musical instruments and lab tops, rotor blades of wind power stations, small boats, and parts of yachts [63].

Future directions: One of the drawbacks of using *Miscanthus* as a biomass crop is its narrow genetic base. However, efforts have been undertaken to broaden the genetic base of *Miscanthus* and maximize the productivity and adaptive range of the crop through traditional breeding as well as modern genetic engineering by the European *Miscanthus* Improvement (EMI) project (www.biomatnet.org/secure/Fair/F659.htm) and research institutes across North America. Even with an unimproved *Miscanthus* crop, the yields achieved so far look very promising. Therefore, yield would be expected to increase dramatically and the cost of production to fall with breeding improvement efforts. A potential hybrid of *M. sinensis* that combines winter hardiness with high biomass potential has been identified through the effort of the EMI project. This hybrid will result in improved crop quality through delayed harvest without significant loss in yield [53]. The high cost of establishment is another major concern associated with cultivating *Miscanthus* as a biomass crop. This concern can be addressed with improvement in farming equipment and farming practices that will help to reduce loss of harvested material, time, and labor cost. The development of new machinery to process rhizomes (that includes lifting, cleaning, splitting, sorting and boxing) and carry out precision rhizome planting has made commercial rhizome multiplication farming and commercial production of *Miscanthus* feasible. Improvement in the crop together with improvement in farming technology and processing of this biomass crop into fuel will undoubtedly make *Miscanthus* a very attractive crop to the biofuel industries.

Switchgrass *Origin and distribution:* Switchgrass (*Panicum virgatum*) is a warm-season grass indigenous to the Central and North American prairie with its northern limit of adaptation at about 51° N [64]. In the USA its adaptive range stretches from the eastern seaboard to as far west as the east side of the Rocky Mountains and from the Texas Coastal Plain to as far north as Hudson Bay [65]. This wide geographic distribution can be seen as the manifestation of the great genotypic and consequently phenotypic variation seen within the species. In addition to its broad adaptation, switchgrass exhibits great adaptability to diverse edaphic conditions. Switchgrass can reach the height of 0.5–3 m or more in wetter areas of the country. Switchgrass has been extensively studied and planted in North America. Historically, switchgrass grown in the USA has been used as forage but over the last 2 decades it has been investigated intensively for its potential as an energy crop. In 1991 switchgrass was identified by the US Department of Energy for development as a model herbaceous energy crop because of its ability to tolerate a wide range of environmental conditions and at the same time offer high biomass yield [66].

Ecotypes: A fair amount of genetic variability exists in the switchgrass populations found across North America. The environment exerts a selective pressure on the population's diverse genotypes. The interaction between environment and genotype has over time created different ecotypes as well as variations within an ecotype (reproductive phenology, cold, heat, and drought tolerance) resulting in varieties with specific genetic and morphological characteristics that provide a good "fit" to a particular region. Through natural selection, two genetically and phenotypically distinct types of switchgrass have emerged, the lowland and the upland varieties (Table 6) [68]. The lowland varieties are vigorous, tall, thick-stemmed and generally found in wetter and more southern habitats. The upland forms are typically shorter and fine-stemmed and mainly found in drier mid- and northern latitudes. The ecotypical differences are generally related to local soil and climatic characteristics, with eastern and southern varieties adapted to higher moisture conditions, and western and northern varieties adapted to drier conditions. The phenotypic and ecotypic variation between the lowland and the upland ecotypes can be explained by their cytotypic diversity. Lowland switchgrass ecotypes are tetraploid, with a base chromosome number of 9 (diploid number 18), leading to 36 chromosomes ($2n = 4x = 36$). Upland ecotypes with the exception of the cultivar Summer, which is tetraploid, are octoploid ($2n = 8x = 72$) and less frequently, hexaploid ($2n = 6x = 54$) [69]. Breeding programs aimed at improving the forage yield have developed cultivars that adapt to specific locales ensuring the success of switchgrass in a large variety of conditions,

Biomass Crops for Biofuels and Bio-based Products.
Table 6 Characteristics of Upland and Lowland switchgrass ecotypes [67]

Upland ecotypes	Lowland ecotypes
Developed on higher "mesic" (moderately moist) sites	Developed in lower lying, "hydric" (considerably moist) sites, more sensitive to moisture stress
Adapted to mid- to northern latitudes	Adapted to lower latitudes
Predominantly octaploid ($2n = 7x = 72$)	Tetraploid ($2n = 4x = 36$)
Longer root length and internodes	Bunch form, larger root diameter
Shoots: originate from more active rhizomes and basal nodes of previous year culms	Shoots: originate from buds on rhizomes
Shorter and fine stems	Taller, coarser, thick stems, long, wide bluish-green leaves with long ligules, large panicles

from arid sites in the shortgrass prairie to brackish marshes and open woods [70].

Growing conditions: Switchgrass will grow in a wide range of soil types from fine to coarse textured soils but prefers soils of finer texture. Loamy and sandy soils will allow the roots and crown to spread more easily than do denser clay soils. Sandy soils dry out quickly potentially limiting the establishment success and biomass yield. Switchgrass can grow in acidic soil with pH as low as 4.3 [71] but optimum growth occurs at a pH between 5.0 and 8.0 [72]. Lowland switchgrass fares better in heavier and wetter soils while the upland types favor drier soils. Within the species, upland types are generally considered more drought tolerant [73]. Switchgrass grows best in association with site-adapted mycorrhizal fungi. The presence of mycorrhizae is thought to enhance phosphorus uptake by the plants [74, 75]. Therefore, mycorrhizae play a key role in moderating switchgrass growth in phosphorus-limited environments as well as reducing fertilizer inputs for biofuels production. Warm soil temperature and moisture are important in the successful establishment of switchgrass. Once established, switchgrass can survive extreme periods of drought. Under nonirrigation conditions switchgrass grows best in areas with greater than 500 mm of average annual rainfall.

Switchgrass seed germination is temperature and pH sensitive [72]. The optimum temperature for germination and growth are cultivar-dependent. Some cultivars such as the southern uplands germinate at about 11°C [76] while other cultivars may require as high as 35°C to germinate [77]. Planting is typically done in spring from mid-March to late May. Dormant seeds require a breaking step for them to germinate. Dormancy-breaking can be achieved by stratification. Planting dormant seeds into a cool soil (10–20°C) and allowing them to stratify in situ has been shown to increase germination [77] but this may lead to weed control problems. The cool season weeds can germinate first and choke out the switchgrass seedlings when the soil warms [78]. Weed control is very important in the early stages of establishment. Unfortunately, there are very few herbicide options available to control the weeds after switchgrass emergence. The herbicides almost universally used for some time as pre- or post-emergent herbicides for switchgrass and other warm-season grasses are triazines [79–82]. However, the types of herbicides and the rates used will best be determined by considering the weed species to be controlled and switchgrass' tolerance to the chemical.

Most research on switchgrass fertility has focused on its use as forage and higher nitrogen applications can ensure high yields and better quality feed. Nonetheless, some researchers have considered nitrogen fertilizer recommendations for switchgrass to be higher than necessary for biomass production. Switchgrass has a remarkable ability to extract nitrogen from unfertilized soils and is inherently thrifty in its use of phosphorus and potassium and often shows little or no response to additions [83, 84]. Mineral cycling within the plant and the presence of mycorrhizae in the soil play an important role in nitrogen and phosphorus nutrition of switchgrass. Switchgrass as a biomass crop in general can be grown without fertilizer or limited addition of fertilizer and still maintain productivity [67]. The nitrogen, phosphorus, and potassium recommendations should ideally be specific to a site or soil.

Harvesting switchgrass for biomass as opposed to forage should preferably be delayed until shoots have essentially all senesced and died which may not be until November or December. This will allow nutrients to be recycled from shoots to below-ground parts at the end of the growing season [85]. Harvesting once per year in late fall or early winter is recommended to maintain the highest sustainable biomass yields in the long term [67]. Harvesting late in the fall or early winter allows moisture content of the crops to drop to 15% or less which will facilitate quick baling and ease of transport as well as improving the quality of the biomass feedstock. For co-firing in coal plants the moisture content should preferably be around 12% to 13% [86]. Harvesting can be carried out with conventional haying equipment.

Yield: Switchgrass becomes fully productive only upon the third year after planting. Unlike other crops where yield data have been available for many years, data for switchgrass as a biomass crop are rather limited and are based mainly on small-plot research. A search across the literature provides switchgrass yield estimates that vary considerably, from less than 0.9 Mg ha^{-1} to almost 36.3 Mg ha^{-1}. Nonetheless, the most frequently observed yield class across all ecotypes, cultivars, soils, and management practices is between 9 and 10.9 Mg ha^{-1}. This great variability in yields is explained by the wide range of ecotypes as well as the strong interactions between genotypes and the environment. Gunderson et al. [70] observed higher yields on average within the lowland cultivars, 11.9 Mg ha^{-1} versus 8.4 Mg ha^{-1} in upland cultivars. Among the lowland varieties Alamo and Kanlow give the highest yield while Cave-in-Rock gives the highest yield for the upland varieties [87].

With newer varieties of switchgrass, yields in excess of 18.2 Mg ha^{-1} have been reported for test plots. Sanderson et al. [88] have reported yields of 13.6–18.2 Mg ha^{-1} in field trials in Texas and Thomason et al. [89] have reported yields in excess of 27.2 Mg ha^{-1} from field work in central Oklahoma. These yields are relatively high and site-specific. In a larger scale study, Parrish and Fike [67] reported average biomass yield in a 10-year study of 12.9 Mg ha^{-1}. Schmer et al. [90] reported on-farm yields ranging from 4.7 to 10.1 Mg ha^{-1} for field trials in the USA. According to the US Agricultural Research Service, growers can expect yields from 15.4 to 36.2 Mg ha^{-1} in the southeast, 10.9–13.6 Mg ha^{-1} in the western Corn Belt, and 2.3–9.1 Mg ha^{-1} in the northern plains [91].

Uses: Switchgrass was originally used as forage, either grazed [92, 93] or for making hay [94, 95]. The use of switchgrass has since been expanded to include nonforage purposes such as for bioenergy, soil stabilization and erosion control in critical areas like strip-mine soils, sand dunes, and dike, and soil improvement in areas degraded by overcropping. "Alamo" switchgrass has also been tested for its ability to remediate soils contaminated with cesium-137 and strontium-90, two radionuclides released during nuclear testing, nuclear reactor accidents, and weapons production. The level of cesium and strontium removed over a 5 months period was reported at 36% and 44%, respectively [96].

Benefits: Benefits associated with switchgrass are numerous. Planting switchgrass, even as a monoculture, is expected to enhance prairie biodiversity by providing forage, habitat, cover, and nesting areas for a diverse prairie wildlife that includes mammals, birds, amphibians, reptiles, invertebrates, and insects. Hohenstein and Wright [97] estimated a 95% reduction in soil erosion rates and a 90% reduction in pesticide use for herbaceous energy crops such as switchgrass relative to annual row crops like corn and soybean. It is also suitable for short windbreak plantings in truck farm fields [98] and it has been shown to improve water and soil quality by reducing carbon emissions through carbon sequestration [99]. Switchgrass can be easily integrated into existing farming operations because conventional equipment for seeding, crop management, and harvesting can be used [100].

Future directions: A significant amount of knowledge of the biology and agronomy of switchgrass has accumulated over the years through research on switchgrass as forage and recently as a biomass feedstock. There is now an understanding of the adaptation of existing cultivars and the development of new cultivars with improved yield and adaptation ability for different agro-ecoregions. However, there are still constraints that limit the use of switchgrass as a bioenergy crop. Problems with seed dormancy, improper or nonuniform planting depth, lack of weed control

options at establishment, and variable weather and soil conditions precluded the development of reliable and economic establishment methods [101]. A better understanding of how nitrogen is used and recycled in switchgrass under different growing conditions will help to develop fertilizer guidance and nutrient management specific to sites and soils [102]. Current research on the genetics, breeding, and molecular biology of switchgrass will result in new switchgrass cultivars with improved yield, greater establishment ability, and altered cell-wall properties for more efficient conversion.

Woody Biomass Crops

Introduction

Biomass, especially woody biomass and energy crops, already contribute substantially to cover energy demands around the world. Dedicated woody crops for biofuels have the potential to be an important energy source and will contribute to the substitution for fossil fuel energy [103]. In fact, the US Department of Energy has a vision to replace 30% of the liquid petroleum fuel for transportation with biofuels and similarly, the European Union Directive 2003/30/EC has targeted 5.75% of all petrol and diesel transport fuels to be derived from biomass by December 2010 [104]. Clearly, a multifaceted approach that includes both agricultural crops and dedicated woody crops will be necessary to attain these goals.

The principal challenge for biomass production is to develop and grow crops with improved physical and chemical traits while increasing biomass yields. Woody perennial plants like trees and shrubs grown for biofuels have the potential to play a central role in providing a renewable source of biomass for conversion to fuels while also providing a wide array of conservation benefits and ecological services, such as favorable habitat for wildlife, clean surface and ground water, conservation of soil and species diversity, that will exceed those associated with conventional annual crops [105].

Poplar

Origin and distribution: Hybrid poplars (*Populus* spp.) are among the fastest-growing trees in North America and among the oldest types of dicotyledonous plants. The genus *Populus* consists of close to 35 species of deciduous flowering plants in the family *Salicaceae*, native to most of the Northern Hemisphere. It includes the cottonwoods, poplars, and aspens, all of which are sometimes termed poplars. The hybrids themselves represent crosses among various cottonwood species [106].

Cottonwood (*Populus deltoides*) was first introduced by early French explorers in North America, which crossed naturally with Black Poplar (*Populus nigra*), creating what is referred to as *Populus* × *euramericana* hybrids (http://www.ag.ndsu.edu). They were first cultivated around fields as windbreaks and were selected for fast-growing characteristics. In 1912, hand-pollinated poplar hybrids were produced in Britain. The shortage of timber after World War II spurred an increase in hybrid poplar plantations in Europe. Even though some of these European varieties were reintroduced to North America in the early 1920s, it was not until the 1970s that commercial planting of hybrid poplar started in the USA. Since then, a national consortium involving government researchers from several agencies, universities, and the private sector has been working on improving hybrid poplar. Research in this area is targeting reduction of production costs by targeting pest and disease resistance, increasing yields and improving management systems. Also, studies are being performed to establish the environmental impact of producing hybrid poplar [107] (http://bioenergy.ornl.gov/main.aspx).

Physiology: Poplars are deciduous trees with alternate leaves, furnished with the appendages known as "stipules." Their flowers are dioecious; the calyx and corolla are replaced by simple scales. The female flower consists of a solitary one-chambered ovary, containing many ovules. Flowers are borne in long, sessile (attached directly to the stem) or pedunculated (growing from a stalk) aments, which are produced from buds formed in the axils of the leaves of the previous year. Leaves are green to dark green and measure 5–12 cm. The fruit is a two- to four-valved capsule, ripening before the full development of the leaf. The seed is light brown and surrounded by a tuft of long, soft, white hairs. Poplars can grow from anywhere between 15 to 50 m, with trunks of up to 2.5 m in diameter They grow upright, with spreading branches

and their root system is shallow and wide-spreading, equal or greater than the height of the tree (Fig. 3). *Populus* species are somewhat susceptible to insects and diseases. Common diseases may include *Melampsora* leaf rust, *Septoria* leaf spot and canker, *Cytospora* canker, wetwood, and stem decay. Common insect pests include poplar borer, aphids, poplar bud gall mite, poplar vagabond aphid, and poplar leaf beetles (http://www.2020site.org/trees/poplar.html).

Culture: Hybrid poplar is a short-rotation woody crop (SRWC). SRWC's are species that usually are planted and harvested in less than 15 years [108]. Hybrid poplar stands are typically planted at 750–1,700 trees ha^{-1} and allowed to grow for 6–12 years before harvest. Hybrid poplars are capable of resprouting from their rootstocks after harvest but it is recommended to reestablish the cultures to reduce the potential of diseases and also to exploit the new improved hybrid varieties. For the production of hybrid poplars, clay loams or sandy-loam, slightly alkaline (pH 5 to 7.5) and medium-textured soils are recommended. They require a moist site and will not tolerate drought on upland sites. The use of herbicides or manual weed removal must be used in the first 3 years, but this is no longer necessary when the canopy closes, creating its own weed control. Furthermore, fertilizer applications are only necessary if the nitrogen level in leaves falls below 3% on a dry weight basis (http://www.ag.ndsu.edu, [107]).

Biomass Crops for Biofuels and Bio-based Products. Figure 3
Hybrid poplar grove

Yield: Hybrid poplars, when grown under short-rotation silviculture, can produce between 8 and 22 Mg ha^{-1} per year and achieve a height of 20 m in as little as 6 years. Average yields in the USA and range of yields by geographic region on hectares currently planted are shown in Table 7 [109].

Hybrid poplar growth and biomass yield could vary greatly depending on the site, the soil properties and weather conditions, as well as the species genotype. The above-ground biomass yield of 4-year-old hybrid poplar stands in Europe (in short-rotation coppice culture) and north central USA averaged between 2 and 11 Mg ha^{-1} per year. In comparison, a recent study at the University of Saskatchewan reported growth and yield data in western Canada of 4-year-old Walker hybrid poplar stands from five locations to average from 0.17 to 0.19 Mg ha^{-1} per year [110]. It has been suggested that once the crop is established, the combination of precipitation and temperature and its

Biomass Crops for Biofuels and Bio-based Products. Table 7 Hybrid poplar yields in regions of the USA [109]

Region	Hybrid poplar yields	
	Average Mg ha^{-1} per year	Range Mg ha^{-1} per year
Lake States	9.9	7.9–11.8
Corn Belt	10.4	8.4–11.7
Southeast	10.1	8.6–11.7
Appalachia	8.0	9.0–11.7
North Plains	8.6	7.3–9.7
South Plains	8.4	7.3–9.0
Northeast	9.0	7.7–10.0
Pacific Northwest	12.9	12.4–13.5

influence on soil moisture becomes the most limiting factor for maximizing biomass production [111].

Advantages: Many advantages can be linked to growing hybrid poplars, from its positive effect on the environment to the fact that they are expected to be grown on agricultural cropland using standard production methods, thus reducing the need for new technology. Environmental benefits are linked to hybrid poplar's perennial nature. Chemical and fertilizer applications are considerably lower and these trees can intercept run-off nutrients to rivers and wetlands close by. Also, wind and water erosion over the life of the rotation is inferior to the erosion caused by annual crops and there is a clear ecological benefit of year-round trees for birds and habitat for small mammals. Their buds provide a source of food for birds, and their twigs and young branches make good forage for wildlife (http://www.ag.ndsu.edu, [107]).

The use of SRWCs for bioenergy production could substantially decrease the overall use of fossil fuels for energy. It would reduce CO_2 emissions into the atmosphere, increase soil organic carbon sequestration, and improve soil erosion control. Additionally, growing woody species like poplar on waste disposal sites and agriculturally marginal lands would definitely benefit rural communities [110].

Uses: Hybrid poplars are grown on plantations mainly for pulpwood used in the manufacture of paper. This wood is also sold as inexpensive hardwood timber, used for pallets and cheap plywood [106]. Wood and wood-derived fuels are a primary energy source in developing countries' domestic households as well as industrial facilities. From a medical point of view, *Populus* species can be a source of salicin, used for fevers and headaches. (http://www.ag.ndsu.edu, [107, 112]). More importantly, they are well suited for the production of bioenergy (e.g., heat, power, transportation fuels) and other bio-based products (e.g., organic chemicals, adhesives).

Poplar as a source of biofuels: Bioethanol is traditionally produced by converting either starch from grains such as corn, or sugar from sugarcane into ethanol. A second technology is based on the hydrolysis of cellulose or lignocelluloses into sugars, followed by fermentation to produce fuel ethanol [113]. The cellulose comes from woody parts of plants or trees, such as hybrid poplar and other short rotation woody crops. The main objective in the production of ethanol from cellulose is to obtain a maximum biomass output with a minimum input. Developing new poplar varieties could expand the biofuel production without incurring the type of environmental problems that intensive agriculture can generate [114]. Major improvements have been achieved through breeding and genetic selection.

Poplars are the first tree for which the entire genome has been sequenced. Its 45,000 genes are being investigated to find ways to improve this tree, from genes that regulate its root system, improving water and nitrogen absorption, to cell wall modification for more extractable cellulose [115, 116]. New varieties focusing on more efficient roots not only would result in higher tolerance to drought but also in bigger trees and thus more biomass for the biofuels industry [115]. Alternatively, modification of cell wall polymers, such as lignin, which interfere with the enzymes needed to degrade cellulose, can benefit the extraction of cellulose from poplar trees for the production of ethanol [116].

To increase vigor and yield of poplar species, new crosses are being performed and examples of studies on new varieties are easy to find. Among these, a cross is found between *Populus trichocarpa* and *Populus deltoides* which has achieved a hybrid with leaves about four times as large as the leaves of either parent at a similar age, expanding their photosynthetic surface area. Other projects are looking at the biochemical indicators for drought tolerance in these hybrids, by growing them with or without irrigation and characterizing biochemical changes. All efforts are focused on fast-growing highly adapted poplar clones [106].

Up to now, traditional row crops like corn have been utilized for ethanol production. Several corn-to-ethanol plants are commercially in use around the world and it is known that they offer an alternative green energy source while minimizing greenhouse gas (GHG) emissions [117]. Nonetheless, poplar trees might have several additional benefits. In fact, corn ethanol reduces GHG emissions by about 13%, while cellulosic ethanol could greatly reduce GHG by 88% [118]. Even though wood from hybrid poplar can produce roughly the same ethanol production per unit biomass (Fig. 4), hybrid poplar generates 40% more excess electrical energy than corn. In addition, fast-growing cellulosic energy crops such as hybrid

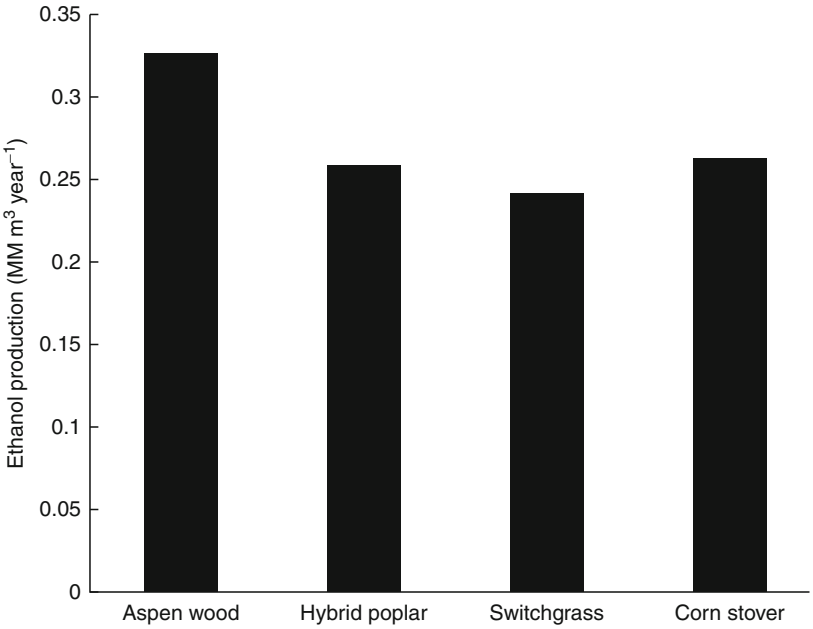

Biomass Crops for Biofuels and Bio-based Products. Figure 4
Comparison of ethanol production utilizing aspen, hybrid poplar, switchgrass, or corn stover

poplar can be grown on a variety of land types, without having to compete with cropland for food and feed needs, as it is necessary for crops such as corn [117]. Poplar plantations do not require intensive inputs and are not harvested every year. There is a wide range of varieties and they could be grown in an equally wide range of climates, from subtropics in Florida to sub-alpine areas in Alaska. It should not be forgotten that the machinery necessary for poplar growth already exists and the infrastructure to handle the trees is already available [116].

The use of dedicated energy crops, such as hybrid poplars will not only address energy security issues, but will also inevitably be beneficial for the environment while addressing global climate change and economic development.

Eucalyptus

Origin and distribution: Eucalyptus is indigenous to Australia, Indonesia, and Papua New Guinea. There are more than 700 species of *Eucalyptus*, almost all (except for two) are native to Australia [119]. Species of *Eucalyptus*, prized globally for excellence in paper and energy production, are cultivated throughout the tropics and subtropics in more than 90 countries worldwide representing 8% of all planted forests (FAO, ftp://ftp.fao.org/docrep/fao/008/A0400E/A0400400.pdf). A few cold-tolerant species and their hybrids grow in the temperate regions of Europe, New Zealand, and South and North America. The global land area under *Eucalyptus* cultivation is estimated at over 20 million hectares and Brazil has emerged as the major global producer and exporter of *Eucalyptus* wood with approximately 4.2 million hectares on plantations followed by India and China with ~3.5 million hectares and 2.9 million hectares, respectively [120]. *Eucalyptus* was first introduced to California as an ornamental plant in 1853. Soon after, it was widely planted throughout the state because it was fast growing and a renewable source of timber and fuel [121]. Its popularity was later replaced with the criticism that *Eucalyptus* forests compete with native plants and do not support native animals. Eucalypt forests in some parts of California were eventually removed [122]. The fuel crisis in the 1970s brought back *Eucalyptus* species as prime candidates for woody biomass cultivated on experimental farms mainly in central California. Two other places in the USA where *Eucalyptus* short-rotation research projects are conducted are located in

Hawaii and Florida [123, 124]. Other regions in the USA considered highly suitable for growing *Eucalyptus* are in Texas, Louisiana, and Georgia. Only four *Eucalyptus* species, *E. grandis (EG), E. urophylla (EU), E. camaldulensis, and E. globulus*, and their hybrids account for nearly 80% of the eucalypt plantations worldwide with *E. grandis* being the most widely used species in tropical and subtropical areas while *E. globulus* is the premier species for temperate zone plantations [125]. *E. grandis* is also used as a parental species in hybrid breeding and is rated worldwide as one of the fastest growing species and has the widest adaptability of all *Eucalyptus* species [125]. The greatest area of plantations of *EG* and its hybrids with other species are in Brazil and several other Central and South American countries.

Importance: *Eucalyptus* species are fast-growing woody perennials with many uses making them economically important trees. Eucalypts are commonly cultivated for the paper and pulp industries because of their high fiber yields and use as fuelwoods. In many poor countries in Africa [126], South America [127], and Asia [128] eucalypts are grown as a cash crop. *Eucalyptus* woods are used as mine props, poles, firewood, and charcoal [119]. The nonwood products derived from eucalypts include essential oils, honey made by bees from its flowers, and tannin [129]. The potential of *Eucalyptus* as a biomass feedstock for cellulosic ethanol has drawn attention to this species of woody perennial. The US Department of Energy (DOE) identified *Eucalyptus* as one of the crops with the potential to contribute to the biomass needed for biofuel to reduce the nation's dependence on imported fossil fuels [1]. *Eucalyptus* has many attributes and advantages that make it suitable as a dedicated energy crop. As a perennial, *Eucalyptus* can be cultivated under the coppice system. The cut stumps resprout to provide another crop. The retained roots with stored carbohydrates and access to soil water and nutrients help sustain rapid regrowth rates [130]. The tree withdraws the mineral nutrients into its roots at the end of a growing season, thus reducing the amount of fertilizer needed and thereby reducing the fertilizer costs and minimizing water pollution caused by run-off. The fact that harvesting only once every few years over a period of 15–20 years reduces the environmental impact created by disturbances at harvesting and planting (soil erosion and nutrient loss) and saves on the cost of establishment (site preparation, seedling, and planting costs). *Eucalyptus* is one of the fastest growing hardwoods which grows well even on environmentally harsh lands (infertile soils, arid lands) [131]. It is a low input crop requiring minimum fertilizer and precipitation. *Eucalyptus* is also the world's most widely planted hardwood species that has multiple end uses, including feedstock for traditional forest products and energy products such as cellulosic ethanol and power generation through direct firing, co-firing or wood pellets in short rotation. In regions of the USA where *Eucalyptus* will most likely be cultivated, infrastructure already exists for planting, harvesting, handling, and processing wood for pulp that could also support the production, processing, and distribution of *Eucalyptus* crops. Last but not least, *Eucalyptus* species have been grown in the USA for many decades and have not demonstrated any invasive characteristics.

Growing conditions: Eucalypts are hardy trees and the majority of *Eucalyptus* species will grow in a range of soils from pH 4.5 to 8.5. They do not require fertile soils and many species naturally occur in shallow, low fertility soils. When grown on deeper more fertile soils they generally grow faster, bigger, and more luxuriant. Some species do require good drainage while others will grow on heavy clay and even on boggy, partially waterlogged sites. Several species grow well on high pH soils, and most species adapt to higher pH soils, although usually with reduced growth rates. *Eucalyptus* will tolerate an annual rainfall of 500–5,000 mm and an annual temperature of 12.3–27.9°C (Table 8). *Eucalyptus* is considered one of the most adaptable plant genuses, and the trees are remarkably hardy in all kinds of weather conditions. Once established the mature trees adapt to the local growing conditions and become very tolerant to drought and prolonged dry periods. However, the young trees of most *Eucalyptus* species do not tolerate frost very well and will succumb to extreme fluctuation of temperatures [132]. Fertilization and nutritional studies of *Eucalyptus spp.* in Australia, Brazil, and Hawaii pointed to a general need for supplementary nitrogen, and sometimes phosphorus, especially at planting and soon thereafter [133, 134]. Fertilizer (N-P-K) is generally applied at planting and again about 6 months later. Subsequently, only nitrogen is needed on most sites. The total amount

Biomass Crops for Biofuels and Bio-based Products. Table 8 Growth requirements of *Eucalyptus* species in USA

Growth requirements	*E. grandis*	*E. saligna*	*E.* camaldulensis	*E. globulus*
Adapted to coarse textured soils	Yes	Yes	Yes	Yes
Adapted to fine textured soils	Yes	No	Yes	Yes
Adapted to medium Textured soils	Yes	Yes	Yes	Yes
Drought tolerance	Low	Medium	Medium	Low
Fertility requirement	Medium	Low	Low	Medium
Frost free days, minimum	340	340	180	240
Moisture USE	Medium	Medium	High	High
pH, minimum	4.0	4.0	5.0	5.0
pH, maximum	6.0	6.0	8.5	6.8
Planting density per acre, minimum	170	170	170	170
Planting density per acre, maximum	1,200	1,200	1,200	1,200
Precipitation, minimum, (mm)	1,016	1,524	508	553.4
Precipitation, maximum, (mm)	1,778	5,080	2,540	1,524
Temperature, minimum (°C)	2–2.2	−6.1°C	−8.3°C	−8.3°C
Coppice potential	Yes	Yes	Yes	Yes
Resprout ability	Yes	Yes	Yes	Yes

(Source: http://www.plants.usda.gov)

required depends on the nitrogen status of the topsoil and may range from 224–673 kg ha^{-1} in four to eight applications (depending on the site quality and rotation length) [123]. The application of nitrogen may be eliminated or reduced with the practice of intercropping with nitrogen-fixing species such as *Leucena* or *Albizia*. Such practices were studied in Hawaii [135], Brazil [136], and India [137] and have shown that it is possible to maintain both the yields and nitrogen status of the soils without using nitrogen fertilizers, or with much reduced fertilizer inputs. *Eucalyptus* can be planted at any time of the year in tropical and subtropical areas but spring time is recommended for colder regions. Young *Eucalyptus* trees do not compete well with weeds; therefore, weed control in the early stages of establishment is very important in the management of *Eucalyptus* cultivation. Weed control is carried out before planting the trees and during the first 2 years of establishment. Pre-emergence and post-emergence herbicides found safe and efficacious for *Eucalyptus* are listed in a report by Elmore [138]. The projected rotation age for bioenergy production is 5 years under optimum growing conditions and a year or two longer under less favorable conditions [125]. However, new and high-yielding varieties have the potential to reduce rotation length to 4 years or less [139].

Yield: The yield of *Eucalyptus* biomass varies widely from species to species and also with provenances (place of seed origin), sites, and management systems around the world. Small plot studies conducted at the University of Massey, New Zealand, comparing the yields of 19 *Eucalyptus* species grown under similar conditions and managed under a coppice regime highlighted the differences in survival rates, the number of shoots per tree, the shoot/tree sizes and ultimately the yields between different species. The yields obtained vary from 4 to 20 Mg ha^{-1} per year and only six species: *E.brookerana*, *E. botryoides*, *E. botryoides* × *saligna*, *E. ovata*, *E. elata*, and *E. oblique* had yields averaging 16 Mg ha^{-1} per year [140]. The yield evaluation of *Eucalyptus* species in small plot trials in Hawaii

Biomass Crops for Biofuels and Bio-based Products. Table 9 *Eucalyptus* biomass yields at five Hawaiian sites after 5 years [141]

Site/Island	Tree species	Elevation (m)	Annual rainfall (mm)	Average temperature (°C)	Agronomic conditions	Planted density (trees/ha)	Annual yield (Mg ha^{-1} per year)
Mountain View, Hawaii	*E. grandis*	296.3	4,623	21.1	Wet, upland	405	20.16
	E. saligna					405	11.2
	E. urophylla					405	20.16
Honokaa, Hawaii	*E. grandis*	232.3	2,057	21.1	Moderately dry, upland	405	29.12
	E. saligna					405	20.60
	E. urophylla					405	31.80
Puunene, Maui	*E. grandis*	7.6	483	25.0	Dry, irrigated, lowland	485	16.57
Kilohana, Kauai	*E. grandis*	256.6	3,023	20.6	Wet, intermediate elevation	405	16.35
	E. urophylla					405	17.47
Hoolehua, Molokai	*E. calmaldulensis*	76.2	711	22.8	Dry, irrigated, intermediate elevation	405	9.85

emphasized the suitability of sites and species (Table 9). *E. grandis* and *E. urophylla* are relatively highly productive at a higher elevation with moderate to high precipitation but not at a lower elevation. *E. camaldulnesis* performed poorly at low elevation even with irrigation. *E. urophylla* has the highest annual yield with ~35 Mg ha^{-1} per year at the moderately upland site [141]. The importance of provenance selection for different sites was brought out in the data for *E. camaldulensis* planted in Afaka, Nigeria. Five-year-old trees had a mean annual increment (MAI) that ranged from 17.3 to 5.1 Mg ha^{-1} per year depending on where in Australia the seed had come from. This demonstrates a possible threefold increase in yield achieved simply by selecting a seed source location [131].

A well-managed *Eucalyptus* plantation will improve the performance of the crop and will maintain a relatively high level of yield throughout the coppice regime. *Eucalyptus* cultivated with irrigation and fertilizer gives a higher yield over *Eucalyptus* grown without these additions. This was demonstrated in a pilot experiment in Brazil under the Brazil *Eucalyptus* Potential Productivity Project (BEPP). The yields of *Eucalyptus* cultivated with no fertilization were 28% lower than yields achieved with fertilization, and the response to irrigation was found to be far larger than that of fertilization. The growth increase from irrigation ranged from a low of 7% at the cooler, higher elevation site to 67% at the driest site [142]. The stand uniformity also has an influence on the yield. Stands with uniform structure (trees in plots planted in a single day) showed 13% greater growth than stands with higher heterogeneity of tree sizes (owing to staggered planting). The yields reported 2 decades ago in field trials in California, Florida, and Hawaii were typically 20–24 Mg ha^{-1} per year [124, 141]. Over the last 10–20 years of intensive research, improved silviculture (site preparation, fertilization and weed control) and superior clones have improved yields, exceeding 37 Mg ha^{-1} per year with the potential to reach ~66 Mg ha^{-1} per year [124]. In Brazil, commonly planted *Eucalyptus* hybrids such as *E. grandis* × *E. urophylla* routinely yield ~24–30 Mg ha^{-1}

per year [142]. Large gains in yield can be achieved by the careful selection of species, sites, provenances, and management system to suit the local conditions.

Economics: Growing biomass and producing bioenergy require a substantial financial investment. Hard numbers on the economics of growing *Eucalyptus* for bioenergy on a commercial scale are unavailable. However, the cost projection from small plot trials in Hawaii for producing and delivering biomass feedstock to the central facility, excluding storage, processing, and biomass conversion ranges from US$30 to US $100 per dry Mg [143]. The estimated cost of producing and delivering *Eucalyptus* in the southern USA ranges from US$50 to US$60 per dry Mg, based on a yield of 28–16.8 Mg ha^{-1} and on a delivery range within 48 Km of the processing site [144]. Factors that contribute to the cost of production are establishment, maintenance, harvesting, transportation, rotation length, and productivity. The cost can be greatly reduced by growing highly productive species, having higher tree stand density and a shorter rotation length. The economic feasibility of growing *Eucalyptus* for biomass can be improved by increasing productivity through improved germplasm, an efficient management system, and improvements in biotechnology. Introducing traits such as improved growth, stress tolerance, reduced lignin composition for easier processing of the biomass, and improved wood quality through increasing cellulose composition will increase productivity and add value to the crop.

Conclusions and Future Directions

Agricultural residues: Residues can contribute as much as 428 million dry Mg per year to biomass harvests for conversion to transportation fuels. Nevertheless, it is clear that although there is a positive energy balance from residue utilization, many factors other than ethanol output have an impact on the use of these residues. Maintenance of soil fertility is paramount to the sustainability of this biomass source. Compensation for the farmer is highly important as well, with potential of their participation in farmer cooperatives (co-op's) to capture part of the value chain and ensure their continued involvement. Additionally, harvest and storage logistics must be explored and resolved. Handling large quantities of loosely packed biomass, transporting it over long distances and storing it in bales or wet stacks are only a few of the logistics issues. Harvesting activities must be coordinated so that the process of grain collection and storage is not slowed with resultant loss in their valuable revenues. However, the potential of this biomass source is important enough for the investments necessary to make these residues a feasible feedstock.

Sweet sorghum and sugar cane: Sugar cane and sweet sorghum are members of same family and share physiological characteristics. Their use as bioenergy crops is almost identical. For the last 40 years, sugar cane has been used as a bioenergy crop in Brazil, which is a successful example of a country that has reduced its gasoline usage by producing bioenergy. Sweet sorghum is considered to be one of the most drought-resistant agricultural crops as it has the ability of remaining dormant during the drought period. de Vries et al. [145] analyzed different biofuel production systems in geographical regions where they are currently important for ethanol. Among the six "first generation" biomass crops, e.g., maize (USA), wheat (Northwest Europe), sugar beet (Northwest Europe), cassava (Thailand), sweet sorghum (China), and sugar cane (Brazil), biofuel production from sugar cane and sweet sorghum delivers substantially more energy per unit energy spent than from the other crops. These two C4 sugar-producing plants appeared to be most sustainable and most efficient in the use of land, water, nitrogen, and energy resources, while pesticide applications were relatively low in relation to the net energy produced. An agronomic and yield comparison of sugar cane and sweet sorghum is presented in Table 10.

Both sugar cane and sweet sorghum are excellent feed stock for first-generation bioethanol production. However, in order to reduce the usage of fossil fuel and attain the goal of sustainability, utilization of lignocellulosic biomass for the production of cellulosic ethanol plays a vital role. Lignocellulosic-rich bagasse from sugar cane and sweet sorghum has the most positive net energy balance among the common feedstocks potentially used for bioethanol production. Sugar cane and sweet sorghum have comparable energy balance, with 8.3 and 8 units of energy produced for every unit of energy invested in their cultivation and production, respectively, especially when compared with 1.8 units for corn grain. On the other hand, only 0.8 unit of

Biomass Crops for Biofuels and Bio-based Products.
Table 10 Comparison of sugar cane and sweet sorghum [146]

	Sugar cane	Sweet sorghum
Crop duration	About 7 months	About 4 months
Growing season	Only one season	One season in temperate and two or three seasons in tropical area
Soil requirement	Grows well in drain soil	All types of drained soil
Water management	36,000 m^3 h^{-1}	12,000 m^3 h^{-1}
Crop management	Requires good management	Little fertilizer required; less pest and disease complex; easy management
Yield (ha^{-1})	70–80 Mg	54–69 Mg
Sugar content on weight basis	10–12%	7–12%.
Sugar yield	7–8 Mg ha^{-1}	6–8 Mg ha^{-1}
Ethanol production directly from juice	3,000–5,000 L ha^{-1}	3,000 L ha^{-1}
Harvesting	Mechanical harvested	Very simple; both manual and through mechanical harvested

energy is produced in fossil fuel production for every unit invested [147]. Currently eight times more energy is produced from sugar cane than what is used in its creation. When bagasse is included in the equation, it is estimated that the number may increase to as much as 16 times. Bagasse is the feedstock with the most positive energy balance available in the near term. Sugar cane bagasse shows significant potential for making the biomass-based ethanol an economically viable solution.

Switchgrass and Miscanthus: Perennial grasses are nonfood crops which can yield high-quality materials for both energy and fiber production. Switchgrass and *Miscanthus* are immense biomass producers and show great potential as bioenergy crops. They can be grown over a wide range of conditions and with minimal agricultural inputs. Switchgrass has deep roots that makes it less susceptible to drought stress and enables it to adapt better in areas where the water precipitation is lower than that required by *M.* × *giganteus*. An analysis of published yields indicates *M.* × *giganteus* produces more biomass per unit area and per unit input than switchgrass but the yields of *M.* × *giganteus* are more strongly influenced by water, while those of switchgrass are more strongly controlled by nitrogen [43]. Therefore, in locations with ample rainfall but with concern over nitrogen contamination of water supplies, it may be better to grow *M.* × *giganteus* while conversely, in arid areas without contamination concerns, greater yields may be obtained growing switchgrass as long as adequate nitrogen fertilization is provided.

Woody crops: Woody crops such as Poplar and *Eucalyptus* represent a critical component of the bioenergy future. They have the potential to be a significant part of the bioenergy solution in the USA and in many other parts of the world. In the USA, perennial woody crops are expected to account for part of the 377 million dry Mg of the 1.37 billion dry Mg total biomass resource potential. The projected yield for the long-term feasibility of renewable energy production defined by DOE is 20 Mg ha^{-1} per year [1]. The projected yield is not only achievable but can be exceeded with improved silviculture, the use of superior clones, and genetic improvement. Investments in research and technology are needed to improve productivity and bring down the cost of production. Recent advances in genetically modified *Eucalyptus* include a freeze-tolerant variety and a low-lignin and high-cellulose variety. The freeze-tolerant variety was developed using a highly productive tropical hybrid, *E. grandis* × *E. urophylla* [139]. A field test of the freeze-tolerant variety demonstrated its ability to maintain its productivity even at temperature as low as −9°C. This has made possible commercial plantings of tropical *Eucalyptus* species in the Southeastern USA where cold winter temperatures would normally restrict such cultivation. The low-lignin and high-cellulose variety with 18% less lignin and 4.5% more cellulose developed by a team of Taiwanese and US scientists (China Post, 2007, http://www.chinapost.com.tw/taiwan/2007/09/14/122524/Gene-modified-eucalyptus.htm) would add value to

the crop by improving efficiency in the pretreatment step utilized in fermentation systems for biofuels production from lignocellulosic raw materials. The authors estimated that an output of 0.9 million Mg of this new variety could generate extra revenues of about US$36 million every year. Advances in research and technology in growing *Eucalyptus* in Brazil over the last 40 years have paid off significantly. Productivity of *Eucalyptus* biomass has increased twofold to fivefold depending on the site quality [148, 149]. Improved new varieties of poplar trees are currently being obtained through genetic engineering and breeding. Varieties with larger leaves, improved root system, and modified lignin are associated not only with higher biomass yields and better net energy balance but they would definitely have a lower environmental impact [115, 116].

Growing *Eucalyptus* and hybrid poplar for biomass is sustainable and will be economically feasible with improved varieties and technology. The use of woody crops for bioenergy offers many benefits with no anticipated long-term environmental impact and may be part of a long-term solution to the nation's energy security.

In order to ensure feedstock availability whether from dedicated crops or from residues, changes in farm and energy policies will need to be made, making sure they are connected to incentivize this new industry.

Bibliography

1. Perlack R et al (2005) Biomass as feedstock for a bioenergy and bioproducts industry: The technical feasibility of a billion-ton annual supply
2. Kadam K, McMillan J (2003) Availability of corn stover as a sustainable feedstock fo bioethanol production. Bioresour Technol 88:17–55
3. Green S (2011) Sustainability: soil. In: Hood E, Nelson P, Powell R (eds) Plant biomass conversion. Wiley-Blackwell, Ames, IA
4. Andrews S (2006) Crop residue removal for biomass energy production: effects on soils and recommendations. USDA – National Resource Conservation Service, Washington
5. Hettenhaus J (2011) Agricultural crop residues for biomass conversion. In: Hood E, Nelson P, Powell R (eds) Plant biomass conversion. Wiley-Blackwell, Ames, IA
6. Wang M, Saricks C, Santini D (1999) Effects of fuels ethanol use on fuel-cycle energy and greenhous gas emissions. Center for Transportation Research, Argonne National Laboratory Argonne, IL, USA
7. Lawrence C, Walbot V (2007) Translational genomics for bioenergy production from fuelstock grasses: maize as the model species. Plant Cell 19:2091–2094
8. Osborne C, Beerling D (2006) Nature's green revolution: the remarkable evolutionary rise of C$ plants. Philos Trans R Soc B Biol Sci 361:173–194
9. Makino A et al (2003) Differences between maize and rice in N-use efficiency for photosynthesis and protein allocation. Plant Cell Physiol 44:952–956
10. Raines C (2006) Transgenic approaches to manipulate the environmental responses of the C3 carbon fixation cycle. Plant Cell Environ 29:331–339
11. de Oliveira M, Vaughan B (2005) Ethanol as fuel: energy, carbon dioxide balances, and ecological footprint. Bioscience 55(7):593–602
12. Bennett AS, Anex RP (2009) Production, transportation and milling costs of sweet sorghum as a feedstock for centralized bioethanol production in the upper Midwest. Bioresour Technol 100(4):1595–1607
13. Reddy BVS, Kumar AA, Ramesh S (2007) Sweet sorghum: a water saving bio-energy crop. In: Linkage between energy and water management for agriculture in developing countries, Hyderabad
14. Gnansounou E, Dauriat A, Wyman CE (2005) Refining sweet sorghum to ethanol and sugar: economic trade-offs in the context of North China. Bioresour Technol 96(9):985–1002
15. Renouf M, Wegener M, Nielsen L (2008) An environmental life cycle assessment comparing Australian sugarcane with US corn and UK sugar beet as producers of sugars for fermentation. Biomass Bioenergy 32:1144–1155
16. Sharpe P (1998) Sugar cane: past and present. Southern Illinois University, Carbondale
17. McIlroy R (1963) An introduction to tropical cash crops. Ibadan University Press, Ibadan, p 163
18. Purseglove J (1979) Tropical crops: monocotyledons. Longman, London, p 607
19. Goldemberg J, Coelho S, Guardabassi P (2008) The sustainability of ethanol production from sugar cane. Energy Policy 36:2086–2097
20. Macedo IC, Seabra JEA, Silva JEAR (2008) Green house gases emissions in the production and use of ethanol from sugarcane in Brazil: the 2005/2006 averages and a prediction for 2020. Biomass Bioenergy 32(7):582–595
21. Dong z et al (1994) A nitrogen-fixing endophyte of sugarcane stems (a new role for the apoplast). Plant Physiol 105: 1139–1147
22. Wrigley G (1982) Tropical agriculture: the development of production, Fourthth edn. Longman, New York, p 496
23. Kim S, Dale B (2004) Global potential bioethanol production from waste crops and crop residues. Biomass Bioenergy 26(4):361–375
24. Destefano S et al (2004) Differentiation of 'Xanthomonas' species pathogenic to sugarcane by PCR-RFLP analysis. Eur J Plant Pathol 109:283–288

25. Laopaiboon P et al (2010) Acid hydrolysis of sugarcane bagasse for lactic acid production. Bioresour Technol 101:1036–1043
26. Reijnders L, Huijbregts M (2009) Transport biofuels: a seed to wheel perspective. Springer, London
27. Banerjee R, Pandey A (2002) Bioindustrial application of sugarcane bagasse: a technology perspective. Int Sugar J 1:3–7
28. Beeharry RP (2001) Carbon balance of sugarcane bioenergy systems. Biomass Bioenergy 20(5):361–370
29. Sun J et al (2004) Isolation and characterization of cellulose from sugarcane bagasse. Polym Degrad Stab 84:331–339
30. Pessoa J, de Manchilha I, Sato S (1997) Evaluation of sugarcane hemicellulose hydroyzate for cultivation of yeasts and filamentous fungi. J Indian Microbiol Biotechnol 18:360–363
31. Halling P, Simms-Borre P (2008) Overview of lignocellulosic feedstock conversion into ethanol – focus on sugarcane bagasse. Int Sugar J 110:191–194
32. Rooney WL et al (2007) Designing sorghum as a dedicated bioenergy feedstock. Biofuels Bioproducts Biorefining (Biofpr) 1(2):147–157
33. Billa E et al (1997) Structure and composition of sweet sorghum stalk components. Ind Crops Prod 6(3–4):297–302
34. Almodares A, Mostafafi D (2006) Effects of planting date and time of nitrogen application of yield and sugar content of sweet sorghum. J Environ Biol 27:601–605
35. Grassi G, Tondi G, Helm P (2004) Small-sized commercial bioenergy technologies as an instument of rural development, in biomass and agriculture: sustainability, markets and policies. OECD Publication Service, Paris, pp 277–287
36. Hunter EL, Anderson IC (1997) Sweet sorghum. Hortic Rev 21:73–104
37. Miller FR, McBee GG (1993) Genetics and management of physiological systems of sorghum for biomass production. Biomass Bioenergy 5(1):41–49
38. Vermerris W et al (2009) Production of biofuel crops in florida: Sweet sorghum. Institute of Food and Agricultural Sciences, University of Florida, Gainesville
39. Belaychi L, Delmas M (1997) Sweet sorghum bagasse: a raw material for the production of chemical paper pulp. Effect of depithing. Ind Crops Prod 6:229–232
40. Corredor D et al (2009) Evaluation and characterization of forage sorghum as feedstock for fermentable sugar production. Appl Biochem Biotechnol 158(1):164–179
41. Bryan W, Monroe G, Caussariel P (1985) Solid-phase fermentation and juice expression systems for sweet sorghum. Trans ASAE 28(1):268–274
42. Sipos B et al (2008) Sweet sorghum as feedstock for ethanol production: enzymatic hydrolysis of steam-pretreated bagasse. Appl Biochem Biotechnol 153:151–162
43. Heaton E, Voigt T, Long SP (2004) A quantitative review comparing the yields of two candidate C4 perennial biomass crops in relation to nitrogen, temperature and water. Biomass Bioenergy 27(1):21–30
44. Finlay R (2004) Mycorrhizal fungi and thier multifunctional roles. Mycologist 18:91–96
45. Beaty E, Engel J, Powell J (1978) Tiller development and growth in switchgrass. J Range Manage 31:361–365
46. Monteith JL (1978) Reassessment of maximum growth rates for C3 and C4 crops. Exp Agric 14(01):1–5
47. Ney R, Schnoor J (2002) Incremental life cycle analysis: using uncertainty analysis to frame greenhouse gas balances from bioenergy systems for emission trading. Biomass Bioenergy 22:257–269
48. Hodkinson T, Renoize S, Chase M (1997) Systematics of *Miscanthus*. Aspects of Applied Biology 49:189–198
49. Greef JM, Deuter M (1993) Syntaxonomy of Miscanthus × giganteus, vol 67. Blackwell, Berlin
50. Linde-Laursen I (1993) Cytogenetic analysis of Miscanthus 'Giganteus', an interspecific hybrid. Hereditas 119(3): 297–300
51. Surlock J (1999) Miscanthus – a review of the European experience with a novel energy crop. Oak Ridge National Laboratory, Oak Ridge
52. Walsh M, McCarthy S (1998) Miscanthus handbook. In: Tenth European bioenergy conference, Wurzburg, 1998. CARMEN Publishers
53. Clifton-Brown J, Long SP, Jorgensen U (2001) Miscanthus productivity. In: Jones MB, Walsh M (eds) Miscanthus for energy and fibre. James & James, London
54. Naidu SL et al (2003) Cold tolerance of C4 photosynthesis in Miscanthus × giganteus: adaptation in amounts and sequence of C4 photosynthetic enzymes. Plant Physiol 132(3):1688–1697
55. Naidu SL, Long SP (2004) Potential mechanisms of low-temperature tolerance of C4 photosynthesis in Miscanthus × giganteus: an in vivo analysis. Planta 220(1):145–155
56. Christian DG, Haase E (2001) Agronomy of Miscanthus. In: Jones MB, Walsh M (eds) Miscanthus for energy and fibre. James & James, London, pp 21–45
57. Lewandowski I et al (2000) Miscanthus: European experience with a novel energy crop. Biomass Bioenergy 19(4):209–227
58. Clifton-Brown J et al (2002) Modelled Biomass production potential of Miscanthus and actual harvestable yield as influenced by harvest time. In: 12th European Biomass conference and exhibition, Amsterdam
59. Heaton EA, Dohleman FG, Long SP (2008) Meeting US biofuel goals with less land: the potential of Miscanthus. Glob Change Biol 14(9):2000–2014
60. Wikberg S (1990) The genus Miscanthus: a summary of available literature. Project Agro-fibre. University of Lund, Sweden
61. Booth E, Batchelor S, Walker K (1996) An evaluation of the potential of fiber crops in Scotland. In: Ninth international conference on Jojoba and its uses and third international conference on new industrial crops and products, Catamarca, 1996
62. Harvey J, Hutchens M (1994) Progress in commercial development of Miscanthus in England. In: Biomass for energy, environment, agriculture and industry – Proceedings of the eighth EC conference, Elsevier Science, Oxford

63. Visser P et al (2001) Utilization of Miscanthus. In: Jones M, Walsh M (eds) Miscanthus for energy and fibre. James & James, London, p 218
64. Jefferson P et al (2002) Performance or American native grass cultivars in the Canadaian prairie provinces. Native Plants J 3:24–33
65. Hitchcock AS, US Department of Agriculture (1935) Manual of the grasses of the United States. Government Printing Office, Washington
66. McLaughlin S (1992) New switchgrass biofuels reserach program for the Southeast. In: Proceedings of the annual automotive technology development contractors' coordination meeting, Dearborn, 1992
67. Parrish DJ, Fike JH (2004) The biology and agronomy of switchgrass for biofuels. Crit Rev Plant Sci 24:423–459
68. Porter CJ (1966) An analysis of varitation between upland and lowland switchgrass (Panicum Virgatum L) in central Oklahoma. Ecology 47:980–992
69. Hopkins A et al (1996) Chromosome number and nuclear DNA content of several switchgrass populations. Crop Sci 36: 1193–1195
70. Gunderson CA et al (2008) Exploring potential U.S. switchgrass production for lignocellulosic ethanol. Oak Ridge National Laboratoy, Oak Ridge
71. Jung G, Shaffer J, Stout W (1988) Switchgrass and bluestem responses to amendment on strongly acid soil. Agron J 80:669–676
72. Hanson J, Johnson H (2005) Germination of switchgrass under various temperature and pH regimes. Seed Technol 27(2): 203–210
73. Stroup J et al (2003) Comparison of growth and performance in upland and lowland switchgrass types to water and nitrogen stress. Bioresour Technol 86:65–72
74. Brejda J et al (1993) Dependence of 3 Nebraska sandhills warm-season grasses in vesicular-arbuscular mycorrhizae. J Range Manage 46:14–20
75. Johnson N (1998) Responses of Salsola kali and Panicum virgatum to mycorrhizal fungi, phosphorus and soil organic matter: implication for reclamation. J Appl Ecol 35:86–94
76. Hsu F, Nelson C (1986) Planting date effects on seedling development of perennial warm-season forage grasses II. Seedling Growth. Agron J 78:38–42
77. Hsu F, Nelson C, Matches A (1985) Temperature effects on germination of perrenial warm-season forage grasses. Crop Sci 25:215–220
78. Vogel K (2004) Switchgrass. In: Moser LE, Sollenberger L, Burson B (eds) Warm-season grasses. ASA-CSSA-SSSA, Madison
79. Cossar R, Baldwin B (2004) Establishment of switchgrass with sorghum-sudangrass. In: Third Eastern native grass symposium, Omnipress, Chapel Hill, 2004
80. Zarnstorff M (1993) Physioecological effects of cultural and pesticide management on no-till establishment of switchgrass and seed dormancy. Dissertation Abstract International. Science and Engineering
81. McKenna J, Wolf D, Lentner M (1991) No-till warm-season grass establishment as affected by atrazine and carbofuran. Agron J 83:311–316
82. Wolf D et al (1989) No-till establishment of perennial, warm-season grasses for biomass production. Biomass 20:209–217
83. Brejda J (2000) Fertilization of native warm-seaon grasses. In: Anderson B, Moore K (eds) Native warm-season grasses: research trends and issues. Crop Science Society of America, Madison, pp 177–200
84. Hall KE, George JR, Riedl RR (1982) Herbage dry matter yields of switchgrass, big bluestem, and indiangrass with N fertilization. Agron J 74(1):47–51
85. Clark F (1977) Internal cycling of 15nitrogen in shortgrass praire. Ecology 58:1322–1333
86. Tin X et al (2006) Switchgrass as an alternate feedstock for power generation: integrated environmental, energy, and economic life-cycle analysis. Clean Technol Environ Policy 8(4):233–249
87. McLaughlin S et al (1999) Developing switchgrass as a bioenergy crop. In: Janick J (ed) Perspectives on new crops and new uses. ASHS Press, Alexandria
88. Sanderson MA et al (1996) Switchgrass as a sustainable bioenergy crop. Bioresour Technol 56(1):83–93
89. Thomason W et al (2004) Switchgrass response to harvest frequency and time and rate of applied nitrogen. J Plant Nutr 27:28
90. Schmer MR et al (2008) Net energy of cellulosic ethanol from switchgrass. Proc Natl Acad Sci 105(2):464–469
91. Comis D (2006) Switching to switchgrass makes sense. In: Agricultural research, USDA-ARS
92. Anderson B (2000) Use of warm-season grasses by grazing livestock. In: Anderson B, Moore K (eds) Native warm-season grasses: research trends and issues. Crop Science Society of America, Madison, pp 147–158
93. Moore K et al (2004) Sequential grazing of cool- and warm-season pastures. Agron J 96:1103–1111
94. McLaughlin SB, Adams Kszos L (2005) Development of switchgrass (Panicum virgatum) as a bioenergy feedstock in the United States. Biomass Bioenergy 28(6):515–535
95. Sanderson MA, Read JC, Reed RL (1999) Harvest management of switchgrass for biomass feedstock and forage production. Agron J 91(1):5–10
96. Entry JA, Watrud LS (1998) Potential remediation of 137Cs and90 Sr contaminated soil by accumulation in alamo switchgrass. Water Air Soil Pollut 104(3):339–352
97. Hohenstein W, Wright LL (1994) Biomass energy production in the United States: an overview. Biomass Bioenergy 6(3):161–173
98. Fike JH et al (2006) Long-term yield potential of switchgrass-for-biofuel systems. Biomass Bioenergy 30(3):198–206
99. Duffy M, Nanhou V (2002) Costs of producing switchgrass for biomass in Southern Iowa. In: Janick J, Whipkey A (eds) Trends in new crops and New Uses. ASHS Press, Alexandria

100. Vogel KP et al (2002) Switchgrass biomass production in the midwest USA: harvest and nitrogen management. Agron J 94(3):413–420
101. Vogel K et al (2006) Switchgrass for biomass: farm-scale production practices affect feedstocck costs and quanitities in the Northern Great Plains. In: Eighth symposium on biotechnology for fuels and chemicals, program abstracts, Nashville, 2006
102. Sanderson M et al (2004) Alternative uses of warm-season grasses. In: Moser L et al (eds) Warm-season (C4) grasses. ASA, CSSA and SSSA, Madison, pp 389–416
103. Parikka M (2004) Global biomass fuel resources. Biomass Bioenergy 27(6):613–620
104. Ragauskas AJ et al (2006) The path forward for biofuels and biomaterials. Science 311(5760):484–489
105. Ruark G et al (2006) Perennial crops for bio-fuels and conservation. USDA Forest Service/UNL Faculty Publications, 2006, p. 18
106. Stettler R et al (1996) Biology of populus and its implications for management and conservation. NRC Researc Press, Ottawa
107. Tuskan G. Popular poplars. trees for many purposes. Available from: http://bioenergy.ornl.gov/main.aspx. Accessed November 28, 2010
108. Demchik M et al (2002) Hybrid poplars as an alternative crop. Natural Resources Special Report
109. Walsh M et al (2003) Bioenergy crop production in the United States. Potential quantities, land use changes, and economic impacts on the agricultural sector. Environ Resour Econ 24:313–333
110. Amicheva BY, Johnston M, Rees KCJV (2010) Hybrid poplar growth in bioenergy production systems: biomass prediction with a simple process-based model (3PG). Biomass Bioenergy 34(5):687–702
111. Labrecque M, Teodorescu TI (2003) High biomass yield achieved by Salix clones in SRIC following two 3-year coppice rotations on abandoned farmland in southern Quebec, Canada. Biomass Bioenergy 25(2):135–146
112. Lattimore B et al (2009) Environmental factors in woodfuel production: opportunities, risks, and criteria and indicators for sustainable practices. Biomass Bioenergy 33(10): 1321–1342
113. Perez-Verdin G et al (2003) Woody biomass availability for bioethanol conversion in Mississippi. Biomass Bioenergy 33: 492–503
114. Pellis A, Laureysens I, Ceulemans R (2004) Growth and production of a short rotation coppice culture of poplar I. Clonal differences in leaf characteristics in relation to biomass production. Biomass Bioenergy 27(1):9–19
115. Goodrich M (2009) From the roots up, developing trees for sustainable biofuel. In: Michigan Tech News, 2009
116. Reidy S (2006) Purdue University Researchers Study poplar trees as feedstock for cellulose ethanol. BioFuels Journal. http://www.biofuelsjournal.com/articles/Purdue_University_Researchers_Study_Poplar_Trees_as_Feedstock_for_Cellulose_Ethanol-37114.html. Accessed November 28, 2010
117. Huang H et al (2009) Effect of biomass species and plant size on cellulosic ethanol: a comparative process and economic analysis. Biomass Bioenergy 33(2):234–246
118. Farrell A, Plevin R et al (2006) Ethanol can contribute to energy and environmental goals. Science 311(5760): 506–508
119. Davidson J (1993) Ecological aspects of Eucalyptus plantations. in regional expert consultation on eucalyptus. RAPA publication 1995
120. Iglesias T, Wilstermann D (2009) Global Eucalyptus Map (v 1.2). In: GIT forestry consulting's eucalyptologics: information resources on Eucalyptus cultivation worlwide, 2009
121. Groenendaal G (1983) History of Eucalyptus in California. In: Proceedings of a workshop on Eucalyptus, Sacramento, 1983. Pacific Southwest Forest and Range Experiment Station, Berkeley
122. Henter H (2005) Tree wars: the secret life of Eucalyptus. In Alumni. 2005, University of California, San Diego
123. Whitesell C et al (1992) Short rotation management of eucalyptus: guidelines for plantations in Hawaii. USDA Forest Service, Pacific Southwest Research Station, Albany
124. Stricker J et al (2000) Short rotation woody crops for Florida. University of Florida, Gainesville
125. Rockwood D et al (2008) Energy product options for Eucalyptus species grown as short rotation woody crops. Int J Mol Sci 9:1361–1378
126. Whitesell C, DeBell D, Schubert T (1988) Six-year growth of eucalyptus
127. Luzar J (2007) The political ecology of a "forest transition": Eucalyptus forestry in the Southern Peruvian. Ethnobot Res Appl 5:85–93
128. Pousajja R (1996) Eucalyptus plantations in Thailand. In: Kashio M, White K (eds) Reports submitted to the regional consultation on eucalyptus
129. Song Y (1992) Utilization of Eucalyptus in China. Appita 45(6):382–383
130. Steinbeck K, McAlpine R, May J (1972) Short rotation culture of sycamore: a status report. J Forest 70(4): 210–213
131. Skolmen R (1983) Growth and yield of some Eucalyptus of interest in California. In: Proceedings of a workshop on eucalyptus in California, Sacramento, 1983. USDA Forest Service, Pacific Southwest Forest and Range Experiment Station, Berkeley
132. Lull G (1908) A handbook for Eucalyptus planters, State Board of Forestry (ed), US Dept of Agriculture, Forest Service
133. Cremer K, Cromer R, Florence R (1978) Stand establishment. In: Hillis W, Brown A (eds) Eucalyptus for wood production. Commonwealth Scientific and Industrial Research Organization, Aulmlia, pp 81–135
134. Knudsen D, Yahner E, Carrea H (1970) Fertilizing Eucalyptus on Brazilian savannah soils. Commonw Forest Rev 49(1): 30–40

135. DeBell D, Whitesell C, Schubert T (1989) Using N_2-fixing Albizia to increase growth of Eucalyptus plantations in Hawaii. Forest Sci 25:64–75
136. De Jesus R, Dias G, Cardoso E (1992) Eucalyptus/leucaena mixture experiment – growth and yields. Biomass and Bioenergy, IPEF, 39:41–46
137. Shailaja R, Ravindranath N, Jagadish K (1991) Experiments in mixed species forestry. In: Annual symposium of bioenergy society, New Delhi, 1991
138. Elmore C (1983) Vegetation management in Eucalyptus. In: Proceedings of a workshop on Eucalyptus in California, Sacramento, 1983. Pacific Southwest Forest and Range Experiment Station, Berkeley
139. Arbogen (2010) Purpose grown trees as an economical and sustainable biomass feedstock. Available from: http://www1.eere.energy.gov/biomass/biomass2010/pdfs/biomass2010_track2_s2_wells.pdf
140. Sims R et al (2008) 1st to 2nd generation biofuel technologies: an overview of current industry and RD&D activites. International Energy Agency, Paris
141. Kinoshita C, Zhou J (1999) Siting evaluation for biomass-ethanol production in Hawaii. National Renewable Energy Laboratory, Golden
142. Stape J et al (2010) The Brazil Eucalyptus potential productivity project: influence of water, nutrients and stand uniformity on wood production. For Ecol Manage 259:1684–1694
143. Hubbard H, Kinoshita C (1993) Investigation of biomass-for-energy production on Molokai. Hawaii Naturall Energy Institute, Honolulu
144. Gonzalez R, Wright J, Saloni D (2010) The business of growing eucalyptus for biomass, Biomass Magazine. http://biomassmagazine.com/articles/3620/the-business-of-growing-eucalyptus-for-biomass. Accessed November 29, 2010
145. de Vries S et al (2010) Resource use efficiency and environmental performance of nine major biofuel crops, processed by first-generation conversion techniques. Biomass Bioenergy 34(5):588–601
146. Almodares A, Hadi M (2009) Production of bioethanol from sweet sorghum: a review. Afr J Agric Res 4:772–780
147. Koppen S, Reinhardt G, Gartner S (2009) Assessment of energy and greenhouse gas inventories of sweet sorghum for first and second generation bioethanol. Food and Agriculture Organization of the United Nations, Rome
148. Santana R, Barros N, Comeford N (2000) Above-ground biomass, nutrient content, and nutrient use efficiency of Eucalyptus plantations growing in different sites in Brazil. NZ J Forest Sci 30:225–236
149. Stape J, Goncalves J, Goncalves A (2001) Relationship btween nursery practices and field performances for Eucalyptus plantations in Brazil: a historical overview and its increasing importance. New Forest 22:19–41
150. Raven P (2009) Biodiversity: What to Do About It in an Age of Rapid Extinction. Presented at the International Plant Molecular Biology Symposium, St. Louis, MO

Biomass Energy Heat Provision for Cooking and Heating in Developing Countries

Ralph P. Overend
Golden, CO, USA

Article Outline

Glossary
Definition of the Subject
Introduction
Biomass Use in Stoves: Environmental Impacts
Combustion Principles and Their Application to Stoves
Health Effects of Biomass Cookstoves
Climate Change and Woodstoves
Findings and Discussion
Future Directions
Bibliography

Glossary

Biomass Biomass is defined as material of biological origin excluding material embedded in geological formations and/or transformed to fossil.

DALY Disability-adjusted life years or DALYs, a measure combining years of life lost due to disability and death.

GIS Geographic Information System which embodies a spatial data base and mapping capability.

GWP Global warming potential, a measure in carbon dioxide equivalent terms of the climate change potential of different compounds in the atmosphere.

HHV Higher heating value or Gross Heating Value (GCV), the energy released on complete combustion including the latent heat of the condensation of water produced in the combustion.

IEA International Energy Agency, a body of the OECD (Organization for Economic Co-operation and Development).

ICS Improved cookstove – a range of technical innovations to improve efficiency and mitigate emissions in an affordable package.

Lambda Symbol λ = mass of air supplied/mass of air required for complete combustion to water and carbon dioxide.

LHV Lower heat of combustion – see HHV, the difference is that the LHV does not include the latent heat of condensation.

LPG Liquefied petroleum gas customarily propane and or butane.

MDG Millennium development goals of the United Nations, an ambitious set of targets for human development of the poorest people in the world.

NMHC Non-methane hydrocarbons or sometimes.

NMVOC Non-methane volatile organic carbon.

PIC Products of Incomplete Combustion which include reactive organic molecules and carbon monoxide, as well as unburnt carbon, which is a particulate often called soot.

WBT Water boiling test, a widely agreed upon laboratory protocol to measure the efficiency of cookstoves under standardized conditions.

Definition of the Subject

Biomass cookstoves are at the nexus of food and energy poverty in developing countries. Superficially, biomass-fueled cookstoves are simple objects that contain a fire and transfer energy to a surface or vessel in which food can be cooked and water boiled. However, the simplicity is illusory because just as in industrial economies the energy needed to service the food chain from farm or garden, to fork or chopstick, is a large and significant burden on the household economy especially in poorer households. This burden is not just economic, but impacts social, humanitarian, and equity issues that directly affect the lives of more than one third of humanity, and impact on the global environment, via the link with climate change gas emissions.

The key challenge is that very low cost biomass-fueled small appliances are an unsatisfactory technology for efficient and nonpolluting combustion. Over 70 years ago the move to improve stoves started in India, with one of the first to reach national distribution being the Magan Chula with a mud and pottery mix construction [1] developed in 1947 by the All India Village Industrial Association (AIVIA), Maganwadi. AIVIA was initiated by Gandhi to further rural development in India [2]. The development was in a context of providing employment opportunity for potters as well as to improve the lives of women through efficiency and cleanliness improvements of biomass-fueled stoves in the kitchen. A similar ethos of multiple objectives is behind the recently announced public-private initiative "Global Alliance for Clean Cookstoves" coordinated by the UN Foundation [3] with the goal of "save lives, improve livelihoods, empower women, and combat climate change by creating a thriving global market for clean and efficient household cooking solutions."

This entry explores the technology background to these issues and the possibility of their amelioration.

Introduction

In the OECD countries, the logistics chain from the farm gate to the fork on the table is a major component of the economy and the energy system. Agriculture itself is a major consumer of energy, but surprisingly it is in the post-harvest system that there is a larger consumption of energy. This is found in the chain: food processing and brand marketing (processing); food and ingredient packaging (packaging); freight services (transportation); wholesale and retail trade and marketing services (wholesale/retail); away-from-home food and marketing services (food service); and household food services (households). Using the national input-output tables exemplarily for the US economy the energy use in an industrial society from the farm to the table is about 15% of the total primary energy use [4]. Processing, food services, and households account for 60% of the food-related energy flows, while agriculture represents less than 15%. With 110 million households in 2002, the food-related energy consumption (after the farm gate) is almost 110 GJ per household. With an average household size of 2.6, the per capita usage is 42 GJ.

In the rural rice economies of Southeast Asia, with populations still preparing most of their food at home, food has its origins locally without the major packaging, transportation, and wholesale/retail components of the chain in industrialized countries, and this results in a food chain demand that is much less than that of industrialized countries. Absent Leontief style input-output tables for developing countries suggests that the

estimates that correspond to the US case are hard to obtain. A 90-country average of 4.1 GJ caput^{-1} for the individual energy use in the post-harvest system was found in the middle of 1980s [5]. However, as would be expected the values varied widely by country with as low as 4 GJ caput^{-1} for Africa, and a high of 7.75 GJ caput^{-1} in Latin America. By far, the largest share of energy in the post-harvest system in developing countries is in cooking – representing 85% in Africa, and only 61% in Latin America, with the average being 74%.

The large difference in the per capita energy consumption post harvest in developing countries versus that of the USA, and the very high proportion that is involved in household cooking serves to emphasize the critical role of cookstoves in development.

The developing country nexus of energy, nutrition, health, indoor and outside air pollution, and degradation of the environment has received considerable attention in the last 60 years. In India, the Magan Chula was a response to indoor air pollution though OECD country interest did not become significant until there were concerns of deforestation [6]. This was then followed by assessments of health, gender issues, social equity, and more recently the global warming potential of the emissions from biomass burning. The impact of these is very dependent on the number and quality of biomass cookstoves and the quantity of fuel that is used. Such data is very hard to obtain and the available estimates are a combination of survey data as well as model assumptions.

The International Energy Agency (IEA) estimates that about half of the population of developing countries, 2.5 billion people, relies on biomass in the form of fuelwood, agricultural residues, and animal dung, and the biofuel charcoal to meet their needs for cooking. In many countries, these fuels meet over 90% of household energy needs. These needs are primarily for cooking, followed by heating, and lighting. The developing country household energy use is estimated at 45 EJ y^{-1}, and the biomass demand is about 32 EJ. This is often described as traditional biomass use, in order to distinguish it from the approximately 15 EJ of "Combustible renewables and waste" an IEA classification that includes municipal solid waste, as well as biomass. The majority of this 15 EJ is used at high efficiency in the heat, power generation, and industrial sectors of the developed economies [7, 8].

Despite the large amount of primary energy going to cookstoves, the efficiency of use is quite low compared with cooking either with natural gas or LPG. The IEA has carried out the thought experiment of replacing biomass cookstoves by LPG estimating that 1.3 billion people would require only 30 Mt of LPG or 1.5 EJ suggesting that replacement of all biomass in cooking by efficient fossil-fueled appliances would have a negligible effect on world fossil hydrocarbon consumption [8]. Another estimate by Goldemberg, quoted by [9], is that 2 billion people would need 120 million tons of oil equivalent or approximately 5 EJ. The efficiency of LPG stoves versus the three-stone stove system is about four times greater with minimal emissions other than carbon dioxide.

Another way to make this biomass fuel estimate is from the bottom up, working from the types of device, and their efficiencies. Cookstoves at the household scale typically have a steady state power output in the range of 1–3 kW, with peak outputs near to 10 kW. Institutions such as schools and hospitals, as well as food vendors and restaurants also use household scale stoves and larger units going up to 50 kW thermal output. The duty cycle for cookstoves ranges from one or two meals a day, say 3 h of usage total, in many households, to much longer for diets that include long cook cycles, as well as in institutional settings.

The estimates of the number of people dependent on solid fueled appliances vary widely. Especially as it has long been recognized that there is an economically driven energy stack [10], such that the poorest at the bottom of the stack will likely use only biomass, while a person much further up the economic ladder may still have a biomass-fueled stove, but will also use electricity, natural gas, LPG, or charcoal. In the business world, the energy stack would be described as a portfolio to reduce risk, since when there is no electricity, or the supply of LPG is unavailable, then there is biomass to fall back on. The World Bank considers that the number using biomass is three billion, with one billion almost totally dependent on biomass fuels [11].

If an average daily duty cycle of 4 h, and assuming a 2 kW output from a 10% efficient stove then with one billion people in an average household of four persons, the annual energy demand is 7.3 PWh or 26 EJ.

This value is of course a floor value for the impact, as many more people with presumably a lower duty cycle will also be using biomass. Thus, both bottom up assumptions and the combination of survey measurements and statistics arrive at a very similar value for the range of primary energy consumption by cookstoves 30–45 EJ.

The need for cooking is integral to the life of modern humans. Evolution over the last 200,000 years has taken the species *Homo*, from a diet of fruits and tubers, with some meat, to a diet in which for many meat is rare and cereals such as rice, corn, and wheat and starch staples such as potato and cassava are the primary source of metabolic energy [12]. Cooking is essential for the modern human to be able to access the energy of hard-to-digest foods, render them more palatable, eliminate toxins, and reduce microbiological risks [13, 14]. The extent or duration of cooking and the temperatures needed for different tasks such as boiling, simmering, frying, and baking unleavened bread are very diverse, and this is reflected in the range of stoves from the Plancha type used for maize foods such as tortillas, to the Chula type used primarily with water boiling and simmering applications.

It has been chosen not to illustrate this entry with any figures showing either the three-stone stove or the various ICS as it is more important to understand the behavior and dynamics of the cookstove as a class. There are literally hundreds of ICS in literature and a good selection of photographs and drawings (some with dimensions) are to be found within the references [1, 15, 16].

To make foods nutritious, the cooking times will also be an important determinant on the fuel consumption. An interesting study of the effect of altitude on the wood consumption when cooking beans highlights the importance of cooking time on the energy consumption in preparing cooked food [17].

Biomass Use in Stoves: Environmental Impacts

The environmental impact of the biomass stove sector ranges from local resource depletion, due to overconsumption, through to indoor and outdoor pollution. Indoor pollution is associated with a horrendous health impact mainly on women and children and is the subject of a separate section, while external pollution has local, regional, and global impacts.

Biomass Resource Impacts

The primary issue is the balance between biomass growth and productivity, and the rate of consumption. The production of wood fuels is generally local and regional with only limited trade between regions on account of the large bulk and low energy density of solid wood. Other biomass fuels such as stalks and straws or dung have even lower energy densities. Local demands depend on population density and have seasonal variations. Access to the wood fuel resource will depend on the availability of land, proximity of woodland and forest, and their access rules. The latter will depend on the nature of the forest land, whether it is for wild life conservation, water catchment protection, and the timber production policies of the national and regional governments.

While there have been many popular press stories of deforestation attributed to fuelwood use – more empirical research has revealed a much more nuanced story with the number of users that are using wood and other biomass resources non-sustainably much less than anticipated. A partnership between the FAO Forest Products Service and the Ecosystem Research Center (CIECO) of the National University of Mexico (UNAM) has generated and tested a GIS based system for identifying and determining priority areas for intervention to support wood energy and bioenergy planning and policy formulation. The tool that was developed WISDOM (Woodfuel Integrated Supply/Demand Overview Mapping) [18] has been applied to Southeast Asia. In combination with poverty data, the tool enabled the identification of areas where poor rural and urban populations that depended primarily on wood fuels for their subsistence energy supply would be likely to suffer severe shortages thus allowing the appropriate poverty alleviation and energy development planning.

The Southeast Asia analysis [19] showed how difficult it is to generalize about both malnutrition and woodfuel; while in 2000 one quarter of the region's population, almost 66 million people live in concomitant conditions of poverty and wood fuel deficit, 35% are in areas of high to medium surplus wood fuels.

The most vulnerable countries in the region are Cambodia and Vietnam, while most other countries had only pockets of poverty and deficit – mostly those with better biomass resources as in Lao PDR, Malaysia, and Yunnan PRC.

Given the land use competition in many regions, there has been extensive research into wood species with characteristics suitable for combustion, with rapid growth and low nutrient requirements being desirable qualities [20, 21].

Much work has been done on the consumption side and in the historical evolution of cookstove development. The initial emphasis was on efficiency for the production of Improved Cookstoves (ICS) in relation to the perceived fuel wood shortages.

Cookstove Efficiencies and the Design of Improved Cookstoves (ICS)

The efficiency of biomass-fired cookstoves is low especially when compared with large scale solid fuel–fired industrial and power generation units.

What exactly is meant by efficiency? There are two stages in the chain from the biomass fuel to the cooked meal. The first stage is the generation of the heat from the chemical energy content of the fuel. The second stage is the transfer of this heat by convection, conduction, and/or radiation to the food or the container in which the food is being cooked. Each of these stages has potential and actual losses, which need to be minimized.

In the first stage, the key is to have complete combustion in which all of the carbon and available hydrogen contents of the fuel are converted to carbon dioxide and water, and all of the resulting energy is transferred to the heat carrier. Combustion of fuels containing carbon and hydrogen in air (oxygen) only takes place in the gas phase, and as will be seen this has serious consequences for how efficient the process will be. This means that solid and liquid fuels, such as wood and oil, have to produce fuel gases either by pyrolytic decomposition or volatilization for the combustion to take place. This is explained from the combustion of gaseous fuels to the combustion of solid fuels.

In the case of a gaseous fuel, the fuel and the air are premixed before going into the combustion chamber. Normally, this premixing will be realized at a specific air to fuel ratio (expressed as Lambda, λ, and defined as mass of air supplied/mass of air required for full combustion to water and carbon dioxide). Typically, the value of λ for a premixed fuel is less than unity. Such a premixed fuel is sometimes described as a rich fuel mixture when λ is below 1.0. Additional air is then supplied in the combustion chamber as secondary air to ensure combustion under conditions of excess air – at which point the combustion is lean with λ above 1.0. A typical gas flame in a domestic appliance is a laminar flow premixed flame in which after ignition, a flame front moves down toward the supply of premixed gas at a very high temperature – the flame is stabilized when it reaches the burner tip. Natural gas flames in air are usually transparent to blue in color, and the heat transfer from the flame is to the heated mass of combustion products that are diluted by the surrounding air. There is little or no radiative heat loss as the flame is not a black body. The chemistry in the flame provides energy to dissociate the fuel into free radicals, which then react with the oxygen in the air to provide heat. So long as the thermal energy provided by the free radical reaction with oxygen exceeds the energy needed to dissociate the fuel, the flame is stable.

When a liquid fuel is burnt, the situation is more complex as the liquid must now be evaporated and the fuel vapor mixed with air prior to ignition. The liquid fuel has to be well dispersed in the air as it evaporates to avoid local areas of fuel rich composition. So most pressurized liquid fuel burners at a small scale have a heated section that serves to evaporate the fuel. Thereafter, the flame is similar in concept to a gas flame. The alternative arrangement is to have a wick to draw the liquid fuel up to a heated area in which the fuel evaporates and is mixed with air to burn. In developing countries both pressurized and wick stoves are commonly fueled with kerosene, with serious safety impacts due to the large boiling point range and relatively low flashpoint of paraffinic fuels which are sometimes diluted with even more volatile gasoline [22].

Solid fuels such as coal and biomass in the form of wood, straw, or dried dung have to undergo an even more significant transformation. The solid fuel has to be heated to a point that it breaks down to generate fuel vapors and fuel gases. Then the flame has to provide heat continuously to the solid to continue generating the fuel that burns. Observation of open wood fires will

show that the flames are strongest when the faces of two burning logs are opposed to each other so that the radiative heat from the combustion is trapped between them. Conversely, if a flaming piece of wood is pulled from the fire, after a short while the flames will be extinguished and the wood will only smoulder producing copious amounts of noxious smoke. This challenge of maintaining a radiative heating environment to burn solid fuels either at a small scale or in an open fireplace has been known for a long time. When open fireplaces were common in the 1960s in the USA, patents to maintain logs in a triangular pitch configuration to enable this radiative trapping to encourage good combustion were quite common [23].

Ignition and combustion of solid fuels is complex, in part because very often the first process that has to take place is drying the material – if the fuel has moisture it has to be removed before the temperature can rise to the point where the solid will pyrolize or break down with heat. Also not all of the wood or biomass is combustible, as it also contains chemical elements that appear after combustion as ash – typically the oxides of calcium, silicon, and aluminum, along with potassium and sodium. In the living biomass, these elements have played a major role in the growth process and some have been picked up from the soil as dust. In any case, they are inert and consume heat without producing fuel gases to burn.

The heating value of a fuel is measured as either the higher (sometimes called gross calorific value) heating value (HHV) or the lower heating value (LHV; i.e., net heating value). The difference between the two is the fate of the water produced in the combustion step. If it is condensed – as happens in the bomb calorimeter that is used to measure fuel energy content. The HHV is greater than the LHV by the heat of condensation of water. Normally combustion systems only yield the LHV energy, as there is no water condensation.

The heating values of fuels are given in Table 1. Here the large effect of water content between green firewood and the air dried versus the bone-dry wood can be seen. This emphasizes the need for dry fuels in biomass combustion. Moisture not only lowers the heating value, but also increases the lambda needed and reduces the maximum flame temperature.

More accurate values of biomass composition and heating values can be obtained from the database (http://www.ecn.nl/phyllis) which enables access to be made to different species, which have different heating values as a result of compositional differences. At the level of cookstove technology such differences will not be crucial in determining performance.

Biomass Energy Heat Provision for Cooking and Heating in Developing Countries. Table 1 LHV of fuels on a mass basis

Fuel type	Heating value (LHV) MJ kg^{-1}
Wet or "Green" firewood; 50–60% moisture	8
Cow dung – dried	10
Tree residues: twigs, leaves, forest duff, etc.	13
Agricultural residues: straws, stalks usually dry	13
Air dried firewood; 20% moisture	15
Densified briquettes: straw, rice husk, bagasse	16
Oven or "Bone" dried firewood; $<$10% moisture	20
Charcoal	28
Charcoaled briquettes	30
Kerosene	44
Biogas (55:45 methane: carbon dioxide volume)	16
LPG – liquid propane gas	46

Adapted from [24]

Combustion Principles and Their Application to Stoves

To get the highest efficiency out of a solid fuel requires that all of the chemical energy is realized by converting all of the carbon and available hydrogen into carbon dioxide and water. At a very large scale, such as industrial boilers, it is possible to construct the combustion section separate from the heat transfer section, even though they are closely coupled. The enclosed combustion section can also be carefully controlled with respect to the addition of air to achieve combustion with the minimum of excess air. It turns out that the

key variables to control are the temperature (T), the duration of the combustion (time = t), and efficient mixing of the air oxidant with the solid fuel derived flammable volatiles (turbulence = τ).

Temperature is very important since the rate of oxidation kinetics of the gaseous fuel species increase with temperature, while the higher temperatures feedback heat by radiation to the solid fuel surfaces encouraging pyrolysis and cracking of the solid fuel, and increasing the rate of surface reactions. Thus, at its simplest, the temperature has to be very high, and under conditions of lambda close to unity, the adiabatic flame temperatures for biomass can be above 1,600°C. Such high temperatures are a challenge to many metals, with softening temperatures of mild steel occurring around 550°C despite a melting point of 1,525°C. Even stainless steel AISI 310 can only operate safely at 1,100°C under small strain. Thus, to maintain high temperatures, it is typical to have refractory lining in boilers and combustors to protect the structural steels used.

While ceramic refractories have high melting points, they have to be specified very carefully against the mineral matter in the solid fuel. Alkali metals (especially potassium and sodium) can form new refractory compositions with different properties including phase changes that spall the refractory thus losing the protection. The mineral matter in biomass can also react to form low melting point eutectics that form fluxes and bond the mineral matter together in a slag or clinker that causes mechanical problems in combustion systems.

Time is the second component of successful combustion, because sufficient time is needed for reactions to go to completion. The time required is a complex relationship with the partial pressure of oxygen and temperature. When both are high, the reaction time is short. At lower temperature conditions, the reactions may well not go to completion, with for example the oxidation of organic compounds resulting in products of incomplete combustion (PIC) which include reactive organic molecules and carbon monoxide, as well as unburnt carbon which is a particulate often called soot.

Turbulence or mixing is essential if individual volumes inside of the combustion zone are not to locally consume the available oxygen (i.e., $\lambda < 1.0$), and result in PIC formation. Turbulence is also an aid to heat transfer after improving the convective heat transfer from the combustion chamber to the cooking vessel or boiler ensuring that the average temperature is as high as possible.

A separate concept related to turbulence is also important, and that is draft. Blowing on the embers of the fire will rapidly increase the temperature from black to bright red and accelerate the combustion. In the industrial scale boilers, there is forced draft with quite high air velocities meeting the solid fuel and combustible gases in the range of 5–10 m s^{-1}. In domestic heating appliances a critical component is the chimney – an insulated tube after the firebox. Here the low density of the hot post combustion flue gases (typically half to one third that of the ambient air) causes the external atmospheric air to enter the firebox and propel the flue gases up the chimney until they are dispersed in the atmosphere. Long chimneys and very high temperatures can create a very high pressure differential and thus a high air flow – controlling the area of the air inlet to the firebox can create high linear velocities or a high draft to enhance the temperature. Kilns to produce lime from limestone ($CaCO_3$) and even iron bloom production has been carried out in dry wood–fired shaft furnaces [25]. The key to high temperatures whether in a kiln or a firebox is to have a high rate of heat release relative to the rate of heat loss through the walls by conduction and radiation, and in the flue gas.

Once the chemical energy of the solid fuel has been released through combustion, the next challenge is to efficiently transfer that heat to the cooking vessel, boiler, or process.

Heat transfer has several modes, namely, radiative, conductive, and convective transfer. A very high temperature source above 1,000°C can radiatively transfer a large amount of heat per unit area of a surface to its surroundings. Heat can also be conducted through the walls of the combustion system to the required application. Finally the heat can be transferred convectively from the combustion gases to the recipient. As an example in an industrial boiler, the water cooled walls remove radiative heat from the combustion volume, and the first bank of boiler tubes are heated both by radiation and by convective heat transfer, while the downstream tubes receive convection heat. Convective heat transfer depends on the velocity of the gas flow, the

exposed surface area, and whether or not the flow is turbulent or laminar.

The Rocket stove [26] is an example of an innovation that responds to the physical and chemical requirements for good combustion and heat transfer at a small scale in an interesting and relatively low tech way. The design starts with a single opening for both fuel and the air for combustion – thus allowing the control of lambda, while the number of sticks (i.e., the rate of fuel) addition to the combustion chamber controls the rate of heat release in a relatively small volume. The combustion chamber is a small insulated volume at the base of an insulated chimney. The chimney provides the draft to draw in the combustion air, and the fuel burn out is completed as the primary combustion products traverse its length. Heat transfer is obtained at the end of the chimney and requires a good fit between the pot and the chimney termination – sometimes aided by a pot skirt (an annulus that channels the flue gases up and along the sides of the pot) to ensure that the hot flue gases transfer their heat by convective heat transfer. Such stoves have a much-improved efficiency and also burn out much more of the PIC resulting in lowered carbon monoxide and particulate emissions.

Biomass Cookstoves

The most frequent form of biomass combustion is in a simple hearth. The fuel, wood, straw, or other material placed on the ground is ignited and then fuel is added to the fire, while some sort of support for a cooking vessel is arranged over the fire to receive the heat to boil water, or provide a surface for cooking breads, or grilling meats and fish. Prehistoric hearths provide evidence of cooking and social life to archeologists, and the carbon remaining in the hearth is often used to carbon date the site as far back as 750,000 years [27].

The hearth can be against a back wall, or free standing with what is a common arrangement of three stones in a triangle, with two of the three stones set in the ground for stability, and the third moveable to accommodate different sizes of cooking vessel. Three-stone stoves are easily assembled, easy to regulate, burn a wide variety of fuels, shapes and sizes, and also provide light, heat, and social focus [6] today as they did in prehistoric times. The power output is controlled by the addition or withdrawal of fuel. If the fuel is wood, then sticks or branches are fed from the edges toward the center where the flame is. While the flames move out from the center to the edges along the sticks, their radial spread is limited as the burning zones get separated and no longer have coupled heat transfer by radiation, and effectively are extinguished. In order to maintain constant power output, fuel has to be constantly moved toward the center of the fire. Since the flame is in the open, windy conditions will cause fluctuations in the output by literally blowing the heat out from under the cooking pot. The low cost of the three-stone stove is because it uses widely available materials, and the efficiency under controlled conditions can be surprisingly high. However, the emissions as smoke and PIC are also very high. In engineering terms, the fuel on the ground with fire in a radius of 5–20 cm is a very small-scale approximation of what is called a pool fire. Since the fuel is confined to a stationary surface, the air supply for combustion has to sweep over the top of the fire and can only be drawn in through the buoyancy of the hot combustion gases. The convective force and the large external area for the fresh air access combine to provide a very small draft velocity. So, temperatures are low, and like in a diffusion flame there are fuel rich (i.e., high in PIC) zones separated from the mixed combustion zones. In nearly all ICS, the fire is supported on a grate with the idea that primary air flows through the fuel bed with λ below 1. Then above the fuel bed, secondary air (sometimes preheated) is added to complete the combustion with λ above 1 to get around the issues of the pool style buoyant combustion of the three-stone fire.

Efficiency of cookstoves is a surprisingly difficult thing to measure and or define. The topic will be returned to later. However, here it is supposed that it is measured by the heat delivered to the pot relative to the heat input to the stove. For example, three-stone efficiencies are described of up to 20–30+% under laboratory conditions in which the rate of fuel supply is controlled and the pot distance to the fire is varied for maximum heat transfer [1, 28].

One of the most widely accepted measurements of stove efficiency, the Water Boiling Test (WBT) originated with VITA [29]. Basically, the test

methods simulate the high power phase needed to bring a food to a boil, followed by a low power (i.e., to simmer) process of cooking while using water to simulate food.

Stove performance is measured by its Percent Heat Utilized (PHU). Alternatively, the Specific Consumption (SC) can be specified. The Percent Heat Utilized of a stove is the percentage of heat released by the fire that is absorbed by the water in the pot. The Specific Consumption is the total quantity of wood used for the simulated cooking process divided by the amount of water "cooked." Results from tests for different stoves can be used to rank the stoves, and more usefully the development of a standardized test was important as researchers tried to understand the effect of different design parameters. Nevertheless, boiling water in a controlled laboratory setting is not likely to reflect the real world situation of cooking different foodstuffs in a home or institutional setting. The current accepted version of the boiling water tests is obtainable from ehs.sph.**berkeley**.edu/hem/hem/. . ./**WBT**_Version_3.0_Jan2007a.pdf. The experience of stove performance in the field can be correlated with the laboratory test. Other more realistic tests have been devised by many research groups under names such as CCT (Controlled Cooking Test) or the KPT (Kitchen Performance Test).

Table 2 summarizes the results not just of the Water Boiling Test (WBT) (3.0) but also of the WBT (4.0), which includes emissions testing of stoves (for WBT (4.0) see http://www.pciaonline.org/testing/wbtcomment).

In a series of tests of stoves without chimneys in five broad classes, the following results were obtained (Table 2).

The detailed results behind Table 2 are the median value and a range. Though, it should be noted that the number of stoves tested in each class is varied, and that outliers have been neglected. Tests on a smaller group of stoves show very similar performance thus showing the value of the WBT as a universal test tool in the design and evaluation of stoves [30]. The value for energy use in charcoal fired stoves is not that which was measured during the WBT, since charcoal is a biofuel with significant energy losses in its production. The measured WBT value of 20 MJ has been multiplied by 2.5 to reflect the energy lost during artisanal charcoal production.

Biomass Energy Heat Provision for Cooking and Heating in Developing Countries. Table 2 Summary of efficiency and emissions performance of several classes of wood-stove data derived from [15]

Stove type	MJ in WBT	CO (g)	PM (g)
Three stone	22+/−8	70+/−25	1.6+/−0.8
Simple ICS	15+/−5	50+/−10	2.5+/−2
Rocket	13+/−3	18+/−3	1.0+/−0.6
Gasifier	20+/−5	22+/−6	0.5+/−0.25
Forced air	10+/−1	5+/−2	0.1+/−0.05
Liquid/gas	8+/−2	5+/−2	< 10 mg
Charcoal	50–60*	100+/−20	0.25

*Correcting for the efficiency of charcoal production from fuelwood

What is clear from the results is that fan-assisted forced air circulation stoves using small wood pieces can achieve nearly the same performance in all three categories as a propane stove. The requirement for fuel preparation to small dry pieces may be a constraint in many circumstances. Typically, the size of the fuel particle should be below 10% of the combustion zone diameter and with the high draft of the forced air circulation stove the combustion zone is quite small with a very high rate of heat release.

Another feature of note is the scatter of performance in the simple stoves. It is known that dimensions for the combustion chamber and the fit with the pot are actually quite critical and that varying manufacturing tolerances can result in stoves that are marginally more efficient, but with very little improvement in the emissions profile over the three-stone stove.

Health Effects of Biomass Cookstoves

The impact of using wood-fired cookstoves indoors has been known for a long time with a strong and direct link to diseases such as COPD (Chronic obstructive pulmonary disease) and weaker links to low birth weights of children and premature cataracts in adults

exposed to open fires such as women and children. The topic did not start to rise to the top of the research agenda until a major analysis was published [31]. This was more fully quantified by the World Health Organization in a paper [32] which ranked indoor air pollution as 8th in the list of disease risk factors being responsible for 2.7% of the global burden of disease. The overall burden due to indoor air pollution from stoves measured in Disability-Adjusted Life Years or DALYs, (a measure combining years of life lost due to disability and death) is five times greater than that of outdoor air pollution. The statistics for high-mortality developing countries show that indoor air pollution is responsible for 3.7% of the overall disease burden.

A major call to action by the WHO [11] outlines in detail what the issues and their impacts have on the United Nations' Millennium Development Goals (MDG). There are no energy topics in the MDG, despite the lack of clean energy availability being the ultimate cause of many problems that are being identified as MGD. The proximate MDG goals affected are: #4 child mortality reduction; #3 gender equality and empowerment of women; #1 opportunities for income generation and extreme poverty eradication; as well as #7 on ensuring environmental sustainability.

The international community has rallied around this cause in the last decade. The Shell Foundation (www.shellfoundation.org) has a major program "Breathing Space" which takes the view that the indoor air pollution challenge has to be solved through market-thinking and private sector involvement. This is a break with former programs in which NGOs and governments have given away or subsidized ICS. There is a partnership with Envirofit International, a US not-for-profit organization to design and market a new range of improved stoves – and to find commercial partners to manufacture and distribute stoves. Their aim is to see 10 million stoves sold in five countries in the next 5 years.

The umbrella organization addressing the cookstove challenge is the Partnership for Clean Indoor Air (PCIA; www.pciaonline.org). Established in 2002 after the Johannesburg World Summit on Sustainable Development, the PCIA has garnered over 400 public and private organizations who contribute resources and expertise to address four critical areas: (1) meeting social and behavioral needs; (2) developing local markets; (3) improving technology design and performance; and (4) monitoring impacts and interventions.

Climate Change and Woodstoves

At first glance, the cookstove impact on global warming is the extent of the emissions of PIC. Many of which have a Global Warming Potential (GWP) many times that of carbon dioxide. However, that would be making the assumption that the entire emission of carbon dioxide from wood combustion in cookstoves was renewable. That is to say the biomass is regrown after harvesting, and without any direct land use change (dLUC) or indirect land use change (iLUC). The evidence presented earlier as well as many field observations show that some proportion of the wood extracted is in fact nonrenewable. In the extreme case of high demand and adverse climate changes almost all of the biomass fuels are nonrenewable as was the case in the Sahel in the 1970 and 1980 decades when population growth and the decadal shift of the tropical inter-convergence zone [33] created famine due to a drought in the Sahel [34]. Food and energy poverty were extreme across the entire southern boundary of the Sahara.

The situation in Africa was the reason for the heightened interest in biomass-fueled cookstoves in that period. Today it is clear that there is some degree of deforestation, and of land degradation in all areas with large scale use of biomass for heating and cooking, due for example to increased soil erosion. The extent of this nonrenewable biomass use is not known with certainty, and has to be estimated. The problem may in fact have a high degree of granularity with communities suffering shortages within a region that has overall a surplus of woodfuels [35]. For India, it is estimated that only 10% of the biomass used is nonrenewable [36].

The emission of PIC is in inverse relationship to the combustion efficiency of the appliance. A linear correlation has been shown with an $R^2 = 0.79$ in different appliances and using different biomass fuels from fuelwood to straw [37]. Also the ratio of carbon monoxide to carbon dioxide produced has been investigated to be a good proxy for the measurement of efficiency, which as described above is not very easy to accomplish.

The PIC themselves range from atmospherically short-lived complex organic molecules (often described

as non-methane hydrocarbons NMHC, or non-methane volatile organic carbon NMVOC), and carbon monoxide with small GWP to long-lived actors with high GWP, substances such as methane.

There are two other biomass combustion sources of GWP, nitrogen oxides (NO_x) and particulates. The major concern on nitrogen oxides is with N_2O di-nitrogen oxide which has a GWP of 386 times that of CO_2. However, it is difficult to correlate NO_x emission from small combustors, as there are contributions from the biomass fuel (Fuel bound nitrogen) and from the temperature and time of combustion oxidizing part of the nitrogen from the air. The temperature and time are related to the actual stove design and its operation with respect to lambda.

Smoke (i.e., particulate emissions) is a major part of the health impact of non-ventilated stoves as well as having significant GWP. The size range of the particulate is very relevant. Large particles above 10 μm do not enter the respiratory system, and are relatively short lived in the atmosphere. Smaller particles (PM2.5; i.e., < 2.5 μm in diameter) can enter the pulmonary system, and are long lived as aerosols in the atmosphere (days to weeks). The atmospheric effects of the carbon in the smoke are still being debated. All biomass combustion with smoke (whether a forest or grass fire, or an open stove with low efficiency) generate organic compounds and black carbon. These agglomerates enter into the atmosphere and become aerosols. Black carbon aerosol absorbs light and contributes to warming, while the organic (white) aerosol reflects and cools the atmosphere. Eventual deposition of black carbon on glaciers will result in increased absorption of solar energy and increase mass loss. A review of black carbon emissions [38] suggests that residential use, primarily in cookstoves burning coal and biomass, is the major source of black carbon and that the region itself is the major contributor of black carbon to the atmosphere. The South Asian atmospheric brown cloud (ABC) covers from the Arabian sea to the Southeast Asian region for the majority of the northern hemisphere winter, and is composed of a large number of aerosols including inorganic dust. However, a major proportion is derived from biomass. The short lifetime of the black carbon in the atmosphere means that it has a short term 20 year-GWP of about 2,200 kg carbon dioxide equivalent while the 100 year-GWP is 500–680 (Table 2 in [38]).

The estimated 30–40 EJ y^{-1} of primary energy in biomass fuel use in cookstoves assuming there are no ICS, and that 10% of the carbon used is nonrenewable will have gross emissions of about 2.4–3.5 Gt CO_2 equivalent, if the cookstove was the three-stone. This is computed based on an overall efficiency from wood input to energy delivered in the pot of 10%. According to [39], the greenhouse gas emissions are about 800 kg GJ¯1 delivered, comprising about half black carbon, one quarter methane, 20% carbon monoxide, and some N_2O. This result is of course very sensitive to the assumptions, the stove performance envelope for efficiency and greenhouse gas emission components.

From Table 2, the general range of ICS efficiency is 1.5 times better than the three-stone while the CO and PM values are only somewhat different. The original data shows that many ICS provide efficiency gains, without a significant improvement in the emissions. Thus the bottom range of ICS stoves would lead to less primary energy consumption, but nearly all of the emission components would remain about the same, leading to a range of 1.3–1.6 Gt CO_2 equivalent. Moving to the rocket stove (at a similar efficiency to the ICS) with its known threefold reduction in CO and its almost halving of PM would change the equation to greenhouse gas emissions of about 350 kg GJ^{-1} delivered, further reducing the emissions to around 0.70–1.0 Gt CO_2 equivalent.

The LPG case with its greater efficiency and ignoring the carbon dioxide equivalent costs of the fuel distribution system needed to replace woodstoves would have an impact of CO_2 equivalent of 181 kg GJ^{-1} of delivered energy – for a total impact in replacing biomass primary energy of about 0.4 Gt CO_2 equivalent. The forced air biomass stove would also achieve LPG like performance on efficiency, methane, and carbon monoxide, though the particulate would still be about 10 times larger than the LPG stove, but one tenth that of the simple ICS.

Table 3 summarizes the assumptions above to arrive at the estimated greenhouse gas emissions of the biomass-fueled cookstove use. Without an accurate basis for estimating the effect of nonrenewable and unsustainable biomass removals, the following assumptions have been made. The delivered energy to the global cook pot is assumed to be 3 EJ y^{-1}. If the entire stove population was the three-stone fire at 10%

Biomass Energy Heat Provision for Cooking and Heating in Developing Countries. Table 3 Estimation of the total emissions of CO_2 equivalent for four different stove scenarios

Stove	Basis Efficiency	Primary energy EJ	Fraction NR	NR-CO_2 Gt	kg CO_2-equivalent per GJ delivered CH_4	N_2O	CO	BC	Total emissions Gt CO_2 equivalent Emissions	Including NR C
3-stone	0.1	30.0	0.30	0.89	189.1	35.5	166	430	2.46	**3.35**
ICS	0.15	20.0	0.20	0.39	89.8	28.4	70.9	106	0.89	**1.28**
Fan-assist	0.5	6.0	0.05	0.03	90	0	8	20	0.35	**0.38**
LPG	0.55	5.5	1.00	0.36	0	10	0	0	0.03	**0.39**

NR nonrenewable biomass resource, *BC* black carbon, *NR C* nonrenewable carbon

efficiency (probably a low estimate) then the 30 EJ of input required would be unsustainable, with 30% of the biomass being nonrenewable. Increasing the efficiency to 15% for the lower end of the ICS population would require only 20 EJ of input and an estimated nonrenewable contribution of 20%. At the efficiency of the fan-assisted stoves only 5% is proposed as nonrenewable due more to local situations of fuel wood deficit rather than regionally.

Findings and Discussion

The domestic biomass cookstove as it exists today is responsible for a wide range of diseases and illnesses that rank it 8th in the list of human health hazards, and for humanitarian reasons this has to be mitigated. The economic cost of the biomass cookstove is also very large both to those directly affected, and through the impacts on the climate system. However, the local effect is hidden when the economy is not monetized. Illness, low productivity, and the time spent in wood and biomass collection by women and children are all components of this cost to the individual and society. And while climate change mitigation is also important, the likely level of greenhouse gas (GHG) is somewhere between 1.3 and 3 Gt of CO_2 equivalent, and this is less than 10% of the most recent global estimate of the total direct fossil fuel emissions of carbon dioxide at 30.8 Gt in 2009 [40]. Like the challenge of reducing the GHG impact of automobile use – the solutions involve the purchasing and use decisions of billions of people and are thus unlikely to be effective without major technological changes in the stove technology. There are advantages in combining society's response to both the health and climate challenges along with meeting the Millennium Development Goals [41].

The thought experiment of replacing all biomass-fired appliances with LPG, if carried out would remove the health impacts, and surprisingly it would also reduce the climate change impact as measured by total GWP of cookstoves by a factor of 4–5 despite the fossil carbon content of LPG. At the same time, the use of LPG would remove pressures on the natural environment due to wood harvesting.

This utopian solution is far away, and may never be realized. Even today, when the UN High Commission for Refugees has to meet humanitarian crises the energy source that is most often used is the biomass and wood resource available locally. The logistics and the direct costs make this the solution of choice for field kitchens and for family use in camps for internally displaced persons or refugees.

With a world population that is gradually urbanizing the number of people without access to modern energy should decrease, as it is much easier to serve the high population densities of cities and the peri-urban areas with electricity and gas. Nevertheless, the rural energy challenge will remain and will require ICS and wherever possible more efficient fuels.

However, as is well known, ICS diffusion has continued to meet many obstacles since the World Bank surveyed this question in 1994 [42]. Even an assessment from 1995 has its echoes today in the many programs that have tried and failed to gain the traction needed for wide scale dissemination [43]. More recent sources (e.g., [44]) emphasize that in less-developed countries

and especially in sub-Saharan Africa the majority, that is, 90% and 83% respectively lack access to modern fuels. Worse still given the initial concerns about the Sahel discussed in the introduction only 6% of those using traditional biomass in these regions have access to ICS.

The 60+ years of attempts to diffuse improved stoves and the extensive technical research of the last 2 decades have arrived at a single conclusion.

Simply put there is no easy low cost technological fix for unvented natural draft biomass-fueled cookstoves.

The theoretical and detailed practical background description above shows that at small scales of average thermal output around 2 kW for solid fuel combustion under natural draft conditions, the efficiencies are poor and emissions are higher than those recommended for 8 h exposures by the World Health Organization (WHO). Miniaturizing forced draft combustion with small particle size fuels can come close to LPG in efficiency and emissions but the fan, its electricity supply and maintenance as well as first cost means that for most of the population needing it, the infrastructure is probably just not there to support the technology. Even the diffusion of LPG stoves in the development context is challenging, and this is for a well defined product, with a very high acceptance by the middle class in urban areas in developing countries [45].

Technology is extremely hard to describe and to define but is clear that ICS technology is much more than just the stove or heating appliance and incorporates many other technologies in the background. The evolution of technology itself relies on technology in associated areas to be successful as outlined by [46]. The Stanford Program on Energy and Sustainable Development has attempted to address the question of stove technology adoption and reasonably enough arrives at three major topics: motivation to acquire new technology; affordability; and the magnitude of the change in lifestyle and attitudes required [47]. Despite going into each of the these areas and producing rational explanations, the Stanford study, and many prior studies omit to make the key observation about the potential community of users of ICS – many of the users are in countries that are failing and are members of the "Bottom Billion" identified by Paul Collier [48]. Curiously, Collier did not actually identify the countries other than they are mostly in Africa and Asia, but what he did identify are the issues that make them fail, the traps of: conflict; natural resources; and being landlocked. Hard-nosed solutions are also proposed that impact on the food and energy poverty issues; their intention is to put the countries on a growth pathway not an aid dependent pathway.

The history of the last 4 decades demonstrates that where stove programs work best is in growth economies such as India and China. The challenge is to translate this to the Bottom Billion who are more likely to be totally dependent on biomass. And the challenge is in many more areas of technology than just energy. The final observation is a quote from a Microsoft pioneer, Kent Toyama who went into the promotion of information technologies in development [49]. His findings clearly cover much more than ICT (information and communication technologies).

"The challenge of international development is that, whatever the potential of poor communities, well-intentioned capability is in scarce supply and technology cannot make up for its deficiency."

"This point may sound reasonable enough when stated in the abstract, but it has an important consequence for anyone expecting to save the world with technology: you can't... at least, not unless the technology is applied where human intent and capacity are already present, or unless you are willing also to invest heavily in developing human capability and institutions..."

Future Directions

Clearly all efforts to improve the kitchen conditions for the large population of women and children exposed to smoke have to be encouraged. The actions of the two major public-private initiatives in this area have to be supported.

Improved statistics on income poverty, food and energy poverty, and the use of GIS to pinpoint and intervene in areas of high environmental stress is needed through the enhancement and maintenance of integrated assessment systems such as WISDOM.

The rapid diffusion of alternatives to natural draft biomass stoves is essential whether it is of forced air biomass stoves or LPG burners. Both will reduce the exposure to pollutants both indoor and to the

atmosphere with respect to PIC and greenhouse gas (GHG) emissions. The natural resource implications are of course minimized while the GHG impact is also reduced significantly. While research to improve user safety and to optimize these systems is needed, even more research is needed in the entire logistics chain. Since experience to date shows that irrespective of cost to the user, and indeed some stove interventions have been highly subsidized, the net envelope of technologies involved require high investments in education and institutions to develop receptor capacity and ensure uptake of the clean burning technology.

The post second world war deployment of ICS has still not developed a universal and successful model for market deployment, nevertheless the current efforts have to be expanded while current and past programs have to be rigorously evaluated for lessons learned. However, it is also evident that natural draft ICS without chimneys have variable performance between different models, especially with respect to PIC and particulate emissions. An internationally recognized performance and certification process is needed if the use of ICS is in fact going to address the health-related problems of using biomass.

For the poorest billion or so users the cookstove problem is just one facet of a much larger problem of poverty and is associated with food and energy poverty and the need for implementation of the Millennium Development Goals to address these.

Bibliography

Primary Literature

1. De Lepeleire G et al (1981) A woodstove compendium. Eindhoven Institute of Technology, Eindhoven, p 377
2. IIT (2001) Detailed project report on setting up of national institute for rural industrialisation. Indian Institute of Technology Delhi, India, p 158
3. Cookstoves, G.A.f.C. 2010 (cited 2011 January); The Global Alliance for Clean Cookstoves is a public-private initiative to save lives, improve livelihoods, empower women, and combat climate change by creating a thriving global market for clean and efficient household cooking solutions. Available from http://cleancookstoves.org/
4. Canning P et al (2010) Energy use in the U.S. food system. USDA, Washington, p 39
5. Parikh JK, Syed S (1988) Energy use in the post-harvest food (PHF) system of developing countries. Energy Agric 6(4): 325–351
6. Eckholm E et al (1984) Fuelwood: the energy crisis that won't go away. Earthscan, London, p 103
7. IEA (2009) Key world energy statistics. OECD/IEA, Paris
8. IEA (ed) (2003) Energy for cooking in developing countries, in world energy outlook 2006. Organisation for Economic Co-operation and Development, Paris, pp 419–455
9. McDade S (2004) Fueling development: the role of LPG in poverty reduction and growth. Energy Sustain Dev 8(3):74–81
10. Masera OR, Saatkamp BD, Kammen DM (2000) From linear fuel switching to multiple cooking strategies: a critique and alternative to the energy ladder model. World Dev 28(12):2083–2103
11. Rehfuess E (2006) Fuel for life: household energy and health. World Health Organization Press, Geneva, p 42
12. Eaton SB (2006) The ancestral human diet: what was it and should it be a paradigm for contemporary nutrition? Proc Nutr Soc 65(1):1–6
13. Carmody RN, Wrangham RW (2009) The energetic significance of cooking. J Hum Evol 57(4):379–391
14. Jansen A et al (2008) Epidemiology of trichinellosis in Germany, 1996–2006. Vector Borne Zoonotic Dis 8(2):189–196
15. MacCarty N, Still D, Ogle D (2010) Fuel use and emissions performance of fifty cooking stoves in the laboratory and related benchmarks of performance. Energy Sustain Dev 14(3):161–171
16. Bhattacharya SC, Albina DO, Abdul Salam P (2002) Emission factors of wood and charcoal-fired cookstoves. Biomass Bioenergy 23(6):453–469
17. Bressani R, Chon C (1996) Effects of altitude above sea level on the cooking time and nutritional value of common beans. Plant Foods Human Nutr Formerly Qualitas Plant 49(1):53–61
18. Masera O et al (2006) WISDOM: a GIS-based supply demand mapping tool for woodfuel management. Biomass Bioenergy 30(7):618
19. Drigo R (2006) Wood-energy supply/demand scenarios in the context of poverty mapping. A WISDOM case study in Southeast Asia for the years 2000 and 2015. Food and Agriculture Organization, Rome, p 136
20. BOSTID (1980) Shrub and tree species for energy production. National Academy of Sciences, Washington, DC, p 234
21. Mead DJ (2005) Forests for energy and the role of planted trees. Crit Rev Plant Sci 24(5&6):407–421
22. Lloyd PJD (2002) The safety of paraffin and LPG appliances for domestic use. J Energy South Afr 13:56–61
23. Thompson AE (1981) Fire array and apparatus. U.S.P. Office, Editor, US Patent No. 4360001, p 4
24. UNHCR (2002) Cooking options in refugee situations: a handbook of experiences in energy conservation and alternative fuels. United Nations High Commissioner for Refugees – Engineering and Environmental Services, Geneva, p 47
25. Rehder JE (2000) The mastery and uses of fire in antiquity. McGill-Queens University Press, Montreal
26. Bryden M et al (2005) Design principles for wood burning cook stoves. EPA, Washington, p 40

27. Alperson-Afil N et al (2009) Spatial organization of hominin activities at Gesher Benot Ya'aqov, Israel. Science 326(5960):1677–1680
28. Bussmann PJT (1988) Woodstoves: theory and applications in developing countries. Technische Universiteit Eindhoven, Eindhoven, p 174
29. Baldwin SF (1987) Biomass stoves: engineering design, development, and dissemination. VITA, and Center for Energy and Environmental Studies, Princeton University, Arlington, p 281
30. Jetter JJ, Kariher P (2009) Solid-fuel household cook stoves: characterization of performance and emissions. Biomass Bioenergy 33(2):294–305
31. Smith K (1987) Biofuels, air pollution and health: a global review. Plenum Press, New York
32. WHO (2002) The world health report 2002: reducing risks, promoting healthy life. World Health Organization, Geneva, p 230
33. Rowell DP (2003) The impact of Mediterranean SSTs on the Sahelian rainfall season. J Climate 16(5):849–862
34. Batterbury S, Warren A (2001) The African Sahel 25 years after the great drought: assessing progress and moving towards new agendas and approaches. Global Environ Change 11(1):1–8
35. Johnson M et al (2009) Quantification of carbon savings from improved biomass cookstove projects. Environ Sci Technol 43(7):2456–2462
36. Venkataraman C et al (2010) The Indian national initiative for advanced biomass cookstoves: the benefits of clean combustion. Energy Sustain Dev 14(2):63–72
37. Edwards RD et al (2003) Models to predict emissions of health-damaging pollutants and global warming contributions of residential fuel/stove combinations in China. Chemosphere 50(2):201–215
38. IRG (2010) Black carbon emissions in Asia: sources, impacts and abatement opportunities. United States Agency for International Development (USAid), Washington, DC, p 72
39. Bond T, Venkataraman C, Masera O (2004) Global atmospheric impacts of residential fuels. Energy Sustain Dev 8(3):20–32
40. Friedlinigstein P et al (2010) Update on CO_2 emissions. Nat Geosci 3(12):811–812
41. Haines A et al (2009) Public health benefits of strategies to reduce greenhouse-gas emissions: overview and implications for policy makers. Lancet 374(9707):2104–2114
42. Barnes DF et al (1994) What makes people cook with improved biomass stoves?: a comparative international review of stove programs, Energy series. International Bank for Reconstruction and Development, Washington, DC, p 60
43. Kammen DM (1995) Cookstoves for the developing world. Sci Am 273(1):72–76
44. Legros G et al (2009) The energy access situation in developing countries a review focusing on the least developed countries and sub-saharan Africa. United Nations Development Programme, New York, p 142
45. Bates L (2009) Making LPG stoves accessible for low income communities in Kassala, Sudan. In: Rai K, McDonald J (eds) Cookstoves and markets: experiences, successes and opportunities. GVEP International, London, pp 31–33
46. Arthur BW (2009) The nature of technology: what it is and how it evolves. Free Press, New York, p 246
47. Slaski X, Thurber M (2009) Research note: cookstoves and obstacles to technology adoption by the poor. Freeman Spogli Institute for International Studies, Stanford University, Stanford, p 8
48. Collier P (2008) The bottom billion: why the poorest countries are faiing and what can be done about it. Oxford, Oxford University Press, p 209
49. Toyama K (2010) Can technology end poverty? Boston Review

Books and Reviews

Babcock and Wilcox Company (2005) Steam its generation and use, 41st edn. Babcock and Wilcox Company, Charlotte
http://lists.bioenergylists.org/mailman/listinfo/stoves_lists.bioenergylists.org and its archives
http://go.worldbank.org/XDCT0ZVU50
The Aprovecho Research Center. http://www.aprovecho.org/lab/home
The HEDON household energy network. http://www.hedon.info/
Partnership for Clean Indoor Air (PCIA). www.pciaonline.org

Biomass Energy Heat Provision in Modern Large-Scale Systems

Ingwald Obernberger[1,2,3], Friedrich Biedermann[1,2]
[1]Bios Bioenergiesysteme GmbH, Graz, Austria
[2]BIOENERGY 2020+ GmbH, Graz, Austria
[3]Institute for Process and Particle Engineering, Graz University of Technology, Graz, Austria

Article Outline

Definition of the Subject
Introduction
Characteristics of Biofuels and Combustion Principles
Industrial Combustion Technologies
Summary
Combustion-Based Power Generation Processes
Emissions from Combustion and Ash-Related Problems
Future Directions
Bibliography

Definition of the Subject

Combustion of solid biomass is the oldest and most mature technology for the production of heat and the main source for the provision of renewable heat today. The applications of biomass combustion comprise a wide range from domestic combustion units with installed capacities of a couple of kW to district heating plants in the MW range and industrial combined heat and power units up to a nominal boiler capacity of 590 MW_{th} [1].

Biomass is the most important renewable energy source in the European Union. In the field of energetic utilization of solid biomass, combustion is the most advanced and market-proven application. Consequently, the energetic use of solid biomass is primarily based on biomass combustion at presence. Biomass combustion technologies cover fixed-bed, fluidized bed, and pulverized fuel combustion systems. They are currently available for different types of biofuels covering a wide range of plant capacities. Concerning plant size, the different applications of biomass combustion can be divided into small-scale biomass combustion systems (capacity range below 100 kW_{th}), medium-scale combustion systems (capacity range between 100 kW_{th} and 20 MW_{th}), large-scale combustion systems (capacity range above 20 MW_{th}), and co-firing of biomass in coal-fired power stations (capacity range usually some 100 MW_{th}).

Emission of pollutants from biomass combustion is due to either incomplete combustion or the release and conversion of fuel-bound elements. Incomplete combustion can lead to high emissions of not fully oxidized pollutants such as CO, C_xH_y, soot, and PAH. Relevant improvements to reduce these emissions have been achieved by optimized furnace design and process control; but there are still further improvements possible in many cases. The release and conversion of pollutants such as NO_x, SO_x, HCl and particles are formed as a result of fuel constituents (e.g., N, K, Na, Pb, Zn, Cl, S). Primary measures such as air staging and fuel staging offer a certain potential for NO_x reduction, which is increasingly used nowadays. Regarding particle emissions, so far only secondary measures (like particle precipitation units) are effective but only economically viable for medium and large-scale units. Further efforts and developments are needed for emission reduction and for plant optimization as well as for the development of combustion technologies for non-wood fuels. In this respect especially energy crops and agricultural as well as industrial biomass residues are of relevance.

This chapter describes the present state of technology and current developments regarding modern medium and large-scale biomass combustion systems.

Introduction

Combustion is the most widely applied technology for heat and power production from solid biofuels at present. Several technologies exist, which are available in the size range from domestic heating of a couple of kW thermal capacity up to industrial combined heat and power production of several hundred MW thermal capacity. The traditional biomass combustion technologies are designed and operated to produce heat. However, the importance of combined heat and power production is increasing [2]. Power production is commercially performed by steam turbines and steam engines in large-scale combustion plants and by organic Rankine cycles for medium-scale applications, while technologies such as Stirling engines and micro-turbines are options for the use in the small scale (below 100 kW_{el}).

The current European utilization of biomass combustion is mainly applied to the following processes:

- Heat generation in small-scale domestic applications for space heating and cooking
- High-temperature heat production in medium- and large-scale applications for district and process heat supply (e.g., district heating networks, wood processing industries, drying purposes)
- Steam production for driving steam turbines as well as for combined heat and power (CHP) applications in large-scale units
- High-temperature heat production for power or combined heat and power supply using heat carriers (e.g., thermal oil, air) in medium and large-scale units.

In recent years, the thermal utilization of solid biomass for heat and electricity production has gained importance. Within the European Union (EU) in particular, biomass is the most relevant renewable energy source and thus contributes substantially to the CO_2 emission reduction targets defined within the Kyoto protocol.

Within the EU, several political measures have been initiated with the aim of supporting the utilization of renewable energies including the Res-e Directive (2001), the EU Biomass Action Plan (2005), Energy and Climate Change Package (March 2007), and the Renewable Energy Directive (June 2009). Within the scope of these measures the following targets have been defined:

- 20% renewables by 2020
- 20% reduction of greenhouse gas emissions by 2020
- 20% increase of energy efficiency by 2020
- 10% increase in biofuels by 2020

Figure 1 shows the estimated primary energy consumption and total turnover of biomass combustion plants in the EU for 2008 as well as the outlook for 2020. The calculations are based on the present market [3–7] and the assumption that the EU 2020 targets will be achieved [8]. The results show that an average market growth rate of approx. 8.3% p.a. is expected. The overall market volume will grow up to 260% and the primary energy consumption from biomass will more than doubled until 2020.

Biomass energy is used for different purposes in various countries. While the markets in Sweden, Denmark, and Finland are directed toward large-scale applications (above 20 MW_{th}), the focus elsewhere in Europe is on small (below 100 kW_{th}) and medium-scale (0.1 till 20 MW_{th}) systems.

This chapter explains relevant characteristics of biomass fuels and combustion principles, summarizes the most common concepts of combustion technology for solid biomass fuels used in medium and large-scale combustion today, and gives a short overview about possible combustion-based technologies for power production. In addition, emissions from combustion of solid biomass fuels and ash-related problems are discussed and research and development trends are presented. Co-combustion of solid biomass with waste or coal is not covered in this report [9, 10].

Characteristics of Biofuels and Combustion Principles

Characteristics of Biofuels

The chemical composition of biofuels can vary concerning both, the concentrations of the main elements (C, H, O, N) as well as the ash content respectively the concentrations of ash-forming elements. The ash content can be seen as a guiding parameter indicating increased ash-related problems with raising ash content. However,

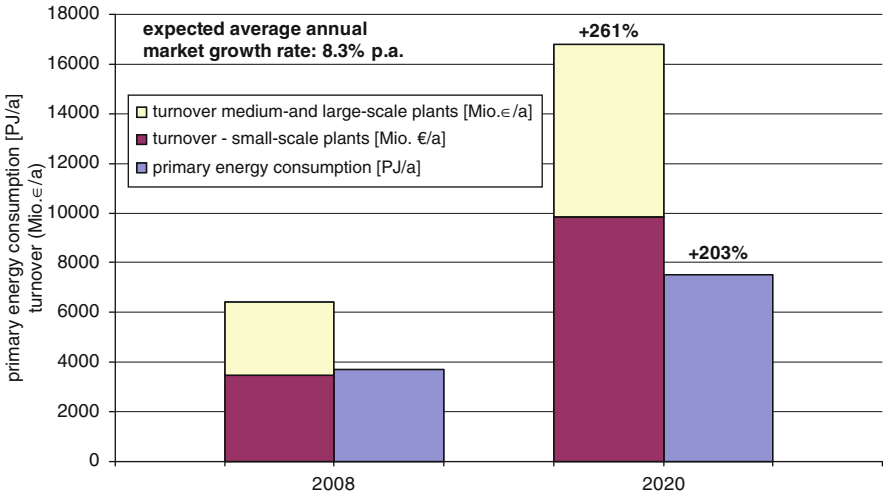

Biomass Energy Heat Provision in Modern Large-Scale Systems. Figure 1
Estimated primary energy consumption and total turnover of biomass combustion plants in the EU for 2008 and outlook for 2020 (Explanations: small, medium, and large-scale plants considered; small-scale plants: nominal boiler capacity below 100 kW_{th}; calculations based on present market and achievement of EU 2020 targets [3–8]

detailed information about the single ash-forming elements is needed in order to evaluate a biofuel with respect to different ash-related problems that can occur. Thereby also interactions between these elements have to be considered. Below some specific characteristic parameters of biofuels, which can be taken as a basis for the evaluation of a fuel are summarized.

Table 1 shows important physical properties of solid biofuels and their effects on the combustion process and the plant design. The moisture content of the fuel provides information concerning the general applicability of a certain fuel in a combustion process and its storability.

Biomass Energy Heat Provision in Modern Large-Scale Systems. Table 1 Combustion-relevant characteristics of solid biomass fuels – physical properties

Properties	Effects
Moisture content	Storability, dry matter losses, NCV, self-ignition, plant design
NCV, GCV	Fuel utilization, plant design
Volatiles	Thermal decomposition behavior
Ash content	Dust emissions, ash manipulation, ash utilization/ disposal, combustion technology
Ash melting behavior	Operational safety, combustion technology, process control system, hard deposit formation
Fungi	Health risks
Bulk density	Fuel logistics (storage, transport, handling)
Particle density	Thermal conductance, thermal decomposition
Physical dimension, form, size distribution	Hoisting and conveying, combustion technology, bridging, operational safety, drying, formation of dust
Amount of fines	Fuel feeding, particle entrainment
Abrasion resistance (wood pressings)	Quality changes, segregation, fine parts

The ash content has to be considered concerning the de-ashing system, ash storage, ash utilization, the grate design as well as the fact that a high ash content lead to higher entrainment of ash particles from the fuel bed with the flue gas and consequently to increased deposit formation, erosion, and particulate matter emissions. Therefore, it is an important parameter to be considered during plant design.

The ash melting behavior of ash mixtures is characterized by the content and by the melting temperatures of the single ash-forming elements respectively their compounds. Si, Ca, and Mg increase and K, Na, and P as well as Cl decrease the ash melting temperature. The ash melting behavior affects the combustion technology and the process control system and is an important factor concerning deposit formation and operational safety.

The bulk density of the fuel has also to be considered concerning fuel transport, storage, and feeding systems.

The amount of fines is relevant concerning the appropriate selection of the combustion technology and the process control. Regarding small-scale systems, the amount of fines is also of big relevance concerning the fuel feeding system (e.g., this is a quality parameter for pellets). In medium and large-scale plants the amount of fines is an important factor regarding particle entrainment (i.e., they can cause strain formation and incomplete burnout).

Table 2 shows combustion-relevant chemical properties of solid biofuels. For a complete characterization of biomass fuel content of C, H, O, and N as well as the gross calorific value (GCV) should be determined since they provide basic information concerning the general applicability of a certain fuel in a combustion process and regarding the energy content of a fuel. The N content is of special relevance concerning NO_x emissions. Moreover, ash-forming elements have to be divided into nonvolatile elements such as Si, Ca, Mg, Al and Fe, semi-volatile elements such as P and Mn, and rather volatile elements such as K and Na. During combustion semi-volatile and especially volatile elements are partly released from the fuel to the flue gas and react with other elements such as S, Cl, or CO_2 in the flue gas. Major ash-forming elements originate either from the biomass (plant) itself or from

Biomass Energy Heat Provision in Modern Large-Scale Systems. Table 2 Combustion-relevant characteristics of solid biomass fuels – chemical properties

Properties	Effects
Carbon (C)	GCV (gross calorific value)
Hydrogen (H)	GCV (gross calorific value), NCV (net calorific value)
Oxygen (O)	GCV (gross calorific value)
Chlorine (Cl)	HCl-, PCDD/F emissions, corrosion, lowering of ash melting temperature
Nitrogen (N)	NO_x-, N_2O-emissions
Sulfur (S)	SO_x- emissions, corrosion
Fluor (F)	HF emissions, corrosion
Potassium (K)	Corrosion (heat exchangers, superheaters), lowering ash melting temperature, formation of aerosols, ash utilization (plant nutrients)
Sodium (Na)	Corrosion (heat exchangers, superheaters), lowering ash melting temperature, formation of aerosols
Magnesium (Mg)	Increase of ash melting temperature, ash utilization (plant nutrients)
Calcium (Ca)	Increase of ash melting temperature, ash utilization (plant nutrients)
Phosphor (P)	Ash utilization (plant nutrient), ash melting, aerosol formation
Heavy metals	Emissions, ash utilization, formation of aerosols

impurities such as soil, stones, and residues from the preprocessing of the fuels. Elements such as P, K, and Na, for example, are part of the cell matrix of plants and elements such as Ca and Si are embedded in the plant fibers. In wood fuels usually Ca is the dominating major ash-forming element while in herbaceous biofuels significantly higher Si contents prevail.

Subsequently, the resulting sulfate, chloride, and also carbonate compounds may form fine particles by nucleation (formation of aerosols) or condense on already formed aerosols and coarse fly ash particles as well as on heat exchanger surfaces (ash deposit formation). In most fuels mainly K and Na are involved in these processes. In P-rich fuels also a part of the organically bound P is released to the flue gas and is involved in aerosol and deposit formation mainly via the formation of KPO_3, P_2O_5, and P_4O_{10} [11].

Minor ash-forming elements (i.e., Zn, Pb, Cd, Cu, Cr, Co, Ni, Mo, As, Sb, Hg, Tl) are mainly of interest concerning problems with too high gaseous and particle-bound heavy metal emissions as well as regarding the ash utilization. Moreover, the presence of heavy metal chlorides in ash deposits can significantly reduce the melting temperatures of the deposits thus leading to increased deposit formation and corrosion rates.

S and Cl are relevant elements concerning gaseous emissions (SO_x, HCl), fine particle (aerosol) formation, as well as ash deposit formation on boiler tube surfaces. Ash deposits are mainly formed by alkali metal salts such as K_2SO_4 and KCl. High Cl-contents of the fuel therefore also increase corrosion-related problems especially due to ash deposits with high Cl-contents. Moreover, Cl reduces the ash melting temperature of deposits. Due to these deposit formation and corrosion-related issues impact of the S- and Cl-contents of the fuel on the superheater surface temperatures (steam temperatures) in steam boilers is given. Furthermore, it has to be taken into account that increasing S and Cl concentrations in the flue gas result in a change of the dew point of the flue gas, which has to be considered concerning possible condensation in the heat exchangers and the flue gas cleaning systems.

Figure 2 exemplary shows how the chemical composition and the ash content of different solid biomass fuels can vary. The ash contents for bark and waste wood are high and even higher for straw while the ash content of pure wood fuels is comparably low. The sulfur content is high in straw and waste wood. The lowest sulfur contents are found in wood chips. The chlorine and potassium content of herbaceous fuels is considerably higher than of woody fuels, which directly affect aerosol formation and ash melting. The big deviation between different biomass fuels concerning their contents of ash-forming elements clearly underlines the relevance of considering the fuel-specific properties during plant design.

Figure 3 shows relevant guiding parameters which can be derived from the chemical compositions of different solid biofuels. An important guiding

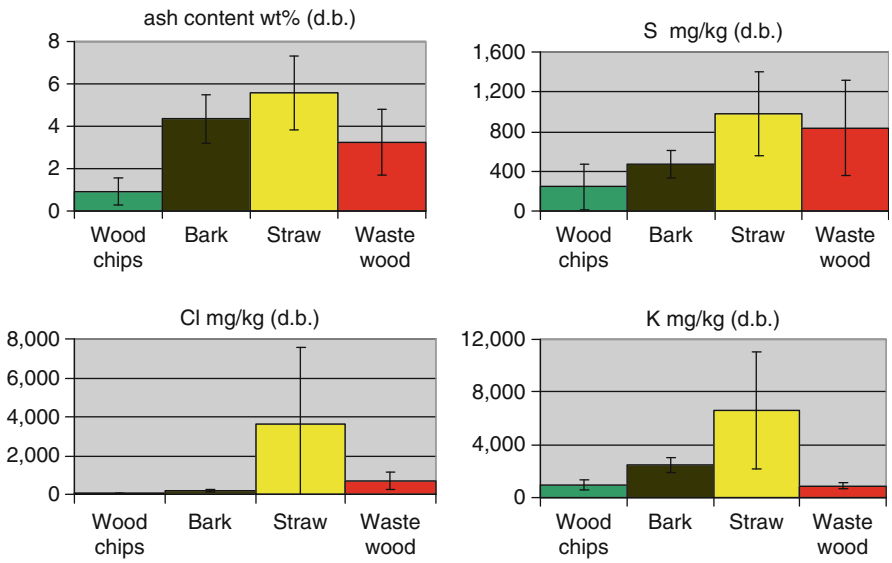

Biomass Energy Heat Provision in Modern Large-Scale Systems. Figure 2
Chemical compositions of different solid biomass fuels – ash, S, Cl, K

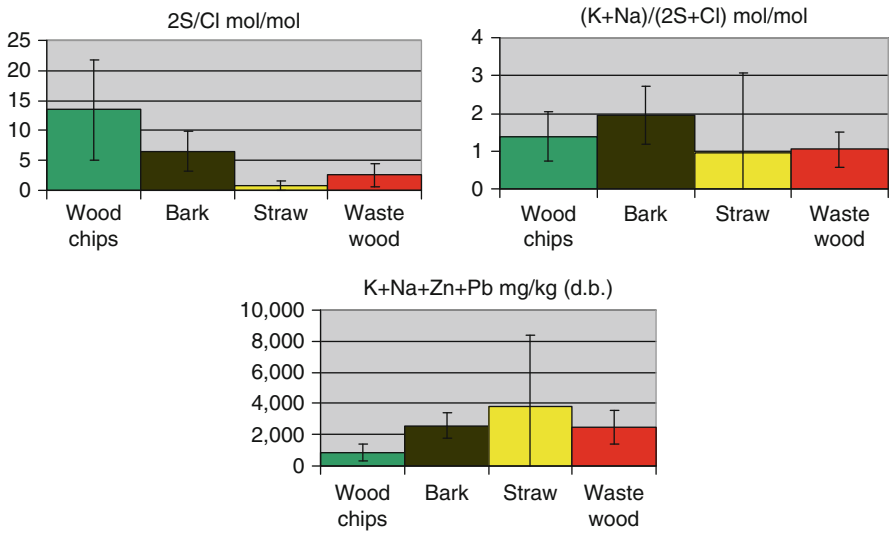

Biomass Energy Heat Provision in Modern Large-Scale Systems. Figure 3
Chemical compositions of different solid biomass fuels – relevant guiding parameters

parameter is the molar ratio (K + Na)/(2S + Cl). During combustion S and Cl preferably form alkaline (K and Na) sulfates and chlorides (S also forms Ca and Mg sulfate). Cl and S, which are not bound by these elements, form gaseous emissions, namely, HCl and SO_x. A molar ratio of (K + Na)/(2S + Cl) > 1 indicates a surplus of alkaline metals. Therefore, for high molar ratios of (K + Na)/(2S + Cl) lower HCl and SO_x emissions have to be expected, since most of the S and Cl is expected to be bound in the ash.

A molar ratio of 2S/Cl > 1 indicates an increased formation of alkaline sulfates, whereas a molar ratio of 2S/Cl < 1 indicates the preferred formation of alkaline chlorides. As corrosion-related problems on heat exchanger surfaces are depending on the Cl content of the ash deposits, a low molar ratio of 2S/Cl increases the risk of corrosion.

The elements K, Na, Zn, and Pb are the most relevant aerosol-forming elements in biomass fuels. With increasing concentration of these elements in a biomass fuel the probability of the release of ash-forming elements during combustion rises and therefore aerosol formation as well as deposit formation increase as well. However, the formation of ash vapors during combustion is not proportional to the concentration of these elements in the fuel since chemical reactions with other elements (e.g., Si) as well as the gaseous atmosphere and the combustion temperature significantly influence the release behavior.

Combustion Principles

In the ideal case, combustion represents a complete oxidation of the solid organic part of the fuel into the gases CO_2 and H_2O. This conversion occurs in different stages or steps, starting with the drying of the fuel particles followed by pyrolysis/gasification and the final oxidation of the charcoal and the flue gases (Fig. 4).

In order to achieve a combustion that is as efficient as possible, each of these combustion steps must be

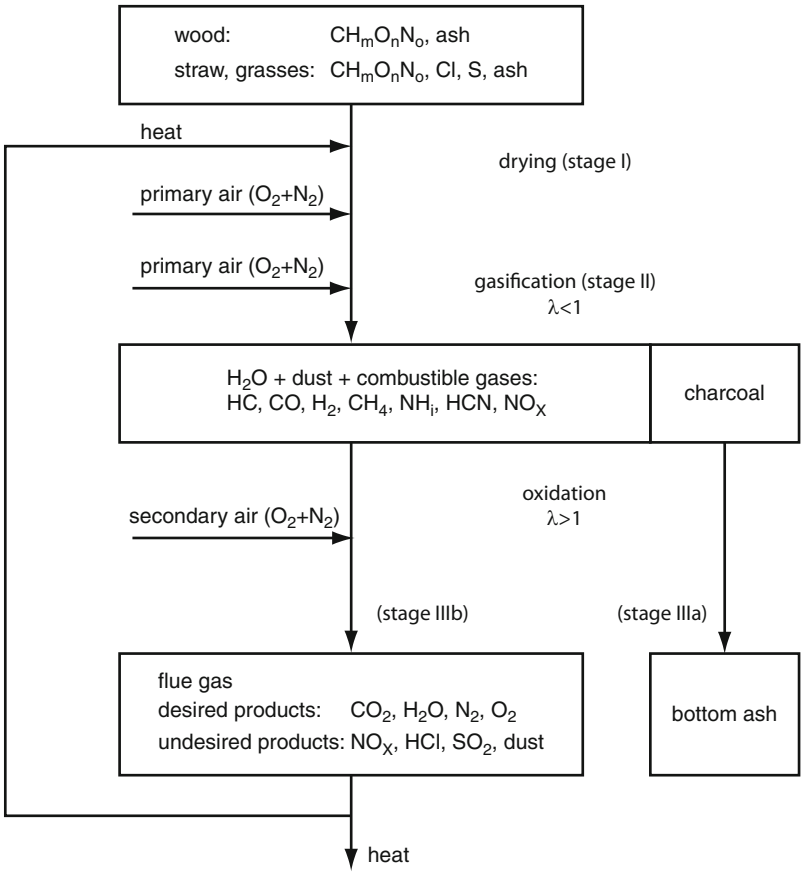

Biomass Energy Heat Provision in Modern Large-Scale Systems. Figure 4
Process of biomass combustion – principle [12]

optimized within the combustion technology implemented. After the step of drying (vaporizing H_2O) the main controlling parameter of the combustion process is the ratio between the amount of air added and the amount of air (oxygen) necessary for a complete combustion of the combustible parts of the fuel, the λ (excess air) factor.

At λ below 1, incomplete oxidation of the fuel (gasification) takes place and only a part of the energy of the fuel is converted into thermal energy. Adding too much air (λ >> 1) will cool down the process, leading to incomplete combustion and thermal losses. Thus the theoretical optimum of the combustion process is at a lambda equal to 1. But in reality this point is difficult to obtain due to mixing constraints between the fuel, flue gas and the air added. Thus, depending on the combustion technology utilized, a total λ between 1.1 to 1.8 in large-scale and 1.5 to 2.0 in medium-scale applications is common in order to achieve a complete combustion.

A lower total λ can be achieved by separating the combustion stages into different locations in the furnace and thereby increasing the retention time for reactions and also the possibility of optimized control. This type of separation, the so-called staged combustion, is shown in Fig. 5, where the drying (I), pyrolysis/gasification (II) and the oxidation of the char (III a) take place in different zones on and above the grate (primary combustion chamber). Then the flue gases are completely oxidized by addition of secondary air in the secondary combustion chamber (III b).

Industrial Combustion Technologies

The characteristics and the quality of biomass as a fuel vary widely, depending on the kind of biomass and the pretreatment technologies applied. For example, the moisture content of the fuel as fed into the furnace may vary from 25 to 60 wt% (w.b.) (bark, sawmill by-products) or drop below 10 wt% (w.b.) (pellets, dry wood processing residues). Also, the ash sintering temperatures of biofuels may extend over a wide range (600–1,200°C) [14, 15] and the particle shapes and sizes can be manifold. Fuel quality can be influenced and improved by suitable (costly) pretreatment technologies, like drying, chopping, and pelletizing.

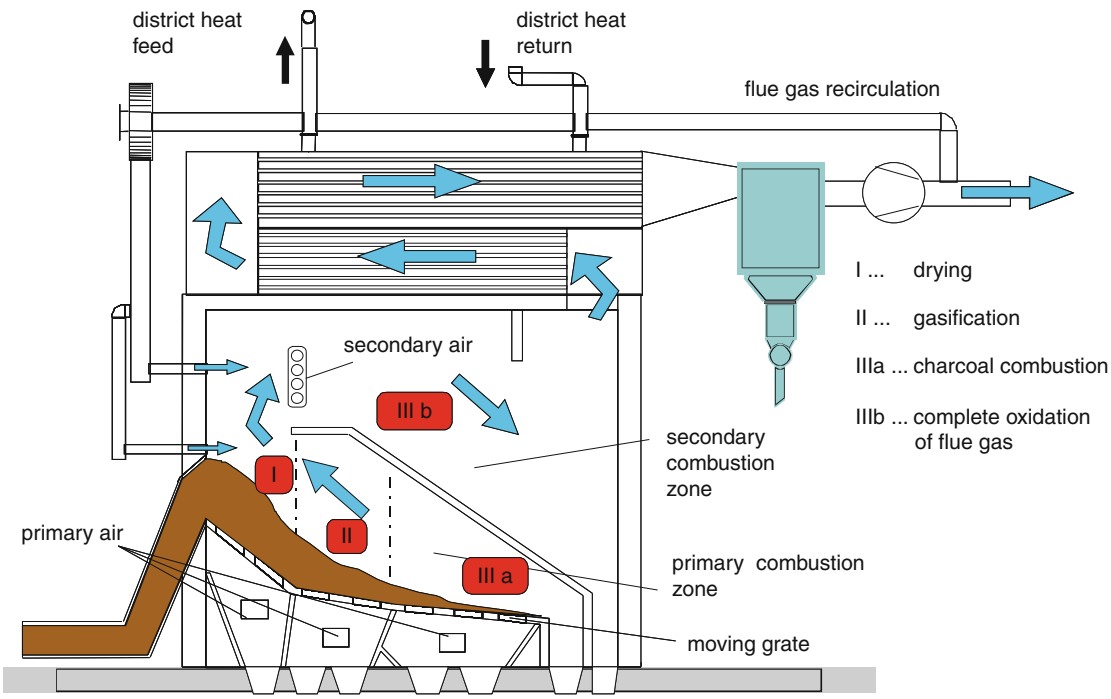

Biomass Energy Heat Provision in Modern Large-Scale Systems. Figure 5
Process of biomass combustion – allocation of the different stages of combustion in a grate furnace [12, 13]

The selection and design of a biomass combustion system is mainly determined by the characteristics of the fuel to be used, the local environmental legislation, as well as by the costs and the performance of the equipment. Another important factor is the size of the plant and the decision whether a heat only or a CHP application should be implemented.

Furthermore, the fuel characteristics can be influenced in order to fulfill the technological and environmental requirements of a given combustion technology by appropriate pretreatment systems. The most suitable technology package therefore can vary from case to case. Generally, due to *economy-of-scale* effects concerning the complexity of the fuel-feeding system, the combustion technology, and the flue gas cleaning system, large-scale systems usually use low-quality fuels (with inhomogeneous fuel characteristics concerning e.g., moisture content, particle size, and ash melting behavior), while high-quality fuels are necessary for small-scale systems in most cases.

While wood is a suitable fuel regardless of the size of the combustion plant, herbaceous biomass is almost entirely used in medium and large-scale plants. The same is true for urban waste wood and demolition wood, in particular due to the need for an efficient flue gas cleaning for the abatement of toxic pollutants (e.g., heavy metals, chlorine compounds).

Accordingly, biomass combustion technologies are divided into

- Small-scale (domestic) combustion, defined as units used for heating or cooking up to a capacity of about 100 kW
- Medium and large-scale industrial combustion, defined as systems used for process heat production, district heating as well as combined heat and power production (CHP) in units larger than 100 kW up to several hundred MW_{th}.

Medium and large-scale combustion systems are typically equipped with mechanical or pneumatic fuel-feeding systems and process control systems supporting fully automatic system operation. In general, the larger the combustion unit the more flexible it becomes regarding the quality of the biofuels used. Thus solid biofuels used in medium and large-scale biomass combustion units comprise not only wood, but also bark, energy crops, agricultural waste products, urban waste wood, and in some cases mixtures of these.

In principle, the following combustion technologies can be distinguished (Fig. 6):

- Fixed-bed combustion
- Bubbling fluidized bed combustion
- Circulating fluidized bed combustion
- Dust combustion

The basic principles of these technologies are shown in Fig. 6 and described below [13, 16].

Fixed-bed combustion systems include underfeed stokers and grate furnaces. Primary air passes through a fixed bed, in which drying, gasification, and charcoal combustion takes place. The combustible gases produced are burned after secondary air has been added, usually in a combustion zone separated from the fuel bed.

Within a fluidized bed furnace, biomass fuel is burned in a self-mixing suspension of gas and solid-bed material into which combustion air enters from below. Depending on the fluidization velocity, bubbling fluidized bed and circulating fluidized bed combustion can be distinguished.

Dust combustion is suitable for fuels available as small particles (average diameter smaller 2 mm). A mixture of fuel and primary combustion air is injected into the combustion chamber where the combustion takes place while the fuel is in suspension. The gas burnout is achieved after secondary air addition. Variations of these basic technologies are also available (e.g., combustion systems with spreader stokers and cyclone burners).

Fixed-Bed Furnaces

Below selected fixed-bed furnaces are discussed in detail.

Underfeed Stokers In underfeed stoker units the fuel is feed into the combustion chamber by screw conveyors from below and is transported upward on an inner or outer grate. Outer grates are more common in modern combustion plants because they allow for more flexible operation and an automatic ash removing system can be attained more easily. Primary air is supplied through the grate, secondary air usually at the entrance to the secondary combustion chamber.

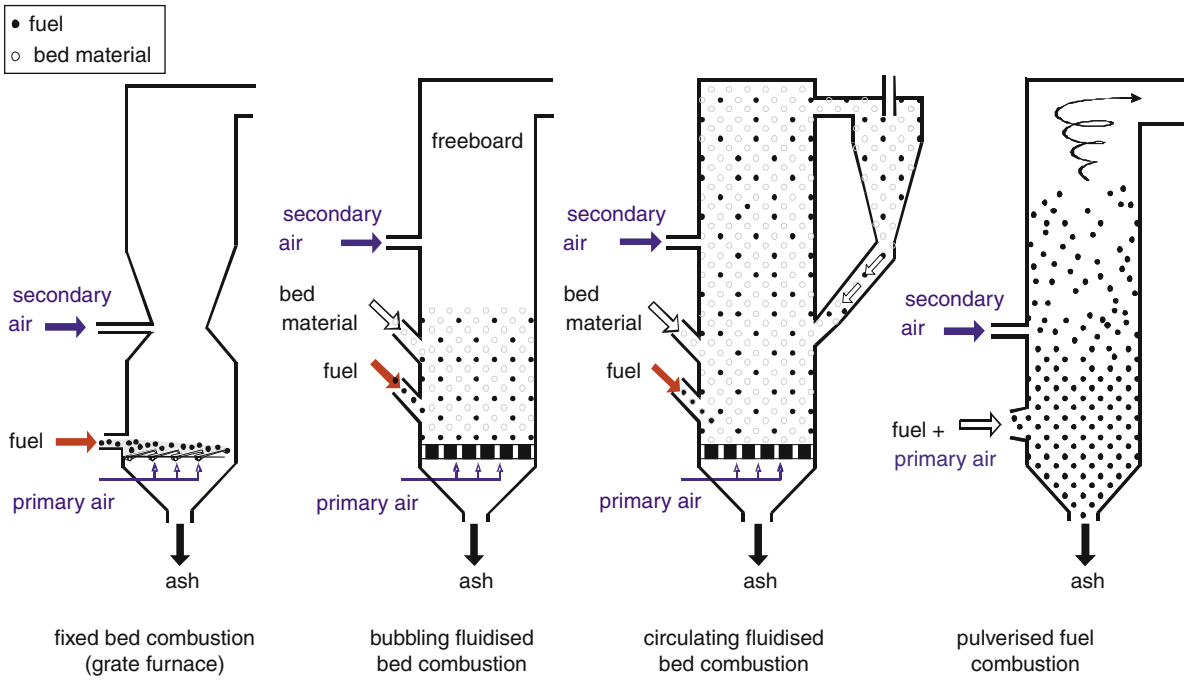

Biomass Energy Heat Provision in Modern Large-Scale Systems. Figure 6
Combustion technologies for biomass [16]

The underfeed technology has been specially developed for fine-grained biomass fuels (below 50 mm) like wood shavings, pellets, or sawdust and is only suitable for fuels with low ash content (because of the limited ash transport from the grate) and with low mineral or metal impurities (as they may block the screw feeders). Moreover, sintered or melted ash particles covering the upper surface of the fuel bed can cause problems in underfeed stokers due to unstable combustion conditions when the fuel and the air are breaking through the ash-covered surface.

Because of the technical limitation of supplying the fuel with screw conveyors, the limiting nominal boiler capacity for this type of units is about 6 MW_{th}. However, in this performance range the investments are typically lower than for other technologies (e.g., grate-fired combustion units) [2]. Another advantage of the underfeed stoker compared to moving grate units (see next section) is the continuous fuel feed which facilitates load regulation for low emissions. A schematic drawing of an underfeed biomass stoker combustion unit is shown in Fig. 7.

Moving Grate Furnaces In moving grate furnaces, the fuel is feed onto the grate either by pushing the fuel horizontally onto the grate or by spreading it onto the grate from above by a spreader stoker. Moving grate furnaces are distinguished by the way the grate is moving (e.g., inclined moving grates, horizontally moving grates, traveling grates, rotating grates, vibrating grates). All of these technologies have specific advantages and disadvantages, depending on fuel properties. Therefore, a careful selection and planning is necessary.

Moving grate furnaces are appropriate for biofuels with a high moisture content (up to 60%), varying particle sizes (with a downward limitation concerning the amount of fine particles in the fuel mixture), and high ash content (up to 50%). Mixtures of wood fuels can be used, but current technology does not allow for mixtures of wood fuels and straw, cereals and grass, due to their different combustion behavior, low moisture content, and low ash melting temperatures. A good and well-controlled grate is designed to guarantee a homogeneous distribution of the fuel and the bed of embers over the whole grate surface. This is important

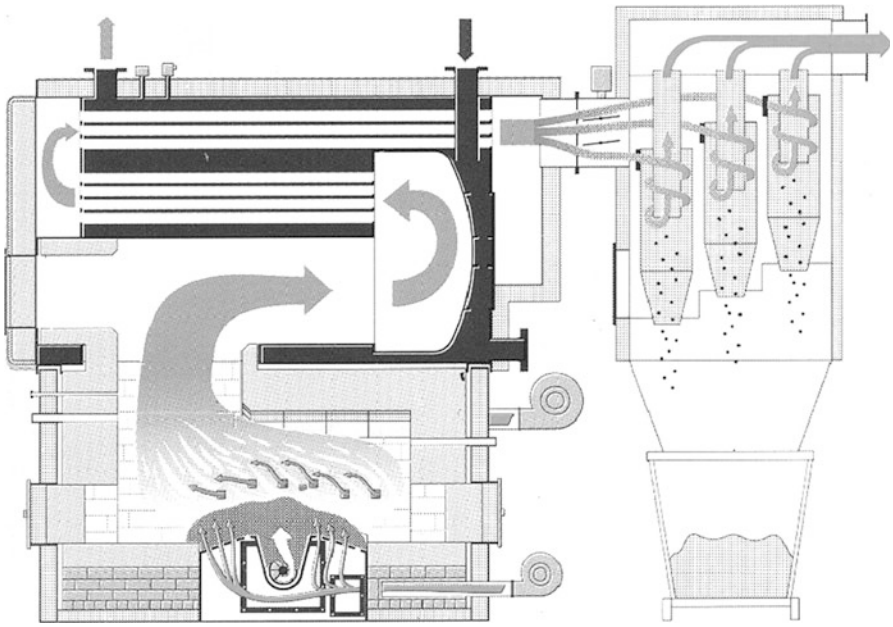

Biomass Energy Heat Provision in Modern Large-Scale Systems. Figure 7
Underfeed stoker furnace [17]

to guarantee a uniform primary air supply over the different grate areas. Inhomogeneous air supply may cause slagging, high fly-ash amounts, and may increase the amount of excess oxygen needed for a complete combustion. Furthermore, the transport of the fuel over the grate must be as smooth and homogeneous as possible in order to keep the bed of embers calm and homogeneous, to avoid the formation of "holes", and to avoid as far as possible the elutriation of fly ash and unburned particles.

The technology needed to achieve these aims includes continuously moving grates, an elaborated control system of the bed of embers (e.g., by infrared beams), and frequency-controlled primary air fans for the different grate sections. The primary air supply divided into physically separated sections below the grate is necessary to be able to adjust the specific air amounts to the requirements of the zones where drying, gasification, and charcoal combustion prevail. These separately controllable primary air supplies also allows a smooth operation of grate furnaces at partial loads of up to a minimum of about 25% of the nominal furnace load and control of the primary air ratio needed (to secure a reducing atmosphere in the primary combustion chamber necessary for low NO_x operation). Moreover, grate systems can be water-cooled to avoid slagging and to extend the lifetime of the materials.

Another important aspect of grate furnaces is that a staged combustion should be obtained by separating the primary and the secondary combustion chambers in order to avoid back-mixing of the secondary air and to separate gasification and oxidation zones. Because the mixing of air and flue gas in the primary combustion chamber is not optimal due to the low turbulence necessary for a calm bed of embers on the grate, the geometry of the secondary combustion chamber and secondary air injection must guarantee a mixture of flue gas and air that is as complete as possible. The better the mixing quality between flue gas and secondary combustion air, the lower the amount of excess oxygen necessary for complete combustion and the higher the efficiency. The mixing effect can be improved with relatively small channels where the flue gas reaches high velocities and where the secondary air is injected at high speed via nozzles that are well distributed over the cross section of this channel. Other means of achieving a good mixture of flue gas and secondary air are combustion chambers with a vortex or cyclone flow.

In order to achieve adequate temperature control in the furnace, flue gas recirculation and water-cooled combustion chamber walls are used. Combinations of these technologies are also possible. Water cooling has the advantage of reducing the flue gas volume, impeding ash sintering on the furnace walls and usually extending the lifetime of insulation bricks. If only dry biomass fuels are used, combustion chambers with steel walls can also be applied (without insulation bricks). Wet biomass fuels need combustion chambers with insulation bricks operating as heat accumulators and buffering moisture content and combustion temperature fluctuations in order to ensure a good burnout of the flue gas.

Below, different types of moving grate constructions are discussed in more detail.

Traveling grate furnaces consist of grate bars mounted on an endless belt (like an escalator) moving through the combustion chamber (Fig. 8a). The fuel is supplied at one end of the combustion chamber onto the grate (e.g., by screw conveyors) or is distributed over the grate by spreader-stokers injecting the fuel into the combustion chamber. The fuel bed itself does not move, but is transported through the combustion

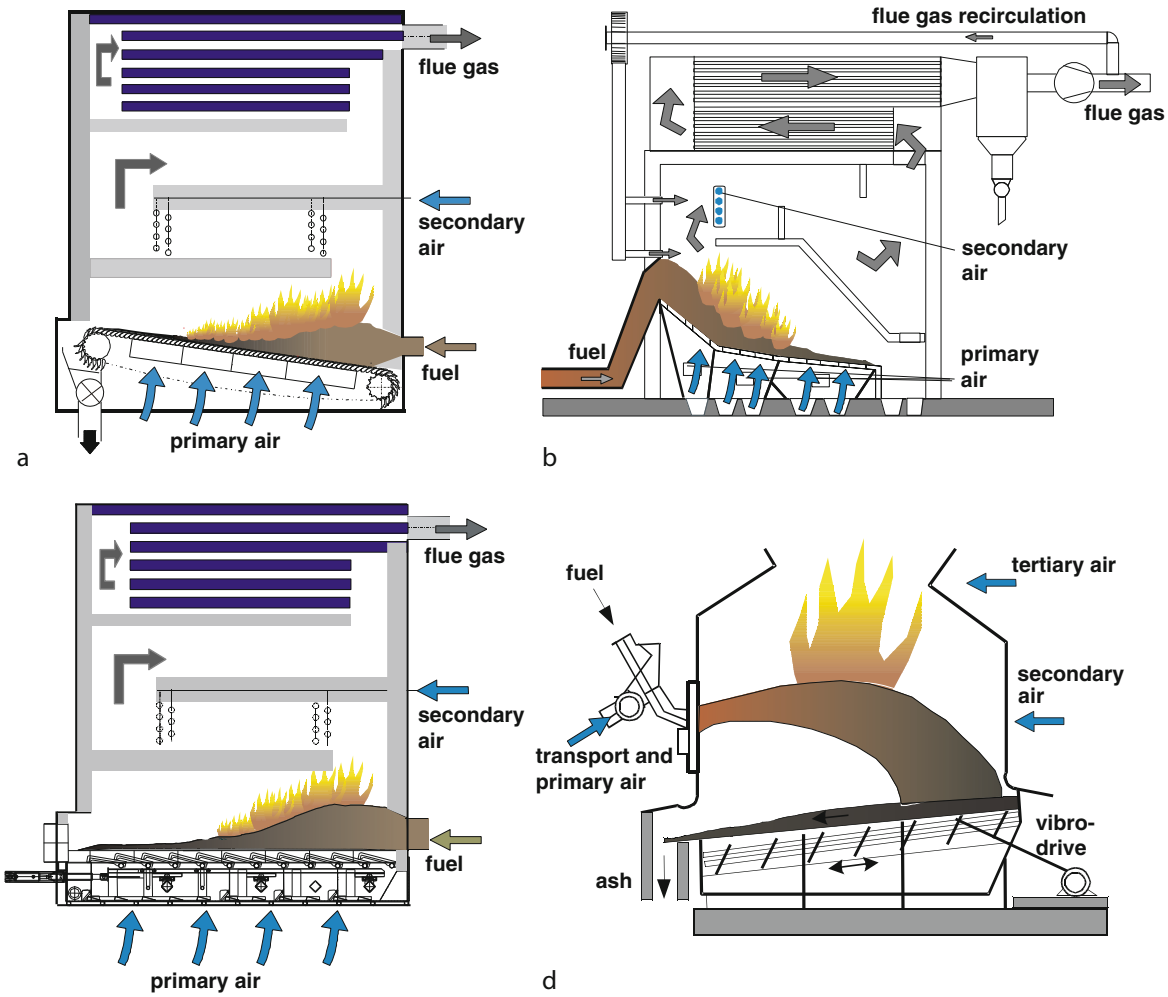

Biomass Energy Heat Provision in Modern Large-Scale Systems. Figure 8
A traveling, an inclined moving, a horizontally moving, and a vibrating grate furnace (**a**) traveling grate [12] (**b**) inclined moving grate [13] (**c**) horizontally moving grate [17] (**d**) vibrating grate [16]

chamber by the grate, contrary to moving grate furnaces where the fuel bed is moved over the grate. At the end of the combustion chamber the grate is cleaned of ash and dirt while the belt turns around (automatic ash removal). On the way back, the grate bars are cooled by primary air in order to avoid overheating and to minimize wear. The speed of the traveling grate is continuously adjustable in order to achieve complete charcoal burnout. The advantages of traveling grate systems are uniform combustion conditions for wood chips and pellets and low emissions of particulate matter, due to the stable and almost unmoving bed of embers. In addition, the maintenance or replacement of grate bars is easy to handle. However, the fact that the bed of embers is not stoked results in a longer burnout time and also may cause bridging of fuel and/or ash particles. Higher primary air input is needed for complete combustion (which implies a lower NO_x reduction potential by primary measures). Moreover, nonhomogeneous biomass fuels imply the danger of bridging and uneven distribution on the grate surface due to lack of mixing. This disadvantage can be avoided by spreader-stokers, which cause a mixing of the fuel bed by the fuel-feeding mechanism applied.

Inclined moving grates have an inclined grate consisting of fixed and movable rows of grate bars (Fig. 8b). By alternating horizontal forward and backward movements of the movable sections, the fuel is transported along the grate. Thus unburned and burned fuel particles are mixed, the surfaces of the fuel bed are renewed, and a more even distribution of the fuel over the grate surface can be achieved (which is important for a uniform primary air distribution across the fuel bed). Usually, the whole grate is divided into several grate sections, which can be moved at different speeds according to the different stages of combustion. The movement of the grate bar is achieved by hydraulic cylinders. The grate bars themselves are made of heat-resistant steel alloys. They are equipped with small channels in their side walls for primary air supply and should be as narrow as possible in order to distribute the primary air across the fuel bed as well as possible. In moving grate furnaces, a wide variety of biofuels can be burned. Air-cooled moving grate furnaces use primary air for cooling the grate and are suitable for wet bark, sawdust, and wood chips, while water-cooled moving grate systems are recommended for dry biofuels or biofuels with low ash-sintering temperatures. In contrast to traveling grate systems, the correct adjustment of the moving frequency of the grate bars is more complex. If the moving frequencies are too high, high concentrations of unburned carbon in the ash or insufficient coverage of the grate will result. Infrared beams situated over the different grate sections allow for adequate control of the moving frequencies by checking the height of the bed. Ash removal takes place under the grate in dry or wet form and a fully automatic operation of the entire system is common.

Horizontally moving grates have a completely horizontal fuel bed (Fig. 8c). This is achieved by the diagonal positioning of the grate bars. This has the advantage that it impedes uncontrolled gravity-induced fuel movements on the grate and increases the stoking effect of the grate movements, thus leading to a very homogeneous distribution of material on the grate surface and impeding slag formation because of hot spots. A further advantage is that the overall height can be reduced. In order to prevent ash and fuel particles from falling through the grate bars, horizontally moving grates should be preloaded so that there is no free space between the bars.

Vibrating grate furnaces consist of a declined finned tube wall placed on springs (Fig. 8d). Fuel is fed into the combustion chamber by spreaders, screw conveyors, or hydraulic feeders. Depending on the combustion process, two or more vibrators transport fuel and ash toward the ash removal unit. Primary air is fed through the fuel bed from below through holes located in the ribs of the finned tube walls. Due to the vibrating movement of the grate at short periodic intervals, the formation of larger slag particles is inhibited. This is the reason why this grate technology is especially applied with fuels showing sintering and slagging tendencies (e.g., straw, waste wood). The disadvantages are the high fly-ash emissions caused by the vibrations, the higher CO emissions due to the periodic disturbances of the fuel bed, and an incomplete burnout of the bottom ash because fuel and ash transport are more difficult to control.

The *cigar burner* is a technology developed for straw and cereal combustion in Denmark (Fig. 9). Straw and cereal bales are delivered in a continuous process

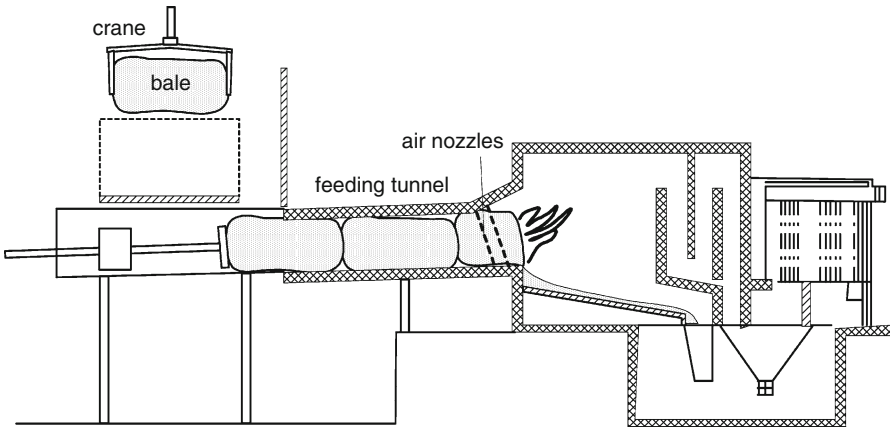

Biomass Energy Heat Provision in Modern Large-Scale Systems. Figure 9
Cigar burner [16]

by a hydraulic piston through a feeding tunnel on a water-cooled grate. Upon entering the combustion chamber gasification of the fuel starts and combustion of the charcoal follows while moving the unburned material over the grate. Grate and furnace temperature control is very important for straw and cereal combustion, due to their low ash melting point and the high adiabatic temperature of combustion caused by the low water content. The combustion chambers must, therefore, be cooled either by water cooled walls or by flue gas recirculation (or by a combination). Furnace temperatures should not exceed 900°C for normal operation. Furthermore, straw and cereal combustion causes very fine and light fly ash particles as well as aerosols to be formed from condensed alkali chlorides/sulfates. This result in the necessity of a regular heat exchanger cleaning system to avoid ash deposits as far as possible. Systems for shredded or cut straw also exist and are operated in a similar way to the technology described. Only the fuel preparation is different. Smaller pieces of straw, slices of straw bales, or shredded straw is preferable to whole bale combustion because smaller particles allow a better combustion control along the grate. Semicontinuous systems like whole bale combustion furnaces where the bales are fed in batch-wise operation into the furnace are not recommended due to the temperature and CO peaks caused when a new bale is delivered. The state-of-the-art process control systems are not able to prevent this unsteady combustion.

Underfeed rotating grate combustion is a Finnish biomass combustion technology that makes use of conical grate sections that rotate in opposite directions and are supplied with primary air from below (Fig. 10). As a result wet and burning fuels are well mixed, which makes the system adequate for burning very wet fuels such as bark, sawdust, and wood chips (with a moisture content up to 65 wt% [w.b.]). The combustible gases formed are burned out with secondary air in a separate horizontal or vertical combustion chamber. The horizontal version is suitable for generating hot water or steam in boilers with a nominal capacity between 1 and 10 MW_{th}. The vertical version is applied for hot water boilers with a capacity of 1–4 MW_{th}. The fuel is fed to the grate from below by screw conveyors (similar to underfeed stokers), which makes it necessary to keep the average particle size below 50 mm. Underfeed rotating grate combustion plants are also capable of burning mixtures of solid wood fuels and biological sludge. The system is computer controlled and allows fully automatic operation.

Fluidized Bed Combustion

Fluidized bed (FB) combustion systems have been applied since 1960 for combustion of municipal and industrial wastes. Since then, over 300 commercial installations have been built worldwide. Regarding technological applications, bubbling fluidized beds (BFB) and circulating fluidized beds (CFB) are distinguished.

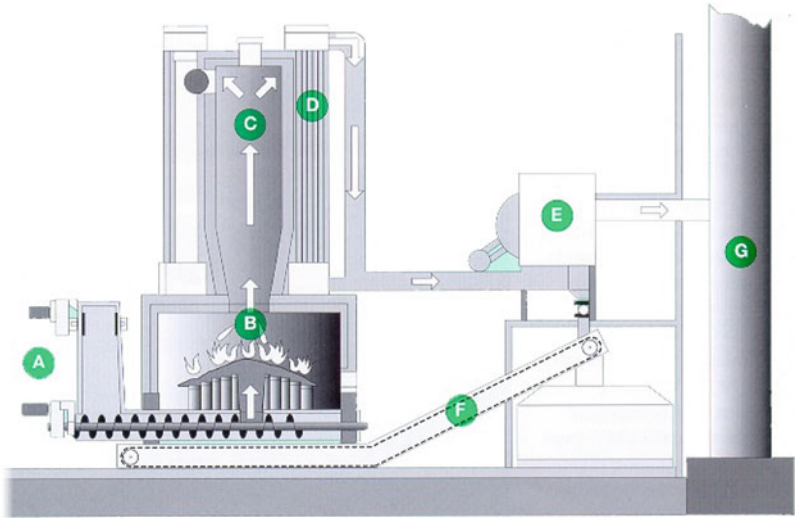

Biomass Energy Heat Provision in Modern Large-Scale Systems. Figure 10
Rotating grate underfeed stoker. (Explanations: 1 fuel feed, 2 rotating grate, 3 bottom of the cone, 4 primary air, 5 air control, 6 ash disposal, 7 ash screw conveyor, 8 burn out zone, 9 secondary air)

A fluidized bed consists of a cylindrical vessel with a perforated bottom plate filled with a suspension bed of hot, inert, and granular material. The common bed materials are silica sand and dolomite. The bed material represents 90–98% of the mixture of fuel and bed material. Primary combustion air enters the furnace from below through the air distribution plate and fluidizes the bed so that it becomes a seething mass of particles and bubbles. The intense heat transfer and mixing provide good conditions for a complete combustion with low excess air demand (λ between 1.1 and 1.2 for CFB plants and between 1.3 and 1.4 for BFB plants). The combustion temperature must be kept low (usually between 800°C and 900°C) in order to prevent ash sintering in the bed. This can be achieved by internal heat exchanger surfaces, by flue gas recirculation, or by water injection (in fixed-bed combustion plants combustion temperatures are usually 100–200°C higher than in FB units).

Due to the good mixing achieved, FB combustion plants can deal flexibly with different fuel mixtures (e.g., mixtures of wood and straw) but are limited when it comes to fuel particle size and impurities contained in the fuel. Therefore, an appropriate fuel pretreatment system covering particle size reduction and separation of metals is necessary for fail-safe operation. Usually a particle size below 40 mm is recommended for CFB units and below 80 mm for BFB units. Moreover, partial load operation of FB combustion plants is limited due to the need of bed fluidization.

Fluidized bed combustion systems need a relatively long start-up time (up to 15 h) for which oil or gas burners are used. Low NO_x emissions can be achieved owing to good air staging, good mixing, and a low requirement of excess air. Moreover, the utilization of additives (e.g., limestone addition for sulfur capture) works well due to the good mixing behavior. The low excess air quantities necessary increase combustion efficiency and reduce the flue gas volume flow. This makes FB combustion plants especially interesting for large-scale applications (normal boiler capacity above 30 MW_{th}). For smaller combustion plants the investment and operating costs are usually too high in comparison to fixed-bed systems. One disadvantage is that they cause high dust loads to be entrained with the flue gas, which makes efficient dust precipitators and boiler cleaning systems necessary. Bed material is also lost with the ash, making it necessary to periodically add new material to the plant.

- Bubbling fluidized bed combustion (BFB) furnaces start to be of interest for plants with a nominal boiler capacity of over 20 MW_{th}. In BFB furnaces

(Fig. 6), a bed material is located in the bottom part of the furnace. The primary air is supplied via a nozzle distributor plate and fluidizes the bed. The bed material is usually silica sand about 1.0 mm in diameter. The fluidization velocity of the air varies between 1.0 and 2.5 m/s. The secondary air is introduced through several inlets in the form of groups of horizontally arranged nozzles at the beginning of the upper part of the furnace (called freeboard) to ensure a staged-air supply to reduce NO_x emissions. Biofuel should not be feed onto, but into, the bed by inclined chutes from fuel hoppers because of the higher reactivity of biomass. The fuel amounts only to 1–2% of the bed material and the bed must be heated (internally or externally) before the fuel is introduced. The advantage of BFB furnaces is their larger flexibility concerning particle size and moisture content of the biomass fuels in comparison to CFB units. Furthermore, it is also possible to use mixtures of different kinds of biomass or to co-fire them with other fuels. One disadvantage (the difficulties at partial load operation) may be solved by splitting or staging the bed.

- By increasing the fluidizing velocity to 5–10 m/s and using smaller sand particles (0.2–0.4 mm in diameter) a circulating fluidized bed combustion (CFB) system is achieved (Fig. 6). The sand particles will be carried along with the flue gas, separated in a hot cyclone or a U-beam separator, and feed back into the combustion chamber (Fig. 6). The bed temperature (800–900°C) is controlled by external heat exchangers cooling the recycled sand, or by water-cooled walls. The higher turbulence in CFB furnaces leads to a better heat transfer and a very homogeneous temperature distribution within the bed. This is of advantage for stable combustion conditions, the control of air staging, and the placement of heating surfaces right in the upper part of the furnace. The disadvantages of CFB furnaces are their large size and therefore high price, the considerable dust load in the flue gas leaving the sand particle separator, the high loss of bed material in the ash, and the small fuel particle size required (between 0.1 and 40 mm in diameter) often requiring a high investment in fuel pretreatment. Moreover, their operation at partial load is problematic. In view of their high specific heat transfer capacity, CFB furnaces start to be of interest for plants of more than 30 MW_{th}, due to their higher combustion efficiency and the lower flue gas flow produced (boiler and flue gas cleaning units can be dimensioned smaller).

Dust Combustion

In dust combustion systems, fuels like sawdust and fine shavings are pneumatically injected into the furnace (Fig. 11). The transportation air is used as primary air. Start-up of the furnace is achieved by an auxiliary burner. When the combustion temperature reaches a certain value, biomass injection starts and the auxiliary burner is shut down. Fuel quality in dust combustion systems needs to be quite constant. A maximum fuel particle size of 10–20 mm must be maintained and the fuel moisture content should normally not exceed 20 wt% (w.b.). The fuel feeding system needs to be controlled very carefully and forms a key technological unit within the overall system due to the explosion-like gasification of the fine and small biomass particles. Fuel/air mixtures are usually injected tangentially into the cylindrical furnace muffle to establish a rotational flow (usually a vortex flow). The rotational motion can be supported by flue gas recirculation in the combustion chamber. The muffle should be water cooled due to the high energy density at the furnace walls and the high combustion temperature. Fuel gasification and charcoal combustion take place at the same time because of the small particle size. Therefore, quick load changes and efficient load control can be achieved.

Besides muffle furnaces, cyclone burners for wood dust combustion are also in use. Depending on the design of the cyclone and the location of fuel injection, the residence time of the fuel particles in the furnace (their burnout) can be controlled well and, if staged combustion is used, also NO_x formation can also be kept low.

A disadvantage of muffle furnaces and cyclone burners is that insulation bricks wear out quickly due to thermal stress and erosion. Other dust combustion systems are thus being built without rotational flow, where dust injection is conducted

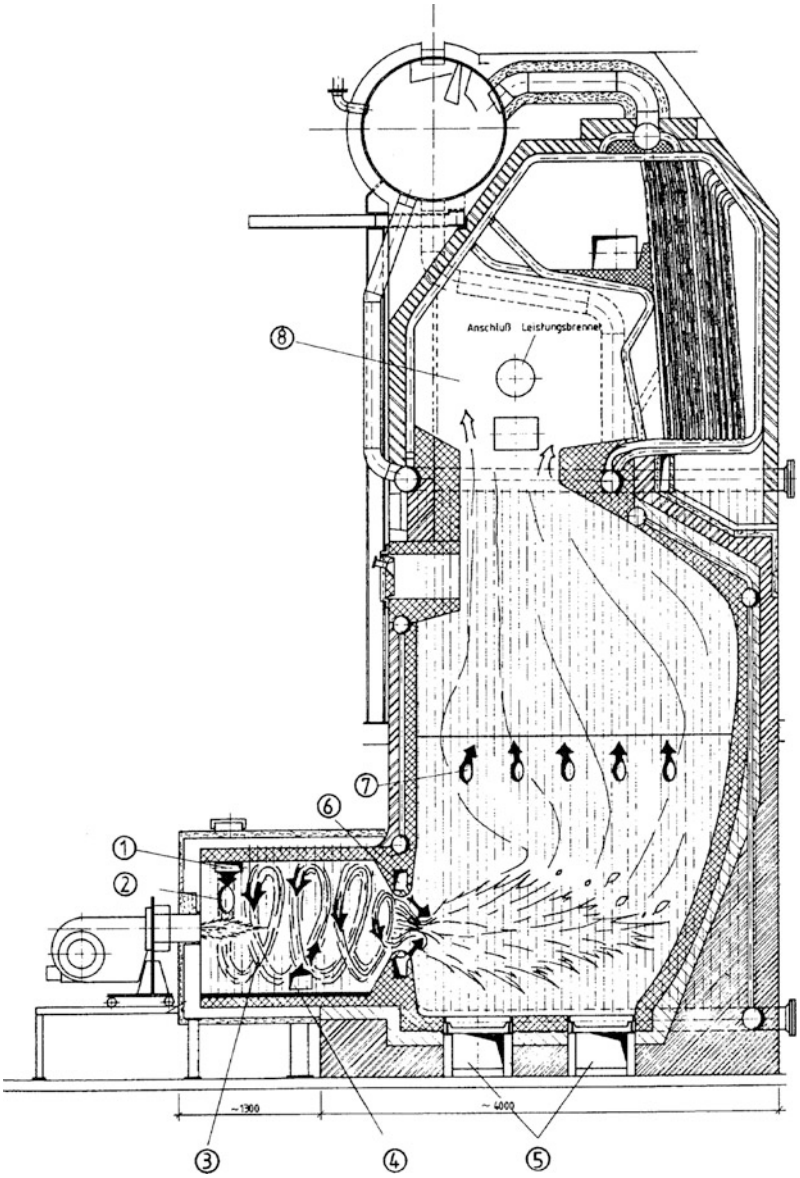

Biomass Energy Heat Provision in Modern Large-Scale Systems. Figure 11
Dust combustion system (muffle furnace) in combination with a water-tube steam boiler [16]. (Explanations: 1 primary air supply, 2 fuel feed, 3 gasification and partial combustion, 4 flue gas recirculation, 5 ash disposal, 6 secondary air supply, 7 tertiary air supply, 8 water tube boiler)

without a swirl in the same way as in a furnace burning fuel oil or natural gas.

Summary

In general, BFB and CFB furnaces show lower CO and NO_x emissions due to more homogeneous and therefore more controllable combustion conditions, while fixed-bed furnaces usually emit less particulate matter and show a better burnout of the fly ash [18, 19].

Table 3 gives a summary of solid biomass combustion technologies and their typical applications and fuel specifications, and Table 4 shows the advantages

Biomass Energy Heat Provision in Modern Large-Scale Systems. Table 3 Summary of solid biomass combustion technologies with typical applications and fuels

Technology	Typical size range	Fuels	Ash content (%)	Moisture content (%)
Underfeed stoker furnaces	10 kW–6.0 MW	Wood chips, wood residues	<2	5–50
Moving grate furnaces	500 kW–50 MW	All wood fuels and most biomass	<10	5–60
Underfeed stoker with rotating grate	2–20 MW	Wood chips, high water content	<10	30–65
Straw furnaces	100 kW–10 MW	Straw bales with bale shredders	<5	<20
Cigar burner	3–5 MW	Straw bales	<5	<20
Dust combustor, or cyclone furnaces	1–10 MW	Various biomass, (dP < 5 mm)	<2	<20
Bubbling fluidized bed	20–50 MW	Various biomass, (dP < 80 mm)	<10	5–60
Circulating fluidized bed	30–100 MW	Various biomass, (dP < 40 mm)	<10	5–60

dP Fuel particle diameter

Biomass Energy Heat Provision in Modern Large-Scale Systems. Table 4 Summary of advantages and disadvantages of different solid biomass combustion technologies

Advantages	Disadvantages
Underfeed stokers	
Low investment costs for plants < 6 MW_{th}	Suitable only for biofuels with low ash content and high ash melting point (wood fuels)
Simple and good load control due to continuous fuel feeding	Low flexibility concerning particle size as well as concerning mineral and metal impurities in the fuel
Low emissions at partial load operation due to good fuel dosing	
Moving grate furnaces	
Low investment costs for plants < 20 MW_{th}	No mixing of wood fuels and herbaceous fuels possible
Low operating costs	Efficient NO_x reduction requires special technologies
Low dust load in the flue gas	High excess air ratio (1.3–1.6) decreases efficiency
Less sensitive to slagging than fluidized bed furnaces	Combustion conditions not as homogeneous as in fluidized bed furnaces
Many options in terms of fuel particle size and moisture content	Low emissions at partial load operation are difficult to achieve
Dust combustion	
Low excess air ratio (1.25–1.4) is possible which increases efficiency	Particle size of biofuel is limited (<10–20 mm)
High NO_x reduction by efficient air staging and mixing possible if cyclone or vortex burners are used	High wear of the insulation brickwork if cyclone or vortex burners are used
Very good load control and fast alternation of load possible	An extra start-up burner is necessary

Biomass Energy Heat Provision in Modern Large-Scale Systems. Table 4 (Continued)

Advantages	Disadvantages
BFB furnaces	
No moving parts in the hot combustion chamber	High investment costs, interesting only for plants >20 MW_{th}
NOx reduction by air staging works well	High operating costs
High flexibility concerning moisture content and type of biomass fuels used (fuel mixing possible)	Low flexibility with regard to particle size (<80 mm)
Low excess air ratio (1.2–1.25) raises efficiency and decreases flue gas flow	High dust load in the flue gas
	Operation at partial load requires special technology
	Medium sensitivity concerning ash slagging
	Loss of bed material with the ash
	Medium erosion of heat exchanger tubes in the fluidized bed
CFB furnaces	
No moving parts in the hot combustion chamber	High investment costs, interesting only for plants > 30 MW_{th}
NO_x reduction by air staging works well	High operating costs
High flexibility concerning moisture content and type of biomass fuels used (fuel mixing possible)	Low flexibility with regard to particle size (<40 mm)
Homogeneous combustion conditions in the furnace if several fuel injectors are used	High dust load in the flue gas
High specific heat transfer capacity due to high turbulence	Partial-load operation requires a second bed
Use of additives easy	High sensitivity concerning ash slagging
Very low excess air ratio (1.05–1.1) raises efficiency and decreases flue gas flow	Loss of bed material with the ash
	Medium erosion of heat exchanger tubes in the furnace

and disadvantages of the different combustion technologies discussed above.

Combustion-Based Power Generation Processes

Electric power production is generally implemented in larger applications such as industrial combustion units or district heating systems. The status of power generation from biofuel combustion is limited to closed thermal cycles. Open processes such as internal combustion engines or direct gas turbines are still in the research stage and not applicable so far mainly due to limitations in separating particles and particle-forming gaseous species (e.g., KCl, K_2SO_4) from the hot flue gas.

In a closed thermal cycle, the combustion of the fuel and the power generation cycle are separated by a heat transfer from the hot flue gas to a process medium used in a secondary cycle. This separation between the fuel and the power-producing engine prevents undesired elements in the fuel and flue gas from causing damage to the engine.

The processes and engine types used or under development today are shortly described here (see [2, 9, 10, 20, 21]).

The available technologies for power production from biomass combustion comprise:

- *Steam turbines* (ST) used as expansion engines in the Rankine cycle with water as a process medium; the water is evaporated under pressure and superheated in heat exchangers in the boiler section of the combustion plant

- *Steam piston engines* (*SPE*) used in the Rankine cycle with or without superheating and transferring the volume work into mechanical work by a piston [22]
- Steam turbines used in *organic Rankine cycles* (ORC) with evaporation of an organic medium in a tertiary cycle separated from the heat production (the combustion heat is transferred to a thermal oil in the boiler which is feed to an external evaporator for the organic medium with a lower boiling temperature than water) [2];
- *Stirling engines* (STE) (indirectly fired gas engines) which are driven by a periodic heat exchange from flue gas to a gaseous medium such as air, helium, or hydrogen [23, 24]
- *Micro-gas turbines* (MGT) using a hot gas cycle with a turbine as an expansion engine.

The most important technical data for power production from biomass combustion are shown in Table 5. The total efficiency indicated within this table is calculated according to Eq. 1.

$$\eta_{\text{tot}} = \frac{P_{\text{el(produced)}} - P_{\text{el(auxiliary)}} + P_{\text{th}}}{P_{\text{fuel input(NCV)}}} \quad (1)$$

The electric efficiency of the plant is calculated according to Eq. 2.

$$\eta_{\text{el-plant}} = \frac{P_{\text{el(produced)}} - P_{\text{el(auxiliary)}}}{P_{\text{fuel input(NCV)}}} \quad (2)$$

Both equations are based on the power supplied with the fuel based on its net calorific value (NCV). The auxiliary electric power is the power needed for the operation of the power or CHP plant and has to be subtracted from the gross electric power produced in order to achieve the net electric power of the plant, which is of relevance for the efficiency calculations stated.

In the column "recommended operation" the best way of operating the plant is shown, i.e., if the plant should be mainly operated for the production of heat (h) or heat and electric power (h/p). The remaining columns give an insight into the current stage of development and experience with the different technologies.

Steam turbines and steam piston engines are available as tested technology for power production through biomass combustion. While steam engines are used with capacities ranging from below 0.1–1.5 MW_{el}, steam turbines exist from 150 kW_{el} upward. The largest purely biomass-fired CHP plant today is equipped with steam turbines and has a nominal electric capacity of 240 MW [1]. Large steam turbine plants are operated with water tube boilers and superheaters making high steam parameters and the use of multistage turbines possible. Furthermore, process measures such as feed water preheating and intermediate tapping are implemented for efficiency improvement. This allows electric efficiencies of about 25% to be achieved

Biomass Energy Heat Provision in Modern Large-Scale Systems. Table 5 Overview of CHP technologies used or under development for the production of electric power based on the combustion of solid biomass [2]

	P_{el} [a] (kW)	$\eta_{el\text{-}plant}$ [b] (%)	η_{tot} [c] (%)	Recommended operation [d]	State of development [e]	Operating experience	Literature sources
ST	150–240,000	8–40	75–90	h/p	Marketable	Marketable	[1, 2, 25]
SPE	<100–1,500	8–16	75–85	h	Marketable	Marketable	[2]
ORC	200–3,000	10–20	75–85	h	Marketable	Marketable	[26–29]
STE	10–150	6.5–17	75–85	h	Demonstration	40,000 h	[30, 31]
MGT	up to 100	8–17	60–65	h/p	Demonstration	2,800 h	[32–36]

ST steam turbine, *SPE* steam piston engine, *SSE* steam screw-type engine, *ORC* organic Rankine cycle, *STE* Stirling engine, *MGT* micro gas turbine

[a]Electric capacity

[b]See Eq. 1

[c]See Eq. 2

[d]p Power-controlled operation recommended, h Heat controlled operation recommended

[e]Possibilities: pilot status, demonstration status, marketable

in the size range of 5–10 MW_{el}. In plants around 50 MW_{el} and larger, the electric efficiency can rise to about 30% in cogeneration mode and more than 40% if operated as a condensing plant.

Small-scale steam plants (<2 MW_{el}) are built with fire tube boilers and hence operated at quite low steam parameters (below 32 bar, below 450°C), which significantly decrease their electric efficiency. Steam plants operated in CHP mode are mainly utilized for the production of process heat or base load district heat, which enables long continuous operation periods with high load.

Steam piston engines can be operated in single- or multistage mode, reaching electric efficiencies between 8–10% and 12–16%, respectively.

Organic Rankine cycles (ORC) are also available as an alternative to conventional steam plants in the range of 0.2 to about 3.0 MW_{el}. These can operate at lower temperatures and pressures, so that a combustion plant with a thermal oil boiler operating at atmospheric pressure can be applied instead of a costly high-pressure steam boiler. Furthermore, the ORC generator can be operated without a superheater because the expansion of the saturated steam of the organic medium leads to dry steam. Furthermore, similar or slightly higher efficiencies are achieved thanks to the availability of well-designed two-stage small-scale turbines for this specific application. ORC plants are a proven technology which has been implemented in biomass combustion plants since 1998 [29, 37].

An option for small-scale power production is the externally fired Stirling engine with air or helium as a medium in a gas-filled heat exchanger coupled to a biomass furnace. A critical component in such plants can be the gas-to-gas heat exchanger operated with hot flue gas from the biomass combustion. Chemically untreated wood is the most suitable fuel so far, since biomass fuels with high ash levels or increased Cl concentrations are a challenge for the heat exchanger. A critical and weak point of the Stirling engine process is also the long-term stability of the engine. At present, not more than 5,000 h have been obtained with a single engine.

Micro-gas turbine (MGT) processes are also being considered in R&D projects for small to medium-scale applications and reached an early demonstration stage. This process offers the possibility of the use of biomass only as well as of the combined use of natural gas (internal combustion) and biomass (external combustion). The combined system offers good electric plant efficiencies and lower maximum temperatures at the air/flue gas heat exchanger compared to a biomass-only application. Moreover, they provide a high degree of automation. However, the technology is not yet proven and shows relatively high investment costs (no serial production yet). Due to thermal stresses in the high temperature air/flue gas heat exchanger only slow load changes are possible. Thus, future operating experiences will have to proof the technological maturity and applicability of such systems.

Emissions from Combustion and Ash-Related Problems

Gaseous Emissions

CO_2 is a major combustion product from all biomass fuels, originating from the carbon content in the fuel. However, these CO_2 emissions are regarded as being CO_2-neutral with respect to the anthropogenic greenhouse gas effect (when a sustainable agriculture/forestry is given) and this is considered to be one main environmental benefit of biomass combustion.

In the case of an incomplete combustion, pollutants such as CO, C_XH_Y, PAH, tar, soot, unburned carbon, NH_3, and N_2O are formed. As shown above, an effective reduction of these pollutants is achieved by an optimized combustion process, providing good mixing between fuel and air, enough retention time (above 1.0 s) at high temperatures (above 850°C), and a low total λ. In modern automated furnaces with effective process control systems the concentrations of unburned pollutants can be reduced to levels close to zero (e.g., $CO < 50$ mg/Nm^3 and $C_XH_Y < 5$ mg/Nm^3 at 11% O_2 [9]).

NO_X emissions from biomass combustion applications are mainly a result of complete oxidation of fuel nitrogen, both from gas-phase combustion and char combustion. Additional NO_X may be formed from nitrogen in the air under certain conditions. However, these reaction mechanisms are not considered to be of significant importance in most biomass combustion applications due to the limited combustion temperatures. The main nitric oxide emitted is NO to be converted to NO_2 within the atmosphere.

Figure 12 shows measured data of NO_X emissions (left) and the percentage of fuel N converted to NO_X (right) versus the N content in the fuel for different biomass fuels. The graphic clearly indicates that NO_X emissions increase with increasing N content in the fuel while the rate of fuel N converted to NO_X decreases.

In order to reduce NO_X emissions from biomass combustion, several primary and secondary measures exist. For the utilization of chemically untreated biomass fuels, secondary measures are usually not necessary [12, 38]. If secondary measures are needed, they should always be combined with primary measures in order to efficiently utilize the NO_X reduction potential available and to reduce operating costs (additive utilization).

Air staging is a widely applied primary measure for NO_X reduction. Here primary and secondary combustion air is injected in separated zones. In order to efficiently reduce NO_X emissions, the air ratio in the primary combustion chamber should be between 0.6 and 0.9 and the residence time of the flue gas in the primary combustion chamber approx. 0.2–0.5 s at temperatures above 800°C. Furthermore, good mixing in the primary combustion zone is of great relevance. This can be achieved by appropriate flue gas recirculation. The potential for NO_X-reduction by air staging is between 30% and 60%.

A second possibility to reduce NO_X emissions by primary measures is fuel staging, where the primary and the secondary fuel is supplied in separate zones. Due to the complexity of the system, fuel staging is usually limited to large-scale applications. Approximately 70% primary fuel and 30% secondary fuel is used. The excess air ratio in the reduction zone following the secondary fuel supply should be between 0.6 and 0.8. Natural gas, biomass producer gas, shavings, or sawdust are usually utilized as secondary fuels. The potential of NO_X reduction by fuel staging amounts to 50–70%.

If primary measures fail to achieve the targeted NO_X reduction, they can be combined with secondary measures. These are selective noncatalytic reduction (SNCR) and selective catalytic reduction (SCR) [12, 39].

- In the SNCR process, ammonia or urea is injected into the flue gas at high temperatures and oxidizing conditions, usually between 850°C and 950°C and a residence time after injection of 0.3–0.5 s [39]. Because of the high temperature, this process does not need a catalyst to initiate the reactions. Ammonia is injected at a rate of between 1:1 and 2.2:1 mole ammonia to mole of NO_X reduced. About 60–70% NO reduction can be realized with

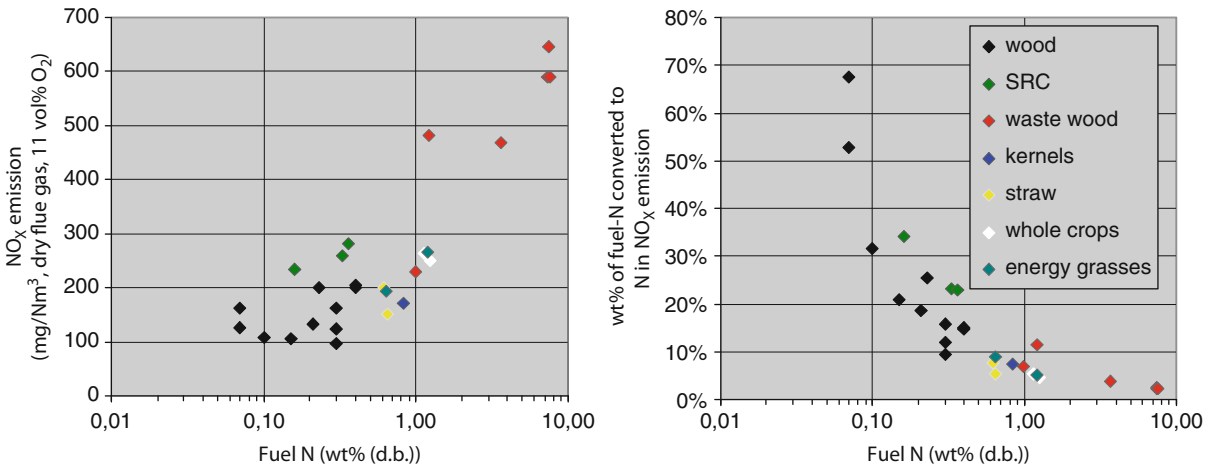

Biomass Energy Heat Provision in Modern Large-Scale Systems. Figure 12
NOx emissions (*left*) and fuel N converted to NOx (*right*) in dependence of the N content in the fuel for different biomass fuels

SNCR. This process requires an accurate temperature control to achieve optimum reduction conditions. If the temperature is too high, ammonia is oxidized to NO and if the temperature is too low, ammonia does not react at all and is emitted together with the NO_X. Additionally, a good mixing is very important. Most SNCR processes have an ammonia slip of some ppm in the flue gas leaving the stack.

- The SCR process reduces NO to N_2 by reactions with usually ammonia or urea in the presence of a platinum, titanium, or vanadium oxide catalyst. SCR operates optimally in a temperature range of 220–270°C using ammonia, and 400–450°C using urea [39]. The stoichiometric coefficient is usually around 1.0. Approximately an 80% NO_X reduction has been reported for SCR in fossil fuel combustion [40], where it is the most widely used secondary NO_X control technology. However, up to 95% NO_X reduction at 250°C without significant slippage of ammonia in a wood-firing system has been reported [39]. For the SCR process in combination with biomass combustion, the long-term behavior of the catalyst can be a problem, as deactivation is likely. In this respect, an efficient dust precipitation stage upstream the SCR unit is an important requirement. SCR systems are considerably more expensive than SNCR systems but can be economically interesting for large-scale applications due to the better conversion efficiency achievable.

Figure 13 shows the relation between fuel N content, NO_X emission reduction measures, and NO_X emissions.

The Cl and S content in different biomass fuels vary in a wide range (Fig. 2) and consequently Cl- and S-related problems may vary considerably for different fuels. In biomass combustion systems usually 40–80 wt% (for wood chips and bark furnaces) and 80–85 wt% (for straw and cereal furnaces equipped with fibrous filters) are embedded in the ashes (related to the total amount of Cl in the biomass fuel). For S the respective values are 40–90 wt% (for wood chips and bark furnaces) and 45–55 wt% (for straw and cereal furnaces equipped with fibrous filters). The remaining Cl and S is emitted as HCl and SO_2

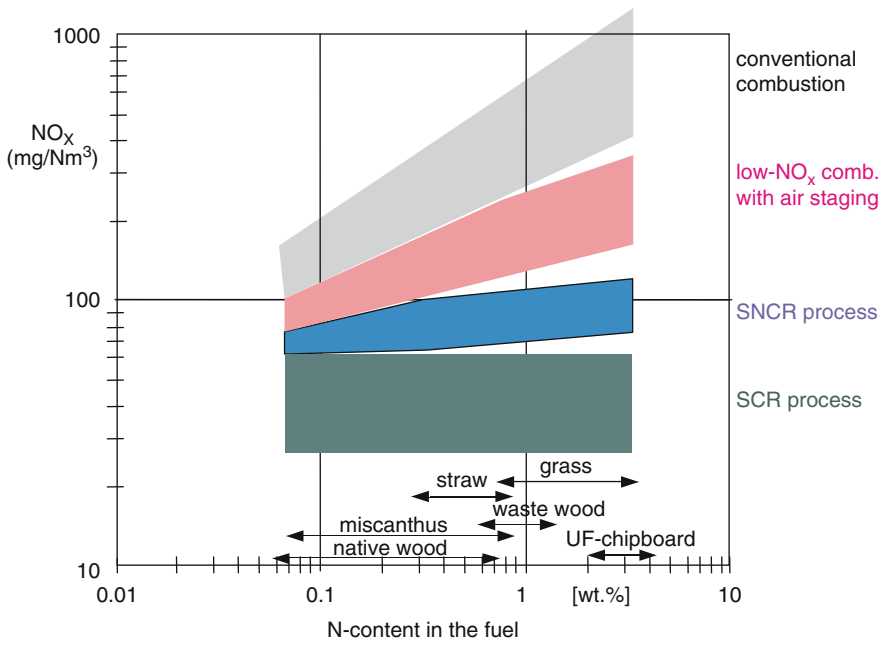

Biomass Energy Heat Provision in Modern Large-Scale Systems. Figure 13
Relation between fuel N content, NO_X emission reduction measures, and NO_X emissions. (Explanations: NO_X calculated as NO_2 and related to dry flue gas and 11 vol% O_2)

(and to a small extent as SO_3). Especially SO_3 emissions may cause corrosion problems in economizers since SO_3 increases the dew point of the flue gas considerably. If high HCl and/or SO_x emissions occur (e.g., for waste wood and straw combustion), the conventional approach to the control of HCl and SO_x emission reduction is the application of dry sorption with calcium hydroxide or sodium bicarbonate in combination with a baghouse filter.

Ash and Aerosol Formation

During the combustion of solid biofuels, the behavior of ash-forming elements follows a general scheme (Fig. 14). Below, a brief description of the basic principles of ash formation during biomass combustion is given.

Upon entering the combustion unit, the fuel is first dried, followed by devolatilization of the volatile organic matter. Subsequently, the remaining fixed carbon is oxidized during heterogeneous gas–solid reactions, which is called charcoal combustion. During these steps, the ash-forming elements behave in two different ways depending on their volatility. Nonvolatile compounds such as Si, Ca, Mg, Fe, and Al are engaged in ash fusion as well as coagulation processes. Once the organic matter has been released or oxidized, these elements remain as coarse ash structures. Semi-volatile species such as K and Na and volatile species such as S, Cl, Zn, and Pb generally behave differently. A certain proportion up to the almost whole amount contained in the fuel of these elements is released to the gas phase due to the high temperatures occurring during combustion. There they undergo homogeneous gas phase reactions and later, due to supersaturation in the gas phase, these ash-forming vapors start to nucleate (formation of submicron aerosol particles) or condense on, respectively, react with the surfaces of existing particles or directly condense on heat exchanger surfaces. The submicron particles, so-called aerosols, form one important fraction of the fly ashes. The second fly ash fraction consists of small coarse ash particles entrained from the fuel bed with the flue gas. Depending on particle size, they are either precipitated from the flue gas in the furnace or boiler mainly by inertial impaction or gravitational settling, or are

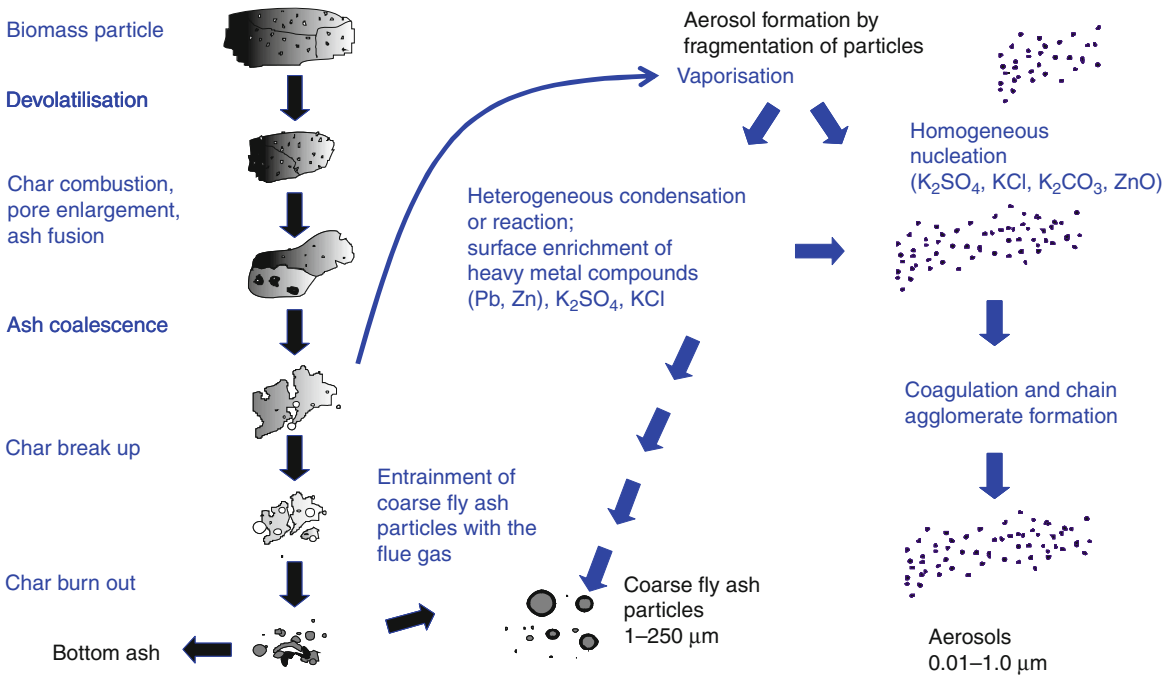

Biomass Energy Heat Provision in Modern Large-Scale Systems. Figure 14
Ash formation during biomass combustion

entrained with the flue gas, forming coarse fly ash emissions. Consequently, the most relevant difference between coarse fly ashes and aerosols is that coarse fly ashes always remain in the solid phase while aerosols undergo phase changes during their formation process (release to the gas phase and gas-to-particle conversion).

A share of the volatile ash-forming elements is not released to the gas phase but undergoes secondary reactions with the nonvolatile species (e.g., Ca, Si), thus being embedded in the coarse ash. The mechanisms of these secondary reactions and the parameters influencing the release of volatile species from the fuel are of great relevance for aerosol and deposit formation [41].

Especially with respect to the utilization of herbaceous biofuels as well as residues from agricultural, food, and biofuel industry, the special role of P has to be mentioned. In conventional wood fuels P is mainly inorganically bound and therefore, almost all P is embedded in the coarse ash fraction. In agricultural biomass as well as biogenic residues from industrial processes a share of the P may also be organically bound. Parts of this organically bound P can also be released to the gas phase and therefore participate in aerosol and deposit formation processes [11, 42].

The bottom ash represents the ash fraction remaining in the furnace after combustion of the fuel and is then removed by the de-ashing system. Coarse fly ash particles, which are entrained from the fuel bed with the flue gas, are partly precipitated on their way through the furnace and the boiler by inertial impaction, gravitational and centrifugal forces and therefore form the so-called furnace or boiler ash. Particles that are small enough to follow the flue gas on its way through the furnace and the boiler finally form the coarse fly ash emission at boiler outlet. The major share of these particles is precipitated in cyclones or filters and forms the cyclone fly ash and parts of the filter fly ash.

Table 6 gives typical data concerning the fractionation of ashes into bottom ashes, cyclone fly ashes and filter fly ashes in modern fixed-bed biomass combustion plants [12]. On the contrary, in fluidized bed and pulverized fuel combustion the amount of bottom ash is low while the fly ash fractions clearly dominate. It is recommended to use a two-stage fly ash precipitation (cyclone plus filter) in order to increase the overall dust precipitation efficiency.

Aerosols are formed by gas-to-particle conversion processes in the furnace and in the boiler. Some of the aerosol particles coagulate with coarse fly ashes due to collisions. Moreover, a smaller part of aerosols is also precipitated in the boiler and therefore contributes to the boiler ash while the major part of this fraction is emitted with the flue gas at boiler outlet. Since aerosols are characterized by particle sizes significantly below 1 μm (ae.d.), precipitation in a cyclone, which usually has a cut diameter of about 5–10 μm, is almost impossible. Thus, aerosols can only be precipitated in more advanced filter systems such as baghouse filters and electrostatic precipitators (ESP). Consequently, aerosols do not contribute to the cyclone fly ashes but to the filter fly ashes as well as to the particulate emissions at filter outlet.

Figure 15 gives the scheme of a typical large-scale grate-fired steam boiler to show where the different ash fractions occur.

The initial step for coarse fly ash formation is the entrainment of small ash, fuel and charcoal particles from the fuel bed with the flue gas. The mass of particles entrained from the fuel bed is influenced by the following parameters:

- The fuel, the ash content and the particle size of the fuel are of major relevance for particle entrainment. The probability that an ash particle is entrained from the fuel bed with the flue gas significantly increases with increasing ash content of the fuel

Biomass Energy Heat Provision in Modern Large-Scale Systems. Table 6 Typical shares of the different ash fractions on the total ashes produced

	Bark combustion	Wood chips combustion	Sawdust combustion	Straw combustion
Bottom ash	65–85	60–90	20–30	80–90
Cyclone fly ash	10–25	10–30	50–70	2–5
Filter fly ash	2–10	2–10	10–25	5–15

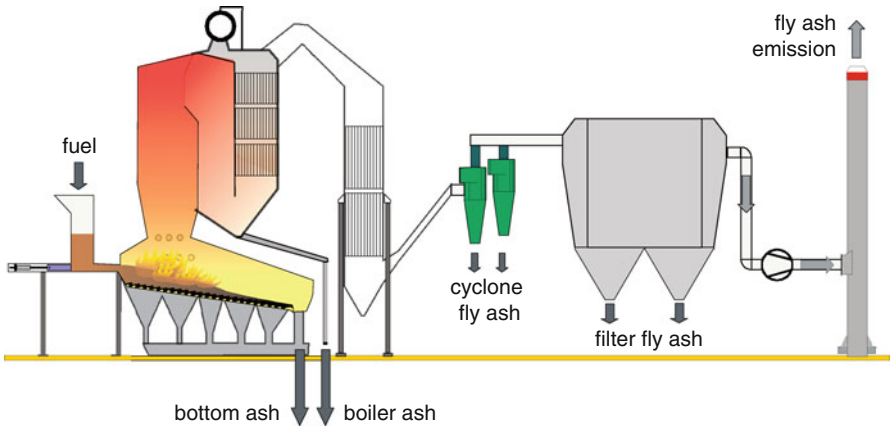

Biomass Energy Heat Provision in Modern Large-Scale Systems. Figure 15
Ash fractions in a biomass combustion unit. (Explanations: typical plant scheme of a large-scale grate-fired steam boiler)

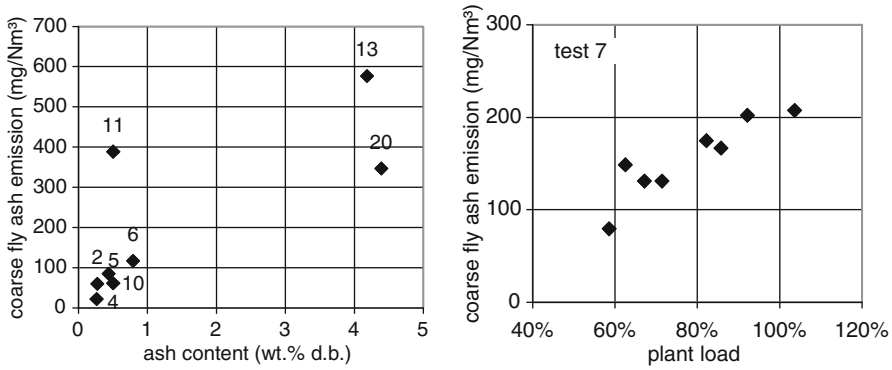

Biomass Energy Heat Provision in Modern Large-Scale Systems. Figure 16
Influence of the ash content of the fuel (*left picture*) and the boiler load (*right picture*) on the total fly ash emissions. (Explanations: emission data related to dry flue gas and 13 vol% O_2, d.b. dry basis, results from tests performed at different grate fired systems, for the results presented on the left picture only measurements at full load (>80% of the nominal boiler capacity) were considered

(Fig. 16, left). Particle entrainment also increases with decreasing particle size of the fuel.

- The boiler load also influences particle entrainment from the fuel bed. Measurements performed show a clear tendency of increasing fly ash emissions with increasing boiler load of the combustion plant (Fig. 16, right).
- In the case of grate-fired systems, the grate system applied as well as the design of the grate have an influence on ash entrainment. Grate systems such as horizontally moving grates, which keep the fuel bed comparably undisturbed during its movement along the grate, show a tendency toward lower ash entrainment than grate systems such as inclined moving grates (due to gravity enforced movements) and vibrating grates. Moreover, the grate design should avoid locally excessive combustion air velocities in the fuel bed, which could lead to channeling and increased fuel and ash entrainment.
- The control system of the combustion plant should be designed in order to achieve a smooth fuel transport on the grate and to minimize disturbances of the fuel bed, which lead to increased particle entrainment.

A considerable number of tests have been carried out to investigate possible parameters influencing the mass of aerosols formed during combustion. Therefore, the combustion air ratio, the furnaces temperature, the moisture content of the fuel, as well as the influence of flue gas recirculation are considered. These parameters are varied during test runs in a range, which is typical for the operation of fixed-bed combustion units. Based on this no significant influences of the parameters mentioned on the mass of aerosols formed during combustion could be identified. This leads to the conclusion that as long as almost complete burnout prevails, the fuel composition, or in more detail, the release of aerosol-forming species from the fuel during combustion, is the most relevant parameter determining the mass of aerosols formed. This statement is confirmed by the data presented in Fig. 17, where the concentrations of the most relevant aerosol-forming elements K, Na, Zn, and Pb in the fuel are plotted against the average aerosol emissions measured at boiler outlet of medium and large-scale fixed-bed combustion plants [43].

Results from test runs including element balances over fixed-bed combustion plants performed with beech, bark, and waste wood have shown that usually 10–40 wt% of K and Na, more than 80% of S, more than 95% of Cl, as well as more than 80% of Zn and Pb are released to the gas phase.

Different particle precipitation technologies are available in order to reduce particle emissions from biomass combustion plants. However, not every technology suits every need. Among the determining factors are the particle size, required collection efficiency, gas flow, allowed time between cleanings, the detailed nature of the particles, and the presence of tars in the flue gas. The following rules of thumb may be helpful in selecting particle control technologies for biomass combustion applications:

- Sticky particles (e.g., tars) must be collected in a liquid (e.g., with a scrubber). Alternatively, a bag filter or an electrostatic filter with coated collecting surfaces is possible. There must also be a way to process the produced contaminated liquids.
- Particles that adhere well to each other but not to solid surfaces are easy to collect. Those that do the reverse often need special surfaces, e.g., Teflon-coated fibers in filters that release collected particles well during cleaning.
- The electrical properties of the particles are of paramount importance in electrostatic filters, and they are often significant in other control devices where friction-induced electrostatic charges on the particles can aid or hinder collection.

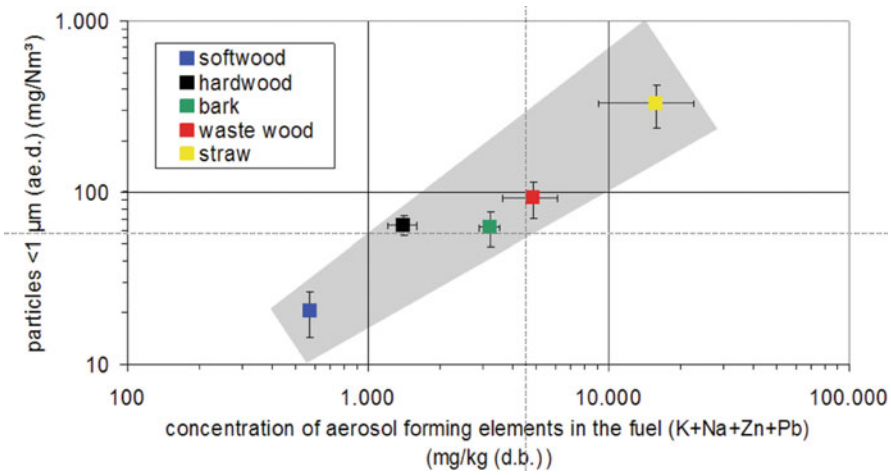

Biomass Energy Heat Provision in Modern Large-Scale Systems. Figure 17
Influence of the fuel used on the mass of aerosols formed

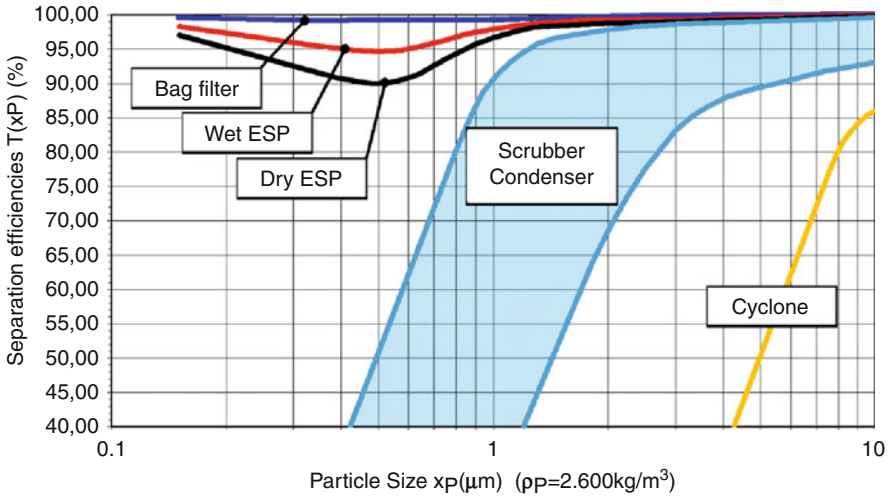

Biomass Energy Heat Provision in Modern Large-Scale Systems. Figure 18
Collection efficiencies for different particle control technologies [44]

- For nonsticky particles larger than about 5 µm, a cyclone separator is probably the only device to consider.
- For particles much smaller than 5 µm normally electrostatic filters, baghouse filters or scrubbers are considered. Each of these can collect particles as small as a fraction of a micron.
- For large flows, the pumping cost makes scrubbers very expensive; other devices are preferable.
- Corrosion resistance and dew point must always be considered.

Figure 18 shows the collection efficiencies for some proven particle precipitation technologies as a function of particle diameter. Table 7 summarizes typical sizes of particles removed by several proven particle control technologies and typical removal efficiencies.

Below, the most important particle precipitation technologies for biomass combustion plants are briefly discussed.

Biomass Energy Heat Provision in Modern Large-Scale Systems. Table 7 Typical sizes of particles removed by various particle control technologies

Particle control technology	Particle size (µm)	Efficiency (%)
Settling chambers	>50	<50
Cyclones	>5	<80
Multicyclones	>5	<90
Electrostatic filters	<1	>99
Bag filters	<1	>99
Spray chambers	>10	<80
Impingement scrubbers	>3	<80
Cyclone spray chambers	>3	<80
Venturi scrubbers	>0.5	<99

- *Cyclones.* Particle separation within a cyclone is based on the principle of gravity in combination with centrifugal forces. Gas and solid particles are exposed to centrifugal forces. Because of the centrifugal forces, particles hit the wall and slide down into a container.
- *Multicyclones.* The separation efficiency of a cyclone can be improved by increasing the centrifugal force through reduction of the cyclone diameter. In order to prevent loss of capacity, several cyclones can be used in parallel.
- *Electrostatic precipitators.* In an electrostatic precipitator, the particles are first electrically charged. Then they are exposed to an electrical field in which they are attracted to an electrode. In practice, separation can be done in one or two

stages. In case of two-stage separation, charging of the particles is first done in a very strong electric field, after which a relatively weak field separates the particles.

- *Baghouse filters.* The construction of a bag filter consists of a filter or cloth, tightly woven from special fibers and hung up in a closed construction through which flue gas passes. The separation efficiency of bag filters is quite high, even with high flue gas flow rates and high particle content. The first layer of particles improves the filtration efficiency. However, as more particles settle on the cloth, the pressure drop increases. Therefore, periodically the cloth is cleaned by vibration or pressurized air. Cloth filters are usually manufactured in cylindrical shapes.
- *Scrubbers.* In scrubbers, particles are scrubbed out from the flue gas by water droplets of various sizes, depending on the type of scrubber used. The particles are removed by collision and interception between droplets and particles. Upon impact, the particles are wetted and carried by the water droplet. The more droplets are formed, the more efficient the unit is. Therefore, the droplets must be small. Smaller-diameter spray nozzles will produce smaller droplets but will also result in higher pressure drops, consuming more energy. Since efficiency increases as the droplet size decreases, efficiency increases with increasing pressure drop.

Slagging, Deposit Formation, and Corrosion

Ash melting, deposit formation, and corrosion are the major internal plant operation–related problems associated to ash-forming elements. Ash melting can occur on the grate and on non-cooled furnace walls. Moreover, fly ash depositions formed on heat exchanger surfaces can also melt. As soon as ashes start partly to melt or fuse, the resulting ash pieces usually called slag.

Deposit formation means the formation of ash layers on furnace and boiler surfaces (furnace walls, radiative and convective heat exchanger surfaces). Thereby it is often distinguished between slagging and fouling. Slagging is the formation of molten or partially fused deposits on furnace walls or convection surfaces exposed to radiant heat. Fouling is commonly defined as the formation of deposits on convective heat exchanger surfaces such as boiler tubes in hot water fire tube boilers and superheaters in water tube steam boilers.

Ash Melting and Slagging Ash melting on the grate can result in problems with the combustion process since slag plates can hinder the primary airflow through the fuel bed. Moreover, larger slag pieces can lead to damages of the grate as well as to problems with blocking the de-ashing system. Slagging and deposit formation in the furnace can lead to increased pressure losses due to smaller flow areas in narrow parts of the furnace, and slagging and deposit formation in the radiative sections of steam boilers can lead to reduced heat transfer. Figure 19 shows typical examples for slagging on a grate and for slag formation in the radiative part of a steam boiler.

Slag formation in biomass furnaces and boilers is always a result of ash melting. Not necessarily, the whole ash has to melt. Usually, single phases which show low melting temperatures start to melt and act as glue between ash particles with higher melting temperatures. Therefore, always different phases of molten and non-molten compounds can be found when analyzing slag pieces or hard deposits. The formation of slag pieces and hard deposits starts at temperatures where about 15 wt% of the ash in a certain ash piece are molten (T_{15}) [45]. At the temperature where the share of molten phases exceeds 70 wt% (T_{70}), the slag/deposit typically starts to flow.

Thermodynamic equilibrium calculations have turned out to be a useful tool to evaluate the melting behavior of biomass ashes. Thereby, thermodynamic equilibrium calculations of multiphase and multicomponent systems simultaneously handling hundreds of chemical species are applied. For combustion systems, both major and minor ash-forming components are taken into account. The reactions of the minor components are usually dependent on the reactions of the major components. However, minor elements (especially Pb and Zn as well as Cl) are also of great relevance, since they usually contribute to a reduction of the ash melting temperatures of ash mixtures. The thermodynamic databases used must be of high quality because small errors and deviations in data for main components give bigger errors on

small components and give wrong results. Especially concerning systems containing P only restricted thermodynamic data are presently available.

One big advantage of thermodynamic equilibrium calculations is that they can be performed for typical grate ash as well as fly ash compositions separately. Therefore, also the significantly differing chemical composition of these fractions can be taken into account when determining their melting behavior (e.g., fly ashes with high amounts of alkaline metal salts show typically considerably lower melting temperatures).

Figure 20 presents results from thermodynamic equilibrium calculations performed for bottom ashes from bark and straw combustion. Here the amount of molten phase in the ash is plotted against the temperature. Since the input data for the calculations have been taken from bottom ash analyses performed during

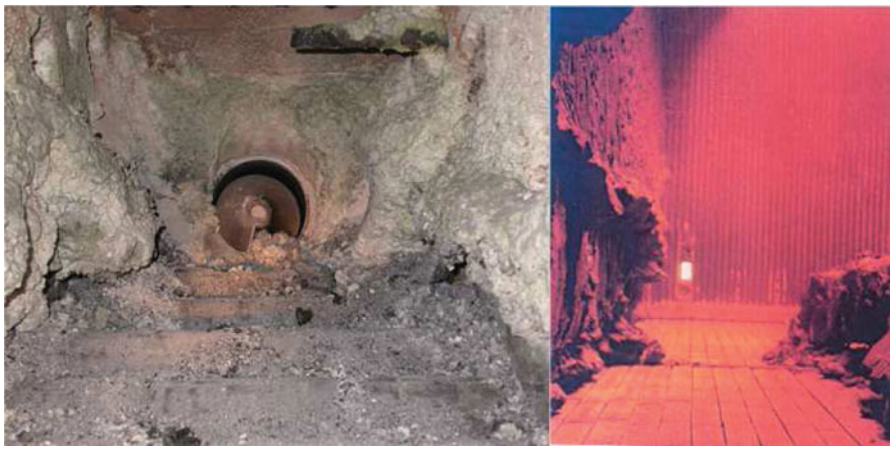

Biomass Energy Heat Provision in Modern Large-Scale Systems. Figure 19
Examples for slag formation. (Explanations: *left* slag formation in a moving grate furnace during combustion of industrial biogenic residues, *right* slag formation in the radiative section of a steam boiler)

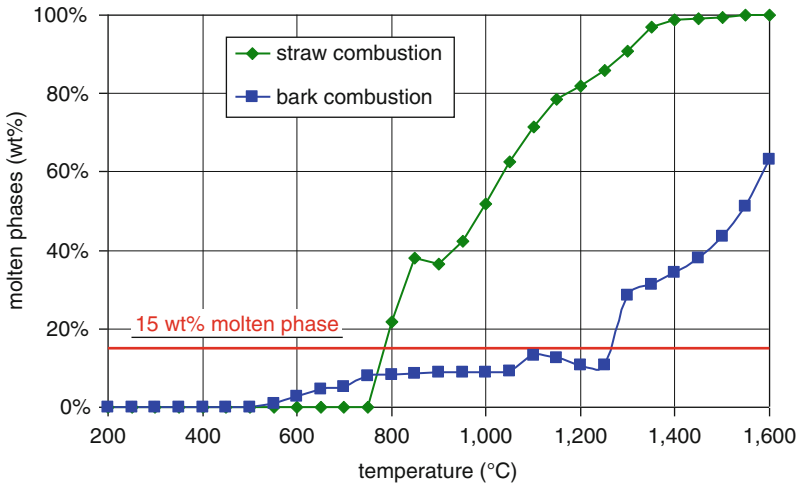

Biomass Energy Heat Provision in Modern Large-Scale Systems. Figure 20
Formation of molten phases in bottom ashes from bark and straw combustion – results from thermodynamic equilibrium calculations [47]

real-scale test runs, realistic ash compositions form the basis for these calculations. In the case of straw combustion a rapid increase of the molten phases at temperatures above 750°C occurs. T_{15} is reached below 800°C. For ashes from bark combustion this effect happens at significantly higher temperatures of about 1,250°C. Moreover, the results of the calculations provide data about the compositions of the molten phases as well as the changes of the compositions depending on temperature.

These results can then also be compared with results from SEM/EDX analyses of molten phases of ash and slag pieces in order the get a more detailed picture of the ash-melting behavior of complex ash mixtures. Such calculations can be useful to indicate relevant trends and differences between various fuels and ash fractions.

Figure 21 shows the influence of heavy metals on the melting behavior of Cl-containing fly ash mixtures. The upper part of the blue line for instance shows the ash melting point of pure K_2SO_4 (melting point: 1,068°C), which is a relevant compound of aerosols formed during biomass combustion. If K-carbonate is formed the first melting point decreases to 940°C, and if K-chloride is formed to 643°C. Small amounts of Na (red curve) decrease the first melting point to 609°C. The presence of Pb and Zn, even in small amounts compared to K and Na, results in molten phases at such low temperatures as 196°C.

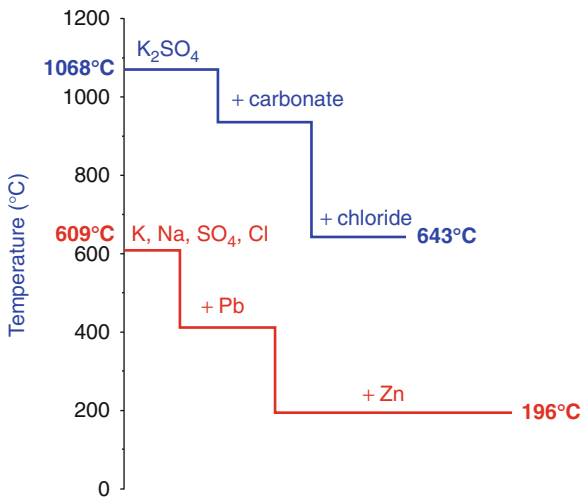

Biomass Energy Heat Provision in Modern Large-Scale Systems. Figure 21
The influence of different K salts as well as of heavy metals on the melting temperatures of ash mixtures.
(Explanations: Source [41])

As it can be revealed from Figs. 20 and 21, ashes from different biomass fuels can show significantly different ash melting behaviors and therefore, measures to reduce problems with ash melting and slagging in combustion plants have always to be adjusted to the chemical composition of the fuel applied. Appropriate measures usually implemented in modern biomass combustion systems are grate cooling, furnace cooling by cooled walls or flue gas recirculation, the appropriate adjustment of the flue gas inlet temperature in convective boiler sections and of the superheater steam temperature, as well as the utilization of additives.

Deposit Formation Deposits are formed by coarse fly ashes as well as condensable gaseous ash-forming compounds present in the flue gas. Under the typical conditions prevailing in biomass hot water, thermal oil, and steam boilers, the direct condensation of ash-forming vapors on heat exchanger surfaces and inertial impaction are of major relevance concerning deposit formation. Thermophoresis has certain relevance, especially when high-temperature gradients between a cooled wall and the flue gas occur. Other mechanisms such as turbulent eddy impaction, Brownian diffusion, and diffusiophoresis are of minor relevance.

With increasing deposit thickness, the heat transfer through the heat exchanger tubes decreases which results in a loss of efficiency. Severe deposit formation (fouling) can block the flue gas pathways through heat exchanger sections. Figure 22 shows deposits on superheater tubes of a waste wood fired steam boiler.

The temperature at the gas side deposit surface increases with increasing deposit thickness (Fig. 23). There, results gained from CFD simulations performed for a superheater tube with a surface temperature of 590°C exposed to a flue gas stream with 1,050°C are presented. From the simulation results, it can be derived that with increasing deposit thickness the surface temperature at the flue gas side significantly increases and finally reaches more than 900°C at

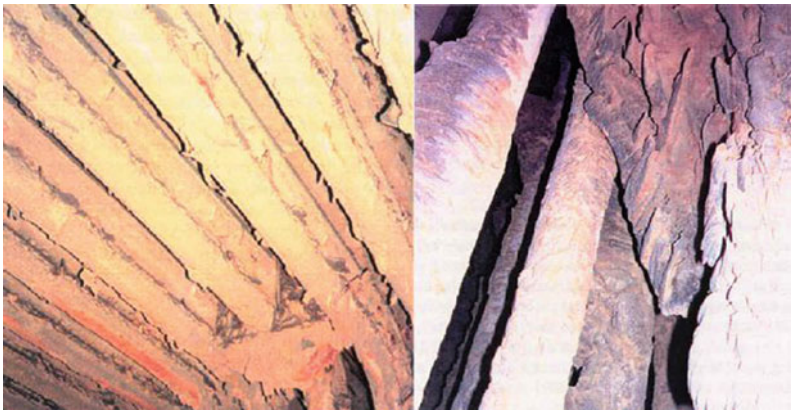

Biomass Energy Heat Provision in Modern Large-Scale Systems. Figure 22
Pictures of deposits formed on superheater tubes of a steam boiler during waste wood combustion. (Explanations: *left* typical deposit formation, *right* severe deposit formation leading to the blocking of heat exchanger pathways)

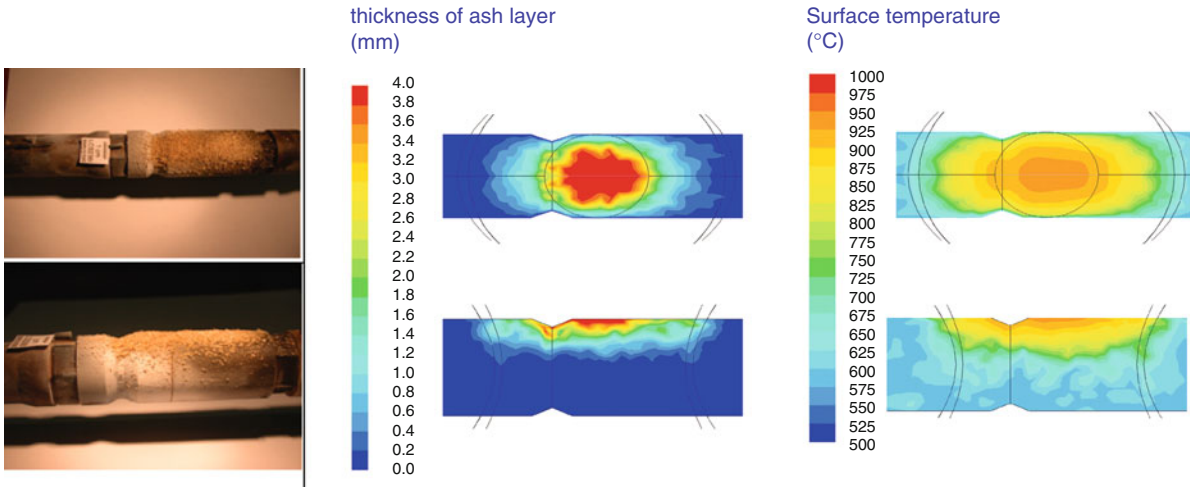

Biomass Energy Heat Provision in Modern Large-Scale Systems. Figure 23
Ash deposit layer on a water-cooled deposition probe (*left*) compared with CFD simulations performed (*middle*) and influence of ash depositions on the surface temperatures (*right*). (Explanations: bulk flue gas temperature 1,050°C, clean probe surface temperature 590°C, figures at the top *top view* figures at the bottom *side view)*

a deposit thickness of about 4 mm. With increasing surface temperature the fraction of molten phases increases and therefore the deposit becomes more sticky and grows faster. Finally, higher amounts of molten phases also lead to the formation of hard deposit layers problematic to be removed.

Consequently, it is important to periodically clean heat exchanger surfaces in order to reduce deposit growth. Therefore, different automatic heat exchanger cleaning systems listed below are usually applied.

- Fire tube boilers can be cleaned by injecting pressurized air into the tubes. Thereby, in an interval of some hours for some milliseconds an air pulse is injected which cleans the boiler tubes. Membrane valves control this air pulse. To protect these valves

from too high temperatures, the cleaning system is usually installed on the wall of the turning chamber between the first and the second duct (cleaning of the first duct in countercurrent and of the second duct in cocurrent flow).

- In water tube steam boilers, usually soot blowers are installed to remove deposits from the superheater surfaces. If there is an increased risk for deposit formation on the tubes in the radiative boiler section, sometimes water canons are also installed. Moreover, shot cleaning by injecting small metal balls into the heat exchanger bundles is sometimes applied.

Besides these secondary measures also primary measures for the reduction of deposit formation should be considered. These measures involve the adjustment of the flue gas and tube surface temperatures to the expected properties of condensing ash-forming compounds (which depend on the composition of the fuel applied) during boiler design as well as a careful control of the flue gas temperatures during operation. Moreover, additives can be used to reduce deposit formation.

Additionally, load changes can lead to changing flue gas and boiler tube temperatures. Due to thermal stresses, deposits can be partly destroyed during phases with load changes. This effect can additionally support the efficiency of automatic cleaning systems.

Corrosion Corrosion is an important issue especially for biomass plants utilizing fuels with high chlorine and sulfur contents. For biomass combustion, three possible corrosion mechanisms are distinguished:

- Active oxidation
- Corrosion due to molten alkaline metal compounds and other salts
- Acid dew point corrosion

The so-called active oxidation (or high-temperature chlorine corrosion) is the most relevant corrosion mechanism in biomass boilers (see Fig. 24). This mechanism is based on the formation of Cl-containing deposit layers on the boiler tube surfaces. The first step of deposit formation is the formation of an ash layer by direct condensation of alkaline metal and heavy metal salts (chlorides and sulfates) on the boiler tube surfaces. The chemical composition of this condensed layer depends on the tube surface temperature and on the fuel composition, respectively, the release behavior of alkaline metals, Cl, S and easily volatile heavy metals from the fuel to the gas phase. If the molar ratio 2S/Cl released from the fuel to the gas phase is high and flue gas temperatures above 850°C occur, mainly alkaline metal sulfate vapors are formed while, if this ratio is low, the formation of alkaline metal chlorides usually dominates.

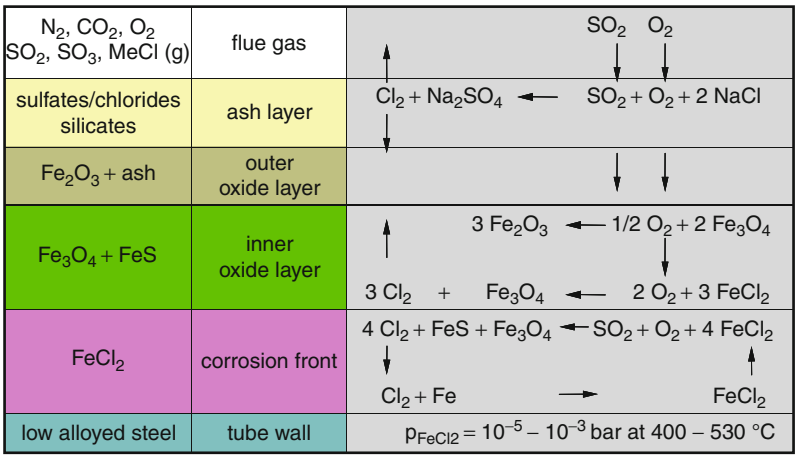

Biomass Energy Heat Provision in Modern Large-Scale Systems. Figure 24
Schematic explanation of the active oxidation mechanism [49]

Combustion tests with chemically untreated wood fuels as well as waste wood have shown, that, when utilizing chemically untreated biomass, at tube surface temperatures above 500°C the Cl-concentration in the deposits starts to significantly decrease [46]. As soon as the surface temperature exceeds 550°C almost no Cl could be found in the deposits. Superheaters of modern steam boilers utilizing chemically untreated biofuels are usually designed for steam temperatures between 480°C and 540°C and thus operate in this temperature range.

In hot water boilers on the other hand, where the tube surface temperatures are rather low (around 100°C) compared with steam boilers, Cl containing deposits are found even when utilizing fuels with very low Cl contents and high 2S/Cl ratios.

To start the process of active oxidation besides Cl-containing deposits also gaseous SO_2 is needed. SO_2 reacts with alkaline metal chlorides under formation of alkali metal sulfate and release of Cl_2. This process happens in the deposit layer and therefore, Cl_2 diffusing toward the inner oxide layer can form $FeCl_2$. $FeCl_2$ has, depending on the temperature, a certain volatility under reducing conditions and can therefore be vaporized. The vapor formed diffuses from the tube wall into the ash layer. There, it is oxidized again (due to the increasing partial pressure of O_2 toward the flue gas) and the Cl_2, which is released, can diffuse back to the tube wall and react there again with iron oxide. Following this process, even small amounts of Cl released in the ash layer have the potential to cause considerable corrosion damages if the residence time of the ash layer on the tube surfaces is high enough.

Three measures to reduce active oxidation can be mentioned:

1. Utilization of fuels with a high molar 2S/Cl ratio to enforce the formation of K_2SO_4 instead of KCl layers.
2. Lower tube surface temperatures considerably reduce the evaporation of $FeCl_2$ and thus slow down the corrosion process.
3. Frequent cleaning of the boiler tubes (implementation of automatic boiler cleaning systems) in order to keep the residence time of ash layers on the tube surfaces low and thus to limit the sulfation reactions.

The second corrosion mechanism depends on the presence of alkaline metal and heavy metal chlorides and sulfates on boiler tube surfaces. These chlorides and sulfates and especially mixtures of them can show comparably low melting temperatures (Fig. 21). Molten salt phases thereby can attack the tube material. This mechanism is of minor relevance for the combustion of chemically untreated fuels. However, in the case of the combustion of waste material such as waste wood, which contains comparably high heavy metal concentrations, it can be of relevance.

During the utilization of chemically untreated woody fuels, usually no problems with acid dew point–induced corrosion are observed. However, when utilizing waste wood or biogeneous residues, this mechanism can become important. If a fuel contains high S concentrations and comparably low K and Caconcentrations, a relevant amount of S will not be embedded into the ashes by the formation of K_2SO_4 and $CaSO_4$ but remains as SO_2 in the gaseous phase. A part of the SO_2 reacts to SO_3 and then with water (flue gas moisture) to form H_2SO_4. The acid dew point temperature (ADT) of H_2SO_4 significantly increases with increasing SO_3-concentrations in the flue gas. If the temperatures of boiler or economizer tube surfaces are below this dew point temperature, H_2SO_4 condensation followed by corrosion takes place. Therefore, an appropriate adjustment of the surface temperatures of economizers and hot water boilers beyond the expected acid dew points is of relevance.

For future technological developments, the main aim is to increase the thermal and electric efficiency by increasing the steam parameters. Thereby, especially fouling and corrosion-related problems have to be considered. For straw combustion for instance, a steam temperature of 542°C leading to an electric efficiency of 31.7% has already been achieved, e.g., in the CHP plant Maribo-Sakskøbing (Denmark). Figure 25 shows a scheme of this CHP plant utilizing wheat straw. Here appropriate technological solutions in order to reduce corrosion particularly in the high-temperature stages of the superheaters have been implemented. The boiler and in particular the superheaters are specially designed to handle the harsh condition from combustion of straw and straw-like biomass fuels in a highly efficient boiler with advanced steam data. The first and second pass superheater stages are operated in the so-called slagging mode.

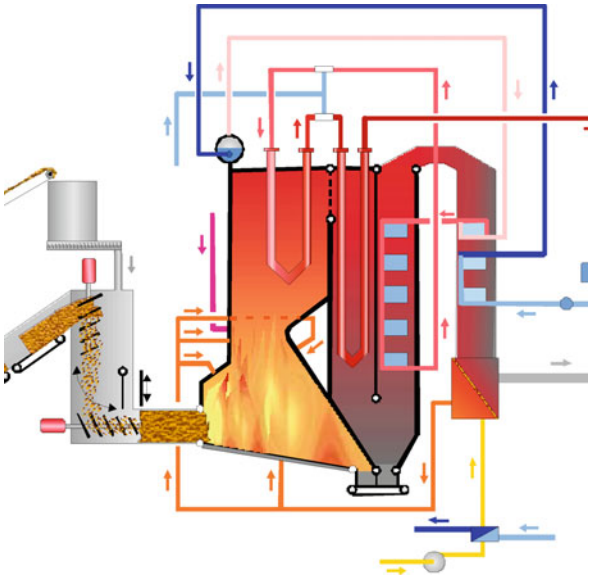

Biomass Energy Heat Provision in Modern Large-Scale Systems. Figure 25
Case study for appropriate technological solutions in order to reduce corrosion-related problems – the CHP plant Maribo-Sakskøbing (Denmark). (Explanations: Source: Bioener ApS; main fuel wheat straw, steam pressure 92 bar, steam temperature 542°C, power output (gross) 10.6 MW, thermal output 20 MW, electric efficiency (gross) 31.7%, thermal plant efficiency 60%, total plant efficiency 91.7%, efficiencies related to fuel power input (NCV))

A continuous K_2SO_4 slag layer on tube surfaces protects the superheater material against high-temperature chlorine corrosion. The slag layer is several cm thick and only removed when the plant is shut down due to thermal stress. By this way, electric efficiencies of more than 31% can be achieved in medium-scale CHP plants at plant availabilities of above 90%.

For CHP plants utilizing wood fuels, even higher steam parameters and consequently efficiencies should be the target for future developments. First R&D results show low corrosion potentials due to decreasing Cl-concentrations in deposits at temperatures above 540°C. However, further long-term tests are needed. For such tests newly developed corrosion probes are a useful development tool [48, 49]. The correct choice of the superheater materials plays an important role for such advanced approaches. Moreover, the application of additives which reduce the Cl-content of deposits can contribute to a further increase of the steam temperatures.

Intelligent Process Control Systems

State-of-the-art control systems for biomass combustion plants usually work with four control circuits which control the load, the furnace temperatures, the pressure in the furnace, and the secondary air ratio. Each of these control circuits is responsible to set respective output parameters based on measured data and defined setpoints. They are to a large extent independent from each other. Dependencies and sometimes highly nonlinear interrelations between the different output parameters are not or only to a small extent taken into consideration. Consequently, conventional control systems work sufficiently efficient at steady state but not efficient in intermediate conditions (e.g., load changes or changes of the fuel quality). The potential of a modern biomass furnace with an optimized furnace geometry and nozzle design is not fully utilized concerning low emission operation and high energetic efficiencies by conventional control systems.

Within recent years control systems implementing neuronal networks, fuzzy logic, and model-based control gained more and more importance but are at the moment not or only to a small extent applied for biomass combustion plants.

With neuronal networks, it is possible to develop a mathematical model in a fast and convenient way directly from experimental data. The major drawback is that the models are not based on the underlying physical relations and are only valid within the scope of the experimental data provided. Consequently, validity is not guaranteed for every state.

Fuzzy control is based on a description of a system based on fuzzy logic, which allows to deduce a mathematical model from a linguistical description of the system behavior. Hence, fuzzy control has the advantage that the operator's expertise can be used to develop a control strategy very quickly. The disadvantage of fuzzy concepts is the fact that states not considered by rules can lead to malfunctions and that there is no deterministic procedure for the design of a fuzzy controller. Consequently, liberties in the realization of

fuzzy controllers can degrade the results significantly. Up to now, fuzzy concepts are partly implemented in control systems for biomass combustion plants but there is no control system available completely based on fuzzy logic.

Model-based concepts require a preferably simple mathematical model that describes the main interrelations of the physical system to be controlled [50–53]. Based on this mathematical model, it is possible to develop a controller taking the nonlinearity and the coupling of the different process variables explicitly into account, wherefore a well-established theory is available. Consequently, the so designed model-based controller is able to react more efficiently on unsteady operating conditions than the currently in combustion plants used control systems. The only disadvantage of the described model based control strategies is that they are very labor intensive in the case that no applicable mathematical model is available. If such models are available, then model based systems are evaluated to be the most suitable and efficient solution.

New control concepts (especially model based control strategies and fuzzy control) will gain more importance for biomass combustion systems in the near future.

Future Directions

Biomass is the most important renewable energy source in the European Union. In the field of energetic utilization of solid biomass, combustion is the most advanced and market-proven application. Consequently, the energetic use of solid biomass is primarily based on biomass combustion at presence. Biomass combustion technologies, like fixed bed, fluidized bed, and pulverized fuel combustion, are currently available for different types of biomass fuels covering a wide range of plant capacities. Concerning plant size, the different applications of biomass combustion can be divided into small-scale biomass combustion systems (capacity range below 100 kW_{th}), medium-scale combustion systems (capacity range between 0.1 and 20 MW_{th}), large-scale combustion systems (capacity range above 20 MW_{th}), and co-firing of biomass in coal-fired power stations (capacity range usually some 100 MW_{th}).

The necessary measures for a complete combustion are well known in principle. But they are still not implemented in all combustion plants operating today. Such improvement would comprise optimized mixing of gases in the furnace as well as implementation of updated and more advanced process control systems. The thermal conversion efficiency of existing combustion plants also has a potential for improvement. These improvement potentials are mainly in the way the plant is operated, like improved maintenance, correct adjustment of excess air ratio, and optimized management of heat distribution. Moreover, process economy for large-scale combustion of biomass fuels with high water contents can be significantly improved by using flue gas condensation.

Regarding plant design, chemical and physical properties of biomass fuels are of great importance. The fuel properties affect fuel transport, storage, and feeding systems as well as the combustion and boiler technology. Especially ash-related problems like aerosol formation, slagging, deposit formation, and corrosion in biomass combustion processes are always strongly associated with the fuel chemistry, in detail, with the concentration and speciation of inorganic compounds in the fuel. Important guiding parameters are, in this respect, the molar ratios (K + Na)/(2S + Cl), 2S/Cl, and the sum of K, Na, Zn, and Pb in the fuel. High molar ratios of (K + Na)/(2S + Cl) indicate lower HCl and SO_x emissions. The molar ratio of 2S/Cl indicates the preferred formation of alkaline sulfates or alkaline chlorides. K, Na, Zn, and Pb are the most relevant aerosol-forming elements. With increasing concentrations of these elements, the probability of aerosol formation as well as deposit formation increase as well. Consequently, if an ash-related problem has to be evaluated always comprehensive knowledge about the fuel is needed.

Beside woody fuels, new feedstocks like annual and perennial energy crops, agricultural and industrial biogenic residues, as well as chemically treated biofuels such as urban waste wood and demolition wood, can significantly contribute to the future energy supply. These types of fuels typically contain higher amounts of nitrogen and volatile ash-forming elements (K, Na, Zn, and Pb) as well as corrosive elements (S and Cl) than the typically chemically untreated woody fuels mainly used today. For this reason, special combustion

and process control systems as well as new processes for efficient energy recovery and emission reduction will be required.

NO_x emissions from biomass combustion applications are mainly due to the oxidization of fuel-bound nitrogen, whereas NO_x formed from air-bound nitrogen is usually of minor relevance in most biomass combustion applications due to moderate combustion temperatures. Primary measures or combinations of primary and secondary measures can efficiently reduce NO_x emissions from biomass combustion. In addition, CFD-modeling of NO_x formation is of great relevance for an improved future plant design.

The reduction of dust and fine particle emissions especially by primary measures is of great relevance for small-scale applications typically not equipped with filter systems. For medium to large-scale plants, efficient filters like ESPs or baghouse filters are state of the art.

CHP technologies based on biomass combustion have reached a high level of development. For large-scale CHP plants (above 2,000 kW_{el}), the steam turbine process is economically and technically feasible. In the medium-scale power range (200–3,000 kW_{el}) the organic Rankine cycle (ORC) process has proven its technological maturity. For small-scale CHP plants (below 100 kW_{el}) the Stirling engine process and the micro gas turbine are in a demonstration phase. However, these technologies have not proven their technological maturity yet.

On going research mainly focuses on the utilization of new biomass fuels (annual crops, short rotation plants, waste materials from the agricultural and the food industry, etc) as well as the further development of combustion technology toward next generation ("zero emissions") systems. The main focus regarding emission reduction is on aerosol emissions as well as on NO_X reduction (for all size ranges). Concerning CHP systems new developments focus on advanced and highly efficient systems. In this respect, increased steam parameters and higher availability are important targets. Regarding process control strategies for combustion plants, new concepts like model based systems will gain more and more importance. Future modeling activities aim at CFD models to simulate the whole biomass combustion plant ("virtual biomass combustion plant") interlinking solid fuel combustion, gas phase reactions, the boiler as well as emissions and ash-related problems.

Bibliography

1. Nickull S (2002) Worlds largest biomass co-generation plant opens in Finland. Co-generation & On-Site Power Production 3(3), May–June 2002
2. Obernberger I, Hammmerschmiedt A (1999) Dezentrale Biomasse-Kraft-Wärme-Kopplungstechnologien Potential, Einsatzgebiete, technische und wirtschaftliche Bewertung. Schriftenreihe "Thermische Biomassenutzung," Band 4. dbv-Verlag der Technischen Universität Graz, Graz, Austria. ISBN3-7041-0261-X
3. Furtner K, Haneder H (2008) Biomasse – Heizungserhebung 2007. NÖ Landes-Landwirtschaftskammer, Abteilung Betriebswirtschaft und Technik (Hrsg.), St. Pölten, Österreich
4. Kopetz H et al (2008) 34 Prozent Erneuerbare machbar. Broschüre, Österreichischer Biomasse-Verband (Hrsg.), Wien, Österreich
5. Obernberger I, Thek G (2009) Herstellung und energetische Nutzung von Pellets – Produktionsprozess, Eigenschaften, Feuerungstechnik, Ökologie und Wirtschaftlichkeit. Schriftenreihe "Thermische Biomassenutzung" des Institutes für Partikel- und Prozesstechnik, Technische Universität Graz, Band 5, Graz, Österreich. ISBN 978-3-9501980-5-8
6. Obernberger I, Thek G (2010) The pellet handbook – the production and thermal utilization of biomass pellets. Earthscan, London
7. Herynkova H (2007) The perspectives of the European heating market. In: Proceedings of the European pellets conference 2007, O.Ö. Energiesparverband, Linz
8. Aebiom (2007) European biomass statistics 2007. European Biomass Association, Belgium
9. Nussbaumer T (2002) Combustion and co-combustion of biomass. In: Proceedings of the 12th European biomass conference, vol I, pp 31–37. ISBN 88-900442-5-X
10. Iea Bioenergy Task 32 (2002) Handbook of biomass combustion and co-firing. van Loo S, Koopejan J (ed) pp 171–213, ISBN 9036517737
11. Zhang L, Ninomiya Y (2007) Transformation of phosphorus during combustion of coal and sewage sludge and its contributions to PM10. Proc Combust Institute 31:2847–2854
12. Obernberger I (1997) Nutzung fester Biomasse in Verbrennungsanlagen unter besonderer Berücksichtigung des Verhaltens aschebildender Elemente. Schriftenreihe "Thermische Biomassenutzung," Band 1, dbv-Verlag der Technischen Universität Graz, Graz, Österreich, ISBN 3-7041-0241-5
13. Obernberger I (2010) The present state and future development of industrial biomass combustion for heat and power generation (keynote lecture). In: Proceedings of the ASME-AIT-UIT 2010 conference on thermal and environmental issues in energy systems, May 2010, Sorento, Italy, vol I. Editione ETS, Pisa, pp 9–25. ISBN 978-884672659-9

14. Hansen L, Frandsen F, dam-Johansen K, Soerensen S (1999) Quantification of fusion in ashes from solid fuel combustion. Thermochim Acta 326(1999):105–117
15. Schmidt A, Zschetzsche A, Hantsch-Linhart W (1994) Analysen von biogenen Brennstoffen. Final report, Bundesministerium für Wissenschaft, Forschung und Kunst, Vienna, Austria
16. Marutzky R, Seeger K (1999) Energie aus Holz und anderer Biomasse. DRW-Verlag Weinbrenner, Leinfelden-Echtlingen, Germany, ISBN 3-87181-347-8
17. Mawera (1996) Company brochure, MAWERA Holzfeuerungsanlagen GmbH & CoKG, Hard/Bodensee, Austria
18. Leckner B, Karlsson M (1993) Gaseous emissions from circulating fluidised bed combustion of wood. Biomass Bioenerg 4(5):379–389
19. Westermark M (1994) Termisk kadmiumrening av träbränsleaskor. report. Vattenvall Utveckling AB, Vällingby, Sweden
20. Nussbaumer T (1999) Stromerzeugung aus biogenen Brennstoffen. Brennstoff Wärme Kraft 51(7/8):51–55
21. Nussbaumer T, Neuenschwander P, Hasler P, Jenni A, Bühler R (1998) Technical and economic assessment of the technologies for the conversion of wood to heat, electricity and synthetic fuels. In: Proceedings of the 10th European Bioenergy Conference, June 1998, Würzburg, Germany. C.A. R.M.E.N., Rimpar, pp 1142–1145
22. Dietler R (1994) Wärme-Kraft-Kopplung mittels Dampfprozess bei Holzfeuerungen. In: Proceedings of the 3 rd Holzenergie-Symposium, October 21, 1994, ETH Zürich, Bundesamt für Energie, Bern, Switzerland, pp 251–274
23. Eder F (1997) Einsatz und Marktchancen von Stirling- und Heissgasmotoren. Brennstoff Wärme Kraft 49(1/2):42–45
24. Carlsen H (1999) Status and prospects of small-scale power production based on Stirling engines – Danish experiences. In: Proceedings of power production from biomass III, Espoo, 14–15 September, 1998. VTT, Espoo, pp 249–264
25. KKK-Kühnle, Kopp and Kausch AG (1998) Company brochure. Kopp & Kausch AG, Frankenthal/Pfalz, Germany
26. Bini R, Manciana E (1996) Organic Rankine cycle turbogenerators for combined heat and power production from biomass. In: Proceedings of the 3 rd Munich discussion meeting 1996. ZAE Bayern, Munich
27. Turboden SRL (1998) Company brochure. Brescia, Italien
28. Scheidegger K, Gaia M, Bini R, Bertuzzi P (2000) Small scale biomass powered CHP plants featuring thermal oil boiler and organic Rankin cycle turbogenerators. In: Proceeding of the 1st World conference and exhibitions on biomass for energy and industry, June 2000, Sevilla
29. Obernberger I, Thonhofer P, Reisenhofer E (2002) Description and evaluation of the new 1,000 kWel Organic Rankine Cycle process integrated in the biomass CHP plant in Lienz, Austria. In: Euroheat & Power, vol 10/2002, pp 18–25
30. Spitzer J, Podesser E, Jungmeier G (1997) Wärme-Kraft-Kopplung (Stirlingmotor, Dampfmotor, ORC-Prozesse). Thermische Biomassenutzung – Technik und Realisierung. VDI report 1319, VDI Verlag GmbH, Düsseldorf, Germany
31. Carlsen H, Bovin J (2000) Biofuel stirling engines for CHP. In: Proceedings of the 1st World conference on biomass for energy and industry, Sevilla, June 2000, vol I. James & James, London, pp 933–936. ISBN 1-902916-15-8
32. Steweag (1997) Forschungsprojekt TINA Thermodynamisch Innovative Nichtnukleare Anlage. Report, Steweag, Graz, Austria
33. de Ruyck J, Allard G, Maniatis K (1996) An externally fired evaporative gas turbine cycle for small scale biomass gasification. In: Proceedings of developments in thermochemical biomass conversion, Banff, Canada, May 1996, vol 2. Blackie Academic and Professional, London. ISBN 0-7514-0350-4
34. Thek G, Brunner T, Obernberger I (2010) Externally with biomass and internally with natural gas fired micro gas turbine – system, furnace and high temperature heat exchanger design as well as performance data from first test runs. In: Proceedings of the 18th European biomass conference and exhibition, Lyon, May 2010. ETA-Florence Renewable Energies, Lyon, pp 1891–1899. ISBN 978-88-89407-56-5
35. Riccio G, Spadi A, Chiaramonti D, Martelli F, Thek G, Brunner T, Obernberger I (2011) Development and test results of an externally biomass-fired micro gas turbine CHP plant. In: Proceedings of the central European biomass conference 2011, Graz, January 2011. Austrian Biomass Association, Vienna
36. Riccio G, Chiaramonti D (2009) Design and simulation of a small polygeneration plant cofiring biomass and natural gas in a dual combustion micro gas turbine (BIO_MGT). Biomass and bioenergy 33:1520–1531, ISSN 0961-9534
37. Hammerschmid A, Obernberger I (2000) Biomasse-Kraft-Wärme-Kopplungen auf Basis des ORC-Prozesses am Beispiel des realisierten EU-THERMIE-Projektes in Admont (Österreich). In: Tagungsband zum 9. Symposium "Festbrennstoffe und umweltfreundliche Energietechnik," Kloster Banz, Deutschland. OTTI Energie-Kolleg (Hrsg.), Regensburg, Deutschland, pp 48–58. ISBN 3-934681-09-3
38. Brunner T, Obernberger I (1996) New technologies for NOx reduction and ash utilization in biomass combustion plants – JOULE THERMIE 95 demonstration project. In: Proceedings of the 9th European bioenergy conference, vol 2. Elsevier, Oxford. ISBN 0 08 0428 495
39. Nussbaumer T (1996) Primary and secondary measures for the reduction of nitric oxide emissions from biomass combustion. In: Proceedings of the international conference "Developments in thermochemical biomass conversion,", Banff, May 1996, vol 2. Blackie Academic and Professional, London. ISBN 0 7514 0350 4
40. de Nevers N (1995) Air pollution control engineering. McGraw-Hill, New York
41. Brunner T (2006) Aerosols and coarse fly ashes in fixed-bed biomass combustion. PhD thesis, book series "Thermal Biomass Utilization," vol 6. Graz University of Technology, Styria. ISBN 3-9501980-3-2
42. Beck J, Brandenstein J, Unterberger S, Hein KRG (2004) Effects of sewage sludge and meat and bone meal Co-combustion on SCR catalysts. Appl Catalysis B 49:15–25

43. Jöller M, Brunner T, Obernberger I (2005) Modelling of aerosol formation. In: Proceedings of the international seminar "Aerosols in Biomass Combustion," Graz, March 2005. Book series "Thermal Biomass Utilization," vol 6. Graz, Austria, pp 79–106. ISBN 3-9501980-2-4
44. Cheremisinoff PN (1993) Air pollution control and design for industry. Marcel Dekker, New York
45. Backman R, Skrifvars B, Yrjas P (2005) The influence of aerosol particles on the melting behaviour of ash deposits in biomass fired boilers. In: Proceedings of the international seminar "Aerosols in biomass combustion," March 2005, Graz, Austria, book series "Thermal biomass utilization", vol 6, Graz, Austria, pp 119–132, ISBN 3-9501980-2-4
46. Obernberger I (2010) The present state and future development of industrial biomass combustion for heat and power generation (keynote lecture). In: Proceedings of the ASME-AIT-UIT 2010 conference on thermal and environmental issues in energy systems, Sorento, May 2010, vol I. Editione ETS, Pisa, pp 9–25. ISBN 978-884672659-9
47. Obernberger I, Brunner T, Frandsen F, Skifvars B, Backman R, Brouwers JJH, van Kemenade E, Müller M, Steurer C, Becher U (2003) Aerosols in fixed-bed biomass combustion – formation, growth, chemical composition, deposition, precipitation and separation from flue gas. Final report, EU project No. NNE5-1999-00114, European Commission DG Research, Brussels
48. Riedl R, Obernberger I (1997) Corrosion and fouling in boilers of biomass combustion plants – active oxidation in boiler tubes. In: Proceedings of the 4th European conference on industrial furnaces and boilers, Porto, April 1997. INFUB, Rio Tinto
49. Waldmann B (2007) Korrosion in Anlagen zur thermischen Abfallverwertung – elektrochemische Korrosionserfassung und Modellbildung. PhD thesis. University Augsburg, Augsburg
50. Haider F, Horn S, Waldmann B, Warnecke R (2007) Korrosionssonden-Ergebnisse zu Messungen in verschiedenen Anlagen. In: VDI-Wissensforum (Hrsg.): Beläge und Korrosion, Verfahrenstech-nik und Konstruktion in Großfeuerungsanlagen – Seminar am 12–13 Juni 2007 in Frankfurt/Main. VDI-Verlag, Düsseldorf
51. Scharler R, Zahirovic S, Schulze K, Kleditzsch S, Obernberger I (2006) Simulationsgestützte Auslegung und Optimierung von Biomassefeuerungs- und Kesselanlagen – Einsatzmöglichkeiten, Stand der Technik und innovative Methoden. In: Österreichische Ingenieur- und Architektenzeitung (ÖIAZ), vol 10–12, pp 296–309. ISSN 0721-9415
52. Obernberger I Scharler R (eds.) (2006) CFD modelling of biomass combustion systems. Progr Comput Fluid Dynamics 6(4/5)
53. Zahirovic S, Scharler R, Obernberger I (2006) Advanced CFD modelling of pulverised biomass combustion. In: Proceedings of the international conference science in thermal and chemical biomass conversion, Victoria, Canada, CPL Press, UK, pp 267–283, ISBN 1-872691-97-8
54. Zahirovic S (2008) CFD analysis of gas phase combustion and NOx formation in biomass packed-bed furnaces – a contribution towards quantitative prediction of CO and NOx formation. PhD thesis, Graz University of Technology, Austria
55. Stubenberger G, Scharler R, Obernberger I (2007) Nitrogen release behavior of different biomass fuels under lab-scale and pilot-scale conditions. In: Proceedings of the 15th European biomass conference & exhibition, Berlin, Germany, ETA-Renewable Energies, Florence, Italy. pp 1412–14120, ISBN 978-88-89407-59-X, ISBN 3-936338-21-3
56. Widmann E, Scharler R, Stubenberger G, Obernberger I (2004) Release of NOx precursors from biomass fuel beds and application for CFD-based NOx postprocessing with detailed chemistry. In: Proceedings of the 2nd World conference and exhibition on biomass for energy, industry and climate protection, Rome, Italy, vol II, ETA-Florence, Italy, pp 1384–1387, ISBN 88-89407-04-2
57. Scharler R, Zahirovic S, Schulze K, Kleditzsch S, Obernberger I (2006) Simulationsgestützte Auslegung und Optimierung von Biomassefeuerungs- und Kesselanlagen – Einsatzmöglichkeiten, Stand der Technik und innovative Methoden. In: Österreichische Ingenieur- und Architektenzeitung (ÖIAZ), vol 10–12 (2006), pp 296–309, ISSN 0721-9415
58. Schulze K, Scharler R, Telian M, Obernberger I (2010) Advanced modelling of deposit formation in biomass furnaces – investigation of mechanisms and comparison with deposit measurements in a small-scale pellet boiler. In: Proceedings of the International Conference "Impacts on fuel quality on power production and environment," Aug 29th–Sept 2nd, Lapland, Finland, EPRI, Palo Alto, CA
59. Schulze K, Scharler R, Obernberger I (2011) Development of biomass fired boilers with an advanced CFD model for ash deposit and aerosol formation. In: Proceedings of the 9th European conference on industrial furnaces and boilers, April 2011, Estoril, Portugal, CENERTEC, Portugal. ISBN 978-972-99309-6-6
60. Scharler R, Kuerten JGM, Schulze K, Obernberger I (2007) Numerical simulation of ash particle impaction in tube bundles – A case study as a basis for a CFD based ash deposit formation model in convective heat exchangers. In: Tagungsband zum 23. Deutschen Flammentag, September 2007, Berlin, Germany, VDI-Bericht Nr. 1988, ISSN 0083-5560, ISBN 978-3-18-091988-1, pp. 299-309, VDI-Verlag Düsseldorf (Hrsg.)
61. Van Kessel L (2003) Stochastic disturbances and dynamics of thermal processes, PhD thesis, Eindhoven Technical University, Eindhoven
62. Bauer R, Gölles M, Brunner T, Dourdoumas N, Obernberger I (2007) Modellierung der Druck- und Volumenstromverhältnisse in einer Biomasse-Feuerung. Automatisierungstechnik 55(8):404–410
63. Bauer R, Gölles M, Brunner T, Dourdoumas N, Obernberger I (2008) Modelling of grate combustion in a medium scale biomass furnace for control purposes. Biomass and Bioenerg 34(4):417–427
64. Gölles M (2008) Development of mathematical models of a biomass grate furnace as a basis for model based control strategies. PhD thesis, Graz University of Technology, Austria

Biomass Energy Heat Provision in Modern Small-Scale Systems

Hans Hartmann[1], Volker Lenz[2]
[1]Technologie- und Förderzentrum im Kompetenzzentrum für Nachwachsende Rohstoffe (TFZ), Straubing, Bavaria, Germany
[2]German Biomass Research Centre (DBFZ), Leipzig, Germany

Article Outline

Glossary
Definition of the Subject
Introduction
Technical Approach
Combustion Principles and Furnace Types
Combustion Efficiency
Flue Gas Emissions
Future Direction
Conclusions
Bibliography

Glossary

Annual efficiency Ratio of useful heat provided and total fuel energy input throughout a full heating season.

Boiler Central heating boilers are designed to avoid the loss of heat to the surrounding space. For this reason, they are equipped with water heat exchangers using hot water central heating circuit through which the transfer of heat to the relevant rooms is realized.

Boiler efficiency Same as combustion efficiency but heat radiation is accounted as a loss.

Combustion efficiency Momentary ratio of useful heat and fuel energy input. Energy losses are free heat in flue gas, fuel residues in ash, and incomplete gas combustion.

Downdraft combustion Wood log combustion principle where the hot gases are not discharged to the top, but the flames instead spread underneath the bottom of the combustion chamber or sideway and the combustion gases released are channeled into a combustion chamber located below or next to the fuel filling space.

Stand-alone furnaces These furnaces (stoves) emit their thermal energy to the surrounding space only.

Updraft combustion Wood log combustion principle where the combustion air (primary air) is channeled upward through the grate or from the bottom of the fire bed and thereby through the whole layer of fuel.

Definition of the Subject

The use of wood for the supply of heat in furnace systems with small to medium capacity has never really gone out of fashion, particularly in rural areas. Especially in recent years, a virtual renaissance in the use of wood for combustion purposes in the most diverse range of furnaces can be observed. Driven by continuously growing fuel costs for oil and gas from fossil resources as well as by public policy promoting the increased use of renewable energies in order to reduce greenhouse gas emissions, more and more already existing furnaces (mainly stoves) are being used more intensively. But also a considerable number of new systems are being installed (size of the market for small-scale furnaces in EU-27 approx. 3–4 million units per annum [3]). In many countries, more than half of the solid biomass used for energetic purposes is used in small-scale furnace systems with a thermal capacity below 1 MW. Small-scale combustion units, however, are at the same time one of the main source of particulate matter emissions. An improvement in existing system technology is therefore an essential challenge for the environmentally sustainable use of solid biomass in small-scale furnaces. For these reasons the present state of technology and current developments are presented in detail within this paper.

Introduction

Solid biomass fuels are used for a variety of reasons and different energetic purposes. Biomass is an energy carrier with a high potential for the reduction of greenhouse gas emissions, compared to fossil fuel energy, provided that the biomass is produced in a sustainable manner. Biomass is often regionally available or can be regionally produced as a source of fuel which can contribute to rural development as well as a more secure energy supply system.

Biomass is used for the supply of electricity, heat, and the production of biofuel. The use of solid biomass fuels – and wood in particular – for the supply of heat is the longest established form of energetic use. Even though the supply of electric power generated from biomass and the production of biofuels has increased considerably in recent years, in most countries of the world the majority of solid biofuels is used for the supply of thermal energy. Nevertheless some tendencies can be noted indicating that the combined generation of heat and power will significantly gain in importance, also in the lower capacity range.

Apart from the environmental debate surrounding the low-tech combustion of biomass in developing countries, emission levels in general and particulate matter emissions from biomass-fueled furnace systems in particular are also increasingly discussed in industrialized countries. Very low levels of emission have already been achieved in the case of large-scale combustion systems with several MW thermal capacity through regulatory stipulations and the corresponding refitting of plants for the implementation of emissions control measures. In contrast to this, there still exists considerable room for improvement in the case of small-scale systems below 1 MW thermal capacity, in particular with regard to stand-alone furnaces and biomass-fueled combustion systems. A number of countries such as Germany, Austria, and Switzerland have already lowered their emission thresholds for this segment of combustion plants, and other European countries and Federal States in the US are also contemplating the imposition of measures aimed at the reduction of emissions.

A comparison of emission levels made during certification of boiler systems in countries where this is a regulatory requirement indicates the gradual development toward lower values. This applies not only in respect of boiler systems but primarily also with regard to the further technological development of stand-alone furnaces (stoves). A significant reduction in the emission of air pollutants can therefore be achieved by using correspondingly advanced technology. Through investigation of the mechanisms leading to the creation of air pollutants and the introduction of specific measures for further reduction, clearly targeted and controlled progress in technical developments already has been and will continue to be achieved.

In this context, the basic principles for optimizing the processes for the combustion of solid biomass in small-scale furnace systems are presented below. Following on from this, the current state of development regarding different systems for combustion is analyzed. Together with an accompanying commentary on current levels of emission, this paper sets out in closing the perspectives concerning potential future developments.

Technical Approach

Combustion Requirements

A major objective should be to accomplish complete oxidation during the combustion process. This can be achieved by physical separation of the phases of pyrolytic decomposition of the fuel and the gasification process of the charcoal (coke) on the one side from the subsequent combustion of the products from the pyrolytic decomposition and gasification on the other side. The most important requirements for a complete conversion of fuel can be summarized as follows:

- Pyrolytic decomposition of the biofuel and gasification of the remaining carbon to CO, H_2, CH_4, C_nH_m, CO_2, and H_2O. This is accomplished through:
  - Complete pyrolytic decomposition of the biomass fuel through sufficiently high temperatures throughout the whole cycle of reaction
  - Complete gasification of the carbon through good distribution and correct dosage in the supply of air (primary air) to the reaction zone
  - As little as possible disturbance to the fire bed being caused as a result of the recharging of fuel and removal of ashes
- Oxidation of the products released by the processes mentioned above; that is, gas phase oxidation of CO, H_2, CH_4 and C_nH_m to CO_2 and H_2O. Complete oxidation of the fuel gases released takes place through:
  - Supply of oxidants (secondary air) in excess,
  - Sufficiently long retention time for the fuel gas/air mixture in the reaction zone
  - Sufficiently high combustion temperatures
  - Good amalgamation of fuel gases and combustion air through high turbulences
  - Limited retention time in the secondary combustion chamber, that is, approximation of the ideal distribution in a so-called plug flow

The requirement concerning the physical separation of the solid materials conversion process (with primary air supply to the fire bed) from the combustion process within the gas phase (with secondary air supply to the secondary combustion chamber) is therefore an essential prerequisite for a controllable combustion process. For this reason both air supply streams should be controlled independently. For solid biofuels, with their high level of volatile compounds, the separation of primary air supply and the secondary air supply into a specific combustion chamber is therefore an essential requirement for system designs. The primary air supply has an impact on combustion power output, whereas secondary air primarily serves to ensure a full oxidation of the combustible gases.

The technical combustion requirements for gas-phase oxidation described above are sometimes also referred to as the "3-T-Rule" for furnace design (time-temperature-turbulence); that is, retention time, combustion temperature, and intensity of amalgamation represent the essential parameters to be optimized [28].

The better the mixture of fuel gases with the combustion air, the lower the amount of excess air required at which the furnace can (almost) be operated without the discharge of noncombusted gases. A lower volume of excess air also results in higher combustion temperatures; surplus amounts of excess air on the other hand would lead to a cooling down of the system (and thus slowing down the reaction speed). To allow for a low volume of excess air it is essential to use slightly moist or wet biomass fuel. Because the energy consumed by the evaporation process of the water will tend to lead to a lowering of temperature levels in the combustion chamber and the resulting water vapor will additionally increase the volume of flue gases discharged and thereby increase further loss of thermal energy from the hot zone. At the lowest possible level of excess air, which is limited by the overriding objective of minimizing the emission of noncombusted elements (i.e., flue gas components that could be further oxidized), the level of efficiency in the performance of the systems would be at the highest [28].

In trying to optimize excess air supplies, a high combustion temperature can also be maintained by avoiding the unnecessary release of heat from the combustion chamber. This is usually accomplished through the installation of thermal insulation refractory lining inside the primary and secondary combustion chambers. Insulation materials used for the lining of surfaces facing the open fire are, for example, fire clay, refractory concrete, lava clay or ceramic fiber materials [28].

As a general rule for most combustion, a principle does apply: The majority of available thermal energy is not (already) obtained in the combustion chamber, but captured later on from the heated combustion gases, in a heat exchanger which is separated from the combustion chamber. Early extraction of heat may be advantageous when using dry fuels, or in special areas of application if, for example, for the control of fire bed temperatures a cooling down effect by way of specific extraction of available thermal energy is desired (e.g., in the case of fuels whose ashes tend to slag). In grate-based furnace systems for such special fuels, water-cooled grates are used sometimes allowing to operate the system without excessive primary air being used for cooling purposes. In the combustion of dry fuels, the encasement of the combustion chamber with water-cooled walls may also be used to allow for the controlled extraction of heat.

Additionally, furnaces have to comply with applicable environmental regulatory requirements, whereby – also in the case of small-scale systems – secondary measures are sometimes introduced (Section on "Emission of Boilers"). The key to arriving at a minimal emission of polluting substances during operations is primarily to maintain optimal operating conditions; this applies in particular with regard to an optimized fuel-air-ratio, and the use of appropriate control mechanisms is required for this purpose. A complete conversion of fuel materials does in most cases go hand in hand with low-emission values.

Differences Between Manually and Automatically Charged Furnaces

Combustion technology distinguishes between manually charged and automatically charged furnaces. Hand-charged furnaces are generally considered systems where fuel is supplied to the combustion chamber intermittently. In contrast to this, the fuel supply in

automatically charged furnaces is transported continuously into the combustion chamber. Thus the furnace is charged as evenly as possible. In the following section, the differences in combustion process between intermittent and continuous charging are initially described in more detail, followed by an introduction of the actual systems technology.

Intermittently charged furnaces demonstrate marked variation of the combustion parameters during the chronological process of a burn-off. This applies in particular for systems without fan ("natural draft furnaces"), which represent the majority of stand-alone furnaces (section on "Stove (Stand-alone Furnaces)"), since the general conditions for combustion between the two recharging intervals do change considerably.

With the loading of every new batch of fuel, the still cold and potentially not yet fully dried new fuel, combined with the opening of the charging trap, the furnace will initially cool down. In the case of updraft combustion, the space available in the combustion chamber decreases during the recharging process and subsequently increases again gradually during the ensuing continuous combustion process. Therefore, this process is also referred to as "batch combustion." With changes in the volume of space available in the combustion chamber, the corresponding retention times for the combustible gases formed through pyrolytic decomposition and gasification also do change in many furnace designs. These constantly changing conditions for combustion can be monitored by reference to the concentration of the meanwhile generated carbon dioxide (CO_2) and carbon monoxide (CO) in the flue gas (Fig. 1, top) [28].

For optimum efficiency in combustion, the air supply needs to be adjusted during the different phases of combustion. The use of a fan system is recommended for this purpose. Through suitable features in the design of furnace systems an attempt is made, furthermore, to achieve a combustion cycle which is as continuous as possible, with constant performance and low levels of emission. The recharging of fuel and the changing volume of space available in the combustion chamber should have as little as possible interfering impact on this process. A combustion principle in which these demands have been met, quite efficiently also in the case of hand-charged furnaces, is the so-called downdraft combustion. In this system, only the lowest layer of the fuel bed takes part in the combustion process (section on "Principles and Operating Systems"). The development of CO_2 and CO

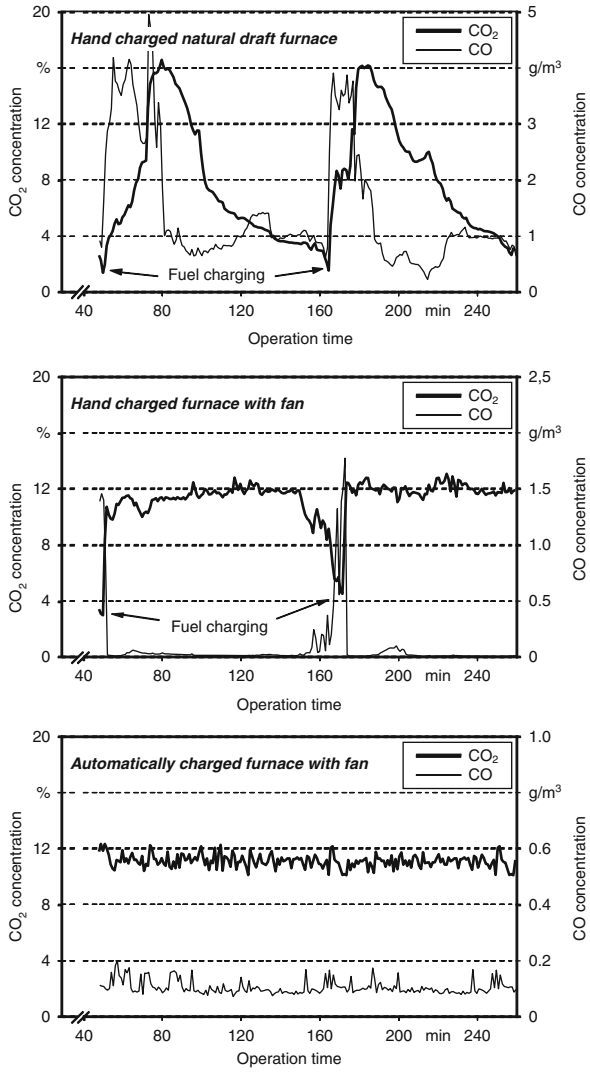

Biomass Energy Heat Provision in Modern Small-Scale Systems. Figure 1
Typical patterns of carbon dioxide (CO_2) and carbon monoxide (CO) concentrations in flue gas during natural draft combustion (masonry heater) (Fig. 1, *top*), a hand-charged furnace with fan (log wood-burning furnace, updraft combustion without grate) (Fig. 1, *middle*) and an automatically charged furnace (wood chip furnace) (Fig. 1, *bottom*) at operating temperature conditions (heating-up phase not illustrated; different scales for CO values in separate illustrations) (see [3])

concentrations in the flue gases (Fig. 1, middle) show, that a largely stable and consistent level of operating conditions, approaching those of automatically charged furnaces, can be achieved based on such a design.

Automatically charged furnaces will generally be fired with fuel easily be formed into batches; such a fuel is produced if necessary through shredding or pelletizing. Usually these fuels are continuously and automatically supplied to the combustion chamber, so that the furnace system can be adjusted to a constant and largely balanced level of performance. Continuity in the supply of fuel allows for an adjustment in the supply of air, specifically adapted to the particular amount of fuel fed into the system, with temperatures in the combustion chamber, at the time, remaining at a constant level [28]. This kind of operating mode ultimately leads to steady and low levels in the emission of noncombusted compounds (Fig. 1, bottom).

Automatic charging, using loose fill fuel materials, also makes it possible to adjust the fuel supply automatically to changing patterns in the demand for thermal energy. As a result of this, automatically charged systems are also capable of operating at only partial load over comparatively long periods (approx. 30 up to 100% of nominal thermal power output). For the bridging of phases with low demand for thermal energy buffer heat storages can therefore be scaled down or – under certain circumstances – be omitted altogether.

Combustion Principles and Furnace Types

Manually Charged Wood Furnaces

Hand-charged furnaces represent the most important group of small-scale systems. Therefore the technical principles and different types of design for this group of systems are described below, in greater detail.

Principles and Operating Systems Hand-charged wood-burning furnaces are fueled at specific intervals – according to capacity and filling space – with smaller or larger charges of solid biofuel. As a result of this, different phases in the combustion cycle do occur and distinctions are made between a start-up phase, the subsequent phase at operating temperatures and finally the phase of combustion of the remaining charcoal. Depending on the system (fan assisted or natural draft) these phases are quite distinct in their characteristics (Fig. 1), and disruptions to continuity in the process of combustion may result in the drawbacks referred to above (e.g., regulation of the optimal amount of air supply).

Nevertheless, manually charged furnaces must be operated at low levels of emission. Apart from optimization of combustion technologies, the correct control and management of the system (i.e., prevention of errors in operating the system) as well as use of the right fuel type are essential prerequisites (i.e., the right choice between untreated, air dried log wood or pellets produced from untreated wood and without additives). The combustion of pieces of particle board remaining from the ordinary production process and treated wood, painted or lacquered wood, as well as combustible waste material (e.g., waste paper, plastic packaging materials) is, generally speaking, not allowed for small-scale furnace systems. Such substances lead not only to high and extremely toxic emissions and toxic residues, but could also reduce the useful lifespan of the plant considerably.

Hand-charged wood-burning furnaces can be distinguished by the following characteristics:

- Construction design: stand-alone furnaces, enhanced stand-alone systems, and central heating boilers
- Draft systems: natural draft or fan-assisted draft
- Grate system: furnaces with or without grate
- Position of grate: shallow combustion or full load combustion
- Combustion principle: updraft combustion with grate, updraft combustion without grate, downdraft combustion, and/or lateral downdraft combustion

The most important distinguishing features are the combustion principles described in more detail below. Their use in the different types of system design is outlined in the subsequent sections on "Stoves (Stand-alone Furnaces)," "Enhanced Stoves," and "Central Heating Boilers."

System designs for the different combustion methods commonly employed in hand-charged furnaces are

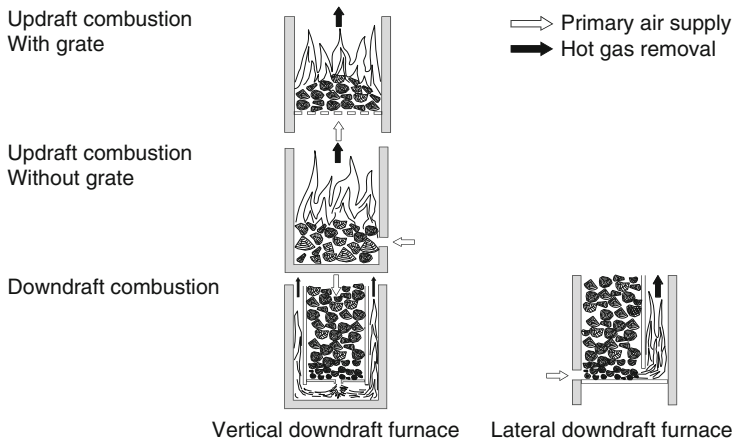

Biomass Energy Heat Provision in Modern Small-Scale Systems. Figure 2
Combustion principles for hand-charged wood-burning furnaces (secondary air flow and secondary combustion chamber not illustrated here)

illustrated in Fig. 2, whereby the two first named systems often cannot be clearly distinguished from one another. They are therefore not always treated as separate individual combustion systems. They are often considered as different operating versions of one and the same system. Since the concepts for updraft combustion with grate and updraft combustion without grate have been developed in different areas – that is, for coal (updraft combustion with grate) and for wood-burning furnaces (updraft combustion without grate) – and different plants with correspondingly varying features are used in practical application, these two combustion principles are covered separately in the following sections.

Updraft combustion with grate. Here the combustion air (primary air) is channeled through the grate or from the bottom of the fire bed and thereby through the whole layer of fuel. Ignition is handled from below and the fire bed develops and spreads over the grate underneath the remaining supply of fuel. Through this process, the entire amount of fuel is heated up and brought simultaneously into a state of reaction (Fig. 2, top). This also represents the major drawback of this system. Because the adjustment of the amount of combustion air supplied to the different levels of combustion gases released proves to be rather difficult. This applies especially if fuel is charged in very large batch sizes and as a result a separation between the zone of the pyrolytic decomposition and the secondary combustion is no longer possible. Therefore these types of furnaces are best operated through frequent charging with small amounts of fuel, in order to achieve an as constant and balanced combustion process as possible. However, the conditions for combustion change with every charging process (as well as throughout the course of the combustion cycle). Therefore, this type of combustion – with grate or without grate – is sometimes also referred to as charge combustion.

Updraft combustion with grate represents the classic combustion principle for short-flamed coal fuels. The proportion of volatile substances ("combustion gases") formed during pyrolytic decomposition is comparatively low for coal, whereas the largest proportion of thermal energy produced is due to the oxidation of carbon. Similarly, the usually missing clear separation between the zone of pyrolytic decomposition and gasification, as well as the oxidation zone, generally turn out to be less disadvantageous in the combustion of coal fuels. In spite of the problems outlined above, the principle of updraft combustion with grate is, so far, used preferably for stand-alone furnaces (especially chimney stoves and fireplaces), even when using wood fuels (characterized by a high content of volatile substances). This is also because easy removal of the ashes is made possible through the grate and ash box. In modern firewood boiler systems, however, the

principle of updraft combustion with grate is usually no longer employed.

Updraft combustion without grate. In contrast to updraft combustion with grate, the combustion air (primary air) in updraft combustion without grate is supplied laterally to the fire bed zone (Fig. 2, middle). The first charge of fuel is ignited from above, and the fire bed is formed in this process during the initial phase of combustion. As the flames and hot gases emitted during the pyrolytic decomposition can rise unhindered, the high operating temperatures required in the secondary combustion chamber for complete combustion are reached comparatively fast, while the fuel supply gradually heats up from the top to the bottom. The release of gaseous substances is therefore slowed down. The wood supply burns more evenly and controlled from the top down to the bottom, that is, the same as would be the case in an updraft furnace with grate. It would be a disadvantage if the furnace is not provided with an appropriate secondary air supply, as the space available in the combustion chamber will vary with the reduction in the level of fuel supplies, so that the retention time for gases (produced by the pyrolytic decomposition and the gasification) in the secondary combustion process will be continuously changing. The longest retention time thus occurs at the end of the combustion cycle and not at the start, as would be desirable from the perspective of looking to achieve an optimum combustion process.

New fuel – if applied – is placed on the remaining fire bed during recharging; and the subsequent combustion cycle is therefore similar to that of updraft combustion with grate furnace system. Small volumes of fuel and frequent intervals in the recharging of the systems are of advantage in updraft combustion without grate, as well. However, since combustion air (primary air) is channeled over and not through the fire bed, excessive rekindling of embers (in the ashes) can be avoided. These furnaces are therefore frequently designed without grate in order to avoid unwanted supply of air. The removal of ashes on the other hand can only be performed when the system has cooled down.

The principle of updraft combustion without grate is commonly used in stand-alone furnaces (e.g., masonry heaters; Fig. 5). As is the case in updraft systems without grate, usually no fans for additional air supply are installed in updraft furnaces without grate ("natural draft operation"). The amount of air supply is regulated by adjustments made to the air supply inlet and chimney flaps.

Furnaces using updraft combustion with or without grate rarely exist as "purebred" systems, but are usually combined in some form or other. For the use of different kinds of fuel (e.g., firewood, wood pellets), these types of stand-alone furnaces (e.g., chimney stoves) can often be switched from one operation mode to another, so that they usually work on the basis of updraft combustion with or without grate. In such combined furnace systems, coal fuels (e.g., briquettes) are used in updraft combustion with grate (predominantly using grate air), whereas for wood fuels the combustion air is supplied laterally or from above while the grate air supply is locked. But small amounts of grate air can also be of advantage in the combustion of wood fuels, as they support the complete combustion of charcoal residue.

Vertical or lateral downdraft combustion. In contrast to the two methods of combustion described above are heat gases in downdraft combustion not discharged to the top, but the flames instead spread underneath the bottom of the combustion chamber or sideway ("downdraft furnaces"). Consequently, the respective lowest layer of fuel takes part in the combustion process. The combustion gases released in the area of primary air supply are channeled into a combustion chamber, located below ("vertical downdraft combustion") or next ("lateral downdraft combustion") to the fuel filling space, by means of fan supported draft, and do reach the stage of complete combustion with the aid of secondary air supply (Fig. 2, bottom). In the case of lateral downdraft combustion, part of the primary air can also enter through a bottom grate, which allows for the removal of ashes and furthermore supports complete conversion of charcoal residues.

The wood placed above the fire bed zone serves as a fuel reserve, which will automatically slip lower during combustion of the charge, thereby allowing for a quasi-continuous recharging with fuel supplies. In contrast to updraft combustion systems, with or without grate, the amount of fuel placed in the combustion space using the downdraft principle is essentially not important. It does, however, have an impact on "operating comfort," as the need for constant recharging can

be eliminated by way of depositing larger amounts of fuel supplies in the filling space; the combustion cycle for a charge in this type of firewood furnace, for example, can run up to 5 h and more.

The downdraft combustion principle allows for relatively continuous pyrolytic decomposition and gasification of fuel materials. This makes it easier to adjust the combustion air flow required for the amount of combustion gases released, allowing for good combustion and high levels of efficiency to be reached.

Due to the advantages outlined above, the downdraft combustion principle is by far the most commonly used system in log wood–fired central heating boilers (section on "Central Heating Boilers"). In contrast to updraft combustion systems with or without grate, however, reinforcement of air supplies through the use of a ventilation system (suction or pressure blowers) is usually an essential requirement. This is one of the reasons – apart from people's esthetic desire to be able to watch the flicker of the flames – why the principle of downdraft combustion is used only rarely in stand-alone furnaces today.

In plants operating on the basis of the downdraft principle, coarse wood chips can generally be used as well, apart from log wood. Unlike updraft combustion, however, there is the risk of hollow combustion (i.e., the formation of "bridges" above the fire bed). This can lead to correspondingly higher levels of emission, as a result of disruptions in the process of complete combustion.

Table 1 summarizes customary hand-charged furnaces, including details concerning typical heating performance, the combustion principle employed and, where appropriate, various distinguishing characteristics. The different types of designs listed are described below in more detail.

The hot combustion gas emitted from the combustion chamber is usually referred to as heat gas, given its hot state. Following the emission of thermal energy into the surrounding space or into the boiler, this combustion gas is referred to as flue gas, once it has cooled down and is discharged into the environment via the chimney (or flue stack).

Stoves (Stand-alone Furnaces) Due to their design, stand-alone furnaces (stoves) emit their thermal energy to the surrounding space only. This usually happens through the radiation of heat and, to a lesser extent, further by way of convection. Stand-alone furnaces which belong to this category of design include open or closed fireplaces, cast iron stoves, chimney stoves, masonry heaters (including masonry convection heaters, tiled stoves), as well as wood-burning kitchen stoves and pellet stoves (see summary in Table 1). They are usually only used occasionally (i.e., as a supplementary source of heating).

One can differentiate between separate types of stand-alone furnaces by way of a variety of criteria (Table 2). For example, they can be grouped into shallow combustion and full-load combustion systems.

- In the case of shallow combustion, only a single layer of firewood is loaded in each recharging process (in the case of kitchen stoves and central heating boilers, shallow combustion is additionally defined by the distance between the grate and the cooking surface [4, 7]). Shallow combustion systems include, for example, open and closed fireplaces, chimney stoves, as well as kitchen stoves and masonry heaters in cooking mode (summer mode, Fig. 8). For these types of furnace systems, the typical load of fuel for each charge ranges between 2 and 5 kg (for cooking mode even less than 2 kg).
- Full-load furnaces are, in contrast to this, suitable for larger fuel charges; this ensures a certain minimum combustion cycle at rated thermal output values ("permanent combustion stoves" [5]; for example, kitchen and masonry stoves in heating or winter mode, or certain types of standard masonry heaters). The volume of individual charges in this case is likely to be in excess of 5 kg fuel per load.

Besides this, there are a large number of further criteria available to differentiate between systems (Table 2). However, they do not always allow a clear distinction between different designs. The reason for this lies in the diversity of modifications made. Also, mixed systems of existing furnace designs are now available, which make a clear and definitive assignment to one category or another somewhat difficult. As a result of this, a variety of names and categories have become common use, and a certain degree of ambiguity, in terms of terminology used in the following remarks, can therefore not be avoided completely.

Biomass Energy Heat Provision in Modern Small-Scale Systems. Table 1 Construction design and characteristics of hand-charged wood furnaces

Type	Heat power output in kW	Combustion principle	Characteristics
Stoves and fireplaces (thermal energy primarily for space of installation – depending on design)			
Open fireplaces	0–5	Updraft combustion with/without grate	With and without hot air circulation, not suitable for permanent heating
Enclosed fireplaces	5–15	Updraft combustion with/without grate	With hot air circulation, display window
Cast iron stoves	3–10	Updraft combustion with/without grate	Free standing wood furnace charged in the domestic/living area where installed
Chimney stoves	4–12	Updraft combustion with/without grate, downdraft combustion (rare)	Same as cast iron stove, with display window
Masonry ("tiled") stoves – slow release thermal storage heaters	3–15	Updraft combustion with/without grate, downdraft combustion (rarely)	Slow radiation of stored heat over a 10–24 h period through radiation (masonry heater), or with convection air supply (hot air masonry heater)
Kitchen stoves	3–12	Updraft combustion with/without grate, downdraft combustion	Heat for cooking (primary use), thermal heat or bench heating (secondary uses)
Pellet stoves[a]	2.5–10	Cup burner/hearth furnace (for wood pellets)	Automatically charged, controlled fuel and air supply (fan), re-charging required approx. every 1–4 days
Enhanced stoves (thermal energy also for areas other than place of installation – depending on design)			
Central heating kitchen stoves	8–30	Updraft combustion with/without grate, downdraft combustion	Supply of thermal energy for cooking, central heating and hot water supply purposes
Enhanced masonry stoves, fireplaces and chimney stoves	6–20	Updraft combustion with/without grate	Water – heating circuit or closed hot air circuit (hypocaust heating system)
Pellet stoves[a] with water jackets	Up to 10	Cup burner/hearth furnace (for wood pellets)	also suitable as sole source for domestic heating (e.g., low-energy construction)
Central heating boilers (use of thermal energy only outside the place of installation)			
Log wood boiler	10–250 (max. 800)	Downdraft combustion, updraft combustion with grate (rare)	Logs up to 1 m in length, natural draft or blower supported boilers, thermal storage (buffer) required

[a]Pellet stoves, in terms of design, would be considered automatically charged furnaces and are therefore reviewed as to characteristics and functions in section "Pellet Furnaces"; however, they have been listed in this section since they belong to the category of typical stand-alone furnaces/room heaters

Although versions with exterior air supply do exist for almost all categories of design, today stand-alone furnaces generally still are operated using air extracted from the room or space where they are installed. Critical operating conditions, as a result of air being extracted from the room, for systems using chimney draft are generally to be expected only if – as it could be the case for modern building designs with tightly

Biomass Energy Heat Provision in Modern Small-Scale Systems. Table 2 Distinguishing features of independently operated stand-alone furnaces (stoves)

Design/ installation	*Assembled (partly using prefabricated components) and installed on site by specialist contractors, fixed permanently*	*Industrially produced complete units, can be moved*
	Open/enclosed fireplaces, masonry heaters (with/ without grate), tiled stoves	Cast iron stoves, chimney stoves, pellet stoves, kitchen stoves
Storage capacity	*Low to medium*	*High ("buffer stoves")*
	Open/enclosed fireplaces, cast iron stoves, chimney stoves, pellet stoves, masonry heaters (with grate), kitchen stoves, enhanced stand-alone furnaces	Masonry heaters/stoves (without grate), cast iron stoves or chimney stoves with large tiled or soapstone exterior surfaces
Charging	*Hand charged*	*Automatically charged*
	Open/enclosed fireplaces, masonry stoves/ convection heaters, cast iron stoves, kitchen stoves	Pellet stoves, pellet boilers for central heating
Typical operating cycles	*Longer operating cycles*[a]	*Usually shorter operating cycles*
	Enclosed fireplaces, cast iron stoves, chimney stoves, pellet stoves, masonry convection heaters, enhanced stand-alone furnaces	Standard masonry heaters (1 h combustion cycle, minimum 12 h release of thermal energy/heat), open fireplaces, kitchen stoves
Supply of thermal energy	*Primarily radiant heat*	*Primarily convection heat transfer*
	Standard masonry stoves, cast iron stoves and chimney stoves without circulation vents, kitchen stoves and pellet stoves	Masonry convection heaters, chimney stoves with circulation vents, stand-alone furnaces with water jackets

[a]Frequent daily or permanent combustion cycles through repeated charging

fitting doors and windows – the otherwise available "combination of combustion air" (i.e., the overall volume of air available from other rooms and spaces connected to the room of installation by way of air circulation; approximately 4 m^3 of ambient air per kW nominal heat power output) should turn out to be insufficient [33]. This is most likely to occur in the case of open fireplaces, which are operated at high levels of excess air.

However, problems may also occur if low-pressure systems are used for the purpose of room ventilation, as they can limit and restrict the natural draft of the chimney (e.g., kitchen vents, controlled ventilation, air-conditioning). In such cases, furnaces without fan need to be supplied additionally with external air.

Open fireplaces. In contrast to all other stand-alone furnaces, an open fireplace has a combustion chamber which is open on one side (exposed to the room or living space where it is installed). The back and partially the sidewalls are usually closed by brickwork (Fig. 3). It is constructed either using fireclay components or

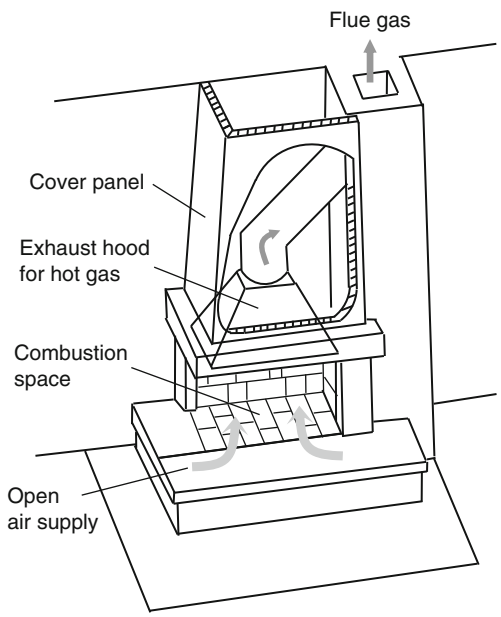

Biomass Energy Heat Provision in Modern Small-Scale Systems. Figure 3
Open fireplace [18]

prefabricated units (e.g., an iron fireplace insert). A controlled and graduated supply of combustion air is not possible for this type of furnace design. In order to prevent the potential emissions of gases into the living space, such furnaces are operated at very high levels of excess air. The necessary combustion air supply is taken from the surrounding living space; in some cases, additional external air is supplied through separate air ducts.

In the case of open fireplaces, the often found use of a stand-alone furnace as an additional source for the provision of heat tends to be only of secondary importance; this type of furnace primarily serves to improve the esthetic "quality of living." Thermal energy is released principally through heat radiation. Due to the significant volume of air, required combustion efficiency generally tends to be poor (i.e., comparatively high combustion temperatures, resulting in low efficiency and a high level of air-pollutant emission); and it is for these reasons that the use of open fireplaces as a source of permanent heating is prohibited, for example, in Germany. The use of open fireplaces, and to some extent of other stand-alone furnaces, has therefore been banned in many residential areas.

Enclosed fireplaces. A fireplace insert can be equipped with an automatically closing glass door or glass screen. Such a system is called enclosed fireplace; other customary names used for this type of installation are "heating place" or "cheminee." These heating inserts comprise a combustion chamber with an ash box, a flue gas collector, hot gas ducts, and an exhaust hood. In contrast to open fireplaces, these furnace designs do have an enclosed combustion chamber (Fig. 4, left), and the supply of combustion air can thereby be better controlled and regulated. Because of this, there will be an increase in room temperature and consequently a significant improvement in heating performance and combustion efficiency; and most importantly, no further increase is caused to air circulation in the room. In order to take advantage of these benefits existing open fireplaces can be refitted with so-called chimney sets.

The thermal energy generated in enclosed fireplaces is largely emitted through radiation. Many enclosed systems are additionally fitted with convection ducts

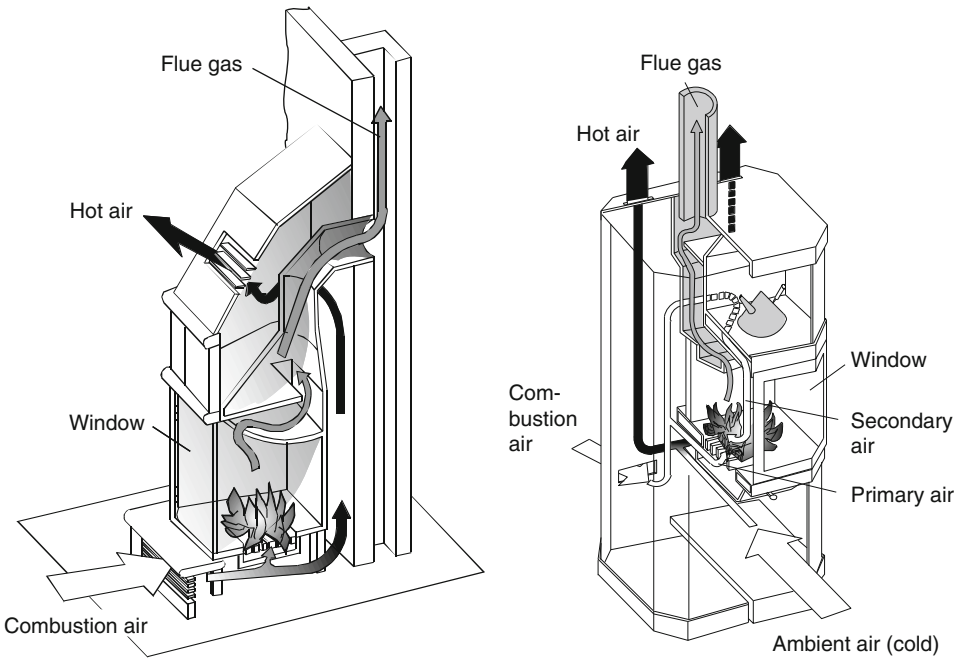

Biomass Energy Heat Provision in Modern Small-Scale Systems. Figure 4
Working principles of an enclosed fireplace (*left*) and a chimney stove (*right*) [32]

and hot air pipes through which air can be distributed – if necessary with the support of a blower system. Thus the supply of heating for adjacent rooms is also possible (section "Enhanced Stoves").

Cast iron stoves. Cast iron stoves differ from open or enclosed fireplaces in as much as they are installed free standing in the living area; they are usually cast iron stand-alone furnaces (also called "iron stoves," although different versions with outside mantling of tiles or soapstone do exist). The fuel is loaded through the upper of usually three doors into the combustion chamber, which generally are lined with fireclay bricks in the lower combustion areas. Ashes having dropped through the grate are caught in the ash box, which can be removed for disposal through the lower door. Cleaning of the grate can be handled via a further door located at the level where the grate is installed. For ease of operation, the design of the grate allows vibrating (manual operation).

Free-standing stoves generally work on the basis of updraft combustion without grate (see Fig. 2). The proportion of air supplied from above can usually be regulated through manually operated flaps or dampers, so that the amount of excess air serving as secondary air supply is predominant. In basic versions of this design, combustion is simply controlled or adjusted by way of a reduction in overall air supply, or by means of a slide damper or rosette installed in the opening designated for the removal of ashes. These stoves may also be clad with tiles or natural stone, thereby increasing buffer mass and at the same time regulating the emission of heat more evenly.

Chimney stoves. The present day version of the cast iron stove is the chimney stove. It can also be installed (free standing) in the living area, but is fitted with a single airtight closing door with screen (Fig. 4, right).

The combustion principle corresponds to that of the cast iron stove. Grate combustion air (primary air) or air from above (secondary air supply) is injected according to the type of fuel used in differing proportions. Air supply from above, however, serves as additional "cleaning air." Therefore, this air is channeled from above alongside the glass screen, in order to counteract the potential precipitation of soot or dust residues.

Similar to cast iron stoves, chimney stoves do release the majority of their heat via radiation (approx. 50%), whereby surface temperatures can be as high as 250°C. In the event that a convection sleeve has been installed (air circulation vents) effective radiation may drop to as little as 10% of the rated thermal energy output [33], whereby the door with glass screen is responsible for the remaining proportion of radiation. The specific burnout rate for chimney stoves has been defined at a maximum value of 4 kW/m^2 [5]. Mass per kW heating performance usually ranges between 13 and 26 and overall loads of 40–80 kg/m^2 heating surface have to be allowed for [33].

Chimney stoves, similar to fireplaces or cast iron stoves, are preferably used during transitional seasonal periods or as auxiliary/supplementary heating. Recharging intervals are short, since only one layer of fuel is loaded – compared to the use of coal briquettes – which will combust in a relatively short period. Stoves which are exclusively designed for the use of wood are therefore considered to be "not suitable for permanent operation" [5].

Masonry stoves/heaters. The main characteristic of masonry slow releasing heaters is the comparatively large volume of storage/buffering capacity in relation to the amount of thermal energy generated by the system. Hot gas is channeled by means of brickwork ducts through the buffering mass, which generally consists of cement plaster, tiles, clay, and mortar – and fireclay or soapstone. Correspondingly, terms like tiled stove, masonry heater, masonry convection stove, and soapstone oven are commonly used in describing these systems. The surface releasing the heat, primarily in the form of thermal radiation, will also be comparatively large so that surface temperatures will usually remain relatively low. For a medium-size masonry heater, these temperatures will range from 70°C to 120°C. Depending on thickness of the walls, the values for thermal radiation will range from 0.7 (heavy duty design) to 1.2 kW/m^2 (compact design) [33]. Although a variety of industrially prefabricated components are used today in the construction of this type of stove, it remains a system requiring considerable amounts of skilled craftsmanship from a stove builder for installation of the brickwork furnace on site.

The original design for a slow heat-releasing stove is the standard masonry heater of brickwork and plaster, with a weight in excess of 1 t [8]. Today's designs mostly use prefabricated sets for the furnace and heating ducts

consisting of special design fireclay brickwork and metal components (front plate for the stove with filling door and openings for air supply, grate insert).

The standard masonry stove (Fig. 5) works according to the principle of updraft combustion without grate principle (Fig. 2). The combustion chamber and size of the secondary heating surfaces (hot gas tracks) have to be adapted to one another in such a way that the temperature of the flue gas emitted through the chimney should typically range between 160°C and 200°C. The storage mass is frequently equivalent to the amount of thermal energy released by one single charge of fuel (fired from above), so that no additional supply of wood has to (nor should it) be placed on top of the gradually reducing fire bed. Due to its substantial storage mass, a cold masonry stove heats up rather slowly. However, the stove also continues to radiate heat long after the embers have died down. Standard masonry stoves are therefore less suitable for "spontaneous use." In modern versions it may be possible to automatically regulate the air supply (e.g., through electronic control of the air vents), but due to the inertia of the system, these means of control remain limited.

Slow heat-releasing stoves typically also require considerable amounts of space. This is why a variety of medium- and smaller-size versions are available on the market, including, among others, the masonry convection heater ("tiled stove") as well (Fig. 6).

In comparison to the conventional slow heat-releasing stove, the warm air convection heater ("tiled stove") usually has less storage mass. This is especially true if it is not fitted with brickwork tracts. A cast iron heating insert (a so-called tiled-stove insert) is used. Around this insert, the brickwork casing (e.g., tiled walls) is installed allowing for a specific distance to the insert. Open-air ducts are installed at the plinth area of the tiled walls, so that cold air from the room can flow behind the tilling of the stove, where it is heated up, rises, and then leaves the air tract through hot air vents installed at the top of the stove. The higher the proportion of thermal energy released through this convection process, the lower the amount of thermal radiation emitted through the tiles. Many masonry convection heaters are additionally fitted with a secondary heating box made of cast iron, sheet steel, or ceramic tiles, which is again enclosed by a back ventilated tile casing and which can account for around 20% of thermal radiation. It often serves also as an additional place for the separation of fly ash. A secondary heating box can also be installed in an adjacent room, so that the stove heater is turned into

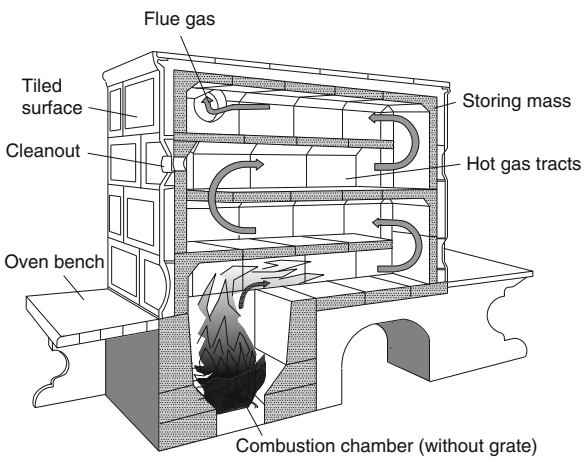

Biomass Energy Heat Provision in Modern Small-Scale Systems. Figure 5
Working principle of a standard masonry heater with lateral brickwork tracts [14] (From KSW Kachelofen GmbH, Germany)

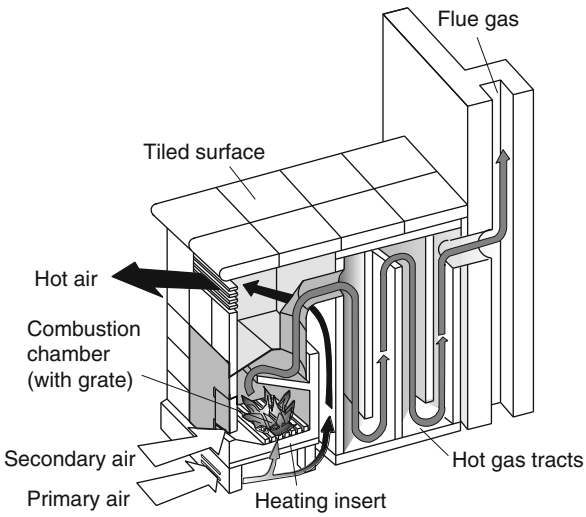

Biomass Energy Heat Provision in Modern Small-Scale Systems. Figure 6
Working principle of a masonry convection heater ("tiled stove") with vertical brickwork tracts [14]

a multiple-room heating system (section "Enhanced Stoves").

Masonry convection heaters fitted with brickwork tracts, however, can also have a comparatively high storage capacity (Fig. 6), so that there is somewhat of a moving transition to radiation-based heating systems. Similar to cast iron and chimney stoves, versions with or without grate can be designed. Tiled stoves can also be fitted with suction fans and flue gas–regulated control of combustion air supplies (microprocessor control system). Modern masonry stoves may also be fitted with glass screens so that they can offer an appearance similar to that of an enclosed fireplace or a chimney stove. In certain design types, the combustion air is supplied via an external air duct in order to allow for heating operations regardless of room air conditions.

Kitchen stoves. The kitchen stove represents a type of design taking in particular care of the needs of such communities and households, where the kitchen is the center of domestic life. Even though the number of newly installed kitchen stoves is meanwhile declining considerably, they are still one of the most important types of stand-alone furnaces. Kitchen stoves are available as industrially produced, complete units, or in the form of more or less prefabricated building-sets ready for on-site installation (e.g., tiled kitchen stoves).

Natural draft–operated kitchen stoves work according to different combustion principles. The latest developments use downdraft systems in the form of vertical downdraft combustion (Fig. 7). For the heating-up stage, an ignition gate is installed which opens up a shortcut for the hot gas from the filling space (underneath the cooking plate) to the flue gas port. During normal operation, the flame is directed downward into the secondary combustion chamber whereby secondary air is supplied through the nozzle. The hot gases flow underneath the cooking plate and around the baking tube, and subsequently pass on in the form of cooled down flue gas into the chimney. In this type of system, the basic principles of efficient combustion can generally be taken into account.

However, the principles of updraft combustion with grate or lateral downdraft combustion (Fig. 2) are also used quite frequently, whereby in these cases the cooking plate is again heated up by the hot gases channeled right underneath the stove-top surface; with the aid of flaps, a potentially fitted baking tube can be heated as well. Some of these stoves can be switched from cooking mode to heating mode, changing from updraft combustion with grate to the downdraft combustion principle (Fig. 8). To ensure that the fire does burn as closely as possible to the cooking plate (in cooking mode) the "cooking combustion chamber" is kept shallow

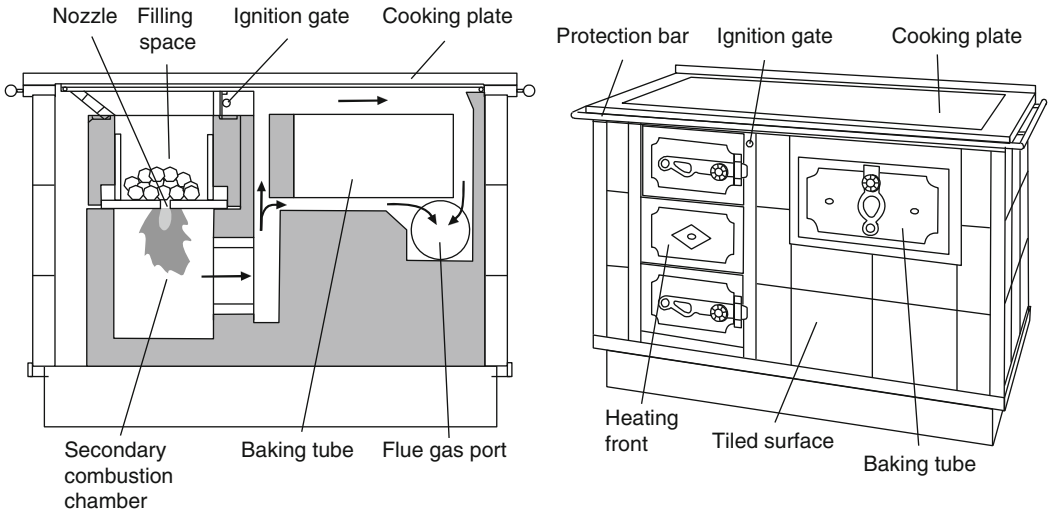

Biomass Energy Heat Provision in Modern Small-Scale Systems. Figure 7
Kitchen stove with downdraft combustion [18]

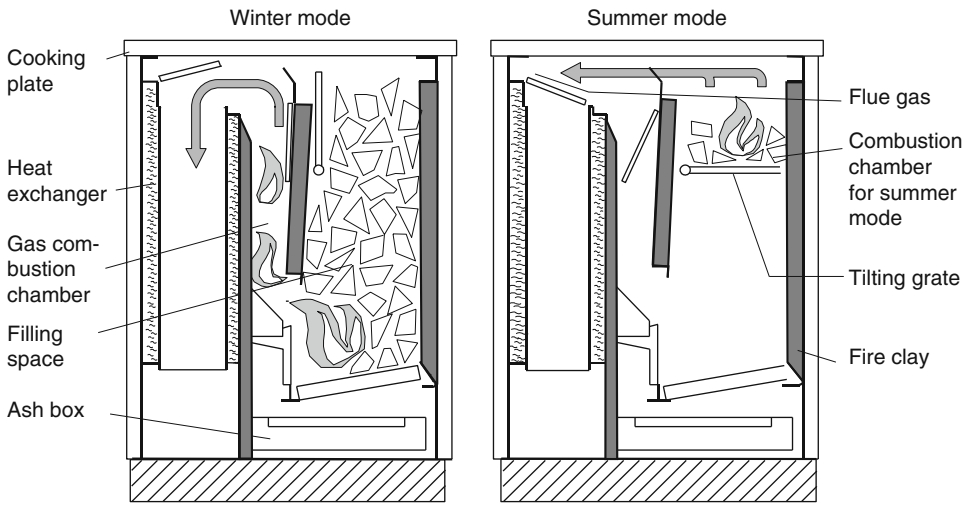

Biomass Energy Heat Provision in Modern Small-Scale Systems. Figure 8
Modern central heating furnace with downdraft combustion: (*left*) winter mode for heating and cooking, (*right*) summer mode for cooking only [18] (From Tiba-Müller AG, Schweiz)

("shallow combustion") through the adjustment of the tilting grate to an appropriate height. If the stove is to be used for heating during winter, the grate is tilted downward, so that the whole of the filling space and/or space of the combustion chamber above the second grate, which is located underneath, can be utilized. This allows for almost doubling the output of heat due to the increased amount of heat exchanger surface now available (Fig. 8). If the stove is fitted with a grate whose position can be changed by means of a lifting device, the switch from summer to winter mode can also be made while the system is in operation.

In winter mode, the enlarged filling space often allows for the use of larger pieces of wood or logs, compared to the restraints imposed by the relatively tight combustion space available during "cooking only mode." Most heating stoves do have separate primary and secondary air supplies as well as other features, albeit limited, for the adjustment of efficiency and performance. Combined kitchen/tiled stove versions are also available where, with the aid of diversion traps, the hot gases are redirected from stove operations into masonry heater tracts (including those potentially located in adjacent rooms).

Enhanced Stoves In the transitional area between stand-alone furnaces and central heating systems, there are a number of hybrid systems and special designs available, which have evolved from stand-alone heaters and stoves. In these systems, only part of the available thermal energy generated is released to the surrounding space and/or utilized for, for example, cooking purposes. By installing an additional water heat exchanger, additional heat can be fed into a heating circuit and/or can be used for tap water heating. If required, thermal energy can also discharged by hot air which is directed via special air ducts, either directly (in the form of convection heat) or acting as a medium for the transfer of thermal energy, to large-scale heating surfaces (e.g., back ventilated tiled walls) in adjacent rooms (hypocaust and/or air central heating systems). These types of enhanced stand-alone furnaces are described in more detail below.

Central heating kitchen stoves. A large proportion of the wood-burning stoves currently in use do not just serve for cooking, baking, and kitchen heating purposes. They also supply hot water for the central heating system and for industrial water. In these types of central heating furnaces, which are available as firewood-burning systems as well as automatically charged pellet central heating boilers, part of the combustion chamber is encased by water jackets and additional heat exchangers are installed inside the hot gas tracts (Fig. 8). Excessive heat can be utilized for heating

up of a heat storage acting as a temporary buffer. The same marginal conditions, essentially, do apply as for hand-charged central heating systems.

Central heating stoves are either used for full-fledged domestic heating systems or as complementary furnaces. They have to be able to meet the safety relevant technological norms and standards applicable for central heating system boilers. They are therefore fitted, for example, with thermal control systems for protection against overheating. These are mechanical devices, controlled by flow temperatures, which will open up the drainage system in the water circulation of a safety heat exchanger connected to the system once a certain level of flow temperature has been reached (overheating), in order to discharge any excess thermal energy.

Central heating stoves can reach an overall efficiency rating of at least 65%, and the thermal radiation in the space where the unit is installed is not accounted for as a loss [4]. Ashes are removed manually.

Enhanced masonry stoves, fireplaces, and chimney stoves. The concept of using water as a medium for the transfer of thermal energy for heating purposes does predominate in the case of central heating stoves. However, special designs incorporating the transfer of heat to adjacent rooms (up to a maximum of approximately four rooms) for heating purposes are more commonly found in the case of enhanced masonry heaters and chimney stoves (Fig. 9). This is accomplished either by means of the partly fan-assisted discharge of hot air (from fresh air, mixed air or circulating air supplies) or by way of circulating hot air in a closed circuit system. The latter is also referred to as the hypocaust system, where the circulating hot air acts as the medium for heat transfer. Air is heated up at the surface of the heating insert's heat exchanger. This hot air is then channeled to one or more hot air canals, through the appropriate adjustment of flaps installed in the system, ultimately reaching the heating surfaces in the relevant rooms. These heating surfaces will be finished in the form of special hypocaust tiles, or as ceramic surfaces, natural stone, or brickwork with plaster and provide the medium for the thermal radiation process. Due to the high level of storage mass, this release of thermal energy can happen slowly and evenly over an extended period. Gravity and buoyancy effects generally maintain circulation in the system.

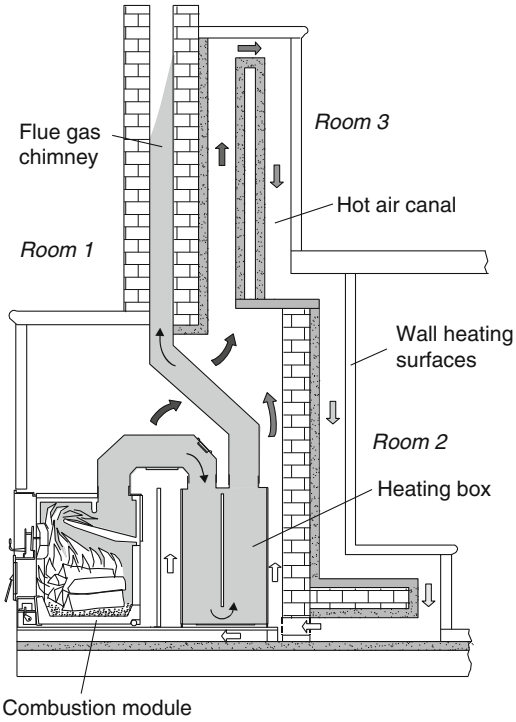

Biomass Energy Heat Provision in Modern Small-Scale Systems. Figure 9
Working principle of a hypocaust system with masonry stove insert [18] (From Brunner GmbH, Eggenfelden)

Masonry heaters, fireplaces, and even chimney stoves can also be utilized for the supply of hot water and are referred to in this context as tiled-stove-heating boilers, fireplace boilers or (water) circulating chimney stoves. Special water-heat exchange adaptors ("water registers" or "water jackets") can be opened up for the circulation of hot flue gases through appropriate adjustment of the diversion flaps, as soon as the furnace has reached operating temperature. This is to release part of the thermal energy generated to the liquid medium of the heat exchanger. Heating water is heated up by this process. This change in operating mode for a masonry stove illustrates Fig. 10. The structural design for a water circulating chimney stove is illustrated in Fig. 11.

For chimney stoves, the heat exchanger can also be installed in the closed cycle of a hot air circulation system. The use of heat buffer storages is advisable, in any event. Masonry heater, chimney stove, or fireplace furnace systems with heat exchangers are used up to a rated thermal energy output of around 20 kW.

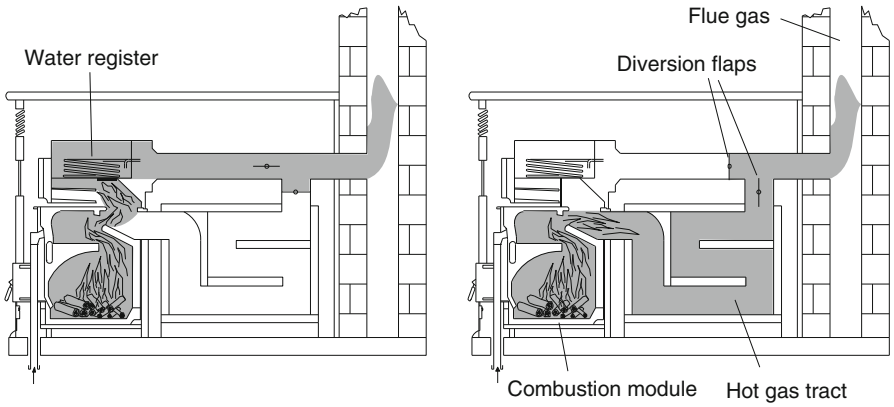

Biomass Energy Heat Provision in Modern Small-Scale Systems. Figure 10
Masonry stove with water heat exchanger; (*left*) additional supply of thermal energy for the heating system, (*right*) supply of space heating for the location where the unit is installed [18] (From Brunner GmbH, Eggenfelden)

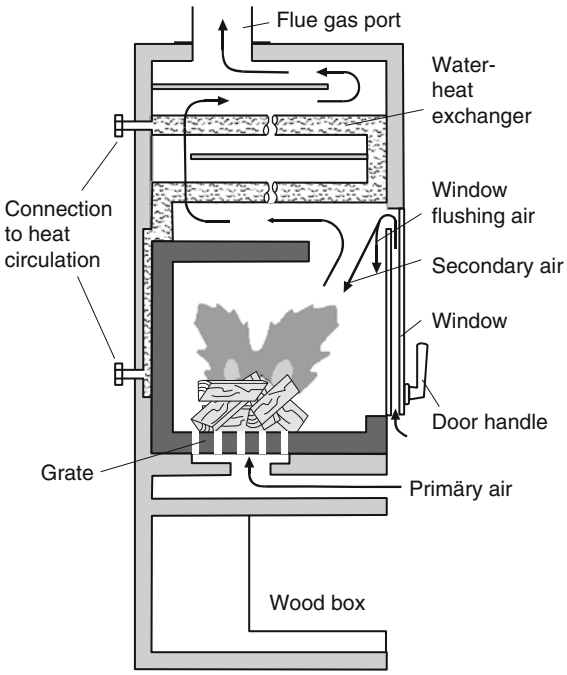

Biomass Energy Heat Provision in Modern Small-Scale Systems. Figure 11
Chimney stove with water heat exchanger [18]

Pellet stoves with water jackets. Since the automatic charging with fuel supplies does allow for a relative wide range in the performance of furnaces (approximately 30% up to 100% of rated thermal power output) the emission of thermal energy from pellet stoves can be particularly well adjusted to the actual demand for heating in residential buildings. This advantage comes to bear especially in the case of systems using water heat exchangers for the heating up of industrial water and water for central heating systems. Additionally, these types of furnaces are increasingly used as a primary source of heating in buildings with low energy design, in combination with other sources of renewable energy (e.g., solar heat) or fossil fuels. In these cases, between 50% and 85% of discharged thermal energy can be generated through water heat exchangers – and at the same time nobody has to miss a clearly visible, flickering flame from the fireplace in the living area.

Central Heating Boilers Other than in the case of stand-alone furnaces or enhanced stoves, central heating boiler are designed to avoid the loss of heat to the surrounding space, since the place of installation will ordinarily not be in a room which needs to be heated and the boiler is unlikely to be needed for cooking purposes. Central heating boilers should therefore be fitted with water heat exchangers (and in exceptional cases with an air heat exchanger) (Fig. 12). Furthermore, they should be connected to a hot water central heating circuit or air circulation system through which the transfer of heat to the heating surfaces in the relevant rooms can be regulated. Surface thermal

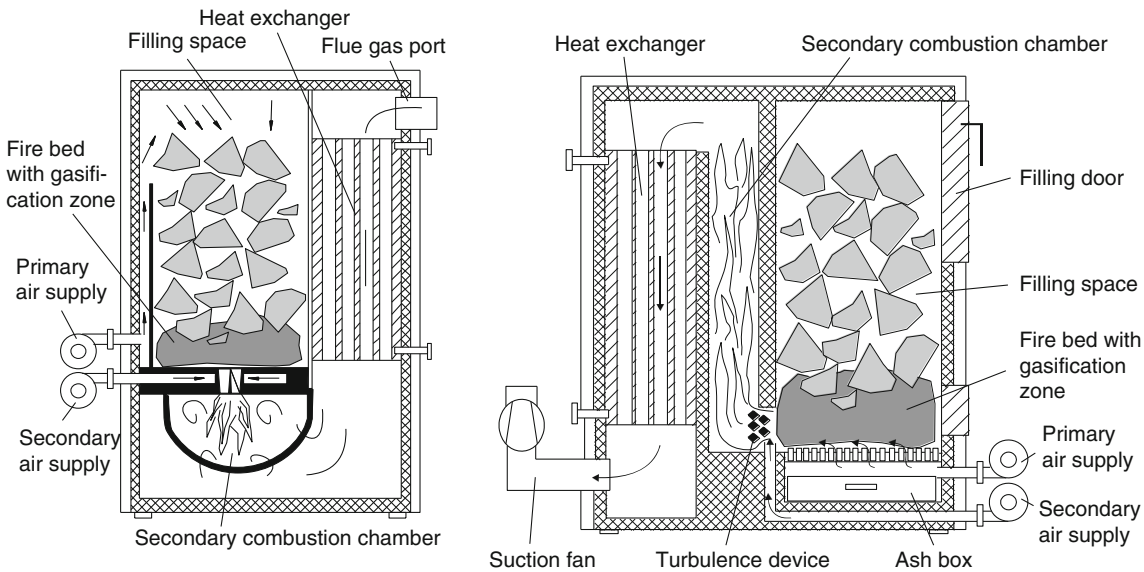

Biomass Energy Heat Provision in Modern Small-Scale Systems. Figure 12
Log wood boiler with vertical downdraft combustion (*left*) and lateral downdraft combustion (*right*) [18]

radiation emitted by such units has to be considered as operational losses and should be minimized through the installation of suitable lining and appropriate thermal insulation measures.

The combustion system used almost exclusively today for hand-charged central heating boilers is based on the downdraft combustion principle (so-called lateral and vertical downdraft furnaces, see Fig. 2) [22]. The filling space is usually loaded with log wood or, less common, with chopped firewood. At a standard thermal energy output rating of 20 to approximately 40 kW, the typical supply of fuel would measure around 30–50 kg in weight per charge. An example of the design for a log wood central heating boiler is shown in Fig. 13.

Combustion air is supplied to the system by way of suction or (less common) pressure blowers, so that the plant can be operated at either high-pressure or low-pressure conditions in the combustion chamber. Boilers working exclusively according to the natural draft principle are less common today. Systems using a blower offer the advantage that the boiler can be operated largely independent of the surrounding conditions (i.e., draft conditions in the chimney). Additionally, a potentially considerable loss in pressure inside the combustion chamber can furthermore be compensated, if appropriate. Such losses in pressure are inevitable if – in order to arrive at a good mixture of combustion air and combustible gases – correspondingly required turbulences are to be created through diminutions or redirection of air and gas flows.

Within thermostatically controlled systems, the amount of thermal energy produced by the boiler is adjusted according to demand and regulated by the water temperature in the boiler (performance control). But flue gas–based systems for the control of combustion air are being used increasingly. Here, the status of flue gases is monitored with the aid of sensors, in order to provide corresponding control variables for adjusting the air supply (e.g., excess air indicators, CO and C_nH_m). This type of flue gas–controlled combustion air management does also lead to improvements in overall operating efficiency [11, 23], so that log wood–fueled boilers can reach efficiency levels in excess of 90% (in some instances) already today.

Through the use of firewood as a fuel, boilers can be operated under partial load conditions up to 50%. However, the installation of a hot water buffer would also be advisable, in this instance, in order to compensate for any potential fluctuations in the demand and supply of thermal energy. Log wood–fueled boilers are occasionally also combined with automatically charged precombustion systems, where the boiler takes over the

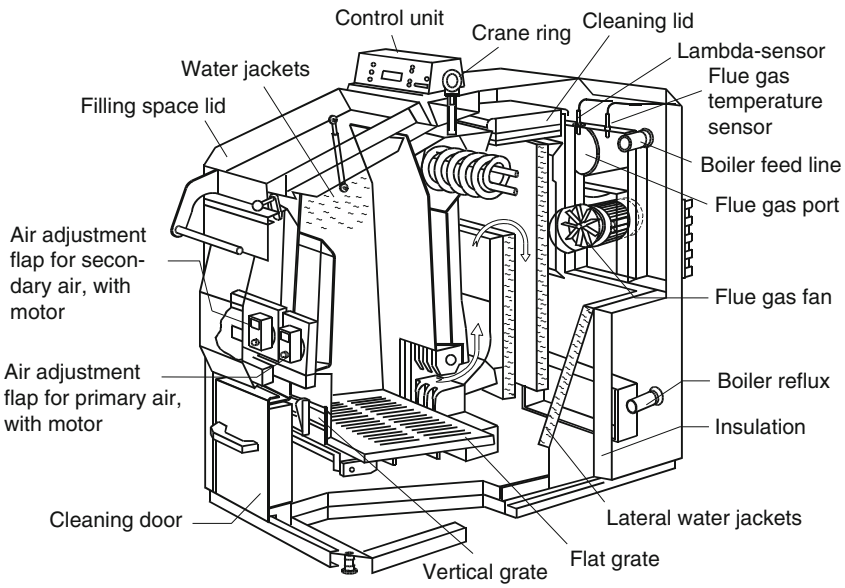

Biomass Energy Heat Provision in Modern Small-Scale Systems. Figure 13
Example of a log wood central heating boiler working on the basis of the of lateral downdraft combustion principle – charged from the top [14] (From HDG Bavaria Kessel- u. Apparatebau GmbH)

function of secondary combustion and acts as a heat exchanger (section "Wood Chip Furnaces").

Hand-charged log wood-burning boilers are predominantly used at ratings up to approximately 50 kW. Their performance spectrum, however, ranges from 10 kW for small-scale domestic boilers (exclusively charged with firewood) up to approximately 250 kW for plants which are commercially used in wood processing industries for the combustion of larger pieces of waste wood from industrial production. Plants with a capacity of up to 800 kW are less common, although the principle of downward combustion is also used in these types of installation. In furnaces operating at such high rates of capacity, it is advisable to make use of mechanical aids for the charging of the system (e.g., push carts and/or small tractors).

In order to reduce the comparatively high level of effort and labor involved in the preparation of firewood, adapted boilers for the use of "one-meter-logs" and rolls are available on the market (above 45 kW nominal heat output). This leads to a reduction of the effort required for charging of the furnace and preparation of the wood fuel.

Some firewood-burning boilers can additionally also be operated using heating oil or gas. If an appropriate burner has to be hinged or swung in front of the wood filling door, the system is referred to as a "conversion combustion boiler." If the switch in fuel can be arranged without conversion of the system, it is referred to as a "convertible combustion boiler" [6]. A special version of the convertible combustion boiler is the "dual combustion boiler," which has two furnace systems, completely separated from one another. These derivative systems for the combined use of wood and fossil fuels are rarely found today, due to stringent emission controls and since a further optimization for different types of fuel is not really possible any longer. Firewood–charged furnaces, however, with a swivel or hook-up wood pellet burner allowing for temporary automatic operation, are becoming increasingly popular; and the ease of use, especially during transitional periods (due to automatic ignition) or during extended periods of absence (by the user), has been increased considerably.

Integration into Residential Energy Systems In order to achieve a high degree of combustion efficiency, hand-charged solid fuel burning furnaces should be operated at maximum load levels in relation to the installed rated thermal energy capacity. Actual utilization

of maximum capacity, however, will be required for a very limited number of heating days only, throughout the course of the year. This is the reason why special measures are needed to ensure an economically and technically efficient integration of the system into the overall structure of energy demand, essentially covering the following aspects:

- Selection of a heating system allowing sufficient flexibility in the adjustment to respective load requirements ("load variation")
- Incorporation of a heat storage device ("heat buffer storage")
- Use of the wood-burning furnace in combination with other sources for the generation of thermal energy (e.g., solar energy, or even in combination with oil and gas-fired systems, using the biomass-fueled boiler to cover base load demand)

The corresponding options are discussed in more detail below.

Load adjustment. Automatically charged wood-burning furnaces and modern firewood boilers are usually available with controls allowing for the automatic adjustment of the amount of thermal energy emitted (i.e., output controls). The technically feasible nominal load range for firewood–charged boilers (at 50–100% of rated thermal energy output) is considerably smaller than that for automatically charged furnace systems (approximately 25–100%). Nevertheless, load reductions should lie significantly above the stated minimum values to prevent increased airborne emissions. These types of load variable furnaces are generally fitted with a pressure or suction fan adjusted by stepwise or infinitely variable control. The performance of systems operating exclusively on the basis of natural draft, however, can usually not be regulated and they should therefore generally be operated at full load. Other than with partial load systems, considerably larger volumes of surplus heat have to be stored in this case on an interim basis.

Heat storage. As soon as the demand for heat drops below the minimum possible level of output achievable in continuous operating mode ("lowest possible output of heat"), the furnace has to be switched off automatically through the interruption of the air and/or fuel supply system. Surplus thermal energy can alternatively be fed into a heat storage tank ("buffer storage") since water temperatures in the boiler would otherwise continue to rise until the safety system of the boiler is activated.

Commonly used heat storage systems are typically steel containers (with thermal insulation) through which the heat transfer medium is circulated during the loading and unloading process. The feed-in system in the upper part of the heat storage device is usually designed to avoid the development of turbulences, in order to ensure that the formation of temperature layers can take place evenly and uninterrupted. This is achieved, for example, through the use of parallel feed lines with deflector baffles (in the case of vertical installation). Another option is a feed-in flow against the flat inside top of the storage tank (lateral connection, Fig. 14). A particularly distinct formation of temperature layers is achieved in so-called layer storage systems, where the reverse flow of heating water is fed back into the system, by way of an integrated uptake, providing for laminar flow back into the different temperature zones. High feed-in temperatures at the boiler favor the formation of temperature layers and increase storage capacity. For the extraction of stored heat, the flow direction is reversed or separate discharge or reverse flow lines are installed.

Different types of storage systems are available depending on whether the heating up of industrial water takes place separately or is integrated into the heat storage system and whether it is intended to serve multiple functions, including the feed-in of solar heat (Fig. 14). In the case of a combined system (i.e., storage with integrated industrial water supply), the effective storage capacity for the heat circuit is reduced by the amount of industrial water feed into the system. Heat storage systems are also available in the form of component parts (i.e., disassembled) for subsequent on-site assembly and installation in inaccessible areas (e.g., basements).

In connection with the hydraulic integration of heat storage into the domestic energy supply system, particular attention should be paid to a properly functioning and well-tuned alignment between the biomass furnace, buffer storage and heat distribution system, as heat losses can otherwise quickly run up to 10–20% of the required available thermal energy. An example of a proper system is illustrated in Fig. 15. During the heating up process, the feed line is "short-circuited"

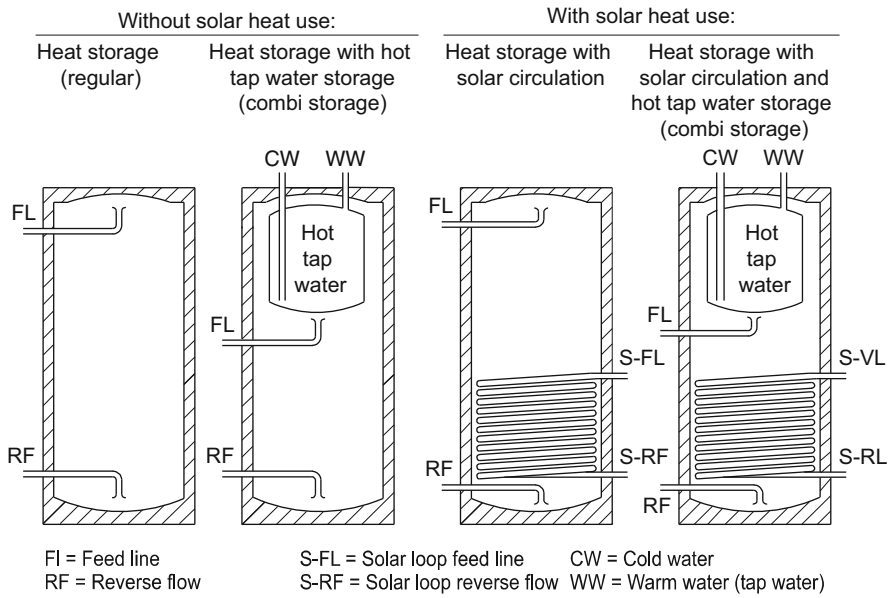

Biomass Energy Heat Provision in Modern Small-Scale Systems. Figure 14
Different types of thermal energy storage systems [14]

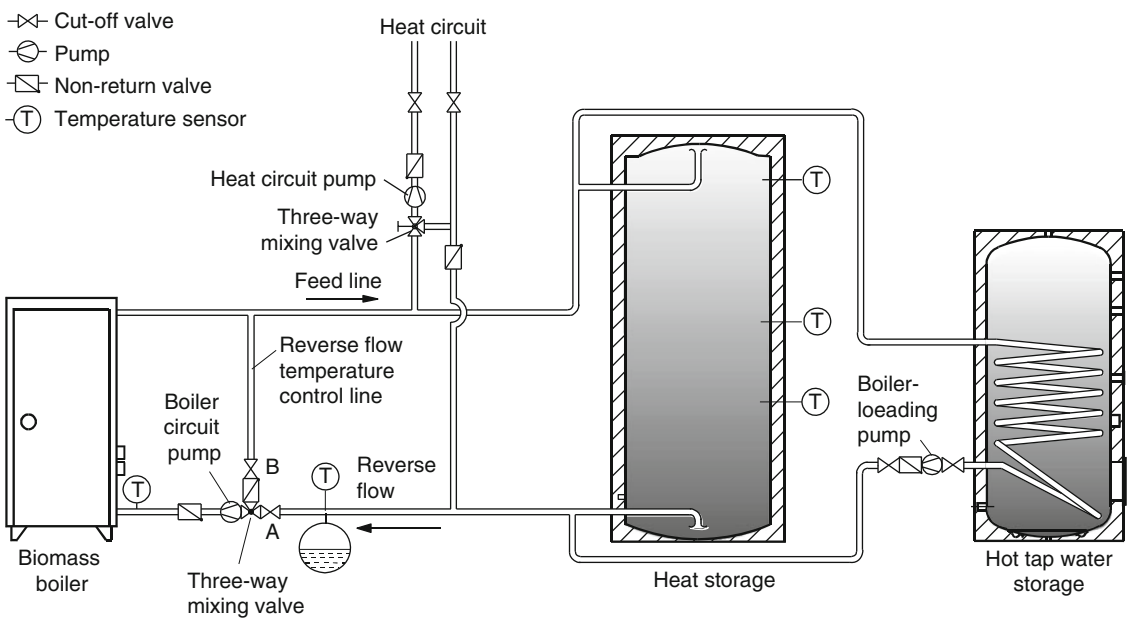

Biomass Energy Heat Provision in Modern Small-Scale Systems. Figure 15
Example of a hydraulic connection system for the storage of thermal energy in a wood-burning heating system [18]

with the reverse flow (valve B open, valve A closed) in order to reach the required operating temperature (usually around 60°C at the boiler's reverse flow) as quickly as possible ("increased reverse flow"). As soon as valve A is opened up, hot water can flow into the heat circuit and the boiler. If there is no or only very low demand for energy, charging of the storage system commences. For this purpose, the heat circuit pump

reduces the flow in such a way, that the surplus volume delivered by the boiler circuit pump is directed into the heat storage system. As soon as the delivery of heat from the boiler is interrupted (e.g., drop in flue gas temperature to below 60°C) both valves close automatically (valves A and B in Fig. 15). Since the boiler circuit pump is now switched off, the heat circuit pump can reverse the flow direction inside the storage system and now extract the heat from the upper section of the storage tank.

The volume of storage capacity required is determined by several factors, including the following:

- Capacity range (variable load or boiler operating exclusively at full load)
- Volume of fuel filling space
- Rated thermal energy output value
- Temperature variations in the buffer system (feed flow/reverse flow)
- Demands in terms of operating comfort/ease of use

Furnaces, which can only be operated at their full thermal energy output rating, require larger storage capacities than variable load furnaces, where the amount of surplus heat will be lower because of automatic heat output adjustments. Larger storage capacities, however, are also required if the system (downdraft combustion) has a comparatively large fuel filling space (charging chamber) and correspondingly high levels of heat energy are produced with each single charge.

In order to simplify the calculation of storage capacity requirements, the rated thermal energy output values can also be taken into account, in addition to the size of the charging duct. Storage capacities of at least around 55 l/kW installed furnace output rating are recommended for hand-charged log wood-burning boilers; the target value to be aimed at lies at around 100 l/kW installed [14]. The same applies for load-adjusted firewood-charged furnaces (partial load operation) which should also be operated in or close to the upper range of their capacity to achieve optimum operating performance at the lowest possible level of air pollutant emissions and the highest possible level of operating efficiency.

The heat storage capacity – and correspondingly the volume of storage required – also depends on the effective difference in buffer and heating circuit feed-in temperatures. Discharge from the heat storage system consequently terminates as soon as the discharge temperature drops below the heating circuit feed-in temperature. Temperature differences arising between the storage (at maximum load) and the heating circuit feed-in range from 25 to 50 K, depending on the design of the heating system. The available capacity of heat storage therefore depends on the heating circuit feed-in temperature, and consequently on the heating system installed. For low-temperature heating systems (e.g., floor or wall heating system), there will consequently be more useable heat available in the buffer system, than would otherwise be the case in conventional radiator systems [14].

Large storage capacities additionally increase operating comfort since fewer start-ups of the system will be required, especially during periods of seasonal transition. Buffering, however, inevitably results in greater heat losses occurring and thus does have an impact on the average annual performance of the overall system. Storage systems should therefore be preferably installed in heated spaces inside the building and/or be equipped with effective thermal insulation.

Combined systems of heat supply. Wood-burning furnace systems, generally speaking, do show relative high levels of emission and low grades of efficiency during summer periods, when they are predominantly used for heating up of industrial water supplies. Alternative solutions in this context are available, for example, by way of a combination with solar systems. Then the use of the biomass boiler may not be necessary at all during the summer and to some extent also during periods of seasonal transition. In the event of such a combined biomass–solar energy system being used, attention must be paid, through the installation of appropriate technical controls and/or monitoring by the user. The biomass-fueled part of the system should not block off storage capacity required by the solar system, if the same heat storage is to be used by both systems. Appropriate intelligent technical control systems, which would also be able to take into account relevant weather forecast, are currently under development.

In providing for peak load demands, especially in the case of larger capacities, it may be advantageous to scale down the biomass-fueled part of the system. This is in order to allow for a substantial reduction in investment costs on the one hand and for a

considerable extension of the period of time during which the biomass boiler can be operated at full load on the other hand. Additionally required supplies to cover peak load demands can then be met, either by means of a cost-efficient oil- or gas-fired boiler (possibly also by way of a boiler integrated into the buffer system), or through the installation of an electric heating rod in the heat storage system.

Automatically Charged Wood Furnaces

The demand for efficient and automated operational processes, combined with a simultaneous increase in the output of thermal energy, has lead to the development of automatically charged furnace systems for solid biofuels. The basic differences and technical advantages, compared to hand-charged furnaces, are discussed in section "Differences between Manually and Automatically Charged Furnaces." Different system technologies are introduced in the following sections.

Automatically charged furnaces are categorized by way of reference to the relative speed of flow of fuel particles and air supply as fixed-bed, circulating bed, and entrained flow combustion systems [19]. However, only fixed-bed furnaces are generally considered suitable for domestic heating systems. According to their respective systems of fuel supply, furnaces can be separated into the following three basic categories: underfed burners, horizontally fed burners, and burners with drop-down fuel supply systems (Fig. 16).

In the case of underfed burner systems, the fuel is supplied to the burner cup (retort) from underneath by means of a feeding screw. Part of the combustion air is injected in form of primary air supply into the retort where drying, pyrolytic decomposition, and gasification of the fuel take place. In order to ensure complete oxidation of the combustible gases formed during these processes, secondary air supply is mixed with the combustible gas prior to entering the secondary combustion chamber. The hot gases subsequently transfer their thermal energy to the heat exchanger. Then they are ultimately released into the atmosphere as flue gas via the chimney system. Fuels to be used in these types of underfed furnaces are low-ash, fine-grade wood chip with a moisture content of 5–35%. Since comparatively high fire bed temperatures are usually reached in this process, this particular form of combustion process is not really suitable for the use of wood bark or straw fuels. The principle of underfed combustion is employed in the majority of small-scale furnace systems designed for the use of wood pellets.

In horizontally fed burner systems, the fuel is charged sideways into the combustion chamber, which may be equipped with or without a grate (Fig. 16). Small-size wood chip fuel supplies (of relative consistent calibration) are usually charged through a conveyor screw system. Coarse and unevenly formed fuels, such as shredded and/or non-sifted wood or wood bark, either require robust screw feeders or can be charged with the aid of a piston installation. Fixed grate systems are predominantly used for furnaces with lower range capacity (<100 kW). Moving grates systems (e.g., pushing floor or roller grates) are increasingly also used for higher capacity furnaces.

Pushing floor combustion systems without a grate (also known as sliding charge furnaces) are based on an operating principle similar to that of an underfed burner system. If they are fitted with a water-cooled combustion chamber, they are – other than for wood chips and wood pellets – also particularly well suited for high ash producing fuels and other combustion materials liable to the formation of slag (e.g., straw fuels, grains). In the case of lateral downdraft furnaces, part of the combustion air is injected into the system in the form of primary air supply channeled through the grate (if installed) via air nozzles inside the burner cup, or in the case of pushing floor furnaces, via front-end air ducts. Under these circumstances, the primary air supply also acts as a cooling agent for the grate, which in turn reduces the risk of slag deposits and overheating of material occurring during the use of critical fuel substances. Secondary air supply is provided either above the grate and/or fire bed, or prior to entry into the secondary combustion chamber.

High-density wood pellets are typically used in furnaces working with drop down feeding of fuel supplies, as well as in underfed burners and (occasionally) grate-based furnace systems. Drop-down feeding systems are a special design developed specifically for the use of wood pellets. They are therefore not suited for the handling of wood chip. The pellets are fed into the system via a conveyor screw and dropped through a pipe or shaft from above onto the fire bed located either in a removable burner cup, on top of a tilting

Principle	Variant	Type	Scheme	Nominal heat power	Fuels
Underfed burners			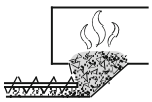	> 10 kW (< 2.5 MW)	Wood chips, wood pellets
Horizontally fed burners	Grate furnace	Fixed grate, partly with ash scraper or tilting grate	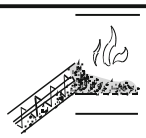	> 35 kW	Wood chips, wood pellets
		Moving grate		> 15 kW < 60 MW	Wood chips, wood pellets, saw dust, bark
		Roller grate	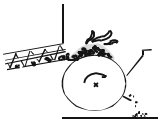	> 40 kW > 450 kW	Wood chips, wood pellets
	Pushing floor furnace		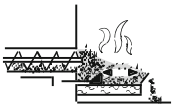	> 25 kW < 800 kW	Wood chips, wood pellets (>15 kW) herbaceous fuels, grain (with water cooling)
Burners with drop down feeding	With grate	Tilting grate burner	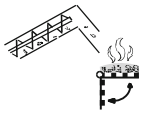	> 15 kW < 30 kW	Wood pellets, precision wood chips
	Without grate	Cup burner	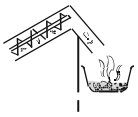	> 6 kW < 30 kW	Wood pellets
		Tunnel burner	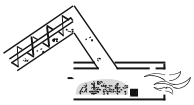	> 10 kW	Wood pellets
		Downdraft burner	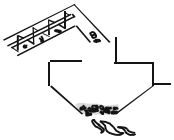	> 14 kW < 60 kW	Wood pellets, wood logs, wood chips (> 20 kW)

Biomass Energy Heat Provision in Modern Small-Scale Systems. Figure 16
Illustration of operating systems for fixed-bed furnaces – according to feeding systems used [14]

grate, or inside a tunnel (Fig. 16). This is where primary and secondary air is injected from underneath or sideways through appropriate nozzles (perforations) arranged in the shape of a ring. Depending on their design, furnaces not using a grate can be separated into cup burners, tunnel burners, and vertical downdraft burners. In addition, there are a variety of other special designs available on the market which can, however, generally be traced back to one of the systems described above.

In horizontally fed furnaces fitted with a grate, the pushing floor is the most commonly used system, although roller grates are sometimes also found. A distinction can furthermore be made between horizontal and tilted grates. More detailed information concerning these different combustion systems (including air supply, feeding of fuel, ash removal, starting controls, and circulation of gas) and the integration of the relevant combustion chambers into the overall furnace systems, in particular, is presented in the following sections and illustrated with selected examples.

Pellet Furnaces A number of special combustion systems do exist for automatically charged pellet-burning furnaces, taking advantage of the fact that pellets can be simply apportioned into the furnace at high energy density. Two of these systems are reviewed in more detail – drop-down feeding with cup burner and drop-down feeding with tilting grate. Additionally, the fuel supply system is explained.

The charging of pellet-fueled furnaces can generally be arranged following the same principles and installation alternatives available for wood chip burning systems (section "Wood Chip Furnaces") whereby, here as well, the more cost-effective solutions are available in the form of inclined floor systems with feeding screws or suction fans.

Pellet boilers are frequently used in combination with interim fuel storage containers (often available in the form of compact systems). In these cases, a fill-level indicator is installed potentially also be able to automatically trigger the recharging process. In contrast to wood chip burning systems, even winding or contorted paths of fuel supply from storage to the actual furnace can be accommodated, since pellets are suitable even for transportation by screw conveyors without axle or pneumatic feeding systems (airflow supported conveyance systems). This provides for considerably more flexibility in the utilization of available space. An example for this type of fuel storage connection by means of an airflow-supported conveyance system is illustrated in Fig. 17. Care needs to be taken, that the space where pellets are stored is served by sufficient passive ventilation, as a minimum requirement.

Drop-down feeding with cup burner. With the introduction of standardized wood pellets, the range of designs for stand-alone furnaces was expanded by the addition of the pellet stove (Table 1). The advantages of automated charging do come to bear even for the low capacity range of systems used for domestic purposes. By using pellets with consistent fuel characteristics (usually 6 or 8 mm in diameter) and low moisture content (<10%), variations in the combustion process are minimized. This is where pellet stoves and chimney stoves differ from one another, even though pellet stoves may also be fitted with a glass screen for the display of the burning fire. Therefore, they are sometimes also referred to as pellet-chimney stoves.

The fuel is placed into a pellet storage bin located at the back of the stove. This storage is usually filled by hand in the case of most stand-alone furnaces. Due to the high bulk density of wood pellets (ca. 650 kg/m^3) comparatively large amounts of fuel can be fed into the system (approximately 20–50 kg), and depending on the operating load status, this supply can last for 1–4 days. Pellets are moved via a conveyor screw into an ascending pipe up to the opening of a dropping shaft through which they are fed into the burner cup (Fig. 18). During the start-up phase, fuel is ignited in the burner cup either by hand (lighter) or more commonly with an electric ignition (hot air ignition fan or heating element). Details of primary and secondary air supplies are illustrated in Fig. 19. A small amount of additional air supply is usually injected into the system through the dropping shaft in order to reduce the risk of backfire occurrence. As is the case for chimney stoves, additional fresh air (cleaning air) has to be channeled from above along the inside of the glass screen in order to prevent the settlement of dust or soot particles, which might otherwise impair visual appearances. From the perspective of achieving an optimum supply of combustion air, however, such "optical measures" always bring with them certain disadvantages. This is true because the cleansing air cannot be specifically used for secondary air supply purposes and, on the contrary, may potentially even contribute toward a rise in emissions and/or reduction of efficiency by further increasing the amount of excess air in the system. But in general the pellet stove – not least of all due to the fuel's high degree of homogeneity – commands a leading position in respect of the following two parameters: Emissions of carbon monoxide are well below the values found in the case of other stand-alone

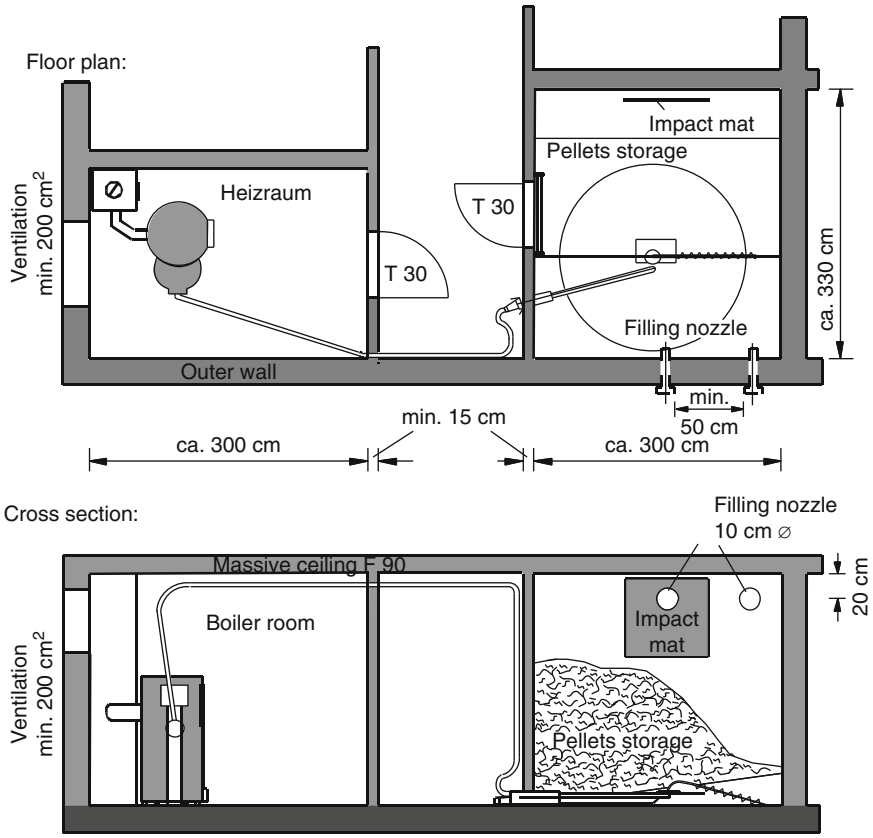

Biomass Energy Heat Provision in Modern Small-Scale Systems. Figure 17
Example of pellet heating installation with pneumatic feeding system [14] (From ÖkoFen GmbH, Austria)

furnaces. The performance efficiency can reach levels of more than 90% (sections "Combustion Efficiency" and "Flue Gas Emissions").

Air is supplied by a low-noise (if possible), graduated or speed-controlled fan system. Air intake is arranged by means of a central inlet manifold, so that pellet stoves with external air supply can largely be operated independently from room air supplies. This operating system is especially relevant for controlled room ventilation systems. Only small amounts of air are still taken from the room of installation (e.g., for cooling of the dropping shaft and the provision of cleansing air).

The flame in the furnace is similar in appearance to that of a gas fire. The release of thermal energy happens partly through radiation, primarily however via convection ducts (Fig. 18). The ashes produced are removed by hand from inside the burner cup and the ash box.

Since pellet stoves are load variable, they are also well suited for continuous operation mode. They are available with capacity ratings up to 10 kW and allow for partial load operations at approximately 30% of rated thermal energy output values, without any significant loss in combustion efficiency.

Details of typical air supply for a cup burner are illustrated in Fig. 19. Primary air is initially channeled into the system through nozzles (perforations) in the bottom of the burner cup, with the aid of a fan (or draft suction), whereas secondary air streams sideways into the burner cup above through a ring-shaped arrangement of air nozzles in the wall of the cup. In other construction designs, secondary air is injected from the side, above the burning fuel or fire bed, through

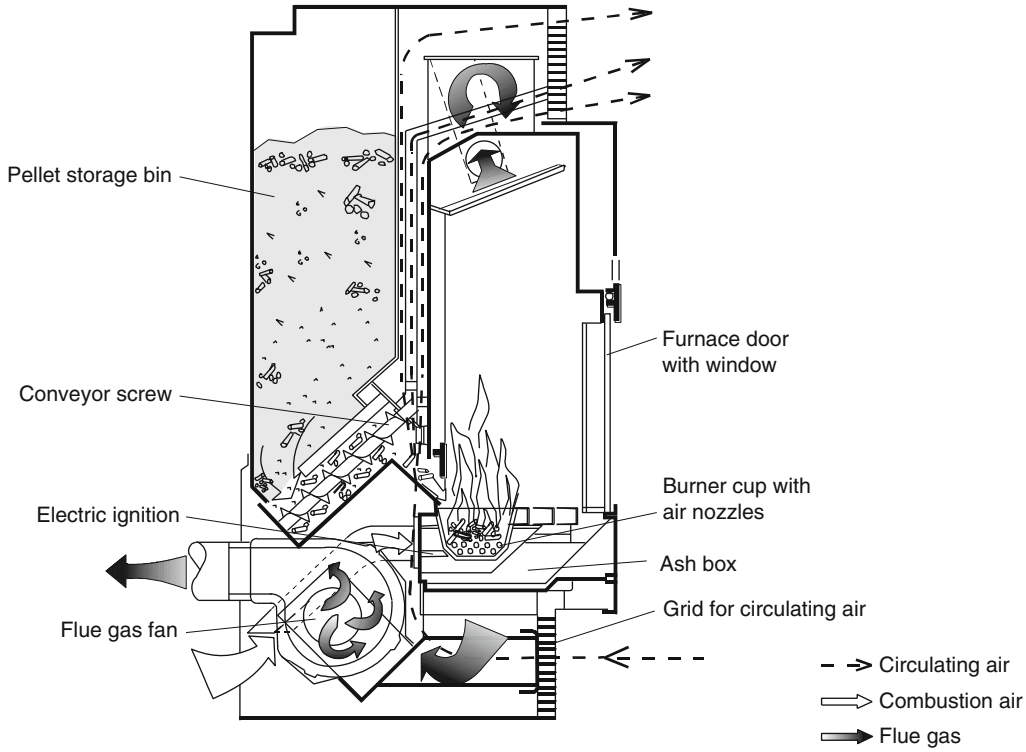

Biomass Energy Heat Provision in Modern Small-Scale Systems. Figure 18
Working principle of a pellet stove with drop down feeding and burner cup [19] (From Wodtke GmbH, Tübingen) [18]

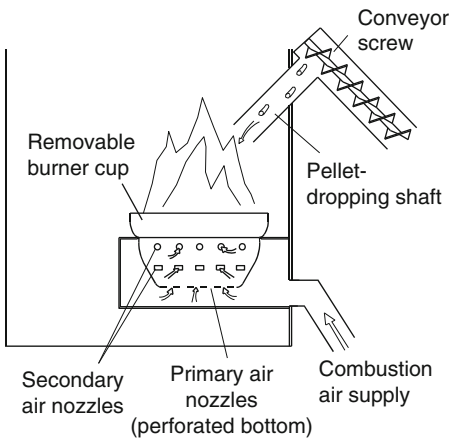

Biomass Energy Heat Provision in Modern Small-Scale Systems. Figure 19
Air supply system for furnaces using burner cups [18]

a ring-shaped arrangement of air nozzles and then mixes with the gases emitted from the fire bed.

Pellet stoves are also available as elements for the refitting of an existing system, similar to the way in which a natural gas or heating oil burner can be mounted onto an existing heating boiler, thereby allowing for conversion of a furnace system already in place. Such plants can be designed as cup burners or alternatively as tunnel burners, where the pellets continuously trickle from above into a combustion pipe, through which the combustion air passes horizontally, so that the flame of the burner can enter sideways into the combustion chamber at the other end.

The principle of drop-down feeding can also be used for pellet boiler systems. The essential difference is the absence of a display window, making it easier to optimize conditions within the combustion chamber. Combustion principle and air flow system are essentially similar.

Drop-down feeding with tilting grate. In this type of design, pellets are fed into the system via a conveyor screw and dropped from above through a dropping pipe or dropping shaft onto the fire bed positioned on a tilting grate. Then primary and/or secondary air is injected from below or sideways through an appropriate ring-shaped arrangement of air supply nozzles (Fig. 20).

In the case of tilting grate systems, the ashes produced are automatically discharged into the grate ash collector located underneath, as and when needed (e.g., every 16 h). In order to ensure that larger ash deposits are completely removed from the grate, the tilting grate, which is designed in form of a perforated plate, is made to collide with a vertical cleaning plate (motor driven) inside the space designated for the collection of grate ashes. This cleaning plate is fitted with spikes arranged in a pattern corresponding to that of the perforations in the tilting grate. Any still glowing embers discharged together with the ashes will burn out in the ash box whilst a new supply of pellets is ignited on the still hot but cleaned grate.

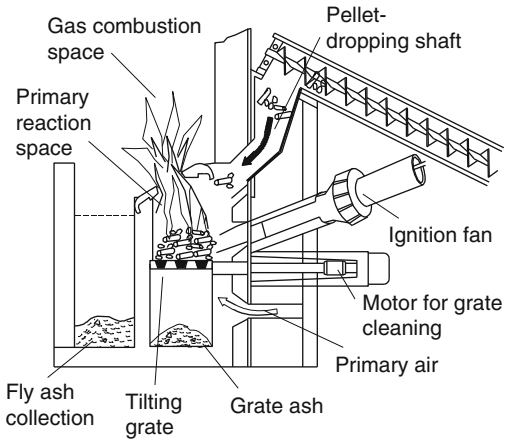

Biomass Energy Heat Provision in Modern Small-Scale Systems. Figure 20
Working principle of a wood pellet furnace with dropping shaft and tilting grate feeding system [18]

Figure 21 provides a representative example of a pellet boiler fitted with a combustion chamber designed according to the system shown in Fig. 20. This illustration also shows the fuel container with feeding screw, the boiler with the necessary cleaning installations, the suction fan and the systems control unit, together with control panel.

Apart from the combustion systems with dropping shaft fuel supply described above, underfed burners as well as inclined grate furnaces with lateral fuel feeder are used in pellet burning appliances (starting at approximately 10 kW rated thermal energy output).

Wood Chip Furnaces Underfed and grate based combustion systems, in the lower capacity range, are generally used for wood chips and wood bark in furnace systems of varying design, which are described in

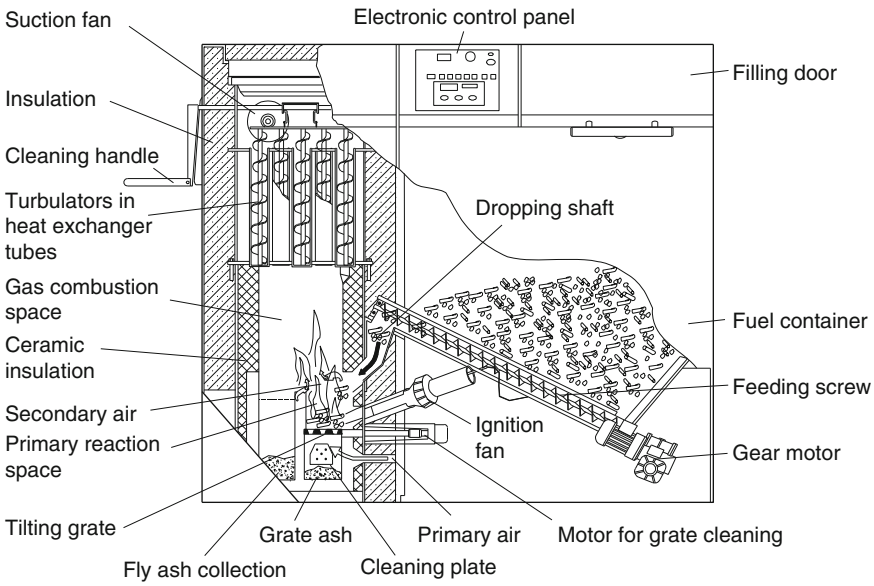

Biomass Energy Heat Provision in Modern Small-Scale Systems. Figure 21
Example of a 15 kW pellet boiler with tilting grate and fuel container [14, 18] (From Guntamatic Heiztechnik GmbH, Austria)

more detail below. Additionally, the fuel supply is discussed.

Wood chip furnaces do usually have a fully automated continuous supply system directly connected to area where the fuel is stored. This is typically done with the aid of a double feeder screw installation, with dropping shaft. In these cases, feeder systems are equipped with leaf spring agitators, conical screw-type conveyors or pushing floors.

The discharge level of silos for wood chip arranged either horizontally or as a tilting level, depending on how access for maintenance and repairs to the moving parts is to be organized. A number of installation layouts commonly used for silo substructures, with leaf spring agitator and conveyor screw, are illustrated in Fig. 22. Similar layouts are essentially also possible for the other conveyor systems referred to in section "Technical Approach".

Underfed burners. In an underfed furnace system (Fig. 23), the fuel supply is delivered to the combustion retort from underneath, by means of a screw conveyor. Part of the combustion air is also injected into the fuel (in form of primary air) through the retort, where the drying process, the pyrolytic decomposition, and the gasification of the charcoal take place. To ensure that the combustible gases are completely oxidized, preheated secondary air is usually mixed with the released gases, if possible, prior to entering the heated secondary combustion chamber. The hot gases subsequently flow through the heat exchanger, where they release their thermal energy, frequently followed by a cyclone separator (in large-scale systems), where particle matter emissions are usually removed.

In small-scale underfed furnace systems, wood chips with a moisture content of 5–30% can be used as a fuel; however, fuel supplies and the control of air flow(s) need to be adapted to the relative quality of fuel – particularly with regard to the moisture content of the fuel – in order to prevent technical failure of the system. A plant laid out, for example, for the combustion of wood chip

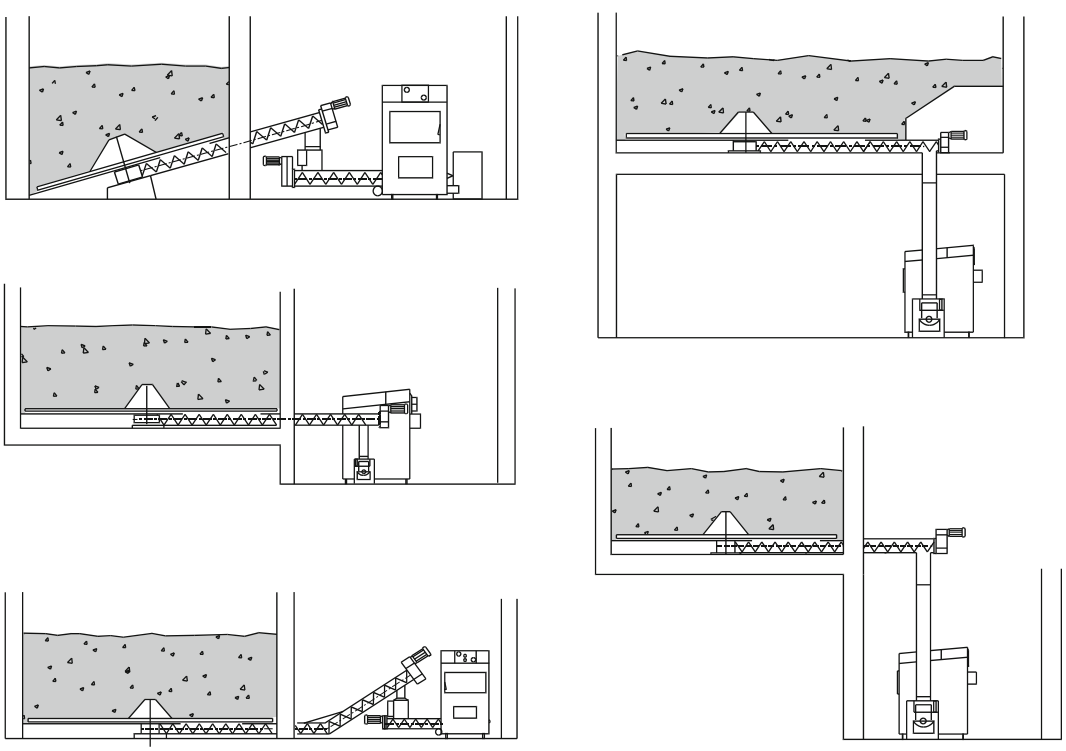

Biomass Energy Heat Provision in Modern Small-Scale Systems. Figure 22
Examples of wood chip boilers with leaf spring agitator and screw-type feeding system [14] (From Herz Feuerungstechnik GmbH, Austria)

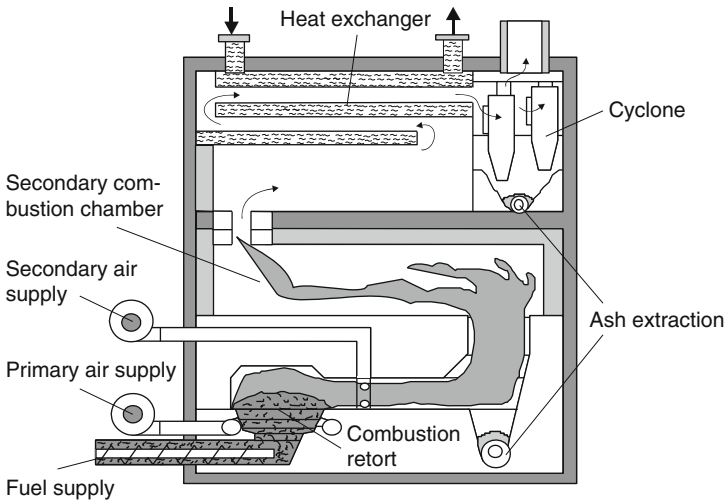

Biomass Energy Heat Provision in Modern Small-Scale Systems. Figure 23
Diagram of an underfed burner system [19]

with comparatively high moisture content would reach too high a level of temperature in the combustion chamber if charged with dry wood. This would ultimately result in material fatigue and the formation of slag residue. For the adjustment of the system to changing types of fuel, generally, skilled service personnel are required. Therefore, it is advisable to maintain a consistent fuel quality.

Figure 23 illustrates the operating principle of a furnace system adapted to the specific combustion properties and characteristics of biomass fuel. The zone where the pyrolytic decomposition and gasification takes place in the fire bed is clearly separated from the combustion of the volatile gaseous substances, which takes place in an appropriately sized secondary combustion chamber. The primary air is injected into the fire bed of the combustion retort and regulates the combustion performance. The usually preheated secondary air is blown in at the entry to the secondary combustion chamber and controls the oxidation and thereby the emission of non-combusted substances in the flue gas.

The mixing of secondary air at the entry point of the secondary combustion chamber (Fig. 23) takes place due to the impulse of the air entering into the system. The secondary combustion chamber is additionally configured as a flow pipe. Through this type of design, specifically adapted to reaction technical requirements, optimal rates of reaction can be achieved for a given volume. Through corresponding regulation of the excess air, the temperature in the secondary combustion chamber can additionally be maintained at the necessary level. This way the stipulations of the "3-T-rule" (section "Combustion Requirements") are well met.

Underfed burner systems are particularly well suited for low ash fuels with low proportions of undersized particles, since the feeding by way of a screw conveyor requires fine grain and even consistency (e.g., wood chip). The principle of underfed burner systems is therefore increasingly used for the combustion of wood pellets (e.g., central heating pellet boilers). The combustion of bark or straw fuels on the other hand is not really sensible, given the high level of ashes produced and/or disruptions to the process potentially occurring as a result of the formation of slag.

Horizontally fed burners. Rigid grate systems are predominantly used for horizontally fed burners. An example for this type of burner is shown in Fig. 24. In plants using fuels with a tendency toward the formation of slag, moving grate systems are also used, starting at around 30 kW. In moving grate systems, the fuel steadily travels downward on the inclined grate, driven by continuous forward and backward movement of grate elements.

The pushing floor furnace (also known as "sliding charge furnace") works similarly to the underfed boiler system. If fitted with a water-cooled burner cup (section "Furnaces for Herbaceous Fuels"), this system is

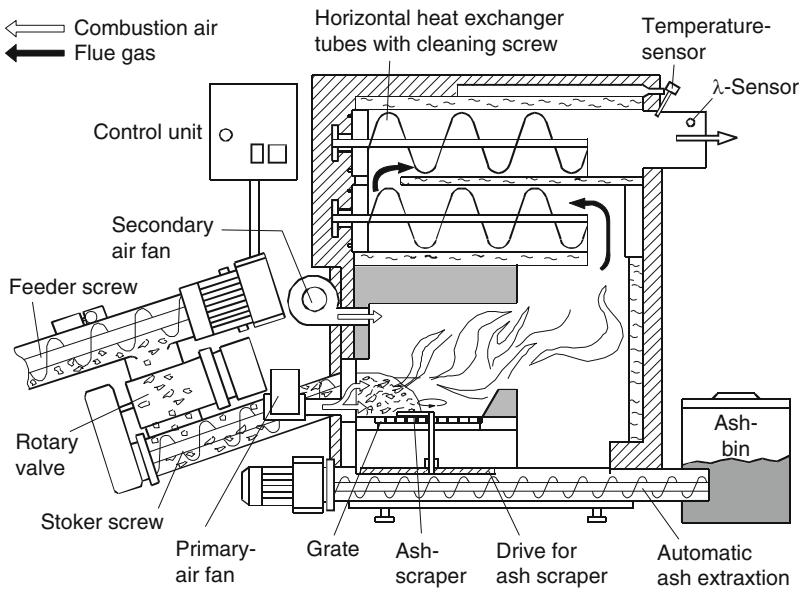

Biomass Energy Heat Provision in Modern Small-Scale Systems. Figure 24
Example of a 50 kW wood chip furnace based on the horizontal feed principle with grate and ash scraper [14] (From Heizomat Gerätebau GmbH, Germany)

specifically also suited for the use of fuels with a tendency toward slag formation.

Part of the combustion air is injected in the form of primary air by means of air nozzles in the sidewalls or, as common for moving grate furnaces, at the front of the grate elements. This way the primary air also serves as cooling for the grate, which reduces the risk of slag deposits and material fatigue during when critical fuels are used.

Secondary air is injected above the grate or the fire bed, or prior to entry into the secondary combustion chamber. The ashes produced drop into an ash box or in some systems removed by hand. In the case of high-ash fuels, however, ashes can also be extracted automatically into a larger disposal unit, by way of a conveyor screw system (Fig. 24).

Furnaces for Herbaceous Fuels

Furnaces for (loose fill) straw and cereal fuels (chaff material, pellets, grains) are generally also suited for wood chip and wood pellets; however, the reverse is not the case. Agrofuels such as straw, grass, whole crop cereals, or grains demonstrate numerous disadvantages compared to wood fuels, since they require elaborate and expensive combustion technologies on the one hand and they make compliance with emission controls currently in force in most countries more difficult on the other hand. These types of fuel are therefore, in practical terms, yet still unimportant, particularly for the segment of small-scale furnace systems.

The disadvantages in combustion properties are numerous. The calorific value is only marginally lower than that for wood; however, the proportion of residual ashes from straw fuels is generally around eight to ten times higher than that for wood fuels. In terms of nitrogen, potassium, and chlorine content straw and grain fuel will again always show significantly higher values than wood (Fig. 25). The aforementioned substances do not only contribute toward the creation of airborne emissions, but also have a negative impact on corrosion and the formation of slag residues in the combustion chamber and on heat exchanger surfaces, which is of particular relevance in the context of furnace system design.

However, the melting properties of the ashes produced are also important, in terms of technical requirements for furnace systems. Here again, ashes from wheat straw with a melting point around 1,000°C are considerably more critical than ashes from the

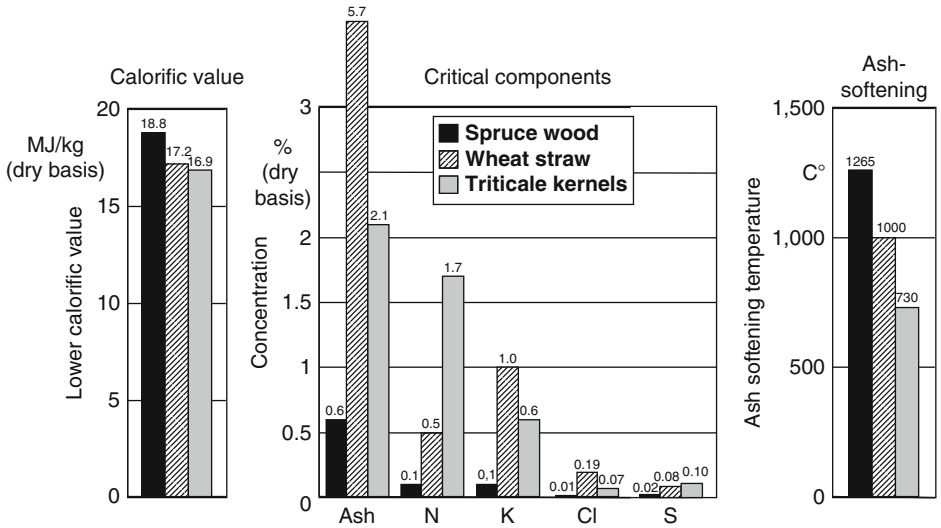

Biomass Energy Heat Provision in Modern Small-Scale Systems. Figure 25
Comparative quality characteristics of spruce wood, wheat straw, and triticale kernels (From [13], triticale: wheat and rye hybrid)

combustion of wood (Fig. 25). In the case of cereal kernels, caking of ashes and the formation of deposits inside the system already do occur at even lower temperatures. Straw- and grain-burning furnaces therefore demonstrate different technical characteristics, in terms of ashes and slag separation, temperature control or the pretreatment of fuels.

- Systems designed for relatively low-ash fuels (e.g., underfed burners) are not suitable for the combustion of straw materials. Retort furnaces equipped with ash scrapers or ash pushers, as well as certain grate furnace systems, can be used for a broader range of fuels and can therefore (to some extent) also be used for straw and grain fuels. The drawback of the strong tendency toward the formation of slag can be counteracted by lowering of combustion temperatures in the fire bed area (e.g., through cooled grate elements, water-cooled outside surfaces for the combustion chamber). The risk of separate slag particles forming deposits can also be partially reduced through constant movement of the fuel and the ashes (e.g., in pushing grate furnace systems (section "Wood Chip Furnaces").
- In the case of straw fuel furnaces, special attention must be paid to the resilience of system components against corrosion and wear (particularly in the heat exchange area). This is to prevent significant limitations to the useful life of such plants. Such risks can, for example, be reduced through the use of stainless steel heat exchangers or silicone carbide for the lining of the inside of combustion chambers. However, there is no real long-term experience available so far. The reason for increases in corrosion is often found in the significantly higher levels of chlorine produced by the combustion of aggressive flue gas substances. But the high potassium content as well, which results in corrosion promoting deposits on system components exposed to flue gases, does contribute to corrosion.
- Compliance with emission control thresholds in the combustion of straw materials can often be safeguarded only through the installation of elaborate secondary flue-gas cleaning systems. Conventional cyclones provide close to zero efficiency in the separation of especially small "submicron" particles, which represent the majority of particulate matter emissions. Effective separation is only possible with the aid of filtrating separators (e.g., through the use of metal netting filters, packed bed filters, cartridge systems) or through electrostatic separation (electrostatic precipitators, section "Secondary Flue Gas Treatment"). Such measures, however, still result in an unacceptable increase in costs for the overall system.

In the combustion of straw fuels, a distinction needs to be made between loose fill combustion systems, using a debaler or already loose, chopped, or pellet material, and systems capable of handling whole bales as fuel. These types of systems are introduced below.

Furnaces for Bulk Material In order to solve and control the special problems arising from the combustion of straw fuels two different ways are used: the adjustment of fuels to the combustion technology, or the adaptation of furnace systems to the different types of fuel.

Adjustment of fuels to the combustion system. The process of slag formation can be counteracted through the addition of additives or the creation of special mixtures of biofuels, as the melting properties of ash from the combustion of biomass fuels depend on the specific composition of the ashes. Based on the present state of knowledge, it would appear that the calcium and potassium content of the fuel are the crucial factors. Calcium containing substances, such as caustic lime or pulverized limestone in particular, act to increase the melting point of ash. Since these are noncombustible additives, the amount of ashes to be removed from the furnace will increase by approximately 15–60%, allowing for the usual addition of aggregates accounting for approximately 0.5–2.0% of overall weight. Special equipment is already available on the market for dosage and mixing of these aggregates; and custom-designed solutions are additionally employed.

Adjustment of the combustion system to fuels. The process of slag formation in special straw burning furnace systems can be avoided by two measures often used in combination:

- Limitation of combustion temperature in the fire bed.
- Keeping fuel and ashes permanently in a state of movement.

Inflowing primary air already contributes toward a reduction of temperatures ("cooling") in the fire bed. However, since the amount of primary air is strictly limited by the requirements for an efficient pyrolytic decomposition and the gasification of the remaining carbon, additional cooling can be achieved through regulating the circulation of flue gas in the combustion chamber. Reliable cooling, at least for the surface areas in small-scale furnaces, however, can only be achieved through cooling down (water-cooled) the surfaces in the fire bed or combustion chamber (e.g., heat exchangers installed underneath the retort in the combustion chamber). In large-scale systems, this can be realized through the use of water-cooled grate components. However, since the formation of slag deposits – without the addition of aggregates – cannot always be avoided, it is important that the slag produced does not settle and can be easily removed.

For the removal of large amounts of ashes, an oscillating ash scraper can be used (Fig. 26). Similar to the pushing floor system sometimes used in fuel storage facilities, the scraper has a wedge-shaped profile allowing for the removal of ashes, with the steep edge facing forward into the direction of the ash disposal system; whereas in reverse motion, the scraper passes underneath the resting bed of ashes. Moving grates can also be used as an alternative solution (Fig. 27). This way it can be avoided, at least partially, that individual slag particles start forming deposits in the system. These movements lead to the fuel entering the combustion chamber being leveled out in the fire bed, through the motions performed by the scraper, grate, or ash removal elements, whilst the ashes produced are moved to an ash box located in the back. If it significant amounts of slag settlement on elements of the combustion chamber cannot be safely avoided, serious disruptions in the supply of combustion air may occur, for example, by the clogging of air nozzles. The disadvantages range from severe disruptions to the combustion process and damage being caused to the plant, up to a complete breakdown of the system or excessive pollutant emissions.

In order to avoid such disruptions, furnaces, in order to be suitable for the combustion of straw fuels, do need an efficient automated ash removal system. An added factor is that under unfavorable conditions, pieces of slag produced may grow to a size, which makes the removal by means of a screw conveyor impossible, and which would therefore cause a disruption to operations. The use of additional agitator systems may turn out to be necessary (e.g., worm-shaft type systems with catches). The removal of ashes, especially in systems with ratings significantly above

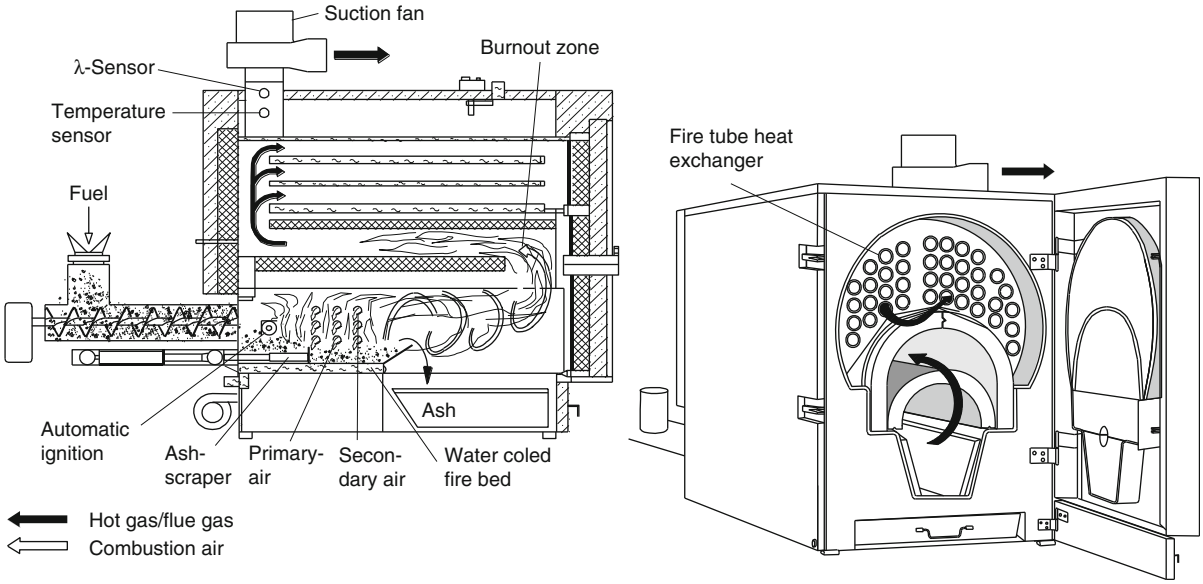

Biomass Energy Heat Provision in Modern Small-Scale Systems. Figure 26
Pushing floor burners suitable for straw fuel supplies (here: 49 kW) with water-cooled fire bed (here without automatic ash scraper) [25]

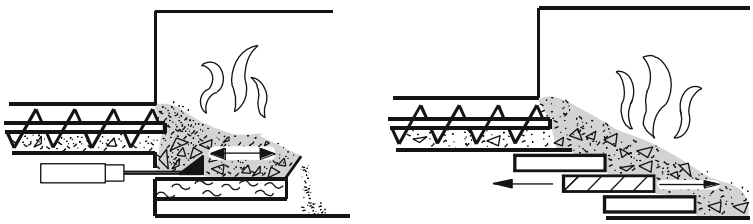

Biomass Energy Heat Provision in Modern Small-Scale Systems. Figure 27
Pushing floor burners with water cooling system in the fire bed (*left*) and moving grate burners for straw fuels (*right*)

100 kW, is sometimes also arranged directly into a fireproof container, located right underneath the combustion area, which can then be easily replaced.

Furnaces for Whole Bales Furnace systems designed for the combustion of whole bales are typically found in plants with ratings above 100 kW. These are usually continuously charged systems (starting at around 2,000 kW) or intermittently charged (i.e., consecutively fed) smaller furnace systems starting at around 350 kW frequently found, for example, in Denmark. In the range of rated thermal energy output levels of below 100 kW, such (bale) systems are only used very rarely.

Given the dimensions of bales, commonly in use today, the charging process is handled mechanically; for example, with the aid of front load tractors, whereby in the largest of these plant layouts up to three big bales (round or square bales) can be charged simultaneously into a water-cooled combustion chamber.

In whole bale furnaces – similar to hand-charged systems – fuel is combusted in charges, with the characteristic phases of initial combustion of volatiles and the subsequent combustion of carbon substances. If such plants do operate on the principle of updraft combustion without grate (section "Principles and Operating Systems") the intermittent and as such difficult to regulate nature of the combustion process is particularly pronounced. The advantage of this combustion principle however is, that these systems are suitable for a wide range of different sizes and shapes of bales. In various markets (e.g., Germany), these systems are not available due to their high levels of pollutant emission.

Recently, the principle of downdraft combustion is also applied in whole bale furnaces (Fig. 28). This involves the selection and subsequent commitment to one specific size and shape of bale to be used for combustion. The advantage of this combustion principle, however, is that the progress in combustion is considerably more evenly balanced, and therefore easier to regulate and control. Nevertheless, more or less major swings in performance, temperature, excess air, and discharge of pollutants (e.g., carbon monoxide) do frequently occur in this type of plant during the course of combustion. This is a feature that these systems have in common with hand-charged wood-burning furnaces. That is why whole bale–charged furnaces, if at all possible, should always be operating under full-load conditions (especially smaller systems); generally these systems will require a relatively large volume of heat storage (section "Integration into Residential Energy Systems").

The system design for a smaller whole bale furnace system is illustrated in Fig. 28. In order to avoid the formation of slag and ash deposits here again – the same as in the case of loose fill furnaces for straw fuels – the critical factor is the reduction of temperatures in the area were fire bed ashes do occur. Cooling of the fire bed therefore is also provided for in these systems. It is typically arranged through the installation of a water jacket enclosing the combustion chamber. The primary air required for combustion is channeled horizontally through the straw via air vents, together with low-temperature carbonization gases (from pyrolytic decomposition) extracted from the upper combustion chamber, to facilitate the combustion of the bale located in the lower section of the combustion chamber. The secondary air is subsequently supplied to the combustion chamber underneath (turbulence chamber), similar to the design found in hand-charged central heating boiler systems.

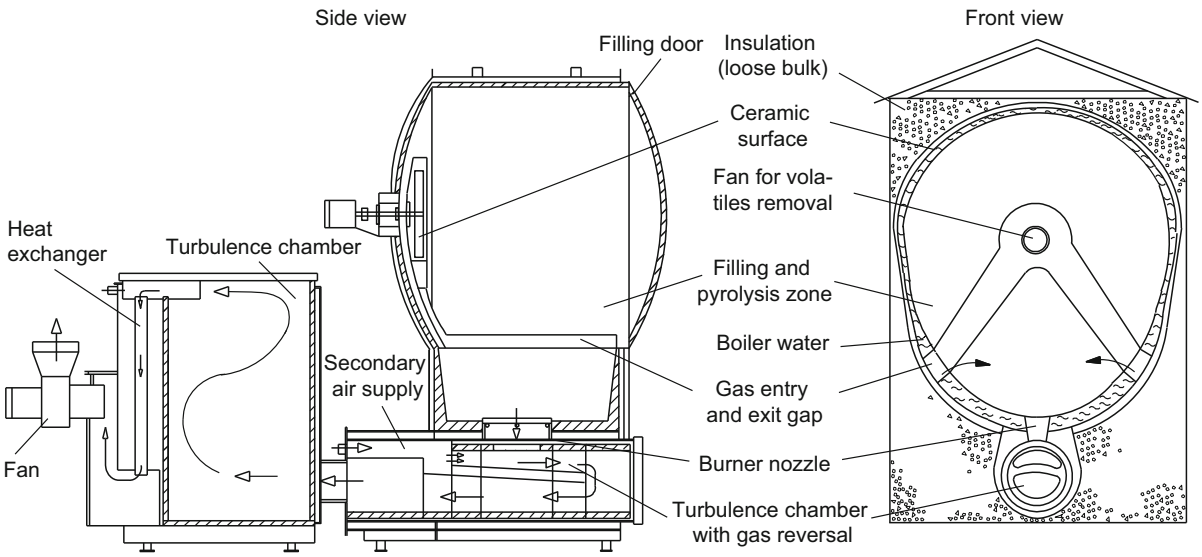

Biomass Energy Heat Provision in Modern Small-Scale Systems. Figure 28
Diagram for round bale furnace (145 kW) for straw-type fuels [14] (From Herlt SonnenEnergieSysteme, Germany)

Combustion Efficiency

When evaluating the efficiency of systems, a distinction is made between combustion efficiency and boiler efficiency. In the case of stand-alone furnaces and enhanced stoves, only the combustion efficiency is specified because the major proportion of available thermal energy is released directly into the surrounding space, and not via a heat transfer medium. A specification of both efficiency ratings is possible only in the case of central heating boilers.

The difference between these two efficiency parameters can be illustrated by the typical flow of thermal energy in a small-scale boiler system (Fig. 29). In calculating the combustion efficiency, the losses due to heat released trough the discharge of flue gas, combustible residues in the ashes and incomplete combustion are taken into account. With regard to boiler efficiency, losses due to thermal energy released by the surface of the boiler still have to be added, so that the boiler efficiency rating for small systems will generally tend to be approximately 3% lower than the combustion efficiency rating.

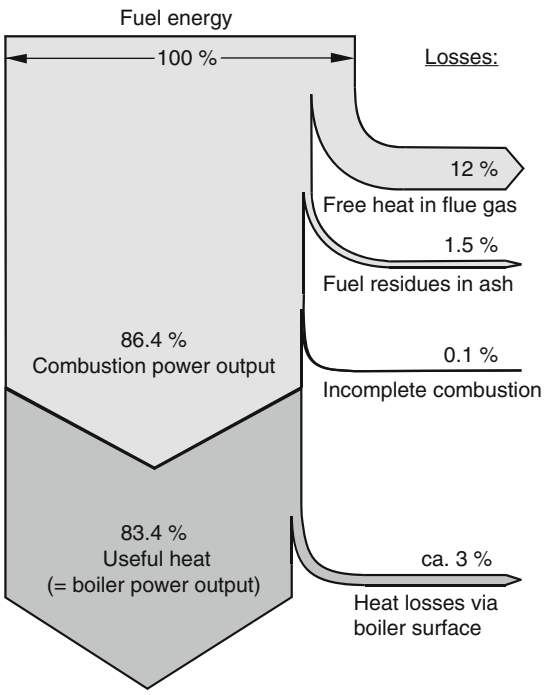

Biomass Energy Heat Provision in Modern Small-Scale Systems. Figure 29
Diagram of typical flows of heat generated by a wood chip boiler (50 kW) at rated thermal energy output values [24]

The flow chart (Fig. 29) demonstrates that the flow of flue gas represents by far largest the contributing factor with regard to the loss of thermal energy. Active measures for the improvement of efficiency are therefore usually aimed at the reduction in flue gas temperatures, whereas improvements in the combustion of gas primarily serve to reduce the emission of pollutants.

The potential for the lowering of flue gas temperatures, however, is limited. In chimney systems liable to be affected by the impact of humidity, temperatures below the dew point are to be avoided. This is true to prevent the formation of condensate, which could not only penetrate the chimney itself, but can also lead to permanent damage occurring to the whole structure of the building (discoloration of brickwork, sedimentation) and increased risks of fire (chimney fire). Additionally, a minimum chimney draft has to be maintained for all chimney systems not equipped with a fume extractor, through the safeguarding of sufficient temperature differences between the flue gases and the surrounding environment.

Efficiency of stand-alone furnace systems. For the segment of hand-charged stand-alone furnaces (stoves), combustion efficiency ratings between 70% and 80% can be expected (Fig. 30). The efficiencies for pellet stoves are likely to be considerably above these values at a rating of approximately 87%. These systems are generally comparable to wood-charged central heating boilers (Fig. 31).

The combustion efficiency values for the different systems shown in Fig. 30 only relate to the actual furnace itself, as flue gas temperatures are always measured at the flue gas connecting pipe of the stove and not the exit point of the chimney. If the system, however, is equipped with a long chimney tract, leading through rooms to be heated, a further cooling down of flue gases is likely to take place. The actual amount of useful heat released would therefore be higher, so that the efficiency rating for the overall system, indeed ought to be set higher.

In type testing performed on furnace test benches today's stand-alone furnaces (stoves) often achieve higher efficiencies, especially since most modern

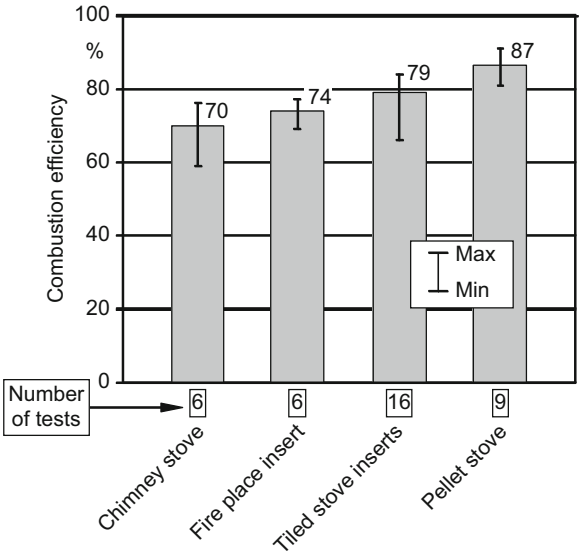

Biomass Energy Heat Provision in Modern Small-Scale Systems. Figure 30
Grades of combustion technology–related performance for stand-alone wood-burning furnaces at rated thermal energy output values [12]

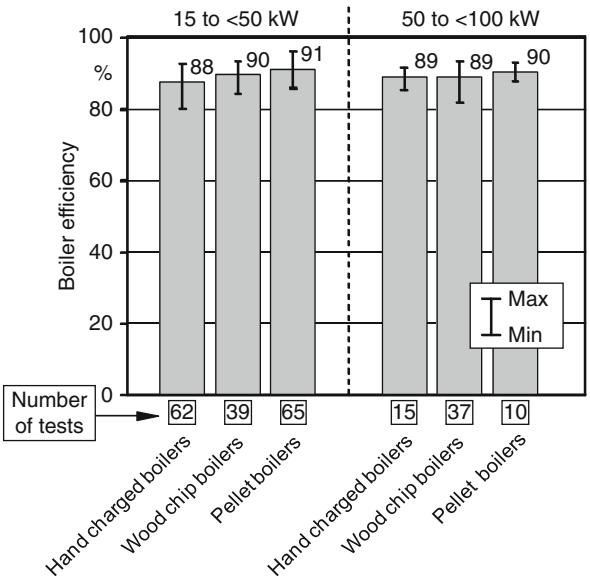

Biomass Energy Heat Provision in Modern Small-Scale Systems. Figure 31
Efficiency rating of central heating wood boilers at rated thermal energy output values; result of 10-year evaluation of tests over the period from 1996 to 2006 [12]

stand-alone furnaces, meanwhile, do have to be able to meet the specific requirements of quality labels (e.g., DIN_{Plus} in Germany). For manually charged stand-alone furnaces it can, nevertheless, be expected that the actual efficiencies achieved in practical day-to-day operations will tend to be somewhat lower than those stated in Fig. 30. Efficient operation of these systems depend to a large degree on the way the system is operated by the user; potential errors in operation (e.g., too high a level of excess air, use of still moist wood fuels, overloading of the combustion chamber, too large or too small pieces of wood) will have a particularly negative impact on performance. These types of errors, however, can generally be avoided if the relevant instructions contained in the operating manual are followed.

The above-mentioned impact of the way in which the system is operated by the user hardly does come to bear in the case of pellet stoves. Since they involve the handling of a uniform standardized fuel material, which additionally can largely also be fed automatically into the system, without user involvement, the efficiency rates shown can also be readily used in practice.

Efficiency of central heating systems. In the case of central heating wood boilers, the combustion efficiency ratings are generally not used as a relevant indicator. Here the boiler efficiency rating is considered, where the performance values are approximately 2–4% lower (Fig. 31). However, almost without exception all values are around a level in excess of 85%; in the case of the most recent boiler designs almost all exceed even the 90% threshold. The simplest way of achieving this result is with pellet central heating boilers, whose ratings tend to be around 2–3% above those for all other types of wood-burning central heating systems. Generally speaking, the variations in efficiency between the different designs and performance categories for any of these systems are rather small.

In the case of the rates of boiler efficiency stated above, the amount of thermal energy released to the surrounding space of the boiler (e.g., radiation) is, by definition, not accounted for as a loss. However, if there is a certain amount of heating required in the space of installation, the overall amount of useful output of heat, from the perspective of the user, is increased. The same applies in respect of the cooling down of flue gases in the chimney tract.

Development of degrees of efficiency. In recent years, further technological developments for wood-burning central heating systems have taken place clearly demonstrated by boiler efficiency ratings. They have improved since the start of the 1980s until the present by approximately 30% (Fig. 32).

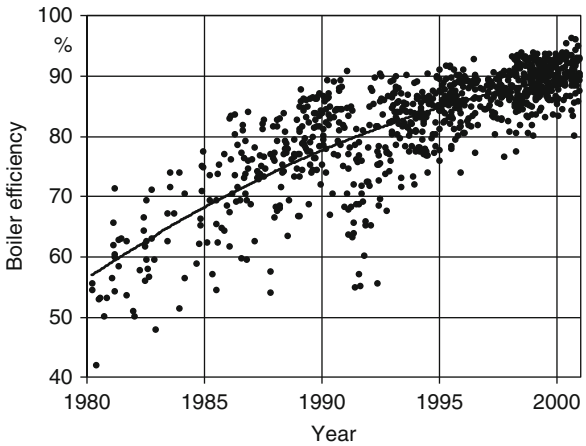

Biomass Energy Heat Provision in Modern Small-Scale Systems. Figure 32
Development of boiler efficiency for hand- and automatically charged wood-burning furnaces at lower capacity ranges since 1980 – results from different boiler-type tests at rated and partial thermal energy output performance [12] (From BLT Wieselburg)

Any significant further increases in rates of efficiency are therefore likely to be achieved only through the introduction of additional condensation heat exchangers. That way flue gases emitted by a wood-burning furnace could be cooled down below the dew point and thermal usage of the latent heat fuel would be increased considerably. This process, which already is standard practice for most natural gas–fired burners ("condensing boiler technology"), could lead to system performance ratings in excess of 100% (based on the lower calorific value H_u, Fig. 33). In the field of biomass fuelling, this effect has so far been used only in the case of larger wood-fired heating plants. But meanwhile this technology has also become available for use in domestic central heating systems. Without any additional consumption of fuel, an increase in performance (and in efficiency) of 18% on average can be achieved. Through the buildup of condensation, particles could be washed out of the flue gas reducing the overall level of air pollutants emitted by the system. In the case of wood fuels, the level of dust separation would reach around 20–40%, depending on the moisture content of the fuel and reverse flow temperatures of the heating cycle [16, 17].

In practical applications of the condensing boiler technology, it will be necessary to find appropriate ways of making use of low-temperature thermal yields (e.g., in low-energy building design with underfloor

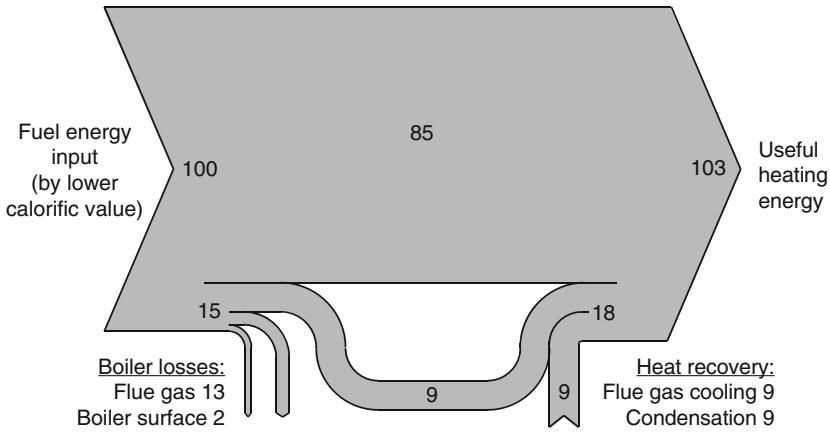

Biomass Energy Heat Provision in Modern Small-Scale Systems. Figure 33
Energy flow diagram for condensation operation. Data given as percentage of total fuel energy input (100%) based on lower calorific value [15]

heating). However, for many users (e.g., old buildings) such conditions do not apply. Opportunities for the economic utilization of the condensing boiler technology are therefore likely to exist primarily in connection with the installation of new heating systems in new buildings, and in respect of pellet boiler systems, where a relative expensive fuel could be saved through an increase in efficiency.

Combustion efficiency versus annual efficiency. The quality of combustion technology, as such, can be quite well defined by reference to its level of combustion or boiler efficiency. But the actual annual operating efficiency of the system is the decisive factor for the user and his annual requirement of fuel supply. This is determined by the user's annual demand for heating in relation to the amount of fuel required for this purpose. Annual operational rates of efficiency for biomass-fueled furnace systems can range from 70% to 85%, depending on the combustion technology, capacity design, supply requirements, size of buffering, and system of controls (Fig. 34). Thus, the optimization of the overall system is essential, also in the case of biomass-fueled furnaces, in order to achieve a high overall efficiency.

Flue Gas Emissions

Below, the emission of pollutants from biomass-fueled furnaces is described depending on the types of design, fuels used, combustion processes, and charging systems. The review is restricted to the limited number of essential pollutants, which are primarily the carbon monoxide components (CO) and particulate matter emissions, as well as emissions of NO_x and volatile organic hydrocarbons. For the latter, controls are not always mandatory for small-scale systems and therefore these parameters are recorded less frequently. Additionally, flue gas treatment technologies are discussed.

Emissions of Stoves

In the case of stand-alone furnace systems (chimney stoves, masonry/tiled stoves and standard masonry heaters, pellet stoves, etc.) the levels of emission are generally not regularly recorded, given the disproportionately high effort that would otherwise be involved. For this reason, the results of type certifications have frequently been used in the evaluation (e.g., from measurements for the quality label). Such type certification procedures, however, are rarely performed under

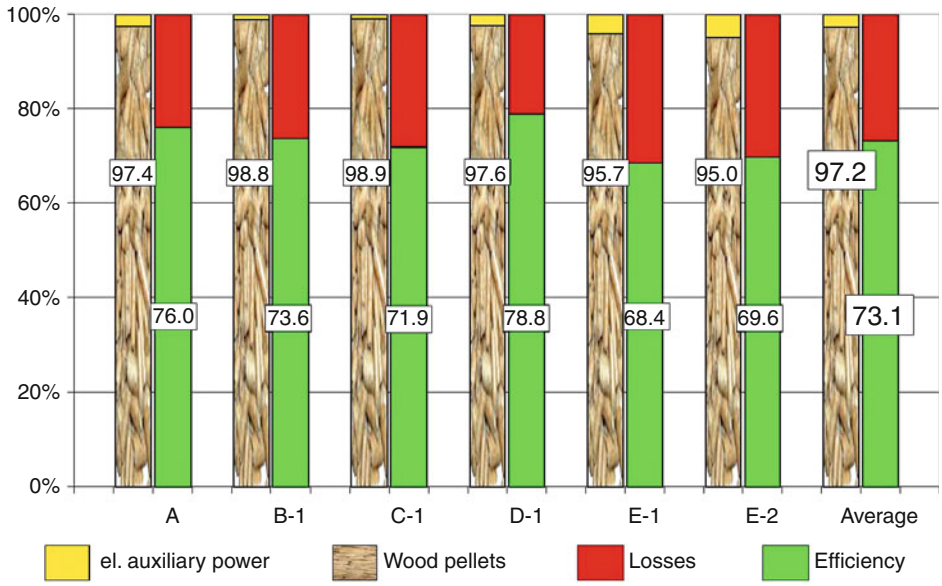

Biomass Energy Heat Provision in Modern Small-Scale Systems. Figure 34
Assessment of annual efficiencies of various wood pellet boiler installations in Germany (wood pellets and electrical auxiliary power as energy input) [21]

real-life conditions, so that the gathering of reliable data concerning the typical operating performance of a stand-alone furnace is only possible through the performance of special trial runs, with test results being recorded throughout the whole of the combustion cycle. Such measurements are usually taken from official public sector commissioned studies (e.g. [9, 12]). The results from such studies show, that average emissions of carbon monoxide, in the case of hand-charged stand-alone furnaces, might stand at a level of around 1,500–5,000 mg/Nm^3, whereby permanently installed furnaces (e.g., masonry tiled stoves) show the most favorable results. A clear exception to this are pellet stoves, which only show one tenth to one twentieth of the emissions recorded for firewood charged stoves. The advantages of pellet stoves become even more clearly visible in relation to volatile organic carbon compounds, commonly also simply referred to as hydrocarbons. The differences in combustion follow the order in the level of CO emissions.

This does not, however, automatically apply with regard to the overall level of emissions, since, in addition to factors such as complete combustion, other processes also do have an impact on the emission of fine particles. High proportions of soot and tar, high flow speeds, and system internal zones with settlement of dust particles are responsible for different kinds of variations. The marginally higher emission of particle dust by chimney stoves could also be the result of several processes, which might increase emissions, taking place simultaneously. The emission levels of NO_x in contrast, are primarily determined by the nitrogen content of the fuel while the impact of combustion technology is rather insignificant in the case of small-scale systems.

Emissions of Boilers

In the case of wood-charged central heating boilers, a considerably lower level of emissions is generally found compared to the levels reached in hand-charged stand-alone furnaces. This does apply in particular in respect of pollutants such as CO, total organic carbon, and partly also for emissions of particulate matter.

CO emissions. The CO emissions of a firewood-charged boiler are, as a rule, around one tenth of the values recorded for a stove charged with firewood (Fig. 36), even though both furnaces are charged in the same way. The range of measured values, however, still remains rather broad, which is due to the wide variety of different types of construction designs (natural draft systems, fan-assisted combustion, lambda-controlled systems). Firewood-charged boilers, with flue gas–regulated supply of combustion air, will typically mark the lower end of the spectrum in terms of CO measurements, which will range here on average between 80 and 250 mg/Nm^3.

A shift from manual to automatic charging will result in significant improvements in the quality of combustion, which is reflected by the overall levels of CO and total organic carbon emissions; whereby the difference between wood-chipfueled and pellet-fueled systems is, in parts, relatively small. In practice, however, greater advantages can be expected from pellet boilers, since pellets constitute a source of fuel characterized by continuously high combustion efficiency (uniform, standardized type of fuel); whereas in the case of wood chips, significant differences in quality frequently do occur, with clear variations from the kind of fuel used during combustion-related technical testing. Measurements taken in field testing therefore often produce significantly differing results from the average type testing values shown here [26].

By way of reference to the relevant levels of CO emissions, the technological development over recent years can be seen quite clearly, and since the beginning of the 1980s they have contributed toward a clear reduction in the emissions of pollutants. This is supported by the evaluation of the results of the type certifications already referred to above (Fig. 35). Concurrent to these improvements in the efficiency, boiler systems for furnaces have been accomplished (section "Combustion Efficiency").

Volatile organic carbon compounds. Similar to the developments in CO emissions, a reduction in the emissions of volatile organic carbon compounds (i.e., TOC – total organic carbon or C_nH_m) from larger systems, with higher nominal thermal energy outputs, can be noticed (Fig. 36). The same applies for the load-related performance of furnace systems, that is, the level of CO and TOC emissions (Fig. 36) does increase significantly, as soon as the system is operated at reduced loads (i.e., in partial load mode) or even at minimum thermal output rating.

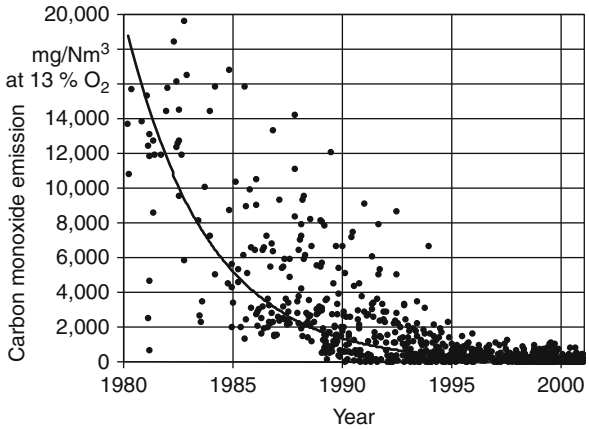

Biomass Energy Heat Provision in Modern Small-Scale Systems. Figure 35
Development of CO emissions for hand- and automatically charged wood-burning furnaces at lower capacity ranges since 1980 – results from different boiler-type tests at nominal and partial thermal energy output performance [12] (From BLT Wieselburg, Austria)

Emission of particulate matter. The connection established in terms of efficiency, between levels of CO and TOC (total carbon) emissions and the relative performance and/or operating loads of systems, does not apply in relation to the emission of particulate matter. These emissions are instead determined by other factors, such as movements in the fire bed, the contents of aerosol-producing substances in the fuel and the existence of potential zones of settlement and/or formation of deposits. Wood chip furnaces will tend to develop higher levels in the overall particulate matter emissions, compared to hand-charged firewood boilers, where the fire bed will ordinarily remain undisturbed. This kind of undisturbed fire bed is frequently also found in pellet-fueled systems, if these are designed in the way of drop-down furnaces, where the area of the fire bed is hardly affected by potential mechanical disruptions. Pellets furthermore do represent a comparatively low-ash-forming fuel.

In the case of residential biomass-fueled furnace systems, it can be assumed that the predominant proportion of particulate matter will occur in the particle size range of below 1 μm (Fig. 37) [2, 9, 25]. All measures aiming at a reduction in the overall emission of particulate matter will simultaneously also represent a measure for the reduction of fine particle emissions.

The possibilities for the achievement of additional reductions in the overall emission of particulate matter (and thereby of very fine particles), through specifically targeted further development of solid fuel combustion technologies (combustion geometries, air supply, other controls) have yet not been exhausted. Specially adapted control of air flows, for example, together with low levels of excess air (particularly within the vicinity of the fire bed) could help to achieve significantly more positive effects in the reduction of air pollutants emissions [30]. It should be possible to transfer the knowledge and experience gained in the introduction of such primary measures to small-scale furnace systems as well.

An additional factor is that, currently, science and industry both work on the development and testing of cost-efficient dust separation technologies as secondary measures. Conventional cyclones today, however, offer close to zero levels of efficiency in the separation of "submicron" particles (<1 μm), which do represent the major proportion of solid fuel emissions (Fig. 37). Current research therefore focuses primarily on the development of new filtering and electrostatic separation devices (e.g., metal netting filters, electrostatic precipitators, packed bed filters). Long-term operating experience with filtration systems for stoves or residential heating boilers, ready for series production, however, is rather scarce.

Even secondary heat exchangers, designed for the condensation of flue gases, do have a certain impact on the reduction of particulate matter emissions. These secondary heat exchangers are meanwhile commercially available on the open market for residential furnaces. In the case of wood chip combustion, the reported degrees of particulate matter separation are in the range of 20–40%, depending on the reverse flow temperatures of the heating system [13].

NO_x emissions. In most countries, there are generally no regulatory thresholds applicable to the emission of NO_x from wood furnaces in the small

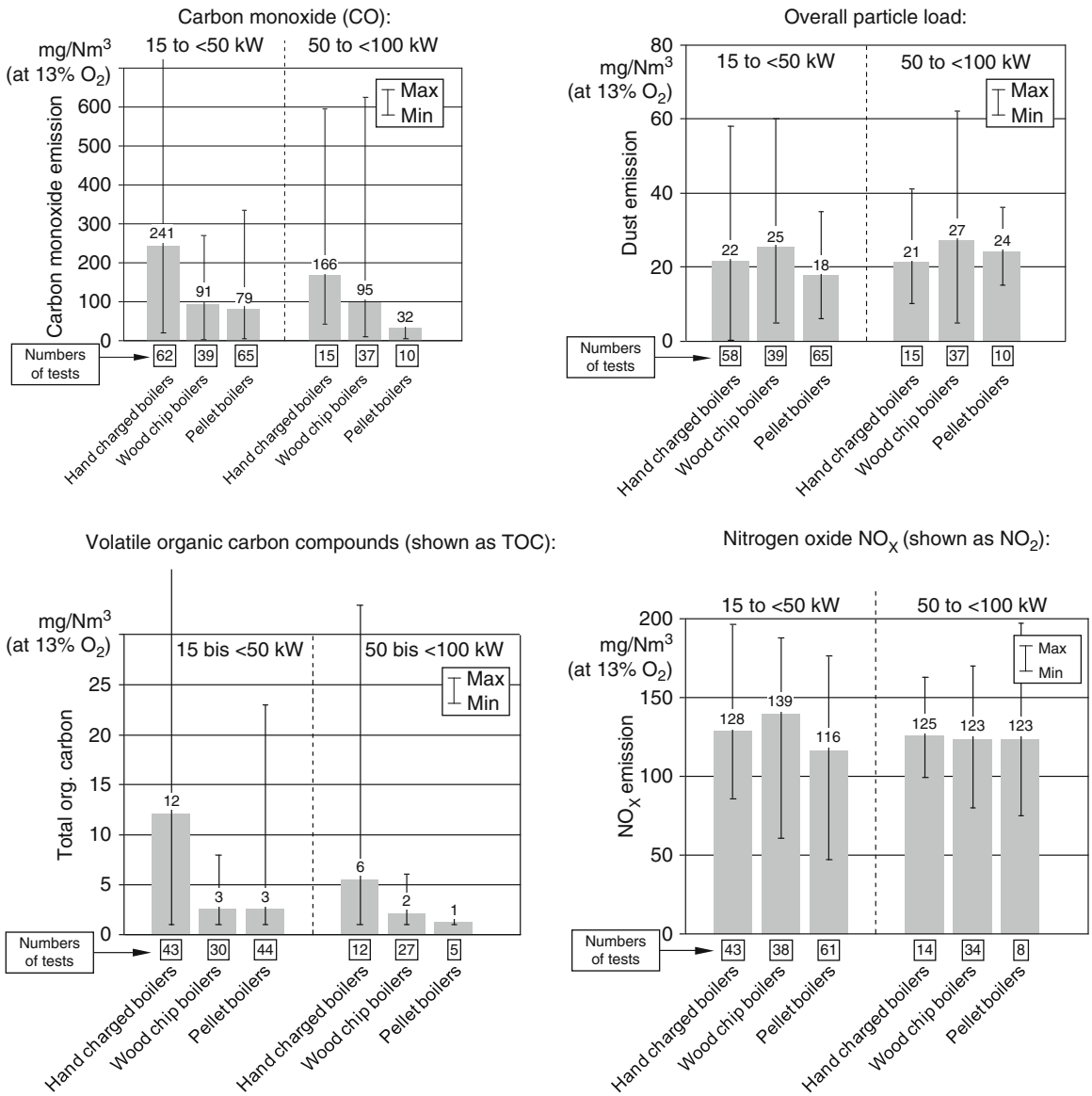

Biomass Energy Heat Provision in Modern Small-Scale Systems. Figure 36
Air pollutant emissions from wood-burning central heating systems – results from different boiler type tests for the 10-year period from 1996 to 2006 [12]

scale. Reference values specified by the German "Clean Air Act" (*TA Luft*) or by the thresholds of the German emission directive (*1.BImSchV*) could for example be complied with, without any problems, since untreated wood would generally be a comparatively low-nitrogen source of fuel. This applies in particular with regard to wood pellets, which are usually produced using sawmill waste wood, and would therefore probably tend to show an even lower level of NO_x emissions, at nominal thermal energy output, than indicated in Fig. 36. This is particularly true since the systems would not be operated permanently at full output capacity. In contrast to the CO and TOC (total carbon) emissions scenarios, as outlined above, a reduction in the combustion

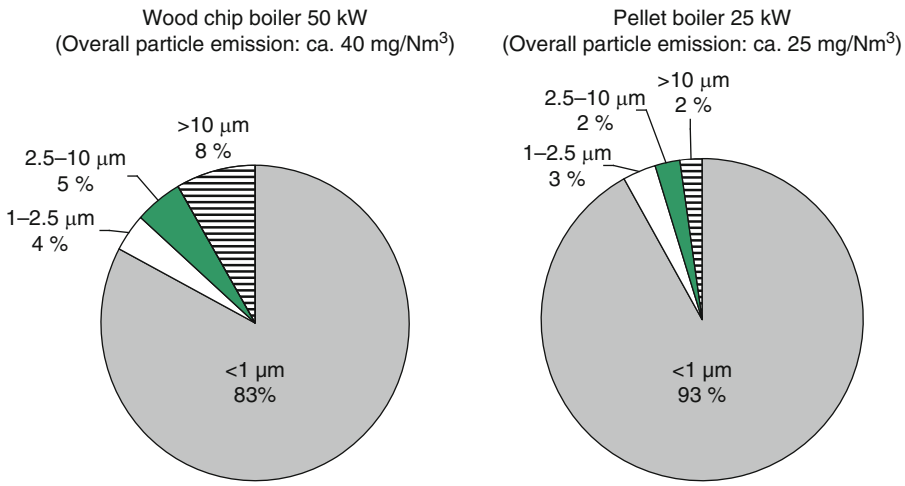

Biomass Energy Heat Provision in Modern Small-Scale Systems. Figure 37
Representative results for the measurement of flue gas particle size distribution, resulting from the combustion of wood chip and wood pellets in residential central heating systems; measurements at nominal thermal energy output values [12]

temperatures, at reduced loads, actually does result in a reduction of NO_x emissions.

Secondary Flue Gas Treatment

In the course of the debate concerning the reduction of particulate matter emissions from biomass furnaces, a need for action has been identified, in particular, with regard to stand-alone furnaces which so far do not have any dust removal systems installed in their flue gas systems. It can be expected that secondary separation systems will increasingly be used in future, especially in connection with the refitting of existing stand-alone furnaces (stoves). A number of different separation technologies can generally be employed in this context and their respective working principles and areas of application are described in the following sections.

Centrifugal collectors. Single-cyclone and multiple-cyclone separators, which remove dusts from the flue gas by way of centrifugal force, are standard fittings for wood chip furnaces in the medium capacity range. They demonstrate good performance ratings in the separation of particles with more than 1 µm diameter. Their performance, however, in the separation of the fine particle fractions does decrease drastically, so that they are not suitable for small-scale heating systems whose emissions consist almost exclusively of fine particle dust.

Filtration collectors. The use of fabric filters (also known as bag house filters) in plants of less than 1 MW capacity is established practice. For small-scale systems starting at 30 kW capacity there are now some initial developments underway concerning the use of metal netting materials as well as cartridges for filtration purposes. A problem, at present, remains how to clean the filters without suffering a rapid increase in the loss of pressure, which would make a continuous operation without the support of additional blowers impossible.

Electrostatic precipitators. In the design of electrostatic precipitators (ESP) for stand-alone furnaces, a thin electrode (e.g., stainless steel wire) can, for example, be installed in the middle of a metal flue pipe (Fig. 38) and be connected to a high voltage supply (up to 30,000 V). The high voltage leads to the dust particles being charged and subsequently deposited on the inside of the metallic flue pipe, which acts as a collecting electrode. The layer of particulate matter created this way on the inside of the flue duct needs to be removed from time to time [31].

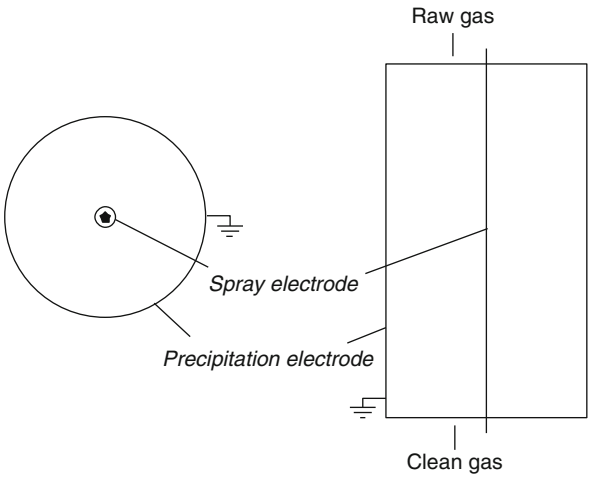

Biomass Energy Heat Provision in Modern Small-Scale Systems. Figure 38
System diagram of an electrostatic precipitator (single-duct electrostatic filter) for stand-alone furnaces [27]

With the use of these types of separators (in field tests), the overall level of emission of particulate matter (including fine particles) could be reduced by 43–66%. In measurements taken under test bench conditions, levels in the reduction of emission of up to 80% have been achieved [9, 10, 20].

In other versions of this type of dust collector, several systems working in parallel are combined into a separate compact filtration unit, which can then also be cleaned periodically by means of a mechanical shaker system and a removable tray for ash residues. This type of dust collector is intended for use in small-scale wood boilers.

A common feature of all electrostatic separator systems is, that the area for the power supply of the spray electrode wire is ventilated by way of a small blower to prevent a short-circuit (i.e., disruptive discharge) caused in the duct through the potential settlement of particles. These types of multiple-duct electrostatic precipitator systems can achieve performance levels of up to 95% in separating efficiency [9, 17].

Electrostatic precipitators belong to the technically most advanced solutions currently available for small-scale furnace systems. Their theoretical operating performance, however, largely depends on three critical factors as demonstrated by Eq. 1:

$$\eta_G = 1 - \exp\left[-v_{eff}\frac{A_{NE}}{\dot{V}}\right] \quad (1)$$

where

$\dot{V}$ is the volume of flue gas streams

A_{NE} is the separation surface of the collecting electrode.

v_{eff} is the flow speed which depends inter alia on particle size, particle load, temperature, pressure, and composition of the gas.

Tests with different combustion technologies using different materials of fuel from renewable energy sources have shown that electrostatic precipitators need to be adapted to the performance of the combustion system and to the fuel to be used, in order to be able to achieve constantly high and sustainable levels of separation efficiency.

An additional complicating factor is that the composition of the particulate matter in the course of the combustion process is constantly changing. During the initial combustion cycle, because of low temperatures, and usually too high a supply of oxygen, significant proportions of tar and condensable hydrocarbons are produced. In the course of the actual main combustion cycle, similar to the case of automatically charged furnaces, sulfides are formed, as well as increasing amounts of black carbon, because of insufficient supply of combustion air during the subsequent carbon combustion process.

The three categories of particulate matter can be differentiated by their respective properties of conductivity. The tar and condensable hydrocarbon substances show low conductivity and therefore produce an insulating layer on the electrodes following the separation process. The soot particles do posses such favorable conductive properties. They can be separated quite easily, and at the same time can be removed again from duct surfaces, where they have agglomerated in the form of coarser dust, so that reductions in the volume of mass are only limited. Only sulfides with a medium level of conductivity do demonstrate good separation and adhesion properties in relation to the collecting electrodes, allowing for efficient separation and discharge [29]. In order to prevent the otherwise particularly problematic buildup of tar and hydrocarbon deposits on electrode surfaces, many separation systems are bypassed during the initial stages of combustion.

Wet scrubbers and condensation systems. These can basically be divided into four different types of scrubbing technologies (Fig. 39).

All four methods demonstrate certain deficits in terms of separation efficiency. In the case of gas streams passing through the scrubbing liquid, for example, separation efficiency depends largely on the size of gas bubbles (Fig. 39, left). In the case of net-coated surfaces being sprayed, the gas channel needs to be kept as flat as possible, in order to ensure a certain level of contact required in this process (Fig. 39, middle – left). The gas stream directed over liquid surfaces essentially follows the principle of inertia, although only with a limited degree of efficiency in the case of fine particles (Fig. 39, middle – right). The method of injection of droplets into to the gas stream, in terms of separation efficiency, also largely depends on the size and density of the droplets (Fig. 39, right).

One feature common to all four scrubbing principles is the additional amount of effort and expenditure required for the handling of the scrubbing liquid. In the first place, it needs to be supplied and pumped to the location where the separation process is to take place, and subsequently it has to be discharged, processed, and disposed after the separation process. Complete separation of dust-loaded droplets from the cleaned stream of gases is generally rather difficult to achieve.

Apart from the use of pure water, alternative scrubbing liquids and additives to scrubbing water are being tested. Special care needs to be taken so that substances likely to facilitate the absorbance of organic flue gas components are not liable to evaporate or ignite at the level of temperatures likely to occur in the separation process.

Whereas the development of a pure scrubbing system is currently still underway, a number of treatment systems have been developed and are close to being introduced to the market, whereby the partial separation of fine particles is achieved by way of flue gas condensation. The corresponding levels of separation efficiency presently still stand at around 20–40%. However, the primary benefits of this technology lie in the recovery of thermal energy from the water vapor contained in flue gas emissions (see section "Combustion Efficiency").

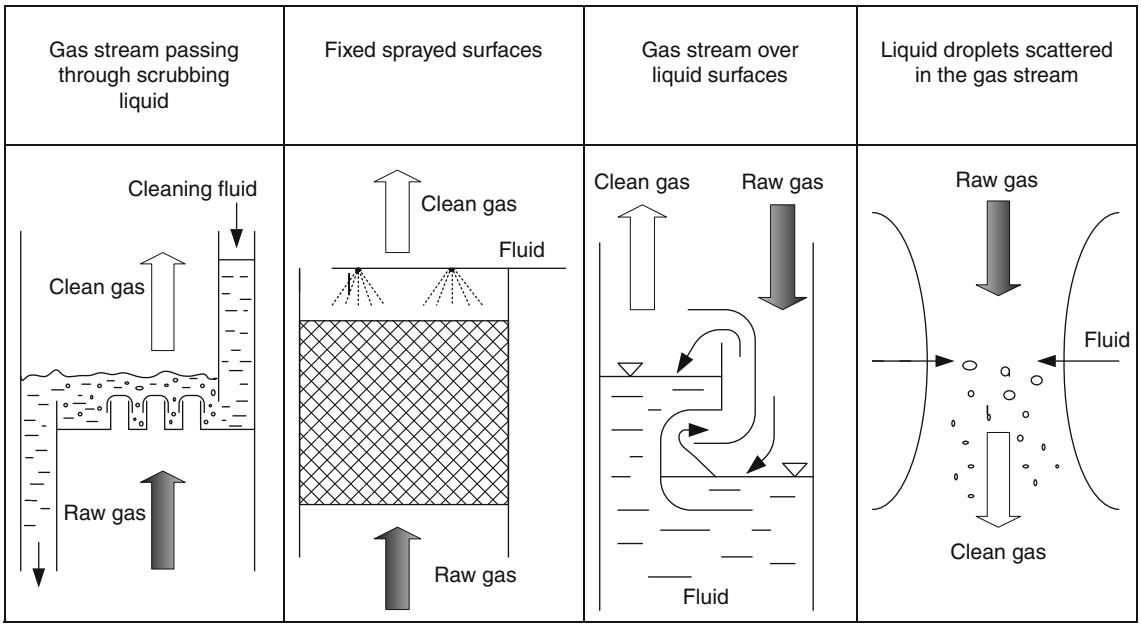

Biomass Energy Heat Provision in Modern Small-Scale Systems. Figure 39
Separation principles used in wet scrubbers

At present, there is no uniform European regulatory framework governing the discharge of condensates produced by this process and regional regulations, in this respect, therefore need to be observed.

Through a combination of condensation and scrubbing technology levels in purification, efficiency in excess of 50% can potentially be achieved in future. With the benefits derived from the simultaneous recovery of thermal energy, these systems could also represent an economically feasible alternative to ensure that even very low thresholds for particulate matter, which may potentially be set for wood furnaces, could still be met in day-to-day operations.

Catalytic converters. In practical terms, however, the methods for secondary flue gas treatment described above generally have no impact on the reduction of gaseous emissions. Catalytic reduction could be an effective process to be employed in this context and a number of different systems for use of this technology are currently under development.

The difficulty for biomass-fueled combustion systems in this respect is that in addition to the gaseous substances resulting from incomplete combustion, significant particle emissions may be produced (condensed hydrocarbon compounds and black carbon), as well as dusts (not containing carbon compounds) resulting from ash forming substances contained in the biomass fuel. Whereas the gaseous components and to some extent also carbon-containing particles can be removed quite efficiently with the aid of catalytic converters, there is a risk that in the case of particulate matter not containing any carbon damage may be caused to the surfaces of the catalytic converter, or that caking may occur. Even with the installation of suitable cleaning systems, the risk of the catalytic layers wearing off cannot be excluded. It is therefore necessary to develop suitable catalysts and carrier materials, adaptable to the relevant ranges in temperature, while at the same time the long-term resilience of catalytic converters needs to be improved. The importance of catalytic separators also being used for the reduction of particulate matter emissions is further demonstrated by the results of current studies, according to which gaseous hydrocarbon emissions do significantly contribute to the overall level of fine particle emission through the creation of secondary aerosols [1].

Overall, it can be expected that in the coming years, integrated separators for small-scale furnace systems as well as separators suitable for the refitting of existing plants will be available on the market at reasonable prices. In the course of this process separator, technology and design will be adapted to the requirements of the relevant combustion systems and the respective types of fuel used, also in order to achieve a high degree of separation efficiency during continuous operations. For furnaces charged with biomass fuel it is likely, that the possibilities for both primary as well as secondary reduction in emissions will be exploited, in order to be able to meet the particularly stringent emission thresholds already imposed in a number of countries.

Future Direction

Based on the current state of technology, as outlined above, one can expect that the admissible levels of emissions – in particular with regard to fine particles – will continue to be lowered in future. Countries with existing emissions control regulations are in the process of severely tightening the relevant threshold values, or have recently done so already. In countries without corresponding regulations for small-scale furnaces, the imposition of threshold levels, or at least the introduction of benchmark values in the context of national standards, is currently under consideration. Europe-wide targets for particulate matter emissions could also be introduced under the recently revised Ecodesign Directive of the European Union.

Upper limits for particulate matter air pollution have already been defined under the EU Directive on Ambient Air Quality currently in force (Directive 2008 [50]EC). However, these limits are already being infringed, as a matter of course, in many densely populated, highly industrialized regions. Past attempts to regulate traffic pollution have rarely resulted in noticeable reductions. At the same time, studies investigating the sources of emissions have clearly identified the significance of wood-burning furnaces in this context. Based on this, it would seem to be merely a question of time until (at regional levels) the targeted reduction of particulate matter emissions from wood combustion will be enforced through regional anti-air pollution action plans. The reduction of dust and nitrogen

monoxide emissions from biomass-charged furnaces must therefore be further pursued, as a matter of urgency.

Complete combustion. The aim must be to achieve complete combustion for all furnace systems and operating conditions. For automatically charged furnaces this can be achieved, at reasonable costs, by means of suitable systems which, apart from oxygen levels in the air, also control temperatures in the combustion chamber and, if appropriate, the level of CO/C_nH_m emissions. However, this is generally unlikely to be the case for hand-charged, stand-alone furnaces with predominantly discontinuous combustion characteristic. For these systems, the use of sensors, electronically controlled flaps, and motor-driven fans will become inevitable in future, even if today the traders still claim that, according to alleged customer demand, these types of furnaces are to be installed without electricity supply. In order to further reduce the impact of the recharging process, the downdraft combustion principle may establish itself as a promising alternative approach for these systems. In the case of chimney stoves, for example, the actual combustion chamber could be fitted with a glass screen to allow for the visual appreciation of flickering flames in the fire (chimney stove based on the design of a firewood-burning boiler with downdraft combustion).

Through the simultaneous achievement of significant improvements in combustion efficiency, the otherwise, in part, extremely high levels of emission of highly toxic polycyclic aromatic hydrocarbons (PAH), as well as large proportions of the constituent substances leading to the formation of secondary particles, would be substantially reduced. In this context, the use of catalytic converters could also serve to ensure low levels of emission in the event of short-term disruptions occurring in the combustion cycle.

Low emission furnaces. Assuming an otherwise largely complete stage of combustion, biomass-fueled furnaces will initially produce inevitable emissions of nitric oxide and fine particles, due to the nitrogen monoxide-forming and ash-forming substances contained in the fuel. Nevertheless, the goal must be to lower emissions to a level approaching that of oil and gas-fired systems. It is therefore also necessary to further improve the quality of fuels used in small-scale furnace systems. Current moves toward standardization provide product norms to be introduced for wood pellets, miscanthus pellets, straw pellets, and reed canary grass pellets, as well as other types of fuel. Through the selective addition of appropriate aggregates, it should furthermore be possible, in future, to make appropriate adjustments for regional and seasonal variations in the relative proportions of trace elements.

In future, furnaces will generally have to show stable systems of separation between the pyrolytic decomposition and gasification zone as well as the zone of the full oxidation of the produced gaseous products. In order to be able to control output performance and/or cope with fluctuating combustion characteristics of the fuel used, methods need to be developed to adjust residence times and temperature levels, by means of the selective supply of air, even under rigid geometry conditions. The amount of primary air supply and fire bed temperature levels should be easily controllable and a suitable exhaust gas recirculation system may be required. The preheated secondary air supply has to be injected in such a way, that a thorough mixture and combination, even with hot combustion gases, can be achieved. Sensor technology and controls will be an essential prerequisite for optimal flow conditions and temperature profiles. For the reduction of NO_x emissions, a low-oxygen, high-temperature zone (approx. 1,000°C) could potentially be interposed between the primary zone and the combustion chamber.

The release of non-carbon-forming particles can be substantially reduced through measures such as optimal composition of fuels (agricultural biomass), low oxygen content, and low temperatures in the primary reaction zone. It should be possible to achieve future levels of particulate matter emissions below 5 mg/Nm and NO_x emissions of less than 100 mg/Nm, without any traceable amounts of hydrocarbon and with CO emissions near the detection limits. This can be supported through the use of integrated dust collection zones and, if appropriate, integrated or downstream fine particle separator systems.

In conjunction with an improvement in combustion performance and flue gas condensation, there will also be an improvement in the level of efficiency of the combustion system. Flue system fans, also if used for stand-alone furnaces, do allow for a noticeable reduction in flue gas temperatures and therefore a significant reduction in flue gas losses. Chimney systems,

therefore, in the future, should be moisture resistant, since the risks of potential occurrence of condensation in the flue system can no longer be safely excluded.

Optimization of systems. Beside improvements to be made to the actual furnaces, optimization of the overall systems is likely to gain importance. In order to be able to achieve low levels of emission and a high level of annual efficiency, boiler systems will need to be adapted specifically to the relevant buildings, existing heaters (e.g., solar thermal installations), and the particular user behavior. Apart from the control systems, which need to be taken into consideration in this context, the user also has to be involved interactively, in the sense of managing supply and demand, by way of consumption meters as well as displays indicating the available supply of renewable thermal energy stored in the buffer system (smart metering).

Alternative concepts need to be explored in order to reduce the heat storage losses during boiler shutdown periods. Thermal insulation to some extent might also be further improved in this context. Possible savings resulting from these measures, however, could potentially still be exceeded through the use of latent heat storage units and/or minimization of storage volumes. Allowing for a continuing decrease in space-specific heating requirements, it seems to be possible that through the use of sensitive demand forecasting tools, industrial water storage, and large-scale storage capacities in buildings (activated floors/ceilings), significantly smaller and more compact biomass-fueled furnaces could be installed. Smaller designs would allow for faster passing through the start-up and shutdown phases, which produce high levels of emission, and at the same time noticeably reduce losses from the cooling down process. This would significantly contribute toward a reduction in emissions, if an increase in the number of starting phases could be prevented by way of an intelligent control.

Operational safety. Excessive levels of emissions from stand-alone furnaces and potential disruptions of the combustion cycle, as well as hazards caused by users otherwise, can be minimized through the increased use of flue gas sensors and other system control mechanisms. The installation of CO and/or C_nH_m sensors in small-scale furnace systems, in combination with the appropriate electronic controls, will always prompt the release of a warning signal. This is true if, for example, the level of humidity of the fuel being charged is likely to cause a disruption to the combustion cycle, with the resulting emission of hazardous concentrations in terms of air pollutants. In such cases, for example, the installation of suction fans could ensure that no potentially hazardous or air-pollutant substances do enter into the living space, particularly when the door to the stove is opened for recharging.

Conclusions

Modern small-scale systems for the supply of heat using solid biomass fuels, and wood in particular, have already reached high standards of quality in terms of combustion efficiency. Further improvements, however, in combustion and furnace technology, including secondary measures for the reduction of emissions, are essential in order to be able to also meet increasing future demands in respect of the reduction of particulate matter and NO_x emissions, as well as allowing for the increased use of biomass fuels, without corresponding increases in the emission of polluting substances. This is technically feasible. Thus the objective must be in the medium to long term not to exceed the levels reached with present day oil- and gas-based combustion technologies. Stand-alone combustion plants, at least, should in the long term not be allowed to operate without an efficient active air control systems. Present priorities concern improvements in the integration of stoves and boilers into the overall heat supply systems of buildings. In the medium term, the simultaneous and combined supply of heat and power, as well as the potential supply of cooling systems during summer temperature conditions, is likely to gain increasingly in importance.

Bibliography

1. Baltensperger U, Heringa MF, Mohr C, Lanz V, DeCarlo PF, Dommen J, Weingartner E, Prévôt ASH (2010) Verhalten der Schadstoffe aus Holzfeuerungen in der Atmosphäre und Beitrag zum Feinstaub. In: 11. Holzenergie-Symposium, Potenzial und Technik zur Holzenergie-Nutzung, pp 59–66
2. Baumbach G, Struschka M (2005) Feinstäube aus Biomassefeuerungen – Herausforderungen an Anlagen sowie an die Mess- und Regeltechnik. In: Arbeitsgruppe Luftreinhaltung der Universität Stuttgart (ed), Jahresbericht 2005, pp 16–27

3. Bio Intelligence Services S.A.S (2009) Solid fuel small combustion installations – Final Stakeholder Meeting, Brussels
4. Deutsches Institut für Normung e.V. (ed) (1988) DIN 18 882 (Heizungsherde für feste Brennstoffe), Beuth, Berlin, p 16
5. Deutsches Institut für Normung e.V. (ed) (1990) DIN 18 890 (Teil 1 und 2 (Entwurf): Dauerbrandöfen für feste Brennstoffe – Verfeuerung von Scheitholz), Beuth, Berlin
6. Deutsches Institut für Normung e.V. (ed) (1990) DIN 4702 (Teil 1: Heizkessel – Begriffe, Anforderungen, Prüfung, Kennzeichnung); Beuth, Berlin, p 25
7. Deutsches Institut für Normung e.V. (ed) (1991) DIN 18 880 (Teil 1 und 2: Dauerbrandherde für feste Brennstoffe), Beuth, Berlin
8. Ebert H-P (1998) Heizen mit Holz in allen Ofenarten, 6th edn. Ökobuch, Freiburg, p 133
9. Ellner-Schuberth F, Hartmann H, Turowski P, Roßmann P (2010) Partikelmissionen aus Kleinfeuerungen für Holz und Ansätze für Minderungsmaßnahmen. Berichte aus dem TFZ (22), Technologie- und Förderzentrum (TFZ) (ed), Straubing, p 134. www.tfz.bayern.de
10. Gaegauf C (2006) Staub- und Partikelanalytik an Klein-Holzfeuerungen mit elektrostatischem Partikelabscheider, Bericht des Ökozentrums Langenbruck
11. Good J, Nussbaumer T (1993) Regelung einer Stückholzfeuerung mit unterem Abbrand, Bundesamt für Energiewirtschaft, Zürich
12. Hartmann H, Höldrich A (2007) Wirkungsgrad, Emissionen, Aschequalität. In: Hartmann H (ed) Handbuch Bioenergie-Kleinanlagen, 2nd edn. Sonderpublikation des Bundesministeriums für Verbraucherschutz, Ernährung und Landwirtschaft (BMVEL) und der Fachagentur Nachwachsende Rohstoffe (FNR), Gülzow, pp 118–130. www.tfz.bayern.de
13. Hartmann H, Launhardt T (2001) Die energetische Nutzung von Stroh und strohähnlichen Brennstoffen in Kleinanlagen. In: Fachagentur für Nachwachsende Rohstoffe (ed) Proceedings "Energetische Nutzung von Stroh, Ganzpflanzengetreide und weiterer halmgutartiger Biomasse", Gülzower Fachgespräche, vol 17. Eigenverlag FNR, Gülzow, pp 62–84
14. Hartmann H, Reisinger K (2007) Feuerungen und Anlagentechnik. In: Hartmann H (ed) Handbuch Bioenergie-Kleinanlagen, 2nd edn. Sonderpublikation des Bundesministeriums für Verbraucherschutz, Ernährung und Landwirtschaft (BMVEL) und der Fachagentur Nachwachsende Rohstoffe (FNR), Gülzow, 2007, pp 75–130. www.tfz.bayern.de
15. Hartmann H, Roßmann P, Link H, Marks A, Müller R, Amann E (2004) Secondary flue gas condensation for domestic wood chip boilers. In: van Swaaii WPM, Fjällström T, Helm P, Grassi A (eds) 2nd world conference and technology exhibition on biomass for energy, industry and climate protection, Rome, 10–14 May 2004. Petten: Energy research Centre of the Netherlands ECN, pp 1334–1337
16. Hartmann H, Roßmann P, Link H, Marks A (2004) Erprobung der Brennwerttechnik bei häuslichen Holzhackschnitzelfeuerungen mit Sekundärwärmetauscher. Berichte aus dem TFZ (2), Technologie- und Förderzentrum, Straubing 2004, p 49. www.tfz.bayern.de
17. Hartmann H, Roßmann P, Turowski P, Ellner-Schubert F, Hopf N, Bimüller A (2007) Getreidekörner als Brennstoff für Kleinfeuerungen – Technische Möglichkeiten und Umwelteffekte. Berichte aus dem TFZ (13), Technologie- und Förderzentrum (TFZ), Straubing, p 126. www.tfz.bayern.de
18. Hartmann H, Nussbaumer T, Hofbauer H (2009) Handbeschickte Feuerungsanlagen. In: Kaltschmitt M, Hartmann H, Hofbauer H (eds) Energie aus Biomasse – Grundlagen, Techniken und Verfahren, 2nd edn. Springer, Heidelberg, pp 468–491
19. Hartmann H, Nussbaumer T, Hofbauer H, Good J et al (2009) Automatisch beschickte Feuerungen. In: Energie aus Biomasse – Grundlagen, Techniken und Verfahren, 2nd edn. Springer, Heidelberg, pp 492–533
20. Kiener S, Turowski P, Hartmann H, Schmoeckel G (2010) Bewertung kostengünstiger Staubabscheider für Einzelfeuerstätten und Zentralheizungskessel. Berichte aus dem TFZ (23), Technologie- und Förderzentrum (TFZ), Straubing, p 141. www.tfz.bayern.de
21. Kunde R et al (2009) Felduntersuchungen an Holzpellet-Zentralheizungskesseln, BWK Das Energie-Fachmagazin, 61(1/2):58–66
22. Launhardt T (1998) Erfahrungen mit Klein-Holzfeuerungen in Prüfstandsmessungen und Ansätze zur Optimierung von Feuerungstechnik und Betrieb. In: Nussbaumer T, Gaegauf C, Völlmin C (eds) 3. Kolloquium Klein-Holzfeuerungen am 20. Nov. 1998 in Klus/Schwiterland, p 17–35
23. Launhardt T, Hurm R, Pontius P, Strehler A, Meiering A (1994) Prüfung des Emissionsverhaltens von Feuerungsanlagen für feste Brennstoffe. Bayerisches Staatsministerium für Landesentwicklung und Umweltfragen (ed), München, Reihe Materialien 109, p 198
24. Launhardt T, Hurm R, Schmid V, Link H (1998) Dioxin- und PAK-Konzentrationen in Abgas und Aschen von Stückholzfeuerungen. Bayerisches Staatsministerium für Landesentwicklung und Umweltfragen (BayStMLU) (ed), München, Reihe Materialien 142, p 149
25. Launhardt T, Hartmann H, Link H, Schmid V (2000) Verbrennungsversuche mit naturbelassenen biogenen Festbrennstoffen in einer Kleinfeuerungsanlage – Emissionen und Aschequalität. Bayerisches Staatsministerium für Landesentwicklung und Umweltfragen (ed), München, Reihe Materialien 156
26. Launhardt T, Hartmann H, Link H (2001) Domestic wood chip boilers – emissions from test stand and practice measurements. In: Proceedings 1st world conference on biomass for energy and industry, 5–9 June 2000, Sevilla. James & James, London, pp 911–914
27. Nussbaumer T (2009) Abgasreinigung und Kondensation. In: Kaltschmitt M, Hartmann H, Hofbauer H (ed) Energie aus

Biomasse – Grundlagen, Techniken und Verfahren, 2nd edn. Springer, Heidelberg, pp 533–551
28. Nussbaumer T, Hartmann H (2009) Direkte thermochemische Umwandlung (Verbrennung): Anforderungen und Besonderheiten. In: Kaltschmitt M, Hartmann H, Hofbauer H (eds) Energie aus Biomasse – Grundlagen, Techniken und Verfahren, 2nd edn. Springer, Heidelberg, pp 463–468
29. Nussbaumer T, Lauber A (2010) Formation mechanisms and physical properties of particles from wood combustion for design and operation of electrostatic precipitators. In: 18th European biomass conference and exhibition, Lyon
30. Oser M, Nussbaumer T (2004) Low-Particle-Pelletfeuerung im Leistungsbereich von 100 bis 500 kW. Bundesamt für Energie (BFE), Bern, Schweiz, p 23
31. Rüegg P (2006) Partikelabscheider. 9. Holzenergie-Symposium, Zürich
32. Schmitz-Günther T (ed) (1998) Lebensräume – Der große Ratgeber für ökologisches Bauen und Wohnen. Könemann Verlagsgesellschaft mbH, Köln, p 479
33. Schramek E-R (ed) (1999) Taschenbuch für Heizung und Klimatechnik ("Reknagel-Sprenger-Schramek"), 69th edn. R. Oldenbourg, München, p 2010

Biomass Energy Small-Scale Combined Heat and Power Systems

Daniel Büchner, Volker Lenz
German Biomass Research Centre (DBFZ), Leipzig, Germany

Article Outline

Glossary
Definition of the Subject
The Global Importance of Micro Cogeneration
Conversion Technologies for Small-Scale Heat and Power Systems
Market Survey
Conclusions
Future Directions
Bibliography

Glossary

Cogeneration Cogeneration (combined heat and power – CHP) describes the use of one source of energy in a plant for the simultaneous supply of heat and electric power.

Plant operating mode The operating mode of CHP plant can be divided into two categories. *Heat-controlled operation* means an operation of the plant according to the thermal energy demand of the heat consumer. In contrast, *power-controlled operation* is determined by the demand for electricity or a maximum power generation. The heat that cannot be used is stored for later usage or is disposed by a cooler.

Small-scale cogeneration unit So far, there is no generally applicable definition of the power range of small-scale CHP plants. In the context of this entry, small-scale or micro CHP plants are Cogeneration units with a maximum electric output capacity of 50 kW.

Status of development Four categories of development stages for cogeneration applications can be defined. *Research and Development* describes the stage of new technologies under laboratory conditions. Plants in *Demonstration* exist as prototypes of their later commercial versions and are subject to field-testing with regard to their suitability for everyday use. Further optimization is under investigation. In case of positive field-testing follows the phase of *Commercialization*. The first produced plants (often also referred to as pilot series) are introduced to the market. Once a plant or technology has been established on the market and has been accepted by the users one refers to *Market Diffusion*.

Definition of the Subject

Combined heat and power (CHP) generation is one of the essential pillar in a modern, sustainable, and environmentally friendly energy generation. This is due to the fact that cogeneration systems are energetically efficient and produce energy where it is needed. There major advantages include a substantially increased fuel efficiency, reduced emissions of CO_2, reduced need for transmission and distribution networks, and a beneficial use of local energy resources (e.g., through the use of waste and biomass).

At present, only approximately 10% of the global electricity generation is done by CHP. Exceptions are some European countries, like Denmark and Finland, which have successfully expanded the use of CHP up to

30–50% of total power generation during the last years (see Fig. 1) [1].

Given that the majority of the CHP plants mostly are driven by fossil fuels (see Fig. 2), it is obvious that the global relevance for biomass-driven combined heat and power generation is still at an extremely low level. In 2007, approximately 5.5% of total energy consumption by end users in the EU, Turkey, and Norway was covered by wood and wood chips, approximately 8% of heating requirements in private households was covered by solid biomass and very few of both in CHP [2, 3]. With a growing world population and increasing economic development in the emerging markets biomass, on the background of climate protection targets, will continue to gain importance worldwide. Due to limited resources, a more efficient use of the potentials available will become of increasing significance in this context.

The supply of heating to private households and the commercial sector by using biomass has gained increasing importance for a number of years. In this field, the demand for and interest in CHP units has also

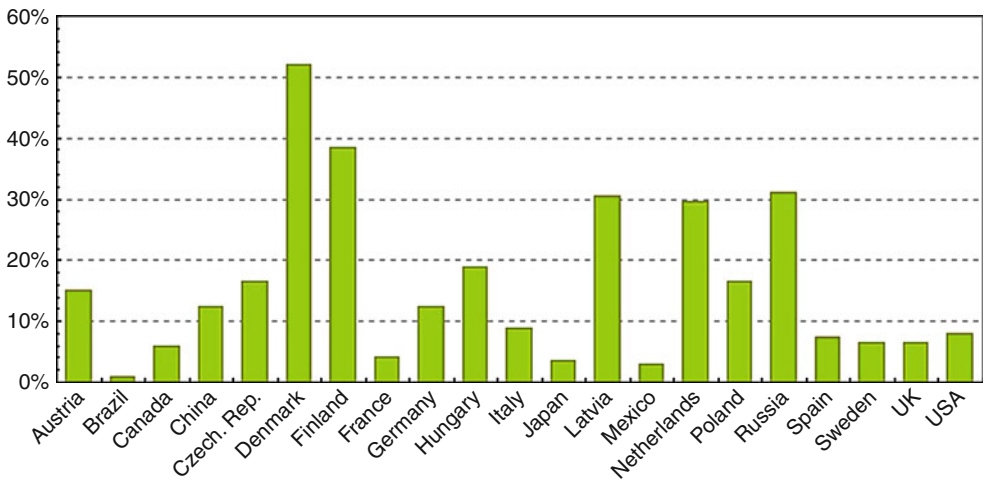

Biomass Energy Small-Scale Combined Heat and Power Systems. Figure 1
CHP share of the national power production [1]

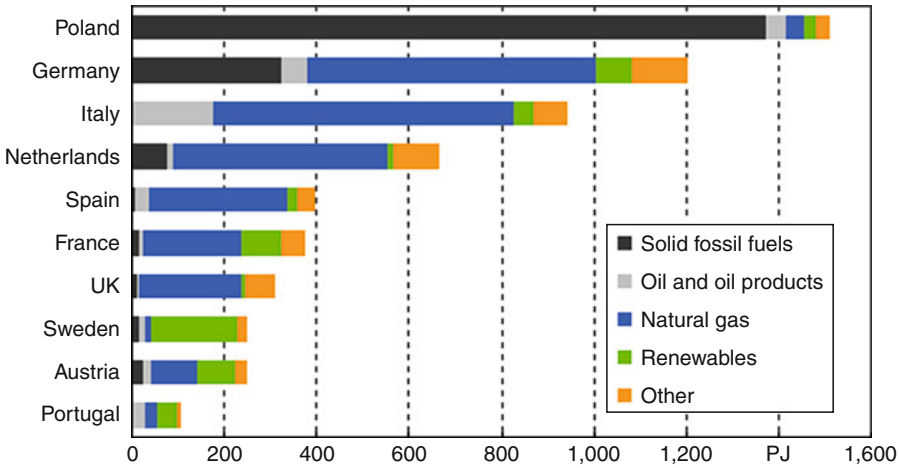

Biomass Energy Small-Scale Combined Heat and Power Systems. Figure 2
Fuel input in CHP by country (selection) [4]

grown significantly, whereby the majority of the already installed micro CHP units are still operating with fossil fuels. For using biomass within small-scale CHP systems, it is therefore of fundamental importance that appropriate cogeneration plants become available on the market.

This entry therefore provides an overview of the global importance of biomass micro cogeneration and the established technological approaches in cogeneration on the basis of solid, liquid, or gaseous biofuels in the range below an electric capacity of 50 kW, subsequently describes selected concepts in their current stage of development (laboratory, demonstration, market introduction, and market ability) and delineates the suitability of biomass-driven micro cogeneration for different areas of application. The presented options are compared and perspectives for future developments are highlighted, also taking into consideration new approaches in technology.

The Global Importance of Micro Cogeneration

Below some examples for the global importance of cogeneration in general are given.

Europe

The landscape of power plants in Europe is currently undergoing a process of change. Reasons for this can be found in the general political environment (e.g., regulation of the energy markets, national and international climate protection targets), in the expected development of the use of renewable energies, and in the expected massive shutdown of fossil fuel power plants exceeding their technical life time in the years to come. The resulting demand for power replacement of up to 14,000 MW in respect of the power plants scheduled to go off the grid for example in Germany by 2020 [5] does represent a major opportunity for the introduction of new technologies.

There are a number of facts determining the development of power demand from private households, small enterprises, and public sector institutions during the next decade. Whereas the utilities expect a continuous growth in the consumption of electricity, due to climate protection reasons the Ministries and the politics assume a decrease in electricity consumption, whereby the greatest potential for this is seen in the industrial sector. There are no noticeable savings expected for private households. If the experiences from the past are transformed to the future, a further increasing electricity demand is more likely than a decreasing demand.

In addition to that, energy-saving measures are more and more implemented within the heating sector through a much better insulation. As a consequence it can be expected that the specific heat demand will continue to decrease in future. For example, the Lead Scenario 2009 commissioned by the German Ministry for the Environment predicts a reduction in average heating requirements within the residential housing sector in Germany by 2020 of approximately 80% referring to the present level taking into account that the average specific living space will grow by around 10% within the same time period (Fig. 3).

Northern America

The establishment of (micro) cogeneration systems on the northern American market is more difficult than it is on the European market. In 2001, the US Environmental Protection Agency (EPA) has established the combined heat and power partnership. The CHP partnership promotes CHP by creating and fostering cooperative relationships with the CHP industry, state and local governments, and other relevant stakeholders. From 2001 to 2009, the program had supported more than 460 projects, representing a total electrical capacity of 4,850 MW [7].

A significant increase of the micro cogeneration is hampered, among others, by the following reasons [8]. In northern America, the distribution of the heat is often done by systems using air, rather than water. The exhaust heat of micro cogeneration systems commonly is recovered in water-filled cooling cycles. Therefore, an additional step is needed to transfer the heat from the hot-water to the air distribution systems. Furthermore, the cost of hot-air heating systems (e.g., stoves) is commonly much lower than the cost of water-filled heating systems (e.g., boiler). This means that the difference between a micro combined heat and power generation system and a heat generation system is much higher than, for example, in Europe. Another important point is the low energy price in many northern American regions, which makes it harder for micro

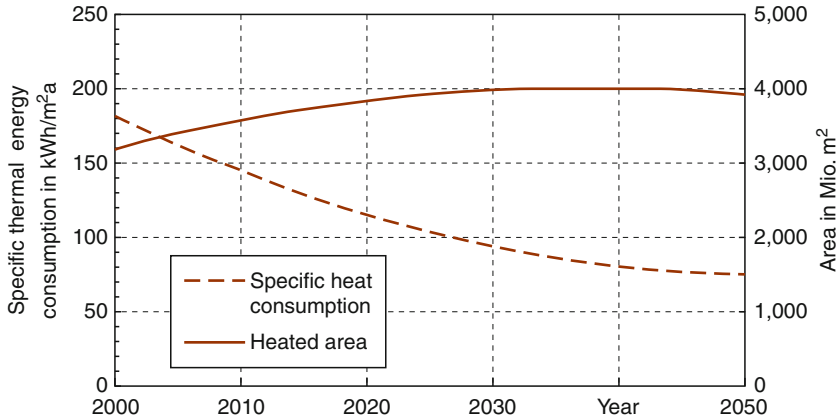

Biomass Energy Small-Scale Combined Heat and Power Systems. Figure 3
Development of the heated area and the specific thermal energy consumption for existing residential buildings exemplarily for Germany [6]

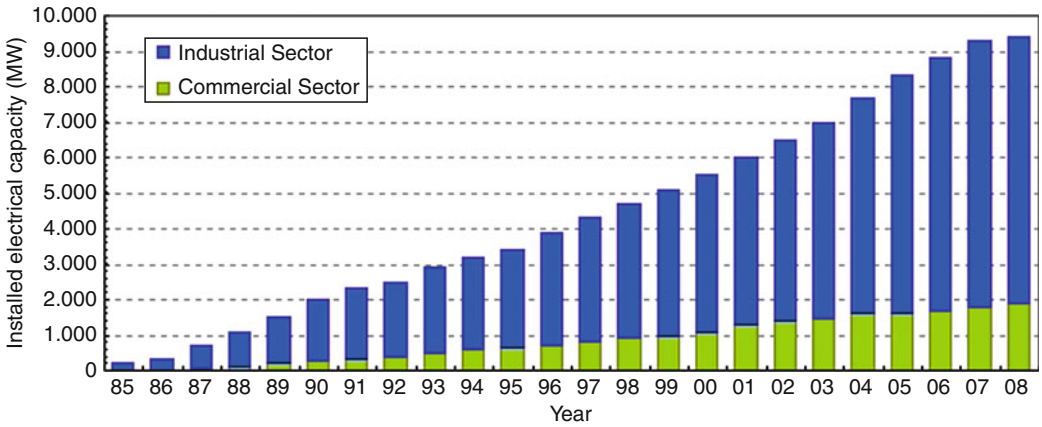

Biomass Energy Small-Scale Combined Heat and Power Systems. Figure 4
Accumulation of installed cogeneration electrical capacity in MWel in Japan, from 1985 to 2008 [9]

cogeneration systems to operate with a clear economic advantage. Despite these reasons, there is a great demand for micro CHP systems being able to work in isolated operation mode.

Japan

The Japanese government has supported ambitious energy targets to reduce the dependency on imports of fossil fuels and to address climate change. As a result, the installed cogeneration capacity has increased substantially over the last 20 years. In 2009, over 9,200 MW_{el} of installed CHP (see Fig. 4) provided around 4% of the country's electricity generation. The major cogeneration technologies used in Japan are gas turbines, diesel engines, and gas engines.

Industrial cogeneration installation represents approximately 80% of the installed electrical capacity. The remaining 20% are commercial and domestic CHP applications. Typical installations are in hospitals, hotels, office buildings, and sport facilities. The electrical capacity of available micro cogeneration systems is typically smaller than 10 kW. One important unit is the gas-engine micro CHP unit Ecowill, with an electrical

capacity of 1 kW and a thermal capacity of around 2.8 kW. In 2010, the worldwide and cumulative sales of the Ecowill have passed the 100,000 mark. The majority of the units were sold in Japan. This has meant that Japan is the world leader in the development and implementation of micro cogeneration technologies at the domestic household level. Japan is also a step ahead of developing Fuel Cells, seeing the market launch of Fuel Cells in 2011–2012.

Conversion Technologies for Small-Scale Heat and Power Systems

In the following, the main technologies for small-scale cogeneration on the basis of solid, liquid, or gaseous biofuels are presented.

The listing starts with piston-cylinder devices (e.g., internal combustion engines, steam piston engines, and stirling engines) as they are the best developed systems for small-scale cogeneration in general, followed by technologies generating electricity using turbines (e.g., steam turbine, hot-air turbines, and micro gas turbines) and concludes with fuel cells and thermoelectric generators.

Internal Combustion Engine

Due to the longstanding experience with engines operating with Diesel, gasoline, or Methane, as well as fossil fuel powered CHP plants, internal combustion engines represent the most proven technology for the cogeneration of heat and power. In a combustion engine the fuel is compressed and then ignited. The subsequent expansion sets the power piston in motion and brings the engine shaft into rotation. A generator converts the mechanical energy of the engine shaft into electric energy (see Fig. 5).

Engine-driven CHP plants with electrical capacities ranging from a few kW up to several MW are available and established on the market. The levels of electrical efficiency thereby range from 25% to 40% and the own internal electricity consumption requirements range between 5% and 10% of the output. From an engine perspective, the quality of the liquid or gaseous fuel is the essential criteria for selection. Due to the high level of noise emission, appropriate sound-insulation measures are necessary. The maintenance requirement for combustion engines lies significantly below that for comparable (micro) gas turbines. The investment costs per installed electrical capacity for combustion engines in the low-capacity segment range from 1,000 to 2,000 €/kW.

Due to the internal combustion, only liquid or gaseous biofuels can be used directly. The use of solid biofuels requires a pre-step gasification. Currently, the majority of biomass micro cogeneration plants available on the market are internal combustion engines operating with biogas (Fig. 6). The major advantages of internal combustion engines are the long history, large production and service infrastructure, and the generally lower power generation costs. Nevertheless,

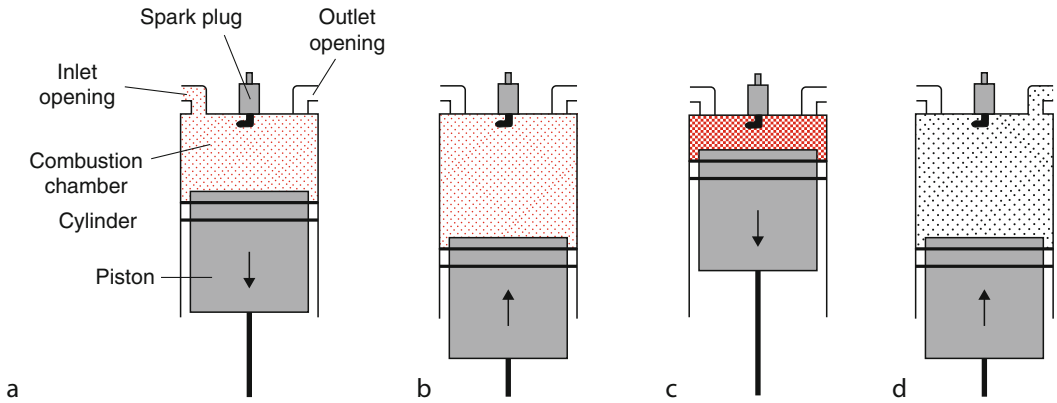

Biomass Energy Small-Scale Combined Heat and Power Systems. Figure 5
Operation principle of an internal combustion engine (**a**) Air-fuel mixture is drawn in; (**b**) Air-fuel mixture is compressed; (**c**) Explosion forces piston down; (**d**) Piston pushes out exhaust

Biomass Energy Small-Scale Combined Heat and Power Systems. Figure 6
PowerTherm® micro-CHP unit (Copyright by PowerTherm Energie Systeme GmbH)

despite these advances most biogas combustion engines are sited on farms and landfill sites with a direct source of biogas feed stocks. For the energy supply of private households and small business and community facilities it currently only plays a subordinate role [10].

Because of technical problems, a heavily fluctuating price of vegetable oil during the last years and the increased public discussion about the direct competition with the food production the use of vegetable oil stagnated on a lower level. Irrespective of these problems there are a few companies (mostly from Germany) that offer solution compatible with vegetable oil.

Steam Piston Engine

Steam piston engines are steam pressure engines where the expansion of steam takes place in a piston engine. Steam piston engines can comprise up to six working cylinders, whereby each cylinder has a piston rod, which controls the required amount of steam through the corresponding stroke. Apart from a two-shaft version also a free-piston steam engine has been developed, comprising two steam cylinders connected by a double free-piston. Since the use of conventional generators for this version is not possible due to the missing shaft rotation, a linear generator has been integrated into the engine (Fig. 7).

At the beginning of the process cycle, steam flows into the cylinder until the valve rod terminates the intake process (Fig. 8). The steam subsequently expands in the working chamber and drives the steam piston. The volume increases and the pressure reduces. Having reached dead-center position, the valve rod releases the outlet valve and the steam is discharged from the cylinder. The energy transferred to the piston is passed on to the output shaft via a connecting rod and converted into electric energy in the generator connected to the system [12].

Steam piston engines, in contrast to steam turbines, can be operated with saturated steam as well as with dry steam. Due to the significantly higher level of usable

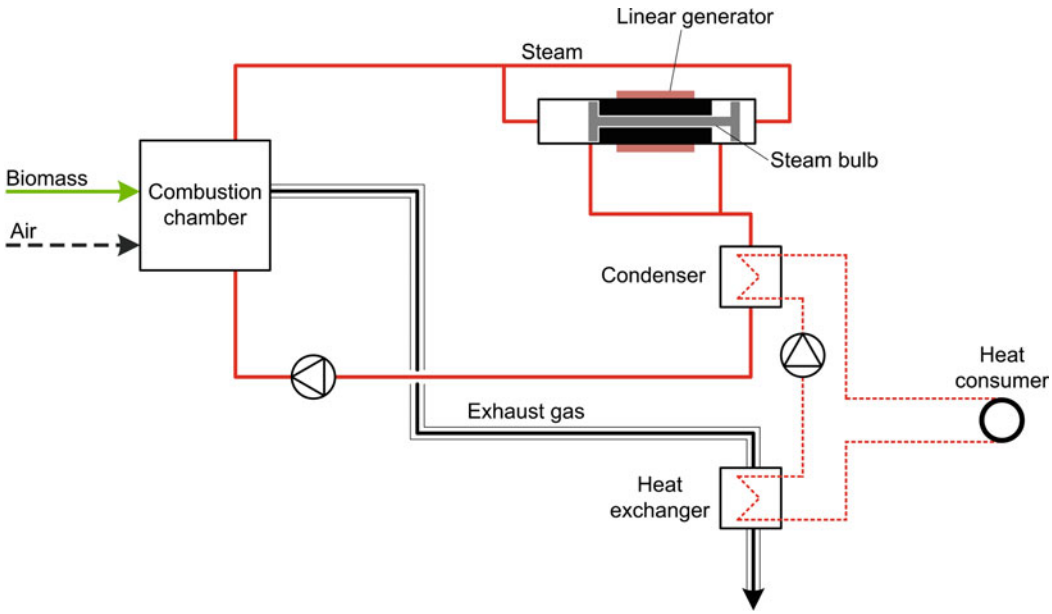

Biomass Energy Small-Scale Combined Heat and Power Systems. Figure 7
System diagram for a biomass CHP unit with free-piston engine and linear generator [11]

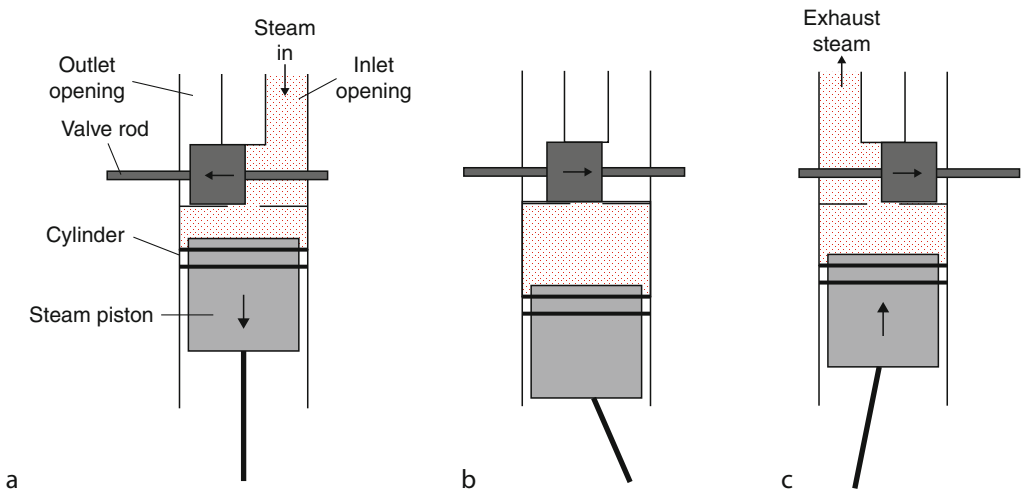

Biomass Energy Small-Scale Combined Heat and Power Systems. Figure 8
Operation principle of a steam piston engine (**a**) Steam intake; (**b**) Pressure reduction and mechanical work; (**c**) Steam outtake [12]

thermodynamic heat content (enthalpy) available through the use of dry steam substantially, higher rates of electrical efficiency can be achieved.

Steam piston engines demonstrate very good rates of electrical partial load performance and in comparison to steam turbines they are less susceptible to any potential contamination of steam. However, the electrical efficiency with 6–15% is rather low. Additionally, steam piston engines show a high level of maintenance for plants requiring lubrication; this is not

necessarily true for plants not requiring lubrication. But such engines show noise emissions of up to 95 dB(A).

Due to the closed steam power cycle in steam piston engines, there are no restrictions on biomass-based fuels, which may be used for steam generation. Steam piston engines can be employed in the range from a couple of 10 kW up to several MW.

Steam Screw-Type Engine

The working principle of the screw-type engine corresponds to the classical steam turbine process with the difference that the expansion of the steam does not take place in a turbine but in a screw-type engine.

Screw-type engines consist of two screw-shaped interlocking rotors that are closely encased by the engine housing (Fig. 9). The working chamber is created by the space between the rotors and changes cyclically during operation. At the beginning of the process cycle, the working medium flows through the intake opening into the space between the rotors. The rotation of the rotors closes off the inlet cross section thereby creating a sealed off working chamber. During the expansion process, the steam flows through the space between the rotors, which widens toward the outlet opening. The steam expands in the process and converts its thermal energy into a rotational movement of the rotors. The mechanical energy generated this way can be converted into electric energy through a directly connected generator [13].

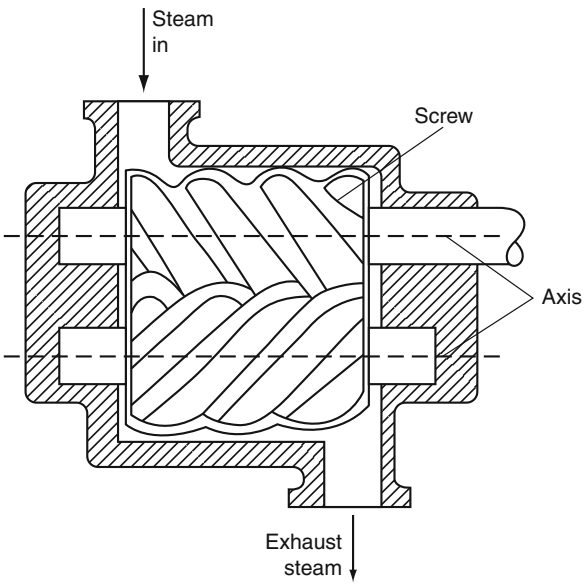

Biomass Energy Small-Scale Combined Heat and Power Systems. Figure 9
Operation principle of a steam screw-type engine [12]

Two types of steam screw-type engines are distinguished: wet and dry operating engines. For wet operating engines, oil is injected into the working chamber for lubrication of the engine and sealing of the rotors. Following discharge from the engine, this oil needs to be separated again from the condensate through appropriate oil extractors. Dry operating engines achieve contact-free movement by means of a special synchromesh transmission. The separately required lubrication of the rotor bearings can be performed through closed labyrinth seals. The advantage of this construction design is that the oil separator does become obsolete. The necessary gap between the two rotors however leads to higher losses of energy compared to wet operating screw-type engines.

For the generation of steam – as is common for systems with external combustion – different sources of heat and fuel can be used. The requirements on fuels thereby increase with declining plant capacities, since smaller plants usually also feature smaller heat exchange surfaces and profiles. As is the case for steam turbines, apart from water also organic fluids may be used as working medium. Steam screw-type engines demonstrate a high level of tolerance with regard to the quality of steam and can be operated with saturated steam as well as with dry and wet steam. In contrast to steam turbines there is no danger of droplet erosion in this case, so that expansion up into the region of wet steam is possible.

Further advantages of steam screw-type engines compared to other heat generating plants are their favorable partial load performance and low maintenance and operational requirements. A disadvantage is the high noise level, which allows for residential housing applications only with the implementation of appropriate sound-insulation measures.

Screw-type engines are generally suitable for the decentralized generation of electricity and heat supplies in the electrical capacity range between 20 and 2,000 kW, whereby no their suitability in the lower

capacity range has not be proven yet. The rates of electrical efficiency are in the range of 10–15% [13, 14].

Stirling Engine

The stirling engine belongs to the hot gas and expansion-driven engines where the piston connected to the generator is not driven directly by the expansion of combustion gases. The power piston and working gas form a closed system whereby the expansion of the working gas is caused through the supply of energy from an external heat source. In this way, stirling engines can generally be used and optimized independent of the type of heat generation process.

Stirling engines are available in a variety of designs, which essentially only differ in the arrangement of the expansion and compression cylinders. Characteristic for all designs is the use of a constant amount of working gas (air, helium, hydrogen, nitrogen) in a closed cycle. Every stirling engine has a high-temperature section and a low-temperature section (in Fig. 10 referred as heater and cooler) between which the working gas is cyclically moved back and forth between the expansion and the compression cylinders (Fig. 11). Depending on the design, the pistons will move at an angle of between 60° and 90° to one another in alternating phases. In single-cylinder systems, by contrast, both pistons are housed in one chamber. The conceptualized process consists of the compression and the expansion phase. During the expansion phase, the working gas expands under the external supply of heat leading to an expansion of the gas. The hot working gas flows through the regenerator toward the compression cylinder and release its thermal energy to the heat sink. In the compression phase, the working gas is once more compressed through the power piston and pushed back through the regenerator into the high-temperature section [15].

The advantage of the stirling engine lies primarily in the use of an external source of heat. This way, the external combustion can be optimized independent of the operational status of the stirling engine. Due to its closed cycle design, the average useful lifespan of a stirling engine will generally also be higher than that of a comparable power generating system. To be set against this are the high demands placed on the seals, which occur with the use of helium as working gas. Regular checking and if appropriate also refilling of the working gas may be necessary, in part. For some models, this leads to a significant increase in operating costs. Additional problems might cause deposits at the heater/heat exchanger. In the case of long servicing intervals, the use of high-quality wood pellets is required for optimized combustion with low particle content within the hot flue gas. In the case that firewood or wood chips are used more frequent servicing intervals are advisable.

Since the combustion does not take place in the stirling engine itself, and since there are no valves, only limited noise emission and vibrations occur during operation. Driven by the growing interest in technical solutions for small-scale power generation the

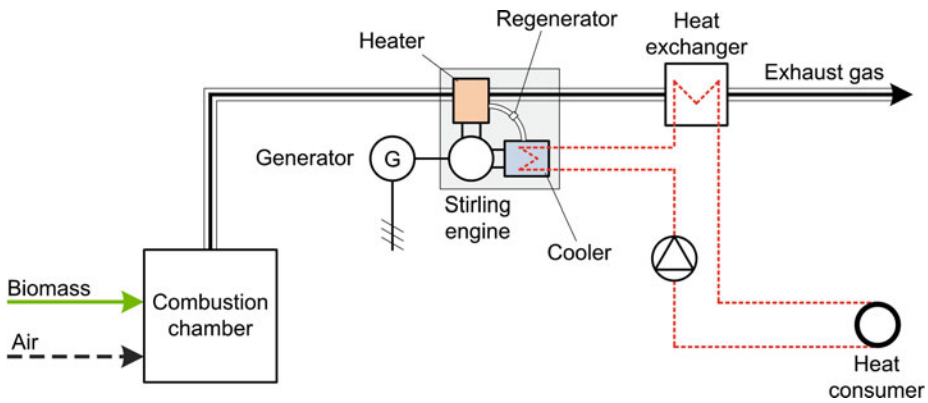

Biomass Energy Small-Scale Combined Heat and Power Systems. Figure 10
System diagram for a biomass CHP unit with a stirling engine [12]

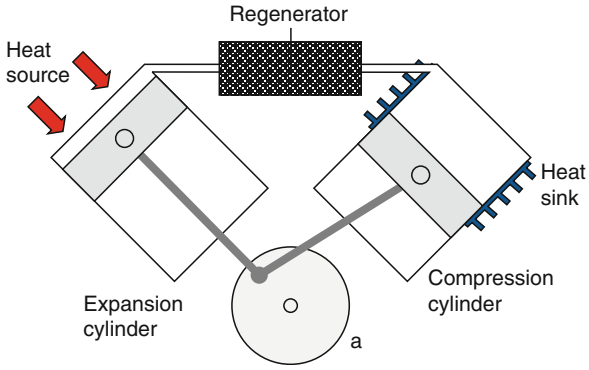

Biomass Energy Small-Scale Combined Heat and Power Systems. Figure 11
Operation principle of an alpha stirling engine with two cylinders

development of market-ready stirling engines has accelerated significantly in recent years. In this context, the latest developments have shown that biomass in form of wood pellets or firewood is well suitable for use. There are currently a number of stirling engines with electrical capacities between 1 and 100 kW in the demonstration and market introduction phase. Provided that a heat sink on a low temperature level and high flue gas temperatures at the heater are available, electrical efficiencies of around 25% can be achieved. However, due to lower flue gas temperatures emitted during biomass combustion the electrical efficiency of biomass-fueled stirling engines tends to be significantly lower. This option is still within the R&D-status.

Steam Turbine

The generation of electric power through steam turbines takes place in a thermodynamic process cycle. Here either water or an organic working medium is circulated within a closed cycle. Common features of all steam turbines are blades on the turbine shaft and casing.

Steam turbines are available in a large variety of construction designs. They can generally be distinguished by their direction of flow. In axial turbines the steam passes through the turbine in parallel to the axis, in radial turbines at a right angle to the axis. Applications for use of both designs can be found in the low electrical capacity range (<100 kW).

In the steam process the working medium is evaporated and subsequently superheated. The superheated steam is channeled between the blades setting the turbine shaft into rotation. The generator connected to the turbine shaft converts the mechanical energy into electrical energy. The steam emitted from the turbine is channeled to a condenser where it discharges most of its still remaining thermal energy into a heating cycle, whereby the steam condenses. The condensate is channeled back into the system.

Water is used as working fluid in the classical steam process. High pressures and high temperatures are required to maximize the energy content of the steam and thus the overall efficiency. In the Organic Rankine Cycle (ORC) process, an organic working medium (usually silicon oil) is used instead of water and an additional thermal oil cycle is often introduced, resulting in increased space requirements and higher costs of investment. In contrast to water, the organic medium has usually significantly lower steam pressure. Therefore, there is no need for the installation of expensive high pressure systems. The thermal oil is heated up to a supply flow temperature of approximately 300°C and then channeled onward into an evaporator where the organic working medium is evaporated through use of the heat transferred by the thermal oil into the ORC process. The steam is expanded in a slow running turbine where it performs mechanical work, which produces electric power within the generator. The expanded steam can afterward be used in a regenerator for the internal recovery of heat. In the downstream-installed condenser the working medium in condensed releasing still remaining heat to external consumers. Following this, the working medium is brought back to operating pressure and again channeled into the evaporator.

Steam turbines in the MW capacity range represent proven technology for the generation of electric power with high levels of electrical efficiency performance of up to 45% (Fig. 13 shows the rotor of a 250 MW industrial steam turbine) [16]. A drawback in the development and market introduction of small-scale steam plants are the much lower electrical efficiencies with a concurrent significant increase in specific costs. In the segment of micro cogeneration units, additional technical problems arise due to the need for miniaturization of turbines, which can be resolved only through increased expenditure in construction. All in all, this has lead to a situation where there are no market-ready

micro steam turbines available in this segment. The capacity range available on the market starts in the range of several MW.

ORC plants for the conversion of waste heat from biomass-fuelled plants in the electrical capacity range of 400 kW to 2.2 MW are today state of the art. But the 10–15% level of electrical efficiency that can be achieved remain significantly below those for steam turbines [17]. Work is currently being done to reduce in power capacities, whereby development activities until now have generally been limited to an assessment of basic technical viability without taking into consideration short-term commercial interests. The partial load performance of ORC plants is comparatively good. The advantage compared to steam turbines lies furthermore in the automated operation without the need for permanent control of the status of the steam cycle and in the possibility of decoupling heat at different temperature levels (condenser and economizer in Fig. 12).

Since steam turbines are closed systems with external heat generation, essentially all available biomass fuels for the generation of steam can be used. Similar to stirling engines, the heat transfer surfaces may need to be formed in such a way that the risk of deposits is minimized. The emission of noise from steam turbines is typically rather significant due to the high rotational speed of the turbine shaft. This makes appropriate sound insulation and vibration control necessary. Due to their slower rotational speeds, ORC plants can be expected to demonstrate lower levels of noise emission.

The investment cost per installed electrical capacity of an ORC module range from 2,000 to 3,000 €/kW. For an ORC plant (including thermal oil boiler, electrostatic precipitator, and thermal oil) the specific costs will increase by around 1,000 €/kW.

Hot-Air Turbine

Within a hot-air turbine, hot air expands inside the gas turbine. The hot flue gas transfers its heat in a high-temperature heat exchanger to the working air, which has already been compressed within the compressor. This compressed working air is heated up to

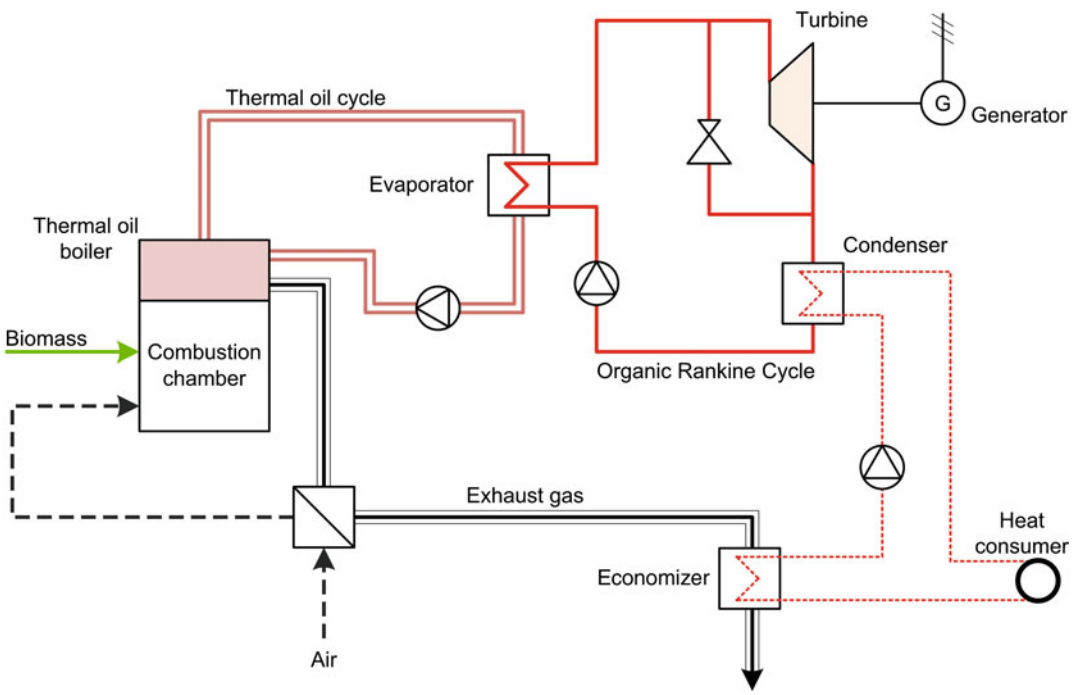

Biomass Energy Small-Scale Combined Heat and Power Systems. Figure 12
System diagram for a biomass CHP unit based on an Organic Rankine Cycle [12]

approximately 800°C. Then it expands in the turbine to ambient pressure and a temperature of approximately 400°C while performing mechanical work. Subsequently the expanded working air is channeled through a heat exchanger, warming up the combustion air needed to provide the thermal energy. The heat remaining in the flue gas at approximately 300°C, can be used for the generation of steam or hot water (Fig. 14). This comparatively high temperature level also allows the generation of electric power by a downstream ORC installation.

Biomass Energy Small-Scale Combined Heat and Power Systems. Figure 13
Steam turbine (Copyright Siemens AG)

Due to the closed air circuit, any type of fuel can generally be combusted in the boiler. The degree of electrical efficiency of hot-air turbines ranges from 10% to 20% [18]. The smallest turbine available, at present, has an electrical output rating of 25 kW with a price of up to 8,800 € per installed electrical capacity in kW. Technically challenging are the high-temperature heat exchangers, which are rather expensive given the high demands placed on the materials used, as well as the limited long-term operating experience available to date. Therefore, this option is basically within the R&D-status.

Inverse Gas Turbine

In contrast to the classical gas turbine process within the inverse gas, turbine process combustion takes place at atmospheric pressure. The flue gas released from combustion at a temperature of around 1,000°C is cleaned in a high-temperature cyclone or hot gas filter and then cooled down to around 700°C through the injection of water or steam. Then the flue gas passes into the gas turbine where it expands from the ambient pressure range into vacuum pressure of approximately

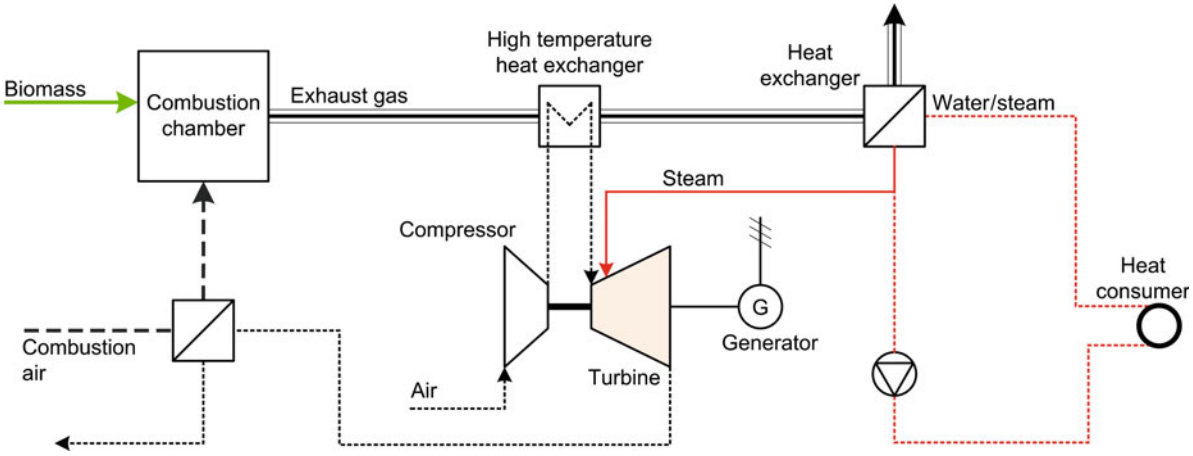

Biomass Energy Small-Scale Combined Heat and Power Systems. Figure 14
System diagram for a biomass CHP unit with hot-air engine and steam injection [13]

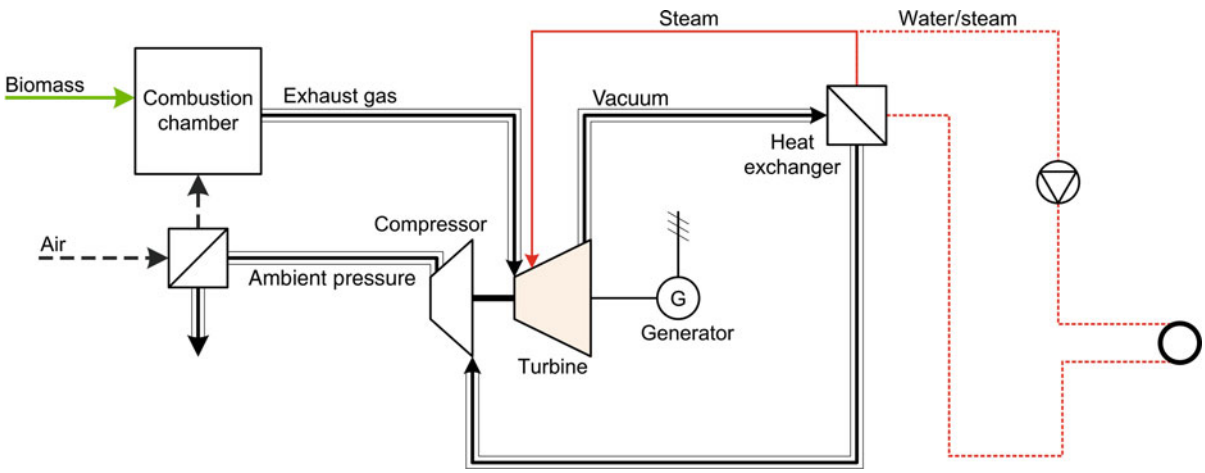

Biomass Energy Small-Scale Combined Heat and Power Systems. Figure 15
System diagram for a biomass CHP unit with inverse gas turbine and steam injection [13]

0.3–0.4 bar and performs mechanical work. The heat of the expanded flue gas can subsequently be used in several steps for the generation of high and low temperature heat. The cooled down exhaust gas, still in the vacuum pressure range, is compressed within a compressor to reach ambient pressure and heated up in the process (Fig. 15). The heat generated this way can, for example, be used for the preheating of the combustion air. The exhaust gas is subsequently released into the atmosphere – if necessary, having first gone through an appropriate cleanup process [19, 20].

Inverse gas turbines can generally be used in an electrical capacity range from only a few kW up to several MW, at rates of electrical efficiency of around 20%. The operating experience necessary for an assessment of maintenance and operational requirements is, at present, not yet available. With the use of standard components for the turbine and peripheral components, it can be assumed that no significant problems should arise. Due to the early stage of the development, no statement about the future price is possible.

An important argument for the development of inverse gas turbines – apart from the advantage derived from atmospheric combustion, which through the use of biomass avoids the otherwise costly fuelling through a pressure vessel – is the possibility to use lean gases with low caloric value and humid biomass. Since the inverse gas turbine process is a modified gas turbine process, similar to the one used for micro turbines, comparable levels of noise emission can be expected. The same applies to the requirement for supporting electric power.

Micro Gas Turbine

Small high-speed gas turbines are referred to as micro gas turbines. The difference between micro gas turbines and conventional gas turbines lies in the power range and the rotation speed.

The combustion air is drawn in through a centrifugal compressor and heated up with the waste heat from the generator, while the generator is cooled at the same time with the cool combustion air. The air heated up this way flows into the combustion chamber, where it is combusted together with the fuel gas. The hot and compressed flue gas expands within the turbine driving the compressor and the generator. The resulting mechanical energy is converted by the generator into electrical energy. In the recuperator, the hot exhaust gases pass on part of their heat to the cooled down combustion air and are discharged from the turbine at a temperature of around 300°C, which can then be used in a downstream heat exchanger to provide process heat (Fig. 16). Micro gas turbines produce high-frequency alternating current of up to 1,600 Hz, which is converted into alternating current with the aid of power electronics [21].

In recent years, natural gas powered micro gas turbines have reached the demonstration and market

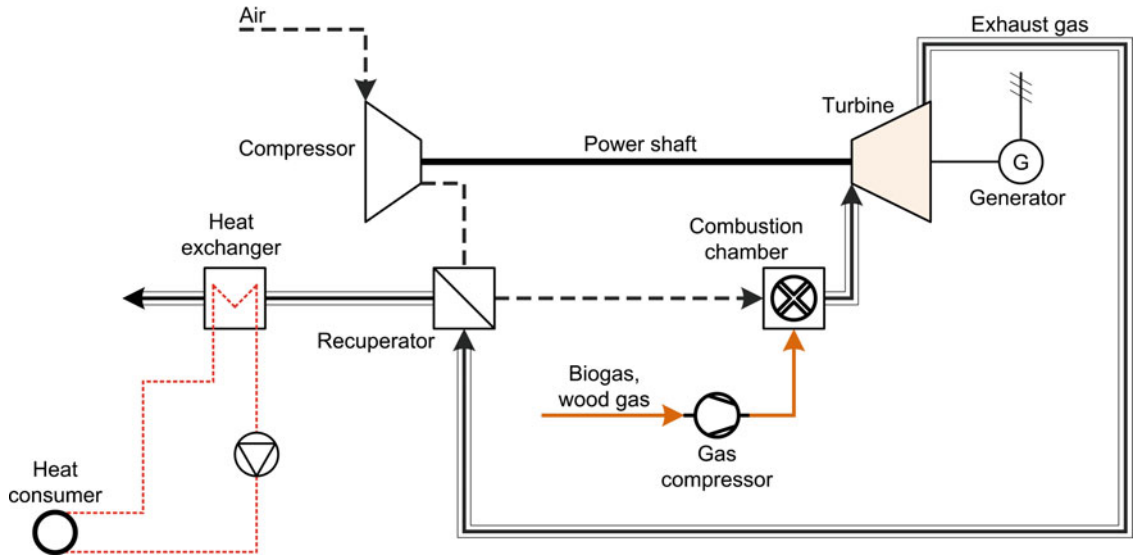

Biomass Energy Small-Scale Combined Heat and Power Systems. Figure 16
System diagram for a biomass CHP unit with a micro gas turbine [22]

introduction phase and are available in the electrical capacity range of 30–200 kW with efficiency rates of 25–30%. The specific costs for micro gas turbines are between 1,000 and 2,000 € per installed electrical capacity in kW. A positive impact on the cost of modules results from the fact that the cooling of the generator and power electronics can still be performed with air up to an electrical capacity of 60 kW. Only at higher capacity ranges, liquid cooling become necessary. Negative impact on the cost of modules is due to the complexity of the frequency conversion unit and the recuperator. Apart from the cost of modules, additional costs for a gas compressor do usually arise.

The maintenance requirements for micro gas turbines are lower than those for piston engines since there are mostly rotating components in the system. Aerostatic bearings used by some manufacturers lead to a further reduction in maintenance requirements. The noise level for some market-ready models up to 100 kW is indicated as approximately 65 dB(A) at a distance of 10 m.

Up to now, most manufacturers have approved the use of landfill gas, sewage gas, and biogas at calorific values between 3.6 and 11.7 kWh/mN^3 [23]. Current research is looking into the development of fuelling systems that allow stable and low emission combustion of gases with low calorific and heating values [24].

Fuel Cell

Fuel cells are one of the future technologies with a high potential of efficiency. In contrast to the thermal power engines, the maximum achievable electric efficiency is not limited by the Carnot limit. For this reason they can achieve substantially higher electric efficiencies than traditional technologies (for this scale up to 45%) with extremely low noise and pollutant gas emissions. The working principle of the fuel cell corresponds to a reversal of water electrolysis, i.e., oxygen and hydrogen react in the fuel cell to form water under release of electrical and thermal energy. Depending on operating temperature and the electrolyte used one can distinguish between different types of electrolyte, all of which are structured similarly.

Fuel cells consist of two electrodes (anode and cathode) separated by a semipermeable membrane. The electrodes are connected to each other through an external electric circuit and thus allow for the flow of electric power to the consumer connected. Since the maximum current of individual cells is limited, technically usable currents are generated through the interconnection of

several single cells into so-called stacks. The electrolyte facilitates the exchange of ions, is impermeable and controls the type of ions exchanged. The choice of electrolyte determines the operating temperature and type of gaseous fuels, which may be used, and thus the areas of application. For the development of new fuel cells as a component of CHP plants, the majority of potential manufacturers opt for PEM technology (polymer electrolyte membrane fuel cell) or the SOFC technology (solid oxide fuel cell).

Depending on the electrolyte used, the range of temperature and the number of stacks outputs of a few kilowatts up to several megawatts can be achieved in fuel cell systems. The electrical efficiency is typically between 25% and 45%. For small-scale decentralized plants, performance rates of 30–35% of electrical energy referred to the used primary energy can be considered as being realistic. Due to the modular structure of the stacks, fuel cells generally demonstrate good control properties and low maintenance requirements. Problem areas still remain the comparatively limited operational experience, the long heat-up period for high-temperature fuel cells, the pending proof of long-term reliability as well as the rather high specific costs [13].

Due to the higher operating temperature of SOFC systems, these are less susceptible to the quality of the fuel gases used. However, for PEM systems this means that the hydrogen required needs to be produced in an upstream reformer and that only high-purity gases may be used. SOFC systems on the other hand are capable of producing hydrogen through an internal reforming process. Hence, high-temperature fuel cells have been identified as better suited for biofuels. For reasons of long-term reliability, sulfur and halogen compounds should essentially be reduced to minimal proportions.

Fuel cell systems could use a wide range of different biofuels. Demonstration projects have been running with biofuels from gasification, landfill, and anaerobic digestion plant. Liquid biofuels, like methanol, ethanol, and dimethylether could also be used. However, presently biogas is the best biofuel for high-temperature fuel cells.

The areas of application for product gases retrieved from solid biomass in SOFC systems have not been explored sufficiently yet. The evaluation of initial research projects however already shows that SOFC systems can generally speaking also be operated using lean gas [25]. Initial trials for the integration of SOFC systems into an allotherm working biomass gasification system have shown that by the use of the TopCycle Process electrical efficiency rates of approximately 43% can be achieved. In application of this principle, the waste heat of the fuel cell is being used as a source of heat for the endothermic gasification process (Fig. 17).

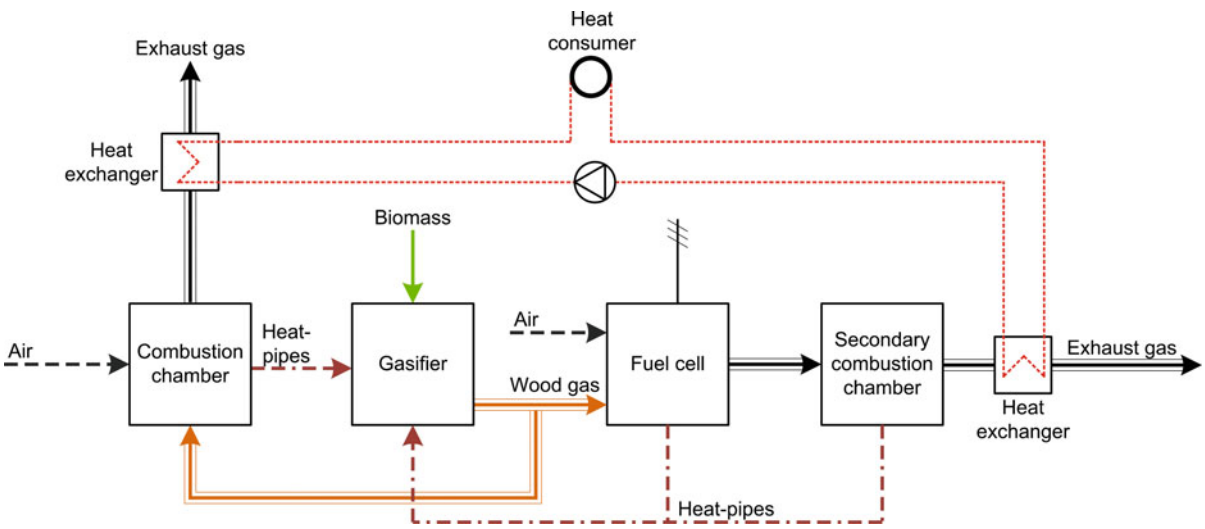

Biomass Energy Small-Scale Combined Heat and Power Systems. Figure 17
System diagram for a biomass CHP unit with fuel cell and TopCycle-System (According to [12, 25])

Through this recycling of waste heat into the gasifier it is possible to achieve a net electric power output of approximately 48 kW derived from a combustion heat output of 113 kW [26]. Based on biomass, this option is still within the R&D-status.

Thermoelectric Generator

Thermoelectric generators are construction elements using the "Seebeck effect" to convert thermal energy supplies into electric power. The working principle corresponds to that of a thermocouple. Figure 18 illustrates the relevant system structure. Through the use of p- and n-type-semiconductor legs, with thermal parallel connection, an electrical serial connection is created.

The rate of efficiency and the performance of thermoelectric generators depend, in addition to the material properties, on the number of interconnected pairs of legs and the difference in temperature between the source of heat and the heat sink. The greater the difference in temperature between the warm and the cold side, the higher the efficiency and the rate of electrical output. However, the two temperature levels may not be chosen arbitrarily. On the warm side, 250°C should not be exceeded – for reasons of material resilience – and on the cold side, the lower temperature range is determined by the temperature of the heating cycle. Due to the lower level of temperatures and flow of heat, the rate of electrical efficiency performance decreases 5–6% in the partial load area. In the future, it might be possible to realize results of 10% and above [28].

A major advantage of this technology is the omission of moving parts, which reduces maintenance and operational demands and results in noise-free operation. Thermoelectric generators are therefore suitable for use in pellet-burning stoves installed in living areas. An additional advantage is that no electrical support power is required.

Due to their homogeneous properties, only wood pellets can be used at the moment. Theoretically, one can consider using any other solid biogenic fuel for the supply of heat; however, with the use of inhomogeneous fuels increasing problems can be expected as a result of fluctuating combustion temperatures and residual ash deposits.

At present the electrical efficiency performance still remains in the rather low range of 400 W, with an efficiency of 2%. For the future a doubling of both these values is aimed [27, 29]. Therefore this option is still within the R&D-status.

Market Survey

Based on the technologies outlined above, the status of these technologies within the bioenergy market is assessed below.

Market-Ready Plants

Gaseous Biomass At present the use of biogas is the most popular renewable fuel for micro cogeneration. Due to a long experience in the use of fossil fuels often standard car engines with necessary technical adaptations

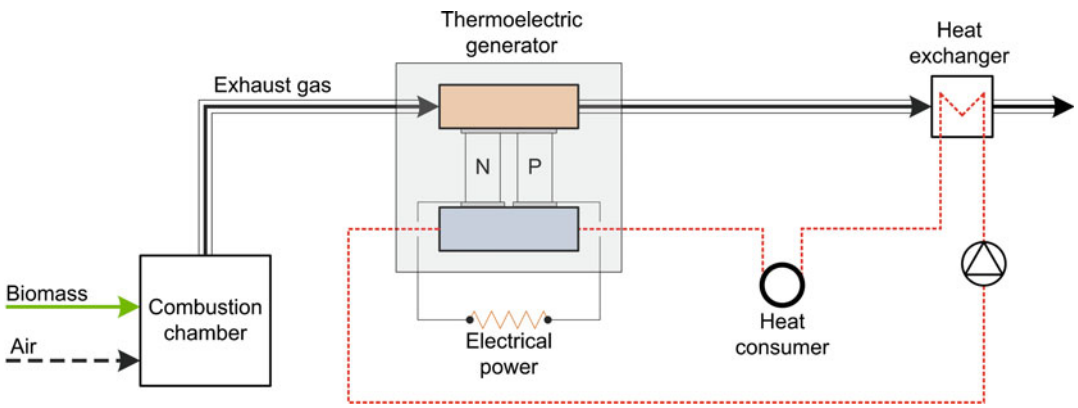

Biomass Energy Small-Scale Combined Heat and Power Systems. Figure 18
Schematic design of a biomass CHP plant with thermoelectric generator (According to [27])

are used. The second important technology for this scale and application is the micro gas turbine. The internal combustion engine is more frequently used than the gas turbine because of its long time experience, large production and service infrastructure, and the generally lower power generation costs. Both technologies are suitable for flexible deployment in synchronized to the grid, isolated, and emergency operation.

Despite these advantages, a further increase in the importance of biogas CHP units in private households or small business and community facilities needs a major improvement in biogas fuel production and supply.

There are several manufacturers offering biogas-fuelled motor CHP units for this scale. Below, some interesting units are shown.

The Italian company *Energia Nova* produces micro CHP units with an electric capacity of 20 kW and a thermal capacity of 44 kW based on a 1,200 cc car engine. The electrical efficiency is specified to be at 29% [10]. Also, the company *Tedom* which is based in the Czech Republic offers biogas-fuelled micro CHP units. The smallest available unit has an electric capacity of 28 kW with a thermal capacity of 50 kW. The unit is driven by the gas combustion engine V3800 and has an electrical efficiency of 30% and a thermal efficiency of 53% [30]. *Spilling*, from Germany, manufactures units with an electric capacity between 5 and 20 kW and a thermal capacity between 10 and 43 kW. The overall efficiency is specified to be at ~90%, depending on the return temperature. The specific investment cost of one unit amount to approximately 2,100 €/kW [31].

The American company *Capstone* offers the only on the market available micro gas turbine with electrical capacities below 50 kW. According to its own information, Capstone has around 5,000 plants installed worldwide [32, 33]. The Capstone models are compact design micro turbines with all rotating parts connected to a single shaft fitted with aerostatic bearings. Due to the air bearings technology employed no lubricants or coolants are required. The turbines are fitted with synchronization equipment, which allows for direct connection to the public grid. The internal controls allow for the parallel operation of up to 20 turbines via a central control centre.

Liquid Biomass The use of liquid biomass for energy has become more popular during the last years. For the combined generation of heat and power, typically the same technologies as for the gaseous biomass are used. Due to the chemical composition of liquid biomass, there are units that cannot work with liquid biofuels directly. Other restraints result from the fuel price, which was very volatile during the last years as well as from the public discussion about the competition with the resource efficiency and the sustainability of liquid biofuels.

One of the major manufacturers of micro CHP units for the use with liquid biofuels in Europe is *SenerTec* from Germany. The 580 cc combustion engine can be used with biodiesel and with rapeseed oil. According to the manufacturers information the electric capacity of the unit is around 5 kW, with a thermal capacity of up to 11.7 kW. The overall efficiency is stated to be at 89% (with an electric efficiency of 29%). The unit works synchronized to the grid and is designed for heat-controlled operation. They reach a maximum flow temperature of 83°C. Through this capability, usage from private households up to small business and community facilities is possible [34]. The investment cost is stated to be at 20,500 € (without value-added tax). The costs will increase for the additional offered accessories (e.g., maintenance kits, condensate pumps, heating circus distributor). The inspection is done according to maintenance plans and is shortened to 1,400 h when using regenerative biofuels [35].

Other manufacturers are *Cogengreen* from Belgium and *KW-Energietechnik* from Germany.

Solid Biomass At present there are no market-ready micro cogeneration units available operating on the basis of solid biofuels. The around 500 micro cogeneration units so far installed in Europe are primarily pilot and demonstration plants or preproduction series installations with customers. The development of market-ready small-scale biomass gasification plants could be a major step toward a considerable market position of solid biomass-driven micro cogeneration units.

Gasification technology offers a number of advantages in the use of biogenic solid fuels – compared to classical combustion. One essential advantage is the fabrication of a specific gaseous product with properties depending primarily on the production process and only secondarily on the type of biomass used. A high level of efficiency can generally be achieved by integration of gasification into the cogeneration process through combustion engines in the segment of

small- and medium-size capacities. For the thermal capacities applied here, only fixed bed gasification technologies are used.

Generally speaking, fixed bed gasification furnaces based on the co-current or counter-current principle are used in the lower capacity range, due to simpler technology. In the counter-current principle the fuel is supplied from above, whereas the gasification medium is injected from below. In the co-current principle, by contrast the fuel and gasification medium are supplied together from above with falling gasification direction.

A successful market introduction of CHP fixed bed gasification plants in the lower capacity range is being hindered by presently still existing significant technical problems. The main ones include relatively low grades of efficiency, often unreliable operating performance of plants due to technological insufficiencies, usually too high emission levels of contaminants, in many cases insufficient purification of gas as well as the sometimes permanent need for control and frequent technical servicing [36].

Demonstration and Pilot Plants

Like described above, there are many liquid or gaseous biofuel-driven micro CHP units with high electrical efficiency commercially available. Due to this situation, there is a considerably lower need for the development of new technologies. The major parts of the research and development activities are invested in systematic improvement of existing systems. The situation is different at the field of micro CHP units based on solid biomass, where the market-ready units are missing but development approaches for almost every conversion technology exist.

Therefore, some important demonstration and pilot plants based on solid biomass are presented below. This selection is realized with the goal to give an overview of the broad variety of the ongoing activities within this area. The order of the listing corresponds approximately with the status of development.

Hoval (1 kW): Stirling Engine Hoval develops biomass powered small-scale CHP plants in which through a combination of a stirling engine and a firewood powered furnace electrical and thermal energy is supplied simultaneously. Since the autumn of 2008, Hoval is offering an initial small run series with 20 CHP plants. The rated thermal output of the logwood-burning furnace AgroLyt is 25 kW, the electrical output rating of the stirling engine is 1 kW (with an electrical efficiency of the stirling engine of around 15–20%). A logwood-burning furnace is used to supply the heat required for the operation of the stirling engine. The stirling engine, as a beta-type (i.e., 2-pistons 1-cylinder system), has been designed with an external regenerator and uses nitrogen with approximately 12 bar as working gas.

For retrofitting of an existing wood burning furnace, the door to the combustion chamber needs to be replaced by a door adapted to the stirling engine (Fig. 19). This way it becomes possible to slide the engine inside the combustion chamber. For the optimal channeling of the exhaust gases through the heat exchanger some of the stone lining inside the combustion chamber needs to be exchanged and the control software needs to be adapted for operation of the stirling engine. Through the use of the stirling engine the space requirements of the biomass furnace increase. Apart from the space required for the furnace and the engine installed, additional space is needed for the installation of a track system. This is necessary since the engine has to be pulled out of the combustion chamber far enough so that the door can be opened without difficulties, in order to allow maintenance works on the furnace. Apart from this track system, a system fixing the engine inside the furnace also is necessary [37, 38].

Since an as effective as possible cooling system for the stirling engine is required in order to achieve a high degree of electrical efficiency, the engine is connected to the existing heating system via a separate cooling circuit. Options are, for example, the integration into the return flow of a low-temperature heating system or a connection to a hot water boiler or buffer. Important for all concepts are that optimal cooling of the stirling engine can be ensured. If this is not the case, suitable heat exchangers need to be installed. The electrical connection can be made through integration into a control cabinet [37].

In the course of the optimization phases carried out to date, many of the original operational problems of the plant have been solved. These concern among others the increase of the availability, the electrical efficiency performance, and the electrical capacity of the stirling engine, as well as a reduction in the demand

Biomass Energy Small-Scale Combined Heat and Power Systems. Figure 19
Stirling engine mounted in the wood burning furnace (Copyright by Hoval)

for supporting electrical power and an improvement in the overall performance rating of the plant. The investment cost of a stirling engine (together with the required fittings and the control cabinet) amount to approximately 8,000 € [38].

Plans for the further development of the stirling engine include an increase in electrical output to 3 kW as well as an integration of the engine into a pellet boiler with greater thermal capacities, starting at around 50 kW [38].

Stirling Danmark (9 and 35 kW_{el}): Stirling Engine
Stirling Danmark currently offers two plants for combined heat and power generation. A stirling engine of the type SD3 with an electrical net output rating of 35 kW and an electrical efficiency of approximately 27% (according to manufacturers' specifications) is used for the generation of electric power.

In one of the models on offer, a counter-current gasifier produces a combustible gas, which is burnt in a specially designed combustion chamber. The stirling engine in this case is integrated into the combustion chamber. The gasifier is charged from below with a mixture of air and flue gas recaptured from the combustion chamber and from above with the fuel (according to the manufacturers data wood chips with a humidity level of up to 55%). Cleaning and reprocessing of the exhaust gas is not provided in this concept. The usable thermal output stands at approximately 145 kW, with a thermal fuel input value of 200 kW [39].

In addition there is another model where the stirling engine is fitted inside the combustion chamber of a wood chips burning furnace. In order to increase the performance rate of the stirling engine the combustion air is already preheated to around 250°C. Using wood chips with a humidity level of up to 50%, a thermal capacity of 215 kW and an electrical efficiency of 35 kW can be supplied by a thermal input rate of 290 kW [40].

Apart from the CHP unit rated at 35 kW electrical capacity Stirling DK is also developing a small-scale CHP plant. The core section of this plant is a beta-stirling engine with an electrical output of 9 kW which, according to the manufacturers, should reach an electrical efficiency rate of approximately 28% [41].

Talbott's (25 kW_{el}): Hot-Air Turbine The company Talbott's Biomass Energy Group Ltd. supplies CHP plants with electrical output ratings ranging from 25 kW up to 100 kW. The humidity levels of the fuels used should not exceed 25%; however, operation at humidity levels up to 40% is possible, in principle. Through the separation of the hot-air turbine process from the supply of heat the operation of furnace and turbine can largely be optimized independent of each other.

The combustion takes place in a stepped grate with automatic ash removal and the plant can be operated with wood chips of G50 quality or wood pellets. A hot-air turbine is used for the generation of electric power, with a manufacturer stated electrical efficiency rate of 20%. The price per installed electrical capacity for the CHP plant is between 6,200 and 8,800 €/kW [42].

Sunmachine (3 kW_{el}): Stirling Engine Sunmachine has also been working for a number of years on the development of a micro cogeneration unit for domestic use as well as small-scale commercial objects. According to manufacturers information, the grid feed-in capacity of the CHP plant ranges from 1.5 to 3 kW, with electrical efficiencies of 20–25%. The thermal capacity is stated as 4.5–10.5 kW. Wood pellets are listed as suitable fuel. The cost per installed electrical capacity of the CHP plant (excluding heat storage, connection, etc.) is around 7,600 €/kW.

Due to governmental subsidies in Germany and the interest in the technological concept, of combining a compact upside-down burner with a newly developed stirling engine, some 400 plants have been sold and installed to date [43]. Partly responsible for the considerable shortfall in meeting the original sales targets is an underestimation of the need for further operational optimization in practice applications. Following restructuring measures (at the end of 2009) and a major reduction in production volumes, resumption of normal production can be expected only once the still remaining technical problems have been solved.

Cleanergy (7.5 kW_{el}): Stirling Engine Already in June 2007, the company SOLO Stirling (the original developer of the stirling engine type V161) had to file for insolvency. The company was subsequently taken over by Stirling Systems and renamed as Stirling Systems. After this company, as well, had meanwhile filed for insolvency, the technical know-how was acquired by the Swedish company Cleanergy. According to a company statement (at the end of 2009), Cleanergy intends to resume production of the stirling engine by 2010 at the latest.

SOLO Stirling had started with the series production of the model V161 in 2002 and had sold around 150 units since the original market launch. Besides the original concept, in which natural gas is used as fuel, tests were also made with the use of biomass. In this context, the direct supply of heat through the combustion of biomass had been investigated, as well as the use of wood gasifier. In operations with a fixed bed counter flow gasifier, the stirling engine V161 achieved an electrical output rating of between 2 and 7.5 kW with a thermal output 8 to 22 kW (i.e., electrical efficiency of around 20%) [41]. It is presently not known whether Cleanergy intends to further pursue the development of a model using biomass.

Bioenergy 2020+ (0.2 kW_{el}): Thermoelectric Generator Austrian Bioenergy Centre (now Bioenergy 2020+) has been exploring the technical viability of using the "Seebeck effect" for the cogeneration of heat and power with a pilot plant since 2006. The objective of the project is to use a modern pellet furnace in isolated operation, regardless of the availability of electric power supplies. As a result of these parameters, the plant is operated in a heat-controlled mode with low electrical output of the power generating unit.

The thermoelectric generator TEG 250 consist of 16 interconnected modules with altogether 288 pairs of legs. In the initial development phase, the thermoelectric generator with an electrical output of 200 W was integrated into a standard wood pellet furnace. The objective was to demonstrate the practical implementation of this combination and to investigate whether the potentials worked out in theory could actually be achieved in practice. During the initial trials, electrical efficiencies of 4% for the generator and 2% for the system as a whole were achieved. As a next step,

the still remaining measures for optimization are to be implemented (e.g., optimizing the heat transfer process, reducing the risk of overheating, ensuring stable, and complete combustion); and the electrical performance of the generator is to be doubled, while reducing the costs by half at the same time [29].

OTAG (3 kW_{el}): Steam Piston Engine Another development is the "lion-Powerblock" from OTAG. Based on the already available natural gas fired "lion" OTAG has been working (since 2007) on a combination suitable for practical application of the "lion-Powerblock" with a wood pellet furnace.

Basis for this is the Linator® – a free-moving piston in a closed process steam operation. The hot gases from the combustion process are used to produce process steam with a temperature of approximately 350°C and a pressure of 5–30 bar. The steam cycle, as is customary for steam piston engines, is a closed system with external combustion.

According to the manufacturers' information, the first plant is undergoing field-testing in monovalent operation since the autumn of 2009. The thermal output modulates in a range between 4 and 14 kW, with an electrical output rating of 3 kW.

Aactor !GT – Ökozentrum Langenbruck (9 kW_{el}): Inverse Gas Turbine Until the end of 2009, the Ökozentrum Langenbruck had been working on the development of a prototype model for an inverse micro gas turbine with a feed-in capacity of approximately 2.4 kW that was to serve as the basis for the design of a prototype turbine powered by atmospherically combusted lean gas. Decisive for the decision to develop such a plant were the results of a market and technology analysis made by the Ökozentrum in which inverse gas turbines were identified as a robust and economically viable technology for the use of lean gases.

Since the first two project phases went rather promisingly, a prototype suitable for field-testing is now to be developed in the next project phase and ultimately the prototype for a lean gas powered inverse gas turbine with a feed-in capacity of 9 kW [19].

Conclusions

Below some conclusions are drawn.

Technological Aspects

The rate of electrical efficiency is one of the main indicators for the evaluation of small-scale CHP plants. This is due to the fact that the economic advantage gained through the feed-in of electricity into the grid and the resulting reimbursement – or through a reduction of the electric energy consumption brought from external sources – generally tend to be significantly higher than those potentially to be gained by the provision of heat.

Below the theoretical electric efficiency together with the current status of development is shown for the conversion technologies and the capacity range described above (Fig. 20). A comparison of these two charts highlights one of the key problems of the use of biofuels for micro cogeneration in general and solid biofuels in particular. On the one hand, the theoretical efficiency potential of most of these technologies is not yet sufficiently exploited. On the other hand, the technology with the highest electrical efficiency rating, (i.e., fuels cells) is currently not available on the market. Applications, on the basis of solid biomass, for the most proven technologies (i.e., steam turbines and micro gas turbines) are presently still missing in the performance range reviewed.

Despite increased research activities over the past few years hardly any commercially operating solid biomass CHP plants can be found up to now in the capacity range under review. An interesting aspect in this context is the fact that two promising developments are not being pursued any further since, from the perspective of the plant manufacturers, an economic operation of the plants is not possible for the time being.

The first of these two is a micro ORC unit with an electric capacity of ~10 kW and a thermal capacity of ~80 kW that was developed by Turboden from Italy. The second one is a four-cylinder stirling engine with an electrical capacity of 1 kW, which uses the hot combustion gases of a wood pellet furnace for the generation of power, developed originally by SPM and later by KWB. After the first plants had already been tested for their practical suitability within a field test, the project was abandoned at the end of 2009. According to statements by KWB it is the presently still rather low actual customer interest that is mainly

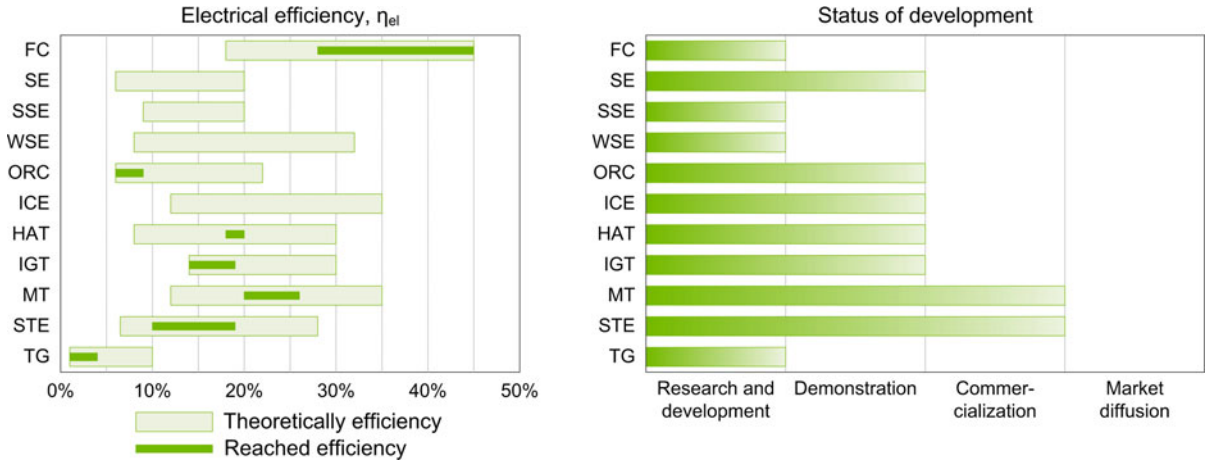

Biomass Energy Small-Scale Combined Heat and Power Systems. Figure 20
Electrical efficiency and status of development of examined conversion technologies for the micro cogeneration on the basis of biomass. For technologies with no real electrical efficiency shown assessable projects are missing. (ICE, Internal combustion engine; SE, Steam piston engine; SSE, Steam screw-type engine; STE, Stirling engine; WSE, Water steam engine; ORC, Organic Rankine Cycle; HAT, Hot-air turbine; IGT, Inverse gas turbine; MT, Micro gas turbine; FC, Fuel cell; TG, Thermoelectric generator)

responsible for this decision. The still ongoing field tests will be completed in order to be able to use the experiences gained for later developments [44].

This also leads to the assumption that either the market for solid biomass micro CHP units is not important enough or the still remaining technical problems, at present, do not justify any further intensive development activities.

Table 1 additionally shows the major advantages and drawbacks of the CHP technologies reviewed. The stated values are to be considered as indications only. In the performance range up to an electrical capacity of 50 kW, internal combustion engines together with micro gas turbines currently represent the most advanced technology for the cogeneration of heat and power by the use of liquid or gaseous biofuels. However, up to now only landfill gas, sewage gas, or biogas with a calorific value between 3.5 and 11.7 kWh/m^3 may be used as fuel. The use of lean gas is still not possible. For the use of solid biofuels the greatest potential for an introduction to the market, in the medium term, is attributed to the stirling engines as these can be integrated into existing furnaces without major reconstruction measures. Nevertheless, the electrical efficiency rates that can be achieved with this technology (up to 20%) are rather low and the technology is still not market mature. Any noticeable market penetration by the remaining technologies over the next 5–10 years would seem at least doubtful.

Among the drawbacks hindering market penetration are first of all the high investment costs for CHP plants, due to low numbers and resulting high unit costs, as well as technical problems related to the inhomogeneous structure of biomass and furthermore, in comparison to gas or oil, the high proportion of non-combustible contaminants. This leads to the currently very low operational lifespan of the plants, low electrical efficiencies, frequent servicing intervals, and a high level of maintenance and operating costs.

Potential Fields of Application

Throughout Europe the greatest potential for micro cogeneration plants is seen in buildings with central heating systems. This means that the conventional generator of heat is replaced by the CHP plant. The heat generated is used for space heating, the supply of hot water and cooling systems for buildings, whereas the electric power generated is primarily used to cover own electricity requirements.

Biomass Energy Small-Scale Combined Heat and Power Systems. Table 1 Key characteristics of the biomass CHP technologies investigated

Conversion technology	Main advantage	Main drawbacks
Internal combustion engines	Well established; wide selection of plants on offer; acceptable costs and grades of efficiency	High level of noise; low exhaust gas temperature; gaseous or liquid fuels required
Steam piston engines	Good partial load performance	High level of noise; very high maintenance requirements
Steam screw-type engines	Good partial load performance	Only limited operating experience; high level of noise
Stirling engines	Adaptable to different furnaces (external combustion); low noise level	Low grade of electrical efficiency; high maintenance requirements
Water steam engines	Proven technology in the higher capacity range	High specific costs for smaller capacity range; low grades of efficiency, high level of noise
Organic Rankine Cycle	Lower inlet temperatures can be used; very good partial load performance	Low grades of efficiency (only limited scope for improvement)
Hot-air turbine	High exhaust gas temperature; high degree of efficiency potential with steam injection; simple process	High cost of high-temperature heat exchanger; complexity of plant system
Inverse gas turbine	Good degree of efficiency potential; wide range of fuel sources	Low grades of efficiency; development just starting; complexity of plant system
Micro gas turbines	High exhaust gas temperature; acceptable grades of efficiency possible	Gas compressor required; use of lean gas not yet possible
Fuel cells (SOFC)	Very high grades of electrical efficiency possible; high exhaust gas temperatures; internal reformation	High internal temperatures; problems with reliability/durability of material; long heating up periods; use of lean gas not yet sufficiently tested
Thermoelectric generator	Noise free; low maintenance requirements; no support energy required; black start possible	Very low grades of efficiency

A positive economic effect in this context comes from applications with a year-round constant demand for heat and the resulting increase in full-load operating hours as well as from applications with a high electric base load, which reduce the amount of external electricity supplies to be purchased and at the same time reduce the amount of power produced that has to be fed into the grid, usually at a lower price.

In addition to the high investment costs an economic operation is currently still impaired by comparatively high servicing and maintenance costs for biomass-based systems, the often low electrical efficiencies of less than 20%, and the resulting unfavorable balance between thermal and electrical output (for biomass micro CHP plants the thermal output is usually greater than the electrical output by a factor of 3.5–10).

Two promising application fields can be distinguished.

Private Household Sector The economic use of micro CHP plants in private households proves to be difficult at the present stage of development despite the high potential for primary energy cost savings. For small single-family dwelling houses, the returns from electricity feed-in or own use are often not sufficient to amortize the high cost of initial investments in the plant.

The heat-controlled operation in combination with increasingly available solar powered hot water supplies often result in full-load operating hours of the CHP plant which allow for the 2,000 h/a to be reached only with the aid of large heat buffers and very low heat output of below 10 kW thermal capacity. An economic operation of a CHP plant will hardly be possible on this basis.

The combined generation of heat and power in single-family dwelling houses is in general economically only viable when the power generated is used to cover own demand, with simultaneous use of the heat. With heat-controlled operation of the plant, the usually rather intermittent demand for heat and in part strongly varying patterns in the demand for heat and power, only a small portion of the own demand for electricity can be covered by micro CHP plants – also as the necessary electric power storage devices are not yet available.

A possible remedy in this respect could be provided by the thermal storage devices available, as a standard, with biomass fuelling and local energy and load management systems. Active load management should be able to offer opportunities to adapt the charging cycle of the heat storage device to the electric load profile in such a way that the CHP plant can produce, if possible, large supplies of electric power during periods of high electric load. Similarly, should the operating periods for major electrical appliances (e.g., washing machines, dryers) be changed in such a way that peak loads do not occur, and that during other times the equipment is operated with otherwise lower electrical and thermal loads, while the heat storage device is being recharged.

In special cases, biomass-based micro CHP in the lower capacity range can already today offer a clear advantage compared to fossil fuel systems. Such applications include, for example, isolated operation in remote regions (e.g., mountain lodges). These often do not have any access to the power grid and as a result often have low electric loads, and due to their location do usually have better access to wood as a fuel than to fossil energy sources. In such cases, a biomass micro CHP designed for isolated operation and without or only low electricity demand offers the possibility for an efficient supply of heat and power.

Small Business and Community Facilities In contrast to single-family dwellings, micro CHP plants can be operated significantly more economically in small manufacturing businesses and office buildings as well as in community objects, such as administrative offices, due to an overall greater supply and often the possibility of being able to significantly better predict the demand for heat and power. Beside the demand profile for heat – which should be evenly distributed over the year, if possible – the demand profile for electric power plays a key role in the evaluation of micro CHP plants under these conditions. Applications with a largely simultaneous demand for heat and power are suitable for cogeneration just as much as those, where the CHP plant can be used to cover the electric base load. The most suitable applications include:

- Community facilities (administration buildings; swimming pools; hospitals)
- Industry and commercial buildings (hotels; office buildings; small supermarkets)

Future Directions

Technologically. In order to be able to capture the existing market potential, the present-day concepts for micro cogeneration need to be further developed in some essential points. In general, developments are required in the electrical output range of 0.5–2 kW, 5–10 kW, and 20–50 kW in order to be able to respond to the different profiles in the demand for heat energy (households, small multiple housing units and small public buildings, medium-sized and larger public and social institutions, as well as small- and medium-sized enterprises).

A high degree of reliability with low maintenance costs is required for all applications. Especially in the two lower performance ranges should servicing be required only once a year (as a maximum) and operations should be running fully automatic. More frequent servicing and controls for larger plants are possible provided if they result in limited work and, most importantly, limited costs. All concepts should be designed in such a way that heat can be provided independent of the supply of power. As the systems are in general operated heat controlled – and only a charging period for the heat storage device can be

stipulated – any additional costs in comparison to a pure heat generator must be limited. Correspondingly, the specific costs per kW thermal energy should only increase (as a maximum) by the amount of savings achieved in the cost of electricity supplies.

For the installation in residential buildings, it is mandatory to provide for a sound-insulation casing and the overall system should be designed in such a way that it requires as little space as possible (including fuel storage), and it should be easy connectable to the existing domestic network (in particular connection to an existing buffer system, with or without solar system). In order to ensure optimal operation – even more so than in the case of biomass furnaces – attention needs to be paid to optimizing controls, including coordination of demand and operating periods of the plant. Subject to these preconditions, micro CHP plants powered by solid biofuels can and will gain in importance in the future – initially only in niche sectors, but with rising costs of energy later on also more widely.

Biofuels. A high tolerance for the quality of the biomass in use is one of the major factors for the future relevance of biomass for micro cogeneration. Systems with high requirements on fuel quality, like it is common for the use of solid biomass, will primarily be established in Central Europe and maybe Northern America. For the remaining regions, the establishment of a market for these fuels is at least very doubtful.

Technologies that could be used with locally available fuels seem to have the greater global potential for decentralized biomass-driven micro cogeneration. Therefore, systems consisting of a conversion stage, in which a fuel gas is produced, and a subsequent use of the gas in the cogeneration unit appear best suited for this. According to the actual stage of deployment, micro anaerobic digestion, and micro gasification could play a particular role in the production of the fuel gas. Ligneous biomass as well as organic waste can be used as raw materials. The combined generation of heat and power can take place in a downstream micro CHP unit. All the technologies mentioned in the section "Market survey" will be usable for this purpose. Due to existing long time experience, large production and service infrastructure and the generally lower specific costs internal combustion engines and micro gas turbines have clear advantages.

Building automation. The future spread of biomass micro CHP plants can be further supported by the increased use of active systems for building automation. In combination with suitable heat storage devices, active systems for building automation allow a power-controlled operation of the CHP plant just as well as electricity storage devices allows a thermal-controlled operation. Both approaches offer the greatest possible reduction in the amount of electricity that needs to be fed into or taken out of the grid.

Such systems – in the course of pending refurbishment measures – can however be retrofitted together with all the associated effects on existing electrical equipment and the building's power supply, particularly in the case of larger buildings. The integration into existing single-family dwelling houses will rather be the exception. Ideally these systems should be taken into consideration already at the planning stage.

Economically. Independent of the political measures taken to improve the economic viability of mini-CHP plants compared with other options, the investment costs for cogeneration units have to decrease substantially, while servicing intervals have to be lengthened significantly also to lower ongoing operating costs. In particular, for plants in which biomass is used the still rather high specific costs and short servicing intervals do obstruct any noticeable market penetration. The high costs and resulting long amortization periods do represent a major obstacle, especially for the private sector.

Politically. In order to achieve the stated climate protection targets, the further development of mini-CHP plants is supported through governmental support programs – at least in European countries that are considered to be the driving force for decentralized cogeneration of heat and power in the lower performance ranges. In Germany a bonus of 0.0511 €/kWh is granted for all electricity produced through cogeneration, and therefore also for the proportion used to cover own demand. Similar programs can currently be found in Great Britain and in The Netherlands. However, the market development during recent years have shown that the market for mini-CHP plants presently still depends on political support; for example, in Germany between autumn 2008 and the end of 2009 approximately 7,000 new mini-CHP plants were installed – following discontinuation of the subsidy program it came to a massive reduction in the number of newly installed units.

Bibliography

Primary Literature

1. International Energy Agency (2009) Cogeneration and district energy: sustainable energy technologies for today and tomorrow. OECD, Paris
2. Eurostat (2009) Energy: yearly statistics 2007. Office for Official Publications of the European Communities, Luxembourg
3. Ecoheatcool (2006) Work package 1: the European heat market – Final report. Euroheat & Power, Belgium
4. Loesoenen P (2009) Combined heat and power (CHP) in the EU, Turkey and Norway: 2008 data. Eurostat, Luxembourg
5. Deutsche Energie-Agentur GmbH (dena) (2010) Aktualisierung der Kurzanalyse der Kraftwerksplanung in Deutschland bis 2020: Schlussfolgerungen und Fazit. dena, Berlin
6. Bundesumweltministerium (BMU) (2009) Langfristszenarien und Strategien für den Ausbau erneuerbarer Energien in Deutschland: Leitszenario 2009. BMU, Berlin
7. U.S. Environmental Protection Agency (2010) Combined heat and power partnership. http://www.epa.gov/chp/partnership/index.html
8. Pehnt M et al (2005) Micro-cogeneration: towards decentralized energy systems. Springer, Berlin/Heidelberg
9. The Center for Promotion of Natural Gas (2010) CHP – Cumulative generation capacity. http://www.cgc-japan.com/web/works/works_0020.html
10. European Renewable Energy Council (EREC) (2007) Cogeneration at small scale: simultaneous production of electricity and heat. EREC, Brussels
11. Kreusch M (ed) (2010) OTAG GmbH: lion-Powerblock.http://www.bhkw-prinz.de/otag-gmbh-lion-powerblock/149
12. Kaltschmitt M, Hartmann H, Hofbauer H (2009) Energie aus Biomasse: Grundlagen, Techniken und Verfahren. 2. Auflage. Springer, Berlin
13. Bundesministeriums für Verkehr, Innovation und Technologie (bmvit) (2002) Technologie Portrait Kraft-Wärme-Kopplung
14. Kötting J (1999) Strom aus fester Biomasse – Der neue Dampfschraubenmotor, klein und wirtschaftlich (Planung und Wirtschaftlichkeit eines Hackschnitzelheiz-(kraft-)werkes mit Nahwärmenetz). Seminar: Bioenergie – gespeicherte Sonnenenergie für den Raum Göttingen, Göttingen
15. Stiglbrunner R, Podesser E (2002) Untersuchung des Stirlingprozesses für eine umweltfreundliche Kälteerzeugung – Systemanalyse. Joanneum Research – Institut für Energieforschung, Graz
16. Müller B (2002) Höhere Wirkungsgrade. Die Macht der kleinen Schritte. Pictures of the Future, München
17. IBS Ingenieurbüro für Haustechnik Schreiner – Heizung-Lüftung-Klima (2010) Kraft-Wärme-Anlagen (BHKW) zur dezentralen Erzeugung von Strom und Wärme aus Biomasse. Dampfturbine, Dampfkolbenmotor, Dampfschraubenmotor, Mischdampf-Kraftwerk, Stirlingmotor, ORC-Prozess, Holzgas-BHKW, Dieselmotor, Gasmotor, Gasturbine. http://energieberatung.ibs-hlk.de/planbhkw_bio.htm
18. Gaderer M (2008) Stromerzeugung aus Biomasse und Abwärme. C.A.R.M.E.N-Fachgesprächsreihe: Wärmeleitungstechnik und Wärmenutzung, Straubing
19. Schmid M (2008) Aactor !GT©; Entwicklung einer Inversen Gasturbine "Aactor" zur Nutzung erneuerbarer Energie und industrieller Abwärme, Phase 2 - Schlussbericht, Ökozentrum Langenbruck, Langenbruck
20. Wellstein J (2010) Gasturbinenprozess: inverted Brayton Cycle. EE-News, www.ee-news.ch
21. Dezentrale Energien Schmalkalden GmbH (DES) (2010) Aufbau und Funktionsweise von Mikrogasturbinen http://www.dezentrale-energien.com/aufbau-funktionsweise-mikrogasturbinen.html
22. Thimsen D (2008) IR250 Micro-turbine case study – technical update, March 2006. Electric Power Research Institute, Palo Alto, CA
23. Wels Strom GmbH (2006) Die Capstone CR30 Mikroturbine; kompakt, extrem tiefe Emissionswerte – Datenblatt
24. Al-Halbouni A et al (2009) Flexibles Feuerungssystem zur Verbrennung von Schwachgasen in Mikrogasturbinen-Brennkammern. Gaswärme-Institut (GWI) e.V, Essen
25. Schweiger A, Hohenwarter U, Karl J (2008) Verstromung von Biomasse-Produktgasen in solid oxide fuel cells. Technische Universität Graz – Institut für Wärmetechnik, Graz
26. Schweiger A, Saule M, Karl J (2008) Thermodynamische Bewertung zur Integration einer SOFC mit Heißgasreinigung in ein Biomasse basierendes Vergasungssystem. Graz
27. Moser W et al. (2008) A biomass-fuel based micro-scale CHP system with thermoelectric generators. Central European Biomass Conference, Graz
28. Moser W, Musil B (2006) Stromerzeugung mit Pellets-Kleinfeuerungen. HLK - Heizung Lüftung Klimatechnik, 6-7/2006
29. Friedl G (2008) Pelletfeuerung mit thermoelektrischer Stromerzeugung, vol 10. Holzenergie-Symposium, Zürich
30. Höfler Blockheizkraftwerke (2010) Klein-BHKW's. http://www.hoefler-bhkw.de/pageID_4806772.html. 07.09.2010
31. Spilling Energie Systeme (2006) PowerTherm® Wirtschaftlichkeitsberechnungen. Spilling Energie Systeme, Hamburg
32. Capstone Turbine Corporation (2009) Press release, photo release: hybrid electric supercar with microturbine technology to debut at LA auto show
33. Greenvironment GmbH (2010) Referenzen: KWK-Anlagen in Deutschland. http://greenvironment.de/referenzen.php
34. SenerTec (2009) Der Dachs: technische Daten. SenerTec, Schweinfurt
35. SenerTec (2010) Produktpreisliste für Endkunden – 2010. SenerTec, Schweinfurt
36. Klemm M, Kaltschmitt M (2010) Perspektiven der Biomassevergasung. In: Energy 2.0-Kompendium 2010, publish-industry Verlag, pp 72–74
37. Hovalwerk AG (2008) Hoval AgroLyt – Stirling BHKW: Infobroschüre/Planungshilfe. Holvalwerk AG, Vaduz
38. Hegele D (2010) Personal correspondence March 2010. Hovalwerk AG, Vaduz

39. Stirling DK (2009) High efficiency small-scale power production. Stirling Danmark, Lyngby
40. Stirling DK (2007) Power production in biomass boiler. Stirling Danmark, Lyngby
41. Steimle F, Lamprichs J, Beck P (2007) Stirling – Maschinen-Technik: Grundlagen, Konzepte, Entwicklungen und Anwendungen. Müller (C.F.), Heidelberg
42. German Power Generators (2009) Talbott's biomass generators BG25 Information pack.
43. Kreusch M (ed) (2010) Sunmachine GmbH: Neustart für Pellets-BHKW http://www.strom-prinz.de/news/article/sunmachine-gmbh-neustart-oder-letztes-aufbaeumen/
44. KWB Germany Southwest branch (2010) Personal correspondence April 2010. KWB Germany Kraft und Wärme aus Biomasse GmbH, Southwest branch – Distribution, Starzach

Books and Reviews

Görner K, Albus R, Dubielzig G (2005) Möglichkeiten der dezentralen Energieerzeugung im Einfamilienhausbereich. GWI, Essen

Pehnt M et al (2005) Micro-CHP: a sustainable innovation? IFEU, Berlin/Heidelberg

Schaumann G, Pohl C, Krebs K (2003) Bewertung von dezentralen Techniken zur Strom- und Wärmeerzeugung (KWK) aus Biomasse in kleinen Leistungsbereichen. Institut für Innovation, Transfer und Beratung GmbH, Bingen

Schmid M, Gaegauf C, Sattler M (2007) Dezentrale Stromerzeugung mit Feststoffbiomasse – zusammengefasstes Wissen für Investoren über den Stand der Technik, die Technologien und die ökonomischen Fakten von gekoppelter Strom- und Wärmeproduktion aus Holz und anderer fester Biomasse bis 1 MW elektrischer Leistung. Ökozentrum Langenbruck, Langenbruck

Soares C (2007) Microturbines: applications for distributed energy systems. Elsevier, London

Thomas B (2007) Mini-Blockheizkraftwerke: Grundlagen, Gerätetechnik, Betriebsdaten. Vogel Buchverlag, Würzburg

Biomass Gasification for Electricity and Fuels, Large Scale

Hermann Hofbauer
Institute of Chemical Engineering, Vienna University of Technology, Vienna, Austria

Article Outline

Glossary
Definition of the Subject
Introduction
Gasification: Principles
Suitable Types of Gasifiers
Producer Gas Composition
Options to Use the Producer Gas
Future Directions
Bibliography

Glossary

AER Adsorption enhanced reforming, dual fluidized bed gasification process for generation of producer gas with high hydrogen content.

Allothermal gasification Heat necessary for the gasification process is generated externally and delivered to the gasifier by a heat exchanger or a heat carrier media.

ASF Anderson Schultz Flory distribution, mathematical model for Fischer Tropsch product distribution.

Autothermal gasification Heat necessary for the gasification process is generated in the same reaction chamber where the gasification reactions take place.

Biofuel Solid biogeneous material used as feed for gasification or fuel for transportation with biogeneous origin.

CHP Technology for combined heat and power production.

CV Calorific value, energy content of a fuel given in MJ/kg or MJ/m^3.

DME Dimethylether, proposed gaseous biofuels for transportation.

Fuel oriented Process for maximizing fuel production.

FT Fischer–Tropsch, synthesis reaction proposed for the production of liquid biofuels.

IGCC Integrated gasification combined cycle, process for maximized electricity production via gasification.

Large scale Large scale refers here to gasification plants with capacities larger than 10 MW fuel input and able to be up-scaled up to or above 100 MW fuel input.

ORC Organic Rankine Cycle, process for electricity production from heat.

Polygeneration Process for generation of at least three different products in one plant at the same time, e.g., heat, electricity, and biofuels.

Producer gas Gas produced in a gasification process.

R&D&D Research and development and demonstration.

SNG Synthetic natural gas, gas produced from solid biomass via gasification with a quality comparable with natural gas.

Syngas (synthesis gas) Producer gas upgraded for synthesis processes.

Synthetic Produced by synthesis reactions.

Synthetic biofuel Biofuel for transportation purpose produced via gasification followed by synthesis processes.

Definition of the Subject

It is commonly agreed that gasification of biomass has a large potential for a more sustainable energy system in the future. However, a lot of research and demonstration efforts have been carried out during the last three decades but there are only a few gasification technologies which are available commercially at the market so far. In the 1980s and 1990s CHP (combined heat and power) production based on gasification has been investigated intensively and several different technologies have been demonstrated in an industrial scale. In the last decade, research and development in biomass gasification have been focused mainly on the production, cleaning, and upgrading of producer gas to synthesis gas (syngas) quality and several synthesis reactions have been studied especially those leading to biofuels for the transportation sector.

This paper gives an overview about the state of development for large-scale biomass gasification and applications of the producer gas for electricity and/or biofuels production. Small-scale gasification is not tackled in this contribution. Large scale refers here to gasification plants with capacities larger than 10 MW fuel input and able to be up-scaled up to or above 100 MW fuel input. In this scale plants for electricity production can be considered as commercially available whereas technologies for biofuels production are still under development or demonstration.

Starting with fundamentals of biomass gasification and basic definitions gasification reactors for biomass proposed or used so far for large scale are described and characterized briefly. The resulting producer gas composition depends on a lot of parameters, therefore, the gas composition of only the most frequently utilized gasifier configurations are discussed. These configurations cover more or less the whole range of gas composition of the different gasifiers used so far. Gas cleaning as a crucial part in each process based on biomass gasification is dealt together with typical applications for electricity or biofuels production. It is neither possible nor useful to describe all configurations which can be found in literature. Therefore, the available information is summarized and typical gas cleaning strategies are presented. Finally, the most important synthesis reactions are described and complex biofuel production routes are shown. These processes are based mainly on catalytic reactions at elevated pressures and temperatures. The requirements for syngas are extreme especially in terms of sulfur contents as these substances are poisons for most of the catalysts used. Furthermore, hydrogen to carbon monoxide ratio has to be in a certain range in order to get high yields of the desired products.

Two different strategies can be followed for biofuels production: fuel orientation or polygeneration. Fuel orientation means to optimize the process for maximizing the yield of biofuels. Polygeneration means the production of at least three different products, normally in case of gasification heat, electricity, and biofuels.

Introduction

In the 1980s and 1990s combined heat and power (CHP) production was the main technology which has been investigated and a lot of different demonstration plants were built and operated [1–3]. A lot of experience could be gained during this time and several plants are able to reach availabilities up to 90%. One of these successful technologies is the dual fluidized bed gasifier which was demonstrated for the first time in Güssing/Austria and is now realized in several other industrial plants at a scale of 10–25 MW fuel input in Austria and Germany [4, 5]. The main obstacles for a broad commercialization are still the lack of sufficient experience and several "negative examples" in the last years. Therefore, for electricity generation, there is still the problem to show a real economic advantage compared with combustion-based technologies for potential investors like, for example, energy utilities.

During the last years R&D efforts have been directed more and more toward synthesis gas (syngas) production from biomass via gasification. Syngas consists mainly of hydrogen and carbon monoxide and is used to produce synthetic materials such as synthetic biofuels. Contrary to CHP, there is no competition with combustion technologies (e.g., production of Fischer–Tropsch fuels) and the market introduction is expected to be much easier. The most advanced and intensively investigated biofuel syntheses are Fischer–Tropsch (FT) synthesis, methanol synthesis, and mixed alcohol synthesis, leading to liquid biofuels. Additionally, synthesis processes leading to synthetic natural gas (SNG) and dimethylether (DME) and thus resulting in a gaseous product are also under intensive investigation. Recently, the first demonstration plant for SNG-production from biomass went into operation in Güssing, Austria.

Figure 1 shows a general process flow sheet for the possibilities of producer gas or syngas utilization. The simplest case is the combustion of producer gas for industrial heat or for co-firing as nearly no producer gas cleaning or upgrading is necessary. Most applications try to produce combined heat and power where a tar and particle reduction has to be foreseen. The production of synthetic products requires a specific gas composition (e.g., hydrogen to carbon monoxide ratio) and an ultra clean gas. Therefore, an extensive gas cleaning and gas upgrading is necessary in most of these cases.

Instead of the generation of single products from producer gas combinations of different products are the more promising way for future applications. Due the fact that CHP (combined heat and power) production is already established, the combined production of heat, power, and even one or more synthetic products are under development. Such concepts are called polygeneration or also biorefineries. The gasification is the key technology for these concepts.

Gasification: Principles

Much work has been published in this field, and a lot of information is available in numerous books and journal papers [3–5, 10, 12]. Therefore, a short summary of the most important principles is presented below to give a review of the current state of the art on gasification reactions and reactor design.

Figure 2 shows the processes which a biomass particle undergoes during gasification. All steps such as drying, devolatilization, and also gasification of the remaining char are endothermic reaction and, therefore, heat has to be supplied to make them running. Another important fact which has to be taken into account for the design of gasification reactors is the release of volatiles. About 80% of the weight of biomass is released during devolatilization and only about 20% remains as char. For one particle, all processes are running consecutively and not in parallel.

In case of pyrolysis, the reaction is stopped after devolatilization (Fig. 2). Then three products are

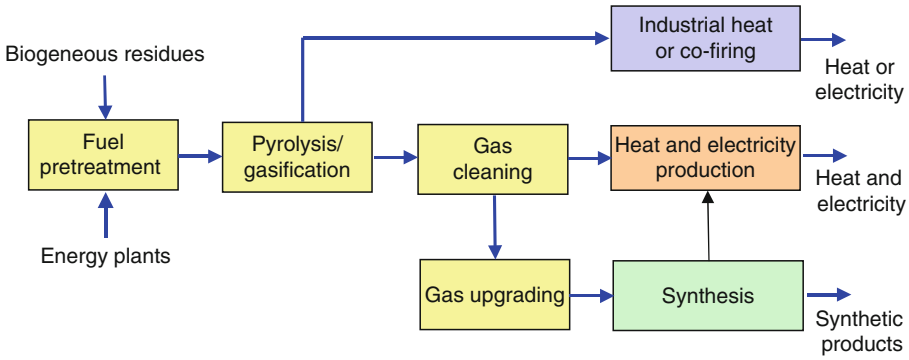

Biomass Gasification for Electricity and Fuels, Large Scale. Figure 1
Possibilities for producer gas utilization

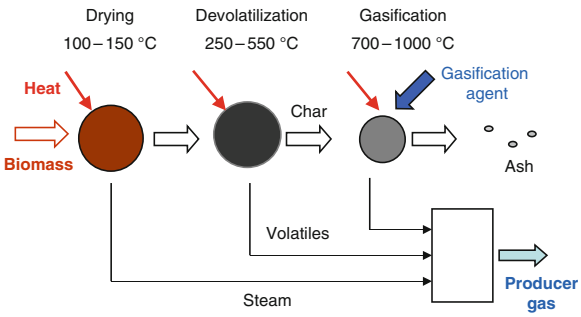

Biomass Gasification for Electricity and Fuels, Large Scale. Figure 2
Processes during gasification of a single particle

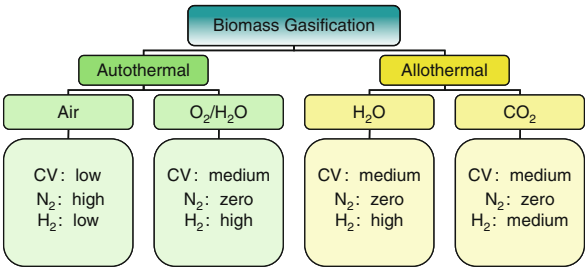

Biomass Gasification for Electricity and Fuels, Large Scale. Figure 3
Classification of gasification processes based on heat supply and gasification agents (CV calorific value)

Biomass Gasification for Electricity and Fuels, Large Scale. Table 1 Gasification agents for char gasification and resulting products

Biomass	Gasification agents	Products
C	½O_2	CO
C	H_2O	CO+H_2
C	CO_2	2CO
C	2H_2	CH_4
C	Air(21% O_2, 79% N_2)	CO+N_2

available: char, condensable volatiles (pyrolysis oil), and gases. Such a pyrolysis is well known as own thermal conversion process but also as pretreatment step for gasification. The latter application is even more important as for most large-scale gasification processes based on entrained flow gasification a pyrolysis step is foreseen.

Table 1 contains basic chemical reactions which take place in each gasification reactor in order to gasify the remaining char after devolatilization. By using a specific gasification agent, the producer gas composition can be influenced. But the most commonly used gasification agent in biomass gasification is still air. This means that the producer gas contains a lot of N_2 which is only a dilution as N_2 cannot be used in any of the presently known applications. Other gasification agents – that lead to high-grade producer gas without N_2 – are pure oxygen, steam, carbon dioxide, and hydrogen (see Table 1 or Fig. 3).

In case of air as gasification agent autothermal gasification is realized. This means that the necessary heat for gasification is produced by partial combustion of the biomass in the same reaction chamber. Another option is a mixture of steam and oxygen to obtain a nitrogen-free producer gas; this possibility is normally applied in large-scale coal gasification (Fig. 3).

To avoid an air separation unit another approach has been established. This process is based on allothermal gasification. This means that the heat necessary for gasification is supplied indirectly via a heat exchanger or a circulating heat carrier. Both types are currently under investigation and also demonstration plants have been built.

In case of poly-generation, the requirements on the syngas quality are defined by the most stringent application. And for the provision of heat, electricity, and biofuels, this is normally the quality defined by the synthesis reactions for the production of biofuels. From such a clean syngas – a mixture of mainly hydrogen and carbon monoxide together with carbon dioxide and other minor components – several interesting synthetic substances can be produced. Currently, the most interesting products are biofuels such as FT-diesel and methanol which are liquid products whereas DME and SNG are gaseous. All four reactions need catalysts which are normally extremely sensible to poisoning, e.g., by sulfur components. Furthermore, the temperatures are in the range of 200–400°C and a pressurized operation is desirable or necessary.

Biomass Gasification for Electricity and Fuels, Large Scale. Table 2 Requirements for syngas

Requirement	Measure
Low content of inert gases (e.g., nitrogen)	Gasification agent steam/oxygen
Optimal H_2/CO ratio	Steam gasification (dual fluidized bed)
	Shift reaction downstream
Low tar content	High-temperature gasification
	Tar removal downstream
Mostly, low methane content	High-temperature gasification
	Methane reforming downstream
Low content of catalysts poisons (e.g., sulfur, chlorine)	Removal downstream (Capture in fluidized bed gasifier)
Mostly, medium or high pressure necessary	Pressurized operation mostly beneficial
	Downstream compression

There are a lot of requirements on the composition of the syngas and the impurities. Table 2 contains some of these requirements. First of all inert gases which are not involved in the reactions should be avoided. For example air as gasification agent leads to about 50% of nitrogen in the syngas which is no educt or reaction agent for none of the synthesis reactions. Therefore, steam or oxygen/steam mixtures are preferable gasification agents. Additionally the different synthesis reactions need different stoichiometric H_2 to CO ratios. Even due to the fact that in practice the ratio differs from these stoichiometric values slightly, in any case a certain H_2 to CO ratio is necessary for an optimal operation. Also low tar contents and mostly also low methane contents (exception methanation) are beneficial. The most serious requirements are the avoidance of poisoning of the catalyst due to sulfur or other undesired components in the syngas. For example, sulfur has to be removed from the syngas down to 50 ppb(v) to reach a long-term operation with sufficient high yields of the desired products [8, 9]. Finally, gasification systems which allow pressurized gasification are well suited for syngas production as almost all synthesis reactions are operated under pressure. An alternative way to the last requirement is a downstream compression of the gas.

Suitable Types of Gasifiers

After definition of requirements for a well-composed producer gas, different types of gasifiers are presented that have been used or currently under development and demonstration for biomass gasification. Gasifiers are normally classified based on fluid mechanic properties in fixed bed, fluidized bed, and entrained flow gasifiers [10]. This classification is used here too. As producer gas from air-blown gasifiers is not suitable for syngas production, these gasifiers are not discussed in detail below.

Fixed Bed Gasifiers

Fixed bed gasifiers are used for producer gas generation from coal, e.g., at Sasol, South Africa. Furthermore, fixed bed gasifiers were also operated at "Schwarze Pumpe," Germany, for gasifying waste. These gasifiers have been shut down recently but a lot of experience is available from the operation over many years.

A schematic figure of a typical fixed gasifier can be seen in Fig. 4. For large-scale gasifiers only an updraft operation has been used. The operation in case of "Schwarze Pumpe" can be characterized as follows [12]:

- Solid waste has been used (e.g., plastics, sewage sludge, fluff from cars, paper and industrial plastics, contaminated wood, municipal solid wastes).
- Solid fuel is required in lumpy form (20–80 mm) to facilitate the counter-current flow of rising producer gases and descending solids.
- Briquetting, pelletizing, or further suitable methods of fuel agglomeration are required.
- Internal diameter within the gasifier has been up to 4.0 m.
- Pressurized operation of the gasifier has been realized (e.g., 25 bar).
- A mixture of steam and oxygen has been used as a gasification agent.

Currently, no intensive research and development efforts are carried out in the field of large-scale fixed bed gasifiers for producer gas generation from biomass.

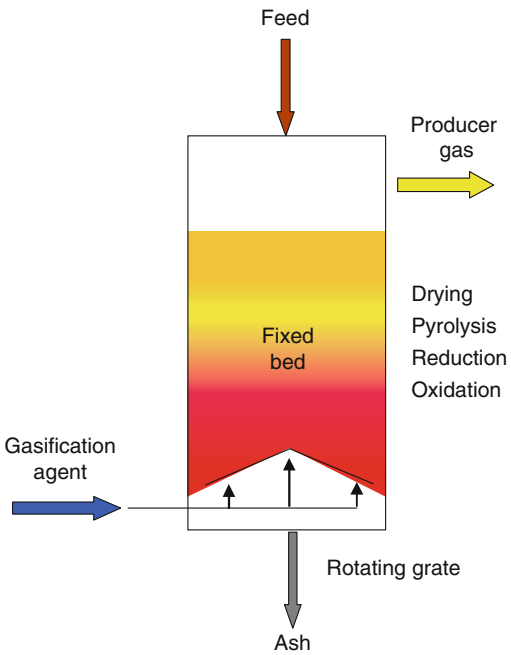

Biomass Gasification for Electricity and Fuels, Large Scale. Figure 4
Typical arrangement for fixed bed gasifiers after [12]

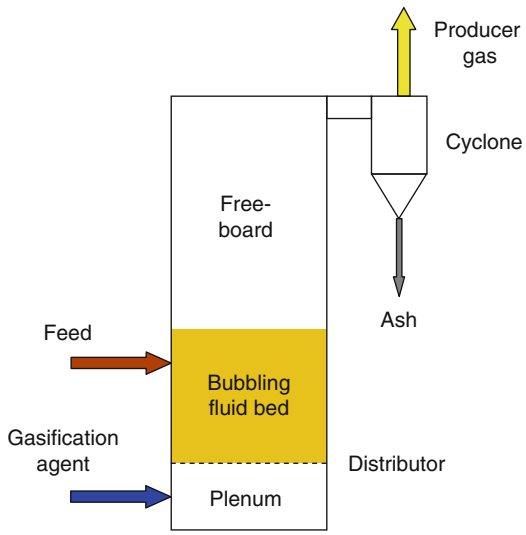

Biomass Gasification for Electricity and Fuels, Large Scale. Figure 5
Stationary (bubbling) fluidized bed gasifier

Fluidized Bed Gasifiers

For fluidized bed gasifiers, a bed material is used which guarantees a stable fluidization and provides excellent heat and mass transfer conditions. This bed material can have further functions; it can act, e.g., as catalyst for the gasification reactions or as a carrier for, e.g., CO_2 in case of the AER (adsorption enhanced reforming) process. The gas necessary for fluidization serves as gasification agent.

Dependent on superficial gas velocities and bed material diameter two types of fluidized beds are distinguished: stationary (bubbling) and fast (circulating) fluidized beds. By combining two of this fluidized bed types dual fluidized bed configurations can offer further advantages for syngas production [3].

Stationary (bubbling) fluidized beds use bed materials with a mean particle diameter between 0.5 and 1 mm und superficial velocities typically between 1.5 and 2.5 m/s. Bed heights range from 0.5 to 2 m followed by a freeboard with a height of several meters. Steam/oxygen mixtures are used as gasification agents. This gaseous mixture is blown via a plenum and distributor into the bed. But also other types of gas introduction into the fluidized bed can be found.

The solid biofuels are fed directly into the fluidized bed or thrown onto the bed to get an intensive contact with the bed material especially in the case of catalytically active materials. The producer gas leaves the gasification reactor via a freeboard where further gas-to-gas reactions take place. The gas is cooled and the fly ash is separated from the gas by a cyclone or any other type of particle precipitator. If ash also accumulates in the bubbling bed, a bed ash removal has to be foreseen. A typical cross-sectional view of a bubbling fluidized bed gasifier is shown in Fig. 5.

Fast (circulating) fluidized bed gasifiers (Fig. 6) operate at superficial velocities between 6 and 10 m/s and use smaller bed particles in the range of 0.2–0.4 mm compared to bubbling fluidized beds. There is no distinct bed height. But the total reactor is filled up with a gas/particle suspension varying in density over height. Bed material is continuously entrained at the top of the gasifier. It is returned again via a (primary) cyclone and a return leg to the reactor. Therefore, this type is also called circulating fluidized bed. Air or steam/oxygen mixtures are used as fluidization as well

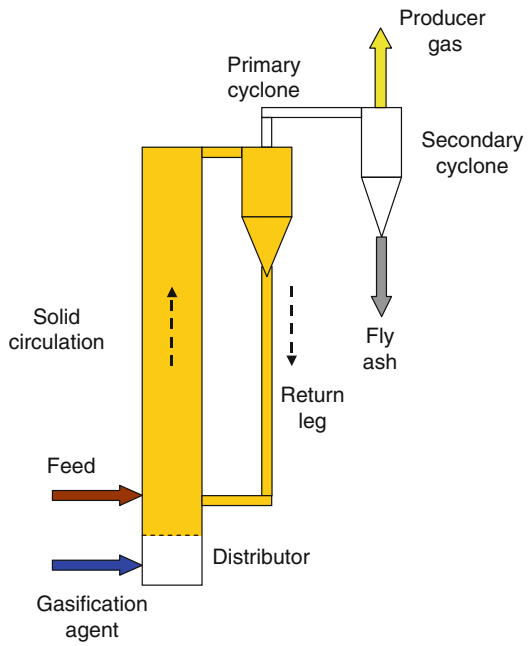

Biomass Gasification for Electricity and Fuels, Large Scale. Figure 6
Fast (circulating) fluidized bed gasifier

as gasification agent. However, the right descritpion of the fluidization state is not circulating fluidized bed but fast fluidization.

Another type of fluidized bed gasifier for large scale is the so-called dual fluidized bed gasifier. This type has got several specific advantages especially for syngas production and is currently investigated in different forms all over the world. By combining the fluidization states (bubbling, fast) three possible configurations of dual fluidized beds are possible: two bubbling beds [14], a bubbling bed/fast fluidized bed [7], and two fast fluidized beds [18]. All these configurations are under development for producer gas generation. In Fig. 7 a dual fluidized bed gaisifier with a bubbling fluidized bed and a fast fluidized bed is presented.

Dual fluidized bed gasifiers allow producing a gas free of nitrogen without the necessity of pure oxygen. One fluidized bed is dedicated for gasification (fluidized with steam) while the other one is designed for combustion (fluidized with air) in order to generate the heat for gasification. The transport of heat from the combustion to the gasification bed is carried out by circulating the bed material.

In addition to this there are also dual fluidized bed systems using alternative heat transport systems with high-temperature heat exchangers (e.g., heat pipe reformer) [11] which is currently rather dedicated to the small and medium scale.

Typical features of fluidized bed gasification can be summarized as follows:

- Temperatures: 700–900°C
- Capacities: 10–200 MW fuel power
- High fuel flexibility
  - Various kinds of fuels, fuel particles size (1–50 (100) mm), large range of ash content and water content
  - Problems with very fine particles and/or low ash melting behavior
- Medium tar content
  - Without measures: 1–20 g/Nm^3 dry gas
  - With measures (catalytically active bed material): <1 g/Nm^3 dry gas
- CH_4 content of about 10% (well suited for SNG production)
- Well suited for co-firing, CHP, and IGCC (integrated gasification combined cycle)

Entrained Flow Gasifiers

Within entrained flow reactors, the gasification of the biomass particles takes place within a few seconds during pneumatic transport through the reactor. This requires small biomass particle diameters and high temperatures to complete the gasification reactions within this short time. Figure. 8 shows a typical configuration of an entrained flow gasifier.

The fuel is typically fed from the top together with the gasification agent (steam/oxygen). In the upper part gasification is carried out, and in the lower part the producer gas is quenched and separated from the ash particles. The ash is withdrawn from the bottom in granulated form. Producer gas is leaving the reactor at the lower part and can be further upgraded to syngas.

The most important characteristics for entrained flow gasifiers are:

- High temperatures (>1,200°C)
- Very small fuel particle diameters are necessary (<1 mm)

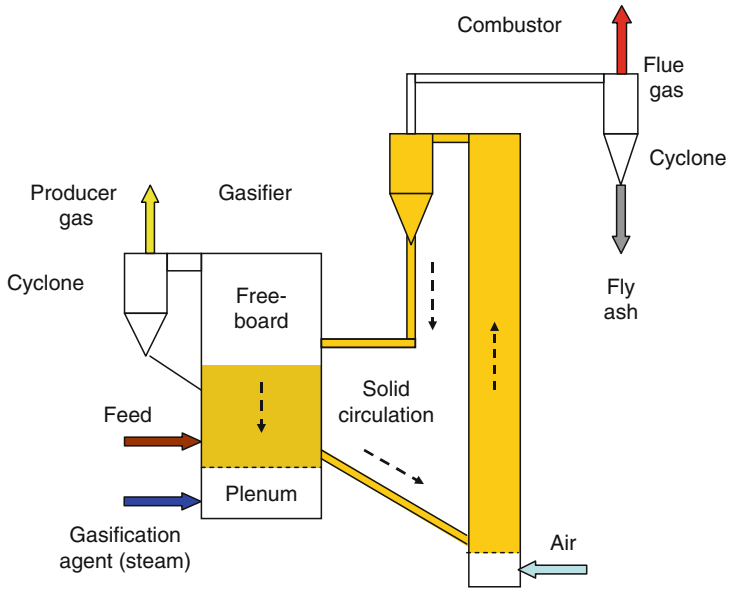

Biomass Gasification for Electricity and Fuels, Large Scale. Figure 7
Dual fluidized bed gasifier

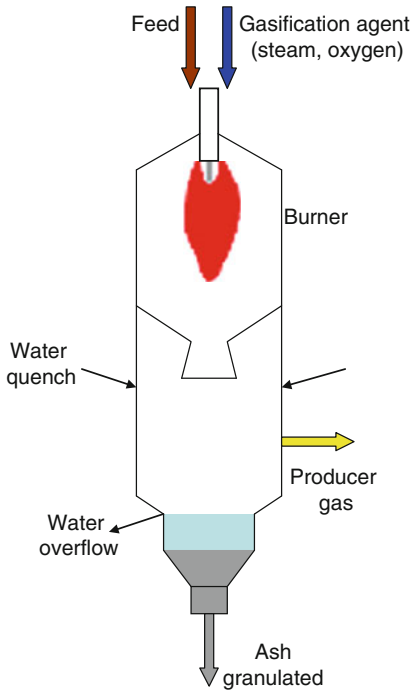

Biomass Gasification for Electricity and Fuels, Large Scale. Figure 8
Entrained flow gasifier after [10]

- Fuel pretreatment necessary (e.g., grinding, torrefaction, pyrolysis)
- Pressurized operation easily possible (e.g., 25 bar)
- Very low tar content within the producer gas (<10 mg/Nm^3 dry gas)
- Low methane content in producer gas (<1%)
- Currently for large scale application and especially for liquid biofuels production (e.g., FT-Fuels or DME from black liquor) under discussion

Producer Gas Composition

The composition of producer gas from biomass via thermal-chemical gasification is mainly dependent on the type of gasification agent and type of reactors presented above. Table 3 contains typical ranges of the syngas composition from an air-blown gasifier, a low-temperature atmospheric steam-blown dual fluidized bed gasifier, low-temperature pressurized oxygen-/steam-blown fluidized bed gasifier, and high-temperature pressurized oxygen-/steam-blown entrained flow gasifier.

The main differences are the nitrogen content, the hydrogen/carbon monoxide ratio, and the methane content. The nitrogen content is high for air-blown

Biomass Gasification for Electricity and Fuels, Large Scale. Table 3 Typical ranges of syngas composition [8]

		Air-blown gasifier	Low-temperature atm. steam-blown fluidized bed gasifier[a]	Low-temperature press. oxygen-blown fluidized bed gasifier[b]	High-temperature press. oxygen-blown entrained flow gasifier[c]
H_2	%	10–15	35–45	23–28	29–35
CO	%	13–17	22–25	16–19	35–44
CO_2	%	13–16	20–23	33–38	17–22
CH_4	%	3–6	9–11	10–13	<1
N_2	%	42–60	<1	<5	<5

[a]Data from Güssing allothermal dual fluidized bed gasifier
[b]Data from Bioflow gasifier
[c]Several data from CHOREN and FZ Karlsruhe

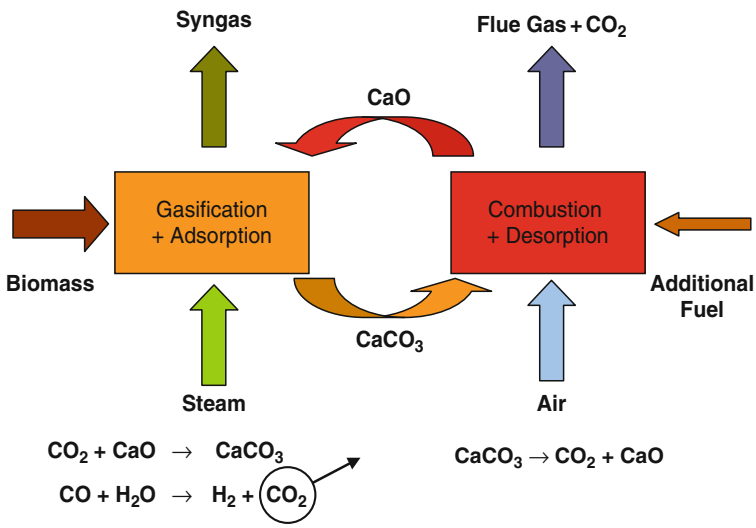

Biomass Gasification for Electricity and Fuels, Large Scale. Figure 9 AER-gas process [22]

gasifiers. This producer gas can only be used for heat and/or electricity production. This producer gas is not beneficial for biofuels production. The hydrogen/carbon monoxide ratio is highest for the dual fluidized bed gasifier and the lowest for the entrained flow gasifier (except air-blown gasifiers). In case of methane, the lowest content can be seen for the entrained flow gasifier and much higher levels for both low-temperature fluidized bed gasifiers. This makes entrained flow gasifiers most suitable for the production of a syngas for, e.g., Fischer–Tropsch (FT) fuels and low-temperature fluidized bed gasifiers have clear advantages for SNG production.

For each of the synthesis reactions, an optimal H_2/CO ratio is necessary to obtain a maximum yield of the desired product. As most of the gasifiers are not able to produce a syngas with the desired H_2/CO ratio, this ratio has to be adjusted before entering the synthesis reactor. This is normally achieved with a water shift reaction that requires an additional step and, therefore, additional costs. In case of a dual fluidized bed reactor, this adjustment can be performed directly in the gasification reactor.

Using calcite (calcium carbonate) as bed material, the so-called AER (absorption enhanced reforming) process can be realized. The process arrangement is shown in Fig. 9. In the combustion reactor operated at

Biomass Gasification for Electricity and Fuels, Large Scale. Table 4 Comparison of conventional dual fluidized bed/AER (absorption enhanced reforming)

Component	Unit	Conventional Olivine 850°C	AER-gas Calcite 650°C
Hydrogen	Vol%	35–45	66–74
Carbon monoxide	Vol%	22–25	5–8
Carbon dioxide	Vol%	20–23	6–8
Methane	Vol%	9–11	10–12
Ethene	Vol%	2–3	1.1
H_2/CO	–	1.6–1.8	8–10

a temperature of about 900°C CO_2 is split off from $CaCO_3$ to form CaO. CaO is circulated to the gasification reactor which is operated typically at temperatures between 640°C and 720°C. In this reactor gasification takes place. Here, the CO_2 produced during the gasification process is captured by CaO to form again $CaCO_3$. By removing CO_2 from the gasification reactor additionally H_2 is produced by the water gas shift reaction. With this process, a hydrogen-rich gas can be produced.

A comparison of typical syngas compositions for the conventional dual fluidized bed process using olivine as bed material and a gasification temperature of 850°C and the AER process using $CaCO_3$ as bed material and a gasification temperature of 650°C can be seen in Table 4. As calcite is catalytically more active for tar reforming than olivine, the tar content is similar in both cases due to a lower temperature in case of calcite as bed material. In the last line of Table 4 the H_2/CO ratio is presented. According to this, the ratio is about five times higher in case of AER operation compared to conventional dual fluidized bed operation.

The AER operation leads to an extremely high H_2/CO ratio which is much higher than necessary for most of the synthesis reactions under discussion so far. By increasing the gasification temperature continuously the CO_2 capturing is reduced and, therefore, also the H_2/CO ratio (Fig. 10). This ends finally at a similar H_2/CO ratio as it is observed with olivine at a temperature of 850°C. Then the CO_2 capture is small and can be neglected.

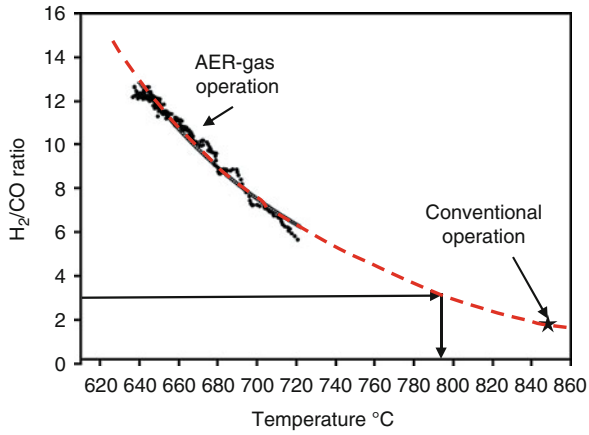

Biomass Gasification for Electricity and Fuels, Large Scale. Figure 10
Adjustment of the H_2/CO ratio by primary measure [22]

Options to Use the Producer Gas

Based on the statements discussed above typical syngas applications for electricity and fuel production are presented below. Electricity production via gasification can be considered as proven technology in large scale whereas for fuel production only demonstration plants are available so far. The chapter follows a very general and systematic approach as too many different plant configurations were proposed in the past. Due the fact that presenting all this different plant configurations would be too confusing, only a few successful technology routes are shown.

Power Production

Gasification offers several advantages for power production from biomass compared to combustion. These advantages are mainly:

- Possibility for utilization of applications of efficient power generation technologies dedicated for gaseous fuels also for solid biomass
- High electrical efficiencies in case of combined heat and power production
- Much easier handling of gaseous fuel compared with solid fuels

Generally, producer gas cleaning is still one crucial point in all gasification applications. Therefore, those

processes using simple and reliable process steps especially for gas cleaning are already more advanced than others.

Co-firing in Coal Power Stations The most basic option of power production via gasification concerning gas cleaning is co-firing of the producer gas in existing power stations. The motivation of this application is the reduction of CO_2 emissions due to replacement of a hard coal or lignite by biomass and/or economic advantages by using cheap waste fuels. In this case, the producer gas is normally not cooled and blown directly (i.e., without any cleaning like, e.g., tar or particle reduction) into the combustion chamber of a pulverized coal-fired power station (Fig. 11a). In such power plants circulating fluidized bed air-blown gasifiers with capacities between 50 and 100 MW fuel input are used. With such biomass or waste gasifiers up to 20% of energy of coal can be substituted by biomass or waste. Several successful plants are in operation and lots of experiences are available (e.g., Lahti plant, more than 70,000 h of operation) [10, 12].

However, there are also other examples where such a very simple solution with no gas cleaning cannot be applied. If, e.g., the fly ash of the coal-fired power plant is used and has to have a certified quality, particles in the producer gas have to be removed before entering the combustion chamber of the power plant. In this case, a gas-cooling device followed by a particle separation could be integrated within the overall concept (Fig. 11b). Here problems might occur due to tar condensation and fouling in the producer gas ducts [23].

Combined Heat and Power Generation Combined heat and power (CHP) generation is applied if high overall energy utilization degrees are desired. Normally, the higher the electrical output at the same overall energy utilization degree the higher is the economic performance of such a plant. Processes using gasification allow comparable high electrical outputs and high overall energy utilization degrees at the same time which is not always the case for combustion-based systems.

For combined heat and power generation, the producer gas is fed into gas engines or gas turbines. Currently, such applications have been implemented in the small as well as in the large scale (e.g., in the capacity range of 10–25 MW fuel input). In general, such plants consist of gasification, gas cooling, gas cleaning (tar and particle separation), and utilization of the clean and cold gas in gas engines. Electrical efficiencies between 20% and 30% and overall energy utilization degrees of 75–80% can be achieved [3].

The most important process chains used currently or proposed for gas cleaning in case of heat and power production are summarized in Fig. 12. The different options are discussed below.

Currently, most installations apply cold gas or wet gas cleaning (Fig. 12a). The producer gas is generated in atmospheric air or steam gasification in fixed bed or fluidized bed gasifiers. After leaving the gasifier, the producer gas is cooled down to 180–200°C. Here the cooler construction as well as the cooler operation conditions have to be selected carefully in order to avoid tar condensation and plugging of producer gas pipes and heat exchangers. At this temperature, particles can be separated from producer gas by fabric filters

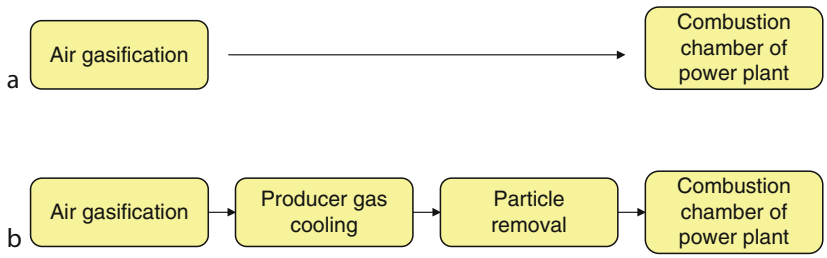

Biomass Gasification for Electricity and Fuels, Large Scale. Figure 11
Typical arrangements for co-firing in coal power stations using biomass gasification

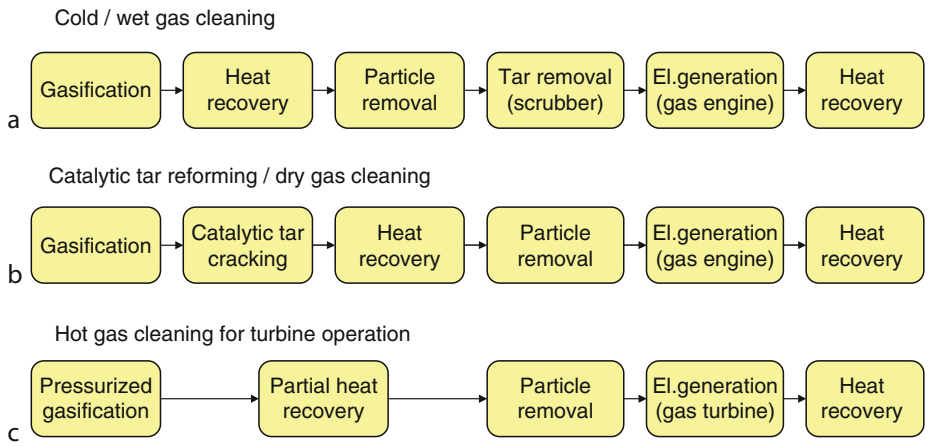

Biomass Gasification for Electricity and Fuels, Large Scale. Figure 12
Typical selected process chains for combined heat and power production

or electrostatic precipitators. In some cases, pre-coated materials are used to protect the filter cloths from plugging with dust/tar mixtures. Another important parameter for a reliable operation of this cooling section is the dust to tar ratio. A certain ratio is necessary to keep the tubes and heat exchanger clean. To control this ratio, in some cases, ash is recycled and fed back into the gasifier together with the fuel.

Scrubbing of the producer gas is carried out to remove most of the tar components. This cleaning step has made enormous technical advances during the last decades. For example, water scrubbers have been replaced by different kinds of solvent scrubbers. The solvent used (e.g., biodiesel) should be cheap and able to absorb high amounts of tar per liter solvent. The saturated solvent have to be withdrawn from the scrubber and can be burnt, e.g., in the combustion part of a dual fluidized bed gasifier. Further developments aim at the regeneration of the solvent to avoid the use of high amounts of scrubber liquids [13]. In such a scrubber, additional heat can be removed to get low temperatures of the producer gas ready for feeding it into the gas engine.

In such an overall process (Fig. 12a), gas engines are used for electricity generation. Electrical efficiencies of gas engines are about 40% referred to the energy content in the producer gas. Offgas temperatures of the gas engines are about 450–500°C. This energy is normally used for operating a district heating system or for industrial heating purposes. In gasification processes, high-temperature levels are also available as heat source as the producer gas has to be cooled down from about 850°C to 200°C and flue gas from the gas engine from 500°C to about 150°C. Therefore, nearly all processes which need heat can be satisfied.

This gas cleaning strategy (Fig. 12a) is also applied at the allothermal dual fluidized bed steam gasification realized at the Güssing plant, Austria.

Another producer gas cleaning strategy applied for combined heat and power generation is based on catalytic tar reforming [6, 21]. This strategy is also sometimes called dry gas cleaning as no scrubber is included into the process chain (Fig. 12b). Within such an overall process, the producer gas is not cooled down after gasification but led to a catalytic cracker for tar reduction. The temperature within such a device has to be above 800°C. The catalytic active compounds used within such a reactor are mostly based on metallic oxides (e.g., nickel, platinum) or nonmetallic oxides such as calcite and dolomite. This catalytic cracking can be carried out in downstream monolithic reactors or even combined in a fluidized bed gasifier using catalytic active bed material. In the latter case, the attrition of the catalysts can become a problem. So, attrition-resistant catalyst particles have to be applied [19].

After catalytic cracking of the tars, the gas can be cooled down without tar condensation problems. At

low temperatures the particles will be removed by conventional particle separation systems according to the requirements defined by the gas engines. Again, the energy in the flue gas can be utilized for district heating or other heat demanding processes (e.g., industrial applications).

Hot gas cleaning is most beneficial for pressurized gasification as it was demonstrated successfully at the Varnamo plant [10, 12]. Furthermore, this gas cleaning strategy has been developed in connection with gas turbine applications because the utilization of gas engines is limited to capacities below 10 MW_{el} (40 MW fuel input) and above this capacity, gas turbines have clear advantages. To avoid thermal energy losses, the producer gas is only partially cooled to temperatures where particle removal is economically possible (about 400–500°C). Particle separation is carried out with ceramic or metallic filter candles. Tar removal is not necessary as the producer gas is fed into a combustion chamber of the gas turbine at temperatures where no condensation takes place. Also, this fact leads to higher energy utilization as the energy content in the tar will be utilized. The heat in the flue gas at the exit of the turbine can be used for heat supply for heating applications but also for a steam process and additional power production in case of an IGCC process (see next chapter).

Power Production with IGCC Processes Highest electrical efficiencies can be obtained by using combined cycles. This means that electricity generation is carried out in two steps typically by a gas turbine process followed by a steam turbine process using the heat from the exhaust gas stream of the gas turbine. Such processes are well established for natural gas but can also be applied to producer gas from biomass gasification. Therefore, if a gasification process has to be integrated to convert solid biomass to a producer gas, the overall process is called integrated gasification combined cycle (IGCC). Due to the high complexity of an IGCC plant, this technology is only economically applicable for large scale (e.g., larger than 60 MW fuel input).

Several different process routes for biomass IGCC plants have been proposed and also demonstrated. The combination of a gas and steam turbine has been realized in two different configurations: one based on pressurized gasification and the other one on atmospheric gasification. Figure 13 shows these two different routes.

The IGCC process based on pressurized gasification (Fig. 13a) has been successfully demonstrated at Varnamo with a capacity of about 18 MW fuel input [10, 12, 6]. Air-blown circulating fluidized bed gasifiers are well suited for IGCC processes. In case of pressurized gasification, a pressure of about 20 bar is suitable. The producer gas is cooled down to about 400–500°C

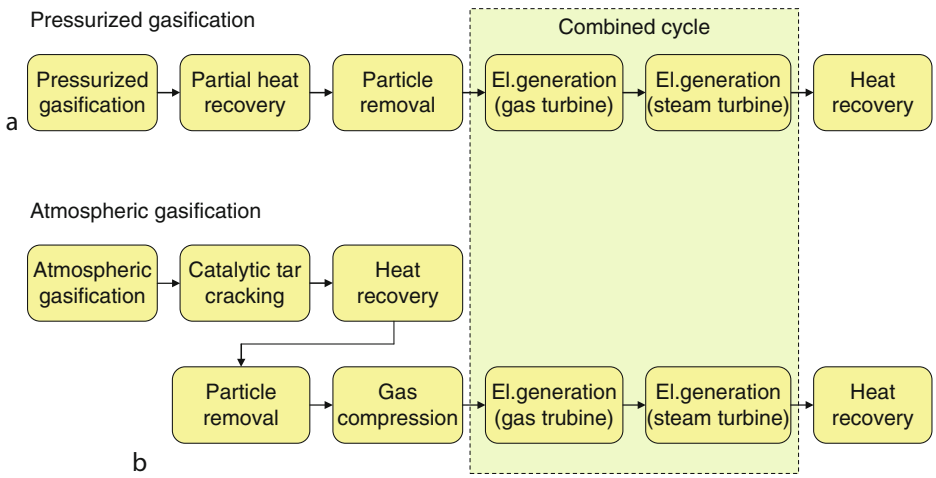

Biomass Gasification for Electricity and Fuels, Large Scale. Figure 13
Two process chains for power production using IGCC

and particles are separated at this temperature level (compare also Fig. 12c). The gas is fed into a gas turbine where about 4 MW_{el} could be obtained from the electricity generator in case of Varnamo. The exhaust gas of the gas turbine is used in a waste heat boiler to generate another 2 MW_{el} with a steam turbine coupled to an electricity generator. Waste heat can be delivered to a district heating system. The overall electrical efficiencies in future plants according to this electricity generation route can be expected in the range of 30–35%.

The IGCC process shown in Fig. 13b avoids pressurized gasification and, therefore, all the problems connected with feeding of solid fuels against a pressure of 20 bars. The gas has to be cleaned (tar, particles) and cooled down to about ambient temperature. The gas cleaning processes shown in Fig. 12a and b can be used for this purpose. This cold and clean producer gas is compressed and fed into the combustion chamber of a gas turbine. The following part can be identical to the case shown in Fig. 13a. The overall electrical efficiencies will be a little bit lower than in case of a pressurized gasification.

During the last years other combined cycles have been proposed and realized for the lower capacity rage of 10–30 MW fuel input. In this case, gas engines are used as explained above. Heat available in the whole process (cooling of producer gas, exhaust gas of the gas engine) are collected with the aid of a thermo-oil and used for operation of an ORC (organic rankine cycle) process. Such plants are already realized with about 30% of overall electrical efficiencies (i.e., gas engine and ORC) [15]. Another process configuration for a combined cycle could consist of a combination of a gas engine with a conventional water/steam process.

Synthesis Applications

Gaseous and liquid biofuels have got a lot of technical advantages compared to solid biofuels. One big advantage is that they could easily be introduced into the market as the existing fossil fuel infrastructure can be used to a certain extent. Therefore, during the last decade, a lot of efforts have been made to develop and demonstrate the generation of synthetic fuel products from solid biomass. Several different synthesis processes are under consideration such as FT-synthesis (Fischer–Tropsch), methanol synthesis, mixed alcohol synthesis, DME synthesis (dimethylether), and production of SNG (synthetic natural gas).

Figure 14 shows an example of a typical process route from solid biomass to a synthetic biofuel. This block diagram contains the most important elements of such processes. Of course, there are processes which don't need all these steps and also others which contain even more steps. Each of the blocks can consist of several steps such as gas cleaning which summarizes particle separation as well as sulfur, nitrogen, and chlorine removal. Such possible steps are written on the right hand side of the figure. But the possibilities shown can be also alternates (e.g., fluidized bed gasifier or entrained flow gasifier). In the following, each of these process steps is discussed separately.

Biomass Pretreatment Normally, biomass has to be pretreated before feeding it into the gasifier. Chipping or grinding and drying are conventional processes to get the right particle size and the right water content for the gasifier under use. To reduce the power consumption for grinding which is necessary for an entrained flow gasifier, torrefaction has been proposed. Results show that the power consumption can be reduced by more than 80% if the biomass is torrefied. However, there is not yet too much experience with torrefaction and no large plant capacities are available.

Another pretreatment step in connection with large-scale entrained flow gasifiers is pyrolysis of the feedstock. Based on such a pyrolysis step, a mixture of pyrolysis oil and char (called slurry) can be produced. Such slurries show a higher energy density than the original biomass and, furthermore, they are quite suitable to be fed into entrained flow gasifiers. By regional distributed pyrolysis plants a large area can be made available for delivering the feedstock for a centrally located large-scale entrained flow gasifier connected, e.g., to an FT-production plant.

Gasification Reactors for Syngas Generation Gasification processes are extremely important for the production of the right producer gas for generating syngas for the respective synthesis process. The most important components in the producer gas are hydrogen (H_2) and carbon monoxide (CO). Depending on the synthesis reaction, a certain H_2 to CO ratio is necessary to get a high product yield (Table 5). From these two

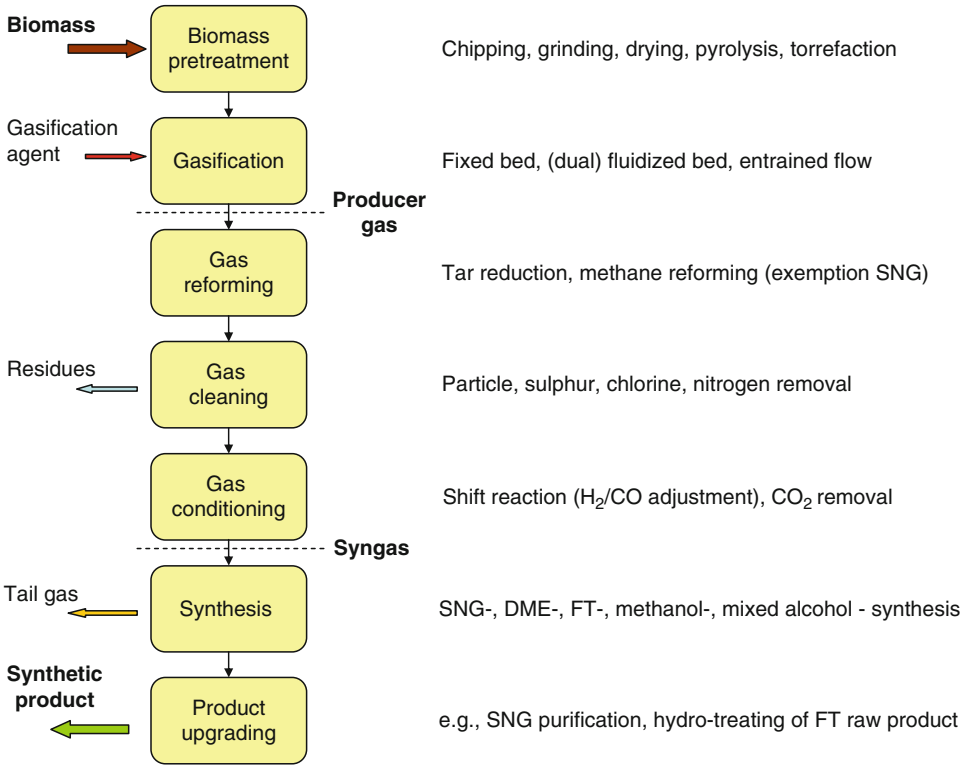

Biomass Gasification for Electricity and Fuels, Large Scale. Figure 14
Example for a typical process chain for synthetic biofuel production

Biomass Gasification for Electricity and Fuels, Large Scale. Table 5 Synthesis reactions [10, 24]

Synthesis	Beneficial H_2/CO ratio	Reactions
Methanol	2.05–2.15	$CO + 2H_2 = CH_3OH$
		$CO_2 + 3H_2 = CH_3OH + H_2O$
Fischer–Tropsch	2.15	$nCO + 2nH_2 = C_nH_{2n} + nH_2O$
Mixed alcohols	1.5	$nCO + 2nH_2 = C_nH_{2n+1}OH + (n-1)H_2O$
		$nCO + (2n+1)H_2 = C_nH_{2n+2} + nH_2O$
DME	2.5 (5)	$CO + 2H_2 = CH_3OH$
		$CO_2 + 3H_2 = CH_3OH + H_2O$
		$2CH_3OH = CH_3OCH_3 + H_2O$
Methanation (SNG)	3	$CO + 3H_2 = CH_4 + H_2O$
		$CO + H_2O = CO_2 + H_2$

requirements gasifier using nitrogen-free gasification agents (O_2, H_2O, CO_2) seem to be the right choice. For example in "Schwarze Pumpe" fixed bed gasifiers were operated many years with oxygen/steam mixtures as gasification agent and methanol was produced. And high-temperature gasifiers such as entrained flow gasifiers lead to a nearly methane and tar free gas (Table 3). These gasifiers are well suited for almost all synthesis

reactions except SNG production. In this case, steam-blown fluidized bed gasifiers have the advantage that part of the producer gas is already methane (9–13%) and this methane has not to be produced anymore downstream (Table 3).

The producer gas provided by the gasifier has to be cleaned and conditioned for the synthesis process.

Hydrocarbon Reforming The producer gas can obtain essential contents of methane and/or other low molecular weight hydrocarbons. This is especially the case for low-temperature (800–950°C) fluidized bed autothermal oxygen/steam gasification or allothermal steam gasification (Table 3). These components can reduce the yield of the desired synthetic product (e.g., FT-diesel) and have to be reformed before entering the gas into the synthesis reactor. Normally, steam reforming is carried out to convert the hydrocarbons into hydrogen and carbon monoxide. For methane, the reaction

$$CH_4 + H_2O = CO + 3H_2 \quad \Delta H = -205.0\ \mathrm{kJ/mol}$$

is carried out at temperatures between 800°C and 1,100°C. Typically nickel is used as a catalyst. Attention has to be drawn to catalyst poison due to sulfur compounds in producer gas. In general it is true that the higher the temperature the lower the poisoning is. Above 950°C sulfur poisoning is nearly negligible [19].

For high-temperature gasification (e.g., entrained flow gasification), the reforming step can be avoided. This is the same for low-temperature gasification and SNG production. In this case, the content of methane already existing within the producer gas is beneficial for the methanation process.

Producer Gas Cleaning Producer gas cleaning is the most crucial part in any synthetic product generation process. This is due to the extremely low concentrations of sulfur (<100 ppb) which have to be obtained to avoid poisoning of the catalysts. Sulfur is not only present within the producer gas in form of H_2S. Additionally, different kinds of organic sulfur compounds can be found in the producer gas. As the total content of sulfur has to be extremely low besides H_2S, most of the organic sulfur has to be removed as well. Methods for sulfur removal are absorption (e.g., different solvents, amines) and adsorption (e.g., ZnO, activated carbon) processes. Similar methods have to be applied to remove nitrogen (NH_3, HCN) and chlorine compounds (HCl) also. Furthermore, particles have to be removed as well (see, e.g., [9]).

Gas Conditioning All synthetic reactions need a certain ratio of H_2/CO in order to get a maximum yield of the desired products. This ratio should be set up before feeding the syngas into the synthesis reactor. This can be carried out by using an AER-process explained above. Normally, the right ratio is obtained by using the water shift reaction described by the following reaction:

$$CO + H_2O = H_2 + CO_2 \quad \Delta H = -40.9\mathrm{kJ/mol}$$

This reaction is performed between 300°C and 450°C and pressures up to 30 bars. Catalysts used for this reaction are based on iron/chromium (Fe_2O_3/CrO). In several cases, this reaction is also running in parallel in the synthesis reactor itself (e.g., SNG, Fischer–Tropsch) without the necessity of a separate step.

Another frequently proposed step for gas conditioning is the separation of CO_2 from the producer gas because producer gas coming out the gasification reactor contains CO_2 due to chemical equilibrium reasons. Further CO_2 is produced by the water gas shift reaction shown above. A too high concentration of CO_2 can be disadvantageous for some synthesis processes. A removal of CO_2 can be carried out by adsorption (e.g., pressure swing adsorption) or absorption (e.g., Rectisol, Selexol) processes.

After these conditioning steps, the producer gas is called syngas as it is now ready for the specific synthesis reactions under consideration.

Synthesis Reactions Currently, several synthesis reaction schemes are under discussion for the production of mostly liquid or gaseous biofuels for the application within the transportation sector. These reactions are summarized in Table 5 where the first three are of liquid nature and the last two led to gaseous biofuels. The reaction equations shown within this table are only the most important ones or the most desired; of course, there are also, more or less, side reactions depending on catalyst performance and reaction conditions which are not shown here.

Gas cleaning and gas conditioning are carried out to satisfy the requirements of the synthesis reactions. The reaction conditions are characterized by temperature levels of 200–400°C, pressures up to 100 bars, and the necessity of catalysts. Typical reaction conditions for these five syntheses are shown in Table 6.

The conversion during these synthesis reactions might not be complete. Therefore, a so-called tail gas containing still some small amounts of the educts will remain after the reaction and leave the synthesis process. There are two strategies to handle this tail gas [2]:

- In a fuel-oriented strategy, the nonreacted part of the tail gas will be recycled back to entrance of the synthesis reactor to maximize the production of the biofuel. This strategy is applied usually in large-scale applications.
- In a polygeneration-oriented strategy, the tail gas will be used to produce heat and power in addition to the biofuel. This strategy is proposed if heat can be used near the location of the plant.

Some of these syntheses are extremely selective such as methanol and methane syntheses. This means that practically only this hydrocarbon molecule is produced. However, this product is still mixed with other components to be separated to get the desired biofuel.

The product in case of, e.g., Fischer–Tropsch synthesis or mixed alcohol synthesis is a mixture of a certain type of molecules. In case of Fischer–Tropsch synthesis, the chain lengths of the C_nH_{2n} molecule can vary between C_1 up to C_{70} following a probability distribution (ASF-probability function).

Biomass Gasification for Electricity and Fuels, Large Scale. Table 6 Ranges of suitable conditions for synthesis reactions [10], [24]

Synthesis	Catalysts	Pressure Bar	Temperature °C
Methanol	$Zn/Cr/Cr_2O_3/Cu$	50–100	250–380
Fischer–Tropsch	Co/Fe	20–40	220–300
Mixed alcohols	MoS_2	100	350
DME (via methanol)	$Cu/ZnO/Al_2O_3$	5–15	250–300
Methanation (SNG)	Ni/Mg	1–10	200–400

However, in order to get a useful biofuel for transportation which can be used in the existing fossil fuel infrastructure upgrading of the product is necessary in all cases.

Product Upgrading Upgrading of the raw synthetic products can be very different depending on the synthesis process itself and its performance. The necessary upgrading steps can be distinguished in cleaning and upgrading. Cleaning steps are mostly only separation processes of undesired components in the raw product to get the necessary final quality of the biofuel (e.g., SNG). During upgrading, the quality of the product is improved by modifying the produced synthetic molecules. Hydro-treating of the FT-raw diesel product or of the waxes is such an example.

Example for a Whole Chain of Biofuel Production Finally, one example for the whole process chain of biofuel production is presented and explained in more detail to get a better view of the complexity of such processes. For this example SNG is selected, as a lot of experience for this process has been gathered during the last decade.

Figure 15 shows a process configuration for SNG production which has been demonstrated recently [20, 16]. The process flow diagram is built up according to the general scheme shown in Fig. 14. As pretreatment steps for the biomass fuels chipping and drying are foreseen. Gasification is carried out in an allothermal dual fluidized bed gasifier as presented in Fig. 7.

The gasification agent is steam, and gasification takes place at a temperature of about 850°C to get a hydrogen-rich gas containing nearly no nitrogen. As the temperature is low, the producer gas consists already of about 10% of methane as shown in Table 3 (column 2).

No steam reforming is foreseen in case of SNG production. Therefore, this step is left out here from the general process route in Fig. 14.

Ultra clean syngas is necessary to carry out the methanation synthesis. Therefore, gas cleaning consists of several steps before the gas can be fed into the synthesis reactor. The producer gas is cooled down to about 180°C and particles are removed

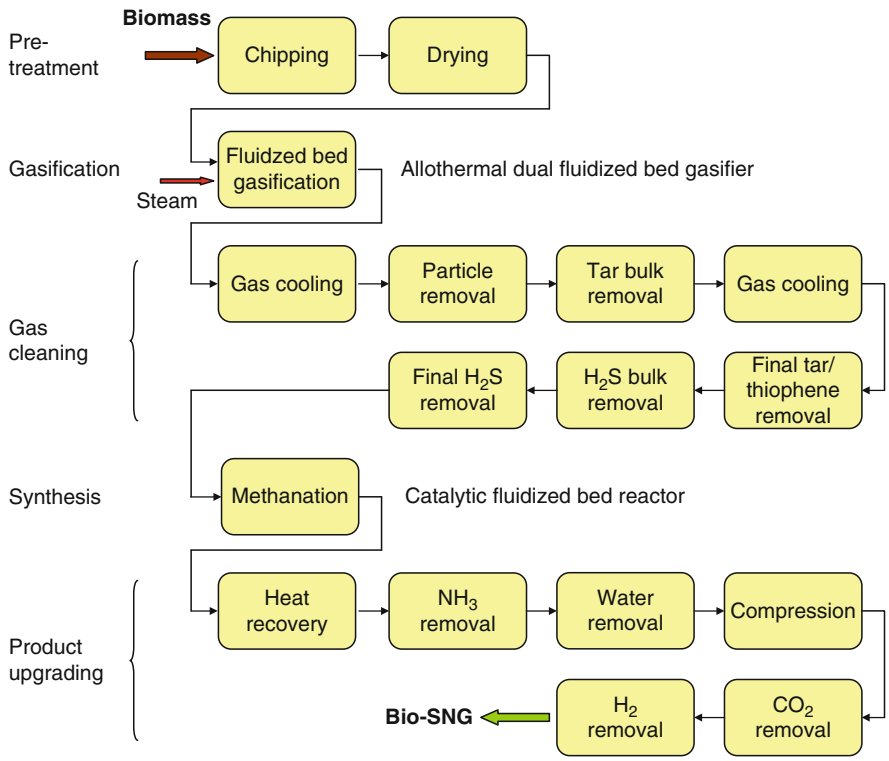

Biomass Gasification for Electricity and Fuels, Large Scale. Figure 15
Process chain for BioSNG production [16]

using a conventional fabric filter. Calcium carbonate is applied as pre-coat material to protect the filter cloths from plugging. A scrubber serves as tar bulk removal device. As fatty acid methyl ester (FAME) is used as scrubber liquid tar is solved and high separation efficiencies are obtained. Particles from fabric filter and saturated scrubber liquid are burnt in the combustion chamber of the allothermal dual fluidized bed gasifier.

The producer gas is cooled down to about 5°C and led to a further scrubber. In this scrubber additional tar components and also thiophene, an undesired sulfur compound, is reduced down to a level which is acceptable for the methanation catalyst. Further two steps are dedicated to H_2S removal applying a H_2S scrubber and a fixed bed adsorption (ZnO) unit.

Now the producer gas has got the quality suitable to be fed into the methane synthesis reactor (syngas). The synthesis is carried out in a fluidized bed reactor with a nickel catalyst as bed material. As the reaction is strongly exothermic, a heat exchanger is located inside the fluidized bed to keep the temperature constant at about 300°C and to obtain a high conversion rate. Alternatively, the reaction can be carried out within a fixed bed where high attention has to be led to the applied cooling strategy [17]. The exit gas of the methanation reactor consists mainly of methane, carbon dioxide, hydrogen, and steam. Methanation is an extremely selective process as nearly no further hydrocarbons are produced. Carbon monoxide is consumed more or less completely. However, this gas is not ready to be fed into a natural gas grid but has to be further upgraded.

Product upgrading in case of SNG is the second complex area besides gas cleaning explained above. Upgrading means separation of undesired gas components from the exit gas of the methanation reactor. NH_3 removal, drying, CO_2 removal and finally H_2 removal have been realized in the process mentioned above. For these steps, conventional scrubbing, adsorption, and membrane technologies are used. At the end of the

process chain, the gas is ready to be fed into the natural gas grid and has got the quality of an H-gas. This upgraded product is called Bio-SNG. The efficiency of such a SNG production can reach up to 65%.

Future Directions

This paper summarizes the state of art of biomass gasification for large-scale electricity and/or biofuels production. This state of the art can be characterized briefly as follows:

- Different gasification reactor systems are available:
  - Fixed bed (autothermal)
  - Fluidized bed (autothermal and allothermal)
  - Entrained flow (autothermal)
- Gasification agent for
  - Autothermal: air only for electricity production, steam/oxygen mixtures for electricity and/or biofuels production
  - Allothermal: steam
- H_2/CO ratio should be adjustable especially for biofuels production. Possible solutions are:
  - Downstream shift reaction
  - Dual fluidized bed (AER-process)
- Electricity production can be considered as commercially available. Main types are:
  - Co-combustion of producer gas in existing coal power stations
  - Combined heat and power production
  - IGCC processes
- Several biofuels production processes are currently under development and/or demonstration.
  - Methanol
  - Fischer–Tropsch fuels
  - Mixed alcohols
  - DME
  - Bio-SNG

Polygeneration (i.e., production of more than two products (e.g., heat, power, and biofuels)) has a great potential for biomass gasification in the future. Furthermore, developments – as far as these can be seen – are the integration and establishment of thermo-chemical platforms in bio-refineries. In nearly all bio-refineries under consideration, there are residues which can be transformed via thermal gasification in more valuable products.

However, there are still a lot of challenges to be overcome in connection with gasification and syngas production. Some important ones are:

- A secure provision and reliable pretreatment processes for biomass
- Reliable, simple, and robust gasification and gas cleaning systems
- Development of robust catalysts for synthesis processes
- Optimization of process chains and overall efficiencies

Bibliography

1. E4Tech (2009) Review of technologies for gasification of biomass and wastes, final report, NNFCC project 09/008
2. Fürnsinn S (2007) Outwitting the dilemma of scale: cost and energy efficient scale-down of the Fischer-Tropsch fuel production from biomass, PhD thesis, Vienna University of Technology
3. Hofbauer H (2007) Fluidized bed gasification – state of technology. In: International conference of biomass gasification for an efficient provision of electricity and fuels – state of knowledge, Leipzig
4. Hofbauer H (2009) Biomass gasification for synthesis gas – overview. In: 17th European biomass conference and exhibition, Hamburg, Germany, 2009
5. Hofbauer H (2009) Necessary conditions for a successful market introduction of gasification technologies – example gasification / polygeneration plant (heat, power, and bioSNG). In: 3rd international conference on application of biomass gasification, CEP – clean energy power, Stuttgart, 2009
6. Hofbauer H (2009) Gasification – technology overview. In: Bridgewater AV et al (eds) Thermal biomass conversion. CPL, Newbury, pp 11–36
7. Hofbauer H, Rauch R, Loeffler G, Kaiser S, Fercher E, Tremmel H (2002) Six years experience with the FICFB-Gasification process. In: 12th European conference on biomass and bioenergy, Amsterdam, 2002, pp 982–985
8. Hofbauer H, Rauch R, Ripfel-Nitsche K (2008) Report on gas cleaning for synthesis applications, final report, EU-ThermalNet
9. Hofbauer H, Rauch R, Ripfel-Nitsche K (2009) Gas cleaning for synthesis applications. In: Bridgewater AV et al (eds) Thermal biomass conversion. CPL Press, Newbury, pp 211–266
10. Kaltschmitt M, Hartmann H, Hofbauer H (2009) Energie aus Biomasse. Springer, Berlin, Heidelberg
11. Karl J (2004) Erzeugung von Synthesegas mit dem Biomass Heatpipe-Reformer - Betriebserfahrungen und Leistungsgrenzen, Tagungsband 6. DGMK-Fachtagung Energie aus Biomasse, Velen
12. Knoef H (2005) Handbook biomass gasification. BTG Biomass Technology Group, The Netherlands
13. Könemann HWJ (2007) OLGA tar removal, 4 MWth commercial demonstration. In: 15th European biomass conference and exhibition, Berlin, May 2007

14. Kunii D, Levenspiel O (1991) Fluidization engineering. Series in Chemical Engineering, Butterworth-Heinemann
15. Madl W, Bosch K, Kotik J (2008) Next dual fluidized bed steam gasifier starts up in Austria. ThermalNet Newsletter, issue 6, pp 19–20
16. Möller, S (2009) The Güssing methanation plant. In: Proceedings of BioSNG09 – synthetic natural gas from biomass, Zürich, 26–27 May 2009
17. Ortwein A, Röntsch S, Klemm M, Kaltschmitt M (2010) Methanation – basics, technologies and integration into thermochemical biorefineries. In: Proceedings of ICPS10, Leipzig, September 2010
18. Paisley MA, Overend RP (2002) Verification of the performance of future energy ressources silvagas biomass gasifier – operating experience in the vermount gasifier. In: 19th International Pittsburgh coal conference, Pittsburgh, 2002
19. Pfeifer C, Koppatz s, Hofbauer H (2010) Catalysts for fluidized bed biomass gasification – overview in recent development and application. In: Proceedings of ICPS10, Leipzig, September 2010
20. Rehling B, Hofbauer H, Rauch R, Tremmel H, Aichernig C, Schildhauer T, Biollaz S, Ulrich, D, Schaub, M (2009) Bio-SNG – first results of the 1MW pilot and demonstration unit at Güssing. In: Proceedings of ICPS09, Vienna, September 2009
21. Salo K (2006) Gasification/gas engine project in Skive, Denmark. ThermalNet Newsletter, issue 1, pp 16–17
22. Soukup G (2009) Der AER-Prozess –Weiterentwicklung in einer Technikumsanlage und Demonstration an einer Großanlage, PhD thesis, Vienna University of Technology
23. Spanjers M, Willeboer W (2010) Biomass gasification for power generation – essent's own developments. In: Proceedings of ICPS10, Leipzig, September 2010
24. Wagner H, Kaltschmitt M (2010) Pathways for synthesis of liquid biofuels – review on conversion efficiency, selectivity and by-products. In: Proceedings of ICPS10, Leipzig, September 2010

Biomass Gasification for Rural Electrification, Small Scale

Marco Klemm
German Biomass Research Centre (DBFZ), Leipzig, Germany

Article Outline

Glossary
Definition of the Subject
Introduction
Generation of Electricity from Biomass via Gasification
Gasification and Gasifiers
Application of the Gas
Gas Treatment
Overall Process Chains
Future Directions
Bibliography

Glossary

Clean gas is the product gas after product gas treatment.

Gasification is the conversion of solid or liquid fuels to gaseous fuels in a reaction with an added reaction agent.

Gasifier is the reactor for the gasification.

Product gas is the burnable gas generated in the gasification, also after gas treatment. If this gas has been adapted to the specification of a downstream synthesis, it is called *synthesis gas* or *syngas*.

Product gas treatment covers all proposed processes for the modification of the product gas properties.

Product gas utilization covers all processes for the use of the product gas, mainly for the provision of other forms of energy. *Product gas application* is synonymous.

Raw gas is the product gas before product gas treatment.

Rural electrification is the mostly decentralized electrical power supply, e.g., single farms, villages, or workshops or small groups of them. The opposite is the electrification of conurbations.

Small scale is the adapted scale for the provision of a single, nonindustrial energy demand. In the case of electrical power supply, often a power range of less than about 1 MW of electrical output is called *small scale*.

Definition of the Subject

Rural electrification confronts the classical, centralized energy economy with several important challenges. The supply system is characterized by little demands scattered in the countryside. To meet each of these demands, an expensive infrastructure is necessary because of the need to connect to the national grid. That is why the costs for the installation can hardly be compensated by the distribution of electricity. Additionally, within developing countries, rural electrification based on national grids is often

not possible due to a nonexisting overall grid, and for the industrialized countries, alternatives are being searched for.

One alternative is the decentralized supply with power generator in an adapted size. Such power generators provide a good opportunity for the utilization of renewable energy. And this is especially true for biomass. Being a product of agriculture and sylviculture, biomass is available in rural areas anyway and that is why the energetic use of biomass is a viable solution, e.g., for the rural electrification.

In such plants for rural electricity supply using biomass, the size of the plants is limited by several restricting factors.

- Firstly, the energy demand is relatively low because single or very few farms, villages, or workshops need to be supplied by one plant.
- Secondly, the biomass provision is easier for small-scale plants. Because biomass is available all over the countryside, large plants of several tens or hundreds of MW of fuel power are not only restricted by the total potential but also by fuel logistic. Transport distances by truck should not be longer than about 50 km in most cases for an economically viable supply. Railway or ship transport on rivers and lakes is limited to very few sites. But biomass provision of rural electrification plants also depends on other criteria. Farms and wood-processing workshops are often anxious to utilize only their own production. Being part of a self-sufficient supply chain, the biomass costs are not of such a high importance to the single user. This biomass provision also requires less organization effort.
- Thirdly, a lot of farms and workshops have a low but year-round heat demand (e.g., for drying, for heating). Because heat supply, especially if realized most time of the year, generates its own financial benefit, the installation of an energy supply plant becomes more economic if it is done in a size corresponding to the heat demand.

Because of these reasons, for rural electrification, often small-scale plants are required. Gasification-based techniques are normally able to generate electricity in the scale of kWs or a few MWs more efficiently than steam cycles. Prospectively, the gasification of biomass enables to use next-generation technology such as the fuel cell.

Apart from electricity generation, biomass gasification technique offers further interesting opportunities like synthesis of liquid and gaseous fuels or natural gas grid integration.

In general, biomass gasification is a key technology for the use of biomass especially for small-scale rural electrification.

Introduction

The basic principle of a biomass gasification plant is that the energy conversion takes place in different steps. This means that the solid biofuel is first converted into a gaseous fuel, which is more easy to utilize. This is realized based on a pure thermochemical process. Such gasification is characterized by reactions between the fuel and a gaseous reactant, the so-called gasification agent. This is also the main difference to pyrolysis which is a thermal degradation of the macromolecules biomass consists of with no additional reactant. In the case of oxygen as gasification agent, the oxygen is used in a substoichiometric amount. If oxygen is added in a stoichiometric amount, the process is called combustion. The production of substances with small molecules and which are gaseous at room temperature (like carbon monoxide, hydrogen, and methane) are the aims of the gasification.

This product, called product gas or producer gas, opens up lots of new opportunities for its application, especially after a product gas treatment. Such opportunities are, for example, the internal combustion in gas engines or gas turbines, the utilization in fuel cells, the synthesis gas chemistry, and the separation of products like hydrogen. Of special importance for rural electrification are processes which enable high efficiency electricity generation also in the small scale, especially in combined heat and power (CHP) production, like the combination of gasification and reciprocating engines.

A thermochemical gasification plant consists of biomass pretreatment, the gasification itself (also called gas generation), the product gas treatment, and the gas utilization, which in this case is electrical energy generation (Fig. 1). For the integration into the energy

Biomass Gasification for Rural Electrification, Small Scale. Figure 1
The basic process chain of a gasification plant for electricity generation

system, also the supply of the solid biofuels to the conversion plant and the distribution of the generated products (i.e., electricity, heat) is necessary, which however will not be a topic of this entry.

The main content of this entry will be the techniques for gasification, product gas treatment, and electricity generation as well as constitutive examples for overall concepts.

The following points are a very brief abstract of the history of biomass gasification:

Centuries BC	Production of charcoal for heating and metallurgy without gas utilization [1, S.93]
Second half of the eighteenth century AC	Start of the development of gas lightening by pyrolysis gases in England, France, the Netherlands, and Germany, involving biomass use [1, p. 244 ff]; [2, p. 241 ff];
1808	First known illuminating gas cleaning activities [2, p. 243]
First half of nineteenth century	Development of internal combustion engines for illuminating gas [1, p. 333 ff]
After 1860	Commercialization of internal combustion engines for illuminating gas by Lenoir and Otto [1, p. 344 ff]
During the nineteenth century	Use of chemicals from illuminating gas production [3] Beginning of a deliberate differentiation between gasification and (auto thermal) pyrolysis
1880	First small and mobile gasifiers by Dawson (England), decentralized gas provision for gas engines [4]
1908	First truck run on gas from wood gasification by Cazes (France) 20 hp, 10–12 km/h, in the following development activities mainly in France [4]
1921	Imbert constructs his first biomass gasifier, start of extensive activities in the following decades [3]
1930s and 1940s	Wood gas for motor vehicles (cars, trucks, etc.) in countries which are cut off from crude oil supply, a several hundred thousands of gasifiers are built in Germany [3–5]
1950s	Nearly all of these systems are replaced by the utilization of gasoline and diesel
From the late 1970s	First restart of biomass gasification activities after the first oil crisis, new focus: power generation, especially in decentralized and small systems (e.g., [6–8])
1990s	Start of the development of a lot of gasification systems driven by the idea of renewable energy supply (e.g., [9–12])
	Start of the research and development work on systems which are currently constitutive, like the Güssing FICFB gasifier [13]
Since about 2000	Start of the commercialization, increased activities in the field of synthetic fuel production

Generation of Electricity from Biomass via Gasification

In comparison with energy conversion chains for the electricity production applying solid fuels like the combustion steam cycle processes, the basic principle of a gasification plant is that energy conversion is realized in different steps. For this reason, a thermochemical gasification plant consists of biomass pretreatment, gasification (also called gas generation), product gas treatment, and gas utilization (here electricity generation). A general survey is shown in Fig. 2. For the

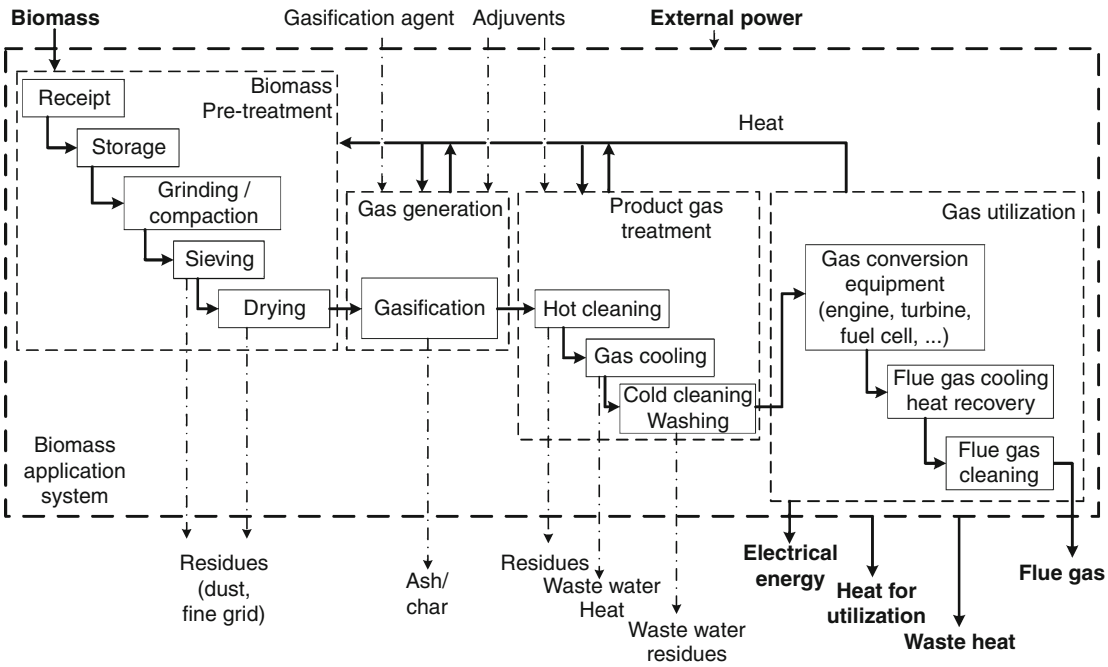

Biomass Gasification for Rural Electrification, Small Scale. Figure 2
General outline of a biomass gasification plant

integration into the energy system also, biomass supply and distribution of the generated products are necessary.

The biomass pretreatment serves for adapting the quality of the biomass delivered to the conversion plant to the requirements of the plant, which are mainly defined by the gasifier. Typical steps of the biomass pretreatment are receipt, storage, grinding, or compaction for the adaptation of the particle size, sieving to ensure that the desired range of fuel size is fulfilled and drying for the adjustment of the required water content. Many different solutions and designs are available for each of these steps. They are similar to the pretreatment for other chains using biomass (e.g., combustion, pyrolysis).

The heart of the conversion plant is the gas generation. In this part, the solid biofuel is converted into a gaseous fuel. The process is straight thermochemical. Thus, the gasification of solid biomass is characterized by reactions between the fuel and a gaseous reactant (i.e., gasification agent). The goal is to produce substances with small molecules gaseous at room temperature (like carbon monoxide, hydrogen, methane).

Because the quality of the provided product gas in most cases is not good enough for the proposed gas utilization, different steps of product gas treatment are necessary (i.e., gas cooling, gas cleaning). The gas cleaning can be realized either before the gas cooling at high temperatures or after gas cooling at low temperatures. In any case, the required product gas treatment is determined by the gap between the gas quality provided by the gasifier and the requirements of the gas utilization.

This product gas opens up lots of opportunities for its application. Such opportunities are, for example, the internal combustion in gas engines or gas turbines and the utilization in fuel cells. Additionally such electricity generation can be combined with a heat provision (i.e., CHP). For the heat supply, different heat flows from product gas treatment and from gas utilization can be used. Due to environmental reasons, often additionally a flue gas cleaning is necessary.

Gasification and Gasifiers

The heart of a gasification plant for electricity supply is the gasification, occurring in a gasifier. This entry deals

with the process of gasification and its partial process and the gasifiers as rectors the gasification occurs in.

Chemical Basics

Biomass gasification is a thermochemical process. The overall process is characterized by the following process steps.

1. Drying
2. Pyrolytic decomposition
3. Oxidation
4. Reduction
5. Gas phase reactions

The importance of the different steps varies depending on the technical frame conditions and their order may change from process to process. Being the reactions employing the gasification the gasification agent, the oxidation, the reduction, and the gas phase reactions can be subsumed as gasification reactions. Regarding this, the gasification can be described as shown in Fig. 3.

The reactions of the gasification process can be summarized as follows.

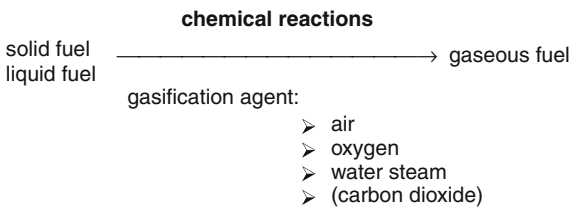

The process steps can be described as follows mainly (see [11, 12]).

Drying The drying is the removal of physically bonded water by vaporization. This is an endothermic process. Drying did not change the chemical properties of the biomass.

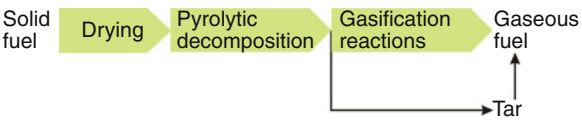

Biomass Gasification for Rural Electrification, Small Scale. Figure 3
Basic steps of gasification

Pyrolytic Decomposition (Degassing, Carbonization) The aim of the pyrolytic decomposition is destroying of organic macromolecules by providing fixed carbon and volatile organic substances (see [14–19]). Products are pyrolysis coke (especially charcoal), pyrolysis gas, and tar. The relative amount of each fraction and its composition strongly depends on the parameters chosen for the pyrolysis process (i.e., reactor type, heating rate, residence time, pressure, and maximum temperature). This is summarized below [20].

$$\text{Complex organic substance} \longrightarrow \text{simple organic substance}$$
$$\text{(cellulose, lignin)} \qquad (CH_4, \text{tar, other hydrocarbon}) + C + H_2 + CO + CO_2 + H_2O$$
$$\text{(coal : endothermic)}$$
$$\text{(biomass : fast process endothermic, slow process exothermic [20]}$$

Pyrolytic decomposition starts with several structural changes within the lignocellulosic biomass. The main reactions at lower temperatures are depolymerization as well as dehydration, decarbonylation, and decarboxylation. As a consequence, water, carbon monoxide, and carbon dioxide are released from the solid biofuel. The hemicelluloses undergo thermal decomposition readily between 200°C and 300°C, while thermal degradation of cellulose dominates at 325–375°C. Lignin decomposition occurs mainly at temperatures above 375°C. However, due to its complex structure, lignin degradation covers a larger temperature interval. In general, at higher temperatures, the solid or liquid product of this pyrolytic decomposition becomes more aromatic.

When the gaseous and vaporous products of pyrolytic decomposition remain in areas with high temperatures, the initially formed tars and other hydrocarbons may be converted into other compounds due to thermochemical processes taking place within the gas phase (e.g., cracking). Otherwise, these substances will stay in the product gas.

Gasification Reactions The gasification reactions (e.g., [21–24]) are these chemical reactions which involve the gasification agent. Such reactions are oxidation and reduction reactions utilizing the fixed carbon as well as homogenous reactions in the gas phase

utilizing gaseous reactants. During these gasification processes, pyrolysis residues react with a gasification agent (e.g., water, carbon dioxide, deficit oxygen/air) to generate a gaseous secondary energy source. Ideally, only carbon monoxide and hydrogen are formed. But due to the chemical equilibrium also, other components such as carbon dioxide, water, methane, and higher hydrocarbons are produced and, thus, ingredients of the gas generated by the gasifier. The carbon monoxide/hydrogen ratio is determined by the choice of gasification agent.

Below the most important reactions are presented:

Oxidation

$$C + {}^{1}/_{2}O_2 \rightarrow CO \quad (\text{Exothermic}, \Delta_R H = -111\text{kJ/mol})$$

$$C + O_2 \rightarrow CO_2 \quad (\text{Exothermic}, \Delta_R H = -394\text{kJ/mol})$$

The main goal of the oxidation step is it to provide the reaction energy for the endothermic reactions. If an oxygen-free gasification agent is used, these oxidation reactions will not take place due to a lack of oxygen. That is why in these cases an external heat input is necessary.

Reduction

$$C + H_2O \rightarrow CO + H_2$$
$$(\text{Endothermic}, \Delta_R H = +131\text{kJ/mol})$$

"heterogeneous water gas reaction"

$$C + CO_2 \rightarrow 2CO$$
$$(\text{Endothermic}, \ \Delta_R H = +172\text{kJ/mol})$$

"Boudouard reaction"

Based on these reduction reactions, carbon monoxide and hydrogen are generated. These are mainly the target products of the gasification.

Homogenous reactions (gas phase)

$$CO + H_2O \leftrightarrow CO_2 + H_2$$
$$(\text{Exothermic}, \Delta_R H = -41\text{kJ/mol})$$

"water gas shift-reaction"

$$CO + 3H_2 \leftrightarrow CH_4 + H_2O$$
$$(\text{Exothermic}, \Delta_R H = -206\text{kJ/mol})$$

"methanation"

Within the gas phase, different secondary reactions of the hydrocarbons, especially of tars, take place. Depending on the reaction conditions, the most important processes are:

- Cracking
- Steam reforming
- Partial oxidation
- Hydrogenation

All reactions involved within gasification are equilibrium reactions. Hence, the temperature has a major influence on the final product composition. As especially oxidation reactions and the methanation are exothermic, these reactions dominate at lower temperatures. In contrast, formation of carbon monoxide and hydrogen from carbon and water according to the heterogeneous water gas reaction as well as the Boudouard reaction is endothermic, and thus these transformations are facilitated by higher temperatures.

Normally, the generated products should continue to react until chemical equilibrium is reached. At typical gasification temperatures, this equilibrium is characterized by a tar-free gas [25]. But such an equilibrium stage is not reached in any single-stage gasifiers. And then equilibration comes to an end (freezes) with decreasing temperatures as it is the case after the producer gas has left the gasifier. That is why often the gas composition generated in biomass gasifiers differs significantly from the equilibrium composition [26]. Because of that, the tar containing gases had to stay within the high-temperature area, preferably more than 1,000°C for several seconds, for complete destruction of tar.

Technical Basics

Being a reaction between fuel and gasification agent, the gasification is mainly determined by the gasification agent. Major gasification agents are:

- Air
- Oxygen
- Water-steam
- Carbon dioxide

Carbon dioxide, however, is hardly used as pure gas but sometimes in flue gas recirculation. Oxygen is unusual in small-scale plants, because there are no adequate small-scale oxygen provision systems. The same is basically true for water-steam. This is

the reason why small-scale gasification systems are usually operated with air.

Important process steps of gasification (like the reduction step), forming the desired products carbon monoxide and hydrogen, are endothermic. This requires a heat supply. Two ways are possible:

- *The allothermic process with heat supply from external sources.* The heat is transferred into the gasifier by recuperation or by hot material flows. Typically, water-steam is used as gasification agent in allothermic processes.
- *The autothermic process.* In this process, the required heat is produced by combustion of a part of the fuel. Therefore, the gasification agent has to contain portions of air or oxygen because the main exothermal (heat delivering) reactions are the oxidation reactions.

In general, the allothermic process is technologically more demanding. For this reason, in the small scale, mostly autothermic processes are realized. Allothermic systems are built mostly with larger thermal capacities.

Reactor Principles

For biomass gasification, lots of different reactors (e.g., [9, 27–31]), in this case called gasifiers, have been developed. An overview is shown in Fig. 4.

These reactors are based on a few principles of gas-solid reactors. Most of the common reactor principles have been considered for the design of gasifiers, both separately and in combination. Therefore, the following cases are discussed:

- Single-stage gasifiers
- Multistage gasifiers

Single-stage gasifiers represent different reactor principles, in particular:

- Fixed-bed gasifiers
- Fluidized-bed gasifiers
- Entrained-flow gasifiers

Multistage gasifiers are characterized by a functional combination of reactor principles for purposeful separation of reactions.

The basic design of a fixed-bed gasifier, a fluidized-bed gasifier, and an entrained-flow gasifier is shown in Fig. 5. Gas velocity, particle size, and residence time are characteristic parameters for these reactor types. The relation of these parameters is also shown in this figure.

Fixed-Bed Gasifiers The main feature of fixed-bed reactors (e.g., [11, 12, 29]) is that the solid phase is placed on a supporting structure, such as grates or fire-proof plates. The force from the fluid phase to the solid phase (resisting force) is low compared with the force of gravity. Even if the resisting force is directed against the gravity force, the solid phase cannot be moved by the resisting force but only by external forces. Being exposed to little movement, the solid phase will mix to a low extent and separated zones can develop, each dominated by a special process step.

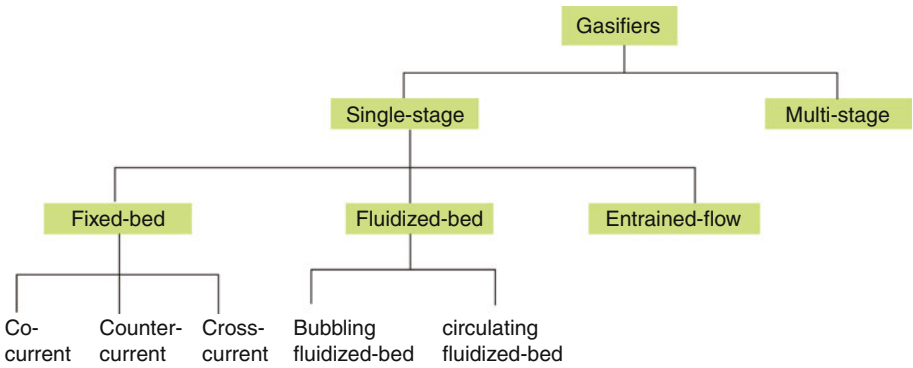

Biomass Gasification for Rural Electrification, Small Scale. Figure 4
Overview of reactor types of gasifiers

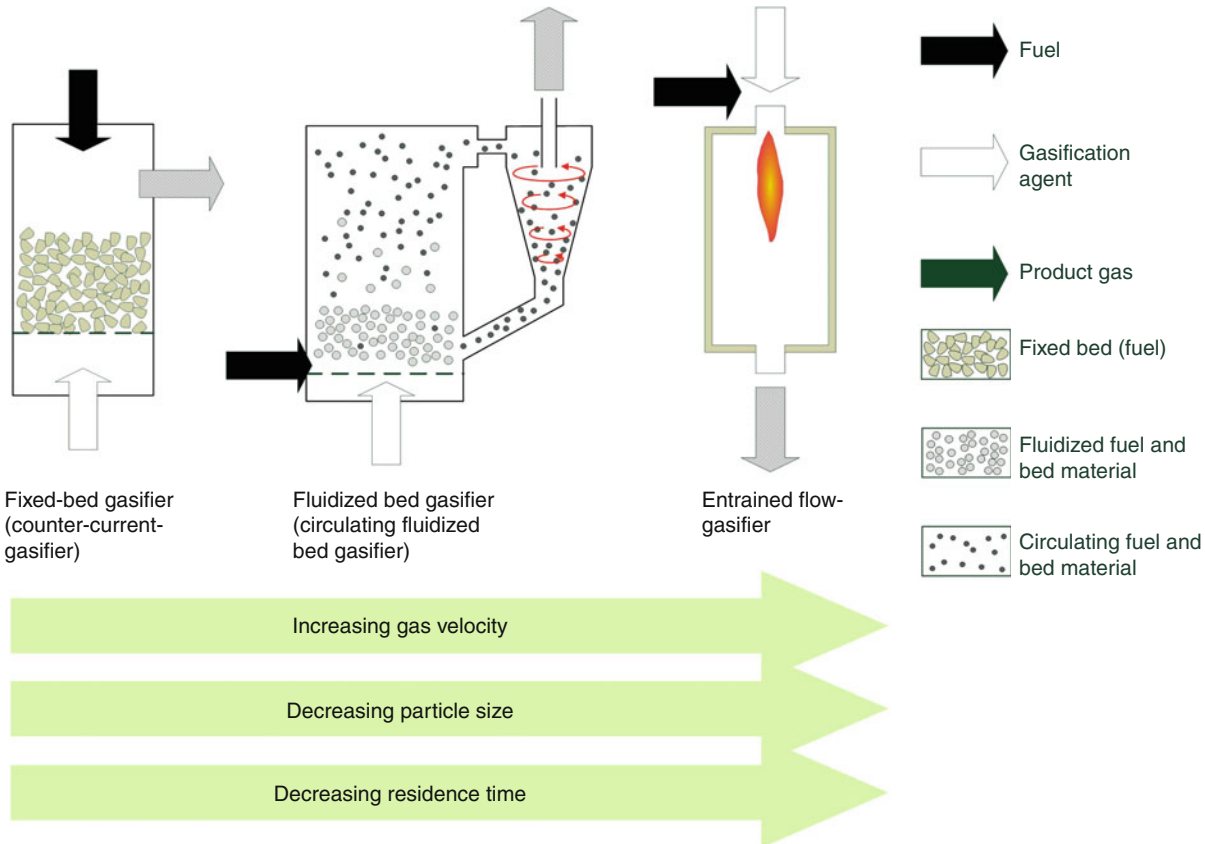

Biomass Gasification for Rural Electrification, Small Scale. Figure 5
The basic reactor types of single-stage gasifiers

There are three types of fixed-bed gasifiers which differ by the direction of movement of the solid fuel and the gases.

Countercurrent gasifier In a countercurrent gasifier (e.g., [7, 8, 32, 33]), the solid fuel and the gases (gasification agent and product gas) move in opposite directions. Normally the solid fuel moves in the direction of the gravity force and the gases rise.

The basic design of a countercurrent gasifier is shown in Fig. 6. Typical is the following order of the process steps from the bottom (grate) to the top of the reactor:

1. Oxidation
2. Reduction
3. Pyrolysis
4. Drying

This means that the hydrocarbons formed during the pyrolytic decomposition, especially the tar, do not flow through a high-temperature area. They only pass through the drying zone. That is why the tar content in the raw product gas is significantly high.

But this principle also has advantages:

- Because of the order of the process steps, the fuel is dried by the heat of the product gas. That is why wet fuels can be used. This is also the reason of its high overall gasification efficiency.
- Fuel with a wide range of particle sizes is less problematic because of a self-regulation of the flow direction.
- As the gasification agent can easily be spread evenly by the grate, the countercurrent gasifier is the fixed-bed gasifier which can most easily be scaled up.
- Because the solid matter is at last in contact with the inserted gasification agent, it is possible to reach a carbon-depleted ash. With the gasification agent air (or oxygen), the ash can become nearly carbon free.

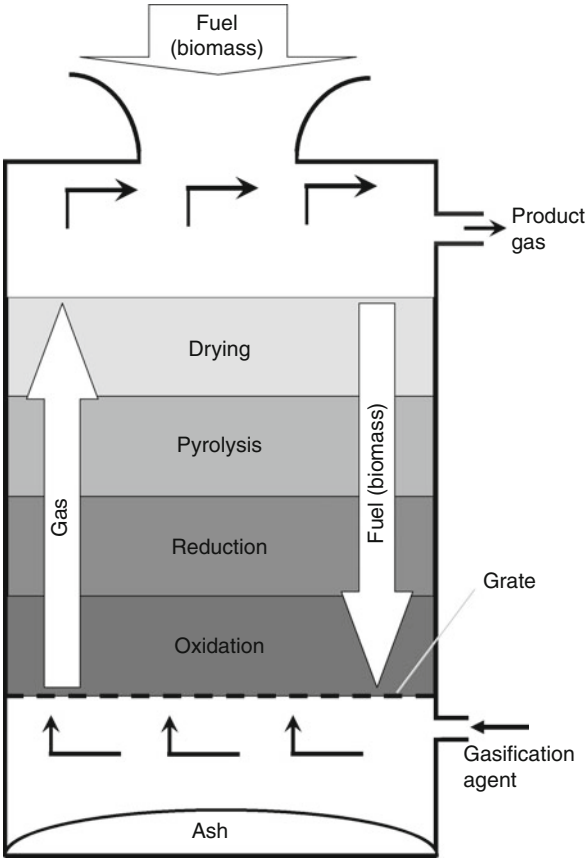

Biomass Gasification for Rural Electrification, Small Scale. Figure 6
Countercurrent gasifier

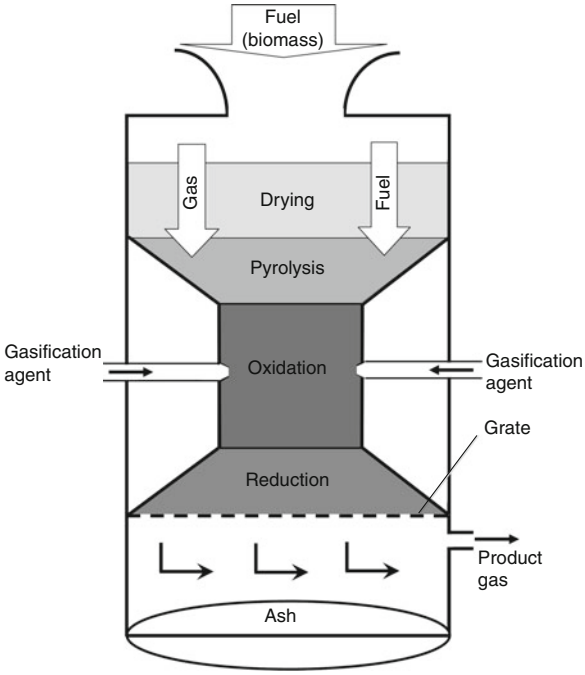

Biomass Gasification for Rural Electrification, Small Scale. Figure 7
Cocurrent gasifier

Basic technical properties of countercurrent gasifiers (reference values) are shown in Tables 1–3.

Cocurrent gasifier In a cocurrent gasifier (e.g., [34, 35]), the solid fuel and the gases move through the whole gasifier, mainly in the same direction. Normally, solid fuel moves in the direction of the gravity force and so do the gases.

The basic design of a cocurrent gasifier is shown in Fig. 7. The gasification agent may be fed from the top of the fuel bed using the whole cross section (open-top gasifier). However, the feed-in of the gasification agent into the oxidation zone through nozzles is more common. Typical is the following order of the process steps from the bottom to the top of the reactor:

1. Reduction
2. Oxidation
3. Pyrolysis
4. Drying

This means that the gases from the pyrolytic decomposition, especially the tar, pass the oxidation and reduction zones while flowing downward. Thereby, the tar is supposed to be cracked by the high temperatures and the tar content in the raw product gas should be very low.

But the flow conditions in commercial scale cocurrent gasifiers, especially in gasifiers with nozzles, are normally not found to be ideal [35]. That is why usually areas with temperatures exist which are too low for cracking of tars. In those parts of the flow, which pass these areas, little or no tar is cracked. That is why a nearly tar-free gas cannot be achieved in a commercial scale cocurrent gasifier.

Although the tar content in the raw product gas is much lower than in a countercurrent gasifier,

Biomass Gasification for Rural Electrification, Small Scale. Table 1 Typical power range, fuel requirements, and efficiencies for the basic principles of gasifiers [38]

	Fixed bed		Fluidized bed
	Countercurrent	Cocurrent	
Common power range [MW][a]	0.1–10	0.02–3	8–100
Fuel requirements			
Grain characteristic	Coarse-grained	Coarse-grained, narrow range of grain size	Fine-grained, narrow range of grain size
Grain size [mm]	5–100	20–100	10–100
Water content [mass-%]	12–40 (60)	12–25	< 40
Ash content [mass-$\%_{wf}$]	< 15	< 5	k. A.
Cold gas efficiency [%]	50–70	65–75	65–85

[a]Fuel input

Biomass Gasification for Rural Electrification, Small Scale. Table 2 Typical gas composition for the basic principles of gasifiers with air as the gasification agent [11, 32, 39]

	Fixed bed		Fluidized bed	
	Cocurrent	Countercurrent	Bubbling	Circulating
Reference water content [% dm]	≈ 6	≈ 50	≈ 15	≈ 15
H_2 [volume-%]	15–21	10–15	≈ 10	15–22
CO [volume-%]	10–22	15–20	≈ 15	13–15
CO_2 [volume-%]	11–13	8–10	≈ 17	13–15
CH_4 [volume-%]	1–5	2–3	≈ 4	2–4
C_nH_m [volume-%]	0.5–2		≈ 1.6	≈ 2
N_2 [volume-%]	Rest	Rest	Rest	Rest
Lower heating value [MJ/Nm^3]	4.0–5.6	3.7–5.1	≈ 4.5	3.6–5.9

the cocurrent principle has still the following disadvantages:

- Leaving the gasifier directly after the reduction zone at high temperature, the heat of the product gas cannot be used in the gasifier (e.g., for drying of the fuel). That is why only relatively dry fuel can be gasified and the gasification efficiency is relatively low.
- The particle sizes have to be within a narrow range.
- The gasification agent is fed into the gasifier through nozzles. This makes it very challenging to spread the gasification agent evenly through the gasifier; because of physical constraints, the gasification agent penetrates only a few centimeters into the fuel bed crosswise to the main flow [35]. That is why a scale-up of cocurrent gasifiers to sizes higher than in test facilities is extremely complicated. For this reason the tar content in the raw product gas rises with increasing gasifier sizes.
- Because the solid matter is at last in contact with the product gas, due to reasons related to the chemical equilibrium, it is not possible to reach

Biomass Gasification for Rural Electrification, Small Scale. Table 3 Comparison of the basic principles of gasifiers [29, 31]

Fixed-bed gasifiers	Fluidized-bed gasifier	Entrained-flow gasifier
+ Suitable for small and very small plants + Unpretentious technique	+ Very good heat and mass transfer + High space and time yield + Low product gas temperature (high chemical efficiency, uncomplex gas cooling)	+ High carbon conversion rate + High reaction velocity + Low start-up and rack out time
○ Reaction zones existing ○ A lot of different concepts	○ No reaction zones	○ Low methane content in product gas
– Slow regulation action – Very long start-up time – Difficult automation	– Limited carbon conversion rate – Carbon-containing ash – Linkage between particle size and fluidization velocity	– Only very small fuel particles possible – Very expensive biomass pretreatment – High product gas temperature (low chemical efficiency, complex gas cooling) – Only very large plants reasonable

a carbon-depleted ash. Thus, the refuse of a single-stage cocurrent gasifier contains several percents of carbon. This lowers the overall efficiency. And, for example, in Germany, the disposal of this ash-carbon-mixture is problematic because the carbon content of material to be dumped on a landfill is limited by law.

Basic technical properties of countercurrent gasifiers (reference values) are shown in Tables 1–3.

Cocurrent gasifiers have been used in the years around World War II in transport applications, especially in trucks. This is one reason for the many newly developed systems based on the principle of cocurrent gasification.

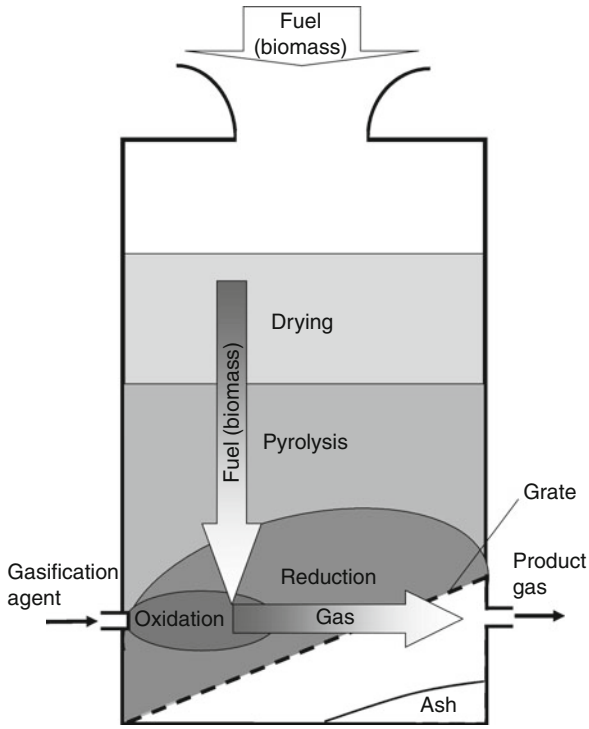

Biomass Gasification for Rural Electrification, Small Scale. Figure 8
Crosscurrent gasifier

But the success under those days' conditions is not sufficient for a successful use in energy applications today. For example, running times of only a few hundred hours and a lot of maintenance work are normally not tolerable nowadays. One of the main requirements for an energy system today is the high availability. This has to be fulfilled also by the gasification processes.

Crosscurrent gasifier In a crosscurrent gasifier (e.g., [9, 36, 37]), the solid fuel and the gases (gasification agent and product gas) move crosswise to each other. Normally, the solid fuel moves in the direction of gravity force. The gasification agent is horizontally injected through a nozzle. And the product gas is also discharged horizontally.

The basic design of a crosscurrent gasifier is shown in Fig. 8. The order of the areas for the process steps is

formed depending on the distance to the nozzle and the shortest way from gas inlet (nozzle) to gas outlet (see Fig. 8).

Because of this special design, the residence time of gases in the gasifier is short. That is why the gas composition can differ from the equilibrium composition, especially the carbon monoxide content can be lower. Only in those parts of the gas, which pass through a high-temperature area, the tars can be cracked. Therefore, the tar content in the raw product gas is higher than in the product gas from cocurrent gasifier.

The crosscurrent gasifier is ready for operation in a short time and enables response to fast variations of load. The gasifier can be built relatively compact.

This type of gasifier has been used in the first half of the twentieth century for transportation purpose. In recent years, there have been some activities for using that gasifier type for renewable energy production in Germany. But, currently, this development is of minor importance.

Fluidized-Bed Gasifiers The main characteristic of fluidized-bed gasifiers (e.g., [11, 12, 29]) is the force equilibrium between the resisting force (the force from the fluid phase to the solid phase) and the force of gravity. Therefore, in a fluidized-bed reactor, the fluid phase has to flow against the force of gravity, that is, vertically upward. This equilibrium of forces depends on the mass of solid particles and the flow velocity of the fluid phase. Particle size is important for unproblematic running of a fluidized-bed reactor. The solid particles float in the fluid flow. Due to the equilibrium of forces, the particles remain in a layer. Particles being too heavy move downward, particles being too light, for example, after a weight-loss during reaction, are blown out of the layer.

The particles in the layer are very well mixed. Causative for the mixing are inhomogeneities in the flow, that is, slight changes in fluid speed and flow direction. Thus, the equilibrium of forces is temporarily disturbed. A resulting force is the outcome. This force changes the direction of the particles. Hence, the particles move chaotically. Another reason is that like in all streamed tubes, also in the fluidized-bed reactor, the velocity near to the wall is lower than in the middle. Because of the force equilibrium, near to the wall, particles go down and in the middle come up. Thus, a circulation is also realized within the particle bed.

In fluidized-bed reactors for combustion and gasification, normally an inert (not reacting) material is used for heat storage and temperature leveling. The leveled temperatures and the stored heat are great advantages of fluidized-bed reactors, because changes in the fuel quality will partly be compensated.

Because of the mixing of the solid phase, no separated zones will develop. All process steps occur simultaneously and close to each other, that is, there are more or less, the same chemical behaviors all over the fluidized bed. Because all gasification reactions are equilibrium reactions, and for this reason, the chemical reaction occurs only up to the equilibrium, the carbon cannot be converted totally. That is way carbon remains in the ash from single-stage fluidized-bed reactors.

There are two main types of fluidized-bed gasifiers outlined below:

- The bubbling-fluidized-bed gasifier (BFB)
- The circulating-fluidized-bed gasifier (CFB)

Basic technical properties of fluidized-bed gasifiers (reference values) are shown in Tables 1–3.

Bubbling-fluidized-bed gasifier (BFB) In a bubbling-fluidized-bed gasifier, nearly all reactions including the solid fuel as reaction partner take place in the fluidized bed. Particles blown out because of too low weight mainly consist of ash because the gas–solid reactions are almost finished when weight of a particle becomes so low. These particles will be separated and disposed of. A recirculation of particles into the reactor is usually not realized. The basic design of a bubbling-fluidized-bed gasifier is shown in Fig. 9.

Circulating-fluidized-bed gasifier (CFB) In a circulating-fluidized-bed gasifier, only a portion of the solid fuel reacts in the fluidized bed. Lighter particles are blown out even if the reactions are not completed and organic matter remains. The target is that a main part not only of the gas phase reactions but also of the gas-solid reactions occurs in the space above the fluidized bed, the so-called free space. At the end of the free space, the remaining particles are separated from the gas. Usually a cyclone is used but also other mechanical gas-solid-separators are possible and tested in different designs. Containing a lot of remaining organic matter which is possible to gasify

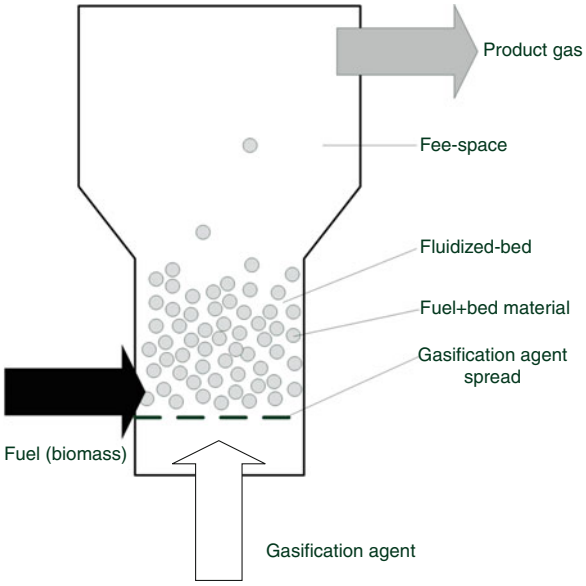

Biomass Gasification for Rural Electrification, Small Scale. Figure 9
Bubbling-fluidized-bed gasifier

a major portion of the separated particles is recirculated into the reactor. The basic design of a Circulating-fluidized-bed gasifier is shown in Fig. 10.

Entrained-Flow Reactor In an entrained-flow reactor (e.g., [30, 31]), the force from the fluid phase to the solid phase (resisting force) is much higher than the force of gravity. The particles are carried along with the fluid phase. The reactions take place while the particles are transported by the fluid phase.

In order to facilitate the transport of fuel particles by the gases, very small fuel particles with a size of less than 1 mm are utilized in entrained-flow gasifiers. Thus the residence time is very short (normally a few seconds or less) and the reaction temperatures are high.

Coal gasifiers in a scale of several hundred MW are often built as entrained-flow reactors. This scale is uncommon for the utilization of biomass. The chopping of biomass to the necessary particle size is expensive and normally only possible with a thermal pretreatment.

A comparison between entrained-flow gasifiers and the other basic principles is presented in Table 3.

Multistage Gasifiers Because of different conditions required by each reaction, it is not possible to optimize all gasification reactions in a single-stage gasifier. Especially the temperature window and residence time for a certain reaction step is often not optimal or appropriate, for example, for tar removal. One idea to solve this problem is to use different reactors for different process steps and reactions. These different reactors can be optimized more easily for reactions taking place in them. On the other hand, the costs may increase by using more than one reactor.

Various combinations have been designed using different types of reactors and dividing the gasification into different sub-processes. Below only a few selected examples are described briefly.

Double fire gasifier This gasifier principle (e.g., [9, 27, 40–42]) got its name, because it is a combination of a cocurrent and a countercurrent gasifier in one shell. Transported by the gravity force, the fuel first passes the cocurrent and then the countercurrent part. The biomass is fed into the cocurrent part. In the zone of the pyrolytic decomposition, volatile substances are released. Like in a single-step cocurrent gasifier, the tar is cracked in the hot zones of this part. For the cocurrent part, there is a first gasification agent inlet with nozzles.

Only the carbon-rich residue from the cocurrent part moves to the countercurrent part. Because of the gasification agent inlet from the bottom (grate), the carbon remaining after the cocurrent stage is utilized in the countercurrent stage. Between the stages, there is no separating device like a grate. Only the position of the product gas outlet defines the gas flow directions and with it also the border of the stages.

A double fire gasifier produces

- Product gas with as little tar as a cocurrent gasifier
- Ash with as little carbon as a countercurrent gasifier

But similar to the cocurrent gasifier, the tar content is still not low enough for a direct utilization.

Viking Gasifier In the Viking Gasifier (e.g., [27, 43–45]), the gasification process takes place in three separated zones. These zones are: firstly, a drying zone and zone with pyrolytic decomposition; secondly, a zone with tar removal by partial oxidation and other gas phase reactions; and thirdly, a gasification, especially reduction, zone.

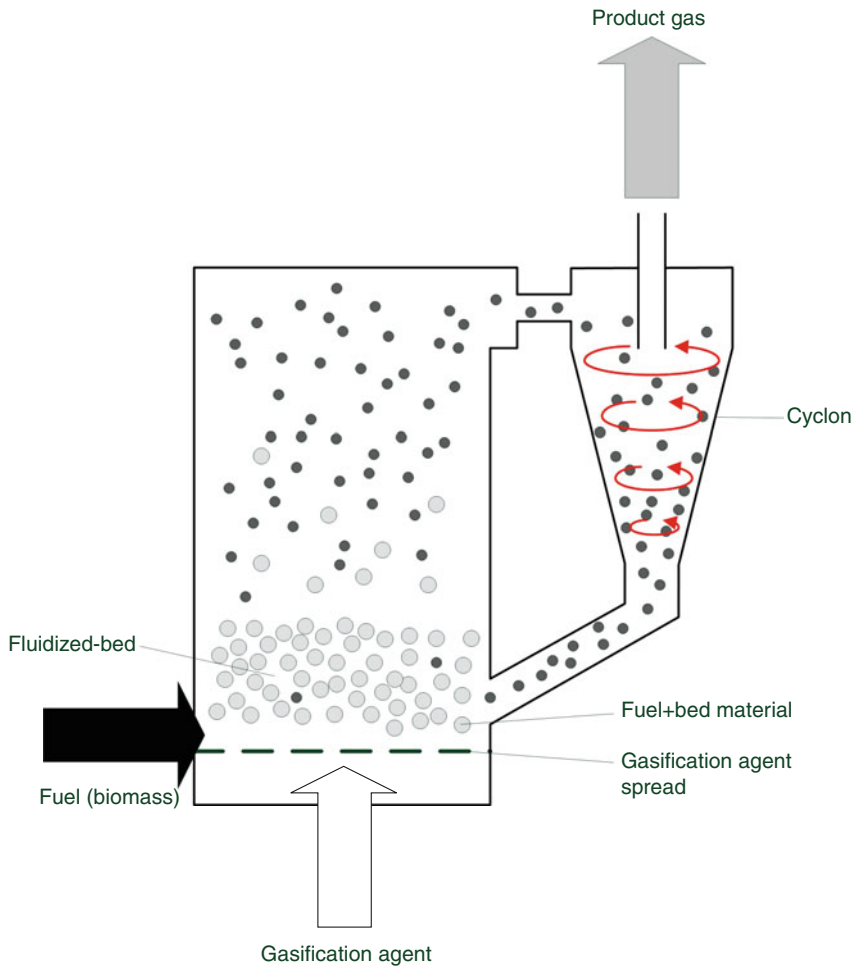

Biomass Gasification for Rural Electrification, Small Scale. Figure 10
Circulating-fluidized-bed gasifier

The drying and pyrolysis zone is designed as a screw reactor. The biomass is transported through this reactor by the screw. The heat for drying and pyrolytic decomposition is transferred through the wall of the reactor. In a plant for electricity generation, mainly the waste heat from the engine can be used for these first process steps and less additional heat is required. The char and the gases leave the reactor at its end. Being a product of pyrolytic decomposition, the gas contains a high amount of tar.

After leaving the screw reactor, the char falls downward and the gases flow downward passing through a free space reactor. In this, air is fed in. The air reacts with the gas, and especially, the tar is removed by partial oxidation. Additionally other fast reactions in the gas phase take place. The char particles with their low reactivity pass through the free space without being largely involved in these reactions. Because of the exothermal oxidation reactions, the gas temperature increases up to about 1,100°C.

Below the free space in the same reactor, the remaining char accumulates. Flowing through this char bed, carbon dioxide and water-steam in the gas react with the char following the reduction reactions described above. In these endothermic reactions, which generate carbon monoxide and hydrogen, the temperature decreases to about 750°C. The gasification efficiency is increased by the reaction zone,

because thermal energy is converted back to chemical energy.

The Viking Gasifier demonstrates that multistage gasifiers can have some advantages:

- Very low tar content in raw product gas.
- High gasification efficiency especially concerning the use of waste heat for drying and pyrolysis.
- Relatively wet biomass can be used.
- Wastewater is hardly contaminated with hydrocarbons.

On the other hand, the technique is much more expensive than single-stage gasifiers.

FICFB process The FICFB process first realized in Güssing/Austria (e.g., [13, 46–49]) is a dual-bed steam gasification working with two reactors (chambers): one for the gasification process with the gasification agent water-steam, and a second one for combustion for heat supply. The reactor principle is based on a circulating-fluidized-bed reactor. The fluidized bed is used for biomass gasification whereas the recirculation part is designed as a combustion chamber. Biomass is fed into the fluidized-bed gasification chamber where it is converted into nitrogen-free syngas and char using steam as gasification agent. The char and additional raw gas for control purpose are burnt with air in the combustion chamber, heating the accompanying fluidized-bed-particles. The hot bed material is then fed back into the gasification chamber, providing the required reaction heat. There are also further constructions available using the dual-bed principle (e.g., [50–55]).

Dual-bed steam gasifiers are developments specifically for biomass. In the German-speaking area, the FICFB process is at the beginning of commercialization, mainly for CHP applications. Several installations are planned, under construction, or recently started operation. Due the fact that the aspired power range of the FICFB technology is above 2 MW electric power according to about 8 MW fuel input power, this technology is not a small-scale technique. But this technique is important, because commercial operation is almost complete and both the technique and the way for solving the occurring problems are exemplary for other ongoing developments.

Application of the Gas

For the complete utilization of the chemical energy, the fuel has to be oxidized to the highest oxidation number (i.e., to carbon dioxide and water). The product gas is only an intermediate product for simplifying the utilization of the solid fuel. Because here the objective is the generation of electricity, other applications of the product gas (like heat supply, e.g., for industrial furnaces, synthesis of bulk chemicals) are not discussed.

Usually, electricity is generated via mechanical power, which is provided from heat in a thermal cyclic process. Currently, the only alternative of some importance is the fuel cell.

The processes for the generation of electricity from the product gas can be sorted into the following categories:

- Electricity generation via heat (thermal cyclic process) and mechanical power (generator)
  - Processes with internal combustion
    - Reciprocation combustion engine
      - Gas engine (Otto principle)
      - Pilot injection engine (Diesel principle)
    - Gas turbines
  - Processes with external combustion
    - Reciprocation engine (Stirling principle)
    - Externally heated gas turbines
    - Utilization in boilers
- Direct electricity generation from chemical energy (i.e., fuel cell)

Currently, the importance of reciprocation engines with internal combustion in small-scale plants is dominating.

Below, the main options for utilization of product gas from thermochemical biomass gasification for electricity generation are discussed.

Reciprocation Combustion Engine

Reciprocating engines (e.g., [27, 29, 56–59]) are common solutions for the transformation of chemical energy into mechanical power in the low and medium power range. Engines for cars, ships, and block heat and power plants are examples. The main characteristic of reciprocation engines is the stepwise work in strokes.

That is why the combustion does not occur continuously (i.e., in one of several strokes). Most common are four-stroke engines.

Gas Engine (Otto Principle) The basic process steps of the gas engine process are as outlined below:

- Mixing of air and gaseous fuel.
- Intake and compression of an air fuel mixture by the piston.
- Ignition of pressurized air fuel mixture; the ignition in an Otto engine occurs by electrical sparks.
- Combustion of the fuel and expansion of the flue gas; the flue gases move the piston and the piston transfers the power via the conrod to the crankshaft.
- The piston ejects the flue gases.

These steps repeat cyclically.

Gas engines can only by operated with cold gas. Because of the thermal expansion of the product gas at higher temperatures, less mass or less normal volume of gas can be delivered into the cylinders. Therefore, the power of the engine decreases with increasing temperature of the gas [60].

The applicability of a product gas from biomass gasification within a gas engine is mainly determined by three parameters:

- Content of pollutants (e.g., tar)
- Laminar flame velocity
- Methane number

Pollutants can damage the engine. The following components are of high importance:

- Tar could cause coking in high-temperature areas and agglutination in cold areas, especially valves and nozzles are in danger.
- Dust is dangerous because of its abrasive properties and the promotion of dirtying by tar.
- Sulfur compounds and ammonia can reduce the resistance time of the lubricating oil.

The common limits of content for these substances are given in Table 4.

Another main property is the laminar flame velocity. If the flame velocity is high enough, also gases with low heating value can be utilized in gas engines. This is important because product gases from biomass gasification normally have a low heating value especially if air is used as gasification agent.

Similar to the octane number in petrol-fired engines, the methane number is a measure of the antiknock properties. But this can be adapted by using lean-burning (e.g., [8, 61–63]).

Pilot Injection Engine (Diesel Principle) The basic process steps of the Diesel engine process (e.g., [58, 59]) are:

- Mixing of air and gaseous fuel.
- Intake and compression of an air fuel mixture by the piston.
- Ignition of pressurized air fuel mixture; the ignition in a pilot injection engine occurs by an injection of a liquid pilot fuel.
- Combustion of the fuel and expansion of the flue gas; the flue gases move the piston and the piston transfers the power via the conrod to the crankshaft.
- The piston ejects the flue gases.

Biomass Gasification for Rural Electrification, Small Scale. Table 4 Gas quality requirements of the gas utilization processes (values for the orientation) [11, 25, 29, 76–80]

Impurity [mg/Nm^3]	Reciprocating combustion engine	Gas turbine	High-temperature fuel cell	Fuel synthesis (as comparison)
Tar	10–100		0.1–1	0.1–1
Dust	10–50	< 30	1–10	0.02–0.5
Sulfur	1,000		0.1–1	0.01–1
Ammonia	50		0.1–1	0.1–1
Alkali (total)		< 30	0.1–1	0.2–1
Halogens (HCl + HF)			0.01–1	0.01–0.1

These steps repeat cyclically.

There are statements in scientific publications pointing out that pilot injection engines emit much more soot than gas engines.

The gas quality requirements of a pilot injection engine are quite similar to those of a gas engine (Otto principle). A low and fluctuating heating value can be compensated by the injected liquid fuel. Also the requirements to laminar flame velocity are not as strict.

Gas Turbine

Gas turbines (e.g., [64–68]) are common solutions for the transformation of chemical energy into mechanical power in large-scale plants. As opposed to the reciprocation engine principle, all process steps in a gas turbine run continuously but in separated zones of the turbine. That is why the combustion can occur without interruptions.

The basic process steps of the gas turbine process are:

- Air intake and air compression in a centrifugal compressor.
- Injection of pressurized fuel; as fuel clean gases and liquids are possible; if the gaseous fuel is not pressurized, like the product gas from most biomass gasifiers, a separate fuel compression is necessary.
- Combustion under pressure in a combustion chamber.
- Expansion: The flue gases drive an expansion turbine and the mechanical power is available at the shaft.

For small-scale plants, only micro gas turbines are interesting. They are used in several facilities but by far not as often as reciprocating engines.

The use of hot producer gas containing tar is basically possible in gas turbines. But due to the pressurized combustion in gas turbine combustion chambers, pressurized gasification or a gas compression is necessary. Pressurized gasifiers are very seldom realized in small scale. Gas compression is not possible with tar containing gas, and it is not efficient with hot gas. Therefore, gas compression requires gas cooling and tar removal just like a reciprocating engine does. Alkalis are very harmful to the materials used in gas turbines and have to be removed also. Because of the very high velocities in a gas turbine, dust particles cause intensive abrasion. Thus, the content of dust which can be tolerated by a gas turbine is very low.

Common orders of magnitude for the gas requirements are given in Table 4.

The lower heating value of the product gas from biomass gasification compared to natural gas requires an adaptation of the gas turbine.

Processes with External Combustion

Common to all processes with external combustion is the separation of the combustion part and the heat utilization. Only heat is exchanged through solid walls. The material flows in the two parts do not mix.

Stirling Engine A Stirling engine (e.g., [29, 69–73]) is a reciprocating engine with an external heat supply via heat exchangers. Basically, a Stirling engine is composed of a heated operating cylinder, a cooled compression cylinder, and a heat regenerator. The heat regenerator serves for temporary heat storage. The operation gas is enclosed in the engine. Typical operation gases are helium, air, nitrogen, and hydrogen.

Generally, the process steps of the Stirling process are as described below:

- The compression piston pushes the cold operation gas through the regenerator into the operation cylinder. The operation gas is heated in the regenerator and in the operation cylinder.
- The compression piston reaches its dead point. The heating of the operation gas is continued in the operation cylinder, with the operating gas expending so that the operation piston is moved. The operation piston transfers the power via the conrod to the crankshaft.
- By passing the dead center, the operation piston moves back. The operation gas is pushed through the regenerator into the compression cylinder. The hot operation gas transfers heat to the regenerator. The compression cylinder starts moving back.
- The cooling of the operation gas is continued in the compression cylinder. The compression cylinder continues moving back.

These steps repeat cyclically.

Externally Heated Gas Turbines The principle of the external heated gas turbine is quite similar to that of a gas turbine. Only the internal combustion under

pressure is replaced by a heat exchanger and an external combustion. Being separated from the gas turbine process, combustion can take place at atmospheric pressure. Because the operation gas is only heated and does not react, it is normally recirculated into the process. In this case, the waste heat after the expansion turbine is dissipated by a heat exchanger. In such closed cycle, similar to the Stirling engine, the operation gas may not only be air but also helium, in particular.

Due to the separation of the combustion and the turbine, a lot of different fuels can be utilized. To reach operation gas temperatures as high as in a gas turbine with internal combustions by a heat exchanger is often the weak point of this technology. At such high temperatures, most materials may easily to be destroyed.

Gas-Fired Boilers The combination of an uncomplex biomass gasifier and a gas-fired boiler can have advantages compared to biomass-fired boilers. These advantages can be low emissions, very basic boiler design, and the possibility of the fuel shift from gaseous or liquid fossil fuel to biomass. Small-scale electricity generation plants using this combination are very uncommon. But this can be a solution for very dirty gases as produced in waste pyrolysis and waste gasification, or for a fuel shift as part of retrofitting action.

Because of the external combustion and the heat provision via recuperation, gas quality requirements are comparatively low. Basically, every combustible gas can be used in such a plant. Even gas with a very low heating value can be used by utilizing this fuel gas in a hot state for combustion and by preheating the air. When using a suitable combustion chamber, tar can be used along with the gas and simultaneously eliminated during combustion. That is why the tar is only a problem in the equipment before the combustion chamber, especially in the pipes, valves, and nozzles. Therefore, tar containing gas is just to be brought to the combustion and fed into the combustion process in a hot state. The temperature must not be lowered between gasification and combustion.

Further gas quality requirements depend on the emission limits and the used construction materials, because corrosion can be a problem. These factors determine the tolerable content of sulfur and chlorine compounds, for example.

Fuel Cell

Fuel cells (e.g., [74–76]) are devices for the electrochemical generation of electricity utilizing the chemical energy of fuels. The fuels are oxidized in electrochemical reactions, releasing charge carriers. These charge carriers cause a current flow.

Because of the utilization of fuel in a chemical process using catalysts and membranes, the gas requirements of a fuel cell are very high. Not only tar and dust but also catalyst poisons are limited to extremely low values. Nevertheless, projects dealing with the utilization of product gas from gasification exist. Estimates for the gas requirements are given in Table 4.

Gas Treatment

Normally, a gap exists between the fuel gas quality generated by the gasifiers and the gas quality requirements of the gas utilization technologies. Thus, the gas quality delivered from the gasifier (Table 5) has to be adapted to the requirement of the gas utilization (Table 4) used in each particular case so as to prevent a deterioration of the gas utilization equipment.

The extent of the necessary gas treatment depends on the techniques used for gasification and gas utilization. For example, a countercurrent gasifier generates gas with a tar content one order of magnitude higher than in the gas produced in other types of single-stage gasifiers, and the gas requirement for some pollutants is several orders of magnitude higher for the use in fuel cells than for a utilization, for example, in gas engines. Different solid fuels used in the gasification can also influence the quality of the raw product gas because of its different content of substances forming gas pollutants. For example, in raw gas from straw gasification, the content of alkalis will normally be higher than in the case of wood gasification.

This means that, for each combination of fuel, gasifier and gas utilization specific demands in terms of gas treatment and suitable gas cleaning technologies exist. Therefore, below common solutions for typical gas treatment tasks are described.

Tar Removal

In most cases, tar removal is imperative to the success of the gas utilization. All single-step gasifiers generate

Biomass Gasification for Rural Electrification, Small Scale. Table 5 Gas quality supplied by the gasifiers (values for the orientation) [11, 32, 76–79]

Impurity [mg/Nm^3]	Fixed bed		Fluidized bed	
	Cocurrent	Countercurrent	Bubbling	Circulating
Tar	10–10,000	10,000–150,000	1,000–30,000	1,000–30,000
Dust	100–8,000	100–3,000	1,000–100,000	8,000–100,000
Sulfur	5–200			
Ammoniac	200–2,000			
Alkali (total)	0,5–5			
Halogens (Hcl + HF)	<500			

tar. And only in the external combustion of hot gas, the tar content is unimportant. High-temperature fuel cells are supposed to be able to use tar containing gas, but the hazard of damage by sooting is obvious.

The tar is a product of the pyrolytic decomposition taking place during biomass gasification. If the tar is not degraded in the following process steps, the tar can be found in the raw gas (Fig. 3). Tar consists of hundreds of different organic species that can add up to an overall tar content of several tens of g/m$_N^3$, for example, in countercurrent gasifiers. During the pyrolytic decomposition, comparatively reactive compounds are generated (so-called primary tars). With increasing temperatures and increasing residence time at these high temperatures, the tar compounds are transformed to more stabile substances (so-called secondary and tertiary tars). The content of polycyclic aromatic hydrocarbons (PAH) rises from primary to tertiary tars [6, 81–84].

The main problems with tar are enumerated below [25, 60, 85].

- Tars are condensing on surfaces and leading to agglutination of components. Causative is the high viscosity of the tars. The agglutination will be increased by dust deposition at these surfaces.
- On hot surfaces, tar can easily react, causing sooting.
- Substances contained in the tar, like polycyclic aromatic hydrocarbons, are carcinogenic and toxic.
- Tar is environmentally harmful.
- Being a mixture of hydrocarbons, tar contains a lot of the chemical energy of the fuel.

That is why tar removal usually is the most important gas treatment step in electricity-generating plants using gasification.

Because of the specific behavior of tar, being a mixture of organic components and having a condensation range from 100°C to 350°C and more, a lot of different technologies can be used for tar removal. Figure 11 gives an overview.

A differentiation of removal processes can be done between tar separation and tar degradation. The term "tar degradation" summarizes chemical processes which consume the tar by forming simple chemical substances like carbon monoxide, hydrogen, methane, and other simple hydrocarbons. Examples for these reactions are cracking, partial oxidation, steam-reforming, and hydrogenation. Tar separation removes tar out of the gas flow without destroying the tar's molecules. In this case, tar remains as by-product or waste. Depending on the condensing temperature range, two principles of tar separation exist: Gaseous tar can be separated above the condensing temperature using absorption and adsorption processes. Alternatively, the tar is condensed and removed in a droplet removal unit. Typical units for droplet removal are quite similar to particulate collection systems. Such techniques are, for example, mechanical separators, washers, and electrical precipitators.

A summarizing overview of tar removal techniques is given in Fig. 11 and Table 6 and a comparison in Table 7.

Tar Degradation Processes Tar degradation processes (e.g., [25, 39, 81, 86, 87]) are waste free and

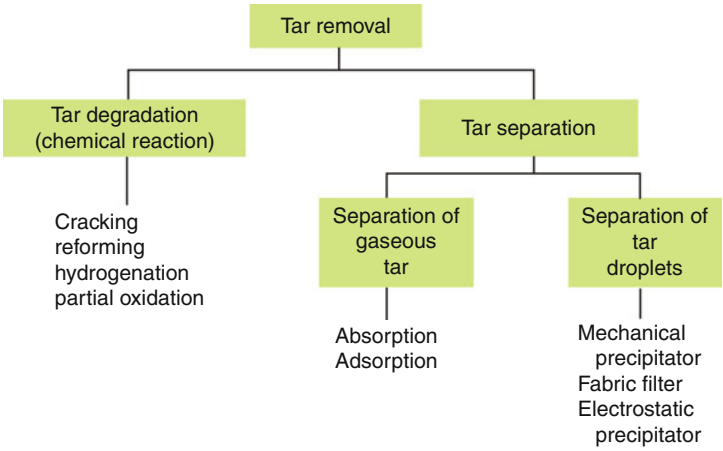

Biomass Gasification for Rural Electrification, Small Scale. Figure 11
Tar removal processes (overview)

Biomass Gasification for Rural Electrification, Small Scale. Table 6 Performance of selected tar removal processes

Technique	Catalytic partial oxidation	RME-scrubber	Electrostatic precipitator	Electrostatic precipitator	Water scrubber
Principle	Tar degradation	Absorption (droplet removal)	Electrostatic droplet removal	Electrostatic droplet removal	Droplet removal (absorption)
Auxiliary material	Air	Biodiesel	–	–	
Tar content raw gas [mg/m_N^3]	4,000–10,000	<4,000	50,000	400	1,000–10,000
Tar content clean gas [mg/m_N^3]	<100	A few	<10	15–35	100–400
Remark	Research	Tested in larger scale	Large scale	Small scale	Small scale

nearly wastewater free and the energy content of the tar can be used. But until today, no sound tar degradation process is available.

Cracking and reforming Cracking is the degradation, normally scission, of organic molecules without a second reacting agent. Its aim is to produce small organic molecules. Reforming means the degradation of organic molecules with water-steam as reacting agent. Target products are hydrogen and carbon monoxide, the most desired gasification products. Because water is contained in the raw product gas, these two reactions occur simultaneously. Both processes run without catalyst if the temperature is high enough.

Because of the necessary high cracking temperatures of more than 1,000°C which exceeds the gasification temperature, thermal cracking downstream biomass gasification causes an efficiency loss. This makes it an unattractive option for biofuel applications. But this efficiency loss can be compensated by several heat recovery processes.

The other alternative is the use of a catalyst. Catalytic cracking and reforming provide more attractive options in terms of chemical efficiency and process economy. The use of catalytic bed materials, like

Biomass Gasification for Rural Electrification, Small Scale. Table 7 Pros and cons of selected tar removal processes

Tar degradation	Absorption (organic solvent)	Electrostatic precipitator
+ No waste + Less wastewater + No cooling before tar removal + No dirtying before tar removal + High overall efficiency	+ Extensive successful tested + Low raw gas tar content permanent reachable + Commercial available	+ Extensive successful tested + Low raw gas tar content permanent reachable + Commercial available + Experience from coke oven plants
– Research and development topic – Catalysts or high temperature required – Catalyst lifetime	– Treatment of tar waste – Wastewater – Cooling before tar removal essential – Consumption of solvent	– Treatment of tar waste – Wastewater – Cooling before tar removal essential

+Advantage
−Disadvantage

dolomite, limestone, or olivine sands in fluidized-bed gasifiers, limits the tar content of biomass product gas typically to less than 10 g/m_N^3. To achieve the required gas purity, further catalytic beds or filters are necessary. Table 1 summarizes the advantages and disadvantages of different catalysts for tar reforming. However, this is a major research and development topic of several companies involved in biomass gasification technology. And so far, these efforts have not reached a development status that makes it suitable for commercial plants.

Catalyst deactivation by sulfur still is a severe constraint for the use of not only Ni-based catalysts but also of a huge number of other highly active catalysts. This problematic underlines the importance of a favorable operating temperature since a sufficient sulfur tolerance of Ni-based catalysts requires temperatures of at least 850–900°C which can hardly be guaranteed because of the strong endothermic tar and methane decomposition.

Another problem is the catalyst deactivation and destroying by sooting. Especially in the cracking process, soot is produced. Soot is a problem in all tar degradation processes except in partial oxidation, because soot production is the energetically preferred process [88–93]. An overview of catalysts is given in Table 8.

Hydrogenation Because of the hydrogen content in the product gas, hydrogenation (e.g., [94, 95]) of tar is also possible without a feed-in of a reaction agent from outside. In a first step, the molecules will be saturated and functional groups can be removed. Afterward with further hydrogen, a so-called hydro cracking can be performed. In this reaction, the molecules will be cracked into smaller ones. But, in contrast to other cracking reactions, no unsaturated components form, because the hydrogen takes part in the reaction and is intercalated in the formed molecules. In a hydrogenation process, using catalysts with reaction temperatures of about 500°C, 50–80% of the tar can be removed. This process is especially used for the reduction of very high-to-medium contents in a first cleaning step, for example, after countercurrent gasifiers.

Partial oxidation So far in the tar degradation processes described above, the required tar content in clean gas cannot be reached and the catalysts are deactivated quickly. An alternative can be the partial oxidation (e.g. [96–100]). Within such a process, air or oxygen is added to the raw product gas. With these reaction agents, the tar components react, forming carbon monoxide, hydrogen, carbon dioxide, and water. Thereby the gasification, as reaction of a solid fuel generating a gaseous fuel composed of only simple substances, is completed in the partial oxidation. Several configurations with and without catalysts are tested.

Such a catalytic-induced partial oxidation with metal catalyst on metal support reaches 95% tar degradation and a clean gas tar content of less than 100 mg/m_N^3 in a test facility [25, 101–103].

Tar Separation The alternative to tar degradation is tar separation. It can be done either in a gas separation process or by tar condensing and droplet removal. The removed tar contains a high amount of chemical energy and is expensive to dispose. That is why a process internal utilization (e.g., recycling within the gasifier) should be preferred.

Biomass Gasification for Rural Electrification, Small Scale. Table 8 Advantages and disadvantages of different catalytic materials for tar reforming [88]

Catalyst	Advantages	Disadvantages
Calcined rocks (dolomite)	Inexpensive and abundant	Fragile materials and quickly eroded from fluidized beds
	Attain high tar conversion	
Olivine	Inexpensive	Lower catalytic activity than dolomite
	High attrition resistance	
Clay minerals	Inexpensive and abundant	Lower catalytic activity than dolomite
	Less disposal problems	Most natural clays do not support temperatures > 800°C
Iron ores	Inexpensive	Rapidly deactivated in absence of hydrogen
	Abundant	Lower catalytic activity than dolomite
Char	Inexpensive	Consumption because of gasification reactions
	Natural production inside the gasifier	Biomass char properties not fixed
	High tar conversion	
Alkali metals	Natural production in the gasifier	Particle agglomeration at high temperatures
	Reduce ash handling problem	Lower catalytic activity than dolomite
Activated alumina	High tar conversion	Quick deactivation by coke
Transition metals	Complete tar reduction at 900°C	Rapid deactivation by sulfur and high tar content
	Increase the yield of CO and H_2	Relatively expensive

Absorption and adsorption processes Tar separation from the gas can be realized by absorption and adsorption processes. Both possibilities are discussed below.

Absorption is defined as a separation process, using different solubilities of substances in liquids. Tars can easily dissolve to be solubilized in several organic solvents such as acetone, tetrahydrofuran, and oils [13, 37, 104]. Because of the properties of the tar, the absorption of tar with a lower condensing temperature occurs normally simultaneously with condensation of other tar components and droplet removal by scrubbing.

Currently, scrubbers with organic solvents (e.g., FAME) as washing solvent are the most common tar removal technologies for small and medium sized biomass gasifiers and are successfully tested at a number of plants. Commercial tar scrubbers are the CTU FAME scrubber [105, 106] used in Guessing and the OLGA tar removal [107–110].

The FAME scrubber is designed for the Guessing gasifier process with a relative moderate tar content of <4 g/m_N. In the typical application, a first tar removal is done by a pre-coated baghouse filter operating at 140°C which removes the previously condensed heavy tars before FAME scrubber. Within the scrubber, the incoming gas is cleaned from tars and other organic impurities by initial quenching and subsequent absorption with FAME. The gas leaves the column with a temperature of 10°C. The solvent is regenerated by stripping with CO_2, but a significant amount of FAME containing the separated tar is fed into the combustion chamber of the dual-bed steam gasifier. Thus, the tar is both, disposed and energetic used. The solution of tar in FAME is much easier to handle than pure tar. Because FAME is also a biofuel, no fossil-based chemical had to combusted. But FAME is more expensive than the wood fuel, by which it is nevertheless important to save FAME. In the Guessing gasification plant, the FAME scrubber was tested successfully with thousands of hours operating time and is still running. This technique is also successfully used with other gasifier types, especially cocurrent fixed-bed gasifiers [111], but the recirculation of tar is difficult if no separated combustion facility exists.

OLGA is based on a multiple stage scrubber in which the gas is cleaned by proprietary scrubbing oil. In the first section, the gas is gently cooled down by the scrubbing oil. Heavy tar condensates, is collected,

separated from the scrubbing oil, and recycled to the gasifier. In the second stage, lighter gaseous tars are absorbed by the scrubbing oil. The saturated oil is regenerated in a stripper. Hot air is used to strip the tars of the scrubbing oil. This air, loaded with light tars, is recycled to the gasifier for combusting and as fluidization medium. Hence, the stripper column design is not only based upon tar removal, but also upon the amount of air that can be used by the gasifier.

The following two aspects of these systems can be highlighted:

- The OLGA scrubber has very low oil consumption and a lower cooling demand and hence is advantageous in terms of operating costs and GHG emissions.
- The FAME scrubber removes a high proportion of thiophenes and hence lowers the further purification effort.

Adsorption (e.g., [39, 112]) is defined as a separation process, using different adhesion forces of substances on surfaces. Usually, solids with very large specific surface are used as adsorbent. Typical adsorbents for tar separation are activated carbon and charcoal. Because of the properties of the tar, the adsorption of tar with a lower condensing temperature normally occurs simultaneously with the droplet removal by the adsorbent bed acting also as packed bed filter. The capacity for the real adsorption is relatively small; that is why these facilities are often run only as packed bed filter. Therefore, the tar removal rate is often not high enough. If the adsorption really occurs, very low clean gas tar contents are reachable [112]. The charcoal produced by cocurrent gasifiers can be used in these packed bed filters.

So far, no processes for the tar desorption and the reactivation of the activated coal are available. Therefore, the charcoal and the tar have to be burnt. Tar removal systems using fire-proof adsorbents are developed. The tar can be removed from this adsorbent by combustion. What remains afterward is a cleaned adsorbent.

Droplet removal For droplet removal, several techniques are available. But the properties causing agglutination and the high viscosity of the tar are often a problem. Tar can also soil tar removal facilities (especially droplet separators) or even destroy then. Crucial for the success of these tar removal processes are the complete tar condensation and the formation of precipitative droplets. Practical experience has shown that these two requirements cannot be easily fulfilled.

Mechanical precipitators use the separation of gas and droplets or particles by centrifugal force, for example, in cyclones and impact separators. The conglomeration of droplets into drops, which are easy to separate from gas, enhances the gas cleaning effect [104, 113]. Impact separators have been the common tar removal techniques in wood gasifiers in the middle of the twentieth century and in decentralized gas works [114]. Nowadays, the reachable clean gas in impact separators tar content is not low enough. Other mechanical precipitators are developed, but they are predominantly used as dust collectors [112].

Electrostatic precipitators employ the effect of the separation of electrically charged particles or droplets. In systems which utilize this principle, smallest droplets can be precipitated [113, 115]. Very low tar contents are reachable, if the tar has been condensed before. Gaseous tar cannot be removed in this way. Such precipitators are currently the commonly used tar removal technique in coke oven plants. Small and medium sized constructions have been developed. This technology is another promising tar separation technique besides the scrubbers for absorption [111, 116–118].

For the removal of particles and droplets, a lot of scrubber designs exist (e.g., [39, 81, 112]). Because absorption is not the primary aim, normally water is used as washing agent. But without the effect of absorption, the reachable clean gas tar content is often not low enough. Because of being quite simple, water scrubbers have been the most implemented tar removal techniques in the recent small-scale gasification activities. But especially systems with water scrubbers are problematic if continuous operation is what is aimed at.

Fabric filters are no usual technique for droplet removal. Moisture and, of course, agglutination and high viscous liquids are able to destroy fabric filters within a short time. Nevertheless, so-called pre-coated filters are used for dust removal in tar containing raw gas and particularly for the separation of tar of high condensing temperature [106, 119, 120]. The answer to this

antagonism is the pre-coating. In this process, powders, for example lime stone, are spread on the fabric filter before the operation and during running as often as necessary. Separated dust and liquids remain in this layer. Then the ratio between particles, that means separated dust as well as pre-coating material, to liquid is high enough to hinder the conglomeration of the layer. This mixture can be removed from the filter.

Other Steps of Product Gas Treatment

Dust Removal Another pollutant normally to be removed before the utilization of product gas from biomass gasification is dust (e.g., [39, 112, 115, 121]). Only in some types of combustion chambers for external combustion, dust is supposed to pose no problem. But, in these cases, the dust has to be removed from flue gas because of emission reduction. Especially gas turbines are very susceptible to deterioration by dust.

Generally, most of the common dust precipitators are applicable for biomass gasification such as

- Mechanical separators
- Fabric filters
- Wet scrubbers
- Electrostatic precipitators

The cleaning of the product gas from the gasification of biomass causes several specific conditions for dust removal. Therefore, the facilities have to be adapted. The most important of these conditions are:

- The gas contains water and especially tar. A dust removal system for that application has to be designed to obviate problems with the condensation of water and tar.
- The gas is combustible. Mixtures containing oxygen in a defined ratio can be explosive. That is why, for example, cleaning of fabric filters with compressed-air is forbidden.

If the gas temperature falls below the maximum condensing temperature of the tar, tar droplets and dust particles will be separated together. This has disadvantages and advantages. On the one hand, tar and dust cannot be separately disposed of or used and the dust separation is complicated by liquids as described above. But, on the other hand, only one device for gas cleaning is necessary.

The following applications are frequently used:

- Dust precipitation with fabric filters at temperatures above the tar condensing range. Sometimes this dust precipitation is accompanied by the separation of the tar with the highest condensing temperature in pre-coated filters.
- Separation of dust and tar together in wet scrubbers or electrostatic precipitators.

Other Pollutants Alkali can deteriorate most gas utilizations, especially gas turbines and fuel cells. But it is normally removed simultaneously during the gas cooling and the dust removal. Often it is adsorbed at the surface of dust particles.

Because product gas from wood contains a lower content of halogen and sulfur compounds, these substances are not relevant for the product gas cleaning for the utilization in electrical energy supply. Exceptions are only the utilization in susceptible devices such as fuel cells and the use of nonstandard fuel like straw.

Fuel Gas Cooling and Water Removal In addition to gas cleaning, gas cooling is an important part of gas treatment. As explained, for example, for the utilization in gas engines, the gas temperature has to stay below a limit defined by engine's behavior. The standard solution is cooling with heat exchangers of recuperator design. This makes heat utilization possible. But these heat exchangers can also be affected by pollution with tar.

Alternatively, quench cooling can be employed where cold water or cold organic liquids are brought in contact with the product gas (e.g., by injection of the liquid into the gas).

If the gas temperature goes below the water dew point during the gas cooling, water will be removed from the gas. A separate gas drying is normally not necessary for small-scale applications for electricity production. If water droplets are problematic for the further equipment, a slight temperature increase after the water separation can solve the problem.

Flue Gas Treatment

Flue gases from reciprocating engines often do not fulfill the emission limits for carbon monoxide and hydrocarbons such as benzol (e.g., [27, 56, 58, 59]).

Oxidizing catalysts and regenerative thermal post-combustion are state-of-the-art techniques for the reduction of these emissions.

Overall Process Chains

Based on the components described, a lot of technical possible process chains, which could be operated, can be set up. For this, only a few conditions have to be fulfilled:

- The gasifier must be able to utilize the biomass fed in and to produce only as much gas as the product gas treatment needs.
- The product gas treatment has to adapt the product gas quality generated by the gasifier to the requirements of the gas utilization.
- The gas utilization must be able to generate the required amount of energy.

In addition, a preferable process chain must also fulfill a number of further conditions:

- High efficiency, especially high overall electrical efficiency
- Low financial and technical input
- High reliability
- Low environmental impact
- Others depending on the specific task

The requirements and operational conditions of gas utilization and gasification determine the necessary additional equipment. In the following, three typical examples for such combinations are explained.

- *Cocurrent gasifier and gas engine*: relatively simple process chain because of relatively clean raw product gas
- *Countercurrent gasifier and gas engine*: complex process chain because of relatively polluted raw product gas
- *Countercurrent and Stirling engine*: simple process chain because of the robust external combustion

Cocurrent Gasifier and Gas Engine

This combination of a cocurrent gasifier and a gas engine (e.g., [119, 120]) is realized in a lot of concepts. The Pyroforce gasification concept is one of the successful examples of the implementation of cocurrent gasification. As shown in Fig. 12, the system consists of biomass supply, gasifier, multistage product gas treatment, gas engine, waste heat recovery, and flue gas treatment.

Applying a cocurrent gasifier, the fuel requirements are quite strict. Only woodchips are allowed to be utilized. The size of pieces has to be between 8 and 63 mm; only 2% fine fraction and 1% coarse fraction

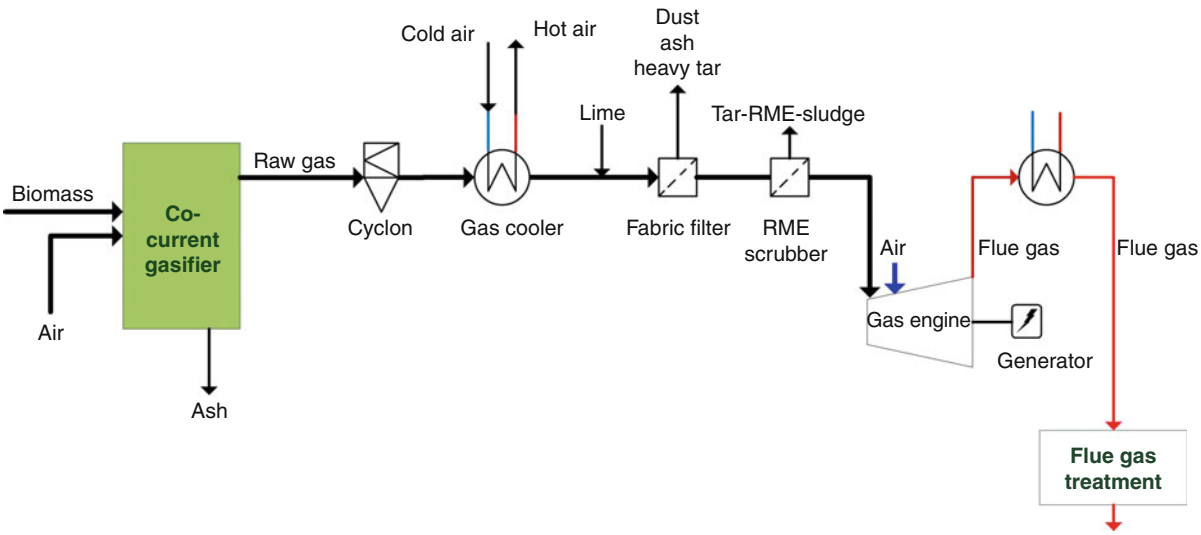

Biomass Gasification for Rural Electrification, Small Scale. Figure 12
Process schema of the Pyroforce process

are tolerable. Also the water content is restricted to 10%. This is the reason why relatively little effort is required for tar removal and handling. The gas treatment consists of a cyclone for the removal of coarse dust, the gas cooling, a pre-coated filter for fine dust precipitation and tar pre-removal, and an FAME-washer for final tar elimination. It has to be considered that this system, which is one of the most reliable small-scale gasification systems available so far, does not use a water washing, but a washing with an organic solvent.

Plants employing the Pyroforce process with an electrical power between 150 and 1,200 kW are running in Austria and Switzerland, where commercial operation has nearly been reached.

Countercurrent Gasifier and Gas Engine

There are also plants operating in practice, which apply a countercurrent gasifier and a gas engine. One successful concept is the Haboøre Updraft Gasification Technology (e.g., [32, 33]). As shown in Fig. 13, the system consists of biomass supply, gasifier, product gas treatment, gas engine, waste heat recovery, flue gas treatment, and extensive condensate treatment system.

Applying a countercurrent gasifier, the fuel requirements are much less strict than for a cocurrent gasifier. Woodchips with 35–55% moisture content can easily be utilized. Also the use of low-grade woodchips and waste fractions is possible. These and the long time experience are the greatest advantages of this technology.

But the high tar content in the raw product gas of countercurrent gasifiers generates a lot of additional effort. The raw product gas of the Haboøre plants contains, in terms of dry gas, 40–100 g/m_N tar and 70–100 g/m_N^3 light hydrocarbons. The raw gas treatment employing a gas cooler with a condensate separator and an electrostatic precipitator is still able to reach a clean product gas tar content of less than 2 mg/m_N^3. But the effort for the condensate treatment is enormous. Several systems have been tested. The standard solution applies a separation of light and heavy fractions, a vaporization for the light fraction, separate combustion chambers for the light and heavy fractions (the second one with raw gas as possible additional fuel), and heat exchangers for the use of the heat from the condensate combustion. This condensate treatment is the major shortcoming of this technology.

Plants employing the Haboøre Updraft Gasification Technology are successfully running under commercial conditions in Denmark and Japan. Especially, the plant in Denmark (Haboøre) has proven its practical performance

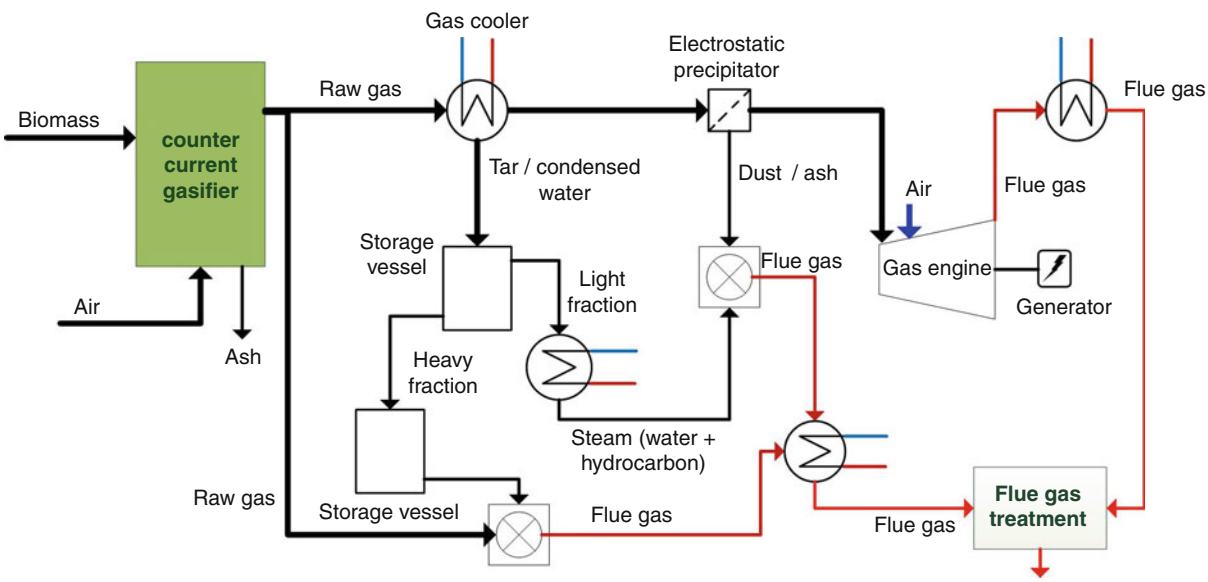

Biomass Gasification for Rural Electrification, Small Scale. Figure 13
Process schema of the Haboøre Updraft Gasification Technology

in more than 55,000 h of operation. The existing plants are a bit larger than 1 MW electrical output. The gasifier, the gas engine, and also the gas treatment can easily be scaled down. But, the issue of an economical condensate treatment increases with the scale being decreased.

Countercurrent Gasifier and Stirling Engine

The combination with a Stirling engine makes it possible to avoid the problem with countercurrent gasifiers described before. Being a gas utilization technique with an external combustion, the Stirling engine is able to use tar containing gas. In an adequately designed combustion chamber, the tar steam can be burned together with the product gas. The tar reacts to carbon dioxide and water. With it, the tar is a valuable energy carrier. Because the tar is used in the combustion chamber of the Stirling engine, no tar removal is necessary to protect the engine and so the whole process chain can be simplified. But, in addition, tar can be a problem in tubes and other devices before burning.

One system using this combination is the BISEA-system developed in Denmark (e.g., [73, 122, 123]). There are two main problems with this combination:

- The reliability is not proven.
- The efficiency of Stirling engines normally is inferior to the efficiency of gas engines.

Gasifiers of simple design combined with Stirling engines are potential solutions for very small-scale applications, if the reliability of these engines can be improved.

Future Directions

In summary, the gasification of solid biomass is a key technology with great prospects for integration in future energy systems. Especially the performance of small-scale electricity generation, for example for rural electrification, can be enhanced. It can be foreseen that high efficiencies in this scale are only possible by employing gasification techniques. The weak points of this technique are currently a global research topic. These activities suggest that gasification can completely play its potential role in the next few years.

To increase the rate of commercialization, the following research topics have to be executed with an enhancement in efforts:

- Investigation of the detailed chemical processes, especially the reaction pathways and kinetics
- Understanding of the behavior of herbaceous biomass as fuel
- Development of gasifiers which
  - Are able to use different and low-grade biomass
  - Produce gas with less tar and other pollutants
  - Have a high efficiency
  - Are inexpensive
  - Can be operated with less effort
- Development of inexpensive but high-efficient product gas cleaning systems
- Minimization of the amount of waste and wastewater, inexpensive but environmentally friendly systems for their recovery
- Further development of the gas utilization technologies with the aim to use low-quality product gases to decrease the effort of gas treatment
- Enhanced system integration
- Increase in reliability and availability together with a reduction of maintenance and operation requirements

All these activities have to be channeled to create demonstration plants which can prove the reliability, availability, and efficiency of gasification technology.

A current problem is that the research and especially development activities in the field of small-scale gasification are dispersed to many minor and largely isolated players. Of major importance for the future of the technology field of small-scale gasification is to pool their efforts and/or to win a big player for the development of the technology.

An alternative approach to high-efficient rural electrification employing biomass is to produce high-quality fuel from the biomass and to utilize this in specialized, decentralized power generators.

Bibliography

Primary Literature

1. Troitzsch U, Weber W (1987) Die Technik – Von den Anfängen bis zur Gegenwart. Georg Westermann Verlag, Stuttgart
2. Gööck R (1993) Die großen Erfindungen –Textil, Bauen und Wohnen, Beleuchtung, Sigloch edn. Künzelsau
3. Fernandez D, Michaelis F (2009) Holzvergasung als Alternativer Brennstoff. In: Kolbenmaschinen. Lecture notes from the Hamburg University of Applied Sciences

4. Danner A Ein klein wenig Wissen über Holzgas. http://verein-fuer-historische-fahrzeuge-und-geraete-uterriexingen.de/app/download/3126344802/Bericht+Holzgas+Alexander+Danner+23+02+05+.pdf. Accessed 14 Aug 2010
5. Lindauer M (2006) Stand der Technik und Wirtschaftlichkeit von Holzver-gasungsanlagen zur Gewinnung von elektrischer Energie. Diploma thesis, Nürtingen-Geislingen University
6. Overend RP, Milne TA, Mudge LK (1985) Fundamentals of thermochemical biomass conversion. Elsevier Applied Science, London/New York
7. Schulze Lammers P, Leuchs M (1985) Vergasung von Biomasse und Nutzung des Gases zum Antrieb von Motoren. Scientific report BMFT-FB-T 85-066, Freising
8. Schulze Lammers P (1984) Kenngrößen der thermischen Gegenstromver-gasung von Weizenstroh und ausgewählten Holzbrennstoffen. Dissertation, Technical University München-Weihenstephan
9. Steinbrecher N, Walter J (2001) Marktübersicht dezentrale Holzvergasung: Marktanalyse für Holzvergasungssysteme bis 5 MW. Öko-Institut, Darmstadt
10. Bühler R (1994) Stand der Technik von Holzvergasungsanlagen. In: Nussbaumer Th (ed) Neue Erkenntnisse zur thermischen Nutzung von Holz, Tagungsband zum 3, Holzenergiesymposium. ETH Zürich, Zürich
11. Nussbaumer Th (2002) Verfahren und Potenzial der Biomasse-Vergasung. In: Nussbaumer Th. (Hrsg.) 7. Holzenergiesymposium, Zürich, 18 Oct 2002
12. Born M (1998) Grundlagen der Vergasung von Abfällen, Verfahren und Prozeß-führung. In: Born M, Berghoff R (eds) Vergasungsverfahren für die Entsorgung von Abfällen. Springer-VDI-Verlag GmbH, Düsseldorf
13. Hofbauer H, Rauch R (2002) Zweibett-Wirbelschichtvergasung in Güssing (A) mit 2 MW_{el}/4,5MW_{th}. In: Nussbaumer Th (ed) 7. Holzenergiesymposium, Zürich, 18 Oct 2002
14. Fu P, Hu S, Xiang J et al (2009) Mechanism study of rice straw pyrolysis by Fourier Transform Infrared Technique. Chin J Chem Eng 17:522–529
15. Yang H, Yan R, Chen H et al (2007) Characteristics of hemicellulose, cellulose and lignin pyrolysis. Fuel 86:1781–1788
16. Britt PF, Buchanan AC, Thomas KB et al (1995) Pyrolysis mechanisms of lignin: surface-immobilized model compound investigation of acid-catalyzed and free-radical reaction pathways. J Anal Appl Pyrol 33:1–19
17. Liu Q, Wang S, Zheng Y et al (2008) Mechanism study of wood lignin pyrolysis by using TG-FTIR analysis. J Anal Appl Pyrol 82:170–177
18. Hosoya T, Kawamoto H, Saka S (2007) Cellulose–hemicellulose and cellulose–lignin interactions in wood pyrolysis at gasification temperature. J Anal Appl Pyrol 80:118–125
19. Hosoya T, Kawamoto H, Saka S (2007) Pyrolysis behaviors of wood and its constituent polymers at gasification temperature. J Anal Appl Pyrol 78:328–336
20. Otschik J (2000) Pyrolyse von Hausmüll – Modellierung am Beispiel der Schweltrommel des Schwelbrennverfahrens. Postdoctoral lecture qualification, Technical University Dresden
21. Kirubakaran V, Sivaramakrishnan V, Nalini R et al (2009) A review on gasification of biomass. Renew Sustain Energy Rev 13:179–186
22. Li C, Suzuki K (2009) Tar property, analysis, reforming mechanism and model for biomass gasification: an overview. Renew Sustain Energy Rev 13:594–604
23. Sutton D, Kelleher B, Ross JRH (2001) Review of literature on catalysts for biomass gasification. Fuel Process Technol 73:155–173
24. Han J, Kim H (2008) The reduction and control technology of tar during biomass gasification/pyrolysis: an overview. Renew Sustain Energy Rev 12:397–416
25. Klemm M (2005) Heißentteerung von Brenngas aus der Vergasung von Biomasse durch katalytische partielle oxidation. VDI Verlag GmbH, Düsseldorf
26. Meyer B (1998) Grundlagen der Vergasung von Abfällen. In: Born M, Berghoff R (eds) Vergasungsverfahren für die Entsorgung von Abfällen. Springer-VDI-Verlag, Düsseldorf
27. Lettner F, Timmerer H, Haselbacher P (2007) Biomass gasification – State of the art description. Report for Intelligent Energy Europe, Grant agreement no. EIE/06/078/SI2.447511
28. Knoef HAM (ed) (2005) Handbook biomass gasification. BTG biomass technology group BV, The Netherlands
29. Obernberger I, Hammerschmid A (1999) Dezentrale Biomasse-Kraft-Wärme-Kopplungstechnologien. dbv - Verlag für die Technische Universität Graz, Graz
30. Berger R, Hein KRG (2003) Verfahrensübersicht: Synthesegaserzeugung aus Biomasse. FVS Fachtagung, Stuttgart
31. Radig W (2007) Vergasung als Option der thermochemischen Nutzung von Biomasse. TerraTec, Leipzig, 5–8 Mar 2007
32. Babcock & Wilcox Vølund (ed) (2009): The gasification process. http://www.volund.dk/technologies_products/gasification/the_gasification_process. Accessed 28 May 2010
33. Lundtorp K (2009) Operational performance and new applications of the Haboøre Updraft Gasification Technology. CEP® Clean Energy Power 2009, Stuttgart, 29–31 Jan 2009
34. Bühler R, Hasler Ph (1997) Stand und Entwicklung der Vergasungstechnik. In: Energietechnik VDI-Gesellschaft (ed) Thermische Biomassenutzung- Technik und Realisierung VDI Berichte 1319. VDI Verlag, Düsseldorf
35. Schneider M (2003) Experimentelle und mathematische Modellierung der Festbettvergasung am Beispiel der Gleichstromvergasung von Holzhackschnitzeln – ein Beitrag zur Erhöhung der Prozeßtransparenz. Dissertation, Technical University Dresden
36. Liebisch G, Topf N (1998) Luft-Querstrom-Vergasung – eine Möglichkeit zur dezentralen Energieerzeugung aus Biomasse und Abfallstoffen. In: Born M, Berghoff R (eds) Vergasungsverfahren für die Entsorgung von Abfällen. Springer-VDI-Verlag, Düsseldorf

37. Topf N, Liebisch G, Hahn D (2001) Innovations: How to transform tar residues into a product. In: First ever meeting of IEA international energy agency thermal gasification of biomass task in Germany, Dresden, 21–23 Nov 2001
38. Zeymer M, Rönsch R, Klemm M (2010) Nutzung fester Brennstoffe in kleintechnischen KWK-Anlagen. In: Workshop Technische Anlagen und Konzepte, Mosbach, 09–10 Mar 2010
39. Hasler Ph, Buehler R, Nussbaumer Th (1998) Evaluation of gas cleaning technologies for biomass gasification. In: 10th European conference and technology exhibition biomass for energy and industry, Wuerzburg, 8–11 June 1998, pp 272 ff
40. Hammerer D (2000) Vergasung von Biomasse zur gekoppelten Strom-, und Wärmeerzeugung. Dissertation, Technical University Graz
41. Hammerer D, Pogoreutz M (2000) Operation experiences with a two-zone fixed-bed gasification system for biomass. In: 1st World conference and exhibition on biomass for energy and industry, Sevilla, 5–9 June 2000
42. Hammerer D, Reetz B (2000) Biomassevergasung in einem Zweizonen-Festbettvergaser. In: Biomassetag des IWT, Graz
43. Biomass gasification Group. DTU The Viking Gasifier. www.bgg.mek.dtu.dk. Accessed 14 Aug 2010
44. Henriksen U et al (2006) The design, construction and operation of a 75 kW two-stage gasifier. Energy 31: 1542–1553
45. Gøbel B et al (2004) Status – 2000 Hours of operation with the Viking Gasifier. In: 2nd World conference and technology exhibition on biomass for energy and industry, Rome
46. Hofbauer H Rauch R et al (2006) Energiezentrale zur Umwandlung von biogenen Roh- und Reststoffen in Wärme, Strom, Bio-SNG und flüssige Kraftstoffe. In: Berichte aus Energie- und Umweltforschung 79, BMVIT, Vienna
47. Hofbauer H, Rauch R et al (2002) Six years experience with the FICFB gasification process. In: Proceedings of the 12th European biomass conference, Amsterdam, pp 982–985
48. Pröll T (2004) Potenziale der Wirbelschichtdampfvergasung fester Biomasse – Modellierung und Simulation auf Basis der Betriebserfahrungen am Biomassekraftwerk Güssing. Dissertation, Technical University Vienna
49. Fuchs M, Rauch R, Hofbauer H (2008) Final report on systematic studies of steam gasification in pilot plant. Bio-SNG Del 5.3. TREN/05/FP6EN/S07.56632/019895. Vienna
50. van der Meijden CM, Veringa HJ et al (2008) The 800 kW_{th} allothermal biomass gasifier Milena. In: 18th European biomass conference, Valencia
51. Smit R (2009) Syngas production from biogas. In: International Freiberg conference on IGCC & XtL Technologies, Dresden
52. Paisley MA, Welch MJ (2003) Biomass gasification combined cycle opportunities using the future energy SilvaGas gasifier coupled to Alstom's industrial gas turbines. In: Proceedings of ASME Turbo Expo, Georgia
53. Paisley MA et al (1989) Gasification of refuse derived fuel in the battelle high throughput gasification system. Report PNL-6998, USA
54. Paisley MA, Overend RP (2002) Verification of the performance of future energy resources' SilvaGas® Biomass Gasifier - operating experience in the Vermont gasifier. In: Pittsburgh coal conference, Pittsburgh
55. Paisley MA (2007) Advanced biomass gasification for the economical production of biopower, fuels, and hydrogen – implementation in Montgomery, New York. 07AIChE. Salt Lake City
56. Herdin G, Wagner M (2000) Erfahrungen mit der motorischen Nutzung von Gasen aus Pyrolyse und sonstigen Vergasungsprozessen. In: DGMK-Fachbereichstagung Energetische und stoffliche Nutzung von Abfällen und nachwachsenden Rohstoffen, Velen/Westfahlen, 10–12 Apr 2000, pp 153 ff
57. Anonymus (1999) Energetische Nutzung von Sondergasen. Company publications Jenbacher Energiesysteme AG
58. Herdin GR (2002) Standesanalyse des Gasmotors im Vergleich zu den Zukunftstechniken (Brennstoffzellen und Mikroturbine) bei der Nutzung von aus Biomasse gewonnenen Kraftstoffen. Jenbacher AG, Jenbach (Austria)
59. Herdin GR (2009) Europäischer Holzgasmotorenmarkt – Notwendigkeiten und Grenzen für die Anpassung von Vergasungsanlagen und Motorentechnik. CEP® Clean Energy Power 2009, Stuttgart, 29–31 Jan 2009
60. Falkenhain GW (2000) Small Bio-Power Plant for Rural Application. In: DGMK-Fachbereichstagung Energetische und stoffliche Nutzung von Abfällen und nachwachsenden Rohstoffen, Velen/Westfahlen, 10–12 Apr 2000, pp 199 ff
61. Christoph K, Cartellieri W, Pfeifer U (1972) Die Bewertung der Klopffestigkeit von Kraftgasen mittels der Methanzahl und deren praktische Anwendung bei Gasmotoren. MTZ Motorentechnische Zeitschrift 33(10):391
62. Schley P, Frieling H (2000) Bestimmung der Methanzahl aus Gasbeschaffenheitskenngrößen. GWF Gas Erdgas 141(1):28
63. Hattingen U (1997) Motorische Nutzung von Holzgas. In: Weingarten J (ed) Holzvergasung Energetische Nutzung von Biomasse in Rheinland-Pfalz, Bingen, 13 Feb 1997, pp 28 ff
64. Cannon MF, Welch MJ (2002) Gas turbines and renewable fuels – the technologies, the risks, and the rewards. In: International conference on renewable bioenergy – technologies, risks, and rewards, London, 29–30 Oct 2002
65. Schmitz W (2001) Konversion biogener Brennstoffe für die Nutzung in Gasturbinen. VDI Verlag GmbH, Düsseldorf
66. Bengtsson S (2006) Pressurized gasification and upgrading to clean hydrogen rich synthesis gas – the EU CHRISGAS project. In: ZAE-Symposium, Freising, 11–12 Dec 2006
67. Waldheim L (2006) GREVE, Arbe and CHRISGAS. IEA Task 33 Workshop, Chicago, Oct 2006
68. Brown Ph, Fadok J, Chan P (2007) Siemens gas turbine H_2 combustion technology for low carbon IGCC. In: 2007

Gasification technologies conference, San Francisco, 14–17 Oct 2007
69. Werdich M, Kübler K (2007) Stirling-Maschinen. Grundlagen – Technik – Anwendung. Ökobuch-Verlag, Staufen
70. Steimle F, Lamprichs J, Beck P (2007) Stirling-maschinentechnik. C. F. Müller-Verlag, Heidelberg
71. Obernberger I, Carlsen H, Biedermann F (2003) State-of the- art and future developments regarding small-scale biomass CHP systems with a special focus on ORC and stirling engine technologies. In: Proceedings of the international nordic bioenergy conference, Jyväskylä (Finland)
72. Biedermann F, Carlsen H, Schöch M, Obernberger I (2003) Operating experiences with a small-scale CHP pilot plant based on a 35 kW_{el} Hermetic four cylinder stirling engine for biomass fuels. In: Proceedings of the 11th international stirling engine conference (ISEC), Rome
73. Stirling Danmark (ed) (2009) Nachhaltige Stromgewinnung - Kleinkraftwerke zur Strom und Wärmegewinnung aus Biomasse mit hohem Wirkungsgrad. http://www.sd.econtent.dk/?download=Stirlingsystem%20mit%20Gegenstromvergaser.pdf. Accessed 28 May 2009
74. McIlveen-Wright DR, Williams BC, McMullan JT (2000) Wood gasification integrated with fuel cells. Renew Energy 19: 223–228
75. Nagel FP, Schildhauer TJ, Biollaz SMA (2009) Biomass-integrated gasification fuel cell systems. Int J Hydrogen Energy 34:6809–6825
76. Hiller R, Schleitzer D (2001) Bewertung von Verfahren zur energetischen Nutzung von Biomasse mittels Brennstoffzellen - Abschlußbericht für die Fachagentur Nachwachsende Rohstoffe e.V., Förderkennzeichen 98 NR047
77. Bandi A, Specht M (2004) Gewinnung von Methanol aus Biomasse. Expertise im Auftrag der Union zur Förderung von Oel- und Proteinpflanzen e.V., UFOP
78. Köppel W (2007) Gasreinigung, Stand der Technik. In: Thermochemische Biomasse-Vergasung für eine effizient Strom-/Kraftstoffbereitstellung, Erkenntnisstand, Leipzig
79. Beer St, Reil St (2010) Betriebserfahrungen bei kleinen Festbettvergasern. In: C.A.R.M.E.N. Fachgespräch Holzvergasung, Straubing, 15 Apr 2010
80. Rösch C, Kaltschmitt M (1998) Vergleich von Systemen zur Stromerzeugung mit integrierter Biomassevergasung. In: DGMK-Fachbereichstagung Energetische und stoffliche Nutzung von Abfällen und nachwachsenden Rohstoffen, Velen/Westfalen, 20–22 Apr 1998
81. Unger Ch, Ising M (2002) Mechanismen und Bedeutung der Teerbildung und Teerbeseitigung bei der thermochemischen Umwandlung fester Kohlenstoff-träger. DGMK-Fachbereichstagung Energetische Nutzung fester Energieträger Velen/Westfahlen, 22–24 Apr 2002
82. Morf Ph, Nussbaumer Th (1998) Grundlagen zur Teerbildung bei der Holz-vergasung. Zwischenbericht Phase 1 im Auftrag des Bundesamtes für Energie, Juni 1998
83. Unger Ch, Ising M (2010) Mechanismen und Bedeutung der Teerbildung und Teerbeseitigung bei der thermischen Umwandlung fester Kohlenstoffträger. www.holzvergasung.info/WWW/UMSICHT/Produkte/ET/pdf/uebersichtsbeitrag_teere_unger_ising.pdf. Accessed 28 Aug 2010
84. Evans RJ, Milne TA (1997) Chemistry of tar formation and maturation in the thermochemical conversion of biomass. In: Bridgwater AV, Boocock DGB (eds) Development in thermochemical biomass conversion. Blackie Academic & Professional, London, p 803
85. Spliethoff H (1998) Gasqualitäten von Biomassevergasern, Stand und Perspektiven. In: Fachagentur nachwachsende Rohstoffe (ed) Gülzower Fachgespräche Energetische Nutzung von Biomasse mit Brennstoffzellen-verfahren, pp 34 ff
86. Dayton D (2002) A review of the literature on catalytic biomass tar destruction. National Renewable Energy Laboratory, Golden (Colorado)
87. Sutton D, Kelleher B, Ross JRH (2001) Review of literature on catalysts for biomass gasification. Fuel Process Technol 73:155–173
88. Zwart R W R (2006) Gas cleaning downstream biomass gasification – status report 2009: ECN-E-08-078, ECN Petten
89. Morf Ph, Hasler Ph, Nussbaumer Th (2002) Mechanisms and kinetics of homogeneous secondary reactions of tar from continuous pyrolysis of wood chips. Fuel 81:843
90. Bajohr S et al (2002) Thermische und katalytische Umsetzung von Kohlenwasserstoffen in Rohgasen aus der Pyrolyse und der Vergasung von Biomasse. DGMK-Fachbereichstagung Energetische und stoffliche Nutzung von Abfällen und nachwachsenden Rohstoffen Velen/Westfalen, 22–24 Apr 2002, pp 167 ff
91. Thomas S et al (2009) Unterschiedliche Verfahren zur Reformierung höherer Kohlenwasserstoffe. Fachsymposium Freiberg, 26–27 Feb 2009
92. Garcia XA, Hüttinger KJ (1990) Mechanism and kinetics of steam gasification of naphthalene. Erdöl und Kohle, Erdgas, Petrochemie – Hydrocarbon Technology 43(3):113
93. Ekström C, Lindman N, Pettersson R (1985) Catalytic conversion of tars, carbon black and methane from pyrolysis/gasification of biomass. In: Overend RP, Milne TA, Mudge LK (eds) Fundamentals of thermochemical biomass conversation. Elsevier, London/New York, p 601
94. Erich E, Klemm M et al (2008) Entwicklung und Erprobung der katalytisch spaltenden Hydrierung und der katalytischen partiellen Oxidation zur Aufbereitung teerhaltiger Brenngase aus der Biomassevergasung. Abschlussbericht zum AIF-Vorhaben Nr. 14398 BG
95. Erich E, Hedfed J (2002) Brenngasaufbereitung in Biomassevergasungs-anlagen. In: VDI-Berichte 1733, VDI-Verlag, Düsseldorf
96. Jönsson O (1985) Thermal cracking of tars and hydrocarbons by addition of steam and oxygen in the cracking zone. In: Overend RP, Milne TA, Mudge LK (eds) Fundamentals of thermochemical biomass conversation. Elsevier, London/New York, p 733

97. Jensen PA, Larsen E, Jörgensen KH (1996) Tar reduction by partial oxidation. In: 9th European bioenergy conference, Copenhagen, pp 1371 ff
98. Brandt P, Henriksen U (1998) Decomposition of tar in pyrolysis gas by partial oxidation and thermal cracking. In: 10th European conference and technology exhibition biomass for energy and industry, Wuerzburg, 8–11 June 1998, pp 1616 ff
99. Susanto H, Beenackers ACM (1996) A moving-bed gasifier with internal recycle of pyrolysis gas. Fuel 75(11):1339
100. Lammers G, Beenackers ACM, Corella J (1997) Catalytic tar removal from biomass producer gas with secondary air. In: Bridgwater AV, Boocock DGB (eds) Development in thermochemical biomass conversion. Blackie Academic & Professional, London
101. Klemm M (2005) Katalytische partielle Oxidation löst Kernproblem der Biomassevergasung. Erdöl Erdgas Kohle 121(H 10):356–359
102. Böhning D, Klemm M (2007) Aufbereitung teerhaltiger Brenngase aus der Biomassevergasung. In: 40. Jahrestreffen Deutscher Katalytiker, Weimar, 14–16 Mar 2007
103. Böhning D, Beckmann M (2009) Dezentrale Biomassevergasung - Teerabbau durch primäre und sekundäre Maßnahmen. In: Thomé-Kozmiensky KJ, Beckmann M (eds) Erneuerbare Energien - Band 2. TK Verlag Karl Thomé-Kozmiensky, Neuruppin
104. Lüdke H (1963) Gasversorgung von A bis Z. Deutscher Verlag für Grundstoffindustrie, Leipzig
105. Hofbauer H, Rauch R, Ripfel-Nitsche K Report on gas cleaning for synthesis application. Del 2E-3, EU ThermalNet
106. Rauch R (2009) Cleaning and usage of product gas from biomass steam gasification. In: SGC Gasification seminar, Stockholm
107. Boerrigter et al (2006) OLGA Optimum. ECN-E–06-046. ECN, Petten
108. Dahlmann Filter Technology (ed) (2008) OLGA tar removal. Technical Information Paper, revision, spring 2008
109. Könemann J W (2009) OLGA tar removal technology. SGC gasification seminar, Stockholm
110. Zwart RWR et al (2009) Oil-based gas washing – flexible tar removal for high-efficient production of clean heat and power as well as sustainable fuels and chemicals. Environ Prog Sustain Energy 28:324–335
111. Bauermeister U (2009) Gaserzeugung aus fester Biomasse – Marktfähigkeit heute. GNS – Gesellschaft für nachhaltige Stoffnutzung mbH, Halle
112. Hasler Ph, Buehler R, Nussbaumer Th (1997) Evaluation of gas cleaning technologies for small scale biomass gasifiers. Swiss Federal Office of Energy and Swiss Federal Office for Education and Science, Zürich and Maschwanden
113. Schmidt J (1970) Verfahren der Gasaufbereitung. Deutscher Verlag für Grundstoffindustrie, Leipzig
114. Oechselhaeuser K (1953) Atlas der Technik des Gasfaches. Verlag Technik, Berlin
115. Bär R (2001) Dust extraction in biomass gasification and incineration plants typical fields of application for various filter typs. In: First ever meeting of IEA international energy agency thermal gasification of biomass task in Germany, Dresden, 21–23 Nov 2001, pp 82 ff
116. Oldenburg H (2010) Reinigung von Brenngasen aus der Vergasung von Biomasse mittels Elektrofilter. DGMK-Fachbereichstagung Konversion von Biomassen, Gelsenkirchen, 10–12 May 2010
117. Klemm M, Ortwein A, Zeymer M, Rönsch St, Schmersahl R (2010) Gasreinigung und -konditionierung – Stand der Technik und Gesamtkonzepte für Methanisierungsanlagen. 1. International biomass conference, Leipzig, 4–5 Mai 2010
118. Anonymus (2010) BETH Teer-Elektrofilter. http://beth-filter.ch/ch-produkte-anzeigen.html?vers=28. Accessed 30 Apr 2010
119. Schaub M, Gemberle H (2007) Die PYROFORCE® – Technologie zur Holzverstromung. Pyroforce Conzepte AG
120. Böcker-Riese B (2008) Orientierungspräsentation zur thermochemischen Vergasung mit dem PYROFORCE®-Verfahren inkl. Grundlagen. Pyroforce Conzepte AG www.pycon.ch. Accessed 11 Mar 2010
121. Fritz W, Kern H (1990) Reinigung von Abgasen. Vogel Buchverlag, Würzburg
122. EHSP Engineering Solutions (ed) (2008) Projekthandbuch – BISEA: Wärme- und Stromerzeugung mit regenerativen Rohstoffen, 2008
123. The Babcock & Wilcox Company (ed) (2001) B&W – Stirling: Power Boiler. www.babcock.com/library/pdf/E1013120.pdf. Accessed 29 May 2009

Books and Reviews

Bridgwater AV (ed) (2001) Progress in thermochemical biomass conversion. Blackwell Science, Oxford

Fachagentur Nachwachsende Rohstoffe (ed) (2006) Analyse und Evaluierung der thermo-chemischen Vergasung von Biomasse. In: Schriftenreihe Nachwachsende Rohstoffe, Landwirtschaftsverlag GmbH, Münster

Guideline for safe and Eco-friendly biomass gasification (2009) Report for Intelligent Energy Europe, www.gasification-guide.eu/gsg_uploads/ documenten/D10_Final-Guideline.pdf

Higman C, van der Burgt M (2008) Gasification, 2nd edn. Gulf Professional, Burlington

Kaltschmitt M, Hartmann H, Hofbauer H (eds) (2009) Energie aus Biomasse. In: Grundlagen, Techniken und Verfahren. Springer, Berlin, 2009

Knoef HAM, Ahrenfeldt J (eds) (2005) Handbook Biomass Gasification. BTG biomass technology group BV, Enschede

Biomass Production

Michaela Ernst[1], Achim Walter[1,2], Ulrich Schurr[1]
[1]IBG-2: Plant Science, Forschungszentrum Jülich, Jülich, Germany
[2]ETH Zürich, Institute of Plant, Animal and Agroecosystem Sciences, Professorship of Crop Science, Zurich, Switzerland

Article Outline

Glossary
Definition of the Subject
Introduction
Generation of Biomass in Plants and Animals
Plant Selection and Plant Breeding
Future Directions
Bibliography

Glossary

Biomass Material derived from recent living organisms.

Bioenergy Energy obtained from fuels derived from biomass.

Bioenergy crops Crops for the production of bioenergy.

Marker-assisted selection (MAS) An indirect selection process in plant breeding. A trait of interest (e.g., shoot biomass) is selected based on a molecular marker (see "molecular marker"), which is linked to the trait.

Molecular marker Molecular markers are identifiable DNA sequences and act as landmarks in the genome. They are inherited by the standard laws of inheritance from one generation to the next.

Trait A genetically determined characteristic or condition. Traits can result from the activity of one single gene or an interaction of the activity of several genes (e.g., shoot biomass is a so-called quantitative trait).

Autotrophic Autotrophic organisms are able to synthesize organic substances from inorganic substances using either light or chemical energy as energy source. These organic molecules are then used to carry out biological functions including cell growth. Autotrophs such as green plants, algae, and certain bacteria are the starting point of the food chain.

Heterotrophic Heterotrophic organisms depend on the organic compounds synthesized by autotrophs and utilize these organic compounds as food. Heterotrophs are animals, fungi, most of the bacteria and protozoa.

Chloroplast Chloroplasts are cell organelles of plant cells in which photosynthesis takes place.

Enzyme Proteins or protein complexes that catalyze a biochemical reaction.

Photosynthetic efficiency The fraction of incident solar energy reaching the surface of the plant that is converted into chemical energy in the form of carbohydrates.

Stomata Tiny pores of the plant surface necessary for transpiration and gas exchange with the surrounding air; their opening and closing is controlled by various factors such as plant hormones and the water status of the plant.

C3-plants C3-plants use the enzyme Ribulose-1,5-bisphosphat-carboxylase/-oxygenase (RuBisCO) to make a three-carbon compound as the first stable product of photosynthesis. Carbon losses through photorespiration are high in contrast to C4- and CAM plants.

C4-plants C4-plants possess biochemical and anatomical mechanisms to raise the intercellular carbon dioxide concentration at the site of fixation and thus reduce carbon losses by photorespiration.

Crassulacean acid metabolism (CAM) plants CAM plants fix CO_2 during the night, store CO_2 as a component of the compound malic acid, and release it from malic acid during the day. Then it is concentrated around and utilized by the enzyme RuBisCO, thereby increasing the efficiency of photosynthesis. The CAM pathway allows plants to remain their stomata shut during the day, which reduces evotranspiration and allows plants to grow in arid climate.

Photorespiration Photorespiration is a very complex side reaction of the main enzyme of photosynthesis (RuBisCO). The catalytic center of RuBisCO is able to bind CO_2 or O_2 in general the enzyme favors CO_2, but if the level of O_2 is increasing, which occur

if stomata are closed – for example, on hot days to avoid evaporation – the competition between CO_2 and O_2 is increased and more O_2 will bound to the enzyme. Photorespiration leads to a net loss of carbon and reduce the photosynthetic efficiency.

Water use efficiency (WUE) The ratio of photosynthetic CO_2 assimilation and evaporation.

Monocotyledonous plants In the traditional plant taxonomic system, monocotyledonous plants, or monocots, are one of the two major groups of flowering plants the other one are the dicotyledonous plants, or dicots. Most members of the monocots have one cotyledon or embryonic leaf, in their seeds, parallel veins, and floral organs arranged in cycles of three.

Dicotyledonous The second major group of flowering plants – see also Monocotyledonous plants. Members are characterized by two embryonic leaves in their seeds, reticulate veins and floral organs arranged in cycles of four or five.

Harvest index The ratio of grain yield to total plant mass.

Ideotype Ideotypes are defined by breeders, specifying the optimal plant for a particular purpose.

Definition of the Subject

The energy of sunlight reaching the earth exceeds global human energy consumption by a factor of several thousand. Plants are equipped with an intrinsic energy conversion system – photosynthesis – allowing them to utilize sun energy directly for the production of biomass. Human mankind has coevolved and profited from this energy conversion system by placing it at the base of its food production chain and by starting the utilization of firewood as its first energy source. Enormous attempts have been made by mankind to optimize food production from plants via targeted agronomical improvements, such as selection of most productive crop species, increasing agronomical output via the measures of the green revolution and by conventional and marker-assisted plant breeding. In contrast to this, practically no attempts have been made to optimize the use of plant material as energy source because access to fossil – plant-derived – energy resources was far easier. In a future energy scenario, dedicated production of plant biomass as an energy source will play a vital role, in concert with other sustainable technologies.

Introduction

Renewable resources convert solar energy, the rotation of the earth and geothermal energy into usable energy. Solar power, hydropower, traditional biomass, wind energy, geothermal heat, and biofuels – bioethanol, biodiesel, and biogas – count as renewable resources. Currently, renewable energies supply more than 10% of global total energy consumption with increasing tendency. Fossil fuels supply 388 EJ (ExaJoule; 10^{18} J) per year – this corresponds to more than 80% of total energy consumption – and biomass 45 +/− 10 EJ per year, including traditional biomass usage. The world's primary demand will grow roughly by 1.6% per year to 714 EJ in 2030 [1]. The relevance of bioenergy from biomass differs from region to region depending on the socioeconomical background of the countries: In industrialized countries biomass contributes to less than 10% of total energy consumption; in developing countries this proportion amounts to 20–30%, and in some countries it can exceed 50% (Bhutan 86%, Nepal 97%). In contrast to the developing countries, where traditional biomass (firewood, sometimes dung) is the main energy source for noncommercial usage of the poorer people (cooking, heating), modern bioenergy in industrialized countries is used for industry (heat, electricity), transport (biofuels), and domestic applications (mainly heat). The interest in transport fuels increased strongly in the industrialized countries (North America, Japan, and Europe) as well as within the rapidly developing Asian nations (China and India) and in Brazil. For example, the production of ethanol was doubled from 2000 to 2009 and the production of biodiesel was increased by a factor of 3. In contrast to this, the production of crude oil increased only by 7% [2, 3].

For this energy provision, biomass is needed. This is true for residues and energy crops. The so-called first-generation bioenergy crops were developed from food crops and therefore they compete for fertile land and external inputs with food crops. For bioethanol production, globally relatively few crop species are used (maize, sugarcane, oil palm, rapeseed). These crops

need a high amount of energy input in form of fertilizer and tillage. Thus, they are of limited value from the point of sustainability. For these reasons, new varieties and species were included – the second-generation of bioenergy plants. The aim was to find plants, which do not compete with food crops and which influence the environment in a mitigating and positive manner. Biomass productivity is the result of different factors, which interact with each other: the genetic background of the variety, the environmental conditions, external factors like the grade of rationalization in agriculture, and the local socioeconomic base.

Generation of Biomass in Plants and Animals

Plants are "autotrophic" organisms that live and grow based on consumption of nonliving matter and energy only. They can acquire energy from sunlight via the light-harvesting complexes of their photosystems and use this energy to produce organic matter from mineral nutrients, atmospheric carbon dioxide, and water. As a by-product they generate and release oxygen, thereby facilitating animal life. Hence, the nutrition and generation of plant biomass does not necessarily depend on the interaction with any other organism, although many plants benefit from symbiotic use of other organisms in their vicinity.

Animals and fungi are different. They have never evolved to "take care of themselves," but they have found successful ways to lead a life and to produce biomass heterotrophically – based on the consumption of dead organic matter. They also have complicated metabolic pathways, converting certain compounds into other compounds. But at the base of these reactions they depend on organic substances (such as carbohydrates, lipids, proteins, vitamins), which have been produced by other organisms and ultimately by plants.

Hence, renewable energy can only be produced in a sustainable and carbon-neutral way mostly from plants. For this reason, this entry will show how plants capture energy from sunlight to produce biomass and it will show the limits and potentials of this process in the context of energy crops for human use. Furthermore, it will elaborate on the ongoing and prospective refinement of plants to quench the human need for food and energy.

Conversion of Light Energy into Chemically Bound Energy

Plants utilize the energy of light quanta to drive biochemical reactions with which they convert anorganic elements and compounds into organic molecules. Both energy conversion (via photosynthesis) and growth processes (via assembly of these organic molecules to biomass) are processes that are characteristic features of plants, which have been optimized in evolution. Intelligent and sustainable production of biomass for renewable energy requires thorough basic process understanding of both processes and directed melioration of photosynthesis and of growth.

Photosynthesis

Photosynthesis converts light energy into chemically bound energy, thereby liberating oxygen from H_2O (to form O_2) and anabolizing carbohydrates from CO_2 and H_2O. Six molecules of carbon dioxide and water are used for the production of one molecule of carbohydrates and six molecules of oxygen. The overall equation for the type of photosynthesis that occurs in plants is shown below (Eq. 1).

$$\underset{\text{Carbondioxide}}{6CO_2} + \underset{\text{Water}}{6H_2O} \xrightarrow{\text{Light}} \underset{\text{Carbohydrates}}{C_6H_{12}O_6} + \underset{\text{Oxygen}}{6O_2} \qquad (1)$$

The primary process in this conversion of energy from one form into another is the acquisition of photons by chlorophyll molecules, thereby lifting the energy status of chlorophyll molecules to higher levels. These acquisition processes occur in two biochemically distinct regions: Photosystem I and Photosystem II.

The Z-scheme is an energy diagram for electron transfer in the "light reactions" of plant photosynthesis. The y-axis shows an energy scale for each molecule's ability to transfer an electron to the next molecule, proceeding from left to right. The source of electrons is water (see on the left side). Plants transform light energy into an electron flow and hence into chemical energy in the form of reduced NADPH and adenosine triphosphate (ATP), which are used in the following Calvin-cycle to drive the production of glyceraldehyde-3-phosphate. Thus, the Z-scheme depicts the sequence of electron flow (oxidation and reduction) from the perspective of plant's energy acquisition. Three major protein complexes are involved

in the Z-scheme: (1) the Photosystem II, (2) the Cytochrome bf complex (containing $Cytb_6$, FeS and Cytf, in the middle of the Z), and (3) the Photosystem I (http://www.life.illinois.edu/govindjee/). Abbreviations from left to right: *Mn* for a manganese complex containing 4 Mn atoms, bound to Photosystem II (PSII) reaction center; *Tyr* for a particular tyrosine in PSII; O_2 for oxygen; *H+* for protons; *P680* for the reaction center chlorophyll (Chl) in PSII: it is the primary electron donor of PSII; Excited (Chl) P680 for $P680^*$ that has the energy of the photon of light; *Pheo* for pheophytin molecule (the primary electron acceptor of PSII; it is like a chlorophyll *a* molecule where magnesium (in its center) has been replaced by two "H"s); Q_A for a plastoquinone molecule tightly bound to PSII; Q_B for another plastoquinone molecule that is loosely bound to PSII; *FeS* for Rieske Iron Sulfur protein; *Cyt. f* for Cytochrome f; $Cytb_6$ (L and H) for Cytochrome b_6 (of Low and High Energy); *PC* for copper protein plastocyanin; *P700* for the reaction center chlorophyll (Chl; actually a dimer, i.e., two molecules together) of PSI; it is the primary electron donor of PSI; Excited (Chl) P700 for $P700^*$ that has the energy of the photon of light; A_0 for a special chlorophyll a molecule (primary electron acceptor of PSI); A_1 for a phylloquinone (Vitamin K) molecule; F_X, F_A, *and* F_B are three separate Iron Sulfur Centers; *FD* for ferredoxin; and *FNR* for Ferredoxin NADP oxido Reductase (FNR).

The photosystems are large complexes composed of a number of different pigments and other molecules that are working together in a very clever way to maximize the use of light energy (Fig. 1). The parts of these pigment complexes that do the job of capturing light quanta are called "light-harvesting complexes"; other parts are responsible to initiate biochemical reactions utilizing the energy of a de-exciting chlorophyll molecule while still other parts are responsible to deal with excessive light energy that cannot immediately be transferred to biochemical reactions. Some of the light energy is used in the end to mobilize "ATP-synthase," a macromolecular protein complex, which is driven by a flux of protons from one side of the membrane to the other and which finally anabolizes the energy-rich molecule adenosine triphosphate (ATP) from adenosine diphosphate (ADP) and phosphate (P) (Fig. 2). ATP is the universal energy currency of all living matter; decomposing ATP to ADP and P drives a plethora of biochemical reactions in both plants and animals.

The conversion efficiency of these reactions is extremely high. Almost 100% of the incoming light energy can be transferred to the primary steps of biochemical reactions, which is decreased by a number of biochemical "downstream reactions" finally resulting in biomass gain via growth processes.

All of the above-mentioned so-called light reactions of photosynthesis (they are driven by the energy of sunlight) take place in the chloroplast. Chloroplasts are organelles contained in each green plant cell. Average leaf tissue contains around 500,000 chloroplasts per mm^2;. The fraction of light energy not used for mobilization of ATP-synthase is providing energy to the so-called dark reactions: The specific biochemical reactions that assemble carbohydrates and oxygen from CO_2 and H_2O (reactions independent of sunlight that can proceed at day or night).

As a central step of these dark reactions, the enzyme Ribulose-1,5-bisphosphat-carboxylase/-oxygenase (RuBisCO) captures CO_2 and releases carbohydrates consisting of three carbon atoms, which are later combined to compounds such as sucrose, starch, and cellulose. The core cycle of dark reactions is called Calvin- or Calvin–Benson cycle (Fig. 3). Its core enzyme, RuBisCO is the most abundant enzyme to be found in all organisms worldwide.

This is the core set of processes performed in nature to convert solar energy into the components of biomass providing human mankind with energy and food. This set of processes is performed by all green plant biomass throughout the entire world, both on land and in the ocean. A map of global photosynthetic productivity (Fig. 4) shows impressively that this process embraces the entire globe, with maxima in tropical regions and boreal biomes. Minima are found in polar regions where temperature is too low, deserts, where water is scarce, and certain ocean regions where lack of mineral nutrients imposes shortages on biomass production.

Photosynthetic Strategies in Plants

There are mainly three photosynthetic strategies in plants. They are characterized by differing processes

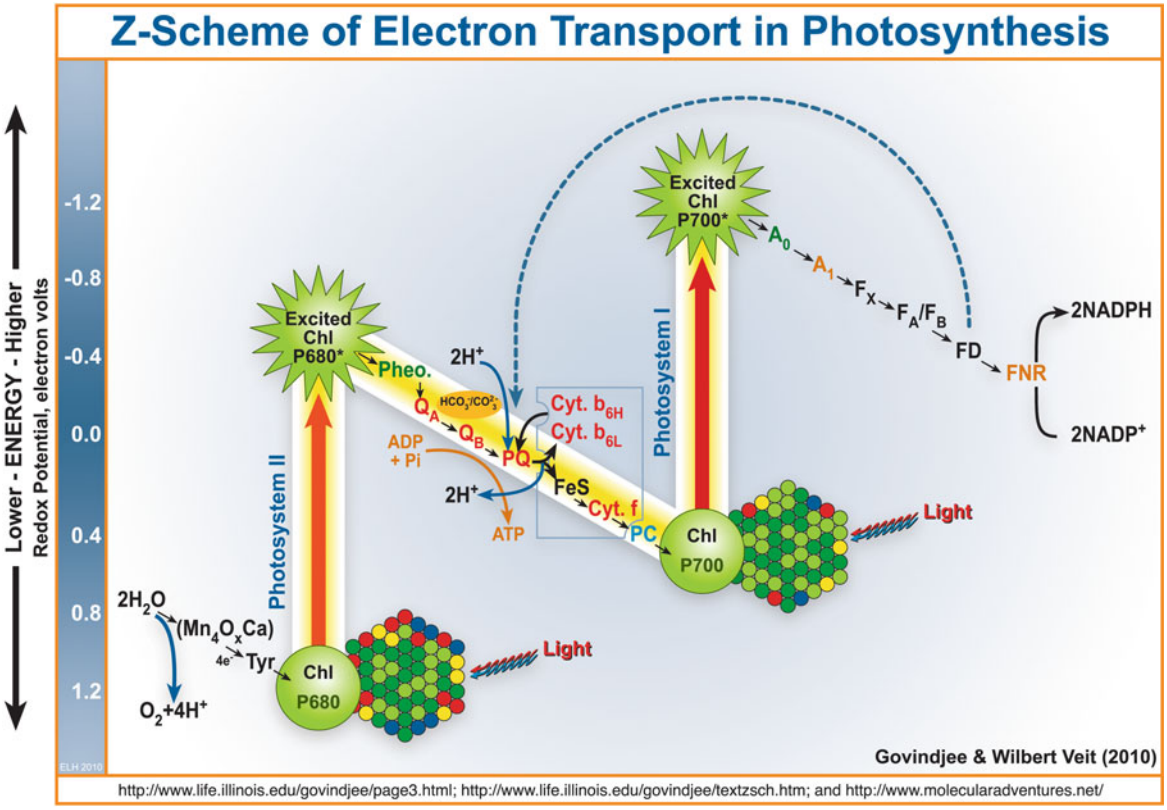

Biomass Production. Figure 1

The Z-Scheme diagram of photosynthesis shows the electron pathway from water to Nicotinamide Adenine Dinucleotide Phosphate, oxidized form ($NAPDH^{+}$); the electrons come from the reduction of water and are used for the production of NADPH. The first Z-Scheme was developed 1960 by Hill [4], many versions of this scheme were developed in the following years. The depicted Z-Scheme was designed by Veit, W. and Govindjee in 2010 (http://www.life.illinois.edu/govindjee/2010_z-scheme.pdf). The Z-scheme is an energy diagram for electron transfer in the "light reactions" of plant photosynthesis. The y-axis shows an energy scale for each molecule's ability to transfer an electron to the next molecule, proceeding from left to right. The source of electrons is water (see on the left side). Plants transform light energy into an electron flow and hence into chemical energy in the form of reduced NADPH and ATP, which are used in the following Calvin-Cycle to drive the production of glyceraldehyde-3-phosphate. Thus, the Z-scheme depicts the sequence of electron flow (oxidation and reduction) from the perspective of plant's energy acquisition. Three major protein complexes are involved in the Z-scheme: (1) the Photosystem II, (2) the Cytochrome bf complex (containing $Cytb_6$, FeS and Cytf, in the middle of the Z) and (3) the Photosystem I (http://www.life.illinois.edu/govindjee/). Abbreviations from left to right: **Mn** for a manganese complex containing 4 Mn atoms, bound to Photosystem II (PSII) reaction center; **Tyr** for a particular tyrosine in PSII; $\mathbf{O_2}$ for oxygen; **H**+ for protons; **P680** for the reaction center chlorophyll (Chl) in PSII: it is the primary electron donor of PSII; Excited (Chl) P680 for **P680*** that has the energy of the photon of light; **Pheo** for pheophytin molecule (the primary electron acceptor of PSII; it is like a chlorophyll a molecule where magnesium (in its center) has been replaced by two "H"s); Q_A for a plastoquinone molecule tightly bound to PSII; $\mathbf{Q_B}$ for another plastoquinone molecule that is loosely bound to PSII; **FeS** for Rieske Iron Sulfur protein; **Cyt. f** for Cytochrome f; $\mathbf{Cytb_6}$ (L and H) for Cytochrome b_6 (of Low and High Energy); **PC** for copper protein plastocyanin; **P700** for the reaction center chlorophyll (Chl;actually a dimer, i.e., two molecules together) of PSI; it is the primary electron donor of PSI; Excited (Chl) P700 for **P700*** that has the energy of the photon of light; $\mathbf{A_0}$ for a special chlorophyll a molecule (primary electron acceptor of PSI); $\mathbf{A_1}$ for a phylloquinone (Vitamin K) molecule; $\mathbf{F_X}$, $\mathbf{F_A}$, and $\mathbf{F_B}$ are three separate Iron Sulfur Centers; **FD** for ferredoxin; and **FNR** for Ferredoxin NADP oxido Reductase (FNR)

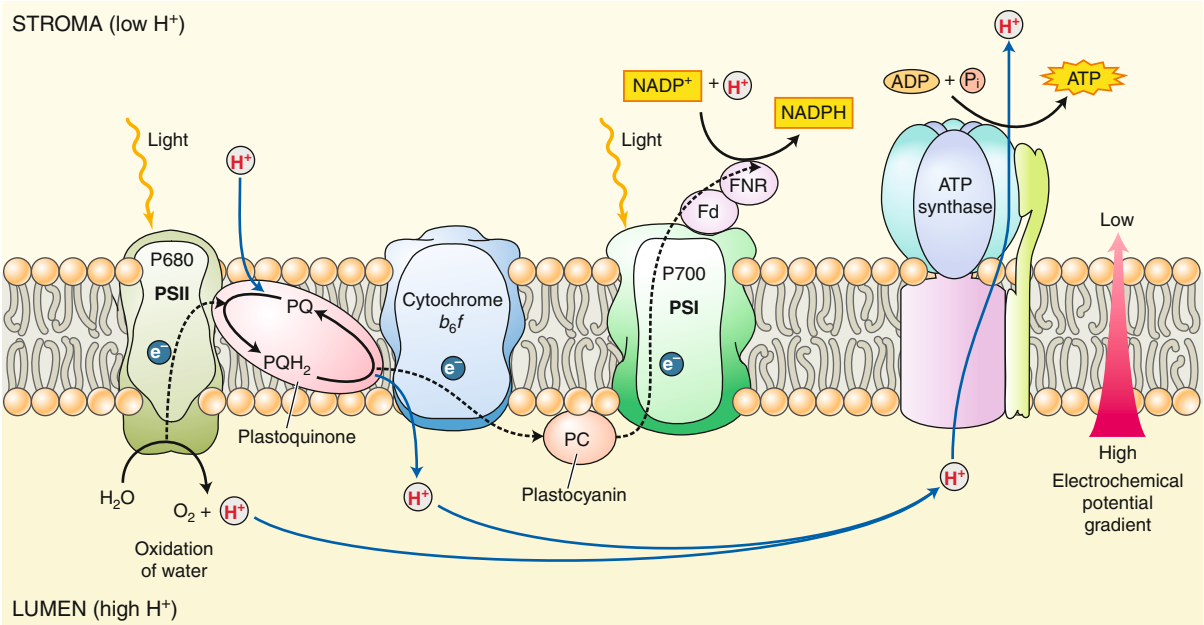

Biomass Production. Figure 2
Light-dependent reactions of photosynthesis at the thylakoid membrane (Taiz and Zeiger, Plant Physiology, 4th edition, ISBN 0-87893-856-7). The figure shows the four protein complexes which are part of the electron- and proton transfer. Inside the lumen water is oxidized and protons are released through the Photosystem II (PS II). In the stroma, $NADP^+$ is reduced to NADPH via Photosystem I (PSI), ferrodoxin (Fd) and Flavoprotein ferrodoxin-NADPH reductase (FNR). Furthermore the cytochrome b_6f complex transports protons into the lumen, which also contribute to a proton gradient. The movement of these protons along the electro-chemical proton gradient through the ATP-synthase is used to produce ATP on the stroma side. Reduced Plastoquinone (PQH2) and Plastoquinone (PC) transfer electrons to the cytochrom-b_6f complex and to the PSI respectively

and metabolic pathways of dark reactions. They are called "C_3 pathway," "C_4 pathway," and "Crassulacean acid metabolism" (CAM). The latter two are specialized and more efficient variations of the basic principles of C_3 photosynthesis depicted above. C_4 and CAM have been evolved in some species by adding some more complexity to the enzymatic machinery and the subcellular localization of photosynthesic processes. C_3 and C_4 plants use different enzymes for capturing the atmospheric CO_2: C_3 plants use RuBisCo to fix CO_2 from the atmosphere and the first primary product is a 3-carbon organic acid: namely 3-phosphoglyceric acid. In contrast, C_4 and CAM (Crassulacean acid metabolism) use phosphoenolpyruvate (PEP) carboxylase to capture the carbon. Their first photosynthesis products are 4-carbon organic acids: malate and aspartate. The C_3 pathway is adapted to operate at optimal rates between 15°C and 20°C. The capturing of CO_2 via RuBisCo is temperature dependent: At higher temperature, relatively less carbon is fixed and more O_2 is generated resulting in rather limited growth. Furthermore, under high temperatures stomata (the pores allowing atmospheric air to get in contact with photosynthetic tissue) are closed, thus less CO_2 reaches the chloroplast and the CO_2/O_2 ratio decreases further. In contrast, C_4 plants are adapted to operate at optimal rates under higher temperatures (30–35°C) and have higher rates of CO_2 exchange; the PEP carboxylase is more efficient in capturing CO_2 independent of temperature, but this way costs more chemical energy in form of ATP. Agriculturally important C_3 species are wheat, rice, and barley. C_4 plants are,

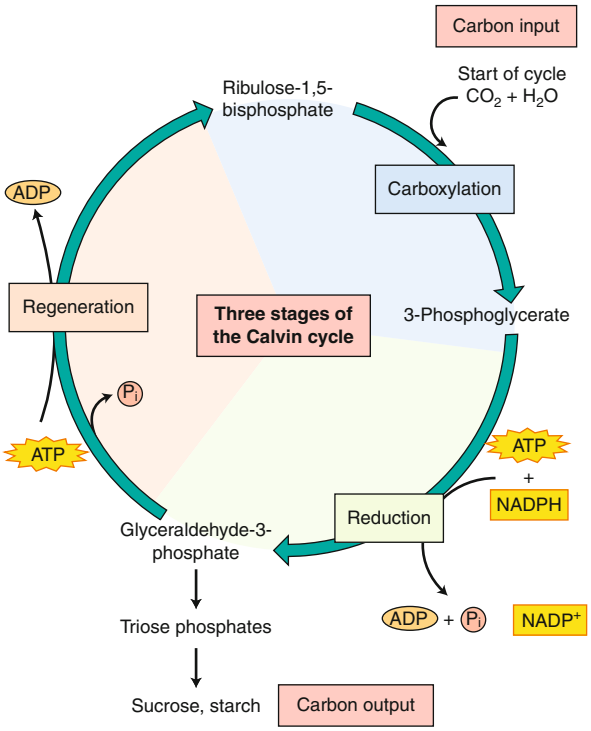

Biomass Production. Figure 3
Overview of the Caclvin cycle and carbon fixation. NADPH and ATP which are produced in the preceding light reaction and the oxidative phosphorylation are used to metabolize glyceraldehyde-3-phosphate into hexose sugars which are the primary products of the metabolism and a source of nutrients for heterotrophs. The enzyme RuBisCo catalyzes the carboxylation of carbon dioxide into two molecules of 3-Phosphoglycerate. One molecule is used for the regeneration of the calvin-cycle and the other one for the central metabolic pathway. In different steps, 3-Phosphoglycerate is converted into Ribulose 5-phosphate, which is regenerated to Ribulose 1,5-bisphosphate through a phosphorylation by the enzyme Phosphoribulose kinase. Then the cycle can start all over again (Taiz and Zeiger, Plant Physiology, 4th edition, ISBN 0-87893-856-7)

for example, maize and sorghum. CAM plants are adapted to very dry conditions; they capture light energy during the day with stomata closed. Only during the night, CAM plants, such as cacti, agave, and pineapple, open their stomata and fix CO_2. Due to this mechanism, they have high water use efficiencies (WUEs) [5, 6]. At a given radiation level, the C_4 species have higher rates of CO_2 exchange than C_3 species: Thus great effort is made to engineer C_4 enzymes into C_3 plants, especially into rice [7–9].

The theoretical maximum photosynthetic efficiency – which is the fraction of the incident solar energy reaching the surface of the plant that is converted into chemical energy in the form of carbohydrates present in the differentiated plant tissue – is calculated as 3.3% for C_3 plants and 6.7% for C_4 plants [10–12]. For C_4 plants, this value originates from the following factorial calculation: 100 times 0.5 times 0.8 times 0.28 times 0.4 = 6.7%, where

- The factor 0.5 represents the 50% of photosynthetically active radiation (PAR) of total energy of the solar radiation that arrive at the earth's surface. The wavelengths used by plants are between 400 and 700 nm.
- Eighty percent (factor 0.8) of PAR are captured by photosynthetically active compounds. The rest is reflected, transmitted, or absorbed by non-photosynthesizing material.
- A theoretical minimum of eight photons of PAR are required to convert the radiation energy to glucose [13], which corresponds to 28% (factor 0.28) of the light energy of these photons.
- Finally, 40% (factor 0.4) of the energy stored in photosynthesis are consumed during dark respiration to sustain all metabolic processes of the plant.

C_3 have a lower photosynthesis than C_4 plants due to an additional loss of about 30% of the CO_2 already fixed during photorespiration – a suite of biochemical reactions coupled to the core activity of RuBisCo. Furthermore, the light-utilizing capacity of C_3 plants becomes light-saturated at lower light intensities than for C_4 plants. In consequence, C_3 plants are unable to utilize approximately 30% of the light absorbed by photosynthetically active compounds, thus the maximum efficiency of energy conversion for C_3 plants is about: 100 times 0.7 times 0.7 times 0.067 = 3.3%.

In the field, the average photosynthetic efficiency is often below 1%, due to unfavorable weather conditions, short vegetation periods in the temperate climates, or due to acute biotic and abiotic stresses. As shown above, C_4 plants have higher photosynthetic efficiencies and thus efforts are made to find bioenergy crops in this group in order to increase biomass and yield. Unfortunately, most of the C_4 plants are not adapted to

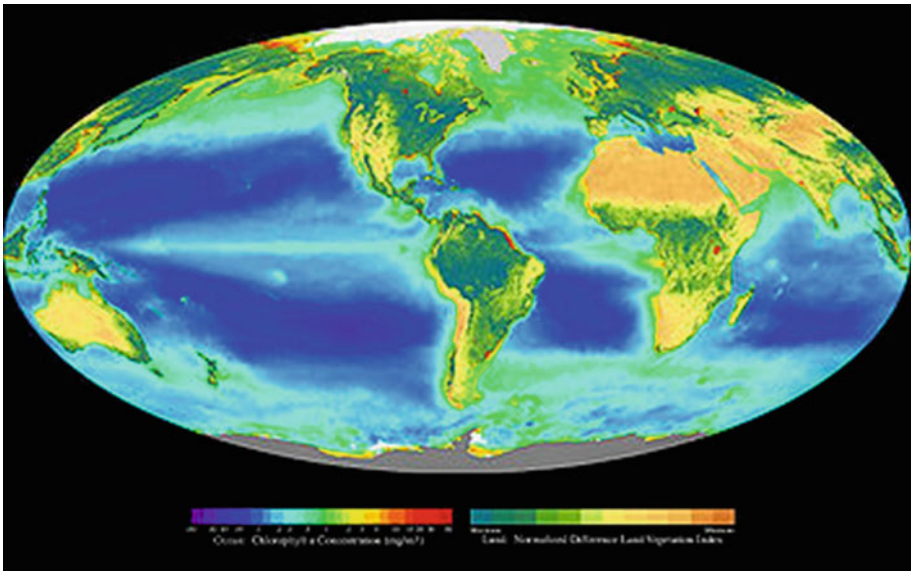

Biomass Production. Figure 4
Composite image showing the global distribution of photosynthesis, including both oceanic phytoplankton and land vegetation (http://en.wikipedia.org/wiki/File:Seawifs_global_biosphere.jpg)

the temperate zones. In order to adapt C_4 bioenergy crops to colder climates, genetic selection of C_4 plants with improved cold tolerance is necessary (e.g., for maize see [14, 15] and for sorghum see [16, 17]).

Biomass Growth and Metabolism

Still it is not fully clear how photosynthetic efficiency and growth processes interact in detail with each other. The way how environmental factors (light, temperature, water), the genetic structure of genotypes and populations and external outputs (fertilizer, irrigation, tillage) and their interactions – the so-called genetic × environment interaction – affect photosynthesis, growth, and final biomass is far from being understood; thus a prediction of final biomass from the theoretical maximum of photosynthetic efficiency is difficult at the moment.

At first glance, plant growth seems to be a trivial process. It is easy to understand that a seedling planted in a flower pot can grow better if placed next to a sunny window compared to the seedling left behind in the dark corner of the basement (provided that both received enough water and the same soil). Yet, it is not possible to explain mechanistically, why the same seedling would have grown much better if it would have been planted in the garden in front of that window at the appropriate time of the year. Plants have evolved not only to withstand a wide range of adverse environmental conditions but also to grow optimally in a certain matrix of dynamically varying environmental conditions to which they are exposed during a typical growth season. Plants are sessile organisms, which has the simple consequence that they cannot escape from unexpectedly cold nights, hot midday hours, dry or wet periods. Moreover, they grow with one half of their body in the atmosphere, being exposed to continually varying light intensity, temperature, herbivore pressure, and other dynamically varying factors – and with their other half in the soil with much more constant temperature regimes but often spatially very heterogeneous supply of water and mineral nutrients. Since their energy and biochemical growth substrates, ultimately provided by photosynthesis, have to be shared between these two parts of their body – the root and the shoot – they are continually facing the dilemma to meet the decision whether to invest into the root or into the shoot, whether to invest the surplus

of energy and metabolites in growth at all or to invest it in storage or in the assembly of more refined, so-called secondary metabolites responsible for protection and defense. Despite the second dilemma, plants need to grow throughout their entire lifetime, since this is their only chance to get access to an increased pool of resources on the background of their sessile lifestyle. Otherwise, their neighbor plants will be faster and steal sunlight, water, or mineral nutrients. The only way out of the constant thrive for increased growth to keep up the success of the plant's body is to invest in "generative growth" – the production of seeds or other forms of offspring that can finally seek their fortune at a different place with less competition or that can endure until times have come that provide better circumstances of living. This prosaic description of the dilemmas, decision processes, and boundary conditions of plant growth and metabolism is far from being put into mechanistic equations, displaying how to engineer the metabolic network of growth processes.

In contrast to photosynthesis, it is not even clear, whether a core pattern of basic principles, such as light and dark reactions in C_3-photosynthesis, exists for the basic processes of plant growth. In recent years, it could be shown that different plant species and different plant organs grow at different times of the day and with a different spatial distribution of growth activity within growing organs [18–24].

It has long been known that the organization of leaf growth differs strongly between two major groups of higher land plants: the dicotyledonous and the monocotyledonous species [18, 25, 26]. An overview of different temporal growth patterns of monocots and dicots is shown in Fig. 5. Monocot leaves show highest growth rates during the day (white background of right panels in Fig. 5) and growth is often directly linked to air temperature. In leaves of dicot plants, there are two major types of growth cycles differing with respect to their phase (occurrence of maxima and minima during 24 h): Type 1 leaves show maximal growth activity at the beginning of the day and have a base-tip gradient of relative growth rate (RGR) over the leaf. This means that there are higher growth rates at the leaf base and lower growth rates at the tip. *Ricinus communis*, *Nicotiana tabacum*, *Nicotiana attenuata*, and *Arabidopsis thaliana* show this pattern. Type 2 leaves show maximal growth rates at the end of the day. *Populus deltoides* and *Glycine max* belong to this Type 2. Furthermore, those two species do not show a base-tip gradient.

Only now, it has been realized that the rules, which different species have to follow in order to produce biomass, differ between species in a way that is difficult to predict from prior plant biology knowledge. Only detailed studies of when and where plants grow in certain environmental conditions will allow biologists to understand better the serendipitous pathways of the metabolic processes that lead from some basic molecules produced in photosynthesis to a fully functional plant to be utilized for human purposes.

Plant Selection and Plant Breeding

Breeding aims for improved biomass crops differ strongly from traditional breeding aims for agricultural crops that are the base of human nutrition. The most successful grain crops are derived from wild relatives characterized by huge seeds and an annual life strategy. From the beginning of agriculture on, these crops were produced with higher efficiency compared to other species (less effort for a certain yield), could be stored for a relatively long time and could be improved rapidly due to their short generation time. With the advent of modern breeding methods, the habitus of these cereal plants changed toward varieties with short stems that were able to put an ever higher fraction of their biomass into their seeds, thus increasing their harvest index – the biomass invested in grain or fruit divided by total shoot biomass. In contrast to food crops, bioenergy plants are mainly harvested for their carbon and not for their nitrogen content. Biomass crops of the second generation such as miscanthus and willow contain only one-tenth of nitrogen compared to cereal crops. For fermentation processes, an improved lignocellulosic accessibility to enzymatic degradation is an advantage because this reduces the energy cost of the refining process. A long growing season is an advantage and biomass crops should have low proportional allocation of dry matter content to reproductive structures, thereby having a low "harvest index" in contrast to cereals. In summary, the ideal attributes of crops for biomass production are quite different from the ones of food crops: So-called new plant "ideotypes" are defined

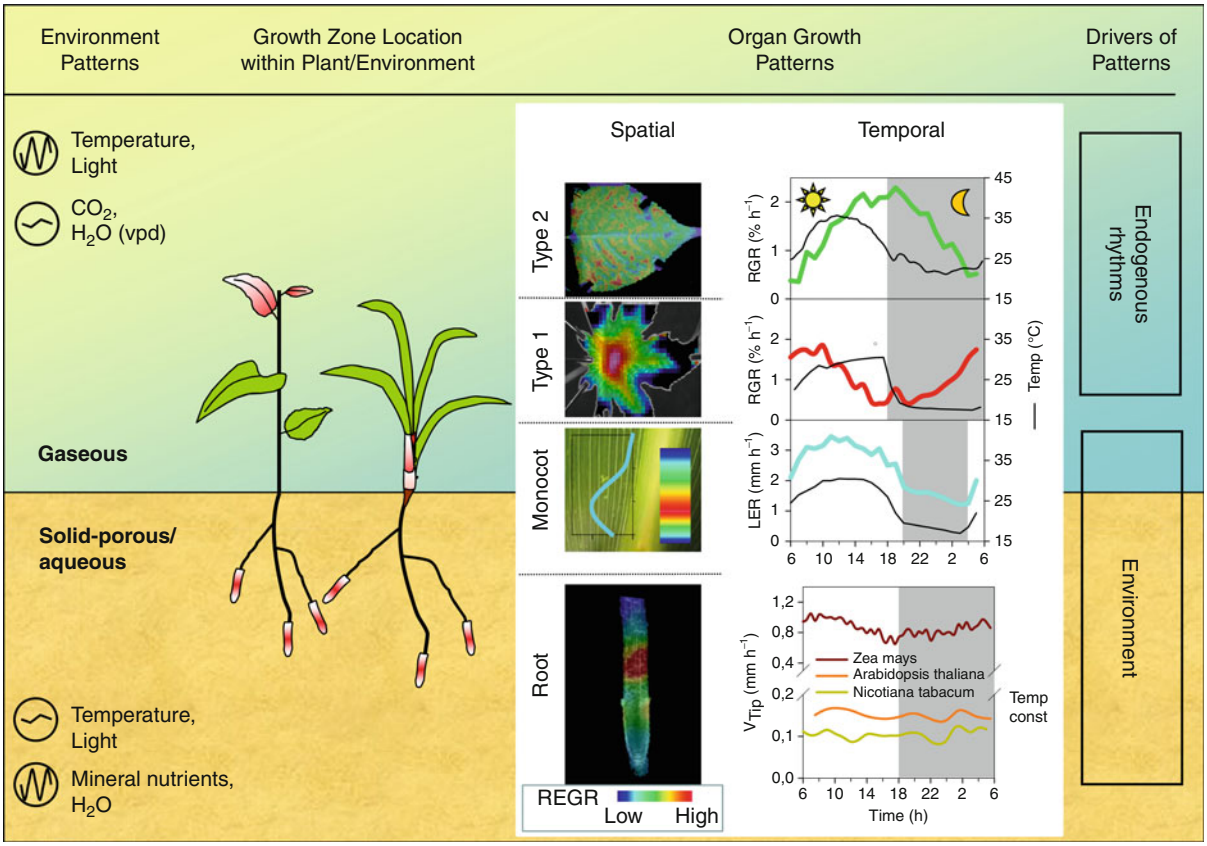

Biomass Production. Figure 5

Different growth patterns of leaves and roots between dicots and monocots. Schematic overview of (from *left to right*) the relationship between environmental dynamics, growth zone positioning, spatiotemporal growth patterns in leaves and roots, and drivers of growth patterns [18]. *REGR* relative elemental growth rate, *RGR* relative growth rate, *LER* leaf elongation rate, V_{tip} velocity of the root tip

by breeders, specifying the optimal plant for a particular purpose. Once the plant model is defined it becomes a breeding target [27, 28]. Searching for new species and varieties such as willow, jatropha, and perennial grasses with new ideotypes is necessary (http://www.fao.org/news/story/en/item/44142/icode/). Today's "first-generation" biomass crops come from a limited number of crop species that are not specifically bred for this purpose such as maize, sugarcane, oil palm, and rape seed [29]. These bioenergy crops are not suitable to mitigate the levels of greenhouse gases and global climate change. Moreover, they compete with food crops for land, water, and nutrients. As specified above, new genetic resources have to be exploited and technological breakthroughs are needed to develop second- and third-generation bioenergy crops, defined by a range of ideotypic traits including improved water-, nutrient-, and light-use efficiencies and improved accessibility of lignocellulose cell wall material to enzymatic degradation. Recent breeding efforts aim to increase vegetative biomass and yield and to improve chemical composition of plant biomass in order to increase conversion efficiency. Many species of this new generation of biofuel plants will be adapted to marginal lands that are unsuitable for most food or feed crops [6, 30].

For the breeding of these new species they need to be domesticated; the inter-annual variability of yield must be reduced. The breeding and genetic modification efforts of these second-generation bioenergy

crops are at the beginning compared to that of food crops. Basic breeding programs must include the collection and evaluation of genetic resources, the genetic analysis and development selection criteria, the genetic improvement for biomass yield and energy-related properties [31–33] through classical selection, genetic modification, and marker-assisted selection. Currently different perennial herbaceous species (C_4 grasses like *miscanthus*), woody plants (such as eucalypthus, jatropha, and poplar), and microalgal systems are analyzed [34–39].

Future Directions

Plant biomass is, and could be even more an important contribution to energy production in future. Potential biomass productivity depends on the genetic background of plants, the specific environmental conditions where plants grow, external factors such as the grade of rationalization in agriculture, and also the specific socioeconomic conditions of the countries in which these crops will be cultivated. These factors interact with each other and therefore there is no single strategy for all countries, but still some points are important to be considered on a global level. It is necessary that the production of energy crops is not in competition with food crops for human nutrition. Energy crops need to be produced in an environmentally mitigating manner while at the same time energy consumption during cultivation must be reduced, thereby increasing and energy efficiency of the crop. New species supply a broad range of available genetic material, which could be the base for breeding and selection. There is a lot of room for more efficient production of plant biomass from available resources. The key to utilizing this potential resides in an improved understanding of plant growth processes that generate usable biomass from the first and very efficient biochemical reactions of photosynthesis.

Bibliography

1. OECD (2008) OECD environmental outlook to 2030. OECD, Paris
2. El Bassam N (2010) Handbook of bioenergy crops: a complete reference to species, development and applications, vol xxvii. Earthscan, London, Washington, 516 p
3. Worldwatch Institute (2007) Biofuels for transport: global potential and implications for energy and agriculture. Earthscan, London, Washington
4. Hill R, Bendall F (1960) Function of the two cytochrome components in chloroplasts: a working hypothesis. Nature 186:136–137
5. Borland AM et al (2009) Exploiting the potential of plants with crassulacean acid metabolism for bioenergy production on marginal lands. J Exp Bot 60(10):2879–2896
6. Somerville C et al (2010) Feedstocks for lignocellulosic biofuels. Science 329(5993):790–792
7. Leegood RC (2002) C_4 photosynthesis: principles of CO_2 concentration and prospects for its introduction into C_3 plants. J Exp Bot 53(369):581–590
8. Taniguchi Y et al (2008) Overproduction of C4 photosynthetic enzymes in transgenic rice plants: an approach to introduce the C_4-like photosynthetic pathway into rice. J Exp Bot 59(7):1799–1809
9. Zhu XG et al (2010) C_4 rice – an ideal arena for systems biology research. J Integr Plant Biol 52(8):762–770
10. Hall DO, Rosillo-Calle F, Williams RW, Woods J (1993) Biomass for energy: supply prospects. In: Johansson TB (ed) Renewable energy: sources of fuels and electricity. Island, Washington, DC, pp 593–651
11. Long SP et al (2006) Can improvement in photosynthesis increase crop yields? Plant Cell Environ 29(3):315–330
12. Carroll A, Somerville C (2009) Cellulosic biofuels. Annu Rev Plant Biol 60:165–182
13. Walker D (1992) Tansley review no. 36 excited leaves. New Phytol 121(3):325–345
14. Soldati A, Stehli A, Stamp P (1999) Temperature adaption of tropical highland maize (Zea maize L.) during early growth and in controlled conditions. Eur J Agron 10:111–117
15. Bhosale SU et al (2007) Chilling tolerance of central european maize lines and their factorial crosses. Ann Bot 100(6): 1315–1321
16. Knoll J, Gunaratna N, Ejeta G (2008) QTL analysis of early-season cold tolerance in sorghum. Theor Appl Genet 116(4):577–587
17. Burow G, Burke JJ, Zhanguo X, Franks CD (2010) Genetic dissection of early-season cold tolerance in sorghum (Sorghum bicolor (L.) Moench). Mol Breeding, doi:10.1007/s11032-010-9491-4
18. Walter A, Silk WK, Schurr U (2009) Environmental effects on spatial and temporal patterns of leaf and root growth. Annu Rev Plant Biol 60:279–304
19. Nozue K et al (2007) Rhythmic growth explained by coincidence between internal and external cues. Nature 448(7151):358–361
20. Poire R et al (2010) Diel time-courses of leaf growth in monocot and dicot species: endogenous rhythms and temperature effects. J Exp Bot 61(6):1751–1759
21. Wiese A et al (2007) Spatio-temporal leaf growth patterns of Arabidopsis thaliana and evidence for sugar control of the diel leaf growth cycle. New Phytol 174(4):752–761

22. Walter A et al (2005) The effect of elevated CO_2 on diel leaf growth cycle, leaf carbohydrate content and canopy growth performance of Populus deltoides. Glob Change Biol 11(8):1207–1219
23. Lai IL et al (2005) Leaf growth dynamics of two congener gymnosperm tree species reflect the heterogeneity of light intensities given in their natural ecological niche. Plant Cell Environ 28(12):1496–1505
24. Walter A et al (2008) Diel leaf growth cycles in Clusia spp. are related to changes between C_3 photosynthesis and crassulacean acid metabolism during development and during water stress. Plant Cell Environ 31(4):484–491
25. Hochholdinger F et al (2004) From weeds to crops: genetic analysis of root development in cereals. Trends Plant Sci 9(1):42–48
26. Osmont KS, Sibout R, Hardtke CS (2007) Hidden branches: developments in root system architecture. Annu Rev Plant Biol 58:93–113
27. Donald CM (1968) The breeding of crop ideotypes. Euphytica 17(3):385–403
28. Dickmann D, Gold M, Flore J (1994) The ideotype concept and the genetic improvement of tree crops. Plant Breed Rev 12:163–193
29. Lobell DB et al (2008) Prioritizing climate change adaptation needs for food security in 2030. Science 319(5863): 607–610
30. Grammelis P et al (2008) Cultivation and characterization of Cynara Cardunculus for solid biofuels production in the mediterranean region. Int J Mol Sci 9(7):1241–1258
31. Bouton JH (2007) Molecular breeding of switchgrass for use as a biofuel crop. Curr Opin Genet Dev 17(6):553–558
32. Dillon SL et al (2007) Domestication to crop improvement: genetic resources for Sorghum and Saccharum (Andropogoneae). Ann Bot 100(5):975–989
33. Casler MD et al (2007) Genetic diversity, plant adaptation regions, and gene pools for switchgrass. Crop Sci 47(6):2261–2273
34. Carpita NC, McCann MC (2008) Maize and sorghum: genetic resources for bioenergy grasses. Trends Plant Sci 13(8):415–420
35. Qing-Zhi M, Wan-Xi P, Dang-Quan Z, Yi-Qiang W, Hong-Chen Q (2009) Study on Bioenergy Utilization Benzene/Ethanol Extractives of Eucalyptus Urophylla Wood by Py-GC/MS. In: Asia-Pacific Power and Energy Engineering Conference, Wuhan
36. Forrest M, Moore T (2008) Eucalyptus gunnii: a possible source of bioenergy? Biomass Bioenergy 32(10):978–980
37. Brittaine R, Lutaladio N (2010) Jatropha: a smallholder bioenergy crop, in integrated crop management, vol 8. FAO, Rome
38. Sannigrahi P, Ragauskas AJ, Tuskan GA (2010) Poplar as a feedstock for biofuels: a review of compositional characteristics. Biofuels Bioproducts Biorefining Biofpr 4(2):209–226
39. Greenwell HC et al (2010) Placing microalgae on the biofuels priority list: a review of the technological challenges. J R Soc Interface 7(46):703–726

Biomass Provision and Use, Sustainability Aspects

Daniela Thrän[1,2], Marek Gawor[1]
[1]German Biomass Research Centre (DBFZ), Leipzig, Germany
[2]Helmholtz–Centre for Environmental Research (UFZ), Leipzig, Germany

Article Outline

Glossary
Definition of the Subject
Introduction
Bioenergy Process Chain
Sustainability Requirements
Summary
Future Directions
Bibliography

Glossary

Agricultural residues Biomass residues originating from production, harvesting, and processing in farm areas [1].

Bioenergy Energy from biomass [1].

Biofuel Fuel produced directly or indirectly from biomass [1].

Biomass Material of biological origin excluding material embedded in geological formations and/or transformed to fossil. (1) Herbaceous biomass: Biomass from plants that has a non-woody stem and which dies back at the end of the growing season. (2) Fruit biomass: Biomass from the parts of a plant which hold seeds. (3) Woody biomass: Biomass from trees, bushes, and shrubs [1].

Biomass residues Biomass originating from well-defined side-streams from agricultural, forestry, and related industrial operations [1].

Carbon leakages Increase of the Greenhouse gas (GHG) emissions in one country as a result of the climate change mitigation activity in another country by, i.e., relocation of the energy-intensive production to the country with less restrictive environmental law. The opposite situation (reduction of the GHG emissions in one country as

a result of climate mitigation policy in another country), known as spill-over, is also possible [2, 3].

Carbon-rich soils Soils with very high carbon content, such as wetlands, peatlands, etc.

Cereal crops Annual crops grown with the main purpose to use the seed for food production. Some cereal crops (barley, wheat, rye, oat) can be used as a solid biofuel [1].

Certification system The system of assuring the sustainable production of the biomass or biomass fuel.

Climate change Change in the state of the climate that can be identified (e.g., using statistical tests) by changes in the mean and/or the variability of its properties, and that persists for an extended period, typically decades or longer. Climate change may be due to natural internal processes or external forcings, or due to persistent anthropogenic changes in the composition of the atmosphere or in land use [2].

CO_2 equivalent (1) Concentration: The concentration of carbon dioxide that would cause the same amount of radiative forcing as a given mixture of carbon dioxide and other greenhouse gases. (2) Emission: The amount of CO_2 emission that would cause the same radiative forcing as an emitted amount of a well-mixed greenhouse gas, or a mixture of well-mixed greenhouse gases, all multiplied with their respective Global Warming Potentials to take into account the differing times they remain in the atmosphere [2].

Energy crops Woody or herbaceous crops grown specifically for their fuel value [1].

Energy forest trees Woody biomass grown specifically for its fuel value in medium to long rotation forestry [1].

Energy (1) Primary energy: Energy forms without technical conversion (e.g., coal, lignite, raw biomass, wind energy). (2) Secondary energy: Energy produced by the conversion of the primary energy carriers (e.g., coal briquettes, gasoline, heating oil, electrical energy). (3) End energy: Energy available for the end-consumer (e.g., heating oil in the oil tank, pellets at the oven, electrical energy before the electricity meter). (4) Useful energy: Energy used by the consumer after the last conversion to satisfy demands such as meal preparation, heating, etc. [4].

Energy efficiency The ratio of energy in the energy carrier to the energy obtained after the conversion.

Fixed carbon Remainder after the percentage of total moisture, total ash, and volatile matter are subtracted from 100 ([1], Adapted from ISO 1213-2:1992).

Forest Defined under the Kyoto Protocol as a minimum area of land of 0.05–1.0 ha with tree-crown cover (or equivalent stocking level) of more than 10–30% with trees with the potential to reach a minimum height of 2–5 m at maturity in situ. A forest may consist either of closed forest formations where trees of various storey and undergrowth cover a high proportion of the ground or of open forest. Young natural stands and all plantations that have yet to reach a crown density of 10–30% or tree height of 2–5 m are included under forest, as are areas normally forming part of the forest area that are temporarily un-stocked as a result of human intervention such as harvesting or natural causes but which are expected to revert to forest [2].

Fuel Energy carrier intended for energy conversion. Fuels may be solid, liquid, or gaseous, and they may originate from biomass, waste, and/or fossil material [1].

Greenhouse gases (GHGs) Gaseous constituents of the atmosphere (natural and anthropogenic) that absorb and emit radiation at specific wavelengths within the spectrum of infrared radiation emitted by the Earth's surface, the atmosphere, and clouds. Most important GHGs are water vapor (H_2O), carbon dioxide (CO_2), nitrous oxide (N_2O), methane (CH_4), and ozone (O_3), as well as purely human-made GHGs: halocarbons, other chlorine- and bromine-containing substances, sulfur hexafluoride, hydrofluorocarbons, and perfluorocarbons [2].

ILUC Indirect Land Use Change, land use change which occurs outside the production boundary of a feedstock, but which is caused by a change in the use or level of output of that feedstock [5].

Landscape management residues Residues of woody, herbaceous, and fruit biomass originating from landscape, park, and cemetery management [1].

LUC Land Use Change (usually understood as direct Land Use Change), change of the land cover

(physical and biological cover over the surface of land, including water, vegetation, bare soil, and/or artificial structures) as a consequence of the human activities such as agriculture, forestry, and building construction that alter land surface processes including biogeochemistry, hydrology, and biodiversity [6].

LULUCF Land use, land use change and forestry, a greenhouse gas inventory sector that covers emissions and removals of greenhouse gases resulting from direct human-induced land use, land use change, and forestry activities [3].

Short rotation plants Woody biomass grown as a raw material and/or for its energy value in short rotation plantations [1].

Sustainability The ability to develop in such a way, that the needs of the present are met without compromising the ability of future generations to meet their own needs (Adopted from [7]).

GJ Gigajoule = 10^9 J.

TJ Terajoule = 10^{12} J.

PJ Petajoule = 10^{15} J.

EJ Exajoule = 10^{18} J.

Definition of the Subject

Biomass is the most relevant renewable energy source covering roughly 12% of the global energy demand [8]. It is usually defined as material of biological origin (i.e., plant and animal) on the Earth's surface, excluding material embedded in geological formations and/or transformed to fossil, which is used directly as a fuel or converted into other forms of energy carrier before combustion. Biomass may be also used for its chemical components [1, 9, 10]. Usually one may include in the term biomass trees, crops, algae, and other plants, as well as agricultural and forest residues. Additionally, many materials are considered to be a biomass, such as wastes including food and drink manufacturing effluents, sludge, manures, industrial (organic) by-products, and the organic fraction of the household waste [10]. Other definitions include also ecological aspects of biomass, defined for example as the amount of living organisms per area, habitat, or region [11, 12]. In this entry, the term biomass will be used in the first meaning as a material of the biological origin.

The sustainable use of the biomass has a very strong relevance, since it may offer several advantages, including:

- *Climate and resource protection*: Biomass use helps to mitigate the climate changes, since GHG emissions from its burning are treated as climate neutral. This is due to the fact, that biomass combustion releases approximately as much carbon dioxide, as the plant removed and accumulated during its growth from the atmosphere and the GHG emitted for the biofuel provision are usually of much smaller magnitude compared to the combustion of fossil fuels. Furthermore, satisfying the energy resources with the biomass helps to save the natural, non-renewable energy sources such as coal or crude oil.
- *Supply safety*: Security of energy supply demands reasonable prices for the energy provision and the diversification of sources, which contribute to the supply. Bioenergy is generated from residues and energy crops spread all over the world and therefore increase the security of supply. Additionally, it may support securing the local communities from the fluctuating prices on the global energy markets.
- *Development of the rural areas*: The provision of bioenergy offers the chance to create added value for the local communities (i.e., farmers, small forest owners, manufacturers) and facilitates the development of the rural areas by, e.g., improving the access to cheap and reliable energy.
- *Poverty abatement and local environmental protection*: Through improved technologies to produce heat, e.g., for cooking purpose, it is possible to reduce air pollution and health problems in the developing countries [13]; the use of the biofuels may also help to reduce traffic-related air pollution in megacities (e.g., Mexico city); furthermore, the cultivation of the biomass on the degraded lands may increase land use efficiency and reduce possible negative competition between food and fuels.
- *Export concerns (raw materials, technologies)*: Increasing biomass use may be associated with the expanding export possibilities, both for the developing countries (as a source of the biomass material), and for the developed countries (which may

export their resource-efficient, high-tech solutions or ready-to-use products, such as Canadian pellets for co-firing in European power plants).

The sustainability is seen as a precondition for the further development of the bioenergy use, since after the initial phase of the enthusiasm and considering the biomass to be a green source of energy it became clear, that its use may create additional, unintended risks for the environment. Such risks were associated, for example, in the case of GHG emission shifts by using carbon-rich soils to produce biofuels. In this case, the carbon released through the land conversion in South-East Asia usually is balanced by the minimized transport-related CO_2-emissions after very long time [14]. Additionally, increased demand on the biomass has revealed that its use may also cause adverse social, environmental, and economic impacts, such as shortening the food supply in case of increasing the use of agricultural areas for energy crops. In many cases, these effects are occurring indirectly as a result of global market mechanism.

In recent years, two main negative impacts have been recognized, namely indirect land use change and competition with food [15]. As an example of the land use change, one may mention the establishment of the agricultural cultivation areas on high-biodiversity tropical areas as a consequence of increased cultivation of the rapeseed for the biodiesel production. This effect occurs as an outcome of undiminished demand for the animal feed and resulting demand for the arable area. Land use change can be caused by energy crop production directly or indirectly. Indirect land use change occurs, if biomass is produced on established arable land, but the former crop production (food or fodder) from this land shifts to forests or high-biodiversity land [16].

These negative impacts may be avoided by applying the sustainability demands and criteria in the provision and use of the biomass. Therefore, the necessity of the sustainable approach may be seen as a prerequisite for an increased biomass use and a worldwide discussion has started, which aimed at working out sustainability criteria and conditions of the biomass use that would allow avoiding above-mentioned negative impacts. According to the current developments and the policy making trends, meeting these criteria will become the prerequisite for labeling the biofuels (like bioethanol, hydrogenated vegetable oil) and eventually being recognized by the international and global institutions as the measures toward climate change mitigation [17].

Such criteria of sustainability should address:

- Type of the impacts occurring, associated with environmental, social, and/or economic spheres of human activities related to biomass.
- The spatial and temporal characteristics of the impacts, taking into consideration the entire biomass and bioenergy use chain, including (where applicable) establishment of the agricultural area, harvesting, transport, preparation, conversion, use and disposal phases of the biomass life cycle.
- The consideration of the future developments with regards to risks and uncertainties.

This entry will analyze various aspects of the sustainability of the biomass provision and use, starting from the description of the possible options of the biomass process chain (conversion of solid, liquid, and gaseous biomass energy carriers into heat, electricity, and power) and addressing the necessary sustainability levels. Subsequently, the current and future potentials of the biomass will be discussed, including the most important influencing factors. The last section of this entry will focus on the proliferation of biomass sustainability standards and tools improving sustainability.

Introduction

The debate about sustainability issues is established since more than 200 years now. The term "sustainability" has been derived from the eighteenth century works of the German nobleman Hanns Carl von Carlowitz, who wrote the handbook on the forestry indicating the need of continuous, steady, and sustained use of the timber resources [18]. Subsequently, the word "sustainable" has been adopted in the English language in the nineteenth century, and finally has being made worldwide known through the reports of the Club of Rome, the Bruntland Commission, and the Earth Summit conference in Rio de Janeiro in 1992 [18].

The modern concept of sustainability is relatively young and still not precisely defined. As a result, there exist many definitions, of which the most

widely known is that created by the Bruntland Commission in 1987 [7]. It states that one may denote sustainability as policies, strategies, and development that meet the needs of the present without compromising the ability of future generations to meet their own needs [7]. This most commonly used definition has been, however, adapted to the needs and points of view of different stakeholders from the public and private sectors. Public stakeholders use the adopted sustainability definition of the Bruntland Commission, namely they define sustainability as the satisfaction of basic economic, social, and security needs now and in the future without undermining the natural resource base and environmental quality on which life depends [19]. The decision makers from the industry underline the minimization of the industry's use of materials and reducing the negative impact on the environment, while increasing long-term shareholder and social value [19]. Both groups recognize, however, the need to support a growing economy, while minimizing its social and economic costs [19], compare also [20]. Within another idea of the sustainability concept [21] it has been defined that "sustainability means that present and future persons have the same right to find, on the average, equal opportunities for realizing their concepts of a good human life." Other sources underline, that definitions of sustainability emphasize different aspects of researchers' interests and activities, including ecological sustainability, economic and social sustainability, land restorativeness, environmental soundness, economic viability, social acceptability, sustainability of all agricultural resources, sustainability from the perspective of the political economy and political ecology, as well as energy sustainability [24]. Summarizing the wide range of possible sustainability definitions, the general concept of sustainability denotes measuring and defining the criteria relating to the social, financial, and environmental spheres of life [19, 22] (Fig. 1).

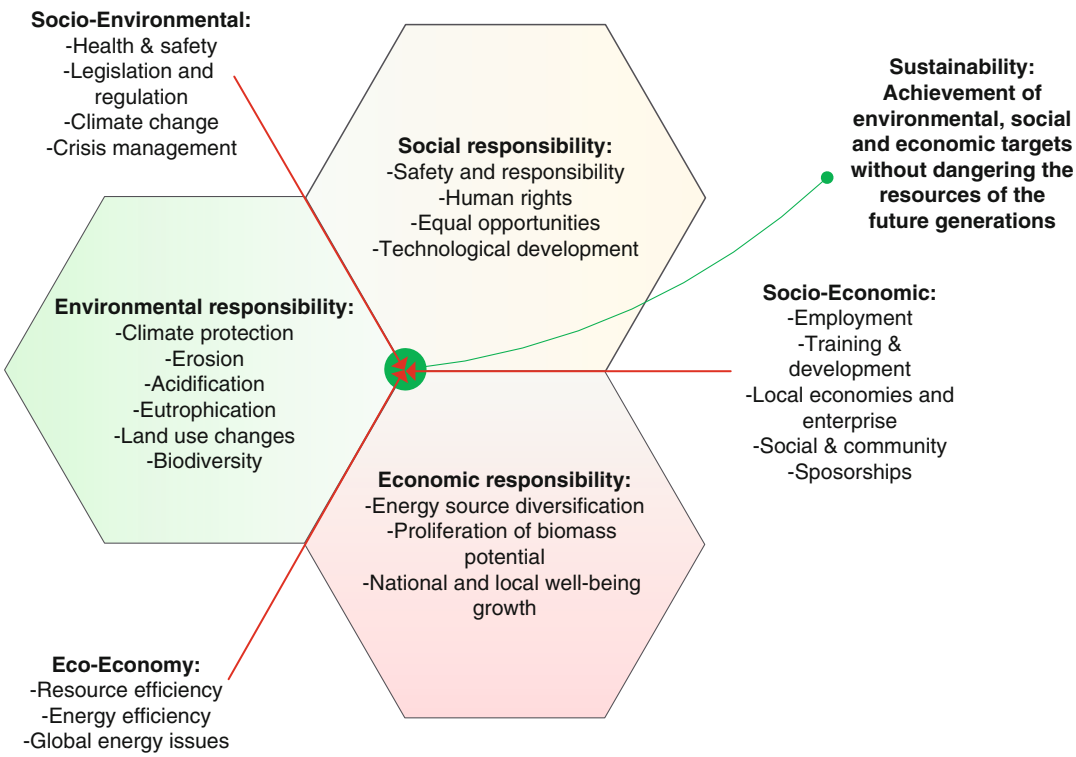

Biomass Provision and Use, Sustainability Aspects. Figure 1
Main areas of sustainability with the special focus on the biomass provision and use (Partially adopted from [23])

Another classification of the various sustainability concepts may be associated with the economy-related perspectives of the weak and strong sustainability. From this point of view, both natural and man-made goods are considered to be a capital. According to the weak concept of the sustainability, both natural and man-made capitals have the same importance and may be used interchangeably. That means that transformation from natural forest to a product (e.g., furniture) does not affect the sustainability, since the future generations may use a man-made capital, which simply substituted the natural capital. The strong sustainability, however, recognizes the unique character of the natural capital, such as clean water, fresh air, and natural landscape. From the perspective of the strong sustainability, it is impossible to substitute lost natural habitats or biodiversity by artificial types of goods [21, 24]. Furthermore, the concept of the weak sustainability is criticized [21] as:

- Being based on the wrong assumptions (i.e., that ecological functions of the environment might be substituted by man-made capital).
- Restricting the right of the future generations to choose the type of capital that is more important for them.
- Assuming that it is possible to substitute the complete and interrelated functions of the complicated ecosystem networks.
- Ignoring the crucial parameters of the human welfare (people want to satisfy not only financial and housing needs, but also lack the contact to the real nature).
- Disregarding the complementarities of several man-made and artificial capitals, such as fishing vessels and fish or sawmills and forests. Thus, disappearance of the natural capital will inevitably mean the termination of the related human activities.
- Rejecting the fact that a minimum stock of natural capital is critical for human survival and well-being, and subsequently missing the possibility of the determination of this critical capital.

The wide perspective and different approaches to the sustainability imply that the use of the biomass does not have to be always sustainable. As an example, the problems related to the indoor air pollution in the developing countries may be mentioned. Stoves operating with solid biofuels, applied incorrectly and having very low efficiencies, are causing many repercussions to the human health and the environment. As a result, poor societies are suffering from problems caused by toxic air pollution and simultaneously depleting the wood reserves in the vicinity of their residential areas [13]. This example shows, that under some conditions, the biomass might be (at least locally) exhausted or its use might damage the natural environment or human beings. In such way, all three target areas of the sustainability are missed:

- From the environmental point of view, burning wood in such insufficient stoves causes the degradation of the local environment and depletion of the wood reserves for the future generation.
- As far as the social aspects are being discussed, the use of the wood for the cooking purposes is influencing significantly the social status of the women realizing the preparation of the meals; the collection of the wood and the cooking itself takes them in most of the cases between 4 and 6 h per day, therefore leaving very restricted time, i.e., for the education purposes [13].
- From an economic point of view, the wood burned stoves are not sustainable, since the pollution-related problems (e.g., lung diseases) are negatively influencing the well-being level of the communities.

To avoid such negative impacts of the biomass provision and use, many institutions and organizations have tried to establish laws, standards, and regulations, allowing to maintain the status of the biomass as a renewable and sustainable energy source, and to possibly minimize its impact on the natural environment. Sustainability and renewability of the bioenergy sources are being treated in the newest laws and regulations as synonyms. For instance, the United Nations Framework Convention on Climate Change (UNFCCC) recognizes few biophysical conditions, under which the biomass may be treated as renewable and of sustainable origin, namely:

- Sustainable management of the area with respect to especially maintaining carbon stocks and

compliance with the national/regional forestry and nature conservation laws is assured.
- Simultaneously, the land retains its original function (the conversion from croplands/grasslands to forest is, however, being allowed).
- In case of biomass residues, there is no decrease in carbon pools, i.e., there is no use of the dead wood, litter, or soil organic carbon that would cause detrimental change of the carbon pool due to the activity.
- It comes from the non-fossil fraction of the municipal or industrial waste [25].

Despite the fact that there are no any single worldwide accepted standards for sustainability, it is still necessary to take into consideration the scientifically accepted sets of sustainability criteria. There are many institutions and committees that work on such criteria. For instance, the WWF listed the following sustainability standards and certification schemes concerning the biomass sustainability:

- American Tree Farm System
- EUGENE: European Green Electricity Network
- EUREPGAP: Protocol for Fresh Fruit and Vegetables
- FLO: Fairtrade Labeling Organizations International
- FLP: Flower Label Program
- FCS: Forest Stewardship Council
- Green Gold Label Program
- Impact Basel Criteria for Responsible Soy Production
- RSPO Principles and Criteria for Sustainable Palm Oil Production
- Sustainable Agricultural Standards
- SFIS: Sustainable Forestry Initiative Standard
- UTZ Kapeh – Codes of Conduct [26], compare also [27].

In recent years, however, the activities in the development of some standards were stopped due to the difficulties with setting generally applicable rules and the complexity of the overall matter as well as the partly conflicting goals (e.g., EUGENE). Other standards are being criticized for being too general and allowing some non-sustainable biomass sources to obtain the sustainability label. Another problem area within the standard development is the coverage of the important environmental problem fields and their definition [28]. This problem is well visible when, e.g., taking into consideration biodiversity loss or indirect land use change, where no international and scientific agreement so far exists with respect to the methodology or modeling factors that shall be applied.

To overcome the misleading abundance of standards and scopes of application, in recent years, the focus of the development has been put on legal and binding laws, set up by countries, e.g., the USA or international bodies, e.g., the EU. These legally binding acts most probably will set the most widely accepted framework for biomass sustainability criteria. Table 1 presents the synopsis of the most important and commonly mentioned groups of the sustainability criteria.

These standards relate to all three main focus areas of sustainability. The question arises about the implementation of the sustainability in the framework of the biomass use, taking into consideration its possible conversion routes as well as the given technical restrictions.

Bioenergy Process Chain

Today biomass can be used with very different process chains. Basically, such process or provision chains depend mainly on the type of biomass, the available technology, and the respective energy demand. Such high variety of possibilities is caused by the fact that biomass differs in many aspects from other renewable sources of energy: It has a price which determines usually 50–90% of the bioenergy production costs (wind turbine operators do not have to pay for the wind), there are one or more provision and conversion steps needed to provide the bioenergy, and finally, biomass as a resource shows naturally lots of variations [31]. As a consequence, in many cases, different provision chains for the same type of biomass resource are possible. Figure 2 shows a simplified diagram of the possible pathways and conversion of bioenergy carriers with respect to the levels of the sustainability and the related potentials (compare with Fig. 4).

There are three major sources of the biomass: forestry (pulp wood, saw timber, tree rests, etc.), agriculture (straw, energy plants, oilseed crops), and wastes (demolition material, industrial wood, sewage sludge, organic household waste). Depending on the type of input material, the biomass has first to be

Biomass Provision and Use, Sustainability Aspects. Table 1 Example of preconditions of the sustainable development and sustainability indicators (Adapted from [29, 26, 30])

Main focus areas	Sustainability targets, aspects and indicators
Land use, land availability, and land use conflicts	Clarification of land ownership, avoiding negative impacts from bioenergy-driven changes in land-use, priority for food supply and food security
Loss of biodiversity and deforestation	No additional negative biodiversity impacts, avoiding deforestation
Greenhouse gas emissions (GHG)	Minimization GHG emissions, substitution of non-renewable energy sources
Soil erosion and degradation	Minimization of soil erosion and degradation, maintaining carbon stocks
Water use and water contamination	Minimization of water use and water contamination, minimizing emissions affecting eutrophication and acidification
Socio-economic problems and standards	Improvement of labor conditions and labor standards, securing employment, ensuring share of proceeds – wage compensation, avoiding human health impacts, especially with respect to the emissions of particulate matter, NO_x, CO, substances producing summer smog, development of fungal spores
Conservation of the cultural function of nature	Protecting natural values of the landscape
Technical aspects	Reducing energy consumption and increasing the efficiency of energy production

collected and prepared. Since the bioenergy sources are not equally distributed on earth, and simultaneously the supply and demand amounts may be different, the use of the bioenergy very often requires the transportation of the biomass through distances exceeding several thousands of kilometers. In such case, one has to take into consideration also preparation processes for the transport and storage (e.g., in the delivery port).

Some of the biomass sources (e.g., demolition wood) may directly be used for energy purposes (usually burned in a furnace). Most of them have, however, to be converted first in order to be used. Here, three basic types of conversion routes may be utilized:

- Thermo-chemical conversion: carbonization, pyrolysis, gasification, or chemical modification
- Physical/mechanical and/or chemical conversion: pressing, extraction, esterification, and transesterification
- Bio-chemical conversion: digestion and fermentation

As a result of these various conversion routes, solid, liquid, and gaseous biofuels are obtained, which subsequently may be burned to obtain heat and/or generate power (in case of the so-called CHP (combined heat and power), both outputs are possible), and in case of automotive fuels may be used to provide a transportation duty.

Since every technology has some advantages and disadvantages, the continuous improvement of the existing and creation of the new technologies is an ongoing process. As it currently seems, one has to take into consideration not only the obstacles relating to the technical side of the conversion, but also other aspects. One of them is definitely the biomass availability. Not every technology may be technically and economically feasible if there will be not enough supply of bioenergy carriers. Figure 3 presents an overview of the technologies currently available on the market, as well as in the middle and in the long time period, and their respective biomass requirement. According to this, the most promising future technologies, including biomethane from synthetic natural gas (SNG), bioethanol from lignocelluloses, or biomass-to-liquid fuel (BtL), require considerable amounts of the biomass inputs. Additionally, the demand on the capital investment is also substantial, becoming an important obstacle in the technological development.

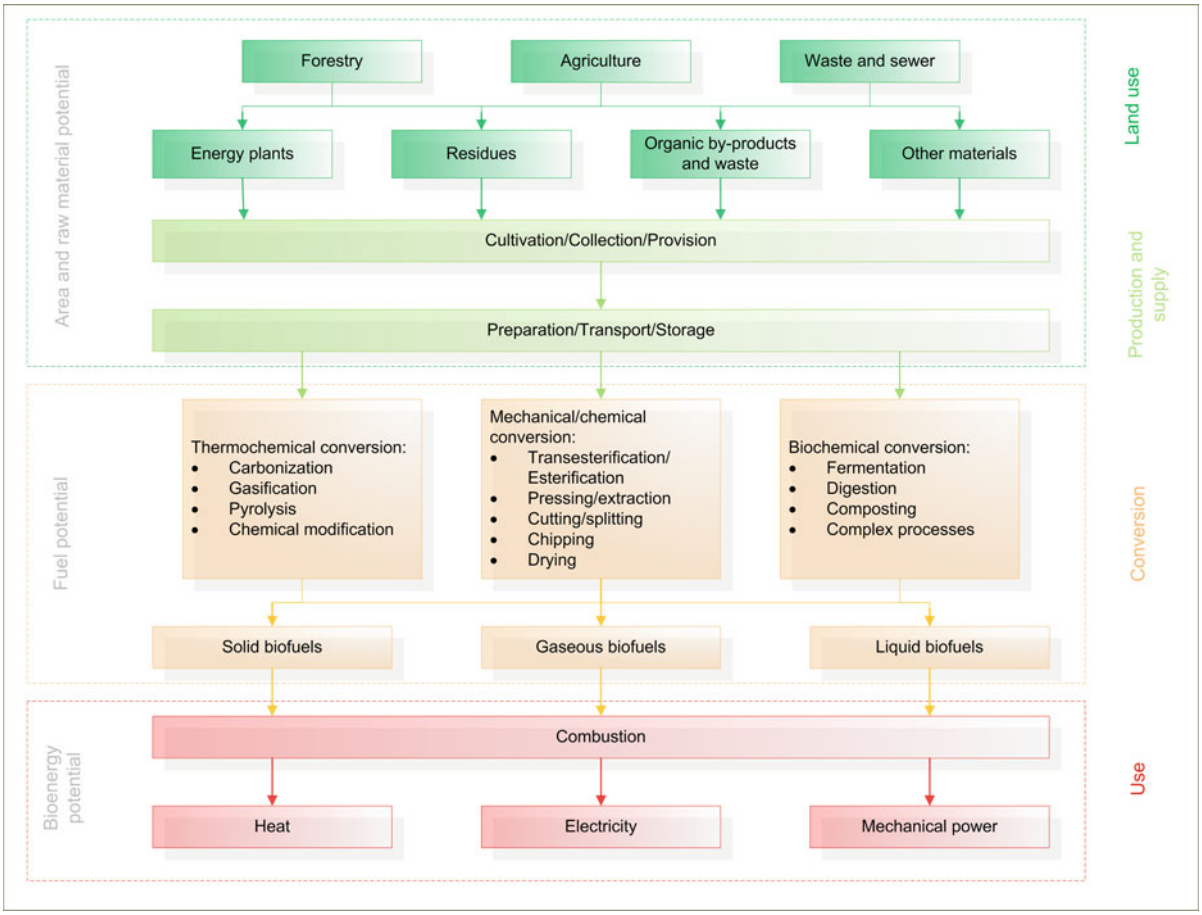

Biomass Provision and Use, Sustainability Aspects. Figure 2
Main conversion pathways of the biomass resources, simplified (Adapted from [32, 33])

Furthermore, the creation of the large-scale industrial plants is partially contradictive to the idea of the local, sustainable biomass use increasing the well-being of the small communities.

Sustainability Requirements

The rapid development of biomass use especially for energy purposes during the last decade revealed competition for resources which may also affect the sustainability targets worldwide. One example is the food-or-fuel debate, which started in 2007 when both energy and food prices increased dramatically. However, other effects of increased biomass use could be also observed. One example may be the situation of several industry branches which experienced difficulties related to the raw material supply (i.e., pulp, paper, or furniture industry). The large-scale production of biomass endangers also the biodiversity (through creation of large monocultures for the biofuel production) and disturbs the natural cycles of carbon in the soil or ground and surface water.

Rules to avoid this wide range of the negative impacts need to cover the whole process or provision chain to ensure that there are no leakage effects [35]. This means that sustainability rules have to be applied on the various levels of the biomass processing, starting from the land use, through processing and conversion, to the biomass use (compare Fig. 2). Another relevant aspect is the application of the various sustainability indicators, relating to the land use changes, soil erosion and degradation, acidification, eutrophication, emissions of the greenhouse gases, etc.

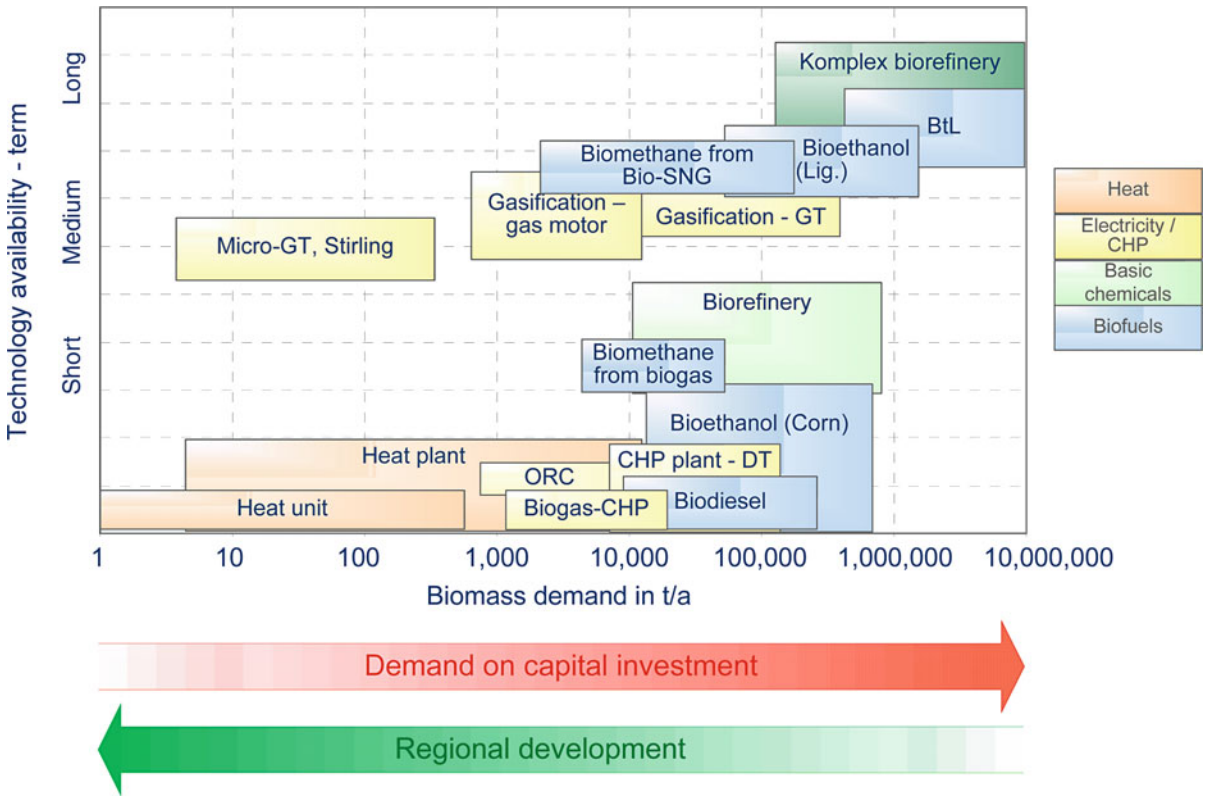

Biomass Provision and Use, Sustainability Aspects. Figure 3
Possible conversions technologies with respect to the biomass use, biomass demand, and temporal availability (Adapted from [34])

This approach is very complex and can only be introduced stepwise. Thus, it becomes clear that the current discussed European and US-American standards do not fulfill this demand yet, because they focus mainly on the GHG emission indicators, omitting other important sustainability indicators (compare [30, 36]).

Figure 4 shows important aspects of sustainability relevant for bioenergy sources. The entire life-cycle chain of the biofuels has to be taken into consideration, including:

- *Land use*: preservation of all land-based functions (ecological and social: like support of the biodiversity, maintenance of the carbon stock and soil productivity, preservation of the land as the habitat for the local communities, etc.).
- *Cultivation and collection*: Greenhouse gas emissions should be minimized during farmland preparation, sawing, tilling, harvesting, transport, and collection; additionally, other environmentally damaging emissions should be avoided.
- *Biomass conversion*: Here, the conversion efficiency is a crucial requirement of sustainability considerations; but some other aspects, e.g., health and safety issues, may also play a significant role; furthermore, the use of the biomass resources demands emission reduction technologies for toxic exhaust (e.g., PM_{10} emissions) and strategies for the limitation of, e.g., noise; last but not least sustainable conversion also demands reasonable GHG savings with regard to the fossil reference energies. The reference systems usually relate to the heat, power, and fuels generated from non-renewable fuels like coal, natural gas, or fossil oil.
- *Biomass use*: Since the biomass resources are limited, they must be used effectively and in an energy-saving way; for the overall sustainability, this can be described as following: The importance of

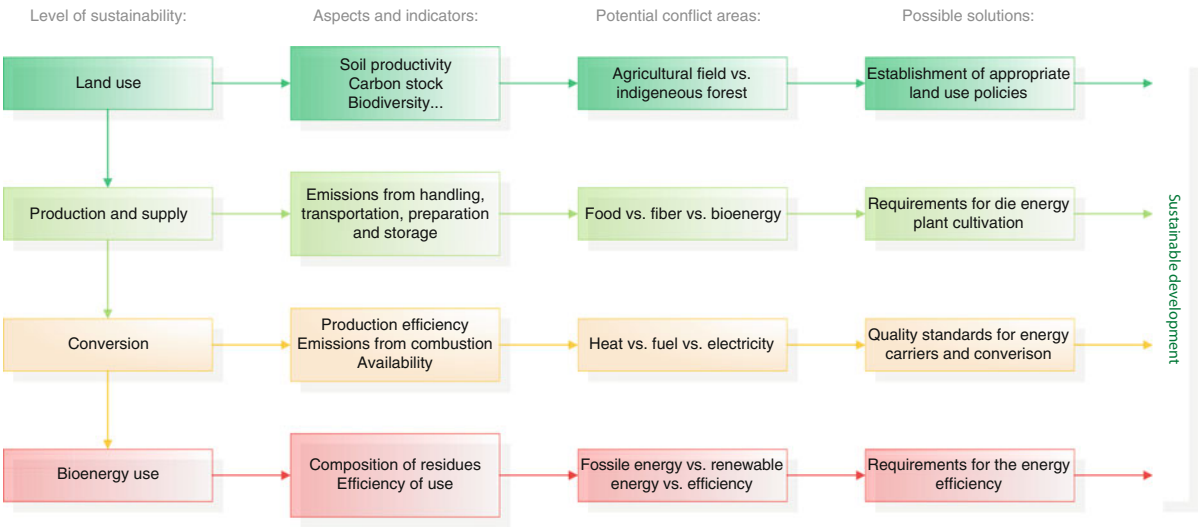

Biomass Provision and Use, Sustainability Aspects. Figure 4
Selected sustainability aspects in relation to the four main pillars of the biomass provision and use (Adapted from [37, 38])

bioenergy for the energy system increases also with a decreasing end energy demand.

- *Residues/ashes*: Remaining materials should be easily integrable in the material flow cycles or (in the case of disposal) inert in the long-term perspective.

Important aspects of the sustainable bioenergy use are discussed in the following sections.

Land Use Change

Recently questions related to land use change (LUC) have become a central part of the discussion concerning sustainability criteria and requirements; this is especially true for the biofuel sector. The term land use change may be defined [39] as environmental change relating to the loss of ecological function, genetic resources, indigenous cultural practices, threatened species' habitats, or even the views and aesthetics of stakeholders, with respect to the given area of consideration. The land-use changes become a critical issue in the discussion about the biofuels, since the intensification of agricultural practices related to the expansion of the biofuels amplified its negative effects on the environment.

Several forms of the LUC have been identified [39], namely:

- Crop changes within agricultural field
- Shift of the fallow land to the cultivation
- Clearing of the natural lands and using them for cultivation purposes
- Displacing of crops from the original areas due to the cultivation of the biofuel crops to the marginal or natural lands

Furthermore, one may identify numerous consequences of the above-mentioned changes, such as loss of habitat for threatened and endangered species or beneficial insects, depletion of the gene reservoirs, increased soil losses through erosion, decreased soil productivity, changes in the hydrological functions of the land (runoff and percolation characteristics), and climate-influencing factors (albedo, evapotranspiration, soil carbon values) [39].

The negative impact of the land use change is relatively well described and quantified in case of the effects occurring in the direct vicinity of the agricultural land (i.e., changes of the carbon stock due to the establishment of the agricultural fields in place of a forest), although such changes (thereafter referred as the direct land use changes, DLUC) have been incorporated in the LCAs of the biofuels recently and basically restricted to the GHG emissions related to the soil carbon release during land conversion [40, 41].

The most controversial discussion in recent years concentrates, however, on the so-called indirect land use changes (ILUC). These changes often are related to

Biomass Provision and Use, Sustainability Aspects. Table 2 Illustrative GHG savings and payback times for biofuel feedstock causing land change [41]

Fuel chain	Assumed country of origin	GHG saving excluding the impacts of land-use change	Carbon payback (years)	
			Grassland	Forest
Palm to biodiesel	Malaysia	46%	0–11	18–38
Soya to biodiesel	USA	33%	14–96	179–481
Sugarcane to bioethanol	Brazil	71%	3–10	15–39
Wheat to bioethanol	UK	28%	20–34	80–140

as the leakage effects, namely, the activity in one place or one country induces the land use changes on the other lands. In this approach, the environmental impacts occur indirectly, outside the boundary of the system in question [39, 40], and thus they are very difficult to assess and to quantify. This difficulty may be related to the spatial (e.g., biomass produced in one location creates pressure on agriculture in other locations) and temporal (e.g., when land cleared for another crop is used for biofuel crop production in successive years) characteristics of the changes, as well as quality of the modeling data [39, 40] and the uncertainty of the results. However, the first modeling approaches have shown that the disadvantages related to the indirect land use changes are causing significant release of carbon stocks. As a result, the GHG savings from the biofuel use are larger than the ILUC-related carbon emissions only after specified time period, so-called payback time (Table 2, [41]).

The large variation of the results relating to the payback times and simultaneously carbon debts (amount of carbon released, that have to be balanced with the GHG savings from the combustion of biofuels) may be seen as a consequence of applying various methods to calculate these quantities, as well as uncertainty of the modeling data. The uncertainties relate to the type, scale, and timing of the indirect effects, and they originate from the following conditions:

- Complex global nature of agricultural markets and uncertainties in predicting the effect of increased production for biofuels.
- Potential for feedstock switching resulting from the possibility of producing the biofuels from various feedstock; producers may switch their feedstock crops more frequently, which creates a potential danger of the increased land use change.
- Production of co-products.
- Commodity price changes [41].

Several models have been created in order to tackle such a complexity of factors influencing ILUC. Four basic groups of the scientific models have been identified [42]:

- Complex multi-layered, numeric macro-economic/econometric, and/or biophysical models: Models such as GTAP, FASOM, FAPRI etc., which are primarily used for legislation in the USA (e.g., California). The models calculate the impact of the additional biomass production on the agricultural markets, on the production methods in the agriculture, and finally the dynamics of the land use change.
- Simplified deterministic approaches, such as the ILUC factor or the bonus according to the European Directive on Renewable Energy (2009/28/EC). In these methods, an assumption is being made that additional biomass production by definition results in additional land use. The models allocate proportionally the land use changes to the increased biomass production.
- Other approaches which strike a balance between these two approaches. Here, a simplified schematic calculation of land-use changes and resulting GHG emissions is performed.
- Approaches that focus on ILUC risk minimization with the help of productions methods, which eliminate or reduce the occurrence of negative environmental effects [42].

Depending on the type of the method chosen, the results may vary – even for the identical conversion pathway and input modeling data – considerably. For example, for bioethanol made from the maize, the calculated results span from 30 g CO_2-eq/MJ energy of the biofuel according to the results supplied by the GTAP model, through 36 g CO_2-eq/MJ for the ILUC factor, 50–65 g CO_2-eq/MJ for the FASOM/FAPRI models, up to 104 g CO_2-eq/MJ calculated by the FAPRI model alone [43]. Furthermore, because the indirect effects are occurring outside the economic and political system of one country, it appears to be very difficult to control and minimize these indirect effects. One possible approach is to apply standards and certification systems or incorporation of the sustainability requirements in the laws and regulations, relating to the biomass production in general and very often to the biofuel production. Within the EU, the indirect land use changes have not been quantified in the regulations yet, although the decision makers have recognized the necessity to include them in the future policy regulations [30]. The US Environmental Protection Agency (EPA) has, however, included ILUC in the newest standards concerning the biofuels, so-called Renewable Fuel Standards (RFS).

One of the most intensively discussed issues concerning the biofuel production recently was the question of the biofuel production impact on the changes of the food prices – so-called food vs. fuel debate – which arose in 2007 when the food prices increased (Fig. 5). A set of main factors responsible for the growing food prices have been identified [44], namely:

- Increased biofuel production driven in the USA and EU by mandates and tax policies, and corresponding demand for biofuel input material: soybeans, maize, wheat, etc
- Rising energy prices
- Declining dollar prices
- Increasing agricultural costs of production
- Export bans and restrictions fuelling the price increase (restricted access to the supplies)

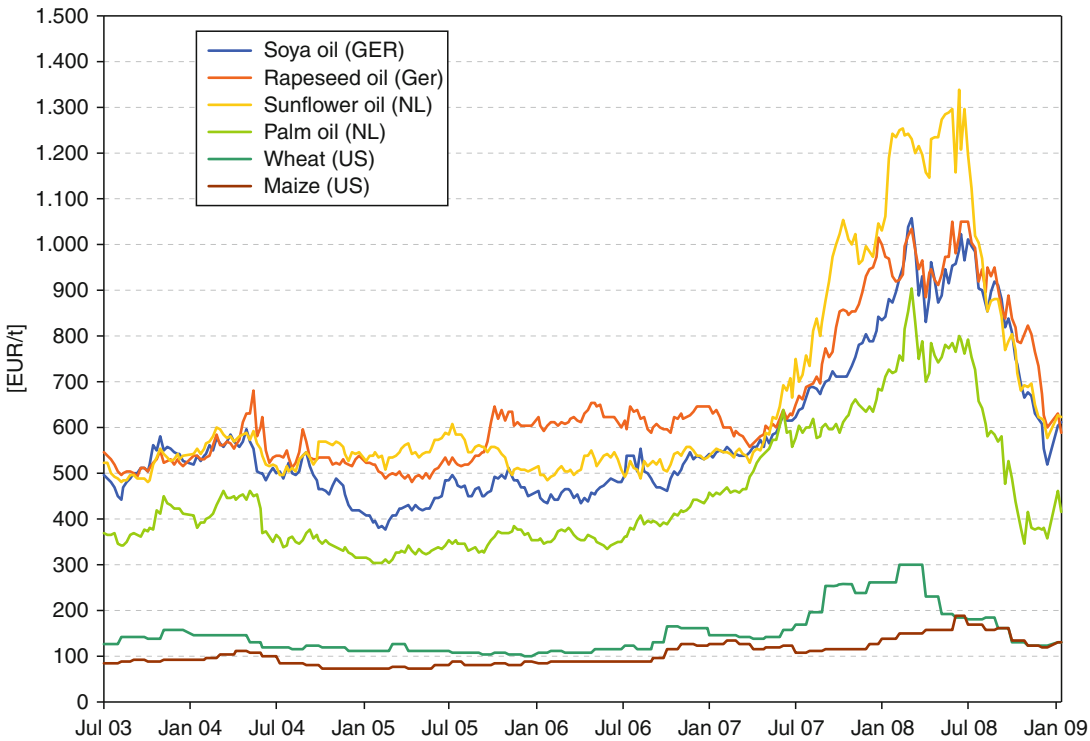

Biomass Provision and Use, Sustainability Aspects. Figure 5
Development of food and biomass prices [45, 46]

- Rapid income growth in developing countries
- Speculative and investor activity

The increase in internationally traded food prices was caused by the confluence of these factors [44]; nonetheless, biofuels played a significant role in this process. However, many studies revealed in the past 2 years a stabilization of the agricultural prices despite constantly increasing share and production of biofuels in the global market. For instance, a recent investigation from the Food and Agricultural Organization (FAO) and the OECD predicts constant, but not sharp increase in the prices during the years 2010–2019. For example the crop prices will be 15–40% higher in comparison to the period 1997–2006, while, e.g., dairy prices will increase by 16–45%. However, biofuel production is not seen as the main factor influencing the prices; other factors shaping the agricultural prices (rising energy prices, demand from developing countries, changes of dietary habits, etc.) are mentioned as well [47]. Nevertheless, from the point of view of the sustainability, one has to analyze and offer solutions, which would minimize the negative impact of the biofuels on the food prices. The problem of the rising food prices may be solved [48], if instead of producing first-generation biofuels (created from the materials which may also be used for nutrition), second-generation biofuels would be introduced into the market. The latter biofuel type is based on crop residues and inedible cellulosic materials, such as leafy steams, stems, stalks, etc. However, the market introduction of second-generation biofuels has to overcome some technical and economic obstacles [48].

Summarizing, the concern about the influence of the biofuel production on the environment seems to be important in the scientific and political discussions. However, blaming the biofuels for the negative effects alone would be too simplistic and would ignore several opportunities created by biofuels, such as bringing particular benefits to the farmers and facilitating the abatement of the poverty worldwide [49]. Nonetheless, attempts to take into consideration and to minimize the possible negative effects were made in the USA with the newest regulations issued by the Environmental Protection Agency (EPA). This regulation, known as the Final Renewable Fuel Standard (also "RFS2"), may be characterized as follows:

- It classifies biofuels on the basis of the life-cycle GHG thresholds as "renewable" (20% GHG savings) or "advanced" (50% GHG savings). Furthermore, for the biomass-based biofuels, a threshold has been set at 50% (renewable biofuels) and 60% (advanced biofuels), respectively.
- "Non-advanced" (renewable) biofuels (mainly corn ethanol) will gain shares until 2022 up to 15 billion gallons (in comparison to the total amount of the renewable biofuel required of 36 billion gallons); then, their blend mandate will remain constant to finally diminish if the technical progress in the advanced biofuels will allow to produce them in larger quantities.
- The EPAs GHG footprint takes into consideration indirect (in the USA also called "international") land use change. As a consequence of this approach, the initial GHG savings of corn ethanol of approximately 52% were reduced to the level of 21%, which not surprisingly become immediately an disputable matter for various groups of interests, such as farmers, fuel producers, investors, and industry players, as well as politicians trying to stop or at least delay applying the ILUC approach within the ongoing decision-making process [50, 36, 51].

For the calculation of the indirect land used changes, a combination of the complex mathematical models have been applied, including remote sensing techniques, based on the historical data (Table 3).

Most of the aspects covered by these models have a significant effect on the final result. But the calculated numbers are still characterized by high uncertainties. Nevertheless, the results are comparable in a better way than those gained with individual approaches [36].

The US Environmental Protection agency has based the assessment of the ILUC on the foundation of the so-called Wheel-To-Wheel (WTW) Life Cycle Assessment (LCA), including each stage of the biofuel production, such as production or extraction of the feedstock, feedstock transportation, fuel production, fuel transportation and distribution, as well as tailpipe emissions. Furthermore, the EPA has made a decision to use a consequential LCA, not the attributional one.

- The attributional LCA provides the information about the emissions and environmental impacts caused by the product or service, emitted during

Biomass Provision and Use, Sustainability Aspects. Table 3 Models and data used for the calculation of the ILUC within RFS2 [42]

Acronym	Name of model	Type of model
DAYCENT		Biophysical model for soil processes
FAPRI	Food and Agriculture Policy Research Institute	Partial equilibrium model (soil)
FASOM	Forest and Agriculture Sector Optimization Model	Partial equilibrium model (USA)
GREET	Greenhouse gases, Regulated Emissions, and Energy use in Transportation Model	Life-cycle model for emissions from the transportation sector
MODIS	Moderate Resolution Imaging Spectroradiometer	Satellite data on land use/cover
MOVES	Motor Vehicle Emission Simulator	Model for vehicle greenhouse gas emissions

its life cycle. The processes taken into consideration are linked in a straight line to the product or service in question by material, energy flows, or services following supply-chain logic. In this type of the LCA, land use impacts are typically confined to direct impacts (e.g., environmental consequences of converting forest areas for the production of corn used within the ethanol production) [36].

- A consequential LCA, however, accounts the GHG emissions or other environmental impacts related to the product or service indirectly, occurring as a consequence of the changes in the demand of the product or service. Here, the changes in the GHG emissions are identified by linking the causes with the effects. For example, if the production of ethanol in the USA increases, the biofuel production may be exported to abroad. As an effect, additional corn or grain production in South American countries has to take place, resulting in, i.e., destroying rain forest for the purpose of establishment of new agricultural fields in Brazil. As a consequence, initial GHG saving by the production of bioethanol will be diminished by cutting off the forests in Amazonia.

The EPA has chosen the consequential LCA as a main research method, since the US administration has decided to take into consideration not only the direct GHG emissions, but also the significant indirect emissions being the effect of the land use changes. Furthermore, the full fuel life cycle has been modeled, including all stages of the fuel and feedstock production and distribution, as well as its use. The Global Warming Potential was estimated using the mass values of the greenhouse gases [36].

The methodology of the RFS2 rulemaking was based on mathematical models created for various purposes. In general, these models have taken into consideration the data estimated for nine land categories in 750 regions across 160 countries worldwide, with a weighted average applied to the rest of the world, covering all significant agricultural producers. The scientific basis for the models was the Economic Input–Output Life Cycle Assessment (EIO-LCA), which estimates the materials and energy resources required for, and the environmental emissions resulting from activities in the overall economy. Furthermore, the following models, modeling factors, approaches, and methods were combined together, in order to obtain comprehensive and reliable results with respect to the various areas of science, needed to estimate ILUC:

- Forestry and Agricultural Sector Optimization Model (FASOM): estimation of the changes in the US agricultural and forest sectors (e.g., changes in crop acres resulting from increased demand for biofuel feedstock or changes in the number of livestock due to higher corn prices) and their associated emissions, as well as land use shifting between crops, and interactions with pasture, and forestry; partial equilibrium economic model.
- Greenhouse gases, Regulated Emissions, and Energy use in Transportation (GREET): spreadsheet analysis tool developed by Argonne National

Laboratories for calculation of the GHG emission factors for fuel and fertilizer production.

- IPCC guidance factors: livestock GHG emission factors.
- CENTURY and DAYCENT: models developed by the Colorado State University to estimate US impacts of the N_2O emissions from the fertilizer application; DAYCENT simulates plant–soil systems and is capable of simulating detailed daily soil water and temperature dynamics and trace gas fluxes (CH_4, N_2O, NO_x, and N_2); CENTURY as a generalized plant–soil ecosystem model simulates plant production, soil carbon dynamics, soil nutrient dynamics, and soil water and temperature.
- Integrated Food and Agricultural Policy and Research Institute international models, as maintained by the Center for Agricultural and Rural Development (FAPRI-CARD): estimation of the impacts of biofuels feedstock production on international agricultural and livestock production; the models capture the biological, technical, and economic relationships among key variables within a particular commodity and across commodities relevant, e.g., for the ILUC.
- Satellite data: used to analyze recent land use changes around the world that have resulted from the social, economic, and political forces that drive land use; EPA has made the assumption that these recent drivers of land use change will remain in relative effect through 2022 modeling time frame such that the recent trends in land use change are indicative of land use changes likely to result in 2022 due to biofuel production; furthermore, the recent land use change patterns were combined with various estimates of carbon stocks associated with different types of land at the state level.
- IPCC Agriculture Forestry and Other Land Use (AFOLU) Guidelines and Winrock International organization: land use change emissions factors [36].

Summarizing, the US EPA has estimated the ILUC on the basis of the economic input–output models. The results of the calculation were combined with the satellite data in order to predict the types of the land converted to cover the increased land demand resulting from the biofuel production. The measurement of the ILUC was done with the help of the GHG emissions, calculated for different types of the land converted. As the EPA underlines, the results of this assessment are characterized with some level of uncertainty which, however, has been taken into consideration and incorporated in the final results of the analysis [36].

The uncertainty of the modeling data and results as well as the complexity of the ILUC issues and factors that have to be taken into consideration are creating the questions about the real impacts of the ILUC and whether or not ILUC should be taken into consideration when setting policy objectives and targets. As already mentioned, ILUC effects are only mentioned but not implemented in the current EU regulations. In the USA, they become a part of the RFS2 standard, but the inclusion of the ILUC as well as the calculated ILUC-related GHG emissions has been extensively criticized. Certainly, the criticism from the farmers and lobbying groups representing industry branches investing and offering, e.g., bioethanol plants may be well understood. However, the critical considerations about the nature and quantification of the ILUC are also noticeable in the scientific discourse. The inclusion of ILUC in GHG balances on the basis of the LCA technique of biofuels is an ad hoc solution to the more fundamental problem of unsustainable agricultural practices in many parts of the world [52]. Furthermore, critics of the ILUC underline that ILUC application in the policy-making process penalizes those that cannot affect the course of land use change while providing no incentives to those that could. The scientific and political debate should concern rather "food vs. feed" instead of "food vs. fuel" debate [53], since about 90% of the human use of arable land is to produce animal feed mostly for the beef cattle. Therefore, the debate should be focused more on the dietary habits and could be also called "beef vs. barrels" debate. Furthermore, the complexity of the models impedes the clarity of the results and the possibilities to check and correct them, if necessary [53]. One has to mention that the criticism of the ILUC incorporation is especially strong in the USA, where the indirect effects were incorporated in the existing standards. Within the EU, on the contrary, scientists and decision makers do not question the nature and existence of the ILUC effects, but focus more on the methods to quantify and subsequently include them in the decision-making process and the binding regulations.

Efficiency

Although the ILUC has drawn a public attention in the last few years and influenced even the legally made thresholds levels for the biofuels in the USA, the land use changes may not be seen as the only one and the most important criterion of the biomass sustainability. A survey among 46 experts being active in the field of the bioenergy in different regions of the world has been carried out [54], asking about the opinion about the most critical sustainability criteria. These 35 criteria mostly mentioned represented social, economic, and environmental spheres of life in the ratio 4:1:4, respectively. The ten most important criteria, obtained from the survey analysis, are presented in Table 4.

As one can see, the efficiency (represented directly and indirectly in several above-mentioned factors) characterizes the crucial part of the sustainability indicators. Simultaneously, increasing the efficiency is the easiest and most feasible option to increase sustainability of biomass and decrease GHG emissions [55]. Therefore, for further consideration, the following sustainability criteria and indicators will be described in detail with respect to the biomass and bioenergy: GHG balances and GHG-saving efficiency, area efficiency, material efficiency and efficiency of use.

In many cases, the various types of efficiencies are strongly related to each other (i.e., material efficiency and GHG reduction efficiency). In some cases, several types of efficiencies may be even combined in one term. For example, the heads of the European Environmental Agencies have defined "resource productivity" as the efficiency, at which energy and materials are used throughout the economy [56]. However, in most of the cases, the political decisions in the field of biomass use are setting targets with respect to the energy and GHG saving efficiencies.

Biofuels are often used in a very unsustainable and inefficient ways mostly due to the lack of capital for the investment in the modern equipment [55]. This fact is easily observed in developing countries, where biomass resources are utilized mainly for cooking and heating purposes. In these countries, increasing the efficiency of fuelwood use would have significant positive effects

Biomass Provision and Use, Sustainability Aspects. Table 4 Identified sustainability criteria and their short description (Adopted from [54])

Rank	Sustainability criterion	Description
1.	Greenhouse gas balance	GHG balance of system covering CO_2, CH_4, O_3, NO_2, H_2O
2.	Energy balance	Conversion efficiencies, energy return on investment, energy return per hectare
3.	Soil protection	Impacts on soil fertility, changes in nutrient cycling, rooting depth, organic matter, water holding capacity, erosion
4.	Participation	Inclusion of stakeholders in decision making; facilitation of self-determination of stakeholders
5.	Water management	Surface and groundwater impacts, riparian buffers, irrigation and cooling cycles and waste water management
6.	Natural resource efficiency	Efficient use of resources at all stages of the system
7.	Microeconomic sustainability	Cost-efficiency incl. start-up costs, internal rate of return, net present value, payback period
8.	Compliance with laws	Complying with all applicable laws and internal regulations like certification principles, countering bribery
9.	Ecosystems protection	Safeguarding protected, threatened, representative, or other valuable ecosystems (e.g., forests); protecting internal energy fluxes/metabolism
10.	Monitoring of criteria performance	Monitoring systems in place for all criteria (e.g., leakage or additionally in GHG accounting)

on greenhouse gas emissions, could reduce the unsustainable exploitation of the natural resources, as well as it may have a positive effect on the indoor air quality. Furthermore, the following categories of GHG emission reductions due to the increase of the energy efficiency have been identified:

- CO_2 emission reductions related to energy inputs into the fuel cycle, mostly during the production and conversion stages.
- Non-CO_2 emission reductions related to end-use efficiency and conversion. In this emission category, increasing the efficiency of, e.g., fuel stoves can result in significant reductions of other pollutants, including non-CO_2 greenhouse gases (CH_4) and other ambient air pollutants, particularly the emissions of unburned components such as VOC (volatile organic compounds), PAH (polyaromatic hydrocarbons), carbon monoxide, and NO_x.
- Land use-related emission reductions (which make up the bulk of GHG emissions from current biomass energy systems) and additional benefits.

In general, the rules implemented in the USA and EU set defined GHG reduction efficiencies as a prerequisite to recognize biomass source (especially valid for the liquid biofuels) at certain defined levels. For the EU, these values vary from 35% to 60%, and for the USA from 20% to 60% (depending on the time frame; the latter values are intended for the advanced biofuels of the next generations introduced around years 2017–2022).

An important remark has to be made with respect to the methodology of accounting the GHG emissions when burning biomass sources. Usually, the renewable sources are considered to provide carbon neutral energy, because the carbon dioxide emissions emitted during combustion are being a part of the natural cycle. As a consequence, re-growing biomass captures the CO_2 emissions released during the combustion. However, the GHG emissions of the biomass burning in the life-cycle perspective may be higher than those in case of the fossil fuel burning; the excess of the emissions is called carbon debt. The numerical value of this debt may depend on various factors, such as type of the energy generated, type of the fossil fuel being displaced (question of the reference system), or the management practices applied when producing the biomass. The difference between the carbon debt, direct GHG emissions, and accounting on the life-cycle basis may lead, however, to misleading interpretations, if oversimplified or interpreted without in-depth analysis [57, 58].

Another type of the efficiency that has to be discussed is area/land use efficiency. One has to treat land as non-renewable and strongly restricted resource, which should be used with a high efficiency, measured, i.e., as the yield rates per area of agricultural land. Another option to increase land use efficiencies from a wider perspective would be to establish plantations of, e.g., short rotation coppice or miscanthus on degraded/abandoned lands. Thus, the area devoted to the crop production is not diminished (reduction of competing use with the food), and simultaneously the overall land use efficiency is increased. In some cases, the land use efficiency strongly correlates to the water-use efficiency [59]. It is, for example, very difficult to improve land use efficiency in the arid and semi-arid regions in the Mediterranean countries, where the water resources are fully exploited and in some cases, even overexploited. Therefore, increasing, e.g., crop yields in these countries is impossible without implementation of the sound water management and irrigation programs.

To increase the land efficiency on existing agricultural areas, a broad variety of different measures may be used, including better agricultural practices, use of fertilizers, irrigation, etc. An interesting possibility of increasing the land efficiency is to use crop and plant residues, not utilized for other purposes. The obstacles with respect to land efficiency, however, may impede in some cases the efforts of efficiency increase in this area.

The next type of the efficiency to be taken into consideration in energetic use of the biomass relates to the materials use and the energy conversion efficiencies [60]. In general, the overall efficiency of the conversion (for instance, in the corn-based ethanol industry or in the area of lumber recovery in the wood industry) has increased in the past 20 years significantly [61]. The question appears, however, how to account the efficiency increase and – specifically in the case of the greenhouse gas emissions – how to decide, whether the efficiencies are high enough or not?

In the other words, what kind of reference systems should be used for the comparison of various existing options?

The most widely used tool for such comparisons between various conversion pathways and options is the Life Cycle Assessment (LCA). The LCA is known since the end of the 1960s; however, it is still considered to be relatively young and immature. As a consequence, there is no widely accepted methodology of conducting LCAs. Thus, the results of the LCA analysis for one product or service may differ according to the method chosen or assumptions made [62].

Another problem with setting the efficiency requirements is the relation between given conversion pathway and the reference or baseline scenario. The choice of the various baseline scenarios may have impact on the calculated GHG saving in the same way as the choice of the LCA method and the respective assumptions. Furthermore, the following assumptions may alter the final results:

- Inclusion or exclusion of the ILUC
- Choice of the historical data about (e.g., deforestation rates vs. biofuel production)
- Choice of the mathematical models
- Choice of the Life Cycle Impact Assessment methods and the modeling factors
- Origin of the biofuel and the production conditions
- The biofuel production technology
- End-use conversion efficiencies

The increasing efficiency is only one factor contributing to the successful and sustainable use of biomass. Another prerequisite of such use relates to the initial availability of the material for bioenergy production, which can be described with the term biomass potential (see below).

Sustainability

In the environmental discussion, the term "sustainable biomass potential" usually refers to the specified amount of raw materials, which may be used for bioenergy provision with simultaneous fulfillment of sustainability requirements. From a technical point of view, biomass potential is defined as the ability to obtain certain amount of the biomass/bioenergy from a given area in a given time period. Usually it is distinguished between the theoretical potential (the total amount of energy that may be created in a given time period by using physically available biomass), the technical potential (part of the theoretical potential of the bioenergy that may be generated taking into consideration technical restrictions), the economic potential (part of the technical potential, amount of bioenergy that may be generated taking into consideration economic restrictions), and the available potential (the bioenergy that may be created in reality, after taking nontechnical and noneconomic constraints into consideration (like the emotional fear from new technologies, emotional barriers to use biomass, etc.) (Adapted from [4]).

Additionally there are also many other approaches toward depicting the possible potentials. For instance, a differentiation can be made according to the availability of biomass (based on the function and position of the material in the entire system) between:

- Area potential (the amount of the material on the given area of land)
- Material potential (amount of material that may be gained from the given area using the available technology)
- Fuel/energy carrier potential (amount of the combustible material that can be made from the raw material)
- Bioenergy potential (amount of the bioenergy that may be created after passing all different conversion routes)

Another aspect that has to be mentioned is the competition between various purposes, for which biomass may be used. This problem may be denoted as the "4F" dilemma. Namely, one has to ask a question: Which need(s) of the mankind should be satisfied first from the available biomass potentials: food, feed, fiber, or fuels? Decision makers and public attention focus currently mostly on the rising food prices as a (supposed) consequence of the growing demand of biomass used for biofuels. However, the system of the interrelationships between those four main purposes seems to be much more complicated and difficult to investigate. Therefore, a system of the different integrated models for assessing and evaluating sustainable biomass potentials should be created.

Sustainable use of biomass demands a clear view of the future biomass potential considering all the relevant sustainability aspects. This includes detailed regional specific information about soil and climate and assumption concerning the expected demand on biomass for food, feed, and materials (fibers).

There are no accepted rules yet to calculate sustainable potentials [63]. Therefore, in the following section, an overview on the debate on biomass potential assessment is given, which already includes sustainability aspects. Simultaneously, the open points of the discussion are described.

Since sustainability relates to many fields of the management and research, an integrated approach seems to be appropriate and necessary to obtain a comprehensive evaluation of the existing potentials. An example of such an integrated model for the biomass potential calculation is shown in Fig. 6. The areas covered by such models range from physics and chemistry (air pollution and climate change), biology and agriculture (land use and its restrictions as well as biophysical conditions), economy (costs and prices), and environmental sciences (Life Cycle Assessment, LCA). LCA studies are currently developing approaches to incorporate indirect land use changes in the results; however, so far there is no widely accepted and applied methodology which might be universally used. The previously mentioned method applied by EPA in the evaluation of the GHG balances of the biofuels may be seen as the first forerunner of such an integrated modeling assessment. However, the models and the data used have still a great potential for improvement.

Factors Influencing the Biomass Potential

Even if a general approach for sustainable potentials is not available yet, the main influencing factors for the future biomass availability can be described. Therefore, in general, the technical biomass potential is analyzed as a realistic maximum. While the technical biomass potential from residues and wastes does mainly depend on human activities and the demographic development, the technical biomass potential from energy crops is linked to available arable land for energy crop cultivation which is influenced by a multitude of different drivers such as policy scenarios (Fig. 7).

The land availability for energy crop production depends on the overall amount of available agricultural land and the demand of land for food and fodder production. But there are various drivers influencing the present and future food and feedstock demand. Their magnitude depends on the climate zone, the soil quality, and specific local conditions. However, the main factors are universally valid in a global context. The following influencing factors may be

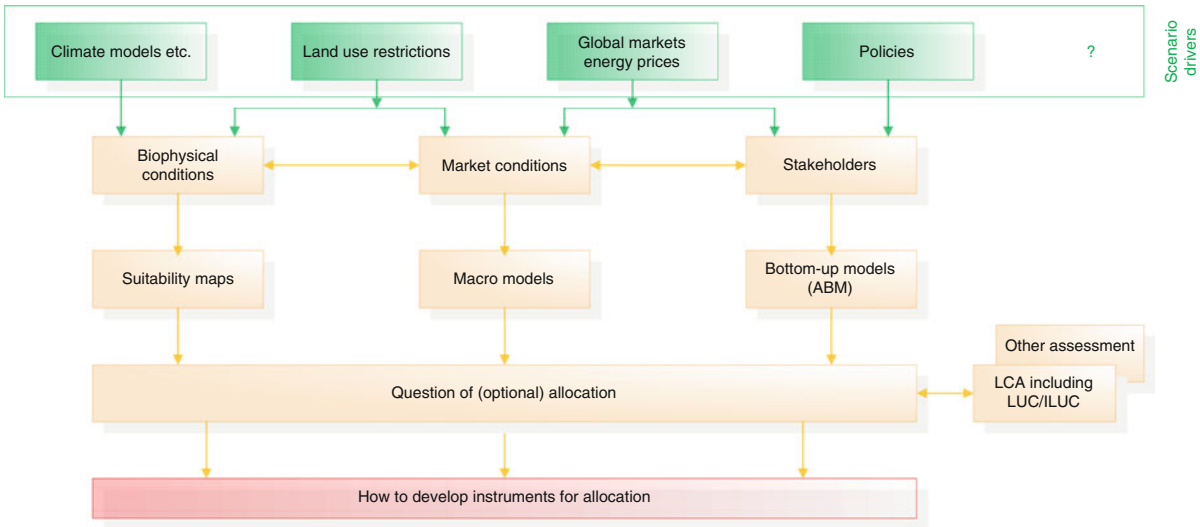

Biomass Provision and Use, Sustainability Aspects. Figure 6
Integrated potential assessment of the energy crops

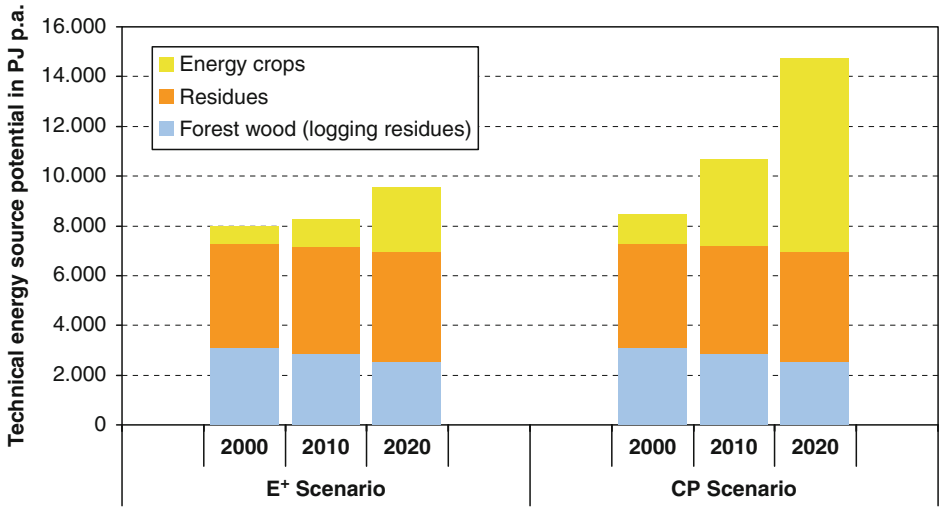

Biomass Provision and Use, Sustainability Aspects. Figure 7
Current and expected technical biomass potentials. Example: European Union considering two different scenarios for the development of environmental standards for the agricultural production. E+: Environmental+scenario, CP: current policy scenario [64]

identified as those playing a crucial role on the worldwide scale [65]:

1. Development of the global population
2. Per capita consumption of food (global per capita consumption of food changes slowly but increasingly; the production of meat needs at least six times the acreage needed for the production of plant products)
3. Increase of harvests by increase of specific yields due to progress in plant breeding
4. Increase of yields by improving the state of the art (real situation in agriculture; i.e., assimilation of production systems particularly in Africa and Asia)
5. Climate change influence the availability of acreage and the development of yields
6. Loss of agricultural acreage by soil degradation (erosion, salinization) and additional need of areas for non-agricultural purposes (infrastructure, restrictions of use, etc.)
7. Competing needs for nature conservation
8. Acreage for flood protection
9. Extensification toward environmental protection
10. Use of resources as raw material in industry
11. Use of resources for attractive non-subsidized exports

Out of these factors, the most important ones are the development of the global population, the future per capita food consumption – both driven by the development of the worldwide economic growth – and the development of the specific yields for food, fodder, and biomass production. Climate change and its impact on the agriculture production will also be an important factor which, however, is very difficult to quantify [66].

Figure 8 shows the main drivers and connections between the different levels of the biomass supply system. According to this, various different factors need to be considered by potential estimates. The assessment of future biomass potentials has to include a range of uncertainties and thus, represents a very complex question.

The previously mentioned influencing factors may have a positive and negative impact on the areas available for biomass production and the biomass potential. The most sensitive drivers are the demand for food (potential reducing factor) and the increase in agricultural yields (potential increasing factor). One has to take into consideration, however, that the potentials and distributions vary largely according to the local conditions. Therefore, information of the biomass potential is necessary on the regional and country-related scale.

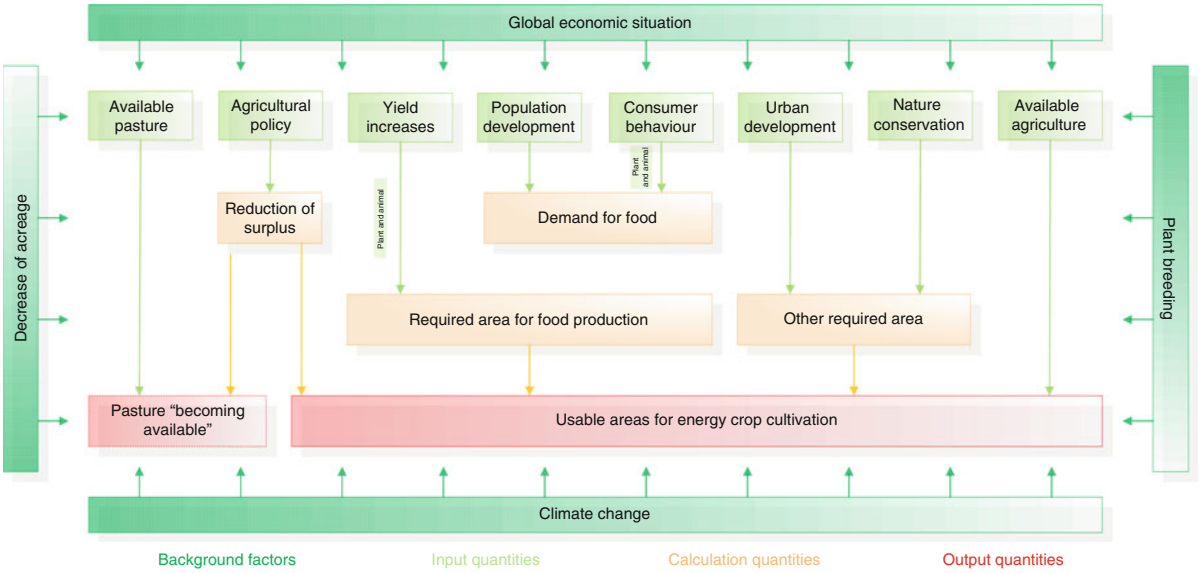

Biomass Provision and Use, Sustainability Aspects. Figure 8
Interrelationships and drivers of the biomass potential for energy crops (Adapted from [34])

Biomass Provision and Use, Sustainability Aspects. Table 5 Potential of agricultural land for energy crops in 2002–2005, in [10^3 ha]

Country	Fallow land	Surplus area from the production of			Sum
		Crops	Milk	Beef	
EU-27	14,145	9,390	4,919	2,140	30,595
Europe others	88,975	5,141	1,837	351	96,336
Europe total	1,03,121	14,531	6,756	2,491	1,26,932
North America	93,373	31,182	−400	373	1,26,123
Central America	15,279	1,241	−4,148	−2,322	17,468
South America	19,100	16,102	5,734	25,904	71,140
America total	1,27,753	49,985	7,604	29,296	2,14,732
Australia	24,909	12,268	65,658	89,925	1,92,760
Oceania	3,219	138	8,197	1,628	13,182
Asia	47,595	13,832	41	675	62,188
Africa	43,337	352	270	65	45,451
Sum (133 countries)	3,49,933	91,105	88,527	1,24,081	6,55,244

Table 5 presents the overview of the available agricultural land for the purposes of the energy crop production (i.e., historical data from 2002 to 2005). As it can be seen, the highest area potential occurs in Australia, Europe, and North America. Most of the land available for energy crop production might be obtained from fallow land, followed by surplus area coming from the production of the beef, other crops, and milk. Nonetheless, in some regions, negative values occur, underlining the missing production capacities and/or

non-advantageous country characteristics. Another surprising fact is the low land availability in Africa and Asia, in relation to the total area of these continents.

The general characteristics of the key regions of the world may be described as follows:

- Europe: relatively large area available for the biomass production; high productivity and efficiency of the production does not leave much space for surplus areas that could be used for the biomass production, especially in so-called old EU member states.
- Russia and the Ukraine: very large area (alone in Russia approximately 216 mn ha of the total agricultural land) available mainly in the form of the fallow land; the current productivity and production efficiency is very low, but may slowly increase in the future; in the middle term, it is estimated that both countries will increase their area potential for bioenergy sources.
- North America: large agricultural area, high yields per hectare, importance of the utilization of the genetically modified organisms (e.g., maize) may be observed; very high area potential.
- Latin America: the growth of agriculturally utilized areas may be observed; Brazil is especially important from the point of view of sustainability, since it is a big ethanol producer.
- Asia: increasing yields per hectare combined with a small area of available land per capita allow to maintain currently the self-provision with food; very small area available for the production of the energy plants; sustainability problems in Malaysia/Indonesia related to the conversion of the carbon-rich soils into palm plantations.
- Australia: one of the highest surplus of the grain exports in the world and approximately 440 mn ha of agricultural land; however, the area potential is expected to decrease due to the growth in population, reduction in yields, and diminishing agricultural land.
- Africa: currently relatively small area potential due to the non-advantageous climate conditions; however, the biomass potential occurring in the other fields of biomass provision.

For the assessment of the sustainable biomass potential, the following areas of the biomass provision pathways, where social, environmental, and economic requirements could be met, are taken into consideration:

- The cultivation of the perennial plants on marginal, idle, or degraded lands abandoned from the agricultural use; in such way, the several negative aspects related to the biomass use are being minimized, namely competition with food crops, direct and indirect land use changes related to the biofuels expansion, which is inevitable associated with the creation of the long-term land clearing–associated carbon debts and biodiversity losses.
- Use of the abandoned crop residues, not utilized for the food production or other purpose. Here, the crucial aspect would be related to the maintenance of the soil fertility (known as humus balance); however, some amounts of the residues might be used, e.g., for energy purpose.
- The sustainable uses of the forest residues, including wood branches, sawmill operation rests, etc.
- Cultivation of the double crops and mixed cropping systems. In the first case, the crops for the bioenergy purposes might be grown between the summer periods, when the traditional crops for the food purposes are cultivated. In the second case, systems which may grow simultaneously for food and energy purposes are summarized.
- Conversion of solid waste streams, rich in organic matter such as municipal and industrial wastes, into, e.g., liquid fuels. Sometimes the declining potential of this source of bioenergy is mentioned due to the minimizing the waste losses in industry and improving the production efficiencies [41, 67, 68].

Concerning these factors, the future potentials for residues are projected to be in a smaller range than the potential for energy crops. Because of the uncertainties mentioned above, energy crop potentials are often assessed with scenario approaches. As a result, various information on the current and future biomass potentials are obtained. Figure 9 presents a comparison of some studies focusing on the current and future potential. As one can see, the difference between the estimation varies from approximately 100 EJ per year up to almost 1,400 EJ per year in 2050.

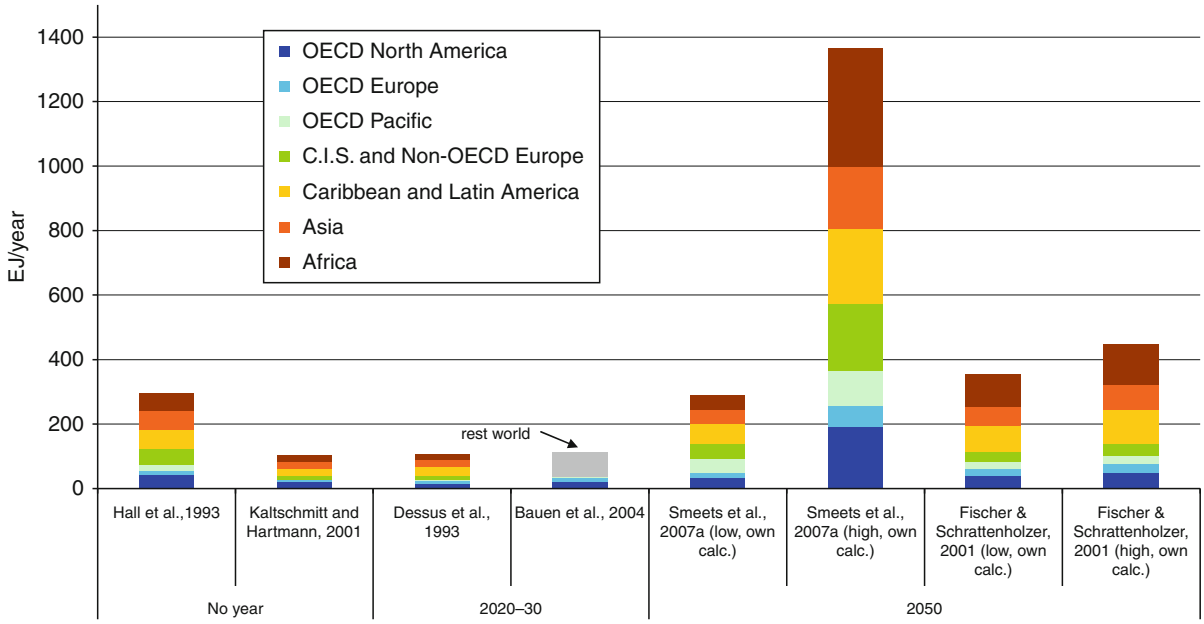

Biomass Provision and Use, Sustainability Aspects. Figure 9
Fuel potential for the various regions of the World (Data of [66, 69–85])

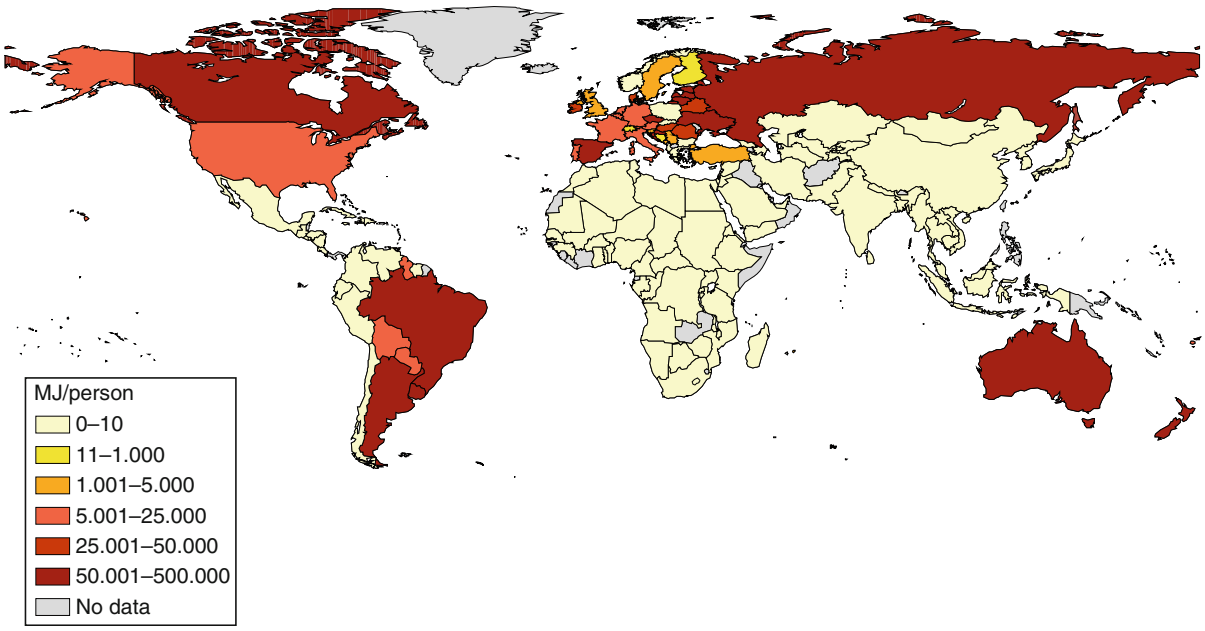

Biomass Provision and Use, Sustainability Aspects. Figure 10
Biomass potential in MJ/person in "business as usual" scenario for the year 2020

The question appears about the role and influence of sustainability standards on the availability of biomass for energy production. As it appears, obeying the "strong" sustainability rules does not automatically result in the reduction of the energy crop potentials. Figures 10 and 11 compare the energy crop potential for a "business as usual" scenario and an "environment and health" scenario, which predict stronger

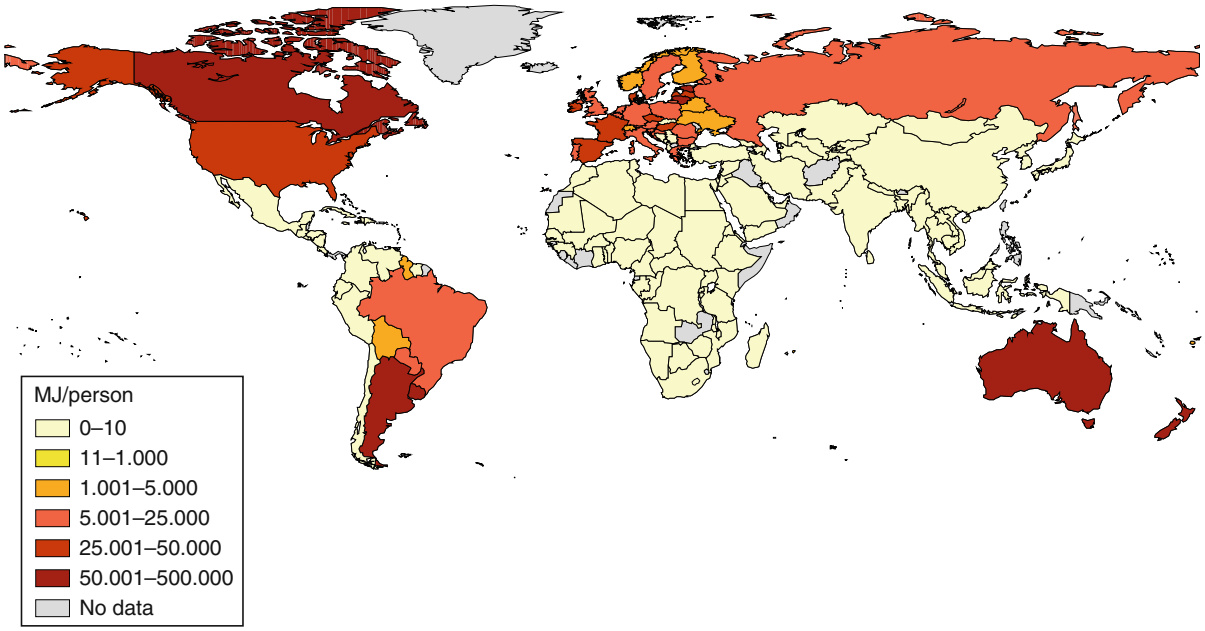

Biomass Provision and Use, Sustainability Aspects. Figure 11
Biomass potential in MJ/person in "environment and health" scenario (ecological approach in agriculture and change in eating habit) for the year 2020

environmental standards (no additional land use change), but also a adoption of the food-consumption-pattern (reduction of meat consumption to a more "healthy" level):

- In the "Business as usual scenario" it was assumed that the legal, economic, and environmental conditions in the future will be exactly the same as today. That means that some negative processes are continuously taking place (e.g., agricultural area degradation, forest clearing, loss of land area for the industrial and residential purposes). Although the ecological agriculture is growing and the fertilizer input is being minimized according to the regulatory trends, the scenario assumes that the conventional production techniques still prevail.
- The environment and health scenario is assuming both: application of the ecological and sustainable land management practices, as well as change in eating habits of the specific countries according to the recommendations of the World Health Organization.

As a result of the "business as usual" scenario calculations, one may see that the global biomass potentials are the highest on the northern hemisphere, in the bigger part of the South America and in Australia. In Africa, Asia, and some countries of the Central and South Africa, the calculated potential is very low (approximately 0 to 1,000 MJ/person, Fig. 10). This is due to the previously mentioned conditions, such as high population number or non-advantageous climatic conditions.

The results of the "environment and health" scenario are in the same range as the "business as usual" scenario. As a result, one may observe an increase in the biomass potentials in most of the industrialized countries and in Russia.

The use of a degraded land, which is also discussed as a relevant biomass potential was not considered in both of the scenarios. Taking those lands for biomass production includes especially social risks, because they are primarily located in developing countries.

Summary

The increasing use of biomass as a consequence of the political decision concerning the minimization of GHG emissions has revealed that the provision and use of

biomass may also have some negative impacts on the environmental, social, and economic spheres of life. As a consequence, various actors and decision makers have decided to employ the concept of sustainability to avoid or minimize potentially negative influence of the biomass use. This entry has discussed the state-of-the art, ongoing developments and the future perspectives in the following areas of the biomass sustainability:

- Sustainability requirements
- Crucial factors to be taken into consideration by sustainability
- Requirements along the biomass process chain
- Life-cycle analyses and the indirect influence of the policies and decision making
- Creation of the standards, certification schemes, and binding laws
- Demands and methodologies for the assessment of sustainable biomass potentials

As it appears, supplying and using biomass in a sustainable manner requires taking into consideration and simultaneously modeling very complex, multi-level interconnected systems. First steps have been done in the last few year, but additional effort has to be taken to include also land use, social aspects, and environmental demands.

Future Directions

The approach toward sustainability depends on the type of stakeholder and its point of view, interests, which subsequently determine different strategies and specific measures. There are four main levels, at which sustainability issues may be developed and proliferated, namely:

- International (e.g., European Union), national, and regional authorities, issuing mandatory laws and standards
- Complementary measures issued on the international, national, and regional levels
- Commercial implementation of sustainability initiatives
- Activities of the non-governmental organizations (NGOs) [86]

The importance of a sustainability approach becomes more important, when creating the binding laws and standards for the biomass market (e.g., biofuel standards). Here, the contradictory interests of biofuel producers (which would like to have their fuel to be recognized as environmentally friendly and being produced in a sustainable manner) and various NGOs and research institutions (which underline, e.g., indirect land use changes) become obvious.

Since the discussion about sustainability of biomass started in the last decade, there are no widely accepted definitions of what sustainability in the context of biomass should mean. Depending on the type of player (international organizations, governments, NGOs, industrial associations, etc.), sustainability is defined in a wider or less detailed perspective. However, it is well visible that the future developments of sustainability requirements will focus on the following issues:

- Protection of highly biodiverse ecosystems and of carbon stocks
- Maintaining carbon balance of the soils
- Emissions from land use, land change, and forestry (LULUCF)
- Reductions of the greenhouse gas emissions in comparison to fossil fuels application
- Reducing energy consumptions and increasing the efficiency [30]
- Not causing any shifts in the GHG emissions (indirect land use changes)

Those targets cannot be successfully achieved within the bioenergy field alone, but demand more complex and comprehensive action and additional efforts in agriculture, energy supply systems, and an international debate on land use in general as well.

Bibliography

Primary Literature

1. European Committee for Standardization (CEN) (2010) Solid biofuels – terminology, definitions and descriptions. Final draft of the norm 14588. Comité Européen de Normalisation, Brussels
2. Metz B, Davidson O, Bosch P, Dave R, Meyer L (eds) (2007) Climate change 2007: mitigation. Contribution of working group III to the fourth assessment report of the intergovernmental panel on climate change. Cambridge University Press, Cambridge, http://www.ipcc.ch/pdf/glossary/ar4-wg3.pdf. Accessed 10 May 2010
3. UNFCC (2010) Glossary of climate change acronyms. http://unfccc.int/essential_background/glossary/items/3666.php. Accessed 29 June 2010

4. Kaltschmitt M, Thrän D (2009) Biomasse in energiesystem. In: Kaltschmitt M, Hartman H, Hofbauer H (eds) Energie aus biomasse: grundlagen, techniken und verfahren. Springer, Dordrecht
5. Tipper R, Hutchinson C, Brander M (2009) A practical approach for policies to address GHG emissions from indirect land use change associated with biofuels. Greenergy, available at http://www.ecometrica.co.uk/wp-content/uploads/Technical_Paper_-_Practical_Approach_to_ILUC_V1.2.pdf. Accessed 29 May 2010
6. Ellis E, Pontius R (2007) Land-use and land-cover change. In: Cutler J et al (eds) Encyclopedia of earth. Environmental Information Coalition, National Council for Science and the Environment, Washington DC, http://www.eoearth.org/article/Land-use_and_land-cover_change. Accessed 29 June 2010
7. United Nations (UN) (2010) Report of the World commission on environment and development: our common future. http://www.un-documents.net/ocf-02.htm. Accessed 10 May 2010
8. International Energy Agency (IEA) (2009) Key world energy statistics. http://www.iea.org/textbase/nppdf/free/2009/key_stats_2009.pdf. Accessed 7 May 2010
9. OECD (2007) Glossary of statistical terms. Paris. http://stats.oecd.org/glossary/download.asp. Accessed 5 Apr 2010
10. International Energy Agency (IEA) (2010) Web page of the Task 29: IEA bioenergy network on socio-economics. http://www.aboutbioenergy.info/. Accessed 5 Oct 2010
11. Merriam-Webster Online Dictionary (2010) Biomass. http://www.merriam-webster.com/dictionary/biomass. Accessed 5 Oct 2010
12. The American Heritage Dictionary of the English Language (2010) Biomass, 4th edn. Houghton Mifflin, Boston. http://dictionary.reference.com/browse/biomass. Accessed 5 May 2010
13. Tangang Yuntenwi EA (2008) Improved biomass cookstoves – a strategy towards mitigating indoor air pollution and deforestation. A case study of the North West Province of Cameroon. BTU Cottbus. http://opus.kobv.de/btu/volltexte/2008/458/. Accessed 5 May 2010
14. Searchinger T, Heimlich R, Houghton RA, Dong F, Elobeid A, Fabiosa J, Tokgoz S, Hayes D, Yu T-H (2008) Use of U.S. croplands for biofuels increases greenhouse gases through emissions from land use change. www.sciencexpress.org. Published online 7 Feb 2008. doi:10.1126/science.1151861. http://www.princeton.edu/~tsearchi/writings/Searchinger_et_al-ScienceExpress.pdf. Accessed 5 Apr 2010
15. Cornelissen S, Dehue B (2009) Summary of approaches to accounting for indirect impacts of biofuel production. http://www.ecofys.com/com/publications/documents/Summaryofapproachestoaccountingforindirectimpactsofbiofuelproduction.pdf. Accessed 29 Apr 2010
16. Fritsche UR, Hennenberg KJ, Hermann A, Hünecke K, Schulze F, Wiegmann K, Fehrenbach H, Roth R, Hennecke A (2009) Sustainable bioenergy: current status and outlook. Federal Environment Agency. http://www.ifeu.org/nachhaltigkeit/pdf/OEKO_IFEU%20(2009)%20Bio-global%20english.pdf. Accessed 29 Apr 2010
17. Eickhout B, van den Born GJ, Notenboom J, van Oorschot M, Ros JPM, van Vuuren DP, Westhoek HJ (2008) Local and global consequences of the EU renewable directive for biofuels. Testing the sustainability criteria. Netherlands Environmental Assessment Agency. http://www.rivm.nl/bibliotheek/rapporten/500143001.pdf. Accessed 29 Apr 2010
18. Grober U (2007) Deep roots – a conceptual history of 'sustainable development' (Nachhaltigkeit). Wissenschaftszentrum Berlin für Sozialforschung (WZB), Berlin, http://bibliothek.wz-berlin.de/pdf/2007/p07-002.pdf. Accessed 7 May 2010
19. Environmental Protection Agency (EPA) (2010a) Sustainability – basic information. http://www.epa.gov/sustainability/basicinfo.htm. Accessed 5 May 2010
20. Benoît C, Mazijn B (2009) Guidelines for social life cycle assessment of products. United Nations Environment Programme. http://www.uneptie.org/shared/publications/pdf/DTIx1164xPA-guidelines_sLCA.pdf. Accessed 29 Apr 2010
21. Ott K (2003) The case for strong sustainability. In: Ott K, Thapa PP (eds) Greifswald's environmental ethics. Steinbeckerverlag Rose, Greifswald, http://umwethik.botanik.uni-greifswald.de/Main/Booklet. Accessed 11 May 2010
22. The Dictionary of Sustainable Management (2010) Sustainability. A project of Presidio High School. http://www.sustainabilitydictionary.com/s/sustainability.php. Accessed 5 May 2010
23. Verify Sustainability (2010) Web page of the company. http://www.verifysustainability.com/. Accessed 12 July 2010
24. Liu L (2009) Sustainability: living within one's own ecological means. Sustainability 1:1412–1430. doi:10.3390/su1041412, http://www.mdpi.com/2071-1050/1/4/1412/pdf. Accessed 11 May 2010
25. UNFCCC/CCNUCC (2006) Definition of renewable biomass. Report from the 23rd meeting of the executive board, Annex 18. http://cdm.unfccc.int/Reference/Guidclarif/ar/methAR_guid03_v01.pdf. Accessed 5 May 2010
26. Fritsche UR, Hünecke K, Hermann A, Schulze F, Wiegmann K (2006) Sustainability standards for bioenergy. World Wide Fund For Nature (WWF) Germany, available at http://www.wwf.de/fileadmin/fm-wwf/pdf_neu/Sustainability_Standards_for_Bioenergy.pdf. Accessed 29 Apr 2010
27. Roundtable on Sustainable Biofuels (2009) Indicators of compliance for the RSB principles & criteria. RSB reference code: [RSB-IND-20-001 (version 1.0)], available at http://cgse.epfl.ch/webdav/site/cgse/shared/Biofuels/Version%20One/Version%201.0/RSB%20Indicators%20V1.pdf. Accessed 29 Apr 2010
28. van Dam J, Junginger M, Faaij A, Jürgens I, Best G, Fritsche U (2008) Overview of recent developments in sustainable biomass certification. Biomass Bioenergy 32:749–780, Elsevier
29. Rösch C, Skarka J, Raab K, Stelzer V (2009) Energy production from grassland – assessing the sustainability of different process chains under German conditions. Biomass Bioenergy 33:689–700. doi:10.1016/j.biombioe.2008.10.008, http://www.itas.fzk.de/deu/lit/2009/roua09a.pdf. Accessed 5 May 2010

30. EU Commission (2010) Report from the commission to the council and the European parliament on sustainability requirements for the use of solid and gaseous biomass sources in electricity, heating and cooling. http://ec.europa.eu/energy/renewables/transparency_platform/doc/2010_report/com_2010_0011_3_report.pdf. Accessed 30 Apr 2010
31. Bauen A, Berndes G, Junginger M, Londo M, Vuille F, Ball R, Bole T, Chudziak C, Faaij A, Mozaffarian H (2009) Bioenergy – a sustainable and reliable energy source. International Energy Agency. http://www.ieabioenergy.com/DownLoad.aspx?DocId=6494. Accessed 29 Apr 2010
32. Scholwin F, Daniel J, Schröder G, Majer S, Müller-Langer F (2008) Energie- und Klimaeffizienz ausgewählter Biomassekonversionspfade zur Kraftstoffproduktion. Institut für Energetik und Umwelt gGmbH, Leipzig, http://www.vanrijn-kws.com/global/show_document.asp?id=aaaaaaaaaafillg&download=1. Accessed 6 May 2010
33. Needham S (2009) Renewable energy technologies update. Parliament of Australia, Department of Parliamentary Services. http://www.aph.gov.au/library/pubs/bn/sci/RenewableEnergy.pdf. Accessed 6 May 2010
34. Thrän D (2007) Energie aus Biomasse – Problemfelder und Forschungsnotwendigkeiten. In: Thomé-Kozmiensky (2007) Energie aus Abfall – Band 3. TK Verlag Karl Thomé-Kozmiensky, Tagung Berlin 24–25th September 07, pp 203–218
35. Junginger M, Faaij A, Schouwenberg PP, Arthers C, Bradley D, Best G, Heinimö J, Hektor B, Horstink P, Grassi A, Kwant K, Leistad Ø, Ling E, Peksa M, Ranta T, Rosillo-Calle F, Ryckmans Y, Wagener M, Walter A, Woods J (2008) Opportunities and barriers for sustainable international bioenergy trade and strategies to overcome them – A report prepared by IEA Bioenergy Task 40. Available at http://www.bioenergytrade.org/downloads/t40opportunitiesandbarriersforbioenergytradefi.pdf. Accessed 09 July 2010
36. Environmental Protection Agency (EPA) (2010c) Renewable Fuel Standard Program (RFS2). Regulatory Impact Analysis. EPA, Office of Transportation and Air Quality, available at http://www.epa.gov/OMS/renewablefuels/420r10003.pdf. Accessed 02 July 2010
37. International Chamber of Commerce (ICC) (2009) International Bioenergy Policy. ICC Paris, available at http://www.iccwbo.org/uploadedFiles/ICC/policy/Environment/213_69%20Bioenergy%20FINAL%20discussion%20paper%2030_04_09.pdf. Accessed 06 May 2010
38. Thrän D (2008) Ressourcen für die Biokraftstoffe von morgen. In: Dettling D (ed) (2008): Die Zukunft der Bioenergie – Herausforderungen und Perspektiven für die globale Nahrungs- und Energiesicherheit. berlinpolis e.V., Berlin
39. Turner BT, Plevin RJ, O'Hare M, Farrell AE (2007) Creating markets for green biofuels: measuring and improving environmental performance. University of California, The Transportation Sustainability Research Center, available at http://www.its.berkeley.edu/publications/UCB/2007/TSRCRR/UCB-ITS-TSRCRR-2007-1.pdf. Accessed 16 June 2010
40. Gnansounou E, Panichelli L, Dauriat A, Villegas JD (2008) Accounting for indirect land-use changes in GHG balances of the biofuels. Review of the current approaches. Swiss Federal Institute of Technology (EPFL) Lausanne, Switzerland, available at http://infoscience.epfl.ch/record/121496/files/Accounting_for_ILUC_in_biofuels_production.pdf. Accessed 16 June 2010
41. Renewable Fuels Agency (RFA) (2008) The Gallagher review of the indirect effects of biofuels production. Available at http://www.renewablefuelsagency.gov.uk/sites/rfa/files/_documents/Report_of_the_Gallagher_review.pdf. Accessed 29 Apr 2010
42. Fehrenbach H, Giegrich J, Reinhardt G, Rettenmaier N (2009) Synopsis of current models and methods applicable to indirect land use change (ILUC). Institut für Energie- und Umweltforschung Heidelberg GmbH, Heidelberg
43. Scheftelowitz M, Majer S, Edel M (2010) Beitrag der Modellierung zur Bewertung der Nachhaltigkeit von Biokraftstoffen – Anforderungen und Zweifelsfragen. Presentation at the expert workshop "Modellierung von direkten und indirekten Landnutzungsänderungen durch Biokraftstoffproduktion," 22 June 2010, Berlin
44. Mitchell D (2008) A note on rising food prices. The World Bank development prospects group, available at http://www-wds.worldbank.org/external/default/WDSContentServer/IW3P/IB/2008/07/28/000020439_20080728103002/Rendered/PDF/WP4682.pdf. Accessed 29 Apr 2010
45. Zentrale Markt- und Preisberichtstelle Zentrale Markt- und Preisberichtstelle für Erzeugnisse der Land-, Forst- und Ernährungswirtschaft GmbH (ZMP) (2002–2009): Agrarrohstoffpreise. Bonn
46. Food and Agriculture Organization of the United Nations (FAOSTAT) (2010) Statistical database on the agricultural prices. Available at http://faostat.fao.org/site/570/default.aspx#ancor. Accessed 12 July 2010
47. OECD-FAO (2010) OECD-FAO Agricultural outlook 2010–2019. Highlights. Available at http://www.agri-outlook.org/dataoecd/13/13/45438527.pdf. Accessed 18 June 2010
48. Inderwildi O, King D (2009) Quo vadis biofuels? Energy & Environmental Science, 2/2009, available at http://www.rsc.org/delivery/_ArticleLinking/DisplayArticleForFree.cfm?doi=b822951c&JournalCode=EE. Accessed 18 June 2010
49. Mastny L (ed) (2007) Biofuels for transport. Global potential and implications for sustainable energy and agriculture. Worldwatch Institute, Earthscan London, Sterling
50. Environmental Protection Agency (EPA) (2010b) EPA finalizes regulations for the National Renewable Fuel Standard Program for 2010 and beyond. EPA, Office of Transportation and Air Quality, available at http://www.epa.gov/oms/renewablefuels/420f10007.pdf. Accessed 21 June 2010
51. Alphonso GR, Cabral NJ, Rieser DL, Sharkey PF, Walls TF (2010) EPA's final renewable fuel standard rule: winners and losers. Available at http://www.martindale.com/energy-law/article_McGuireWoods-LLP_922038.htm. Accessed 21 June 2010

52. Brown R, Hayes D, Brown T, Gibbons J (2009) Carbon in the economy. Presentation given at Biofuels Science and Sustainability Tour. Iowa State University, Ames, IA, available at http://www.iowarfa.org/documents/BrownTourGHGPanel.pdf. Accessed 18 June 2010
53. Dale BE (2009) Biofuels & indirect land use change: a debate on the issues. Michigan State University, available online at http://everythingbiomass.org/Portals/EB/Biofuels%20and%20Indirect%20Land%20Use%20Change_Debate%20Sept%2009.pdf. Accessed 18 June 2009
54. Buchholz T, Luzadis VA, Volk TA (2009) Sustainability criteria for bioenergy systems: results from an expert survey. J Clean Prod 17(Suppl 1):S86–S98, available at http://www.glogov.org/images/doc/Buchholz.pdf. Accessed 24 June 2010
55. Schlamadinger B, Jürgens I (2004) Bioenergy and the clean development mechanism. Available at http://www.fao.org/sd/dim_en2/bioenergy/docs/policy2_en.pdf. Accessed 24 June 2010
56. German Federal Environmental Agency (UBA) (2006) Delivering the sustainable use of natural resources. Available at http://www.umweltbundesamt.de/energie/archiv/EPA_resourcespaper_2006.pdf. Accessed 24 June 2010
57. Walker T, Cardellichio P, Colnes A, Gunn J, Kittler B, Perschel B, Recchia C, Saah D (2010) Biomass sustainability and carbon policy study. Manomet Center for Conservation Sciences, Manomet, available at http://www.manomet.org/sites/manomet.org/files/Manomet_Biomass_Report_Full_LoRez.pdf. Accessed 06 July 2010
58. Manomet Center for Conservation Sciences (Manomet) (2010) Statement from Manomet on the biomass study. Available at http://www.manomet.org/sites/manomet.org/files/Manomet%20Statement%20062110b.pdf. Accessed 06 July 2010
59. El-Beltagy A, Oweis T (1998) Efficiency: key to sustainability in water scarce areas. Conference paper, presented in Paris at the International Conference "Water and sustainable development" Available at http://www.oieau.fr/ciedd/contributions/at2/contribution/beltagy.htm. Accessed 24 June 2010
60. International Air Transport Association (IATA) (2008) 2nd Generation biomass conversion efficiency. Available at http://www.iata.org/SiteCollectionDocuments/Documents/IATAConversionTechnologiesFinalv2.pdf. Accessed 24 June 2010
61. Ackom EK, Mabee WE, Saddler JN (2010) Industrial sustainability of competing wood energy options in Canada. Appl Biochem Biotechnol. doi:10.1007/s12010-010-9000-6, available at http://www.springerlink.com/content/u42658777t823354/fulltext.pdf. Accessed 28 June 2010
62. Gawor M (2010) Application of life cycle assessment in the context of classical environmental management system and with respect to the implementation of the EuP Directive. BTU Cottbus, available at http://opus.kobv.de/btu/volltexte/2010/1435/. Accessed 28 June 2010
63. Rettenmaier N, Reinhardt G, Schorb A, Köppen S, von Falkenstein E, Berndes G, Christou M, Dees M, Eleftheriadis I, Goltsev V, Kunikowski G, Lakyda P, Lehtonen A, Lindner M, Röder J, Vasylyshyn R, Vesterinen P, Wirsenius S, Zhelyezna TA, Zibtsev S (2008) Biomass energy Europe. Status of biomass resource assessments. Version 1. Available at http://www.eu-bee.com/_ACC/_Components/ATLANTIS-DigiStore/Download.asp?fileID=132813&basketID=837. Accessed 12 July 2010
64. Thrän D (2006) Sustainable strategies for biomass use in the European context. Analysis in the charged debate on national guidelines and the competition between soild, liquid and gaseous biofuels. Institut für Energetik und Umwelt, Leipzig
65. Thrän D, Seidenberger T, Zeddies J, Offermann R (2010) Global biomass potentials – Resources, drivers and scenario results. Energy Sustain Dev 14:200–205, doi:10.1016/j.esd.2010.07.004
66. Kaltschmitt M, Hartmann H (eds) (2001) Energie aus Biomasse: Grundlagen, Techniken und Verfahren. Springer, Berlin
67. Tilman D, Socolow R, Foley JA, Hill J, Larson E, Lynd L, Pacala S, Reilly J, Searchinger T, Somerville C, Williams R (2009) Beneficial biofuels – The food, energy, and environment trilemma. Science 325(5938):270–271, doi:10.1126/science.1177970
68. International Energy Agency (IEA) (2007) Good practice guidelines: bioenergy project development & biomass supply. Available at http://www.iea.org/textbase/nppdf/free/2007/biomass.pdf. Accessed 29 Apr 2010
69. Bauen A, Woods J, Hailes R (2004) Bioelectricity vision: Achieving 15% of electricity from biomass in OECD countries by 2020. Imperial College London, Centre for Energy Policy and Technology. Available at http://www.wwf.de/fileadmin/fm-wwf/pdf_misc-alt/klima/biomassereport.pdf. Accessed 06 May 2010
70. Dessus B, Devin B, Pharabod F (1993) World potential of renewable energies. World Solar Summit, Paris. Available at http://unesdoc.unesco.org/images/0009/000948/094849mb.pdf. Accessed 06 May 2010
71. Faaij A (2007) Global outlook on development of sustainable biomass resource potentials. In: Presentation held at the 1st conference of European Biomass Co-firing Network, Budapest, Hungary July 2–4, 2007. Available at http://www.netbiocof.net/pdf_presentations/Copernicus-institut_A.Faaij_Biopotentials_Conf-Budapest_July-2007.pdf. Accessed 10 May 2008
72. Fischer G, Schrattenholzer L (2001) Global bioenergy potentials through 2050. Biomass Bioenergy 20:151–159
73. Hall D, Rosillo-Calle F, Williams R, Woods J (1993) Biomass for energy: supply prospects. In: Johansson T, Kelly H, Reddy A, Williams R (eds) Renewable energy: sources for fuels and electricity. Island Press, Washington, DC
74. Hoogwijk M, Faaij A, Eickhout B, de Vries B, Turkenburg W (2005) Potential of biomass energy out to 2100, for four IPCC SRES land-use scenarios. Biomass Bioenergy 29:225–257
75. Hoogwijk M, Faaij A, van den Broek R, Berndes G, Gielen D, Turkenburg W (2003) Exploration of the ranges of the global potential of biomass for energy. Biomass Bioenergy 25:119–133
76. Johansson T, McCormick K, Neij L, Turkenburg W (2004) The potentials of renewable energy. In: Thematic background paper for the International conference for renewable energies 2004. Bonn, Germany

77. Lightfoot HD, Green C (2002) An assessment of IPCC working group III findings in climate change 2001: mitigation of the potential contribution of renewable energies to atmospheric carbon dioxide stabilization. Available at http://www.geog.mcgill.ca/gec3/wp-content/uploads/2009/02/Report-no.-2002-5.pdf. Accessed 12 June 2010
78. Moomaw W, Moreira J (eds) (2001) Technological and economic potential of greenhouse gas emissions reduction. In: Metz B, Davidson O, Swart R, Pan J (eds) Climate change 2001: mitigation. Contribution of working group III to the third assessment report of the intergovernmental panel on climate change. Cambridge University Press, Cambridge. Available at http://www.ipcc.ch/ipccreports/tar/wg3/089.htm. Accessed 06 May 2010
79. Sims R, Schock R, Adegbululgbe A, Fenhann J, Konstantinaviciute I, Moomaw W, Nimir H (2007) Energy supply. In: Metz B, Davidson O, Bosch P, Dave R, Meyer L (eds) (2007) Climate change 2007: mitigation. Contribution of working group III to the fourth assessment report of the intergovernmental panel on climate change. Cambridge University Press, Cambridge. Available at http://www.ipcc.ch/pdf/assessment-report/ar4/wg3/ar4-wg3-chapter4.pdf. Accessed 06 May 2010
80. Smeets E, Faaij A (2007) Bioenergy potentials from forestry in 2050: an assessment of the drivers that determine the potential. Clim Change 81:353–390
81. Smeets E, Faaij A, Lewandowski I, Turkenburg W (2007) A bottom-up assessment and review of global bio-energy potentials to 2050. Prog Energy Combust Sci 33:56–106
82. Swisher J, Wilson D (1993) Renewable energy potentials. Energy 18(5):437–459
83. Wolf J, Bindraban P, Luijten J, Vleeshouwers L (2003) Exploratory study on the land area required for global food supply and the potential global production of bioenergy. Agric Syst 76:841–861
84. Yamamoto H, Fujino J, Yamaji K (2001) Evaluation of bioenergy potential with a multi-regional global-land-use-and-energy-model. Biomass Bioenergy 21:185–203
85. Yamamoto H, Yamaji K, Fujino J (1999) Evaluation of bioenergy resources with a global land use and energy model formulated with SD technique. Appl Energy 63:101–113
86. Agronomica Ltd (2003) Approaches to sustainability. Available at http://www.agronomica.org/ApptoSF.htm. Accessed 05 May 2010

Books and Reviews

Al-Riffai P, Dimaranan B, Laborde D (2010) Global trade and environmental impact study of the EU biofuels mandate. International Food Policy Institute (IFPRI), available at http://www.ifpri.org/sites/default/files/publications/biofuelsreportec.pdf. Accessed 29 Apr 2010

Berndes G, Hoogwijk M, van den Broek R (2003) The contribution of biomass to the future global energy supply: a review of 17 studies. Biomass Bioenergy 25:1–28

Bundesamt für Naturschutz (2010) Bioenergie und Naturschutz. Synergien fördern, Risiken vermeiden. Bundesamt für Naturschutz, Bonn

Bundesministerium für Bildung und Forschung (2009) Forschung für nachhaltige Entwicklungen. Rahmenprogramm des BMBF. Berlin, Bonn, available at http://www.fona.de/pdf/publikationen/forschung_nachhaltige_entwicklungen.pdf. Accessed 30 Apr 2010

Bundesministerium für Umwelt, Naturschutz und Reaktorsicherheit (2008) Megatrends der Nachhaltigkeit. Unternehmensstrategie neu denken. Available at http://www.bmu.de/files/pdfs/allgemein/application/pdf/broschuere_csr_megatrends.pdf. Accessed 30 Apr 2010

Cornelissen S, Dehue B, Wonink S (2009) Summary of approaches to account and monitor indirect impacts of biofuel production. Available at http://www.globalbioenergy.org/uploads/media/0910_Ecofys_-_Summary_of_approaches_to_account_for_and_monitor_indirect_impacts_of_biofuel_production.PDF. Accessed 29 Apr 2010

Cotula L, Dyer N, Vermeulen S (2008) Fuelling exclusion? The biofuels boom and poor people's access to land. International Institute for Environment and Development and Food and Agriculture Organization of the United Nations, available at http://www.iied.org/pubs/pdfs/12551IIED.pdf. Accessed 29 Apr 2010

Cowie A, Bird N, Woess-Gallasch S (2009) Sustainability of bioenergy. A statement resulting from a joint IEA bioenergy meeting. International Energy Agency, available at http://ieabioenergy-task38.org/publications/Joint_Task_Paper_on_Sustainability_updated_Sept_2009.pdf. Accessed 30 Apr 2010

Die Bundesregierung (2002) Perspektiven für Deutschland. Unsere Strategie für nachhaltige Entwicklung. http://www.bundesregierung.de/nsc_true/Content/DE/__Anlagen/2006-2007/perspektiven-fuer-deutschland-langfassung,property=publicationFile.pdf/perspektiven-fuer-deutschland-langfassung. Accessed 30 Apr 2010

Dornburg V, Faaij A, Verweij P, Langeveld H, van de Ven G, Wester F, van Keulen H, van Diepen K, Meeusen M, Banse M, Ros J, van Vuuren D, van den Born GJ, van Oorschot M, Smout F, van Vliet J, Aiking H, Londo M, Mozaffarian H, Smekens K (2008) Assessment of global biomass potentials and their links to food, water, biodiversity, energy demand and economy. Bilthoven MNP. Available at: http://www.bioenergytrade.org/downloads/wabbiomassmainreportbiomassassessment.pdf. Accessed 06 May 2010

Elliot Campbell J, Lobell DB, Genova RC, Field CB (2008) The global potential of bioenergy on abandoned agriculture lands. Available at http://www.globalbioenergy.org/uploads/media/0806_Campbel_et_al_-_The_global_potential_of_bioenergy_on_abandoned_agricultural_lands.pdf. Accessed 29 Apr 2010

Fargione J, Hil J, Tilman D, Polasky S, Hawthorne P (2008) Land clearing and the biofuel carbon debt. Science 319:1235, doi:10.1126/science.1152747

Food and Agriculture Organization of the United Nations (FAO) (2004) Unified Bioenergy Terminology. Available

at ftp://ftp.fao.org/docrep/fao/007/j4504e/j4504e00.pdf. Accessed 10 May 2010

Fritsche UR, Hünecke K, Wiegmann K (2005) Kriterien zur Bewertung des Pflanzenanbaus zur Gewinnung von Biokraftstoffen in Entwicklungsländer unter ökologischen, sozialen und wirtschaftlichen Gesichtspunkten. Öko-Institut e.V., Darmstadt, available at http://www.oeko.de/oekodoc/232/2004-023-de.pdf. Accessed 29 Apr 2010

Kaltschmitt M, Lenz V, Thrän D (2008) Zu energetischen Nutzung von Biomasse in Deutschland – Potenziale, Stand und Perspektiven. Available at http://www.leibniz-institut.de/archiv/kaltschmitt_25_04_08.pdf. Accessed 13 July 2010

Kaltschmitt M, Thrän D, Weber M (2007) Perspektiven und Szenarien für eine nachhaltige Biomassenutzung. In: Banse G, Kiepas A (eds) Nachhaltige Entwicklung in Polen und Deutschland. edition sigma, Berlin

Melillo JM, Reilly JM, Kicklighter DW, Gurgel AC, Cronin TW, Paltsev S, Felzer BS, Wang X, Sokolov AP, Schlosser CA (2009) Indirect emissions from biofuels: how important? Science 326(5958):1397–1399. doi:10.1126/science.1180251

Moreira, J (2006) Global biomass energy potential. Mitig Adapt Strat Global Change 11:313–342

Ozinga S, Krul L (2004) Footprints in the forest. Current practice and future challenges in forest certification. FERN, available at http://www.fern.org/sites/fern.org/files/media/documents/document_1890_1900.pdf. Accessed 30 Apr 2010

Ravindranath NH, Manuvie R, Fargione J, Canadell JG, Berndes G, Woods J, Watson H, Sathaye J (2009) Greenhouse gas implications of land use and land conversion to biofuel crops. In: Howarth RW, Bringezu S (eds) Biofuels: environmental consequences and interactions with changing land use. Cornell University, Ithaca

Searchinger TD (2009) Government policies & drivers of world biofuels, sustainability criteria, certification proposals and their limitations. In: Howarth RW, Bringezu S (eds) Biofuels: environmental consequences and interactions with changing land use. Cornell University, Ithaca

Smeets E, van Dam J, Faaij A, Lewandowski I (2006) Bottom-up methodologies for assessing technical and economic bioenergy production potential. In: Brouwer F, McCarl BA (eds) Agriculture and climate beyond 2015: a new perspective on future land use patterns. Springer, Dordrecht

Sugrue A (2008) Bioenergy production on marginal and degraded land: the potential social impacts. Available at http://www.uneptie.org/energy/activities/mapping/pdf/social.pdf. Accessed 29 Apr 2010

Thrän D, Kaltschmitt M (2007) Competition - Supporting or preventing an increased use of bioenergy? Biotechnol J 2(12):1514–1524

Thrän D, Scheuermann A, Fuchs G, Weber M (2006) Weltweite Biomassepotenziale: datenrecherche und -bewertung. Institut für Energetik und Umwelt gGmbH, Leipzig

Thrän D, Weber M, Scheuermann A, Fröhlich N, Zeddies J, Henze A, Thoroe C, Schweinle J, Fritsche U, Jenseit W, Rausch L, Schmidt K (2006) Nachhaltige Biomassenutzungsstrategien im europäischen Kontext. Erstellt im Auftrag des Bundesministeriums für Umwelt, Naturschutz und Reaktorsicherheit, BMU, Berlin

Trinnaman J, Clarke A (2004) 2004 Survey of energy resources. Elsevier, Amsterdam, available at http://www.worldenergy.org/documents/ser2004.pdf. Accessed 06 May 2010

United Nations (UN) (2008) Making certification work for sustainable development: the case of biofuels. United Nations, New York and Geneva, available at http://www.unctad.org/en/docs/ditcted20081_en.pdf. Accessed 30 Apr 2010

van Dam JMC (2009) Sustainability of bioenergy chains: the result is in the details. PhD thesis, available at http://igitur-archive.library.uu.nl/dissertations/2009-0504-200337/dam.pdf. Accessed 30 Apr 2010

Vis MW, Vos J, van der Berg D (2008) Sustainability criteria & certification systems for biomass production. Biomass Technology Group, Enschede, available at http://ec.europa.eu/energy/renewables/bioenergy/doc/sustainability_criteria_and_certification_systems.pdf. Accessed 30 Apr 2010

von Lampe M (2006) Agricultural market impacts of future growth in the production of biofuels. OECD, available at http://www.oecd.org/dataoecd/58/62/36074135.pdf. Accessed 29 Apr 2010

WBGU (2008) Welt im Wandel: Zukunftsfähige Bioenergie und nachhaltige Landnutzung. Mercedes Druck, Berlin, available at http://www.wbgu.de/wbgu_jg2008.html. Accessed 29 Apr 2010

Woods J, Black M, Murphy R (2009) Future feedstocks for biofuel systems. In: Howarth RW, Bringezu S (eds) Biofuels: environmental consequences and interactions with changing land use. Cornell University, Ithaca

Zah R, Faist M, Reinhard R, Birchmeier D (2009) Standardized and simplified life-cycle assessment (LCA) as a driver for more sustainable biofuels. J Clean Prod 17:102–105

Biomass Pyrolysis

Andreas Hornung
European Bioenergy Research Insitute – EBRI, Aston University, Aston Triangle, Birmingham, UK

Article Outline

Glossary
Definition and Importance of the Subject
Introduction
Kinetic Parameters and Degradation Mechanisms
Fast Pyrolysis
Intermediate Pyrolysis
Slow Pyrolysis

Comparison of Different Pyrolysis Techniques
Future Directions
Annex 1: Example: Haloclean Pyrolysis and Gasification of Straw
Bibliography

Glossary

Fast pyrolysis Heat up of the sample within 1–2 s and the condensation of products within seconds.

Intermediate pyrolysis Heat up of the sample within minutes (1–10) and the rapid condensation of products within seconds.

Pyrolysis Pyrolysis is the thermochemical conversion of feed material under the absence of oxygen; usually products of pyrolysis are char, liquid, and gas.

Slow pyrolysis Heat up of the sample within hours or days.

Thermochemical conversion Treatment of material at elevated temperature and which is causing chemical conversion reactions like cracking, radical reactions, decarboxylation, and so on.

Definition and Importance of the Subject

Pyrolysis is the oxygen free thermochemical conversion of materials. Pyrolysis turns a feed like biomass into three major products: gases, liquids, and char. The char contains the ash and is often called biochar. Pyrolysis is able to condition or liquefy biomass. For most of the processes and feedstock materials the liquid contains of two phases, a water rich and organic rich fraction.

By means of pyrolysis, several types of biomass feedstock can be made suitable for gasification or combustion. A solid feed is turned into gas and liquid, or a slurry, which is a mixture of liquid and char. For combustion purpose, the char is very suitable which is in most cases bridle and possible to use in a coal-fired power plant or a biomass power plant.

Introduction

Pyrolysis in general is the thermochemical conversion of feed material under the absence of oxygen. Pyrolysis reactors exist in various designs and for various pyrolysis conditions as fast, intermediate, or slow. Traditionally, the slow pyrolysis is known, for example, for charcoal production. This chapter is dealing with the more advanced pyrolysis types for fast and intermediate pyrolysis. It will give an overview of reactors and technical applications and the related state of the art. The final sections will deal with the numerical simulation of the processes as well as the post treatment of pyrolysis chars to activated carbon.

Pyrolysis of biomass is of a different kind in terms of feedstock, applied reactors, as well as applied type of pyrolysis – fast, intermediate, or slow pyrolysis. The classical approach on slow pyrolysis leads to charcoal or even finally to activated carbon, starting from wood. The opposite of this is fast pyrolysis of wood in creating a maximum of liquid phase for this specific feedstock and usually tar containing chars.

More difficult as the pyrolysis of wood is the pyrolysis of nonwoody biomass and the application of its products. A new type of pyrolysis is the intermediate pyrolysis. In between the reaction conditions of slow and fast pyrolysis, it offers much different product qualities of liquids, gases, and of the biochars, the residue from pyrolysis. The distribution of product phases is affected as well as the composition of the liquid phase. It is of importance that the reaction conditions for intermediate pyrolysis offer a wide range of variation for the process optimization.

Kinetic Parameters and Degradation Mechanisms

Biomass essentially can be converted to energy and clean fuels via thermochemical processes. In every thermochemical process, pyrolytic degradation plays a significant role. Attempts were made to correlate the characteristics of biomass pyrolysis with those of its components using overall kinetic models [1–3]. The agreement of these models was only at a specific heating rate, and the reason could be related to influence of heating rate on char formation. Understanding the physical dynamics (weight loss behavior, morphological and structural changes with respect to time and different heating rates) may lead to improved methods of conversion. Among various approaches to obtain the kinetics, the simplest ones are to use empirical and employ global kinetics, by using the Arrhenius expression and to correlate the rates of mass loss with temperature [4].

Increasing applications of lignocellulosic materials for energy production have increased the need to know

its detailed reaction mechanisms and thermal behavior. From energy economic point of view for control over product generation and their composition, the thermal behavior studies of lignin is very crucial. Lignin in general is more thermally stable, produces more char and higher fraction of aromatics in the liquid product compared to cellulose and hemicellulose under similar conditions. In this study, the TG-MS techniques are used to evaluate the thermal characteristics and formal kinetic parameters for pyrolysis of different kinds of lignin. A mathematical model for basic studies under integration with the experimental data is realized.

Experiments were carried out using different kinds of lignin. Tests were carried out with technical lignins, hydrolytic and organosolv. The hydrolytic lignin is typically a G type lignin. Organosolv lignin was of the H type lignins. The structures of these lignins are shown in Fig. 1.

The branched macromolecular structure of hydrolytic lignin contains primary and secondary aliphatic as well as phenolic OH groups. The methoxyl content is in the range of 9–11%. It is linked to neighboring phenyl propane repeat units via C–C and C–O–C bonds. C=O groups are also present, and the phenolic OH groups were predominant over the aliphatic OH groups compared to the presence of the methyl groups. The hydrolytic lignin has an ash content of 2–3% with an average molecular weight of 19,300 gM^{-1}.

Organosolv lignin contains primary and secondary aliphatic as well as phenolic OH groups. It has an elemental composition of Carbon 66.5%, Hydrogen 6.1%, OCH_3 18.9%, sugars <0.5%, and ash <1%.

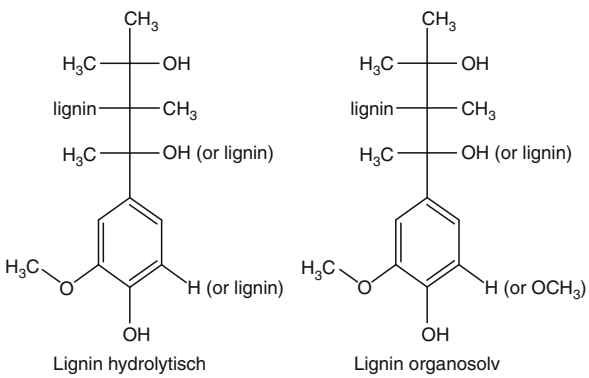

Biomass Pyrolysis. Figure 1
Structure of hydrolytic and organosolv lignin

This type of lignin also has C=O groups, and the amounts of the phenolic and aliphatic OH groups are almost equal with an average molecular weight of 3,500 gM^{-1}.

In order to understand the degradation mechanisms of lignin, it is important to understand the structure of lignin; in the sense, what kind of linkages and reactive groups are present. The lignin structure constitutes peripheral groups, aromatic nuclei, labile bridges, and char links. The chemical structure (CS) comprises:

- The nature of the repeating units
- The nature of end groups
- The composition of possible branches and cross-links
- The nature of defects in the structural sequence

The chemical reactions can occur at the principal polymer backbone and also at the sites of repeated units. The propagation of the chemical reactions can affect both the molecular weight distribution and the chemical structure of the polymer [5].

The releasing of gas and tar components in the vapor phase with the simultaneous carbonaceous residue formation is determined by an enormous number of chemical reactions. These involve different precursors and intermediates in the condensed phase. The evolution of a specific product is strongly affected by the structures of the corresponding precursors. Tar is generally defined as the volatiles that condense at room temperature. Many tar components are recognized to be directly derived from the starting repeated unit of a specific macromolecular constituent of biomass. Volatiles are made of noncondensable gases with high heating value, light oils suitable as fuels and feed stocks, and high boiling tars for subsequent refining.

In lignin, the aromatic groups can be considered as refractory nuclei, which remain intact both in tar and char formation. Chemical constitution and reactivity of the linkages between the monomers has strong affects on the shortening process of the polymer chain and on the tar and char formation. The description of reacting phase is completed by overall characterization of the peripheral groups. They promote bimolecular reactions and affect the permanent gas formation in pyrolysis process. The diverse variety of lignin is rendered with four structural components: non-reacting carbon (aromatic nuclei), labile bridges, char links, and

peripheral groups. Repeated units are interconnected by labile bridges or char links. Labile bridges represent aliphatic, alicyclic, and heteroatomic functionalities, not distinct chemical bonds. Peripheral groups are the remains of broken bridges on fragments ends that have the same composition. Labile bridges that decompose into char links during devolatilization leave a fraction of their oxygen in the char link. The residual oxygen is released as CO at high temperature.

The numerical kinetic analysis extends the interpretability of temperature-programmed conversion of biomasses, and it is potentially useful for the elucidation of fundamental reaction mechanistic information. The TG analysis represents the starting base for the computation of the main kinetic parameters. The numerical results in comparison with the experimental results are shown in the Fig. 2.

The increasing in complexity of the model allows monitoring the time/temperature evolution of the main families of components. The model is able to reproduce the main trend with the increasing of the overall heating rates as established by the mass spectrometric investigations. As shown in Fig. 3, the developed model is also able to predict the lignin thermal behavior for high heating rates giving useful information for operative conditions, which are not easily achieved, in the lab-scale level. The total amount of char, tar, and permanent gas at different pyrolysis temperatures and different overall heating rates, which are not easy to realize in lab scale, are done by numerical methods.

Fast Pyrolysis

Pyrolysis is thermal decomposition occurring in the absence of oxygen. During pyrolysis, the feed is cracked and not oxidized or partially oxidized like in gasification or combustion. During pyrolysis, always a set of products is resulting: charcoal, liquids, and gas.

By means of fast pyrolysis, thermal energy is transferred within seconds into the organic material

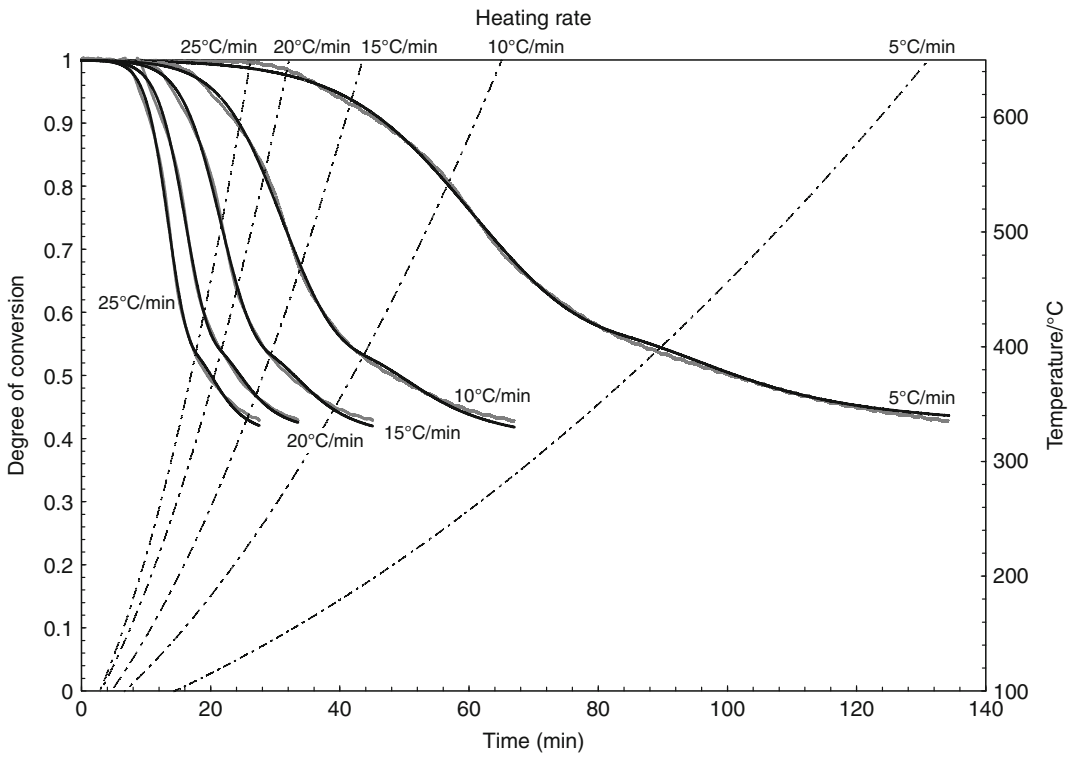

Biomass Pyrolysis. Figure 2
Pyrolysis of hydrolytic lignin at different heating rates model development (*gray*) and experiments (*black*)

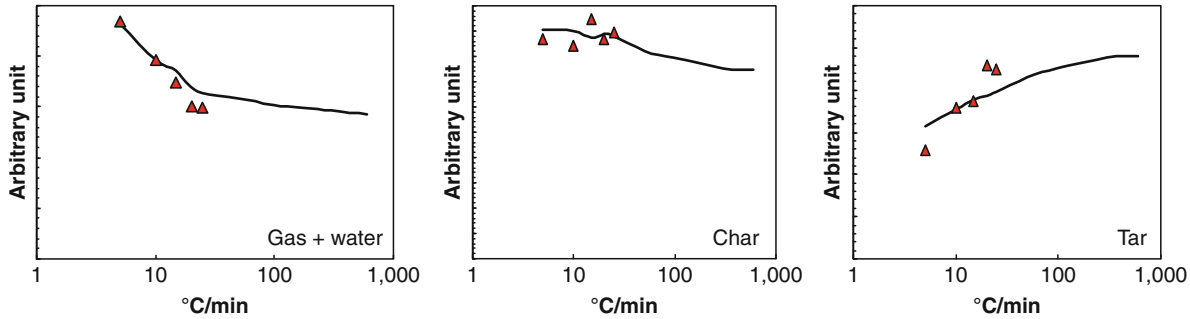

Biomass Pyrolysis. Figure 3
Total yields of the main products families from pyrolysis of hydrolytic lignin at different heating rates and at a final temperature of 500°C. Comparison and predictions (marks = experimental data). The *y* axis stands for arbitrary yields given as a function of the heating rate used

and the resulting vapors are removed from the hot reaction zone within seconds. Both parts of the process usually have residence times of 0.5–2 s, and the character of the products is mainly defined by the high energy flow into the sample. Typical for fast pyrolysis is therefore a higher tar formation during pyrolysis. Especially during fast pyrolysis of nonwoody biomasses, the liquids are higher in viscosity and tar content compared to those from intermediate pyrolysis.

In terms of woody biomass, the fast pyrolysis is of interest for liquid production, as the liquid is received in very high quantity, up to 75% (compare Table 1).

Principles

Below the most important principles are summarized:

- Very high heating rates, up to 1,000°C/s
- Fine-grounded materials, particles of several millimeters down to several 10 μm
- Typical reaction temperatures from 400°C up to 550°C, higher or lower temperatures are given in literature
- Short vapor residence times of 1–2 s
- High cooling rates for the vapors to reduce thermal post decomposition

Process Technology

Bubbling Fluid Bed Reactor The bubbling fluidized bed is a simple and well-understood technology (Fig. 4). The advantages are good temperature control and efficient heat transfer due to high particle density. Pilot (approx. 250 kg/h) and technical scale (up to 200 t/day) units are available (e.g., [1–3]).

Circulating Fluid Bed Reactor Circulating fluid bed reactors are more complex than bubbling fluid bed reactors (Fig. 5). Compared to bubbling fluid bed reactors, the residence time of the char is almost the same as the residence time of the gases and vapors. Due to higher gas velocity, the char is transported rapidly through the reactor which usually leads to higher char contents in the pyrolysis oil. A counter measure is the involvement of filters to keep back the particles. The circulating fluid bed is very popular especially because of it high throughput. The heat for the process is realized by burning the char while heating the sand in a separate reactor unit and recirculation of the hot sand into the circulating fluid bed (for examples of this technology see [5–7]).

Ablative Pyrolysis Reactor At the ablative pyrolysis, the heat transfer is optimized by having a huge heat transfer surface and a small sample surface pressed against it (Fig. 6). The biomass, usually wood, is pressed mechanically against the hot surface and the hot surface is passing by. The reaction rates are not limited by heat transfer. Therefore, larger wood particles can be used or a solid compressed stick of wood chips is pressed against a hot rotating plate (hydraulically fed wood rods) [8, 9]. Within an alternative approach, fine particles are pressed with supersonic velocities (high tangential pressure) against the inside of a cylindrical reactor [10]. Within another

Biomass Pyrolysis. Table 1 Pyrolysis of wood under fast and slow pyrolysis conditions

	Fast pyrolysis 500°C	Slow pyrolysis 420°C	Slow pyrolysis 500°C	Slow pyrolysis 600°C
Total liquid, wt% on dry feed	75	51.9	52.8	51.9
Char yield, wt% on dry feed	8.5	33.6	31.9	32
Gas yield, wt% on dry feed	10.9	13.4	11.3	11.4
Closure, wt% on dry feed	94.4	98.9	96	95.3
Heating rate (°C/min)	–	14.5	13.7	12.6
		(Slow pyrolysis liquid from dry ice and acetone condenser-water and light ends)		
Water content (%)	20.8	45.9	48.2	43.8
Char content (%)	0.04	0.02	0.03	0.03
Viscosity (cP)	53.8	1.4	1.1	1.8
PH	2.4	2.3	2.5	2.4
Elemental analysis (%)				
C	43.9	28.13	28	27.39
H	7.4	9.38	9.38	9.55
N	0.07	0.03	–	–
O by difference	48.6	62.5	62.7	63.1
HHV (wet) (MJ/kg)	14.4	6.8	6.4	7.1
		(Slow pyrolysis liquid from EP – heavy organic fraction)		
Water content (%)	–	8.6	11.3	7.8
PH	–	2.8	2.6	2.6
Elemental analysis (%)				
C	–	54.8	53.75	55.30
H	–	7.14	7.41	7.23
N	–	0.10	0.13	0.16
O by difference	–	38	38.72	37.32
HHV (wet) (MJ/kg)	–	21.3	20.4	21.8

Source: Bridgwater et al. [32].

development pressure and motion is derived mechanically within a rotating blade reactor [11].

Twin Screw Reactor – Mechanical Fluidized Bed Here, fast pyrolysis is accomplished in a twin screw mixer reactor heated by a solid heat carrier. Central parts of the fast pyrolysis system are a reactor with twin screws rotating in the same direction, cleaning each other with intertwining flights and a heat carrier loop which can be designed in several ways [12]. The heat carrier can consist of sand or steel shot (Fig. 7).

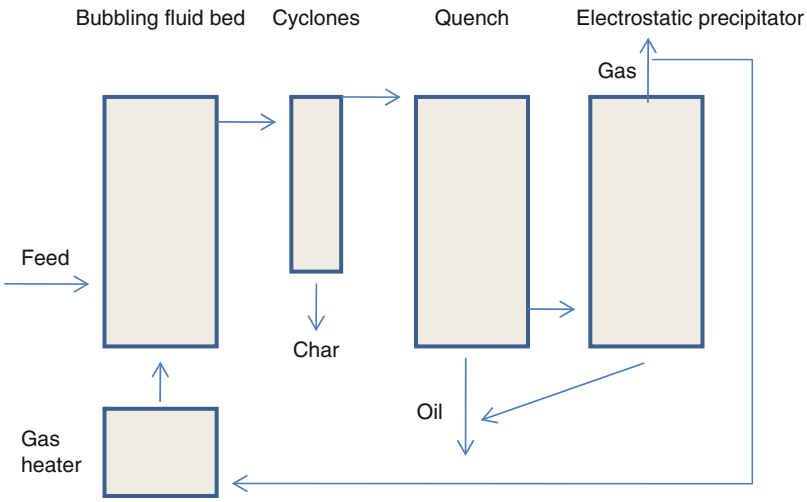

Biomass Pyrolysis. Figure 4
Bubbling fluid bed reactor

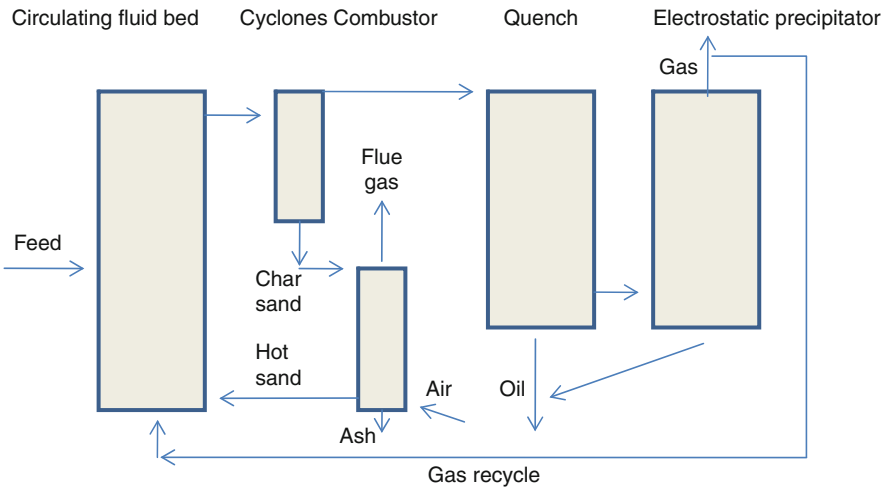

Biomass Pyrolysis. Figure 5
Circulating fluid bed reactor

The abrasive character of rapid moved sand or steel shot results in high amounts of char dust and is usually making it difficult to separate the vapors from the char after pyrolysis. Measures like cyclones and hot gas filtration have to be taken to improve the quality of the pyrolysis liquid.

Rotating Cone The rotating cone reactor [13, 14] effectively operates as transported bed reactor. The transport is affected by centrifugal forces in a rotating cone. The heat transfer is realized by hot sand, generated in a bubbling bed char combuster, where the remaining char from pyrolysis is oxidized to heat up the sand [10] (Fig. 8). The char application is integrated to heat the sand, and the rotating cone is improving the heat transfer, but is less abrasive than the twin screw system described in Sect. "Twin Screw Reactor – Mechanical Fluidized Bed". Finally, the system has been applied successfully for the conversion of open fruit bunches from palm in Malaysia by [13].

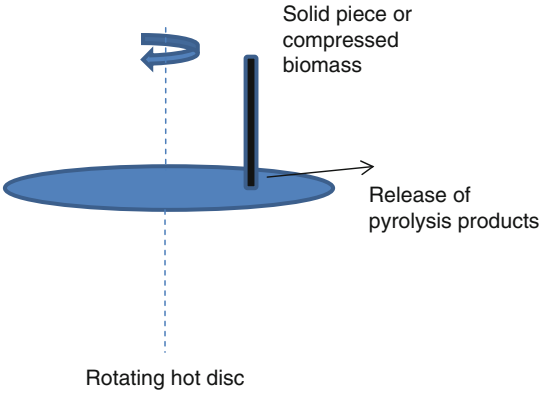

Biomass Pyrolysis. Figure 6
Ablative pyrolysis reactor

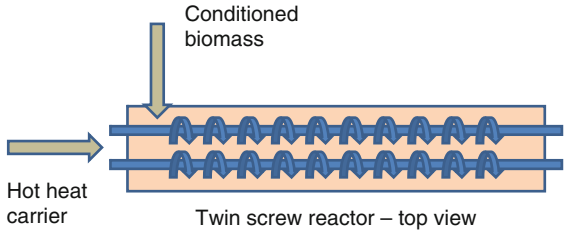

Biomass Pyrolysis. Figure 7
Twin screw reactor

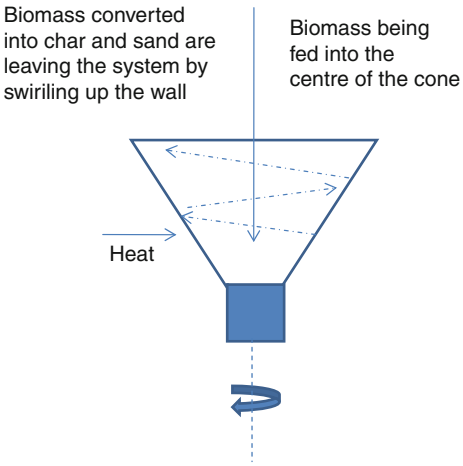

Biomass Pyrolysis. Figure 8
Rotating cone reactor

Intermediate Pyrolysis

Intermediate Pyrolysis differs from fast pyrolysis in terms of the heat transfer to the feed. The heating rates are much lower, in the range of 100–500°C/min. This leads to less tar formation during the pyrolysis process as more controlled chemical reactions are taking place instead of thermal cracking of the biopolymer. The vapor residence times are very much dependant on the reactor type, but can be like in case of fast pyrolysis as low as 2 s.

In terms of the pyrolysis of woody materials, intermediate pyrolysis is producing much lower liquid fractions, about 55% compared to 75%. Nevertheless, this is valid only for the pyrolysis of woody feeds and changes to a more equal scenario in case of other biogenic materials.

Principles

Below the most important principles are summarized:

- Moderate heating rates, up to 200–300°C/min
- Residence times of several minutes, up to 10 min
- Coarse, shredded, chopped, or fine-grounded materials can be used as single feed or in mixtures, particles of several centimeters down to dust can be used
- Water content of the feed up to 40 wt%
- Typical reaction temperatures from 400°C up to 550°C, lower temperatures down to 350°C are possible
- Short vapor residence times of 2–4 s
- High cooling rates for the vapors to reduce thermal post decomposition

Process Technology

Typically, two major types of rotary kilns are used for intermediate pyrolysis processes: internally or externally heated systems. For internal heated kilns, a heat exchanger based on steam or gas powered tubes or electrical heaters are used. For externally heated systems, there exist steam, gas (direct or indirect), or electrical-powered systems. The following examples show engineering solutions for processing of high volatile feeds or relevance in processing.

Conrad Process The Conrad recycling process uses a horizontal auger kiln reactor that applies heat to the

feedstock [15–17]. The control of the pyrolysis process is decided by temperature, and especially auger speed and temperature.

Double Rotary Kiln Pyrolysis The double rotary kiln pyrolysis is designed for mechanical coupling of a pyrolysis unit and a combustion unit. The coaxial system of two rotary kilns opens up the possibility to evaporate organics from the feed material in the inner kiln, while the carbonaceous residues are transported through the external kiln to a combustion zone. The process heat of combustion is used to heat the inner kiln while the ashes are leaving the system [18]. Both kilns can be equipped with lifters or spiral lifters.

Low-Temperature Carburization Process The low-temperature carburization process (LTC) meets the need for a process, which economically reduces petrochemical and hydrocarbon residues into recyclable products, feedstocks, or clean fuels. The indirectly fired rotary kiln system can be operated up to 850°C. The throughput varies in between 800 and 2,000 kg/h.

The LTC kiln sealing system allows operating the system under positive pressure, assuring no leakage of air which can produce an explosive mixture.

For cleaning the kiln wall from carbonaceous materials and feed, a cyclindrical cleaning device has been developed lying on the bottom of the rotary kiln, equipped with high-temperature bearings effective even a temperature range up to 1,100°C, running up to 8,000 h/a without lubrication. The cylindrical unit is mounted on the infeed side of the kiln and ends in the carburization zone of the kiln. A cone segment connects to the infeed zone.

Haloclean-Gas Tight Rotary Kiln Haloclean rotary kiln is especially designed for the pyrolysis of high amount of inert and/or thermosetting containing materials. The invention is based on the experience with a vertical reactor system for pyrolysis, the so-called Cycled-Spheres Reactor [19]. A system has been developed [20] improving the heat transfer to poorly heat transferring materials like plastics and biomass, ensuring that decomposition in laboratory scale can also be described with micro kinetic analysis [21]. The usage of a spheres-filled reaction vessel improves the heat conductivity by order of magnitude at least one [9]. The system used a screw cycling metal spheres. The idea of heat transferring metal spheres and a screw which not only transports spheres but also feed material was kept and transferred into an industrial-like reaction system, a rotary kiln [22]. To keep the performance in low rates of consecutive reactions of the pyrolysis gases as well as low residence times of the pyrolysis gases in the system at all, the hollow screw shaft has been equipped with 200 sintered metal plates. These plates are permanently cleaned by the material passing their surface, thus keeping the inner core of the screw clean from pyrolysis products, and they are introducing the purge gas directly where the pyrolysis products are evolved (Fig. 9).

By the screw the residence time control of the rotary kiln is completely different to existing kiln types. Feed and heat transferring spheres are transported in

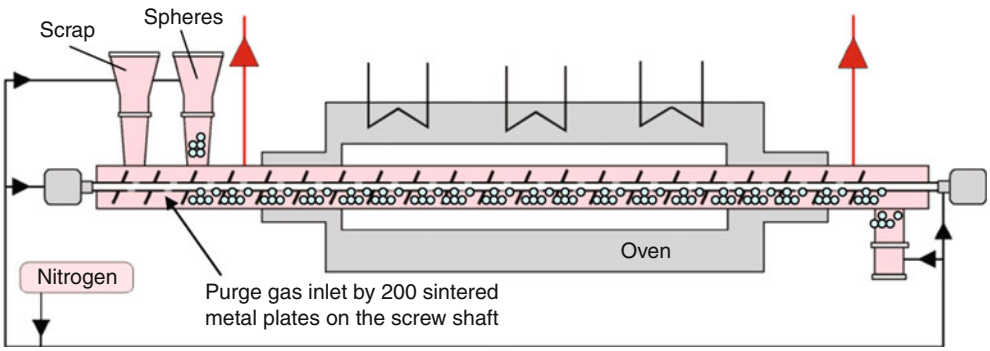

Biomass Pyrolysis. Figure 9
The Halocean reactor

distinct volumes through the kiln. By using the screw in forward and backward movements, the residence time can be shifted to very long times, keeping the material permanently in motion and mixing. The system is indirect electrically heated by an outer oven and by the screw. Up to now the system is realized in pilot scale [23–25] and has been transferred to technical scale (20,000 t/a) in 2009 (see Annex 1 for an example).

The Pyroformer The Pyroformer [26] combines pyrolysis with enhanced char catalyzed reforming and is increasing the gas production. Higher gas productions rates are favorable especially if the pyrolysis is coupled to a gasification system. The reactor consists of two coaxial screw units (Fig. 10). The inner auger transports the biomass through the reactor and the outer screw transports the char back to the inlet zone, where the char is mixed together with the fresh biomass. The char is therefore heat carrier and reaction partner.

Slow Pyrolysis

Slow pyrolysis is the oldest way of treating biomass under oxygen free conditions and the most traditional. The production of barbeque charcoal is the best known example. Together with the production of charcoal, related products can be achieved like acetic acid or alcohols. Usually the pyrolysis vapors are used to deliver the heat for pyrolysis in a direct or indirect mode, which means either to heat the kiln from outside or to heat the biomass by getting it in contact with the combustion gases from pyrolysis gases. A third way is to go for a partial oxidation, but this is outside the theme of pyrolysis.

Principles

The material used for this type of pyrolysis is shaped from briket size to whole logs. Usually the feed material is traditionally wood, recent literature also shows cashew nut shells and palm [27–29].

The residence time of the solid phase is usually hours, up to weeks. For almost ash-free materials, the residue goes down to 15%, usually around 30% are found.

The heating rates are several degrees per minute.

A slow pyrolysis taking place within 1–2 h and at a heating rate of approximately 5 K/min will have a nearly even distribution between char, liquid, and gas.

Process Technology

A modern batch process with recirculation of the combustion gases is the Degussa process.

The process is based on a large retort with a capacity of 100 m^3. The retort is fed by a belt conveyer from the top. After charging, hot gases are reaching the feed and over 16–20 h carbonization takes place. The pyrolysis gases are leaving the retort. The condesables are removed in a cooler and scrubber unit, noncondensables go to a heat exchanger, where the gas is heated by using the remaining pyrolysis gas fraction. The temperature for carbonization is about 450–550°C. The charcoal is discharged from the bottom and fall into air-tight bunkers for cooling (Fig. 11). The production rate is about 24,000 t/year of charcoal from beech wood in seven retorts of this type. Typical

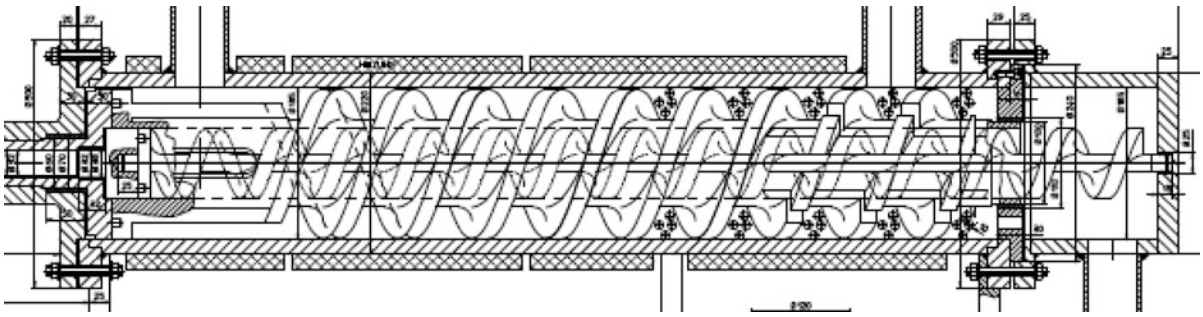

Biomass Pyrolysis. Figure 10
Scheme of a pyroformer

charcoal yield obtained from beech wood is 34%. In addition, 500 t/year of very pure acetic acid can be recovered from this process as well as smoke flavors [30].

An example for an indirect-heated continuous process is the O.E.T. Calusco process.

Wood is transported by trolleys through a horizontal tunnel. The tunnel, 45 m long, is U-shaped. The tunnel is divided in three chambers where the wood is firstly predried, secondly carbonized, and finally cooled down. Each trolley contains 12 m^3. The carbonization process is energetically self-sufficient as long as the moisture content of the feedstock is below 45–50% (dry basis). The pyrolysis gases are used to run the process (Fig. 12). The total residence time within the tunnel is 25–35 h depending on moisture content and feedstock used. The typical production capacity of such a plant is about 6,000 t/year of charcoal [31].

A further selection of charcoal processes is given in [31].

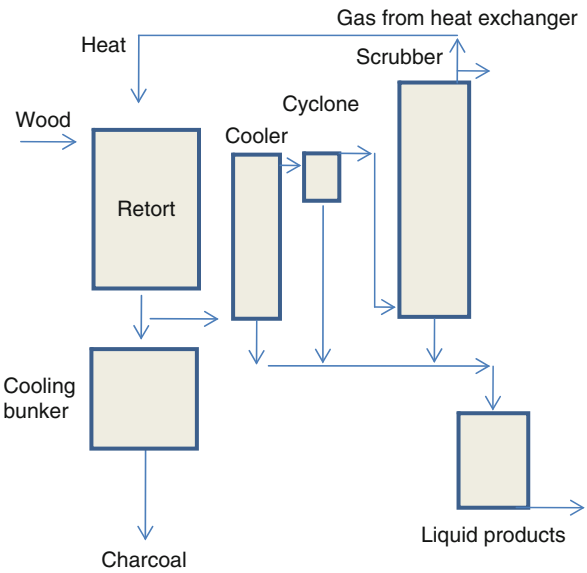

Biomass Pyrolysis. Figure 11
Degussa process – Chemviron [30]

Comparison of Different Pyrolysis Techniques

Literature is generally pointing out fast pyrolysis as the measure to turn biomass into maximum amount of liquid and minimum amount of gases. This is true for sure (Table 1 and arrows), but only for wood and is usually leading to one phase liquids high in water, acids, and tars.

In terms of other feedstock like straw, grass, or industrial residues from agricultural products like husks, the picture is much more different. The intermediate pyrolysis offers working conditions preventing formation of high molecular tars and offering dry and bridle chars suitable for different applications like fertilization or combustion. An advantage of this type of processing is the non-milling character and the applicability of larger sized feedstock, which offers the opportunity to separate easily the char from the vapors and to reach a coupled gasifier with low ash feed independent of the ash content of the material before pyrolysis.

Figure 13 shows the typical behavior of wood during fast pyrolysis at different temperatures. The blue marker (a) shows that even under intermediate pyrolysis conditions, almost similar results can be achieved. Even if two liquid phases are obtained, the total is quite similar. Only if the gas and char yield varies, less char and more gas is produced. Looking at wheat straw, the yellow marker (b) for intermediate pyrolysis and the white marker (c) show a very similar behavior, no longer matching the slopes for wood. The comparison with the gray marker (d) for slow

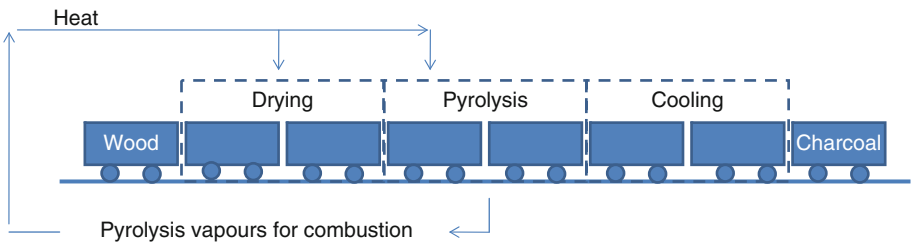

Biomass Pyrolysis. Figure 12
Principle drawing of the O.E.T Calusco

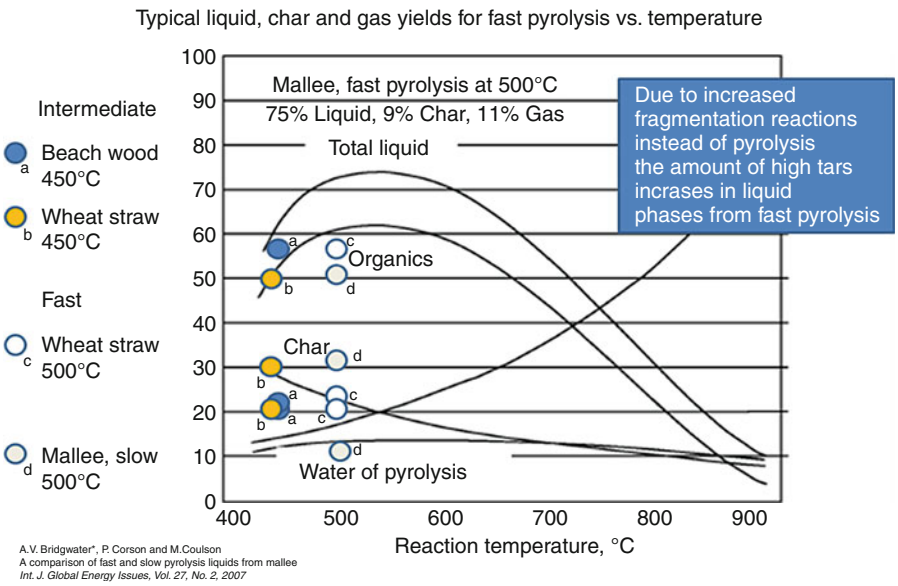

Biomass Pyrolysis. Figure 13
Comparison of the yields of liquids from fast, slow, and intermediate pyrolysis [32]

pyrolysis of mallee shows that the intermediate pyrolysis offers a new treatment variety. Compared with fast and slow pyrolysis, similar or more advantageous products can be achieved with less sophisticated technological approaches and therefore lower costs of investment.

Future Directions

Pyrolysis of biomass is an important process or process element to turn biomass into liquid and gaseous products. Worldwide companies are searching for solutions to liquefy wood and other biomasses to get an intermediate product higher in energy per volume. The sought applications ranging from co-firing and firing in biomass boilers, fuel for gas engines and dual fuel engines to feed of gasifiers. Furthermore, the chemical in the liquids are of interest for bio-refineries as high-value products can be extracted. Finally, the char from pyrolysis is of increasing importance as it can be used to deliver the so-called biochar. Biochar is suitable to fertilize agricultural land and, in addition, sequesters carbon instead of carbon dioxide. Today, the most promising chars for biochar application are delivered by intermediate pyrolysis [33, 34].

Annex 1: Example: Haloclean Pyrolysis and Gasification of Straw

Pyrolysis of straw is still an issue for most of the existing pyrolysis units in the field of fast and slow pyrolysis. The Haloclean process has already been tested in 2005 in a campaign of 5 weeks for the conversion of 15 t of straw into liquids, gas, and char. Later on, the liquids and the char have been successfully converted to synthesize gas in a commercial-scale gasifier [35].

The Haloclean-reactor has been used in a temperature range of 320–500°C. Typical for this reactor are short residence times (1–10 min for the solid residues) for pyrolysis of chaffed straw, finely ground straw, and straw pellets with variable residence times of about 0.3–60 s for the gas phase and gaseous pyrolysis liquids. The Haloclean-reactor consists of a rotary kiln equipped with an internally nitrogen purged and heated screw. During the pyrolysis, metal spheres are transported through the rotary kiln for a better heat transfer.

A very important result of this test is that the shape and size of the feed can be variable without changing the performance of the reactor.

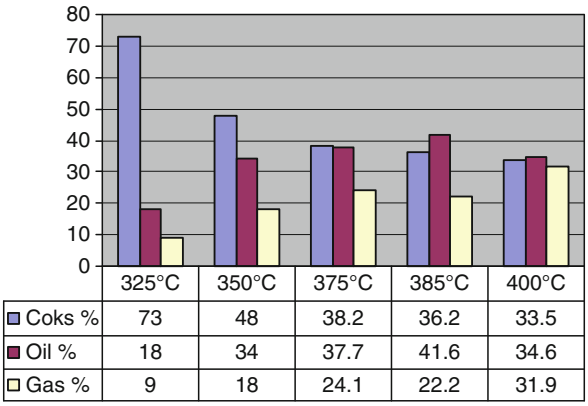

Biomass Pyrolysis. Figure 14
Yield of pyrolysis products – powdered straw

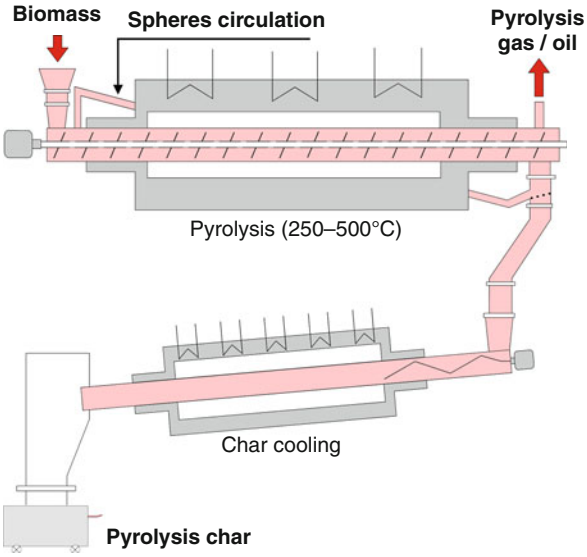

Biomass Pyrolysis. Figure 15
Scheme of the Haloclean-pyrolysis pilot plant

Figure 14 shows that at low temperature (325°C), the coke yield is much higher than the yield of oil (73:18), while at higher temperature (375°C), the ratio coke/oil is 38:37 (1:1). At a pyrolysis temperature of 385°C, the ratio coke/oil is at an optimum of 36:41.6. Therefore, it is possible to obtain with the Haloclean pyrolysis up to 5% more oil than coke.

Generally one can see that the amount of pyrolysis gas is increasing with increasing temperature; at 400°C, the amount of pyrolysis oil is decreasing due to the fact that more and more pyrolysis oil is degraded to pyrolysis gas.

The dimensions of the Haloclean-pyrolysis pilot plant are shown in Fig. 15. Below the dimensions of such a plant are given exemplarily.

- Diameter of the pipe: $d_o = 273$ mm, $d_i = 253$ mm
- Length of the oven: 2,200 mm
- Total length: 4,500 mm
- Diameter of the screw: 116 mm
- Draft of the screw: 150 mm
- Heat transfer medium: Spheres $m = 70$ g, $d = 25$ mm

Below, results of the pyrolysis of straw are shown as an example.

- *Pyrolysis Char*: H_o = 26 MJ/kg; H_o is the upper heating value
  C: 63%, H: 3.7%, N: 1.1%, O: 12.9%
  Ash content of the Char: SiO_2: 59%, Al_2O_3: 0.3%, Fe_2O_3: 0.7%, CaO: 7.3%, MgO: 2.1%, P_2O_5: 3.4%, Na_2O: 0.4%, K_2O: 23.8%, SO_3: 3.1%
- *Pyrolysis Liquid*: H_o = 7 MJ/kg (approx. 50% water phase) and 18% highly phenolic phase (H_o = 24 MJ/kg)

Bibliography

Primary Literature

1. Cuevas A, Reinoso C, Scott DS (1995) Pyrolysis oil production and its perspectives. In: Proceedings of the power producition from biomass II, Espoo, 29–30 March 1995. VTT, Espoo
2. Robson A (2001) PyNe newsletter no. 11. Aston University, Birmingham, pp 1–2. ISSN 1470-3521
3. McLellan R (2000) PyNe newsletter no 10. Aston University, Birmingham, p 12. ISSN 1470-3521
4. Hornung A, Sagi S, Marongiu A, Seifert H (2008) Evaluation of the formal kinetic parameters and degradation mechanisms for the pyrolysis of lignin by thermogravimetry mass-spectrometry. In: Proceedings of the international conference 16th European biomass conference and exhibition, Feria Valencia, 2–6 June 2008
5. Trebbi G, Rossi C, Pedrelli G (1997) Plans for the production and utilisation of biooil from biomass fast pyrolysis. In: Bridgwater AV, Boocock DGB (eds) Developments in thermo-chemical biomass conversion. Blackie Academic, London, pp 378–387
6. Rossi C, Graham RB (1997) Fast pyrolysis at ENEL. In: Kaltschmitt MK, Bridgwater AV (eds) Biomass gasification and pyrolysis. CPL Scientific, Newbury, pp 300–306

7. Boukis L, Gyftopoulou ME, Papamichael I (2001) Biomass fast pyrolysis in an air-blown circulating fluidised bed reactor. In: Bridwater AV (ed) Progress in thermochemical biomass conversion. Blackwell Science, Oxford, pp 1259–1267
8. Meier D (2005) New ablative pyrolyser in operation in Germany. PyNe newsletter 17. Aston University, Birmingham, pp 1–3
9. Lede J, Panagopoulos J, Li HZ, Villermaux J (1985) Fast pyrolysis of wood: direct measurement and study of ablation rate. Fuel 64:1514–1520
10. Diebold JP, Scahill J (1987) Production of primary pyrolysis oils in a vortex reactor. In: Ratcliff CT, Suuberg EM, Vorres KS (eds) Production analysis and upgrading of oils from biomass (pyrolysis oils from biomass: producing, analyzing, upgrading), vol 32(2). American Chemical Society, Washington, DC, pp 21–28
11. Bridgwater AV (2009) Fast pyrolysis of biomass. In: Bridgwater AV, Hofbauer H, van Loo S (eds) Thermal biomass conversion. CPL Press, Newbury, pp 42–45
12. Dahmen N, Dinjus E, Henrich E (2007) Erdöl – Erdgas – Kohle 123(3):OG31
13. Prins W, Wagenaar BM (1997) Review of rotating cone technology for flash pyrolysis of biomass. In: Kaltschmitt MK, Bridgwater AV (eds) Biomass gasification and pyrolysis. CPL Scientific, Newbury, pp 316–326
14. Wagenaar BM, Venderbosch RH, Carrasco J, Strenziok R, Van der Aa BJ (2001) Rotating cone bio-oil production and applications. In: Bridgwater AV (ed) Progress in thermochemical biomass conversion. Blackwell Science, Oxford, pp 1268–1280
15. Oeck RC (1982) US Patent 4,412,889
16. Meszaros MW (1996) Advanced recycling technologies for plastics. In: Khan MR (ed) Conversion and utilization of waste materials. Taylor & Francis, Washington, DC
17. Meszaros MW (1995) Advances in plastics recycling. Thermal depolymeriation of thermoplastic mixtures, vol 609, ACS symposium series. American Chemical Society, Washington, DC, pp 170–182
18. McIntosh MJ, Arzoumanidis GG (1995) US Patent 5,662,052
19. Hornung A (1997) Entwicklung eines Verfahrens zur fraktionierten thermischen Zersetzung von Kunststoffgemischen, Fortschritt-Berichte VDI, 3, 484. VDI Verlag, Düsseldorf
20. Hornung A, Hornung U, Bockhorn H (1996) DE 196 20 721
21. Hornung U (1996) Bestimmung der Vergasungskinetik von Kunststoffen mit Hilfe eines isotherm betriebenen Kreislaufreaktors. Fortschritt-Berichte VDI, 3, 485. VDI Verlag, Düsseldorf
22. Sea Marconi Technologies (2000) EP 00830831.4
23. Hornung A, Koch W, Schöner J, Furrer J, Seifert H (2002) Stepwise pyrolysis of electronic scrap. In: Björkman B, Samuelsson C, Wikström JO (eds) TMS fall 2002 extraction and processing division meeting on recycling and waste treatment in mineral and metal processing: technical and economic aspects, vol 2. GTC-Print AB, Lulea, pp 103–108
24. Hornung A, Seifert H (2004) Pyrolyse von E-Schrott. In: Pyrolyse- und Vergasungs-verfahren in der Energietechnik – Bio-Fuel-Konzepte. Saxonia Standortentwicklungs- und –verwaltungsgesellschaft mbH, Freiberg, 16, pp 237–251
25. Hornung A, Donner S, Koch W, Schöner J, Seifert H (2004) Haloclean/Pydra – thermal-chemical recycling of WEEE. In: Hornung A, Schöner J, Seifert H (eds) MoDeSt workshop on recycling of polymeric material. Wissenschaftliche Berichte, FZKA 7005
26. Hornung A, Apfelbacher A (2009) Patent GB 246,0156
27. Khor KH, Lim KO (2008) Slow pyrolysis of oil palm EFB. Int Energy J 9:181–188
28. Das P, Ganesh A (2004) Bio-oil from pyrolysis of cashew nut shell-a near fuel. Biomass Bioenergy 27:265–275. doi:10.1016/S0961-9534(02)00182-4
29. Abdullah N, Gerhauser H (2008) Bio-oil derived from empty fruit bunches. Fuel 87:2606–2613. doi:10.1016/j.fuel.2008.02.011
30. Brocksiepe H-G (1986) Charcoal. In: Ullmann's encyclopedia of industrial chemistry, 5th edn, vol A6. VCH, Weinheim
31. Domac J, Trossero M (2008) Industrial charcoal production. TCP/CRO/3101 (A) Development of a sustainable charcoal industry. Zagreb, Croatia
32. Bridgwater AV, Carson P, Coulson M (2007) A comparison of fast and slow pyrolysis liquids from mallee. Int J Global Energy Issues 27(2):204–216
33. Hornung A (2008) High integrative, CO_2 negative, high efficient power generation from ash rich biomass in power plants of 10 MW and coupled production of algae based bio oils as well as black earth (dark soil) avoiding effluents at Hainhaus/Odenwald – "ICONE Power nach dem BtVB Prozess. Bioenta Reichelsheim, Germany
34. Hornung A (2009) Bio-thermal valorisation of biomass: the BtVB process at Hainhaus/Odenwald. In: Proceedings of the 2nd international congress on biodiesel, AOCS, Munich, 15–17 Nov 2009
35. Hornung A, Apfelbacher A, Seifert H (2005) Thermo-chemical conversion of straw – Haloclean, an optimised low temperature pyrolysis. In: 14th European biomass conference and exhibition, biomass for energy, industry and climate protection, Paris, 17–21 Oct 2005

Books and Reviews

Ahmedna M, Marshall WE, Rao RM (2000) Production of granular activated carbons from select agricultural by-products and evaluation of their physical, chemical and adsorption properties. Bioresour Technol 71:113–123

Finch HE, Redlick R (1969) Rice hull method, apparatus and product. US Patent 3,451,944

Hornung U, Schneider D, Hornung A, Tumiatti V, Seifert H (2009) Sequential pyrolysis and catalytic low temperature reforming of wheat straw. J Anal Appl Pyrol 85:145–150

Huang S, Jing S, Wang J, Wang Z, Jin Y (2001) Silica white obtained from rice husk in a fluidized bed. Powder Technol 117:232–238

Oh GH, Park Ch R (2002) Preparation and characteristics of rice-straw-based porous carbons with high adsorption capacity. Fuel 81:327–336

Sun R, Thomkinson J, Mao FC, Sun XF (2001) Physiochemical characterization of lignins from rice straw by hydrogen peroxide treatment. J Appl Polym Sci 79:719–732

Yun ChH, Park YH, Park ChR (2001) Effects of pre-carbonization on porosity development of activated carbons from rice straw. Carbon 39:559–567

Biomass Resources, Worldwide

André Faaij
Copernicus Institute, Department of Science, Technology and Society, Utrecht University, Utrecht, The Netherlands

Article Outline

Glossary
Definition of the Subject
Introduction
Analysis of Existing Studies
Integration of the Findings
Discussion of the Results
Conclusions and Future Directions
Note
Bibliography

Glossary

Biodiversity The variability among living organisms from all sources including, inter alia, terrestrial, marine, and other aquatic ecosystems and the ecological complexes of which they are part, which includes diversity within species, among species, and of ecosystems.

Bio energy Energy derived from biomass.

Biofuel Any liquid, gaseous, or solid fuel produced from plant or animal organic matter (e.g., soybean oil, alcohol from fermented sugar, black liquor from the paper manufacturing process, wood as fuel, etc.). Second-generation biofuels are products such as ethanol and biodiesel derived from lignocellulosic biomass by chemical or biological processes.

Biomass The total mass of living organisms in a given area or of a given species usually expressed as dry weight. Organic matter consisting of, or recently derived from, living organisms (especially regarded as fuel) excluding peat. Biomass includes products, by-products, and waste derived from such material. Cellulosic biomass is biomass from cellulose, the primary structural component of plants and trees.

Deforestation The natural or anthropogenic process that converts forest land to non-forest.

Ecosystem A system of living organisms interacting with each other and their physical environment. The boundaries of what could be called an ecosystem are somewhat arbitrary, depending on the focus of interest or study. Thus, the extent of an ecosystem may range from very small spatial scales to the entire planet.

Forest Defined under the Kyoto Protocol as a minimum area of land of 0.05–1.0 ha with tree-crown cover (or equivalent stocking level) of more than 10–30% with trees with the potential to reach a minimum height of 2–5 m at maturity in situ. A forest may consist either of closed forest formations where trees of various story and undergrowth cover a high proportion of the ground or of open forest. Young natural stands and all plantations that have yet to reach a crown density of 10–30% or tree height of 2–5 m are included under forest, as are areas normally forming part of the forest area that are temporarily unstocked as a result of human intervention such as harvesting or natural causes but which are expected to revert to forest.

Governance The way government is understood has changed in response to social, economic, and technological changes over recent decades. There is a corresponding shift from government defined strictly by the nation-state to a more inclusive concept of governance, recognizing the contributions of various levels of government (global, international, regional, local) and the roles of the private sector, of nongovernmental actors, and of civil society.

Integrated assessment A method of analysis that combines results and models from the physical, biological, economic, and social sciences, and the interactions between these components in a consistent framework to evaluate the status and the consequences of environmental change and the policy responses to it.

Land use The total of arrangements, activities and inputs undertaken in a certain land-cover type (a set of human actions). The social and economic purposes for which land is managed (e.g., grazing, timber extraction, and conservation). Land-use change occurs when, for example, forest is converted to agricultural land or to urban areas.

Models Models are structured imitations of a system's attributes and mechanisms to mimic appearance or functioning of systems, for example, the climate, the economy of a country, a crop. Mathematical models assemble (many) variables and relations in computer code to simulate system functioning and performance for variations in parameters and inputs. Bottom-up models aggregate technological, engineering, and cost details of specific activities and processes. Top-down models apply macroeconomic theory, econometric and optimization techniques to aggregate economic variables, like total consumption, prices, incomes, and factor costs. Hybrid models include bottom-up approaches or results in top-down models.

Potential Several levels of biomass supply potentials can be identified, although every level may span a broad range.

Market potential The amount of bioenergy output expected to occur under forecast market conditions, shaped by private economic agents and regulated by public authorities. Private economic agents realize private objectives within given, perceived, and expected conditions. Market potentials are based on expected private revenues and expenditures, calculated at private prices (incorporating subsidies, levies, and rents) and with private discount rates. The private context is partly shaped by public authority policies.

Economic potential The amount of bioenergy output projected when all social costs and benefits related to that output are included, there is full transparency of information, and assuming exchanges in the economy install a general equilibrium characterized by spatial and temporal efficiency. Negative externalities and co-benefits of all energy uses and of other economic activities are priced. Social discount rates balance the interests of consecutive human generations.

Sustainable development potential The amount of bioenergy output that would be obtained in an ideal setting of perfect economic markets, optimal social (institutional and governance) systems, and achievement of the sustainable flow of environmental goods and services. This potential is distinct from economic potential by explicitly addressing inter- and intragenerational equity (distribution) and governance issues.

Technical potential The amount of bioenergy output obtainable by full implementation of demonstrated and likely to develop technologies or practices. No explicit reference to costs, barriers, or policies is made. In literature, analysts often adopt practical constraints in that context they implicitly take into account for instance socio-geographical and socio-political considerations (also called resource potential).

Theoretical potential This potential is derived from natural and climatic (physical) parameters. The theoretical potential can be quantified with a reasonable accuracy, but the information is of limited practical relevance. It represents the upper limit of what can be produced from biomass from a theoretical point of view based on current scientific knowledge. It does not take into account energy losses during the conversion process necessary to make use of the resource nor any kind of barriers.

Price elasticity of demand The ratio of the percentage change in the quantity of demand for a good or service to 1% change in the price of that good or service. When the absolute value of the elasticity is between 0 and 1, demand is called inelastic; when it is greater than 1, demand is called elastic.

Reforestation Direct human-induced conversion of non-forested land to forested land through planting, seeding, and/or the human-induced promotion of natural seed sources, on land that was previously forested but converted to non-forested land. For the first commitment period of the Kyoto Protocol, reforestation activities will be limited to reforestation occurring on those lands that did not contain forest on December 31, 1989.

Scenario A plausible description of how the future may develop based on a coherent and internally consistent set of assumptions about key

relationships and driving forces (e.g., rate of technological change, prices) on social, economic, energy, etc. Note that scenarios are neither predictions nor forecasts, but are useful to provide a view of the implications of developments and actions.

Definition of the Subject

The role of biomass as a sustainable source for energy and materials has been heavily debated in recent years. In 2008, when food prices peaked (just as oil and many other commodities), biofuels were blamed for starving the poor, disturbing markets, making unsustainable use of land and water and, especially due to indirect land-use change, resulting in poor or even negative greenhouse gas (GHG) balances. In the meantime, a large amount of literature has been produced providing pieces of insight in various fields, but integral analyses on the matter are scarce. This article provides an extensive assessment of what is known and what is not known about the possibilities to realize a sustainable resource base for bio-based energy carriers and materials. The work looked at energy potentials in conjunction with key factors affecting its sustainability (biodiversity, water, competition with the food production system, soil quality, and energy demand) and deployed integrated assessment modeling plus a detailed evaluation of uncertainties. Biomass energy potentials are found to range between 200 and 500 EJ/year in 2050. Crucial in these figures is that water limitations, biodiversity protection, and food demand are taken into consideration. Improvements of agricultural efficiency and crop choice (especially perennial cropping systems offer the best perspectives) are essential preconditions to reach the higher end of the range.

Introduction

In a wide variety of scenarios, policy strategies, and studies that address the future world energy demand and the reduction of greenhouse gas emissions, biomass is considered to play a major role as renewable energy carrier. Over the past decades, the modern use of biomass has increased rapidly in many parts of the world and many countries have ambitious targets for further biomass utilization in the light of the Kyoto GHG reduction targets. Rising oil prices have also increased the level of interest in bioenergy.

Biomass is the most important renewable energy source, providing about 10% (46 EJ) of the annual global primary energy demand. A major part of this biomass use (37 EJ) is noncommercial and relates to charcoal, wood, and manure used for cooking and space heating, generally by the poorer part of the population in developing countries. Modern bioenergy use (for industry, power generation, or transport fuels) is making already a significant contribution of approximately 9 EJ, and this share is growing. Today, biomass (mainly wood) contributes some 10% to the world primary energy mix, and is still by far the most widely used renewable energy source (Fig. 1). While bioenergy represents a mere 3% of primary energy in industrialized countries, it accounts for 22% of the energy mix in developing countries, where it contributes largely to domestic heating and cooking, mostly in simple inefficient stoves.

The expected deployment of biomass for energy on medium to longer term differs considerably between various studies. A key message from the review of currently available insights on large-scale biomass deployment is that its role is largely conditional: deployment will strongly depend on sustainable development of the resource base and governance of land use, on development of infrastructure, and on cost reduction of key technologies, for example, new generation biofuels.

Due to rising prices for fossil fuels (especially oil, but also natural gas and to a lesser extent coal), the competitiveness of biomass use has improved considerably over time. In addition, the development of CO_2 markets (emission trading), as well as ongoing learning and subsequent cost reductions for biomass and bioenergy systems, have strengthened the economic drivers for increasing biomass production, use, and trade. Sufficient biomass resources and a well-functioning biomass market that can assure reliable, sustainable, and lasting biomass supplies are crucial preconditions to realize such ambitions. To date, various countries have considerable experience with building biomass markets and linking available resources with market demand. Examples are found in Brazil, Sweden, Finland, Canada, and the Netherlands. Relatively recently, international trade in biomass resources has become part of the portfolio of market dealers and volumes traded worldwide have

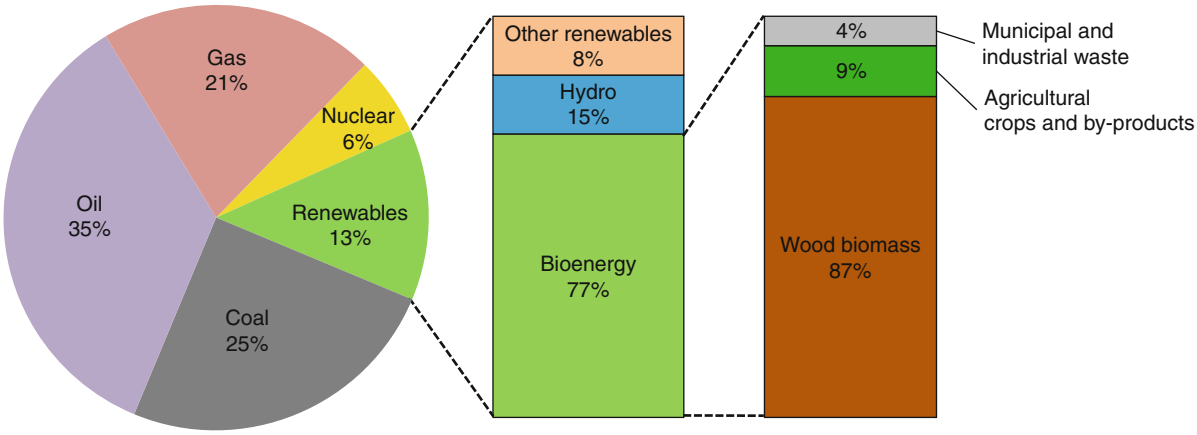

Biomass Resources, Worldwide. Figure 1
Share of bioenergy in the world primary energy mix [1, 2]

increased at a very rapid pace with an estimated doubling of volumes in several markets over the past few years [3].

Because of the "globalization of bioenergy" and the steeply increased demand for both liquid and solid biofuels, biomass supplies (e.g., pellets from agricultural and forest residues, vegetal oils such as palm oil and rapeseed, bio-ethanol) from other continents are now used in various markets. This triggered a heated debate on the sustainability of those developments, because biomass production is now also associated with increased competition with food production and land, loss of forest cover, and the like. Besides such competition, also the net reduction in GHG emissions is questioned in case land use for biomass is associated with clearing (virgin) forest, conversion of peat land, as well as high fossil energy inputs for machinery, fertilizers, and other agrochemicals.

If biomass is to contribute to levels representing up to one third of the global future energy supply during this century, this implies that land-use implications are very significant. Views on such potential developments differ from "utterly destructive" to feasible and possible to develop biomass potentials in synergy with rural development and sustainable management of natural resources. The latter, more positive views, are supported by the fact that rationalization of agriculture has beneficial effects and biomass may also be produced on marginal and degraded lands not suited for production of food, with possible ecological benefits.

Proper standardization and certification procedures to ensure sustainable biomass production and use are currently being developed. Currently, this is a priority for various governments, market players, and international bodies. In particular competition between production of food, preservation of forests and nature, and the use of land for biomass production should be avoided. It is often stated that this may be possible by using lignocellulosic biomass resources that can come from residues and wastes or are grown on non-arable (e.g., degraded) lands and in particular by increased productivity in agricultural and livestock production. Demonstration of such combined development where sustainable biomass production is developed in conjunction with more efficient agricultural management is a challenge and it is questioned to what extent strict sustainability demands will influence biomass resource potentials over time.

The potential for energy crops depends largely on land availability considering that worldwide a growing demand for food has to be met, combined with environmental protection, sustainable management of soils and water reserves, and a variety of other sustainability requirements. Given that a major part of the future biomass resource availability for energy and materials depends on these complex and related factors, it is not possible to present the future biomass potential in one simple figure.

Focusing on the more recent estimates of biomass resource potentials, energy farming on current

agricultural (arable and pasture) land could, with projected technological progress, contribute 100–300 EJ annually, without jeopardizing the world's future food supply. A significant part of this potential (around 200 EJ in 2050) for biomass production may be developed at low production costs in the range of 2 €/GJ assuming this land is used for perennial crops [4, 5]. Another 100 EJ could be produced with lower productivity and higher costs, from biomass on marginal and degraded lands. Regenerating such lands requires more upfront investment, but competition with other land uses is less of an issue and other benefits (such as soil restoration, improved water retention functions) may be obtained, which could partly compensate biomass production costs. Combined and using the more average potential estimates, organic wastes and residues could possibly supply another 40–170 EJ, with uncertain contributions from forest residues and potentially a significant role for organic waste, especially when biomaterials are used on a larger scale.

Key to the introduction of biomass production in the suggested orders of magnitude is the rationalization of agriculture, especially in developing countries. There is room for considerably higher land-use efficiencies that can more than compensate for the growing demand for food [6].

Available studies already indicate that the results are sensitive to assumptions about crop yields and the amount of land that could be made available for the production of biomass for energy uses, including biofuels. Critical issues include:

- *Competition for water resources*: Although the estimates mentioned above generally exclude irrigation for biomass production, it may be necessary in some countries where water is already scarce.
- *Use of fertilizers and pest control techniques*: Improved farm management and higher productivity depend on the availability of fertilizers and pest control. The environmental effects of heavy use of fertilizer and pesticides could be grave.
- *Land use*: More intensive farming to produce energy crops on a large scale may result in losses of biodiversity. Perennial crops are expected to be less harmful, or even able to achieve positive effects compared to conventional crops such as cereals and seeds. More intensive cattle-raising would also be necessary to free up grassland currently used for grazing.
- *Competition with food and feed production*: Increased biomass production for biofuels out of balance with required productivity increases in agriculture could drive up land and food prices.

Although available studies give a reasonable insight in the importance of various parameters, the integration between different arenas is still relatively limited. This causes confusion in public as well as scientific debate, with conflicting views on the possibilities for sustainable use of biomass as a result. These explanations aim to tackle this problem by providing a more comprehensive assessment of the current knowledge with respect to biomass resource potentials.

The main objectives of this work are outlined below.

1. Provide clear insights in the linkages between the impacts of (large-scale) use of biomass for energy and material on food supplies, water use, nature and biodiversity, and in macroeconomic terms.
2. Provide insight in regional and site-specific elements in the above-mentioned issues.
3. Translate the results of the assessment into an overview of the more and less certain issues with respect to biomass resource potentials and to policy-relevant recommendations on how to develop and use biomass resources in a sustainable way, including research and development needs.

To reach these goals the work is set up as follows.

- The first part comprises an assessment of recent literature on the key areas distinguished: biomass potentials, food production, water, biodiversity, energy demand, and analyses of agricultural economics. Furthermore, greenhouse gas (GHG) balances of biomass use for energy are distinguished as a separate topic. Distinction is made between various biomass resource-technology combinations and different settings for biomass production.
- The second part is an integration component, which describes the linkages between the different key areas and quantifies the consequences of the results of the assessment to the extent that available models and tools allow doing so. A limitation is that no new models are developed.

- The third part translates the results of the assessment and the integration activities into an extensive assessment of the uncertainties of future biomass resource potentials and which factors are of major and which of lesser importance. Based on this, policy recommendations and further steps to reduce uncertainties and fill gaps in knowledge are identified.

Analysis of Existing Studies

Here, a summary is given of the review of recent studies in the field of biomass potentials, biodiversity, water, food demand, energy demand, and agricultural economics. These are main relevant areas for estimating the potentials of biomass for energy and material purposes.

The review describes the most important aspects and parameters that should be taken into account in an "ideal study." Common to all areas is that global trends on population growth and economic development are an important basis to estimate future development. Within the review, the key parameters on the current situation and on the future developments that resulted from the various studies are presented. Finally, conclusions are drawn regarding important relations of the separate areas with biomass potentials and possible knowledge gaps.

Biomass Potential Studies

Earlier analyses of biomass potential studies had shown large ranges of outcomes that were based on differences in methodologies and assumption on crop yields and available land and in the case of economic potentials on differences in the estimated production costs [7].

An "ideal" study to evaluate biomass potentials should take into account global and regional trends and specific local conditions such as soil types, water availability, possibility of irrigation, and land-use planning taking biodiversity and soil quality into account. It is expected that moving to the large-scale use of biomass for energy and materials will change land-use patterns and energy systems significantly. Such changes would influence supply and demand of (agricultural) land as well as those of food, materials, wood products, and energy carriers in a dynamic way. The economic relationships between the demand and the supply of biomass, especially taking into account changes of land and food prices on a regional to local level, should therefore be considered.

This section focuses on the potential availability of biomass resources for energy and materials. It briefly discusses the various resource categories: residues from forestry and agriculture, various organic waste streams and, most important, the possibilities for active biomass production on various land categories (e.g., for wood plantations or energy crops such as sugar cane) (Fig. 2).

Biomass residues potential availability is discussed below. These may be divided into:

1. Primary residues: residues generated pre- and at harvest of main product, for example, tops and leaves of sugar cane
2. Secondary residues: residues generated in processing to make products, for example, bagasse, rice husks, and black liquor
3. Tertiary residues: residues generated during- and post end use (+ non-used products), for example, demolition wood and municipal solid waste

In general, biomass residues (and wastes) are intertwined with a complex of markets. Many residues have useful applications such as fodder, fertilizer and soil conditioner, and raw material, for example, for particle board, medium density fiber board (MDF), and recycled paper. Net availability as well as (market) prices of biomass residues and wastes therefore generally depend on market demand, local as well as international markets for various raw material, and on the type of waste treatment technology deployed for remaining material. The latter is particularly relevant when waste treatment is paid for giving some organic waste streams a (theoretical) negative value. Typically, the net availability of organic wastes and residues can fluctuate and is influenced by market developments, but also can depend on climate (high and low production years in agriculture) and other factors.

Energy crops are planted on agricultural or other lands for energy and material purposes. In practice there exists a competition between land used for energy crops, animal grazing, forestry, and food. However, synergy exists between these sources; the growth in food and forestry products directly implies increased amounts of crop residues with potential use for energy purposes.

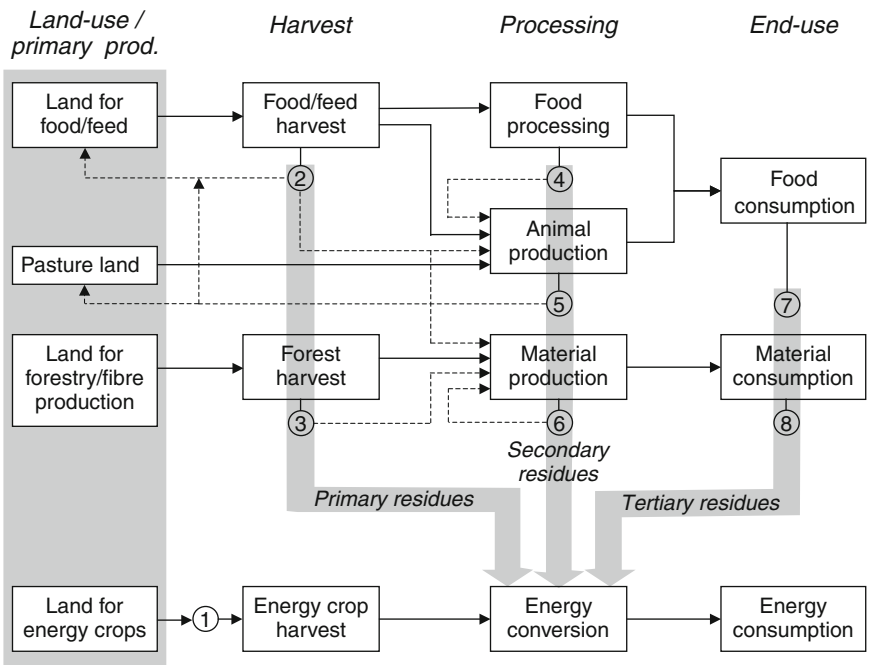

Biomass Resources, Worldwide. Figure 2
Schematic overview of the present terrestrial biomass flows in the food, materials, and bioenergy sectors, as well as in final end use. The *gray arrows* denote: (1) energy crops, (2) agricultural residues, (3) forest residues, (4) food residues, (5) manure, (6) non-food organic waste, (7) food consumption waste, and (8) non-food consumption waste [9]

Residues and Wastes Vast amounts of biomass residue exist that could potentially be used as feedstock for biofuel production. Much of the plant matter produced by common crops is left on the fields after harvest, and a large portion of this decomposes into carbon dioxide rather than returning to the soil. Similarly, forestry practices leave behind large quantities of unharvested wood, and fire mitigation practices have allowed forest underbrush to accumulate. Of the biomass that is already being harvested, large amounts of residues are generated at agricultural processing facilities and forestry mills, including sugar cane bagasse, rice hulls, nut shells, saw dust, and black liquor (at paper mills). In urban areas, cellulosic residues include portions of municipal solid waste, grass clippings, and wood from tree trimmings and land clearing activities.

Residues and wastes have several advantages over dedicated energy crops. Most of them would require no additional land acreage, as they are typically pre-collected into piles at large agricultural and forestry facilities and often represent "waste" that must otherwise be disposed of. As a result, this feedstock is cheaper and is likely to be the first source of biomass to be tapped. Already, the wood products industry uses most lumber residues and much of the forestry residue in Europe and the USA for processing purposes and to generate coproducts such as wood chips, fiberboard, etc.

For sustainability reasons, however, estimates of potential bioenergy from waste and residues would likely be lower than those suggested above. In general, it is a good idea to retain some portion of biomass residue in the field or forest to hold carbon, water, and other nutrients in the soil, and to provide habitat for various species. Leaving a protective amount of residue behind is especially important on steep slopes or on ecologically sensitive sites that have particularly erodible soils, or are near riparian areas.

Residues from Agriculture The production potential for agricultural residues depends on the various yields of different agricultural products, the total agricultural

land area, and the type of production system. Less-intensive management systems require the reuse of residues for maintaining soil fertility, reducing the total amount that can be sustainably removed. More intensively managed systems, meanwhile, allow for higher use rates of residues but also typically rely on crops with lower crop-to-residue ratios, such as corn.

Estimates are available from various studies. Potential depends on yield/product ratios and the total agricultural land area as well as type of production system. Less-intensive management systems require reuse of residues for maintaining soil fertility. Intensively managed systems allow for higher utilization rates of residues but also usually deploy crops with lower crop-to-residue ratios. Estimates vary between some 15 and 70 EJ/year. The latter figure is based on the regional production of food (in 2003) multiplied by harvesting or processing factors and the assumed recoverability factors [6]. These figures do not subtract the potential alternative use for agricultural residues. But, competing applications can reduce the net availability of agricultural residues for energy or materials significantly [8].

Dung This category especially concerns the use of dried dung. Total estimated contribution could be 5–55 EJ/year worldwide. The low estimate is based on global current use, and the high estimate is the technical potential. Utilization (collection) in the long run is uncertain because this is particularly considered a poor man's fuel [9]. There are also sociocultural constraints in waste utilization, which explain somewhat the wide differences in waste utilization across different regions and cultures.

Organic Wastes This category includes the organic fraction of municipal solid waste (MSW) and waste wood (e.g., demolition wood). Organic wastes are a particularly attractive source of biomass energy because they can have a "negative" price. In other words, collecting and utilizing can result in savings from landfill tipping fees. Estimates on the basis of literature values strongly depend on assumptions regarding economic development, consumption, and the use of biomaterials; the ranges projected for MSW in the long run (e.g., beyond 2040) amount to 5–50 EJ/year. Higher values are possible when more intensive use is made of biomaterials [9, 10].

Forest Residues The (sustainable) energy potential of the world's forests is partly uncertain. A recent evaluation of forest reserves and development of demand for wood products concluded that even in the case of the highest wood demand projections found in literature, the demand can (in theory) be met without further deforestation. The bioenergy potential from forestry can contribute 1–98 EJ/year of surplus natural forest growth and 32–52 EJ/year harvesting and processing residues in 2050. The most promising regions are the Caribbean and Latin America, the former Soviet Union, and partially North America. Key variables are the demand for industrial round wood and fuel wood, plantation establishment rates, natural forest growth, and the impact of technology and recycling [11].

Despite this potential, the amount of energy that can be obtained from forest residues and other waste biomass resources will be limited in comparison to energy crops; moreover, these reserves will likely be depleted first as demand for bioenergy grows. Finland, which has focused on harnessing biomass energy for many years, has already used a large part of its accessible residues and wastes and is now importing wood energy.

Energy Crops Biomass production requires land. Conservatively, the productivity for a perennial crop (like Willow, Eucalyptus, or Switchgrass) lies between 8 and 12 t dry matter per hectare per year. The heating value of dry clean wood amounts to about 18 GJ/t (LHV). One hectare of planted area can therefore produce about 140–220 GJ/(ha year) (gross energy yield, energy inputs for cultivation, fertilizer, harvest, etc., amount to about 5%).

One petajoule would require 4,500–7,000 ha; 1,500 MW_{th} (the amount of fuel needed to fire a base load power plant with 40% efficiency of 600 MW_e) would require 140,000–230,000 ha; and 100 EJ (about one quarter of the world's current energy use) would ask 450–700 Mha.

The potential for energy crops therefore largely depends on land availability considering that worldwide a growing demand for food has to be met, combined with nature protection, sustainable management of soils and water reserves, and a variety of other sustainability criteria. Given that a major part of the

future biomass resource availability for energy and materials depend on these (intertwined, uncertain, and partially policy dependent) factors, it is impossible to present the future biomass potential in one simple figure.

Review of Studies In this assessment, the focus is laid on the relation between estimated biomass potentials and the availability and demand of water, the production and demand of food, influence on biodiversity, and economic mechanisms. For this purpose, eight recent studies are analyzed (Table 1). None of these studies covers the whole range of issues, but they all have strong points at certain issues.

The scope of the studies, in terms of biomass resources included, varies as well as the scenario assumptions. As a consequence, global biomass potentials vary widely. The high biomass potential for 2050 determined by Smeets et al. [6] shows potentials under intensive, very high technologically developed agriculture. On the contrary, the low biomass potential for 2050 calculated by Wolf et al. [17] is caused by high population growth, high food demands, and extensive agricultural production systems. The study of Hoogwijk et al., 2005, refers to production of energy crops on abandoned, marginal, and rest land assuming global and regional trends as described in the IPCC SRES scenarios, under increasing agricultural efficiency over time [13]. Finally, the study of Rokityanski et al. determines economic potentials of afforestation and reforestation, excluding other types of biomass and assuming extensive forestry management [16]. As a result, the economic potentials for 2100 are rather low.

Most earlier assessments of biomass resource potentials used rather simplistic approaches to estimating the potential of biomass plantations [7], but the continuous development of modeling tools that combine databases containing biophysical information (soil, topography, climate) with analytical representations of relevant crops and agronomic systems has resulted in improvements over time (see, e.g., [18, 19, 20, 21, 22]).

Table 2 shows ranges in the assessed resource potential year 2050, explicit for various biomass categories. The ranges (based on [6, 9, and 13]) provide a summary of the biomass categories discussed. A large number of studies (e.g., [23, 24, 25]) were reviewed that assess the global and regional potential, and on selected additional studies not included in these reviews ([6, 10, 19, 26–29]).

The wide ranges in Table 2 are because the studies differ in their approach to considering different determining factors, which are in themselves uncertain: Population, economic, and technological development can go in different directions and pace; biodiversity and nature conservation requirements set limitations that are difficult to assess; and climate change as well as land use in itself can strongly influence the biophysical capacity of land. Biomass potentials can also not be determined exactly as long as uncertainty remains about agreed trade-offs with respect to additional biodiversity loss or intensification pressure in food production as well as potential synergies in land use.

Conclusions Summarizing, both the technical and economic potential of biomass resources for energy and material use can be very large, up to over two times the current global energy demand, without competing with food production, protection of forests and nature. Besides residues from agriculture and forestry (which are significant, but also limited due to competing applications), organic waste and the active production of biomass (e.g., energy crops) are the two main factors responsible for these potentials. Key, however, to the development of competitive energy cropping systems is the rationalization of agriculture, especially in developing countries, which can result in considerably higher land-use efficiencies for agriculture and, thus, a surplus of productive land. Perennial crops (such as Eucalyptus, poplar, grasses as *Miscanthus* and sugar cane) provide the most favorable economics and environmental characteristics for biomass production. Table 2 provides a summary of the biomass categories discussed in this section.

In theory, energy farming on current agricultural land could, with projected technological progress, contribute over 800 EJ, without jeopardizing the world's food supply. Organic wastes and residues could possibly supply another 40–170 EJ, with uncertain contributions from forest residues and potentially a very significant role for organic waste, especially when biomaterials are used on a larger scale. In total, the upper limit the of bioenergy potential could be over

Biomass Resources, Worldwide. Table 1 Overview and evaluation of selected biomass potential studies

Study	Subject	Biomass potential	Evaluation
Fischer et al. [12]	Assessment of ecophysiological biomass yields	CEE, North and Central Asia; EC (poplar, willow, *Miscanthus*); TP	*Strong:* detailed differentiation of land suitability for biomass production of specific crops on a grid-cell level (0.5 degree) *Weak:* not considering interlinkages with food, energy, economy biodiversity, and water demands
Hoogwijk et al. [13]	Integrated assessment based on SRES scenarios	Global, EC (short-rotation crops); TP	*Strong:* integrated assessment considering food, energy material demands including a scenario analyses based; analyses of different categories of land (e.g., marginal, abandoned) *Weak:* crop yields not modeled detailed for different species and management systems
Hoogwijk et al. [4]	Cost-supply curves of biomass based on integrated assessment	Global; EC (short-rotation crops; TP, EP (as cost-supply curve)	*Strong:* establishes a global cost-supply curve for biomass based on integrated assessment *Weak:* linkage land/energy prices not regarded
Obersteiner et al. [14]	Biomass supply from afforestation/ reforestation activities	Global; F (incl. short-rotation); EP	*Strong:* modeling of economic potential by comparing net present value of agriculture and forestry on grid-cell level *Weak:* yields of forestry production not dependent on different technology levels
Perlack et al. [15]	Biomass supply study based on outlook studies from agriculture and forestry	USA; EC, F, FR, AR, SR, TR; TP	*Strong:* detailed inclusion of possible advances in agricultural production systems (incl. genetic manipulation) *Weak:* no integrated assessment, e.g., demands for food and materials not modeled
Rokityanski et al. [16]	Analysis of land-use change mitigation options; methods similar to Obersteiner et al. [14]	Global; F (incl. short-rotation); EP	*Strong:* policy analysis of stimulating land-use options including carbon prices *Weak:* agricultural land not included
Smeets et al. [6]	Bottom-up assessment of bioenergy potentials	Global; EC, F, AR, FR, SR, TR; TP	*Strong:* detailed bottom-up information on agricultural production systems including animal production *Weak:* yield data for crops only regionally modeled
Wolf et al. [17]	Bottom-up assessment of bioenergy potentials mainly analyzing food supplies	Global; EC; TP	*Strong:* various scenarios on production systems and demand showing a large range of potentials *Weak:* yields of energy crops not specified for different species and land types

Biomass: *EC* energy crops, *F* forestry production, *FR* primary forest residues, *AR* primary agricultural residues, *SR* secondary residues, *TR* tertiary residues
Potentials: *TP* technical potential, *EP* economic potential

Biomass Resources, Worldwide. Table 2 Overview of the global potential bioenergy supply on the long term for a number of categories and the main preconditions and assumptions that determine these potentials

Biomass category	Main assumptions and remarks	Potential bioenergy supply up to 2050
Energy farming on current agricultural land	Potential land surplus: 0–4 Gha (more average: 1–2 Gha). A large surplus requires structural adaptation of intensive agricultural production systems. When this is not feasible, the bioenergy potential could be reduced to zero as well. On average higher yields are likely because of better soil quality: 8–12 dry t/ha year is assumed[a]	0–700 EJ (more average development: 100–300 EJ)
Biomass production on marginal lands	On a global scale a maximum land surface of 1.7 Gha could be involved Low productivity of 2–5 dry t/ha year[a]. The supply could be low or zero due to poor economics or competition with food production	(0) 60–150 EJ
Biomaterials	Range of the land area required to meet the additional global demand for biomaterials: 0.2–0.8 Gha (average productivity: 5 dry t/ha year) This demand should come from category I and II in case the world's forests are unable to meet the additional demand. If they are, however, the claim on (agricultural) land could be zero	Minus (0) 40–150 EJ
Residues from agriculture	Estimates from various studies. Potential depends on yield/product ratios and the total agricultural land area as well as type of production system: Extensive production systems require reuse of residues for maintaining soil fertility. Intensive systems allow for higher utilization rates of residues	Approx. 15–70 EJ
Forest residues	The (sustainable) energy potential of the world's forests is unclear. Part is natural forest (reserves). Range is based on literature data. Low value: figure for sustainable forest management. High value: technical potential. Figures include processing residues	(0) 30–150 EJ
Dung	Use of dried dung. Low estimate based on global current use. High estimate: technical potential. Utilization (collection) on longer term is uncertain	(0) 5–55 EJ
Organic wastes	Estimate on basis of literature values. Strongly dependent on economic development, consumption, and the use of biomaterials. Figures include the organic fraction of MSW and waste wood. Higher values possible by more intensive use of biomaterials	5–50 (+) EJ[b]
Total	Most pessimistic scenario: no land available for energy farming, only utilization of residues. Most optimistic scenario: intensive agriculture concentrated on the better quality soils (more average potential in a world aiming for large-scale utilization of bioenergy)	40–1,100 EJ (250–500 EJ)

[a]Heating value: 19 GJ/t dry matter

[b]The energy supply of biomaterials ending up as waste can vary between 20 and 55 EJ (or 1,100–2,900 Mt dry matter per year (see Table 4); biomass lost during conversion, such as charcoal is logically excluded from this range). This range excludes cascading and does not take into account the time delay between production of the material and "release" as (organic) waste

1,000 EJ/year [6, 9]. This is considerably more than the current global energy use of about 500 EJ.

Latin America, sub-Saharan Africa, and Eastern Europe clearly are the most promising regions, as well as Oceania and East and Northeast Asia (in the future). The latter can in particular be explained by the projected demographic developments (possibly declining population in China after 2030) and fast technological progress in agriculture, leading to substantial productivity increases.

These analyses also show that a large part of the technical potential for biomass production may

be developed at low production costs of around 2 USD/GJ [4]. Major transitions are however required to exploit this bioenergy potential, especially improving agricultural efficiency in developing countries (i.e., increasing crop yields per hectare). It is still uncertain to what extent and how fast such transitions can be realized in different regions. Under less favorable conditions, the (regional) bioenergy potential(s) could be quite low.

Also, it should be noted that technological developments in conversion, as well as long distance biomass supply chains (i.e., comprising intercontinental transport of biomass derived energy carriers), can dramatically improve competitiveness and efficiency of bioenergy. Increased competitiveness is logically a driver to develop the production potentials of bioenergy.

The recent biomass potential studies give more detailed and well-founded insights into future biomass potentials, but none of the studies does include all critical aspects. Important issues that remain unresolved are:

- The competition for water with other economic sectors, as well as the possibilities of irrigation, has not been included in the biomass potential studies.
- Human diets and alternative protein chains have been included to a limited extent only in the potential estimates, while the impacts of different animal production systems need to be studied in more detail and applied to more biomass potential studies.
- The demand for wood products and other biomaterials has been simplified in most studies and has not been modeled based on economic scenario analysis.
- The impact of large-scale biomass production on the prices (and subsequently) demands of land and food has not been sufficiently studied.
- The impact of specific biodiversity objectives on biomass potentials has not been investigated in detail.

These issues are discussed in more detail in the following sections.

Biodiversity

The global number of species has shown a fast decrease in the last few centuries, mostly through habitat loss and land-use change. The raised policy interest has led to two global UN Conventions that contain targets on preventing further biodiversity decline. The CBD Convention wants to reduce the rate of further loss by 2010, and is focused on a broad range of causes for the decline, among which land use changes. The Climate Convention (UNFCCC) has a long-term goal to prevent damage to biodiversity from climate change effects, next to mitigating climate change itself.

Designing policy options and measures that may help to reach these short- and long-term targets (such as climate change mitigation through use of bioenergy) depend on the way the concept of biodiversity is implemented. Biodiversity includes the variability of all living organisms and all ecosystems. It is a complex phenomenon and cannot be simply defined and measured. All possible indicators are imperfect to capture the full complexity, but they are useful if they can be monitored and explained, related to human impact, and modeled to show future developments and the effects of policy choices. Several complementary indicators are therefore used within the CBD framework. Different indicators might give different messages because of different definitions and implicit valuation of biodiversity, for instance when indicators based on “naturalness” or contrarily on “agro-biodiversity” are used.

Bioenergy potential studies conducted so far mostly neglect the effects of biofuel production on different biodiversity indices. An ideal study should take all relevant biodiversity aspects and scales into account, and should not only show local effects, but possible shifts and trade-offs to other locations as well. Several types of impact assessment studies can be distinguished:

1. Assessing local and present impacts of bioenergy cultivation
2. Assessing integral, global impacts of bioenergy in an LCA-approach, comparing the effects of biofuels and fossil fuels over the whole production chain on greenhouse gas emissions, land use, and biodiversity effects
3. Regional and global scenario studies, showing the integral and future effects of bioenergy, in combination with other global developments in

population growth, food demand, diets, and agricultural productivity

Review of Studies For local impact studies, locally specific aspects like irrigation, fertilizer and pesticide use, former land use, and landscape structure are important. When still natural areas are converted for bioenergy production, natural biodiversity is obviously lost. In case energy crops are just an additional element in agricultural rotation systems local short-term effects are negligible. On the other hand, agro-biodiversity is at risk when extensively used low input farmlands are converted to biomass crops. In Europe, protecting this type of biodiversity is a policy objective in its own. Positive effects for local biodiversity are also possible, for instance when replacing intensively managed agricultural systems by extensively managed perennial crops; or when replacing monocultures by extensively used mixed systems (agroforestry, mixed cropping, organic farming).

In LCA-studies, the global and integral impact of biofuels on biodiversity depends strongly on the following aspects:

- The integral reduction of greenhouse gas emissions (with fossil fuels as a reference, but also comparing different applications of the same biomass) per hectare of land used, depending on technology, soil characteristics, and climate. Liquid biofuels based on perennial and woody crops as well as sugarcane ethanol and palm oil generally provide better results than European crops. However, changes in land use might lead to an increase of CO_2 emissions in case carbon is released from the soil.
- The loss of biodiversity related to specific land-use changes. In general the cultivation of natural areas leads to significant loss. In case of the cultivation of abandoned land the effect in time depends on the restoration time of biodiversity values. The values of cultivated land depend on management practices and crop type.
- The (reduced) long-term effect of climate change on biodiversity, which is hard to quantify because of high uncertainties on the long term. For most liquid biofuels the overall impact on biodiversity is very likely to be negative. For none of the biofuels a positive impact can be guaranteed.

There are no global scenario studies that take all relevant aspects of the biofuel debate into account. Several issues were treated in a global study [30, 31]. The analysis contained an ambitious climate change option with a broad measure portfolio, including large-scale use of bioenergy. The aggregated indicator MSA ("mean abundance of original species") was applied to express global biodiversity loss, which can be interpreted as a measure of naturalness or ecosystem intactness. The indicator is not intended to highlight individual species, agro-biodiversity, or the specific value of protected areas. The analysis indicated that increased land use of mainly abandoned land and marginal grounds for growing bioenergy crops leads to biodiversity losses on the short term (as compared to a baseline scenario, in which abandoned lands will restore to a more-or-less natural situation). By 2050, the increased loss is not yet counteracted by biodiversity gains through avoided climate change. In determining whether short-term losses can be balanced by long-term gains, uncertainty should be taken into account. Long-term effects are based on modeling exercises that are surrounded with considerable conceptual and data uncertainty. The local and specific characteristics and biodiversity values of the economically defined "marginal grounds" are also not well known. Further, there is uncertainty on the assumption on fast and complete biodiversity restoration on abandoned land.

Conclusions Published studies on the biodiversity effects of growing bioenergy crops are very diverse and show opposite results. These differences are the result of using different time horizons (short and/or long term), different scales of observation (local, regional, or global), and the different biodiversity definitions (for instance naturalness or agro-biodiversity). More often than not, the used biodiversity indicators are not explicitly defined.

The integral global impacts of biofuels on biodiversity depend mainly on the long-term positive effect of reduced future climate change and the short-term negative effect of land-use change for large-scale energy crop cultivation instead of nature. In determining whether short-term losses can be balanced by long-term gains, uncertainties should be taken into account. The short-term effects have a high degree of confidence

as the effects of local land-use change are based on monitored effects, while long-term effects are based on modeling exercises that are surrounded with considerable conceptual and data uncertainty. This finding shows that it is not easy to combine both the short-term CBD biodiversity goals and the long biodiversity goals of the Climate Convention.

In all cases a negative impact results from additional land use for large-scale biomass production. European annual agricultural crops do worse at the local level than tropical and perennial and woody crops. Further, not all biodiversity indicators might show the same results, especially when agro-biodiversity and naturalness are confronted. Specifically, the uncertainties about the future beneficial effects of reduced climate change on biodiversity make it hard to draw definite conclusions about the long-term impact of biofuels.

Water

Quantification of the spatial and temporal distribution of river runoff and assessing the influence of humans form the backbone for decisions on optimal use of water resources. A common classification of water resources is the classification into blue and green water flows. Blue water refers to water in rivers, lakes, and groundwater. Green water refers to water in the rooted zone of the soil originating directly from rainfall that is available to plants. Globally around 80% of agricultural evapotranspiration (crop water depletion) originates from green water, while the remaining 20% is provided through irrigation (blue water withdrawals) [32]. Twenty to fifty percent of blue water, depending on the local situation, is required for environmental requirements and services. In addition, water is required for industrial and domestic use.

At the regional and local scale, for blue water irrigation efficiency is a major determinant of water use. It is often defined as the net crop water requirement for evapotranspiration as part of the water withdrawn from a water source. A typical value would be 40%. Most of the other 60% is captured and recycled somewhere else in the system. As reuse loops of water are very common in river basins, improving irrigation efficiency becomes a very complex issue. Water productivity (WP) indicates the efficiency of water use, including blue water, if irrigated, and green water. Crop water productivity (CWP) is an indicator of crop yield per unit of water consumed (evapotranspiration). This implies crop water productivity depends on the main product. If the plant parts used for energy and food are not the same, crop water productivity of a crop differs for both purposes. Water use by crops can be estimated based on weather data and crop growth modeling or by a crop-specific water use efficiency (WUE) that varies among crops and crop types (C_3–C_4 crops, annuals – perennials, herbaceous – woody species) and also with weather (rainfall, temperature, radiation) and agricultural management, such as input use and other practices. Water use efficiency can refer to evapotranspiration, transpiration, total crop yield, economic product, etc. Hence, caution is required when using data from literature [33].

The ideal study does not exist as several very divergent aspects have to be considered with respect to water. Water availability and water use can be assessed at crop, farm, river basin, continental, and global scales. Each scale has its own crucial parameters for reliable calculations and estimates and its own assessment targets. Water use for bioenergy production has to be compared with actual water (and nutrient) use and existing or expected bottle necks for water availability have to be identified. As priority is often given to the other uses (food, domestic and industrial water use), all uncertainties and inaccuracies are accumulating in the final assessment of the scope for energy crops.

Review of Studies Expected future water use by industry and domestic sectors differs between different sources, as assumptions on technological development (efficient systems), economy, and lifestyle vary among these sources. Some studies expect it to be more or less constant [34] and others expect it to increase by 60–220% [35]. However, the largest part of this use (80%) flows back to rivers, lakes, or groundwater. For agricultural water withdrawal, estimates vary considerably depending on the scenarios on population growth, human diet, and input levels used. However, in all scenarios total water use is increasing. Energy crops are not considered explicitly in most studies.

The effect of expanding the area under biomass crops taking into account both rain-fed and irrigated agriculture can be estimated [13, 17]. If the area available for energy crops varies between 0% and 45% of the

present agricultural land (depending on the assumed scenario; i.e., human diet, input level, and population growth [36]), under a biomass-intensive scenario similar trends can be expected for energy crops as other studies showed for food crops. But the effect is stronger: increasing water scarcity in most regions, with the largest effects in the regions that are already water scarce. Increasing evapotranspiration is the main factor and irrigation of energy crops would increase water scarcity.

Total blue water requirements and availability, including the environmental water requirements (EWR) have been expressed in a water stress indicator (Fig. 3) [32, 35, 37].

All studies give solutions or directives for improving water use efficiency at given scales, both for irrigated and rain-fed agriculture. It is generally acknowledged that considerable improvements can potentially be realized. Measures to alleviate water stress include increased recycling of industrial and domestic water, change of diets toward less-water-consuming foods and less meat, improve agricultural water productivity by reducing runoff, water harvesting, supplemental irrigation, and better maintenance of irrigation systems; the latter measures specifically increase the use efficiency of blue water.

At the field scale, high water use efficiency (WUE) of crops can only be achieved if other factors (nutrient availability, incidence of pests and diseases, appropriate and timely management) are not limiting crop production to a larger extent than water. In that case, evaporation (unproductive water loss) is minimized and transpiration (productive water use) is maximized. Hence, optimal input use and soil management increase the efficiency of green (and blue) water use. In different regions of the world large variations in actual crop water use efficiency are reported resulting from variations in these factors [32]. Hence, in estimating opportunities for energy crops, the strong interaction between water, nutrients, and management has to be taken into account. In practice, crop production systems in a region, steered by local climatic, edaphic, economic, and social conditions, show large differences in input use and efficiency as compared to otherwise comparable systems in other regions.

Climate change is very likely to change rainfall patterns while increasing temperatures will influence water transpiration and evaporation. The net effect is not easy to predict and will show large variations among different regions of the world. Especially, semi-arid and arid areas are expected to suffer from reduced water availability caused by a combination of increasing precipitation variability, increased water use by crops, and reduced groundwater recharge. Problems are further expected in river basins depending on glacier or snowmelt-fed rivers while sea-level rise may lead

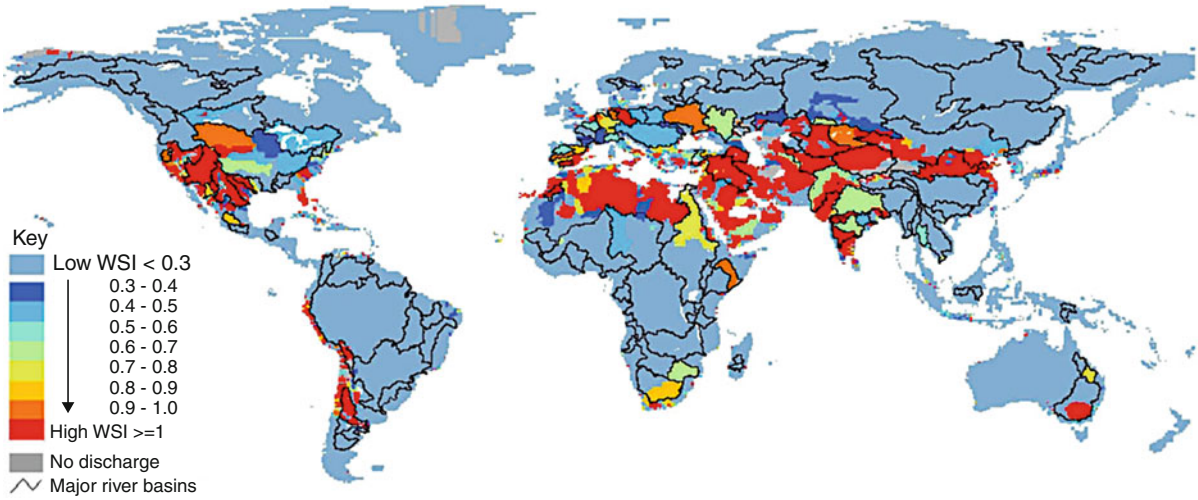

Biomass Resources, Worldwide. Figure 3
Water stress indicators [37]

to increased salinization of groundwater and estuaries. While positive effects of climate change on freshwater systems will occur, on the whole, negative effects will outweigh the benefits. There are signs that the impact on irrigation systems may be very strong, generally limiting irrigation water potential.

Conclusions Comparing the different analyses shows that problems are analyzed at a higher scale than the solutions formulated. The large variability in regional climate and hydrology asks for a detailed and local analysis of the biophysical possibilities for crop production. The studies analyzed show that conditions show large differences among different regions. In some regions abundant water availability provides ample opportunities for energy crop production, while water scarcity in other regions is seriously restricting any opportunity for energy crops.

To determine water availability for energy crop production a basin scale seems most appropriate in order to assure that the interaction between upstream and downstream water availability and use is taken care of. A suggestion is to execute the following steps:

- Estimate renewable water resources on the scale of a "river basin" area.
- Determine how much water is required for food and feed crop production related to local production systems and regional developments and estimate future projections.
- Estimate the environmental water requirements.
- Verify the available land area for additional (energy) crop production.
- Assess the regional and crop(type) specific water use efficiency of the energy crops to be cultivated.
- Assess whether water availability or land area is a limiting factor for bioenergy production for different parts of the river basin.

This procedure favors a multi-scale approach taking into account the influence of local measures on the larger regional scale and vice versa. It does not require just straightforward aggregation but a more detailed analysis of relations to arrive at an optimal water distribution. The local situation should be analyzed to assess the scope for energy production. However, to date, studies at this resolution have only been done incidentally, and global figures give a misleading picture.

A rough estimate of available blue water for energy crops, based on global water flows, is 1,300–5,000 km^3, depending on the share required for EWR (50–20%). However, where this water is available and if it can really be used cannot be determined based on available studies. Future change in rainfall patterns will regionally have a large impact, especially in regions that are already water scarce.

Food

Technologically speaking, producing enough food for even ten billion people seems feasible [38]. In contrast, doing so without compromising sustainability – both by pollution and by resource depletion – will be a formidable challenge [39]. Currently, food production appropriates about 75% of the available freshwater and 35% of the global land area [40]. While the world population doubled during the second half of the twentieth century, in consequence of increasing incomes, its appetite for meat quadrupled, requiring 40–50% of the world grain harvest to be fed to livestock [38]. Within the food domain, meat production has a disproportionate environmental impact [41] and, therefore, environmental impacts of food production are strongly coupled to actual diets.

The key metric with regard to food demand is elusive. For example, in the Netherlands the food consumption is about 20% lower than the food production [42]. This difference can only be approximated, since the quality of FAO food supply data is poor. Furthermore, food prices are hard to predict.

The ideal study estimating food demand takes at least into consideration (1) world population, (2) economic aspects (including income and food prices), (3) production systems, and (4) diet characterization, in sufficient geographic and temporal detail.

The principal food demand projections [43] address world population growth, diet changes (increased use of animal products), yield increases (including those due to use of GMOs), and economic aspects. Freshwater resources are taken into account, but biofuel production is not addressed. Projections are at a general, aggregate level and quite optimistic with regard to yield increases and the effects of climate

change. In general, these studies seem to implicitly and explicitly favor further intensification of agriculture, without paying much attention to the potential of organic production.

The real drawbacks of FAO data [43] are that it regards supply (production + imports - exports) per country, per commodity. That is not a very firm basis and, furthermore, everything after primary production, such as food processing, transport, refrigeration, etc., is lacking, and so is innovation in the latter part of the chain.

Primary production systems underlying FAO projections are described in sufficient detail. The majority of farming systems are small-scale operations, particularly in developing countries. Although an inventory of such production systems has been made available by the FAO and the World Bank [44], detailed projections of their development and future contributions to world food production are lacking altogether. The direction and rate of innovation of primary production is taken into account in the FAO projections, but evidently hard to model. Furthermore, availability of food is interrelated to other products, such as feed, fuel, and materials derived from crops and livestock, in a very complex way.

In striving for sustainable food production and consumption, the protein chain is an excellent starting point [45–47], as on average, 6 kg of plant protein is required to yield 1 kg of meat protein [48, 49]. In theory, a promising solution may be offered by partial replacement of meat proteins with plant protein products (so-called Novel Protein Foods, NPFs) in the human diet. It is estimated, conservatively, that – without putting a healthy nutrition in jeopardy – world meat supply could easily be cut by *one third*, that is, from 140% to 166% to 100%. Even then, the average protein consumption would be 20% over the RDI (recommended daily intake) and one third of protein consumption would still be derived from meat. Life cycle assessment showed that a partial transition from animal to plant protein (abolishing feed production but keeping extensive livestock, i.e., feeding on grass and agricultural waste) might result in a three- to fourfold lower requirement of agricultural land and freshwater to start with. Moreover, worldwide there is potential for a 30–40-fold reduction in water use [41]. Several economic arguments [50, 51] indicate, however, that actual practice may not be as straightforward as theory suggests, due to status and cultural trends.

The principal food demand projections are those by the FAO, which are based on supply (production + imports - exports) per country, per commodity. They are the best available, but the descriptive data is crude and so are the projections based on them. The largest knowledge gap in the available models and data is probably in consumer preferences. Studies of diet change show that in addition to availability and price, status aspects and cultural trends play an important role.

Biomass Demand for Energy

In order to put the assessment of biomass potentials and their interrelations with other land-claiming functions into perspective, an assessment is also made of future energy demand development and the foreseen role of biomass therein. (Note that almost all of these demand-side models also need to make assumptions on availability and cost of biomass, in order to compare competitiveness of biomass and other supply options. As such, it is not possible to make a clear-cut distinction between biomass supply and biomass demand assessments.)

Earlier demand projections for primary biomass for production of transportation fuel were largely based on the World Energy Outlook (WEO) of the International Energy Agency of 2006 [52], with a relatively wide range of about 14–40 EJ of primary biomass, or 8–25 EJ of fuel. However, higher estimates were also included, ranging between 45 and 85 EJ demand for primary biomass in 2030 (or roughly 30–50 EJ of fuel).

Demand for biomass for heat and power was stated to be strongly influenced by (availability and introduction of) competing technologies such as CCS, nuclear power, wind energy, solar heating, etc. The projected demand in 2030 for biomass would be around 28–43 EJ according to the data used in the 2007 IPCC report [2]. These estimates focus on electricity generation. Heat is not explicitly modeled or estimated in the World Energy Outlook, therefore underestimating total demand for biomass.

Also potential future demand for biomass in industry (especially new uses as biochemicals, and also

expansion of charcoal use for steel production) and the built environment (heating as well as increased use of biomass as building material) was highlighted as important, but no quantitative projections were included in potential demand for biomass on medium and longer term.

The results of the review of studies with respect to bioenergy deployment under different scenarios as presented in the scenario study review of the IPCC Special Report on Renewable Energy [53] are summarized in Figs. 4 and 5. For medium term (2030), estimates for primary biomass use range (rounded) between 7 and 180 EJ for the full range of results obtained. The 25–75% quantiles deliver a range of 30–117 EJ. This is combined with a total final energy delivered of 0–61 EJ. For 2050, these ranges amount for primary biomass supplies 10–305 EJ for the full range and 22–184 EJ for the 25–75% quantiles and 0–76 EJ (22–57 EJ for the 25–75% quantiles) for the final energy delivered.

A first striking finding from this review is that the overall conversion efficiency from primary energy to final energy delivered appears to be 25% on average in 2050. Final energy is not defined in those aggregate results and a breakdown of biomass use for power, heat, fuels, and materials is not available. Given that the technology portfolio on medium and longer term allows for conversion efficiencies of over 90% for CHP and over 60% for production of some biofuels, the final energy delivered seems therefore grossly underestimated in the scenario range considered.

In the reference scenario of the WEO 2009 of the IEA [1], biomass is expected to contribute 66 EJ in 2030 (compared to 48 EJ in 2007). This includes traditional biomass use. Biofuels contribute 5% of world road transport energy demand; this is an almost fourfold increase compared to current production. Biomass for power increases from 259 TWh in 2007 (about 1 EJ_e) to 839 TWh (about 3 EJ_e) in 2030, mostly from CHP, as well as co-firing.

In the 450 ppm scenario, the contribution of biomass is projected to be 81 EJ, a 22% difference compared to the reference scenario. In addition it should be noted that in this scenario a decreased contribution of traditional biomass is assumed and the relative increase of modern bioenergy is larger than the 22% compared to modern biomass use in the reference scenario. Use of

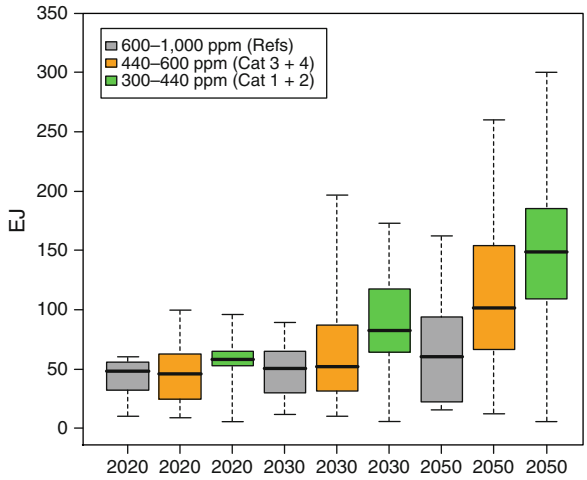

Biomass Resources, Worldwide. Figure 4
The primary biomass utilization according to the scenario review the IPCC SRREN report, divided into projections for reference scenarios, scenarios that target 440–600 ppm, and scenarios that target 330–440 ppm. The *colored bars* represent the 25–75% quantiles of the obtained results. The *dotted bars* represent the full range of estimates

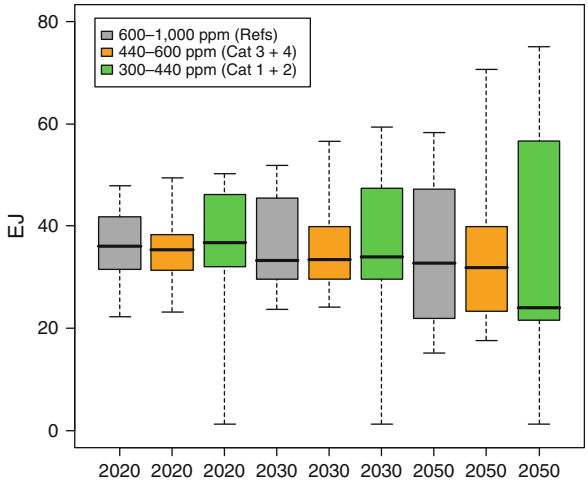

Biomass Resources, Worldwide. Figure 5
The final energy delivered via biomass utilization according to the scenario review of the IPCC SRREN report, divided into projections for reference scenarios, scenarios that target 440–600 ppm, and scenario's that target 330–440 ppm. The *colored bars* represent the 25–75% quantiles of the obtained results. The *dotted bars* represent the full range of estimates

biomass in CHP and electricity only increases by 67% compared to the reference scenario. Biofuel production is more than doubled compared to the reference scenario.

This is also confirmed by the results of the IEA Energy Technology Perspectives study of 2008 [54]. The analysis on biofuels projects a rapid penetration of second-generation biofuels after 2010 and an almost complete phase out of cereal- and corn-based ethanol production and oilseed-based biodiesel after 2030. This was a sharp contrast to the World Energy Outlook studies of 2006 and 2007 [52, 55], where second-generation biofuels were excluded from the scenario analysis and thus biofuels at large played a marginal role in the projections for 2030. This is a clear example of the importance of high quality data on performance prospects (and thus learning potential and rates) of energy technologies and in general for such strategic studies.

Agricultural Economics

Economics occupies a special position in the study, because it integrates costs and values. Ideally, it shows "what the society wants." An ideal economic study on food and bioenergy production takes into account the effects bioenergy use on prices, production, and markets of all other crops. It compares the net-return of all possible crops which a farmer can grow. The competition with other markets (food, feed) – determining the output prices of competing markets and crops – is decisive for the economic feasibility of biofuels. The ideal study is able to deal with the interaction between the agro markets worldwide. This is essential due to the fact that (a) bioenergy can be produced using by-products and (b) the production of bioenergy often leads to by-products. Moreover, the ideal study is able to deal with the competing claims of food, feed, and fuel on production factors in order to estimate a real economic feasible production of biomass for fuel.

Agro-economic models that use the agro-economic principles described above have especially covered the possible price impacts of deployment of biofuels produced from food crops, simply because the current CGE models are equipped for that. To date, no full macroeconomic (scenario) analysis exists that includes large-scale use of lignocellulosic resources, second-generation biofuels, power, heat, and (advanced) biomaterials. Therefore, no overall overview of consequences and no overview of economic feasible production can be given yet. Furthermore, the economic studies which have been done yet focus on first-generation biofuels. The second-generation biofuels and the use of by-products is the second step in the economic models and not implemented yet.

From the other studies found in the literature (i.e., based on the POLYSYS model from the University of Tennessee, the AGLINK model of the OECD, the Ethanol model from Iowa State University) it is clear that the discussions about the fuel sources need to take into consideration impacts on the world agricultural markets.

The driving forces behind agro-production are: demography, global change, political administrative regime, macroeconomics, agro-technology, and changes in value in society, consumer concerns, and behavior. In studies conducted by the FAPRI, OECD, and EU the link with the most relevant data sources (FAO, OECD, and EUROSTAT) have been made [56, 57]. It should be noted that those driving forces are influenced by many dynamic developments worldwide. This requires scenario analyses as is used in most economic studies.

The agro-economic studies that have been carried out often deal with agricultural land and do not take into account forestry land. They also do not deal with second-generation biofuels. The studies carried out illustrate the necessity of including competition and interactions between agricultural markets. The production of biofuels affects prices of feed and food. Those effects have to be taken into account in order to present a realistic picture of available biomass for biofuel. These effects are also relevant to assess the social sustainability of bioenergy, especially the effects on regional incomes and food security.

Methods used to estimate the global land-use impacts of bioenergy utilization are under continuous development to address discovered weaknesses. Field measurements and model validation are needed to reduce uncertainties of analyses and models [58]. Existing methods for determining ILUC (often grouped with LUC) can be divided into two methods employing macroeconomic/econometric and/or

biophysical models and deterministic methods allocating global land-use change to respective fuels/feedstocks grown in a few specified land types [59]. If specified land types were altered or key types absent, different carbon stock values (above and below ground) would be obtained over time [60]. Various studies use a combination of macroeconomic/econometric models and/or biophysical models/data. Some government studies implement policies to encourage the increased use of biofuels that can be shown to achieve GHG reductions as measured through direct and indirect impacts. One case uses absolute values of carbon intensity (CARB) while others set GHG emissions reductions thresholds relative to fossil fuels.

Implementation of the use of these modeling systems generally proceeds in two phases. Global land-use change as derived from scenarios with and without policy-induced increases in bioenergy use is calculated. Then the impacts of ILUC are attributed to the appropriate fuel/feedstock as linked to via the economic system. Macroeconomic/econometric models combined with biophysical models/data are complex and resource intensive; they can be viewed as lacking transparency to non-modelers. Two studies utilizing these methodologies have conducted significant uncertainty analysis [61, 62].

The recently released EPA results (2010) resulted from a series of peer reviews and comments on initial modeling data (a similar review process is underway with CARB for ILUC determinations) [63]. Among improvements EPA updated the Brazilian land-use data, considering information provided by the Brazilian Land Use Model [64] combining remote sensing data, field data, and micro-regional modeling for inputs into a partial equilibrium model (FAPRI). With this inclusion, changes in the elasticities of multiple crops across several land types were obtained for a series of larger regions for a more detailed picture of the dynamics of land use within Brazil. The major land-use change has been pasture intensification with use of degraded pastureland for biofuels derived from soya and sugarcane; also occurring are crop substitutions in the Cerrado and other regions [64]. Earlier modeling exploring the land-use consequences of increased use of US corn for ethanol production used lower spatial resolution and did not include pastureland among land types covered, resulting in the conversion of forests to cropland for food and fuel production [65]. LUC estimates vary depending on model and scenario assumptions. Corn LUC results are converging with improvements in the models and their input data. Initial dynamic results are shown in EPA's results.

This method assumes that additional biomass production will inherently lead to an increase in land-use change, perform a calculation of total LUC impact using census/spatial data/measurements, and then allocate ILUC impacts among energy feedstocks/fuels. ILUC can be divided over a period and converted to various functional units to determine the impact of a feedstock or fuel on ILUC. Example approaches are reported in [66, 67]. The benefits of these deterministic methods are that they are simpler and more transparent to potential users. These methods are less resource intensive, but the simplified methodology might lead to the loss of important details of geographic scope and currently lack dynamic capabilities.

The assessment of available literature showed that initial models were lacking in geographic resolution leading to higher proportions of assignments of land use to deforestation than necessary as the models did not have other kinds of lands such as pastures in Brazil that could be used. First an ILUC factor of 1 (losing 1 ha of forest land for each hectare of land used for bioenergy) has been claimed [65]. Later macroeconomics coupled to biophysical model studies tuned that down to 0.3–0.15 and more detailed evaluations (e.g., [68, 69]) suggest that any ILUC effect strongly (up to fully) depends on the rate of improvement in agricultural and livestock management and the rate of deployment of bioenergy production. This balance in development is also the basis for the recent European biomass resource potential analysis, for which expected gradual productivity increments in agriculture are the basis for possible land availability [70, 71] and that take avoidance of competition with food (or nature) as a starting point. Increased model sophistication to adapt to the complex type of analysis required and improved data on the actual dynamics of land distribution in the major biofuel-producing countries is now producing results that are converging to lower overall land-use change impacts and acknowledgement that land-use management at large is key.

Integration of the Findings

In the first part of this entry, existing literature on bioenergy potentials and consequences of bioenergy use for issues such as biodiversity, food prices, and water use were assessed. This assessment not only provided information on these issues, but also showed key uncertainties. Many of these uncertainties originate from the fact that existing studies have only partly dealt with the linkages between bioenergy use and other issues. For instance, none of the studies on potential for bioenergy considered potential impacts on water use.

An important reason for the conclusion that studies mostly look only at a part of the relevant issues is that the relationships between these issues are complex and therefore cannot be captured in detail by a single study or model. In this context, Fig. 6 highlights some of the key relationships and assumptions that could determine an overall assessment of bioenergy (in blue).

In this entry, some insights are provided into the impacts of more integrated considerations by performing some sensitivity analysis using existing models. The aim of these analyses is not to provide quantitative answers, but instead to assess the possible impacts of some key uncertainties (selected on the basis that they could be analyzed within the scope of this assessment).

The analysis concentrates on the following main issues:

1. The role of bioenergy use in energy models; in particular to identify which factors can limit penetration of bioenergy (potential for bioenergy, long-term cost-supply curve, energy use in specific sectors); and the sensitivity of bioenergy potential estimates to issues such as uncertain development

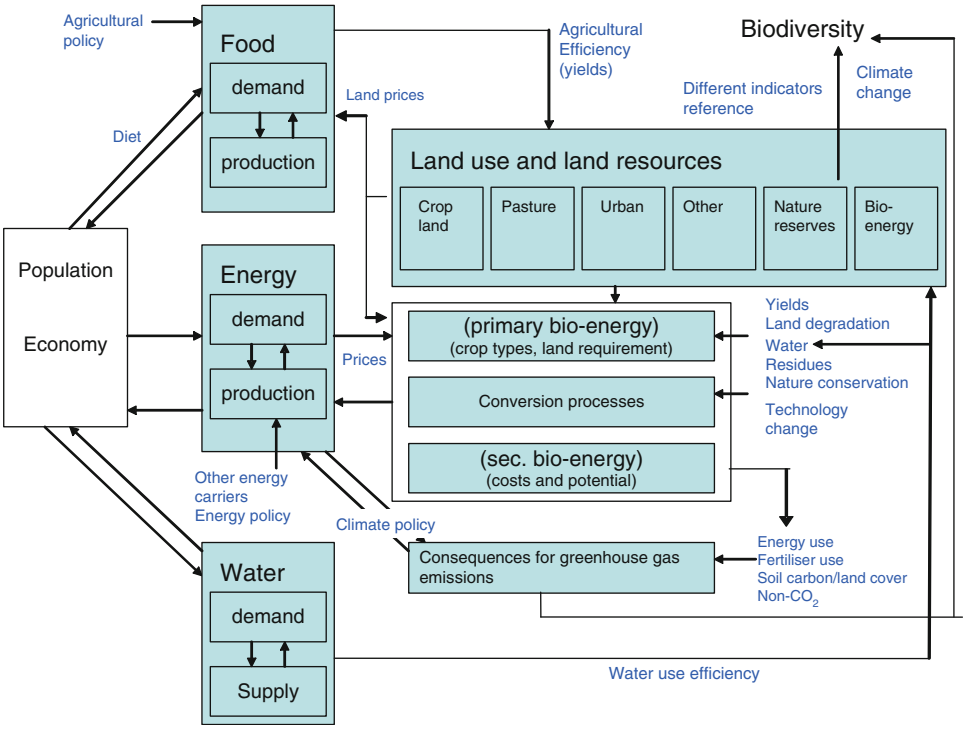

Biomass Resources, Worldwide. Figure 6
Overview of some key relationships and assumptions relevant to assess potential bioenergy supply. The figure is only meant as an indication (e.g., other relationships also exist and scientific disciplines may order to information differently) [25]

of agriculture technologies, land use, water scarcity, land degradation, and nature reserves
2. Key uncertainties in assessing biodiversity losses as a result of land conversion for bioenergy
3. The economic link between food, feed, and fuel

Impacts of Key Uncertainties

In the inventory part, it has been looked into various estimates for potentials for bioenergy – one of them by Hoogwijk [4, 13]. Compared to others the estimates of Hoogwijk are relatively elaborate – but do not consider issues such as water scarcity or greenhouse gas impacts. In that context, the methodology of Hoogwijk is implied but some sensitivity analysis to estimate the potential impacts of alternative assumptions are included.

Hoogwijk's method is indicated in Fig. 7. First, suitable areas for bioenergy are identified on the basis of land-use scenarios that do not include bioenergy. In the calculations all areas required for food production are excluded. On the remaining areas (1) a land-specific exclusion factor (between 0% and 100%), (2) the rain-fed potential energy crop productivity (depending on crop, soil, and climate), and (3) the assumed state of agricultural management (% of potential production) determine the potential. In the calculation presented here, the exclusion factor for forests and nature reserves is 100%, and 50% for natural grassland ecosystems (e.g., steppe, savannah, and grasslands). The total potential is equal to the sum of all areas.

The potential for bioenergy determined thus concentrates on two areas:

- Abandoned agriculture land (in the short term mainly in developed regions; but later on also in some developing regions)
- Natural grass ecosystems (an exclusion factor of 50% is used here, leading to an expansion of total arable area, but outside forest)

Finally, also areas with a very low potential yield (part of tundra and desert ecosystems) are excluded.

Below, the Hoogwijk method is applied and the following uncertainties are analyzed:

- Different scenarios
- Different crops and land areas
- Water scarcity
- Land degradation
- Nature reserves

Many global land-use scenarios show potential land abandonment in parts of the world (e.g., the Millennium Ecosystem Assessment, several scenarios assessed in the recent IPCC AR4 report, the IPCC SRES scenarios). Nevertheless, from an economic perspective this feature is sometimes questioned as lower land prices would slow down the incentive for agricultural yield improvement. The scenario taken here as central case does have the feature of land abandonment.

Finally, in Hoogwijk's original application nature reserves existing in 2000 were excluded from potential biomass production. Here, to explicitly analyze the influence of biodiversity restrictions this assumption has only been added in the discussion on nature reserves.

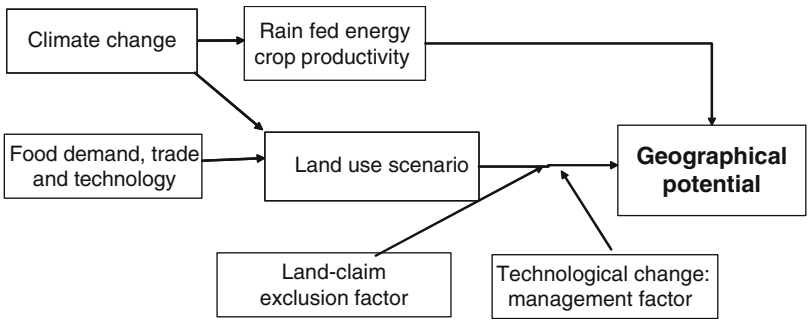

Biomass Resources, Worldwide. Figure 7
Methodology of assessing bioenergy potentials

Different Scenarios The analysis of Hoogwijk concentrated on the geographic and economic potential of woody biofuels – using the IMAGE implementation of the IPCC SRES scenarios as a basis. Given new insights into possible future changes, here instead the reference scenario of the Netherlands Sustainability Outlook and the OECD Environmental Outlook (DV-2 or OECD baseline) [57] is used. (The reference scenario of the DV-2 is based on work that has been performed jointly by the OECD and MNP, and also forms the reference scenario of the OECD Environmental Outlook [57].) This scenario should be regarded as a "medium-development" type of scenario (in terms of population and economic change, but also agricultural productivity change). GDP per capita grows globally by about 2% per year, while the global population reaches a level of 9.4 billion people in 2050. Changes in agricultural yield and consumption patterns are based on the FAO projections [72]. The resulting agricultural land worldwide (including extensive grassland) increases from 4.9 Gha in 2000 to 5.5 Gha in 2050 (excluding extensive grassland; these numbers are 3.8 and 4.4 Gha). The extension of agriculture land occurs almost exclusively in developing countries, while land use in OECD countries remains more or less stable. Compared to the IPCC scenarios, in terms of most assumptions, the scenario lies in between the A1b (high economic growth) and B2 (medium assumptions) scenarios. Scenario-related assumptions (such as for population growth, food demand, agricultural trade, and technology change [6, 13]) are very important for the potential for bioenergy.

The potential as calculated using the methodology indicated in Fig. 8 on the basis of the OECD-baseline scenario in 2050 is around 200 EJ. (In other words, the total area of abandoned agricultural area and natural grass ecosystems, taking into account the 50% exclusion factor, could produce 200 EJ of primary bioenergy). Using the land-use patterns of the IPCC SRES scenarios (but keeping other factors, such as assumed bioenergy yields and land-claim exclusion factors the same as under the OECD-baseline scenario) would lead a range from 120 to over 325 EJ (with low potentials in A2 as a result of a high population growth, low yields, and little trade; and high potentials in A1 and B1 as a result of low population growth and rapid yield change).

An important factor in these calculations is the assumed changes in yields. This is also shown in Fig. 8 by indicating the two alternative cases that look into a more compact agriculture compared to the OECD-baseline (DV-2) scenario (and thus higher yields). In the first, agricultural yields are improved for all crops and regions by 12.5% compared to the base case. The value of an additional increase of 12.5% is equal to half the suggested improvement potential compared to baseline in the International Assessment of Agriculture Science and Technology Development (IAASTD). The second scenario of more compact agriculture applies the same convergence in agriculture

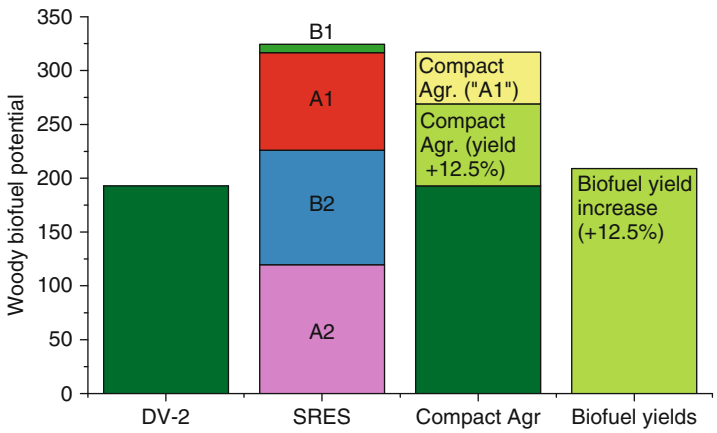

Biomass Resources, Worldwide. Figure 8
Potential for primary woody bioenergy (not including residues) and using different scenario assumptions

yields worldwide as in the A1 scenario, that is, bringing 2050 technology levels in developing countries close to current Western European levels – while keeping the baseline improvement for developed countries. Both cases lead to a considerable increase in potential compared to the OECD-baseline scenario: 40% for the first case and about 65% for the second. In other words, assumed yield changes for agriculture in general critically determine the potential for bioenergy. Assuming a more compact agriculture could possibly lead to about 300 EJ of primary woody bioenergy in 2050. It should be noted, however, that yield improvement could obviously also be slower than our base case assumptions. Furthermore, these calculations are single-factor variations: the changes in yields discussed here are likely to impact land and food prices, and could therefore lead to indirect effects.

Obviously, the yield increases for biofuel crops also are uncertain. The assumed increase in the base case is based on yield estimates by [13] and strongly varies per region (as 2000 yields are very different for different regions). Globally, these values lead to a 100% improvement for woody biofuels (assuming a low 2000 starting value). Assuming an additional improvement in yields of 12.5% (now without improving the yields of other crops above the baseline) leads to an increase of total potential compared to the OECD-baseline scenario by 12.5%. This implies that in general the yield increases for food crops have a stronger impact on bioenergy potentials than the yield increases for bioenergy crops specifically.

Different Crops and Land Areas In addition to woody bioenergy, also other crops are already applied as feedstock for bioenergy. Woody bioenergy can be applied as feedstock into electricity and heat power plants and as feedstock for biofuels. Other, more conventional agriculture crops, such as sugar, maize, oil crops, and cereals, can also be converted into ethanol or biodiesel. Finally, agricultural residues also can be used.

Here, only the (primary) potential for woody crops and sugar is estimated, shown in Fig. 9 on both abandoned agriculture land and natural grassland. The potential on abandoned agriculture land increases over time – with more abandoned land becoming available. The potential on natural grassland is mainly a function of yields as the area of natural grassland is more constant. Worldwide, the potential for woody and sugar bioenergy is considerable. Sugar has very high yields in developing regions. The type of fuel chosen does obviously depend strongly on relative prices of crops, animal feed and food. In most cases, woody biofuel seem to become the most dominant feedstock worldwide of the two options evaluated here.

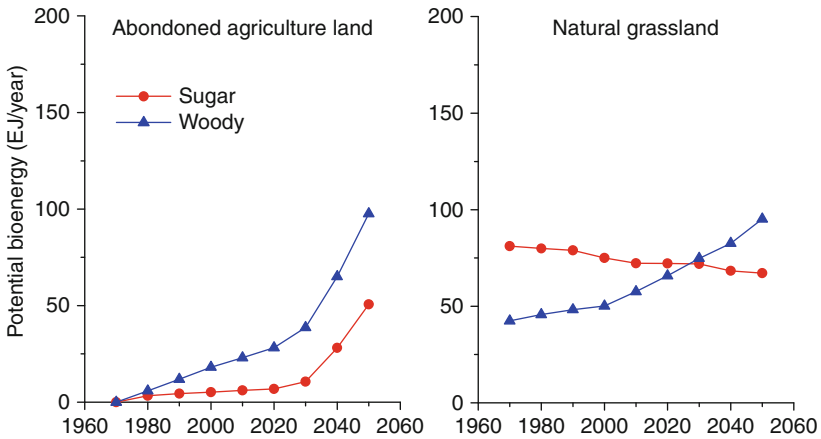

Biomass Resources, Worldwide. Figure 9
Potential for primary bioenergy on different crops and land types in the OECD-baseline (DV-2) scenario (potential cannot be added, as the same grid cell might be used for both the sugar and woody bioenergy potential). Natural grassland comprises natural ecosystems that would be converted into agricultural land [24]

Water Scarcity All calculations on bioenergy potential have been carried out assuming rain-fed production conditions. This can be regarded as an underestimation given the fact that irrigation could increase yields. However, IMAGE calculations do not take into account that other sectors than agriculture may also use (the same) water resources. In order to assess the potential impact of water scarcity on bioenergy potentials, here a map of the water stress indicator is used as calculated by the University of Kassel using the WaterGap model [34] on the basis of the same scenario as used for the bioenergy calculations (thus based on the same socioeconomic, land-use, and energy scenario). The water stress indicator is defined as the total actual water withdrawals as proportion of the maximum available runoff minus environmental water requirements. Values of this index of 0.2 and higher is defined as modest water scarcity, while values above 0.4 are defined as severe water scarcity [37]. Some authors have earlier tried to assess the impacts of water scarcity on bioenergy potential, showing that while impacts are not dramatic on a global scale, on a more local scale water scarcity may clearly limit bioenergy potential.

To assess the possible impact, here a simple overlay is made between the bioenergy map with the water stress indicator maps of the WaterGap model. This overlay suggests that about 15% of the total potential for bioenergy is in severe water-scarce areas (and might therefore be excluded), and another additional 5% in modest water scarcity areas (Figs. 10 and 11). It should be noted that to fully analyze the potential impacts of bioenergy on water scarcity, a better approach would be to calculate the water demand of potential bioenergy areas (using the water demand factors discussed in the integration analysis) and evaluate the impact of increased water demand at grid or watershed level.

Land Degradation Degraded areas form an important topic in the discussion on bioenergy for two reasons:

- First, while abandoned agriculture areas are mentioned as a source for land for bioenergy, some of these areas are likely to suffer from land degradation. In fact, dependent on the degree of the degradation the soil might lose its function for biomass production or its function as substrate for natural vegetation. Reclamation of degraded soils into suitable land for production or into natural vegetation can be difficult.
- For less severely degraded areas, some people argue that by using these areas extensively (for bioenergy production), it is possible to enhance soil recovery. In this case, these areas would be prime expansion areas with little biodiversity impact as original vegetation cannot automatically recover. Whether this is actually possible needs to be looked into further, but using degraded land for production might need considerable inputs and investments, while it also might lead to benefits in view of recovery, biodiversity, and biomass production.

The IMAGE model does not model land degradation. In order to make a rough estimate of the impact of degraded land use on biomass potentials here, data from the GLASOD database have been used. The GLASOD database has classified land worldwide in terms of soil degradation. Two main criteria were used: the severity of degradation (category 1–4) and degree of degradation (0–100%). Next, these two axes for various degradation types have been combined into one final score again going from cat.1 to cat. 4. (Light degradation of soils means that there is a somewhat reduced productivity of the terrain and moderate degradation of soils requires major improvements often beyond the means of the local farmers. Strongly degraded soils are not reclaimable at farm level for food production and are virtually lost. Extremely degraded soils are considered irreclaimable and beyond restoration. The strongly and extremely degraded soils together cover about 300 million hectares. The total area of degraded soils is about 1964 million hectares, which is about 15% of the total land surface. The four main types of soil degradation, in order of importance, are water erosion (56%), wind erosion (38%), chemical deterioration (12%), and physical deterioration (4%). The degradation is in almost all cases human induced.) Using the GLASOD maps of soil degradation, three categories of degradation are distinguished: no-to-minor degradation (GLASOD cat. 1–2), serious degradation (GLASOD cat. 3), and severe degradation (GLASOD cat. 4). The last category is too severely degraded to include in bioenergy potentials because it

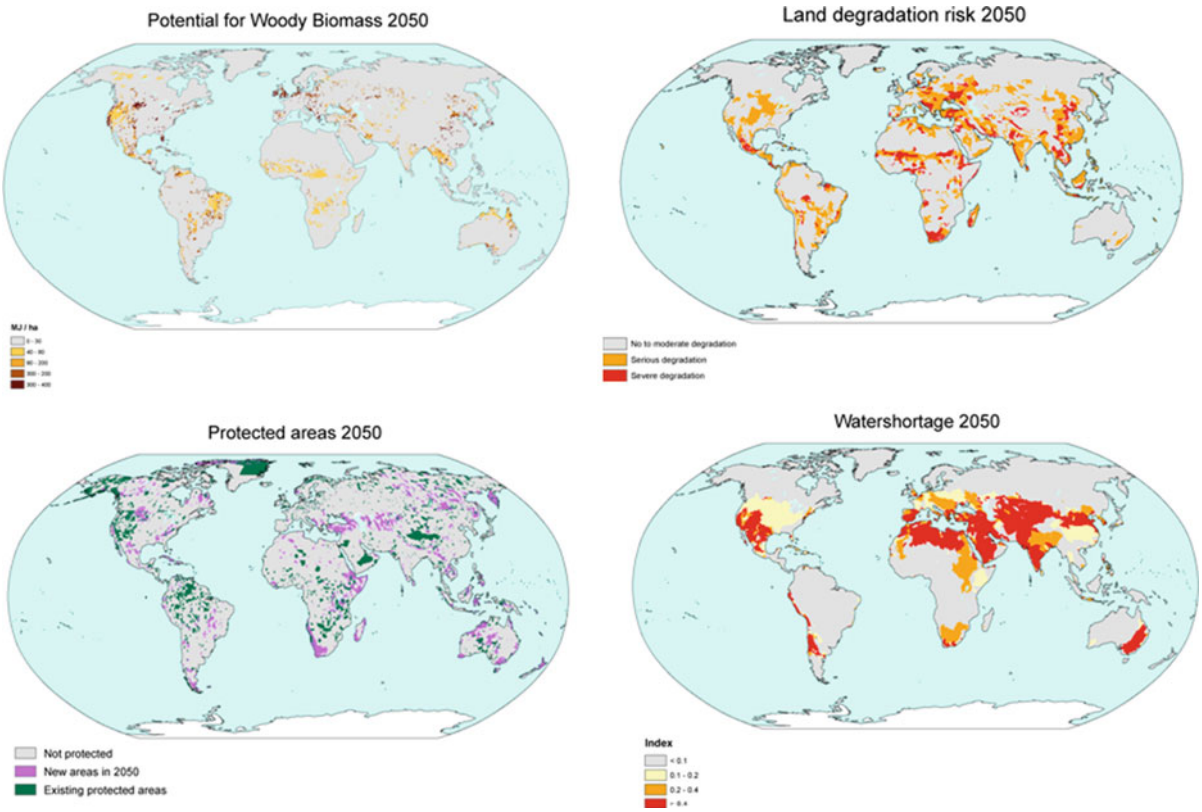

Biomass Resources, Worldwide. Figure 10
Maps of potential for woody bioenergy production in 2050, land degradation (map from the GLASOD database), protected areas (Sustainability First scenario GEOIV) and the water stress index (WaterGap results for 2050) as used in the analysis

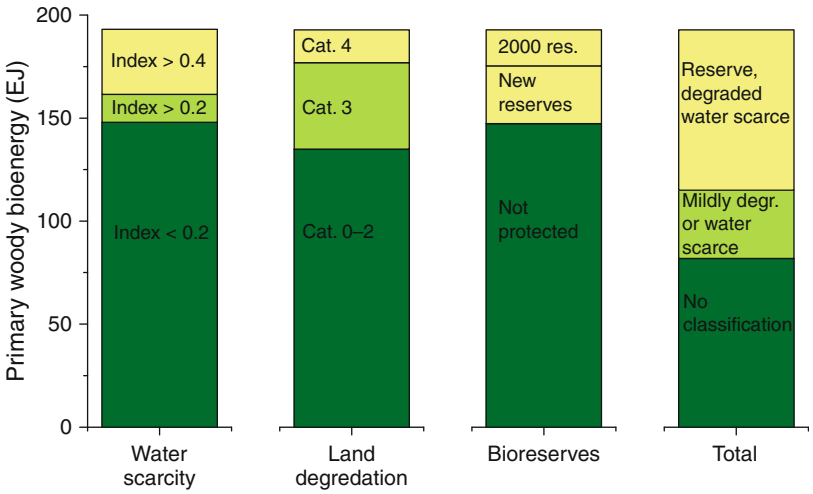

Biomass Resources, Worldwide. Figure 11
Impacts of sensitivity analysis on 2050 potential for woody biofuels [24]

will not be feasible in practice due to high costs, while the second category could potentially include useful areas to target to combine soil restoration and bioenergy production. As much more analysis is required to assess whether such combination is possible, the overlay made here should be regarded as indicative. No assumptions have been made on lower yields and/or higher costs of exploitation.

The results show that biomass potentials would be about 8% higher in the OECD-baseline scenario (DV-2) if severely degraded land areas could be used. Another 22% could be gained in modestly degraded areas.

Nature Reserves Another important relationship exists between conservation of biodiversity and bioenergy use. It should be noted that already in all calculations so far, forest areas and 50% of natural grasslands (implemented for each grid cell) have excluded for reasons of biodiversity conservation. However, still bioenergy use could lead to a reduction of biodiversity (converting natural grass land to bioenergy crop area for instance). In order to provide some insight into the impact of further biodiversity restrictions on bioenergy potential, maps have been used of (1) nature reserves in the year 2000 and (2) areas designated to become nature reserves under the Sustainability First scenario of the Global Environmental Outlook of UNEP (it should be noted that in the original work of Hoogwijk and other IMAGE applications, nature reserves existing in 2000 are mostly already excluded from estimates on bioenergy potential). Under the Sustainability First scenario, most of the biodiversity hot spots are brought under protection – while the scenario also aims to protect sufficient areas of different eco-regions. Impact on bioenergy potential is considerable. Excluding reserve areas in 2000 reduces the total bioenergy potential by around 10% – while excluding the (very ambitious) expansion of reserves by 2050 would reduce the potential by another 15%. In total, this may lead to a reduction of bioenergy potential by 25%.

All Factors Together In Fig. 11, the combined impact of protected areas, degraded land, and water availability in sensitivity analysis (last column) is shown. As indicated, a considerable part of the original potential either in severely water-scarce areas, in areas with severe land degradation, or in potential nature reserve areas. This part of the potential, that is, 40%, may be considered as not available. A second category is either found on soils with mild degradation or in areas with mild water stress. The question whether this part of the total potential (20%) can be used (or even maybe an attractive area to use, see soil degradation) remains open.

Figure 12 summarizes the findings of the analysis in a different way by showing the 2020 and 2050 total potential for biofuels and electric power using a crop mix that leads to maximal potentials for the production of biofuels or electric power. Results are given in terms of primary (before conversion) and secondary energy content after conversion: the actual energy produced in the form of biofuels or electric power. In each case, the first column indicates the most optimistic estimate for potential assessed here assuming the compact agriculture case and the 12.5% increase in yields for bioenergy crops. The second column shows the potential under the default OECD-baseline (DV-2) scenario case and finally the third column provides an indication of the potential after conversion. For each column, the white area indicates the part of the potential that might be excluded as it is either (1) severely degraded, (2) under severe water stress, or (3) potential nature reserve, while the green area indicates the remaining potential (for the individual impact of these factors see Fig. 11). The total potential for biofuels slightly exceeds that of electric power as here in some cases more productive crops are used (sugar; selection on lowest production costs).

For the OECD-baseline scenario, the remaining primary potential for bioenergy varies in 2020 somewhere around 70–100 EJ (for power and transport) and in 2050 somewhere around 100–175 EJ. Using more optimistic assumptions for development of agricultural yields, these numbers change into around 75–125 EJ in 2020 and around 200–275 EJ in 2050.

Obviously, the potential for bioenergy is pretty meaningless without an assessment of the associated production costs. On the basis of additional assumptions on capital and labor costs for production and conversion of bioenergy and transport costs, it is also possible to estimate the cost curves for both biofuels and (bio)electric power [4, 73]. The formula (a Cobb–Douglas production function) are here applied at the grid level – calculating production costs as a function of

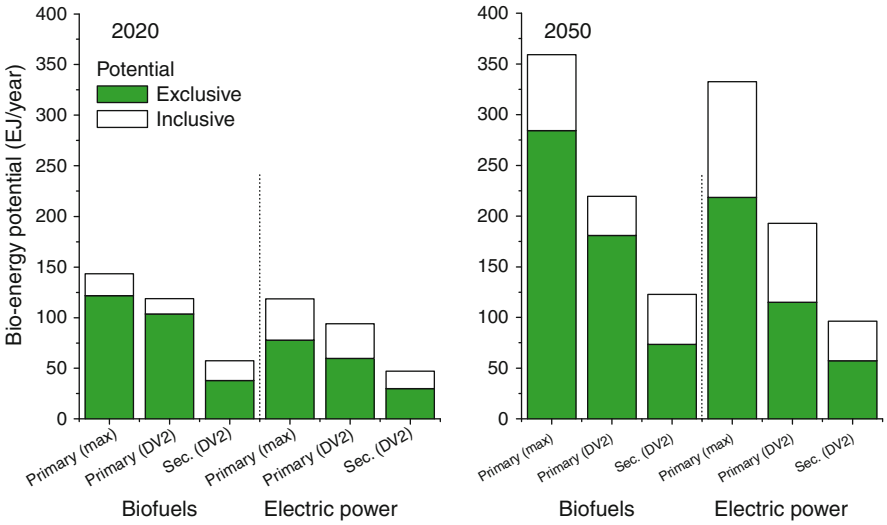

Biomass Resources, Worldwide. Figure 12

Potential for bioenergy, primary and secondary. Inclusive refers to the original estimates not accounting for restrictions discussed in the previous sections (i.e., soils with degradation or water stress). The exclusive potential does exclude severely degraded soils, areas under severe water stress, and nature reserves. The potential for secondary energy takes into account the conversion from primary energy into secondary energy carriers (fuels and electricity). Note that the potential for biofuels and electric power cannot be added as they refer to the same area [24]

GDP per capita (as proxy of labor costs), capital inputs, and yields [4]. Both yields and GDP are assumed to improve with time (consistent with the scenario discussed so far). The curves move out over time (as potential increases) and tend to move along the y-axis. The latter shows both an increase (as a result of labor costs increase) on the low side and a decline (as a result of technology progress on costs) on the high side. The curves assessed on the basis of the information presented here are shown in Fig. 13. It should be noted that adoption of bioenergy in the energy system will not be based on primary bioenergy costs (as calculated here) but on the basis of the costs of different fuel types. The cost of conversion is often more dominant in this.

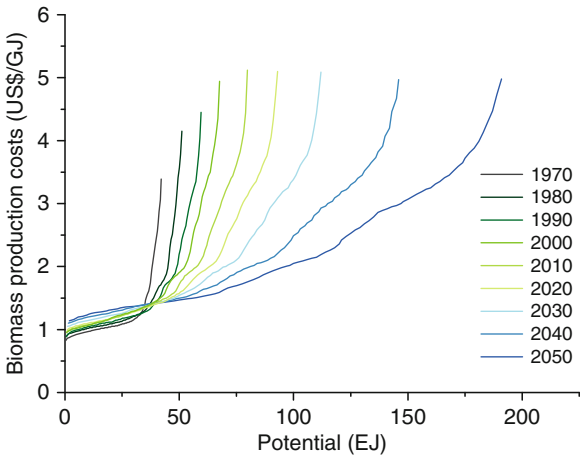

Biomass Resources, Worldwide. Figure 13

Cost curves for biofuels following from the modeling based analysis [24]

Biodiversity Consequences

From a biodiversity point of view (as expressed in CBD and IPCC goals), the effects of growing bioenergy crops are the response to several (global) environmental developments. On the short term, land-use dynamics are dominant, while on the long term the contribution to reducing climate change becomes important. Assessing both opposite effects of bioenergy is surrounded with considerable uncertainty, and is influenced by many other modeling exercises that are involved. For instance, projecting climate change will set the required mitigation efforts, while estimating

the biomass potential in mitigation will determine land use.

A complete sensitivity and uncertainty assessment should ideally consider: uncertainty in definitions (using different indicators), data uncertainty (land-use data), model parameter uncertainty (responses of climate change and other pressures), conceptual model uncertainty, and scenario assumptions. Only a few sources of uncertainty could be investigated, and are presented as first-order estimates of possible effects of scenario choices and model sensitivities.

The OECD scenario for the Environmental Outlook [57] serves as a background for this exercise. In the OECD-baseline scenario, biodiversity declines by 11% between 2000 and 2050 (expressed in MSA). For an ambitious 450 ppm option for climate change mitigation, large-scale bioenergy production is implemented with mainly woody biofuels. For this, 1.8 million square kilometers of abandoned agricultural land is used, and a further 3 million square kilometers of extensively used grasslands (considered having a seminatural character) are converted. Compared to the baseline, the total biodiversity decline in the option is 1% less (relative difference of 10%).

Local Biodiversity of Different Crops Important for the local biodiversity of production areas are the specific crop types used, and the type of land allocated for biofuel production. Three different hypothetical cases can be compared: using converted natural areas, using abandoned agricultural areas, or using agricultural areas. The resulting differences of several percentages at most are relevant compared to the complete 450 ppm option effect of ±1%.

1. Growing bioenergy crops on natural areas (converted forests and natural grasslands) will lead to large biodiversity losses. Agricultural crops lead to a loss of −3.1%, woody biofuels to −2.7%, and agroforestry systems to −1.8%.
2. Using abandoned areas will lead to lower local biodiversity losses. Here it is assumed that these areas would otherwise be used for nature restoration (leading to partially recovered nature in 2050). Using these abandoned areas will then lead to losses of −1.3% for agricultural bioenergy crops, −0.9% for woody biofuels, and no net loss for agroforestry. In the OECD climate change option, a large part of bioenergy production is allocated on extensively used seminatural grasslands. These grasslands may contain valuable biodiversity, as is the case for European High Nature Value farmlands (mostly grasslands) that are important for conserving agro-biodiversity. Temperate grasslands present a category that is underrepresented and falls short of the 10% target for global Protected Areas [74]. More knowledge on the global extent and biodiversity status of extensive grasslands and their attractiveness for biofuel production is needed to better assess this subject.
3. Agricultural areas contain a relatively low local (residual) biodiversity. Replacing these crops with woody biofuels leads to a local biodiversity increase of +0.5%, and using mixed land-use systems (agroforestry) leads to an increase of +1.4%. However, this local biodiversity effect neglects the possible shift in production area for food production. The total effects of land-use dynamics on a global level will therefore be different.

The mean MSA values for different land-use categories are sufficiently known for application in global land-use assessment, but there is considerable variation in values between individual studies. These can be the result of, for instance, different time scales (years after conversion), landscape structure, and specific management. A further analysis on these sources of variation can possibly give insights into (local) practices that are favorable for combining biodiversity and human use at local scales.

For these exercises, a constant area for bioenergy production is taken for comparative reasons. This leaves the specific contribution of crops to reducing atmospheric carbon out of consideration that will determine the required area for the different crops. Further, when agricultural and abandoned areas are used, shifts in food production regions can be expected and consequently further biodiversity losses. The exact effect of different crops and allocation can only be investigated by global and integral modeling exercises.

Uncertainty in the Climate Change Response Different model concepts and indicators may give different results for future effects of climate change on

biodiversity. For instance, the MSA indicator presents changes in local species abundance. Other often-used indicators focus on the risk of ultimate species extinction [75]. Different outcomes will not easily converge with more research, but must be seen as complementary information on the complexity of the biodiversity issue, and the mechanisms underlying biodiversity change.

The GLOBIO implementation of stable areas with suitable environmental conditions shows relatively little variation in the calculated parameters. More variation can be found in different climate models that give future environmental conditions, and in the sensitivity of the climate system to rising atmospheric CO_2-eq concentrations. With extreme values for climate sensitivity and assuming linear responses of biodiversity, a biodiversity response from −1.8% to −4.5% is estimated. This range in values is comparable to the values found for the different crop types and land allocation.

In integral models, several different global developments take place simultaneously. This makes it hard to exactly assess the effect of biofuels alone and the factors that may tip the balance between losses and gains. The bioenergy effects can be better assessed by implementing hypothetical scenarios, varying the implementation of biofuels only. Assuming linear responses between emission reductions and biodiversity effects, a first exercise shows that the total balance between land-use changes and climate change effects will probably be negative (total effect of −0.8% to −1.4%). In the 450 ppm options, the reduced climate change effects are the result of a complete package of mitigation measures, while woody biofuels are responsible for about a third of the effect.

Including Species Richness in the MSA Indicator An important characteristic of the MSA approach is the integration of different impacts in one and the same indicator, and the possibility to aggregate the biodiversity values over countries and regions. This allows comparing and balancing different pressures and time scales. As a consequence of this approach, MSA is not sensitive to all aspects of biodiversity. It is not sensitive to the species richness of different biomes, and all different ecosystem types (whether species rich or poor) are treated equally.

To explore the possibilities of including species richness in the indicator, the weighing was complemented by species weighing. This was done by using species richness numbers compiled for each distinguished eco-region (64 in total [76]). The species weighted MSA accentuates species-rich regions, such as Latin America, Africa, and parts of Asia. The global biodiversity decline for the OECD baseline is now somewhat larger (−1%). However, the same happens in the 450 ppm option, and the net result hardly differs from the usual MSA.

Conclusions With the presented and discussed sources of uncertainties and assumptions, a limited range of sensitivities was presented for the IMAGE-GLOBIO approach for assessing biofuel effects.

Ultimately, the effects are determined by the balance between land-use changes and climate change effects. Specific used crop types and land-use dynamics exert an important influence on this net outcome. Using still natural areas obviously leads to the highest losses, while using abandoned lands might reduce this loss. Using agricultural areas gives the lowest local impacts, but neglects shifts to other food production regions. The most important scenario uncertainty lies in the assumptions on agricultural land use versus abandoned and converted land use. Biodiversity responses to climate change remains a subject for further investigation, but will undoubtedly give different results, depending on the models and concepts used.

The exact conditions under which abandoned areas will be available for biofuel production remain a matter of discussion. Trade and cost mechanisms usually determine the regional allocation of abandoned and natural areas. As such, land abandonment is independent from biofuel production, stimulated by liberalization and differences in regional production costs. But bioenergy production can also be considered as a stimulating factor through land competition.

Making a balance between global land-use changes and climate responses must be done by integral modeling, as the specific crop potentials determine the required area for biofuels and the contribution to reduced atmospheric CO_2 concentrations. Including both elements (land-use changes and CO_2 reduction) in one life-cycle-analysis type of indicator may prove useful to summarize the balance. A first estimation of

this net biofuel effects, separated from other scenario developments, indicates that the biodiversity loss through land-use change is larger than the reduced climate change effects, brought about by bioenergy production alone.

It can be concluded that for biodiversity considerable scientific uncertainty exists due to ongoing debate on methodologies on how to quantify biodiversity impacts in general. Clearly, large-scale monocultures that would go at the expense of nature areas are detrimental for biodiversity (e.g., highlighted in [30]). However, as discussed, bioenergy can also lead to positive effects such as the environmental benefits that can be derived from integrating different perennial grasses and woody crops into agricultural landscapes, including enhanced biodiversity, soil carbon increase and improved soil productivity, reduced shallow landslides and local "flash floods," reduced wind and water erosion, and reduced volume of sediment and nutrients transported into river systems. Forest residue harvesting improves forest site conditions for replanting and thinning generally improves the growth and productivity of the remaining stand. Removal of biomass from over dense stands can reduce wildfire risk. Again, biomass production and its specific location, level of land-use planning and zoning, and effective environmental impact and management systems can lead to low-impact biomass production systems. This is also an area that deserves considerably more research, data collection, and proper monitoring, as exemplified by ongoing activities of governments and roundtables in case or pilot studies [77–79].

The Economic Link Between Food, Feed, and Fuel

Worldwide production of biofuels is rapidly growing. Worldwide production of ethanol tripled from 20 billion liters to 50 billion liters (Fig. 14) and world biodiesel production has grown from 200 million gallons to almost 1,000 million gallons in the period 2001–2005. In the European Union in 2004, about 0.4% of the EU cereal and 0.8% of the EU sugar beet production was used for bio-ethanol, and more than 20% of oilseed production was processed into bio-diesel. The growth rate over the previous 2 years (2002–2004) was 27% and 70% for bio-ethanol and bio-diesel, respectively [81].

The production of biofuels started after the high oil prices in the 1970s which were due to supply restrictions by the OPEC cartel (Fig. 14). High oil prices induced innovations that saved oil or replaced oil by cheaper or more reliable substitutes, such as biofuels. World bio-ethanol production grew to about four billion gallons in 1985. In the early 1980s, the oil prices collapsed to their original level and stayed there until the beginning of the new millennium. The level of biofuel production, however, did not collapse but remained almost constant and increased only

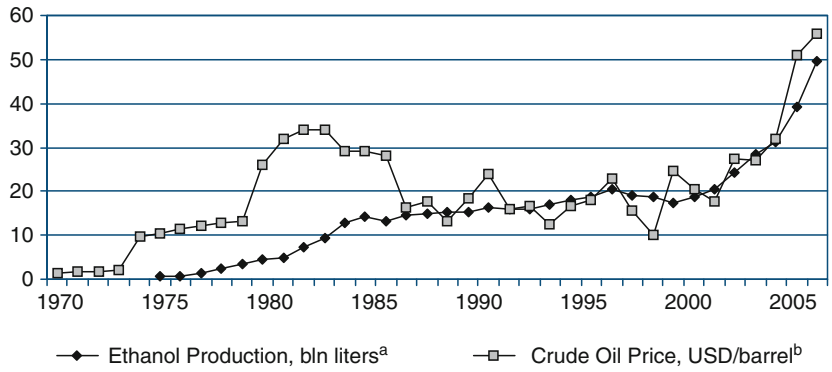

[a]F.O. Licht (2007)
[b]Nominal prices. Saudi-Arabian Light-34°API.

Biomass Resources, Worldwide. Figure 14
World fuel ethanol production and crude oil prices: 1970–2005 [80]

marginally after 1985. The recent rise in oil prices in combination with environmental concerns lead to the recent biofuel boom.

The only integrated biofuel market in practice is Brazil's cane-based ethanol market. In their ethanol/electricity cogeneration system sugar cane becomes a competitive energy provider at petrol prices of about $ 35/bbl [82]. The driver for biofuel production in the EU, the USA, and Canada is mainly political, including tax exemptions, investment subsidies, and obligatory blending of biofuels with fuels derived from mineral oil, while high energy prices further enhance biofuels production and consumption in other countries and regions. Arguments for biofuel promoting policies are reduction of greenhouse gas emissions in the light of climate change, diversification of sources of energy, improvement of energy security, and a decreased dependency on unstable oil suppliers, benefits to agriculture and rural areas, etc.

The growing integration of food and energy markets increases the ability to channel agricultural supply either to food, feed, or fuel processing. If this trend continues one can expect that the agricultural raw material price implied by future energy prices will either act as a ceiling – as long as it is profitable to use biofuel crops for energy production – or, if agricultural prices go above such threshold, demand for bio-based products for energy production will become negligible. This basic price transmission from energy to agricultural prices depends on various factors, which are (a) conversion technologies and costs, (b) carbon prices, (c) legislation, for example, mandatory blending obligations, and (d) economic incentives such as subsidies or tax exemptions.

Until now biofuels have been produced by processing agricultural crops using available technologies. These so-called first-generation biofuels can be used in low percentage blends with conventional fuels in most vehicles and can be distributed through existing infrastructure. Advanced conversion technologies are needed for the next generation of biofuels. This generation will use a wider range of biomass resources – agriculture, forestry, and waste materials – and promises to achieve higher reductions in greenhouse gas emissions and the costs of fuel production [24, 83].

Given the current policy developments and the availability of just first-generation biofuels, an increased biofuel production either due to "pure" market forces and/or "policy" might have significant impacts on agricultural markets, including world prices, production, trade flow, and land use. The fact that demand elasticities for energy are much higher compared to most food products also contributed to the strong dynamics agri-food market shows during recent years. Linkages between food and energy production include the competition for land, but also for other production inputs. The effect of an increasing supply of by-products of biofuel production such as oil cake and gluten feed also affect animal production for instance.

Liquid biofuel production creates additional demand for agricultural commodities, including foodstuffs that place additional pressure on natural resources such as land and water and thus raise food commodity prices. Biofuels from lignocellulosic biomass can reduce it but not eliminate competition. To the extent that domestic food markets are linked to international food markets, even countries that do not produce bioenergy will be affected by the higher prices.

The OECD-FAO Agricultural Outlook (2008) model [56] found that if biofuel production were to be frozen at 2007 levels, coarse grains prices would be 12% lower and vegetable oil prices 15% lower in 2017 compared to expected biofuels increases. World maize prices would be 26% higher under a scenario of continued biofuel expansion according to the then-existing national development plans [84]. They would be more than 70% higher under a drastic biofuel expansion scenario where biofuel demand is double compared to the first scenario (these scenarios are relative to a baseline of modest biofuel development where biofuel production remains constant at 2010 levels in most countries). World prices for wheat, sugar, and other crops would increase with greater biofuels production, but would be less than in the case of maize and oilseeds. IFPRI (2008) estimated that 30% of the weighted average increase of world cereal prices was attributable to biofuels between 2000 and 2007 [85]. The eventual impact of biofuels on prices will depend on the specific technology used, the strength of government mandates for biofuel use, the nature of trade policies that can

favor inefficient methods of biofuel production, and the level of oil prices.

The impact of higher prices on the welfare of the poor depends on whether the poor are net sellers of food (benefit from higher prices) or net buyers of food (harmed by higher prices). The poor are a heterogeneous group, with some being net sellers of food while others are net buyers. On balance, the evidence indicates that higher prices will adversely affect poverty and food security, even after taking account of the benefits of higher prices for farmers [86, 87]. A major study of FAO on the socioeconomic impacts of the expansion of liquid biofuels [88] indicates that poor urban consumers and poor net food buyers in rural areas are particularly at risk. The number of malnourished children would increase by 4.4–9.6 million under the two above-mentioned scenarios [84].

Higher food prices will have negative consequences for net food-importing developing countries. Especially for the low-income food-deficit countries, higher import prices can severely strain their balance of payments. Food exporting countries will benefit from higher prices, but the number of such countries is limited and they tend to be more developed (e.g., Thailand, Brazil, and Argentina).

A significant increase in the cultivation of crops for bioenergy implies a close coupling of the markets for energy and food [89]. As a result, food prices may become more closely linked to the dynamics of world energy markets. Political crises that affect energy markets would thus affect food prices. For around one billion people in the world who live in absolute poverty, this situation poses additional risks to food security.

Meeting the food demands of the world's growing population will require an increase in global food production of 70% by 2050 [90]. This FAO study also estimates that the increase in arable land between 2005/2007 and 2050 will be just 4%. Given this limited increase, there could be significant competition for the use of agricultural land because biomass production is land intensive. Increased biofuels production could also reduce water availability for food production (as more water is diverted to production of biofuel feedstock). Cash crops can represent an additional incomes source and do not necessarily compete with food crops, and may contribute to improving food security [91]. However, there are instances of negative effects of cash crops on food security [91–93].

Growing demand for biofuels and the resulting rise in agricultural commodity prices can present an opportunity for promoting agricultural growth and rural development in developing countries. The development potential critically depends on whether it is economically sustainable without government subsidies. If long-term subsidies are required, there will be fewer government funds available for investment in a wide range of public goods that are essential for economic and social development, such as agricultural research, rural roads, and education. Even short-term subsidies need to be considered very carefully, as once subsidies are implemented they can be difficult to remove. Experience from Latin America shows that governments that utilize agricultural budgets for investment in public goods instead of subsidies experience faster growth, more rapid poverty alleviation, and less environmental degradation [94].

Bioenergy may reduce dependence on fossil fuel imports and increase energy supply security, although the benefits are not likely to be large [88]. Case studies for several Caribbean countries have been completed and indicate large potential benefits. Recent analyses of the use of indigenous resources implies that much of the expenditure on energy provision is retained locally and recirculated within the local/regional economy, but there are trade-offs to consider. For example, the increased use of biomass for electricity production and the corresponding increase in demand for some types of biomass (e.g., pellets) could cause distortions leading to the temporary lack of supply of biomass during periods of high demand. Households are particularly vulnerable in this regard.

The technology and institutions used for biofuels production will also be an important determinant of rural development outcomes. For example, private investors in some instances will look to the establishment of biofuel plantations to ensure security of supply. If plantations are established on nonproductive land without harming the environment, then there should be benefits to the economy. It is essential not to overlook the uses of land that is important to the poor. Governments need to establish clear criteria for determining marginal or productive land, and criteria must aim to protect vulnerable communities and

female farmers who may have less secure land rights [88]. Research in Tanzania suggests that an outgrower approach to producing biofuels is more pro-poor, due to the greater use of unskilled labor and accrual of land rents to smallholders in this system, compared with a more capital-intensive plantation approach [95].

Increased investment in rural areas will be crucial for making biofuels a positive development force. If governments rely exclusively on short-term farm-level supply response, the negative effects of higher food prices will predominate. If higher prices motivate greater investment in agriculture (e.g., rural roads and education, research and development) from public and private sectors, there is tremendous potential for sparking medium- and long-term rural development. As one example, proposed biofuel investments in Mozambique could increase annual economic growth by 0.6%-points and reduce the incidence of poverty by about 6%-points over a 12-year period [96].

The increased use of residues for some feedstocks – such as pellets or used cooking oil – requires careful analysis. While residues are presently inexpensive, as the market expands or as other uses are found, the price could change dramatically. For example, used cooking oil in Europe went from a waste product to a valuable commodity. One must also assess the long-term supply picture. For example, beetle-killed timber in British Columbia, Canada, is a large source material for pellet manufacture for the European market, but it is not clear for how long it will be available.

Social impacts from a large expansion of bioenergy are very complex and difficult to quantify. In general, bioenergy options have a much larger positive impact on job creation in rural areas than other energy sources. Also when conventional agriculture would rationalize to "free up land" for bioenergy, the total job impact and value added generated in rural regions increases when bioenergy production increases [97]. For many developing countries, the potential bioenergy has for generating employment and economic activity in rural regions is a key driver. In addition, expenditures on fossil fuel (imports) can be (strongly) reduced. However, whether such benefits end up with rural farmers depends largely on the way production chains are organized and how land use is governed. In case (too) rapid bioenergy deployment competes with food production, increases in food prices can be significant as shown by many recent studies that focused on implications of rapid expansion of first-generation biofuels produced from food crops: impacts on food prices – and more in general on food security – may be significant, particularly for poor people. It is also acknowledged in many analyses that when such competition is avoided, and value chains are properly organized (e.g., with cooperatives with proper ownership structures and using agroforestry systems), farmers and local economies can be major beneficiaries of additional biomass production for energy (see, e.g., [95]).

The way bioenergy is developed, under what conditions, and with what options will have a profound influence on whether those impacts will largely be positive or negative (see, e.g., [78, 79] with examples of such scenarios for Argentina). Bioenergy has the opportunity to contribute to climate mitigation, energy security and diversity goals, and economic development in developed and developing countries alike but the effects of bioenergy on environmental sustainability may be positive or negative depending upon local conditions, how criteria are defined, how actual projects are designed and implemented, among many other factors.

Discussion of the Results

From a review of recent literature, several issues evolved that influence the amount of biomass that will be available for energy and materials. For some of these issues, ranges of biomass potentials had been analyzed by means of scenario analysis in the studies reviewed. Furthermore, an indicative analysis of some of these main issues and their linkage to bioenergy potentials has been carried out using several energy demand and economic models. The issues analyzed were those that are relatively easy to integrate (even though on a rough level).

- *Improvement agricultural management.* Yields for food and energy crops as well as animal production system are a key issue in determining technical biomass potentials. It has been shown (e.g., [6]) that, depending on different medium to highly efficient agricultural management systems, the potentials for bioenergy crops vary from 200 to 1,400 EJ/year. Modeling in IMAGE has shown that increasing yield levels of food and energy crops by

about 12.5% and bringing 2050 technology levels in developing countries close to current Western European levels leads to an increase of 40–60% of biomass potentials. For comparison, global average increase in cereal yields between 1961 and 1998 was about 2.2%/year (FAOSTAT). (Extrapolating this global average rate of learning until 2050 would lead to an increase by a factor 2.5, while probably learning rates in developed countries that already learned a large part historically would be lower than in developing countries for which a large learning potential still exists.) An important aspect of improving agricultural management is the rate of deployment of more efficient agricultural management practices in the developing countries, which itself depends on many factors that are often included in scenario analysis, such as socioeconomic developments, policies, resource endowment, infrastructure, power, etc.

- *Choice of crops.* As yields, agricultural inputs, and suitability of different types of climate and soil can be very different for different crops, the choice of energy crop is very important for overall biomass potentials. In this context, the developments in biofuels are crucial. Most recent studies assume the use of perennial lignocellulosic energy crops that can be used for heat and power applications, second-generation biofuels, but not for first-generation biofuels for which sugar, starch, and oilseed crops are required. Perennial lignocellulosic crops, such as herbaceous and woody crops, usually have higher total energy yields than annual starch, sugar, and oilseed crops. The amount of biofuel that can be gained from these annual crops via first-generation processes from 1 ha is typically lower than the amount of biofuel that can be gained from lignocellulosic crops via second-generation processes. However, once second-generation technologies become commercially available, lignocellulosic agricultural residues of annual starch, sugar, and oilseed crops can also be used for biofuel production. Another advantage of lignocellulosic crops is the fact that they are usually better suited to marginal lands (i.e., lands on which crop yields are very low) than annual crops. However, some of these marginal lands might not be suited to biomass production at all. It should be noted that some perennial crops that are suited to the production of first-generation biofuels such as sugar cane and palm oil have rather high yields too.
- *Bioenergy demand versus supply.* Typically, supply and demand of biomass are investigated in separate models leading to estimates of geographical – what can be produced given land availability – and economic – what will be produced and used from an economic point of view – biomass potentials. Most studies on geographical biomass supply estimate only total amounts of available biomass, while some also analyze cost-supply curves of biomass. Dynamic adaptations of biomass supply to demand are, however, not considered in recent studies. Comparing scenario analysis of available biomass supplies with bioenergy demands shows that demands are typically lower than supply, even though the gap depends on the costs of biomass as well as on the assumption on global energy demand. The global demand for biomass for the use for energy as modeled with TIMER is about 15–20% of the possible supply. However, no result of integrated modeling supply and demand is available considering price effects. It should be noted that energy demand depends on cost-supply curves of biomass as well as learning in energy conversion.
- *Use of degraded land for biomass production.* An important question for the total biomass potentials and the availability of land is if and which degraded land areas can be used for biomass production. Most recent studies include agricultural land without explicitly defining whether and what type of degraded agricultural land has been included. For example, [13] uses "low-productive lands" which produce about 1–3% of the global potential for energy crops. Here the potential of using severely degraded land has been estimated to increase potentials by about 30–45% compared to not using severely degraded lands. This estimate has been made using soil quality and climate as a basis of yield estimates. However, it is unknown whether the assumed yields are realistic as it is difficult to assess the impact of soil degradation on the productivity of the soil. This depends on many local conditions. In general, one can conclude that yield levels on degraded soils are often far below the levels of the undisturbed soil. Another issue is the

potential value of degraded lands for biodiversity. This value depends on whether and during which timeframe this land restores itself to pristine nature. Restoration of the original vegetation on degraded soils has problems similar to biomass production since most of the original conditions of the soil have been changed (lower nutrient levels, lower water holding capacity). However, it has been shown that taking biodiversity recovery into account presents a factor to consider for the net option effect in terms of biodiversity.

- *Competition for water.* The use of water for biomass production (rain-fed as well as irrigated production) competes with other industrial, domestic, and agricultural uses. In general, the impacts of water availability on biomass potentials could be large as water use for industrial and domestic purposes as well as for agricultural food production is projected to increase strongly in the coming years. The evaluation of the potentials shows that water scarcity (as estimated in the WaterGAP model and not based on a river basin scale) decreases the area available for energy crops by 15–20% and decreases the estimated biomass potential by 15–25% compared to the DV-2 scenario. The increasing variability of rainfall due to climate change is expected to decrease the area further, while an increase in water use efficiency of agriculture and the use of perennial lignocellulosic crops (that might increase water retention in some areas) could increase the biomass potential based on water availability. However, the review of studies on water has shown that the demand and availability of water cannot be analyzed on an adequate scale to evaluate biomass potentials for regions with possible water scarcity. At least an analysis on a river basins scale is needed, but these data are not systematically available.
- Learning in biomass conversion and competing technologies. The comparison of costs and efficiencies of biomass options with other options for energy supply is important for the use of fossil or biomass technologies for energy supply. This performance of energy conversion technologies can be influenced by "technological learning," and a cost-reducing effect that occurs more strongly in newer technologies, for example, hydrogen fuel cells or biomass conversion, than in more conventional (fossil and renewable) technologies. The results discussed, which assume different rates of learning, show that shares of bioenergy could vary strongly, but, for example, in energy model run with overall faster learning rates for selected conversion technologies, the role of bio-based is affected [54, 98].
- *Protected areas expansion.* In current biomass potential studies, usually nature conservation areas are excluded from biomass potentials, but besides little or no land is reserved for biodiversity conservation. The issue of which land can be used for biomass production without substantially decreasing biodiversity and nature conservation values and which land has to be excluded has not been resolved completely. The analysis indicates that excluding existing nature reserves – even though part of these could legally be used for biomass production – and future nature reserves does decrease estimated biomass potentials by about 25%.

The following issues are not covered within the quantitative analyses.

- *Food demands and human diets.* Assumptions on the future demand for food are crucial for estimating biomass potentials as in most studies it has been assumed that only land that is not needed for the production of food is available for biomass production [76]. Most estimates of biomass potentials that consider food demand and human diets are based on food demand projections of the FAO, representing a large range of possible future demands, depending on population developments and economic growth. Using these FAO projections estimate the difference between a scenario assuming low food demands and a scenario assuming high food demands to be about 130 EJ/year, while keeping other factors constant. Other studies [13] estimate this difference to be about 50 EJ/year.
- *Market mechanism food-feed-fuel.* If the use of biomass as fuel or as feedstock increases, prices of agricultural land and food will increase in the short term in addition to autonomous price increased due to population and income growth. This effect influences in turn supply costs of biomass and subsequently economic potentials, but also has impacts on food security issues that are

core of current biomass discussions. Some price effects have been calculated for first-generation biomass crops. For example in [99], world prices for first-generation biofuel crops increase between 6.5% for cereals and 10% for sugar under a mandatory blending according to the EU Biofuels Directive. However, the increase in biofuel use leads to a decline in crude oil prices by around 2%. Due to the fact that agricultural land is more or less a fixed factor, agriculture land prices react stronger on higher demand for biofuel crops as input for biofuel production. First results show that land prices in the EU increase strongly as a consequence of the biofuel directive. Land prices rise between 5% in the Netherlands and 15% in the UK. But further analysis needs to be done to achieve a more profound analysis of the key variables for the driving forces behind agro-production related to market developments such as price changes, technical progress, and policies.

- *Costs of biomass supply.* The costs of biomass supplies are important for the amount of biomass that can be used economically, that is, for the bioenergy demand. However, in energy demand models either static costs are used or cost-supply curves based on the availability of land after reserving land for other functions. In [4, 13] this was analyzed using the latter method, the amount of energy crops available at prices below 2 €/GJ which is about the price of coal. This amount is about 30–40% lower than the overall technical potentials. Given the nature of biomass supply curves used, no price effects of competition between resources (biomass for materials, food, agricultural land, water, nature conservation) are taken into account in the cost-supply curves that determine energy demands, even though they are relevant for modeling.
- *Use of by-products from agriculture and forestry.* By-products from food and wood production, for example, lignocellulosic residues, and from their processing, for example, rapeseed press cake, can be used for the production of bioenergy and for the production of animal feed. As second-generation conversion technologies are able to cope with lignocellulosic by-products from agriculture and forestry, a wider range of sources for bioenergy becomes available increasing biomass potentials significantly. Additional to this potential of energy crops, thus, a considerable amount of about 76–96 EJ of residues from forestry, agriculture, and food and wood processing as well as secondary wastes are available at low costs [6]. Moreover, in the discussion of competition between food, feed, and fuel, the use of by-products as an animal feed has to be taken into account in order to assess the final effects on the feed market. This use of by-products potentially decreases the amount of biomass available.
- *Water use efficiency of crops.* The water use efficiency of crops depends on the type of crops as well as on agricultural management. For example, water use efficiencies in gram biomass per kilogram of water are about 1.7–2.2 for wheat, 2.5–3.8 for sugar beet, 4.0–6.4 for sugar cane, and 1–9.5 for lignocellulose crops [36]. Increasing water use efficiency of food crops as well as energy crops could reduce the competition for water resources between agricultural production and other uses, especially for irrigation-type systems. This increased water efficiency might in turn lead to higher biomass potential. To determine this effect, quantitative research on the amount of biomass available in rain-fed and irrigated agriculture depending on water availability and realized water on a regional and global level would be needed. However, only studies on a field level addressing these issues are so far available.
- *Climate change.* Climate change can influence the suitability of a certain area for biomass production as well as their "biodiversity value," but limited research on the relationship between biodiversity, biomass production, and future climate change has been carried out. The GBO2 study shows a negative effect of climate change on biomass production and biodiversity [30]. These negative relations depend on the use of agricultural land that is not needed for food production and its restoration value as well as on the use of "more natural" areas. However, a decrease in the possibilities of annual crop production might lead to larger possibilities for perennial energy crops. Research into these complex correlations and feedback mechanisms has not been sufficient to quantify the impact of climate change on biodiversity and biomass potentials.
- *Alternative protein chains.* The production of proteins from animal farming uses large amounts of

land and other resources. Life-cycle assessment showed that a transition from animal to plant protein might result in a 3–4-fold lower requirement of agricultural land and about a 30–40-fold lower water use [41]. The land and water resources that could be made available by such a transition could then be (partly) used for biomass production and for relieving the pressure on biodiversity. The influence of changing protein sources for human consumption on biomass potentials could not be quantified within this study and has not been studied in the reviewed biomass potentials studies, but might be potentially large. An area of 25 Mha of soy would yield an amount of protein equivalent to livestock presently fed by 400 Mha of feed crops (300 Mha grains plus 100 Mha oilseeds), thus setting 375 Mha free [41]. (Even in this rough estimate, meat from grazing animals [beef, lamb, and goat] and from animals fed agricultural waste [pork] would still be available.) Changing protein sources requires technological change as well as a change of consumption patterns. Present trends, however, suggest meat demand to be increasing, rather than decreasing.

- *Demand for biomaterials.* Wood and fiber products (pulp, timber, boards, etc.) are the largest group of biomaterials currently produced. In studies considering all types of biomass resource, the demand for wood products is included, that is, the wood products demand is subtracted from the future biomass potentials. Smeets et al. [6] estimated the difference between high and low future demands for wood products in 2050 to be about 30 EJ/year. Chemicals and other biomaterials might become another important area for biomaterial use and are usually not included in biomass potentials estimates. However, demands for biomaterials are comparatively low (e.g., results from a scenario analysis on bio-based chemicals indicate that even in a scenario with high market potentials of bio-based chemicals not more than 10% of agricultural land in the EU-25 in 2050 will be used for bulk chemical production – assuming lignocellulosic feedstock [104]) and do not exclude the use of biomass for energy as cascading strategies, that is, first using biomass for food, feed, materials and then converting organic wastes to energy can be applied. In energy demand models, the use of biomass as feedstock material is typically not included and the only global model that does take it into account predicts a limited, but not insignificant amount of biomass to be allocated to materials. As a consequence, coupling and integration of sector modeling (e.g., wood products, chemicals, forestry) to biomass potential estimates and is necessary.
- *GHG balances of biomass chains.* The biomass potential studies regarded do include biomass options regardless of their greenhouse gas balance. GHG emission reduction is an important driver of biomass use and might increase actual biomass demands, while on the other hand excluding biomass chains with low or negative reductions could lower biomass potentials. However, the possible influence of this latter aspect is small, as most potential studies are already based on lignocellulosic biomass and, thus, disregard unfavorable biomass chains such as first-generation fuels from annual crops and land-use changes from wetland and forests to energy crop production [101, 102].

In Table 3, the key uncertainties discussed are summarized and evaluated in view of their importance (column 2). Also the impact on biomass potentials as estimated in the literature reviewed is presented (column 3). For example, for the improvement of agricultural management it is indicated that biomass potentials increase or decrease compared to the estimates in recent studies. This means that the reviewed biomass potential studies used different values for agricultural efficiency that are within the ranges that were derived from our review. As a consequence, biomass potentials estimated in the recent studies could increase or decrease if other assumption on agricultural management improvements would be assumed. However, for protected areas it is indicated that biomass potentials decrease compared to the ranges estimated in recent studies, meaning that if the recent studies would have included protected areas, the estimated potentials would be lower.

In addition to these results of the inventory, the results of the integrating analysis are also presented (column 4) and percentages of supply refer to the DV-2 scenario in IMAGE that estimates biomass potentials of about 200 EJ/year. However, it should be

Biomass Resources, Worldwide. Table 3 Overview of uncertainties and their impact on biomass resource potentials [24]

Issue/effect		Impact on biomass potentials compared to	
Supply potential of biomass	Importance	*Supply as estimated in recent studies*	*OECD-baseline scenario in IMAGE*
Improvement agricultural management[a]	***	↑↓	↑ 40–65%
Choice of crops	***	↓	↓ 5–60%
Food demands and human diet	***	↑↓	n/a
Use of degraded land[b]	***	↑↓	↑ ca. 30–45%
Competition for water[c]	***	↓	↓ 15–25%
Use of agricultural/forestry by-products	**	↑↓	n/a
Protected area expansion[d]	**	↓	↓10–25%
Water use efficiency	**	↑	n/a
Climate change	**	↑↓	n/a
Alternative protein chains	**	↑	n/a
Demand for biomaterials	*	↑↓	n/a
GHG balances of biomass chains	*	↑↓	n/a
Demand potential of biomass		*Demand as estimated in recent studies*	*Biomass supply as estimated in TIMER*
Bioenergy demand versus supply[e]	**	↑↓	↓ 80–85%
Cost of biomass supply	**	↑↓	n/a
Learning in energy conversion	**	↑↓	n/a
Market mechanism food-feed-fuel	**	↑↓	n/a

Importance of the issues on the range of estimated biomass potentials: *** – large, ** – medium, * – small

Impact on biomass potentials: potentials as estimated in recent studies would: ↑ – increase, ↓ – decrease, ↑↓ increase or decrease – if this aspect would be taken into account

n/a: no quantitative analysis has been carried out in this study

[a]Increasing yield levels of food and energy crops by about 12.5% compared to the baseline (half the suggested improvement potential in the International Assessment of Agriculture Science and Technology Development) leads to an increase of about 40% of biomass potentials. Moreover, bringing 2050 technology levels in developing countries close to current Western European levels leads to an increase of up to 60% of potentials in 2050

[b]The potential of using severely degraded land (cat. 3 and cat. 4 of the GLASOD classification [103]) has been estimated to increase potentials by about 30% (cat. 3) and 45% (cat. 3 and 4)

[c]Other main uses that compete with biomass production for water are agricultural, industrial, and domestic uses. Excluding areas with a water scarcity of >0.4 and of >0.2, respectively, leads to a decrease of estimated biomass potentials of about 15–25% in the analysis in section "Integration of the Findings." However, due to climate change, in future the number of regions with water scarcity will increase and competition for water will become more important

[d]Reserving nature reserves in areas designated to become nature reserves under the Sustainability First scenario of the Global Environmental Outlook of the UNEP leads to a reduction of up to 25% of biomass potentials

[e]The economic biomass potentials based on energy demand modeling is much smaller than the possible technical biomass supply. Starting from a biomass cost-supply curve with a maximum supply of 700 EJ/year in 2050, the energy demand at carbon taxes of 0–300 €/tC is only about 15–20% of the possible supply, that is, the economic potential is 80–85% lower than possible supply

noted that the results of the integration analysis provide an order of magnitude but are not based on an integrated modeling analysis.

In recent discussions about the large-scale development of biomass use for energy and materials, many issues around biomass potentials and linked areas such as water, biodiversity, food, energy demands, and economic developments play an important role. Below, a summary of knowledge and knowledge gaps concerning biomass potentials are given. Note that social impacts of biomass use and impacts on energy security – though of large political relevance – have not been an explicit part of this study. Also policies and their effects on biomass potentials have only been analyzed on a very limited level, that is, investigating the effects of carbon taxes on energy demand.

1. Are biomass potentials sufficient to supply a large part of future energy demands? (In the assessment of the German Advisory Council on Global Change that assumes a very limited availability of land due to nature protection and high food consumptions with at the same time very low crop yields, only about 70 EJ from residues and about 40 EJ from energy crops are estimated to be available [100].)

   In principle, biomass potentials are likely to be sufficient to allow biomass to play a significant role in the global energy supply system. Under the assumption that food demands of future population are met, most recent studies estimate global biomass potentials of 300–800 EJ/year in 2050 for various scenario conditions. The analysis reported in this entry showed that under negative circumstances concerning land availability (i.e., excluding large areas for nature protection, mild to strong water-scarce areas, and mildly and severely degraded land from biomass production) only about 80 EJ/year from energy crops might be available, while an additional amount of about 80 EJ/year from residues and an additional amount about 60–100 EJ/year of surplus forest growth is likely to be available. At the same time, scenario analyses predict a global primary energy use of about 600–1,040 EJ/year [5].

   Energy demand models that calculate the amount of biomass used if energy demands are supplied cost-efficiently at different carbon tax regimes estimate that in 2050 about 50–250 EJ/year of biomass are used, a range that is significantly lower than the estimated supply potential. For determining future economic potentials of bioenergy more exactly, however, an advanced integration of demand models with cost-supply curves of biomass and extended knowledge about technological learning in energy conversion technologies would be necessary.
2. What drives the economic competitive use of bioenergy and materials?

   Most important in the economic part in the discussion around bioenergy is the fact that feedstock crops such as cereals, oilseeds, or sugar cane are in direct competition with food on the consumption side. For biomass such as willow or switchgrass, this competition is less stringent, but also in this case biomass production is in direct competition for scarce resources, especially land. Changes in relative prices between different crops and between different energy sources, that is, energy crop prices versus fossil energy prices, are the key drivers in future use of biomass. The economic analysis of biofuel use clearly shows that apart from direct policy measures, for example, mandatory blending commitments, this price ratio is the most significant driver in the use of biofuels. Any analysis of biofuel potentials which also takes economics into account must consider this key element. However, the dynamics are also important, because shifts in relative prices also trigger investments and technical progress in the biofuel sector which lowers in the long-term production costs and increases the long-term profitability of biofuel production.
3. What are the main sources of biomass?

   Biomass for energy and material in 2050 is derived from three major sources: (1) residues and waste (about 5–20%), (2) surplus forest growth (about 5–15%), and (3) energy crops (about 60–80%). In the biomass potential studies, it is assumed that biomass is grown on surplus agricultural land that is not needed for food

production and partly on other types of land. This surplus land depends on the demands for food and material and the subsequent price effects.

4. What role might degraded lands play in biomass production?

   Another question in determining future biomass potentials is whether degraded lands – of which productive capacity has declined temporarily or permanently – can be used for biomass production. At this moment the potential of the large area of degraded soils – classified as light and moderately degraded and covering about 10% of the total land area – to contribute to the production of biomass is not yet clearly assessed. This is because of the unknown impact of two possible drawbacks: firstly the large efforts and long time period required for the reclamation of degraded land and secondly the low productivity levels of these soils. In the integration analysis it has been shown that using severely degraded land would increase biomass potentials from energy crops by about 30–45%, assumed that in principle it would be possible. However, using severely degraded land for annual crop production might require large investments and many attempts for reclaiming degraded land for food production have failed. Other attempts with, for example, reforestation and agroforestry might be more promising for biomass production and some projects in the past on, for example, saline soils have been successful. Further research on the potential of degraded soils for biomass production is needed. Preferably, other mitigation options (carbon storage in soils and vegetation) and adaptation options should be integrated in the research on the potential of degraded soils for biomass production.

5. What determines biomass yields?

   It should be noted that the conclusion that future biomass potentials are large enough to play a relevant role in supplying a significant part of future energy demands depends on land availability (see above) and on biomass yields. Ranges of assumptions on land availability in the reviewed literature influence total technical biomass potentials more strongly than the estimated ranges of biomass yields. Biomass yields depend mainly on the development of agricultural management and the choice of crops. First, most recent biomass potentials studies assume that the efficiency of agricultural production improves in the coming decades assuming low to high technology development rates. (For illustration, extreme scenarios that assumed extensive agriculture or high advanced technologies with landless animal production resulted in estimated future global biomass potentials of about 0 EJ/year and 1,500 EJ/year, respectively.) Practice, however, shows that deployment of agricultural technologies in developing countries can be a difficult task and implementation strategies need to be studied very well. Second, all estimates of future biomass potentials discussed are based on the use of perennial lignocellulosic biomass in 2050. This necessitates the availability of second-generation conversion technologies for the production of biofuels and most chemicals. Perennial lignocellulosic crops have in general higher yields than annual sugar, starch, and oilseed crops, while perennial sugar and oil crops (e.g., sugar cane, palm oil) have high yields too. Calculations in the integration part of this study indicate that potentials for annual biomass crops, that is, maize, might be very low and not sufficient to provide a large part of energy demands.

6. Is water a limiting factor for biomass potentials?

   In general, water availability can be a limiting factor for the production of biomass and food. A simple and rough analysis in this study has shown that excluding water-scarce areas decreases the biomass potentials by about 15–25% for woody bioenergy crops in 2050, in a scenario with biomass potentials about 200 EJ/year (and thus excluding residues and learning in agricultural management). Water availability, however, has not been analyzed on a sufficiently detailed spatial level to estimate regional biomass potentials in water-scarce areas. Another remaining point of uncertainty is the possibility to increase water use efficiency in agriculture and as such increasing biomass potentials. A regional to local analysis is necessary to further evaluate this

possibility. Finally, climate change will increase variability of rainfall patterns. It is expected that in the subtropics and some already water-scarce areas rainfall will decrease, while at high latitudes it will increase. For the tropics, estimates of future rainfall vary.

7. What is the relation between biodiversity conservation and using bioenergy?

   Studies that estimate biomass potentials assume that nature conservation areas are excluded from biomass production, as such estimated biomass potentials consider biodiversity conservation on a base level. Assuming that larger parts of land should not be used for biomass production for reasons of biodiversity conservation, potentials would decrease accordingly.

   In most cases perennial lignocellulosic crops have lower impacts on biodiversity than annual sugar, starch, and oilseed crops and are, thus, better suited for combining biodiversity and biomass production. Important open questions in this area are:

   - To what degree is the potential energy production on a certain piece of land related to the (potential) biodiversity value of the same piece of land if reserved for nature?
   - How to measure biodiversity, realizing that different available indicators tell different stories?
   - What are the effects of future climate changes on biodiversity (very uncertain) and areas for biomass production (more certain)?

8. What is the effect of biomass use on food prices?

   Economic analyses indicate clearly that food prices increase with an increased demand for biomass, but the magnitude of this increase is uncertain. In the long term, price increases might accelerate agricultural efficiency leading to larger potentials of food and biomass production and mitigating price increases. For example, OECD and FAO project a price increase of coarse grains prices of about 30% in the short term and about 10–20% in the medium term (2010–2016) compared to the 1996 level. At the same time, prices of sugar are projected to increase by about 30–40% and then even to decrease compared to the 1996 level [56]. Only part of these projected price developments is due to the increase of biofuel production, while other parts are due to low recent harvests and increasing other demands. This analysis indicates clearly that land, food, and energy demand are linked via prices. Thus, a priori not a certain area will be reserved for food production, but economic mechanisms determine the distribution of land uses. For annual crops that are used for the production of first-generation biofuels, the linkage between food prices and biofuel demands is probably larger than perennial lignocellulosic crops used for second-generation biofuel production. This is due to direct competition. However, currently agricultural models do not include and analyze second-generation biofuels and knowledge on the impacts of second-generation biofuels on food prices is lacking. Finally, while large amounts of biomass can be used without jeopardizing future global food demands, it should be noted that food availability and affordability are very regional and that these future regional distributions of food and energy supplies are not sufficiently known yet. Here, further knowledge including the influence of policies and subsidies on food security especially in developing countries is needed.

9. How should the available biomass be used?

   Energy demand models show that the optimal use in terms of cost-efficient energy supply depends on future technological development of bioenergy technologies as well as alternative technologies. Other major drivers found for directing biomass use are greenhouse gas emission reductions, carbon taxes, and oil prices. Thus, cost-efficient optimal biomass use strongly depends on future developments. From a greenhouse gas perspective, second-generation biofuels are in most cases more efficient than first-generation biofuels, while the comparison between second-generation biofuels and electricity depends on energy conversion technologies as well as fossil references for electricity production. Using biomass for materials, for example, for construction and chemicals, and the cascading of these materials can be attractive from a greenhouse gas reduction perspective. Compared to energy, however, markets for biomaterials are rather small.

10. What types of analyses are still needed?

    This review gives an overview of the most important linkages between the areas of water, food, biodiversity, economic effects, energy demands, and biomass potentials. While knowledge and knowledge gaps in these areas have been discussed above an integrated analysis of these areas is still missing. Important issues in such an integrated analysis are as follows:
    - Drivers and barriers in the food-feed-fuel nexus that could be used to refine modeling and scenario analysis of geographical and economic biomass potentials
    - Linkages between the availability and prices of water, the availability and prices of land, the demand for food and feedstock, the demand for energy, and between the cost-supply curves of biomass
    - Regional analysis that analyzes the relation between food security, biomass potentials, water availability, and land-use changes on a spatially explicit level
    - Mechanisms of changes and the implications of policy instruments in different parts of the world

Conclusions and Future Directions

Current understanding of the potential contribution of biomass to the future world's energy supply indicates that the total supplies could amount from a minimal 100 up to 1,500 EJ theoretical potential (compared to some 450 EJ current global primary energy demand). This assessment gave a much more sophisticated view on the factors and biomass resource categories that explain the ranges, which are particularly caused by the way food demand and agricultural management develops and by uncertainties to what extent more marginal and degraded lands may be deployed for biomass production. The potential consists of three main categories of biomass:

1. Residues from forestry and agriculture and organic waste, which in total represent between 40 and 170 EJ, with a mean estimate of around 100 EJ. This part of the potential biomass supplies is relatively certain, although competing applications may push the net availability for energy applications to the lower end of the range. The latter needs to be better understood, for example, by means of improved models including economics of such applications.
2. Biomass produced via cropping systems on possible surplus good quality agricultural and pasture lands. This part of the potential biomass supplies is the most significant and can amount up to over 300 EJ for the high-level improvement for agricultural efficiency included in the SRES scenario range. It is also a more uncertain category. The key factor determining net availability of land is improvement in efficiency in agriculture and livestock production systems. From a technical perspective, potential efficiency increases are very large seen on a global basis, especially in developing countries as is highlighted in [6]. However, the speed at which such improvements may be realized is uncertain and depends on a wide variety of factors which are partly poorly understood and manageable. In particular the economic drivers for such developments require further attention. The lower estimate given in this study based on the OECD scenario results in biomass supplies from energy crops up to 120 EJ (which includes corrections for water scarcity, land degradation, and new land claims for nature reserves; see also the third category below). A "compact agriculture scenario" (roughly similar to the A1 and B1 SRES scenarios) would add some 140 EJ to that estimated 120 EJ, resulting in a range of 120–260 EJ.
3. The use of marginal and degraded lands that are not used for food production. This aspect is addressed in some more detail in this assessment. Although it should be recognized that data quality on such soils is fairly weak, that land-use scenarios in this respect are crude, and that knowledge to what extent different types of vegetation can be established has seen limited study, some global estimates have been compiled. The potential contribution could add about 70 EJ to the production of energy crops EJ, but this would include a large area where water scarcity provides limitations and soil degradation is more severe. The lower estimate, covering more limited degradation and water scarcity, represents the 120 EJ discussed above. This lower estimate also incorporates estimated additional demand for new nature reserves.

The key uncertainties for this category are the extent to which such lands can really be utilized for biomass production from a technical and economic perspective and to what extent nature and biodiversity conservation may conflict with the partial use for biomass harvesting, since marginal and abandoned lands do represent varying levels of biodiversity. Management, harvest, and trade-offs with biodiversity need to be assessed on a regional scale. Another important element is to what extent increased food demand may make it more attractive to use marginal lands for food production in the future and thus compete with bioenergy. Such dynamics can still not be investigated by current modeling tools.

The level of knowledge on this category is relatively poor and the lands in question in fact cover a wide variety of different settings, from semiarid lands to degraded lands in various degrees to soils affected by salinity, etc. On the one hand, use of such lands for biomass may be very attractive because conflicts with food production are far less up to absent compared to arable lands. Furthermore, important co-benefits may be achieved such as regeneration of soils, improved water retention, and (some) regained economic activity, which may prove even more important drivers than biomass production for energy alone. On the other hand, obtaining sustained biomass production, be it with low productivity, may bring higher costs.

Overall (Fig. 15), this assessment tuned the broad range of estimates of global biomass resource potentials down to a range of minimally 200 EJ up to more than 500 EJ.

Another result of this assessment (but also confirmed by the IPCC fourth assessment report and the new IPCC report on Renewable Energy Sources [2, 53]) is that current energy scenarios which include GHG mitigation strategies following IPCC guidelines indicate that the demand for bioenergy until 2050 could in fact be limited compared to the potential biomass supplies, because various other options are more competitive in terms of specific mitigation costs. This may in particular be true for the use of biomass for power generation because other alternatives (such as wind energy, fossils with CCS, and nuclear energy) are more attractive at marginal biomass costs above ca 3 US$/GJ. The estimated demand for primary biomass reported in this assessment (based on MARKAL and TIMER model results) amounts maximally ca. 150 EJ, with ranges in other models of about 50–250 EJ. This is basically within the range of the indicated biomass resource potentials. In particular, the residues and wastes can cover a very significant part of the demand to start with. Specifically, production of transport fuels (based on lignocellulosic biomass via second-generation technologies) is expected to play a dominating role on medium term. Biomass use for materials and feedstock adds to the demand, but is a minor factor in total demand based on most current model results, although this area has still received limited attention. It should be noted though that the indications given by the IPCC, MARKAL, and TIMER are based on relative cost-effectiveness (e.g., costs per ton of CO_2 emission avoided). Other drivers, such as energy security and rural development could result in sustained policy support in particular for biofuels. This may increase demand for biomass considerably. In addition, the total energy demand is uncertain and in the higher projections, biomass demand may rise well over the indicated 150 EJ.

It should be noted that the energy model results are in particular sensitive to assumptions on the expected performance of advanced conversion technologies (such as second-generation biofuel production processes). It should also be noted that there is a wide range of energy models available which may yield different results than listed here. The main drivers for biomass demand though will not be different using other models.

The key studies that provided an important basis for the potential estimates mentioned are [4, 6, 13]. Given that those are among the most recent studies available and that in particular the Hoogwijk study already incorporated various limitations with respect to nature areas, low-productive areas, etc., these played an important role. The IPCC SRES scenarios used in the Hoogwijk analyses were used as a basis for this assessment as well, varying agricultural efficiency and using the base land-cover simulations of the IMAGE model. This assessment has provided several corrections of the available results to date, especially with respect to water availability, soil quality, and protected areas (which were excluded from the potentials for biomass production). These are significant and led to

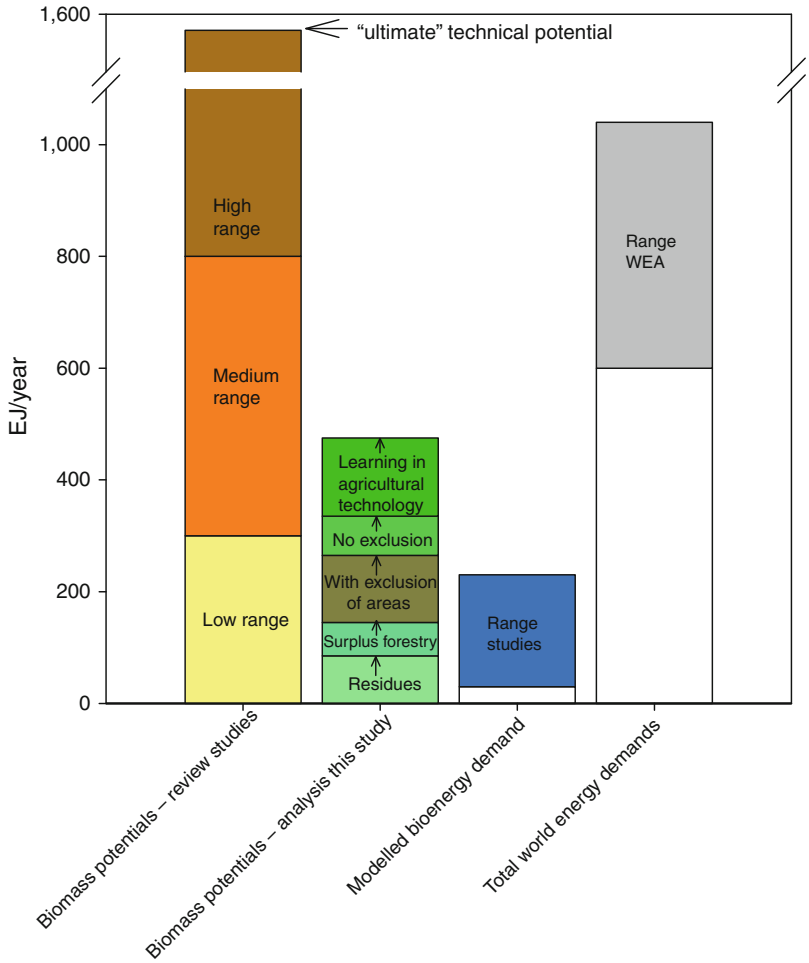

Biomass Resources, Worldwide. Figure 15

Comparison of technical biomass potentials with bioenergy demands in 2050. Biomass potentials as analyzed in this study refer to the OECD-baseline scenario of IMAGE. (Exclusion of areas is the exclusion of mildly and severely degraded and water-stressed areas as well as the exclusion of areas designated as current and future nature reserves, while learning in agricultural technology reaches levels as assumed in the SRES A1 scenario.) [25]

corrections to earlier estimates of the resource potentials as argued above. Table 4 lists the key factors that influence that size of the potential.

This assessment also showed different trade-offs from biomass/bioenergy production on biodiversity. From a perspective of global biodiversity targets, different spatial scales and both short- and long-term effects must be taken into account. On a local scale, biodiversity may benefit from growing biomass, when intensive agricultural practices are replaced by low-intensity biomass production systems (such as short-rotation forestry, mixed land-use systems). The large variation recorded in local effects deserves further attention for defining favored management practices. On a global scale, however, agricultural lands may only become available when food production regions will shift, for instance through trade liberalization. Thus, the short-term global biodiversity effects are intimately related to global land-use dynamics and especially the different causes of land abandonment. On the long term, biomass production is expected to contribute to reduced greenhouse gas emissions and, therefore, reduced climate change effects on biodiversity. A first-order estimate indicates that the balance between

Biomass Resources, Worldwide. Table 4 Overview of uncertainties and their impact on biomass resource potentials and recommended activities to reduce uncertainties

Issue/effect	Importance	Recommended activities to reduce uncertainties
Supply potential of biomass		
Improvement agricultural management	***	Research to better understand how efficiency and livestock can be increased in a sustainable manner and for different settings. Insight in development pathways and feasible rates of improvement need to be integrated in modeling frameworks. Improved insights in preconditions for improvements can provide a basis for targeted policies
Choice of crops	***	There are clear recommendations on the importance of lignocellulosic biomass production systems for different settings. Under certain conditions, sugar cane and palmoil could still be feasible options on longer term as well. Much more market experience with such production systems needed in different settings, including degraded and marginal lands, intercropping schemes (e.g., agroforestry), and management of grasslands. The latter is an important land-use category on which current understanding and data needs improvement
Food demand	***	Increases in food demand beyond the base scenarios (e.g., up to nine billion people in 2050) that were the focus in this study will strongly affect possibilities for bioenergy. Vice versa, limited population growth will mean the opposite
Use of degraded land	***	Represents a significant share of possible biomass resource supplies. Experiences with recultivation and knowledge on these lands (that represent a wide diversity of settings) are limited so far. More research is required to assess the cause of marginality and degradation and the perspectives for taking the land into cultivation. Research and demonstration activities required to understand the economic and practical feasibility of using degraded/marginal land is needed. This land-use category also requires attention (e.g., via better databases) in modeling efforts
Competition for water	***	Increased water demand for conventional agriculture, domestic, and industrial use is a concern in various world regions, with agriculture being by far the most important sector in this respect. This assessment provided a first-order insight in how (energy) crop production potentials may be constrained by water availability, which is significant already in some regions and will increase in the future. Constraints in water supplies and sustainable management need ultimately to be studied at water basins scale, in interaction with local scales
Use of agricultural/ forestry by-products	**	Residues are an important resource category. The net availability for energy purposes can in the future in particular be affected negatively by competing applications (e.g., biomaterials and traditional biomass use). Their net availability can be improved by better infrastructure and logistics. Key areas for research and sustainable management are maintaining sound organic matter levels in soils and nutrient balances. To some extent (especially for residues in tropical regions) more research and field experience to determine such levels is desired
Protected area expansion	**	Increased ambition levels for nature reserves on a global scale can have a significant impact on net land availability for biomass production. Land exclusion assumptions in the available studies, however, seem to overlap with the potential future land claims for nature and further modeling work and improved databases are desired. Furthermore, more insights are desired in how land-use planning including new bioenergy crops can maximize biodiversity benefits. Evaluating biodiversity impacts on regional level is still a field under scientific development and more fundamental work is needed in this arena

Biomass Resources, Worldwide. Table 4 (Continued)

Issue/effect	Importance	Recommended activities to reduce uncertainties
Water use efficiency	**	See above under competition for water. An important factor in the equation is improvement of water use efficiency in both current agriculture (that could be achieved through efficient management adapted to the local production situation, increasing resource use efficiency) and in biomass production itself. Technical improvement potentials are considerable compared to current average practice. This suggests that for various areas water management is a prime design parameter for sustainable biomass production and land-use management. This area deserves considerable further research efforts, preferably linked to field experience and the socioeconomic environment
Climate change	**	The impact of climate change on agricultural production and productivity of lands could be significant, but exact effects are also uncertain. Effective mitigation strategies, of which large-scale bioenergy deployment could be a significant element, will limit the influence of this factor. At this stage, this is still the objective of the governments that have signed the Kyoto Protocol Varying reported effects of climate change on natural systems and their biodiversity deserve further attention. Especially, variation due to using different indicators and modeling concepts should be better explained. This will influence the balance between land-use dynamics and avoided climate change effects Furthermore, although agriculture may face serious barriers due to climate change, this may also enhance the need for alternative adaptation measures to avoid soil losses and maintain vegetation covers. Biomass production (again especially via perennial systems) may then play a role as adaptation measure. Such strategies (under different climate change scenarios) are so far hardly studied and deserve further attention in future research efforts and scenario analyses
Alternative protein chains	**	See above under food demand. Possible but very uncertain reversal of current diet trends, i.e., introduction of more novel plant protein products (as alternative for meat) could on the longer term strongly reduce land and water demand for food. Such options and the feasibility in terms of implementation are, however, insufficiently studied. Further work in this area is recommended
Demand for biomaterials	*	Demand for biomass to produce biomaterials (both conventional as building material as new ones as bulk bio-based chemicals and plastics) can be a significant factor, but is limited due to market size (compared to demand for energy carriers). Furthermore, biomaterials will also end up as (organic) waste material later in their lifecycle, indirectly adding to increased availability of organic wastes. In many cases this "cascaded use" of biomass increases the net mitigation effect of biomass use. For some biomaterial markets specific cropping and plantation systems may be required due to demands of the biomass composition. Biomaterials are so far poorly integrated as a factor in energy models and as mitigation option. This can be improved in further work to understand the interactions between different flows and markets better (also in macroeconomic terms)
GHG balances of biomass chains	*	The net GHG performance of biomass production systems is not identified as a limiting factor for the potential, provided perennial cropping systems are considered. Also, striving for biomass production that is similar or better than previous land use (e.g., grasslands that remain grasslands or trees that replace annual crops) generally improves the overall carbon balance. This can also be true for replanting of degraded lands. The key factor in the net carbon balance is leakage. Avoiding leakage is directly related to increased efficiency in agriculture and livestock and net carbon impacts of biomass production should include this dimension. Such dynamics should ideally also be incorporated in future modeling exercises

Biomass Resources, Worldwide. Table 4 (Continued)

Issue/effect	Importance	Recommended activities to reduce uncertainties
Demand potential of biomass		
Bioenergy demand versus supply	**	The data on potential biomass demand in future energy scenarios reported in this study hint that biomass demand may in fact be lower than the biomass supplies that could be generated in baseline scenarios used (as "OECD Baseline"). At ambitious levels of climate change abatement, the key demand factor is likely to be the use of biomass for transport fuels due to the very few alternatives available for oil and reducing CO_2 emissions in the transport sector. Nevertheless, long-term energy demand projections are also characterized by considerable variability (especially caused by GDP and population growth and the rate of deployment of energy efficiency measures at large). Demand for transport fuels, e.g., could therefore also be significantly higher than projected in this report and this could be further enhanced when policies target increased energy security and rural development as other priorities that are likely to favor biomass and biofuels It is recommended to incorporate (dynamic) biomass supply projections and a more diverse portfolio of conversion options (e.g., including hydrogen production from biomass and combined with CCS) in current models to obtain more coherent analyses and scenarios
Cost of biomass supply	**	The costs of biomass supplies are influenced by the degree of land-use competition, availability of (different) land (classes), and optimization (learning) in cropping and supply systems. The latter is still relatively poorly studied and incorporated in scenarios and (energy and economic) models, which can be improved. Nevertheless, the variability of biomass production costs seems far less than that of oil or natural gas, so uncertainties in this respect are relatively limited
Learning in energy conversion	**	See remarks on energy models and costs of biomass supply; better insights in development potentials of key technologies (second-generation systems) and biomass supplies will improve the quality of scenario results with respect to the relative role of biomass for energy (and materials)
Market mechanism food-feed-fuel	**	To date, limited modeling efforts are available to fully interlink macroeconomic/market models with biomass potential studies, especially when lignocellulosic biomass is concerned. To date, price dynamics and, longer-term, responses of agriculture (in terms of increased land use and/or increased efficiency) are also addressed to a limited extent. Although the long-term impacts on actual physical biomass resource potentials may be limited, understanding the economic responses to increased demand for food and bioenergy and how these affect the relative competitiveness of bioenergy compared to other energy supply options is extremely important for defining balanced policy strategies Linked to this, socioeconomic implications (such as impacts on rural income, rural employment) should be further understood

Importance of the issues on the range of estimated biomass potentials: *** – large, ** – medium, * – small

global biodiversity losses from increased land use and reduced climate change effects from biomass production alone is not beneficial for biodiversity within 50 years. However, this conclusion is surrounded by considerable uncertainty, especially on climate change effects and also with respect to net biodiversity values of vegetation patterns and cropping systems. The latter may be strongly influenced by good practices and governance of land use. This element deserves further research.

As summarized, the size of the biomass resource potentials and subsequent degree of utilization depend on numerous factors. Part of those factors are (largely) beyond policy control. Examples are population growth

and food demand. Factors that can be more strongly influenced by policy are development and commercialization of key technologies (such as conversion technology for producing fuels from lignocellulosic biomass and perennial cropping systems), for example, by means of targeted RD&D strategies. Other areas are:

- Sustainability criteria, as currently defined by various governments and market parties.
- Regimes for trade of biomass and biofuels and adoption of sustainability criteria (typically to be addressed in the international arena, e.g., via the WTO).
- Infrastructure; investments in infrastructure (agriculture, transport, and conversion) is still an important factor in further deployment of bioenergy.
- Modernization of agriculture; in particular in Europe, the Common Agricultural Policy and related subsidy instruments allow for targeted developments of both conventional agriculture and second-generation bioenergy production. Such sustainable developments are, however, crucial for many developing countries and are a matter for national governments, international collaboration, and various UN bodies (such as FAO).
- Nature conservation; policies and targets for biodiversity protection determine to what extent nature reserves are protected and expanded and set standards for management of other lands.
- Regeneration of degraded lands (and required preconditions) is generally not attractive for market parties and requires government policies to be realized.

Although this assessment was not specifically targeting formulation or further design of sustainability criteria for biomass production, the results provide leads for further steps for doing so. For criteria framework as developed in many places, it is evident that a number of important criteria require further research and design of indicators and verification procedures. This is in particular the case for the so-called macro-themes (land-use change, biodiversity, macroeconomic impacts) and some of the more complex environmental issues (such as water use and soil quality) [105].

This study has confirmed that in principle technical and economic biomass resource potentials could be very large on a global scale (up to one third of global energy demand following more average projections for energy demand as well as biomass resource potentials). However, only a smaller part of the larger potential estimates will be almost certainly available (namely, the biomass residues and organic wastes). The larger part of the potential has to be developed via cultivation and has to meet a wide variety of sustainability criteria to avoid conflicts with respect to water use, land-use competition, protected areas, biodiversity, soil quality, and socioeconomic issues. Based on the findings in this assessment, for large parts of the resource potentials the indications are that such conflicts can indeed be avoided or may in parts even result in co-benefits. The latter could be true for using some categories of degraded lands (impacts on soils, water use, and biodiversity), combined strategies for modernization of agriculture, and diversification of cropping patterns (e.g., intercropping, agro forestry systems).

Both in size and in terms of meeting this wide array of criteria, annual food crops may not be suited as a prime feedstock for bioenergy. Perennial cropping systems, however, offer very different perspectives. These cannot only be grown on (surplus) agricultural and pasture lands, but also on more marginal and degraded lands, be it with lower productivity. Such cropping system represent a very diverse set of possible production systems, from low-intensity forestry and managing existing grasslands to highly productive plantations with short-rotation coppice systems or energy grasses like *Miscanthus*. At this stage, there is still limited (commercial) experience with such systems for energy production, especially considering the more marginal and degraded lands and much more research and demonstration work is needed to develop feasible and sustainable systems suited for very different settings around the globe. This is a prime priority for agricultural policy.

Most challenging in harnessing biomass production potentials in a sustainable way is probably the design of governance and implementation strategies. Such strategies should allow for gradual introduction of biomass cropping systems into rural regions and simultaneously increasing agricultural and livestock productivity. As confirmed by this study, those productivity increases are an essential component to avoid conflicting claims on land and to strong competition (e.g., via increased prices for food). This assessment as

a whole points out that policies targeting development of bioenergy use and biomass production should incorporate a variety of targets and boundaries. Fulfilling a strict GHG criterion (e.g., 90% compared to reference fossil energy use) will lead to different choices for crops and land management compared to a situation where no criterion is formulated. This is also true for sustainable management of water resources, biodiversity, as well as rural development. Clearly, the balance of objectives will be different from setting to setting (e.g., compare rural Africa with the EU) and trade-offs have to be made. It is argued here that such trade-offs should be explicit, balanced, and should incorporate clear boundaries that should be respected and used as a starting point for developing biomass production in a given region. Governance and deployment of incentives (such as subsidies or obligations) could then also be designed to achieve just that. This is a fairly sharp contrast to some of the current biofuel policies implemented in the EU and the USA.

Note

This entry is to a considerable extent based on a reworked version of the following publication: Veronika Dornburg, André Faaij, et al. *Biomass Assessment*: *Assessment of global biomass potentials and their links to food, water, biodiversity, energy demand and economy – Main Report*, Netherlands Research Programme on Scientific Assessment and Policy Analysis for Climate Change. Report no: WAB 500102012, January 2008, p 85 + Appendices.

Bibliography

1. IEA (2009) World energy outlook 2009. IEA/OECD, Paris, France
2. IPCC (2007) Climate change 2007: mitigation. In: Metz B, Davidson OR, Bosch PR, Dave R, Meyer LA (eds) Contribution of working group III to the fourth assessment report of the intergovernmental panel on climate change. Cambridge University Press, Cambridge
3. Junginger M, Bolkesjø T, Bradley D, Dolzan P, Faaij A, Heinimö J, Hektor B, Leistad Ø, Ling E, Perry M, Piacente E, Rosillo-Calle F, Ryckmans Y, Schouwenberg P-P, Solberg B, Trømborg E, da Silva WA, de Wit M (2008) Developments in international bioenergy trade. Biomass Bioenergy 32(8):717–729
4. Hoogwijk M, Faaij A, de Vries B, Turkenburg W (2009) Exploration of regional and global cost–supply curves of biomass energy from short-rotation crops at abandoned cropland and rest land under four IPCC SRES land-use scenarios. Biomass Bioenergy 33(1):26–43
5. WEA (2000) World energy assessment: "energy and the challenge of sustainability". UNDP, UNDESA and WEC, New York
6. Smeets EMW, Faaij APC, Lewandowski IM, Turkenburg WC (2007) A bottom-up assessment and review of global bio-energy potentials to 2050. Prog Energy Combust Sci 33(1):56–106
7. Berndes G, Hoogwijk M, van den Broek R (2003) The contribution of biomass in the future global energy supply: a review of 17 studies. Biomass Bioenergy 25(1):1–28
8. Junginger M, Faaij A, Koopmans A, van den Broek R, Hulscher W (2001) Setting up fuel supply strategies for large scale bio-energy projects – a methodology for developing countries. Biomass Bioenergy 21(4):259–275
9. Hoogwijk M, Faaij A, van den Broek R, Berndes G, Gielen D, Turkenburg W (2003) Exploration of the ranges of the global potential of biomass for energy. Biomass Bioenergy 25(2):119–133
10. Fischer G, Schrattenholzer L (2001) Global bioenergy potentials through 2050. Biomass Bioenergy 20:151–159
11. Smeets E, Faaij A (2007) Bioenergy potentials from forestry to 2050, an assessment of the drivers that determine the potentials. Clim Change 81:353–390
12. Fischer G, Prieler S, van Velthuizen H (2005) Biomass potentials of miscanthus, willow and poplar: results and policy implications for Eastern Europe, Northern and Central Asia. Biomass Bioenergy 28(2):119–132
13. Hoogwijk M, Faaij A, Eickhout B, de Vries B, Turkenburg WC (2005) Potential of biomass energy out to 2100, for four IPCC SRES land-use scenarios. Biomass Bioenergy 29(4):225–257
14. Obersteiner M, Alexandrov G, Benítez PC, McCallum I, Kraxner F, Riahi K, Rokityanskiy D, Yamagate Y (2006) Global supply of biomass for energy and carbon sequestration from afforestation/reforestation activities. Mitig Adapt Strateg Glob Change 11(5–6):1003–1021
15. Perlack RD, Wright LL, Turhollow AF, Graham RL, Stokes BJ, Erbach DC (2005) Biomass as feedstock for a bioenergy and bioproducts industry: the technical feasibility of a billion-ton annual supply. Oak Ridge National Laboratory, Oak Ridge. ORLN/TM-2005/66
16. Rokityanski D, Benitez P, Kraxner F, McCallum I, Obersteiner M, Rametsteiner E, Yamagata Y (2007) Geographically explicit global modeling of land-use change, carbon sequestration and biomass supply. Technolo Forecast Soc 74(7):1057–1082
17. Wolf J, Bindraban PS, Luijten JC, Vleeshouwers LM (2003) Exploratory study on the land area required for global food supply and the potential global production of bioenergy. Agric Syst 76:841–861
18. Fischer G, Nachtergaele F, Prieler S, Teixeira E, van Velthuizen HT, Verelst L, Wiberg D (2008) Global agro-ecological zones assessment for agriculture (GAEZ). IIASA, Laxenburg, and FAO, Rome
19. van Vuuren D, van Vliet J, Stehfest E (2009) Future bioenergy potentials under various natural constraints. Energ Policy 37:4220–4230

20. Wise MA, Calvin KV, Thomson AM, Clarke LE, Bond-Lamberty B, Sands RD, Smith SJ, Janetos AC, Edmonds JA (2009) The implications of limiting CO_2 concentrations for agriculture, land use, land-use change emissions and bioenergy. Pacific Northwest National Laboratory, Richland
21. Melillo JM et al (2009) Indirect emissions from biofuels: how important? Science 326:5958
22. Lotze-Campen H, Popp A, Beringer T, Müller C, Bondeau A, Rost S, Lucht W (2009) Scenarios of global bioenergy production: the trade-offs between agricultural expansion, intensification and trade. Ecol Modell. doi:10.1016/j.ecolmodel.2009.10.002
23. IEA bioenergy: ExCo: 2009:05/bioenergy – a sustainable and reliable energy source. A review of status and prospects/Bioenergy%20a%20sustainable. . .pdf
24. Dornburg V, Faaij A, et al (2008) Biomass assessment: assessment of global biomass potentials and their links to food, water, biodiversity, energy demand and economy – Main Report, Netherlands Research Programme on Scientific Assessment and Policy Analysis for Climate Change. Report no: WAB 500102012, January 2008, p 85 + Appendices
25. Dornburg V, van Vuuren D, van de Ven G, Langeveld H, Meeusen M, Banse M, van Oorschot M, Ros J, van den Born GJ, Aiking H, Londo M, Mozaffarian H, Verweij P, Lysen E, Faaij A (2010) Bioenergy revisited: key factors in global potentials of bioenergy. Energy Environ Sci 3:258–267
26. Field CB, Campbell JE, Lobell DB (2008) Biomass energy: the scale of the potential resource. Trends Ecol Evol 23:65–72
27. Hakala K, Kontturi M, Pahkala K (2009) Field biomass as global energy source. Agric Food Sci 18:347–365
28. Metzger JO, Huttermann A (2009) Sustainable global energy supply based on lignocellulosic biomass from afforestation of degraded areas. Naturwissenschaften 96:279–288
29. Wirsenius S, Azar A, Berndes G (2010) Preserving natural ecosystems and global biodiversity: how much land can be spared for nature by dietary changes and livestock productivity increases? Agricultural Systems, under review
30. CBD & MNP (2007) Cross-roads of life on earth. Exploring means to meet the 2010 biodiversity target. Solution-oriented scenarios for global biodiversity oulook 2. Report nr. CBD Technical Series no. 31/MNP report nr. 555050001, Secretariat of the Convention on Biological Diversity (sCBD) and Netherlands Environmental Assessment Agency (MNP), Montreal & Bilthoven
31. CBD (2006) Global biodiversity outlook 2. Secretariat of the Convention on Biological Diversity, Montreal
32. Molden D, Frenken K, De Fraiture Ch, Barker R, Mati B, Svendsen M, Sadoff C, Finlayson CM (2007) Trends in water and agricultural development. In: Molden D (ed) Water for food, water for life: a comprehensive assessment of water management in agriculture. Earthscan, London, pp 57–89
33. Bessembinder JJE, Leffelaar PA, Dhindwal AS, Ponsioen TC (2003) Which crop and which drop, and the scope for improvement of water productivity. Agric Water Manage 73:113–130
34. Alcamo J, Döll P, Henrichs T, Kaspar F, Lehner B, Rösch T, Siebert S (2003) Development and testing of the WaterGAP 2 global model of water use and availability. Hydrol Sci J 48(3):317–338
35. Shiklomanov IA (2000) Appraisal and assessment of world water resources. Water Int 25:11–32
36. Berndes G (2002) Bioenergy and water – the implications of large-scale bioenergy production for water use and supply. Global Environ change 12:253–271
37. Smakthin VU, Revenga C, Döll P (2004) Taking into account environmental water requirements in global-scale water resources assessments. Research Report of the CGIAR Comprehensive Assessment of Water Management in Agriculture. No. 2, International Water Management Institute, Colombo, Sri Lanka, p 24
38. Evans LT (1998) Feeding the ten billion: plants and population growth. Cambridge University Press, Cambridge. ISBN 0-521-64081-4
39. Tilman D, Cassman KG, Matson PA, Naylor R, Polasky S (2002) Agricultural sustainability and intensive production practices. Nature 418:671–677
40. Smil V (2002) The earth's biosphere: evolution, dynamics, and change. MIT Press, Cambridge. ISBN 0-262-19472-4
41. Aiking H, De Boer J, Vereijken JM (eds) (2006) Sustainable protein production and consumption: pigs or peas? vol 45, Environment and Policy. Springer, Dordrecht, The Netherlands. ISBN 1-4020-4062-8
42. Quist J (2000) Towards sustainable shopping, cooking and eating in the Netherlands. Background report, Delft University of Technology, Delft, The Netherlands. Available on CD ROM at www.sushouse.tudelft.nl
43. von Braun J, Rosegrant M, Pandya-Lorch R, Cohen MJ, Cline SA, Brown MA, Bos MS (2005) New risks and opportunities for food security: scenario analyses for 2015 and 2050, 2020 Discussion paper 39. IFPRI, Washington, DC
44. Dixon J, Gulliver A, Gibbon D (2001) Farming systems and poverty; improving farmers' livelihoods in a changing world. FAO and World Bank, Rome/Washington, DC
45. Grigg D (1995) The pattern of world protein consumption. Geoforum 26(1):1–17
46. Millstone E, Lang T (2003) The atlas of food: who eats what, where and why. Earthscan, London. ISBN 1-85383-965-5
47. Smil V (2002) Worldwide transformation of diets, burdens of meat production and opportunities for novel food proteins. Enzyme Microb Technol 30:305–311
48. Pimentel D, Pimentel M (2003) Sustainability of meat-based and plant-based diets and the environment. Am J Clin Nutr 78:660S–663S
49. Smil V (2000) Feeding the world: a challenge for the twenty-first century. MIT Press, Cambridge. ISBN 0-262-19432-5
50. Seidl A (2000) Economic issues and the diet and the distribution of environmental impact. Ecol Econ 34:5–8
51. White T (2000) Diet and the distribution of environmental impact. Ecol Econ 34:145–153

52. IEA-WEO (2006) World energy outlook 2006. International Energy Agency, Paris
53. IPCC (2011) Special report on renewable energy sources. (forthcoming)
54. IEA-ETP (2008) Energy technology perspectives report, Paris-France
55. IEA-WEO (2007) World energy outlook 2007. International Energy Agency, Paris
56. OECD and FAO (2007) Agricultural outlook 2007–2016. Organisation for Economic Co-operation and Development, Paris, France
57. OECD (2008) OECD environmental outlook to 2030. Report, OECD – Organisation for Economic Co-Operation and Development, Paris
58. Dale V, Efroymson R, Kline K, Goss Eng A, Haq Z (2009) Land-use change and bioenergy: workshop, Vonore, May 2009. http://www.ornl.gov/sci/besd/cbes/workshops/LandUse_Report.pdf
59. Fehrenbach H, Giegrich J, Reinhardt G, Rettenmaier N (2009) Synopsis of current models and methods applicable to indirect land use change (ILUC). Report Commissioned by Bundesverband der deutschen Bioethanolwirtschaft e.V. (BDBe) http://www.bdbe.de/studien.html
60. Amaral W et al (2008) Environmental sustainability of sugarcane ethanol in Brazil. In: Zuurbier P, van de Vooren J (eds) Sugarcane ethanol. Wageningen Academic Publishers, Wageningen, pp 113–138
61. EPA (2010) Renewable fuel standard program (RFS2) regulatory impact analysis, EPA-420-R-10-006, February 2010. http://www.epa.gov/otaq/renewablefuels/420r10006.pdf
62. Hertel TW, Tyner WE, Birur DK (2010) Global impacts of biofuels. Energy J 31:75–100
63. CARB (2010) January 10, 2010, Final regulation order, subchapter 10. Climate change, article 4. Regulations to achieve greenhouse gas emission reductions, subarticle 7. Low carbon fuel standard, http://www.arb.ca.gov/regact/2009/lcfs09/lcfs09.htm
64. Nassar A, Harfuch L, Moreira MMR, Bachion LC, Antoniazzi LB, Sparovek G (2009) Impacts on land use and GHG emissions from a shock on Brazilian sugarcane ethanol exports to the United States using the Brazilian land use model (BLUM). The Brazilian Institute for International Negotiations, ICONE, Report to the U.S. Environmental Protection Agency regarding the proposed changes to the renewable fuel standard program, http://www.iconebrasil.org.br/arquivos/noticia/1873.pdf. EPA-HQ-OAR-2005-0161-1958
65. Searchinger T, Heimlich R, Houghton RA, Dong F, Elobeid A, Fabiosa J, Tokgoz T, Hayes D, Yu T (2008) Use of US croplands for biofuels increases greenhouse gases through emissions from land use change. Science 319:1238
66. Fritsche U et al (2008) The ILUC factor as a means to hedge risks of GHG emissions from ILUC associated with bioenergy feedstock provision, Oeko Institute
67. Tipper R et al (2009) A practical approach for policies to address GHG emissions from ILUC associated with biofuels, Arbeit für Ecometrica für Greenergy, Technical Paper – TP-080212-A; Jan 2009
68. Lapola DM, Schaldach R, Alcamo J, Bondeau A, Koch J, Koelking C, Priess JA (2010) Indirect land-use changes can overcome carbon savings from biofuels in Brazil. Proc Natl Acad Sci USA 107(8):3388–3393
69. Al-Fiffai P, Dimaranan B, Laborde D (2010 March) Global trade and environmental impact study of the EU biofuels mandate study prepared by IFPRI
70. Fischer G, Prieler S, van Velthuizen H, Berndes G, Faaij A, Londo M, de Wit M (2010) Biofuel production potentials in Europe: sustainable use of cultivated land and pastures, Part II: land use scenarios. Biomass Bioenergy 34(2):173–187
71. de Wit M, Faaij A (2010) European biomass resource potential and costs. Biomass Bioenerg 34(2):188–202
72. Bruinsma J (2002) World agriculture: towards 2015/2030, an FAO perspective. FAO, Rome. ISBN 9251048355
73. Vuuren DP van (2007) Energy systems and climate policy. Ph.D. thesis, Utrecht University
74. IUCN & UNEP/WCMC (2003) United Nations list of protected areas report, the world conservation union (IUCN) and world conservation monitoring centre (UNEP/WCMC). Gland, Switzerland/Cambridge, UK
75. IPCC 4th assessment report WG II report, 2007
76. WWF (2006) WildFinder: online database of species distribution, version 01.06. http://www.worldwildlife.org/wildfinder
77. DOE (2010) Department of energy, golden field office, impact assessment of integrated biorefinery projects. http://www.biorefineryprojecteis-abengoa.com/Home_Page.html
78. van Dam J, Faaij APC, Hilbert J, Petruzzi H, Turkenburg WC (2009) Large-scale bioenergy production from soybeans and switchgrass in Argentina. Part A: potential economic feasibility national international markets. Renew Sust Energy Rev 13:1710–1733
79. van Dam J, Faaij APC, Hilbert J, Petruzzi H, Turkenburg WC (2009) Large-scale bioenergy production from soybeans and switchgrass in Argentina. Part B: environmental and socio-economic impacts on a regional level. Renew Sust Energy Rev 13(8):1679–1709
80. http://www.eia.doe.gov/emeu/aer/txt/ptb1107.html. Accessed 17 July 2007
81. WWI (2006) Biofuels for transportation – global potential and implications for sustainable agriculture and energy in the 21st century. Worldwatch Institute, Washington, DC
82. Schmidhuber J (2005) The nutrition and the energy transition of world agricultural markets. Plenary presentation at the German association of agricultural economists (GeWiSoLa), Göttingen, October 2005
83. Hamelinck C, Faaij A (2006) Outlook for advanced biofuels. Energ Pol 34(17):3268–3283
84. Rosegrant MW, Cai X, Cline SA, Nakagawa N (2002) The role of rainfed agriculture in the future of global food production, EPTD discussion papers 90, International Food Policy Research Institute (IFPRI)

85. IFPRI (2008) High food prices: the what, who, and how of proposed policy actions. Policy brief. http://www.ifpri.org/sites/default/files/publications/foodpricespolicyaction.pdf. Accessed 30 March 2008
86. Ivanic M, Martin W (2008) Implications of higher global food prices for poverty in low-income countries. Agric Econ 39:405–416
87. Zezza A, Davis B, Azzarri C, Covarrubias K, Tasciotti L, Anriquez G (2008) The impact of rising food prices on the poor. FAO ESA Working Paper 08-07
88. FAO (2008) State of food and agriculture. Biofuels: prospects, risks and opportunities
89. Schmidhuber J (2007) Impact of an increased biomass use on agricultural markets, prices and food security: a longer-term perspective
90. Bruinsma J (2009) The resource outlook to 2050: by how much do land, water and crop yields need to increase by 2050? Expert Meeting on how to feed the world in 2050, Food and Agriculture Organization of the United Nations, Economic and Social Development Department, Rome
91. Tefft J (2010) Mali's White Revolution: Smallholder Cotton. In: Haggblade S, Hazell P (eds) Successes in African agriculture: lessons for the future., International Food Policy Research Institute, Washington, DC, pp 1960–2006
92. Binswanger HP, von Braun J (1991) Technological change and commercialization in agriculture: the effect on the poor. World Bank Res Obser 6(1):57–80
93. von Braun J (1994) Production, employment, and income effects of commercialization of agriculture. In: von Braun J, Kennedy E (eds) Agricultural commercialization, economic development, and nutrition. The Johns Hopkins University Press, Baltimore
94. López R, Galinato GI (2007) Should governments stop subsidies to private goods? Evidence from rural latin America. J Public Econ 91(5–6):1071–1094
95. Wiskerke W, Dornburg V, Faaij A, Malimbwi RE, Rubanza CDA (2010) Towards a sustainable biomass energy supply for rural households in semi-arid conditions in Tanzania – a cost/benefit analysis. Renew Sust Energy Rev 14(1):148–165
96. Arndt C et al (2010) Biofuels, poverty, and growth: a computable general equilibrium analysis of Mozambique. Environ Dev Econ 15(1):81–105
97. Wicke B, Smeets E, Faaij A, Tabeau A, Hilbert J (2009) Macroeconomic impacts of bioenergy production on surplus agricultural land – a case study of Argentina. Renew Sust Energy Rev 13(9):2463–2473
98. de Wit M, Junginger M, Lensink S, Londo M, Faaij A (2010) Competition between biofuels: modeling technological learning and cost reductions over time. Biomass Bioenergy 34(2):203–217
99. Banse M, Tabeau A, Woltjer G, van Meijl H (2007) Impact of EU Biofuel policies on world agricultural and food markets. Paper presented on the 10th Annual GTAP Conference, 07–09 June 2007, Purdue University, Indiana
100. WBGU – German Advisory Council on Global Change (2003) Towards sustainable energy systems. Earthscan, London. http://www.wbgu.de/wbgu_jg2003_engl.html
101. Larson ED (2007) A review of LCA studies on liquid biofuel systems for the transport sector. Energy Sust Dev X (2):109–126
102. Hoefnagels R, Smeets E, Faaij A (2010) Greenhouse gas footprints of different biofuel production systems. Renew Sust Energy Rev 14(7):1661–1694
103. Oldeman LR, Hakkeling TRA, Sombroek WG (1991) GLASOD, world map of human-induced soil degradation. ISRIC/UNEP, ISRIC, Wageningen
104. Patel MK, Crank M, Dornburg V, Hermann BG, Roes L, Hüsing B, Overbeek L van, Terragni F, Recchia E (2006) Medium and longterm opportunities and risks of the biotechnological production of bulk chemicals from renewable resources. E.C.G.P.D. research. Utrecht, The Netherlands
105. van Dam J, Junginger M, Faaij A (2010) From the global efforts on certification of bioenergy towards an integrated approach based on sustainable land use planning (submitted to Renew Sust Energy Rev 2010)

Biomass to Liquid (BtL), Concepts and Their Assessment

Franziska Mueller-Langer[1], Niels Jungbluth[2]
[1]German Biomass Research Centre gGmbH (DBFZ), Leipzig, Germany
[2]ESU-services, Uster, Switzerland

Article Outline

Glossary
Definition of the Subject
Introduction
Production Pathways on Synthetic Fuels
Technical Assessment
Economic Assessment
Environmental Assessment
Conclusions
Future Directions
Bibliography

Glossary

ADP Abiotic depletion potential
AP Acidification potential
bf Biomass feedstock

BtL Biomass to liquid
CAPEX Capital expenditures
CED Cumulative energy demand
CH_4 Methane
CHP-F Combined heat, power, and fuel generation
CML Centrum voor Milieukunde Leiden
CO Carbon (mono-)oxide
CO_2 Carbon dioxide
CtL Coal to liquid
DE Diesel equivalent
DME Dimethylether
EP Eutrophication potential
eq Equivalent
EU European Union
€ Euro
FOW Forest wood
FT Fischer–Tropsch
GtL Gas to liquid
GWP Global warming potential
H_2 Hydrogen
LCA Life cycle assessment
LCI Life cycle inventory analysis
LCIA Life cycle impact assessment
MeOH Methanol
MF Maximum fuel
MISC Miscanthus
MJ MEGA Joule
NMVOC Non-methane volatile organic compounds
OPEX Operational expenditure
P Power
pkm Passenger kilometer
POCP Photochemical oxidation
R&D&D Research and development and demonstration
SNG Synthetic natural gas
SP Starting point
SRC Short-rotation coppice
SS Self-sufficient
STR Straw
TCI Total capital investment
ZnO Zinc oxide
η Efficiency

Definition of the Subject

To meet future policy and technical targets, biofuels of the next generation need to be developed in parallel to the existing biofuel generation. However, there is no silver bullet yet that of the various discussed options for next generation biofuels (e.g., bioethanol, synthetic biofuels, biohydrogen based on lignocelluloses, biomethane) will become widely accepted within the future transportation sector. BtL fuels (biomass to liquid) are one option of future biofuels that has center stage of discussion due to favorable fuel properties. Therefore different concepts for BtL provision have been analyzed and compared by technical, economic, and environmental criteria. This is done to perform a consistent comparison of BtL concepts being currently under development (e.g., [1, 2]).

Introduction

Despite national trends due to a strong increase of mobility of goods and persons, the energy demand for transportation purpose will increase significantly in Europe, America, and Asia (globally about 26% until 2020 compared to 2005) [3]. Although this sector will continue to primarily ask for crude oil products, hope is given for increased energy efficiency and maybe electro mobility in the years to come. Biomass is of particular interest within the ongoing discussion on sustainable mobility due to its advantages concerning, e.g., climate relevance and security of supply. In developed and developing countries, fossil fuel price fluctuations, climate change issues, as well as supply security aspects have resulted in significant growth in the interest on biofuels. This development will probably increase independently from the also ongoing debate on food security and sustainability issues.

To meet future targets, besides other promising biofuel options, BtL (i.e., biomass to liquid, especially Fischer–Tropsch fuels) have taken a center stage in the ongoing discussion due to its favorable fuel properties as synthetic designer fuel (e.g., regarding heating value, high cetane number, promising cloud point, low aromatic and polyaromatic content) and thus the opportunity to implement BtL fuels without any adaptation into the existing infrastructure of fuel distribution and use.

Within this paper selected BtL options are analyzed and assessed under European frame conditions. Different concepts for BtL provision are compared by technical, economic, and environmental criteria. This is done to perform a consistent comparison of BtL

concepts currently under development and to show both pros/cons as well as prospects/risks of the BtL systems from different viewpoints.

Production Pathways on Synthetic Fuels

XtL is a synonym for the production of synthetic liquid fuels from different raw materials. Gas to liquids (GtL) or coal to liquids (CtL) are currently the most important industrial processes for synthetic (liquid) fuel production. Concerning the fuel synthesis part, XtL use similar technologies (basically Fischer–Tropsch (FT) synthesis) but the raw materials and synthesis gas production – and therewith also technical aspects – are different. Due to historic and economic reasons, commercial XtL plants show different sizes and plant capacities. So far, primarily Fischer–Tropsch technologies have been implemented at industrial scale and are being further developed in new industrial GtL projects mostly in Qatar. The differences in the plant sizes between BtL and GtL/CtL do not obligatorily lead to completely new process designs along the BtL provision chain. There are many similarities of the production routes of current commercial XtL and future BtL plants. The relation of typical capacities of XtL plants being installed or planned as well as the diesel fuel demand in Europe is shown in Fig. 1 [4].

BtL Production Pathways

The production of synthetic fuels and intermediate products (i.e., "designer fuels" with clearly defined properties) is characterized by three main steps after appropriate biomass pretreatment: (1) gasification of lignocellulosic biomass to a raw gas, (2) cleaning and conditioning of raw gas to synthesis gas, (3) catalytic synthesis of this gas to synthetic biofuels (e.g., FT, MeOH, DME, and SNG), and (4) final product treatment. The principle is shown in Fig. 2.

Regarding biomass pretreatment for gasification, the mechanical-thermal biomass treatment (e.g., chipping and drying of solid biofuels) is technically mature. But processes to produce intermediate products that can be easier transported and handled for gasification (i.e., pyrolysis and torrefaction) are in the pilot/demonstration stage. Despite the scale of a gasifier, no gasification system is a priori appropriate for biomass. Among other criteria, chemical characteristics, physical and mechanical properties of the utilized biomass are important. However, basically all

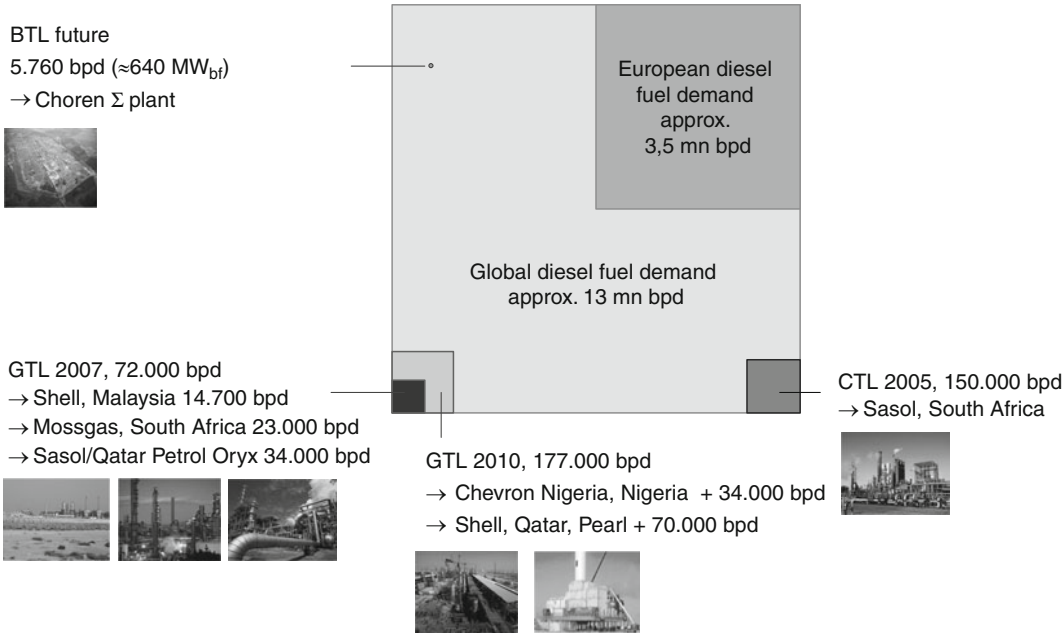

Biomass to Liquid (BtL), Concepts and Their Assessment. Figure 1
XtL capacities (>1,000 bpd) worldwide

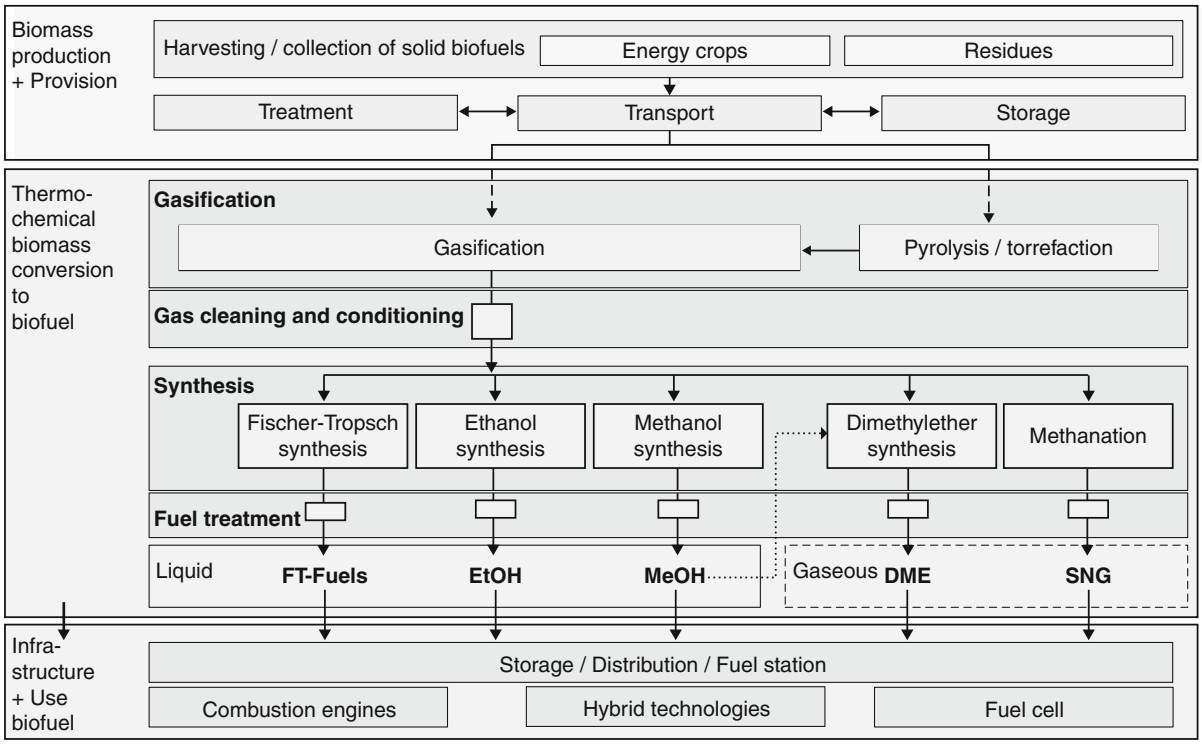

Biomass to Liquid (BtL), Concepts and Their Assessment. Figure 2
General overview of synthetic biofuel routes

types of gasification reactors for biomass (e.g., fluidized bed and entrained flow reactor) are still under development up to now. Furthermore, previous developments on gasification were mostly not focused on synthesis gas production but rather on the use of product gas for CHP generation [5–10].

Primarily with regard to the gas purity and the H_2/CO ratio, specific qualities of synthesis gas at constant compositions and large amounts have to be achieved depending on fuel synthesis (e.g., for the production of 100–1,000 m^3_{STP}/h of FT). Because no gasifier system meets these requirements so far, appropriate gas cleaning and conditioning systems have to be applied. During gasification, in addition to the main components (CH_4, H_2, CO, CO_2), impurities also are generated such as tars, coarse and fine particles, sulfur compounds, alkalis, halogen and nitrogen compounds, as well as heavy metals. Their quantities vary depending on the gasification process. For raw gas cleaning alternatively low temperature wet gas cleaning or hot gas cleaning can be used. The effectiveness of wet gas cleaning (e.g., cyclone and filter, scrubbing based on chemical or physical absorption) has been well proven for large-scale coal gasification systems. Different to that, not all elements of hot gas cleaning (e.g., tar cracking, granular beds and filters, physical adsorption or chemical absorption, ZnO-bed, physical absorption) are technically mature yet. Nevertheless, hot gas cleaning offers benefits for the overall energy balance with regard to the avoidance of contaminated sewage. Available system components can be applied for gas conditioning: Hydrocarbons in the product gas can be converted by means of a steam or autothermal reforming step resulting in a higher H_2/CO ratio. To achieve the required quality for fuel synthesis the water gas CO shift conversion is conducted as final step of synthesis gas production [8, 11–18].

Promising BtL Concepts

At present the provision of synthetic biofuels is under discussion for various processes and technologies

related to biomass feedstock treatment, kind of gasification, gas treatment, synthesis and product upgrading. Further on, different scales are possible using different types of solid biofuels and different potential integration schemes into existing industrial facilities (e.g., pulp and paper production, crude oil refinery, petrochemicals). In Europe currently discussed BtL developments focus on FT diesel and DME (e.g., [13, 19–23]).

Considering this variety of potential technologies, the most relevant BtL production concepts in Europe have been analyzed for a reference plant size of up to 500 MW_{bf} biomass input power. This has been done to enable a qualitative comparison. Therefore the biofuel supply chains are virtually scaled. This can be realized by one or several plants. The decision whether one 500-MW_{bf} plant or several smaller plants will be realized is taken based on recommendations given by the respective technology developer. Table 1 provides an overview about the different technologies [4].

Technical Assessment

Each of the concepts has been developed within a specific technical and economic background that leads to a specific optimization of the process conditions. Considering that fact, differences in the technical performance are observed. In order to compare the most relevant differences, a multi-criteria assessment methodology has been adapted and applied (e.g., [4, 24]). This method allows evaluating different pros and cons on (1) efficiency, (2) flexibility, and (3) industrial

Biomass to Liquid (BtL), Concepts and Their Assessment. Table 1 Overview of assessed BtL concepts (European conditions)

Concept	1	2	3	4	5
Pretreatment					
Mechan./thermal	Drying		–	Drying + pelletizing	Drying
Thermochemical	Carbonization	Fast pyrolysis	Residue: black liquor from pulp mill[a]	–	
Location	Plant	Decentral	Plant		
Gasification	Entrained flow			Circulating fluidized bed	
	Chemical quench	Quench		Autothermal	Allothermal
Main gas cleaning/ conditioning	Conventional physical absorption			Dedicated technologies	
	Selexol	Rectisol			
Synthesis (reactor, catalyst)	Tubular fixed bed reactor, Co	Slurry bubble column reactor, Co	Conventional indirect MeOH-DME	Tubular fixed bed reactor, Fe	Slurry bubble column reactor, Fe
Fuel upgrading	Distillation, hydrocracking		Distillation	External upgrading in refinery	
Main fuel product	FT diesel	FT raw product	DME	FT raw product	
By-products	Naphtha, electricity	Electricity	–	Electricity	Electricity
Plant scale[b]	Medium	Large	Medium	Medium	Small/medium
Industrial integration[c]	Stand alone/ location specific	Refinery integration	Pulp mill	Refinery upgrading	District heat and refinery

[a]No explicit thermochemical product: residue of pulp mill
[b]Plant scale focused by the concept developers
[c]Integration of mass and energy flows of the BtL plant with other industrial plants/consumers

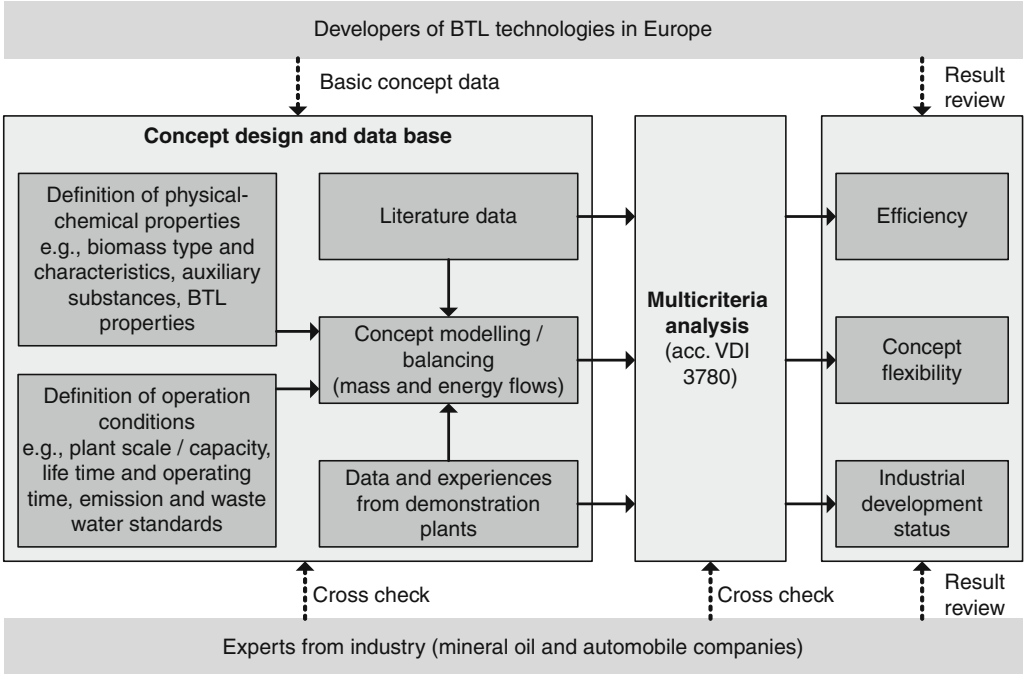

Biomass to Liquid (BtL), Concepts and Their Assessment. Figure 3
Simplified approach for the assessment of technical aspects

development status of selected BtL concepts. A simplified approach of this analysis is shown in Fig. 3. The analysis serves as a preliminary evaluation of selected questions (like a pre-feasibility study) rather than a comprehensive study.

The quality of such an assessment is limited by the quality of the data. Thus, for all concepts the most relevant parameters for indicator calculations were fixed (e.g., properties and operation conditions; Fig. 3). Data for the concept design have been taken from engineering and operating experiences of existing concepts and demonstration plants as well as GtL and CtL plants. Both methodical approach and data have been reviewed by industry [25]. It has to be noted that the data and information applied for the analysis origins from different sources (simulation, estimation, or detailed engineering) and different development status of the BtL concepts (pilot plants, laboratory experiments, or literature).

Based on this approach selected results about overall efficiencies as well as development status and R&D&D demand are summarized in the following.

Overall Efficiencies

One of the main process indicators (also with high relevance for economic and environmental issues) is the overall efficiency of the conversion plant. To calculate efficiencies different definitions are possible and legitimate in so far as coherent boundary definition is ensured (cf. [4]). Figure 4 summarizes the results of the efficiency calculation based on the so-called CHP-F method (cf. Eq. 1); the appropriate shares reflect the sum of single efficiencies, whereby the shares are representing the parts listed in the legend of the figure.

$$\eta = \frac{P_{\mathrm{BTL}} + P_{\mathrm{co-fuels}} + P_{\mathrm{by-products}}}{P_{\mathrm{input\ streams}}} \tag{1}$$

The CHP-F method is based considering co-fuels and by-products fuel as target power (i.e., BtL). They are useful for other applications and have not to be generated by another conversion process. Therefore by-product powers are added to the target power and equal to another.

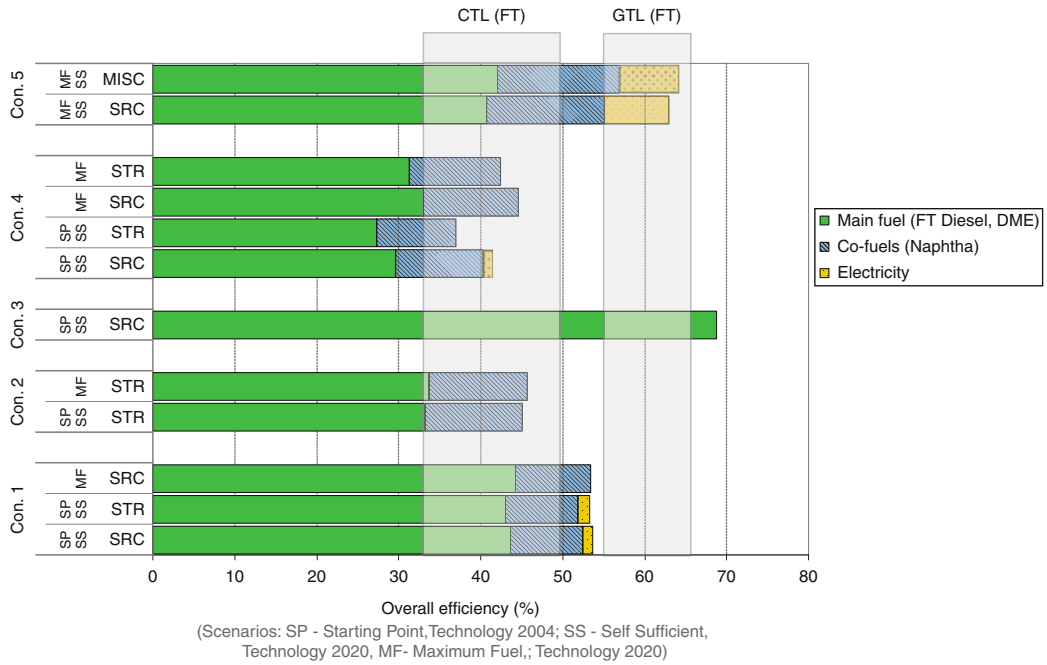

Biomass to Liquid (BtL), Concepts and Their Assessment. Figure 4
Overall efficiencies of assessed BtL concepts and efficiency ranges of CtL and GtL concepts

According to that, significant differences exist between the concepts that are mainly influenced by the choice of synthesis and the integration of mass and energy flows of the BtL plant with other industrial plants/consumers (i.e., development focus/design specificity). Related to the produced fuel the production of DME as annex concept of a pulp and paper mill (concept 3) is the most efficient. This is due to a higher efficiency of the DME synthesis compared to the other synthesis routes (like Fischer–Tropsch hydrocarbon production) and the process integration of heat and power provision within a pulp and paper mill.

With today's design and technology for FT diesel production (scenario "starting point" (SP)), the highest efficiency could be achieved by the entrained flow gasification concept (concept 1). In the future, a CFB gasification concept (concept 5) shows promising opportunities to achieve one of the best diesel efficiencies. Reasons for this are optimized energetic integrations (e.g., heat or tail gas recovery) within these concepts. The technical measures shown with these concepts are possible in principal (theoretically) but have to be confirmed within future demonstration plants.

Development Status and R&D&D Demands

In addition to efficiency and flexibility, the technical assessment of the different concepts has been extended to a preliminary qualitative evaluation of the development status of the technologies involved. This has been done based on an industrial perspective. A selection of criteria relevant to industry have been applied to analyze the overall concept, the gasification, the gas cleaning, and gas conditioning as well. The selected criteria (e.g., feedstock flexibility, scale-up issues, process design, and energy integration issues) allow addressing some of the most critical challenges in the implementation of new and complex technologies. However, they are based on qualitative assessment and should not be considered as a quantitative measurement of relative maturity of the different concepts.

Considering these indicators, there are significant differences between BtL concepts under development in Europe. This is mainly caused by the different time frames of process developments of the technology providers (i.e., more than 10 years up to only 3 years) and the development focus (i.e., from research institutes up to industrial enterprises with different departments for engineering, construction). Regardless these large differences, it has to be pointed out that none of the concepts can be called "proven technology" and can be bought off-the-shelf. Some of the concepts show a promising maturity justifying the development of a first industrial demonstration project in, e.g., 50 MW_{bf} range together with (industrial) monitoring. Others need further development and demonstration in pilot scale (<10 MW_{bf} range) also including monitoring.

Based on such an analysis and evaluation of BtL concepts in Europe, the research, demonstration, and monitoring demands have been identified as key issues (e.g., [1]). The focus of these works can be summarized as follows:

1. Feedstock flexibility. Only certain biomass feedstock have been already tested in pilot plants; for direct gasification technology the ongoing development is focused basically on woody biomass. For practical reasons (e.g., diversification of biomass origin with regard to biomass supply including storage, conditioning, and transport issues and costs) commercial plants will be adapted to few defined biomass types.
2. Gasification. Basically biomass-based CFB gasifier show a higher maturity than the EF gasifiers. Therefore they are more suited for near-future industry application. There is a further need for R&D activities in the promising and generally advantageous EF gasifier. Feedstock preparation concerns aspects like integration of feedstock with a low ash melting point into CFB gasifier (cf. concept 4, 5), thermochemical pretreatment for EF gasifier (cf., e.g., concept 2), handling of feedstock of different qualities, and feeding into pressurized reactors.
3. Gas cleaning and conditioning. Despite that some of the concepts will apply high maturity gas treatment technologies, they need to be adapted to biogenous raw gases of different gas qualities. The concepts 1–3 apply the well-adapted and commercially proven Selexol or Rectisol unit. The other concepts include technologies that are adapted for tolerant synthesis but not yet proven commercially. This is especially true for low temperature gasifier (i.e., CFB in concept 4, 5).
4. Synthesis, raw product upgrading including refinery integration of syncrude. Basically synthesis reactors are available commercially. For concept developers large-scale commercial BtL production is expected to be realized with difficulties without the support of the mineral oil and gas industry, which has the knowledge on large-scale synthesis and product upgrading. Pilot and demonstration projects can also fail because of lacking licences for synthesis and other units.
5. Energetic integration. Since of important influence on overall plant efficiency and thus costs, process integration is one key issue for future plant developments. However, due to the dependency of local conditions at plant site this aspect is less limited by available BtL technologies rather than by identifying suitable plant locations. For instance, the high-process integration of annex plants (cf. concept 3 integrated into pulp mills) favor high efficiencies, however, only for niche applications.

In addition to that for further development of BtL plants, the most important technical issue is to develop scale-up strategies. These strategies have to include the integration of the different process steps along the whole supply chain (i.e., biomass feedstock to transportation biofuel) for demonstrating the effective process performances and reliability. Particularly concerning economic issues, industrial reliability, technical performance, and operability, respectively, have to be demonstrated. To achieve these targets, most of the technical concepts analyzed and further developed in, e.g., [4] could be useful in some context and are basically predisposed by project- and location-specific frame conditions. For each process unit (like, e.g., gasifier) industrial applications exist, however, in a different setting (e.g., in terms of feedstock, size, and final product). In order to leverage maximum learning and progress from the current pilot and demonstration activities, a detailed scientific support, modelling and monitoring in the above-mentioned fields is required.

Economic Assessment

Typically, economic assessment is intended to evaluate different cost alternatives in order to identify relative advantages, to compare different options with regard to omission, and to determine important influencing factors. Especially with regard to assess biofuel production costs, dynamic partial models (e.g., based on annuity) can be favorably applied since the accuracy is higher compared to static partial models due to a periodic accounting (VDI 6025, [26]). According to this, based on the different costs and revenues the annuities can be determined. Taking the annual production rate into account, the specific BtL fuel production costs can be calculated. The calculation approach is summarized in Fig. 5.

Knowledge or assumption of several framework parameters is required for calculating biofuel production costs at the base case 2004 (SP scenario). Listed for the various cost categories, an overview is given as follows (cf. also [27]):

- Capital-related costs. The determination of TCI costs is based on study estimation (accuracy of approx. 20–30%) including the method of additional or overhead costs. Maintenance costs are included by servicing costs.
- Consumption-related costs. For the calculation of base case BtL production costs biomass supply costs

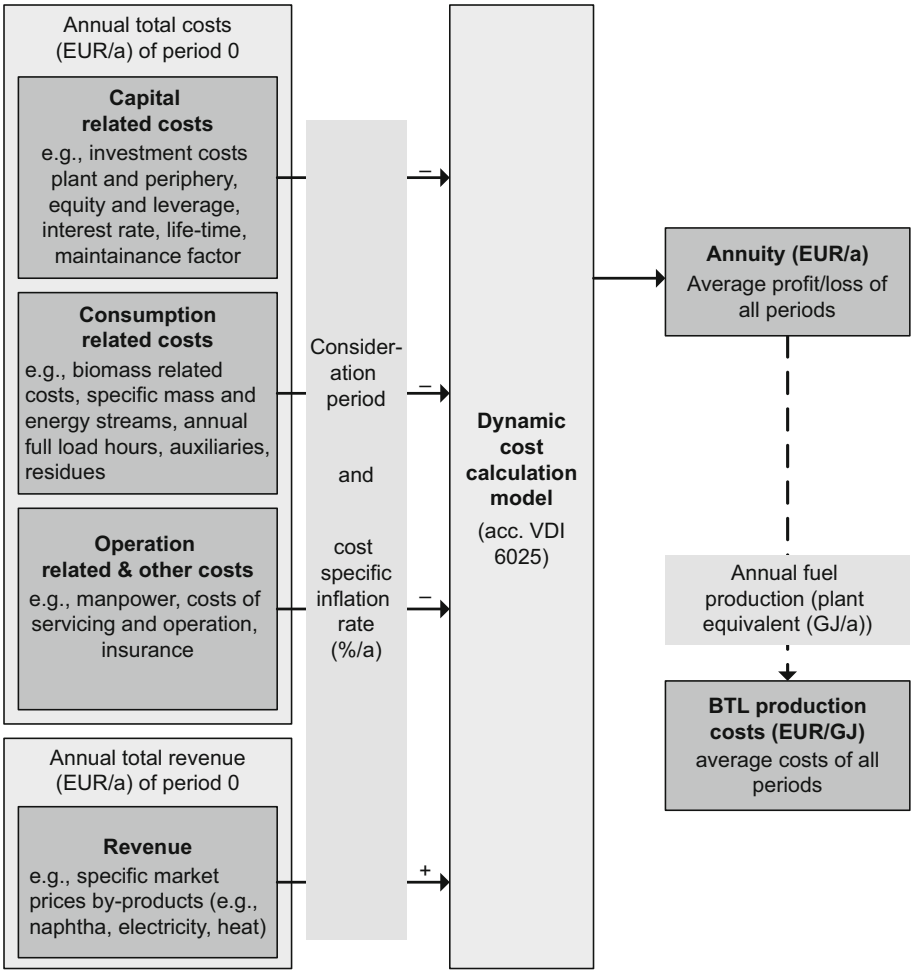

Biomass to Liquid (BtL), Concepts and Their Assessment. Figure 5
Model for calculating BtL production costs

of 5 €/GJ_{LHV} have been used [28, 29]. Annual full load is assumed to be 8,000 h/a. Costs for process energy such as natural gas about 40 €/MWh_{NG}, for electricity about 60 €/MWh_{el} are assumed.

- Operation-related and other costs. Average personnel costs of 50,000 €/(a employee) are assumed. Servicing costs amount annually 3% of TCI. Other costs are related to TCI as well: insurance and contingencies of 1%/a, administration of 0.5%/a, and others (e.g., continuous costs, fees, or testing costs) of 0.75%/a.
- Revenues. Depending on amount and quality for by-products, revenues can be received free plant. Therefore, for naphtha about 400 €/t, for electricity 60 €/MWh_{el}, and about 30 €/MWh_{th} for heat are assumed.

Moreover, a consideration period of 20 years and an interest rate of 10% (related to leverage and equity) are assumed. The annual inflation rate amounts to 2% for capital related, other costs and revenues; for consumption and operation-related costs about 3%.

Total Capital Investment

Total capital investment (TCI) requirements of biofuel production plants are highly important with regard to financial risks and – as it is the case for more complex biofuel concepts – regarding the biofuel production costs. The determination of TCI costs is based on study estimation (accuracy of approx. 20–30%) including the method of additional or overhead costs. According to this, plant equipment costs have been determined by up- or down-scaling (typical scale factor of approx. 0.7) of existing costs data for similar devices. Moreover, component-specific installation factors (e.g., 1.54 for large-scale to 1.66 for small-scale plants) are taken into account [14]. The investment cost figures given were calculated with particular references from literature dating from 2004 or before (e.g., [11, 14, 15, 30–33]) and for others (e.g., that are currently in pilot stage) only rough estimations of technology developers are considered. An overview of rough estimation on TCI is summarized in Fig. 6.

However, TCI for BtL plants (especially for FT fuels) are expected to be much higher compared to other existing biofuel technologies like less complex technologies for biodiesel based on transesterification or premium diesel based on hydrogenation of vegetable oils. They typically show TCI in a range of 190–470 €/$kW_{biofuel}$ and are thus related to less capital risk than BtL [34].

With regard to economy of scale, specific TCI typically decrease with increasing plant capacity. However, there is a continuous cost increase in the engineering

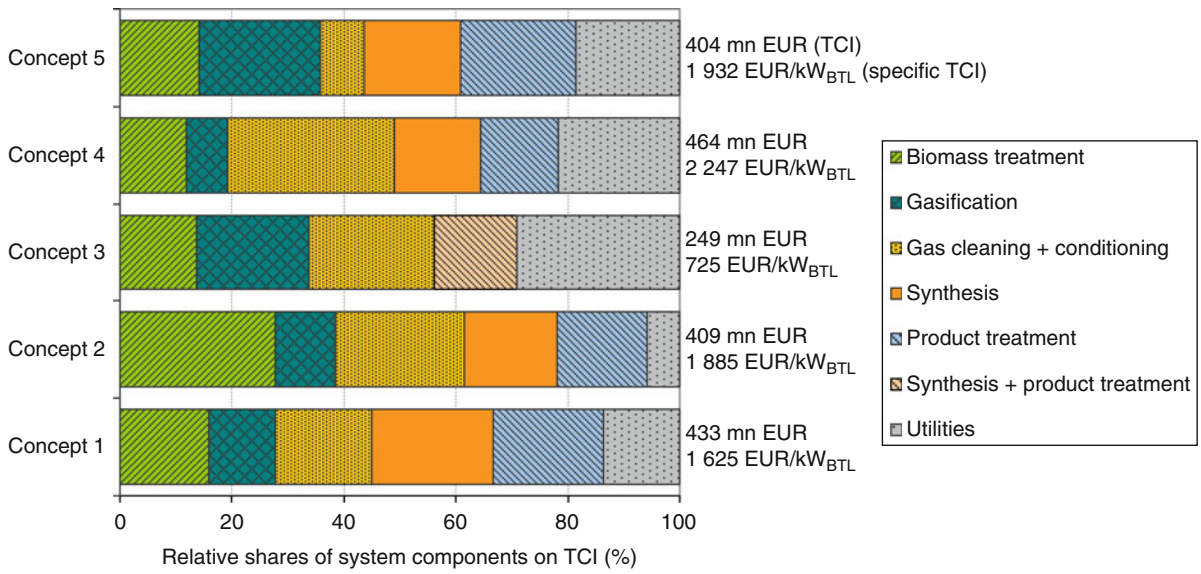

Biomass to Liquid (BtL), Concepts and Their Assessment. Figure 6
Overview of TCI, specific TCI, and relative share of system components for BtL concepts (EUR = €)

and construction industries, which cannot be reflected at all. The price development of chemical plants and machinery (that also refers to biofuel production plants) is commonly indexed by means of the so-called Kölbel–Schulze methodology. According to this price index [35], the TCI for chemical plants has been increased by approx. 35% in the period from 2000 to 2007. This effect will be considered within the sensitivity analysis.

BtL Production Costs

Production costs of future biofuels have been analyzed for exemplary concepts at the shown data base of the time horizon of 2004. The results are summarized in Fig. 7. As the results of the economic analysis reveal, BtL production costs show significant differences, whereby the biomass costs at plant gate are the main influencing factor. Due to this fact, plant efficiency is of strong importance. Furthermore, capital-related costs, in this relation full load hours, become relevant.

Moreover, comparing the calculated BtL production costs with consolidated results on biofuel production costs from other studies (e.g., [15, 36–42]), no significant cost reduction can be expected for FT fuels (8–47 €/GJ) and DME (13–32 €/GJ) compared to currently available biofuels such as biodiesel (4–34 €/GJ) and bioethanol (9–45 €/GJ).

Sensitivity Analyses

The sensitivity analyses have been carried out for the determination and optimization of influencing cost components to the total biofuel production costs for the annual full load hours of the plant, biomass costs, and TCI impact parameters. The results are briefly discussed as follows.

- Annual full load hours. For an economic and competitive operation of commercial BtL plants running hours at full load are strongly important (cf. Fig. 8). Even a reduction of annual hours of about 2,000 h/a results in an increase of BtL

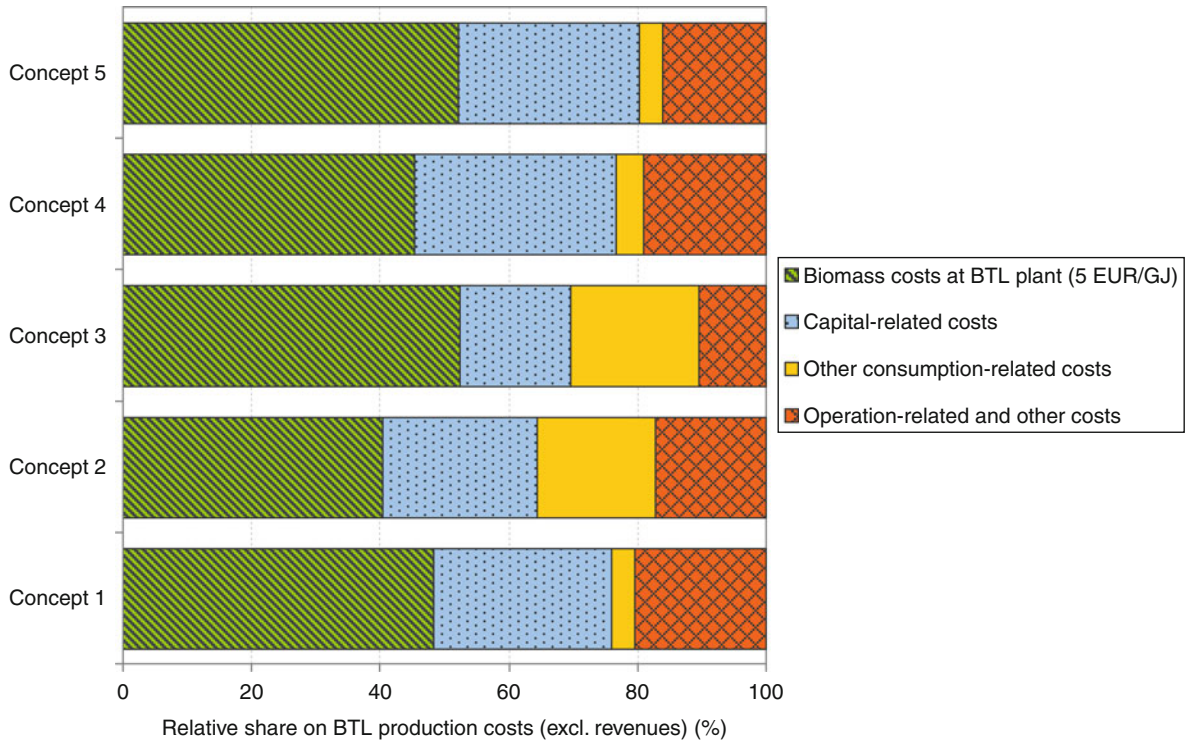

Biomass to Liquid (BtL), Concepts and Their Assessment. Figure 7
Relative comparison of BtL production costs (excl. revenues for by-products) (EUR = €)

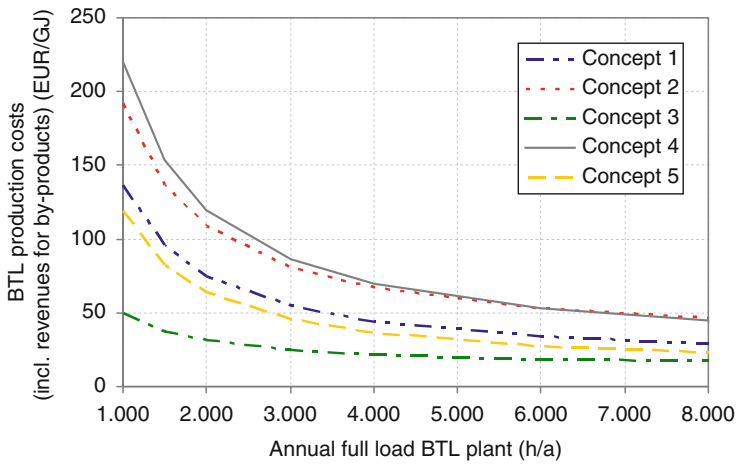

Biomass to Liquid (BtL), Concepts and Their Assessment. Figure 8
Influence of concept-specific annual full load hours (1 €/l_{DE} = 1 €/l/0.0357 GJ/l_{DE} = 28 €/GJ_{BtL}) (EUR = €)

production cost of about 9–20% compared to the base case. Following Fig. 7, BtL concepts with comparably lower fixed costs (i.e., capital- and operation-related costs) or higher consumption–related costs (incl. biomass supply costs), respectively, are less dependent on annual running hours (e.g., concept 3, 5).

- Biomass costs. As shown in Fig. 9, BtL concepts with a high biomass conversion efficiency will be able to produce BtL at favorable costs at a broader biomass costs level; e.g., to produce BtL at a cost level of up to approx. 30 €/GJ biomass costs for the concept 1 can be in a range of up to 5.5 €/GJ, for the concept 4 biomass should not cost more than 2.0 €/GJ. Nevertheless, it is expected that biofuel production costs will moderately increase in future due to rising energy prices with expected price effects for feedstock during broad implementation of biofuel strategies.
- TCI and learning curves of BtL plant. As exemplarily shown for one concept (Fig. 10), doubling of TCI will result in nearly about 50% higher BtL production costs (assumed that all other cost components will be the same). In general, it can be anticipated that costs for BtL production technologies will decrease over time because of improvements in technology and therefore annual full load. Hence, some estimates can be made using the long-term experience of similar technologies (e.g., power generation). Cost reductions of technologies (i.e., reduction of capital investment based on cumulative installed capacity and development stage) within a certain time period (e.g., present to 2020) can be estimated using learning curves. Experiences have shown that technologies display different capital investment reduction factors with regard to their development stages (i.e., R&D, commercialization, and further improvement); the assumed digression factor for commercial BtL plants is 0.9. Taking this so-called learning curve effect into account, BtL production costs can only be slightly reduced in future.

Environmental Assessment

Assessment of BtL Concepts

The environmental assessment of the different BtL concepts is done by means of a life cycle assessment (LCA). This takes into account not only greenhouse gas emissions or energy uses, but all types of environmental problems caused in the life cycle, e.g., eutrophication or land occupation issues.

The LCA method aims to investigate and compare environmental impacts of products or services that occur from cradle to grave. All environmental impacts caused by a product, e.g., 1 MJ of biofuel, are assessed in a standardized way. It includes all the stages during the life cycle: the production of pesticides and fertilizers, the necessary transports, the conversion of the biomass to fuel, and all emissions in the life cycle are

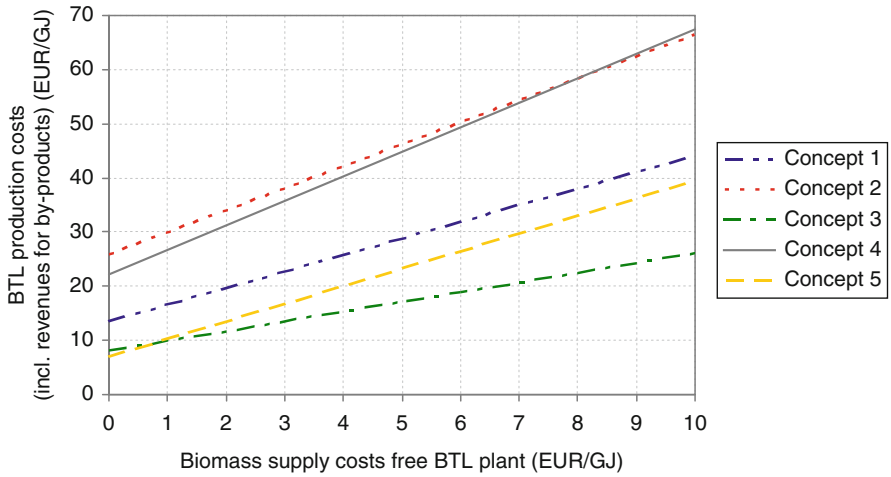

Biomass to Liquid (BtL), Concepts and Their Assessment. Figure 9
Influence of concept-specific efficiency and role of biomass costs to the total BtL production costs (1 €/l_{DE} = 1 €/l/0.0357 GJ/l_{DE} = 28 €/GJ_{BtL}) (EUR = €)

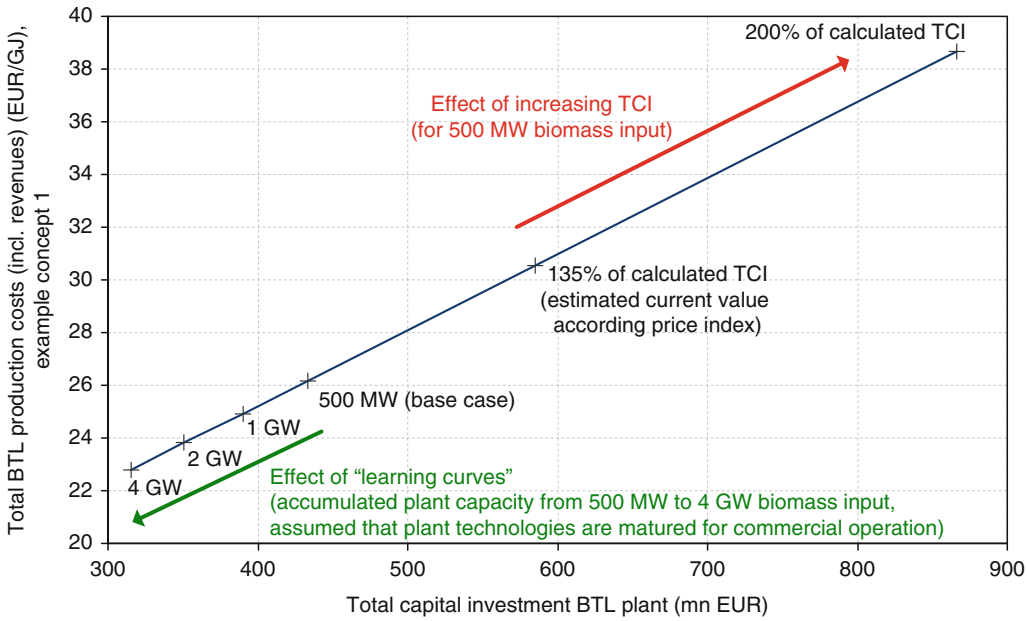

Biomass to Liquid (BtL), Concepts and Their Assessment. Figure 10
Influence of TCI and learning curves to the total BtL production costs (EUR = €)

investigated in the LCA. The method has been standardized by the International Organization for Standardization (ISO) [43].

- Goal and scope definition. The goal of the LCA is to compare different production concepts of BtL fuels (cf. Table 1) [44]. The assessment includes all process stages from well-to-tank (WTT), i.e., biomass production and provision, BtL production, BtL distribution to end use. The reference flow describes in a physical unit the final product or service delivered by the investigated product systems. It is the appropriate unit for analyzing

different products or production routes. Therefore, the function of interest is the supply of chemically bound energy (BtL) to powertrains. The reference flow used in the comparison of BtL fuel production routes is defined as the energy content expressed as the "lower heating value of the fuel delivered to the tank." Figure 11 shows the major stages of the fuel production and supply part of the product system. The conversion processes are divided into different subprocesses (e.g., gasification, gas treatment, synthesis). The LCA relies on the recursively modelled background data of the ecoinvent database v2.01 [44, 45].

The LCA assigns the environmental impacts of foreseen production chains to the produced products. The attribution approach is used that aims at describing the environmentally relevant actual physical flows to and from a life cycle and its subsystems. Thus, it considers only environmental impacts of the running processes and not the impacts caused by a change from one technology to another. Results are stable over time and resistant to changes in other parts of economy. This type of analysis does not reflect that production patterns might be changed due to a decision supported by the LCA.

There is no standardized way or best solution of how to solve problems of by-products and further functions in life cycle inventory modelling. The ISO standard leaves different choices for the problem. Depending on the solution chosen, the results of an LCA might be quite different.

In this assessment, multi-output processes are divided into subsystems (where possible). If this is not possible, the approach of allocation based on different relationship principles is used as far as possible. The allocation between wheat straw and wheat grains is based on prices. The allocation between heat and electricity in the conversion power plant is based on the exergy content. Irrespective of the allocation approach chosen, it is intended that mass balances are correct in all cases. The biomass input to the

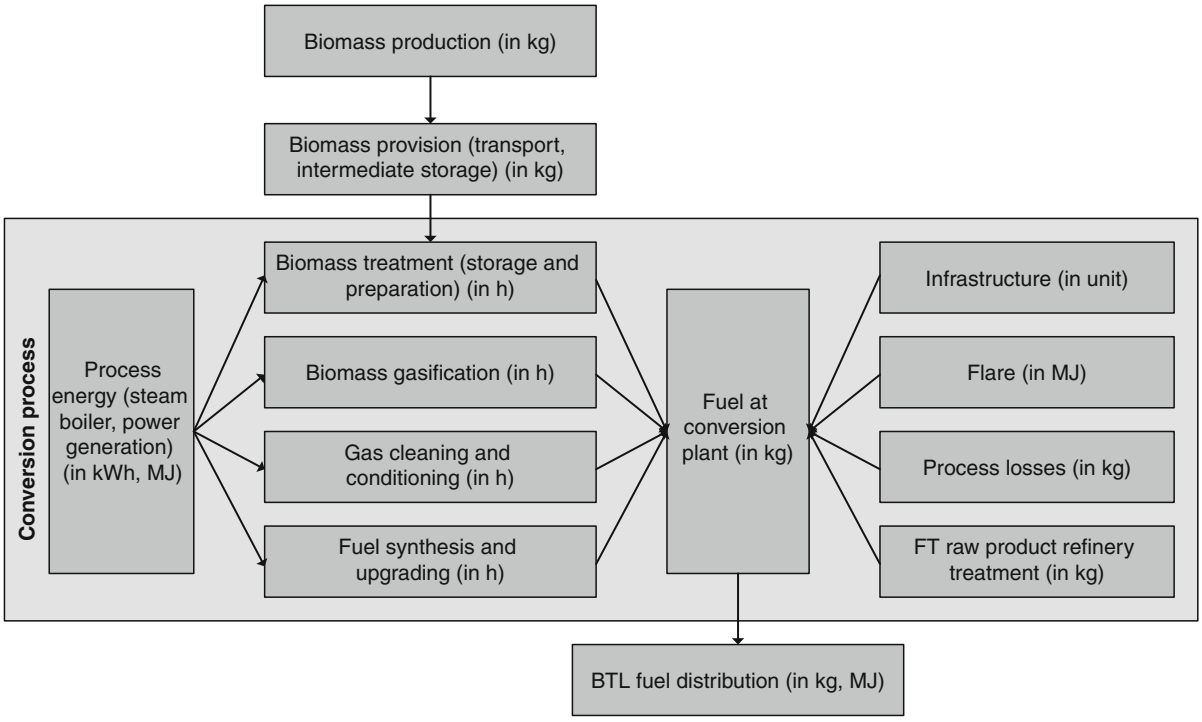

Biomass to Liquid (BtL), Concepts and Their Assessment. Figure 11
Flowchart/subsystems of the product system of BtL fuels

conversion process is fully allocated to fuel production. No part of the biomass is allocated to the generation of heat and electricity, which might be produced as a by-product.

- Life cycle inventory analysis. The second report describes the life cycle inventory analysis (LCI) for the LCA study [46]. In this step of the LCA, data are collected for all inputs and outputs in different stages of the life cycle of BtL fuels.
  - Biomass production and supply. Three types of biomass inputs are used in the conversion to BtL fuels. These are SRC (short-rotation wood such as willow-salix or poplar), MISC (miscanthus), and STR (wheat straw). The life cycle inventory data are based on regional information investigated for Northern, Eastern, Southern, and Western Europe. A critical issue in the inventory of, e.g., wheat straw is the allocation between wheat straw and wheat grain. In the base case, this allocation is made with today's market prices. This gives an allocation factor of about 10% to the produced straw (on a per kilogram basis). A sensitivity analysis is calculated based on the energy content, which leads to an allocation factor of 43% to the produced straw.
  - BtL production and distribution. Data of the conversion processes were provided by the different plant developers. The data are mainly based on technical modelling of such plants, which is based on experiences and knowledge gained from the research work done in the project. The data are crosschecked as far as possible during the technical assessment of the conversion concepts [4]. Where so far no reliable first-hand information is available (e.g., emission profiles of power plants, concentration of pollutants in effluents, or the use of catalysts), assumptions are based on literature data. Thus, sometimes it is difficult to distinguish between different process routes because differences could not be investigated.

All inventory data investigated are recorded in the EcoSpold data format. The format follows the ISO-TS 14048 recommendations for data documentation and exchange formats. It can be used with all major LCA software products [47]. All background data, e.g., on fertilizer production or agricultural machinery are based on the ecoinvent database v2.0 [45]. They were investigated according to the same methodological rules as used here. The quality of background data and foreground data is on a comparable and consistent level and all data are fully transparent.

Overall Results Following the methodical approach, the part on results focuses on the life cycle impact assessment (LCIA) and the interpretation of the life cycle assessment [48]. The data describing emissions and resource uses are calculated over the full life cycle and aggregated to the list of category indicators before interpretation.

The elementary flows from the life cycle inventory analysis are characterized according to commonly accepted methodologies. The life cycle impact assessment (LCIA) covers several impact category indicators (cf. Table 2). These indicators characterize and summarize the contribution of individual emissions or resource uses to a specific environmental problem. The higher the figure, the higher is the potential environmental impact resulting from emissions and resource uses over the life cycle of the investigated product. There is no weighting used across the category indicators. This life cycle impact assessment evaluates the use of primary energy resources, the emission of greenhouse gases, and the potential contribution of elementary flows to photochemical oxidant formation, acidification, and eutrophication. Besides the LCIA results, two cumulative results of elementary flows are presented. The water use sums up all demands of water in the life cycle including rainwater but excluding turbine water. For land competition, all surface land uses are summed up as square meter used over 1 year.

The main drivers regarding all environmental category indicators have been analyzed [44]. They can be summarized as follows:

- The major elementary flow regarding the cumulative energy demand is the energy bound in harvested biomass. Thus, the biomass production process accounts for 80–90% of the cumulative energy demand.
- Crude oil (50–60%) and natural gas use are the major contributions to abiotic depletion. The use of uranium has only a small contribution within

Biomass to Liquid (BtL), Concepts and Their Assessment. Table 2 Category indicators investigated in this assessment [49, 50]

Category indicator	Description of the problem and relevance for the processes investigated
Cumulative energy demand (CED)	The cumulative energy demand of biomass, other renewable, fossil, and nuclear energy resources is characterized and summed up with the reference unit MJ_{eq} (MJ equivalents).
Abiotic depletion potential (ADP)	Important is the use of nonrenewable energy resources. The depletion of other abiotic resources is included in this indicator as well. The use of uranium for electricity generation is included with a smaller characterization factor compared to the CED.
Global warming potential (GWP)	Contribution to the problem of climate change evaluated with the global warming potential. Main reason for promotion of BtL fuels.
Photochemical oxidation potential, non-biogenic (POCP, non-biogenic)	Evaluation of potential contribution to the formation of summer smog. The production processes and agriculture have some relevance. It has to be noted that only a small part of NMVOC gets a characterization factor according to the CML methodology. All unspecified NMVOC are not assessed. Biogenic emissions from plant growing are not evaluated, but other biogenic emission, e.g., CO from biomass burning.
Acidification potential (AP)	Emission of acid substances contributing to the formation of acid rain. Relevant are air emissions from agriculture and fuel combustion in transport processes.
Eutrophication potential (EP)	Overfertilization of rivers and lakes due to human-made emissions. High relevance for the use of fertilizers in agricultural processes.
Inventory results for resources	
Water use	Water is a scare resource especially in Southern European countries. The indicator includes all types of water use including rainfall on the agricultural area, irrigation water, and direct uses of water in conversion processes.
Land competition	Fertile land area is the most important resource for production of biomass and there are differences between different biomass types. It is recorded in m^2/a (square meter occupied for 1 year).

this category indicator. The resource extraction takes place in many different unit processes of the life cycle.

- Fossil carbon dioxide (50–70%) and dinitrogen monoxide (20–40%) are the major elementary flows with respect to climate change. Methane from off-gases and emissions of the internal power plant in the conversion plant accounts for up to 15% of the total greenhouse gas emissions.
- A range of different substances is important with regard to the photochemical oxidation. The most important ones are sulfur dioxide, carbon monoxide, and different NMVOC. DME emissions are relevant in the fuel distribution.
- Acidification is caused by ammonia, sulfur dioxide, and nitrogen oxides in about equal shares. The emissions of acidifying substances can be attributed to the biomass production, direct air emissions of these conversion processes that release off-gases, and emissions from the internal power plant. The operation of transport devices and tractors is also an important source of such emissions.
- Eutrophication is caused by nitrates, phosphates, ammonia, and nitrogen oxides. A share of more than 50% of the release of eutrophication emissions can be attributed in most cases directly to the agricultural production process. Other important sources of emissions are the direct air emissions from the conversion process and power plant. The

production of fertilizers contributes in smaller amounts.

- The water use is fully dominated by rainwater used in agriculture. Other water uses, e.g., in the conversion plant or for irrigation are not very important.
- The results for land competition are dominated by the agricultural biomass production, which accounts for about 90% of all land uses. For the conversion routes based on straw, this share is reduced to 80%. Because of the allocation procedure, only a small part of the land used for wheat cultivating is attributed to straw. Several wood-consuming background processes, e.g., storage facilities, get a share of up to 20% in the land occupation of straw conversion routes.

In the following, the category indicator results of different conversion concepts are compared from well to tank. They are summarized in Figs. 12 and 13. Many category indicators like acidification, eutrophication, water use, and land competition show an absolutely dominating influence of the agricultural production of biomass. Thus, the type of biomass and the conversion rate are important in the comparison.

The conversion rate plays a major role in the formation of air emissions from the conversion plant. It is assumed that the higher the conversion rate, the lower is the share of biogenic carbon dioxide and thus also other pollutants that are released to the ambient air. Therefore, the improvement of the conversion rates and the reduction of the environmental burdens of the biomass production itself are the main drivers for further environmental improvements of the BtL chains.

The BtL concepts 1 and 3 have the lowest environmental impacts in the assessment with regard to the environmental indicators cumulative energy demand, global warming, photochemical oxidation, acidification, eutrophication, and abiotic resource depletion. They are followed by concept 4 and 2 process. Concept 5 shows the highest environmental impacts due to a process design with a considerably high amount of electricity production and thus a lower biomass to fuel conversion rate.

In the case of the conversion of wood, concept 1 has between 15% and 30% higher impacts than concept 3 with regard to the category indicators cumulative energy demand, abiotic depletion, global warming, eutrophication, water and land use. This can mainly be explained with the higher conversion rate of the DME process. However, the concept 1 has 35% lower impacts in the category indicator photochemical oxidation, because the emissions in the DME distribution are higher. Concept 4 has more than 65% higher impacts than concepts 1 and 3. Concept 5 has a rather

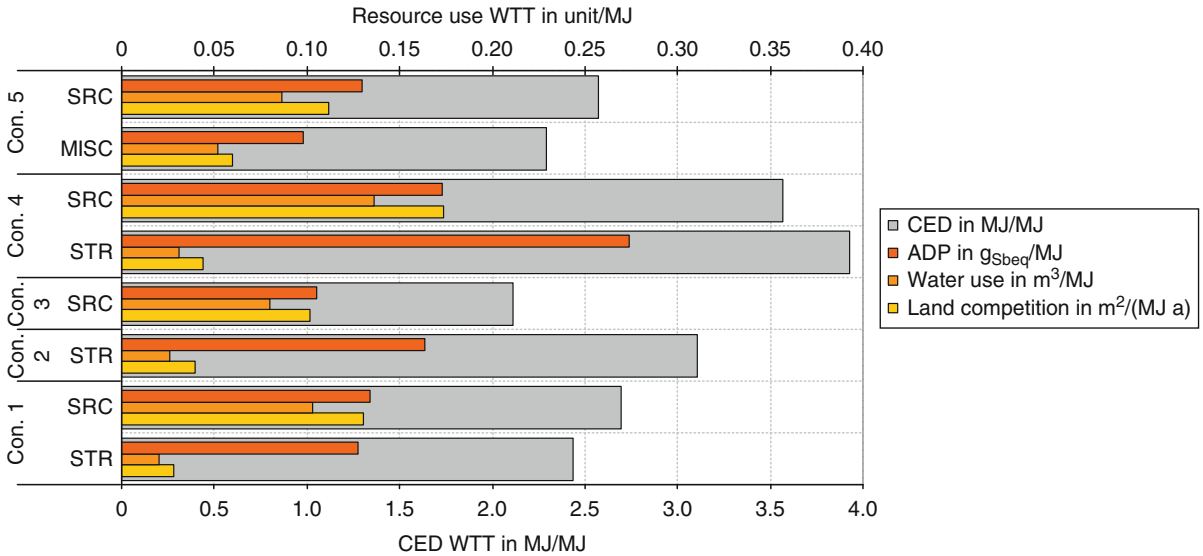

Biomass to Liquid (BtL), Concepts and Their Assessment. Figure 12
Cumulative energy demand and other resource uses based on the energy content of BtL delivered to the tank

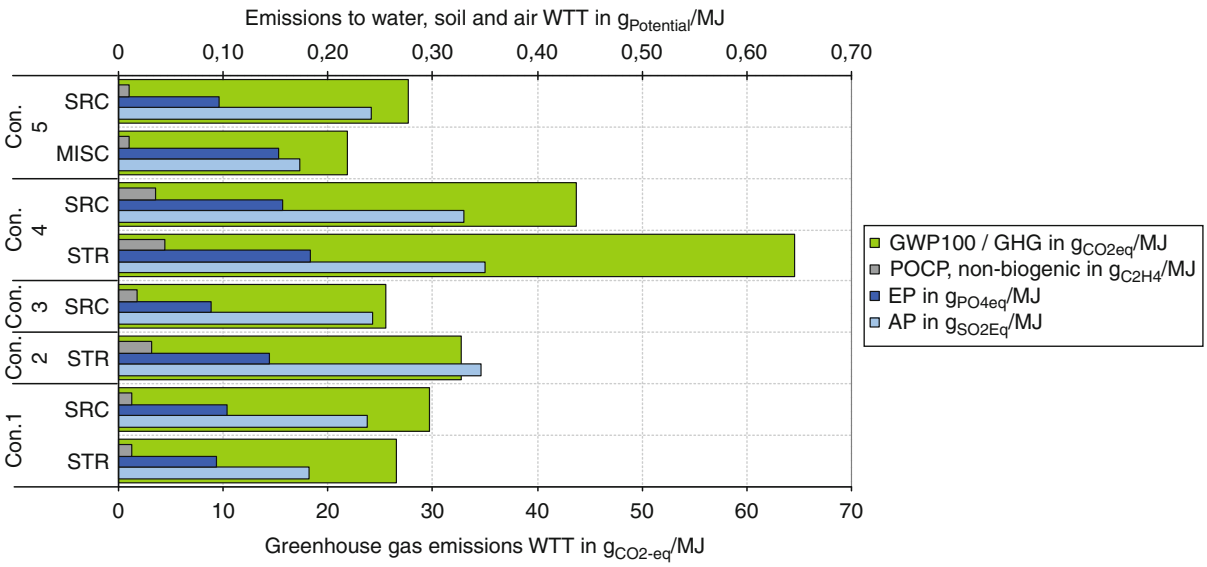

Biomass to Liquid (BtL), Concepts and Their Assessment. Figure 13
Greenhouse gas emission (global warming potential) and other emissions to water, soil, and air based on the energy content of BtL delivered to the tank

low conversion rate and thus has higher impacts in all category indicators except photochemical oxidation, which does not include biogenic emissions.

The comparison of processes based on wood or straw depends not only on the type of biomass, but also on the difference in the conversion rate. The CFB-D process based on wood performs slightly better than processes based on straw regarding the category indicators of cumulative energy demand, abiotic depletion, global warming potential, and eutrophication potential. For concept 1, the process with straw has lower environmental impacts than the conversion of wood. In the case of straw conversion, concept 1 has the lowest impacts fin all category indicators followed by concept 2 and 4 process. There is only one conversion process using Miscanthus (concept 5). Thus, a direct comparison with other conversion concepts is not possible.

Sensitivity Results The data of biomass conversion have been investigated in detail for different subprocesses of the process. The aim was to compare also different subprocesses and to see the relative share of subprocesses in relation to the total environmental impacts.

In general, many category indicators' results of the subprocesses of the conversion process are quite dependent on the biomass input. The share of biomass production and provision is in most cases higher than 90% with respect to the cumulative energy demand, water use, and land competition. The second most important factor is the air emissions with off-gases or due to the energy production in the on-site power plant. This is especially important for the release of substances contributing to photochemical oxidation. Thus, the subprocesses using more heat and electricity contribute more to the total environmental impacts.

The detailed analysis shows that it is difficult to compare different conversion concepts based on the detailed results of single process stages, because the allocation of environmentally relevant streams within the plant might be quite different. Thus, the importance of the different subprocesses might be distinctly different even if the overall results are quite similar.

The allocation criterion between straw and wheat grains has an important influence on the total impacts of all processes that use straw as an input. Allocation by energy content results in up to three times higher environmental impacts per MJ of fuel produced from straw as compared to allocation by actual market prices.

A sensitivity analysis of concept 5 was made. Heat and electricity produced simultaneously are accounted for as equal products to liquid fuels according to their

exergy content. The results of different category indicators are reduced by 10–30%, if the wood input for concept 5 is reduced by about 30% according to the exergy shares of fuel, heat, and electricity production.

Different improvement options are identified from an environmental point of view. The most important one is the increase of the biofuel yield from a given amount of biomass. This reduces the input of biomass and decreases the losses, e.g., in form of air pollutants or effluents. Another conclusion is to improve the environmental profile of the biomass production itself, because this analysis shows that the biomass production has a dominating influence on most of the environmental indicators. Using wastes and by-products is therefore preferable with respect to some category indicators, but not always possible. Possibilities for such an improvement have not been evaluated in detail. Detailed studies of agricultural production show that improvements are not easy to achieve. Different influencing factors, e.g., fertilizer and pesticide use, diesel consumption, and level of yields, have to be balanced out to find an optimum solution. Also the use of wood from forests, produced without using fertilizers and pesticides, might be a viable option for the provision of biomass not yet investigated.

For some processes, auxiliary inputs, e.g., quicklime, are found to be an important contribution to some category indicators. Thus, further focus should be put on reducing the necessary input. In addition, a separate refinery treatment of FT raw products can increase the environmental impacts slightly. Nutrients, which are bound in the biomass, such as phosphorous, are lost with the disposal of ashes, sludge, slag, or effluents. Recovering these nutrients and recycling them for a use in agriculture might be another option to improve the overall performance.

Comparison with Fossil Fuels

A second study has investigated the use of BtL fuels and compared it with fossil diesel [51]. The study has been elaborated as a follow-up study of a recent investigation on several types of biofuels [52, 53]. In that study the environmental impacts of several biofuel options like biogas, plant oil methyl ethers, ethanol, and methanol have been investigated from a Swiss market perspective. The study investigated mainly renewable fuels, which are directly produced from a biomass resource by a physical, chemical, or biological process like oil pressing, chemical reaction, fermentation, or anaerobic digestion. The former study concluded that with many biofuels it would be possible to reduce the emissions of greenhouse gases. But, on the other side there are severe disadvantages regarding several other environmental problems if biofuels are compared with fossil fuels.

- Goal and scope definition. The goal is the investigation of the transport service provided by passenger cars and this is compared with the fossil references natural gas, diesel, and petrol. This includes the necessary infrastructure for roads and its maintenance and the production, maintenance, and disposal of cars. Thus, this is the evaluation of the full life cycle of transport services, which is also commonly referred to as "cradle to grave."
- Life cycle inventory analysis. The inventory for fuel production is based on the data mentioned above and ecoinvent data v2.0 [48, 45]. The inventory of the fuel use emissions is based on information published by automobile manufacturers on reductions due to the use of BtL fuels (cf. Table 1, here except concept 3). Passenger cars fulfilling the EURO 3 emission standards are the basis for the comparison. The use of DME produced from black liquor was not considered in the assessment because it does not seem a realistic option for the Swiss market and it is mainly meant to be used in trucks.

The Swiss study [53] compared the environmental impacts of several biofuels with using fossil fuels (i.e., low sulfur diesel and gasoline, natural gas) in conventional cars. The authors used two single score impact assessment methods for their evaluation, namely, the Eco-indicator 99 (H, A) and the ecological scarcity 2006 method [54, 55] as well as the cumulative energy use and the global warming potential [56]. With these methods, impacts of toxic substances like pesticides are also taken into account.

Comparison of BtL Fuels with Fossil Fuels Figure 14 shows a comparison of transports with passenger cars operated with BtL fuel and fossil fuel. The comparison is presented for the use of nonrenewable energy resources. The ranking of the different types of fuels is

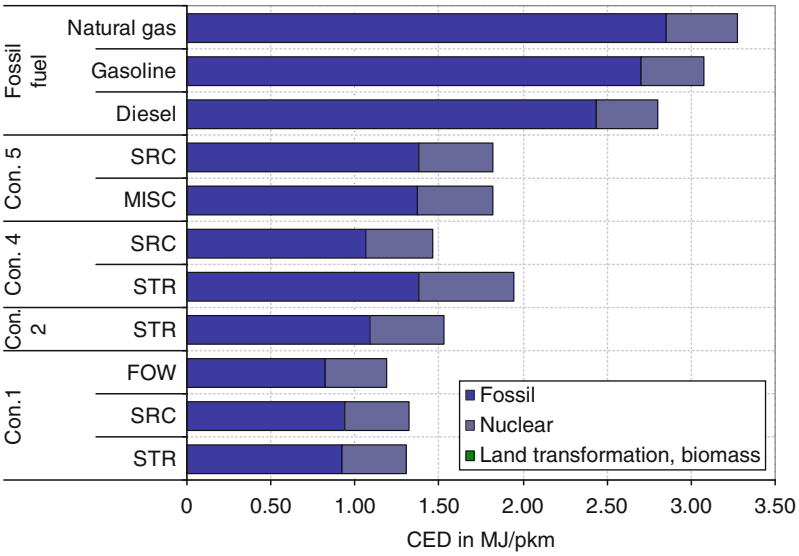

Biomass to Liquid (BtL), Concepts and Their Assessment. Figure 14
Nonrenewable cumulative energy demand of the transport services

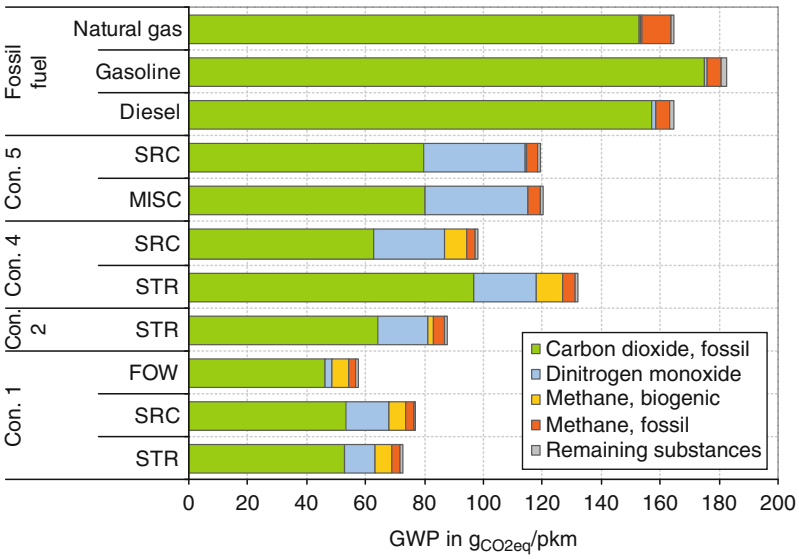

Biomass to Liquid (BtL), Concepts and Their Assessment. Figure 15
Global warming potential of transport services

the same as already discussed on the basis of 1 MJ of fuel delivered to the tank [48]. Of interest is the difference between the transport with cars operated on BtL fuel and the reference cars operated with petrol. The inventory of a EURO 3 passenger car is taken as the baseline. The use of nonrenewable energy resources can be reduced by 37–61% due to the use of the investigated BtL fuels.

Figure 15 compares the emission of greenhouse gases (global warming potential over a time horizon of 100 years) in the life cycle of BtL fuels and fossil fuels. The emission of greenhouse gases is reduced between

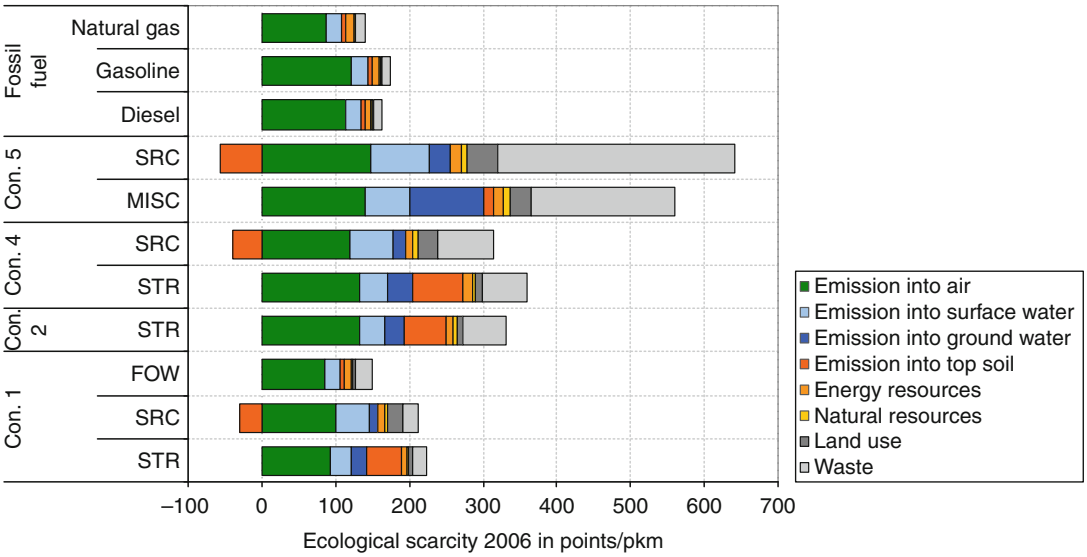

Biomass to Liquid (BtL), Concepts and Their Assessment. Figure 16
Ecological scarcity (2006) points of the transport services with different fuels

28% and 60% compared to the petrol car if BtL fuels from agricultural biomass are used. The best option with forest wood can reduce the global warming potential by even 69%.

Figure 16 shows the results with the method ecological scarcity 2006 [54]. Also here some heavy metals are removed from the agricultural soil during plant growing and thus results in the category emissions into topsoil are negative. All BtL fuels made from agricultural biomass have higher environmental impacts than the fossil reference. The emissions of nitrate are comparably higher for Miscanthus. This is the reason for the relatively higher contribution from emissions into groundwater.

For some fuels environmental impacts due to waste management are quite important. This is due to the disposal of ashes and slag from the conversion process. It might be possible to further improve the disposal or even to reuse the remaining as fertilizers in biomass production. So far such options have not been considered in the modelling of the conversion plants.

The total environmental impacts of the best option using forest wood are about the same as for the fossil reference. Thus, it is possible to produce BtL fuels competitive to fossil fuel as long as they do not use agricultural biomass such as short-rotation wood.

Comparison with Other Biofuels A comparison with other biofuels is possible based on the data investigated earlier [52, 53]. In comparison to other already available biofuels, e.g., rape methyl ether, the results are in the same order of magnitude. These results confirm the findings of a detailed LCA on existing biofuels [53]. Many biofuels derived from agricultural biomass are not preferable from an environmental point of view if the full life cycle is taken into account. But, BtL processes may also use wood from forestry or biomass residues. In comparison to short-rotation wood or other energy crops, this would substantially reduce the environmental impacts.

It is not possible to draw general conclusions for the comparison of synthetic BtL fuels with, e.g., plant oils, ethanol, or methyl ethers. For all types of renewable fuels, the used biomass type is an important factor for the environmental impacts. Thus, better and worse fuels exist in each category. Neither a general advantage nor a general disadvantage of BtL fuels compared to other biofuels is confirmed here.

The best BtL process achieves fuel yields, which allow driving about 50,000 km from the short-rotation wood grown on 1 ha. This is about the same as for sweet sorghum and in the upper range of the biofuels investigated [53]. On the other side also greenhouse gas emissions per hectare are relatively high compared to

the renewable fuels investigated in a previous study. The best option is again forest wood, but this fuel achieves slightly lower mileage per hectare than short-rotation wood. Concerning fuel yields per hectare, there is no general advantage or disadvantage compared to other types of biofuels. Again type of biomass and the large range of efficiencies lead to a wide range of possible results.

Conclusions

Synthetic fuels are of strong interest because of their designable fuel properties in order to provide premium fuels that on the one hand contribute to meet current and future exhaust emission standards and on the other hand allow the use of several raw materials for their production. BtL fuels are one option of future biofuels. There are various concepts to provide liquid synthetic biofuels based on solid biomass. So far it is open that conversion route will be implemented into the market on the background of given techno-economic constraints and necessary environmental benefits. Within this paper five different concepts for BtL provision being currently developed (i.e., FT diesel and DME) have been compared consistently by specific technical and economic criteria under European frame conditions. The results can be summarized as follows.

- The technical assessment has shown that none of the BtL concepts discussed so far has reached an industrial production level. Rather each of these concepts represents a technology leader in terms of specific aspects. An operation of the existing pilot and demonstration projects could be demonstrated in few cases and made know-how available for detailed engineering of BtL plants on the large scale. The technical measures shown for these concepts are possible in principal (theoretically) but have to be confirmed within future demonstration plants. The overall efficiencies could reach a range of 37–64%. They are mainly influenced by the choice of synthesis (here concept 3 shows favorable results) and the integration of mass and energy flows of the BtL plant (as the favorable results present for concept 1 and 5). Important issues that need to be addressed for further R&D&D covers aspects like feedstock flexibility and preparation for biomass gasification (e.g., regarding feedstock qualities and pressurized reactors) and commercial prove of gas cleaning and conditioning (e.g., for CFB gasifiers). Moreover support of the mineral oil and gas industry is important for synthesis, raw product upgrading including refinery integration of syncrude (especially for FT fuels) as well as energy integration for high efficiencies are necessary.
- From the economic assessment it can be concluded that BtL technologies are much more capital intensive than for, e.g., conventional biodiesel fuels, and thus of high capital risk concerning financing investors attractively. BtL production costs strongly depend on biomass costs and therewith on the biomass to biofuel conversion efficiency. Thus, favorable options are concepts with high conversion efficiency (e.g., concept 3), process integration (e.g., concept 1 and 5), and/or the conversion of low-cost biomass residues. Moreover – according to high TCI – parameters like capital-related costs and thus annual full load hours are of importance for an economic plant operation. Considering TCI costs reduction due to learning curves and increasing experiences for commercial technology application, the overall BtL production costs can only be reduced slightly. Thus, BtL costs are expected to be higher compared to other biofuels.
- The environmental assessment confirms that BtL fuels promise positive effects only regarding greenhouse gas emissions and use of nonrenewable energy resources, depending on their concept and frame conditions. The type of biomass input and the conversion rate to the final fuel are quite important. The emissions of greenhouse gases due to transport services can be reduced by about 60% with the best BtL processes using short-rotation wood or straw as a biomass input. This is comparable to other types of biofuels made from agricultural biomass resources. With forest wood, reductions up to 69% are possible. On the other side, there are severe disadvantages from an environmental point of view if fuels are produced from agricultural biomass. The introduction of BtL fuels made from energy crops would further increase environmental problems mainly caused due to today's agricultural practice. Emissions of substances contributing to eutrophication and acidification are much higher than those of transport services based on fossil fuels. Direct emissions of

the conversion plant and transport issues are less relevant as long as legal limits are maintained and biomass is not transported over very large distances.

Future Directions

So far all data for the conversion processes are based on modelling and not on commercial plants. Due to the variety of conversion concepts and possible biomass resources, it is not possible to make generally valid statements concerning the overall impacts of BtL fuels compared to other types of renewable or fossil fuels. All the aspects, however, especially the environmental impacts of BtL fuels have to be reevaluated when BtL fuels are introduced to the market in a commercial way. To quantify the real impacts it is necessary to know the type of biomass used and key figures of the conversion plant, in particular the conversion efficiency, amount and revenues of by-products, emissions and wastes.

In order to leverage maximum learning and progress from the current development activities for BtL, a detailed scientific support, modelling and monitoring of the overall process, and its integration into the energy system is strongly required in the years to come if BtL should contribute to cover the energy demand in a sustainable way.

Bibliography

1. Vogel A, Müller-Langer F, Kaltschmitt M (2008) Analysis and evaluation of technical and economic potentials of BtL-fuels. Chem Eng Technol 31(5):755–764
2. Jungbluth N, Frischknecht R, Tuchschmid M (2008) Life cycle assessment of BTL-fuels, conversion concepts and comparison with fossil fuels. In: 16 European biomass conference + exhibition, Valencia, 2–6 June 2008
3. International Energy Agency (2007) World energy outlook 2007. International Energy Agency, Paris. ISBN 978-92-64-02730-5
4. Vogel A, Thrän D, Muth J, Beiermann D, Zuberbühler U, Hervouet V, Busch O, Biollaz S (2008) Comparative assessment of different production processes. Scientific report WP5.4. Technical Assessment, SES6-CT-2003-502705 RENEW – renewable fuels for advanced powertrains
5. Boerrigter H, Van der Drift A (2004) Biosyngas – description of R&D trajectory necessary to reach large-scale implementation of renewable syngas from biomass. Energy research Centre of the Netherlands (ECN), Petten
6. Henrich E et al (2005) Gaserzeugung aus Biomasse. Final report, Forschungszentrum Karlsruhe
7. Kaltschmitt M, Hartmann H, Hofbauer H (2009) Energie aus Biomasse. Grundlagen, Techniken und Verfahren. Springer, Berlin
8. Knoef H (2005) Handbook biomass gasification. BTG Biomass Technology Group, Enschede
9. Rudloff M (2004) Presentation at the congress, Synthetische Biokraftstoffe – Techniken, Potenziale, Perspektiven. CHOREN Industries, Wolfsburg
10. Zanzi R (2006) Torrefied wood an alternative to charcoal for reducing deforestation. Royal Institute of Technology, Department of Chemical Engineering and Technology, Stockholm
11. Boerrigter H et al (2003) Production of FT transportation fuels from biomass; technical options, process analysis and optimisation and development potentials. Energy 29:1743–1771, Utrecht
12. Cheng WH, Kung HH (1994) Methanol production and use. Marcel Decker, New York
13. Ekbom T, Lindblom M, Berglin N, Ahlvik P (2003) Technical and commercial feasibility study of black liquor gasification with methanol/DME production as motor fuels for automotive uses – BLGMF. Nykomb Synergetics AB, Chemrec, Volvo, Ecotraffic, OKQ8, STFi; Methanex, Final Report, Altener Programme
14. Faaij A, Hamelinck C (2001) Future prospects for production of methanol and hydrogen from biomass. Utrecht
15. Hamelinck C (2004) Outlook for advanced biofuels. PhD thesis, University Utrecht
16. Hoehlein B et al (2003) Methanol als Energieträger. Forschungszentrum Jülich GmbH, Institut für Werkstoffe und Verfahren der Energietechnik (IWV), Schriften des Forschungszentrums Jülich Reihe Energietechnik Band 28, ISBN 3-89336-338-6, Jülich
17. Saller G (1999) Technisch-wirtschaftliche Bewertung der Methanolerzeugung aus Biomasse mit Hilfe von Prozessmodellen. Universität Siegen, Dissertation
18. Tijmensen M, Faaij A, Hamelinck C, Van Hardeveld M (2002) Exploration of the possibilities for production of Fischer-Tropsch liquids and power via biomass gasification. Biomass and Bioenergy 23:129–152, Elsevier, Amsterdam
19. Deutsche Energie-Agentur GmbH (2006) Biomass to liquid – BtL realisierungsstudie. Zusammenfassung, Berlin
20. Henrich E (2007) Economic aspects of biosynfuel production via bioslurry gasification. In: Proceedings of the 15th European biomass conference, Paris
21. Rudloff M (2007) First commercial BTL production facility – the Choren ß-Plant Freiberg. In: Proceedings of the 15th European biomass conference, Paris
22. Nitsche R (2007) BTL- biomass to liquid (Fischer Tropsch process at the biomass gasifier in Güssing). In: Proceedings of the 15th European biomass conference, Paris
23. Gebhard R (2006) Black Liquor Gasification – large scale production of green transportation fuels, presentation. Energy Technology Centre, Sweden

24. VDI 3780 (2000) Technikbewertung, Begriffe und Grundlagen. Verein Deutscher Ingenieure, Düsseldorf 2000. Beuth Verlag GmbH, Berlin
25. Syncom (2008) Renewable fuels for advanced power trains, final report of the integrated project RENEW, contract no: SES6-CT-2003-502705
26. VDI 6025 (1996) Betriebswirtschaftliche Berechnungen für Investitionsgüter und Anlagen. VDI-Gesellschaft Technische Gebäudeausrüstung. Beuth Verlag GmbH, Berlin
27. Mueller-Langer F, Vogel A, Brauer S (2008) Overall costs. SES6-CT-2003-502705 Renewable fuels for advanced powertrains. WP5.3 Deliverable D 5.3.8 IEE Germany
28. Mueller-Langer F, Vogel A, Thrän D (2007) Suitable logistic concepts for biomass provision to BtL plants. In: 2nd generation biomass-to-liquids biofuels – technology & commercialisation outlook, BTLtec, Vienna
29. Mueller-Langer F, Thrän D, Gańko E, Jaworski Ł (2007) Biomass provision costs – Final report. SES6-CT-2003-502705 renewable fuels for advanced powertrains. WP5.3 Deliverable D 5.3.6 EC BREC Poland, IEE Germany
30. Chiesa P (2003) Co-production of hydrogen, electricity and CO_2 from coal using commercially-ready technology. In: Second annual conference on carbon sequestration, Washington
31. Ekbom T, Berglin N, Lögdberg S (2005) Black liquor gasification with motor fuel production – BLGMF II, A techno-economic feasibility study on catalytic Fischer-Tropsch synthesis for synthetic diesel production in comparison with methanol and DME as transport fuels. Nykomb Synergetics AB, STFi-Packforsk, KTH Royal Institute of Technology, Statoil, Structor Hulthén Stråth, Final Report, Sweden
32. Munson C, Adams J (2003) Cost allocation targets for vision 21 plant modules, Presentation, San Francisco
33. Swedish National Energy Administration (2002) The Bio-DME-Project Phase 1. Non-confidential version, Report, Stockholm
34. Mueller-Langer F, Oehmichen K (2009) Economic and environmental aspects of Bio-SNG compared with other biofuels. In: Bio-SNG '09 – synthetic natural gas from biomass; international conference on advanced biomass-to-SNG technologies and their market implementation, Zürich
35. Huerthig GmbH (2007) Price index for chemical plants and machinery. published quarterly in journal "Chemie Technik". Hüthig Fachverlag, Heidelberg
36. Doornbosch R, Steenblik R (2007) Biofuels: Is the cure worse than the disease?. Round table on sustainable development, Organisation for Economic Co-operation and Development, OECD, SG/SD/RT(2007)3, Paris
37. Gangl C (2004) Ethanolerzeugung aus stärkehaltigen Rohstoffen zur Treibstoffzwecke. Wien
38. Kavalov B, Peteves SD (2005) Status and perspectives of biomass-to-liquid fuels in the European Commission. European Commission, Directorate General Joint Research Centre (DG JRC), Institut for Energy, Petten
39. Quirin M, Gärtner SO, Pehnt M, Reinhardt GA (2004) CO_2-Studie – CO_2-neutrale Wege zukünftiger Mobilität durch Biokraftstoffe: Eine Bestandsaufnahme. Institut für Energie- und Umweltforschung Heidelberg GmbH (IFEU), Studie im Auftrag der Forschungsvereinigung Verbrennungskraftmaschinen (FVV), Heft 789, Frankfurt am Main
40. Schmitz N, Henke J, Keppler G (2006) Biokraftstoffe eine vergleichende Analyse. Fachagentur Nachwachsende Rohstoffe e. V. (Hrsg.) mit finanzieller Förderung des Bundesministeriums für Ernährung, Landwirtschaft und Verbraucherschutz, Gülzow
41. Thuijl EV, Roos CJ, Beurskens LWM (2003) An overview of biofuel technologies, markets and policies in Europe. Energy Research Centre of the Netherlands, Petten
42. Wakker A et al (2006) Biofuel and bioenergy implementation scenarios. Final report of VIEWLS WP5, modelling studies. Senter Novem, Petten
43. International Organization for Standardization (2006) Environmental management – Life cycle assessment – Principles and framework, 2nd edn. ISO 14040:2006, 2006-06: Geneva
44. Jungbluth N, Frischknecht R, Faist Emmenegger M, Tuchschmid M (2007) Life cycle assessment of BTL-fuel production: goal and scope definition (revised). RENEW – renewable fuels for advanced powertrains. Sixth framework programme: sustainable energy systems, deliverable: D 5.2.2. ESU-services, Uster. Retrieved from www.esu-services.ch
45. ecoinvent Centre (2007) ecoinvent data v2.01, ecoinvent reports No. 1–25. 2007, CD-ROM, Swiss Centre for Life Cycle Inventories, Duebendorf. Retrieved from www.ecoinvent.org
46. Jungbluth N, Frischknecht R, Faist Emmenegger M, Steiner R et al (2007) Life cycle assessment of BTL-fuel production: inventory analysis. RENEW – renewable fuels for advanced powertrains. Sixth framework programme: sustainable energy systems, deliverable: D 5.2.7. ESU-services, Uster. Retrieved from www.esu-services.ch/renew.htm
47. Jungbluth N, Schmutz S (2007) Inventory dataset: EcoSpold/Gabi/Excel. RENEW – renewable fuels for advanced powertrains. Sixth framework programme: sustainable energy systems, deliverable: D 5.2.9. ESU-services, Uster. Retrieved from www.esu-services.ch/renew.htm
48. Jungbluth N, Frischknecht R, Faist Emmenegger M, Steiner R et al (2007) Life cycle assessment of BTL-fuel production: life cycle impact assessment and interpretation. RENEW – renewable fuels for advanced powertrains. Sixth framework programme: sustainable energy systems, deliverable: D 5.2.10. ESU-services, Uster. Retrieved from www.esu-services.ch/renew.htm
49. Guinée JB (final editor), Gorrée M, Heijungs R, Huppes G et al (2001) Life cycle assessment; an operational guide to the ISO standards, parts 1 and 2. Ministry of Housing, Spatial Planning and Environment (VROM)/Centre of Environmental Science (CML), Den Haag/Leiden
50. Frischknecht R, Jungbluth N, Althaus H-J, Bauer C et al (2007) Implementation of life cycle impact assessment methods. CD-ROM, ecoinvent report No. 3, v2.0, Swiss Centre for Life Cycle Inventories, Dübendorfz Retrieved from www.ecoinvent.org

51. Jungbluth N, Büsser S, Frischknecht R, Tuchschmid M (2008) Ökobilanz von Energieprodukten: life cycle assessment of biomass-to-liquid fuels. programm biomasse, 280006, ESU-services Ltd. im Auftrag des Bundesamt für Energie, Bundesamt für Umwelt und Bundesamt für Landwirtschaft, Berne
52. Jungbluth N, Chudacoff M, Dauriat A, Dinkel F et al (2007) Life cycle inventories of bioenergy. Ecoinvent report No. 17, v2.0. ESU-services, Uster. Retrieved from www.ecoinvent.org
53. Zah R, Böni H, Gauch M, Hischier R, et al (2007) Ökobilanz von Energieprodukten: Ökologische Bewertung von Biotreibstoffen. Schlussbericht, Abteilung Technologie und Gesellschaft, Empa im Auftrag des Bundesamtes für Energie, des Bundesamtes für Umwelt und des Bundesamtes für Landwirtschaft, Bern
54. Frischknecht R, Steiner R, Jungbluth N (2009) The Ecological Scarcity Method – Eco-Factors 2006: A method for impact assessment in LCA. Federal Office for the Environment FOEN, Zürich und Bern
55. Goedkoop M, Spriensma R (2000) The Eco-indicator 99: A damage oriented method for life cycle impact assessment. Methodology Report, 2nd rev edn. PRé Consultants, Amersfoort
56. Frischknecht R, Jungbluth N, Althaus HJ, Bauer C et al (2007) Implementation of life cycle impact assessment methods. CD-ROM, ecoinvent report No. 3, v2.0, Swiss Centre for Life Cycle Inventories, Dübendorf. Retrieved from www.ecoinvent.org
57. PRé Consultants (2007) SimaPro 7.1. Amersfoort. www.simapro.com
58. Jungbluth N, Frischknecht R, Faist Emmenegger M, Steiner R et al (2007) Life cycle assessment of BTL-fuel production: Final Report. 2007, RENEW – renewable fuels for advanced powertrains. Sixth framework programme: sustainable energy systems, deliverable: D 5.2.15. ESU-services, Uster. Retrieved from www.esu-services.ch/renew.htm

Biomass Use on a Global Scale

Ausilio Bauen, Raphael Slade
Centre for Energy Policy and Technology, Imperial College, London, UK

Article Outline

Glossary
Definition of the Subject
Introduction
Bioenergy Routes to Different End Uses
Overview of Current and Future Biomass Use
Biomass Use for Heat and Electricity
Biomass Use for Transport Fuels
Future Directions
Bibliography

Glossary

Anaerobic digestion Decomposition of biological wastes by microorganisms, usually under wet conditions, in the absence of air (oxygen), to produce biogas.

Biodiesel Biodiesel refers to a diesel-type fuel produced by transesterification of vegetable oils or animal fats.

Bioenergy Energy produced from the conversion of organic matter.

Bioethanol Alcohol with a two carbon structure and the molecular formula C_2H_5OH.

Biofuel A liquid or gaseous transport fuel produced from biomass.

Biogas A combustible gas derived from decomposing biomass under anaerobic conditions. Biogas normally consists of 50–60% methane, 25–50% carbon dioxide, and other possible elements such as nitrogen, hydrogen, or oxygen.

Biomass Non-fossilized organic material of plant and animal origin.

Bio-SNG Bio Synthetic Natural Gas is a gas that meets the quality standard of natural gas derived from syngas produced from the gasification of biomass.

Butanol Alcohol with a four carbon structure and the molecular formula C_4H_9OH.

Combustion (of biomass) The process of converting biomass fuel into heat, water, and carbon dioxide, though reaction with oxygen present in air.

Energy crops Crops grown specifically for energy. These include food crops such as corn and sugarcane, and nonfood crops such as poplar trees and switchgrass.

Fermentation Conversion of carbon-containing compounds by microorganisms for production of fuels and chemicals such as alcohols, acids, or energy-rich gases.

Fischer–Tropsch (FT) process Catalyzed chemical reaction in which syngas from gasification is converted into a liquid biofuel for gasoline, diesel, or kerosene displacement.

Gasification A thermochemical process at elevated temperature and reducing conditions to convert a solid fuel to a gaseous form (CO, H_2, CH_4, etc.), with char, water, and condensibles as minor products.

Hydrotreating Process which consists of the addition of pairs of hydrogen atoms to a molecule.

Lignocellulosic ethanol Ethanol produced from lignocellulosic material.

Organic Rankine cycle (ORC) A Rankine cycle is a closed circuit steam cycle to convert heat into mechanical energy in an engine. An organic Rankine Cycle uses an organic fluid with a high molecular mass instead of steam, allowing heat recovery from low temperature sources.

Pyrolysis The thermal decomposition of biomass at moderate temperatures (greater than 400°F, or 200°C) in the absence of air.

Stirling engine Closed-cycle regenerative heat engine with a gaseous working fluid. The working fluid, the gas which pushes on the piston, is permanently contained within the engine's system.

Syngas Syngas (from the contraction of synthesis gas) is a mixture of mainly carbon monoxide (CO) and hydrogen (H_2), which is the product of high temperature steam or oxygen gasification of organic material such as biomass.

Torrefaction Mild pretreatment of biomass at a temperature between 200°C and 300°C, resulting in carbonization.

Transesterification Process of exchanging the alkoxy group of an ester compound with another alcohol.

Definition of the Subject

Biomass is an extremely diverse resource that can be converted to multiple energy end uses (heat, electricity, transport fuels) through a range of mature and prospective technologies. Understanding the various options available to use biomass for energy, and their relative technical, economic, and environmental merits is important in understanding how biomass can be most effectively used. This understanding needs to be complemented by an understanding of the drivers (e.g., competing technologies, economic value, relative environmental benefits) for using biomass in different applications, and how these may change in the future. This chapter describes the different ways in which biomass can be used to produce heat, electricity, and transport fuels, covering a range of feedstock, conversion technologies, and intermediate products, and discusses the current and prospective use of biomass in different applications.

Introduction

Biomass can be broadly defined as any non-fossilized organic material of plant and animal origin. A range of biomass products can be used for energy, including products and by-products from forestry, agriculture and aquaculture, as well as a range of agricultural, industrial, and municipal residues and wastes.

Biomass is the oldest fuel used by mankind and has been its main source of energy for cooking and keeping warm from the dawn of civilization to the industrial revolution [1]. Until the eighteenth century, humans were almost completely reliant on wood and charcoal for all of their energy needs, and it was not until the early 1800s that easily accessible coal became more prevalent as it drove Europe's industrial revolution. Over the last century, biomass has been supplanted by higher energy density, easier to handle and cheaper fossil fuels such as coal, oil, and gas.

However, while fossil fuel has mostly replaced the use of biomass, it still accounts for some 50 EJ per year globally, which represents roughly 10% of global annual primary energy consumption. While it represents a mere 3% of primary energy in industrialized countries, it accounts for 22% of the primary energy mix in developing countries, where it contributes largely to domestic heating and cooking, mostly in simple inefficient stoves. Least developed countries still rely on biomass for over 90% for their energy needs [2, 3].

At present, forestry, agricultural, and municipal residues and wastes are the main feedstocks for producing heat and electricity from biomass. In addition, a small share of sugar, grain, and vegetable oil crops are used as feedstocks for the production of liquid biofuels.

The biomass resource base is potentially large, and so are the opportunities for its increased use in different energy segments in both industrialized and developing countries. There is significant potential to expand biomass use by tapping the large volumes of

unused residues and wastes. The use of conventional crops for energy use can also be expanded, with careful consideration of land availability and food demand. In the medium term, lignocellulosic crops (both herbaceous and woody) could be produced on marginal, degraded, and surplus agricultural lands and provide the bulk of the biomass resource. In the longer term, aquatic biomass (algae) could also make a significant contribution.

Over the last 3 decades, issues of energy security, increasing prices of fossil fuels, and global warming have triggered a renewed interest in biomass for the production of heat, electricity, and transport fuels. Many countries have introduced policies to support bioenergy, not least as a means of diversifying their agricultural sectors, which has stimulated sustained growth in the sector. This has been accompanied by significant developments in conversion processes, with many technologies introduced in the market and several cleaner, more efficient technologies, capable of producing a broader range of products, at the research, development, and demonstration stage. Bioenergy has become increasingly diversified in terms of final uses, and in terms of resources, with new conversion technologies being developed to account for the varied physical nature and chemical composition of the feedstocks available, as well as the energy service required. There is also growing interest and research in the production of chemicals from biomass, possibly in conjunction with the production of energy. The multifunctional role of biomass, in terms of both the products and services it might provide, offers an opportunity to generate value beyond energy products.

Projected world primary energy demand by 2050 is expected to be in the range of 600–1,000 EJ (compared to about 500 EJ in 2008). Scenarios looking at the penetration of different low-carbon energy sources indicate that future demand for bioenergy could be up to 250 EJ/year [2]. This projected demand falls well within the estimates of sustainable biomass supply potential, so it is reasonable to assume that biomass could sustainably contribute between a quarter and a third of the future global energy mix. The contribution from bioenergy that is actually realized will depend on the cost competitiveness of bioenergy and on future policy frameworks, such as greenhouse gas emission reduction targets.

Biomass is currently the largest global contributor of renewable energy in developed and developing countries, and has significant potential to expand in the production of heat, electricity, and fuels for transport. Further deployment of bioenergy, if carefully managed, could provide an even larger contribution to global primary energy supply; significant reductions in greenhouse gas emissions, and potentially other environmental benefits; improvements in energy security and trade balances, by substituting imported fossil fuels with domestic biomass; and opportunities for economic and social development in rural communities.

Bioenergy Routes to Different End Uses

There are many bioenergy routes that can be used to convert raw biomass feedstock into a final energy product. Several conversion technologies have been developed that are adapted to the different physical nature and chemical composition of the feedstock, and to the energy service required (heat, power, transport fuel). Biomass upgrading technologies (e.g., pelletization, torrefaction, pyrolysis) are also available and being developed to convert bulky raw biomass into denser and more practical energy carriers, thereby enabling more efficient transport, storage, and convenient use in subsequent conversion processes.

The production of heat by the direct combustion of biomass is the leading bioenergy application throughout the world and is often cost-competitive with fossil fuel alternatives. Technologies range from rudimentary stoves to sophisticated modern boilers. For a more valuable and efficient use of the biomass resource, modern, large-scale heat applications are often combined with electricity production in combined heat and power (CHP) systems.

Different technologies exist or are being developed to produce electricity from biomass. Co-combustion (also called co-firing) of biomass in coal-based power plants is the lowest cost option for solid biomass conversion to electricity. Dedicated biomass combustion plants, including MSW combustion plants, are also in successful commercial operation, and many are integrated with industrial or district heating CHP facilities. Anaerobic digestion is well suited for producing

electricity and heat from wet organic materials, via the production of biogas. All these technologies are well established and commercially available. Gasification technology promises greater efficiency, better economics at both small and large scale and lower emissions compared with other biomass-based power generation options. However, reliable and cost-effective operation needs to be more widely demonstrated. Other technologies (such as Organic Rankine Cycle and Stirling engines combined with combustion systems) are currently in the demonstration stage and could prove economically viable in a range of small-scale applications, especially for CHP.

In the transport sector, biofuels are widely deployed in several countries – mainly bioethanol from starch and sugar crops and biodiesel from oil crops and residual oils and fats. Their production costs vary significantly depending on the feedstock used (and their volatile prices), and on the scale of the plant. The potential for further deploying these biofuels is high, subject to sustainability criteria, including sustainable land use criteria, being met. Methane derived from biogas is also used in several countries (e.g., Sweden), mainly as a fuels for vehicle fleets, such as municipal buses. Many other biofuel routes are under investigation or being demonstrated based on a wide range of feedstocks (different types of residues and wastes and novel crops) and on biological and thermochemical conversion routes. These biofuel routes could lead to a wider range of fuels which could more easily displace greater quantities of fossil fuels.

Further development of bioenergy technologies is needed mainly to improve the efficiency, reliability, and sustainability of bioenergy chains. In the heat sector, improvement could lead to cleaner, more reliable systems linked to higher quality fuel supplies such as pellets. In the electricity sector, the development of smaller cost-effective electricity or CHP systems could better match local resource availability. In the transport sector, improvements could lead to a wider range of higher quality and more sustainable biofuels, expanding their use across different transport sectors (e.g., aviation). Ultimately, bioenergy production may increasingly occur in biorefineries where transport biofuels, power, heat, chemicals, and other marketable products could all be coproduced from a mix of biomass feedstocks.

Combustion

Combustion is the simplest means of generating heat from relatively dry biomass. Technologies range from open fires and simple stoves rated at a few kW (3–50 kW) to sophisticated installations that combine heat and electricity production (CHP) which can service the needs of an entire community or industrial complex, to large plants of hundreds of megawatt capacity.

Burning biomass in an open fire has a low efficiency (∼10–15%) and, in developing countries, where this is the primary source of heat for cooking, there have been major efforts to replace open hearths with simple stoves in order to conserve limited supplies of fuel and improve living conditions [4]. In industrialized countries, there is also a major market for biomass for domestic heating. Modern domestic biomass boilers can provide efficiencies of 70–90% and may include automated fuel feed, catalytic gas cleaning, and increasingly make use of standardized fuel such as pellets [5]. Biomass heating is well developed in European countries with good resource availability. In Sweden, in particular, a large and growing market has developed for biomass pellets, which are fired in automated systems [5].

Pellets are more expensive than the wood chips from which they are derived due to the processing. But, they have a number of advantages: they offer greater energy density, are comparatively easy to transport and have lower moisture content (below 8%) compared to wood chips. Pellets can provide a uniform product, resulting in reliable and consistent performance when burnt. This uniformity is defined within product standards, which can also prove important in facilitating the trade of biomass feedstocks [6].

Domestic heat may also be provided by district heating, where biomass is burnt in a large-scale facility and the heat distributed via a network of pipes. In general, the bigger the combustion plant the lower the capital cost per unit energy supplied, and the greater the thermal efficiency [7]. Larger facilities can also accommodate more easily the use of lower quality or contaminated biomass (e.g., waste derived fuels). These fuels are lower cost but may necessitate pretreatment or flue-gas cleaning that are generally only economically viable at a larger scale [7].

While domestic installations produce low-grade heat (<100°C), large boilers produce high-pressure steam that can be used to generate electricity via steam cycles before residual heat is distributed. Such combined heat and power (CHP) systems can be very efficient (60–90%), but for maximum efficiency, they require large and stable heat loads. They are therefore economic in colder climates where district heating is installed, or where there is an industrial heat demand. Heat may also be used to provide chilling via adsorption chillers, which when combined with the supply of electricity and heat is known as tri-generation [8]. In the lower capacity range, the Stirling Engine (10–100 kW_e) and the Organic Rankine Cycle (ORC) (50–2,000 kW_e) are suitable technologies for distributed cogeneration.

A boiler combined with a steam cycle is currently the cheapest and most reliable route to produce power from biomass. While there are many relatively small-scale plants (e.g., 5–10 MW_e) that use low-cost sources of biomass local to them, the importance of economies of scale for steam cycle plants means that dedicated biomass power plants will need to be of a certain size to be economically viable (e.g., >30 MW_e), depending on the cost of biomass. The size of a plant is also generally limited by the availability of biomass or the cost of transporting biomass to it. But, the development of biomass trade is facilitating the development of larger-scale biomass power plants of hundreds of MW, generally located in port areas where biomass can be shipped in at relatively low cost.

The co-combustion of biomass with fossil fuels for heat and power production can be relevant to all scales of operation. Biomass co-firing activities have expanded rapidly in recent years, particularly in Northern Europe, and the most popular approach has involved the direct co-firing of solid biomass with coal in existing large power station boilers. This has proved to be the most cost-effective and efficient large-scale means of converting biomass to electricity, because of the scale and infrastructure associated with coal plants.

One of the largest, most advanced, and most efficient biomass CHP plants in the world is the Igelsta plant in Södertälje, near Stockholm, Sweden [9]. Commissioned in March 2010, the plant produces 200 MW of heat and 85 MW of electricity, sufficient to heat around 50,000 homes and provide power for around 100,000 homes.

The fuel used in the Igelsta plant is a combination of wood chips from forest residues (75%) and solid recovered fuels (25%). When running at full capacity, the plant uses approx. 17,000 t of fuel per week. Keeping the plant supplied is a major logistical operation and requires approx. 200 ship-loads, 200 train deliveries, and 12,000 road shipments per year. Wood chips from forestry operations are transported by road, rail, and boat from all over Sweden and neighboring Baltic countries. The recovered fuels include scrap paper, wood, and plastic that is not suitable for recycling and is sourced from offices, shops, and industries in the Stockholm region. Pelletized waste from similar sources is imported by boat from Germany and the Netherlands. Also imported is over 100,000 t of waste wood from Norway, Belgium, and the UK. The municipality that owns the plant considers that such fuel flexibility will be critical as competition for biomass increases.

The combustion technology used at Igelsta is a circulating fluidized bed boiler, incorporating state of the art flue-gas cleaning. The heat it produces is used to raise steam: used first for electricity production (85 MW) and then to deliver low-grade heat to the local district heating network (140 MW). By condensing the steam in the flue gas, the plant is able to deliver an additional 60 MW heat to the heating network, and this gives the combined system an overall efficiency in excess of 90%.

Gasification

Gasification involves the partial oxidation of dry biomass at high temperatures (>500°C) and produces a combustible mixture of carbon monoxide and hydrogen, along with some methane, carbon dioxide, water, and small amounts of nitrogen and heavier hydrocarbons (tar) [10].

Heat production using small gasifiers is commercially established with gasification-boiler systems predominantly used to retrofit natural gas or heating-oil boilers at industrial sites that have easy access to woody residues as fuel, such as wood manufacturing sites. The systems typically produce space heat, and/or process heat or steam and can also be combined with downstream equipment such as absorption chillers and

steam turbines to produce cooling and electricity, respectively [10].

Small- and large-scale gasifier-boiler systems have been developed to supply heat into district heating networks. In Finland, "Bioneer" gasifiers, with an output approximately 5 MWth, were commercialized in the 1980s (following on from a research program initiated during the 1970s), and were coupled to district heating boilers, but faced stiff competition from simple combustion technologies [115, 11]. Also in Finland, a gasifier was built in Lahti in 1997 to provide low-calorific value gas to an existing pulverized coal boiler. This gasifier has a design capacity of 45–70 MWth, and the feedstock is 50% biomass and 50% recycled wood and refuse derived fuel, although demolition wood and shredded tires have also been used.

A potentially interesting future option for delivering renewable heat is to produce a synthetic natural gas from biomass (Bio-SNG) by catalytically converting gas produced from the gasification of the biomass into methane and upgrading (the gas may also need to be enriched to ensure that the calorific value meets the specification required by the network) it to remove water and CO_2. This gas can then be injected into national gas networks and used in domestic and industrial boilers. The technology for producing SNG from coal is mature, and a commercial scale gasifier has operated in North Dakota since 1984. Production from biomass, however, is still at a pre-commercial stage. Interest is growing, however, and large-scale demonstration projects are currently being planned in the Netherlands (10 MWth) and Gothenburg, Sweden (approx. 30 MWth) [12, 13].

Cogeneration of heat and power on a small scale has been attempted using fixed bed gasifiers coupled to modified diesel engines (100–200 kW_e). The principle motivation has been to provide small-scale electricity supply to rural locations in developing countries, though several other demonstration projects have been developed elsewhere (e.g., in Europe and the USA), with the aim to develop a low-cost small-scale electricity generation system. In India, it has been reported that 1,844 biomass gasifier systems with an aggregate capacity of 62 MW_e were deployed by 2004 [14]. Costs, maintenance, and automation requirements have hindered the deployment of such systems outside a developing country context.

A plant in Güssing, Austria, provides a larger-scale example of a gasifier coupled with a gas engine to produce electricity and provide heat to the local district heating system. This plant runs on wood chips from the local area and has a fuel capacity of 8 MW and an electrical output of about 2 MW_e [15]. In 2010, total operating hours since commissioning in 2002 were reported as 43,000 h for the engine and 53,000 h for the gasifier, making this one of the most successful biomass gasification demonstrations [16].

Combining intermediate scale (approx. 10 MWth) gasification with a combined cycle gas turbine was the focus of significant attention in the 1990s. This concept (known as Biomass Integrated Gasification Combined Cycle (BIGCC)) is theoretically appealing because it could provide a greater ratio of electricity to heat and allow for larger-scale electricity generation from gasification systems. Demonstration projects were initiated and undertaken in Sweden, the UK, and the USA, but the technology has proven difficult to commercialize so far: costs remain very high and cleaning the gas to the specification required by the turbine has proved more difficult than expected. Thus far, the technology as a whole remains pre-commercial [5].

Gasification is an important component of several of the proposed new biofuel production routes, such as catalytic routes to diesel, gasoline, naphtha, methanol, ethanol and other alcohols, and syngas fermentation routes to ethanol. Many of the component technologies for some of these routes, such as feedstock preparation, gasification, and Fischer–Tropsch or methanol synthesis are commercially viable or technically mature for other applications. However, the systems as a whole are at the early demonstration stage worldwide, with further development and learning needed to achieve commercially viable fuel production [10].

Anaerobic Digestion

Wet and green biomass can be used to produce biomethane via anaerobic digestion (AD). This technology is fully mature and has been commercially applied at scales ranging from household digesters (approx. 2 m^3) to large municipal waste treatment facilities. All types of biomass can be used as substrates for biogas production as long as they contain a high proportion of carbohydrates, proteins, fats, cellulose,

and hemicelluloses. Highly lignified biomass – e.g., wood – is not suitable without pretreatment due to the fact that lignin cannot be anaerobic decomposed by existing bacteria [17].

Anaerobic digestion produces biogas and digestate. The digestate comprises residual indigestible material (e.g., lignin) and dead microorganisms; it contains valuable plant nutrients like nitrogen and potassium and can be used as a fertilizer and soil conditioner [18]. The biogas is a mixture of methane (ca. 60%), carbon dioxide (ca. 40%), and trace contaminant gases such as hydrogen sulfide; it can be burnt to provide heat, electricity, or both. The biogas can also be stripped of the carbon dioxide, and the methane purified and compressed or liquefied to be used as a fuel for vehicles. Alternatively, the methane can also be injected into the natural gas grid, and several countries, such as Germany, Sweden, and Switzerland, have defined quality standards for biogas injection into the grid [19].

The world's biggest biogas producer is China, where, in 2007, there were an estimated 26.5 million biogas plants, with a gas output of 10.5 billion m^3 [20]. The construction of biogas digesters has also been a key part of the development of renewable energy sources in India where an estimated 3.9 million digesters were installed by 2006; the vast majority of these are family-scale digesters based on cow dung and used for producing fuel for cooking [21].

In Europe, biogas generation for electricity production has grown rapidly. In early 2010, about 5,900 biogas plants with an installed electrical capacity of 2,300 MW_e were operational, and it is predicted that more than 3,000 biogas plants with an electrical capacity of more than 1,700 MW_e will be constructed between 2009 and 2013. Germany is the country with the largest installed capacity, but an increasing number of EU Member States are creating the necessary regulatory frameworks to encourage growth of the national biogas industries [22]. Germany also hosts the world's largest biogas plant at Güstrow. This plant started in 2009 and has a capacity of 50 MWth. The plant can digest 450,000 t of biomass (maize, grain, and silage) per year. The gas is upgraded and injected into the gas grid, and the digestate is returned to the fields [23].

Anaerobic digestion is little developed in the USA, and as of 2010, there were only 151 digesters with a capacity of about 37 MW_e (and 6 MWth). The majority (80%) of these plants are located at dairy farms [24].

Fermentation and Other Microbial Routes

Sugar from crops such as sugarcane and sugar beet is easily fermented to ethanol using yeast in a process known for millennia by mankind. Starches from crops such as corn and wheat can also be easily converted to sugars that can then be fermented to ethanol. Ethanol production using fermentation is the cheapest and most commonly used production route for biofuels for transport. The main producing countries are the USA, based on corn/maize, and Brazil, based on sugarcane. There are around 200 ethanol plant is the USA for a total production capacity of around 50 billion liters, and around 400 plants in Brazil for a total production capacity of around 25 billion liters. In Brazil, ethanol plants coproduce ethanol and sugar for the food market. Corn ethanol plants coproduce dry distillers grains and solubles (DDGS) that are used as animal feed.

Cellulose and hemicellulose, which together with lignin make up most forms of plant biomass, can be broken down into sugars, which can then be fermented into ethanol. Lignocellulosic materials, such as straw, grass, and wood, are more difficult to break down than starch, and therefore require more complex pretreatment to release the constituent sugars from the biomass. Lignocellulosic ethanol conversion technology is at the demonstration stage, with demonstration plants being developed globally. The USA is where most lignocellulosic ethanol activity is centered, and 28 projects are under development.

Sugars can also be converted by microbial processes into higher alcohols, e.g., butanol, and into longer hydrocarbon chains, that could replace gasoline, diesel, and jet fuel. Microbial butanol production is commercial, but the majority of alternative processes are at an early stage of development.

Transesterification and Hydrotreating

Vegetable oils are converted to biodiesel by reacting them with an alcohol in the presence of a base or acid catalyst, a process known as transesterification, which improves the fuel properties of the biodiesel compared

to a straight vegetable oil. Biodiesel is produced globally by transesterifying a range of vegetable oils such as rapeseed, sunflower, soy and palm oil, as well as used cooking oils and animal fats. Most biodiesel production occurs in Europe, with a production capacity of around 20 million tons.

An alternative commercial process for the production of renewable diesel is hydrogenation, which consists of reacting the vegetable oil with hydrogen in the presence of a catalyst. It produces a renewable diesel of superior quality (with higher blending potential) to that obtained via transesterification, and could also be used to produce renewable jet fuel. However, hydrogenation is a more complex process that requires large-scale installations, and as such, is less deployed to date, with a few plants in Europe and South-East Asia.

Alternative sources of oils to conventional oil crops are being developed which could extend vegetable oil production to areas less suitable or not suitable for food crops and which would not compete with them. Examples of these alternative sources of oil are crops like jatropha and algae.

Pyrolysis and Other Thermochemical Processes

Pyrolysis is the controlled thermal decomposition of solid biomass occurring at around 500°C in the absence of oxygen (anaerobic environment) and produces a liquid bio-oil, gas (syngas), and charcoal (biochar) mix. Bio-oils can also be produced by liquefaction in the presence of water, and possibly additional solvents (e.g., methanol), at high pressure (120–200 bar) and relatively mild temperatures (300–400°C) in a process is known as hydrothermal upgrading (HTU). One attractive feature of this process is that wet biomass can be used directly and yields a bio-oil that is less soluble in water.

Compared to raw solid biomass, bio-oil should be cheaper to handle, store, and transport. Also, the energy density (per unit volume) of bio-oil is higher than that of pellets or torrefied biomass, which gives it a competitive advantage in terms of transport cost.

Bio-oil could be upgraded and used as a transport fuel, providing an efficient route to fuels that could be closely integrated with a petroleum infrastructure. It could also be used as fuel for heating and electricity generation, or to produce valuable chemicals.

In spite of these advantages and recent advances, these technologies are at the demonstration stage. Only a few successful pyrolysis demonstration units have been realized (e.g., in Finland and Canada), and both economic and technical issues around quality, consistency, and long-term stability of the bio-oil, which tends to degrade over time, remain to be addressed.

Overview of Current and Future Biomass Use

The predominant use of biomass today consists of fuel wood used in noncommercial applications, in simple inefficient stoves for domestic heating and cooking in developing countries, where biomass contributes some 22% to the total primary energy mix. The IEA [3] estimates that about 2.7 billion people will still be dependent on biomass for cooking in 2030. There is significant scope to improve the efficiency of this use and its environmental performance, and thereby help reduce biomass consumption and related impacts.

In industrialized countries, the total contribution of modern biomass is on average only about 3% of total primary energy and consists mostly of heat-only and heat and power applications [2]. Current heat and electricity market segments which are experiencing growth include domestic heat supply (e.g., pellet boilers), large-scale industrial and community CHP generation (particularly where low-cost feedstocks such as forest residues, bagasse, MSW, etc., are available), and co-firing in large coal-based power plants. The deployment of dedicated electricity plants has been mainly confined to low-cost feedstocks in relatively small-scale applications, such as the use of biogas and landfill gas from waste treatment. However, several relatively large-scale dedicated plants (of up to a few hundred megawatts) fuelled with wood chips are being developed around the world, generally because of a strengthening in national renewable energy policies.

Transport biofuels are currently the fastest growing bioenergy sector, receiving a lot of public attention. They represent only 1.5% of total road transport fuel consumption and only 2% of total bioenergy, but are expected to play an increasing role in meeting the demand for road transport fuel [2].

Overall, world primary energy demand from biomass and waste is expected to grow from 1,176 Mtoe (1 Mtoe = 0.042 EJ) in 2007 to 1,604 Mtoe in

2030 in the IEA's Reference Scenario [3], representing 10% of total primary energy. Biomass use for power generation goes from 84 Mtoe in 2007 to 257 Mtoe in 2030 (4% of electricity), corresponding to 259–839 TWh (1 TWh = 3.6 PJ) of electricity produced and an installed capacity of 46–146 GW. Biomass use for biofuels goes from 34 Mtoe in 2007 to 133 Mtoe in 2030 (4% of transport fuels).

In the IEA's 450 Scenario (where CO_2 in the atmosphere is stabilized at 450 ppm in the period to 2050), biomass use is higher than in the Reference Scenario in 2030 (350 Mtoe higher), representing 16% of total primary energy demand. Major increases in the use of biomass are predicted in all sectors, with use in combined heat and power production and in electricity-only power plants up by 67% (172 Mtoe) compared to the Reference Scenario in 2030 (contributing 5% of electricity), and the contribution of biofuels more than doubling, reaching 278 Mtoe in 2030 (contributing 9% of energy for transport). The eightfold increase over the 2010–2030 period is estimated to occur mainly in those regions that already have the strongest support for biofuels, led by the USA and followed by the European Union, Brazil, and China. Biofuels also make a significant appearance in aviation, with volumes reaching 42 Mtoe globally by 2030 at a global blending ratio of 15% (compared to a mere 1% in the Reference Scenario).

Biomass Use for Heat and Electricity

Biomass can be used to generate heat at all scales required, ranging from a single household to a large industrial complex, and using all types of biomass. Biomass-to-heat systems are commercial, and in many cases, they are also cost-competitive with their fossil fuel alternatives, particularly in locations not connected to a natural gas grid [2]. The principal technologies used to deliver modern biomass heat are combustion, gasification, and digestion.

Globally, around 2.6 billion people are still reliant on traditional uses of biomass and burn wood, straw, charcoal, and dung to provide basic energy services such as cooking and heating [25]. This use is dominant in rural areas of developing countries and is associated with poverty and deforestation [26, 27]. Traditional conversion technologies, such as simple combustion in open hearths, also tend to be inefficient and contribute to indoor air pollution which can damage health [28]. Using biomass in this way accounts for about 13% of global final energy consumption and about 87% (39 EJ) of global bioenergy [2], though the extent of biomass use is difficult to estimate accurately.

Biomass is also extensively used for domestic heating in industrialized countries. While biomass continues to be used in open fireplaces, mainly for aesthetic reasons, where biomass is the main source of heating modern biomass conversion technologies are used, which provide high-quality energy services that are clean, efficient, and comparable in convenience with their fossil fuel alternatives. Estimating how much heat is provided via modern systems in industrialized countries is also difficult because the heat market is captive to the buildings, industrial processes, and locations being supplied. Government statistics tend only to record large systems, such as district heating networks and power plants.

Small appliances such as log burning stoves are only visible at point of sale, or if they use biomass that appears in retail statistics. Nevertheless, there is evidence of a growing market for modern boilers and stoves in the OECD. Within the USA, for example, it is estimated that approximately 800,000 households use wood as their primary heat source, whereas in the top nine European countries (Austria, Belgium, Denmark, Finland, France, Germany, Italy, Spain, and Sweden), the number of domestic stoves and boilers is estimated to exceed 1.3 million and accounts for the majority of solid biomass sold in Europe [25, 29].

In OECD countries, the volume of biomass for residential heat is expected to grow by 40–90% to reach 3.2–4.3 EJ in 2030 [3], as a result of a growing share of biomass in district heating systems and the growing market for modern boilers and stoves in buildings. Scandinavian countries – Sweden, Finland, and Denmark – are leaders in biomass residential heating, with large systems producing more than two thirds of the biomass heat. In Sweden, biomass is now the primary energy source for the district heat sector and in 2009 the share of energy production from biomass exceeded oil for the first time [25]. Sweden is the leader with biomass contributing close to 50% of its large-scale residential heat production, followed by Austria (24%), Finland (17%), Denmark (14%), and Norway (10%).

On average 5% of large-scale heat is provided by biomass in the USA and 7% in the IEA member countries [30].

Biomass is also used to provide process heat to a variety of industries, mainly agricultural and forestry product processing industries, where electricity is often produced in combination with heat. Other industries too use biomass fuels for their processes (e.g., the use of charcoal in the Brazilian steel industry). Industrial use of biomass was about 189 Mtoe in 2007 and is expected to grow to 292 Mtoe in 2030 according to the IEA's Reference Scenario [3].

Worldwide, the installed capacity for biomass-based power generation was about 46 GW in 2007 [3], with an estimated electricity production of some 259 TWh (roughly the annual total power consumption of Spain). This power production occurs mostly in:

- Co-firing plants in countries with coal power stations
- Combustion-based CHP plants linked to district heating systems (Nordic countries in Europe), and in large pulp and paper or food industries (e.g., Brazil, USA)
- Landfill gas units and MSW incineration and anaerobic digestion plants
- Dedicated biomass combustion plants fuelled with wood chips and agricultural residues (e.g., straw)

Biomass Use for Transport Fuels

Biofuels are a fast growing bioenergy sector. While Brazil has been producing bioethanol from sugarcane since the 1970s, it is only in the last decade that biofuel production has acquired global production significance. Biofuels, though, still represent only about 1.5% of total road transport fuel consumption and only account for some 2% of the final bioenergy mix (in energy terms) [2].

Bioethanol production has grown dramatically over the last decade. Nearly 80% of the global supply of biofuels is bioethanol from Brazil (from sugar-cane) and the USA (from corn/maize), where plants with capacities up to more than 500 million liters per year are found. Global biodiesel production has also grown significantly, with most production based in Europe, and companies in Germany and Austria having established themselves as leading technology providers. China and India also produce significant quantities of biofuels, mostly of bioethanol.

Bioethanol is used as a gasoline substitute and is generally blended with gasoline to different extents depending on fuel and vehicle specifications at levels between 5% and 10%. In Brazil, the ethanol blend level is higher (25%) and neat ethanol is also sold for use in vehicles. In the past, the use of neat ethanol required dedicated vehicles, but the successful and rapid introduction of flex-fuel vehicles now allows for switching between bioethanol and conventional gasoline, and any blend in between. In Europe and the USA, the introduction of flex-fuel vehicles has also led to the uptake of E85, a blend of 85% ethanol and 15% gasoline.

Biodiesel is used as a diesel substitute and is generally blended up to between 5% and 7% with diesel, mainly because of limitations imposed by fuel and vehicle specifications. Higher biodiesel blends are used in fleet vehicles (e.g., trucks and buses), generally in the form of B30, a blend of 30% biodiesel and 70% diesel. In Germany, 100% biodiesel has been used in vehicles, through a dedicated network of refueling stations.

Biomethane derived from biogas is used as a fuel, mainly for compressed natural gas (CNG) fleet vehicles. There were nine million vehicles in operation in 2007 compared with four million in 2004. Sweden, with a fleet of 15,000 CNG vehicles, has a share greater than 55% of biomethane in natural gas for transport, and Switzerland over 35%. Germany and Austria are both aiming for 20% by 2020 [31].

Global biofuels supply reached about 0.8 million barrels per day in 2008, with most of the use and growth in production in North America and Europe. Biofuels growth remains largely driven by energy security and climate change policies, with agricultural policy also playing an important role. The industry, however, is subject to the vagaries of the oil price and agricultural commodity prices, with dips in oil prices and rises in the prices of sugar, starch, and vegetable oil commodities cutting the profitability of biofuel production and placing financial strain on producers. The growth of the biofuels industry will also depend on its environmental and social sustainability.

The use lignocellulosic feedstocks promises access to a greater resource and greater GHG reduction potential than current ethanol and biodiesel production from sugar, starch, and oil crops. But routes based on lignocellulosic material are in the early days of

commercialization. New biofuel technologies also allow biofuels to penetrate other transport fuel markets such as aviation fuel (e.g., production of jet fuel from Fischer Tropsch or hydrotreating routes).

Future Directions

Energy security and climate change policy are the main drivers for the expansion of bioenergy use. Agricultural policy has been – and continues to be – an important driver. Rising fossil fuel prices also mean that bioenergy is increasingly competitive in heat, electricity, and transport applications. However, bioenergy will compete for economic resources with other low-carbon and oil-substituting technologies in the different sectors.

The best use of biomass depends on how it can best contribute to overall energy system goals. There are likely to be trade-offs between the different attributes bioenergy may contribute to meeting these goals in the different sectors. For example, appreciating where bioenergy can have the greatest impact on GHG emissions reduction relies on both an understanding of the emissions savings which could result from different bioenergy routes and the importance of bioenergy in reducing emissions in a particular sector relative to other low-carbon options.

The potential for innovation in bioenergy remains large, and so is its potential to contribute effectively to the future energy system across heat, electricity, and transport applications.

Bibliography

1. James SR (1989) Hominid use of fire in the Lower and Middle Pleistocene: a review of the evidence. Curr Anthropol 30:1–26
2. Bauen A, Berndes G, Junginger M, Londo M, Vuille F (2009) Bioenergy – a sustainable and reliable energy source a review of status and prospects. IEA bioenergy. international energy agency, Paris. www.ieabioenergy.com
3. IEA (2009) World energy outlook 2009. International Energy Agency, Paris
4. Barnes DF, Openshaw K, Smith KR, van-der-Plas R (1994) What makes people cook with improved biomass stoves? A comparative international review of stove programs. World Bank technical paper #242. http://www-wds.worldbank.org/external/default/WDSContentServer/WDSP/IB/1999/08/15/000009265_3970311122727/Rendered/PDF/multi_page.pdf. Accessed Dec 2010
5. Faaij APC (2006) Bio-energy in Europe: changing technology choices. Energy Policy 34:322
6. Perry M, Rosillo-Calle F (2006) Sustainable international bioenergy trade: securing supply and demand – UK Task 40 Co-firing report. Imperial College of Science Technology & Medicine, London
7. Dornburg V, Faaij A (2001) Efficiency and economy of wood-fired biomass energy systems in relation to scale regarding heat and power generation using combustion and gasification technologies. Biomass Bioenerg 21:91–108
8. BEC (2010) Information sheet no. 4: combined heat and power (CHP). Biomass energy centre (BEC). www.biomassenergycentre.org.uk/pls/portal/docs/PAGE/RESOURCES/REF_LIB_RES/PUBLICATIONS/4.%20CHP%20V5%209-2009.PDF. Accessed Dec 2010
9. Söderenergi (2010) The Igelsta CPH plant – Sweden's largest bio-fuelled cogeneration facility. www.soderenergi.se. Accessed Dec 2010
10. E4tech (2009) Review of technologies for gasification of biomass and wastes. UK National Non-Food Crop Centre (NNFCC)
11. OPET (2002) Review of Finnish biomass gasification technologies. Technical Research Centre of Finland/organisations for the promotion of energy technologies (OPET)
12. Goteborgenergi (2010) Gothenburg biomass gasification project: GoBiGas Göteborg Energi. http://www.goteborgenergi.se/English/Projects/GoBiGas__Gothenburg_Biomass_Gasification_Project. Accessed Dec 2010
13. Meijden CMVD, Veringa H, Vreugdenhil BJ, van-der-Drift A, Zwart RWR, Smit R (2009) Production of bio-methane from woody biomass. Energy research Centre of the Netherlands (ECN). www.ecn.nl/docs/library/report/2009/m09086.pdf. Accessed Dec 2010
14. Nounia MR, Mullickb SC, Kandpalb TC (2007) Biomass gasifier projects for decentralized power supply in India: a financial evaluation. Energ Policy 35:1373–1385
15. Bolhàr-Nordenkampf M, Hofbauer H (2004) Gasification demonstration plants in Austria. International Slovak Biomass Forum, Bratislava
16. Repotec corporate webpage, Repotec (Renewable power technologies). www.repotec.at. Accessed Dec 2010
17. Weiland P (2010) Biogas production: current state and perspectives. Appl Microbiol Biotechnol 85:849–860
18. BEC (2010) Anaerobic digestion, Biomass energy centre (BEC). http://www.biomassenergycentre.org.uk/portal/page?_pageid=75,17509&_dad=portal&_schema=PORTAL. Accessed Dec 2010
19. Grid N (2009) The potential for renewable gas in the UK. National grid. http://www.nationalgrid.com/NR/rdonlyres/E65C1B78-000B-4DD4-A9C8-205180633303/31665/renewablegasfinal.pdf. Accessed Dec 2010
20. Chen Y, Yang G, Sweeney S, Feng Y (2010) Household biogas use in rural China: a study of opportunities and constraints. Renew Sustain Energy Rev 14:545–549
21. Bhattacharya SC, Jana C (2009) Renewable energy in India: historical developments and prospects. Energ Policy 34:981–991
22. Agrobiomass (2010) Biomass market grows throughout Europe, agrobiomass: agricultural bioenergy and bioproducts. www.agrobiomass.com/. Accessed Dec 2010

23. Nawaro Güstrow BioEnergie Park, NAWARO BioEnergie AG. www.nawaro.ag/en/company/projects/guestrow-bep/. Accessed Dec 2010
24. EPA (2010) U.S. Anaerobic digester status report. US Environmental Protection Agency (EPA)
25. REN21 (2010) Renewables 2010: global status report. Renewable energy policy network for the 21st century (REN21)
26. Ludwig J, Marufu LT, Huber B, Andreae MO, Helas G (2003) Domestic combustion of biomass fuels in developing countries: a major source of atmospheric pollutants. J Atmos Chem 44:23–37
27. Hall DO, Moss PA (1983) Biomass for energy in developing countries. Geo J 7.1:5–14
28. WRI (1998) Burning biomass fuels pollutes indoor air (adapted from World health organization (WHO), Health and environment in sustainable development: five years after the earth summit, WHO, Geneva, Table 4.4, p. 87). World Resources Institute (WRI). www.wri.org/publication/content/8464. Accessed Dec 2010
29. AEBIOM (2010) AEBIOM European biomass statistics, European biomass association (AEBIOM). www.aebiom.org. Accessed Dec 2010
30. IEA (2007) Renewables for heating and cooling: untapped potential. International Energy Agency, Paris
31. IANGV (2008) Time for EU action on natural gas vehicles to support fuel policy. NGV global news. International association for natural gas vehicles, 17 Sept 2008
32. Peterson D, Haase S (2009) Market assessment of biomass gasification and combustion technology for small- and medium-scale applications. Technical report NREL/TP-7A2-46190, National Renewable Energy Laboratory. http://www.nrel.gov/docs/fy09osti/46190.pdf. Accessed Dec 2010
33. Bridgwater T (2010) Pyrolysis and gasification of biomass. Workshop: development of multi-product lignocellulose biorefinery technology with focus on residues (pentoses, lignin) from cellulose ethanol production – results of the integrated project biosynergy. Aston University: Bioenergy Research Group, Reims, France
34. Granatstein DL (2002) Case study on Lahden Lampovoima gasification project Kymijarvi power station – Lahti – Finland for IEA bioenergy task 36. Natural resources Canada/CANMET Energy Technology Centre (CETC)
35. Seiffert M, Kaltschmitt M, Miranda JA (2009) The biomethane potential in Chile. Biomass Bioenerg 33:564–572
36. Cozens P, Manson-Whitton C (2010) Bio-SNG feasibility study: establishment of a regional project. Progressive energy & CNG services. http://www.cngservices.co.uk/assets/Bio-SNG-Feasibility-Study.pdf. Accessed Dec 2010
37. DECC (2009) Biomethane into the gas network: a guide for producers. Department of energy and climate change (DECC), London
38. ISPRE Research and development on renewable energies: a preliminary global report on biomass. International Science Panel on Renewable Energies (ISPRE), Paris

Biomethane from Anaerobic Processes

Frank Scholwin[1], Jörgen Held[2]
[1]University Rostock, Germany
[2]Swedish Gas Centre, Malmö, Sweden

Article Outline

Glossary
Definition of the Subject and Its Importance
Introduction
History of Biomethane Production and Utilization
Framework for Biomethane Production and Utilization
Technologies for Biomethane Production
Economics of Biomethane Production and Utilization
Future Directions
Bibliography

Glossary

Biomethane Biomethane is produced in technical processes from biogenic resources. It can be generated via the biochemical pathway (from biogas) and via the thermochemical pathway (Bio-SNG). Through upgrading processes, its composition, focusing mainly on the methane content, is adapted to natural gas quality.

Biogas upgradation Biogas upgradation is the process which adapts the biogas quality to natural gas quality after cleaning the biogas from trace gases (H_2S, NH_3, water vapor, and others). Within this process, mainly carbon dioxide is removed from the biogas.

Biogas Biogas is a gas that is produced as waste product during anaerobic microbiological breakdown of organic substances.

Landfill gas Landfill gas is a special type of biogas produced in landfills from the degradation of the organic constituents of wastes. It is characterized by many organic long chain trace gases.

Sewage sludge gas Sewage sludge gas is a special type of biogas that is produced at wastewater treatment plants during the anaerobic treatment of sewage sludge. It is characterized by the content of siloxanes.

Definition of the Subject and Its Importance

This entry focuses on the development, its reasons, and the perspectives of biomethane supply from biogas through anaerobic digestion. This option becomes more and more important due to the political requirements for reduction of greenhouse gases as well as for raised independency on fossil fuels coming from abroad. Thus, a detailed analysis of market development as well as technology development of this sector with about 10 years experiences is done to discuss the possibilities and the challenges of biomethane supply and its contribution to reach these targets.

Introduction

Biomethane can generally be produced following two pathways. The first and more established one is the upgradation of biogas from anaerobic digestion of wet biomass. The second one is the cleaning and upgradation of gas derived from thermochemical treatment (gasification) of solid dry biomass (e.g., wood). This is illustrated in Fig. 1.

This entry will only focus on the anaerobic digestion pathway of biomethane supply having more than 10 years history in industrial scale application and a strong technological development during this time. The development depends on several factors – the main two are the reduction of greenhouse gas emissions from energy supply on the one hand and the supply of a decentralized available energy carrier independently from international markets on the other hand.

The main technological challenge of biomethane supply is the energy-efficient separation of almost pure methane from biogas containing a large share of carbon dioxide and shares of nitrogen, oxygen, hydrogen, hydrogen sulphide, ammonia, and other trace gases. Due to the market development today, a lot of technologies are available and under research.

The economic challenge of biomethane supply is the cost effectiveness in comparison with fossil and renewable fuels. In most cases, this is still not given today and governmental measures are in place in many countries to force the development of this technology.

Based on this background the following description will bring some light into the history of biomethane production including some examples of biomethane plants in the world. Furthermore the reasons for this development will be analyzed looking

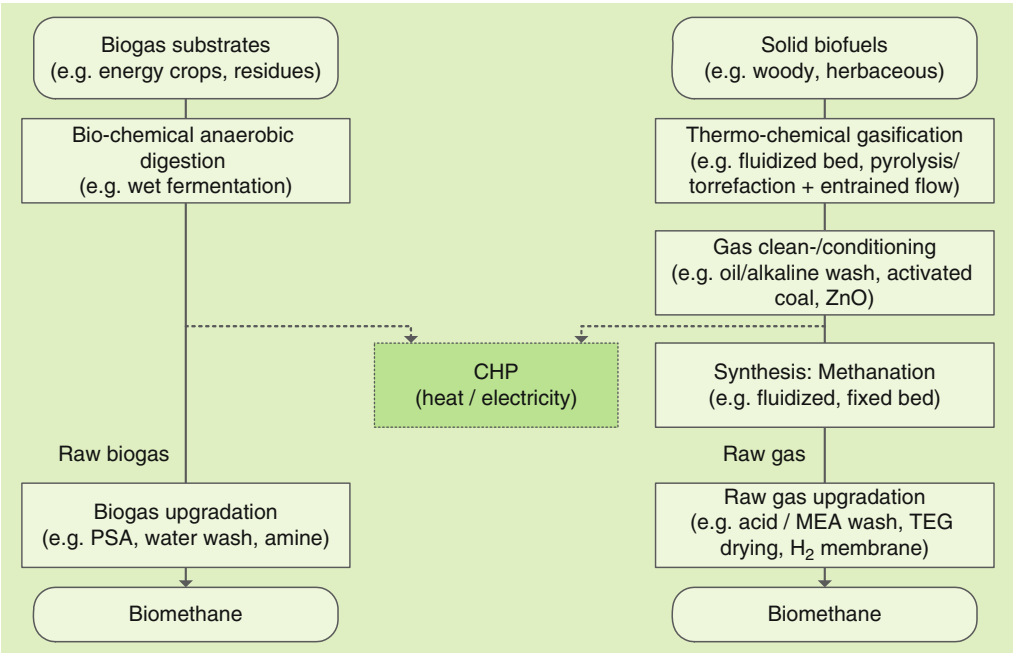

Biomethane from Anaerobic Processes. Figure 1
Pathways of biomethane production

into the realized and necessary framework conditions for the technology. This will be followed by an overview on the technologies applied and under research with their development potentials. The explanations are continued with an economic outlook for this technology. Finally some conclusions are drawn on the future research demand and the overall perspectives of the technology.

History of Biomethane Production and Utilization

Biogas has been produced for decades in industrial scale for various reasons (e.g., as means to reduce and stabilize sewage sludge and other wastes, to stabilize landfills, to reduce eutrophication within the agricultural sector, and last but not least, in times of energy supply limitations for decentralized energy provision). Usually the produced biogas is used to cover the need for cooking energy, for heat, or for electricity at the production site. However, mismatch between the biogas production and the local heat demand normally results in flaring, which from a resource and energy efficiency perspective is devastating. The increased environmental concern and the possibility to take advantage of the energy that otherwise would be burnt off in a flare have resulted in new solutions such as biogas upgrading and grid injection.

The biogas upgrading development took off in the 1980s and early 1990s through demonstration and industrial scale plants in France, Sweden, Switzerland, The Netherlands, and the USA. While the focus in The Netherlands and the USA was on upgrading of landfill gas for grid injection, the focus in Sweden and Switzerland was on upgrading biogas to vehicle fuel.

Figure 2 illustrates the development of the number of upgrading plants worldwide, and Fig. 3 visualizes the installed capacity of upgrading plants. Both figures show the exponential growth of the sector. The capacities are with about 50% dominated by relatively few very large landfill upgrading plants, located preponderant in the USA. The worldwide distribution of the plants is illustrated in Fig. 4.

As examples of the variety of applications below are some of the early plants described.

Tilburg, The Netherlands

The upgrading plant based on water scrubbing was built in 1986, when utilization of the gas from landfills began. The landfill facility was later complemented with a biogas plant where vegetable, fruit, and garden (VFG) waste are digested. The capacity of the upgrading plant is 2,000 m^3/h of raw gas from the landfill and the VFG-digester. The upgraded biogas has a methane content of 88% which gives a heating value and a Wobbe index similar to the natural gas produced in Groningen/The Netherlands. The upgraded biogas is injected into the Tilburg City distribution network [1].

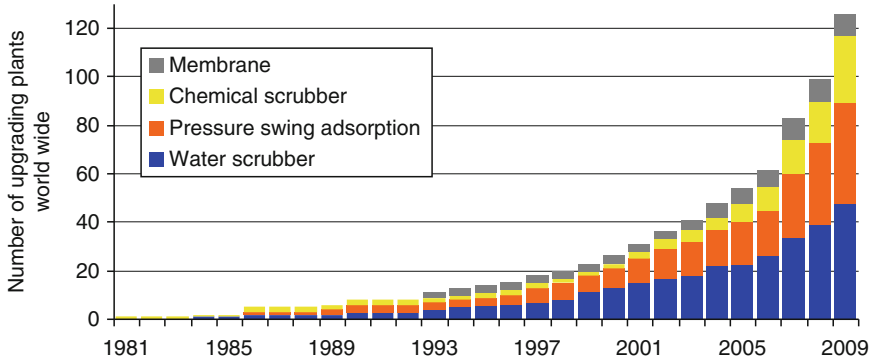

Biomethane from Anaerobic Processes. Figure 2
Development of biogas upgrading plants in operation worldwide

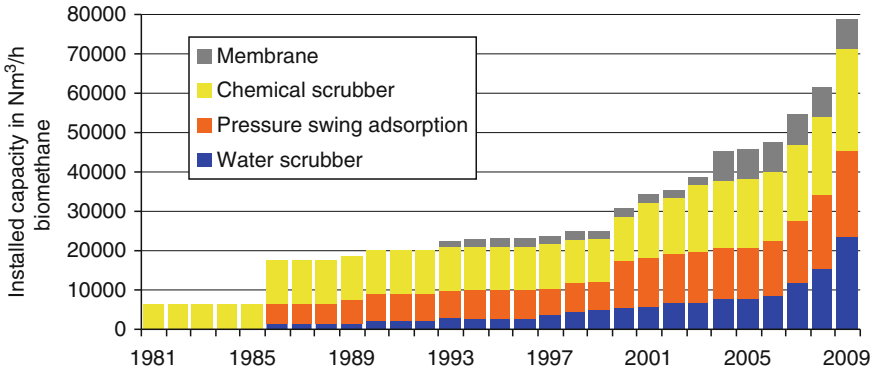

Biomethane from Anaerobic Processes. Figure 3
Development of the capacity of biogas upgrading plants in operation worldwide

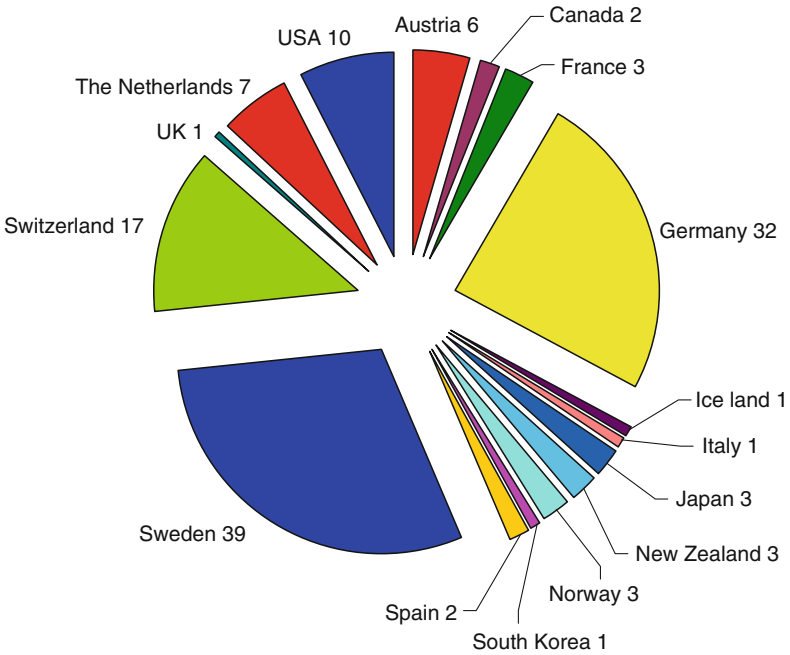

Biomethane from Anaerobic Processes. Figure 4
Distribution of biogas upgrading plants in operation worldwide 2009

New York, USA

In 1982 an upgrading plant based on Selexol-washing technology has been installed at the Fresh Kills landfill on Staten Island, New York City. With a capacity of 13,000 m^3/h raw gas, this was the first large-scale commercial application of landfill gas upgraded to pipeline quality and injected on a gas grid [2].

Lille, France

Up to 1990, 20% of the biogas produced by the wastewater treatment plant was burnt off and the rest used to supply heat and power to the treatment plant. With a production of 15,000 m^3 per day, in average 3,000 m^3 biogas (equivalent to 1,200 L of petrol) was flared every day.

To take advantage of the biogas surplus, the Urban Community of Lille decided by the end of 1990 to launch a project. The primary objectives of the project were to:

- Build a pilot site for the production of upgraded biogas
- Convert a conventional diesel bus into a biogas-powered bus

The biogas upgrading plant based on water scrubbing was commissioned in June 1995, and a distribution terminal was installed at the Marquette production site. The washing unit was designed to treat 100 m^3/h raw gas. A new facility with a capacity of 1,200 m^3 upgraded biogas was built in 2007. Compressed natural gas has been used to allow expansion of the gas bus fleet prior to the new facility was in place and to manage fluctuations in biogas production [3, 4].

Rümlang, Switzerland

The first upgrading plant in Switzerland was built in Rümlang by Kompogas in 1992. It was a pilot plant with a capacity of about 30 m^3/h raw gas. The digester was fed with biowaste. Initially the upgrading system was based on water scrubbing. This has been changed in 1995 to a PSA. The upgraded biogas is used as vehicle fuel (A. Wellinger, 2009, Personal communication by e-mail 26-11-2009) [5].

Linköping, Sweden

In 1992, some of the biogas produced at the sewage treatment plant was upgraded in a small plant using the PSA technique. The capacity was 150 m^3/h raw gas, and the plant supplied five city buses with fuel. A full-scale biogas plant was built at Åby, near Linköping, which started to operate in spring 1997. The upgrading, based on water scrubbing, has a capacity of 500 m^3/h raw gas, and the upgraded biogas is used as vehicle fuel. A third plant, using the same upgrading technology, was built in 2002, with a capacity of 1,400 m^3/h raw gas. Including the gas from the sewage treatment plant, approx. 65 million cubic meters of upgraded biogas is produced every year, which through a local gas grid supplies fuel to city buses, garbage trucks, and a number of filling stations. As Linköping has no natural gas pipeline, liquefied natural gas (LNG) is used as backup. A train was converted from diesel to biogas in 2006. The train operates on the line between Linköping and Västervik and can run 600 km between each refueling [5].

Framework for Biomethane Production and Utilization

The development of application of the technology still depends on political support. In most cases the product biomethane is not economically competitive compared to natural gas. Thus the realization of biomethane projects requires financial support. Therefore in different countries different support schemes have been implemented. Therefore the situation in Sweden, Switzerland, Germany, and Luxemburg will be discussed due to the fact that the development is the most important worldwide (except Luxemburg as a special case).

Sweden

In Sweden most biomethane is used as green gaseous vehicle fuel. In fact the rapid development has led to a situation where the use of biomethane has surpassed natural gas in this sector. Due to the fact that the production cost of biomethane is relatively high compared to fossil fuels, biomethane is targeted for sectors where the benefits of a renewable high-quality fuel with low carbon dioxide footprint are valued. Thus the situation developed that large amounts of biomethane are used as fuel for cars, heavy vehicles, and buses. Additionally the largest grid operator is really interested in biomethane production and supply so that there were almost no reservations on biomethane.

The Swedish government supports through various subsidy schemes the investment into biomethane plants to raise the interests in the technology. This support system in combination with the very high strategic aims for greenhouse gas reduction in Sweden has led to a good development of the biomethane supply.

Germany

In Germany biomethane is used for different applications. Due to the fact that the German gas industry has published a self-commitment to supply from 2010 10% of the gas which is sold as fuel for vehicles, some biomethane is used on this pathway. The largest share of the gas is for sure used as fuel for combined heat and

power plants due to interesting feed-in-tariffs for electricity from biomass based on the so-called Renewable Energy Entry Act (German feed-in law). There it is stated that new plants for electricity production from biogas receive between 0.09 and about 0.2 €/kWh electricity fed into the electricity grid guaranteed for the next 20 years. These tariffs are no subsidies; they are defrayed by all German electricity consumers according to their electricity demand.

An increasing amount of biogas is also sold to private households, which can buy biomethane at market prices.

An additional support for biomethane use is the so-called Gas Entry Act. In this act, conditions for gas grid connection and a tariff for reduction of the grid use costs for the grid operator due to local gas feed-in (0.006 €/kWh_{gas}) are defined. Additionally, regulations for the priority feed-in of biomass-based gases in comparison with fossil gases are given.

Switzerland

In Switzerland the associations of gas industry and biogas suppliers agreed on a voluntary system of feed-in-tariffs where specific remunerations for the gas amount per kilowatt hour are defined. On this basis the gas production is financed. The biomethane is prevailing used as vehicle fuel.

Luxembourg

In Luxembourg a guideline for direct feed-in-tariffs for biomethane into the natural gas grid in combination with clear rules for gas grid access will be implemented soon. Totally independent on the final use of the gas, these tariffs shall be economically sufficient for biomethane production processes. Tariffs will cover different financial efforts for biomethane production from different feedstock (e.g., sewage sludge, organic wastes, energy crops) as well as the economy of scale.

Conclusions

The first and most important framework condition is the opening of the gas grids and/or the possibilities for biomethane trading to force the development of biomethane production and use. Evaluating the effectiveness of the very different incentive models for biomethane production especially systems which enable guaranteed refinancing of the investments over long periods seem to be most promising. An example is the system under establishment in Luxembourg [6]. From the administrative point of view, systems on the basis of voluntary agreements of the industry are probably the fastest way to introduce some incentives. Finally the level of inducement of plant construction and operation depends clearly on the absolute height of financial incentives. In the case of high incentives (subsidies or feed-in-tariffs), it has to be taken into account that the market could overreact so that after a first boom of plant construction, lots of companies could get into troubles with a very fast growth what could be seen in Germany in 2008 and 2009. Thus the incentives should be chosen very carefully to get a sustainable market development for biomethane production and use.

Technologies for Biomethane Production

Generally it has to be differentiated between two mains steps of biomethane production using biochemical processes. That is biogas production and biogas upgradation.

Biogas Production

Biogas production has to be seen as state of the art. A huge variety of different technologies are available on the market depending on the feedstock characteristic. An economically efficient biomethane supply requires a minimum plant size. This has some influence on the substrates to be used for biochemical biogas generation. Based on analysis done for German conditions and considering the feed-in of biomethane into the gas grid, an economic biomethane supply requires a plant capacity of at least 200 m_N^3 biomethane. Experiences show that this capacity requires very large amounts of municipal and/or industrial organic wastes (about 30,000 t/a and more) or energy crops (about 15,000 t/a and more). Also sewage sludge from municipal wastewater treatment plants of large towns or huge landfills can be the source for the biogas. Excrements from animal breeding play due to the low energy content no important role for biomethane supply.

Biomethane from Anaerobic Processes. Table 1 Composition of biogas (from residues, waste, and energy crops digestion) wastewater treatment plant gas (from sewage sludge digestion) and natural gas

Component	Biogas	WWTP gas	Natural gas
Methane	50–70%	60–70%	93–98%
Carbon dioxide	25–40%	30–40%	1%
Nitrogen	<3%	4%	1%
Oxygen	<2%	1%	–
Hydrogen	Traces	Traces	–
H_2S	Up to 10,000 ppm	Up to 1,000 ppm	–
NH_3	Traces	Traces	–
Ethane	–	–	<3%
Propane	–	–	<2%
Siloxanes	Traces	<6 mg/m^3	–

The most important obstacle of biogas utilization as a substitute for natural gas is the content of different compounds (e.g., CO_2, H_2S, NH_3). Table 1 shows the average composition. Biogas has due to its different composition to be differentiated into biogas from residues, waste, and energy crops and biogas from wastewater treatment plants where sewage sludge is digested.

Biogas Upgradation to Biomethane

The market share of the different technologies can be taken from Figs. 2 and 3. Upgrading technologies for biogas result mainly from technological applications from the natural gas sector where partly comparable upgrading tasks have to be solved, but at a by far larger scale. Until today, some technologies show long time experiences and others are relatively new.

Generally it has to be stated that all upgrading plants pledge to reach a biomethane quality of more than 96% methane content and a methane loss less than 3%. Additionally a very high availability for all technologies is promised. This has been confirmed in practice with an availability of about 95% at most plants [7]. Practical measurements have shown different results, but more or less independent of the used technology. Especially it seems to be necessary to care about the methane losses which are reported with at maximum up to 10% (typical range 0.1–3%), because they influence environmental and economic parameters of such plants very strongly.

For all the described technologies, current research activities are reported with some focus on membrane technologies due to essential development successes at membrane processing. Technologies under research are the so-called process internal methane enrichment (or in situ methane enrichment) using the absorption of carbon dioxide in the liquid phase of fermentation and external reduction of the carbon dioxide concentration from this phase as well as the so-called ecological lung using the enzymatic dissolution of carbon dioxide with the enzyme carboanhydrase in a comparable process as in the lung [8].

Water Scrubbing One of the mainly used technologies for biogas upgrading is the water scrubbing process which shows a very long history of experiences.

This process is based on sorption of carbon dioxide in water at high pressures (about 10 bar) and desorption of carbon dioxide at lower pressures in another vessel to separate carbon dioxide and methane. At the same time, most trace gases (e.g., H_2S) are separated during this process. As water source circulated, fresh water or cleaned wastewater without circulation can be used. Advantages of wastewater use are compensated by biofouling in the scrubbers due to the relatively high organics content.

Due to the long research and development period, the technology has reached a very high level of development and is proven in practice. Thus, it has to be expected that the technology has to compete with other technologies in economic questions but is seen as technological state of the art.

Pressure Swing Adsorption The pressure swing adsorption technology is based on high-pressure adsorption of carbon dioxide at molecular sieves or activated charcoal in at least two steps. Other trace gases have to be separated, e.g., in filter systems before carbon dioxide adsorption. Adsorption materials have long operation durations but have to be exchanged from time to time.

This technology shows long time experiences and is well established and competes as solid and reliable technology in the market.

Chemical Scrubbing Chemical scrubbing is possible with a number of substances (e.g., Selexol, MEA, DEA), which are capable to absorb carbon dioxide at ambient or low pressures mostly combined with heat demand for desorption. Available information about efficiencies of the processes is very different, but a lot of experiences exist and research is going on. The advantage of chemical scrubbing is that used substances are selective for carbon dioxide (and sometimes for H_2S too, most times H_2S-separation is done before upgrading), and thus no methane will be absorbed resulting in high methane concentrations in the purified gas and low methane emissions. Adsorption processes under pressure seem to be of comparable behavior as water scrubbing processes. Ambient pressure systems promise less electrical energy demand for the continuous process and could be of high interest for applications where only low pressure is required after upgrading and heat is available [7].

For the time being, some chemical scrubbing technologies are reliable and well established and others are under development.

Membrane Technologies Due to the different molecule sizes of methane and carbon dioxide, it is generally possible to separate both gases through membranes. The smaller methane molecules can pass through a membrane, and a gas with very high methane content and a gas with very high carbon dioxide content can be produced. Technologies were developed for dry separation (transport through the membrane is forced by very high pressure) and for wet separation (transport is forced by a very low concentration of methane in a fluid which methane is absorbed in). Both technologies are known from long running plants and improved technologies from pilot plants. Efficiencies regarding methane losses and energy demand of improved technologies are subject of ongoing evaluation. The most important challenge is to reach comparable high methane concentrations and low methane losses as reached by the established technologies.

Cryogenic Upgrading Additionally it is possible to use the differences in dew and condensation points of methane and carbon dioxide. Therefore it has been shown in small scale as well in large scale that both gas components can be separated by cooling down of biogas to less than −45°C at about 80 bar pressure.

Economics of Biomethane Production and Utilization

Economics of biomethane supply will predominantly affect its future utilization. At production costs between 0.05 and 0.08 €/kWh$_{gas}$, biomethane is not really competitive with natural gas at import costs of 0.02–0.03 €/kWh$_{gas}$.

Looking in the different cost positions of biomethane at a German example of a plant based on energy crops digestion (which show the highest potential for the growth of this sector in the future), the costs result from raw biogas production including the costs for substrate supply (about 50% of this position), costs for biogas upgradation to biomethane, and the costs for gas grid injection, transportation as well as feed-out (Fig. 5).

Looking into the future, it is expected that energy prices will still increase. So it has to be assumed that biomethane prices and natural gas prices will cross any time. But for sure this will not happen before the natural gas prices have doubled. Although there are many activities for improvements of raw biogas

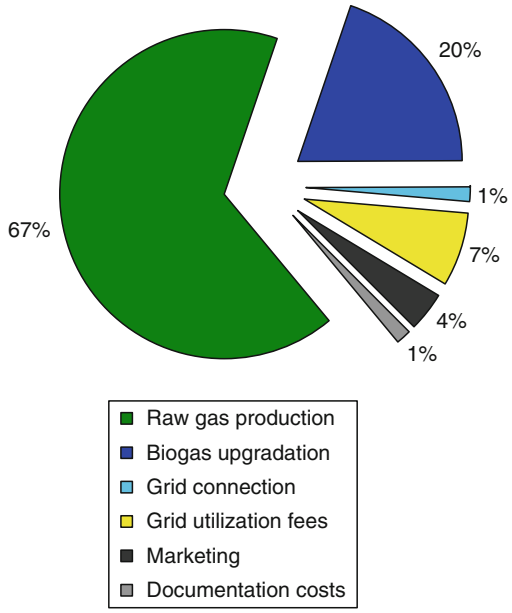

Biomethane from Anaerobic Processes. Figure 5 Distribution of biomethane supply costs at the point of feed-out from the gas grid under German conditions for a plant at 1,500 Nm^3/h biomethane supply from energy crops digestion

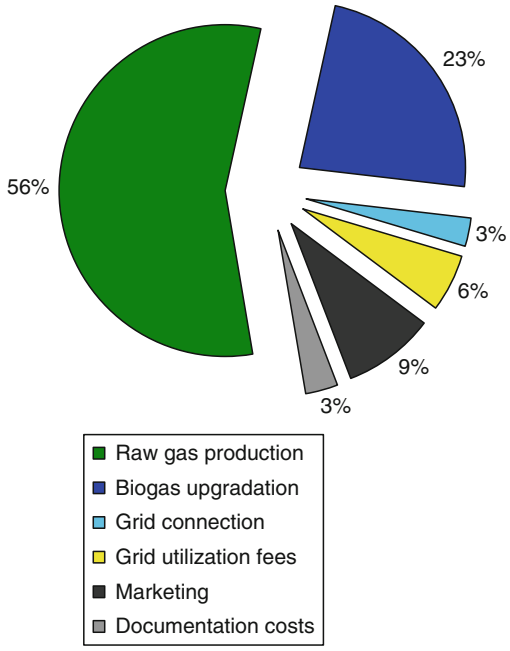

Biomethane from Anaerobic Processes. Figure 6 Distribution of biomethane supply costs at the point of feed-out from the gas grid under German conditions for a plant at 500 Nm^3/h biomethane supply from energy crops digestion

production and biogas upgradation, in the short term, improvements can be expected allowing achieving up to 20% cost efficiency. But this will partly be compensated by the general price increase.

Looking into the cost distribution of a smaller plant (Fig. 6), it is visible that the total share of raw biogas production and upgradation decreases. Thus, cost efficiency in these sectors will have smaller effects.

Contradictory the share of the costs for gas grid access and transportation grow due to the fact that absolute costs for the gas grid access are not dependent on the capacity of the plants.

As a result, it must be stated that cost reduction potentials at gas grid distribution of biomethane should be more investigated and reduced for further growth of the biomethane industry. It would additionally be necessary to achieve significant cost reductions to optimize the biomethane production. This could be realized with reductions of requirements for biomethane feed-in plants and sharing the costs of feed-in with the gas grid operators.

Future Directions

It is expected that the trend of the last decades will be rapidly continued in the future regarding plant numbers and capacities worldwide with a special focal point in Europe. Due to effects of the economy of scale and the limited availability of cost-effective small-scale technologies for gas upgradation and gas feed-in the size of plants for gas grid injection will still be relatively large in the range of 200 m_N^3 biomethane and more.

Depending on the crude oil and natural gas price development, the speed of the growth will vary. But international targets for greenhouse gas reductions and financial measures to support the use of renewable

energies will force a wide use of this technology. Full economic competitiveness regarding profits from natural gas trading and utilization within the next few years is not to be expected. But the current development in some countries shows that economic models for biomethane production and use are applicable.

Moreover, biomethane is the only renewable energy carrier which can – due to its high quality – substitute gaseous fuels without technical adaptations of the consuming applications. And it has the full flexibility of utilization for heat, electricity, and fuel supply that can be distributed and traded on a global market.

Research activities for technology improvement are still going on so that the challenges of decrease of environmental negative effects (energy consumption, greenhouse gas emissions) of increased gas quality as well as decreased costs will be solved in the years to come.

Bibliography

1. Energie-Cités (2000) Biogas, Tilburg. http://www.agores.org/Publications/CityRES/English/Tilburg-NL-english.pdf
2. McCarron GP, Pierce JL (2005) Pipeline quality gas, an LFG utilization alternative ready to come in from the cold, 9th LMOP conference. http://www.epa.gov/lmop/documents/pdfs/conf/9th/mccarron.pdf. Accessed January 2006
3. BioNETT (2006) Bio-methane in Lille – a case study. http://www.bio-nett.org/Bio-methane-in-Lille-Case-Study.pdf. Accessed January 2009
4. Energie-Cités (1999) Biogas – Biofuel, Lille, France. http://www.agores.org/Publications/CityRES/English/Lille-FR-english.pdf
5. Held J, Mathiasson A, Nylander A (2008) Biogas from manure and waste products – Swedish case studies, Swedish Gas Association. http://www.energigas.se/sv-SE/Publikationer/~/media/Files/www_energigas_se/Publikationer/Rapporter/BiogasinfoEngGodaExempel.ashx
6. Scholwin F, Hofmann F, Plättner A, Ebert M (2007) Förderung der Biogaseinspeisung in Luxemburg; Project of the Institute for Energy and Environment for Le Gouvernement du Grand-Duche de Luxembourg Ministere de l Èconomie et tu Commerce exterieur
7. Persson M (2003) Utvärdering av uppgraderingstekniker. för biogas; SGC-Rapport 142; Lunds Tekniska Högskola. http://www.sgc.se/dokument/SGC142.pdf
8. Petersson A, Wellinger A (2009) Biogas upgrading technologies – developments and innovations; Report for the IEA Task 37 Group – Energy from biogas and landfill gas. http://www.iea-biogas.net/Dokumente/upgrading_rz_low_final.pdf

Bioremediation and Mitigation

Ralph J. Portier
Department of Environmental Sciences, School of the Coast & Environment, Louisiana State University, Baton Rouge, LA, USA

Article Outline

Glossary
Definition of the Subject
Introduction
Bioremediation Technologies Available for Sustainable Mitigation
Mitigation Case Studies with Petroleum and Related Hydrocarbons
Future Directions
Conclusions
Bibliography

Glossary

Bioremediation Bioremediation can be defined as a process using a microbial community and/or the related enzymes to return the natural environment altered by contamination to its original condition. Bioremediation can also be considered an industry that uses these techniques to solve real-world problems. Bioremediation is an applied field of science that combines advanced biotechnology and engineering approaches with basic microbiology to solve complicated challenges in soil water and groundwater contamination [1].

Biodegradation/biomineralization The process in the carbon cycle of using a microbe/microbial community (bacteria, fungi, yeasts, actinomycetes) or plants to convert complex carbon-based chemicals (organic matter) to simpler structures and biomass. The complete conversion of said chemical to its mineral form, namely, biomass, water, and CO_2 is called biomineralization. The process is described as aerobic if oxygen is required by the biological community and anaerobic if it is not required or present [1].

Mitigation The effort to eliminate or reduce loss and/or impact to habitat, life, property, or natural

resources. Hazard mitigation means any action taken to reduce or eliminate the long-term risk to human life and property from natural hazards (Stafford Act 44: CFR 206: 401) [1, 2].

Polycyclic aromatic hydrocarbons (PAHs) Lipophilic, fused, aromatic rings typically found in compounds of oil, coal, tar deposits or residuals from burning any fossil fuel. Also known as polynuclear aromatic hydrocarbons, several are considered to be potential human carcinogens by USEPA. Benzo(a)pyrene is considered a benchmark regulatory toxicant for bioremediation of most hydrocarbon-contaminated sites [1].

Sustainable remediation Practices or multitasked approaches for restoring a site to its native state with a frugal use of available resources so as to benefit human health and the environment [1].

Definition of the Subject

The high costs involved with conventional remedial techniques and frequently, the liability associated with the use of such techniques, has encouraged industry to search for innovative remediation technologies. The use of innovative technologies that provide a cost-effective and permanent treatment method is gaining the attention of regulatory agencies, the public, and, most importantly, the industries responsible for cleanup. In order to address these needs, research organizations and engineering firms are testing various innovative technologies in the laboratories and in the field. One such technology, bioremediation, is currently gaining more and more acceptance and has proven to be a cost-effective mitigation strategy [3].

The US Environmental Protection Agency has been at the forefront in promoting bioremediation as an innovative solution for addressing risk-based regulatory challenges for the cleanup of contaminated soils, sediments, groundwater, and industrial effluent. The establishment of specific criteria for acceptable levels of exposure in soils and sediments, groundwater, and/or discharge into rivers and streams has hastened the recognition of applying specific microbial cultures and/or communities to mitigate in a sustainable effort [4–6].

Introduction

The practice of using microorganisms to clean up contamination can be traced back as early as 600 BC. It was common practice to treat municipal wastewater by building intricate sewage systems that would transport wastewater to collection vats and lagoons where microbes would aid in the biodegradation of organic wastes. Today, this same principal can be used to clean up modern pollution problems like chemical spills and tank leaks [6]. This process is the utilization of a consortium of microbes to degrade organic pollutants. Through bioremediation, toxic pollutants can be broken down into nontoxic byproducts such as CO_2 and water. Aerobic heterotrophs have enzymatic systems capable of oxidizing suitable substrates by transfer of electrons to molecular oxygen. To put it in simple terms, this process is performed through the following reaction:

$$\text{Substrate} + O_2 \rightarrow \text{Biomass} + CO_2 + H_2O + \text{Other Organics}$$

Typically, in an aerobic or oxygen-requiring bioremediation, the contaminant degrading potential of these microorganisms is enhanced through the addition of essential reactants (inorganic and organic nutrients, water, and oxygen) [6, 7]. Biodegradation of complex organic pollutants may require a series of concerted metabolic events involving several species of bacteria or coupled interactions with bacteria and fungi [8]. Slader and Godwin [9] described the basic reactions in microbial metabolism as:

- Enzymatic catalyzed degradation of aliphatic hydrocarbons where the end products of beta-oxidation are organic alcohols and acids
- Enzymatic catalyzed hydrolysis, acidification, and ring cleavage of the benzene ring
- Production of homeostatic enzymes which regulate the well-being of the organisms by coordinated responses that automatically compensate for environmental changes
- Cometabolism, which involves use of readily degradable hydrocarbons in combination with fortuitous transformation of a desired pollutant

Microbial Parameters for Successful Mitigation

Bioremediation is clearly an interdisciplinary field involving expertise from engineering, geology, chemistry, and ecology [10]. Numerous approaches to soil and

sediment remediation have been developed and implemented on an international basis. A common goal in all of the processes is to create the necessary environment for the growth of an optimal microbial community which can, in an effective manner, biodegrade contaminants of concern [11, 12].

The rate and extent of contaminant biodegradation using any natural process can be affected by numerous factors including, the actual structure of the contaminants of concern, its solubility and water bioavailability, co-oxidation/cold metabolism potential, relative toxicity, and its interaction with other properties in soil and sediment. Oxygen plays a dominant role in the selection of appropriate microbial communities for biodegradation to proceed. Water content in either bound water or groundwater is equally important in that water serves not only as a universal solvent but also has as a facilitator of movement of important nutrients and buffers for microbial biodegradation process initiation. Other limiting factors which affect the efficacious use of microorganisms to remediate contaminated soils or sediments include but are not limited to temperature, pH, organic and inorganic soil content, and the presence of metals such as arsenic, lead, and mercury [13–15].

Contaminated sites present the problem of attempting to biodegrade a diverse mixture of contaminants. A typical example is oil, the mixture of chemicals with different molecular weights, latent heat of vaporization, and relative water solubility. This necessitates the requirement of careful characterization of all constituents within the mixture. Therefore, remediation approaches are often dictated by the relative quantity of the most recalcitrant chemical in the mixture [14].

Bioremediation as a mitigation tool has the additional problem of project specificity, that is, requiring a case-by-case evaluation of the suitable bioremediation approach as dictated by the challenges of each specific site. Thus no one all-encompassing bioremediation tool or remedy will work for all contaminated sites. The remediation services market represents less than 5% of the $250 billion annual environmental industry market and is limited in its further expansion by the requirement of designing site-specific solutions using an adapted microbial community. However, the significant savings to both the public and private sector in using a microbiological approach to cleanup sites continues to be the major driver for looking at mature and evolving bioremediation technologies as a solution to mitigation challenges.

Candidate Contaminants for Bioremediation

Candidate contaminants for bioremediation processes have been successfully used to remediate petroleum hydrocarbons such as gasoline, diesel fuel, crude oil and creosote; pesticides and their derivatives such as phenoxyacetate herbicides, carbamates, and organophosphates; chlorinated solvents such as methylene chloride, trichloroethylene, and vinyl chloride; and halogenated aromatic hydrocarbons such as pentachlorophenol, chlorinated benzenes, and even some polychlorinated biphenyls (PCBs) [16–18].

Because of the nature of bioremediation, it is most applicable toward detoxification of organic wastes, most of which are at least theoretically biodegradable [19–21]. Among the most recalcitrant organic contaminants are the organohalogens, which, because of their rarity in nature, are persistent, as few biological systems have evolved to degrade them [19]. In contrast, petroleum hydrocarbons (PHCs) are relatively easily degraded [20, 21]. Historically PHCs entered the environment only via sporadic seepage and erosion, which allowed for the development of some natural microbial biodegradative pathways. In recent history, however, man's increasing reliance on fossil fuels has resulted in dramatic increases in petroleum hydrocarbon pollution [21]. Currently the combined chronic marine and terrestrial discharges of PHCs account for greater than 90% of anthropogenic environmental pollution [21].

Advantages of Bioremediation

Microbiological processes can be used as the keystone technology to develop cost-effective remediation systems for hazardous/nonhazardous waste sites. Bioremediation can be much cheaper than other technologies, approximately one third to one half the cost of transport and incineration of similar volumes of waste. In addition, byproducts that require landfilling such as incineration ash are not produced [23]. As the technology of bioremediation methods advances, the market for bioremediation products has also increased.

Microbial pollution products to be used in remediation projects, including dried or liquid microbial inocula with or without nutrient additives, have annual sales of $7–10 million and the potential market may reach $200 million [13].

Additionally, in situ bioremediation reduces the risk of exposure during cleanups by avoiding the need for excavation [22]. Bioremediation shows promise for further reducing the low levels of contaminants left after excavation of high level contaminants [22]. Bioremediation is a natural process that has the potential of degrading toxics and other wastes to harmless products – carbon dioxide, water, and fatty acids – when the process is completed [17, 22]. An in situ bioremediation system can serve as a permanent in-place management system. The installation of an in situ bioremediation system can be accomplished with minimal site/business disruption and public exposure [23]. Bioremediation is currently applied to a wide range of site conditions and contaminants, from oil-contaminated beaches in Alaska to PCB-contaminated soils in Florida [24]. It is at the forefront of a larger group of innovative remediation technologies.

Bioremediation depends on the natural selection of organisms that have the capacity to metabolize xenobiotic chemicals. Many of these organisms occur naturally in contaminated areas, and the growth of these populations can be enhanced by the addition of nutrients and oxygen. Degradation of contaminants that resemble natural compounds is more rapid than with complex organic molecules such as dieldrin [6, 25].

Disadvantages of Bioremediation

Contaminated sites may differ greatly in terms of both microbiological and physiochemical parameters. Previous biodegradation at long-standing sites may result in increased proportions of components of greater recalcitrance. Greater assessment details are required for proposed biological treatment prior to cleanup to determine the impact of the chosen methodology upon the microbial population [26].

Actual experience with the bioremediation technology is limited when compared to conventional remediation technologies such as incineration, and competing technologies can usually be completed in less time. The present body of knowledge on bioremediation is widely dispersed and often inaccessible, since much of it is considered proprietary. Bioremediation is not effective in the destruction of metals [27–29].

Soils and sediments are extremely complex mixtures with many microenvironments and vast arrays of living organisms. This complexity and other factors enhance the efficient chemical or physical attack on a molecule, leading to its degradation. Consequently, it is often difficult to distinguish between the microbial, chemical, and physical factors that contribute to the removal or transformation of a molecule [17, 30, 31].

Environmental limitations to biodegradation include: (1) toxic levels of waste, (2) lack of oxygen, (3) unfavorable pH, (4) lack of nutrients, (5) lack of moisture, and (6) unfavorable temperatures [17, 32]. These limitations can be circumvented by environmental manipulation either ex situ as in a bioreactor or in situ using appropriate amendment strategies. Parameters such as waste loading, pH, nutrients, and size of organism populations can be controlled and lead to maximum degradation rates. This type of manipulation is most effective for liquid wastes. Groundwater containing the organochlorine, toxaphene, and the organophosphates dioxathion and methyl parathion have been biologically treated ex situ using two reactors containing adapted *Acinetobacter* spp. immobilized on a support material. The bioreactors were operated over a 90-day period at a flow rate of 80 gallons per day. The microorganisms degraded 60% and 35% of the chlorinated and phosphate wastes, respectively [33].

The physicochemical bioavailability of any polluting chemical mixture in soils/sediments can be affected by its sorption equilibrium, irreversible sorption, and degree of incorporation into humic material. Mass transfer limitations can include oxygen diffusion and solubility, the relative rate of diffusion of nutrients, and the solubility/miscibility with water. Oxidation/reduction potential and the availability of electronic receptors as dictated by the presence or absence of oxygen plays a role in microbial population speciation and density [4]. Finally, not only is the chemical structure of the contaminants of concern and its relative solubility important in the overall efficiency of the mitigation process, the net concentration of the chemical itself plays an important role [5]. The induction of

suitable enzymes for effective bioremediation and subsequent growth and enrichment of a capable microbial community is often dictated by the limits of detection of each chemical in the mixture at the cellular level [17].

Single Species Versus Community Approaches

Many studies evaluating the microbial degradation of chemicals and soil, sediment and groundwater usually follow a reductive approach into a single microbial strain characterized on a chemical constituent basis [34]. Each organism is identified by either traditional selective culture approaches or amplified rDNA restriction (a simple method of identifying microbial community structure by characterizing DNA sequences indicative of temporal changes in the indigenous microbial population).

Simple screening studies of site soils/water for important microbes at the species level, which may be effective, and degrading chemicals of concern are evaluated in shaker flash studies or microcosm studies (a variable specific simulation of the complex field remediation challenge). Data sets generated can give an indication as to the appropriate degradation pathway necessary for site remediation. The screening data sets at the single species level also sets the stage for optimizing site conditions to insure a multiple species or community approach will be viable [34].

The issue of releasing genetically engineered microorganisms (GEM) whose genetic material has been altered into an ecosystem has become a controversial one. Critics contend that an ecosystem imbalance caused by a genetically adjusted organism could lead to disastrous consequences. The genome of the microbial population would be altered and the results of the genetic manipulation, when known, would be too late and could not be changed [34]. There are questions of economics, production, quality control, application, host specificity, and safety. It may not be economically feasible to develop a stable population, ensure integrity by quality control and apply microbial pesticides on a large scale. These organisms should only affect a target population, but in many cases it is difficult to predict whether a microbial pesticide could affect non-target organisms [35]. Engineered organisms can lose or alter the gene(s) that allow them to degrade a specific toxicant after several generations, rendering them useless in bioremediation [36]. The advantages of isolating an organism which has adapted naturally to the degradation of waste products are many, and eliminates the issues with using GEM.

Economics

There are several remedial technologies that may be considered when determining corrective action for any site. The technologies discussed are nonbiological approaches like soil venting (including vacuum extraction), soil flushing, hydraulic barriers, and excavation. The first three methods are considered in situ treatment methods, remediation of those soils in their original location. The fourth method, excavation, is normally combined with off-site disposal, incineration, soil washing, or enhanced volatilization. A comparison of costs associated with each of these technologies is shown in Table 1. When considering each of these technologies, costs as well as site-specific variables must be considered in determining the most effective method [37].

In situ and Ex situ Bioremediation Approaches

Bioremediation methods and/or technologies are broadly classified as either ex situ or in situ processes.

Bioremediation and Mitigation. Table 1 An economic comparison of remediation approaches

Remedial methods	Treatment costs[a]
Soil venting (including vacuum extraction)	\$130–180/yd^3
Land farming	\$60–123/yd^3
Soil flushing	\$200/yd^3
Hydraulic barriers	\$67–88/ft^2
Off-site disposal (including excavation and backfill)	\$155–275/yd^3
Incineration (including excavation and backfill)	\$235–675/yd^3
Soil washing (including excavation and backfill)	\$185–235/yd^3
Enhanced volatilization (including excavation and backfill)	\$300/yd^3

[a]US Dollars, 2010

Ex situ methods require the physical removal of contaminated material prior to the initiation of the treatment process. In situ approaches involve treatment of contaminated soil sediment and or groundwater "in place." Since bioremediation is a mitigation tool used for treating contamination in heterogeneous environments with complex phase separation of many materials by relative water solubility, the ability to successfully mitigate without physical removal and transportation to another location with its inherent risks of recontamination is desirable. The treatment of the Alaskan shoreline of Prince William Sound from the Exxon Valdez oil spill is an example of the successful use of an in situ approach to bioremediation [39].

Bioremediation Technologies Available for Sustainable Mitigation

The following technologies have been effectively used for sustainable remediation and are recognized as approved technologies by USEPA and other national environmental agencies [37, 40, 41]:

- *Bioaugmentation or Enhanced Bioremediation*: a process of amending contaminated media with microorganisms (bioaugmentation) and or nutrients (biostimulation) to degrade/immobilize/accumulate contaminants of concern.
- *Natural Attenuation (NA) or Monitored Natural Attenuation (MNA)*: the use of natural attenuation processes, that is, biodegradation/biomineralization, to achieve site-specific remediation objectives within a time frame that is reasonable compared to those offered by more active methods. As a natural biological and chemical process, NA is considered a natural process in achieving the goal of reducing mass, toxicity, mobility, concentration, and net total volume of a contaminant or mixture of contaminants in soil or groundwater. Risk assessment guidelines are used to ascertain whether remediation objectives are realized.
- *Bioventing*: an in situ remediation technology that uses indigenous microorganisms to biodegrade organic constituents absorbed to soils in unsaturated zones. Soils in the capillary fringe and the saturated zone are not affected. In bioventing, the activity of the indigenous bacteria is enhanced by inducing air or oxygen flow into the unsaturated zone using extraction or injection wells and, if necessary, by adding nutrients.
- *Bioplugs and Bioconduits*: an in situ technology that uses preselected acclimated microorganisms permanently immobilized or attached to a porous matrix and inserted into soils/sediments as a seeding device for both saturated and unsaturated zones. Microbial activity is maintained by using contaminated site water or ground water as a carbon nutrient source.
- *Biopiles*: also known as biocells, biomounds, or bioheaps; are excavated soils/sediments amended with minerals, nutrients, and water so as to reduce concentrations of contaminants in with indigenous microflora.
- *Composting or Compost Piles*: a variation of bioplies in which organic contaminants (e.g., PAHs) are mixed with lignocellulosic materials so as to biodegrade and/or cometabolize the recalcitrant constituents as the acclimated microbial population converts simpler carbon (under aerobic and anaerobic conditions) to innocuous, stabilized residuals.
- *Landfarming*: one of the oldest full-scale bioremediation technologies dating back to the treatment of process residuals from oil refinery operations. Also known as land treatment or land application, it is an above-ground remediation technology in which contaminated soils, sediments, or sludges are tilled or "turned" using standard farm cultivation equipment and allowed to slowly biodegrade as the acclimated soil microbial populations reduce the concentration of contaminants over time. It is one of the more widely used processes for handling large volumes of contaminated soils/sludges but requires significant acreage for repeated dispersal in layers or "lifts" over time.
- *Bioslurry or Liquid Solids Contact (LSC) Reactors*: an aqueous slurry in either a tank or lined impoundment that is created by combining soil, sediment, or sludge with water and other additives. The slurry is mixed to keep solids suspended (at a ratio of 30–40% volume:volume in water) and microorganisms in contact with the soil contaminants. Upon completion of the process, the slurry is dewatered and the treated soil is distributed in a land farm for

further biodegradation and dewatering by evaporation.

- *Online Bioreactor Systems*: the treatment of contaminants in extracted ground water that are put into contact with microorganisms in attached biological contractors (e.g., rotating and trickling filters) or suspended growth biological reactors (e.g., activated sludge). The technology is sometimes referred to as "pump & treat" technology.
- *Phytoremediation*: the use of plants to remediate contaminated soil and groundwater. However, different plant systems have individual mechanisms by which they extract (or accumulate), stabilize, volatilize, and/or degrade the contaminants, which is discussed in detail below.
- *Constructed Wetlands or "Rock and Reed" Systems*: treatment systems that have been designed and constructed to utilize the natural processes involving rock, clays, and specific wetland vegetation with a large root rhizosphere so as to allow surface and subsurface attached, associated microbial population to assist in treating contaminated water.

Mitigation Case Studies with Petroleum and Related Hydrocarbons

Over the past several decades, humans have grown more and more reliant on fossil fuels. Many of the comforts that humans enjoy today are possible largely because of fossil fuels such as petroleum. This intensification in use has resulted not only in an increased dependence but an increase in petroleum-related pollution. It has been estimated that petroleum contamination into the environment is between 1.7 and 8.8 million metric tons annually, most from anthropogenic sources. The manufacturing, transportation, and distribution of petroleum-based products over the past century have led to an increase in the amount of petroleum hydrocarbon pollution. Leaks, spills, and other accidents have all contributed to the contamination of air, soils, and water bodies by petroleum. Pollution can come from oil tankers, pipelines, and above and below ground storage tanks [42].

The pollution poses risk to human health and the environment. Although considered a nonhazardous waste by law, petroleum is a regulated contaminant. Most of the danger associated with petroleum-contaminated sites comes from lighter weight hydrocarbons such as BTEX (benzene, toluene, ethylbenzene, and xylenes) and from fire hazards caused by vapors. Petroleum or any other type of contamination also makes initiating new construction projects on contaminated sites more challenging. It can impede the construction process as cleanup must occur and environmental standards must be met before construction begins. Petroleum hydrocarbons, as pollutants, fall into an intermediate category in their degradation between highly biodegradable, biogenic, and highly recalcitrant xenobiotics. Fortunately, these hydrocarbons can usually be readily degraded by microorganisms present in the environment. This fact makes treatment of petroleum hydrocarbon–contaminated areas more feasible [33].

Many treatment methods, however, are expensive and not complete in cleaning up petroleum waste. Partial contamination may still reside in soil or groundwater. Consequently, new techniques, such as bioremediation, are required to clean up petroleum wastes more completely and at a cheaper cost.

Categories of Petroleum Hydrocarbons

Petroleum hydrocarbons (PHCs) can be divided into four structural categories: saturated or aliphatic, aromatic, asphaltic or polar, and resins [18, 20, 24]. Aliphatic and saturated constituents can either be cyclic or acyclic compounds with or without carbon–carbon multiple bonds. Examples include pentene, pentane, and cyclohexane. Aromatic components are unsaturated cyclic compounds such as benzene and its derivatives [44]. Asphaltenes are highly condensed partially oxygenated compounds that occur in crude petroleum and are particularly resistant to biodegradation. Resins include oxygen, nitrogen, and sulfur-containing compounds that are for the most part recalcitrant [18, 23, 24]. Various characteristics of PHCs affect their inherent biodegradability; the chemical structure of individual components of petroleum products is most important, but physical state, toxicity, influence of other compounds, and presence of additives are also factors [18, 24]. Rates of biodegradation are the greatest for saturates, followed by light aromatics, high molecular weight aromatics and finally polar compounds. Increasing numbers of carbons in alkanes

(homology), variations in chain length and ring condensation account for the wide variety of hydrocarbons that occur in crude petroleum [18, 43]. Because of these variations, the biodegradability of PHCs will differ from site to site. In general, PHCs are ranked in the following order of susceptibility to biodegradation: straight chain alkanes > branched alkanes > low molecular weight aromatics > cyclic alkanes [20].

Fate of Petroleum upon Entering Soils

Petroleum waste usually enters the ground via accidental spills, leaks, or through permitted or illegal dumping [20]. Once spilled onto the soils, infiltration into the vadose zone is likely. Infiltrated soils move vertically downward through unsaturated soils, where they may dissolve into the gaseous phase, or be otherwise dispersed, diluted, or sorbed onto particulate matter, then spread out laterally over the soil water table [18, 43]. Absorption of petroleum components onto particulate matter decreases the toxicity to microorganisms, but adds to PHC persistence [20, 43]. In cases where infiltration cannot occur, for example, freezing or saturated soils, evaporation and photooxidative losses contribute greatly to PHC removal [18]. Contaminants within the vadose zone may also undergo chemical and microbiological transformations that can influence partitioning [45].

Simple aliphatic compounds are biodegraded by enzymes catalyzing oxidation, reduction, and oxidative coupling reactions. Normal alkane biodegradation is initiated by complex monooxygenase enzyme systems, which oxidize the alkane to the corresponding primary alcohol [46]. The primary alcohol is oxidized via the aldehyde to the corresponding carboxylic acid by alcohol and aldehyde dehydrogenases. Beta-oxidation enzymes convert the acid to a simpler alcohol and acetic acid. The new alcohol is further degraded with the same sequence of enzymes to form a simpler aliphatic hydrocarbon with fewer carbons [47].

The Toxic Component of Petroleum

Simple polycyclic aromatic hydrocarbons or PAHs are considered by national environmental agencies as the toxic component of petroleum. PAHs are the basis for risk assessment-based mitigation approaches for environmental remediation. They constitute by volume only 0.2–7.0% of oil mixtures. PAHs, such as benzene, toluene, naphthalene, anthracene, and phenanthrene, and their alkyl-substituted derivatives are catalyzed by a class of enzymes known as dioxygenases. The products of initial metabolism of simple aromatic hydrocarbons are commonly catechols or substituted catechols [47]. Ring cleavage of these compounds occurs by one of two pathways depending on the species and the substrate. The ortho-pathway involves cleavage of the ring between the hydroxyl group while the meta-pathway involves cleavage of a bond between a carbon atom bearing a hydroxyl and an adjacent, non-hydroxylated carbon atom [20]. Both ortho- and meta-pathways are involved in aromatic hydrocarbon degradation, but substituted catechols are generally degraded via the meta-pathway [5].

Benzo(a)pyrene and similar high-molecular weight compounds are initially metabolized by the enzymatic catalyst monoxygenase, which converts the parent compound into a 7,8-epoxide [5]. An epoxide hydrase then catalyzes the epoxides to dihydrodiols; arylhydrocarbon hydroxylase in turn tranforms the dihydrodiols to phenols [35, 43]. The diastereomeric benzo(a)pyrene, 7,8-dihydrodiol and 9,10-epoxides, are presumed to be the ultimate carcinogens of benzo (a)pyrene, since they are (1) highly carcinogenic for newborn mice, (2) mutagenic and cytotoxic for both mammalian and bacterial cells, and (3) chemically reactive in binding to DNA [12].

Due to the large size and extreme insolubility of such PAHs as benzo(a)pyrene or benzo(a)anthracene, few soil/sediment microorganisms have the capability to utilize aromatic hydrocarbons containing more than three aromatic rings as the sole source of carbon and energy [48–50]. The chemical and physical characteristics of the seven key PAHs of interest are shown in Table 2.

Ex situ Approach for Soils/Sediments

Land Treatment Unit (LTU) Along an Active Railway
Rail operations have been and continue to be in the mainstream of industrial activity. Unfortunately, the use of fuels for rail operations is not without its environmental costs. At every stage of fossil fuel shipment and utilization, waste is generated and released. Ecosystems along transportation corridors have been

Bioremediation and Mitigation. Table 2 Chemical and physical properties of seven key PAHs

Compound	Rings	MW	Solubility
Naphthalene	2	128	31.70
Phenanthrene	3	178	1.0
Anthracene	3	178	0.045
Pyrene	4	202	0.132
Benzo(a)anthracene	4	228	0.006
Chrysene	4	228	0.002
Benzo(a)pyrene	5	252	0.001

MW molecular weight
Solubility (mg/L) is aqueous solubility at room temperature

damaged by exposure to the accumulation of high concentrations of petroleum hydrocarbon materials in soils and ballast material. One strategy for dealing with broadcast railroad lubricants is to apply adapted microbial consortia to the contaminated soil/ballast matrix. This procedure is called land treatment and is used to degrade waste hydrocarbons into the nontoxic, naturally occurring end products CO_2 and H_2O. Over a 12-month period, this soil remediation strategy was used to remediate diesel-contaminated soils at an active rail yard in McGehee, Arkansas. A LTU was designed and constructed to optimize petroleum hydrocarbon biodegradation rates and prevent waste mobilization into subsoils and groundwater [52, 53] (Fig. 1). The LTUs had the following features:

- Compacted clay subgrade and 40-mm HDPE (high density polyethylene) geomembrane liner leachate collection system comprised of a sand drainage layer, a gravel, and perforated pipe drain; a gravel sump and standpipe; and an 80,000-l leachate storage tank
- Leachate collection/irrigation pump, mobile sprinkler, and piping/hose
- 19-mm HDPE geomembrane cover and surface water outlet for the recycling of leachate collected from the LTU when the water content was above optimum conditions

Lifts of contaminated soil/ballast layered to 0.4-m depth were loaded into the LTU and treated until a target cleanup concentration of <200 mg/kg soil dry weight was reached. Approximately 7,500 m^3 of contaminated soil were successfully treated over a 6-month time frame. Soil total petroleum hydrocarbon (TPH) levels were reduced from an initial concentration of 2,500 ± 485 mg/kg soil dry weight to less than 140 ± 62 mg/kg soil dry weight in each of three lifts. Mean petroleum hydrocarbon reduction rates ranged from 17.3 mg/kg soil dry weight per day for cooler months to 42.5 mg/kg soil dry weight per day for warmer months. The data generated under varying climatic conditions demonstrate that the mitigation strategy of employing an adapted microbial population can be used to remediate rail TPH soils to acceptable regulatory levels for typical rail operations [55].

Ex situ Approaches for Groundwater

Recovery and Biological Treatment of Wood Preservatives in Groundwater Well-recovery networks coupled to immobilized microbe bioreactors (IMBRs) were installed at a 172-acre former wood preserving process facility in Baldwin, Florida in 1995 for the bioremediation of toxic organic wood preservatives, both free phase and soluble, present in site groundwater. The well-recovery network was designed to recover contaminated components in two steps: (1) a pumping system to remove free phase creosote from the hardpan at 10–14 m below the surface and (2) a system for recovering subsurface-clarified groundwater to a holding tank, where trace creosote fractions and pentachlorophenol were further gravity separated. Immobilized microbial isolates evaluated in earlier laboratory and field pilot tests were established into two 40,000-l bioreactors for the biodegradation of all targeted constituents [56, 57]. Microbial growth, DO, pH, flow rate and temperature were monitored in this combined in situ/ex situ bioremediation system.

The immobilized packed bed reactor (IMBR) system is filled with bio-support media, and contains adapted microbes with enzymatic capability of mineralizing the organic compounds of interest [58]. The packed bed provides a large surface area for microbial colonization [59, 60]. The bio-support media is usually a chemically inert and physically stable quartz-based diatomaceous earth material, which has a good pore morphology and high surface area. Adsorption or

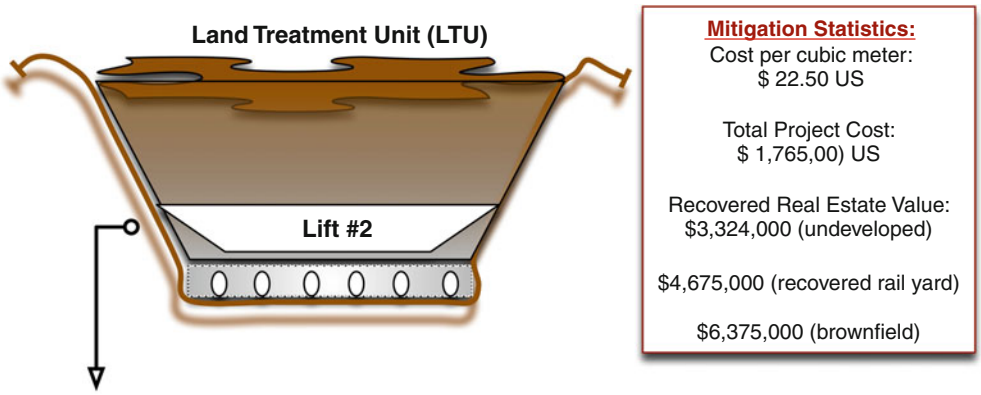

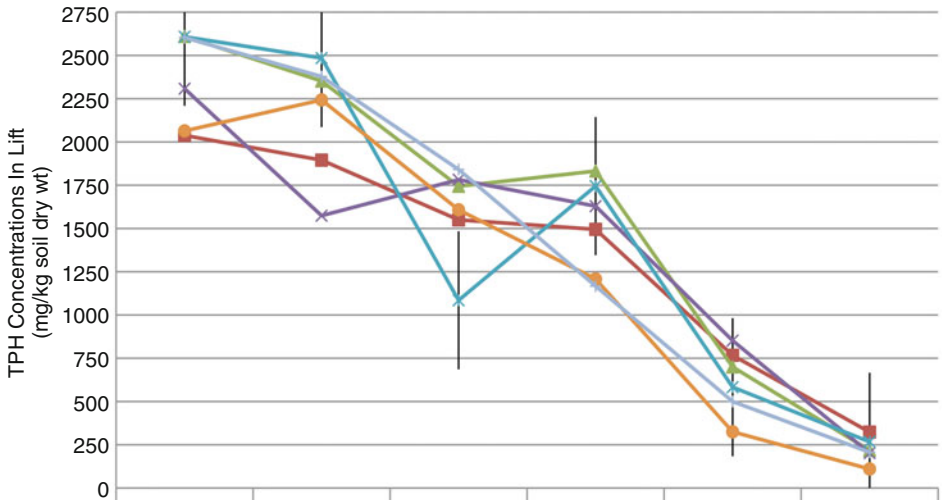

Time (days)	0	14	30	45	60	90
Treatment Zones A	2038	1895	1550	1495	767	323
B	2610	2352	1744	1832	700	218
C	2308	1574	1782	1629	852	202
D	2608	2485	1085	1745	583	267
E	2064	2243	1608	1208	325	110
F	2603	2378	1841	1167	500	207

Bioremediation and Mitigation. Figure 1
Ex situ mitigation strategy for treatment of petroleum-based contamination along an active railway

covalent bonding to this media is the primary mechanism for immobilization. Bacterial immobilization involves the entrapment of cells onto the matrix. Once bound, the cells are then readily accessible to the surrounding substrate.

Ten-year operational data sets have indicated successful biodegradation of the clarified feed composed primarily of pentachlorophenol (PCP), targeted polycyclic aromatic hydrocarbons (PAHs), and minor amounts of other chlorinated phenols and nitrophenols. The recovery system retention time of approximately 3.2 days satisfied federal and state NPDES target levels (Fig. 2). Flow rates of 34.5 ± 3.8 L/min were maintained throughout the treatment time

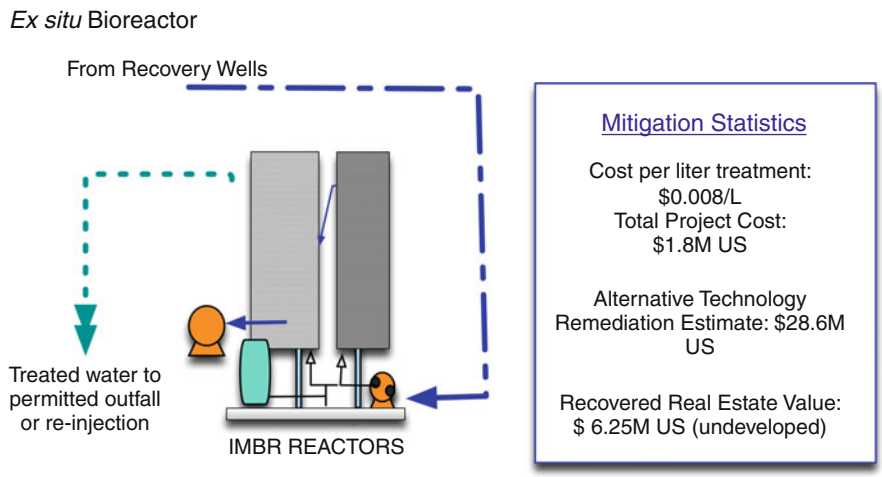

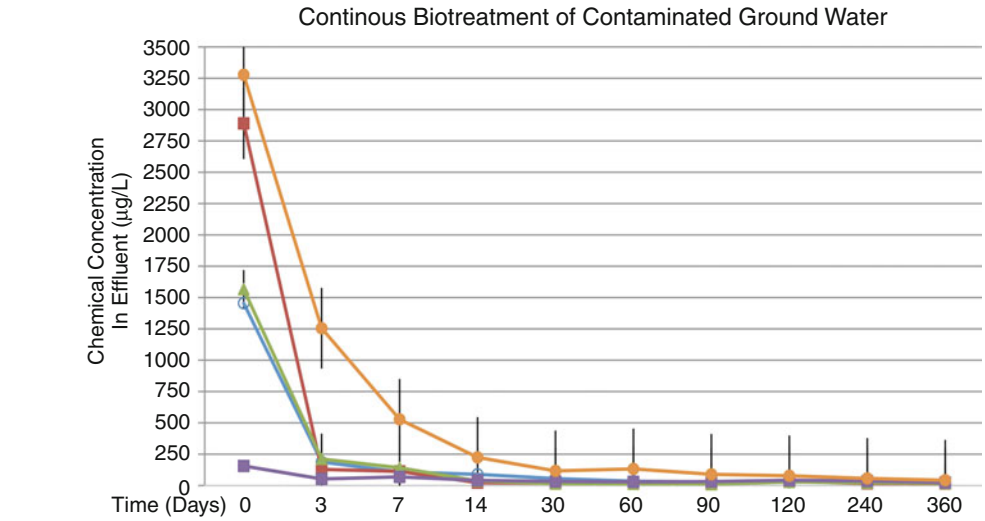

Time (Days)	0	3	7	14	30	60	90	120	240	360
Napthalene	1455	188	108.5	89.2	55.6	34.5	28.8	26.6	32.8	22.5
Phenanthrene	2890	129	112.8	22.5	18.5	28.8	12.5	32.5	16.8	15.9
Chrysene	1567	212	141.5	36.5	14.8	13.5	10.5	28.7	22	18.8
Benzo(a)pyrene	156	52.5	68.9	41.5	32.5	29.5	31.5	42.2	36.2	24.5
Pentachlorophenol	3278	1255	528.2	224.5	116.8	132.5	89.5	77.8	56.8	42.4

Bioremediation and Mitigation. Figure 2
Ex situ mitigation approach for continuous treatment and hydraulic control of a contaminated groundwater bloom in an urban area

frame. Treated effluent was used during drought years to irrigate surface vegetative cover and allow for perculation down to the hardpan [59]. The site received a national award in 1996 for the innovative control and treatment of a groundwater plume from the American Forest and Paper Association. The site is currently zoned recreational and is close to meeting groundwater MCLs.

In situ Approaches for Soils, Sediments, and Groundwater

In situ remediation approaches are targeted at reducing groundwater concentrations without employing a "pump and treat" approach. Earlier technology approaches allowed for passive treatment of a contaminated plume as it moved through a biological barrier or trench. The concept has proven to be marginally successful for plume control, that is, preventing toxic groundwater from moving beyond the legal boundaries of the affected site, but does not address the real problem of the source of contamination in soils/sediments [55, 59].

Newer technologies attempt to focus treatment on the soil/sediment itself using direct addition of free microbial cells to the contaminated soil/sediment lens (bioaugmentation) or providing nutrients and allowing for the indigenous microflora to reduce soil concentrations over time. This approach, called natural attenuation, models the rate of kinetic biodegradation/mineralization of soil/sediment contamination and provides an estimate for reaching MCLs [37, 39].

A variation of both approaches is to treat the subsurface groundwater and redirect a preferred acclimated biomass to the point sources of contamination in soils/sediments. The same immobilized microbe bioreactor concept mentioned for ex situ groundwater treatment has been used for treatment of petroleum contaminated soils and groundwater, in situ. Soil seeding bioreactors called bioplugs are installed vertically using conventional drilling equipment; bioconduit*s* are horizontally placed bioreactors installed using directional drilling equipment [61].

Adapted indigenous microbial strains are used for immobilization in the bioreactors, having been identified as able to degrade the specific compounds/contaminants of interest. The use of indigenous microflora, a concept combining the positive aspects of bioaugmentation and natural attenuation, reduces the time of microbial acclimation to surrounding soil/sediment conditions and lowers the rejection rate of viable biomass in close proximity to areas of elevated contamination. Once placed on the subsurface, the reactors contain and sustain selected microbial populations required for effective degradation of highly contaminated soils. The in situ soil bioreactors are designed with ports for nutrient and air/oxygen amendment to maintain optimum conditions. The operational flow is maintained by initiating a pressure gradient in the reactors using compressed air/oxygen or nitrogen for anaerobic applications. The aeration flow rate is designed based on the site-specific conditions and the contaminants (volatile organic compounds or semi-volatile organic compounds) to be remediated [60, 61].

The use of contaminated groundwater or site water through the immobilized bed results in mineralization of organics in the water phase to biomass and generates whole cell bleed-off from the bed. The elevated biomass is allowed to escape from the bioplugs/bioconduits, thus introducing an enriched, adapted microflora moving layer into the surrounding soil/sediment strata in a radial pattern. Over time the biomass fronts, by physical movement and chemotaxis, infiltrate contaminated areas and reduce concentrations of chemical constituents in the soil/sediment matrix. The point source of the contaminated groundwater plume is therefore eliminated [60, 62].

Hydraulic control of the treatment area is quite important [62]. The bioplugs generate a hydraulic gradient at a targeted site, either as a result of the injection of water through the bioplugs or the injection of air, which can modify the pressure gradient. Hydraulic control generally consists of some method of collecting the water down gradient from the region of influence, that is, a recovery trench, and recycling it back to the site trough the bioplugs. There are two major reasons for recycling the water: (1) recycling will control the migration of contaminants from the affected area and (2) recycling will help maintain the nutrient concentration in the injection water and reintroduce adapted microorganisms back to the affected area while treating the groundwater to meet MCLs [62].

In situ Remediation of Contaminated Groundwater and Site Soils at a Natural Gas Pipeline Compressor Station Over the last 30 years, leakage and accidental discharge of petroleum-based lubricating oil used to maintain the pipeline and related equipment of a gas transmission facility have resulted in petroleum hydrocarbon (PHC) contamination of the soil. The site evaluation conducted by a private engineering firm identified fifty areas at four different sites exhibiting

PHC concentrations greater than regulatory acceptable levels. All fifty areas were successfully remediated using bioremediation techniques. Due to the depth of the contamination and soil conditions, fifteen areas were remediated by installing approximately 550 in situ immobilized bioreactors (bioplugs) (Fig. 3a). A monitoring protocol developed for the site was implemented during the remediation period to maintain optimal conditions and make operational adjustments, as required. Only one of the areas targeted for remediation is discussed in this case study [61].

The bioplug system was designed to facilitate petroleum hydrocarbon mineralization by placing PHC-degrading microorganisms in close contact with the contaminants [61]. Initial total petroleum hydrocarbon concentrations as analyzed by EPA Method 418.1 at the subject area were as high as 16,000 mg/kg with an average concentration of 4,400 mg/kg soil dry weight. Samples were collected at different radial distances (1, 2, and 3 m) and depths (1, 2, and 3 m below ground surface) from each bioplug location within the subject area. The samples were analyzed to determine the effective radius of influence for each plug. Analysis of covariance indicated that TPH degradation at 2-, 4-, and 5-m radial distances and depths occurred at an equivalent rate throughout the degradation period [64].

Changes in polycyclic aromatic hydrocarbon (PAH) composition were monitored by gas chromatography/mass spectrometry. Samples were analyzed for PAH content and concentration. Fourteen PAH compounds were identified in varying concentrations during the day-14 sampling. By day-90, PAHs with three or fewer rings were completely degraded. However, low concentrations of flouranthene, benzo(a)pyrene, benzo(b) flouranthene, and indeno(1,2,3cd)pyrene were identified after 90 days of remediation. The presence of 4+ ring PAHs was expected because of the fact that the ability of microbes to mineralize PAHs decreases with increasing ring number [60, 62, 63].

The assays were coupled with microbial measurements of total heterotrophic and total petroleum-degrading bacteria, and direct measurements using acridine orange florescent staining. Changes in the population of PHC-degrading microorganisms over time in the subject area were determined by averaging the values obtained from all samples collected within the area. The microbial growth and the degradation of the contamination occurred exponentially within the first 30 days. The microbial growth was observed decreasing after 30 days, when the majority of the easily degraded petroleum hydrocarbons, saturated alkanes and PAHs containing fewer than three rings had been depleted (approximately by 72%). Sampling and analysis during the remediation period indicated an increase in the heterotrophic and petroleum-degrading microbial population by 75% and 57%, respectively, from day 14 to 90. Within 180 days from the activation of the remediation system, targeted compliance TPH concentrations (100 mg/kg soil dry weight) were attained. The reduction of PAH concentrations for soils and groundwater over time is shown in Fig. 3b.

Future Directions

Improved Mitigation Drivers

In the past few years, the goal of establishing US cleanup standards using bioremediation approaches has made significant progress as cities, municipalities, state agencies, and the federal government have focused on establishing bioremediation actions linked to accepted numerical metrics within a defined cost structure or economic price tag. The US Environmental Protection Agency has used maximum contamination level goals (MCLGs) and maximum contaminant levels (MCLs) as tools for establishing the highest allowable level of contamination in drinking water [40]. With the use of the MCL rules and MCLGs, US-EPA has set in place a framework for deciding "how clean is clean" for contaminated soils and sediments and affected groundwater under the Resource Conservation and Recovery Act (RCRA) program for contaminated industrial sites and Comprehensive Environmental Response, Compensation Liability Act (CERCLA), or "Superfund," for abandoned hazardous waste sites. Linking the MCL and MCLG criteria to "Best Available Remediation Technology," or BART, has become the driver for risk-based bioremediation mitigation [65]. Legal judgments and records of decision (RODs) now involve decisions affecting not only environmental protection, land use, and related economics, but human health and quality of life [66]. Risk-based cleanup standards have made significant progress in the past 10–15 years; most states now have in place a series of decision tiers

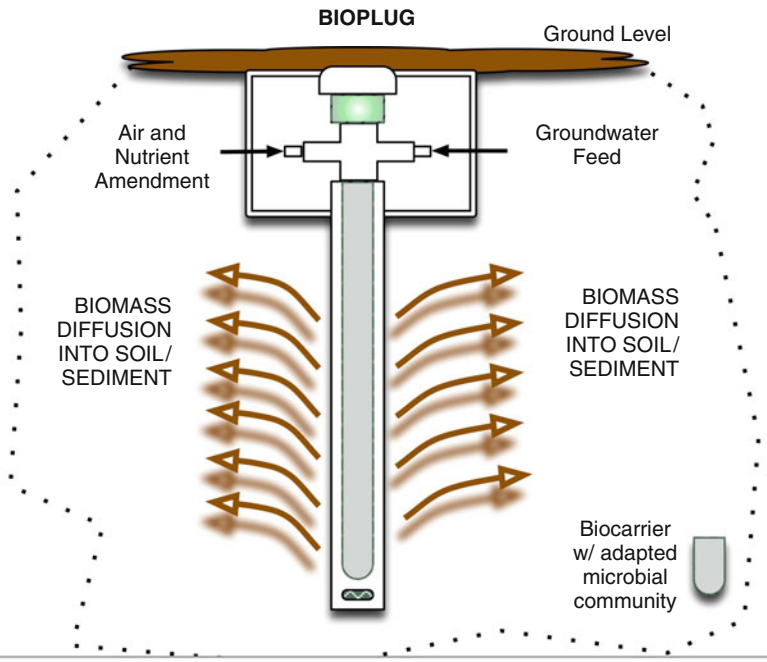

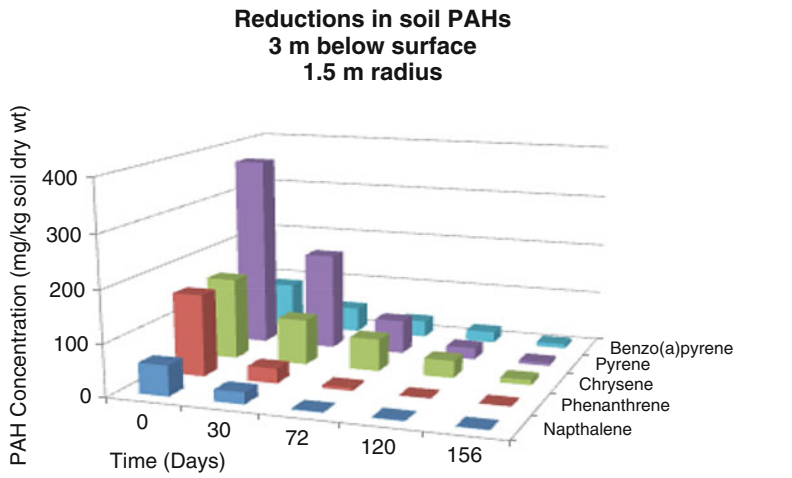

	0	30	72	120	156
Napthalene	58.8	22.5	1.8	2.1	1.2
Phenanthrene	158.2	28.5	5.5	0.5	0.5
Chrysene	158.5	88.4	62.5	33.5	9.6
Pyrene	370.5	188.4	65.8	22.5	6.2
Benzo(a)pyrene	88.5	48.5	32.2	21.5	8.2

a

Bioremediation and Mitigation. Figure 3
(Continued)

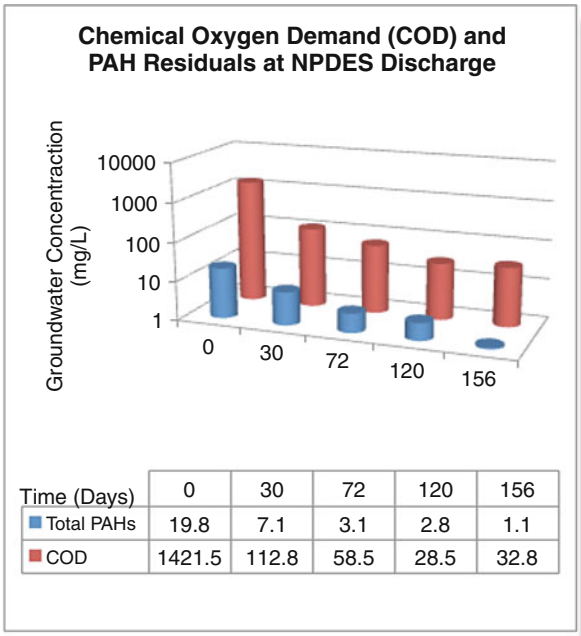

Mitigation statistics

Cost per cubic meter remediation: $12.50 US

Cost per liter Groundwater treatment: $0.0004 per liter

Projected Site Remediation Cost" Excavation: $ 12.8 M US

Actual Site Remediation Cost: Bioplug System: $2.1M

Total cubic meters remediated: estimated 168,230

Coastal Restoration Benefit: estimated $11.2 M US

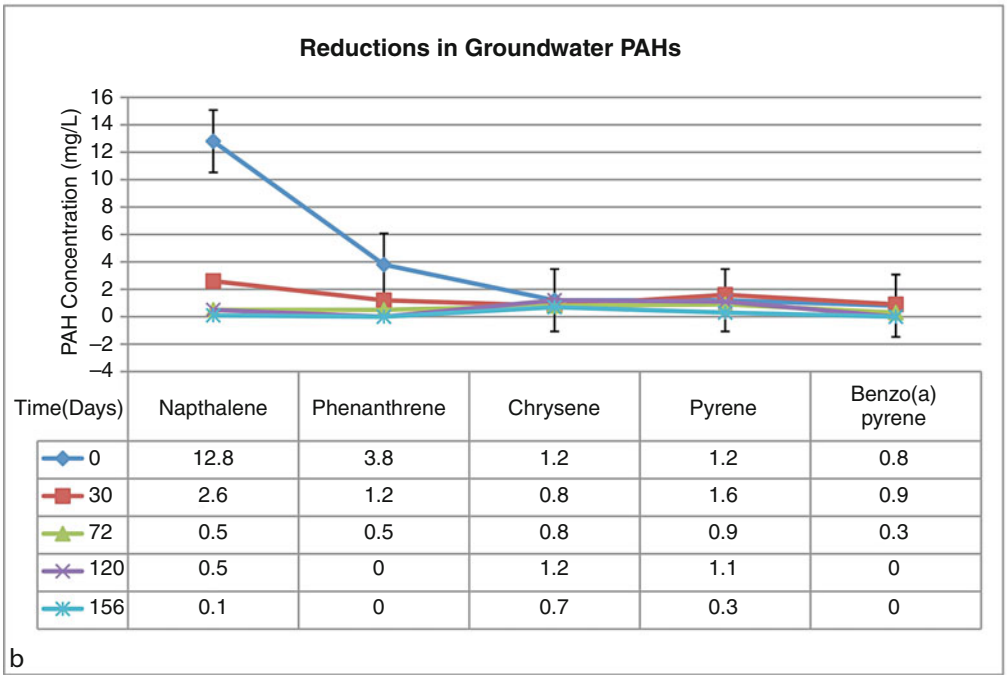

Bioremediation and Mitigation. Figure 3
(**a**) The application of an in situ mitigation strategy to reduce soil PAH concentrations with depth at a natural gas compressor station. (**b**) Reductions in groundwater PAH and total COD concentrations in a combined in situ mitigation approach to remediate a natural gas pipeline compressor station

(usually in the form of tables by specific contaminant) for assessing risk and reaching legally acceptable cleanup criteria for soil and groundwater in specific residential, light industry, or heavy commercial locations [67]. As mitigation criteria become more focused on the quality of life in determining "how clean is clean," Risk-Based Corrective Action Plans (RBCAs) will have additional social and economic mitigation criteria separate from technical engineering and economic indices in establishing sustainable remediation cleanup standards [68, 69].

Defining Stakeholders

Over the past decade, the selection of mitigation goals and remediation technologies has been driven by technical criteria and acceptance by regulatory agencies [70]. Only in recent years has a health and health protection criteria played the more dominant role in decision making. The development of the Internet and access to information has not only affected site owners, state and municipal agencies, and board industry, but has also led to an expansion in a broader inclusion of the general public as stakeholders in any bioremediation approach. Thus the concept of sustainable remediation, practices or multitask approaches for restoring a site to its native state with a frugal use of available resources, involves stakeholders at the regional, national, and international level [70–72].

Developing National and International Bioremediation Mitigation Programs

Executive Order 13123, "Greening of the Government Through Efficient Energy Management," by the US-EPA Office of Solid Waste and Emergency Response provided definable environmental goals for state and local municipalities in initiating sustainable mediation [65]. Smart energy resources management and green remediation can be incorporated into sustainable environmental practices. Remediation management practices of contaminated sites are outlined by Diamond et al., in which future initiatives and sustainable mitigation-based bioremediation are based [73]. State initiatives in Minnesota, California, Illinois, and Louisiana are early indications of how important federal tools are being assimilated into state and local programs [65, 74, 75]. The Canadian Environmental Protection Act implemented in 2,000 forms the basis for establishing risk-based criteria for contaminated soil and groundwater and air blue emissions in the various provinces of the country [76, 77]. The province of Québec has made significant progress in establishing written guidelines or soil protection and contaminated site restoration. Key components of this guideline include the concept of prevention, the necessity of reclamation and rehabilitation, and most importantly the idea of the polluter pays principle. However, Québec has achieved only modest success with many sites remaining under the category of off-site disposal [77].

The European Union adopted the Environmental Technology Action Plan in 2004 to demonstrate sustainable remediation practices at specific field locations in an attempt to follow US-EPA initiatives for standardization of risk-based criteria based on human health considerations [71, 78].

Asian countries have seen record economic growth over the past 2 decades which has resulted in significant progress in quality of life improvements at the expense of the deterioration of natural resources, increased pollution, and threat to human health [79]. Japan has made significant progress with the implementation of the soil contamination countermeasures law of 2003. China and India are attempting to emulate both the US-EPA initiatives and the European Union as they struggle to make difficult public health decisions within the world's fastest-growing economies [80].

Conclusions

One of the key axioms mentioned in Executive Order 13123 is that of "sustainability means change" [81]. Leadership at the local, state, national, and international level will be needed so as to realize the public perceptions as to what successful mitigation put into practice really means [70, 82]. Remediation selection and optimization assessments have become the norm in making good decisions for restoring impacted sites [83]. However, sustainability does not rank as the highest priority in making decisions on-site remediation. As market and government forces continue to seek economically efficient but socially responsible approaches to site cleanup, sustainability has been the driving criterion for mitigation-based bioremediation to become the norm [70].

Bioremediation mitigation strategies can be effectively designed by incorporating vadose zone and groundwater modeling [84]. Based on the availability of site hydrogeologic data and conditions, analytical modeling and/or numerical modeling can be used in designing the in situ bioremediation of the saturated zone.

An effectively designed, operated, and maintained bioremediation system offers an added advantage over conventional strategies like "pump and treat" by reducing the time of remediation. An advantage of using a technology such as the in situ immobilized bioreactors is to effectively increase the petroleum degrader population by placement of the adapted microorganisms in close contact with the organic residue. The in situ immobilized bioreactors can also be used to provide a cometabolite for degradation of hazardous byproducts produced during the degradation process of some of the chlorinated solvents [57]. Also, the frequently encountered problem of ineffective indigenous microorganisms and/or low indigenous microbial population can be avoided [56].

The use of bioremediation mitigation approaches in conjunction with physical/chemical systems, that is, excavation, solidification, or vapor extraction, can provide a combination of mass reduction phenomenon and mass transfer phenomenon, thus reducing the time of remediation and the cost of cleanup. In many cases, due to the complex nature of the surface and subsurface conditions, a combination of in situ remediation techniques is recommended [83]. With rigorous engineering design, bioremediation technologies can be economical, viable, and safe solutions to real-world contamination problems [84].

Bibliography

Primary Literature

1. U.S. Environmental Protection Agency (2004) Terms of environment: glossary, abbreviations and acronyms. EPA 175-B-001 (Last Revised December 1997). http://www.epa.gov/OCEPAterms/
2. Robert T (2000) Stafford disaster relief and emergency assistance act, as amended by public law, pp 106–390, 30 October 2000. United States Code Title 42. The Public Health and Welfare
3. Bradford ML, Krishnamoorthy R (1991) Consider bioremediation for waste sitecleanup. Chem Eng Prog 12(1):80–85
4. Sayler GS, Fox R, Blackburn J (eds) (1991) Environmental biotechnology for waste treatment. Springer, New York
5. Tabak HH, Quave SA, Mashni CI, Barth EF (1981) Biodegradability studies with organic priority pollutant compounds. Water Qual 53(10):1503–1517
6. National Research Council (2005) Contaminants in the subsurface: source zone assessment and remediation. The National Academies Press, Washington, DC
7. Understanding Bioremediation: A Guidebook for Citizens (1991) United states environmental protection agency. Office of Research and Development, Office of Environmental Engineering and Technology
8. Worth M, Fernandes AL, Freshner R (1991) Bioremediation of contaminated soil: a case study in Canada, pp 326–343. Environmental Pollution, Canada.
9. Slater JH, Godwin D (1980) Contemporary microbial ecology. Academic, London
10. Carberry JB, Lee SW (1990) Care and transport of petroleum in the unsaturated soil zone under biotic and abiotic conditions. Water Sci Technol 22(6):45–52
11. Hughes JB, Neale CN, Ward CH (2000) Encyclopedia of microbiology, 2nd edn. Academic, New York
12. Prince RC (1998) Kirk-Othmer encyclopedia of chemical technology. Wiley, New York
13. Srinivasan U (2003) U.S. bioremediation markets. Frost and Sullivan research report, no. 7857. Frost and Sullivan, Palo Alto, CA
14. Portier RJ (1988) Enhanced biotransformation and biodegradation of polychlorinated biphenyls in the presence of aminopolysaccharides. Aquat Toxicol 10:503–516
15. Vance OB (1991) Onsite bioremediation of oil and grease contaminated soils. Nat Environ J 1(1):26–30
16. Roos D, Stroo HF, Bourquin AW, Sikes DJ (1988) Bioremediation of hazardous waste sites in the USA: case histories. The Association Dedicated to Air Pollution Control and Hazardous Waste Management, vol 38.6, pp 2–9
17. Walker WW, Cripe CR, Pritchard PH, Bourquin AW (1988) Biological and abiotic degradation of xenobiotic compounds in vivo estuarine water and sediment/water systems. Chemosphere 17(12):2255–2270
18. Bartha R (1986) Biotechnology of petroleum pollutant biodegradation. Microb Ecol 12:155–172
19. Frederickson JK, Bolton H Jr, Brockman FJ (1993) In Situ and on-site bioreclamation. Environ Sci Technol 27(9):1711–1716
20. Lyman WJ, Noonan DC, Reidy PJ (1990) Cleanup of petroleum contaminated soils at underground storage tanks. Pollut Technol Rev No.195: 38–65
21. Musts for USTs (1995) United States environmental protection agency. Office of Underground Storage Tanks. EPA 510-k-95-002
22. Skinner JH (1991) Bioremediation research issues. In: Sayler GS, Fox R, Blackburn JW (eds) Environmental biotechnology for waste treatment, vol 41. Plenum, New York, pp 61–70
23. Gabriel PF (1991) Innovative technologies for contaminated site remediation: Focus on bioremediation. Air Waste Manage Assoc 41(12):1657–1660

24. Riser-Roberts E (1992) Bioremediation of petroleum contaminated sites. CRC Press, Washington, DC
25. Iwamoto T, Nasu M (2001) Current bioremediation practice and perspective. J Biosci Bioeng 92(1):1–8
26. Grady L (1985) Biodegradation: its measurement and microbiological basis. Biotechnol Bioeng 27(5):660–674
27. States use of bioremediation: advantages, constraints, and strategies (1991) Natural resources policy studies center for policy research. National Governors' Association
28. Portier RJ, Friday DD (1991) Development of an immobilized microbe bioreactor for VOC applications. Environ Prog 10(1):30–39
29. Portier RJ (1982) Correlative field and laboratory microcosm approaches in ascertaining xenobiotic fate and effect in diverse aquatic environment. Ph.D. Dissertation, Louisiana State University, Baton Rouge, LA, 205 p
30. Grommen R, Verstraete W (2002) Environmental biotechnology: the ongoing quest. J Biotechnol 98(1):113–123
31. Ward OP, Singh A, VanHamme J (2003) Accelerated biodegradation of petroleum hydrocarbon waste. J Ind Microbiol Biotechnol 30(5):260–270
32. Halvorson HO, Pramer D, Rogul M (eds) (1985) Engineered organisms in the environment: scientific issues. American Society of Microbiology (ASM), Washington, DC
33. Atlas RM, Bartha R (1987) Microbial ecology: fundamentals and application, 2nd edn. The Benjamin/Cummings Publishing Company, Inc, Menlo Park, CA
34. Begley S, Waldrop T. (1989) Microbes to the rescue. Newsweek, June 19, pp 56–57.
35. McFarland MJ, Sims RC, Blackburn JW (1991) Use of treatability studies in developing remediation strategies for contaminated soils. In: Sayler G, Fox R, Blackburn JW (eds) Environmental biotechnology for waste treatment. Plenum, New York, pp 163–174
36. Johnson LM, McDowell CS, Krupha M (1985) Microbiology in pollution control from bugs to biotechnology. Dev Ind Microbiol 26:365–376
37. Van Hamme J, Singh A, Ward OP (2003) Recent advances in petroleum microbiology. Microbiol Mol Biol Rev 67(4): 503–549
38. U.S. Environmental Protection Agency (2008) Green remediation: incorporating sustainable environmental practices into remediation of contaminated sites. Office of Solid Waste and Emergency Response, EPA 542-R-08-002. http://www.brownfieldstsc.org/pdfs/green-remediation-primer.pdf. Accessed 5 May 2009
39. Brune H, Schaat H (1991) Organic pollutants in soil and food chain. In: Nath B (ed) International conference on environmental pollution. Inderscience Enterprises, Ltd, Geneva, Switzerland, pp 335–343
40. Atlas RM (1984) Diversity of microbial communities. Adv Microb Ecol 7:1–47
41. Atlas RM (1984) Microbiology, fundamentals and applications. Macmillan, New York
42. Bond PL, Druschel GK, Banfield JF (2000) Comparison of acid mine drainage microbial communities in physically and geochemically distinct ecosystems. Appl Environ Microbiol 66(11):4962–4971
43. Morrison BA (1992) On-site bioreclamation of creosote-contaminated soil at the Scott Lumber site. Air Waste Manage Assoc 92(27):2–12
44. Diamond ML, Page CA, Campbell M, McKenna S, Lall R (1999) Life-cycle framework for assessment of site remediation options: method and generic survey. Environ Toxicol Chem 18:788–800
45. U.S. Environmental Protection Agency (1996) Semi-volatile organic compounds by gas chromatography/mass spectrometry (GC/MS). In: SW-846. Test methods for evaluating solid wastes physical/chemical methods (Method 8270C), 3rd edn, EPA Revision 3. Office of Solid Waste, Washington, DC
46. Venosa AD, Haines JR, Nisamaneepong W, Govind R, Pradhan S, Siddique B (1991) Protocol for testing bioremediation products against weathered Alaskan crude oil. Proceedings of 1991 international oil spill conference. American Petroleum Institute, Washington, DC, pp 563–570
47. U.S. Environmental Protection Agency (1999) Monitored natural attenuation of petroleum hydrocarbons, EPA 600-F-98-021. Office of Research and Development
48. Portier RJ, Martin AM (eds) (1991) Applications of adapted microorganisms for site remediation of contaminated soil and water biological degradation of wastes. Elsevier Science, New York
49. Ward OP, Singh A (2004) Applied bioremediation and phytoremediation, vol 1, Soil biology series. Springer, New York
50. Nelson CH (1993) A natural cleanup. Civil Engineering, American Society of Civil Engineers (ASCE), 63(3):57–59.
51. Bianchini MC, Henry D, McMillin, Portier R (1986) Contribution to toxicant biotransformation by commercially available mutated bacterial cultures as compared to adapted indigenous microflora in the degradation of aromatic and aliphatic hydrocarbons. Abstract. American society for Microbiology/Canadian society for Microbiology symposium on environmental insult and recovery of stressed systems, Toronto, Canada
52. Portier RJ, Ahmed SI (1988) A marine biotechnical approach for coastal and estuarine site remediation and pollution control. Mar Technol Soc J 22(2):34–42
53. Portier RJ, Bianchini M (1988) Comparison of effective toxicant biotransformation by autochthonous microorganisms and commercially available cultures in the 'in situ' reclamation of contaminated sites. Biotechnologische In-Situ Sanierung. Gustav Fishscher Verlag, pp 273–292
54. Portier RJ (2003) Trends in soil science, technology and legislation in the USA. J Soils Sediments 3(4):257
55. Friday DD, Portier RJ (1989) Evaluation of a packed bed immobilized microbe bioreactor for the continuous biodegradation of halogenated-contaminated ground waters. AWMA/EPA international symposium on hazardous waste treatment: biosystems for pollution control, pp 97–112.

56. Sattler DL, Hoover DG, Davis TM, Portier RJ (1997) Recovery and biological treatment of organic wood preservatives in groundwater. In: In situ and on-site bioremediation, vol 5. Batelle Press, Columbus, OH
57. Portier RJ, Sattler DL, Hoover DG, Davis TM, Williams SE (1998) Recovery and microbial remediation of organic wood preservatives in groundwater at a former wood treating plant. Remediation 8(4):95–108
58. Portier RJ, Barton K, Koury J (1995) Low intervention soil bioremediation approaches. Remediation 5(2):57–75
59. Portier RJ, Metosh-Dickey C, Anas D (2004) Biological treatment of wood preservatives in site soils/sediments and associated groundwater: a 5-year study. Proceedings: session, WA1. Biorestoration strategies for contaminated sediments fourth SETAC world congress, Portland, OR, 3 p
60. Metosh-Dickey C, RJ Portier (2004) In situ bioremediation of contaminated soils and sludges. Presented at CPBR 2004 symposium, Washington, DC (poster and extended abstract)
61. Morgan P, Watkinson RJ (1990) Assessment of the potential for in situ biotreatment of hydrocarbon-contaminated soils. Water Sci Technol 22(6):63–68
62. Morris MS, Novak JT (1989) Mechanisms responsible for the biodegradation of organic compounds in the subsurface. J Hazard Mater 22(3):393–405
63. Einarson MD (2006) The practical handbook of environmental site characterization and ground-water monitoring, 2nd edn. CRC Press, Boca Raton, FL
64. Efroymson RA, Nicolette JP, Suter GW II (2004) A framework for net environmental benefit analysis for remediation or restoration of contaminated sites. Environ Manage 34:315–331
65. Interstate Technology and Regulatory Council (2008) Use of risk assessment in management of contaminated sites. ITRC Risk Assessment Resources Team. http://www.itrcweb.org/Documents/Risk Docs/RISK2 ExSum.pdf. Accessed 5 May 2009
66. Diamond ML, Page CA, Campbell M, McKenna S, Lall R (1999) Life-cycle framework for assessment of site remediation options: method and generic survey. Environ Toxicol Chem 18:788–800
67. Dresner S (2002) The principles of sustainability. London, Earthscan. Economist Intelligence Unit. http://a330.g.akamai.net/7/330/25828/20080208181823/graphics.eiu.com/upload/Sustainability allsponsors.pdf. Accessed 5 May 2009
68. Brundtland Commission (1987) Report of the world commission on environment and development: our common future. http://www.un-documents.net/wced-ocf.htm. Accessed 5 May 2009
69. Favara P, Nicolette JP, Rockel M (2008) Combining net environmental benefit analysis with economics to maximize remediation sustainability and value. Presented at the sixth international conference on the remediation of chlorinated and recalcitrant compounds, Monterey, CA
70. Diamond ML, Page CA, Campbell M, McKenna S (1998) Life cycle framework for contaminated site remediation options: final report. Prepared for Ontario Ministry of Environment and Energy
71. Ellis DE, Ei TA, Butler PB (2008) Sustainability analysis for improving remedial action decisions. Presented at the sixth international conference on remediation of chlorinated and recalcitrant compounds, Monterey, CA
72. Elkington J (1994) Towards the sustainable corporation: win-win-win business strategies for sustainable development. Calif Manage Rev 36(2):90–100
73. Environment Canada (2008) Turning the corner: regulatory framework for industrial greenhouse gas emissions. http://www.ec.gc.ca/doc/virage-corner/2008-03/541eng.htm. Accessed 5 December 2008
74. Environment Canada (2008) Turning the corner: Canada's offset system for greenhouse gases. http://www.ec.gc.ca/doc/virage-corner/2008-03/526eng.htm. Accessed 5 December 2008
75. HOH Water Technology A/S, NIRAS Consulting Engineers and Planners A/S, Revisorsamvirket/Pannell Kerr-Forster, ScanRail Consult (2000) Environmental/economic evaluation and optimising of contaminated sites remediation. Prepared for Danish National Railway Agency and Danish State Railways
76. Nielsen DM, Nielsen GL, Preslo LM (2006) The practical handbook of environmental site characterization and groundwater monitoring, 2nd edn. CRC Press, Boca Raton, FL
77. Beinat E (1997) Value functions for environmental management. Kluwer, Dordrecht, Germany
78. Office of the Federal Environmental Executive (2007) Leading by example: Federal government environmental and energy efficiency accomplishments for 2004–2006. http://ofee.gov/leadingbyexample/LeadingbyExample2004–2006.pdf. Accessed 5 May 2009
79. Economist Intelligence Unit (2008) Doing good: business and the sustainability challenge. http://a330.g.akamai.net/7/330/25828/20080208181823/graphics. eiu.com/upload/Sustainability allsponsors.pdf. Accessed 9 May 2009
80. Volkwein S, Hurtig HW, Klopffer W (1999) Life cycle assessment of contaminated sites remediation. Int J Life Cycle Assess 4(5):263–274
81. Efroymson RA, Nicolette JP, Suter GW II (2004) A framework for net environmental benefit analysis for remediation or restoration of contaminated sites. Environ Manage 34(3):315–331

Books and Reviews

Atlas RM, Phlip J (eds) (2005) Bioremediation, applied microbial solutions for real-world environmental cleanup. ASM Press, Washington, DC

Baltz RH, Demain AL, Davies JE (eds) (2010) Manual of industrial microbiology and biotechnology, 3rd edn. ASM Press, Washington, DC

Sutter GW II (ed) (2007) Ecological risk assessment, 2nd edn. CRC Press/Taylor & Francis, Boca Raton, FL

U.S. Environmental Protection Agency (2005) Groundwater sampling and monitoring with direct push technologies. Office of Solid Waste and Emergency Response, EPA 540-R-04-005. http://www.clu-in.org/download/char/540r04005.pdf. Accessed 8 December 2008

Biosensors and Bioassays for Ecological Risk Monitoring and Assessment

Scott D. Soelberg, Clement E. Furlong
Departments of Medicine-Division of Medical Genetics and Genome Sciences, University of Washington, Seattle, WA, USA

Article Outline

Glossary
Definition of the Subject and Its Importance
Introduction
Principles of SPR Sensors
Direct Detection of Protein Analytes
Subtractive Inhibition Assays for Large Molecules (Whole Cells)
Future Directions
Bibliography

Glossary

Analyte The molecule or microorganism that is the detection target in an analytical procedure.

Recognition element A protein or other biomolecule that can bind to an analyte with specificity and affinity.

ELISA Enzyme Linked Immunosorbent Assay. An assay using an antibody immobilized on a solid phase, (usually microtiter plate) to capture analyte and a second antibody coupled to an amplifier to detect the specific analyte.

Lateral flow assay An immunoassay in which a liquid sample is added to a dry porous carrier and wicked by capillary action to a recognition element immobilized on a specific area of the support material. A colored nanoparticle is used to detect the presence of analyte.

Nanoparticle A particle with dimensions between 1 and 100 nm.

Hapten A small molecular weight molecule (usually <1,000 Da) that cannot elicit an immune response by itself and must be attached to a larger carrier molecule prior to injection into the host animal.

Paramagnetic Magnetism induced in the presence of an externally applied magnetic field.

Definition of the Subject and Its Importance

This article describes the development and use of portable recognition element (RE)-based assays for environmental biosensing. It will focus on using portable optical biosensors; specifically surface plasmon resonance (SPR)-based biosensors for detecting a wide variety of analytes that may pose environmental risks. Portable SPR-based biosensor systems are suitable for real-time environmental monitoring as well as for many other applications including biodefense, medical diagnostic applications, food safety, and general laboratory research. Many of the detection strategies described here can also be used across other detection platforms that use recognition elements as the fundamental detection event, including lateral flow [1] and ELISA assay platforms [2].

Introduction

This article will provide an overview of portable SPR biosensor applications, including a description of the fundamental technology used in SPR biosensing, the assay development process including preparation of the sensor surface for specific analyte detection, environmental sample collection, and the many different protocols and approaches used for analyte detection and signal amplification. Examples of detection of environmental pathogens and pollutants as well as the limits of detection for these examples will also be illustrated.

Biosensor Introduction

A biosensor is generally made up of four component subsystems, (1) a means to deliver the sample (fluidics system) is a requirement for most aqueous-based biosensor systems; (2) a biological sensing component (recognition element), sometimes including a signal amplifier; (3) an electronic signal transducer to convert the detection event to a signal interpretable by the user; and (4) a user interface to display the result. Figure 1 shows a flow chart of a typical biosensor system. Portable SPR biosensors function by introducing a liquid sample via a fluidics delivery system to a sensor surface containing an immobilized bio-recognition element.

Most other RE-based assay systems require the addition of secondary REs attached to amplifiers to create detectable signals. Signal amplifiers include

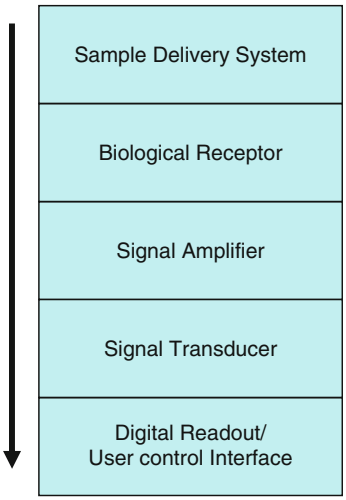

Biosensors and Bioassays for Ecological Risk Monitoring and Assessment. Figure 1
Biosensor flow diagram. Arrow indicates the flow of information as the signal is acquired

enzymes coupled to an RE that can convert a reporter substrate into a measurable colorimetric, luminescent, or fluorescent output. Fluorometric, luminometric, or spectrophotometric readers are then required to convert the signal to digital output. SPR-based biosensors convert molecular binding events directly to a detectable signal in real time, thus a signal amplifier step is not always required for detecting the presence of analyte.

Commercial SPR systems first became available in the mid 1980s. Large bench-top instruments were developed for determining the binding rates of interaction between biomolecules in real time without the requirement for amplification. Currently most commercial SPR-based sensor systems are still used for this purpose, as well as for the study of interaction analyses in drug discovery. Detection strategies and protocols developed with bench-top SPR systems are readily implemented for use in portable devices. Bench-top SPR systems, however, are large and have delicate optical components that require sensitive calibrations and regular maintenance, precluding their use as portable devices. In addition, most commercially available SPR instruments are prohibitively expensive for use in environmental monitoring. In the late 1990s Texas Instruments developed a miniature, integrated SPR module (Spreeta) [3–5]. The robust nature and small size of this integrated chip made possible the development of portable SPR biosensor systems. Naimushin et al. [6] described a temperature-controlled SPR system based on an early Spreeta three-channel SPR module manufactured by Texas Instruments. The importance of temperature control and the use of reference channels were noted in this publication. Chinowsky et al. [7] described a portable 24-channel SPR-based system that could detect as many as 24 different analytes. This system is based on eight miniature 3-channel Spreeta sensor chips (further described in Soelberg et al. [8]).

Principles of SPR Sensors

SPR sensors are optical sensors that exploit the interaction of light with a gold surface for the signal transduction event. Figure 2 shows the Kretschmann [9] configuration of an SPR-based detector (Fig. 2a). Polarized light illuminating a thin (50 nM) gold surface at varying angles (or wavelengths) is reflected back to a detector element (Fig. 2b). Light of a specific angle (or wavelength) is not reflected, but couples to surface plasmon electrons to generate a surface plasmon wave across the metal surface of the sensor. This coupling angle or wavelength is dependent on the refractive index (RI) of the solution adjacent to the gold surface. SPR curves are shown in Fig. 1b. The coupling angle or coupling wavelength is dependent on the refractive index (RI) of the solution adjacent to the gold surface (Fig. 2b). The reflected light intensity reaches a minimum at a specific coupling angle or wavelength. Specific recognition elements (REs) (e.g., antibodies, receptors, nucleic acids, or small molecular weight analytes) are attached to the sensor surface. The blue "Y" shapes in Fig. 2a represent recognition elements. Binding of analyte to a surface-bound recognition element causes a change in RI at the sensor surface, and a resulting shift in the SPR angle or wavelength of minimum intensity (Fig. 2c). Analyte binding is followed in real time as the system software converts the shift in the coupling angle or wavelength to an RI value as a function of time.

For a general discussion of SPR principals, the reader is referred to the following excellent books on SPR technology [10–12].

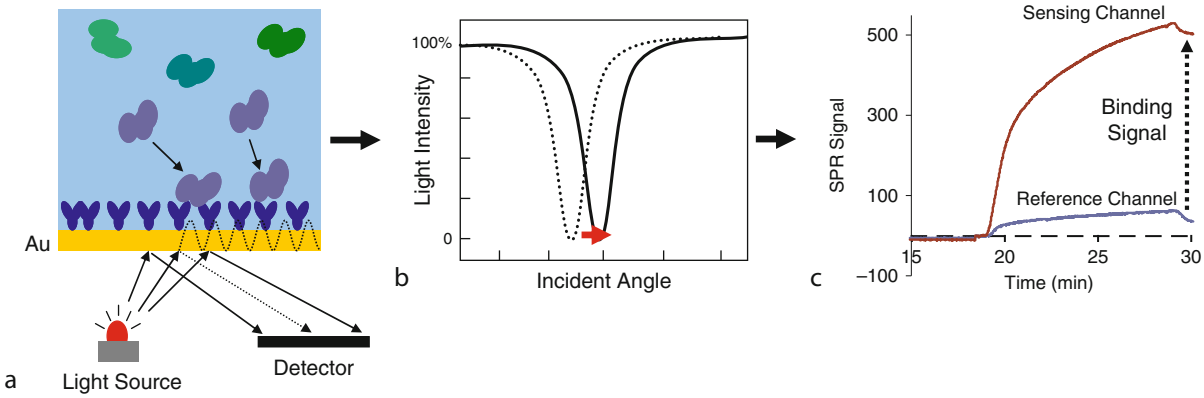

Biosensors and Bioassays for Ecological Risk Monitoring and Assessment. Figure 2
The fundamentals of SPR detection. (**a**) Specific analyte molecules bind to the REs immobilized on the gold surface. (**b**) This binding causes a shift in the coupling angle. (**c**) Plotting the change in coupling angle (SPR signal) as a function of real time generates a sensorgram. Red line = sensing (detection) channel. Blue line = reference (nonspecific) channel

Sensor Surface Preparation

Modifying the Gold Surface for Covalent Attachment of Recognition Elements There are several methods for attaching recognition elements to sensor surfaces. The different approaches to surface attachment of the RE can result in different levels of interferent binding, and several attachment methods should be evaluated to determine the optimal conditions for specific assays and sample matrices. The methods outlined below will be restricted to attaching recognition elements to gold surfaces, as most SPR sensors use gold as the surface metal. Several examples of surface functionalization are described below.

Self assembling monolayers (SAMs). Various SAMs have been described for use in coupling recognition elements to gold surfaces. Most exploit the strong affinity of sulfhydryl (thiol) or disulfide groups that can interact with the gold surface to form strong and stable bonds (also called chemisorption). The sulfur gold interaction is semi-covalent with a binding energy of 45 kcal/mol [13]. For a comprehensive review of these methods, the reader is referred to [14–16].

Examples of SAMs Used for SPR Sensors

Mixed alkane thiols. Alkane thiols are molecules with sulfhydryl head groups for binding to the gold surface, a carbon chain as the back bone, with a functional terminal group for attachment chemistries or passivation. Mixed alkane thiols are terminated at the tail end with either a hydroxyl (to reduce nonspecific binding (NSB) to the sensor surface) or with a functional group (R-NH_2 or R-C00$^-$) at a fixed percentage to allow even spacing of the functional groups to which an RE can be attached by standard coupling chemistries. For example, EDC/sulfo-NHS activate surface carboxyl groups, which in turn couple to amine groups of the RE [17]. Attachment of the alkane thiols to the gold surface is achieved by soaking the clean gold surface in mixtures of alkane thiols [18].

Hydrogel surfaces. One of the most widely used SPR surfaces is a carboxy-dextran hydrogel to which multiple receptors or ligands can be attached per strand of dextran [19, 20]. This protocol has the advantage of a fairly dense three-dimensional decoration of the sensor surface with receptors or ligands, but can have issues with bulkier analytes since the matrix can slow mass transfer to the receptors located throughout the hydrogel matrix. The carboxy-dextran layer can be built on a SAM to form a very stable surface for protein or ligand immobilization (Fig. 3).

Gold-binding peptide (GBP). GBP is an engineered protein domain with repeat sequences that binds tightly to gold surfaces [21]. This small peptide can be used as a foundation layer on the gold surface to which REs can be attached via standard EDC-NHS protein coupling [17]. A description of the protocols involved

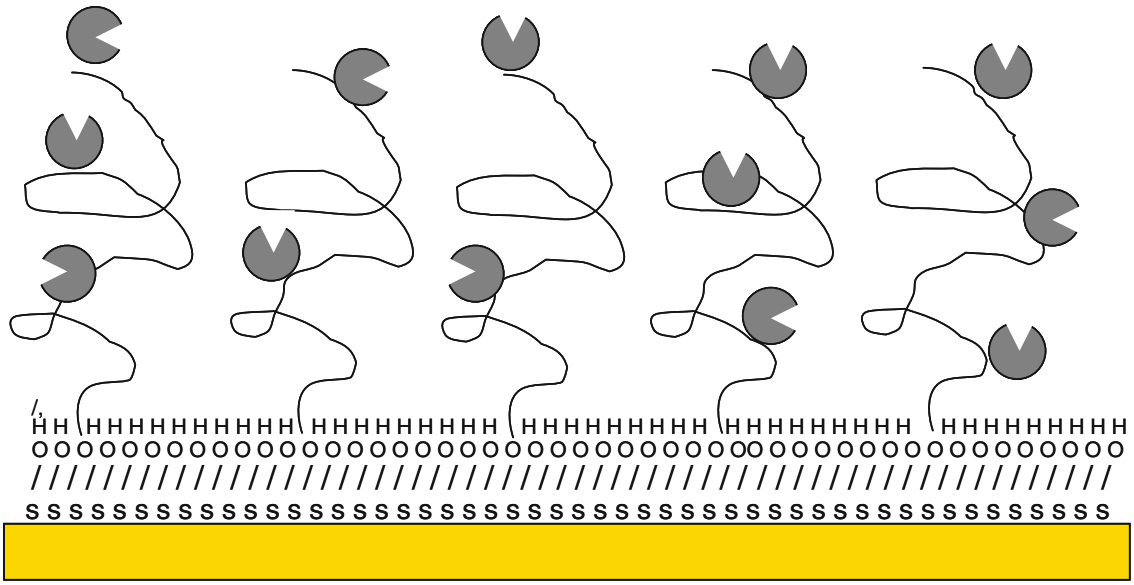

Biosensors and Bioassays for Ecological Risk Monitoring and Assessment. Figure 3
Alkane thiol with terminal OH groups and functional groups with recognition elements attached

in using the gold-binding peptide for sensor surface preparation can be found in Woodbury et al. [22].

Physical adsorption of recognition elements. Antibodies and other proteins can also be directly adsorbed (also called physisorption) through charge interactions between the gold and protein surfaces without specific chemical modification. For this procedure, antibodies in solution are simply introduced in concentrated form (>1 mg/mL) to a gold surface cleaned with nitric acid and ethanol. The orientation of the antibody is not controlled in this procedure; therefore not all the antibodies will have the functional arms oriented outward. However, this method has been shown to produce a surface that is robust and capable of sensitive detection and regeneration [7]. This simple approach to surface coating can be useful for many sensor applications.

Covalent attachment of recognition elements to modified sensor surfaces. Sensor surfaces modified by SAMs terminated with free amino or carboxyl groups can then be modified to covalently couple recognition elements (e.g., protein molecules) through standard protein coupling procedures. The most commonly used reaction is the amino to carboxyl protein coupling using the chemicals EDC or EDC/sulfo-NHS for carboxyl group activation and protein coupling [17].

Attachment of "adapter molecules." Generic surface foundation layers may be attached by adsorption or covalently coupled to SAM-modified sensor surfaces followed by binding of the RE to generic adapter molecules. Some examples of these generic receptor molecules include avidin or streptavidin to which can be attached biotin-labeled recognition elements such as antibodies, DNA, protein nucleic acids (PNAs) [23], locked nucleic acids (LNAs) [24], ligand receptors, or other biotin-labeled recognition elements [25] (Fig. 4, *Right*). Other types of receptors that can be attached to the sensor surface include proteins A or G. The bacterial proteins A and G that bind specifically to the Fc domain of immunoglobulins (Igs) (most notably many IgGs) can be adsorbed or covalently attached to a modified gold surface and used for construction of regenerable sensor surfaces for repeat assays. These surface-adsorbed molecules provide "sockets" for antibody binding to sensor surfaces. The Igs can be removed with regeneration buffer (e.g., low pH), and new antibodies, for example, with different specificity, can be added to the surface "sockets" (see Fig. 4, *Left*) [26, 27]. Covalent attachment of antibody receptor molecules to robust surfaces such as SAMs should provide longer-lasting regenerable surfaces.

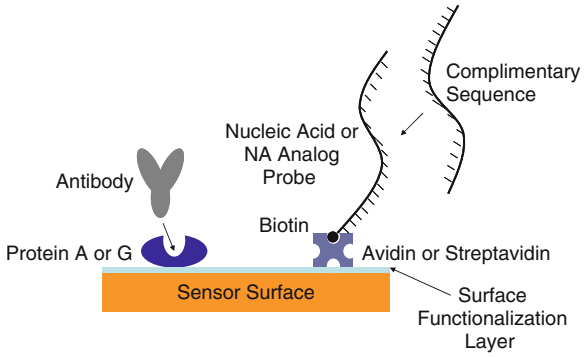

Biosensors and Bioassays for Ecological Risk Monitoring and Assessment. Figure 4
Adaptor molecules allow for replaceable antibody surface (*left*) or binding of biotinylated probes (*right*)

Surface functionalization for competition assays. For the competition-based assays described below in the section entitled "Small Molecule Detection," small molecular weight ligands are often conjugated directly to a SAM surface or to a carrier protein [28, 29] that can either be covalently attached to a SAM, adsorbed to the sensor surface, or chemically coupled to a surface foundation layer in a similar manner as with the antibody attachment protocols.

Surface passivation with blocking proteins. Another important aim in preparing a sensor surface for analyte detection is to generate a sensor surface that has a low degree of nonspecific, or background binding from the sample. Additional steps to passivate the sensor surface and minimize nonspecific binding may be required after attaching the RE [30]. For example, when analyzing a serum sample, proteins may nonspecifically bind to the sensor surface and interfere with or overwhelm the analyte-specific binding signals. By pretreating the sensor surface with serum proteins such as albumin or other blocking agents, nonspecific sample matrix proteins can be blocked from interaction with the sensor surface.

Referencing

Referencing is another way to compensate for the effects of nonspecific interactions in bioassays. Referencing involves monitoring an additional channel with an RE that is not specific for the analyte of interest. It is important to include a reference channel with the same antibody type, such as a rabbit polyclonal or mouse monoclonal, and use the signal from this channel to correct for nonspecific binding. In the example shown in Fig. 2c, the light blue line shows that there was little nonspecific binding signal during the sensing step. With proper reference channel treatment, subtraction of the reference channel value from the signal of the analyte-specific channel provides an accurate measure of the specific binding.

Sensor Storage and Preservation

It is important to make use of stable recognition elements and to develop protocols for maintaining activity of the sensor REs during storage. There is relatively little information in the literature regarding preservation of recognition elements on sensor surfaces. Drying a specific carbohydrate glass such as a trehalose and high molecular weight dextran layer over the RE has been shown to preserve antibody function for at least 1 year without the need for vacuum packing the sensor element [28].

Sample Acquisition from the Environment and Removal of Interferents

SPR-based biosensors for environmental monitoring require that the analytes are contained in an aqueous solution, often with some preprocessing to concentrate the sample and/or reduce the level of interferents and enhance the specific signal from the target analyte. The protocols for sample collection/processing are highly dependent on the target analyte and the sample matrix. An environmental sample will generally fall into one of three general classes: sample in liquid form, sample in solid form, such as in dirt or on a solid surface, and sample dispersed in air, such as aerosolized pesticides, microbes, or nerve agents. Once the sample is collected or transferred to an aqueous phase, it can be delivered to the biosensor for detection of the specific target analyte.

Airborne samples. For bioaerosols and airborne chemical samples, a number of collection systems have been described or are commercially available. Because the immunoassay SPR-based assays depends on the sample being in liquid form, the two most practical collectors for this medium are wetted-wall cyclonic collectors [31] and glass impingers [32, 33].

Samples can also be obtained by directing air flow through a filtration system; however the filter must be stripped with aqueous buffer to suspend the trapped particulates for analysis.

Bioaerosol wetted-wall cyclone collectors are those in which air samples are directed over a high-surface-area sample collecting liquid making use of cyclonic action. Environmental sampling using a cyclonic collector to analyze long distance airborne transport of both viral and bacterial porcine pathogens was demonstrated by Dee et al. [31]. In their example, aerosolized porcine reproductive and respiratory syndrome virus (PRRSV) and *Mycoplasma hyopneumoniae* were collected using a liquid cyclonic collector from as far as 4.7 km from the source of the swine pathogens.

Glass impingers are the simplest types of air-to-liquid sample collectors. Impingers are commercially available and operate by simply directing a stream of air into a liquid sample (Fig. 5). There are a number of examples in the literature of using impingers for collecting airborne particles into a liquid for analysis, including for the detection of airborne nitrophenols (see, e.g., Bishop and Mitra, 2007) [32] and airborne bacterial spores dispersed in an aerosol chamber (see, e.g., Rosen, 2006) [33].

Filter sampling and resuspension in liquid medium is another approach to sample introduction for environmental biosensing. In these samplers, an air or water stream is driven through a filter device, and the filter will trap the small target analyte particles. Mixed cellulose ester (MCE), Teflon, poly-tetra fluoroethylene (PTFE) filters, and gelatin filters can trap particles such as bacteria and viruses from aerosolized or aqueous samples. The concentrated samples are then suspended in an aqueous solution for analysis. Fabian in 2009 [34] demonstrated a comparison of four aerosol collectors, including two types of filter collectors (gelatin and Teflon) for airborne influenza virus collection and viability analysis. Burton et al. in 2005 [35] compared the MCE, PTFE, and gelatin filter materials for detection of the *Bacillus anthracis* stimulant *B. subtilis* in bioaerosols. Filtration in which the filtrate is analyzed for specific molecules or organisms smaller than the filter pore size can also be employed. Figure 6 shows an example of a small molecule detection filter device that excludes larger protein molecules in a saliva sample, and smaller molecules that pass through the filter are then delivered to a sensor surface [29]. This approach has the advantage of eliminating components of the matrix that may bind nonspecifically to the sensor surface, such as mucins in saliva or biofilm forming molecules from seawater.

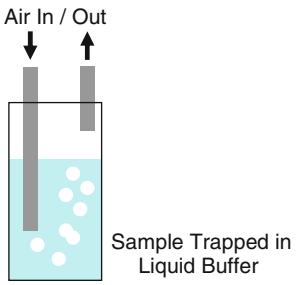

Biosensors and Bioassays for Ecological Risk Monitoring and Assessment. Figure 5
Glass impinger for converting aerosolized samples to aqueous samples

Liquid samples. Samples already in liquid such as freshwater or seawater samples are relatively easy to process and are amenable to processing with automated systems. Liquid collection systems can be as simple as a collection tube dipped by hand into the water for manual collection or a pump delivery system to the sensor. Filtration can also be an efficient way to collect a sample if the analyte of interest is large enough to be trapped with a filter. For example, *Giardia duodenalis* and *Cryptosporidium* species present in low levels in drinking water were filtered and detected via polymerase chain reaction (PCR) by Plutzer et al. [36]. In cases where the analyte may be present at low concentrations or where the matrix may contain many interferents, filtration can be a way to concentrate samples and select for specific sizes of particles through low or high molecular weight cutoff filters. The analytes can be washed from a filter with a buffer that is optimal for detection, or a hollow fiber flow-filter can be used to change out buffer conditions in real time (Fig. 6). More complex ocean sample collection makes use of a suspended-particle multi-sampler (called a rosette) for obtaining discrete samples from given depths and locations [37].

Solid surface samples. Collecting environmental samples from surfaces for analysis can be as simple as swiping the surface with a moistened swab. The swab can then be added to a liquid buffer solution and

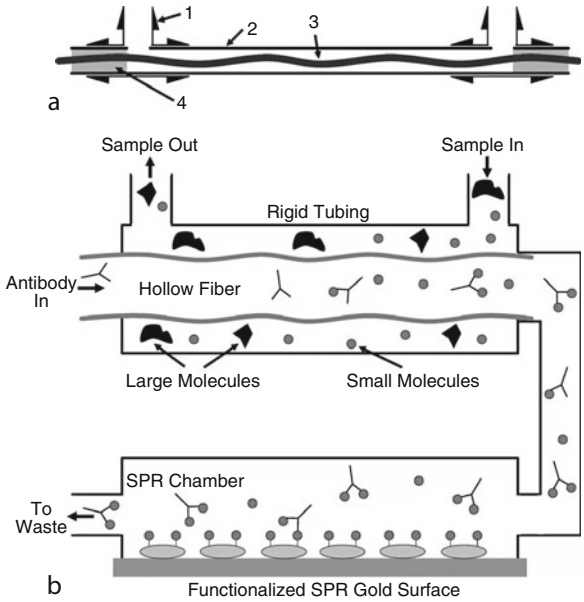

Biosensors and Bioassays for Ecological Risk Monitoring and Assessment. Figure 6
An example of in-line filtration of samples to remove interferents before competition assay analysis with a portable Surface Plasmon Resonance biosensor. External, in-line filtering flow cell, which directs flow into the SPR system. (**a**) Construction of the in-line filtering flow cell required sliding a 1.6-mm Tee connector (1) (T210-1, Valve Plastics, Fort Collins, CO) over the ends of 0.75-mm inner diameter PEEK tube (2) (1533, Upchurch Scientific, Oak Harbor, WA), followed by drilling a hole into the PEEK tube to allow sample flow, and then sealing the PEEK tube to the tee with urethane adhesive (Lord Corp., Cary, NC). A hydrophilic hollow fiber (3) (Minntech, Minneapolis, MN) with a molecular weight cutoff of 20,000 was inserted into the PEEK tube, and both ends were sealed with urethane adhesive (4). Following sealing of the hollow fiber into the PEEK tube, the ends of the hollow fiber were cut flush with the tee preserving the opening to the hollow fiber. (**b**) Salivary samples were diluted 1:2 with buffer and flowed through tubing external to the hollow fiber. The antibody solution was flowed countercurrent through the hydrophilic hollow fiber and then through the SPR biosensor system. Diffusion may also be aided by bulk flow across the hollow fiber wall controlled by a pressure differential created by higher flow rates outside the hollow fiber (not drawn to scale). (From [29])

vortexed to resuspend the sample in liquid. Particulates such as soil samples can be measured or weighed, then resuspended in liquid buffer. In "Surface Sampling of Spores in Dry-Deposition Aerosols" Edmonds et al. compared different swab materials used on four surfaces with different surface properties for sampling of bacterial spores [38]. Once the target analyte(s) has been collected in or transferred to an aqueous solution, a number of different strategies have been used for the specific detection of the target analyte. These strategies are outlined in the following section.

Immunomagnetic Particle Purification of Specific Analyte

Paramagnetic antibody-conjugated particles can be used to rapidly concentrate and purify an analyte from a complex matrix of particles commonly found in environmental samples. Figure 7 shows an example of this type of cleanup procedure. Immunomagnetic beads (IMBs) decorated with analyte-specific antibodies are added to a sample and mixed. The IMBs bind the analyte of interest, then are immobilized in a magnetic field, and all impurities and potential interferents are washed away with analysis buffer. The IMBs with bound analyte in analysis buffer are then released by removal of the magnetic field and introduced to the sensor for detection [8]. Once the concentrated, purified target analyte(s) is collected in or transferred to analysis buffer, a number of different strategies have been used for the specific detection of the target analyte. These strategies are outlined in the following section.

Detection Strategies

Development of an SPR-based assay requires consideration of several factors that will affect the SPR signal: (1) the type and properties of the surface-immobilized recognition or specificity element; (2) size of the analyte of interest, reflecting its ability to generate a RI change large enough to be detected when bound by the RE immobilized on the sensor surface; (3) the specificity of the recognition element for target analyte and related analytes; (4) strategies for reducing nonspecific binding of other components of the matrix, and (5) any strategy for amplifying the signal from bound analyte.

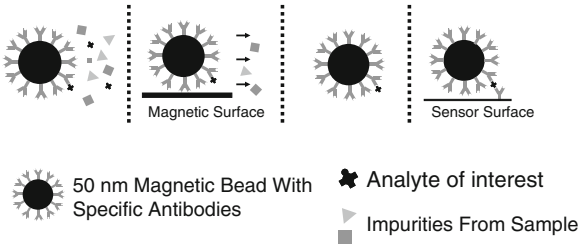

Biosensors and Bioassays for Ecological Risk Monitoring and Assessment. Figure 7
Magnetic bead cleanup of sample matrix. Each frame (separated by a dotted line) is a separate step in the cleanup and detection process

Properties of the recognition element. A recognition element is any molecule that can bind with high specificity and affinity to the target analyte. The recognition element should be stable and ideally be capable of regeneration for many cycles of analyte binding and surface regeneration. Antibodies have been found to fulfill these requirements and have been used for many different sensing applications [39]. Receptors with high specificity and affinity for analyte such as metallothioneins binding to heavy metal ions (Cd^{2+} and Hg^{2+}) can also serve as suitable recognition elements [40]. The use of molecular imprinted polymers (MIPs) can also be used, for example, ochratoxin A, an *Aspergillus* that produced mycotoxin, was detected with a MIP surface with SPR at concentrations down to 0.05 ppm [41]. Nucleic acids or nucleic acid analogs such as peptide nucleic acids (PNAs) can be used on a biosensor surface to detect complementary sequences of nucleic acids such as ribosomal RNA (rRNA) from *Escherichia coli* [42]. Locked nucleic acids (LNAs) are other analogs with increased thermal stability and resistance to nuclease activity, which can also be used as recognition elements for detection of DNA or RNA [24].

There are several issues to consider when preparing an SPR sensor surface for the detection of a specific analyte. First, the recognition element that is attached to the sensor surface should be very specific for the target analyte. This specificity is often provided by the immobilization of an antibody raised with against all or part of the target analyte. Specificity can be determined by testing the antibody for cross reactivity with closely related molecules or microorganisms. It is important to test the specificity of the chosen recognition element against analytes with structures similar to those of the target analytes, particularly if related analytes may be present in the sample matrix. For example a bacterial antibody raised to *B. anthracis* spores can be tested against other Bacillus species for cross reactivity. This example is demonstrated in the multi-analyte detection shown in Fig. 13. Here *B. subtilis* (BG) spores are tested against *B. anthracis* spores, and against many other unrelated antigens. The specificity of the antibody for the bacterial analyte of interest, but not for a closely related bacterial species, is shown in this figure. The extent of cross reactivity with other antigens, especially related antigens, determines usefulness of a given antibody preparation for specific applications.

REs with high affinity are also desirable for achieving high sensitivity of analyte detection. Antibody target affinities can vary by as much as four orders of magnitude [43]. SPR and ELISA analysis can be used for determining the antibody association and dissociation rates (K_a and K_d) and thus determine the usefulness of the antibody for high sensitivity detection assays [44]. For example, SPR can be used to screen for high affinity monoclonal antibodies from a pool of different clones [45, 46]. The primary goal when developing a detection assay is to have a sensor surface that binds the target with very high affinity and specificity without binding other interferents present in the sample matrix.

Consideration of antibody properties and purity. The choice of an analyte-specific antibody may require evaluation of several different polyclonal or monoclonal antibody preparations. Significant differences in both specificity and affinity of analyte binding will greatly affect the ability of a given protocol to provide the levels of sensitivity and specificity required for a given application. Often, it may require the generation of monoclonal or polyclonal antibodies to the target analyte if the appropriate antibodies are not available from commercial sources or from collaborators/colleagues. An additional factor affecting the quality of signal is the extent of purity of the antibody being used for the assay. It is important to note that with a surface interaction method such as SPR, the greater the purity of the specific antibody on the SPR surface, the more robust will be the response to analyte binding.

Affinity purified polyclonal or monoclonal antibodies are essential for optimal SPR-based protocols. When making use of amplification protocols, either monoclonal or polyclonal antibodies, or monoclonal antibodies with different epitope specificity may be useful. The amplification antibodies may be of lesser purity since any unrelated antibodies will wash through the system. Similar considerations will be obtained for other types of recognition elements.

Detection Limit by Analyte Type

Once a suitable recognition element has been acquired, the next step is determining the detection limit for the analyte of interest. Dividing analytes into four general classes is helpful for discussion. The categories of analyte detection with SPR are usually broken down into groups based on size. Small molecules do not usually affect generate a significant change in RI directly when bound to the sensor surface; very large analytes (e.g., whole cells) can be larger than the effective probing range of the plasmon wave, and thus only a fraction of the particle will affect the SPR signal. The categories for detection are usually classified as (1) small molecules such as organic pollutants, chemical toxins, and heavy metals (below MW 5,000) [14, p. 476] usually undetectable by direct SPR measurement (2) protein molecules >5,000 Da (e.g., protein toxins, protein biomarkers, or antibodies), which diffuse easily and are large enough to generate a significant surface change in RI, (3) viruses, and larger particles such as (4) microbes, and (5) single-celled eukaryotic organisms (algae and fungi). Whole cells, whether bacteria or eukaryotes, often diffuse slowly to the sensor surface, may not bind easily to surface recognition elements due to shear forces, and fall at least partly outside of the penetration depth of most SPR instruments (approximately 100–600 nm) [14], p 463. Figure 8 shows the sizes of several proteins and microorganisms relative to the antibody surface and SPR penetration depth. A *Cryptosporidium* oocyst [47], an *E. coli* cell [48], a norovirus particle [49], an SEB protein toxin molecule [50], and an IgG detection antibody [51] are displayed in relation to the probing distance from the SPR surface. Detection limits from direct detection protocols (no amplifiers) as well as with those using additional amplification steps are compared below.

Small Molecule Detection

Direct detection of small molecules with SPR. There are a few examples of SPR biosensors being used to directly detect the binding of metal ions. Wu et al., 2004 [52] used the heavy metal binding protein metallothionein immobilized on an SPR surface as a sensor for metal ions such as cadmium (Cd^{++}), zinc (Zn^{++}), and nickel (Ni^{++}). With this system, concentrations of Cd^{++} as low as 2 μM were detectable.

Competition (inhibition) for detection of small molecules. Since the binding of small analytes does not generally result in large changes in RI at the sensor surface, detection of small molecular weight analytes often makes use of an indirect assay in which the analyte itself is immobilized on the sensor surface,

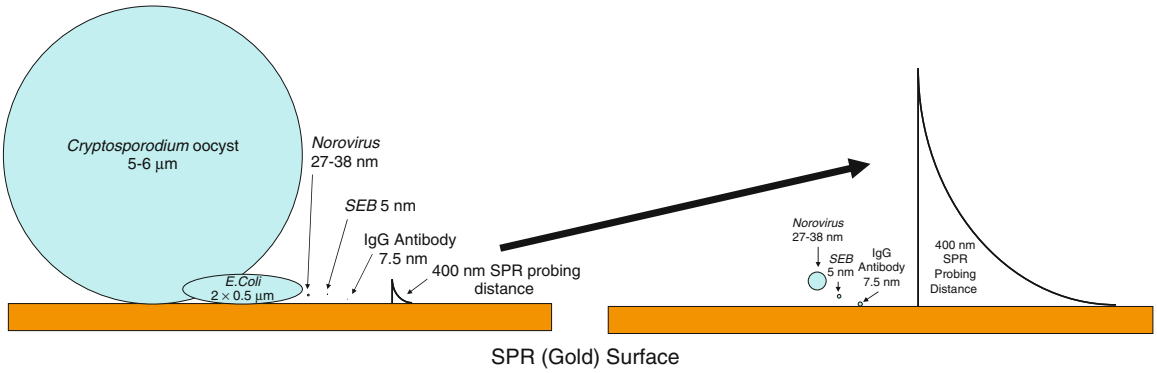

Biosensors and Bioassays for Ecological Risk Monitoring and Assessment. Figure 8
Some examples of the size variation of different classes of analyte detectable by SPR biosensor assay compared to the effective detection range of an SPR sensor

often through coupling to a carrier protein or tethered to the surface covalently. The most common method of antibody-based detection of small molecules is referred to as a competition or inhibition assay. The target analyte (hapten) molecule is attached to the sensor surface using one of the protocols described above in the sensor surface preparation section. Antibody in solution is then allowed to bind to the surface-immobilized target analyte, establishing a rate of antibody binding in the absence of analyte. Samples containing the target analyte are introduced, inhibiting antibody binding at levels proportional to the concentration of target analyte in the sample (Fig. 9a). As an alternative to rate determination, total binding signal can also be measured, and this signal is also inversely proportional to the concentration of analyte over a specific concentration range [53]. Another protocol (Fig. 9b) can be used in which anti-analyte antibody is immobilized on the sensor surface. With this protocol, sample containing the small molecule is first added and allowed to bind to the surface antibody. Analyte-protein conjugate is then introduced to the surface. The signal from this binding step is again inversely proportional to the amount of analyte bound to the surface from the original sample. This protocol is beneficial when antibody needs to be conserved due to low availability or high cost.

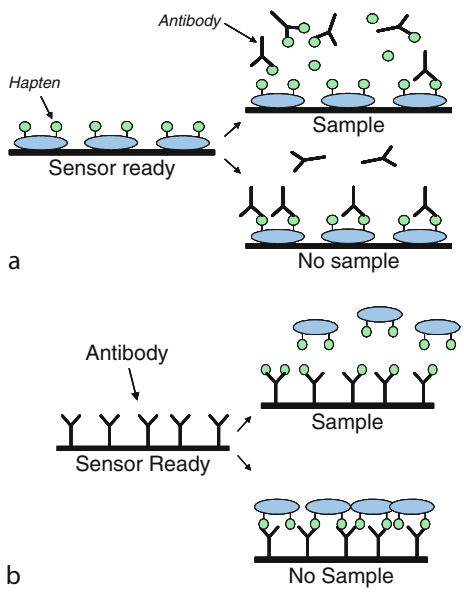

Biosensors and Bioassays for Ecological Risk Monitoring and Assessment. Figure 9
(**a**) Competition detection of a small molecule using SPR. A schematic of the sensor surface shows the hapten-conjugated protein on the surface of a sensor in the "sensor ready" state. The quantity of antibodies that bind to the surface during exposure to sample is inversely correlated to the amount of analyte in the sample.
(**b**) Alternatively, small molecule binds to the antibody on the sensor surface and inhibits binding of the larger carrier protein derivatized with the same small molecule. This protocol will conserve antibody if it is costly or scarce

There are many examples in the literature of small molecule detection using the competition assay. For example, domoic acid (MW 311), a toxin produced by the algae *Pseudo-nitzschia* that can accumulate in marine filter feeders, was detected using a competition assay in both laboratory buffers and in spiked clam samples at levels as low as 4 ng/mL [28]. Yu et al. [53] described a domoic acid competition assay with a detection limit of 0.1 ng/mL in laboratory buffers using an SPR-based detection system. The organophosphate insecticide chlorpyrifos (MW 250) was detected in a variety of environmental water samples by SPR using a competition assay with a detection limit of 45–64 ng/mL [54]. TNT (Trinitrotoluene), a component of land mines and other explosive devices (MW 227) was detected by SPR analysis at concentrations ranging from 0.008 ng/mL (8 ppt) to 30 ng/mL (30 ppb) [55].

Direct Detection of Protein Analytes

One of the primary advantages of SPR-based systems is the ability to detect direct binding of analytes quickly and without amplifier reagents or other manipulation of the sample (Fig. 10). If the concentration of a larger analyte (>5,000 Da) such as a protein toxin is at an adequate level, and if there are not significant interferents in the sample, it is possible to not only directly detect the analyte, but also to quantify the analyte from either the initial rate of binding or the maximum shift in RI on binding of the target analyte to the surface RE. Figure 11 shows the direct detection of *Staphylococcal* enterotoxin B (SEB) in buffer solution at several different analyte concentrations [56]. At low analyte concentrations (Fig. 11b, inset), the concentration of analyte is linearly dependent

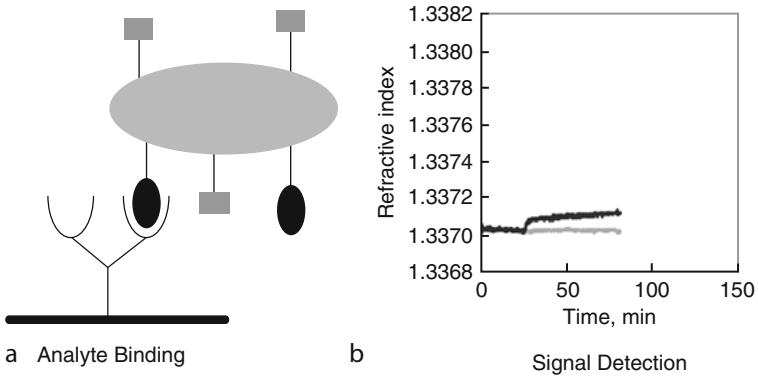

Biosensors and Bioassays for Ecological Risk Monitoring and Assessment. Figure 10
(**a**) Binding of protein analyte to antibody immobilized on the gold sensor surface. (**b**) Real-time signal (refractive index) generated during the binding event

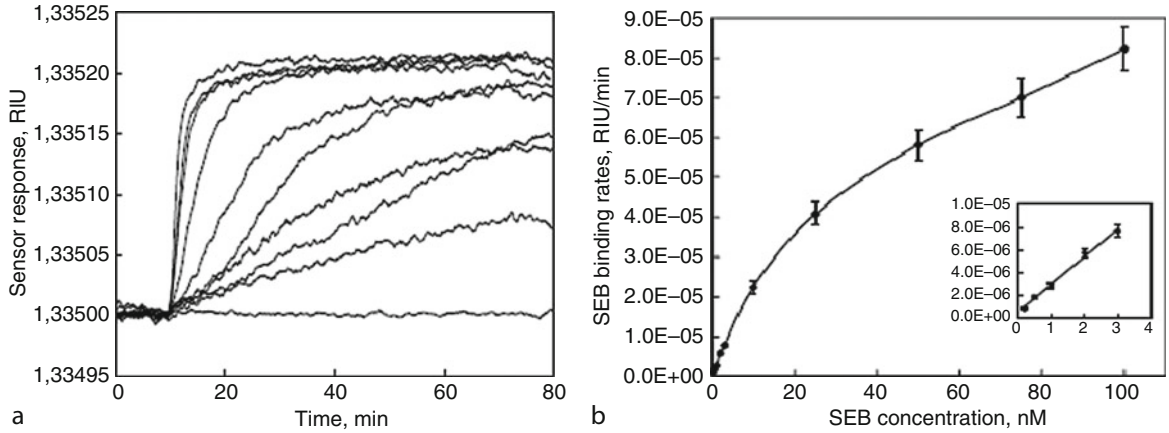

Biosensors and Bioassays for Ecological Risk Monitoring and Assessment. Figure 11
(**a**) Binding of *Staphylococcal* enterotoxin B (SEB) to sensor surface at different concentrations of SEB (0.2, 0.5, 1, 2, 3, 10, 25, and 75 nM). (**b**) Plot of initial rates of binding of SEB as a function of SEB concentration (inset, expanded scale for the indicated low concentrations of SEB). (From [56])

on the initial rate of binding of SEB to the surface-immobilized antibodies.

Amplification strategies. Amplification is generally carried out with addition of a second recognition element prior to or after the analyte is bound to the surface (Fig. 12). Also called a sandwich assay, this second element can be an antibody, or an antibody coupled to a larger particle to affect a greater increase in the SPR signal. Sensitivity of analyte detection can be dramatically increased by using amplifiers. Proteins, including antibodies like the fish iridovirus antibody [57], microbial toxins (SEB) [56, 58], and many others are detected with amplification steps to increase the binding signal.

To increase the sensitivity of detection and at the same time validate the identity of analyte, a second, particle-bound antibody specific for an analyte epitope different than that of the surface-immobilized antibodies may be used. Nano-immunomagnetic particles or nano-gold particles have been used for this application. The advantage of the nano-immunomagnetic particles is that they may be used in sample processing steps to purify and concentrate the target analyte before introduction to the sensor [8]. Figure 13 shows an integrated amplification protocol, where the SEB is bound first to a magnetic particle and then allowed to bind to the SPR surface. The resulting signals for 10 ng

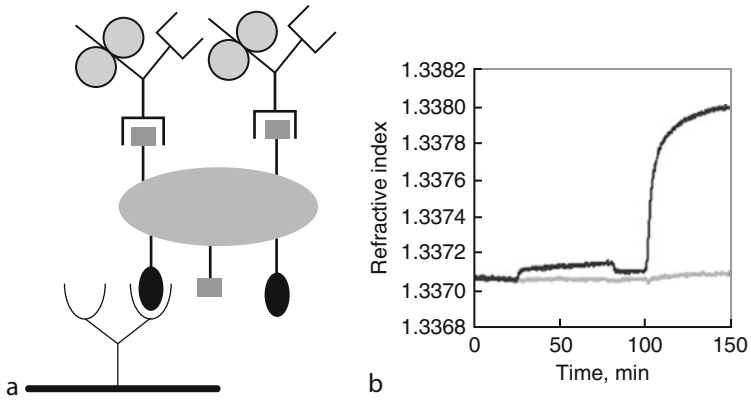

Biosensors and Bioassays for Ecological Risk Monitoring and Assessment. Figure 12
(**a**) Binding of secondary antibodies with different epitope specificity coupled to amplifier particles to captured analyte. (**b**) Signals generated upon binding of analyte to the sensor surface followed by binding of the secondary antibody/bead complex

and 1 ng/mL SEB are much larger than SEB alone. These amplifiers can be the same magnetic particle used for purification of the sample shown in Fig. 6. The concentration/purification step provides a significant increase in the sensitivity of the detection protocol and eliminates possible interferents from the sample stream at the same time. Larger micron-sized particles conjugated with the secondary antibodies diffuse too slowly to the sensor surface to be useful in real-time detection. Nano-gold and nano-magnetic particles can also be coupled to nucleic acids for amplification of DNA or RNA binding to a sensor surface. A sulfur group-derivatized nucleic acid or a biotinylated nucleic acid can be attached to the gold or magnetite particles.

This sandwich protocol is useful for the detection of microbes, spores, viruses, and toxic proteins [7]. Figure 14 also shows sandwich type amplification of several different types of analytes.

Subtractive Inhibition Assays for Large Molecules (Whole Cells)

To detect large molecules (i.e., whole cells) that lie mostly outside the SPR evanescent wave (Fig. 8) a technique similar to the small molecule competition can be employed. This technique involves addition of antibody to a suspension of bacteria or other larger particles, and then removal of the antibody-complexed particles by centrifugation or filtration and quantification of the remaining antibodies by binding to anti-antibody RE or immobilized target epitope on the SPR surface. Depletion of antibody signal is proportional to the concentration of analyte in the sample. Simplifying the protocol by eliminating the filtration/centrifugation step and relying on the difference in diffusion rate between the large particles and the antibody can also be employed, although the sensitivity may be affected.

Multiplex Detection

For many environmental biosensing applications it is useful to be able to detect a number of different analytes from a single sample. These include testing for threats from deliberate contamination, from the many potential pathogens in water supplies, testing for different strains of a similar microbial organism, and testing for different chemical pesticides [59] in the field. Figure 14 provides an example of detecting eight different analytes with sequential injections into the same sensor system. The system incorporated eight 3-channel sensors with the same recognition elements on all three channels of each sensor element. This configuration provided binding data in triplicate in real time.

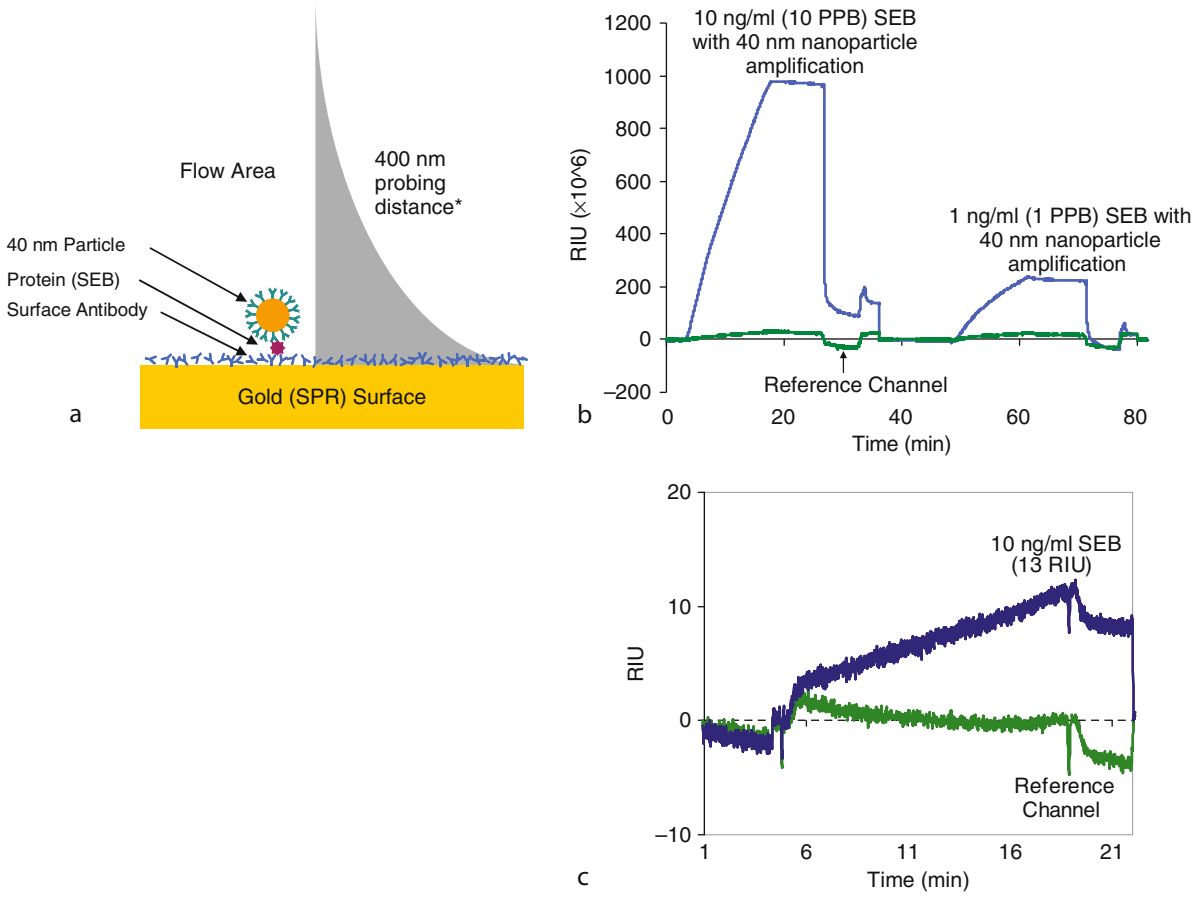

Biosensors and Bioassays for Ecological Risk Monitoring and Assessment. Figure 13
(**a**) Cartoon of protein (SEB) detection with amplifier in relation to the SPR sensor probing distance. (**b**) Detection of SEB with amplifier at two different concentrations with a low pH wash to reset the sensor between detection events. Protein (SEB) was mixed with 40 nm particles prior to injection for amplification of the signal. (**c**) The 10 ng/mL signal without nanoparticle amplification is approximately 13 RIU. Nanoparticle amplification resulted in a 70-fold increase in the SPR signal

Future Directions

The future directions of portable environmental SPR biosensing have been partially defined with the development of the SPR microscope or imager. SPR imagers are a variation of the SPR sensor described here in which light incident at a fixed angle or wavelength illuminates a much larger surface area. The ability of the SPR imaging systems to interrogate multiple different spots or REs on a single chip surface in an array format can also be performed in real time, allowing for hundreds and even thousands of samples to be analyzed simultaneously. A 1,000-spot bench-top array system has been demonstrated [60], and a prototype portable SPR array imager has also been described [61]. The challenge will be to produce systems that are sufficiently small to be used as portable devices or small, inexpensive bench-top systems. For general laboratory use, the binding partners of interest will include a vast array of different biomolecules, drugs, and other small molecules.

Future enhancements of portable systems will depend on further development of microfluidic and nanofluidic systems, including microvalves and pumps, simplification of the user interface, smaller processors and control electronics, and perhaps the

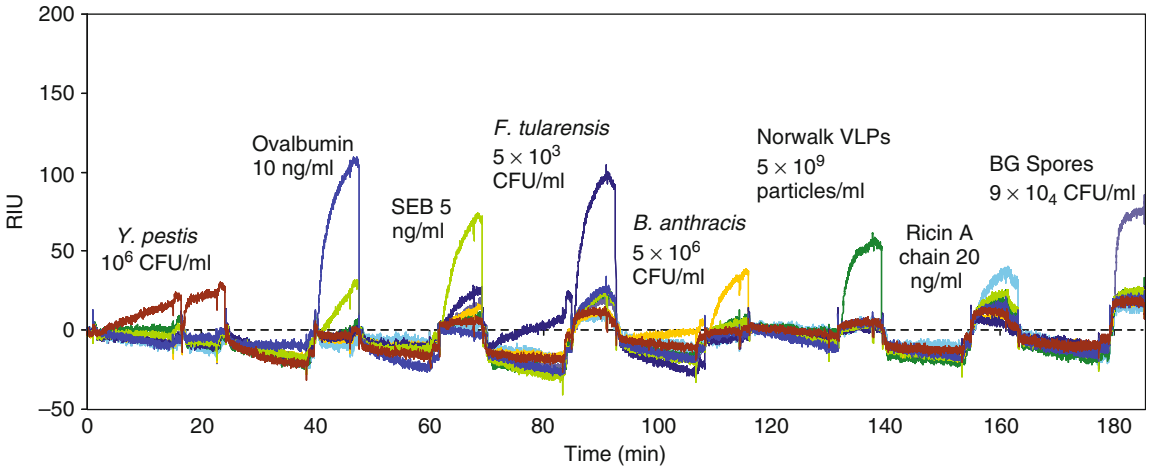

Biosensors and Bioassays for Ecological Risk Monitoring and Assessment. Figure 14
Serial detection of *Yersinia pestis*, Hen egg ovalbumin, *Staphylococcal* enterotoxin B (SEB), *Francisella tularensis*, *Bacillus anthracis* spores, Norwalk virus-like particles (VLPs), ricin A chain, and *B. subtilis* (BG) spores at the indicated concentrations with single steps of antibody amplification after each direct binding step

further reduction in size of the sensing element. The currently available SPREETA biosensor element is only about one-fourth the size of the original devices. Refractive index is highly sensitive to small temperature changes, and reduction in the size of the temperature control circuitry will allow for further miniaturization of portable sensor systems. Simply reducing the size of the existing portable systems to hand-held devices will provide instruments with a broad range of applications.

The continued development of recombinant antibody selection and expression systems such as recombinant *E. coli* single chain camelid antibodies [62] will be important for generating both wild-type and variant recombinant proteins that will be useful as inexpensive sensor recognition elements. This is an area that can benefit from increased efforts and funding. The reduction in antibody costs will be especially important for protocols that consume reasonable quantities of antibodies, such as those utilizing amplification approaches.

Bibliography

1. Ngom B et al (2010) Development and application of lateral flow test strip technology for detection of infectious agents and chemical contaminants: a review. Anal Bioanal Chem 397(3):1113–1135
2. Lequin RM (2005) Enzyme immunoassay (EIA)/enzyme-linked immunosorbent assay (ELISA). Clin Chem 51(12):2415–2418
3. Melendez J et al (1996) A commercial solution for surface plasmon sensing. Sens Actuators, B 35(1–3):212–216
4. Melendez J et al (1997) Development of a surface plasmon resonance sensor for commercial applications. Sens Actuators, B 39(1–3):375–379
5. Elkind JL et al (1999) Integrated analytical sensors: the use of the TISPR-1 as a biosensor. Sens Actuators, B 54(1–2):182–190
6. Naimushin AN et al (2003) A portable surface plasmon resonance (SPR) sensor system with temperature regulation. Sens Actuators, B 96(1–2):253–260
7. Chinowsky TM et al (2007) Portable 24-analyte surface plasmon resonance instruments for rapid, versatile biodetection. Biosens Bioelectron 22(9–10):2268–2275
8. Soelberg SD et al (2009) Surface plasmon resonance detection using antibody-linked magnetic nanoparticles for analyte capture, purification, concentration, and signal amplification. Anal Chem 81(6):2357–2363
9. Kretschm E (1971) Determination of optical constants of metals by excitation of surface plasmons. Z Phys 241(4):313
10. Davies J (1996) Surface analytical techniques for probing biomaterial processes, CRC series in chemistry and physics of surfaces and interfaces. CRC Press, Boca Raton, p 178
11. Homola J (2006) Surface plasmon resonance based sensors, Springer series on chemical sensors and biosensors. Springer, Berlin, p xii, 251
12. Schasfoort RBM, Tudos AJ (2008) Handbook of surface plasmon resonance. RSC Pub, Cambridge
13. Love JC et al (2005) Self-assembled monolayers of thiolates on metals as a form of nanotechnology. Chem Rev 105(4): 1103–1169

14. Homola J (2008) Surface plasmon resonance sensors for detection of chemical and biological species. Chem Rev 108(2): 462–493
15. Mrksich M, Whitesides GM (1996) Using self-assembled monolayers to understand the interactions of man-made surfaces with proteins and cells. Annu Rev Biophys Biomol Struct 25:55–78
16. Rusmini F, Zhong Z, Feijen J (2007) Protein immobilization strategies for protein biochips. Biomacromolecules 8(6): 1775–1789
17. Staros JV, Wright RW, Swingle DM (1986) Enhancement by N-hydroxysulfosuccinimide of water-soluble carbodiimide-mediated coupling reactions. Anal Biochem 156(1):220–222
18. Bain CD, Evall J, Whitesides GM (1989) Formation of monolayers by the coadsorption of thiols on gold: variation in the head group, tail group, and solvent. J Am Chem Soc 111(18): 7155–7164
19. Lofas S, Johnsson B (1990) A novel hydrogel matrix on gold surfaces in surface-plasmon resonance sensors for fast and efficient covalent immobilization of ligands. J Chem Soc Chem Commun 21:1526–1528
20. Leidberg BaL (1993) Principles of biosensing with an extended coupling matrix and surface plasmon resonance. Sens Actuators, B 11:62–73
21. Brown S (1997) Metal-recognition by repeating polypeptides. Nat Biotechnol 15(3):269–272
22. Woodbury RG et al (1998) Construction of biosensors using a gold-binding polypeptide and a miniature integrated surface plasmon resonance sensor. Biosens Bioelectron 13(10): 1117–1126
23. Joung HA et al (2008) High sensitivity detection of 16s rRNA using peptide nucleic acid probes and a surface plasmon resonance biosensor. Anal Chim Acta 630(2): 168–173
24. Mohrle BP, Kumpf M, Gauglitz GN (2005) Determination of affinity constants of locked nucleic acid (LNA) and DNA duplex formation using label free sensor technology. Analyst 130(12):1634–1638
25. Yang N et al (2007) Evaluation of two- and three-dimensional streptavidin binding platforms for surface plasmon resonance spectroscopy studies of DNA hybridization and protein-DNA binding. Biosens Bioelectron 22(11):2700–2706
26. Jung Y et al (2007) Self-directed and self-oriented immobilization of antibody by protein G-DNA conjugate. Anal Chem 79(17):6534–6541
27. Bae YM et al (2005) Study on orientation of immunoglobulin G on protein G layer. Biosens Bioelectron 21(1):103–110
28. Stevens RC et al (2007) Detection of the toxin domoic acid from clam extracts using a portable surface plasmon resonance biosensor. Harmful Algae 6(2):166–174
29. Stevens RC et al (2008) Detection of cortisol in saliva with a flow-filtered, portable surface plasmon resonance biosensor system. Anal Chem 80(17):6747–6751
30. Huber D et al (2009) Effectiveness of natural and synthetic blocking reagents and their application for detecting food allergens in enzyme-linked immunosorbent assays. Anal Bioanal Chem 394(2):539–548
31. Dee S et al (2009) Evidence of long distance airborne transport of porcine reproductive and respiratory syndrome virus and *Mycoplasma hyopneumoniae*. Vet Res 40(4):39
32. Bishop EJ, Mitra S (2007) Measurement of nitrophenols in air samples by impinger sampling and supported liquid membrane micro-extraction. Anal Chim Acta 583(1):10–14
33. Rosen DL (2006) Airborne bacterial endospores detected by use of an impinger containing aqueous terbium chloride. Appl Opt 45(13):3152–3157
34. Fabian P et al (2009) Airborne influenza virus detection with four aerosol samplers using molecular and infectivity assays: considerations for a new infectious virus aerosol sampler. Indoor Air 19(5):433–441
35. Burton NC et al (2005) The effect of filter material on bioaerosol collection of *Bacillus subtilis* spores used as a *Bacillus anthracis* simulant. J Environ Monit 7(5):475–480
36. Plutzer J, Torokne A, Karanis P (2010) Combination of ARAD microfibre filtration and LAMP methodology for simple, rapid and cost-effective detection of human pathogenic *Giardia duodenalis* and *Cryptosporidium* spp. in drinking water. Lett Appl Microbiol 50(1):82–88
37. Breier JA et al (2009) A suspended-particle rosette multisampler for discrete biogeochemical sampling in low-particle-density waters. Deep Sea Res I 56(9):1579–1589
38. Edmonds JM et al (2009) Surface sampling of spores in dry-deposition aerosols. Appl Environ Microbiol 75(1):39–44
39. Conroy PJ et al (2009) Antibody production, design and use for biosensor-based applications. Semin Cell Dev Biol 20(1): 10–26
40. Zhang Y et al (2007) Studies of metal ion binding by apo-metallothioneins attached onto preformed self-assembled monolayers using a highly sensitive surface plasmon resonance spectrometer. Sensor Actuator B Chem 123(2):784–792
41. Yu JCC, Lai EPC (2005) Interaction of ochratoxin A with molecularly imprinted polypyrrole film on surface plasmon resonance sensor. React Funct Polym 63(3):171–176
42. Joung HA et al (2008) High sensitivity detection of 16s rRNA using peptide nucleic acid probes and a surface plasmon resonance biosensor. Anal Chim Acta 630(2):168–173
43. Wark KL, Hudson PJ (2006) Latest technologies for the enhancement of antibody affinity. Adv Drug Deliv Rev 58(5–6):657–670
44. Nieba L, Krebber A, Pluckthun A (1996) Competition BIAcore for measuring true affinities: large differences from values determined from binding kinetics. Anal Biochem 234(2): 155–165
45. Friguet B et al (1985) Measurements of the true affinity constant in solution of antigen-antibody complexes by enzyme-linked immunosorbent-assay. J Immunol Meth 77(2):305–319
46. Pope ME et al (2009) Anti-peptide antibody screening: selection of high affinity monoclonal reagents by a refined surface plasmon resonance technique. J Immunol Meth 341(1–2): 86–96

47. Achi R, Mata L (1997) Oocyst size of *Cryptosporidium* sp. (Apicomplexa: Cryptosporidildae) suggest the presence of *C. parvum* in Costa Rican children. Rev Biol Trop 45(1B):615–618
48. Kubitschek HE (1990) Cell-volume increase in *Escherichia coli* after shifts to richer media. J Bacteriol 172(1):94–101
49. Prasad BVV et al (2001) Structural studies on gastroenteritis viruses. In: Chadwick D, Goode JA (eds) Gastroenteritis viruses, pp 26–46
50. Papageorgiou AC, Tranter HS, Acharya KR (1998) Crystal structure of microbial superantigen staphylococcal enterotoxin B at 1.5 angstrom resolution: implications for superantigen recognition by MHC class II molecules and T-cell receptors. J Mol Biol 277(1):61–79
51. Ban N et al (1994) Crystal-structure of an idiotype antiidiotype Fab complex. Proc Natl Acad Sci USA 91(5):1604–1608
52. Wu CM, Lin LY (2004) Immobilization of metallothionein as a sensitive biosensor chip for the detection of metal ions by surface plasmon resonance. Biosens Bioelectron 20(4): 864–871
53. Yu QM et al (2005) Detection of low-molecular-weight domoic acid using surface plasmon resonance sensor. Sens Actuators, B 107(1):193–201
54. Mauriz E et al (2006) Real-time detection of chlorpyrifos at part per trillion levels in ground, surface and drinking water samples by a portable surface plasmon resonance immunosensor. Anal Chim Acta 561(1–2):40–47
55. Kawaguchi T et al (2007) Fabrication of a novel immunosensor using functionalized self-assembled monolayer for trace level detection of TNT by surface plasmon resonance. Talanta 72(2):554–560
56. Naimushin AN et al (2002) Detection of *Staphylococcus aureus* enterotoxin B at femtomolar levels with a miniature integrated two-channel surface plasmon resonance (SPR) sensor. Biosens Bioelectron 17(6–7):573–584
57. Cho HS, Kim TJ (2007) Comparison of surface plasmon resonance imaging and enzyme-linked immunosorbent assay for the detection of antibodies against iridovirus in rock bream (*Oplegnathus fasciatus*). J Vet Diagn Investig 19(4):414–416
58. Hodnik V, Anderluh G (2009) Toxin detection by surface plasmon resonance. Sensors 9(3):1339–1354
59. Hennion MC, Barcelo D (1998) Strengths and limitations of immunoassays for effective and efficient use for pesticide analysis in water samples: a review. Anal Chim Acta 362(1): 3–34
60. Boozer C et al (2006) Looking towards label-free biomolecular interaction analysis in a high-throughput format: a review of new surface plasmon resonance technologies. Curr Opin Biotechnol 17(4):400–405
61. Chinowsky TM et al (2007) Compact, high performance surface plasmon resonance imaging system. Biosens Bioelectron 22(9–10):2208–2215
62. Alvarez-Rueda N et al (2007) Generation of llama single-domain antibodies against methotrexate, a prototypical hapten. Mol Immunol 44(7):1680–1690

Biosynthetic Natural Gas

Michael Seiffert, Stefan Rönsch
German Biomass Research Centre (Deutsches BiomasseForschungsZentrum gemeinnützige GmbH), Leipzig, Germany

Article Outline

Glossary
Definition of the Subject
Introduction
Biomass Resources
Biomass Supply
Bio-SNG Conversion Technology
Distribution Infrastructure
Assessment of Bio-SNG Provision Pathways
Future Directions
Bibliography

Glossary

Biomass gasification Thermochemical conversion process, where the gasification media (pretreated solid fuel) is converted into a gaseous fuel (called raw gas).

Bio-SNG Biosynthetic Natural Gas is a gaseous biofuel provided via thermochemical conversion including the steps biomass gasification and subsequent methanation.

Methanation Methanation is a catalyst-based synthesis with the aim to provide methane from a syngas. Therefore, the gas components hydrogen and carbon monoxide occurring within the syngas are converted to methane and water-steam.

Tri-generation Technology for the parallel production of the energy carrier heat, electricity, and fuel (e.g., conversion of biomass into heat, electricity, and Bio-SNG) with varying shares according to the given demand.

Definition of the Subject

Since the discussion on climate protection started and numerous countries declared defined goals for the use of renewable sources of energy in the heat, electricity as well as in the transportation sector, the request to

develop promising and sustainable nonfossil energy pathways gain more and more importance on the political agenda. Under the various renewable sources of energy biomass and especially solid biofuels contribute already significantly within the global energy system mainly due to the easy availability of solid biomass and the ability to cover the given demand anytime (e.g., application for cooking purposes in developing countries, provision of heat in countries with a cold season). Beside these established pathways, new routes for an efficient and sustainable biomass use are under development. One promising example of such a new provision chain is the conversion of solid biofuels via gasification and subsequent methanation into Biosynthetic Natural Gas (Bio-SNG) to be used as a substitute for Natural Gas. This provision pathway allows the use of local available lignocellulosic biomass for the efficient production of a well-known gaseous energy carrier (i.e., Bio-SNG). Thus, this energy carrier can substitute Natural Gas and can help to reduce the energy-related greenhouse gas (GHG) emissions. With the use of Bio-SNG in the mobile and stationary sector, the already existing infrastructure can be used. Based on this, the aim of the following explanations is to present such Bio-SNG provision chains in detail and to assess them concerning technical, economic and environmental aspects.

Introduction

Within the global energy system, Natural Gas is an important energy carrier. Related to the overall primary energy consumption Natural Gas contributes currently with a share of 20.5%. And the demand for Natural Gas is projected to increase until 2030 by more than 50%. For the sectors residential, services, and agriculture as well as industry, an annual growth rate between 1.2% and 1.4% is expected globally. In contrast, the power sector is characterized by a projected growth rate of 2.4% and an overall market share of 45% by 2030 [1]. Additionally, the infrastructure to distribute and store Natural Gas is fully available and has been improved continuously during recent years. Beside a highly efficient energetic utilization for stationary and mobile application, Natural Gas can be used as a raw material, e.g., within the chemical industry [2].

Since numerous countries introduced legislative frame conditions to implement the Kyoto Protocol (e.g., European guideline 2009/28/EG) or to reduce CO_2-emissions (e.g., EU wide CO_2-control for passenger cars and light-duty vehicles), the substitution of fossil energy gains more and more importance. Beside this, selected countries dominate the supply of fossil energy carriers like Natural Gas and create therewith a substantial import dependency. The substitution of Natural Gas through biomethane is therefore an option allowing solving several problems and facing some important challenges at once.

For the production of biomethane, two conversion pathways are market ready respectively under development at the moment [3]. Beside the biogas pathway (i.e., the biochemical biomass conversion), the thermochemical conversion of solid biomass is another promising option to produce biomethane (here called: Biosynthetic Natural Gas or Bio-SNG to avoid a misunderstanding with biomethane from anaerobic processes).

The entire provision chain of Bio-SNG is characterized by some advantages compared to other biomass conversion routes. Relatively, small production systems (starting from a few 10 MW thermal capacity) enable the use of locally available biomass without too long transport distances. The possibility of tri-generation (i.e., the production of heat, power, and fuels) allows high overall efficiencies and therewith a high CO_2 mitigation potential. Due to a more market-ready technology and smaller conversion units, fewer risks are given in comparison to the production of BtL-fuels. Bio-SNG can be distributed and stored with the very well-developed Natural Gas grid that makes it possible to transport the biomethane together with Natural Gas from the source to the end user [4].

The production of Bio-SNG can be carried out via steam gasification of woody biomass, gas cleaning, subsequent methanation, and raw gas upgrading (Fig. 1). The steam gasification and a subsequent gas cleaning have been demonstrated successful in a technical scale of 8 MW thermal capacity at the biomass combined heat and power (CHP) gasification plant in Güssing/Austria since 2002. Steam gasification leads to a producer gas with a relatively high content of hydrogen and methane. These properties are necessary for an efficient SNG production [5].

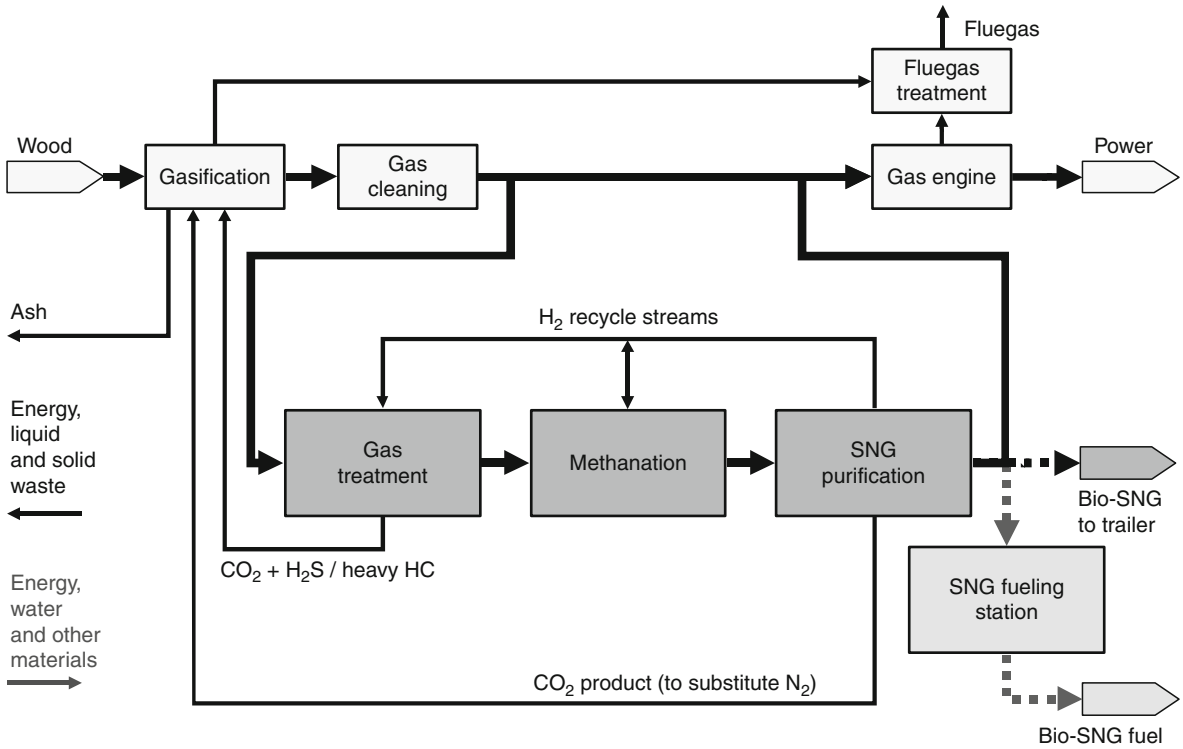

Biosynthetic Natural Gas. Figure 1
Basic process flow diagram

Biomass Resources

Taking into consideration the technical requirements of the conversion technology (e.g., gasifier requirements), solid biofuels seem to be promising for the production of Bio-SNG from the current point of view. Thus, woody and herbaceous biomass material streams are favorable resources. Based on the CEN classification standard (i.e., European Committee for Standardization), the following solid biofuels are of great importance [6]:

1. Forest and plantation wood
2. Wood processing industry by-products and residues
3. Used wood
4. Herbaceous biomass from agriculture and horticulture
5. Herbaceous processing industry by-products and residues

Based on the gathered experiences in the field of biomass pretreatment and biomass gasification, the qualitative requirements can be defined in accordance to the standard ÖNORM M 7133. Table 1 gives an exemplary overview to qualitative requirements on woody biomass suitable for the production of Bio-SNG [7].

Biomass Supply

The decentralized availability of biomass develops partially complex provision structures as well as numerous capacity-related bottlenecks along the entire biomass supply chain closing the gap between the place of biomass production and use. In this context, it is necessary to integrate efficient provision concepts into the local and regional frame conditions (e.g., biomass potential, infrastructural aspects) in order to achieve a high logistic performance and low provision costs free plant gate as well as low environmental effects.

Biosynthetic Natural Gas. Table 1 Selected specifications for solid biofuels for the Bio-SNG production

Criteria	Unit	Specification
Origin	–	Woody biomass from forest residues and short rotation coppices
Product	–	Wood chips
Water content	In%	20 up to 30
Size	In mm	30 up to 50
Share of impurities	–	Rough impurities (like stones, metal pieces, and other contaminants) as well as the addition of combustible impurities (like abrasive dust) are not permitted
Ash content	In%	<2

Concerning the configuration of biomass supply chains a wide range of approaches are possible. The overall objective of the provision of solid biofuels to Bio-SNG production plants (and in general to biomass conversion plants) is the optimized combination of the preconditions at the source with the requirements of the sink (respectively conversion plant) along the entire supply chain. This includes the adjustment of the qualitative and quantitative fuel requirements as well as further technical, spatial, and time-related criteria.

Beside a high technical biomass potential for a certain fuel assortment aspects like the catchments area, the necessity of a fuel conditioning, transport distances as well as the distribution of storages are of importance for the configuration of the overall supply chain. Depending on the conversion plant size, different transport modes seem favorable and can be divided into the (a) road, (b) rail, and (c) water way transport. The latter can be distinguished into the inland water way and overseas transport. Beside a straight supply of the biomass to the Bio-SNG facility, the provision of the relevant biofuels is also possible through numerous intermediate steps.

The solid biofuel provision to Bio-SNG plants is characterized by fully mechanized concepts. Via road transport, the supply is usually carried out with swap bodies. For the provision of biomass assortments with intermodal systems, relying on train transport as main mode, the preliminary run (road transport) and the main run is integrating swap bodies as well. To overcome medium distances the use of container systems is promising, since the handling process is more efficient and the down times of the transport media can be reduced. The provision of solid biofuels via inland waterway or overseas is based on the bulk transport. This is true, because the transport is carried out over longer distances and is due to the transport mode more time consuming. Therefore, it is necessary to exploit the load unit by using bulk goods.

Between the different supply approaches significant differences with regard to the logistic efficiency, the complexity of the supply chain as well as the infrastructural flexibility exist. While the logistic efficiency for the road-based supply is the highest, this alternative is limited in terms of transport distances. The intermodal transport is in general characterized through higher complexity and lower logistic efficiency, whereas it is more convenient for the long-distance biomass supply. In the field of infrastructure flexibility, direct supply via road transport is in most cases the most convenient alternative [8].

Bio-SNG Conversion Technology

The thermochemical production pathway of synthetic Natural Gas aims to convert solid biofuels into gas with high methane content (approx. 95%). The conversion from solid biomass to Bio-SNG at a certain location can be subdivided into five process steps:

1. Biomass pretreatment
2. Biomass gasification
3. Gas cleaning
4. Methanation
5. Raw-SNG upgrading (Fig. 2)

In the following, the technology of these process steps is described in detail.

Biomass Pretreatment

Due to its inhomogeneous characteristic, solid biofuels have to be pretreated before gasification to ensure a reliable feeding into the gasification reactor on the one hand and to allow for optimal gasification conditions inside the gasification reactor on the other. Thereby, in

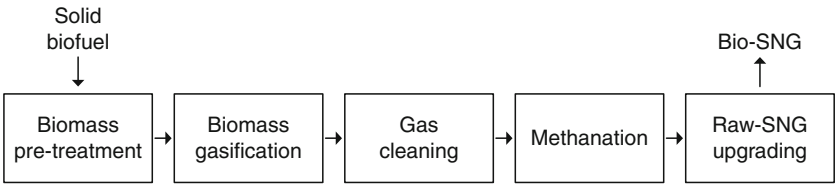

Biosynthetic Natural Gas. Figure 2
Scheme of Bio-SNG conversion pathways

general, the pretreatment focuses on an adaption of the biomass size to meet the demands of the feeding system and on the drying of the biomass to reduce the energetic losses within the gasification process [9]. As entrained-flow gasifier requires a pumpable or dispersible fuel, their application demands a special biomass pretreatment (e.g., pyrolysis, torrefaction) [10].

The pretreatment of the solid biofuel necessary for the reasons outlined above can be realized with mechanical, thermal, and thermochemical processes.

Mechanical Pretreatment Mechanical biomass pretreatment processes comprise primarily process steps like size reduction, sieving, and/or pressing of the fuel to ensure a homogeneous particle size and particle form [11] to prevent locking of the gasifier's feeding system and to ensure a uniform flow regime inside the gasification reactor.

Thermal Pretreatment The thermal biomass pretreatment comprises biomass drying in order to increase the biomass' quality and heating value and to reduce its weight [11]. Such drying processes can be distinguished in natural and technical drying. For Bio-SNG production pathways, technical drying processes are – due to the disposability of process heat and the need for low biomass water contents (approximately 10–20%) permitting an energy-efficient gasification process [9] - of particular interest.

Thermochemical Pretreatment With regard to Bio-SNG production pathways, thermochemical pretreatment methods primarily aim to meet the demands of entrained-flow gasification systems. Regarding the biomass pretreatment to allow for their use in entrained-flow gasification systems, two methods are under discussion: torrefaction [12] and pyrolysis [13]. Both methods operate under absence of external oxygen. While torrefaction processes deaerate water and volatile components [11, 14], pyrolysis processes decompose the biomass into three products: gas, condensable hydrocarbons (pyrolysis oil after condensation), and char. Thereby, here the flash pyrolysis is of particular interest as this process allows to achieve high pyrolysis oil yields [15]. The use of torrefaction and pyrolysis products in entrained-flow gasifier is still under investigation and cannot be considered as state of the art.

Biomass Gasification

Gasification is a thermochemical conversion process, where the gasification media (pretreated fuel) is converted into a gas (called raw gas) with the main components CO_2, CO, H_2O, H_2, and – depending on the gasification parameters – certain amounts of CH_4. As the process is endothermic, heat has to be supplied. Beside the main gas components mentioned above, the raw gas may contain different impurities like particles, tars, sulfur compounds, nitrogen compounds, halogens, and alkali compounds. The amount of these impurities within the raw gas depends on multiple process conditions and can be influenced to a certain degree by gasification technology and conditions [10, 11, 16, 17].

The available gasification processes can be distinguished according to the (a) gasification agent, (b) gasification pressure level, (c) heat supply, and (d) reactor design. The reactor design is related to different scale potentials and therewith characteristic for the subsequent gas usage. According to the fluid-dynamic behavior of the fuel in the gasifier, the following reactor designs can be used in general for the provision of a raw gas (Fig. 3).

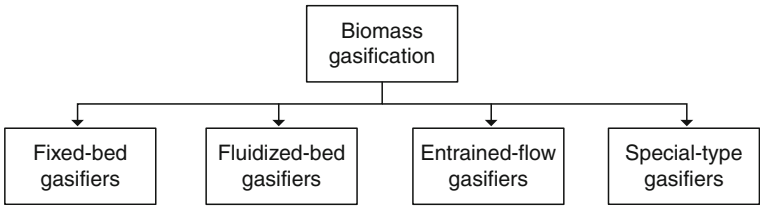

Biosynthetic Natural Gas. Figure 3
Reactor designs of biomass gasification systems

Regarding the Bio-SNG production, in general the following two reactor designs are most important according to current knowledge.

Fluidized-Bed Gasifier Fluidized-bed gasifier (Fig. 4) is characterized by the fluidization of fine-grained inert material (e.g., sand) and solid feedstock particles inside the reactor. Thereby, the mixture of inert material and feedstock particles behaves similar to a fluid. Due to the homogeneous feedstock allocation inside the reactor, there are no separated reaction zones, the temperature level (between 700°C and 950°C) is easily to be adjusted, and the heat and mass transfer within fluidized-bed reactors can be optimized in comparison to fixed-bed gasifier. However, the dust content of the raw gas is relatively high [11, 18]. Fluidized-bed gasifier is distinguished as (a) stationary, (b) circulating, and (c) twin-bed fluidized-bed gasifier.

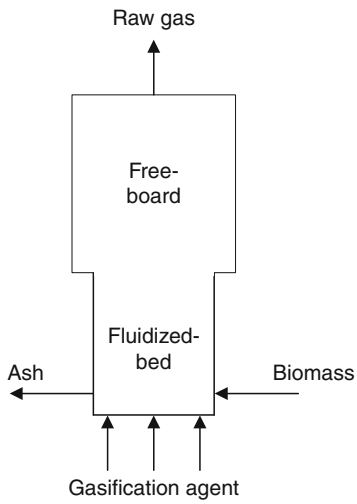

Biosynthetic Natural Gas. Figure 4
Scheme of stationary fluidized-bed gasifier

Entrained-Flow Gasifier Entrained-flow gasifier (Fig. 5) is commonly applied for coal gasification. Here the gasification media consisting of (very) small particles is gasified within seconds at temperatures of 1,300–1,600°C and pressures up to a 60 bars [10]. In general, oxygen is used as a gasification agent. The resulting raw gas is free of tars and has a low methane content - in comparison to the fluidized-bed gasifier where the raw gas is characterized by a high tar and methane content.

The main advantages of entrained-flow gasifier are high carbon conversion rates and a tar-free raw gas. The effort on gasification and handling of the process parameters (high temperatures and pressures) are disadvantages of this design. Entrained-flow gasifier is under discussion for plant sizes of several hundred megawatts [10, 19].

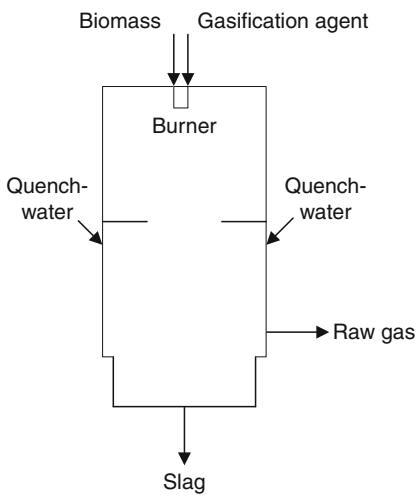

Biosynthetic Natural Gas. Figure 5
Scheme of entrained-flow gasifier

Gas Cleaning

Depending on the gasification parameters (e.g., reactor design, gasification pressure, gasification temperature, and gasification agent), the raw gas contains different impurities as (Fig. 6) [20]:

- Particles (e.g., char, dust, ash, bed material)
- Tars (e.g., C_7H_8, $C_{10}H_8$)
- Sulfur compounds (e.g., H_2S, COS, thiophenes)
- Nitrogen compounds (e.g., NH_3, HCN)
- Halogens (e.g., HCl)
- Alkali compounds (e.g., Na- and K-compounds)

To avoid catalyst poisoning in the subsequent synthesis (e.g., caused by organic sulfur) and damage at other plant components (e.g., corrosion at heat-exchanger surfaces), the raw gas has to be cleaned after leaving the gasifier. To remove the impurities mentioned above, various cleaning methods are available at the market.

Particles Particles can be removed from gas streams by cyclones, filters, electrostatic precipitators, or washing systems. Cyclones are applied for a rough particle removal. They separate particles above 5 μm by centrifugal forces and characterized by robust and simple design and low-pressure drop within the gas. Filters are appropriate for a fine particle separation even of particles below 5 μm. However, a drawback of filters is the pressure drop especially for increased separation rates. Electrostatic precipitators achieve a high particle separation in combination with low-pressure drops. They operate either dry or wet. But they need a high technical effort in comparison to cyclones and filters. Washing systems (e.g., Venturi washers) are able to remove even smaller particles as well as additional gas impurities. However, the technical effort of washing systems for particle removal is very high as a subsequent separation of withdrawn particles from the solvent is usually necessary [11, 17].

Tars Tars can be removed from the gas by catalytic or thermal tar cracking as well as by washing with organic medium and water. At high temperatures, tars are cracked into small molecules like CO and H_2. For this process, high temperatures (around 1,200°C) or/and long residence times are necessary. However, the provision of such a high temperature level lowers the process efficiency. Compared to this catalytic tar cracking requires lower temperatures (around 850°C). But so far no cheap catalysts with a long technical lifetime are available on the market. Tar can also be washed out from the gas with water. Thereby, the raw gas is cooled down to condense the tars. But then the contaminated washing water has to be cleaned. Therefore, in recent years washing systems using organic washing media have been developed. The advantage is that the contaminated solvent can be burnt. Therewith, purities of about 10 mg/m^3 (i.N.) can be achieved [11, 17].

Sulfur Compounds Sulfur can be removed by adsorptive and/or absorptive methods. ZnO and active carbon beds are commercially available adsorptive processes for sulfur removal. Both systems have to be regenerated from time to time. To reduce the respective effort and to ensure high sulfur separation rates, active carbon bed and ZnO-bed can be combined: with active carbon beds a rough and with ZnO

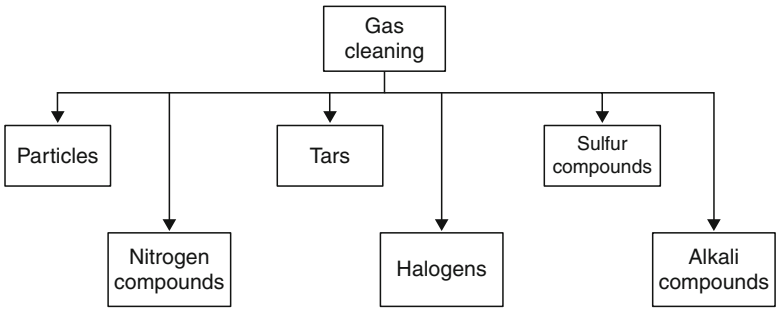

Biosynthetic Natural Gas. Figure 6
Categories of raw gas impurities

a fine sulfur removal is achieved. If larger amounts of sulfur have to be removed from the gas, technically complex systems known from coal gas cleaning can be used (e.g., Rectisol washing, Selexol washing, Amine washing) [11, 17].

Nitrogen Compounds, Halogens, and Alkali Compounds Nitrogen compounds and halogens are separated from the gas by adsorptive and absorptive methods mentioned above. To improve the separation rate, these methods can be adapted to the impurity to be removed (e.g., by the addition of sodium hydroxide to water solvent). A common way to remove alkali compounds from the gas is to condense them (below 600°C) and remove them by conventional filter techniques [11, 17].

Methanation

The process step methanation comprises a catalyst-based synthesis with the aim to increase the methane content of the cleaned gas. Thereby, the gas components hydrogen and carbon monoxide are converted to methane and water vapor (Eq. 1).

$$CO + 3H_2 \leftrightarrow CH_4 + H_2O \quad (1)$$

In principle, all metals of the eighth main group catalyze the methane synthesis. However, due to their availability and price stability the use of nickel catalyst is of particular interest [21]. This catalyst operates within a wide pressure (1–80 bar) and temperature range (250–650°C), but the desired formation of methane is enhanced at low temperatures and high pressures. To ensure a high carbon monoxide conversion, a H_2/CO-ratio of at least 3/1 is advisable. However, as raw gases from biomass gasification processes are typically characterized by H_2/CO-ratios of 0.3–2.0, in general an adjustment of this ratio is foreseen either by adding additional hydrogen or by converting carbon monoxide and water vapor into hydrogen and carbon dioxide according to the water gas shift reaction (Eq. 2).

$$CO + H_2O \leftrightarrow H_2 + CO_2 \quad (2)$$

As nickel catalysts catalyze the water gas shift reaction as well at elevated temperatures and pressures, the water gas shift reaction can be integrated in the methanation reactor instead of an upstream shift-reactor before the methanation.

Basically, methanation reactors can be distinguished according to the fluid-dynamic behavior of their catalysts in fixed-bed reactors and fluidized-bed reactors.

Fixed-Bed Reactors Due to the exothermal methanation reaction and limited axial and radial heat transfer rates of fixed-bed reactors, an isothermal operation is only possible with low conversion rates or high technical and operational effort [21]. For a reasonable heat management, multiple fixed-bed reactors with limited conversion and thus limited heat transfer rates are combined with each other in series, parallel or mixed arrangements.

Fluidized-Bed Reactors In contrast to fixed-bed reactors, fluidized-bed reactors are characterized by a fluidized-bed of the catalyst inside the reactor. To realize a quasi-isothermal operation, the reaction heat can be managed with help of an internal heat exchanger. Therefore, even high gas and heat flows can be handled with a single methanation reactor [22, 23].

Raw-SNG Upgrading

To feed Bio-SNG into the Natural Gas grid, it has to fulfil the quality requirements of the grid. Therefore, after the methanation an upgrading of the raw Bio-SNG is necessary. This includes the separation of carbon dioxide, water, and – depending on the raw-SNG quality – other gas components (e.g., hydrogen). Thereby, beside the Bio-SNG composition and purity, the Wobbe index is of particular interest.

For all raw-SNG upgrading steps, several technologies are available at the market and in operation for treatment processes of SNG from coal, Natural Gas treatment processes, and biogas upgrading processes. However, due to their different technical and operational effort, selected technologies are advisable for small-scale applications and others for large-scale applications. In the following, the most important techniques – with regard to Bio-SNG production – for raw-SNG drying and carbon dioxide removal are described.

Carbon Dioxide Removal Considering the carbon dioxide removal, absorptive and adsorptive processes are available.

A relevant adsorption process for Bio-SNG production systems is the pressure swing adsorption (PSA) for the adsorption of carbon dioxide on an active carbon bed [24]. Absorption processes can be realized based on physical and chemical processes. While physical absorption processes only based on the solubility of the absorptive in the solvent, within chemical absorption processes a chemical reaction between solvent and absorptive takes place to separate the gaseous components from a gas flow. Examples for physical absorption process are the Rectisol process [25] and the Selexol process [26].

Drying For the raw-SNG drying, in general, the gas is cooled down below the water dew point. For further drying, adsorptive and absorptive methods can be applied [27].

Distribution Infrastructure

The Natural Gas grid is classified into four different grid levels. The international pipeline system (level 1) for long-distance transport of Natural Gas is operated on a pressure level of 80 up to 120 bars. An average standard gas volume for such a grid is about 1.0 up to 2.5 mn m^3_{gas}/h. For the national transport of gas (e.g., within Germany, the Netherlands or Austria), a high-pressure grid for the long-distance transport is available (level 2). Such a pipeline system is usually in operation with a grid pressure of 25 up to 80 bars. The connection between long-distance pipeline networks and local gas grids is realized by a regional pipeline system (level 3). These networks are characterized through a wide bandwidth of the pressure level (from 1 up to 70 bars). With the help of the local gas grid, the Natural Gas is distributed to the final consumer (level 4). The lowest pressure level of such a pipeline system is in the range of 30 up to 100 mbar.

From the technical point of view, the feed-in of upgraded biomethane with a defined gas quality is possible in high-pressure gas grid. For medium- and low-pressure grids are in general the required floats not necessarily sufficiently given [28]. But locally a different situation might be given.

The technologies for the feed-in of biomethane into the Natural Gas grid (e.g., compressors) are market ready and commercially available. For the injection of the biomethane in the pipeline, a lifting of the pressure above the grid pressure is required [28].

Therewith the possibility is given to produce Bio-SNG for instance at a place where the plant site requirements are fulfilled (e.g., biomass availability, favorable infrastructure for the provision of biomass and distribution of the produced energy, and heat sink) and to distribute the biomethane via the existing gas pipeline system to the final consumer. The decoupling of the production and utilization allows the efficient application for the generation of heat and electricity. Beside this, Bio-SNG is a favorable alternative for mobile applications (e.g., passenger cars, light heavy-good vehicles).

Assessment of Bio-SNG Provision Pathways

According to the multitude of available technologies, different Bio-SNG production pathways are currently under discussion. Thereby, aspects like (a) the biomass assortment, (b) the plant capacity, or (c) the biomass conversion and especially the gasification system have major influence on the overall system. Therefore, below selected reference concepts are defined and assessed with regard to technical, economic, and environmental criteria.

Reference Concepts

Here are concepts for the provision of Bio-SNG defined (Table 2). Both pathways can be assigned to different time frames. While the concept "fluidized-bed" is oriented on the short term (2015), the "entrained-flow" concept is an alternative for a medium term (2020–2025). The described capacity, operation hours, etc., create the frame conditions of the investigated system and the base for the assessment of the Bio-SNG provision pathways.

The concept "fluidized-bed" represents the "state-of-the-art" technology based on fluidized-bed gasification. This concept is analyzed for a plant scale of 30 MW. It is assumed that forest wood is used as a raw material.

The "entrained-flow" concept represents a future concept with torrefaction as a biomass pretreatment

Biosynthetic Natural Gas. Table 2 Reference concepts and their frame conditions

Criteria	Unit	Concept "fluidized-bed"	Concept "entrained-flow"
Capacity	MW_{bf}	30	200
Operation hours	h/a	8,000	
Fuel demand	t_{dm}	50,000	350,000
Bio-SNG output	m^3_{SNG}/h	2,000	13,333
Pressure level gas grid	bar	25	70

step realized at the conversion plant site. This concept is analyzed for a plant scale of several hundred megawatts. Beside wood from forest services, additionally woody biomass from short rotation coppices is foreseen as a biomass feedstock.

The system boundary is defined by the biomass provision step harvest/collection and through the upgrading of Bio-SNG on Natural Gas quality ready for to be feed-in into the gas grid.

For the biomass supply, a full mechanized provision chain is assumed. The storage process is carried out with air tube ventilation systems that allow a reduction of the water content up to 30% (free plant gate). Chipping is performed with truck-mounted chippers at the forest road. For the handling process, discontinuous conveyors are chosen and finally the solid biofuels are transported directly by truck to the Bio-SNG plant. The conversion technology [29] assumed here is based on an atmospheric fluidized-twin-bed biomass gasifier operating with water-steam as gasification agent. Heat for the endothermic gasification reaction is supplied by bed material circulating between the gasification reactor and a combustion chamber [30]. Char and recycled gasification raw gas are used as fuel for the combustion chamber. Tars are removed from the raw gas by a wet washing system using biodiesel as solvent. A fraction of the tar-loaded biodiesel is pumped into the combustion chamber and used as fuel. The methanation is realized within a fluidized-bed methanation reactor [23] and consists of an active carbon and a ZnO-bed. Afterward the raw-SNG is dried, carbon dioxide is separated from the gas with the help of an amine washing, and hydrogen is removed by membrane technique. The overall system is shown in Fig. 7.

For the reference concept "entrained-flow," forest and short rotation wood is harvested and collected fully mechanized. At the field or forest, the biomass is stored and chipped for the following transport. The handling from the storage or chipping place into the freight hold of a truck is done with discontinuous conveyor. With the preliminary run, the distance between biomass site and the handling site for the subsequent main run is bridged. With the railway-based transport the main run to the conversion plant is carried out, whereas for the loading process, continuous conveyors are selected. The biomass is provided at the conversion plant with this reference pathway. Here the biomass is torrefied at 250°C before gasification with oxygen as gasification agent [12] takes place. After water quench, the raw gas is cleaned from particles by a Venturi-washing system, conditioned with regard to the H_2/CO-ratio in a water gas-shift reactor and separated from sulfur compounds and carbon dioxide with help of a Rectisol washing. The methanation is realized in an arrangement of fixed-bed methanation reactors. Thereby, additional steam is used to avoid carbon deposition at the catalyst surface. Finally, the raw-SNG is dried by cooling the gas down [27]. The reference concept "entrained-flow" is shown in Fig. 8.

Technical Assessment

In the following, both Bio-SNG production pathways are analyzed and compared from a technical point of view. The technical analysis focuses on the process efficiency of the Bio-SNG provision pathways at plant gate.

The methodological basis for the technical assessment is the calculation of mass and energy balances with a flow sheet simulation. Based on these calculations, the energetic gross and net efficiencies are determined representatively for the technical competitiveness of the process. The efficiencies are defined according to Eqs. 3 and 4.

$$\eta_{gross} = \frac{|P_{SNG}|}{|P_{Biomass}|} \quad (3)$$

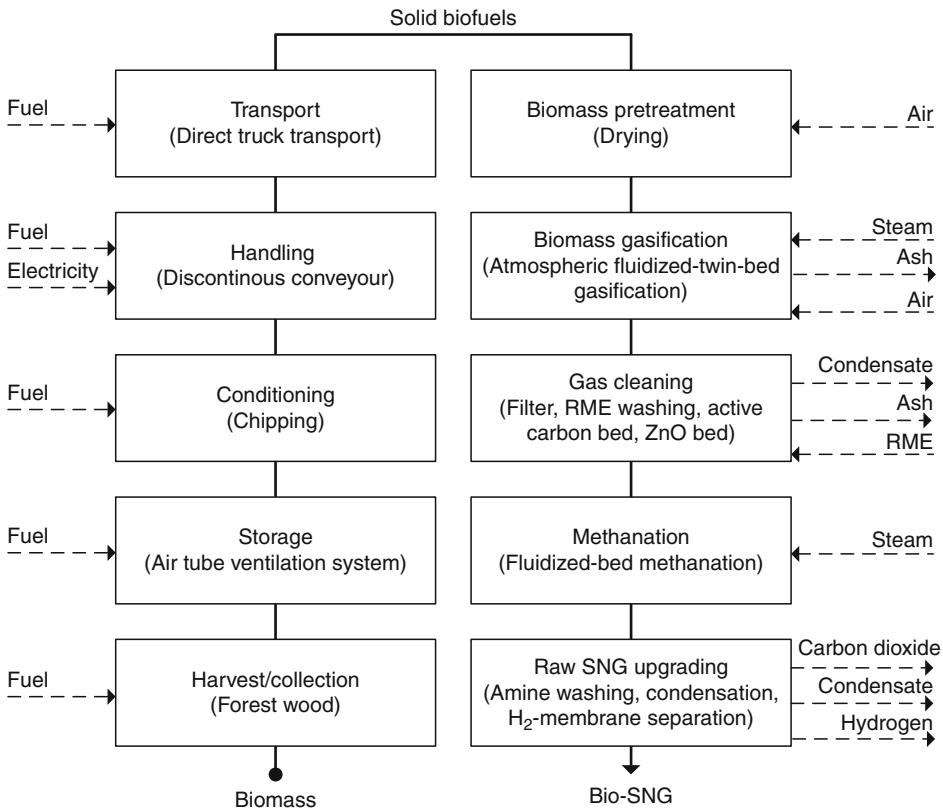

Biosynthetic Natural Gas. Figure 7
Schematic overview of Bio-SNG reference concept "fluidized-bed"

$$\eta_{\text{net}} = \frac{|P_{\text{SNG}}|}{|P_{\text{Biomass}}| + |P_{\text{Electricity consumption}}|} \quad (4)$$

According to different frame conditions and assumptions concerning plant site and process modelling, for each process different efficiencies are calculated. Typical ranges of these values of gross and net efficiency are shown in Fig. 9.

Regarding the results shown in Fig. 9, both Bio-SNG production chains are characterized by net efficiencies in a similar range between 58% and 65%. However, due to process units with a high electrical power demand (e.g., air separation unit, biomass pretreatment), the reference concept "entrained-flow" shows a lower net efficiency than the reference concept "fluidized-bed."

Considering the calculated process efficiency, the overall Bio-SNG conversion chain is characterized by a high biomass-to-SNG rate. Even by including the plant's electricity consumption, net efficiencies of more than 58% can be achieved. Major losses occur within the process step "biomass gasification" (cold gas efficiency of about 70–80%) and the process step methanation (cold gas efficiency of about 80–90%).

Economic Assessment

For a successful market implementation of Bio-SNG (for instance as a transportation fuel), the production costs are an important indicator. Therefore, the specific Bio-SNG production costs are calculated here based on the annuity method [31]. The annual costs for capital, raw material, and auxiliaries will be allocated with the annual credits for by-products (e.g., heat). Depending on the yearly produced Bio-SNG the specific Bio-SNG production costs can be calculated. They refer to the lower heating value. An overview to the bandwidth of these costs from the regarded concepts is given in Fig. 10.

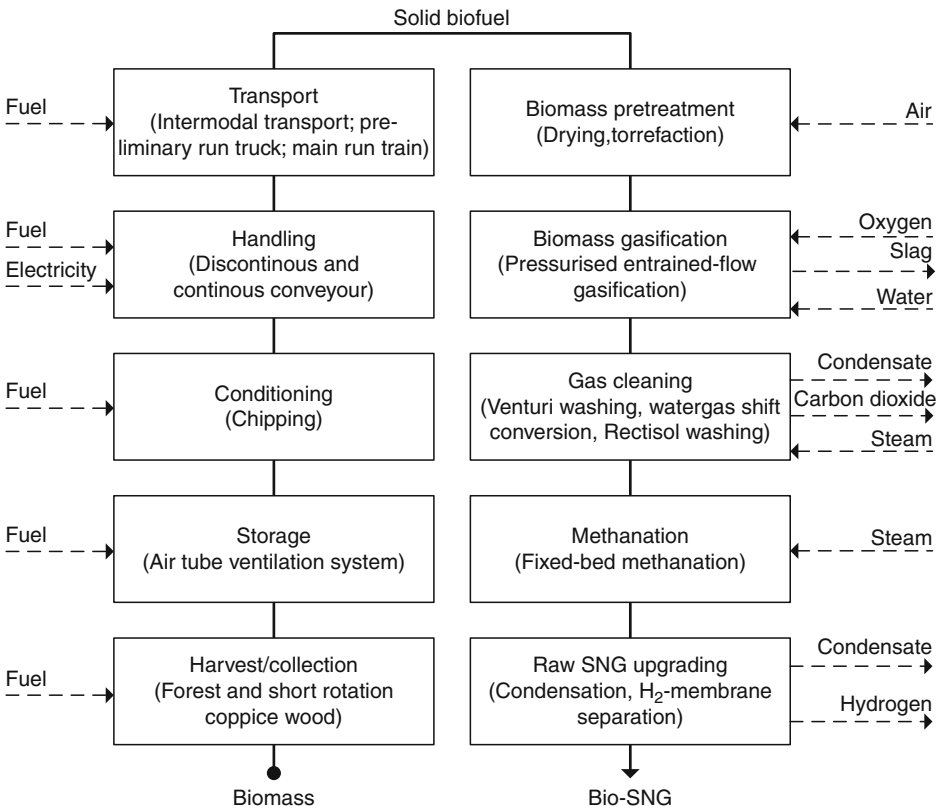

Biosynthetic Natural Gas. Figure 8
Schematic overview of Bio-SNG reference concept "entrained-flow"

The calculations show Bio-SNG production costs between 0.07 and 0.12 €/kWh$_{Bio\text{-}SNG}$. However, a cost reduction potential is given due to improvement and upscale of the plant concepts. Plants with the "entrained-flow" concept allow a lowering of the specific production costs about 0.01 €/kWh$_{Bio\text{-}SNG}$, mainly due to the economy of scale effect. This is true due to beneficial effects related to the higher capacities (e.g., lower specific costs for investment, maintenance, insurance).

Environmental Assessment

For the environmental evaluation of the defined reference concepts, the specific greenhouse gas (GHG) emissions are calculated in accordance to the allocation method described in the RES Directive [32].

For all steps of the Bio-SNG provision, the relevant inputs of energy or auxiliaries are assessed. The greenhouse gas (GHG) emissions allocated to the products Bio-SNG and heat according to the lower heating values. Greenhouse gas emissions for electricity consumption have been calculated based on the European electricity mix. The results are referred to the defined functional unit 1 GJ$_{Bio\text{-}SNG}$. The results of the regarded concepts "fluidized-bed" and "entrained-flow" are shown in Fig. 11.

For the regarded Bio-SNG provision concepts, specific greenhouse gas emissions between 20 and 35 kg CO_2/GJ$_{Bio\text{-}SNG}$ have been determined. The results show that the concept "fluidized-bed" has with 25 kg$_{CO2}$/GJ$_{Bio\text{-}SNG}$ significant lower emissions. In comparison, the concept with entrained-flow gasification is

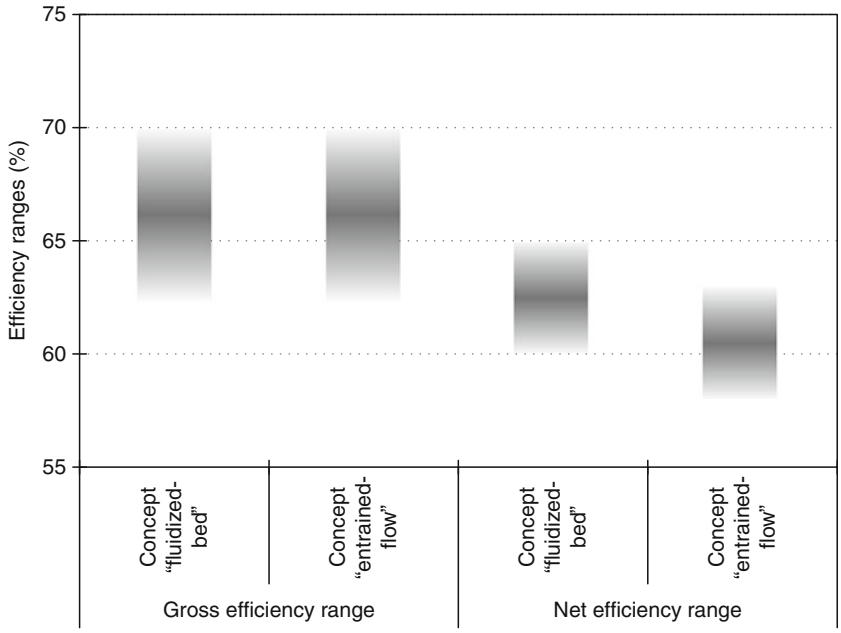

Biosynthetic Natural Gas. Figure 9
Gross and net efficiency range for regarded reference concepts

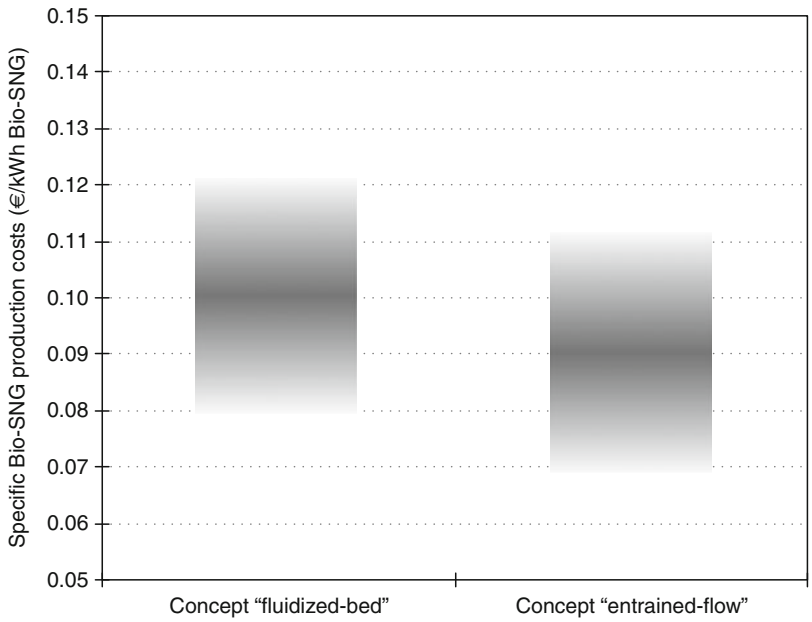

Biosynthetic Natural Gas. Figure 10
Specific Bio-SNG production costs for the regarded reference concepts

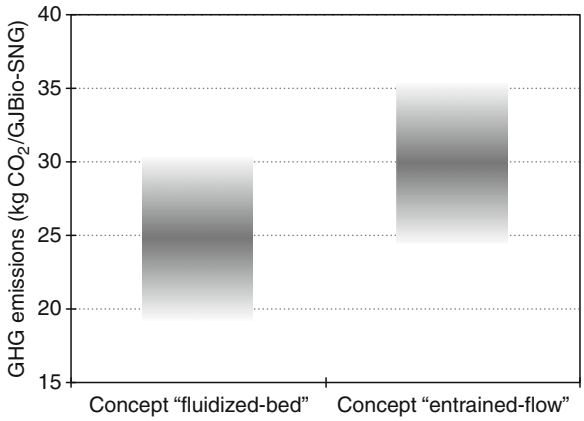

Biosynthetic Natural Gas. Figure 11
Bio-SNG GHG emission for the regarded reference concepts

characterized by about 5 $kg_{CO2}/GJ_{Bio\text{-}SNG}$ higher emissions. This is due to a more complex biomass supply (e.g., longer transport distances, higher number of handling processes), additional efforts within the conversion process (e.g., air separation unit) as well as a lower net efficiency of the conversion.

Overall Assessment

Below, the results of the technical, economic, and environmental evaluations are comprehensively discussed. Beside this, the possible implementation of the relevant Bio-SNG plant concepts will be analyzed with regard to the aspect flexibility.

Both production pathways are characterized by similar gross energetic efficiency, while the concept "fluidized-bed" shows a higher net efficiency. Additional, this production concept is advantageous in terms of environmental aspects. This is mainly due to a less complex supply structure for biomass and shorter transport distances than for concepts with several hundred megawatts fuel input, like for the "entrained-flow" concept. In contrast, the latter concept is beneficial regarding the Bio-SNG production costs (primarily due to the economy of scale effect). Furthermore, it has to be taken into account that with an increase of the scale from the conversion plant a raise of the economic risk in terms of investment costs is given.

For the establishment of a Bio-SNG plant beside infrastructural aspects (e.g., biomass provision – access to traffic infrastructure; distribution of energy carrier – access to gas grid, heat sink) also biomass-related criteria are of importance. Between plants with varying scales, significant differences in terms of site requirements exist. For conversion plants with approximately 30 MW (e.g., concept "fluidized-bed"), the regional availability of biomass is important and a connection to the road network for the biomass supply is sufficient. Compared to this, large-scale concepts need favorable logistic conditions (e.g., access to railway and inland waterway or oversea), while the regional biomass availability is of minor importance. Due to these frame conditions, the site flexibility of Bio-SNG plants with smaller scale is significantly higher.

Summing up, the implementation of Bio-SNG plants with a regional biomass supply seems to be favorable from the technical, environmental, and location-related point of view with plant concepts in the smaller scale (e.g., "fluidized-bed" concept). Only at outstanding sites, an establishment of large-scale production facilities for Bio-SNG is justified.

Future Directions

The demand for Natural Gas is increasing for mobile and stationary application. Due to climate protection reasons (e.g., to reduce greenhouse gas emissions) as well as for energy related reasons (e.g., to diversify supply sources) the substitution of Natural Gas through biomethane is a favorable alternative.

With the production of Bio-SNG, a technically efficient solution is available to provide biomethane in an efficient way in the medium term in significant dimensions. The specific production costs as well as the resulting greenhouse gas emissions depend strongly on the local conditions of a potential conversion plant site and the structure of the biomass provision. However, they are relatively low.

Through a systematic technical enhancement of the entire process chain, the specific Bio-SNG production costs can be reduced and the greenhouse gas mitigation potential can be improved even further.

For a successful market implementation of Bio-SNG, further research and development steps are required. In parallel, the consumer interest has to be raised for this sustainable and alternative biofuel.

Bibliography

1. International Energy Agency (2008) World energy outlook, Paris
2. Di Pascoli S, Femia A, Luzzati T (2001) Natural gas, cars and the environment A (relatively) 'clean' and cheap fuel looking for users. Ecol Econ 38:179–189
3. Mozaffarian M, Zwart RWW, Boerrigter H, Deurwaarder EP, Kersten SRA (2004) "Green Gas" as SNG (synthetic natural gas) a renewable fuel with conventional quality. In: Contribution to the science in thermal and chemical biomass conversion conference, Victoria, Vancouver Island, BC, Canada, 30 Aug – 2 Sep 2004
4. Seiffert M, Kaltschmitt M, Hofbauer M, Müller-Langer F (2009) Demonstration of the production and utilization of synthetic natural gas from solid biofuels presentation of the European project "Bio-SNG". International conference on polygerneration strategies, Vienna, 2009
5. Biollaz S (2009) The SNG technology platform in Güssing, A. Status report of Bio-SNG project, Villigen
6. European Committee for Standardization (2005) Solid biofuels – fuel specification and classes CEN/TS 14961. CEN, UK
7. Austrian Standard Institute (2003) ÖNORM M 7133 – Hackgut für energetische Zwecke - Anforderungen und Prüfbestimmungen
8. Seiffert M, Pätz C, Müller-Langer F (2009) Economic-ecological optimisation of biomass logistics for Bio-SNG conversion plants. In: 17th European biomass conference and exhibition, Hamburg, 2009
9. Bolhàr-Nordenkampf M, Hofbauer H (2004) Biomass gasification combined cycle thermodynamic optimisation using integrated drying. In: Proceedings of ASME Turbo Expo 2004: power for land, sea and air, Vienna, 14–17 June 2004
10. Knoef HAM (2005) Handbook biomass gasification, 1st edn. BTG biomass technology group BV, Enschede
11. Kaltschmitt M, Hartmann H, Hofbauer H (2009) Energie aus Biomasse – Grundlagen, Techniken und Verfahren, 2 Aufl. Springer, Berlin
12. Prins MJ (2005) Thermodynamic analysis of biomass gasification and torrefaction. Dissertation, Eindhoven
13. Lange S (2008) Systemanalytische Untersuchung zur Schnellpyrolyse als Prozessschritt bei der Produktion von Synthesekraftstoffen aus Stroh und Waldrestholz. Dissertation, Karlsruhe
14. Bergman PCA, Kiel JHA (2005) Torrefaction for biomass upgrading. ECN report, ECN-RX—05-180, Petten
15. Bridgwater AV, Meier D, Radlein D (1999) An overview of fast pyrolysis of biomass. Org Geochem 30:1479–1493
16. Higman C, van der Burgt M (2003) Gasification, 1. Aufl. Gulf professional publishing, Elsevier science, Burlington
17. Vogel, A, Bolhàr-Nordenkampf, M, Kaltschmitt, M, Hofbauer, H (2006) Analyse und Evaluierung der thermo-chemischen Vergasung von Biomasse. Schriftenreihe "Nachwachsende Rohstoffe", Band 29, Teil 1: Technologische und verfahrenstechnische Untersuchungen, Landwirtschaftsverlag GmbH, Münster
18. Hofbauer, H (2007) Wirbelschichtvergasung – Stand der Technik. Internationale Tagung Thermo-chemische Biomasse-Vergasung für eine effiziente Strom-/Kraftstoffbereitstellung – Erkenntnisstand 2007, Leipzig
19. Meyer B (2007) Entwicklungsdefizite und –perspektiven der großtechnischen Gaserzeugung-/reinigung. Internationale Tagung Thermo-chemische Biomasse-Vergasung für eine effiziente Strom-/Kraftstoffbereitstellung – Erkenntnisstand 2007, Leipzig
20. Köppel W (2007) Gasreinigung – Stand der Technik. Internationale Tagung Thermo-chemische Biomasse-Vergasung für eine effiziente Strom-/Kraftstoffbereitstellung – Erkenntnisstand 2007, Leipzig
21. Hedden K, Anderlohr A, Becker J, Zeeb H-P, Cheng Y-H (1986) Gleichzeitige Konvertierung und Methanisierung CO-reicher Gase. Forschungsbericht der DVGW-Forschungsstelle am Engler-Bunte-Institut der Universität Karlsruhe (TH), T 86-044, Karlsruhe
22. Friedrichs G, Proplesch P, Wismann G, Lommerzheim W (1985) Methanisierung von Kohlevergasungsgasen im Wirbelbett Pilot-Entwicklungsstufe. Forschungsbericht der Thyssengas GmbH, T 85-106, Duisburg
23. Seemann M (2006) Methanation of biosyngas in a fluidized bed reactor – development of a one-step synthesis process, featuring simultaneous methanation, watergas shift and low temperature tar reforming. Dissertation, Zurich
24. Ullmann's Encyclopedia of Industrial Chemistry (2006) Gas production. Wiley-VCH Verlag GmbH & Co. KGaA, Weinheim
25. Lurgi GmbH (2009) Rectisol®-Verfahren. http://www.lurgi.com/website/fileadmin/user_upload/pdfs/11_Rectisol-DE.pdf, State. Accessed 11 Dec 2009
26. UOP LLC (2009) UOP Selexol™ process. http://www.uop.com/objects/Selexol.pdf, State. Accessed 11 Dec 2009
27. Kohl AL, Nielsen, RB (1997) Gas purification, 5 Aufl. Gulf Publishing Company, Elsevier Science, Houston
28. Cerbe G (2004) Grundlagen der Gastechnik – Gasbeschaffung, Gasverteilung, Gasverwendung. Carl Hanser Verlag, München/Wien
29. Rehling B, Hofbauer H, Rauch R, Tremmel H, Aichernig C, Schildhauer T, Biollaz S, Ulrich D, Schaub M (2009) Bio-SNG – first results of the 1MW pilot and demonstration unit at Güssing. In: International conference on polygeneration strategies, Vienna, 2009
30. Hofbauer H, Rauch R, Loeffler G, Kaiser S, Fercher E, Tremmel H (2002) Six years experience with the FICFB-gasification process. In: 12th European conference and technology exhibition on biomass for energy, industry and climate protection, Amsterdam, 2002
31. Verein Deutscher Ingenieure e. V. (VDI) (2000) VDI 2067: Wirtschaftlichkeit gebäudetechnischer Anlagen – Grundlagen und Kostenrechnung. Blatt 1, Beuth Verlag GmbH, Berlin
32. Commission of the European communities (2008) Proposal for a directive of the European parliament and of the council on the promotion of the use of energy from renewable sources. COM(2008) 19, Brussels

Biotechnology and Nutritional Improvement of Crops

Gemma Farre[1], Sonia Gomez-Galera[1], Shaista Naqvi[1], Chao Bai[1], Georgina Sanahuja[1], Dawei Yuan[1], Uxue Zorrilla[1], Laura Tutusaus Codony[1], Eduard Rojas[1], Marc Fibla[1], Richard M. Twyman[2], Teresa Capell[1], Paul Christou[3,4], Changfu Zhu[1]
[1]Department of Vegetal Production and Forestry Science, ETSEA, University of Lleida, Lleida, Spain
[2]Department of Biological Sciences, University of Warwick, Coventry, UK
[3]Department de Produccio Vegetal i Ciencia Forestal, Universitat de Lleida/ICREA, Lleida, Spain
[4]Institució Catalana de Recerca i Estudis Avançats (ICREA), Barcelona, Spain

Article Outline

Glossary
Definition of the Subject and Its Importance
Introduction
Overview of Essential Nutrition in Humans
Nutrient Deficiencies
Responses to Malnutrition
Biotechnology Strategies to Increase Nutritional Content
Future Directions
Bibliography

Glossary

Antinutrients Substances that interfere with the absorption of nutrients.

Bioavailability The amount of a nutrient in food that can be absorbed and utilized.

Biofortification Any fortification strategy that improves nutritional content at source (before harvest).

Conventional breeding Any process used to create new plant varieties without recombinant DNA technology (e.g., introgression, mutagenesis, and hybridization).

Gene silencing Prevention of gene expression, usually through epigenetic means such as antisense RNA, RNA interference, or de novo DNA methylation.

Genotype The total genetic constitution of an organism.

Inbred Progeny produced as a result of breeding between genetically similar parents.

Introgression The introduction of a new allele from one species into the gene pool of another by repeated backcrossing of an interspecific hybrid with one of its parents.

Locus The position of a gene or other genetic marker on a chromosome.

Macronutrient A nutrient required at levels exceeding 100 mg/day (includes carbohydrates, fats, proteins, water, and fiber as well as certain minerals).

Malnutrition The situation resulting from a nutrient imbalance in the diet, usually referring to a lack of one or more nutrients but equally applicable to nutrient excess.

Micronutrient A nutrient required in minute amounts (typically less than 10 mg/day); includes vitamins and many minerals.

Mineral An inorganic nutrient, usually represented by a soluble ion.

Phenotype The sum of observable characteristics of an organism.

Phytate (phytic acid) A phosphorus-containing compound in the outer husks of cereal grains that, in addition to limiting the bioavailability of phosphorous itself, binds to other minerals and inhibits their absorption.

Promoter The DNA sequence upstream of a gene that regulates transcription.

Quality protein maize (QPM) A variety of maize (corn) developed by CIMMYT that contains 70–100% higher levels of lysine and tryptophan in the grain compared to normal varieties.

Transgene A gene from one species that has been incorporated into the genome of another organism using recombinant DNA technology.

Transgenic plant A plant that carries integrated exogenous DNA in the nuclear genome.

Vitamin An organic micronutrient.

Definition of the Subject and Its Importance

Food insecurity is one of the most important social issues faced today, with nearly one billion people enduring chronic hunger and an additional two billion people suffering from nutrient deficiencies, mostly in

the developing world. Strategies to address food insecurity must ultimately address underlying problems such as poverty and poor governance/infrastructure, but the improvement of agricultural productivity in the developing world is an important goal, and biotechnology is one of a raft of measures being considered to achieve it. Genetically engineered plants provide one route to sustainable higher yields, which will increase the quantity of food available. However, genetic engineering can also increase the nutritional quality of crops, and this is the definition elaborated in this article. In particular, the focus is on biotechnology-based methods to increase the availability of essential nutrients, which are often limiting in human diets and lead to specific deficiency diseases.

Introduction

Food security is taken for granted in the industrialized world, where stable political and social structures ensure that everyone has access to enough safe and nutritious food. In contrast, almost one billion people are chronically undernourished in the developing world, regularly consuming less than 2,000 calories per day [1]. There are also a further two billion people who, despite having access to an adequate source of calories, nevertheless lack essential nutrients; perhaps surprisingly, a significant number of these people are citizens of industrialized countries. This means that up to half the world's population at any one time may suffer from malnutrition [1].

The underlying causes of food insecurity in the developing world are complex but poverty is one of the main factors, reflecting the fact that more than one billion people live on less than US $1 per day and another two billion are only marginally better off. The world's poorest people tend to be rural farmers in developing countries, depending entirely on subsistence agriculture, whereas less than 1% of the population in the industrialized world are farmers and they tend to farm for profit. Because of limited purchasing power, the poorest farmers cannot irrigate their crops or buy fertilizers, herbicides, and pesticides. This leads to soil exhaustion, falling yields and quality, and the crops become susceptible to pests, diseases, and natural disasters such as drought. In the industrialized world, malnutrition can reflect poverty on the fringes of society, but is also an educational/lifestyle issue that needs to be approached differently [1].

Any long-term strategy to address food insecurity in the developing world must tackle the underlying problem of poverty by providing rural employment–based income through increased agricultural productivity. Given projected increases in the world's population, the higher cost of oil, falling reserves of fresh water, and greater urbanization, it will certainly be necessary to increase the quality, quantity, and diversity of major food crops. A variety of strategies have been proposed, including the efficient use of organic and inorganic fertilizers, irrigation strategies, soil and water conservation, pest and disease management, and the production of improved plant varieties with higher yields or novel products. Biotechnology provides a range of tools that can be used to improve agriculture in the developing world by lifting yields or increasing food quality, and the latter aspect of biotechnology is considered in this article – the use of biotechnology for nutritional improvement [2, 3].

Overview of Essential Nutrition in Humans

Nutrients and Their Roles in Human Health

Nutrients are chemical substances in food that are necessary for humans to have healthy and active lives. Humans require at least 49 defined nutrients to meet their metabolic needs (Table 1), some highly specific and some represented by families of related molecules. Inadequate consumption of even one of these nutrients will result in adverse metabolic effects leading to poor health, impaired development in children, and (if this is a population-wide problem) an economic impact on society. Table 2 lists the daily guideline amounts in adults for some of these nutrients, as reported by the Food and Agricultural Organization (FAO) of the United Nations and the World Health Organization (WHO) [4]. Table 3 shows some common dietary sources of different nutrients. Generally, nutrients are divided into two broad categories: macronutrients (needed in gram or hundred milligram quantities per day, mainly for energy, structural components of body tissues, and bulk composition of body fluids) and micronutrients (needed in microgram or milligram quantities per day, for many diverse functions).

Biotechnology and Nutritional Improvement of Crops. Table 1 The 49 nutrients essential for sustaining human life [37]

Water and energy	Protein (amino acids)	Lipids-fat (fatty acids)	Macro-elements	Micro-elements	Vitamins
Water	Isoleucine	Linoleic acid	Na	Fe	A
Carbohydrates	Leucine	α-Linolenic acid	K	Zn	D
	Lysine		Ca	Cu	E
	Methionine		Mg	Mn	K
	Phenylalanine		S	I	C (ascorbic acid)
	Threonine		P	F	B1 (thiamine)
	Tryptophan		Cl	B	B2 (riboflavin)
	Valine			Se	B3 (Niacin)
				Mo	B5 (pantothenic acid)
				Ni	B6
				Cr	B9 (folate)
				V	Biotin
				Si	B12 (cobalamin)
				As	Choline
				Sn	
				Co	

Source: [37]

Macronutrients include carbohydrates, fats, proteins, certain mineral ions, water, and fiber, whereas micronutrients include a range of inorganic ions (minerals) and organic molecules (vitamins) [4].

Macronutrients

Carbohydrates and fats consist only of carbon, hydrogen, and oxygen. They are primarily used to derive energy, although they also contribute to some structures in the body, such as the carbohydrates heparan sulfate, chrondoitin sulfate, and hyaluronic acid in the extracellular matrix, and various lipid components of cell membranes. Carbohydrates range from simple monosaccharides (e.g., glucose, fructose, and galactose) to complex polysaccharides (e.g., starch, glycogen, the matrix carbohydrates listed above, and cellulose, the predominant component of plant cell walls). All polysaccharides are polymers of monosaccharide units. Therefore, carbohydrates that can be digested by humans are broken down into monosaccharides and metabolized for energy, used as substrates to synthesize other molecules, or reassembled into energy-storing or structural polymers. Many carbohydrates cannot be broken down in the human digestive system because the corresponding enzymes are not present (e.g., cellulose, inulin) and these are collectively known as dietary fiber. Insoluble fibers such as cellulose help the digestive system function properly (preventing constipation and diarrhea), but there are also many soluble forms of fiber such as inulin which have positive roles in digestion, slowing the movement of food through the gut and facilitating nutrient absorption. Both insoluble and soluble fibers are thought to help prevent colon cancer and cardiovascular disease. Although carbohydrates as a general class of compounds are essential nutrients, no specific carbohydrate is essential because the human body can synthesize all the carbohydrates it needs from simple sugars.

In contrast, fats in the diet include both essential and nonessential molecules. The majority of dietary fat

Biotechnology and Nutritional Improvement of Crops. Table 2 Recommended nutrient intakes for males and females between the ages of 25 and 50 years [37]

Nutrient	Assessment	Male	Female
Energy (kcal)	AEA[a]	2,900	2,200
Protein (g)	AEA	63	50
Vitamin A (mg retinol equivalent)	RDA[b]	1,000	800
Vitamin D (mg)	RDA	5	5
Vitamin E (mg α-tocopherol equivalent)	RDA	10	8
Vitamin K (mg)	RDA	80	65
Riboflavin (mg)	RDA	1.7	1.3
Niacin (mg niacin equivalent)	RDA	19	15
Thiamine (mg)	RDA	1.5	1.1
Pantothenic acid (mg day^{-1})	ESADDI[c]	4–7	4–7
Vitamin B6 (mg)	RDA	2	1.6
Vitamin B12 (mg)	RDA	2	2
Biotin (mg day^{-1})	ESADDI	30–100	30–100
Folate (mg)	RDA	200	180
Vitamin C (mg)	RDA	90	60
Ca (mg)	RDA	800	800
P (mg)	RDA	800	800
Mg (mg)	RDA	350	280
Na (mg)	MR[d]	500	500
K (mg)	MR	2,000	2,000
Cl (mg)	MR	750	750
Fe (mg)	RDA	10	15
Zn (mg)	RDA	15	12
Cu (mg)	ESADDIC	1.5–3	1.5–3
Se (mg)	RDA	70	55
I (mg)	RDA	150	150
Mn (mg)	ESADDI	2 ± 5	2 ± 5
Mo (mg)	ESADDI	75 ± 250	75 ± 250
Cr (mg)	ESADDI	50 ± 200	50 ± 200
F (mg)	ESADDI	1.5 ± 4	1.5 ± 4

Source: [37]

[a]AEA, average energy allowance

[b]RDA, recommended dietary allowances

[c]ESADDI, estimated safe and adequate daily dietary intakes

[d]MR, minimum requirement

Biotechnology and Nutritional Improvement of Crops. Table 3 Sources of some essential nutrients [4, 5]

Component	Examples of sources
Carbohydrates	Cereal grains and potato
Insoluble fiber	Whole grain barley and vegetable peels
Soluble fiber	Fruits, vegetables, and legumes
Essential fatty acids	Fish, flax seed oils, soybeans, pumpkin seeds, sunflower seeds, walnuts, most vegetables, nuts, seeds, and marine oils
Dietary protein	Tofu and other soy-products, eggs, grains, legumes, and dairy products such as milk and cheese, meat, fish
Vitamin A	Carrots, yams, pumpkins, yellow or orange fruits, fish, eggs, and tuna
Vitamin B1	Whole grains, rice bran, lean meats, legumes, wheat germ, oranges, poultry, fish, and enriched pastas
Vitamin B2	Fortified grains and cereals, leafy green vegetables, poultry, fish, yogurt, milk, and cheese
Vitamin B3	Fortified breads and cereals, brewer's yeast, broccoli, carrots, cheese, dandelion greens, eggs, fish, milk, peanuts, potatoes, tomatoes, tuna, beef liver, and chicken breast
Vitamin B6	Whole grain breads and cereals, fish, chicken, and bananas
Vitamin B9	Pinto beans, navy beans, green leafy vegetables, beef, brown rice, bran, cheese, lamb, liver, milk, mushrooms, oranges, pork, and tuna
Vitamin B12	Ham, clams, cooked oysters, king crab, herring, salmon, tuna, lean beef, liver, and low fat dairy products
Vitamin C	Citrus fruits, strawberries, broccoli, melons, peppers, collards, dandelion greens, onions, radishes, and watercress
Vitamin D	Sun exposure, sardines, salmon, fortified milk, fortified cereals, herring, liver, tuna, margarine, and cod liver oil
Vitamin E	Whole grains, wheat germ, nuts, spinach, and sunflower seeds
Vitamin K	Dark-green leafy vegetables and the skins of fruit and vegetables
Calcium	Dairy products and green leafy vegetables
Magnesium	Fish, dairy products, nuts, soybeans, and cocoa
Phosphorus	Milk, cheese, meats, fish, and eggs
Sulfur	Meats, fish, dairy products, eggs, and garlic
Potassium	Legumes, whole grains, and bananas
Sodium	Table salt (sodium chloride, the main source), milk, and spinach
Chlorine	Table salt and unprocessed foods
Iron	Red meat, and leafy vegetables (especially spinach)
Zinc	Wheat germ, pine nuts, sesame seeds, sunflower seeds, and beefsteak
Manganese	Avocados, berries, nuts, egg yolks, whole grains, green leafy vegetables, and legumes
Iodine	Seafood, dairy products, and iodized salt (table salt)
Fluorine	Drinking water, seafood, teas, and toothpaste
Selenium	Nuts, lamb's kidney, mushrooms, and sunflower seeds
Molybdenum	Legumes, dark green leafy vegetables, and grains
Nickel	Chocolate, nuts, fruits, and vegetables
Chromium	Whole grain breads, brown rice, cheese, and lean meats

Biotechnology and Nutritional Improvement of Crops. Table 3 (Continued)

Component	Examples of sources
Vanadium	Seafood, mushrooms, olives, whole grain breads, carrots, and vegetable oils
Cobalt	Vitamin B12, red meat, fish, eggs, cheese, and milk
Silicon	Whole grain breads and cereals, beets, bell peppers, and legumes
Copper	Beans, almonds, broccoli, garlic, soybeans, peas, and seafood

Source: Revised and updated from [4, 5]

is in the form of triacylglycerides (fatty acid esters of glycerol) and the fatty acids can be interconverted or converted into more specialized phospholipids and sphingolipids that have numerous roles in the body, such as cell membrane components and signaling molecules. Other lipids are derived from cholesterol, which is synthesized in the liver. There are several essential fatty acids as well as fat-soluble vitamins that the body cannot synthesize de novo, and these are discussed in detail below.

Proteins are the third major class of macronutrients and these contain nitrogen in addition to carbon, oxygen, and hydrogen. Many proteins also contain sulfur (see below). Fibrous proteins form the structural and mechanical components of tissues (e.g., muscles owe their contractile ability to the proteins actin and myosin, hair and nails are comprised predominantly of keratin, and skin contains large amounts of collagen and elastin). In contrast, most globular proteins are enzymes, the biological catalysts that ensure chemical reactions can take place at the body's ambient temperature. Other proteins fulfill a range of biological functions – signaling molecules and receptors, transmembrane conduits such as ion channels, components of the immune system, effectors of blood clotting, transport and storage of other molecules (e.g., hemoglobin, oxygen, ferritin, and iron), and the control of gene expression. Proteins are linear polypeptides derived from a panel of 20 "standard" amino acids specified by the genetic code (as well as two specialized variants encoded through unique mechanisms), plus a range of posttranslational forms that are generated by chemical modification after protein synthesis. Many of the standard amino acids can be synthesized de novo by humans but some cannot, and these are known as essential amino acids (see below). Proteins are described as "complete" in the sense of nutritional completeness if they provide a source of all the essential amino acids but this designation refers to the sum of all proteins in a meal, not an individual protein molecule.

Essential Amino Acids

Of the 20 standard amino acids, eight (isoleucine, leucine, lysine, methionine, phenylalanine, threonine, tryptophan, and valine) (Table 1) are described as essential because the human body cannot synthesize sufficient amounts de novo so they must be obtained from food [5]. A diet that contains adequate amounts of essential amino acids is particularly important during pregnancy, lactation, early development, and following injury. Most plants are deficient in at least one essential amino acid but a balanced diet provides adequate quantities of all. For example, cereal storage proteins are generally deficient in lysine and threonine whereas legumes lack the sulfur-containing amino acids methionine and cysteine. A diet solely comprising one of these protein sources will therefore be deficient for one or more essential amino acids, but it is possible to combine two incomplete protein sources (e.g., rice and beans) to make a complete protein meal, and such characteristic combinations are the basis of distinct cultural cooking traditions. Food from animals, such as meat, eggs, fish, milk, and cheese, provide all the essential amino acids.

Essential Fatty Acids

Fats are more correctly described as triglycerides (three fatty acids attached to one glycerol backbone), and most fatty acids are nonessential in that the body can synthesize them by interconverting other fatty acids. The exceptions are the omega-3 and omega-6 polyunsaturated fatty acids (PUFAs), so named because the first double-bond is found at the third (or sixth) carbon from the terminal CH_3 group. These cannot be synthesized de novo from saturated fats, nor interconverted,

and must be obtained from the diet [6]. There are several essential fatty acids in each category, but the body can synthesize any omega-3 fatty acid given a source of one of them (ditto for the omega-6 fatty acids) and therefore only the group is defined as essential. The simplest source of omega-3 is α-linolenic acid and the simplest source of omega-6 is linoleic acid. Good sources of both these molecules include fish, shellfish, seeds, nuts, and leafy vegetables.

Macrominerals

Minerals are inorganic molecules, and those required at levels exceeding 100–200 mg/day (calcium, chlorine, magnesium, phosphorus, potassium, sodium, and sulfur; see Table 2) are known as macrominerals [4]. Their function is generally structural and/or electrolytic/osmotic, although they may also perform additional specialized roles. For example, calcium is an important electrolyte in muscles and in the digestive system, but is also a structural component of bones and teeth, and furthermore acts as a signaling molecule and as a trigger for the transmission of nerve impulses. Sodium, potassium, and chlorine are key electrolytes that maintain osmotic balance in cells. Magnesium is an important buffer and stabilizer for organic phosphates including nucleic acids, and is absolutely required for the activity of adenosine triphosphate (ATP). It is also part of the active site of many enzymes. Phosphorus is the key energy currency in cells (as part of ATP). It is also an important structural component of nucleic acids and some proteins, the basis of a key regulatory mechanism in signal transduction pathways, a component of membrane lipids, and (along with calcium) forms the mineral structure of bones and teeth. Finally, sulfur is found in two essential amino acids (methionine and cysteine) as well as two post-translational variants with central roles in core metabolism (homocysteine and taurine). The ability of cysteine residues to form disulfide bridges is critical to the structural integrity of many proteins. Sulfur is also found in coenzyme A, which is needed for carbohydrate and fatty acid metabolism, as well as providing the thiol group in many other reactions.

Micronutrients

Micronutrients are required in small quantities (generally less than 100 mg/day) and are divided into organic molecules (vitamins) and inorganic molecules (microminerals). Vitamins are organic substances that (a) are not carbohydrates, amino acids, or fats, and (b) cannot be manufactured by the body in sufficient amounts in all circumstances and must therefore be obtained from the diet. There are 13 human vitamins, although some are represented by a small family of interconvertible molecules rather than a single substance. Most are required because humans lack the metabolic capability to produce them, although vitamin D is an exception because it is produced in the skin during exposure to UVB irradiation albeit not always in sufficient quantities to make dietary sources unnecessary. Vitamins are classified as either water soluble or fat soluble. In humans, there are four fat-soluble vitamins (A, D, E, and K), which are transported throughout the body in fat globules and stored in the liver and other fatty tissues, and nine water-soluble vitamins (eight B vitamins and vitamin C) that are not stored in the body and must be replaced every day.

Minerals that are required at levels below 100–200 mg/day are known as microminerals or trace minerals (Table 2) and these are required in minute amounts usually because they are required for the catalytic activity of a small number of specific enzymes. However, certain microminerals have more significant roles [4]. For example, iron can act as both an electron donor and acceptor, and in this context forms the functional core of the heme complex, which is found in the oxygen-binding molecules hemoglobin and myoglobin, and in the catalytic center of cytochromes (enzymes that carry out redox reactions). Iron is therefore required for oxygen transport in the body and for energy metabolism, also contributing to the catalytic activity of a range of nonheme enzymes such as ribonuclease reductase. Zinc also has multiple functions – it is an essential component of hundreds of enzymes (e.g., carboxypeptidase, liver alcohol dehydrogenase, and carbonic anhydrase) as well as transcription factors (zinc fingers and related molecules) and signaling proteins. The roles of other microminerals are more specialized and are discussed below.

Facultative Nutrients

The eight essential amino acids are needed by everyone. In addition, cysteine, tyrosine, histidine, and arginine

are essential for infants and children because they are required in large amounts for growth and development, and that demand cannot be satisfied without a dietary source [5]. For the same reason, children have greater requirements for the essential fatty acids than adults, although these are not facultative because they are also essential nutrients in adults despite being required in lower quantities. The amino acids arginine, cysteine, glycine, glutamine, histidine, proline, serine, and tyrosine are also considered conditionally essential, meaning they are not normally required in the diet, but must be supplied to specific populations that do not synthesize them in adequate amounts [7].

It is sometimes more convenient to define the essentialness of amino acids on a group basis in the same way as the essential fatty acids, since interconversion is possible within a group but no member of that group can be synthesized de novo. This applies to the sulfur-containing amino acids methionine, homocysteine, and cysteine, and to the aromatic amino acids phenylalanine and tyrosine. Likewise, arginine, ornithine, and citrulline, which are interconvertible within the urea cycle, can be considered as a group for nutritional purposes.

Nutrient Deficiencies

The lack of essential nutrients causes widespread malnutrition, a hidden problem in many communities because its effects are often subclinical or affect physical and cognitive development in a cumulative manner. Micronutrient deficiencies in particular have been referred to as "hidden hunger"; such deficiencies occur on a population-wide basis when the diet lacks diversity or is overly dependent on a single staple food [4], but in individual cases may reflect a genetic abnormality that prevents nutrient absorption or metabolism. Some important nutrient deficiencies and disorders are discussed below.

Macronutrient Deficiencies and Disorders

A lack of carbohydrates in the diet leads to a calorie deficit and results in hunger, then eventually catabolysis and atrophy as the body uses its own tissues as a source of energy to maintain essential functions. These are the early signs of starvation, and can result in permanent organ damage and ultimately death. Besides this general process, there are several specific disorders of carbohydrate metabolism such as galactosemia and glycogen storage diseases, which reflect an inability to break down or synthesize particular carbohydrates. As in the case for carbohydrates, a general deficiency in fats results in a calorie deficit, which if prolonged results in the symptoms of starvation. Deficiencies for essential fatty acids occur rarely, and mostly in infants. The symptoms include scaly dermatitis, alopecia, hair loss, thrombocytopenia, and stunted growth. The symptoms can be reversed by supplying adequate quantities of omega-3 and omega-6 fatty acids in the diet.

The essential amino acids are components of many proteins, so the symptoms associated with deficiency are often quite general. In adulthood, amino acid deficiencies may result in tiredness, inability to concentrate, irritability, bloodshot eyes, and in the longer term stunted growth, hair loss, anemia, connective tissue defects, inefficient wound healing, and reproductive problems. Acute amino acid deficiencies in childhood are more severe and result in a disease called kwashiorkor which involves swelling of the feet and abdomen, anorexia, ulcerating dermatoses, loss of hair, nails, and teeth, an enlarged fatty liver, and irritable behavior. It is possible that the symptoms of kwashiorkor may also be caused in part by concomitant micronutrient deficiencies and in some cases by poisoning. The disease also affects the immune system, often rendering children incapable of producing antibodies against vaccines.

As well as deficiency diseases, there are also several disorders of amino acid metabolism that need special dietary provisions. These include phenylketonuria (PKU), in which the enzyme phenylalanine hydroxylase is missing so phenylalanine cannot be converted into tyrosine, and maple syrup urine disease (MSUD), in which the body is unable to use the amino acids isoleucine, leucine, and valine.

Vitamin A Deficiency

Vitamin A in its reduced form (retinal) is required for the production of rhodopsin in the eyes, and helps to maintain epithelial and immune cells (making it necessary for a healthy immune system). In its acidic form (retinoic acid), it is a morphogen in development. Although many foods are said to be good sources of

vitamin A, it should be noted that these generally do not contain retinal itself but derivatives that can be converted into retinol and then into either retinal or retinoic acid. Meat and dairy sources of vitamin A primarily contain an esterified form called retinyl palmitate, whereas plants produce pro-vitamin A carotenoids such as β-carotene that are cleaved to produce retinol. These are abundant in a wide variety of dark green, yellow, and orange fruits; and vegetables such as oranges, broccoli, spinach, carrots, squash, sweet potatoes, and pumpkins [8].

Vitamin A deficiency (VAD) causes night blindness, i.e., the deterioration of light sensitive cells (rods) essential for vision in low light intensity and it can also damage the cornea resulting in a total form of blindness called xerophthalmia. The lack of vitamin A has a particularly severe effect on the immune system leaving individuals susceptible to infections [4]. More than four million children worldwide exhibit signs of severe VAD, including 250,000–500,000 per year that become partially or totally blind [9]. During pregnancy, women have a higher demand for vitamin A, and VAD in pregnancy causes nearly 600,000 deaths every year [9].

Vitamin B Group Deficiencies

The vitamin B complex comprises eight distinct molecules with different properties and functions. Vitamin B_1 (thiamine) is a coenzyme in carbohydrate metabolism, with the triphosphate derivative particularly active in neurons. Deficiency causes beriberi, a nervous system disorder resulting in weight loss, various degrees of amnesia and psychosis (in its severest form known as Korsakoff's syndrome), impaired perception, limb weakness, arrhythmia, and swelling, possibly leading to heart failure and death.

Vitamin B_2 (riboflavin) is the central component of the important enzyme cofactors flavin adenine dinucleotide (FAD) and flavin mononucleotide (FMN), whereas vitamin B_3 (niacin) is converted into the cofactors nicotinamide adenine dinucleotide (NAD) and its phosphate derivative NADP. Therefore, both vitamins are required in many enzymes that take part in carbohydrate, fat, and protein metabolism as well as other functions. Riboflavin deficiency causes ariboflavinosis, which is characterized by sensitivity to light, cracked lips, dermatitis, and swelling of the tongue, pharyngeal and oral mucosa, and genitals. Niacin deficiency causes pellagra, which has varied symptoms including diarrhea, dermatitis, insomnia, fatigue, and mental confusion leading in severe cases to dementia. Vitamin B_5 (pantothenic acid) is needed for the synthesis of coenzyme A (CoA), and is therefore critical in the metabolism and synthesis of carbohydrates, proteins, and fats. Deficiency is rare and complete deficiency in humans has not been observed. Vitamin B_6 (pyridoxal, pyridoxine, or pyridoxamine) helps to balance sodium and potassium levels; it is also the precursor of pyridoxal phosphate, a cofactor required for the synthesis of heme and several important neurotransmitters. Deficiency may therefore lead to anemia due to the lack of heme, depression due to its impact on neurotransmitter production, high blood pressure and water retention due to the impact on electrolyte balance, and also elevated levels of homocysteine. Vitamin B_7 (biotin) is a coenzyme in the metabolism of fatty acids and leucine, and it plays a role in gluconeogenesis. Deficiency may lead to stunted growth and neurological disorders in infants. Vitamin B_9 (folic acid) is the source of tetrahydrofolate which is essential in DNA synthesis and many other core metabolic reactions. Deficiency in adults causes macrocytic anemia and elevated levels of homocysteine, but the impact in pregnant women is much more severe, leading to neural tube defects in the fetus. Spina bifida, in which bones of the spine do not completely enclose the spinal cord, is the most common congenital abnormality associated with folate deficiency [10]. Vitamin B_{12} (cobalamin) is involved in the regeneration of folate, which means that deficiency in many cases mimics folic acid deficiency and can be alleviated by folate in the diet. However, it is also the cofactor for two specific (non-folate-dependent) enzymes, methylmalonyl coenzyme A mutase (MUT), and 5-methyltetrahydrofolate-homocysteine methyltransferase (MTR). Therefore, even in the presence of adequate folate, cobalamin deficiency can result in the failure of these reactions, leading to the accumulation of metabolites that weaken and destabilize myelin, resulting in neurological symptoms associated with demyelination. Finally, choline is a B vitamin that has three primary roles: structural integrity and signaling in cell membranes, cholinergic neurotransmission (acetylcholine synthesis), and the provision of methyl

groups via its metabolite, trimethylglycine (betaine), for the synthesis of S-adenosylmethionine. Choline deficiency is rare because, like vitamin D, humans can synthesize some choline although not always adequate amounts.

Vitamin C Deficiency

Vitamin C (ascorbic acid) is a powerful electron donor (antioxidant) and a cofactor in several metabolic pathways, including those forming the mature form of collagen. It plays an important role in the synthesis and stabilization of neurotransmitters, and also reduces iron compounds, enhancing the gastrointestinal absorption of dietary nonheme iron [11]. Insufficient vitamin C in the diet causes scurvy, which involves the breakdown of connective tissue fibers and muscular weakness [11]. High levels of vitamin C are found in citrus fruits and green vegetables [4].

Vitamin D Deficiency

Vitamin D is required for normal calcium and phosphorus homeostasis. It is a ligand that, when bound to its receptor, acts as a transcription factor controlling genes that affect calcium and phosphorus absorption; it is therefore particularly important for bone growth and maintenance. Deficiency results in impaired bone mineralization, which leads to bone-softening diseases such as rickets, a childhood disease characterized by stunted growth and deformity of the long bones, and osteomalacia, an adult bone-thinning disorder characterized by proximal muscle weakness and bone fragility, with chronic musculoskeletal pain.

Vitamin E Deficiency

Vitamin E is a group of compounds with powerful antioxidant activity. It protects fatty acids, low-density lipoproteins (LDLs), and other components of cell membranes from oxidation by free radicals [4]. Although it protects all cells, vitamin E is particularly important in red blood cells and neurons, so severe vitamin E deficiency results in anemia and neurological problems associated with nerve degeneration in the hands and feet. Vegetable oils, nuts, and green leafy vegetables are the major sources of vitamin E, and the consumption of foods rich in vitamin E is thought to reduce the risk of cancer, cardiovascular disease, and cataracts [4].

Vitamin K Deficiency

Vitamin K is a group of fat-soluble vitamins derived from 2-methyl-1,4-naphthoquinone that are needed for γ-carboxylation, a form of protein posttranslational modification. This is particularly important for the formation of the calcium-binding Gla domain, which is present in several blood-clotting proteins and osteocalcin. Vitamin K deficiency therefore affects blood coagulation as well as bone mineralization. Vitamin K1 (phylloquinone) needs to be sourced from the diet whereas vitamin K2 (menaquinone) is produced by bacteria in the large intestine and deficiency is rare except in maladsorption disorders or in patients with reduced gut flora (e.g., after treatment with broad-spectrum antibiotics). There are also several synthetic forms of the vitamin.

Iron Deficiency and Toxicity

Iron is the component of heme that binds oxygen, allowing oxygen to be transported from the lungs to peripheral tissues as part of oxyhemoglobin and carbon dioxide to be transported in the opposite direction. Iron also acts as an intracellular electron transporter to transfer energy (especially to the mitochondria) and it is a part of enzyme systems involved in the synthesis of hormones and neurotransmitters [4]. Iron deficiency is the most widespread nutritional disorder in the world, affecting an estimated 1.2 billion people [12]. In children, low iron intake is associated with cognitive dysfunction whereas in adults it causes iron deficiency anemia (IDA), oxidative DNA damage, reduced immunity, and (in pregnant women) premature births/low birth weight [12]. The true prevalence of iron deficiency in a population is greater than the level of clinically detectable IDA because most individuals are likely to be iron deficient long before a detectable drop in hemoglobin levels [12]. Iron deficiency is often caused by inadequate intake, but it can also result from the consumption of antinutritional molecules such as phytic acid/phytate which inhibit the uptake of bioavailable iron even if sufficient amounts are present in the diet. Foods rich in phytate include many cereal grains, so people with cereal-rich diets are particularly susceptible to iron-deficiency diseases.

The upper limit for iron consumption is 25–50 mg/day. Symptoms of iron toxicity include fatigue,

anorexia, dizziness, nausea, vomiting, headache, weight loss, shortness of breath, and possibly a grayish color to the skin [13]. Chronic excess iron intake results in symptoms such as liver cirrhosis, diabetes, and heart failure, and can promote some cancers. Acute overdose (e.g., iron supplements) is toxic and may induce gastrointestinal side effects as well as causing secondary hemochromatosis [13].

Zinc Deficiency and Toxicity

Zinc is a key functional component of over 300 enzymes and also coordinates the functional domains of numerous transcription factors. Zinc deficiency therefore affects many aspects of metabolism and gene expression, and has notable detrimental effects on the immune system, basal metabolism, and development, particularly spermatogenesis and testosterone steroidogenesis [14]. Severe and prolonged zinc deficiency in humans reduces appetite and bone growth, delays sexual maturation, causes skin lesions, diarrhea, and alopecia (hair loss), and reduces the ability of the cellular immune system to fight infections [14]. Zinc, like iron, is affected by the amount of phytate in the diet, so deficiency is particularly prevalent in populations that subsist on cereal-rich diets.

The upper level of Zn intake in adults is 45 mg/day, although tolerance is lower in women, children, and the elderly. Excessive long-term zinc intake interferes with iron and copper metabolism, so the symptoms of zinc toxicity overlap with those of iron and copper deficiency, e.g., anemia, neurological symptoms, and lower immunity [14]. Excessive levels of zinc also affect the relative levels of LDL and HDL cholesterol and increase the risk of cardiovascular disease [14].

Iodine Deficiency and Toxicity

Iodine is an essential component of the thyroid hormones thyroxine (T4) and triiodothyronine (T3), whose function is to increase the basal metabolic rate (therefore affecting carbohydrate, fat, and protein metabolism), stimulate protein synthesis, regulate long bone growth in concert with growth hormone, stimulate neuronal maturation, and regulate how cells respond to catecholamines [15, 16]. For some of these functions, iodine acts in concert with iron, zinc, and selenium [16]. Iodine deficiency disorder (IDD) generally reflects a lack of iodine in the soil, which places more than 1.5 billion people in the world at risk, particularly children and pregnant or lactating women [4, 15]. The initial effects of IDD are to suppress the synthesis of thyroid hormones, which leads the pituitary gland to produce more thyroid-stimulating hormone and causes the thyroid to enlarge in an attempt to capture more iodine from the blood. This condition, known as goiter, can be reversed by iodine supplementation (see below). The effects of long-term iodine deficiency in pregnancy and childhood cannot be reversed – these include stunted physical and mental development, resulting in a condition known as cretinism [16].

Iodine toxicity is unusual because a daily intake of 1 mg or more appears to be safe. However, where there is prolonged excessive consumption or an underlying disease that prevents iodine metabolism, the excess iodine can inhibit thyroid hormone synthesis, a phenomenon known as the Wolff–Chaikoff effect [4].

Selenium Deficiency and Toxicity

Selenium is a component of the nonstandard amino acids selenocysteine and selenomethionine, which are required for the activity of a number of enzymes (selenoenzymes) such as glutathione peroxidase, tetraiodothyronine 5′ deiodinase, thioredoxin reductase, formate dehydrogenase, and glycine reductase. Its presence in thyroid hormone deiodinase means that selenium is necessary for the normal function of the thyroid gland. Many of the other selenoenzymes act as antioxidants with a range of protective roles in the body, helping to prevent cancer and cardiovascular disease, often in concert with vitamin E [4, 16, 17]. Selenium may also play a role in the regulation of other micronutrients, such as iron and zinc [16].

Selenium deficiency can lead to Keshan disease, a potentially fatal cardiomyopathy associated with increased susceptibility to infectious diseases, and also Kashin–Beck disease (usually if selenium and iodine deficiency occur concurrently) which is characterized by cartilage atrophy and necrosis leading to damaged joints [4, 18]. Selenium deficiency is unusual, but occurs where the mineral is particularly scarce in the soil, as in some parts of China. Interestingly, in other parts of China, the soil is so rich in selenium

(>9% selenium content) that eating corn grown on this soil can result in acute selenium toxicity (selenosis). The maximum safe dietary intake of selenium is thought to be 400–800 μg/day, and most people consume only 10% of this amount, but in villages surrounding this selenium-rich area, a typical diet yields 3,200–6,690 μg of selenium per day, which is 100-fold the normal level. In these villages, morbidity can approach 50% with typical symptoms including a garlic-like odor to the breath, gastrointestinal disorders, loss of hair and nails, fatigue, irritability, and progressive neurological damage, leading eventually to liver cirrhosis and death [4, 18].

Other Microminerals

Whereas iron, zinc, iodine, and selenium are the "big four" micronutrients with diverse functions in the body, a variety of additional mineral ions are required for specific purposes. Copper is an essential component of several enzymes including cytochrome c oxidase, cobalt is a component of vitamin B_{12}, manganese is an essential cofactor for enzymes such as the antioxidant superoxide dismutase, molybdenum is a component of several redox enzymes, and nickel is present in urease. Fluorine is a special case in that it is not essential for life, but the addition of fluoride to drinking water helps to prevent dental caries, so it certainly contributes to human health and well-being. Other minerals, such as boron, vanadium, silicon, and arsenic, are thought to have biological roles although this has yet to be demonstrated in humans. Many of these microminerals are known to cause rare deficiency disorders as well as toxicity effects. Chronic copper deficiency, e.g., has multiple effects on metabolism because the corresponding enzymes cannot function, and also leads to anemia because copper is required for efficient iron absorption. Excess copper competes with zinc so the symptoms overlap with zinc deficiency, but acute copper toxicity is rare other than in individuals with metabolic disorders due to the efficiency of copper secretion.

Responses to Malnutrition

The most effective intervention to alleviate micronutrient malnutrition is the implementation of a varied diet including fresh fruit, vegetables, fish, and meat. This is impractical in many countries because food is not widely available, but even where fresh food is abundant, there can be compliance issues that result in persistent low-level malnutrition. Where infrastructure allows, micronutrient nutrition can be improved using supplements (usually in tablet/sachet form) or conventional fortification (where micronutrients are added to processed foods, such as packaged cereals). Unfortunately, such strategies have been largely unsuccessful in developing countries because of insufficient funding, poor governance, and a poor distribution network. There has been some success in a limited number of cases discussed later, including mineral fortification (iodized salt) and vitamin supplementation (vitamin A), although coverage has been incomplete. Developing country governments must address the risk of micronutrient malnutrition and should actively participate in the establishment of intervention programs, seeking international expertise and assistance where necessary. A more recent development is biofortification, where intervention takes place before plants are harvested. Different strategies to alleviate micronutrient malnutrition have been ranked according to their cost-effectiveness by the Copenhagen Consensus, a panel of expert economists that decide the most cost-effective strategies for addressing global challenges (Table 4). In this section, the different interventions for improving micronutrient nutrition are summarized, mainly in the context of developing countries where malnutrition has the greatest impact.

Emergency Measures (Short-Term Relief): Supplementation Programs

Supplementation is the distribution of pills or mineral solutions for immediate consumption and is the most effective short-term intervention to improve nutritional health. Supplementation helps to alleviate acute mineral shortages but is unsustainable for large populations and should be replaced with fortification at the earliest opportunity [19]. In developed countries, where mineral malnutrition is rare, supplementation is focused on a small subset of the population with specific deficiencies resulting from medical conditions. In developing countries, where acute and chronic deficiencies are commonplace, supplementation is highly recommended as a complement to the diet (fortified or otherwise) for the entire population. Supplementation

Biotechnology and Nutritional Improvement of Crops.
Table 4 Copenhagen Consensus Center strategies [23]. The Copenhagen Consensus Center is a think-tank based in Denmark that advises governments and philanthropists about the best ways aid and development money can be used to address the world's greatest challenges. Currently, strategies to address malnutrition represent five of the top ten strategies providing the best value

Rank	Solution	World's greatest challenges
1	Micronutrient supplements for children (vitamin A and zinc)	Malnutrition
2	The Doha development agenda	Trade
3	Micronutrient fortification (iron and salt iodization)	Malnutrition
4	Expanded immunization coverage for children	Diseases
5	Biofortification	Malnutrition
6	Deworming and other nutrition programs at school	Malnutrition and Education
7	Lowering the price of schooling	Education
8	Increase and improve girls' schooling	Gender equality
9	Community-based nutrition promotion	Malnutrition
10	Provide support for women's reproductive role	Gender equality

has also been recommended by WHO, the World Food Program (WFP), and UNICEF [20] for extreme situations such as refugee camps, where it can also help to address diseases such as acute diarrhea.

The distribution of vitamin A supplements has been one of the most cost-effective and successful acute intervention programs in the developing world [19], but this is a rarity. Like fortification, successful supplementation strategies require a robust infrastructure and a government determined to improve the nutritional health of its population [19]. Supplementation requires compliance monitoring because people often neglect to take regular supplements at prescribed intervals. For example, in some communities with both chronic iodine deficiencies and no access to iodized salt, the distribution of iodine capsules to women is a short-term but more expensive measure to avoid IDD [21]. Many studies have shown that zinc supplements are beneficial, particularly in areas with zinc-depleted soil [4, 22]. Zinc supplementation has been adopted by WHO and UNICEF in their guidelines for the treatment of acute diarrhea [20]. Zinc supplements are normally formulated as tablets or as oral rehydrated solutions, requiring the active compliance of families and communities. The supplements must be administered frequently, and may be more efficient when other micronutrients such as vitamin A are administered simultaneously [14, 19].

Long-Term Measures (Sustainable Relief): Fortification Programs

Food fortification is one of the most cost-effective long-term strategies for micronutrient nutrition [23] and ranks third in terms of cost-benefit balance according to the Copenhagen Consensus (Table 4). Fortification takes place during food processing and increases the product price. These factors make fortified products unaffordable to the most impoverished people living in remote rural areas. Even in more accessible areas, fortification requires government awareness and policies for implementation and compliance monitoring. The Flour Fortification Initiative (FFI) claims that food fortification must be implemented at a national level to be successful, and must involve the public, private business and government sectors. The FFI supports mandatory fortification based on scale, equity, business, cost, and sustainability. The creation of partnerships among countries with established fortification policies would help other countries to establish their own infrastructure. Although the implementation of mandatory fortification would take time, there are enormous benefits for the country and its population [24].

Before considering case studies, it is important to note that food fortification targets must be selected carefully. Research must be carried out to identify the best vehicles to deliver micronutrients, i.e., those with the widest and most frequent consumption reflecting the staple diet of individual countries and/or regions. Also, a suitable fortification agent must be identified – one

that is stable but easily mobilized in the gut, one that does not alter the quality of the food to which it is added, and one that can be stored and distributed easily. Since many parts of the world suffer from multiple deficiencies, strategies must also be developed to fortify foods simultaneously with several micronutrients, without adverse interactions among them. The addition of a single micronutrient would have approximately the same cost implications as the addition of several, but more research is needed to determine the most cost-effective way to make nutritionally complete foods [23, 24].

Iodization of Salt Iodine fortification of salt is one of the nutrition success stories of the twentieth century, helping to eliminate IDD in many parts of the world. Even though alternative food vehicles have been proposed, salt is thus far the most economical and sustainable fortification target. In 1990, 20% of households in the developing world consumed iodized salt. In 1994, WHO and UNICEF recommended mandatory salt iodization in all countries to ensure consumption and prevent access to unfortified salt. By the year 2000, iodized salt had reached 70% of households in the developing world. Although some countries still lack access to iodized salt, the reach is improving all the time, with many countries becoming self-sufficient and no longer needing donations to support their fortification programs [25]. Countries with no nutrition policies or monitoring are the main challenges for intervention strategists, because fortification requires external funding and IDD reappears if salt iodization is discontinued.

Organizations such as WHO, UNICEF, and The International Council for the Control of Iodine Deficiency Disorders (ICCIDD) have created and distributed guidelines for the implementation of iodine fortification. They work together to eliminate iodine deficiency through the Universal Salt Iodization (USI) in partnership with the Micronutrient Initiative (MI), the World Bank, Kiwanis International, and with public and private sector involvement including consumer organizations, schools, and medical authorities around the world.

Iron and Folate Fortification of Wheat Flour Another successful fortification approach is the inclusion of minerals in wheat flour, so that widely consumed products such as bread become nutritionally beneficial as well as providing calories. Indeed, bread is often double fortified with iron and folate, most recently in Iran [26]. The mandatory fortification of wheat flour has been established in several developing countries in Latin America, leading to a reduction in IDA [19]. The FFI has created a network that involves the participation of public, private, and government sectors, resulting in an increase in the global prevalence of iron-fortified wheat flour from 18% in 2004 to 27% in 2007, helping 540 million people to avoid IDA [26]. The MI also supports this strategy and works with FFI in developing countries.

Iron fortification can be technically challenging because iron compounds that are easily absorbed by the gut tend to leach easily and also change the taste of food, whereas those with less impact on taste are the most difficult to absorb [27, 28]. Encapsulation has been investigated as a potential solution and this is an active area of current research [29].

Other Examples Zinc fortification has been implemented in the industrialized world but rarely in developing countries. One exception is zinc-fortified wheat and corn flour in Mexico, which is used to make bread and tortillas, the two principal staples [30]. Organizations such as the Zinc Task Force (ZTF) and the International Zinc Nutrition Consultative Group (IZINCG) are fighting zinc deficiency by promoting diverse strategies to eliminate it. As zinc and iron deficiency tend to go hand in hand, it has been suggested that double fortification would be effective with little additional cost, particularly if iron fortification were already in place.

Selenium-fortified products such as salt, margarine, cereals, and soft drinks have been produced although not widely distributed [18]. Salt fortified with selenium has been used in parts of China where the soil is naturally depleted but it has not been supported to the same degree as iodized salt [17]. The multi-micronutrient fortification of biscuits with iron, zinc, iodine, and vitamin A has been implemented with Vietnamese schoolchildren, reducing the risk of IDA, IDD, and VDA, and increasing the effectiveness of deworming [31].

Long-Term Measures (Sustainable Relief): Biofortification

Conventional interventions have a limited impact, so biofortification has been proposed as an alternative long-term approach for improving nutrition [23, 32]. Biofortification focuses on enhancing the micronutrient qualities of crops *at source*, encompassing processes that increase both micronutrient levels and their bioavailability in the edible parts of staple crops. The former can be achieved by agronomic intervention (in the case of minerals), plant breeding or genetic engineering, whereas only plant breeding and genetic engineering can influence nutrient bioavailability.

Plant breeding and genetic engineering are often regarded as similar means to achieve a common goal because, in contrast to agronomic interventions, both involve changing the genotype of a target crop. The two processes are similar in aim, albeit different in scope. Both attempt to create plant lines carrying genes that encourage the efficient accumulation of bioavailable micronutrients – plant breeding achieves this by crossing the best-performing plants and selecting those with favorable traits over many generations, whereas genetic engineering accesses genes from any source and introduces them directly into the crop. Plant breeding is restricted to genes that can be sourced from sexually compatible plants and the limited amount of genetic variability therein, whereas genetic engineering has no taxonomic constraints and even synthetic genes can be used.

The main advantage of genetic engineering and plant breeding approaches for mineral enhancement is that investment is only required at the research and development stage, and thereafter the nutritionally enhanced crops are entirely sustainable. Furthermore, as stated above, mineral-rich plants tend to be more vigorous and more tolerant of biotic stress, so the overall yields are likely to improve in line with mineral content [27]. Unlike conventional intervention strategies, genetic engineering and plant breeding are both economically and environmentally sustainable. A combination of both strategies has also been proposed [33] and can produce significant synergic improvements compared to each strategy applied individually [34]. Although there are no commercial nutritionally enhanced plants derived from either method at the current time, this approach has the greatest cost-effectiveness in the long term and is likely to have the most important impact over the next few decades.

Biofortification is also likely to be more accessible than conventional interventions in the long term because it removes hurdles such as the reliance on infrastructure and compliance. Moreover, plants assimilate minerals into organic forms that are naturally bioavailable and contribute to the natural taste and texture of the food. Economic studies have shown the many potential health benefits of biofortification, especially in combination with conventional strategies [35].

Nutritional Improvement Through Agronomic Approaches Farmers have applied mineral fertilizers to soil for hundreds of years in order to improve the health of their plants, but within certain limits the same strategy can also be used to increase mineral accumulation within cereal grains for nutritional purposes. This strategy only works if the mineral deficiency in the grain reflects the absence of that mineral in the soil, and if the mineral fertilizer contains minerals that can be mobilized rapidly and easily. Also, even if plants can absorb minerals efficiently from the soil, they may store the mineral in inedible organs (e.g., leaves but not fruits or seeds), or they may accumulate the mineral in a form that is not bioavailable, thus having no impact on nutrition [27].

In industrialized countries such as Finland and New Zealand, this strategy has been applied successfully to increase the amount of selenium in the diet [18]. It is difficult to apply to iron, because most of the inorganic iron in the soil is inaccessible to plants. Like supplements and fortification, agronomic intervention is probably best applied in niche situations or in combination with other strategies [36].

One drawback of agronomic intervention in developing countries is the cost and impact of fertilizers. Fertilizer use increases the cost of food, thus reducing its availability to the most impoverished people. To be effective, fertilizers must be applied regularly, but impoverished farmers would be under financial pressure to "cut corners" to save costs, even though seeds produced from mineral-rich soil tend to germinate more vigorously than those in poor soils, thus increasing yields [36].

Iodine fertilizers have received comparatively little attention due to the success of fortification programs,

but they have been used in regions of China where the soil has low iodine levels. The addition of iodine to irrigation water (fertigation) in China has successfully increased the level of iodine in rice, but despite the technical success such projects have not addressed IDD due to poor infrastructure [16]. Iron has a very low mobility in soil because it binds rapidly to soil particles when applied as fertilizer in the form of $FeSO_4$. It is converted rapidly from Fe^{2+} to Fe^{3+} under these circumstances, rendering it unavailable for absorption [27]. In poor soils lacking the macronutrients nitrogen, phosphorus, and potassium, the application of NPK fertilizers can promote the capture of iron, although this also depends on the soil pH. Alkaline conditions in the rhizosphere prevent the uptake of iron and zinc, whereas slightly acidic soil promotes the absorption of these minerals [27]. Foliar sprays of $FeSO_4$ or chelates allow the direct uptake of iron.

Unlike iron, zinc is very mobile in soil and is easily absorbed, especially under slightly acidic conditions. Zinc fertilizers such as $ZnSO_4$ can increase the yield of cereals and legumes in zinc-deficient soils, and can also increase zinc levels in the grain (although this is dependent on genotype). Zinc fertilization has been used in Turkey, where NPK fertilizers are enriched with zinc and applied normally for crop production. Soils in Turkey are extremely deficient in zinc and this program has successfully increased plant growth and yield. Although it is likely that the population has benefited from the nutritional properties of crops grown with zinc fertilizers, no population studies have yet been carried out to determine the impact on human health [36].

Finally, selenium provides probably the most successful example of agronomic intervention by mineral fertilization because it fulfills the three major requirements for such a strategy to work: (1) sodium selenate is highly mobile in many soil types; (2) it is absorbed easily by plants and, in the case of cereals, accumulates in the grain; and (3) it accumulates in a readily bioavailable form, selenomethionine [17]. As is the case for zinc, selenium added to NPK fertilizers has been used successfully in Finland and New Zealand to increase the selenium content of grains, with a positive impact on the general health and well-being in the population [18].

Nutritional Improvement Through Conventional Breeding Plant breeding programs focus on improving the level and bioavailability of nutrients in staple crops using their natural genetic variation [37]. The HarvestPlus program was established by the Consultative Group on International Agricultural Research (CGIAR) to improve human nutrition by breeding new varieties of the staple food crops consumed by the poor. It is a global alliance of institutions such as the International Rice Research Institute (IRRI), the Centro Internacional de Mejoramiento de Maíz y Trigo (CIMMYT), the Centro Internacional de Agricultura Tropical (CIAT) and the International Institute of Tropical Agriculture (IITA) and other academic institutions world-wide. Its aims include the discovery of genetic variation affecting heritable mineral traits, verification of its stability under different conditions and the feasibility of breeding to increase mineral content in edible tissues without affecting yields or other quality traits. Feasibility data, mainly for iron and zinc, has been collected and a summary has been published [38].

Although breeding for increased mineral levels is more sustainable than conventional interventions, no high-mineral varieties have been introduced to the market thus far. This reflects the long development times, particularly if the mineral trait needs to be introgressed from a wild relative. Breeders utilize molecular biology techniques such as quantitative trait locus (QTL) maps and marker-assisted selection (MAS) to accelerate the identification of high-mineral varieties, but they have to take into account differences in soil properties (e.g., pH, organic composition) that may interfere with mineral uptake and accumulation. For example, the mineral pool available to plant roots may be extremely low in dry, alkaline soils with a low content of organic matter [36].

Conventional breeding could also be useful for the enhancement of organic nutrients, although there has been no coordinated international effort to achieve progress in this area. Even so, crosses between inbred lines have been used to identify QTLs affecting carotenoid and tocopherol levels in corn [39], as well as carotenoid levels in carrot and tomato [40], and these could be used in the future for nutritional improvement programs. Recently, natural genetic variation at several loci in corn has been

exploited to generate lines with increased levels of specific carotenoids [41, 42].

Although some variation in iodine content has been found in staple crops [43], the focus remains on manual intervention strategies because salt iodization has been so successful. However, the HarvestPlus initiative has proposed the inclusion of iodine in its program because of widespread iodine deficiency in some countries and the interaction between iodine and other micronutrients (mainly iron, zinc, and vitamin A [16]). Iron and zinc levels vary significantly in many crops, and CGIAR is looking into the possibility of breeding high-mineral varieties of cereals using this genetic diversity. The amount of iron in rice grains varies between 6 and 22 mg kg^{-1}, whereas in corn it varies between 10 and 160 mg kg^{-1}, and in wheat the range is 15–360 mg kg^{-1} [44]. Zinc levels are similarly broad – between 14 and 61 mg kg^{-1} in rice, 14 and 190 mg kg^{-1} in wheat, and between 12 and 96 mg kg^{-1} in corn [43, 44]. Despite this natural variation, commercial varieties of wheat still have low mineral levels compared to wild wheat, where the grain may contain up to tenfold the normal amount of zinc. Furthermore, wild emmer wheat accessions have been identified in which the seeds contain up to 139 mg kg^{-1} zinc, up to 88 mg kg^{-1} iron, and up to 380 g kg^{-1} protein, as well as showing strong tolerance of drought stress and low zinc levels in the soil [44]. There also appears to be moderate genetic variation in the selenium content of modern cereals although wild wheat varieties, with higher selenium levels, are potential sources of additional diversity [43, 44].

Nutritional Improvement Using Biotechnology

The major advantages of genetic engineering over conventional breeding are the diversity of the potential sources of genetic information, the speed with which improved elite varieties can be generated and, perhaps most important, the fact that nutritional traits for different vitamins and minerals can be stacked in the same plant without highly complex breeding programs [32]. Genetic engineering currently offers the only opportunity to produce nutritionally complete staple foods.

Despite these advantages, there are no high-micronutrient, genetically engineered crops on the market thus far. Whereas with conventional breeding this reflects the long development phase, in the case of genetic engineering this reflects the current uncertain regulatory environment, particularly trade barriers and differences in national regulatory systems that inhibit the production, transport, and use of transgenic products. Trade barriers for transgenic crops have been established de facto in the EU because of the precautionary approach to regulatory oversight, so developing countries (such as China and India) are pressured not to grow such products for export even though they may still benefit the domestic population by improving health and wealth [2, 3].

Biotechnology Strategies to Increase Nutritional Content

Many biotechnology strategies can be used to enhance the nutritional value of crops and these offer a rapid way to introduce such traits into elite varieties. The best approach for a given nutrient depends predominantly on whether the plant synthesizes the nutritional compound de novo or obtains it from the environment. Organic molecules such as amino acids, fatty acids, and vitamins are synthesized by the plant, and increasing the nutritional content therefore requires some form of metabolic engineering with the aim of increasing the amount of the desirable compound, decreasing the amount of a competitive compound (e.g., one that uses the same precursors but diverts them into a different pathway) or even extending an existing metabolic pathway to generate a product that is not usually made in that species [32]. In contrast, mineral nutrients are obtained from the environment and mineral enhancement therefore involves strategies to increase uptake, transport and/or to increase accumulation in harvestable tissues [23].

Increasing the Availability of Essential Amino Acids

Among the eight essential amino acids discussed above, methionine, lysine, and tryptophan are the most limiting in legumes and cereals, and since these are the major types of staple crops they are also the primary targets for nutritional enhancement. Generally, four strategies have been applied to increase the content of essential amino acids in plants: (1) mimicking natural mutants, (2) the expression of recombinant storage proteins with desirable amino acid profiles, (3) genetic engineering to enhance the free amino acid pool, and (4) combination approaches.

Mimicking Natural Mutants The naturally occurring *opaque2* mutant in corn has higher lysine and tryptophan levels than wild-type corn but has a soft, chalky kernel which is unsatisfactory for cooking. The higher content of essential amino acids in the mutant results from lower levels of certain storage proteins (e.g. α- and β-zeins) allowing other proteins (e.g. 27-kDa γ-zein) to replace them and increase the prevalence of the two limiting amino acids. Breeding programs have resulted in the development of quality protein maize (QPM) which benefits from the higher lysine and tryptophan levels of the *opaque2* mutant but combines this with a hard kernel for superior cooking qualities [45]. Although QPM has lower levels of α- and β-zeins compared to wild-type corn, it has higher levels of γ-zein. Zarkadas et al. [46] showed that QPM may provide up to 73% of human protein requirements, compared to 28–50% for common corn. Success with *opaque2* corn has stimulated extensive research to identify similar mutants in other cereals such as barley (*Hordeum vulgare*) and sorghum (*Sorghum bicolor*).

The *opaque2* corn mutants have inferior agronomic traits that cannot be overcome easily, but the laborious breeding program that gave rise to QPM can be replicated much more rapidly by genetic engineering. The transformation of corn with an RNAi construct to suppress target storage protein genes resulted in a phenocopy of the *opaque2* phenotype; transgenic seeds contained less α-zein than normal but higher levels of lysine [47, 48].

Expression of Recombinant Storage Proteins The main source of essential amino acids in sink tissues such as developing seeds is the storage proteins; therefore, one reason for the lack of certain amino acids in some staple crops is the absence of major storage proteins containing them. Thus, one of the main strategies for improving the levels of limiting amino acids is to express heterologous storage proteins that are rich in these specific amino acids.

One of the earliest attempts using this approach was the expression of pea legumin, which is rich in lysine, in rice endosperm, where lysine is limiting; in the best lines, heterologous legumin represented up to 4.2% of the total protein content [49]. Similarly, Stöger et al. [50] generated transgenic wheat plants expressing pea legumin using the low molecular weight (LMW) glutenin promoter, with legumin representing 1.5% of total soluble protein in the best transgenic lines. More significant increases in lysine content have been achieved by modifying cereal storage protein genes before deployment to increase the number of lysine codons. For example, Jung and Carl [51] modified the barley hordothionine protein to include 12 lysine residues (hordothione-12, HT12) and the barley high lysine protein to include eight lysine residues (barley high lysine-8, BHL8) and expressed them in corn along with the bacterial enzyme dihydrodipicolinate synthase (DHPS, see below). This resulted in a total lysine content of nearly 0.8%, about four times the level in wild-type seeds. The expression of HT12 in sorghum increased the lysine content by 50% compared to wild-type grain, and the expression of *sb401*, encoding another high-lysine storage protein, increased lysine levels in corn by 54.8% and total protein content by up to 39% [52].

Lysine levels can also be increased by expressing the animal equivalent of storage proteins, such as the nutritional proteins found in milk. The principle was established when porcine α-lactalbumin was expressed in corn and either targeted for secretion to the apoplast or for retention in the endoplasmic reticulum (ER), but individual amino acid levels were not reported [53]. More recently, Bicar et al. [54] repeated the experiment and showed that α-lactalbumin expression in corn increased the lysine content up to 47%. The lysine content of transgenic corn has also been increased up to 26% by expressing a heterotypical Arabidopsis lysyl tRNA synthetase, which inserts lysine residues in place of other amino acids during the synthesis of seed-storage proteins [55].

The expression of heterologous storage proteins has also been used as a strategy to increase the levels of methionine in transgenic crops, focusing on the 2S storage proteins which are unusually methionine rich. For example, expression of Brazil nut 2S albumin in soybean and narbon bean doubled the methionine content of the seeds, and increased methionine content by 33% in canola [56]. Similarly, the expression of sunflower 2S albumin increased total methionine content by up to sevenfold in potato tubers [57]. This approach does not always work well, e.g., the expression of the sunflower albumin SFA8 in rice and chickpea [58] merely redistributed the sulfur-containing amino acids (more methionine, less cysteine) with no

net improvement in nutritional properties. The 2S sulfur-rich albumins are allergenic in some human populations, reducing their usefulness for improving nutritional quality [59].

Ideally, a single protein would provide nutritional completeness in terms of essential amino acids. Grain from the pseudo-cereal amaranth (*Amaranthus hypochondriacus*) not only has a high protein content compared to traditional crops (17–19% of seed dry weight (DW) compared to ~10%), but that protein is rich in essential amino acids such as lysine (5%, more than twice the amount in wheat flour), threonine (2.9%), tyrosine (3.4%), and the sulfur-containing amino acids cysteine and methionine (4.4%). This provides a nutritional composition fairly close to the ideal as recommended by WHO, and the protein is not allergenic [5]. The cDNA for this protein has therefore been expressed in a number of crops with nutritionally incomplete proteins to increase overall protein levels and provide greater amounts of limiting amino acids. Rascón-Cruz et al. [60] expressed amaranthin in corn using the rice glutelin-1 promoter and increased the amount of protein by up to 32% while simultaneously boosting the levels of the three most limiting amino acids, lysine, tryptophan, and isoleucine. Chakraborty et al. [57] expressed the protein in potato tubers using the granule-bound starch synthase (GBSS) promoter, and increased total protein levels by up to 45%. Most recently, the protein was expressed in wheat using the LMW glutenin promoter with the amaranthin protein representing nearly 2.5% of total seed protein in some lines, increasing the levels of lysine to 6.4%, and tyrosine to 3.8% [61].

As well as natural heterologous storage proteins, completely synthetic proteins (i.e., proteins designed from first principles) can also be expressed to boost the levels of particular amino acids. For example, a synthetic protein matched to human amino acid requirements was expressed in cassava [62]. Even in these ideal cases, however, the levels of essential amino acids in the resulting transgenic crops tend to fall below expectations given the composition of the heterologous proteins. The inability of heterologous proteins to change the essential amino acid content of target crops abruptly and predictably often reflects the limited free amino acid pool, which provides the substrates for protein synthesis.

Engineering the Free Amino Acid Pool

In higher plants, lysine, threonine, and methionine are synthesized from aspartic acid via a pathway that is highly branched and under complex feedback control (Fig. 1) [63]. Two key enzymes are aspartate kinase (AK), which functions early in the pathway and is inhibited by both lysine and threonine, and dihydrodipicolinate synthase (DHPS), which is the first enzyme specifically committed to lysine biosynthesis and is inhibited by lysine alone. Feedback-insensitive versions of the bacterial enzymes have been expressed in model plants with encouraging results, e.g., the free lysine

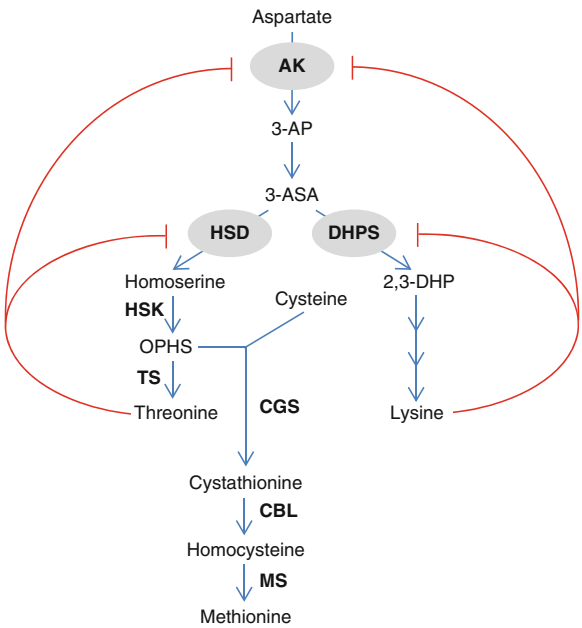

Biotechnology and Nutritional Improvement of Crops. Figure 1
Synthesis of the essential amino acids lysine, threonine, and methionine [63]. The three key enzymes (*gray circles*) are aspartokinase (AK), dihydrodipicolinate synthase (DHPS), and homoserine dehydrogenase (HSD), all of which are subject to end-product feedback inhibition (*red arrows*). Abbreviations for substrates: 3-AP, aspartyl-3-phosphate; 3-ASA, aspartate semialdehyde; OPHS, *O*-phosphohomoserine; 2,3-DHP, 2,3- dihydrodipicolinate. Abbreviations for other enzymes: HSK, homoserine kinase; TS, threonine synthase; CGS, cystathionine-γ-synthase; CBL, cystathionine β-lyase; MS, methionine synthase. Multiple arrows indicate several unspecified reactions

content in tobacco and Arabidopsis seeds was increased by expressing feedback-insensitive DHPS [63]. Similarly, the expression of feedback-insensitive DHPS in corn embryos increased the levels of free lysine from <2% to almost 30% of the free amino acid pool, with concomitant increases in threonine [64]. Analogous approaches have increased the lysine levels in canola and soybean [65, 66]. However, high levels of lysine in all plant tissues can cause abnormal vegetative growth and flower development that reduce seed yield [63].

The increased accumulation of lysine in tobacco seeds correlated with the enhanced activity of a bifunctional enzyme, lysine-ketoglutarate reductase/saccharopine dehydrogenase (LKR/SDH), which controls the first two reactions of the α-amino adipic acid pathway of lysine catabolism (Fig. 2) [67, 68]. To determine the impact of lysine catabolism on the levels of free lysine in the amino acid pool, a feedback-insensitive DHPS was expressed in wild-type Arabidopsis seeds and those of a LKR/SDH knockout mutant [69]. Whereas transgenic seeds without the mutation contained 12 times the normal levels of lysine, transgenic mutant seeds contained 80 times normal lysine levels, showing the importance of lysine catabolism in strategies to increase the accumulation of this amino acid. Similarly, it has been possible to cross transgenic corn lines where one parent expresses a feedback-insensitive enzyme for lysine synthesis that doubles the amount of free lysine [70] and the other expresses an RNAi construct against LKR/SDH thus inhibiting lysine catabolism [71]. In the double transgenic progeny, the amount of lysine was 40 times the level present in wild-type corn [64].

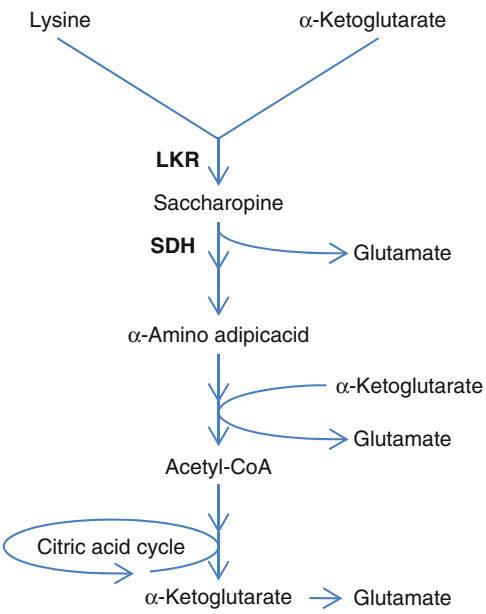

Biotechnology and Nutritional Improvement of Crops. Figure 2
Lysine catabolism in plants, showing the production of three glutamate molecules for every molecule of lysine [63]. Enzyme abbreviations: LKR, lysine-ketoglutarate reductase; SDH, saccharopine dehydrogenase. Multiple arrows indicate several unspecified reactions

The major enzyme-controlling methionine synthesis is cystathionine γ-synthase (CGS), and its activity in Arabidopsis is under feedback control reflecting the abundance of the important metabolic intermediate S-adenosylmethionine (SAM) [72]. Mutations in the N-terminal portion of CGS that affect this feedback regulation result in methionine overproduction [72, 73], and this can be combined with the expression of a feedback-insensitive AK to increase methionine levels even further [74].

The expression of feedback-insensitive AK also increases the abundance of threonine. In some cases, the increases in threonine levels were matched by smaller, although still significant, increases in the levels of isoleucine, methionine, and lysine, indicating that AK activity is more important for threonine synthesis than it is for lysine synthesis [63].

Tryptophan synthesis in plants is strongly regulated by high levels of tryptophan inhibiting the enzyme anthranilate synthase, which catalyzes the conversion of chorismate to anthranilate. As is the case for other amino acids, a preferred strategy to overcome this limitation is the expression of a feedback-insensitive version of this key enzyme, as has been achieved in tobacco leaves and the roots of the forage legume *Astragalus sinicus* [75]. A mutant anthranilate synthase from rice has been shown to increase the amount of free tryptophan in transgenic rice seeds by over 400-fold [76], in potato tubers by approximately 30-fold [77], and in soybean seeds by approximately 20-fold [78]. A similar mutant gene from tobacco increased free tryptophan levels by sixfold in transgenic soybean leaves and twofold in seeds [79].

Tabe et al. [80] have recently shown that cysteine levels can be increased by up to 26-fold in developing lupin seeds by expressing a feedback-insensitive serine acetyltransferase (SAT). The levels of glutathione were also higher in developing seeds, but methionine levels were unaffected. Interestingly, the overall levels of cysteine and methionine in mature seeds did not change, suggesting feedback to counter the accumulation of cysteine later in development. The above strategy was also combined with the overexpression of a seed storage protein by crossing transgenic lines expressing the SAT enzyme with those expressing a sunflower albumin gene. Again, this resulted in higher levels of cysteine during development but no change in the amount of methionine; there was no significant change in either amino acid in mature seeds [80].

Increasing the Availability of Essential Fatty Acids

Polyunsaturated fatty acids (PUFAs) are synthesized from saturated fats through an alternating sequence of desaturation and elongation reactions, each requiring a different class of enzymes (Fig. 3). Humans are unable to synthesize PUFAs because they lack the necessary Δ12 and Δ16 desaturases to convert oleic acid into α-linolenic acid (omega-3) and linoleic acid (omega-6). However, they do possess Δ6 and Δ5

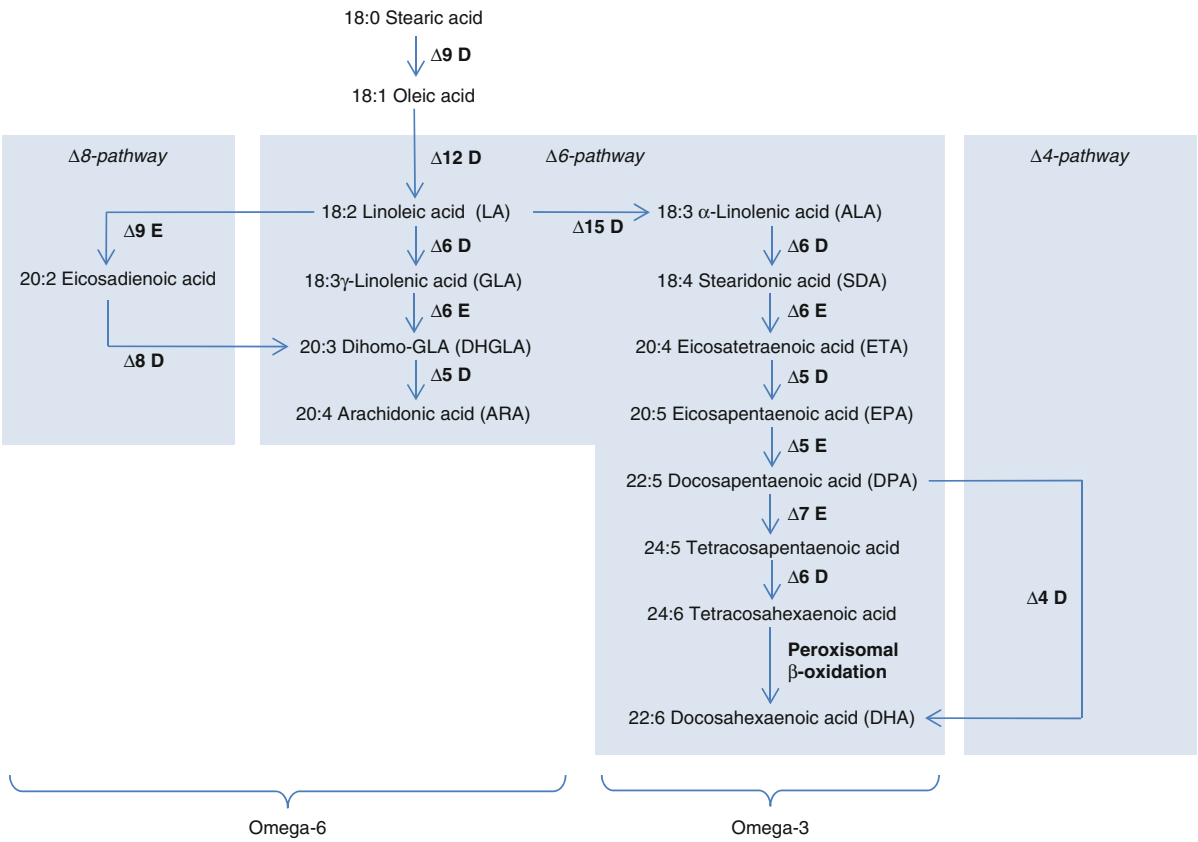

Biotechnology and Nutritional Improvement of Crops. Figure 3
Overview of very-long-chain polyunsaturated fatty acid synthesis focusing on the strategies that have been used in transgenic plants either by enhancing the standard Δ6-pathway or importing enzymes from the alternative Δ8-pathway and microbial Δ4-pathway [82]. Enzymes identified by "D" and "E" are desaturases and elongases, respectively. Humans lack the Δ12 desaturase that converts oleic acid into linoleic acid

desaturases, so if adequate amounts of α-linolenic acid and linoleic acid can be sourced in the diet they can be converted into longer-chain molecules in the liver, yielding the very-long-chain (VLC) PUFAs eicosapentaenoic acid (EPA), docosahexaenoic acid (DHA), and arachidonic acid (ARA) [81]. Even so, this is a slow process because the Δ6 and Δ5 desaturases are inefficient, and these molecules can become limiting. Strategies to increase the availability of essential fatty acids in plants therefore not only concentrate on the accumulation of α-linolenic acid and linoleic acid but also on the VLC-PUFAs EPA, DHA, and ARA.

As shown in Fig. 3, the synthesis of EPA and ARA requires three enzyme activities: Δ6-desaturase, Δ6-elongase, and Δ5-desaturase; DHA synthesis requires an additional β-oxidation step which occurs in peroxisomes [82]. The elongation steps require an acyl-CoA substrate, whereas the desaturations require the presence of phosphatidylcholine. The switching of fatty acids between the phosphatidylcholine and CoA pools is facilitated by acyltransferases and these are often the limiting step in VLC-PUFA synthesis [83] (Fig. 4). However, this bottleneck can be alleviated using the alternative Δ8-pathway, in which the elongation and saturation steps are realized by a Δ9-elongase, Δ8-desaturase, and Δ5-desaturase [84] (Fig. 3). This pathway is more efficient for ARA and EPA synthesis because there is less reliance on acyl exchange [82].

Four main strategies have been used to enhance VLC-PUFA biosynthesis in plants: expressing enzymes that increase the availability of precursors for α-linolenic acid and linoleic acid synthesis, enhancing the typical Δ6-pathway, introducing the alternative Δ8-pathway and importing the microbial Δ4-pathway (Fig. 3). Thus far, enhancing the Δ6-pathway has been most successful (Table 5), increasing the levels of ARA, EPA, and DHA by up to 25%, 15%, and 0.5%, respectively [85, 86]. However, Kinney et al. [87] showed that the levels of EPA and DHA could be increased by 19.5% and 3%, respectively, in soybean by enhancing the Δ4- and Δ6-pathways simultaneously, and Qi et al. [88] increased EPA levels to 3% and ARA levels by 6.6% in *Arabidopsis* by importing the Δ8-pathway and removing the acyl exchange bottleneck.

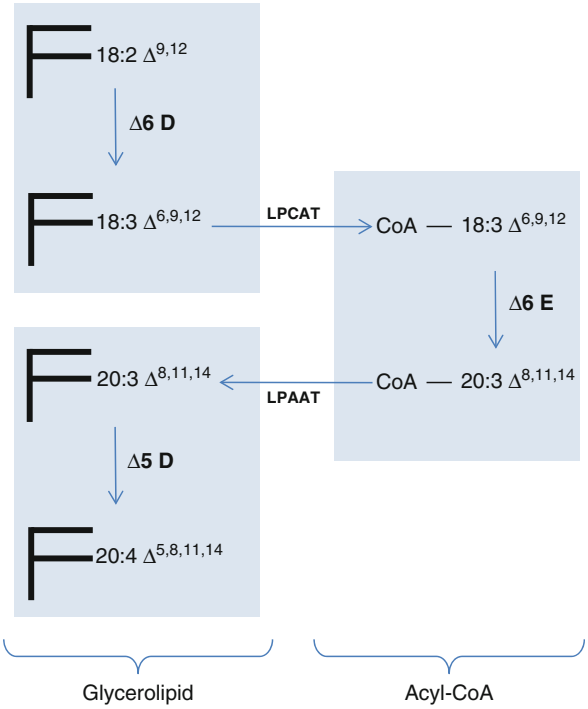

Biotechnology and Nutritional Improvement of Crops. Figure 4
Fatty acid desaturation in plants requires glycerolipid substrates, whereas elongation requires acyl-CoA substrates. Successive desaturation and elongation steps therefore require substrates to be shuttled between phosphatidylcholine and coenzyme A (CoA) using enzymes known as acyltransferases. Enzymes identified by "D" and "E" are desaturases and elongases, respectively. Abbreviations: 18:2 $\Delta^{9,12}$, linoleic acid; 18:3 $\Delta^{6,9,12}$, γ-linolenic acid; 20:3 $\Delta^{8,11,14}$, dihomo-γ-linolenic acid; 20:4 $\Delta^{5,8,11,14}$, arachidonic acid; LPCAT, lysophosphatidylcholine acetyltransferase; LPAAT, lysophosphatidic acid acyltransferase

Increasing Vitamin Levels

Vitamin A In plants, carotenoids such as β-carotene (pro-vitamin A) are synthesized in the plastids via the methylerythritol-4-phosphate (MEP) pathway, also known as the non-MVA pathway. Initially, pyruvate and D-glyceraldehyde-3-phosphate are converted into 1-deoxy-D-xylulose-5-phosphate (DXP) by DXP synthase (DXS), and DXP is then converted into the isomeric C5 precursors isopentenyl diphosphate (IPP) and dimethylallyl pyrophosphate (DMAPP). Three

Biotechnology and Nutritional Improvement of Crops. Table 5 Transgenic plants with enhanced levels of essential fatty acids [82]

Species	Genes (source)	Promoters	% Fatty acids
Arabidopsis (*Arabidopsis thaliana*)	*Δ9-elongase* (*Isochrysis galbana)*	Constitutive	ARA: 6.6
	Δ8-desaturase (*Euglena gracilis)*	CaMV 35S	EPA: 3
	Δ5-desaturase (*Mortierella alpine*)		
Arabidopsis	*Δ5/Δ6-desaturase* (*Danio rerio*)	Seed-specific	ARA: 1.2
	Δ6-elongase (*Caenorhabditis elegans*)	Napin	EPA: 2.5
	Δ4-desaturase (*Pavlova salina*)		
	Δ5-elongase (*P. salina*)		
Linseed (*Linum usitatissimum*)	*Δ6-desaturase* (*Phaeodactylum tricornutum)*	Seed-specific	ARA: 1.5
	Δ6-elongase (*Physcomitrella patens*)	USP	EPA: 1
Tobacco (*Nicotiana tabacum*)	*Δ5-desaturase* (*P. tricornutum*)		ARA: 2
Soybean (*Glycine max*)	*Δ6-desaturase* (*Saprolegnia diclina)*	Different seed-specific promoters	EPA: 19.5
	Δ6-elongase (*M. alpina*)		ARA: 5.3
	Δ5-desaturase (*M. alpina*)		
	Fad3 (Arabidopsis)		
	Δ17-desaturase (*Saprolegnia diclina*)		
	Δ4-desaturase (*Syzygium aggregatum*)		
	Elongase (*P. salina*)		
Mustard (*Brassica juncea*)	*Δ6-desaturase* (*Pythium irregulare)*	Seed-specific	ARA: 25
	Δ6-elongase (*P. patens*)	Napin	EPA: 15
	Δ5-desaturase (*Thraustochytrium* sp.)		
	Δ12-desaturase (*Calendula officinalis*)		
	Elongase (*Thraustochytrium* sp.)		
	ω3-desaturase (*Phytophthora infestans*)		
Marchantia polymorpha	*Δ6-desaturase (Marchantia polymorpha)*	Constitutive	ARA: 11.4 (3.6-fold)
	Δ6-elongase (M. polymorpha)	CaMV35S	EPA: 12.1 (2-fold)
	Δ5-desaturase (M. polymorpha)		
Tobacco	*Δ6-desaturase (M. polymorpha)*	Constitutive modified CaMV35S	ARA: 13.4
	Δ6-elongase (M. polymorpha)		EPA: 3.2
	Δ5-desaturase (M. polymorpha)		
Soybean	*Δ6-desaturase (M. polymorpha)*	Seed-specific α′subunit of β-conglycin	ARA: 3
	Δ6-elongase (M. polymorpha)		EPA: 0.3
	Δ5-desaturase (M. polymorpha)		

Source: Data updated from [82]

molecules of IPP condense with one molecule of DMAPP to form the C20 precursor geranylgeranyl diphosphate (GGPP), which is used for the synthesis of carotenoids, tocopherols, chlorophylls, plastoquinones, and gibberellins [89]. The first committed reaction in carotenoid biosynthesis is the conversion of GGPP to phytoene by phytoene synthase (PSY). In plants, phytoene then undergoes four desaturation steps catalyzed by phytoene desaturase (PDS) and ζ–carotene desaturase (ZDS) to generate the first colored carotene, *cis*-lycopene, which is converted to all-*trans*-lycopene by carotene isomerase (CRTISO) [90]. Lycopene is the substrate for two different enzymes – lycopene β-cyclase (LYCB), which adds β-ionone rings to both ends generating β-carotene; and lycopene ε-cyclase (LYCE), which adds an ε-ionone ring to one end, the other being cyclized by LYCB to generate α-carotene [90]. Both molecules can be hydroxylated to produce xanthophylls such as lutein, zeaxanthin, and violaxanthin (Fig. 5) although these do not have pro-vitamin A activity [90].

The amount of β-carotene produced by plants can be enhanced by increasing the availability of carotenoid precursors, by expressing enzymes in the common part of the pathway (between GGPP and lycopene), by biasing the pathway toward the β-branch through the expression of LYCB at the expense of LYCE, or by increasing the storage capacity for carotenoids (Table 6) [90].

The first approach has been successful in producing plants that synthesize high levels of GGPP, but because this is used in several pathways not all of the flux is directed toward carotenoid synthesis. For example, the overexpression of DXP synthase in tomato and potato increased the total carotenoid content by up to 1.6-fold compared to wild type, but the levels of tocopherols and plastoquinones were also affected [91].

The expression of enzymes in the committed part of carotenoid pathway is a more targeted approach, and is particularly necessary in cereal grains where the pathway is blocked at the first committed step. In rice endosperm, the carotenoid pathway terminates at GGPP because there is very limited PSY activity. "Golden Rice" is a transgenic variety expressing daffodil PSY and LYCB as well as the multifunctional bacterial enzyme CrtI, which carries out all the desaturation steps between phytoene and lycopene. The β-carotene content of the original Golden Rice was 1.6 μg/g DW [92], but the replacement of daffodil PSY with the more active corn enzyme resulted in Golden Rice 2, in which the β-carotene levels reached 31 μg/g DW [93]. Similar results have been achieved in corn endosperm. For example, Aluru et al. [94] expressed the bacterial enzymes CrtB (PSY) and CrtI under the control of an enhanced seed-specific promoter, increasing the total carotenoid level to 33.6 μg/g DW and the β-carotene level to 9.8 μg/g DW. More recently, Zhu et al. [95] used a combinatorial transformation strategy to introduce up to five carotenogenic transgenes into corn, with the best-performing line (Ph-3, expressing PSY and CrtI), producing over 60 μg/g DW of β-carotene. Another recent breakthrough in this area was the creation of transgenic corn plants transformed with four genes enabling the simultaneous modulation of three metabolic pathways [96]. As above, the carotenoid pathway was engineered with the genes encoding PSY and CrtI, resulting in a 169-fold increase in β-carotene levels to 57 μg/g DW. These combinatorial and stacked transgene approaches are discussed later in detail.

Similar progress has been made in the brassicas. The expression of bacterial CrtB (PSY) in canola resulted in a 50-fold increase in total carotene levels compared to wild-type seeds (1,617 μg/g fresh weight (FW)), with a β-carotene content of 949 μg/g FW [97]. Ravanello et al. [98] achieved 1,341 μg/g FW total carotenoids with the same gene. The combined expression of CrtB (PSY) and CrtI boosted levels to 1,412 μg/g FW, but further addition of CrtY (LYCB) reduced total carotenoid levels to 1,229 μg/g FW although it increased the relative amount of β-carotene to 846 μg/g FW. Recently, Fujisawa et al. [99] introduced seven bacterial transgenes into canola encoding the enzymes isopentenyl pyrophosphate isomerase (which interconverts IPP and DMAPP), CrtE (GGPP synthase), CrtB (PSY), CrtI (carotene desaturase), CrtY (LYCB), and two additional enzymes (CrtZ and CrtW) that catalyze downstream steps converting β-carotene into ketocarotenoids. Although this resulted in the production of several ketocarotenoids, the predominant carotenoid was still β-carotene, which accumulated to 214.2 μg/g FW, 1,074-fold higher than in wild-type seeds.

Diretto et al. [100, 101] expressed CrtB, CrtI, and CrtY in potato tubers, increasing total carotenoid levels to 114 μg/g DW and β-carotene levels to 47 μg/g DW.

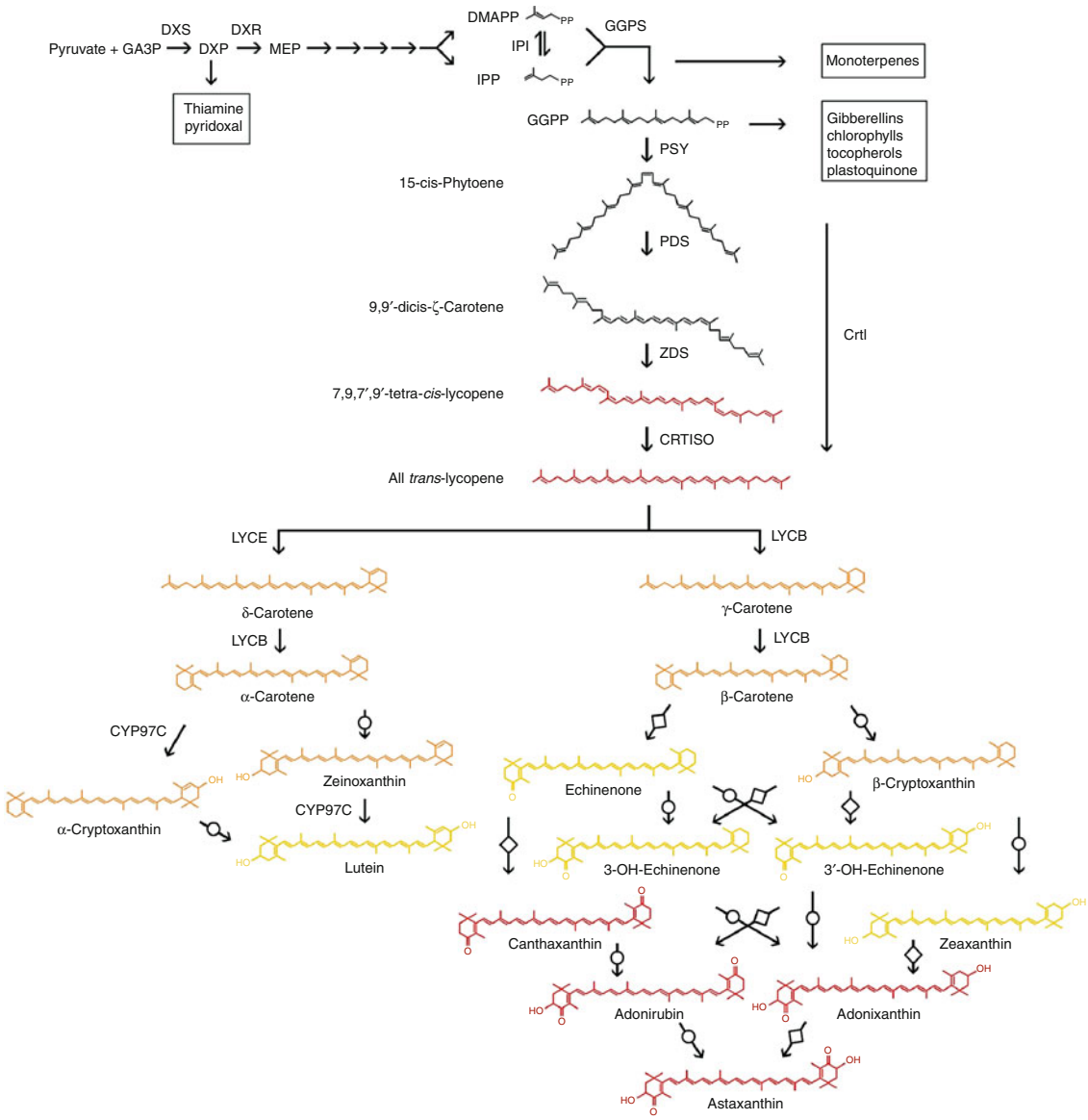

Biotechnology and Nutritional Improvement of Crops. Figure 5

The extended carotenoid biosynthetic pathway in plants [171]. The precursor for the first committed step in the pathway is GGPP (geranylgeranyl pyrophosphate), which is converted into phytoene by phytoene synthase (PSY, CrtB). GGPP is formed by the condensation of IPP (isopentenyl pyrophosphate) and DMAPP (dimethylallyl pyrophosphate), which are derived predominantly from the plastidial MEP (methylerythritol 4-phosphate) pathway as shown in the upper part of the figure. The pathway is linear until lycopene, involving three steps catalyzed by separate enzymes in plants but by the single, multifunctional enzyme CrtI in bacteria. Lycopene is the branch point for the α- and β-carotene pathways, which usually end at lutein and zeaxanthin, respectively, through the expression of β-carotene hydroxylases (*arrows* with *circles*). An elaborated ketocarotenoid pathway can be introduced by expressing β-carotene ketolases (*arrows* with *diamonds*) since these compete for substrates with β-carotene hydroxylases and generate diverse products. Other abbreviations: GA3P, glyceraldehyde 3-phosphate; DXP, 1-deoxy-D-xylulose 5-phosphate; DXS, DXP synthase; DXR, DXP reductoisomerase; IPI, IPP isomerase; GGPPS, GGPP synthase; PDS, phytoene desaturase; ZDS, ζ-carotene desaturase; CRTISO, carotenoid isomerase; LYCB, lycopene β-cyclase; LYCE, lycopene ε-cyclase; HydE, carotene ε-hydroxylase

Biotechnology and Nutritional Improvement of Crops. Table 6 Transgenic plants with enhanced carotenoid levels [171]

Species	Genes (source)	Promoters	Carotenoid levels in transgenic plants
Rice (*Oryza sativa*)	*psy1* (daffodil; *Narcissus pseudonarcissus*)	CaMV35S (constitutive)	0.3 μg/g dry weight (DW) phytoene in seeds
		Gt1 (seed specific)	0.74 μg/g DW phytoene in seeds
	psy1 and *lycb* (daffodil)	Gt1 (*psy1* and *lycb*) and CaMV35S (*crt*I)	1.6 μg/g DW total carotenoids in endosperm
	*crt*I (*Pantoea ananatis*)		
	psy1 (corn)	Gt1	37 μg/g DW total carotenoids in seeds
	*crt*I (*P. ananatis*)		
Canola (*Brassica napus*)	*crt*B (*P. ananatis*)	Napin (seed specific)	1,617 μg/g fresh weight (FW) total carotenoids in seeds (50-fold)
	*crt*B (*P. ananatis*)	Napin	1,341 μg/g FW total carotenoids in seeds
	*crt*E and *crt*B (*P. ananatis*)		1,023 μg/g FW total carotenoids in seeds
	*crt*B (*P. ananatis*)		1,412 μg/g FW total carotenoids in seeds
	*crt*I *(P. ananatis)*		
	*crt*B and *crt*Y (*P. ananatis*)		935 μg/g FW total carotenoids in seeds
	*crt*B and *β-cyclase* (*B. napus*)		985 μg/g FW total carotenoids in seeds
	*crt*B and *crt*Y (*P. ananatis*)		1,229 μg/g FW total carotenoids in seeds
	*crt*I *(P. ananatis)*		
	idi, *crt*E, *crt*B, *crt*I, and *crt*Y (*P. ananatis*)	CaMV35S, napin and Arabidopsis *FAE1* (seed specific)	412–657 μg/g FW total carotenoids in seeds (30-fold)
	*crt*Z , *crt*W (*Brevundimonas* sp.)		60–190 μg/g FW total ketocarotenoids in seeds

Biotechnology and Nutritional Improvement of Crops. Table 6 (Continued)

Species	Genes (source)	Promoters	Carotenoid levels in transgenic plants
Tomato (*Solanum lycopersicum*)	*psy1* (tomato)	CaMV35S	3,615 μg/g DW total carotenoids in vegetative tissue (1.14-fold)
	psy1 (tomato)	CaMV35S	2,276.7 μg/g DW total carotenoids in fruit (1.25-fold)
			819 μg/g DW β-carotene in fruit (1.4-fold)
	*crt*I (*P. ananatis*)	CaMV35S	520 μg/g DW (1.9-fold) β-carotene in fruit
	lycb (Arabidopsis) *chyb* (pepper; *Capsicum annuum*)	pds	63 μg/g FW β-carotene in fruit (12-fold)
	*crt*B (*P. ananatis*)	Polygalacturonase (fruit specific)	825 μg/g DW β-carotene in ripe fruit (2.5-fold)
	dxs (*Escherichia coli*)	Fibrillin	7,200 μg/g DW total carotenoids in fruit (1.6-fold)
	det-1 (tomato, antisense)	P119, 2A11, and TFM7 (fruit specific)	130 μg/g DW β-carotene (8-fold) in red-ripe fruit (assuming a water content of 90%)
	CRY2 (tomato)	CaMV35S	1,490 μg/g DW total carotenoids ripe fruit pericarps (1.7-fold)
			101 μg/g DW β-carotene ripe fruit pericarps (1.3-fold)
	chrd (cucumber; *Cucumis sativus*)	CaMV35S	Reduced carotenoid levels in flower
	*crt*Y (*P. ananatis*)	aptI	286 μg/g DW β -carotene in fruit (4-fold)
	Fibrillin (pepper)	Fibrillin	150 pg/g FW β -carotene in fruit
	lycb (Arabidopsis)	pds (fruit specific)	546 μg/g DW FW total carotenoids in fruit (7-fold) (assuming a water content of 90%)
	lycb (tomato)	CaMV35S	2,050 μg/g DW total carotenoids in fruit (31.7-fold) (assuming a water content of 90%)
	lycb (daffodil)	Ribosomal RNA	950 μg/g DW β-carotene in fruit

Biotechnology and Nutritional Improvement of Crops. Table 6 (Continued)

Species	Genes (source)	Promoters	Carotenoid levels in transgenic plants
Potato (*Solanum tuberosum*)	*ZEP* (Arabidopsis)	GBSS (tuber specific)	60.8 μg/g DW total carotenoids in tubers (5.7-fold)
	*crt*B (*P. ananatis*)	Patatin (tuber specific)	35 μg/g DW total carotenoids in tubers (6.3-fold)
			11 μg/g DW β-carotene in tubers (19-fold)
	lyce (potato, antisense)	Patatin	12.27 μg/g DW total carotenoids in tubers (2.5-fold)
			0.043 μg/g DW β-carotene in tubers (14-fold)
	*crt*O (*Synechocystis* sp.)	CaMV35S	39.76 μg/g DW total carotenoids in tubers
			ketocarotenoids represented 10–12% of total carotenoids in tubers
	dxs (*E. coli*)	Patatin	7 μg/g DW total carotenoids in tubers (2-fold)
	*crt*B (*P. ananatis*) *bkt1* (*Haematococcus pluvialis*)	Patatin	5.2 μg/g DW total carotenoids in tubers
			1.1 μg/g DW total ketocarotenoids in tubers
	bkt1 (*H. pluvialis*)	Patatin	30.4 μg/g DW total carotenoids in tubers
			19.8 μg/g DW total ketocarotenoids in tubers
	or (cauliflower; *Brassica oleracea* var *botrytis*)	GBSS	25 μg/g DW total carotenoids (6-fold) in tubers
	or (cauliflower)	GBSS	31 μg/g DW total carotenoids in tubers (5.7-fold)
	crtB, *crtI*, and *crtY* (*P. ananatis*)	Patatin	114 μg/g DW total carotenoids in tubers (20-fold)
			47 μg/g DW β-carotene in tubers (3,600-fold)
	bch (potato, antisense)	Patatin	21.7 μg/g DW total carotenoids in tubers (4.5-fold)
			0.085 μg/g DW β-carotene in tubers (38-fold)
	bch (potato, antisense)	GBSS and CaMV35S	3.31μg/g DW β-carotene in tubers

Biotechnology and Nutritional Improvement of Crops. Table 6 (Continued)

Species	Genes (source)	Promoters	Carotenoid levels in transgenic plants
Corn (*Zea mays*)	*psy1* (corn)	Wheat LMW glutelin, barley (*Hordeum vulgare*) D-hordein, corn γ-zein, rice prolamin (all endosperm-specific)	146.7 μg/g DW total carotenoids in seeds
	*crt*I (*P. ananatis*)		35.85 μg/g DW total ketocarotenoids in seeds
	*crt*W (*Paracoccus* spp.)		
	lycb (*Gentiana lutea*)		
	*crt*B *and crt*I (*P. ananatis*)	super γ -zein	33.6 μg/g DW total carotenoids in seeds (34-fold)
	psy1 (corn)	Wheat LMW glutelin and barley D-hordein	163.2 μg/g DW total carotenoids in seeds (112-fold)
	*crt*I (*P. ananatis*)		59.32 μg/g DW β-carotene in seeds (169-fold)
Lotus japonicus	*crt*W (*Agrobacterium aurantiacum*)	CaMV35S	387 μg/g FW total carotenoids in flower petals (1.5-fold)
			89.9 μg/g FW total ketocarotenoids in flower petals (2.2-fold)
Carrot (*Daucus carota*)	*bkt1* (*H. pluvialis*) *chyB* (Arabidopsis)	CaMV35S and *Agrobacterium rhizogenes rol*D (root specific)	345.5 μg/g FW total carotenoids in root
			2,400 μg/g root DW novel ketocarotenoids
	psy (Arabidopsis)	CaMV35S	858.4 μg/g DW total carotenoids in roots
Tobacco (*Nicotiana tabacum*)	*crt*W and *crt*Z (*Paracoccus* sp.)	CaMV35S	1,275 μg/g DW total carotenoids in leaves
			64 μg/g FW total ketocarotenoids in leaves
	*crt*O (*Synechocystis* sp.) *crt*Z (*P. ananatis*)	CaMV35S	839 μg/g DW total carotenoids in leaves (2.5-fold)
			342.4 μg/g DW total ketocarotenoid in leaves
	*crt*O (*Synechocystis* sp.)	CaMV35S	429 μg/g DW total carotenoids in leaves
			156.1 μg/g DW total ketocarotenoid in leaves
	*crt*W and *crt*Z (*Brevundimonas* sp.)	*rrn*	7,380 μg/g FW total carotenoids in leaves (2.1-fold)
			7,290 μg/g FW total ketocarotenoids in leaves
Wheat (*Triticum aestivium*)	*psy1* (corn) *crt*I (*P. ananatis*)	CaMV35S and 1D × 5 (constitutive)	4.96 μg/g DW in seeds

Biotechnology and Nutritional Improvement of Crops. Table 6 (Continued)

Species	Genes (source)	Promoters	Carotenoid levels in transgenic plants
Arabidopsis (*Arabidopsis thaliana*)	*bkt1* (*H. pluvialis*)	Napin	4-keto-lutein, canthaxanthin, and adonirubin seeds up to 13-fold
	bch (Arabidopsis)	CaMV35S	2,274.8 nmol/g DW total carotenoids
	psy (Arabidopsis)	Napin	260 μg/g FW β-carotene in seeds
	psy (Arabidopsis)	CaMV35S	1,600 μg/g DW (10-fold) in seed-derived calli and 500 μg/g DW (100-fold) of total carotenoids in roots
	chyB (Arabidopsis)	CaMV35S	285 mmol/chl a(mol) violaxanthin (2-fold)
			728 mmol/chl a(mol) of total carotenoid
	AtB1 (Arabidopsis)	CaMV35S	38.2 μg/g β-carotene leaf tissue
	CYP97A3 (Arabidopsis)	CaMV35S	41.7 μg/g β-carotene leaf tissue
	CYP97B3 (Arabidopsis)	CaMV35S	36.7 μg/g β-carotene leaf tissue
	CYP97C1 (Arabidopsis)	CaMV35S	41.3 μg/g β-carotene leaf tissue

Source: Data updated from [171]

They also silenced the endogenous *lyce* and *bch* genes, thereby eliminating competition at the branch point between the α- and β-carotene pathways and preventing the further metabolism of β-carotene.

Ripening tomatoes accumulate low levels of β-carotene and in order to address this deficiency, several investigators have attempted to overexpress either the endogenous *lycb* gene or equivalent heterologous genes [102–106]. D'Ambrosio et al. [103] have been the most successful with this approach, achieving a 32-fold increase in β-carotene levels and generating orange-colored tomato fruits. Another successful strategy was the suppression of the endogenous *DET1* gene, which regulates photomorphogenesis. The expression of a *det1* RNAi construct in tomato chromoplasts increased β-carotene levels eightfold to 130 μg/g DW [107].

An alternative strategy to achieve β-carotene accumulation in plants is to modify the storage capacity of chromoplasts, where β-carotene accumulates in specialized lipoprotein-sequestering structures. A spontaneous mutation in the cauliflower *Orange* (*Or*) gene resulted in deep orange cauliflower heads associated with the hyperaccumulation of carotenoids in chromoplasts [108, 109] and the mutant allele has been cloned and expressed in potato tubers, where it increased the level of β-carotene tenfold and turned the tuber flesh orange [110].

Vitamin E Vitamin E is a collection of four tocopherols and four tocotrienols (each as α, β, γ, and δ derivatives), collectively known as tocochromanols [111]. All eight isomers can be absorbed equally efficiently during digestion but the hepatic α-tocopherol transfer protein (α-TTP) shows preferential retention of α-tocopherol, making it the most important form in terms of vitamin E activity in the human body [111].

Tocochromanol biosynthesis in higher plants (Fig. 6) occurs in the plastids and requires precursors from the cytosolic shikimate pathway and the plastidial

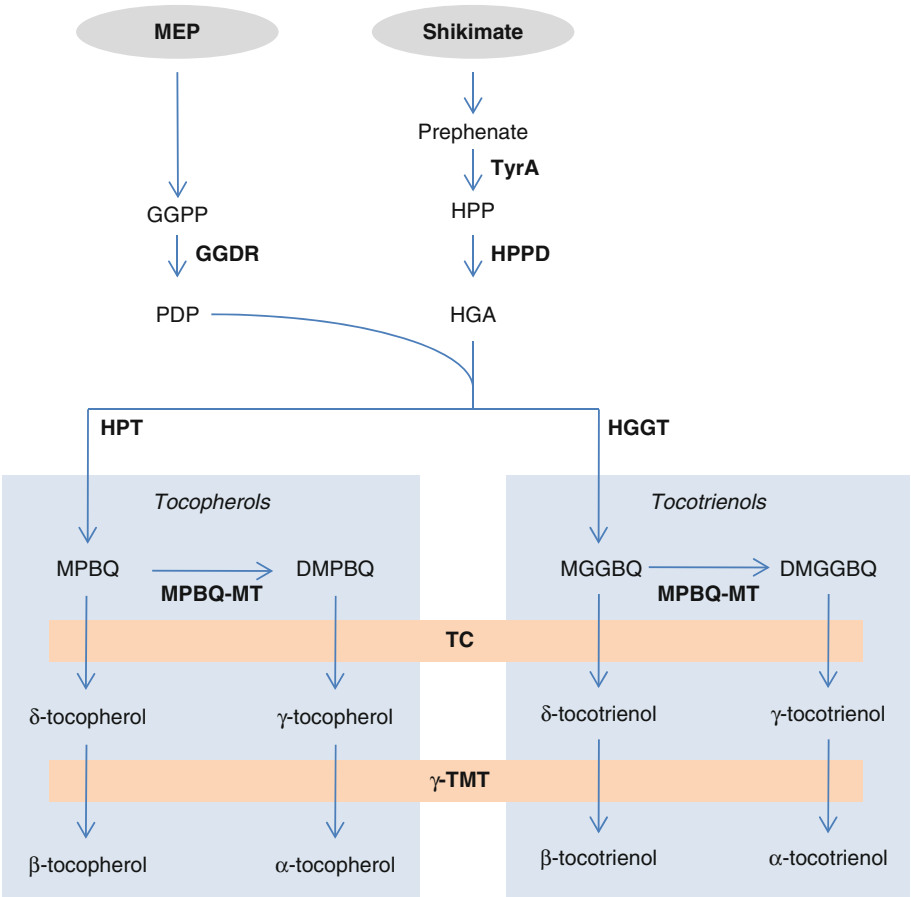

Biotechnology and Nutritional Improvement of Crops. Figure 6
Vitamin E synthesis in plants [111]. The pathway involves the prenylation of homogentisic acid (HGA), derived from the shikimate pathway, with phytyldiphosphate (PDP), derived from the methylerythritol phosphate (MEP) pathway. Prenylation may be carried out by two different enzymes – HPT (homogentisate phytyltransferase) or HGGT (homogentisate geranylgeranyl transferase) – to generate alternative intermediates that give rise to the tocopherol and tocotrienol branches of the pathway, respectively. These intermediates are substrates for the same three enzymes, yielding eight different products. Additional substrate abbreviations: GGPP, geranylgeranyl pyrophosphate; HPP: ρ-hydroxyphenylpyruvic acid; MPBQ, 2-methyl-6-phytylbenzoquinol; DMPBQ, 2,3-dimethyl-5-phytylbenzoquinol; MGGBQ, 2-methyl-6-geranylgeranylplastoquinol; DMGGBQ, 2,3-dimethyl-5-geranylgeranylplastoquinol. Additional enzyme abbreviations: GGDR, geranylgeranyl diphosphate reductase; HPPD, HPP dioxygenase; MPBQ-MT: MPBQ methyltransferase; TC, tocopherol cyclase; γ–TMT: γ-tocopherol methyltransferase

MEP pathway [111]. The tocochromanol head group is derived from the shikimate pathway, and this involves the conversion of p-hydroxyphenylpyruvic acid (HPP) to homogentisic acid (HGA), by HPP dioxygenase (HPPD); the MEP pathway contributes the side chain [111]. The first committed step in tocochromanol biosynthesis is the prenylation of HGA. There are two enzymes that carry out this reaction. If prenylation is carried out by homogentisate phytyltransferase (HPT), the product is 2-methyl-6-phytylplastoquinol (MPBQ), which leads to the synthesis of tocopherols. Alternatively, HGA can be prenylated by homogentisate geranylgeranyl transferase (HGGT), producing 2-methyl-6-geranylgeranylplastoquinol (MGGBQ), which leads to the synthesis of tocotrienols [111].

The eight isomers form through a complex series of reactions involving enzymes with multiple substrates at each stage. Both MPBQ and MGGBQ are substrates for tocopherol cyclase (TC), leading to the production of δ-tocopherol and δ-tocotreinol, respectively. They are also substrates for the enzyme MPBQ methyltransferase (MPBQ-MT), which adds a second methyl group to form 2,3-dimethyl-5-phytyl-1,4-benzoquinone (DMPBQ) and 2,3-dimethyl-5-geranylgeranyl-1,4-benzoquinone (DMGGBQ), respectively. These methylated derivatives are also substrates for TC, leading to the production of γ-tocopherol and γ-tocotreinol, respectively. Finally, all four of these products (the δ- and γ-tocopherols, and the δ- and γ-tocotrienols) can be methylated by γ-tocopherol methyltransferase (γ-TMT) to produce their β- and α- counterparts [111].

Plants can be engineered to accumulate higher levels of vitamin E by overexpressing the genes involved in tocochromanol synthesis, and this can be achieved either by increasing the total tocochromanol content or skewing tocochromanol synthesis toward the more potent vitamers, particularly α-tocopherol (Table 7). In the first approach, the overexpression of HPT increased tocopherol levels by up to 1.6-fold in the seeds and 4.4-fold in the leaves of transgenic Arabidopsis plants [112]. The overexpression of HPPD increased tocotrienol levels tenfold in Arabidopsis leaves [113], twofold in tobacco leaves, and 1.5-fold in tobacco seeds [114]. In the second approach, the expression of Arabidopsis γ-TMT in lettuce increased the α/γ tocopherol ratio but had no effect on the total tocopherol content [115]. However, by crossing the lines expressing HPT and γ-TMT, both the total tocopherol content and the α/γ tocopherol ratio were increased [115]. In canola, total tocochromanol levels have been doubled by expressing genes encoding HPT, HPPD, and TC [116].

The impact of HPPD expression can be enhanced by the simultaneous expression of TyrA, the enzyme responsible for the synthesis of HPP from prephenate (Fig. 6). TyrA expression has little effect on its own, but when combined with HPPD in tobacco, tocochromanol levels in the leaves increased eightfold [117]. Similar results have been achieved in Arabidopsis, canola, and soybean seeds using the same combination of genes, although the total tocochromanol content increased only 2–2.5-fold in these cases [118]. The expression of HPT, HPPD, and TyrA increased the tocochromanol content of seeds fivefold, and the further addition of geranylgeranyldiphosphate reductase (GGDR), which provides

Biotechnology and Nutritional Improvement of Crops. Table 7 Transgenic plants with enhanced tocochromanol levels [111]

Species	Genes (source)	Promoters	Tocochromanol levels in transgenic plants
Tobacco (*Nicotiana tabacum*)	*hppd* (barley; *Hordeum vulgare*)	CaMV 35S	50 μg/g DW in seeds (1.5–2-fold)
	tyrA (*Erwinia uredovora*)	Arabidopsis histone gene H4748	67 μg/g DW in leaf (1.3-fold)
	tyrA (*E. uredovora*), *hppd* (Arabidopsis)		14.3 μg/g DW of α-tocotrienols
			551 μg/g DW in leaf (10-fold)
Corn (*Zea mays*)	*hggt* (barley)	Embryo-specific	>800 nmol/g DW in seeds (6-fold)
	hppd and *vte3* (Aradidopsis)	CaMV 35S	9.5 μg/g DW (3-fold)
Lettuce (*Lactuca sativa*)	*vte4* (Arabidopsis)	CaMV 35S	Improved α-/γ –tocopherol ratio up to 0.4–544 as compared to α/γ ratio in wild type, which is 0.6–1.2
Mustard (*Brassica juncea*)	*vte4* (Arabidopsis)	CaMV 35S	62.29 μg/g of α-tocopherol levels in seeds (6-fold)

Biotechnology and Nutritional Improvement of Crops. Table 7 (Continued)

Species	Genes (source)	Promoters	Tocochromanol levels in transgenic plants
Canola (*Brassica napus*)	*hppd* (Arabidopsis)	DC3Ω	819 μg/g oil in seeds (1.2-fold)
	hppd, *hpt1*, *vte1* (Arabidopsis)	DC3Ω (*hppd*), napin (*hpt1*, *vte1*)	1,850 μg/g oil in seeds (2-fold)
	tyrA (*E. uredovora*)	Lac	540 μg/g of total tocochromanols in seeds (2.3-fold)
	tyrA (*E. uredovora*), *hppd*, *hpt1* (Arabidopsis)	Lac	3.7-fold increase in seeds
	vte1 (Arabidopsis)	Napin	1,018 μg/g oil of total tocochromanols in seeds (20–50% increase)
	vte1 (corn)	Napin	1,159 μg/g oil of total tocochromanols in seeds
Soybean (*Glycine max*)	*tyrA* (*E. uredovora*), *hppd*, *hpt1* and *ggh* (Arabidopsis)	Lac	4,806 μg/g of total tocochromanols in seeds (15-fold)
	vte3 (Arabidopsis)	7Sα	The majority of the tocopherol accumulated as γ-tocopherol (75–85%) with increased α-tocopherol as well. By contrast, these seeds had very low levels of β- and δ-tocopherol, only 0.5–1.5% of total tocopherols
	vte4 (Arabidopsis)	7Sα	100% of α-tocopherols in seeds
	vte3 and *vte4* (Arabidopsis)	7Sα	8-fold increase in α-tocopherol in seeds
	vte4 (*Perilla frutescens*)	Vicilin	390 nmol/g FW of α-tocopherol content in seeds (10.4-fold)
			52 nmol/g FW of β-tocopherol content in seed (14.9-fold)
Arabidopsis (*Arabidopsis thaliana*)	*vte4* (Arabidopsis)	DC3	328 μg/g α-tocopherol in seeds (86-fold)
	hppd (Arabidopsis)	CaMV 35S, DC3	37% and 28% increase of tocopherol levels in leaf and seed respectively
	hpt1 (Arabidopsis)	CaMV 35S	4.4-fold increase in total leaf tocopherol content (mainly α-tocopherols)
	hpt1 (Arabidopsis)	Napin	2-fold increase of tocopherols in seed

Source: Data updated from [111]

the precursor phytyldiphosphate, increased the tocochromanol content by up to 15-fold [118].

The seed-specific expression of Arabidopsis MPBQ-MT and γ-TMT in soybean resulted in a complete conversion of β-, γ-, and δ-tocopherols to α-tocopherol, with a fivefold enhancement in the vitamin E activity of soybean oil [119]. Similarly, Tavva et al. [120] achieved a 10.4-fold increase in α-tocopherol levels and a 14.9-fold increase in β-tocopherol levels in soybean seeds expressing *Perilla frutescens* γ-TMT.

Vitamin C Most vitamin C (ascorbic acid) in plants is synthesized through the L-galactose pathway [121], although other routes through galacturonic acid, L-glucose, and *myo*-inositol have been proposed [122]. Oxidation of ascorbic acid produces the short-lived radical monodehydroascorbate (MDHA), which is either converted to ascorbic acid by MDHA reductase (MDHAR) or undergoes spontaneous degradation into ascorbic acid and dehydroascorbate (DHA). DHA is then either recycled to ascorbic acid by dehydroascorbate reductase (DHAR), using

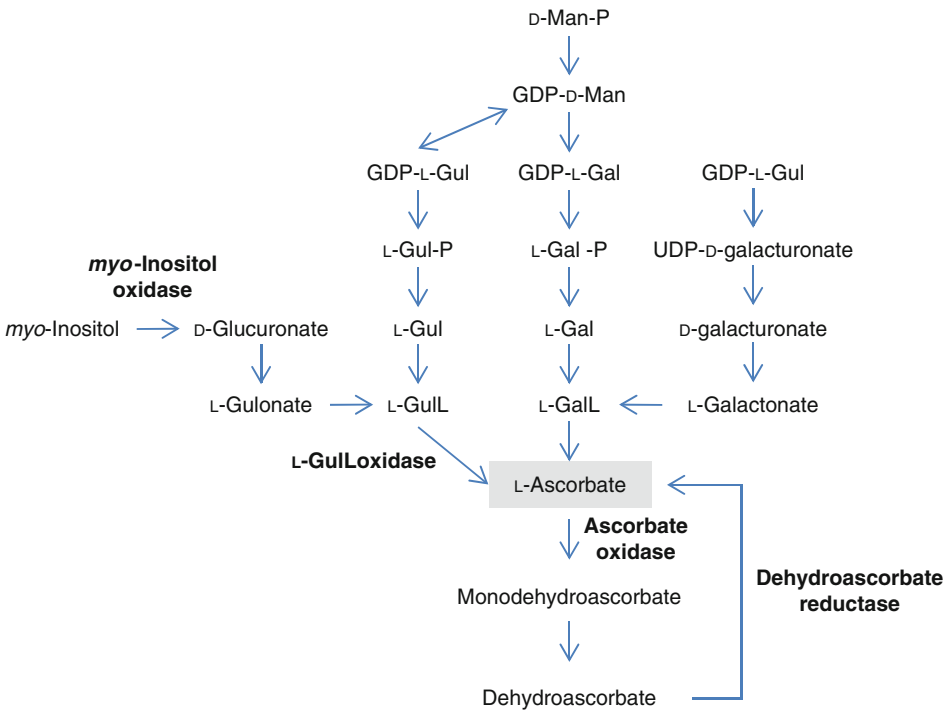

Biotechnology and Nutritional Improvement of Crops. Figure 7
Synthesis of ascorbic acid in plants [96]. Abbreviations: Gal, galactose; GalL, galactonolactone; GDP guanidine diphophate; Gul, gulose; GulL, gulonolactone; Man, mannose; P, phosphate; UDP, uridine diphosphate

glutathione as the reductant, or undergoes irreversible hydrolysis to generate 2,3-diketogulonic acid (Fig. 7).

Since at least three separate metabolic pathways are involved in the biosynthesis of ascorbic acid in plants in addition to the recycling of oxidation products, three different strategies have been used to enhance ascorbate levels: overexpression of enzymes involved in ascorbate biosynthesis, overexpression of recycling enzymes (such as DHAR) to enhance regeneration, and antisense suppression of ascorbate oxidase (Table 8). Enhancing ascorbate regeneration has been the most successful approach [122]. The expression of wheat DHAR increased ascorbate levels by twofold in transgenic corn seed and fourfold in transgenic tobacco leaves, with concomitant reductions in the levels of DHA [123], whereas the expression of rice DHAR in corn increased the level of ascorbate in the seeds by more than sixfold [96].

Jain and Nessler [124] achieved a sevenfold increase in ascorbate levels by expressing L-gulono γ-lactone oxidase (GLOase) in tobacco and lettuce (the lack of this enzyme accounts for the inability of primates to synthesize their own ascorbic acid). Transgenic tobacco plants expressing phosphomannomutase (PMM) or GDP-D-mannose pyrophosphorylase (GMP) also accumulated double the normal levels of ascorbate [125].

Plants of the genus *Actinidia* are particularly rich in ascorbic acid, so genes from the ascorbate biosynthesis pathway in *Actinidia* species have been expressed in model plants to ascertain if this can be used to boost ascorbate levels. Transgenic tobacco plants expressing *Actinidia chinensis* GDP-L-galactose guanyltransferase contained threefold the normal levels of ascorbate in the leaves [126] whereas Arabidopsis plants expressing the equivalent enzyme from *Actinidia eriantha* contained 4.2-fold more ascorbate than normal. Expressing this enzyme in concert with GDP-L-mannose-3′,5′-epimerase achieved a 12-fold increase in ascorbate revealing an important bottleneck in the L-galactose pathway [127].

Biotechnology and Nutritional Improvement of Crops. Table 8 Transgenic plants with enhanced ascorbate levels [122]

Species	Genes (source)	Promoters	Ascorbate levels in transgenic plants
Corn (*Zea mays*)	*dhar* (wheat; *Triticum aestivum*)	Corn Ubi-1 (constitutive)	~150 nmol/g FW in kernel (1.9-fold)
	dhar (rice; *Oryza sativa*)	Barley (*Hordeum vulgare*) D-hordein	607.2 nmol/g FW (6.1-fold)
Tomato (*Solanum lycopersicum*)	*mMDH*	CaMV 35S (constitutive)	(5–6-fold)
Lettuce (*Lactuca sativa*)	*GLOase* (rat; *Rattus norvegicus*)	CaMV 35S	430–580 nmol/g FW (4–7-fold)
Tobacco (*Nicotiana tabacum*)	*GLOase* (rat)	CaMV 35S	480 nmol/g FW (7-fold)
	dhar (wheat)	CaMV 35S	2,800 nmol/g FW (2.4-fold)
	GalLDH (tobacco)	CaMV 35S	(1.5–2-fold)
	GMP (*Malpighia glabra*)	MgGMP	800–1,000 nmol/g FW (2-fold)
	GGT (GDP-L-galactose D- mannose-1-phosphate guanyltransferase) (*Actinidia chinensis*)	CaMV 35S	1,000 μg/g FW (3-fold)
	PMM (*M. glabra*)	MgGMP	700 μg/g FW (2-fold)
Arabidopsis (*Arabidopsis thaliana*)	*GalUR* (strawberry; *Fragaria* × *ananassa*)	CaMV 35S	~600 nmol/g (3-fold)
	miox4 (Arabidopsis)	CaMV 35S	~500 nmol/g FW (2–3-fold)
	GGT (GDP-L-galactose guanyltransferase) (*Actinidia eriantha*)	CaMV 35S	8.6–12-fold
	GME (GDP-L-mannose-3′,5′-epimerase) (*A. eriantha*)	CaMV 35S	

Source: Data updated from [122]

Folate Folic acid is a tripartite molecule combining pterin, p-aminobenzoate (PABA), and one or more glutamate moieties. The three parts of the molecule are produced separately in different subcellular compartments (plastids, cytosol, and mitochondria) and then joined together. Pterin is formed from guanosine triphosphate (GTP) in the cytosol and PABA is formed from chorismate in the plastids. These moieties are then transported to the mitochondria, where they condense to form dihydropteroate and are converted to polyglutamates (Fig. 8). Metabolic engineering can be used to increase folate levels in plants but the compartmentalization of the pathway adds a degree of complexity (Table 9).

Initial strategies involving modulation of individual branches of the pathway have been moderately successful. For example, expressing GTP cyclohydrolase 1 (GCH1) enhances the cytosolic (pterin) branch of the pathway and increases pterin levels, which ensures that the other two branches become rate limiting. In tomato, this approach doubled the normal levels of folate in the fruit [128]. Similar results were achieved by enhancing the PABA branch of the pathway by overexpressing aminodeoxychorismate synthase

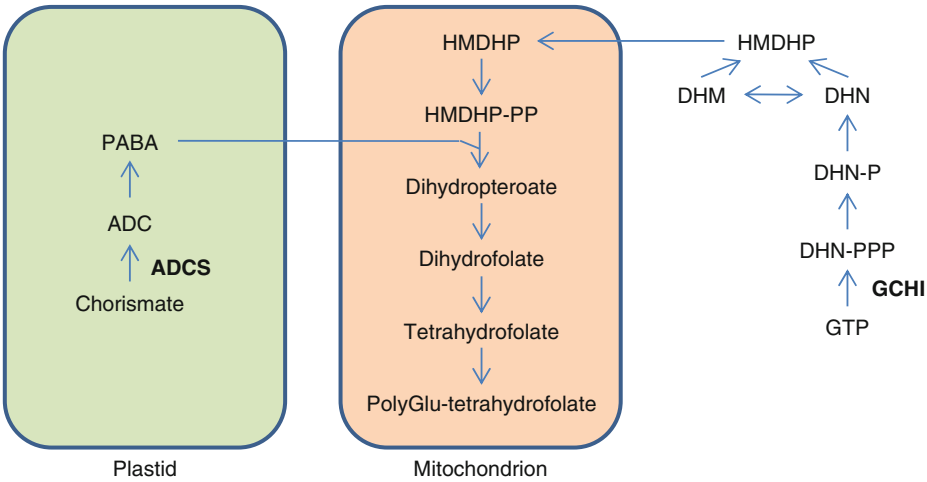

Biotechnology and Nutritional Improvement of Crops. Figure 8
Synthesis of folate in plants [96]. Abbreviations: aminodeoxychorismate (ADC), GTP cyclohydrolase I (GCHI), ADC synthase (ADCS), DHN, dihydroneopterin; -P/-PP/-PPP, mono/di/triphosphate; DHM, dihydromonopterin; HMDHP, hydroxymethyldihydropterin

Biotechnology and Nutritional Improvement of Crops. Table 9 Transgenic plants with enhanced folate levels [172]

Species	Genes (source)	Promoters	Folate levels in transgenic plants
Tomato (*Solanum lycopersicum*)	*gtpchI* (mammalian)	Tomato E8	0.8–2.3 nmol/g FW (2-fold)
	gtpchI (mammalian) and *adcs* (Arabidopsis)	Tomato E8	8.4 μg/g DW (25-fold)
Corn (*Zea mays*)	*folE* (*Escherichia coli*)	Barley (*Hordeum vulgare*) D-hordein	1.94 μg/g DW (2-fold)
Arabidopsis (*Arabidopsis thaliana*)	*folE* (*E. coli*)	CaMV 35S	2.27–4.70 nmol/g FW (2–4-fold)
Rice (*Oryza sativa*)	*gtpchI* (Arabidopsis)	Rice endosperm-specific globulin (glb-1)	38.3 nmol/g (100-fold)
	adcs (Arabidopsis)		
Lettuce (*Lactuca sativa*)	*gtpchI* (chicken; *Gallus gallus*)	CaMV 35S	1.9 μg/g (5.4-fold)

Source: Data updated from [172]

(ADCS) [129]. Each of these experiments revealed the limitations of the other pathway branches, but by crossing the two transgenic lines, the enhanced pathways were combined resulting in complementation between them and the creation of transgenic tomato fruits containing 25-fold the normal levels of folate [129]. The strategy has been replicated in other crops with similarly impressive results: the expression of Arabidopsis GCH1 and ADCS in rice endosperm, e.g., increased folate levels by up to 100-fold [130].

Pantothenate Although most work in the area of vitamin enhancement in plants has focused on vitamins A, B_9 (folate), C, and E, there have been a small number of studies addressing other vitamins. Fouad and Rathinasabapathi [131] expressed the *E. coli*

*pan*D gene encoding L-aspartate-α-decarboxylase (ADC) in tobacco and increased the level of pantothenate (vitamin B_5) in the leaves by up to 4.1-fold. Similarly, Chakauya et al. [132] expressed the *E. coli pan*B gene encoding ketopantoate hydroxymethyltransferase (KPHMT) in canola, increasing levels of pantothenate in leaves, flowers, siliques, and seeds by 1.5–2.5-fold compared with the wild type.

Increasing Mineral Levels

In contrast to the situation with vitamins and essential amino acids and fatty acids, the mineral content of plants cannot be increased by metabolic engineering because minerals are not synthesized de novo by plants; instead they are taken up from the environment. Therefore, increasing the mineral density of plants using biotechnology involves a different set of strategies, focusing on the introduction of genes that improve the efficiency of mineral extraction from the soil (through improved mobilization and/or improved uptake), improve the efficiency of transport from the roots to storage organs such as seeds and fruits, and increase the capacity of storage organs to store minerals in a form that is available in the diet and not toxic to the plant [23, 32]. In addition, these strategies can be supplemented with those seeking to reduce the abundance of antinutritional compounds such as phytate, which inhibits mineral absorption in the gut, and/or to increase the abundance of nutritional enhancer compounds such as inulin, which facilitate mineral absorption by slowing down the progress of food through the gut (Table 10).

Biotechnology and Nutritional Improvement of Crops. Table 10 Some examples of mineral nutritional enhancers and antinutrients in plant foods [37]

Nutritional enhancers	Major dietary source
β-Carotene (pro-vitamin A)	Green and orange vegetables
Certain amino acids (cysteine, lysine, etc.)	Animal meats
Certain organic acids (ascorbic acid, citrate, etc.)	Fresh fruit and vegetables
Hemoglobin	Animal meats
Inulin	Chicory, garlic, onion, wheat, artichoke
Long-chain fatty acids	Human breast milk
Antinutrients	**Major dietary source**
Phytic acid (phytate)	Whole legume seeds and cereal grains
Goitrogens	*Brassicas* and *Alliums*
Hemagglutinins	Most legumes and wheat
Oxalic acid (oxalate)	Different vegetables (spinaches, beet, linseed, oca)
Tannins and other polyphenolics	Tea, coffee, beans, sorghum

Source: Adapted from [37]

Mineral Uptake and Transport The efficiency with which minerals are taken up from the soil depends on their accessibility, which in turn reflects their solubility and interactions with soil particles. Iron is present in the soil mainly as Fe^{3+}, an insoluble form with the tendency to bind strongly to inert particles. Therefore, plants have evolved two distinct strategies to facilitate iron absorption (Fig. 9). Strategy I is used by non-graminaceous plants and involves acidifying the rhizosphere through the secretion of protons, reducing Fe^{3+} to Fe^{2+} using reductases and then absorbing the soluble Fe^{2+} using specific transporters. Strategy II is used by graminaceous plants and involves the direct acquisition of Fe^{3+} by secreting chelating agents (phytosiderophores) into the rhizosphere, followed by adsorption of the chelated iron complexes. Specific root transporters are then required for the uptake of the soluble Fe^{3+}-phytosiderophore complexes [133]. Zinc is present in soil as Zn^{2+} and can be directly absorbed in this form. Many of the genes required for zinc uptake, sequestration, and redistribution in plants have been identified [44] and it is thought that zinc-hyperaccumulating plants sequester large amounts of zinc in the vacuole, a strategy that confers zinc tolerance. However, Zn^{2+} can also form chelates with phytosiderophores, and the Zn^{2+}-phytosiderophore complexes share the same channels as those used for iron chelates. Therefore, some strategies that have been developed to improve the uptake of iron also improve the uptake of zinc as a beneficial by-product, and vice

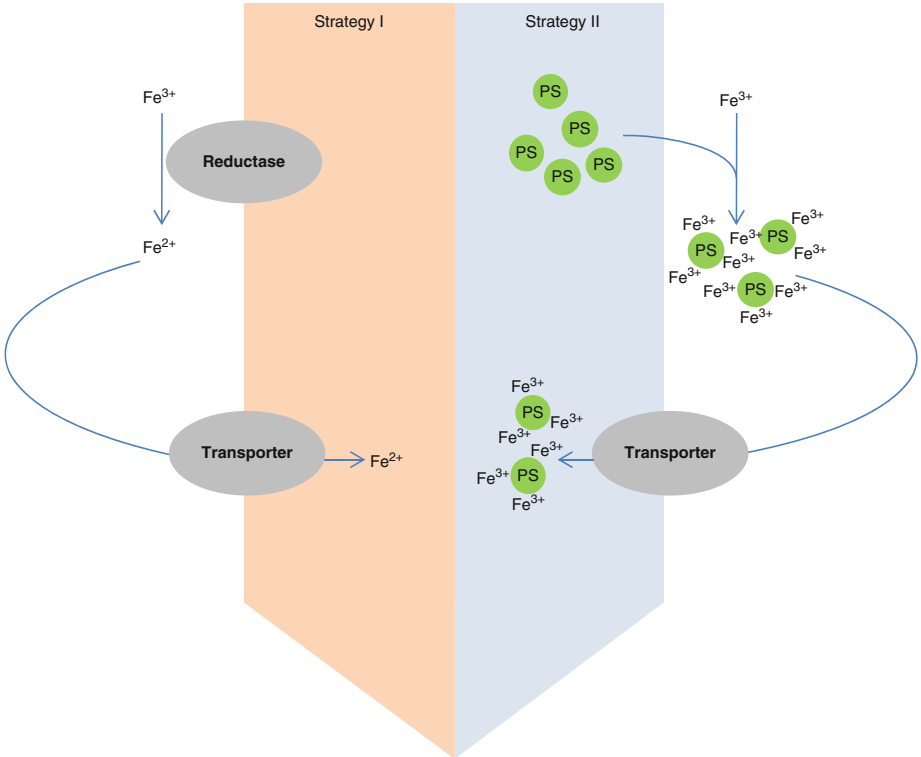

Biotechnology and Nutritional Improvement of Crops. Figure 9
Strategies for iron acquisition by plants [134]. Strategy I, as used by non-graminaceous plants, involves the acquisition of Fe^{2+} after reduction of Fe^{3+} in the rhizosphere by secreted reductases. Strategy II, as used by graminaceous plants, involves the secretion of phytosiderophores (PS) which chelate Fe^{3+}, allowing absorption of the chelated complexes

versa, although this depends on the genes involved [134]. Other minerals are taken up through specific transporters, e.g., plants take up selenium from the soil in the form of selenate (via sulfate transporters), selenite (via phosphate transporters), or as organic compounds (selenoproteins), and they take up calcium via specific Ca^{2+}/ H^{+} antiporters (CAX). Once inside the plant, minerals may also share transport mechanisms – e.g. Fe^{2+}, Zn^{2+}, and Ca^{2+} may all form complexes with nicotianamine for transport through the phloem to sink tissues.

In order to improve iron uptake from the soil, transgenic plants have been created expressing heterologous iron transporters, reductases, and enzymes involved in phytosiderophore biosynthesis (Table 11). For strategy I plants, such approaches have usually involved the expression of iron transport proteins, whereas for strategy II plants, iron accumulation can be enhanced by the production of higher levels of phytosiderophores, with the anticipated collateral effects on zinc absorption [23]. In rice, e.g., iron and zinc uptake was improved by the expression of the barley *naat-A* and *naat-B* genes encoding nicotianamine aminotransferases, which are involved in phytosiderophore biosynthesis [135]. Similarly, the overexpression of barley nicotianamine synthase in tobacco doubled the iron and zinc concentrations in leaves [136]. Transgenic barley expressing the Arabidopsis ZIP1 iron/zinc transporter, despite having smaller seeds, accumulated twice the amount of zinc and iron as wild-type plants [137]. In contrast, constitutive overexpression of barley ZIP7 increased the zinc content of the grain by 50%, but had negligible effect on the iron content regardless of the abundance of zinc in the soil, showing that iron and zinc are not always co-absorbed [138]. Interestingly, expression of the Arabidopsis putative zinc transporter MTP1 in barley led to a dramatic short-term increase in the amount of

Biotechnology and Nutritional Improvement of Crops. Table 11 Transgenic plants with enhanced mineral levels [23]

Species	Genes (source)	Promoters	Mineral content in seeds (and increase relative to wild type)
Iron			
Corn (*Zea mays*)	*ferritin* (soybean; *Glycine max*) + *phytase (Aspergillus niger)*	Rice glutelin-1	38 μg/g DW (2-fold)
Rice (*Oryza sativa*)	*ferritin* (soybean),	Rice gluB-1	38.1 μg/g DW (3-fold)
		Corn Ubi-1	No increase in seeds
		Rice GluB-1	34.7 μg/g DW (4.4-fold)
		Rice Glb-1	27 μg/g DW (3-fold)
	ferritin (pea; *Pisum sativum*),	CaMV-35S	31.3 μg/g DW (4.82-fold)
	ferritin (common bean; *Phaseolus vulgaris*) + *phytase (Aspergillus fumigatus)*	Rice glutelin-1	22.07 μg/g DW (2-fold)
	nas1 (Arabidopsis; *Arabidopsis thaliana*) + *ferritin* (common bean)	CaMV35S + rice globulin	7 μg/g DW (6.3-fold) (in polished rice)
Tobacco (*Nicotiana tabacum*)	*nas1* (barley; *Hordeum vulgare*)	CaMV35S	(2.3-fold in leaves)
	nas1 (Arabidopsis)	CaMV35S	(1.5-fold in leaves)
Calcium			
Carrot (*Daucus carota*)	sCAX 1 (Arabidopsis)	CaMV35S	3.9 mg/g DW (1.6-fold) (in carrot)
Lettuce (*Lactuca sativa*)	sCAX 1 (Arabidopsis)	Cell division cycle (cdc2a)	18.9 mg/g DW
Potato (*Solanum tuberosum*)	sCAX 1 (Arabidopsis)	CaMV35S	1.7 mg/g DW (3-fold) (in tuber)
	CAX2B chimeric (Arabidopsis)	CaMV35S	2.5 mg/g DW (3-fold) (in tuber)
Rice	sCAX 1 (Arabidopsis)	CaMV35S	not determined
Tomato (*Solanum lycopersicum*)	CAX 4 (Arabidopsis)	CaMV35S	1.8 mg/g DW (in fruit)

Source: Data updated from [23]

zinc stored in the roots under high zinc loads, but no difference in the amount of zinc in the seeds over the long term [139].

Several different approaches can be envisaged to enhance the uptake and storage of selenium, based on the multiple inorganic and organic sources of selenium in the soil and the manner in which they are interconverted [140]. ATP-sulfurylase (APS) is rate limiting for selenate reduction and accumulation in most plants, so the overexpression of this enzyme can increase the uptake of selenate [141]. Selenocysteine methyltransferase (SMT) converts selenocysteine into selenium-methylselenocysteine (MetSeCys), a nontoxic form found at high levels in the selenium-hyperaccumulator, *Astragalus bisulcatus*, so the overexpression of this enzyme would be a suitable approach for increasing the accumulation of organic selenium.

Pilon-Smits et al. [141] expressed Arabidopsis APS in Indian mustard, resulting in a threefold increase in selenium levels in leaves and greater tolerance for high selenate levels in the soil. The levels of organic selenium also increased because of the increased capacity for selenate reduction [141, 142]. Indian mustard plants

overexpressing both APS and SMT accumulated 10-fold more MetSeCys than normal, reflecting the increased uptake of selenate and its conversion to MetSeCys as well as the reduction of selenite [143]. More recently, McKenzie et al. [144] expressed *Brassica oleracea* APS and *Astragalus bisulcatus* SMT in tobacco plants supplied with selenate. The expression of SMT increased total selenium levels up to 4-fold, and whereas the expression of APS did not increased total selenium level, when combined with the SMT, a greater proportion of selenium was converted into MetSeCys.

The calcium content of crops has been enhanced by expressing specific Ca^{2+}/ H^{+} antiporters located in the vacuolar membrane (Table 11). For example, the Arabidopsis cation exchanger 1 antiporter (sCAX1) [145], enhances the level of bioavailable calcium when expressed in transgenic potato tubers and carrot taproots [33, 146–148]. The same protein has been expressed in transgenic lettuce, which accumulated higher levels of calcium than wild-type leaves without impacting on flavor or crispness [149]. Kim et al. [150] constructed a chimeric Arabidopsis gene (*CAX2B*) by combining a truncated N-terminal portion of *CAX2* with the "B" domain from *CAX1*. Transgenic potatoes expressing this recombinant construct accumulated calcium without affecting the levels of related cations such as Mn^{2+}. Transgenic tomatoes expressing the Arabidopsis *CAX4* gene also accumulated higher levels of calcium than wild-type fruits [150].

Mineral Storage in Sink Tissues In cereal grains, minerals are predominantly stored in the bran (embryo and aleurone layer) rather than the endosperm, which means that much of the nutritional value of cereals is lost during polishing [151]. Encouraging plants to absorb more minerals from the soil is therefore not sufficient to increase the nutritional value of *food*. In addition to improving mineral uptake, cereals must be engineered to accumulate minerals in the endosperm.

Minerals in plants are found both as free ions in solution and as complexes with dedicated proteins that have evolved for the specific function of mineral transport and storage (protecting the plants against both mineral deficiency and overload). Ferritin, e.g., is a 450-kDa protein consisting of 24 subunits that form a shell, enabling the storage of up to 4,500 Fe^{3+} ions as crystallites with hydroxide and phosphate. Recombinant soybean ferritin has been expressed in the endosperm of several cereals allowing the accumulation of iron in the endosperm [152–155] and pea ferritin has also been constitutively expressed in rice [156]. In the best cases, the level of bioavailable iron exceeded 35 mg kg^{-1}.

Combined Strategies to Increase Mineral Density in Cereal Grains Although increasing the uptake of iron and the ability of plants to accumulate iron both work as individual strategies to improve the mineral content of cereal crops, there are limitations when each strategy is applied alone. Increasing the uptake of iron without considering its distribution will result in the hyperaccumulation of iron in vegetative tissues as well as the seeds, eventually resulting in overload and toxicity. Conversely, the overexpression of ferritin without compensating for the increased iron storage capacity results in the sequestration of free iron needed by plant cells for normal physiological functions, inhibiting photosynthesis and causing chlorosis even if plenty of iron is available in the soil [154]. These issues can be overcome by combining the strategies, i.e., increasing both uptake and storage capacity in the same plant. For example, the combined expression of Arabidopsis nicotianamine synthase and soybean ferritin in rice resulted in rice grains with 6.3-fold more iron in the polished endosperm than wild-type plants (and also elevated levels of zinc), but no adverse effects [157].

Strategies to Ensure Stored Minerals Are Bioavailable Increasing the levels of minerals in plants does not necessarily increase their bioavailability, i.e., the proportion of the mineral that can be absorbed in the human gut [23]. In some cases, bioavailability depends on the chemical form in which a mineral is presented. For example, selenomethionine is a more bioavailable form of selenium than any inorganic source [18], and heme iron is more bioavailable than nonheme iron [158]. For cereals in particular, bioavailability reflects the presence of antinutritional compounds that inhibit absorption, such as phytate and oxalic acid, which chelate divalent cations (Table 10). It has been shown that high levels of such compounds can reduce mineral bioavailability to the extent of causing marginal deficiency diseases even if absolute mineral levels are adequate [159]. This can easily be overcome with a varied

diet, but is particularly challenging in developing country settings where a monotonous diet of staple cereals in commonplace.

Strategies to tackle the presence of antinutritional compounds include conventional breeding to reduce the level of phytate in cereals, and biotechnology-based approaches to either reduce phytate levels or increase the levels of nutritional enhancers that counteract the effect of phytate. For example, natural variation in levels of the nutritional enhancer inulin has been investigated to increase the bioavailability of zinc [160]. Mutagenesis and conventional breeding have been used to generate low-phytate corn, barley, rice, and soybean [161, 162], which have 66%, 95%, 64%, and 80% less phytate, respectively, than corresponding wild-type lines, as well as beans with a 90% reduction of the normal levels of phytate but with no adverse effects on plant growth and development [163]. A *Medicago truncatula* mutant has also been bred with low levels of oxalic acid and therefore 22.87% higher calcium bioavailability [164]. Phytate levels have also been reduced in transgenic cereals by expressing a recombinant fungal enzyme (phytase) that degrades the compound. This strategy has been used to increase iron bioavailability in wheat (86% reduction in phytate [165, 166]) and corn (23% reduction in phytate [167]). The combined expression of ferritin and phytase was used in rice [168] and corn [169] (95% reduction of phytate) to increase iron levels and bioavailability in simulated digestion/absorption trials.

Stacking Nutritional Enhancement Traits The vast majority of transgenic plants engineered for nutritional enhancement have been created with the specific intention of tackling one particular nutrient (or class thereof). In many cases, this has involved the transfer of a single gene. In others, discussed above, two transgenic lines have been crossed to combine enhancements in an additive or synergistic manner, e.g., enhancing iron uptake and accumulation, or enhancing two branches of a metabolic pathway to increase the levels of folate. An alternative approach is supertransformation (the transformation of transgenic plants with additional transgenes), which has been used to produce VLC-PUFAs in Arabidopsis [88]. Both methods have two major drawbacks – the long and labor-intensive development process involving several breeding generations, and the fact that the different transgenes are unlinked, leading to segregation in subsequent generations [170]. Cotransformation refers to the simultaneous introduction of two or more transgenes, and its major advantages are that plants carrying multiple transgenes are produced in one generation and all the transgenes are likely to integrate at the same locus, thus preventing segregation. Cotransformation has been used to introduce up to seven transgenes simultaneously for the purpose of nutritional enhancement, in this case, the enhancement of carotenoid synthesis in canola [99], but even in this case, the aim was to modulate the levels of a single nutrient, β-carotene.

It is clear that, regardless of the success of experiments involving individual nutrients, the deployment of a transgenic plant line enhanced for a single nutrient will only serve to shift the problem of nutrient deficiency onto a different compound. In order to address the challenge of micronutrient deficiency in a global manner, the next objective must be to enhance staple crops for all essential nutrients simultaneously. Zhu et al. [95] reported a unique and surprisingly straightforward approach to this challenge based on combinatorial nuclear transformation in corn. They chose the carotenoid biosynthetic pathway and transformed corn with a collection of five transgenes encoding the enzymes phytoene synthase, phytoene desaturase, lycopene β-cyclase, β-carotene hydroxylase, and β-carotene ketolase. Unlike other transformation experiments where the aim is to achieve a defined outcome, here the aim was to generate maximum diversity, i.e., a library of transformants expressing different combinations of transgenes. Transgenic plants expressing different enzyme combinations and showing distinct metabolic phenotypes were generated, allowing the identification and complementation of rate-limiting steps in the pathway. Individual transgenic lines were identified with extraordinarily high levels of β-carotene (as discussed earlier) and other carotenoids, providing the mechanism to generate plants with high levels of different nutrients in the same experiment. The same group expanded this principle by breeding selected transgenic lines with selected non-transgenic cultivars to generate lines with unprecedented levels of zeaxanthin [34] and by repeating the process with additional

transgenes to identify plants simultaneously enhanced for multiple vitamins. Using four transgenes encoding enzymes from three metabolic pathways (corn PSY and bacterial CrtI for carotenoid synthesis, rice DHAR for ascorbate synthesis, and *E. coli* GCH1 for folate synthesis), Naqvi et al. [96] generated transgenic corn lines with a 407-fold increase in β-carotene (57 μg/g DW), a 6.1-fold increase in ascorbate (106.94 μg/g DW), and a 2-fold increase in folate (200 μg/g DW) compared to the non-transformed control plants.

Future Directions

Biotechnology has the potential to address some of the major elements of food insecurity both by increasing the availability of food and making that food more nutritious. The nutritional properties of plants can be improved by increasing the levels of essential amino acids, PUFAs, and vitamins, and by favoring the accumulation of minerals in a bioavailable form. Golden Rice and Multivitamin Corn are key developments in the history of nutritional enhancement, providing models for the development of crops that will particularly benefit subsistence farmers in developing countries. It is imperative that the focus shifts away from single gene strategies and single nutrients and toward the introduction of multiple genes that simultaneously enhance multiple pathways, leading ultimately toward the creation of transgenic crops that are in every sense of the word nutritionally complete.

Bibliography

Primary Literature

1. FAO (2006) The state of food insecurity in the world 2006. FAO, Rome
2. Christou P, Twyman RM (2004) The potential of genetically enhanced plants to address food insecurity. Nutr Res Rev 17:23–42
3. Ramessar K, Naqvi S, Dashevskaya S, Peremarti A, Yuan D, Gomez-Galera D, Velez SMR, Farre G, Sabalza M, Miralpeix B, Twyman RM, Zhu C, Bassie L, Capell T, Christou P (2009) The contribution of plant biotechnology to food security in the 21st century. In: Amsel L, Hirsch L (eds) Food science and security. Nova Science, New York
4. FAO/WHO (2002) Human vitamin and mineral requirements. Report of a joint FAO/WHO expert consultation. FAO/WHO Press, Rome/Geneva
5. FAO/WHO/UNU (2007) Protein and amino acid requirements in human nutrition. Report of a joint WHO/FAO/UNU Expert Consultation. FAO/WHO Press, Rome/Geneva
6. Burr GO, Burr MM, Miller E (1930) On the fatty acids essential in nutrition. III. J Biol Chem 86:1–9
7. Fürst P, Stehle P (2004) What are the essential elements needed for the determination of amino acid requirements in humans? J Nutr 134:1558S–1565S
8. Harrison EH (2005) Mechanisms of digestion and absorption of dietary vitamin A. Annu Rev Nutr 25:87–103
9. UNICEF (2006) Vitamin A deficiency. http://www.childinfo.org/areas/vitamina/
10. Scott JM, Kirke P, Molloy A, Daly L, Weir D (1994) The role of folate in the prevention of neural tube defects. Proc Nutr Soc 53:631–636
11. Basu TK, Dickerson JWT (1996) Vitamin C (ascorbic acid). In: Basu TK, Dickerson JWT (eds) Vitamins in health and disease. CAB International, Oxford, UK, pp 125–147
12. WHO (2003) Battling iron deficiency anemia: the challenge. WHO Press, Geneva
13. Schümann K (2001) Safety aspects of iron in food. Ann Nutr Metab 45:91–101
14. Maret W, Sandstead HH (2006) Zinc requirements and the risks and benefits of zinc supplementation. J Trace Elem Med Biol 20:3–18
15. WHO (2004) Iodine status worldwide: WHO global database on iodine deficiency. WHO Press, Geneva
16. Lyons GH, Stangoulis JCR, Graham RD (2004) Exploiting micronutrient interaction to optimize biofortification programs: The case for inclusion of selenium and iodine in the HarvestPlus Program. Nutr Rev 62:247–252
17. Lyons GH, Lewis J, Lorimer MF, Holloway RE, Brace DM, Stangoulis JCR, Graham RD (2004) High-selenium wheat: agronomic biofortification strategies to improve human nutrition. Food Agric Environ 2:171–178
18. Combs GF (2001) Selenium in global food system. Br J Nutr 85:517–547
19. Shrimpton R, Schultink W (2002) Can supplements help meet the micronutrient needs of the developing world? Proc Nutr Soc 61:223–229
20. WHO/WFP/UNICEF (2007) Preventing and controlling micronutrient deficiencies in populations affected by an emergency. Joint statement by the World Health Organization, the World Food Programme and the United Nations Children's Fund. WHO Press, Geneva
21. Allen LH, Gillespie SR (2001) What works? A review of the efficacy and effectiveness of nutrition interventions. ACC/SCN/Asian Development Bank, Geneva/Manila
22. Black RE (2003) Zinc deficiency, infectious disease and mortality in the developing world. J Nutr 133: 1485S–1489S
23. Gomez-Galera S, Rojas E, Sudhakar D, Zhu C, Pelacho AM, Capell T, Christou P (2010) Critical evaluation of strategies for mineral fortification of staple food crops. Transgenic Res 19:165–180

24. Underwood BA, Smitasiri S (1999) Micronutrient malnutrition: policies and programs for control and their implications. Annu Rev Nutr 19:303–324
25. UNICEF (2008) Sustainable elimination of iodine deficiency. UNICEF, New York
26. Sadighi J, Mohammad K, Shikholeslam R, Amirkhani MA, Torabi P, Salehi F, Abdolahi Z (2009) Anaemia control: lessons from the flour fortification programme. Public Health 123:794–799
27. Frossard E, Bucher M, Mächler F, Mozafar A, Hurrell R (2000) Potential for increasing the content and bioavailability of Fe, Zn and Ca in plants for human nutrition. J Sci Food Agric 80:861–879
28. Li Y, Diosady LL, Jankowski S (2008) Effect of iron compounds on the storage stability of multiple-fortified Ultra Rice®. Int J Food Sci Technol 43:423–429
29. Zimmermann MB, Wegmueller R, Zeder C, Chaouki N, Biebinger R, Hurrell RF, Windhab E (2004) Triple fortification of salt with microcapsules of iodine, iron, and vitamin A. J Clin Nutr 80:1283–1290
30. IZINCG (2007) Zinc fortification (technical brief 4). http://www.izincg.org/index.php
31. Nga TT, Winichagoon P, Dijkhuizen MA, Khan NC, Wasantwisut E, Furr H, Wieringa FT (2009) Decreased prevalence of anemia and improved micronutrient status and effectiveness of deworming in rural Vietnamese school children. J Nutr 139:1013–1021
32. Zhu C, Naqvi S, Gomez-Galera S, Pelacho AM, Capell T, Christou P (2007) Transgenic strategies for the nutritional enhancement of plants. Trends Plant Sci 12:548–555
33. Jeong J, Guerinot ML (2008) Biofortified and bioavailable: The gold standard for plant-based diets. Proc Natl Acad Sci USA 105:1777–1778
34. Naqvi S, Zhu C, Farre G, Sandmann G, Capell T, Christou P (2010) Synergistic metabolism in hybrid corn reveals bottlenecks in the carotenoid pathway and leads to the accumulation of extraordinary levels of the nutritionally important carotenoid zeaxanthin. Plant Biotechnol J. doi:10.1111/j.1467-7652.2010.00554.x.
35. Stein AJ, Meenakshi JV, Qaim M, Nestel P, Sachdev HPS, Bhutta ZA (2008) Potential impacts of iron biofortification in India. Soc Sci Med 66:1797–1808
36. Cakmak I (2008) Enrichment of cereal grains with zinc: agronomic or genetic biofortification? Plant Soil 302:1–17
37. Welch RM, Graham RD (2004) Breeding for micronutrients in staple food crops from a human nutrition perspective. J Exp Bot 55:353–364
38. White PJ, Broadley MR (2005) Biofortifying crops with essential mineral elements. Trends Plant Sci 10:586–593
39. Wong JC, Lambert RJ, Wurtzel ET, Rocheford TR (2004) QTL and candidate genes phytoene synthase and zeta-carotene desaturase associated with the accumulation of carotenoids in maize. Theor Appl Genet 108:349–359
40. Santos CA, Simon PW (2002) QTL analyses reveal clustered loci for accumulation of major provitamin A carotenes and lycopene in carrot roots. Mol Genet Genomics 268: 122–129
41. Harjes CE, Rocheford TR, Bai L, Brutnell TP, Kandianis CB, Sowinski SG, Stapleton AE, Vallabhaneni R, Williams M, Wurtzel ET, Yan J, Buckler ES (2008) Natural genetic variation in lycopene epsilon cyclase tapped for maize biofortification. Science 319:330–333
42. Yan J, Kandianis CB, Harjes CE, Bai L, Kim EH, Yang X, Skinner DJ, Fu Z, Mitchell S, Li Q, Fernandez MG, Zaharieva M, Babu R, Fu Y, Palacios N, Li J, Dellapenna D, Brutnell T, Buckler ES, Warburton ML, Rocheford T (2010) Rare genetic variation at *Zea mays crtRB1* increases beta-carotene in maize grain. Nat Genet 42:322–327
43. Graham RD, Welch RM, Bouis HE (2001) Addressing micronutrient malnutrition through enhancing the nutritional quality of staple foods: principles, perspectives and knowledge gaps. Adv Agron 70:77–142
44. White PJ, Broadley MR (2009) Biofortification of crops with seven mineral elements often lacking in human diets – iron, zinc, copper, calcium, magnesium, selenium and iodine. New Phytol 182:49–84
45. Prasanna BM, Vasal SK, Singh NN (2001) Quality protein maize. Curr Sci 81:1308–1319
46. Zarkadas C, Hamilton R, Yu Z, Choi V, Khanizadeh S, Rose N, Pattison P (2000) Assessment of the protein quality of 15 new northern adapted cultivars of quality protein maize using amino acid analysis. J Agric Food Chem 48:5351–5361
47. Segal G, Song R, Messing J (2003) A new opaque variant of maize by a single dominant RNA-interference-inducing transgene. Genetics 165:387–397
48. Huang S, Frizzi A, Florida C, Kriger D, Luethy M (2006) High lysine and high tryptophan transgenic maize resulting from the reduction of both 19- and 22-kD α-zeins. Plant Mol Biol 61:525–535
49. Sindhu AS, Zheng ZW, Murai N (1997) The pea seed storage protein legumin was synthesized, processed and accumulated stably in transgenic rice endosperm. Plant Sci 130:189–196
50. Stöger E, Parker M, Christou P, Casey R (2001) Pea legumin overexpressed in wheat endosperm assembles into an ordered paracrystalline matrix. Plant Physiol 125:1732–1742
51. Jung R, Carl F (2000) Transgenic corn with an improved amino acid composition. In: Müntz K, Ulrich W (eds) The 8th international symposium on plant seeds. Institute of Plant Genetics and Crop Plant Research, Gatersleben
52. Yu J, Peng P, Zhang X, Zhao Q, Zhu D, Sun X, Liu J, Ao G (2004) Seed-specific expression of a lysine rich protein *sb401* gene significantly increases both lysine and total protein content in maize seeds. Mol Breed 14:1–7
53. Yang S, Moran D, Jia H, Bicar E, Lee M, Scott M (2002) Expression of a synthetic porcine α-lactoalbumin gene in the kernels of transgenic maize. Transgenic Res 11:11–20
54. Bicar E, Woodman-Clikeman W, Sangtong V, Peterson J, Yang S, Lee M, Scott M (2008) Transgenic maize endosperm containing a milk protein has improved amino acid balance. Transgenic Res 17:59–71

55. Wu XR, Kenzior A, Willmot D, Scanlon S, Chen Z, Topin A, He SH, Acevedo A, Folk WR (2007) Altered expression of plant lysyl tRNA synthetase promotes tRNA misacylation and translation recoding of lysine. Plant J 50:627–663
56. Muntz K, Christov V, Saalbach G, Saalbach I, Waddell D, Pickardt T, Schieder O, Wustenhagen T (1998) Genetic engineering for high methionine grain legumes. Nahrung 42:125–127
57. Chakraborty S, Chakraborty N, Datta A (2000) Increased nutritive value of transgenic potato by expressing a nonallergenic seed albumin gene from *Amaranthus hypochondriacus*. Proc Natl Acad Sci USA 97:3724–3729
58. Chiaiese P, Ohkama-Ohtsu N, Molvig L, Godfree R, Dove H, Hocart C, Fujiwara T, Higgins TJ, Tabe LM (2004) Sulphur and nitrogen nutrition influence the response of chickpea seeds to an added, transgenic sink for organic sulphur. J Exp Bot 55:1889–1901
59. Pastorello EA, Pompei C, Pravettoni V, Brenna O, Farioli L, Trambaioli C, Conti A (2001) Lipid transfer proteins and 2S albumins as allergens. Allergy 56:45–47
60. Rascón-Cruz Q, Sinagawa-García S, Osuna-Castro JA, Bohorova N, Paredes-Lopez O (2004) Accumulation, assembly, and digestibility of amarantin expressed in transgenic tropical maize. Theor Appl Genet 108:335–342
61. Tamás C, Kisgyorgy BN, Rakszegi M, Wilkinson MD, Yang MS, Láng L, Tamás L, Bedo Z (2009) Transgenic approach to improve wheat (*Triticum aestivum* L.) nutritional quality. Plant Cell Rep 28:1085–1094
62. Zhang P, Jaynes JM, Potrykus I, Gruissem W, Puonti-Kaerlas J (2003) Transfer and expression of an artificial storage protein (*asp1*) gene in cassava (*Manihot esculenta* Crantz). Transgenic Res 12:243–250
63. Galili G, Höfgen R (2002) Metabolic engineering of amino acids and storage proteins in plants. Metab Eng 4:3–11
64. Frizzi A, Huang S, Gilbertson LA, Armstrong TA, Luethy MH, Malvar TM (2008) Modifying lysine biosynthesis and catabolism in corn with a single bifunctional expression/silencing transgene cassette. Plant Biotechnol J 6:13–21
65. Falco SC, Guida T, Locke M, Mauvais J, Sandres C, Ward RT, Webber P (1995) Transgenic canola and soybean seeds with increased lysine. Biotechnol (NY) 13:577–582
66. Mazur B, Krebbers E, Tingey S (1999) Gene discovery and product development for grain quality traits. Science 285:372–375
67. Karchi H, Shaul O, Galili G (1994) Lysine synthesis and catabolism are coordinately regulated during tobacco seed development. Proc Natl Acad Sci USA 91:2577–2581
68. Karchi H, Miron D, Ben-Yaacob S, Galili G (1995) The lysine-dependent stimulation of lysine catabolism in tobacco seeds requires calcium and protein phosphorylation. Plant Cell 7:1963–1970
69. Zhu X, Galili G (2003) Increased lysine synthesis coupled with a knockout of its catabolism synergistically boosts lysine content and also transregulates the metabolism of other amino acids in Arabidopsis seeds. Plant Cell 15:845–853
70. Huang S, Kruger DE, Frizzi A, D'Ordine RL, Florida CA, Adams WR, Brown WE, Luethy MH (2005) High-lysine corn produced by the combination of enhanced lysine biosynthesis and reduced zein accumulation. Plant Biotechnol J 3:555–569
71. Houmard NM, Mainville JL, Bonin CP, Huang S, Luethy MH, Malvar TM (2007) High-lysine corn generated by endosperm-specific suppression of lysine catabolism using RNAi. Plant Biotechnol J 5:605–614
72. Hacham Y, Avraham T, Amir R (2002) The N-terminal region of Arabidopsis cystathionine gamma-synthase plays an important regulatory role in methionine metabolism. Plant Physiol 128:454–462
73. Hacham Y, Schuster G, Amir R (2006) An in vivo internal deletion in the N-terminus region of Arabidopsis cystathionine gamma-synthase results in CGS expression that is insensitive to methionine. Plant J 45:955–967
74. Hacham Y, Matityahu I, Schuster G, Amir R (2008) Overexpression of mutated forms of aspartate kinase and cystathionine gamma-synthase in tobacco leaves resulted in the high accumulation of methionine and threonine. Plant J 54:260–271
75. Cho HJ, Brotherton JE, Song HS, Widholm JM (2000) Increasing tryptophan synthesis in a forage legume *Astragalus sinicus* by expressing the tobacco feedback-insensitive anthranilate synthase (*ASA2*) gene. Plant Physiol 123:1069–1076
76. Wakasa K, Hasegawa H, Nemoto H, Matsuda F, Miyazawa H, Tozawa Y, Morino K, Komatsu A, Yamada T, Terakawa T, Miyagawa H (2006) High-level tryptophan accumulation in seeds of transgenic rice and its limited effects on agronomic traits and seed metabolite profile. J Exp Bot 57: 3069–3078
77. Yamada T, Tozawa Y, Hasegawa H, Terakawa T, Ohkawa Y, Wakasa K (2004) Use of a feedback-insensitive a subunit of anthranilate synthase as a selectable marker for transformation of rice and potato. Mol Breed 14:363–373
78. Ishimoto M, Rahman SM, Hanafy MS, Khalafalla MM, El-Shemy HA, Nakamoto Y, Kita Y, Takanashi K, Matsuda F, Murano Y, Funadashi T, Miyagawa H, Wakasa K (2010) Evaluation of amino acid content and nutritional quality of transgenic soybean seeds with high-level tryptophan accumulation. Mol Breed 25:313–326
79. Inaba Y, Brotherton JE, Ulanov A, Widholm JM (2007) Expression of a feedback insensitive anthranilate synthase gene from tobacco increases free tryptophan in soybean plants. Plant Cell Rep 26:1763–1771
80. Tabe L, Wirtz M, Molvig L, Droux M, Hell R (2009) Overexpression of serine acetlytransferase produced large increases in O-acetylserine and free cysteine in developing seeds of a grain legume. J Exp Bot 61:721–733
81. Goyens P, Spilker M, Zock P, Katan M, Mensink R (2005) Compartmental modeling to quantify γ-linolenic acid conversion after longer term intake of multiple tracer boluses. J Lipid Res 46:1474–1483
82. Napier JA (2007) The production of unusual fatty acids in transgenic plants. Annu Rev Plant Biol 58:295–319

83. Robert SS (2005) Production of eicosapentaenoic and docosahexaenoic acid-containing oils in transgenic land plants for human and aquaculture nutrition. Mar Biotechnol 8:103–109
84. Truksa M, Vrinten P, Qiu X (2009) Metabolic engineering of plants for polyunsaturated fatty acid production. Mol Breed 23:1–11
85. Wu G, Truksa M, Datla N, Vrinten P, Bauer J, Zank T, Cirpus P, Heinz E, Qiu X (2005) Stepwise engineering to produce high yields of very long-chain polyunsaturated fatty acids in plants. Nat Biotechnol 23:1013–1017
86. Kajikawa M, Matsui D, Ochiai M, Tanak Y, Kita Y, Ishimoto M, Kohzu Y, Shoji S, Yamato KT, Ohyama K, Fukuzawa H, Kohchi T (2008) Production of arachidonic and eicosapentaenoic acids in plants using bryophyte fatty acid Δ6-desaturase, Δ6-elongase and Δ5-desaturase genes. Biosci Biotechnol Biochem 72:435–444
87. Kinney AJ, Cahoon EB, Damude HG, Hitz WD, Kolar CW, Liu Z-B (2004) Production of very long chain polyunsaturated fatty acids in oilseed plants. WO 2004/071467 A2
88. Qi B, Fraser T, Mugford S, Dobson G, Sayanova O, Butler J, Napier JA, Stobart AK, Lazarus CM (2004) Production of very long chain polyunsaturated omega-3 and omega-6 fatty acids in plants. Nat Biotechnol 22:739–745
89. Eisenreich W, Schwarz M, Cartavrade A, Arigoni D, Zenk MH, Bacher A (1998) The deoxyxylulose phosphate pathway of terpenoid biosynthesis in plants and microorganisms. Chem Biol 5:221–233
90. Zhu C, Naqvi S, Capell T, Christou P (2009) Metabolic engineering of ketocarotenoid biosynthesis in higher plants. Arch Biochem Biophys 483:182–190
91. Enfissi E, Fraser P, Lois L, Boronat A, Schuch W, Bramley P (2005) Metabolic engineering of the mevalonate and non-mevalonate isopentenyl diphosphate-forming pathways for the production of health-promoting isoprenoids in tomato. Plant Biotechnol J 3:17–27
92. Ye X, Al-Babili S, Klöti A, Zhang J, Lucca P, Beyer P, Potrykus I (2000) Engineering the provitamin A (β-carotene) biosynthetic pathway into (carotenoid-free) rice endosperm. Science 287:303–305
93. Paine J, Shipton C, Chaggar S, Howells R, Kennedy M, Vernon G, Wright S, Hinchliffe E, Adams J, Silverstone A, Drake R (2005) Improving the nutritional value of Golden Rice through increased pro-vitamin A content. Nat Biotechnol 23:482–487
94. Aluru M, Xu Y, Guo R, Wang Z, Li S, White W, Wang K, Rodermel S (2008) Generation of transgenic maize with enhanced provitamin A content. J Exp Bot 59:3551–3562
95. Zhu C, Naqvi S, Breitenbach J, Sandmann G, Christou P, Capell T (2008) Combinatorial genetic transformation generates a library of metabolic phenotypes for the carotenoid pathway in corn. Proc Natl Acad Sci USA 105:18232–18237
96. Naqvi S, Zhu C, Farre G, Ramessar K, Bassie L, Breitenbach J, Conesa D, Ros G, Sandmann G, Capell T, Christou P (2009) Transgenic multivitamin corn through biofortification of endosperm with three vitamins representing three distinct metabolic pathways. Proc Natl Acad Sci USA 106:7762–7767
97. Shewmaker CK, Sheehy JA, Daley M, Colburn S, Ke DY (1999) Seed-specific overexpression of phytoene synthase: increase in carotenoids and other metabolic effects. Plant J 20:401–412
98. Ravanello M, Dangyang K, Alvarez J, Huang B, Shewmaker C (2003) Coordinate expression of multiple bacterial carotenoid genes in canola leading to altered carotenoid production. Metab Eng 5:255–263
99. Fujisawa M, Takita E, Harada H, Sakurai N, Suzuki H, Ohyama K, Shibata D, Misawa N (2009) Pathway engineering of *Brassica napus* seeds using multiple key enzyme genes involved in ketocarotenoid formation. J Exp Bot 60:1319–1332
100. Diretto G, Welsch R, Tavazza MF, Pizzichini D, Beyer P, Giuliano G (2007) Silencing of beta-carotene hydroxylase increases total carotenoid and beta-carotene levels in potato tubers. BMC Plant Biol 7:11
101. Diretto G, Al-Babili S, Tavazza R, Papacchioli V, Beyer P, Giuliano G (2007) Metabolic engineering of potato carotenoid content through tuber-specific overexpression of a bacterial mini-pathway. PLoS ONE 2:e350
102. Rosati C, Aquilani R, Dharmapuri S, Pallara P, Marusic C, Tavazza R, Bouvier F, Camara B, Giuliano G (2000) Metabolic engineering of beta-carotene and lycopene content in tomato fruit. Plant J 24:413–419
103. D'Ambrosio C, Giorio G, Marino I, Merendino A, Petrozza A, Salfi L, Stigliani A, Cellini F (2004) Virtually complete conversion of lycopene into beta-carotene in fruits of tomato plants transformed with the tomato *lycopene beta-cyclase* (t*lcy-b*) cDNA. Plant Sci 166:207–214
104. Dharmapuri S, Rosati C, Pallara P, Aquilani R, Bouvier F, Camara B, Giuliano G (2002) Metabolic engineering of xanthophylls content in tomato fruits. FEBS Lett 519:30–34
105. Apel W, Bock R (2009) Enhancement of carotenoid biosynthesis in transplastomic tomatoes by induced lycopene to provitamin A conversion. Plant Physiol 151:59–66
106. Wurbs D, Ruf S, Bock R (2007) Contained metabolic engineering in tomatoes by expression of carotenoid biosynthesis genes from the plastid genome. Plant J 49:276–288
107. Davuluri GR, van Tuinen A, Fraser PD, Manfredonia A, Newman R, Burgess D, Brummell DA, King SR, Palys J, Uhlig J, Bramley PM, Pennings HM, Bowler C (2005) Fruit-specific RNAi-mediated suppression of DET1 enhances carotenoid and flavonoid content in tomatoes. Nat Biotechnol 23:890–895
108. Li L, Paolillo DJ, Parthasarathy MV, Dimuzio EM, Garvin DF (2001) A novel gene mutation that confers abnormal patterns of beta-carotene accumulation in cauliflower (*Brassica oleracea* var. botrytis). Plant J 26:59–67
109. Lu S, Eck J, Zhou X, Lopez A, O'Halloran D, Cosman K, Conlin B, Paolillo D, Garvin D, Vrebalov J, Kochian L, Küpper H, Earle E, Cao J, Lia L (2006) The cauliflower *Or* gene encodes a DNAJ cysteine-rich domain-containing protein that mediates high levels of β-carotene accumulation. Plant Cell 18:3594–3605
110. Lopez AB, Eck JV, Conlin BJ, Paolillo DJ, O'neill J, Li L (2008) Effect of the cauliflower *Or* transgene on carotenoid

accumulation and chromoplast formation in transgenic potato tubers. J Exp Bot 59:213–223
111. DellaPenna D, Pogson B (2006) Vitamin synthesis in plants: tocopherols and carotenoids. Annu Rev Plant Biol 57: 711–773
112. Collakova E, DellaPenna D (2003) The role of homogentisate phytyltransferase and other tocopherol pathway enzymes in the regulation of tocopherol synthesis during abiotic stress. Plant Physiol 133:930–940
113. Tsegaye Y, Shintani D, DellaPenna D (2002) Overexpression of the enzyme p-hydroxyphenylpyruvate dioxygenase in Arabidopsis and its relation to tocopherol biosynthesis. Plant Physiol Biochem 40:913–920
114. Falk J, Brosch M, Schäfer A, Braun S, Krupinska K (2005) Characterization of transplastomic tobacco plants with a plastid localized barley 4-hydroxyphenylpyruvate dioxygenase. J Plant Physiol 162:738–742
115. Cho EA, Lee CA, Kim YA, Baek SH, Reyes BG, Yun SJ (2005) Expression of γ-tocopherol methyltransferase transgene improves tocopherol composition in lettuce (*Latuca sativa* L.). Mol Cells 19:16–22
116. Raclaru M, Gruber J, Kumar R, Sadre R, Luhs W, Zarhloul K, Friedt W, Frentzen M, Weier D (2006) Increase of the tocochromanol content in transgenic *Brassica napus* seeds by overexpression of key enzymes involved in prenylquinone biosynthesis. Mol Breed 18:93–107
117. Rippert P, Scimemi C, Dubald M, Matringe M (2004) Engineering plant shikimate pathway for production of tocotrienol and improving herbicide resistance. Plant Physiol 134:92–100
118. Karunanandaa B, Qi Q, Haoa M, Baszis S, Jensen P, Wong Y, Jiang J, Venkatramesh M, Gruys K, Moshiri F, Beittenmiller D, Weiss J, Valentin H (2005) Metabolically engineered oilseed crops with enhanced seed tocopherol. Metab Eng 7:384–400
119. Van Eenennaam A, Lincoln K, Durrett T, Valentin H, Shewmaker C, Thorne G, Jiang J, Baszis S, Levering C, Aasen E, Hao M, Stein J, Norris S, Last R (2003) Engineering vitamin E content: from Arabidopsis mutant to soy oil. Plant Cell 15:3007–3019
120. Tavva V, Kim Y, Kagan I, Dinkins R, Kim K, Collins G (2007) Increased α-tocopherol content in soybean seed overexpressing the *Perilla frutescens* γ-tocopherol methyltransferase gene. Plant Cell Rep 26:61–70
121. Wheeler GL, Jones MA, Smirnoff N (1998) The biosynthetic pathway of vitamin C in higher plants. Nature 393:365–369
122. Ishikawa T, Dowdle J, Smirnoff N (2006) Progress in manipulating ascorbic acid biosynthesis and accumulation in plants. Physiol Plant 126:343–355
123. Chen Z, Young T, Ling J, Chang S, Gallie D (2003) Increasing vitamin C content of plants through enhanced ascorbate recycling. Proc Natl Acad Sci USA 100:3525–3530
124. Jain AK, Nessler CL (2000) Metabolic engineering of an alternative pathway for ascorbic acid biosynthesis in plants. Mol Breed 6:73–78
125. Badejo A, Eltelib H, Fukunaga K, Fujikawa Y, Esaka M (2009) Increase in ascorbate content of transgenic tobacco plants overexpressing the acerola (*Malpighia glabra*) phosphomannomutase gene. Plant Cell Physiol 50:423–428
126. Laing WA, Wright MA, Cooney J, Bulley SM (2007) The missing step of the L-galactose pathway of ascorbate biosynthesis in plants, an L-galactose guanyltransferase, increases leaf ascorbate content. Proc Natl Acad Sci USA 104:9534–9539
127. Bulley SM, Rassam M, Hoser D, Otto W, Schünemann N, Wright M, MacRae E, Gleave A, Laing W (2009) Gene expression studies in kiwifruit and gene over-expression in Arabidopsis indicates that GDP-L-galactose guanyltransferase is a major control point of vitamin C biosynthesis. J Exp Bot 60:765–778
128. Díaz de la Garza RI, Quinlivan EP, Klaus SM, Basset GJ, Gregory JF III, Hanson AD (2004) Folate biofortification in tomatoes by engineering the pteridine branch of folate synthesis. Proc Natl Acad Sci USA 101:13720–13725
129. Díaz de la Garza R, Quinlivan EP, Klaus SM, Basset GJ, Gregory JF, Hanson AD (2007) Folate biofortification in tomatoes by engineering the pteridine branch of folate synthesis. Proc Natl Acad Sci USA 104:4218–4222
130. Storozhenko S, De Brouwer V, Volckaert M, Navarrete O, Blancquaert D, Zhang GF, Lambert W, Van Der Straeten D (2007) Folate fortification of rice by metabolic engineering. Nat Biotechnol 25:1277–1279
131. Fouad W, Rathinasabapathi B (2006) Expression of bacterial L-aspartate-α-decarboxilase in tobacco increases β-alanine and pantothenate levels and improves thermotolerance. Plant Mol Biol 60:495–505
132. Chakauya E, Coxon K, Wei M, MacDonald M, Barsby T, Abell C, Smith A (2008) Towards engineering increased pantothenate (vitamin B5) levels in palnts. Plant Mol Biol 68:493–503
133. Ishimaru Y, Suzuki M, Tsukamoto T, Suzuki K, Nakazono M, Kobayashi T, Wada Y, Watanabe S, Matsuhashi S, Takahashi M, Nakanishi H, Mori S, Nishizawa NK (2006) Rice plants take up iron as an Fe^{3+}-phytosiderophore and as Fe^{2+}. Plant J 45:335–346
134. Ghandilyan A, Vreugdenhil D, Aarts MGM (2006) Progress in the genetic understanding of plant iron and zinc nutrition. Physiol Plant 126:407–417
135. Takahashi M, Nakanishi H, Kawasaki S, Nishizawa N, Mori S (2001) Enhanced tolerance of rice to low iron availability in alkaline soils using barley nicotianamine aminotransferase genes. Nat Biotechnol 19:466–469
136. Takahashi M, Terada Y, Nakai I, Nakanishi H, Yoshimura E, Mori S, Nishizawa NK (2003) Role of nicotianamine in the intracellular delivery of metals and plant reproductive development. Plant Cell 15:1263–1280
137. Ramesh SA, Choimes S, Schachtman DP (2004) Overexpression of an Arabidopsis zinc transporter in *Hordeum vulgare* increases short-term zinc uptake after zinc deprivation and seed zinc content. Plant Mol Biol 54:373–385
138. Tiong J, Genc Y, McDonald GK, Langridge P, Huang CY (2009) Over-expressing a barley ZIP gene doubles grain zinc content in barley (*Hordeum vulgare*). In: Proceedings of the

international plant nutrition colloquium XVI. UC Davis, California
139. Van der Zaal BJ, Neuteboom LW, Pinas JE, Chardonnens AN, Schat H, Verkleij JA, Hooykaas PJ (1999) Overexpression of a novel Arabidopsis gene related to putative zinc-transporter genes from animals can lead to enhanced zinc resistance and accumulation. Plant Physiol 119:1047–1055
140. Sors TG, Ellis DR, Salt DE (2005) Selenium uptake, translocation, assimilation and metabolic fate in plants. Photosynth Res 86:373–389
141. Pilon-Smits EAH, Hwang S, Lytle CM, Zhu Y, Tai JC, Bravo RC, Chen Y, Leustek T, Terry N (1999) Overexpression of ATP sulfurylase in Indian mustard leads to increased selenate uptake, reduction and tolerance. Plant Physiol 119:123–132
142. Terry N, Zayed AM, de Souza MP, Tarun AS (2000) Selenium in higher plants. Annu Rev Plant Physiol Plant Mol Biol 51:401–432
143. LeDuc DJ, AbdelSamie M, Móntes-Bayon M, Wu CP, Reisinger SJ, Terry N (2006) Overexpressing both ATP sulfurylase and selenocysteine methyltransferase enhances selenium phytoremediation traits in Indian mustard. Environ Pollut 144:70–76
144. McKenzie MJ, Hunter DA, Pathirana R, Watson LM, Joyce NI, Matich AJ, Rowan DD, Brummell DA (2009) Accumulation of an organic anticancer selenium compound in a transgenic Solanaceous species shows wider applicability of the selenocysteine methyltransferase transgene from selenium hyperaccumulators. Transgenic Res 18:407–424
145. Mei H, Zhao J, Pittman JK, Lachmansingh J, Park S, Hirschi KD (2007) In planta regulation of the Arabidopsis Ca^{2+}/H^{+} antiporter CAX1. J Exp Bot 58:3419–3427
146. Park S, Kim CK, Pike LM, Smith RH, Hirschi KD (2004) Increased calcium in carrots by expression of an Arabidopsis H^{+}/Ca^{2+} transporter. Mol Breed 14:275–282
147. Park S, Kang TS, Kim CK, Han JS, Kim S, Smith RH, Pike LM, Hirschi KD (2005) Genetic manipulation for enhancing calcium content in potato tuber. J Agric Food Chem 53:5598–5603
148. Connolly EL (2008) Raising the bar for biofortification: enhanced levels of bioavailable calcium in carrots. Trends Biotechnol 26:401–403
149. Park S, Elless MP, Park J, Jenkins A, Lim W, Chambers E IV, Hirschi KD (2009) Sensory analysis of calcium-biofortified lettuce. Plant Biotechnol J 7:106–117
150. Kim CK, Han JS, Lee HS, Oh JY, Shigaki T, Park SH, Hirschi K (2006) Expression of an *Arabidopsis CAX2* variant in potato tubers increases calcium levels with no accumulation of manganese. Plant Cell Rep 25:1226–1232
151. Sellappan K, Datta K, Parkhi V, Datta SK (2009) Rice caryopsis structure in relation to distribution of micronutrients (iron, zinc, beta-carotene) of rice cultivars including transgenic indica rice. Plant Sci 177:557–562
152. Goto F, Yoshihara T, Shigemoto N, Toki S, Takaiwa F (1999) Iron fortification of rice seeds by the soybean ferritin gene. Nat Biotechnol 17:282–286
153. Drakakaki G, Christou P, Stöger E (2000) Constitutive expression of soybean ferritin cDNA in transgenic wheat and rice results in increased iron levels in vegetative tissues but not in seeds. Transgenic Res 9:445–452
154. Qu LQ, Yoshihara T, Ooyama A, Goto F, Takaiwa F (2005) Iron accumulation does not parallel the high expression level of ferritin in transgenic rice seeds. Planta 222:225–233
155. Vasconcelos M, Datta K, Oliva N, Khalekuzzaman M, Torrizo L, Krishnan S, Oliveira M, Goto F, Datta SK (2003) Enhanced iron and zinc accumulation in transgenic rice with the ferritin gene. Plant Sci 164:371–378
156. Hong-Xia Y, Mei L, Ze-Jian G, Qing-Yao S, Xiao-Hui X, Jin-Song B (2008) Evaluation and application of two high-iron transgenic rice lines expressing a pea ferritin gene. Rice Sci 15:51–56
157. Wirth J, Poletti S, Aeschlimann B, Yakandawal N, Drosse B, Osorio S, Tohge T, Fernie AR, Günther D, Gruissem W, Sautter C (2009) Rice endosperm iron biofortification by targeted and synergistic action of nicotianamine synthase and ferritin. Plant Biotechnol J 7:631–644
158. Theil EC, Briat JF (2004) Plant ferritin and non-heme iron nutrition in humans, HarvestPlus technical monographs 1. International Food Policy Research Institute/International Center for Tropical Agriculture (CIAT), Washington, DC/California
159. Karunaratne AM, Amerasinghe PH, Sadagopa Ramanujam VM, Sandstead HH, Perera PAJ (2008) Zinc, iron and phytic acid levels of some popular foods consumed by rural children in Sri Lanka. J Food Compos Anal 21:481–488
160. Welch RM, Graham RD (2005) Agriculture: the real nexus for enhancing bioavailable micronutrients in food crops. J Trace Elem Med Biol 18:299–307
161. Raboy V (2002) Progress in breeding low phytate crops. J Nutr 132:503S–505S
162. Liu QL, Xu XH, Ren XL, Fu HW, Wu DX, Shu QY (2007) Generation and characterization of low phytic acid germplasm in rice (*Oryza sativa* L.). Theor Appl Genet 114:803–814
163. Campion B, Sparvoli F, Doria E, Tagliabue G, Galasso I, Fileppi M, Bollini R, Nielsen E (2009) Isolation and characterization of an *lpa* (low phytic acid) mutant in common bean (*Phaseolus vulgaris* L.). Theor Appl Genet 118:1211–1221
164. Morris J, Nakata PA, McConn M, Brock A, Hirschi KD (2007) Increased calcium bioavailability in mice fed genetically engineered plants lacking calcium oxalate. Plant Mol Biol 64:613–618
165. Brinch-Pedersen H, Hatzack F, Sørensen LD, Holm PB (2003) Concerted action of endogenous and heterologous phytase on phytic acid degradation in seed of transgenic wheat (*Triticum aestivum* L.). Transgenic Res 12:649–659
166. Brinch-Pedersen H, Hatzack F, Stöger E, Arcalis E, Pontopidan K, Holm PB (2006) Heat-stable phytases in transgenic wheat (*Triticum aestivum* L.): deposition pattern, thermostability, and phytate hydroslysis. J Agric Food Chem 54:4624–4632
167. Chen R, Xue G, Chen P, Yao B, Yang W, Ma Q, Fan Y, Zhao Z, Tarczynski MC, Shi J (2008) Transgenic maize plants

expressing a fungal phytase gene. Transgenic Res 17: 633–643
168. Lucca P, Hurrell R, Potrykus I (2002) Fighting iron deficiency anemia with iron-rich rice. J Am Coll Nutr 21:184S–190S
169. Drakakaki G, Marcel S, Glahn RP, Lund EK, Pariagh S, Fischer R, Christou P, Stöger E (2005) Endosperm specific co-expression of recombinant soybean ferritin and *Aspergillus* phytase in maize results in significant increases in the levels of bioavailable iron. Plant Mol Biol 59:869–880
170. Halpin C, Barakate A, Askari BM, Abbott JC, Ryan MD (2001) Enabling technologies for manipulating multiple genes on complex pathways. Plant Mol Biol 47:295–310
171. Farré G, Sanahuja G, Naqvi D, Bai C, Capell T, Zhu C, Christou P (2010) Travel advice on the road to carotenoids in plants. Plant Sci 179:28–48
172. Bekaert S, Storozhenko S, Mehrshahi P, Bennett MJ, Lambert W, Gregory JF III, Schubert K, Hugenholtz J, Van Der Straeten D, Hanson AD (2008) Folate biofortification in food plants. Trends Plant Sci 13:28–35

Books and Reviews

Lemaux PG (2008) Genetically engineered plants and foods: a scientist's analysis of the issues (Part I). Annu Rev Plant Biol 59:771–812

Lemaux PG (2009) Genetically engineered plants and foods: a scientist's analysis of the issues (part II). Annu Rev Plant Biol 60:511–559

Mène-Saffrané L, DellaPenna D (2009) Biosynthesis, regulation and functions of tocochromanols in plants. Plant Physiol Biochem 48:301–309

Rosati C, Diretto G, Giuliano G (2009) Biosynthesis and engineering of carotenoids and apocarotenoids in plants: state of the art and future prospects. Biotechnol Genet Eng Rev 26:139–162

Breeding in Beef Cattle

Matthew L. Spangler
Department of Animal Science, University of Nebraska, Lincoln, NE, USA

Article Outline

Glossary
Definition of the Subject
Introduction
Structure of the Beef Industry
Basic Principles of Genetic Improvement
Basics of an EPD
Multiple-Trait Selection
Breed Selection
Crossbreeding
Molecular Information
Future Directions
Bibliography

Glossary

Beef Improvement Federation (BIF) accuracy A metric of accuracy that is more conservative than true accuracy. It is linearly related to prediction error variance.

Bio-economic index A collection of EPD that are relevant to a breeding objective whereby each EPD is multiplied by an economic weight.

Composite A crossbred animal. Generally thought of in terms of a pedigreed seedstock animal that is a cross of two or more breeds.

Expected progeny difference Equivalent to half of a breeding value.

Molecular breeding value The sum of marker effects multiplied by the number of copies of a given marker.

Definition of the Subject

The beef cattle industry represents a diverse and unique sector of animal agriculture with varying breeds, production climates, and marketing objectives. The industry is not vertically integrated and thus breeding and selection decisions are controlled by individual farmers and ranchers. In the United States, the average herd size is less than 30 cows. However, there exists sound tools from which to make genetic selection decisions to ultimately make genetic change and improve profitability. These tools, some of which have been utilized for decades, are available to all beef cattle producers. The utilization of current genetic selection tools can aid in the profitability and ultimately the sustainability of beef enterprises.

Introduction

The beef cattle industry is comprised of seedstock and commercial producers. In general, genetic improvement, or accumulation of breeding value, occurs in the seedstock sector and flows to the commercial

industry via the purchase of bulls and/or semen. Less than 10% of producers in the United States utilize artificial insemination (AI). Selection decisions can be made based on a plethora of information, but the most informative are breeding values or expected progeny differences (EPDs) in the US and economic index values. There are several EPD and index values across multiple breeds.

There have also been an increasing number of commercially available genomic tests made available for multiple traits. Some of these have undergone independent validation, while others have not. This technology holds the promise to increase the rate of genetic progress and to allow for selection on those traits that are expensive or challenging to measure routinely. However, there still exist several caveats to solve before this is completely brought to fruition.

Sustainability from a beef perspective will depend on economics and consumer perception. Genetic selection will need to focus on tools that aim solely at the genetic component of phenotypes and tools that apply economic parameters need to be quantified such that a return on investment can be determined. Consumer demand will ultimately be dictated by price and product quality suggesting that efficient genetic selection is needed and that selection tools need to evolve to improve end-product quality.

Structure of the Beef Industry

In other species, such as swine and poultry, the breeding pyramid is much more clearly defined than in beef cattle given formalized breeding companies. However, it still exists in beef cattle (Fig. 1) as some purebred producers have a much larger influence over the gene pool of a breed compared to others. At the nucleus level, animals (particularly sires) are produced for use at the multiplier level although some nucleus animals are sold directly to commercial herds. The nucleus herds are the drivers of genetic change. The multiplier herds, as the name implies, multiply genes from the nucleus populations to produce animals for use in the commercial sector. It is possible, and does occur, for animals from multipliers to enter into nucleus herds.

There are four main pathways from which herds can influence the rate and direction of genetic change: producing sires of sires, sires of dams, dams of sires, and dams of dams. The most influential is sires of sires. As an example, Marquez et al. [1] characterized the population structure of the Red Angus breed and found that indeed it could be divided into nucleus and multiplier herds and that only 30% of the total herds produced sires of sires.

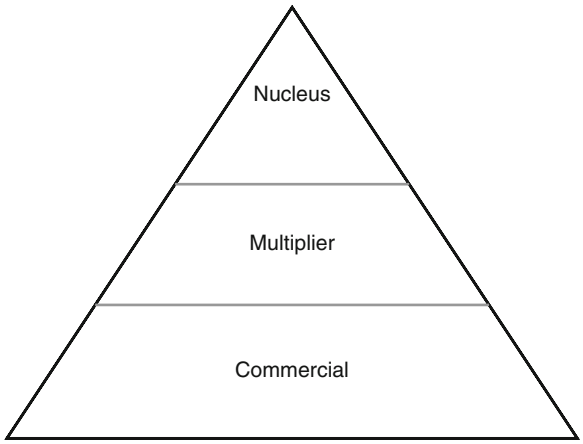

Breeding in Beef Cattle. Figure 1
The breeding pyramid representing the three broad segments of the beef industry

Basic Principles of Genetic Improvement

In order to make genetic improvement the target trait (s), observable or measureable characteristics of an animal, must display variation. The goal of genetic improvement is to improve the phenotype, observed category or measured level of performance for a trait, by improving the genotype or genetic makeup of an animal to best fit the system and to make the best product for consumers. The phenotype (P) of an animal is comprised of both genetic (G) and nongenetic factors such as the environment (E) such that

$$P = G + E$$

These two primary factors, G and E, can be further divided into additive (A), dominance (D), and epistatic (I) genetic effects and both permanent (E_P) and temporary (E_T) environmental effects such that

$$P = G_A + G_D + G_I + E_P + E_T$$

Temporary genetic effects can be thought of as differences in feeding regime or climate and are generally accounted for by contemporary groups whereas PE

are long lasting changes that influence future performance (i.e., the loss of one-quarter of the udder). Contemporary groups are considered to be a group of animals that have been subjected to the same environmental effects or managed alike such as being born in the same year, season, and herd, being of the same sex, and fed the same diet.

Trait Types

There are two broad categories of traits, simply inherited and polygenic traits. Simple traits are expressed qualitatively, controlled by only one or two genes, and are typically influenced little by environment. In contrast, polygenic traits are controlled by many genes, are greatly influenced by the environment, and are quantitative in nature (i.e., they are expressed numerically or on a continuous scale).

Simple Traits

In beef cattle, the phenotype of horns is controlled by dominance wherein the horned allele is recessive. If a heterozygous male is mated to a heterozygous female the resulting calf has a 25% chance of being horned and a 75% chance of being polled (absence of horns). This is illustrated in the Punnett Square below where P denotes the polled allele, and p represents the horned allele.

	P	p
P	PP	Pp
p	pP	pp

Black and red coat color is controlled in the same manner where black is dominant to red such that homozygous (BB) and heterozygous (Bb) animals are black and only homozygous animals for the recessive allele (bb) are red.

Similarly, many genetic defects in cattle are also recessive in nature. A list of known genetic defects in beef cattle can be found in Table 1. Use the example of Neuropathic Hydrocephalus (NH), a recessive lethal mutation found in Angus cattle. If a heterozygous bull (Nn) is mated to a homozygous normal female (NN) then the resulting offspring would be 100% normal (i.e., not afflicted) with 50% of them being homozygous and the other 50% heterozygous.

	N	N
N	NN	NN
n	nN	nN

Breeding in Beef Cattle. Table 1 Genetic defects currently monitored by US breed associations

Genetic abnormality	Primary breed(s) of incidence	Lethal or nonlethal	Mode of inheritance	DNA test available
Alpha (α)-mannosidosis	Red Angus	Lethal	Simple recessive	Yes
Arthrogryposis multiplex (AM)	Angus and derivatives	Lethal	Simple recessive	Yes
Beta (β)-mannosidosis	Salers	Lethal	Simple recessive	Yes
Fawn calf syndrome (FCS)	Angus	Nonlethal	Simple recessive	Yes
Neuropathic hydrocephalus (NH)	Angus	Lethal	Simple recessive	Yes
Hypotrichosis (hairless calf)	Hereford	Nonlethal	Simple recessive	No
Idiopathic epilepsy	Hereford	Nonlethal	Simple recessive	Yes
Osteopetrosis	Angus and Red Angus	Lethal	Simple recessive	Yes
Protoporphyria	Limousin	Nonlethal	Simple recessive	Yes
Pulmonary hypoplasia and anasarca (PHA)	Maine-Anjou and Shorthorn	Lethal	Simple recessive	Yes
Tibial hemimelia (TH)	Shorthorn and Maine-Anjou	Lethal	Simple recessive	Yes

Coat color in shorthorn cattle is controlled by co-dominance. There are three possible phenotypes that can result from the pairing of two alleles, red (R) and white (W). When two R or two W alleles pair together the resulting animals is either red (RR) or white (WW), respectively. However, the heterozygous animals (RW or WR) or an intermediate color, a mixture of both red and white called "roan." The example below illustrates the genotypes and phenotypes that would be expected from the mating of a roan bull to a roan cow. In this example there is a 25% chance the calves will be red, 50% chance they will be roan, and 25% chance the will be white.

	R	W
R	RR	RW
W	WR	WW

Sex-influenced traits have different expressions in different sexes given the same genotype. A classic example of a sex-influenced trait in beef cattle is the presence or absence of scurs. Here the scured allele (Sc) would appear to be dominant in males but recessive in females.

Males	Females
SS = no scurs	SS = no scurs
SSc = scurs	SSc = no scurs
ScSc = scurs	ScSc = scurs

Polygenic Traits

The number of gametes that an individual can produce is equal to 2^n where n is the number of heterozygous loci. The number of possible genotypes that can be produced from any one mating is equal to $3^n \times 2^m$ where n is the number of loci where both parents are heterozygous and m is the number of loci where only one parent is heterozygous. From this, it is obvious that from a single mating there can arise numerous possible genotypes.

	Individual heterozygous at every loci	Both individual heterozygous
Number of genes	Number of gametes	Number of genotypes
1	2 (2^1)	3 (3^1)
2	4 (2^2)	9 (3^2)
10	1,024 (2^{10})	54,049 (3^{10})

Basics of an EPD

A breeding value (BV) is cumulative additive value of an animal. A transmitting ability (TA) is the average of gametes an individual passes to offspring.

$$TA = 1/2BV$$

In beef cattle, a TA is referred to as an expected progeny difference (EPD).

EPDs allow for the comparison of animals within a breed for their genetic potential as parents for a given trait. EPDs have existed in the beef industry for decades and their use has produced intended genetic change in many traits.

Many traits (e.g., weaning weight, yearling weight (YW), ultrasound measurements, etc.) must be recorded within certain age windows (ranges when it is acceptable to measure animals). Animals measured outside of defined age windows will not have their own record incorporated into an EPD calculation. This allows for a fair comparison of animals. Specific age windows can be found on the corresponding breed association Web site. Records are then adjusted to a constant endpoint, most generally age (Table 2).

Too often, seedstock producers and bull buyers focus on actual weights and ultrasound data when selecting sires. Expected progeny differences provide a measure by which animals within a breed can be compared to one another for their genetic potential as parents for specific traits. EPDs incorporate multiple

Breeding in Beef Cattle. Table 2 Beef Improvement Federation (BIF) standard adjustment factors for birth and weaning weight

AOD	Birth weight	Male	Female
2	+8	+60	+54
3	+5	+40	+36
4	+2	+20	+18
5–10	0	0	0
11 and older	+3	+20	+18

sources of information, including full pedigree, an animal's own record, and progeny information. As additional sources of information become available, the accuracy of the EPD value increases. Prior to a National Cattle Evaluation (NCE), animals are given interim EPDs. During a genetic evaluation, all pedigree information would be included.

Pedigree estimate:

$$\text{Sire EPD} = 0.20 \quad \text{Dam EPD} = 0.10$$

$$\searrow \qquad\qquad \swarrow$$

$$\text{Progeny EPD} = \left(\frac{0.20 + 0.10}{2}\right) = 0.15$$

Pedigree estimate + animal record:

$$EPD_{\mathrm{I}} = (0.5 * \mathrm{EPD_S}) + (0.5 * \mathrm{EPD_D}) + (0.5 * \phi)$$

Where $\mathrm{EPD_I}$ is the EPD for some individual I, $\mathrm{EDP_S}$ is the EPD for the sire of animal I, $\mathrm{EPD_D}$ is the EPD for the dam of animal I, and ϕ is the Mendelian Sampling effect. The phenomena of Mendelian sampling arises due to the fact that each parent passes a sample half of its alleles to its offspring and every allele has an equal likelihood of being passed on. This effect can be quantified using contemporary group deviations and is a measure of how much better or worse an animal is compared to the average of his parents. One could envision a scenario where an animal could receive only the most desirable alleles from both parents resulting in a favorably large Mendelian sampling effect or the exact opposite which could result in an unfavorably large sampling effect. Perhaps the best example is a set of flush mates. Although all of them have the same pedigree estimate, they differ considerably in terms of performance and consequently their EPD, once they have a record, differ due to Mendelian sampling.

When using EPD it is important to understand that the role of EPD is to provide a measure of comparison within a breed. To compare animals across breeds, estimates from the US Meat Animal Research Center (MARC) can aid in determining differences between EPD of different breeds (Table 3). These across breed adjustment factors, adjusted to an Angus basis, are updated annually and can be found at http://www.beefimprovement.org/proceedings.html.

Example:

If a Hereford bull has a birth weight EPD of 1.5 and a Simmental bull has a birth weight EPD of 1.0 these adjustment factors can be used to approximate what these two bulls birth weight EPD would be on an Angus basis so that they can be compared. On an Angus basis, the Hereford bull would have a birth weight EPD of 4.2 (1.5 + 2.7) and the Simmental bull would have a birth weight EPD of 6.4 (1.0 + 5.4). Therefore, it can be expected in this scenario that the Hereford bull would sire calves that are 2.2 lbs. lighter at birth. This table can be an effective tool to determine differences in weight and milk potential between major US breeds. This information can be used to help determine which breed(s) are better suited to different environments. For instance, in a low input environment, breeds with a negative adjustment factor for milk might be more desirable.

Breeding in Beef Cattle. Table 3 2008 Adjustment factors for comparison of expected progeny difference (EPD) across various breeds

Breed	Birth weight	Weaning weight	Yearling weight	Milk
Angus	0.0	0.0	0.0	0.0
Charolais	9.6	39.0	47.3	2.9
Gelbvieh	4.4	5.0	−22.4	7.0
Hereford	2.7	−2.9	−12.8	−15.3
Limousin	4.0	−3.8	−27.8	−11.9
Red Angus	2.8	−5.2	0.9	−3.9
Simmental	5.4	23.3	16.9	13.9

Source: Adapted from Kuehn et al. [2]. More breeds and more traits are available in the full results from the US Meat Animal Research Center

Breed Average and Percentile Ranks

Table 4 illustrates a percentile rank table. These will be different for every breed and will change yearly with the addition of new animals with performance information recorded. The 50th percentile represents breed average. If an animal is in the top 1% for a given trait then it can be said that 99 animals in a hundred are "worse" for that trait. Conversely, if an animal is in the 95th percentile then it can be said that 94 in 100 animals will be better than him/her for that trait. Knowledge of percentile table gives you an idea of how an individual ranks within a breed for a specific trait or index. However, it may

Breeding in Beef Cattle. Table 4 Percentile rank

Top %	CED	BW	WW	YW	Milk
1	14	−2.5	67	117	34
5	11	−.9	59	105	30
10	10	−.1	55	99	28
20	9	.7	50	92	25
50	6	2.2	42	79	20
75	3	3.4	36	69	16
95	-2	5.2	26	50	10

CED calving ease direct, *BW* birth weight, *WW* weaning weight, *YW* yearling weight, *Milk* maternal milk (maternal component of weaning weight)

not be beneficial to choose extreme animals. For instance, even though a sire might be in the top 1% of the breed for Milk, his Milk value may be too extreme for your production environment.

EPD Definitions

	BULL A	BULL B
Calving ease direct	10	6
Birth weight	+2.0	+3.5
Weaning weight direct	20	+22
Yearling weight	+40	+52
Yearling height	.3	.6
Milk	+3	−2
Maternal weaning weight	+13	+9
Gestation length	−.1	+1.1
Calving ease maternal	4	6
Mature daughter height	+.5	+1.0
Mature daughter weight	0	+30
Scrotal circumference	+.1	−.45
Heifer pregnancy	6	9
Carcass weight	+2.0	+20
Percent retail cuts	0	+.2
Marbling	0	−.3
Ribeye area	+.06	+1.6
Fat thickness	−.01	−.09
Tenderness	−.1	.1
Days to finish	15	10
Stayability	10	6
Maintenance energy	0	10
Docility	6	2

Calving ease direct – Bull A should have 4% more unassisted births from first-calf heifers than Bull B. While birth weight is an indicator of calving ease, it does not tell the whole story. Calving ease is an economically relevant trait. Producers should not use both birth weight and calving ease EPD together since the birth weight EPD is already used in the calculation of calving ease.

Birth weight – Bull B's calves would be on the average 1.5 lb heavier at birth. Normally, producers should select bulls for use on heifers that are at or less than the breed average for birth weight. Keep in mind that when crossing breeds, heterosis or hybrid vigor can increase birth weights 10–15% over a straight-bred average.

Weaning weight direct – Calves from Bull B should average 2 lb more on adjusted weaning weights because of additional growth. Because of the low accuracy associated with yearling bulls, the amount of emphasis placed on such a small difference should be limited. These EPDs are virtually the same even if the accuracies were high.

Yearling weight – Bull B's calves should average 12 lb heavier at 1 year of age.

Yearling height – Bull B's calves should be 0.3 in. taller on average at a year of age compared to the offspring of Bull A. Height measurements are taken at the hip. Height (the actual measurement and not the EPD), along with age, is used to calculate frame score.

Milk – Daughters from Bull A should produce calves that are 5 lb (the difference between +3 and −2) heavier at weaning. This is not a measure of pounds of milk but rather weaning weight due to milk production. This 5 lb, unlike the weaning weight figure attributed to growth from the bull, is the result of differences in the daughters' milk production and mothering ability. Excessively high milk levels in low input environments should be discriminated against due to increased nutrient requirements of cows.

Total maternal (maternal weaning weight) – Daughters from Bull A will produce calves that are 4 lb heavier at weaning because of their combined genetics for growth and milk. This is a calculated figure of one-half the bull's weaning weight direct EPD plus his milk EPD. For example, Bull A has a maternal weaning weight value of 13 which is equal to half of his weaning weight direct EPD (20/2 = 10) plus his milk EPD [3].

Gestation length – Calves from Bull A should have a 1-day shorter gestation.

Calving ease maternal – Bull B's daughters should calve as first-calf heifers with 2% more unassisted births (6–4) than the daughters of Bull A.

Mature height – Bull B's daughters should be.5 in. taller at maturity.

Mature weight – Bull B's daughters should be 30 lb heavier when mature.

Scrotal circumference – Bull calves from Bull A should have.55 cm larger adjusted scrotal circumferences. Scrotal circumference is an indicator of the age of maturity of a bull's daughters. Bulls with larger scrotal circumference should have daughters that reach puberty earlier.

Heifer pregnancy – Daughters of Bull B are 3% more likely to become pregnant as heifers.

Carcass weight – Bull B should produce calves that have 18 lb more adjusted carcass weight.

Percent retail product – The calves from Bull B should yield 0.2% more closely trimmed, boneless retail cuts from the round, loin, rib, and chuck. Some breeds may report a Yield Grade (YG) EPD. The same factors (back fat, ribeye area, and carcass weight) would be included but a lower YG is more desirable as opposed to percent retail product where a higher value is more desirable. In either percent, retail product or YG fat thickness contributes the most to these two calculations. Consequently, selecting for decreased YG or increased percent retail product will lead to leaner animals so caution should be used to avoid extremely lean replacement females.

Marbling – Calves from Bull A should have a marbling (MARB) score of >0.3. Marbling scores range from 1.0 which is devoid of marbling and a utility quality grade to 10.9 which is abundant marbling and a prime + quality grade. For example, if calves sired by Bull B had a marbling score of 5.0 then calves sired by Bull A are expected to have a marbling score of 5.3. Ultrasound EPDs were calculated for a number of breeds for traits of ribeye area (REA), fat, and intramuscular fat (IMF), which is correlated to marbling, but now the majority of breeds use these ultrasound measurements in the calculation of carcass EPDs. Therefore, instead of seeing both an IMF EPD and a marbling EPD you just see the marbling EPD but it has ultrasound measurements included in the calculation.

Ribeye area – At a given end point, calves from Bull B should have ribeye areas that are 1.54 square inches larger than Bull A's calves.

Fat Thickness – At a given end point, calves from Bull A should be.08 in. fatter when measured at the 12th rib. This would be less desirable on a carcass animal, but extremely lean females going back into a cowherd may also be undesirable.

Tenderness – Calves sired by Bull A should produce meat that is more tender than that of calves sired by Bull B by 0.2 lbs. of shear force. Tenderness is measured by Warner Bratzler Shear Force (WBSF) that is reported in the pounds of force required to cut through a one inch thick piece of meat. A lower value is more desirable.

Days to finish – Calves sired by Bull B should spend 5 fewer days on feed to reach a constant fat endpoint.

Stayability – A measure of reproductive longevity. Daughters of Bull A are 4% more likely to stay productive in the herd to age 6.

Maintenance energy – The Red Angus Association of America calculates a Maintenance Energy (ME) Expected Progeny Difference (EPD) that indicates differences in the Mcal/month needed for maintenance due to mature size (corrected for body condition score) and milking ability (The Rancher's Guide to EPD available at www.redangus.org). A much simpler way to think of it is that a bull with a ME EPD of +10 compared to one that is +0 will produce daughters that will require approximately 11 more pounds of average quality forage per month (assuming average quality forage =.86 Mcal/lb.).

Docility – Bull A should sire 4% more calves that have a temperament in the most docile score than Bull B. The actual measurement of docility is recorded either at weaning or at yearling (depending on the breed association) and is categorized as the

animals' behavior as they enter, are restrained in, and exit the chute.

Beef Improvement Federation (BIF) temperament scoring system.

1. Docile – Mild disposition – gentle and easily handled. Stands and moves slowly during processing, undisturbed, settled, and somewhat dull and does not pull on the headgate when in the chute – exits the chute calmly.
2. Restless – Quieter than average but slightly restless, might be stubborn during processing, might try to back from the chute, pulls back on the headgate, some tail flicking, exits the chute promptly.
3. Nervous – Typical temperament – manageable but nervous and impatient with a moderate amount of struggling, movement, and tail flicking as well as repeated pushing and pulling on the headgate – exits the chute briskly.
4. Flighty – Wild, jumpy and out-of-control, quivers and struggles violently, might bellow and froth at the mouth, continuous tail flicking, defecates and urinates during processing, frantically runs the fence line and might jump when penned individually, exhibits long flight distance, and exits the chute nervously.
5. Aggressive – Similar to Score 4 but with added aggressive behavior, fearful, extreme agitation, continuous movement that might include jumping and bellowing while in the chute, exits the chute frantically, and might exhibit attack behavior when handled alone.
6. Very Aggressive – Extremely aggressive temperament. Thrashes about or attacks wildly when confined in small, tight places. Pronounced attack behavior.

Accuracy

The uncertainty surrounding early predictions of genetic merit are a result of Mendelian sampling. Every animal is passed a random sample of alleles from each parent, half coming from the dam and half from the sire. An estimate of the average effect of what was passed from parent(s) to offspring in the form of pedigree estimates can be calculated, but the certainty of how correct this estimate is (i.e., the accuracy) is low. As more information is collected, such as an individual's own record and data from progeny, accuracy increases. For lowly heritable traits, like measures of reproduction, it can take a considerable number of offspring to reach high BIF accuracy levels, given that the BIF scale is more conservative than true accuracy (r) as illustrated in Table 5. To calculate r in the context of progeny test sires the following equation can be used where n is the number of progeny:

$$r = \sqrt{\frac{nh^2}{4 + (n-1)h^2}}$$

To convert BIF accuracy to true accuracy (r) the following equation can be used:

$$r = \sqrt{1 - (1 - \mathrm{BIF})^2}$$

Theoretically, accuracy is the correlation between an animal's predicted EPD and its true EPD. However, it is much simpler to think of it as a measure of risk indicating how much an animal's EPD may change with the inclusion of additional information. Accuracy is not an indication of how variable a particular sire's calves will be but rather how the estimate of an animal's EPD is likely to change. As the accuracy value increases, the amount by which an EPD is likely to change

Breeding in Beef Cattle. Table 5 Approximate number of progeny needed to reach accuracy levels (true (r) and the Beef Improvement Federation standard) for three heritabilities (h^2)

Accuracy		Heritability levels		
R	BIF	h^2 (0.1)	H^2 (0.3)	h^2 (0.5)
0.1	0.01	1	1	1
0.2	0.02	2	1	1
0.3	0.05	4	2	1
0.4	0.08	8	3	2
0.5	0.13	13	5	3
0.6	0.2	22	7	4
0.7	0.29	38	12	7
0.8	0.4	70	22	13
0.9	0.56	167	53	30
0.999	0.99	3,800	1,225	700

decreases. Possible change values differ for every trait and for every breed (e.g., an Angus bull with an accuracy of 0.30 may have a different possible change value than a Limousin bull with the same accuracy value for the same trait). Possible change tables are available on breed association Web sites.

Example: Possible Change in the Marbling EPD of a Limousin Sire

Assume that a young Limousin sire has a marbling EPD of 0.10 with an accuracy of 0.20. Using the values in Table 6, it is expected that 2/3 of the time his true EPD would fall within +/− 0.20 (one standard deviation) of his printed EPD or between −0.10 and 0.30. If there is 2 in 3 chance that the true EPD is between −0.10 and 0.30 then there must be 1 in 6 chance that his true EPD is below −0.10 and a 1 in 6 chance that his true EPD is above 0.30.

Multiple-Trait Selection

Through genetic correlations, selection for one trait can influence other traits. This knowledge is useful when practicing multiple-trait selection. There are three primary methods of multiple-trait selection: tandem selection, independent culling levels (ICLs), and selection indexes.

Breeding in Beef Cattle. Table 6 Accuracy related to possible change in Limousin cattle

BIF accuracy	Ribeye area EPD possible change	Marbling score EPD possible change
0.0	0.46	0.24
0.1	0.41	0.22
0.2	0.37	0.20
0.3	0.32	0.17
0.4	0.28	0.14
0.5	0.23	0.12
0.6	0.18	0.10
0.7	0.14	0.07
0.8	0.09	0.05
0.9	0.05	0.02

Source: www.nalf.org

Tandem selection. Tandem selection is the process of placing selection pressure on one trait and once the desired level of the trait under selection has been reached. Then selection for a new trait would begin. This is the simplest form of multiple-trait selection and the most inefficient. The two (or more) traits involved are selected for independently such that progress made in one trait could be eroded once selection for another trait becomes the focus of the breeding scheme. This is the poorest way to select for multiple traits.

Independent culling levels. Independent culling levels (ICLs) describe the process where threshold criteria for multiple traits are set and any animal not meeting all criteria (threshold levels for all traits) are excluded as candidates for selection. Although this ensures a certain level of superiority across multiple traits it may cull a particular animal that is just below the threshold level for one trait.

Economic Index

An economic index is a collection of EPDs that are weighted by their economic value such that traits with a greater impact on a production goal have a larger economic weight associated with them. Assume that there is an index centered on improving profit potential of terminal animals sold on a grid. In this particular index, the traits of economic importance might be yearling weight (YW), ribeye area (REA), marbling (MARB), and external fat (BF). Below is an example of how this index might look.

$$I = EPD_{YW} \times a_{YW} + EPD_{REA} \times a_{REA} + EPD_{MARB} \times a_{MARB} + EPD_{BF} \times a_{BF}$$

Where I is the index value, EPD_{YW} is the animal's EPD for yearling weight, and a_{YW} is the economic weight associated with trait yearling weight. The same approach is used for the other traits in this index, MARB and BF, where the animal's EPDs for these traits are multiplied by an economic weight. The economic weights are derived by computer simulation work to determine the economic value of changing particular traits.

Several breeds publish economic indexes including Angus, Hereford, Gelbvieh, Charolais, Simmental, and

Limousin. Each index has an intended purpose and is catered toward particular breeding objectives.

An addition the breeding objective of beef cattle in the future will likely be some measure of environmental impact, such as green house gas (GHG) emissions. There are conflicting estimates of how much beef cattle production contributes to worldwide GHG production, but there are convincing estimates that suggest that per unit of product, beef cattle production is more environmentally friendly now that at any time point in the past despite decades of artificial selection to increase output. Figure 2 illustrates that in 30 years, from 1977 to 2007, beef production has increased while the number of cows has decreased. During the same three decades, the resources needed for beef production (land, water, feed) decreased along with gas emissions and the carbon footprint [3].

Breed Selection

Correct breed selection is the critical first step to initializing a crossbreeding system. Choosing a breed(s) is dependent upon:

1. Production and marketing goals
2. Production environment
3. Available feed and labor resource

Choosing a breed that is best suited to your production environment is dependent on several factors including the availability of feed, and level of stress (temperature, amount of moisture, etc.). Table 7 outlines the biological type of cattle that are best suited for particular levels of feed resources and stress.

The decision of whether or not to utilize a particular strategic system of crossbreeding depends upon individual production goals. In order to take advantage of breed complementarity, breeds must be paired such that they excel in different areas that are critical to the overall production goal(s). For instance, if the goal were to sell calves at weaning then it would make sense to use a breed, most likely Continental, which will maximize direct weaning weights. However, this purebred system will maximize outputs, but may require large inputs as well. With that in mind, perhaps it would make more sense from an economic perspective to use a British breed as the genetic base for all dams and use a continental breed for sires thus minimizing the input costs from the female side yet still capturing added growth in the calves due to the direct growth provided by the sire breed. This would be a very simple example of a crossbreeding system.

Matching Biological Type to Environment

Benefits of heterosis make it important for producers to have a crossbreeding program. It is just as important that the producer match the type of crossbred cow to the environment and management system. This can be viewed as the foundation of a crossbreeding program. If the biological type does not match the resources, the system will fail, regardless how perfect the end product may be.

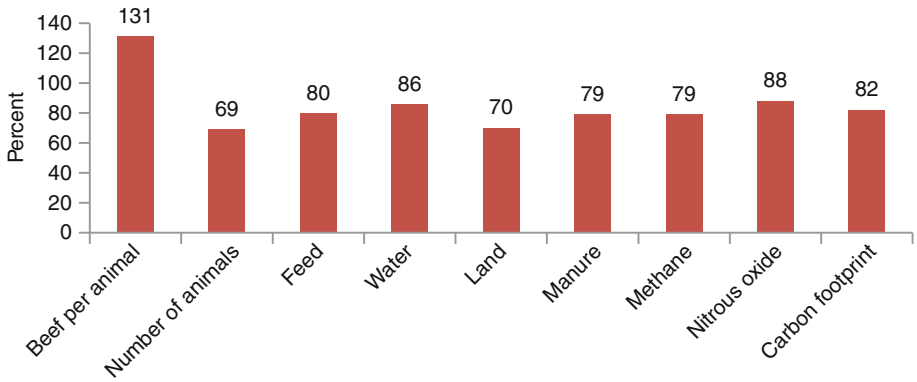

Breeding in Beef Cattle. Figure 2
Changes in metrics of beef production from 1997 to 2007 in the United States

Breeding in Beef Cattle. Table 7 Matching genetic potential for different traits to production environments

Production environment			Traits				
Feed availability	Stress[a]	Milk	Mature size	Ability to store energy[b]	Resistance to stress[c]	Calving ease	Lean yield
High	Low	M to H[d]	M to H	L to M	M	M to H	H
	High	M	L to H	L to H	H	H	M to H
Medium	Low	M to H	M	M to H	M	M to H	M to H
	High	L to M	M	M to H	H	H	H
Low	Low	L to M	L to M	H	M	M to H	M
	High	L to M	L to M	H	H	H	L to M

Source: Adapted from Gosey [4]
[a]Heat, cold, parasites, disease, mud, altitude, etc.
[b]Ability to store fat and regulate energy requirements with changing (seasonal) availability of feed
[c]Physiological tolerance to heat, cold, internal and external parasites, disease, mud, and other factors
[d]*L* low, *M* medium, *H* High

Cow weight is probably easier to understand than milk production, but research has shown that cows with the genetic propensity to milk heavily require more nutrients year round, not just when they are milking. The National Research Council (NRC) data shows that a cow producing 25 lbs. of milk at peak lactation requires 10% more feed energy than a cow producing 15 lbs. of milk at peak lactation. To see a 10% difference in feed energy with regards to mature weight it would require moving from a 1,000 lb. cow to a 1,200 lb. cow, or a change of 200 lbs. of body weight. There are breed differences in lactation yields so breed selection is critical when matching genetics to your environment. These breed differences can be found in literature from research at the Meat Animal Research Center (MARC). Moderating mature cow size and selecting for an optimal window of milk production is beneficial when it comes to cutting costs regardless of your production environment. However, in limited feed environments females with high maintenance energy requirements may also have difficulty maintaining an acceptable body condition score and rebreeding. Nugent et al. [5] determined that with limited nutrient availability, breeds with a high genetic potential for milk production had longer anestrous periods which lead to lower conception rates during a fixed breeding season. Other researchers have concluded that selection for increased milk production past an adequate threshold is not economically or biologically efficient [6]. It can be challenging to determine if cows within a herd have too much milking potential. Other than knowledge of the genetics of sires used in the past, it is important to note the body condition score of females. Extremely thin females fed the same as those with an acceptable body condition score may produce too much milk for their environment. If a producer is constantly supplementing females to maintain body condition to ensure they will successfully breed back, this might be an indication that bulls you buy in the future should have a more moderate value of milk genetics.

Another critical aspect of fitting genetics to the production environment is regional adaptation. If natural selection is allowed to play a large role in selecting the parents for the next generation, indigenous breeds should be well suited to their production environment. An example of an indigenous breed that has thrived in number is the Nelore breed in Brazil. The Nelore breed makes up roughly 65% of the world's bovine population and is well suited to tropical conditions. With adaptation in mind, indigenous breeds can be used as the base and exotic (foreign) breeds used in strategic crossbreeding systems to change target traits such as growth or carcass attributes. A case study [7] in Zimbabwe compared indigenous breeds of Afrikaner (a breed developed in South Africa), Tuli, Nkone, and

Mashona, to breeds developed outside of the African Continent such as Brahman, Charolais, Hereford, Simmental, Aberdeen Angus, and Sussex. The results showed that indigenous breeds excelled in fitness traits (fertility and survivability) while the foreign breeds excelled in growth, feed conversion, and carcass attributes.

Crossbreeding

Heterosis

Too often heterosis (hybrid vigor) is thought to be the exclusive goal of crossbreeding. Heterosis is nothing more than an unexpected and often beneficial deviation from the average of the two parental lines. Hybrid vigor can also be thought of as the "anti-inbreeding." Inbreeding increases uniformity by increasing homozygosity but also creates "inbreeding depression" or a general decrease in survival and reproductive traits that can be caused by a decrease in heterozygosity. Percent heterosis can be calculated as:

$$\%\,\text{Heterosis} = \left[\frac{(\text{crossbred average} - \text{straightbred average})}{\text{straight bredaverage}}\right]\text{x}100$$

A simple example would be the percent heterosis realized in the average weaning weight from breeding a herd of Breed A cows to a group of Breed B bulls. Let 525 lb be the average weaning weight of the F1 calves, 450 lb be the average weaning weight of the Breed A population, and 550 lb be the average weaning weight of the sire's population.

The pounds of heterosis would be:

$$\text{Pounds of heterosis} = 525 - \left[\frac{(450 + 550)}{2}\right] = 25\ \textit{pounds}$$

and the percent of heterosis would be:

$$\%\ \text{heterosis} = \frac{25}{[(450 + 550)/2]} = .05 \text{ or } 5\%$$

The amount of heterosis that is realized for a particular trait is inversely related to the heritability of the trait. This is logical since traits that are lowly heritable have a small additive component (proportionally speaking) and crossbreeding takes advantage of dominance and epistatic effects. With that in mind, traits of low heritability (e.g., reproductive traits) generally benefit from heterosis the most (Table 8). They generally have a heritability of less than 10% and can be improved through the adequate use of crossbreeding systems. End-product traits on the other hand that benefit from heritability in the moderate to high range benefit less from heterosis. Another benefit of crossbreeding may be a decrease in methane production per unit of beef produced. In a comparison of the methane production per ton of live weight weaned from a 16,000 ha farm in Australia, changing from Shorthorns (mean cow weight 422 kg) to composite breed cattle in (mean cow weight 507 kg), reduced methane production per ton of weight weaned by 31%. This was largely due to higher weaning rates of composite breed females (80 vs 55%) [8].

Breeding in Beef Cattle. Table 8 Individual heterosis: advantage of the crossbred calf

Trait	Observed improvement	% Heterosis
Calving rate	3.2	4.4
Survival to weaning	1.4	1.9
Birth weight	1.7	2.4
Weaning weight	16.3	3.9
ADG	0.08	2.6
Yearling weight	29.1	3.8

Source: Adapted from Cundiff and Gregory [9]

There are three main types of heterosis:

1. Individual
2. Maternal
3. Paternal

Retained Heterosis Unfortunately there exists a popular misconception that heterosis exists only in the first generation of crossbreds (F1). Heterosis is *retained* in the breeding of crossbred animals and is related to the probability of alleles from different parental lines joining together. For instance, if two F1 animals are mated, heterosis in the corresponding

offspring is called *retained heterosis* and is equal to the following:

$$\text{Heterosis retained} = 1 - [(P_{S1}P_{D1}) + \ldots + (P_{Sn}P_{Dn})]$$

Where P_{S1} is the proportion of the sire from breed 1 and P_{D1} is the proportion of the time from breed 1 and n is equal to the total number of breed involved.

Maternal Heterosis The offspring of an F1 female will benefit from maternal heterosis (Table 9), thought of as realized heterosis of milk production.

Paternal Heterosis Fewer examples of paternal heterosis exist and consequently crossbred sires have often been ignored. The benefit of crossbred or composite sires lies in their ability to inject heterosis and breed complementarity into a herd with greater ease than the rotational crossbreeding systems described above.

Composites

Some of the first such animals are the American Breeds, or Brahman Derivatives. Perhaps there is no greater example of breed complementarity (breeding animals to adapt to a specific environment) and consequently of heterosis.

The American Gelbvieh Association, North American Limousin Foundation, and American Simmental Association are three breed associations that have implemented new programs to introduce composites such as the Balancer, Lim-Flex, and SimAngus, respectively. There is no doubt that some of these programs have met with opposition from within the respective associations due to an ignorant stance that purebred animals are superior. I greatly admire those who have pushed, pulled, and prodded these programs through.

Crossbred females have proven to be very profitable and well accepted from a commercial standpoint. The use of crossbred bulls has not been accepted so easily. Some common fears have been the perception of larger amounts of variation within composite populations and the lower accuracy of EPDs of composite animals. In a study of three composite lines at MARC and their parental purebreds, there were no statistical significant differences in the coefficient of variation for reproduction, production, or carcass traits measured (Table 10).

Breed Complementarity

In addition to heterosis, crossbreeding programs can increase production efficiency by using additive (highly heritable) traits through *complementarity*. Differing breeds can be matched to complement traits, more closely fitting the genetic goals for biological type.

Complementarity is fully exploited under a system when crossbred cows of lower frame size, and optimum milk are crossed with a large framed terminal breed, noted for rapid growth and carcass leanness in order to produce market animals [11].

Simulation work by Lamb et al. [12] shows that generally English breeds are more biologically efficient, while Continental breeds are more economically

Breeding in Beef Cattle. Table 9 Maternal heterosis: Advantage of the crossbred cow

Trait	Observed improvement	% Heterosis
Calving rate	3.5	3.7
Survival to weaning	0.8	1.5
Birth weight	1.6	1.8
Weaning weight	18.0	3.9
Longevity	1.36	16.2
Cow lifetime production		
No. Calves	0.97	17.0
Cumulative weaning weight, lb.	600	25.3

Source: Adapted from Cundiff and Gregory [9]

Breeding in Beef Cattle. Table 10 Coefficients of variation for purebred versus composite steers

Trait	Purebreds	Composites
Birth weight	0.12	0.13
Wean weight	0.10	0.11
Carcass weight	0.08	0.09
Retail product %	0.04	0.06
Marbling	0.27	0.29
Shear force	0.22	0.21

Source: Adapted from [10]

efficient. The English X Continental cross was the most biologically and economically efficient. In some environments, heat and disease tolerance of the Brahman (*Bos Indicus*) may be required to complement the carcass traits, disposition, and age at puberty of an English breed [13].

Crossbreeding Systems

There are many other crossbreeding systems that vary significantly in terms of difficulty. Items that can influence the success of a crossbreeding system include:

1. Number of cows in the herd
2. Number of available breeding pastures
3. Labor and management
4. Production and marketing system
5. Availability of high-quality bulls of the various breeds

Terminal Cross All offspring from a terminal cross are sold. The sire used is usually from a breed noted for high growth, and desirable carcass end product. Under this system, genetic differences between maternal and terminal breeds can be exploited through complementarity. Individual heterosis is improved an additional 5% from this type of cross [11]. If female replacements are not generated, little emphasis needs to be placed upon milking genetics of the sires used. By purchasing crossbred F1 females, maximum maternal heterosis can also be achieved.

Two-Breed Terminal In this simple situation, cows of breed A are bred to bulls of breed B and all offspring are sold. In this system, the offspring are F1s and will benefit from 100% of the possible individual heterosis.

Three-Breed Terminal In this situation, cows that are F1 females comprised of ½ breed A and ½ breed B are mated to bulls of breed C for the production of terminal offspring. In this system, calves not only benefit from 100% of the possible individual heterosis, but maternal heterosis is realized as well. In general, the females should be a cross of two maternal breeds that emphasize efficiency and milking ability while the sire breed should inject growth.

Rotational Systems The three-breed rotation is similar to the two-breed rotation. A third breed is added to this system, thus a third breeding pasture is needed, unless AI is utilized. Management of this system is patterned after the two-breed rotation. If the maximum amount of heterosis is 23.3% (14.8% + 8.5%) then the expected level of heterosis is higher with a three-breed than two-breed rotation, 86% versus 67% [14].

Two-Breed Rotation A two-breed rotation is a simple crossbreeding system requiring two breeds and two breeding pastures. The two-breed rotational crossbreeding system is initiated by breeding cows of breed A to bulls of breed B. The resulting progeny (A*B) chosen as replacement females would then be mated to bulls of breed A for the duration of their lifetime. The service sire is the opposite breed of the female's own sire. These progeny are then one-quarter breed A and three-quarters breed B. Since these animals were sired by breed B bulls, they are mated to breed A bulls. Each succeeding generation of replacement females is mated to the opposite breed of their sire. Initially only one breed of sire is required. Following the second year of mating, two breeds of sire are required. After several generations, the amount of retained heterosis stabilizes at about 67% of the maximum heterosis, resulting in an expected 16% increase in the pounds of calf weaning weight per cow exposed above the average of the parent breeds [14]. In this system, a minimum of two breeding pastures and 50 cow units are required.

Three-Breed Rotation A three-breed rotational system achieves a higher level of retained heterosis than a two-breed rotational crossbreeding system does. After several generations, the amount of retained heterosis stabilizes at about 86% of the maximum heterosis, resulting in an expected 20% increase in the pounds of calf weaning weight per cow exposed above the average of the parent breeds [14]. Like the two-breed system, distinct groups of cows are formed and mated to bulls of the breed that represents the smallest fraction of the cows breed makeup. A cow will only be mated to a single breed of bull for her lifetime.

A minimum of three breeding pastures is required for a three-breed rotational system. Replacement females must be identified by breed of sire to ensure proper matings. The minimum herd size is approximately 75 cows with each one-third being serviced by

one bull of each breed. Scaling of herd size should be done in approximately 75 cow units to make the best use of service sires, assuming one bull per 25 cows. Replacement females are mated to herd bulls in this system, so extra caution is merited in sire selection for calving ease to minimize calving difficulty. The progeny produced from these matings that do not conform to the breed type of the herd should all be marketed. Breeds used in rotational systems should be of similar biological type to avoid large swings in progeny phenotype due to changes in breed composition. The breeds included have similar genetic potential for calving ease, mature weight and frame size, and lactation potential to prevent excessive variation in nutrient and management requirements of the herd.

When choosing a crossbreeding system it is critical to consider more than the amount of heterosis retained. After all, each system requires different levels of input (pastures, etc.) and differing levels of difficulty. Table 11 describes the advantages and requirements for the above mentioned crossbreeding systems.

Molecular Information

Molecular Information: Paternity and Simply Inherited Traits

Molecular-based tools are another source of information that has received considerable attention by producers throughout the beef industry and by both the academic community and the private sector. These tools initially came in the form of candidate genes but have now grown to the inclusion of multiple markers called Single Nucleotide Polymorphisms (SNPs). The use of molecular information has grown from simple applications such as identifying animals that are carriers of the red allele to identifying animals that are carriers of lethal genetic defects, to paternity assignment, and a growing number of diagnostic tests for a suite of complex traits ranging from reproduction to carcass.

Genotyping to determine parentage allows for a sire to be correctly linked to a corresponding calf. The identification of an animal's sire via DNA marker technology can be advantageous in multi-sire breeding pastures, or for ascertaining if a calf is the product of an artificial insemination (AI) mating or a clean-up bull. This promotes knowledgeable culling and breeding decisions by determining which sire(s) are contributing the most (or least) to a particular breeding objective. In the case of commercial ranch settings, for example, it may be beneficial to determine the sire that is responsible for calving difficulties.

Because paternity identification is a process of excluding potential sires on the basis of their genotype, it is important that DNA from all possible sires be included in paternity tests. It will be more difficult to

Breeding in Beef Cattle. Table 11 Summary of crossbreeding systems by advantage and other factors

Type of system		Advantage[a]	Retained heterosis[b]	Minimum no. of breeding pastures	Minimum herd size	No. of breeds
2-breed rotation	A*B rotation	16	67	2	50	2
3-breed rotation	A*B*C rotation	20	86	3	75	3
Terminal cross with straightbred females[c]	T*A	8.5	0	1	Any	2
Terminal cross with purchased F1 females	T*(A*B)	24	100	1	Any	3
Rotating unrelated F1 bulls	A*B x A*B	12	50	1	Any	2
	A*B x A*C	16	67	1	Any	3
	A*B x C*D	19	83	1	Any	4

Source: Adapted from Ritchie et al. [14]
[a]Measured in percentage increase in lb of calf weaned per cow exposed
[b]Relative to F1 with 100% heterosis
[c]Cundiff and Gregory [15]

definitively make paternity assignments on closely related bulls in a multiple-sire breeding pasture, given they are likely to share a similar genotype. Although microsatellites have typically been the marker of choice for paternity analysis, the use of SNP markers is becoming more common for a number of reasons including their abundance, high potential for automation, low genotyping error rates, and ease of standardization between laboratories.

Although identifying carriers of genetic defects is a rather simple application of DNA technology, it is an important tool when making mating decisions. It is known that afflicted animals can only arise if two carrier animals are mated. In this scenario, there exists a 25% chance that the corresponding calf will have the defect. Unfortunately, this added information has been used as the primary selection tool whereby carrier animals are automatically discarded. If a producer potentially has carrier females, then carrier bulls should be avoided. However, if this is not the case, then it could be beneficial to use the best available bull, regardless of his status as a carrier. As an industry, there is the ability to make informed decisions based on science concerning this issue and not throw away animals that are superior across the remainder of their genome because they have a flaw that can be effectively managed around.

Molecular Information: Complex Traits

Several advancements in molecular technology have occurred with regard to complex traits (i.e., production, carcass, and reproduction traits). Including the number of markers included in a given panel, reporting styles of the results, and the number of traits for which a diagnostic test exists. Recently, this information is included in the Angus National Cattle Evaluation (NCE) for the first time.

The promise of the inclusion of marker information into EPD calculations holds three primary benefits:

1. Increased accuracy for young animals (i.e., yearling bulls), which is particularly beneficial when selecting on traits that are measured late in life (e.g., stayability)
2. Shortened generation intervals
3. EPD values for novel traits (i.e., efficiency, end-product healthfulness, disease susceptibility) that may have, at best, sparse collection of phenotypes

However, the magnitude of these benefits will depend on the proportion of variation explained by a given marker panel. At present, the best objective source of information regarding this is the National Beef Cattle Evaluation Consortium (NBCEC) Web site (www.nbcec.org). Pertinent information from this Web site includes population, trait, regression coefficient (b), and the p-value (p). The population defines what breed(s) were used to validate the test. If the test was validated in *Bos taurus* animals then it is possible that the test will not explain the same proportion of variation in *Bos indicus* animals. The trait defines what the test was validated for. If it is a metric of efficiency like residual feed intake (RFI) then it will explain how the trait is defined. Generally, a p-value of less than 0.05 suggests that the test is a statistically significant predictor of differences in phenotypes. The regression coefficient is equal to the regression of phenotypes for the trait of interest on the molecular score. It explains the units of change in the phenotype that would be expected for a one-unit change in the molecular score (i.e., MBV). Ideally, these b values should be 1. For example, if two animals have molecular scores for RFI of −1.5 and 1.0, respectfully, the difference between those scores is 2.5. Normally it is expected that, on average, these two animals' phenotypes would differ by 2.5 lb of RFI. However, if the regression coefficient is 0.4 then their phenotypes are expected to differ by 1 lb (2.5*0.4).

Without the seamless integration of this technology into EPD calculations, the industry is faced with two disjoined pieces of information: traditional EPD and marker panel results. In this scenario, it is impossible to directly compare EPD to marker panel results even if the results come in the form of molecular breeding values (MBVs). This is because the molecular scores only explain a portion of the additive genetic variation. Further, some of the marker panel results have a metric of accuracy associated with them. At the current time, this metric is not comparable to the Beef Improvement Federation accuracy value associated with EPD simply due to differences in the way they are computed. While it is logical that the accuracy value of a MBV should be related to the proportion of additive genetic variation

explained by the test there is not a standardized metric that is being used. Thallman et al. [16] analyzed different methods of calculating this proportion for MBV in light of the fact that there is not a standardized method and recommended the use of the square of the additive genetic correlation between the MBV and the trait of interest.

In contrast to the thought process of DNA marker panel results being a separate and disjoined piece of information, these test results should be thought of as a potentially useful indicator that is correlated to the trait of interest. As such, the MBV can be included in NCE as a correlated trait following methods of Kachman [17]. Other methods have been proposed including using large (50,000 +) SNP panels to form a genomic relationship matrix that could allow for known relationships between animals based on genotypes across SNP loci. Combining these sources of information, molecular tools and traditional EPDs, has the potential to allow for the benefits of increased accuracy and increased rate of genetic change as discussed earlier.

MacNeil et al. [18] utilized Angus field data to look at the potential benefits of including both ultrasound records and MBVs for marbling as correlated traits in the evaluation of carcass marbling score. MacNeil and colleagues used a 114 SNP marker panel that was developed using 445 Angus animals and calculated to have a genetic correlation (r) of 0.37 with marbling (i.e., the test explained $(0.37)^2 = 0.137$, or 13.7%, of the additive genetic variation). For animals with no ultrasound record or progeny data, the marker information improved the BIF accuracy of the Angus marbling EPD from 0.07 to 0.13. Assuming a heritability of 0.3 for marbling, a BIF accuracy of 0.13 is equivalent to having approximately 5 progeny carcass records on a young animal or an ultrasound record on the individual itself. In this particular study, both ultrasound records and MBV were found to be beneficial indicators of carcass marbling. The genetic correlation between MBV and ultrasound was found to be 0.80. Some breeds have begun to integrate this technology and it is likely that more will do so in the future.

Considerations

Current marker panels are likely to work best in the populations where discovery occurred, but will potentially decrease in predictive power as the target population becomes more genetically distant from the discovery population [19]. Below is an example of scenarios where the discovery population is close to the target population and progresses to more distant populations.

Discovery	Target	
Angus	Angus	Closest relationship
Angus	Charolais	
Angus	*Bos indicus*	Most distant relationship

Marker panels are likely to become larger in the future with the possibility of whole genome selection (WGS). Currently, genome selection in beef cattle is in its infancy. Although preliminary data from the dairy industry look promising [20], the structure of the beef industry offers unique challenges. It is not known how well this approach will work in beef cattle with its diversity of breeds, diverse sector-specific selection goals, and less extensive phenotype and data collection resources.

Future Directions

Undoubtedly, molecular discoveries and their seamless integration into existing infrastructures and genetic selection tools will aid in the increased rate of genetic change and hopefully profitability of producers. These molecular tools will be in the form of larger (770 K) SNP panels and genome sequences. At the same time, a suite of reduced marker panels will be commercialized for use on progeny while the larger panels are used for herd bulls. These molecular tools will be integrated into breeding value estimations allowing for higher accuracy values on younger animals and allowing for genetic predictions of traits that have not yet been exploited such as the nutrient content of beef, feed efficiency, and susceptibility to disease. Effort will also be placed on precision mating, or specific combining ability, when developing composite animals, aided by molecular technology. One final area of effort includes the robustness of marker effects across breeds and environments, and how to accommodate these differences in national cattle evaluations. All of this has the potential to allow for selection on total profitability and not just production, ultimately aiding in the sustainability of the beef industry worldwide.

Bibliography

Primary Literature

1. Marquez GC, Speidel SE, Enns RM, Garrick DJ (2010) Genetic diversity and population structure of American Red Angus cattle. J Anim Sci 88:59–68
2. Keuhn LA, Van Vleck LD, Thallman RM, Cundiff LV (2008) Across-breed EPD tables for the year 2008 adjusted to breed differences for birth year of 2006. In: Proceedings of beef improvement federation annual meeting. Calgary, Alberta, June 30–July 3, pp 53–77
3. Capper JL (2010) Comparing the environmental impact of the US beef industry in 1977 to 2007. J Anim Sci 88:(Suppl 2)
4. Gosey J (1994) Composites: a beef cattle breeding alternative. In: Proceedings of beef improvement federation annual meeting. West Des Moines, 1–4 June 1994, p 93
5. Nugent RA III, Jenkins TG, Roberts AJ, Klindt J (1993) Relationship of post-partum interval in mature beef cows with nutritional environment, biological type and serum IGF-1 concentrations. Anim Prod 56:193–200
6. Oijen M, Montano-Bermudez M, Nielsen MK (1993) Economical and biological efficiencies of beef cattle differing in level of milk production. J Anim Sci 71:44–50
7. Mpoful N (2002) Comparison of indigenous and foreign cattle for beef production at Matopos Research Station in Zimbabwe. In: Proceedings of the 7th world congress on genetics applied to livestock production, Montpellier, France
8. Bently D, Hegarty R, Alford A (2008) Managing livestock enterprises in Australia's extensive rangelands for greenhouse gas and environment outcomes: a pastoral company perspective. Aust J Exp Agric 48:60–64
9. Cundiff LV, Gregory KE (1999) What is systematic crossbreeding? In: Proceedings of NCBA Cattleman's College, Charlotte, Feb 1999
10. Cundiff LV, Gregory KE, Koch RM (1994) Breeding cattle for improved product consistency. Presented 1994 national cattlemen's convention and trade show, Reno, 26–29 Jan 1994
11. Cundiff LV (1981) Evaluation of maternal breeds. In: Proceedings of the beef cow symposium VII, Rapid City, 7–9 Dec 1981
12. Lamb MA, Tess MW, Robinson OW (1992) Evaluation of mating systems involving five breeds for integrated beef production systems: I. Cow-calf segment. II. Feedlot segment. III. Integrated system. J Anim Sci 70:689
13. Winder JA, Rankin BJ, Bailey CC (1992) Maternal performance of Hereford, Brangus, and reciprocal crossbred cows under semidesert conditions. J Anim Sci 70:1032
14. Ritchie H, Banks D, Buskirk D, Cowley J (1999) Crossbreeding systems for beef cattle. Michigan State University Extension Bulletin E-2701
15. Gregory KE, Cundiff LV (1980) Crossbreeding in beef cattle: evaluation of systems. J Anim Sci 51:1224–1242
16. Thallman RM, Hanford KJ, Quaas RL, Kachman SD, Templeman RJ, Fernando RL, Keuhn LA, Pollak EJ (2009) Estimation of the proportion of genetic variation accounted for by DNA tests. In: Proceedings of the 41st beef improvement federation, Sacramento
17. Stephen K (2008) Incorporation of marker scores into national cattle evaluations. In: Proceedings of the 9th genetic prediction workshop, Kansas City, pp 88–91
18. MacNeil MD, Nkrumah JD, Woodward BW, Northcutt SL (2010) Genetic evaluation of Angus cattle for carcass marbling using ultrasound and genomic indicators. J Anim Sci 88:517–522
19. de Roos APW, Hayes BJ, Spelman RJ, Goddard ME (2008) Linkage disequilibrium and persistence of phase in Holstein-Fresian, Jersey, and Angus cattle. Genetics 179:1503–1512
20. VanRaden PM, Van Tassell CP, Wiggans GR, Sonstegard TS, Schnabel RD, Taylor JF, Schenkel FS (2009) Invited review: reliability of genomic predictions for North American Holstein dairy bulls. J Dairy Sci 92:16–24

Books and Reviews

Beef Improvement Federation (2002) Guidelines for uniform beef improvement programs. Beef Improvement Federation, Athens, Georgia

National beef cattle evaluation consortium (2010) Sire selection manual. National beef cattle evaluation consortium, Lexington, Kentucky

Breeding in Developing Countries and Tropics

SWP Cloete
Department of Animal Sciences, University of Stellenbosch, Matieland, South Africa
Institute for Animal Production, Elsenburg, South Africa

Article Outline

Glossary
Definition of the Subject and Its Importance
Introduction
Setting the Scene
Animal Resources
The Most Important Livestock Products for Ensuring Food Security
Challenges
The Technological Age
Future Directions
Conclusion and Recommendations
Bibliography

Glossary

Fitness A measure of the ability of an organism to survive and reproduce in a particular environment.

Genetic resource Genetic material of plants or animals of value as a resource for future generations of humanity.

Genomics The study of the genomes of organisms, including intensive efforts to determine the entire DNA sequence of organisms as well as fine-scale genetic mapping.

Phenotype The appearance of an organism based on an interactive combination of genetic traits and environmental factors.

Selection Choosing organisms with desirable genetic characteristics for propagation from candidates available.

Sustainability The capacity to endure, that is, the ability of biological systems to remain diverse and productive over time.

Definition of the Subject and Its Importance

Species breeding has led to marked genetic improvement of production by livestock in the developed world over the past decades. Selection has been so successful that the emphasis in the breeding objective has been changed to welfare, behavior, and other consumer-orientated objectives. The same level of progress has not been achieved in the developing world. Current and projected future population growth requires that food production from farm animals in these regions be improved markedly from the present inadequate levels. Limitations in the institutional infrastructure and the unique challenges of livestock production in the emerging world and the tropics were discussed in detail. This led to recommendations on how these challenges can be overcome and how "new" issues like global warming and animal welfare should be handled in a sustainable manner. Focus should be on the phenotyping of individuals for production and particularly for traits associated with fitness. Data should be linked to pedigree information where possible, to generate a broad-based institutional environment where the genetic improvement of animals in the developing countries can be strived for. Samples for the acquisition of DNA should be obtained from phenotyped individuals, for possible later genomic studies. Continued further learning and the accrual of information as well as collaboration to mutual benefit across institutional and national boundaries are needed to enable this. Sustainable livestock improvement in the developing world could accrue if these prerequisites are met.

Introduction

It is fair to say that the past decades have been marked by rapid change. Mankind had to adapt to immense technological progress, rapid urbanization, instability on monetary markets, as well as becoming part of the global village. The changes listed above are by no means exhaustive and many other challenges to the current generation can also be noted.

Yet it is important to note that there is still immense poverty in parts of the world, despite groundbreaking scientific breakthroughs as well as rapid progress in communication systems allowing easy access to the information that are generated elsewhere in the global village. While the developed world appears to be going from strength to strength in the acquisition and application of knowledge, the developing countries are lagging behind. In the Millennium Development Goals Report [1], Kofi Annan (the then secretary general of the United Nations) stated: "We will not enjoy development without security, we will not enjoy security without development, and we will not allow either without respect for human rights. Unless all these causes are advanced, none will succeed."

As a point of departure it has to be observed that the fundamental human rights of millions of people in the developing world are closely interwoven with livestock and the meat, milk, or fiber they produce [2–5]. The livestock industry is inextricably linked with the eradication of extreme poverty and hunger (Goal 1) and the ensuring of environmental sustainability (Goal 7) [1]. Improved and sustainable levels of animal production could not only contribute to improved household food security, but also to an increased household income in the developing world. This could lead to spinoffs indirectly benefitting other millennium development goals, such as the achievement of universal primary education (Goal 2), the reduction of infant mortality (Goal 4), and an improved maternal health (Goal 5). The benefits of including meat in diets of vulnerable groups are becoming evident now [6, 7].

During an exercise where livestock and poverty in the developing world were mapped by Thornton et al. [4] it became evident that large areas of the developing countries are only fit for rangeland-based livestock production. Considerable other areas are also utilized by livestock in combination with cropping in rainfed or irrigated mixed production systems. Ruminant livestock strongly depends on crop residues and the intercrops planted in the ley-farming systems which are preferred at present [8].

Against this background, it is reasonable to assess the contribution of livestock breeding to the sustainability of livestock production systems. This topic is addressed by providing background information leading to thoughts on global food security, information pertaining to farm animal genetic resources and livestock products contributing to food security, and external and internal challenges, the advent of the technological age and challenges stemming from it. These topics culminate in proposed future directions to place sustainable farm animal breeding in the developing world and the tropics on a solid foundation, before some concluding remarks.

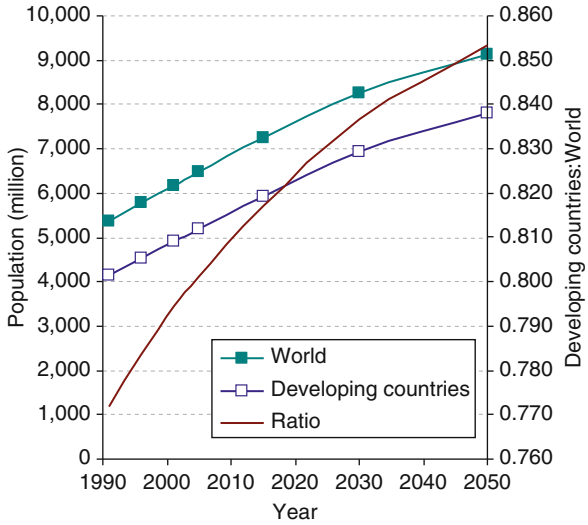

Breeding in Developing Countries and Tropics. Figure 1 The population growth of the developing countries relative to the entire human population of the world from 1990–1992 to 2004–2006, and extrapolated beyond that to 2050. The human population in the developing countries is also expressed as a ratio of the world population (Source: FAO [9])

Setting the Scene

World Population

The world population grew steadily from 1990–1992 to 2004–2006 (Fig. 1). Extrapolation beyond the data to 2050 suggests sustained population growth from 5,358 million people in 1990–1992 to 9,136 million people in 2050, an increase of 71%. In the case of the developing world, this increase amounts to 89%, from 4,135 million people in 1990–1992 to 7,797 million people in 2050. Expressed as a ratio, 0.77 of people were living in the developing world in 1990–1992, compared to an estimated 0.85 in 2050. The impact of this change of population structure on the available resources in terms of plant and animal production is evident.

Global Food Production

Given the increase in the global population and the even faster population growth in the developing countries, it is imperative to have a look at global food production. The production of grain in the developing world has increased from ~1.3 million kilotons in 1995 to just below 1.6 million kilotons in 2007 (Fig. 2).

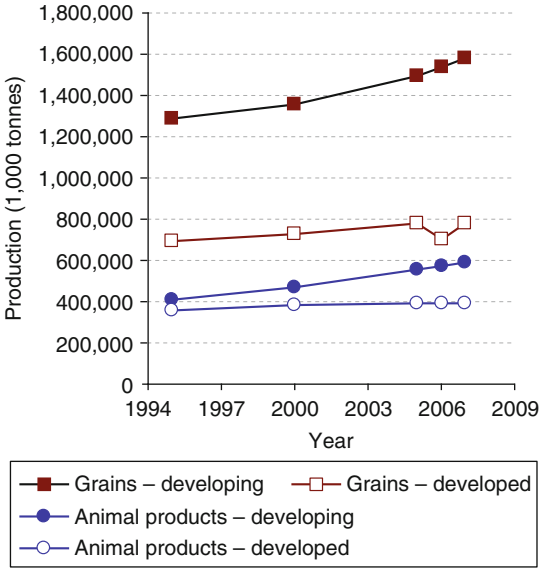

Breeding in Developing Countries and Tropics. Figure 2 The production of grains and animal products (meat, milk, and eggs) in countries of the developing world and the developed world (Source: FAO [10])

Expressed relative to 1995 production, this increase amounted to 23%. Grain production in the developed world amounted to just below 0.69 million kilotons in 1995 and 0.78 million kilotons in 2007, an increase of about 12%. Animal products (meat, milk, and eggs) in the developing world increased from 0.41 million kilotons in 1995 to 0.59 million kilotons in 2007, an increase of 44%. Animal products in the developed world, in contrast, remained fairly stable at between 0.36 and 0.40 million kilotons over the entire period. There thus seems to be an effort on the part of the developing world to compensate for the faster population growth by a higher food production. However, this increase has to be seen in relation to the relative size of the respective populations in the developing and developed countries. Grain production per head of the developed world increased by 8.5% from 563 kg/head in 1995 to 611 kg/head in 2005 (Table 1). Grain production per head in the developing world, in contrast, remained relatively stable at a substantially lower level of between 275 (during 2000) and 286 (during 2005) kg/head (a difference of 4.0%). The output of animal products accordingly ranged from 293 to 308 kg/head in the developed world, compared to between 90 and 107 kg/head in the developing world.

Breeding in Developing Countries and Tropics. Table 1
Per capita production of grain and animal products (meat, milk, and eggs) in developing and developed countries during 1995, 2000, and 2005

Product type and regions	Year		
	1995	2000	2005
Grains			
Developing regions	281.9	275.4	286.0
Developed regions	563.1	582.8	611.3
Livestock products			
Developing regions	90.4	95.0	107.4
Developed regions	293.4	306.5	308.2

Source: FAO [10].

The lower per capita production of food in the developing world results in the need for imports to contribute to the food supply of the local population. The global importation of food in relation to total imports is provided in Fig. 3. It is evident that food imports exceed 5% of overall imports in many countries in the developing world. Africa and the Middle East are particularly dependent upon imports of food to contribute to local food security, with food imports

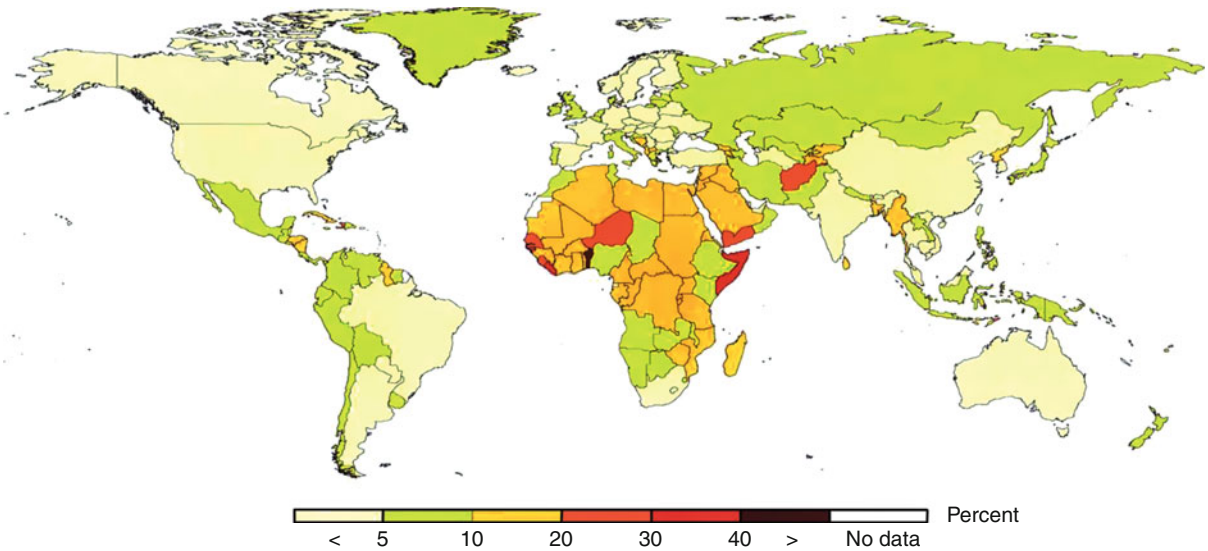

Breeding in Developing Countries and Tropics. Figure 3
The share of food imports in relation to total imports on a global basis (Source: FAO [10])

exceeding 10% of total imports in most countries. On the upper end of the scale, food imports contribute more than 30% to total imports in some countries in these regions.

Products of an Animal Origin

Table 1 suggests substantial differences between the developing world and the developed world in terms of per capita animal production. As this entry deals with animal products, this topic needs to be elucidated further. In terms of quantity, milk was the most important animal product, followed by meat and eggs (Fig. 4).

The same ranking applied both in developing and developed countries. It is evident that the production of all livestock products increased substantially over the past decade in the developing world (Fig. 4). Production in the developed world, on the other hand, remained stagnant or increased by smaller increments. These trends are set to continue in the future [11]. However, it needs to be considered that the population of the developing world exceeded 80% of the global population during 2005. It is thus evident that the somewhat higher animal production in these regions is canceled by the larger population density, hence the almost threefold lower per capita output of animal products in Table 1.

Against this background, local meat production is balanced against overall food supply for this commodity in developing countries and developed countries in Fig. 5. It is seen that there is a clear deficit in local production in the developing countries, as opposed to an oversupply in the developed countries. The deficit in own production in the developing countries is negated by imports, while only a small proportion of meat is exported. Developed countries are more likely to export meat, but also import relatively more meat than developing countries. The proportion of meat affected by stock changes and other purposes (mostly cultural) is relatively small, but appears to be somewhat higher in developing countries.

Table 1 suggests a substantially lower per capita production of animal products in developing countries relative to developed countries. In Fig. 6, this tendency is quantified for the top ten animal products globally. Per capita energy consumption from small stock (sheep and goat) meat in the developing regions amounted to 79% of that in the developed world. Other products where per capita energy consumption of the developing

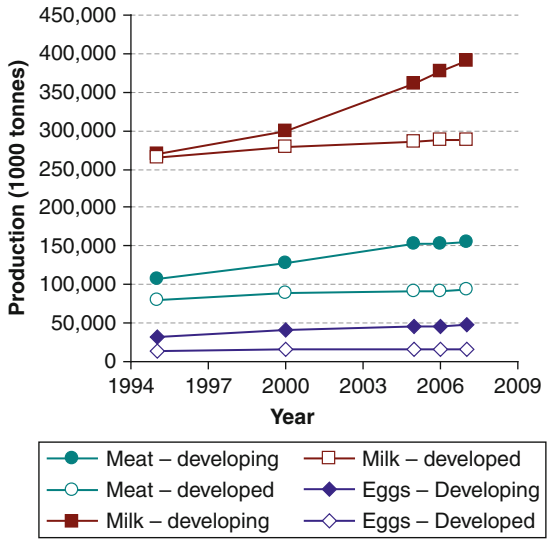

Breeding in Developing Countries and Tropics. Figure 4 Relative quantities of the most important livestock products in developing and developed countries (Source: FAO [10])

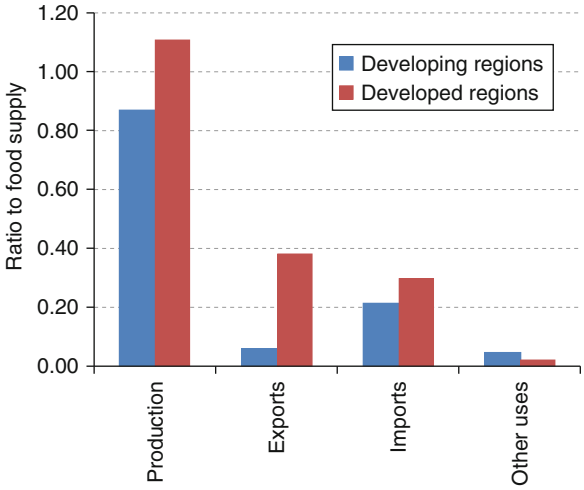

Breeding in Developing Countries and Tropics. Figure 5 A food balance for animal meats for the developing world and the developed world relative to the overall food supply in kiloton (Source: FAO [10])

world exceeded 50% of the corresponding figure in the developed world are poultry (67%), offal (67%), beef (65%), and milk (57%). Inhabitants of the developing world consumed energy from eggs (39%), honey (38%), pork (24%), animal fats (21%), and cheese (12%) at much lower quantities than their counterparts in the developed world.

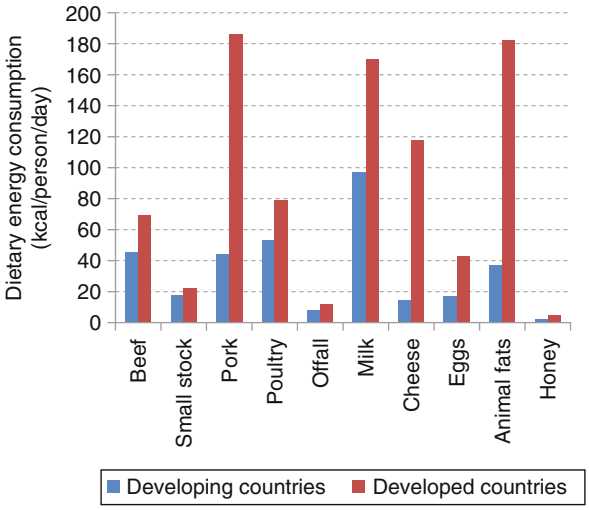

Breeding in Developing Countries and Tropics. Figure 6
Per capita energy consumption of the top ten animal products in the developing world and in the developed world (Source: FAO [10])

Global Food Security

It is evident from Fig. 6 that inhabitants of the developing world consume substantially less energy from animal products than their counterparts in the developed world. It is thus important to consider relative food security of both groupings in view of these results. It is estimated that ~854 million people in the world lack adequate nourishment for a healthy and productive lifestyle, a figure that remained fairly stable over the last two decades [9]. The number of people dependent on one or other form of food aid for a livelihood is estimated at ~73 million worldwide. It is notable that the most insecure areas in terms of the provision of food are in developing countries in Asia and the Pacific, Latin America and the Caribbean, and Near East and Sub-Saharan Africa. Figure 7 depicts the frequency of undernourishment in different areas of the world as a percentage of the total population. It is evident that people in the central part of Africa are particularly at risk from undernourishment, but that variable levels of

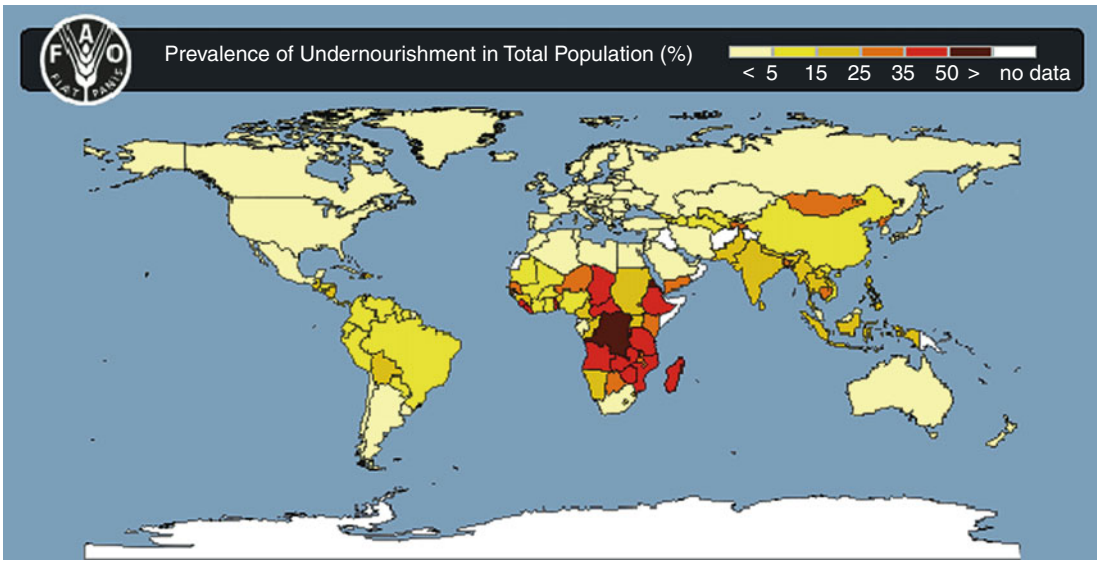

Breeding in Developing Countries and Tropics. Figure 7
The prevalence of undernourished people as a percentage of the total population in different countries throughout the world (Source: FAO [9])

undernourishment also occurs in South and Central America, in South and central Asia, and in Oceania.

The percentage of undernourished people worldwide was estimated at 16% in 1990–1992, 14% in 1995–1997, 14% in 2002–2004, and at 13% in 2004–2006 [10]. It is notable that less than 5% of the total population suffered from undernourishment in the developed world. Less than 5% of the population of the developing states in Northern Africa correspondingly suffers from undernourishment. The occurrence of undernourishment is compared for other regions in the developing world over time from 1990–1992 to 2004–2006 in Fig. 8.

It is notable that most regions reported a slight decline in food insecurity, but that it still remains at unacceptably high levels. Sub-Saharan Africa and Southern Asia were the regions where the population was most at risk during recent years (Fig. 8).

So far the discussion has centered around trends in the global human population, livestock products, as well as the issue of food security. The animal resources at the disposal of the global community for the alleviation of food insecurity need to be considered next.

Animal Resources

Domestication

Present-day production systems depend on Livestock species domesticated in the distant past. Fifteen out of 148 non-carnivorous species weighing more than 45 kg were domesticated, while only 10 out of an estimated 10,000 avian species were domesticated [12]. The time lapses since domestication of mammal livestock (in ascending order) is estimated at 10,000 years for goats, 8,500 years for sheep, 7,000–9,500 years for cattle, 6,500 years for horses and the South American camelids, 6,000 years for donkeys, 4,500–5,000 years for camels, 4,500 years for yaks and 4,000–4,500 years for water buffalo [12]. Chickens were domesticated between 5,000 and 7,500 years ago.

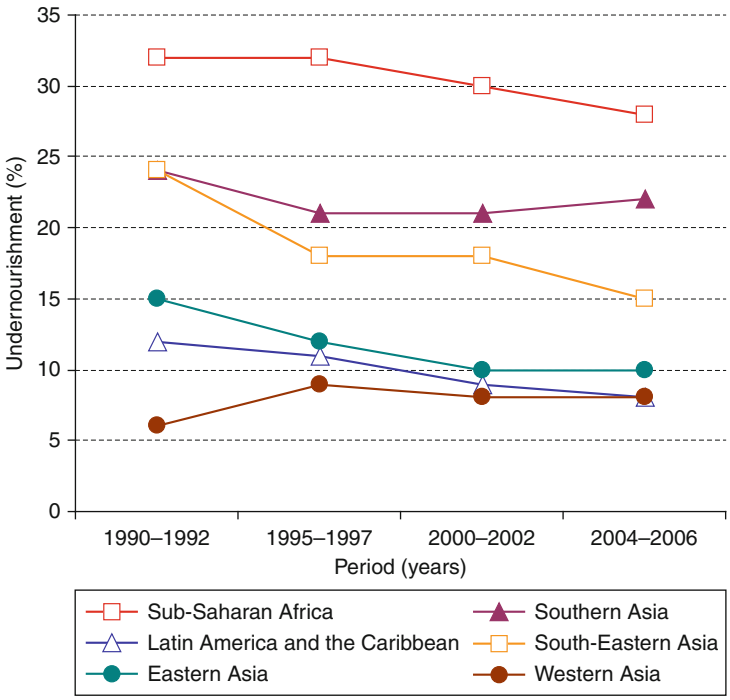

Breeding in Developing Countries and Tropics. Figure 8
The frequency of undernourishment in regions within the developing world over time from 1990–1992 to 2004–2006 (Source: FAO [9])

Distribution of Livestock Domestication, the resultant controlled breeding and selection, and the dispersal of domesticated livestock by human migration resulted in a wealth of diverse animal genetic resources. These livestock species are widely dispersed and adapted to a wide variety of environments and production systems. The percentages of countries in regions throughout the world that reported the presence of a specific domesticated mammalian species are listed in Table 2.

The wide representation across countries among the mammalian livestock species traditionally used for food production (cattle, sheep, goats, and pigs) is evident from Table 2. The exceptions are sheep that are somewhat underrepresented in the Southwest Pacific at 31%, and pigs that are underrepresented in the Near and Middle East at 8%. Species like buffaloes, rabbits, and deer are important contributors to food security in some regions. Other species (yaks, camels, South American camelids, and guinea pigs) also contribute to regional food security, but are extremely localized in their distribution.

Domestic chickens are the most important avian livestock species by far (Table 3). Livestock species like turkeys, ducks, geese, Muscovy ducks, pigeons, quails, and guinea fowl also contribute in most regions of the world, but are nowhere close to the role played by domestic chickens. Other species (partridges, pheasants, peacocks, and the ratite species) also contribute to regional food security, but are fairly to extremely localized in their distribution.

At ~1.35 billion head, cattle have to be considered as the most important mammalian livestock species in the World (Table 4). Cattle are closely followed by sheep (1.08 billion head), pigs (0.96 billion head), and goats (0.81 billion head). The only other species exceeding half a billion head are rabbits at 0.54 billion head. Regions housing more than 10% of the world

Breeding in Developing Countries and Tropics. Table 2 The percentage of countries in different regions of the world reporting the presence of specific mammalian livestock species

Mammalian species	Region						
	Africa	Asia	Europe and the Caucasus	Latin America and the Caribbean	Near and Middle East	North America	Southwest Pacific
Cattle	98	96	100	94	75	100	77
Sheep	92	86	100	91	100	100	31
Goats	96	96	93	94	83	100	69
Pigs	70	82	91	91	8	100	92
Horses	46	93	91	64	58	100	23
Donkeys	38	46	36	39	50	50	–
Buffalo	8	57	25	27	25	0	0
Deer	2	25	14	9	0	50	15
Rabbit	38	39	39	48	8	0	0
Dromedary	32	25	2	0	58	0	8
Bactrian camel	0	25	5	0	0	0	0
Yak	0	32	2	0	0	0	0
Guinea pig	8	0	0	15	0	0	0
Alpaca	2	0	0	12	0	0	0
Llama	0	0	0	15	0	0	0
Vicuňa	0	0	0	12	0	0	0

Source: Adapted from Rischkowsky et al. [13].

Breeding in Developing Countries and Tropics. Table 3 The percentage of countries in different regions of the world reporting the presence of specific avian livestock species

Avian species	Region						
	Africa	Asia	Europe and the Caucasus	Latin America and the Caribbean	Near and Middle East	North America	Southwest Pacific
Chicken	78	93	86	70	50	100	85
Turkeys	24	43	57	30	17	100	8
Ducks	32	61	50	33	17	0	46
Geese	16	39	61	21	17	50	8
Muscovy ducks	16	39	20	18	17	0	62
Guinea fowl	28	18	11	9	8	0	0
Pigeons	10	21	9	6	17	0	15
Quails	2	39	14	6	0	50	0
Partridges	4	7	7	0	0	0	0
Pheasants	0	7	9	6	0	0	0
Ostriches	12	11	7	0	0	0	8
Emus	2	4	2	3	0	0	0
Cassowary	0	4	2	0	0	0	0
Peacocks	0	0	0	2	0	0	0

Source: Adapted from Rischkowsky et al. [13].

Breeding in Developing Countries and Tropics. Table 4 The world's population of the most important mammalian livestock species, with the relative contribution of the different world regions as percentages

Species	Region							World population (billion head)
	Africa (%)	Asia (%)	Europe and the Caucasus (%)	Latin America and the Caribbean (%)	Near and Middle East (%)	North America (%)	Southwest Pacific (%)	
Cattle	14	32	11	28	3	8	3	1.355
Sheep	16	36	18	7	9	1	14	1.081
Pigs	2	62	20	8	0	8	0	0.960
Goats	22	62	4	4	8	0	0	0.808
Rabbits	0	74	24	1	2	0	0	0.537
Buffalo	0	97	0	1	2	0	0	0.174
Horse	6	25	13	44	0	11	1	0.055
Donkeys	27	38	4	20	12	0	0	0.041
Camels	40	20	2	0	38	0	0	0.019
Camelids	0	0	0	100	0	0	0	0.006

Source: Adapted from Rischkowsky et al. [13].

cattle population are Asia (32%), Latin America and the Caribbean (28%), Africa (14%), and Europe and the Caucasus (11%). Sheep are mostly found in Asia (36%), Europe and the Caucasus (18%), and Africa (16%). Asia (62%) and Europe and the Caucasus (20%) house the majority of the global pig population, while the most important goat-rearing regions are Asia (62%) and Africa (22%). Rabbits are mostly found in Asia (74%) and Europe and the Caucasus (24%). Most of the world's camels are found in Africa (40%), the Near and Middle East (38%), and Asia (20%). Table 4 confirms the status of buffaloes and South American camelids as truly regional livestock species.

Domestic chickens are by far the most important avian livestock species, with a more than tenfold advantage above ducks in the second place (Table 5). Most chickens are found in Asia (48%), while Latin America and the Caribbean (15%), Europe and the Caucasus (14%), and North America (13%) also house more than 10% of the world population.

Turkeys are found in Europe and the Caucasus (43%), North America (33%), and Latin America and the Caribbean (18%). Ducks and geese are almost exclusively found in Asia, where 90% of the world population can be found for both species.

It is also notable that most livestock can be found in the developing countries of Asia, the only exceptions being horses, camels, camelids, and turkeys (Tables 4 and 5). This is not surprising, given the high population density in this region, and the need for food produced by mammalian and avian farm animal genetic resources.

Biodiversity as Reflected by Breed Animal biodiversity is also illustrated by the number of distinct breeds that are identifiable in domestic livestock. The mammalian livestock species with the highest number of distinct breeds is sheep, followed by cattle, horses, pigs, goats, and rabbits (Table 6).

About half of the sheep breeds are found in Europe and the Caucasus, a quarter in Asia and about 12% in Africa. Regions with more than 10% of the cattle breeds are Europe and the Caucasus (31%), Asia (26%), Africa (19%), and Latin America and the Caribbean (14%). Most pig breeds are found in Asia (41%), followed by Europe and the Caucasus (32%), and Latin America and the Caribbean (12%). The regions with the most goat breeds are Asia (35%), Europe and the Caucasus (33%), and Africa (18%). Domestic chickens are the most diverse avian livestock species in terms of breed, with nearly five times as many distinct breeds than ducks in the second place (Table 7). Most chicken breeds are found in Europe and the Caucasus (58%) and Asia (22%). None of the other regions had more than 10% of the chicken breeds of the world. Regions with more than 10% of the world's duck breeds are Asia (38%), Europe and the Caucasus (36%), and Latin America and the Caribbean (11%). Goose breeds mostly originate from Europe and the Caucasus (65%) and Asia (24%). Most turkey breeds are found in Europe and the Caucasus (42%), with Africa, Asia, Latin America and the Caribbean, as well as North America all contributing 13% to the global animal diversity in terms of breeds The contribution of Europe and the Caucasus to biodiversity, as reflected by distinct

Breeding in Developing Countries and Tropics. Table 5 The world's population of the most important avian livestock species, with the relative contribution of the different world regions as percentages

Species	Region							World population (billion head)
	Africa (%)	Asia (%)	Europe and the Caucasus (%)	Latin America and the Caribbean (%)	Near and Middle East (%)	North America (%)	Southwest Pacific (%)	
Chicken	6	48	14	15	3	13	1	16.740
Duck	1	90	7	2	1	1	0	1.046
Turkey	3	1	43	18	1	33	1	0.280
Geese	1	90	6	0	3	0	0	0.302

Source: Adapted from Rischkowsky et al. [13].

Breeding in Developing Countries and Tropics. Table 6 The biodiversity, as reflected by distinct breeds, of the most important mammalian livestock species, with the relative contribution of the different world regions as percentages

Species	Region							Number of breeds
	Africa (%)	Asia (%)	Europe and the Caucasus (%)	Latin America and the Caribbean (%)	Near and Middle East (%)	North America (%)	Southwest Pacific (%)	
Sheep	12	25	48	4	5	3	3	1,129
Cattle	19	26	31	14	4	3	3	990
Horses	7	24	48	11	2	4	4	633
Pigs	9	41	32	12	0	3	2	566
Goats	18	35	33	5	6	1	2	559
Rabbits	7	8	76	7	2	0	0	207
Donkeys	14	28	28	15	11	3	2	150
Buffalo	2	73	9	9	6	0	2	132
Camels	47	24	3	0	24	0	2	97
Camelids	0	0	0	100	0	0	0	13

Source: Adapted from Rischkowsky et al. [13].

Breeding in Developing Countries and Tropics. Table 7 The biodiversity, as reflected by distinct breeds, of the most important mammalian livestock species, with the relative contribution of the different world regions as percentages

Species	Region							World Population (billion head)
	Africa (%)	Asia (%)	Europe and the Caucasus (%)	Latin America and the Caribbean (%)	Near and Middle East (%)	North America (%)	Southwest Pacific (%)	
Chicken	8	22	58	8	2	1	2	1,132
Ducks	9	38	36	11	2	0	0	234
Geese	6	24	65	3	1	0	1	166
Turkeys	13	13	42	13	4	13	2	85

Source: Adapted from Rischkowsky et al. [13].

breeds, is higher than suggested by the contribution of this region to the overall livestock populations (Tables 4 and 5). The only exception in this respect is the turkey, where the contribution of the region to the population size and the number of breeds are roughly equal. It has been suggested that many of the breeds in this region are recognized as separate entities, while being quite similar genetically [13]. In contrast, breed recording and characterization may be constrained by technical and human resources in parts of the developing world, such as Sub-Saharan Africa. This topic will be addressed later.

The Most Important Livestock Products for Ensuring Food Security

From the foregoing, it is possible to rank the domestic livestock species in terms of their importance to human food security, based on their population size and breed

diversity. There is little doubt that chickens, cattle, pigs, sheep, and goats need to be regarded as the most important livestock species in this context. More attention will thus be given to these species in the subsequent text. The importance of other regional species also needs to be considered. However, this would involve substantial additional information, which cannot be accommodated within the constraints of the present study.

Meat products are seen as important dietary sources of protein, iron, zinc, and vitamin b12 among others [7]. Meat products were related to increased live weight gains and improved cognitive function in children [14]. Meat thus has to be considered as an extremely important product for both the developed world and the developing world. Milk also provides calcium, phosphorus, vitamin B12, desirable fatty acids, and good-quality protein, and was also reported to have similar benefits to live weight and height of children under conditions where food supply is marginal [14]. The outlook for animal products (meat and dairy products) is subsequently provided per species for the major species listed above.

Meat from avian origin in this section is termed as poultry meat. However, with domestic chickens constituting more than 90% of avian livestock in the world (Table 5), it is safe to assume that the trends would also hold true for this species. Data were obtained from the outlook document of the OECD-FAO [11], and the results are provided for OECD-member states (representing the developed world) and non-OECD countries (representing the developing world). After considering production and consumption figures per species, attention is focused upon the per capita consumption of the various species meats.

Poultry

Poultry meat production in the non-OECD countries is forecast to increase steadily by 45% from ~43,600 kt carcass weight equivalent (cwe) in the early 2000s to ~63,300 kt cwe in 2017 (Fig. 9). The corresponding increase in the OECD countries is forecast to be more modest, namely, an increase of 17% from ~26,400 to ~42,400 kt cwe. Poultry consumption, on the other hand, is seen to increase by 17% from ~34,600 to ~40,400 kt cwe in OECD countries, while the concomitant increase in non-OECD countries is expected to amount to 45% (from 45,100 to 65,300 kt cwe). A deficit in non-OECD countries is evident from Fig. 9, which can be partly offset by a surplus in production in the OECD countries.

Pigs

The production of pork is expected to increase from ~63,200 kt cwe in 2004 to ~85,500 kt cwe in 2017 in

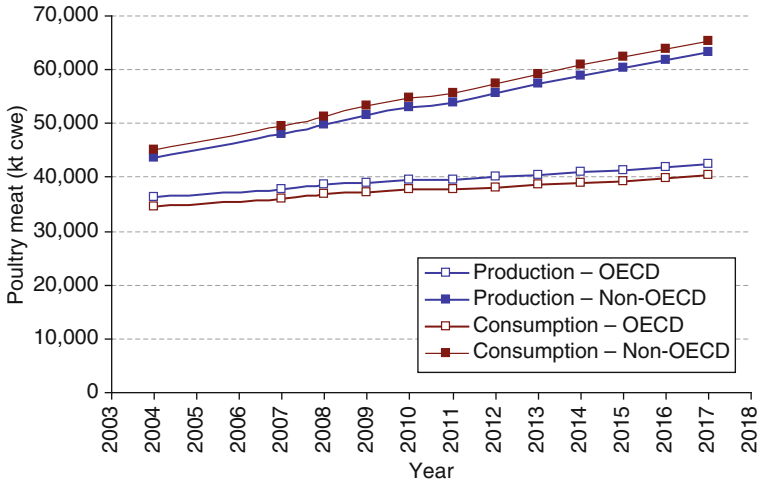

Breeding in Developing Countries and Tropics. Figure 9
Poultry meat production and consumption in kiloton carcass weight equivalent (cwe) in OECD and non-OECD countries (Source: OECD-FAO [11])

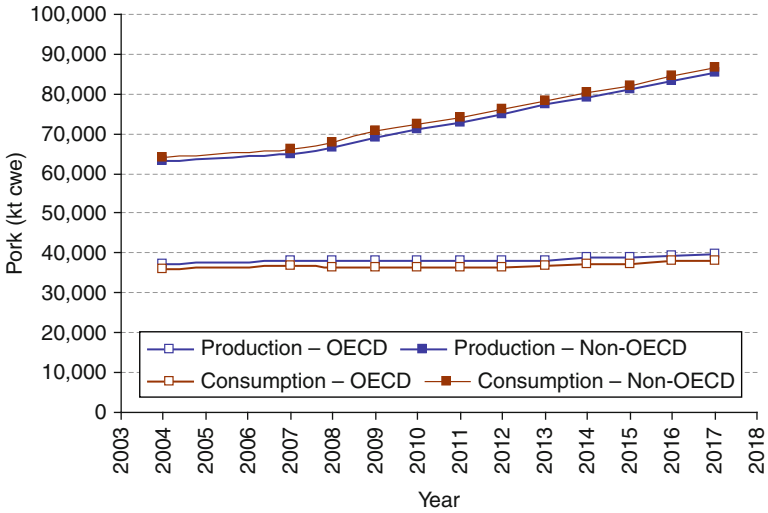

Breeding in Developing Countries and Tropics. Figure 10
Pig meat production and consumption in kiloton carcass weight equivalent (cwe) in OECD and non-OECD countries (Source: OECD-FAO [11])

the non-OECD countries, an increase of 35% (Fig. 10). OECD countries are likely to record a comparatively small increase, from ~37,100 to ~39,800 kt cwe. This increase only amounts to 7%. Consumption in the non-OECD countries is seen to increase by 36% from 63,900 to 86,900 kt cwe, while a modest increase of 7% was predicted for OECD countries (~35,800 to ~38,200 kt cwe). As for poultry meat, it was noted that a slight overproduction in OECD countries can once again be of value to counter a deficit in the non-OECD countries.

Cattle

Beef and veal production is expected to increase by 41% in the non-OECD countries, from ~37,000 kt cwe in 2004 to 52,200 kt cwe in 2017 (Fig. 11). In contrast, production in OECD countries is forecast to be relatively stable at between 26,500 and 27,200 kt cwe. As with production, consumption of beef and veal in the non-OECD region is expected to increase by 41%, from 36,500 to 51,500 kt cwe over the period from 2004 to 2017. A slight increase of about 5% is expected in the consumption of beef and veal in the OECD countries (from 26,800 to 28,000 kt cwe). Production and consumption seem to be in closer correspondence in both regions for this commodity.

Small Stock

Global production of sheep meat (mutton and lamb) is modest compared to the other types of meat. Production in non-OECD countries is expected to increase by 22% from ~10,900 kt cwe in 2004 to ~13,500 kt cwe in 2017 (Fig. 12). No increase in sheep meat production is forecast for OECD countries, and figures are expected to remain stable at 2,300–2,400 kt cwe over the entire period. Consumption of sheep meat is expected to increase by 25% in non-OECD countries (from ~11,300 to ~14,100 kt cwe), while sheep meat consumption is expected to decline by 3% in OECD countries (from 2,417 to 2,340 kt cwe). As for other meats, surplus production of sheep meat in the OECD countries may play a role in alleviating the deficit expected in non-OECD countries.

Global goat meat (chevron) production all but doubled from 2.05 million ton in 1985 to 4.05 million ton in 2005 [15]. This trend could mostly be ascribed to a 2.5-fold increase in goat meat production from 1.3 million ton in 1985 to 3.3 million ton in 2005 in

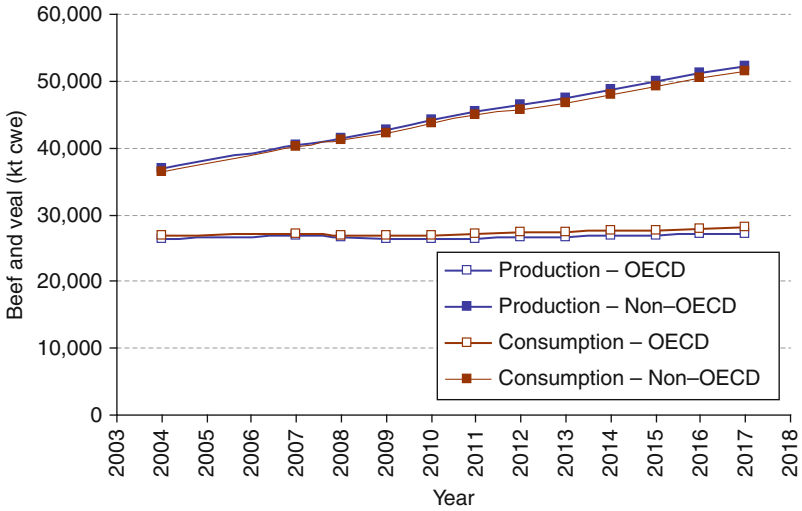

Breeding in Developing Countries and Tropics. Figure 11
Beef and veal production and consumption in kiloton carcass weight equivalent (cwe) in OECD and non-OECD countries (Source: OECD-FAO [11])

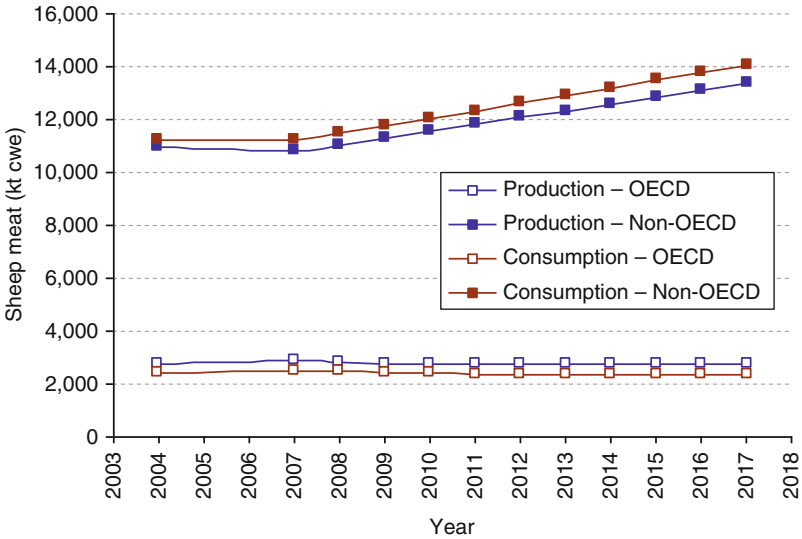

Breeding in Developing Countries and Tropics. Figure 12
Sheep meat production and consumption in kiloton carcass weight equivalent (cwe) in OECD and non-OECD countries (Source: OECD-FAO [11])

Asia. Less spectacular increases from 1985 to 2005 were reported for other countries in the developing world, namely, from 0.53 to 0.86 kt in Africa and from 0.59 to 0.83 kt in South America. In the developed world, Europe led the way with a 33% increase in chevron production from 0.09 to 0.12 kt. In contrast, goat meat production in Oceania declined markedly from 0.12 kt in 1985 to 0.02 kt in 2005 [15].

Per Capita Meat Consumption

Per capita consumption of pork as well as of beef and veal is forecast to remain largely stable up to 2017 in the OECD countries, at respectively ~23 and ~15 kg/person/year (Fig. 13). The per capita consumption of poultry meat is expected to increase by 9% from 25.4 to 27.8 kg/person/year. In contrast, the consumption of sheep meat is predicted to decline by 11% from 1.8 to 1.6 kg/person/year. The ranking of the meat from the various species is consistent over years, the sequence being poultry, pork, beef and veal, and finally sheep meat. The per capita consumption of all meat types, with the exception of sheep meat, is forecast to be lower in non-OECD countries (Fig. 13). Per capita consumption of meat from all the different species is predicted to increase over time in the latter grouping. In sequence of the importance of the different types of meat, per capita consumption is expected to rise by 15% for pork (from 9.5 to 10.9 kg/person/year), by 22% for poultry (from 7.6 to 9.3 kg/person/year), by 18% for beef and veal (from 4.9 to 5.8 kg/person/year), and by 5% for sheep meat (from 1.9 to 2.0 kg/person/year).

It is evident from Fig. 13 that the wealthier OECD countries are able to sustain high levels of protein intake from livestock. With the exception of sheep meat, developing countries are lagging behind, suggesting that there is almost unlimited scope for the improvement of livestock productivity for meat production in these regions. When the relatively small contribution of sheep meat in both regions is considered, it is tempting to discard this industry as an important contributor to food security. However, it is recognized that the sheep industry is able to thrive under marginal conditions where other livestock species find it difficult to adapt. Because of this, expansion in numbers (and thus product quantity) is not always easy to achieve. It is thus important to recognize the importance of this species to local food security, and also to the sustainable utilization of resources in marginal areas [8].

Dairy Products

The outlook is for both the OECD countries and non-OECD countries to increase their production and consumption of cheese in the immediate future (Fig. 14). Production is expected to increase from respectively ~14,200 and ~4,000 kt product weight (pw) in 2004 to respectively ~17,000 and ~5,300 kt pw in 2017. When expressed relative to 2004 production, these changes amount to respectively 20% and 35%. Corresponding increases in consumption amount to respectively 21% and 31%, from ~13,700 kt pw in OECD countries and ~4,300 kt pw in non-OECD countries to respectively ~16,600 and ~5,700 kt pw. As for other commodities, the surplus in OECD countries is forecast to be able to assist in alleviating the deficit in non-OECD countries.

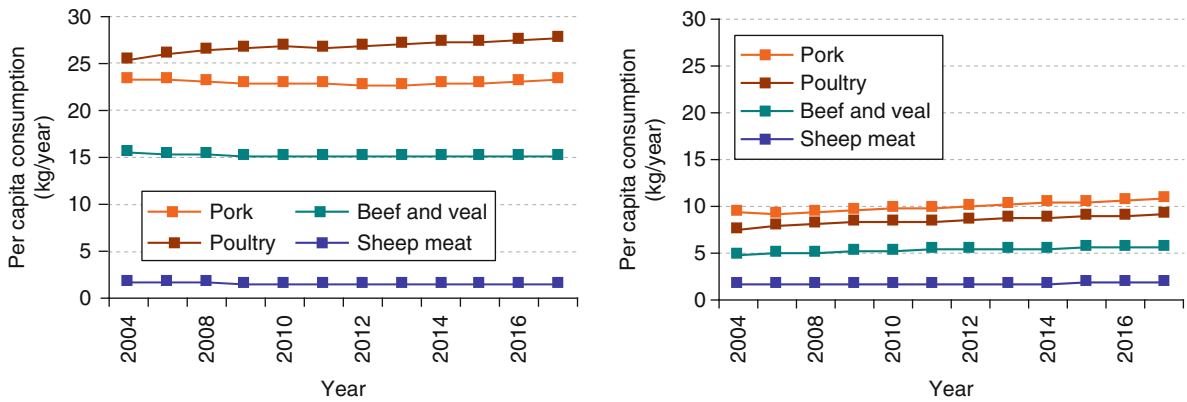

Breeding in Developing Countries and Tropics. Figure 13
Per capita consumption of meat from the various species in the OECD countries (*left*) and in the non-OECD countries (*right*) for the period from 2004 to 2017 (Source: OECD-FAO [11])

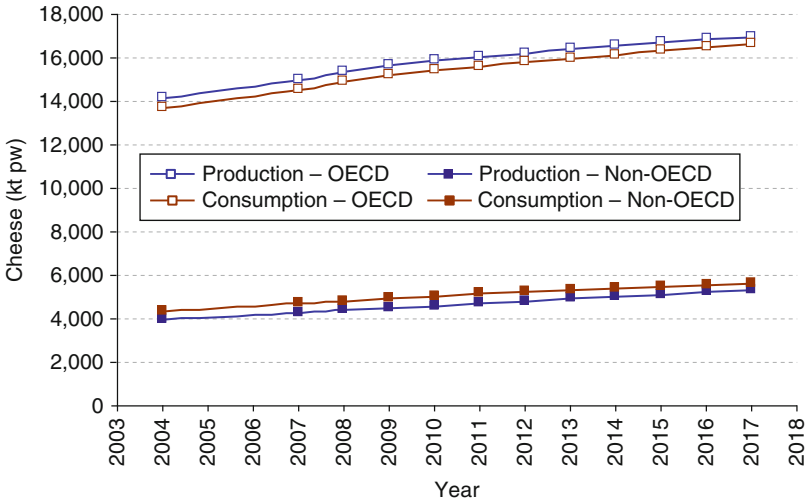

Breeding in Developing Countries and Tropics. Figure 14
Cheese production and consumption in kiloton product weight (pw) in OECD and non-OECD countries (Source: OECD-FAO [11])

World production of goat cheese increased by 28% from 343 kt in 1985 to 438 kt in 2005 [15]. Regional production in the developing world more than tripled from 35 kt in 1985 to 122 kt in 2005, stayed constant at ~4 kt in South America, and declined by 13% from 114 kt in 1985 to 99 kt in 2005. In the developed world, European goat cheese production rose by 36% from 132 kt in 1985 to 180 kt in 2005, while production in northern and central America halved from 34 kt in 1985 to 18 kt in 2005. According to Dubeuf and Boyazoglu [15], selection of goats is limited to milk goats in developed countries. There thus seems ample scope to improve performance at all levels of the dairy goat industry in developing countries.

When butter is considered, it is evident that production and consumption are predicted to remain constant at respectively between 3,600 to 3,700 kt pw and 3,100 to 3,200 kt pw in OECD countries (Fig. 15). In the case of the non-OECD countries, production of butter is expected to increase by 68% from ~4,700 kt pw in 2004 to ~7,800 kt pw in 2017. Consumption is forecast to increase by 61% from ~5,100 to ~8,300 kt pw over the same period.

Milk powder production (the sum of skim milk powder production and whole milk powder production) is projected to increase by 58%, from ~2,560 kt pw in 2004 to 4,060 kt pw in 2017, in non-OECD countries (Fig. 16). Consumption of milk powder is forecast to increase by 46%, from 4,140 to 6,030 kt pw over the same period. Both milk production and milk consumption remained fairly constant in OECD countries over the same period. The deficit between milk powder production and milk powder consumption in non-OECD countries is quite marked in this case. Fortunately the forecasted surplus of milk powder produced in the OECD countries will go a long way to alleviate this deficit in the non-OECD countries, as have been found for most of the other commodities.

It is evident that the production of butter and milk powder is substantially lower in OECD countries, compared to their non-OECD counterparts. In contrast, cheese production is much higher in OECD countries. This trend is understandable if it is considered that cheese is a prestigious, high-value product.

Challenges

It needs to be considered that livestock production in developing regions is faced with a number of challenges

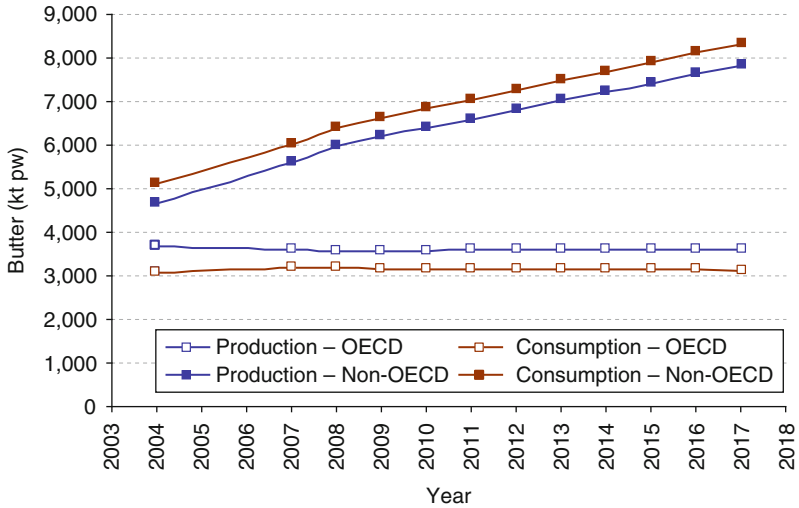

Breeding in Developing Countries and Tropics. Figure 15
Butter production and consumption in kiloton product weight (pw) in OECD and non-OECD countries (Source: OECD-FAO [11])

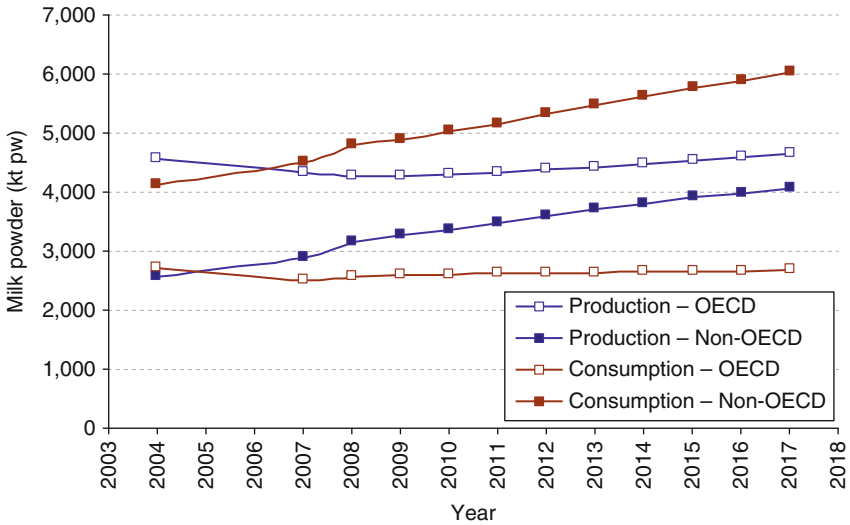

Breeding in Developing Countries and Tropics. Figure 16
Milk powder production and consumption in kiloton product weight (pw) in OECD and non-OECD countries (Source: OECD-FAO [11])

to ensure sustainability [16, 17]. These challenges need to be overcome to ensure sustainable breeding programs. A broad subdivision can be considered as challenges imposed by the environment (or external challenges) and those related to infrastructure and capacity (indicated as internal challenges).

External Challenges

Production under Various Systems It should be considered that the natural and/or cultivated plant resources form the basis for all types of livestock production. The more industrialized livestock sector relies on feedstuffs (concentrates, and roughages for dairy cows) that are in many cases imported from elsewhere for the sustenance of farmed animals. In contrast, natural and cultivated pastures are particularly important for the grazing ruminants that are able to convert low-quality roughage to nutritious protein for human consumption. Owing to a lack of control over pasture conditions in farming systems reliant on natural precipitation, periods of nutrient undersupply may occur. Persistent droughts may occur from time to time, adding to the challenges faced by tropical livestock [18]. Moreover, tropical pastures are known to have a high lignin content, particularly at the end of the growing season [19].

These afore-mentioned factors may act as constraints to efficient livestock production in developing and tropical regions. Low-potential extensive natural rangeland sustains a large portion of the well-developed sheep sector in South Africa [8]. Seasonal and unprecedented longer-term droughts are the rule rather than the exception. According to Mirkena et al. [19], adaptation of farm animals to such periods of feed scarcity can be achieved in a number of ways. Animals may develop a reduced metabolic requirement, or an ability to slow down metabolism. Digestive efficiency could be improved, while an improved utilization of low-quality roughage could be enabled. An alternative strategy could be to deposit adipose body reserves to act as a safeguard against periods of inadequate nutrient supply. As pertaining to a reduction in metabolic requirement, Silanikova [20] demonstrated that desert Bedouin goats have lower energy requirements than suggested by their body size, while they are also able to utilize low-quality roughage with a high fiber content. The latter type of goat also tolerated intake levels of ~50% below ad lib intake, compared to ~20% in Saanen goats. Localized fat reserves are found in a number of species adapted to harsh environments. Tail fat reserves of Horro and Mentz lambs were proportionally more reduced in comparison to other fat depots during periods of food scarcity and resultant loss of body condition [21].

On the other hand, Fig. 13 clearly indicates that an increasingly large portion of per capita meat consumption is expected to be produced by poultry and pigs under more intensive production systems, also referred to as industrial systems [22]. This development leads to some challenges in itself. The intensification of animals on smaller areas is feared to lead to unprecedented spinoffs, like an increase in the transmission of diseases between animals and mankind [23]. This topic is dealt with in the next section, with a number of appropriate examples. However, it is important to note that some doubts exist about the governance of some countries in the developing world to adequately deal with this potential threat [23]. According to Gummow [23], this problem is compounded by a poor immune status in many countries because of diseases like HIV/AIDS. Additionally, child nutrition was found to be inadequate in many developing countries, leading to complications like stunting and retarded growth [6], as can also be inferred from Fig. 8.

Disease It is important to recognize that disease plays an important role in livestock production throughout the world, both in developing and developed regions. There is evidence that local, indigenous cattle developed tolerance to tsetse and trypanosomis challenge in parts of Africa infested by the tsetse fly [19]. A study by Van der Waaij [24] suggested that several quantitative trait loci (QTL) have a role to play in the tolerance of trypanosomis of cattle in the African tropics. Animals imported to these regions are not likely to survive, unless a high level of husbandry and the usage of appropriate chemical treatments are applied. Infestation of farm animals with ticks in developing countries often results in death owing to tick-borne diseases [25]. Local breeds of cattle, sheep, and goats are often tolerant to the challenge provided by such diseases [19]. In this respect, it has been shown that local Small East African goats were less likely to be affected by ticks and abscesses caused by ticks than imported Toggenburg goats in Tanzania [26]. Consistent differences in favor of the local Small East African goats were found for all three species of ticks that were considered in the study.

Analyses conducted on the national database of the Bonsmara breed in the South African National Beef Recording and Improvement Scheme indicated useful genetic variation in tick numbers, particularly when the data were structured to involve environments with a higher level of tick infestation [27]. Genetic variation on the underlying liability scale was also reported for the ability of Merino sheep to resist breech strike by the sheep blowfly, *Lucilia cuprina* [28–30]. The significant genetic variation was supported by distinct line differences between Merino lines divergently selected for their ability to rear multiple offspring [31]. The challenge of animals with breech strike is controversial from an ethical viewpoint, while the transient nature of breech strike makes an adequate natural challenge under all conditions infeasible. Alternatively, it has been suggested that indicator traits should receive some attention. Traits that are considered include breech fold score, dag score, breech cover score, and crutch cover score. A number of studies suggested that all these indicator traits show significant genetic variation [28, 29, 32, 33]. In general, the indicator traits were not unfavorably related to wool and fleece traits. There is also some evidence that dag score [28, 29], breech cover score [29], and breech fold score [30] are genetically related to breech strike. Earlier work also suggested a genetic basis for body strike in sheep, as reviewed by Morris [34]. Selection for combined resistance to body strike and fleece-rot also resulted in genetic gains that accorded with expectations [35]. Infestation with the sheep body louse, *Bovicola ovis*, was accordingly reported to be heritable in a New Zealand study [36]. However, lice infestation was not conclusively associated with susceptibility to gastrointestinal nematodes.

Most species of farmed livestock are also affected by internal parasites. In this respect, marked breed differences in resistance to *Haemonchus contortus* were reported between the indigenous Kenyan Red Maasai sheep compared to the Dorper breed, an import from South Africa. Indigenous Red Maasai sheep had lower parasite burdens (as reflected by fecal worm egg counts), higher packed cell volumes as well as an improved lamb survival compared to Dorpers [37]. A later study reported small breed differences in a more arid environment with an inherently lower parasite challenge [38]. The relative advantage of the Red Maasai became evident in an environment conducive to helminth infestation, as reflected by a threefold advantage in levels of production on Red Maasai sheep compared to Dorpers [38]. Nimbkar et al. [39] reported corresponding differences in crosses of the Garole breed with the Banmur and Deccani breeds in India. These breed differences are supported by ample evidence of genetic variation in fecal worm egg counts as a measure of resistance to gastrointestinal roundworms in sheep [40, 41], as well as realized genetic progress [34, 41, 42]. Selection for lower fecal worm egg counts resulted in lower outputs of larvae on the pasture by reproducing ewes [43] and concomitant economic gains [44].

Genetic parameters and progress in other diseases of sheep were reviewed by Morris [34]. Apart from four mycotoxic diseases, the review also considered bacterial diseases like mastitis, footrot, and pneumonia. All diseases have shown moderate genetic variation, and realized genetic gains were reported for facial eczema and ryegrass staggers. Mastitis and footrot also formed part of the review by Bishop [45], indicating how the epidemiology of transmittable diseases affects options to utilize genetic variation in disease resistance in a number of species. In dairy cattle, improved modeling and revised trait definitions are being investigated for usage in the genetic improvement of resistance to mastitis on a national scale, as based on readily available somatic cell count data [46, 47]. Similar studies are underway as pertaining to bovine Johne's disease [48] and bovine tuberculosis [49].

Additionally, cognizance should be taken of new diseases of a noninfectious nature. Gummow [23] pointed out that increased industrialization and pollution also impacted on livestock farming, and listed chronic copper and vanadium overdose as an important source of livestock deaths in the Mpumalanga province of South Africa. Other examples of noninfectious conditions listed in the latter review were the impact of environmental contaminants on the life expectancy of humans in Russia as well as air pollution in the United States. These conditions need to be understood better, while pollution needs to be brought down to manageable levels [23].

The previous discussion dealt with the importance of disease, as well as heritable resistance to known pathogens. The complexity of selection for resistance to known pathogens, as reviewed by Bishop [45], is also recognized. The relevance of the above-mentioned to the eventual outcome of the chapter will become clear in the section on future directions.

It is important to note that intensification in the more industrialized livestock species (poultry, pigs, and dairy cows) are likely to be conducive to an increased risk of infection by some diseases [23]. Owing to close contact with mankind, the transmission of some animal diseases to humans (also referred to as zoonoses) places a further dimension on the importance of livestock disease. A number of recent and historic epidemics, resulting in loss of life among animals and humans alike, have been listed by Gummow [23]. The transmission of animal diseases to humans falls beyond the scope of this review, and will not be dealt with in detail. However, it is necessary to refer briefly to recent occurrences of Bovine Spongiform Encephalopathy (better known as BSE), foot and mouth disease, and Avian Influenza to get an indication of the impact of such diseases on mankind. Avian Influenza in particular has led to recent scares, associated with a loss of approximately 200 human lives [22]. An outbreak of Rift Valley Fever during the summer and autumn of 2010 similarly resulted in substantial livestock losses [50], as well as at least 17 human fatalities in South Africa during the past year [51]. This has resulted in the suspension of raw wool exports worth an estimated 1 billion South African Rand (ZAR) to the Chinese market on August 16, 2010 [52]. The impacts of such events on livestock, humans, and the economy should be clear from the foregoing.

Heat Stress and Water Requirements The climate can influence animal production in many ways. The impact of low and unreliable rainfall patterns already received attention previously. One of the other main stressors of livestock in the developing world, and particularly in the tropics, is heat [19]. Heat stress is reflected in increases in a number of physiological responses that result in impaired production and reproduction [53]. Heat stress is aggravated by an increased humidity [19]. According to Marai et al. [53], the following temperature humidity index (THI) can be an indication of the amount of heat stress experienced by animals:

$$\mathrm{THI} = \mathrm{db}^{\circ}\mathrm{C} = [(0.31 - 0.31\,\mathrm{RH})\mathrm{db}^{\circ}\mathrm{C} - 14.4]$$

With db°C = the dry bulb temperature in °C
RH = the relative humidity (RH%/100w)

Values below 22.2 suggest an absence of heat stress, a value from 22.2 to <23.3 is indicative to moderate heat stress, a value from 23.3 to <25.6 suggests severe heat stress and a value exceeding 25.6 reflects extreme heat stress. It is suggested that adapted animals are able to increase their sweating rate under adverse conditions in terms of heat stress, while they are able to control heart rate and rectal temperature better than their poorly adapted contemporaries.

A Brazilian study compared a number of physiological responses of five naturalized Brazilian cattle breeds (Curraleiro, Crioulo Lageano, Pantaneiro, Junqueira, and Mocho Nacional – the former four breeds from a *Bos taurus ibericus* origin and the latter from a *B taurus ibericus* x *B taurus aquitanicus* origin), as well as the commercially available Holstein (*B taurus taurus*) and Nellore (*B taurus indicus*) breeds [54]. Of the latter two breeds, it was thought that the Holstein would be poorly adapted to heat stress, while the Nellore was thought to be well adapted. Physiological traits measured on the animals are reported in Table 8.

The temperatures were not extreme during the duration of the study. Maxima ranged from just above 20°C to just below 30°C, while minima ranged from ~12°C to ~22°C. Humidity ranged from ~50% to 90% in the mornings and from ~25% to ~58% in the afternoons. Although all physiological traits in Table 8 were within normal ranges for cattle, it is notable that Nellore cattle consistently had a lower rectal temperature, respiration rate, sweating rate, serum cortisol concentration, and packed cell volume compared to their Holstein contemporaries. Rectal temperature of Holstein cattle differed by 1.4°C from the morning to the afternoon, whereas all the other breeds differed by less than 1.1°C. The respiration rate of Holstein cattle also differed by 5.7 movements/min from the morning to the afternoon, compared to 0.4 movements/min in the Junqueira breed. Based on the packed cell volume and total plasma protein

Breeding in Developing Countries and Tropics. Table 8 Means for physiological traits of five naturalized Brazilian cattle breeds, as well as the Holstein and Nellore breeds

Breed	Physiological trait						
	RT	RR	HR	SR	Cort	PCV	TPP
Crioulo Lageano	38.7	33.8	64.4	242	14.8	32.1	7.34
Curraleiro	38.8	31.0	70.7	251	11.6	34.3	7.34
Junqueira	38.7	26.4	69.9	234	14.7	32.7	7.40
Mocho Nacional	38.8	38.8	70.6	259	13.6	35.0	7.23
Pantaneiro	38.8	33.3	69.9	252	15.9	36.8	7.50
Holstein	39.0	32.7	62.6	258	13.8	37.7	7.34
Nellore	38.6	27.7	68.9	225	12.0	33.1	6.99

RT Rectal Temperature (°C), *RR* Respiration rate (movements/min), *HR* Heart rate (movements/min), *SR* Sweating rate (g/m/h), *Cort* Serum cortisol concentration (ng/mL), *PCV* Packed cell volume, *TPP* Total plasma protein
Source: Adapted from McManus et al. [54].

concentration, it was suggested that Holstein cattle were more dehydrated than the other breeds, and the Nellore breed in particular. The clear breed differences in Table 8 clearly suggest that the Holstein would be less adapted to heat than the Nellore breed, as anticipated. Of the naturalized breeds, the Junqueira seemed to be best adapted. In contrast, adaptation of the Mocho Nacional breed appeared to be the worst among the naturalized breeds.

The impact of heat stress on sheep was reviewed by Marai et al. [53]. Lambs borne by heat-stressed ewes had lower birth weight than those of ewes not subject to heat stress. The impact seems to be brought about by a reduction in embryo cell number and placentome size. Heat stress also depressed lamb growth, with solar radiation together with heat stress aggravating the situation. Exposure of sheep to heat stress conditions leads to impaired feed intake levels, as well as increases in respiration rate, body temperature, and water intake. The digestion of forage is also impaired by the exposure of sheep to heat stress conditions [53].

The physiological response of a temperate sheep breed (Rambouillet) was compared to those of two Indian breeds (Malpura and Chokla) at ambient temperatures of 24°C and 40°C in a study by Singh et al. [55]. The better adaptation of the Indian breeds to the ambient temperature of 40°C is evident in Fig. 17, as reflected by reduced respiration rates and rectal temperatures.

Very similar results were reported for Suffolk sheep, as representative of a temperate breed relative to local Egyptian breeds (the Barki and Rahmani) in the study of El-Sheikh et al. [56]. In this study, respiration rate and rectal temperature were studied at exposure to elevated temperatures (0 h), and after 2 and 4 h of exposure to high temperatures (respectively +2 h and +4 h). The better adaptation of the two local breeds compared to the Suffolk is evident from Fig. 18.

The better adaptation of local breeds to conditions of excessive heat is evident from the foregoing. It could therefore be expected that animals from temperate breeds could find it difficult to adapt and thrive under such conditions. Menjo et al. [16] reported that 25% of Holstein-Friesian heifers born from artificial insemination in Kenya were lost to involuntary culling prior to their first calving. It is notable that the survival of heifers bred from semen of Kenyan, South African, and Israeli bulls had an improved survival relative to those bulls originating from Australia, New Zealand, the United States, and Canada. Conditions in terms of ambient temperature in the dairy producing areas of the latter countries are arguably cooler than those experienced in Kenya, while harsher conditions are expected in South Africa and Israel. Unfortunately, the relative milk yields of the heifers that originated from semen from the respective regions were not reported and could, thus, not be considered. Boonkum et al. [57] accordingly reported that days open were

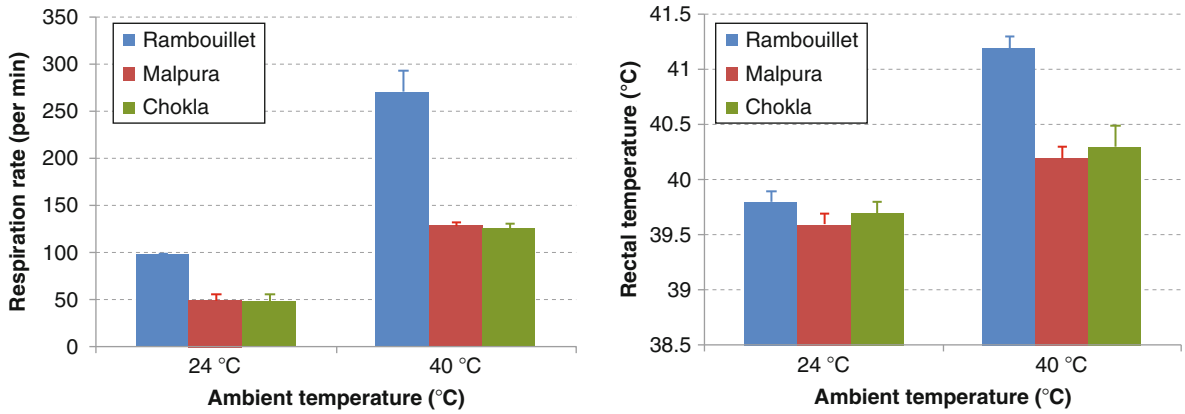

Breeding in Developing Countries and Tropics. Figure 17
Means for respiration rate (*left*) and rectal temperature (*right*) of animals from the Rambouillet, Malpura, and Chokla sheep breeds at ambient temperatures of 24°C and 40°C (Adapted from Singh et al. [55])

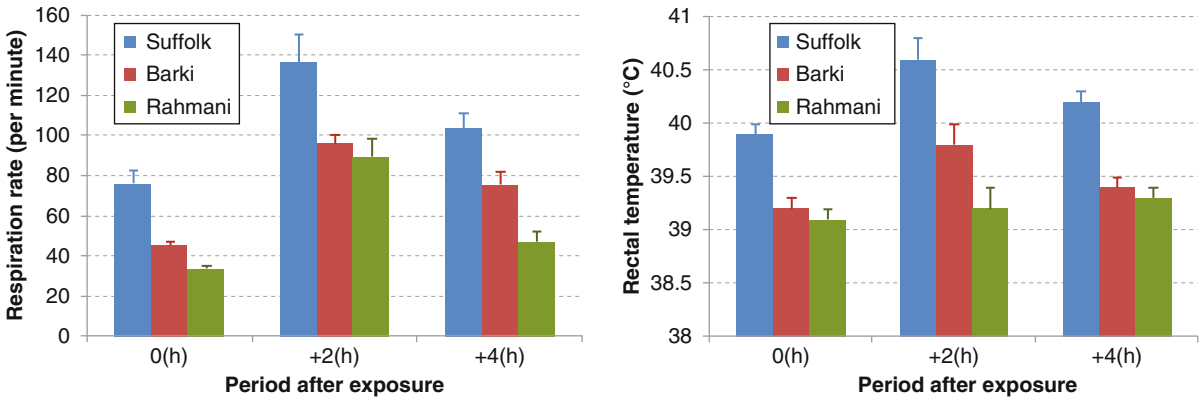

Breeding in Developing Countries and Tropics. Figure 18
Means for respiration rate (*left*) and rectal temperature (*right*) of animals from the Suffolk, Barki, and Rahmani sheep breeds after 2 and 4 h of exposure to elevated temperatures (adapted from El-Sheik et al. [56])

increased with an increased proportion of Holstein genes in Thai Holstein and Holstein cross cows. The heritability of days open was slightly higher for summer calvings compared to late rainy season calvings. Susceptibility to heat stress increased with increasing parities, possibly leading to the observed high erosion rates of cows from first to third parity [58]. Whereas genetic trends for milk yield was favorable from first to third parity, second and third lactation cows became more susceptible to heat stress with time. These effects are expected to be aggravated with global warming. It is reassuring that statistical methods are sufficiently robust to rank animals for heat tolerance for selection purposes. Genomic selection is expected to improve the accuracy of evaluating young animals for selection purposes.

Many developing countries are in water-scarce areas of the world. It is therefore important to consider adaptation of livestock to water scarcity. Mirkena et al. [19] noted that breeds originating from arid countries can withstand water deprivation for longer periods than their counterparts from temperate countries. Camels are extremely well adapted in this sense, being able to withstand water deprivation for 17 days

on dry feed [59] and for 30–60 days on green feed [60]. There are also donkey, goat, sheep, and some cattle breeds that are able to go without water for several days [61]. Black Bedouin and Barmer goats in the Middle East may go for 4 days without water [20]. Adapted breeds minimize water losses in urine and feces and are able to produce milk despite low water intakes. Because of the increasing strategic importance of water, production practices for the future should adopt water conservation practices [62].

The adaptation of local tropical breeds to extreme conditions was discussed in this section. The importance of this adaptation to breeding in the developing world will become clear in subsequent sections.

Internal Challenges

Infrastructure and Capacity Regions in the developing world were shown to lack infrastructure and capacity for the management of animal genetic resources (Table 9).

Between 71% and 100% of African countries had limited or no capacity in the seven categories that were considered. The situation in Asia was more variable. The central and southeastern parts had limited capacity, while conditions in the east and south were somewhat better. The capacity of the Southwest Pacific, Central America, and the Near and Middle East was also limited with 78–100% of the countries having

Breeding in Developing Countries and Tropics. Table 9 Assessment of regional capacities for the management of animal genetic resources for food production

Region	Physical infrastructure		Intellectual infrastructure		Policy development		
	Capacity	Participation	Research	Knowledge	Awareness	Laws	Implementation
Africa							
North and West Africa	92	96	87	87	87	96	96
East Africa	71	100	71	86	71	86	100
Southern Africa	82	82	100	100	91	91	100
Asia							
Central Asia	100	100	100	100	100	100	100
East Asia	50	50	75	25	50	50	50
South Asia	43	71	43	85	43	71	86
Southeast Asia	75	100	75	75	75	50	75
Southwest Pacific	91	91	91	91	91	91	91
Europe and the Caucasus	31	31	36	33	31	36	46
Latin America and the Caribbean							
Caribbean	33	67	33	33	33	67	67
Central America	78	78	78	78	78	78	78
South America	30	70	30	50	50	60	50
North America	0	0	0	0	0	50	0
Near and Middle East	86	100	85	86	86	100	100

Source: Adapted from Brockhaus [63].
The percentage of countries having no or limited capacities are listed with reference to physical infrastructure, intellectual infrastructure, and policy development. The balance of countries would have medium to high scores in these respects.

limited or no capacity in the categories that were considered. The capacity of the South American and the Caribbean regions were intermediate in this respect, with between 30% and 70% of the countries having no or limited capacity in one or more of the categories under consideration. In contrast, the developed countries in Europe and the Caucasus and North America consistently had moderate to good capacities in 50% or more of the categories under consideration. The situation in North America in particular is good, with 100% of the countries having medium to good capacity in all categories except for the existence of laws and political programs.

The scenario set out in Table 9 led to an assessment by Brockhaus [63] that the strategic action as pertaining to genetic resource management has a sound basis in North America, Europe and the Caucasus, and, to a lesser extent, in Latin America and the Caribbean. Legislation in the former regions is well underway to regulate animal genetic resources. Weaknesses in the developing world are not only present at a strategic level but also at the basic operational and organizational levels. It thus seems that efforts to improve the vast and diversified livestock genetic resource of the developing world are constrained by several factors [64]. On the positive side, a growing level of awareness is present in the other regions [63]. This provides an opportunity to identify countries and stakeholders that may act as catalysts of development in other countries of the regions lagging behind. Local, regional, and international stakeholders that could play a role in this respect were listed by the latter literature source.

Structured Programs From Table 9 it is evident that the capacities to ensure structured livestock improvement may be lacking in most countries of the developing world. The emphasis placed on structured breeding programs for the livestock species of interest in the different regions must thus be considered next. The species most likely to be involved in structured breeding programs worldwide is cattle, followed by sheep, goats, pigs, and chickens (Table 10). Breeding of both dairy and beef cattle is also considered as a priority by the largest number of countries. Regions with below 50% countries involved in structured cattle breeding programs are Africa (31%), the Near and Middle East (14%), the Caribbean and Central America (17%), and the Southwest Pacific (13%). Structured sheep and goat breeding is practiced less widely, with the only regions where programs are in place in 50% or more of the countries being Europe and the Caucasus, as well as North America in the developed world, and only the Near and Middle East in the developing World. The situation for structured goat breeding is much the same except for fewer than 50% of the countries in the Near and Middle East having programs in place. It is of interest that sheep and goat breeding was only considered as a priority in four African countries [65]. This

Breeding in Developing Countries and Tropics. Table 10 Percentages of countries reporting structured livestock breeding programs per species in the regions of interest

Region	Chickens	Cattle	Sheep	Goats	Pigs
Africa	2	31	10	10	6
Asia	16	58	30	32	19
Near and Middle East	14	14	57	43	0
Europe and the Caucasus	23	74	59	54	62
Caribbean and Central America	8	17	17	8	8
South America	20	60	10	10	10
North America	50	100	50	50	100
Southwest Pacific	9	13	40	0	18
World	14	47	33	27	27

Source: Adapted from Thieme [65].

situation is perplexing, as Africa is the continent with the third highest sheep population and the second largest goat population worldwide (Table 4). Structured pig breeding is basically only being practiced in the developed world countries in the Europe and Caucasus and North American regions. The North American region is basically the only region where structured poultry breeding is practiced by 50% of the countries. The lack of activity in pig and poultry breeding in most regions can be related to breeding in these species being mostly entrusted to international breeding companies with worldwide marketing capabilities.

Tools and Strategies in Livestock Breeding Breeding in pigs and poultry is mostly centralized and practiced at low levels in the developing world. These species will thus not be covered in this section.

There is clearly a lack of activities associated with animal genetic resource management of cattle in Africa, Asia, as well as in the Near and Middle East, when compared to the situation in the developed countries of Europe and the Caucasus (Table 11). Countries in Latin America and the Caribbean are well situated as far as identification, performance recording, and artificial insemination of cattle are concerned. However,

Breeding in Developing Countries and Tropics. Table 11 The percentage of cattle and sheep breeds applying tools integral to livestock breeding during the process of breed improvement

Region	Africa	Asia	Near and Middle East	Europe and the Caucasus	Latin America and the Caribbean
Cattle breeds with:					
Breeding goal	18	28	14	44	4
Strategy implemented	13	24	9	44	1
Individual identification	11	12	9	44	58
Performance recording	12	16	9	42	45
Artificial insemination	23	12	23	38	69
Genetic evaluation	9	12	5	38	24
Sheep breeds with:					
Breeding goal	14	33	16	52	5
Strategy implemented	9	33	8	50	5
Individual identification	9	2	8	45	31
Performance recording	8	2	8	45	14
Artificial insemination	2	17	0	12	35
Genetic evaluation	5	18	0	21	37
Goat breeds with:					
Breeding goal	21	12	13	28	12
Strategy implemented	15	12	13	25	12
Individual identification	18	3	6	33	27
Performance recording	21	3	13	30	22
Artificial insemination	5	3	0	5	31
Genetic evaluation	16	3	0	10	27

Source: Adapted from Thieme [65].

most cattle breeds in this region lack a breeding goal and a breeding strategy.

Genetic resource management of sheep breeds in Africa, Asia, and the Near and Middle East is clearly hampered by a lack of identification of individuals and performance recording (Table 10). A third of Asian sheep breeds have a breeding goal and selection strategy in place. This is in contrast with Latin America and the Caribbean, where these aspects of animal resource management are lacking. However, the latter region performs better for the recording of individual animals, artificial insemination, and genetic evaluation. Artificial insemination and genetic evaluation of sheep are in fact better placed in Latin America and the Caribbean than in the developed regions of Europe and the Caucasus. About half the sheep breeds in these developed regions have breeding goals, selection strategies, as well as individual identification and recording in place.

The situation regarding goat breeds are quite similar to that in sheep, but with generally higher levels of uptake of genetic strategies and tools in African goat breeds (Table 11). In contrast, goat genetic resource management in the developed countries of Europe and the Caucasus are generally on lower levels compared to sheep. The lower uptake of artificial insemination in small ruminants compared to bovines is notable. This trend is probably related to the lack of a reliable trans-cervical insemination protocol in the small ruminant species.

The most important stakeholder in determining breeding goal definition was identified as research organizations in all regions [65]. The identification of individual animals also appears to be mostly driven by research institutions. The exception to this rule was in Europe and the Caucasus, where it was mostly driven by breeders and governments. Recording of animal performance is mostly driven by research organizations in Africa, by governments and breeders in Asia, by nongovernmental organizations in the Near and Middle East, and by breeders in Europe and the Caucasus. Genetic evaluation is seen as the responsibility of research organizations in all regions.

Crossbreeding programs to complement pure-breeding efforts were reported in all species and all regions [65]. Crossbreeding seems to be more prevalent in cattle and goats compared to sheep.

Research Expenditure The importance of research organizations in the evaluation of animal genetic resources has been highlighted in the previous section. It is therefore relevant to consider the state of research funding in countries of the developing world and in the developed world (Fig. 19). The developing countries (orange bars) with the highest research expenditure in terms of gross domestic product (GDP) is China at 1.49%. Other developing countries are Brazil (1.02%), South Africa (0.95%), India (0.71%), Turkey (0.58%), and Mexico (0.46%). Research expenditure of countries in the developed world (dark red bars) ranged from 0.47% of the GDP for the Slovak Republic to 3.63% of the GDP for Sweden. The average research expenditure for OECD countries (blue bar) amounted to 2.26% of GDP.

Figure 19 provides information on research in general. Agricultural research is often not the area of scientific development attracting the highest level of funding. Information on South Africa as an example of a fairly prosperous developing economy is provided to demonstrate this point. Of a total research budget of ~ZAR 16.5 billion in 2006/2007, funding of research and development in Agricultural Sciences amounted to 6.9% [67]. This figure was substantially lower than those for Engineering Sciences (21%), Medical and Health Sciences (15%), Information, Computer and Communication Sciences (14%), Applied Sciences and Technologies (11%) and Social Sciences (9.4%). Of the ~ZAR 1.14 billion invested in Agricultural Sciences, only ~ZAR 0.34 billion are dedicated to research on animal production and animal primary products. This amounts to approximately 2% of the overall research and development budget.

During 2006/2007, the contribution of different sectors of the South African economy to agricultural research and development (the gross value of research and development is provided in Table 12) amounted 3.0% for the business sector, 16.7% for the governmental sector, 4.6% for the higher education sector, 8.1% for nonprofit organizations and 19.0% for science councils. Compared to 2004/2005 figures, research and development expenditure increased by 37% in the business sector, by 98% in the government sector, by 30% in the higher education sector, and by 38% for science councils. No consistent increase was evident in the research and development expenditure of nonprofit

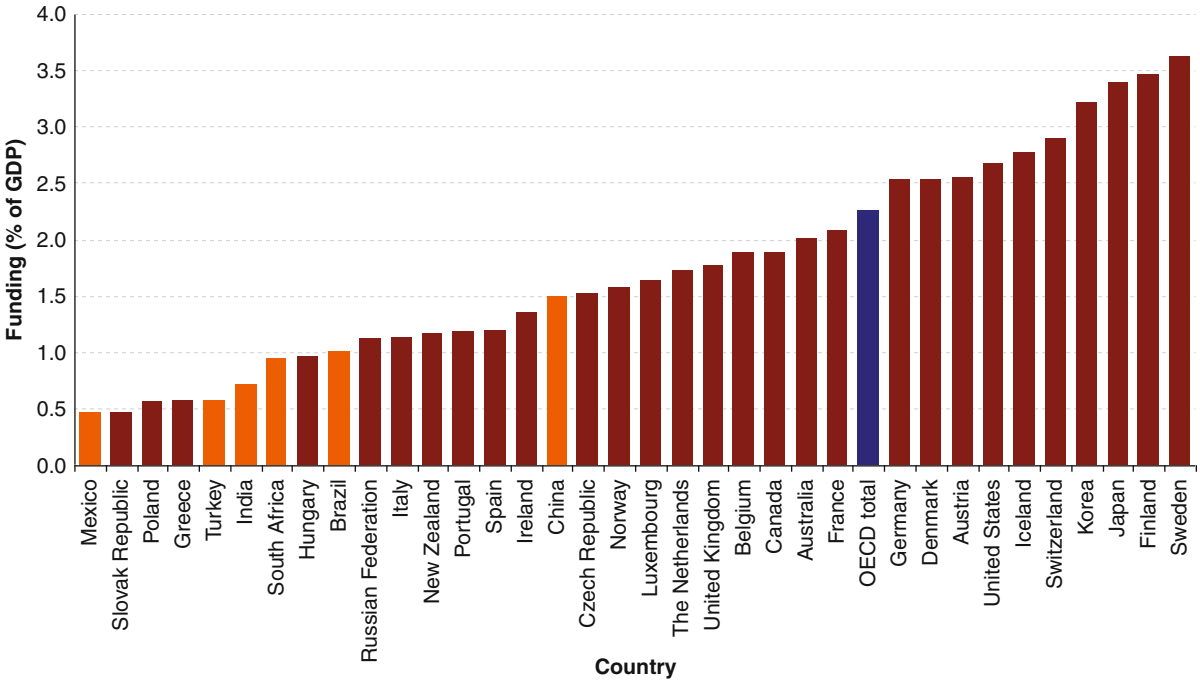

Breeding in Developing Countries and Tropics. Figure 19
Research funding expressed as a percentage of the gross domestic product (GDP) for a number of countries. Developed countries are depicted in dark red, developing countries in orange, while the blue bar depicts the average of the OECD countries (Source: OECD [66]).

organizations. The share of agricultural research remained relatively stable in the business and higher education sectors as well as in the science councils. In contrast, the percentage of governmental research and development funds devoted to agricultural research halved over the same period (Table 12). The gross value of governmental research on animal production and animal primary products increased slightly from ZAR 0.058 billion during 2004/2005 to ZAR 0.067 billion during 2006/2007. However, the percentage of the total budget devoted to these study fields declined from 11.2% to 7.0% over the same period [67]. A modest increase in the share of agricultural research was recorded for nonprofit organizations. The contribution of this sector is probably not that important if it is considered that research by nonprofit organizations attract a relatively small fraction of the overall research funding (according to Table 12 only 1.2% of the overall research and development budget).

Given the importance of governments and other stakeholders in research in decision-making pertaining to livestock breeding [65], the reduction in the percentage of governmental funds allocated to agricultural research and development is disconcerting. If it is considered that South Africa has been identified as an emerging economy along with Brazil, Chile, China, India, Russia, and Ukraine [68], it is evident that the situation may be worse in other countries in the developing world. There thus seem to be a need for a concerted effort to consolidate funding for research pertaining to livestock genetic resources in the countries of the developing world.

Intellectual Capacity The previous heading was concerned with the funding of research in the developing world. Apart from the monetary needs, the functioning of all research organizations also depends on the number and quality of the researchers employed. The number of researchers per 1,000 members of the population in a number of developed and developing countries thus needs to be considered. It is clear that developing countries (orange bars) have substantially

Breeding in Developing Countries and Tropics.

Table 12 Changes in South African research and development expenditure for Agricultural Sciences in the recent past, expressed relative to the total expenditure on research and development in the business, governmental, and higher education sectors, as well as nonprofit organizations and science councils

Sector and expenditure	Year		
	2004/2005	2005/2006	2006/2007
Business			
Total R&D (ZAR billion)	6.766	8.244	9.243
Agriculture (%)	2.8	3.1	3.0
Governmental			
Total R&D (ZAR billion)	0.515	0.844	1.021
Agriculture (%)	33.9	18.5	16.7
Higher education			
Total R&D (ZAR billion)	2.534	2.732	3.299
Agriculture (%)	3.8	5.2	4.6
Nonprofit organizations			
Total R&D (ZAR billion)	0.198	0.227	0.212
Agriculture (%)	6.4	7.3	8.1
Science councils			
Total R&D (ZAR billion)	1.996	2.102	2.745
Agriculture (%)	19.7	18.4	19.0

Source: Adapted from Anon [67].

fewer researchers in employment per 1,000 population members when compared to developed countries (Fig. 20). The numbers of researchers per 1,000 population members in developing countries ranged from 0.3 in India to 1.9 in Turkey. In contrast, between 3.6 (Italy) and 15.7 (Finland) researchers were employed per 1,000 population members in the developed world, giving an average of 7.3 researchers per 1,000 population members for OECD member countries. The number of researchers per 1,000 population members in the developed world is thus substantially higher than in the developing world.

The discrepancy in the number of researchers per 1,000 population members is evident from Fig. 20. It is of interest to note the trend in the employment of researcher fulltime equivalents in a developing country like South Africa. Firstly, it is important to note that close to 50% of all the researcher fulltime equivalents in South Africa were employed by the business sector in 2006/2007 (Table 13). The higher education sector accounted for another 29%, science councils for 16%, the governmental sector for 6%, and nonprofit organizations for 1.6%. Overall, the number of researcher fulltime equivalents increased by 15% from 11,080 in 2004/2005 to 12,739 in 2006/2007 [67]. A similar increase was noted in the business sector, while the number of researcher fulltime equivalents in the governmental sector increased by a substantial 60%. The number of researcher fulltime equivalents in the higher education sector was fairly stable, while nonprofit organizations suffered a 13% decline in researcher fulltime equivalents. The number of researcher fulltime equivalents in science councils decreased by 15% from 2004/2005 to 2005/2006, but recovered to a level 28% higher than in 2004/2005 during 2006/2007. It is notable that researchers contributed about 50% to all research related personnel in the business sector (Table 13). Researchers formed a more commanding part of the personnel corps in the higher education sector (71–77%) and in nonprofit organizations (56–69%). In contrast, the support personnel appeared to have the lion's share of the personnel corps at the expense of researchers in the government sector (30–44%) and in science councils (31–40%). The latter similarity is not surprising, as the science councils are parastatal organizations receiving part of their budgets from the government coffers.

From the aforegoing, it can be deducted that scientists in the developed world are often faced with particular challenges relative to their counterparts in the developed world. One of these should be a heavier workload, to make up for the deficit in manpower as reflected in Fig. 20. It is therefore not surprising that South African professionals were found to spend longer times at the office compared to their colleagues in the United States, United Kingdom, and Australia in a survey conducted between June 2010 and July 2010 [69].

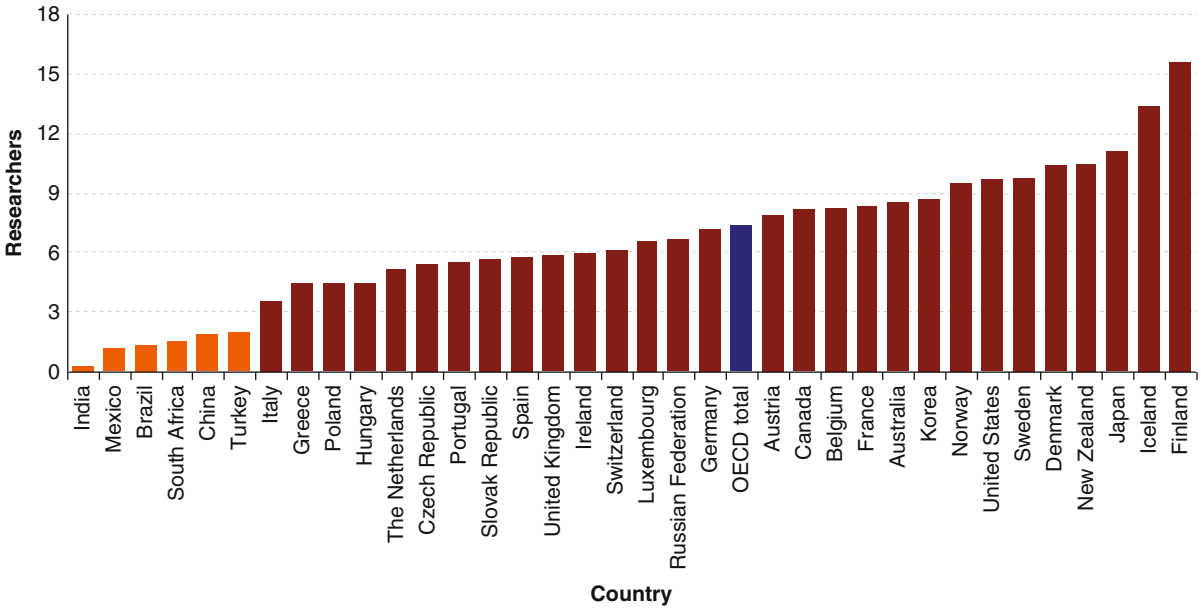

Breeding in Developing Countries and Tropics. Figure 20
The number of researchers expressed per 1,000 population members for a number of countries. Developed countries are depicted in dark red, developing countries in orange, while the blue bar depicts the average of the OECD countries (Source: OECD [66]).

In 25% of the professionals interviewed, this situation was aggravated by inconsistent internet access. In view of South Africa's assessment as a developing economy [68], it is expected that the situation in many other developing countries could be worse.

It needs to be stated that the results provided in Fig. 19 and in Table 13 are for research in general and not for agricultural research in particular. Unfortunately, the information pertaining to researcher fulltime equivalents was not broken down to the level of research field as for the expenditure on research reported in Table 12. The increase in the number of researchers has to be viewed positively, noting that research and development in a country is needed for sustained growth and global competitiveness [67]. On the other hand, it has already been shown that the emerging economy of South Africa invested only 6.9% of the total research and development budget in agricultural research (Table 12). As high-level researchers are often attracted to better funding opportunities, it is likely that the agricultural sector could find it difficult to recruit and retain the most promising young scientists. Moreover, the increase in the number of researcher full time equivalents is unlikely to be met with immediate success, as its impact still needs to filter through with time.

Against this background, it is not surprising that animal resource management is suboptimal in most countries in the developing world, as depicted in Tables 9–11. Therefore it is important to consider ways to ensure that services with respect to animal resource management are delivered to producers in these regions, given the important contribution of livestock to food security and rural sustainability. In this process it is fitting to have a look at how the developing world contributes to the global science output.

The Contribution of Developing Countries to Global Science The recent 9th World Congress on Genetics Applied to Livestock Production (WCGALP) was held from August 1 to August 6, 2010, in Leipzig, Germany. WCGALP provides an opportunity to take stock of global research efforts involving livestock production every 4 years. The relative contribution that stemmed

Breeding in Developing Countries and Tropics. Table 13 Changes in the number of South African researchers (expressed in full-time equivalents – FTE) in the recent past, expressed relative to the total number of FTE active within research and development (R&D) in the business, governmental, and higher education sectors, as well as nonprofit organizations and science councils

Sector and researcher fulltime equivalents	Year		
	2004/2005	2005/2006	2006/2007
Business			
Researcher fulltime equivalents (n)	5,300	5,896	6,111
Percent of personnel involved in R&D	46.9	48.2	48.5
Governmental			
Researcher fulltime equivalents (n)	491	651	784
% of personnel involved in R&D	29.5	43.9	37.9
Higher education			
Researcher fulltime equivalents (n)	3,506	3,555	3,658
Percent of personnel involved in R&D	77.1	72.1	70.8
Nonprofit organizations			
Researcher fulltime equivalents (n)	234	198	203
Percent of personnel involved in R&D	64.5	69.2	55.9
Science councils			
Researcher fulltime equivalents (n)	1,549	1,323	1,983
Percent of personnel involved in R&D	31.0	32.2	40.0

Source: Adapted from Anon [67].

from scientists in the developing world can be assessed simultaneously. The country of origin of the first author of each abstract of oral contributions during concurrent sessions and of posters displayed during poster sessions was recorded and summarized in Table 14. None of the eight plenary lectures that were presented during the congress was by scientists or groups of scientists from the developing world. The contribution of the developing world to papers presented during concurrent sessions will be considered next. The contribution of scientists from the developing world ranged from 4% in the case of the topic "genetics of trait complexes" to 12.5% for the topics "genetic improvement programs" and "special topics" (Table 14). Cases where contributions from the developing world exceeded 10% of all contributions within subtopics will be noted subsequently. Within the topic of "species breeding," the developing world contributed most toward "small stock breeding" (33.3% of 21 papers), "poultry breeding" (20.0% of 20 papers), and "aquaculture" (18.8% of 16 papers). The contribution of scientist groups in the developing world to small stock breeding should probably be seen in context with the projected and current trends in sheep meat in Fig. 12. Pertaining to the topic "Genetics of trait complexes" one of nine papers on "behavior" (11.1%) was presented by scientists from the developing world. The developing world does not seem to be active on the topic "methods and tools" as no subtopic attracted 10% of more of the papers in this case. When the topic "genetic improvement programs" was considered, groups from the developing world contributed most papers to the subtopic "breeding objectives and economics of selection schemes" (40% of 10 papers), "management of genetic resources" (26.1% of 23 papers) and "selection for harsh environments

Breeding in Developing Countries and Tropics. Table 14 Contributions to the concurrent paper or poster sessions of the 2010 World Congress on Genetics Applied to Livestock Production per topic, with the contributions from developing countries as percentage

Topic	Papers[a]		Posters[a]		Total[a]	
	N	%	*N*	%	*N*	%
Species breeding	164	11.0	181	49.2	345	31.0
Genetics of trait complexes	101	4.0	79	27.8	180	14.4
Methods and tools	90	4.4	46	30.4	136	13.2
Genetic improvement programs	96	12.5	52	32.7	148	19.6
Special topics	24	12.5	2	0	26	11.5

[a]Number of contributions within categories (*N*) and percentage contributed by the developing world (%).
Source: Adapted from WCGALP [70].

(e.g., the tropics)" (11.1% of 9 papers). Given the location of most developing countries, it is somewhat surprising that the major contribution of the latter subtopic still seemed to originate from the developed world. A notable lack of activity was observed for the subtopics "advances in selection theory, including experimental demonstrations" (0 of 7 contributions), "selection using molecular information" (1 out of 39 contributions) and "design of selection schemes exploiting additive and/or nonadditive effects" (0 out of 8 contributions). Within the "special topics" category, scientists from developing countries contributed to the subtopics of "animal breeding and the environmental challenges" (22.2% of 9 contributions) and "education and training" (14.3% of 7 contributions). Overall scientist groups from the developing world contributed 41 out of 475 papers during concurrent sessions, or 8.6% of the total number of papers. Developing countries contributing three or more of these papers were Brazil (8), South Africa (5), Iran (4), Israel (4), and Kenya (3).

The contributions of scientist groups from the developing world to the poster sessions are much more evident (Table 14). About half of the posters on the topic "species breeding" originated in the developing world, while between 27.8% (genetics of trait complexes) and 32.7% (breeding objectives and economics of selection schemes) of contributions were made by scientist groups in the developing world. Both posters on special topics were presented by scientist groups of the developed world.

Subtopics with more than 30% contributions from the developing world are listed next. The contribution of the developing world to posters on the topic of "species breeding" amounted to 73.7% for "poultry breeding" (of 19 contributions), 71.4% for "beef cattle breeding" (of 42 contributions), 62.5% for "small stock breeding" (of 16 contributions), 58.7% of "dairy cattle breeding" (of 46 contributions), and 38.5% for "aquaculture" (of 13 contributions). When the topic "genetics of trait complexes" was considered, it was found that posters originating from the developing world exceeded 30% for the subtopics "growth, development, feed intake and efficiency" (55.6% of 18 contributions), "lactation" (42.9% of 7 contributions), and "behavior" (33.3% of 3 contributions). Under the topic "methods and tools," the contributions of scientists from the developing world exceeded 30% for "functional genomics and systems biology" (37.5% of 8 contributions), "statistical methods – linear and nonlinear models" (33.3% of 15 contributions) and "software and bioinformatics" (33.3% of 6 contributions). When the topic of "genetic improvement programs was considered, contributions from developing world exceeded 30% for "breeding objectives and economics of selection schemes" (50% of 10 contributions) and "management of genetic resources" (33.3% of 15 contributions). It is evident that scientists from the developing world were more likely to make their contributions by the way of posters. It could be by own choice in many instances, while the available slots for oral presentations could simply have been filled by

contributions from developed countries in other cases. Of the 142 posters presented by scientists from the developing world, five or more posters were contributed by Brazil (57), China (17), Mexico (14), South Africa (12), Iran (11), and Kenya (5). The overall contribution of developing countries thus ranged from 11.5% for the topic "special topics" to 31.0% for the topic "species breeding" (Table 14).

Of the 837 contributions presented in concurrent sessions or as posters during WCGALP, 183 (or 21.9%) originated from the developing world. Most of these contributions were from Brazil (65), China (19), South Africa (17), Iran (15), Mexico (14), and Kenya (8). In total, 1,382 delegates from 60 countries attended the Congress. Of these, 229 delegates (or 16.6%) were from 32 developing countries. Developing countries represented by more than 10 delegates were Brazil (67), China (39), South Africa (19), and Mexico (19). It is notable that the average number of contributions per delegate were 183/229 = 0.799 for the developing world and 654/1,153 = 0.567 for the developed world. It thus seemed as if the scientists from the developing world were at least as willing to contribute to the scientific program as their peers from developed countries. Alternatively, a contribution at the congress could be a prerequisite for attendance for many of these scientists, given the limited funds that are available for these scientists (see Fig. 19).

From the aforegoing it is evident that the quantity and depth of research in the developing world make it difficult for scientists from these countries to compete with peers in the developed world. Kahi [64] also noted that studies from the developing world were underrepresented at the WCGALP. The fact that science groups in the developing world were much less likely to contribute papers on molecular genetics and genomic selection was also highlighted in the latter paper. More than a third of contributions at the WCGALP reported results of genomic selection [71]. The trend toward an increased investment in genomic selection is discussed later under the section "The technological age." However, the role of scientists in the developing world is anticipated to decline if they are not able to become involved in this study field. As noted before, the disparity in research funding and the availability of high-quality manpower (Fig. 20) doubtlessly contribute to this finding. However, it is also clear that a number of dedicated scientists from the developing world (based on the average number of contributions per delegate) still present their research findings at international forums. The capacity for change thus exists with such scientists acting as catalysts for the application of sound scientific applications in the developing world.

The Case for Conserving Animal Genetic Resources

It is estimated that 190 of approximately 7,600 livestock breeds became extinct over the past 15 years [72]. Roughly 60 breeds of cattle, goats, pigs, horses, and poultry were lost in the past 5 years. This section asks whether this should be a cause of concern or not. Moreover, it should be debated whether the livestock breeds of the developed world should be treated as a strategic resource, and if so, why?

As an initial comment, it needs to be stated that the share of the developing world in global animal genetic resources trading is minimal [73]. Detailed records were available for trade flows of cattle semen, live cattle, and live pigs. Data for poultry, small ruminants, and aquaculture species are unfortunately scant. The bovine semen trade is dominated by OECD countries. Bovine semen is mostly exported by the United States (32.6% of the trade), Canada (31.5%), the Netherlands (7.4%), France (6.2%), Germany (5.6%), the United Kingdom (3.8%), Italy (2.5%), and other OECD countries (9.2%). In contrast, the share of developing countries in bovine semen exports is minimal at just over 1% of global trade. Developing countries exporting bovine semen are South Africa (0.5%), Argentina (0.3%), Brazil (0.3%), and others (0.2%). Much the same situation is in place for live cattle for breeding, where the contribution of the developing world amounts to only 7.5% of the global trade [73]. The contribution of the developing world to the trade of live pigs for breeding amounts to approximately 5%. The bulk of gene flow in farm animal genetic resources takes place between developed countries (60–70%). The rationale is that farming in these countries developed to depend on high-performance operations, operating at high levels of intensity and accuracy and at a reduced environmental variability [73]. It is argued that farm animal genetic resources from these systems should be adaptable to production systems worldwide. Based on this assumption, it is not surprising that gene

flow from the developed countries to the developing countries constitutes the second most important trade pathways, accounting for between 20% and 33% in the trade of farm animal genetic resources. The exportation of genetic material from the developing world to the developed world constitutes between 1% and 2% of the global trade. There is also modest trade in farm animal genetic resources among developing countries, particularly with reference to low-input production systems [73].

A number of instances where genetic material from developing countries has been introduced to developed countries were reviewed by Blackburn and Gollin [74]. Neither Chinese Meishan pigs nor Zimbabwean Tuli cattle were able to penetrate the commercial livestock market in the United States. Although the Meishan pigs were prolific, unwanted growth and body composition traits led to a realization among pig geneticists in the United States that they could select for prolificacy within local pig breeds, without a need to cater for the unwanted characteristics of the Meishan. Tuli cattle similarly did not perform satisfactorily in terms of growth and feedlot performance, despite a good ranking for biological efficiency compared to Angus/Hereford cows. Interest in the breed thus dwindled, with only 150 registrations in 2000. In contrast, the South African Boer goat gained a foothold in the commercial goat market based on an improved body size, faster growth rate, and an improved conformation compared to local Spanish goats, which formed the basis of United States chevron production prior to the importation of Boer goats [74]. Adoption of the breed is supported by ~45,000 registrations in 2005, but Boer does were found to have a lower reproduction capacity than Spanish and Kiko does [75].

Against this background, it does not seem as if farm animal genetic resources of the developing world have a major role to play in the high-output production systems of the developed world. It even seems worthwhile to consider replacing the relatively low output farm animals of the developing world with more productive genotypes from the developed world. However, it has clearly been shown that these genotypes do not always perform according to expectations because of susceptibility to heat conditions [53–56], and typical diseases [24, 26, 37, 38] in the developing world. The often unpredictable environmental conditions inherent to farming systems in the developing world also contribute to a lack of adaptation of exotic genotypes [16, 19] under typical farming conditions in the developing regions. Samdup et al. [76] recently established that the crossing of indigenous dairy cattle in Bhutan with high-yielding Jersey cattle, as well as purebred Jersey cattle, resulted in a milk off-take of 2.4–4.6 times that achieved by local cows. However, the higher production levels of Jersey and Jersey crossbreds were offset by poor survival as well as low reproduction rates. Although crossbreeding contributed to higher livestock gross margins in the intensive areas, it has not yet resulted in meeting the demand for dairy products in Bhutan.

The downside of uncontrolled crossbreeding in farm animal genetic resources in the developing world is that the valuable adaptation traits like disease resistance may be lost. Based on the analysis of microsatellites, there is evidence that the genetic basis of the gastrointestinal nematode–tolerant Red Maasai breed is being eroded by crossing, predominantly with the exogenous Dorper breed [17, 77]. Based on the results of Baker et al. [37, 38], the ability of the Red Maasai to tolerate internal parasites may be lost in this way. Urgent intervention to halt the process has been advocated by Ole Kwallah et al. [77]. Fortunately, a nucleus flock under governmental control is still available to use in this process [17]. When Scholtz et al. [78] surveyed the South African beef cattle population in the communal sector, a high percentage (35%) of bulls that were used for breeding purposes were classified as nondescript or crossbred. This classification included the highest percentage of bulls, followed by the Nguni (22.5%), Brahman (18.2%), Afrikaner (9.9%), Bonsmara (5.1%), Drakensberger (2.8%), Simmentaler (2.1%), and various other breeds (4.4%). This observation also draws attention to a possible loss of genetic diversity because of random crossbreeding in the communal resource herds.

In this context, it is important to draw attention to fears that global livestock biodiversity will be compromised by the present animal breeding practices. These fears are supported by many breeds in different parts of the world with a lack of complete population data, as summarized in Table 15. It is clear that population data are not available for many breeds in the developing regions. Among the developing countries,

Breeding in Developing Countries and Tropics.
Table 15 The percentage of breeds with population data in the respective world regions according to class (*Mammalia* or *Aves*), and in total

Region	*Mammalia*	*Aves*	Total
Africa	32.5	21.4	30.5
Asia	55.9	41.4	52.5
Europe and the Caucasus	67.2	58.4	64.6
Latin America and the Caribbean	12.9	13.7	13.1
Near and Middle East	42.5	23.3	39.3
North America	61.3	97.8	69.3
Southwest Pacific	22.1	15.2	20.4
World	**47.2**	**44.2**	**46.5**

Source: Adapted from Cardellino and Boyazoglu [79].

information for Asia does not lag as far behind the developed world as for other developing regions, like Latin America and the Caribbean. The implication of this is that conservation status of many breeds is doubtful, simply because there is no information. According to Cardellino and Boyazoglu [79], the risk of extinction is not known for 30.0% of cattle breeds, 33.8% of goat breeds, 30.4% of pig breeds, and 29.6% of sheep breeds. Between 3.1% (goat) and 18.9% (pig) of breeds in all these species are already extinct, while between 12.7% (sheep) and 18.0% (pig) breeds are classified as at risk. The classification of no risk applies to 38.1% of cattle breeds, 49.5% of goat breeds, 32.6% of pig breeds, and 44.9% of sheep breeds. Against the background of these realities, it is important to consider ex situ conservation in the form of embryos and semen in some cases [80, 81]. The Brazilian animal germplasm bank has 60,000 doses of semen, more than 250 embryos, as well as over 700 DNA samples at present [81].

It is hypothesized that biodiversity in farm animal genetic resources is needed to ensure that it is possible to react to major changes possibly brought about by major events, like global warming. Against this background, a plan was drawn up to conserve the existing animal genetic resources, and to ensure that adapted genetic resources remain available for the smallholder systems typical of the developing world [82]. In accordance with this quest, Villanueva et al. [83] developed an indicator of farm animal biodiversity. The system was applied to British sheep and cattle breeds, and allowed inferences that the biodiversity in cattle at least actually increased from 2001 to 2008. A similar trend in sheep was negated somewhat by an increased variability in the data. It has also been reported by Djemali et al. [84] that the Sicilo-Sarde Tunisian dairy sheep breed has actually been resurrected in the recent past, after having been on the verge of extinction.

These arguments lead to the important topic of conserving farm animal genetic resources in the developing world. According to Cardellino and Boyazoglu [79], such efforts should incorporate the recording of phenotypic performance in local breeds. According to the latter authors, the use of molecular information has possibly been overemphasized in conservation efforts of genetic resources in the developing world in the past. The role that molecular characterization may play in the conservation of farm animal genetic resources is well understood, and described by Toro et al. [85]. The point made by Cardellino and Boyazoglu [79], however, is that efforts for animal breeding for the genetic improvement of populations have been compromised to some extent. The basic principles of recording phenotypic data and pedigree information in livestock production systems have been known for a long time [86], so there is no need to elaborate on this. However, this is not done on a routine basis in the developing world. While major gains have been achieved in livestock production systems in the developed world, the same cannot be said for the developing world. Aspects like routine recording of phenotypes and pedigrees become a major effort under communal and smallholder production systems [79]. This results in little genetic gain being achieved. This may be a blessing in disguise, as there are many burning questions in this respect that still need to be answered [79]. Some of these questions pertain to the following:

- Standard interventions aimed at improving production may be counterproductive.
- Genetic and environmental effects may not be adequately researched in harsh environments.
- The magnitude and direction of genotype by environment interactions in unfavorable environment may differ from those in good environments.

- All the crucial adaptive traits may not be recognized.
- Selection could move populations off their adaptation equilibrium and make matters worse.

These challenges should be addressed before major interventions are applied. There are thus a number of research opportunities to address these challenges in future [79]. Before these can be addressed, however, it is necessary to have a closer look at the successes and failures of programs that were implemented in developing countries in the past.

Animal Breeding in the Developing World: Successes and Failures This section summarizes existing breeding programs, and what could be learned from them. It was attempted to cite most examples from the developing regions, but comparisons with the developed world are unavoidable. Readers will notice that this section is biased toward experience with farm animal genetic resources in South Africa. The reason for this is that a well-developed commercial sector exists in South Africa alongside low-input systems with communal land use. With a producer support estimate of approximately 4% in comparison to the range of estimates from below 5% (in Australia and New Zealand) to more than 70% (in Iceland, Norway, and Switzerland) in OECD countries [8], the South African commercial livestock industry is relatively efficient and in many ways comparable to livestock industries in the developed world.

As a point of departure, it has been established that animal breeding in developed countries has resulted in major and verifiable contributions in improved livestock production, resulting in the demands of consumers being met in a cost effective and sustainable manner [87]. Genetic advances in the more intensive pig, poultry, and dairy industries are often cited as examples of what can be achieved by a structured breeding program for well-defined selection objectives. Recent results pertaining to the well-established Sheep Genetics Australia scheme indicated that participants make progress at an average rate that is comparable to what is attainable in theory in the dual-purpose and terminal sire schemes [88]. Wool sheep farmers are less successful and are progressing at a rate of ~30% of what is attainable in theory. Advances such as those reported by Swan et al. [88] for dual-purpose and terminal sire sheep breeds have led to selection objectives in developed countries having changed from production traits to traits associated with animal welfare, product safety, and preferences by consumers [65].

It is evident from the foregoing discussion that such advances have not been realized in the developing world. However, there are examples of animal improvement schemes in developing countries that are benchmarked with international schemes. An example is the South African dairy cattle scheme participating in Multiple Across-Country Evaluations (MACE). Test-day databases for the South African Ayrshire, Guernsey, Holstein, and Jersey breeds were harmonized with those of other participating countries [89, 90], to allow participation of the local dairy industry in MACE. Bovine semen produced in South Africa has a small international market share of 0.5% [73].

In contrast, dairy contributed only about 10% to the reason why emerging and communal farmers keep cattle [91]. Communal farmers mostly milked non-dairy breeds like the Nguni (34%), Brahman (22%), Afrikaner (20%), and Bonsmara (10%) under free-ranging conditions. Traditional dairy breeds like Friesians and Jerseys only contributed 3% to communal cattle used for milk production. Herd size averaged 6 for dairy cattle and 11 for dual-purpose breeds. At 16%, the percentage of traditional dairy cows was somewhat higher for emerging farmers, but most of the cows milked were still from nondairy breeds. Herd size averaged 39 head for dairy cattle and 42 head for dual-purpose cattle in this sector [91]. Details of levels of production were not provided but it is assumed to be fairly low. In this respect, McDermott et al. [2] identified the dairy and small stock enterprises in small-scale farming systems as amenable to intensification.

There is evidence that breeding decisions peculiar to regions and managerial capacity of farmers may hold advantages in the dairy production enterprises of developing countries. In this respect, it was demonstrated that the continuous importation of semen may not be economically viable in the Kenyan dairy production system, where smallholders living below the poverty line own 70% of the dairy cattle [92]. Systems where semen from local bulls was used were consistently more profitable than those relying predominantly on imported semen. Arguably this effects

could result from better adaptation to environmental conditions, as more daughters of Kenyan, Israeli, and South African artificial insemination bulls survived involuntary culling under Kenyan conditions [16], as discussed previously. Based on the parameters of the mechanistic lactation functions, it was contended that lower-yielding Ayrshire cows were better adapted to low- and medium-input systems in Kenya than Holstein-Friesian cows [93]. In contrast, the latter breed would have distinct advantages in high-input production systems where the levels of management and husbandry were high. Finally, it should be noted than India became the world's largest producer of milk, mostly through smallholding systems [94]. It is thus clear that substantial quantities of milk could be produced by small-scale farmers. This appears to be the case particularly in countries like Kenya and India, where there is also substantial private sector involvement [94].

The bulk of agricultural land in South Africa is not arable. Large areas are thus suitable only for extensive grazing, mostly by beef cattle in the north-eastern part and by sheep in the southwestern part [8]. The commercial breeding sector of the South African beef industry is serviced by the National Beef Recording and Improvement Scheme managed by the Agricultural Research Council (ARC), as described by Bergh [95]. After a peak of ~450,000 weights in the mid-1980s, this Scheme annually recorded between ~170,000 and ~260,000 weights since 1992. Breeding values for a range of growth/production, size, and reproduction traits are available to breeders [96]. Additional reproduction traits have been developed for inclusion in the Scheme recently [97], indicative of continuous development according to consumer specifications. It is estimated that nine beef breeds (Afrikaner, Beefmaster, Bonsmara, Braford, Charolais, Drakensberger, Gelbvieh, Angus, and Sussex) have at least 80% of the available females participating in the recording scheme [78]. As for other schemes managed by the ARC, real-time information to producers is available on the Internet [95]. Other beef breeds in South Africa are being provided by similar services by Breedplan® International [98], providing a link to international genetics. At 0.8%, South Africa controls a small portion of the international trade in live cattle exports for breeding [73], placing the country in the third position after Panama (4.1%) and Lithuania (1.0%) among developing countries.

At 47%, the sale of live animals and beef was listed as the most important reason for keeping cattle in the communal cattle sector of South Africa [78]. Cattle were also listed as being important for investment (15.4%) and cultural and ceremonial practices (13.3%), while the production of milk (10.2%), draft power (4.1%), and other reasons (4.5%) were of secondary importance. The average herd size in the communal/emerging sector was 19 head, as compared to 413 head in the commercial sector [78]. The most important attributes looked for a bull by communal farmers were size (33.1%), followed by conformation (22.0%) and performance (18.9%). When ranked by emerging farmers, the attributes were ranked somewhat differently, being performance (30.3%), size (23.5%), and conformation (19.3%). Corresponding attributes in the commercial sector were performance (33.2%), conformation (11.1%), and temperament (9.8%). Only 1.9% of communal and 36.8% of emerging farmers used a controlled mating season, compared to 88.6% in the commercial sector. Artificial insemination was used by 0.1% of communal farmers, 6.3% of emerging farmers, and 21.9% of commercial farmers [78]. Guidelines for the participation of communal farmers to the National Beef Recording and Improvement Scheme are available [99], but uptake is low.

In sheep, across flock genetic evaluation results have been reported for the South African Dorper breed [100], the South African Merino breed [101], and the South African Dohne Merino breed [102]. The South African Small Stock Scheme has recently been compared to the evaluation scheme provided by Sheep Genetics Australia to Australian livestock producers [8]. The schemes do not differ appreciably for the basic production traits (live weights, wool and fiber traits, as well as for reproduction), which are recorded on farm by livestock producers. Differences between the schemes involve traits associated with disease resistance (fecal worm egg counts and traits associated with blowfly challenge) and carcass quality traits (ultrasonic muscle and fat dimensions) which are recorded on a national basis in Australia, but not in South Africa. The personnel to record these traits are not available in the South African scheme [8], and it is therefore only recorded in experimental flocks. The shortage in

qualified personnel is not unexpected if the trend in terms of researchers are compared (Fig. 20 and Table 13). Australia boasts 8.5 researchers per 1,000 community members, compared to 1.5 researchers in South Africa. With almost a sixfold advantage it is not surprising that the former country has the capacity to allow the recording of the additional traits on a national basis. Moreover, if it is considered that the investment in research on animal production and animal primary products constitutes only 2% of the national research budget in South Africa [67], it is clear that scientists in South Africa are under immense pressure to deliver services comparable to that in developed countries like Australia.

Still there is reason for positive thinking. Overall, the South African scheme recorded ~81,000 weights and ~33,000 wool records (including a fleece testing service) for 2006-born animals with four professional staff and 10 auxiliary staff [103]. It was also shown that the recording of weights increased by about 50% from 2003 to 2006 in the scheme. These records were derived from 13 breeds, but slightly more than half came from the two major wool breeds (Merino – 31.4% and Dohne Merino – 23.9%) and a further quarter from the Dorper meat breed (24.2%) [8].

Sustained improvements in the relative economic value of breeding animals have been reported in the South African Merino breed [101] and in other South African breeds [103]. Leading studs in almost all breeds showed additive genetic gains comparable to those achieved elsewhere in the world. It is important to note that similar sheep breeding schemes are operative elsewhere in the developing world. Across-flock breeding values are thus available on the Internet for several sheep-producing countries in South America (see review by Cardellino and Mueller [104]). Similar reports were forthcoming from developing countries in South America, Western Africa, and India [105]. Kosgey et al. [18] reviewed a number of small stock projects in the tropics. Objectives strived for mostly involved growth, live weight, disease resistance, and traits associated with reproduction. An Indian project that was highlighted, involved the introgression of the fecundity gene from the Garole breed into the Deccani breed. Failed programs mostly lacked farmer participation [18]. Predicted rates of genetic gain from simulations in Ethiopian sheep breeds were generally in good agreement with actual responses in on-station research [106]. These predictions are in the process of being validated in four communities from different Ethiopian agroecological systems, based on community participation. Traditional Brazilian sheep breeding systems generally used appearance as the main criterion for selection. Recently a recording and genetic evaluation scheme named Ovigol® was launched to provide progressive breeders with the option of selection for traits linked to the profitability of their operations [107]. Uptake during the first 18 months was good, with records of 5,195 performance recorded animals of 13 breeders having been entered into the system.

The genetic merit of rams from the South African commercial sheep breeding sector was compared to that of the communal sector on commercial and communal properties [108]. Fleece weight of progeny from commercial rams exceeded that of communal rams by about 15%, while the fiber diameter of lambs sired by communal rams was between 7% and 9% broader than that of commercial rams (Table 16). This resulted in

Breeding in Developing Countries and Tropics. Table 16 Relative performance of commercial and communal rams on properties in the commercial and communal areas of South Africa

Trait	Commercial properties		Communal properties	
	Commercial rams	Communal rams	Commercial rams	Communal rams
Clean fleece weight (kg)	2.8 (100)	2.4 (86)	2.0 (100)	1.7 (85)
Fiber diameter (μm)	18.4 (100)	20.0 (109)	19.4 (100)	20.5 (107)
Clean yield (%)	76.3 (100)	68.5 (90)	66.9 (100)	60.5 (90)
Wool income (ZAR/head)	92.67 (100)	60.09 (65)	54.87 (100)	37.53 (68)

Source: Adapted from Marais [108].
Figures in brackets are expressed as a percentage of performance of commercial rams.

wool income from the progeny of commercial rams being about 35% higher than that of lambs sired by communal rams. This trend was fairly consistent at both localities, with performance at the commercial properties being improved relative to that at communal properties.

In another study, Marais [109] studied the reproduction of ~1,200 communal ewes on four locations either mated to commercial or communal rams under communal production conditions. Reproduction was low, with the lambing percentages (lambs born per 100 ewes mated) being 30% and 47% for ewes mated to commercial and communal rams respectively. The corresponding means for weaning percentage (lambs weaned per 100 ewes mated) were 27% and 37% respectively, while lamb survival (lambs weaned per 100 lambs born) averaged 88% and 79% respectively. It is clear that reproduction of ewes mated to communal rams were substantially better than that of ewes mated to commercial rams, while the progeny of commercial rams had a slight advantage in terms of survival. The poor mating performance of commercial rams possibly suggest that they were not adequately adapted to the low-input communal conditions. The progeny of commercial rams were 7.2% heavier than those of communal rams at an age of 7 months. Lambs marketed per 100 ewes mated averaged 34.2% in a Western Cape study on properties of emerging farmers, with ranges between 9.5% and 56.7% [110]. In contrast, lamb marketing percentage ranged from 90% to 116% in a study where five commercial Merino-type ewe lines were mated to Dormer or Suffolk rams in a terminal crossbreeding experiment [111]. Even if it is considered that no replacements were kept in the latter study (ewe replacements need to be bought in) the improvement is evident. Additionally, the percentage of lambs docked per 100 ewes mated (range in brackets) on commercial properties in the Western Cape amounted to 88% for Merinos (63–103%), 93% for Dohne Merinos (76–113%), and 113% for South African Mutton Merinos (105–124%) in the study of Fourie and Cloete [112]. Even if losses between docking and marketing are considered, it is evident that reproduction on commercial properties would be superior to that on communal properties.

Based on the above information, the South African wool industry embarked on a program to improve conditions in the communal small stock production areas in the Eastern Cape in the early 2000s. The dual focus was on the upgrading of existing communal shearing sheds as well as the genetic improvement of the local animal resources [113]. Approximately 20,000 breeding rams have been introduced from the commencement of the program in 2003. It was furthermore independently established that 28% of such communal sheds realized prices of better or equal to the national average in 2008/2009, compared to 9% in 2005/2006. Socioeconomic studies also indicated that undernutrition of children in the region was reduced from 43% in 2004 to 28% in 2009. This change results from an improved product (meat and wool) income, which initially contributed 47% to total household income compared to 65% at present.

As pertaining to substitution of animals from a local population with animals from the same breed but from another region to ensure a higher output, it was shown that Turkish Awassi dairy sheep had an improved milk yield compared to local Awassi ewes maintained in Syria [114]. Crossbreeding with and substitution by Turkish breeding stock were thus advocated as avenues for the improvement of Syrian dairy sheep breeding stock. Selection based on performance in the current flock also resulted in immediate gains, demonstrating that these principles are robust for extension to the Syrian environment.

The performance testing of meat and dairy goats in South Africa and other regions were reviewed by Olivier et al. [115]. The bulk of meat goat weaning weight data was derived from the Boer goat breed, with 11,679 records. The vast majority of dairy goat lactations were derived from the Saanen breed, with 14,688 out of a total of 16,148 lactation records. Data from these two breeds (Boer and Saanen) combine pedigree information and performance and form part of the National Livestock Improvement Scheme in South Africa. A study of small-scale goat keepers revealed that uncontrolled mating practices were followed by 98.3% of communal farmers and 92.3% of emerging farmers, at respective doe to buck ratios of 11:1 and 30:1 [116]. The reasons for keeping goats in the communal sector were for cash or investment (43.0%), products (37.6%), and cultural purposes (18.7%). Corresponding figures for emerging goat farmers were, respectively, 34.4%, 40.7%, and 24.8%.

Communal farmers mostly kept unimproved veld goats (53.3%), Angora goats (28.3%), and Boer goats (15.4%). Emerging farmers had a lower percentage of unimproved veld goats (1.0%), and more Angora and Boer goats (62.8% and 36.1% respectively). Flock sizes ranged from 9 to 29 in the communal sector and from 18 to 91 in the emerging sector. High mortality of kids and females was listed as a major constraint to goat farming in these sectors [116].

The South African commercial poultry industry is highly industrialized, with little information on performance in the public domain. It would suffice to say that approximately 16 billion ZAR out of a total livestock income of 37 billion ZAR was derived from this sector in 2005/2006 [8]. In contrast, the communal sector kept an average of 10.9 chickens per household, with a range from 9.7 to 17.0 [117]. The number of hens per household averaged 6.1, with ranges from 5.4 to 8.4. Chicks per household amounted to 1.3, with ranges from 1.0 to 2.3. Egg output was estimated at between 35 and 45 eggs per hen per year. Chickens were mostly kept for household meat (89.8% of cases) and eggs for home consumption (64.2% of cases). Minor reasons for keeping chickens were for selling to other parties, ceremonies, culture, and manure [117]. Indigenous chicken production is considered important throughout Africa, despite relatively low levels of output [118]. However, the latter reference still demonstrated significant genetic variation in egg weight and body weights to be exploited in well-designed breeding programs. Genetic progress can thus be achieved, even though production conditions are less than optimal.

Based upon arguments presented under the previous headings, it was expected that animal improvement in most of the developing countries will be constrained by a lack of capacity. However, success in the commercial livestock sector of South Africa and in other developing countries has been reported above. Relative information on small-scale farming operations in South Africa is also reported for comparison. The latter production systems are comparable with small-scale production elsewhere. However, it is clear that commercial successes are not common in such systems. Production is mostly focused on home consumption, while levels of production are relatively poor. Yet successes have been reported throughout the world, as reviewed by Kahi et al. [119]. Moreover, socioeconomic drivers leading to success in these case studies were listed by the latter study. These guidelines could be used as a blueprint for future schemes wanting to embark on successful breeding programs in the communal livestock resource.

From the foregoing it seems that sustainable animal genetic resource management is feasible in the developing world. Strategies to operate within the constraints imposed by capacity problems and other limitations in this region need to be considered, while the improvement of production in small-scale, low-input systems should receive serious attention. It is suggested that this will be easier to achieve in the presence of a strong commercial sector.

The Technological Age

It is common knowledge that the available technology improved rapidly over the past couple of decades. Analyses on animal breeding and genetics data that required a mainframe computer 20 years ago for a series of single-trait analyses are now routinely run as a single multi-trait analysis on a laptop computer.

Data Capturing, Analysis, and Dissemination

Computing power and data storage capacities increased markedly over the past few years. Software for the on-farm capture of animal records is readily available. This software enables operators with only basic computer skills to effectively collect data for entrance in national or regional databases. The recording system can easily be managed to use open-source software for routine data entry, data editing, and genetic analyses [120, 121]. Custom-made software for a specific enterprise can also be used for routine recordings [122]. Moreover, excellent research tools for data manipulation, the assessment of environmental effects, genetic parameter estimation, as well as the computation of animal solutions are readily available [123–126]. It seems quite feasible to adapt existing software used for breeding value estimation to include a genomic relationship matrix for the estimation of genomic breeding values in a single step approach [127, 128]. The available software packages allow for the analysis of various traits, which could consist of normally distributed linear data or traits with more challenging distributions (for instance, binary traits

or discrete scores with multiple thresholds) in single- or multiple-trait analyses. The partitioning of random effects in direct and maternal genetic components as well as maternal permanent environmental effects have also become commonplace, while standard genotype by environment interactions is easily modeled. Analyses of longitudinal data, for example, growth data, lactation test-day records or reaction-norm analyses to model genotype by environment interactions, by using random regression methods have also become routine [129–132]. Interactive systems, where participants can access information on their animals directly from the Internet, have also become commonplace [95, 104, 121]. As this process takes place in real time, delays are effectively dealt with. This infrastructure is at the disposal of all livestock producers, including those of the emerging/communal sectors, provided that all relevant information is recorded.

Genomic Selection

If progress can be considered as rapid in computer support systems and specialist software for genetic analysis, this probably applies in the superlative to progress in DNA-based marker systems and marker-assisted selection. The bovine genome has recently been completely mapped and allows the study of the genetic structure of cattle breeds worldwide [133]. High-density Single Nucleotide Polymorphism (SNP) chips of thousands of SNP markers evenly spaced across the genome are readily available for pigs [134, 135], sheep [136, 137], cattle [138–140], and poultry [141, 142]. It has indeed been suggested that full genome information may become as commonplace as SNP technology at the next WCGALP to be held in Vancouver in 2014 [143]. The utilization of the genomic information linked to phenotypes has recently been reviewed by Goddard et al. [144], to give an overview of methods and the future of the technology. Information on SNPs was used in a BLUP or BayesA framework to attain genomic breeding values for Australian progeny testing sires [145]. Compared to the tradition sire pathway EBV, the BLUP-based system improved the accuracy of selecting dairy sires for progeny testing from 0.38 to 0.44 for the Australian selection index, from 0.35 to 0.53 for the Australian profit ranking, from 0.28 to 0.45 for protein yield, from 0.20 to 0.29 for protein percentage, and from 0.16 to 0.18 for fertility. The BayesA method resulted in further improvements of 0.04, 0.02, 0.03, 0.05, and −0.04, respectively [145]. There is consensus among analysts that genomic information can greatly enhance genetic progress in dairy cattle breeding [144, 146–148]. However, it needs to be stated that price considerations at present will only allow males and elite females to be genotyped [147]. Naturally, this may change in future as the technology becomes more affordable.

The above advances will have a marked impact on animal breeding in the developed world. The question remains if it will become sufficiently affordable for routine use in the countries of the developing world, given the financial constraints in these countries (Fig. 19). The human capacity needed to make full use of these innovations is another topic that needs to be debated, given the dearth of people with adequate scientific training in these countries (Fig. 20). These and other issues will be debated in the next section.

Future Directions

Future of Livestock Breeding in the Developing Regions and Tropics

Breeding Objectives Given the environmental challenges faced by animals in the developing world and the tropics, there is little doubt that elements of adaptability, robustness, and fitness should form part of the selection objective in those areas. Fitness and/or adaptability can be defined in many ways as was reviewed by Barker [149], but a definition like "a measure of the ability of an organism to survive and reproduce in a particular environment" is probably a good compromise. Naturally, the concept includes stressors that are inherent to the particular environment maintaining the animals, for instance, climatic conditions and disease. As the prospects of breeding for resistance to disease as well as adaptation to stressful environments in terms of heat, water scarcity, and a variable food supply have already been discussed, they will not be revisited here. It is, however, important to mention that records pertaining to susceptibility to a disease are highly incidence dependent [150], which should be considered during analysis. The importance of assessing the genetic resources from the developing world and the tropics for disease resistance has been highlighted by

Gauly et al. [151], while some guidelines as to how to proceed with the process were also presented. Bath and Van Wyk [152] recently proposed a practical check for helminth infestation of small ruminants, which was easily applied by both commercial and small-scale farmers. It was suggested that this check can be used to guide decisions pertaining to the selective treatment of animals for internal parasites.

The remaining elements of fitness are therefore survival and reproduction, as was defined by Goddard [153]. According to the latter author, these elements of fitness have largely been ignored during selection of farm animals, despite obvious economic value. Arguments against reproduction and survival are a low heritability, while it was also considered difficult to record. Reproduction is also sex-limited and usually assessed later in the life of animals than other production traits. The omission of including fitness traits in the breeding objective led to a general decline of fitness in those farm animals that were intensely selected for (say) milk production. Yet the genetic coefficient of variation of 6-week pregnancy rate in dairy cattle equals that of milk yield [153]. The latter author suggests that the correct way to handle this situation would thus be to include fitness traits together with the traits of interest for a particular livestock species in a selection index, with appropriate economic weights.

It is also appropriate to consider selection for reproduction and survivability in a number of livestock species farmed with in developing countries. A number of indicators of reproduction (days from calving to first service, days open, artificial inseminations per conception, and pregnancy rate) in South African Holstein cattle of 14 herds were considered by Muller et al. [154]. Heritability estimates ranged from 0.06 to 0.08, as was also reported by other authors from developed countries. Selection for number of lambs weaned per ewe mated of South African Merino ewes (a trait with a similar low heritability as that quoted above) resulted in a genetic response of ~2% per annum, which is of the same magnitude as is expected for other traits of economic importance [155]. This realized improvement was consistent with expectations based on the review of Snowder and Fogarty [156]. Stayability of South African Angus cattle was similarly shown to be heritable [157]. From these results from the developing world it is evident that selection for reproduction and herd life in farm animals should be attainable, should it be desired. Appreciable progress has in fact been demonstrated in the national analysis of the South African Merino breed [101]. Total weight of lamb weaned per ewe mated (as measure of reproduction) improved at a rate of 0.73% per annum in the best performing flock, while the average flock gained at 0.14% per annum. At the same time, fiber diameter was reduced by 0.48% per annum in the best flock and by 0.42% per annum in the national flock. During the same period, relative economic values increased by 2.80 ZAR per annum in the best performing flock ($R^2 = 0.94$) and by 1.17 ZAR per annum in the national flock ($R^2 = 0.98$).

How to Achieve the Objective of Improving Fitness and Adaptability Having discussed the state of animal agriculture in the developing world, as well as successes and failures of projects in that region, the issue remains whether the capacity to allow sustained improvement in those regions exists. It needs to be stated that research priorities for this venture has been clearly outlined by Cardellino and Boyazoglu [79]. The proposed needs are summarized in Table 17 and include the development of suitable information systems, the characterization of resources, as well as a sound knowledge of genetic diversity, functional genetics, and animal breeding. The collection of phenotypic data is a prerequisite for the system to be successful. If these data could be linked to pedigrees it would be an added bonus. This objective may seem nearly unattainable at present. However, traceability based on individual identification is increasingly seen as a good agricultural practice for the assurance of safety and quality in global trade [158]. It is foreseen that the developing world will in future have to comply with such prerequisites for continued market access. It should thus not be seen as far-fetched to start to apply a principle like individual identification in the near future. Data containing phenotypes linked to pedigree information can initially be used for routine genetic improvement. If it is affordable it could also be linked to genomic information in future. Goddard et al. [144] stressed the importance of being able to link genomic information to phenotypes for the accurate prediction of genomic breeding values. It should be noted that recommendations on animal welfare have been left out from Table 17 as it will be dealt with separately at a later stage.

Breeding in Developing Countries and Tropics. Table 17 Research priorities to enable the breeding of livestock in developing regions to increasingly contribute to local food security and poverty relief

Area	Specific needs
Information systems	Upgrading of the existing farm animal genetic resources (FAnGR) information system
	Acquisition of data on population size and structure
	The geographical referencing of FAnGR
Characterization	Define traits and record adaptation and performance of indigenous populations
	Describe the environment to evaluate genotype x environment interactions
Genetic diversity	Define and determine the risk of extinction for FAnGR
	Adopt measures to halt the decline of genetic diversity
	Assess genetic diversity by using molecular markers
	Integrate data on phenotypes with molecular information
	Acquire global information on specific markers associated with production and fitness
Functional genetics	Ensure that the genetic basis of adaptation traits are properly understood, including disease resistance, fitness, and adaptability to challenging environments
	Apply the most recent tools for conventional genetic improvement and marker-assisted selection (MAS)
Animal breeding	Assess impact of selection under low-input conditions
	Study the consequences of introducing exotic breeds
	Devise breeding structures for a low impact environment where little or no organizational structure exists
	Research stable crossbreeding systems with a role for indigenous breeds
	Implement MAS selection where applicable, that is, in the case of disease resistance
	Gain insight in genetics of adaptation to systems with a low and variable nutrient supply

Source: Adapted from Cardellino and Boyazoglu [79].

The challenges of such a venture will be enormous. The requirements and structure of performance recording and genetic evaluation for low-input agriculture have been well documented [159] but their application in practice is lagging behind. Open nucleus breeding systems have often been advocated as a solution to the lack of sustainable genetic improvement in the developing regions [18, 160]. This solution will only be feasible if the nucleus herds/flocks are under central control of accomplished scientists at a governmental, academic, or parastatal research institution. Having said this, it is equally important to have the support of the stockowners at grassroots level. Failure of livestock breeding projects in the developing world has commonly been attributed to a lack of community involvement [18], whereas successful efforts generally benefitted from community involvement [119]. The importance of close involvement with the community stems from the multifunctional role of livestock in communities in the developing world [94]. Broad stakeholder involvement has been suggested, with collaboration of local committees, researchers and development practitioners [161]. Close interaction of these diverse partners are considered to be critical for success. The importance of participatory development approaches was also stressed by Nesamvuni et al. [162]. According to the latter authors, the integration of coexisting research and development programs is highly preferable to research and development programs operating in isolation.

Using the Kenyan Boran breed as an example, Rewe et al. [163] assessed open and closed nucleus systems of registered breeders with or without gene influx from commercial breeders to ensure that adaptation traits (mainly disease tolerance) are not compromised. The introduction of germplasm from the commercial breeders was profitable in both schemes. The study demonstrated that the success of a breeding program depended on the production system, and that adaptation could be introduced from the indigenous herd, as was suggested in Table 17.

It will be a bonus if a strong commercial sector, operating on par with conditions in the developing world, can be included in the genetic evaluation system. The successful establishment of public–private partnerships to enable the system to work is a further prerequisite for success. This blueprint seems to be effective in the South African small stock sector, as was described previously. It also appears to be relevant to dairy production in Kenya [94]. The real success with it will, however, only become known with the passage of time.

It needs to be stressed that this whole process can be orchestrated with existing tools for quantitative genetics, using known theory for the sustained genetic improvement of livestock. The emphasis on fitness traits may depart slightly from what has been practiced traditionally. Yet the approach to select for adaptation and fitness would be fairly similar to what has been proposed by Goddard [153] for general application across the globe.

Table 17 also refers to the possible role that crossing with indigenous livestock may play in commercial production. The benefits of well-planned crossbreeding systems in terms of direct and maternal heterosis are well known [164]. Structured studies are needed to apply these to livestock breeds in the developing world, where it needs to be balanced with the need to conserve the indigenous genetic resources. The substantial differences between breeds that form part of the genetic resource, as well as the relative advantage of crossbred ewes under challenging conditions in France compared to purebreds was confirmed in the literature [165, 166]. More structured research on this topic is needed for the optimal utilization of local, adapted farm animal genetic resources in the developing world. The role of cortisol and the functioning of the hypothalamic-pituitary-adrenocortical axis in breeding for an increased robustness have been highlighted recently [167]. Future studies should thus focus on the underlying causes of genetic variation at this level.

It is also important to consider the role that molecular genetics and marker-assisted selection may play in this process [167]. Constraints in monetary resources, infrastructure, and suitably qualified scientists place immediate earth-shattering breakthroughs beyond the ability of developing countries at present. Further issues like intellectual property rights also complicate immediate application on a wide scale in the developing world [168, 169]. However, scientists in the developing world should take cognizance of progress in the application of marker-assisted selection in the developed world. The rapid development of technology may allow for inputs from this part of the world in future, as the technology becomes more affordable. Fitness traits like disease resistance and reproduction, which need to be selected for in the emerging regions, is particularly well suited to marker-assisted selection [168, 170]. The provision here is that sufficient monetary investment in the genotyping of animals should be available at that stage. Therefore it is also recommended that DNA samples from phenotyped animals in the nucleus flocks/herds be collected and stored for possible future usage. The general concept has been applied in the Australian Information Nucleus flock [171–173], which has already produced a number of outcomes [174]. Scientists in the developing world are well aware of the importance of combining genetic and environmental information for selection decisions [64]. It should thus be feasible for these scientists to adapt to the requirements listed above, should the opportunity arise.

Readers will notice that most of the examples listed in this section involved grazing ruminants. It is conceded that pigs and poultry played an important role in the production of protein in both the developing and developed world, and will continue to do so in the future (see Fig. 13). However, these industrialized livestock systems are in many cases served by multinational breeding companies, as stated previously. Moreover, the prospects of selecting for "robustness" or "fitness" in poultry and pigs have been covered in some detail in other entries in this encyclopedia [175, 176]. The issues dealt with in the latter entries

are complex, and it would have been impossible to deal with them comprehensively in this entry.

Finally, it is clear that the system that is proposed would not only need monetary inputs, but also the human capacity to successfully orchestrate the flocks/herds [119]. In case of severe threat to some genetic resources, the option of ex situ conservation should also be an option [80, 81]. The need for collaboration across institutional and national boundaries, to ensure that the various forms of information generated in this way are optimally utilized, cannot be overstressed [168, 169]. It is therefore appropriate to ensure that the intellectual capacity to drive all the processes is available, as discussed under the following heading.

Broadening the Knowledge Base It is evident that the objectives above are unlikely to be achieved without a sound knowledge base. Based on the disadvantage of developing countries in terms of human capacity (Fig. 20), it is obvious that the people active on research and development of farm animal genetic resources should be well-trained. The limitation in human resources results in several challenges for scientists in this region, such as an increased workload in terms of teaching, and a reduced capacity for conducting research [177]. Sustainable farming and the improved use of farm animal genetic resources were targeted in a joint venture between the International Livestock Research Institute (ILRI) and the Swedish University of Agricultural Sciences. Training by the project team reached 137 university lecturers and researchers in developing countries so far [177]. Agriculture is not a favored study direction, as it is associated with poverty and an inability to improve the livelihood of families. A typical curriculum for students in animal science in South Africa (as an example of a developing country) was provided by Casey [178]. The intention with the training of students is to prepare them for a professional career in animal production, with appropriate registration. It is also noted that Sub-Saharan Africa has many universities that teach animal production. However, there is a lack of communication and collaboration between these role players [178]. In contrast, six European universities joined hands to form the 2-year European Master of Science program in Animal Breeding and Genetics [179]. The intention of the course is to assist in increasing livestock and fish production, development of sustainable animal breeding programs, the improvement of health and welfare, and the preservation of natural resources. The program also draws students from developing countries, but with ~20 scholarships per year, the impact is limited. Of students starting the program between 2007 and 2009, 46% were from Asia, 31% from Africa, 9% from the Americas, and 13% from within Europe. In Latin America, two universities from Peru, Bolivia, Mexico, and Spain each collaborate with universities in Argentina and Austria to present a master degree in Animal Science [180]. Original assessment indicates that there is heterogeneity in the curricula, grading systems, and duration. A program for harmonization has been proposed.

In view of the challenges listed above, steps need to be taken to rectify the situation in the developing world. The obvious prerequisite is to ensure a skilled and motivated core of senior mentors, to pass on knowledge to the next generation. This will be facilitated by closer collaboration between role-players, both among institutions in the developing world and with institutions in developed countries [64, 119, 168, 169, 177]. Joint appointments of senior researchers at science and technology institutions at higher education institutes could also benefit training in farm animal genetic resources, by making better use of expertise [181]. To assist in these quests, there is a wealth of Internet-based training modules that can easily be accessed [182–184]. Collaboration between research groups and those involved in training is also proposed [177]. This approach will ensure that the studies embarked upon will be relevant. It is also important to attempt to recruit and retain well-qualified and dynamic persons for careers in animal agriculture, both in training and research. The so-called brain-drain from developing countries needs to be stopped and preferably turned around. This will only become feasible if scientists see a future for themselves in animal agriculture in developing countries, both in monetary terms and in job satisfaction. Alternatively, well-trained international scientists could be used as trainers when they return to their home countries for holiday or familial responsibilities [177]. There ought to be opportunities for improving the local knowledge base in developing countries when all these avenues are fully exploited.

"New" Issues

Finally, it is necessary to give attention to issues that have not previously impacted on animal agriculture in the developing world. Both topics are specialized study fields, worthy of an exhaustive discussion in their own right. However, this chapter will only briefly deal with the new challenges, within the developing world context.

Climate Change There is consensus that the global temperatures are on the increase, and that it is probably related to higher atmospheric concentrations of the so-called greenhouse gases. It is expected that global warming will affect extensive pasture systems to a greater extent than intensive, industrialized systems [62]. This implies that animal production in the developing world will be more vulnerable than in the developed world [4]. The carbon dioxide emissions of the developing world, in particular, are modest compared to emissions in the developed world [2]. Hoffman [80] pointed out that livestock production is contributing to global warming, but also that it will be affected by the consequences of the phenomenon. It is estimated that agriculture produces between 10% and 12% of the total global anthropogenic greenhouse gas emissions [185]. Between 50% and 60% of methane and nitrous oxide could be derived from livestock activities. The review by Eckard et al. [185] focuses on the possibility to reduce greenhouse gas emissions by ruminants through the manipulation of the animals, their diet, and their rumen microbes. Manipulation of animals is centered about breeding (the focus of this entry) and on changing managerial systems. Eckard et al. [185] cited sources that quoted differences between animals in methane production, hinting at possible genetic differences. These allegations were substantiated by Robinson et al. [186], reporting that methane production in sheep were repeatable (0.47) and heritable (0.30). Adjustment for live weight resulted in these parameters being reduced to respectively 0.32 and 0.13. Adjustment for live weight also eliminated the effect of sire breed upon methane production, while correlations with rumen volatile fatty acids did not support a contention that the latter could be used as a proxy for methane production. Cassandro et al. [187] predicted methane production of dairy cows from dry matter intake, and derived a heritability of 0.12, with upper and lower confidence limits of respectively 0.03 and 0.28. Genetic correlations of methane production with milk yield and butterfat content were high (respectively 0.92 and 0.67), but protein content and somatic cell count were not genetically correlated to predicted methane production (0.14 in both instances).

Alternatively, selection for an improved efficiency would also indirectly benefit methane excretions per unit product from ruminants, as reviewed by Eckhard et al. [185], Hegarty and McEwan [188], and Herrero et al. [189], as would improvements in feed conversion and residual feed intake. Lamb production systems based on crossbreeding would be more effective in terms of methane produced per unit product than a wool and hogget production system [188]. Alternatively, methane emissions per unit product could also be reduced by an improved reproduction rate, the early disposal of unproductive animals and the longer retention of productive animals in flocks or herds. As dairy products are produced at lower levels of greenhouse gas emissions than beef, there may be a shift to dairy in a situation where greenhouse gasses need to be reduced [80].

Possibly more relevant to conditions in the developing world is the adaptation of animals to higher ambient temperatures and to more frequent severe climatic events, which are predicted to be a consequence of climate change [80]. The possible genetic improvement of adaptability, robustness, and heat tolerance has already been discussed and will not be reiterated here. Unforeseen catastrophic climatic episodes like floods, droughts, and heat waves could have a major and unpredictable impact on local farm animal genetic resources. For instance a heat wave in 1995 in the Midwestern United States resulted in an economic loss of $31 million in the state of Iowa alone [62]. Such events should be managed when they occur, as it is impossible to plan for them. However, the need for a disaster strategy to be in place in areas likely to be affected cannot be overemphasized. Thornton and Gerber [4] suggested that up-to-date weather information will play a role in mitigating the effects of climate change. State-supported schemes reminiscent of a sort

of insurance scheme may have a role to play in disastrous events, while species substitution toward more hardy animals may be contemplated (i.e., from cattle to camels in dry parts of Kenya).

Animal Welfare Pressure on output traits, particularly regarding the more intensive livestock industries, resulted in the welfare of farm animals being compromised [189]. This topic is also extensively covered by Knap [175] in this issue, and interested readers are also referred to this paper. Because of this, discerning consumers have ensured that animal welfare is among the important considerations in production systems in developed countries, like Europe [190, 191]. Welfare in farm animals are usually defined as freedom from hunger, thirst, discomfort, pain, injury, fear, and distress, as well as an ability to express normal behavior [189]. Several routine husbandry procedures are considered to infringe on these fundamental freedoms, for example, the Mules operation in Australia [28, 30]. In this case, popular opinion has prevailed that the pain, fear, and distress of the operation outweighs the possible later advantages in terms of better resistance of animals to breech strike. This has resulted in pressure on Australian livestock producers to phase out the procedure. The same reasoning applies to tail docking of lambs. An alternative genetic solution was thus sought to enable the abolishment of this practice in the Netherlands in the two sheep breeds where conditional approval to dock tails are still granted [192]. Genetic variation seems to exist for tail length and selection for shorter tails may thus be possible. Issues in the developed world mostly involve the quality of life of farm animals in more intensive systems [193]. Aspects like survival, adequate nutrition, and protection against intense cold or heat are more important under extensive conditions. Sørenson and Fraser [193] proposed a self-regulatory process of auditing livestock operations for animal welfare, agreed on by all role-players.

Aspects of importance to this discussion are the impact breeding for welfare traits could have on genetic gains in other traits. First of all, it is fair to say that animals, where welfare is compromised, will in many cases not be capable of high levels of production. Because of the emphasis of herd health in dairy cattle selection schemes in Norway along with production traits, cows are much more likely to reconceive than in European countries. In response to this, longevity as well as health and fertility became much more important in the United Kingdom dairy indexes as well [189, 190]. Impaired mobility of dairy cattle because of poor claw health also leads to direct and indirect costs. Claw health traits of Finnish Ayrshire cows were lowly heritable [194]. Some leg conformation traits had favorable genetic correlations with claw health, and could serve as indicator traits.

A simulation study on outdoor pig production indicated that genetic gains had to be compromised when welfare traits (leg conformation, mothering ability, and longevity) were included in the selection index [195]. Apart from a slightly slower growth rate and a reduced fat depth, free-range pigs performed as well as pigs in a conventional housing system [196]. The former system produced pork of a similar quality as that observed in a conventional system. Observations made at lambing were evaluated as possible indicators of ovine lamb survival by Brien et al. [174] and Lemmon et al. [197]. Although some observations were favorably related to survival, none were obvious candidates for immediate industry application in the former study. The latter study suggested that alternative methods of improving lamb survival should be investigated. It is however, notable that divergent selection for the ability of sheep to rear multiple offspring led to divergence in age-specific lamb survival in South Africa [198]. Hatcher et al. [199] also reported scope for the improvement of lamb survival by selection, although low direct and maternal heritability estimates were derived.

Animal welfare of the mostly free-ranging animals in the developing world is probably not compromised to the same extent as those animals in more industrialized systems. The exceptions are probably freedom of hunger and thirst, which cannot be guaranteed. It is nonetheless important for scientists in developing countries to take cognizance of the emphasis on welfare, and ensure that information on the impact of the selection strategies for livestock (that were previously discussed) on animal welfare are also considered. Intuitively, selection for adaptability, robustness, and fitness is unlikely to compromise welfare. However, challenge

of animals by environmental stressors (heat, parasites, and uncertain food supply) typical of the developing world may lead to some ethical concerns. It is reassuring that the need to ensure a value system throughout the entire production chain is also recognized in the developing world [200].

Conclusion and Recommendations

From the foregoing it is evident that livestock industries in the developing world are faced by numerous challenges involving the environment, infrastructure, funding, and the availability of a sufficient number of well-trained scientists specializing in breeding and farm animal genetic resources. Despite these drawbacks, scientists in the developing world seem to be willing to contribute to the advancement of science in the region in spite of the considerable odds against them.

Within the constraints in terms of funding and manpower, it is proposed that major efforts should be put into obtaining phenotypic records from the farm animal genetic resource managed in the developing world. Wherever possible these records should be linked to pedigree information, which could follow on from the identification of animals for traceability purposes. Should this vision prove to be impossible to implement on a wider scale, it should be applied to genetic resources maintained by governmental, academic, and parastatal institutions within the developing world. The decision as pertaining to broader community involvement will largely be determined by local conditions, and need to be considered with care on the grassroots level. A prerequisite is that supportive institutional research actions should be conducted in environments conforming to those used by those resource-poor stockkeepers standing to benefit from it. Secondly, it has to be ensured that all initiatives involving the latter groups must have their full support for the intended projects to be successful. This structure will form the basis for simple animal recording and genetic evaluation schemes under communal and emerging farm systems. These schemes are highly unlikely to be cost effective and need to be subsidized from funds supplied by local government, higher education institutions or external sources. However, such evaluation is integral for local food security, sustainable development, and rural stability, thereby increasing leverage for the acquisition of funds dedicated to this cause. Should the envisaged scheme become successful and gather momentum, it would be easy to integrate into existing livestock improvement schemes for commercial agriculture, should the infrastructure exist.

Being in the developing world and the tropics, breeding should focus on traits associated with fitness and adaptability. However, traditional production and product quality traits should also be recorded, to monitor the impact of selection decisions on these traits.

It is not foreseen that genomic selection will change the way animal genetic resources in the developing world are selected in a drastic way in the immediate future. However, it is advised that samples for the extraction of DNA are acquired for as many animals with phenotypes as possible in the system. After the extraction of DNA, these samples should be kept under safe conditions for possible future use. Given the appreciable advances in the technology, it may be possible to utilize DNA-based methods for the evaluation and selection of farm animal genetic resources in the developing world in the foreseeable future. Should this vision become a reality, the scene should be set for the immediate application of this technology on a broader basis. The need for adequate phenotypic data to link to genomic information cannot be overemphasized.

Finally, it is conceded that new issues such as global warming and the insistence of customers on assurance of traceable and welfare-based production systems are likely to affect animal breeding and genetics in the developing world in future. The animal breeding sector in developing countries should preempt these possible challenges, and react to it in a constructive way. Modern societies embrace change. Animal breeders in the developing world thus need to ensure that the challenges imposed by these issues are turned into opportunities.

Bibliography

1. Millennium Development Goals Report, 2005. United Nations, New York
2. McDermott JJ, Staal SJ, Freeman HA, Herrero M, Van der Steeg JA (2010) Sustaining intensification of smallholder livestock systems in the tropics. Livest Sci 130:95–109
3. Pilling D, Rischkowsky B, Cuesta ML (2007) Uses and values of animal genetic resources. In: Rischkowsky B, Pilling D (eds)

Part 1: The state of agricultural biodiversity in the livestock sector – The state of the World's Animal Genetic Resources for Food and Agriculture. Food and Agriculture Organization of the United Nations, Rome, pp 77–100
4. Thornton PK, Gerber PJ (2010) Climate change and growth of the livestock sector in developing countries. Mitig Adapt Strateg Glob Change 15:169–184
5. Thornton PK, Kruska RL, Henninger N, Kristjanson PM, Reid RS, Atieno F, Odero AN (2002) Mapping poverty and livestock in the developing world. ILRI (International Livestock Research Institute), Nairobi, 124 p
6. Faber M (2010) Nutrition in vulnerable communities in economically marginalized societies. Livest Sci 130:110–114
7. McAfee AJ, McSorley EM, Cuskelly GJ, Moss BW, Wallace JMW, Bonham MP, Fearon AM (2010) Red meat consumption: an overview of the risks and benefits. Meat Sci 84:1–13
8. Cloete SWP, Olivier JJ (2010) South African sheep and wool industries. In: Cottle DJ (ed) The international sheep and wool handbook. Nottingham University Press, Nottingham, pp 95–112
9. FAO (2010) Food security statistics. http://www.fao.org/economic/ess/food-security-statistics/en/. Accessed 6 July 2010
10. FAO (2009) FAO Statistical yearbook for 2009. http://www.fao.org/economic/ess/publications-studies/statistical-yearbook/en/. Accessed 6 July 2010
11. OECD-FAO (2008) Agricultural outlook 2008–2017. The Organization for Economic Co-operation and Development and the Food and Agricultural Organization of the United Nations. OECD Publications, Paris
12. Hanotte O (2007) Origin and history of livestock diversity. In: Rischkowsky B, Pilling D (eds) Part 1: The state of agricultural biodiversity in the livestock sector – The state of the world's animal genetic resources for food and agriculture. Food and Agriculture Organization of the United Nations, Rome, pp 5–22
13. Rischkowsky B, Pilling D, Scherf B (2007) Status of animal genetic resources. In: Rischkowsky B, Pilling D (eds) Part 1: The state of agricultural biodiversity in the livestock sector – The state of the world's animal genetic resources for food and agriculture. Food and Agriculture Organization of the United Nations, Rome, pp 23–49
14. Ndlovu L (2010) The role of foods of animal origin in human nutrition and health. In: Swanepoel F, Stroebel A, Moyo S (eds) The role of livestock in developing communities: enhancing multifunctionality. Technical Centre for Agricultural and Rural Cooperation (CTA), Wageningen, pp 77–92
15. Dubeuf J-P, Boyazoglu J (2009) An international panorama of goat selection and breeds. Livest Sci 120:225–231
16. Menjo DK, Bebe BO, Okeyo AM, Ojanjo JMK (2009) Survival of Holstein-Friesian heifers on commercial dairy farms in Kenya. Appl Anim Husb Rural Dev 2:14–17. www.sasas.co.za/aahrd/
17. Muigai AWT, Okeyo AM, Kwallah AK, Mburu D, Hanotte O (2009) Characterization of sheep populations of Kenya using microsatellite markers: implications for conservation and management of indigenous sheep populations. S Afr J Anim Sci 39(Suppl 1):93–96
18. Kosgey IS, Baker RL, Udo HMJ, Van Arendonk JAM (2006) Successes and failures of small ruminant breeding programmes in the tropics: a review. Small Rumin Res 61:13–28
19. Mirkena T, Duguma G, Haile A, Tibbo M, Okeyo AM, Wurzinger M, Sölkner J (2010) Genetics of adaptation in domestic farm animals: a review. Livest Sci 132:1–12
20. Silanikova N (2000) The physiological basis of adaptation in goats to harsh environments: a review. Small Rumin Res 35:191–193
21. Nigussie E, Rottman OJ, Pirchner E, Rege JEO (2000) Allometric growth coefficients and partitioning of fat depots in indigenous Ethiopian Menz and Horro sheep breeds. In: Merkel RC, Abebe G, Goetsch AI (eds) Proceedings of the Conference on the opportunities and challenges of enhancing goat production in East Africa, Debub University, Awassa, 10–12 November 2000, pp 151–163
22. Otte J, Roland-Holst D, Pfeiffer D, Soares-Magalhaes R, Ruston J, Graham J, Silbergeld E (2007) Industrial livestock production and global health risks. Research Report, Pro-Poor livestock policy initiative, a living from livestock. RR Nr 07–09, June 2007. http://www.fao.org/AG/AGAINFO/programmes/en/pplpi/docarc/rep-hpai_industrialisationrisks.pdf. Accessed 18 May 2010
23. Gummow B (2010) Challenges posed by new and re-emerging infectious diseases in livestock production, wildlife and humans. Livest Sci 130:41–46
24. Van der Waaij EH (2001) Breeding for trypanotolerance in African cattle. PhD dissertation, Wageningen Institute of Animal Sciences, Waginingen
25. Bigalke RD (1980) The control of ticks and tick-borne diseases of cattle in South Africa. Zimb Vet J 11:20–21
26. Schwalbach LMJ, Greyling JPC, David M (2003) The efficacy of a 10% aqueous Neem (*Azadirachta indica*) seed extract for tick control in Small East African and Toggenburg female goat kids in Tanzania. S Afr J Anim Sci 33:83–88
27. Budeli MA, Nephawe KA, Norris D, Selapa NW, Bergh L, Maiwashe A (2009) Genetic parameter estimates for tick resistance in Bonsmara cattle. S Afr J Anim Sci 39:321–327
28. Greeff JC, Karlsson LJE (2009) Opportunities to breed for resistance to breech strike in Merino sheep in a Mediterranean environment. Proc Assoc Adv Anim Breed Genet 18:272–278
29. Greeff JC, Karlsson LJE, Schlink AC (2010) Genetic parameters of breech strike and its indicator traits in Merino sheep in a Mediterranean environment. In: Proceedings of the 9th world congress on genetics applied to livestock production, Leipzig, 1–6 August 2010, 4 p. ISBN 978-3-00-031608-1. http://www.kongressband.de/wcgalp2010/assets/pdf/0954.pdf. Accessed 20 Jan 2011
30. Scholtz AJ, Cloete SWP, Van Wyk JB, Misztal I, Du Toit E, Van der Linde TCdeK (2010) Genetic (co)variances between wrinkle score and absence of breech strike in mulesed and unmulesed Merino sheep, using a threshold model. Anim Prod Sci 50:210–218

31. Scholtz AJ, Cloete SWP, Van Wyk JB, Kruger ACM, Van der Linde TCdeK (2010) Influence of divergent selection for reproduction on the occurrence of breech strike in mature Merino ewes. Anim Prod Sci 50:203–209
32. Brown DJ, Swan AA, Graser H-U (2010) Genetic relationships between indicator traits for fly strike resistance and production traits in Merino sheep. In: Proceedings of the 9th world congress on genetics applied to livestock production, Leipzig, 1–6 August 2010, 4 p. ISBN 978-3-00-031608-1. http://www.kongressband.de/wcgalp2010/assets/pdf/0924.pdf. Accessed 20 Jan 2011
33. Pickering NK, Dodds KG, Blair HT, Hickson RE, Johnson PL, McEwan JC (2010) Heritability of dags and its genetic relationships with fleece traits and live weights. In: Proceedings of the 9th world congress on genetics applied to livestock production, Leipzig, 1–6 August 2010, 4 p. ISBN 978-3-00-031608-1. http://www.kongressband.de/wcgalp2010/assets/pdf/0294.pdf. Accessed 20 Jan 2011
34. Morris CA (2009) Review of genetic parameters for disease resistance in sheep in New Zealand and Australia. Proc Assoc Adv Anim Breed Genet 18:263–271
35. Mortimer SI, Atkins KD, Raadsma HW (1998) Responses to selection for resistance and susceptibility to fleece rot and body strike in Merino sheep. In: Proceedings of the 6th world congress on genetics applied to livestock production, Armidale, vol 27, pp 283–386
36. Pfeffer A, Morris CA, Green RS, Wheeler M, Shu D, Bisset SA, Vlassoff A (2007) Heritability of resistance to infestation with the body louse, *Bovicola ovis*, in Romney sheep bred for differences in resistance or resilience to gastro-intestinal nematode parasites. Int J Parasit 37:1589–1597
37. Baker RL, Mwamachi DM, Audho JO, Aduda EO, Thorpe W (1999) Genetic resistance to gastro-intestinal parasites in Red Maasai, Dorper and Maasai x Dorper ewes in the sub-humid tropics. Anim Sci 69:335–344
38. Baker RL, Mugambi JM, Audho JO, Charles AB, Thorpe W (2002) Comparison of Red Maasai and Dorper sheep for resistance to gastro-intestinal nematode parasites, productivity and efficiency in a humid and semi-arid environment in Kenya. In: Proceedings of the 7th world congress on genetics applied to livestock production, Montpellier, 19–23 August 2002, vol 31, pp 639–642
39. Nimbkar C, Ghaisasi PM, Swan AA, Walkden-Brown SW, Kahn LP (2003) Evaluation of growth rates and resistance to nematodes of Deccani and Banmur lambs and their crosses with Garole. Anim Sci 76:503–515
40. Cloete SWP, Olivier JJ, du Toit E, Dreyer FH (2007) Genetic analysis of faecal worm egg count in South African Merinos under natural challenge. S Afr J Anim Sci 37:237–247
41. Karlsson LJE, Greeff JC (2006) Selection response in worm egg counts in the Rylington Merino parasite resistant flock. Aust J Exp Agric 46:809–811
42. Woolaston RR, Piper LR (1996) Selection of Merino sheep for resistance to *Haemonchus contortus*: genetic variation. Anim Sci 62:451–460
43. Williams AR, Greeff JC, Vercoe PE, Dobson RJ, Karlsson LJE (2010) Merino ewes bred for parasite resistance reduce larval contamination onto pasture during the peri-parturient period. Animal 4:122–127
44. Greeff JC, Karlsson L, Underwood N (2006) Breeding Merino sheep for worm resistance increases profit in a Mediterranean environment. In: Proceedings of the 8th world congress on genetics applied to livestock production, Bello Horizonte, Brazil. Communication 15–08
45. Bishop SC (2009) Interpretation and prediction in disease genetics. Proc Assoc Adv Anim Breed Genet 18:255–262
46. Eding H, De Jong G (2010) Predicting Mastitis resistance breeding values from somatic cell count indicator traits. In: Proceedings of the 9th world congress on genetics applied to livestock production, Leipzig, 1–6 August 2010, 4 p. ISBN 978-3-00-031608-1. http://www.kongressband.de/wcgalp2010/assets/pdf/0437.pdf. Accessed 20 Jan 2011
47. Urioste JI, Franzen J, Strandberg E (2010) Genetic characterization of new candidate traits derived from test-day somatic cell counts. In: Proceedings of the 9th world congress on genetics applied to livestock production, Leipzig, 1–6 August 2010, 4 p. ISBN 978-3-00-031608-1. http://www.kongressband.de/wcgalp2010/assets/pdf/0121.pdf. Accessed 20 Jan 2011
48. Van Hulzen K, Nielen M, Koets AP, De Jong G, Van Arendonk J, Heuven HCM (2010) Within herd test prevalence affects genetic variation in antibody response to *Mycobacterium avium* subspecies paratuberculosis in milk of Dutch Holstein Friesians. In: Proceedings of the 9th world congress on genetics applied to livestock production, Leipzig, 1–6 August 2010, 4 p. ISBN 978-3-00-031608-1. http://www.kongressband.de/wcgalp2010/assets/pdf/0301.pdf. Accessed 20 Jan 2011
49. Bermingham M, More S, Good M, Cromie A, Higgins I, Berry D (2010) Genetic correlations between susceptibility to *Mycobacterium bovis* infection and performance in Irish Holstein Friesian dairy cows. In: Proceedings of the 9th world congress on genetics applied to livestock production, Leipzig, 1–6 August 2010, 4 p. ISBN 978-3-00-031608-1. http://www.kongressband.de/wcgalp2010/assets/pdf/0766.pdf. Accessed 20 Jan 2011
50. Anon (2010) Free state: rift valley fever spreads. http://www.health24.com/news/Infectious_diseases/1-922,55166.asp. Accessed 11 Aug 2010
51. Anon (2010) 17 dead from rift valley fever. http://www.news24.com/SouthAfrica/News/17-dead-from-Rift-Valley-Fever-20100507. Accessed 11 Aug 2010
52. Anon (2010) SA wool exports to China stopped. http://www.fin24.com/Business/SA-wool-exports-to-China-stopped-20100817?pageNo=1. Accessed 18 Aug 2010
53. Marai IFM, El-Darawany AA, Fadiel A, Abdel-Hafez MAM (2007) Physiological traits as affected by heat stress in sheep – A review. Small Rumin Res 71:1–12
54. McManus C, Prescott E, Paluda GR, Bianchini E, Louvandini H, Mariante AS (2009) Heat tolerance in naturalized Brazilian cattle breeds. Livest Sci 120:256–264

55. Singh M, Rai AK, More T, Dhaliwal JS (1980) Note on comparative physiological response of sheep and goats to high ambient temperature. Indian J Anim Sci 50:202–205
56. El-Sheikh AS, Salem MH, Ibrahim II, Mohamed AA, El-Sherbini AA, Yousef MK (1981) Relative adaptability of some local and foreign breeds of sheep to Sahara desert. Egypt J Anim Prod 21:109–120
57. Boonkum W, Misztal I, Tsuruta S, Duangjinda M, Pattarajinda V, Tumwasorn S, Sanpote J, Buaban S (2010) Genetics of days open in Thai crossbred Holsteins. In: Proceedings of the 9th world congress on genetics applied to livestock production, Leipzig, 1–6 August 2010, 4 p. ISBN 978-3-00-031608-1. http://www.kongressband.de/wcgalp2010/assets/pdf/0255.pdf. Accessed 20 Jan 2011
58. Misztal I, Aguilar I, Tsuruta S, Sanchez JP, Zumbach B (2010) Studies on heat stress in dairy cattle and pigs. In: Proceedings of the 9th world congress on genetics applied to livestock production, Leipzig, 1–6 August 2010, 4 p. ISBN 978-3-00-031608-1. http://www.kongressband.de/wcgalp2010/assets/pdf/0625.pdf. Accessed 20 Jan 2011
59. Schmidt-Nielsen B, Schmidt-Nielsen K, Houpt TR, Jarnum SA (1956) Water balance of the camel. Am J Phys 185:185–194
60. Schmidt-Nielsen K (1955) Investigations on the Physiology of the Camel: Preliminary report. http://unesdoc.unesco.org/images/0014/001486/148616eb.pdf. Accessed 27 July 2010
61. Bayer W, Feldman A (2003) Diversity of animals adapted to smallholder systems: conservation and sustainable use of agricultural biodiversity. http://www.eseap.cipotato.org/UPWARD/Agrobio-sourcebook.html. Accessed 21 Aug 2010
62. Nardone A, Ronchi B, Lacetera N, Ranieri MS, Bernabucci U (2010) Effects of climate changes on animal production and the sustainability of livestock systems. Livest Sci 130:57–69
63. Brockhaus M (2007) Institutions and stakeholders. In: Rischkowsky B, Pilling D (eds) Part 3: The state and capacities in animal resource management – The state of the world's animal genetic resources for food and agriculture. Food and Agriculture Organization of the United Nations, Rome, pp 187–214
64. Kahi AK (2010) Developing countries and the 9th world congress on genetics applied to livestock production. J Anim Breed Genet 127:333
65. Thieme O (2007) Structured breeding programmes. In: Rischkowsky B, Pilling D (eds) Part 3: The state and capacities in animal resource management – The state of the world's animal genetic resources for food and agriculture. Food and Agriculture Organization of the United Nations, Rome, pp 215–241
66. OECD (2009) OECD Factbook 2009: Economic, environmental and social statistics, Paris. ISBN 92-64-05604-1
67. Anon (2009) National survey of Research and Experimental development (R & D): 2006/2007. Compiled by the Centre for Science, Technology and innovation indicators and the Human Sciences Research council for the Department of Science and Technology. The Department of Science and Technology, Pretoria, South Africa
68. OECD (2009) Agricultural policies in emerging economies: monitoring and evaluation. http://www.oecd.org/tad/support. Accessed 14 Oct 2009
69. Anon (2010) South Africans at work longer – survey. http://www.fin24.com/printArticle.aspx?iframe&aid=b17e6777-d714. Accessed 20 Dec 2010
70. WCGALP (2010) Book of abstracts. In: Proceedings of the 9th world congress on genetics applied to livestock production, Leipzig, 1–6 August 2010. http://www.wcgalp2010.org/download/wcgalp_hauptprogramm-web.pdf. Accessed 20 Jan 2011
71. Habier D (2010) More than a third of the WCGALP presentations on genomic selection. J Anim Breed Genet 127:336–337
72. Cardellino RA (2009) Editorial: introduction and overview to the special issue on animal genetic resources. Livest Sci 120:163–165
73. Gollin D, Van Dusen E, Blackburn H (2009) Animal genetic resource trade flows: economic assessment. Livest Sci 120:248–255
74. Blackburn H, Gollin D (2009) Animal genetic trade flows: the utilization of newly imported breeds and gene flow of imported animals in the United States of America. Livest Sci 120:240–247
75. Browning R, Leite-Browning ML, Byars M (2010) Reproductive and health traits among Boer, Kiko, and Spanish meat goat does under humid subtropical conditions of the southeastern United States. J Anim Sci 89:648–660
76. Sandup T, Udo HMJ, Eilers CHAM, Ibrahim MNM, Van der Zijpp E (2010) Crossbreeding and intensification of smallholder crop-cattle farming systems in Bhutan. Livest Sci 132:126–134
77. Ole Kwallah ABO, Okeyo AM, Mburu D, Hanotte O, Muigai AWT (2010) Genetic diversity and relationships of sheep breeds of Kenya: preliminary results and evidence of dilution of the indigenous Red Maasai. In: Proceedings of the 9th World Congress on Genetics Applied to Livestock Production, Leipzig, 1–6 August 2010, 4 p. ISBN 978-3-00-031608-1. http://www.kongressband.de/wcgalp2010/assets/pdf/0828.pdf. Accessed 20 Jan 2011
78. Scholtz MM, Bester J, Mamabolo JM, Ramsay KA (2008) Results of the national cattle survey undertaken in South Africa, with emphasis on beef. Appl Anim Husb Rural Dev 1:1–9. www.sasas.co.za/aahrd/
79. Cardellino RA, Boyazoglu J (2009) Research opportunities in the field of animal genetic resources. Livest Sci 120:166–173
80. Hoffmann I (2010) Climate change and the characterization, breeding and conservation of animal genetic resources. Anim Genet 41(Suppl 1):32–46
81. AdaS M, MdoSM A, Egito AA, McManus C, Lopes MA, Paiva SR (2009) Present status of the conservation of genetic resources in Brazil. Livest Sci 120:204–212
82. FAO (2007) Report of the technical conference on animal genetic resources for food and agriculture. Interlaken, Switzerland, 3–7 September 2007, ITC-AnGR/07/REP. http://www.fao.org/AG/againfo/programmes/en/genetics/ITC_docs.htm. Accessed 18 May 2010
83. Villanueva B, Sawalha RM, Roughsedge T, Rius-Vilarrasa E, Wooliams JA (2009) Development of a genetic indicator of biodiversity for farm animals. Livest Sci 129:200–207

84. Djemali M, Bedhiaf-Romdhani S, Iniguez L, Inounou I (2009) Saving threatened native breeds by autonomous production, involvement of farmer organization, research and policy makers: the case of the Sicilo-Sarde breed in Tunisia, North Africa. Livest Sci 120:213–217
85. Toro MA, Fernandez J, Caballero A (2009) Molecular characterization of breeds and its use in conservation. Livest Sci 120:174–195
86. Holst PJ (1999) Recording and on-farm evaluations and monitoring: breeding and selection. Small Rumin Res 34: 197–202
87. Djemani M, Wrigley J (2002) Tayloring genetic improvement to meet the overall livestock development objective. In: Proceedings of the world congress on genetics applied to livestock production, Montpellier, 19–23 August 2002, vol, 33, pp 299–306
88. Swan AA, Brown DJ, Banks RG (2009) Genetic progress in the Australian sheep industry. Proc Assoc Adv Anim Breed Genet 18:326–329
89. Mostert BE, Theron HE, Kanfer FHJ, Van Marle-Köster E (2006) Comparison of breeding values and genetic trends for production traits estimated by a lactation model and a fixed regression Test-day Model. S Afr J Anim Sci 36:71–78
90. Mostert BE, Theron HE, Kanfer FHJ, Van Marle-Köster E (2006) Test-day models for South African dairy cattle for participation in international evaluations. S Afr J Anim Sci 36:58–70
91. Grobler SM, Scholtz MM, Bester J, Mamabola JM, Ramsay KA (2008) Dairy production systems in the emerging and communal sectors of South Africa: Results of a structured survey. Appl Anim Husb Rural Dev 1:25–30. www.sasas.co.za/aahrd
92. Okeno TO, Kosgey IS, Kahi AK (2010) Economic evaluation for improvement of dairy cattle in Kenya. In: Proceedings of the 9th world congress on genetics applied to livestock production, Leipzig, 1–6 August 2010, 4 p. ISBN 978-3-00-031608-1. http://www.kongressband.de/wcgalp2010/assets/pdf/0610.pdf. Accessed 20 Jan 2011
93. Wasike CB, Magothe TM, Peters KJ, Kahi AK (2010) Describing the lactation process in Ayrshire and Holstein Friesian cattle in Kenya using a mechanistic lactation function. In: Proceedings of the 9th world congress on genetics applied to livestock production, Leipzig, 1–6 August 2010, 4 p. ISBN 978-3-00-031608-1. http://www.kongressband.de/wcgalp2010/assets/pdf/0402.pdf. Accessed 20 Jan 2011
94. Moyo S, Swanepoel FJC (2010) Multifunctionality of livestock in developing communities. In: Swanepoel F, Stroebel A, Moyo S (eds) The role of livestock in developing communities: enhancing multifunctionality. Technical Centre for Agricultural and Rural Cooperation (CTA), Wageningen, pp 1–11
95. Bergh L (2010) The national beef recording and improvement scheme. In: Scholtz MM (ed) Beef breeding in South Africa, 2nd edn. Agricultural Research Council, Pretoria, pp 55–70
96. Rust T, Theron HE, Scholtz MM, Bergh L (2010) The practical use of breeding values in beef cattle breeding. In: Scholtz MM (ed) Beef breeding in South Africa, 2nd edn. Agricultural Research Council, Pretoria, pp 115–128
97. Rust T, Schoeman SJ, Van der Westhuizen J, Van Wyk JB (2009) Non-linear model analysis of categorical traits related to female reproduction efficiency in beef cattle. S Afr J Anim Sci 39:260–266
98. Anon (2010) Performance information for breeds that do not participate in the national beef recording and improvement scheme. In: Scholtz MM (ed) Beef breeding in South Africa, 2nd edn. Agricultural Research Council, Pretoria, pp 267–291
99. Nenghovela NB, Maiwashe A, Matjuda LE (2010) Breeding principles and guidelines for the emerging beef farmer. In: Scholtz MM (ed) Beef breeding in South Africa, 2nd edn. Agricultural Research Council, Pretoria, pp 139–148
100. Olivier JJ, Cloete SWP (2006) Genetic analysis of the South African Dorper sheep. In: Proceedings of the 7th world congress on genetics applied to livestock production, Bello Horizonte. Communication 04–10
101. Olivier JJ, Cloete SWP (2007) Genetic change in some South African Merino studs participating in the Merino plan. Proc Assoc Adv Anim Breed Genet 17:324–327
102. Van Wyk JB, Swanepoel JW, Cloete SWP, Olivier JJ, Delport GJ (2008) Across flock genetic parameter estimation for yearling body weight and fleece traits in the South African Dohne Merino population. S Afr J Anim Sci 38:31–37
103. Schoeman SJ, Cloete SWP, Olivier JJ (2010) Returns on investment in sheep and goat breeding in South Africa. Livest Sci 130:70–82
104. Cardellino RC, Mueller JP (2009) Fibre production and sheep breeding in South America. Proc Assoc Adv Anim Breed Genet 18:366–373
105. Madalena FE, Agyemang K, Cardellino RC, Jain GL (2002) Genetic improvement in medium to low-input systems of animal production. Experiences to date. In: Proceedings of the world congress on genetics applied to livestock production, Montpellier, 19–23 August 2002, vol 33, pp 299–306
106. Tadele M, Duguma G, William A, Haille A, Iňiguez L, Wurzinger M, Sölkner J (2010) Indigenous sheep genetic improvement schemes for Ethiopian smallholder farmers and pastoralists. Proceedings of the 9th world congress on genetics applied to livestock production, Leipzig, 1–6 August 2010, 4 p. ISBN 978-3-00-031608-1. http://www.kongressband.de/wcgalp2010/assets/pdf/0937.pdf. Accessed 20 Jan 2011
107. Amer PR, Santos BFS, Byrne TJ, Campbell AW (2010) Breeding objectives for a developing sheep industry in Brazil. In: Proceedings of the 9th world congress on genetics applied to livestock production, Leipzig, 1–6 August 2010, 4 p. ISBN 978-3-00-031608-1. http://www.kongressband.de/wcgalp2010/assets/pdf/0523.pdf. Accessed 20 Jan 2011
108. Marais PG (2007) Evaluation of the genetic potential for growth and wool production of typical Transkei ewes and rams. Research report of the Grootfontein Agricultural Development Institute, 2007, Middelburg, pp 33–34
109. Marais PG (2006) Evaluation of the genetic potential for growth and wool production of typical Transkei ewes and rams. Research report of the Grootfontein Agricultural Development Institute, Middelburg, pp 33–34

110. Grobler HJF (2008) How are our LRAD farmers doing? AgriProbe 5(2):4–5. Research and news magazine of the Western Cape Department of Agriculture, Elsenburg
111. Cloete SWP, Cloete JJE, Herselman MJ, Hoffman LC (2004) Relative performance and efficiency of five Merino and Merino-type dam lines in a terminal crossbreeding system with Dormer or Suffolk sires. S Afr J Anim Sci 34:135–143
112. Fourie AJ, Cloete SWP (1993) Reproductive performance of commercial Merino, Dohne Merino and SA Mutton Merino flocks in the Southern Cape. S Afr J Anim Sci 23:104–110
113. Cape Wools SA (2010) Annual report 2008/2009. http://www.capewools.co.za/index.php?option=com_docman&task=cat_view&gid=36&Itemid=92. Accessed 2 Sept 2010
114. Iñiguez L, Hilali M (2009) Evaluation of Awassi genotypes for improved milk production in Syria. Livest Sci 120:232–239
115. Olivier JJ, Cloete SWP, Schoeman SJ, Muller CJC (2005) Performance testing and recording in meat and dairy goats. Small Rumin Res 60:83–93
116. Bester J, Ramsay KA, Scholtz MM (2009) Goat farming in South Africa: findings of a national survey. Appl Anim Husb Rural Dev 2:9–13. www.sasas.co.za/aahrd/
117. Mtleni BJ, Muchadeyi FC, Maiwashe A, Phitsane PM, Halimani TE, Chimonyo M, Dzama K (2009) Characterisation of production systems for indigenous chicken genetic resources in South Africa. Appl Anim Husb Rural Dev 2:18–22. www.sasas.co.za/aahrd/
118. Magothe TM, Muhuyi WB, Kahi AK (2010) Genetic parameter estimates for egg and body weights of indigenous chicken in Kenya. In: Proceedings of the 9th world congress on genetics applied to livestock production, Leipzig, 1–6 August 2010, 4 p. ISBN 978-3-00-031608-1. http://www.kongressband.de/wcgalp2010/assets/pdf/0195.pdf. Accessed 20 Jan 2011
119. Kahi AK, Bett RC, Rewe TO (2010) Socio-economic drivers of successful breeding programs in developing countries. In: Proceedings of the 9th world congress on genetics applied to livestock production, Leipzig, 1–6 August 2010, 8 p. ISBN 978-3-00-031608-1. http://www.kongressband.de/wcgalp2010/assets/pdf/0011.pdf. Accessed 20 Jan 2011
120. Newman SAN, Amyes N, Cruickshank GJ, Young MJ (2002) Sheep Improvement Limited – the national sheep performance scheme in New Zealand. In: Proceedings of the 9th world congress on genetics applied to livestock production, Montpellier, 19–23 August 2002, vol 33, pp 733–736
121. Szkotnicki WJ, Kennedy D, Miller SP, Schaeffer LR (2010) A web 2.0 system for managing sheep records and genetic evaluations. In: Proceedings of the 9th world congress on genetics applied to livestock production, Leipzig, 1–6 August 2010, 4 p. ISBN 978-3-00-031608-1. http://www.kongressband.de/wcgalp2010/assets/pdf/0447.pdf. Accessed 20 Jan 2011
122. Olivier JJ (2003) Shepherd. Sheep breeding support software. http://gadi.agric.za/software/shepherd/shepherd.htm. Accessed 24 Aug 2010
123. Gilmour AR (2009) Mixed models in animal breeding: where to now? Proc Assoc Adv Anim Breed Genet 18:394–397
124. Gilmour AR, Gogel BJ, Cullis BR, Thompson R (2006) ASReml User Guide. Release 2.0. VSN International, Hemel Hempstead
125. Gianola D, de los Compos G, Gonzalez-Recio O, Long N, Okut H, Rosa GJM, Weigel KA, Wu X-L (2010) Statistical learning methods for genome based analysis of quantitative traits. In: Proceedings of the 9th world congress on genetics applied to livestock production, Leipzig, 1–6 August 2010, 8 p. ISBN 978-3-00-031608-1. http://www.kongressband.de/wcgalp2010/assets/pdf/0014.pdf. Accessed 20 Jan 2011
126. Misztal I (2008) Reliable computing in estimation of variance components. J Anim Breed Genet 125:363–370
127. Aguilar I, Misztal I, Legarra A, Tsuruta S (2010) Efficient computations of genomic relationship matrix and other matrices used in the single step evaluation. In: Proceedings of the 9th world congress on genetics applied to livestock production, Leipzig, 1–6 August 2010, 4 p. ISBN 978-3-00-031608-1. http://www.kongressband.de/wcgalp2010/assets/pdf/0768.pdf. Accessed 20 Jan 2011
128. Misztal I, Aguilar I, Legarra A, Tsuruta S, Johnson DL, Lawlor TJ (2010) A unified approach to utilize phenotypic, full pedigree, and genomic information for genetic evaluation. In: Proceedings of the 9th world congress on genetics applied to livestock production, Leipzig, 1–6 August 2010, 16 p. ISBN 978-3-00-031608-1. http://www.kongressband.de/wcgalp2010/assets/pdf/0050.pdf. Accessed 20 Jan 2011
129. Nephawe KA (2004) Application of random regression models to the genetic evaluation of cow weight in Bonsmara cattle in South Africa. S Afr J Anim Sci 34:166–173
130. Cardoso FF, Alencar MM, Tempelman RJ (2010) Genotype by environment interaction and prediction of genetic merit. In: Proceedings of the 9th world congress on genetics applied to livestock production, Leipzig, 1–6 August 2010, 8 p. ISBN 978-3-00-031608-1. http://www.kongressband.de/wcgalp2010/assets/pdf/0015.pdf. Accessed 20 Jan 2011
131. Lewis CRG, Hermesch S, Bunter KL (2010) A random regression analysis of sow lactation feed intake and the effect of temperature on intake. In: Proceedings of the 9th world congress on genetics applied to livestock production, Leipzig, 1–6 August 2010, 4 p. ISBN 978-3-00-031608-1. http://www.kongressband.de/wcgalp2010/assets/pdf/0670.pdf. Accessed 20 Jan 2011
132. Wolc A, Barczak E, Wòjtowski J, Ślòsarz P, Szwaczkowski T (2010) Variance components of growth in Polish sheep described by random regression models. In: Proceedings of the 9th world congress on genetics applied to livestock production, Leipzig, 1–6 August 2010, 4 p. ISBN 978-3-00-031608-1. http://www.kongressband.de/wcgalp2010/assets/pdf/0408.pdf. Accessed 20 Jan 2011
133. The Bovine Hapmap Consortium (2009) Genome-wide survey of SNP variation uncovers the genetic structure of cattle breeds. Science 324:528–532
134. Onteru S, Fan B, Garrick D, Stalder K, Rothschild M (2010) Whole- genome association analysis for sow lifetime

production, reproduction and structural soundness traits using the porcine SNP60 beadchip. In: Proceedings of the 9th world congress on genetics applied to livestock production, Leipzig, 1–6 August 2010, 4 p. ISBN 978-3-00-031608-1. http://www.kongressband.de/wcgalp2010/assets/pdf/0273.pdf. Accessed 20 Jan 2011

135. Souza CA, Ramayo Y, Megens HJ, Rodriguez MC, Loarca A, Caal E, Soto H, Melo M, Revidatti MA, De la Rosa SA, Shemereteva IN, Okumura N, Cho, IC, Delgado JV, Paiva SR, Crooijmans RPMA, Schook LB, Groenen MAM, Ramos-Onsins SE, Pėrez-Enciso M (2010) Porcine colonization of the Americas: a 60K SNP story. In: Proceedings of the 9th world congress on genetics applied to livestock production, Leipzig, 1–6 August 2010, 4 p. ISBN 978-3-00-031608-1. http://www.kongressband.de/wcgalp2010/assets/pdf/0510.pdf. Accessed 20 Jan 2011
136. Dodds KG, Auvray B, Pickering N, McEwan JC (2009) Quality control for ovine SNP50 beadchip genotypes. Proc Assoc Adv Anim Breed Genet 18:296–299
137. Magee DA, Park SDE, Scraggs S, Murphy AM, Doherty ML, Kijas JW, International Sheep Genomics Consortium, MacHugh DE (2010) High fidelity of whole-genome amplified sheep (*Ovis aries*) deoxyribonucleic acid using a high-density single nucleotide polymorphism array-based genotyping platform. J Anim Sci 88:3183–3186
138. Khatkar MS, Tier B, Hobbs M, Khatkar D, Cavanagh JAL, Crump R, Moser G, Raadsma HW (2009) Genome structure in Australian Holstein Friesian cattle revealed by combined analysis of three high density SNP panels. Proc Assoc Adv Anim Breed Genet 18:247–250
139. Raadsma HW, Zenger KR, Khatkar MS, Crump R, Moser G, Solkner J, Cavanagh JAL, Hawken RJ, Hobbs M, Barris W, Nicholas FW, Tier B (2007) Genome wide selection in dairy cattle based on high density genome-wide SNP analysis: from discovery to application. Proc Assoc Adv Anim Breed Genet 17:231–234
140. Vinet A, Touze JL, Bichot R, Hestault O, Bellayer C, Boussaha M, Fritz S, Guillaume F, Sapa J, Bodin L, Phocas F (2010) Genome-wide scan for bovine ovulation rate using a dense SNP map. In: Proceedings of the 9th world congress on genetics applied to livestock production, Leipzig, 1–6 August 2010, 4 p. ISBN 978-3-00-031608-1. http://www.kongressband.de/wcgalp2010/assets/pdf/0459.pdf. Accessed 20 Jan 2011
141. Avendaňo S, Watson KA, Kranis A (2010) Genomics in poultry breeding – from Utopias to deliverables. In: Proceedings of the 9th world congress on genetics applied to livestock production, Leipzig, 1–6 August 2010, 8 p. ISBN 978-3-00-031608-1. http://www.kongressband.de/wcgalp2010/assets/pdf/0049.pdf. Accessed 20 Jan 2011
142. Gärke C, Ytournel F, Bed'hom B, Gut I, Lathrop M, Weigend S, Simianer H (2010) Differentiation power of SNPs for assessing the phylogenetic structure of populations. In: Proceedings of the 9th world congress on genetics applied to livestock production, Leipzig, 1–6 August 2010, 4 p. ISBN 978-3-00-031608-1. http://www.kongressband.de/wcgalp2010/assets/pdf/0722.pdf. Accessed 20 Jan 2011
143. Perez-Enciso M (2010) Leipzig: the dawn of the genomes era. J Anim Breed Genet 127:338
144. Goddard ME, Hayes BJ, Meuwissen THE (2010) Genomic selection in farm animal species – Lessons learn and future perspectives. In: Proceedings of the 9th world congress on genetics applied to livestock production, Leipzig, 1–6 August 2010, 8 p. ISBN 978-3-00-031608-1. http://www.kongressband.de/wcgalp2010/assets/pdf/0701.pdf. Accessed 20 Jan 2011
145. Hayes BJ, Bowman PJ, Chamberlain AJ, Goddard ME (2009) Invited review: genomic selection in dairy cattle: progress and challenges. J Dairy Sci 92:433–443
146. Liu Z, Seefried F, Reinhardt F, Thaller G, Reents R (2010) Dairy cattle genetic evaluation enhanced with genomic information. In: Proceedings of the 9th world congress on genetics applied to livestock production, Leipzig, 1–6 August 2010, 8 p. ISBN 978-3-00-031608-1. http://www.kongressband.de/wcgalp2010/assets/pdf/0009.pdf. Accessed 20 Jan 2011
147. Weigel KA, De los Campos G, Vazquez AI, Van Tassell CP, Rosa GMJ, Gianola D, O'Connell JR, VanRaden PM, Wiggans GR (2010) Genomic selection and its effects on dairy cattle breeding programs. In: Proceedings of the 9th world congress on genetics applied to livestock production, Leipzig, 1–6 August 2010, 8 p. ISBN 978-3-00-031608-1. http://www.kongressband.de/wcgalp2010/assets/pdf/0119.pdf. Accessed 20 Jan 2011
148. Wiggans GR, Cooper TA, VanRaden PM, Silva MV (2010) Increased reliability of genetic evaluation for dairy cattle in the United States from use of genomic information. In: Proceedings of the 9th world congress on genetics applied to livestock production, Leipzig, 1–6 August 2010, 4 p. ISBN 978-3-00-031608-1. http://www.kongressband.de/wcgalp2010/assets/pdf/0476.pdf. Accessed 20 Jan 2011
149. Barker JSF (2009) Defining fitness in natural and domesticated populations. In: van der Werf J, Graser H-U, Frankham R, Gondro C (eds) Adaptation and fitness in farm animal populations: evolutionary and breeding perspectives on genetic resource management. Springer, Dordrecht, pp 3–14. www.springer.com
150. Bishop SC, Woolliams JA (2010) Understanding field disease data. In: Proceedings of the 9th world congress on genetics applied to livestock production, Leipzig, 1–6 August 2010, 4 p. ISBN 978-3-00-031608-1. http://www.kongressband.de/wcgalp2010/assets/pdf/0401.pdf. Accessed 20 Jan 2011
151. Gauly M, Besbes B, Pinard-van der Laan MH, Hoffman I, Greeff J, Thevenon S, Baker L, Tibbo M, Bishop S, Mugambi J, Dempfle L, Sidibe I, Mandonnet N, Amarande AFT, Miller JE (2010) Ruminant genetic resources and their resistance/tolerance to parasitic diseases. In: Proceedings of the 9th world congress on genetics applied to livestock production, Leipzig, 1–6 August 2010, 4 p. ISBN 978-3-00-031608-1. http://www.kongressband.de/wcgalp2010/assets/pdf/0445.pdf. Accessed 20 Jan 2011

152. Bath GF, Van Wyk JA (2010) The Five Point Check© for targeted selective treatment of internal parasites in small ruminants. Small Rumin Res 86:6–13
153. Goddard M (2009) Fitness traits in animal breeding programs. In: van der Werf J, Graser H-U, Frankham R, Gondro C (eds) Adaptation and fitness in farm animal populations: evolutionary and breeding perspectives on genetic resource management. Springer, Dordrecht, pp 41–52. www.springer.com
154. Muller CJC, Cloete SWP, Potgieter JP and Zishiri, OT (2010) Genetic parameters for fertility traits in South African Holstein cows. In: Proceedings of the 9th world congress on genetics applied to livestock production, Leipzig, 1–6 August 2010, 4 p. ISBN 978-3-00-031608-1. http://www.kongressband.de/wcgalp2010/assets/pdf/0734.pdf. Accessed 20 Jan 2011
155. Cloete SWP, Gilmour AR, Olivier JJ, Van Wyk JB (2004) Genetic and phenotypic trends and parameters in reproduction, greasy fleece weight and live weight in Merino lines divergently selected for multiple rearing ability. Aust J Exp Agric 44:745–754
156. Snowder GD, Fogarty NM (2009) Composite trait selection to improve reproduction and ewe productivity. Anim Prod Sci 49:9–16
157. Maiwashe A, Nephawe KA, Theron HE (2009) Analysis of stayability in South African Angus cattle, using a threshold model. S Afr J Anim Sci 39:55–60
158. GLOBALGAP (2010) Control points and compliance criteria – integrated farm assurance: All livestock base. English version V.3.0-4_Mar10. GLOBALGAP, Köln (Cologne), Germany. http://www.globalgap.org/cms/upload/The_Standard/IFA/English/CPCC/GG_EG_IFA_CPCC_LB_ENG_V3_0_4_Mar10.pdf. Accessed 2 Sept 2010
159. Olivier JJ, Moyo S, Montaldo HH, Thorpe W, Valle Zarate A, Trivedi KR (2002) Integrating genetic improvement into livestock development in medium- to low-input productions systems. In: Proceedings of the world congress on genetics applied to livestock production, Montpellier, 19–23 August 2002, vol 33, pp 365–372
160. Philipsson J, Rege JEO, Okeyo AM (2006) Sustainable breeding programmes for tropical farming systems. In: Ojango JM, Malmfors B, Okeyo AM (eds) Animal Genetics Training Resource, version 2. International Livestock Research Institute, Nairobi, Kenya/Swedish University of Agricultural Sciences, Uppsala, Sweden
161. Pell AN, Stroebel A, Kristjanson P (2010) Livestock development projects that make a difference: what works, what doesn't and why. In: Swanepoel F, Stroebel A, Moyo S (eds) The role of livestock in developing communities: enhancing multifunctionality. Technical Centre for Agricultural and Rural Cooperation (CTA), Wageningen, pp 13–29
162. Nesamvuni EA, Swanepoel FJC, Stroebel A (2010) Interactions between gender, environment, livelihoods, food, nutrition and health. In: Swanepoel F, Stroebel A, Moyo S (eds) The role of livestock in developing communities: enhancing multifunctionality. Technical Centre for Agricultural and Rural Cooperation (CTA), Wageningen, pp 93–105
163. Rewe TO, Herold P, Kahi AK, Valle Zarate A (2010) Genetic improvement and monetary returns in alternative closed and open nucleus breeding programs for Boran cattle reared in the semi-arid tropics. In: Proceedings of the 9th world congress on genetics applied to livestock production, Leipzig, 1–6 August 2010, 4 p. ISBN 978-3-00-031608-1. http://www.kongressband.de/wcgalp2010/assets/pdf/0850.pdf. Accessed 20 Jan 2011
164. Fogarty NM (2006) Utilization of breed resources for sheep production. In: Proceedings of the 8th world congress on genetics on applied livestock production, Bello Horizonte, Brazil. Communication 04–10
165. Bouix J, Jacquin M, Foulquiė D, Autran P, Guillouet P, Hubert D, Bibė B (2002) Genetic effects on sheep production in harsh environment and extensive management system. In: Proceedings of the world congress on genetics on applied livestock production, Montpellier, 19–23 August 2002, vol 29, pp 441–444
166. Francois D, Boissy A, Jacquiet P, Allain D, Bibė B, Rupp R, Moreno CR, Bodin L, Hazard D, Bouix J (2010) Genetics of adaptation traits for harsh environment in sheep. In: Proceedings of the 9th world congress on genetics applied to livestock production, Leipzig, 1–6 August 2010, 4 p. ISBN 978-3-00-031608-1. http://www.kongressband.de/wcgalp2010/assets/pdf/0453.pdf. Accessed 20 Jan 2011
167. Mormėde P, Foury A, Terenina E, Knap PW (2010) Breeding for robustness: the role of cortisol. Animal 5:651–657
168. Naqvi AN (2007) Application of molecular genetic technologies in livestock production: potentials for developing countries. Adv Biol Res 1:72–84
169. Robinson J, Ruane J (2007) Marker-assisted selection as a potential tool for genetic improvement in developing countries: debating the issues. FAO invited book. In: Guimaraes EP, Ruane J, Scherf BD, Sonnino A, Dargie JD (eds) Marker-assisted selection: current status and future perspectives in crops, livestock, forestry and fish. FAO, Rome, pp 427–440. ftp://ftp.fao.org/docrep/fao/010/a1120e/a1120e04.pdf. Accessed 28 July 2010
170. Van der Werf JHJ (2007) Marker-assisted selection in sheep and goats. FAO invited book. In: Guimaraes EP, Ruane J, Scherf BD, Sonnino A, Dargie JD (eds) Marker-assisted selection: current status and future perspectives in crops, livestock, forestry and fish. FAO, Rome, pp 229–247. ftp://ftp.fao.org/docrep/fao/010/a1120e/a1120e04.pdf. Accessed 28 July 2010
171. Fogarty NM, Banks RG, Van der Werf JHJ, Ball AJ, Gibson JP (2007) Te information nucleus – a new concept to enhance sheep industry genetic improvement. Proc Assoc Adv Anim Breed Genet 17:29–32
172. Mortimer SI, Pearce KL, Jacobs RH, Hopkins DL, Warner RD, Geesink GH, Hocking Edwards JE, Pethick DW, Van der Werf JHJ (2009) The information nucleus – genetically improving Australian lamb production. Proc Assoc Adv Anim Breed Genet 18:426–429

173. Van der Werf JHJ, Banks RG (2010) A genomic information nucleus flock to accelerate rates of genetic improvement in sheep. In: Proceedings of the 9th world congress on genetics applied to livestock production, Leipzig, 1–6 August 2010, 8 p. ISBN 978-3-00-031608-1. http://www.kongressband.de/wcgalp2010/assets/pdf/0046.pdf. Accessed 20 Jan 2011
174. Brien FD, Hebart ML, Hocking-Edwards JE, Greeff JC, Hart KW, Refshauge G, Gaunt G, Behrendt R, Thomson K, Hinch GN, Geenty KG, Van der Werf JHJ (2009) Genetics of lamb survival: preliminary studies on the information nucleus flock. Proc Assoc Adv Anim Breed Genet 18:108–111
175. Knap PW (2011) Pig breeding for sustainability. Encyclopedia for Sustainability, Science and Technology, Springer, Germany (in press)
176. Eitan Y, Soller M (2011) Poultry breeding: the broiler chicken as harbinger of the future. Encyclopedia for Sustainability, Science and Technology, Springer, Germany (in press)
177. Ojango JM, Panandam JM, Bhuiyan AKFH, Khan MS, Kahi AK, Imbayarwo-Chikosi VE, Halimani TE, Kosgey IS, Okeyo AM (2010) Higher education in animal breeding in developing countries – challenges and opportunities. In: Proceedings of the 9th world congress on genetics applied to livestock production, Leipzig, 1–6 August 2010, 6 p. ISBN 978-3-00-031608-1. http://www.kongressband.de/wcgalp2010/assets/pdf/0073.pdf. Accessed 20 Jan 2011
178. Casey NH (2009) Integrated higher learning – an investment in intellectual capital for livestock production. Livest Sci 130:83–94
179. Van Arendonk JAM, Malmfors B, Verrier E, Thaller G, Solkner J, Klemetsdal G, Lont DE (2010) European Master in Animal Breeding and Genetics: international collaboration to face future needs. In: Proceedings of the 9th world congress on genetics applied to livestock production, Leipzig, 1–6 August 2010, 4 p. ISBN 978-3-00-031608-1. http://www.kongressband.de/wcgalp2010/assets/pdf/0561.pdf. Accessed 20 Jan 2011
180. Wurzinger M, Toro M, Villaroel M, Serradilla JM (2010) Reform and desighn of Masters programs "Animal Science" at seven Universities in four Latin American countries. In: Proceedings of the 9th world congress on genetics applied to livestock production, Leipzig, 1–6 August 2010, 4 p. ISBN 978-3-00-031608-1. http://www.kongressband.de/wcgalp2010/assets/pdf/0868.pdf. Accessed 20 Jan 2011
181. Ojango JMK, Malmfors B, Okeyo AM, Philipsson J (2009) Capacity building for sustainable use of animal genetic resources in developing countries. Appl Anim Husb Rural Dev 2:23–26. www.sasas.co.za/aahrd
182. Bullock D, Lewis R, Weaber R, Lockee B, Strohbehn D, Garrick D, Pollak J (2010) Distance education: A short time solution to training graduates and producers with a shrinking population of quantitative geneticists. In: Proceedings of the 9th world congress on genetics applied to livestock production, Leipzig, 1–6 August 2010, 4 p. ISBN 978-3-00-031608-1. http://www.kongressband.de/wcgalp2010/assets/pdf/0916.pdf. Accessed 20 Jan 2011
183. Lewis R, Lockee B, Krishnamurthy L, Meese J, Boynton D (2010) Experiential learning online: Cyber sheep. In: Proceedings of the 9th world congress on genetics applied to livestock production, Leipzig, 1–6 August 2010, 4 p. ISBN 978-3-00-031608-1. http://www.kongressband.de/wcgalp2010/assets/pdf/0930.pdf. Accessed 20 Jan 2011
184. Van der Waaij L, Oldenbroek JK (2010) Teaching Animal Breeding digitally in professional Agricultural education. In: Proceedings of the 9th world congress on genetics applied to livestock production, Leipzig, 1–6 August 2010, 4 p. ISBN 978-3-00-031608-1. http://www.kongressband.de/wcgalp2010/assets/pdf/0980.pdf. Accessed 20 Jan 2011
185. Eckard RJ, Grainger C, De Klein CAM (2010) Options for the abatement of methane and nitrous oxide from ruminant production. Livest Sci 130:47–56
186. Robinson DL, Goopy J, Hegarty R (2010) Repeatability, animal and sire variation in 1-hour methane emissions and relationships with rumen volatile fatty acid concentrations. In: Proceedings of the 9th world congress on genetics applied to livestock production, Leipzig, 1–6 August 2010, 4 p. ISBN 978-3-00-031608-1. http://www.kongressband.de/wcgalp2010/assets/pdf/0712.pdf. Accessed 20 Jan 2011
187. Cassandro M, Cecchinato A, Battagin M, Penasa M (2010) Genetic parameters of methane production in Holstein Friesian cows. In: Proceedings of the 9th world congress on genetics applied to livestock production, Leipzig, 1–6 August 2010, 4 p. ISBN 978-3-00-031608-1. http://www.kongressband.de/wcgalp2010/assets/pdf/0837.pdf. Accessed 20 Jan 2011
188. Hegarty R, McEwan JC (2010) Genetic opportunities to reduce methane emissions from ruminant livestock. In: Proceedings of the 9th world congress on genetics applied to livestock production, Leipzig, 1–6 August 2010, 8 p. ISBN 978-3-00-031608-1. http://www.kongressband.de/wcgalp2010/assets/pdf/0515.pdf. Accessed 20 Jan 2011
189. Herrero M, Thornton PK, Gerber P, Van der Zijpp A, Van de Steeg J, Notenbaert AM, Lecomte P, Tarawali S, Grace D (2010) The way forward for livestock and the environment. In: Swanepoel F, Stroebel A, Moyo S (eds) The role of livestock in developing communities: enhancing multifunctionality. Centre for Agricultural and Rural Cooperation (CTA), Wageningen, pp 51–76
190. Conington J, Gibbons J, Haskell MJ, Bünger L (2010) The use of breeding to improve animal welfare. In: Proceedings of the 9th world congress on genetics applied to livestock production, Leipzig, 1–6 August 2010, 12 p. ISBN 978-3-00-031608-1. http://www.kongressband.de/wcgalp2010/assets/pdf/0057.pdf. Accessed 20 Jan 2011
191. Veissier L, Butterworth A, Bock B, Roe E (2008) European approach to ensure good animal welfare. Appl Anim Behav Sci 113:279–297
192. Bohte-Wilhelmus DI, De Haas Y, Veerkamp RF, Windig JJ (2009) Genetic selection as alternative to tail docking in Hampshire Down and Clun Forest. In: Proceedings of the 9th world congress on genetics applied to livestock production, Leipzig, 1–6 August 2010, 4 p.

ISBN 978-3-00-031608-1. http://www.kongressband.de/wcgalp2010/assets/pdf/0205.pdf. Accessed 20 Jan 2011
193. Sørenson JT, Fraser D (2010) On-farm welfare assessment for regulatory purposes: issues and possible solutions. Livest Sci 131:1–7
194. Häggman J, Juga J, Sillanpää MJ, Thompson R (2010) Genetic parameters for claw health an leg conformation traits in Finnish Ayrshire cows. In: Proceedings of the 9th world congress on genetics applied to livestock production, Leipzig, 1–6 August 2010, 4 p. ISBN 978-3-00-031608-1. http://www.kongressband.de/wcgalp2010/assets/pdf/0308.pdf. Accessed 20 Jan 2011
195. Gourdine JL, De Greeff KH, Rydmer L (2010) Breeding for welfare in outdoor pig production: a simulation study. Livest Sci 132:26–34. doi:10.1016/j.livsci.2010.04.017
196. Hoffman LC, Styger E, Muller M, Brand TS (2003) The growth and carcass and meat characteristics of pigs raised in a free-range or conventional housing system. S Afr J Anim Sci 33:166–175
197. Lemmon KL, Hebart ML, Brien FD, Hynd PI (2009) The genetics of temperament traits in Merino sheep. Proc Assoc Adv Anim Breed Genet 18:96–99
198. Cloete SWP, Misztal I, Olivier JJ (2009) Genetic parameters and trends for lamb survival and birth weight in a Merino flock divergently selected for multiple rearing ability. J Anim Sci 87:2196–2208
199. Hatcher S, Atkins KD, Safari E (2010) Lamb survival in Australian Merino sheep: a genetic analysis. J Anim Sci 88: 3198–3205
200. Mushi DE, Mtenga LA, Eik LO (2007) Some factors affecting the quality of meat from ruminants and their relevance to the Tanzanian meat industry. Tanz J Agric Sci 8:173–192

Breeding in Horses

Thorvaldur Árnason
Agricultural University of Iceland, Borgarnes, Iceland
International Horse Breeding Consultant,
Morgongava, Sweden

Article Outline

Glossary
Definition of the Subject
Introduction
Horse Breeding
Selection and Genetic Progress
Future Directions
Bibliography

Glossary

Animal model (AM) Statistical models that are used for evaluation of breeding values of all individuals in the population of interest.

Best linear unbiased prediction (BLUP) Standard statistical method for estimating breeding values in populations. BLUP adjusts for systematic fixed environmental effects and accounts for genetic relationships among animals.

Breeding value (BV) Mean additive genetic value of an individual relative to all members of the (base) population.

Effective population size (N_e) Number of individuals that would give rise to calculated sampling variance, or rate of inbreeding, if they bred in the manner of the idealized population with complete random mating, no selection, no migration, and no mutations.

Estimated breeding value (EBV) Estimate of the mean additive genetic value of an individual for a quantitative trait.

Generation interval (L) Average age of the parents when their progenies that will replace them in breeding are born.

Heritability (h^2) Measures the extent to which the phenotypes are determined by genetic factors. It is expressed as the ratio between additive genetic variance and the total phenotypic variance.

Inbreeding coefficient (F) Measure of the probability that two genes at any locus in an individual are identical by descent. It refers to an individual and expresses the degree of genetic relationship between the individual's parents.

Riding horse The narrow definition of riding horse or sport horse refers to horses of "Warmblood" breeds or Thoroughbred crosses, which compete in the classical equestrian sporting events of dressage, show jumping, and eventing. However, the broad definition of a riding horse refers to a horse used for any type of riding and will be used here.

Selection Any natural or artificial process favoring the survival and propagation of certain individuals in a population.

Selection intensity (i) Function of the proportion of animals selected for breeding relative to the total number of animals available for selection.

The smaller the proportion selected, the higher the selection intensity.

Timeform handicap ratings An estimate of racing capacity of Thoroughbred horses (in Great Britain). Express racing merit as weights in pounds that the compiler believes the horse should carry in an average free handicap race.

Trotter A horse trained for harness racing. The horse races in trot, which is a two-beat springing gait with a suspension phase (no ground contact) between two diagonal supporting pair of legs.

Definition of the Subject

Animal breeding can be defined as a human activity with the deliberate purpose to change existing populations of animals in some desired directions, so that future generations of these animals become more valuable in some sense. A prerequisite for successful animal breeding is that there is a genetic variation in the population in the traits one want to improve in future generations. Other requirements are: clear definitions of the breeding goals, good pedigree files, valid measures of the desired traits, methods of genetic evaluations that can combine information from the pedigree and the measured trait, and finally effective selection of breeding animals with high estimated genetic values (BV = breeding values) and therefore presumably with relatively large proportion of valuable genes affecting the desired traits.

The selected parents will transmit their genes to the next generation, and depending on the amount of genetic variation in the traits, accuracy of estimated genetic evaluations, and the selection intensity, the average level of the offspring generation will be raised as compared with the parent generation.

All general principles and methods of animal breeding obviously apply equally to the breeding of horses. There are however few structural and demographic characteristics specific to horse breeding that should be highlighted:

- Thorough registration of pedigree files
- Low rate of reproduction
- Long generation intervals
- Important traits are recorded on both males and females
- Wide overlapping of age groups among breeding candidates
- Considerable nonrandom mating practiced
- Extremely large differences in economic value depending on assumed genetic merit

All these factors support the use of methods for genetic evaluations that combine all pedigree information in an optimal way. In particular, the use of animal models (AMs) to obtain best linear unbiased predictions (BLUP) for genetic evaluation of breeding animals has become an important tool in modern horse breeding.

Introduction

Humans began to breed horses when the horse was domesticated some 6,000 years ago. Tamable animals were then selected from wild flocks and broken in. Stallions and mares with suitable temperament and desired characteristics were spared and got offspring in their new environment. The fitness measure of natural selection in the wild life was replaced by a selective value in the new role of serving humans. This artificial, and to lesser degree natural selection, of horses over 6,000 years has resulted in gradual genetic changes and subdivision into breeds adapted to different purposes [1, 2].

Throughout the history horses have been used for variety of purposes, such as riding, driving, carrying packs, and pulling agricultural equipments. Horses were also for a long time the most important means of transport in wars and have played a great role in the political and social development of many civilizations and even for the conquest of whole continents. Horses have also played a major role in the mythology of many religions but have as well been kept for their grace and were commonly used as a symbol of material status. The Vikings even used stallions for fighting contests. In many cultures, horses have been used for milk and meat production. The life of nomads in central Asia, of cowboys grazing and driving big herds of cattle, and of Indians hunting wild buffalos on the savannas in North America would have been impossible without horses. In brief, the human history would have been very much different without the company of the horse [3].

Today there are about 60 million horses in the world [4]. While horses are still used for agricultural work

and transportation in many parts of the world, the main role of horses in modern societies is to serve humans as pleasure or sport companions. The economic and social impact of the worldwide horse sector is tremendous and often underrated. In Europe, three to six horses (varies between countries) create full employment for one person. So within the European Union alone, with almost six million horses, about one million people are directly or indirectly employed in horse-related activities. About 4% of European agricultural land is dedicated to horse breeding [5].

Horses are used and will undoubtedly be used in the future for various competitive performance events, sport events, and pleasure riding or driving. Modern knowledge of animal breeding, genetics, statistics, reproduction technology, and computer science will certainly be used for adapting the different horse populations of the world to their intended purpose.

Horse Breeding

Breeds

Horses are members of *Equus ferus caballus*. In fact, there is no strict scientific definition of the term breed, but the elusive concept of breed as a definition of a population of "purebred" animals is commonly used among horse breeders. The classic definition of a autochthonous breed refer to a distinctive set of animals associated with a restricted geographical area in which it was developed to meet human needs under particular local conditions [6]. Often horse breeds are defined by breeding societies or registries that record pedigrees and maintain a studbook for a selected subset of horses based on geographical origin, phenotype, or function [3]. New synthetic horse breeds have been created by genetic selection according to a common breeding goal across several older horse breeds. As an example, many European Warmblood breeds have evolved this way. At the Web site "Breeds of Livestock: Horse Breeds" (http://www.ansi.okstate.edu/breeds/horses) detailed description on over 300 different horse breeds all over the world can be accessed.

Breeding Goals

Horse breeding, as all animal breeding, starts with a clear definition of breeding goals that usually includes many traits. The breeding objectives are a statement of the relative values of genetic change in all the desired traits that are included in a breeding plan. The overall objective (aggregate genotype) can be expressed as $H = \alpha_1 A_1 + \alpha_2 A_2 + \ldots + \alpha_n A_n$, where α_i is the relative (economic) weight and A_i is the animal's breeding value for the ith trait. The α_i values are often linear or nonlinear functions of the profit (return – cost) [7, 8]. Horse breeders often have a rather clear idea as to which traits they want to improve by genetic selection. However, the exact definitions of the relative weights on the different traits included in the breeding goal are often vague and determined by preferences of the individual breeder. Meanwhile, it is important that breeders should be provided with genetic evaluations for all the major traits that might be included in the breeding goal [9].

Registration of Pedigree Files

Unique identification of all members of a population has become a prerequisite for all rational breeding schemes using modern animal breeding methodology. The same identification number must refer to the same horse anywhere in the comprehensive pedigree files and in all files containing the registered traits. As horse breeding becomes increasingly more internationalized, the communication between horse registers in different countries is vital for successful breeding schemes. It is important that the identification number given to a newborn foal follow the individual animal throughout its entire life, even if the animal is exported to, or competes in, another country. It should contain codes for the country of birth, year of birth, and possibly the sex of the animal. The Web-based "universal equine life number" (UELN) system (www.ueln.net) offers a solution to this problem.

Measured Traits and Estimation of Genetic Parameters

An important part of a horse breeding scheme is to develop and use measures with good correlations with the traits in the breeding goal. The measurements need to be collected on a large or a random part of the population to be used in the selection and breeding process. Most traits that are important in breeding of horses are governed by a large number of genes and

many environmental factors. They may therefore be analyzed with genetic and statistical methods that apply to quantitative traits [10]. Measurements of performance traits in horses are often not normally distributed and need to be transformed to approach the normal distribution. Sometimes conversion to ranks is more favorable [11]. Measures of performance in racing and other equine competition sport events are frequently based on functions of earnings, ranks, or racing times. Occasionally, the measures are summarized in handicap ratings or cumulated competition points.

In many populations, the recorded traits are scored on a linear scale, often by subjective judgment, in special field or station tests. These traits may involve measurements of conformational details, temperament, performance in special gaits, or performance at various ranch tasks.

Before the registered traits can be used as a basis for genetic evaluations, the genetic parameters (variation, heritability, genetic correlations, and environmental correlations) among the traits must be estimated. The methods used for estimating genetic parameters in horse populations are usually based on maximum likelihood techniques for mixed animal models [12, 13]. In some recent cases, Bayesian Markov Chain Monte Carlo (MCMC) methods have been applied [14, 15].

Heritability of racing performance traits based on earnings and rank functions have frequently been estimated in the range of 0.3–0.4. Time measures in trotter races and shorter gallop races generally show heritability estimates of nearly the same magnitude (0.2–0.4), while heritability estimates of racing time in longer Thoroughbred races are usually considerably lower or in the region 0.1–0.2 [12, 13].

Heritability estimates of competition variables for jumping and dressage performance in riding horses have been found to be lower than in racing or about 0.1, on average. Data on competition results in riding horses is often subjected to strong preselection, which can be the main reason for the low heritability estimates [13].

The average heritability estimates for field test traits measuring gaiting ability and free jumping in riding horses are in the range of 0.2–0.3. Corresponding average heritability estimates of traits registered at station tests for stallions are generally much higher or in the range of 0.4–0.6 [13].

Heritability estimates of sport competition scores in Icelandic horses were found to be around 0.2–0.3, while heritability of field test traits within the same breed was estimated in the range 0.2–0.4 with the average value of 0.34 [16, 17].

Heritability of cutting performance in Western riding competitions has been estimated in the range of 0.04–0.19 [18].

This brief summary confirms that genetic variation and thus scope for genetic improvement has been found in the most important traits in many horse breeds.

Genetic Evaluations and Selection

Traditionally, selection of horses was for a long time based on phenotypic observations on performance and body conformation in combination with subjective evaluation of the pedigree. Since mid-1980s, the BLUP method with animal model (AM) has gained popularity as a superior and standard method for combining information from phenotypic observations and pedigree [19]. Estimated breeding values (EBVs) obtained by AM-BLUP are now used as the main selection criteria in many horse populations.

Estimation of breeding values in a population begins with definition of a linear statistical model. The model should fit the data as well as possible but it should also include as few parameters as possible. The model should account for all major factors affecting variation in the data in a systematic way. In the simplest form, the model may be written for a single trait as

$$y_{ij} = \mu + b_i + a_j + e_{ij}$$

where y_{ij} is the phenotypic observation on the jth horse belonging to the ith class of fixed (systematic) effects affecting the trait; μ represents the overall mean of the (base) population; b_i represents the deviation from the population mean caused by the ith class of fixed effects; and a_j represents the breeding value of the jth horse. The breeding values are random normally distributed deviations from the genetic mean of the base population and have the variance $\mathbf{A}\sigma_A{}^2$, where $\mathbf{A}$ is the additive genetic relationship matrix. Finally e_{ij} denotes the remainder of the model, which is assumed to include

independent and randomly distributed environmental effects pertaining to the *j*th horse.

Practical application of AM-BLUP in horse populations are usually based on far more complicated models than that shown above. They often include many fixed environmental factors, which affect systematically the variation in phenotypic records. As the breeding goal usually includes many correlated traits, multiple trait (MT) AM-BLUP procedures are commonly used for genetic evaluation of horses. Sometimes additional random factors are included in the model. This may be for genetic evaluation of repeated records on the same trait, or in other cases for better estimation and adjustment of genetic or environmental effects. As an example, the model may include both permanent environmental and genetic effects of the dam (maternal effects), or permanent environmental effects of riders, drivers, or trainers. Random regression models as an alternative to repeatability models for genetic evaluation of traits of longitudinal nature have good prospect in horse breeding [20, 21]. The trajectories may for example represent age development, racing distance, or competition classes.

Important traits in horse breeding are commonly scored on an ordered categorical scale. If there are at least several categorical classes and histograms of the distribution show good approximation to the normal distribution then the data can be analyzed by linear models without any significant loss in precision. If, however, there are as few as 2–4 classes, then nonlinear threshold models may be more appropriate. This particularly applies to binary traits with low or variable frequency across the fixed effect classes of the model. But sometimes linear models (AM-BLUP) are used in such cases in large data, since the computations in the linear models are much simpler.

With the AM-BLUP method, the effects of fixed factors and the breeding values are estimated simultaneously by solving a large set of mixed model equations (MME) with equally as many unknown solutions as there are equations. The estimated breeding values become adjusted for fixed effects that are correspondingly adjusted for differences in breeding values of the horses with records in the various fixed effect subclasses. The use of the additive genetic relationship matrix inverse ($\mathbf{A}^{-1}$), computed from the pedigree list, ensures that sharing of genes between related animals is correctly accounted for in the model. In addition, the EBVs of animals that are parents of recorded animals are adjusted for in the EBVs of the mate. That is a very important property in horse breeding where the allocation of mares to breeding stallions is generally far from random in terms of genetic merit.

The pedigree file used as data for computing $\mathbf{A}^{-1}$ is a list of all registered animals in the population. Each row consists of unique identification number of the individual animal and both parents. First, the inbreeding coefficients are calculated for all animals with one of the several efficient algorithms (e.g., [22, 23]) that have been developed from the original algorithm of Quuas [24]. Then the elements of $\mathbf{A}^{-1}$ are build up by simple rules depending on the number of identified parents of each animal [25]. Animals without identified parents build the base population. In most horse populations, pedigrees are well filled and the pedigree of the youngest animals can be traced back through many generations. In such situations, one common base population can reasonably be assumed. Sometimes horse populations are either: mixtures from many base populations (e.g., synthetic breeds), or there is importation of breeding stock from other countries or populations, or there are many animals with incomplete pedigrees. In such cases, an appropriate genetic grouping by creating several base populations becomes essential [26].

The AM-BLUP method has been applied for genetic evaluations in many horse breeds throughout the world. Most applications have been within Europe, where AM-BLUP methods are routinely used for genetic evaluations in riding horses, trotters, Icelandic horses, and Thoroughbreds in many countries. In some breeds, the method has been in practical application for up to more than 2 decades. The published index values for the most important traits of the breeding goals have been widely used by breeding organizations, and by individual breeders, for facilitating their selection decisions. In many cases, the breeders have access to Web applications where BLUP indices can be searched and listed in various ways. These have become valuable tools for the breeders and a large help in their mating plans. Analysis of genetic trends in these populations have invariably shown that the rate of genetic progress have been boosted by the introduction of the AM-BLUP method.

As an alternative to the BLUP method, Ricard [13] has developed a nonlinear approximate Bayesian animal model method for genetic evaluation of horses based on ranks in competitions. The method provides estimated breeding values for an underlying normally distributed liability variable from the likelihood of ranking according to some phenotypic observations in any single race or competition event. The estimated breeding values are obtained as the mean (or mode) of the marginal joint posterior density of the combined prior information and the likelihood function according to Bayesian principles. A statistical inference drawn from the resulting EBVs can be given by probability statements in Bayesian fashion. The method adjusts the likelihood for systematic environmental effects and utilizes additive genetic relationship between animals in the same way as the AM-BLUP method does. The method has only been applied for genetic evaluation of trotters and riding horses in France [27, 28]. The method is computationally demanding and general software for the method is not yet readily available. Developments of the concept of ranks (Thurstonian model) into full Bayesian analyses using MCMC Gibbs sampler methods have recently been proposed [29, 30]. The development of this methodology and modeling will continue and seems to have great potential in horse breeding.

Genetic evaluations of horses are often biased due to censoring of records [31, 32]. Horses are frequently preselected before they enter races, riding competitions, or field testing events. Information on the preselection criterion is usually lacking. However, in horse populations pedigree information is generally available on all horses, even on those without records. Therefore, the trait racing-status or test-status can be defined as an all-or-non trait, with the value one for tested animals and zero for culled or non-tested horses. Test-status has been confirmed a highly heritable trait in several horse populations (e.g., [32–34]). Environmental correlations between test-status and the recorded traits are not estimable because all animals with test-status equal to zero lack phenotypic records on the tested traits. However, genetic correlations between test-status and the recorded traits can be estimated if environmental covariances are constrained to some predefined values (e.g., zero). Indications of moderate to high genetic correlations between test-status and performance traits in horses have been confirmed in some populations [32, 33]. Inclusion of test-status in a multiple trait AM-BLUP framework was shown to increase the accuracy of selection and increase the rate of genetic progress in Swedish trotters, where the procedure has been routinely applied for a long time [33]. Ignorance of the problem with censoring of records results undoubtedly in bias in genetic evaluations and substantial loss of genetic progress in many horse populations.

International Genetic Evaluations

Breeding of sport horses has become a big global industry. Many breeding organizations of Warmblood riding horses in Europe have implemented modern methods for genetic evaluation of breeding horses on a national scale. The increased international trade with valuable breeding horses has led to important exchange of genetic material across populations having similar breeding goals.

The Interstallion project (http://www.interstallion.org) was established in 1998 to harmonize and improve exchange of information between Warmblood breeding organizations within Europe. The main aims have been to: (a) describe breeding objectives, test procedures, and genetic evaluation methods, (b) recommend improvements of national genetic evaluation systems, and (c) study methods of comparing genetic evaluations across countries. The project has resulted in several publications on these subjects [35–40].

Genetic evaluations for the global population of the Icelandic horse are computed regularly and published on the Internet (http://www.worldfengur.com) [41].

Selection and Genetic Progress

Factors Affecting Genetic Progress

The rate of genetic improvement by genetic selection in horse populations depends on:

1. Additive genetic variability in the selected traits (σ_A)
2. Intensity of selection (i)
3. Accuracy of selection (correlation between the true and the estimated breeding value, R_{TI})
4. Generation interval (L)
5. Inbreeding depression (d)

The genetic improvement per year can be expressed as

$$\Delta G/\text{year} = \sigma_A i R_{TI}/L - \Delta d$$

Increased intensity and accuracy of selection will increase the rate of genetic improvement if it is not leading to longer generation intervals nor increased homozygosity in loci affecting the traits and the general vigor (inbreeding depression). Generation intervals are generally very long in horse breeding (8–12 years). Shortening of the generation interval often means reduction in the accuracy in genetic evaluations (R_{TI}) but the selection intensity is usually affected in positive direction. The selection intensity, generation interval, and accuracy of selection are often different for stallions and mares. Therefore, the formula above is often modified to include two or four paths [42].

Multistage Selection in Horses

In horse breeding, large increase in the rate of response to selection can often be gained by an effective scheme for genetic evaluation of young horses that is based on pedigree information and early performance testing [43, 44]. The selection of stallions and usage for breeding is usually of a multistage nature as they are selected repeatedly within the same generation [45]. The first step in stallion selection is based on pedigree information (ancestry and collateral relatives) and determines which colts get performance tested and thus undergo the second and the most important selection step for traits having medium to high heritability. Selection intensity should be high at the second selection stage, but unfortunately testing capacity is often limited, especially for riding horses. The cost and labor of keeping stallions instead of geldings is usually high and many colts are castrated at a young age before they can express their abilities. The third and final selection step is based on EBVs when the offspring results provide the main source of information. The value of the progeny information increases for traits with low heritability.

Effect of Selection on Effective Population Size and Inbreeding

Several generations of constant directional selection, in large populations with moderate selection intensity, will lead to a measurable reduction (10–30%) in the genetic variability (σ_A), which thereafter is assumed to stay reasonably constant due to an equilibrium between the reduction in genetic variance and the variation rebuilt by recombination [46]. Therefore, in large populations with negligible inbreeding, selection is expected to be effective for changing the population mean in the desired direction over many generations.

Intense selection in closed populations (no migration) will build up increased relationship among the future members of the population. That corresponds to reduction in the effective population size (N_e) and leads to mating of related individuals, which is defined as inbreeding. Small N_e and consequently heavy inbreeding results in random change in gene frequencies across generations and a general reduction in the Mendelian sampling variance term and thus decreased genetic variability (σ_A). Accumulation of inbreeding (Δd) in small closed populations will reduce the scope for genetic improvement in the selected traits. In addition, increased homozygosity in many loci in the population will presumably affect fitness traits negatively (fertility, health, vigor, etc.) and increase frequency of genetic diseases in the population [10].

Many horse populations are at risk of getting small effective population size, due to small actual population size, intensive selection on EBVs alone, and large variation in family size. In such populations, the risk of reduced genetic variability and inbreeding depression should not be ignored and the breeding schemes should aim at sustainable long-term progress, where breeding animals are to be selected in an optimum way such that genetic improvement in the breeding goal traits and effects on future inbreeding are simultaneously considered [47–49]. Sustainable breeding plans aiming at maintenance of genetic variation should direct the selection such that future inbreeding is avoided at the cost of some loss in short-term genetic progress.

Obtainable and Observed Genetic Progress in Horse Populations

The rate of genetic response in large horse populations depends mainly on how accurately the traits reflecting the breeding goal can be measured (heritability), the amount of variation in the aggregate genotypes (genetic variability), the quality of the method used

for genetic evaluation (accuracy of selection), the testing capacity (selection intensity), and the age when the trait comes to an expression and can be measured (generation interval) [10].

In horse populations with onset of testing or racing performance at 3–6 years of age, and a conventional breeding scheme, the generation intervals are normally about 8–10 years for males and 10–12 years for the females. The selection intensity could correspond to ca 5% (1–10%) for males and ca 60% (40–80%) for females. When the selection criteria are EBVs that are obtained from the AM-BLUP method, then the source of information is a combination of pedigree, own performance, and offspring results. The average accuracy of selection on the male side (R_{TI}) could be about 0.8 for trait with $h^2 = 0.2$ and about 0.9 for trait with $h^2 = 0.4$. Higher accuracy would normally require more emphasis on progeny performance, which would prolong the generation interval. The accuracy of selection on the female side depends heavily on how large proportion of mares is tested for their own performance. A reasonable assumption could be $R_{TI} = 0.45$ for trait with $h^2 = 0.2$ and $R_{TI} = 0.63$ for $h^2 = 0.4$.

Given the assumptions above, the annual genetic progress in horse populations could correspond to 4–4.5% of the phenotypic standard deviation for traits (or combination of traits) with $h^2 = 0.2$ and to 6.5–7.5% for traits with the higher heritability of $h^2 = 0.4$. For readers interested in evaluation of different combinations of factors affecting the genetic progress in large populations, where inbreeding is ignored, a Java applet is available free at the following link: www.ihbc.se/web/contents/ihbcWebApplets/GenResponseApplet.html.

Estimates of genetic trend have been reported in several horse populations. The estimated annual genetic gain has been ranging from zero up to 6% of the phenotypic standard deviation of selected traits. Estimates of genetic trend in three different horse populations may serve as examples (Fig. 1). The Swedish Standardbred Trotter (SST) is a synthetic breed originating from imported American Standardbred Trotters and French Trotters. About 5,000 foals are born annually in the SST breed. The Nordic Trotter (NT) is a heavier type (cold-blood) originating from Norway and northern part of Sweden. About 1,300 Nordic Trotter foals are born annually (850 in Norway, 450 in Sweden). The Icelandic Horse is a closed population of small, compact, and strong horses that has been purebred in Iceland for more than thousand years. It is the only horse breed in Iceland where about 7,000

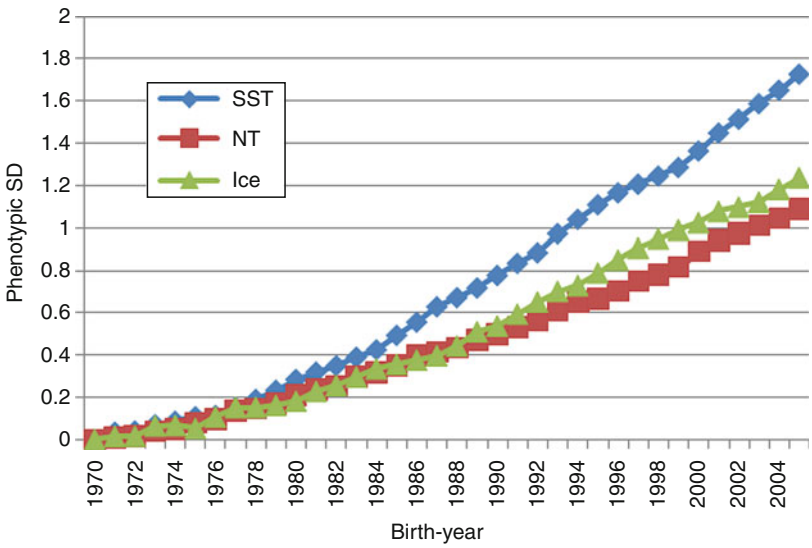

Breeding in Horses. Figure 1
Realized progress in the aggregate genotype, expressed in phenotypic standard deviation (σ_P) units, in three horse populations (*SST* Swedish Standardbred Trotter, *NT* Nordic Trotter, Ice Icelandic horse)

foals are born annually. Both the trotter breeds are used for harness racing and the breeding goal consists of several traits expressing racing performance ability and sustainability. The Icelandic Horse is used for riding and is known for its gaiting abilities, willingness, good character, and hardiness. The breeding goal for the Icelandic Horse consists of a linear function of 16 traits (8 conformation traits and 8 traits measuring riding ability [gaits and temperament]). The traits are registered at special field tests.

Genetic evaluations based on BLUP methods have been available as a guide for selection in these three breeds since mid-1980s. Between 1970 and 2005, the mean of the aggregate genotype (weighted mean of EBVs for several racing variables) in the SST population has been raised by 1.73 σ_P units, corresponding to the average annual ΔG/year = 0.049 over the entire period. The rate of genetic gain has increased gradually over the period as seen by the increased steepness in the slope showing the trend. For the last 10 years, the rate of genetic gain has been ΔG/year = 0.062, or 6.2% of the phenotypic standard deviation. In the smaller population of Nordic Trotter, the population average level has lifted 1.09 σ_P units since 1970. That corresponds to ΔG/year = 0.031 over the entire period and to ΔG/year = 0.042 for the last 10 years. The population mean of Icelandic horses has been raised to 1.73 σ_P units over the 35-year period or by 3.5% σ_P per year. The average rate of response over the last decade has increased by 1% of the phenotypic standard deviation, or to 4.5% σ_P per year.

In the comparison of the three breeds, the efficiency of the selection has apparently been largest in the Standardbred Trotter. This larger genetic progress can mainly been attributed to higher selection intensity, particularly on the male side, where relatively few stallions are selected on the basis of results from races where many colts compete. The high selection intensity in SST is obtained by high testing capacity (races), widespread use of artificial insemination so that each selected stallion is able to cover more mares, and excessive use of information on results and pedigree. This is clearly reflected in the larger short-term response. However, the long-term sustainability of the breeding plan in the SST breed may be questioned as explained below when considering inbreeding and effective population size.

Long-Term Genetic Progress

An important aspect of sustainable animal breeding plans aiming at long-term genetic progress is to maintain genetic diversity (i.e., variation) within the population. In closed populations, gene frequencies fluctuate randomly from one generation to another as a result of the finite sampling of gametes. This phenomenon, called genetic drift, is quantified by the term effective population size, N_e [10, 50]. In a closed population, with no migration, the N_e is dependent on the number of parents in each generation, the variance of parental family sizes and selection. One way to estimate N_e is to measure the rate of increase of inbreeding over the different generations: $1/2N_e = \Delta F = (F_t - F_{t-1})/(1 - F_{t-1})$, where F_t is the mean coefficient of inbreeding for generation t (e.g., [10]).

The development of inbreeding in the three horse populations shows different levels that have evolved since the respective base populations (Fig. 2). The figure demonstrates difference in the rate of increase of inbreeding over time across the populations and thus gives a measure of their effective population sizes. According to the rate of inbreeding and the corresponding generation intervals, the effective population size (N_e) is approximately 40 for the Swedish Standardbred Trotter (SST), 50 for the Nordic Trotter (NT), and 100 for the Icelandic horse (Ice). The rate of inbreeding per generation, ΔF, is 1.3% in SST, 1.0% in NT, and 0.5% in Ice. In guidelines from FAO [51], the minimum recommended N_e is 50 corresponding to ΔF = 1.0% in livestock populations. Otherwise there is a great risk of loss in genetic variation, which will suppress long-term genetic progress and increase the risk for homozygosity of deleterious alleles, thus affecting health and fitness traits negatively. The SST breed is not only showing alarmingly high level of inbreeding (F ≈8%), but clearly surpassing the recommended rate of inbreeding per generation. The genetic constitution of the current generation of the SST breed is 94% of American Standardbred Trotter origin, while the remaining 6% can be traced to French Trotter base animals [33]. The American Standardbred Trotter is highly inbred with average inbreeding coefficient above 10%. The inbreeding in American Standardbred trotters and pacers is mainly due to remote inbreeding, where the horses are connected to one another by

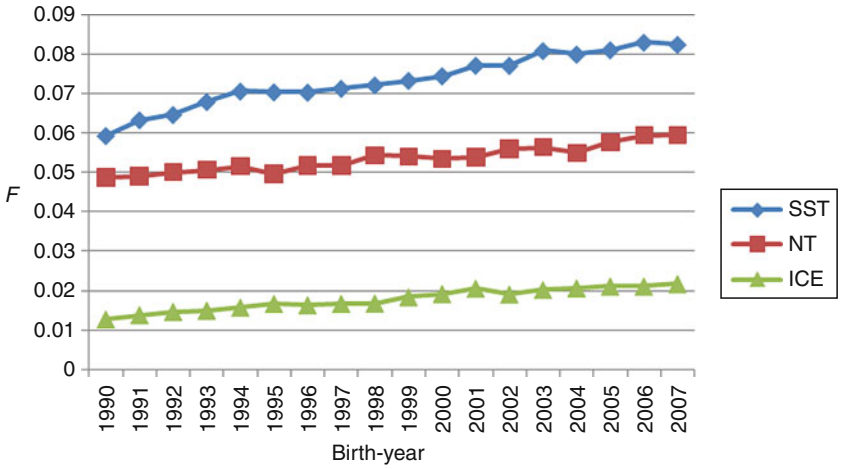

Breeding in Horses. Figure 2
Trend and level of inbreeding coefficients (*F*) in three horse populations (*SST* Swedish Standardbred Trotter, *NT* Nordic Trotter, Ice Icelandic horse)

numerous paths through a small number of remote common ancestors. At the same time, breeders have deliberately avoided close consanguineous mating [52, 53]. Swedish breeders of Standardbred trotters have followed the same strategy. The average relationship among SST born in 2000 was R = 16.4% with a standard deviation of 5.2% [54]. Random mating within the population will result in average inbreeding coefficient above 8%. In order to reduce the rate of increase in inbreeding in the future, the variation in relationship among breeding candidates must be utilized in the mating strategy. Criteria for selection of breeding animals that involve EBVs modified such that the average relationship between selected animals is restricted have been proposed [47–49]. Increased migration of genetic material of French origin is also a recommended option for the breeders of Standardbred trotters in Sweden.

Breeders of the Nordic trotters have become increasingly aware of the risks associated with inbreeding in small closed populations. Negative effects of inbreeding (inbreeding depression) have been confirmed for reproductive traits, health traits, and racing performance in the Nordic trotter [55, 56]. Quotas for maximum number of mares that can be mated to each stallion have been put into effect and the rate of increase in inbreeding has reduced considerably compared with the period of 1970–1990, when the rate of inbreeding corresponded to N_e = 32 [57].

The inbreeding in the Icelandic horse is still at a low level and the rate of increase in the rate of inbreeding (ΔF) is yet not alarming. The breeding goal is broad as it includes very many traits, which helps keeping broad genetic variation among selected breeding individuals. However, awareness of the importance of maintaining low average genetic relationship among the selected parents is vital for the future of this breed, since import of genetic material to the closed horse population in Iceland is not a feasible option.

Genetic Progress in Racing Speed

One of the most interesting and debated questions concerning horse breeding is the "paradoxical" lack of improvement in winning times in the classical races for Thoroughbred horses over the last 50 years, in spite of significant genetic variation in racing performance variables and intense selection on racing performance [58–65].

The wild ancestors of modern horses were grazing flight animals and natural selection for speed and ability to traverse long distances were certainly important factors for the survival of the fittest. The Thoroughbred horses were founded by English and African horses screened for galloping speed and have been subject to an intense artificial selection on racing performance for over three centuries (30 horse generations). As a consequence, Thoroughbred horses are the fastest racehorses in the world galloping over distances of

1 to 2 miles. The breeding animals have not been selected directly on racing speed or racing time. Rather they have been selected on some function of ranks in races and special weight has been put on the ability to win races. Thoroughbred horses racing in the classical races all belong to the fastest segment of horses in the population.

Gaffney and Cunningham [61] estimated genetic change in Timeform handicap ratings of Thoroughbred horses in Great Britain. They confirmed effective selection on Timeform ratings and estimated annual genetic gain corresponding to almost 5% of the phenotypic standard deviation of 3-year-old Timeform ratings. This genetic progress is not reflected in winning times of the classic races, but the authors concluded that correlated genetic improvement in speed had been achieved in the Thoroughbred population as a whole but the fastest individuals in the population had reached the physiological limits for racing speed over the distance of the classic races. This conclusion assumes asymmetry in the distribution of racing speed.

The genetic evaluations of the Swedish Standardbred Trotter involve several variables that are functions of ranks in races (earnings, order at finish in the race) and racing time. As ranks in races are measures of racing performance that are relative to contemporaries racing at the same time, a genetic progress in these variables cannot be projected to any observable scale with clear physical meaning. On the other hand, the genetic progress in racing performance should be reflected in faster racing times. The best average racing time over 1 km has indeed improved continuously for the Swedish Standardbred Totter since recording started for the horses born in 1976 (Fig. 3). The limits for racing speed in trotters have apparently not been reached yet. However on the observed untransformed scale (s/km), the rate of improvement has slightly reduced over time and it seems increasingly harder to break the records. The dispersion of the slowest and fastest racing time records in the population around the average is also apparently asymmetrical. Arnason [66, 67] has previously argued that genetic evaluation of racing time records should be based on scaled logarithmic transformation of racing time records as $y^*_i = \ln(y_i - x)$, where y_i is the observed racing time record on the ith horse in s/km units, x is the asymptotic physiological limits for trotting racing speed in s/km in races over the traditional distance of 1 mile. When x is equal to 68.2 the distribution of y^*_i is almost perfectly normal in the population of Swedish Standardbred male trotters and the trend in average log transformed racing time records is linear.

The trend in statistics (mean, minimum (fastest), maximum (slowest)) of fastest racing time records of 3–5-year-old males in the population of Swedish Standardbred Trotter can be described with the

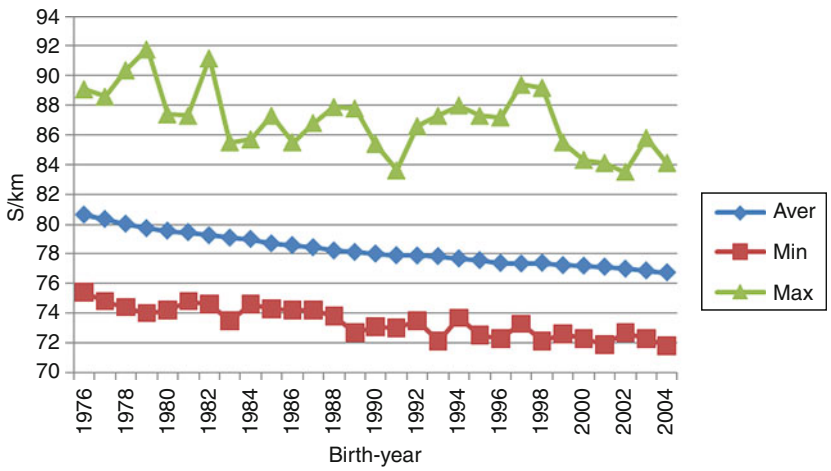

Breeding in Horses. Figure 3
Observed trend in best average racing time records as 3–5-year-olds over 1 km for the average (aver), fastest (min), and slowest (max) Standardbred male trotters born in Sweden

expression: $s/km = x\,(1 + e^{-pt})$, where x is the ultimate asymptotic limit for the fastest racing time records in the population as defined above, p is a positive constant, and t = birth-year – z, where z is a time scaling constant [67]. The constants p and z were estimated from recent data on racing results in the population of SST leading to the following equations for prediction of the development of the trend in the average, fastest, and slowest racing times in the population:

$$s/km_{(aver)} = 68.2\left(1 + e^{(-0.013(\text{birth-year}-1843)}\right)$$
$$s/km_{(min)} = 68.2\left(1 + e^{(-0.021(\text{birth-year}-1867)}\right)$$
$$s/km_{(max)} = 68.2\left(1 + e^{(-0.008(\text{birth-year}-1829)}\right)$$

The predicted trend is revealed in Fig. 4. The racing time records in the population are expected to improve (become faster) at a linear rate on the logarithmic transformed scale, but at a diminishing rate on the untransformed linear scale of racing time (s/km). The presented racing times refer to "volt start," which is the most common starting procedure for trotting races in Sweden. Records from the flying "auto start" are adjusted by adding 2 s to the racing time.

The history of selection for trotting racing performance in Standardbred trotters is much shorter than that of selection for gallop racing performance in Thoroughbreds, and probably reflects a difference of at least 20 generations. If genetic variation can be maintained in the trotter population and the selection for trotting racing performance will be continued in the same manner over the next 200 years, the prediction equations above give the following estimates: Average racing time record for males born 2210 = 68.78 s/km; fastest racing time = 68.25 s/km; and slowest racing time = 71.44 s/km. This can be compared with the corresponding observed average, minimum, and maximum racing times of males born 2004 in the SST population: 76.74, 71.8, and 84.1 s/km. A parallel between this expected scenery for the development of racing speed in trotters and that already observed in Thoroughbreds is highly tempting. The average records (and the slowest) will continue to improve, however at ever decreasing rate, far after an apparent stagnation in the improvement of the fastest records. A slight improvement of the best records will be increasingly harder to identify due to the inappropriate scale. The small difference in racing speed between the fastest horses becomes less important as relative to fighting spirit and the mental and physical ability of the horse to react to the signals of the driver (or jockey) and to variations in speed at different phases of the race.

If there are some asymptotic limits to racing speed, they must relate to a nonlinear accumulation of biological and physical constraints on racing performance. Such factors might be: energy supply, energy

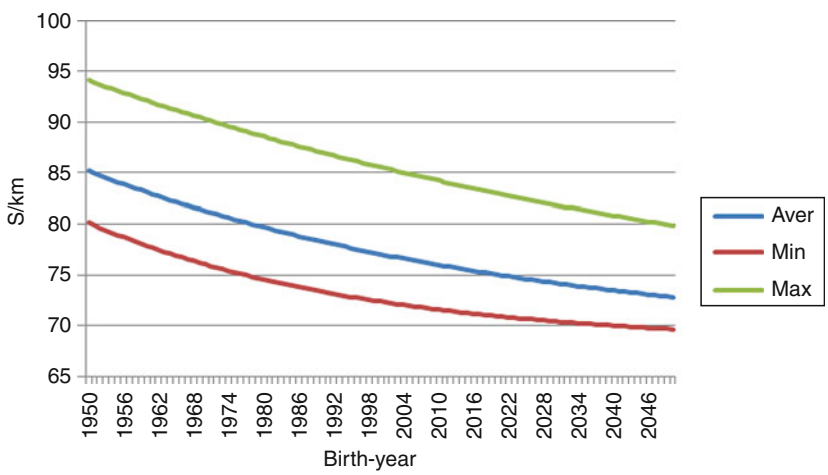

Breeding in Horses. Figure 4
Predicted trend in best average racing time records as 3–5-year-olds over 1 km for the average (aver), fastest (min), and slowest (max) Standardbred male trotters born in Sweden

transport rate, neural functions, oxygen supply, oxidative enzyme activity, accumulation of lactic acid in the blood, exponential increase in energy requirement for overcoming air resistance, and generally a nonlinear risk of stress on the locomotion (tendons, bones and ligaments), respiratory and cardiovascular systems, with increasing racing speed [13, 68].

Hypothetically, an insertion of a gene with positive effect on racing performance on an inferior racing horse would be likely to have more marked effect on its racing performance than if the same gene was inserted into an outstanding racer, which would already carry many genes with positive effects on racing performance. Such scale effects can often be removed by appropriate transformation and traditional quantitative genetic analysis methods may apply. Alternatively, a nonlinear polynomial genetic model for finite number of independent loci (geometric progression) might be attempted [66, 67]. The geometric progression model assumes constantly diminishing marginal substitution effects of the alleles affecting the trait.

In conclusion, the fact that racing times in classic Thoroughbred races have not improved markedly in more than a half century in spite of available genetic variation and selection is not necessarily a "paradox." It could merely be a result of the use of improper scale for measuring racing times in horses approaching their biological limits.

Future Directions

Methods of organized animal breeding using BLUP animal models and selection on EBV for important traits have proved useful in many horse populations worldwide. Genetic progress at the annual rate of 3–6% of the phenotypic standard deviation has been reported in several populations. Sustainable breeding schemes yielding this rate of constant response over a long period and at the same time maintaining sufficient genetic variability in the population can be accomplished with established knowledge and relatively cheap technical equipments.

In many parts of the world are rational and organized breeding plans still lacking in large and locally important horse breeds. In some societies, this can be explained by poverty and lack of higher level of education. In others is the social culture, including reluctant conservatism, a hindrance to the introduction of new technique and scientific influence on the traditional horsemanship and "horse culture." This will certainly change and introduction of new and modern organized breeding plans for horses will undoubtedly be seen in many countries in near future.

The increased international trade with valuable breeding horses and exchange of genetic material across horse populations has created need for international genetic evaluations, where EBVs can be fairly compared across countries. The need for international genetic evaluations will certainly grow in the near future.

Methodological developments in genetic evaluation procedures and statistical models will undoubtedly enhance future breeding in horses. Of particular foreseen interest is genetic evaluation of ranks in competitions based on Bayesian Thurstonian models [29, 30] and use of random regression models for evaluation of traits with repeated measurements [20, 21].

Recently, the horse genome has been fully sequenced and the results are available to the scientific community [69, 70]. This has created optimism that genomic selection, which is selection on genomic breeding values (GEBVs), might revolutionize future horse breeding. The GEBV are calculated as the sum of the effects of dense genetic markers across the entire genome on the trait of interest. The genetic (DNA) markers are in the form of a large collection of chromosome fragments, so-called SNP (single nucleotide polymorphism) chips. Since GEBV can be obtained already in young foals, the possibility to shorten the long generation intervals in traditional horse breeding and to hinder castration of genetically valuable individuals is obvious. Genomic selection has the most potential for genetic improvement of traits that are manifested late in life and of traits with low heritability. Breeding for performance traits in sport horses, longevity, and various health traits in horses could benefit enormously if genomic selection can be practiced in a cost-effective way.

More methodological as well as technical development is required before genomic selection can gain widespread practical application in horse breeding. The first step is the development of a sufficient number of high-density SNPs across the entire horse genome and the second step is to genotype large reference populations in different horse breeds with phenotypic

records so that the effects of the markers on the phenotypes can be analyzed. In subsequent generations, a large number of horses will need to be genotyped for the markers to determine which chromosome segments they carry. Then the estimated effects of the segments can be summed across the whole genome to predict the GEBV [71]. This new technology is already revolutionizing dairy cattle breeding in several countries [72, 73] and an efficient algorithm for computing the relationship matrix by use of genomic information has been invented [74]. A combination of a traditional selection on EBVs and a selection on GEBVs is likely to be adapted soon in the most valuable sport and racing populations, where the cost of genotyping is little in relation to the value of the breeding animals and organized breeding plans with registration of data on phenotypes and pedigrees are already in function. As a dramatic reduction in the cost of genotyping can be anticipated in the future, a practical and widespread use of genomic selection may become reality in breeding of horses throughout the world sooner than expected in the light of current status and prizes. An important challenge will be to meet unforeseeable snags that may rise from the use of the new technique and difficulties in managing future genetic variation and long-term genetic gain.

Bibliography

Primary Literature

1. Anthony D, Telegin DY, Brown D (1991) Origin of horseback riding. Scientific Am 225:44–48
2. Bökönyi S (1984) Horse. In: Mason IL (ed) Evolution of domesticated animals. Longman, London, pp 162–173
3. Bowling AT, Ruvinsky A (2000) Genetic aspects of domestication, breeds and their origins. In: Bowling AT, Ruvinsky A (eds) The genetics of the horse. CABI Publishing, Wallingford, pp 25–51
4. FAOSTAT Database (2008) faostat.fao.org
5. EU Equus (2009) www.equus2009.eu
6. Mason IL (1996) A world dictionary of livestock breeds, types and varieties, 4th edn. CAB International, Wallingford
7. Hazel LN (1943) The genetic basis for constructing selection indexes. Genetics 28:476–490
8. Amer PR, Fox GC, Smith C (1994) Economic weights from profit equations: appraising their accuracy in the long run. Anim Prod 58:11–18
9. Árnason T, Van Vleck LD (2000) Genetic improvement of the horse. In: Bowling AT, Ruvinsky A (eds) The genetics of the horse. CABI Publishing, Wallingford, pp 473–497
10. Falconer DS, Mackay TFC (1996) Introduction to quantitative genetics, 4th edn. Longmans Green, Harlow
11. Ricard A (1998) Developments in the genetic evaluation of performance traits in horses. In: Proceedings of the 6th world congress on genetics applied to livestock production, Armidale, NSW. University of New England, Armidale, vol 24, pp 388–395
12. Tolley ES, Notter DR, Marlowe TJ (1985) A review of the inheritance of racing performance in horses. Anim Breed Abstr 53:163–185
13. Ricard A, Bruns E, Cunningham EP (2000) Genetics of performance traits. In: Bowling AT, Ruvinsky A (eds) The genetics of the horse. CABI Publishing, Wallingford, pp 411–438
14. Correa MJM, Mota MDS (2007) Genetic evaluation of performance traits in Brazilian Quarter Horse. J Appl Genet 48: 145–151
15. Stock KF, Distl O, Hoeschele I (2007) Bayesian estimation of genetic parameters for multivariate threshold and continuous phenotypes and molecular genetic data in simulated horse populations using Gibbs sampling. BMC Genet 8:19
16. Albertsdóttir E, Eriksson S, Nasholm A, Strandberg E, Árnason T (2007) Genetic analysis of competition data on Icelandic horses. Livest Sci 110:242–250
17. Albertsdóttir E, Eriksson S, Nasholm A, Strandberg E, Árnason Th (2008) Genetic correlations between competition traits and traits scored at breeding field-tests in Icelandic horses. Livest Sci 114:181–187
18. Burns EM, Enns RM, Garrick DJ (2004) The status of equine genetic evaluation. In: Proceedings, Western Section, American Society of Animal Science, pp 82–86
19. Kennedy BW, Schaeffer LR, Sorensen DA (1988) Genetic properties of animal models. J Dairy Sci 71(suppl 2):17–26
20. Bugislaus AE, Roehe R, Willms F, Kalm E (2006) The use of a random regression model to account for change in racing speed of German trotters with increasing age. J Anim Breed Genet 123:239–246
21. Menendez-Buxadera AM, Mota MDS (2008) Variance component estimations for race performance of thoroughbred horses in Brazil by random regression model. Livest Sci 117:298–307
22. Meuwissen THE, Luo Z (1992) Computing inbreeding coefficients in large populations. Genet Sel Evol 24: 305–313
23. Sigurdsson Á, Árnason T (1995) Predicting genetic trend by uni- and multitrait models. Acta Agric Scand Sect A 45:1–10
24. Quaas RL (1976) Computing the diagonal elements and inverse of a large numerator relationship matrix. Biometrics 32:949–953
25. Henderson CR (1976) A simple method for computing the inverse of a numerator relationship matrix used in prediction of breeding values. Biometrics 32:69–83
26. Westell RA, Quaas RL, Van Vleck LD (1988) Genetic groups in an animal model. J Anim Sci 66:2817–2825
27. Tavernier A (1990) Estimation of breeding value of jumping horses from their ranks. Livest Prod Sci 26:277–290

28. Tavernier A (1991) Genetic evaluation of horses based on ranks in competition. Genet Sel Evol 23:159–173
29. Gianola D, Simianer H (2006) A thurstonian model for quantitative genetic analysis of ranks: a Bayesian approach. Genetics 174:1613–1624
30. Ricard A, Legarra A (2010) Validation of models for analysis of ranks in horse breeding evaluation. Genet Sel Evol 42:3
31. Klemetsdal G (1992) Estimation of genetic trend in racehorse breeding. Acta Agric Scand 42:226–231
32. Albertsdóttir E, Eriksson S, Sigurdsson Á, Árnason T (2009) An all-or-none trait to account for pre-selection in Icelandic horse breeding. In: Book of Abstracts of the 45th annual meeting of the European association of animal production, 24–27 August 2009, Barcelona. Universityof Wisconsin, Madison, p 217
33. Árnason T (1999) Genetic evaluation of Swedish standardbred trotters for racing performance traits and racing status. J Anim Breed Genet 116:387–398
34. Bugislaus AE, Roehe R, Willms F, Kalm E (2005) Multivariate genetic analysis to account for preselection and disqualified races in the genetic evaluation of racing performances in German trotters. Acta Agric Scand Sect A 55:49–56
35. Koenen EPC, Aldrige LI, Philipsson J (2004) An overview of breeding objectives for warmblood sport horses. Livest Prod Sci 88:77–84
36. Thorén-Hellsten E, Viklund A, Koenen EPC, Ricard A, Bruns E, Philipsson J (2006) Review of genetic parameters estimated at stallion and young horse performance tests and their correlations with later results in dressage and show-jumping competition. Livest Sci 103:1–12
37. Ruhlman C, Bruns E, Fraehr E, Koenen EPC, Philipsson J, Janssens S, Quinn K, Thorén-Hellsten E, Ricard A (2009) Genetic connectedness between seven European countries for performance in horse jumping competitions of warmblood riding horses. Livest Sci 120:75–86
38. Thorén-Hellsten E, Jorjani H, Philipsson J (2008) Connectedness among five European sport horse populations. Livest Sci 118:147–156
39. Thorén-Hellsten E, Jorjani H, Philipsson J (2009) Genetic correlations between similar traits in the Danish and Swedish Warmblood sport horse populations. Livest Sci 124:15–20
40. Ruhlman C, Janssens S, Philipsson J, Thorén-Hellsten E, Crolly H, Quinn K, Manfredi E, Ricard A (2009) Genetic correlations between horse show jumping competition traits in five European countries. Livest Sci 122:234–240
41. Árnason T, Sigurdsson Á, Lorange JB (2006) Global genetic evaluations of the Icelandic horse and genetic connectedness between countries. In: Proceedings of the 8th world congress on genetic applied to livestock production, Belo Horizonte, 13–18 August 2006, CD-ROM communication 24-16
42. Rendel JM, Robertson A (1950) Estimation of genetic gain in milk by selection in a closed herd of dairy cattle. J Genet 50:1–8
43. Strom H, Philipsson J (1978) Relative importance of performance tests and progeny tests in horse breeding. Livest Prod Sci 5:303–332
44. Hugason K, Árnason T, Norell L (1987) Efficiency of three-stage selection of stallions. J Anim Breed Genet 104:350–363
45. Cochran WG (1951) Improvement by means of selection. In: Proceedings of Second Berkely Symposium on Mathematical, Statistics and Probability. University of California Press, Berkeley, pp 440–470
46. Bulmer MG (1971) The effect of selection on genetic variability. Am Nat 105:201–211
47. Wray NR, Goddard ME (1994) Increased long-term response to selection. Genet Sel Evol 26:431–451
48. Meuwissen THE (1997) Maximizing the response of selection with a predefined rate of inbreeding. J Anim Sci 75: 934–940
49. Grundy B, Villanueva B, Wooliams JA (2000) Dynamic selection for maximizing response with constrained inbreeding in schemes with overlapping generations. Anim Sci 70: 373–382
50. Wright S (1931) Evolution in Mendelian populations. Genetics 16:97–159
51. Woolliams JA, Gwaze GP, Meuwissen THE, Planchenault D, Renard JP, Thibier M, Wagner H (1998) Secondary guidelines for the development of national farm animal genetic resources management plans. Management of small populations at risk. Food and Agricultural Organization of the United Nations (FAO), Rome
52. MacCluer JW, Boyce AJ, Dyke B, Weitkamp LR, Pfennig DW, Parsons CJ (1983) Inbreeding and pedigree structure in Standardbred horses. J Hered 74:394–399
53. Cothran EG, MacCluer JW, Weitkamp LR, Pfennig DW, Boyce AJ (1984) Inbreeding and reproductive performance in Standardbred horses. J Hered 75:220–224
54. Árnason T (2001) Inbreeding – threat to trotting horses. In: Papers, 2001 World Trotting Conference, 6th to 15th July 2001, Suomen Hippos, Helsinki & Mikkeli
55. Klemetsdal G (1993) Demographic parameters and inbreeding in the Norwegian trotter. Acta Agric Scand Sect A 43:1–8
56. Anderson E, Nasholm A, Gerber E, Árnason Th (1998) Inbreeding and its impact on racing performance in Swedish and Norwegian coldblooded trotters. In: Book of Abstracts of the 49th annual meeting of the European association of animal production, 24–27 August 1998, Warsaw. Wageningen Publishers, Wageningen, pp 314
57. Klemetsdal G, Johnson M (1989) Effect of inbreeding on fertility in Norwegian trotter. Livest Prod Sci 21:263–272
58. Cunningham EP (1976) Genetic studies in horse populations. In: Proceedings of the international symposium on genetics and horse breeding. Royal Dublin Society, Dublin, pp 2–8
59. Robertson A (1976) What has genetic to contribute to horse breeding. In: Proceedings of the international symposium on genetics and horse breeding. Royal Dublin Society, Dublin, pp 64–70
60. Langlois B (1980) Heritability of racing ability in thoroughbreds – a review. Livest Prod Sci 7:591–605

61. Gaffney B, Cunningham EP (1988) Estimation of genetic trend in racing performance of thoroughbred horses. Nature 332: 722–724
62. Hill WG (1988) Why aren't horses faster. Nature 332:678
63. James JW (1990) Selection limits in thoroughbred horses. In: Proceedings of the 4th world congress on genetics applied to livestock production, Edinburgh, 23–27 July 1990, vol 16, pp 221–224
64. Langlois B (1994) An introduction to genetic analysis in the Thoroughbred. In: Book of abstracts of the 45th annual meeting of the European association of animal production, Rome 5–8 September 1994, Edinburgh, Rome, p 358
65. Langlois B (1996) A consideration of the genetic aspects of some current practices in thoroughbred horse breeding. Ann Zootechnie 45:41–51
66. Árnason T (1994) Simple (plausible) non-linear model for inheritance of racing speed and corresponding genetic changes from selection. In: Book of abstracts of the 45th annual meeting of the European association of animal production, Rome 5–8 September 1994, Edinburgh, Rome, p 360
67. Árnason T (2001) Trends and asymptotic limits for racing speed in standard bred trotters. Livest Prod Sci 72:135–145
68. Cunningham EP (1998) The genetics of track performance in thoroughbreds. In: Book of abstracts of the 49th annual meeting of the European association of animal production, 24–27 August 1998, Warsaw, Wageningen Pers, Wageningen, p 309
69. Wade CM, Giulotto E, Sigurdsson S, Zoli M, Gnerre S, Imsland F, Lear TL, Adelson DL, Baily E, Bellone RR, Blocker H, Distl O, Edgar RC, Garber M, Leeb T, Mauceli E, MacLeod JN, Penedo MCT, Raison JM, Sharpe T, Vogel J, Andersson L, Antczak DF, Biagi T, Binns MM, Chowdhary BP, Coleman SJ, Della Valle G, Fryc S, Guérin G, Hasegawa T, Hill EW, Jurka J, Kiialainen A, Lindgren G, Liu J, Magnani E, Mickelson JR, Murray J, Nergadze SG, Onofrio R, Pedroni S, Piras MF, Raudsepp T, Rocchi M, Roed KH, Ryder OA, Searle S, Skow L, Swinburne JE, Syvanen AC, Tozaki T, Valberg SJ, Vaudin M, White JR, Zody MC, Broad Institute Genome Sequencing Platform, Broad Institute Whole Genome Assembly Team, Lander ES, Kindblad-Toh K (2009) Genome sequence, comparative analysis and population genetics of the domestic horse. Science 326:865–867
70. Gu J, Orr N, Park SD, Katz LM, Sulimova G, MacHugh DE, Hill EW (2009) A genome scan for positive selection in Thoroughbred horses. PLoS ONE 4(6):e5767. doi:10.1371/journal.phone.0005767
71. Meuwissen THE, Hayes BJ, Goddard ME (2001) Prediction of total genetic value using genome-wide dense marker maps. Genetics 157:1819–1829
72. Hayes BJ, Bowman PJ, Chamberlain AJ, Goddard ME (2009) Invited review: genomic selection in dairy cattle: progress and challenges. J Dairy Sci 92:433–443
73. VanRaden PM, Sullivan PG (2010) International genomic evaluation methods for dairy cattle. Genet Sel Evol 42:7
74. Legarra A, Aguilar I, Misztal I (2009) A relationship matrix including full pedigree and genomic information. J Dairy Sci 92:4656–4663

Books and Reviews

Bowling AT (1996) Horse genetics. CAB International, Wallingford
Bowling AT, Ruvinsky A (eds) (2000) The genetic of the horse. CABI Publishing, Wallingford
Mrode RA (2005) Linear models for the prediction of animal breeding values, 2nd edn. CABI Publishing, Wallingford
Van Vleck LD, Pollak EJ, Oltenacu EAB (1989) Genetics for the animal sciences. Freeman, New York

Bus Rapid Transit and Light Rail Transit Systems: State of Discussion

Cliff Henke
Parsons Brinckerhoff, Newark, NJ, USA

Article Outline

Glossary
Definition of the Subject and Its Importance
Introduction
BRT Developments
Light Rail Developments
Current and Future Trends
Conclusion
Bibliography

Glossary

Bus rapid transit (BRT) An integrated bus-oriented public transport service composed of six basic elements: higher-quality, more styled buses; a well-designed service plan, including route structure is faster and more frequent transit service than typically experienced with regular route local bus service; upgraded, appealing passenger stations; roadway infrastructure that gives BRT priority in mixed traffic or separated from other traffic entirely to help ensure faster travel times; intelligent transportation technologies, not only for traffic priority as mentioned above but also for real-time passenger information and vehicle tracking to ensure more ambitious service schedule; and clear, distinct branding and marketing [1].

Bus rapid transit vehicle A bus used in BRT service, typically with advanced features such as

aerodynamic styling, hybrid electric drive or other advanced propulsion, and real-time tracking systems, similar to what are now used in rail transit systems.

Buy America Provisions of federal transit law that govern purchases of goods with federal surface transportation assistance grants. Certain aspects of this policy date back to protectionist sentiments of the 1930s. In 1978, Congress stipulated that for purchases of rolling stock, these would be considered to be US made if they were assembled with at least 60% of components and materials by value supplied by US sources. The rules have been subsequently refined and subject to controversy several times since [3].

Capital assistance/expenditures Government subsidies for expenses related to the purchase of equipment and facilities, such as stations, buses, and trains; maintenance facilities; and support systems. Such equipment typically means property that has a useful life of more than 1 year. Capital expenses do not include operating expenses that are eligible to use capital funds.

Commuter rail service Regional-distance, usually locomotive-hauled passenger train service often sharing tracks with freight railroads. Chicago's Metra service is an example.

Federal Transit Administration A sub-cabinet-level government agency of the US Department of Transportation that administers a variety of grant programs that help fund bus and rail transit projects in US cities, Puerto Rico, and the US territories, as well as rural areas and federal lands.

Fixed-route bus service Traditional form of transit bus service, typically with frequent stops along a defined route. The bus services of the Chicago Transit Authority are an example.

Light rail transit (LRT) A form of urban rail public transportation that generally has a lower capacity and lower speed than metro (also known as heavy rail) systems, but higher capacity and higher speed than traditional streetcar systems. These rail systems are typically electrically powered, usually by overhead catenary. They ideally operate their own rights-of-way separated from other traffic but if necessary can also operate in mixed traffic on city streets [2].

Modal split Term of art in public transportation for market share. That is, the percentage of journeys taken with the various forms of public transportation, as compared with walking, bicycling, or the private automobile.

Operating assistance/expenditures Government subsidies for expenses associated with the operation of the transit agency and its passenger services, including vehicle operations (e.g., bus, train, "dial-a-ride," and vanpool services), vehicle and facility maintenance, and general administration (e.g., marketing, top management, insurance, and finance). Operating expenses also include salaries, wages, and benefits as well as outsourced services under contract.

Privatization In its strictest definition, it is the return of publicly owned and operated public transport services to the private sector. However, in the USA, it is also defined as the contracting of publicly owned services to private companies, private participation in the capitalization or ownership of these publicly owned services, or the franchising of these services to private firms.

Public transport service Bus and rail services operated either by public or private organizations on a scheduled or on-demand basis. These services are distinct from charters, which are hired for groups such as tours.

Public–private partnerships/models Synonymous with most definitions of privatization except the complete return of transit services to private ownership and operation with minimal oversight.

Purchased transportation services Bus and train service provided by others through a contract; also called contract service.

Rolling stock Industry term for buses and trains and other vehicles used in public transport service.

Transit-oriented development Land use patterns such as higher densities around BRT and rail stations that also contribute to greater transit usage on these systems.

Transportation Equity Act for the 21st Century Also known as TEA 21, the landmark surface transportation assistance law passed in 1998 that ended operating assistance for agencies that served urbanized regions with fewer than 200,000 residents. It also for the first time guaranteed a stream of funding for capital assistance over the 6-year period

in which the law was effective, which helped public transportation agencies better manage and plan their capital expenditures.

Travel time savings Industry term for the average estimated savings per trip on new transit systems as compared with the average travel time from a commute taken by an automobile or by the previous bus network serving the route.

Urban Mass Transportation Act The 1964 federal law that began the federal government's involvement in the oversight and financial assistance of regional, state, and local public transport services.

Vehicle maintenance Activities associated with bus, railcar, and support vehicle (e.g., fueling and repair trucks) maintenance (repairs and routine replacement of parts) and servicing (cleaning, fueling, etc.), also including inspection and oversight of these activities. In addition, vehicle maintenance includes repairs due to vandalism and accidents.

Vehicle operations Those activities associated with providing scheduled and on-demand passenger services, such as vehicle dispatching and scheduling, driver and technician training, ticketing and fare collection management, and system security.

Definition of the Subject and Its Importance

Increasingly, light rail transit (LRT) and bus rapid transit (BRT) are the two solutions cities throughout the world most often turn to in a broad variety of urban public transport applications to address a wide range of mobility challenges. While regional rail schemes (also called commuter rail in the USA and Canada) are also experiencing rapid growth, and many cities that have metros (also known as heavy rail in the USA and Canada) continue to expand their networks, LRT and BRT are even faster growing modes.

Whether LRT, BRT, metros, or commuter railroads, virtually all large cities in the developed world now boast at the very least starter urban passenger rail systems, in many instances restoring only partly the networks these cities had a century or more ago. Many of these have since supplemented the initial segments with a second wave of lines to build out their networks. Meanwhile, a growing number of midsize cities in the developed world, including a rapidly growing list of cities in developing countries, have also added networks. Call these stages the first two waves of the worldwide public transport renaissance. Now public transport infrastructure investment is entering a third wave of the renaissance, in which the growth of public transport investment becomes an essential and integral part of a nation's or a region's balanced transport strategy.

BRT is perhaps the fastest growing public transport mode in a century. Only 12 years ago, 17 US cities were selected by the then Federal Transit Administrator Gordon Linton to participate in his BRT Consortium. Just 5 years later, according to congressional sources, more than 50 and as many as 75 communities have a BRT project in some stage of development. Today, virtually every project seeking federal financial support, regardless of mode, also studies a BRT alternative, thus putting the mode on equal policy consideration with other public transport strategies.

The simplest and most often used definition of BRT is a public transport concept that "thinks like rail but uses buses." The interest in it is borne out of desire to offer increasingly congested cities a flexible, relatively inexpensive alternative to more highways or more expensive and longer-to-implement transit alternatives. Applications range from feeder systems to rail lines (e.g., Los Angeles) to downtown circulators (e.g., Orlando and Denver) to urban transport spines in their own right that can change the region's modal split and stimulate transit-oriented investment (e.g., Bogotá, Curitiba and Eugene, Oregon).

Similarly, applications of LRT range from spines for smaller cities that cannot justify the expense of metro systems to feeder systems to metros or regional passenger railways to circulators that often run in the street with other traffic. These last systems are often called trams or streetcars, as well. The flexibility of LRT also results in systems that operate in their own rights-of-way either underground, in elevated structures or at grade, as well as combinations of all of the above.

Since 1975, 23 cities in North America alone have fueled the rebirth of LRT development. Prior to that year, only seven cities had such services, as most were discontinued in favor of road and highway investments. LRT services now operate in 24 US cities, as well as three each in Canada and Mexico. Still more are under construction or in various other stages of development [4].

Introduction

BRT and LRT systems are being planned, constructed, and opened for service at a faster pace than previously, because these projects today tend to be smaller projects than metros, and as such are better suited for smaller applications, such as network spines for small cities, lines for suburb-to-suburb commutes – long the overwhelming share of journeys to work in the USA and a growing trend elsewhere as well – and for smaller-scale feeders to previously established systems.

In addition, these systems, particularly smaller, often street-running LRT lines known as trams or streetcars, but also BRT in a growing number of instances as well, serve as outstanding reshapers of the built environment and as economic catalysts.

They also help provide solutions to another worldwide trend: the aging of the population in the developed world. It has already taken hold in Japan, Europe, and Canada, and is becoming an increasing challenge of the USA. Older persons generally prefer to drive less, and they require smaller homes. Many also prefer to live nearer to better health-care services, nearer educational, cultural, and arts institutions, and otherwise "where the action is," or where their extended families are – that is, in cities.

This third wave is also driven by other powerful demographic forces. These include the population growth worldwide, as well as the concentration of that population in cities. This urbanization includes not simply the teeming populations of the developing nations, but also in the USA and other developed economies.

As a consequence, this current wave of public transport investment could be the largest expansion yet. However, as will be explained below, this third wave will require a different approach to project development and management.

BRT Developments

There are two major reasons why BRT has been so attractive to city planners. First, BRT projects are typically a fourth of the cost of comparable light rail projects. In addition, BRT can be implemented in roughly a third of the time – or even less – to design and build [5].

For example, the Los Angeles County Metropolitan Transportation Authority (MTA) built and opened its Orange Line BRT in the West San Fernando Valley to light rail standards (to enable a future conversion if it so chose) for $330 million; it took 3 years to design and construct, even with court-ordered stoppages to address neighborhood lawsuits that were concerned about noise, as well as delays caused by construction interruptions from one of the rainiest winters on record in the region. A roughly comparable LRT line in the service area, the Gold Line, took more than a decade to develop and opened at a cost of approximately $1 billion. Moreover, the Orange Line carries more weekday passengers than the Gold Line [6].

According to the US Senate's Banking Committee staff analyses, more than 50 American communities are developing BRT projects; that number grew with the addition of roughly 2 dozen BRT earmarks in SAFETEA-LU. The accompanying table provides a list of these projects.

Based on a BRT market study performed for the FTA in fall 2002 and updated in 2007 by the advanced transportation research consortium WestStart – CALSTART (Pasadena, CA), as many as five new BRT systems per year and/or ten new BRT corridors could open each year between 2007 and 2010 [7].

Interest in BRT outside the USA is even stronger. Based on success of the TransMilenio, which carries nearly two million boardings per weekday in Bogotá, the government of Colombia has launched a new policy to develop BRT in six other cities. Nearby Ecuador is also planning BRT lines in at least three of its cities. Cities in Peru and Chile are also planning systems.

These successes in many ways emulate the achievements of Curitiba, Brazil, which many point to where BRT began. Despite having the second highest automobile ownership rates in Brazil (only after the country's capital, Brasilia), approximately 70% of weekday journeys are on public transport, mostly on the city's BRT network.

In Asia, Beijing is in the throes of building a six-line network, which began as part of its preparations for the 2008 Summer Olympics; as many as a hundred more cities in China are studying networks, as the government there has included BRT as a transport solution for corridor applications whose volumes warrant less than a tram or light rail investment. The Korean Ministry of

Transport is not only involved in assisting several cities in network planning and construction, it is working with a manufacturing consortium to design and commercialize a next-generation BRT vehicle.

Several African cities view BRT as a cost-effective mobility solution in their plans to cope with rapid population growth, most of which is urbanization. Accra, Ghana as well as Johannesburg and Cape Town in South Africa have opened new systems (the latter two in preparation for hosting the FIFA World Cup this past summer).

India's Ministry of Urban Development has issued a new report, "National Urban Transport Policy," which encourages its lower-density cities to develop BRT. Accordingly, the ministry has approved BRT projects in Ahmedabad, Indore, Jaipur, and Pune.

Like South America, Europe and Australia were at the forefront of BRT and continue to witness new projects. In the UK, projects are part of Quality Bus Corridor projects, many of which featuring guided bus systems, including two in Leeds, and one each in Edinburgh, Ipswich, and Bradford. The next to open will be the world's longest guided busway, the 26-km Cambridgeshire Guided Busway built on an abandoned railway right-of-way between Cambridge and St. Ives. Manchester and Luton have also schemes in development.

The industry publication METRO has been tracking the growth of BRT in its annual "BRT 25" survey. Its most recent survey [8] found that the average project cost for BRT networks under development is $143.8 million for new projects.

Light Rail Developments

Though not as fast as BRT in recent years, growth in LRT systems around the world has also been impressive. In the USA, only 11 cities operated modern LRT or their historic counterparts, streetcar services. Today, more than 30 do, and many of those have opened additional lines to build out their networks [9].

In other North American and South American countries, the growth rate has not been as high as in the USA, but most either continue to operate the networks they started or have expanded them. In Mexico, LRT is available in Guadalajara, Monterrey, and Mexico City. In Canada, five cities operate such systems, including Toronto, Edmonton, Calgary, Ottawa, and Vancouver. A sixth, Waterloo, Ontario, is planning such a system.

A recent phenomenon has been the growth in planning, constructing, and opening streetcar lines (also called trams in Europe and some parts of Asia). Interest in streetcars represents a return to an old idea, mainly because of their history in attracting and focusing strong economic development adjacent to their lines. Indeed, the Smithsonian Institution's recent exhibit on public transport history explained that interurban streetcar lines were built throughout the USA to connect new real estate developments [10]. Henry Huntington became rich not just because of his Pacific Electric rail empire in Southern California but also because of similar, though smaller, enterprises in other parts of the nation [11].

Today's applications comprise either modern technology, such as the systems recently opened in Portland, Oregon, Seattle and Tacoma, Washington, and Nottingham, England, or the one opened in the early 1990s in Strasbourg, France; or heritage (or vintage) systems, such as the one in Kenosha, WI. However, most streetcar lines in the USA and elsewhere in the world employ modern vehicles and other technologies.

Interest in these two modes in recent years has been more intense than that surrounding light rail in the late 1970s and early 1980s and commuter rail in the 1990s, the last emerging markets in public transport. In fact, BRT and streetcars very likely will exceed the other US rapid transit markets not only in project cost but also in the number of projects, even at a time when these other public transport modes are also growing robustly.

In most of the developing nations, BRT will likely be the favored mode, while in many European nations light rail-based systems will be favored. Rail will also continue to be preferred in more densely populated cities of Japan, Korea, and China, though in these countries the mode of choice will just as likely be metro systems as LRT, particularly for the "backbone" lines of networks. However, BRT and tram systems will increasingly become surface network supplements even in these cities, creating stronger networks than benefit all modes of public transport – what telecoms and IT experts call "network effects."

This trend will continue if not accelerate for four fundamental reasons. First, throughout the world, there is a growing recognition that greater investment in public transport improvements is needed to cope with worsening congestion and increasing urbanization throughout the world. Shanghai, Bangkok, Abidjan, Sao Paulo, Mexico City, Cairo, and even Paris and London face ever-increasing metropolitan growth and its attendant problems. Indeed, a recent study found that every other person on the globe lives in a city and that by 2030 60% of the population will live in cities, 23 of them with more than 10 million in population [12]. Only a handful could be characterized as high density.

Second, BRT and streetcars are now considered legitimate tools in urban transport planners' toolkit. Third, BRT, but particularly rail-based public transport modes, are increasingly viewed as good catalysts for economic development, which can also attract private capital to build and operate these systems. Finally, growing fiscal pressures make smaller-scale and faster-to-implement projects more viable relative to more expensive and longer-to-deploy alternatives.

Each of these modes shares some characteristics, but each also has strengths and weaknesses relative to the other modes. For example, BRT is more flexible and typically faster-to-implement, more scalable, and less risky from a project management perspective. On the other hand, streetcars can attract private capital more easily, because their return on investment tends to be much higher – as much as 2–3 times higher – than BRT.

Current and Future Trends

Both rail-based and road-based public transport investments present a much different set of opportunities for policy-makers and thus will continue to require different strategies. These are briefly summarized below and elaborated upon later:

First, BRT and LRT projects in the future will tend to be smaller but many more will be developed. Each project will be smaller than the transit projects in the past, but there will be many more such investments than traditional, larger rail projects, even though all public transportation investments continue to grow rapidly. Implementation and management of these requires a more nimble and flexible oversight, one that is able to respond to changing conditions more quickly.

Second, such smaller systems will be implemented with much more interdisciplinary interaction not only within the project team but also with some different stakeholders. Often because they are far more likely to be built in smaller cities that have less technical expertise than their larger counterparts, BRT and streetcar systems will be implemented for project sponsors that will tend to rely more heavily on turnkey and concession-based project delivery methods, such as design-build, design-build-operate-maintain, and build-operate-transfer techniques to transfer project risk to private sector experts, accelerate or even help finance projects than with larger urban rail transport projects. This will require project sponsors and their contractors and other consultants, as well as city officials, professional planners, the business community, and other project stakeholders to analyze opportunities in a more interdisciplinary, collaborative approach.

Third, smaller projects will shift financing of them away from central government funding to more decentralized sources, including state, regional, and local governments and, increasingly, even private sources. The progress of this trend will depend on how each country's government is structured. In the USA, even though federal public transport assistance programs have recently been modified to better assist BRT and streetcar projects, they will likely rely less on federal support and more on state, local, or even private sources of funding, which will require different project management, outreach, government affairs, and financial planning strategies than larger projects. This is partly because the explosive growth in interest in such projects has already outstripped available funding. This resource competition combined with lower-average project costs and faster implementation for BRT and streetcars prompts many localities to bypass centralized funding and approval processes altogether.

In many countries, this is already the norm. For example, the central governments of Germany and France contribute well less than 50% of project cost. Moreover, private concessions are responsible for designing, constructing, and operating most new urban transport projects outside the USA [13].

Meanwhile, another interesting trend that has emerged has been the consideration of BRT designs

that can be converted at a future date to LRT. Although many cities have designed busways and bus rapid transit running ways that can be converted to future light rail operation, few cities have done so. Seattle's Downtown Transit Tunnel is the most recent such example.

Several cities, however, are beginning to look at BRT as an incremental step to future LRT, whether as political cover against criticism of rail advocates who see BRT as a lower quality investment or as a way to lay groundwork for an incremental strategy, when ridership and political support warranted a higher-capacity solution.

Various scenarios for designing BRT running ways to accommodate future light rail have been advocated and studied. An interesting recent experience occurred in San Francisco, where city planners there examined how its Geary Avenue Corridor BRT Project could be designed to accommodate light rail transit (LRT) at some point in the future. San Francisco County's Proposition K specifically envisioned that Geary, one of the busiest corridors in the city, accommodate a "BRT service with exclusive lanes and dedicated stations... designed and built to rail-ready standards." The San Francisco County Transportation Authority (SFCTA) staff concluded earlier that light rail was not financially possible within the provisions of the referendum's 30-year Expenditure Plan and thus drafted the plan in a way that required all center-running BRT design alternatives for Geary to be "rail-ready" [14].

Two center-running alignments with exclusive lanes were selected for detailed "rail-readiness" evaluation using three definitions of rail readiness. The first definition is a minimal package of design guidelines that would produce an alignment that does not preclude a future conversion to light rail; such an approach would use LRT-standard horizontal and vertical clearances, grades, adjacent tangents, and turning radii, as well as stations sited at locations that can accommodate a light rail platform (typically 180 ft vs. a typical 120 ft BRT platform).

The second definition goes well beyond this approach, to comprise a series of investments that would lead to LRT conversion much more quickly, with less incremental financial expenditure and fewer impacts to nearby businesses and transit riders. This definition includes the design criteria of the first definition, but would also provide additional design detail for surface and subsurface infrastructure, including all trackwork (rail, fasteners, and concrete supportive slab); all electrical and communications ductbanks, manholes, catenary pole and substation foundations for traction power cables and train control wiring; ductbanks and concrete boxes for stray-current protection against corrosion; any necessary drainage work; and utilities relocation needed, including work to preserve access by these utilities so as not to interrupt BRT service. This definition considerably narrows the differences between this version of BRT and the cost and construction considerations for light rail. The third definition used in San Francisco is between these extremes in the range of investments, though closer to the first definition.

Because of budget constraints as well as the fact that light rail for this corridor was not likely in the near future or even two decades after revenue opening of BRT, the first definition of rail readiness was selected by city planners. They were concerned that even though the other definitions' additional up-front investment obviated some construction when any decision was made to convert to LRT, the remaining construction needed for LRT would still require a great deal of development time as well as create disruptions to neighborhood businesses and residences [15].

This analysis comports with the experiences of other cities seeking to design BRT running ways for a future LRT. For example, the staff of the Metropolitan Transit Authority of Harris County, Texas (known locally as Houston Metro) returned to a policy that committed to LRT for all five of its future rapid transit lines, after it initially considered "rail-ready" BRT (which was even given a new term, "guided rapid transit") on four of these five lines under development.

Houston Metro staff had repeatedly made representations to the public that the lines can be converted without disruption to service, to include the rail embedded into the corridor and all systems except for the electric traction system [16]. In the end, however, it abandoned any "rail-readiness" strategy and opted to eliminate the incremental step [17].

The difficulties of designing BRT for a future LRT are underscored by the initial design of Seattle's Downtown Transit Tunnel. It was designed to accommodate LRT at some point in the future, and even

included rails embedded in the tunnel's roadway. Other important rail transit design elements were incorporated at that time, including rail-oriented horizontal and vertical geometry requirements, tunnel clearances for LRVs, station platform lengths to accommodate four-car LRV trains, station widths, and sizing of structural elements to support LRV loads.

However, LRT technology has changed significantly since the original tunnel's design in the late 1980s, in many ways which were not anticipated when the tunnel was designed roughly two decades ago. For example, the conversion, which was completed in late summer 2007, included a new LRT traction power system (with attendant retrofit of grounding and other corrosion protection), track and platform modifications to accommodate low-floor LRVs not available in North America at the time the tunnel was designed, upgraded fire/life safety systems to comply with toughened regulations, and improved train control and communications systems to support an integrated joint bus and rail operation. Importantly, the tunnel bed was also lowered to accommodate both low-floor LRVs and buses [18].

In addition, the bus service that used the DSTT was rerouted to the surface streets of the area during tunnel reconstruction. To minimize these adverse impacts, additional police officers were assigned at key intersections who supplement the police force that was also reassigned to surface bus operations. A large public information campaign was also launched to explain the transition. The cost of these measures combined with the retrofit work exceeded $100 million [19].

In all three scenarios of rail readiness studied in San Francisco, the most minimal "does not preclude LRT" approach would have cost $2.8 million more than the baseline cost estimate for a two-lane BRT center-running exclusive running way, or slightly less than a 3% premium. For the second scenario, total project costs would have approached nearly 100% more than a comparable baseline center-running BRT running way cost estimate. The third scenario of rail convertibility studied for the Geary Corridor, which includes more features than the first definition but not as many as the second, would have been approximately 10% more than the baseline design [20].

Importantly, some significant costs are excluded from these comparisons, however. For example, vehicles, commissioning and testing costs, and any necessary retrofit of maintenance facilities to accommodate future LRV designs, catenary and substation technologies are not included, because these technologies have been undergoing the most rapid evolution and are thus more difficult to project in the future [20].

Conclusion

When modern light rail systems were developed, the mode represented the avant-garde of the public transport renaissance, as a growing number of cities throughout the world planned and constructed LRT systems. That wave of the renaissance gave way to subsequent, more rapidly accelerating phases involving BRT and streetcars, as cities increasingly looked upon public transport and strategies that were central to addressing urbanization, congestion, sustainable mobility, and economic revitalization. Because those challenges will be no less daunting tomorrow, the public transport renaissance, particularly the part that includes BRT and street-running light rail, continues to be bright.

Bibliography

Primary Literature

1. Federal Transit Administration (2008) Bus rapid transit. Government Printing Office, Washington, DC
2. American Public Transportation Association (2005–2010) Fact book. American Public Transportation Association, Washington, DC
3. Committee on Rules, United States House of Representatives, U.S. Congress (2005) Safe, accountable, flexible and efficient transportation equity act: a legacy for users: report of the conference committee. U.S. G.P.O, Washington, DC
4. Schumann JW (2010) Status of North American light rail transit systems: year 2009 update, joint international light rail conference: growth and renewal, 19–21 Apr 2009, Los Angeles, California. Transportation Research Board, Transportation Research Circular E-C145, July 2010, p 3
5. U.S. General Accounting Office (2001) Mass transit: bus rapid transit shows promise: report to Congressional Requesters, GAO report #GAO-01-984. GAO, Washington, DC
6. Metropolitan Transportation Authority (MTA) (2005) FY03-FY07 metro strategic performance plan (Updated FY05). Metropolitan Transportation Authority, Los Angeles
7. Kantor D, Peak M, Wnuk L (2008) Analysis of BRT vehicle market and ridership trends. WestStart-CALSTART, Pasadena
8. Schlosser N (Apr 2010) New BRT projects gather momentum across the U.S. Metro, p 22

9. Schumann, ibid, p 4
10. Smithsonian Institution (2005) American on the move: streetcar city, Washington, DC: growth of the capital's suburbs. http://americanhistory.si.edu/onthemove/exhibition/exhibition_4_7.html. Accessed 12 Sept 2005
11. Richmond J (2005) Transport of delight: the mythical conception of rail transit in Los Angeles. The University of Akron Press, Akron
12. Union of International Public Transport (2003) Ticket to the future: three stops to sustainable mobility. Union of International Public Transport, Brussels, March
13. Henke C (1996) The french answer. Metro, May–June
14. San Francisco County Transportation Authority (2006) Geary corridor bus rapid transit design principles & guidelines, approved by Geary Citizens Advisory Committee, 1 Dec 2006
15. Kirschbaum J, Chang T (2005) ACTION – adopt a motion to approve the proposed approach to the concept of rail-ready design in the Geary BRT study and the proposed Q&A language, memorandum to the Geary Citizens Advisory Committee, 18 Feb 2005
16. (Aug 2005) Convertible transit. Railway Age
17. Sallee R (2005) Metro told using buses over rail hurts credibility. Houston Chronicle, 28 June 2005
18. Parsons Brinckerhoff Quade, Douglas Inc. (2005) Sound transit long-range plan update, issue paper no.5: convertibility of BRT to light rail, prepared for sound transit, Mar 2005
19. Wood E, Shelton DS, Shelden M (2005) Designing BRT for LRT convertability: an introduction for planners and decision-makers, presented at the annual meeting of the transportation research board, Washington DC, final version Nov 2005
20. Parsons Brinckerhoff Inc., Technical Memorandum to San Francisco County Transportation Authority (Feb 2008) Geary BRT rail readiness analysis

Books and Reviews

Bill Millar (president of APTA) (2004) Testimony before the subcommittee on transportation, treasury & independent agencies, committee on appropriations, U.S. house of representatives, 19 Mar 2004

Congressional Budget Office (1981) The effect of OPEC oil pricing on output, prices and exchange rates in the United States and other industrialized countries. Government Printing Office, Washington, DC, February

Cudahy BJ (1990) Cash, tokens and transfers: a history of urban mass transit in North America. Forham University Press, New York

Dittmar H, Ohland G (2004) The new transit town: best practices in transit-oriented development. The Island Press, Washington, DC

Jackson RJ, Kochtitzky C (2002) Creating a healthy environment: the impact of the built environment on public health. Sprawl Watch Clearinghouse, Washington, DC

Shapiro RJ, Hassett KA, Arnold FS (2002) Conserving energy and preserving the environment: the role of public transportation. American Public Transportation Association, Washington, DC

Shelby RC et al (2003) Bus rapid transit and other bus service innovations: hearing before Senate banking, housing and rban affairs committee. U.S. G.P.O, 24 June 2003

Small K (2005) Unnoticed lessons from London: road pricing and public transit. Access 26(Spring):10–15

U.S. Department of the Treasury and Council of Economic Advisers (2010) An economic analysis of infrastructure investment. Government Printing Office, Washington, DC, October 11

Bus Rapid Transit, Institutional Issues Related to Implementation

Mark A. Miller
California Partners for Advanced Transit and Highways (PATH) Program, Institute of Transportation Studies, University of California, Berkeley, CA, USA
Institute of Transportation Studies, School of Public Affairs, University of California, Los Angeles, CA, USA

Article Outline

Glossary
Definition of the Subject
Introduction
Institutional Issues: A Broad Perspective
Institutional Issues: Stakeholder Experience
Future Directions
Acknowledgments
Bibliography

Glossary

Dual-mode buses Buses that operate under both manual and partially-to-fully automated control.

Intelligent transportation systems A system or service designed to make the movement of people or goods more efficient, safer, more economical, and less polluting. Such systems work by applying advanced and emerging technologies in information processing, communications, and electronics to surface transportation needs. People can use these systems or experience their influence at home, at work, driving in his/her automobile, waiting at a bus stop, crossing a street, riding on

a bus, or looking for a parking space. Examples of ITS technologies with transit applicability either already deployed in particular settings or at least under investigation, include advanced vehicle identification systems, electronic fare payment systems, interactive trip planning systems (kiosk, personal computer), transit signal priority systems, safety and security systems, intelligent vehicle systems (e.g., collision warning systems (frontal, side, and rear), precision docking, and lane-keeping assistance systems) and operations management systems (e.g., computer-aided dispatch system, automatic vehicle location systems, automated scheduling and dispatch software, automatic passenger counter systems, and vehicle component monitoring systems).

Multimodal Involves more than one mode of transport for passengers.

Quality of service The overall measured or perceived performance of transit service from the passenger's point of view.

Stakeholders A person, group, or organization that has direct or indirect stake in an organization or enterprise because it can affect or be affected by that organization's or enterprise's actions, objectives, and policies. Key stakeholders in the implementation of a bus rapid transit system include public transit agencies and municipal or state departments of transportation.

Technology push/market pull A term customarily used in a company's business strategy for a new product or innovation that implies that a new invention is pushed through research and development (R&D), production, and sales functions onto the market without proper consideration of whether or not it satisfies a user need. On the contrary, an innovation based upon market pull has been developed by the R&D function in response to an identified market need.

Transit choice riders Riders who choose to use transit for their trip making, particularly during peak travel time periods for work-related trips, even though they have other means of travel, especially a motor vehicle, available to them. Such riders may choose transit over other modes for a variety of reasons, including saving money, avoiding driving in congested traffic, being able to use travel time productively for other activities, and helping the environment.

Transit-oriented development (TOD) A mixed-use residential or commercial area designed to maximize access to public transport and often integrates features to encourage transit ridership.

Definition of the Subject

Bus rapid transit (BRT) is an innovative, high-capacity, lower-cost public transit travel mode that can improve urban mobility to help make bus transit more attractive by enhancing customer quality of service with an ultimate goal of increasing ridership that contributes to relieving traffic congestion. BRT systems can easily be customized to community needs and incorporate state-of-the-art, low-cost technologies as part of their flexible and incremental implementation approach.

For purposes of this entry, the following definition of bus rapid transit taken directly from [1, 2] is used:

- Bus rapid transit is a flexible, rubber-tired form of rapid transit that combines stations, vehicles, services, running ways, and intelligent transportation systems into a fully integrated system with a strong image and identity. Bus rapid transit applications are designed to be appropriate to the market they serve and their physical surroundings, and they can be incrementally implemented in a variety of environments (from rights-of-way totally dedicated to transit to streets and highways where transit is mixed with traffic).

Running ways for BRT include mixed traffic lanes, curbside bus lanes, and median busways on city streets; reserved lanes on freeways; and bus-only roadways, tunnels, and bridges. Most stations are located curbside or on the outside of bus-only roadways and arterial median busways. Similarly, BRT stations have low platforms since many are already being served or are planning to be served by low-floor buses. Conventional standard and articulated diesel or compressed natural gas buses are in wide use for BRT operations, and there is a continuing trend toward innovations in vehicle design, including environmentally clean or green vehicles; dual-mode operations in particularly appropriate settings such as tunnels; low-floor buses; more and wider doors; and use of distinctively branded bus rapid transit vehicles and stations. Service innovations

include fare-collection procedures and station design. Intelligent transportation systems range from existing and more customary automatic vehicle locations systems, transit signal priority systems, and passenger information systems to more advanced systems including intelligent vehicle systems.

Introduction

Though there has been renewed interest in its use, bus rapid transit is not a new concept. A brief discussion of the beginnings of bus rapid transit is presented in this section of the entry to provide an historical context of BRT to better appreciate from where their institutional issues derive (section "Institutional Issues: A Broad Perspective").

The Origins of the Bus Rapid Transit Concept

As early as the 1930s in the USA, bus rapid transit was suggested in a transportation plan for Chicago, Illinois, that called for converting rail rapid transit lines to express bus operation on certain highways with on-street distribution in the central business district (CBD) [1]. In the late 1950s, transportation agencies looked for ways to implement high-quality, low-cost transit service; for example, in a 1957 study [3], California investigated high-speed bus operations for commuter travel in the San Francisco Bay Area. The proposal called for using a freeway – then under construction – for high-speed bus service utilizing what was then considered modern improvements including park-and-ride lots, pedestrian friendly designs, and improved amenities. The report acknowledged that BRT was the "most economic form of rapid transit that can be operated in this area under present conditions" [3].

Design studies for bus rapid transit within freeway medians were developed in the late 1950s in the Washington D.C. area, which recommended that "in planning of future radial freeways a cross section . . . be provided to afford maximum flexibility and reserve capacity for vehicles as well as for the mass movement of people" [1]. In 1959, the St. Louis, Missouri transportation plan included an 86-mile bus rapid transit system, of which 42 miles were to be special grade-separated bus roadways. The focus of this proposal was an elevated loop road circling downtown St. Louis [1].

In 1963, Crain [4] presented a BRT concept, calling for transportation planners to devise new transit services that replicate the high performance, door-to-door service offered by automobiles, while remaining within the economic reach of most cities. Such a system, Crain states, "combine(s) the best features of rail rapid transit and conventional bus operations by retaining the flexibility of one while obtaining some of the speed and capacity of the other" [4]. Crain also described the use of exclusive lane use and preferential traffic controls for the rapid bus concept. People-throughput capacity of such a service was also emphasized in order that this concept be effectively sold to politicians and the public [4].

Crain promoted most of the features that are being incorporated into today's BRT systems including exclusive lanes, transit signal priority, rapid fare-collection techniques, quick boarding and alighting, and enclosed pre-boarding payment stations. His preliminary cost estimates showed BRT producing high-capacity service (10,000–20,000 passengers per hour) at a fraction of the cost of rail. His estimates also showed that BRT would cost only 2% of the cost of rail for at-grade BRT service and only 10% the cost of rail for an elevated BRT system [5]. He also discussed the importance of providing up-to-the-minute schedule information to passengers (a precursor to today's automated vehicle location systems and passenger information systems technologies), the importance of overcoming the negative sentiments of transit (bolstering its image), and the need to properly sell the service (marketing). All of these concepts have been incorporated into what we today know as bus rapid transit.

In 1970, Milwaukee, Wisconsin, proposed a transitway plan that included 107 miles of express bus routes over the freeway system and an 8-mile, east–west transitway equipped with 39 stations (excluding downtown) and 33,000 parking spaces [6].

Dual-Mode Systems

Several additional reports from the 1960s outlined many of the same goals and operational characteristics sought in today's BRT but envisioned an even more sophisticated system. Many of the BRT concepts that were explored during the late 1960s and early 1970s focused on providing BRT with, at least, partial system

automation. The most common concept involved the use of dual-mode buses. The idea was to combine the flexible collection and distribution capabilities of a bus system with the high line haul performance of an exclusive right-of-way rail system, all with a single seat trip and utilizing automation technologies. The most emphasized features of the systems during this period tended to be full bus automation (for a portion of the route) and exclusive right-of-way of the line haul segment. The hope was that this automation component would permit a reduction in operating costs by eliminating the need for a driver for a portion of the trip, while providing greater line haul capacity than could be achieved through manual driving alone. Meanwhile, exclusive right-of-way (busway or bus lane) would remove the vehicle from the most heavily congested portions of the trip, and permit higher operating speeds, making the transit trip more attractive. Interest in the dual-mode concept at the time declined due to (1) insufficient technological capabilities for cost-effective automation of vehicles, (2) operational savings based on the assumption that the vehicle would be "driverless" for the trip's line haul portion was problematic, and (3) costs of grade separations envisioned for busways greatly reduced the capital-cost savings as compared to a rail system [6].

Early Busways

During the 1960s and early 1970s, bus rapid transit projects were implemented in several regions within the USA, though appeared to be diluted versions of Crain's original concept. Most bus services that were implemented utilized exclusive bus lanes on freeways, but none really utilized a mix of multiple strategies. These projects, therefore, functioned merely as express bus services, whose effectiveness depended primarily on congestion free bus lanes to provide most of the operational improvements. The most notable projects during this period were the (1) Shirley Busway in Washington D.C. [7, 8], (2) El Monte Busway in Los Angeles, California, (3) Holland Tunnel bus lanes in New Jersey and New York, and (4) bus lanes on various bridges in the San Francisco Bay Area. Most of these facilities were eventually converted into high occupancy vehicle (HOV) facilities to improve their utilization. Primary factors that contributed to these systems not utilizing the entire BRT toolbox of strategies include (1) insufficiently developed or cost-effective technologies and (2) lack of political will to champion their use. Domestically, during the following two decades interest in BRT generally waned as the US transit industry's mode of choice for high traffic corridors tended toward rail-based projects [6].

International Experience

During the 1960s, Curitiba, Brazil, experienced rapid population growth of approximately 3% per year due to large in-migration from rural surroundings resulting in overwhelming traffic congestion. A 1965 regional plan called for the establishment of developmental policies for transportation whose goal was to encourage growth patterns that would be sustainable and supportive of a viable public transit system. The plan called for a mono-centric city with four radial corridors that would bear most of the burden of growth and development in the region. Lacking adequate financial resources for a rapid rail "Metro" system, an approach taken by many of its larger neighboring Latin cities, Curitiba opted for a Bus rapid transit system. Whereas, an underground Metro was priced at approximately $60–$70 million dollars per kilometer ($97–$113 million dollars per mile) (*1,965 $US*), the express bus roadways were only $200,000 per kilometer ($323,000 per mile) [9–11].

The busway opened for service in 1972, and incorporated many, if not most, of the features outlined in Crain's paper [4, 5]. The system relied on features such as a high or raised boarding platform to match the vehicle floor height [12], pre-boarding fare payment, signal priority, onboard automated announcement systems [12] and high-frequency service to ensure high-quality Metro-like service. Over the last 30 years, Curitiba has been able to incrementally expand and upgrade the system as funding allowed and demand warranted. Instituting strong land use controls, the government has also been able to effectively guide growth to encourage development patterns along structural axes that reinforce and encourage use of the bus system. This has kept Curitiba's central city both a vibrant and a pleasant urban environment.

With the success in Curitiba, several other developing Latin American cities such as Sao Paulo, Brazil,

Porto Alegre, Brazil, and Quito, Ecuador, have since implemented systems based on the Curitiba public transit model.

Similarly, Ottawa, Canada also turned to the Bus rapid transit concept when it decided to upgrade its transit system. Ottawa made the decision to use the bus as the backbone of the city's transit system, and started its "Transitway" in 1973 with approximately 6.8 miles of bus lanes. By 1983, the first of several busways were opened providing buses with exclusive, grade-separated right-of-way. By 2000, the system utilized 16 miles of exclusive right-of-way, approximately 7.8 miles of priority lanes, and 2 miles in mixed traffic with nearly 200,000 trips per day capable of carrying 10,000 riders per hour in each direction [6, 13].

The Transitway has features that make it special. In the outlying areas away from the urban core, the Transitway's right-of-way is an exclusive bus lane that is at- and above-grade depending on location usually with one lane per direction. At each station, the right-of-way expands to two lanes per direction to allow for buses to stop without blocking other buses. Moreover, at some locations, the exclusive right-of-way is directionally separated by barrier or a grassy median. In a few locations, the bus uses the freeway for short distances (1–2 miles) in an exclusive bus lane. This lane is the freeway's right-most lane that is an exit-only lane for use only by Transitway buses. It is separated by means of a virtual barrier with diamond symbols painted on the bus lane. Some of the Transitway's stations have similarities to rapid rail stations, not in the sense that they are underground (in fact, there is only one tunnel station on the Transitway's route), but that they are infrastructurally extensive. For example, some of these stations are adjacent to commercial office development and are linked together via enclosed walkway bridges. At one location, the Transitway has a stop immediately outside a major department store that is part of a suburban mall. The extensively built stations are fully enclosed to accommodate Ottawa's winter weather with multiple stops for entry onto and exit from buses. Also, bus routes for non-Transitway lines converge at several of the Transitway's stations. In addition to the Transitway's connection with Ottawa's International Airport, it also connects with Ottawa's central train station via an enclosed walkway bridge linking the two stations [6].

Ottawa is typically heralded as another shining success story for bus rapid transit and several other Canadian cities have since embraced this concept. Though most do not use exclusive right-of-way, projects in cities such as Montreal, Quebec, and Vancouver, British Columbia have turned toward advanced technologies, in lieu of exclusive facilities, to achieve higher bus performance.

The Return of Bus Rapid Transit to the USA

During the late 1970s, BRT made a comeback to the USA with the implementation in Pittsburgh, Pennsylvania of the first of three major segments of its busway system. In 1977, the 4.3-mile South busway became operational followed in 1983 by the 6.6-mile East Busway with a 2.3 mile extension in 2003; in 2000, the West busway – 5 miles in length – officially opened. This busway system, combined with several new Light Rail Transit projects, has produced an integrated, multimodal system for the greater metropolitan Pittsburgh area [14]. Bus rapid transit success stories in cities such as Curitiba, Ottawa, and Pittsburgh, coupled with continuing congestion and air pollution in urban areas have sparked a renewed interest in the bus rapid transit concept. In 1998, the US Department of Transportation's Federal Transit Administration initiated support for ten BRT demonstration projects, which helped generate further interest in bus rapid transit [15–17].

Contents of This Entry

This entry begins with a discussion of institutional issues associated with the implementation of bus rapid transit systems from a macroscopic perspective. Initially, issues were organized into categories including, for example, intergovernmental and interorganizational, political will, and land use. The subsequent discussion of each category follows with a listing of specific institutional issues within each category.

The entry then turns to a more focused look at specific institutional issues that, based on experience, stand out from other issues relative to the following two criteria: level of importance and level of difficulty to resolve. Specific examples are provided in this section of the entry to illustrate issues.

Institutional Issues: A Broad Perspective

The implementation of bus rapid transit systems traverses numerous stages consisting of system design, development, testing, evaluation, and deployment culminating in a completed and fully operational system. Moreover, all these activities take place in a context with organizational stakeholders participating at various levels. In fact, an overriding theme running through the BRT implementation process is the notion of stakeholders, their agendas, and the relationships among them. As each stage of BRT implementation proceeds through its more technological, design, and operational aspects, questions may arise concerning the effects of actions taken or policy decisions made, which are often of a nontechnical nature and usually referred to as *institutional issues*. These less-technical and less-operational issues, which are numerous and diverse, need to be considered and effective arrangements made that address them to successfully implement a bus rapid transit system.

Bus rapid transit systems will not necessarily experience the same set of institutional issues because each BRT deployment will be affected by local and regional factors. Moreover, even when the same issues arise in different settings, there will likely be local and regional site-specific differences. The importance of identifying and working out such issues should not be underestimated as they do contribute to the overall success of implementing bus rapid transit systems in terms of how transit operations and quality of service for passengers are enhanced.

Institutional issues may be grouped into the following general categories [6]:

- Intergovernmental and Interorganizational
- Intra-agency
- Political Will
- Public Relations and Marketing
- Funding and Finance
- Labor and Human Factors
- Safety and Liability
- Land Use and Planning
- Physical Environment

Intergovernmental and Interorganizational

It is rarely the case that a transit agency can develop a bus rapid transit system without the coordination and cooperation of multiple agencies and often overlapping governmental jurisdictions. Even if this were possible, there is benefit in seeking the cooperation and support of other agencies. However, the multi-jurisdictional and/or multi-stakeholder aspects can make the process of decision-making and implementation more complex as each stakeholder usually brings their own philosophies, priorities, and agendas to the table. Achieving agreement among all affected stakeholders – whether political jurisdictions or other transportation organizations – often proves to be a difficult task. To have a system that works effectively requires the transit agency to achieve agreement with localities and other agencies on infrastructure, operations, and responsibilities.

When planning for the deployment of bus rapid transit systems, there are, at a minimum, two distinct types of stakeholders with primary roles. One is the local and/or regional transit agency whose interest lies foremost in reducing its own costs while also enhancing the quality of transportation services that it delivers to its passengers. The other primary stakeholder is the local and/or regional highway and traffic department along the route the transit agency's bus runs and this latter stakeholder could include multiple operators depending on whether the bus runs through multiple political jurisdictions. Other stakeholders with a role to play in the implementation of bus rapid transit might also include the following agencies and/or organizations [18]:

- Municipal environmental, health, and urban development and public works departments
- Construction industry and other potential industry supporters
- Regional and/or metropolitan planning organizations
- State or provincial department of transportation
- Relevant national or federal transportation agencies, for example, in the USA such agencies include the Federal Transit Administration and Federal Highway Administration
- Advocacy groups, for example, proponents of competing or complimentary rail projects
- Motorists and their representative organizations
- Economic development agencies
- Business and merchant associations

- Neighborhood or corridor resident associations
- Traffic and transit law enforcement
- Public transportation experts and consultants
- Nongovernmental organizations
- Public transportation passengers, for example, the Bus Riders Union in Los Angeles, California
- Nonmotorized transportation users
- General public

The significance of these stakeholders' roles and influence depends on local and regional conditions encompassing the bus route/traffic corridor where the bus rapid transit system is to be implemented.

Typically, a public transit agency will interface with other government agencies during regular service discussions; however, these interfaces become more critical with the development of a bus rapid transit system; it is typical for a public transit agency to need to coordinate with an organization it had not worked with prior to the bus rapid transit project. These agreements should set out agency and staff responsibilities giving particular attention to the clarification of roles. Achieving consensus, let alone agreement, among all affected stakeholders, whether political jurisdictions or other transportation organizations may at times prove to be a challenging and possibly difficult task. To have a system that works effectively requires the transit agency to achieve agreement with localities and other agencies on infrastructure, operations, and assignment of responsibilities. However, the primary objectives of transit agencies – to provide high-level, high-quality service for their customers at minimum cost – may conflict with the objectives of highway and traffic agencies whose performance is often judged more on enhancing vehicle-moving than people-moving capacity. These often-competing objectives can complicate the implementation of bus rapid transit strategies and may require significant coordination and cooperation if multiple transportation and traffic agencies are involved. An example of conflict of objectives occurs when a BRT project is planned to operate in mixed traffic on public running ways such as when working to achieve the operational benefits of BRT service, preferential treatment on the running way is often required.

The selection and incorporation of new BRT infrastructure may also prove difficult. For many projects, public transit agencies are "tenants" of streets or highway departments, often dependent on the cooperation of the roadway operator for the right to use their infrastructure such as the roadway, signal poles and boxes, etc. Many BRT strategies also utilize infrastructure, which not only needs to be incorporated into the existing roadway facilities, but must be operated and maintained as well. With new infrastructure come additional financial responsibilities. Reaching agreement on acceptable designs, and operational and maintenance responsibilities would likely involve coordination among these agencies.

Bus rapid transit operations will be effective only if laws and regulations regarding transit prioritization are enacted, adhered to, and enforced. Effective enforcement carries with it financial responsibilities that may be thrust reluctantly upon local jurisdictions. Infrastructure and enforcement are two factors vital to the success of BRT, which often lie outside the control of the transit agency. Enlisting the support of the affected parties in these two areas may ultimately determine the success and effectiveness of the BRT system.

Bus rapid transit prioritization may also occur at the expense of other roadway users such as in the case of queue jump lanes. This issue will require discussion and agreement on where and how these preferences should be given, while considering its impact on existing roadway operations. Any impacts to existing services will require the consent and support of highway agencies or street departments, and local governments.

Finally, in attempting to make a seamless transit system, BRT services should be coordinated with neighboring transit agencies. This may require them to revise their operations and schedules to provide better feeder services for the BRT system.

The number and complexity of the agreements will depend upon the type of facility and the governmental organization(s) in the area. There are generally a number of elements of the system that are out of the control of the transit agency. Cooperation among agencies is critical to the successful introduction and operation of a BRT system. In these cases, it is necessary to define and codify these responsibilities. Intergovernmental agreements will be required with a number of different agencies covering items such as right of use (how long, conditions for extension or termination of agreement, state in which the facility is returned to the

appropriate agency, legal responsibility, watering maintenance of landscaping, maintenance of running ways, trash collection, graffiti removal, advertising, enforcement, signal timing, lighting). In some cases, local or state laws may be enacted, repealed, or modified to implement various BRT elements or practices, such as the use of the BRT facility by emergency service vehicles.

A specific example to illustrate this type of institutional issue brings together technological aspects, operational plans, and institutional concerns of implementing bus rapid transit. For Los Angeles' Wilshire-Whittier Boulevard Metro Rapid service, which opened in 2000, the Metropolitan Transportation Authority (MTA) implemented a number of bus rapid transit features as elements of its Metro Rapid service including transit signal priority along the heavily traveled corridor, which traverses the cities of Santa Monica, Beverly Hills, and Commerce in addition to the city of Los Angeles and each of these municipalities controls traffic signal operation within their respective jurisdictions. Moreover, along the corridor, the municipal boundaries are such that the city of Los Angeles is interspersed among the other three municipalities in a noncontiguous fashion. Thus, for the Wilshire-Whittier corridor, MTA and the four traffic signal operators, that is, the local municipalities, are the primary stakeholders. Initially, transit signal priority was implemented only within the city of Los Angeles as the other cities wanted demonstrative proof of transit signal priorities' benefits before relinquishing control over the operation of traffic signals in their jurisdictions. To date, transit signal priority still remains implemented only in the city of Los Angeles while negotiations between MTA and the other jurisdictions continue.

The following list summarizes intergovernmental/interorganizational institutional issues:

- Integration of multiple priorities, objectives, and agendas
- Impacts of BRT on roadway operations
- Streets/highway departments "relinquishing" control of their infrastructure
- Agreement on performance measures
- Maintenance responsibilities for shared infrastructure and hardware/software
- Responsibility for enforcement on bus lanes/busways
- Institutional fears of new technologies
- Coordination on selection and implementation of technologies
- Coordinating other transit agencies' services and BRT operations

Intra-agency

Institutional issues may arise not only among transit agencies, political jurisdictions, and highway traffic agencies, but also internally within an individual transit agency. Concerns over preferences in funding and scarce resources, the delegation of responsibilities, and increased responsibilities for staff may result in internal resistance and morale issues for a transit agency. Unless there are additional funding sources available, increased spending on one route will usually mean decreased funding on others.

Bus rapid transit systems may require additional resources to support the service offered. Additional operations, new technologies, new vehicles, and new infrastructure will require training and maintenance. Achieving agreement on roles and responsibilities may be difficult if employees are merely required to shoulder additional duties and responsibilities for BRT without additional compensation or support.

Many transit agencies may still be unfamiliar with at least a portion of available BRT strategies and agencies may need time and resources to locate or develop both design and operational standards for many of these strategies. Initiating BRT service may also require additional work to reschedule existing services to support the BRT system. As many BRT systems will operate as trunk lines, feeder services will need to be coordinated to achieve the full benefit of the system.

Even gaining internal agreement on what strategies should be implemented, what fare structures should be used, and what technologies are appropriate will again require time and resources. Many agencies will need additional time to identify and digest best industry practices for these issues. Even then, identifying and attempting to accommodate a transit agency's departments' needs may cause internal conflict. As new strategies may affect the duties of department staff, it is vital

that they are consulted and strategies are selected with their concerns in mind.

The following list summarizes intra-agency institutional issues:

- Concerns (or perceptions) that BRT is given special preference over other transit services
- Defining and agreeing on new roles, responsibilities, and organizational structures to support BRT
- Creation of design and operational guidelines for BRT
- Determining an appropriate fare structure and medium
- Internal coordination on selection of technology
- Coordinating schedules of other transit routes with BRT operations
- Insufficient understanding of the "state of the art" of technologies and how they can be used in BRT operations

Political Will

The deployment of a bus rapid transit system is one of many stages in the process of design, development, testing, evaluation, and finally deployment of a completed system. At each stage, decision-making stakeholders are involved in a variety of ways that impact the specific deployment path a particular bus rapid transit system will take. The decision-makers are by definition major players in the political arena that govern the local jurisdictions in which the bus rapid transit system would operate. The commitment to bus rapid transit by such major players is of crucial importance to the success of a bus rapid transit system.

One concern in the political arena may be whether a proposed bus rapid transit system is a solution in search of a problem, whether appropriate technologies are being used, and whether there is a market for these enhanced bus transit services. Does it result from a technology push or market pull?

To establish and sustain a high level of interest and commitment to BRT, a political champion will likely be required. Whether it is an individual or organizational entity, a political champion would aid in coalition building and sustaining interest in BRT, which could wax and wane with the whims of the political process. The strength and capability of the political champion would help determine if the project could weather the political storms of opposition arising from various quarters, for example, the local business community, the mass media, or local residents. However, gaining such championing decision-makers often requires proof of the operational and quality-of-service benefits of BRT, but political support is required to perform the testing that could result in the quantifiable benefits, resulting in a chicken-or-the-egg dilemma requiring resolution.

There may also be issues regarding legislative restrictions on the procurement of new vehicles that could delay or slow deployment of BRT. Legal issues may also arise as a result of changes in service associated with BRT operation. For example, route changes, the elimination of stops, or lengthening the distance between consecutive stops could potentially present legal challenges.

Many political officials may be reluctant to undertake a bus rapid transit project due to the perceived risks, especially in relation to upsetting powerful special interest groups. For example, motorists and existing public transportation operators may tend to resist such change. Thus political officials may end up playing it safe by avoiding any type of major public transportation initiative that will risk alienating specific stakeholders. However, when officials take the perceived low-risk path of inaction or very slow action, the ensuing political rewards will certainly be reduced [18].

The following list summarizes politically related institutional issues:

- Concerns of BRT being a top down solution
- Perceived or actual competition of BRT with rail transit
- Lack of domestic BRT success stories
- Lack of empirical evidence of BRT's operational effectiveness
- Finding political champions to support BRT
- Concerns over long-term level of interest, potential for waning
- Local and business community opposition to the removal of, or restrictions on, parking spaces for BRT use
- Local and community opposition to BRT

- Concerns over the distribution of the costs and benefits of BRT
- Legal issues associated with service changes
- New vehicle procurement

Public Relations and Marketing

The success of implementing a bus rapid transit system, as with nearly any new product, service, or system, largely depends on how well it is sold to the public, which often requires setting expectations. Setting high, yet realistic expectations is crucial to gain support for BRT. Failure to produce what was promised could lead to disappointment and a loss of public confidence and support. Bus rapid transit may also require a significant public education campaign on interacting with new transit agency strategies, features, and technologies such as bus lanes, signal priority systems, queue jump lanes, and new fare-collection systems. Moreover, the transit agency needs to consider public views about its current performance. Before taking on the additional responsibilities of a BRT system a transit agency must ensure it is performing satisfactorily, or it could face political and public opposition as it embarks on new ventures [19].

The following list summarizes public relations and marketing institutional issues:

- Educating the public on BRT, and managing perceptions and expectations
- Concerns over transit agency's existing performance and reputation
- Concerns over effects of BRT on existing roadway operations
- Educating pedestrians and motorists on interacting with BRT
- Educating users on changes in and uses of multiple fare structures

Funding and Finance

During the 1960s and 1970s, interest in BRT in the USA waxed and waned. Though there is renewed interest, the fear of history repeating itself in the USA may still cause concern among transit agencies considering BRT for their communities and lead to their reluctance to embrace bus rapid transit. Though the up-front capital costs for most BRT projects are relatively small compared to other capital-intensive modal alternatives such as rail, transit agencies will still be responsible for the operations and maintenance of the new system. With continued fiscal pressures facing transit agencies, concerns may arise over the long-term financial commitment to bus rapid transit. Similarly, bus rapid transit will also require additional financial commitments for staff, training, and enforcement [19].

The following list summarizes funding- and finance-related institutional issues:

- Concerns over long-term funding commitments to BRT at the state and federal levels
- Concerns about BRT redirecting funds away from existing service or other routes
- Lack of understanding of funding mechanisms available for BRT
- Agency reluctance to expand services due to current fiscal constraints
- Ability to use existing buses or need for new fleet
- Capital costs of BRT
- Cost of operating and maintaining (O&M) new technologies and infrastructure
- Cost of additional staff and/or training to support BRT
- Cost of additional facilities to support BRT
- Cost of and responsibility for enforcement, for example, proof of payment

Labor and Human Factors

Another important stakeholder group that must be considered for bus rapid transit is the transit agency staff, especially bus drivers. What will be the impact of bus rapid transit on bus drivers? With the implementation of bus rapid transit, there could be concerns over additional work and responsibilities without assurances of additional staff, needed resources, and/or pay. Bus drivers would have a direct and potentially the closest connection of all agency employees to any new technologies implemented as part of a bus rapid transit system. How would such technologies affect bus drivers? Would it mean any change in the roles and responsibilities of their job? Could the implementation of a bus rapid transit system mean that some bus drivers would lose their jobs or be replaced by individuals with more familiarity with and experience in the use of certain technologies? Will there be assurances to

retrain and reeducate bus drivers to use these new systems?

Another concern of bus drivers could be the use or perceived misuse of technology by transit agency management for driver performance monitoring. Drivers may fear their employers using "Big Brother" privacy-threatening tactics under the guise of improving transit operations and service [19].

The following list summarizes labor-related institutional issues:

- Lack of support from transit agency staff
- Changing role of drivers
- Use of technology, for example, automated vehicle location systems for monitoring schedule adherence
- Different responsibilities between bus rapid transit and non-BRT routes

Safety and Liability

Bus rapid transit may involve new procedures, technologies, or personnel tasks. The potential thus exists for system components not to function as anticipated, raising safety and liability issues. Stakeholders need to consider whether bus rapid transit changes the assignment of risk and responsibility if technologies or strategies do not function as intended. Safety issues regarding pedestrians and motorists and their interaction with bus rapid transit components, such as signal prioritization and queue jump lanes, will also need to be considered and addressed [19].

The following list summarizes safety- and liability-related institutional issues:

- Insurance industry–initiated changes in assignment of risk and responsibility for bus transport
- Potential changes in liability associated with technological and/or operational malfunctions of BRT systems
- Safety issues arising from changing interaction of pedestrians and motorists with new technologies and/or strategies
- Safety concerns of residents along BRT corridors

Land Use and Planning

Large-scale public transportation projects often influence travel patterns and surrounding land uses, over both the short and the long term. Bus rapid transit would be no different, as high-level transit services, which BRT attempts to replicate, have often significantly altered surrounding land uses. However, bus rapid transit may raise concerns over how it fits into a region's overall transportation planning environment and how it will affect local land uses.

Anecdotally most transit planners believe that fixed guideway systems have a positive impact on land use, particularly around the station areas, whereas bus-based systems have at best a neutral impact. Bus-based systems have been shown to have a beneficial impact at a community level; however, property adjacent to stops/stations is considered less desirable.

One of the biggest concerns of communities developing bus rapid transit systems is convincing them that BRT will provide the benefits that they associate with fixed guideway modes. The advent of BRT systems has challenged this premise. The new BRT systems that have chosen to incorporate a fixed guideway element have demonstrated that bus-based transit systems can have a positive impact on urban form and land values. Although the BRT concept is still relatively new in the USA with only a handful of systems in operation, there is a growing body of evidence that suggests that BRT systems can support existing land users and promote higher density residential, office, and commercial land use, particularly around BRT stations. North American examples of this trend include Boston, Pittsburgh, and Ottawa, where $1,250 million, $302 million, and $675 million of new or improved development, respectively, has occurred. The continuing development of more BRT systems will provide further evidence of this effect; however, as land use improvements tend to lag transit investment, examples of this trend may take a while to be realized [20].

Some BRT systems have benefited by initially developing a number of key stations where land use development potential exists and linking them with transit facilities which incrementally increase to fully exclusive busways. In this way, they could make strategic infrastructural investments at specific locations without the need to improve the whole corridor to the same level.

The following list summarizes land-use- and planning-related institutional issues:

- Coordinating a BRT project with local planning agencies' land use policies
- Gaining community support for transit-oriented development
- Possible reluctance of potential developers to invest along BRT corridors due to a perceived lack of permanence as compared to rail
- Integrating BRT projects into the metropolitan planning process
- Planning requirements such as transportation improvement programs that could delay implementation of a bus rapid transit system
- Need for strong community involvement in planning phases builds support

Physical Environment

The physical imposition of a BRT system may also raise political and institutional challenges. Many project areas, especially in older city centers, may simply lack the physical space to accommodate certain BRT strategies. In other areas, transit agencies may encounter opposition if BRT competes with, or at least is viewed as competing with, other interests for high-value real estate. This may inflate costs or overly complicate operational requirements. Though eminent domain is an option, it usually is an undesirable, drawn-out process. Ensuring there is adequate and obtainable physical space could present problems for certain projects.

Secondly, image is a strong marketing tool for BRT. Many design guidelines suggest making the system unique and easily identifiable. Many projects are included as part of their systems station area improvements. However, these improvements are usually being inserted into existing urban design. Finding station area designs that promote a strong image, while being acceptable to local interests, may be a challenge.

The following list summarizes physical-environment-related institutional issues:

- Availability and acquisition of right-of-way or physical space
- Reaching agreement or consensus on bus stop/station area enhancements
- Need to educate and address public concerns regarding the potential effects of BRT on the physical environment

Institutional Issues: Stakeholder Experience

Transit agency experience has shown that there are specific institutional issues that are primary and stand out from others with respect to the criteria of level of importance and ease of resolution. Eight primary issues are listed below (in no particular order) [21]:

1. Local and business community opposition to the removal of/restrictions on parking spaces for BRT use
2. Availability and acquisition of right-of-way or physical space
3. Integration of multiple priorities, objectives, and agendas
4. Concerns over long-term funding commitments to BRT
5. Impacts of BRT on roadway operations
6. Finding political champions to support BRT
7. Gaining community support for transit-oriented development
8. Educating the public on BRT and managing perceptions and expectations

Integration of Multiple Priorities, Objectives, and Agendas

The integration of multiple priorities, objectives, and agendas often lies at the heart of institutional issues. When several institutions come together to discuss issues of common interest, each brings its own organizational experiences, cultures, and goals. A "win-win" strategy might not always be achievable, but BRT project members need to acknowledge and be thoughtful of other agencies' issues and concerns. Modal biases and agendas have historically infiltrated transportation planning. However, in recent years, with the recognition that multimodal transportation systems tend to be the healthiest, there are greater levels of cooperation. Many transportation organizations, however, still have responsibilities to their respective agencies or jurisdictions, and are still expected to protect their own interests. Though greater cooperation nevertheless must also be accompanied by continuous dialogue to discuss and better understand stakeholders' concerns and by attempts to address them throughout the BRT development and implementation process.

For example, close working arrangements between traffic engineers and transit planners are essential in developing busway and bus lane designs, locations of bus stops and turning lanes, and application of traffic controls. A good program of traffic controls and signage will help ensure safe vehicle and pedestrian crossings of busways and bus lanes. Excessively long traffic signal cycle lengths to accommodate exclusive bus phases should be avoided.

Los Angeles's successful Metro Rapid bus operations on its Wilshire-Whittier and Ventura Boulevard lines are a direct result of cooperation between the MTA and the city's Department of Transportation (DOT). These two agencies found that (1) a modest "advance" or "extension" of the traffic signal green time (or a delay of the red signal time) of up to 10 s per cycle can reduce bus delays with negligible impacts on cross street traffic, (2) bus headways should not be less than 2.5–3.0 min to enable major cross streets to "recover" from the time lost, and (3) far-side stops are essential.

An at-grade busway has fewer traffic impacts on intersecting roads than a typical arterial street. However, relatively light bus volumes require traffic control strategies that ensure safety at grade crossings. Positive protection, such as bus-actuated traffic signals, is essential. However, if accidents persist, gating of bus crossings may be appropriate. The busway should be treated as though it were a high-speed light rail line on a private right-of-way. If there is sufficient conflict among various modes (i.e., vehicles, transit vehicles, and pedestrians), it is important to incorporate gates to reduce these conflicts [1].

Finding Political Champions to Support Bus Rapid Transit

Though public support is critical in implementing a BRT system, it is usually not attainable through transportation agencies alone. Finding a political champion to support a BRT initiative may be critical in gaining public support. Politicians are typically the final decision-makers and often have the clout to produce results. Gaining the ear and voice of influential politicians is one of the most often-cited means of achieving results [19].

Roadway-Related Issues

The following three issues may be covered under the umbrella of *roadway-related issues*:

- Local/business community opposition to removal of/restrictions on parking spaces for BRT use
- Availability and acquisition of right-of-way or physical space
- Impacts of BRT on roadway operations

Bus rapid transit intends to provide the high-quality service associated with rail transit at a much lower cost. In many BRT projects, this is accomplished by providing buses with exclusive or nearly exclusive right-of-way, so operations are not affected by urban street congestion. However, obtaining the required right-of-way may be difficult. Most BRT projects operate, for at least a portion of their route, in developed urban areas where physical space for transportation improvements is typically not in abundance. In several projects, this space comes from currently utilized roadway lanes or from existing parking lanes. Operators of the roadway facilities (typically municipal streets departments or state departments of transportation) used for BRT projects will be interested in how BRT operations would affect their facilities. In cases where projects look to utilize roadway space that is currently on-street parking, businesses and residents may be opposed to the "loss" of parking, even if it is only for peak-period directions and times. For example, at BRT stops/stations the use of queue jump lanes and/or bus bulbs may also be considered. The use of these design attributes in order to improve the level of service may, however, conflict with concerns of the local business community over its opposition to the removal of or restrictions placed on parking space availability that may be necessary to accommodate such operational and service plans for BRT. Therefore one of the major institutional considerations in assessing where BRT is a realistic alternative for specific corridors or roadway facilities is the availability of physical space to accommodate BRT operations. Proper consideration must be given to identify whether there are competing interests for space and how BRT operations may impact these facilities [19].

Concerns over Long-Term Funding Commitments to BRT

Concerns over long-term funding commitments to BRT include it merely being the popular favorite and the implications for transit agencies should the BRT concept fall out of favor. Some BRT projects will require a great deal of capital investment, often

requiring transit agencies to shoulder the risk of having greater capital to maintain without recovering sufficient additional revenue to cover those costs. Whether these are items that a transit agency can afford to operate and maintain, may cause reluctance on the part of transit agencies to embrace BRT [19].

Gaining Community Support for Transit-Oriented Development

Allaying the fear of the unknown is often a responsibility that must be borne when presenting an untested concept to the public. Many BRT projects have incorporated land use strategies to encourage and reinforce transit usage. However, for most outside of the transportation and planning communities, the concept of transit-oriented development (TOD) is new. For many, higher density and mixed use equals more crowding and greater congestion. Attempting to obtain public support for TOD may be a challenging undertaking, especially if there are not many local examples to aid the public's understanding. Proactively educating the public on the underlying objectives of TOD may assist a transit agency in avoiding public opposition to it [19].

Educating the Public on Bus Rapid Transit, and Managing Perceptions and Expectations

This issue may be critical in maintaining continued support of and interest in bus rapid transit. Agencies must perform a balancing act on this issue. For BRT to be embraced by both the public and the decision-makers, the concept must be "sold" to them but it must be sold in the correct manner and amount. Setting unrealistically high expectations can lead to disappointment and a loss of support both from the public and from the decision-makers. It is important that balance be maintained between the "hype" and actual results.

Future Directions

Throughout the world, bus rapid transit systems continue to be implemented, with more than 135 systems in over 28 countries on 6 continents and 90 cities in North and South America, Europe, Asia, Australia, and Africa in both the developed and developing worlds. In the USA alone, there are nearly 60 existing BRT systems with significant progress made in the number of implemented systems in the last 12 years alone, which marks a special milestone year in the history of BRT in the USA because 1998 was the start of the most recent resurgence of interest in the USA in bus rapid transit with the US Department of Transportation's formal initiation of and support for a US BRT Demonstration Program.

BRT has shown that it is indeed a viable rapid transit mode within the USA. The strength of the mode lies in its diverse range of BRT strategies and its flexible and incremental character of deployment that allows transit agencies to customize their BRT system to the local environment including institutional concerns, available right-of-way, or traffic conditions.

For example, agencies with both budget and time resource constraints and little, if any, additional right-of-way capacity may consider a BRT system modeled after Los Angeles's Metro Rapid service. The Metro Rapid uses lower-cost strategies including ITS technologies (transit signal priority systems), frequent headway-based service, a branded and unique identity for the buses and bus stops, low-floor buses, real-time passenger information systems, and a simple route structure with fewer stops to minimize total travel time and enhance travel time reliability on mixed traffic urban arterials. If additional right-of-way capacity is available, agencies may want to consider implementing services on dedicated bus lanes within existing roadways, such as the EmX Line along the Franklin Avenue corridor between Eugene and Springfield, Oregon, where a traffic lane was converted for BRT use. Another example is the Healthline BRT system along the Euclid Avenue corridor in Cleveland, Ohio, where one traffic lane per direction along its 4.5 mile long corridor was removed to build a bus lane within the median. With still more available right-of-way, on the high end of the roadway capacity continuum are exclusive running ways, such as the Metro Orange Line in Los Angeles built along a 14-mile former rail right-of-way owned by MTA. Such systems offer the greatest potential for achieving high speeds and high levels of travel time reliability required for and desired by public transit choice riders.

The next decade will continue to see more BRT systems implemented on an international scale especially in the developing world. In the USA, BRT will continue playing a major role in transit systems throughout the country. Cain A, et al. [22] have suggested that if current trends continue in pioneering BRT cities such as Los Angeles, which has already

implemented a network of approximately 25 Metro Rapid BRT Lines beginning with its initial deployment of the Wilshire-Whittier and Ventura Boulevard Lines in 2000, the next major challenge will be transitioning from individual BRT corridors into integrated networks of BRT routes. Such expansion offers transportation planners and engineers the opportunity to increase the benefits of BRT from the corridor level to the city or regional level, enhancing public transit ridership that helps improve mobility and air quality, reduce congestion, and promote economic growth. Careful integration of such networks with existing BRT and conventional bus services as well as non-bus transit modes will be crucial to achieving a successful transition. Nonetheless, in the context of a BRT network as opposed to an individual BRT corridor, the institutional structure may experience changes and it is possible that additional institutional issues heretofore not identified may arise or already existing issues may be exacerbated, which of course will need to be addressed as part of any successful BRT network implementation process.

Acknowledgments

Portions of sections "Public Relations and Marketing" to "Safety and Liability" and "Finding Political Champions to Support Bus Rapid Transit" to "Gaining Community Support for Transit-Oriented Development" above use material from citation [19] and are the copyright of the National Academy of Sciences, Washington, D.C., 2001; and are reproduced with permission of the Transportation Research Board.

Bibliography

Primary Literature

1. Levinson HS et al (2003) Bus rapid transit volume 1: case studies in bus rapid transit. TCRP Report 90, Transit Cooperative Research Program. Transportation Research Board, Washington, DC
2. Levinson HS et al (2003) Bus rapid transit volume 2: implementation guidelines. TCRP Report 90, Transit Cooperative Research Program. Transportation Research Board, Washington, DC
3. California Public Utilities Commission, Transportation Division, Traffic Engineering Section (1957) Report on bus rapid transit between Concord and Oakland-San Francisco. California Public Utilities Commission, San Francisco, p 6
4. Crain JL (1963) The rapid transit bus concept. Stanford Research Institute, Menlo Park, p 1
5. Crain JL (1963) The rapid transit bus concept. Stanford Research Institute, Menlo Park, p 16
6. Miller MA, Buckley SM (2000) Institutional aspects of bus rapid transit: a macroscopic examination. California PATH Working Paper, UCB-ITS-PWP-2000-07, California PATH Program, University of California, Berkeley
7. National Capital Transportation Agency (1963) A study of bus rapid transit operations of the national capital region. National Capital Transportation Agency, Washington, DC
8. Metropolitan Washington Council of Governments (1970) Feasibility study for bus rapid transit in the Shirley highway corridor. Metropolitan Washington Council of Governments, Washington, DC
9. Rabinovitch J, Hoehn J (May 1995) A sustainable urban transportation system: the 'surface metro' in Curitiba, Brazil. Environmental and Natural Resources Policy and Training Project, Working Paper No. 19
10. Rabinovitch J (1996) Innovative land use and public transportation policy: the case of Curitiba, Brazil. Land Use Policy 13(1):51–67
11. Rabinovitch J, Leitman J (1996) Urban planning in Curitiba. Sci Am 274:26–33
12. Diaz R, Schneck, D. (2000) Bus Rapid Transit Technologies in the Americas: An Overview. Transport Res Rec 1731:3–9
13. Bonsall JA (1989) Transitways: the Ottawa-Carleton experience. Ottawa-Carleton Regional Transit Commission, Ottawa
14. Web site: http://pittsburgh.pahighways.com/busways/. Accessed 21 May, 2010
15. Federal Transit Administration (1998) Bus rapid transit demonstration program. United States Department of Transportation, Federal Transit Administration, Washington, DC
16. Federal Transit Administration (1999) Proceedings of the bus rapid transit demonstration program. United States Department of Transportation, Washington, DC
17. Federal Transit Administration (1999) Bus rapid transit demonstration program kick off workshop. United States Department of Transportation, Washington, DC
18. Wright L, Hook W (2007) Bus rapid transit planning guide, 3rd edn. Institute for Transportation & Development Policy, New York, pp 189–190
19. Miller MA, Buckley SM (2001) Bus rapid transit institutional issues: the route from research to experience. Transit: bus transit and maintenance, paratransit, and new technology. Transportation Research Record, No. 1760. Transportation Research Board National Research Council, National Academy Press, Washington, DC, pp 34–41
20. Miller MA, Carey G, McNamara I, Zimmerman S (2006) Development of bus rapid transit information clearinghouse. California PATH Research Report, UCB-ITS-PRR-2006-7, California PATH Program, University of California, Berkeley
21. Miller MA, Buckley SM (2001) Institutional aspects of bus rapid transit operation. California PATH Research Report,

UCB-ITS-PRR-2001-09, California PATH Program, University of California, Berkeley
22. Cain A, Darido G, Thole C, Flynn J (2007) BRT update: an overview of bus rapid transit in the United States. Mass Transit Magazine

Books and Reviews

Diaz RB, Hinebaugh D (2009) Characteristics of bus rapid transit for decision-making (CBRT). Federal Transit Administration, FTA-FL-26-7109-2009.1

Eccles KA et al (2007) Design, operation, and safety of at-grade crossings of exclusive busways. Report 117, Transit Cooperative Research Program. Transportation Research Board, Washington, DC

ECONorthwest, Parsons Brinckerhoff Quade & Douglas, Inc., et al (2002) Estimating the benefits and costs of public transit projects: a guidebook for practitioners. In: Report 78, Transit Cooperative Research Program. Transportation Research Board – National Research Council, National Academy Press, Washington, DC

General Accounting Office (2001) Mass transit: bus rapid transit shows promise, GAO-01-984. U.S. General Accounting Office, Washington, DC

Kittelson & Associates, Inc. et al (2003) Transit capacity and quality of service manual, 2nd edn. Transit Cooperative Research Program, Report 100. Transportation Research Board, Washington, DC

Kittelson & Associates, Inc. et al (2007) Bus rapid transit practitioner's guide. Transit Cooperative Research Program, Report 118. Transportation Research Board, Washington, DC

Levinson HS et al (1973) Bus use of highways: state of the art. National Highway Cooperative Research Program, Report 143. Transportation Research Board, Washington, DC

Levinson HS et al (1975) Bus use of highways: planning and design guidelines. National Highway Cooperative Research Program, Report 155. Transportation Research Board, Washington, DC

Miller MA et al (2006) Development of deployment strategy for an integrated bus rapid transit system. California PATH Research Report, UCB-ITS-PRR-2006-09, California PATH Program, University of California, Berkeley

Peak M, Henke C, Wnuk L (2005) Bus rapid transit ridership analysis. Federal Transit Administration, U.S. Department of Transportation, FTA-CA-26-7068-2004.1

St. Jacques K, Levinson HS (1997) Operational analysis of bus lanes on arterials. Transit Cooperative Research Program, Report 26. Transportation Research Board, Washington, DC

Thole C, Samus J (2009) Bus rapid transit and development: policies and practices that affect development around transit. Federal Transit Administration, U.S. Department of Transportation, FTA-FL-26-7109.2009.5

Wilbur S et al (1975) Bus rapid transit options in densely developed areas. U.S. Department of Transportation, Washington, DC

Bus Rapid Transit: Worldwide History of Development, Key Systems and Policy Issues

Dario Hidalgo
EMBARQ, The World Resources Institute Center for Sustainable Transport, Washington, DC, USA

Article Outline

Glossary
Definition of the Subject and Its Importance
Introduction
BRT Components, Characteristics, and Impacts
BRT Status Around the World
BRT in the United States and Canada
BRT in Latin America
BRT in Europe
BRT in Asia
BRT in Australia and New Zealand
BRT in Africa
Future Directions
Bibliography

Glossary

Alternatives analysis Evaluation of different transit choices available, usually requiring cost-benefit analysis, life cycle costing, and sensitivity analysis.

Branding Name, term, design, symbol, or any other feature that identifies a service or product.

Bus corridor A street or highway featuring bus priority measures, such as bus lanes or busways or traffic signal priority.

Bus lane Street or highway lane(s) with priority designation for bus public transport services.

Bus priority Infrastructure or traffic signal measures to speed up bus public transport services, especially at intersections or junctions.

Busway Street or highway lane(s) exclusively designated for bus public transport services.

Comfort The capacity to give physical ease and well-being. In public transport, it is usually related to the provision of adequate space, soft ride, easy circulation, and adequate information for passengers.

Commercial speed Distance traveled divided by the time, as perceived by the passengers of the public transport system. It includes time spent at bus stops or stations, intersections or junctions, and the time traveling between them.

Externalities An economic effect that is not reflected in market prices. In public transport, this term usually refers to travel time, air pollution, road fatalities and injuries, and other effects on people and the environment.

Fare collection Collection of entrance fee in a public transport service. It may include direct access to the service or tickets or passes to travel.

Headway Time interval between two consecutive transit vehicles.

Intelligent transport system (ITS) Is an umbrella term for a range of technologies including processing, control, communication, and electronics that are applied to a transportation system.

Paratransit Is an alternative mode of flexible passenger transportation that does not follow fixed routes or schedules. It includes informal services as well as formal services provided for users with special needs, such as elderly and disabled.

Passenger capacity Number of passengers that can be accommodated in a vehicle, station, service, or section of the transport system. Can be measured in units of space (passengers per square meter), vehicles (passengers per bus), or time (passengers per hour per direction).

Peak section load Number of passengers riding inside the transit vehicles in the heaviest section of the public transport system and direction per unit of time, usually 1 h.

Public transport Is a shared passenger transportation service which is available for use by the general public. Also known as public transportation or transit.

Public–private partnership Describes a government service or private business venture which is funded and operated through a partnership of government and one or more private sector companies. These schemes are sometimes referred to as PPP or P3. In public transport, this term usually describes the service or concession contract for transit provision, which may include development of infrastructure and vehicles.

Rapid transit A system of public transport in an urban area, using a combination of infrastructure, vehicles, operations, and information technologies to provide fast and reliable service.

Reliability Capability of being relied on; dependability. In public transport, this refers to the provision of timely services, with low variance in arrival and travel times.

Service operation plan Public transport routes, schedules, and itineraries, preferably planned in advance and centrally controlled to provide service according to the user needs.

Traffic signal Signaling devices positioned at road intersections, pedestrian crossings, and other locations to control competing flows of traffic. Also known as traffic lights, stoplights, traffic lamps, traffic signals, or semaphores.

Transit-oriented development (TOD) Urban area designed to maximize access by public and nonmotorized transportation to encourage transit ridership. A typical TOD has a rail or bus station at its center, surrounded by relatively high-density and mixed used development. It usually has adequate facilities and attractive street conditions for walking and cycling, good connectivity, and uses traffic calming and parking management measures.

Definition of the Subject and Its Importance

Bus rapid transit (BRT) can be defined as a flexible, rubber-tired form of rapid transit that combines stations, vehicles, services, running ways, and information technologies into an integrated system with strong identity [1]. Complete BRT systems offer fast, comfortable, and low-cost urban mobility [2]. BRT is an evolution of bus priority measures, such as designated busways and bus lanes, which were proposed, and in some cases implemented, as early as 1937 throughout the world [3]. The expression BRT was initially used in the United States in a 1966 study [4]. The concept gained popularity in Latin America after the successful upgrade of busways in Curitiba, Brazil, to full-featured BRT in 1982 [5]. The high performance, low cost, and rapid implementation of this system, and its adaptations to Quito, Bogotá, Mexico City, Beijing, Jakarta, Los Angeles, Beijing, Istanbul, and Guangzhou, among other cities, made the idea attractive for urban

transport planners throughout the world. As of January 2011, there were about 118 cities with BRT or bus corridors, with 97 of the cities entering into the list in the last 10 years, and at least 80 cities building, designing, or planning BRT systems [6]. BRT is an attractive option for public transport delivery, applicable to a wide variety of conditions – from very low to very high passenger throughput, and should be considered in alternatives analysis in most transit corridors. Critics of BRT indicate that these systems are not permanent, use precious surface space, and exhibit operational and cost issues as compared with rail [7]. BRT implementation requires strong political leadership, sound technical planning, and adequate funding levels [2, 8].

Introduction

The concept of BRT is not new [3], but it has only being extensively deployed around the world in the last decade [6]. The growth may be attributed in part to the success of Curitiba [5] and its adaptations in different parts of the world [2, 3]. In general, BRT systems exhibit low cost, rapid implementation, and high performance, with significant positive impacts [2, 9].

Interesting trends are emerging in the BRT industry [6], such as the implementation of citywide integrated bus systems based on BRT, improved processes for private participation in operations, increased funding from national governments, and growth of bus manufacturers and technology providers. Technological developments in vehicles and information systems are also improving the quality, performance, and impact of BRT [9].

Despite the growth, there are some outstanding issues: BRT does not have a single meaning and image and it is often regarded as a "second best" as compared to rail alternatives [2]. Its ability to foster urban development and the use of space designated for cars are often questioned, as well as its actual costs and impacts [7]. In addition, several systems in the developing world suffer problems resulting from poor planning, implementation, and operation, due to financial, institutional, and regulatory constraints [8].

This entry discusses the concept, its history, and expected trends. In the first section the concept of BRT is developed. The following sections show the history and current status of BRT in different geographical regions of the world – the United States and Canada, Latin America, Europe, Australia and Oceania, and Asia. The final section indicates future directions.

BRT Components, Characteristics, and Impacts

Components of BRT include [9], running ways, stations, vehicles, fare collection, intelligent transport systems (ITS), service operation plans, and branding elements. There could be different degrees of complexity of each one of these elements, resulting in varied system performance characteristics and system impacts. Performance characteristics include commercial speed, passenger capacity, capital and operational productivity, and costs. Impacts of BRT encompass user perception, travel time, reliability, comfort, and externalities – air pollution, road safety, physical activity, and urban development, among others.

Advanced BRT systems typically involve integration of (see Fig. 1, list adapted from [1, 2, 9]):

- Median running ways for exclusive use of the BRT system buses which are separated from the rest of the traffic through raised curbs (right of way A or B, according to the classification by Vuchic [10]).
- Stations with off-board payment and platforms with level access for boarding to the buses.
- Large buses with multiple doors, special design features, and lower emission levels than conventional buses.
- Use of advanced electronic ticketing systems, such as contactless fare cards, integrated to other applications.
- Several information technology applications for centralized control – such as automatic vehicle location (AVL) and dispatch systems, and improved user information systems – variable message signs in stations and buses to indicate next bus and next station in real time, and provide public announcements; online and personal data appliance providing routing and schedule information, among other applications.
- Combined service plans according to the passenger demand characteristics, including high frequency trunk line services combined with feeder services, as well as accelerated and express bus services.

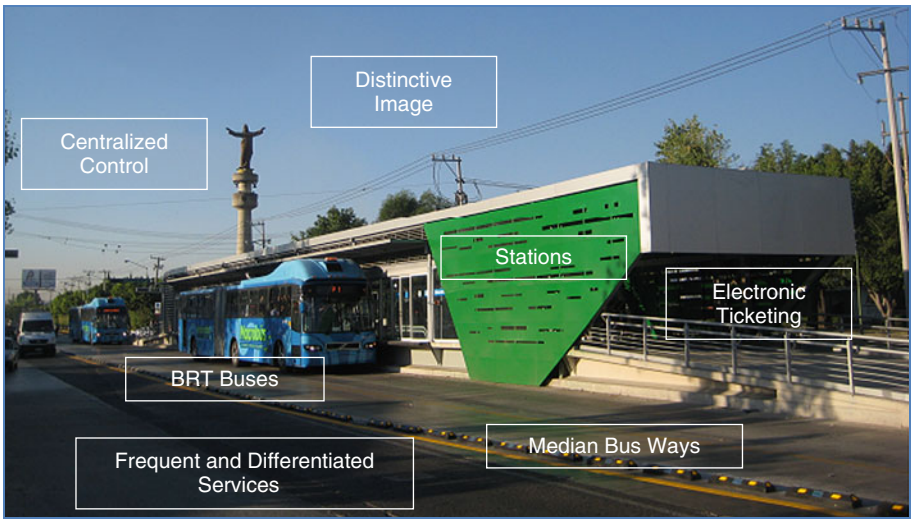

Bus Rapid Transit: Worldwide History of Development, Key Systems and Policy Issues. Figure. 1
BRT system characteristics (Guadalajara, México, Macrobus BRT system, CTS Mexico 2010)

- Distinctive image differentiating running ways, stations, buses and overall service from other bus services and transit applications in the city.

Few systems encompass all these components. Each component is adapted to the local conditions and the service needs [1], as well as budgetary constraints. As a result, performance characteristics are varied. Table 1 presents the maximum values of some performance indicators observed:

BRT capital costs are in the range of one tenth to one third of comparable rail systems [2, 14]. BRT costs depend on the selection of system components and performance requirements. Figure 2 shows comparison of capital costs for some systems in the developing world; most systems have been built and equipped at a cost between 1 and 5 million USD per kilometer. The higher cost of the Bogotá BRT system reflects the investment to achieve very high peak load (45,000 pphpd) and commercial speed (28 km/h) [8].

Regarding system impacts, most systems have resulted in higher passenger demand than expected [2, 9, 14]; user satisfaction is frequently high [15, 16]; travel times are usually reduced as a result of higher commercial speeds than buses in mixed traffic [2, 8, 9], reliability increased due to the supporting infrastructure and communication technologies [9], and there is documentation on positive impacts for several systems regarding reduction of crashes, pollutant emissions, and improved urban environments [9, 14, 17, 18] Concerning comfort, most systems in developing countries use very high occupancy standards and may not be considered comfortable [8]; this is a result of financial restrictions that require most transit operations in developing cities to be self sustainable. As a result, productivity levels need to be very high. Critics of BRT often cite comfort issues when comparing bus systems with rail [7].

BRT Status Around the World

BRT is currently a key component of an effective urban transport policy to address congestion, pollution, and road accidents. A survey of BRT around the world [6] indicates that there are about 118 cities with BRT or bus corridors. The existing BRT and bus corridors as of January 2011 comprise about 280 corridors, 4,300 km, 6,700 stations, and use 30,000 buses, serving about 28 million passengers per day [6]. As of January 2011, about 49 new cities were building BRT systems, 16 cities were expanding their corridors, and 31 cities indicated they were at in initial planning stages [6]. What used to be unusual in the early 1990s became common in 2010. Most cities have either developed BRT or bus corridors, or have considered their inclusion in their transportation improvement plans.

Bus Rapid Transit: Worldwide History of Development, Key Systems and Policy Issues. Table 1 Maximum values for some performance indicators in selected BRT systems

Performance indicator	Definition	Value (year)	System, city (date)	System features
Commercial speed	Distance/time as perceived by the user on board (km/h)	42 km/h (2011)	Metrobüs, Istanbul, Turkey	Fully segregated busway on expressway, stations every 1.1 Km [11]
Peak section load	Passengers/hour/ direction (pphpd)	45,000 pphpd (2011)	TransMilenio, Bogotá, Colombia	Median busway, level access stations with five platforms, overtaking lanes and combined services –local, express, seven standees per square meter, dense urban area [12]
Infrastructure productivity	Passengers/kilometer of busway	35,800 (2011)	Guangzhou BRT, China	Median busway, with long station, overtaking lanes, open operation 40 routes, very dense urban area [13]
Capital productivity	Passenger boardings/ bus/day	3,100 (2010)	Macrobús, Guadalajara, México	Median busway, overtaking lanes relatively dense, mixed use urban area [8]
Operational productivity	Passenger boardings/ bus kilometers	13.2 (2010)	Metrovía, Guayaquil, Ecuador	Median busway, dense urban area, very low fare (USD 0.25 per trip) [8]

Table 2 presents a regional distribution of BRT and bus corridors around the world, which shows its presence in all continents. Latin America has about one fourth of the cities in the world, but concentrates two thirds of the ridership. There are a very high number of cities and kilometers in Asia, which is the fastest urbanizing region in the world. Usage in Europe, the USA, and Canada is comparatively low in relation with the total kilometers reported. Only two cities in Africa have introduced BRT: Johannesburg, South Africa, and Lagos, Nigeria. The only intercontinental BRT is in Istanbul, Turkey, crossing the Bosphorus Strait.

Figure 3 shows the number of cities introducing BRT or bus corridors since 1970, as well as the total cumulative number of cities. Most cities in the list (97), introduced BRT or bus corridors in the first decade of the twenty-first century. The highest number of cities introducing BRT or bus corridors in the last decade is in China, followed by Indonesia, and the Latin American region.

Some trends are emerging in the BRT Industry:

- Implementation of integrated transit systems based on BRT: The initial phase of implementing isolated corridors is evolving toward citywide systems integration, often including other modes of transport like Metro (Sao Paulo [19], Santiago [20], and Guangzhou [13]); Light Rail Transit (Guadalajara [21], Monterrey); and conventional buses (Sao Paulo [19], Santiago [20], and Bogotá [22]).
- Improved processes for private participation in operations: Most BRT systems in developing countries operate under public–private partnership agreements, using performance-based concession contracts which are awarded either through competitive tendering – with some provisions to include incumbent operators, or direct negotiations of new concessions with existing private providers [8].
- Increased funding from national governments: BRT systems are eligible for funding from the national or federal governments in several countries, like Mexico – through the national fund of infrastructure FONADIN [23]; Brazil – through the Program for Growth Acceleration PAC 2 Mobility in Large Cities [24]; and India – through the Jawaharlal Nehru National Urban Renewal Mission JnNURM [25] and the National Urban Transport Policy [26], among others.
- Growth of bus manufacturers and technology providers: Commercial vehicle manufacturers and

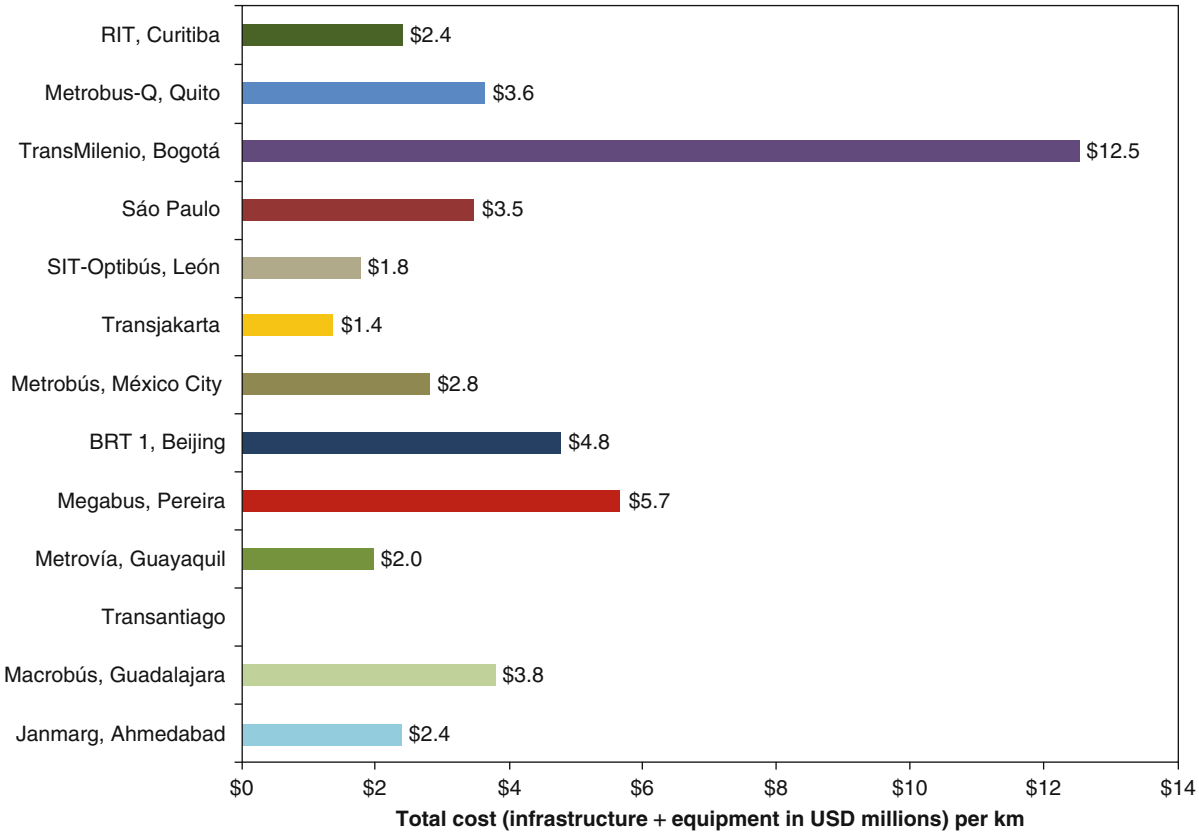

Bus Rapid Transit: Worldwide History of Development, Key Systems and Policy Issues. Figure. 2 Capital costs per kilometer for selected BRT systems (2009) (Source: Hidalgo and Carrigan [8])

Bus Rapid Transit: Worldwide History of Development, Key Systems and Policy Issues. Table 2 Regional distribution of BRT and bus corridors as of January 2011

	Cities	Corridors	Kilometers	Stations	Buses	Passengers/day
Africa	2	2	47	63	363	290,000
Asia	33	85	1,306	1,658	6,590	6,289,531
Europe	25	32	291	609	781	629,369
Europe/Asia	1	2	43	33	300	700,000
Latin America and the Caribbean	32	90	1,330	2,687	18,656	17,591,945
Oceania	5	12	324	142	1,411	345,800
USA and Canada	20	57	993	1,485	1,993	1,013,901
Total	118	280	4,335	6,676	30,094	26,860,546

Source: EMBARQ BRT/Bus Corridors Database [6]

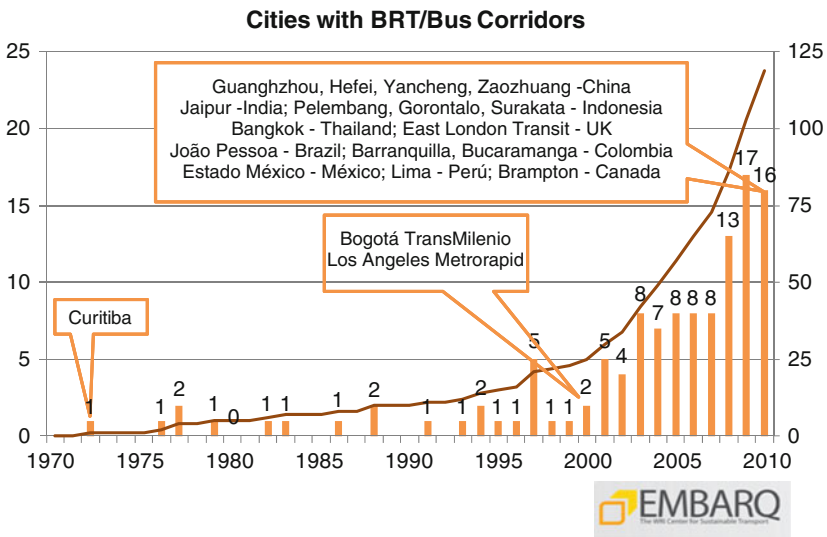

Bus Rapid Transit: Worldwide History of Development, Key Systems and Policy Issues. Figure. 3 Cities with BRT/bus corridors 1970–2010 (Source: EMBARQ BRT/Bus Corridors Database [6])

information technology providers are increasing their activity, especially in emerging economies like Brazil, China, India, and Indonesia.

- Technological developments in vehicles and information systems are also improving the quality, performance, and impact of BRT [9]. Advanced technologies include cleaner fuels – Compressed Natural Gas CNG, Ultra Low Sulfur Diesel ULSD, Biofuels, Hydrogen; improved propulsion technologies – hybrid drive trains, electric; emissions posttreatment – catalytic converters, particulate filters; improved central dispatch and real-time control systems – automatic vehicle location (AVL) and operations control; enhanced fare collection systems using electronic ticketing and contactless fare cards; improved user information systems – variable message signs, communication with personal wireless devices for routing, information of next buses and public announcements, among others.

Despite the growth, there are some outstanding issues:

- BRT does not have a single meaning and image – a broad spectrum of applications, from improved bus service on mixed traffic to totally segregated systems, are considered BRT [1, 2, 9].
- It is often regarded as a "second best" as compared to rail alternatives without a fair evaluation or alternatives analysis [2, 7, 10, 14].
- Its ability to foster urban development and the use of space designated for cars are often questioned, as well as its actual costs and impacts [7].

Several systems in the developing world suffer problems like [8]

- Rushed implementation – several components incomplete at the time of commissioning, but gradual improvement over time has been observed
- Very tight financial planning – user fares are not defined technically generating risks in some systems
- Very high occupancy levels – the adopted standard of 160 passengers/vehicle for articulated buses is not acceptable by the users
- Early deterioration of infrastructure – lack of road surface reinforcement or problems in design and construction result in maintenance issues
- Delayed Implementation of fare collection systems, which often require longer timetables than initially expected and need very tight supervision
- Insufficient user education for initial implementation and system changes

These issues are often the result of poor planning, implementation, and operation, due to financial, institutional, and regulatory constraints; they are not intrinsic to the BRT concept [8].

BRT in the United States and Canada

According to Levinson et al. [3], the idea of using buses to provide mass transit is not new. Plans for bus systems, displaying the current understanding of BRT, were proposed as early as 1937, when a "plan called for converting three west side rail rapid-transit lines to express bus operation on super highways with on-street distribution in central areas and downtown," in Chicago. Similar major initiatives for buses on reserved lanes on freeways were proposed in a 1956–1959 Washington D.C. Plan, a 1959 St. Louis Plan, and a 1970 Milwaukee Plan [3].

Several research studies, indicating the potential of BRT and suggesting guidelines for the design of bus facilities were completed between 1966 and 1975. Levinson et al. [3] indicate that "most of these planning studies focused on the facility aspects of BRT, often as an adjunct to urban freeways. Little or no attention was given to the station, service, and image/identity aspects of BRT."

The planning emphasis changed in the late 1970s, from bus use of streets and highways toward the provision of high-occupancy vehicle (HOV) lanes and light rail transit (LRT) due to environmental and performance considerations [3]. LRT tended to be considered more fully in alternative analyses, due to lack of information on the potential benefits and costs of BRT [3]. More recently, BRT recaptured interest of planners and funding agencies [3]. The Federal Transit Administration (FTA) sponsored a BRT conference in 1998, using Curitiba's BRT system as a model, published major documents highlighting BRT, established a BRT Consortium with 17 supporting cities in 1999, and launched a BRT "Demonstration Program" involving 15 cities [3].

The most important BRT systems and bus corridors in the United States and Canada by January 2011 are presented in Table 3, including date of initial implementation, some features, and estimated ridership. There are 20 cities, featuring 57 corridors and 993 km, serving about 1,013,901 passengers per weekday.

Systems in the United States are not usually displaying full BRT features. The most advanced applications are the Orange Line (Los Angeles, California, 2007, Fig. 4), EmX (Eugene, Oregon, 2008), and the HealthLine (Cleveland, Ohio, 2009). Evaluations of these and other applications in the United States are available in the FTA document "Characteristics of BRT for Decision Makers" [9] and the National BRT Institute [27], a federal funded program.

In Canada, the City of Ottawa, implemented a very interesting concept, the Transitway, a fully segregated corridor with services coming in and out, allowing for direct trips without transfers [9, 28]. Plans to partially replace the Transitway system with Light Rail are underway [29]. The suburban communities of York (2005) and Brampton (2010), in Ontario, also improved transit using BRT.

BRT in Latin America

Many Latin American cities have embraced bus rapid transit as a key component of their transit systems. Curitiba, Brazil, can be considered the cradle of modern BRT [5]. Since the 1970s, Curitiba's administrators have introduced constant innovations to the city's bus-based transit system. Originally, the bus system evolved from conventional buses in mixed traffic to busways, which were fitted with at-level boarding, prepayment, and articulated buses, creating the first full BRT system in the world in 1982 [5]. Later on, the city introduced high capacity bi-articulated buses and the electronic fare ticketing systems.

In 2009, the Curitiba integrated bus system was upgraded, again, with the introduction of the Green Line, its sixth BRT corridor which includes the operation of 100% bio-diesel articulated buses [5]. In 2010, the city also introduced capacity enhancements for one of its existing corridors (Fig. 5). Capacity expansions are underway in all the original corridors.

The success story of Curitiba has been replicated in several cities through the region, with adaptation to the local conditions [34]. Quito replicated the Curitiba concept in 1995, with the use of electric trolleybuses to preserve the environment in its historic downtown [34]. Bogotá, expanded the concept in 2000, using very large stations with passing lanes, combined local and express services, electronic ticketing system and

Bus Rapid Transit: Worldwide History of Development, Key Systems and Policy Issues. Table 3 Most relevant BRT systems and bus corridors in the United States and Canada by January 2011

City	Initial year	Name	Corridors	Kilometers	Stations	Buses	Passengers/ day (year)	Source
Pittsburgh, Pennsylvania	1977	South, MLK East, West Busways	3	31.3	50	103	51,700 (2009)	[6, 9]
Ottawa, Ottawa	1983	Transitway	3	30.0	37	195	97,739 (2008)	[6, 9]
Miami, Florida	1997	South Miami-Dade Busway	1	34.0	30	46	23,000 (2009)	[6, 9]
Orlando, Florida	1997	LYNX Lymmo	1	5.1	22	9	4,475 (2009)	[6, 9]
Chicago, Illinois	1998	Express	3	62.4	154	109	54,742 (2009)	[6, 9]
Los Angeles, California	2000	Metrorapid	21	390.2	650	893	464,600 (2009)	[6, 9]
Oakland, California	2003	San Pablo Rapid	1	23.8	52	26	13,000 (2009)	[6, 9]
Albuquerque, New Mexico	2004	Rapid Ride	1	23.5	30	25	12,430 (2009)	[6, 9]
Boston, Massachusetts	2004	Silver Line	2	11.7	61	62	30,874 (2009)	[6, 9]
Las Vegas, Nevada	2004	MAX	1	12.75	22	20	10,000 (2009)	[6, 9]
Halifax, Nova Scotia	2005	Metrolink	3	39.4	16	15	7,266 (2008)	[6, 9]
York, Ontario	2005	VIVA	5	63.6	59	71	35,300 (2008)	[6, 9, 30]
Los Angeles, California	2007	Orange Line	1	24.65	28	125	62,597 (2009)	[6, 9]
Eugene, Oregon	2008	EmX	1	6.8	18	13	6,200 (2009)	[6, 9]
Phoenix, Arizona	2008	LINK	4	128.0	92	5	2,372 (2009)	[6, 9]
Cleveland, Ohio	2009	HealthLine	1	12.1	36	21	10,591 (2009)	[6, 9]
Kansas City, Kansas	2009	MAX	1	10.2	42	9	4,450 (2009)	[6, 9]
New York, New York	2009	Bx Select Bus	2	26.4	52.7	220	110,187 (2010)	[6, 31]
Snohomish County, Washington	2009	Swift	1	28.9	16	10	4,878 (2010)	[6, 32]
Brampton, Ontario	2010	Züm	1	28.5	17	15	7,500 (2010)	[6, 33]

centralized control, achieving extremely high peak loads – over 45,000 passengers per hour per direction (Fig. 6) [35].

The Curitiba, Quito, and Bogotá successes were then replicated, with adaptations, to at least 29 cities (Table 4). As of January 2011, there were at least 91 BRT and bus corridors; 1,300 km; 2,700 stations; and 18,000 buses, serving more than 17 million passengers per day [6]. Latin America has one fourth of the world cities with BRT or bus corridors, serving two thirds of the estimated global ridership [6].

Many other cities in the region, like Buenos Aires, Medellin, Cartagena, Cúcuta, Arequipa, Asunción, Chihuahua, Querétaro, San Juan, and Panamá City, were building corridors or in final planning stages as of January 2011 [6].

The highest concentration of BRT and bus corridors is in Brazil with 16 cities and 828 km [6]. It is important

Bus Rapid Transit: Worldwide History of Development, Key Systems and Policy Issues. Figure. 4
Orange Line, Los Angeles, North Hollywood station (Source: Gary Leonard, http://www.metro.net/press/2005/10_october/metro_160a.htm#North)

Bus Rapid Transit: Worldwide History of Development, Key Systems and Policy Issues. Figure. 5
Boqueirao busway in Curitiba integrated system after capacity expansion in 2010 (Source: Municipality of Curitiba 2010)

Bus Rapid Transit: Worldwide History of Development, Key Systems and Policy Issues. Figure. 6
Bogotá TransMilenio BRT system peak section in Avenida Caracas – station with five platforms, prepayment, level boarding and overtaking lanes for local and express services (Source: TRANSMILENIO S.A. 2001)

Bus Rapid Transit: Worldwide History of Development, Key Systems and Policy Issues. Table 4 Most relevant BRT systems and bus corridors in Latin America and the Caribbean by January 2011

City	Initial year	Name	Corridors	Kilometers	Stations	Buses	Passengers/ day (year)	Source
Curitiba, Brazil	1972	Rede Integrada de Transporte	6	72	376	2,200	2,260,000 (2010)	[5, 6]
Goiania, Brazil	1976	Rede Metropolitana de Transporte Coletivo	3	35	70	200	200,000 (2010)	[6, 36]
Porto Alegre, Brazil	1977	Prioridade Transporte Colectivo	10	57.2	103	1,300	1,170,000 (2010)	[6, 36]
Sao Paulo, Brazil	1979	Prioridade Transporte Colectivo	10	301.3	602.6	7,604	6,843,664 (2010)	[6, 36]
Juiz de Fora, Brazil	1982	Av. Visconde do Rio Branco	1	5	10	83	75,000 (2010)	[6, 36]
Campinas, Brazil	1988	Prioridade Transporte Colectivo	3	13.4	9	178	160,000 (2010)	[6, 36]
Mauá – Diadema, Brazil	1988	Corredor Metropolitano ABD	1	33	66	233	273,000 (2010)	[6, 36]
Campo Grande, Brazil	1991	Sistema Integrado de Transportes	1	3.2	6.4	89	80,000 (2010)	[6, 36]

Bus Rapid Transit: Worldwide History of Development, Key Systems and Policy Issues. Table 4 (Continued)

City	Initial year	Name	Corridors	Kilometers	Stations	Buses	Passengers/ day (year)	Source
Fortaleza, Brazil	1994	Sistema Integrado de Transportes	1	3.6	7.2	86	77,000 (2010)	[6, 36]
Quito, Ecuador	1995	Metrobus-Q	3	42.2	82	531	440,000 (2010)	[6, 8]
Uberlândia, Brazil	1997	Sistema Integrado de Transportes de Uberlândia	1	17	13	78	70,000 (2010)	[6, 36]
Bogota, Colombia	2000	TransMilenio	7	84	144	1,769	1,700,000 (2010)	[6, 37]
Natal, Brazil	2001	Sistema Integrado de Transportes	2	5	19	200	180,000 (2010)	[6, 36]
Leon, Guanajuato, México	2003	Optibus	4	31	61	90	700,000 (2010)	[6]
Monterrey, México	2003	Metrobus	3	101	201	85	125,281 (2010)	[6]
Belo Horizonte, Brazil	2004	Prioridade Transporte Colectivo	2	23.7	47.4	483	435,000 (2010)	[6, 36]
Feira de Santana, Brazil	2005	Sistema Integrado de Transportes	2	3.5	7	83	75,000 (2010)	[6, 36]
Mexico City	2005	Metrobus	3	67	108	275	620,000 (2011)	[6]
Salvador, Brazil	2005	Sistema de Transporte Coletivo por Ônibus	2	4	8	167	150,000 (2010)	[6, 36]
Guayaquil, Ecuador	2006	Metrovia	2	63	60	215	300,000 (2010)	[6, 38]
Guatemala City	2007	Transmetro	2	35.0	70	400	400,000 (2010)	[6]
Merida, Venezuela	2007	Transmerida	2	30	34	8	8,000 (2010)	[6, 39]
Pereira, Colombia	2007	Megabus	3	19.15	37	137	115,000 (2010)	[6, 40]
Recife, Brazil	2007	Sistema Estrutural Integrado (L-O)	1	9	28	444	400,000 (2009)	[6, 41]
Santiago, Chile	2008	Transantiago	3	26	52	130	130,000 (2010)	[6]
Cali, Colombia	2009	MIO	6	179.0	358	470	215,000 (2010)	[6, 40]
Guadalajara, Mexico	2009	Macrobus	1	16	27	144	130,000 (2010)	[6]
Barranquilla, Colombia	2010	Transmetro	1	13.4	15	92	32,000 (2010)	[6, 40]

Bus Rapid Transit: Worldwide History of Development, Key Systems and Policy Issues. Table 4 (Continued)

City	Initial year	Name	Corridors	Kilometers	Stations	Buses	Passengers/ day (year)	Source
Bucaramanga, Colombia	2010	Metrolinea	1	8.9	24	131	75,000 (2010)	[6, 40]
Estado Mexico	2010	Mexibus	1	16	32	63	63,000 (2010)	[6, 42]
João Pessoa, Brazil	2010	Corredor de Ônibus de João Pessoa	1	2.5	5	111	100,000 (2010)	[6, 43]
Lima, Perú	2010	Metropolitano	2	27	35	627	160,000 (2010)	[6, 44]

Bus Rapid Transit: Worldwide History of Development, Key Systems and Policy Issues. Figure. 7
Expresso Tiradentes, Sao Paulo, Brazil (Source: Sao Paulo Transportes SPTrans 2008)

to indicate that most cities in Brazil, outside Curitiba and Goiania, keep the general model of busways, rather than full BRT systems. There was a major upgrade of the integrated system in Sao Paulo in 2005 [19], which included the introduction of an elevated fully segregated busway – Expresso Tiradentes (Fig. 7). Similarly, Santiago, Chile introduced a major reform in bus services in 2008, which includes several busways, and prepayment in selected stations, but keeps most fare collection off board and has few segregated busways [20].

BRT in Europe

European cities have preserved and enhanced their transit systems in high capacity corridors using metros and tramways mainly, with buses only considered in

medium capacity corridors. Heddebaut et al. [45] consider that high capacity BRT configurations do not suit the European context (lack of available space, undesirable urban cuttings, and low demand). These authors prefer the term "Bus with a High Level of Service (BHLS)," rather than BRT, to refer to the European applications introduced in several cities (Table 5). Most applications have bus lanes in congested areas (downtown), sharing the road with taxis and bicycles, and in few cases lanes in expressway (High-occupancy vehicle lanes in Madrid and Grenoble, Metrobüs in Istanbul).

Case studies compiled by the European Union project COST [46] indicate that BHLS corridors are well adapted to new urban zones, small towns, and medium-sized conurbations [45]. They also allow for a variety of configurations (feeder-trunk and direct services), and permit transformation into tramway systems once there is sufficient demand. Some applications used advanced vehicles, including optical or magnetic or physical guidance (e.g., Castellón de la Plana, Eindhoven, Leeds).

Outside the European Union, the most widely used application is the Istanbul Metrobüs, which connects Europe and Asia in the only intercontinental BRT system (Fig. 8). This system has central busways on expressway (fully segregated BRT), very long platforms, low floor buses (articulated and bi-articulated), and achieves very high commercial speed (42 km/h) and peak throughput (30,000 passengers/hour/direction) [11]. It carries 700,000 passengers per day in a 45 km corridor, under expansion in 2011.

Table 5 shows the most relevant corridors in Europe, including Turkey. There are at least 27 cities in Europe with bus corridors, 35 corridors, 335 km, and 1,083 buses, serving 1.3 million passengers per day (53% in Istanbul) [6].

BRT in Asia

BRT is evolving very rapidly in several Asian countries, such as China [49], Indonesia [50], India [51], and Iran [6]. Applications are very varied, from very basic bus corridors (e.g., Delhi and Pune) to very complete systems (e.g., Ahmedabad and Teheran). Table 6 lists the most relevant corridors as of January 2010.

There are at least 33 cities, with 85 corridors, 1,306 km, 1,720 stations, 6,590 buses, serving 6.3 million passengers per day. Forty-five percent of the cities started operation in 2009 and 2010 and many other cities are building and planning BRT and bus corridors across the region.

One important advance in BRT development is the application in Guangzhou, China (Fig. 9), which uses direct services, with large stations, overtaking lanes and the use of advanced technologies for control and user information [49]. This system features very high throughput (30,000 passengers per hour per direction), with small number of transfers.

BRT in Australia and New Zealand

Australia has a long tradition on BRT, as one of the first world systems, the Adelaide North East Busway started operation in 1986 [55]. Brisbane, Melbourne, Sydney, and Auckland introduced bus corridors between 2001 and 2005 (Table 7). Bus corridors in Australia and New Zealand have very diverse design features, from guided busways (Adelaide) and fully grade-separated bus-only roads (Brisbane, sections of Sydney), to on-street busways (Auckland) and bus lanes (Melbourne) [55].

According to Currie and Delbosc [55], the BRT concept continues to be very attractive in the region with rapid increase in kilometers and ridership, especially on established systems. The authors identify risks in the provision of vehicles and accommodating high patronage growth, but highlight the relative cost-effectiveness. BRT development in Australia and New Zealand has exceeded rail in the last decade; nevertheless, rail has received greater attention lately [55].

Brisbane (Fig. 10), exhibits very advanced design features, and recently completed a downtown tunnel.

BRT in Africa

Infrastructure and service development in African cities is beginning to pick up attention by the local authorities, as urbanization and GDP increase. Governments are beginning to recognize the need for organized transit, to replace low-quality informal paratransit services [56].

Two cities, Lagos, Nigeria, and Johannesburg, South Africa, started operations of BRT systems in 2009. Lagos implemented a corridor on the parallel

Bus Rapid Transit: Worldwide History of Development, Key Systems and Policy Issues. Table 5 Most relevant bus corridors in Europe as of January 2010, including Istanbul, which extends to Asia

City	Initial year	Name	Corridors	Kilometers	Stations	Buses	Passengers/day (year)	Source
Paris, France	1993	TVM	1	19.5	29	33	65,000 (2009)	[6, 47]
Ipswich, UK	1994	Ipswich Rapid Transit	1	0.5	1	1	739 (2010)	[6]
Leeds, UK	1995	Superbus	2	4.2	8.4	62	31,000 (2005)	[6, 48]
Dublin, Ireland	1997	QBC	1	8.4	17	68	34,000 (2009)	[6, 46]
Rouen, France	2001	TEOR	3	13	52	64	45,000 (2009)	[6, 47]
Utrecht, The Netherlands	2001	TVM	2	8.2	16	42	33,500 (2005)	[6]
Caen, France	2002	Twisto TVR	1	15.7	34	24	48,000 (2009)	[6, 47]
Nancy, France	2002	TVR (GLT)	1	8	30	18	37,000 (2009)	[6, 47]
Amsterdam, The Netherlands	2002	Zuidtangent BRT	1	33	66	80	40,000 (2009)	[6, 46]
Bradford, UK	2002	Manchester Road	1	3.7	7.4	7	5,467 (2005)	[6, 48]
Eindhoven, The Netherlands	2003	Phileas	1	15	30	12	28,500 (2009)	[6, 9]
Crawley, UK	2003	Fastway	2	24	48	23	6,000 (2005)	[6, 46]
Prato, Italy	2004	LAM	1	15	30	120	60,000 (2009)	[6, 46]
Edinburgh, Scotland	2004	Fastlink	2	5	10	55	44,000 (2005)	[6, 48]
Lyon, France	2006	C-Lines	1	4	10	5	4,700 (2009)	[6, 47]
Nantes, France	2006	BusWay (Line 4)	1	7	15	20	21,000 (2009)	[6, 47]
Kent, UK	2006	Fastrack	1	15	30	14	5,726 (2005)	[6, 48]
Luton, UK	2006	FTR train to plane	1	5	2	4	30,000 (2010)	[6]
York, UK	2006	FTR First York	1	5	10	11	5,500 (2010)	[6]
Lorient Triskell, France	2007	BHLS	1	5	15	13	15,000 (2009)	[6, 47]
Maubeuge, France	2008	BHLS - Viavil	1	7.5	14	20	5,000 (2009)	[6, 47]
Toulouse, France	2008	Toulouse BSP	2	11	17	11	13,300 (2009)	[6, 47]
Istanbul, Turkey	2008	Metrobus	2	43	33	300	700,000 (2010)	[6, 11]
Castellon de la Plana, Spain	2009	TVRCAS	1	1	4	2	4,000 (2010)	[6]
Cambridge, UK	2009	Guided Busway	1	25	50	46	36,938 (2005)	[6, 48]
Swansea, UK	2009	FTMetro	1	13.5	27	10	5,000 (2010)	[6]
London, UK	2010	East London Transit	1	20	40	18	9,000 (2010)	[6]

Bus Rapid Transit: Worldwide History of Development, Key Systems and Policy Issues. Figure. 8 Istanbul Metrobüs, intercontinental BRT system (Source: Dario Hidalgo, EMBARQ, March 2010)

Bus Rapid Transit: Worldwide History of Development, Key Systems and Policy Issues. Table 6 BRT and bus corridors in Asia as of January 2010

City	Initial year	Name	Corridors	Kilometers	Stations	Buses	Passengers/day (year)	Source
Taipei, China Taiwan	1996	Busways	10	30.3	143	1,680	1,680,000 (2008)	[6, 52]
Kunming, China	1999	Busways	5	46.7	63	156	156,000 (2010)	[6, 53]
Nagoya, Japan	2001	Yutorito Line	1	6.5	9	52	26,000 (2010)	[6]
Seoul, North Korea	2003	Median bus lanes	5	43	73	500	400,000 (2009)	[6, 53]
Jakarta, Indonesia	2004	TransJakarta	10	172.2	241	520	276,643 (2010)	[6, 50]
Beijing, China	2005	Beijing BRT	3	34.5	60	200	200,000 (2008)	[6, 53]
Batam, Indonesia	2005	Bus Pilot Project	2	36	20	22	1,472 (2010)	[6, 50]
Hangzhou, China	2006	Hangzhou BRT	2	18.8	50	104	153,000 (2010)	[6, 53]
Pune, India	2006	Pune BRTS	2	16.5	33	54	54,000 (2010)	[6]
Bogor, Indonesia	2007	Trans Pakuan	2	60	56	30	2,978 (2010)	[6, 50]

Bus Rapid Transit: Worldwide History of Development, Key Systems and Policy Issues. Table 6 (Continued)

City	Initial year	Name	Corridors	Kilometers	Stations	Buses	Passengers/day (year)	Source
Tehran, Iran	2007	Tehran BRT	5	91	114	1,125	1,440,000	[6]
Changhzou, China	2008	Changhzou BRT	2	41	51	240	240,000 (2010)	[6, 53]
Chongqing, China	2008	Chongqing BRT	1	6	9	10	1,500 (2010)	[6, 53]
Dalian, China	2008	Dailan BRT	1	9	13	87	87,000 (2010)	[6, 53]
Jinan, China	2008	Jinan BRT	4	34.4	46	165	162,750 (2010)	[6, 53]
Xiamen, China	2008	Xiamen BRT	3	48.9	40	177	177,750 (2010)	[6, 53]
New Delhi, India	2008	Delhi BRTS	1	5.8	9	96	95,565 (2010)	[6]
Yogyakarta, Indonesia	2008	Trans Jogja	3	90	76	75	12,702 (2010)	[6, 50]
Zhengzhou, China	2009	Zhengzhou BRT	1	26.6	38	170	84,000 (2010)	[6, 53]
Ahmedabad, India	2009	Janmarg	3	39	61	60	102,013 (2010)	[6, 54]
Bandung, Indonesia	2009	Trans Metro Bandung	1	16	15	10	589 (2010)	[6, 50]
Manado, Indonesia	2009	Trans Kawanua	2	51	39	27	108 (2010)	[6, 50]
Pekanbaru, Indonesia	2009	Trans Metro Pekanbaru	2	74	58	20	5,691 (2010)	[6, 50]
Semarang, Indonesia	2009	Trans Semarang	1	30	53	20	2,560 (2010)	[6, 50]
Guangzhou, China	2010	Guangzhou BRT	1	22.5	26	800	800,000 (2010)	[6, 53]
Hefei, China	2010	Hefei BRT	2	12.7	14	65	65,250 (2010)	[6, 53]
Yancheng, China	2010	Yancheng BRT	1	8	21	20	20,000 (2010)	[6, 53]
Zaozhuang, China	2010	Zaozhuang BRT	1	33	24	20	20,000 (2010)	[6, 53]
Jaipur, India	2010	Jaipur bus	1	7.1	10	20	6,200 (2010)	[6]
Gorontalo, Indonesia	2010	Trans Hulonthanlangi	3	90	84	15	1,920 (2010)	[6, 50]
Palembang, Indonesia	2010	Trans Musi	2	60	106	15	1,920 (2010)	[6, 50]
Surakarta, Indonesia	2010	Batik Solo Trans	1	30	53	15	1,920 (2010)	[6, 50]
Bangkok, Thailand	2010	Bangkok BRT	1	15.9	12	20	10,000 (2010)	[6, 53]

Bus Rapid Transit: Worldwide History of Development, Key Systems and Policy Issues. Figure. 9 Guangzhou, China, BRT corridor (Source: Karl Fjelstrom [49] http://www.transportphoto.net/photo.aspx?id=7599&c=Guangzhou&l=en)

Bus Rapid Transit: Worldwide History of Development, Key Systems and Policy Issues. Table 7 BRT and bus corridors in Australia and Oceania as of January 2010

City	Initial year	Name	Corridors	Kilometers	Stations	Buses	Passengers/ day	Source
Adelaide, Australia	1986	O-Bahn	1	12	3	138	28,000 (2009)	[6, 55]
Brisbane, Australia	2001	Brisbane Busway	3	23.8	21	1,002	242,000 (2009)	[6, 55]
Melbourne, Australia	2003	SmartBus	4	233	56	122	36,200 (2009)	[6, 55]
Sydney, Australia	2003	Busways	3	49.1	58	140	32,400 (2009)	[6, 55]
Auckland, New Zealand	2005	Northern Busway	1	5.9	4	9	7,200 (2009)	[6, 55]

roads of an existing expressway with a length of 22 km, 26 stations, and 220 buses, carrying 220,000 passengers per day [57]. However, it is not considered a full BRT, as the bus lanes are on the kerb side, with some sections on mixed traffic and access to the buses requires stairs [56].

Johannesburg launched a full BRT system in preparation to the Football World Cup in 2009 (Fig. 11). The system is 25 km long (out of 122 km planned), with 33 stations and 143 buses. It connects the high-density community of Soweto with the central business district and carries 70,000 passengers per day [58].

Bus Rapid Transit: Worldwide History of Development, Key Systems and Policy Issues. Figure. 10
Brisbane BRT (Source: Karl Fjelstrom December 2004, http://www.transportphoto.net/photo.aspx?id=1303&c=Brisbane&l=en)

Bus Rapid Transit: Worldwide History of Development, Key Systems and Policy Issues. Figure. 11
Rea Vaya, Johannesburg's BRT, South Africa (Source: Rea Vaya (2010) http://www.reavaya.org.za/photo-gallery/state-of-the-art/category/1)

Cape Town (South Africa) started operations of its BRT in 2011. There are systems in intermediate planning stages in Port Elizabeth and Pretoria (South Africa); Dar es Salaam (Tanzania) and Accra (Ghana) [56]. Other cities considering BRT include Kampala (Uganda), Nairobi (Kenya), and Bloemfontein – Ethekwini, East London – Buffalo City, Ekurhuleni, Polokwane, and Rustenburg (South Africa) [56].

The main challenges for African cities are the creation of local capacity to oversight and operate systems, transforming the paratransit informal services and funding the capital costs (infrastructure and buses) [56].

Future Directions

BRT will evolve in several directions, namely:

1. BRT will gradually become an integral part of most transit systems, as the cities grow their corridors into networks and integrate BRT services with other modes of transport (metro, regional rail, and standard buses). Pedestrian and bicycle access will be improved, and bike- and car-sharing services will be incorporated around BRT stations.
2. Automatic guidance systems, using video, magnetic or physical devices, will evolve to ensure optimal docking at stations. In some cases, priority lanes will be intermittent; only a few meters ahead and behind the bus will be reserved using advanced signal and communications technologies, at other times the lanes may be used for general traffic [59]. This will eliminate the perception of "empty lane" in systems with headways beyond 2 min.
3. The buses will have several advanced technology components: hybrid buses, plug-in hybrids, or fully electric with high autonomy or extra-fast battery charging systems at each station. Alternative technologies will evolve, such as solar recharging hydrogen fuel cell, biofuels from sustainable feedstock, among others.
4. Programming and operations will improve due to the availability of intelligent transport systems (ITS), including the integration into the signal networks (advanced transit signal priority [TSP]). Improved control (Global Positioning System [GPS], Automatic Vehicle Location [AVL], and Operations Support Systems) will allow optimal regulation and dynamic equilibrium of the supply (buses) and the travel demand (passengers). Very advanced routing systems will be possible, including super express, express, and local, services, as well as direct services, to reduce transfers.
5. Fare collection systems will be integrated into cell phones and turnstiles will no longer be required. Tickets will be deducted automatically from electronic wallets, which will have other multiple applications, just as debit cards. User fares will be differentiated by time of day, day of week, and length according to the supply and demand conditions of the system, increasing efficiency and service quality.
6. User information systems will be dynamic, with electronic panels that indicate the next bus and public announcements, helping users to navigate the system in advanced screens or cell phones.
7. Land use along the corridors will include good accessibility, high-density, and mixed uses (Transit-Oriented Development [TOD]). BRT will support urban development and vice versa.
8. Contracts with private operators will be based on performance, with dynamic adjustment formulas of their revenue according to changes in input costs.
9. Infrastructure, technology, training, education, and control will ensure safety, with a vision of zero tolerance of severe injuries and fatalities.
10. BRT will facilitate physical activity, low or zero emissions, and universal accessibility (disabled people).

Many of these advances are already applied in several systems around the globe or under research and development. Integration into future BRT systems will happen in the next few years.

Bibliography

1. Levinson H, Zimmerman S, Clinger J, Gast J, Rutherford S, Bruhn E (2003) Bus rapid transit, vol 2: implementation guidelines. Transit cooperative research program – report 90, vol II. Transportation research board, National Academies, Washington, DC
2. Wright L, Hook W (eds) (2007) Bus rapid transit planning guide, 3rd edn. Institute for Transportation and Development Policy, New York

3. Levinson H, Zimmerman S, Clinger J, Rutherford S, Smith RL, Cranknell J, Soberman R (2003) Bus rapid transit, vol 1: case studies in bus rapid transit. Transit cooperative research program – report 90, vol I. Transportation research board, National Academies, Washington, DC
4. Wilbur Smith and Associates (1966) Under commission from American Automobile Manufacturers Association (Levinson HS, Principal Investigator). Transportation and parking for tomorrow's cities, New Haven, Cited by 3
5. Lindau LA, Hidalgo D, Facchini D (2010) Curitiba, the cradle of bus rapid transit. Built Environ 36(3):274–282, http://www.atypon-link.com/ALEX/toc/benv/36/3
6. Hidalgo D (2011) The global bus rapid transit (BRT) industry, EMBARQ, The world resources institute center for sustainable transport, Washington, DC, Jan 2011. http://www.embarq.org/en/the-global-bus-rapid-transit-brt-industry. Accessed 10 May 2011
7. Light Rail Now (2011) Bus rapid transit analyses. http://www.lightrailnow.org/facts/fa_brt.htm. Accessed 10 May 2011
8. Hidalgo D, Carrigan A (2010) Modernizing public transportation, Lessons learned from major bus improvements in Latin America and Asia, World Resources Institute, Washington, DC. http://www.embarq.org/en/modernizing-public-transportation. Accessed 10 May 2011
9. Diaz RB (ed), Hinebaugh D (2009) Characteristics of BRT for decision makers (CBRT), 2nd edn. Publication FTA-FL-26-7109.2009.1, Federal Transit Administration, United States Department of Transportation, Washington, DC
10. Vuchic VR (2007) Urban transit systems and technology. Wiley, Hoboken
11. IETT (2011) Istanbul public transport authority, Istanbul Metropolitan Administration, Turkey. http://www.iett.gov.tr/en/section.php?sid=58. Accessed 11 May 2011
12. TRANSMILENIO SA (2011) Empresa de Transporte del Tercer Milenio S.A., Alcaldía Mayor de Bogotá, D.C., Colombia. http://www.transmilenio.gov.co/WebSite/Default.aspx. Accessed 11 May 2011
13. ChinaBRT (2011) Guangzhou BRT. http://www.chinabrt.org/en/cities/guangzhou.aspx. Accessed 11 May 2011
14. Hensher D (1999) A bus-based transitway or light rail? Continuing the saga on choice versus blind commitment. Road Transp Res 8(3):3–21
15. CTS Mexico (2011) Usuarios aprueban Macrobús, identifican temas por resolver, Centro de Transporte Sustentable de México, México. http://www.ctsmexico.org/node/426. Accessed 11 May 2011
16. CTS Mexico (2011) V Encuesta de Opinión al Usuario de Metrobús, Centro de Transporte Sustentable de México, México. http://www.ctsmexico.org/node/160. Accessed 11 May 2011
17. INE (2008) The benefits and costs of a bus rapid transit system in Mexico City, Instituto Nacional de Ecología, México. http://www.epa.gov/ies/pdf/mexico/Metrobus%20Mexico%20Phase%20III.pdf. Accessed 11 May 2011
18. Hidalgo D, Pereira L, Estupiñan N, Jiménez PL (2010) TransMilenio de Bogotá, Un Sistema de Alto Desempeño e Impacto Positivo – Principales Resultados de Evaluación Ex-Post de las Fases I y II. XVI Congreso Latinoamericano de Transporte Público y Urbano –CLATPU, México, 6–8 Octubre 2010
19. Hidalgo D (2009) Citywide transit integration in a large city: the Interligado system of São Paulo, Brazil. Transp Res Rec J Transp Res Board 2114:19–27 (Developing countries)
20. Muñoz JC, de Ortúzar JD, Gschwender A (2009) Transantiago: the fall and rise of a radical public transport intervention. In: Saleh W, Sammer G (eds) Travel demand management and road user pricing: success, failure and feasibility. Ashgate, Farnham, pp 151–172 (Chapter 9)
21. Hidalgo D, Voukas Y, Freiberg G, Lopez A, Alveano S (2010) The Macrobus system of Guadalajara, Mexico: an evolved concept in BRT planning and implementation for medium capacity corridors, XVI Pan-American conference of traffic and transportation engineering and logistics – Lisbon, 16–18 July 2010
22. TRANSMILENIO SA (2010) Sistema Integrado de Transporte Público SITP. http://www.transmilenio.gov.co/WebSite/Contenido.aspx?ID=AcercaDelSITP. Accessed 11 May 2011
23. Mier y Terán C (2009) PROTRAM federal mass transit program, World Bank transport forum 2009, 31 March 2009. http://siteresources.worldbank.org/INTENERGY/Resources/335544-1232567547944/5755469-1239633250635/Carlos_Mier_Y_Teran.pdf. Accessed 11 May 2011
24. Ministerio das Cidades (2010) PAC 2 Mobilidade Grandes Cidades, Governo do Brasil. http://www.cidades.gov.br/index.php?option=com_content&view=article&id=776:pac-2-mobilidade-grandes-cidades&catid=68&Itemid=103. Accessed 11 May 2011
25. Ministry of Urban Development, Government of India (2010) Jawaharlal Nehru National Urban Renewal Mission JnNURM. http://jnnurm.nic.in/. Accessed 11 May 2011
26. Ministry of Urban Development, Government of India (2007) National Urban Transport Policy. http://www.urbanindia.nic.in/policies/TransportPolicy.pdf. Accessed 11 May 2011
27. National BRT Institute (2011) http://www.nbrti.org/. Accessed 12 May 2011
28. Hofman A (2011) Advanced network planning for bus rapid transit: the "Quickway" model as a modal alternative to "Light Rail Lite", Federal transit administration, FTA-FL-26-7104.2007.4. http://www.nbrti.org/docs/pdf/BRT%20Network%20Planning%20Study%20-%20Final%20Report.pdf. Accessed 12 May 2011
29. OC Transport (2011) Ottawa's light rail future. http://www.octranspo1.com/routes/ottawas_light_rail_futurem. Accessed 12 May 2011
30. http://www.yrt.ca/. Accessed 10 Jan 2011
31. http://www.nyc.gov/html/dot/downloads/pdf/ssi09_projects/ssi09_fordham_sbs.pdf. Accessed 10 Jan 2011
32. http://www.commtrans.org/News/New.cfm?id=1386. Accessed 10 Jan 2011

33. http://en.wikipedia.org/wiki/Z%C3%BCm. Accessed 10 Jan 2011
34. Hidalgo D, Carrigan A (2010) BRT in Latin America – high capacity and performance, rapid implementation and low cost. Built Environ 36(3):283–297
35. Hidalgo D, Lleras G, Hernández E (2010) Capacidad en Sistemas de Transporte Masivo en Buses - Desarrollo de Fórmulas y Aplicación al Caso de TransMilenio de Bogotá, XVI Congreso Latinoamericano de Transporte Público y Urbano –CLATPU, México, 6–8 Octubre 2010
36. ANTP (2011) http://portal1.antp.net/site/simob/Lists/MrsCdds09/Mcidades.aspx. Accessed 10 Jan 2011
37. TRANSMILENIO SA (2010) http://www.transmilenio.gov.co/WebSite/Contenido.aspx?ID=TransmilenioSA_TransmilenioEnCifras_EstadisticasGenerales. Accessed 10 Jan 2011
38. Fundación Metrovía (2010) www.metrovia-gye.com/start.htm. Accessed 10 Jan 2011
39. Trolebús Mérida (2010) http://www.venezuelavanza.es.tl/TROLEBUS–g-MERIDA-g-.htm. Accessed 10 Jan 2011
40. Ministerio de Transporte (2010) Sistemas de Transporte Masivo en Colombia. Unidad Especial de Transporte Masivo, Bogotá
41. Municipalidad de Recife (2010) http://www.recife.pe.gov.br/pr/secplanejamento/caxanga.html. Accessed 10 Jan 2011
42. http://es.wikipedia.org/wiki/Mexib%C3%Bas. Accessed 10 Jan 2011
43. http://www.agenciat1.com.br/4101-onibus-ganham-faixa-exclusiva-em-joao-pessoa/. Accessed 10 Jan 2011
44. Menckhoff G, Ochoa C, Ardila A (2010) El Metropolitano de Lima: Implementación y Primeros Resultados de un Nuevo Sistema BRT. Congreso Latino Americano de Transporte Público y Urbano, CLATPU, Ciudad de México, Octubre 2010
45. Heddebaut O, Finn B, Raubel S, Rambaud F (2010) The European bus with high level of service (BHLS): concept and practice. Built Environ 26(3):307–316
46. COST BHLS (2010) www.bhls.eu. Accessed 10 Jan 2011
47. Rabuel S (2010) Buses with high level of service: choosing and implementing the right system, centre for the study of urban planning, transport and public facilities, CERTU. http://www.nbrti.org/docs/pdf/buseshighlevelofservice_bhns_2009_english.pdf. Accessed 10 Jan 2011
48. http://www.ashford.gov.uk/pdf/Planning_Pentland_6c_WS_11.pdf. Accessed 10 Jan 2011
49. Fjelstrom K (2010) Bus rapid transit in China. Built Environ 26(3):363–374
50. Ernst JP, Sutomo H (2010) BRT´s influence on public transport improvements in Indonesian cities. Built Environ 26(3):344–352
51. Tiwari G, Jain D (2010) Bus rapid transit projects in Indian cities: a status report. Built Environ 26(3):353–362
52. Chang M (2008) BRT in Taiwan. http://ce11012.ce.ntu.edu.tw/paper%5CBeijing%20skchang.pdf. Accessed 10 Jan 2011
53. ITDP (2011) BRT in China and Asia. http://www.chinabrt.org/. Accessed 10 Jan 2011
54. CEPT University (2010) Janmarg 14th month report, CEPT University Ahmadabad, 4 Dec 2010
55. Currie G, Delbosc A (2010) Bus rapid transit in Australasia: an update on progress. Built Environ 26(3):328–343
56. Gauthier A, Weinstock A (2010) Africa: transforming paratransit into BRT. Built Environ 26(3):317–327
57. Moberola D (2010) The Lagos BRT system, LAMATA. http://siteresources.worldbank.org/EXTAFRSUBSAHTRA/Resources/DP09-Lagos-BRT.pdf. Accessed 10 Jan 2011
58. Mcaul C (2010) Rea Vaya, the Johannesburg BRT. http://www.sutp.org/documents/Armin-Nairobi-event/BRT%20Joburg%20Presentation_McCaul.pdf. Accessed 10 Jan 2011
59. Viegas J, Baichuan L (2004) The intermittent bus lane signals setting within an area. Transp Res C Emerg Technol 12(6):453–469

Bus Rapid Versus Light Rail Transit: Service Quality, Economic, Environmental and Planning Aspects

Vukan R. Vuchic[1], Richard M. Stanger[2], Eric C. Bruun[1]
[1]Department of Electrical & Systems Engineering, University of Pennsylvania, Philadelphia, PA, USA
[2]Los Angeles, CA, USA

Article Outline

Glossary
Definition of the Subject
Introduction
Process and Controversies in Selecting Transit Modes
Negative Trends in the Application of Urban Transit Modes Between 1945 and 1975
Inherent Differences Between Industrialized and Developing Countries
Light Rail Transit
Upgrading Bus Services into Bus Transit Systems and Bus Rapid Transit
Comparison of LRT and BRT Modes
Trends and Expected Future Directions
Bibliography

Glossary

Access time The component of door-to-door travel time spent leaving the point of trip origin to a transit stop.

Annualized operating cost The direct cost of operating and maintaining a transit route or set of routes over a whole year; an average value.

Articulated bus A bus vehicle with three (exceptionally four) axles and two (exceptionally three) body sections connected by body joints that provide a continuous interior for passengers. Body articulations allow the bus to make turns occupying a moderately wider body profile than a regular, two-axle bus.

At-grade BRT Bus rapid transit that is predominantly on ROW B and has most of the following elements: signal priority at intersections and other preferential treatments elsewhere; well-spaced stops like stations, with good passenger amenities; regular, reliable services throughout the day; off-board fare collection; real-time arrival information; large, distinctive buses allowing rapid passenger exchange; and a clear, branded image.

Automated guided transit (AGT) Automated vehicles, operated on ROW A, in either a shuttle or loop configuration, typically serving internal circulation needs of large institutions or downtowns. Vehicles may be either steel wheel or rubber tired.

Average operating speed A performance indicator computed by dividing the length of a route or line by the travel time required.

Bogie or truck (United States) Frame containing axle, motor, and brake assemblies and pivots under the body/chassis of a rail vehicle.

Build-operate-transfer (BOT) A project implementation method where one single entity is responsible for building transit infrastructure, procuring all needed equipment and managing the operations for an initial period time before the eventual handover to public ownership.

Bus lane Traffic lane for exclusive (or dominant) use by buses. It may be:

Contraflow – Operating in the opposite direction from other traffic.

Exclusive – Physically separated lanes (usually two) for bus use only.

High Occupancy Vehicle (HOV) Lane – A traffic lane open only to vehicles with more than a minimum number of persons onboard.

Regular – Lane on urban street or motorway reserved only for buses, separated by markings, signs, or cones but not physically separated.

Bus rapid transit (BRT) or bus transit with high level of service (BHLS) Bus transit system with mostly ROW B, long spacings between stops, signal priorities, vehicles with distinct image, and other rail-like components for high performance.

Bus transit system (BTS) A bus service designed as a coordinated system with average stop spacings of at least 300 m, some bus lanes, passenger-friendly vehicle design, operations control, passenger information, etc., for higher speed, reliability, and efficiency.

Consist A set of rail vehicles coupled into a train.

Cross-subsidization The concept of using excess revenues (profits) from one line or route and using them to support another line that earns revenues less than its costs.

Deadheading Moving a transit unit to a line from a depot or storage location or repositioning a vehicle to another line without passengers.

Design-build model An approach to major projects making the same firm/consortium responsible for both the design and construction phases.

Design-build-operate-maintain (DBOM) model An approach to major projects in which the same firm/consortium is responsible for the design, construction, operation, and maintenance phases.

Diametrical line (or route) A transit line that has a radial alignment from a suburb to center city, crosses it, and continues into another suburb.

Economy of scale The unit cost of output decreases with the quantity of output.

Elasticity of demand The percentage change in ridership over the percentage change in some other quantity (e.g., fare or frequency)

Frequency The rate at which transit units pass a fixed point, usually expressed per hour; it is the inverse of headway but usually expressed in minutes.

Global positioning system (GPS) The currently dominant vehicle location system, based on taking position fixes from multiple satellites.

Guideway A travel way (rail track, guide beam, and other guiding surfaces) that physically guide vehicles. Guideways for nonrail vehicles always require ROW A.

Headway The time interval between transit units passing a fixed point, usually expressed in minutes. It is

the inverse of frequency, which is usually expressed as departures per hour.

High occupancy vehicle (HOV) lane A traffic lane open only to vehicles with more than a minimum number of persons onboard.

Hybrid vehicle A bus or rail transit vehicle that combines two different forms of propulsion like an internal combustion engine and an electric motor, which operate in optimum combination for each regime, such as in acceleration, low or high speed, etc.

Intelligent transportation system (ITS) A package of hardware and software specifically designed for improving transportation operations, information to the public, and/or information for service planning.

Interlining The practice of having a vehicle continue onto another line or route rather than reversing at a terminus.

Level of service (LOS) The combined service characteristics experienced by the user.

Light rail transit (LRT) A transit mode utilizing predominantly ROW B, sometimes A or C, on different network sections. Its electrically powered vehicles operate in one- to four-car transit units. The mode has a wide range of LOS and performance characteristics.

Light rail vehicle (LRV) An electric rail transit vehicle, powered or unpowered, with up to seven body sections and overall length of 20–50 m capable of operating on ROW A, B, and C.

Line capacity The maximum throughput of transit units (TUs) or spaces measured at one point on a line on a per-unit time basis; it has a wide range of values depending upon safety regime and assumed crowding standards.

Linked trip A trip that includes all segments a user makes on public transport vehicles.

Load factor or coefficient of utilization Ratio of passengers in a vehicle/transit unit and its total capacity in spaces.

Locally preferred alternative The project alternative selected locally that is then submitted to the federal government for further review and a funding decision (specific to the United States).

Marginal cost The cost to carry one more vehicle on a roadway, one more person in a transit vehicle, or, in general, the cost of providing one more unit of service output.

Maximum load section (MLS) The segment of a line or route on which the maximum number of passengers is carried.

Metropolitan planning organization (MPO) A governmental body legally required to do transportation forecasting and to propose a transportation improvement/investment plan for a metropolitan region (specific to the United States).

Modal split The fraction of trips by a particular mode along a route or line, between two points, or across an entire region.

Monorail An urban transit technology that operates exclusively on right-of-way A using in most cases tires for both lateral and vertical support on a beam with a special cross section, typically a proprietary design.

National Transit Database (NTD) A source of operating statistics and cost information for each transit agency receiving federal funds that is broken into categories used for cost modeling and estimating (United States only).

No-build scenario A project alternative used to compare what may happen if no action is taken. The no-build alternative may sometimes include modest Transportation Systems Management investments.

O-Bahn Bus transit technology in which buses have two horizontal wheels and roadway has two lateral surfaces; the buses can operate on regular streets or enter sections where guiding wheels stretch out and provide guidance against the lateral surfaces so that the driver does not steer.

Operating speed Average speed on a line or network including times for stops, but not terminal times and deadheading.

Opportunity cost The forgone possibilities when resources are committed to a particular project alternative.

Pantograph A spring-loaded mechanism mounted atop electric vehicles that glides along and collects current from a suspended high-voltage catenary.

Paratransit In the narrow definition, services provided as a public service on a demand-responsive basis; in the broader definition any for-hire services that are not fixed route (e.g., taxis, jitneys, vanpools, airport shuttles, etc.).

People mover The informal name for Automated Guided Transit (AGT) system.

Public–private partnership (PPP) A method of project development in which responsibilities and finances are divided amongst various parties in recognition of the benefits each can receive, hopefully to the mutual benefit of all parties.

Radial line (or route) A line or route that begins in CBD or at a center of activity and goes to suburbs, in the direction of lower demand density.

Real-time passenger information (RTPI) The estimated arrival time for a vehicle at a particular stop based on tracking of actual location versus scheduled location; it can be delivered with signs in the field over the Internet, over Personal Digital Assistants (PDAs), cell phones, etc.

Regular Lane on urban street or motorway reserved only for buses, separated by markings, signs, or cones but not physically separated.

Right-of-way (ROW) Broadly speaking, any path or way on which a transit vehicle travels. Transit rights-of-way (ROW) are classified in three categories:

Category A Right-of-Way (ROW A) – Fully controlled ROW without (or with fully protected) grade crossings or any legal access by other vehicles or persons; also called "grade-separated" or "exclusive" ROW. It can be a tunnel, aerial, or at-grade level.

Category B Right-of-Way (ROW B) – ROW horizontally separated from other traffic (by curbs, barriers, grade-separations, etc.), but with grade crossings for vehicles and pedestrians usually at regular street intersections.

Category C Right-of-Way (ROW C) – Surface streets with mixed traffic. Transit may have preferential treatment, such as reserved lane but not physically separated lanes, or it may travel in general traffic lanes.

Short turning Transit line on which some transit units turn back at a station closer than the outlying terminal.

Shuttle A route that consists of only two stops, one at each terminus.

Space-averaged load factor A performance indicator used to measure vehicle space consumption efficiency over the length of a route, computed as the ratio of total space-distance consumed over total space-distance offered.

Streetcar A rail transit mode consisting of electrically powered rail vehicles operating in one- to three-car transit units, usually on ROW B or C.

Sustainable Development The concept that economic development should take place so that nonrenewable resources are not depleted and natural systems of restoration and pollution mitigation are not overloaded.

Tangential route (or Line) A route or line that does not enter into a central area, but instead connects peripheral locations, generally having the property of more even loading because demand does not increase continually as with radial routes.

Timed-transfer system (TTS) A network consisting of transit lines and one or several transit centers or focal points at which transit units from intersecting lines arrive simultaneously, allowing easy passenger transfer in all directions.

Tramway See Streetcar

Transit signal priority (TSP) The control of traffic signal timing, and possibly street layout, designed to favor transit vehicles over private vehicles.

Truck See Bogie

Unlinked trip A trip counted separately, even if it may actually be a transfer between two transit vehicles.

Zonal service Transit service in which trains operate express or local along different sections of the route, with connections between zones only at a few joint stations.

Definition of the Subject

The term "urban public transit" encompasses a family of modes each serving a particular transport market. These modes can be arrayed by their costs and the quality of service they provide. Toward one end of the spectrum is the typical urban bus mode. At the other end are the regional rail systems with their high speeds and high capacities. In between, urban transit modes have ranges of cost and performance that overlap, and choosing between them may be difficult. Over the last several decades, the modes most often seen as competing for selection are bus rapid transit (BRT) and light rail transit (LRT).

This debate between the BRT and LRT advocates has too often been destructive, pitting two important urban transit modes against each other when the real "enemy" is the overuse and overfunding of the private car. Policymakers are often left more confused as they listen to the different opinions of their transit advisors. Sometimes they are led to believe that they will be able to save money with BRT yet get the same level of transit service and capacity as with LRT; in other cases they realize that an LRT solution is the better one even if it requires higher investment because of its stronger passenger attraction, permanence, and stronger positive impacts on the city.

What would be useful is to understand why and how the BRT and LRT modes evolved and what roles they play within a public transit network. Important in this context is to see BRT as several distinct services, each important, but few providing the speed and capacity of light rail transit.

Introduction

There has long been an ongoing debate in urban transportation on the role of bus and rail modes in urban transportation. That debate is actually a "subproblem" of the overall urban transportation problem – the relationship between public transit, private cars, pedestrians, and other modes. This problem occurs in all countries when auto ownership increases rapidly. The debate eventually defines the main issue: medium and large cities face the "collision of cities and cars." The excessive traffic congestion caused by cars, which is wasteful, environmentally damaging and degrading to a city's livability, can be solved either by extensive construction of highways and parking facilities or by controlling the use of private cars and offering competitive transit systems.

The policies of "adjusting cities to cars" were particularly strong in the United States. From 1945 to 1970, there was massive financial support for highway construction with negligible support for transit and the total neglect of pedestrians.

This wave of "auto mobilization" of cities also encompassed transit planning. A campaign swept the country against rail modes and for the replacement of streetcars by "flexible buses" in mixed traffic. This campaign, fueled by highway, car manufacturers, and the oil industry, also actively worked against rail rapid transit systems. A major consulting firm developed an all-bus plan for Washington, D.C., a city that obviously needed rapid transit. The plan showed buses in huge underground stations with insufficient capacity, lack of signalization, and unacceptable exhaust gases. Moreover, the system would have required higher investment and operating costs than the rail. There was even a campaign alleging that "flexible" paratransit was more efficient for car-based cities than "fixed" rail transit.

Yet, even as the construction of metro and light rail transit lines intensified in dozens of cities in North America and around the world over the last 4 decades, extreme anti-rail transit views continue in some countries. In the United States, through the 1950–1970 period, the only urban transit modes to choose from were low-investment buses and trams (streetcars), and very high-investment rail rapid transit (metros or subways). The evolution of the tram into light rail transit (LRT), first introduced in Europe in the 1960s and then in the United States by 1980, gave urban planners a rail mode with some of the attributes of rapid transit that was more cost-effective in medium-density corridors and medium-size cities. This evolution was made possible by relocating trams from city streets and mixed traffic onto their own, separated (generally) at-grade rights-of-way.

Over the last 2 decades, a similar evolution has occurred with buses. Early on freeway bus lanes were introduced. Later, select bus routes on urban streets were upgraded through a series of smaller steps including longer bus stop spacing and preferential lane and signal treatments. As the ultimate step in this evolution, several cities have built largely grade-separated busways (e.g., Ottawa and Bogotá). This wide range of bus improvements was given the single label bus rapid transit (BRT) (Fig. 1).

However, the introduction of the BRT concept has again ignited a campaign that BRT can provide the same service as rail transit but at a much lower cost. As further discussion will show, BRT offers a different set of features than rail transit and it differs considerably from LRT, so that services of the two modes are by no means fully comparable. Nor are their permanence and impact on cities comparable.

Bus Rapid Versus Light Rail Transit: Service Quality, Economic, Environmental and Planning Aspects. Figure 1 Two BRT vehicles in Bogota, Colombia can carry all the people in the cars shown in six highway lanes

The debate between BRT and LRT advocates is important because policymakers who want to improve their transit systems often do not understand what each mode is able to deliver. The ongoing arguments among their advisors on the merits of BRT versus LRT are destructive for two reasons: they waste time and too often further delay already long-delayed decisions, and they play into the hands of those who are against any improvements to public transit.

This section reviews the evolution of both LRT and BRT and explains how each might meet the transit needs of cities. It defines the subcategories of bus services that fall under the umbrella term "BRT" in an effort to separate bus systems which have many LRT features (primarily separated ROW B, signal priority, and long lengths between stops) from buses which have only a few operational improvements.

Process and Controversies in Selecting Transit Modes

Civic leaders, transportation planners, and the public in general are increasingly recognizing that urban transportation policies, specifically the selection of transit modes, have a major impact on the type and quality of transportation, as well as on the entire city's character and quality of life.

Selection of transit modes is therefore a major step in urban transportation planning. Many factors that should be considered in comparing and selecting transit modes can be grouped into several categories:

- *System performance*: transporting capacity, speed, reliability, safety, comfort, and other elements.
- *Economic aspects*: investment and operating costs estimated for the projected quality of service, volume of attracted passengers, and applied fares.
- *Direct and indirect impacts*: The effects of the planned transit system on the area it serves and the entire city.
- *Role of transit on the livability, sustainability, and global impacts on weather change, energy consumption, and other broad aspects*: The planned transit line or network must analyze these long-term aspects, which are gaining increasing importance.

- *Quality and permanence*: Numerous other factors, such as the ability to protect the transit right-of-way from use by other vehicles.
- *Local preference*: The preference of the population for different transit modes.
- *Influences by different lobbies*: Groups (e.g., labor unions, business interests), often driven by financial interests rather than public interest, often wish to influence major transit decisions.

To compare transit modes systematically, it is very helpful to consider the elements that define modes. They are:

- *ROW category*: There are three types of ROW: A (fully grade separated), B (separated from other traffic), and C (within mixed traffic).
- *Technology*: Its main components are support (road or rail), guidance (steered or guided), propulsion (diesel or electric), and method of driving and control (manual or signalized).
- *Type of service*: This characteristic includes line length and functional role (short-haul, regular city service or regional).

While planning and attention to mode selection must be performed carefully, excessive controversies can be very harmful because they often cause long delays and lead to incorrect decisions, such as selection of a mode without sufficient capacity, with an inferior ability to attract passengers, or a mode that is later degraded by a failure to protect its ROW.

The "family of transit modes" can be formed by listing the modes from the lowest capacity minibuses on ROW C through medium-capacity modes on ROW B, including BRT and LRT, and AGT, metros and regional rail systems with long trains on ROW A providing the highest capacity and performance. When the average investment of these modes per kilometer of line is plotted on the ordinate, the diagram of the family of modes in Fig. 2 shows three areas with their increasing performance and investment costs.

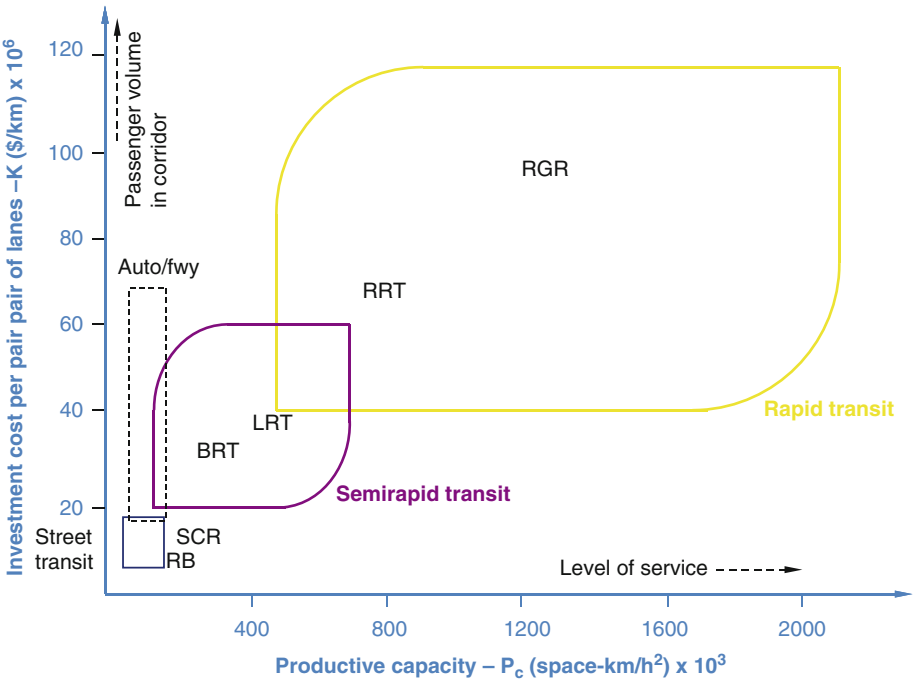

Bus Rapid Versus Light Rail Transit: Service Quality, Economic, Environmental and Planning Aspects. Figure 2 Relationship between system performance (productive capacities) and investment cost of different generic classes of transit modes

Negative Trends in the Application of Urban Transit Modes Between 1945 and 1975

This entry discusses many of the factors that led to the creation of the distinct BRT and LRT modes.

Impact of Auto-highway Expansion on Selection of Transit Modes

Public transport companies, facing heavily subsidized highway construction for private vehicles and virtually no public assistance for transit investments and operations, were forced to convert their systems from electric streetcars and trolleybuses to motorbuses. Part of this conversion was logical when diesel buses were upgraded so that they became more economical and required less investment than streetcars on lightly traveled lines. However, conversion of heavily traveled streetcar lines, particularly those which had separated rights-of-way (category B), was made with explanations that streetcars were obsolete, buses were "more flexible" to mix with general traffic, their lines could be easily changed, etc. Such conversions were mistakes that led to downgrading of transit services in general.

If urban transportation is analyzed as a multimodal system, the nearly complete conversion of streetcars/tramways that was done in the United States, United Kingdom, France, and a number of other countries, had the following results:

+ Lower investment cost for line infrastructure (tracks and overhead cables)
− Loss of transit ROW B and the operation of "flexible" transit vehicles in general traffic, which resulted in reduced speed, reliability, and loss of distinct image of transit services
− Change from rail to bus vehicles which are smaller, less comfortable, have fewer doors, and cannot be coupled in trains (lower line capacity)
− Change from electric to diesel traction, which downgrades performance, generates exhaust gases and noise, and prevents operation in tunnels

Downgrading of Transit Services

There were secondary impacts of the conversion from rail to bus transit. In many cities conversion to buses was followed by the belief that "flexibility" of buses should be used to replace a single heavily traveled line with high frequency of service by a large number of bus routes that provide better area coverage but have longer headways, lower speed, and reliability of service. Such extensive networks, which still exist in many cities, require less transferring, but offer services that have long headways and irregular alignments, resulting in low recognition and image. The belief was that copying services private cars offer would increase transit ridership. However, the opposite happened. Extensive networks of bus services with long and irregular headways attracted significantly fewer passengers than a smaller number of streetcar lines with frequent services.

Replacement of Streetcars by Buses Led to Major Losses of Passengers

The substitution of networks of rail lines having frequent, fast, and reliable services with extensive networks of infrequent bus services was not only less attractive, but in the long run its lower image and permanence diminished the role of transit and made it supplementary to private cars, particularly in small- and medium-sized cities. This was demonstrated by the fact that the number of passengers carried by buses in US cities consistently decreased even during the period between 1950 and 1970, when buses were introduced in many cities to replace streetcars.

Decreasing transit ridership, increasing traffic congestion and deterioration of cities led many cities to search for higher quality of transit services. The experience with "flexible" buses led to realization that making transit vehicles independent of general traffic is the basic element in achieving transit competitive with private cars.

Many cities tried to introduce reserved bus lanes, but found little support from traffic engineers, and great difficulties getting the police to enforce lane separation. The concept of LRT with tracks physically separated from other traffic by curbs was a logical solution to this problem, and since the late 1970s, about 20 cities in North America have introduced LRT systems with separated and protected ROW on their main lines. With the introduction of rail vehicles with greater comfort, more space, and higher speed than buses, many cities were very successful in reversing downward trend of transit ridership.

Two Major Trends in Transit Role Definition and Mode Selection: "Flexible Buses" or Upgrading Streetcars into LRT

Between the 1950s and the 1970s, policies on the selection of transit modes varied among cities depending on local conditions, methods of decision-making, financing sources, and the expertise of transportation planners and transit agencies. Nevertheless, a review of trends during this period of rapid car ownership increase in North America and Europe showed two distinctly different major groups of cities.

Cities with Policies That Encouraged Automobile Use: These policies facilitated unlimited private car use. They were followed in most US, UK, French, and Spanish cities, and they resulted in massive replacements of streetcars/tramways by buses in mixed traffic as well as extensive construction of freeways in urbanized areas. Metro was considered the only alternative for high-performance transit competitive with private cars.

Cities with Policies That Fostered Balanced Intermodal Transportation: These policies implemented *parallel improvements* of streets/highways and transit systems to achieve a balanced urban transportation system. They were the basic transportation policies in most cities in Germany, Switzerland, Austria, Benelux, and most Scandinavian countries as the only solution leading to livable cities. The main element in achieving transit competitive with private cars was recognized to be physical separation of transit, that is, the provision of ROW B and A. Selection of these separated ROWs made LRT the logical choice, because rail offers significantly higher performance, comfort, and image in the city, as well as greater permanence of transit ROW. These advantages were given more weight as, since the 1970s, most busways in the United States were downgraded into HOV facilities, greatly diminishing the priority of buses over other types of vehicles (Fig. 3).

The results of the two sets of urban transportation policies were drastically different with respect to mode selection as well as livability of cities. The cities which followed balanced transportation policies systematically upgraded tramways and buses on streets into semi-rapid transit modes to counter the increasing

Bus Rapid Versus Light Rail Transit: Service Quality, Economic, Environmental and Planning Aspects. Figure 3 Initially an exclusive bus roadway, the El Monte Busway in Los Angeles, USA has been degraded into an HOV facility, even allowing single driver hybrid cars

attraction of private cars, and to make transit independent of traffic congestion. The cities attempting to accommodate the increasing volumes of auto traffic found themselves with low-quality transit buses in ROW C facilities and with an inability to build extensive metro networks due to its high investment cost. Eventually, many of these cities realized that they needed transit modes that offer much higher performance than do buses on streets, but at significantly lower investment costs than metro systems. The LRT mode met this requirement, and it has been built in dozens of cities in the United States, France, United Kingdom, Spain, Canada, and others. Later development of the BRT mode provided another opportunity for these cities to build medium-capacity modes, narrowing the "gap" between buses on streets and metro systems.

Inherent Differences Between Industrialized and Developing Countries

What follows is a generalization. There are, of course, wide differences between particular nations, and even cities within the same nation. Moreover, some economies have such rapid development that the context for planning transport is continually changing. While rapid change increases the need for dramatic action, it also increases the risk of unforeseen consequences from implementing a project. The following are conditions that make the selection of modes in developing countries different than their selection in industrialized countries.

Demographics: Richer countries, by definition, have a population with more travel mode and destination choices. Thus, most new public transportation enhancements in such countries must pay heed to the needs and desires of so-called "choice" riders. While the fare levels are not unimportant, they are less important than creating attractiveness for persons who can afford the high investment and operating costs of auto ownership.

By contrast, in developing countries a large percentage of the population is "captive" riders. They will be either walking or using public transportation. They are much more sensitive to the fare level. If the fare level can be kept very low by allowing greater crowding, this option is often employed even at the expense of losing many choice riders.

In rapidly developing countries there is a need for public transport investments that address both choice and captive riders. On the one hand, suppressing auto use by affluent persons becomes an important goal. On the other hand, an increasing population of lower and medium-income persons and higher development densities demands a goal of providing high capacities with moderate fares. The question then arises whether one mode can address both goals simultaneously or whether different systems must be built for different passenger segments.

Wage levels: Public transport systems in the developed world typically use 70–80% of their operating budget for salaries, wages, and fringe benefits. Thus, it becomes of vital importance to identify and employ technologies that increase worker productivity. Some well-capitalized public transport systems have seen continuing increases in service output with little increase in staff size. The ability to increase consist size without additional drivers is one of the main reasons for upgrading high-demand bus corridors to rail modes. Furthermore, state-of-the-art self-service fare collection like pay-by-phone, computer-aided dispatching for field supervision, Internet-based itinerary planning services, and other advanced technologies can pay for themselves. The ultimate productivity gain is conversion of rail lines to full automation to remove the driver.

By comparison, well-organized transit agencies in developing countries often pay a small fraction of the hourly labor rate paid in richer countries, and with fewer benefits. At the same time, funds to purchase advanced technologies are likely to be scarce. In such an environment, the case to go to rail technologies, or even to larger buses, is not as compelling.

Employment policies and labor regulation: In many developing countries, governments view public transport as a significant source of employment. In some cases, publicly owned services are overstaffed. In many more cases, the vast majority of transport services are provided by owner-operators or persons renting or leasing vehicles from owners of bus fleets. In such situations, attempts to build public transport networks on high-capacity corridors using very large vehicles often meet strong opposition. A recent and dramatic case is the entirety of South Africa. Efforts to design BRT networks in Gauteng (Johannesburg-Pretoria),

Cape Town, and Nelson Mandela Bay all met intense, and even violent, opposition from minibus syndicates.

While it may be logical to suggest that the mobility of millions of persons is more important than the employment of a few thousand persons, it is a fact that politicians can be very wary of labor opposition, particularly in the context of high unemployment. In such cases, the higher labor productivity of rail or large BRT buses is not a particularly strong selling point. (Actually, rail systems do have a lot of other employment in track, station, and vehicle maintenance.)

Financing capacity: The ability to finance major construction projects can be a problem for many cities even in the richer countries. For many poorer cities and countries, it means increasing taxes or depending upon international investment banks that attach conditions to their grants and loans. Either option can be unattractive to politicians.

One of the consequences of the difficulty to finance transit projects is the controversy between building BRT and metros. This is true even for very large cities that need the capacity of a metro due to large populations, long travel distances, and severe street congestion. The choice in such cases is often between the lower investment costs per kilometer of lower-performance BRT, or the higher investment for a higher performance and more permanent rail system.

Organizational capacity and effectiveness: In many developing countries, the existing institutions at the city, regional, and/or national level do not have the ability to design, build, or manage modern high-capacity public transport systems. This lack of capability acts as a deterrent to even consider many projects. One case is instructive. A need for a metro network in Delhi was recognized in 1997, but neither the national government nor prospective international lenders believed that the existing public agency could design, build, or manage such a system given its record of gross overstaffing and inefficiency. Thus a new corporation to be headed by a proven manager was created. In the end, the corporation not only built an excellent metro rail system, but it was well poised to compete against international firms for future projects in other Indian cities.

Public participation: Most of the industrialized countries have public participation laws designed to allow affected parties as well as the average citizens to influence the design process. These laws are a democratic response to cases where citizens receive a new transportation project that they would not have selected had there been more input. This process slows down the design effort, but it also presumably results in a more beneficial and just project in the long run.

Many developing countries, even with well-intentional planners, do not have formal public participation processes. Thus, planners must design systems with less knowledge of the needs and desires of potential users. The technical expertise of planners and engineers is therefore of primary importance.

On the other hand, in some developing countries governments have greater powers than in democratic industrialized countries. This can make the design and build steps far easier, quicker, and more efficient.

Right-of-way acquisition: Obtaining reserved ROW B is the basic element determining the feasibility of semi-rapid transit, BRT or LRT. The possibility of getting a protected ROW depends on many factors, often different in developing and industrialized countries. Advocates of BRT claim that 8–10 m strips of land can be obtained easily in many developing countries because auto traffic volumes are lower than in industrialized countries. However, in numerous cases the expected acquisition of such rights-of-way has proven to be unrealistic.

The reasons for this discrepancy of theoretical claims and real-world implementation are many. Although car ownership in those countries is still low, street traffic congestion is often even more acute than in industrialized countries because their streets are even more congested by trucks, minibuses, rickshaws, taxis, bicycles, pedestrians, and other participants. The diversity of modes makes traffic conditions even more chaotic and difficult to regulate. This makes acquisition of protected traffic lanes extremely difficult. For example, in several cities, fleets of buses that were bought for planned BRT systems had to be stored in expectation that the BRT infrastructure will be built later. In Jakarta, there were legal challenges of exclusion of

other traffic from bus lanes, while in New Delhi regulations allowing and prohibiting taxis from BRT lanes was changed several times.

In industrialized countries there is also a major difference between BRT systems in theory and in practice, but for different reasons. A number of successful reserved busways with most BRT elements were downgraded by their conversion to high occupancy vehicle (HOV) lanes. The decisions for these changes were made by judges in courts (discontinuance of HOV lanes on the Santa Monica Freeway in Los Angeles), by city councils (discontinuance of a bus mall in Philadelphia), by state legislatures (conversion of the El Monte Busway in Los Angeles to HOV lanes), and by other bodies which have no professional expertise in urban transportation.

Decisions to retain the exclusive use of busways by buses or to allow other vehicles vary among cities and countries. In the United States, many exclusive busways have been downgraded to HOV facilities, in many cities taxis are allowed to share busways, and most recently hybrid passenger cars are given this privilege. In Madrid, motorcycles are permitted in busways.

Modal integration: In the more developed countries, it is common for one agency to either provide all services, regardless of mode, or else manage them under one coordinated fare structure. The operator of a particular vehicle in no way depends upon the fares collected (or not) from boarding passengers. In such an environment, it is possible to institute significant or even total network reorganization with the advent of a new mode. Thus the lower income person is not unduly penalized for needing to transfer between services.

By contrast, most developing countries have cash-based operators that depend on retaining all or part of the money collected. At the same time, riders are forced to pay a full fare each time they switch between vehicles or modes. Thus, both the operators and riders have reason to oppose the imposition of a new higher-capacity mode within their existing network. The former sees a revenue loss and the latter sees paying additional fares to use the new service.

Traffic enforcement: Police control and enforcement of exclusive transit rights-of-way is very different for the two semi-rapid transit systems. LRT requires very little police control, mostly limited to intersections. A BRT lane, when it is immediately adjacent to other traffic lanes, is always attractive to road vehicles traveling in other lanes, so that police enforcement must always exist at intersections and bus lanes between intersections.

Police enforcement depends on local police effectiveness, which varies among cities. For example, cities like Singapore and New York have stricter controls than Boston and Moscow. Similar variations exist among cities in developing countries, but in many of their cities the practice of bribing policemen degrades the traffic discipline even more.

Light Rail Transit

Cities which adopted policies of implementing balanced transportation concentrated on upgrading transit by developing rail transit networks on ROW categories B and A. This has been the most important measure making transit independent of street traffic congestion and therefore competitive with the private automobile. Transit on exclusive ROW logically led to the development of advanced articulated rail vehicles, increased operating speeds, reliability, comfort, and safety.

Major changes in medium-capacity rail transit, most of which took place in Germany, The Netherlands, Belgium, and several other European countries, created a transit mode that is actually more similar in its performance and efficiency to metro/rapid transit than to conventional streetcars/tramways, so that it was given a new name: light rail transit, LRT, or Stadtbahn in German (Figs. 4–6).

Development of LRT Mode

Following several decades of system design, rights-of-way development, and technical and operational innovations, LRT has become a very diversified mode. The most significant innovations that led to the creation of LRT and its introduction in dozens of cities are listed in the box below.

It is interesting to note that during the 1970s and 1980s many cities built tunnels for center-city sections of LRT to make their operations as close to the metro as

Bus Rapid Versus Light Rail Transit: Service Quality, Economic, Environmental and Planning Aspects. Figure 4
Tramway on ROW category C in Milan, Italy

Bus Rapid Versus Light Rail Transit: Service Quality, Economic, Environmental and Planning Aspects. Figure 5
LRT on ROW category B in Paris, France

possible. This was the case, for example, in Frankfurt, Stuttgart, Edmonton, and Hannover. Since 1990, however, an increasing number of cities have designed LRT systems that run through pedestrian zones with decreased or eliminated general traffic. For example, in cities like Strasbourg, Calgary, Denver, Barcelona, and Istanbul, LRT trains travel through central cities at lower speeds than tunnels would allow, but that often

Bus Rapid Versus Light Rail Transit: Service Quality, Economic, Environmental and Planning Aspects. Figure 6
LRT on aerial structure in Los Angeles, USA

Bus Rapid Versus Light Rail Transit: Service Quality, Economic, Environmental and Planning Aspects. Figure 7
LRT within a pedestrian zone in Karlsruhe, Germany

does not result in longer passenger trips because it eliminates for passengers the time and effort of walking two levels into and out of underground stations (Fig. 7). Heavily traveled lines with longer trips and a need for higher speed are, however, still being placed in tunnels, on aerial structures or other types of exclusive ROW, as is the case in Dallas (Fig. 8), Cologne, Copenhagen, St. Louis and Rouen.

Bus Rapid Versus Light Rail Transit: Service Quality, Economic, Environmental and Planning Aspects. Figure 8
High-capacity high-speed LRT train in Dallas, USA

Major Steps in the Development of LRT and Its Role as the Leading Medium-Capacity Transit Mode

- Consolidation of extensive tramway networks into fewer, high-performance LRT lines.
- Systematic replacement of ROW C (street running) by ROW B and A, that is, separated ROW.
- Use of street medians, tunnels, or aerial alignments on the same lines.
- Intermodal integration with bus and metro lines through construction of joint transfer stations.
- Development of high-quality rails and switches that provide quiet and virtually perfect riding comfort, far superior to buses and rubber-tired AGT systems.
- Articulated vehicles offering spacious comfort, operated as one- to four-car trains up to 90 m long with capacities as high as 750 spaces.
- Change from unidirectional tramway-type to bidirectional metro-type rolling stock.
- Self-service fare collection allowing rapid boarding/alighting of passengers on all doors and use of any type of fare.
- Low-floor (0.25–0.35 m above top of rails) vehicles facilitate boarding/alighting of all passengers and meet the needs of the disabled.
- Because of increased TU capacity, one-person crews, and increased operating speeds, the productivity of operating personnel (expressed as passenger-km/h/driver) has increased about 20 times from tramways. Productivity is also about five times greater than on the highest capacity BRT (750 vs 150 spaces per driver, not considering typically higher operating speeds of LRT than BRT).
- Operation of LRT in central cities is performed effectively in tunnels, or, in many cities, by running directly in pedestrian malls and zones (with lower operating speeds on such sections).
- Integration (track sharing) of LRT with regional rail lines for services to suburbs and nearby cities.

Major Types of LRT Applications

Successful construction of LRT in many European cities led to numerous professional conferences and the adoption of LRT as the leading medium-capacity transit mode in many countries which had eliminated streetcars/tramways during the 1950–1970 era: United States, Canada, France, United Kingdom, Spain, and a number of others. During this new wave of building LRT since the 1970s, about 100 cities have either expanded or built new lines and networks. In many cities one or several new LRT lines have become the main transit system carriers with significant increases

in transit ridership. This was the case, for example, in San Diego, Calgary, Sacramento, Portland, Strasbourg, Bordeaux, Sevilla, Birmingham, Denver, and many others.

The successful introduction of LRT in so many cities of different sizes and characters is largely due to the extreme diversity of characteristics of the LRT mode. An analysis of the present broad family of tramway/LRT modes has defined ten categories of this mode by its physical, operational features and role it plays in the city's transportation. They are listed in the box below.

Ten Categories of LRT and Its "Neighbors": Tramways and Mini-metro Modes

1. Conventional tramway mostly with ROW B and C: Melbourne, Moscow, St. Petersburg, Toronto
2. Modernized tramways with signal priority, improved stops, prepaid fares, etc.: Amsterdam, Oslo, Prague, Vienna, Zurich
3. New tramways built in redesigned pedestrian-oriented city centers (some also using historic vehicles as center-city shuttles): Grenoble, New Orleans, Nice, Portland Streetcar
4. LRT developed from upgraded tramways: Berlin, Cologne, Rotterdam, San Francisco, Stuttgart
5. LRT with metro network: Boston, Brussels, Philadelphia
6. LRT systems in suburbs of megacities: Hong Kong (Tuen Mun), London (Croydon), New York (Hudson-Bergen), Paris (lines T1, T2, and T3)
7. New high-performance LRT systems: Birmingham, Calgary, Dallas, Denver, Nantes, Portland, San Diego
8. Light Rail Rapid Transit (LRRT): LRT on ROW A only, also referred to as a "mini-metro": Kuala Lumpur, Manila, Philadelphia (Norristown Line)
9. Automated LRT: same as #8, but fully automated and without driver: Copenhagen, Kuala Lumpur, London (Docklands), New York (JFK Airport), Vancouver (Skytrain)
10. LRT/Regional Rail integrated systems, popularly (although incorrectly) known as "Tram-Train": Bern, Karlsruhe, Kassel, Manchester, Saarbrucken

Review of LRT Characteristics

An analysis of the development and broad deployment of LRT in many cities shows that this transit mode has many characteristics that make it an optimal solution for cities that need medium-capacity transit systems, that is, those that perform much better than regular buses on streets, but require a substantially lower investment cost than metro systems. Main characteristics of LRT are summarized in the following box.

LRT has several other physical characteristics that distinguish it from road vehicles. First, being a guided system, LRT uses considerably wider and longer vehicles than buses and it can operate in trains. With the high capacity of transit units, LRT can provide a higher line capacity per track than road vehicles can provide per lane. Second, electric propulsion gives LRT systems better performance (acceleration, grade-climbing ability, braking with regeneration of energy), no exhaust or noise along the line, and the ability to operate in tunnels, which vehicles with internal combustion engines do not have. Finally, rail technology makes signalization, automatic train protection (ATO), and other automated safety features possible, so that LRT can operate at higher speeds and at a higher degree of safety than road vehicles.

Positive and Negative Characteristics of Light Rail Transit Compared to Its Peer Medium-Capacity Modes

+ Rail guidance technology has a simple basic mechanism: four to eight wheels per vehicle running on two steel rails.
+ The simplest, fastest, fail-safe switching of all guidance technologies.
+ Steel-wheel-on-steel-rail contact produces extremely low rolling resistance, so that rail modes require the lowest energy consumption per ton of weight of all presently operational transit modes for any given dynamic performance.
+ Rail is the only guidance technology that allows not only at-grade crossings, but also on-street running.

+ Its simplicity and ruggedness give rail technology low maintenance requirements and high durability.
+ It copes better with adverse weather conditions (rain, snow, and ice) than rubber-tired technologies.
+ Modern rail vehicles provide virtually the ultimate in stable, smooth riding comfort.
– Investment cost of rail lines is higher than that for buses, but lower than the cost of other guidance technologies, such as Rubber-Tired Rapid Transit and Maglev.
– The lower adhesion coefficient of steel-on-steel than rubber on dry concrete surfaces gives LRT and other rail modes two relative disadvantages.
– Rail systems cannot negotiate as steep gradients as can rubber-tired systems.
– They must be operated with higher degree of safety because of their longer stopping distance.
– Although modern rail vehicles run extremely quietly on straight sections and mild curves, when negotiating sharp curves, rail vehicles produce more noise and vibration than do rubber-tired vehicles.

Roles and Impacts of Light Rail Transit

The interaction of transit systems with land use planning, physical form, and quality of life in cities is mainly dependent on the infrastructure of the transit system. While transit modes with flexible routings, such as buses on streets, do not have much impact on city planning and form, permanent infrastructure of guided systems provides the certainty that investment decisions require, so that LRT can be used to influence the form and character of a city.

Mayors of several cities which have recently built LRT systems, including Portland, Denver, and Salt Lake City, have often pointed out in their speeches that the introduction of LRT did not only improve transportation services, but it changed the character and increased the livability of their cities as well. Similarly, many cities in France, Spain, Ireland, and other countries have used the construction of new LRT systems as the pivotal project for the reconstruction of entire corridors or central urban areas to make them more pedestrian-oriented rather than car-dominated. Good examples of this are Strasbourg, Lyon, Toulouse, Nice, Dublin, and Valencia (Spain).

Upgrading Bus Services into Bus Transit Systems and Bus Rapid Transit

Local bus routes are the workhorses of the transit industry, and must operate under challenging conditions. They operate in mixed traffic like all other vehicles. They have no signal priority, and only rarely any reserved bus lanes. They serve many bus stops, often 150–200 m apart, which vary from a small sign on the side of the road to shelters and benches. The driver does fare payment and control at the front door. And local bus routes necessarily serve both short, local trips and long, commuter trips.

Over time, a number of measures that incrementally improve local bus services have been developed and gained increasing acceptance. Taken together, they provide a level of service that has become popularly known as bus rapid transit. Unfortunately, BRT is a term that has been too loosely used to describe too wide a range of bus service enhancements. This has somewhat tarnished the term.

This chapter will first review efforts to make buses act more like light rail within their own guided rights-of-way and within their own tunnels. Concurrently, bus planners began to focus on taking the bus mode and greatly improving its physical and operating environment. The next section will discuss those measures that have given buses preferential treatment in its ongoing struggle with all other vehicles using the streets.

Guided Buses and Buses in Tunnels

In the late 1970s and early 1980s, there were a number of guided busways proposed and a few were built. These efforts were attempts to provide the bus mode some of the attributes of rail transit, or at least make them appear to have the attributes of rail transit: speed, safety, and exclusive, narrow rights-of-way. Other applications used various mechanical arms or wheel assemblies to allow buses to track a raised, guiding curb. Anything raised, of course, made it difficult to move across intersections, and interrupting the contact with the raised curb proved too unsafe. Other designs used electronic or optic sensors to guide the vehicle.

The most lasting of these guided buses was the German O-Bahn concept that was initially built in Essen, Germany, but that test track did not get extended and has been superseded by light rail.

Bus Rapid Versus Light Rail Transit: Service Quality, Economic, Environmental and Planning Aspects. Figure 9
Sole major O-Bahn system in Adelaide, Australia

An O-Bahn was also built in Adelaide, Australia, and it is still operating there. This concept uses concrete beams with guiding curbs within its own, fully grade-separated right-of-way. This design proved successful to install, if expensive. It has not been replicated elsewhere, except for a few short sections of bus lines (Fig. 9).

Several bus tunnel projects were built to allow buses to avoid surface congestion. The first such project in America was Pittsburgh's original South Busway opened in 1977. It made use of an old tramway tunnel that was converted to serve both buses and light rail trains. There are, however, no stops or stations in the tunnel. The 2.1-km Seattle Bus Tunnel began construction in 1987 and cost $450 M to complete. Operations began in 1990 using dual-mode diesel-electric trolleybuses. It became a joint bus and light rail tunnel in 2007. The older buses, which cannot operate with the light rail overhead catenary system, have been replaced with new diesel-electric battery hybrid buses. Thus, tunnels for BRT have cost in some cases more than tunnels for rail modes, including LRT and metro systems.

By far the longest bus tunnel built in North America has been a section of the Silverline near South Station in Boston. The project was poorly conceived and represents an extremely expensive facility with very poor results. This bus tunnel cost about $500 million per mile ($350 million per km) to build. To solve the problem of diesel motor exhaust, dual-mode (diesel/electric) buses have been introduced. The tunnel has curves with limited sight distances, but has no signal protection, so that speed is limited on different sections to 10–20 km/h. At the exit of the tunnel, there is a traffic signal that further delays trolleybuses 1–2 min. The line then continues to the airport, where buses stop along a frequently congested four-lane roadway. Picking up passengers with luggage who have to pay fares on board also slows the service down.

The Silverline in Boston demonstrates that claims that BRT is always much cheaper to build than LRT is not correct. Actually, in many cases (Seattle, Boston) BRT tunnels have involved much higher investment cost and provided much lower system performance than rail tunnels.

The Development of Bus Preferential Treatments

For many decades buses were treated no differently than any other street vehicle. The result was slow service and poor reliability. Gradually, planners began to realize that providing preferential treatment for buses increased transit speeds, attracted riders, and lowered operating costs. These have increasingly been incorporated into street designs, but there is still a reluctance to provide buses with the priority that their higher passenger loads warrant.

Intersections are where a number of improvements can be made. One basic improvement is to allow buses to go through an intersection from a right-hand turn lane where there is often a bus stop. Providing a lead "queue jumping" green signal from this lane or a "bypass" lane through the intersection also reduces travel time.

The separation of buses onto their own lanes provides much more benefit, but this if often quite difficult in a congested city and is done, even now, only rarely. Reserving the curb lanes for buses is the most common approach because bus stops can still be on sidewalks. Bus lanes can also be located in the center of streets. This is usually an expensive proposition, however, because streets may need to be further widened for bus stops, turn lane storage, etc. Contraflow bus lanes take advantage of wide streets or street pairs to carve out the necessary travel way for buses; in the proper place they can be useful.

Finally, buses have begun to be given (by traffic engineers) various levels of traffic signal priority (TSP). TSP for bus transit usually comes in the form of a "green wave", or "green extension/red truncation" which is limited, for example, to less than 10% of the cycle length. While traffic engineers may give signal priority to buses at many intersections along the route, they are rarely given at all intersections.

A higher level of transit signal priority is traffic signal *preemption*. Light rail trains are almost always given traffic signal preemption when operating faster than 35 mph and preemption often comes with crossing gate protection. These gates are justified because the weight, speed, and long stopping distances of trains require stronger protection and allow higher transit speeds than buses.

Express Bus Services

The first step often taken by transit agencies to enhance local bus services is to supplement the route with limited-stop service. Fewer bus stops means shorter travel times for passengers going longer distances. This is especially appealing during peak commuting hours, which is when many limited-stop bus services operate. Reducing bus stops is a prerequisite for all higher levels of bus operations.

Other than fewer stops, however, many of the features of local bus services remain: no preferential treatment, no dedicated bus lanes, onboard fare payment and control, and no special amenities or service branding.

Enhanced Bus Transit Service

These services add further travel time savings to limited-stop bus services. They retain and even reduce the number of bus stops of limited-stop bus services. They included bus stops with improved shelters and seating, arrival-time message boards, and if possible extended-curb bus stops that remove the time buses lose moving out of, and then back into, the flow of traffic. Special bypass lanes at intersections, lead "queue jumping" green signals, and special turning lanes can help give buses an advantage at busy intersections. Priority signal treatment that gives approaching buses an extended green signal can be a significant travel time improvement. The ultimate improvement is to give the buses their own bus lanes separated from other traffic. However, as noted above, rarely are designated street lanes of any length given over to bus operations.

Bus services with enough of these enhancements are often branded to reflect their special status and service quality. Often newer, articulated, cleaner-energy buses with special paint schemes and catchy names are used to differentiate these services. For example, this network is called Metro Rapid Bus in Los Angeles, Special Bus Services (SBS) in New York, and the Silverline in Boston.

Although these types of services are often given the label BRT, they usually do not include enough enhancements to warrant the label. Enhanced bus services typically lack three key timesaving features: fully separated bus roadways, off-bus fare collection, and traffic signal preemption.

At-Grade Busways

There are at least two major at-grade busways in the United States: the South Miami-Dade Busway and the Los Angeles Orange Line. The Eugene, Oregon's Emerald Express busway may be another, although it does not have the same level of treatment the others do. (Seattle has an approximately 2 km long busway segment south of the bus tunnel.) The first two facilities appear to have all of the ingredients needed to provide service comparable to light rail. They operate over

Bus Rapid Versus Light Rail Transit: Service Quality, Economic, Environmental and Planning Aspects. Figure 10
The Orange Line BRT in Los Angeles on ROW category B uses articulated buses to increase line capacity

separate bus roadways; they have off-vehicle fare collection; they have traffic signal priority at most intersections they cross; and they have only limited service over city streets. To make up for the inability to train-line buses, these busways use longer, articulated buses to provide more line capacity (Fig. 10).

That being said, the service provided is not comparable to light rail operations. The main reason is that neither the Orange Line nor the South Miami Busway has crossing gates and therefore both must slow to below 32 km/h (20 mph) at each intersection, even with signal priority [1]. The use of crossing gates with at-grade busways has not been allowed by traffic engineers because their operation takes too much green time away from cross traffic [2]. At some intersections the buses on the Orange and South Miami-Dade Busways have no signal priority at all.

Crossing gates are mandatory for LRT above a certain speed typically 55 km/h (35 mph). Because of them, ROW B for LRT can act like a ROW A by providing full protection for the light rail train.

Bus Transit System: BTS

As mentioned above, regular bus services in many cities, including most US cities, are operated very inefficiently: they have stop spacings of 150–300 m (at every intersection), passengers board and alight at any door, colliding with those who are boarding and trying to pay through a single channel door; many buses do not stop close to the curb; there are few bus lanes and nearly no signal priorities at any intersections. Recent efforts to improve such operations have been rather liberally given the term "bus rapid transit." This trend has resulted in downgrading the BRT concept and caused confusion.

This text uses three definitions of bus systems. Regular, conventional (and often inefficient) bus services are referred to as "Regular Bus – RB." Bus services which are improved in station spacings, operations, etc., similar to many bus services in European countries and those in US cities which have been upgraded, are designated here as "Bus Transit System – BTS." Finally, "bus rapid transit – BRT" are the systems which have distinctly higher performance with elements defined rather precisely in the following section.

Bus Rapid Transit

Definition of Bus Rapid Transit There is a consensus [3] that bus rapid transit is a bus system that has the following elements superior to regular bus systems:

1. Reserved (physically separated) lanes or roadway – ROW B or A not shared with other vehicle categories (taxis, HOVs, and others)

2. Distinctive lines with frequent, reliable service and regular headways during all daily hours
3. Distinctive stops with passenger information and protection spaced at least 300–600 m
4. Distinctively designed bus vehicles with large door-to-capacity ratios, low floor, or high platforms
5. Bus preferential treatment at all signalized intersections
6. Use of ITS technology for monitoring vehicle movements, passenger information, and fare collection

However, this definition is rather "idealistic," because there is virtually no bus system in the world that has all these elements. Therefore, it is considered that BRT is a system that has most of these elements.

Several bus systems in the world have achieved an exceptionally high quality and fall in this definition of BRT. Often cited are Bogotá's TransMilenio (Fig. 11), Brisbane's Busways, and Ottawa's Busways. Pittsburgh's Busways could be among them if its image and other elements (station amenities, off-board fare collection) were improved.

The most important requirement for a busway to be comparable to an LRT line is to give it a similar right-of-way and, therefore, a similar operating speed. Because at-grade busway buses will not get the same signal preemption as do light rail trains, greater emphasis – and investment – must be made to give busways more grade-separation at intersections. The need to provide a high level of priority is particularly true in the central business district when a 90 km/h (55 mph) approach on a busway can degenerate into an 15 km/h (9 mph) slog through congested downtown streets. Successful BRT systems try to make this investment (Fig. 12).

BRT stops are also well spaced and more like stations with good weather protection, seating, a sense of security, and real-time bus arrival information. These elements are common with LRT stations, but are too often short-changed on busway lines.

BRT systems use large buses with wide doors for easy and rapid passenger exchange. Articulated buses are common and even double-articulated buses are used. To help market the better BRT service(s), its buses have special bus colors and logos.

BRT systems try to provide BRT buses any preferential treatment necessary through any at-grade intersections or bottlenecks off the ROW A. A number of such measures were discussed in the preceding section. It does little good to have great service only on that portion of the bus route that is fully

Bus Rapid Versus Light Rail Transit: Service Quality, Economic, Environmental and Planning Aspects. Figure 11
Bogotá TransMilenio BRT line

Bus Rapid Versus Light Rail Transit: Service Quality, Economic, Environmental and Planning Aspects. Figure 12 Bogotá's BRT distribution through central city pedestrian area

grade-separated if the overall experience of the passenger is mediocre.

BRT systems monitor all aspects of their operation to make sure buses are on time and safe, to provide the traveling public with real-time arrival information and respond to their questions, and to process quickly and efficiently the collection of fares.

BRT systems have robust bus operations with several types of services available. While there is typically the busway-only service equivalent to a light rail line, there may also be express bus services and services typical of a freeway busway with suburban bus routes using the common busway trunk segment. Two things make such a complex operation possible: the design of the busway that allows buses traveling in the same direction to pass each other and the full grade-separation of the busway. This mix of bus operations is beyond the abilities of almost all light rail systems. The extra tracks needed for trains to pass other trains traveling in the same direction are rarely built. Express trains may skip-stop or be scheduled to just catch up with a local train ahead, but do not pass the local train.

True BRT is not "cheap LRT" or "LRT Lite" [4]. Building a substantially grade-separated busway with well-designed stations can be very expensive, particularly within the congested central city. But with a robust and well-conceived service plan using several types of bus routes the resulting service can have some advantages over LRT with respect to easier introduction of line connections, branches, and express/local services if stops have four lanes (see Fig. 11). It is, however, doubtful that a BRT line can achieve on any given ROW width (two tracks/lanes, or four tracks/lanes) the capacity of a light rail line capable of coupling multiple cars into a single unit.

BRT Evaluation: Successes and Failures At this time (2011), the broad experiences of recent decades achieved by dozens of cities – and demonstrated by cities recognized as leaders in efficient transportation that contributes to their livability and sustainability – can be summarized in the following major points:

- Balanced intermodal transportation is greatly superior to transportation systems based on car dependency, meaning excessive restrictions on certain major modes such as transit, walking, or bicycling, or impracticalities on their use.
- Balanced transportation must incorporate and favor public transit systems which consist, particularly in medium and large cities, of different integrated modes, such as buses, BRT, trolleybuses, LRT, metro, and regional rail.

- Large cities, with more than one million people, usually have rail modes as their main carriers, but rail systems cannot achieve their full potential if they are not complemented by and integrated with buses.

There have always been promoters of individual modes claiming that they are superior to other modes. The strongest such pressures have been for private cars, and their political successes have created car-dependable cities that are inferior to intermodal cities with respect to quality of life, economic vitality, and sustainability. Single-mode promoters have also caused "waves" of discussions that the most efficient modes are paratransit, monorails, various automated guided systems (AGT), including the totally infeasible personal rapid transit (PRT, now reappearing under the name "Pod cars"). These extremist views that a single mode is the dominant or only solution for all cities have eventually been discredited. Intermodal transit systems utilizing the diverse family of transit modes, from historic streetcars to BRT and regional rail systems, are obviously the trend for the future.

To be fair, promoters of single modes have fostered some useful innovations. Paratransit has become more diversified since the 1970s. Some 2 dozen monorails have been built in various cities, and AGT systems are used in an increasing number of airports as well as for transit lines in some cities, particularly as downtown circulators.

It is unfortunate that BRT, which has brought very significant progress to many cities, is promoted by some organizations, government bodies, and individuals as the single mode superior to all other modes. This fringe of extremist BRT promoters is actually causing considerable harm by weakening the concept of intermodal transit and by actually strengthening the already dominant pro-automobile lobbies. Finally, these "BRT evangelists" harm the cause of BRT by promising that this mode can solve all transport problems, so that its problems or failures in different cities lead to questioning the value of the entire BRT concept.

Many elements of BRT were introduced during the 1970s and 1980s in several cities, although the term "BRT" had not yet been coined. São Paulo developed several high-density corridors with high-frequency service by buses and trolleybuses utilizing four-lane stations with overtaking of buses, platooning of buses from different branches for increased capacity on the joint trunk, etc. Pittsburgh, Washington (Shirley Highway), and Los Angeles (El Monte) introduced busways, although more for commuter services than for regular transit. Ottawa built a network of busways and made more integration of their services with land use planning around their stations. (The limitation of this system has been that its busways lead into downtown streets, which represent a capacity bottleneck for the entire network.)

To clarify the strengths and limitations of the BRT mode, several leading BRT projects are evaluated here.

Curitiba: Following innovations in bus system design in various cities, Curitiba in Brazil built a network of BRT lines which is still considered the best planned one because it was designed as an integrated part of the city's land use plan. The BRT lines represent the spines of major corridors with high-density buildings throughout the city.

In addition to the planning aspects, Curitiba became the leader in designing high-level platforms and high-floor buses for level boarding/alighting through wide doors on articulated and double-articulated buses. Fare collection at the entrance to specially designed stations in the median of the busway was another element that increased line speed and capacity. Curitiba is considered as a leader in the development of the BRT concept.

Bogotá's TransMilenio BRT System: This BRT system has drawn great publicity and is called by some the "Gold Standard of BRT." It is therefore useful to examine its strengths and achievements, as well as its limitations and shortcomings.

The city of Bogotá, capital of Colombia, suffered from chronic congestion that was getting steadily worse with its growth of population and car ownership. It was served by remarkably primitive transit services consisting mostly of 8- and 10-m long private bus lines without any coordination, integration, or joint fares among hundreds of companies and individuals who owned and operated them. The city faced two problems: how to organize transit services into a coordinated system, and then how to build a network of high-capacity semi-rapid (mostly independent) or rapid (fully separated) transit lines.

Rail rapid transit was planned for a long time, but problems in coordinating, organizing, and financing the project stalled progress. Then, under the leadership of Mayor Enrique Penalosa, a BRT system was built for a major corridor, opening in December 2000. This was followed by other lines, which now represent a network of high-capacity lines.

The achievements of TransMilenio are quite remarkable. The system represents a huge leap forward over the chaotic, low-quality and low-capacity disintegrated bus lines. These small-bus services still carry the majority of trips in Bogotá and still represent a serious problem because of their poor service quality and inability to attract choice riders. The TransMilenio system has successfully attracted a substantial portion of trips and provided them with much faster and more reliable services. Now, finally, the city with a population of about seven million persons and growing has an increasing network of fast lines largely independent from street congestion, which also reduce the traffic loads and congestion on existing streets.

Along with these significant achievements, TransMilenio has several serious limitations, which should be carefully considered in further transit planning for the city. They are:

- The success in attracting very large passenger volumes is overwhelming the system. TransMilenio operates at and beyond its capacity for long periods of the day. That results in extremely low passenger comfort and lower service reliability than the system could provide with below-capacity passenger volumes.
- TransMilenio busways are located in the median of corridors with 8–12 traffic lanes that can be crossed by pedestrians only via long overpasses provided at distances of several hundred meters. This design provides only a single access to every bus station, so that walking distances from the closest buildings and streets to a bus station entrance amount in many cases to several hundred meters and involves crossing ramps and bridges unprotected from the weather. This design is very unattractive to users, reduces the competitiveness of transit services for car owners, and represents a major divide between streets and buildings on its opposite sides. This is the opposite impact on a city's livability from the impacts that LRT services have when they go through pedestrian zones.
- While electrically powered rail transits (LRT or metro) provide quiet vehicles without exhaust and long-term sustainability, buses with diesel or other internal combustion engines represent a much less attractive alternative. Thus, in the choice between BRT and LRT or metro, buses represent a major step backward with respect to a city's livability and sustainability (Figs. 13–16).

These limitations explain why there is so much interest in building a metro in Bogotá. Low- and medium-capacity BRT lines represent the optimal, most economic solution when matched with similar passenger demand. However, a BRT line operating beyond its capacity requires a major investment in a line that provides a higher quality of service, attracts more choice riders, and enhances the city's livability. Bogotá is a city with a steadily increasing population that brilliantly converted uncoordinated midi-bus services into a coordinated network of regular buses and BRT lines. It has used taken advantage of corridors that allowed the four-lane busway, but now must invest in rail transit to further improve its quality of transit service, economic vitality, and sustainability. The question is actually not whether Bogotá's higher-capacity transit system should be BRT or LRT/metro: the city obviously needs both, rail for its most heavily loaded lines, BRT serving a network of medium-capacity lines.

Mexico City's Insurgentes BRT: Similar to Bogotá, the Insurgentes corridor was served by uncoordinated minibuses with erratic, unreliable service. The first 20 km and 36 stations of the Insurgentes BRT facility opened in 2005; in 2008 an additional 9 km opened. As with the TransMilenio BRT system this line operates in the median of a major arterial road requiring passengers to access stops only through one entrance after long walks. Buses stop one at a time and cross many signalized intersections one at a time, so that the maximum capacity obtained using one articulated bus per signal cycle amounts to 5,000–6,000 persons/h.

The BRT line was so much better than the minibuses that the line attracted 280,000 persons/day, which exceeded its capacity and resulted in extreme, sometimes dangerous, overcrowding.

Bus Rapid Versus Light Rail Transit: Service Quality, Economic, Environmental and Planning Aspects. Figure 13
Back-up of buses at TransMilenio station reduces service reliability

Bus Rapid Versus Light Rail Transit: Service Quality, Economic, Environmental and Planning Aspects. Figure 14
Long overpasses are only access to many TransMilenio stations

Also similar to TransMilenio, the Insurgentes line was built faster and at lower investment cost than an LRT line would have required. However, while its current operation can be deemed a success based on its daily ridership, its capacity limit was reached at the time the line opened. An upgrade to rail technology could allow double or triple the capacity still maintaining only one transit unit (train) per signal cycle through intersections. Only the street block length would limit the potential train length. Safety

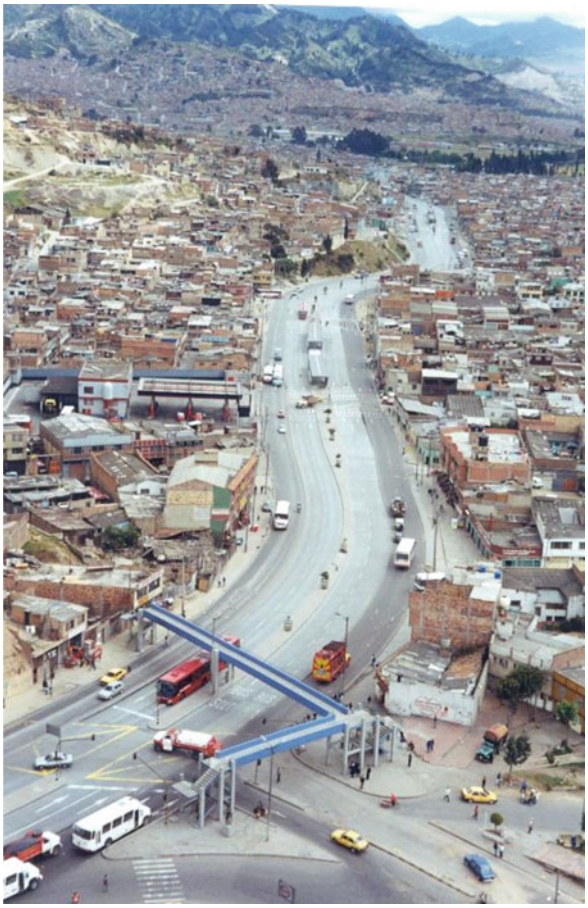

Bus Rapid Versus Light Rail Transit: Service Quality, Economic, Environmental and Planning Aspects. Figure 15
TransMilenio corridor is a major barrier to pedestrians in Bogota

would also be increased with the decrease in the number of bus braking and accelerating cycles and with the added signal protection on any segment where train speed exceeds 70 km/h. LRT would have provided so much greater capacity, resulting in correspondingly greater riding comfort. Given the present ridership levels, one could argue that conversion to a metro line would even have merit.

The Bogotá and Mexico City examples show fairly typical decisions many cities face as they ponder how to improve their transit services. If there is an avenue in which ROW B can be obtained, BRT usually requires a lower investment and simpler/shorter implementation. However, LRT would provide a much higher capacity, better riding comfort and passenger attraction over the long term. Moreover, with respect to the city's livability and sustainability LRT is clearly superior to diesel (or even CNG) buses, particularly in sensitive inner city areas.

Istanbul Freeway Median BRT: Istanbul is by any definition a megacity spanning a very large region. Due to the long travel distances and extremely heavy congestion, the traveling public wastes much time. Even the limited access highways can be chaotic with thousands of buses stopping along the roadside, thus resembling ROW C much more than ROW A in character. In 2007, the first 18 km and 14 stations within one such freeway opened as a BRT system (Phase I). Typically, its stops and dedicated lanes were located in the middle of the limited access highway. In 2008, an additional 29 km and 25 stations were added (Phase II). At that time it was projected that an additional 11 km would be built for a total of 50 km at a relatively modest total cost of $125 M (Fig. 17).

Phases I and II already carry 858,000 passengers per day, and many passengers are saving over 1 h per day in commuting times. Thus, it would seem to be a major success. However, this very success indicates that the conditions are strong for an upgrade to rail technology. There are close to 2,500 bus trips made per day on this busway with headways often down to 20 or 30 s of separation. Consequently, there is a significant amount of air pollution and fuel consumption from the enormous volume of buses. Furthermore, bus speeds and passenger comfort are limited and safety is compromised due to hundreds of thousands of accelerating and braking cycles per day at highway speeds.

The ready availability of the right-of-way and the long station spacings due to their location at overpasses would allow for the running of large high-capacity trains that accelerate faster and obtain higher speeds than do buses. The high demand and ROW A clearly justifies rapid transit technology, not LRT technology. Headways would still be short while time savings and passenger comfort would be greatly increased. Safety would be enhanced by automatic train protection. Total energy consumption and both air and noise pollution would be reduced. Operating cost savings would

Bus Rapid Versus Light Rail Transit: Service Quality, Economic, Environmental and Planning Aspects. Figure 16
Exhaust pollution from TransMilenio operations

Bus Rapid Versus Light Rail Transit: Service Quality, Economic, Environmental and Planning Aspects. Figure 17
BRT with ROW category A in Istanbul, Turkey

be substantial and could be used to bolster other parts of Istanbul's network including more feeder services.

It is true that far fewer bus drivers would be needed, but this decrease in employment would be far offset by the increase in economic vitality and job opportunities opened with the corridor's faster travel times. (There would also be some offsetting employment created to maintain and repair the guideway and vehicles.)

Comparison of LRT and BRT Modes

Light rail transit and bus rapid transit (but not Bus Transit Systems) are functionally similar modes. As semi-rapid transit (mostly independent of street traffic), both provide much higher service performance and have more positive impacts than the basic street transit mode – regular (conventional) buses (RB). Both require investments that are significantly higher than those for RB, but much lower than for metro systems. However, LRT and BRT are drastically different in their technology, operations, quality of service, and their short- and long-term impacts on the city. In most cases, they typically provide different "investment cost/performance packages" so that their comparison is very complex.

Applications of the two modes vary between two extremes. In medium-sized cities or corridors BRT can fully meet the capacity and performance needs at lower cost than LRT. At the other extreme, in many medium- or large-size cities LRT offers far superior performance, operates efficiently in pedestrian-oriented areas or in short tunnels under city centers, and has many more positive impacts for a city's livability than does BRT. Between these two poles, where BRT and LRT are, respectively, obviously the superior choices, are many applications with different trade-offs so that either one of the two systems may be the preferred mode.

Review of Modal Characteristics

Table 1 presents a comparison of the basic characteristics of RB, as the most widely used street transit mode, BRT and LRT. The characteristics are grouped in three categories: system components, lines and operational components, and system characteristics.

As Table 1 shows, the elements in which BRT differs from RB are ROW category, larger vehicle capacity if double-articulated buses are used, different line designs and stop spacings, higher investment costs, and its greater passenger attraction.

Focusing on the BRT and LRT modes, their comparison can be summarized in a number of characteristics, as presented in the following box [5].

Some of these comparisons are factual and obvious, proven in real-world situations. Several of the major differences will be discussed here.

Advantages (+) and Disadvantages (−) of LRT over BRT

- + Separate ROW (B or A) for LRT is easier to achieve because LRT uses rail tracks instead of roadway lanes, and due to its different technology requires no physical protection and police enforcement, as do busways (Fig. 18).
- + LRT has better vehicle performance than BRT because of its electric traction.
- + LRT produces no exhaust along the line and much lower noise than BRT (except that in a few cities, trains are required to use horns at grade crossings).
- + LRT is often designed to serve as the central element for access and image of pedestrian areas in central cities; a busway with high-frequency bus services is much less compatible with "pedestrianized" areas.
- + LRT can use tunnels, BRT cannot.
- + LRT vehicles are more spacious and comfortable and have better riding quality than buses.
- + LRT has a stronger image; it is more popular and attracts more riders.
- + LRT has a stronger positive impact on urban development than BRT.
- − Investment costs for LRT are higher than those for BRT.
- − For the first LRT line in a city, introduction of a new technology requires more extensive construction of infrastructure as well as new equipment, and it involves longer implementation.

Diesel Bus Technology Versus Electric Rail Technology

The basic benefits and drawbacks of diesel and electric traction, and rubber-tired and rail technology are inherent in the BRT and LRT modes. All BRT systems use the internal combustion engine for propulsion. In the past the fuel was diesel. Recently, new BRT systems in the industrialized world use less polluting liquid natural gas (LNG) or compressed gas (CNG) as fuel sources, but engine performance does not fundamentally change.

More detailed analysis of BRT and LRT characteristics caused by their different types of traction and

Bus Rapid Versus Light Rail Transit: Service Quality, Economic, Environmental and Planning Aspects. Table 1
Comparison of regular bus, bus rapid transit, and light rail transit characteristics

Characteristic▼ / Mode▶	Regular bus(RB)	Bus rapid transit (BRT)	Light rail transit (LRT)
System components:			
ROW	C	B (C, A)	B, (A, C)
Support	Road	Road	Rail
Guidance	Steered	Steered	Guided
Propulsion	ICE	ICE	Electric
TU control	Driver/visual	Driver/visual	Driver/signal
Vehicle capacity (spaces)	80–120	80–180	100–250
Max TU size	Single vehicle	Single vehicle	1–4 car trains
Max TU capacity	120	180	$4 \times 180 = 720$
Lines/operational elements:			
Lines	Many	Few	Few
Headways	Long/medium/short	Long/medium/short	Medium/short
Stop spacings (meters)	80–250	200–400	250–600
Transfers	Few	Some/many	Many
System characteristics:			
Investment cost/km	Low	High	Very high
Operating cost/sp	Medium	Medium	Low
System image	Variable	Good	Excellent
Pass. attraction	Limited	Good	Strong
Impacts on land use and city livability	Least	Moderate	Strongest

road/rail technology are given in the following two boxes, respectively [6].

Several relevant points from the above comparisons deserve some discussion here.

- LRT in most cases costs more to construct initially. Although rail equipment and facilities last longer, the required higher initial investment is often a major problem. An exception to LRT costing more than BRT might be where ridership demand requires a category A BRT to avoid at-grade crossings, but LRT can provide that capacity with a less expensive category B design.
- LRT has much more capacity because rail technology allows the coupling of railcars into trains; coupling cannot be done with buses. This is particularly important for transit projects using category B rights-of-way. Traffic engineers limit the amount of green time given to transit. If the expected ridership demand on the line is high, the transit unit used must carry the most passengers. In this regard, LRT has the added advantage of requiring crossing gates for safety.
- BRT has the potential to offer more service options, not just the end-to-end operation typical for LRT. A BRT line can offer end-to-end service, but can

Bus Rapid Versus Light Rail Transit: Service Quality, Economic, Environmental and Planning Aspects. Figure 18 Recently opened LRT line in Dublin, Ireland on a ROW category A section

supplement it with express bus services or multiple route-to-trunk line services typical of freeway bus operations.

- If capacity and service quality require that ROW A is used, that is usually more complicated for buses than rail vehicles and results in bus services which are much inferior to rail. The best example is the Silverline BRT in Boston, where a 1-mile long tunnel required an investment cost of about $500 million, and buses now operate in it at speeds limited to 10–25 km/h. Capacity of buses operating in single-lane tunnels is only a fraction of the capacity LRT would provide.
- Road and rail technologies also have a direct impact on operations of their rights-of-way. Separation of ROW for LRT needs no enforcement because in most designs road vehicles cannot use tracks because they are not paved. BRT's advantage, that it uses the same road surface as other street lanes, is actually a serious disadvantage with respect to control of their use. Many bus lanes and busways have been first downgraded by allowing other vehicles to share them (first taxis and vehicles making turns at intersections, then HOVs, any cars who pay tolls in such lanes, and then even hybrid private cars). In many cases these steps led to eventual losing of ROW B for buses and discontinuation of the BRT system (see Fig. 3).

Electric Rail Traction Compared with the Internal Combustion Engines of Buses

+ Produces higher, smoother acceleration (limited by passenger comfort)
+ Produces far less noise and vibration
+ Produces no local air pollution
+ Can easily use tunnels due to absence of pollution and good dynamic performance
+ Allows for regenerative braking, thus reducing energy consumption
+ Is much cleaner to operate and maintain
– Requires additional investment for electrification of lines and construction of substations
– Overhead power lines are sometimes criticized for aesthetic reasons, although many passengers like the distinct identity the catenary gives the line
– Is susceptible to power failure that stops all vehicles on a section of line

Rail Technology Compared with Rubber-Tired Buses

+ Makes coupling of cars into trains possible, drastically increasing line capacity
+ Rail guidance allows use of wider and longer cars and requires narrower free profile
+ Has much higher safety because of automatic signal control, although at additional investment and maintenance costs
+ Provides a far more stable, smoother ride quality
+ Is far more energy-efficient due to steel wheels on steel rails
+ Can better cope with adverse rain, ice, and snow conditions
– Requires substantially higher investment, although the vehicles and guideways are more durable and require lower ongoing maintenance
– Cannot negotiate as steep a gradient, nor as sharp curves as buses
– Requires a higher degree of safety because of longer stopping distances
– Can be much louder when going through sharp curves
– Is normally slower around any given radius of curvature and may therefore have a slower travel time between stations than bus technology

Line Capacities

An extensive debate has been going on with respect to the line capacity of different transit modes. To check the validity of various claims of modal capacities, two values will be quoted for each mode: the first, for the bus mode, assumes regular buses with 90-space capacity (6 persons/m^2) and with single stops with fast boarding/alighting, allowing average headways as short as 1 min. Such a system provides a line capacity of 5,400 spaces/h.

The second value for bus line capacity assumes that each stop has four lanes, allowing overtaking and "leapfrogging" of buses. In this way, capacity can be increased significantly. This is seldom possible in urban areas, but some examples exist. Portland, Oregon, organized a pair of bus streets with two lanes for buses and overtaking of buses in stop areas, which achieved capacity of 180 buses/h or average headways of only 20 s. With an average capacity between regular and articulated buses of 110 spaces, this results in a line capacity of 19,800 spaces/h.

The Comonor project, a high-capacity bus corridor in São Paulo, Brazil, claimed to have achieved capacity of 24,000 spaces/h by operating buses in platoons overtaking each other at stops along the line. However, that description turned out to be theoretical, and actual capacity provided on São Paulo streets was considerably lower.

New claims of much higher capacities for new BRT systems came particularly with the opening of the TransMilenio system in Bogotá, Colombia. That system was systematically designed for high capacity: most buses are articulated and double-articulated, all fares are collected at station entrances, and the system has two lanes on some sections, but four lanes in station areas allowing bypassing and overtaking of buses. This is particularly the case on the main line built in a wide median of a very wide freeway right-of-way. However, the line has a number of signal-controlled intersections, which limit the green time for the BRT line.

Even if it is assumed that all buses are double-articulated and occupied with an extremely high average density of 6 persons/m^2, and that it is possible to have an average headway of buses crossing signalized intersections of 20 s, such an operation would amount to about 28,000 spaces/h. Although these assumptions are higher than in real world (for one, not all buses are double-articulated), advocates of BRT systems have claimed capacities exceeding 30,000, later 35,000 and even as high as 53,000 persons/h. The latest revisions to a couple of prominent BRT design manuals written for applications to developing countries appear to be correcting these overblown numbers downward, toward lower, although still unrealistic values of over 30,000 persons/h.

For comparison, the capacity of LRT lines operated with trains consisting of two articulated cars (such as in Manila) with realistically achievable 2-min headways is about 15,000 spaces/h. With more optimistic assumptions, corresponding to those used by BRT promoters, LRT lines using four-articulated car trains as operated in several cities and 1.5 min headways would achieve an offered capacity of 32,000 spaces/h. With four tracks for bypassing in stations, this capacity could be

increased further, but the critical locations would be at intersections. As the measurements of actual operations of the Orange Line BRT (Los Angeles) show, LRT can provide substantially higher capacity at street crossings than buses because of the higher capacity of LRT trains compared to individual buses, even double-articulated ones.

Under similar assumptions, ten-car trains of a metro system operating at 1.5-min headways would provide a capacity in the order of 60,000 spaces/h, while the four-track metro line in New York carried 89,000 persons/h in the 1940s (presently, passenger numbers are smaller, because trains in most of the industrialized countries are operated with higher comfort levels which result in 4–5 persons/m^2).

Another deceptive feature of these claims of BRT capacities is that they represent the obsolete, simplistic measure of line capacity as a single number, without regard to service quality and level of service. With respect to highway capacity, it was already in 1950 realized that capacity in terms of vehicles per hour should be related to the level of service (LOS), which was defined as LOS A through F. Capacity of transit lines is now also related to performance and LOS. For example, if one transit line carries 14,000 persons/h with an operating speed of 16 km/h and another line carries 14,000 with a speed of 24 km/h, their performance is by no means the same. Lehner [7] introduced the concept of productive capacity – product of transporting capacity and speed – to include this characteristic. It can be insightful to plot the productive capacity against investment cost. Vuchic [8] specified that evaluation of transit capacity should include the following five factors:

- Offered line capacity in spaces/h
- Operating speed in km/h
- Load factor or capacity in persons/space, where spaces include both seated and standing spaces assuming a certain degree of crowding
- Comfort standard in square meters/person (or degree of crowding in persons/m^2)
- Reliability of service in percent of departures on time

Consequently, capacity of transit modes cannot be evaluated only by hourly throughput of persons; it must include level of service.

Comparisons of capacities of different modes must also be made for comparable conditions and assumptions. For example, comparing capacities of BRT and LRT must assume that both modes have either two lanes/tracks, or four lanes/tracks in stations. Thus, the Insurgentes BRT line in Mexico City should be compared with a two-track LRT line, such as in Cologne or Manila. The TransMilenio BRT line in Bogotá should be compared with a four-track LRT line, which would have capacity well over 40,000 spaces/h.

Compared modes must also have the same load factors and comfort standards. Reliability and operating speed would then have to be measured or predicted on the basis of characteristics of each mode.

Recent Studies Comparing Different Modes of Real-World Transit Systems

Studies comparing transit modes generally fall into two categories. The first compares modes that are being planned or hypothesized, that is, not in operation. These types of studies are needed, of course, when doing major planning work, but they must use projections of ridership and costs rather than actual ridership and costs. The alignments and operational assumptions made for each alternative should be as similar as the characteristics of different modes allow.

The second category of studies compares modes operating in one or more cities. A major problem with these types of studies is that each system operates in a different cultural, economic, and operational context, but their great advantage is that their features and numerical values are realistic, not hypothetical and subjective.

One recent study that looked at one city with several bus and rail modes operated by a single agency is described below.

Case Study: Comparison of Transit Modes in Los Angeles Over the past 25 years Los Angeles' metro transit network has evolved from an all-bus system to a network of many transit services and modes. As of spring 2008, this network included a rapid transit line, three light rail lines, three busways, 19 enhanced bus transit routes, and 95 local bus routes. For the first time the opportunity exists to compare a variety of transit modes all operated by the same agency within the same

urbanized area eliminating differences in labor costs between urban areas, in operating and management practices, in efficiencies of scale, and in time and methods of data collection [9].

Various performance and cost measures were calculated for each mode operated by the Los Angeles metro. The results of this analysis are shown in Table 2 for performance measures, in Table 3 for cost measures.

The Orange (BRT) Line is much slower than the average of the LRT lines. This is because it does not have full signal priority and catches red lights at a third of its intersections. Its buses must also slow below 32 km/h (20 mph) at all crossings. It also has nowhere near the carrying capacity of the light rail lines and is nearing capacity with about 25,000 daily riders. One LRT Line (Blue) has had a weekday ridership above 80,000 for a number of years.

On the other hand, the Orange Line was built for less than half of the capital cost per kilometer of the Gold (LRT) Line during the same period. Time will tell whether that investment was prudent given the much slower speed and the looming capacity limit of the busway. The Orange Line may be an example of a BRT line that should have been built fully grade-separated for higher speed and capacity, but if it had been, its cost might have exceeded the cost of an equivalent light rail line operating on the existing ROW B.

Summary Comparison of BRT and LRT Modes

Table 4 gives a summary comparison between the BTS, BRT, and LRT modes. Overall, the two bus modes have advantages with respect to investment cost, construction time, and the complexity of system implementation. However, LRT demonstrates superiority in most measures of service efficiency and level of service: speed, comfort, image, and passenger attraction. Even more important may be that LRT is superior in its positive impacts on land use planning, urban form, livability, and sustainability. Focusing on the BRT-LRT comparison, BRT tends to be a faster and usually (but not always) lower investment solution, but LRT provides higher service quality, stronger passenger attraction, and a more powerful step in increasing the city's quality of life and sustainability.

Trends and Expected Future Directions

City populations in many developing countries are growing rapidly. Those countries that also have growing economies and rising income levels are seeing ominous growth in auto ownership. One defense against the inevitable, debilitating congestion that these new cars bring is to invest in attractive urban transit systems capable of meeting future demands.

Bus Rapid Versus Light Rail Transit: Service Quality, Economic, Environmental and Planning Aspects. Table 2 Performance measures of Los Angeles metro transit modes (2008)

Performance measure	Local bus	Rapid bus	Orange Line BRT	Light rail	Rapid transit
Ave. peak hour speed (km/h)	20.6	24.0	29.3	41.4	51.8
Ave. trip length (km)	5.7	7.3	9.4	11.3	8.0
Daily riders: (experienced) (possible max)	30,000 30,000	30,000 30,000	25,000 35,000	84,000 100,000	140,000 300,000

Bus Rapid Versus Light Rail Transit: Service Quality, Economic, Environmental and Planning Aspects. Table 3 Cost measures of Los Angeles metro transit modes (2008$ unless noted)

Cost measures	Local bus	Rapid bus	Orange Line	Light rail	Rapid transit
Capital cost ($M/km)	N/A	$ 0.15 (2000)	$17.3 (2005)	$ 38.9 (2003)	$130 (2000)
Operating cost per pass-km	$0.60	$0.39	$0.30	$0.31	$0.27
Operating subsidy per pass-km	$0.47	$0.29	$0.22	$0.25	$0.20

Bus Rapid Versus Light Rail Transit: Service Quality, Economic, Environmental and Planning Aspects. Table 4
Summary comparisons of the BTS, BRT, and LRT modes

Mode characteristic	Bus transit system BTS	Bus rapid transit BRT	Light rail transit LRT	Superior mode
Investment cost	Medium	High	Very high	BTS
Implementation Complexity and time	Short	Medium	Long	BTS
Operating cost	Lower for low passenger volumes	Lower for low passenger volumes	Lower for high passenger volumes	Depends
Operating speed	Medium	High	High	Depends
Ability to accommodate service options	Low	Some with four-lane stops	Low except with four-track stops	BRT
Capacity	Low	Medium	High	LRT
Type of energy and traction	Internal comb. engine	Internal comb. engine	Electric	LRT
Vehicle performance	Good	Good	Excellent	LRT
Air pollution and noise	Poor	Poor	No local pollution, low noise	LRT
System image and passenger attraction	Fair	Good	Excellent	LRT
Potential to influence land development	Limited	Fair	Very good	LRT
Contribution to livable urban environment	Some	Limited	Excellent	LRT

For large cities with many million inhabitants, high population densities, and heavily traveled corridors, rail rapid transit (metro) is clearly the most efficient transit mode for the basic network. Megacities like Tokyo, Beijing, and São Paulo will have to extend their metros as the population continues to grow.

The trend of developing medium-capacity modes, which started with the growth of LRT and later BRT, will continue. These modes are being introduced to supplement metros in suburban areas and as transitional solutions when metros cannot be built fast enough for financial or physical reasons.

The two modes most capable of meeting the need in many cities in developing countries are LRT and true BRT. Both, however, are costly investments. One future direction is therefore to convey to transit policymakers that the investment decision they face is between these two modes, not the false promise of inexpensive, inadequate lower-cost bus modes.

In developed countries, a future direction for study is to appraise honestly the cost and performance of true BRT systems and their more comprehensive service options. In some applications the LRT model of a high-capacity rail line fed through transfers from connecting bus routes may not provide the most attractive, convenient service. In other cases, if a BRT would be loaded to capacity as soon as it is opened (which is the case with some lines in Bogotá and Insurgentes in Mexico), a rail system – LRT or metro – would obviously be a more efficient and permanent solution. Understanding where each of these options works best will be quite useful.

Finally, the damaging argument within the transit community between BRT and LRT must subside if transit is to compete most aggressively with the private car. In a world that needs to have far fewer private cars depleting our oil reserves, strangling our cities, and fouling our air, the focus must be to provide the most

Bus Rapid Versus Light Rail Transit: Service Quality, Economic, Environmental and Planning Aspects. Figure 19
Five-section low-floor LRT vehicle provides high capacity and can make sharp turns on ROW category B in urban streets in Helsinki, Finland

Bus Rapid Versus Light Rail Transit: Service Quality, Economic, Environmental and Planning Aspects. Figure 20
Buses and light rail trains share ROW category B in Helsinki

attractive, cost-effective transit, bus, or rail for a given circumstance. It should not be to have one mode to the exclusion of another. A good example for this is Bogotá, where the debate should not be BRT versus LRT, but BRT *and* a rail system (LRT or metro). This is particularly the case with lines where volumes are very high and environmental aspects are very important. In such cases the transit system must enhance the livability of the city, minimize its air and noise pollution, and join rather than divide its neighborhoods (Figs. 19 and 20).

Bibliography

Primary Literature

1. Eccles KA (2007) Design, operation, and safety of at-grade crossings of exclusive busways. TCRP Report 117. TRB, National Research Council, Washington, DC, pp 19–20
2. Stanger R (2007) An evaluation of Los Angeles's orange line busway. J Public Transp 10(1):103–119 (Center for Urban Transportation Research, Tampa)
3. Kittelson & Associates (2007) Bus rapid transit practitioner's guide. TCRP Report 118. TRB, National Research Council, Washington, DC
4. Hoffman A (2008) Advanced network planning for bus rapid transit: the "Quickway Model" as a modal alternative to "Light Rail Lite". Department of Transportation, Federal Transit Administration, Washington, DC
5. Vuchic VR (2007) Urban transit systems and technologies. Wiley, Hoboken, p 541
6. Vuchic VR (2007) Urban transit systems and technologies. Wiley, Hoboken, p 116
7. Lehner F (1978) Der maximale Wirkungsgrad des Personaleinsatzes; (Maximum efficiency of personnel assignment). Alba Buchverlag, Dusseldorf
8. Vuchic VR (2005) Urban transit operations, planning, and economics. Wiley, Hoboken, p 88
9. Stanger R (2010) Comparative performance of Los Angeles' transit modes. Presented at the 11th joint light rail conference, 9 Apr 2009. Transportation Research Board and American Public Transportation Association, Los Angeles, Transportation Research Board Circular 143

Books and Reviews

Bruun E (2005) BRT versus LRT operating costs: comparisons using a parametric cost model. Transportation Research Record No. 1927. Transportation Research Board of the National Academies, Washington, DC, pp 10–20

Grava S (2003) Urban transportation systems: choices for communities. McGraw Hill, New York

Hess D, Taylor B, Yoh A (2005) Light rail lite or cost-effective improvements to bus service?: evaluating costs of implementing bus rapid transit. In: Transportation Research Record: Journal of the Transportation Research Board, No. 1927. Transportation Research Board of the National Academies, Washington, DC, pp 22–30

Kittelson & Associates (2007) Bus rapid transit practitioner's guide. TCRP Report 118. TRB, National Research Council, Washington, DC

Koonce P, Ringert J, Urbanik T, Rotich W, Kloos B (2002) Detector range setting methodology for signal priority. J Public Transp 5(2):115–135 (Special edition on BRT, Center for Urban Transportation Research, Tampa)

Kühn F (2002) Godard & Fatorzoun (eds) Urban mobility for all – La Mobilité Urbane pour Tous. Swets & Zeitlinger, Lisse, pp 357–365

Levinson H, Zimmerman S, Clinger J, Rutherford S, Smith R, Cracknell J, Soberman R (2003) Bus rapid transit, volume 1: case studies in bus rapid transit. TCRP Report 90. TRB, National Research Council, Washington, DC

Levinson H, Zimmerman S, Clinger J, Gast J, Rutherford S, Bruun E (2003) Bus rapid transit, volume 2: implementation guidelines. TCRP Report 90. TRB, National Research Council, Washington, DC

Newman P, Kenworthy J (1999) Sustainability and cities. Island Press, Washington, DC

Sislak KG (2000) Bus rapid transit as a substitute for light rail transit: a tale of two cities (CD-ROM). Presented at the eighth joint conference on light rail transit, Dallas

Stutsman J (2002) Bus rapid transit or light rail transit – how to decide? Los Angeles Case Study. In: Transportation Research Record: Journal of the Transportation Research Board, No. 1973. Transportation Research Board of the National Academies, Washington, DC, pp 55–61

TCRP (Transit Cooperative Research Program) (2005) Innovations in bus, rail and specialized transit. Research Results Digest 70. Transit Cooperative Research Program, National Academy Press, Washington, DC

Thompson GL, Matoff TG (2003) Keeping up with the Joneses: planning for transit in decentralizing regions. J Am Plann Assoc 69(3):296–312

Vuchic Vukan (2005) Planning and selection of medium and high performance transit modes. In: Urban transit: operations, planning and economics. Wiley, Hoboken (Chap. 12)

Bus Versus Rail Implications for Transit-Oriented Development

Ming Zhang
Graduate Program in Community and Regional Planning, School of Architecture, The University of Texas at Austin, Austin, TX, USA

Article Outline

Glossary
Definition and Importance
Introduction
Transit Technologies
Cost Characteristics of Bus Versus Rail Mass Transit
Capacity of Bus Versus Rail Transit
Transit Impacts on Property Values
Density for Bus and Rail Transit

Best Practice of Bus- Versus Rail-Based TOD
Conclusions
Future Directions
Bibliography

Glossary

BRT Bus rapid transit (BRT) refers to a variety of mass transit systems that utilize buses to provide faster, more efficient services than a conventional bus line. BRT runs on existing roadways or dedicated rights-of-way and offers such operational features as high-capacity, low-floor bus vehicles, traffic signal prioritization, and real-time information services.

LRT Light rail transit (LRT) refers to electrically propelled rail vehicles operating singly or in trains. It obtains power from overhead cables and runs on reserved but not necessarily grade-separated rights-of-way. LRT provides service capacities and speeds typically lower than metro rail.

Metro rail Metro rail typically consists of steel-wheeled, electric-powered vehicles operating in trains of two or more cars on a fully grade-separated right-of-way. Alternative names for metro rail include subway and heavy rail. It offers higher capacities and speeds than light rail.

New urbanism New urbanism refers to an urban design movement led by a group of architects and urban planners in the USA since the early 1980s. New urbanism promotes walkable neighborhoods and attacks suburban sprawl through nonconventional physical planning and design approaches. Traditional neighborhood design (TND) and transit-oriented development (TOD) are two examples of new urbanist practice.

TOD Transit-oriented development (TOD) refers to mixed-use, medium- to high-density development around the transit station with pedestrian- and cyclist-friendly environmental design. The term was coined by Architect Peter Calthrope while other terms, for example, Transit-Focused Design and Transit Villages, have also been used to describe similar development concepts.

Transit ridership The quantity of passengers riding on the transit over a given period of time, for instance, a day or a year.

Transit value capture Transit value capture refers to the process by which all or a portion of increments in land value attributed to public transit investments are recaptured by the public sector. The idea can be traced back to the thinking of Henry George and his followers. The rationale states that transportation projects improve accessibility to the adjacent land. This improved accessibility is capitalized in property values, generating a windfall for private landowners. Public agencies can capture a portion of that windfall by utilizing a variety of methods. The captured value can then be used to finance transportation or other public infrastructure.

VMT Vehicle miles traveled (VMT) measures the distance in miles that vehicles are driven over a given period of time, for instance, a day or a year.

Definition and Importance

Transit-oriented development (TOD) refers to mixed-use, medium- to high-density development around the transit station with pedestrian- and cyclist-friendly environmental design oriented to transit services. Integrating transit with land use has been a common practice in most European, Asian, and Latin American cities. It is not a brand-new idea in the USA either. In the streetcar era, for example, developments largely concentrated along transit corridors in Boston, Chicago, San Francisco, and many other streetcar communities. TOD began to regain popularity in the early 1990s when the US Architect Peter Calthorpe coined the term in his book *The Next American Metropolis: Ecology, Community, and the American Dream* [1]. Other terms have been used by transportation professionals, urban planners, and the real estate industry to express similar development concepts, for example, "transit-sensitive land use" [2], "transit-oriented design" [3], "transit-focused development" [4], and "transit villages" [5]. TOD represents these multi-professional interests in developing around transit. Amid a worldwide trend of rising motorization and growing vehicle miles traveled (VMT), TOD is being widely promoted as a strategy to achieve sustainable transportation. Currently, there are over 4,000 transit sites in the USA offering significant potential to practice TOD [6].

At the center of TOD is transit. There are a variety of transit technologies; broadly they can be grouped as bus-based or rail-based. Bus- versus rail-based transit presents distinctive operational and service characteristics and involves quite different levels of public investments. Accordingly, bus-TOD versus rail-TOD entails different planning and design considerations. Whether to develop bus- or rail-based mass transit has long been a topic of policy debate. Recent developments in bus rapid transit (BRT) and light rail transit (LRT) throughout the world add to existing heated discussions on the advantages of bus- versus rail-based transit systems. This entry describes the comparative characteristics of bus- versus rail-based transit and discusses their implications for TOD.

Introduction

Transit-oriented development (TOD) is a strategy to integrate transportation with land use by focusing development on transit. A number of factors have motivated many communities in the USA to pursue TOD. Fighting sprawl and sprawl-induced problems is among the top. Community development in the USA after World War II can be largely characterized as low-density, strictly separated land uses, and car-oriented design. In a sprawling built environment, transit becomes operationally unviable and driving becomes a necessity. The consequences are ever-growing vehicle miles of travel (VMT) and increasing roadway congestion, energy consumption, and vehicle emissions. TOD offers potentials to curb sprawl and to help reduce the driving-related problems. Many state and local governments are encouraged to implement TOD by the recent steady increase in federal funding for transit. For example, the three transportation bills in the less than 20 years, namely, ISTEA to TEA21 to SAFETEA-LU, authorized increase in transit funding from $25 to $36 to $52.6 billions, respectively.

TOD is being widely advocated in Europe, Asia, and Latin America as well although their cities have traditionally developed in relatively high densities and rich mixed uses. The TOD interest grows out of the concern that new developments in many of these cities tend to depart from the traditional urban form. Amid rising income and associated growth in private motorization, neighborhoods and workplaces are becoming increasingly car oriented and pedestrian/cyclist hostile. Densities in these cities are high relative to the North American cities; yet the high density may not function well if it is not fully integrated with the transit. Dysfunctional density likely leads to what the New Urbanist Andres Duany called "high-density sprawl" [7]. Careful TOD planning, design, and implementation are essential for transit and its surrounding built environment in order to benefit from density.

A TOD typically has five attributes: transit access, a district of walking distance from the transit, mixture of different compatible urban functions, medium to high development density, and pedestrian- and cyclist-friendly environmental design in the TOD district. These attributes are interrelated and their composition for a specific TOD will vary by the spatial, socioeconomic, and technological context in which the TOD is proposed. TOD planners have created TOD typologies, specifying variations in design attributes for TODs in different spatial context, for instance, downtowns, urban neighborhoods, employment centers, and other regional locations [8]. As transit is at the center of TOD, TOD attributes will also vary by transit technologies.

Transit Technologies

Transit technologies evolve along with advances in vehicle technologies, information and communications technologies, as well as power and energy technologies. Table 1 shows the most commonly seen urban transit modes grouped into two categories: bus-based and rail-based. A comprehensive list and characterization of urban transit can be found in Vuchic [9].

TOD attributes and the ways in which these attributes interact will differ depending on the specific transit that the TOD is proposed for.

- A particular type of transit technology is associated with certain levels of cost. In general, the cost consists of two parts: capital and operation. Capital costs include vehicle cost and infrastructure cost (land acquisition and clearance and system complexity). Operating cost includes labor, insurance, fuel, administration, and others.
- Different transit technologies and operating plans deliver various levels of service capacities. Main

Bus Versus Rail Implications for Transit-Oriented Development. Table 1 Transit technologies and descriptions

System technology and description	Example systems	Service geography	Average speed	Station spacing	Typical headway	Guideway	Typical power source
Bus-based							
Regular bus: A road vehicle designed to carry multiple passengers. Buses vary in capacity from a dozen to several hundred passengers.	Cities with transit services	Urban	15–30 km/h	0.2–1.0 km	8–20	On street	Gasoline
Trolley bus A passenger *bus* operating on tires and having an electric motor that draws power from overhead wires.	New Orleans	Urban	15–30 km/h	0.2–1.0 km	8–15	On street	Electric
Bus rapid transit BRT is a relatively new umbrella term for urban mass transportation services utilizing buses to perform premium services on existing roadways or dedicated rights-of-way.	Pittsburg, Curitiba, Bogota, Beijing	Urban, Regional	25–50	0.4–1.5	10–20	Shared or exclusive ROW	Gasoline
Rail-based							
Streetcar Bus on rails typically operating on city streets	Portland	Urban	15–25	0.4	8–15	On street	Electric
Light rail With an overhead power supply and LRT utilizes predominantly reserved but not necessarily grade-separated rights-of-way. Electrically propelled rail vehicles operate singly or in trains. LRT provides a wide range of passenger capabilities and performance characteristics at moderate costs.	Dallas: DART; Denver:	Urban, Regional	30–60	1–1.5	5–30	Exclusive or shared ROW	Electric
Heavy rail	Washington, D.C. Metro; San Francisco: BART; New York City: MTA Boston: MBTA Chicago: CTA	Urban, Regional	80–130 km/h	1–3	3–10	Grade-separated, Exclusive ROW	Electric

Bus Versus Rail Implications for Transit-Oriented Development. Table 1 (Continued)

System technology and description	Example systems	Service geography	Average speed	Station spacing	Typical headway	Guideway	Typical power source
Commuter rail	Boston Purple Lines: MBTA; New York Long Island Railroad San Jose: CalTrain	Regional	50–120 km/h	3–10 km	15–30 min.	Exclusive ROW	Diesel or hybrid

factors affecting service capacities include vehicle size, service frequency, and road conditions.

- Carrying capacity, along with other operational and contextual factors, determines the level of services (LOS). Existing empirical studies have shown that the extent of land-use impacts of transit development is positively associated with LOS. In other words, higher capacity systems such as metro likely have stronger positive impacts on the value of land near the station.
- More expensive land leads to higher development intensity, which will result in higher population or employment density.
- Higher population and job density provides a larger pool of transit ridership. If there are more people riding on the transit, farebox revenue will increase. Higher density also provides a larger basis for economic activities and a larger tax base for the local community. The farebox and tax income help reduce cost burden of building and operating transit systems. Ridership increases, however, may trigger a greater need for expanded services, which can lead to increases in operating and potentially capital costs.

Cost Characteristics of Bus Versus Rail Mass Transit

The main topic of debate on bus versus rail transit development is cost. Recent discussions largely focus on cost comparisons between BRT and LRT due to a number of performance similarities between them. On a per user basis, rail transit systems generally cost more to build than bus transit but less to operate owing to relatively higher capacities associated with rail. Still, within each type of transit, there are large variations in technical specifics and operational characteristics.

Capital Cost Comparison Between Bus and Rail Transit

Table 2 shows the average capital cost per route mile for BRT, LRT, and MRT based on selected systems reviewed by USDOT [10], GAO [11], and BAH [12]. On average, BRT costs $10.24 millions (in 1990 dollars) per mile to build, less than half of LRT ($26.4 million) and less than one-tenth of MRT ($128.2 million). Nevertheless, average cost–based comparisons between bus and rail will likely generate controversies [13]. Table 2 also shows the ranges of capital costs of the transit systems studied. Notably, within same type of transit technology, capital costs vary considerably. For instance, the BRT in Miami, FL costs $5.6 million per mile to build, whereas the West Busway BRT in Pittsburgh, PA costs $41.7 per mile, higher than the average capital cost of LRT. The most expensive LRT among the 21 projects reviewed by USDOT [2] is in Buffalo, NY, which costs $90.19 per mile, over 40% higher than the per-mile capital cost of the metro in Miami.

Many factors contribute to the large variations in the capital costs of transit systems. Costs of BRT projects, for example, include vehicles (regular or articulated), the roadway cost (busways or bus lanes), station structures, park-and-ride facilities, communications, and traffic signal systems. For rail transit systems, guideway elements may take a large share of capital costs, depending on types of structure (e.g., tunnel or elevated). Different ways of accounting the costs by including (or excluding) various capital cost elements will change the average cost figures quite significantly. Hence, when comparing different types of transit systems with respect to capital costs, it is important to maintain consistency in cost reporting

Bus Versus Rail Implications for Transit-Oriented Development. Table 2 Capital cost comparisons of bus versus rail (in 1990 US$)

	BRT	LRT	MRT
Average cost per route mile (millions)	$10.2	$26.4	$128.2
Cost range (millions)	$5.6 ~ $41.7	$9.4 ~ $90.2	$63.9 ~ $169.6
Number of projects reviewed	9	21	4

Sources: Calculated from [10–12]

Bus Versus Rail Implications for Transit-Oriented Development. Table 3 Per mile capital cost breakdown of bus versus rail (in 1990 US$1,000s)

	BRT		LRT		MRT	
	$	%	$	%	$	%
Land (right-of-way)	3,018	15.0	1,520	7.8	7,436	5.8
Guideway	6,495	33.5	4,289	22.0	33,333	26.0
Trackwork or special conditions	983	8.5	1,686	8.7	5,385	4.2
Stations	1,387	9.1	1,094	5.6	33,333	26.0
Power and control	113	2.7	2,047	10.5	10,513	8.2
Facilities (yards and shops)	192	1.9	974	5.0	2,820	2.2
Eng./Mgt./Test (soft costs)	2,948	20.3	5,581	28.6	19,230	15.0
Vehicles	1,483	9.0	2,295	11.8	16,154	12.6
Total	16,620	100	19,486	100	128,203	100

Sources: Calculated from [10–12]

and to examine/compare specific cost elements whenever data is available. Such itemized comparisons allow clear identification of specific factors driving up the system development cost.

Table 3 shows the breakdown of capital cost by subsystems for the three types of rapid transit technologies. Data for LRT and MRT come from a USDOT study of nine completed projects [2], whereas cost data for BRT are for two proposed systems in Atlanta, GA and Abuquerque, NM. Note that, although BRT costs less on average than LRT ($16.6 and $19.5 million per mile, respectively), for several items BRT costs exceed those of LRT. For instance, the average land acquisition cost (right-of-way) for the BRT projects ($3.018 million per mile) is almost twice as much as that of LRT project ($1.52 million per mile). This is partly because BRT requires a wider right-of-way than LRT. BRT guideway cost ($6.495 million per mile) is much higher than that of LRT ($4.289 million per mile) due to construction of dedicated busways. Station cost for BRT is also slightly higher than that of LRT. In most cases, a BRT station is located in highway median areas and requires elevated structure for passengers to access the station from both sides of the road. Capital cost for conventional bus is not reported here because it runs mostly on existing roadways free-of-charge and does not require guideways.

Operating Cost Comparison Between Bus and Rail Transit

Table 4 below compares operating costs between the bus and the rail transit modes. Cost per vehicle revenue mile measures the average cost of operating individual vehicles. It is the annual cost of operating a vehicle

Bus Versus Rail Implications for Transit-Oriented Development. Table 4 Operating costs (1990$)

	BUS	BRT	LRT	MRT
$ per vehicle revenue mile	3.1	3.6	9.3	6.5
$ per vehicle revenue hour	45.0	78.8	125.0	152.0
$ per 1,000 place mile	60.0	72.3	96.0	49.2
$ per 1,000 passenger mile	616.4	496.9	578.0	282.0

Sources: Calculated from [10, 11]

divided by the total annual number of miles traveled while the vehicle is in revenue service (e.g., excluding the miles traveled to/from the maintenance yard). Among the four transit modes listed in the table, LRT exhibits the highest cost at $9.3 per vehicle revenue mile. MRT has a relatively lower cost than LRT mainly because it can operate with as long as ten or more cars per train. Standard bus and BRT have the lowest vehicle-mile costs. Operating cost per vehicle hour is another way of measuring the cost of transit operation regardless of the number of passengers carried. MRT, which typically operates at a higher speed than other transit modes, displays the highest vehicle-hour cost. BUS and BRT once again rank the lowest in operating cost measured on the per vehicle revenue hour basis.

The other two measures of operating costs – cost per thousand place mile (where places account for total number of seats and permitted standings) and cost per thousand passenger mile – take into consideration the differences in vehicle capacity and system usage among the transit modes. Notably, MRT has the lowest cost at $49.2 per thousand place mile, whereas LRT's place-mile cost is the highest at $96. If usage is considered, BUS has the highest cost at $616.4 per thousand passenger mile. Again, MRT is the least expensive at $282 per thousand passenger mile. It should be noted that figures for BRT in the table above are derived from data in the GAO study [3]. The study does not report cost per passenger mile. The figure of BRT's $496.9 per thousand passenger mile was estimated based on the assumption that average trip distance of BRT passengers was half of the BRT route length.

Overall, figures in the table above indicate that BRT outperforms LRT in all of four operating cost categories. Nevertheless, cautions should be exercised when interpreting these averages. Tennyson [13] has challenged that GAO's study was unevenly biased against LRT – the bus costs were reported too low due to possible inconsistency and errors in the reported data. As with the capital costs reviewed earlier, a wide range of figures exist in each of the four operating costs. The use of alternative measures may give different results on the cost performance of bus versus rail. Operating costs for light rail systems vary widely depending upon the system operating environment [14]. For example, operating costs in Buffalo were $67 million dollars a year for an on-street system and $87 million dollar/year for an in-tunnel system [5]. The cost per average weekday boarding on Los Angele's Orange LRT line is $16,743 and $45,762 for the Gold Line Extension [15].

The US National Transit Database reports that, between 1998 and 2007, the operating cost per unlinked trip has increased for all but MRT (Fig. 1) [16].

Capacity of Bus Versus Rail Transit

Bus and rail transit technologies differ in their design capacities. Under different system operational plans, their trunk line capacities may vary significantly. Table 5 provides a reference to the line capacities of standard bus, BRT, LRT, and MRT [17]. The basic capacity of a standard bus serves as a benchmark for line capacity comparisons among these transit modes.

Standard buses can operate in short headways with relatively high frequencies. Unit capacity may vary depending on the bus seating configuration and comfort standard. On average, standard buses can achieve a line capacity of 3,800–5,400 places per hour. Articulated buses have vehicle capacities approximately 50% greater than standard buses. Operating in slightly longer headways and lower frequencies than standard buses, articulated buses can offer a line

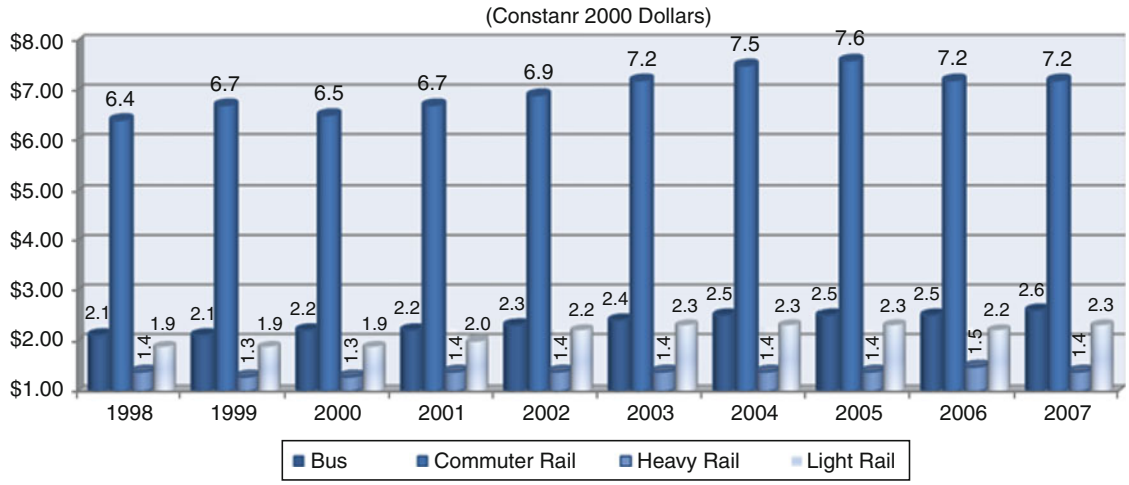

Bus Versus Rail Implications for Transit-Oriented Development. Figure 1
Trends of operating cost per unlinked passenger trip for bus and rail modes 1998–2007 [16]

Bus Versus Rail Implications for Transit-Oriented Development. Table 5 Maximum line capacities of transit modes

Mode	Vehicle dimensions (L × W m)	Transit unit capacity (Seat + standing spaces)	Minimum headway (s)	Maximum frequency (Transit units per hour)	Line capacity
Standard bus	12.00 × 2.50	75	70–50	51–72	3,800–5,400
Articulated bus	18.00 × 2.5	120	80–60	45–60	5,400–7,200
High-capacity bus (BRT)	22.00 × 2.50	160	30–12	120–300	9,000–30,000
LRT (partially separated ROW)	24.00 × 2.65	3 × 170 = 510 or 2 × 280 = 560	150–75	24–48	12,200–26,900
MRT	21.00 × 3.15	10 × 240 = 2,400	150–120	24–30	67,200–72,000

Source: [17]

capacity between 5,400 and 7,200 places per hour. High-capacity buses are used by many BRT systems in the world. Examples include Sao Paulo and Curitiba, Brazil, and Transmillennio in Bogota, Colombia. They can achieve a line capacity level more than four times the basic bus capacity. Sao Paulo, Curitiba, and Bogota operate high-capacity buses along well-planned bus corridors. Special operating features such as bus convoys and off-board fare collection allow a total throughput of about 300 buses per hour. At such a high frequency, line capacities were reported to achieve 24,000 and 30,000 places per hour in Sao Paulo and Bogota, respectively.

LRT line capacities are close to those attained by high-capacity BRT at 4.2 times that of basic bus capacities. An LRT with fully separated ROW will achieve line capacities higher than figures provided above. MRT systems have a great diversity of features that determine MRT line capacities. For instance, dimensions of metro cars in Paris (15.00 × 2.5 m) are much smaller than in Toronto and Hong Kong (21.00 × 3.23 m). Maximum train lengths also vary,

from four cars in Boston to ten or more cars in New York, Tokyo, and San Francisco. In these cities with large-profile systems, line capacities often exceed 70,000 places per hour.

Table 5 provides a reference of transit line capacities under design conditions. In reality, the capacities of these transit systems vary dramatically due to such factors as operational techniques, facility constraints, transit demand, and road conditions. Current debate on BRT-LRT capacity comparisons centers around methods where these constraints are taken into consideration. For example, the communication-based train technology (CBTC) creates very small virtual blocks to allow trains to approach one another in closer intervals. CBTC can increase capacity by 10–15%. Automatic train operation is an operating technology that allows the train to optimize speed, which can increase line capacity by 2–4%. Another factor differentiating the line capacities of bus from train systems is the number of lanes. Typically, BRT travels in a single lane per each direction, whereas rail can follow multiple track lanes. For example, New York has several three- and four-track trunk lines.

Like cost variations, bus and rail transit each offers a wide range of service capacities. Generally speaking, rail transit offers larger capacities than bus transit. In real-world applications, however, it is common to see an overlapping range of capacity offerings by bus and rail transit systems. For instance, BRT in Curitiba achieves far greater higher capacities than the LRT in Buffalo. Vehicle technologies, operation/management efficiencies, and station/street conditions all have significant effects on achievable capacities. Table 6 shows the range of peak-hour capacities suggested by the literature for four aggregated transit modes [18].

Transit Impacts on Property Values

Analyzing rail transit's effects on land use/land development can be built upon the urban location theories, which suggest, in a most succinct form, that transportation defines the urban spatial access pattern and accessibility determines the worth of land. In making location decisions, households (or firms) bid for locations by trading housing (and/or land) consumption against commuting costs to the urban center (e.g., the CBD). The closer to the center, the better the access, and the higher the bid rent. Therefore, we would expect a downward sloping accessibility curve from the urban center. Parallel to the accessibility curve is a downward gradient bid-rent curve. Measuring price or rent levels associated with the proximity to rail transit will provide quantified information on the *magnitude* of rail transit's influence on land value and land use.

Research on property/land value impacts of transit has accumulated a large volume of literature. A number of meta-studies have been published [19, 20]. RICS [19] reviewed about 150 references in the topical area. Most of those reviewed are studies from the USA, Canada, the UK, and Europe. Residential properties have been the focus of the existing studies, while commercial, retail, and office properties were also examined.

Table 7 compiles findings of the reviewed studies of transit impacts on property values. Due to differences in methods used in the studies, direct comparisons of the study findings are quite challenging. This entry groups the studies by property types (residential, commercial, or others) and by transit technologies. The focus is on the magnitude of transit proximity effects measured in monetary terms. Due to limited

Bus Versus Rail Implications for Transit-Oriented Development. Table 6 Capacity comparison among transit modes

	BUS	BRT	LRT	MRT
Typical peak-hour capacity	1,000–3,000	2,000–10,000	3,000–18,000	13,000–41,000
Ratio to BRT capacity	0.35	1.0	1.65	5.3
Highest observed in the USA or Canada	3,000	11,000	10,000	50,000

Source: [18]

Note: (1) The BRT mode shown here combines those mixed with street traffic and those with dedicated busways. (2) BRT is used for ratio calculation is for consistency with cost comparison shown in previous section.

Bus Versus Rail Implications for Transit-Oriented Development. Table 7 Transit impacts on property values

Study	Transit system	Findings	Standardized proximity premium in present US$	Standardized proximity premium in 1990 US$
Apartment (monthly rent in dollars per square meters for every meter closer to the station)				
Rodriguez and Targa (2004) [21]	BRT: Bogota	6.8–9.3% increase for every 5 min walk closer to the station; or in 2002 US$439–653/0.1 km	0.07	0.05
Cervero and Duncan (2002) [22]	LRT: LA County	No significant effects found	0	0
Cervero and Duncan (2002) [23]	LRT: San Diego	East line: within 1/2 mile; 2000 $104,827 more than other locations	0.27	0.21
Benjamin and Sirmans (1996) [24]	MRT: Washington, D.C.	Rents decrease by 2.4–2.6% for each one-tenth mile increase of distance from a metro station. 1992 mean month rent $797	(1.24)	(1.15)
Single-family homes (dollars per home for every meter closer to the station)				
Munoz-Raskin (2006) [25]	BRT: Bogota	In most cases, negative impacts are reported for properties location within 5-min distance to the system		
Landis et al. (1995) [26]	LRT: San Diego Trolley	The typical home sold for 1990 $272 more for every 100 m closer to a light rail station.	2.72	2.72
Landis et al. (1995) [26]	LRT: Sacramento	No effects found	0	0
Landis et al. (1995) [26]	LRT: San Jose	The typical house was worth $197 less for every 100 m it was closer to light rail.	(1.97)	(1.97)
Al-Mosaind et al. (1993) [27]	LRT: Portland MAX, Eastside	The typical house sold for $663 more for every 100 ft nearer a light rail station.	21.74	24.02
Chen et al. (1998) [28]	LRT: Portland MAX, Eastside line	Beginning at a distance of 100 m from the station, each additional meter away from decreases average house price by 1992 $32.20.	32.20	30
Dueker and Bianco (1999) [29]	LRT: Portland MAX, Eastside line	Median house values increase at increasing rates as move toward an LRT station. The largest price difference (1990 $2,300) occurs between the station and 200 ft away.	37.70	37.70
Lewis -Workman and Brod (1997) [30]	LRT: Portland MAX, Eastside line	On average, property values increase by $75 for every 100 ft closer to the station (within the 2,500 ft–5,280 ft radius).	2.25	1.83
Knaap et al. (1996) [31]	LRT: Portland MAX, Westside line	The values of parcels located within ½-mile of the line rise with distance from the lines, but fall with distance from the stations.		
Landis et al. (1995) [26]	MRT: BART	1990 single-family home prices decline by $1–2 per meter of distance from a BART station in Alameda and Contra Costa Counties.	1.50	1.50
Lewis -Workman and Brod (1997) [30]	MRT: BART	Average home prices decline by about $1,578 for every 100 ft further from station.	51.74	43.11

Bus Versus Rail Implications for Transit-Oriented Development. Table 7 (Continued)

Study	Transit system	Findings	Standardized proximity premium in present US$	Standardized proximity premium in 1990 US$
Lewis -Workman and Brod (1997) [30]	MRT: New York City MTA	Average home prices decline by about $2,300 for every 100 ft further from the station areas.	75.41	62.84
Voith (1993) [32]	MRT: Philadelphia SEPTA	Finds a premium for single-family homes with access to rail stations of 7.5–8.0% over the average home value.	7.75%	
Cervero and Duncan (2002) [23]	CRT: San Diego	Price increases by 17% in ½ mile of non-downtown Coaster station	84	63.75
Landis et al. (1995) [26]	CRT: CalTrain	Did not find a significant impact on house values from proximity to a rail station. Houses within 300 m of a CalTrain right-of-way sold at a $51,000 discount.	(170)	(170)
Armstrong (1994) [33]	CRT: Boston MBTA, Fitchburg Line	Single-family residences located in communities that have a rail station have a market value approximately 6.7% greater than those that do not. Also found a property value loss of about 20% for properties located within 400 ft of a commuter or freight rail right-of-way.	6.70%	
Commercial property (dollars per square meter for every meter closer to the station)				
Landis et al. (1995) [26]	LRT: San Diego Trolley	No effect found for commercial impacts	0	0
Weinberger (2001) [34]	LRT: Santa Clara, County Guadalupe line	Commercial space within a ¼-mile of a station received an average of 2.3¢ to 5.0¢ more per square feet than space located more than ¾-mile from a station. Office space sold within a ¼-mile of a station received an average of $4.87 per square feet more per gross building square feet compared to space located more than ¾-mile from a station.	0.36	0.27
Landis et al. (1995) [26]	MRT: BART	Found no effect for commercial property.	0	0
Nelson (1998) [35]	MRT: Atlanta MARTA	Price per square meter falls by $75 for each meter away from transit stations. Price rises by $443 for location within special public interest districts.	75.00	61.07
FTA (2000) [36]	MRT: Washington, D.C.	Price per square foot decreases by about $2.30 for every 1,000 ft further from station.	0.07	0.05
Fejarang et al. (1994) [37]	MRT: Los Angeles	Commercial space within ½-mile of the rail corridor had an additional $31 increase in mean sale price per square feet over the mean sales price of a comparable control group outside of the rail corridor, between 1980 and 1990.	0.39	0.34

information provided by some of the studies, only part of the reported proximity effects could be converted to 1990 US dollars in comparable units.

Mixed results have been reported on transit proximity premiums associated with apartment rents [21–24]. Results vary mainly depending on the types of transit technologies. Most studies have found positive transit proximity premiums for single-family homes, with a few reporting negative impacts [25–33]. For instance, Armstrong [33] found that single-family home prices were 6.7% higher in communities with a commuter rail station than in communities without. However, a statistically significant property value loss of roughly 20% was found for properties located within 122 m (400 ft) of the right-of-way. Weinberger [34] argues that the presence of transit is a nuisance and may drive down adjacent property values. They cite the noise generated by transit and believe that transit access allows undesirable people easy access to their neighborhoods. Chen et al. [28] tested the nuisance hypothesis in their study of light rail in Portland, Oregon, but found that the benefits to property values attained from proximity to light rail outweighed the negative effects. As shown in Table 7, most studies have identified positive effects of rail transit on nearby properties although some reported negative effects.

LRT tends to have mixed impacts on commercial properties [22, 23, 26, 34], contrasting to mostly positive effects associated with MRT [26, 35–37]. Nelson's [35] study of the Atlanta MARTA heavy rail line showed a negative gradient of $75 reduced property value per meter from a transit station, indicating a positive benefit associated with access to transit. Weinberger's study suggest positive impacts on commercial property values resulting from proximity to light rail stations, though no specific capitalization rate is provided. The study by Cervero and Duncan shows that in Santa Clara County, commuter rail had a greater impact on commercial property values than the light rail line. Weinstein and Clower's [38] study of the DART light rail system also suggests appreciable effect on commercial properties in the Dallas area from proximity to light rail.

Data on the effects of BRT on property values are quite limited. Rodriguez and Targa [21] estimated that, in Bogota, Columbia, every additional 5 min of walking time to a BRT station reduced rental price by 6.8–9.3%, which translates to a premium of US$0.05 per m^2 for every meter closer to the station after controlling for the distance to (i.e., the nuisance effect of) the system right-of-way. Also studying Bogota's BRT, Munoz-Raskin [25] confirmed that, in most cases, property values were lower within 5-min distance of the system than those beyond. Cervero and Duncan's [22] study of BRT in Los Angeles found that residential properties near BRT stops sold for less while commercial properties for more. The reason for this negative price effect, according to them, is that the majority of BRT stops are located in redevelopment areas of Los Angeles. In another study looking at how income serves as a determinant in communities' valuing transit, Nelson [10] found that the elevated MARTA heavy rail in Atlanta had positive effects on home values in low-income neighborhoods but negative effects in high-income neighborhoods.

One factor that may partly explain the varying empirical findings above is system maturity [12, 14]. Studies conducted on newly constructed transit systems may not capture the positive valuation of transit on property values because housing markets have not had time to react to transit's presence. Transit ridership may serve as an indication of the magnitude that transit can add to property values, since low ridership indicates that transit is not an amenity to be used [14]. Transit technology also matters, with reliability and speed adding value to the system and in turn being capitalized in property values. Unwanted adjacent uses such as freight or industry will also play an important role by reducing neighborhood quality of life [13].

Density for Bus and Rail Transit

A question of general interest is what land-use densities are needed in order to support specific transit operations. The work by Pushkarev and Zupan [39] remains one of the most influential publications on density and transit uses. They plotted with the logarithmic values of population and trip densities on the horizontal and vertical axis, respectively. The log-log graph exhibits virtually a straight line. Specifically, in the New York Region, trips per square mile by MRT increase from 12 at a residential density of 0.8 dwelling units per acre (or du/ac) to more than

Bus Versus Rail Implications for Transit-Oriented Development. Table 8 Transit supportive densities

Mode	Service	Minimum necessary residential density (dwelling units per acre)	Remarks
Dial-a-bus	Many origins to many destinations	3.5–5	Lower figure if labor costs twice those of taxis; higher if thrice those of taxis
Local bus	Minimum to frequent services; 1/2 mile route spacing; 20–120 buses per day	4–15	Average, varies as a function of downtown size and distance from residential area to downtown
Express bus (BRT) – walk access	Five buses during 2 h peak period	15 Average density over 2 mile^2 tributary area	From 10 to 15 miles away to largest downtowns only
Express bus (BRT) –drive access	Five to ten buses during 2 h peak period	3 Average density over 20 mile^2 tributary area	From 10 to 20 miles away to downtowns larger than 20 million square feet of nonresidential floorspace
Light rail (LRT)	Five-minute headways or better during peak hour.	9 Average density for a corridor of 25–100 mile^2	To downtowns of 20–50 million square feet of nonresidential floorspace
Metro rail (MRT)	Five-minute headways or better during peak hour.	12 Average density for a corridor of 100–150 mile^2	To downtowns larger than 50 million square feet of nonresidential floorspace

Source: From [39, 40]

60,000 at a density of 200 du/ac. Table 8 shows a typical range of transit supporting densities [39, 40].

Recent studies have confirmed the pattern that Pushkarev and Zupan found 3 decades ago: the closer people live to transit and other services such as shops, the more likely it is that they will utilize the transit and drive less [41, 42]. The study by Frank and Pivo [43] compared travel mode choice among different census tracts with differing levels of employment and population density. They found that transit usage and walking increase as density and land-use mix increase, whereas travel by single-occupancy vehicle (SOV) declines. The relationship between density (employment and population) and mode choice for SOV, transit, and walking displays a nonlinear pattern for both work and shopping trips. Significant modal shifts from SOV to transit and walking occur when employment density increases from 20 to 75 employees per acre or reaches 125 or more employees per acre. Population density needs to exceed approximately 13 persons per acre in order to achieve major modal shifts from SOV to non-driving modes for shopping travel.

The Institute of Transportation Engineers in its 1989 publication suggests that, to support bus service with headways of an hour, 4–6 du/ac and 5–8 million square feet of commercial/office space in the corridor is needed; for bus service with 30 min headways, 7–8 du/ac and 8–20 million square feet of commercial/office space is needed; and for light rail and feeder bus service density of 9 du/ac and 35–50 million square feet of commercial/office space is desired [44]. Newman and Kenworthy found that densities of at least 12–16 persons/acre are needed to support urban transit [45]. Similarly, another study found that transit use increases sharply when residential density moves from 7 to 16 du/ac [46]. Levinson [47] found that a relationship between mode choice and density was significant only in densities greater than 10,000 persons per square mile. As much as 93% of the transit demand in Portland, OR can be explained by employment and housing densities [48]. Residential densities of more than 80 du/ac were considered highly supportive, those from 46–80 du/ac medium high, those from 20–45 du/ac medium, 6–19 du/ac medium low, and 0–5 du/ac as low in support of transit [49]. Standard bus service can be maintained at 7 du/ac, and significant transit use increases can occur at 10 du/ac and higher [46, 50]. Lawton has also shown that the higher the density found in an area, the more likely

people will walk or take transit and produce less vehicle miles traveled [51].

Some have argued that certain densities of office and other industries can support transit without high-density development [52–54]. Cervero [55] investigated suburban employment densities and found that ride sharing increased by 3.5% for every 5,000 jobs added. Retail and services located near places of employment reduce VMT and prompt workers to utilize transit [56]. Barnes and Davis [57] maintain that commercial land use exerts much more influence on travel choices than do residential densities. Additional work by Cervero has found that suburban employment centers, especially when mixed use is incorporated, prompt the employees to commute via different modes. Furthermore, those living near transit stations are much more likely than others to commute to work by transit [58–60].

Others have emphasized the link between transit usage, car ownership, and centrality instead of transit usage to density [61]. It has been shown that a 10% increase in population centrality (corresponding with higher densities) lowers the chance that a worker drives to work by a margin of 2.1% [62]. Johnson concluded that not only density but density and its spatial relation to the transit stop are both important when evaluating ridership potential [63]. Schimek [64] has argued that, while density matters, its affects are minimal – only providing a 0.7% reduction in auto travel with a 10% rise in density. Another study noted that while density seemed to explain bus usage significantly, it was difficult to properly identify densities, and that destination as well as departure points should be taken into account [65].

Specific densities needed for BRT operation have not been sufficiently identified, although figures for the standard bus-based operations can be borrowed and extrapolated. BRT may perform better in lower-density areas than LRT [66]. In corridors with several medium-density cores but with an overall low-density landscape, BRT's flexibility may make it more suitable than LRT [67].

Transit analysis conducted by the Florida Department of Transportation has ranked densities as to how they may support public transit (Table 9). Residential densities at 80 dwelling units or more per acre are considered highly supportive, whereas less than five dwelling units per acre are not transit supportive [68].

Bus Versus Rail Implications for Transit-Oriented Development. Table 9 Florida DOT's assessment of transit supportive densities

Dwelling units per acre	*Support level*
>80	High
46–80	Medium high
20–45	Medium
6–19	Medium low
0–5	Low

Source: [68]

Best Practice of Bus- Versus Rail-Based TOD

Curitiba is the capital city of the Brazilian state of Paraná in Brazil. It presents one of the most successful corridor-type TODs on BRT in the world. Curitiba's BRT system is featured with exclusive rights-of-way, biarticulated buses, tube stations, and land-use zoning coordinated with high-capacity bus corridors (Fig. 2). The system plan is known as the Trinary Model. The model has a two-lane street at the center where the express buses have their exclusive lane. Adjacent to the express lane are two one-way streets moving in the opposite directions. Lots on both sides of the central streets are zoned to develop at high densities. One block from the one-way street on each side of the corridor is a regular two-way street that carries a mix of private vehicle flow and conventional bus services. Five of these roads form a star that converges to the city center. Land farther from the roads is zoned for lower-density developments.

The success of Curitiba's bus-based corridor TOD is shown by a number of key statistics: as of 2008, there were 340 bus lines, 58 km of busways, 1,100 km bus routes, and 26 terminals. Daily the system serves 380,000 passengers by the corridors and 2.4 million by the network. The BRT operates at a less than 1 min headway in the peak hour, peak directions, with an average speed of 30 km/h for the trunk line and 20 km/h for other routes. More than 70% of commuters ride the bus to work.

Bus Versus Rail Implications for Transit-Oriented Development. Figure 2
BRT-based TOD in Curitiba, Brazil

Bus Versus Rail Implications for Transit-Oriented Development. Figure 3
LRT-based TOD node, Mockingbird Station, Texas, USA

The Mockingbird Station TOD represents the best practice of TODs implemented around a single node of LRT (Fig. 3). Located four miles north of downtown Dallas, the Mockingbird Station is one of the largest on the Dallas Area Rapid Transit (DART) rail line. Developer Ken Hughes of UC Urban of Dallas initiated and developed the 4-ha project in 2000–2001. Main functions of the TOD site contains 16,536 m^2 of retail,

restaurant, and cinema space; 12,727 m^2 of office space, 211 loft apartments; and parking for 1,580 vehicles. The main features of the Mockingbird Station TOD include its combination of adaptive use of historical warehouses with new construction, fine design of streetscape and public arts, and careful organization of pedestrian paths and public as well as private vehicle movement. The success of the Mockingbird Station TOD has proven that a properly conceived TOD can succeed and flourish by serving the adjacent communities, increasing transit use while acting as a catalyst for place making.

Hong Kong's Mass Transit Railway Corporation (MTRC) is one of few successful cases in the world that the rail transit agency is able to fully self-finance system construction and operation by practicing a Hong Kong model of TOD, namely, "Rail + Property" or "R + P" (Fig. 4). Its central idea is to integrate property development with rail operation and construction such that the profit gained from property development pays the operational and capital costs of the rail system. The main working procedures are as follows. First, MTRC studies development potentials in the area of approximately 500-m distance to the proposed stations. It then obtains land development right from the government for the (re)developable properties. The land cost to MTRC (i.e., land premium income to the government) is estimated based on the no-rail scenario. Next, MTRC specifies development plan for the properties in terms of use composition (residential, retail, green space, transportation, etc.), density (i.e., FAR), and other needed facilities. After the government's approval of the plan, MTRC develops the rail system and the station area in partnership with developers. Because of rail transit availability, property value increases. MTRC then sells properties to individuals or firms, sharing the profits with developers and the government. The MTRC's earnings will be used for maintenance and expansion of rail services as well as other expenses or investments.

Bus Versus Rail Implications for Transit-Oriented Development. Figure 4
Tsingyi station: example of Hong Kong's "Rail + Property" TOD model

MTRC's R + P model proves to offer an all-win solution, at least in the scope of MTRC's services. MTRC benefits from guaranteed funds for service delivery and expansion. To the community, ordinary citizens enjoy high-quality rail services while the share of household expenditure in transportation remains low (9%) [69]. To the developer, MTRC plays a coordinator role, helping reduce start-up costs. The government is a big winner as well. Since 2000 when MTRC went public, the R + P practice has enabled MTRC to operate high-quality rail services without asking subsidy from the government. Furthermore, the Hong Kong government has received a profit (net initial equity contribution) of over HK$103 billion from its 76% MTRC shares.

Conclusions

Table 10 summarizes modal characteristics of bus- and rail-based transit systems. Main categories of features for comparison include capacity, cost (capital and operating), land-use impacts, and transit supportive densities. For easy reference, their attributes are normalized by using BRT as the main reference.

Bus Versus Rail Implications for Transit-Oriented Development. Table 10 Comparison among major transit modes

	BUS	BRT	LRT	MRT
Capacity: typical peak-hour passengers	1,000–3,000	2,000–10,000	3,000–18,000	13,000–41,000
Capital cost (1990$ per route mile, millions)		$10.24	$26.4	$128.2
Operating cost ($ per vehicle revenue mile)	$3.1	$3.6	$9.3	$6.5
Operating cost ($ per unlinked passenger trip)		$1.51	$2.03	$1.23
Property impacts: apartment (1990$ per square meter for every meter away from transit)		$0.05	$0.3	$1.15
Property impacts: single-family home (1990$ per home for every meter away from transit)			$0–38	$43–62
Minimum density (dwelling units/acre)	4	9	9	12
Ratio to BRT				
Capacity	0.35	1	1.65	5.30
Capital cost		1	2.58	12.52
Operating cost (per vehicle revenue mile)	0.86	1	2.58	1.81
Operating cost (per unlinked trip)		1	1.34	0.82
Minimum density	0.44	1.00	1	1.33

The comparisons depicted above indicate that, on average, BRT has the potential to outperform LRT in providing a moderate to high level of service capacity at a moderate level of capital and operating costs in neighborhoods with moderate population and job densities. MRT, although most expensive to build, can achieve over five times the capacity of BRT or LRT and has demonstrated the largest positive impacts on property values in the vicinity of rail stations.

The reviews provided in this entry on the comparative costs, capacities, and land-use impacts of various rapid transit technologies suggest that no simple answer exists to the question. Perhaps no single form of transit will fit all market needs of a community. Each transit technology is efficient when it is in the right place serving the right market. It is more likely the case that all forms of transit systems coexist, each serving a particular market niche. The key is to propose context-sensitive TODs for integrated development transit with land use.

Future Directions

Current TOD practices and studies have largely focused on nodal TODs, that is, the stand-alone TODs around individual bus stops or train stations. However, many community objectives, for instance, affordable housing provision, job-housing balance, and congestion relief, cannot be well addressed at the individual TOD basis. From a traveler's perspective, whether she/he uses transit depends not only on what the origin can offer but also on what amenities the destination provides. Hence, an important direction for future study is Corridor TOD, which formulates development and implementation strategies at the corridor scale along bus or rail transit routes.

Another future direction is TOD-based value capture for transit financing. Existing TOD initiatives are mostly concerned with physical planning and design of TODs as well as legal and political barriers to TOD implementation. There are successful examples as mentioned above on TOD-based value capturing through integrated transit-land development. How the successful experience can be transferred to cities and countries with different legal, institutional, and financial settings remains a challenge and warrants future research.

Furthermore, the current urban TOD practice can be expanded to other modes of transportation for intercity travel, for example, air, ferry, and high-speed

rail. Stations and terminus for intercity transportation typically have more complex traffic operations than those of intracity transit. A new trend is to develop the station or terminal areas as multifunctional places rather than traditionally as single-function transportation hubs. TOD principles can be applied to these cross-region modes, while their technological complexities require specific consideration.

Bibliography

1. Calthorpe P (1993) The next American metropolis: ecology, community and the American dream. Princeton Architectural Press, New York
2. Beimborn E, Rabinowitz H, Gugliotta P, Mrotek C, Yan S (1991) Guidelines for transit-sensitive suburban land use design. Report No. DOT-T-91-13. U.S. Department of Transportation, Urban Mass Transportation Administration, University Research and Training Program, Washington, DC
3. Urban Land Institute (1994) Transit-oriented design. Working Paper 635, June 1994, The Urban Land Institute, Washington, DC
4. Porter DR (1998) Transit-focused development: a progress report. J Am Plann Assoc 64(4):475–488
5. Bernick M, Cervero R (1997) Transit villages in the 21st century. McGraw-Hill, New York
6. Reconnecting America, 2006. http://www.reconnectingamerica.org
7. Gordon D (2003) New urbanism and smart growth: twins separated at birth? Places - Forum Environ 15(2). http://www.escholarship.org/uc/item/8wp02013. Accessed 10 March 2010
8. Dittmar H, Ohland G (2004) The new transit town: best practices in transit oriented development. Island Press, Washington, DC
9. Vuchic V (2007) Urban transit-systems and technology. John Wiley, Hoboken, NJ
10. USDOT (1993) Characteristics of urban transportation systems, revised edn. U.S. Department of Transportation, Washington, DC
11. GAO (2001) Mass transit: bus rapid transit shows promise. U.S. General Accounting Office, Washington, DC
12. BAH (Booz-Allen & Hamilton, Inc.) (2003) Light rail capital cost study update. Federal Transit Administration, Washington, DC
13. Tennyson E (2008) Analysis of the general accounting office report "Bus Rapid Transit Shows Promise." http://www.lightrailnow.org/myths/m_brt002.htm. Accessed 30 July 2008
14. Pickrell D (1992) A desire named streetcar. J Am Plann Assoc 58(2):158–177
15. Vincent W, Callaghan L (2007) Evaluating the Los Angeles orange line BRT. In: Presented at 86th annual meeting of the transportation research board, Washington, DC
16. U.S. Federal Transit Administration (2008) National transit database. At URL: http://www.ntdprogram.gov/ntdprogram/pubs/NTST/2007/HTML/Operating_Costs_and_Performance_Measures.htm. Accessed 10 March 2010
17. Vuchic V (2005) Urban transit: operations, planning and economics. John Wiley & Sons, Hoboken, NJ
18. Kittelson & Associates (2003) TCRP report 100: transit capacity and quality of service manual, 2nd edn. Transportation Research Board, Washington, DC
19. RICS (2007) Land value and public transport. RICS policy unit. http://www.rics.org/NR/rdonlyres/567DF930-261E-4B2A-89E4-D466FEB84436/0/land_report4.pdf. Accessed December, 2007
20. Debrezion G, Pels E, Rietveld P (2007) The impact of railway station on residential and commercial property value: a meta-analysis. J Real Estate Finance Econ 35:161–180
21. Rodriguez DA, Targa F (2004) Value of accessibility to Bogota's bus rapid transit system. Transp Rev 24(5):587–610
22. Cervero R, Duncan M (2002) Land value impacts of rail transit services in Los Angeles County. Report prepared for National Association of Realtors, Urban Land Institute, Washington, DC
23. Cervero R, Duncan M (2002) Land value impacts of rail transit services in San Diego County. Report prepared for National Association of Realtors, Urban Land Institute, Washington, DC
24. Benjamin JD, Stacy Sirmans G (1996) Mass transportation, apartment rent and property values. J Real Estate Res 12(1):1–8
25. Munoz-Raskin R (2007) Walking accessibility to bus rapid transit in Latin America: Does it affect property values? The case of Bogota, Columbia. In: Presented at 86th Annual Meeting of the Transportation Research Board, Washington, DC
26. Landis J, Guhathakurta S, Huang W, Zhang M (1995) Rail transit investments, real estate values, and land use change: a comparative analysis of five California rail transit systems. UCTC Working Paper No. 285. University of California Transportation Center, Berkeley
27. Al-Masaind MA, Duecker KJ, Strathman JG (1993) Light-rail transit stations and property values: a hedonic price approach. In: Transportation research record: Journal of Transportation Research Board, No. 1400, TRB, National Research Council, Washington, DC, pp 90–94
28. Chen H, Rufolo A, Dueker KJ (1997) Measuring the impact of light rail systems on single family home values: a hedonic approach with GIS application. Discussion paper 97–93, Center for Urban Studies, Portland State University, Portland
29. Dueker KJ, Bianco MJ (1999) Light rail transit impacts in Portland: the first ten years. In: Presented at the 78th annual meeting of the transportation research board, Washington, DC
30. Lewis-Workman S, Brod D (1997) Measuring the neighborhood benefits of rail transit accessibility. In: Transportation research record: Journal of Transportation Research Board, No. 1576, TRB, National Research Council, Washington, DC, pp 147–153
31. Knaap GJ, Ding C, Hopkins L (2001) Do plans matter?: the effects of light rail plans on land values in station areas. J Plann Educ Res 21(1):32–39
32. Voith R (1993) Changing capitalization of CBD-oriented transportation systems: evidence from Philadelphia, 1970–1988. J Urban Economics 33(3):361–376

33. Armtrong RJ (1993) Impacts of commuter rail service as reflected in single-family residential property values. In: Transportation Research Record: Journal of Transportation Research Board, No. 1466, TRB, National Research Council, Washington, DC, pp 88–98
34. Weinberger R (2001) Light rail proximity: benefit or detriment in the case of Santa Clara County, California? In: Transportation Research Record: Journal of Transportation Research Board, No. 1747, TRB, National Research Council, Washington, DC, pp104–113
35. Nelson AC (1998) Transit stations and commercial property values: a cast study with policy and land-use implications. J Public Transp 2(3):77–95
36. FTA (Federal Transit Administration) (2000) Transit benefits 2000 working papers: a public choice policy analysis. Federal Transit Administration, Office of Policy Development, Washington, DC
37. Fejarang R (1994) Impact on property values: a study of the Los Angeles metro rail. In: Presented at the 73rd annual meeting of the transportation research board, Washington, DC
38. Weinstein BL, Clower TL (2002) An assessment of the DART LRT on taxable property valuations and transit-oriented development. Center for Economic Development and Research, University of North Texas, TX
39. Pushkarev B, Zupan J (1977) Public transportation and land use policy. Indiana University Press, Bloomington, IN
40. Calthorpe P (1993) The next American metropolis: ecology, community, and the American dream. Princeton Architectural Press, New York
41. Handy S, Cao X, Buehler TJ, Mokhtarian PL (2005) Link between the built environment and travel behavior: correlation or causality. In: Presented at 84th Annual meeting of the transportation research board, Washington, DC
42. Handy S, Mokhtarian PL (2005) Which comes first: the neighborhood or the walking? ACCESS 26:16–21
43. Frank LD, Pivo G (1995) Impacts of mixed use and density on utiliation of three modes of travel: Single-occupant vehicle, transit and walking. In: Transportation Research Record: Journal of Transportation Research Board, No. 1466, TRB, National Research Council, Washington, DC, pp 44–52
44. Holtzclaw J (2008) Using residential patterns and transit to decrease auto dependence and costs, Natural Resources Defense Council. http://www.smartgrowth.org/library/cheers.html. Accessed October 30, 2008
45. Newman P, Kenworthy J (1989) Cities and automobile dependence: an international sourcebook. Gower, Aldershot
46. Smith W (1984) Mass transit for high-rise high-density living. J Transp Eng 110(6):521–535
47. Levinson HS (1996) Cities, transportation and change. Transp Q 50(4):67–85
48. Nelson/Nyggard Consulting Associates (1995) Land use and transit demand: the transit orientation index. Primary Transit Network Study, Tri-Met, Portland, OR
49. Florida DOT (2008) South Florida East Coast corridor transit analysis study alternatives development. http://www.sfeccstudy.com/. Accessed 30 July 2008
50. Dittmar H, Ohland G (2004) The new transit town: best practices in transit oriented development. Island Press, Washington, DC
51. Lawton K (2008) The urban structure and personal travel: an analysis of Portland, Oregon Data and some national and international data, E-Vision 2000 conference. www.rand.org/scitech/stpi/Evision/Supplement/lawton.pdf. Accessed 30 July 2008
52. Ewing R (1998) Transportation and land use innovations. APA Press, Chicago
53. Loukaitou-Sideris A, Banerjee T (2000) The blue line blues: why the vision of transit village may not materialize despite impressive growth in ridership. J Urban Des 5(2):101–125
54. Kim S, Ulfarsson G, Gudmundur T (2007) Analysis of light rail rider travel behavior: impacts of individual, built environment, and crime characteristics on transit access. Transp Res A Policy Pract 41(6):511–522
55. Cervero R (1989) America's suburban centers: the land-use–transportation link. Unwin Hyman Inc, Winchester, MA
56. Chatman DG (2003) How density and mixed uses at the workplace affect personal commercial travel and commute mode choice. In: Transportation Research Record: Journal of Transportation Research Board, No. 1831, TRB, National Research Council, Washington, DC, pp 193–201
57. Barnes G, Davis G (2001) Land use and travel choices in the twin cities. Center for Transportation Studies, University of Minnesota (www1.umn.edu/cts), Report #6 in the Series: Transportation and Regional Growth Study, Minneapolis
58. Cervero R (1994) Rail-oriented office development in California: how successful? Transp Q 48(1):33–44
59. Cervero R (1998) The transit metropolis: a global inquiry. Island Press, Washington, DC
60. Cervero R (2006) Office development, rail transit, and commuting choices. J Public Transp 9(5):41–55
61. Miller E, Ibrahim A (1998) Urban form and vehicle usage. In: Transportation Research Record: Journal of Transportation Research Board, No. 1617, TRB, National Research Council, Washington, DC
62. Bento A, Cropper ML, Mobarak AM, Vinha K (2008) The impact of urban spatial structure on travel demand in the United States, World Bank group working paper 2007. http://econ.worldbank.org/files/24989_wps3007.pdf. Accessed 30 July 2008
63. Johnson A (2003) Bus transit and land use: illuminating the interaction. J Public Transportation 6(4):21–39
64. Schimek P (1997) Understanding the relatively greater use of public transit in Canada compared to the USA. Unpublished Ph.D. dissertation. Massachusetts Institute of Technology. Cambridge, MA
65. Messenger T, Ewing R (1996) Transit-oriented development in the sunbelt. In: Transportation Research Record: Journal of Transportation Research Board, No. 1552, TRB, National Research Council, Washington, DC, pp 145–152
66. Currie G (2006) Bus rapid transit in Australasia. J Public Transport (BRT special edition), 1–22

67. Falbel S, Rodriguez P, Levinson H, Younger K, Misiewicz S (2006) Bus rapid transit plans in New York's capital district. J Public Transport (BRT special edition), 23–49
68. Florida DOT (2009) South Florida East coast corridor study. URL http://www.sfeccstudy.com/index.html. Accessed 10 March 2010
69. Tang BS, Chiang YH, Baldwin AN, Yeung CW (2004) Study of the integrated rail-property development model in Hong Kong, Research Center for Construction & Real Estate Economics, the Hong Kong Polytechnic University, Hong Kong

C

Carbon Dioxide Sequestration, Weathering Approaches to

R. D. Schuiling
Department of Earth Sciences – Geochemistry, Institute of Geosciences, Utrcht University, Utrecht, The Netherlands

Article Outline

Glossary
Definition of the Subject
Introduction
Materials
Modes of Application
Weathering
Weathering Reactions of Olivine
Enhanced Weathering: What Does It Involve?
Rate of Weathering of Olivine
Costs
Mitigating Environmental and Social Costs
Applications of the Olivine Option
Collateral Benefits
Geopolitical Implications of the Olivine Option
Future Directions
Bibliography

Glossary

CO_2 capture Any process whereby CO_2 is sustainably removed from the atmosphere for a long period.

Dunite Common rock type consisting for more than 90% of the mineral olivine.

Enhanced weathering Any process whereby weathering reactions are sped up, like crushing the rock into fine particles and spreading these in suitable climates.

Laterite Iron-rich tropical soil, which is the insoluble residue left after the weathering of the rock.

Mineral carbonation The reaction of CO_2 with minerals (particularly Mg or Ca silicates), leading to the formation of solid and stable carbonates. This carbonation is preceded by the transformation of CO_2 gas to bicarbonate solutions.

Olivine A silicate which is a mixed crystal of Mg_2SiO_4 and Fe_2SiO_4. It is the fastest weathering common silicate.

Weathering The process whereby rocks are decomposed by reaction with water and acid (usually carbonic acid).

Definition of the Subject

The aim of enhanced weathering is to capture CO_2 by the carbonation of silicates, or by dissolution of these silicates during which the greenhouse gas CO_2 is converted to bicarbonate in solution. Research in this field is still focused on increasing the rate of reaction, but the required additional technologies add considerably to the cost of the process. In this entry, the focus is on the optimization of the weathering conditions, by selecting the most reactive abundantly available minerals, grinding them, and spreading the grains over land. Thereafter nature takes its course. Since its formulation in the late 1990s, more and more people realize that this simple and natural approach may well turn out to be one of the most promising and environmentally friendliest ways to counteract climate change and ocean acidification.

Introduction

CO_2 is a greenhouse gas. The rising concentration of CO_2 in the atmosphere by the burning of fossil fuels is considered by many to be the main cause of climate change. Most efforts on carbon sequestration so far have focused on the physical removal of CO_2, by locking it up as a supercritical fluid in available spaces in the subsoil, like abandoned oil and gas fields or aquifers. Sequestration by mineral carbonation*

Robert A. Meyers (ed.), *Encyclopedia of Sustainability Science and Technology*, DOI 10.1007/978-1-4419-0851-3,
© Springer Science+Business Media, LLC 2012

has long been neglected, as it was deemed to be too slow or too costly. The main arguments for a slow rate of reaction stem from an extrapolation of abiotic experiments in the laboratory. Observations from the "real world" only now begin to show that weathering rates are often 1–2 orders of magnitude faster than rates determined in the laboratory. Arguments based on the apparent high-cost aspect are due to the fact that almost all researchers assume that mineral carbonation must be coupled to a technology to speed up the reaction. This may involve thermal treatment of the mineral, a chemical or mechanical pretreatment or a technology based on subjecting the mineral to high pressures and temperatures in autoclaves. Most of these approaches are successful to some extent, but their high cost makes such mineral carbonation technologies unattractive [1], and some produce large amounts of CO_2. If there is no objection to the reaction taking a few months or a few years to run to completion, then there is no need for the use of expensive equipment, which must meet minimum throughput rates for financial reasons. Given these conditions, chemical weathering in favorable environments becomes an attractive proposition. It can be applied on a world scale, it is a low-cost operation per ton of CO_2 captured, it is sustainable, it provides employment opportunities in developing countries, and unpleasant environmental surprises are unlikely, as the same process has already operated over the entire geological history.

This entry, therefore, will focus on the enhancement of the process of chemical weathering, by which a mineral is converted to a bicarbonate solution. These bicarbonate solutions are transported by rivers to the oceans, where they will be captured as carbonate rocks, which are the ultimate sink for CO_2. During the precipitation of solid carbonates, half of the CO_2 is released again, but this process takes on average several hundreds to thousands of years, so the bicarbonate step is the relevant step for climate change mitigation.

Materials

Most materials to be used for carbonation are naturally occurring rocks or minerals, although residues from industrial processes are also considered. Industrial residues have the advantage of being readily available and sometimes need to be removed or treated anyhow. However, their total volume is too small to make more than a small dent in the CO_2 problem, but they may provide an easily accessible and cost-effective part of the solution. Some of the materials in this category are (coal) fuel ashes, oil shale ashes, metallurgical slags, including slags from the production of elementary phosphorus, red mud from the alumina industry, and wastes from the demolition of concrete buildings [2, 3]. It was shown that wastes from the demolition of concrete are rapidly carbonated in soils, and their carbonation compensates for decarbonation during manufacture.

Among the naturally occurring materials for carbonation, olivine and olivine rocks, called dunites, take a prominent place because olivine weathers fast and is abundantly available (see Fig. 1). Other candidate materials include basalts and basaltic tuffs, and possibly anorthosites. A mineral that is also frequently mentioned is wollastonite ($CaSiO_3$). Wollastonite does react quickly with CO_2 and water, but wollastonite deposits are rare and small. It is evident that priority will be given to material that is already crushed or milled, as this saves mining and milling costs. Many ore deposits of chromite, nickel, magnesite, peridot (a semiprecious variety of olivine), or even diamond have olivine-rich host rocks. Billions of tons of such rocks can be found in crushed form as mine tailings. Later on, in the section on rate of weathering, some spectacular evidence on the rate of weathering of powdered olivine or serpentine (the hydration product of olivine) on mine dumps will be presented.

Modes of Application

a. In dedicated industrial installations
b. In situ injection in suitable rock types
c. Ex situ after crushing and spreading suitable rock types

a. Industrial installations. These require an input of fairly pure CO_2 to reach a maximum efficiency. This means that they can be dependent on point sources of pure CO_2, or on more dilute sources of CO_2 from which the CO_2 must first be captured and purified. Industrial treatments, involving thermal or chemical activations, or large autoclaves through which the mineral powders must pass as fast as possible have significant energy requirements. It is doubtful that

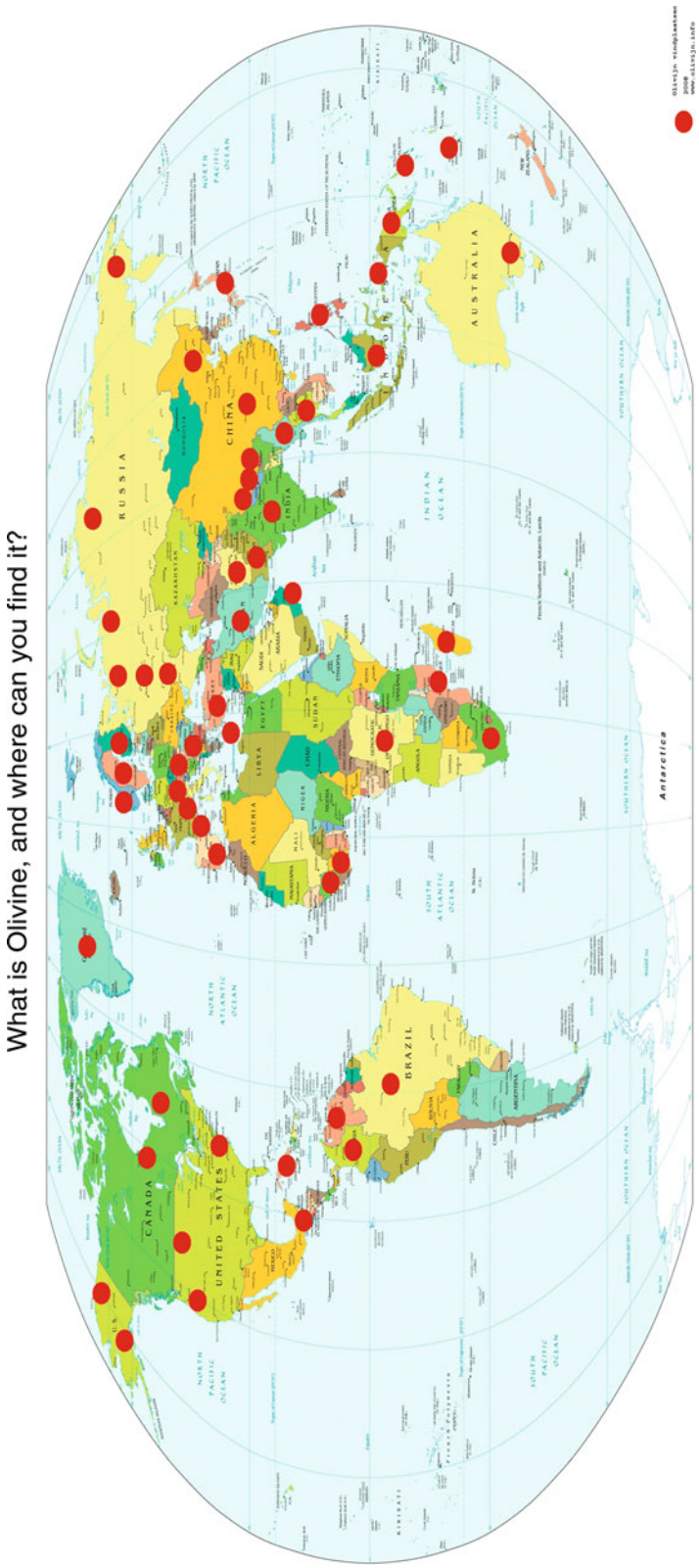

Carbon Dioxide Sequestration, Weathering Approaches to. Figure 1
Distribution of dunites in the world. *One dot* in a country may represent several dunites

large-scale application of thermal or chemical treatment of olivine, for instance, can be carried out at the required scale of 25 billion tons of olivine annually, let alone in a cost-effective way.

b. In situ injection in suitable rock types. The major distinction between this type of injection and the most commonly proposed CCS (Carbon Capture and Storage) is that injection in flood basalts or olivine rocks aims at converting the injected CO_2 gas into carbonate rock by reaction with the host rock. This reaction produces some heat, which may further speed up the reaction. In oil and gas fields, or in saline aquifers, the CO_2 remains in the reservoir as a gas (or more correctly as a supercritical fluid), with the inherent risk of leakage, or even explosive escape. The main conditions for a reservoir rock in which the CO_2 will be injected and converted to solid carbonates are reactivity and, what can be called, "selective" permeability. Thick sections composed of many superimposed volcanic flows with a horizontal extension of sometimes more than 1 million km^2, so-called flood basalts, may be an option. A number of features of lava flows, including flows that are separated from the overlying flow by a rubble zone, which can have high permeability, often finding a high concentration of bubbles near the top of the flow where these bubbles contribute to the accessibility of the rock for rock/fluid interaction; and some lava flows vertical structure with more or less hexagonal columnar jointing that originates from shrinkage during cooling, which permits easy access for fluids throughout the basalt flow. The combination of these properties makes piles of basalt flows almost ideal targets for injection, although their reactivity is considerably lower than that of olivine-rich rock types. Flood basalts can occupy enormous volumes, in several cases in excess of 1 million km^3. Well-known examples are the Deccan traps in India, the Siberian traps, the Karroo basalts, and the flood basalts of the Parana basin, each covering more than 1 million km^2. The Columbia River flood basalts and the Deccan traps are presently under investigation on how they can be used for carbon capture [4]. Logistics of CO_2 transport and its associated cost, as well as the rate at which it can be injected, and the reactivity of the rock will probably limit their use as a CO_2 trap to locations close to voluminous point sources of CO_2. They potentially constitute a safer storage than aquifers or abandoned oil and gas fields because after reaction with the rock, the CO_2 is no longer stored as a gas but as a solid carbonate.

The situation with direct injection into olivine-rich rocks is more or less the reverse of injection into basalt piles. Permeability is often much smaller, as most dunites (dunite is the rock type that consists for more than 90% of olivine) are massive rocks. They may contain joints, but these are often sealed with a thin veneer of serpentine or magnesite ($MgCO_3$). On the other hand, their reactivity is considerably better. Spectacular examples (Fig. 2) of carbonation of olivine-rich rocks in Oman were presented by [5]. These authors propose that annually up to one billion tons of CO_2 can be injected into these rocks in Oman. Transport of such volumes of CO_2 from industries and coal-fired power plants in the industrialized world, as well as purifying it and bringing it to a remote site, poses, however, a huge logistical problem. Even if the logistical problems are not insurmountable in terms of cost, there remains the problem that the rocks must be intensely fracced for injection. Kelemen and Matter suggest that the considerable heat of reaction from the hydration [5] and carbonation [6] may help to crack the rocks further. Although from the reactivity point of view direct injection of CO_2 + water into dunites is an attractive proposition, the likely high costs may limit its use to locations where a coal-fired power plant is situated at

Carbon Dioxide Sequestration, Weathering Approaches to. Figure 2
Multiple generations of carbonate cement around dunite pieces in alluvial terraces in Oman [5]

short distance from a dunite massif like near Orhaneli/Turkey [7], or where, like in Oman, the CO_2 produced by the installations on oil and gas fields can be injected directly into the dunites nearby.

c. Ex situ after crushing and spreading suitable rock types. This option is better known as enhanced weathering [8]. This is probably the most promising solution for the sustainable capture of CO_2 on the scale of billions of tons of CO_2 annually. It is only for this option that a more complete description of the proposed process will be given, as well as some quantitative estimates of its costs and energy requirements. Furthermore, the possible collateral benefits of the method will be considered.

Weathering

It is estimated that the Earth produces around 0.5 billion tons of CO_2 each year, mainly from volcanic sources [9]. Other important sources of CO_2 are carbonate rocks that decompose after having been transported to great depth and subjected to high temperatures in subduction zones [10], or limestones and dolomites in the contact aureole of intrusive rocks, or marbles or siliceous dolomites undergoing high-grade regional metamorphism. If there were no feedback mechanism or mechanisms by which this CO_2 is constantly removed from the atmosphere and sustainably stored in rocks, the Earth would now have an atmosphere similar to Venus, where the CO_2 pressure of the atmosphere is 80 bars, and the surface temperature of the planet is 450°C, due to the excessive greenhouse effect. The major feedback mechanism is the weathering of silicate minerals, in particular Ca and Mg silicates, which is only possible thanks to the presence of liquid water on Earth, whereas it is absent on Venus. A smaller feedback mechanism is the storage of CO_2 as organic carbon (oil and natural gas, coal, and organic carbon dispersed in sediments). Chemical weathering can be described as the neutralization of an acid by rocks. H_2CO_3 is the dominant acid during weathering. It is converted to bicarbonate in solution. The rock is partly dissolved. A residue of clay minerals can form as the solid end product. Weathering has been a life-saving process for our planet. Not only has the interaction of CO_2 and water with rocks saved us from a greenhouse problem as found on Venus, but it has provided us also with fertile soils, without which it would have been impossible for any evolved life forms to develop, and it has released the mineral nutrients from the rocks which are a basic requirement for plant life.

Some typical weathering reactions are as follows, weathering of olivine:

$$Mg_2SiO_4 + 4CO_2 + 4H_2O \rightarrow 2Mg^{2+} + 4HCO_3^- + H_4SiO_4 \quad (1)$$

and weathering of anorthite:

$$CaSi_2Al_2O_8 + CO_2 + 2H_2O \rightarrow CaCO_3 + Al_2Si_2O_5(OH)_4 \quad (2)$$

The first reaction, the weathering of olivine, describes an intermediate step in the weathering process. After this dissolution step, the Mg-bicarbonate solution is transported to the sea, where ultimately it will precipitate in the form of carbonate sediments (limestones and dolomites). That process, however, takes on average hundreds, if not thousands of years, so the first step, the formation of Mg- or Ca-bicarbonate waters is the relevant step for CO_2 capture on a time scale of a few tens of years. The second reaction (Eq. 2) demonstrates the formation of a carbonate and a clay mineral by the weathering of anhydrous silicates.

Many nongeologists think that the CO_2 that is dissolved in the oceans, present as CO_2 in the air, or contained in biomass plays the major role in the CO_2 balance of the Earth. In fact, these reservoirs are only short-lived and minor transitory storage rooms. The major part of the geochemical CO_2 cycle is represented by emission of CO_2 from the Earth, its transformation by weathering into a bicarbonate solution, followed by its transport to the oceans and deposition as carbonate rocks. These carbonate sediments form the ultimate sink on a human time scale. Geologically speaking, even these solid carbonate sinks are not eternal, but are recycled as well, albeit with time scales of hundreds of millions of years. The relations can be demonstrated with the following table (Table 1) [11].

The process of chemical weathering has always provided the main mechanism to keep the CO_2 levels of the atmosphere within reasonable bounds. Of course, there have been fluctuations in the course of geological

Carbon Dioxide Sequestration, Weathering Approaches to. Table 1 Distribution of carbon on Earth. Modified after [11]

	Amount of carbon ($\times 10^{15}$ kg)	Relative amount (%)
Limestone ($CaCO_3$)	35,000	46.6
Dolomite	25,000	33.3
Sedimentary carbon	15,000	20
Recoverable fossil fuels	4	0.005
Oceanic CO_2	42	0.056
Atmospheric CO_2	3	0.004
Biomass	0.056	0.0007
Anthropogenic emission	0.03/year	
Input from Earth's interior	0.002/year	

history because the available surface area where reactive rocks were exposed to the atmosphere varied; during or shortly after major orogenic periods, or after large-scale volcanic activity, the area of fresh rocks available to weathering was larger than in periods where the landscape was more mature, and where many easily weatherable rocks were covered by a thick weathering crust, which virtually stopped their interaction with CO_2 and water. At the same time, it is likely that the annual emissions of CO_2 from the Earth were also subject to large variations caused by the intensity of volcanism, related to the rate of plate spreading.

To a certain extent, such variations are counteracted by the CO_2 concentration of the atmosphere itself, which acts as its own negative feedback. The higher the CO_2 pressure, the more acidic the water, and the faster the weathering which removes that same CO_2 from the atmosphere.

There is geological evidence that factors like mountain building or massive volcanism, through their effects on rates of weathering and emission of CO_2, have influenced the CO_2 pressures of the atmosphere in the past and may have led to periods of glaciation [12–14]. Since the industrial revolution, atmospheric CO_2 levels have risen rapidly (from 260 to 392 ppm), largely due to mankind burning in a few 100 years the fossil fuels that took hundreds of millions of years to form. If weathering is going to be used as a tool to counteract this rise in CO_2, caused by mankind annually emitting more than ten times as much CO_2 than the Earth normally emits, then the weathering process must also be made more than ten times more effective than normal to reach a new balance. The process as discussed here is to select widely available rock types that weather easily, mine them and increase their reactive surface area by crushing them, and spread the crushed rocks over land or along beaches in areas with the most suitable climate for weathering.

In subsequent sections, only olivine and olivine rocks will be discussed. Other rock types can also be used, but they are less effective or less available, although locally, there may be good reasons to use other rock types, such as basalts, anorthosites, or nepheline syenites. In the following weathering reactions, the formula of olivine will be simplified to Mg_2SiO_4, although olivine normally is a mixed crystal of Mg_2SiO_4 and Fe_2SiO_4, with the Mg-endmember usually dominant. One finds a number of ways in which the weathering reaction of olivine is described. As this affects the amount of CO_2 that can be captured for a given amount of olivine, these different weathering reactions will be briefly discussed, and the major reaction that takes place in nature will be identified. A common way is the reaction in which during weathering two new solid minerals are formed, namely, magnesite ($MgCO_3$) and serpentine ($Mg_3Si_2O_5(OH)_4$).

Weathering Reactions of Olivine

$$2Mg_2SiO_4 + CO_2 + 2H_2O \rightarrow MgCO_3 + Mg_3Si_2O_5(OH)_4 \quad (3)$$

In this reaction, 2 olivine moles capture 1 CO_2 mole.

A second reaction is

$$Mg_2SiO_4 + 2CO_2 + xH_2O \rightarrow 2MgCO_3 + SiO_2\ xH_2O \quad (4)$$

In this reaction, 1 olivine mole captures 2 CO_2 moles.

The reaction that occurs normally in places with sufficient rainfall

$$Mg_2SiO_4 + 4CO_2 + 4H_2O \rightarrow Mg^{2+} + 4HCO_3^- + H_4SiO_4 \quad (5)$$

In seawater, it is convenient to split the reaction into

$$Mg_2SiO_4 + 4H_2O \rightarrow 2Mg_2^{+} + 4OH^- + H_4SiO_4 \quad (6a)$$

followed by

$$4OH^- + 4CO_2 \rightarrow 4HCO_3^- \quad (6b)$$

In reactions (5) and (6a and 6b), each olivine mole captures 4 moles of CO_2. Evidence will be presented that reaction (5) is the common weathering reaction. It has been mentioned already before that the resulting Mg-bicarbonate waters will ultimately form carbonate rocks in the oceans. During the precipitation of those carbonates, half of the captured CO_2 returns to the atmosphere, but as this process may take thousands of years, we will neglect it as far as it affects climate change in the short run.

In order to find out what is the normal reaction mechanism for olivine weathering, a suite of springwaters issuing from olivine rocks in Turkey were collected [15]. One can distinguish the following steps during the formation of such springwaters:

1. Rainwater falls on the ground.
2. It infiltrates the soil. The CO_2 concentration in soil atmospheres is usually around a 100 times larger than in the open air, because litter in the soil decays and soil fauna respires, both contributing to a high concentration of CO_2 in the soil [16, 17].
3. After equilibration with this CO_2-rich soil atmosphere, the water infiltrates the underlying rock and reacts with it (the weathering step).
4. Finally, the water emerges again as a spring at some lower point.

Olivine-rich rocks contain generally, next to the dominant mineral olivine, some other silicates, including calcium silicates. From Fig. 3, it is evident that there is a close relation between the (Mg + Ca) content of the water, expressed in milliequivalents, and the amount of CO_2 that has been converted to bicarbonate. This close

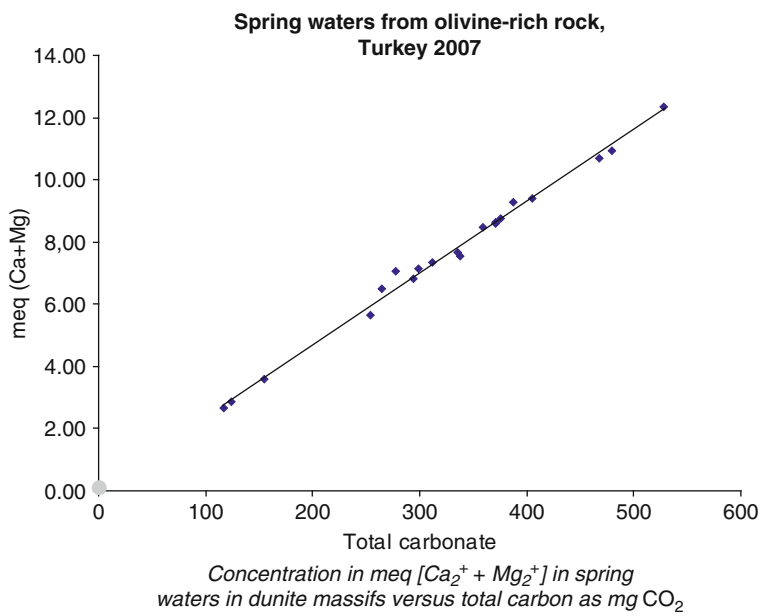

Carbon Dioxide Sequestration, Weathering Approaches to. Figure 3
Relationship between calcium + magnesium extracted from the rock and amount of CO_2 captured as bicarbonate in springwaters issuing from olivine rocks in Turkey

relation has been confirmed in a number of cases all over the world, and it can be concluded that the reaction leading to bicarbonate in the solution is the major pathway in which CO_2 is removed from the air, taken up as bicarbonate in the water and transported to the oceans.

Even when the problem is considered on the scale of the whole Earth, the picture remains essentially the same. All rivers together transport annually 3.6×10^{16} kg of water to the oceans. The weighted average of their concentration of Ca is 11 ppm, of Mg 2.6 ppm, and of HCO_3 42.4 ppm. Expressed again in milliequivalents, this means that Ca + Mg make up 0.77 meq and bicarbonate 0.7 meq, so, despite all complications, there is still a satisfactory agreement. If we calculate from these figures the amount of CO_2 that is annually brought to the sea by rivers, this comes out as 1.1 billion tons of CO_2, the same order of magnitude as the annual emission of CO_2 by the Earth, which is obviously larger, as emissions of CO_2 from the seafloor are only partly taken into account. Some of this CO_2 returns to land, takes part in weathering reactions, and returns as bicarbonate to the oceans.

Enhanced Weathering: What Does It Involve?

Having established that the principal weathering reaction is reaction (5), the formation of magnesium bicarbonate solutions, it can now be calculated from the stoichiometry of this reaction how much olivine is required each year to sequester all the emitted CO_2 by enhanced weathering, under the assumption that energy savings, switching to green energy and change of lifestyle, will not lead fast enough to a lowering of the world's CO_2 emissions, and other technologies for CO_2 capture will remain negligible. In this scenario, the required volume turns out to be approximately 7 km^3 of olivine rock. This is, of course, large because it must match the carbon contained in all the oil, gas, and coal that is burnt. It is, however, within the range of modern large-scale mining. This volume of olivine is equivalent to 10 km^3 of oil. It is worthwhile to come to grips with the scale of this mitigation effort (Fig. 4). The largest mine in the world, the copper mine at Bingham, Utah, USA, has an excavated volume of 25 km^3. Olivine mining at this scale, however, means that olivine moves up from a modest commodity to third place in the mining industry, after construction materials and

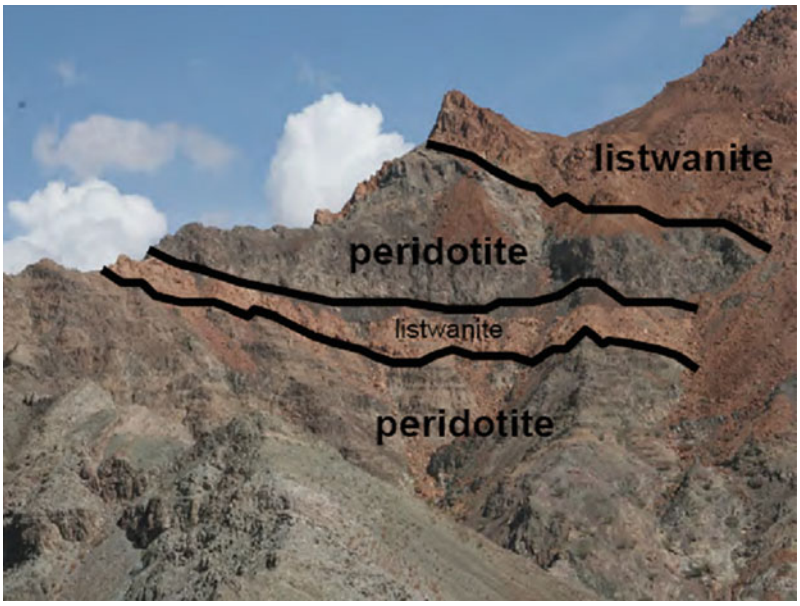

Carbon Dioxide Sequestration, Weathering Approaches to. Figure 4
It is a sobering thought that these huge bands of listwanite (completely carbonated dunites consisting of magnesite + quartz) in Oman, containing 500 million tons of CO_2, are equivalent to only 1 week of the world's anthropogenic CO_2 emissions [4]

coal. One should, obviously, not open only one single, huge olivine mine but spread the mining operations over 30–50 open-pit olivine mines. In order to profit from the most suitable climatic conditions for weathering, these mines should be strategically spread along the tropical zone. A larger number of olivine mines will be able to service wider areas without requiring large transport. Each of the selected sites for olivine mining must produce in the order of 500 million tons of olivine each year to reach the required 7 km^3 per year. It may well turn out that it is more favorable both economically and environmentally to increase the number of olivine mines and decrease their size. At the same time, this will spread the economical benefits of olivine mining over a larger number of countries and further limit the required transport distances. This volume of olivine rock must be crushed and milled to grains of around 100 μm in diameter. If 7 km^3 is spread over an area of 10 million km^2, it will occupy a layer of 0.7-mm thickness. In the section on rate of weathering, it will be shown that grains of olivine of 100 μm will weather in approximately 5 years in tropical soils. It will, therefore, be cheaper to spread a layer of 3.5-mm thickness each year over an area of 2 million km^2, shift to the next area in the following year, and come back to the first after 5 years.

In a few instances outside the tropical zone, conditions may be so favorable that large olivine exploitations can be located there. For example, a possible site for an olivine mine outside the tropical zone might be Oman, which has the largest ophiolite zone in the world and a long coastline along the Indian Ocean. Deeply weathered sections of dunite, dating from earlier more humid periods, can be found, but in its present desert climate, the olivine does not weather, but forms huge talus deposits on the slopes of the mountains, at a short distance from the Indian Ocean. These scree deposits have no overburden which must first be removed, like in most tropical dunite deposits. In Oman, the loose pieces, after some additional crushing, can be loaded into ships that have direct access to the Indian Ocean.

Rate of Weathering of Olivine

Much of the debate on the potential of enhanced weathering using olivine grains to counteract climate change centers on the problem of the rate of weathering. The rate of weathering is enhanced in hot humid conditions, hence why this idea is focused on the application of crushed olivine in the wet tropical regions.

There are a number of reasons to focus on the wet tropics for large-scale applications:

- Weathering is faster under hot, humid, climatic conditions.
- Tropical soils are usually very poor and can benefit from the addition of mineral nutrients.

This does not mean that the olivine option is useless in temperate climates, it is just that the rate of weathering will be slower.

In abiotic laboratory experiments, it was found that the surface of olivine grains retreats at a few tenths of a micron per year [18]. This is described by the shrinking-sphere concept. Such low rates would make it difficult to use enhanced weathering to mitigate the greenhouse effect. Fortunately, there is observational evidence on rates of weathering of olivine in the real world (see below), which shows that the rates are more than tenfold, and probably 100-fold larger, than those found in the laboratory. Qualitative information on fast rates of weathering is obtained from volcanic terrains with rocks containing olivine. When volcanism started in the Eifel/Germany, synchronous Rhine sediments downstream in the Netherlands immediately started to contain a wealth of volcanic minerals, but *no olivine*, despite the fact that these volcanic rocks contain plenty of that mineral. Contrary to the other minerals of volcanic origin, olivine has not survived the short trip from Bonn to the Dutch border. Similar observations are reported from many other volcanic terrains in the world. Although suggestive of fast weathering, this evidence is difficult to quantify.

In contrast, the rate of weathering of dunite massifs in the tropical zone can be quantified, or at least a minimum rate of weathering can be firmly established. The first example is the dunite massif of Conakry/Guinea. This dunite occupies the entire peninsula on which Conakry, the capital of Guinea, is situated. It has an approximate length of 50 km and an average width of 5 km. Over its entire surface, it is covered by a thick lateritic weathering crust, which is very clearly visible as a purplish red area on satellite

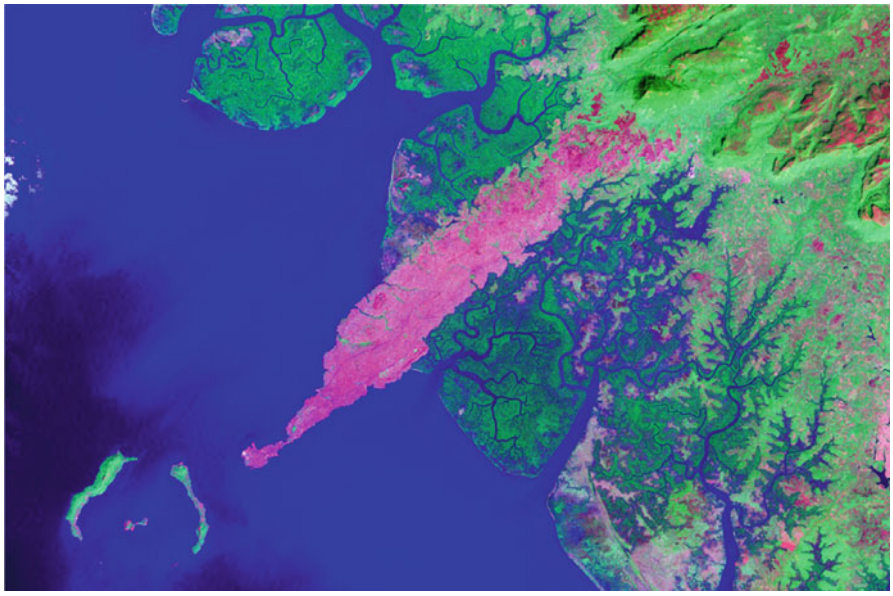

Carbon Dioxide Sequestration, Weathering Approaches to. Figure 5
The dunite massif of Conakry, Guinea. The length of the dunite massif (in *purplish red*) is approximately 50 km

pictures (see Fig. 5). This lateritic crust, which is the iron-rich insoluble red residue of the dunite after deep tropical weathering, contains virtually no silica, magnesium or calcium oxides which were completely leached out during the weathering process [19]. These components make up around 90% of the original dunite. This means that 1 m of laterite is equivalent to 10 m of dunite, or even more if the remaining components of the laterite were not completely immobile but have also been leached to some extent. The same author presents evidence that iron has in fact been fairly mobile and was partially leached out as well, which means that 1 m of laterite is equivalent to more than 10 m of dunite. The weathering crust has a thickness between 30 and 100 m. The age of the dunite (that is to say the time at which this dunite intrusion formed) has been determined as 195 million years. From these data, it is simple to calculate the minimum rate of weathering as follows: 50 m of laterite is equivalent to 500 m of dunite, 500 m (= 500 million microns) divided by 195 million years is 2.6 μm/year. This is already ten times faster than deduced from laboratory experiments, but the real rate of weathering must have been considerably faster. The rock is an *intrusion*. That means it was emplaced between rocks at some depth and covered by other rocks, which had to be removed first by erosion before the dunite became exposed and could start its weathering process. If the dunite intrusion has taken place at 2 km depth, it would take 100 million years before the dunite massif was entirely laid bare by erosion at an estimated erosion rate of the order of 1–2 cm/1,000 years [20]. This is the average erosion rate for all continents. This correction alone more than doubles the calculated rate of weathering. That is not the only positive correction that must be made. In more recent times, the weathering process, under such a thick weathering crust, has virtually come to a standstill, as the thick laterite crust effectively shields the underlying rock from further interaction with the atmosphere. This shortens again the time span over which weathering was active, and thereby increases the rate of weathering.

A further positive correction concerns the difference between weathering of a solid rock as opposed to loose grains. A rock is attacked by weathering from above along a two-dimensional front, whereas loose olivine grains in soil are attacked from all sides. It seems certain that olivine grains in tropical soils dissolve at least at a rate of 10 μm/year, but most likely even faster. Even when their surface retreats only by 10 μm/year, a grain of 100 μm will disappear in 5 years. A similar calculation can be made for the dunite body

at Jacupiranga, Brazil [21]. Here, the rock has an age of 130 million years, and it is covered by a weathering crust of >40 m (this is where the drill hole stopped, but at 40 m, the drill was still in lateritic weathering crust). The minimum rate of weathering turns out to be >3.1 μm/year, but the same positive corrections have to be applied as in the Conakry case.

From a global balance of weathering and erosion, similar minimum rates of weathering emerge. The average rate of erosion of the continents is 1–2 cm in a 1,000 years [20]. As olivine grains from the interior of the continents do not make it to the oceans, this means that olivine rocks dissolve (= weather) at least at the same speed, which is 10–20 μm/year. The most dramatic evidence for fast weathering of crushed magnesium silicate rocks comes from observations of weathering rates of mine dumps of such rocks [22]. By measuring the amount of a suite of newly formed Mg carbonates, it was shown that the mine tailings of two abandoned asbestos mines in British Columbia weather extremely fast. In this case, it does not involve fresh olivine, but its hydration product serpentine ($Mg_3Si_2O_5(OH)_4$) that weathers and produces carbonates. This carbonation proceeds as follows:

$$Mg_3Si_2O_5(OH)_4 + 3CO_2 + 2H_2O \rightarrow 3MgCO_3 + 2H_4SiO_4 \quad (7)$$

At low temperatures, magnesite seldom forms, but in its place, hydrated magnesium carbonates, like nesquehonite $Mg(HCO_3)(OH)\cdot 2H_2O$, are found instead (Fig. 6).

In order to make sure that these carbonates have indeed newly formed, ^{14}C analyses were performed on these carbonates which gave an age of about 0, showing that the carbon in these minerals really represents the sequestration of present-day atmospheric carbon [23]. In one of the cases, the mine dump, occupying a surface area of 0.5 km^2, had captured 82,000 t of CO_2 between 1978 and 2004, more than 50 times the maximum ever recorded for natural weathering under the most favorable conditions. The real rate of weathering is even higher because the authors have only taken the solid products into account, whereas the waters that percolate through the mine dumps carry an additional load of dissolved weathering products. These waters become quite alkaline, and their high silica content leads to small diatom blooms in a pool at the foot of the tailings dump and in at least one of the mine pits [23–25].

Carbon Dioxide Sequestration, Weathering Approaches to. Figure 6
Efflorescence of nesquehonite on the serpentinite tailing heap at Clinton Creek (Photograph by S.A. Wilson)

One may wonder why there is such a large discrepancy between laboratory experiments, showing low rates of weathering, and the real world, where weathering rates are 100 times larger. The answer is relatively simple. Higher plants live in symbiosis with mycorrhizal fungi in and around their root system. These fungi secrete low molecular organic acids like acetic acid, malic acid and oxalic acid that rapidly attack mineral grains in the soil [26]. This liberates mineral nutrients that are subsequently taken up by the higher plants. In turn, the higher plants "reward" the fungi by providing them sugars. Lichens act in a similar way by secreting oxalic acid that "eats" the underlying rock [27]. In the laboratory, mycorrhizal fungi and lichens are absent, and this is the reason why the abiotic reaction rates that were found in the laboratory are much lower than weathering rates in nature.

This all refers to weathering rates of olivine on land. Much less information is available for olivine on beaches, in the surf zone, shallow seas, and tidal flats. To understand what happens to olivine upon weathering we must distinguish between the chemical reaction of olivine with seawater and mechanical impacts during grain transport. To measure quantitatively the chemical weathering rate of olivine in seawater, one could use a so-called olivine reactor (see Fig. 7),

Carbon Dioxide Sequestration, Weathering Approaches to. Figure 7
The olivine reactor (artist's impression)

a concrete box 50 m long and 4 m wide, constructed perpendicular to the coast and filled with olivine sand. To obtain even more information from this experiment, the reactor can be partitioned lengthwise, and the two compartments can be filled with olivine sand of different grain sizes. On its coastal side, there is a low inlet, permitting seawater to enter the box during high tide. The seawater will drain from the other side toward the sea during ebb, after having passed through 50 m of olivine sand. By analyzing the water before and after it has passed the olivine reactor, one can calculate how much olivine reacts during each tidal cycle, how much CO_2 it captures, and if and when the reaction starts to be hampered by reaction products attached to the grains. Once the CO_2 that is transformed into bicarbonate arrives in the seawater, it will take time before it is transformed into carbonates in the form of shells and corals, but no figures are available for this final uptake. Upon the formation of carbonate, half of the captured CO_2 is liberated again, but that may take centuries by when CO_2-neutral energy production may have been well established. It is reported that olivine dissolves somewhat faster in saline water than in fresh water [28].

The mechanical action, the grinding down of olivine grains, by waves and currents largely determines the rate of weathering of olivine on beaches and in shallow seas with strong bottom currents. There is a paper in which the rate of weathering of olivine grains on beaches is calculated [29], but that is based on theoretical modeling and overlooks the mechanical consequences of the surf, where grains are wearing down by the constant rubbing and bumping against each other. Olivine beaches are practically restricted to places where cliffs of olivine-rich rocks overlook the beach. Like on any other beach sand, the olivine grains are rounded, which means that they have lost little slivers of olivine due to bumping and scraping against each other. This has the advantage that one does not need to mill the olivine at high cost to very small grain sizes because the sea takes the place of the ball mill. These little slivers will quickly disappear by chemical weathering. In a recent experiment, this surf action was reproduced [30]. Grains of olivine were rotated in conical flasks. Within 24 h, the crushed olivine grains that were originally angular, with a rough surface, had transformed into rounded and polished grains (Fig. 8).

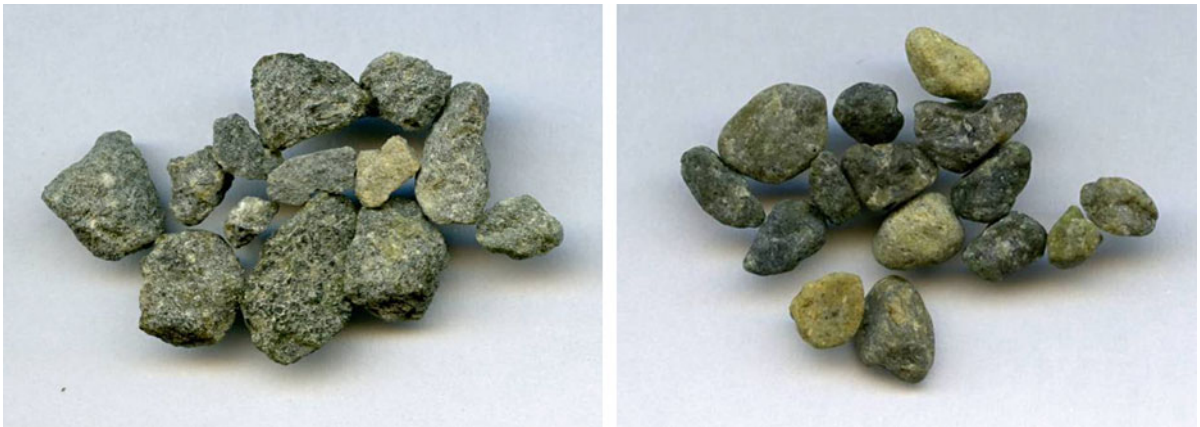

Carbon Dioxide Sequestration, Weathering Approaches to. Figure 8
Simulation of surf action. *Left*: Olivine grit (2–5 mm) at start. *Right*: Olivine grit, rounded and polished after 3 days shaking

The clear water at the start had become an opaque white suspension of very tiny olivine slivers, half of which had a grain size of less than 5 μm. The system reacts fast, the pH shoots up to 9.4, and a clay-type magnesium mineral is newly formed. The surf is clearly the world's largest, most efficient and cheapest ball mill. The experiments also showed that a mixture of different grain sizes of olivine wears down more quickly than single grain sizes. There are strong currents along the bottom of the Southern North Sea, the Channel, and the Irish Sea. If one would cover this sea bottom with a layer of 1 cm of crushed olivine, this would compensate 5% of the global CO_2 emissions, more than the combined CO_2 emissions of the adjacent countries, England, France, The Netherlands, Belgium, and Ireland, which together produce about 4% of the world's emission.

For tidal flats, a very different picture emerges. Tidal flats are inhabited by huge populations of lugworms (*Arenicola maritima*). The upper few centimeters of the mud pass on average three times each year through the guts of the lugworm. In its digestive system, weathering is 700–1,000 times faster than outside [31]. In experiments in which lugworms were fed with small fragments of basaltic rock, these pieces came out as small heaplets of clay [32]. As basalt weathers much slower than dunite, it can be expected that spreading of olivine grains over tidal flats is a very effective application of enhanced weathering/sequestration of CO_2.

Costs

Except in cases where the required olivine-rich rock is already available in crushed form on mine dumps, the application of enhanced weathering implies mining and milling of solid dunite rock from large open-pit mines. In 2002, two Swedish mining engineers calculated the cost of mining and milling of bulk rocks in large open-pit mines [33]. This turns out to be 6 Euros/t. After passing the primary and secondary crushers at the mine site, the granulated material must then be transported from the mine to the points of use. If we restrict the transport distance to a maximum of 300 km around the mine, this adds on average 6 Euros/t for transport. From the stoichiometry of reaction (5), one can calculate that 1 t of olivine will sequester 1.25 t of CO_2. This brings the price for the sequestration of CO_2 to slightly under 10 Euros/t, making it by far the cheapest method to sustainably capture CO_2. In comparison, CCS, the most commonly discussed technology for the sequestration of CO_2, costs between 70 and 100 Euros/t of CO_2 [34]. Even though the costs are modest, compared to other options that are considered, the cost to sequester all man-made CO_2 emissions by enhanced weathering of olivine still comes to around 250 billion US$/year worldwide.

The energy costs, expressed in terms of the CO_2 expenditure for mining, milling, and transport, have been calculated in an LCA (life cycle analysis) [35]. The total CO_2 requirement for the operation as a whole

turns out to be 4% of the CO_2 that will later be captured by the extracted olivine. In order to bring the olivine grains from the mine to the point of use, several transport systems can be considered, including road, railroad, river, or sea. Making maximum use of the opportunities provided by local conditions will keep costs lower.

Mitigating Environmental and Social Costs

(*This section is mainly based on a personal communication by Mrs. Gwendolyn Wellmann, community development specialist, Port Elizabeth, S.A.*)

There are, however, also environmental costs (and benefits) to the olivine option. Every mining operation has a negative impact on the natural and social environment, even if the mining is done for the purpose of solving a worldwide environmental problem. Fortunately, there are ways to overcome the environmental damage, or at least diminish it. All dunite bodies in the tropical zone are covered by a thick laterite (laterite is the typical red soil of tropical countries, an iron-rich residue that is left after the weathering of rocks in tropical climates). Dunites contain on average 0.2–0.3% nickel, which is not very soluble during weathering. As most of the major components (SiO_2, MgO, CaO) are leached out during weathering, the Ni content of the residue rises accordingly and may reach 2% to sometimes over 3% Ni, making these nickel laterites a rich nickel ore [36]. In a number of countries (e.g., Brazil, Cuba, Philippines, Indonesia, New Caledonia, Madagascar, Malawi), these Ni laterites are mined, or mining options are being studied. By continuing the mining below the laterite crust and also mining the underlying dunite, one can avoid the impact of clearing a new mining site; the infrastructure for mining is already in place at such locations, and there is a local population that depends on mining for their living. The removal of the overburden consisting of Ni-laterite ore is an additional financial bonus for the mining of dunite below. This way, one can save the environment, help the people, and at the same time make olivine mining cheaper.

Even though mining brings with it many positives to an area, including employment opportunities, infrastructure development, and local economic development; and even if it is an olivine mine that will benefit the earth, mining also brings with it many negatives, such as an influx of job seekers, the increase of HIV/AIDS, violence, and discontent. In terms of mitigating the negative impact on the social fabric in a mining area, what is most important is the attitude of the mining company. The majority of mining companies adhere to the International Council on Mining and Metals' *Sustainable Development Principles* [37], with its underlying message that the overall success of any mining venture in a populated area is to consult, consult, consult with the local people. This requires the company from the onset, which might mean as early as the time of exploration activities, to meet with the local people; gain their views; understand their concerns; seek first to understand what makes the local community tick, before expecting them to understand your needs; and to devise long-term mitigating actionable plans for the rehabilitation of the area.

Should an olivine mine be established in a poor, developing country, it is vital that as the mining company starts to invest in the community, whether through infrastructure, local economic development, or alternative livelihood projects, it also invests in the development and promotion of a functional local government. This is important because the management and maintenance of these projects will ultimately be the responsibility of the local government. A weak, nearly nonexistent local government will lack the correct policies, procedures, structures, and systems to ensure sustainability of any project invested in by the local mine. The result of this is that there is a tendency for both the affected communities and the government to rely on the mine to assume local government roles. This can be problematic as implementing local governance is not the mine's expertise or responsibility, and as has been demonstrated numerous times in many countries – when the community feels the lack of service delivery – they will express their discontent by attacking the mine. One of the ways of investing in local governance is to expand the skills base of local government officials through training. The skills that are most frequently lacking in these areas are those needed for planning, budgeting, project implementation, and public consultation. Once olivine mining is a certified means of obtaining carbon credits, it is recommended that it is supervised by a special international body.

Applications of the Olivine Option

It should be emphasized that the presence of liquid water is essential. This rules out all countries with a desert climate except along their coasts, where olivine grains will disintegrate in the surf and be spread by wind and currents. The rate of reaction is increased by a high temperature. There are a number of arguments to focus on the wet tropics for *large-scale* applications:

- Weathering is fastest under these climatic conditions.
- Tropical soils are usually very poor, and can benefit from the addition of mineral nutrients.

For all mines, not just the ones in the wet tropics, the following arguments hold:

- Large mines profit from the economy of scale.
- Olivine rocks sometimes contain marginal chromite, nickel, or magnesite deposits, and the related rock kimberlite is the normal host rock for diamonds. If the host rock itself is also put to good use, and brings a profit in the form of carbon credits, instead of being dumped as a mining waste, this may make such marginal deposits economical.
- Once the olivine option is accepted as a legitimate means of carbon capture, the olivine mines can sell carbon credits.

There may be additional novel or niche applications suitable to certain regions, such as using olivine sand instead of quartz sand to strew into Astroturf playing fields, using olivine gravel on tennis fields, spreading olivine grains on lawns to reduce the growth of moss, using olivine as the top layer on footpaths or bicycle paths, adding a layer of olivine as roof covering, using olivine instead of quartz in sandblasting, using olivine grit on icy roads, adding olivine powder to digesters to improve the quality of the biogas by transferring the CO_2 part of the biogas to bicarbonate in the liquid, and using olivine sand in sound barriers along main roads. These are all fairly minor applications, although taken together they are not negligible.

A larger application that can be used in the tropics as well as in temperate climates is to cover beaches that are subject to erosion or tidal flats by olivine sand. Olivine is considerably heavier than quartz and will not be eroded and transported away from the beach as easily as quartz sands. The tides will alternately wet the beach and drain the pore water. During such a tidal cycle, the olivine will react with the seawater, thus adding alkalinity to the sea, which makes it possible to store more CO_2 as bicarbonate in the seawater without acidifying it. The olivine grains bump into each other or scratch each other when they are moved by the surf. They become rounded, and the tiny slivers that have come off the grains will very rapidly weather [38]. If marine constructions (dams or artificial reefs) are built with olivine blocks and sand, this will conceivably lead to well-cemented structures after some time. Seawater is saturated with $CaCO_3$. If the water between the olivine pieces is only slowly replaced, it can react with the olivine for some time. This raises the pH of the interstitial seawater, causing a shift in the carbonate equilibria. This leads to a supersaturation of calcite which precipitates as a cement between the olivine. This process is similar to the formation of beach rocks. Filling the solution holes left by underground solution mining of salt with olivine powder serves two, possibly three purposes. After the cavity is filled with olivine, it is no longer necessary to keep the brine-filled hole permanently pressurized to prevent it from collapsing because the olivine will support the cavity. By injecting CO_2 into the mixture of olivine and brine, one captures CO_2 as bicarbonate. The heat of reaction of carbonatation + hydratation may heat the water sufficiently to use it for warm thermal medicinal baths, or swimming pools.

There are possible ideas for large-scale or economical applications of olivine. One such novel idea is the application of olivine in biodigesters. Biodigesters are installations where agricultural waste, urban sewage sludge, and organic waste stream from industry are anaerobically digested; during digestion, the organic material is turned into biogas. The biogas that is produced consists for around 2/3 of methane and 1/3 of CO_2. By adding olivine powder to the digester, part of the CO_2 gas will be converted to bicarbonate in solution, so the quality of the biogas will improve. As yet unpublished experiments at the Wageningen Agricultural University have shown that this is indeed the case, but there were two unexpected additional positive results. Most of the smell disappears. This can be explained by the fact that the FeO that is liberated

when the iron part of the olivine dissolves reacts immediately with H_2S and forms solid iron sulfides. A second effect was even more unexpected. The methane increased not only in relative amount but also in absolute amount. In nature, serpentinization of olivine under exclusion of free oxygen is often accompanied by methane emissions. These are due to the following reaction:

$$6Fe_2SiO_4 + CO_2 + 14H_2O \rightarrow CH_4 + 6H_4SiO_4 + 4Fe_3O_4 \quad (8)$$

Sometimes this leads to methane flames, like in the Turkish Yanartasi (the rock that always burns), where a peridotitic rock is being serpentinized at some depth and in Los Fuegos Eternos (the eternal fires) in the Zambales ophiolite complex on the main island of the Philippines, Luzon. The increase in methane production in the biodigesters is probably due to the same reaction.

Collateral Benefits

It was already pointed out in the report entitled "Geoengineering the climate" of the commission on geoengineering to the Royal Society that the consequences of enhanced weathering could be benign in principle [39]. One of the most obvious advantages of enhanced weathering is that it has the potential to mitigate ocean acidification, the decrease of pH in response to rising atmospheric CO_2 concentrations [40]. The ongoing lowering of the pH endangers the growth of coral reefs and likely affects marine life in general. A number of other collateral benefits of the olivine option can be mentioned.

Improvement of Soil Productivity

Tropical soils, except in areas with recent volcanism, are generally very poor, as they lack important mineral nutrients like magnesium, calcium, potassium, and phosphate. A limited amount of these nutrients is recycled by the standing forest, but once this is cut, the trees are removed and the soil is used for agricultural crops, it loses its productivity very fast. Spreading crushed dunite rock will solve the magnesium problem, and the calcium problem as well to some degree. Kimberlites, the host rock of diamonds, are also olivine-rich, but in addition they contain a potassium mineral (phlogopite) as well as often some phosphate. In order to provide a more balanced mixture of major nutrients, one should spread the crushed kimberlite of which hundreds of millions of tons are lying on the mine dumps of diamond mines. At the request of the author, seepage waters from kimberlite tailings in India and South Africa were analyzed. It was found that the waters that seep through these kimberlite tailings have a high pH and sequester large amounts of CO_2 as bicarbonate. Moreover, they can contain significant concentrations of potassium (data from the de Beers mine tailings in South Africa and the Panna diamond mine in India, Schuiling, unpublished). Again, one should avoid as much as possible mining wastes that contain chrysotile, although this white asbestos is considerably less dangerous than crocidolite (blue asbestos) or amosite (brown asbestos), which are not associated with dunites or peridotites. Recent research by Arcadis has shown that chrysotile weathers quite fast, and thereby loses its fibrous character [41].

Mindful of the beneficial effects of volcanic rock on the fertility of soils, it may also be a good idea to spread mixtures of crushed dunite and rock meal, like volcanic tuffs in areas with poor soils. Although the rock meal weathers considerably slower than dunite powder, and thus contributes much less to CO_2 sequestration, the combination is likely to increase productivity of the soil for a number of years, by which it can contribute to world food production. In view of the scarcity of potash fertilizer and its high price, it is recommended [42] to use powdered nepheline syenites to provide potassium to poor tropical soils, as the nepheline $(Na,K)AlSiO_4$ weathers considerably faster than potash feldspar. Acid sulfate soils form another problem that can be solved by spreading olivine. The Mekong delta, as well as a number of soils in estuaries along the East coast of Australia, suffers from high acidity, once the soil is plowed in preparation for agriculture. This exposes the pyrite in these soils to the oxygen in the air. The pyrite oxidizes and produces sulfuric acid, which reduces their rice productivity (Mekong) or sugarcane production (Australia) considerably [43]. If crushed olivine is spread on these acid sulfate soils, its weathering will neutralize the acid and thus increase their productivity. If the neutralization reaction is simplified to

$$2FeS_2 + 2Mg_2SiO_4 + 7.5O_2 \rightarrow 4MgSO_4 + Fe_2O_3 + 2SiO_2 \quad (9)$$

this would mean that 1 t of soil with 1% of pyrite would require close to 12 kg of olivine for complete neutralization.

Production of Biofuels from Siliceous Algae

In a very different manner, olivine can help to produce biofuel from algae instead of from land-based crops which use up land that is thereby lost for world food production and cost large amounts of scarce irrigation water [44, 45]. Diatoms (siliceous algae) grow very fast and are a proven raw material for the production of biodiesel, as they have a lipid content around 50%. Their growth, unfortunately, is often limited by the availability of silica, which they need to build their silica skeletons. During weathering, olivine releases large amounts of silica in solution. If one constructs a lagoon, preferably where the coastal waters carry large loads of urban or agricultural waste, diatoms can be grown in the following manner. The lagoon should be along a coastal stretch where the beach can be covered by olivine sand. A dam must be constructed around the lagoon to separate it from the open sea, except for one or a few U tubes through this dam. These U tubes permit the exchange of water between the lagoon and the open sea. The opening on the lagoon side of each tube should be covered by a perforated metallic plate, which acts as a support for a plankton net. During high tide, the water will flow into the lagoon and wet the olivine sand on the beach. During low tide, there will be an outflowing current of the water, including the part that formed the pore water between the olivine grains on the beach that is drained during ebb. This outflow will also carry the diatoms, but these are retained on the plankton net, where they can be harvested to be used as the raw material for biodiesel production. It is expected that in such diatom farms almost pure diatom cultures will form, as they have a competitive edge over organisms that do not use silica.

The growth of diatoms might also be stimulated for quite a different purpose. More and more often, coastal waters are threatened by poisonous dinoflagellate blooms ("red tides"), causing massive fish kills, and threatening human health. The main reason is believed to be the supply of untreated urban waters that contain high levels of nutrients. If one could stimulate the growth of fast-growing and nonpoisonous diatoms to consume the contained nutrients in these coastal waters, this may reduce or eliminate the dinoflagellate blooms. Besides, diatoms are an excellent fish food. The stimulation can be done by applying the same method, covering the beaches with olivine sand which will provide the silica that is necessary for the growth of the diatoms.

Geopolitical Implications of the Olivine Option

Although many scientists realize that CCS is a very costly operation [34], and is unlikely to solve the CO_2 problem at the required volumes, it is still the most widely discussed and preferred option, particularly among Western politicians and those that may benefit from the uptake of the technology. This can make for a powerful lobby. Many scientists urgently call for a reduction of CO_2 emissions, by increasing efficiency, changing our lifestyles, and switching to sustainable energy (wind, water, solar power, biomass, geothermal energy, or even nuclear energy). In the long run, mankind will be obliged to make the change to renewable energy anyhow, as our reserves of oil and gas are dwindling. Although there are still vast reserves of coal, these too are not endless. It is evident that the world should reduce its carbon footprint as quickly as possible. Some are concerned that the possibility of CO_2 sequestration may provide an excuse not to change current lifestyles, sometimes called the "moral hazard" argument. Trying to change people's attitudes and lifestyles is necessary, but it may be a slow process, whereas the danger of climate change requires immediate action. The two sides have a different time frame, and both are needed to avoid the imminent climate change caused by rapidly rising CO_2 levels in the atmosphere.

The picture is complicated by the fact that the largest industrializing nations (such as China, India, Brazil, South Africa, and Indonesia) all possess vast coal reserves and want to lift the standard of living of their people as quickly as possible. One requirement to reach that goal is the unlimited access to cheap energy. Reduction of emissions is, therefore, not necessarily a top priority. Enhanced weathering ideas may be a way to break this deadlock by providing a means of compensating their emissions by using olivine. All five industrializing nations mentioned also possess vast reserves of olivine rocks. They can exploit these with

their own workforce for 10% of the cost of CCS for the same amount of CO_2 sequestered, and it will give them large employment opportunities. Moreover, if they produce more olivine than required to meet their own agreed quota, they can sell surplus carbon credits to the other countries for 15 Euros/t of CO_2, and still make a profit. This will permit them to continue to use their cheap energy based on coal, while still doing their part to counteract climate change.

Future Directions

A number of niche applications of the concept of enhanced weathering of olivine have already been set into motion, like the inclusion of olivine in roof coverings, the addition of olivine to fertilizers or potting soil, or the covering of (bicycle) paths with olivine sand. Several other niche applications are under development. A breakthrough, though, depends on the certification of the olivine option for carbon credits, and the start of large-scale olivine mining. In the global climate debate, enhanced weathering can play a major role to reconcile the views and aims of the West and those of the emerging economies (China, India, Brazil, South Africa), if it is accepted that these countries may continue to use their vast coal reserves as a source of cheap energy, on condition that they compensate their CO_2 emissions by enhanced weathering of olivine.

Bibliography

Primary Literature

1. Huygens WJJ, Comans RNJ (2005) IEA Greenhouse Gas report 2005/11
2. Renforth P, Manning DAC, Lopez-Capel E (2009) Carbonate precipitation in artificial soils as a sink for atmospheric carbon dioxide. Appl Geochem. doi:10.1016/j.apgeochem.2009.05.005
3. Manning DAC (2008) Biological enhancement of soil carbonate precipitation: passive removal of atmospheric CO_2. Mineral Mag 72(2):639–649
4. Charan SN, Prasad PSR, Sarma DS, Archana KB, Chavan CD (2010) Evaluation of Deccan continental flood basalts. India, for geological sequestration of CO_2. J Appl Geochem 12(4):560–565
5. Kelemen PB, Matter J (2008) In situ carbonation of peridotite for CO_2 storage. Proc Natl Acad Sci U S A 105(45):17295–17300
6. Schuiling RD (1964) Serpentinization as a possible cause of high heat-flow values in and near oceanic ridges. Nature 201(4921):807–808
7. Schuiling RD (2006) Mineral sequestration of CO_2 and recovery of the heat of reaction. In: Badescu V, Cathcart RB, Schuiling RD (eds) Springer
8. Schuiling RD, Krijgsman P (2006) Enhanced weathering: an effective and cheap tool to sequester CO_2. Clim Change 74(1–3):349–354
9. Hards VL (2005) Volcanic contribution to the global carbon cycle. British Geological Survey, occasional report 10, 26 pp
10. Schuiling RD (2004) Thermal effects of massive CO_2 emissions associated with subduction volcanism. C R Geosci 336(12): 1053–1059
11. Dunsmore HE (1992) A geological perspective on global warming and the possibility of carbon dioxide removal as calcium carbonate mineral. Energy Convers Manag 33: 565–572
12. Raymo ME, Ruddiman WF (1992) Tectonic forcing of late Cenozoic climate. Nature 359(6391):117–121
13. Saltzman MR, Young SA (2005) Long-lived glaciation in the late Ordovician. Isotopic and sequence-stratigraphic evidence from western Laurentia. Geology 33:109–112
14. Young SA, Saltzman MR, Foland KA, Linder JS, Kump LR (2009) A major drop in seawater $^{87}Sr/^{86}Sr$ during the Middle Ordovician (Darriwilian): links to volcanism and climate? Geology 37(10):951
15. Schuiling RD, Praagman E (2011) Olivine Hills. Mineral water against climate change. In: Brunn S (ed) Engineering earth. Springer, Dordrecht
16. Sumner ME (2000) Handbook of soil science. CRC Press, London/New York/Washington, DC
17. Kling GW, Evans WC, Tanykele G, Kusakabe M, Ohba T, Yoshida Y, Hell JV (2005) Degassing Lake Nyos and Monoun: defusing certain disaster. Proc Natl Acad Sci U S A 102(40):14185–14190
18. Olsen AA (2007) Forsterite dissolution kinetics: applications and implications for chemical weathering. PhD thesis, Virginia Polytechnic Institute and State University, Blacksburg
19. Percival FG (1965) The lateritic iron deposits of Conakry. Trans Inst Min Metall 74:429–462
20. Middelburg JJ, Soetaert K, Herman PMJ (1997) Empirical relationships for use in global diagenetic models. Deep-Sea Res J 44(2):327–344
21. Oliveira SMB, Melfi AJ, Carvalho A, Friedrich G, Marker A, Kanig M (1988) Lateritic evolution of the Jacupiranga complex, S.P. Geochimica Brasiliensis 2(2):119–126
22. Wilson SA, Raudsepp M, Dipple GM (2006) Verifying and quantifying carbon fixation in minerals from serpentine-rich mine tailings using the Rietveld method with X-ray powder diffraction data. Am Mineral 91:1331–1341
23. Wilson SA, Dipple GM, Power IM, Thom JM, Anderson RG, Raudsepp M, Gabites JE, Southam G (2009) Carbon dioxide fixation within mine waste of ultramafic-hosted ore deposits: examples from the Clinton Creek and Cassiar chrysotile deposits, Canada. Econ Geol 104:95–112
24. Power IM et al (2011) Modern carbonate microbialites from an asbestos open pit pond, Yukon, Canada. Geobiology 9: 180–195

25. Schuiling RD, Wilson SA, Power IM (2011) Silicic acid saturation is unlikely to limit the geoengineering potential of enhanced silicate weathering. Proc Natl Acad Sci USA 108:E41
26. Van Schöll L, Kuyper ThW, Smits MM, Landeweert R, Hoffland E, Van Bremen N (2008) (2008) Rock-eating mycorrhizas: their role in plant nutrition and biogeochemical cycles. Plant Soil 303: 35–47
27. Wilson MJ, Jones D, McHardy WJ (1981) The weathering of serpentinite by *Lega atra*. Lichenologist 13:167–176
28. Garcia B, Beaumont V, Perfetti E, Rouchon V, Blanchet D, Oger P, Dromart G, Huc A-Y, Haeseler F (2010) Experiments and geochemical modeling of CO_2 sequestration by olivine. Potential, quantification. Appl Geochem 25:1383–1396
29. Hangx SJT, Spiers CJ (2009) Coastal spreading of olivine to control atmospheric CO_2 concentrations: a critical analysis of viability. Int J Greenhouse Gas Control 3:757–767
30. Schuiling RD, de Boer PL (2011) Fast weathering of olivine in shallow seas for cost-effective CO_2 capture. Earth Syst Dyn 2:551–568. Discussion
31. Needham SJ, Worden SH, Cuadros J (2006) Sediment ingestion by worms and the production of bio-clays: a study of macrobiologically enhanced weathering and early diagenetic processes. Sedimentology 53:567–579
32. Worden RH, Needham SJ, Cuadros J (2006) The worm gut; a natural clay mineral factory and a possible cause of diagenetic grain coats in sandstones. J Geochem Explor 89:428–431
33. Steen B, Borg G (2002) An estimate of the cost of sustainable production of metal concentrates from the Earth's crust. Ecol Econ 42(3):401–413
34. McKinsey & Company (2008) Carbon capture & storage: assessing the economics. Report 22 Sept 2008
35. Koornneef JM, Nieuwlaar E (in prep.) Environmental life cycle assessment of CO_2 sequestration through enhanced weathering of olivine. Working paper, Group Science, Technology and Society, Utrecht University
36. Golightly JP (1981) Nickeliferous laterite deposits. Economic geology 75th anniversary volume, pp 710–735
37. ESMAP, World Bank, ICMM (2005) Community development toolkit. ESMAP, World Bank, ICMM, Washington, DC
38. Schuiling RD, de Boer PL (2010) Coastal spreading of olivine to control atmospheric CO_2 concentrations: a critical analysis of viability. Int J Greenhouse Gas Control 4:855–856, Comment: Nature and laboratory experiments are different. Short Comm
39. Royal Society (2009) Geoengineering the climate: science, governance and uncertainty. RS Policy document 10/09, Sept 2009 RS1636
40. Schuiling RD, Tickell O (submitted) Olivine against climate change and ocean acidification
41. Arcadis (2011) Voortgang proef biologische asbestsanering, nieuwsbrief 3 (Progress report biological asbestos sanitation, newsletter 3)
42. Manning DAC (2010) Mineral sources of potassium for plant nutrition. A review. Agron Sustain Dev 30:281–294
43. Van Breemen N (1976) Genesis and solution chemistry of acid sulfate soils in Thailand. PhD thesis, Agricultural University of Wageningen, 263 pp
44. Bozarth A, Maier U-G, Zauner S (2009) Diatoms in biotechnology: modern tools and applications. Appl Microbiol Biotechnol 82(2):195–201
45. Dismukes GC, Carrieri D, Bennette N, Posewitz MC (2008) Aquatic phototrophs: efficient alternatives to land-based crops for biofuels. Curr Opin Biotechnol 19:235–240

Books and Reviews

MacKay DJC (2008) Sustainable energy – without the hot air. UIT, Cambridge, UK

Carrying Capacity for Aquaculture, Modeling Frameworks for Determination of

Joao G. Ferreira[1], Jon Grant[2], David W. Verner-Jeffreys[3], Nick G.H. Taylor[3]
[1]Departamento de Ciências e Engenharia do Ambiente, Faculdade de Ciências e Tecnologia Universidade Nova de Lisboa, Monte Caparica, Portugal
[2]Department of Oceanography, Dalhousie University, Halifax, NS, Canada
[3]Cefas Weymouth Laboratory, Weymouth, Dorset, UK

Article Outline

Glossary
Definition of the Subject and Its Importance
Introduction
Modeling Frameworks for Carrying Capacity
Future Directions
Acknowledgments
Bibliography

Glossary

Dynamic models Models that incorporate a time-varying element. Such models may have no spatial dimension or extend to modeling spatial variation in all three dimensions.

Integrated multi-trophic aquaculture (IMTA) Cocultivation of aquatic species at different trophic levels, such as salmon, mussels, and kelp or scallop

and sea cucumber, in order to maximize yield and minimize the environmental footprint.

Modeling framework Models are a representation of reality, which they aim to reproduce in terms of generality, realism, accuracy, and simplicity. As a rule, generality and simplicity are maximized. A model framework usually consists of two or more models, which are combined to address different levels of complexity.

Research models Models that are more detailed, usually complex to develop, implement, and apply. Aimed mainly at the scientist, rather than the manager.

Screening models Models that use a limited set of inputs, and provide highly aggregated outputs, such as an index of suitability or an environmental score card.

Virtual technology for aquaculture Any artificial representation of ecosystems that support aquaculture, whether directly or indirectly. Such representations, exemplified by mathematical models, are designed to help measure, understand, and predict the underlying variables and processes, in order to inform an Ecosystem Approach to Aquaculture.

Definition of the Subject and Its Importance

Aquaculture, defined simply as the cultivation of aquatic organisms, has many similarities to agriculture, most notably that it is based on the interaction between humans and other elements of the natural system, converting the latter (at least in part) into a *managed* system.

In parts of the world, such as Southeast Asia, the distinction between the two types of cultivation becomes increasingly fuzzy, especially if they take place on land. Cocultivation of rice and tilapia in paddy fields [1] or the combination of penaeid shrimp (e.g., the whiteleg shrimp *Penaeus vannamei*) and water spinach (*Ipomoea aquatica*) in earthen ponds is common, as are many other combinations (Fig. 1). Carrying capacity in such intensive systems, whether in monoculture or in integrated multi-trophic aquaculture (IMTA), might at first glance seem equivalent to assimilative capacity.

Aquaculture in open water, whether in reservoirs, lakes, or coastal systems, must take into account the complexities of water circulation, together with the harmonization of different uses. In the context of organically extractive open-water culture, Bacher et al. [2] and Smaal et al. [3] defined carrying capacity as:

Carrying Capacity for Aquaculture, Modeling Frameworks for Determination of. Figure 1
Pigs might fly? Cocultivation of pigs and fish such as carp or rohu in India http://harfish.gov.in/technology.htm

The standing stock at which the annual production of the marketable cohort is maximized.

Although this definition was proposed for bivalve shellfish culture, it is sufficiently broad to be relevant for production in open freshwater, coastal, and offshore environments, as well as in land-based systems using ponds or raceways. However, production carrying capacity needs to be further qualified, because in economic terms the maximization of annual production is not the objective function, and brings with it increased environmental costs. Commercial production must seek to achieve optimal *profit*, well before the inflection point in the production function, where total physical product (TPP) maximizes *income* (e.g., [4, 5]).

This production-oriented view of carrying capacity for aquaculture, whether in terms of assimilative capacity for fed aquaculture such as finfish or shrimp or with respect to food depletion in the case of shellfish such as oysters, clams, or abalone, has been expanded over the last decade into a four pillar approach based on physical, production, ecological, and social carrying capacity [6, 7]. These pillars encompass the three elements of sustainability, viz., planet, people, and profit.

The terms carrying capacity and assimilative capacity are frequently associated with models of aquaculture impacts. Because these terms attempt to define the

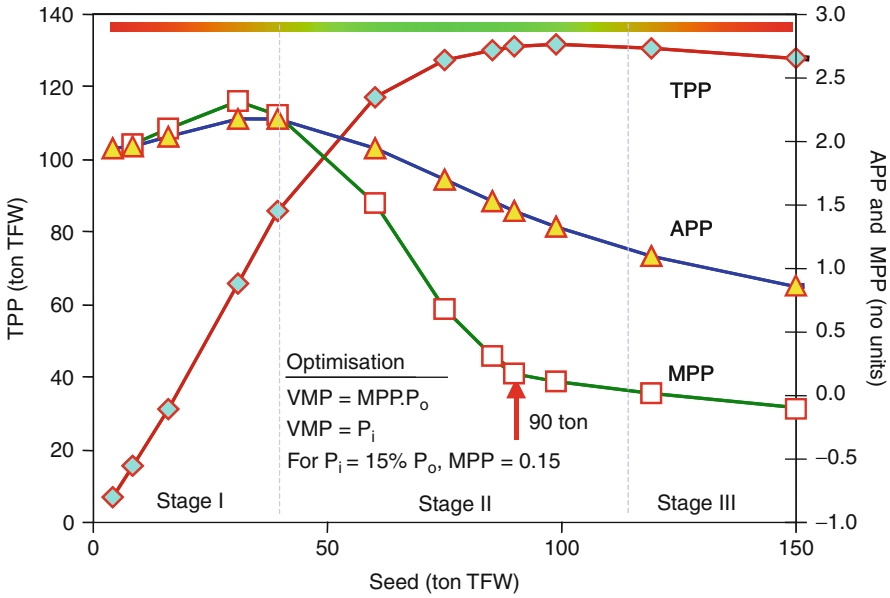

Carrying Capacity for Aquaculture, Modeling Frameworks for Determination of. Figure 2
Marginal analysis indicates that the seed that provides maximum profit (*red arrow*) falls well to the left of the maximum production, shown by the *dotted line*. Production beyond the optimal profit point adds no value and potentially increases environmental pressure (Results from the FARM model, Adapted from [4])

limits of sustainable aquaculture, predictive capability is highly sought (Fig. 2).

This chapter reviews the state of the art in modeling frameworks that assist with that prediction and support proactive management of aquaculture.

Introduction

The establishment of aquaculture activities in different geographical areas has historically been a bottom-up process, without any systemic planning or definition of a zoning framework. This is seen throughout the world, from the development of salmon cage culture in Scottish lochs to the incremental destruction of mangroves for construction of shrimp farms (Fig. 3).

This approach to licensing (or in many cases just to development) has been based on space availability and limits to production rather than on any environmental criteria, and has led to undesirable ecosystem effects, including habitat destruction both on land and in open waters, coastal eutrophication through increased nutrient loading from land, organic enrichment of sediments, loss of benthic biodiversity, and major outbreaks of disease.

In the last decade, better regulatory frameworks have led to a more stringent approach to licensing, most notably in the European Union, the United States, and Canada. The European Union's Marine Strategy Framework Directive (EU MSFD – EC [80]), together with guidelines for an Ecosystem Approach to Aquaculture (EAA – [8]), highlights the ecological component and aims to optimize production without compromising ecosystem services. Part of the challenge of determining carrying capacity is the quantification of negative externalities as a first step toward improved management.

In Brazil, for instance, where aquaculture has grown very rapidly over the past decade (Fig. 4), environmental permitting of new tilapia farms in reservoirs is determined through the application of the Dillon and Rigler [9] phosphorus loading model, a rather simplistic view of carrying capacity.

A maximum limit of 30 μg L^{-1} of P has been established for reservoir waters, 5 μg L^{-1} of which is reserved for fish farming, to allow for multiple uses including cattle ranching, sugar cane production, urban discharges, and the natural background.

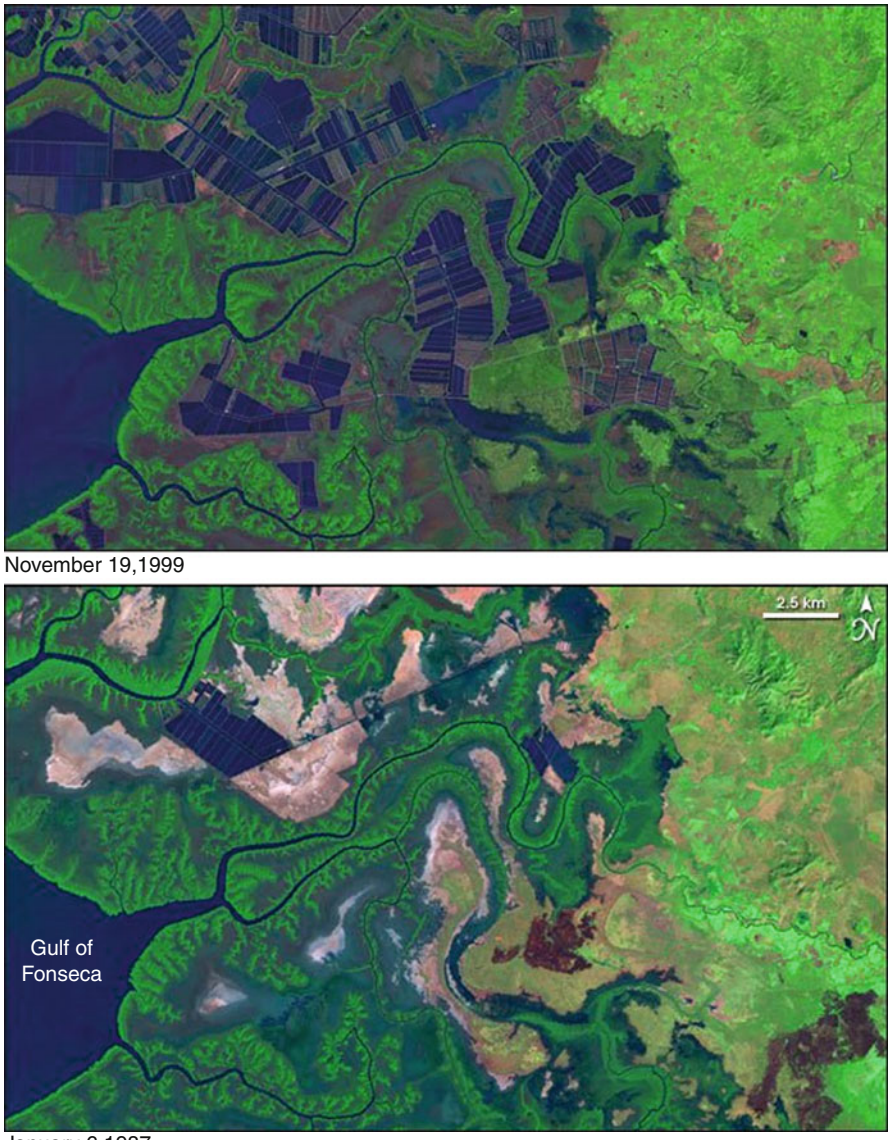

Carrying Capacity for Aquaculture, Modeling Frameworks for Determination of. Figure 3
Expansion of shrimp ponds over a 13-year period in Estero Real, Nicaragua [83]

Fish farms are licensed sequentially, based on the contribution to P loading of their declared production.

Although this approach does address carrying capacity at the system scale (i.e., $\Delta P = 5\ \mu g\ L^{-1}$), it does not consider any spatial or temporal variation, nor does it account for factors such as organic enrichment, disease, or impacts on biodiversity – all of which may be linked.

Whereas production and social (e.g., tourism) impacts are often local, ecological impacts *of* aquaculture can have far broader scales, as can large-scale effects *on* aquaculture, such as advection of harmful algae from offshore [10]. Sustainability is "easier to plan than to retrofit," [10] which makes a case for the analysis of carrying capacity at the system scale (e.g., Nobre et al. [11]), i.e., defining and quantifying the overall potential for different types of aquaculture prior to local-scale assessment (e.g., [12]) of new operations. Simulation models of varying degrees of complexity must play a role in the determination of

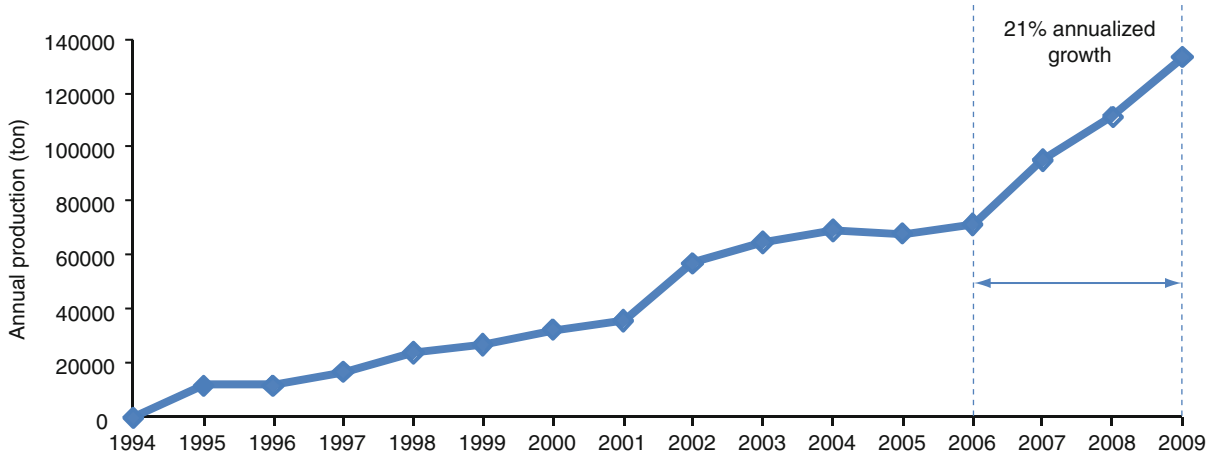

Carrying Capacity for Aquaculture, Modeling Frameworks for Determination of. Figure 4
Production of farmed tilapia in Brazil (MPA, personal communication, 2011)

carrying capacity for aquaculture, often combined as model frameworks, given the range of time and space scales and the number of processes involved.

Over the next decades, the growth of aquaculture will take place in developing nations [13–15], which makes it paramount that the digital divide, which is already considerable (as is the legal divide; see [16]), does not become wider.

Simulation technology that can support planning should be close to the production centers and be able to deal with data-poor environments and limited computational access and skills.

Modeling Frameworks for Carrying Capacity

The concept of carrying capacity in aquaculture, based on four pillars of sustainability, has been adapted in Fig. 5 to include governance [16, 17]. This is considered more relevant than the physical element, which in many respects is encapsulated in the production pillar. Governance, on the other hand, is clearly missing from the original model of Inglis et al. [6], and the quality of balanced regulation, stakeholder involvement, and community-based management [18] often constitutes the difference between sustainable aquaculture and an environmental time bomb.

The social (here used in the context of social opposition to visual or other impacts of aquaculture development, such as conflict with leisure areas) pillar is at

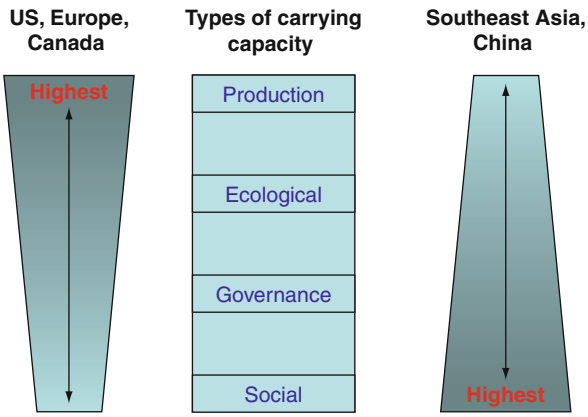

Carrying Capacity for Aquaculture, Modeling Frameworks for Determination of. Figure 5
The relative importance of the four pillars of carrying capacity (Adapted from [17])

the forefront of decision-making for aquaculture in the EU, the US, and Canada and can frequently be identified as the single most important criterion for carrying capacity assessment and site selection (Fig. 5). By contrast, in Asia and other parts of the world where food production is the paramount concern, licensing criteria are more frequently based on the production pillar, with ecological considerations assuming less relevance. In China and Southeast Asia, the social component acts as a driver for increased aquaculture, for reasons of economy and food security. Governance is not usually

limited by a lack of legal instruments [16] but often by their adequacy and acceptance by stakeholders.

Two of the pillars illustrated in Fig. 5, production and ecology, are amenable to mathematical modeling, and two are not. This does not mean that those mathematical models will be entirely successful in describing growth, environmental effects, and particularly ecosystem responses, but they do make a significant contribution to the improved evaluation of carrying capacity. Part of the difficulty lies with our understanding of the relevant processes, parameters, and rates, part with other factors, such as the lack of a paradigm in ecology to support prediction. For instance, in the EU MSFD, as in other legal instruments, there are complex descriptors of ecosystem health such as biodiversity, and the scientific community struggles to establish meaningful classification systems and their relationship to anthropogenic pressures.

There are also interactions with the human component of cultivation that constitute simulation challenges. Culture practice, for instance, is widely variable and can generally only be modeled in average terms [19].

Issues related to disease, which fall squarely between production and ecology and are extremely difficult to model, are a huge challenge in aquaculture and often include a significant element of poor governance, such as relaying of infected animals to hitherto uncontaminated areas.

Rearing large numbers of animals of the same species in close proximity to each other favors the establishment and spread of infectious diseases within those farmed populations [84]. Disease can affect both survival and growth of animals. Outbreaks of highly virulent bacterial and viral diseases can result in high mortality of an affected farm stock. For example, outbreaks of white spot syndrome virus (WSSV) in farmed whiteleg shrimp can result in greater than 60% mortality, with an attendant dramatic impact on the farms and regions dependent on farming this species.

Additionally, with ever increasing demands from consumers for high-quality products, the effects that disease can have on product quality are of increasing importance. For example, tilapia that have survived outbreaks of *Francisella* often have unsightly lesions in the fillets. There are also examples of diseases, such as Red Mark Syndrome in rainbow trout [85], that do not result in any significant mortality or morbidity, but still result in the product being downgraded or rejected by processors after harvest, imposing significant economic costs on the farmer.

The ecological effects of disease in aquaculture can also be profound. This includes spread of pathogens from farmed fish to wild fish and vice versa [86]. Disease agents that affect aquaculture species generally have their origins in wild aquatic animals [86]. Many systems (e.g., salmonid netcage and bivalve culture) involve rearing the farmed animals in relatively open systems where the reared animals are in direct contact or close proximity with wild animals. Water is an ideal medium for the dissemination of many pathogens, leading to a high risk of transfer. For instance, in Norway and Scotland, exchange of sea lice *Lepeophtheirus salmonis* between farmed Atlantic salmon and wild salmonids has been implicated in causing significant declines in populations of wild Atlantic salmon and sea trout.

In order to examine modeling frameworks, the following sections review the definitions of, and distinctions between, the pillars of carrying capacity that are more amenable to mathematical modeling.

Assimilative Capacity and Carrying Capacity

Assimilative capacity is sometimes considered a subclass of the more general term carrying capacity, but other more specific definitions have been applied. We make a distinction as detailed below. Assimilative capacity refers to the ability of biological systems in the water column or sediments to process organic matter, nutrients, therapeutants, or contaminants without alteration of ecosystem state or function.

Carrying capacity refers to the biomass of cultured organisms that can be supported without altering system state or function measured by water or sediment quality standards and processes [20, 21]. The latter is thus determined by aquacultured biomass [22], where the former is independent of aquaculture and determined by biological properties of the habitat.

The application of standards to models of impact takes two forms:

1. Absolute criteria determined by regulatory bodies such as the Water Framework Directive of the EU (EU WFD – EC [79])

2. Relative standards compared to reference conditions or the range of variation observed in the environment

In both cases, there is an attempt to use these values as sustainability criteria. In the case of absolute standards, the background of the environmental conditions is not considered. For example, naturally eutrophic waters may show higher nutrient levels, with no relationship to aquaculture. This is particularly true of chlorophyll impacted by shellfish depletion. It may be more realistic to consider depletion in the context of the range of values observed in the environment as a means of establishing whether aquaculture signals can be detected against background noise. This type of standard has been applied to shellfish depletion of chlorophyll by Filgueira and Grant [20] and to shellfish biodeposits by Grant et al. [23].

Tett et al. [22] formalize both carrying capacity and assimilative capacity as the result of dose–response curves, couched in the terminology of DPSIR (Drivers-Pressure-State-Impact-Response; see also [24]; Fig. 6), where pressure is the farmed biomass and state is the system response modeled as a water quality standard. By comparing physical and geochemical rate processes, a net balance is determined, whereby the quantity of interest displays an increase (e.g., ammonia) or decrease (e.g., dissolved oxygen) relative to a water quality standard. When two of these processes are balanced, an index is created, constituting some of the earliest models in this research area, sometimes referred to as screening models.

A further distinction is that assimilative capacity be a function only of biological processing. Tett et al. [22] use the net results of water quality models which include advection–diffusion as well as biological processing to define assimilative capacity. Following bioenergetic lexicon, assimilation is a metabolic process involving digestion and/or decomposition, but excluding physical exchange.

There has been some decoupling of the measurements used to characterize aquaculture impacts in sediments (redox, sulfides; [25]) with models that are based on oxygen fluxes. Brigolin et al. [26] used a more classical early diagenesis model to examine coupled redox reactions at fish farm sites. This is one of the few cases where the field measurements used in regulation could be compared to model output including total sulfides and seabed oxygen consumption.

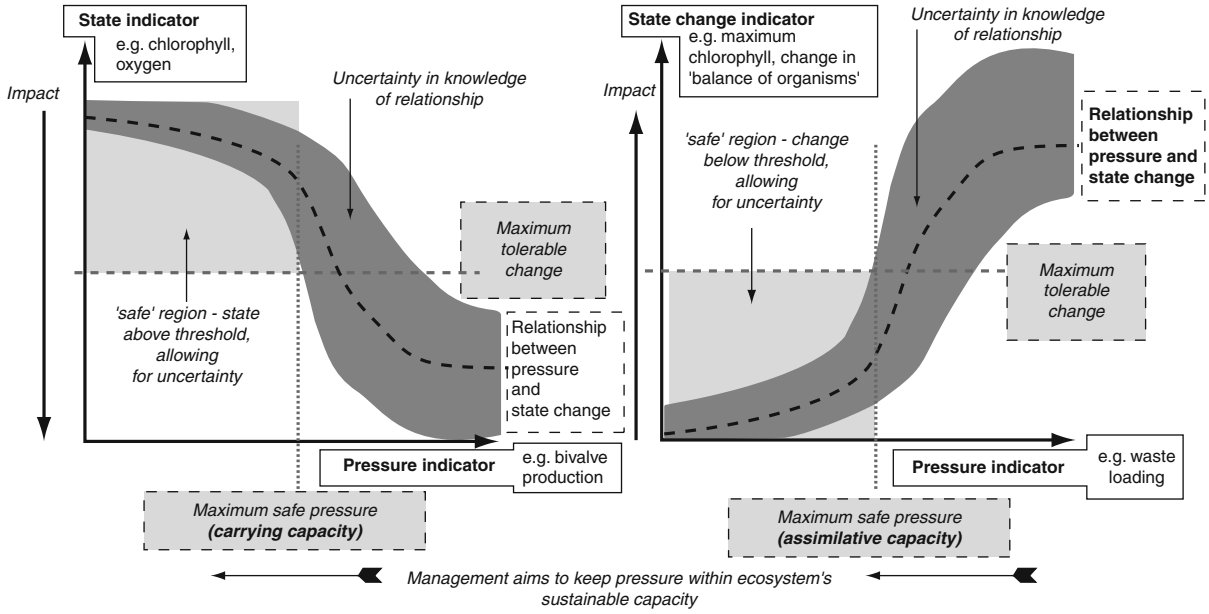

Carrying Capacity for Aquaculture, Modeling Frameworks for Determination of. Figure 6
Conceptual framework of assimilative and carrying capacities [22]

In terms of benthic impacts, assimilative capacity as the ability of sediments to accept some degree of organic enrichment without generating anoxic crises is well grounded conceptually. A comparison of benthic carbon supply via fish feed and fecal input to oxygen demand of the sediment forms the basis of some the original models of benthic impact [27] including the long-standing Norwegian MOM approach [21]. This concept was widely applied to multiple salmon sites by Morrisey et al. [28]. De Gaetano et al. [78] produced a more sophisticated version of the model for Mediterranean fish culture.

The intermediate disturbance hypothesis (e.g., [29]) provides a functional form to the model by suggesting a parabolic response of benthic diversity and activity to organic loading. Stimulation of aerobic demand occurs at low enrichment, peaking at intermediate levels and declining at high levels (Fig. 7; [30]).

The latter authors define "acceptable aquaculture" as keeping sediment oxygen demand at or below the peak. They produced a numerical model which included a 3D circulation component, organic deposition, and decomposition based on a sediment diagenesis model using oxygen fluxes and anaerobic processes. Output is in the form of mapped values of organic loading based on fish stocking density that produces maximum aerobic oxygen concentration (Fig. 8).

The map shows that farms within the inner parts of the inlet have less permissible organic sedimentation due to reduced flushing. We suggest that this example is the appropriate approach to assimilative capacity since it models system function and its response to organic loading based on the capacity of the benthos to absorb organic matter while maintaining oxic conditions. In addition, inclusion of a spatial diffusion–advection model allows incorporation of nonlocal processes and provides mapped output. Results are inherently inclusive of far-field effects and include interaction of multiple farms. Although the paper did not have the context of marine spatial planning, it is clearly applicable in terms of both the approach and the results. The comprehensive nature of this study and its faithfulness to the concept of assimilative capacity make it noteworthy in the literature.

Models of assimilative capacity, like those for shellfish carrying capacity, differ in spatial resolution. The original index models are 1-box, 0D models treating any body of water as a single basin. Physical exchange is thus averaged over the entire domain. This is often problematic since estuaries or other embayments are places with strong gradients in flushing. In addition, aquaculture sites are averaged in this scheme, so no questions regarding optimal location can be addressed.

One hybrid approach which solves some of these problems is the use of a full circulation model whose

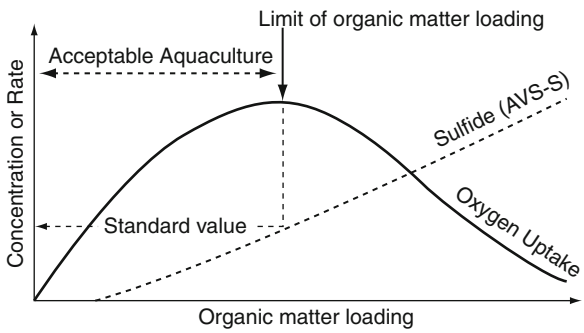

Carrying Capacity for Aquaculture, Modeling Frameworks for Determination of. Figure 7
Acceptable limits for organic matter loading from fish farms and the relationship to benthic oxygen uptake and sediment sulfide content [30]

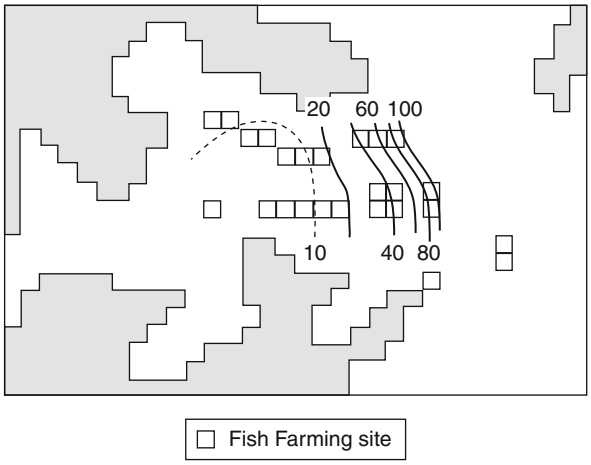

Carrying Capacity for Aquaculture, Modeling Frameworks for Determination of. Figure 8
Isopleths of the limit values of the organic matter loading rate ($\mu mol O_2/cm^2/day$) in Gokasho Bay, estimated by a numerical model [30]

output is applied to local models. In this case, at least the physics is location specific, and subregions of the system may be considered without the 0D averaging.

Lee et al. [31] applied this approach to yellowtail culture in Hong Kong Harbour by comparing oxygen delivery to fish oxygen consumption and determining net oxygen concentration relative to water quality standards for different levels of stocked biomass. Similar schemes have been used for finfish culture in Scotland [22].

Models for Finfish, Shrimp, and Bivalve Culture

Models for Open Water Culture Models for organic loading by finfish include submodels of circulation, particle transport, and benthic response [21]. Models may also include a phytoplankton-nutrients-zooplankton (PNZ) component, simulating trophodynamics in the water column. This may be necessary due to the importance of phytoplankton and the microbial loop as nutrient processors [22]. For either finfish or shellfish, some version of a farm production or bioenergetics model is essential to estimate waste outputs from cultured animals. Benthic models applied to aquaculture are typically diagenetic, aimed at resolving sediment decomposition and nutrient regeneration [78].

For finfish, benthic deposition of farm wastes and consequent impacts are the primary emphasis; since fish are not dependent on the environment for food, trophodynamics are less relevant. Similarly, the models are usually localized since much of the waste material remains near the cage site (e.g., DEPOMOD). Nonetheless, there is concern that wastes reach the far field and produce negative benthic impacts. Despite this potential, far-field models of finfish cage culture are uncommon. Some early examples used 3D circulation models to examine waste dispersal over kilometer scales [87].

In a more recent example, Symonds [32] compared near-field models such as DEPOMOD to a far-field model based on a 3D circulation. He found that the dependence of near-field models on limited current meter observations was subject to the noise and uncertainty inherent in those measurements. In addition, the far-field model had the potential for bidirectional transport of waste, whereas the near-field model had permanent escape from its limited domain causing potential underestimation of benthic impacts. In addition, the far-field model allows consideration of multiple farms and their interaction. Skogen et al. [33] used a 3D circulation model coupled to a full ecosystem model to study the effects of fish farms on far-field oxygen, nutrients, and primary production, concluding that eutrophication in the far field of a Norwegian fjord was not enhanced by the farm.

The goal of most bivalve shellfish models is to understand seston depletion as a limiting food resource for farmed animals. This requires a trophodynamic model which includes primary production, bivalve grazing, and advection–diffusion. Because farmed shellfish feed on phytoplankton from distant sources, recent examples involve models which include the far field. Nevertheless, there are many examples of 1-box, 0D models in which the physics and biology are averaged over the basin. Environmental impact of biodeposition to the benthos has been considered in several models including spatial examples [30, 34], but this is less frequently addressed compared to seston depletion. The opposite is true for field studies where benthic impacts are emphasized, and seston depletion is rarely addressed due to the difficulty in observing it. Because seston depletion occurs first at a farm scale, models of the depletion process have also been created at the local scale, prominently the FARM model [4]. Far-field models of seston depletion are increasingly common [20, 35].

It may be concluded that models of finfish aquaculture impacts would benefit from more spatial realism and far-field content, as well as further emphasis on assimilative capacity. Similarly, shellfish models would benefit from inclusion of benthic impact prediction in association with existing focus on seston depletion. The development of assimilative capacity models would be identical for both finfish and shellfish culture. This also places the context to that of ecosystem function. The present context of faunal indices based on carbon deposition in local models is important [36, 37], but is predicted on the basis of somewhat tenuous empirical relationships which are a departure from the more quantitative nature of the models.

Models for Land-Based Culture Models that simulate land-based culture taking place in ponds, tanks, or

raceways use many of the biogeochemical features described above, but the physics is simplified to a reactor type of system and serves to determine water exchange and effluent loading to adjacent water bodies. Such models are cheaper to develop and implement than the examples given for open waters (here including lakes and estuaries, where water circulation should also be accounted for). According to the latest figures from FAO, over 70% of freshwater aquaculture in China takes place in ponds, corresponding to an area the size of New Jersey and an annual production of over 15 million tons [88].

This number is triple the total aquaculture production of America, Europe, and Africa combined, which suggests that substantial emphasis should be placed on models that can assist with site selection, optimization of carrying capacity, and evaluation of negative environmental externalities of pond culture.

Various examples of this type of approach exist (e.g., [38, 77]. Figure 9 shows mass balance results obtained with the Pond Aquaculture Management and Development (POND) model [39], which simulates the production and environmental effects of shrimp, fish, and bivalves cultivated in ponds, in monoculture or IMTA.

The model was run for a site at 23°N, with a daily water renewal of 3% of the pond volume, and estimates an environmental discharge of about 45 kg of nitrogen (mostly dissolved, but also as algae), roughly 14 population equivalents (PEQ) per year for the 90-day cultivation cycle. The cost of offsetting these emissions is over 500 USD [40]. In developing countries, these

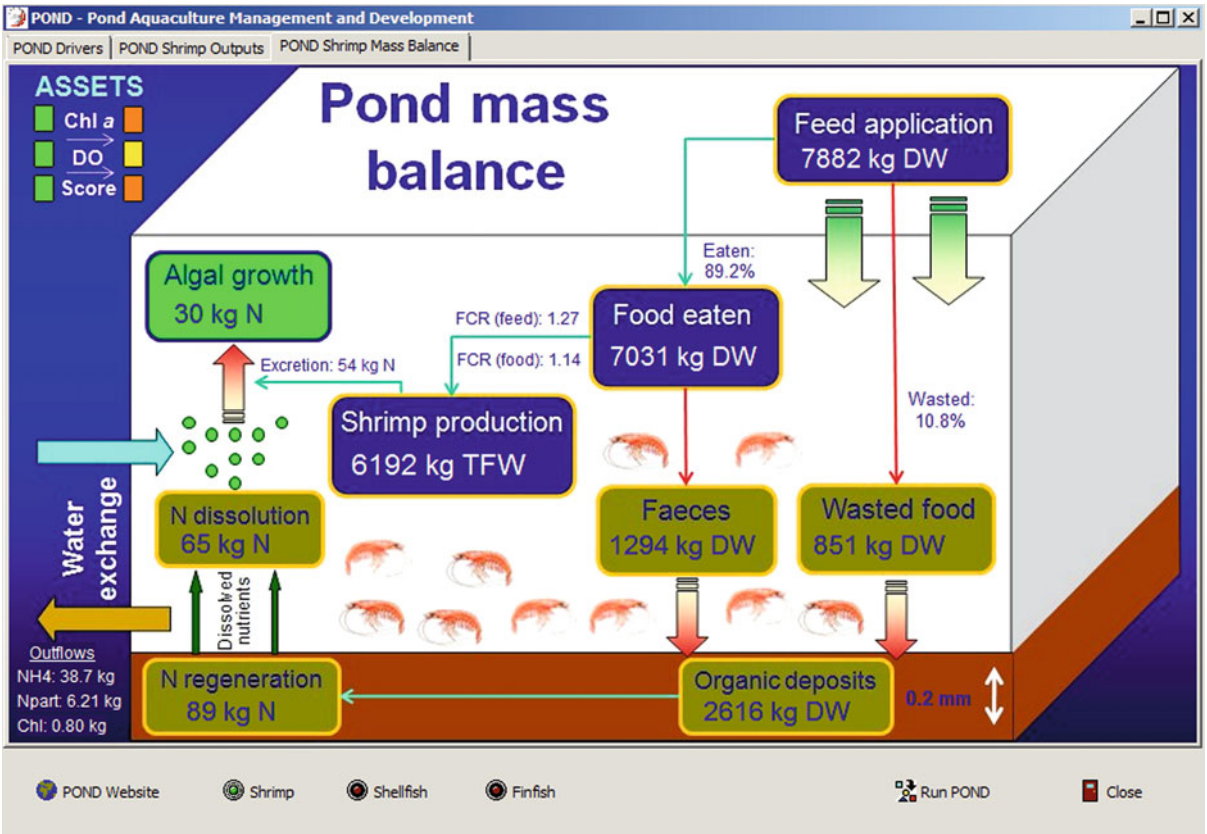

Carrying Capacity for Aquaculture, Modeling Frameworks for Determination of. Figure 9
Mass balance of whiteleg shrimp (*Penaeus vannamei*) culture, including production and environmental externalities for a 1-ha pond

waste costs are not internalized but rather imposed on to the environment, contradicting the first principle of the ecosystem approach to aquaculture [8] that:

- Aquaculture should be developed in the context of ecosystem functions and services (including biodiversity) with no degradation of these beyond their resilience.

By contrast, pond production in the United States already requires a National Pollutant Discharge Elimination System (NPDES) permit [41]. Often, this means that large agro-industrial companies from developed countries price-leverage the lack of environmental regulation and/or implementation in the developing world.

Models of this kind can be coupled with a range of other models to provide a decision support framework. POND uses the well-tested Assessment of Estuarine Trophic Status (ASSETS) model [42], providing a color-coded assessment (Fig. 9) of the degradation of water quality over the culture cycle.

Models for Integrated Multi-trophic Aquaculture IMTA has been practised in Asia for thousands of years. In the fifth century B.C., the Chinese aquaculturalist Fan Lee [81] wrote:

- You construct a pond out of six mou of land. In the pond you build nine islands. Place into the pond plenty of aquatic plants that are folded over several times. Then collect twenty gravid carp that are three chih in length and four male carp that are also three chih in length. Introduce these carp into the pond during the early part of the second moon of the year. Leave the water undisturbed, and the fish will spawn. During the fourth moon, introduce into the pond one turtle, during the sixth moon, two turtles: during the eighth moon, three turtles. The turtles are heavenly guards, guarding against the invasion of flying predators.

A substantial proportion of Asian aquaculture currently takes place in cocultivation, improving production, optimizing resources, and reducing environmental waste [14]. Despite this oriental wisdom, multi-trophic aquaculture is still rare in North America and Europe, although commercial interest is growing rapidly. This is reflected in research (e.g., [43, 44]), with the annual number of scientific publications on IMTA doubling from 2007 to 2010 (SCOPUS).

The combinations of species, relevant proportions, and culture practice are key to successful IMTA. There is traditional knowledge in China and other parts of Asia on what works best, but advances in mathematical modeling can make a substantial contribution by quantifying energy flows, production, and environmental externalities ([45], Nobre et al. [11], [16]).

Figure 10 shows a simulation of IMTA for a shrimp farm, with cocultivation of the Pacific oyster *Crassostrea gigas* at different densities, using the POND model. As the oyster density in the ponds increases, the net primary production (NPP) of phytoplankton is reduced due to top-down control, although NH_4^+ increases due to bivalve excretion. The model is not simulating macroalgae or other aquatic plants, which if added would significantly reduce the output of ammonia.

The ASSETS score is best at the higher oyster density, but at a density of 10 oysters m^{-2}, the shrimp culture cycle would yield a harvestable oyster biomass of over 500 kg to provide an annualized extra income of over 10,000 USD. The removal of algae and detritus by the filter-feeding bivalves corresponds to three PEQ per year, about 15% of the discharge. At the higher densities, the bivalves are performing a bioextractive function and do not reach market size in a short cycle due to food depletion. A more detailed analysis can be made by simulating oyster growth continuously over multiple cycles of shrimp culture. Such interactions can also be modeled for other combinations, for example, tilapia and shrimp or salmon and mussels.

Models for Disease Spread and Control In determining the carrying capacity of aquaculture operations, it is important to ensure aquaculture production practices and systems within a farm, managed region, or zone are resilient to the effects of disease. Modeling provides a means of investigating the interactions occurring among the four pillars and the spread and establishment of pathogens; however, to date, most models have ignored the influence of society on aquatic disease. Many different models have been derived to investigate the spread and impact of particular pathogens: In aquatic systems, two of the most

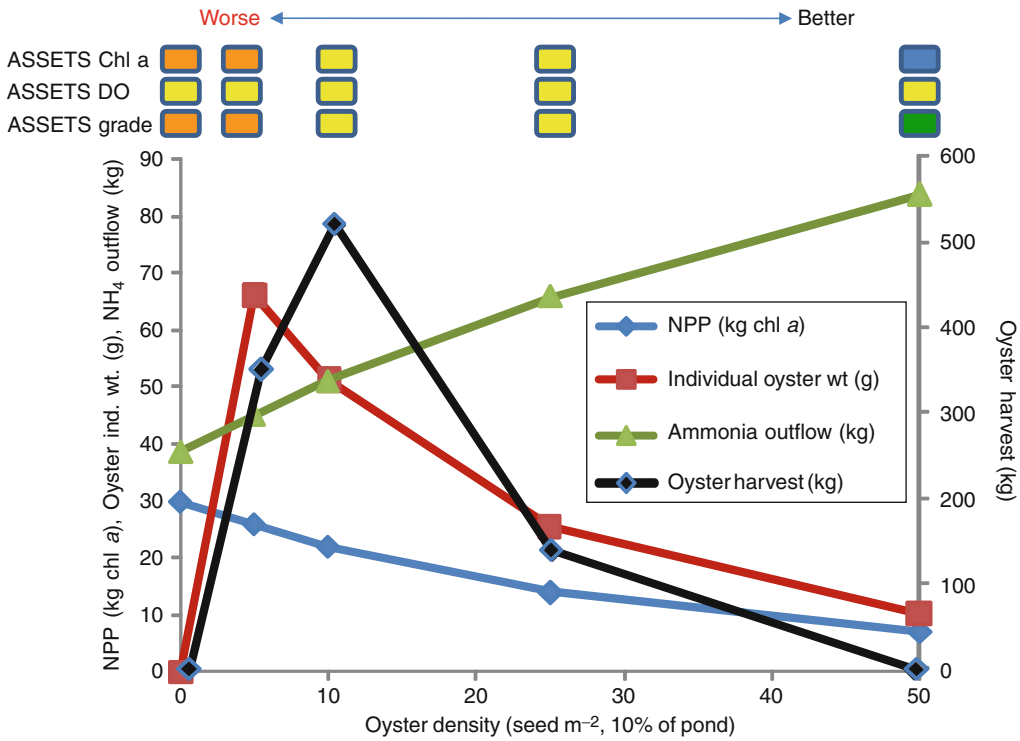

Carrying Capacity for Aquaculture, Modeling Frameworks for Determination of. Figure 10
Analysis of IMTA production and externalities by means of the POND model

common approaches are (1) compartment-based models and (2) network models.

Compartment-based models assume that individuals transition through a series of states from susceptible (S) to infected (I), and potentially back, or through a series of other states such as resistant (R). These models are often referred to as SIR models [46] and are usually based on continuous time, and therefore use differential equations; however, stochastic and discrete time approaches are also used. SIR models do not track individuals but assume the population follows a set of behavior rules, and that at each point in time, a proportion of the population leaves one state to enter another according to these rules. In aquatic systems, these models are generally used to track disease through a population of animals, but they have also been applied to look at spread through a population of sites. Simple implementations are often analytically tractable, allowing conditions under which thresholds and equilibria occur to be found without the need to run simulations.

One of the key pieces of information that can be derived from these models is a maximum (susceptible) host carrying capacity for which a pathogen cannot persist. Such carrying capacities used in the context of pathogens are often referred to as a critical threshold (N_T) and may be useful to wildlife and farm managers when attempting to control or prevent disease. This threshold is however largely dependent on the assumptions made regarding the way a pathogen is transmitted, and obviously does not apply if transmission is not dependent on host density, but is frequency based (as is often assumed to be the case when modeling sexually transmitted infections). It is therefore important that the correct form of transmission is used in a disease model to avoid false inference. The most commonly used form of model assumes that transmission occurs by contact between animals or sites, that the number of contacts is density dependent, and that mixing between individuals occurs equally and at random. This is often referred to as a "density-dependent transmission" or "pseudo mass action" model [47, 48].

Under these assumptions, one method by which N_T can be derived is by determining the conditions under which the basic reproductive number, R0, is equal to 1. In simple terms, R0 is the number of secondary infections that arise if an infected individual enters a wholly susceptible population. If greater than 1, the pathogen will establish; if less than 1, it will die out. R0 is governed by the total population density, the period over which an infected animal sheds pathogen, and the transmission rate β (the rate of contacts between individuals and that the probability that given a contact, infection occurs). Both environmental conditions and management/husbandry decisions can influence this number, and therefore the critical threshold for establishment. Understanding the influence of each of the four pillars of carrying capacity on R0 is therefore critical in order to predict and manipulate N_T. Omori and Adams [49] illustrate the application of compartment-based models to assess the influence of the ecology and production pillars on the dynamics of Koi herpesvirus in farmed carp populations *(Cyprinus carpio)*. Their approach showed that temperature and on-farm production processes used in conjunction with this could be used to immunize a population, preventing clinical disease expression.

The assumption of random mixing of a population is often not reasonable, as in reality some individuals will be more social or isolated than others, and individuals tend to have discrete groups of contacts that may or may not be connected to other groups within a population. Under these circumstances, the assumption of random mixing can lead to substantial overprediction of the epidemic process. Social network analysis (SNA) and modeling approaches provide a means of incorporating the contacts that occur between individuals, and therefore the consequence this may have on pathogen spread. In the case of agriculture and aquaculture, these models tend to be based at the level of the site, rather than the animal in question.

A major advantage of this modeling approach is that much epidemiologically useful information can be obtained merely by examining the network properties, without parameterizing for a particular disease. For example, in order to develop generic surveillance and control strategies, it may be useful to identify:

- Clusters of connected individuals within the network and whether it is possible to make them epidemiologically distinct through the removal of a few connections.
- Long chains of connection that join the network throughout and thus allow disease spread.
- Super-spreaders, which are individuals that contact a high number of other individuals and can thus rapidly spread pathogens.
- Super-sinks, which are individuals that receive from a lot of other individuals. Though they may not spread a pathogen, they are most likely to receive one and may therefore be useful for surveillance purposes.

Many statistics can be generated to summarize different properties of a network. Although R0 can also be estimated, other statistics such as the degree of centrality or clustering coefficient may provide more useful means of assessing the likelihood of spread through a network. Green et al. [50] demonstrated the application of such statistics using SNA applied to the Scottish network of trout and salmon farms. The analysis showed how much transmission was likely to occur in the network as it stood but also used a variety of methods to remove the most influential connections to reduce transmission.

In addition to examining the network properties, stochastic simulations can be run over the network. In such simulations, the network is randomly seeded with infected individuals and, at each subsequent time point, connected individuals change state from susceptible to infected at a given probability and given the likelihood of a contact. This approach is often useful when evaluating rates of spread and the effectiveness of control strategies but also has the potential to be used as a real-time tool during an outbreak, if it can be parameterized for the pathogen of interest. Further useful information may be gained from these models by making network models spatially explicit, as this facilitates the designations of control zones.

Werkman et al. [51] used stochastic network simulations to good effect to determine the efficacy of different fallowing strategies in eradicating disease from areas producing different amounts of fish. Thrush and Peeler [52] used a simulation of movements over the English and Welsh trout industry network to

investigate the potential spread of *Gyrodactylus salaris*. This demonstrated that in 95% of the simulations run, less than 63 of 193 river catchments would be at risk of getting the pathogen in the 12 months following introduction. Jonkers et al. [53] developed this model further into a strategic tool that could be used to evaluate the effectiveness of different control and surveillance efforts on disease spread.

One of the major limitations of network approaches is that they rely on knowledge of the complete network of connections and assume that this remains stable over time. Missing connections or changes to the network with time could lead to misdirected efforts. For many aquatic systems, reliable network data are not available or are difficult to compile. Under these circumstances, simpler compartment-based approaches may still be of value in informing control policies. One such application was demonstrated by Taylor et al. [54] to evaluate the effectiveness of different control options in reducing the spread of Koi herpesvirus in the UK between sites holding carp.

Most models applied to aquatic systems to date tend to be based at either the level of the site or animal, with few attempting to combine the two approaches. There is, however, substantial scope to develop future models that incorporate multiple levels that account for transmission between individual animals in a unit, the influence this has on the transmission between units on a farm, and the subsequent effect on between-farm spread (Fig. 11).

Where attempts to link these two levels together have been made, useful results have been obtained. Hydrodynamic models have been applied to look at the spread of sea lice between Norwegian salmon cages in fjord systems [55]. These models track the number of lice generated and monitor their dispersal and decay over time and space to see whether they reach and infect other sites. Green [56] combined compartment-based and network approaches to incorporate the influence of within-site processes on network spread and found that differences in site biomass influenced the rate of between-site transmission if density-dependent transmission was assumed. One of the major advantages of models that link the within-site epidemic with between-site spread is that they allow for the consequences of different detection (or action) rates to be assessed, allowing more efficient resource planning.

The primary goal of all of the approaches described above is often to apply changes to the system to understand their influence on pathogen spread. In

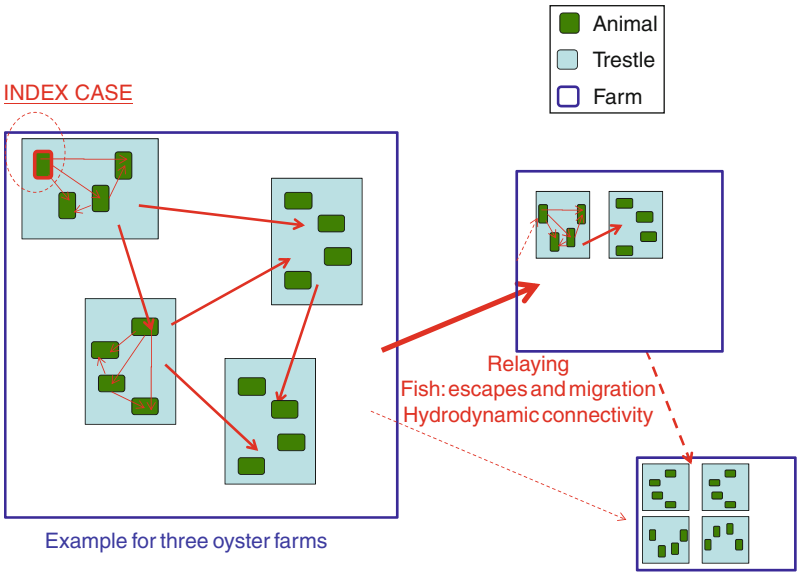

Carrying Capacity for Aquaculture, Modeling Frameworks for Determination of. Figure 11
Network models working at different scales in time and space

application to aquaculture systems, this may be conducted to establish how best to maximize N_T (either in the number of animals produced within a site or the number of sites in an area) and thus increase carrying capacity. Generally speaking, N_T can be increased by reducing the amount of connectivity between individuals (restrictions in movements), changing their susceptibility to disease (e.g., by vaccination) or reducing the period over which an individual is able to transmit a pathogen (e.g., through good surveillance and rapid culling). Other important disease management tools that have or could be evaluated by the modeling approaches described above include:

- The use of management areas in which aquaculture activities such as harvesting or treatment are coordinated between all farms in an area
- Fallowing of sites between production cycles to allow pathogens present to die out and potentially reduce the infection pressure other sites are exposed to
- Year class separation, where only one age class is present at a time causing all animals to be harvested prior to stocking new animals
- Removal of high-risk contacts between sites that are likely to spread disease widely
- Biomass limits to reduce the maximum amount of pathogen that could be discharged from a site
- Minimum distances between sites to reduce transmission via hydrographic connectivity

Building a Framework

Screening Models and Research Models The models reviewed above address different components of aquaculture carrying capacity, focusing mainly on production and environmental effects, including disease aspects. Additionally, they consider different scales in time and space and range from statistical models to spatially discrete representations, which may (e.g., hydrodynamic models) or may not (GIS) be time varying. It is useful in this context to distinguish between screening models and research models.

Screening models typically use a limited set of inputs and provide highly aggregated outputs, such as an index of suitability or an environmental scorecard. Examples include a comparison of ammonia excretion by caged salmon compared to tidal flushing [57] and the production of biodeposits compared to tidal removal for suspended mussel culture [23].

Models of this type (e.g., FARM, [4]; POND; Fig. 9) are easy to use by the management community and provide a quick diagnosis for a specific site, or a generic overview comparison for multiple areas.

Models that are complex to apply (and usually lengthy and complex to develop and implement) may be termed research models and are of limited practical use in day to day management. Partly, this is due to the knowledge required for parameterization, volumes of data involved, and substantial requirements in processing and interpreting results. This does not mean that the results of such models do not have a clear application for management, but operating them may be beyond the scope of many institutions.

The concept of a single overarching model, able to provide answers across a range of space and time, has been shown repeatedly to be unsound. Just as software suffers from feature creep [58, 59], stand-alone models tend to become increasingly overparameterized, partly in an effort to better match reality and partly in an attempt to solve per se what should really be approached with a combination of models.

A more promising alternative is to combine GIS, dynamic models, network models, and remote sensing tools as appropriate to deal with questions that range from the impact of a HAB event on a salmon cage at the scale of days to the economic success of 10 years of mussel farming.

An increase in model complexity does not necessarily equate to increased accuracy [60], whether in physical or biological models. In both cases, the scale at which predictions may be made is limited by our incapacity to accurately predict the weather. As a consequence, model resolution and accuracy are limited by key drivers such as river flows, salinity patterns, and water and air temperature, which impact metabolic rates, algal blooms, turbidity, spawning, or larval dispersal.

Models in the Context of Integrated Coastal Zone Management Carrying capacity models for aquaculture are useful in their predictive capability and therefore in management of both cultured biomass as well as location. Spatially resolved models are particularly notable in this context. Within the catchment, this

may be addressed by means of GIS (see, e.g., [61]) and can be enhanced through a combination of dynamic simulations and spatially resolved models.

Aguilar-Manjarrez and Nath [89] performed an extended analysis of the potential for fish aquaculture in Africa, based on GIS models, using a resolution of 3 arc minutes (25 km^2 at the equator). For small-scale operations, suitability was based on water requirements, soil and terrain, availability of feed inputs, and farmgate sales projections. This analysis was also carried out for larger, commercial farming and concluded that for the three species considered (Nile tilapia, African catfish, and carp), about 23% of the area of continental Africa scored very suitable for both types of farming. These authors did not explicitly consider environmental effects of fish farming, probably because that analysis is best performed regionally or locally, as part of detailed site selection, but the modeling tools for addressing these impacts are available today.

GIS models have also been combined with remote sensing to assess aquaculture opportunities, for example, for crab and shrimp in the Khulna region of Bangladesh [62]. In this case, the focus was on gross production, economic output, and employment, and discussed species suitability with respect to factors such as salinity distribution and freshwater availability. Once again, the environmental externalities of the different types of culture were not included but can be modeled to provide a more complete picture for decision support, including externality costs.

Figure 12 shows the Jaguaribe estuary, in the state of Ceará, northeast Brazil. As part of the application of the ASSETS model to determine the eutrophication status of the estuary (Eschrique and Braga, personal communication, 2011), the nitrogen loading from 1,200 ha of shrimp farms, located between the city of Aracati and the dunes fringing the beach, was determined using POND.

The contribution of shrimp farming to the nitrogen load was estimated to be of the order of 60 t $year^{-1}$, roughly equivalent to 20% of the total loading, or about 15,000 PEQ.

Screening models of this kind are simple to use and help water managers in developing countries to address the challenge of multiple uses and nutrient sources to the coastal zone and to make better decisions with respect to site selection and waste treatment. They can also be included in a more general catchment modeling approach, combining their outputs with hydrological models such as the Soil and Water Assessment Tool (SWAT) model (e.g., Nobre et al. [11]).

In open water, including semi-enclosed systems such as estuaries and bays, because spatially resolved models incorporate physical circulation, they are potentially useful for other aspects of coastal zone management.

There are of course a variety of possibly impactful activities in the coastal zone including eutrophication, fisheries and fish processing, contaminant input, resource extraction, and transportation. There are inevitably competing uses of the water and bottom, and making predictions about aquaculture in isolation is insufficient. Water and sediment quality standards applied over large spatial scales help to apply objectives that may be seen as ecosystem-based management. The implementation of these objectives is achieved through marine spatial planning. The implication of planning is that predictions can be made to anticipate overlaps, conflicts, and cumulative impacts of various activities.

Although models exist for these other activities, particularly those acting through eutrophication, the models need to interact coherently, and their outputs should be tied together in a way that is useful for management decisions. Two essential features of this integration are physical models that unify the transport of materials common to almost every process in the ocean and GIS to maintain data layers. The physical model establishes the spatial domain which can be either conserved, collapsed, or expanded within the GIS. At present, models run within GIS are necessarily simple and based on averaged values. For example, the AKVAVIS tool developed in Norway [63] utilizes a GIS with calculation of shellfish growth as well as fish farm effects on water quality at any location based on an inline model using depth, temperature, and other spatially located characteristics within the GIS [63].

Tironi et al. [24] utilized an open source circulation model to predict far-field deposition for Chilean salmon culture. An essential feature of their work was a GIS interface used to depict other coastal activities in light of hydrodynamics and dispersal of farm waste. Nobre et al. [11]) combined models of watersheds, aquaculture, and eutrophication to look at mitigation strategies for improving nutrification in Chinese bays.

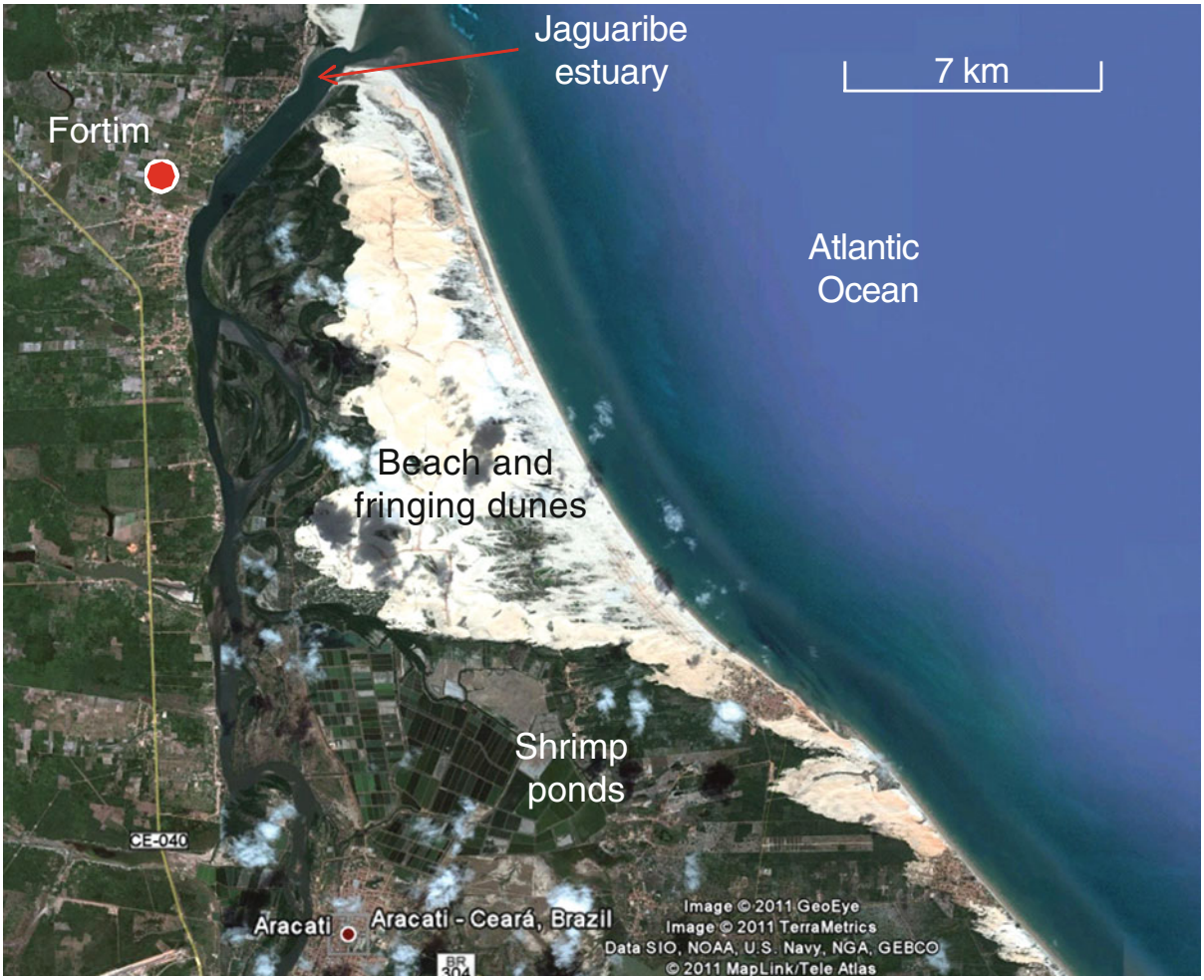

Carrying Capacity for Aquaculture, Modeling Frameworks for Determination of. Figure 12
The Jaguaribe estuary, in Ceará, NE Brazil. Shrimp farms occupy an area of about 12 km^2 and discharge the effluent into the estuary

In marine systems with aquaculture but lacking other activities (e.g., some Norwegian fjords), the culture model may form the basis of the decision support system. In Lysefjord (southern Norway), a pump was used to transport water to depth where it enhanced diffusion of nutrient from below the thermocline to the euphotic zone [90]. The increase in primary production was used as a food source for cultured mussels. A model was employed to determine the best location for the upweller as well as the mussels in order to benefit from increased primary production, balancing the increase in new production with mussel removal to maintain chlorophyll within its natural limits. This example is of interest because the ecosystem was truly managed in terms of bottom-up nutrient supply, new production, grazing in terms of mussel culture, and marine spatial planning optimized for the extent and level of shellfish culture.

As more types of activities are added to decision support tools, one approach is to use GIS as a wrapper for model outputs produced as layers. Decision support comes from ancillary software with features such as portrayal of alternative land uses, exclusion of protected areas, weighting of valued features and habitats, and economic analyses. Several initiatives have been undertaken in this vein, with the incorporation

of simulation models mostly in the initial stages of progress. Examples which have freely available ArcGIS extensions include NatureServe Vista (natureserve.org) and Marine InVEST (naturalcapitalproject.org). There are different emphases in the various projects, including conservation, community engagement, ecosystem services, and land use, in addition to water quality issues.

Among these, Marine InVEST seeks to maintain ecosystem services in the context of activities such as fisheries, aquaculture, renewable energy, and recreation [64]. Input information ranging from oceanographic data to species distribution is used in various models to consider outputs in terms of ecosystem services provided, traditional model results (e.g., water quality), and socioeconomic valuation (Fig. 13).

We note the importance of models other than those based on eutrophication and water quality. For example, some of the same spatial data used to model aquaculture impacts can be used to predict the location of sea grasses or species at risk [65, 66]. Protected areas or buffer zones may then become part of the plan. In this way, critical habitat and biodiversity are also considered along with aquaculture siting. Moreover, these decision-support frameworks can be used in public forums to incorporate community input, as has been done with protected area planning via MARXAN GIS [67]. In practice, these are few examples of models used to this extent, but it provides a very useful management shell in which to consider aquaculture submodels.

The Other 50% of the Problem At present, two major components of carrying capacity, the social and governance aspects, are not amenable to mathematical modeling (Fig. 5); they are nevertheless fundamental areas for aquaculture management.

The social pillar, from the perspective of social acceptance of aquaculture and, in particular, of the definition of limits to industry growth, has been discussed, for example, by Byron et al. [18]. Stakeholder dialogue, understanding of terms and concepts, and the simple fact that opinions can be voiced during the decision-making process are major contributors to generate consensus. The tools employed include

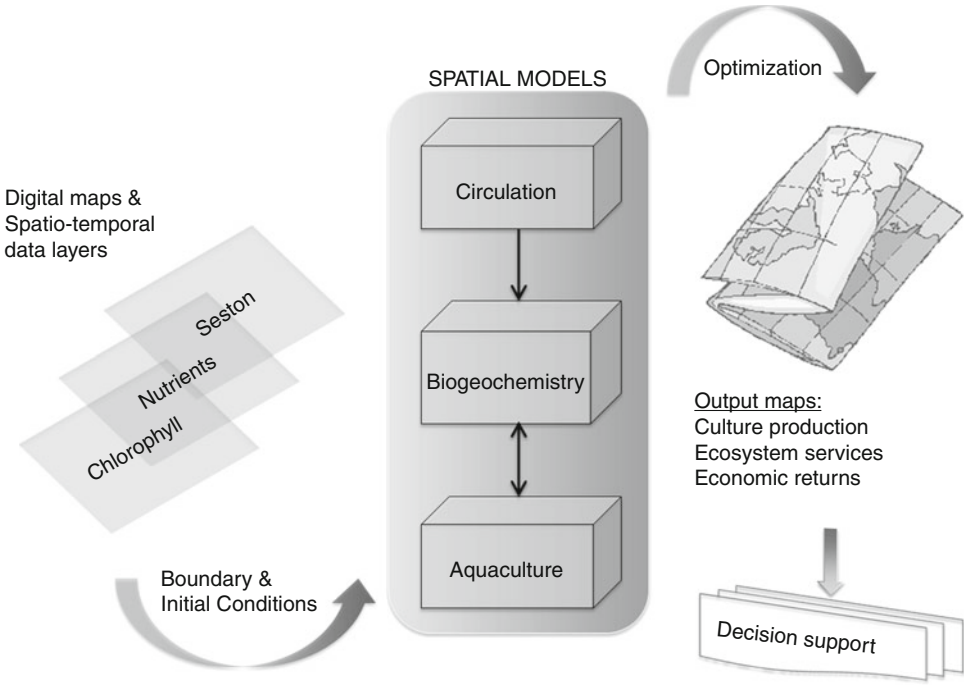

Carrying Capacity for Aquaculture, Modeling Frameworks for Determination of. Figure 13
Models for different purposes are linked through input data layers that are used to build scenarios about management actions (e.g., restoration of eelgrass, increase in aquaculture) and climate change (e.g., sea-level rise, water temperature)

questionnaires, meetings, and presentations of different sides of the issue. Simulation models can help inform those discussions by, for example, providing quantitative data on development scenarios but social positions often have a strong emotional component.

The governance pillar plays a major role in the assessment of carrying capacity. Table 1 shows key aspects of the human interaction in aquaculture and highlights the consequences of poor practices and governance.

The issues identified have consequences that vary in severity, from a reduction in revenue and profit to major outbreaks of disease and the loss of aquaculture resources across large areas.

Because the effects of human mismanagement can be so far reaching, it is important to discuss to what extent modeling frameworks can be used to assist the farmer and the water manager. The eight topics in Table 1 fall under the heading of governance (here taken to include self-regulation by farmers and farmers' associations, as well as legal instruments, policy, and implementation), but only three (dark blue) can benefit directly from recommendations from

Carrying Capacity for Aquaculture, Modeling Frameworks for Determination of. Table 1 Key issues in culture practice, time frames, and potential consequences (color coding reflects the extent to which models can be applied: *black* – substantial; *dark red* – reasonable; *light red* – inapplicable)

N°	Topic	Time frame	Issues/consequences	Examples
1.	Species selection	Prior to cultivation	Imported exotics, disease, proliferation	Pacific oyster, now considered invasive in the Netherlands; *Perkinsus* (dermo) and MSX, U.S. East Coast
2.	Seed purchase	Start of cultivation	Disease from imports, stable broodstock	Herpes virus spreading in oysters across Europe
3.	Relaying	Variable	Disease spread	Transmission of Herpes in oysters across Europe, ISA in Chilean salmon
4.	Stocking (farm or pond scale)	Critical periods	Overstocking can lead to: mass mortalities due to dissolved oxygen depletion, other environmental factors, and stress-related disease outbreaks	Whitespot Syndrome Virus (WSSV) in Penaeid shrimp, *Perkinsus* in clams
5.	System-wide carrying capacity	Months to years	If carrying capacity is significantly exceeded: harvest reductions, disease outbreaks, economic hardship, system collapse, long recovery cycles, long-term loss of resource	Marennes-Oléron, France, longer oyster culture cycles; Sacca di Goro, Italy, mass mortality of Manila clam; Qinshan, Fujian province, China, 50,000 fish cages (yellow croaker), mass mortality
6.	Feeding practice	Culture cycle	Ecologically damaging practices with ecosystem consequences, e.g., overfeeding of caged fish and benthic hypoxia	Fertilization of intertidal/subtidal areas in China to promote seaweed growth, increasing yields of commercial products (seaweed, gastropods); use of juvenile fish as fish meal for cage culture in parts of Asia
7.	Spatial distribution of culture	Culture cycle	If inappropriate, e.g., by combining year classes in shellfish, more labor-intensive, greater impacts on the ecosystem, e.g., through sediment reworking	Clam culture in southern Portugal
8.	Lease structure	–	Fragmented/inexistent lease structure, smallholdings governance issues, due to multiple stakeholders	Pond culture in Thailand (average freshwater pond: 0.28 ha); Clam culture in southern Portugal (average lease: 0.15–0.5 ha)

simulation models, addressing stocking density and feeding practices.

Five of the issues identified introduce disease-related problems, and whereas procedures such as relaying, or seed import from contaminated sources, are strictly within the remit of good governance, models can to some extent assist in predicting the likelihood (i.e., risk), spread, and establishment of diseases, if present within an aquaculture area.

Regulations enacted to control spread of diseases can directly mandate what species and culture practices, stocking densities, etc., are permitted within a zone/region. Firstly, this would include planning applications assessments that would consider, among other factors, how siting a farm may potentially adversely affect other aquaculture operations located in that area, as well as potential effects on wild animal populations. In some cases, e.g., in Chile, regulations have been enacted that specify minimum distances between farms.

There is also an increasing move by some large-scale industries, as part of developing common codes of practice, to manage farms to minimize the effects of disease on production. These codes can include restricting stocking densities, production on farms, specifying minimum allowable distances between farms, and introduction of mandatory fallowing periods between production cycles. All these are measures that would theoretically constrain carrying capacity, at least in the short term, but might well increase the overall sustainability of the industry in the zone or region in the longer term. Although these may not be enforced by government regulations when first developed (e.g., they are often "voluntary codes"), those signing up may be entering legally binding agreements. These codes may then be used as the basis to develop more formal regulatory frameworks in the future at the local, national, and even supranational level.

Regulation can also influence the carrying capacity of a zone or region both directly and indirectly. In particular, to help control the spread of diseases between countries, the OIE aquatic animal code [91] lists a number of infectious aquatic animal diseases that are generally considered untreatable, pose a significant threat to aquaculture and/or wild fish populations, and are not widely distributed (e.g., are exotic to most countries where the species they affect are farmed). Countries and regions also have laws and regulations to prevent the entry and, where pathogens do gain entry, specify measures for their control and eradication. For instance, Directive 2006/88/EC lays down, for European Member States, the required minimum animal health requirements, disease prevention, and control measures for aquaculture animals and products.

Eradication of a disease from a country or zone may involve extensive depopulation of affected farms and not restocking them until it is confirmed that the risk from disease is significantly reduced. This has obvious short- and long-term consequences on the carrying capacity of the affected species in the affected areas. For example, following detection of the notifiable viral disease Infectious Salmon Anemia (ISA) on an Atlantic salmon farm in Chile in 2007, the disease spread throughout the salmon industry [92]. The effects were dramatic. It is estimated that salmon production in 2010 was little more than 98,000 t, down from 386,000 t in 2006 [93]. With the 1.5–2.5-year production cycle for salmon, these effects will be felt for years to come, with estimated smolt release in 2009 only 10% what it was in 2007 [94]. It is estimated that, compared to production in 2007, levels will be reduced cumulatively by at least 700,000 tons during the period 2009–2011, with their value reduced by more than two billion USD.

Disease controls can restrict the types of aquaculture activity that are permitted, or are practically possible, within a zone or region. Here, the constraints to carrying capacity are often opportunity costs, with fish not reared in a particular area because of potential disease risks. The effects can be quite subtle. For instance, in the UK, controls in place to restrict the spread of bacterial kidney disease are considered by some sectors of the rainbow trout farming industry to adversely affect their operations at the expense of the larger Atlantic salmon industry that has generally supported the maintenance of these controls. This would also include the effects of restrictions placed on the movements of live fish and ova between countries that limit the opportunities to farm those species in other countries.

Finally, societal acceptance of aquaculture activities may be influenced by disease risk concerns, particularly to wild fish stocks. This is perhaps best illustrated by sea lice spread to wild fish. There is additional public

concern as to the effects on the environment of use of chemical treatments. In particular, there is strong resistance to fish farming in many remote and pristine environments due to fears they may adversely affect local ecosystems. Increased public awareness of welfare issues in aquaculture may also lead to practices that reduce the incidence of disease as a consequence.

Blueprint for a Model System

There are considerable challenges in selecting and combining different types of models, each of which plays a particular role, for carrying capacity assessment. A number of models are available, many of which reviewed above, but the level of usability varies widely, as does the capacity of one model to "speak" to another. This comes about through the "one tool" syndrome: If your only tool is a hammer, all your problems are nails. One tool, i.e., one model, may be fine for a particular level of analysis, but it will be incapable of doing all the work.

For instance, a local-scale model such as DEPOMOD [36], MOM [68], or FARM [4] will need current velocity fields supplied either by field measurements or by other types of models. Equally, it will not provide a robust answer with respect to system-scale carrying capacity. Even at the farm scale, such models do not consider the interactions among farms, although the siting of a new farm in a region will inevitably affect environmental conditions and production in existing farms. These changes will then feed back, so that the original farm-scale assessment will change because the model input data will change.

Figure 14 illustrates this difference for mussel culture in Killary Harbour, Ireland, by comparing two models at differing scales [35]. EcoWin2000 (E2K) is an ecological model applied at the system scale, whereas FARM simulates production and environmental carrying capacity at the local scale. Both models can be used to perform a marginal analysis [4] to determine stocking densities that lead to optimal profitability. This is extremely useful for licensing purposes since farms often maximize income rather than profit (i.e., aim for the highest TPP). It can be seen that for a coastal or semi-enclosed system, there appear to be significant differences between the results for the system-scale model, where the dotted line indicating highest TPP (which exceeds the seeding density of maximum profit) occurs at a density 7–8 times greater than the present situation. FARM, however, which deals only with the local scale, determines the end of stage 2, i.e., highest TPP, as around X15 density. This is because (1) E2K runs multiple production cycles, typically for periods of 10–20 years, i.e., the ecosystem model reports what is actually harvested, whereas

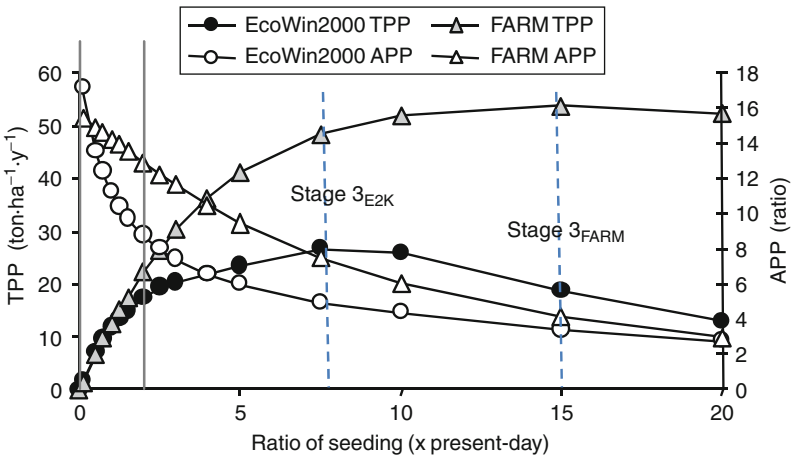

Carrying Capacity for Aquaculture, Modeling Frameworks for Determination of. Figure 14
Impacts of different mussel-stocking densities on total physical product (TPP, harvestable biomass) and average physical product (APP, the ratio between seeded and harvested biomass) as simulated by EcoWin2000 (system scale, per unit of cultivated area) and FARM (single farm) for Killary Harbour, Ireland (Adapted from [35])

FARM reports what is harvestable over one cycle, and (2) FARM does not account for interactions among farms, whereas E2K considers the farms in the whole water body.

The following set of properties is desirable when assembling a modeling system to address aquaculture carrying capacity:

1. No single model solves all problems. Overparameterization and code bloat only make matters worse.
2. Models should only be as complex as the problem requires. In other words, as simple as possible. Increased computational power is no excuse for unnecessary complexity.
3. Models should be able to work independently, present value in doing so, and add further value when working in conjunction with other models.
4. Models should define exactly what problems they can address, as part of the overall questions for an ecosystem, rather than the opposite.
5. Any model in the system must be able to receive input from data or from other models and be able to supply outputs in a form that can be easily used by other models.
6. Different models are appropriate for different scales in space and time. Carrying capacity assessment may require scales as short as a tidal cycle (e.g., for intertidal culture of clams) and as long as a decade (e.g., for coupling ecological models with economic models).
7. Models share a challenge with field sampling with respect to the conversion of data (measured or modeled) into information that is useful for managers; the use of screening models, or other approaches that help to distil data into meaningful information, is a vital component of any system.

Figure 15 shows an example of such a multi-model framework for investigating the role of bioextraction by oysters, clams, and ribbed mussels as part of a nutrient control strategy for Long Island Sound. The various models chosen conform to the seven properties described above.

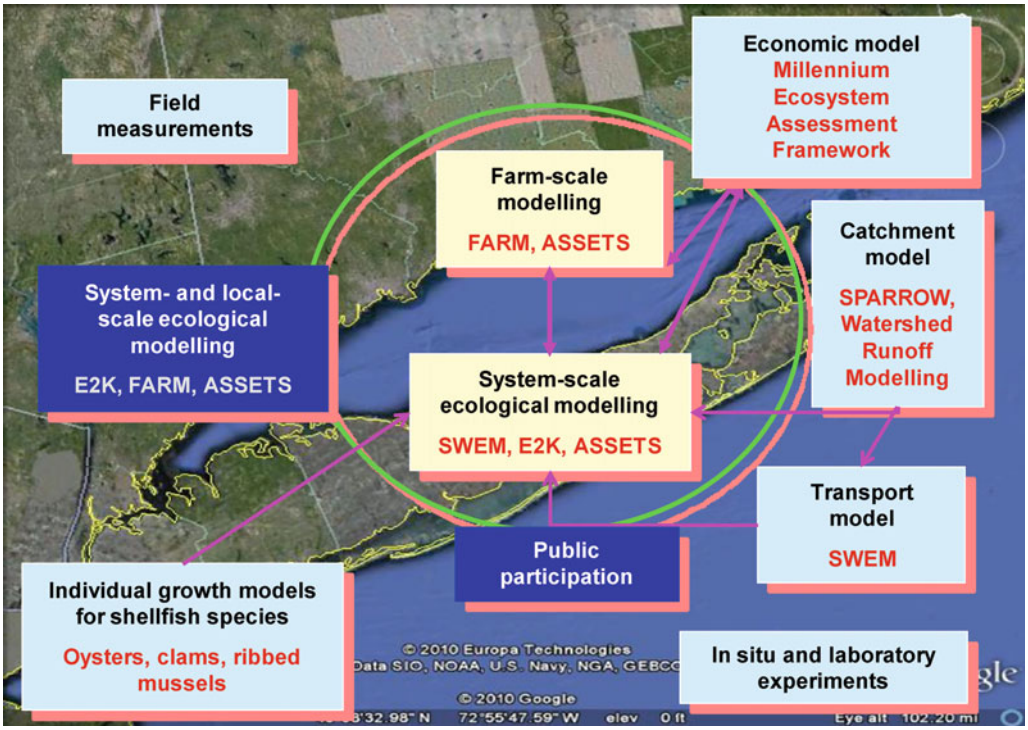

Carrying Capacity for Aquaculture, Modeling Frameworks for Determination of. Figure 15
Modeling framework: the REServ shellfish bioextraction project, Long Island Sound, USA (NOAA/EPA REServ Project)

Previous applications of this kind of framework include the SMILE project in Northern Ireland [19] and the SPEAR project in China ([69], Nobre et al. [11]).

A different kind of multi-model framework has been developed by Kapetsky et al. [70], through the application of various types of remotely sensed data in a GIS system, incorporating variables such as sea surface temperature, current speed, and chlorophyll *a*. In the example shown in Fig. 16, current speeds of 0.1–1 m s^{-1} are combined with suitable depth ranges for fish cages and shellfish longlines. High current speeds are problematic for both culture structures, due to excessive hydrodynamism, and finfish production, due to higher metabolic costs and lower yields; very low current speeds may cause sediment organic enrichment and quality loss for certain species.

Quantification of suitable areas indicates that 123 countries have at least 100 km^2 within their exclusive economic zone that meet these criteria.

For an annual production of 1 kg m^{-2} $year^{-1}$, this corresponds to 10^7 t $year^{-1}$ of aquatic products. This analysis has been further refined by considering distance to port, a key economic consideration for offshore aquaculture, which will considerably reduce this estimate. The same applies to other factors, such as marine protected areas. An assessment of spatial potential (a component of *production* carrying capacity) was executed at a finer scale for selected areas in Canada, Chile, Ireland, and Norway (Fig. 17). For a number of specific locations (farms) in these four countries, the time required for growing an adult salmon was then determined using a dynamic model [71], forced by remotely sensed sea surface temperature. In this case, the model end point was a particular fish biomass, rather than a specific cultivation period.

It is easy to see how this kind of coupling can be leveraged, for example, by introducing the effect of current speeds on metabolic requirements, using economic models to analyze the trade-offs between biomass and market price (lower yield, higher product

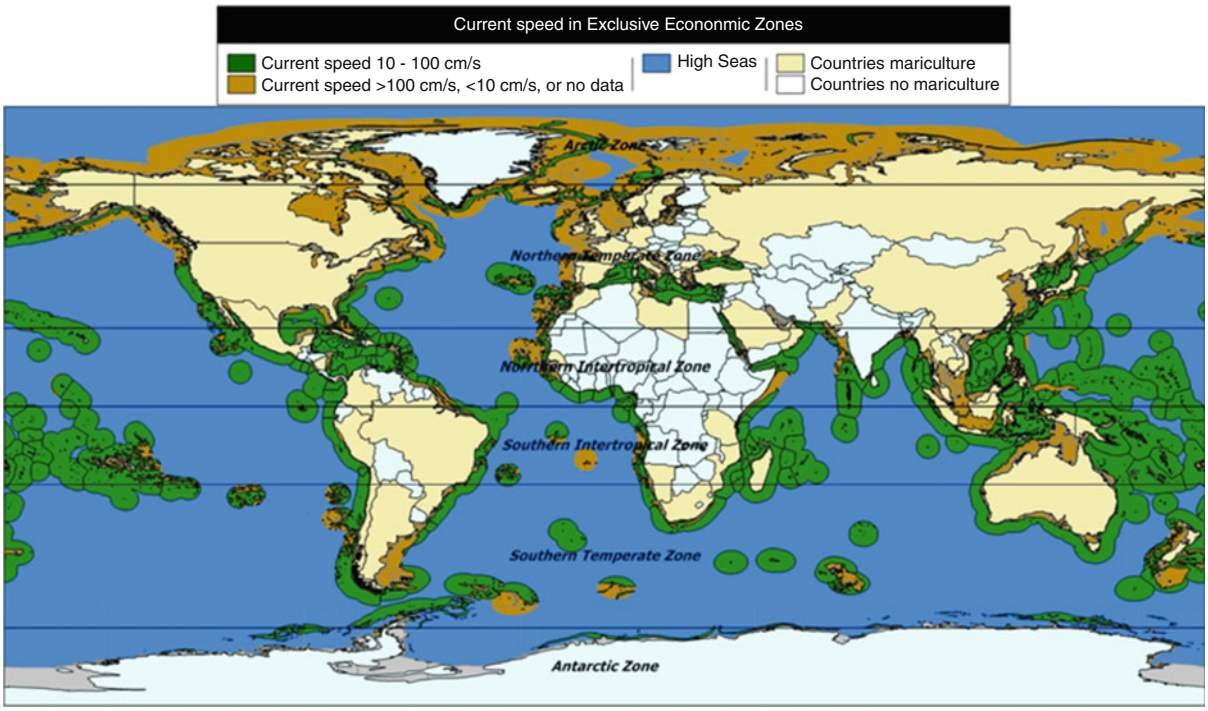

Carrying Capacity for Aquaculture, Modeling Frameworks for Determination of. Figure 16
World ocean areas suitable for offshore aquaculture (From [70])

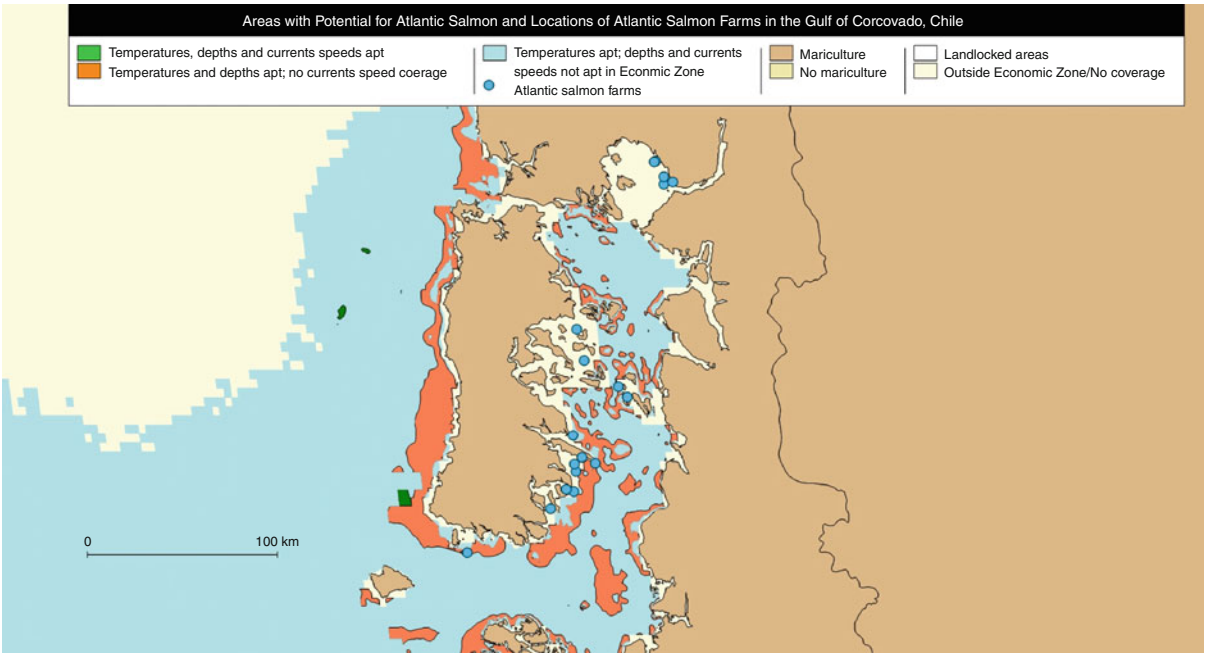

Carrying Capacity for Aquaculture, Modeling Frameworks for Determination of. Figure 17
Areas in Chiloé Island, Chile, with temperature apt for Atlantic salmon mariculture (22–32°C) and depths (25–100 m) and current speeds (10–100 cm/s) apt for submerged cages (From [70])

quality), and using models such as FARM to quantify environmental effects, considering factors such as current speed and depth of site, both of which are readily available.

It is clear from this discussion that different modeling products and services are required for different markets. Water managers or planners may for instance be concerned with bay-scale carrying capacity, taking into account the multi-sectorial context of aquaculture, i.e., integrating ecological models with marine spatial planning. Those types of models will help inform decisions on the conservation of wild populations and biodiversity and also provide support for licensing, legislative compliance, and source apportionment for managing pressures.

On the other hand, a farmer will probably be more focused on optimization of production, improvement of feed conversion ratios, and business profits. But increasingly, the environmental footprint of the farm, together with potential positive impacts, such as the role of shellfish in reducing eutrophication symptoms, will be of interest. In the European Union, with legislative requirements for Good Ecological Status by 2015 in all EU water bodies and Good Environmental Status in all marine waters by 2020, some of the modeling approaches and tools described above will undoubtedly be in demand to perform self-assessments and to resolve conflicts.

As models of disease risks evolve, and become better integrated with other types of models, these too will be in demand for siting decisions.

Some of these models will be products, some will be services, and some will be a combination of both. The ways in which those markets develop and the future directions in which the science and technology may evolve will be discussed in the final section of this entry.

Future Directions

Support for an Ecosystem Approach to Aquaculture

Application of the EAA on a worldwide scale requires the harmonization of (1) environmental, (2) social, and (3) multi-sectorial planning objectives [8]. These three principles and their relative weights differ substantially across world regions, and it is not feasible

from a social and political standpoint to establish uniform compliance with respect to limits and thresholds.

The only solution is to define appropriate approaches, which within particular world regions define a gradient in relative terms, assessing EAA in terms of the principles stated above. The three principles of EAA can be mapped onto the four pillars of carrying capacity and illustrated as the overlap of these [16]. The importance of each theme represented will vary regionally and will evolve through time based on societal cues.

It is clear that aquaculture in Europe and North America is more closely aligned with EAA, and the present effort in marine spatial planning will only reinforce that. It is also clear that aquaculture production in developed countries will grow little, and that consumer demand in these regions is satisfied in large part through imports (Fig. 18).

In the United States, 84% of aquatic products are presently imported, of which 50% are from aquaculture. This has resulted in a nine-billion-USD seafood trade deficit [82]. Table 2 presents a summary of the main issues that are presently considered in aquaculture carrying capacity and site selection, together with what may constitute future components for assessment. Models play a key role.

Since developing nations supply the bulk of farmed aquatic products, will continue to do so, and will probably increase their contribution, it is critical that state-of-the-art tools are available to ensure sustainability in the countries where they are most needed.

Which developing countries and which types of culture should be priorities for the application of such models? From an EAA perspective, those that have the highest impact on the environment are the most promising candidates. Kapetsky et al. [73] used FAO production statistics at country environment level (freshwater, brackish water and marine) to estimate the intensity at which aquaculture was practised in each of those environments. A knowledge of the species being cultured can reveal the production systems and their associated impacts in a very general way. The approach outlined above can be refined to focus more closely on modeling needs by considering the potential impacts by species and culture systems in countries in which production data by species are reported.

Dissemination of models can be passive (e.g., packages freely accessible via the Internet) or active

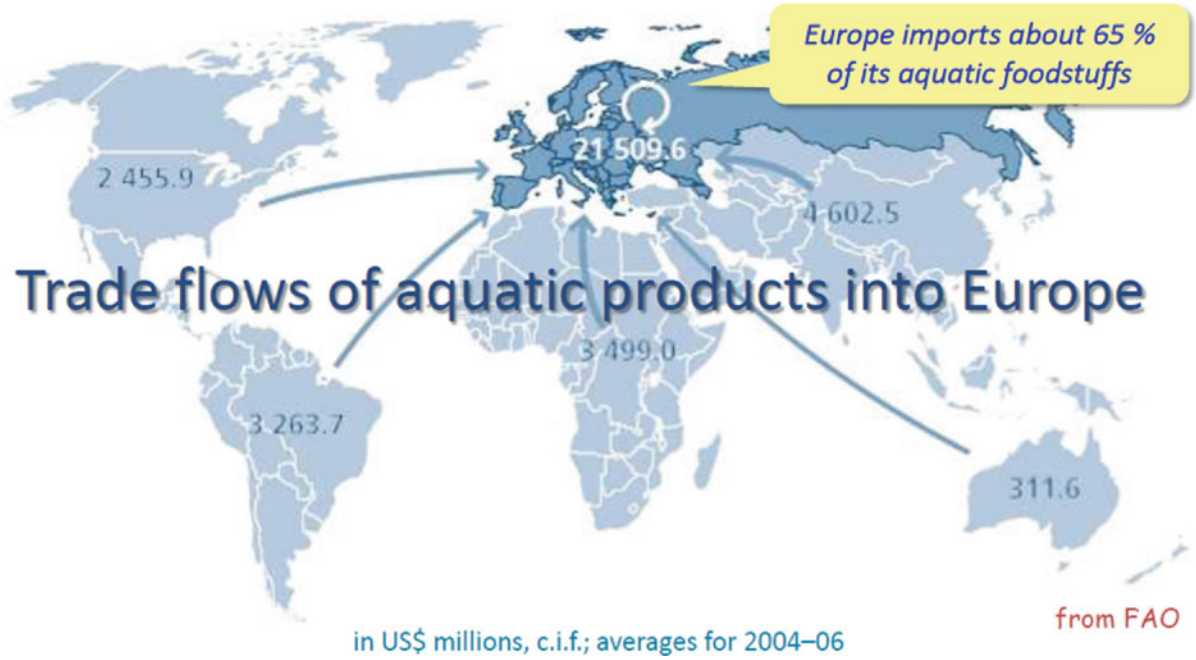

Carrying Capacity for Aquaculture, Modeling Frameworks for Determination of. Figure 18
Trade flows of aquatic products into Europe [72]

Carrying Capacity for Aquaculture, Modeling Frameworks for Determination of. Table 2 Novel management approaches (Adapted from [10])

Topic	Now	Tomorrow
Feed based (cage, pond)	Site selection based on holding capacity (cages), wastewater minimization (ponds)	Integrated model systems, risks, welfare, and disease. Holistic indicators
		LCA: inefficiencies and eco-labeling
		Mechanistic and statistical models
		Data assimilation models
Shellfish farming	Large areas	Economic sustainability, ecology and economics, disease
	Focus on production and social carrying capacity NIMBY, (Not in my backyard) NIMTO (Not in my term in office)	Coupled GIS expert systems including xenobiotics, HAB, etc.
		Model uncertainties in yield
		Early warning
Integrated multi-trophic aquaculture	Optimize production	Integrated coastal zone management
	Reduce negative externalities	Simulate species combinations
		Full economic assessment
		Combine GIS, remote sensing, and modeling

(training courses and workshops by region or by country). In both cases, it is essential to establish the technical capacity, level of interest, and financial commitment of the audience and the status of the Internet as a communications and data pipeline for technical support in each country. The focus should not be on developing countries alone because (1) virtual technology specialists in developed countries may be in a position to aid dissemination and (2) companies established in developed countries often have aquaculture operations in developing countries, and could therefore also help to bridge the gap.

Looking into the Crystal Ball

The Thematic Review "Virtual Tools for Aquaculture," presented at the FAO Global Aquaculture Conference in 2010 [10], encapsulates much of our thought on the future of models in aquaculture. The final points in this entry are drawn from that review.

The aquaculture industry is going to be affected by many different issues and trends over the coming years, often operating concurrently, sometimes in unexpected ways, and producing changes in the industry that may be very rapid indeed. Mathematical models will play an important role in addressing many of these, particularly in the following areas:

1. Information exchange and networking are going to accelerate the use of virtual technology and decision-making for problem solving to support industry growth. Web-based access to real-time information will further accelerate this growth.
2. Links between industry and research centers will become more effective responding to objective-led demand for virtual technology-driven RTD.
3. Strategic alliances will need to be reinforced or created for the implementation of virtual technology for aquaculture in developing countries, for example, FAO and WorldFish Center are working in many of the same target countries, and this could facilitate the transfer of research outcomes on virtual technology to end users. The same applies to collaborative research with third countries mediated, for example, by the European Union, the United States of America, and Canada.
4. Many virtual technology tools will need to be more production and management oriented. And even if

attractive and promising, these tools will have to be adapted to local realities and conditions to really become useful (and used) in the future. This requires a compromise with respect to ease of use, data requirements, and scientific complexity. Many such tools will evolve from service to product, requiring academic developers to accept a loss of control in conditions of application, as a natural trade-off (and inherent risk) of product maturity.

A number of key thematic and technical areas where models for aquaculture are currently incipient, and expected to develop strongly in the next decade or so, have been identified below. In all the examples, such models will contribute to an overall modeling framework, by integrating and complementing existing tools.

Disease Disease in cultivated aquatic species is a major source of concern, yet disease modeling is still relatively underutilized in these systems though its worth has clearly been demonstrated in several studies. However, while epidemiological theory predicts that host density thresholds may be an important part of host–parasite dynamics, clear empirical examples are rare, as much in aquaculture as in other studied agricultural systems. It is suggested that this is not evidence that host thresholds do not exist, rather that statistical difficulties arise with confounding factors or inadequate data. Evidence here is afforded from much better-understood and more data-rich systems, for example, human measles [95–97], where there is compelling evidence on the effects of host density on the likelihood of disease outbreaks taking place within populations.

One of the major limitations in aquatic systems, however, is that the routes by which pathogens are transmitted and their relative contributions to an epidemic are often not understood. If transmission is incorrectly specified, there can be substantial consequences to estimates of N_T. Additional experimental and field data are required to identify and quantify transmission routes for many aquatic animal pathogens, if prediction of the effects of host density on disease incidence is to be made through modeling. To facilitate this, increasing emphasis is required on the use of real-time data acquisition combined with models for real-time analysis and short-term prediction of animal welfare. It is expected that such systems will become cheaper and more generalized, and that some of the indicators and trends will find application at longer timescales, albeit by means of a probabilistic approach.

A further potential limitation of the models currently used is their inability to predict across and link scales from the processes occurring within a tank to the transmission across and then between sites. Methods of investigating disease processes through these metapopulation approaches should be investigated further.

To date, only a few models have been developed to simulate pathogenic infections of shellfish with respect to physiology, for example, Powell et al. (1996) for the American oyster *C. virginica*, but with widespread concerns about relaying, susceptibility, and mortality, models focusing on a more mechanistic approach will undoubtedly appear over the next decade.

Harmful Algal Blooms This is another area where little predictive capacity exists, except in the short term through the use of operational oceanography, relying on bloom identification and tracking. Management is at present reactive, and modeling of appearance and development of such blooms is in its infancy, due to the lack of an appropriate paradigm. Sensors such as targeted RNA probes (e.g., [74]), integrating handheld devices, or potentially deployed in situ and used in a networked framework will both help in early detection and management and contribute to the understanding of the underlying triggers. Considerable developments are also expected in remote sensing algorithms able to discriminate (at least) between HAB and nontoxic blooms (S. Bernard, personal communication, 2010).

Certification and Traceability The arrays of sensors that can be deployed at the farm scale to enable coupled monitoring and modeling are important for both product certification and traceability. The number, reliability, and accuracy of underwater sensors will increase, and the cost will decrease, both with technological developments and market growth.

Real-time data acquisition and interpretation will make it possible for consumers to visualize the whole "cradle to grave" cycle of an aquaculture product. For

instance, a batch of oysters may be "bar coded" to reveal the origin of seed and the entire environmental interaction over the culture period, including metadata and measured data on water quality, HAB events, condition (meat ratio) of the animals, and impact on their environment, for example, in terms of reduction of eutrophication symptoms through the indirect removal of nitrogen and phosphorus, or conversely the addition of particulate organic material due to biodeposition. Such sensors will typically be queried at a sub-hourly frequency, particularly if they are also used for welfare monitoring; this will easily allow importers, health inspectors, or consumers to perform verification and certification, and will provide an important contribution to both food safety and environmental awareness.

For the farmer, the existence of this kind of integrated coding will also help improve various aspects of culture practice and increase attractiveness of the business model to the key sector of insurance. For the consumer, such data will need to be presented in a comprehensible format, for example, in the form of a few indicators (Fig. 19).

Carrying Capacity for Aquaculture, Modeling Frameworks for Determination of. Figure 19
QR code for farmed shellfish, readable on any smart phone

Modeling with Data Scarcity Good data are required to support acceptable model predictions. The acquisition of high-quality data, with appropriate spatial and temporal resolution, is expensive and often beyond the scope of developing countries, except on a fairly limited scale. This, together with an often fragmented approach to the study of interacting ecosystems, in many cases driven by institutional barriers, presents a challenge to the application of models.

Improved mechanisms for data access, particularly for remotely sensed data, together with models that deal with uncertainty and risk, will contribute to conversion of sparse data into more meaningful information – although such an approach may be considered unsuitable in parts of the developed world, in many countries it will be a much better basis for decisions than the options that are presently used. In addition, it will promote a "virtuous cycle" toward more informed decision support and promote the use of better data and more sophisticated models, as the data become available to drive them.

A wide variety of models will benefit from this development because many models developed and tested for temperate systems need adjustment with respect to parameters, thresholds, and equations, when applied to tropical and subtropical systems.

Information Technology The last 5 years have seen a huge leap in various areas of distributed computing, all of which are expected to develop significantly in the coming years.

Three examples are presented here:

1. Web 2.0 now provides a large diversity of community- and corporation-based resources. Currently, over 7,000 items exist for aquaculture on YouTube – at the time of presentation of the VITAL Thematic Review [10] there were 1,800. For aquaculture modeling, that number has also quadrupled since 2010 and now stands at 75.
2. There is a strong trend toward the development and use of *Software as a Service* (SAAS), deployed on the web and competing with traditional desktop applications. This is incipient in the aquaculture world but can be seen, for example, in the WinShell application (http://longline.co.uk/winshell), which allows users to simulate individual shellfish growth

Carrying Capacity for Aquaculture, Modeling Frameworks for Determination of. Figure 20
Tidal prediction for the port of Mumbai using the Oceanus21 smart phone app (http://longline.co.uk/oceanus21). Ports can be automatically selected based on GPS coordinates and phone location

on line. Central to the development of this kind of application are Rich Internet Applications (RIA), which provide a full user experience and are an area of rapid growth [75]

3. Mobile computing is increasingly ubiquitous, and it is now possible to use models on many handheld devices, as illustrated in Fig. 20, which shows a tide prediction model for Mumbai, India. This kind of model might be used to help predict the yield in intertidal culture of bivalve shellfish.

The trend toward the increasing use of such devices, including for various real-time applications in aquaculture management, will increase. In parallel, the stand-alone server is rapidly being replaced by cloud computing, which will tend to make the circulation of data both easier and cheaper. Both elements will contribute to bridge the information divide between richer and poorer nations.

Computer access, literacy, and internet connectivity are significant barriers to entry for the population in the rural areas in developing countries, where aquaculture takes place. Over the coming decade, many aquaculture farmers will have their first contact with the World Wide Web by means of smart phones. Cell phones are ubiquitous even in remote areas and are much better adapted to local language and alphabet, which constitute other barriers in accessing technology.

The future of aquaculture is promising. It needs to be, given the world population growth expected in the next decades. Simulation models, particularly when used within appropriate frameworks, show enormous potential to inform and guide the future development of aquaculture, toward a world which is more socially responsible, more equitable, and more sustainable.

Acknowledgments

We are grateful to the EU FP7 COEXIST project, and to FAO, for the opportunity to develop many of the ideas presented here. We would like to thank B. Costa-Pierce for the opportunity to contribute to this volume, all our coauthors in the Virtual Tools for Aquaculture FAO report presented at the FAO Global Aquaculture Conference 2010, E.S. Braga and S. Eschrique for data on the Jaguaribe estuary, Ceará, Brazil, and S.B. Bricker and L. Ramos for comments on the draft. We thank H. Mildmay-White for design work on figures.

Bibliography

1. Frei M, Razzak MA, Hossain MM, Oehme M, Dewan S, Becker K (2007) Performance of common carp, *Cyprinus carpio* L. and *Nile tilapia*, *Oreochromis niloticus* (L.) in integrated rice–fish culture in Bangladesh. Aquaculture 262(2–4):250–259
2. Bacher C, Duarte P, Ferreira JG, Héral M, Raillard O (1998) Assessment and comparison of the Marennes–Oléron Bay

(France) and Carlingford Lough (Ireland) carrying capacity with ecosystem models. Aquat Ecol 31(4):379–394
3. Smaal AC, Prins TC, Dankers N, Ball B (1998) Minimum requirements for modelling bivalve carrying capacity. Aquat Ecol 31:423–428
4. Ferreira JG, Hawkins AJS, Bricker SB (2007) Management of productivity, environmental effects and profitability of shellfish aquaculture – the farm aquaculture resource management (FARM) model. Aquaculture 264:160–174
5. Jolly CM, Clonts HA (1993) Economics of aquaculture. Food Products, New York, 319 pp
6. Inglis GJ, Hayden BJ, Ross AH (2000) An overview of factors affecting the carrying capacity of coastal embayments for mussel culture. NIWA Client Report CHC00/69, Christchurch, New Zealand
7. McKindsey CW, Thetmeyer H, Landry T, Silvert W (2006) Review of recent carrying capacity models for bivalve culture and recommendations for research and management. Aquaculture 261(2):451–462
8. Soto D, Aguilar-Manjarrez J, Hishamunda N (eds) (2008) Building an ecosystem approach to aquaculture. In: FAO/Universitat de les Illes Balears Expert Workshop. 7–11 May 2007, Palma de Mallorca, Spain. FAO Fisheries and Aquaculture Proceedings, No 14, Rome, FAO, 2008, 221 p
9. Dillon PJ, Rigler FH (1974) A test of a simple nutrient budget model, predicting the phosphorus concentration in lake water. J Fish Res Can 31:1771–1778
10. Ferreira JG, Aguilar-Manjarrez J, Bacher C, Black K, Dong SL, Grant J, Hofmann E, Kapetsky J, Leung PS, Pastres R, Strand O, Zhu CB (2010a) Expert panel presentation V.3. Progressing aquaculture through virtual technology and decision-making tools for novel management. In: Book of abstracts, global conference on aquaculture 2010, 22–25 Sept 2010. FAO/NACA/Thailand Department of Fisheries, Bangkok, Thailand, pp 91–93
11. Nobre AM, Ferreira JG, Nunes JP, Yan X, Bricker S, Corner R, Groom S, Gu H, Hawkins A, Hutson R, Lan D, Lencart e Silva JD, Pascoe P, Telfer T, Zhang X, Zhu M (2010) Assessment of coastal management options by means of multilayered ecosystem models. Estuarine, Coastal Shelf Sci 87:43–62
12. Ferreira JG, Sequeira A, Hawkins AJS, Newton A, Nickell TD, Pastres R, Forte J, Bodoy A, Bricker SB (2009) Analysis of coastal and offshore aquaculture: application of the FARM model to multiple systems and shellfish species. Aquaculture 289:32–41
13. Silva C, Ferreira JG, Bricker SB, DelValls TA, Martín-Díaz ML, Yañez E (2011) Site selection for shellfish aquaculture by means of GIS and farm-scale models, with an emphasis on data-poor environments. Aquaculture 318:444–457
14. Sorgeloos P (2010) Resources, technologies and services for future aquaculture: a needs assessment for sustainable development. In: Book of abstracts, global conference on aquaculture 2010, 22–25 Sept 2010. FAO/NACA/Thailand Department of Fisheries, Bangkok, Thailand, pp 29–31
15. Swaminathan MS (2010) Aquaculture and nutritional security in a warming planet. In: Book of abstracts, global conference on aquaculture 2010, FAO/NACA/Thailand Department of Fisheries, Bangkok, Thailand, 22–25 Sept 2010, pp 4–6
16. Ferreira JG, Ramos L, Costa-Pierce BA (2010b) Key drivers and issues surrounding carrying capacity and site selection, with emphasis on environmental components. In: FAO expert workshop on aquaculture site selection and carrying capacity estimates for inland and coastal waterbodies. Institute of Aquaculture, University of Stirling, Stirling, UK, 6–8 Dec 2010
17. Byron C, Costa-Pierce BA (2010) Carrying capacity tools for use in the implementation of an ecosystems approach to aquaculture. In: FAO expert workshop on aquaculture site selection and carrying capacity estimates for inland and coastal waterbodies. Institute of Aquaculture, University of Stirling, Stirling, UK, 6–8 Dec 2010
18. Byron C, Bengtson D, Costa-Pierce B, Calanni J (2011) Integrating science into management: ecological carrying capacity of bivalve shellfish aquaculture. Marine Policy 35:363–370
19. Ferreira JG, Hawkins AJS, Monteiro P, Moore H, Service M, Pascoe PL, Ramos L, Sequeira A (2008) Integrated assessment of ecosystem-scale carrying capacity in shellfish growing areas. Aquaculture 275:138–151
20. Filgueira R, Grant J (2009) A box model for ecosystem-level management of mussel culture carrying capacity in a coastal bay. Ecosystems 12:1212–1233
21. Stigebrandt A (2011) Carrying capacity: general principles of model construction. Aquac Res 42:41–50
22. Tett P, Portilla E, Gillibrand P, Inall M (2011) Carrying and assimilative capacities: the acexr-lesv model for sea-loch aquaculture. Aquac Res 42:51–67
23. Grant J, Cranford P, Hargrave B, Carreau M, Schofield B, Armsworthy S, Burdett-Coutts V, Ibarra D (2005) A model of aquaculture biodeposition for multiple estuaries and field validation at blue mussel (*Mytilus edulis*) culture sites in eastern Canada. Can J Fish Aquat Sci 62:1271–1285
24. Tironi A, Marin VH, Campuzano J (2010) A management tool for assessing aquaculture environmental impacts in chilean patagonian fjords: integrating hydrodynamic and pellets dispersion models. Environ Mgmnt 45:953–962
25. Hargrave B (2010) Empirical relationships describing benthic impacts of salmon aquaculture. Aquacult Environ Interact 1:33–46
26. Brigolin D, Pastres R, Nickell TD (2009) Modelling the impact of aquaculture on early diagenetic processes in sea loch sediments. Marine Ecol Prog Ser 388:63–80
27. Findlay R, Watling L (1997) Prediction of benthic impact for salmon net-pens based on the balance of benthic oxygen supply and demand. Mar Ecol Prog Ser 155:147–157
28. Morrisey D, Gibbs M, Pickmere S, Cole R (2000) Predicting impacts and recovery of marine-farm sites in Stewart Island, New Zealand, from the Findlay-Watling model. Aquaculture 185:257–271
29. Probert PK (1984) Disturbance, sediment stability, and trophic structure of soft-bottom communities. J Mar Res 42:893–921
30. Abo K, Yokoyama H (2007) Assimilative capacity of fish farm environments as determined by the benthic oxygen uptake

rate: studies using a numerical model. Bull Fish Res Agen 19:79–87
31. Lee J, Choi K, Arega F (2003) Environmental management of marine fish culture in Hong Kong. Mar Pollut Bull 47:202–210
32. Symonds A (2011) A comparison between far-field and near-field dispersion modelling of fish farm particulate wastes. Aquacult Res 42:73–85
33. Skogen MD, Eknes M, Asplin LC, Sandvik AD (2009) Modelling the environmental effects of fish farming in a Norwegian fjord. Aquaculture 298:70–75
34. Chapelle A, Lazure P, Souchu P (2001) Modelling anoxia in the Thau Lagoon(France). Oceanol Acta 25:79–86
35. Nunes JP, Ferreira JG, Bricker SB, O'Loan B, Dabrowski T, Dallaghan B, Hawkins AJS, O'Connor B, O'Carroll T (2011) Towards an ecosystem approach to aquaculture: assessment of sustainable shellfish cultivation at different scales of space, time and complexity. Aquaculture 315:369–383
36. Cromey CJ, Nickell TD, Black KD (2002) DEPOMOD – modelling the deposition and biological effects of waste solids from marine cage farms. Aquaculture 214:211–239
37. Cromey CJ, Nickell TD, Black KD, Provost PG, Griffiths CR (2002) Validation of a fish farm waste resuspension model by use of a particulate tracer discharged from a point source in a coastal environment. Estuaries 25:916–929
38. Funge-Smith SJ, Briggs MRP (1998) Nutrient budgets in intensive shrimp ponds: implications for sustainability. Aquaculture 164:117–133
39. Ferreira JG, Zhu CB, Saurel C, Bricker SB, Vale C (2011) Modelling the role of bivalve shellfish in IMTA. Examples for shrimp ponds and offshore finfish cage culture. In: 103rd Meeting of the National Shellfish Association, Baltimore, March 2011
40. Lindahl O, Hart R, Hernroth B, Kollberg S, Loo L, Olrog L, Rehnstam-Holm A (2005) Improving marine water quality by mussel farming: a profitable solution for Swedish Society. Ambio 34(2):131–138
41. Boyd CE (2009) Advances in technologies and practice for land-based aquaculture systems: ponds for finfish production. In: Burnell G, Allan G (eds) New technologies in aquaculture: improving production efficiency, quality and environmental management, Chapter 32. CRC/Woodhead, Oxford, pp 984–1009
42. Bricker SB, Ferreira JG, Simas T (2003) An integrated methodology for assessment of estuarine trophic status. Ecol Model 169(1):39–60
43. Chopin T, Troell M, Reid G, Knowler D, Robinson S, Neori A, Buschmann A, Pang S, Fang JG (2010) Integrated-multi-trophic aquaculture (IMTA) – a responsible practice providing diversified seafood products while rendering biomitigative services through its extractive components. Aquaculture Europe 2010, Porto, October 2010
44. Neori A, Chopin T, Troell M, Buschmann AH, Kraemer GP, Halling C, Shpigel M, Yarish C (2004) Integrated aquaculture: rationale, evolution and state of the art emphasizing seaweed biofiltration in modern mariculture. Aquaculture 231:361–391
45. Ferreira JG, Zhu CB, Bricker SB (2009b) Eutrophication and aquaculture: la vie en rose? Eutrophication, integrated multi-trophic aquaculture, and top-down control. In: ASLO Aquatic Sciences Meeting, Nice
46. May RL, Anderson RM (1991) Infectious diseases of humans: dynamics and control. Oxford University Press, Oxford [Oxfordshire]. ISBN 0-19-854040-X
47. Begon M, Bennett M, Bowers RG, French NP, Hazel SM, Turner J (2002) A clarification of transmission terms in host-microparasite models: numbers, densities and areas. Epidemiol Inf 129:147–153
48. McCallum H, Barlow N, Hone J (2001) How should pathogen transmission be modelled? Trends Ecol Evol 16:295–300
49. Omori R, Adams B (2011) Disrupting seasonality to control disease outbreaks: the case of koi herpes virus. J Theor Biol 271:159–165
50. Green DM, Gregory A, Munro LA (2009) Small- and large-scale network structure of live fish movements in Scotland. Prev Vet Med 91:261–269
51. Werkman M, Green DM, Murray AG, Turnbull JF (2011) The effectiveness of fallowing strategies in disease control in salmon aquaculture assessed with an SIS model. Prev Vet Med 98:64–73
52. Thrush M, Peeler E (2006) Stochastic simulation of live salmonid movement in England and Wales to predict potential spread of exotic pathogens. Dis Aquat Organ 72:115–123
53. Jonkers ART, Sharkey KJ, Thrush MA, Turnbull JF, Morgan KL (2010) Epidemics and control strategies for diseases of farmed salmonids: a parameter study. Epidemics 2:195–206
54. Taylor NGH, Norman RA, Way K, Peeler EP (2011) Modelling the koi herpesvirus (KHV) epidemic highlights the importance of active surveillance within a national control policy. J Appl Ecol 48:348–355
55. Asplin L, Boxaspen K, Sandvik AD (2004) Modelled distribution of salmon lice in a Norwegian fjord. ICES CM/P:11,12 pp
56. Green DM (2010) A strategic model for epidemic control in aquaculture. Prev Vet Med 94:119–127
57. Gillibrand P, Turrell W (1997) The use of simple models in the regulation of the impact of fish farms on water quality in Scottish sea lochs. Aquaculture 159:33–46
58. Brooks FP (1995) The mythical man-month. Essays on software engineering. Addison-Wesley, London, 322 pp
59. McConnell S (1995) Achieving leaner software. IEEE Software, Nov/Dec 1995, 127–128
60. Uncles RJ, Peterson DH (1996) The long-term salinity field in San Francisco Bay. Cont Shelf Res 16(15):2005–2039
61. Nath SS, Bolte JP, Ross LG, Aguilar-Manjarrez J (2000) Applications of geographical information systems (GIS) for spatial decision support in aquaculture. Aquac Engin 23:233–278
62. Salam MA, Ross LG, Beveridge M (2003) A comparison of development opportunities for crab and shrimp aquaculture in southwestern Bangladesh, using GIS modelling. Aquaculture 220:477–494
63. Ervik A, Agnalt A-L, Hansen AA, Aure J, Bekkvik T, Døskeland I, Hageberg A, Hansen T, Karlsen Ø, Oppedal F, Strand Ø (2008)

AkvaVIS–dynamic GIS-tool for sitting of fish farms for new aquaculture species. Environmental quality requirements for new aquaculture species and Atlantic salmon. Tech Rep 10/2008. Institute of Marine Research, Bergen, Norway, in Norwegian, 90 pp
64. Lester SE, Mcleod KL, Tallis H, Ruckelshaus M et al (2010) Science in support of ecosystem-based management for the US west coast and beyond. Biol Conserv 143:576–587
65. Fonseca M, Whitfield PE, Kelly NM, Bell SS (2002) Modeling seagrass landscape pattern and associated ecological attributes. Ecolog Applic 12:218–237
66. Franklin J (2010) Mapping species distributions: spatial inference and prediction (Ecology biodiversity and conservation). Cambridge University Press, Cambridge, 338 pp
67. Watts ME, Ball IR, Stewart RR, Klein CJ, Wilson K, Steinback C, Lourival R, Kircher L, Possingham HP (2009) Marxan with Zones: software for optimal conservation based land- and sea-use zoning. Environ Modell Software 24:1513–1521
68. Ervik A, Kupka-Hansen P, Aure J, Stigebrandt A, Johannessen P, Jahnsen T (1997) Regulating the local environmental impact of intensive marine fish farming. I. The concept of the MOM system (Modelling-ongrowing fish farms-monitoring). Aquaculture 158:85–94
69. Ferreira JG, Andersson HC, Corner RA, Desmit X, Fang Q, de Goede ED, Groom SB, Gu H, Gustafsson BG, Hawkins AJS, Hutson R, Jiao H, Lan D, Lencart-Silva J, Li R, Liu X, Luo Q, Musango JK, Nobre AM, Nunes JP, Pascoe PL, Smits JGC, Stigebrandt A, Telfer TC, de Wit MP, Yan X, Zhang XL, Zhang Z, Zhu MY, Zhu CB, Bricker SB, Xiao Y, Xu S, Nauen CE, Scalet M (2008b) Sustainable options for people, catchment and aquatic resources. In: IMAR (ed) The SPEAR project, an international collaboration on integrated coastal zone management, Institute of Marine Research/European Commission, 180 pp. http://www.biaoqiang.org/documents/SPEAR book.pdf
70. Kapetsky J, Aguilar-Manjarrez J, Jenness J, Ferreira JG (2010a) Spatial analysis for the sustainable development of off-the-coast and offshore aquaculture from a global perspective. FAO Rome, (in press)
71. Stigebrandt A (1999) Turnover of energy and matter by fish – a general model with application to salmon. Fisken and Havet No. 5, Institute of Marine Research, Norway, 26 pp
72. FAO (2009) The state of world fisheries and aquaculture 2008. Food and Agriculture Organization of the United Nations, Rome
73. Kapetsky JM, Aguilar-Manjarrez J, Soto D (2010b) Status and potential of spatial planning tools, decision-making and modelling in implementing the ecosystem approach to aquaculture. In: Aguilar-Manjarrez J, Kapetsky JM, Soto D (eds) The potential of spatial planning tools to support the ecosystem approach to aquaculture. FAO/Rome. Expert Workshop. 19–21 Nov 2008, Rome, Italy. FAO Fisheries and Aquaculture Proceedings, No 17, Rome, FAO. pp 19–176. www.fao.org/docrep/012/i1359e/i1359e00.htm
74. Greenfield DI, Marin R III, Jensen S, Massion E, Roman B, Feldman J, Scholin C (2006) Application of the environmental sample processor (ESP) methodology for quantifying pseudo-nitzschia australis using ribosomal RNA-targeted probes in sandwich and fluorescent in situ hybridization. Limnol Oceanogr Meth 4:426–435
75. Anderson J, McRee J, Wilson R (2010) Effective UI – the art of building great user experience in software. O'Reilly Media, USA, 294 pp
76. Aguilar MJ, Nath SS (1998) A strategic reassessment of fish farming potential in Africa. Food and Agriculture Organization, Rome
77. Burford MA, Lorenzen K (2004) Modeling nitrogen dynamics in intensive shrimp ponds: the role of sediment remineralization. Aquaculture 229(1–4):129–145
78. De Gaetano P, Doglioli A, Magaldi M, Vassallo P, Fabiano M (2008) Foam, a new simple benthic degradative module for the lamp 3d model: an application to a mediterranean fish farm. Aquacult Res 39:1229–1242
79. European Commission (2000) Directive 2000/60/EC of the European Parliament and of the council of 23 October 2000 establishing a framework for Community actions in the field of water policy. Off J Eur Commun L327:1, 22 Dec 2000
80. European Commission (2008) Directive 2008/56/EC of the European parliament and of the council of 23 october 2000 establishing a framework for community action in the field of marine environmental policy (Marine strategy framework directive). Off J Eur Communs L164:19, 17 June 2008
81. Moo TSY, Undated. Excerpts from Chinese fish culture, by Fan Lee. Contribution No. 459, Chesapeake Biological Laboratory. University of Maryland, Solomons, MD, USA
82. National Oceanic and Atmospheric Administration (2011) NOAA aquaculture program: aquaculture in the U.S. http://aquaculture.noaa.gov/us/
83. United Nations Environment Programme, undated. Remote sensing images of mangrove destruction. http://www.grid.unep.ch/activities/global_change/atlas/images/honduras_s.jpg
84. Krkošek M (2010) Host density thresholds and disease control for fisheries and aquaculture. Aquac Environ Interact 1:21–32
85. Verner-Jeffreys DW, Pond MJ, Peeler EJ, Rimmer G, Oidtmann B, Way K, Mewett J, Jeffrey K, Bateman K, Reese RA, Feist SW (2008) Emergence of coldwater strawberry disease of rainbow trout, Oncorynchus mykiss Walbaum in England and Wales: outbreak investigations and transmission studies. Dis Aquat Org 79:207–218
86. Johansen LH, Jensen I, Mikkelsen H, Bjørn PA, Jansen PA, Bergh Ø (2011) Disease interaction and pathogens exchange between wild and farmed fish populations with special reference to Norway. Aquaculture 315:167–186
87. Dudley RW, Panchange VG, Newell CR (2000) Application of a comprehensive modeling strategy for the management of net-pen aquaculture waste transport. Aquaculture 187: 319–349
88. Food and Agriculture Organization (2011) The state of world fisheries and aquaculture 2010. Fisheries Department, Food

and Agriculture Organization of the United Nations, Rome, 218 pp
89. Aguilar-Manjarrez J, Nath SS (1998) A strategic reassessment of fish farming potential in Africa. CIFA Technical Paper 32, FAO, Rome, 196 pp
90. Filgueira R, Grant J, Strand O, Asplin L, Aure J (2010) A simulation model of carrying capacity for mussel culture in a Norwegian fjord: role of induced upwelling. Aquaculture 308:20–27
91. OIE World Organisation for Animal Health (2011) Aquatic animal health code. http://www.oie.int/international-standard-setting/aquatic-code/access-online/
92. Mardones FO, Perez AM, Carpenter TE (2009) Epidemiologic investigation of the re-emergence of infectious salmon anemia virus in Chile. Dis Aquat Org 84:105–114
93. Asche F, Hansen H, Tveteras R, Tveteras S (2010) The salmon disease crisis in Chile. Mar Resour Econ 24:405–411
94. Carvajal P (2009) ISA and the reshaping of Chile's Salmon Industry. Intrafish Industry Report, May. Intrafish, Bergen
95. Keeling MJ, Grenfell BT (1997) Disease extinction and community size: modeling the persistence of measles. Science 275:65–67
96. Grenfell BT, Bjornstad ON, Finkenstadt BF (2002) Dynamics of measles epidemics: scaling noise, determinism, and predictability with the TSIR model. Ecol Monogr 72:185–202
97. Bjørnstad ON, Finkenstädt BF, Grenfell BT (2002) Dynamics of measles epidemics: estimating scaling of transmission rates using a time series sir model. Ecol Monogr 72:169–184

Carrying Capacity for Sustainable Bivalve Aquaculture

Christopher W. McKindsey
Ocean and Environmental Sciences Division, Fisheries and Oceans Canada, Institut Maurice-Lamontagne Fisheries and Oceans Canada, Mont-Joli, Québec, Canada

Article Outline

Glossary
Definition of the Subject
Introduction
Functional Categories of "Carrying Capacity"
Decision Framework to Determine Carrying Capacity
Knowledge Gaps and Future Directions
Bibliography

Glossary

Benthic Pertaining to the sea floor.

Carrying capacity The intensity of a practice that a given environment can sustain indefinitely given the availability of various necessities in that environment and the various pressures on them.

Ecosystem approach to aquaculture (EAA) A strategy to integrate aquaculture into context of the wider ecosystem such that it promotes sustainable development, equity, and resilience of interlinked social and ecological systems.

Ecosystem-based management (EBM) A process that highlights the need to use the best available knowledge about the marine ecosystem to manage marine resources, with an emphasis on maintaining ecosystem service functions.

Integrated coastal zone management (ICZM) A process for managing coastal zones that uses an integrated approach and considers all aspects of the coastal zones, including biological, geographical, and political boundaries, to achieve sustainability.

Model A simplified description, conceptual or mathematical, of a system or process, to assist in calculations, predictions, and understanding.

Pelagic Pertaining to the water column.

Definition of the Subject

Bivalve aquaculture is one of the fastest growing sectors of the food industry, raising concerns about the influence of the activity on the environment. This is true at two levels: First, farmers must make sure that the bivalves that they raise do not deplete resources in a given area to such an extent that bivalve production is decreased. Second, society in general wishes that such activities have an acceptable impact on the environment and are sustainable. There is also intense competition for space and its use in many coastal zones, making siting of many farms contentious. Thus, many organizations have stressed the importance of determining the carrying capacity of different areas for bivalve culture. There are a number of ways that "carrying capacity" may be defined, including physical, production, ecological, and social, and the first three categories are to lesser or greater degrees related to social expectations and standards. A number of methods have been developed to calculate these

different categories of carrying capacity for bivalve culture. This entry outlines some advances to estimate the different categories of carrying capacity and suggests a framework that may be followed to encourage the development of a sustainable bivalve aquaculture industry. An emphasis is placed on the latter two categories as these are the ones for which knowledge is the most lacking, are arguably the most complex, and for which advances are the most pressing.

Introduction

Aquaculture is the fastest growing sector of the food industry. Since the 1970s, production in the sector has increased at a rate of about 7% per year and by 2008 accounted for 43% of the total annual fisheries production of 160 million tons and projections by the UN [1] suggest that this production will increase greatly in the future. This increase in production has raised concerns about the impacts of the activity on local environments, (e.g., [2]) and much work has been focused on understanding the interactions between aquaculture and the ecosystem, (e.g., [3, 4]). Although concerns were initially largely directed at the influence of finfish cage culture on the environment (e.g., nutrient loading, disease issues, and interactions due to escapes), concerns have also been raised about the influence of farmed bivalves.

As for aquaculture in general, production of farmed bivalves has increased greatly over the past few years and as of 2008, 11.7 million tons of the total 13.5 million tons of worldwide bivalve captures was from aquaculture production. This includes the culture of over 4 million tons each of clams and oysters and about 1.5 million tons each of scallops and mussels. The greatest concerns relating to farmed bivalves include enhanced localized biodeposition [5], food depletion in the water column due to bivalve grazing [6], alteration of nutrient and oxygen fluxes [7], and the transfer of disease and hitchhiking species [8]. Recent reviews on the environmental interactions associated with bivalve culture have been done for oysters [9], clams [10], and mussels [11].

Increasingly, regulators and other groups are looking to science to determine whether sites have reached their carrying capacity for bivalve culture. Moreover, a number of standards – performance standards, best management practices, certification standards, etc. – have been or are being developed to ensure that bivalve production is being done in a manner that is consistent with a global environmental ethic [12–14]. Some of these codes have been developed by industry groups and are voluntary in nature, some have been developed and are used by public authorities and regulatory agencies, and others are being developed by a variety of organizations (e.g., buyers, nongovernmental organizations, marketing groups) as a means of informing consumers about a product with the goal of influencing farm practices through consumer choice and market forces [15]. In all cases, the idea is that such criteria will encourage the development of a sustainable bivalve aquaculture industry such that the carrying capacity of a given area has not been exceeded and impacts are minimized. Recently, the National Research Council [15] suggested that performance standards based on the carrying capacity of sites be developed and implemented at the ecosystem level. Similarly, the FAO [16] has suggested that an Ecosystem Approach to Aquaculture (EAA) be followed to ensure the "integration of the activity within the wider ecosystem in such a way that it promotes sustainable development, equity, and resilience of interlinked social and ecological systems." Many advances have been made in the estimation of carrying capacity for bivalve culture over the past few years. The broad aim of this entry is thus to update an earlier paper on the subject [17] and to discuss a number of ideas that have been developed in the interim. It focuses on the outgrowing stage of bivalve culture as this stage is arguably the most important in terms of its interactions with the environment. Many other activities related to bivalve culture exist (see list below) and these are discussed by McKindsey et al. [17].

Abbreviated selection of activities related to bivalve culture that may influence the ecological carrying capacity of coastal areas. (Modified from McKindsey et al. [17].)

1. Seed collection
   (a) Dredging
      (i) Disturbance of benthic communities, especially the removal of long-living species

(ii) Removal of juveniles from wild populations of target species
(iii) Collection of non-target species
(iv) Suspension of sediments
(v) Depletion of food resources for other species
(vi) Release of H_2S and reduction of dissolved oxygen in the water due to oxygen-consuming substances, release of nutrients

(b) Artificial collectors
(i) Removal of juveniles from wild population of target species
(ii) Increasing target and non-target species recruitment success
(iii) Alteration of the hydrodynamic regimes
(iv) Acting as FAD
(v) Risk of entanglement for large vertebrates (e.g., marine mammals, sea birds, turtles, sharks)
(vi) Foci for nuisance species

(c) Hatcheries
(i) Chemical pollution (e.g., pharmaceuticals)
(ii) Genetic selection
(iii) Spread of diseases

(d) Importation
(i) Introduction of alien species
(ii) Genetic pollution
(iii) Spread of diseases

2. Ongrowing
(a) Effects common to all techniques
(i) Organic enrichment of seafloor
(ii) Providing reef-like structures
(iii) Alteration of hydrodynamic regime (current speed, turbulence)
(iv) Food web effects: competition with other filter feeders, increasing recycling speed of nutrients, removal of eggs and larvae of fish and benthic organisms
(v) Spawning: release of mussel larvae
(vi) Providing food for predators of bivalves
(vii) Control of predators and pests

(b) Bottom culture
(i) Activities to prepare the culture plots, e.g., dredging for predator removal
(ii) Placement of protective structures (netting, pipes)
(iii) Removal of associated organisms by dredging and relaying
(iv) Competition for space with wild benthos organisms

(c) Artificial structures for suspended and off-bottom culture (trestles, poles, rafts, longlines)
(i) Acting as artificial reef or FAD (attraction/displacement or enhancement of animals)
(ii) Risk of entanglement for large vertebrates (e.g., marine mammals, sea birds, turtles, sharks)
(iii) Foci for nuisance species

3. Harvesting
(a) Effects common to all techniques
(i) Removal of biomass, nutrients
(ii) Removal of filtration capacity
(iii) Removal of non-target species
(iv) Competition with predators

(b) Dredging
(i) Disturbance of benthic communities, especially removal of long-living species
(ii) Suspension of sediments
(iii) Release of H_2S and decrease of dissolved oxygen in the water due to oxygen-consuming substances, release of nutrients

(c) Collection of off-bottom structures

4. Processing
(a) Dumping of by-catch
(b) Relaying near auction houses
(c) Depurating
(d) Dumping of shells
(e) Effluents from processing plant
(f) Spread of alien species or diseases

As a first step, it is important to understand what is meant by "carrying capacity." A number of definitions have been suggested that consider a variety of physical, biological, and social criteria. In this entry, the four functional categories of "carrying capacity" as outlined by Inglis et al. [18] and McKindsey et al. [17] are used:

1. *Physical carrying capacity* – the total area of marine farms that can be accommodated in the available physical space.

2. *Production carrying capacity* – the stocking density of bivalves at which harvests are maximized.
3. *Ecological carrying capacity* – the stocking or farm density above which unacceptable ecological impacts become apparent.
4. *Social carrying capacity* – the level of farm development above which unacceptable social impacts are manifested.

The specific aims of this entry are to (1) provide an overview and update of different categories of carrying capacity, (2) give a more in-depth review of factors that could be considered for the determination of *ecological* and *social carrying capacity* as these categories are the least developed conceptually and in terms of modeling, (3) outline a decision framework for incorporating all four categories of bivalve carrying capacity into the determination of the overall carrying capacity of a given area for bivalve culture, and (4) outline research to address knowledge gaps for carrying capacity studies.

Functional Categories of "Carrying Capacity"

Physical Carrying Capacity

The physical carrying capacity of a site (embayment, inlet, offshore area, etc.) is simply the geographic area in which conditions are suitable for the production of a given species using a given method. It is a function of the overlap of the requirements of the species being harvested and the physical resources (e.g., depth, substrate type, salinity, hydrodynamics) in the site. The physical carrying capacity of a site may differ greatly between species and culture methods being employed. For example, an embayment may have an extensive area that is suitable for on-bottom clam culture but relatively little area that is appropriate for suspended oyster culture. Likewise, modification of an area (e.g., by the addition of a species-specific appropriate substrate) may extend the physical carrying capacity of an area.

Traditionally, the physical carrying capacity of sites was determined by building knowledge of an area using hydrographic charts as the base layer, adding other appropriate layers (e.g., temperature and salinity) as available, and analyzing the layers using formal or *ad hoc* Geographic Information Systems (GIS), (e.g., [19, 20]). With the expansion of culture sites in more remote regions where such information may not be readily available, the use of remote sensing methods to estimate various physical parameters (e.g., depth, salinity, temperature, as well as chlorophyll levels and related biological parameters that are needed to estimate production carrying capacity – see further) may be used in combination with GIS to facilitate site selection [21]. Although more of a social factor (see further), an additional advantage of using GIS for aquaculture site selection is that it can be used within a coastal management framework to include other activities so as to avoid user conflicts [22, 23].

Production Carrying Capacity

The production carrying capacity of a site is the stocking density at which harvests are maximized. Given that trade-offs between bivalve growth rates, market tastes, and economic returns, etc., would likely encourage selection of a specific bivalve size and type (see further), production carrying capacity is often not necessarily the greatest biomass. This category of carrying capacity is what most people think about when they consider "carrying capacity" and is the best studied. The production carrying capacity of a given site is strongly related to hydrodynamic and food regimes and its physical carrying capacity. Indeed, various "habitat suitability models" have been developed that combine both categories of data to predict the best areas for bivalve production, (e.g., [24]). Models to predict production carrying capacity have three main components: (1) a hydrodynamic model that transports food, nutrients, and other wastes; (2) a biogeochemical component that describes processes that influence food production and consumption; and (3) a physiological component that determines the rate of food consumption and growth of the farmed bivalves [25].

Bivalve culture systems are hierarchical, with individual bivalves and their associated fouling organisms nested within culture units (socks, cages and stacks of cages, pearl nets and strings of pearl nets, etc.), these being nested within culture gear (longlines or rafts), which are nested within farms, and so on [26–28]. An understanding of processes operating at each scale as well as the relations between these scales is needed to predict hydrodynamics and how this influences

biogeochemical and physiological processes within culture systems and to understand cascading effects on the greater ecosystem.

In its simplest form, the production carrying capacity of a given location is a function of the available food resources and the rate at which they are renewed via in situ production and/or flushing relative to their rate of removal (filtration) by the farmed bivalves. This type of approach has been developed for mussel culture in eastern Canada [29]. However, such models commonly under- or overestimate flushing and a number of authors have suggested that their use be avoided for production carrying capacity studies, (e.g., [30]). Despite this, a number of groups have advocated calculating the ratio of clearance time by farmed bivalves to flushing rate or water residence times (as calculated by such methods) to evaluate the sustainability of sites for bivalve culture [31] and as a rough first step in evaluating whether carrying capacity is potentially exceeded for ecological certification standards [32]. In the latter case, if the ratio between clearance and renewal times is less than unity, then further analyses based on primary productivity are required.

More encompassing approaches to calculating production carrying capacity based on hydrodynamic and mathematical models that include spatially and temporally explicit feedbacks between the farmed bivalves, phytoplankton, zooplankton, detritus, and physical (e.g., temperature, nutrients, see Fig. 1) parameters are becoming the standard. Models vary greatly in complexity. Although a simple box model for a location may be sufficient for some situations, it is likely unsuitable for embayments with some degree of environmental heterogeneity [33]. The next level of complexity is a simple 1-D hydrodynamic transport model, (e.g., [34]), which may be expanded upon to include vertical transport for suspended culture, (e.g., [35]). More complex models include multiple coupled boxes within an area driven by a 2-D hydrodynamic model (with tidal and meteorological forcings). The most complex models, fully refined 3-D finite-element hydrodynamic models, generally provide a much more

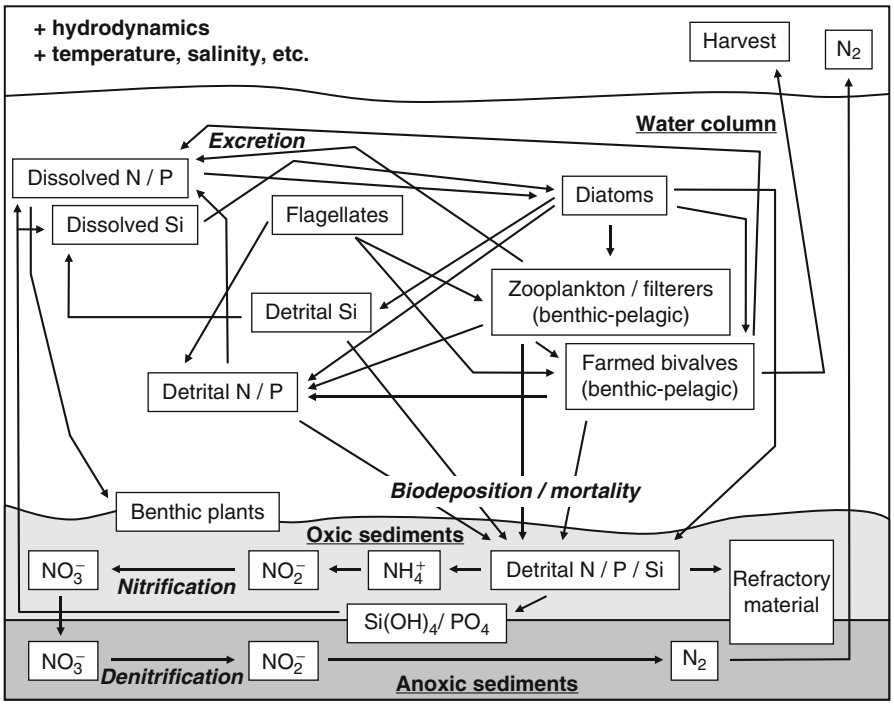

Carrying Capacity for Sustainable Bivalve Aquaculture. Figure 1
Conceptual diagram of bivalve aquaculture interactions in coastal ecosystems considered in production carrying capacity estimations. Only main pathways are indicated

accurate estimation of hydrodynamics and may be used to drive the biological models. Historically, computational power has limited the broad application of complex models [36] but this is no longer the case as powerful computers are now readily available [25]. However, increased development time and sampling requirements to validate more complex models make the use of simpler box models a good approximation for understanding the hydrodynamics of an area and slow ecological processes [37] and for carrying capacity modeling [38].

Production carrying capacity models require data on biogeochemical components which include a large number of variables related to the flux of nutrients and primary production and interactions between different food sources for the farmed bivalves. This includes nutrient fluxes due to excretion by the farmed bivalves and associated organisms and organic matter in trapped sediments in culture structures [39–41], nutrient uptake by and production of phytoplankton [42–44], zooplankton and detritus components, and a benthic component that includes biological and chemical processes [45–47]. This latter submodel is of particular importance in shallow areas [33]. Figure 1 gives an example of the types of processes that are included within such models.

Bivalves graze on and may impact plankton and other suspended components in the water column [48]. These components and environmental factors (e.g., temperature) in turn greatly influence the growth of the farmed bivalves. Models to predict the physiological response and growth of bivalves vary greatly in their complexity. Models may be divided into statistical and more mechanistic approaches that include bioenergetics [49, 50]. Today, many studies use an approach based on dynamic energy budget (DEB) models that were developed by Kooijman, (e.g., [51–53]). In these models, energy budgets are partitioned into core processes: structural volume, reserves, and a reproductive buffer, and forced by food and physical parameters. Examples include work on a variety of bivalves, (e.g., [25, 54–56]) and have been incorporated into general models for bivalve production carrying capacity [35, 57]. A generalized set of DEB models for a few of the most commonly farmed bivalve species has been assembled and is available (http://www.shellsim.com). Production carrying capacity models based on this latter suite of components have been successfully used in a number of studies, (e.g., [35]). Although these types of models are attractive in that they include logical mechanistic processes, their complexity makes them difficult to apply at times and requires substantial ground truthing and simpler models will often yield acceptable results.

Ultimately, the different sub-models must be put together to estimate production carrying capacity. An important advance in modeling production carrying capacity is the development of Graphical User Interface (GUI) modeling environments that allow users to link different sub-models fairly easily through a visual environment rather than with text commands. An example of this is the use of object-oriented modeling environment, as promoted for the FARM model developed by Ferreira et al. [35, 57]. This model links together various components forced by a 1-D hydrodynamic model, or 1-D with horizontal mixing for off-bottom bivalve culture, to estimate production carrying capacity and eutrophication assessment (see further) at the farm-scale based on a limited number of parameters. It may also be used to guide the selection of growing sites, culture layouts, production densities, farmed species, and to maximize production or economic returns. The model has been shown to be useful in a number of locations and for a number of species [57] and is available as a client–server application (www.farmscale.org; www.longline.co.uk/winshell). Simile [58] is an object-based GUI modeling environment that has been used extensively by Grant and colleagues [25, 33, 38, 54, 59]. This environment is well suited to constructing carrying capacity models for bivalve culture because of its inherent ability to represent spatial elements and specify hydrodynamic connections between them and, because of its GUI environment, it is transferable to nonexperts [38].

Models for production carrying capacity usually consider only the farmed bivalves as consumers of plankton. However, in some situations, particularly shallow sites with large densities of natural bivalves, grazing by natural bivalves may also exert a large pressure on plankton communities [60–62]. Thus Sequeira et al. [63] have recently developed a model that includes natural benthic communities as a forcing function on plankton communities and suggest that these populations may significantly reduce production

carrying capacity. Similarly, Cugier et al. [64] found that wild native and exotic filter-feeding organism had a greater effect on the control of primary productivity than did the farmed bivalves in Mont Saint Michel Bay, France (Fig. 2). The biomass of filter-feeding fouling organisms, particularly tunicates, on farmed bivalves and infrastructure may be considerable, at times greater than that of the farmed bivalves [65]. Given that they may have similar grazing rates to that of farmed bivalves [66], these should be included within production carrying capacity models where fouling is great. This has been attempted for the Thau Lagoon [67] and the Oosterschelde Estuary [68].

Ecological Carrying Capacity

The definition the "ecological carrying capacity" of a system is greatly dependent on social values as what is considered to be an "unacceptable" impact is dependent on the values of a given society. A society or their representatives must select which components (e.g., species or habitats) of a given area are important and set acceptable limits of change for each. Often, information on specific parameters may not be available and managers may choose to consider components for which information is available or more easily obtained. As pointed out by McKindsey et al. [17], this may be a logical choice given that components that have a high societal value are also likely to have been studied.

While production carrying capacity focuses on the farmed bivalves themselves and the organisms that support their production, ecological carrying capacity also includes other organisms and habitats in the ecosystem. There are three main categories of ecological carrying capacity: (1) that related to the pelagic habitat; (2) that related to the benthic habitat; and (3) that which employs ecosystem function approaches. The first category is largely related to plankton depletion due to grazing by farmed bivalves. The second category is related to increased sedimentation within culture sites due to biodeposition by the farmed bivalves. The third category considers both these issues and changes in biomass and energy flow in a system. Ecological carrying capacity is strongly related to both the physical carrying capacity and the production carrying capacity of a site, particularly with respect to that related to the pelagic habitat.

Models to estimate the production carrying capacity of a site contribute to determining the ecological carrying capacity of a site for organisms that are dependent on the delivery of food from the water column. Presumably, if the farmed filter-feeding bivalves impact themselves by overgrazing the available resources, then they are also likely impacting other organisms that feed in a similar manner [69]. Indeed, some recent production carrying capacity models explicitly included benthic filter-feeding organisms [63, 64] and some work has suggested that overgrazing by farmed bivalves may impact other suspension feeders in the surrounding ecosystem [70]. The calculation of carrying capacity for other planktivores in the water column may be similarly evaluated. Sedimentation rates to the bottom are a function of the plankton communities in an area (e.g., [71]). Thus, as has been shown for natural systems with bivalves [72, 73], depletion of the water column via grazing by farmed bivalves may influence sedimentation rates within a given area and thereby benthic communities, potentially enhancing differences between benthic communities within and outside of culture sites [11].

With respect to the benthic habitat, research has largely focused on the impact of increased sedimentation due to biodeposit production by farmed bivalves on infaunal communities [9–11]. Research on the ecological carrying capacity of benthic habitats has likewise been focused on predicting how increased sedimentation due to biodeposit production by farmed bivalves influences infaunal communities. Grant et al. [74] predicted benthic loading rates from biodeposits from farmed mussels (*Mytilus edulis*) at a bay scale as a balance between biodeposit production, as calculated using a simple physiological model, and flushing, as calculated based on a simple tidal prism model (validated using a finite-element 2-D hydrodynamic model and field work). Although there was some variation between modeled and observed biodeposition for both studied bays, the authors suggest that the approach is valuable as a screening tool to develop relative ranking of different systems and identify potential issues. A number of approaches have also been evaluated that couple spatially explicit hydrodynamic-dependent particle tracking models to predict flux of

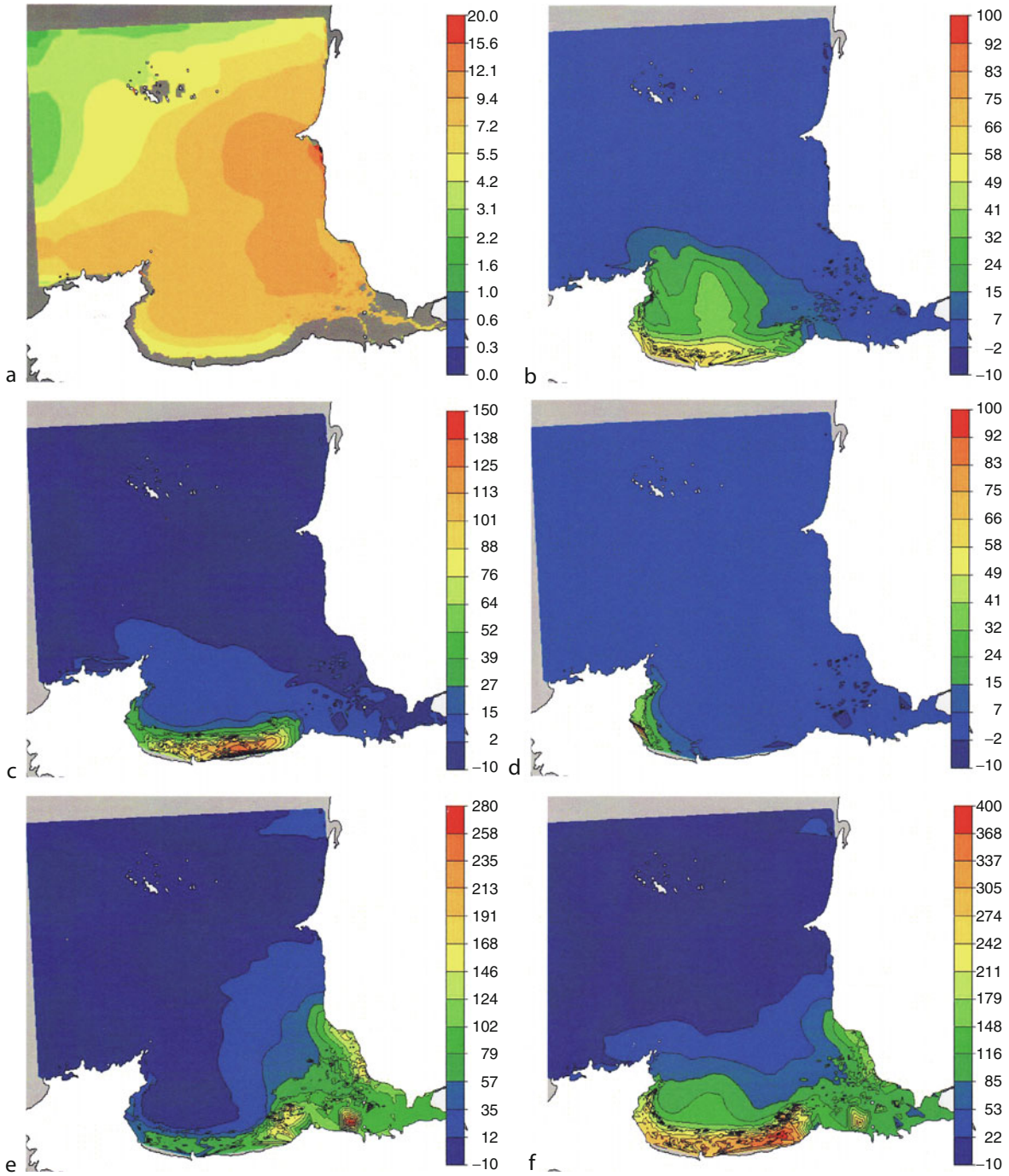

Carrying Capacity for Sustainable Bivalve Aquaculture. Figure 2

Simulated annual maximum chlorophyll a for the reference case (A – current situation with all filter feeders included) and differences with the reference case (in%) for five scenarios of with different filter feeders removed, (B – without exotic slipper-limpets, C – without farmed mussels, D – without farmed oysters, E – without native filter feeders, F – with no filter feeders in the bay). Because of the wide range of differences between the scenarios, the scale bar is not the same for each sub-figure (From Cugier et al. [64])

biodeposits from farmed bivalves to the bottom to predict benthic loading footprints and associated benthic community changes. A simple approach is to modify the existing DEPOMOD model, which was developed to this end for finfish cage culture but for which individual bivalve culture structures (e.g., mussel longlines, see Fig. 3) or groups of structures in a system may be modeled [75]. However, this approach has a number of limitations. First, the model assumes a homogenous flow field, an assumption that is unlikely to be true for extensive culture sites. Second, the module for resuspension of sedimented biodeposits is not fully developed and remains one of the greatest sources of uncertainty for biodeposition/impact models [74]. Although resuspension may be negligible in areas with weak currents [75], Giles [76] used a more advanced hydrodynamic model to drive a biodeposit dispersion model and stressed the importance of this aspect for predicting the dispersal of biodeposits in areas with strong currents. A number of recent studies have started to address this issue and supply data to better parameterize this module, (e.g., [75, 77, 78]). Although general relationships exist for benthic organic loading and infaunal community structure [79], predictive dose-dependent relationships between organic loading from bivalve biodeposits and faunal responses are largely lacking, making predictions difficult [80]. Similarly, there is no universal metric available to describe benthic responses although a large number of indices have been developed, some showing good relationships with aquaculture [81]. As noted above, the biomass of tunicates and other fouling organisms on farmed bivalves and infrastructure may be considerable, and these likely contribute greatly to organic loading to the sea bottom in some cases [65, see Fig. 3] and thus must be considered when determining the biodeposition-related ecological carrying capacity of an area for the benthic habitat.

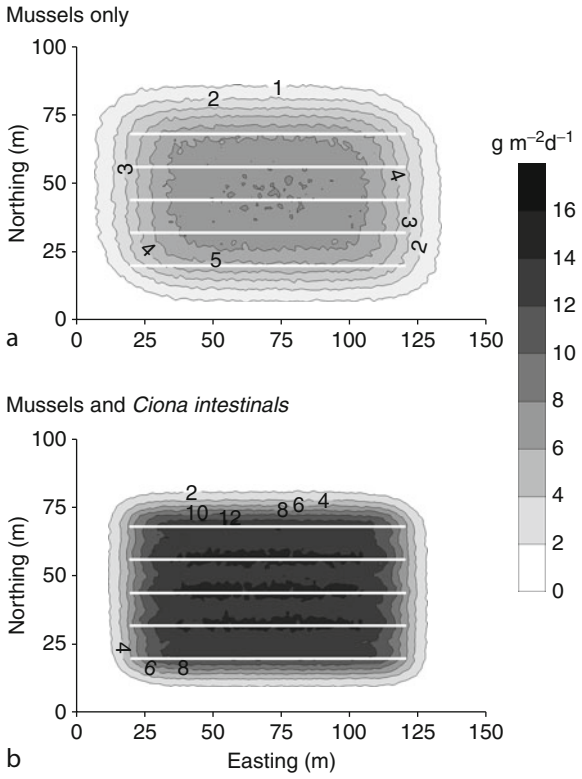

Carrying Capacity for Sustainable Bivalve Aquaculture. Figure 3
Modeled biodeposition footprint (g m^{-2} d^{-1}) within an idealized suspended mussel farm with (**a**) mussels only and (**b**) mussels fouled with *Ciona intestinalis*. Biodeposition rates were modeled for five backlines (white lines in figure) measuring 100 m each based on currents measured during a 24 h period in St. Marys Bay, eastern Canada (Modified from McKindsey et al. [65])

Tenore et al. [82] used a mass-balance approach to examine the influence of bivalve culture as a part of a coastal ecosystem but specifically to predict ecological carrying capacity. Gibbs [83] used food web analysis to estimate the level of bivalve culture that could develop before it dominated the energy flow in a marine system and impacted fisheries resources. More recent work has used Ecopath with Ecosim [84] to determine the trophic functioning of various areas that include bivalve culture [85–88]. These models differ considerably in their complexity (i.e., number of trophic groups included) and have generally found that bivalve culture promotes short energy pathways with high trophic efficiency and energy cycling. However, the aim of these studies was not specifically to determine the ecological carrying capacities of the studied areas. Research [69] to evaluate the carrying capacity of an area for mussel culture in New Zealand using Ecopath found that the ecological carrying capacity of the area (defined as the level of culture that would not significantly change the major energy fluxes or structure of the food web) was much less than the production

carrying capacity (defined as the level of production at which the ecosystem collapses down to a nutrient–phytoplankton–culture–detritus-dominated system) of the area. More recent research in the eastern United States based on the same approach but for coastal lagoons with oysters also found that the stocking density calculated for ecological carrying capacity was less than that calculated for production carrying capacity [89]. Although the original version of Ecopath was limited in its applicability because it could not be used to simulate changes to flows with time, the new version does not assume a steady state. Rather, it bases the parameterization on an assumption of mass balance over an arbitrary period, often a whole year, and biomasses of any given trophic group need not be at equilibrium. A component of Ecopath, Ecosim, accepts time series data for different trophic groups and may be appropriate to evaluate different management (i.e., stocking and harvesting) options. These approaches have some limitations. Perhaps the most important for bivalve culture is that the models are not spatially explicit. Thus, the model may not be used to identify near-field and far-field effects and exchanges between areas are assumed to be instantaneous. This is not logical in complex coastal areas where most bivalve culture is done. This issue has been addressed to some extent with the development of Ecospace, a dynamic, spatial version of Ecopath that incorporates the key elements of Ecosim [84]. This review found no studies that use either Ecosim or Ecospace to estimate ecological carrying capacity for bivalve culture; information to do this is usually not available and when such spatially explicit temporal data are not available, Ecopath provides a standardized methodology for developing a model [89]. As it is, data on many specific biological variables (life history values, interactions, etc.) are lacking for most systems. If default values are used, these must not be simply accepted without critical evaluation [90]. Even when data is available to guide the determination of variable values, many must be adjusted to make the model balance [69]. Perhaps most importantly, Ecopath uses a largely top-down mass-balance approach and thus poorly represents bottom-up effects [91], a situation that will be problematic for bivalve culture given that it largely impacts nutrients and lower trophic levels.

In sum, most potential measures of ecological carrying capacity consider only a single or a restrained number of ecosystem components [92]. Little research has been directed at understanding the impact of biodeposition (of biodeposits and of farmed bivalves and associated organisms) on the productivity or sustainability of benthic infaunal communities or the communities of larger invertebrates and fishes that may prefer to associate with culture sites to profit from the biodeposition. Likewise, little research has addressed the impact of the modification/addition of physical structure associated with bivalve culture (i.e., both the infrastructure and the farmed product, as well as removal of seagrass, etc.) [11]. The addition of structure may attract and create suitable habitat for a large variety of organisms, such as fish and decapods, but also of fouling organisms that may otherwise not have appropriate habitat in a given area. In contrast, the removal of some features for bivalve culture may repel other organisms. Thus, flexible approaches to evaluating ecological carrying capacity need to be developed to incorporate our evolving understanding of the functioning of marine ecosystems and their interactions with bivalve culture [17, 89].

Social Carrying Capacity

The social carrying capacity of a site is the most complex of all types of carrying capacity to determine. It depends on not only the three above categories of carrying capacity but also on trade-offs between stakeholders to meet the demands of both the population (socioeconomic factors such as traditional fisheries, employment in other sectors, and recreational use) and the environment (protected habitats, species, etc.) [22, 31, 83, 93–95]. Moreover, social issues often inform other categories of carrying capacity (see further in "Decision Framework" section). This category is at the heart of Marine Ecosystem-Based Management (EBM) and Integrated Coastal Zone Management (ICZM) and must be fully developed so that responsible management decisions may be made [96]. That being said, the techniques for determining the social carrying capacity of a site are the least developed of all carrying capacity categories [97].

Despite these limitations, a number of criteria are common to each of the different methods:

representativeness, independence, and involvement/buy-in of the groups involved in the process, and transparency [98].

One method that has been developed to manage natural resources is the concept of "limits of acceptable change," or LAC. Although originally developed to define the limit of recreational activities in terrestrial wilderness areas, it may also be applicable to a wider range of natural resource management issues [99, 100]. More recently, it has been applied to bivalve aquaculture in New Zealand [101]. It was recognized that LAC was not a tool to determine the level of bivalve culture that was ecologically sustainable. Rather, it provided an adaptive management framework to prevent significant negative effects due to the activity. Through a collaborative process, LAC provides a framework to identify indicators of change, setting levels of changes of indicators that are acceptable, and identifying management responses that are to be undertaken if these levels are exceeded. The selected indicators must be relevant and practical to measure. Although in the New Zealand example ecological indicators were selected (spatial extent of phytoplankton depletion, also done recently in eastern Canada [25]), the approach could also be used for other types of indicators derived from other categories of carrying capacity evaluations. The important aspect is that the selected indicators are chosen in a collaborative way [102], including input and discussions with members of the public, environmental managers, scientists, members of the industry, groups with conflicting interests, etc. In addition to the process being representative, it must also be transparent and adaptive so that new information may be easily included in the decision-making process. Indeed, much work has shown that collaborative efforts between all stakeholders are essential to ensuring satisfaction in the consultation process and developing policy [103].

A recent example of this is the evaluation of the ecological carrying capacity of lagoons in Rhode Island, eastern United States, for oyster culture [97]. This involved the development of the Working Group on Aquaculture Regulations (WGAR), which guided and oversaw the development of a mass-balance modeling approach to calculate both the ecological and social carrying capacities of the area for oyster culture. Whereas it is usually left up to the modelers to determine what constitutes an acceptable or an unacceptable impact [97], it was considered that the process would be much more transparent and inclusive by including input from all stakeholders, following the criteria outlined by Soto et al. [104] stating that an ecosystem approach to aquaculture (EAA) should:

1. Be developed in the context of ecosystem functions and services with no degradation of these beyond their resilience capacity
2. Improve human well-being and equity for all relevant stakeholders
3. Be developed in the context of (and integrated to) other relevant sectors

The above strategies to evaluate the social carrying capacity of locations may be considered as social-ecological systems (SESs) where all of the potential stakeholders participate. Walker et al. [105] outline four general steps in the process:

1. Stakeholder-led development of a conceptual model of the system, including its history and preliminary assessments of the drivers of key ecosystem goods and services.
2. Identification of the range of drivers of the system, stakeholder visions for the future, and contrasting possible future policies, to identify a limited set of future scenarios.
3. Identify the resilience of the system by examining the results from i and ii. This is generally done through the development of models of the system's dynamics to identify important attributes that affect resilience.
4. Stakeholder evaluation of the process and outcomes in terms of policy and management implications.

Ostrom [106] recently developed a framework to evaluate the sustainability of management strategies for SESs. It is a nested approach with four first-level core subsystems. In bivalve culture systems, these may include (1) resources systems – a given embayment or other logical management area; (2) resource units – such as phytoplankton biomass or physical space; (3) governance systems – the specific rules related to culture activities that manage resource use; and (4) users – the various groups that use the resource for sustenance, recreation, etc. Each core subsystem is made up of a series of secondary subsystems and

interacts with other core subsystems. One of the main findings was that, although many researchers have predicted that users of a system will not self-organize to create a sustainable SES and thus regulation by governments is needed, this prediction was not supported when stakeholders were enabled to discuss management options. Monitoring and enforcement were other key components that determined the success of the studied SESs.

A further method to determine the social carrying capacity of a site is by attaching a monetary value to the different categories of impact due to aquaculture [15]. However, this is a complex undertaking and must include both positive and negative effects of the operations [107]. Moreover, acceptability of different effects is quite variable among locations and groups, further complicating the goal of attaining consensus for different variables.

The use of fuzzy expert systems has also been advocated to determine the social carrying capacity of an area for bivalve culture [17]. This approach has been shown to be useful when data types are disparate and uncertainties are great or simply unknown. In short, instead of stating that a given level of production is acceptable or unacceptable, a given level is treated as being, say, 50% acceptable. It is rather more like dealing with varying shades of gray rather than cases that are black and white. This has the important effect of inducing less conflict between stakeholders on issues that may be contentious.

In sum, methods to determine social carrying capacity for bivalve culture remain poorly developed. In general, few methods have been developed specifically for aquaculture although methods developed for other sectors may be adapted. Analysis of the attempts to use SESs in other systems has shown that some approaches work; such approaches may be looked to for determining social carrying capacity for bivalve culture.

Decision Framework to Determine Carrying Capacity

A hierarchical approach to determine the carrying capacity of an area for bivalve culture is proposed (Fig. 4). The first level, the physical carrying capacity, relates to the available natural conditions and the needs

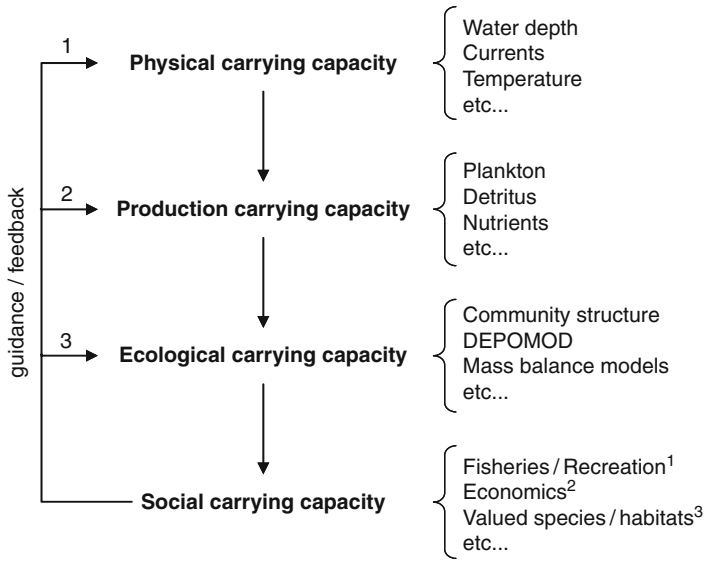

Carrying Capacity for Sustainable Bivalve Aquaculture. Figure 4
Hierarchical structure to determine carrying capacity of a given area. Note that social carrying capacity provides guidance to choosing pertinent response variables and on establishing limits for these. Superscripts indicate examples of the type of information that informs the selection of response variables for other carrying capacity categories (Modified from McKindsey et al. [17])

of the operation and bivalves to be cultured. The second level, the production carrying capacity, is a function of the supply of food to the farmed bivalve in an area and is determined using modeling efforts. At the third level, the ecological carrying capacity of an area is estimated using modeling or by following a logical framework to evaluate the range of possible outcomes for production estimates varying between none (and/or the current level) and the maximum calculated production carrying capacity; there is little use to go beyond this point as it is assumed that this level will not be surpassed knowingly. Finally, managers weigh and balance the different scenarios based on the outcomes from each of the preceding categories of carrying capacity and make a decision as to what level of productivity is acceptable – the social carrying capacity.

It must be understood that the three first categories of carrying capacity are a function of social values. For example, a given coastal area in which bivalve culture may be done is often valued for myriad competing activities, such as water quality, visual aesthetics, competition for limited space, other species, etc. For the first category, physical carrying capacity, competition for physical space may be direct or indirect. For example, direct competition may result as there may be multiple demands to use the same area for different purposes, such as bivalve culture as well as fishing or recreational boating. Indirect competition may arise because of visual aesthetics or the not-in-my-backyard factor where waterfront owners or users do not want their views affected by aquaculture installations. Production carrying capacity is likely rarely maximized because of economic costs related to production. Thus, Nobre et al. [108] developed a modeling approach that considers both ecological and economic aspects and their interactions to maximize profit and EAA as focusing aquaculture management on maximizing output is likely economically inefficient and carries unnecessary ecological risks. In fact, this approach addresses all four categories of carrying capacity with an emphasis on maximizing economic returns. The ecological carrying capacity of an area is also clearly a function of social values as what is valued varies among populations (e.g., specific bird and fish populations, water clarity, eelgrass, or specific rare habitats).

Consultation with stakeholders throughout the process of defining the carrying capacity for a given area will identify the appropriate (given the social values of the population) response variables or indices to be examined [97]. Ideally, the scientists should then be able to select suitable tools from a toolbox (e.g., models, GIS, and comparisons with previous studies) to predict the form of the response curves of the selected response variables to a range of production-level scenarios. It is important to note that although it is the role of scientists to describe the form of the responses to a range of production-level scenarios (see Fig. 5), their role ends once they have done this. It is then up to managers, in consultation with the various stakeholders, to use all available scientific information to inform regulations and policy [17, 97]. Again, this should be done within the context of EBM and ICZM, given that there is likely a paucity of information about a number of factors that are needed to make informed judgments [96]. Thus managers will likely have to rely on instinct, local knowledge, extrapolation from studies done elsewhere, contributions from various stakeholders, etc., to make management and policy decisions. Even faced with an absence of some types of information, this does not remove the logic of the hierarchical nature of the decision

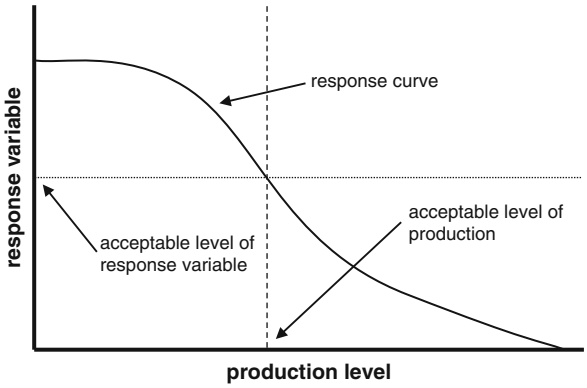

Carrying Capacity for Sustainable Bivalve Aquaculture. Figure 5
Hypothetical response curve of an environmental variable under the influence of varying levels of bivalve culture production. The dotted line indicates the level of the indicator that has been determined to be acceptable and the dashed line the corresponding level of production (Modified from McKindsey et al. [17])

framework outlined above. Indeed, it could be argued that this is precisely when the process is most useful and should be followed using all available information – so that an unbiased view of the situation may be formed and thus promoting appropriate management decisions. As pointed out by McKindsey et al. [17], failure to follow the process (e.g., by stating at the outset of the process that certain types of development or developments in certain areas are not permitted) will likely result in otherwise feasible bivalve culture installations not being initiated. It is also contrary to the notion of effective and transparent processes in the establishment of ICZM or EBM.

Knowledge Gaps and Future Directions

This entry concludes with a brief discussion of knowledge gaps and directions for future research to better estimate the carrying capacity of areas for sustainable bivalve culture, except for the estimation of physical carrying capacity for which methods are fairly well developed and are currently used extensively to this end.

While it is generally true that "existing models must be made spatially explicit" [17], this is currently being done. However, models to this end require much information that is often not easily available. So, perhaps a better knowledge gap to address is to determine when such models are needed and when can general models be used.

Similarly to the first point, although temporal variation must be included in models to consider seeding and harvesting activities, some generalized models to this end have already been developed [35, 57, 108, 109]. These should be expanded upon and evaluated in several locations to fully assess their generality.

Far-field impacts for the benthic environment need to be evaluated. For example, is sedimentation outside of culture sites decreased due to grazing and, if so, what is the influence of this on the benthic environment? How does this influence our interpretation of "impacts" on the benthic environment within farm sites?

Work is needed on how nonlinear or unexpected results may be incorporated into carrying capacity models. For example, how can the provision of bivalve culture-related structure in the environment – which may increase the abundance of fouling organisms and thus filtration capacity or attract various other organisms – be included in carrying capacity estimates?

Methods need to be developed to include both "positive" and "negative" effects into the decision-making process. For example, while suspended bivalve culture may increase organic loading locally, it may also mitigate the effects of eutrophication (and models have been developed to assess this, e.g., 35) or increase the abundance of commercially important species locally [11].

Despite the growing prevalence of certification standards and ecolabeling for aquaculture products, it is not clear that such processes are improving conditions in the field [14]. Although such standards are often elaborated within a multi-stakeholder framework, it is not clear under which conditions they are necessary and how the three previous points are considered in their development or application.

Given that many groups promote including the notions of reversibility or resilience in the definition of carrying capacity, (e.g., [16]), surprisingly little work has actually addressed this for the benthic environment [but see 110]. Work on evaluating the resilience of benthic systems to bivalve culture is needed.

Appropriate management tools, such as methods for combining disparate data types, need to be developed to incorporate the information needed to estimate various aspects of carrying capacity to aid in decision making and policy development.

Bibliography

Primary Literature

1. FAO Fisheries and Aquaculture Department (2010) Global datasets, FishStat Plus – Universal software for fishery statistical time series. http://www.fao.org/fishery/statistics/software/fishstat/en. Accessed 6 Feb 2011
2. Black KDE (2001) Environmental impacts of aquaculture. CRC Press, Boca Raton
3. Holmer M, Black K, Duarte CM, Marbà N, Karakassis I (2008) Aquaculture in the ecosystem. Springer, New York
4. Davenport J, Black K, Burnell G, Cross T, Culloty S, Ekarante S, Furness B, Mulcahy M, Thetmeyer H (2003) Aquaculture: the ecological issues. Blackwell, Oxford
5. Mattsson J, Lindén O (1983) Benthic macrofauna succession under mussels, *Mytilus edulis* L. (Bivalvia), cultured on hanging long-lines. Sarsia 68:97–102
6. Troost K, Gelderman E, Kamermans P, Smaal AC, Wolff WJ (2009) Effects of an increasing filter feeder stock on larval

abundance in the Oosterschelde estuary (SW Netherlands). J Sea Res 61:153–164
7. Prins TC, Smaal AC, Dame RF (1998) A review of the feedbacks between bivalve grazing and ecosystem processes. Aquat Ecol 31:349–359
8. McKindsey CW, Landry T, O'Beirn FX, Davies IM (2007) Bivalve aquaculture and exotic species: a review of ecological considerations and management issues. J Shellfish Res 26:281–294
9. Forrest BM, Keeley NB, Hopkins GA, Webb SC, Clement DM (2009) Bivalve aquaculture in estuaries: review and synthesis of oyster cultivation effects. Aquaculture 298:1–15
10. Dumbauld BR, Ruesink JL, Rumrill SS (2009) The ecological role of bivalve shellfish aquaculture in the estuarine environment: a review with application to oyster and clam culture in West Coast (USA) estuaries. Aquaculture 290:196–223
11. McKindsey CW, Archambault P, Callier MD, Olivier F (in press) Influence of suspended and off-bottom mussel culture on the sea bottom and benthic habitats: a review. Can J Zool
12. Young JA, Brugere C, Muir JF (1999) Green grow the fishes-Oh? Environmental attributes in marketing of aquaculture products. Aquacult Econom Manage 3:7–17
13. Lee D (2008) Aquaculture certification. In: Ward T, Phillips B (eds) Seafood ecolabelling: principles and practice. Wiley-Blackwell, Oxford, pp 106–133
14. Tlusty MF (2011) Environmental improvement of seafood through certification and ecolabelling: theory and analysis. Fish Fisher. doi: 10.1111/j.1467-2979.2011.00404.x
15. National Research Council (2009) Ecosystem concepts for sustainable bivalve mariculture. National Academies Press, Washington
16. Soto D, Aguilar-Manjarrez J, Hishamunda N (2008) Building an ecosystem approach to aquaculture. In: FAO/Universitat De Les Illes Balears expert workshop, 7–11 May 2007, Palma De Mallorca, Spain. FAO Fisheries and Aquaculture proceedings, vol 14. Rome
17. McKindsey CW, Thetmeyer H, Landry T, Silvert W (2006) Review of recent carrying capacity models for bivalve culture and recommendations for research and management. Aquaculture 261:451–462
18. Inglis GJ, Hayden BJ, Ross AH (2000) An overview of factors affecting the carrying capacity of coastal embayments for mussel culture. NIWA Client Report CHC00/69, National Institute of Water & Atmospheric Research Ltd, National Institute of Water & Atmospheric Research Ltd, pp vi + 31
19. Nath SS, Bolte JP, Ross LG, Aguilar-Manjarrez J (2000) Applications of geographical information systems (GIS) for spatial decision support in aquaculture. Aquacult Eng 23:233–278
20. Longdill PC, Healy TR, Black KP (2008) An integrated GIS approach for sustainable aquaculture management area site selection. Ocean Coast Manage 51:612–624
21. Meaden GJ, Kapetsky JM (1991) Geographical information systems and remote sensing in inland fisheries and aquaculture. FAO Fish. Tech. paper no. 318, FAO, Rome, pp 262
22. Dempster T, Sanchez-Jerez P (2008) Aquaculture and coastal space management in Europe: an ecological perspective. In: Holmer M, Black K, Duarte CM, Marbà N, Karakassis I (eds) Aquaculture in the ecosystem. Springer, The Netherlands, pp 87–116
23. Goulletquer P, Le Moine O (2003) Shellfish farming and coastal zone management (CZM) development in the Marennes-Oléron Bay and Charentais Sounds (Charente Maritime, France): a review of recent developments. Aquacult Int 10:507–525
24. Vincenzi S, Caramori G, Rossi R, De Leo GA (2007) A comparative analysis of three habitat suitability models for commercial yield estimation of *Tapes philippinarum* in a North Adriatic coastal lagoon (Sacca di Goro, Italy). Mar Pollut Bull 55:579–590
25. Guyondet T, Roy S, Koutitonsky VG, Grant J, Tita G (2010) Integrating multiple spatial scales in the carrying capacity assessment of a coastal ecosystem for bivalve aquaculture. J Sea Res 64:341–359
26. Fréchette M (2008) Hierarchical structure of bivalve culture systems and optimal stocking density. Aquacult Int. doi:10.1007/s10499-008-9198-2
27. Stevens C, Plew D, Hartstein N, Fredriksson D (2008) The physics of open-water shellfish aquaculture. Aquacult Eng 38:145–160
28. Plew DR, Stevens CL, Spigel RH, Hartstein ND (2005) Hydrodynamic implications of large offshore mussel farms. IEEE J Oceanic Eng 30:95–108
29. Carver CEA, Mallet AL (1990) Estimating the carrying capacity of a coastal inlet for mussel culture. Aquaculture 88:39–53
30. Guyondet T, Koutitonsky VG, Roy S (2005) Effects of water renewal estimates on the oyster aquaculture potential of an inshore area. J Mar Syst 58:35–51
31. Gibbs MT (2007) Sustainability performance indicators for suspended bivalve aquaculture activities. Ecol Indic 7:94–107
32. WWF (2009) Bivalve aquaculture dialogue: environmental and social standards for bivalve aquaculture. http://www.worldwildlife.org/what/globalmarkets/aquaculture/WWFBinaryitem13945.pdf. Accessed 3 May 2011, pp 22
33. Grant J, Bacher C, Cranford PJ, Guyondet T, Carreau M (2008) A spatially explicit ecosystem model of seston depletion in dense mussel culture. J Mar Syst 73:155–168
34. Bacher C, Grant J, Hawkins AJS, Fang J, Zhu M, Besnard M (2003) Modelling the effect of food depletion on scallop growth in Sungo Bay (China). Aquat Living Resour 16:10–24
35. Ferreira JG, Hawkins AJS, Bricker SB (2007) Management of productivity, environmental effects and profitability of shellfish aquaculture – the farm aquaculture resource management (FARM) model. Aquaculture 264:160–174
36. Duarte P, Meneses R, Hawkins AJS, Zhu M, Fang J, Grant J (2003) Mathematical modelling to assess the carrying capacity for multi-species culture within coastal waters. Ecol Eng 168:109–143
37. Ménesguen A, Cugier P, Loyer S, Vanhoutte-Brunier A, Hoch T, Guillaud J-F, Gohin F (2007) Two- or three-layered box-models versus fine 3D models for coastal ecological modelling? A comparative study in the English Channel (Western Europe). J Mar Syst 64:47–65

38. Grant J, Curran KJ, Guyondet TL, Tita G, Bacher C, Koutitonsky V, Dowd M (2007) A box model of carrying capacity for suspended mussel aquaculture in Lagune de la Grande-Entrée, Iles-de-la-Madeleine, Québec. Ecol Eng 200:193–206
39. Mazouni N, Gaertner JC, Deslous-Paoli JM (2001) Composition of biofouling communities on suspended oyster cultures: an in situ study of their interactions with the water column. Mar Ecol Prog Ser 214:93–102
40. Richard M, Archambault P, Thouzeau G, Desrosiers G (2006) Influence of suspended mussel lines on the biogeochemical fluxes in adjacent water in the Îles-de-la-Madeleine (Quebec, Canada). Can J Fish Aquat Sci 63:1198–1213
41. Nizzoli D, Bartoli M, Viaroli P (2007) Oxygen and ammonium dynamics during a farming cycle of the bivalve *Tapes philippinarum*. Hydrobiologia 587:25–36
42. Souchu P, Vaquer A, Collos Y, Landrein S, Deslous-Paoli JM, Bertrand Bibent B (2001) Influence of shellfish farming activities on the biogeochemical composition of the water column in Thau lagoon. Mar Ecol Prog Ser 218:141–152
43. Cugier P, Ménesguen A, Guillaud JF (2005) Three-dimensional (3D) ecological modelling of the Bay of Seine (English Channel, France). J Sea Res 54:104–124
44. Cranford PJ, Strain PM, Dowd M, Hargrave BT, Grant J, Archambault MC (2007) Influence of mussel aquaculture on nitrogen dynamics in a nutrient enriched coastal embayment. Mar Ecol Prog Ser 347:61–78
45. Alonso-Pérez F, Ysebaert T, Castro CG (2010) Effects of suspended mussel culture on benthic-pelagic coupling in a coastal upwelling system (Ría de Vigo, NW Iberian Peninsula). J Exp Mar Biol Ecol 382:96–107
46. Nizzoli D, Welsh DT, Fano EA, Viaroli P (2006) Impact of clam and mussel farming on benthic metabolism and nitrogen cycling, with emphasis on nitrate reduction pathways. Mar Ecol Prog Ser 315:151–165
47. Richard M, Archambault P, Thouzeau G, McKindsey CW, Desrosiers G (2007) Influence of suspended scallop cages and mussel lines on pelagic and benthic biogeochemical fluxes in Havre-aux-Maisons Lagoon, Îles-de-la-Madeleine (Quebec, Canada). Can J Fish Aquat Sci 64: 1491–1505
48. Dame RF, Prins TC (1998) Bivalve carrying capacity in coastal ecosystems. Aquat Ecol 31:409–421
49. Beadman HA, Willows RI, Kaiser MJ (2002) Potential applications of mussel modelling. Helgol Mar Res 56:76–85
50. Grant J, Bacher C (1998) Comparative models of mussel bioenergetics and their validation at field culture sites. J Exp Mar Biol Ecol 219:21–44
51. Kooijman SALM (2010) Dynamic energy budget theory for metabolic organisms, 3rd edn. Cambridge University Press, Cambridge
52. Sousa T, Domingos T, Poggiale J-C, Kooijman SALM (2010) Dynamic energy budget theory restores coherence in biology. Philos Trans R Soc B 365:3413–3428
53. Saraiva S, Van Der Meer J, Kooijman SALM, Sousa T (2011) Modelling feeding processes in bivalves: a mechanistic approach. Ecol Eng 222:514–523
54. Filgueira R, Grant J, Strand Ø, Asplin L, Aure J (2010) A simulation model of carrying capacity for mussel culture in a Norwegian fjord: role of induced upwelling. Aquaculture 308:20–27
55. Bacher C, Gangnery A (2006) Use of dynamic energy budget and individual based models to simulate the dynamics of cultivated oyster populations. J Sea Res 56:140–155
56. Rosland R, Strand Ø, Bacher C, Alunno-Bruscia M, Strohmeier T (2009) Applying dynamic energy budget (DEB) theory to predict growth and bio-energetics of blue mussels under low seston conditions. J Sea Res 62:49–61
57. Ferreira JG, Sequeira A, Hawkins AJS, Newton A, Nickell TD, Pastres R, Forte J, Bodoy A, Bricker SB (2009) Analysis of coastal and offshore aquaculture: application of the FARM model to multiple systems and shellfish species. Aquaculture 289:32–41
58. Muetzelfeldt R, Massheder J (2003) The simile visual modelling environment. Eur J Agron 18:345–358
59. Filgueira R, Grant J (2009) A box model for ecosystem-level management of mussel culture carrying capacity in a coastal bay. Ecosystems 12:1222–1233
60. Cloern JE (1982) Does the benthos control phytoplankton biomass in south San Francisco Bay? Mar Ecol Prog Ser 9:191–202
61. Officer CB, Smayda TA, Mann R (1982) Benthic filter feeding: a natural eutrophication control. Mar Ecol Prog Ser 9:203–210
62. Klepper O, van der Tol MWM, Scholten H, Herman PMJ (1994) SMOES: a simulation model for the Oosterschelde ecosystem. Part 1: Description and uncertainty analysis. Hydrobiologia 282–283:437–451
63. Sequeira A, Ferreira JG, Hawkins AJS, Nobre A, Lourenço P, Zhang XL, Yan X, Nickell T (2008) Trade-offs between shellfish aquaculture and benthic biodiversity: a modelling approach for sustainable management. Aquaculture 274:313–328
64. Cugier P, Struski C, Blanchard M, Mazurié J, Pouvreau S, Olivier F, Trigui JR, Thiébaut E (2010) Assessing the role of benthic filter feeders on phytoplankton production in a shellfish farming site: Mont Saint Michel Bay, France. J Mar Syst 82:21–34
65. McKindsey CW, Lecuona M, Huot M, Weise AM (2009) Biodeposit production and benthic loading by farmed mussels and associated tunicate epifauna in Prince Edward Island. Aquaculture 295:44–51
66. Petersen JK (2007) Ascidian suspension feeding. J Exp Mar Biol Ecol 342:127–137
67. Gangnery A (2003) Etude et modélisation de la dynamique des populations de bivalves en élevage (*Crassostrea gigas* et *Mytilus galloprovincialis*) dans le bassin de Thau (Méditerranée, France) et des ascidies solitaires associées. PhD thesis. Universite de Montpellier II - Sciences et Techniques du Languedoc, Montpellier, France
68. van der Tol MWM, Scholten H (1998) A model analysis on the effect of decreasing nutrient loads on the biomass of benthic

suspension feeders in the Oosterschelde ecosystem (SW Netherlands). Aquat Ecol 31:395–408
69. Jiang WM, Gibbs MT (2005) Predicting the carrying capacity of bivalve shellfish culture using a steady, linear food web model. Aquaculture 244:171–185
70. van Stralen MR, Dijkema RD (1994) Mussel culture in a changing environment: the effects of a coastal engineering project on mussel culture (*Mytilus edulis* L.) in the Oosterschelde estuary (SW Netherlands). Hydrobiologia 282(283):359–379
71. Wassmann P (1998) Retention versus export food chains: processes controlling sinking loss from marine pelagic systems. Hydrobiologia 363:29–57
72. Strayer DL, Smith LC, Hunter DC (1998) Effects of the zebra mussel (*Dreissena polymorpha*) invasion on the macrobenthos of the freshwater tidal Hudson River. Can J Zool 76:419–425
73. Connell SD (2005) Assembly and maintenance of subtidal habitat heterogeneity: synergistic effects of light penetration and sedimentation. Mar Ecol Prog Ser 289:53–61
74. Grant J, Cranford P, Hargrave B, Carreau M, Schofield B, Armsworthy S, Burdett-Coutts V, Ibarra D (2005) A model of aquaculture biodeposition for multiple estuaries and field validation at blue mussel (*Mytilus edulis*) culture sites in eastern Canada. Can J Fish Aquat Sci 62:1271–1285
75. Weise AM, Cromey CJ, Callier MD, Archambault P, Chamberlain J, McKindsey CW (2009) Shellfish-DEPOMOD: modelling the biodeposition from suspended shellfish aquaculture and assessing benthic effects. Aquaculture 288:239–253
76. Giles H (2009) Modelling the dispersal of biodeposits from mussel farms: the importance of simulating biodeposit erosion and decay. Aquaculture 291:168–178
77. Giles H, Pilditch CA (2004) Effects of diet on sinking rates and erosion thresholds of mussel *Perna canaliculus* biodeposits. Mar Ecol Prog Ser 282:205–219
78. Walker TR, Grant J (2009) Quantifying erosion rates and stability of bottom sediments at mussel aquaculture sites in Prince Edward Island, Canada. J Mar Syst 75:46–55
79. Pearson TH, Rosenberg R (1978) Macrobenthic succession in relation to organic enrichment and pollution of the marine environment. Oceanogr Mar Biol Annu Rev 16:229–311
80. Callier MD, Richard M, McKindsey CW, Archambault P, Desrosiers G (2009) Responses of benthic macrofauna and biogeochemical fluxes to various levels of mussel biodeposition: an in situ "benthocosm" experiment. Mar Pollut Bull 58:1544–1553
81. Borja Á, Rodríguez JG, Black K, Bodoy A, Emblow C, Fernandes TF, Forte J, Karakassis I, Muxika I, Nickell TD, Papageorgiou N, Pranovi F, Sevastou K, Tomasetti P, Angel D (2009) Assessing the suitability of a range of benthic indices in the evaluation of environmental impact of fin and shellfish aquaculture located in sites across Europe. Aquaculture 293:231–240
82. Tenore KR, Boyer LF, Cal RM, Corral J, Garcia-Fernandez C, Gonzalez N, Gonzalez-Gurriaran E, Hanson RB, Iglesias J, Krom M, Lopez-Jamar E, McClain J, Pamatmat MM, Perez A, Rhoads DC, de Santiago G, Tietjen J, Westrich J, Windom HL (1982) Coastal upwelling in the Rias Bajas, NW Spain: contrasting the benthic regimes of the Rias de Arosa and de Muros. J Mar Res 40:701–772
83. Gibbs MT (2004) Interactions between bivalve shellfish farms and fishery resources. Aquaculture 240:267–296
84. Christensen V, Walters CJ, Pauly D (2005) Ecopath with Ecosim: a user's guide. Fisheries Centre, University of British Columbia, Vancouver
85. Wolff M (1994) A trophic model of Tongoy Bay – a system exposed to suspended scallop culture (Northern Chile). J Exp Mar Biol Ecol 182:149–168
86. Lin HJ, Shao KT, Kuo SR, Hsieh HL, Wong SL, Chen IM, Lo WT, Hung JJ (1999) A trophic model of a sandy barrier lagoon at Chiku in southwestern Taiwan. Estuar Coast Shelf Sci 48: 575–588
87. Wolff M, Koch V, Isaac V (2000) A trophic flow model of the Caeté Mangrove Estuary (North Brazil) with considerations for the sustainable use of its resources. Estuar Coast Shelf Sci 50:789–803
88. Brando VE, Ceccarelli R, Libralato S, Ravagnan G (2004) Assessment of environmental management effects in a shallow water basin using mass-balance models. Ecol Eng 172: 213–232
89. Byron C, Link J, Costa-Pierce B, Bengtson D (2011) Modeling ecological carrying capacity of shellfish aquaculture in highly flushed temperate lagoons. Aquaculture 314:87–99
90. Plaganyi EE, Butterworth DS (2004) A critical look at the potential of ECOPATH with ECOSIM to assist in practical fisheries management. S Afr J Mar Sci 26:261–287
91. Steele JH (2009) Assessment of some linear food web methods. J Mar Syst 76:186–194
92. Broekhuizen N, Zeldis J, Stephens SA, Oldman JW, Ross AH, Ren J, James MR (2002) Factors related to the sustainability of shellfish aquaculture operations in the Firth of Thames: a preliminary analysis. NIWA client report EVW02243. NIWA, New Zealand, pp vi + 106
93. Hoagland P, Jin D, Kite-Powell H (2003) The optimal allocation of ocean space: aquaculture and wild-harvest fisheries. Mar Resour Econ 18:129–147
94. Dolmer P, Frandsen RP (2002) Evaluation of the Danish mussel fishery: suggestions for an ecosystem management approach. Helgol Mar Res 56:13–20
95. Stead SM, Burnell G, Goulletquer P (2003) Aquaculture and its role in integrated coastal zone management. Aquac Int 10:447–468
96. Nobre AM, Ferreira JG, Nunes JP, Yan X, Bricker S, Corner R, Groom S, Gu H, Hawkins AJS, Hutson R, Lan D, Lencart e Silva JD, Pascoe P, Telfer T, Zhang X, Zhu M (2010) Assessment of coastal management options by means of multilayered ecosystem models. Estuar Coast Shelf Sci 87:43–62
97. Byron C, Bengtson D, Costa-Pierce B, Calanni J (2011) Integrating science into management: ecological carrying capacity of bivalve shellfish aquaculture. Mar Policy 35:363–370

98. Norton BG (2005) Sustainability: a philosophy of adaptive ecosystem management. University of Chicago Press, Chicago
99. Cole DN, Stankey GH (1997) Historical development of limits of acceptable change: conceptual clarifications and possible extensions. In: McCool SF, Cole DN (eds) Proceedings – limits of acceptable change and related planning processes: progress and future directions: from a workshop held at the University of Montana's Lubrecht Experimental Forest. Gen. Tech. Rep. INT-GTR-371. U.S. Department of Agriculture, Forest Service, Rocky Mountain Research Station, Ogden, UT, pp 5–9
100. McCool SF (1996) Limits of acceptable change: a framework for managing national protected areas: experience from the United States. In: Workshop on impact management in marine parks, Maritime Institute of Malaysia, August 13–14. Kuala Lumpur, Malaysia, pp 1–15
101. Zeldis J, Felsing M, Wilson J (2006) Limits of acceptable change: a framework for managing marine farming. Water Atmosphere 14:16–17
102. Krumpe E, McCool SF (1997) Role of public involvement in the limits of acceptable change wilderness planning system. In: McCool SF, Cole DN (eds) Proceedings – limits of acceptable change and related planning processes: progress and future directions: from a workshop held at the University of Montana's Lubrecht Experimental Forest. Gen. Tech. Rep. INT-GTR-371. U.S. Department of Agriculture, Forest Service, Rocky Mountain Research Station, Ogden, UT, pp 16–20
103. Weible CM, Pattison A, Sabatier PA (2010) Harnessing expert-based information for learning and the sustainable management of complex socio-ecological systems. Environ Sci Policy 13:522–534
104. Soto D, Aguilar-Manjarrez J, Brugère C, Angel D, Bailey C, Black K, Edwards P, Costa-Pierce B, Chopin T, Deudero S, Freeman S, Hambrey J, Hishamunda N, Knowler D, Silvert W, Marba N, Mathe S, Norambuena R, Simard F, Tett P, Troell M, Wainberg A (2008) Applying an ecosystem-based approach to aquaculture: principles, scales and some management measures. In: Soto D, Aguilar-Manjarrez J, Hishamunda N (eds) Building an ecosystem approach to aquaculture. FAO/Universitat De Les Illes Balears expert workshop, 7–11 May 2007. Palma De Mallorca, Spain; FAO Fisheries and Aquaculture proceedings, vol 14. Rome, pp 15–35
105. Walker B, Carpenter S, Anderies J, Abel N, Cumming G, Janssen M, Lebel L, Norberg J, Peterson GD, Pritchard R (2003) Resilience management in social-ecological systems: a working hypothesis for a participatory approach. Conserv Ecol 6:1–14
106. Ostrom E (2009) A general framework for analyzing sustainability of social-ecological systems. Science 325:419–422
107. Whitmarsh D, Palmieri MG (2009) Social acceptability of marine aquaculture: the use of survey-based methods for eliciting public and stakeholder preferences. Mar Policy 33:452–457
108. Nobre AM, Musango JK, de Wit MP, Ferreira JG (2009) A dynamic ecological-economic modeling approach for aquaculture management. Ecol Econ 68:3007–3017
109. Ferreira JG, Hawkins AJS, Monteiro P, Moore H, Service M, Pascoe PL, Ramos L, Sequeira A (2008) Integrated assessment of ecosystem-scale carrying capacity in shellfish growing areas. Aquaculture 275:138–151
110. Lu L, Grant J (2008) Recolonization of intertidal infauna in relation to organic deposition at an oyster farm in Atlantic Canada – A field experiment. Estuar Coasts 31:767–775

Books and Reviews

Department of Marine and Natural Resources (2001) Guidelines for landscape and visual impact assessment of marine aquaculture. Department of Marine and Natural Resources, Dublin, pp 1–65

GESAMP (2008) Assessment and communication of environmental risks in coastal aquaculture. GESAMP reports and studies no 76. FAO, Rome, pp 198

Hewitt CL, Campbell ML, Gollasch S (2006). Alien species in aquaculture. Considerations for responsible use. IUCN, Gland and Cambridge, UK, pp viii + 32

Marques JC, Salas F, Patrício J, Teixeira H, Neto JM (2009) Ecological indicators for coastal and estuarine environmental assessment. WIT Press, Southampton

Ward T, Phillips B (2008) Ecolabelling of seafood: the basic concepts. Wiley-Blackwell, Oxford, p 472

WWF (2010) Bivalve aquaculture dialogue standards. http://www.worldwildlife.org/what/globalmarkets/aquaculture/WWFBinaryitem17872.pdf. Accessed 3 May 2011, pp 22

CdTe Solar Cells

Stephan Buecheler, Lukas Kranz, Julian Perrenoud, Ayodhya Nath Tiwari
Laboratory for Thin Films and Photovoltaics, EMPA – Swiss Federal Laboratory for Materials Science and Technology, Duebendorf, Switzerland

Article Outline

Glossary
Definition of the Subject
Introduction
State-of-the-Art of CdTe Solar Cells
Industrial Production
Processing and Properties

Environmental and Material Resource Issues
Further Directions
Abbreviations
Bibliography

Glossary

CdTe Inorganic compound semiconductor with high absorption coefficient (larger than 10^4 cm^{-1}) and almost ideal energy bandgap (1.49 eV) for terrestrial photovoltaic applications.

Conversion efficiency Ratio between the useful electrical power of the solar cell or module to the incoming sunlight power (here called efficiency). The conversion efficiency of solar cells and modules depends on external parameters such as temperature, irradiation intensity, and spectrum. For comparable results the conversion efficiency has to be measured under standard test conditions (STC). If not otherwise mentioned the presented efficiency values are measured under STC.

Heterojunction A pn-junction where the p- and n-type semiconductors are different materials such as a junction in the CdTe/CdS stack.

Photovoltaic (effect) Direct conversion of the sunlight into electricity, first discovered by A. E. Becquerel in 1839.

pn-junction Combination of p- and n-type semiconductors for the separation of charge carriers generated by the photovoltaic effect.

Solar cell Electronic device for direct conversion of solar energy into electrical energy using the photovoltaic effect (also called photovoltaic cell).

Solar module Interconnection of a number of solar cells in series for increasing the output voltage or in parallel for increasing the output current.

Standard test conditions (STC) Definition of the external parameters for the device under test during determination of the photovoltaic performance. These include a defined irradiation intensity of 100 mW/cm^2, a reference illumination spectrum AM1.5 G, and device temperature of 25 °C.

Thin film Layer of material with thickness between sub-nanometer and few micrometers. Thin film solar cells consist of a stack of several thin films with different properties and functions.

Definition of the Subject

CdTe thin film solar cells and modules are currently the driving force for production cost reduction in the whole photovoltaic sector. The device concept is simple consisting of multilayer stack of metal and semiconducting thin films. For the deposition of these layers a variety of large area and high-speed deposition methods are available. The CdTe solar cell as it is known today was first described in 1969 by Adirovich et al. [1]. In the beginning of the twenty-first century CdTe solar modules dominated the PV market in terms of production volume and lowest cost. This chapter is a review of more than 40 years of research and development activities and hot topics in the field of CdTe thin film photovoltaics.

Introduction

Still today the photovoltaic (PV) market is dominated by silicon wafer-based solar modules; however, in 2009 the annual production volume of CdTe thin film solar modules increased to above 10% of the total annual PV production [2]. The enormous increase of the CdTe-based PV in the market share in the recent history is induced by the company First Solar Inc. By the end of 2009, they reached a production capacity of 1.4 GWp and announced production costs as low as 0.76$/Wp as well as a plan for further growth of the capacity toward 2.2 GWp by end of 2012 [3]. This makes the leading producer of CdTe PV technology First Solar Inc. to be the largest solar cell manufacturer worldwide (2010).

In CdTe compound semiconductor-based solar cells CdTe is the absorbing material with direct energy bandgap of 1.49 eV at 300K [4] and an absorption coefficient larger than 10^4 cm^{-1} for photons with energy above the bandgap [5]. In the Shockley-Queisser model these are almost ideal properties for the application of terrestrial solar energy conversion [6]. The theoretical efficiency limit of CdTe-based solar cells is about 30% under AM1.5 G irradiation (reference spectrum of the sun under an angle of 48.2°, the spectrum is specified in the international standard IEC60904-3 Ed.2 2008) [6, 7].

CdTe solar cell research started with the investigation of pn-homojunctions by RCA Laboratories, USA, in the late 1950s; Paul Rappaport at RCA Lab reported an efficiency of 2.1% (100 mW/cm^2, unknown

spectrum) for a p-type CdTe single crystal-based cell with one-sided n-type doping by indium in 1959 [8]. Twenty years later in 1979, active area efficiency of 6% (90 mW/cm^2, tungsten lamp) was reported by French National Center for Scientific Research (CNRS) in France for a homojunction device with a p-type CdTe layer grown by close space vapor transport deposition onto a n-type single crystalline CdTe substrate [9]. In 1982, CNRS reported improved efficiency of 10.7% (107 mW/cm^2, AM1 spectrum) with the same deposition method [10]. The main problems of the single crystal CdTe solar cells based on the concept of shallow pn-homojunction are linked to the difficulties in achieving high doping concentration in the thin p-type conducting layer that is deposited onto the n-type single crystal and also the diffusion of compensating dopants from the thin layer into the CdTe substrate [11].

CdTe heterojunction solar cells were investigated in two approaches according to the CdTe conductivity type. Work on n-type CdTe was mainly done in combination with p-type Cu_2Te. This investigation started in the 1960s and the best cell efficiency of about 7% (60 mW/cm^2, unknown spectrum) was reported in 1973 by Justi et al. [12]. In those devices light enters through the p-type Cu_2Te layer and is absorbed in the n-type CdTe and a metal mesh is used as front contact. A major problem in further increasing the efficiency was the lack of p-type transparent conductors.

The work on p-type CdTe solar cells also started in the 1960s by depositing a thin layer of n-type semiconductor on p-type CdTe single crystals [13]. In this configuration the highest efficiency of 13.4% (100 mW/cm^2, AM1.5) with remarkable high open circuit voltage of 892 mV was obtained with a n-In_2O_3/p-CdTe junction [14].

Thin film CdS/CdTe solar cells as they are known today were first demonstrated by Adirovich et al. in 1969 with efficiency of about 1% (100 mW/cm^2, unknown spectrum) [1]. A comprehensive description of CdS/CdTe solar cells including fundamental issues some of which are still open challenges today was presented by Bonnet and Rabenhorst in 1972 [15]. They reported an efficiency of up to 6% (50 mW/cm^2, xenon arc lamp using UV and IR filters). The CdS/CdTe thin film solar cells have been intensively studied by many research groups worldwide. Major previous reviews on CdTe thin film photovoltaics include the pioneer work of R.H. Bube [16], the book chapters of McCandless & Sites [17] and of Burgelman [18], a special issue on CdTe in Solar Cells [19], and several other contributions such as a comparison between CIGS and CdTe technology [20]. In the following sections a review of the achievements, results, and challenges of thin film CdS/CdTe solar cell research and development is presented.

State-of-the-Art of CdTe Solar Cells

State-of-the-art high-efficiency CdTe solar cells are multilayer devices with CdS and CdTe thin films as n-p heterojunctions sandwiched between front and back electrical contacts. Figure 1 shows the schematic cross-section of such a CdS/CdTe thin film solar cell in superstrate configuration (layer stacks are always given in sequence of the deposition). The superstrate configuration means that the light enters the device through the substrate which has to be a transparent material for optical photons. In this configuration a transparent and electrically conducting front contact is deposited first on the substrate. Typical materials used for this purpose in CdTe solar cells are transparent conductive oxide (TCO) layers such as tin oxide doped with fluorine (FTO), indium oxide doped with tin (ITO), zinc oxide doped with aluminum (AZO), and cadmium stannate Cd_2SnO_4 (CTO). In most highly efficient CdS/CdTe solar cell configurations the TCO layer is

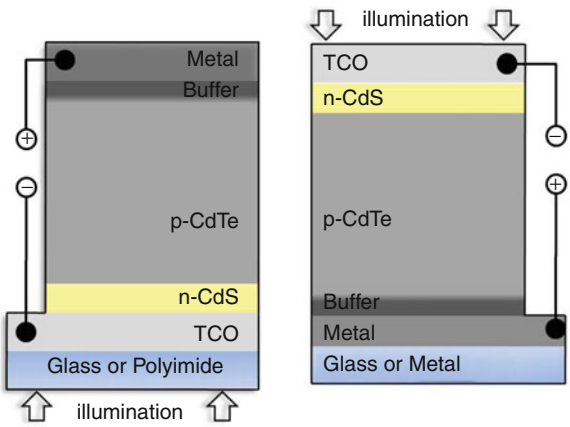

CdTe Solar Cells. Figure 1
Schematic cross-sections of CdS/CdTe thin film solar cells in superstrate (*left*) and substrate (*right*) configuration

covered by a highly resistive and transparent (HRT) layer. The function of that HRT layer is discussed in section Highly Resistive and Transparent Layer.

A thin layer of CdS is deposited as n-type semiconductor onto the TCO followed by the p-type CdTe absorber. The TCO/CdS/CdTe layer stack is annealed in a chlorine and oxygen containing ambient, which is commonly referred to as "activation treatment" or "$CdCl_2$ treatment." For low resistive ohmic electrical back contact formation, a chemical etching process for modification of the CdTe surface is commonly applied. The necessity of that surface treatment process prior to the metal back contact deposition is because of the problems associated with high electron affinity and energy bandgap of CdTe. The requirements, properties, and functionality of each layer and CdTe surface modifications are described in section Processing and Properties. The very first CdS/CdTe thin film solar cell in superstrate configuration was presented already in 1969 by Adirovich et al. [1] with efficiency of about 1% under low illumination intensity. They deposited the CdS and subsequently CdTe layers onto conductive SnO_2 coated glass substrates and used Cu as back electrical contact. Figure 2 shows the schematic energy band diagram for state-of-the-art CdS/CdTe solar cells. In this schematic the light is entering the device from the left side.

Broadly, the CdTe solar cell processing technology can be categorized based on high or low deposition temperatures used for the deposition of the CdTe layer. High-temperature methods (above 550°C) include close space sublimation (CSS), vapor transport deposition (VTD), and modifications of those, while low-temperature methods (below 450°C) include sputtering, electro deposition (ED), and high vacuum evaporation (HVE). Table 1 shows a summary of achieved solar cell efficiencies on rigid glass and flexible polyimide substrates with CdTe layer deposited by different methods.

The certified record efficiency for CdS/CdTe solar cells on glass is 16.5% on cell level achieved by the

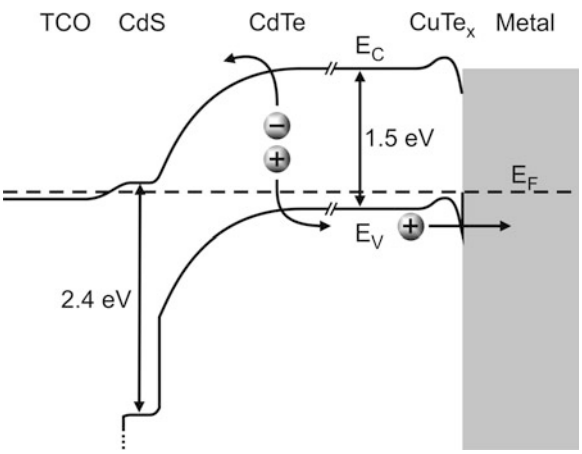

CdTe Solar Cells. Figure 2
Schematic energy band diagram of CdS/CdTe solar cells

CdTe Solar Cells. Table 1 PV performance of CdS/CdTe solar cells in superstrate configuration deposited by various methods on rigid glass and flexible polymer substrate. The given temperature is the maximum temperature of the complete process. If not otherwise mentioned, the PV performance was measured under standard test conditions

Method	Temp (°C)	Substrate/TCO/HRT	Eff. (%)	V_{OC} (mV)	J_{SC} (mA/cm^2)	FF (%)	Area (cm^2)	Lab	Ref.
CSS	660	BSG/CTO/ZTO	16.5	845	25.9[a]	75.5	1.03	NREL	[21, 22]
VTD	550	SLG/SnO_2/Ga_2O_3	13.6	810	23.7	70.8	–	IEC	[23]
Sputter	390	ASG/AZO	14.0	814	23.6	73.3	0.15	Toledo	[24]
HVE	420	BSG/AZO/i-ZnO	15.6	834	24.7[a]	75.9	0.15	Empa	[25]
ED	400	Glass/FTO	14.2	819	23.5[b]	74	0.02	BP Solar	[26]
HVE	420	PI/AZO/i-ZnO	12.4	823	19.6	76.5	0.15	Empa	[27]
Sputter	390	PI/AZO	10.7	768	19.5	69.8	–	Toledo	[28]

BSG borosilicate glass, *ASG* aluminosilicate glass, *SLG* soda-lime glass, *PI* polyimide
[a]With antireflection (AR) coating
[b]Measured under ELH lamp with 84 mW/cm^2 intensity

National Renewable Energy Laboratory (NREL), USA, using a complex process to minimize various optical and electrical losses and deposition/annealing process temperatures to well above 600°C [21]. Efficiency of 15.6% was achieved with the low-temperature (below 450°C) HVE process [25]. It can be seen in Table 1 that for high- and low-temperature processed devices comparable open circuit voltages and fill factors are obtained. This indicates that the process temperature for the CdTe deposition may not have a major impact on the electrical quality of the polycrystalline semiconductor as far as their relevance for the highest reported efficiencies are concerned. The largest difference of the compared devices is visible in the short circuit current density depending on the optical properties of the used TCO material, the CdS layer thickness, and the substrate material itself.

The limited transmittance through the substrate material can also impose a major limitation in the CdS/CdTe solar cells in superstrate configuration. While borosilicate glass (BSG) has 3–5% higher transparency compared to standard soda-lime glass (SLG) the low transparency of polyimide (PI) is particularly a problem for the development of flexible, lightweight solar cells. Polyimide has been currently identified as the most promising material for the development of flexible CdS/CdTe solar cells in superstrate configuration.

The PI material is chemically stable and processing temperatures of 450°C in vacuum can be applied without significant changes of the material properties. With flexible and lightweight substrate highest efficiency of 12.4% was obtained using a low-temperature HVE process [27]. The rather low J_{SC} of that device results from the optical losses in the PI film while V_{OC} and FF of flexible devices on PI are comparable to cells on glass substrates (see Table 1).

Optical losses in the substrate material are not an issue in CdTe/CdS devices grown in the substrate configuration. This configuration was first described by Bonnet and Rabenhorst in 1972 [15]. They used a conductive molybdenum foil as substrate material covered with a thin layer of Cu. The CdTe layers were deposited by high-temperature vapor phase deposition (HTVPD) at 650°C followed by the CdS layer grown with vacuum evaporation and contacted with indium. With this configuration they reached device efficiencies between 5% and 6% (50 mW/cm^2, xenon arc lamp using UV and IR filters). The role of the thin Cu layer between the Mo foil and the CdTe was for the formation of a heavily doped Cu_xTe interlayer as tunneling contact.

In Table 2, various CdTe/CdS devices in substrate configuration on rigid glass and flexible substrate are compared. The highest efficiency of 9.9% was reported by Romeo et al. already in 1992 [29]. They used a BSG substrate covered with a thin layer of Cu followed by a Mo layer as electrical back contact. They argued that the Cu diffuses through the Mo and forms a Cu_xTe interlayer which acts as a tunneling contact between the Mo and the CdTe. The CdTe layer was deposited by HVE method followed by a sputtered CdS layer. The cell was finished with a 3 μm thick AZO layer. In 2010, Empa developed a completely Cu-free CdTe solar cell in

CdTe Solar Cells. Table 2 PV performance of CdS/CdTe solar cells in substrate configuration deposited by various methods on rigid and flexible substrates. The given temperature is the maximum temperature of the complete process

Method	Temp (°C)	Substrate	Eff. (%)	V_{OC} (mV)	J_{SC} (mA/cm^2)	FF (%)	Area (cm^2)	Lab	Ref.
HVE	500	BSG/Cu/Mo	9.9	690	28[a]	51	0.3	Parma	[29]
HVE	420	BSG/Mo/Sb_2Te_3	8.6	658	21.4	61	0.15	Empa	[30]
HTVPD	650	Mo foil/Cu	5			45		BI	[15]
CSS	570	Mo foil	3.5	500	10.6	40	–	UNAM	[31]
HVE	500	Mo foil	5.3	629	22.0	38	–	El Paso	[32]
HVE	450	PI/Au/Cu	7.3	692	21.6	49	–	ETHZ	[33]
Sputter	390	Mo foil/ZnTe	7.8				0.05	Toledo	[34]

[a]Spectrum and intensity of artificial illumination not reported

substrate configuration using a Mo/Sb_2Te_3 back contact structure with efficiency of 8.6% measured under standard test conditions. In this device the CdTe layer was deposited by HVE followed by CBD-CdS and finished with a sputtered i-ZnO/AZO bilayer electrical front contact [30].

With flexible CdTe/CdS devices in substrate configuration highest efficiency of 7.8% was obtained with a nitrogen doped ZnTe tunneling contact between a Mo foil and a sputtered CdTe layer [34]. Without tunneling enhancing interlayer efficiency of 5.3% was reported by Singh et al. [32]. Romeo et al. achieved an efficiency of 7.3% on polyimide in substrate configuration using a lift-off process [33]. The difficulty in formation of a low resistive and ohmic contact to the p-type CdTe – which does not contribute to diffusion of back contact elements across the pn-junction during cell processing and lifetime of the device – is the major limitation of the substrate configuration. The physical aspects of the ohmic contact formation are discussed in more detail in section Processing and Properties.

Industrial Production

For solar electricity generation CdTe solar cells are interconnected to large area solar modules in order to yield high voltage and power. For thin film solar modules commonly monolithical interconnection is used where the layers are patterned during the growth of the multilayer stack for serial connection of adjacent cells. Figure 3 shows the principle of the monolithic interconnection.

The industrial production of CdTe thin film solar modules started in the 1980s. At that time several companies located in USA, Japan, and Germany started large-scale production with different deposition technologies. Golden Solar Inc., USA, developed a production plant based on spray deposition technique with annual capacity of 2 MWp [35]. Solar Cells Inc., USA (now First Solar Inc.), worked on the industrialization of the high rate vapor transport technique [36]. BP Solar, USA, used electrodeposition for the growth of the CdTe layer and achieved module efficiency of 10.9% [37]. Matsushita Battery Company Ltd., Japan, developed screen printing as well as CSS technologies for large-scale CdTe deposition [38]. Both, BP Solar and Matsushita Battery built pilot-production plants for CdS/CdTe thin film solar modules, however, stopped their activities in 2002. Antec Solar GmbH, Germany, worked on the industrialization of a CSS technique based on the work of the solar pioneer Dieter Bonnet [39].

The key players in CdTe solar module commercialization are listed in Table 3. Today the company First Solar Inc. dominates not only the production of thin film solar modules but the whole PV market in terms of large production volume and lowest cost of production. With annual production capacity of 1.4 GWp in 2010, First Solar Inc. has a total PV market share of more than 10%. Abound Solar, USA, is on the way of becoming the second largest producer of CdTe thin film modules with an annual production capacity target of 200 MWp in 2010 [46]. The third company, which offers a CdTe solar module on the market is Calyxo GmbH, a subsidiary of the company Q-Cells SE in Germany. The annual production capacity target of Calyxo is 110 MWp by 2011 [42]. Arendi, a start-up company in Italy announced to set up a production plant for annual production capacity of 15 MWp. PrimeStar Solar, a company in USA with involvement of General Electric, announced an annual production capacity of tens of MWp. Roth&Rau AG together with CTF company in Germany is involved in developing

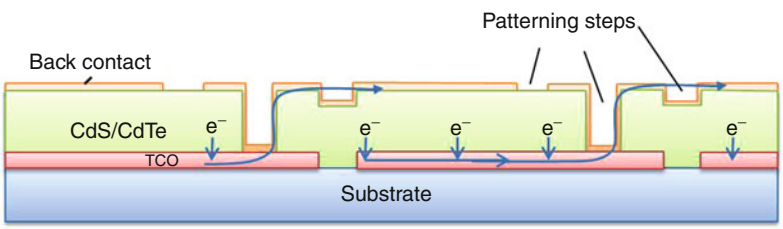

CdTe Solar Cells. Figure 3
Principle of monolithic interconnection of single cells to solar modules

CdTe Solar Cells. Table 3 Summary of industrial activity on CdS/CdTe solar modules

Company	Eff. (%)	V_{OC} (V)	J_{SC} (A)	FF (%)	Area (m^2)	Method	Ref.
Abound Solar	10.1	47.8	2.28	66.8	0.72		[40]
Antec Solar[a]	6.9	85.0	1.11	52.8	0.72	CSS	[41]
Arendi						CSS	
BP Solar[a]	10.9	26.2	3.24	62.3	0.49	ED	[37]
Calyxo[b]	9.0	90.7	1.16	61.9	0.72	APVTD	[42]
First Solar Inc.	11.1	61.7	1.76	73.8	0.72	VTD	[43]
Golden Photon[a]	8.5				0.33	Spray	[44]
Matsushita[a]	9.3				0.12	Printing	[38]
Matsushita[a]	11.0				0.54	CSS	[38]
Roth&Rau[c]	9.9	121	2.39		1.92		[45]
Prime Star Solar	–					CSS	
Xunlight 26 Solar[d]						Sputtering	
Solexant[d]						Printing	
von Roll Solar[d]						Printing	

[a]Currently no activity
[b]Announced module efficiency of 10.8% in July 2010
[c]Development of turnkey CdTe production plants
[d]Development of flexible CdTe solar modules

and offering turnkey CdTe production plants with an annual capacity of 80 MWp [47].

Most of the mentioned companies with currently running production plants of significant volume develop modules on rigid glass substrates. Substituting a flexible substrate for the rigid glass can further increase the low-cost potential of this technology. Flexible CdTe solar cells and modules offer several advantages in the production of devices as well as on the final product in terrestrial and space applications. A cost-effective and fast roll-to-roll deposition process is possible with the use of a flexible substrate material. Also faster heating and cooling are applicable for thin flexible substrate material and there is no need for cost intensive robotics as needed for handling of fragile and heavy glass. This approach will not only lower the production cost but also the energy payback time significantly.

Due to the light-weightiness and flexibility of the final product new markets become attractive. The building integrated architecture will enter new dimensions for energy production on roofs and facades not only for flat surfaces but also for complex curved shapes as well as for lightweight industrial and rural buildings. Other applications include the portable source of power for mobile and electronic applications. Flexible CdTe solar cells have been already developed in the superstrate and substrate configurations. Efficiencies of 3.5–7.8% have been reported for the substrate configuration using molybdenum foil as substrate material [15, 31, 32, 34]. The highest reported efficiencies of flexible CdTe solar cells in superstrate configuration on PI are 10.7% by sputtering [28] and 12.4% by high vacuum evaporation [27]. Using the later technology a flexible 31.9 cm^2 CdTe solar module of 8.0% total area efficiency was developed at Empa, Switzerland, with 11 cells monolithically interconnected by all laser-based scribing [48].

The company Xunlight 26 Solar, USA, is currently developing flexible CdS/CdTe solar modules using an all-sputtering approach based on the technology developed by Compaan et al. at Toledo University [28] while

a few start-up companies have announced pilot plants based on proprietary printing technologies, e.g., Solaxant, USA, and von Roll Solar, Switzerland.

Processing and Properties

In this section processing and properties of the individual layers in the multilayered state-of-the-art CdTe thin film solar cells are described in detail.

Window Layer

The most commonly used CdTe thin film solar cells are pn-heterojunction devices. The junction is formed between the p-type CdTe compound semiconductor and a n^+-type window layer stack. This is a one-sided abrupt junction resulting in an almost complete shift of the depletion region into the p-type absorber material. Photons with energy above the energy bandgap of the n-type semiconductor stack are absorbed in the window material. Carriers generated within the diffusion length from the junction in the window material are collected and contribute to the photocurrent. However, because of the high recombination rate in the window layer and the asymmetric depletion region across the junction, most of the carriers generated in the window material are lost. Since photons absorbed in the window layer do not contribute to the overall current it is essential to reduce the parasitic light absorption in the window material or layers to improve the performance of such devices.

For optimum flow of minority charge carriers across the junction a continuous band alignment is desired. In heterojunction devices the pn-junction forming partners most often have different energy bandgaps resulting in energy band discontinuities. In such heterojunction devices the band offset in the conduction band between the p-type absorber and the n-type window material should be small in order to prevent a barrier formation for photogenerated electrons [49].

The requirements for the n-type window stack can be summarized as follows (cf. [49–51]):

- Sufficiently large bandgap and negligible absorption of light with energy below the energy bandgap of the window material in order to reduce parasitic absorption losses.
- Conduction band offset ΔE_C with p-type counter part of the heterojunction should be small; a negative ΔE_C enhances interface recombination of electron hole pairs and a positive ΔE_C forms a potential barrier for electrons.
- Formation of no or only minimum number of interface traps (deep defects) at the junction. A large interface trap density increases the recombination velocity at the interface.
- Fermi level close to the conduction band in order to reach a high built in potential and high recombination barrier for holes at the interface.
- High conductivity for efficient electron transport from the heterojunction to an external circuit.

In state-of-the-art CdTe-based solar cells a stack of three layers is used to meet the above-mentioned requirements of the window material. The stack is composed of a TCO layer for electronic transport of the generated charge carriers and a HRT layer in order to prevent shunting and current flow back into weak diodes. Both the TCO and the HRT layers are high bandgap materials with low parasitic absorption losses, however, with an unfavorable conduction band offset if directly applied onto the absorber layer which results in rather low efficiency devices [25]. In order to improve the band alignment between the n-type window material and the p-type absorber layer a thin CdS buffer layer is essential. An additional requirement of the CdS layer is the reduction of the interface trap (deep-defect) density.

Transparent Conductive Oxide Layer The transparent conductive oxide has to combine high transparency in the wavelength range between 300 and 850 nm with high electrical conductivity. As the presence of free carriers, which is needed for the current transport, leads to free carrier absorption there is always a trade of between conductivity and transparency. The most commonly used metal oxides for TCO materials are FTO, ITO, AZO, and CTO. Deposition techniques for thin film TCO include spray pyrolysis, chemical vapor deposition (CVD), rf- and pulsed dc-sputtering, and pulsed laser deposition. The method used for the deposition influences the layer properties as well as the production costs of the TCO layer. In superstrate device configuration it is an inevitable requirement that the

TCO layer needs to withstand the subsequent layer depositions and treatments during CdTe solar cell production. Hence the suitability of the TCO material is predetermined by the selection of the CdTe solar cell production processes. For example, ZnO-based TCOs are incompatible with the ammonium hydroxide containing chemical bath deposition (CBD) solution often used for CdS deposition as well as with heat treatments above 300°C in the presence of oxygen due to increasing resistivity [52].

The optical and electrical performance of the TCO layer directly influences the J_{SC} and FF of the device [53]. To quantify and compare the optical and electrical performance of different TCOs, Roy Gordon [54] proposed the expression $\sigma/\alpha = R_s * ln(\mathrm{T} + \mathrm{R}) - 1$ as figure of merit, where σ is the conductivity, α the absorption coefficient (average value in the visible range), R_s is the sheet resistance in ohm square, and T and R are the total transmittance and reflectance (in the visible range). The highest figure of merit will be achieved by the TCO with the largest product of effective electron mass and mobility, while film thickness and doping concentration are less important parameters [55]. In Table 4, commonly used TCO materials are compared according to this figure of merit. It should be noted that the defined figure of merit does not take the specific plasma frequency and transparency cut of band-to-band transitions into account (usually in the UV part). For CdTe solar cells, where the response of the device (300–850 nm) is close to the visible range of the solar spectrum (380–780 nm), this figure of merit is a meaningful value. Absorption in the glass which is mainly caused by iron impurities is also a source of optical loss in commercially available low-cost glasses.

CdTe Solar Cells. Table 4 Figure of merit (As proposed by Gordon [55]) of some TCO materials used for CdTe solar cells. The higher the figure of merit value the higher will be the expected achievable solar cell efficiency

Material	Sheet resistance (Ω/square)	Visible abs. coeff. alpha	Figure of merit (Ω^{-1})	Ref.
CTO	10	0.01	10	[21]
ZnO:F	5	0.03	7	[55]
AZO (CVD)	3.8	0.05	5	[55]
AZO (sputtered)	4.5	0.04	5	[30]
ITO	6	0.04	4	[55]
FTO	8	0.04	3	[55]

Other aspects that can play an important role for the choice of the TCO material are the minimum required deposition temperature, diffusion barrier properties, chemical durability, morphology and nucleation properties, and toxicity. A discussion of these and other aspects can be found in the work of Gordon [55].

For CdTe solar cell production FTO is one of the favored TCO materials as it is chemically and thermally stable and low-cost deposition processes, such as spray, are suitable for large-scale deposition. The highest figure of merit is achieved with CTO. With this layer processed at 660°C the highest reported CdTe solar cell efficiency of 16.5% has been achieved in conjunction with ZTO as highly resistive and transparent interlayer [21]. As shown in Table 4 also, AZO is an excellent material due to its figure of merit. Low cost of the raw material, low required deposition temperature, low toxicity, and low plasma frequency compared to competitive materials are other advantages of this material. The lower thermal and chemical stability compared to FTO and CTO are however problematic when conventional high-temperature production processes (like CSS) are used for CdTe solar cells. However, using low-temperature deposition techniques (below 450°C) several research groups have succeeded in producing highly efficient CdTe solar cells on ZnO-based TCOs [25, 56].

Highly Resistive and Transparent Layer In high-efficiency CdTe devices a highly resistive and transparent (HRT) layer is added between the TCO and the CdS in order to limit electrical losses at local shunts and grain boundaries which can occur especially in solar cells with reduced CdS layer thickness. Commonly used materials include SnO_2 [57], In_2O_3 [58], Ga_2O_3 [17], ZnO [25], and Zn_2SnO_4 (ZTO) [21]. Because of possible nonconformal layer deposition of CdS on TCO and recrystallization during the $CdCl_2$ treatment of the CdS/CdTe stack, direct contacts between the TCO and the CdTe can locally occur due to island formation of the CdS and/or sulfur diffusion into the CdTe.

This means that locally the pn-junction can be formed between the TCO and the CdTe semiconductors [59]. Those TCO-CdTe diodes are connected in parallel with the CdS/CdTe diodes and adversely influence the device performance mainly reducing the V_{OC} and FF and hence the efficiency.

Rau et al. developed a model through which the beneficial effect of the i-ZnO layer in polycrystalline Cu(In,Ga)Se_2 (CIGS)-based solar cells can be explained by the conduction band offset at the HRT-buffer interface enabling self-limitation of electrical losses due to electrical potential differences between the n-type window material and the single grains in the CIGS absorber [60]. The offset barrier limits current flowing into the diodes with poor quality and thus improves the performance of parallel connected diodes. A similar role is envisaged for the HRT layer in CdTe-based devices. Additionally, the HRT layer can reduce diffusion from the TCO into the CdTe of metallic elements such as indium or aluminum which are potential compensating donors in the p-type CdTe.

CdS Buffer and Alternatives In state-of-the-art high-efficiency CdTe solar cells CdS is used as a buffer between the n-type transparent oxide bilayer and the p-type CdTe layer. The main role of the CdS layer is the proper alignment of the conduction and valence band in the heterojunction as well as reduction of interface traps. The CdS layer can be deposited with various techniques like CBD [21, 37, 61], sputter deposition [24], CSS [22], and HVE [62]. This variety of growth possibilities allows choosing a deposition technique which is compatible to the subsequent CdTe growth by either vacuum or non-vacuum-based processes. CdS grows intrinsically n-type and no relevant conduction band offset between CdS and CdTe is formed as calculations [63] and measurements [64] revealed. If a thick CdS layer is used (above 200 nm), nearly all photons with wavelength below 517 nm are absorbed in the CdS. As the electron hole pairs in the CdS layer are barely collected this leads to losses in the J_{SC} in the order of about 5 mA/cm^2 which translates into an efficiency loss of approximately 20% relative. The CdS absorption losses can be reduced by reducing the CdS layer thickness and simultaneously introducing the HRT layer to compensate for possible inhomogeneous coverage (see Fig. 4). Table 5 illustrates the effects of CdS thickness reduction and application of HRT layer on the PV properties of CdTe solar cells.

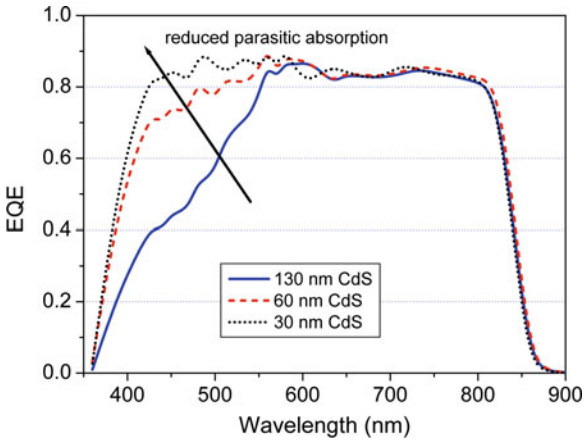

CdTe Solar Cells. Figure 4
External quantum efficiency (EQE) of CdS/CdTe devices with varied CdS layer thickness. The higher photo current of devices with thin buffer (below 100 nm) is compromised by decreasing V_{OC} and FF. Optimum efficiency for lab cells is obtained with 50–80 nm thick CdS and HRT layers

CdTe Solar Cells. Table 5 Impact of CdS window layer thickness and the use of HRT layers on solar cell performance [65]. The given CdS thickness is measured before the annealing treatment of the CdS/CdTe stack in $CdCl_2$ ambient

Window layer (thickness) (nm)	HRT layer (thickness) (nm)	V_{OC} (mV)	J_{SC} (mA/cm^2)	FF (%)	Eff (%)
CdS (240)	No	803	18.4	73.8	10.9
CdS (120)	No	699	19.9	47.6	6.6
CdS (120)	i-ZnO (200)	844	21.0	72.3	12.8

In large area module production, however, a certain thickness of CdS is needed to maintain high production yield; hence a significant J_{SC} loss due to parasitic light absorption is inevitable in industrially produced CdTe solar modules. Although the application of HRT layer helps in improving the reproducibility and processing robustness, there is still an interest to search for alternative materials to CdS, primarily to reduce optical losses. Promising candidates to replace CdS are wide bandgap oxides or sulfides. The requirements for

an alternative material are proper conduction band alignment to CdTe, sufficient temperature stability, and no out diffusion, especially of n-doping elements into CdTe (like Al, In, Ga), during subsequent CdTe deposition and annealing treatment. The ZnO/CdTe heterojunction has already been studied in 1988 [66] and is reported to yield solar cell efficiencies close to 10% [25]. This heterojunction system suffers from unfavorable band alignment and a large lattice mismatch [67, 68]. ZnS and $Zn_xCd_{1-x}O$ grown by CBD have been tested as n-type partner to CdTe leading to 3% efficient CdTe thin film devices [69]. ZnS deposited by spray pyrolysis and $ZnO_{1-x}S_x$ deposited by atomic layer deposition (ALD) were investigated leading to nearly 10% efficient CdTe thin film devices [70]. The external quantum efficiency of such a ZnS/CdTe device is shown in comparison with a conventional CdS/CdTe device with 120 nm thick CdS layer in Fig. 5. Also shown are the transmittance (corrected for reflectance by T + R) of TCO and the HRT layers. The areas between the curves labeled with the numbers 1, 2, and 3 indicate the dominant optical loss mechanisms due to parasitic light absorption in the CdS layer, reflection at the various interfaces, and the free carrier absorption in the TCO, respectively. The $ZnO_{1-x}S_x$ ternary compound is especially promising as it allows tuning the band alignment to CdTe via engineering the sulfur to oxygen ratio [71].

CdTe Absorber Layer

The compound semiconductor CdTe has a bandgap of 1.49 eV at 300 K and an absorption coefficient of $>10^4$ cm^{-1}. This makes CdTe an ideal absorber material in thin film solar cells.

Another big advantage of CdTe is its simple phase diagram (Fig. 6) compared to other compound semiconductors. CdTe evaporates congruently. The compound has a considerably higher fusion temperature and lower vapor pressure than the single elements. Excess tellurium and cadmium have a low solubility in CdTe. This facilitates stoichiometric growth and allows the utilization of a variety of different deposition techniques. Commonly used deposition techniques are described in the following subsections. A comprehensive review of CdTe deposition and properties can be found in [17].

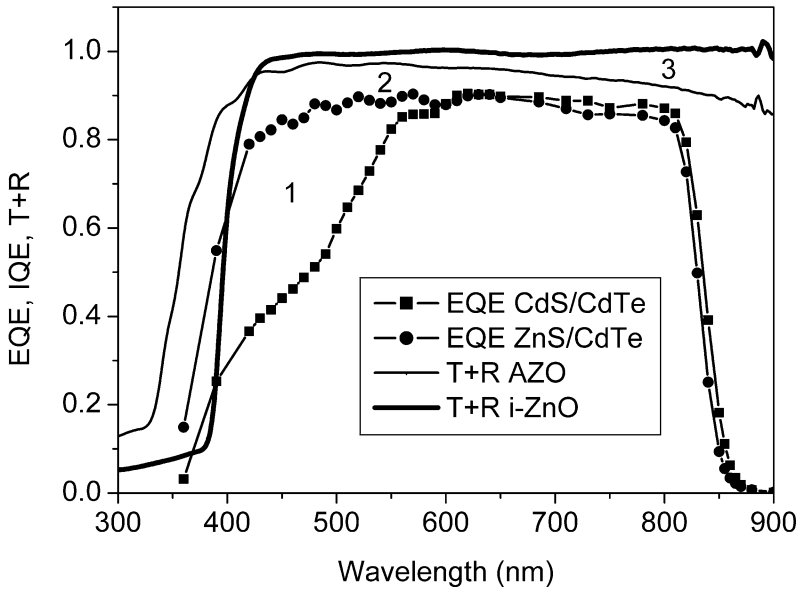

CdTe Solar Cells. Figure 5
Comparison of external quantum efficiency of CdS/CdTe and ZnS/CdTe solar cells. The other *curves* shown are transmittance plus reflectance (T + R) of the AZO TCO layer and the i-ZnO HRT layer. The areas between the curves labeled by the numbers 1, 2, and 3 indicate the dominant loss mechanisms due to CdS absorption, reflection, and TCO free carrier absorption, respectively

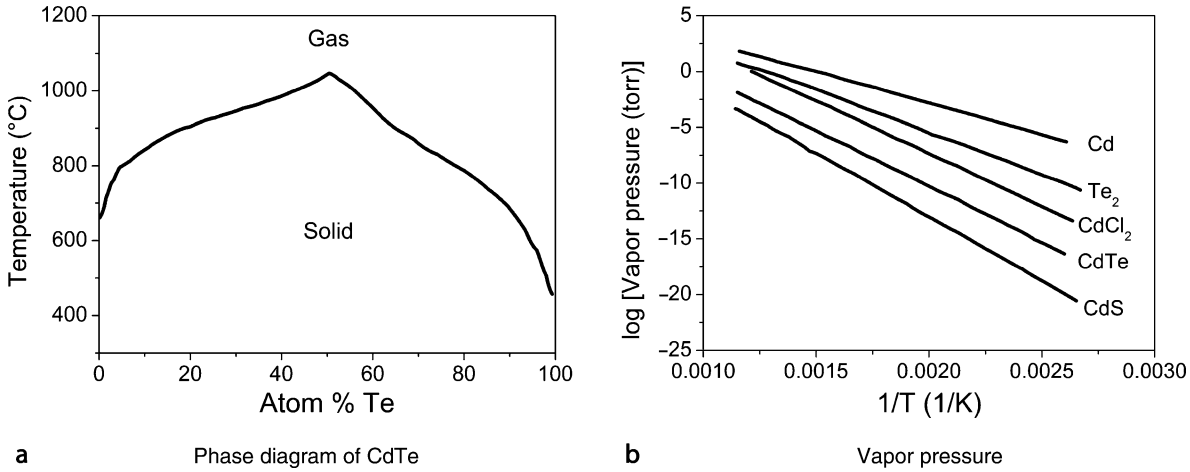

CdTe Solar Cells. Figure 6

(**a**) T-x Phase Diagram of CdTe at 1 atm. (**b**) Vapor pressures of different materials used for the production of CdTe solar cells. Due to the simple phase diagram of CdTe and the higher vapor pressures of the single elements compared to the compound, the growth of CdTe is relatively simple (Data from [17])

CdTe Deposition Techniques

Close Space Sublimation (CSS) CdTe is evaporated out of the compound in an ambient of inert gas (Ar) with pressures in the order of 1 mbar [21, 39]. A small amount of oxygen is commonly added in order to reduce the formation of pinholes and to improve junction quality. A small source-substrate distance of a few millimeters is used to allow the sublimated material to reach the substrate at the rather high pressure. With this method growth rates on the order of µm/min are achieved. Substrate and source temperatures of approximately 600°C and 700°C are used, respectively. Grains of as-deposited layers exhibit nearly random orientation and are commonly 1–10 µm in size. A typical scanning electron microscopy (SEM) picture of the CdTe surface is shown in Fig. 7a. The current efficiency record for CdTe solar cells of 16.5% has been produced using this method [21].

Vapor Transport Deposition (VTD) A carrier gas (argon and oxygen) saturated with Cd and Te vapor is transferred to the heated substrate (500–600°C) where supersaturation and subsequent reaction to CdTe happens [72–74]. Grain sizes and orientation are comparable to CSS-deposited films. First Solar Inc., the largest producer of CdTe modules, is using this technique in its production plants [75].

High Vacuum Evaporation (HVE) CdTe is deposited either by co-evaporation from elemental sources or by evaporation from the compound source in high vacuum (10^{-6} mbar) [20, 25, 76]. Figure 7b shows that as-deposited grains have sizes of approximately 0.5–1 µm with a strong preferential orientation in (111) direction. In spite of using a growth temperature as low as 350°C this technique has proven to yield efficiencies up to 15.6% [25]. The low-temperature process also allows the growth of flexible and lightweight cells on polyimide film (section "State-of-the-Art of CdTe Solar Cells").

Sputtering A CdTe target is sputtered by Ar-ions at a pressure of about 10 mtorr [56, 77, 78]. Cd and Te are transferred to the sample where condensation and film growth takes place. CdTe films are grown at substrate temperatures of 200–400°C and as-sputtered CdTe with grain sizes of 100–200 nm are obtained [79]. With this method, 14% efficient cells on glass have been produced [56]. Sputtering has also been used for flexible cells on polymer films.

Metal Organic Chemical Vapor Deposition (MOCVD) Cd and Te containing metal-organic precursors are transferred to the substrate by a carrier gas where the precursors decompose and reaction to

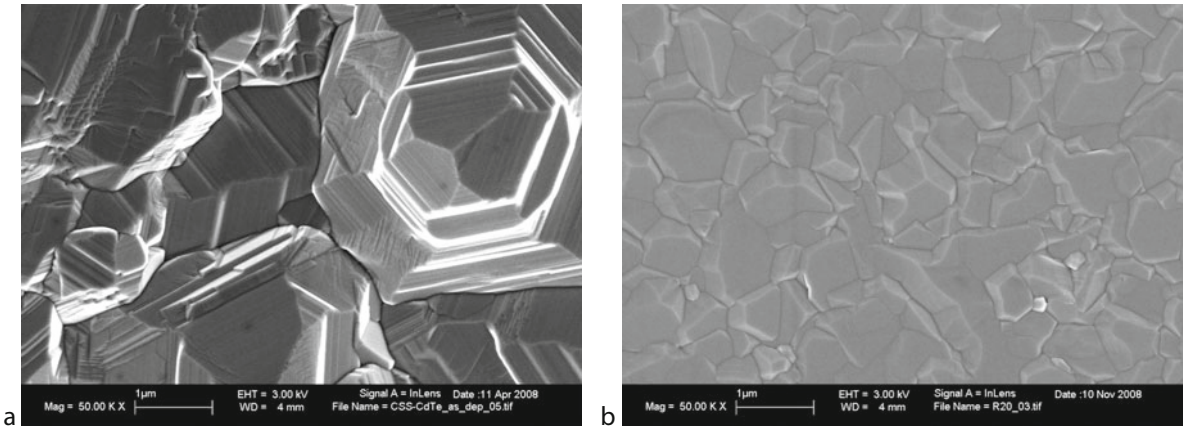

CSS-CdTe HVE-CdTe

CdTe Solar Cells. Figure 7
Scanning electron microscope (SEM) pictures of as-deposited CSS-CdTe and HVE-CdTe

CdTe occurs [80]. An atmospheric pressure and a growth temperature of 300–400°C are used. With a MOCVD-grown CdTe/CdZnS solar cell, 13.3% efficiency has been achieved [80].

Electrodeposition The cathodic electrodeposition of CdTe is carried out from acidic solutions containing Cd^{2+} and $HTeO_2^+$ [81]. The ions are reduced at the substrate and reaction to CdTe occurs. The temperature of the bath is approximately 90°C. Grain sizes of as-deposited CdTe films are of the order of 0.1–0.5 um. Subsequent annealing leads to recrystallization and conversion of the CdTe layer from n-type to p-type.

Screen Printing A paste containing CdTe, $CdCl_2$, and a binder is deposited onto the substrate through a mesh at atmospheric pressure [82, 83]. After heating to remove the binders, the layer is annealed at 600–700°C to recrystallize the film and activate the junction. With this method, 12.8% solar cells have already been produced in 1984 [83].

Spray Deposition A solution containing precursors of Cd and Te and complexing agents is sprayed at atmospheric pressure onto a substrate [84–86]. Dissolved CdTe nanoparticles are also used for spraying CdTe films. After removal of the solvents by heating, the layer is annealed at temperatures up to 600°C.

Spin-Casting of Dissolved Nanocrystals A solar cell based on CdTe or CdSe nanoparticles has been introduced by the group of P. Alivisatos [87]. Dissolved CdTe or CdSe nanoparticles are spin-cast from solution on a TCO. The company Solexant is currently bringing this technology to market.

$CdCl_2$ Annealing Treatment In order to obtain highly efficient CdTe solar cells, a heat treatment of the CdS/CdTe stack in a chlorine containing ambient is mandatory. This annealing treatment is commonly referred to as $CdCl_2$-treatment or activation treatment. The treatment is crucial for highly efficient CdTe solar cells produced with any method. Figure 8 shows that the treatment improves all cell parameters. The details of the ambient, temperature, and duration may differ from group to group, depending on the process. Many investigations of the influence of the treatment on the structural and electronical properties of solar cells have been carried out. Comprehensive reviews can be found in [88, 89].

Annealing Treatment Methods The annealing treatment is performed in the presence of chlorine and oxygen at temperatures of 400–500°C [88, 89]. Chlorine can be introduced in various ways, but the most common way is by using $CdCl_2$. CdTe films produced by screen printing of spray deposition, e.g., are treated with additives of $CdCl_2$. In the case of

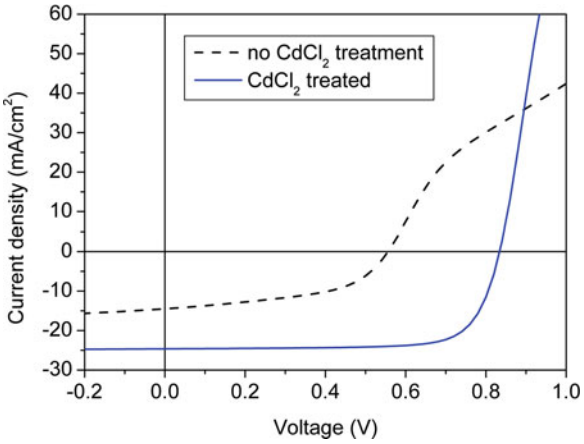

CdTe Solar Cells. Figure 8
Photovoltaic performance of a HVE-grown CdTe solar cell heat treated at 420 °C with and without the presence of $CdCl_2$

HVE- or CSS-CdTe, $CdCl_2$ is usually added after deposition. It can be done by dipping the cell into a solution of $CdCl_2$ in methanol, but because of problems for large-scale manufacturing, other methods have been developed like vacuum deposition of $CdCl_2$ and subsequent annealing in air or annealing the sample in a vapor containing $CdCl_2$ [90–92]. Alternatively to $CdCl_2$ one can use other Cl-containing chemicals to perform the treatment of CdTe. A gas from the Freon© family has been also used to fabricate CSS-CdTe solar cells with efficiency up to 15.8% [93, 94]. Apart from replacing the $CdCl_2$ in the treatment, the Freon© treatment has the advantage of eliminating the need of an etching step, which is difficult to implement into in-line production [95]. However, some environmental concerns are raised about using this gas, but a close cycle loop can help to overcome this problem. Other possible chlorine sources include HCl or Cl_2 [91, 96]. The different treatments showed similar effects on the structural and electronic properties.

Structural Effects The $CdCl_2$-treatment can have a strong influence on the structural properties of CdS and CdTe layers and interfaces depending on the growth conditions and the properties of the as-deposited layers.

As-deposited HVE-CdTe grows heteroepitaxially on the CdS grains with a columnar structure with many stacking faults and a (111) preferred orientation especially when grown at low temperatures as it can be seen in Fig. 9 [62, 97]. The $CdCl_2$ treatment leads to recrystallization of the CdTe layer which starts from the surface of CdTe [97]. $CdCl_2$ acts as a sintering flux, enhancing grain growth and coalescence of grains. After the treatment HVE-CdTe grain sizes have grown to sizes of a few micrometers [62, 97]. The treatment reduces the preferential orientation in (111) direction, the orientation relationship between CdTe and CdS is lost, and the number of stacking faults is strongly reduced (Fig. 9). When the treatment in air is performed without the presence of chlorine, the increase in grain size is diminished and less reduction in stacking fault density is observed [97].

As-deposited CdTe layers grown with the high-temperature CSS-method exhibit large grain sizes, which increase with increasing distance from the CdS junction in addition to a few smaller CdTe grains close to the CdS junction. In this case no grain growth upon heat treatment is observed for large grains, while grain growth has been found for small grains close to the junction (Fig. 10) [97, 98].

As-deposited CdTe layers by electrodeposition method have rather small grains but after the annealing treatment significantly enlarged grain size is observed. In that case no extra $CdCl_2$ is added since the precursors contain the elements that are needed for the recrystallization.

In conclusion, small grains become larger after recrystallization while no significant change is observed for initially large grains. CdTe grain sizes, which can differ for different deposition methods, have comparable sizes after the treatment.

The lattice mismatch between CdTe and CdS is ~10% [99], which can lead to a large number of defects at the interface [97]. This lattice mismatch can partly be compensated by intermixing of CdS and CdTe in the interface region, forming $CdS_{1-x}Te_x$. The bandgap of the compound changes from 1.49 eV for CdTe to 2.4 eV for CdS with a bowing which has its minimum at about 1.4 eV for a S content of about 25%. The ternary compound has a miscibility gap, which was determined for temperatures above 650°C [100] and expanded to conditions relevant during activation treatment [101]. The solubility limit of S in CdTe and of Te in CdS at 415°C was determined to be 5.8% and 3%, respectively.

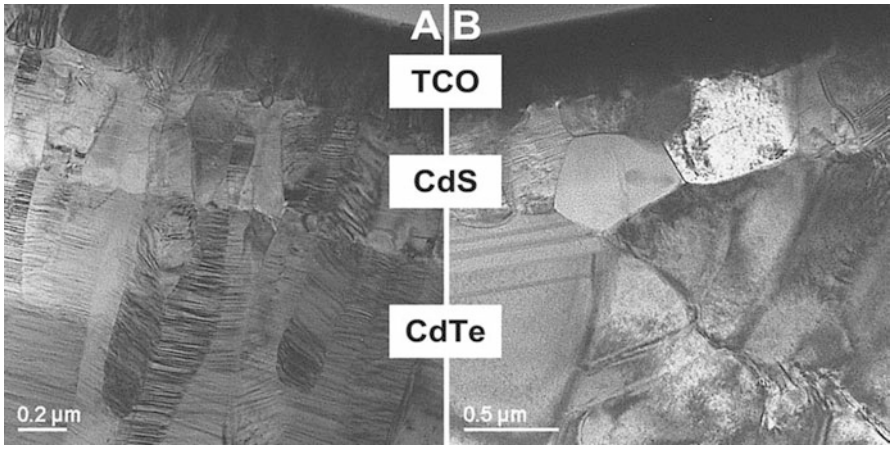

CdTe Solar Cells. Figure 9
Transmission electron microscopy (TEM) pictures of as-deposited and treated CdTe solar cells deposited by HVE [59]

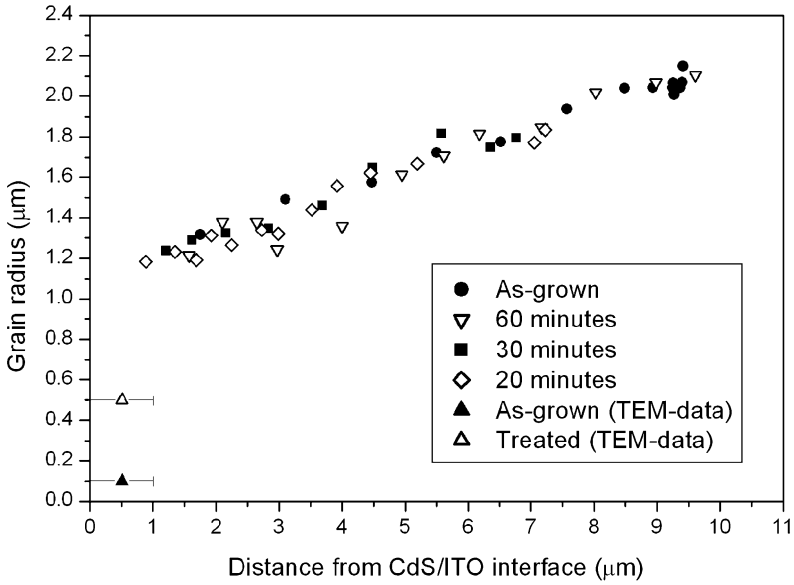

CdTe Solar Cells. Figure 10
As-deposited CSS-CdTe has large grains in the order of 1–3 µm with smaller grains close to the junction. CSS-CdTe does not show growth of large grains upon $CdCl_2$ treatment, but small grains close to the junction exhibit grain growth (Adapted from [98])

The highest S concentration observed in CdTe is close to the solubility limit [89, 97].

After the $CdCl_2$ treatment, intermixing of CdTe and CdS is observed as illustrated in Fig. 11. The extent of intermixing depends on the deposition methods used for CdS and CdTe layers. Intermixing has beneficial as well as detrimental effects. As already mentioned, it facilitates lattice relaxation between CdTe and CdS, which can reduce defects in the interface region and improve the junction formation. It leads to a partial consumption of the CdS layer; due to this consumption the spectral response in the short wavelength region is

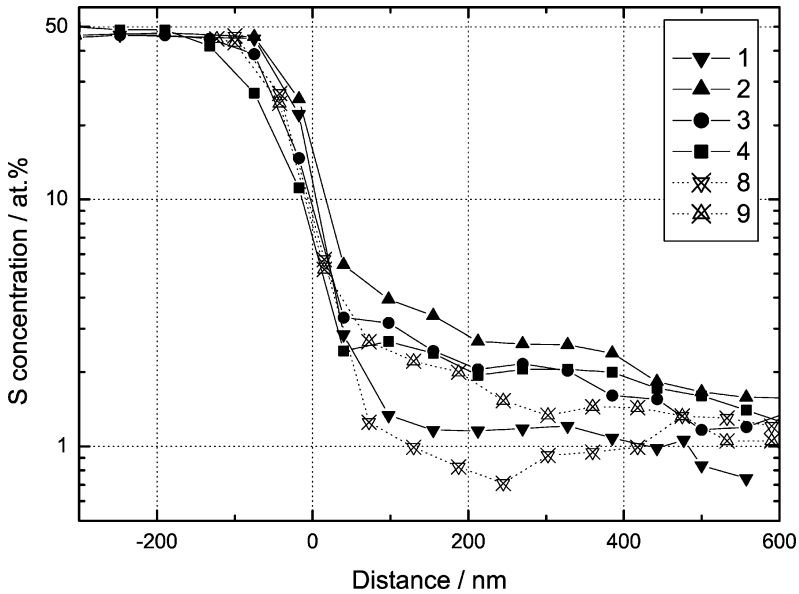

CdTe Solar Cells. Figure 11
Concentration profiles of sulfur across the CdS/CdTe interface for both HVE- and CSS-grown cells after deposition and after heat treatment with different amounts of $CdCl_2$. 1: As-deposited by HVE. 2,3,4: 30 min treated at 430 °C with 400, 150, and 70 nm $CdCl_2$, respectively. 8,9: As-deposited by CSS and treated with 100 nm $CdCl_2$ for 15 min at 420 °C [97]

enhanced (section "CdS Buffer and Alternatives"). However, if all CdS is consumed, the junction will be built between $CdTe_{1-x}S_x$ and the TCO, which has inferior junction properties compared to CdTe/CdS and yields lower V_{OC} and fill factor. A complete CdS consumption can also occur locally, if the CdS layer thickness is too small due to nonuniformity or because the CdS layer recrystallizes nonuniformly. This results in many CdTe/CdS and CdTe/TCO junctions connected in parallel, also decreasing the V_{OC} and FF of the cell. In order to minimize the effect of a reduced voltage with decreasing CdS thickness, a HRT layer is introduced between CdS and the TCO, as it builds a more effective junction to CdTe than the TCO [25] (section "CdS Buffer and Alternatives"). A negative effect of CdS/CdTe intermixing is the decrease of the window layer bandgap by diffusion of Te into CdS. It shifts the absorption of the window layer to longer wavelengths. On the other hand, S diffusion into CdTe reduces the bandgap of CdTe, shifting the cutoff of the spectral response to a larger wavelength which is shown in EQE plot in Fig. 12. This yields a slightly higher quantum efficiency in the wavelength region close to the CdTe bandgap.

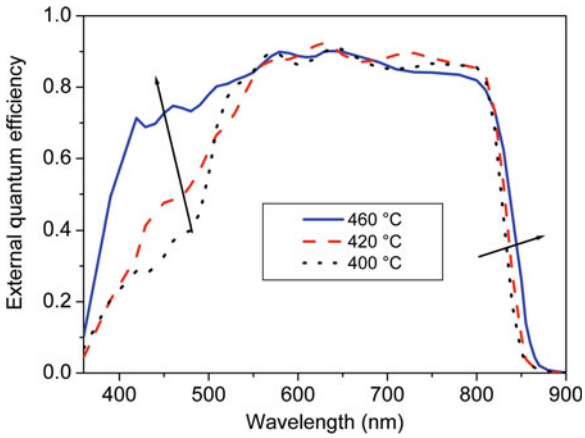

CdTe Solar Cells. Figure 12
Effect of variation of treatment temperature on the quantum efficiency. More CdS is consumed at higher treatment temperatures. The cutoff at the absorber band edge is slightly shifted to larger wavelengths for higher temperatures

Electronic Effects The treatment has pronounced effect on the electrical properties of the CdTe layer causing conductivity type conversion from n- to p-type and further enhancing the p-type conductivity

of the CdTe layer. This is not obvious at first glance, as Cl_{Te} is an n-dopant in single crystalline CdTe, but the V_{Cd}-Cl_{Te} complex, the so-called A-center is a shallow acceptor [102, 103]. The p-type doping with Cl cannot be achieved in the presence of Cd overpressure, but only with excess Te [104]. This is achieved by the presence of oxygen during annealing. The presence of oxygen further increases the effective acceptor concentration in the annealed CdTe layer and the V_{OC} of the finished cells [105]. These electronic changes might be explained by a surface-type conversion through the formation of a Cd-deficient surface layer by the preferential oxidation of Cd. Oxidation thus leads to deviation from stoichiometry and Cd-vacancies are generated below the surface, enhancing p-type conductivity [104, 106]. Additionally, isoelectronic oxygen can act as a shallow acceptor in CdTe [107]. The annealing treatment also leads to an efficient passivation of the grain boundaries, which reduces recombination at trapping states associated with the grain boundaries. However, several studies also found an increased number of deep defects after treatment, which might limit the performance [108–111].

Influence of Polycrystallinity The polycrystalline nature of the absorber influences the performance of a CdTe solar cell. Grain boundaries can induce a large number of trapping states [112], which can serve as recombination centers for the photogenerated charges, decreasing cell performance. Grain boundaries can also lead to local band bending, which builds a potential barrier and therefore hinders charge transport across grain boundaries [113]. However, polycrystalline CdTe solar cells exhibit a very good performance and even outperform its single crystalline counterpart [114]. The high performance of polycrystalline devices is possible because of an efficient passivation of the grain boundaries after the absorber treatment. According to a model by Visoly-Fisher et al. [115] the better performance of polycrystalline devices can be explained by hole depletion along grain boundaries which occurs after the annealing treatment of the absorber. The hole depletion results in local downward band bending close to the grain boundaries, which assists in the separation of photogenerated charge carriers (Fig. 13). Holes are transported through the grain bulk to the back contact, while electrons are transported along the depleted grain boundaries to the junction. Due to this depletion the recombination of minority carriers is reduced. On the one hand, depleted grain boundaries enhance charge separation and transport but on the other hand the cell voltage is reduced as depleted grain boundaries ending at the junction are connected in parallel with the main junction of the CdTe/CdS cell.

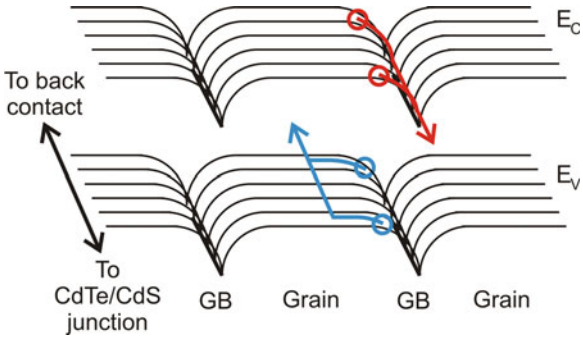

CdTe Solar Cells. Figure 13
According to a model by Visoly-Fisher, grain boundaries assist in separation of generated electron hole pairs. Hole depletion along grain boundaries leads to band bending. Holes are drawn toward the grain boundaries and are transported along grain boundaries, while electrons are transported in the grain bulk (Redrawn from [114])

CdTe Thickness Reduction Due to the high absorption coefficient only 1 μm of CdTe is needed to convert 92% of the sunlight with energies larger than the bandgap into electricity. Nevertheless, thicker CdTe (2–10 μm) is commonly employed to avoid pinholes and grain boundary recombination pathways originating from weak control on film morphology, microstructure, and device structure. Currently R&D efforts are being made to decrease the CdTe thickness without negative effect on the cell performance, as less material consumption would further decrease the cost of CdTe solar modules. Especially a decreased amount of Te due to thinner CdTe could enable an increase of the market share of CdTe modules [116]. By re-optimizing the post-deposition treatment and the back contact annealing and using a mild etchant for CdTe, it is possible to achieve comparable efficiencies with absorbers of about 1 μm thickness [106, 117].

Doping of CdTe The short circuit current density in highly efficient CdTe solar cells is quite close to its theoretical limit (26 mA/cm^2 vs. 30 mA/cm^2), while the open circuit voltage is well below its theoretical limit. In spite of a comparable bandgap of CdTe and GaAs, the V_{OC} of CdTe is about 200 mV lower than the V_{OC} of single crystalline GaAs devices and also the FF is slightly lower. The low voltage of CdTe solar cells is caused by a rather low carrier lifetime of about 1 ns and low hole density of about 10^{14} cm^{-3} [118]. A way to increase the open circuit voltage would be by increasing the shallow acceptor density. For this purpose doping of p-CdTe is essential. However, substitutional doping of p-type II–VI semiconductors is generally challenging because of self-compensation [119, 120]. Self-compensation denotes the spontaneous formation of defects, which partly or completely compensate the doping of the intentionally incorporated dopants. Especially in large bandgap semiconductors the spontaneous formation of compensating defects can be energetically favorable. These compensating defects can be spontaneously formed through native defects like vacancies, interstitials, antisites, or dopant-vacancy pairs. Also the added impurity can compensate itself if it has amphoteric behavior, i.e., its electrical activity depends on the position in the lattice. To overcome these problems, nonequilibrium techniques like low-temperature growth, ion-implantation, or quenching from high temperature can be used. However for solar cell manufacturing these methods are not attractive.

Most II–VI semiconductors can be doped efficiently to either n- or p-type, depending on the covalent radius ratio of II- to VI-atoms [119]. CdTe is an exception, as single crystals of CdTe can be doped to both p- and n-type although with limited maximum carrier concentration. Moderate acceptor densities of about 10^{17} cm^{-3} have been achieved in single crystal CdTe by doping with group I impurities substituting Cd or group V impurities substituting Te. Also controlled deviation from stoichiometry to Te-rich CdTe can lead to p-conductivity by native defects like V_{Cd} [121–123]. In polycrystalline CdTe solar cells p-doping with hole densities of about 10^{14} cm^{-3} is achieved by the absorber treatment in the presence of Cl and O (section "CdCl2 Annealing Treatment"). Also Cu, which is used in the back contact, can partly diffuse into CdTe and contribute to p-type doping [124, 125]. But Cu has a relatively large activation energy (Table 6) and is often associated with stability problems of CdTe solar cells (section "Electrical Back Contact"). Attempts to additionally dope the absorber have been less successful [135–137]. A reason might be a more pronounced self-compensation in polycrystalline material because of an increased number of defects due to grain boundaries. Not only are deliberately added impurities present in CdTe solar cells, but also impurities that originate from the source materials or from interdiffusion during processing steps from other layers or the substrate, especially in the case of high-temperature deposition methods. Many of these impurities are potentially active and can affect the photovoltaic properties [138].

Electrical Back Contact

One of the main challenges in CdTe solar cell technology is related to the difficulty of formation of an ohmic and stable electrical back contact to the CdTe layer. Because of a large electron affinity of 4.3 eV and a relatively large bandgap of 1.49 eV of CdTe, a metal with a work function of >5.8 eV would theoretically be needed to form an ohmic contact to p-CdTe (Fig. 14); however, such materials are rare. Additionally, surface states of CdTe cause Fermi level pinning and an abrupt metal contact will result in barrier heights above 0.8 eV, independent of the work function of the metal [50]. A barrier at the back contact can significantly affect the I–V curve by blocking the hole transport from CdTe to the metal. It results in a blocking behavior of the current at large positive bias, an effect commonly referred to as rollover. An I–V curve with rollover can be modeled by a series connection of two diodes with opposite polarity – the CdTe/CdS junction and the CdTe-metal back contact Schottky diode [139]. The rollover can cause a decrease of fill factor, which is significant for barrier heights above 0.5 eV [140]. Therefore alternative concepts to the abrupt CdTe-metal contact are being developed to form quasi-ohmic tunneling contacts. A common way is to implement a highly doped buffer layer between p-CdTe and the secondary metallic contact for reducing the width of the depletion layer. This leads to a very thin barrier of a few nanometers, allowing holes to tunnel through the barrier as shown in Fig. 14.

CdTe Solar Cells. Table 6 Donor and acceptor levels of different impurities, native defects, and impurity-native defect complexes in CdTe

Element	Acceptors			Donors		
	Lattice position	E_A	Reference	Lattice position	E_D	Reference
Li	Li_{Cd}	57.8	[126]	Li_i	13.9	[127]
Na	Na_{Cd}	58.8	[126]			
Cu	Cu_{Cd}	146	[128]			
Ag	Ag_{Cd}	107.5	[128]			
Au	Au_{Cd}	263	[129]			
Al				Al_{Cd}	14.05	[130]
Ga	$Ga_{Cd} - V_{Cd}$	131	[131]	Ga_{Cd}	13.88	[130]
In	$In_{Cd} - V_{Cd}$	142	[131]	In_{Cd}	14.15	[130]
N	N_{Te}	56	[132]			
P	P_{Te}	68.2	[132]			
As	As_{Te}	92	[132]			
Sb	Sb_{Te}	280	[133]			
Bi	Bi_{Te}	300	[134]			
O	O_{Te}	46	[107]			
Cl	$Cl_{Te} - V_{Cd}$	125	[131]	Cl_{Te}	14.48	[130]
	V_{Cd}	130	[134]			
	Te_i	570	[134]			

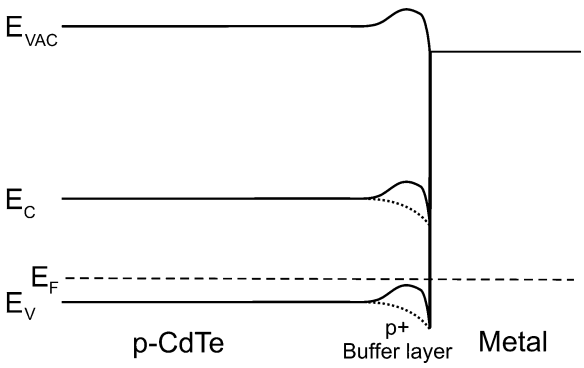

CdTe Solar Cells. Figure 14
Band diagram of the p-CdTe-back contact. Due to the high electron affinity of CdTe it forms a Schottky junction with metals. By increasing the CdTe acceptor density close to the metal or by introducing a thin buffer layer with high acceptor density, a thin quasi-ohmic tunneling contact can be formed

A conventionally used buffer layer is Cu_xTe since it has p-type conductivity with a high acceptor density. It can be produced by selectively etching the surface of CdTe, depositing a few nanometers of Cu and subsequent annealing. The etching produces a Te-rich CdTe surface and can be obtained by using a diluted bromine methanol (BM) solution [141] or a mixture of nitric and phosphoric acid (NP) [142]. The BM etch is a milder etchant and it affects the morphology of CdTe less than the NP etch. Figure 15 shows that the NP etching smoothens the surface and widens grain boundaries (GBs). Preferential etching along GBs can produce shunting pathways as depicted in Fig. 16. Figure 17 shows the evolution of a Te layer with increasing etching time with a NP etch as determined by X-ray diffraction (XRD). Cu can be added by evaporation or by applying a Cu doped paste, which itself serves as the secondary contact. Alternatively, Au can be used as the secondary contact but it can diffuse with time and

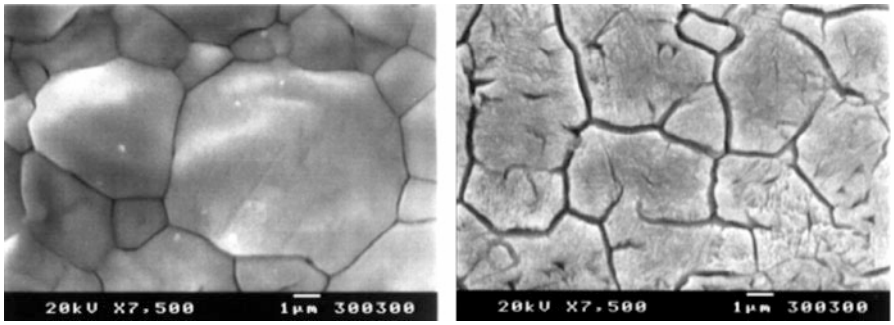

CdTe Solar Cells. Figure 15
SEM images of the CdTe morphology after etching. The BM etch (*left*) affects the morphology less than the NP etch (*right*) which smoothens the surface and widens GBs [143]

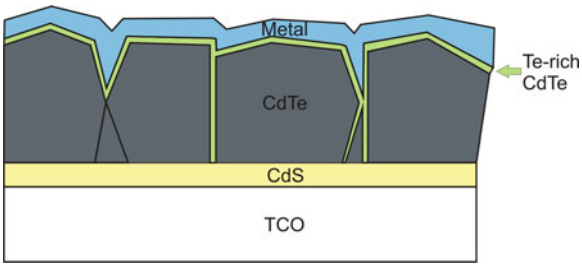

CdTe Solar Cells. Figure 16
Schematics of a CdTe solar cell with shunting paths along grain boundaries. Overetching can lead to strong etching along grain boundaries, leaving conducting Te-rich CdTe all along from the CdTe top surface to the CdS interface

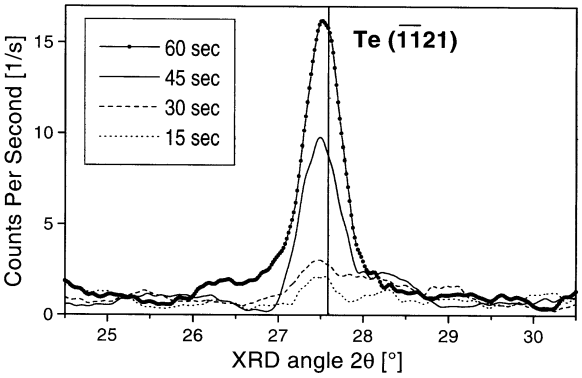

CdTe Solar Cells. Figure 17
XRD patterns of NP-etched CdTe with different etching times. Etching produces a Te-rich layer [144]

cause efficiency degradation. Therefore other metals, e.g., Mo, are applied. Cu_xTe-based contacts form low resistive quasi-ohmic contacts, but diffusion of Cu preferably along the grain boundaries in CdTe can lead to a fast degradation of the cells. This makes the contact suitable for research purposes but not for the use in commercial products. However, efforts have been made do develop stable contacts by carefully optimizing the thickness and composition of Cu_xTe for long-term stable performance. Promising alternative buffer layers to Cu_xTe have been developed. These buffer layers include Sb_2Te_3 [145], Sb [144], ZnTe [146], As_2Te_3 [94], HgTe [147], and Ni:P [148].

Sputtered Sb_2Te_3/Mo have been applied to CdTe solar cells and efficiencies up to 15.8% [149] have been achieved. The use of electrodeposited Sb_2Te_3 as back contact buffer layer has also yielded reasonable efficiencies above 11% [150]. In spite of these convincing efficiencies, the band alignment is claimed to be rather unfavorable [151]. Figure 18 illustrates that CdTe solar cells with Sb- or Sb_2Te_3-buffer and Mo metal layer have proven to show stable performance for a long period of time [143, 152].

A negligible valence band offset was measured between CdTe and ZnTe [153, 154], which results in a good contact between these two semiconductors. A highly p-type doped ZnTe forms a tunneling contact to metals like Ti. A high doping density of more than 10^{20} cm^{-3} can be achieved by doping with Cu [155]. With ZnTe.Cu based back contact, solar cells with efficiency of 12.9% have been produced [146, 156].

ITO is also well suited for the use as contact to etched p-CdTe [157]. Due to its transparency it can

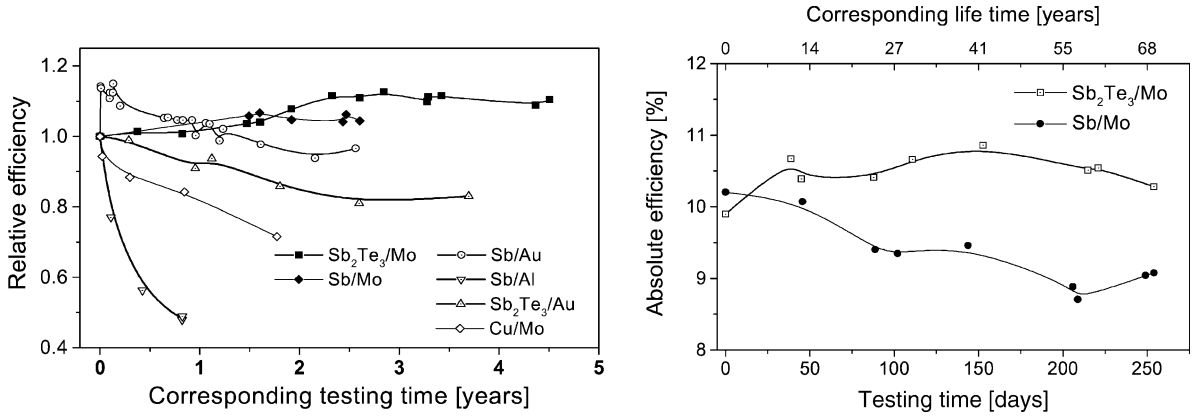

CdTe Solar Cells. Figure 18

Stability of CdTe solar cells with different back contacts under light soaking at elevated temperatures. Sb_2Te_3/Mo and Sb/Mo back contacts show stable performance over a very long period of time [143]

be applied for use in bifacial CdTe solar cells (see also Alternative Device Structures).

The performance stability problem of CdTe solar cells is generally connected to the back contact and especially to the diffusion of elements that form the back contact including the buffer layer. A comprehensive review on the stability of CdTe cells can be found in [158]. On the one hand, Cu helps creating an ohmic back contact and can increase the acceptor density in CdTe, but on the other hand it is a mobile element in CdTe. Excess Cu can easily diffuse along grain boundaries and accumulate at the junction and in the CdS, as found by SIMS measurements [143]. This results in deterioration of the solar cell performance. Degradation is commonly observed by the development of a rollover of the IV-curve at high forward bias and a decrease of V_{OC} and FF. The short circuit current density usually stays unaffected [158]. Both the $CdCl_2$ treatment [159] as well as the etch process [144] have influences on the stability of the cells in addition to the choice of the metal and buffer materials.

Alternative Device Structures

The conventionally used cell design has shown good performance, but also performance limitations as the highest efficiency of 16.5% is still below the theoretical limit of 30%. Therefore alternative device configurations that can possibly enhance the efficiency of CdTe solar cells should be considered.

Although highest efficiency CdTe solar cells are grown in superstrate configuration, cells in substrate configuration are attractive for reducing the losses in the window layer. Such configuration is currently reconsidered because of its potential use on flexible substrates. It would enable the use of flexible metal foils and solve the problem of parasitic light absorption of superstrate CdTe solar cells on polyimide foils. In order to achieve highly efficient CdTe solar cells in substrate configuration, the problems of forming an efficient ohmic contact to CdTe which withstands the subsequent high-processing temperatures remains a challenging issue.

a-Si solar cells are commonly grown in a p-i-n structure in order to reduce recombination. A similar concept might also be applied to CdTe solar cells, where CdS is used as n-layer, CdTe as intrinsic layer, and a highly doped p-type semiconductor-like ZnTe as p-layer and electron reflector. This would lead to higher open circuit voltage without the need of an increased doping acceptor concentration in CdTe [118, 160]. At the same time this would enable the use of thinner absorber layers.

Bifacial CdTe solar cells with a transparent back contact have been developed by using ITO as a contact to CdTe [157]. This structure enables illumination from both sides and can be used for the application in tandem solar cells. A CdTe solar cell with transparent back contact and 2.5 μm absorber thickness yielded a stable efficiency of 10.3% for front-side illumination and 2.1% in back-side illumination [161].

By reducing the CdTe thickness to 1 μm and adapting the $CdCl_2$ treatment, the performance of back-side illumination could be increased to 3.2%, still maintaining a relatively high efficiency of 8% for front-side illumination (Fig. 19).

Environmental and Material Resource Issues

Environmental, Health, and Safety Issues

The CdTe thin film technology has demonstrated excellent potential for cost-effective production of solar electricity. The energy payback time of CdTe modules compared to other PV technologies is significantly lower [162–164]. The environmental, health hazard, and safety (EH&S) issues of CdTe solar modules have been extensively investigated by several independent agencies in the USA and Europe (e.g., Brookhaven National Laboratory, USA, Fraunhofer Institut fuer Festkoerpertechnolgie, Germany, etc.). The studies prove that the Cd emission during the total life cycle of a CdTe module is lower compared to other PV and conventional energy production technologies [165]. Despite this scientific fact and the technological proofs, the CdTe PV technology has suffered from the perception of toxicity of elemental Cd, even though it is used in the form of a stable compound in thin film modules.

Referring to the perception and concerns on Cd issues, the studies of V. Fthenakis (Sr. Chemical Engineer, Brookhaven National Laboratory) and K. Zweibel (Former Manager, Thin Film Partnership Program, NREL, USA) confirm that CdTe modules would be almost benign with zero emission, without associated health hazards and they gave a clean chit to CdTe technology.

A peer review, organized by the European Commission's Joint Research Center and moderated by the German Federal Ministry of Environment (Berlin 2005), has studied the major published data on the environmental profile of CdTe PV provided by the leading institutes and companies. A summary of the outcome is given below:

- Cd is produced as a by-product of Zn and can either be put to beneficial uses or discharged to the environment posing another risk.
- CdTe used in PV is a chemically stable compound that does not leak into the environment during normal use or foreseeable accidents.
- Air emissions of Cd from the whole life cycle of CdTe PV (mining to end of life) are 100–360 times lower than Cd emitted into air from coal and oil power plants that PV displaces.

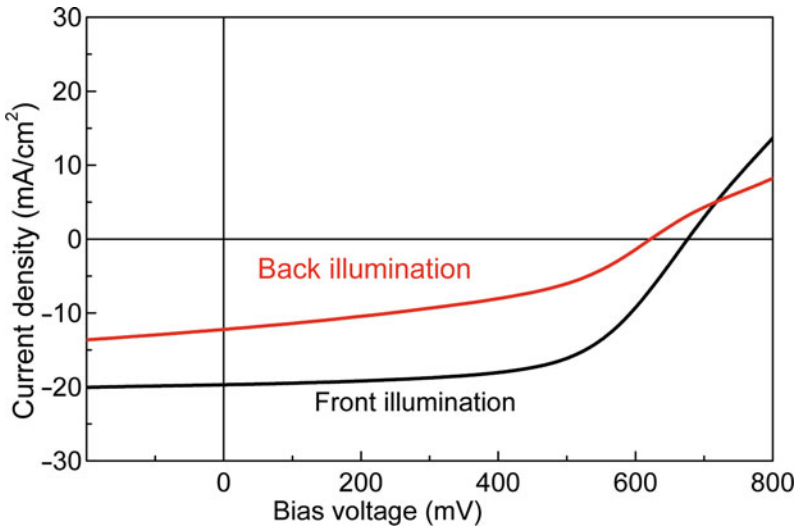

CdTe Solar Cells. Figure 19
Performance of a CdTe solar cell with transparent back contact and a CdTe thickness of 1 μm upon front- and back-side illumination

- Absolutely no pollutant emission during normal operation. "Every energy source or product may present some direct or indirect environmental health and safety hazards but the CdTe industry is proactive in controlling them, and these issues should by no means be considered a problem for CdTe PV modules."
- CdTe modules have shorter energy payback time and lower life-cycle emission of CO_2, SO_2, and NO_x than all other PV technologies.
- A low production cost technology like CdTe will accelerate the growth of the share of all PV technologies in the energy market.

The conclusion of the peer review was that the environmental risks of CdTe PV are minimal if materials are recycled and/or end-of-life systems and policies are in place.

Reduction of CdTe layer thickness and increase of efficiency with EH&S conform processes are expected to have a major impact on the life cycle of CdTe PV, although the significant cost saving may not be felt at production capacities below 50 MWp. In state-of-the-art CdTe modules (average CdTe layer thickness of 4 μm) the amount of Cd per unit area is approximately 12 g/m^2. Reducing the CdTe layer thickness toward 1 μm will reduce the Cd amount per unit area to 3 g/m^2. Assuming a module efficiency of 10%, an average annual energy yield of 900 kWh/kWp, and a lifetime of 25 years, the energy produced per unit weight of Cd will increase with reduced CdTe layer thickness from about 190 to 770 kWh/g. It has to be emphasized that there is neither consumption nor emission of Cd or Te during production and operation of the solar modules. At the end of life the material is still inside the module and can be recycled, which closes the chain of the raw material.

Resources of Raw Materials

Among the required elements for the production of CdTe thin solar modules tellurium is the least abundant. Tellurium is a scarce material that is expected to have a share of 0.01 ppm in the earth's crust. The majority (above 90%) of its current production is stemming from anode slimes collected from electrolytic copper refining [166]. From this source about 430–500 metric tons of tellurium are available per year [167, 168]. The refined tellurium is consumed as a metallurgical alloying element, as catalyst in chemistry, in blasting caps, and as pigment for blue and brown colors in ceramics. Purified tellurium is used in thermal imaging, thermoelectric devices, phase change memories, and CdTe thin film solar cells [169]. The demand of tellurium in PV applications has increased significantly in the past decade. Ken Zweibel estimated the consumption of tellurium for 1 GWp of state-of-the-art CdTe module technology being 91 metric tons [116]. This means that First Solar Inc. would consume about 25–30% of the annual tellurium production per year (assuming that the factories are running at the announced production capacity). With increasing concern in tellurium supply on the one hand other sources such as gold tellurium, lead-zinc ores with higher concentrations of tellurium, or bismuth telluride ores are investigated and an increased annual production is expected [116, 166]. On the other hand intensive R&D effort is expected to reduce the tellurium demand per output power (Wp) in CdTe solar modules by increased module efficiency and reduced absorber layer thickness. Such a scenario with increased module efficiency to 15% and reduced absorber thickness to 0.67 μm was presented by Ken Zweibel leading to a reduction of tellurium consumption to 15 metric tons per GWp [116]. Zweibel further calculated that with the mentioned technological improvement and today's annual tellurium production about 6–7% of the global electricity demand can be covered by CdTe solar modules in 2030. This is a significant contribution and justifies further financial and R&D investments in this technology.

Further Directions

Even though the CdTe solar technology has already been successfully transferred from the research laboratory to the industrial production, there are still challenges and major problems to be solved for further efficiency improvement, cost reduction, as well as novel applications. An important point of consideration is the large difference between the theoretically achievable efficiency of close to 30% and the practically achieved 16.5% up to now. Among the open problems are (1) increasing the transmittance of the substrate-TCO stack while maintaining high conductivity using

simple processing techniques; (2) reducing the CdS thickness well below 100 nm or using alternative material of higher bandgap and/or lower absorption for minimization of absorption loss, without adversely affecting the fill factor and cell voltage; (3) reducing the self-compensation effect in the polycrystalline CdTe material to increase the net acceptor density; (4) increasing the raw material utilization by reducing the CdTe layer thickness and applying optical confinement effects as well as by alloying CdTe with Se in order to reduce the Te consumption; (5) forming a low resistive ohmic and stable back contact onto p-type CdTe by an all-vacuum deposition process; (6) developing highly efficient CdTe solar cells in substrate or p-i-n configurations; (7) developing low-temperature processes; (8) developing low-cost, large area scalable processes of high material utilization; and (9) adapting roll-to-roll processing. Also important for technological and production cost reduction point of view is to further enhance the solar module efficiency thereby closing the gap between highest cell and module efficiencies. R&D to overcome these challenges will help to further increase the conversion efficiency and to reduce the production costs.

Abbreviations

ALD	Atomic layer deposition
APVTD	Atmospheric pressure vapor transport deposition
AR	Antireflection
ASG	Aluminosilicate glass
AZO	Aluminum doped zinc oxide
BI	Battelle-Institute e.V
BM	Bromine methanol
BSG	Borosilicate glass
CBD	Chemical bath deposition
CIGS	Copper indium gallium diselenide
CNRS	French National Center for Scientific Research
CSS	Close space sublimation
CTO	Cadmium stannate
CVD	Chemical vapor deposition
ED	Electrodeposition
EH&S	Environmental, health hazard, and safety issues
EQE	External quantum efficiency
ETHZ	Swiss Federal Institute of Technology Zurich
FF	Fill factor
FTO	Fluorine doped tin oxide
GBs	Grain boundaries
HRT	Highly resistive and transparent oxide
HTVPD	High-temperature vapor phase deposition
HVE	High vacuum deposition
IEC	Institute for Energy Conversion, University of Delaware
IQE	Internal quantum efficiency
ITO	Tin doped indium oxide
Jsc	Short circuit current density
NP	Nitric-phosphoric acid
NREL	National renewable energy laboratory
PI	Polyimide
PV	Photovoltaic
R	Reflectance
R&D	Research and Development
SEM	Scanning electron microscopy
SLG	Soda-lime glass
STC	Standard test condition
T	Transmittance
TCO	Transparent conductive oxide
UNAM	Centro de Investigacin en Energa, Solar Materials Department, Temixco, Morelos 62
V_{OC}	Open circuit voltage
VTD	Vapor transport deposition
XRD	X-ray diffraction
ZTO	Zinc stannate

Bibliography

1. Adirovich EI, Yuabov YM, Yagudaev GR (1969) Photoelectric effects in film diodes with CdSCdTe heterojunctions. Sov Phys Semicond 3:61
2. Osborne M (2009) First Solar's market share set to soar. www.pv-tech.org. Accessed 6 Oct 2010
3. First Solar Inc. (2010) Corporate overview Q2 2010, www.first-solar.com. Accessed 6 Oct 2010
4. Hansen GL, Schmit JL, Casselman TN (1982) Energy gap versus alloy composition and temperature in $Hg_{1-x}Cd_xTe$. J Appl Phys 53:7099
5. Rothwarf A, Ber KW (1975) Direct conversion of solar energy through photovoltaic cells. Prog Solid State Chem 10:71
6. Shockley W, Queisser HJ (1961) Detailed balance limit of efficiency of p-n junction solar cells. J Appl Phys 32:510
7. DeVoc A, Parrott JE, Baruch P, Landsberg PT (1994) Bandgap effects in thin-film heterojunction solar cells. In: Proc of 12th European Photovoltaic Solar Energy Conf, Amsterdam, The Netherlands, pp 1315–1318

8. Rappaport P (1959) The photovoltaic effect and its utilization. Sol Energy 3:8
9. Mimila-Arroyo J, Marfaing Y, Cohen-Solal G, Triboulet R (1979) Electric and photovoltaic properties of CdTe pn homojunctions. Sol Energy Mater Sol Cells 1:171
10. Cohen-Solal G, Lincot D, Barbe M (1988) High efficiency shallow p(+)nn(+) cadmium telluride solar cells. Sol Cells 23:1
11. Goren D, Amir N, Khanin E, Asa G, Nemirovsky Y (1996) Single crystalline CdTe solar cells grown by MOCVD. Sol Energy Mater Sol Cells 44:341
12. Justi EW, Schneider G, Seredynski J (1973) Investigations on CdTe thin film solar cells. Energy Convers Manag 13:53
13. Muller RS, Zuleeg R (1964) Vapor-deposited, thin-film heterojunction diodes. J Appl Phys 35:1550
14. Nakazawa T, Takamizawa K, Ito K (1987) High efficiency indium oxide/cadmium telluride solar cells. Appl Phys Lett 50:279
15. Bonnet D, Rabenhorst H (1972) New results on the development of a thin film p-CdTe/n-CdS heterojunction solar cell. In: Proc of 9th Photovoltiac Specialist Conf, Freiburg, pp. 129–131
16. Bube R (1998) Photovoltaic materials. Imperial College, London
17. McCandless BE, Sites JR (2003) Cadmium telluride solar cells. In: Luque A, Hegedus S (eds) Handbook of photovoltaic science and engineering. Wiley, Chichester/Hoboken, pp 617–662
18. Burgelman M (2006) Cadmium telluride thin film solar cells. In: Poortmans J, Arkhipov V (eds) Thin film solar cells: fabrication, characterization, and application. Wiley, Chichester
19. Coutts T, Kazmerski L, Wagner S (1988) Special issue on cadmium tellunde. Sol Cells 23:1
20. Romeo A, Terheggen M, Abou-Ras D, Baetzner DL, Haug F-J, Kaelin M, Rudmann D, Tiwari AN (2004) Development of thin-film Cu(In, Ga)Se2 and CdTe solar cells. Prog Photovoltaics Res Appl 12:93
21. Wu X, Keane JC, Dhere RC, DeHart C, Albin DS, Duda A, Gessert TA, Asher S, Levi DH, Sheldon P (2001) 16.5%-efficient CdS/CdTe polycrytalline thin-film solar cell. In: Proc of 17th European Photovoltaic Solar Energy Conf, Munich, Germany, p 995
22. Wu X (2004) High-efficiency polycrystalline CdTe thin-film solar cells. Sol Energy 77:803
23. McCandless BE, Buchanan WA, Birkmire RW (2005) High throughput processing of CdTe/CdS solar. In: Proc of 31st IEEE Photovoltaic Specialist Conf, Lake Buena Vista, USA, pp 295–298
24. Gupta A, Compaan AD (2003) All sputtered 14% CdS/CdTe device with ZnO: Al front contact. In: Kurokawa K, Kazmerski L, McNelis B, Yamaguchi M, Wronski C, Sinke W (eds) Proc of 3 rd World Conf on Photovoltaic Energy Conversion, Osaka, Japan, pp 352–355
25. Perrenoud J, Kranz L, Buecheler S, Pianezzi F, Tiwari AN (2010) The use of aluminum doped ZnO as transparent conductive oxide for CdS/CdTe solar cells. Thin Solid Films. doi:10.1016/j.tsf.2010.12.234
26. Woodcock JM, Turner AK, Ozsan ME, Summers JG (1991) Thin film solar cells based on electrodeposited CdTe. In: Proc of 22nd IEEE Photovoltaic Specialist Conf, Las Vegas, USA, pp 842–847
27. Perrenoud J, Buecheler S, Tiwari AN (2009) Flexible CdTe solar cells and modules: challenges and prospects. In: Proc SPIE Vol. 7409, San Diego, USA, p. 74090 L
28. Vasko AC, Liu X, Compaan AD (2009) All-sputtered CdS/CdTe solar cells on polyimide. In: Proc of 34th IEEE Photovoltaic Specialist Conf, Philadelphia, USA, pp 001552–001555
29. Romeo N, Bosio A, Canevari V (1992) A new method to prepare efficient CdTe/CdS thin film solar cells. In: Proc of 11th European Photovoltaic Solar Energy Conf, Montreux, CH, pp 972–974
30. Perrenoud J (2010) Empa, Switzerland, unpublished results
31. Pantoja-Enriquez J, Mathew X, Hernandez G, Pal U, Magana C, Acosta DR, Guardian R, Toledo JA, Contreras-Puente G, Chavez-Carvayar JA (2004) CdTe/CdS solar cells on flexible molybdenum substrate. Sol Energy Mater Sol Cells 82:307
32. Singh VP, McClure JC, Lush GB, Wang W, Wang X, Thompson GW, Clark E (1999) Thin film CdTe-CdS heterojunction solar cells on lightweight metal substrates. Sol Energy Mater Sol Cells 59:145
33. Romeo A, Khrypunov G, Kurdesau F, Arnold M, Baetzner DL, Zogg H, Tiwari AN (2006) High-efficiency flexible CdTe solar cells on polymer substrates. Sol Energy Mater Sol Cells 90:3407
34. Matulionis I, Han S, Drayton JA, Price KJ, Compaan AD (2001) Cadmium telluride solar cells on molybdenum substrates. In: MRS Proc, San Francisco, USA, vol 668, pp H8.23.1–H8.23.6
35. Brog TK (1997) Commercial production of thin film CdTe photovoltaic modules, final report. NTIS, Springfield
36. Nolan JF, Meyers PV (1993) Fabrication of stable large-area thin-film CdTe photovoltaic modules. Annual subcontracting report, NREL/TP-413-5740
37. Cunningham D, Davies K, Grammond L, Mopas E, O'Conner N, Rubcich M, Skinner D, Trumbly T (2000) Large area apolloTM module performance and reliability. In: Proc of 28th IEEE Photovoltiac Specialist Conf, pp 13–18
38. Aramoto T, Tsuji M, Yamamoto T, Nishio T, Veluchamy P, Higuchi H, Kumazawa S, Shibutani J, Nakajima S, Nishiyama Y, Arita T, Hanafusa A, Hibino T, Omura K (2000) Highly efficient large area thin film CdS/CdTe sub-module solar cells. In: Proc of 28th IEEE Photovoltiac Specialist Conf, pp 436–439
39. Bonnet D (2000) Manufacturing of CSS CdTe solar cells. Thin Solid Films 361–362:547
40. Abound Solar (2009) Data sheet AB1-2009-05-13
41. Antec Solar, Data sheet ATF 50
42. www.calyxo.com/en/manufacturing_company/index.html. Accessed 24 Aug 2010
43. First Solar (2010) Data sheet FS Series 3™ PD-5-401-03 NA JUN 2010
44. Schulz DL, Pehnt M, Rose DH, Urgiles E, Cahill AF, Niles DW, Jones KM, Ellingston RJ, Curtis CJ, Ginley DS (1997) CdTe thin films from nanoparticle precursors by spray deposition. Chem Mater 9:889

45. Roth & Rau Data sheet (2010) www.roth-rau.de/datenbanken_de/photovoltaic/12542138682.pdf. Accessed 25 Aug 2010
46. Groom N (2009) Abound, U.S. solar startup, takes on first solar, Thomson Reuters, press release 14 Apr 2009
47. Fischer KH (2009) Produktion von CdTe-Modulen. Energie 2.0, 12 Sept 2009
48. Perrenoud J, Schaffner B, Buecheler S, Tiwari AN (2011) Fabrication of flexible CdTe solar modules with monolithic cell interconnection. Sol Energy Mater Sol Cells 95:S8
49. Sze SM (1981) Physics of semiconductor devices. Wiley, New York
50. Klein A, Saeuberlich F, Spaeth B, Schulmeyer T, Kraft D (2007) Non-stoichiometry and electronic properties of interfaces. J Mater Sci 42:1890
51. Klenk R (2001) Characterization and modelling of chalcopyrite solar cells. Thin Solid Films 387:135
52. Hansen GL, Schmit JL, Casselman TN (1990) Preparations of ZnO: Al transparent conducting films by d.c. magnetron sputtering. Thin Solid Films 193–194:721
53. Koishiyev GT, Sites JR (2009) Impact of sheet resistance on 2-D modeling of thin-film solar cells. Sol Energy Mater Sol Cells 93:350
54. Gordon RG (1996) Preparation and properties of transparent conductors. In: MRS Proc, San Francisco, USA, pp 419–429
55. Gordon RG (2000) Criteria for choosing transparent conductors. In: MRS Bulletin, pp 52–5
56. Gupta A, Compaan AD (2004) All-sputtered 14% CdS/CdTe thin-film solar cell with ZnO: Al transparent conducting oxide. Appl Phys Lett 85:684
57. Li X, Ribelin R (1998) The effect of high-resistance SnO_2 on the CdS/CdTe device performance. In: National Center for Photovoltaics Program Review Meeting, pp 1–8
58. Takamoto T, Agui T, Kurita H, Ohmori M (1997) Improved junction formation procedure for low temperature deposited CdS/CdTe solar cells. Sol Energy Mater Sol Cells 49:219
59. Terheggen M, Heinrich H, Kostorz G, Baetzner DL, Romeo A, Tiwari AN (2004) Analysis of bulk and interface phenomena in CdTe/CdS thin-film solar cells. Interface Sci 12:259
60. Rau U, Schmidt M (2001) Electronic properties of ZnO/CdS/Cu (In, Ga)Se2 solar cells – aspects of heterojunction formation. Thin Solid Films 387:141
61. Chu T, Chu S (1993) Recent progress in thin-film cadmium telluride solar cells. Prog Photovoltics Res Appl 1:31
62. Romeo A, Baetzner DL, Zogg H, Tiwari AN (2000) Recrystallization in CdTe/CdS. Thin Solid Films 361–362:420
63. Wei SH, Zhang SB, Zunger A (2000) First-principles calculation of band offsets, optical bowings, and defects in CdS, CdS, CdTe, and their alloys. J Appl Phys 87:1304
64. Fritsche J, Schulmeyer T, Kraft D, Thissen A, Klein A, Jaegermann W (2002) Utilization of sputter depth profiling for the determination of band alignment at polycrystalline CdTe/CdS heterointerfaces. Appl Phys Lett 81:2297
65. Perrenoud J (2010) Empa, Switzerland, unpublished results on TEC15 glass from Pilkington
66. Tomar MS (1988) Photovoltaic properties of ZnO/p-CdTe thin film heterojunctions. Thin Solid Films 164:295
67. Wei SH, Zunger A (1998) Calculated natural band offsets of all IIVI and IIIV semiconductors: chemical trends and the role of cation d orbitals. Appl Phys Lett 72:2011
68. Meyer BK, Poklity A, Farangis B, He Y, Hasselkamp D, Krae-mer T, Wang C (2004) Structural properties and band gap bowing of $ZnO_{1-x}S_x$ thin films deposited by reactive sputtering. Appl Phys Lett 85:4929
69. Contreras-Puente G, Vigil O, Ortega-Lopez M, Morales-Acevedo A, Vidal J, Albor-Aguilera ML (2000) New window materials used as heterojunction partners on CdTe solar cells. Thin Solid Films 361362:378
70. Perrenoud J, Buecheler S, Kranz L, Fella C, Skarp J, Tiwari AN (2010) Application of $ZnO_{1-x}S_x$ as window layer in CdTe solar cells. In: Proc of 35th IEEE Photovoltaic Specialist Conf, Hawaii, USA, pp 000995–001000
71. Platzer-Bjorkman C, Torndahl T, Abou-Ras D, Malmstrom J, Kessler J, Stolt L (2006) Zn(O, S) buffer layers by atomic layer deposition in Cu(In, Ga)Se2 based thin film solar cells: band alignment and sulfur gradient. J Appl Phys 100:044506
72. Powell RC, Dorer GL, Reiter NA, McMaster HA, Cox SM, Kahle TD (1999) US patent No 5945163
73. McCandless BE, Birkmire RW, Buchanan WA, Fields S, Hanket GM (2002) Vapor transport deposition of cadmium telluride films. In: Proc of 29th IEEE Photovoltaic Specialist Conf, New Orleans, USA, pp 547–550
74. Hanket GM, McCandless BE, Buchanan WA, Fields S, Birkmire RW (2006) Design of a vapor transport deposition process for thin film materials. J Vaccum Sci Technol A 24:1695
75. First Solar Inc. (2003) News Releases. www.first-solar.com. Accessed 10 Nov 2010
76. Khrypunov G, Romeo A, Kurdesau F, Baetzner DL, Zogg H, Tiwari AN (2006) Recent developments in evaporated CdTe solar cells. Sol Energy Mater Sol Cells 90:664
77. Shao M, Fischer A, Grecu D, Jayamaha U, Bykov E, ContrerasPuente G, Bohn RG, Compaan AD (1996) Radio-frequency-magnetron-sputtered CdS/CdTe solar cells on soda-lime glass. Appl Phys Lett 69:3045
78. Compaan AD, Gupta A, Lee S, Wang S, Drayton J (2004) High efficiency, magnetron sputtered CdS/CdTe solar cells. Sol Energy 77:815, Thin Film PV
79. Compaan AD, Plotnikov V, Liu X, Paudel N, Kwon D, Wieland K (2010) Thin-film CdTe cells: reducing the CdTe. Thin Solid Films. doi:10.1016/j.tsf.2010.12.179
80. Irvine SJC, Barrioz V, Lamb D, Jones EW, Rowlands-Jones RL (2008) MOCVD of thin film photovoltaic solar cells-next-generation production technology? J Cryst Growth 310:5198
81. Basol BM (1988) Electrodeposited CdTe and HgCdTe solar cells. Sol Cells 23:69, Special issue on cadmium telluride
82. Nakayama N, Matsumoto H, Nakano A, Ikegami S, Uda H, Yamashita T (1980) Screen printed thin-film CdS-CdTe solar-cell. Jpn J Appl Phys 19:703

83. Matsumoto H, Kuribayashi K, Uda H, Komatsu Y, Nakano A, Ikegami S (1984) Screen-printed CdS/CdTe solar cell of 12.8% efficiency for an active area of 0.78 cm^2. Sol Cells 11:367
84. Albright SP, Ackerman B, Jordan JF (1990) Efficient CdTe CdS solar-cells and modules by spray processing. IEEE Trans Electron Dev 37:434
85. Curtis CJ, van Hest M, Miedaner A, Hersh A, Leisch J, Ginley DS, Nekuda J (2008) Spray deposition of high quality $CuInSe_2$ and CdTe films. In: Proc of 33 rd IEEE Photovoltiac Specialist Conf, San Diego, USA, pp 1–4
86. Krishna KV, Dutta V (2003) Spray deposition of CdTe-Te thin films using ethylene-diamine-tetra-acetic acid as a complexing agent in the precursor solution. Sol Energy Mater Sol Cells 80:247
87. Gur I, Fromer NA, Geier ML, Alivisatos AP (2005) Air-stable all-inorganic nanocrystal solar cells processed from solution. Science 310:462
88. McCandless BE, Birkmire RW (1991) Analysis of post deposition processing for CdTe/CdS thin film solar cells. Sol Cells 31:527
89. McCandless BE, Moulton LV, Birkmire RW (1997) Recrystallization and sulfur diffusion in $CdCl_2$-treated CdTe/CdS thin films. Prog Photovoltaics Res Appl 5:249
90. McCandless BE, Dobson KD (2004) Processing options for CdTe thin film solar cells. Sol Energy 77:839
91. Zhou TX, Reiter N, Powell RC, Sasala R, Meyers PV (1994) Vapor chloride treatment of polycrystalline CdTe/CdS films. In: Proc of 224th IEEE Photovoltaic Specialist Conf, Waikoloa, USA, pp 103–106
92. Zhao H, Palekis V, Selvaraj P, Morel DL, Ferekides CS (2002) Vapor chloride treatment studies of CdTe/CdS solar cells. In: Proc of 29th IEEE Photovoltaic Specialist Conf, New Orleans, USA, pp 668–671
93. Romeo N, Bosio A, Romeo A, Mazzamuto S, Canevari V (2006) High efficiency CdTe/CdS thin film solar cells prepared by treating CdTe films with a Freon gas in substitution of CdCl2. In: Proc of 21st European Photovoltaic Solar Energy Conference, Dresden, Germany, pp 1857–1860
94. Bosio A, Menossi D, Mazzamuto S, Romeo N (2010) Manufacturing of CdTe thin films PV modules. Thin Solid Films. doi:10.1016/j.tsf.2010.12.137
95. Romeo A, Buecheler S, Giarola M, Mariotto G, Tiwari AN, Romeo N, Bosio A, Mazzamuto S (2009) Study of CSS- and HVE-CdTe by different recrystallization processes. Thin Solid Films 517:2132
96. Qu Y, Meyers PV, McCandless BE (1996) HCl vapor post-deposition heat treatment of CdTe/CdS films. In: Proc of 25th IEEE Photovoltaic Specialist Conf, Washington, USA, pp 1013–1016
97. Terheggen M, Heinrich H, Kostorz G, Romeo A, Baetzner D, Tiwari AN, Bosio A, Romeo N (2003) Structural and chemical interface characterization of CdTe solar cells by transmission electron microscopy. Thin Solid Films 431–432:262
98. Durose K, Cousins MA, Boyle DS, Beier J, Bonnet D (2002) Grain boundaries and impurities in CdTe/CdS solar cells. Thin Solid Films 403–404:396
99. Chiarotti G (1993) 1.6 Crystal structures and bulk lattice parameters of materials quoted in the volume. Springer-Materials – The Landolt-Brnstein Database. http://www.springermaterials.com. doi:10.1007/10086066_6
100. Nunoue S-Y, Hemmi T, Kato E (1990) Mass spectrometric study of the phase boundaries of the CdS-CdTe system. J Electrochem Soc 137:1248
101. Jensen DG, McCandless BE, Birkmire RW (1996) Thin film cadmium telluride-cadmium sulfide alloys and devices. In: Conference record of the twenty fifth IEEE photovoltaic specialists conference, Washington, DC, 13–17 May 1996. pp 773–776
102. Hofmann DM, Omling P, Grimmeiss HG, Meyer BK, Benz KW, Sinerius D (1992) Identification of the chlorine A-center in CdTe. Phys Rev B 45:6247
103. Valdna V, Buschmann F, Mellikov E (1996) Conductivity conversion in CdTe layers. J Cryst Growth 161:164
104. Marfaing Y (2001) Impurity doping and compensation mechanisms in CdTe. Thin Solid Films 387:123
105. Zhao H, Farah A, Morel D, Ferekides CS (2009) The effect of impurities on the doping and V_{OC} of CdTe/CdS thin film solar cells. Thin Solid Films 517:2365
106. McCandless BE, Buchanan WA (2008) High throughput processing of CdTe/CdS solar cells with thin absorber layers. In: Proc of 33 rd IEEE Photovoltaic Specialist Conf, San Diego, USA, pp 1–6
107. Akimoto K, Okuyama H, Ikeda M, Mori Y (1992) Isoelectronic oxygen in II-VI semiconductors. Appl Phys Lett 60:91
108. Ringel SA, Smith AW, MacDougal MH, Rohatgi A (1991) The effects of $CdCl_2$ on the electronic properties of molecular-beam epitaxially grown CdTe/CdS heterojunction solar cells. J Appl Phys 70:881
109. Burgelman M, Nollet P, Degrave S (1999) Electronic behaviour of thin-film CdTe solar cells. Appl Phys A 69:149
110. Versluys J, Clauws P, Nollet P, Degrave S, Burgelman M (2003) DLTS and admittance measurements on CdS/CdTe solar cells. Thin Solid Films 431:148
111. Seymour FH, Kaydanov V, Ohno TR (2006) Simulated admittance spectroscopy measurements of high concentration deep level defects in CdTe thin-film solar cells. J Appl Phys 100:033710
112. Seto JYW (1975) The electrical properties of polycrystalline silicon films. J Appl Phys 46:5247
113. Werner J, Jantsch W, Froehner KH, Queisser HJ (1982) Transport across silicon grain boundaries. In: Grain Boundaries in Semiconductors. Elsevier Science
114. Visoly-Fisher I, Cohen SR, Ruzin A, Cahen D (2004) How polycrystalline devices can outperform single-crystal ones: thin film CdTe/CdS solar cells. Adv Mater 16:879
115. Visoly-Fisher I, Cohen S, Gartsman K, Ruzin A, Cahen D (2006) Understanding the beneficial role of grain boundaries in polycrystalline solar cells from single-grain-boundary scanning probe microscopy. Adv Funct Mater 16:649
116. Zweibel K (2010) The impact of tellurium supply on cadmium telluride photovoltaics. Science 328:699

117. Gupta A, Parikh V, Compaan AD (2006) High efficiency ultra-thin sputtered CdTe solar cells. Sol Energy Mater Sol Cells 90:2263
118. Sites J, Pan J (2007) Strategies to increase CdTe solar-cell voltage. Thin Solid Films 515:6099
119. Desnica UV (1998) Doping limits in II-VI compounds – challenges, problems and solutions. Prog Cryst Growth Charact Mater 36:291
120. Panchuk O, Fochuk P (2010) Doping. In: Triboulet R, Siffert P (eds) CdTe and related compounds; physics, defects, hetero- and nano-structures, crystal growth, surfaces and applications. Elsevier, Amsterdam, pp 309–362
121. Fochuk P, Grill R, Panchuk O (2006) The nature of point defects in CdTe. J Electron Mater 35:1354
122. Lyahovitskaya V, Chernyak L, Greenberg J, Kaplan L, Cahen D (2000) n- and p-type post-growth self-doping of CdTe single crystals. J Cryst Growth 214–215:1155
123. Berding MA (1999) Annealing conditions for intrinsic CdTe. Appl Phys Lett 74:552
124. Grecu D, Compaan AD, Young D, Jayamaha U, Rose DH (2000) Photoluminescence of Cu-doped CdTe and related stability issues in CdS/CdTe solar cells. J Appl Phys 88:2490
125. Gessert TA, Metzger WK, Dippo P, Asher SE, Dhere RG, Young MR (2009) Dependence of carrier lifetime on Cu-contacting temperature and ZnTe: Cu thickness in CdS/CdTe thin film solar cells. Thin Solid Films 517:2370
126. Molva E, Chamonal JP, Pautrat JL (1982) Shallow acceptors in cadmium telluride. Physica Status Solidi B 109:635
127. Bhargava RN (1982) The role of impurities in refined ZnSe and other II-VI semiconductors. J Cryst Growth 59:15
128. Molva E, Chamonal JP, Milchberg G, Saminadayar K, Pajot B, Neu G (1982) Excited states of Ag and Cu acceptors in CdTe. Solid State Commun 44:351
129. Molva E, Francou JM, Pautrat JL, Saminadayar K, Dang LS (1984) Electrical and optical properties of Au in cadmium telluride. J Appl Phys 56:2241
130. Francou JM, Saminadayar K, Pautrat JL (1990) Shallow donors in CdTe. Phys Rev B 41:12035
131. Stadler W, Hofmann DM, Alt HC, Muschik T, Meyer BK, Weigel E, Muller-Vogt G, Salk M, Rupp E, Benz KW (1995) - Optical investigations of defects in $Cd_{1-x}Zn_x$Te. Phys Rev B 51:10619
132. Molva E, Saminadayar K, Pautrat JL, Ligeon E (1983) Photoluminescence studies in N, P, As implanted cadmium telluride. Solid State Commun 48:955
133. Nikonyuk ES, Zakharuk ZI, Shlyakhovyi VL, Fochuk PM, Rarenko AI (2001) Mechanism of incorporation of an antimony impurity into cadmium telluride crystals. J Semicond 35:405
134. Wei SH, Zhang SB (2002) Chemical trends of defect formation and doping limit in II-VI semiconductors: the case of CdTe. Phys Rev B 66:155211
135. Chin KK (2010) p-Doping limit and donor compensation in CdTe poly-crystalline thin film solar cells. Sol Energy Mater Sol Cells 94:1627
136. Vigil-Galn O, Brown M, Ruiz CM, Vidal-Borbolla MA, Ramrez-Bon R, Snchez-Meza E, Tufio-Velzquez M, Estela-Calixto M, Compaan AD, Contreras-Puente G (2008) On the doping problem of CdTe films: the bismuth case. Thin Solid Films 516:7013
137. Proskuryakov YY, Durose K, Al Turkestani MK, Mora-Sero I, Garcia-Belmonte G, Fabregat-Santiago F, Bisquert J, Barrioz V, Lamb D, Irvine SJC, Jones EW (2009) Impedance spectroscopy of thin-film CdTe/CdS solar cells under varied illumination. J Appl Phys 106:044507
138. Emziane M, Durose K, Halliday DP, Bosio A, Romeo N (2005) Efficiency improvement in thin-film solar cell devices with oxygen-containing absorber layer. Appl Phys Lett 87:261901
139. Niemegeers A, Burgelman M (1997) Effects of the Au/CdTe back contact on IV and CV characteristics of Au/CdTe/CdS/TCO solar cells. J Appl Phys 81:2881
140. Demtsu SH, Sites JR (2006) Effect of back-contact barrier on thin-film CdTe solar cells. Thin Solid Films 510:320
141. Danaher WJ, Lyons LE, Marychurch M, Morris GC (1986) Chemical etching of crystal and thin film cadmium telluride. Appl Surf Sci 27:338
142. Sarlund J, Ritala M, Leskelae M, Siponmaa E, Zilliacus R (1996) Characterization of etching procedure in preparation of CdTe solar cells. Sol Energy Mater Sol Cells 44:177
143. Baetzner DL, Romeo A, Zogg H, Wendt R, Tiwari AN (2001) Development of efficient and stable back contacts on CdTe/CdS solar cells. Thin Solid Films 387:151
144. Baetzner DL, Wendt R, Romeo A, Zogg H, Tiwari AN (2000) A study of the back contacts on CdTe/CdS solar cells. Thin Solid Films 361–362:463
145. Romeo N, Bosio A, Tedeschi R, Romeo A, Canevari V (1999) Highly efficient and stable CdTe/CdS thin film solar cell. Sol Energy Mater Sol Cells 58:209
146. Gessert TA, Sheldon P, Li X, Dunlavy D, Niles D, Sasala R, Albright S, Zadler B (1997) Studies of ZnTe back contacts to CdS/CdTe solar cells. In: Proc of 26th IEEE Photovoltaic Specialist Conf, Aualein, USA, pp 419–422
147. Yan Y, Jones KM, Wu X, Al-Jassim MM (2003) Formation of $Cd_xHg_{1-x}Te$ layers on CdTe after NP-etching and HgTe-graphite pasting. In: MRS Proc, San Francisco, USA, vol 763
148. Duke S, Miles RW, Pande P, Spoor S, Ghosh B, Datta PK, Carter MJ, Hill R (1996) Characterisation of in-situ thermally evaporated CdS/CdTe thin film solar cells with NiP back contacts. J Cryst Growth 159:916
149. Romeo N, Bosio A, Canevari V, Podest A (2004) Recent progress on CdTe/CdS thin film solar cells. Sol Energy 77:795
150. Leimkhler G, Bartelt O, Reineke-Koch R (2001) Electrodeposited antimony and antimony telluride as back contact interlayer for cadmium telluride thin film solar cells. In: Proc of 17th European Photovoltaic Solar Energy Conf, Munich, Germany, pp 1169–1171
151. Kraft D, Spaeth B, Thissen A, Klein A, Jeaegermann W (2003) Chemical and electronic properties of metal/Sb_2Te_3/CdTe contacts for CdTe thin film solar cells studied by photoelectron spectroscopy. In: MRS Proc, San Franscico, USA, pp 450–453

152. Baetzner DL, Romeo A, Terheggen M, Doebeli M, Zogg H, Tiwari AN (2004) Stability aspects in CdTe/CdS solar cells. Thin Solid Films 451–452:536
153. Rioux D, Niles DW, Hoechst H (1993) ZnTe – a potential interlayer to form low-resistance back contacts in CdS/CdTe solar cells. J Appl Phys 73:8381
154. Spaeth B, Fritsche J, Klein A, Jaegermann W (2007) Nitrogen doping of ZnTe and its influence on CdTe/ZnTe interfaces. Appl Phys Lett 90:062112
155. Gessert TA, Mason AR, Reedy RC, Matson R, Coutts TJ, Sheldon P (1995) Development of rf sputtered, Cu-doped ZnTe for use as a contact interface layer to p-CdTe. J Electron Mater 24:1443
156. Tang J, Mao D, Feng L, Song W, Trefny J (1996) The properties and optimization of ZnTe:Cu back contacts on CdTe/CdS thin film solar cells. In: Proc of 25th IEEE Photovoltaic Specialist Conf, Washington, USA, pp 925–928
157. Tiwari AN, Khrypunov G, Kurdzesau F, Baetzner D, Romeo A, Zogg H (2004) CdTe solar cell in a novel configuration. Prog Photovoltaics Res Appl 12:33
158. Dobson KD, Visoly-Fisher I, Hodes G, Cahen D (2000) Stability of CdTe/CdS thin-film solar cells. Sol Energy Mater Sol Cells 62:295
159. Enzenroth RA, Barth KL, Sampath WS, Manivannan V, Kirkpatrick AT, Noronha P (2009) Stable Cu-based back contacts for CdTe thin film photovoltaic devices. J Sol Energy Eng 131:021012
160. Meyers P (1988) AMETEKS CdTe solar module development program. Sol Cells 24:35
161. Romeo A, Khrypunov G, Galassini S, Zogg H, Tiwari AN (2007) Bifacial configurations for CdTe solar cells. Sol Energy Mater Sol Cells 91:1388
162. Fthenakis VM, Alsema E (2006) Photovoltaics energy payback times, greenhouse gas emissions and external costs: 2004 early 2005 status. Prog Photovoltaics Res Appl 14:275
163. Raugei M, Bargigli S, Ulgiati S (2007) Life cycle assessment and energy pay-back time of advanced photovoltaic modules: CdTe and CIS compared to poly-Si. Energy 32:1310
164. Fthenakis VM, Raugei M, Held M (2009) Update of environmental impacts and energy payback times of photovoltaics. In: Proc of 24th European Photovoltaic Solar Energy Conf, Hamburg, Germany, p 6DO.10.5
165. Fthenakis VM, Kim HC, Alsema E (2008) Emission from photovoltaic life cycles. Environ Sci Technol 42:2168
166. Georg MW (2010) Tellurium in U.S. Geological Survey, mineral commodity summaries, Jan 2010
167. Green MA (2006) Improved estimates for Te and Se availability from Cu anode slimes and recent price trends. Prog Photovoltaics Res Appl 14:743
168. Lifton J (2009) The tellurium supply conjecture, published in Resource Investor on 9 Jul 2009
169. Selenium and Tellurium in 2008 Minerals Yearbook of USGS, 2009

CERCLA, Sustainability and Public and Environmental Health

Robert Davis Jewett, Michael W. Wascom
Department of Environmental Sciences, Louisiana State University, Baton Rouge, LA, USA

Article Outline

Glossary
Definition of the Subject
Introduction to CERCLA
Understanding CERCLA
SARA Revisions of CERCLA
Citizen Roles
NCP, NPL, and Site Procedures
Remediation Priorities and ARARs
ATSDR and the CERCLA List
Liability Scheme
Defenses
Enforcement Tools
States and Local Governments under CERCLA
Case Study: Agriculture Street Landfill Project
Criticisms of CERCLA
Future Directions
Bibliography

Glossary

One of the most useful ways to begin a study of the Comprehensive Environmental Response, Compensation, and Liability Act (CERCLA) is to engage the intriguing lexicon the act provides. As is demonstrated by the definitions below, terms are often defined under CERCLA in ways that are remarkably broad, granting a great deal of elbow room and flexibility for the US Environmental Protection Agency (EPA) to go about the work of protecting the public from hazardous materials, no matter when or how they have come to present a threat.

Environment Under CERCLA, the term "environment" is defined broadly in a manner that is distinctly multimedia. An environment is anywhere or anything that can become contaminated with a hazardous substance, including all surface and ground waters, land surfaces or subsurface strata,

or the ambient atmosphere. Any release of a hazardous material into any sort of environment is potentially covered under CERCLA.

Facility The term "facility" usually brings to mind an image of a building or series of buildings, but CERCLA defines the term more broadly. A "facility" under CERLCA includes any site or area where a hazardous material has been deposited, placed, stored, disposed of, or has somehow come to be located. It is just as likely to refer to a faulty storage tank or a leaking pipe as to a building or similar structure.

Hazardous substance In defining hazardous substances, CERCLA makes use of all other definitions and lists of such substances in previous US environmental legislation. However, there is one important exception: petroleum and petroleum products, natural gas and synthetic gas used for fuel. This is the so-called Petroleum Exception. Interestingly, the definition of a hazardous substance does not refer to any particular or minimum amount of a material that must be present for it to become hazardous. In theory, there is no lower limit of materials that must be present or must have been released before a remedial action is authorized, or liability is imposed.

Contaminant or pollutant CERCLA also authorizes cleanups of categories of substances that are broader than materials judged to be hazardous according to the standards of earlier federal regulations. Contaminants or pollutants, under CERCLA, are materials that may cause adverse health effects. While CERCLA allows the EPA to respond to sites polluted by these lesser threats, it authorizes recovery of cleanup costs from responsible parties only in cases of contamination by a documented hazardous substance.

Release Again, a release of a hazardous substance is broadly defined. CERCLA authorizes response to any sort of a release, including all manner of spills, leaks, and discharges into the air, as well as leaching, dumping, injecting, emitting, or disposing. Certain exceptions are made, generally for releases that are covered under other federal laws. As an example, motor vehicle emissions are excluded from CERCLA but are covered by federal emission standards and other regulations.

Removal Removal is also broadly defined, creating more potential opportunities to assess liability. Removal may refer to certain actions directly involved in cleanup of a site, such as removing the hazardous material from the area, or transporting waste to an authorized disposal facility. However, it may also refer to actions such as monitoring, assessing, and evaluating releases or potential releases. This allows the EPA to take preventive action to prevent a potential release.

Remedy or remedial action As in the case of removal, the construction of the terms "remedy" or "remedial action" in CERCLA allows for response to both actual or potential or threatened releases. The terms are also broadly construed to allow for a wide range of response actions, including public health or environmental monitoring, transportation of hazardous materials, implementation of an alternative water supply, and even removal or relocation of communities to safe locations.

Potentially responsible party or PRP Remedial actions that occur through CERCLA are often conducted not by the EPA directly, but by parties that are judged to be in some way accounle for the release. These parties, known as Potentially Responsible Parties, or PRPs, fall into four categories: owners, operators, arrangers or generators, and transporters. For more information on these categories and their responsibilities and liabilities under CERCLA, see section "Liability Scheme" below.

CERCLA Is also a distinctly creative act, which has also introduced new entities and terms into the knowledge base of environmentally conscious people, those affected by CERCLA actions and even CERCLA's critics.

The Superfund The Superfund has become a common name for all of CERCLA, but it also refers to the Hazardous Substance Superfund, established to provide financial resources to clean up hazardous sites. The Superfund was established by taxes imposed upon the chemical and petroleum industries and an environmental tax on corporations. It has since been supported by allocations from the federal general fund and through additional legislation, such as the American Recovery and Reinvestment Act.

The National Priority List or NPL The NPL was added to an existing resource, the National Contingency Plan (NCP), which was brought into being under the Clean Water Act to address the containment and removal of spilled oil and other hazardous substances. Under CERCLA, the NCP was revised to include direct provisions for responding to releases of hazardous substances, pollutants, and contaminants, including those released on land or in the air. CERCLA also revised the NCP to include a list of sites that were considered to be top priorities for response. This is the National Priority List, or NPL. Criteria for placement on the NPL are discussed in section "NCP, NPL, and Site Procedures" below.

Finally, CERLA brought into being a new federal agency The Agency for Toxic Substances and Disease Registry or ATSDR. ATSDR is charged under CERCLA with assessing the presence and nature of health hazards at specific Superfund sites, as well as working to prevent or reduce further exposure and the illnesses that result from exposures. It compiles and maintains a prioritized list of hazardous materials at Superfund sites, the CERCLA Priority List of Hazardous Substances. ATSDR also has a range of other duties, including health surveillance and the development and distribution of information on toxic substances. For more information, see section "ATSDR and the CERCLA List" below.

Definition of the Subject

The Comprehensive Environmental Responses, Compensation, and Liability Act of 1980, or CERCLA, also known as the Superfund Act, is a landmark piece of environmental legislation [1]. Its notably bold design, discussed in detail below, fits the daunting work it was established to perform, the remediation of the worst and most dangerous releases of hazardous materials in the history of the USA. CERCLA also plays a role in the prevention of threatened releases. While it is subject to criticism and may not function perfectly, or even quite as intended, CERCLA remains an essential safeguard of environmental and public health in the USA.

Introduction to CERCLA

Sustainability may be defined as the capacity to endure. The achievement of sustainability suggests a relationship to time, in which the past is never so bad as to doom the present or erase the future. CERCLA is unique among the central pieces of environmental legislation in the USA in that it is largely oriented to the past, and ensuring that the legacy of environmental destruction that accompanied the growth of industrialism in the USA does not continue to jeopardize the future of the nation, its people, or the environment. As a practical measure, CERCLA casts environmental disasters and hazardous releases as problems that can be solved. These problems, however, are often of a scope and gravity that defy inexpensive or easily realized solutions. This is why CERCLA operates not only through the use of a public "Superfund" but also through partnerships, sometimes coerced, with other parties, who are held to be responsible for hazardous releases, even those that occurred many years ago.

Early in 2010, approximately 1,280 sites were listed on the National Priority List, either in the midst of a CERCLA remediation or awaiting one. An additional 340 sites had been delisted in the history of CERCLA since 1980, with more than 60 sites under consideration to be added to the list [2]. However, it was only a small group of well-publicized releases of hazardous substances that originally inspired CERCLA.

CERLCA was enacted by Congress in response to environmental and public health disasters, including, inter alia: (a) the environmental contamination at a site in Kentucky that came to be known as "The Valley of the Drums"; a site of dioxin contamination in Times Beach, Missouri, that eventually caused the abandonment of the town; and, most notably, (b) the Love Canal contamination near Niagara Falls, New York.

The Love Canal incident is one of the more famous environmental disasters to occur in the USA. In the summer of 1977, 200 families were evacuated from the area of Love Canal when waste chemicals began to seep into the basements of homes in the community. In 1980, the US government filed suit, under the Resource Conservation and Recovery Act and the Safe Drinking Water Act, against the company that had dumped tens of thousands of tons of hazardous chemicals at the Love Canal site and then abandoned it, years before.

CERCLA was designed to address cases such as Love Canal, in which the past intervenes into the present, clouding the future of an area and its people. As noted above, CERCLA is, in large measure, retroactive in nature, allowing the government to go back in time to find responsible parties for current environmental contaminations. In 1980, during the closing days of the 96th Congress, the original CERCLA legislation passed. It was signed by President Jimmy Carter as one of his last official acts in office.

This entry will review CERCLA, including its initial provisions and later revisions. It will focus on issues that include liability under CERCLA, defenses against liability, site selection including technical review of sites, and the CERCLA Priority List of Hazardous Materials under ATSDR.

Understanding CERCLA

Original CERCLA and Basic Elements

The original CERCLA legislation included four basic elements:

1. A system for gathering and analyzing information concerning potential or actual releases of hazardous materials, pollutants, or contaminants
2. Federal authority to respond to control and clean up releases of hazardous materials, pollutants, or contaminants
3. The Hazardous Substance Response Trust Fund, or Superfund, to underwrite response and cleanup activities
4. A strict liability scheme for those judged to be responsible for releases of hazardous substances

In the matter of notification of a release, CERCLA functions in concert with other regulations, including the Emergency Planning and Community Right to Know Act, in requiring any person in charge of a facility (as uniquely defined under CERCLA as noted above) who has knowledge of a release of a hazardous substance to notify the National Response Center, a federal clearinghouse for hazard and public and environmental health information, as well as other appropriate state, federal, or local agencies.

CERCLA permits the EPA to request from any individual or party information deemed relevant to a release of hazardous materials. As with many federal authorities under CERCLA, this power is broadly construed. As an example, the EPA can obtain financial information to discover a party's ability to pay for the costs of a cleanup, as well as information that more directly relates to the handling of hazardous materials or the cause or scope of the release [3].

The second basic authority under CERCLA is the authority to clean up a site at which a release has occurred or is occurring. CERCLA authorizes two different types of response actions to releases or threatened releases, removal actions, and remedial actions:

- Removal actions are short-term response actions for cases in which releases or threatened releases require prompt response. These actions may be emergency actions, time-critical actions, or non-time-critical actions. Removal responses are generally used to address localized risks; for instance, the removal of drums containing hazardous materials that have been found on a site may be necessary to reduce or eliminate a contamination and mitigate risks posed to public health. Removal may also prevent contamination from compromising other elements of the environment; for example, topsoil removal may prevent further contamination of the water supply.
- Remedial actions are generally longer-term actions, designed to permanently reduce the risks associated with a release or threatened release. While these actions may have some urgency, they may constitute a long-range project rather than a time-intensive emergency response. For instance, a remedial action may involve taking actions to contain a hazardous substance or neutralize a toxin. Only sites listed on the National Priority List (NPL) are eligible for remedial action under CERCLA.

On some occasions, the type of response selected under CERCLA is subject to controversy: As one example, see the case of the Agriculture Street Landfill in New Orleans as discussed below, where a partial removal action may not have been sufficient to remediate a complex site.

CERCLA also created the Superfund, and is sometimes known as "The Superfund Act." This fund supports response, removal, and remediation activities.

However, it is not the only source of funds for these activities. Despite its nickname, the Superfund lacks sufficient funds to clean up all the sites on the National Priority List, or even those that are being cleaned up at any particular time. Instead, the preferred federal strategy is to conserve Superfund resources and compel or persuade other parties to clean up a site themselves. These additional parties, known as "Potentially Responsible Parties" or PRPs, are held responsible under the CERCLA liability scheme. These parties may also sue or reach agreements with other PRPs concerning which parties are responsible for the cleanup and in what proportion. See section "Liability Scheme" below.

SARA Revisions of CERCLA

In 1986, CERCLA was revised by the passage of the Superfund Amendments and Reauthorization Act, or SARA [4]. SARA added standards for an acceptable cleanup, provisions concerning the legal settlement process, and rights for state and citizens including some of those listed under Citizen Roles above.

Before SARA, CERCLA did not include any particular standards regarding cleanup operations. SARA provides guidelines on matters such as the type of cleanup action, compliance with the National Contingency Plan, and cost-effectiveness. SARA also provides criteria for assessing proposed remedies. These are discussed in section "NCP, NPL, and Site Procedures" below.

SARA also engages the issue of how to promote voluntary settlements EPA claims against PRPs. SARA provides substantial guidance on issues such as contributions among PRPs, how to address shares of unknown PRPs, and what to do about PRPs who are responsible only for very small quantities of hazardous material. SARA also added the "Innocent Landowner" defense for potential PRPs, which is discussed under Liability Scheme below.

CERCLA was also revised by the Small Business Liability Relief and Brownfields Revitalization Act of 2002 [5]. Some of the changes made by this act are noted throughout the entry below.

Citizen Roles

SARA also established a series of important roles for citizens to play in legal actions under CERCLA. First, citizens or citizens groups affected by a Superfund site may apply for a Technical Assistance Grant. These grants are used by citizens to hire their own independent technical consultants to advise them about health and environmental issues and monitor the work of the EPA and others regarding the site.

Citizens may sue any party, except the EPA, that is alleged not to be in compliance with any order, standard, condition, or requirement that is in force under CERCLA. The EPA may choose to intervene in the suit and prosecute the alleged offender. In such a case, the citizen suit is barred.

Citizens may also petition for a preliminary assessment at a site if that site is not scheduled for response actions. This method may be useful in making a certain site a higher priority for a remediation [3]. Another central right reserved for citizens is the right to comment. For instance, citizens can comment on any settlement agreements or consent decrees prior to judicial approval.

In addition, citizens have the right to know about the chemical and substance hazards they may face. Specifically, this requirement includes emergency notification of chemical releases; notification of chemical use, storage, and production activities in a community; emission reporting requirements; state and local emergency planning, and the development of emergency response plans.

NCP, NPL, and Site Procedures

As mentioned in the Glossary above, CERCLA substantially revised the National Oil and Hazardous Substances Pollution Contingency Plan (NCP). The NCP provides guidelines and procedures governing the response to releases or threatened releases of hazardous substances, pollutants, or contaminants. Under CERCLA, NCP criteria for the remediation of a hazardous release include a preference for permanent solutions, as well as cost-effectiveness and a practical ability to implement the solution.

Under CERCLA, the NCP was also revised to include a National Priority List (NPL), which serves as an information and management tool to help the EPA prioritize sites for cleanup. Inclusion of a site on the NPL does not in itself assign liability or require potentially liable parties to initiate action to clean up

the site. The NPL serves primarily informational purposes, identifying for the states and the public those sites, facilities, or releases that appear to warrant remedial actions.

Upon notification of a potentially hazardous release, or when a potentially hazardous site or release is otherwise discovered, the site is listed in the Comprehensive Environmental Response and Liability Information System (CERCLIS) for subsequent evaluation. EPA then assembles information on the site and conducts a Preliminary Assessment/Site Inspection (PA/SI) to determine the scope of any contamination or potential contamination. This process involves a review of records regarding the site and any hazardous substances associated with it, interviews of potentially knowledgeable parties, visual inspections by qualified personnel, and limited field sampling. The PA recommends further investigation, if warranted.

If the site is thought to present a threat to public or environmental health or safety, additional investigations are performed concerning the hazardous materials at the site, their potential for contacting humans, and possible migration pathways for spreading contamination. Information gathered in the investigative review process is then subject to a hazard analysis, using criteria that include the toxicity of hazardous substances, the location of possible receptors, and threats to the human food chain or the watershed or atmosphere. This analysis culminates in the development of a score on the Hazard Ranking System (HRS). A HRS score above 28.5 results in placement of the site on the NPL.

Sites that score at or above the threshold are then subject to a Remedial Investigation (RI) and Feasibility Study (FS). The RI includes an extensive sampling program and risk assessment in order to define the extent and degree of the contamination and the associated risks. It is designed to be a thorough analysis but can take years to complete. Typically, reports are compiled that describe the site's geology and hydrogeology, the sources of contamination, the type and degree of mobility of the contaminants, and all aspects of the threat to the public health or the environment. Any part of these data is potentially useful in developing and studying possible methods of remediation.

The next step is the FS, which is used to develop and evaluate various remediation alternatives. The FS details several remedial methods and analyzes each in light of the data from the RI. The work is often broken down into phased components, called Operable Units, to separate the remediation process, and often the physical or geographic area of the contamination, into more manageable units [6].

The preferred alternative identified by the FS is presented in a proposed plan for public review and comment. If the EPA stays with the proposed solution after this comment period, the selected alternative is approved in a Record of Decision (ROD). The site then enters into a Remedial Design phase and then the Remedial Action phase. Many sites require Long-Term Monitoring and 5-year reviews once the Remedial Action has been completed. If a site is not considered sufficiently hazardous for inclusion on the NPL, the EPA may still order a removal action to address an imminent threat.

EPA's nationwide strategic plan for addressing hazardous sites is found in another document, the Superfund Comprehensive Accomplishment Plan (SCAP). This document provides a list of those activities that are expected to occur at each site during a fiscal quarter. Information often appears in the SCAP before it is announced to the public [6].

Remediation Priorities and ARARs

As the EPA works toward a feasible solution for a site, various factors may become important. One is the level or degree of cleanup necessary. The central issue here is often what level of risk or remaining contamination is acceptable. As the EPA generally works with PRPs with a financial stake in the cleanup process, levels of remediation often become controversial. See the section on the "Agriculture Street Landfill site" for an example of a case where no real agreement was reached between affected citizens, the EPA and the PRPs, resulting in a lengthy court battle.

Section 121 of CERCLA is especially significant with respect to decisions about methods of remediation as it sets forth requirements for cleanup standards [7]. Remedial actions under CERCLA are consistent with the precepts of the NCP when possible. This section states that actions should be cost-effective. The guidelines also state a preference for permanent solutions that reduce the volume, toxicity, or mobility

of the contamination. Less permanent solutions, such as the construction of barriers, are not favored.

For hazardous materials left on site, remedies under CERCLA are required to achieve all Applicable or Relevant and Appropriate Recommendations (ARARs). The level or degree of the hazard must remain less than any standard, requirement, criterion, or limit under any federal environmental law or any state or facility siting law that is more stringent than the federal guidelines. This means that the site must achieve the cleanup level (or safety level) set by the most stringent laws that are applicable. The NCP includes criteria for determining whether a law or standard applies. Laws or standards may not apply, for instance, if they target a certain medium, such as water, and the hazardous material at the site is found in a different medium, such as soil. Other differences include (a) the activities regulated by the regulation versus those undertaken at the site and (b) the type of facility considered in the regulation versus that at which the proposed remedial action is to take place.

Once determined to apply, an ARAR generally must be met unless it is waived. CERCLA does provide a few circumstances in which a remedy may be selected that does not meet an ARAR, for instance, if the remedy is only part of a larger solution that will meet the ARAR or if meeting the ARAR would lead to greater risks to human health or the environment than would alternative actions [6].

ATSDR and the CERCLA List

Another important aspect of site selection and development of remedial responses is the CERCLA Priority List of Hazardous Substances maintained by the Agency for Toxic Substances (ATSDR). This list established, in order of priority, the substances most commonly found at facilities on the NPL and which are determined to pose the most significant potential threat to human health due to their known or suspected toxicity and potential for human exposure. The list is revised and published every 2 years, with a yearly review and revision to reflect additional information on hazardous substances.

This priority list is not a list of "most toxic" substances, but rather a prioritization of substances based on their frequency, toxicity, and potential for human exposure at NPL sites. This priority list and the order of the materials on it are based on an algorithm that relies on three components: frequency of occurrence at NPL sites, toxicity, and potential for human exposure to the substances found at NPL sites. Some substances included on the list are low in toxicity but often appear at NPL sites. The items high on the list are subjects of toxicological profiles prepared by ATSDR [8].

Liability Scheme

The liability scheme in force under CERCLA is novel and contradicts even some conventional canons of common law. For instance, a party cannot avoid liability under CERCLA simply by entering into a contract with another party, such as the new owner of a site, that transfers liability or indemnity. CERCLA supersedes such agreements.

CERCLA delineates four classes of "Potentially Responsible Parties," or PRPs, any of which may be liable for the cleanup of a Superfund site. These four classes are:

- The current owners or operators of the facility
- Owner or operators of the facility at the time of disposal of any hazardous substance
- Any person who arranges for the disposal, treatment, or transport of a hazardous substance at the facility
- Any person who transported a hazardous substance, pollutant, or contaminant to a facility, or accepted the material for transport, if that person selected the facility

Within these categories, the liability is broad. As an example, both the current owner and the owner at the time of contamination may be held liable. Does this mean that an owner who knows nothing about the dumping of materials years before on a property the new owner purchased just last year may be held liable for the cleanup of the material? In some cases, the answer is "yes," although such an owner is not entirely without defenses. Owners have a better opportunity to avoid liability if the release did not occur during the time they owned the property, and if they performed due diligence in purchasing the property, handled any hazardous materials discovered with care, and cooperated fully with EPA inquiries. See section "Defenses" below.

The operator is generally defined as the party who controls the operations at a site or facility. Parties that hold a security stake in a facility or site but are not technically its owners may be considered operators if they make any control decisions about a business or property.

Transportation companies that move materials from place to place may or may not be held liable under CERCLA. Courts have ruled that transporters who select the site where the materials are brought (generally the Superfund site) are liable, while those simply moving materials to a site picked by another party, such as the generator, are not liable. However, in actual practice, generators have often hired transporters simply to remove the materials from the site, without knowing where the materials would go. In these cases, the transporter is liable for selecting the disposal site, and the generator is also liable under the category of "Arranger."

Arrangers, often referred to as "generators," are the largest category of parties held liable under CERCLA. Arrangers contract for the removal, disposal, or treatment of hazardous materials, which may or may not be owned or produced by the arranger. This category has somewhat fuzzy boundaries – for instance, what if the arranger sells the material to another party for a legitimate business reason, such as for use in an industrial process? Is this "arranger" liable when the material later is dumped at an unmarked site? However, what if this "sale" was simply a ruse to cover for an illegal dumping operation? Such questions are subject to careful investigation and often litigation.

Defenses

Defenses against liability under CERCLA are limited. CERCLA is considered a "strict liability" law, meaning that mitigating factors such as negligence or an absence of negligence are not always considered in reaching determinations of liability. Even the defenses provided for potential PRPs under the law may not be viable in actuality. As one example, the law makes a provision for an Act of God defense; in actual practice, however, this remedy has not been upheld. Courts have ruled that all the usual "acts of God," hurricanes, tornadoes, earthquakes, etc., are foreseeable, and the resulting release of hazardous materials is avoidable with the proper precautions. Similarly, an act of war provides a defense only when the act is demonstrated to be the sole cause of the release [9].

A more viable defense that is frequently raised is the "Omission of a Third Party" defense whereby a defendant attempts to escape liability by claiming that the release was solely the act of a third party, for which the PRP is not responsible. However, for this defense to be applicable, the PRP may not have an articulated relationship with the third party; for instance, the third party may not be a rogue employee of the PRP company, or a party working under a contract with the defendant.

Another related defense is referred to as the "Held Only for a Security Interest" defense, or the "Secured Creditor Exception," which may protect parties that hold a stake in a property only for a security interest, without participating in the management of the property. Lenders are among those who may be eligible for this defense.

The revisions of CERCLA under SARA codified an emerging defense related to the Omission of a Third Party defense, the "Innocent Landowner" defense. To qualify for this defense in most cases, the landowner must establish a justifiable ignorance of the contamination. For instance, it is not enough simply to have purchased the property and then discovered only afterward that the site was contaminated. Instead, owners are required to show that they did due diligence, including undertaking all appropriate inquiry into the conditions of the property before purchase. Landowners may also rely on an "innocent landowner" defense in cases in which a property is acquired through inheritance or bequest.

Under the Small Business Liability Relief and Brownfields Revitalization Act, another defense for another class of "innocent landowners" is designated. To qualify, a number of provisions have to be demonstrated, including:

- All disposal or release of hazardous materials occurred before the landowner purchased the property
- All appropriate inquires into the previous ownership and use of the facility were made
- Appropriate care was taken regarding the hazardous materials, including appropriate action to stop the release

The landowner is also required to cooperate fully with the EPA's investigation into the property, the release of hazardous materials, and any response actions.

The Small Business Liability Relief and Brownfields Revitalization Act also provided another category of defense for PRPs, called the "De Micromis Party Exception." This defense is for parties who have generated, transported, or arranged for transport of only small amounts of hazardous material. The exemption applies when amounts are below 110 gal of liquid materials or 200 lb of solid materials. However, the exemption only applies when these materials do not figure heavily in the cost of remediation or restoration of the site. This exemption also protects a "de micromis" party from other PRPs seeking contributions toward the expense of remedies: A PRP suing another potential PRP must show that the "de micromis" defense does not apply [3].

Enforcement Tools

The EPA has several powerful enforcement tools to direct toward PRPs. Two of these, civil judicial injunctive actions and unilateral administrative orders, fall under the "imminent hazard" section of CERCLA, which authorizes the EPA to act if it determines that a release or threatened release poses an "imminent hazard" to public health [10]. An administrative order, in particular, can be compelling, as courts have held that PRPs have no right to a hearing or review before the order is issued. Willful violation of a unilateral EPA order makes the PRP subject to a fine of up to $25,000/day [3].

Litigation is another potential remedy. Under CERCLA, monies that can be recovered through litigation include costs incurred by state or federal governments, costs incurred by another party, and damages to natural resources including the expense of damage assessment. Under these broad categories, the EPA has recovered expenses for investigation, monitoring, and testing of a site; planning a response; staff costs; attorney fees; as well as expenses related more directly to remedial actions at the site [3].

The EPA prefers not to take remedial action on its own and then attempt to recoup the costs of its actions from PRPs. The preferred response is for PRPs themselves to conduct the remediation, under the monitoring and supervision of the EPA or relevant state agencies. Further, the EPA prefers that these actions be taken "voluntarily," which generally means under threat of a potential administrative order or another action. The EPA has several advantages that make its consultations with PRPs likely to be convincing. If the PRP complies with the EPA, it may escape the fines imposed under administrative orders, the damages granted by courts, and the legal fees entailed in court battles. It may also reduce any negative publicity or quell the complaints of angry citizens. Rather than battle the EPA, a route that many PRPs find more fruitful is to engage in discussions with, or legal actions against, other PRPs involved with the same release or facility to attempt to spread fiscal responsibility for the cleanup.

States and Local Governments Under CERCLA

States are responsible for the future management of all removal and remedial actions, once those actions are judged to be complete. States must also provide at least one federally licensed hazardous waste disposal facility to receive wastes removed from the Superfund sites within the state. The facilities may also be privately owned or operated and contracted to the state.

Under SARA, states were given additional roles in federal cleanup actions. States have the opportunity to review and comment on many federal actions involved in a remediation, including the Remedial Investigation and Feasibility Study, the proposed remedial action, the engineering design of the action, technical data and reports related to the remedy, and any decisions to waive standards.

States and local governments may also be held liable under CERCLA if they have acted in the roles of the PRP categories. However, governmental agencies acting purely in a regulatory manner are generally exempt from liability.

Case Study: Agriculture Street Landfill Project

The Agriculture Street Landfill in the Ninth Ward of New Orleans was operated as a landfill for approximately 50 years, ending in 1958. In 1965, it was briefly reopened to receive a massive amount of debris from Hurricane Betsy. The landfill was locally referred to as Dante's Inferno because its contents often caught fire,

and the area was frequently smoldering. It was a toxic environment to be sure.

In 1967, the city of New Orleans and the Housing Authority of New Orleans decided to develop the area as a community for low-income residents. Between 1969 and 1971, the Press Park townhomes were developed. Later, Gordon Plaza, a development of single-family homes was constructed. Several playgrounds were also built in the area. A tract of land was set aside for an elementary school, and, in 1986, Mouton Elementary School opened for its first group of students. Residents and employees working in the area often complained of unusual smells and illnesses.

The record of environmental testing at the site has been contested. According to the area citizens' group and the law firm that eventually filed a class action suit on behalf of area citizens, the results have often been kept from residents. The city of New Orleans tested the site in the late 1970s in anticipation of the development of Gordon Plaza. After the testing, the city required the builders to add topsoil to the building site, but the results of the tests themselves have never been made public. Before the construction of Mouton School, another round of testing revealed the presence of lead, mercury, and arsenic. The Orleans Parish School Board received a recommendation that topsoil be brought in and a clay barrier used to contain the contamination. However, no barrier was established when the school was built. Instead, during construction area residents were subjected to dusts that may have included hazardous materials [11].

In 1986, the EPA tested the area, but area residents said that they were never shown the results of the test. In 1993, the EPA tested again . This time, they reported to area residents that the former Agriculture Street Landfill was contaminated with approximately 150 different hazardous substances, including almost 50 that were known to cause cancer. In 1994, the EPA declared the area a potential Superfund site and placed it on the National Priority List.

In 1994, area residents formed Concerned Citizens of Agriculture Street Landfill. Utilizing an important provision of CERCLA, the group requested a technical assistant grant from the EPA, to fund an independent environmental consultant. The group lobbied for the closing of the Mouton school, and the school was soon closed.

In the mid-1990s, the city government broke ranks with the federal authorities; led by Mayor Marc Morial, the city joined residents in arguing for federal support for relocating area residents. The EPA believed that the site could be remediated and from 1998 to 2001 took action, including replacing topsoil from open areas, but without excavating structures or streets. Residents were given certificates stating that their properties had been partially remediated, and were also given written restrictions on what they could do with their properties [11].

A lawsuit filed on behalf of the residents was granted class action status in 1999. The case went to trail in 2004, with the residents prevailing. The landfill area was ruled to be unreasonably dangerous under state law. The residents were awarded damages and market value of their properties. Employees and students also received awards. The judge in the case used discretionary powers to increase the monies received by 100%. Upon appeal, judgments for emotional distress were halved, but the rest of the decision stood. As of 2010, residents were applying to receive their claims, some 40 years after the regrettable residential development of the former landfill began [11].

As for the landfill site, it is believed that Hurricane Katrina removed much of the new topsoil deposited in remedial actions and may have dispersed contaminants throughout the area. It may be that the EPA's efforts in this area, which many believe were not of sufficient boldness to respond effectively to the severity of the contamination, have come largely to naught [12].

Criticisms of CERCLA

CERCLA cuts a board swath through American society. It is an ambitious federal regulation that was designed to engage the enormous and complex problem of releases of hazardous materials. It also imposes new and in some ways novel legal requirements on those who may be deemed in any manner responsible for a release or threatened release, even in cases in which they would not be held responsible under conventional canons of common law. It is little wonder that CERLCA is controversial and comes under criticism from a range of viewpoints and for myriad reasons.

Business owners, industry and corporate interests have complained that the strict liabilities imposed by CERLCA inhibit economic growth, not only by tying

up money in expensive remediations, but also by creating a chilling effect that prevents the purchase for redevelopment of any sites that could prove to be contaminated. One of the main charges laid against CERCLA from this perspective is that it simply is not "fair." It is unfair, for instance, for owners or operators who exercised all due caution in handling a material to be held liable for a release that occurred due to the unsafe actions of another party. It is also unfair to expect today's generation of business owners or shareholders to remediate a site that was contaminated years ago.

A particular sticking point has been the extension of liability to parties that may have sent only a small quantity of materials, comprising a hazard that is limited in scope and degree, to a disposal facility where a hazardous release eventually occurred. For instance, cases that involved pizzerias, donut shops, fitness facilities, and a local Elks Club have been publicized [13]. The revisions of defense provisions of CERCLA under the Small Business Liability Relief and Brownfields Revitalization Act were directed at ensuring that small business and other parties who are not large owners, operators, generators, handlers, or transporters of hazardous materials may escape liability.

Simultaneously, environmentalists and citizens' groups have criticized CERCLA on other grounds. These parties have argued that CERCLA remains tied to corporate interests, that the EPA is hesitant or unwilling to take on controversial projects, and that its preferred remedial actions often do not go far enough to solve the problem. The slow progress of cleanup projects is another common complaint [6].

As a large public project that uses taxpayer money, CERCLA has also drawn criticism from taxpayers and watchdog groups that have raised objections to what is perceived as inefficient use of public funds. However, other critics and public officials argue that the real problem is that there is simply not enough money in the system to perform the ambitious work CERCLA calls for, especially since the industry tax that originally funded the Superfund expired in 1995 and has not been renewed.

In the absence of public funding, private funding for remedies under CERCLA is all the more essential. However, businesses have also found a way to circumvent the law: declaring bankruptcy to avoid legal or financial responsibility [14]. The use of the legal system to settle questions of CERCLA liability, whether between PRPs and the EPA or among different PRPs, has also been criticized as a drain on resources [15].

Critics from a variety of perspectives have also argued over issues involving the intersection of science and politics, including methods for assessing and rating sites and placing certain projects of the National Priority List. Some have claimed that the risks of some sites are greatly exaggerated by the EPA, while the risks posed by other sites may be overlooked. Questioning the objective, scientific basis for placement on the NPL, some critics have said that there is no evidence that those projects included on the NPL are more hazardous than those that are not. Similarly, some critics have claimed that due to improper risk assessments, the EPA has performed unnecessary actions on sites, beyond those needed to control the hazards [15]. In the matter of the Agriculture Street Landfill, however, the opposite claim borne out by the courts is seen: that the EPA's actions did not go nearly far enough to ensure public health.

Perhaps one of the most resonant criticisms of CERCLA, offered over the years by people from different political persuasions and economic or social interests, is that its provisions make the revitalization or rehabilitation of older, often abandoned, industrial sites much less attractive. Not only have potential developers or owners been reluctant to take control of such properties for fear of liability, lenders are also reluctant to make loans for the purchase or redevelopment of the property. Provisions of the Small Business Liability Relief and Brownfields Revitalization Act address this issue.

Future Directions

While criticisms of CERCLA are many, they have not yet reached a pitch that would put the future of CERCLA into radical question. Americans are too concerned with issues of sustainability, public health, and the condition of the environment to allow hazardous sites to go without remediation. Alternative schemes have been proposed – for instance, market-based systems that would allow for the remediation and redevelopment of sites by private parties under market conditions [15]. However, such alternatives have not so far been seriously engaged in the political system,

suggesting that at this point, Americans want governmental agencies to have a strong hand in remediation efforts, as well as the prevention of threatened hazardous releases.

The most pressing issues as CERCLA heads into the future appear to be funding cleanups and maximizing the effectiveness of funds spent. Historically, approximately 70% of cleanup activities under CERCLA have been paid for by PRPs. However, as parties find avoidance methods, whether through legal exceptions or by declaring bankruptcy, the federal share may increase. Originally, federal monies were provided through taxes on industry, but these have since expired. The Superfund is now increasingly dependent on general fund appropriations. The Superfund did receive a boost in funding under the American Recovery and Reinvestment Act of 2009, the federal stimulus meant to alleviate a recession. This act provided $600 million that was directed toward 50 Superfund sites, approximately doubling the federal investment in these cleanup operations. However, it is not clear how or if this level of funding can be sustained when the Recovery Act expires [16]. One hopeful sign, however, may be a decrease in litigation and resultant expenses [17]. President Obama has also proposed reinstating the corporate taxes that originally funded the Superfund [18].

Even as commitment to CERCLA wavers, at least some degree in the USA, the act is seen worldwide, in some instances, as an intriguing method for funding other environmental and sustainability projects. As one example, the proposed International Climate Change Fund, an alternative to the climate agreement set by the Kyoto Protocol, would use a trust fund similar to the Superfund to pay for the development and purchase of "clean" or low-carbon technologies for developing countries. All countries would be required to pay into the fund, with the payment based on their own carbon emissions, including greenhouse gases and "flow" emissions [19].

CERCLA is still a relatively young law, especially given the scale of the work it engages in the world. It is also novel, in purpose, orientation, and form. Even after 30 years, one may still be in the mode of adjusting to it and striving to understand if it is the right means for the job it set out to do. Thus, revisions of CERCLA to date, such as SARA and the Small Business Liability Relief and Brownsfield Revitalization Act, have performed formative functions, reshaping the law to be more effective and fair, rather than supplanting CERCLA altogether. CERCLA was boldly constructed for an enormous undertaking. Whether it can complete this work is unknown and under dispute. However, it seems fair to say that lesser or more conventional legislation would be even less likely to succeed.

Bibliography

Primary Literature

1. Comprehensive Environmental Response, Compensation, and Liability Act of 1980. United States Public Law, 96–510
2. National Priority List Site Totals by Status and Milestone. EPA. Retrieved 22 Mar 2010
3. Ferrey S (2007) Environmental law, 4th edn. Wolters Kluwer, Austin, pp 362–382
4. Superfund Amendments and Reauthorization Act. United States Public Law 99–499
5. Small Business Liability Relief and Brownfields Revitalization Act. United States Public Law 107–118
6. Sullivan TFP (ed) (2009) Environmental law handbook, 20th edn. Government Institutes, Lanham, pp 510–528
7. Cleanup standards. 42 United States Code § 9621
8. ADSTR http://www.atsdr.cdc.gov/cercla/. Retrieved 20 Mar 2010
9. Switzer CS, Gray P (2002) CERCLA, 2nd edn, Basic practice series. American Bar Association, Chicago, pp 42–43
10. 42 United States Code § 9606(a)
11. Bagneris Law Firm. http://www.bagnerislawfirm.com/landfill_litigation_history. Retrieved 19 Mar 2010
12. Knickerbocker B (2005) Katrina Lays Bare Superfund Woes. Christian Science Monitor, 15 Sept 2005
13. Steinzor R (1998) The legislation of unintended consequences. Duke Environ Law Policy Forum 95:95–113
14. Borgardus K (3 May 2007) Bankrupt companies avoid more than $700 million in cleanup costs. Center for Public Integrity. http://projects.publicintegrity.org/superfund/report.aspx?aid=867. Retrieved 22 Mar 2010
15. DeLong J (2010) Privatizing superfund: how to clean up hazardous wastes. Cato Institute. http://www.cato.org/pubs/pas/pa-247es.html. Retrieved 19 Mar 2010
16. EPA (2010) http://www.epa.gov/superfund/eparecovery/faq.html. Retrieved 22 Mar 2010
17. Should the U.S. resurrect superfund? (2 Mar 2009). Natl J. http://energy.nationaljournal.com/2009/03/should-the-us-resurrect-superf.php. Retrieved 27 Mar 2010
18. Superfund: Litigation has decreased and EPA needs better information on site cleanup and cost issues to estimate future program funding requirement (15 July 2009). United States Government Accounting Office
19. International Climate Change Fund. http://climatelab.org/International_Climate_Change_Fund. Retrieved 25 Mar 2010

Books and Reviews

Airst RL (1994). Fair Assessment for Contaminated Properties, Urban Land.

Applegate JS, Laitos JG (2005) Environmental law: RCRA, CERCLA and the management of hazardous waste. Foundation, New York

Austrian Z, Eichler H (1994) Urban brownfields site survey: preliminary analysis. Cleveland State University, Levin College of Urban Affairs, Cleveland

CERCLA/Superfund Orientation Manual (1992). EPA, Washington

Chemical Waste Litigation Reporter (Information Service)

Cooke SM (ed) (1992) Law of hazardous waste: management, clean-up, liability and litigation (updated annually). Michael Bender, Stony Brook, NY

Davis TS (ed) (2002) Brownfields: a comprehensive guide to redeveloping contaminated property, 2nd edn. American Bar Association, Chicago

Federal Environmental Laws 2009 edn. (2009). West, New York.

Fogelman V (1992) Hazardous waste cleanup, liability, and litigation: a comprehensive guide to superfund law. Quorum, Westport

Garrett TL (ed) (1992) The environmental law manual. American Bar Association, Chicago

Gochfeld M (1995) Hazardous waste. In: Rosenstock L, Cullen M (eds) Textbook of occupational and environmental medicine. W.B. Saunders, Philadelphia

Gochfeld M, Burger J (1995) Assessment and mediation of hazardous waste sites. In: Brooks S et al (eds) Environmental medicine. Mosby, St. Louis

Initial guidance for implementing the superfund remedial program provisions of the American reinvestment and recovery act of 2009 (2009). EPA, Washington

Introduction to the Hazard Ranking System EPA, Washington. http://www.epa.gov/superfund/programs/npl_hrs/hrsint.htm. Accessed 27 Mar 2010

LaGrega MD, Buckingham PL, Evans JC (2001) Hazardous waste management, 2nd edn. McGraw-Hill, New York

Preliminary Assessment/Site Inspection. EPA, Washington. http://www.epa.gov/superfund/cleanup/pasi.htm. Retrieved 27 Mar 2010

Robinson N, Reilly KA (1992) Environmental regulation of real property. Law Journals Seminar Press, New York

Rodgers WH (2001) Environmental law. West Group, New York

Spranking JG, Weber GS (1997) Law of hazardous wastes and toxic substances in a nutshell. West, New York

Stern C, McKinney JA, Graham DB (1996) CERCLA enforcement: a practitioner's compendium of essential EPA guidance and policy documents. American Bar Association, Chicago

Stever DW (2010) Law of chemical regulation and hazardous waste. West, New York

Sullivan TFP (ed) (1995) Environmental law handbook. Government Institutes, Rockville

Superfund 20th Anniversary Report (2000) EPA, Washington

Switzer CS, Gray PL, McCullough MS (2000) CERCLA enforcement: a practitioner's compendium of essential EPA guidance and policy documents, Vol 2. ABA, Chicago

Watts RJ (1997) Hazardous wastes: sources, pathways, receptors. Wiley, New York

Chemicals in the Environment, Diffusive Transport

Edward Cussler

Department of Chemical Engineering, University of Minnesota, Minneapolis, MN, USA

Article Outline

Glossary

Definition of the Subject

Introduction

Basic Diffusion

Dispersion

Diffusion Coefficients

Diffusion Across Interfaces

Important Special Cases

Future Directions

Bibliography

Glossary

Convection Mass transfer effected by flow due to applied forces like pressure (forced convection) or to density differences (free convection).

Diffusion Mixing caused by molecular motion.

Diffusion coefficient The negative of the flux per concentration gradient.

Diffusivity Another name for the diffusion coefficient.

Dispersion Mixing caused by diffusion and simultaneous flow.

Flux Mass or moles transferred per area per time.

Mass transfer Diffusion and dispersion, especially across interfaces.

Mass transfer coefficient The flux per concentration difference, especially near an interface.

Overall mass transfer coefficient The flux per virtual concentration difference from one phase across an interface into a second phase.

Definition of the Subject

Diffusion is mixing without stirring. It is mixing caused by Brownian motion, that is, by thermally induced random motion of molecules or small particles. Because diffusion is often slow, it frequently limits the overall rate of the process. Diffusion has the reputation of being a difficult subject, which it can be; however, the difficulty most often comes from complicated units, from interfaces, or from the combination of diffusion and convection. By itself, diffusion is not hard. It is easier than viscous flow and much easier than ideas like entropy or chemical potential.

Two other phenomena, closely related to diffusion, are also reviewed in this entry. Dispersion is mixing caused by the interaction of flow and diffusion. Often, it is described using mathematics similar to those which describe diffusion. In environmental problems, these two phenomena are sometimes treated without distinction and without penalty. Mass transfer, an alternative description of diffusion, assumes that all concentration changes occur near interfaces. While it is used largely to describe chemical processing, it has considerable value in environmental problems.

Introduction

This entry is organized as four sections. The first section gives the mathematical description of diffusion itself. The second reviews dispersion, a different phenomenon that is mathematically similar to diffusion but which is caused by different physical effects. The third section, "Diffusion Coefficients," reviews values of the diffusion coefficients themselves; and the fourth section "Diffusion Across Interfaces," explains mass transfer across interfaces, especially air–water interfaces. Finally, the section "Important Special Cases" reports some common situations which have important features.

Basic Diffusion

The basic mathematical description of diffusion is Fick's Law, suggested by Adolph Fick (1829–1910) when he was just 26 years old. For a dilute solution, Fick's Law is:

$$j_1 = -D\frac{dc_1}{dz} \tag{1}$$

where j_i is the flux of a solute "1," and dc_1/dz is the concentration gradient, that is, the change of the solute concentration with position. The diffusion coefficient D is a proportionality constant which is nearly constant in almost all situations. The flux is the amount of solute moving per cross-sectional area per time and so has the dimensions of mass (M) per area (length squared L^2) per time (t). The concentration gradient has dimensions of concentration (M/L^3) per distance (L). Thus the diffusion coefficient has dimensions of (L^2/t).

The form of Fick's Law in Eq. 1 has some hidden implications. First, it is a one-dimensional equation of what is actually a more general vector relation. Because at least four out of five diffusion problems are one-dimensional, this is often not a major issue. Second, the concentration can be expressed in different units. If it were expressed in moles per volume, then the flux would be in moles per area per time. If it were expressed as a mole fraction or a mass fraction or a partial pressure, then unit conversions would be necessary and annoying, but not difficult. Third, the minus sign in Eq. 1 is arbitrary, stuck in to make the diffusion coefficient positive. The only difficult implication of Eq. 1 is the restriction to dilute solutions, explored in more detail at the end of this section. The restriction is rarely important because solutions in the environment are so often dilute. For example, liquid water contains 55 mol/l, so almost every aqueous solution is dilute.

The most important case of Fick's law is diffusion across a thin film, described next. Other important cases and concentrated solutions are reviewed later.

Diffusion Across a Thin Film

The simplest case, steady diffusion across a film, is also the most important. Imagine a thin film separating two well-stirred solutions, as shown in Fig. 1. On the left, the solution has a concentration c_{10}; on the right, the concentration is $c_{1\ell}$. The key parts of this case are the variation of concentration across the film $c_1(z)$ and the flux j_1. Finding these requires a mass balance on a differential volume Δz thick and located at an arbitrary position z within the film:

$$(\textit{mass accumulation}) = (\textit{mass diffusing in} - \textit{out})$$

$$\frac{\partial}{\partial t}(c_1 A \Delta z) = (j_1 A)_z - (j_1 A)_{z+\Delta z} \tag{2}$$

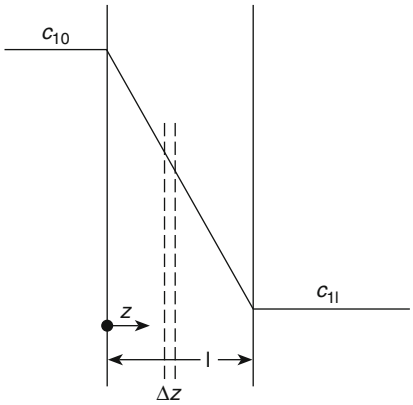

Chemicals in the Environment, Diffusive Transport. Figure 1
Concentration profile across a thin film

where A is the constant cross-sectional area of the film. Because diffusion is steady, the concentration does not change with time, the left-hand side of Eq. 2 is zero, and

$$0 = \frac{j_1|_z - j_1|_{z+\Delta z}}{(z+\Delta z) - z}$$

$$0 = -\frac{dj_1}{dz} \tag{3}$$

This restates the assumption of steady-state diffusion, independent of time. Combining this relation with Fick's Law (Eq. 1) yields:

$$0 = D\frac{d^2 c_1}{dz^2} \tag{4}$$

This is subject to two boundary conditions:

$$z = 0 \quad c_1 = c_{10} \tag{5}$$

$$z = \ell \quad c_1 = c_{1\ell} \tag{6}$$

This is enough to solve this important problem.

Equation 4 may be integrated once to find:

$$\frac{dc_1}{dz} = A \tag{7}$$

where A is an integration constant. Integrating a second time gives:

$$c_1 = Az + B \tag{8}$$

where B is a second integration constant. Evaluating A and B from Eqs. 5 and 6 gives:

$$\frac{c_1 - c_{10}}{c_{1\ell} - c_{10}} = \frac{z}{\ell} \tag{9}$$

The flux can now be found by combining this result with Fick's Law:

$$\begin{aligned} j_1 &= -D\frac{dc_1}{dz} \\ &= \frac{D}{\ell}(c_{10} - c_{1\ell}) \end{aligned} \tag{10}$$

If the concentration difference across the film is doubled, the flux doubles. If the diffusion coefficient is twice as big, the flux will be twice as big, too. If the film thickness increases two times, the flux will be cut in half.

This important example is so simple mathematically that many novices tend to skip over it. This is a mistake. Its nuances are explored by the following questions:

1. *How does the flux change if the film is chemically different than the adjacent solutions?*

In this case, the boundary conditions in Eqs. 5 and 6 change to:

$$z = 0 \quad c_1 = Hc_{10} \tag{11}$$

$$z = \ell \quad c_1 = Hc_{1\ell} \tag{12}$$

where H is a partition coefficient, the ratio at equilibrium of the concentration inside the film to that in the adjacent solution. Paralleling the arguments above,

$$j_1 = \frac{(DH)}{\ell}(c_{10} - c_{1\ell}) \tag{13}$$

The diffusion coefficient D in Eq. 10 is replaced with the product (DH), which is called the permeability. (The term (DH/ℓ) is called the permeance.) As will be shown later, diffusion coefficients in gases and liquids do not vary much, but partition coefficients vary a lot. Thus partition is often the key to permeability.

2. *How is the flux changed by a fast reversible reaction giving an immobile product?*

This case occurs surprisingly frequently in, for example, adsorption in soil or dyeing of wool. The answer is that at steady state, the flux does not change. Every point crossing the film has a different concentration which is in equilibrium with a different absorbed

amount. Still, at steady state, the reaction is at local equilibrium and does not affect the flux. This is not the case for unsteady state, for irreversible reactions, or for mobile reaction products.

Other Important Cases

Many diffusion problems are not thin films. Surprisingly, many do behave as if they were thin films. For example, for a sphere of radius R slowly dissolving in a stagnant fluid with a concentration of $c_{1\infty}$, the flux is:

$$j_1 = \frac{D}{R}(c_{10} - c_{1\infty}) \tag{14}$$

where c_{10} is the concentration in solution at the surface of the sphere. For diffusion from a solution of c_{10} through a very thin, impermeable film with a cylindrical orifice of radius R, and into a solution at $c_{1\infty}$, the flux is:

$$j_1 = \frac{D}{\frac{\pi}{2}R}(c_{10} - c_{1\infty}) \tag{15}$$

The fluxes in these cases are strong mathematical parallels to that in Eq. 10. The mathematics in these cases is different, but the final result is remarkably similar. The thin film limit is a good guide about 80% of the time.

For unsteady state diffusion, this is not true. Fluxes and concentration profiles for a wide variety of unsteady cases have been calculated and are tabulated in a few clear texts. One of these cases, useful in perhaps 10% of all cases, is unsteady diffusion into a semi-infinite slab, shown in Fig. 2. In this case, a mass balance gives:

$$\frac{\partial c_1}{\partial t} = D\frac{\partial^2 c_1}{\partial z^2} \tag{16}$$

where t is the time. For this semi-infinite slab, the initial and boundary conditions are:

$$t = 0 \quad \text{all } z \quad c_1 = c_{1\infty} \tag{17}$$

$$t = 0 \quad z = 0 \quad c_1 = c_{10} \tag{18}$$

$$t = 0 \quad z = \infty \quad c_1 = c_{1\infty} \tag{19}$$

The concentration profile in this case is:

$$\frac{c_1 - c_{1\infty}}{c_{10} - c_{1\infty}} = 1 - erf\,\frac{z}{\sqrt{4Dt}} \tag{20}$$

where *erf* is the error function. The flux at the edge of the slab, that is, at $z = 0$, is:

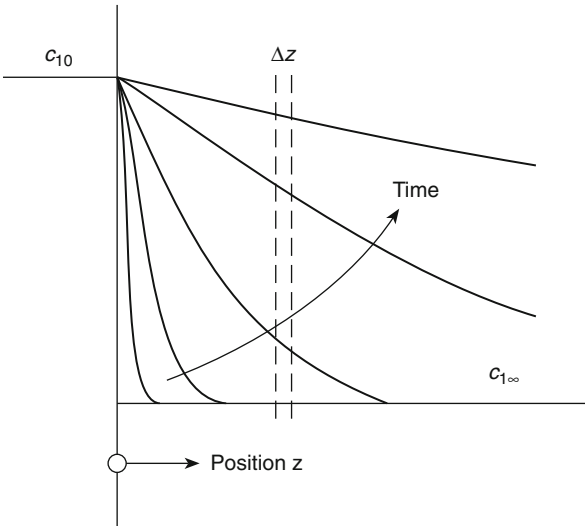

Chemicals in the Environment, Diffusive Transport. Figure 2
Concentration profile into a semi-infinite slab

$$j_1 = \left(\sqrt{\frac{D}{\pi t}}\right)(c_1 - c_{1\infty}) \tag{21}$$

This is the key result for this case.

The cases of a thin film and a semi-infinite slab are especially important because they bracket observed behavior. More specifically, the result in Eq. 21 for a semi-infinite slab is compared with the flux across a thin film in Table 1. In both cases, the flux will double if the concentration difference doubles. If the diffusion coefficient doubles, the flux across a thin film doubles, but the flux into the semi-infinite slab increases $\sqrt{2}$ times. If the film's thickness doubles, the flux drops two times for the film, but is unchanged for the slab. If diffusion occurs for twice as long, the flux for the thin film keeps its steady value, but that for the slab drops by a factor of $1/\sqrt{2}$. These limits will usually bracket all diffusion behavior because all shapes will be between the film and the slab. These two cases are key to understanding the mathematics of diffusion.

A third special case is especially important for environmental engineering. This is the decay of a pulse. In this case, a large amount of solute is released at a particular plane at $z = 0$. Solute diffuses away from this position in only one dimension. The solute

Chemicals in the Environment, Diffusive Transport.

Table 1 Flux across a film or into a slab. These two cases are important because they bracket almost all diffusion problems. In this table, K is the equilibrium constant of the rapid chemical reaction

	Thin film	Semi-infinite slab
Concentration difference	Δc_1	Δc_1
Diffusion coefficient	D	$\sqrt{D}$
Thickness	ℓ^{-1}	–
Time	–	t^{-1}
Flux without reaction	$j_1 = \frac{D}{\ell}\Delta c_1$	$j_1 = \sqrt{\frac{D}{\pi t}}\Delta c_1$
Flux with fast reversible reaction	$j_1 = \frac{D}{\ell}\Delta c_1$	$j_1 = \sqrt{\frac{D(1+K)}{\pi t}}\Delta c_1$

concentration as a function of position z and time t gives the details of any environmental impact.

The mathematics follows the same route as the slab: a mass balance is subject to initial and boundary conditions, which are combined with Fick's Law and solved to give the concentration profile. The mass balance is:

$$\frac{\partial c_1}{\partial t} = D\frac{\partial^2 c_1}{\partial z^2} \tag{22}$$

This mass balance, identical with the mass balance for the slab (Eq. 16), occurs so frequently that some just call it "the diffusion equation." The initial and boundary conditions are different from Eqs. 17–19 for the slab:

$$t = 0 \quad \text{all } z \qquad c_1 = \frac{M}{A}\delta(z) \tag{23}$$

$$t = 0 \quad z = 0 \qquad \frac{dc_1}{dz} = 0 \tag{24}$$

$$z = \infty \qquad c_1 = 0 \tag{25}$$

In these conditions, M is the total solute injected, A is the cross-sectional area, and $\delta(z)$ is the Dirac function, equal to zero everywhere except at $z = 0$, where it is infinity. While the mathematical solution of Eqs. 22–25 is tricky, the answer is simple:

$$c_1 = \left[\frac{M/A}{\sqrt{4\pi Dt}}\right] e^{-\frac{z^2}{4Dt}} \tag{26}$$

In this Gaussian concentration profile, the quantity in square brackets is the maximum concentration, which drops as time grows. The mathematical form of this important result is also observed for other environmental problems which do not depend only on diffusion, as described in the section "Dispersion."

Concentrated Diffusion

One reason that diffusion has the reputation of being difficult comes from the major complexities of concentrated solutions. These complexities are rarely important in environmental engineering and so should be ignored unless there are good experimental reasons not to do so. These complexities are mentioned here only to illustrate when they are important.

To explore this, imagine putting a pot of room temperature water of 25°C on a stove that is turned off. The flux of any evaporating water will be given by Eq. 10. If the air above the stove were dry, $c_{1\ell}$ would be zero. Because the water at 25°C has a vapor pressure of about 25 mmHg, c_{10} is about:

$$\begin{aligned} c_{10} &= \left[\frac{25\text{ mm Hg}}{750\text{ mm Hg}}\right]\frac{1\text{ mol}}{22.4\times10^{-3}\text{ m}^3} \\ &= 1.5\frac{\text{mol}}{\text{m}^3} \end{aligned} \tag{27}$$

If the liquid water in the pot is 0.1 m below the rim and the diffusion coefficient of water vapor in air is about 2.8×10^{-5} m^2/s, the flux is:

$$\begin{aligned} j_1 &= \frac{D}{\ell}(c_{10} - c_{1\ell}) \\ &= \frac{2.8\times10^{-5}\text{m}^2/\text{s}}{0.1\text{m}}\left(1.5\frac{\text{mol}}{\text{m}^3} - 0\right) \\ &= 4\times10^{-4}\frac{\text{mol}}{\text{m}^2\text{s}} \end{aligned} \tag{28}$$

Now imagine heating the liquid water in the pot to boiling. If the heat flux q is 20 kJ/m^2 s, then the molar flux caused by boiling is:

$$\begin{aligned} n_1 &= \frac{q}{\Delta\tilde{H}_{vap}} \\ &= \frac{20\text{kJ/m}^2\text{s}}{48\text{kJ/mol}} \\ &= 0.4\frac{\text{mol}}{\text{m}^2\text{s}} \end{aligned} \tag{29}$$

The boiling flux n_1 is 1,000 times greater than the diffusion flux at room temperature, but it is not a function of D. Thus slow dilute evaporation is a function of the diffusion coefficient; but boiling depends not on diffusion but on heating rate.

But what about intermediate cases? For example, how fast will evaporation take place at 50°C?

Answering this question requires a more complete form of Fick's Law. Unfortunately, there is no single way to do this. One choice is the following:

$$[\text{Total flux}] = [\text{Diffusion flux}] + [\text{Convective flux}]$$

$$\begin{aligned} n_1 &= c_1(v_1 - v) + c_1 v = j_1 + c_1 v \\ &= -D\frac{dc_1}{dz} + c_1 v \end{aligned} \tag{30}$$

where v is most often a volume average velocity. The most common alternative form of Fick's law, strongly advocated by a few zealots, may be approximated as:

$$\nabla c_1 = \frac{c_1 c_2}{cD}(v_2 - v_1) \tag{31}$$

where c_2 and v_2 are the concentration and velocity of the solvent. This form avoids choosing a convective velocity, but it can cloud the physical significance of the problem.

Fortunately, the result for a problem like the water evaporation given above is the same for both forms of Fick's Law given in Eqs. 30 and 31. If water at 50°C is evaporating from the pot above into dry stagnant air, the total flux is:

$$\begin{aligned} n_1 &= -\frac{Dc}{\ell}\ln\left(1 - \frac{c_{10}}{c}\right) \\ &= \frac{-2.8 \times 10^{-5}\text{m}^2/\text{s}\left(\frac{1\text{mol}}{22.4\times10^{-3}\text{m}^3}\right)}{0.1\text{m}}\ln\left(1 - \frac{92.5}{760}\right) \\ &= 1.62 \times 10^{-3}\text{mol}/\text{m}^2\text{s} \end{aligned} \tag{32}$$

This is about 7% greater than the result would be if calculated from Eq. 10 for a dilute solution at 50°C. The moral is clear: the effects of concentrated diffusion will only rarely be important in the atmospheric and aquatic environments.

This completes our basic description of the three cases key to understanding diffusion. These are the thin film (80% of the cases), the semi-infinite slab (10% of the cases), and the decay of a pulse (5% of the cases). Other cases with different boundary conditions do occur, and solutions for these are tabulated in the literature. However, these other cases are not as common in practice. Similarly, diffusion in concentrated solutions is complicated but infrequently important. The simple form of Fick's Law in these three cases is the best way to get started.

Dispersion

We now turn to an environmentally important problem mathematically similar to diffusion but with a different physical origin. To make this problem specific, imagine dealing with the spill of a single toxin on the ground. Imagine the concentration of the toxin spreads in one dimension with time and groundwater flow, producing a roughly Gaussian concentration profile. We want to know how the spread of this toxin varies with the diffusion coefficient of the toxin.

The answer is surprising: if the diffusion coefficient increases, the spread of the toxin may be bigger, smaller, or unchanged. The toxin's concentration profile is:

$$c_1 = \frac{M/A}{\sqrt{4\pi Et}}e^{-\frac{(z-vt)^2}{4Et}} \tag{33}$$

where M is the total amount of toxin, A is the cross-sectional area across which the dispersion occurs, and v is the velocity of any flow through the soil. The dispersion coefficient E has the same units as the diffusion coefficient but will often be much larger. This result, a complete analogue to Eq. 26, can be derived from parallels to Eqs. 22–25 by replacing the diffusion coefficient D with the dispersion coefficient E. However, while this mathematical parallel is complete, it does not explain the physics responsible for dispersion.

To explore the physics involved, imagine the toxin is injected as a pulse into a small tube of diameter d. The toxin's dispersion will be a strong function of how much flow is in the tube. If there is absolutely no flow, then the dispersion coefficient equals the diffusion coefficient:

$$E = D \tag{34}$$

Increasing diffusion increases dispersion. If there is a small, laminar flow of velocity v, then:

$$E = \frac{v^2 d^2}{192D} \tag{35}$$

Increasing diffusion decreases dispersion. The velocity where Eq. 35 becomes dominant is when:

$$\frac{v^2 d^2}{192D^2} >> 1 \tag{36}$$

For non-absorbing soil with the equivalent of 500 μm particles and diffusion in water liquid, D is about 10^{-9} m^2/s, so v must be much greater than 30 μm/s or 2 m/day for Eq. 35 to swamp Eq. 34. If there is a large, turbulent flow ($dv/v > 2{,}000$), then:

$$E = \frac{dv}{2} \tag{37}$$

Dispersion, now independent of diffusion, is due to the coupled turbulent fluctuations of concentration and velocity. The physical basis of Eqs. 33–37 is associated with G.I. Taylor.

Those with a more practical bent may correctly be skeptical of modeling flow through a soil as occurring in a straight tube. Others sharing this skepticism have extended this analysis to flow in packed beds. The key results involve two new quantities:

$$\bar{t} = t(1 + k') \tag{38}$$

$$k' = \left[\frac{\text{Soil concentration}}{\text{Solution concentration}}\right]\left(\frac{1-\varepsilon}{\varepsilon}\right) \tag{39}$$

where ε is the void fraction available for flow. In physical terms, $\bar{t}$ is the time corrected for any absorption by the soil, including material that diffuses into the soil's pores. The quantity k' is a type of equilibrium constant between the soil and the solution, lumping together adsorption and absorption. In this case, a pulse of toxin may still be dispersed to give the Gaussian concentration profile in Eq. 24, but with time t replaced by $\bar{t}$. The dispersion coefficient E is now given by:

$$E = D(1 + k') + \frac{d^2 v^2}{192D}\left(\frac{1 + 6k' + 11(k')^2}{1 + k'}\right) + \frac{\delta^2 v^2}{3D'}\left(\frac{k'}{1 + k'}\right) \tag{40}$$

where δ is an equivalent thickness of an absorbent and D' is the diffusion coefficient in the absorbent, not in the solution. The first term on the right-hand side of Eq. 40, the parallel of Eq. 34, is due to diffusion in the direction of flow. The second term, the analogue of Eq. 37, comes from Taylor dispersion and is often the most important. The third term is new, the result of the rate of absorption.

This overview of dispersion is intended as a caution and a starting point. The caution is that many Gaussian concentration profiles are due to diffusion coupled with other phenomena. The starting point in understanding these profiles is recognizing that their spread can depend inversely on diffusion. In other words, slow diffusion may result in wide dispersion.

Diffusion Coefficients

Diffusion is an important process because it is slow, and diffusion coefficients thus often control the overall rate of processes involving diffusion, flow, and chemical reaction. Typical values of diffusion coefficients, shown in Table 2, are chosen from the wide number of references in the literature but corrected to a temperature of 25°C. This wide literature is much less extensive than studies of other physical properties like viscosity or Young's modulus, because diffusion coefficients are relatively difficult to measure.

The values in Table 2 show diffusion in gases is about 10,000 times faster than diffusion in liquids, which is in turn over a billion times faster than diffusion in solids. Diffusion coefficients in gases fall around 10^{-5} m^2/s. Diffusion coefficients in liquids fall around 10^{-9} m^2/s. Diffusion coefficients in solids are much more variable, but are so slow that most of the mass transport occurs in fluid-filled gaps and pores within the solid. For example, in a bed of sand, most transport occurs in the spaces between sand grains and relatively little within the bulk of the grains themselves. In environmental problems, diffusion in gases and liquids is more important.

The diffusion coefficients, given in Table 2 for 1 atm and 25°C, do change with process variables, as outlined in Table 3. The variation with temperature in gases and liquids is small. For example, the temperature must be increased from 25°C (= 298° K) to 200°C (= 473° K) to double the diffusion coefficient in gases. Because the viscosity of a liquid drops as the temperature rises, the diffusion coefficient in a liquid changes faster with temperature, but the change is still modest. In contrast, diffusion coefficients in solids usually change more rapidly with temperature, doubling every 10°C or so.

Chemicals in the Environment, Diffusive Transport.
Table 2 Diffusion coefficients. Values given are in m^2/s and at 298 K and 1 atm

Gases	
Gas pair	Diffusion coefficient
Air-H_2O	2.6×10^{-5}
CO_2-O_2	1.6×10^{-5}
H_2-N_2	7.8×10^{-5}
H_2-O_2	8.9×10^{-5}
N_2-O_2	2.2×10^{-5}
N_2-H_2O	2.9×10^{-5}
O_2-H_2O	2.8×10^{-5}
O_2-octane	0.7×10^{-5}
Solids	
	Diffusion coefficient
C in Fe (BCC)	6×10^{-25}
Fe in Fe (BCC)	3×10^{-52}
B in Si	7×10^{-33}
He in SiO_2	4×10^{-14}
Na^+ in NaCl	1×10^{-36}
Ag^+ in AgCl	1×10^{-19}
Liquids	
Solute-solvent	Diffusion coefficient
O_2-H_2O	2.10×10^{-9}
CO_2-H_2O	1.92×10^{-9}
H_2S-H_2O	1.41×10^{-9}
HCl-H_2O	3.33×10^{-9}
NaCl-H_2O	1.61×10^{-9}
CaCl-H_2O	1.33×10^{-9}
NH_3-H_2O	1.64×10^{-9}
Urea-H_2O	1.38×10^{-9}
Sucrose-H_2O	0.52×10^{-9}
Albumin-H_2O	0.08×10^{-9}
H_2O-C_2H_5OH	1.24×10^{-9}
Benzene-butanol	0.99×10^{-9}
Hexane-heptane	4.21×10^{-9}

Chemicals in the Environment, Diffusive Transport.
Table 3 Variations of diffusion coefficients

	Gases	Liquids	Solids
Typical value, m^2/s	10^{-5}	10^{-9}	Much smaller
vs. T	$T^{3/2}$	T	Large
vs. p	p^{-1}	–	–
vs. solute diameter	size^{-2}	size^{-1}	size^{2}
vs. viscosity μ	μ^{1}	μ^{-1}	–

Other process variables also have relatively small effects. The diffusion coefficient in gases does vary inversely with pressure; but the gas concentration varies directly with pressure; so the flux, related to the diffusion coefficient times the concentration, may remain more constant. The diffusion coefficient does vary inversely with the size of the diffusing species. While these effects are usually modest for gases and liquids, they can be much larger for solids. These generalizations are justified by the approximate physical arguments given next.

Gases. The diffusion coefficients in gases can be predicted with reasonable accuracy from kinetic theory. This theory assumes that a gas contains individual molecules moving with thermal motion and colliding with each other only as pairs. Under these cases, the diffusion coefficient is given by:

$$D = \frac{1}{3}\lambda v \tag{41}$$

where λ is the distance between collisions and v is the molecular velocity. For a monatomic gas, this velocity is kinetic, related to the thermal energy:

$$\frac{1}{2}mv^2 = k_B T \tag{42}$$

where m is the molecular mass and k_B is Boltzmann's constant. Keep in mind that here v is a molecular velocity. It is the sonic velocity; it is much greater than the average velocity v used in Eqs. 30 and 31.

We must now estimate the distance between collisions λ. There are two cases. First, for the bulk gas, λ is found from the volume occupied by one molecule:

$$[\text{Volume of one molecule}] = [\text{Distance between collisions}] \times [\text{Area swept out between collisions}]$$

$$\frac{k_B T}{p} = \lambda\left[\frac{\pi}{4}\sigma^2\right] \tag{43}$$

where σ is the molecular diameter. Equations 41–43 can be combined to find:

$$D = \left(\frac{4\sqrt{2}}{3\pi}\right)\frac{(k_B T)^{\frac{3}{2}}}{p\sigma^2\sqrt{m}} \tag{44}$$

This approximate relation is close to that found from more complex theories: D does vary inversely with p, σ^2, and $\sqrt{m}$; it does vary with T to a power greater than one and less than two.

The second important limit of Eq. 41 occurs only for a gas diffusing in small pores of diameter d. In this case, the diffusing species is much more likely to collide with the pore walls than with other molecules. Thus the combination of Eqs. 41 and 34 becomes:

$$D = \frac{\sqrt{2}}{3} d\sqrt{\frac{k_B T}{m}} \tag{45}$$

This case, called Knudsen diffusion, has a diffusion coefficient which depends on the pore diameter d, but not on the molecular diameter σ. Now, the diffusion coefficient is independent of pressure, though it does vary inversely with the square root of solute mass. Under ambient temperature and pressure, Knudsen diffusion is important when the pores are much less than 0.1 μm.

Liquids. Diffusion in liquids is normally not described by a kinetic theory but as the motion of a rigid, spherical solute diffusing in a continuum of solvent. Despite the major approximations obviously made by this simple model, it gives remarkably good results. It is the standard against which new predictions are always judged.

The model begins by describing the friction on a solute sphere:

$$\text{Force} = [\text{Coefficient of friction } f] \times \text{Velocity } v_1 \tag{46}$$

The velocity v_1 now is the average and not the sonic value v used for gases. The coefficient of friction f is given by Stokes Law:

$$f = 6\pi\mu R \tag{47}$$

where μ is the solvent velocity and R is the solute radius. The force was suggested by Einstein to be the negative of the gradient of the chemical potential μ_1. Thus:

$$\begin{aligned} -\frac{d\mu_1}{dz} &= [6\pi\mu R]v_1 \\ &= -\nabla(k_B T \ln c_1) = -\frac{k_B T}{c_1}\frac{dc_1}{dz} \end{aligned} \tag{48}$$

Rearranging:

$$-c_1 v_1 = \left(\frac{k_B T}{6\pi\mu R}\right)\frac{dc_1}{dz} \tag{49}$$

But $(c_1 v_1)$ is the total flux n_1, equal in dilute solution to the diffusion flux j_1. Comparing this with Eq. 33 gives:

$$D = \frac{k_B T}{6\pi\mu R} \tag{50}$$

The diffusion coefficient in liquids varies inversely with solute size and with solvent velocity. This simple relation is called the Stokes–Einstein equation.

Equation 50 often gives good estimates of diffusion in liquids. Its simplicity is an invitation to attempt improvements. These include assuming the sphere is not solid but gas, replacing the sphere with an ellipsoid, allowing the sphere to spin, and putting it in a small pore. Other attempts at improvement allow for nonideal solutions, assigning different friction coefficients to solute and solvent, and considering changes close to the spinoidal. While none of these efforts is definitive, each can clarify the perspective of a particular chemical system. Still, the simple Stokes–Einstein equation is the best place to start for understanding diffusion in liquids.

Solids. As explained above, the diffusion in solids is so slow that most transport usually occurs in any fluid-filled flows and voids within the solid. Some solid processes are certainly dramatically affected by diffusion – metallic welds and doped semiconductors are two good examples – but the diffusion of chemicals in the environment is usually through fluids.

The relative unimportance of diffusion in solids is fortunate, because diffusion coefficients in solids scatter. These coefficients do not cluster around a single value, and they depend strongly on crystal structures. For example, the diffusion of carbon in body-centered cubic iron is 10^{10} times faster than the diffusion of carbon in face-centered cubic iron. Sometimes, an anomalously high coefficient reflects different types of

vacancies in the solid crystals. For example, silver ion diffuses 10^{17} times faster in AgCl than sodium ion diffuses in NaCl.

Estimates of diffusion in solids, which normally begin with a face-centered cubic lattice, assume a coefficient given by:

$$D = R^2 N\omega \tag{51}$$

where R is now the distance between atoms or ions in the crystal; N is the dimensionless fraction of vacant sites; and ω is the jump frequency, the number of atomic or ionic movements per time. The size of R is estimated from crystal structure, and the fraction N from the free energy of mixing. The jump frequency ω is often felt to have an Arrhenius temperature dependence. Arguments like this are not predictions but are rationales to organize data.

Diffusion Across Interfaces

Diffusion from one phase to another is an important and complex limit, a source of confusion for many. In this case, there are two limits that are close parallels to the cases of a thin film and a semi-infinite slab discussed above in the sections "Diffusion Across a Thin Film" and "Other Important Cases." One case is exemplified by the so-called infinite couple, when two alloy bars of different but homogeneous composition are closely joined together. In this case, each atomic species can diffuse between the two bars, giving concentration profiles that are known. This limit is rarely important in environmental science and engineering.

The second, much more important limit occurs when solutes diffuse from one relatively well-mixed phase across a phase boundary to a second relatively well-mixed phase. This limit approximates what happens when sulfur dioxide in the air diffuses into a lake. In this case, bulk air is often well-mixed, and the bulk water in the lake is, too. However, this good mixing does not extend all the way to the air–water interface. About the last one millimeter of air and about the last one-tenth millimeter of the water are not well-mixed. Diffusion across these two films, one in air and the other in the water, is what governs the rate of sulfur dioxide dissolution in the lake.

We develop these ideas below. "The Mathematics of Mass Transfer" derives the mathematical framework. "Concentration Units" details transport across interfaces. "The Meaning of $c_1{}^*$" uses this framework to calculate the mass transfer in several environmentally relevant situations.

The Mathematics of Mass Transfer

To begin our study of mass transfer, imagine a small volume of air containing hydrogen sulfide at concentration c_{10} that is suddenly contacted with a large volume of water. The sulfide dissolves in the water so that its concentration c_1 drops with time. Predicting this concentration change with the diffusion equations given above is possible, but difficult. Often, an easier prediction is to use an alternative tool, a mass transfer analysis, which is more suitable for engineering applications.

This mass transfer analysis begins by writing a mass balance on the H_2S in the air:

[Accumulation in the air] =
[Amount dissolved in water]

$$V\frac{dc_1}{dt} = -AK(c_1 - c_1{}^*) \tag{52}$$

where V is the air volume, A is the interfacial area between air and water, and $c_1{}^*$ is proportional to the concentration of the H_2S in the water. When there is a lot of pure, well-mixed water present, this concentration is zero. The rate constant K in Eq. 52 is an overall mass transfer coefficient, a function of H_2S diffusion in both the water and the air. It has the units of velocity, that is, of length L per time t. This mass balance is subject to the initial condition:

$$t = 0 \quad c_1 = c_{10} \tag{53}$$

Integrating, Eq. 52 becomes:

$$\frac{c_1}{c_{10}} = e^{-K\left(\frac{A}{V}\right)t} \tag{54}$$

The H_2S concentration in the air decays exponentially with time, as if it were undergoing a first-order chemical reaction. The rate constant of this reaction (KA/V) has units of reciprocal time. However, the concentration in air is not dropping because of a chemical reaction but because of diffusion of H_2S from the air into the water.

As a second example, imagine absorbing carbon dioxide from flue gas. The flue gas is steadily flowing upward in a small absorption tower. Excess strong base is steadily flowing downward through the tower. A mass balance on the carbon dioxide in a small differential volume dV in the tower results in:

$$[\text{Accumulation in } dV] = [CO_2 \text{ Flow in} - \text{out}] + [CO_2 \text{ Absorbed by base}]$$

$$0 = Q\frac{dc_1}{dV} - Ka(c_1 - c_1{}^*) \tag{55}$$

where Q is the volumetric flow rate of flue gas, a is the interfacial area per volume in the tower, and $c_1{}^*$ is about zero because the base is strong and there is a lot of it. As before, K is an overall mass transfer coefficient describing the rate of reaction. This mass balance is subject to a boundary condition:

$$V = 0 \quad c_1 = c_{10} \tag{56}$$

Integration gives:

$$\frac{c_1}{c_{10}} = e^{-Ka\left(\frac{V}{Q}\right)} \tag{57}$$

The CO_2 concentration exiting the absorption column decreases exponentially as the column volume V is increased or as the column flow Q is decreased. Note that Eqs. 54 and 57 are complete mathematical parallels, even though the former describes unsteady dissolution without flow, and the latter describes steady absorption with flow.

Interfacial mass transfer is not hard. It is just an alternative description of diffusion which complements that given by Fick's Law. The three features do make interfacial mass transfer complicated. These three complications are the units of concentration, the detailed meaning of $c_1{}^*$, and the values of the mass transfer coefficient K. Details of these features follow.

Concentration Units

The first issue, concentration units, results because the units used for clearly explaining the ideas are not always those easiest to use in practice. The concentration units implied in this essay are of the amount per volume, for example, moles per liter or grams per cubic meter. The concentration units used in practice are different. In gases, the units are sometimes partial pressures; in liquids, the units are often mole fractions.

Expressing concentrations as partial pressures or mole fractions leads to different definitions of mass transfer coefficients. In particular, the total flux across the interface N_1 from one dilute gaseous solution into another dilute liquid solution may be defined as:

$$N_1 = n_1|_{\text{interface}} = j_1|_{\text{interface}} = K(c_1 - c_1{}^*) \tag{58}$$

where c_1 is the concentration of species "1" in the gas. The restriction to dilute solution is not a major constraint. Alternatively, the interfacial flux can be defined as:

$$N_1 = K_p(p_1 - p_1{}^*) \tag{59}$$

where p_1 is the partial pressure of solute "1" in the gas, and K_p is a new, different overall mass transfer coefficient. But from the ideal gas law:

$$p_1 = \frac{n_1 RT}{V} = c_1 RT \tag{60}$$

Comparing the two equations shows:

$$K_p = \frac{K}{RT} \tag{61}$$

If K has units of meters per second, then K_p may have units of moles per square meter per second per pascal.

Similarly, for mass transfer from a liquid into a gas, an alternative definition is:

$$N_1 = K(c_1 - c_1{}^*) \tag{62}$$

where c_1 is now the concentration of species "1"in the liquid, and K is an overall mass transfer coefficient different from that in Eq. 58. Alternatively,

$$N_1 = K_x(x_1 - x_1{}^*) \tag{63}$$

where x_1 is the mole fraction of species "1" in the liquid, and K_x is still another overall mass transfer coefficient. Because

$$c_1 = cx_1 \tag{64}$$

where c is the total concentration in the liquid, the two overall coefficients are related:

$$K_x = cK \tag{65}$$

For example, if K is in meters per second, and c is in moles per meter cubed, then K_x will have units of moles per square meters per second. Other definitions of coefficients are also possible, but are no harder.

The Meaning of $c_1{}^*$

The meaning of the concentration $c_1{}^*$ appearing in Eqs. 52, 55, 58, 59, and 62 is the hardest step in this description. These flux equations all assert that the flux is proportional to a concentration difference. The flux will be zero when the concentration is zero. Thus, $c_1{}^*$ must be the hypothetical gaseous concentration of species "1" that is in equilibrium with species "1" dissolved in the liquid. This is harder than interfacial heat transfer: there, the heat flux is proportional to the temperature on one side of the interface minus that on the other side. Here, the mass flux is proportional to a concentration difference which equals to one real concentration that does exist minus a second one which is hypothetical.

To be more specific, imagine the case in Eq. 58, where c_1 is the actual concentration of species "1" in the well-mixed, bulk gas on one side of the interface. The concentration $c_1{}^*$ is equal to the concentration in the well-mixed, bulk liquid times some type of Henry's Law constant, which describes equilibrium between gas and liquid. Sometimes, those studying this point for the first time can be helped by silently chanting

- $c_1{}^*$ is the concentration that would be in the gas if it were in equilibrium with the liquid (which it isn't).

Remembering this chant may help mastering this difficult point.

To try to make this point clearer, imagine in calculating the flux of oxygen in air into wastewater with a concentration of 1×10^{-4} mol/ℓ. At equilibrium,

$$c_1(\text{gas}) = 30c_1(\text{liquid}) \tag{66}$$

Thus,

$$c_1{}^*(\text{gas}) = 30 \times 10^{-4}\ \text{mol}/\ell \tag{67}$$

As a result,

$$\begin{aligned} c_1 - c_1{}^* &= \frac{0.21\ \text{mol}}{22.4\ell} - 30 \times 10^{-4}\frac{\text{mol}}{\ell} \\ &= 64 \times 10^{-4}\ \text{mol}/\ell \end{aligned} \tag{68}$$

Understanding problems like these is often helped by always checking what happens when the system is at equilibrium.

Values of Mass Transfer Coefficients

We now turn to the variations of the overall mass transfer coefficient with quantities like the diffusion coefficient in the adjacent phases. The most common case is that of transfer from a gas into a liquid. The concentration in the gas is expressed as a partial pressure, and the concentration in the liquid is expressed as a mole fraction. The flux N_1 across the interface is then:

$$\begin{aligned} N_1 &= K_p(p_1 - p_1{}^*) \\ &= k_p(p_1 - p_{1i}) \\ &= k_x(x_{1i} - x_1) \end{aligned} \tag{69}$$

where p_1 and x_1 are the average concentrations in the gas and liquid, respectively; and p_{1i} and x_{1i} are the corresponding but unknown gas and liquid concentrations at the interface. The mass transfer coefficients k_p and k_x describe transport in the gas and in the liquid. Sensibly, the individual mass transfer coefficient k_p is a function of diffusion in the gas, but not of diffusion in the liquid; and the individual mass transfer coefficient k_x is the reverse.

The concentrations across the interface will normally be in equilibrium, so that:

$$p_{1i} = Hx_{1i} \tag{70}$$

where H is a Henry's Law constant. Combining this constraint with Eq. 69 gives:

$$N_1 = \left[\frac{1}{\frac{1}{k_p} + \frac{H}{k_x}}\right](p_1 - Hx_1) \tag{71}$$

By comparing this with the overall mass transfer coefficient K_p yields:

$$K_p = \frac{1}{\frac{1}{k_p} + \frac{H}{k_x}} \tag{72}$$

$$p_1{}^* = Hx_1 \tag{73}$$

These are the results sought. Obviously, similar equations are possible for other concentrations and other equilibria analogous to Henry's Law.

The way in which k_p and k_x vary with the diffusion coefficients can be estimated either from experiments or from theories. The experiments are summarized as correlations, most often in terms of dimensionless numbers. For example, for mass transfer into a liquid flowing through a packed tower with packing of size d, the most widely accepted correlation is:

$$k_x = k(\text{liquid})c(\text{liquid}) \tag{74}$$

$$k(\text{liquid})\left(\frac{1}{vg}\right)^{\frac{1}{3}} = 0.0051\left(\frac{v}{av}\right)^{0.67}\left(\frac{D}{v}\right)^{0.50}(ad)^{0.4} \tag{75}$$

where v is the kinematic viscosity of the liquid, g is the acceleration due to gravity, v is the superficial liquid velocity, a is the surface area per volume of the packing, and D is the diffusion coefficient in the liquid. The quantity (v/av) is one form of the dimensionless Reynolds number; the quotient (v/D) is the dimensionless Schmidt number. Correlations like this, which are based on extensive experiments, should be used for estimates whenever possible.

In many cases, however, appropriate correlations may not be reliable, or may not be available at all. In these cases, estimates for liquids can be made by assuming that:

$$k(\text{liquid}) = \frac{D}{\ell} = \frac{D}{10^{-4}\text{m}} \tag{76}$$

where D is the diffusion coefficient in the liquid and ℓ is often called the film thickness or the boundary layer. This casual description can be confusing, because these terms are more specifically defined in theories of mass transfer. A corresponding estimate for gases is:

$$k(\text{gas}) = \frac{D}{\ell} = \frac{D}{10^{-3}\text{m}} \tag{77}$$

where D is now the diffusion coefficient in gases, typically 10^4 times larger than that in liquids. Equations 76 and 77 are major approximations to be used only in desperation.

Important Special Cases

The sections above describe the mathematics of diffusion and dispersion. They have summarized characteristics of diffusion coefficients and listed some typical values. They have discussed mass transfer coefficients as an alternative description of interfacial diffusion frequently valuable in environmental engineering. None of the ideas presented are especially difficult to understand.

However, actually putting these ideas into practice can be complicated, largely because of difficult units and subtle definitions. This final section considers specific chemical examples that illustrate the ideas involved. These examples are approximate but can serve as a warning of where trouble can occur.

Overall Mass Transfer Coefficient of Oxygen (Case #1)

Imagine wanting to estimate the mass transfer coefficient K_p of oxygen from air into water. From Table 2 and Eq. 77,

$$k(\text{gas}) = \frac{D}{\ell} = \frac{2\times10^{-4}\ \text{m}^2/\text{s}}{10^{-3}\text{m}} = 0.02\ \text{m/s} \tag{78}$$

The coefficient k_p is found from this by a unit conversion:

$$k_p = \frac{k(\text{gas})}{RT} = \frac{0.02\ \text{m/s}}{\left(8.2\times10^{-6}\frac{\text{m}^2\ \text{atm}}{\text{mol}^\circ\text{K}}\right)298^\circ\text{K}} = 8\frac{\text{mol}}{\text{m}^2\text{s atm}} \tag{79}$$

Similarly, from Table 3 and Eq. 76,

$$k(\text{liquid}) = \frac{2\times10^{-9}\ \text{m}^2/\text{s}}{10^{-4}\ \text{m}} = 2\times10^{-5}\ \text{m/s} \tag{80}$$

The coefficient k_x has a different conversion:

$$k_x = k(\text{liquid})c = \left(2\times10^{-5}\ \text{m/s}\right)\left(\frac{1\ \text{mol}}{18\times10^{-6}\ \text{m}^3}\right) = 1.1\frac{\text{mol}}{\text{m}^2\text{s}} \tag{81}$$

Henry's Law for this system is (cf. Eq. 70):

$$p_1 = \left(4.3\times10^4\ \text{atm}\right)x_1 \tag{82}$$

Thus from Eq. 72,

$$K_p = \frac{1}{\frac{\text{m}^2\text{s atm}}{8\ \text{mol}} + \frac{4.3\times10^4\ \text{atm m}^2\text{s}}{1.1\ \text{mol}}} = 2.6\times10^{-5}\frac{\text{mol}}{\text{m}^2\text{s atm}} \tag{83}$$

This coefficient describes oxygen transport between air and water when the concentration difference is expressed as partial pressures of oxygen.

Overall Mass Transfer Coefficient of Oxygen (Case #2)

The example above is straightforward because it matches the detailed equations given earlier. The same problem can be solved in different units. Thus, the flux N_1 is:

$$N_1 = K_c(c_1{}^* - c_1) \tag{84}$$

where c_1 is the actual oxygen concentration in water, $c_1{}^*$ is the oxygen concentration in water that is in equilibrium with air, K_c is a different overall mass transfer coefficient given by:

$$K_c = \frac{1}{\frac{m}{k(\text{gas})} + \frac{1}{k(\text{liquid})}} \tag{85}$$

and m is a different form of Henry's Law constant, defined by the equilibrium:

$$c_1(\text{liquid}) = mc_1(\text{gas}) \tag{86}$$

Comparing Eqs. 81 and 82 gives:

$$\begin{aligned} m &= \frac{c(\text{liquid})RT}{H} \\ &= \left(\frac{\text{mol}}{18 \times 10^{-6}\text{m}^3}\right)\left(8.2 \times 10^{-6}\frac{\text{m}^3\text{atm}}{\text{mol}^\circ\text{K}}\right) \\ &\quad \left(\frac{298^\circ\text{K}}{4.3 \times 10^{-4}\text{atm}}\right) \\ &= 0.03 \end{aligned} \tag{87}$$

The numerical value of Henry's Law constant is completely different. The combination of Eqs. 78, 80, 85, and 87 gives:

$$\begin{aligned} K_c &= \frac{-1}{\frac{0.03}{0.02\ \text{m/s}} + \frac{3}{2\times10^{-5}\ \text{m/s}}} \\ &= 2 \times 10^{-5}\ \text{m/s} \end{aligned} \tag{88}$$

In both this formulation and that in Eq. 83, diffusion in the liquid dominates the mass transfer. This is often taken as a consequence of the slower diffusion in the liquid. This is not completely true, as the next example shows.

Overall Mass Transfer Coefficient of Ammonia from Air into Water

This example illustrates how the rate at which ammonia is dissolved in water can be estimated. The individual mass transfer coefficients of ammonia are easily found:

$$k(\text{gas}) = \frac{D(\text{gas})}{\ell} = \frac{2.3 \times 10^{-5}\text{m}^2/\text{s}}{10^{-3}\text{m}} = 0.023\ \text{m/s} \tag{89}$$

and

$$\begin{aligned} k(\text{liquid}) &= \frac{D(\text{liquid})}{\ell} = \frac{1.6 \times 10^{-9}\text{m}^2/\text{s}}{10^{-4}\text{m}} \\ &= 1.6 \times 10^{-4}\text{m/s} \end{aligned} \tag{90}$$

One Henry's Law constant for dilute acid is given in the literature as:

$$p_1(\text{atm}) = \left(7000\frac{\text{atm}\,\ell}{\text{mol}}\right)c_1(\text{liquid, molar}) \tag{91}$$

Converting the pressure into a molar concentration:

$$\begin{aligned} c_1(\text{gas, molar}) &= \left(7000\frac{\text{atm}\ \ell}{\text{mol}}\right)\left(\frac{\text{mol}^\circ\text{K}}{0.082\ \text{atm}\ \ell}\right) \\ &\quad \left[\frac{c_1(\text{liquid, molar})}{298^\circ\text{K}}\right] \\ &= 290c_1(\text{liquid, molar}) \end{aligned} \tag{92}$$

Combining these results with Eq. 85 gives:

$$\begin{aligned} K_c &= \frac{1}{\frac{290}{0.023\ \text{m/s}} + \frac{1}{1.6\times10^{-5}\ \text{m/s}}} \\ &= 1.3 \times 10^{-4}\ \text{m/s} \end{aligned} \tag{93}$$

The much higher solubility of ammonia in dilute acid means the mass transfer is now more affected by diffusion in air.

Toxin Diffusion in a Biofilm

The final example imagines a dilute toxin dissolved in water and metabolized irreversibly by microorganisms immobilized in a biofilm. This example, which is not as chemically specific as the first three, also assumes that the concentration of dissolved oxygen is much greater than the concentration of the toxin. Thus, the rate per

biofilm area N_1 is given by the overall rate of diffusion of the toxin to the biofilm, followed by the diffusion and reaction of the toxin within the biofilm.

This overall rate is mathematically equivalent to mass transfer across an interface, where the solute diffused through the gas to reach the interface, quickly crossed the interface, and then diffused into the liquid. In fact, the biofilm case is often easier because most biofilms are largely water and hence their partition coefficient m is one. Thus,

$$N_1 = \frac{c_1}{\frac{1}{k(\text{liquid})} + \frac{1}{k(\text{biofilm})}} \tag{94}$$

The coefficient k (liquid) can often be found from mass transfer correlations; Equation 76 provides a first guess. The value in the biofilm depends on the details of the reaction. However, delightfully, most theories give the same result:

$$k(\text{biofilm}) = \left[\frac{D(\text{biofilm})}{\tau}\right]^{\frac{1}{2}} \tag{95}$$

where τ is the half-life of the reaction. While beyond the scope of this entry, this result is carefully derived in most books on diffusion and reaction. This result underscores the value of the simple ideas of diffusion and reaction presented here.

Future Directions

After 150 years of concentrated effort, diffusion is an established subject. Active research does continue on, for example, semiconductors and polymer membranes, but this does not have major environmental application.

Diffusion is an important tool for describing environmentally significant mass transfer. In many cases, this transfer can be described in terms of diffusion coefficients. In many air pollution problems, mass transfer can be described in terms of dispersion, which is mathematically similar to diffusion but due to coupled diffusion and flow.

The underused description of mass transfer, especially across interfaces, is in terms of mass transfer coefficients. These are functions of diffusion coefficients and of other parameters, like velocity and viscosity. Exploiting this topic offers potential gain for environmental engineering.

Bibliography

Books and Reviews

Aris R (1999) Mathematical modeling. Academic, San Diego. ISBN 0-12-604585-1

Astarita G, Savage DW, Bisio A (1983) Gas treating with chemical solvents. Wiley, New York. ISBN 0-471-057681

Berg HC (1993) Random walks in biology. Princeton University Press, Princeton. ISBN 0-691-000646

Bird RB, Stewart WS, Lightfoot EN (2002) Transport phenomena, 2nd edn. Wiley, New York. ISBN 0-471-41077-2

Carslaw HS, Jaeger JC (1976) Conduction of heat in solids. Oxford University Press, New York. ISBN 0-19-853303-9

Crank J (1980) The mathematics of diffusion. Oxford University Press, New York. ISBN 0-19-853411-6

Cussler EL (2009) Diffusion: mass transfer in fluid systems, 3rd edn. Cambridge University Press, Cambridge. ISBN 0-521-56477-8

Dutta BK (2009) Mass transfer and separation processes. PHI Learning, New Delhi. ISBN 978-81-203-2990-4

Seader JD, Henley EJ (2006) Separation processes principles, 2nd edn. Wiley, New York. ISBN 0-471-46480-5

Seinfeld JH, Pandis S (2006) Atmospheric chemistry and physics, 2nd edn. Wiley, New York. ISBN 0-471-72018-6

Sherwood TK, Pigford RL, Wilke CR (1975) Mass transfer. McGraw Hill, New York. ISBN 0-070-566929

Taylor GI (1953) Dispersion of soluble matter in solvent flowing slowly through a tube. Proc R Soc London Ser A 219:186–203

Taylor GI (1954) The dispersion of matter in turbulent flow through a pipe. Proc R Soc Lond Ser A 223:446–468

Taylor R, Krishna R (1993) Multicomponent mass transfer. Wiley, New York. ISBN 0-47-157417-1

Treybal RE (1980) Mass transfer operations, 3rd edn. McGraw-Hill, New York. ISBN 0-070-651760

Chemicals in the Environment, Dispersive Transport

John S. Gulliver
Department of Civil Engineering, University of Minnesota, Minneapolis, MN, USA

Article Outline

Glossary
Definition of Dispersive Transport in the Environment
Introduction
Solutions to Transport with Convection
Dispersion in Groundwater Flow
Dispersion in Rivers

Example Applications
Conclusion
Future Directions
Bibliography

Glossary

Convection The movement of a constituent with movement of the fluid.

Diffusion The spreading of fluid constituents through the motion inherent to atoms and molecules.

Diffusion coefficient A coefficient that describes the tendency of molecules to spread a constituent mass.

Dirac delta An impulse of a given quantity (mass) that occurs over an infinitely short time or space.

Dispersion The process of mixing caused by a variation in velocity and transverse diffusion or turbulent diffusion.

Dispersion coefficient A coefficient that can describe the mixing caused by a transverse velocity profile and transverse diffusion or turbulent diffusion. A dispersion coefficient means that some sort of spatial mean velocity is being used to describe the flow. Then, the mixing lateral or longitudinal to the spatial mean velocity due to a combination of a velocity profile and diffusion or turbulent diffusion is described by the dispersion coefficient. The coefficient's location in the mass transport equation is similar to diffusion coefficients, and the units are similar.

Laminar flow Flow that has no turbulent eddies, where the fluid flows in laminas and diffusion creates the mixing of the fluid.

Turbulent diffusion The mixing of fluids through turbulent eddies created by convection.

Turbulent diffusion coefficient A coefficient that comes from the multiplication of two turbulent velocities of the flow, divided by density of the fluid. The coefficient's location in the mass transport equation is similar to diffusion coefficients, and the units are similar, so it is called a "turbulent diffusion coefficient."

Definition of Dispersive Transport in the Environment

Dispersion is the enhanced mixing of material through spatial variations in velocity. When it is of interest (when we are not keeping track of the three-dimensional mixing), dispersion is typically one or two orders of magnitude greater than turbulent diffusion. The process of dispersion is associated with a spatial mean velocity, the assumption of plug flow, and a velocity profile. The means used in association with diffusion, turbulent diffusion, and dispersion are identified in Table 1.

The means by which diffusion and possibly turbulent diffusion are combined with a spatial mean velocity to result in dispersion is illustrated in Fig. 1. A velocity profile over space with mixing due to diffusion (and possibly turbulent diffusion) is combined into a cross-sectional mean velocity and a dispersion coefficient. Without the cross-sectional mean velocity, there *is no* dispersion coefficient.

Introduction

Dispersion was first developed as a means of dealing with reactors, where there was little interest in the processes creating mixing inside of the reactor, but

Chemicals in the Environment, Dispersive Transport. Table 1 Temporal or spatial means and scales used in association with various mixing processes

Process	Variable representing *process*	Mean	Scale of mean
Diffusion	Diffusion coefficient	Temporal	Molecular
Turbulent diffusion	Turbulent diffusion *coefficient*	Temporal	Minutes
Dispersion	Dispersion coefficient	Spatial	Scale of flow

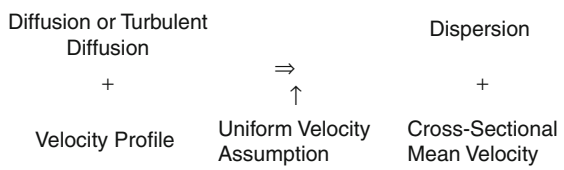

Chemicals in the Environment, Dispersive Transport. Figure 1
Representation of the process by which diffusion or turbulent diffusion is related to dispersion

great need to appropriately describe the output from the reactor. The physics of the mixing process is lost in the conversion to a spatial mean velocity profile, but the end result can still be modeled by dispersion.

A similar spatial mean velocity (bulk mean velocity) is used for the plug flow reactor model. Thus, plug flow with dispersion is a natural match, where the mixing that truly occurs in any reactor or environmental flow is modeled as dispersion. This is the model that will be applied to utilize dispersion as a mixing model.

Dispersion in Laminar Flow

Any flow with a nonuniform velocity profile will, when spatial mean velocity and concentration are taken, result in dispersion of the chemical. For laminar flow, the well-described velocity profile means that we can describe dispersion analytically for some flows. Beginning with the diffusion equation in cylindrical coordinates (laminar flow typically occurs in small tubes):

$$\frac{\partial C}{\partial t} + U\frac{\partial C}{\partial x} = D\left[\frac{\partial^2 C}{\partial r^2} + \frac{1}{r}\frac{\partial C}{\partial r} + \frac{\partial^2 C}{\partial x^2}\right] + S \qquad (1)$$

where the x-coordinate is aligned with the flow velocity, and $v = w = 0$. We will outline the development of a dispersion coefficient for a fully developed laminar pipe flow. This means that we are far enough from the entrance that the velocity profile is essentially in equilibrium with the loss of pressure along the pipe. This flow has a velocity profile (developed in most fluid mechanics texts):

$$U = U_{\max}(1 - r^2/R^2) \qquad (2)$$

as illustrated in Fig. 2.

To convert Eq. 1 to cross-sectional mean values, we will assign:

$$\hat{C} = \frac{1}{\pi R^2}\int_0^R C 2\pi r\ dr \qquad (3)$$

$$U = \frac{1}{\pi R^2}\int_0^R U\, 2\pi r\, dr = \frac{U_{\max}}{2} \qquad (4)$$

Then, in Eq. 1:

$$C = \hat{C} + C'(r) \qquad (5)$$

and

$$u = U + u'(r) \qquad (6)$$

Now, if we equate Eq. 2 and 6, we get

$$u'(r) = u_m\left(\frac{1}{2} - \frac{r^2}{R^2}\right) \qquad (7)$$

Substituting Eqs. 5, 6, and 7 into Eq. 1:

$$\frac{\partial \hat{C}}{\partial t} + \frac{\partial C'}{\partial t} + (U + u')\frac{\partial(\hat{C} + C')}{\partial x} = D\left[\frac{\partial^2(\hat{C} + C')}{\partial r^2} + \frac{1}{r}\frac{\partial(\hat{C} + C')}{\partial r} + \frac{\partial^2(\hat{C} + C')}{\partial x^2}\right] + S \qquad (8)$$

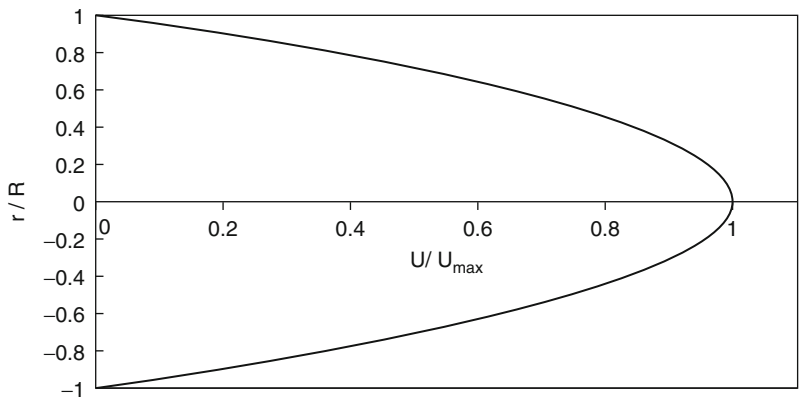

Chemicals in the Environment, Dispersive Transport. Figure 2
The velocity profile in a fully developed tubular flow is a paraboloid

An order of magnitude analysis will tell us that $\partial^2/\partial r^2 >> \partial^2/\partial x^2$. In addition, $\partial \hat{C}/\partial r = 0$, by definition. Now, if we put everything that is known on the left-hand side of Eq. 8, the result will be:

$$\frac{\partial \hat{C}}{\partial t} + U\frac{\partial \hat{C}}{\partial x} = -\left[\frac{\partial C'}{\partial t} + U\frac{\partial C'}{\partial x} + U'\frac{\partial \hat{C}}{\partial x} + U'\frac{\partial C'}{\partial x}\right] + D\frac{\partial^2 C'}{\partial r^2} + \frac{D}{r}\frac{\partial C'}{\partial r} + S = D_L\frac{\partial^2 \hat{C}}{\partial x^2} + S \tag{9}$$

The second equality in Eq. 9 is a definition of longitudinal dispersion coefficient, D_L. G. I. Taylor [1] assumed that some of the terms in Eq. 9 would cancel and that longitudinal convective transport would achieve a balance with transverse diffusive transport. He then solved the second equality in Eq. 9 for a fully developed tubular flow, resulting in the relation,

$$D_L = \frac{R^2 U^2}{48\,D} = \frac{d^2\,U^2}{192\,D} \tag{10}$$

A similar relation can be developed for laminar flow down an inclined plate:

$$D_L = \frac{32\,h^2\,U^2}{945\,D} \tag{11}$$

The longitudinal dispersion coefficient is proportional to the square of the flow scale (d or h), proportional to the square of the velocity scale (U), and *inversely* proportional to the diffusion coefficient. The greater the diffusion, the less severe the spread of the chemical by the velocity profile because of local mixing, and the smaller the longitudinal dispersion coefficient. This result may seem illogical, but can be explained by the following: Longitudinal dispersion describes mixing only in terms of the cross-sectional mean concentration, and transverse mixing actually slows down longitudinal dispersion. The governing Eq. 9 does not concern itself with local mixing issues.

Knowing the relations given in Eqs. 10 and 11, we no longer need the more cumbersome middle portion of Eq. 8, and we can work to solve the equation,

$$\frac{\partial \hat{C}}{\partial t} + U\frac{\partial \hat{C}}{\partial x} = D_L\frac{\partial^2 \hat{C}}{\partial x^2} + S \tag{12}$$

In expressing the equations for longitudinal dispersion, we will drop the "hat" above the cross-sectional mean values. Thus, if D_L is involved, we are discussing cross-sectional mean concentrations.

Dispersion in Turbulent Flow

The dispersion that occurs in turbulent flow can also be calculated, as long as the velocity profile is given. This was done by Taylor [2] for a tubular flow and by Elder [3] for a two-dimensional, open-channel flow. Both investigators assumed that a logarithmic velocity profile would apply in the entire flow field. The logarithmic velocity profile is a fairly good description where shear stress can be assumed constant. It is a good assumption for a fully developed turbulent flow field, because the locations where the logarithmic profile applies are those with the greatest change in velocity.

For a fully developed tubular flow, assuming a logarithmic velocity profile, Taylor derived the equation,

$$D_L = 5.05\ d\ u_* \tag{13}$$

where u_* is the shear velocity at the wall. Elder [3] derived the following equation for a two-dimensional, open-channel flow:

$$D_L = 5.93\ h\ u_* \tag{14}$$

It is interesting to compare Eqs. 13 and 14 with those for a fully developed laminar flow, Eqs. 10 and 11. In the chapter on Turbulent Transport, eddy diffusion coefficient in a turbulent boundary layer was found to be linearly dependent upon distance from the wall and on the wall shear velocity. If we replace the diffusion coefficient in Eq. 11 with an eddy diffusivity that is proportional to $h\ u_*$, we get,

$$D_L \sim \frac{h^2\ U^2}{hu_*} \tag{15}$$

Noting that for a given boundary roughness we can generally say that $U \sim u_*$, Eq. 15 becomes,

$$D_L \sim hu_* \tag{16}$$

which is what we have in Eq. 14.

The relations developed for longitudinal dispersion coefficient are given in Table 2. The experimental results in rivers tend to have a large range because of the variety of lateral velocity profiles that exist in natural rivers and streams.

Chemicals in the Environment, Dispersive Transport. Table 2 Relationships for longitudinal dispersion coefficient in pipes and channels developed from theory and experiments

Flow conditions	D_L	Notation
Laminar flow in a pipe [1]	$\frac{R^2 U^2}{48 D}$	R = radius of tube U = cross-sectional mean velocity D = diffusivity h = depth V_p = velocity of upper plate Δ_z = spacing of plates u_* = shear velocity
Laminar flow down an inclined plate	$\frac{32h^2 U^2}{945 D}$	
Laminar flow-linear velocity profile (Couette Flow)	$\frac{V_p^2 \Delta_z^2}{120 D}$	
Turbulent flow in a pipe, assuming logarithmic velocity profile [2]	$10.1Ru_*$	
turbulent flow down an inclined plate, assuming logarithmic velocity profile [3]	$5.93hu_*$	
Open flume (experimental)	8–400 hu_*	
Canals (experimental)	8–20 hu_*	
Rivers (experimental)	8–7,500 hu_*	

Solutions to Transport with Convection

Diffusive transport with convection occurring simultaneously can be solved more easily if we orient our coordinate system properly. First, we must orient one axis in the direction of the flow. In this case, we will choose the x-coordinate so that u is nonzero and v and w are zero. Second, we must assume a uniform velocity profile, $u = U =$ constant with y and z. Then Eq. 30 of the Transport in the Environment chapter becomes

$$\frac{\partial C}{\partial t} + \frac{U}{R}\frac{\partial C}{\partial x} = \frac{D}{R}\left[\frac{\partial^2 C}{\partial x^2} + \frac{\partial^2 C}{\partial y^2} + \frac{\partial^2 C}{\partial z^2}\right] + \frac{S}{R} \tag{17}$$

where S is a source or sink term other than adsorption or desorption. In Eq. 17, we are assuming that chemical reaction does not take place on the surface of a solid, i.e., while the chemical is sorbed to solids. Now, we will convert our Eulerian (fixed) coordinate system to one that moves (Lagrangian) with velocity U/R and assign an independent variable

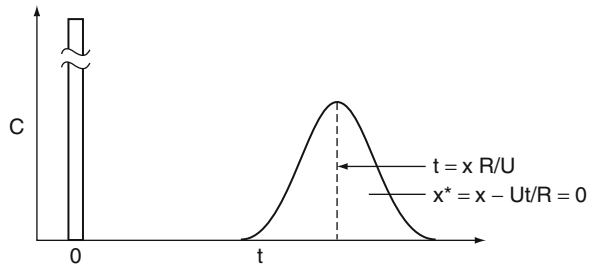

Chemicals in the Environment, Dispersive Transport. Figure 3
Pulse response in fixed and moving coordinate systems

$$x^* = x - Ut/R \tag{18}$$

such that $x^* = 0$ at $x = U\ t/R$. The response of the system to a conservative pulse, given in Fig. 3, indicates that in the Lagrangian coordinate system specified, there is no convection term, only diffusion. Then Eq. 17 becomes

$$\frac{\partial C}{\partial t} = \frac{D}{R}\left[\frac{\partial^2 C}{\partial x^{*2}} + \frac{\partial^2 C}{\partial y^2} + \frac{\partial^2 C}{\partial z^2}\right] + \frac{S}{R} \tag{19}$$

Determination of Dispersion Coefficient from Tracer Clouds

The one-dimensional mass transport equation for plug flow with dispersion, and a retardation coefficient of 1, is

$$\frac{\partial C}{\partial t} + U\frac{\partial C}{\partial x} = D_L\frac{\partial^2 C}{\partial x^2} + S \tag{20}$$

We will convert our fixed coordinate system to a coordinate system moving at velocity U through the change of variables, $x^* = x - Ut$. Then Eq. 20 is given as

$$\frac{\partial C}{\partial t} = D_L\ \frac{\partial^2 C}{\partial x^{*2}} + S \tag{21}$$

Now, if we are determining the dispersion coefficient through the use of a pulse tracer cloud, the boundary conditions are those of a Dirac delta:

1. At $t = 0$, a pulse of mass M is released at $x^* = 0$.
2. As $t \Rightarrow \infty$, $C \Rightarrow 0$.

The solution to Eq. 21 with these boundary conditions [4] is:

$$C = \frac{M/A}{\sqrt{4\pi\ D_L t}}\, e^{\frac{-(L-Ut)^2}{4 D_L t}} \tag{22}$$

or, in dimensionless variables,

$$\frac{C}{C_0} = \frac{C}{M/(AL)} = \frac{1}{\sqrt{4\pi\, Cou/Pe}} \exp\left[-\frac{(1-Cou)^2}{4\, Cou/Pe}\right] \tag{23}$$

Where $Cou = U\ t/L = t/t_r$ is a Courant number and $Pe = U\ L/D_L$ is a Peclet number. Comparing Eq. 23 to a Gaussian probability distribution,

$$P(\phi) = \frac{1}{\sigma\sqrt{2\pi}} \exp\left[-\frac{\phi^2}{2\sigma^2}\right]$$

we can see that the plug flow with dispersion, when $Pe > 10$, can be fit to a Gaussian distribution in terms of C/C_0 and $(1-\theta)$, with the relationships,

$$\sigma^2 = \frac{\sigma_t^2}{t_r^2} = 2\, Cou/Pe \tag{24}$$

where

$$\sigma_t^2 = \frac{\int_0^\infty t^2\, C/C_0\, dt}{\int_0^\infty C/C_0\, dt} - t_r{}^2 \tag{25}$$

and

$$t_r = \frac{\int_0^\infty t^2\, C/C_0\, dt}{\int_0^\infty C/C_0\, dt} \tag{26}$$

In addition, if we could measure the tracer cloud over distance at one time, we would use the relation,

$$\sigma^2 = \frac{\sigma_x^2}{U^2 t_r{}^2} \tag{27}$$

where

$$\sigma_x^2 = \frac{\int_0^\infty x^2\, C/C_0\, dx}{\int_0^\infty C/C_0\, dx} - \bar{x}^2 \ \ and \ \ \bar{x} = \frac{\int_0^\infty x\, C/C_0\, dx}{\int_0^\infty C/C_0\, dx} \tag{28}$$

The response of a plug flow with dispersion model to a pulse input, Eq. 23, is given in Fig. 4 for various values of the Peclet number, $Pe = U\ L/D_L$.

Dispersion in Groundwater Flow

Dispersion in a flow through porous media occurs due to heterogeneity in the media, i.e., the conductivity of the soil varies with space. This is shown on three levels in Fig. 5. On the particle scale, a thread of tracer will be split a number of times as it moves through the media. Each split of the tracer thread will move through the media at a speed corresponding to the resistance that it encounters. If you take a number of tracer threads coming out of the media at different times, and collected them in an outlet pipe, what you would see at the

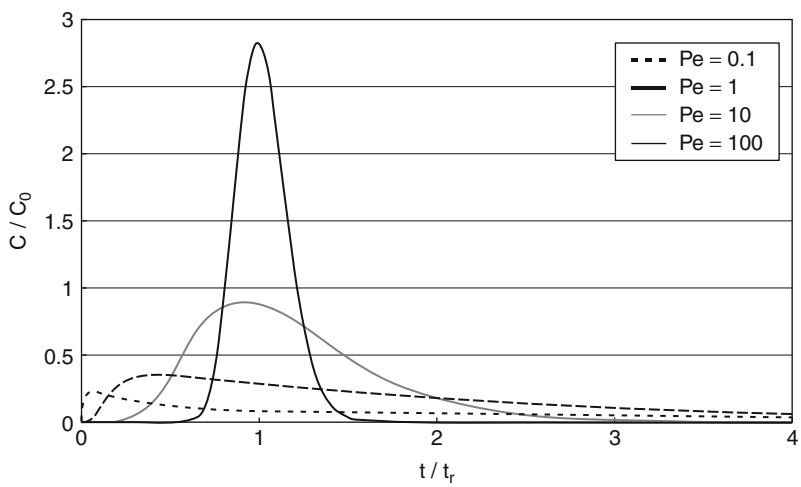

Chemicals in the Environment, Dispersive Transport. Figure 4
Response of the plug flow with dispersion model to a pulse input

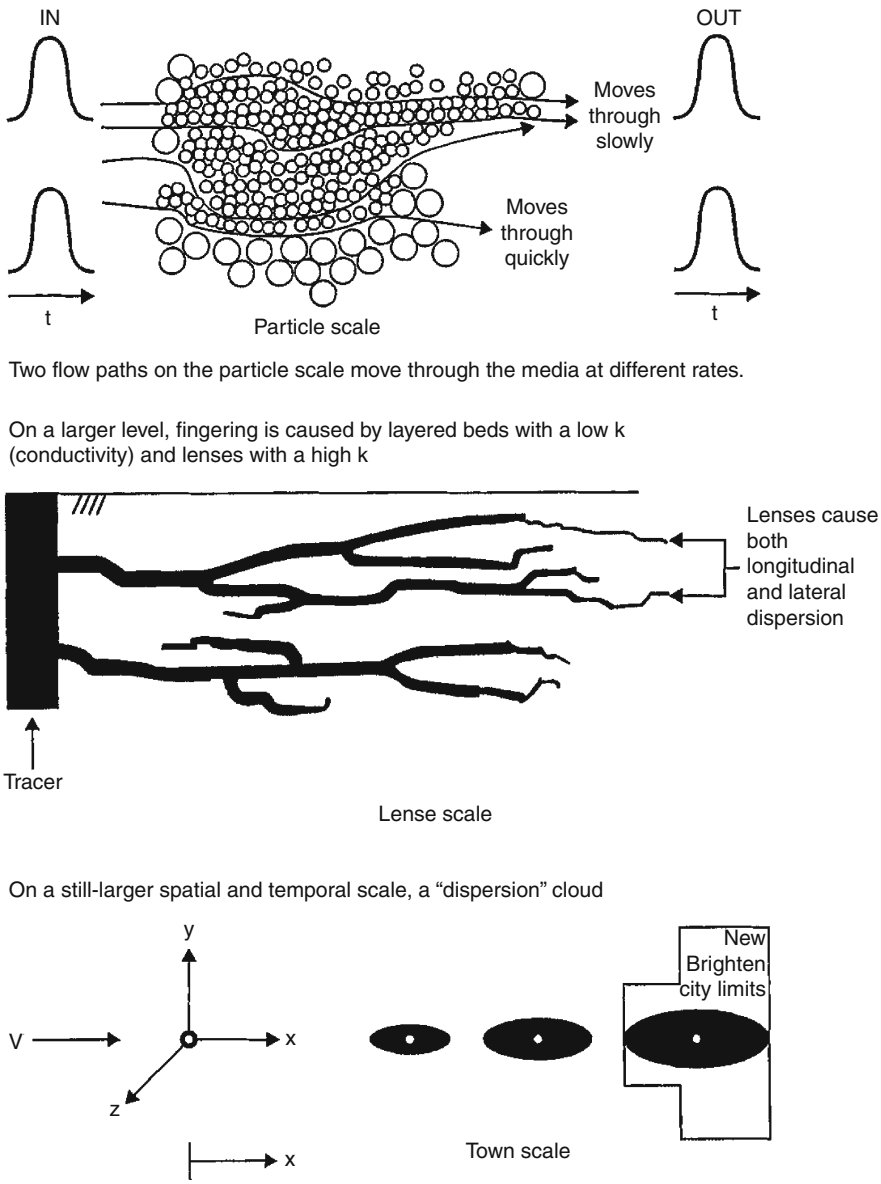

Chemicals in the Environment, Dispersive Transport. Figure 5
Illustration of dispersion in groundwater flow at various scales (From [5])

end of the pipe would be a dispersed pulse. This dispersion would be much greater than the diffusion that would occur. A lateral dispersion would also occur because the media would move some of the tracer threads laterally. Thus, in groundwater flow, there generally is longitudinal and lateral dispersion, created by the character of the media.

On a larger scale, a similar process can occur. Fingering of the tracer is created by layered beds with a low conductivity and lenses with a high conductivity. The tracer that ends up in a lens travels at a relatively high speed. Those tracer molecules will reach the measuring point sooner than the tracer molecules stuck in the low conductivity beds, creating longitudinal dispersion. As the lenses are not all parallel to each other, they will also create a lateral dispersion of the tracer.

Finally, on a still larger scale, about the scale of a small town, there will be isopleths (lines of constant

concentration) of our tracer that look something like those given in the last illustration of Fig. 4. If enough particle and lens effects have occurred with an apparent randomness to our tracer cloud, then the cloud disperses in a manner similar to that illustrated.

Incorporating the retardation coefficient for the chemical, discussed in the chapter on Transport in the Environment, the mass transport equation is then written as:

$$\frac{\partial C}{\partial t} + U/R\frac{\partial C}{\partial x} = \frac{(D+D_x)}{R}\frac{\partial^2 C}{\partial x^2} + \frac{(D+D_y)}{R}\frac{\partial^2 C}{\partial y^2} + \frac{(D+D_z)}{R}\frac{\partial^2 C}{\partial z^2} \tag{29}$$

where R is a retardation coefficient, and D_x, D_y, and D_z are the dispersion coefficients in the x-, y-, and z-directions, respectively.

The dispersion coefficients are dependent upon the character of the media and the flow velocity. It is difficult to predict these coefficients within an order of magnitude, so they are normally measured or fit to measured data in the field. For example, if a concentration variance in the x, y, and z directions can be measured in response to a pulse release, then an approximate solution would be:

$$C = \frac{MR^{1.5}}{8(\pi^3 t^3 D_x D_y D_z)^{0.5}} \exp\left[\frac{-Rx^{*2}}{4 D_x t}\frac{-Ry^2}{4 D_y t}\frac{-Rz^2}{4 D_z t}\right] \tag{30}$$

where x^* is $x - Ut/R$. Comparing Eq. 30 to that for a three variable Gaussian distribution, we can see that:

$$D_x = 9\ R\sigma_x{}^2/(2t) \tag{31a}$$

$$D_y = 9R\ \sigma_y{}^2/(2t) \tag{31b}$$

$$D_z = 9\ R\sigma_z{}^2/(2t) \tag{31c}$$

where σ_x^2, σ_y^2 and σ_z^2 are the variance of concentration in the x, y, and z directions, respectively. They are given by the equations,

$$\sigma_x^2 = \frac{\int x^2\, C\, dx}{\int C\, dx} - \left(\frac{\int x\, C\, dx}{\int C\, dx}\right)^2 \tag{32a}$$

$$\sigma_y^2 = \frac{\int y^2\, C\, dx}{\int C\, dx} \tag{32b}$$

$$\sigma_x^2 = \frac{\int z^2 C\, dx}{\int C\, dx} \tag{32c}$$

The last term in Eq. 32a is the distance to the center of mass. In the diffusion equation, it is equal to Ut/R.

Dispersion coefficients in groundwater flow. In a uniform media of particles, the longitudinal dispersion coefficient, D_L, and the transverse dispersion coefficient, D_t, are both functions of the grain diameter and velocity. (In our previous example, D_L was D_x, and D_t would indicate D_y and D_z). The relevance of longitudinal and transverse dispersion relative to diffusion may therefore be *very roughly* characterized by a Peclet number, Pe:

$$Pe = Ud/D \tag{33}$$

where d is the grain diameter and U is a bulk velocity, Q/A, where the cross section includes porous media. If the consideration is not of uniform media but is for a heterogeneous region of high and low groundwater flow permeability, then the appropriate length scale would be the size of these permeability regions, normal to the flow. The characterization is [6];

$$D_L/D \sim Pe \tag{34}$$

Koch and Brady [7] have characterized transverse dispersion coefficient as a fraction of longitudinal dispersion coefficient:

$$D_t/D_L \sim\ 0.1 \tag{35}$$

Thus, longitudinal dispersion coefficient is roughly 10 times the value of transverse dispersion coefficient in a uniform media.

In the field, however, all media are heterogeneous, resulting in far greater dispersion than in uniform porous media. Because of the heterogeneities, the velocity profile can be highly variable over long distances, creating a much greater dispersion. Gelhar et al. [8] provided a plot of field data that can be manipulated to result in an equation that applies between a scale of 1 and 100,000 m:

$$Pe_{D_L} = \frac{UL}{D_L} = 2.5\ X\ 10^{1\pm1.4} \tag{36}$$

where L is the horizontal scale of the measurement. The field data are given in Fig. 6, with the curves of Eq. 36.

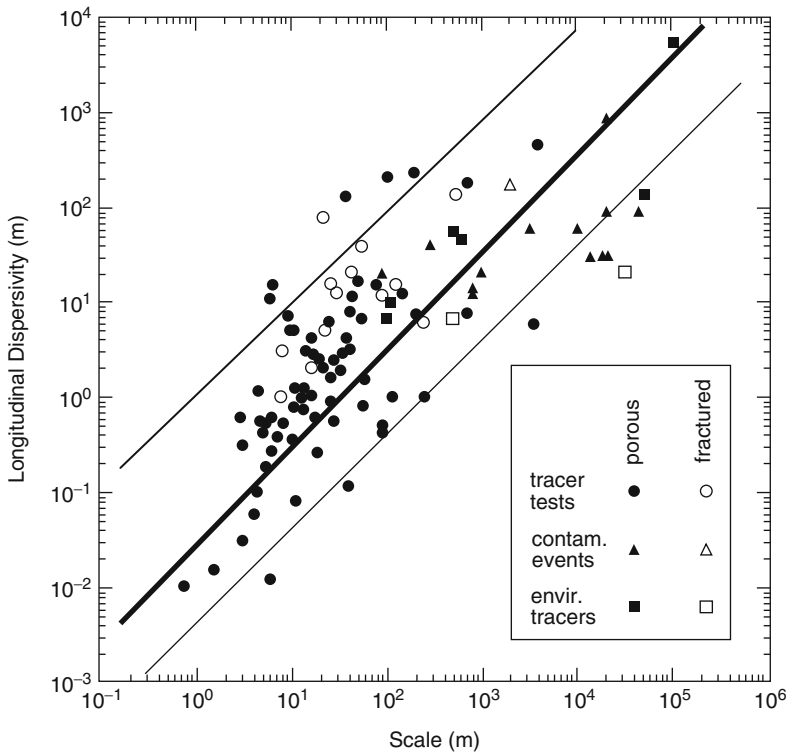

Chemicals in the Environment, Dispersive Transport. Figure 6
Field data on dispersion coefficients, taken from Gelhar et al. [8] with Eq. 36 added. Longitudinal dispersivity is D_L/U

Dispersion in Rivers

Rivers are an excellent environmental flow for describing the flow as a mean velocity with dispersion. The flow is confined in the transverse and vertical directions, such that a cross-sectional mean velocity and concentration can be easily defined. In addition, there is less variation in rivers than there is, for example, in estuaries or reactors, both of which are also described by the plug flow with dispersion model. For that reason, the numerous tracer tests that have been made in rivers are useful to characterize longitudinal dispersion coefficient for use in untested river reaches. A sampling of the dispersion coefficients at various river reaches which were determined from tracer tests is given in Table 2. Also given are the relevant mean parameters for each reach.

The question that we need to ask ourselves is whether the longitudinal dispersion can be predicted accurately for these rivers. Equation 16, which predicts that $D_L/(u_* h)$ = constant, is shown in Table 2 to have a large range of constants, probably because of the variations in cross section and morphology seen in natural streams. Fischer [9] observed that this constant seemed to depend upon mean surface width, W, and substituted W for h in the numerator of Eq. 16 to develop the following empirical equation to characterize longitudinal dispersion coefficient in rivers:

$$D_{LP} = 0.011 \frac{U^2 \; W^2}{u_* h} \tag{37}$$

where D_{Lp} is the predicted value of D_L, h the mean depth, U the cross-sectional mean velocity, and u_* the mean shear velocity of the river reach. When compared to the data given in Table 3 the root mean square error relative to the measurement, given by the equation,

$$\underset{\text{rms Errors}}{\text{Relative}} = \sqrt{\frac{1}{n}\sum_n \left(1 - \frac{D_{LP}}{D_L}\right)^2} \tag{38}$$

where n, the number of measurements, is 1.71. This relative rms error means that roughly 67% of the

Chemicals in the Environment, Dispersive Transport. Table 3 Measurements of longitudinal dispersion coefficient in laboratory flumes and rivers (after Fisher et al., 1979)

References	Channel	Depth. h(m)	Width. *W*(m)	Mean velocity, *U* (m/sec)	Shear velocity, *u** (m/sec)	Observed despersion coefficient, D_L (m^2/sec)	D_L/(hu*)	D_{LR} predicted by Eq. (37) (m^2/sec)
Thomas (1958)	Chicago Ship Canal	8.07	48.8	0.27	0.0191	3.0	20	12.4
State of California (1962)	Sacramento River	4.00		0.53	0.051	15	74	
Owens et al. (1964)	River Derwent	0.25		0.38	0.14	4.6	131	
Glover (1964)	South Platte River	0.46		0.66	0.069	16.2	510	
Schuster (1965)	Yuma Mesa A Canal	3.45		0.68	0.345	0.76	8.6	
Fischer (1967)	Trapezoidal laboratory channel with roughened sides	0.035	0.40	0.25	0.0202	0.123	174	0.156
		0.047	0.43	0.45	0.0359	0.253	150	0.244
		0.035	0.40	0.45	0.0351	0.415	338	0.298
		0.035	0.34	0.44	0.0348	0.250	205	0.202
		0.021	0.33	0.45	0.0328	0.400	392	0.248
		0.021	0.19	0.46	0.0388	0.220	270	0.103
Fischer (1968b)	Green-Duwamish River, Washington	1.10	20		0.049	6.5–8.5	120–160	
Yotsukura et al. (1970)	Missouri River	2.70	200	1.55	0.074	1500	7500	3440
Godfrey and Frederick (1970)	Copper Creek, Virginia (below gauge)	0.49	16	0.27	0.080	20	500	5.24
		0.85		0.60	0.100	21	250	15.1
		0.49	16	0.26	0.080	9.5	245	4.86
	Clinch River, Tennessee	0.85	47	0.32	0.067	14	235	22
		2.10	60	0.94	0.104	54	245	73
		2.10	53	0.83	0.107	47	210	28

Chemicals in the Environment, Dispersive Transport. Table 3 (Continued)

References	Channel	Depth. h(m)	Width. *W*(m)	Mean velocity, *U* (m/sec)	Shear velocity, *u** (m/sec)	Observed despersion coefficient, D_L (m^2/sec)	D_L/(hu*)	D_{LR} predicted by Eq. (37) (m^2/sec)
	Copper Creek, Virginia (above gauge)	0.40	19	0.16	0.116	9.9	220	2.19
	Powell River, Tennessee	0.85	34	0.15	0.055	9.5	200	6.12
	Cinch River, Virginia	0.58	36	0.21	0.049	8.1	280	22.1
	Coachella Canal, California	1.56	24	0.71	0.043	9.6	140	47.6
McQuivey and Keefer (1974)	Bayou Anacoco	0.94	26	0.34	0.067	33	520	13
		0.91	37	0.40	0.067	39	690	38
	Nooksack River	0.76	64	0.67	0.27	35	170	98
	Wind Bighorn Rivers	1.10	59	0.88	0.12	42	330	232
		2.16	69	1.55	0.17	160	440	340
	John Day River	0.58	25	1.01	0.14	14	170	88
		2.47	34	0.82	0.18	65	150	20
	Comite River	0.43	16	0.37	0.05	14	650	16
	Sabine River	2.04	104	0.58	0.05	315	3090	330
		4.75	127	0.64	0.08	670	1760	190
	Yadkin River	2.35	70	0.43	0.10	110	470	44
		3.84	72	0.76	0.13	260	520	68
Gulliver (1977)	MERS Experimental Streams	0.32	32	0.95	0.52	0.11	17	0.61

predictions are within a factor of 1.71 (within 71%) of the observed.

Tracer Determination of Longitudinal Dispersion Coefficient in Rivers Tracers are generally used to determine longitudinal dispersion coefficient in rivers. Some distance is required, however, before the lateral turbulent diffusion is balanced by longitudinal convection, similar to Taylor's [1] analysis of dispersion in a laminar flow. This transport balancing distance, X^* is given by the equation:

$$X^* = \frac{0.2\ UW^2}{\varepsilon_y} \tag{39}$$

The region $x < x^*$ can be visualized as a mixing region, which can skew the results of a tracer study. Downstream of this region, where turbulent diffusion is balanced by longitudinal convection, the variance of a tracer pulse grows linearly with distance. It is best to begin the measurements a distance X^* below the tracer release. Once dispersion coefficient at one or more river discharges have been measured, Eq. 37 can be used to adjust the dispersion coefficient to all discharges:

$$\frac{D_{LQ_1}}{D_{LQ_2}} = \left(\frac{U^2W^2}{u_* h}\right)_{Q_1}\left(\frac{u_* h}{U^2W^2}\right)_{Q_2} \tag{40}$$

The technique used to perform the analysis of tracer studies will be the subject of Example 4.

Example Applications

Example 1: Determination of retardation coefficient. As part of a forensic investigation of a continuous Malathion spill, you need to determine the retardation coefficient of the soil at the site for Malathion. You have decided to do so in a column experiment with the soil, illustrated in Fig. 7. Also given in the figure are the results of a pulse test with the non-sorptive tracer, chloride, and the results of a pulse test with Malathion. What is the retardation coefficient, R?

Chloride:

$t_r = t_{r1} = 20$ min.

$\sigma_{t1} = 3$ min.

Malathion:

$t_r = t_{r2} = 400$ min.

$\sigma_{t2} = 66$ min.

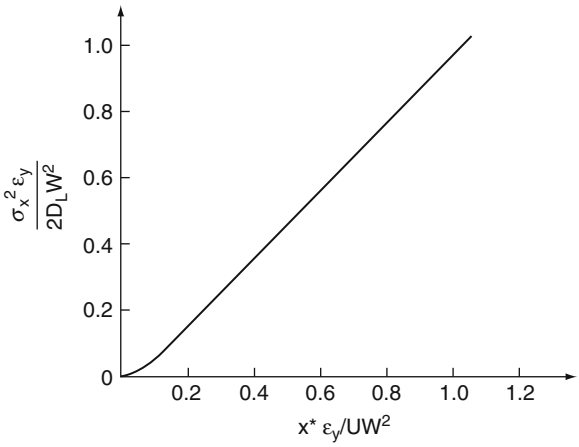

Chemicals in the Environment, Dispersive Transport. Figure 7
Illustration of the column test for retardation coefficient and results of the tracer tests

This test can result in a retardation coefficient from a comparison of both residence times and the variance.

Residence times: The residence time of the chloride can be given as $t_{r1} = L/U$, and the residence time of the Malathion can be given as $t_{r2} = R\ L/U$. Thus,

$$R = \frac{tr_2}{tr_1} = \frac{400\ \text{min}}{20\ \text{min}} = 20$$

Variance of tracer curves: Eq. 27 provides the relationships:

$$\sigma^2 = \sigma_t{}^2/t_r{}^2 = 2D_L Cou/(UL).$$

Therefore, assuming that $Cou = 1$,

$$\sigma_{t2}^2 = \frac{2D_L}{LR}\frac{R}{U}tr_2^2 = \frac{2D_L}{UL}tr_2^2 = \sigma_{t1}^2\frac{tr_2^2}{tr_1^2} = R^2\,\sigma_{t1}^2$$

or,

$$R = \sigma_{t2}/\sigma_{t1} = 66\ \text{min}/3\ \text{min} = 22$$

Our two means of determining the retardation coefficient in the column gave $R = 20$ and $R = 22$. We can also check whether the organic carbon content of the soil fits what is generally known from the literature. First, there is the relation for R:

$$R = 1 + \frac{\rho_B}{\varepsilon}K_d \tag{41}$$

Second, we have the equation from Karikhoff et al. [10]:

$$k_d = 0.41\left(\frac{\text{cm}^3}{\text{g}}\right) f\, K_{ow} \tag{42}$$

Combining Eqs. 29 and 30 results in an equation for the organic fraction:

$$f = \frac{(R-1)\varepsilon}{0.41\,\rho_B\,(\text{g/cm}^3)\,K_{ow}} = 0.030 - 0.033 \tag{43}$$

For Malathion, $K_{ow} = 230$. From soil tests, $\varepsilon = 0.3$, and $\rho_\beta = 2.0$ g/cm^3. Then Eq. 43 gives $f = 0.030 - 0.033$. This number is about right for the organic-rich soil that was tested. Thus, we know that our column tests are of the right order.

Example 2: Atrazine spill into an irrigation well (three-dimensional dispersion with convection). Three kilograms of 1,000 g/m^3 Atrazine pesticide is accidentally dumped down an old farm irrigation well, placed to pump water out of porous sandstone, as illustrated in Fig. 8. Estimate the movement of the Atrazine plume over time and the concentrations in the plume.

Given:

$U = 10$–4 m/s	d (sandstone) $\cong 1$ mm
$f = 10$–4 (not soil)	$D = 10$–1^0 m^2/s
$\varepsilon = 0.3$	$\rho_b/\varepsilon = 6$ g/cm^3

Our solution is [4]:

$$C = \frac{M}{8\varepsilon(\pi t/R)^{3/2}\sqrt{D_x D_y D_z}} \exp\left[-\frac{R\left(x - \frac{U}{R}t\right)^2}{4\,D_x t} - \frac{Ry^2}{4\,D_y t} - \frac{Rz^2}{4\,D_y\,t}\right] \tag{44}$$

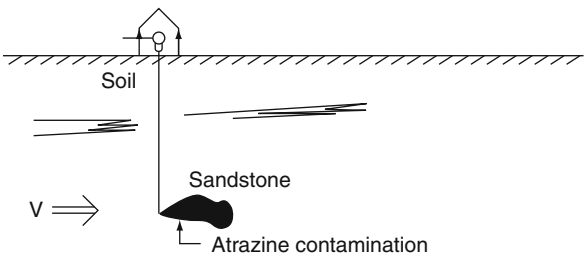

Chemicals in the Environment, Dispersive Transport. Figure 8
Illustration of well and Atrazine spill (From [5])

Now, estimate the maximum concentration location of this maximum and spread of the Atrazine cloud as a function of time.

Dispersion coefficients: As a first guess, let us use the empirical relations provided in Eqs. 34 and 35. We will assume no heterogeneity in rock porosity and no lenses.

$$\frac{D_x}{D} = \frac{D_L}{D} \cong Pe = \frac{Ud}{D} \quad \text{or}$$
$$D_x = (10^{-4}\,\text{m/s})(10^{-3}\text{m}) = 10^{-7}\,\text{m}^2/\text{s}$$

$$\frac{D_y}{D} = \frac{D_z}{D} \cong 0.1\,Pe \quad \text{or}$$
$$D_y, D_z = 0.1\,(10^{-7}\,\text{m}^2/\text{s}) = 10^{-8}\,\text{m}^2/\text{s}$$

Retardation Coefficient:
Lehman et al. [11] gives:
$\log(K_{0w}) = 2.75$ for Atrazine
$\therefore K_{0w} = 10^{2.75} = 562$
Using Karikhoff et al. [10] relationship:
$K_d = \beta f K_{0w}$ where $\beta = 0.41$ cm^3/g and $f = 10^{-4}$
Then

$$K_d = 0.41\ \text{cm}^3/\text{g}\ (10^{-4})(562) = 0.023\ \text{cm}^3/\text{g}$$

and

$$R = 1 + \frac{\rho_b}{\varepsilon}K_d = 1 + 6\,\frac{\text{g}}{\text{cm}^3}(0.023\ \text{cm}^3/\text{g}) = 1.14$$

Even with a fairly sorptive organic compound, the retardation coefficient in rock is not much different from 1.0. Eq. 44 gives a maximum at $y = 0$, $z = 0$, $x = U\,t/R$. Thus,

$$C_{\max} = \frac{M}{8\varepsilon(\pi t/R)^{3/2}\sqrt{D_x D_y D_z}}$$

and

$$X_{\max} = \frac{Ut}{R} = 0.88 \times 10^{-4}\,(m/s)\,t\,(s)$$

We will indicate spread by 4σ, which corresponds to 95% of the total mass of the cloud, for a Gaussian distribution like this equation provides.

For 1-D diffusion: $\sigma^2 = 2\,Dt/R$
For 3-D diffusion: $\sigma^2 = \frac{2}{9}\,Dt/R \quad \sigma = \frac{\sqrt{2\,Dt/R}}{3}$
and

$$4\sigma_x = \frac{4\sqrt{2D_x\,t/R}}{3}$$

Chemicals in the Environment, Dispersive Transport.
Table 4 Estimated concentration over time and space with transport through a uniformly porous sandstone

Time	C_{max} (g/m^3)	X_{max} (m)	$4\sigma_x$ (m)	$4\sigma_y$ (m)
1 hr	4.0×10^8	0.32	0.04	0.014
1 day	3.4×10^6	7.6	0.17	0.054
1 month	2.1×10^4	229	0.90	0.29
1 year	500	2,800	3.1	0.98
2 years	180	5,500	4.4	1.39
10 years	16	27,000	9.9	3.13

Chemicals in the Environment, Dispersive Transport.
Table 5 Estimated concentration over time and space with transport through a sandstone media with 1 m heterogeneities

Time	C_{max} (g/m^3)	X_{max} (m)	$4\sigma_x$ (m)	$4\sigma_y$ (m)
1 hr	1.25	0.32	1.3	0.4
1 day	.011	7.6	5.5	1.7
1 month	6.6×10^{-5}	229	29	9.2
1 year	1.57×10^{-6}	2,800	99	31
2 years	5.6×10^{-7}	5,500	140	44
10 years	5.0×10^{-8}	27,000	320	99

$$4\sigma_z = 4\sigma_y = \frac{4\sqrt{2D_y\ t/R}}{3}$$

Note that in Table 4, the concentrations at 1 h, 1 day, and 1 month are above the initial Atrazine concentration (1,000 g/m^3). This is one problem with Dirac delta boundary conditions because they initially have no volume, only mass. At greater elapsed time, however, the inaccuracies of the Dirac delta solution have a minimal impact on the resulting concentration.

However, virtually all media have heterogeneities of high and low porosity regions, as well as lenses that form around cracks. If we assume that the spacing of these regions is a mean of 1 m, instead of the 1 mm grain size, then our estimated dispersion coefficients are increased by a factor of 10^3. Applying the above equations to these parameters results in a reduction in C_{max} by a factor of 3.2×10^4 and an increase in both 4σ values by a factor of 32. The resulting estimates of the pertinent parameters are given in Table 5. These values are likely to be more realistic for transport through a groundwater aquifer.

The unknown dispersion coefficient is not uncommon in groundwater transport problems. It is typically one of the parameters fitted to measurements in groundwater transport.

Example 3: Drinking water pollution by trichloroethylene (steady state groundwater transport with lateral dispersion). A military ammunition plant in Arden Hills, Minnesota, used trichloroethylene (TCE) as a metal cleaning solvent for many years. Trichloroethylene is currently believed to be a carcinogen. Unaware of the hazardous nature of TCE, plant personnel placed the waste grease and TCE in a trench to burn (the grease) or soak into the ground (the TCE) and disappear from sight for many years. What was not known, however, is that they were placing the TCE into an aquifer that surfaces near the armory. Four kilometers downstream, the City of New Brighton used this aquifer as a source of municipal water supply. What is the expected TCE concentration in the New Brighton water supply and what should be done in the adjacent cities? Is the TCE plume sufficiently captured by the New Brighton wells? The following conditions were approximated from available data:

Supply of TCE = 100 kg/day
$U = 1.6 \times 10^{-5}$ m/s
Aquifer thickness, $H = 30$ m
$R \cong 1.0$ in the aquifer for TCE.
Aquifer porosity, $\varepsilon = 0.3$
New Brighton extraction, $Q = 0.25$ m^3/s
Drinking water recommended limit for TCE = 5 μg/L (5×10^{-3} g/m^3)

As a first assumption, we will assume that the New Brighton well was located in the center of the plume, compute the capture zone, and then the concentrations within this capture zone. The capture zone is given by:

$$Y = \frac{Q}{\varepsilon HU} = 1740\ m \tag{45}$$

At a velocity of 1.6×10^{-5} m/s, the 4 km distance would be covered in 8 years, which is short compared to the ~40 years of dumping TCE. We will therefore assume that the system is at steady state. We have these boundary conditions:

At $x = 0$, $\dot{M} = 100\,\text{kg/day} = 1.2\,\text{g/s}$
At $y = \infty$, $C = 0$
At $x = \infty$, $C = 0$.

The solution with these boundary conditions is:

$$C = \frac{\dot{M}}{H\varepsilon\,(4\pi x U D_t)^{1/2}}\,\exp\left(\frac{-Uy^2}{4\,D_t\,x}\right)$$

with a capture zone mean of

$$\bar{C} = \frac{2}{Y}\int_0^{Y/2} C dy$$

where Y is the width of the capture zone, and a leakage from the capture zone, M_L of

$$M_L = 2\varepsilon H \int_{Y/2}^{\infty} C dy$$

Using the rough approximations of Eqs. 35 and 36, we get

$$D_{\mathrm{L}} = 0.0026\mathrm{m}^2/\mathrm{s}$$

and

$$D_t = 2.6\,\mathrm{X}\,10^{-4}\mathrm{m}^2/\mathrm{s}.$$

Note that Eq. 36 gives $D_{\mathrm{L}} = 0.0026$ m^2/s with a 67% confidence interval of between 0.064 and 1×10^{-4} m^2/s, or 1.4 orders of magnitude. This variation would need to be considered in any preliminary analysis of this problem.

The solution for this application is given in Fig. 9 at various lateral distances from the peak concentration.

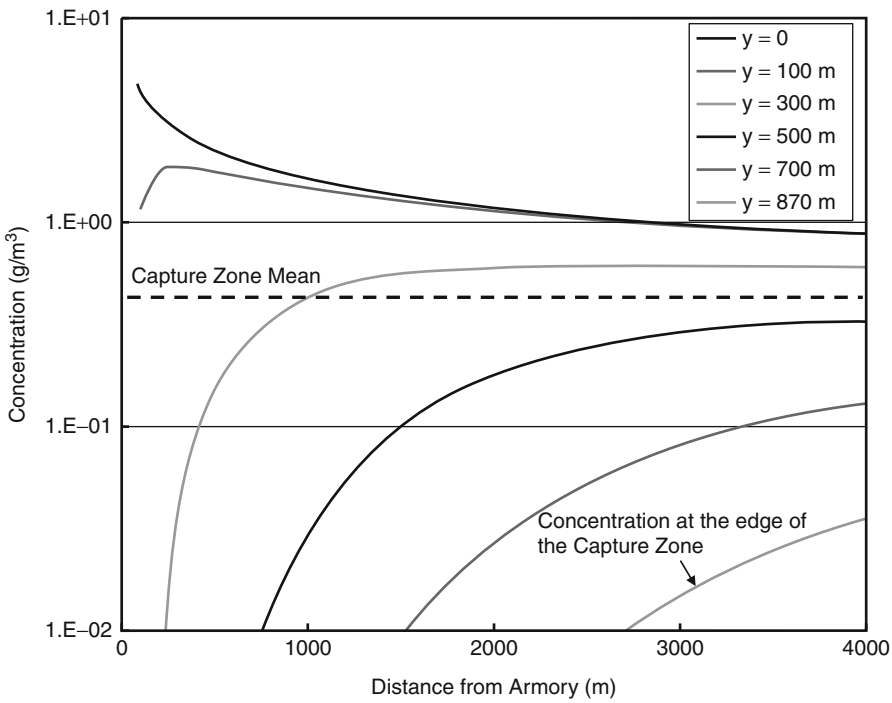

Chemicals in the Environment, Dispersive Transport. Figure 9
Predicted concentration of trichloroethylene in groundwater plume versus distance for the ammunitions plant release – City of New Brighton case study

The capture zone mean is 0.42 g/m^3, or almost 100 times the recommended limit, which would raise concern in New Brighton. The leakage from the capture zone at $x = 4{,}000$ m for this scenario is computed to be 47 g, or sufficient mass to result in a concentration of 9×10^{-4} g/m^3 for a similar capture zone. It is possible, then, that almost all of the plume was captured by the City of New Brighton, so the problem may not cover a wider area than the immediate downstream cities. This, at least, is one positive result of the low transverse dispersion of groundwater plumes.

Example 4: Determination of D_L in a river. A tanker car carrying a solvent derailed on a bridge and fell into the Nemadji river, Wisconsin. The forensic investigation team has a computational model that will simulate the spill, if some coefficients are determined, including D_L and t_r. The most cost-effective means of determining these parameters would be to perform a conservative tracer pulse test and adjust the parameters from discharge on the day of the tracer test (30 m^3/s) to discharge on the day of the spill (70 m^3/s) with some predictive equations that have been developed.

The location of the pulse input is identified as $x = 0$. The measured tracer concentrations and other relevant data are given in Fig. 10. From this data, determine the D_L and t_r parameters on the day of the test for the reach from $x = 8{,}000$ m to $x = 35{,}000$ m.

Because the variance of the tracer curve grows linearly with distance after $x = x^*$, we can make the following statements:

$$\Delta t_r = t_{r_2} - t_{r_1}$$

and

$$\Delta\sigma_t^2 = \sigma_t^2|_2 - \sigma_t^2|_1$$

and finally,

$$\frac{\Delta\sigma_t^2}{\Delta t_r^2} = \frac{2D_L}{U\Delta x} = \frac{2D_L\,\Delta t_r}{\Delta x^2}$$

At $x = 8{,}000$ m,

$$t_{r_1} = \frac{\int Ct\,dt}{\int C\,dt} \cong \frac{\sum Ct\,\Delta t}{\sum C\,\Delta t}$$

Using all of the Δt values set equal to 0.1 h, Δt can be cancelled out of the equation, and

$$t_{r_1} = \frac{1.30\,\text{h g/m}^3}{0.67\,\text{g/m}^3} = 1.94\,\text{h}$$

Also,

$$\sigma_t^2|_1 = \frac{\int Ct^2\,dt}{\int C\,dt} - t_{r1}^2 \cong \frac{\sum Ct^2\,\Delta t}{\sum C\,\Delta t} - t_{r1}^2$$

or, again cancelling the equal Δt's:

$$\sigma_t^2|_1 = \frac{2.59\,\text{h}^2\text{g/m}^3}{0.666\,\text{g/m}^3} - (1.94\,\text{h})^2 = 0.125\ \text{h}^2$$

We have assumed that the location 8,000 m downstream of the pulse injection will be out of the "mixing" region, as specified by Eq. 39. We are now ready to check this assumption with the parameters of the stream flow at $x = 8{,}000$ m. First, $U = Q/A = 8$ m^3/s/10.8 m^2 = 0.74 m/s, and from the chapter on Turbulent Transport:

$$\varepsilon_y \cong (0.6 \pm 0.3)\,u_* h \tag{46}$$

where

$$u_* = \sqrt{ghS} = \sqrt{(9.8\,\text{m/s}^2)(0.6\,\text{m})(10^{-3})} = 0.077\,\text{m/s}$$

Then,

$$\begin{aligned}\varepsilon_y &= (0.6 \pm 0.3)\,(0.077\,\text{m/s})(0.6\,\text{m})\\ &= 0.028 \pm 0.014\ \text{m}^2/\text{s}\end{aligned}$$

and Eq. 41 gives,

$$X_* = \frac{0.2\,(0.74\,\text{m/s})\,(30\,\text{m})^2}{0.028\,\text{m}^2/\text{s}} = 4760\,\text{m}$$

With the approximations in Eq. 39, $x = 8{,}000$ m will be assumed sufficient to begin our determination of D_L, especially since that is one of the few access points (a bridge) into this reach of the river.

We will now perform a similar calculation on the tracer cloud at $x = 35{,}000$ m.

$$t_{r_2} = 11.54\ \text{hr}$$

$$\sigma_t^2|_2 = \frac{1\,4\ \text{hr}^2\,\text{g/m}^3}{0.105\,\text{g/m}^3} - (11.54\ \text{hr})^2 = 0.162\ \text{hr}^2$$

$$\Delta x = 35{,}000\ \text{m} - 8{,}000\ \text{m} = 27{,}000\ \text{m}$$

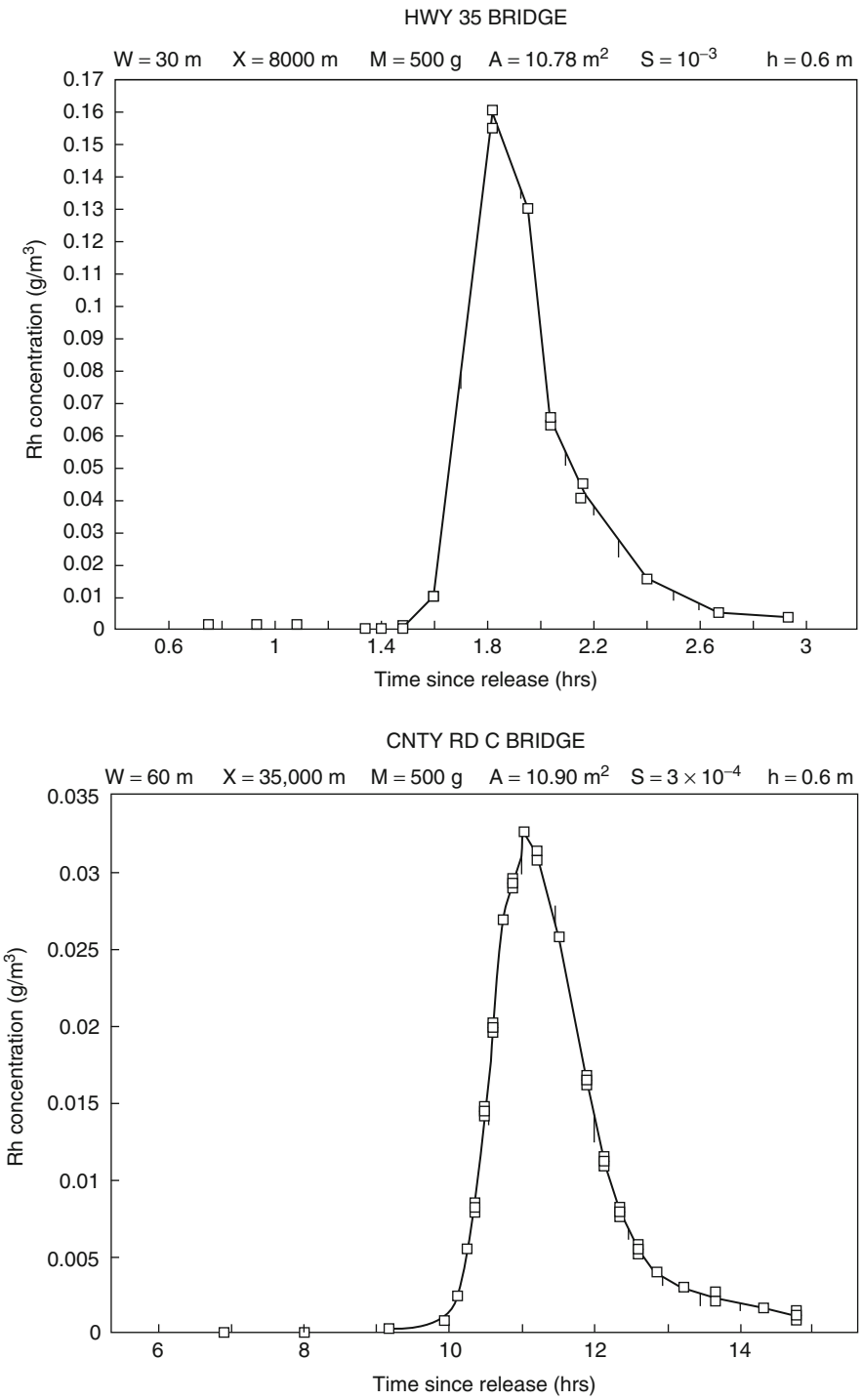

Chemicals in the Environment, Dispersive Transport. Figure 10
Tracer measurements taken at the Highway 35 and County Road C bridges

Now,

$$D_L = \frac{\Delta\sigma_t^2\,\Delta x^2}{2\Delta t_r^3} = \frac{(0.162 - 0.125)\,\mathrm{hr}^2\,(27,000\,\mathrm{m})^2}{2\,(11.54 - 1.94)^3\,\mathrm{hr}^3}$$

or,

$$D_L = 15,200\mathrm{m}^2/\mathrm{hr} = 4.2\mathrm{m}^2/\mathrm{s}$$

We can use Eq. 37 to adjust our dispersion coefficient from the 8 m^3/s with 0.6 m mean depth on the day of the tracer test to the 3 m^3/s with 0.4 m mean depth that existed as the river discharge on the day of the spill:

$$D_L = 0.011\,(Q/Wh)^2\;W^2/(\sqrt{ghS}\,h) \tag{47}$$

and then, assuming that the slope does not change and that the banks are fairly steep, such that $dA = W\,dh$, and assigning the subscripts t and s to indicate tracer and spill:

$$D_{LS} = D_{Lt}\left(\frac{Q_s}{Q_t}\right)^2\left(\frac{h_t}{h_s}\right)^{7/2}$$
$$= 4.2\,\frac{\mathrm{m}^2}{\mathrm{s}}\left(\frac{3\,\mathrm{m}^3/\mathrm{s}}{8\,\mathrm{m}^3/\mathrm{s}}\right)\left(\frac{0.6\,\mathrm{m}}{0.4\,\mathrm{m}}\right) = 2.4\;\mathrm{m}^2/\mathrm{s}$$

In addition, t_r can be adjusted as well:

$$\Delta t_{rs} = \Delta t_{r_t}\,\frac{Q_t}{Q_s}\frac{h_s}{h_t} = (11.54 - 1.94)\,\mathrm{h}\,\frac{8\mathrm{m}^3/\mathrm{s}}{3\,\mathrm{m}^3/\mathrm{s}}\frac{0.4\,\mathrm{m}}{0.6\,\mathrm{m}}$$

so

$$\Delta t_{r_s} = 17\,\mathrm{h}$$

The use of an empirical relation, such as Eq. 37, to adjust parameters for discharge is more accurate than simply using the equation itself, because the coefficient and other variables that can have substantial uncertainty are eliminated from the equation.

Conclusions

Dispersive transport is handled in a manner similar to turbulent diffusion and diffusion, with almost the same equations and solutions. The primary difference is that a dispersion coefficient is one or two orders of magnitude greater than turbulent diffusion coefficients and about 10 orders of magnitude greater than diffusion coefficients. Assuming that the dispersion coefficient will result in a Gaussian distribution of a chemical is only a rough approximation, however, which can be inaccurate at the trailing edge of the chemical cloud.

Future Directions

As computational power of our computers continues to improve, less attention will be paid to dispersive transport in the environment. The merging of velocity profiles and mixing to make a dispersion coefficient will be of less value when a more exact solution is available on desktop computers. The simplicity of the analysis, however, still will make the dispersion equations valuable in developing an understanding of mixing and transport problems in environmental settings.

Bibliography

Primary Literature

1. Taylor GI (1953) Dispersion of soluble matter in solvent flowing slowly through a tube. Proc R Soc Lond Ser A 219:186
2. Taylor GI (1954) The dispersion of matter in turbulent flow through a pipe. Proc R Soc Lond Ser A 223:446
3. Elder JW (1959) The dispersion of marked fluid in turbulent shear flow. J Fluid Mech 5:544
4. Crank J (1975) The mathematics of diffusion, 2nd edn. Oxford University Press, Oxford
5. Gulliver JS (2007) An introduction to chemical transport in the environment. Cambridge University Press, Cambridge
6. Freeze RA, Cherry JA (1979) Groundwater. Prentice-Hall, Englewood Cliffs
7. Koch DL, Brady JF (1985) Dispersion in fixed beds. J Fluid Mech 154:399
8. Gelhar L, Welty C, Rehfeldt KR (1992) A critical-review of data on field-scale dispersion in aquifers. Water Resour Res 28(7):1955
9. Fisher HB (1973) Longitudinal dispersion and turbulent mixing in open-channel flow. Ann Rev Fluid Mech 5:59
10. Karikhoff SW, Brown DS, Scott TA (1979) Sorption of hydrophobic pollutants on natural sediments. Water Res 13:241
11. Lehman WJ, Reehl WF, Rosenblatt DH (1990) Handbook of chemical property estimation. American Chemical Society, Washington, DC

Books and Reviews

Fisher HB, List JE, Koh RCY, Imberger J, Brooks NH (1979) Mixing in inland and coastal waters. Academic, San Diego

Kreyszig E (1982) Advanced engineering mathematics, 4th edn. Wiley, New York

Levenspiel O (1962) Chemical reaction engineering. Wiley, New York

Chemicals in the Environment, Turbulent Transport

John S. Gulliver
Department of Civil Engineering, University of Minnesota, Minneapolis, MN, USA

Article Outline

Glossary
Definition of Turbulent Transport in the Environment
Introduction
Mass Transport Equation with Turbulent Diffusion Coefficients
Prandtl's Mixing Length Hypothesis for Turbulent Flow
Example Applications
Conclusion
Future Directions
Bibliography

Glossary

Diffusion The spreading of fluid constituents through the motion inherent to atoms and molecules.

Diffusion coefficient A coefficient that describes the tendency of molecules to spread a constituent mass

Dirac delta An impulse of a given quantity (mass) that occurs over an infinitely short time or space.

Kinematic viscosity The fluid viscosity divided by the fluid density, resulting in units that are similar to a diffusion coefficient, or length squared per time.

Laminar flow Flow that has no turbulent eddies, where the fluid flows in laminas and diffusion creates the mixing of the fluid.

Prandtl's mixing length The mean length that the turbulence in the flow will transport mass, momentum, or energy.

Reynolds number The ratio of inertial to viscous forces, resulting in a meaningful velocity times a meaningful distance divided by kinematic viscosity.

Turbulent diffusion The mixing of fluids through turbulent eddies created by convection.

Turbulent diffusion coefficient A coefficient that comes from the multiplication of two turbulent velocities of the flow, divided by density of the fluid. The coefficient's location in the mass transport equation is similar to diffusion coefficients, and the units are similar; so it is called a "turbulent diffusion coefficient."

Definition of Turbulent Transport in the Environment

It is fairly safe to state that, except for flow through porous media, the environment experiences turbulent flow. To emphasize this point, the constriction of a water flow or airflow that would be required will be considered to have the other option, laminar flow.

An experimentally based rule of thumb is that laminar flow typically occurs when the pipe Reynolds number, Vd/ν, is less than roughly 2,000, or when an open-channel Reynolds number, Vh/ν, is less than roughly 500, where V is the cross-sectional mean velocity, d is the pipe diameter, ν is the kinematic viscosity of the fluid, and h is the channel depth. The diameter or depth that would not be exceeded to have laminar flow by these experimental criteria is given in Table 1.

Table 1 shows that with the boundary conditions present in most environmental flows, that is, the earth's surface, ocean top and bottom, river or lake bottom, etc., turbulent flow would be the predominant condition. One exception that is important for interfacial mass transfer would be very close to an interface, such as air–solid, solid–liquid, or air–water interfaces, where the distance from the interface is too small for turbulence to occur due to the high viscous

Chemicals in the Environment, Turbulent Transport.
Table 1 Maximum diameter or depth to have laminar flow, with the transition Reynolds number for a pipe at 2,000

Water ($\nu = 10^{-6}$ m^2/s)		Air ($\nu \sim 2 \times 10^{-5}$ m^2/s)	
V (m/s)	D (m)	h (m)	d (m)
10	2×10^{-4}	5×10^{-5}	0.004
3	7×10^{-4}	1.5×10^{-4}	0.014
1	0.002	0.0005	0.04
0.3	0.007	0.0015	0.14
0.1	0.02	0.005	0.4
0.03	0.07	0.015	1.4
0.01	0.2	0.05	4.0

dissipation. Because turbulence is an important source of mass transfer, the lack of turbulence very near the interface is also significant for mass transfer, where diffusion once again becomes the predominant transport mechanism.

Introduction

What is turbulent flow? The simple illustration of a free-surface flow given in Fig. 1 is used to describe the essential points of the turbulence phenomena. Turbulent open-channel flow can be described with a temporal mean velocity profile which reaches a steady value with turbulent eddies superimposed upon it. These turbulent eddies are continually moving about in three dimensions, only restricted by the boundaries of the flow, such that they are eliminated from the temporal mean velocity profile, $\bar{u}$ in Fig. 1. It is this temporal mean velocity profile that is normally sketched in turbulent flows.

There will also be a temporal mean concentration. If there is a source or sink in the flow, or transport across the boundaries as in Fig. 1, then the temporal mean concentration profile will eventually reach a value such as that given in Fig. 1. This flux of compound seems to be from the bottom toward the top of the flow. Superimposed upon this temporal mean concentration profile will be short-term variations in concentration caused by turbulent transport. The concentration profile is "flatter" in the middle of the flow because the large turbulent eddies that transport mass quickly are not as constrained by the flow boundaries in this region. Now, if a concentration-velocity probe is placed into the flow at one location, the two traces of velocity and concentration versus time would look something like that shown in Fig. 2.

Turbulent diffusion is thus not really diffusion, but the mixing of chemicals through turbulent eddies created by convection. Turbulent diffusion is thus a form of convection. Although it has the appearance of diffusion in the end, that is, random mixing similar to diffusion, the causes of diffusion and turbulent diffusion are very different. Since the end products are similar, diffusion coefficients and turbulent diffusion coefficients are often simply added together.

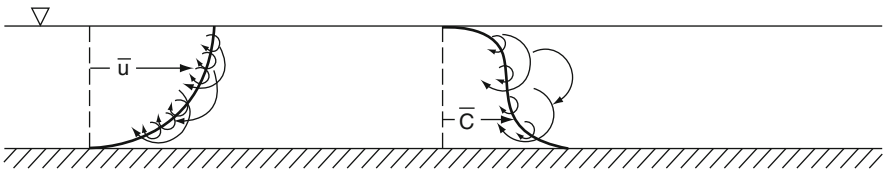

Chemicals in the Environment, Turbulent Transport. Figure 1
Turbulent eddies superimposed on a temporal-mean velocity and temporal-mean concentration profiles (From Gulliver [1])

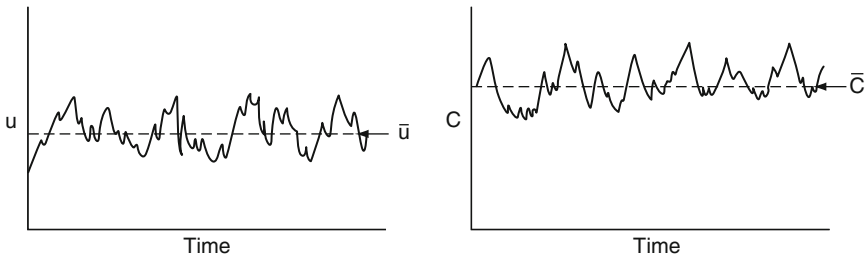

Chemicals in the Environment, Turbulent Transport. Figure 2
Time traces of typical measurements of velocity and concentration in a turbulent flow

It is convenient to divide the velocity and concentration traces into temporal mean values and fluctuating components:

$$u = \bar{u} + u' \tag{1}$$

and

$$C = \bar{C} + C' \tag{2}$$

where $\bar{u}$ is the temporal mean velocity at a point location, u' is the fluctuating component of velocity (variable over time), $\bar{C}$ is the temporal mean concentration at a point location, and C' is the fluctuating concentration component of concentration which is also variable over time. Formal definitions of $\bar{u}$ and $\bar{C}$ are as follows:

$$\bar{u} = \frac{1}{\Delta t}\int_0^{\Delta t} u\,dt \tag{3}$$

and

$$\bar{C} = \frac{1}{\Delta t}\int_0^{\Delta t} C\,dt \tag{4}$$

where Δt is long compared to the time period of the oscillating components.

Mass Transport Equation with Turbulent Diffusion Coefficients

In this section the most common equations for dealing with mass transport in a turbulent flow will be derived. Beginning with the mass transport equation developed in the entry "► Transport in the Environment,"

$$\frac{\partial C}{\partial t} + \frac{\partial(uC)}{\partial x} + \frac{\partial(vC)}{\partial y} + \frac{\partial(wC)}{\partial z} = \frac{\partial}{\partial x}\left(D\frac{\partial C}{\partial x}\right) + \frac{\partial}{\partial y}\left(D\frac{\partial C}{\partial y}\right) + \frac{\partial}{\partial z}\left(D\frac{\partial C}{\partial z}\right) + S \tag{5}$$

the temporal mean of the entire equation will be taken and eventually one will end up with an equation that incorporates turbulent diffusion coefficients.

In a turbulent flow field, Eq. 5 is difficult to apply because C, u, v, and w are all highly variable functions of time and space. Osborne Reynolds [2] reduced the complexities of applying Eq. 5 to a turbulent flow by taking the temporal mean of each term (e.g., the entire equation). Then, the mean value of a fluctuating component will be equal to zero, or

$$\overline{\frac{\partial C}{\partial t}} = \overline{\frac{\partial(\bar{C} + C')}{\partial t}} = \overline{\frac{\partial \bar{C}}{\partial t}} + \overline{\frac{\partial C'}{\partial t}} = \frac{\partial \bar{C}}{\partial t} + 0 \tag{6}$$

Equation 6, the change of a temporal mean over time, may seem like a misnomer, but it will be left in to identify changes in $\bar{C}$ over a longer time period than Δt. Continuing,

$$\overline{\frac{\partial C}{\partial x}} = \overline{\frac{\partial(\bar{C} + C')}{\partial x}} = \overline{\frac{\partial \bar{C}}{\partial x}} + \overline{\frac{\partial C'}{\partial x}} = \frac{\partial \bar{C}}{\partial x} \tag{7}$$

$$\overline{\frac{\partial C}{\partial y}} = \overline{\frac{\partial(\bar{C} + C')}{\partial y}} = \overline{\frac{\partial \bar{C}}{\partial y}} + \overline{\frac{\partial C'}{\partial y}} = \frac{\partial \bar{C}}{\partial y} \tag{8}$$

$$\overline{\frac{\partial C}{\partial z}} = \overline{\frac{\partial(\bar{C} + C')}{\partial z}} = \overline{\frac{\partial \bar{C}}{\partial z}} + \overline{\frac{\partial C'}{\partial z}} = \frac{\partial \bar{C}}{\partial z} \tag{9}$$

However, the temporal mean value of two fluctuating components, multiplied by each other, will not necessarily be zero:

$$\overline{u'C'} \neq \bar{u}'\bar{C}' \tag{10}$$

This is similar to a least-square regression, where the mean error is zero, but the sum of square error is not. The x-component of our convective transport terms will be dealt with first:

$$\overline{uC} = \overline{(\bar{u} + u')(\bar{C} + c')} = \overline{\bar{u}\bar{C}} + \overline{\bar{u}C'} + \overline{u'\bar{C}} + \overline{u'C'} \tag{11}$$

Three of the four terms in Eq. 11 may be reduced to something known:

$$\overline{\bar{u}\bar{C}} = \bar{u}\bar{C} \tag{12}$$

$$\overline{\bar{u}C'} = 0 \tag{13}$$

$$\overline{u'\bar{C}} = 0 \tag{14}$$

but, the fourth term will take some additional consideration, because it is not equal to zero:

$$\overline{u'C'} \neq 0 \tag{15}$$

By inference, the following can be written for all three convective transport terms:

$$\overline{uC} = \bar{u}\bar{C} + \overline{u'C'} \tag{16}$$

$$\overline{vC} = \bar{v}\bar{C} + \overline{v'C'} \tag{17}$$

and

$$\overline{wC} = \bar{w}\bar{C} + \overline{w'C'} \tag{18}$$

Finally, applying continuity $(\bar{u} + \bar{v} + \bar{w} = 0)$ to Eq. 5 and taking the temporal mean results of Eqs. 6, 7, 8, 9, 16, 17, and 18

$$\begin{aligned}\frac{\partial \bar{C}}{\partial t} + \bar{u}\frac{\partial \bar{C}}{\partial x} + \bar{v}\frac{\partial \bar{C}}{\partial y} + \bar{w}\frac{\partial \bar{C}}{\partial z} \\ = -\frac{\partial}{\partial x}\overline{u'C'} - \frac{\partial}{\partial y}\overline{v'C'} - \frac{\partial}{\partial z}\overline{w'C'} + \frac{\partial}{\partial x}\left(D\frac{\partial \bar{C}}{\partial x}\right) \\ + \frac{\partial}{\partial y}\left(D\frac{\partial \bar{C}}{\partial y}\right) + \frac{\partial}{\partial z}\left(D\frac{\partial \bar{C}}{\partial z}\right) + \bar{S}\end{aligned} \tag{19}$$

where the turbulent convective transport term can be moved to the right-hand side, because the concentration distribution that results from these terms looks similar to diffusion.

With this temporal mean process, we have reduced the terms for which we will have difficulty defining boundary conditions in turbulent flow fields from seven in Eq. 5 to three in Eq. 19. We will now deal with these three terms.

The diffusion equation is a useful and convenient equation to describe mixing in environmental flows, where the boundaries are often not easily defined. It also lends itself to analytical solutions and is fairly straightforward in numerical solutions. Although an alternative technique for solutions to mixing problems is the mixed cell method described in the entry "▶ Chemicals in the Environment, Dispersive Transport," there are complications when applied to multiple dimensions and to flows that vary with space and time. Finally, we are comfortable with the diffusion equation, so we would prefer to use that to describe turbulent mixing if possible.

Therefore, let us consider the following thought process: if the end result of turbulence, when visualized from sufficient distance, looks like diffusion with seemingly random fluctuations, then we should be able to identify the terms causing these fluctuations in Eq. 19. Once identified, they can be related to a "turbulent diffusion coefficient" that describes the diffusion caused by turbulent eddies. Looking over the terms in Eq. 19 from left to right, we see an unsteady term, three mean convective terms, the three "unknown" terms, the diffusive terms and the source/sink rate terms. The "unknown" terms are the only possibility to describe turbulent diffusion.

In the late nineteenth century, Boussinesq [3] probably went through something similar to the thought process described above. The end result was the *Boussinesq eddy diffusion coefficient*:

$$-\overline{u'C'} = \varepsilon_x \frac{\partial \bar{C}}{\partial x} \tag{20a}$$

$$-\overline{v'C'} = \varepsilon_y \frac{\partial \bar{C}}{\partial y} \tag{20b}$$

$$-\overline{w'C'} = \varepsilon_z \frac{\partial \bar{C}}{\partial z} \tag{20c}$$

where ε_x, ε_y, and ε_z are the turbulent (or eddy) diffusion coefficients, with units of m^2/s similar to the (molecular) diffusion coefficients.

Then Eq. 19 with Eqs. 20a, 20b, and 20c becomes

$$\begin{aligned}\frac{\partial \bar{C}}{\partial t} + \bar{u}\frac{\partial \bar{C}}{\partial x} + \bar{v}\frac{\partial \bar{C}}{\partial y} + \bar{w}\frac{\partial \bar{C}}{\partial z} = \frac{\partial}{\partial x}\left[(D+\varepsilon_x)\frac{\partial \bar{C}}{\partial x}\right] \\ + \frac{\partial}{\partial y}\left[(D+\varepsilon_y)\frac{\partial \bar{C}}{\partial y}\right] + \frac{\partial}{\partial z}\left[(D+\varepsilon_z)\frac{\partial \bar{C}}{\partial z}\right] + \bar{S}\end{aligned} \tag{21}$$

Turbulent diffusion is created by the flow field, which can vary with distance. Hence, turbulent diffusion coefficient cannot be assumed constant with distance. Removing that assumption leaves turbulent diffusion coefficient inside of the brackets.

Character of Turbulent Diffusion Coefficients

A turbulent eddy can be visualized as a large number of differently sized rotating spheres or ellipsoids. Each sphere has sub-spheres, and so on until the smallest eddy size is reached. The smallest eddies are dissipated by viscosity, which explains why turbulence does not occur in narrow passages: there is simply no room for eddies that will not be dissipated by viscosity.

The cause of the rotation is shear forces created by solid boundaries or variations in velocity lateral to the primary flow direction. A buoyant plume of smoke or steam, for example, will have a temporal mean velocity profile develop laterally to the plume, as the rising

plume mixes with the ambient air. Turbulent eddies are formed by this velocity gradient, and can be seen at the edge of the smoke or steam plume. The magnitude of turbulent diffusion coefficients is primarily dependent upon the scale of turbulent eddies and the speed of the eddy rotation. As illustrated in Fig. 3, a large eddy will have greater eddy diffusion coefficient than a small eddy because it will transport a compound (or solute) farther in one rotation. Likewise, a faster spinning eddy will have a larger eddy diffusion coefficient than one which is the same size but spinning more slowly because the solute simply gets there faster. These two facts provide meaning to the following observations:

1. The largest scale of turbulence is roughly equal to the smallest overall scale of the flow field. This may be seen in comparing the size of eddies at the edge of the smoke or steam plume to the width of the plume.
2. The rotational eddy velocity is roughly proportional to the velocity gradient times the eddy scale.
3. Eddy size decreases near boundaries to the flow field. Since the eddy size is zero at a solid boundary, and often close to zero at a fluid density interface (like an air–water interface), the turbulent eddy size has to decrease as one approaches the boundaries. In addition, since the flow cannot go through a boundary, the largest eddy size cannot be greater than the distance from the center of the eddy to the boundary.
4. Turbulent diffusion occurs because turbulent eddies are transporting mass, momentum, and energy over the eddy scale at the rotational velocity. This transport rate is generally orders of magnitude greater than the transport rate due to molecular motion. Thus, when a flow is turbulent, diffusion is normally ignored because $\varepsilon >> D$. The exception is very near the flow boundaries, where the eddy size (and turbulent diffusion coefficient) decreases to zero.

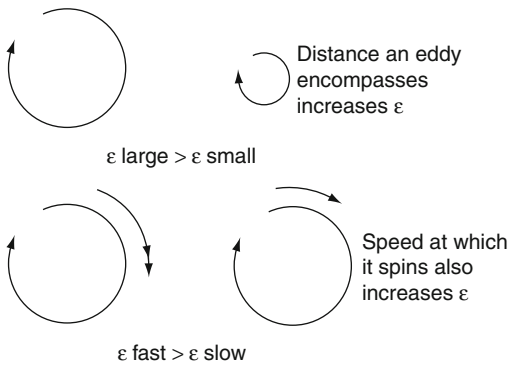

Chemicals in the Environment, Turbulent Transport. Figure 3
Character of turbulent diffusion coefficients (From Gulliver [1])

Thus, what influences the velocity and scale of eddies? For the most part, it is the velocity gradients and scale of the flow. Velocity gradients are the change in velocity over distance. If we have a high velocity, we typically have a large velocity gradient somewhere in the flow field. At solid walls, for example, the velocity must go to zero. Thus, *the large velocity difference results in large velocity gradients, which results in faster spinning eddies and a larger turbulent diffusion coefficient*. This process is illustrated in Fig. 4.

The scale of the flow field is also important because *the larger eddies perform most of the transport*. The small eddies are always there in a turbulent flow, and their existence is important for local mixing. It is the large eddies, however, that are the most responsible for transport, as illustrated in Fig. 5.

The four observations, listed above, were enough for Ludwig Prandtl [4] to hypothesize a simple model for describing turbulent transport that works

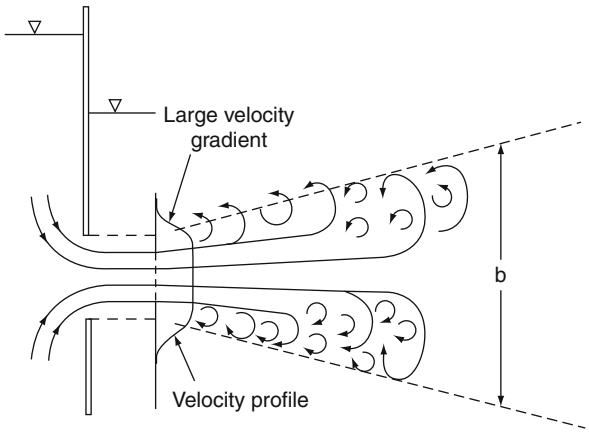

Chemicals in the Environment, Turbulent Transport. Figure 4
Eddy formation at the edge of a jet issuing into a tank illustrates the importance of velocity gradients in eddy diffusion coefficient (From Gulliver [1])

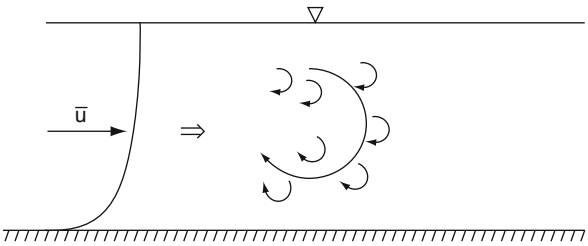

Chemicals in the Environment, Turbulent Transport. Figure 5
Large and small eddies in an open-channel flow. The large eddies perform most of the top-to-bottom transport (From Gulliver [1])

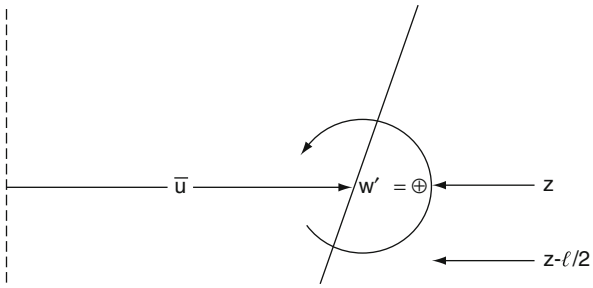

Chemicals in the Environment, Turbulent Transport. Figure 6
Illustration of the relationship between velocity profile, turbulent eddies, and mixing length

surprisingly well, considering the complexity of turbulent flow.

Prandtl's Mixing Length Hypothesis for Turbulent Flow

Prandtl's mixing length hypothesis was developed for momentum transport, instead of mass transport. The end result was a turbulent viscosity, instead of a turbulent diffusivity. However, since both turbulent viscosity and turbulent diffusion coefficient are properties of the flow field, they are related. Turbulent viscosity describes the transport of momentum by turbulence, and turbulent diffusivity describes the transport of mass by the same turbulence. Thus,

$$\varepsilon_x = \mu_{tx}/\rho,\ \varepsilon_y = \mu_{ty}/\rho,\ \text{and}\ \varepsilon_z = \mu_{tz}/\rho$$

where μ_{tx}, μ_{ty}, and μ_{tz} are the turbulent viscosity in the x, y, and z directions. Now, for the x-component of momentum (ρu), the Boussinesq approximation is

$$-\rho\ \overline{u'u'} = \mu_{tx}\frac{\partial \bar{u}}{\partial x} \tag{22}$$

$$-\rho\ \overline{v'u'} = \mu_{ty}\frac{\partial \bar{u}}{\partial y} \tag{23}$$

$$-\rho\ \overline{w'u'} = \mu_{tz}\frac{\partial \bar{u}}{\partial z} \tag{24}$$

Let us consider the fully developed velocity profile in the middle of a wide-open channel, with x-, y-, and z-components in the longitudinal, lateral, and vertical directions, respectively. It is fully developed because $\partial\bar{u}/\partial x$ is close to zero. The fact that it is a wide channel means that $\partial\bar{u}/\partial y$ also is very small in the middle. From Eqs. 22 and 23, we can see that the turbulent transport of momentum in the x- and y-directions will be small because the gradients are small. Equation 24 indicates that there will be a net turbulent transport of momentum in the z-direction.

$$-\overline{w'u'} = \varepsilon_z\frac{\partial \bar{u}}{\partial z} \neq 0 \tag{25}$$

Now, half of the w' values will be positive, and the other half will be negative. We will use this criterion to divide them into two parts:

$$\overline{w'u'} = \overline{w'u'}^{+} + \overline{w'u'}^{-} \tag{26}$$

where $w'u'^{+}$ has a value when w' is positive and is equal to zero when w' is negative. $w'u'^{-}$ has a value when w' is negative and is equal to zero when w' is positive. Consider the cases when w' is positive. Then Eq. 26 becomes

$$\overline{w'u'} = \overline{w'u'}^{+} + 0 \tag{27}$$

Let us assume that an eddy of length L is pulling a blob of fluid upward, as illustrated in Fig. 6. On average, the blob will have an x-component of velocity equal to $\overline{u}(z - L/2)$, where z is the location where u' is to be estimated. Thus, the eddy pulls up, on average, the u value that is at $z - L/2$. This will become the deviation from the temporal mean velocity at location z:

$$u' = u - \bar{u} \approx \bar{u}(z - L/2) - \bar{u}(z) \cong \frac{1}{2}(\bar{u}(z - L) - \bar{u}(z)) \tag{28}$$

Equation 28 is a relation for a difference in velocity, which can be written as a velocity gradient times a distance:

$$u' = -\frac{\partial \bar{u}}{\partial x}\left(\frac{L}{2}\right) \tag{29}$$

Velocity difference = velocity gradient × distance

Then,

$$\overline{w'u'}^{+} \approx \overline{\frac{w'}{2}[\bar{u}(z-L)-\bar{u}(z)]} \approx -\frac{\overline{w'}}{2}L\frac{\partial \bar{u}}{\partial z} \tag{30}$$

the development is similar for $\overline{w'u'}^{-}$:

$$\overline{w'u'}^{-} \approx \overline{w'u'}^{+} \approx -\frac{\overline{w'}}{2}L\frac{\partial \bar{u}}{\partial z} \tag{31}$$

Now combining Eqs. 26, 30, and 31 gives

$$\overline{w'u'} = -\overline{w'L\frac{\partial \bar{u}}{\partial z}} \tag{32}$$

Because turbulent eddies tend to be close to spherical in shape:

$$|w'| \approx |u'| \tag{33}$$

and from Eq. 29:

$$w' \sim L\frac{\partial \bar{u}'}{\partial z} \tag{34}$$

If we substitute Eq. 34 into Eq. 32, and then substitute the result into Eq. 24, we get

$$-\overline{w'u'} = \varepsilon_z\frac{\partial \bar{u}}{\partial z} = L^2\left(\frac{\partial \bar{u}}{\partial z}\right)^2 \tag{35}$$

or

$$\varepsilon_z = L^2\left|\frac{\partial \bar{u}}{\partial z}\right| \tag{36}$$

Equation 36 is Prandtl's *mixing length hypothesis*, and it works well, considering that the basis for the equation is so empirical. However, Eq. 36 does present a challenge for us that mixing length, L, still needs to be specified. Measurements have shown us the following:

1. Near a wall, $L = \kappa z$, where κ is von Kármán's constant [5] and is very close to 0.4, and z is the distance from the closest wall.

   Prandtl also made another assumption in this region, that $w'u'$ could be approximated by a constant equal to the mean wall shear stress, or

   $$-\overline{w'u'} = \tau/\rho = u_*^2 \tag{37}$$

   Then, eliminating $\overline{w'u'}$ from Eqs. 35 and 37 results in the well-known *logarithmic velocity profile*:

   $$\frac{\bar{u}}{u_*} = \frac{1}{k}\ell n\left(\frac{z}{z_0}\right) \tag{38}$$

   where u_* is the shear velocity at the wall, τ is the wall shear stress, and z_0 *is* an integration constant, often *called the dynamic roughness*. Table 2 provides some typical dynamic roughness lengths for atmospheric boundary layers. Applying Eq. 36 to 37 results in an equation for ε_z in this region:

   $$\varepsilon_z = \kappa u_* z \tag{39}$$

2. Very near a wall (approaching the laminar sublayer where the turbulence is so small that it is eliminated by the viscosity of the fluid), that is, for $zu_*/\nu < 35$, $L \sim y^2$ [6].

   Making the same assumption that $u'w'$ is approximately equal to wall shear stress, this relation for L results in the following relation for velocity profile very near the wall:

   $$\frac{\bar{u}}{u_*} = \beta\frac{\nu}{u_{**}z} \tag{40}$$

Chemicals in the Environment, Turbulent Transport.

Table 2 Dynamic roughness lengths, z_0, for typical atmospheric surfaces (Turner [7])

Surface Type	z_0 (m)
Urban	1.-3
Forest	1.3
Deciduous forest in winter	0.5
Desert shrubland	0.3
Wetland	0.3
Cropland (summer)	0.2
Cropland (winter)	0.01
Grassland (summer)	0.1
Grassland (winter)	0.001
Water	~0.0001

Equation 40 is not used in mass transport calculations near a wall or interface because the unsteady character of mass transport in this region is very important, and Eq. 39 is for a temporal mean velocity profile.

3. Away from a wall, where the closest wall does not influence the velocity profile, L is a function of another variable of the flow field (Prandtl [8]). For example, consider the jet mixer given in Fig. 4. In this case, the mixing length, L, is a function of the width of the jet or plume. As the jet/plume grows larger, the value of L is larger.

   Here, it is easier to simply give the experimental relation for eddy diffusivity:

$$\varepsilon_z = \beta\, u_{\max} b \tag{41}$$

   where b is the width of the mixing zone, β is a constant, and $u_{\max}$ is the maximum velocity in the jet at the given location, x.

Figure 7 gives some relationships for eddy diffusion coefficient profiles under different conditions that will be handy in applications of turbulent diffusive transport.

Example Applications

Example 5.1: Profile of eddy diffusion coefficient. Estimate the eddy diffusivity profile for a wind velocity of 18 m/s measured at 10 m over a large lake (Fig. 8), and calculate the elevation above the water surface where $\varepsilon_z = D$ for water vapor.

There is only one assumption needed:

1. The wind fetch is sufficient so that $\overline{U}_{10}$ is influenced by shear at the water surface (10 m is inside the boundary layer of the lake surface at this point).

Then, mixing length theory may be used with momentum transport to derive:

$$\frac{\partial \bar{u}}{\partial z} = \frac{u_*}{\kappa z} \tag{42}$$

and,

$$\varepsilon_z = \kappa\, u_* z \tag{43}$$

Now, Wu [9] has provided the following equation from a fit of field data:

$$u_* = 0.01\, \overline{U}_{10}\left(8 + 0.65\, \overline{U}_{10}\right)^{1/2} \tag{44}$$

which indicates that as the waves get larger at high wind speeds the boundary roughness effect upon u_* increases by the factor $\left(8 + 0.65\, \overline{U}_{10}\right)^{1/2}$, where $\overline{U}_{10}$ is given in m/s.

Then,

$$\varepsilon_z(\mathrm{m}^2/\mathrm{s}) = 0.01\, \kappa\, \bar{u}_{10} z (8 + 0.65\, \bar{u}_{10})^{1/2} = 0.32\, z$$

when z is given in meters. Now, the diffusion coefficient of water vapor in air is calculated to be $D = 2.6 \times 10^{-5}$ m^2/s. Then, the elevation at which the diffusivity of water vapor would equal eddy diffusivity in this case would be,

$$0.32z = 2.6 \times 10^{-5}$$

or,

$$z = 8 \times 10^{-5}\ \mathrm{m} = 0.08\ \mathrm{mm} = 80\ \mu\mathrm{m}$$

Thus at $z = 80$ μm elevation above the water surface, eddy diffusivity will be equal to the diffusivity of water. A similarly small elevation would result for almost any environmentally relevant compound. We can thus see that both ε and D need to be considered simultaneously in Eq. 20 only very close to surfaces in turbulent flow, where ε approaches the diffusion coefficient. Otherwise, diffusivities can be ignored in solving turbulent flow transport problems, since $\varepsilon + D$ is essentially equal to ε.

Example 5.2: Concentration profile of suspended sediment in a river (assuming ε_z is constant). We will apply Eq. 20 to solve for the concentration profile of suspended sediment in a river, with some simplifying assumptions. Suspended sediment is generally considered similar to a solute, in that it is a scalar quantity in Eq. 20, except that it has a settling velocity. We will also change our notation, in that the bars over the temporal mean values will be dropped. This is a common protocol in turbulent transport, and will be followed here for conformity. Thus, if an eddy diffusion coefficient, ε, is in the transport equation,

u means $\bar{u}$

v means $\bar{v}$

w means $\bar{w}$ and

C means $\bar{C}$

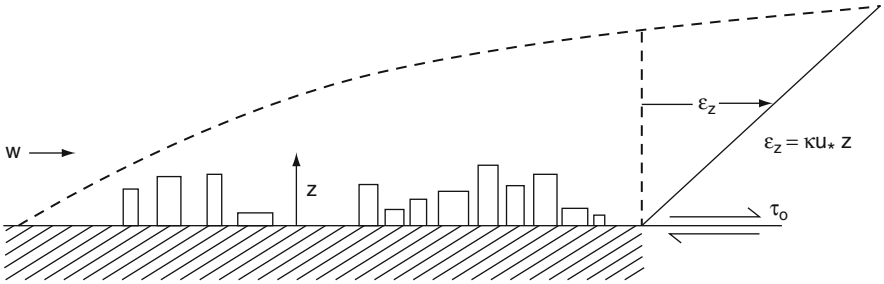

a Unconfined boundary layer

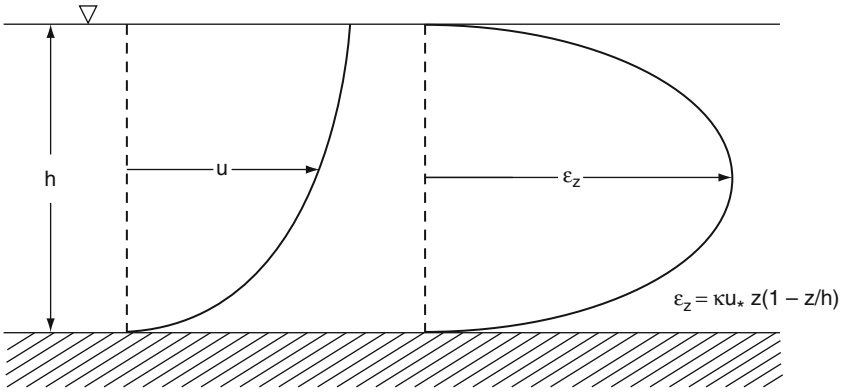

b Flows with a free surface

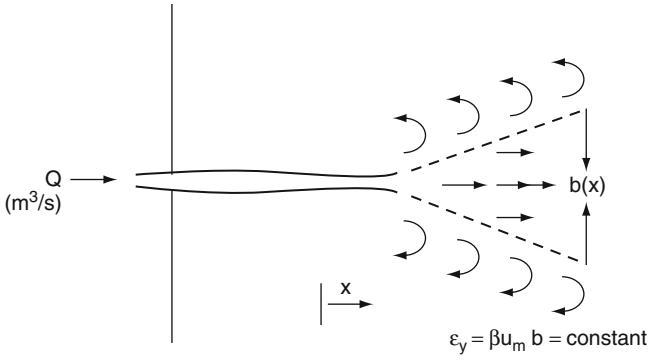

c Jetlike flows (not close to a boundary)

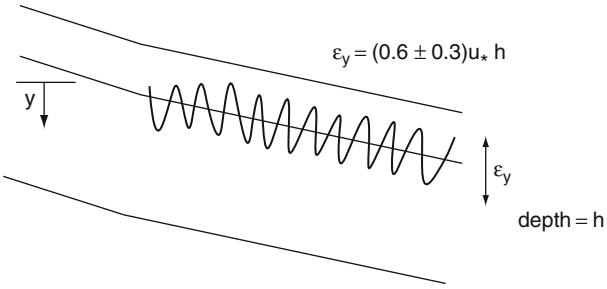

d Depth averaged transverse turbulent diffusion in a river

Chemicals in the Environment, Turbulent Transport. Figure 7
Profiles of eddy diffusion coefficient for various types of applications (From Gulliver [1])

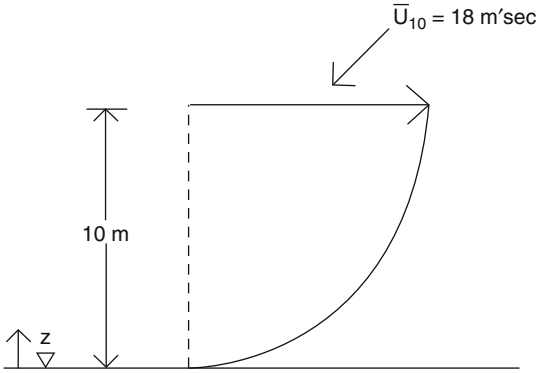

Chemicals in the Environment, Turbulent Transport. Figure 8
Velocity profile over a large lake

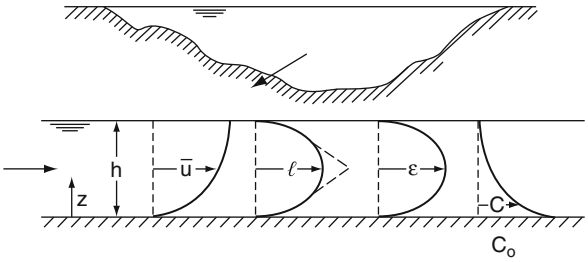

Chemicals in the Environment, Turbulent Transport. Figure 9
Lateral and longitudinal cross sections of a typical river

throughout the remainder of this entry. Fig. 9 gives a longitudinal and lateral cross section of our river. We will make the following assumptions:

1. The flow is steady over the long term, so that $\partial C/\partial t = 0$.
2. The flow is fully developed, such that any gradient with respect to x is equal to zero ($\partial C/\partial x = 0$).
3. The river can be divided into a series of longitudinal planes with no significant interaction, such that $v = 0$ and $\varepsilon_y = 0$ (this is the assumption of the stream-tube computational models).
4. The vertical eddy diffusivity, ε_z, is a constant value.

Assumptions 3 and 4 are more difficult to justify.

The solute will have a vertical velocity, $w = -v_s$, where v_s is the settling velocity of the suspended sediment.

Then, Eq. 20 becomes

$$-v_s \frac{\partial C}{\partial z} = \frac{\partial}{\partial z}\left[(D + \varepsilon_z)\frac{\partial C}{\partial z}\right] \tag{45}$$

where we have not yet applied assumption 4. We can move the settling velocity into the partial term:

$$\frac{\partial(-v_s C)}{\partial z} = \frac{\partial}{\partial z}\left[(D + \varepsilon_z)\frac{\partial C}{\partial z}\right] \tag{46}$$

and since both sides of Eq. 46 are a gradient with respect to z, the terms inside of the gradients must also be equal:

$$-v_s C = (D + \varepsilon_z)\frac{dC}{dz} \tag{47}$$

Equation 47 is converted to an ordinary differential equation because all variables are only a function of z. Now, we will deal with assumption 4. Fig. 7 gives the equation developed by Rouse [10] for ε_z:

$$\varepsilon_z = \kappa\, u_* z(1 - z/h) \tag{48}$$

where u_* is the shear velocity at the bottom of the channel, or

$$u_* = \sqrt{\tau/\rho} \tag{49}$$

where τ is the shear stress at the wall. For a fully developed open-channel flow in a wide channel, the following relation is easily derived:

$$u_* = \sqrt{ghS} \tag{50}$$

This derivation can be found in a text on fluid mechanics or open-channel flow. Assumption 4 states that $\varepsilon_z = \bar{\varepsilon}_z$ for all values of z, where ε_z is the depth average, or

$$\bar{\varepsilon}_z = \frac{1}{h}\int_0^h \varepsilon_z dz = \frac{\kappa u_*}{h}\int_o^h z(1 - z/h)dz = 0.067\, u_* h \tag{51}$$

where h is the depth of the stream. The term $\bar{\varepsilon}_z$ is almost always much greater than D in a turbulent flow. Thus,

$$D + \overline{\varepsilon_z} \cong \overline{\varepsilon_z}$$

Now, substituting these equations into Eq. 47 results in

$$\overline{\varepsilon_z}\frac{dC}{dz} + v_s C = 0$$

We will solve this by separating variables,

$$\frac{dC}{C} = \frac{-v_s}{\bar{\varepsilon}_z} dz$$

integrating, and taking both sides of the solution to the power of e:

$$C = \beta_1 \, e^{\frac{-v_s}{\bar{\varepsilon}_z} z}$$

Now, we need a boundary condition to determine β_1. This is difficult with suspended sediment profiles. We can develop a fairly good estimate of the distribution of suspended sediment once we have a known concentration at some location in the flow field. In the sediment transport field bed load and suspended load are often discussed. The relation between the two, and some experience and measurements of both simultaneously, can be used to predict an equivalent suspended sediment concentration at the bed. Then, the relevant boundary condition is

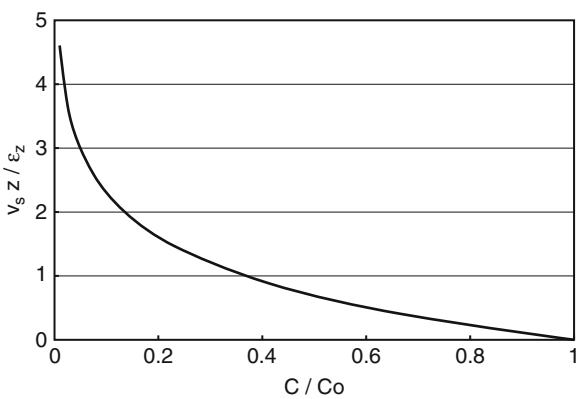

Chemicals in the Environment, Turbulent Transport. Figure 10
Suspended sediment concentration profile for Example 2

1. At

$$z = 0, \; C = C_0.$$

where C_0 is the concentration that has been determined from the bed load–suspended load relationship. Applying this boundary condition gives $\beta_1 = C_0$, and our solution is

$$C = C_0 \, e^{-v_s z/\bar{\varepsilon}_z}$$

The result is illustrated in Fig. 10. This problem can also be solved *without* assumption 4 [10].

Example 5.3: Concentration of organic compounds released into the air by an industrial plant (application of the product rule to error function solutions). There is some concern about the emissions from the adhesives produced in an industrial plant. Specifically, the town of Scream Hollow is 1 km away from the plant, where citizens have begun to complain about odors from the plant and of headaches. One culprit, aside from a haunting, may be the release of Acrolein, C_3H_4O, a priority pollutant that is an intermediary of many organic reactions. The average release from the 200 m × 200 m × 10 m plant sketched in Fig. 11 is assumed to be 20 g/h. If the wind is blowing directly toward Scream Hollow, at 3 m/s measured at 3 m height, with a dynamic roughness of 0.2 m for the farmland, what concentrations will the Scream Hollow inhabitants experience? Is this above the EPA threshold limit of 0.1 ppm(v)?

We will need to make some assumptions to formulate this problem. They are:

1. The Acrolein release is distributed over the most downwind plane of the building. With the important concentration being 1 km away, this is not a bad assumption. Then, the Acrolein will be

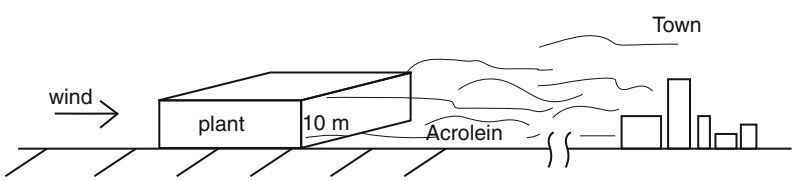

Chemicals in the Environment, Turbulent Transport. Figure 11
Illustration of toxic chemical release into the atmosphere, with the wind blowing toward a town

released over the plane that is 200 m × 10 m. If 20 g/h = 0.0056 g/s are released into a wind moving at 3 m/s, the initial concentration is

$$C_0 = \frac{0.0056\ \text{g/s}}{3\ \text{m/s}(200\ \text{m})(10\ \text{m})} = 9.3 \times 10^{-7}\ \text{g/m}^3$$

2. We will use a cross-sectional mean velocity of $U = \bar{u}$ at 3 m height, or $U = 3$ m/s.
3. We will use $\bar{\varepsilon}_z = \bar{\varepsilon}_y = \varepsilon_z$ at 3 m height.
4. We will not consider any of the source or sink terms for Acrolein.

We will also set up the coordinates so that $(x,y,z) = (0,0,0)$ occurs on the ground at mid-plant width, and will orient the wind in the x-direction.

With these assumptions, the governing equation becomes

$$U\frac{\partial C}{\partial x} = \bar{\varepsilon}_y \frac{\partial^2 C}{\partial y^2} + \bar{\varepsilon}_z \frac{\partial^2 C}{\partial z^2} \tag{52}$$

The boundary conditions are

1. At $(x,y,z) = (0, -100\ \text{m} \Rightarrow 100\ \text{m}, 0 \Rightarrow 10\ \text{m})$, $C = C_0$.
2. As $x \Rightarrow \infty$, $y \Rightarrow \infty$, or $z \Rightarrow \infty$, $C \Rightarrow 0$.
3. Zero mass flux at $z = 0$.

These boundary conditions, illustrated in Fig. 12, will give us a concentration front, but in two dimensions. In addition, we have a zero flux condition that will require an image solution. We will use the solution of Example 5 in the entry "► Transport in the Environment" to develop a solution for this problem. The solution, before applying boundary conditions, was

$$C = \beta_o + \beta_1 erf\left(\frac{z}{\sqrt{4Dt}}\right)$$

Now, we need an image to the concentration front about the $z = 0$ plane. In the y-direction we have a step-up at $y = -\Delta y$ and a step down at $y = \Delta y$. We will also use the product rule (Example 3, ► Transport in the Environment) to indicate that the solution to our governing equation for the y-direction should be multiplied times the solution in the z-direction. Then the solution can be given as

$$\frac{C}{C_o} = \beta_o + \left[\beta_1\, erf\left(\frac{(z+\Delta z)}{\sqrt{4\bar{\varepsilon}_z x/U}}\right) + \beta_2\, erf\left(\frac{(z-\Delta z)}{\sqrt{4\bar{\varepsilon}_z x/U}}\right)\right] \times \left[\beta_3\, erf\left(\frac{(y+\Delta y)}{\sqrt{4\bar{\varepsilon}_y x/U}}\right) + \beta_4\, erf\left(\frac{(y-\Delta y)}{\sqrt{4\bar{\varepsilon}_y x/U}}\right)\right]$$

where $\Delta y = 100$ m and $\Delta z = 10$ m.

Now, to see if our boundary conditions can be satisfied with the form of the solution:

$$@\, x \Rightarrow \infty, C \Rightarrow 0. \quad \text{Thus } \beta_0 = 0.$$

$$@\, z \Rightarrow \infty, C \Rightarrow 0. \quad \text{Thus } \beta_1 = -\beta_2.$$

$$@\, y \Rightarrow \infty, C \Rightarrow 0. \quad \text{Thus } \beta_3 = -\beta_4.$$

$$@\, x \Rightarrow 0, \text{and } (y,z) = (0,0), C/C_0 = 1.$$

With the last boundary condition, Eq. E5.5.3 becomes

$$1 = (\beta_1 - \beta_2)(\beta_3 - \beta_4)$$

or,

$$1 = 2\beta_1 \times 2\beta_3$$

or,

$$1 = 2\beta_2 \times 2\beta_4$$

Finally, @ $x \Rightarrow 0$ and $(y,z) = (0,\Delta z)$, $C/C_0 = ½$. Thus $\beta_1 = ½$.

Applying this last boundary condition results in $\beta_3 = ½$, $\beta_2 = -½$, and $\beta_4 = -½$. Thus, the solution to Eq. 52 is

$$\frac{C}{C_o} = \frac{1}{2}\left\{erf\left(\frac{(z+\Delta z)}{\sqrt{4\bar{\varepsilon}_z x/U}}\right) - erf\left(\frac{(z-\Delta z)}{\sqrt{4\bar{\varepsilon}_z x/U}}\right)\right\} \times \left\{erf\left(\frac{(y+\Delta y)}{\sqrt{4\bar{\varepsilon}_y x/U}}\right) - erf\left(\frac{(y-\Delta y)}{\sqrt{4\bar{\varepsilon}_y x/U}}\right)\right\} \tag{53}$$

Now, if we use $\Delta z = 10$ m, $\Delta y = 100$ m, $U = 3$ m/s, the only remaining parameter to find is $\bar{\varepsilon}$. Using Eq. 43 given in Example 1:

$$\bar{\varepsilon}_z = \bar{\varepsilon}_y = \kappa u_* z \tag{43}$$

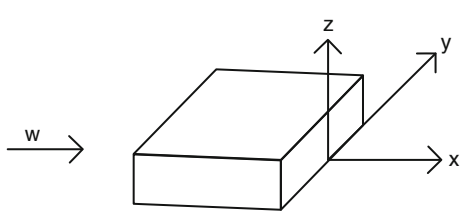

Chemicals in the Environment, Turbulent Transport. Figure 12
Illustration of the coordinate system for Example 5

Note that the logarithmic boundary equation can be written as

$$\frac{\bar{u}}{u_*} = \ell n\left(\frac{z}{z_o}\right) \tag{54}$$

where z_0 is the dynamic roughness, assumed to be 0.2 m for the crop land between the plant and Scream Hollow. Then,

$$u_* = \frac{\bar{u}}{\ell n(z/z_o)} = \frac{3\,\mathrm{m/s}}{\ell n\left(\frac{3\,\mathrm{m}}{0.2\,\mathrm{m}}\right)} = 1.1\ \mathrm{m/s}$$

and

$$\bar{\varepsilon}_z = 0.4(1.1m/s)(3m) = 1.3\ m^2/s$$

If we now plug all of the parameters for the industrial plant into Eq. 53, we get $C = 0.25\ \mu\mathrm{g/m^3} = 2.5 \times 10^{-7}\ \mathrm{g/m^3}$. In terms of ppm(v), we will use $\rho_{\mathrm{air}} = 1.2\ \mathrm{g/m^3}$, and the molecular weights of air and Acrolein of 29 and 56 g/mole, respectively. Then,

$$\begin{aligned} C &= \frac{2.5 \times 10^{-7}\,\mathrm{g/m^3}}{\rho_{\mathrm{air}}} \frac{MW_{\mathrm{air}}}{MW_{C_3H_40}} \\ &= \frac{2.5 \times 10^{-7}\,\mathrm{g/m^3}}{1.2\,\mathrm{g/m^3}} \frac{20\,\mathrm{g/mole}}{56\,\mathrm{g/mole}} \\ &= 1.08 \times 10^{-7} \frac{\mathrm{moles}\ C_3H_40}{\mathrm{mole\ air}} \end{aligned}$$

This is right at the threshold for continuous exposure, and the pollution from the plant should be investigated in more detail.

Conclusions

1. Although turbulent diffusion is a convection transport, and not a diffusive transport, the result looks similar to diffusion, and can be described by a turbulent diffusion coefficient.
2. Most environmental flows are turbulent. The exceptions are flow through porous media and flows that are very close to an interface.
3. Reynolds averaging and the Boussinesq assumption result in a turbulent transport equation that contains many features of the diffusive mass transport equation, and can be solved by similar techniques.
4. Prandtl's mixing length is a relatively accurate simplification for many turbulent flows.

Future Directions

The future for turbulent transport in the environment is in the direction of computational mass transport. This requires a simultaneous fluid dynamics–mass transport solution. On typical environmental scales, the computational power of our computers still must be advanced to solve these large problems while resolving the scale of the smallest turbulent eddies. Direct numerical simulation cannot deal with the scale of these problems, and large eddy simulation cannot keep both the scale and grid refinement required.

Bibliography

Primary Literature

1. Gulliver JS (2007) Introduction to chemical transport in the environment. Cambridge University Press, Cambridge, UK, 288 pp
2. Reynolds O (1895) On the dynamical theory of incompressible viscous fluids and the determination of the criterion. Philos Trans R Soc 186:123–164
3. Boussinesq J (1877) Essai sur la théorie des eaux courantes. Mem Pres Acad Sci Paris 23:46
4. Prandtl L (1925) Bericht iiber Untersuchungen zur ausgebildeten Turbulenz. Z Angew Math Mech 5:136–139
5. von Kármán T (1930) Mechanische Ahnlichkeit und Turbulenz. Nachr Ges Wiss Gottingen 5:58–76. Also Proceedings of third international congress on applied mechanics, vol I, Stockholm, pp 85–93, 1930
6. Reichardt H (1951) Vollstandige Darstellung der turbulenten. Geschwindigkeitsverteilung. Ann Angew Math Mech 31:7
7. Turner DB (1994) Workbook of atmospheric dispersion estimates, 2nd edn. Lewis, Boca Raton
8. Prandtl L (1942) Bemerkungen zur Theorie der freien Turbulenz. Z Angew Math Mech 22:241–243
9. Wu J (1980) Wind-stress coefficients over sea surface. J Geophys Res 74:444
10. Rouse H (1937) Modern conceptions of the mechanics of fluid turbulence. Trans Am Soc Civil Eng 102(1965):463–543

Books and Reviews

Nezu I, Nakagawa H (1993) Turbulence in open channel flow. Balkema, Rotterdam

White FM (1974) Viscous fluid flow. McGraw-Hill, New York

Climate Change and Global Water Sustainability

Harry X. Zhang
Associate Editor on Sustainability, Journal of Water Science and Technology, IWA, Reston, VA, USA

Article Outline

Glossary
Definition of the Subject
Introduction
Global Water Sustainability and Climate Change
Future Directions
Acknowledgment
Bibliography

Glossary

CO_2 Carbon dioxide is the predominant greenhouse gas. Anthropogenic CO_2 emissions are created largely by the combustion of fossil fuels.

GCM General circulation model, a term commonly used to describe climate models maintained at large research centers.

GHG GHG is a greenhouse gas such as CO_2 and methane. These gases contribute to global warming by capturing some of the outgoing infrared radiation before it leaves the atmosphere.

IPCC The Intergovernmental Panel on Climate Change was formed in 1988 by the World Meteorological Organization and the United Nations Environmental Program. It reports research on climate change. Their assessments are closely watched because of the requirement for unanimous approval by all participating delegates.

Sustainability The most widely quoted definition of sustainability and sustainable development is that by the Brundtland Commission of the United Nations in 1987: "sustainable development is development that meets the needs of the present without compromising the ability of future generations to meet their own needs."

Definition of the Subject

Climate change is one of many dynamic processes impacting global water sustainability. Other processes (e.g., change in population size and location, economic development and land use, aging infrastructure, and changing social values) also have major influences on water sustainability and must be considered along with climate change in a holistic approach to global water resources management [1].

Climate change has the potential to affect many public and private sectors in which water managers play an active role, including water availability, water quality, flood risk reduction, ecosystems, coastal areas, navigation, other key industrial sectors such as power and energy, food and beverage. These changes may have adverse or positive impacts on one or more sectors. Any or all of these changes could occur gradually or abruptly [1].

Increases in temperature can affect the amount and duration of snow cover, which in turn, can affect timing of streamflow. Glaciers are expected to continue retreating, and many small glaciers may disappear entirely. Peak streamflow may move from late spring to early spring/late winter in those areas where snowpack is important in determining water availability. Changes in streamflow have important implications for water and flood management, irrigation, and planning. If supplies are reduced, off-stream users of water such as irrigated agriculture and in-stream users such as hydropower, fisheries, recreation, and navigation, could be most directly affected [2, 3].

Besides more well-known impact of climate change on water quantity and water supply, climate change will affect ambient water quality. In its 2009 *National Water Program Strategy*: *Response to Climate Change*, the US Environmental Protection Agency (USEPA) notes that it expects more waterbodies will be labeled "impaired" even if pollution levels remain stable, because warmer air temperatures will result in warmer water, which will hold less dissolved oxygen and therefore be more likely to foster harmful algal blooms and change the toxicity of some pollutants. Likewise, projected increases in intense rainfall and extreme water events would wash more nutrients, pathogens, and toxins into

waterbodies. Such changes may significantly deteriorate aquatic ecosystem health in various areas over the next 50 years [4].

The objective of this entry is to link climate change and water sustainability with a global view, from both public/government and private/business perspectives. In addition, this entry summarizes future research needs for global water sustainability in the context of climate change based on literature review.

Introduction

Definition of Global Water Sustainability

Sustainability has become a wide-ranging term that can be applied to almost every facet of life on Earth, from local to a global scale and over various time periods. There are certain conceptual foundations that have been developed to aid in understanding sustainability. The importance of the 1987 Brundtland Commission definition is recognized "*sustainable development is development that meets the needs of the present without compromising the ability of future generations to meet their own needs*," which relies on maintaining equity between generations to help define terms. Beyond this, however, systems analytic concepts are embraced to sharpen the definition. For example, the Brundtland definition assumes that future generations will need the same mix and share of resources that are enjoyed at present. This may not be so if technology changes to require less of X and more of Y than is used at present [5, 6].

Sustainability has been defined as a property of a system that can be maintained in a certain state indefinitely. As used with regard to the environment, it refers to the potential longevity of human cultures that are supported by critical external factors, such as agriculture, forestry, and fisheries, all of which have a water component. History includes many examples of earlier societies that have eventually died out, sometimes as a result of their failure to successfully relate to their environment. In modern terms, a case of use of resources by increasing demand can be seen, and a fixed supply provided by a single world. The challenge is to determine how to create long-term sustainability [5, 6].

Daly [7] suggests the following three operational rules defining the condition of sustainability:

- Renewable resources such as fish, soil, and ground water must be used no faster than the rate at which they regenerate.
- Nonrenewable resources such as minerals and fossil fuels must be used no faster than renewable substitutes for them can be put into place.
- Pollution and wastes must be emitted no faster than natural systems can absorb them, recycle them, or render them harmless.

The short way to describe sustainability requires that human activity, at a minimum, only uses nature's resources at a rate at which they can be replenished naturally.

Definition of Climate Change

Climate is the average weather in a given place, usually over a period of more than 30 years. While the weather can change in just a few hours, climate changes occur over longer timeframes. Climate is defined not only by average temperature and precipitation, but also by the type, frequency, and intensity of weather events such as heat waves, cold waves, storms, floods, and droughts. Climate has natural year-to-year variations, and extremes in temperatures and weather events have occurred throughout history.

Climate change refers to any significant change in measures of climate (such as temperature, precipitation, or wind) lasting for an extended period (decades or longer). Climate change might result from natural factors and processes or from human activities [8].

The term "climate change" is often used interchangeably with the term global warming. Global warming refers to an average increase in the temperature of the atmosphere near the Earth's surface, which can contribute to changes in global climate patterns. However, rising temperatures are just one aspect of climate change. The phrase "climate change" is growing in preferred use to "global warming" because it helps convey that there are changes in addition to rising temperatures [9].

The Earth's climate depends on the balance between the amount of energy received from the sun and the

amount of energy that is absorbed or radiated back into space. Natural influences can alter how much heat is reflected or absorbed by the Earth's surface, including changes in the sun's intensity, volcanic eruptions, and multiyear climate cycles. Human activities such as deforestation and the production of greenhouse gases also affect this balance. These alterations, in turn, affect climate on local, regional, and global scales [8].

Key Characteristics of Water Sustainability Solutions

Water sustainability solutions are characterized by certain systems analysis properties that may indicate the overall stability of the system. It is important for sustainability that solutions to problems should be viable for long durations; that the system should not be required to undergo extreme change in short periods of time to reach the desired solution; that the solution sought is often a compromise of available options, and not some extreme case; and, is not overly complex. Even with these precautions, the most successful solutions often possess the additional property of reversibility. Only actual experience can tell if the right track is being followed, and if not, changes should be made. Whether the geographic scale is a local water problem or a national system, these rules tend to produce sustainable solutions [6, 10].

Water sustainability solutions are characterized by certain systems analysis properties that may indicate the overall stability of the system. It is important for sustainability

- That solutions to problems should be viable for long durations
- That the system should not be required to undergo extreme change in short periods of time to reach the desired solution
- That the solution sought is often a compromise of available options and not for some extreme case
- And is not overly complex

One can imagine far more concepts than can be captured as indicators. Some are quantitative, but others qualitative and not readily measured. Therefore, some limited number of indicators has to be chosen. Too many will overwhelm the policy-making process and may paralyze decision-making. Too few will fail to describe issues in sufficiently comprehensive manner. There is no single set of criteria for what makes a good indicator. However, perhaps a simple checklist will make it possible to at least begin this difficult selection process [6].

Solutions to water sustainability problems are characterized by properties that may indicate the overall stability of the system. Selecting the right indicator is a complicated process. Some indicators are quantitative, but others are qualitative and not readily measured. Choosing the number of indicators to track is a delicate balance; too many will overwhelm the policy-making process, while too few will fail to describe issues sufficiently [6]. Table 1 is based on the US General Accounting Office (GAO) Report "Environmental Indicators: Better Coordination Is Needed to Develop Environmental Indicator Sets That Inform Decisions" [11].

Climate Change Indicators by USEPA

In 2010, USEPA has published a report entitled "*Climate Change Indicators in the United States*" to help readers interpret a set of important indicators to better understand climate change. The report presents 24 indicators, each describing trends in some way related to the causes and effects of climate change. The indicators focus primarily on the United States, but in some cases global trends are presented in order to provide context or a basis for comparison. The indicators span a range of time periods, depending on data availability.

For each indicator, this report presents one or more graphics showing trends over time; a list of key points; and text that describes how the indicator relates to

Climate Change and Global Water Sustainability.
Table 1 Ten criteria used to select indicators most frequently cited by GAO Survey Respondents [11]

Measurable	Data quality
Relevant	Importance
Appropriate geographic scale	Appropriate temporal scale
Understandable	Data comparability
Data available	Trend data available

climate change, how the indicator was developed, and any factor that might contribute to uncertainty in the trend or the supporting data.

USEPA selected the 24 indicators presented in this report from a broader set of 110 indicators, many of which were identified at an expert workshop in 2004 on climate change indicators convened by the National Academy of Sciences and funded by USEPA. The indicators in this report were chosen using a set of screening criteria that considered usefulness, objectivity, data quality, transparency, ability to show a meaningful trend, and relevance to climate change.

All of the indicators selected for this report are based on data that have been collected and compiled by following rigorous protocols that are widely accepted by the scientific community. Various government agencies, academic institutions, and other organizations collected the data.

Global Water Sustainability and Climate Change

Outlook of Global Water Sustainability in Year 2050

A recent report [12] entitled "Vision 2050" by World Business Council for Sustainable Development (WBCSD) addresses three questions: What would a sustainable world look like in 2050? What are the pathways and solutions for achieving sustainability? What are the roles business can play in ensuring more rapid progress toward that world?

As "Vision 2050" has perceived, it should be strived to build a world in which around 9 billion people are not just living on the planet, but living well and within the limits of the planet in 2050 [12]. By "living well," WBCSD is describing a standard of living where people have access to and the ability to afford education, health care, mobility, the basics of food, water, energy and shelter, and consumer goods. By "living within the limits of the planet," WBCSD means living in such a way that this standard of living can be sustained with the available natural resources and without further harm to biodiversity, climate, and other ecosystems.

Vision 2050 seeks to provide a common understanding so leaders can make the decisions that deliver the best outcomes possible for human development over the next 4 decades. The guiding principle is an attempt to help leaders across governments, businesses, and civil society avoid repeating mistakes of the past such as making decisions in isolation that result in unintended consequences for people, the environment, and planet Earth. It is also a platform for ongoing dialogue, so the important questions that need to be answered can be raised continuously in order to make progress in this uncharted territory.

Although distinct, the elements also show the interconnectedness of issues such as water, food, and energy – relationships that must be considered in an integrated and holistic way, with trade-offs that must be understood and addressed.

The top three critical pathways listed in "Vision 2050" include:

- Addressing the development needs of billions of people, enabling education and economic empowerment, particularly of women, and developing radically more eco-efficient solutions, lifestyles, and behavior
- Incorporating the cost of externalities, starting with carbon, ecosystem services, and water
- Doubling of agricultural output without increasing the amount of land or water used

The "Vision 2050" or similar documents provide an outlook on how a sustainable world would like in 2050 and a forward-looking perspective on strategic pathways toward global water sustainability. The following sections discuss the interlinkage between global water sustainability and climate change from both public/government and private/business perspectives.

Global Water Sustainability and Climate Change from Public Perspective

The most recent report by the Intergovernmental Panel on Climate Change states that global warming will lead to "*changes in all components of the freshwater system*," and concludes that "*water and its availability and quality will be the main pressures on, and issues for, societies and the environment under climate change*."

The future effects of climate change on water resources in the United States and other parts of the world will depend on trends in both climatic and non-climatic factors. Evaluating these impacts is challenging because water availability, quality, and streamflow are sensitive to changes in temperature and precipitation.

Other important factors include increased demand for water caused by population growth, changes in the economy, development of new technologies, changes in watershed characteristics, and water management decisions.

All regions of the world show an overall net negative impact of climate change on water resources and freshwater ecosystems. Areas in which runoff is projected to decline are likely to face a reduction in the value of the services provided by water resources. The beneficial impacts of increased annual runoff in other areas are likely to be tempered in some areas by negative effects of increased precipitation variability and seasonal runoff shifts on water supply, water quality, and flood risks [2].

In addition to the typical impacts on water management, climate change introduces an additional element of uncertainty about future water resource management. Water resources in the United States are heavily managed and supplies are scarce in some regions of the country. Strategies have been developed and continue to evolve to address these issues. Implementation of adaptation measures, such as water conservation, use of markets to allocate water, and the application of appropriate management practices will have an important role to play in determining the impacts of climate change on water resources [13, 14].

Water Availability Generally, increases in the Earth's surface temperature will increase evaporation from the oceans and land, leading to more overall precipitation. However, this additional precipitation will not be distributed evenly, and shifting storm patterns will likely cause some areas to experience more severe droughts. Scientists have suggested that extreme weather events such as storms, floods, and hurricanes will likely also become more intense. There is natural variability in the intensity and frequency of such events, however, so care must be taken to determine whether observed trends reflect long-term changes in the Earth's climate system.

Changes in temperature, precipitation patterns, and snowmelt can have impacts on water availability. Temperature is predicted to rise in most areas, but is generally expected to increase more in inland areas and at higher latitudes. Higher temperatures will increase loss of water through evaporation. The net impact on water supplies will depend on changes in precipitation (including changes in the total amount, form, and seasonal timing of precipitation). Generally speaking, in areas where precipitation increases sufficiently, net water supplies may not be affected or they may even increase. In other areas where precipitation remains the same or decreases, net water supplies would decrease. Where water supplies decrease, there is also likely to be an increase in demand, which could be particularly significant for agriculture, which is the largest consumer of water, and also for municipal, industrial, and other uses.

Increases in temperature can affect the amount and duration of snow cover, which in turn, can affect timing of streamflow. Glaciers are expected to continue retreating, and many small glaciers may disappear entirely. Peak streamflow may move from late spring to early spring/late winter in those areas where snowpack is important in determining water availability. Changes in streamflow have important implications for water and flood management, irrigation, and planning. If supplies are reduced, off-stream users of water such as irrigated agriculture and in-stream users (such as hydropower, fisheries, recreation, and navigation) could be most directly affected [2].

In summary, the cause–effect impact analysis represents four major chains of causation that may be expected to result from global warming [15].

- First, as temperatures rise, it is expected that sea levels will rise due to warmer ocean temperatures and melting of land ice such as glaciers.
- Next, warmer overall temperatures are expected to produce two important changes in seasonal conditions over most of the continental United States. Warmer and shorter winters are expected.
- Third, warmer and drier summers are expected.
- Lastly, warming is expected to accelerate and amplify the functioning of the hydrologic cycle to produce, among other things, more intense rainfall events.

Water Quality Higher water temperatures and changes in the timing, intensity, and duration of precipitation can affect water quality. Higher temperatures reduce dissolved oxygen levels, which can have an effect on aquatic life. Where streamflow and lake levels fall, there will be less dilution of pollutants. However, increased frequency and intensity of rainfall will produce more pollution and sedimentation due to runoff [2].

Flood magnitudes and frequencies will very likely increase in most regions, mainly a result of increased precipitation intensity and variability. Increasing temperatures are expected to intensify the climate's hydrologic cycle and melt snowpacks more rapidly [2]. Flooding can affect water quality, as large volumes of water can transport contaminants into water bodies and also overload storm and wastewater systems.

Higher temperatures, particularly in the summer, earlier snowmelt, and potential decreases in summer precipitation could increase risk of drought. The frequency and intensity of floods and droughts could increase, even in the same areas.

Sea level rise may also affect freshwater quality by increasing the salinity of coastal rivers and bays and causing saltwater intrusion, movement of saline water into fresh ground water resources in coastal regions.

Changes in water quality could have implications for all types of uses. For example, higher temperatures and changes in water supply and quality could affect recreational use of lakes and rivers or productivity of freshwater fisheries. Certain species of fish could find temperatures too warm and migrate to more northern or higher altitude locations where water is cooler.

Case Studies: Lower Low Flows Expected from Climate Change and Its Impact on Water Quality Climate change is expected to make low flows more common in some areas, resulting in less contaminant-dilution capacity and higher pollutant concentrations. In many arid or semiarid areas (places with overall decreased runoff), water quality deterioration will be even more pronounced.

Cruise et al. [16] assessed current and future water quality conditions in the US Southeast. Results showed that in many southeastern areas, streamflow was projected to decline over the next 30–50 years, exacerbating water quality problems. Between 2020 and 2039, water quality conditions might worsen because of drier late springs, summers, and falls.

Changes in low flows could affect Total Maximum Daily Load (TMDL) implementation and water quality compliance. Eheart et al. [17] showed that the assumed climate change scenarios could substantially affect low-flow standards in the US Midwest. For example, a 25% decrease in mean precipitation cut critical low flows by 63% (without irrigation) to 100% (with irrigation). The frequency of single low-flow violations increased several-fold with irrigation. Likewise, the frequency of multiple low-flow violations in a 3-year period rose from about 20% to nearly 100% as climate change became more severe. The paper also noted that existing TMDLs for rivers and streams may become obsolete due to worsening low-flow events in the future.

The extra pressures that climate change may place on waterbodies could increase treatment costs; however, the magnitude of such costs greatly depends on the response elsewhere in the watershed. A 2003 study by USEPA's Office of Research and Development [18] examined how climate change could affect the cost of water quality compliance and TMDL implementation. It focused on 235 publicly owned treatment works (POTWs) discharging to impaired streams or rivers due to organic enrichment and low dissolved oxygen in the Great Lakes region. These POTWs will probably be required to meet TMDLs more stringent than current discharge levels, and the effect of climate change on streamflow could result in even more stringent discharge limitations. This screening study suggests that even a small reduction in the design flow would have significant cost implications, that is, holding all other factors constant, climate change may make it significantly more costly to meet water quality goals in the Great Lakes region.

A related study assessed the potential costs of reducing TMDL-driven effluent limits for biochemical oxygen demand (BOD) to maintain ambient water quality due to climate change for the water industry in England and Wales under the European Union's Water Framework Directive [19]. Under the climate change impact, the low flow within receiving waters collecting water treatment facility effluent is expected to further decline. This study found that costs were highly sensitive to increases in stringency of effluent limits and the changes in design flow due to climate change factors added significantly to the costs of TMDL implementation and overall water quality management.

Water Resources Planning Under Uncertainty Traditionally, water resource managers have accumulated significant experience successfully planning and operating their systems in the face of uncertainty regarding future hydrology, weather,

available water supply, and projected water demand. In recent years, however, it has become clear that today's planning approaches may no longer be adequate. Dynamic population and economic growth have placed increasing pressure on water supplies and concerns about environmental impacts have grown [1].

In addition, the potential for climate change has confronted water managers with an additional novel challenge. While in any particular service area the precise impacts of climate change for temperature, precipitation, evaporation, storm water capture, and imported supplies remain deeply uncertain, it has become increasingly clear that past weather and hydrological records no longer provide an accurate guide to future weather and hydrology.

The linkage between the rate of temperature rise and the timing and location of these other more complex effects on Earth systems is where the science is most challenged and the uncertainties are greatest [1]. Many effects may be expected to advance gradually as a function of gradual temperature rise, and yet the same phenomena may be subject to stochastic influences that could produce extreme events much sooner than implied by the gradual trend.

Climate change presents a much greater degree of uncertainty than is typically encountered in facilities and operations planning. How do you prepare for changes of unknown magnitude on an unknown timeline? There is a great temptation to wait and see if climate science can be improved to provide a better basis for action. But, it would be a mistake to just ignore climate change and resume a business as usual approach to planning.

The uncertainty in climate forecasts is magnified many times by the complexities of tracing climate effects through the subsequent hydrologic and environmental processes that produce the changed operating conditions that wastewater and storm water agencies will have to face [15].

The familiar risk management paradigm consists of three steps: (1) risk identification, (2) risk assessment/characterization, and (3) risk management. The application to climate change adaptation planning is quite unique. It is necessary to first take the problem apart and examine it piece by piece to perform a thorough risk identification analysis. The possible impacts of increasing temperatures are far reaching when all the secondary effects on hydrologic and environmental processes are taken into account.

Near-Term and Long-Term Climate Risks for Water Infrastructure Climate variations can directly or indirectly affect many aspects of human society – in both positive and disruptive ways. For example, warmer temperatures might reduce heating costs and improve conditions for growing some crops; yet, extreme heat can cause illness or death among vulnerable populations. Precipitation can replenish water supplies and nourish crops, but intense storms can damage property, cause loss of life and population displacement, and temporarily disrupt essential services such as transportation, telecommunications, and energy and water supplies.

Climate change certainly involves some near-term threats to existing assets that will call for protective measures to sustain them. However, the current infrastructure configuration (including water infrastructure) may not be the most sustainable choice for the long term. Future generations may need a different type of infrastructure that is designed from the start to be more sustainable in a changing environment, involving nontraditional types of investments such as decentralized treatment, green infrastructure, watershed buffers, and wetlands [15].

The prospect of climate change sometimes evokes a misperception that the sky is falling and leads people to skip right over the risk characterization step and begin evaluating adaptation options as though everything is happening at once. It is prudent to first undertake a vulnerability analysis to assess how soon the impacts may materialize at a level that represents a meaningful threat to existing or planned facilities and operations in order to define the most appropriate adaptive responses. In some instances, adaptation may become a multigenerational strategy where the responsibility of current water managers is limited to laying the right planning foundation to enable selection and implementation of the best adaptations by future generations [15].

Climate Change Indicators Relating to Global Water Sustainability Environmental indicators are a key tool for evaluating existing and future programs and supporting new decisions with sound science. In the years to come, the indicators in this report will provide

data to help the federal agencies decide how best to use its policy making and program management resources to respond to climate change. Ultimately, these indicators will help government agencies evaluate the success of their climate change efforts.

USEPA selected the 24 indicators presented in this report from a broader set of 110 indicators, many of which were identified at an expert workshop in 2004 on climate change indicators convened by the National Academy of Sciences and funded by USEPA. The indicators in this report were chosen using a set of screening criteria that considered usefulness, objectivity, data quality, transparency, ability to show a meaningful trend, and relevance to climate change [8].

The climate change indicators are divided into five categories:

- *Greenhouse Gases*: The indicators characterize the amount of greenhouse gases emitted into the atmosphere through human activities, the concentrations of these gases in the atmosphere, and how emissions and concentrations have changed over time.
- *Weather and Climate*: This entry focuses on indicators related to weather and climate patterns, including temperature, precipitation, storms, droughts, and heat waves. These indicators can reveal long-term changes in the Earth's climate system.
- *Oceans*: The world's oceans have a two-way relationship with climate. The oceans influence climate on regional and global scales, while changes in climate can fundamentally alter certain properties of the ocean. The indicators in this category examine trends in ocean characteristics that relate to climate change, such as acidity, temperature, heat storage, and sea level.
- *Snow and Ice*: Climate change can dramatically alter the Earth's snow- and ice-covered areas. These changes, in turn, can affect air temperatures, sea levels, ocean currents, and storm patterns. The indicators in this category focus on trends in glaciers; the extent and depth of snow cover; and the freezing and thawing of oceans and lakes.
- *Society and Ecosystems*: Changes in the Earth's climate can affect public health, agriculture, energy production and use, land use and development, and recreation. Climate change can also disrupt the functioning of ecosystems and increase the risk of harm or even extinction for some species.

Among the major categories of climate change indicators mentioned above, oceans and snow and ice are closely related to water sustainability, besides weather and climate. Summary finding and more detailed discussions are given as follows based on USEPA [8].

The oceans and the atmosphere interact constantly, both physically and chemically, exchanging heat, water, gases, and particles. This relationship influences the Earth's climate on regional and global scales. It also affects the state of the oceans.

Covering nearly 70% of the Earth's surface, the oceans store vast amounts of energy absorbed from the sun and move this energy around the globe through currents. As greenhouse gases trap more energy from the sun, the oceans will absorb more heat, resulting in an increase in sea surface temperatures, rising sea levels, and possible changes to ocean currents. These changes will very likely lead to alterations in climate patterns around the world. For example, warmer waters promote the development of more intense storms in the tropics, which can cause property damage or loss of life.

The oceans are also a key component of the Earth's carbon cycle. Over geological time, much of the world's carbon has come to reside in the oceans, either within plants and animals or dissolved as carbon dioxide. Although the oceans can help lessen climate change by storing a significant fraction of the carbon dioxide that human activities emit into the atmosphere, increasing levels of dissolved carbon dioxide can change the chemistry of seawater and harm certain organisms. These effects, in turn, could substantially alter the biodiversity and productivity of ocean ecosystems.

Changes in ocean systems generally occur over much longer time periods than in the atmosphere, where storms can form and dissipate in a single day. The interactions between ocean and atmosphere occur slowly, over many years, even decades. For this reason, even if greenhouse gas emissions are stabilized tomorrow, it will take many more years, decades or centuries, for the oceans to adjust to the climate changes that have already occurred.

Even if greenhouse gas emissions are stabilized tomorrow, it will take many more years – decades or

centuries – for the oceans to adjust to the climate changes that have already occurred.

Example climate change indicators related to oceans include:

- *Sea Surface Temperature*: The surface temperature of the world's oceans increased over the twentieth century. Even with some year-to-year variation, the overall increase is statistically significant, and sea surface temperatures have been higher during the past 3 decades than at any other time since large-scale measurement began in the late 1800s.
- *Sea Level Rise*: When averaged over all the world's oceans, sea level has increased at a rate of roughly six-tenths of an inch per decade since 1870. The rate of increase has accelerated in recent years to more than an inch per decade. Changes in sea level relative to the height of the land vary widely because the land itself moves. Along the US coastline, sea level has risen the most relative to the land along the Mid-Atlantic coast and parts of the Gulf Coast. Sea level has decreased relative to the land in parts of Alaska and the Northwest.
- *Ocean Acidity*: The ocean has become more acidic over the past 20 years, and studies suggest that the ocean is substantially more acidic now than it was a few centuries ago. Ocean acidification already is degrading seawater quality and adversely affecting marine ecosystems. A 2004 report on ocean acidification by the United Kingdom's Royal Society estimates that pH will average 7.65 by 2100. Rising acidity is associated with increased levels of carbon dioxide dissolved in the water. Changes in acidity can affect sensitive organisms such as corals.
- In 2007, environmental group in the United States filed petitions asking eight coastal states to address the effects of climate change on ocean water quality (such as ocean acidification), list certain segments of the Atlantic and Pacific Oceans as impaired for pH, and establish TMDLs for carbon dioxide. This is a creative approach to reducing air emissions of carbon dioxide. USEPA formally responded in early 2009, setting out a public process to evaluate ocean acidification's effects on water quality and determine whether the current pH criterion should be modified. If USEPA strengthens the pH criterion for oceans, then states will have to follow suit because the Clean Water Act requires state standards to be at least as protective as USEPA ones. Moreover, states are required to designate waterbodies that do not meet water quality standards as "impaired" and take action to limit their pollution. Stronger water quality standards for pH could translate into measures that regulate pollution from carbon dioxide, the primary cause of ocean acidification.

Furthermore, climate change can dramatically alter the Earth's snow- and ice-covered areas. Unlike other substances found on the Earth, snow and ice exist relatively close to their melting point and can change from solid to liquid and back again. As a result, prolonged warming or cooling trends can result in observable changes across the landscape as snow and ice masses shrink or grow over time.

Changes in snow and ice cover, in turn, affect air temperatures, sea levels, ocean currents, and storm patterns. For example, melting polar ice caps add fresh water to the ocean, increasing sea level and possibly changing currents that are driven by differences in temperature and salinity. Because of their light color, snow and ice reflect more sunlight than open water or bare ground, so a reduction in snow cover and ice causes the Earth's surface to absorb more energy from the sun.

Changes in snow and ice could not only affect communities and natural systems in northern and Polar Regions, but also have worldwide implications. For example, thawing of frozen ground and reduced sea ice in the Arctic could affect biodiversity on local and global scales, leading to harmful effects not only on polar bears and seals, but also on migratory species that breed or feed in these areas. These same changes could affect human societies in several ways, such as by compromising food availability. Reduced snow cover could diminish the beneficial insulating effects of snow for vegetation and wildlife, while also affecting water supplies, transportation, cultural practices, travel, and recreation for millions of people.

Example climate change indicators related to snow and ice include:

- *Glaciers*: Glaciers in the United States and around the world have generally shrunk since the 1960s, and the rate at which glaciers are melting appears to have accelerated over the last decade. Overall,

glaciers worldwide have lost more than 2,000 cubic miles of water since 1960, which has contributed to the observed rise in sea level.

– *Snow Cover*: The portion of North America covered by snow has generally decreased since 1972, although there has been much year-to-year variability. Snow covered an average of 3.18 million square miles of North America during the years 2000–2008, compared with 3.43 million square miles during the 1970s.
– *Snowpack*: Between 1950 and 2000, the depth of snow on the ground in early spring decreased at most measurement sites in the western United States and Canada. Spring snowpack declined by more than 75% in some areas, but increased in a few others.

Global Water Sustainability and Climate Change from Business Perspective

Business Risks of Water and Climate Change Despite a growing consensus among climate experts that freshwater is one of the resources most vulnerable to long-term climate change, there is little awareness and discussion about the potential consequences for businesses and their shareowners. For all of its importance, to sustain the fast-growing global population and to ensure future prosperity, few companies and investors are thinking strategically about the profound business risks that will exist in a world where climate change is likely to exacerbate already diminishing water supplies [20]. Climate change is likely to exacerbate water availability and quality, which will have a wide range of implications for business (Table 2).

It should be noted that climate change will likely exacerbate all three types of risks: physical, reputational, and regulatory [20].

Physical Risks Water scarcity directly affects business operations, raw material supply, intermediate supply chain, and product use in a variety of ways. Declines or disruptions in water supply can undermine industrial and manufacturing operations where water is needed for production, irrigation, material processing, cooling, washing, and cleaning. Drought attributable in significant part to climate change is already causing acute water shortages in large parts of Australia, Asia, Africa, and the United States.

Water quality risks are often overlooked but may have significant financial implications. The quality of process water is critical in many industrial production systems, and contaminated water supply may require additional investment and operational costs for pretreatment.

Water scarcity, changes in precipitation patterns, and glacier melt caused by climate change directly

Climate Change and Global Water Sustainability. Table 2 Business impacts from climate change and water sustainability (Adapted from [20, 21])

	Climate change impact on water sustainability	Business impacts could include
1	Increasing water demand	– Higher costs for water – Regulatory caps for water use – Conflicts with local communities and other large-scale water users – Growing demand for water-efficient products and technologies
2	Water scarcity and unsustainable supply	– Impacts on future growth and license to operate – Decreased amount of water available for business activities – Operational disruptions and associated financial loss – Increased costs for water
3	Declining water quality	– Increased costs for pretreatment to obtain desired water quality – Increased costs for wastewater treatment to meet more stringent regulations – Regulatory restrictions for specific industrial activities and investments – Increased responsibility (and costs) to implement community water infrastructure and watershed restoration projects to mitigate reputational risks – Increased health costs for employees in the countries that are impacted

affect power generation, curtailing hydro-based power production, and also impacting any power plants that run steam turbines. Whether powered by coal, natural gas, or nuclear energy, electricity generation relies on having an adequate supply of cooling water. Businesses that depend on highly reliable energy from these power sources will be at risk.

Physical water resource constraints make companies more susceptible to reputational risks. Declines in water availability and quality can increase competition for clean water. In water-scarce regions, tensions can arise between businesses and local communities, particularly in developing countries where local populations often lack access to safe and reliable drinking water. Community opposition to industrial water withdrawals and perceived or real inequities in use can emerge quickly and affect businesses profoundly.

Reputational Risks Reputational risks increase as people become more aware of their rights to access water. The concept of "access to clean water as a human right" is gaining more recognition globally. However, international and local businesses may find themselves using copious amounts of water in regions where people lack sufficient water to meet basic needs.

Growing awareness around the ecological impacts of water withdrawal and discharge increases both reputational and regulatory risks. Healthy freshwater ecosystems are an essential part of local communities and livelihoods, not only by serving as a source of clean drinking water, but also by providing cultural, social, aesthetic, and economic value. As a result, significant water withdrawal or wastewater discharge, regardless of the extent of actual impacts on the neighboring communities or ecosystems, inevitably increases the risk of conflict with local communities. Moreover, the vulnerability of ecosystems is expected to increase due to climate change.

Regulatory Risks Physical and reputational pressures affecting water availability and wastewater discharge can result in more stringent water policies. Water scarcity, coupled with increased concern among local communities about water withdrawals, will put pressure on local authorities and policymakers to consider water reallocations, regulations, and development of water markets that cap usage, suspend permits to draw water, and lead to stricter water quality standards.

Water scarcity will increase water prices. Among other factors, water scarcity is driving shifts toward full-cost pricing aimed at providing economic incentives for efficient water use. In many places, artificially low water prices are rising as subsidies are phased out.

Utilities in industrial countries are increasingly implementing tiered rate system, where water users pay more for increased consumption. These tariff structures are specifically designed to encourage commercial and industrial users to use water efficiently.

Water-intensive products and services face increased sociopolitical risks. As water scarcity becomes a serious problem in many parts of the world, there may be corollary pressure, both regulatory and reputational, on products that require a significant quantity of water. Products and services that require large amounts of water or energy to produce or to use may be phased out by law, lose market share to less water-intensive products, or cause reputational damage for the company.

Taken together, this means that businesses will face vastly increased uncertainty about the availability and quality of their water supplies. One of the strongest conclusions in the latest IPCC report is that "*climate change will challenge the traditional assumption that past hydrological experience provides a good guide to future conditions*." Therefore, it will become increasingly crucial for businesses to incorporate climate change factors when assessing and managing their water risks.

Example of Climate Change Impact on Industrial Sectors For most industry sectors, the largest portion of their water footprint is embedded in the production of raw materials such as food crops, fibers, and metals. Many companies' raw material production lies far upstream from direct operations. As a result, they typically fail to assess water-related risks in this segment of their value chains, according to Ceres and Pacific Institute (2009). Severe drought, flooding, or changes in precipitation patterns due to climate change can decrease agricultural yields and quality, which may increase input costs. In addition, water scarcity and increased competition for freshwater resources can change pricing structures or subsidies for irrigation water for crop or livestock production, which can also drive up costs.

Beverage Sector Potable water is the primary and most important ingredient for the majority of beverage products, making beverage companies' direct operations especially vulnerable to water availability and quality concerns. Beverage manufacturing requires high-quality source water, putting the water use of this industry in direct competition with local populations and their drinking water needs. Large water withdrawals can result in controversies in regions where water is scarce and local populations lack access to affordable drinking water.

In cases of severe shortages or contamination of drinking sources, bottling and manufacturing facilities risk shutdowns, as PepsiCo and Coca-Cola bottlers experienced in Kerala, India. Public concern about clean water access is impacting bottled water sales. Consumer demand is soaring in developing countries, but falling in large developed countries such as the United States.

Food Sector The industry's most significant water-related exposure is in raw material production (i.e., precipitation and irrigation needed to grow food and maintain pastureland for grazing). Many of the world's croplands are in semiarid areas that are expected to become drier due to climate change.

Among the regions at risk is the High Plains aquifer that provides water for 27% of the irrigated land in the United States and 70–90% of the irrigation water for three of the country's top producing grain states – Texas, Kansas, and Nebraska. Human-induced stresses on the aquifer have already resulted in water table declines greater than 100 ft in some areas.

Increased temperature and dry weather due to climate change will raise water requirements for livestock whose numbers are growing as global demand for meat increases. As water problems become more severe, the impacts of agriculture generally will draw even more attention.

Higher water temperature due to climate change may increase the concentration and variety of waterborne pathogens. As a result, food supplies may face greater risk of contamination and recall, disrupting the supply of ingredients for food manufacturers and negatively affecting consumer confidence in food products.

Electric Power/Energy Sector The electric power industry requires a consistent supply of water. Thermoelectric-power withdrawals account for 48% of total water use, 39% of total freshwater withdrawals for all categories in the United States [22]. Furthermore, heated discharges from power plants have a harmful effect on water quality and local ecosystems, which is only exacerbated as water levels drop.

Hydropower plants are at increased risk due to decreases or changes in water flow caused by climate change. Hydropower generation is likely to be most directly affected by climate change because it is sensitive to the amount, timing, and geographical pattern of precipitation and temperature. For example, in parts of the United States such as Alaska and the Rocky Mountains, natural water storage in snowpack and glaciers has been reduced. Climate change may also increase evaporation rates of reservoirs in arid parts of the United States such as Lake Mead and Lake Powell on the lower Colorado River [23].

The sector has significant water-related risks embedded in raw material supply. Extraction and processing of fossil fuels require large volumes of water. Water scarcity or a change in water supply due to climate change may disrupt fuel supply or increase the cost of fuel for power generation.

What Businesses Can Do to Manage Water-Climate Risks Strategically The impacts of companies' water use vary greatly depending on local hydrological, social, economic, and political factors. Unlike greenhouse gas emissions, which have the same impacts regardless of where the emissions are generated, one unit of water is not equal to another. The same amount of water withdrawn in an arid urban area versus a rural wet region has completely different impacts and associated risks for companies. The absolute volume of water used is often less important than the timing of its use. Because of water's regional and timing-specific character, companies need to convert water footprint data into actual water impacts and risks.

As mentioned earlier, three main types of water-related risks include:

1. Physical risks: Local hydrological conditions (potential shortage risks, water quality risks, flooding risks, and possible impacts of climate change on future water supply and demand)
2. Regulatory risks: Socioeconomic conditions as they relate to water (trends in regional demand, local

water governance capacity, and regional water pricing) and potential regulatory costs
3. Reputational risks: Potential impacts of a company's water withdrawal or wastewater discharge on local communities and ecosystems, and disparities or inequities in local and regional water access

To evaluate and effectively address water and climate change risks, business and private sectors can take the following actions, based on a synthesis of [20, 21, 24].

1. Measure the company's water footprint (i.e., water use and wastewater discharge) throughout its entire value chain, including suppliers and product use. Companies can only mange what they measure, so in order to accurately assess risks and opportunities, a first step for companies is to conduct a comprehensive and integrated water and carbon accounting. By aligning measurement of water and carbon/energy, businesses can identify how the three are interlinked, providing key basic information for developing a holistic management strategy.
2. Assess physical, regulatory, and reputational water risks associated with climate change. Explicit attention should be paid to understanding any potential competing demands the company may have for water and energy. If possible, companies should also seek to align their water and climate risk assessments. Regardless, having a detailed understanding of local water conditions, including hydrological, social, economic, and political factors, can give companies room to anticipate and plan for a wide range of scenarios.

   For key areas of operation and sourcing in high-risk regions, contingency plans should be developed to respond to risks such as decreasing water availability and quality, higher water prices, extreme hydrologic events, and local economic development. Potential climate-related impacts should be explicitly considered in contingency plans. Contingency plans should also include demand-side and supply-side strategies. For example, conservation and efficiency improvement measures or process modifications that reduce or eliminate water use will decrease the company's dependency on freshwater supplies. Supply-side measures include collaboration with local authorities and stakeholders to improve local water security and participation in integrated water management or ecosystem restoration to protect local water sources.
3. Integrate water and climate issues into strategic business planning and governance structures. When developing water management plans, companies will need to consider and integrate the potential impacts of climate change on water supplies and water quality. Climate-related impacts on water should also be considered when making a range of strategic business decisions from factory design and siting to new product development. Companies should also evaluate the energy implications of water management plans and strategies and seek combined and integrated solutions to water and energy.
4. Engage key stakeholders as a part of water and climate risk assessment, long-term planning, and implementation activities. When developing a corporate water and climate change management plan, managers can benefit from sharing information with employees, investors, customers, local communities, and other key stakeholders in order to gain valuable feedback. Through early and continuous engagement with concerned stakeholders, companies can better understand, anticipate, and respond to emerging issues and expectations. Open dialogue with water providers and local communities may also be helpful in preventing and reducing the risk of future water and climate change–related disputes or disruptions. Such discussions may also identify pivotal inputs that help prioritize action steps.
5. Disclose and communicate water performance and associated risks. Companies should publicly report management activities and key metrics on their water and energy performance. This information can help shareholders and stakeholders assess how companies are addressing their water and climate change risks. Such metrics are also a useful tool for engaging employees across the enterprise.
6. Seek opportunities for collective action, including public and private partnership. Because water is a shared resource, its management can be a sensitive social, cultural, and environmental issue, particularly in times of drought and water restrictions. Companies can rarely achieve the best water management outcomes on their own, as most

solutions to water supply, quality, and sanitation issues require comanagement approaches involving collective action and partnerships. Such approaches can give companies competitive advantages through alignment of their corporate water strategies with public policy goals and multi-stakeholder initiatives. These activities can include collaborations with local communities, NGOs, and government agencies, as well as peer-to-peer collaborations with other businesses.

The United Nations, in concert with national governments, has established a set of goals, known as the Millennium Development Goals. One of these goals is to reduce by half the number of people worldwide without access to clean water or adequate sanitation by 2015. There is a growing recognition that businesses are well positioned to play a role in achieving these goals. The public, in turn, has growing expectations that the private sector, often perceived as complicit in global water threats, should do its part regionally and internationally to address these challenges. Especially in regions under high water stress, or where substantial populations lack safe and affordable water, there is increased pressure for companies to work with local stakeholders, including water agencies, community groups, and other industry water users to share and manage limited resources more equitably and efficiently.

In addition, The CEO Water Mandate established in 2007 is one of the most comprehensive and visible cross-sectoral, public–private partnerships on water. It represents both a call-to-action and a strategic framework for responsible water management by business. It is voluntary in nature, but is built around six core areas of responsibility with which its endorsers must commit to and demonstrate improvement: direct operations, supply chain and watershed management, collective action, public policy, community engagement, and transparency.

Future Directions

Climate change has the potential to have adverse or positive impacts on many sectors in which water resource managers play an active role, including water availability, water quality, floods, ecosystems, coastal areas, power and energy, and other industrial sectors [1].

Data Needs for Climate Change Projection

Water resources planning involves making assumptions about future plausible hydroclimatic conditions (e.g., temperature, precipitation, and river flows). The choice of information supporting these assumptions is affected by a changing climate. While science is not capable of predicting the exact magnitude of the changes, there are methods to characterize the range of possible changes [1].

The instrumental record has historically been vital in planning for both norms and extremes, as it provides information on the conditions under which water resource systems may operate. Given a changing climate, it may be appropriate to evaluate the system response for a range of hydroclimatic variability wider than in the historical record.

Paleoclimate information and stochastic modeling can be useful for developing climate scenarios that include a wide range of potential hydroclimatic conditions. The expanded variability may allow a more robust evaluation of planning alternatives, particularly when there is concern that study outcomes and decisions may be sensitive to climate assumptions.

Current expectations about future climate may indicate a need to supplement historical climate information. Planning assumptions might instead be related to projections of future temperature and precipitation. This can be accomplished using a multitude of approaches, although a best approach has yet to be determined. Incorporating climate projections generally involves surveying available climate-projection information, deciding what portion to relate to planning assumptions, and conducting the intervening impact analysis on natural and social systems. These results are then related to planning assumptions about supplies, demands, and operating constraints. In many planning studies, assumptions are developed relative to a stationary reference climate.

Those engaged in planning need to share information, plan together, and collaboratively modify existing policies and procedures to ensure efficient and effective solutions. The exchange of information, resources, best practices, and lessons learned across jurisdictional lines and among different groups of stakeholders is a key element of successful adaptation planning [25].

Adaptive Management Approaches for Decision-Making

Water resource managers make decisions in the face of uncertainty associated with varying space and time scales, and they make assumptions about supplies, demands, weather, climate, and operational constraints at those scales. However, current planning approaches have generally assumed that future climate conditions will be similar to the historical record, an assumption that may be suspect if climate is changing. A robust decision criterion supports selection of plans that will perform well over a wide range of possible future scenarios, although uncertainties will remain no matter how future scenarios are generated. A sequential decision process allows alternative courses of action, given different possible future conditions, and can be changed as new information becomes available.

Adopting alternatives that perform well over a wide range of future scenarios could improve system flexibility. These approaches are not mutually incompatible and can be used in conjunction with current water management planning methods that primarily employ cost-benefit analysis and sensitivity analysis.

Adaptive management is an approach where decisions are made sequentially over time and allows adjustments to be made as more information is known. Incorporation of adaptive management can build in flexibility and reevaluation of decisions that evolve over time in response to new information. The use of multiple scenarios in the context of robust and adaptive planning will enhance decision-making, particularly if the scenarios span a wide range of possible outcomes.

Adaptation options include operational, demand management, and infrastructure changes. Because climate has such a large effect on water resource system design and operations, it is apparent that climate change would translate into modified design and operational assumptions for determining resource supplies, system demands, system performance requirements, and operational constraints. Several water management or system development options might be considered to facilitate adaptation under climate change, including operational, demand management, and infrastructure changes. Options should be evaluated across appropriate spatial areas; specific options will vary from system to system, as will the preference among these options.

Business action on climate change has primarily focused on managing the risks and opportunities associated with emerging regulations and changing market demands. But as recognition grows that some climate impacts are already occurring, and many more are likely inevitable, companies are beginning to develop adaptation plans to complement existing climate strategies.

Incorporating the Concept of Non-stationarity

Non-stationarity presents many challenges to the water resource managers. The assumption of stationarity has been used throughout the development of infrastructure for managing water resources. Many other types of analyses are also integrally linked to stationary concepts (e.g., hydrologic statistics such as flood frequency, low-flow frequency, and flow duration, and design criteria). Widely accepted methods for incorporating non-stationarity do not yet exist. While research proceeds, efforts can be made to bring analyses up to date, so that they use the most recently available data.

Climate change is expected to make certain aspects of water availability and water quality estimation more uncertain. For example, "*stationarity*, the idea that natural systems fluctuate within an unchanging envelope of variability, is dead and should no longer serve as a central, default assumption in water-resource risk assessment and planning," according to US Geological Survey and National Oceanic and Atmospheric Administration scientists in a February 6, 2008, *Science* article [26].

Nonstationary hydrologic variables can be modeled stochastically to describe the temporal evolution of their probability distributions, with uncertainty estimates. For example, water management professionals could define plausible planning futures based on climate projection data and then expand the set of such futures via stochastic modeling. However, such downscaled projections only should be used in water quality management programs when the planning horizon extends at least several decades into the future and the projections contain information reliable enough for planning purposes.

Using such projection techniques and data implies that the reference period underlying the stochastic

model is relevant to the planning period. If there is a lot of uncertainty about how a particular factor might affect a decision that could produce undesirable outcomes, then stakeholders should conduct activities to reduce that uncertainty.

Changes to planning and analysis that better accommodate non-stationarity will improve water management. Collaboration in all these activities may allow more rapid results and improved communication both within the water resources community and to other stakeholders.

For example, if non-stationarity is incorporated into water quality management, water management professionals should adopt a more innovative approach for accepting the growing list of impaired waters that will require a TMDL because of climate change. They should assess the TMDL, its implementation plan, and the effectiveness of both under projected climate-change scenarios and related management responses. If "*stationarity should no longer serve as a central, default assumption in water-resource risk assessment and planning*," then trade-offs need to be made between ambient water quality simulations based on long-term historical data and those based on stochastic models of such data. By better understanding how to define critical conditions and worst-case scenarios, water management professionals can formulate appropriate strategies to control point and nonpoint source pollution to meet TMDL standards.

Meanwhile, TMDL and National Pollutant Discharge Elimination System (NPDES) permit regulators will need to adapt by considering the long-range implications of climate change on waterbody impairment and revising permit limits and guidance accordingly. Some water quality standards and pollutant-specific goals may have to change to provide the environmental protection needed in an altered climate. Ongoing studies should give policymakers the information and tools needed to adapt cost-effectively [4].

Opportunities for Future Research

There are significant gaps in knowledge, monitoring, and practice that limit incorporation of climate change considerations into water resources planning and management. Research and monitoring are both needed to fill knowledge gaps and set up advances in planning capabilities. Although neither will eliminate all uncertainties, they will provide significant improvements in understanding the effects of climate change on water resources, including quantity and quality, and in evaluating associated uncertainties and risks required for more informed decision-making [1].

Many uncertainties remain with respect to climate change and its potential impacts on water resources. Major gaps must be bridged to achieve success in addressing the effects of climate change. Additional research may narrow uncertainties, provide information in more useable forms, or develop more robust strategies for incorporating uncertainty into decision-making. However, additional research will not eliminate uncertainty entirely, and robust and flexible operations and planning approaches can be used to help manage water resources effectively despite this uncertainty.

Recognize that adaptation must happen at local and regional levels. Climate changes and their associated impacts vary greatly from location to location. Although national and international action is essential, many important decisions about how best to manage systems affected by climate change are made at local and regional levels.

At press time, there was no "best" procedure for considering projected climate information in either class of long-range decision-making. Until there is less uncertainty or time reveals which methods best characterize future conditions, an array of reasonable approaches exist.

However, many of the prioritized gaps address themes common to multiple-resource management issues [1]:

- Developing downscaled climate-projection information at finer spatial–temporal resolutions than what is already available (e.g., sub-monthly and less than 1/8° resolution), for more variables, and using methods that do not rely on "stationarity" between the relation of large-scale atmospheric circulation and local land-surface climate
- Improving the ability to assess and anticipate region-specific impacts of climate change on land cover and ecosystems and potentially land-cover feedbacks on climate

– Improving the ability to assess the potential response of regional precipitation and hydrologic extremes to global climate change
– Improving the understanding of how social systems mediate climate change impacts and establish expectations for water resource system performance and reliability, which would presumably need to be preserved under a changing climate

Climate change must be quantified with respect to the myriad of other natural and cultural issues that face the water managers. Sound water management is built on long-term hydrological and meteorological monitoring networks that provide sound, accurate, timely, and consistent data that can be used readily to develop and assess decision-making tools needed to quantify uncertainty, forecast change, and create the multiphase, multilevel climate scenarios that will provide reasonable and relevant management. Changes to planning and analysis that better accommodate non-stationarity will improve water management. Collaboration in all of these activities may allow more rapid results and improved communication, both within the water resources community and to other stakeholders.

In summary, climate change is one of many dynamic processes impacting water resources management. A holistic approach must be considered on climate change impact on water resources management. Adaptation services are emerging as governments, businesses, and communities worldwide are recognizing the need to address current and potential climate change impacts. The journey toward global water sustainability needs to include the consideration of climate change impact in the planning and implementation over a long period of time.

Acknowledgment

The author thanks Dr. Ethan T. Smith (US Geological Survey, retired) for his joint collaboration and support on water sustainability publications over years.

Bibliography

Primary Literature

1. USGS (US Geological Survey), Brekke LD, Kiang JE, Olsen JR, Pulwarty RS, Raff DA, Turnipseed DP, Webb RS, White KD (2009) Climate change and water resources management: a federal perspective, U.S. Geological Survey Circular 1331. US Geological Survey, Reston
2. IPCC (Intergovernmental Panel on Climate Change) (2007). Summary for Policymakers. In: Climate change (2007) The physical science basis (Fourth Assessment Report). Cambridge University Press, Cambridge, UK
3. IPCC (Intergovernmental Panel on Climate Change), Bates BC, Kundzewicz ZW, Wu S, Palutikof JP (eds) (2008) Climate change and water, Technical paper VI of the Intergovernmental Panel on Climate Change. IPCC, Geneva
4. Zhang HX (2010) Changes ahead: water management professionals should account for climate change when working with TMDLs. Water Environ Technol February 2010:37–40
5. Smith ET, Zhang HX (2004) How do we know it's sustainable? Measuring water sustainability effectively is challenging. Water Environ Technol June 2004:37–41
6. Smith ET, Zhang HX (2007) Taking the long view: the journey toward sustainable water resources management begins by determining the most important water issues and indicators. Water Environ Technol June 2007:63–70
7. Daly HE (1996) Beyond growth: the economics of sustainable development. Beacon, Boston. ISBN 0-8070-4709-0
8. USEPA (2010) Climate change indicators in the United States. Environmental Protection Agency, Washington, DC
9. The National Academies (2008) Understanding and responding to climate change. National Academies Press, Washington, DC
10. Smith ET, Zhang HX (2009) Water sustainability indicators and biofuels production, WEFTEC 2009, 10–14 Oct 2009. WEFTEC, Orlando
11. General Accounting Office (GAO) (2004) Environmental indicators: better coordination is needed to develop environmental indicator sets that inform decisions, Report GAO-05-52. GAO, Washington, DC
12. WBCSD (World Business Council for Sustainable Development) (2010) Vision 2050 – the new agenda for business. Geneva, Switzerland
13. USEPA (2008) National water program strategy: response to climate change, Report EPA 800-R-08-001. USEPA, Washington, DC
14. USEPA (2009) Climate Change and Water Resources. http://www.epa.gov/climatechange/effects/water/. Accessed 28 April 2010
15. WERF (Water Environment Research Foundation) (2009) Implications of climate change for adaptation by wastewater and stormwater agencies. Alexandria, VA
16. Cruise JF, Limaye AS, Al-Abed N (1999) Assessment of impacts of climate change on water quality in the southeastern United States. J Am Water Resour Assoc 35(6):1539–1550
17. Eheart JW, Wildermuth AJ, Herricks EE (1999) The effects of climate change and irrigation on criterion low streamflows used for determining total maximum daily loads. J Am Water Resour Assoc 35(6):1365–1372
18. Mortsch L, Alden M, Scheraga JD (2003) Climate change and water quality in the Great Lakes Region – risks, opportunities and responses. A report prepared for the Great Lakes Water Quality Board of the International Joint Commission. Washington, DC

19. ICF International, RPA (2007) The potential costs of climate change adaptation for the water industry. Final report submitted to Environment Agency, UK
20. Ceres, Pacific Institute (2009) Water scarcity and climate change: growing risks for businesses and investors. CERES, Boston
21. Pacific Institute (2009) Climate change and the global water crisis: what businesses need to know and do. Pacific Institute, Oakland
22. US Geological Survey, Hutson SS, Barber NL, Kenny JF, Linsey KS, Lumia DS, Maupin MA (2004) Estimated use of water in the United States in 2000, US Geological Survey Circular 1268. US Geological Survey, Reston
23. USCCSP (U.S. Climate Change Science Program) (2007) Effects of climate change on energy production and distribution in the United States. USCCSP, Washington, pp 29–48
24. Barton B (2010) Murky waters? Corporate reporting on water risk – a benchmarking study of 100 companies. Ceres, Boston
25. Pew Center on Global Climate Change (2009) Climate change 101: understanding and responding to global climate change. Pew Center on Global Climate Change, Arlington
26. Milly PCD, Betancourt J, Falkenmark M, Hirsch RM, Kundzewicz ZW, Lettenmaier DP, Stouffer RJ (2008) Stationarity is dead: whither water management? Science 319(5863):573–574

Climate Change Impacts on Emerging Contaminants

Shane A. Snyder[1], Yongrui Tan[2], James W. Udy[3], Michael E. Bartkow[4], Sylvain Merel[1], Benoit Roig[5], Olivier Thomas[5]
[1]Department of Chemical and Environmental Engineering, University of Arizona, Tucson, AZ, USA
[2]Applied Research and Development Center, Southern Nevada Water Authority, Las Vegas, NV, USA
[3]Seqwater, Queensland, Australia
[4]Seqwater, c/- National Research Centre for Environmental Toxicology (Entox), Queensland, Australia
[5]Environment and Health Research Laboratory, French School of Public Health, Rennes, France

Article Outline

Glossary
Definition of the Subject
Introduction
Case Studies
Future Directions
Bibliography

Glossary

Climate change Changes in the statistical distribution of weather over periods of time that range from decades to millions of years. It can be a change in the average weather or a change in the distribution of weather events around an average (e.g., greater or fewer extreme weather events).

Emerging contaminants Synthetic or naturally occurring chemicals or microorganism that is not commonly monitored in the environment but has the potential to enter the environment and cause known or suspected adverse ecological and (or) human health effects.

Endocrine disrupting compounds Exogenous substances that act like hormones in the endocrine system and disrupt the physiologic function of endogenous hormones.

Potable water Water of sufficiently high quality that can be consumed or used without risk of immediate or long-term harm.

Water quality The physical, chemical, and biological characteristics of water. It is a measure of the condition of water relative to the requirements of one or more biotic species and or to any human need or purpose. It is most frequently used by reference to a set of standards against which compliance can be assessed.

Water reuse The practice of using wastewater or reclaimed water from one application for another application. The deliberate use of reclaimed water or wastewater must be in compliance with applicable rules for a beneficial purpose.

Definition of the Subject

Because of the rapid economic development and the subsequent population growth and urbanization, the freshwater supply in some regions of the world is experiencing a shortage due to increasing demand and decreasing replenishment. The water quality in these regions is often deteriorating as a result of heavy pollution and lack of adequate wastewater treatment. It is also realized that climate change and the consequent impact to drought and precipitation conditions may have severed this shortage. This has put pressure on water utilities to adopt new technologies to treat and deliver water resources that were previously not

considered to be amenable for such purpose, for example, desalination and water reclamation. For metropolitan areas that are not in close vicinity of ocean, water reclamation and reuse has become an increasingly attractive option to supplement existing water resources and to meet consumer demand. However, recent research has suggested potential health risk associated with water reuse for increased concentrations of pollutants that are not effectively removed by treatment processes. Such concern is especially heightened with the discovery of a group of "emerging contaminants" that are previously unknown or not commonly monitored in the water environment. With the rising public awareness and the potential of regulation of these contaminants by governmental agencies, research has been conducted to study the effects of anthropogenically driven processes, such as climate change, on the environmental concentrations of these compounds. This article is a review of such efforts. In addition, two case studies are discussed in detail to demonstrate the impacts of climate change on water use patterns and the subsequent effect on water quality.

Introduction

Population Growth/Urbanization

Since the industrial revolution, the world's urban population has experienced significant growth, largely due to the growing demand for concentrated labors in factories and buildings. This growth is more significant during the twentieth century, during which time the world's urban population increased more than tenfold, while rural population increased about twofold [1]. Today, half the world's population lives in urban centers, compared to less than 15% in 1,900 [1]. This growth trend is expected to continue and possibly accelerate in the foreseeable future (Fig. 1). However, the rate of growth varies greatly among different regions of the world. After the World War II, the increase of urban population happened mostly in Africa, Asia, and Latin America, while Europe and North America have seen more people moving out of the city centers (Fig. 2). This trend of urbanization, in addition to the increasing importance of large cities, was a result of the transformations of national economies and employment patterns, as more employment opportunities were created in urban-based industry and services. Virtually all nations experienced an employment shift away from agriculture, and most of the growth in those working in industry and services were in urban areas.

The trend toward more urbanized societies and the growing number of people living in large cities has very large implications for freshwater use and wastewater management. On a global scale, about 3,800 cubic kilometers of water per year are withdrawn to meet societal needs. The total available volume of renewable freshwater is several times more than is needed to sustain the current world population. However, population centers can access only about 31% of the

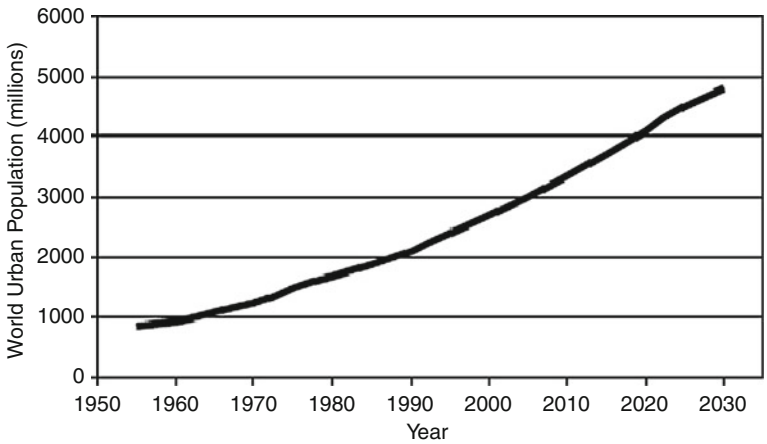

Climate Change Impacts on Emerging Contaminants. Figure 1
Estimated and projected urban population in the world (adapted from [1])

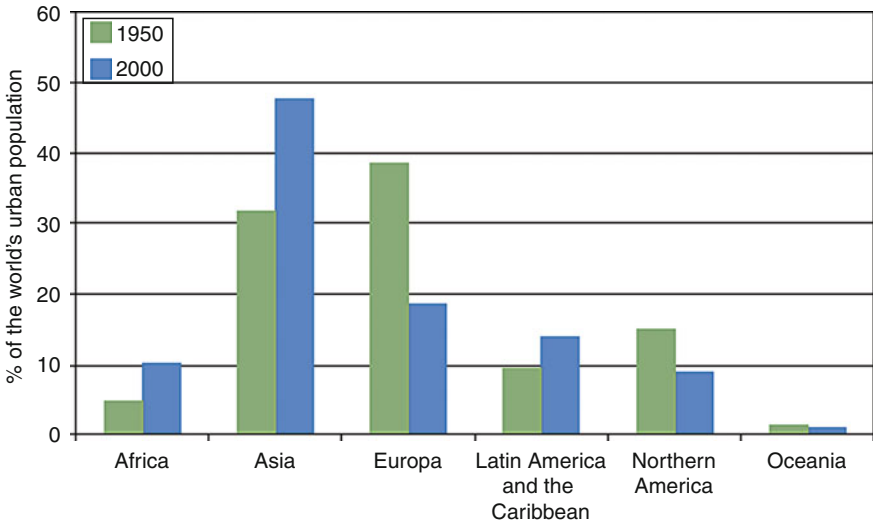

Climate Change Impacts on Emerging Contaminants. Figure 2
Comparative distribution of the world's urban population, 1950–2000 (adapted from [1])

renewable water because of geographical constraints and seasonal variations [2]. In addition, although agriculture remains the largest user of freshwater resources, the water demands from city enterprises and consumers have become increasingly important. At the same time, there has also been a rapid growth in the contribution of city-based enterprises and consumers to water pollution. As a result, many major cities have had to draw freshwater from increasingly distant watersheds, as local surface and groundwater sources no longer meet the demand for water, or as they become depleted or polluted [2].

The main water-related urban challenge in low- and middle-income nations is to provide adequate access to stable and safe water supply for drinking and sanitation. Currently, about one-third of the world's population lives in countries that face moderate to severe water shortages [3]. In order to meet the need of increasing urban population over the next century, the quantity of available water must increase by 25–60% from current level. However, as indicated by United Nations, urban populations have grown more rapidly than the capacity of developing countries to manage them, including putting into place institutional structures to ensure good provision for water, sanitation, and wastewater management within each locality [4]. This discrepancy will only become more significant with the continuing process of industrialization and urbanization in these countries.

Climate Change

There is empirical evidence of impacts on water resources from global warming. Land-based and mountain glaciers have generally experienced a worldwide retreat and thinning during the last century. Notably, glacier melting has considerably accelerated on a global basis during recent years [5, 6]. The mean mass balance decrease that took place during the period 1990–1999 was three times greater than that of the previous decade [7]. The Intergovernmental Panel on Climate Change (IPCC), in cooperation with new partners, has begun to address this issue in addition to their more traditional focus on greenhouse gases and temperature changes [8].

On the other hand, global warming should also enhance extreme events like floods and droughts [9–14]. However, the increasing occurrence and magnitude of drought periods associated with intense evaporation would favor water scarcity and hydraulic stress. Consequently, the lower water renewal (through melting glacier or rainy periods) due to climate change directly jeopardizes freshwater availability, particularly when water withdrawal (through irrigation, industrial

or domestic use) is simultaneously increased by anthropogenic activities.

Global weather patterns are major controlling factors in the climate and water balance for both southwest United States and northeast Australia. In southwest United States, one of the major factors in determining the water balance is total winter precipitation that falls as snow in the Rocky Mountains and the subsequent meteorological factors that influence the timing and rate of snowmelt. The subsequent runoff has a direct influence on water yield to the Colorado River, which directly or indirectly supplies water to meet potable or irrigation needs for more than 30 million people. In contrast the water budget for northeast Australia, specifically the subtropical region of southeast Queensland is determined by a combination of the global influence of the Southern Oscillation Index (El Niňo/La Niňa – ENSO) and more regional factors that influence the frequency and magnitude of precipitation in the coastal catchments (e.g., orographic rainfall as well as other influences including sea breezes, land use/vegetation cover influencing transpiration, and the availability of moisture in the atmosphere).

A number of studies over the last 20 years have suggested that there will be a decrease in runoff over the Southwestern United States because of global warming [15–18]. The Colorado River will be greatly impacted by this decrease as most of its water comes from snowmelt and subsequent runoff. The decrease will be caused by increasing temperatures, evaporation, and decreasing precipitation. The statistical/empirical studies, as well as climate model studies of the last few years all show a decrease in runoff to the Colorado River [19–22]. The estimates of runoff reduction from these studies are remarkably similar, and range between 10% and 30% over the next 30–50 years (Fig. 3). Given the agreement about both size and timing of runoff reduction, it is important to examine its impact on regional population in terms of water supply and water quality. In its recent report on Colorado River Basin water management, the National Academy of Sciences notes future potential problems with availability of water in the region. It calls for a comprehensive analysis of water needs and uses in the region.

Southeast Queensland has a subtropical coastal climate that is influenced by occasional monsoonal weather patterns, resulting in cyclones and tropical rain depressions providing large amounts of precipitation over several days or weeks. However, the climate is generally dominated by regional influences associated with weather patterns that provide southeast winds and sea breezes in summer and lighter westerly winds in winter. This results in winters being predominantly dry periods with the majority of precipitation being delivered in summer storms with hot dry weather periods between storms. Although there has always been large inter annual variability in precipitation, the water supply for this region has always relied on its storage

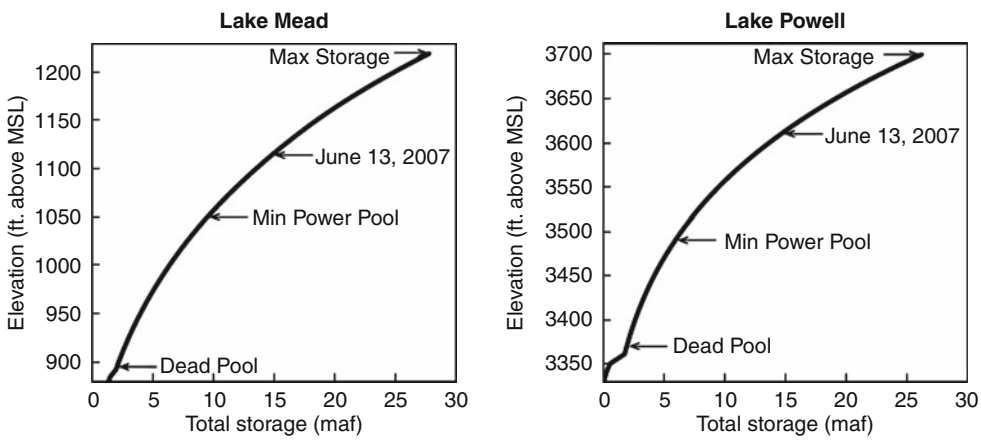

Climate Change Impacts on Emerging Contaminants. Figure 3
Total reservoir storage in Lakes Mead and Powell (million acre feet) as a function of lake surface elevation above mean sea level (feet) (adapted from [80])

capacity being large enough to meet demand between the large tropical storms, which usually return the reservoirs to full supply.

Climate change predictions for southeast Queensland only predict a small net reduction in total annual average precipitation. However, the pattern of delivery for this precipitation is likely to have a large impact on both total water yield from the catchments and transport of emerging contaminants. The impact of climate change is predicted to increase the period between large storms, with longer more severe droughts between events as well as increase the severity of the tropical storms when they do occur. This will potentially result in more mobilization of pollutants, including emerging contaminants.

The combined effect of changes in the frequency and magnitude of large storms and precipitation events in general is expected to reduce the total water yield to reservoirs, but also increase the pollutant loads delivered to reservoirs during large events. The lack of any large precipitation/flow events between 2000 and 2008 and long periods of rainless days between small precipitation events resulted in the worst drought in the last century and very low soil moisture readings in the catchments.

Water Reuse

The need for a dependable water supply is crucial, particularly for large cities with limited water resources in the surrounding area. However, as the population continues to grow, coupled with the impact to existing water supply by climate change, more and more cities are in need of supplemental sources of water. New sources may include water transfer from neighboring regions, internal water sources developed by optimizing the city's water use, water conservation, and water reclamation and reuse. San Diego County in California is an example of projected changes in the distribution of water sources in an urban setting. Currently, about 90% of the municipal water supply is obtained from a wholesale water provider. However, water demands are projected to increase by 50%, as a result of growing development and urbanization [23]. Increased use of reclaimed water and desalination of seawater will have to make up the difference. At inland locations or where desalination would cost too much, reclaimed water may contribute even more significantly to the overall water supply. It may be used for irrigation or industry, and it can replenish groundwater and surface water resources.

As the size of cities and their population expand, the quantity of wastewater increases proportionally. Wastewater treatment has gained much advance during twentieth century due to rapid growth of urban population and the consequent needs for sanitation and clean environment. Historically, wastewater was collected from industrial and residential discharge and went through a series of physical, chemical, and biological treatment before discharging into receiving water or for land disposal. However, over the past few decades, people have recognized the potential for recovering and reusing water from wastewater. The advances in wastewater treatment technology, such as membrane filtration, also helped to make this potential a reality by providing end water with better quality. These processes can now effectively remove biodegradable material, nutrients, and pathogens so the treated waters have a wide range of potential applications (Table 1).

Over the past 2 decades, the amount of municipal wastewater recovered for reuse has increased throughout the world [24]. The technique of water reuse is being applied in many countries including the United States, Mexico, Germany, Mediterranean and Middle Eastern countries, South Africa, Australia, Japan, China, and Singapore. The primary incentives for implementing water reuse are augmentation of water supplies and/or pollution abatement. Water reuse can be categorized as "direct" or "indirect," depending on whether the reclaimed water is used directly or mixed with other sources. On an international scale, direct non-potable water reuse is currently the dominant mode for supplementing public water supplies for irrigation, industrial cooling water, river flow augmentation, and other applications [25].

On the other hand, unplanned, indirect potable water reuse, through wastewater effluent disposal to streams, rivers, and groundwater basins, has been an accepted practice around the world for centuries. Communities situated at the end of major waterways have long histories of producing potable water from river water sources that have circulated through multiple cycles of withdrawal, treatment, and discharge.

Climate Change Impacts on Emerging Contaminants.
Table 1 Potential application for reclaimed water

Application settings	Examples
Urban use	
Unrestricted	Landscape irrigation (parks, playgrounds, school yards), fire protection, construction, in-building uses (toilets, air conditioning)
Restricted	Irrigation of areas where public access is infrequent and controlled (golf courses, cemeteries, residential, greenbelts)
Agriculture irrigation	
Food crops	Crops grown for human consumption and consumed uncooked
Nonfood crops	Fodder, fiber, seed crops, pastures, commercial nurseries, sod farms, commercial aquaculture
Recreation use	
Unrestricted	No limitations on body contact (lakes and ponds used for swimming, snowmaking)
Restricted	Fishing, boating, and other noncontact recreational activities
Environmental use	Artificial wetlands, enhanced natural wetlands, and sustained stream flows
Groundwater recharge	Groundwater replenishment, saltwater intrusion control, and subsidence control
Industrial reuse	Cooling system makeup water, process waters, boiler feed water, construction activities, and washdown waters
Potable reuse	Blending with municipal water supply (surface water or groundwater)

Similarly, riverbeds or percolation ponds may recharge underlying groundwater aquifers with wastewater-dominated water, which, in turn, is withdrawn by down-gradient communities for domestic water supplies. The safeguards for this unplanned indirect potable reuse are often carried out by advanced water treatment technologies. Planned indirect water reuse involves linking the discharge of treated wastewater with potential downstream water uses. For example in Los Angeles County, Calif., a groundwater recharge program has reclaimed water for indirect potable use since 1962 [26, 27], and in northern Virginia, the discharge of highly treated municipal wastewater by the Upper Occoquan Sewage Authority to the upper reaches of the Occoquan Reservoir has been in effect since 1978. Virginia's reservoir serves as the principal drinking water supply source for approximately one million local residents [28].

Recent documents from World Health Organization (WHO) [29] and the United States Environmental Protection Agency (EPA) [30] address the state-of-the art aspects and future trends in water use, both of which predict increased development and use of the above-mentioned practice to augment water supply sources in order to meet demands. The WHO guidelines for wastewater reuse first published in 1995 are being updated with a planned release date of 2006 [29]. According to water reuse surveys, the best water reuse projects in terms of economic viability and public acceptance are those that substitute reclaimed water in lieu of potable water for use in irrigation, environmental restoration, cleaning, toilet flushing, and industrial uses [31, 32].

Water Quality

While most of the studies have addressed the impact of climate change on water availability, recent research programs tend to focus on water quality. Indeed, the declining quality of surface and groundwater resources could imply the declining quality of drinking water with potential risk for human health [11]. In this context, the direct and indirect impact of climate change on emerging contaminants is particularly considered.

Water Reuse and Emerging Contaminants The term emerging contaminants refers to a group of heterogeneous substances that have been recently detected in the environment [33, 34]. They usually enclose pharmaceuticals and personal care products (PPCPs), hormones, endocrine disrupting compounds (EDCs),

flame retardants and algal toxins. However, the word "emerging" indicates that these substances are recently monitored but it does not necessarily imply that their occurrence in water is new [33, 35]. For example, some emerging substances occur in water for decades but they could not be detected in the past due to the technological limits.

Although reclamation and reuse of wastewater is beneficial for communities to supplement existing surface or ground water supply, the increasing public awareness and regulation over water quality pose great challenge to the water reuse industry. Over the last half of the twentieth century, the increasing availability of chemical products for industrial, medical, and household uses resulted in subtle but consistent changes in the characteristics of the wastewater that is produced in urban environments. As a result, pharmaceuticals and endocrine disrupting compounds (EDCs) have been detected in many water bodies around the world and are now considered ubiquitous wastewater contaminants [36, 37]. Undoubtedly, the major contributor of such widespread contamination is municipal wastewater discharge. In many cases, surface water with some degree of wastewater influence is used as source waters for drinking water treatment facilities leading to the presence of these compounds in finished drinking water. Thus, the propensity for surface water or drinking water contamination could grow with the increase of water reuse applications, unless appropriate controls or planned water supply systems are implemented.

Snyder et al. [38, 39] surveyed the occurrence of 36 pharmaceuticals and EDCs in the source and finished drinking water of 20 US DWTPs (Table 2). Twelve compounds were detected in at least 50% of the source water samples: atrazine, caffeine, carbamazepine, DEET, gemfibrozil, ibuprofen, iopromide, meprobamate, naproxen, phenytoin, sulfamethoxazole, and TCEP. Median concentrations of detected pharmaceuticals and EDCs in source drinking water were low and usually less than 10 ng/L, except for atrazine (28 ng/L), caffeine (27 ng/L), fluorene (13 ng/L), galaxolide (28 ng/L), metalochlor (15 ng/L), musk ketone (16 ng/L), and TCEP (13 ng/L). It is important to note that median concentrations of fluorene, galaxolide, and musk ketone were biased by low frequencies of detection. Eight compounds were detected in at least 50% of the finished drinking water samples: atrazine, caffeine, carbamazepine, DEET, ibuprofen, iopromide, meprobamate, and phenytoin. Median concentrations of detected pharmaceuticals and EDCs in finished drinking water were also less than 10 ng/L, except for atrazine (29 ng/L), caffeine (23 ng/L), metalochor (86 ng/L), and triclosan (43 ng/L). Again, median concentrations of metalochlor and triclosan were biased by low frequencies of detection.

Recent studies in environmental toxicology and pharmacology have suggested that long-term health risks may be associated with chronic exposure to trace chemical compounds, such as PPCPs, pesticides, and disinfection by-products (DBPs) in reclaimed water [36, 40–42]. Recently, many of these compounds have been classified as endocrine disrupters that can interfere with the functioning of natural hormones. Exposure to endocrine disrupters can impact the growth of amphibians, fish, and other wildlife at levels as low as parts per trillion [43].

Understanding the prevalence of these compounds and how to control them in the context of wastewater treatment is an active area of research. A number of articles have investigated the fate of trace hormones and pharmaceuticals through water treatment processes [38, 39, 44–55]. The ability of a particular treatment process to remove organic contaminants depends mostly on the structure and concentration of the contaminant. Chemical oxidation (during drinking water applications), biological removal/transformation (during wastewater applications), or nanofiltration/reverse osmosis are the water treatment technologies most responsible for pharmaceutical and EDC removal, though the operational parameters of the process (e.g., oxidant dose and contact time) will also determine the degree of attenuation of a particular contaminant.

Climate Change and Harmful Algal Blooms With optimal environmental conditions such as nutrient concentration and temperature, the photosynthetic biomass contained in surface water tends to multiply faster. In fact, spring streaming usually reloads water resources with nutrients (N and P), then summer provides favorable water temperature (20–25°C) and light intensity for an optimal photosynthesis. Consequently, most of algae and cyanobacteria (also known as blue-green algae) reach a maximum growth rate. In some

Climate Change Impacts on Emerging Contaminants. Table 2 Concentrations of pharmaceuticals and EDCs in the US source and finished drinking water (adapted from [38, 39])

	Source (n = 20)				Finished (n = 20)		
	MRL (ng/l)	Max.	Med.	#	Max.	Med.	#
Acetaminophen	1.0	9.5	1.6	7	< MRL	< MRL	–
Androstenedione	1.0	1.9	1.9	1	< MRL	< MRL	
Atrazine	1.0	570	28	17	430	29	15
Caffeine	1.0	87	27	14	83	23	12
Carbamazepine	1.0	39	3.1	18	5.7	2.8	11
DEET	1.0	28	6.9	20	30	5.1	18
Erythromycin	1.0	3.5	2.2	8	1.3	1.3	1
Estrone	1.0	1.4	1.2	2	2.3	1.7	2
Fluorene	1.0	13	13	1	< MRL	< MRL	–
Galaxolide	1.0	30	28	3	< MRL	< MRL	–
Gemfibrozil	1.0	11	4.8	13	6.5	4.2	5
Hydrocodone	1.0	1.9	1.9	1	< MRL	< MRL	–
Ibuprofen	1.0	24	4.2	16	32	3.8	13
Iopromide	1.0	46	7.6	14	31	6.5	13
Meprobamate	1.0	16	5.9	16	13	3.8	15
Metalochlor	1.0	170	15	7	160	86	4
Musk ketone	1.0	17	16	3	17	17	1
Naproxen	1.0	16	2.2	10	8	8	1
Oxybenzone	1.0	7.4	2.9	4	1.1	1.1	1
Phenytoin	1.0	13	3.2	18	6.7	2.3	14
Progesterone	1.0	1.1	1.1	1	1.1	1.1	2
Sulfamethoxazole	1.0	44	8.1	17	< MRL	< MRL	–
TCEP	–	66	13	15	19	5.5	7
Triclosan	1.0	30	1.9	6	43	43	1
Trimethoprim	1.0	2.3	2.2	3	1.3	1.3	1

cases their excessive growth leads to the appearance of a thin green layer at the water surface, a phenomenon called bloom and illustrated in Fig. 4a.

Nowadays, the occurrence of cyanobacterial blooms in surface water is a growing environmental and public health concern. Indeed, some blooms can be potentially harmful according to the prevailing species. For example some cyanobacteria can perform the biosynthesis of a wide range of substances called cyanotoxins. Based on their toxicological properties, these ones are usually considered as hepatotoxins (acting on the liver), neurotoxins (acting on the nervous system) and dermatotoxins (acting on the skin). Humans are potentially exposed to cyanotoxins through recreational waters but also through drinking water produced using a contaminated resource. For instance, several intoxications have been reported after exposure to the widespread hepatotoxin

a

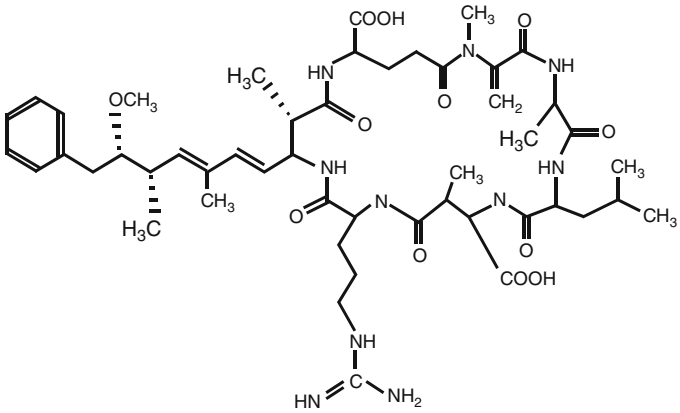

b Microcystin-LR

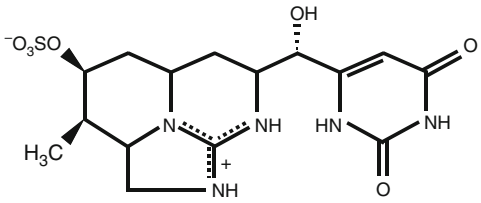

c Cylindrospermopsin

Climate Change Impacts on Emerging Contaminants. Figure 4
Occurrence of algal bloom in a french pond (**a**) and structure of 2 cyanotoxins (**b** and **c**)

microcystin-LR illustrated in Fig. 4b. Most of them were limited to gastro-enteritis [56], but more than 50 patients died in the Brazilian dialysis center of Caruaru [57–59].

A few studies indicate that climate change should directly increase the frequency and magnitude of cyanobacterial blooms [60–62]. On the one hand, global warming would allow the bloom to occur sooner. However, the blooms are more intense when they occur sooner, as indicated in Fig. 5 [62]. On the other hand, global warming would allow the bloom to collapse later. Consequently, the amount of cyanobacteria in water should be higher the year after. However, the blooms are more intense when the initial number of cells is high, as indicated in Fig. 5. In addition, one could also suppose that the increasing floods associated with climate change should bring higher amount of nutrients in surface waters, which would also favor the intensity of algal blooms. On the contrary, the statistical data are not yet sufficient to conclude on the impact of climate change on the frequency of blooms. This could be attributed to the lack of specific database for algal blooms monitoring. Indeed, such phenomenon is not necessarily reported to the administration in charge of the environment, and their management strongly varies according to the country.

Climate change may also influence the distribution of cyanotoxins. For example, the hepatotoxin cylindrospermopsin illustrated in Fig. 4c was mostly reported in Australia [63–65], New Zealand [66], Thailand [67, 68], and in southern states of the USA, like Florida [69]. Therefore, it has long been considered a tropical toxin [70]. However, since a few years, cylindrospermopsin has been characterized in

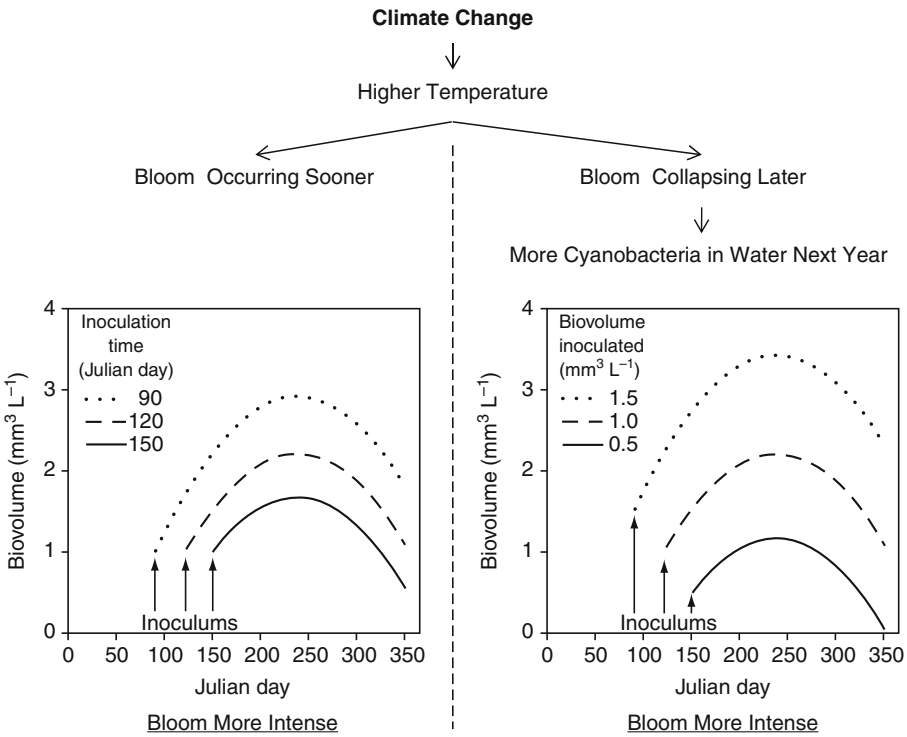

Climate Change Impacts on Emerging Contaminants. Figure 5
Impact of climate change on harmful algal blooms (adapted from [62])

temperate countries, such as Germany [70–73] and France [74, 75], and even in boreal environments, like in Finland [76]. One possible explanation for this change in cylindrospermopsin distribution might be the global warming but there is not yet scientific evidence to confirm this hypothesis.

Case Studies

Two reservoirs within subtropical zone were chosen to study the impact of climate change on emerging contaminants, where recycled wastewater is or will be used to supplement the water supply: Lake Mead in southwest United States and Lake Wivenhoe in northeast Australia. Since these water supplies provide raw drinking water to millions of people, there is a need to understand the various contaminant loads received by each reservoir – to ensure public health and public acceptance. The main impacts that require quantification and management are: (1) changes in water chemistry that can be attributed to an increase in the proportion of recycled water relative to natural surface water flow; and (2) processes that mobilize pollutants during extreme storm events. Climate change has the potential to affect both of these scenarios.

Lake Mead, United States

Lake Mead is a man-made reservoir residing on the Lower Colorado River, about 25 miles from Las Vegas, Nevada, a major metropolitan area in southwest United States. It was established by the construction of Hoover Dam in 1920s. Lake Mead and the lower Colorado River serve the water needs for more than 30 million Americans, or roughly 10% of the US population [77]. Las Vegas has been one of the fastest growing US cities over the last decade, and its current population is approximately two million. Yet, Las Vegas is located in one of the most arid climates on earth, with only 8 cm of annual rainfall and more than 2 m of evaporation per annum. Lake Mead serves as both the source for the area's drinking water and the sink for its wastewater. Approximately 900 million gallons per day (MGD) of water is withdrawn during peak summer months for

potable use, industrial use, and irrigation. Approximately half of that water is returned to Lake Mead as treated wastewater via the effluent-dominated Las Vegas Wash (the remainder is lost to groundwater or evaporation). Though the flow of the Wash is small, historically averaging just 1.4% of the total flow into Lake Mead, it mainly consists of (85%) treated wastewater. There are no other major urban areas discharging wastewater into the Colorado River or Lake Mead.

During the twentieth century, the average flow of the Colorado River dropped by a factor of 2, from approximately 1.9 × 1,013 L (15 million acre-ft) in 1900, to approximately 8.6 × 1,012 L (7 million acre-ft) in 2000 (USGS 2004). Barnett et al. [78] concluded that 60% of the observable climate-related trends (including snow-pack on the western Rocky Mountains, which serves as the source of the Colorado River) between 1950 and 1999 were attributed to human-induced climate change. Moreover, researchers predict that this trend will continue in the coming decades further straining water resources in the American Southwest [79–81]. The link between insufficient water supplies and slowing patterns of surface water flow partially attributed to climate change has been observed in the US Great Plains [82].

In 1996, the US Geological Survey issued the first report in the United States indicated that fish below wastewater outfalls showed evidence of impact to estrogenic compounds [83]. Since 1997, extensive monitoring of Lake Mead for pharmaceuticals and suspected EDCs has been underway [37, 84–86].

In 2000, the Colorado River Basin began to experience prolonged drought. Between 2000 and 2008, the volume of Lake Mead dropped from 100% to less than 50% its full capacity, and the lake had lost more than 35 m in elevation. Figure 6 shows the Hoover Dam at full capacity as compared to the dam today highlighting the loss of lake elevation. During this time, the flow of the Las Vegas Wash and the concentrations of pharmaceuticals and EDCs within the Wash did not significantly change [87]. The net effect was that there was less dilution of wastewater and an apparent increase in concentrations of wastewater contaminants (including atrazine, carbamazepine, DEET, diazepam, diclofenac, dilantin, estradiol, estrone, ethynylestradiol, fluoxetine, gemfibrozil, meprobamate, naproxen, progesterone, sulfamethoxazole, testosterone, and trimethoprim) in source drinking water (Fig. 7).

Similar trends are observed for both nitrate and conductivity. Nitrate concentrations in the Las Vegas Wash did not change at a rate statistically different from zero ($p = 0.4$) between January 1, 2003 and December 31, 2007. Nitrate concentrations decreased in the Colorado River at a rate of 0.00007 mg L^{-1} d^{-1}

Climate Change Impacts on Emerging Contaminants. Figure 6
Photographs of Lake Mead at full capacity in 1983 and again following drought in 2007 – Lake Mead was at full capacity as recently as 2000 (adapted from [87])

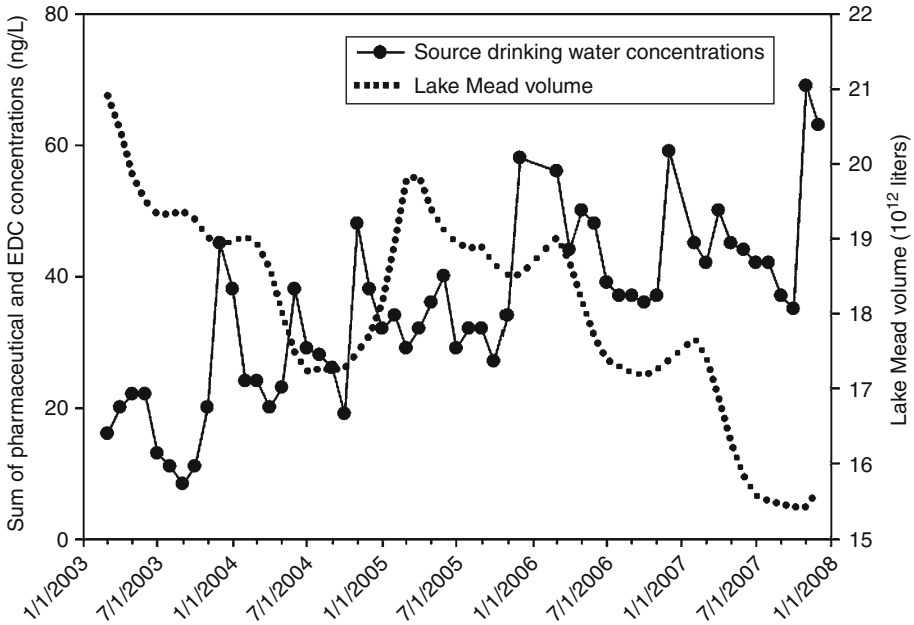

Climate Change Impacts on Emerging Contaminants. Figure 7
Summed concentrations of seventeen pharmaceuticals, endocrine disrupting compounds (EDCs), and other wastewater contaminants in Las Vegas' source drinking water as well as the volume of Lake Mead between March 2003 and December 2007 (adapted from [87])

($p < 0.0001$), yet increased in source drinking water at a rate of 0.0002 mg L^{-1} d^{-1} ($p < 0.0001$) over this same time period. Conductivity in the Las Vegas Wash did not change at a rate statistically different from zero ($p = 0.03$) between January 1, 2003 and December 31, 2007. Yet, conductivity decreased in the Colorado River at a rate of 0.04 μS cm^{-1} d^{-1} ($p < 0.0001$) and increased in source drinking water at a rate of 0.05 μS cm^{-1} d^{-1} ($p < 0.0001$) over this same time period. As was the case with concentrations of pharmaceuticals and EDCs, the increased loading associated with the slight increase in flow of the Las Vegas Wash over this time period does not alone account for the concomitant increase in nitrate and conductivity in source drinking water. This is especially true when one considers that historically, source drinking water is largely composed of water from the Colorado River [77], where concentrations of nitrate and conductivity actually decreased over this time period. Thus, the discrepancy between loading and source water concentration is not explained by a hydrological explanation of a system at steady state. The increase in pharmaceutical and EDC concentrations, nitrate concentrations, and conductivity in source drinking water is due to the decline in volume of Lake Mead between January 1, 2003 and December 31, 2007. During this time, the volume of Lake Mead declined from approximately 65% capacity, to almost 50% capacity (Fig. 6) at an average rate of 0.00007 d^{-1} ($p < 0.0001$).

Lake Wivenhoe, Australia

Lake Wivenhoe is the major drinking water supply for over a million people in the city of Brisbane, in subtropical Queensland, Australia. Unlike Lake Mead, which receives the majority of its water from snowmelt from the Rocky Mountains, Lake Wivenhoe receives all its water from precipitation in its surrounding catchments (5,400 km^2). Lake Wivenhoe catchments have a high proportion of agriculture, resulting in significant loads of pollutants into the lake during the large and highly episodic inflow events [88]. The reservoir itself is a eutrophic system with regular blooms of toxic algal species, in particular the cyanobacterium *Cylindrospermopsis raciborskii* [89]. Other land use in the

catchments includes both urban and industrial activities. In recent years, considerable research effort has been focused on characterizing the occurrence of trace organic contaminants in the lake and its tributaries prior to the introduction of recycled water.

A recent drought, described as the worst on record and a rapidly growing population in southeast Queensland, Australia, have been placing pressure on surface water supplies. This region is the fastest growing in Australia with the population forecast to more than triple by 2026 with commercial and industrial demand for water also increasing [90]. The region has few accessible groundwater resources and until recently, has relied on surface reservoirs to store water for potable treatment. The largest such reservoir is Lake Wivenhoe which was formed by damming the Brisbane River and is fed by the surrounding watershed as well as the Somerset Dam on an upstream tributary. The storage capacity of this reservoir is 1.2×109 m^3 and the major potable water treatment plant in the area is located on the Brisbane River downstream of Wivenhoe Dam [91].

There is now little scope for further large dams in the region, and recently a 1.25×105 m^3/d capacity desalination plant was commissioned as an additional climate independent source of potable water [90]. A further initiative to address the potable water situation in the region is the construction of a water reclamation project that will be the largest in the Southern Hemisphere and the third largest in the world once completed [91]. This project takes treated wastewater from six existing wastewater treatment plants in the South-East Queensland area. These plants all practice biological nutrient removal and deliver disinfected water of secondary standard to advanced water treatment plants (AWTPs) [90, 92]. The AWTPs adopt a dual membrane approach, using microfiltration and reverse osmosis, followed by advanced oxidation (H_2O_2/UV) and finally stabilization and disinfection with chlorine.

A monitoring campaign of the reclaimed water produced by the AWTPs was carried out from May to November 2008. It was undertaken for disinfection by-products (DBPs), pharmaceuticals and personal-care products (PPCPs), and pesticides together with other organic micropollutants as well as inorganic and microbial analytes that were detected in source wastewaters [92]. Over 300 chemicals were monitored for in secondary treated effluent with 114 organic chemicals detected. On this basis, 114 chemicals were monitored in AWTP effluent, with 99 not detected and 15 chemicals detected and quantified at least once. Of the detected compounds, bromodichloromethane, dibromochloromethane, chloroform, dichoroacetic acid, and NDMA (N-Nitrosodimethylamine) are categorized as DBPs. Paracetamol (N-(4-hydroxyphenyl) ethanamide), salicylic acid, and DEET (N,N-Diethyl-m-toluamide) are categorized as PPCPs. Triclopyr ([(3,5,6-Trichloro-2-pyridinyl)oxy]acetic acid) and dalapon (2,2-dichloropropionic acid) are pesticides (subclass herbicides), and cholesterol and caffeine are consumer products categorized under "others". The remaining detected compounds, 4-t-octylphenol, bisphenol A, and nonylphenol are regarded as good indicators of industrial contribution to wastewater [92]. Due to their weak estrogen-like activity, they are considered an environmental hazard.

Results showed the sporadic occurrence of the herbicides atrazine and simazine, triclopyr, 2,4-dichlorophenoxyacetic acid (2,4-D) and Dichlorprop (2,4 DP), and PPCPs such as caffeine, DEET, salicylic acid, and carbamazepine (Table 3). Industrial organics included 4-t-octylphenol, nonylphenol, and bisphenol A. Typically water concentrations were close to the detection limit of 10 ng/L. Possible sources of these chemicals in the catchments include urban sources (e.g., WWTPs, unsewered homes, stormwater runoff, landfills) and agricultural activities (e.g., weed control).

A wider range of chemicals were detected in samples from flow events with water concentrations typically exceeded levels measured in the lake. Bisphenol A was typically detected at the highest concentrations at most sites with water concentrations ranging up to >1,400 ng/L at Cooyar Creek and over half the sites exceeding 500 ng/L. The water concentrations of 4-t-octylphenol ranged from 28 ng/L to 500 ng/L. The highest concentrations were recorded at O'Reilly's Weir and Cooyar Creek. Caffeine, DEET, and salicylic acid were detected in at least half of the samples, typically between 10 and 30 ng/L. On some occasions DEET was measured at higher concentrations, particularly in Cooyar Creek (290 ng/L) and Emu Creek (200 ng/L). Ibuprofen was measured at the high water concentrations in Coal and Esk Creeks (2,280 ng/L and 2,270 ng/L, respectively). Herbicide profiles were

Climate Change Impacts on Emerging Contaminants. Table 3 Concentrations of pharmaceuticals, EDCs, and pesticides in reclaimed waters from wastewater treatment plants in the South-East Queensland area

		Sites											
		Apr–May 2008						Jan–May 2009					
		Esk offtake		Logan's inlet		Dam wall		Esk offtake		Logan's inlet		Dam wall	
	Chemical name	Max	Med	Max	Med	Max	Med	Max	Med	Max	Med	Max	Med
Known EDCs	4-t-octylphenol	<MRL	<MRL	<MRL	<MRL	<MRL	<MRL	27	12	38	10	26	4
	Nonylphenol	<MRL	<MRL	<MRL	<MRL	<MRL	<MRL	35	10	54	13	38	6
	Bisphenol A	11	11	<MRL	<MRL	<MRL	<MRL	1	1	6	2	4	3
PPCPs	Caffeine	<MRL	<MRL	20	20	<MRL	<MRL	50	35	60	60	60	35
	Carbamazepine	<MRL	<MRL	<MRL	<MRL	<MRL	<MRL	20	20	40	40	<MRL	<MRL
	DEET	30	30	30	20	30	30	10	10	10	10	10	10
	Salicylic acid	<MRL	<MRL	10	10	10	10	<MRL	<MRL	10	10	<MRL	<MRL
Herbicides	Atrazine	<MRL	<MRL	10	10	10	10	10	10	<MRL	<MRL	<MRL	<MRL
	Simazine	10	<MRL	<MRL	<MRL	10	10	<MRL	<MRL	<MRL	<MRL	<MRL	<MRL
	Triclopyr	10	10	<MRL	<MRL	<MRL	<MRL	<MRL	<MRL	<MRL	<MRL	<MRL	<MRL
	2,4-D	<MRL	<MRL	<MRL	<MRL	<MRL	<MRL	10	10	<MRL	<MRL	<MRL	<MRL
	2,4-DP	<MRL	<MRL	<MRL	<MRL	<MRL	<MRL	20	20	<MRL	<MRL	<MRL	<MRL

MRL for herbicides and PPCPs = 10 ng/L; known EDCs = 1 ng/L
MRLs were not included in the calculation of median values

dominated by different chemicals depending on where the sample was collected 2,4-Dichlorophenoxyacetic acid (2,4-D) and 2,4-Dichlorophenoxybutyric acid (2,4-DB) were measured in a sample from the O'Reilly's Weir at 1,000 ng/L each. Hexazinone was measured at 670 ng/L in a sample from Cooyar Creek and tebuthiuron was measured at 130 ng/L in Capt. Logan's Creek.

Overall, the monitoring of chemicals in flow events has shown that water concentrations in tributaries during such events can exceed levels in the lake by ten times or more. Clearly these inflows can have impacts on water quality, although dilution and attenuation of chemicals are likely to occur. For example, ibuprofen was not detected in samples collected from the lake in May 2008, after flow event monitoring detected at the chemical at concentrations exceeding 1 ug/L. This chemical is known to degrade relatively quickly in natural water systems.

There was a significant rain event in May 2009, the bulk of which had fallen between May 19 and 21. The net result was that Lake Wivenhoe capacity rose from 43% (5.25×10^5 ML) on May 18 to 63% (7.32×10^5 ML) on May 27. Monitoring flow events of lower magnitude in early 2008 had shown that significant chemical loads could enter the lake from different tributaries hence it was possible that flow events of the scale that occurred in May 2009 could impact on lake water quality.

Sampling was undertaken at three sites in Lake Wivenhoe on May 27, 2009. Samples were subjected to the same analysis as previously. Interestingly, the occurrence of herbicides and PPCPs remained sporadic and in most cases below detection limits. Levels of the industrial organics remained in the range detected during sampling from earlier in 2009 and no hormones were detected. These results indicated that even though flow events are capable of delivering a load of contaminants to the lake, the combined effects of dilution and attenuation appear to result in minimal impact on water quality.

Future Directions

With increasing demand from population growth and dwindling availability due to urbanization and pollution, water has become a more precious and limited resource in many areas of the world. For the past few decades, water industry has been searching for new means of producing fresh water, such as direct and indirect reuse of wastewater, to supplement existing and traditional sources. The advances in water treatment technologies, together with more efficient water management practices, have greatly improved reused water quality and expanded the acceptance and adoption of water reclamation and reuse across the industry. However, research has suggested that there is increasing concern regarding the safety of reused water to human and aquatic species, because of the detection of some emerging contaminants in water systems receiving wastewater discharge. Although the concentrations of these contaminants are usually low, there are evidences that they can cause adverse health conditions to population after long-term consumption. The increasing public awareness has pressured governmental agencies to consider regulating these contaminants, which in turn poses great challenges to water treatment facilities.

Climate change as a result of human activities since industrial revolution has been suggested to associate with the changes in global water systems through a number of influencing factors, such as glacier melting, changes in precipitation, and evaporation patterns. The impact of climate change to local water resources is especially significant for arid regions that depend on large water reservoirs to regulate and balance seasonal water supply. The intake water quality in local water treatment plants is greatly affected by wastewater discharge and runoff from surrounding catchments, which can be impacted by changes in precipitation and upstream water volume. More research is needed to understand the long-term effect of climate change on water quality, including the levels of regulated and emerging contaminants. Such knowledge will help water industry to prepare and make long-term plans to address water safety and meet future regulations.

Bibliography

Primary Literature

1. United Nations (2004) World urbanization prospects: The 2003 Revision. New York, United Nations Population Division, Department of Economic and Social Affairs, ST/ESA/SER.A/237
2. Postel SL (2000) Entering an era of water scarcity: the challenges ahead. Ecol Appl 10:941–948

3. World Bank (2001) Water and Sanitation Program, 99-00 Report. World Bank water and sanitation program. Washington, DC
4. UNESCO (2006) Water, a shared responsibility. United Nations Educational, Scientific and Cultural Organization and Berghahn Books, Paris, France and New York
5. Arendt AA, Echelmeyer KA, Harrison WD, Lingle CS, Valentine VB (2002) Rapid wastage of Alaska glaciers and their contribution to rising sea level. Science 297(5580):382–386
6. Dyurgerov M (2003) Mountain and subpolar glaciers show an increase in sensitivity to climate warming and intensification of the water cycle. J Hydrol 282:164–176
7. Frauenfelder R, Zemp M, Haeberli W, Hoelzle M (2005) World-Wide glacier mass balance measurements: trends and first results of an extraordinary year in Central Europe. Ice and Climate News, No 6. pp 9–10
8. IPCC (2004) Expert Meeting on the Science to Address UNFCCC Article 2 including Key Vulnerabilities. Buenos Aires, Argentina 18–20 May 2004, Short Report
9. Bates BC, Kundzewicz ZW, Wu S, Palutikof JP (2008) Climate change and water. Technical paper of the intergovernmental panel on climate change, Geneva
10. Beniston M, Stephenson D, Christensen O, Ferro C, Frei C, Goyette S, Halsnaes K, Holt T, Jylhä K, Koffi B, Palutikof J, Schöll R, Semmler T, Woth K (2007) Future extreme events in European climate: an exploration of regional climate model projections. Clim Chang 81(suppl 1):71–95
11. Delpla I, Jung AV, Baures E, Clement M, Thomas O (2009) Impacts of climate change on surface water quality in relation to drinking water production. Environ Int 35(8):1225–1233
12. Kundzewich Z, Hirabayashi Y, Kanae S (2010) River floods in the changing climate – observations and projections. Water Resour Manage 24(11):2633–2646. DOI:10.1007/s11269-009-9571-6
13. Ward P, Renssen H, Aerts J, Balen R, Vandenberghe J (2008) Strong increases in flood frequency and discharge of the river Meuse over the late Holocene: impacts of long term anthropogenic land use change and climate variability. Hydrol Earth Syst Sci 12:159–175
14. Wigley T (2009) The effect of changing climate on the frequency of absolute extreme events. Clim Chang 97:67–76
15. Revelle R, Waggoner P (1983) Effects of carbon dioxide-induced climatic change on water supplies in the western United States. In: Changing Climate, Report of the carbon dioxide assessment committee, National Academic, Washington, DC
16. Nash L, Gleick P (1991) The sensitivity of stream flow in the Colorado Basin to climatic changes. J Hydrol 125:221–241
17. Nash L, Gleick P (1993) The Colorado Basin and climate change. EPA 230-R-93-009, Policy, Planning and Evaluation, Environmental Protection Agency, Washington, DC
18. Hoerling M, Eischeid J (2007) Past peak water in the West. Southwest Hydrology vol 6, Issue 1, pp 8–19
19. Milly P, Dunne K, Vecchia A (2005) Global pattern of trends in streamflow and water availability in a changing climate. Nature 438:347–350
20. Christensen NS, Wood AW, Voisin N, Lettenmaier DP, Palmer RN (2004) Effects of climate change on the hydrology and water resources of the Colorado basin. Clim Change 62: 337–363
21. Christensen N, Lettenmaier D (2006) A multimodel ensemble approach to climate change impacts on the hydrology and water resources of the Colorado River Basin. Hydrol Earth Syst Discuss 3:1–44
22. Seager R (2007) Model projections of an imminent transition to a more arid climate in southwestern North America. Science 316:1181–1184
23. San Diego County water authority (2002) San Diego County Water Authority 2001–2002 annual report. San Diego County Water Authority, San Diego, CA
24. Levine AD, Asano T (2004) Recovering sustainable water from wastewater. Environ Sci Tech 38(11):201A–208A
25. Asano T (1998) Wastewater reclamation and reuse: water quality management library, vol 10. CRC Press, Boca Raton
26. Nellor MH (1984) Health effects study. County sanitation districts of Los Angeles County, Los Angeles
27. Crook J, Asano T, Nellor MH (1990) Groundwater recharge with reclaimed water in California. Water Environ Technol 24:42–49
28. National Research Council (1998) Issues in potable reuse: the viability of augmenting drinking water supplies with reclaimed water. National Academy Press, Washington
29. World Health Organization (2005) Guidelines for the safe use of wastewater, excreta and greywater in agriculture and aquaculture. World Health Organization, Geneva
30. United States environmental protection agency (2004) Guidelines for water reuse. EPA 625/R-04/108
31. Lazarova L (2001) Recycled water: technical-economic challenges for its integration as a sustainable alternative resource. In: Proceedings of UNESCO International Symposium. Les frontiéres de la gestion de l'eau urbaine: impasse ou espoir? Marseilles, 18–20 June 2001
32. Mantovani P, Asano T, Chang A, Okun DA (2001) Management practices for non-potable water reuse. Water Environment Research Foundation Report 97-IRM-6
33. Erickson BE (2002) Analyzing the ignored environmental contaminants. Environ Sci Technol 36(7):140–145
34. Snow DD, Bartelt-Hunt SL, Saunders SE, Cassada DA (2007) Detection, occurrence, and fate of emerging contaminants in agricultural environments. Water Environ Res 24:1061–1084
35. Daughton CG (2004) Non-regulated water contaminants: emerging research. Environ Impact Asses Rev 24(7–8):711–732
36. Kolpin DW, Furlong ET, Meyer MT, Thurman EM, Zaugg SD, Barber LB, Buxton HT (2002) Pharmaceuticals, hormones, and other organic wastewater contaminants in US streams, 1999–2000: a national reconnaissance. Environ Sci Technol 36(6): 1202–1211
37. Vanderford BJ, Pearson RA, Rexing DJ, Snyder SA (2003) Analysis of endocrine disruptors, pharmaceuticals, and personal care products in water using liquid chromatography/tandem mass spectrometry. Anal Chem 75(22):6265–6274

38. Snyder SA, Adham S, Redding AM, Cannon FS, DeCarolis J, Oppenheimer J, Wert EC, Yoon Y (2007) Role of membranes and activated carbon in the removal of endocrine disruptors and pharmaceuticals. Desalination 202(1–3):156–181
39. Snyder SA, Wert EC, Lei HX, Westerhoff P, Yoon Y (2007) Removal of EDCs and pharmaceuticals in drinking and reuse treatment processes. AWWA Research Foundation, Denver, p 331
40. Drewes JE, Heberer T, Reddersen K (2002) Fate of pharmaceuticals during indirect potable reuse. Water Sci Technol 46(3):73–80
41. Gold LS (1999) Supplement to the Carcinogenic Potency Database (CPDB): Results of animal bioassays published in the general literature in 1993 to 1994 and by the National Toxicology Program in 1995 to 1996. Health Perspect 107:527–600
42. Tanaka H (2001) Comparison between estrogenicities estimated from DNA recombinant yeast assay and from chemical analyses of endocrine disruptors during sewage treatment. Water Sci Technol 43:125–132
43. Daughton CG, Ternes TA (1999) Pharmaceuticals and personal care products in the environment: Agents of subtle change? Environ Health Perspect 107:907–938
44. Ternes TA, Kreckel P, Mueller J (1999) Behaviour and occurrence of estrogens in municipal sewage treatment plants—II. Aerobic batch experiments activated sludge. Sci Total Environ 225(1–2):91–99
45. Ternes TA, Stumpf M, Mueller J, Haberer K, Wilken RD, Servos M (1999) Behavior and occurrence of estrogens in municipal sewage treatment plants I. Investigations in Germany, Canada and Brazil. Sci Total Environ 225(1–2):81–90
46. Zwiener C, Frimmel FH (2000) Oxidative treatment of pharmaceuticals in water. Water Res 34(6):1881–1885
47. Adams C, Wang Y, Loftin K, Meyer M (2002) Removal of antibiotics from surface and distilled water in conventional water treatment processes. J Environ Eng–ASCE 128(3): 253–260
48. Drewes JE, Amy G, Reinhard M (2002) Targeting bulk and trace organics during advanced membrane treatment leading to indirect potable reuse. In: Water Sources Conference Proceedings REU vol 5, pp 1–18
49. D'Ascenzo G, Di Corcia A, Gentili A, Mancini R, Mastropasqua R, Nazzari M, Samperi R (2003) Fate of natural estrogen conjugates in municipal sewage transport and treatment facilities. Sci Total Environ 302(1–3):199–209
50. Huber MM, Canonica S, Park GY, Von Gunten U (2003) Oxidation of pharmaceuticals during ozonation and advanced oxidation processes. Environ Sci Technol 37(5):1016–1024
51. Snyder SA, Westerhoff P, Yoon Y, Sedlak DL (2003) Pharmaceuticals, personal care products, and endocrine disruptors in water: implications for the water industry. Environ Eng Sci 20(5):449–469
52. Snyder SA, Wert EC, Rexing DJ, Zegers RE, Drury DD (2006) Ozone oxidation of endocrine disruptors and pharmaceuticals in surface water and wastewater. Ozone Sci Eng 28(6):445–460
53. Huber MM, Korhonen S, Ternes TA, von Gunten U (2005) Oxidation of pharmaceuticals during water treatment with chlorine dioxide. Water Res 39(15):3607–3617
54. Westerhoff P, Yoon Y, Snyder S, Wert E (2005) Fate of endocrine-disruptor, pharmaceutical, and personal care product chemicals during simulated drinking water treatment processes. Environ Sci Technol 39(17):6649–6663
55. Yoon Y, Westerhoff P, Snyder SA, Wert EC, Yoon J (2007) Removal of endocrine disrupting compounds and pharmaceuticals by nanofiltration and ultrafiltration membranes. Desalination 202(1–3):16–23
56. Kuiper-Goodman T, Falconer I, Fitzgerald J (1999) Human health aspects. In: Chorus I, Bartram J (eds) Toxic cyanobacteria in water: a guide to their public health consequences, monitoring and management. E&FN Spon, London, pp 113–153
57. Pouria S, Andrade de A, Barbosa J, Cavalcanti RL, Barreto VTS, Preiser W, Poon GK, Neild GH, Codd GA (1998) Fatal microcystin intoxication in haemodialysis unit in Caruaru, Brazil. Lancet 352(9121):21–26
58. Azevedo SMFO, Carmichael WW, Jochimsen EM, Rinehart KL, Lau S, Shaw GR, Eaglesham GK (2002) Human intoxication by microcystins during renal dialysis treatment in Caruaru – Brazil. Toxicology 181–182:441–446
59. Yuan M, Carmichael WW, Hilborn ED (2006) Microcystin analysis in human sera and liver from human fatalities in Caruaru, Brazil 1996. Toxicon 48:627–640
60. Dale B, Edwards M, Reid PC (2006) Climate change and harmful algal blooms. In: Granéli E, Turner JT (eds) Ecology of harmful algae. Springer, New York, pp 367-378. Griffiths DJ, Saker ML (2003) The Palm Island mystery disease 20 years on: a review of research on the cyanotoxin cylindrospermopsin. Environ Toxicol 18(2):78–93
61. Paul VJ (2008) Global warming and cyanobacterial harmful algal blooms. In: Hudnell KH (ed) Cyanobacterial harmful algal blooms: state of the science and research needs. Springer, New York, pp 239–257
62. Wiedner C, Rücker J, Brüggemann R, Nixdorf B (2007) Climate change affects timing and size of populations of an invasive cyanobacterium in temperate regions. Oecologia 152(3):473–484
63. Saker ML, Thomas AD, Norton JH (1999) Cattle mortality attributed to the toxic cyanobacterium *Cylindrospermopsis raciborskii* in an outback region of North Queensland. Environ Toxicol 14(1):179–182
64. Stewart I, Seawright AA, Shaw GR (2008) Cyanobacterial poisoning in livestock, wild mammals and birds – an overview. In: Hudnell KH (ed) Cyanobacterial harmful algal blooms: state of the science and research needs. Springer, New York, pp 613–637
65. Fristachi A, Sinclair JL (2008) Occurrence of cyanobacterial harmful algal blooms workgroup report. In: Hudnell KH (ed) Cyanobacterial harmful algal blooms: state of the science and research needs. Springer, New York, pp 45–103

66. Stirling DJ, Quilliam MA (2001) First report of the cyanobacterial toxin cylindrospermopsin in New Zealand. Toxicon 39(8):1219–1222
67. Li R, Carmichael WW, Brittain S, Eaglesham GK, Shaw GR, Mahakhant A, Noparatnaraporn N, Yongmanitchai W, Kaya K, Watanabe MM (2001) Isolation and identification of the cyanotoxin cylindrospermopsin and deoxy-cylindrospermopsin from a Thailand strain of *Cylindrospermopsis raciborskii* (Cyanobacteria). Toxicon 39(7):973–980
68. Carmichael WW, Azevedo SMFO, An JS, Molica RJR, Jochimsen EM, Lau S, Rinehart KL, Shaw GR, Eaglesham GK (2001) Human fatalities from cyanobacteria: chemical and biological evidence for cyanotoxins. Environ Health Perspect 109(7):663–668
69. Burns J (2008) Toxic cyanobacteria in Florida waters. In: Hudnell KH (ed) Cyanobacterial harmful algal blooms: state of the science and research needs. Springer, New York, pp 127–137
70. Rücker J, Stüken A, Nixdorf B, Fastner J, Chorus I, Wiedner C (2007) Concentrations of particulate and dissolved cylindrospermopsin in 21 Aphanizomenon-dominated temperate lakes. Toxicon 50(6):800–809
71. Fastner J, Heinze R, Humpage AR, Mischke U, Eaglesham GK, Chorus I (2003) Cylindrospermopsin occurrence in two German lakes and preliminary assessment of toxicity and toxin production of *Cylindrospermopsis raciborskii* (Cyanobacteria) isolates. Toxicon 42(3):313–321
72. Fastner J, Rücker J, Stüken A, Preußel K, Nixdorf B, Chorus I, Köhler A, Wiedner C (2007) Occurrence of the cyanobacterial toxin cylindrospermopsin in northeast Germany. Environ Toxicol 22(1):26–32
73. Wiedner C, Rücker J, Fastner J, Chorus I, Nixdorf B (2008) Seasonal dynamics of cylindrospermopsin and cyanobacteria in two German lakes. Toxicon 52(6):677–686
74. Bernard C, Harvey M, Briand JF, Biré R, Krys S, Fontaine JJ (2003) Toxicological comparison of diverse *Cylindrospermopsis raciborskii* strains: evidence of liver damage caused by a French *C. raciborskii* strain. Environ Toxicol 18(3):176–186
75. Brient L, Lengronne M, Bormans M, Fastner J (2009) First occurrence of cylindrospermopsin in freshwater in France. Environ Toxicol 24(4):415–420
76. Spoof L, Berg KA, Rapala J, Lahti K, Lepistö L, Metcalf JS, Codd GA, Meriluoto J (2006) First observation of cylindrospermopsin in *Anabaena lapponica* isolated from the boreal environment (Finland). Environ Toxicol 21(6):552–560
77. Fogg GE (1969) The physiology of an algal nuisance. Proc R Soc Lond B Biol Sci 173:175–189
78. Barnett TP, Pierce DW, Hidalgo HG, Bonfils C, Santer BD, Das T, Bala G, Wood AW, Nozawa T, Mirin AA, Cayan DR, Dettinger MD (2008) Human-induced changes in the hydrology of the western United States. Science 319(5866):1080–1083
79. Barnett T, Malone R, Pennell W, Stammer D, Semtner B, Washington W (2004) The effects of climate change on water resources in the West: Introduction and overview. Clim Change 62(1–3):1–11
80. Barnett TP, Pierce DW (2008) When will Lake Mead go dry? Water Resources Res 44(3): W03201
81. McCabe GJ, Wolock DM (2007) Warming may create substantial water supply shortages in the Colorado River Basin. Geophys Res Lett 34:L22708. doi:10.1029/2007GL031764
82. Brikowski TH (2008) Doomed reservoirs in Kansas, USA? Climate change groundwater mining Great Plains lead unsustainable surface water storage. J Hydrol 354(1–4):90–101
83. Bevans HE, Goodbred SL, Miesner JF, Watkins SA, Gross TS, Denslow ND, Choeb T (1996) Synthetic organic compounds and carp endocrinology and histology in Las Vegas Wash and Las Vegas and Callville Bays of Lake Mead, Nevada, 1992 and 1995. US Geological Survey, Nevada
84. Roefer P, Snyder S, Zegers RE, Rexing DJ, Fronk JL (2000) Endocrine-disrupting chemicals in a source water. J Am Water Works Assoc 92(8):52–58
85. Snyder SA, Villeneuve DL, Snyder EM, Giesy JP (2001) Identification and quantification of estrogen receptor agonists in wastewater effluents. Environ Sci Technol 35(18):3620–3625
86. Trenholm RA, Vanderford BJ, Holady JC, Rexing DJ, Snyder SA (2006) Broad range analysis of endocrine disruptors and pharmaceuticals using gas chromatography and liquid chromatography tandem mass spectrometry. Chemosphere 65(11): 1990–1998
87. Benotti MJ, Stanford BD, Snyder SA (2010) Impact of drought on wastewater contaminants in an urban water supply. J Environ Qual 39(4):1196–1200
88. Burford MA, Johnston SA, Cook AJ, Packer TV, Taylor BM, Townsley ER (2007) The relative importance of watershed and reservoir characteristics in promoting algal blooms in subtropical reservoirs. Wat Res 41:4204–4114
89. Burford MA, O'Donohue MJ (2006) A comparison of phytoplankton community assemblages in artificial and naturally mixed subtropical water reservoirs. Freshw Biol 51:973–982
90. Traves WH, Gardner EA, Dennien B, Spiller D (2008) Towards indirect potable reuse in South East Queensland. Water Sci Technol 58:153–161
91. Freeman S, Bates J, Wallis-Lage C, McEvoy J (2008) Drought relief in South-East Queensland, Australia provided by membrane-reclaimed water. J Am Water Work Assoc 100:40–52
92. Queensland Water Commission (2009) Interim water quality report February 2009. Queensland Government, Brisbane

Climate Change Modeling Methodology, Introduction

Philip J. Rasch
Pacific Northwest National Laboratory, Richland, WA, USA

In the early 1980s, Eugene F. Stoermer began informally using the term "anthropocene" to refer to a time in the history of the Earth in which humans introduce

impacts that at times rival natural processes in the global functioning of the planet [7]. While there is some uncertainty about when the anthropocene began (with some dating it as far back as 8,000 years ago), there is little doubt that humans are affecting the planet today, and one of the ways is through our impact on the Earth's climate.

Concern about the possible impact of mankind on climate dates back at least as far as 1896, when Svante Arrhenius [1] suggested that mankind might inadvertently warm the planet by increasing the concentration of carbon dioxide, and the idea that man might have an impact on the Earth's climate has been studied ever since. Concern about the matter has been increasing since the 1970s, and in 1995, a very large group of climate scientists, in an assessment produced by the Intergovernmental Panel on Climate Change [2], wrote that "*the balance of evidence suggests a discernible human influence on global climate*." That statement, based on a careful evaluation of observational evidence, theory, and model studies, ignited a firestorm of comment and controversy. There is little doubt that the vast majority of climate scientists were concerned then, and study since that time has made the arguments that man is affecting climate even more compelling. In February of 2007, the IPCC released its fourth assessment [3], which found that "*human actions are 'very likely' the cause of global warming*," with "very likely" specifically defined to mean a 90% or greater probability of explaining an increase in average global temperatures over the last 100 years, with many other attendant changes. Some debate continues about these conclusions to this day, with a few scientists and more non-scientists indicating doubt that mankind is responsible for the changes, but almost no doubt that the warming is real.

There are many reasons for skepticism about climate change: some scientific, some not. It is not my intention that this section provides much information about climate change itself. The assessment report, the "synthesis document," and the "summaries" intended for policymakers, laypersons, and scientists from other fields [2–5] provide much more detail than could possibly be included here.

Instead, these entries are designed to introduce readers to the "methodologies" used in climate science. What are the tools used for? How is confidence gained in the use of those tools? It is impossible to provide a thorough review with the few entries, and few pages of each entry in this section, but it is hoped that they provide readers with an introduction to the science, and methodology, and pointers to places where more detail can be found.

Climate science is a complex field. Climate is governed by processes that interact and operate on a vast array of time and space scales. The processes involving radiative transfer, chemistry, and phase changes of water are most easily described at atomic and molecular scales; the influence of ice sheets, continents, and planetary scale circulations controlling the basic energy balance of the planet operate at continental scales; even planetary orbital and solar variations operating at millennial time scales cannot be ignored. Many of those processes are well understood; other less so.

Models are the means that scientists use to express their knowledge about a process, or a set of processes using equations that can be solved on a computer. It is impossible to represent everything known about all the processes that govern climate in detail on today's computers because it is simply beyond the computer power currently available to us, and approximations must be made. There are also many things scientists recognize that are "not known" that may be important in understanding climate change. It is hoped that these entries will provide hints on how climate models are constructed, how they are assessed and tested, and how they are used to provide insight into the changing climate of the past, and the possible changes that will take place in the future.

Here is a brief description of the entries of this section, and the rationale for their inclusion.

A broad overview of coupled climate system modeling is provided in ► Coupled Climate and Earth System Models by Gent. This entry introduces the components of a coupled model, how they work together, and the kind of scientific problems that they are designed to address.

The individual component models are described in more detail in the next set of entries. Each of these component models can be used on its own to study a piece of the climate system by essentially "prescribing" the behavior of the other components, or they can be used as a part of the bigger model to explore interactions. Bitz and Marshall describe treatments of

the cryosphere (ice and snow in the Earth System) in the entry ► Cryosphere, Modeling of; Yoon and Ma cover ocean processes in ► Oceanic General Circulation Models. Bacmeister discusses global atmospheric models from a weather modeling point of view in ► Weather Prediction Models, and Rasch discusses these models from a climate perspective in the entry ► Atmospheric General Circulation Modeling. Niu and Zeng provide an introduction to land surface models in ► Earth System Model, Modeling the Land Component of. These models provide scientists with a picture of how physical components of the climate system respond to "forcing" from other components.

It is also interesting to explore the interaction between the physical system and society. ► Integrated Assessment Modeling by Edmonds et al. describes "Integrated Assessment" modeling and climate change that begin to assess how humans affect climate and how climate affects humans.

Some aspects of climate change are most easily explored at a very high resolution with more detail than can be afforded on today's computer systems. This motivates the entry on ► Regional Climate Models by Leung. Methods used to assess uncertainties in climate change studies are outlined in ► Climate Change Projections: Characterizing Uncertainty Using Climate Models by Sanderson and Knutti.

Climate varies on many time scales. The entry by Goddard on ► Climate Predictions, Seasonal-to-Decadal provides a very nice introduction to the issues of prediction of climate processes on multi-decadal time scales. The climate section concludes with an example by Wang and Lau of one way that the mankind may be influencing a very important feature of the Earth system that influences the lives of billions of people, the Indo-Asian monsoon (► Monsoon Systems, Modeling of).

It is hoped that scientists and engineers find the entries interesting, and that they stimulate additional study in this important topic in Sustainability Science.

Bibliography

1. Arrhennius S (1896) On the influence of carbonic acid in the air upon the temperature of the ground. Philos Mag 41:237–276
2. IPCC (1996) Climate change 1995: the science of climate change. In: Houghton JT, Meira Filho LG, Callander BA, Harris N, Kattenberg A, Maskell K (eds) Contribution of working group I to the second assessment report of the intergovernmental panel on climate change. Cambridge University Press, Cambridge. ISBN 0-521-56433-6 (pb: 0-521-56436-0)
3. IPCC (2007-SRM) Climate change 2007: synthesis report. In: Core Writing Team, Pachauri RK, Reisinger A (eds) Contribution of working groups I, II and III to the fourth assessment report of the intergovernmental panel on climate change. IPCC, Geneva, 104 pp
4. IPCC, 2007-WG1: Climate change 2007: The physical science basis. In: Solomon S, Qin D, Manning M, Chen Z, Marquis M, Averyt KB, Tignor M, Miller HL (eds) Contribution of working group I to the fourth assessment report of the intergovernmental panel on climate change. Cambridge University Press, Cambridge/New York
5. IPCC 2007-WGII, Barker T, Bashmakov I, Bernstein L, Bogner JE, Bosch PR, Dave R, Davidson OR, Fisher BS, Gupta S, Halsnæs K, Heij GJ, Kahn Ribeiro S, Kobayashi S, Levine MD, Martino DL, Masera O, Metz B, Meyer LA, Nabuurs G-J, Najam A, Nakicenovic N, Rogner H-H, Roy J, Sathaye J, Schock R, Shukla P, Sims REH, Smith P, Tirpak DA, Urge-Vorsatz D, Zhou D (2007) Technical summary. IPCC-WGIII, climate change 2007: mitigation. In: Metz B, Davidson OR, Bosch PR, Dave R, Meyer LR (eds) Contribution of working group III to the fourth assessment report of the intergovernmental panel on climate change. Cambridge University Press, Cambridge/New York
6. Parry ML, Canziani OF, Palutikof JP, Co-authors (2007) Climate change 2007: impacts, adaptation and vulnerability. In: Parry ML, Canziani OF, Palutikof JP, van der Linden PJ, Hanson CE (eds) Contribution of working group II to the fourth assessment report of the intergovernmental panel on climate change. Cambridge University Press, Cambridge, pp 23–78
7. Steffen W, Grinevald J, Crutzen P, McNeil J (2011) The anthropocene: conceptual and historical perspectives. Philos Trans R Soc 369:842–867. doi:10.1098/rsta.2010.0327

Climate Change Projections: Characterizing Uncertainty Using Climate Models

Ben Sanderson[1], Reto Knutti[2]

[1]National Center for Atmospheric Research, Boulder, CO, USA

[2]Institute for Atmospheric and Climate Science, ETH, Zürich, Switzerland

Article Outline

Glossary

Definition of the Subject and Its Importance

Introduction
Projection Uncertainty and the Need for Ensembles
Multi-model and Perturbed Physics Ensembles
Model Validation and Tuning
Statements of Probability
Future Directions
Bibliography

Glossary

Bayes' Theorem A law in probability theory relating the probability of a hypothesis given observed evidence to the often easier to characterize probability of that evidence given the hypothesis. The theorem states that the conditional "posterior" probability of an event A given an event B is equal to the "prior" probability of A multiplied by the likelihood of B given A is true, normalized by the prior probability of B.

Climate sensitivity The equilibrium global mean near surface air temperature response in Kelvin to a sustained doubling of the atmospheric carbon dioxide concentration.

CMIP-3 The Coupled Model Intercomparison Project Phase 3, a set of coordinated model experiments using General Circulation Models from the world's major modeling centers.

Detection and attribution A process whereby spatial "fingerprints" associated with individual climate forcing factors (such as aerosol or greenhouse gas concentrations) are identified and used to quantify whether an observed change exceeds the range of natural internal climate variability (detection) and to attribute it to different causes, that is, different forcings (attribution).

Empirical model A model based on fitting empirical data, and thus makes no attempt to justify its representations of the system with any physical basis.

General circulation model (GCM) A three-dimensional mathematical model for the atmosphere and possibly the ocean, land, and sea ice.

Initial condition ensemble A number of simulations using a single climate model, each with a small, unique perturbation to the initial state.

Last glacial maximum (LGM) A period in the most recent ice age lasting several 1,000 years, peaking approximately 20,000 years ago at the maximum extent of the ice sheets.

Lead time The period in between the time at which the forecast is made and the time to be forecasted.

Multi-model ensemble (MME) A collection of structurally different models from a range of institutions used to perform a coordinated set of experiments.

Parameter space The multidimensional domain created by considering the possible values of a number of parameters within a model.

Perturbed physics ensemble A set of climate simulations generated by taking a single physical model and altering uncertain parameters within a range of plausibility.

Prior probability (marginal probability) The probability of an event before any additional data is considered in a Bayesian sense.

Posterior probability The probability of an event after considering additional relevant evidence in a Bayesian sense.

Systematic error The difference between a model simulation and observations or a poorly represented process which is not reducible by parameter tuning.

Definition of the Subject and Its Importance

The atmosphere, ocean, land surfaces, and ice sheets of the Earth are highly complex and coupled systems, with physical laws which describe behavior from the microscopic to the planetary scale. General Circulation Models are computational analogs for these physical systems, which can be used to study how these systems might behave when boundary conditions are changed (e.g., by increasing the concentration of atmospheric greenhouse gases).

Inherent in the design of such models are a myriad of choices when deciding which components of the system are to be modeled and how to represent processes which cannot be currently modeled explicitly. In order to have any confidence in the ability of our models to have value for simulating aspects of future climate change, it is necessary for those models to reproduce observable properties of the physical system. However, model errors in the simulation of the past or present are likely to be smaller than errors in future projections because model developers can use

observations and historical records in the development of their code. Additionally, some processes may not be observable or testable yet, because they might only take place in a warmer (or otherwise changed) world.

One way to characterize at least some of the uncertainty in future projections is to produce an ensemble of climate simulations, each making different but reasonable assumptions about their representation of physical processes.

In recent years, a number of groups in the international climate science community have produced General Circulation Models of the earth system, each making different choices about model complexity, resolution, and parameterization of processes which occur at scales finer than those resolved. By conducting coordinated experiments with each of these models, it has become possible to examine some of the effect that such choices have on uncertainty in future climate simulations. However, the sheer volume of data and range of models available from such an ensemble presents a new challenge for the science to address: How can a spread of non-independent "best guesses" be combined to produce meaningful statements of uncertainty which are relevant to climate-related policy decisions?

Introduction

In 1979, Jule Charney chaired a committee on anthropogenic global warming, producing a report [1] providing a brief overview of the state of the science of climate change. At the time, two General Circulation Models were available for consideration, one led by Syukuro Manabe and the other by James Hansen. The report produced an estimate for the climate sensitivity (the equilibrium global mean temperature change to a doubling of the atmospheric carbon dioxide concentrations) based on the mean result of these two models. In comparing the predicted future climate of these two models, the report stated:

- We conclude that the predictions of CO_2-induced climate changes made with the various models examined are basically consistent and mutually supporting. The differences in model results are relatively small and may be accounted for by differences in model characteristics and simplifying assumptions.

This, in many ways, represents the first effort to combine multiple results from an ensemble of climate model simulations, and the statements made using those models are still relevant to ensemble modeling. A better understanding in the uncertainties in the simulations and increased confidence can be claimed if an ensemble of somewhat independent models produces common features in its simulations, and if the origins of the differences between simulations may be traced back to physical characteristics.

When presented with a range of simulations of future climate, one must make judgments on many levels on how that ensemble should be interpreted: How should model agreement, or lack of it, translate into a degree of confidence in the simulations? Should all models be treated equally, and if not then how should one distinguish between them? If some processes are absent from some or all of the simulations, how can the projections be updated to account for these "known and unknown unknowns"? Should each ensemble member be interpreted to be an estimate of the "truth" with some unknown error, or should the "true" earth system be considered as a potential member of the ensemble? Although some of these questions verge on the philosophical, the judgments made in answering them can have large effects on the results themselves that are obtained and the degree of uncertainty in those results.

In recent years, there have been systematic efforts to explore and characterize uncertainty using large ensembles of increasingly complex models of the earth system. These model simulations have been coordinated and analyzed to help in characterizing climate change in a series of assessment reports for the Intergovernmental Panel on Climate Change (IPCC). In 1990, 1995, 2001, and 2007, a selection of GCMs were assembled from various major modeling groups around the world to compare simulations of past, future, and other idealized scenarios of climate change. Through the successive decades, model complexity and scope have increased; the early GCMs of Manabe [2] and Hansen [3] modeled atmospheric dynamics and radiative transfer, with a simplistic representation of the hydrological cycle. By the time of the First Assessment Report of the IPCC [4] (FAR) in 1991, models included clouds, a land surface model, and prescribed

ice cover. For the Second Assessment Report [5] (SAR), some models also included a representation of the ocean and interactive sea ice. In the Third Assessment Report [6] (TAR), some models considered the effects of volcanic eruptions and aerosol emissions, with a fully dynamical representation of the oceans. By the time of most recent Fourth Assessment Report [7] (AR-4), some models were beginning to include an explicit representation of the carbon cycle in the earth system. Today's models continue to model additional components of the earth system, such as interactive vegetation, dynamically resolved ice sheets, a coupled carbon-nitrogen cycle and full atmospheric chemistry. In parallel with all of these improvements, the last few decades have also seen a continued increase in model resolution. Where the models used in the FAR split the earth into cells as large as 500 km on a side, models for the AR4 can resolve at a scale of a few tens of kilometers.

This entry focuses on the advantages and additional complexities which one must consider when studying a range of different model simulations. Rather than giving a comprehensive description of the results of the models assessed in the successive generations of the IPCC, this entry will discuss the added technical and conceptual challenges encountered when considering the results of a range of non-independent models and how a range of simulations may be combined into best estimates and uncertainties for future climate evolution.

Projection Uncertainty and the Need for Ensembles

Empirical and Physical Models

In 150 AD, Ptolemy devised a model of the motion of planets in the solar system by describing a system of concentric, geocentric circles (or "*deferents*") on which were mounted smaller circles ("*epicycles*") on which the planets themselves were mounted. This system thus had a large number of degrees of freedom (the diameters and speeds of rotation of each of the deferents and epicycles), which could be finely tuned to reproduce the motions of the bodies in the night sky. Such was the predictive power of this approach, that variations of this simple model were accepted until Copernicus' heliocentric model was published in 1543. Although Copernicus' model fits the established view of the universe more closely, both of these models were *empirical* in that they were not based on any physical principles at that time. However, even without a physical basis, Galileo was able to validate the Copernican model by studying the phases of the planet Venus – which was only consistent with the heliocentric formulation. It was not until Newton's law of universal gravitation that the model could be given a physical underpinning.

Any model of a physical system is an approximate representation of the truth. It should be able to reproduce some behavior of that system, and it might do this empirically like Ptolemy's model or by explicitly simulating physical processes within the true system like an orbital system based upon Newtonian gravitation. A model, whether empirical or physical, cannot ever be validated in the strict sense of showing it to be a wholly correct representation of the true system; it can only be evaluated by reproducing some output not used in the tuning of the model itself. This was true of Galileo's observation of the phases of Venus – information not used in the tuning of the Ptolemic model. However, any empirical model becomes very sensitive to changing boundary conditions. For example, if the mass of the Sun were to instantly double, the Copernican model of the solar system would be a very poor approximation of planetary motion, whereas a model based upon Newtonian mechanics would capture enough of the necessary physics to remain useful.

These fundamental principles are relevant to methodologies for simulating the climate today. If the simplest, zero dimensional empirical model of the climate is taken to be:

$$C\frac{dT'}{dt} = F' - \lambda T'$$

where T' is the global mean temperature difference from an equilibrium state, F' is the additional radiative forcing to the planet (i.e., the change in the top of atmosphere radiative balance caused by a forcing, e.g., increased CO_2), C is the effective heat capacity of the system, and λ is the global sensitivity parameter. This equation has two free parameters, C and λ which may be tuned such that the model can fit an observed past time series of F' and T', that of the twentieth century, for example. The model can then be evaluated by predicting a previously unseen time period, such as the last glacial maximum. This evaluation, if successful,

would give more confidence in the model but would not necessarily make it trustworthy for a prediction of the future – where the boundary conditions are outside those seen in both the training and validation period.

The added advantage of using a GCM to simulate future climate is that model simulations are in theory more trustworthy because they are based upon physical principles, which it is believed can reproduce observed climate by coupling underlying physical laws that are known to be true. However, this view is often overoptimistic; although some components of the modeled climate, such as the equations of motion in the atmosphere or the instantaneous radiative forcing due to a change in atmospheric carbon dioxide concentrations are well understood and consistently implemented in different GCMs, there are other processes such as convection which cannot explicitly be resolved with current computing resources. These processes and their effects on the large scale climate must be approximated with uncertain parameters that must be estimated by tuning the model to reproduce some observed features of the climate. What this means, in practice, is that a GCM is neither only an empirical nor an explicitly physical model; it is a hybrid of the two where model developers face many arbitrary choices in parameterizing processes which cannot be explicitly resolved. The necessity for the tuning process reintroduces some of the problems encountered with an empirical model, with the possibility of false confidence in model performance by over-tuning the model to reproduce past climate. The ambiguity in these parameterizations justifies the existence of multiple models for the same purpose [8]; each of these models is seen as a plausible approximation of the climate system given the imperfect understanding, the uncertainties in observations and the computational constraints.

Types of Uncertainty and the Need for Ensembles

Although weather and climate simulations share some properties (sometimes they are conducted with the same model), the limiting uncertainties are very different. Climate represents the distribution of all possible states in which one expects to find a system, whereas weather is the specific evolution of the system from a given initial state. A model-based weather forecast is a *prediction*, in that the initial state of the simulation is as close as possible to observations and the absolute errors grow rapidly afterwards. In weather prediction, these errors occur as specific weather systems evolve from the initial state. Because the atmosphere is a chaotic system, very small errors in the estimate of the initial state can result in very large differences in the distributions of weather systems a few days later. Initial condition uncertainty is evaluated by repeating simulations with a range of slightly different initial conditions to form "Initial Condition Ensembles." The spread of these ensembles initially grows rapidly but eventually saturates when the "memory" of the initial state is lost (this timescale is longer in the oceans, perhaps up to 10 years for North Atlantic ocean temperatures [9]).

On decadal to century timescales, the mean and spread of an initial condition ensemble represents a *projection* of the future climate state, although this spread is only a small fraction of the total error (sometimes known as "uncertainty of the first kind"). The second kind of uncertainty relates to the boundary conditions of the problem, some of which are naturally occurring such as the level of incoming solar radiation or volcanic activity, while others are dependent on anthropogenic factors such as the future emissions of greenhouse gases or aerosols. To address this uncertainty, one must perform a range of simulations using different plausible scenarios for changes in boundary conditions. The results of any simulation are therefore conditional on assumptions made about future human behavior. There is currently little real skill in forecasting future volcanic activity and changing solar activity so simplistic but plausible scenarios for these quantities are often used (such as repeating past values). However, in most future scenarios these represent a relatively small fraction of the total anthropogenic climate forcing.

Figure 1 shows the relative sources of error in a climate model projection as a function of the lead time [11]. For lead times of less than a decade, the uncertainty in the initial state combined with chaotic error growth and natural patterns of variability are the dominant sources of error but on the scale of several decades or more, it is the future emissions scenario which dominates the uncertainty. Predictions on all timescales, however, are subject to model

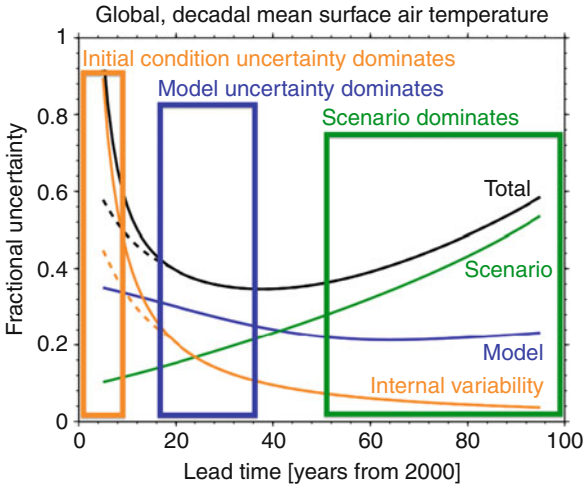

Climate Change Projections: Characterizing Uncertainty Using Climate Models. Figure 1
A figure showing the fractional sources of uncertainty in a climate model projection as a function of time. The *orange* "internal variability" *line* shows the errors due to uncertain knowledge of the initial state of the system, while the *dotted line* shows the potential reduction in error if effort is made to assimilate ocean observations into the model at the start of the simulation. The *green line* shows the fractional error due to the unknown future emissions of climate altering gases, while the *blue line* shows the error due to the model imperfections. The *boxes* show where different types of uncertainty are dominant for a projection of future climate (Reproduced from [10])

uncertainties. These arise when a climate model contains parameterizations for unresolved or missing processes. Parameterizations take large-scale quantities resolved by the model, such as temperature, wind speed, and humidity, and relate them to unresolved processes, such as convective mass flux and cloud profiles. Although these parameterizations are usually constructed from physical underpinnings and evaluated with observed data, they introduce some unavoidable uncertainty when a range of parameter values might be physically plausible. GCMs are often subject to a tuning of parameter values to reproduce features of the observed climate, but with tens or hundreds of uncertain parameters this process is time consuming and can yield multiple solutions because of the computational cost, a systematic tuning of all parameters is unfeasible.

One method of quantifying the parameter uncertainty problem is to construct a "Perturbed Physics Ensemble" (PPE) using a single GCM. This process has been attempted using several major climate models [11–13] and involves taking a subset of important unknown parameters within the GCM and perturbing them within the bounds of physical plausibility. Such experiments might perturb, for example, a parameter which states the necessary humidity required for the formation of cloud. By varying this parameter, one can change dramatically how the model distributes clouds both in the present day and the future. These changes can affect the strength of global feedbacks which can change, for example, the amount of warming that the model predicts for a given rise in greenhouse gases. An example of a PPE is the "climateprediction.net" experiment [13], which used idle time in volunteer's computers to perform perturbed simulations of future climate. Incorporating this range into an uncertainty estimate for predictions of future climate requires a framework for joint consideration of each model's performance in simulating past and present climate as well as its future response.

The remaining model uncertainties are due to so-called "systematic" or structural errors arising from the model design, that is, the choices of which processes to model, the resolution of the model, the numerical schemes, and the specific form of the parameterization scheme. The structural differences between different GCMs provide a lower bound on the extent of the structural difference between any one GCM and the true climate system, but in reality the models in an ensemble such as those used for the IPCC reports share many common properties in terms of resolution, numerical methods, missing components, and parameterization schemes which might make all the models subject to similar errors. Nevertheless, considering a range of GCMs which make different modeling assumptions is an essential step when evaluating the robustness of any prediction of future climate change because it places a lower bound on the uncertainty arising from the choices made by model developers.

Multi-model and Perturbed Physics Ensembles

When making predictions of a future climate state, there is a wealth of evidence to suggest that considering

a combined prediction using multiple, somewhat independent models yields more accurate results than any single model [14–16]. Additionally, the spread of simulations provides a measure of robustness in the prediction. The following section describes some reasons for the increased performance of multi-model and perturbed physics ensemble forecasts, together with some of the complexities arising from their analysis.

Range of Ensemble Responses

The spread of results from an ensemble of climate simulations is dependent upon the experimental design, or lack of it. A perturbed physics ensemble (PPE) has the luxury of allowing some control of the distribution of models in the parameter space of the model, though the structure of the underlying model places a fundamental limit on the range of observable behavior in the ensemble. For example, if a PPE is created by perturbing cloud parameters in a GCM which has no parameterization for cirrus clouds formed by gravity waves, then there is no way that such an ensemble can include uncertainty about that process. Designers of such experiments must also be aware that the decisions of how to sample the parameter space of a model will directly influence the distribution of future climate simulations [17]. In contrast, multi-model ensembles (MMEs) such as the Coupled Model Intercomparison Project (CMIP-3), explore "systematic" model differences, which sample models with different representations of the physical system, rather than simply varying parameters in a single model. These are "ensembles of opportunity" where multiple modeling groups run coordinated experiments but the ensemble itself is not sampled in any systematic fashion. Nor is the ensemble randomly sampled because each modeling group will tune their model to minimize model differences from observations, thus creating an ensemble of "best-guesses." This is quite different from the PPE case where the model is intentionally detuned to produce a wide range of behavior. Evidence for this can be seen by examining the spread of climate sensitivity in both a multi-model and a perturbed physics ensemble (Fig. 2). When considering a range of observational constraints on climate sensitivity, it is apparent that the multi-model values tend to cluster about the most likely value, whereas the perturbed physics ensemble contains models which span the full range of uncertainty in climate sensitivity. Although impossible to verify, it also is possible that there is also a component of social anchoring [18] which draws multi-model sensitivities toward the mean value as any group which finds their model to be an outlier may have to defend why this is the case, whereas a model with the consensus value of sensitivity is less likely to be questioned.

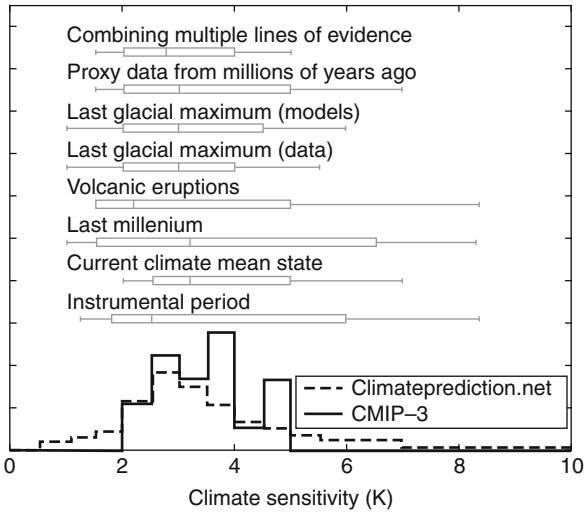

Climate Change Projections: Characterizing Uncertainty Using Climate Models. Figure 2
Distribution functions of climate sensitivity (an estimate of the equilibrium response of a model to a doubling of CO_2) for models in the CMIP-3 ensemble (hinting at the range of responses from an MMF analysis), compared with a selection of models from the climateprediction.net project (hinting at the range of uncertainty from a PPE analysis). *Box and whisker plots* show estimates of the most likely values, together with 66th and 90th percentiles of likelihood for climate sensitivity taken from various lines of observational evidence (Adapted from [19]). *Histograms* represent the fraction of models in each 0.5 K bin of climate sensitivity for the atmosphere-only components of 19 models in the CMIP-3 archive and for a 2,000 member subset of the climateprediction.net ensemble [13]

The Ensemble Mean State

In various fields, it has been shown that the combined performance of multiple models can exceed that of an individual ensemble member. Examples of this can be

seen in models of crop yield [20], disease modeling [21], and even in the optimization routines used for movie recommendations based upon past viewing choices [22]. Similarly in seasonal climate predictions, it has been shown that the multi-model ensemble means yield better forecasts, in general, than using only initial condition ensembles from a single model [16]. A multi-model study incorporating a set of initial conditions for each model is often referred to as a "super-ensemble." The accuracy of the model mean often performs best in multivariate applications, that is, a single model may show increased skill in predicting one particular diagnostic, but when many variables are considered in the same metric the ensemble mean prediction tends to show greater skill than any individual model [23].

This effect can also be seen in GCM simulations of recent past climate. Figure 3 shows successive generations of the CMIP ensemble evaluated using a multivariate error metric comparing twentieth century observations to model simulations of that period for a variety of model diagnostics. The figure shows that model errors in simulating the current climate have decreased over time but also that for each generation of the ensemble, the multi-model mean results in a model-data discrepancy almost as good, or better than the best performing ensemble member. Various studies have found that both in detection and attribution studies [24] and in simulations of recent climate [25] that a multi-model mean provides a better multivariate simulation than any individual model.

This approach is common in the reports of the IPCC, where an unweighted mean of future model simulations is used to show a "best-guess" simulation of future climate, while the degree of model spread is used to estimate some measure of the significance of the result. There are more sophisticated methodologies that one may use for model combination, involving Bayesian methodologies [27] or model weighting [28], but the correct implementation and interpretation of such studies is subject to some debate. It has been shown that the ranking of model performance within a multi-model ensemble such as CMIP-3 is often highly dependent on the choice of metric used to evaluate the model. A metric based on the model's ability to reproduce observed variability will produce a different ranking than a metric which evaluates the model simulation of the mean state [30], and the performance of different models on these two metrics are very weakly correlated (Fig. 4). In addition, violation of the model "democracy" (one model, one vote) in the IPCC process is potentially controversial, as choices of

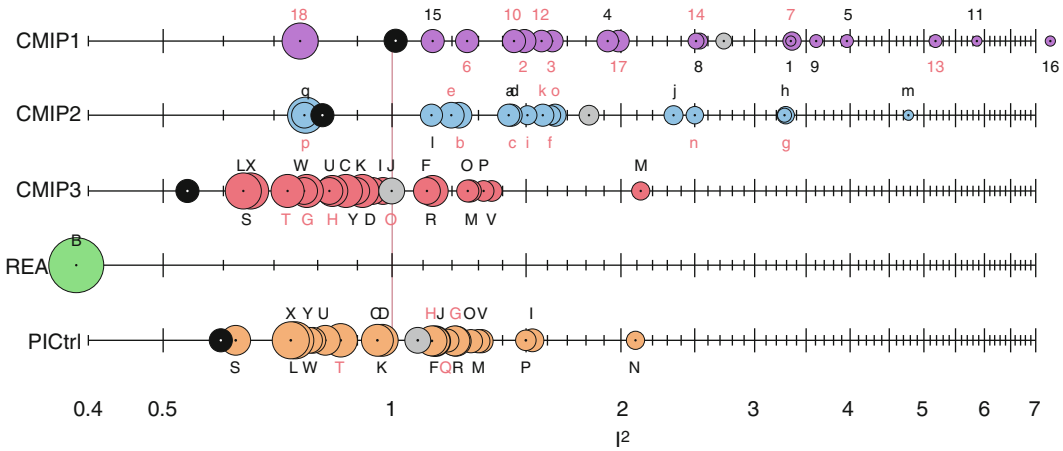

Climate Change Projections: Characterizing Uncertainty Using Climate Models. Figure 3
A comparison of model errors reproduced from Reichler and Kim ([26], corrigendum) multivariate errors are evaluated for successive generations of the coupled model intercomparison project (CMIP). *Colored circles* represent individual models in the ensemble, whereas *black circles* show the performance of the multi-model mean. REA represents the NCEP reanalysis and the CMIP-3 PICNTRL is the performance of the preindustrial control simulations when evaluated against present-day observations

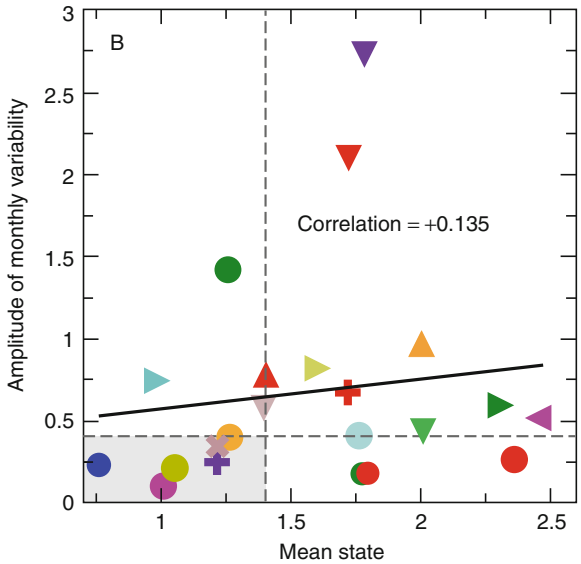

Climate Change Projections: Characterizing Uncertainty Using Climate Models. Figure 4
The relationship between model skill in reproducing the mean climate state and skill in reproducing patterns of natural variability for models in the CMIP-3 ensemble. Each point represents a single model in the CMIP-3 archive, and errors are averaged over a large number of diagnostics. The *black line* shows the fitted least-squares regression (Reproduced from [29])

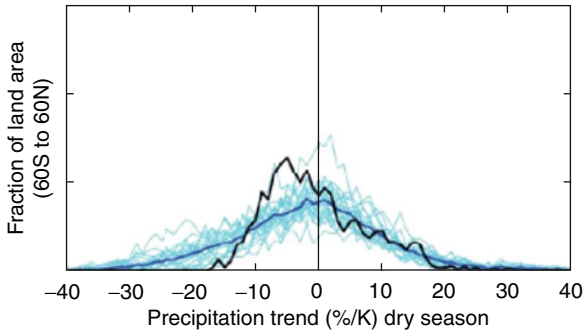

Climate Change Projections: Characterizing Uncertainty Using Climate Models. Figure 5
This plot, from Knutti [31] shows the fraction of land area between 60°N and 60°S experiencing a given change in precipitation in the dry season. Precipitation change is measured in percent per unit global temperature rise in Kelvin measured over the period 1900–2100 relative to the 1900–1950 average. Each *light blue line* represents a single CMIP3 ensemble member, the *dark blue line* marks the average of all distributions. The *black line* shows the precipitation change in the multi-model mean. The expected absolute precipitation change in the multi-model mean is about 30% smaller than in any single model

how to weight models could be interpreted as a political statement [31].

The question of why multi-model means perform better than individual models is a complex one. Certainly, the mean is not in itself a self-consistent representation of a physical system and is therefore not subject to many of the restrictions that apply when tuning one model to reproduce an observed climate. As an example, a single model may be tuned in different ways to reproduce two different observed values "A" and "B," but it might be impossible to tune the model to reproduce "A" and "B" simultaneously. However, if different models in the ensemble make different choices about the relative importance of "A" and "B," it is likely that the ensemble mean will be close to the observed values in the case of a large ensemble. Clearly, real GCMs have a large number of observable diagnostics to reproduce and a large number of tuning parameters, but it remains true that the multi-model mean is less restricted by model structure than any individual model in the ensemble. Another interpretation is that some of the model biases are random perturbations about the truth (i.e., each model reproduces the observations with some pattern of bias that is characteristic to that model and but different in each model), such that averaging many models reduces the magnitude of the biases. In the limit of completely random independent biases, the average would be perfect for an infinite number of models.

In some cases, the multi-model mean can indicate behavior unrepresentative of any of the models within the ensemble. Figure 5 shows the distribution of expected percentage precipitation change per unit global temperature increase in the current dry season for various models within the CMIP3 archive. Each individual model shows a wide distribution of change with some regions showing up to 30% decrease in precipitation for every degree rise in global mean temperature. If the models are averaged together in advance, however, the resulting multi-model mean has no region which displays this extreme decrease in

precipitation in the dry season. The multi-model mean is thus not representative of the findings of the individual ensemble members in the respect that it fails to recover the extremes of the distribution of precipitation change. The reason for this discrepancy is, at least partially, a difference of the spatial representation of precipitation patterns in different ensemble members. Different models have different resolution, representations of orography, and parameterizations for precipitation. When combined this gives each models unique spatial modes of variability for precipitation. This allows each model to display extreme future drying in some specific regions, but critically those regions are not necessarily identical in all models in the ensemble, effectively smearing out the small scales and the extremes of the distribution. Thus, although the mean result of a large ensemble may provide a reduction in model bias, the averaging process itself may create an unrepresentative forecast.

Model Independence

Given a set of truly independent models distributed about the truth, one would always be able to improve simulation quality by increasing the number of models in the ensemble as truly independent errors would tend to cancel. Any study which treats CMIP ensemble members as independent realizations of a possible future is implicitly making this assumption, but one can make statistical arguments to show that the models are not distributed in a way which would be consistent with this assumption [36]. To illustrate this visually, Fig. 6 shows maps of temperature and precipitation from a selection of models in the CMIP-3 archive, all of which could be used with equal weight in producing a multi-model mean. However, one can see instantly that the two GFDL models have very similar biases in surface temperature, even though they are submitted as separate models to the archive. The temperature biases in the other two models shown have very different spatial patterns. The precipitation plots, however, show that there are some common biases in all four of the models. There are many reasons why these common biases might exist; all models in the CMIP-3 ensemble cannot explicitly resolve features smaller than about half a degree, which renders them incapable of simulating behavior such as atmospheric blocking or the response to local orography. Models may also share parameterization schemes and be tuned to reproduce the same observations [32], and in some cases the same model can be submitted to the ensemble at multiple resolutions meaning that models can share considerable parts of code, making it very likely that model biases will be correlated. In summary, it is both expected and evident that the current generation of climate models does not provide an independent sample of estimates distributed about an underlying truth, and it is unlikely that increasing the number of similar models in the ensemble would drastically increase the accuracy of combined predictions.

Model Validation and Tuning

GCMs are frequently tuned by minimizing differences between simulations of the past century and observations. The observations can be in the form of data from satellites and in situ measurements or may be expressed as reanalyzed products which attempt to incorporate information from both of these. Simulations of earlier periods may also be evaluated against proxy data (estimates of temperature or rainfall etc., produced from tree rings, ice cores, etc.), although the long simulations and necessary model reconfiguration for these periods often mean they do not form part of the active model development process. Because models are tuned to agree with data over the twentieth century, they tend to agree with each other for this time period. There is little spread in the model simulations over the twentieth century. Figure 7 taken from the IPCC AR-4 report shows that the models behave similarly throughout the twentiethcentury when compared to any one of the scenarios for the twenty-first century. The reader should not attach any significance to the absolute values of the global mean temperature time series, which are expressed as anomalies with respect to the 1980–2000 mean for all models.

The remarkable consistency of the global mean temperature evolution in the twentiethcentury in the current generation of GCMs is made possible through the various degrees of freedom the models have in fitting this well-observed period. The response of any model is governed by a combination of transient ocean heat uptake, climate sensitivity, and the radiative forcing to the system, which effectively makes the problem

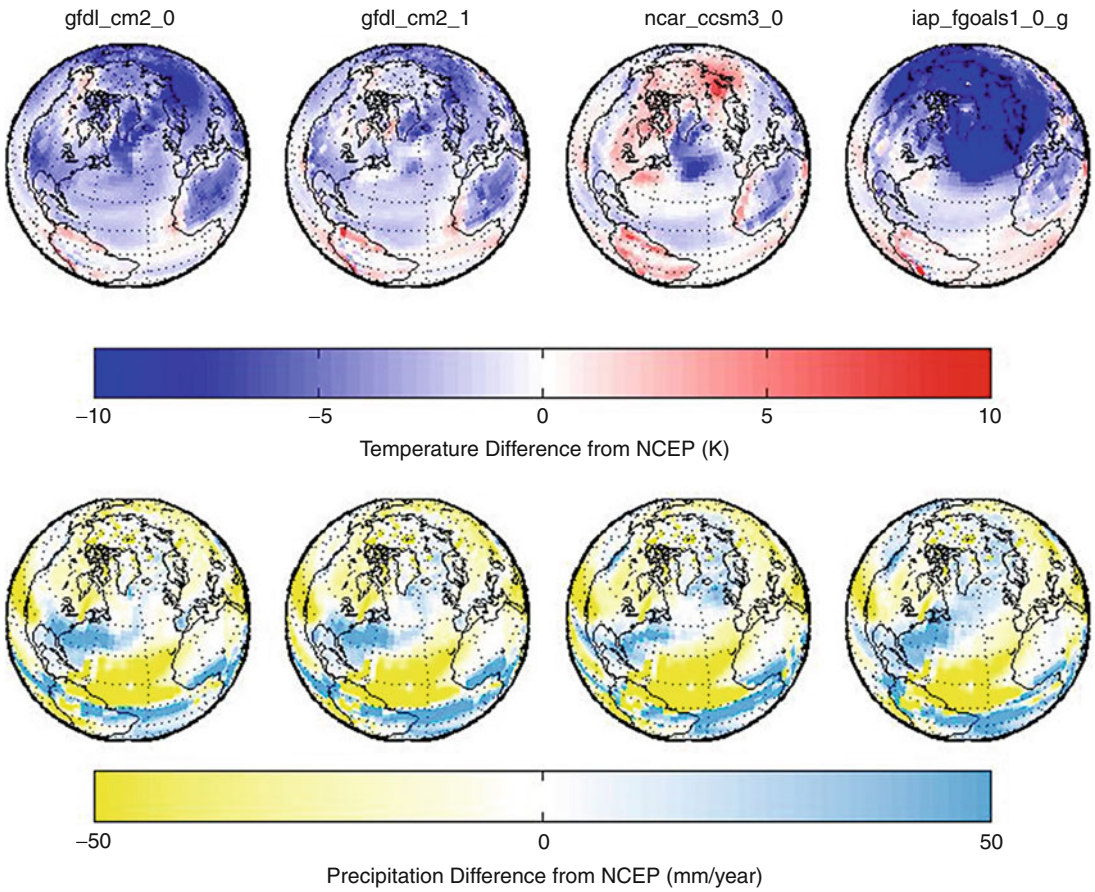

Climate Change Projections: Characterizing Uncertainty Using Climate Models. Figure 6
Temperature and precipitation maps of the North Atlantic region from four models submitted to the CMIP-3 archive. Each map shows the 1980–2000 averages for June, July, and August – expressed as a difference between the model simulation and the NCEP reanalysis for the same period. The *top row* shows the anomaly for surface temperatures, while the *bottom row* shows the anomaly for annual total precipitation

poorly constrained with multiple ways to fit the twentieth century global mean temperature time series [33]. A study by Kiehl (2007) concluded that models produced this agreement by compensating between differences in climate sensitivity with differences in aerosol forcing. Figure 8 shows both the climate sensitivities and the later twentieth century anthropogenic forcing of climate in a selection of GCMs [34]. It is apparent that those models with a larger anthropogenic climate forcing in the twentieth century have a smaller climate sensitivity, allowing the models to successfully reproduce the twentieth century temperature record (a weak correlation between aerosol forcing and climate sensitivity is also seen in the CMIP-3 archive used for the AR4 report [35]).

In each of the twenty-first century scenarios illustrated in Fig. 7, the aerosol concentrations are predicted to decrease as increasingly stringent clean air legislation comes into effect. Meanwhile, all the scenarios show a continuing increase in greenhouse gases throughout the twenty-first century, which makes the climate sensitivity of the models the primary factor influencing their future evolution as the total anthropogenic forcing increases. The differing climate sensitivities amongst the CMIP3 models thus cause a larger spread in the twenty-first century simulations than for the

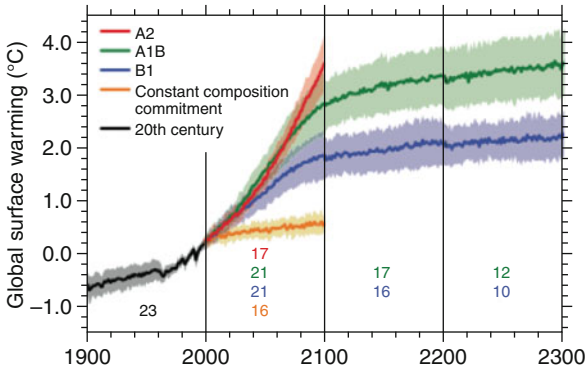

Climate Change Projections: Characterizing Uncertainty Using Climate Models. Figure 7
A figure reproduced from the IPCC AR-4 report (Fig. 10.4) showing the mean and inter-model spread of simulations in the CMIP-3 model archive for simulations of the twentieth century, together with the simulations of three different scenarios for periods after the year 2000. Global mean temperatures are shown relative to the 1990–2000 mean. In each case, the *line* represents the multi-model mean and the shading shows the 1 standard deviation ensemble spread

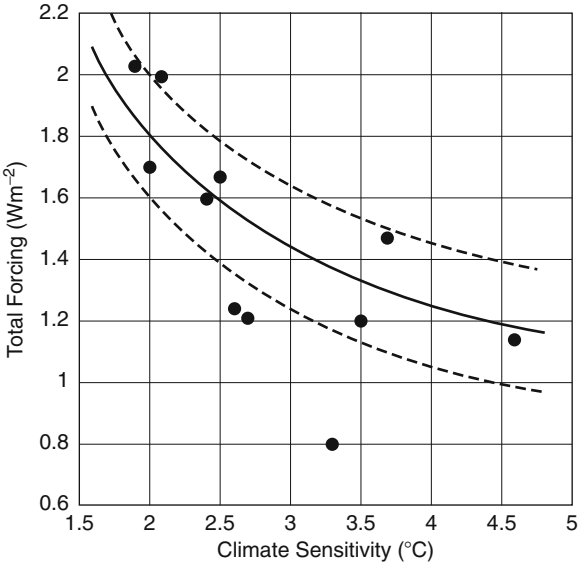

Climate Change Projections: Characterizing Uncertainty Using Climate Models. Figure 8
A figure reproduced from Kiehl [35] which shows the relationship between climate sensitivity and total anthropogenic forcing of climate in the late twentieth century in a set of GCMs, represented by the *black dots*. The *solid line* represents a theoretical relationship between the two quantities necessary to produce the warming observed over the twentieth century, the *dashed lines* show the uncertainty in this relationship due to uncertainty in transient ocean heat uptake

twentieth century simulations. However, it should be noted that most AR4 models included the "direct" radiative effect of aerosols, but not their indirect effect on cloud properties. This means that eliminating the correlation between climate sensitivity and aerosol forcing would not necessarily reduce projection uncertainty, and the success of most models in simulating the twentieth century may be partly spurious [36].

An additional problem lies in the lack of independent data with which to tune and verify the models. In many cases, model quality metrics are based upon mean state and variability data from the latter twentieth century data, which is very likely to be used in the development of parameterizations and tuning of the model. For example, most models use satellite data products to tune the top of atmosphere energy fluxes, and these products are often considered to be one of the more robust constraints when evaluating a model quality metric. In addition, models may often be evaluated against reanalyses, rather than the observational data itself. Reanalysis products are model simulations strongly "nudged" to reproduce an incomplete set of observations, effectively filling in the gaps with self-consistent model data output. This process introduces an additional layer of complexity, because the reanalysis climate will contain features both of the constraining observations and the underlying model. For fields where real data is sparse or where data is not assimilated directly (such as precipitation metrics), the reanalysis output might have much more dependence on the underlying model than on any real-world data. As a result, when using reanalysis data as a constraint for multiple models, those models with a similar representation of the hydrological cycle to that used in the reanalysis will appear to perform better.

The model development process involves a considerable amount of value judgment, as a model serves many purposes and some compromise between the

many different plausible performance metrics must be made. The relatively small number of degrees of freedom available to model developers makes it impossible to perfectly match a large number of observable quantities simultaneously, which means that there may be multiple possible parameter combinations which are equally valid. Each of these combinations, although they fit historical observations equally well, may have different projections of future climate change if they exhibit different climate sensitivities or aerosol responses.

In the past, model tuning has largely been a time-consuming process of expert judgment and trial and error, which leads to some uncertainty of what errors in a simulation are irreducible through parameter adjustment. Although not yet used operationally, various techniques have been proposed to automate this tuning process. One technique uses an optimal gradient descent approach to minimize some multivariate error metric [34]. This approach can yield multiple solutions, as the response surface in the parameter space of the model may show local minima. Another approach involves using a preexisting perturbed physics ensemble and fitting a nonlinear response surface [37] to interpolate between the sampled points in the parameter space. This effectively produces a "model emulator" which can predict the point in parameter space which minimizes model error, but the result is dependent on the parameter space being sufficiently densely sampled to capture the dominant features. One can also combine the predictions from a range of plausible perturbed models. The ensemble Kalman filter [38] approach has been used [39] to create a set of valid perturbed versions of a single climate model, but is subject to uncertainty that there is an unknown systematic error in the climate model which cannot be corrected by parameter modification.

A final problem lies in the incompleteness of the model representation of the climate. Many current models, for example, cannot simulate the indirect effect of aerosols on cloud amounts. Tuning an incomplete model to reproduce the observed radiative balance at the top of the atmosphere therefore involves overcompensating the cloud amounts by artificially enhancing other processes, which arguably makes the representation of the current and future state less accurate.

Statements of Probability

Multi-model Ensembles

As indicated throughout this entry, the production of a probabilistic statement for future climate from a multimember or perturbed physics ensemble has no clearly established methodology and requires a priori assumptions to be made. Arguably the simplest assumption that can be made is one of model equality, using the democratic "one model, one vote" approach [40]. In such a method, the probability of a future event is estimated by the fraction of models in which the event happens. This hypothesis can be tested by cross-validation within an unused subset of the ensemble. However, this approach is limited by the implicit assumption that the ensemble is a random sample of plausible estimates of the true climate, where the various arguments in section "Projection Uncertainty and the Need for Ensembles" suggest this assumption may not be valid.

The next logical step is therefore to consider some measure of model skill as a weighting for each model, producing an estimate of future climate as a median of model predictions, such that models with a small bias are given a greater weight [41]. Such approaches are always highly dependent on the exact choice of metric used to evaluate the model weighting [29].

Many studies have adopted Bayesian methodologies, where prior beliefs about the range of future climate change are updated with information from models and/or observations. One example [42] takes a prior probability distribution for current and future regionally averaged climate signal (or the corresponding climate change signal) and updates this using information from models and observations. Priors can be chosen to be uninformative (flat over a large range of possible values) so that the final PDF shape is mainly influenced by the information from models and observations. The likelihood of each model simulation of the past and the future is then represented as the realization from PDFs centered around the unknown "true" present and future climate, as if the ensemble were a sample from a large idealized population of possible models. The width of the PDFs is in turn estimated jointly with the climate signals. Its magnitude depends on that model bias compared to the consensus estimate of the present day and future

state. Markov Chain Monte Carlo techniques are used to approximate the result of Bayes theorem applied to priors and likelihood, allowing a joint probability distribution for the "true" climate states and the unknown parameters characterizing the model distributions to be estimated. From it, the PDF of the regional climate change signal is also straightforward to derive.

A Bayesian approach has been also applied at the grid-point scale by representing the entire field of future climate anomaly for each model in terms of a truncated set of basis functions combined with some noise estimate [43], such that each model has its own low-dimensional set of coefficients to describe the pattern of climate change. The advantage of this approach is that a similar Bayesian methodology may be applied to derive estimates for the "true" values of the coefficients, which when recombined with the basic functions results in PDFs for climate change at the grid-point level.

An issue with both traditional weighting schemes and the Bayesian approaches is the way in which outliers are treated – the so-called "convergence criterion". In the case of a large PPE, such as the climateprediction.net experiment, the logic in down-weighting outliers assumes that there is some significance in the consensus mean projection, errors are distributed randomly and that models which deviate strongly from the consensus are somewhat less trustworthy. However, in a small ensemble of best-guesses such as CMIP-3, this argument is subject to question. It is possible that a single model in the ensemble is able to simulate processes which are not simulated in other models. This model is arguably more trustworthy than the rest of the ensemble and yet it would be down-weighted through the application of a simple convergence criterion.

Another issue with all of the methods discussed thus far is the assumption of model independence. It can be shown [44] that the width of the final PDF using a Bayesian methodology is inversely proportional to the number of the models considered in the ensemble. Whilst this would be true if all models were independent estimates of a true climate, it has been demonstrated that this not a valid assumption [32]. Although some statistical methodologies have endeavored to artificially reduce the more obvious interdependencies of the CMIP-3 ensemble [45], there is at present no generally accepted methodology for doing so. The Bayesian techniques that have been developed so far tend to produce a PDF narrower than the spread of the original ensemble, as the independence assumption causes uncertainties to decrease with added ensemble members.

A completely different approach to producing model projections is to statistically "calibrate" models, where a relationship is established between model simulations and observations over an observed period. Once this relationship has been determined, it may be applied to future climate projections to produce a "calibrated" estimate of the true future response. This approach assumes, of course, that the relationship between the projections and the true response will remain constant in the future. This approach has been applied to large scale metrics such as past and future sea-ice loss [46], as well as more complex statistical multivariate approaches which find the best fitting relationship between modes of variability in model simulated and observed past climate, again using those relationships to produce a calibrated future projection [47, 48].

Finally, some "detection and attribution" studies [49] determine spatial patterns of climate changes associated with different atmospheric forcings, using observations to determine whether models are over- or under-representing those changes in past simulations. This allows future model projections to be rescaled in light of the observations. One of the major uncertainties in such approaches is in the derivation of the calibration coefficients themselves, and whether the calibration is valid when applied to a future planet in a very different state. These uncertainties tend to result in wider PDFs than Bayesian methodologies [33].

Perturbed Physics Ensembles

While "one model, one vote" may be a questionable assumption in a multimodel ensemble, it is quite ostensibly wrong in a perturbed physics ensemble where some models have vastly inaccurate simulations of the mean climate [50]. PDFs of future climate derived from a perturbed physics ensemble have therefore often been forced to take a different approach.

Most studies thus far arising from PPEs have focused on producing PDFs for climate sensitivity, and have broadly fallen into three categories: weighting

of the parameter space, using the ensemble to establish relationships between observable quantities and unknowns such as climate sensitivity, or a traditional Bayesian technique. An example of the first approach [11] takes a PPE and ascribes each model a weighting, based upon model skill in reproducing the observed climate. By interpolating between the sampled points in the parameter space, one can then produce a weighted integral of the unknown quantity (e.g., climate sensitivity). It is argued, however [51], that the PDF obtained from such an approach is fundamentally dependent upon the prior assumptions made in sampling the original parameters.

A second approach of finding relationships between observable and unknown quantities has been demonstrated using both linear [52] and nonlinear [53] transfer functions. In each case, the ensemble is used to derive some predictors which internally estimate the climate sensitivities of ensemble members. These regression coefficients can then be used together with observations of the true climate state to make a prediction of the true climate sensitivity. Clearly, these predictions are subject to uncertainty in the observational state and in the internally derived prediction error, both of which may be estimated relatively easily. The major "unknown unknown" in such an approach is the systematic or irreducible error of the underlying model, that is, how much additional uncertainty arises when the predictor is applied to the real world. A lower bound of this quantity may be obtained by examining the skill of the predictor when applied to a multimodel ensemble such as CMIP-3, but this will not account for common errors arising from lack of resolution or simulated processes.

The final approach to be considered is the use of an ensemble Kalman filter [40]. The ensemble is used together with observations to update prior beliefs about several unknown model parameters. The ensemble Kalman filter then involves an iterative process forming an idealized ensemble of plausible perturbed models. Once again the methodology is sensitive to assumptions about model error, which scale the relative importance of the model-observation discrepancies forming the overall cost function. By assuming model errors are small, the resulting idealized ensemble will be more tightly clustered about the observed state. The distribution of climate sensitivities in this idealized ensemble is then deemed to approximate a PDF for the sensitivity. One advantage of such a technique is that the predictions may be validated by producing a hindcast for the past (the Last Glacial Maximum, in this case). The LGM simulation can then be used to produce an out of sample weighting for the optimized ensemble.

Future Directions

The analysis of climate simulations from multiple models is still a problem in its relative infancy. Various techniques have been proposed in this entry, each making different assumptions about model independence, prior distributions, systematic model errors, and about what statistical framework is appropriate. These choices remain, at present, somewhat subjective and often yield different probability distributions for unknown climate variables. The apparent contradictions between the methodologies can be understood, however, in light of the assumptions made. In contrast to a numerical weather forecast where thousands of verification cases are available to test the forecast skill, the climate projections for a century into the future are making a statement about a situation never observed before and where no model evaluation is possible. Because there is only a single realization of the future, any statement of probability expresses a degree of belief in a Bayesian sense of how different future outcomes are supported by current evidence (models, data, methods), and is therefore inherently subjective.

Clearly, any projection (and the uncertainty associated with it) must be tailored in a fashion useful to decisions on policy and planning for a changing climate. Policymakers tend to push for increases in precision, but this can lead to decreases in real accuracy if predictions are overconfident [54]. There is arguably little point in providing PDFs of future change for planning purposes if the width of those PDFs are massively sensitive to either subjective decisions or unknown errors, and the raw collection of "best-guesses" from the different models is as useful a way as any to present the ensemble of forecasts. One inherent danger with this approach, however, is the tendency to see the multi-model distribution as a discrete probability distribution for future climate. As is seen, the lack of model independence, the fact that all models are neglecting certain sources of uncertainty (e.g., the

carbon cycle climate feedback uncertainty) and the fact that every modeling group will tend to submit only a best-guess climate together implies that the true uncertainty may be larger than that indicated by the spread of model simulations.

Future generations of multi-model ensembles are also likely to introduce more complex "Earth System Models," at least for some ensemble members. These models, in addition to atmosphere, ocean, land, and sea ice components are likely to introduce fully coupled carbon–nitrogen cycles, chemistry, urban, and ecosystem models into the simulation. These components of future uncertainty have not been thoroughly explored in previous generations of the CMIP experiments, and are likely to increase the spread of simulation response for the coming century. Although this could be perceived to indicate an increase in uncertainty, it is more accurately converting an "unknown unknown" into a parametric uncertainty. If different models include different components of the earth system in their models, it will also become more difficult to compare them on a like-with-like basis, as is mostly possible today. However, this underlines the importance with each generation of climate models of recognizing the uncertainties associated with what is omitted, as well as those arising from the simulations themselves.

Although there may be some use in overall metrics of model skill [55], it is likely that projections of specific phenomena will benefit from tailored metrics to rank the performance of different models (e.g., El Niño or future sea ice extent). This will also require a proper assessment of which subset of models to use for each particular application based upon both past model skill and physical plausibility [31]. In addition, the community may benefit more from a diverse range of model predictions, where each model may be evaluated on its own performance, in place of a group of models which are artificially clustered toward a mean response leaving no way of simulating the extremes or boundaries of future climate change.

In this entry both multi-model ensembles and perturbed physics ensembles have been discussed, but there is little discussion on how the information from the two may be combined. Indeed, at present there is little to no literature on how one may combine the parametric uncertainty sampled in a PPE with the inter-model systematic differences in a multi-model ensemble. This presents a fundamental problem in that current PDFs from both of these techniques cannot incorporate the best estimates of systematic and parametric uncertainty. Future analyses must combine these various uncertainties in order to make statements about model robustness. Currently, the ability to conduct such an analysis is limited because only a small subset of the models in the CMIP-3 archive have produced a perturbed physics ensemble, and for those ensembles which do exist, the experiments have not been conducted in any coordinated fashion.

Despite all of the challenges associated with combining and interpreting results from multiple climate models, the presence of coordinated ensembles of projections provides an invaluable insight into the magnitude of some of the uncertainties which are inherent in every simulation conducted, and the ensemble provides a unique opportunity to understand why models differ. As time goes on, the length of good quality observations will increase allowing better evaluation of the transient behavior of the models (a better metric for future transient response than those based upon the model simulation of the base climate [56]). In addition, as more components of the climate system are simulated, although model convergence is not expected (at least in the short term), one can be confident that at least "unknown unknowns" in future predictions can be represented in the form of parametric uncertainty.

Finally, possibly the greatest single uncertainty in future climate remains that of human behavior. Certainly in the case of the CMIP-3 ensemble, the spread in twenty-first century simulations due to different emission scenarios generally exceeded that of the inter-model spread to any particular scenario. Simple models of the climate have already been coupled to socioeconomic models [57–59], but little progress to date has been made in coupling socioeconomic models to GCMs. As a result, potential complex feedbacks between climate change and human behavior have not been sampled in any systematic framework. Nevertheless, although an integrated treatment of uncertainty in future climate projections may seem some way off, the use of multi-model ensembles will continue to frame at least some of those uncertainties in a systematic framework, providing a robustness which would be impossible with any single model, however complex that model may become.

Bibliography

Primary Literature

1. Ad Hoc Study Group on Carbon Dioxide and Climate (1979) Carbon dioxide and climate: a scientific assessment. National Academy of Sciences, Washington, DC
2. Manabe S et al (1979) A global ocean-atmosphere climate model with seasonal variation for future studies of climate sensitivity. Dyn Atmos Oceans 3:393–426
3. Hansen JE et al (1983) Efficient three-dimensional global models for climate studies: models I and II. Mon Weather Rev 111:609–662
4. Houghton JT, Jenkins GJ, Ephraums JJ (eds) (1991) Scientific assessment of climate change – report of working group I. Cambridge University Press, Cambridge, p 365
5. Houghton JT, Meira Filho LG, Callender BA, Harris N, Kattenberg A, Maskell K (eds) (1995) Contribution of working group I to the second assessment of the Intergovernmental Panel on Climate Change. Cambridge University Press, Cambridge, p 572
6. Houghton JT, Ding Y, Griggs DJ, Noguer M, van der Linden PJ, Xiaosu D (eds) (2001) Contribution of working group I to the third assessment report of the Intergovernmental Panel on Climate Change (IPCC). Cambridge University Press, Cambridge, p 944
7. Solomon S, Qin D, Manning M, Chen Z, Marquis M, Averyt KB, Tignor M, Miller HL (eds) (2007) Contribution of working group I to the fourth assessment report of the Intergovernmental Panel on Climate Change, 2007. Cambridge University Press, Cambridge/New York
8. Parker WS (2006) Understanding pluralism in climate modeling. Found Sci 11:349–368
9. Collins M, Allen MR (2002) Assessing the relative roles of initial and boundary conditions in interannual to decadal climate predictability. J Climate 15:3104–3109
10. Hawkins E, Sutton R (2009) The potential to narrow uncertainty in regional climate predictions. BAMS 90:1095–1107
11. Murphy JM et al (2004) Quantifying uncertainties in climate change from a large ensemble of general circulation model predictions. Nature 430:768–772
12. Stainforth DA et al (2005) Uncertainty in predictions of the climate response to rising levels of greenhouse gases. Nature 433:403–406
13. Annan J, Hargreaves J (2006) Using multiple observationally-based constraints to estimate climate sensitivity. Geophys Res Lett 33(4):L06704
14. Palmer TN, Doblas-Reyes FJ, Hagedorn R, Weisheimer A (2005) Probabilistic prediction of climate using multi-model ensembles: from basics to applications. Philos Trans R Soc B 360:1991–1998
15. Weigel AP, Liniger MA, Appenzeller C (2008) Can multi-model combination really enhance the prediction skill of probabilistic ensemble forecasts? Q J R Meteorol Soc 134:241–260
16. Hagedorn R, Doblas-Reyes FJ, Palmer TN (2005) The rationale behind the success of multi-model ensembles in seasonal forecasting. Part I: basic concept. Tellus 57A:219–233
17. Frame DJ, Booth BBB, Kettleborough JA, Stainforth DA, Gregory JM, Collins M, Allen MR (2005) Constraining climate forecasts: the role of prior assumptions. Geophys Res Lett 32: L09702. doi:10.1029/2004GL022241
18. van der Sluijs J et al (1998) Anchoring devices in science for policy: the case of consensus around climate sensitivity. Soc Stud Sci 28(2):291–323
19. Knutti R, Hegerl GC (2008) The equilibrium sensitivity of the Earth's temperature to radiation changes. Nat Geosci 1:735–743
20. Cantelaube P, Terres J-M (2005) Seasonal weather forecasts for crop yield modelling in Europe. Tellus Ser A 57:476–487. doi:10.1111/j.1600-0870.2005.00125.x
21. Thomson MC, Doblas-Reyes FJ, Mason SJ, Hagedorn R, Connor SJ, Phindela T, Morse AP, Palmer TN (2006) Malaria early warnings based on seasonal climate forecasts from multi-model ensembles. Nature 439:576–579. doi:10.1038/nature04503
22. Schclar A et al (2009) Ensemble methods for improving the performance of neighborhood-based collaborative filtering. In: Proceedings of the third ACM conference on recommender systems, ACM, New York, 23–25 Oct 2009, pp 261–264
23. Hagedorn R, Doblas-Reyes FJ, Palmer TN (2005) The rationale behind the success of multi- model ensembles in seasonal forecasting – I. Basic concept. Tellus A57:219–233. doi:10.1111/j.1600-0870.2005.00103.x
24. Gillett NP, Zwiers FW, Weaver AJ, Hegerl GC, Allen MR, Stott PA (2002) Detecting anthropogenic influence with a multi-model ensemble. Geophys Res Lett 29:1970. doi:10.1029/2002GL015836
25. Lambert SJ, Boer GJ (2001) CMIP1 evaluation and intercomparison of coupled climate models. Clim Dyn 17:83–106. doi:10.1007/PL00013736
26. Reichler T, Kim J (2008) How well do coupled models simulate today's climate? Bull Am Meteorol Soc 89:303–311
27. Robertson AW, Lall U, Zebiak SE, Goddard L (2004) Improved combination of multiple atmospheric GCM ensembles for seasonal predition. Mon Weather Rev 132:2732–2744. doi:10.1175/MWR2818.1
28. Krishnamurti TN, Kishtawal CM, Zhang Z, Larow T, Bachiochi D, Williford E, Gadgil S, Surendran S (2000) Multimodel ensemble forecasts for weather and seasonal climate. J Climate 13:4196–4216. doi:10.1175/1520-0442(2000)013!4196:MEFFWAO2.0.CO;2
29. Santer BD, Taylor KE, Gleckler PJ, Bonfils C, Barnett TP, Pierce DW, Wigley TML, Mears C, Wentz FJ, Brüggemann W, Gillett NP, Klein SA, Solomon S, Stott PA, Wehner MF (2009) Incorporating model quality information in climate change detection and attribution studies. PNAS 106:14778–14783
30. Knutti R (2010) The end of model democracy? Clim Change 102(3–4):395–404. doi:10.1007/s10584-010-9800-2
31. Knutti R, Furrer R, Tebaldi C, Cermak J, Meehl GA (2010) Challenges in combining projections from multiple climate models. J Climate 23:2739–2758

32. Tebaldi C, Knutti R (2007) The use of the multi-model ensemble in probabilistic climate projections. Philos Trans R Soc A 365(1857):2053–2075
33. Knutti R, Stocker TF, Joos F, Plattner G-K (2002) Constraints on radiative forcing and future climate change from observations and climate model ensembles. Nature 416:719–723. doi:10.1038/416719a
34. Jackson C et al (2004) An efficient stochastic Bayesian approach to optimal parameter and uncertainty estimation for climate model predictions. J Climate 17(14):2828–2841
35. Kiehl JT (2007) Twentieth century climate model response and climate sensitivity. Geophys Res Lett 34:22710
36. Knutti R (2008) Why are climate models reproducing the observed global surface warming so well? Geophys Res Lett 35(18):5
37. Sanderson BM et al (2008) Constraints on model response to greenhouse gas forcing and the role of subgrid-scale processes. J Climate 21(11):2384–2400
38. Evensen G (2003) The Ensemble Kalman Filter: theoretical formulation and practical implementation. Ocean Dyn 53:343
39. Annan JD et al (2005) Parameter estimation in an intermediate complexity earth system model using an ensemble Kalman filter. Ocean Model 8:135
40. Raisanen J, Palmer TN (2001) A probability and decision-model analysis of a multimodel ensemble of climate change simulations. J Climate 14(15):3212–3226
41. Giorgi F, Mearns LO (2002) Calculation of average, uncertainty range, and reliability of regional climate changes from AOGCM simulations via the 'reliability ensemble averaging' (REA) method. J Climate 15:1141
42. Tebaldi C et al (2004) Regional probabilities of precipitation change: a Bayesian analysis of multimodel simulations. Geophys Res Lett 31:24213
43. Furrer R, Sain S, Nychka D, Meehl G (2007) Multivariate Bayesian analysis of atmosphere–ocean general circulation models. Environ Ecol Stat 14:249–266
44. Lopez A et al (2006) Two approaches to quantifying uncertainty in global temperature changes. J Climate 19:4785
45. Smith R, Tebaldi C, Nychka D, Mearns L (2009) Bayesian modeling of uncertainty in ensembles of climate models. J Am Stat Assoc 104:97–116
46. Boé J et al (2009) September sea-ice cover in the Arctic ocean projected to vanish by 2100. Nat Geosci 2(4):1–3
47. Greene AM et al (2006) Probabilistic multimodel regional temperature change projections. J Climate 19:4326
48. Buser CM et al (2009) Bayesian multi-model projection of climate: bias assumptions and interannual variability. Clim Dyn 33(6):849–868
49. Stott PA, Kettleborough JA (2002) Origins and estimates of uncertainty in predictions of twenty first century temperature rise. Nature 416:723–726
50. Sanderson BM et al (2008) Towards constraining climate sensitivity by linear analysis of feedback patterns in thousands of perturbed-physics GCM simulations. Clim Dyn 30(2–3):175–190
51. Frame DJ et al (2005) Constraining climate forecasts: the role of prior assumptions. Geophys Res Lett 32(9):L09702
52. Piani C et al (2005) Constraints on climate change from a multi-thousand member ensemble of simulations. Geophys Res Lett 32(23):L23825
53. Knutti R et al (2006) Constraining climate sensitivity from the seasonal cycle in surface temperature. J Climate 19(17):4224–4233
54. Dessai S et al (2008) In: Adger N, Lorenzoni I, O'Brien K (eds) Climate prediction: a limit to adaptation. Living with climate change: are there limits to adaptation. Cambridge University Press, Cambridge, pp 49–57
55. Gleckler PJ et al (2008) Performance metrics for climate models. J Geophys Res 113:D06104
56. Allen MR, Frame DJ (2007) ATMOSPHERE: call off the quest. Science 318:582–583
57. Edmonds J, Wise M, Pitcher H, Richels R, Wigley T, MacCracken C (1997) An integrated assessment of climate change and the accelerated introduction of advanced energy technologies. Mitig Adapt Strateg Glob Change 1:311–339
58. Messner S, Strubegger M (1995) User's guide for MESSAGE III, WP-95-69. International Institute for Applied Systems Analysis, Laxenburg
59. Bouwman AF, Kram T (2006) Integrated modelling of global environmental change. An overview of IMAGE 2.4. Netherlands Environmental Assessment Agency (MNP), MNP publication number 500110002/2006, Bilthoven

Books and Reviews

Kharin VV, Zwiers FW (2002) Climate predictions with multimodel ensembles. J Climate 15(7):793–799

Knutti R et al (2008) A review of uncertainties in global temperature projections over the twenty-first century. J Climate 21:2651–2663

Climate Change Remediation, Introduction to

Timothy M. Lenton[1], Naomi E. Vaughan[2]
[1]University of Exeter, Hatherly Laboratories Biosciences, College of Life and Environmental Sciences, Exeter, UK
[2]School of Environmental Sciences, University of East Anglia, Norwich, UK

Article Outline

Sunlight Reflection (SR)
Carbon Dioxide Removal
Broader Issues

This section focuses on ideas to deliberately remedy anthropogenic climate change, either by actively removing greenhouse gases from the atmosphere or by decreasing the amount of sunlight absorbed at the Earth's surface. The technologies discussed are commonly grouped under the term "geoengineering," defined in a 2009 report by the Royal Society as the "deliberate large-scale manipulation of the planetary environment to counteract anthropogenic climate change." Geoengineering methods can be contrasted with more conventional approaches to mitigating climate change that involve reducing the emissions of greenhouse gases, especially carbon dioxide (CO_2). However, there is some overlap as enhancing the sinks of greenhouse gases, for example, by afforestation, can be described as both geoengineering and mitigation. (The Intergovernmental Panel on Climate Change (Working Group III) states that "mitigation means implementing policies to reduce greenhouse gas emissions *and enhance sinks*" [our emphasis].)

Failure by the international community to make substantive progress in reducing CO_2 emissions, coupled with recent evidence of accelerating climate change, have brought urgency to the search for additional means of tackling climate change. This has fueled much recent debate about geoengineering and a flurry of mostly model-based research studies. There is widely expressed concern that undertaking, or even discussing, geoengineering poses the "moral hazard" of reducing efforts to tackle the root cause of climate change, namely, greenhouse gas emissions. However, few of those researching geoengineering advocate it as an alternative to reducing greenhouse gas emissions. Instead, current discussions are usually framed in terms of the possible use of geoengineering *in addition to* reducing greenhouse gas emissions in order to limit the magnitude of climate change, for example, to stay within the widely discussed policy "threshold" of limiting global warming to 2°C above preindustrial.

The technologies discussed herein can be subdivided into those involving carbon dioxide removal (CDR) from the atmosphere, and those involving reflecting sunlight, referred to by the Royal Society as "solar radiation management" (SRM) (although the word "management" implies a high level of understanding of the system in question that is probably not justified for the climate). The distinction can also be thought about in terms of wavelengths of radiation; short-wave geoengineering tries to reduce incoming sunlight, while long-wave geoengineering tries to reduce the return flux of heat to the surface from the increased blanket of heat-absorbing gases in the atmosphere. Sunlight reflection can never perfectly counterbalance an increased greenhouse effect because the two types of downwelling radiation have different spatial and seasonal patterns.

The section presents some of the more widely discussed geoengineering options, without being comprehensive. Here, we try to fill some of the gaps as well as introduce the entries herein.

Sunlight Reflection (SR)

Sunlight reflection can act rapidly to cool the climate if deployed on a sufficiently large scale. It could, in principle, be deployed to return the Earth to its preindustrial temperature, to hold it at some level of warming that has already occurred, or to lower future global warming. A popular framing is that sunlight reflection could "buy time" for decarbonising the economy and allowing greenhouse gas concentrations to stabilize and then come down. Alternatively, potent methods of sunlight reflection might be reserved for use "in emergency" should dangerous climate change become apparent, but it is as yet unproven that such a deployment after a threshold had been passed would prevent the change that was already underway.

Methods of sunlight reflection can be distinguished in terms of the altitude at which they are applied. They start outside the Earth's atmosphere with the idea of placing mirrors or sunshades in space to reduce the amount of sunlight reaching the Earth (D. J. Lunt "► Sunshades for Solar Radiation Management"). To counteract a doubling of atmospheric carbon dioxide would require a roughly 2% reduction in the amount of sunlight reaching the top of the Earth's atmosphere. To achieve this, one proposal is to put tiny "flyers" (each about 0.3 m^2) between the Earth and the Sun at the first Lagrangian (L1) point. The roughly 5 million km^2 of sunshade required at this distance (around 1.5 million km) means the method will probably remain in the realm of science fiction for the foreseeable future. However, the model studies that have been conducted to

examine the effects on the climate provide useful information on the effects of a uniform reduction in incoming sunlight, which might be achieved by other means.

Currently, the leading candidate for geoengineering a reduction in incoming sunlight is to inject tiny particles into the Earth's stratosphere which will scatter (or in some cases absorb) sunlight (B. Kravitz "► Stratospheric Aerosols for Solar Radiation Management"). (The stratosphere is the thermally stratified layer of the Earth's atmosphere between about 10 and 50 km altitude, separated from the well-mixed troposphere below by the tropopause.)

A natural analogue here is a volcanic eruption, such as Mt. Pinatubo in 1991, which injected sulfate aerosol into the stratosphere and measurably cooled the climate (by around 0.5°C in the following year, followed by a tailing off). The stable thermal structure of the stratosphere means that aerosols stay aloft for much longer than in the troposphere below, and therefore, a much smaller loading of particles is required to have a given cooling effect. An estimated 1.5–5 MtS year^{-1} would need to be deliberately injected into the stratosphere to offset a doubling of CO_2, which is much less than the 50–100 MtS year^{-1} that human activity currently adds as pollution to the troposphere. The main unanswered questions surround how to inject sulfate aerosols into the stratosphere in a way that stops them from coagulating, because if the tiny particles combine to become larger particles, this can profoundly alter their radiative properties, at the extreme, turning a cooling effect into a warming effect. Other types of aerosol, notably soot, and engineered metal nanoparticles are also being discussed as possible candidates for stratospheric injection.

Moving down into the lower atmosphere, clouds are a major contributor to the reflectivity of the planet, and low-level clouds in particular have a net cooling effect at the surface. Hence, it has been proposed to cool the planet by making marine stratocumulus clouds more reflective (S. H. Salter "► Solar Radiation Management, Cloud Albedo Enhancement"). This can be achieved by distributing the same amount of cloud water over more but smaller droplets, which requires a source of the tiny particles known as cloud condensation nuclei on which water condenses. Sea salt is the most obvious and ubiquitous candidate aerosol, and a means of spraying it from the ocean using wind-powered boats with Flettner rotors is described by Salter. An alternative is to enhance the source of cloud condensation nuclei from the biological production and air-sea exchange of the gas dimethyl sulfide. The methods may also suppress rainfall, increasing the lifetime of clouds and giving a further cooling effect. They should be most effective far from sources of human pollution (which also provide condensation nuclei), such as in the Southern Ocean. However, this means the cooling effects on the climate would inevitably be patchy, which in turn can cause unexpected climate changes far away, for example, in some model simulations, the Amazon gets drier.

Finally, a number of proposals have been made to enhance the reflectivity of the Earth's surface, focusing on deserts, grasslands, croplands, and human settlements. Here, the total area altered and the change in surface reflectivity (albedo) are the key determinants of the global cooling effect. As the land comprises only 29% of the Earth's surface, to achieve a significant global cooling effect would require major overcooling of parts of the land. Instead, these approaches are best thought of as means of achieving significant localized cooling. In the case of more reflective croplands, cooling effects would be largest just before the crop is harvested, so this could provide a means of, for example, cooling future European summers. However, there remain unanswered questions regarding the effects on crop yield. Reflective roof surfaces are now legislation in California and more widespread adoption of this approach could become an important adaptation strategy in tackling urban heat islands, even though its global cooling effect will be negligible.

Carbon Dioxide Removal

Current total CO_2 emissions from fossil fuel burning, land-use change, and cement production are rapidly approaching 10 billion tons of carbon per year ($\sim$10 PgC year^{-1}). Just to stop CO_2 concentration from rising in the atmosphere, the net anthropogenic source of CO_2 has to be reduced first by about 50% to match natural sinks and, then on, down to zero as the natural sinks decay. To help achieve this, carbon dioxide removal (CDR), and subsequent storage, is a clear complement to reducing CO_2 emissions. Doing both together could stabilize atmospheric CO_2

concentration sooner and at a lower level. Ultimately, CDR could be used to bring the concentration of atmospheric CO_2 down faster than natural sinks, to whatever is deemed a safe level. However, like reducing emissions, CDR will act relatively slowly to alter the rate and magnitude of climate change when compared to potent methods of sunlight reflection. To achieve significant global CO_2 removal, even with the most effective CDR methods, will require global deployment for decades. Furthermore, the Earth system actually works against deliberate CDR by always trying to maintain a balanced apportioning of CO_2 between the ocean, atmosphere, and land surfaces. Hence, if CO_2 is removed from the atmosphere, some leaks out from the ocean and/or land to partly compensate, meaning that the effect on atmospheric CO_2 concentration decays over time. (This is simply the opposite of the well-known land and ocean carbon sinks, which are generated by the addition of CO_2 to the atmosphere.)

Carbon dioxide removal covers a wide range of methods and pathways to storage. CO_2 can be removed from the air by photosynthesis (by plants, algae, or cyanobacteria) or by physical and chemical means, which are related to natural weathering reactions. The ease of removal varies with the pathway. The carbon may ultimately be stored as liquid CO_2 (in geological reservoirs or the deep ocean), in charge-balanced solution in seawater, as carbonate rocks, as charcoal, or as buried or standing biomass. The different forms of storage have differing stability in terms of thermodynamics, kinetics of reactions, and ease with which CO_2 might be returned to the atmosphere.

Photosynthesis is effectively solar-powered carbon capture for free (to us), although it is remarkably inefficient (~0.5% efficiency, compared to solar photovoltaic cells capable of ~20% efficiency), and biomass is the least stable form of carbon storage because it is a source of energy to other organisms. However, in the ocean, some of the carbon fixed in photosynthesis can sink to depths where it has a lifetime of up to 1,000 years. The amount exported to depth depends crucially on the supply of limiting nutrients to the surface ocean. Hence, several geoengineering proposals consider adding limiting nutrients, especially iron, to the surface ocean to stimulate biological productivity (P. W. Boyd "► Ocean Fertilization for Sequestration of Carbon Dioxide from the Atmosphere"). Iron fertilization is unusual in being a form of geoengineering that can draw on a series of 12 experiments to investigate its biogeochemical consequences (though not geoengineering specifically). However, what those experiments have shown is that it is remarkably difficult to increase the sinking flux of carbon to the deep ocean. Model studies add that even with global iron fertilization maintained for a century, the potential impact on atmospheric CO_2 concentration is modest, lowering it by, at most, around 30 parts per million.

Land-based photosynthesis has the potential to fuel larger carbon dioxide removal fluxes, despite the smaller surface area of the land compared to the ocean and the need not to take land from natural ecosystems or to interfere with food production. The potential is greater because of the high productivity that can be achieved on land. The simplest method is afforestation, but it only works as a means of carbon dioxide removal if the conversion to forest is permanent and the carbon that is lost as trees decay is replaced by new trees. Still, afforestation is already underway at a global scale, with around 250 million hectares having been planted in recent decades, and this is creating a sink of circa 0.3 PgC $year^{-1}$, canceling roughly 3% of current total CO_2 emissions.

Carbon dioxide removal can also be achieved by converting waste biomass from farming and forestry into longer-lived forms for storage, although the long-term potential will depend more on the supply of deliberately cultivated biomass energy crops. Several conversion pathways are available. Biomass energy combustion coupled with capture and storage of the CO_2 given off (often referred to as BECS or BECCS) is more cost-effective than chemical methods of CO_2 air capture, although there are still energy penalties in capturing and compressing CO_2. Fermentation of biomass, for example, to produce liquid biofuels, yields a near-pure stream of CO_2 reducing the capture cost. Alternatively, pyrolysis of biomass (in the presence of little or no oxygen) produces charcoal, which can be returned to the soil as biochar (S. Shackley et al. "► Biochar, tool for climate change mitigation and soil management"). Although the energy yield from pyrolysis is somewhat less than from combustion, biochar has a range of cobenefits, including improving soil water retention and fertility, which make it an attractive option. Energy remains in the biochar, but

it is hard for organisms to break the material down, making much of it long-lived in soil.

Carbon dioxide can also be captured from the air by chemical means, using, for example, a strong alkali solution. When CO_2 has been captured into concentrated form in this way, or from combusting or fermenting biomass, it can be stored in liquid form. However, it is safer and more permanent to neutralize carbonic acid to form carbonate rocks or aqueous bicarbonates by mirroring natural rock weathering processes. Carbonate weathering brings CO_2 into solution as bicarbonate (although, ultimately, on a ~10,000-year timescale when carbonates are redeposited in the ocean, the CO_2 will be returned to the atmosphere). Silicate weathering followed by carbonate deposition is a permanent removal process for atmospheric CO_2. However, these reactions are generally rather slow, even when applied to a CO_2-rich gas stream. Heating to speed up the reactions is too costly; hence, better methods for accelerating carbonation are needed, and some work on using electrochemical energy to accelerate the reactions is underway.

Finally, CO_2 can be removed from the air by mining, crushing, and spreading on the land silicate minerals that weather rapidly such as serpentine or olivine (R. D. Schuiling "► Carbon Dioxide Sequestration, Weathering Approaches to"). This represents a direct attempt to accelerate silicate weathering, which should be most effective in wet regions of the tropics under vegetation, because plants and their associated mycorrhizal fungi produce organic acids that accelerate dissolution. Olivine has relatively large deposits in the tropics, making it a promising candidate, although estimates are needed of the energy and CO_2 costs of mining, grinding, and distributing the rock on appropriate land. Weathering rates can be limited by factors other than substrate supply, and current estimates suggest this CDR method may be limited to at most around 1 PgC year^{-1}.

Broader Issues

The concept of geoengineering and the particular proposals, both CDR and SRM, provoke a plethora of social concerns ranging from specific questions of economical or political feasibility for each proposed method to broader ethical and philosophical debates about our relationship with nature.

Efforts are underway to establish a framework for governing geoengineering, particularly SRM. This poses a host of questions, relating both to research and possible implementation (S. Low et al. "► Geoengineering Policy and Governance Issues"). Historical efforts at weather modification provide some past precedent (albeit at a smaller scale), but they offer little in the way of existing governance frameworks to draw on. Given the rapidly evolving nature of the field, flexibility and adaptability will be key requirements for whatever governance framework emerges.

The use of any geoengineering method as a response to climate change will ultimately be made by societies. Therefore, the public perception of, and engagement with, this group of emerging technologies is of critical importance in determining their future usefulness. Concepts of upstream engagement and responsible innovation can help incorporate a range of societal values into research at an early stage (and they are both, in different ways, built into two current UK Research Council–funded projects on geoengineering).

Early public engagement (e.g., "Experiment Earth" conducted by the UK Natural Environment Research Council) has already yielded unexpected responses to geoengineering. In particular, the "moral hazard" argument that geoengineering will suppress efforts to reduce greenhouse gas emissions has not been clearly borne out. Some members of the public responded to information on geoengineering with the opposite response; that if things are so bad that scientists are considering geoengineering, then efforts to reduce the root cause of climate change, namely, greenhouse gas emissions, must be strengthened.

Moving forward, the ethical and philosophical debate about geoengineering needs to distinguish SRM and CDR techniques. SRM only deals with the symptoms of climate change, notably rising temperatures. CDR, on the other hand, like conventional emissions reduction, tackles the root cause of climate change: rising greenhouse gas concentrations. Specific methods still raise specific concerns. But as research on geoengineering continues to escalate, we hope this section provides a stimulating introduction to the methods and the debates surrounding them.

Climate Predictions, Seasonal-to-Decadal

Lisa Goddard
Forecasting and Prediction Group, International Research Institute for Climate Society (IRI), The Earth Institute of Columbia University, Palisades, NY, USA

Article Outline

Glossary
Definition of the Subject and Its Importance
Introduction
Seasonal-to-Interannual Prediction
Decadal Prediction (Experiments)
Future Directions
Bibliography

Glossary

Climatology Reference period used to describe the characteristics of the climate, such as the mean annual cycle, or the expected statistics of weather or of year-to-year climate variability. The World Meteorological Organization recommends the most recent three full decades; e.g., in 2009, the WMO climatology period would cover 1971– 2000.

External forcing Factors that influence the climate system but are not explicitly driven by the climate system, such as human emissions of greenhouse gases, changes in the sun's radiation, and volcanic emissions.

Forecast The guidance offered by a forecaster or forecast center on the future climate conditions. A forecast could be based on a single prediction, but typically is a distilled product that involves recalibrated model predictions and often multiple prediction inputs.

Internal variability The chaotic evolution of a fluid, such as the ocean or atmosphere, due to nonlinear dynamics that are sensitive to small uncertainties or variations in initial conditions. Depending on timescale, internal variability may refer to that generated internally to the atmosphere, to the ocean, or due to ocean–atmosphere interaction. It is the part of the seasonal-to-decadal climate that is not deterministically predictable.

Prediction The future climate conditions indicated by a single prediction model, which could be statistical or dynamical. These differ from climate change projections in that information of the climate state at or near the initial time of the forecast is highly relevant to its future evolution.

Teleconnections Climate variability in one region that is driven remotely by climate variability in another region. This typically refers to regional patterns of climate anomalies over land and/or oceans that result from specific ocean phenomena, such as during El Niño events.

Definition of the Subject and Its Importance

Seasonal-to-decadal climate prediction seeks to quantify the likely evolution or change of the climate system over a specific time horizon of months to years. Climate predictions based on dynamical models incorporate all relevant processes to the extent possible, including anthropogenic climate change, but most importantly those processes that govern the likely evolution of natural climate variability. The predictions, if well calibrated, describe the probability of a given magnitude of change in the mean climate or changes in the characteristics of the weather over the forecast period. For example, a seasonal forecast for next winter might indicate a greater likelihood for the seasonal mean temperatures to be colder than usual, or might indicate the likelihood for more frequent storms over the 3-month period.

Seasonal prediction is a fairly well-established enterprise with a number of forecast centers around the world issuing real-time seasonal predictions–based dynamical models [1]. Increasingly, national meteorological and hydrological services create seasonal forecast products based on their own statistical or dynamical prediction tools and/or incorporate predictions from the international centers. Decadal prediction is a much newer endeavor and is still considered experimental [2]. Only a few groups have attempted decadal-scale climate predictions intended to capture the evolution of natural decadal variability for the coming decade from a global circulation model [3–5], and although the results indicate there may be added information from these predictions relative to the more familiar climate change projections of the

Intergovernmental Panel on Climate Change (IPCC), it is not clear that the added information results from better prediction of the decadal-scale climate variability that would exist even in the absence of increasing greenhouse gases.

Climate forecasts are potentially valuable to society on seasonal-to-interannual timescales to inform resource management, planning decisions, and on decadal timescales to inform longer-term plans and infrastructure investment. Even in the climate change context, decadal prediction could prove important, as the climate experienced regionally for the coming decade(s) will likely be some combination of anthropogenic climate change and natural decadal variability. Decisions and investments related to climate change adaptation typically apply to the next 10–20 years into the future, rather than 80 years into the future. Thus better information on evolution of the climate and changes in risks of climate extremes can lead to more appropriate planning. However, climate predictions are necessarily probabilistic, and in the case of decadal predictions are yet to be established as skillful. Thus it is important that decision systems be designed and optimized to account for the inherent uncertainty in future climate, that can still allow benefits to be realized in times of favorable climate and losses to be mitigated in times of adverse climate.

Introduction

Climate varies on all timescales, from seasonal variations to millennial ice ages. Prediction of the climate at timescales that are relevant to societal decisions, but extending beyond weather forecasts, has been roughly broken into three classes: seasonal-to-interannual prediction that addresses the changes in seasonal climate and its weather characteristics a couple months to a year in the future, decadal prediction, sometimes referred to as near-term climate change prediction that addresses changes in the mean climate and its characteristics for a couple years to a couple decades into the future, and climate change projections that consider changes in the mean climate and its characteristics 50–100 years in the future.

The seasonal-to-interannual timescale dominates the climate that is experienced locally. On a local-to-regional scale, year-to-year variability almost always explains the majority of the variance in the observed climate (e.g., Fig. 1). Year-to-year variability is where most impacts are experienced. However, it is the superposition of the three climate timescales that can lead to changes or trends in the frequency of adverse years. Extreme examples are potentially the protracted drought conditions in the western United States from the mid-1990s to the early twenty-first century [6], the 2003 European heat wave [7], or the extremely active hurricane season 2005 [8], which was accompanied by many land-falling hurricanes in the United States such as Katrina.

The primary difference between prediction of climate variability on different timescales is the drivers, or phenomena, associated with those impacts. This leads to differences in the way prediction systems are designed to predict the climate fluctuations and associated impacts on different timescales. Seasonal-to-interannual prediction is an initial value problem; by initializing the climate system close to the observed state at the beginning of the prediction, a dynamical model will aim to capture the likely evolution of the climate system. At the other end of the time spectrum, climate change projection is a boundary value problem, which means that the driver of the climate change is external to the climate system and imposed upon it. Anthropogenic increases in greenhouse gases are due to man's activities and are not part of the natural climate system. Climate change projections depend on correctly projecting the changes in the Earth's atmospheric composition and the subsequent changes in the Earth's energy balance. Decadal prediction lies at the intersection between seasonal-to-interannual prediction and climate change projection; it is an initial value as well as a boundary value problem. Decadal prediction depends both on initializing the climate system close to the observed state, especially the slowly evolving components, and on correctly representing the changes in Earth's energy budget.

This is not to say that predictions on longer timescales do not contain the higher frequency phenomenon. However, there is a predictability limit for natural climate variability, which refers to how far into the future some aspect of climate variability can be predicted before the uncertainty, or range of possibilities, approaches the climatological uncertainty. At that point little to no predictive information remains.

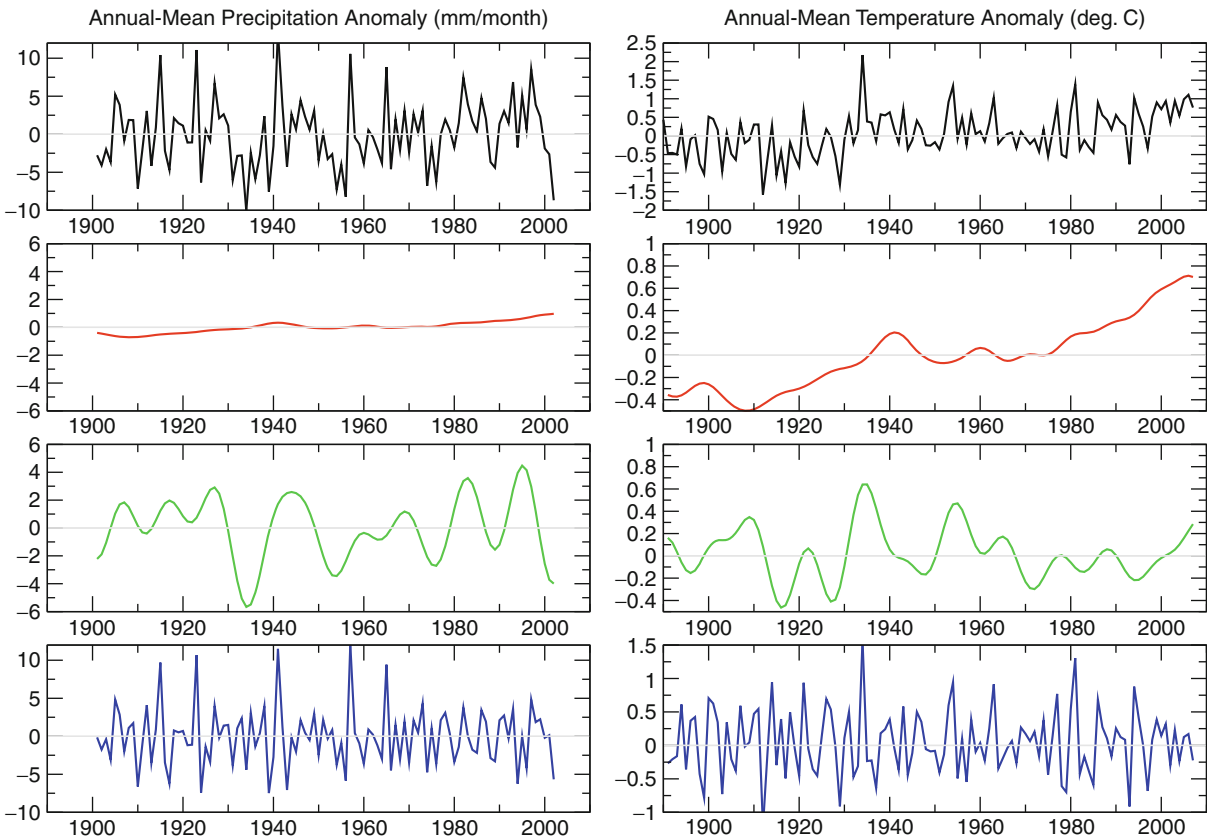

Climate Predictions, Seasonal-to-Decadal. Figure 1

Example of simple decomposition of (**a**) temperature and (**b**) precipitation averaged over the state of Colorado in the United States. The *top* panels (*black*) show the observed annual mean time series. The second panels (*red*) represent "climate change" time series, in which the climate changes are consistent with the globally averaged temperature, obtained by decadally filtering the time series and regressing it against a similar low-frequency filtered time series of globally averaged temperature. The *third* panels (*green*) represent the "natural decadal variability," which is low-frequency time series that is not coincident with globally averaged temperature changes, obtained as the difference between the low-frequency filtered time series and the "climate change" time series. The *bottom* panels (*blue*) represent the year-to-year variability on top of the low-frequency changes, which is the difference between the full time series and the low-frequency filtered time series. Note that there is no attribution to anthropogenic changes or physical phenomena in any of these time series. Details are likely to change with different filtering parameters and with different approaches to estimate global warming

The limit of predictability is not necessarily a fixed quantity. It changes with the phenomenon, but also changes with time, meaning that at some times a phenomenon will be more predictable than others and thus the evolution can be predicted farther into the future. It is not possible to determine what the true limit of predictability is or should be [9]. The model(s) that can predict the phenomenon with the greatest fidelity when compared to observations over some long history containing many realizations of the phenomenon determine the *current* limit of predictability.

In order to make a prediction one must first determine what is to be predicted. If the aim is to predict local-to-regional scale climate over land, one must know the driver of that climate variability. Numerous research and prediction studies have demonstrated that it is the large-scale variability in the pattern of surface temperature, and in particular the sea surface

temperatures that drive the predictable aspect of changes in the atmospheric circulation and thus regional temperature and precipitation. But what drives that sea surface temperature variability? The sea surface temperatures must be predicted if it is hoped to predict the associated terrestrial climate impacts. Once the ocean phenomena or processes relevant to sea surface temperature variations are identified, the climate models must be capable of simulating those. Furthermore, if the prediction of some phenomenon from a particular model is to provide actionable information, then the phenomenon must be predictable above the other ongoing processes in the climate system; in other words, the signal of the phenomenon must be predictable above the background noise of the climate system. In the next section, an example of this process of identification, model validation, and prediction based on the El Niño-Southern Oscillation (ENSO) phenomenon and seasonal climate prediction is presented.

Brief History of ENSO Prediction: Impacts of the ENSO phenomenon have been experienced for centuries, long before the phenomenon itself was identified. The peoples of Peru used the term El Niño to refer to the expected changes in the local climate and fish stocks associated with a seasonal reversal of the current system off the coast of western South America, because these changes occur near the end of the year at a time near Christmas (El Niño is Spanish for the Christ child). However, they also noted that warm seasonal waters associated with the change of currents, would occasionally be very warm and would also bring abundant rainfall. It is these extreme years, which recur about every 3–7 years that are now called El Niño events. Farmers in drought-prone regions of the Andes even developed a method to predict the coming of the increased rainfall during these events by monitoring the visibility of a star in the Pleiades constellation [10]. What they were observing was the shift of convection from the western tropical Pacific into the central Pacific in concert with the development of an El Niño event (Fig. 2).

Sir Gilbert Walker could be said to be the pioneer of seasonal forecasting as he sought to quantify the atmospheric component of ENSO, the Southern Oscillation, and its relationship to regional climate variability, such as the devastating droughts in India [11]. To accomplish this he examined correlations between 32 stations across the world for fields of sea level pressure, temperature, rainfall, and riverflow. He discovered that negative excursion of the Southern Oscillation Index was associated with increased likelihood for drought over India; his empirical model has not been much improved upon over the last century for that region.

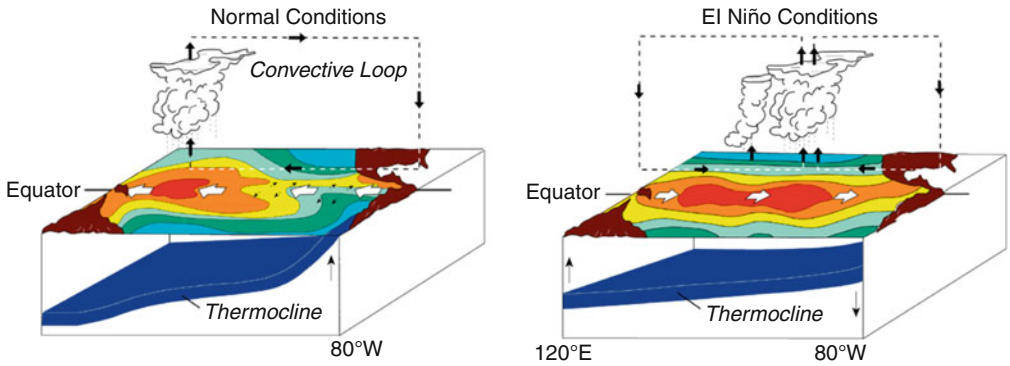

Climate Predictions, Seasonal-to-Decadal. Figure 2
Schematic drawing of the tropical Pacific ocean–atmosphere state during (**a**) average or neutral conditions in which trade winds blow east to west, pushing warm surface waters to the western Pacific, which pushes down the thermocline (separation between warm upper ocean and cold deep ocean) and concentrates the deep convection in the western Pacific; (**b**) El Niño conditions in which the thermocline becomes deeper in the eastern Pacific and warm water moves westward, which weakens the east–west Trade Winds and allows the convection to move into the central Pacific (Source: http://www.tao.noaa.gov/proj_overview/tao_tour_ndbc.shtml)

Researchers have continued to improve upon the foundation that Walker laid for ENSO teleconnections (Fig. 3). Maps that show significant correlation between regional temperature and precipitation changes to ENSO events for specific 3-month average seasons are widely used to illustrate ENSO's global reach [12, 13]. However, these teleconnection patterns represent expectations based on statistics and are not guaranteed to occur in any specific event; the probabilistic likelihood of a regional impact [14] is a further refinement of the climate anomalies due to ENSO, and something that climate prediction models should be expected to replicate in their ensemble distributions over time.

It was not until the second half of the twentieth century that researchers discovered that the Southern Oscillation was associated with changes in the large-scale sea surface temperature pattern over the tropical Pacific; it was the coupled interaction between the east–west sea surface temperature gradient and the low-level winds between the high and low pressure centers of the Southern Oscillation that led to the growth of Niño events [15]. It was soon after recognized that the change in the winds due to the changes in sea surface temperatures, associated with the Southern Oscillation, modified the distribution of the upper-ocean mass field below the surface [16], and that the adjustment of these perturbations to the mass field could lead to the eventual decay of the El Niño event and possible initiation of the opposite phase, La Niña.

In the 1980s simple dynamical models [17–19] were developed that simulated the coupled air-sea processes central to ENSO and reinforced the theory that had been informed primarily by observations. The first experimental El Niño forecast was published in 1986 [20], using one of these simplified dynamical models. Since then more complex models have been built that capture not only the dominant processes behind ENSO but also provide a more complete representation of the climate system to better capture uncertainties in ENSO. These models also simulate the atmospheric teleconnections that lead to changes in sea surface temperatures of other ocean basins and to changes in the terrestrial climate. These are the impacts that served as the initial motivation for the study of ENSO. Finally, through the process of identification of a primary driver of seasonal climate variability and the dominant physical processes behind it, and the development of models that could simulate and predict this driver and its teleconnections, seasonal prediction was born.

The prediction of decadal-scale climate variability is a much more recent endeavor. Although research on decadal climate variability through the use of observations and models is not new [21–26], a community-wide effort in this area is new. The motivation to predict decadal climate variability has arisen in part from a desire to use the climate change projections that appear in the Working Group 1 report of the Intergovernmental Panel on Climate Change [27] to inform sectoral decision making, [28] as well as plans and investments toward climate change adaptation. For these societal needs, climate information for the next 5–20 years becomes more relevant than that for the next 100 years. The other side to the motivation behind experimental decadal predictions is the realization that there are processes inherent in the natural climate system evolving at decadal-to-multidecadal timescales, and the mounting evidence that dynamical models have some ability to simulate some aspects of the observed variability [29, 30].

As the successes and failures in climate prediction are considered, it must be borne in mind that climate predictions are necessarily probabilistic. They indicate the likelihood of a range of possible outcomes. The magnitude of this range of outcomes, often referred to as the uncertainty or probability distribution, is sensitive to uncertainties in the initial conditions from which the predictions evolve, to uncertainties in external forcings, and to errors in prediction models. The value about which the uncertainty is centered is sensitive to the external forcings and to information in the initial conditions that may lead to specific, robust evolution of the climate system. Particularly in the case of decadal prediction, which is still in the experimental phase, success refers to relative performance, or agreement between prediction and observations, compared to the state of predictions beyond the seasonal timescale, namely, climate change projections. In other words, much of the judgment of decadal prediction in these early experiments focuses on the added forecast quality from the initial conditions relative to that from the boundary conditions, or external forcing. Therefore, success in the eyes of the climate community may

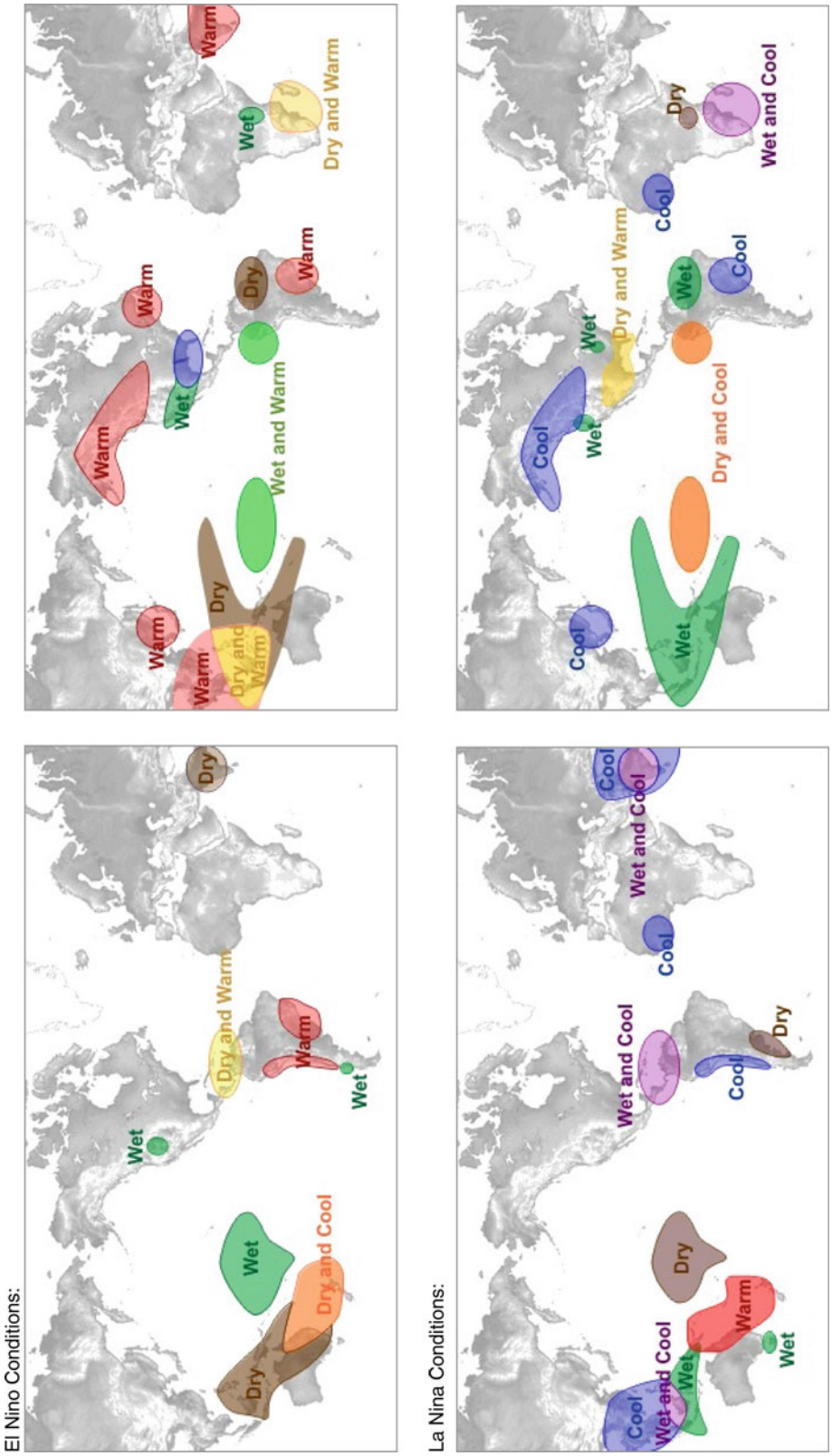

Climate Predictions, Seasonal-to-Decadal. Figure 3
Expected climate anomalies for (**a**) El Niño events during northern hemisphere summer when events are developing, and (**b**) El Niño events during northern hemisphere winter when events are mature; and for (**c**) La Niña events during northern hemisphere summer, and (**d**) La Niña events during northern hemisphere winter (Source: http://www.srh.noaa.gov/jetstream//tropics/enso_impacts.htm)

not constitute information that is accurate enough or specific enough to be actionable.

Although both seasonal prediction and decadal prediction experiments, and climate change projections for that matter, use the same type of dynamical models, substantial differences exist between their application for these different timescales of prediction. The following sections contain discussions of Drivers of Variability, Model Fidelity, Prediction Systems, and Internationally Coordinated Efforts, first for the seasonal-to-interannual timescale, followed by a similar analysis for the decadal prediction problem. The only difference in the structures is that the section on seasonal-to-interannual prediction also contains a discussion of Forecast Skill. The echoed structure is intentional in that many of the issues and approaches will be similar for both timescales. However, there are important differences in what is known about the drivers of climate variability at these different timescales as well as differences in the maturity of the prediction systems.

Seasonal-to-Interannual Prediction

Seasonal-to-Interannual Prediction: Drivers of Interannual Variability

Seasonal-to-interannual prediction derives from initial conditions of the climate system. Unlike weather forecasts, where the relevant initial condition is the atmospheric state and the sea surface temperatures are approximately constant, seasonal forecasts depend more on the initial condition of the ocean. The evolution of the ocean state, particularly the density structure and the currents, leads to changes in the pattern of sea surface temperatures that can then influence the atmospheric circulation.

The dominant pattern of surface temperature variability, after accounting for global warming, is that of the El Niño-Southern Oscillation (ENSO) (e.g., [31]). For this reason ENSO has received a great deal of attention in studies of climate prediction on seasonal-to-interannual timescales. Changes in winds and precipitation are associated with these global temperature pattern changes.

El Niño events recur about every 3–7 years on average, and are somewhat locked to the annual cycle in that they tend to develop and grow through the middle of the year and tend to peak near the end of the year. During an El Niño event when much of the warm water in the western equatorial Pacific moves eastward, the region of deep convection also moves eastward into the central Pacific (Fig. 2), and in some cases reaches as far as the coast of South America. Since the equatorial Pacific spans nearly half the circumference of the Earth, a shift of the largest region of deep convection from the far western Pacific to the central equatorial Pacific represents a huge spatial shift in where the tropical atmosphere is heated.

In the tropics, where the effect of Earth's rotation is weaker, the atmospheric response to the pattern of sea surface temperatures is thermally direct. The low-level winds converge toward the warmest water, or equivalently, to the region of lower pressure. This is true of the mean conditions as well as the anomalous conditions. Since the lower atmosphere is very humid in the tropics, the regions of converging low-level winds produce an upward flow of very moist air and heavy precipitation with a very large latent heat release to the atmosphere associated with water vapor condensation. Near the top of the troposphere, relatively dry air is expelled from these regions of strong deep convection, and that air then sinks. The sinking dry air suppresses convection. The regions of warmest sea surface temperatures and associated strong deep convection are located typically over the western Pacific warm pool and the western hemisphere warm pool, which encompasses the northeastern tropical Pacific extending to the northwestern tropical Atlantic. Variations in these warm pool regions have direct impacts on the climate in the neighboring regions, but changes in the strength and location of those convective centers can also impact regional climate remotely though changes in atmospheric circulation.

The resulting changes in the atmospheric circulation can lead to warmer conditions in the other tropical oceans [32, 33], which carry additional regional climate impacts. For prediction of the regional climate due to tropical sea surface temperature changes outside the Pacific, it is important to be able to predict those sea surface temperatures. For example, the tendency for northeastern Brazil to be drier than normal during an El Niño event (Fig. 3) is due in part to the anomalous subsidence from the shift in deep convection over the central Pacific, but it is also due to associated warming

of the sea surface temperatures over the north tropical Atlantic [34]. Similarly, wetter conditions in eastern Africa associated statistically with El Niño events are now known to result from the warming of SSTs in the western Indian Ocean that are also associated with El Niño events [35]; an El Niño event that is not accompanied by warm SST anomalies in the western Indian Ocean leads to drier conditions over East Africa due to anomalous subsidence resulting from El Niño's enhanced convection in the central Pacific.

El Niño can affect weather and seasonal climate outside the tropics through changes in the position and strength of the storm tracks. When the warm water that normally resides in the western Pacific extends across the Pacific, it changes the large-scale temperature differences between the tropical and the midlatitudes. This allows the storm track associated with the subtropical jet stream to strengthen over the central and eastern subtropical Pacific where it is usually weaker and more variable. Additionally, the warming of the equatorial Pacific region as a whole allows the amount water vapor in the lower atmosphere to increase. The combination brings more frequent and stronger storms into the southern tier of the United States during El Niño events. This impact on extratropical climate is seen in the winter hemisphere because this is when the jet stream is strongest. So although a similar influence can be discerned for storm track headed toward South America, the impact is less robust, since El Niño events are typically growing during southern hemisphere winter in the middle of the year. During the northern hemisphere winter is closer to the time when El Niño events are mature.

It is the large-scale changes in the patterns of low-level heat and moisture that drive changes in the atmospheric circulation. El Niño happens to be the dominant phenomenon influencing that and the focus of those changes is primarily over the tropical oceans. However, changes in land-surface conditions, such as soil moisture or ice, can also influence regional climate. Soil moisture influences the overlying atmosphere primarily through evaporation, which can then influence precipitation as well as near-surface air temperature during certain times of the year [36]. Dry soil conditions, and thus a reduced ability of the surface to cool itself through evaporation, are likely to have contributed to the 2003 European heat wave [37]. Changes in patterns, extent, and timing of snow cover can also impact the atmospheric circulation through changes in land atmosphere energy exchange and may impart predictability to northern hemisphere wintertime temperatures [38] and also the strength of the East Asian monsoon [39].

Seasonal-to-Interannual Prediction: Model Fidelity

Once the main drivers of seasonal-to-interannual climate variability are identified, it is then necessary to ascertain whether the model to be used for seasonal-to-interannual prediction can replicate the drivers with sufficient realism. Change in patterns of SSTs is the dominant driver of seasonal-to-interannual climate variability worldwide. However, the regional terrestrial climate will only be predictable if the relevant SSTs are predictable [40]. Given that the El Niño phenomenon represents the majority of year-to-year variance in SSTs, including influencing the global ocean outside the tropical Pacific [41], most studies of the suitability of a model to predict seasonal-to-interannual climate will focus on the model's ability to predict El Niño. Of course, such studies of model fidelity help further elucidate the processes behind such phenomena.

The first attempt to predict El Niño employed a very simple model of the tropical Pacific Ocean that consisted of a warm, lighter, upper ocean overlying a cold, heavier deep ocean [17]. The depth of the upper layer determined the temperature at the surface in the eastern and central equatorial Pacific where upward currents are known to bring cold water from the deeper ocean into the upper layer and cool the surface; the more shallow the upper layer, the easier for the upwelling currents to bring cold water to the surface. The surface temperature anomalies in the east influence the east–west temperature gradient, which affects the strength of the trade winds, which affect the slope of the interface between the upper and lower ocean layers, and thus affects the eastern equatorial surface temperature. This describes the classic Bjerknes feedback mechanism [15] that maintains the mean state as well as the coupled air-sea feedbacks that can evolve an El Niño or La Niña event. Off the equator in the western Pacific the anomalous winds create depth anomalies of the opposite sign to those in the

eastern equatorial Pacific, which can then adjust via equatorial wave dynamics, eventually causing the decline of the current event (e.g., El Niño) and potentially initiating an event of the opposite sign (e.g., La Niña). The positive feedback growth together with the delayed negative feedback that can cause the turnabout from one phase to the next was named the Delayed Oscillator mechanism [19]. Variants on this central idea, such as the Recharge Oscillator [42] have since been formulated as observations of the tropical Pacific became available [43] and as the tropical Pacific air-sea variability was studied in more models.

Although the first models to successfully predict El Niño in the late 1980s were very simplified compared to the complexity of the real ocean–atmosphere system, they still remain viable prediction tools. It is very difficult to represent all the physical processes in the tropical ocean–atmosphere system precisely, and because of the strong interconnectedness of these processes, small errors in the representation of one process leads to associate errors in others. Thus it was not until the early twenty-first century that coupled ocean–atmosphere models of full complexity clearly demonstrated parity with simpler prediction models (Fig. 4) [44]. The metric most commonly presented to represent a model's ability to predict El Niño is the NINO3.4 index of sea surface temperature, which is the average of the temperature anomaly over the central equatorial Pacific from 5S–5N and 170W to 120W, as this is the region that exhibits the highest correlation with terrestrial climate anomalies worldwide [45].

However, this simple index does not capture all of the characteristics of El Niño. The timing and spatial structure of El Niño-related sea surface temperature anomalies can also influence the resulting teleconnections [46]. Additionally, single metrics such as correlation or mean error can mask the conditions under which El Niño is predictable. Most dynamical systems, particularly those with a chaotic component, exhibit conditional predictability meaning that there are times when the system is more predictable than others [47]. Thus it is also common to present the

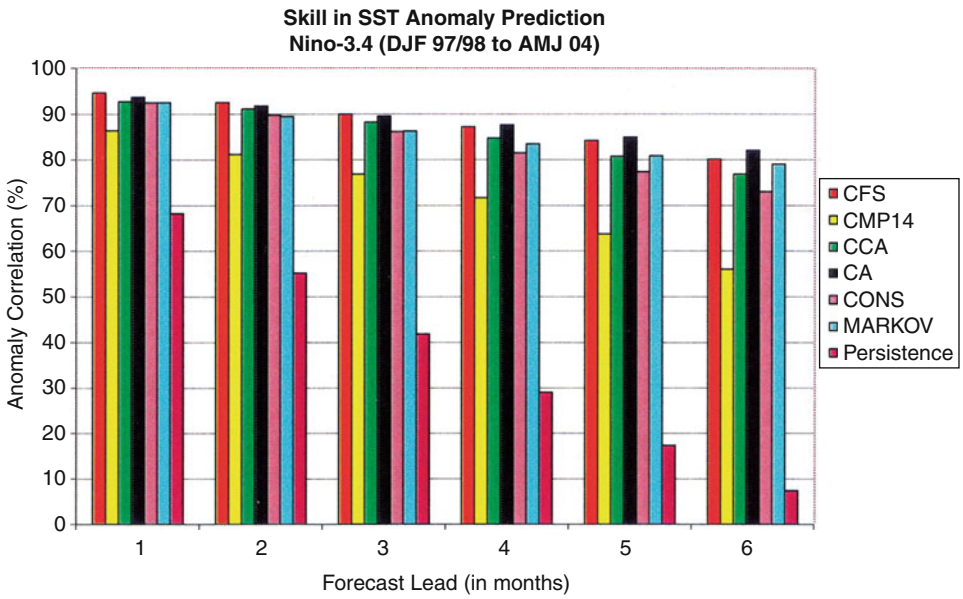

Climate Predictions, Seasonal-to-Decadal. Figure 4

Anomaly correlation (%) by various methods of the seasonal mean Niño-3.4 SST as a function of lead (horizontal; in months). The results are accumulated for all seasons in the (target) period DJF 1997/1998 to DJF 2003/2004. Except for CFS (the Climate Forecast System) coupled ocean–atmosphere model of the National Weather Service's Climate Prediction Center (CPC), all forecasts were archived in real time at CPC from 1996 onward. CMP14 is the previous coupled model, *CCA* is canonical correlation analysis, *CA* is constructed analog, *CONS* is a consolidation (a weighted mean), and MARKOV is an autoregressive method (From [44])

prediction history of models, to show how observed sea surface temperatures along the equator vary compared to the predictions as a function of lead time [48]. A common finding from such qualitative examination is that although models may do well in predicting the occurrence of an El Niño event, they have difficulty predicting the magnitude of large events or locating the variability far enough east during strong events [49, 50]. Such biases have repercussions for predicting the associated climate anomalies.

Predicting the driver of the climate anomalies is the first step. Next is to predict the associated climate anomalies. Biases in prediction of the drivers, such as El Niño events that do not exhibit the strength or structure of observed events, lead to biases in regional climate prediction. One way to circumvent some of the error in predicted SSTs is to statistically correct them before providing this information as boundary conditions to the atmospheric model. This approach is known as two-tier forecasting because the SSTs are predicted first and the climate is predicted second using an atmospheric GCM. Changes in the atmospheric circulation do not feed back onto the SST anomalies. Because El Niño is the largest driver of climate anomalies, and El Niño teleconnections are driven by the ocean variability, this is a viable approach. However, outside the tropical Pacific a notable fraction of the ocean variability is driven by the atmosphere, and thus in those regions heat and momentum fluxes will not be properly represented by two-tier forecasts.

One-tier forecasts, where the ocean and atmosphere evolve together, allow for a more physically consistent evolution of the ocean–atmosphere system. Coupled ocean–atmosphere models are increasingly the prediction tools of choice at operational forecast centers around the world [1]. However, due to model biases over some parts of the tropical ocean, regional climate prediction remains problematic with coupled models. In particular coupled models have great difficulty in representing the mean state of the tropical Atlantic, with the warmer water occurring in the western instead of the eastern equatorial Atlantic [51]. As a result, the tropical Atlantic SST variability is not predicted with any skill for most seasons by the current generation of coupled models, and the potential predictability of climate variability over western Africa and northeastern Brazil is substantially degraded compared to what it would be with skillful SST predictions [40].

Other biases that have been known for decades still persist in coupled ocean–atmosphere models and limit the quality of climate predictions. Such systematic biases include a double intertropical convergence zone over the Pacific, poor representation of regions of stratus clouds over the eastern subtropical and extratropical oceans, and vertical temperature gradients that are too diffuse in the equatorial Pacific where the warm upper ocean transitions to the cold deep ocean. The processes responsible for these features in Nature and how they are represented in models are active areas of research. Recent modeling experiments using models with a spatial resolution of tens of kilometers rather than hundreds of kilometers does reduce some of these biases by better resolving certain climate processes.

Seasonal-to-Interannual Prediction: Prediction Systems

Prediction systems are based on observations, models, and their connection through data assimilation systems. The three together form the three-legged chair of prediction systems [9]. Any weak leg compromises the system, and improvements in one leg often lead to improvements in the other legs.

Predictability of seasonal-to-interannual climate variability arises from the initial conditions of the ocean, particularly those conditions in the tropical Pacific Ocean that carry some signal of future El Niño conditions. Observations of upper ocean heat content anomalies in the other tropical oceans are also important for prediction as they can influence the persistence of local sea surface temperature anomalies as well as moderate the impacts of El Niño-related teleconnections in the region. Therefore, it is important to adequately observe the tropical ocean state. However, since models have errors in their representation of the real world, using the observations too faithfully to describe the initial conditions for model forecasts can cause problems. This is where data assimilation is essential to prediction systems.

Data assimilation is the process used to produce initial conditions for a dynamical model by combining observations with other information from a previous

simulation of the model. If this is not done carefully, the introduction of the observations into the models can lead to initialization shock when the prediction is started. Initialization shock is a term used to identify the rapid development of model errors when a simulation is started. One approach to minimizing this problem is called anomaly initialization in which observed anomalies of the ocean state rather than the full state are added to the model's mean state to arrive at initial conditions. Other data assimilation methods address the mismatch between the spatial and temporal characteristics of the variability between Nature and the model. Currently, the atmosphere, ocean, and land components of prediction models are initialized separately. The data assimilation efforts are separate, and thus consistency in the initial states and tendencies of these components is not ensured. Methods to assimilate observational data into the coupled model as a whole are being investigated starting with the coupled ocean–atmosphere system [52].

Recent advances in El Niño prediction skill at the European Centre for Medium-Range Weather Forecasts in the United Kingdom were accomplished by both improvements to their model and improvements to the ocean data assimilation system [53]. Additionally, retrospective forecasts, also called "hindcasts," of the NINO3.4 El Niño index from 1960 to present from that forecast system have demonstrated the value of the observations provided by the Tropical Atmosphere–Ocean array of data buoys that measure temperatures of the upper 500 m of the tropical Pacific Ocean, some at the equator also measuring ocean currents, as well as temperature, winds, and humidity at the surface. At the time when the array of buoys was completed in the early 1990s, the forecast error of the NINO3.4 index dropped dramatically [54]. This result is most clearly demonstrated in forecasts that are initiated in February, when the biases in the model are at a minimum. This echoes the connected nature of these three elements of forecast systems; observations and their assimilation into models are crucial for prediction, but better models better elucidate the value of the observing network.

Even at that point when models, the observing network, and the use of those observations for forecast initial conditions becomes essentially perfect, climate forecasts will still contain uncertainties. Small, almost imperceptible, uncertainties in the initial state or the detailed evolution of some small-scale processes will lead to some divergence in the future state. This is the chaotic element of the climate system, sometimes referred to as the "butterfly effect." Where uncertainty is due to errors, there is the potential to reduce it. However, it is not necessarily the goal of forecasters to eliminate uncertainty, as this would be unrealistic, but to quantify it to the extent possible. Better models that can capture the random nature of processes, such as turbulence or convection, would improve process-related contributions to uncertainty. Better representation of such processes may actually increase the uncertainty in forecasts, relative to what models now indicate. Better observations, more complete observational networks, and improved data assimilation techniques can better indicate the uncertainties that arise from initial conditions [55, 56].

The uncertainty in climate forecasts should thus be considered as a range of possible outcomes. Typically the range of possible outcomes, or probabilities, are presented relative to the past climate history of the last several decades. A common format used by many operational forecast centers is tercile classes. For example, the precipitation for a given location over the last 30 years is used to quantify the above-normal category as the wettest 10 years, the below-normal category as the driest 10 years, and the near-normal category as those in between. In this case, the climatological probabilities are 33.3% for any category without any further knowledge. This should be the forecast probability for each category if there is no signal in the current prediction or if the prediction tools have no skill in that region and/or season. If skill and signal exists, then the forecast probabilities will differ from the climatological probabilities (Fig. 5). If the signal in the forecast indicates likelihood for wetter conditions, then the probability for above-normal precipitation will be higher than 33.3% and the probability for below-normal precipitation will be less. Alternatively, the forecast can be represented as the probability for exceeding or not exceeding some quantitative value.

One of the most important qualities of probabilistic forecasts is that the probabilities are reliable, or representative of the frequency of occurrence. The other important quality is that they are sharp, or differ substantially from the climatological probabilities.

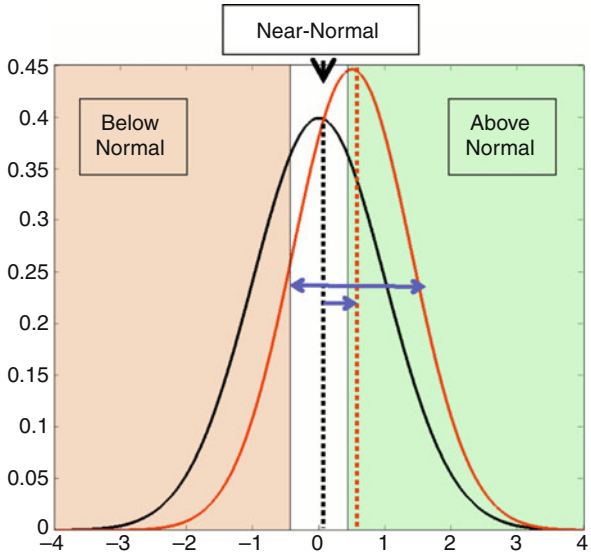

Climate Predictions, Seasonal-to-Decadal. Figure 5 Schematic of a probabilistic forecast distribution relative to a distribution of the historical climate observations. The values (*horizontal axis*) have been normalized with a mean of 0. The *shaded* regions represent the above-normal tercile (*green*) and the below-normal tercile (*brown*) of the historical distribution

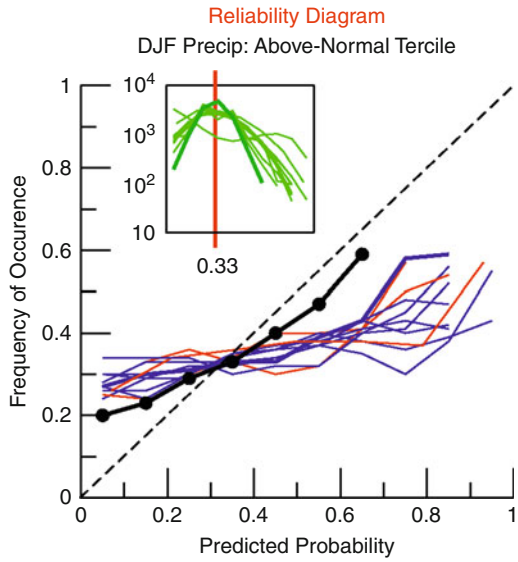

Climate Predictions, Seasonal-to-Decadal. Figure 6 An example of a reliability diagram, which indicates the skill of probabilistic forecasts. The diagram compares the forecasted probability of an event (in this case, above-normal winter rainfall in North America) to its observed frequency. A perfect forecast is represented by the *dashed line*, a *horizontal line* represents a forecast identical to climatology, and *sloped lines* are potentially skillful. The *blue* and *red lines* correspond to individual CGCMs and AGCMs, respectively, and are more horizontal than the *black line*, which represents the mean of these models. While the mean of the models is more reliable than any of the individual models, it tends to be underconfident for rare events (the *black line* lies above the perfect forecast line for low-probability events). Typically, a histogram accompanies a reliability diagram (*inset*), indicating the number of times that forecasts of various confidence levels were issued (Source: Adapted from [58])

Diagnostics of these forecast characteristics can be visualized through reliability and attributes diagrams (Fig. 6) and quantified through reliability and resolution skill scores, respectively [57]. A reliability diagram shows the complete joint distribution of forecasts and observations for a probabilistic forecast of an event or forecast category (such as the above-normal tercile). In a reliable forecast system, the probability assigned to a particular outcome should be the frequency with which – given the same forecast – that outcome should be observed. The information supplied by reliability diagrams includes calibration, or what is observed given a specific forecast (e.g., under and overforecasting), as well as resolution and refinement which is the frequency distribution of each of the possible forecasts giving information on the degree of aggregate forecaster confidence (small inset graph in Fig. 6). Reliability diagrams can further indicate whether there are systematic biases in the forecasts, such as not predicting enough occurrences of above-normal temperatures. Such probabilistic verification, such as reliability diagrams also can be useful for estimating event-specific prediction skill, for example if El Niño events were better predicted than La Niña events or drought conditions were better predicted than very wet seasons. A distinction in prediction skill between the cases of high and low variability calls for further examination of the physical causes of the discrepancy and whether it is inherent to the climate system dynamics or a shortcoming of the model(s).

It is a common feature of dynamical model predictions to be overconfident, indicated by a reliability curve that is more horizontal than the 45° angle that would indicate a reliable prediction system. For example, an overconfident forecast would be one in which a forecast that indicates above-normal rainfall is 80% likely in a given season, but overtime that forecast is followed by observations of above-normal rainfall 40% of the time. Such overconfidence can arise from errors in both the forecast signal and the forecast uncertainty.

Recalibration of predictions and multi-model ensembling are two approaches used to improve forecast reliability. Multi-model ensembling, which combines the prediction of several dynamical models, can improve the reliability and overall skill of predictions in two ways. First, although all models have errors, they do not necessarily have the same errors, thus combining the models reduces the systematic errors that would exist in the prediction from a single model. This can lead to reduced error and thus increased correlation skill in El Niño predictions, for example (Fig. 7) [59]. Similarly, it can increase the spatial coverage for where there is skill in capturing the predictable signals in the climate. The second advantage is the improvement in uncertainty estimation by considering the random errors and different parameterizations of random processes that give rise to the range of possible outcomes.

Multi-model ensembling can lead to overall better information on the climate signal and its uncertainty [60], and thus on forecast reliability (Fig. 8). Different approaches exist to combine models. The most straightforward is to treat all models equally. Particularly for prediction systems with short retrospective forecast histories of about 25 years or less, it will be difficult to discern differences in forecast quality between comparable models. This is the typically situation with one-tier prediction systems that use coupled ocean–atmosphere models, because the ocean observations used in the forecast initialization is only available since the late 1980s. For two-tiered forecast systems that use atmosphere-only models the ocean temperatures can be predicted statistically, which allows for longer histories of retrospective forecasts. In these systems, it becomes possible to discern differences in regional forecast performance and to use that information to give more weight to better performing models, which can lead to further improvements in forecast reliability [61, 62].

An alternative approach to performance-weighting models is to recalibrate the models prior to combination [63]. Recalibration has the advantage of improving forecast quality of individual models. It is also more viable for prediction systems with limited retrospective forecast histories, although a minimum of about 25 years is still required to identify systematic biases in seasonal-to-interannual variability. The recalibration of predictions is an attempt to account for systematic biases in both the signal and uncertainty in the predictions at a given location. Recalibration can also be used to account for spatial biases in the forecasts by comparing observed and predicted seasonal climate over several decades [9].

Reliable forecast information may still not provide enough specificity for those who wish to include seasonal-to-interannual climate forecasts in their decision models, such as those in the agricultural or water sectors. The spatial mismatch of the information, the fact that decision makers in sectors such as agriculture and water require information at much higher resolution, even if it means greater uncertainty, is a commonly cited reason for not using the operational forecasts [64]. There may also exist the desire for greater temporal resolution, such as the characterization of the weather within the climate that might predict the likely number of dry spells of a given duration. In some cases, certain weather characteristics of the seasonal climate may be more predictable than the seasonal totals (e.g., [65]). One way to address the information mismatch between the coarse spatial resolution, or the quality of the higher temporal variability, from global seasonal climate forecasts and the more detailed needs of the end user is through downscaling techniques. In statistical downscaling, the global climate forecast provides the input parameters for an empirical model with high spatial resolution. Statistical techniques can also be used to infer the signal in the weather characteristics relative to the seasonal mean, based on changes in the large-scale background climate, such as those empirically related to ENSO [66, 67], or to changes in atmospheric circulation [65]. In the dynamical downscaling, the global forecast is used to provide lateral boundary conditions to

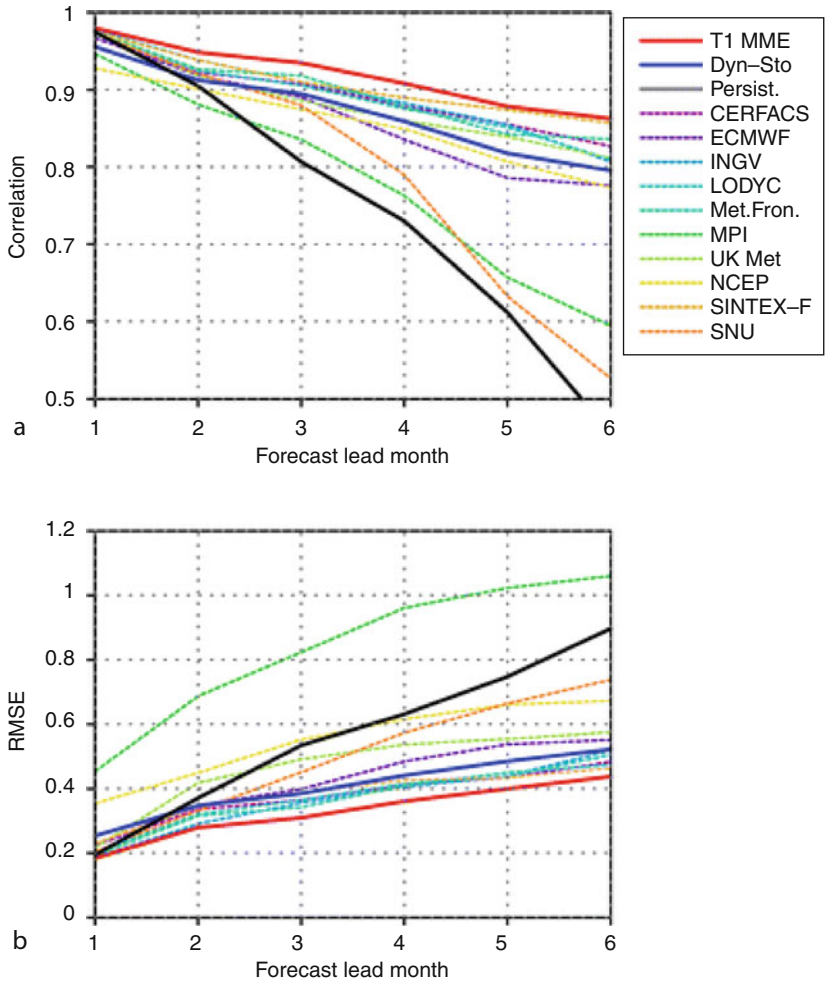

Climate Predictions, Seasonal-to-Decadal. Figure 7
(**a**) Anomaly correlation coefficients and (**b**) RMSE of NINO3.4 index during 1980–2001 with respect to lead time after removing the mean bias. The mean skill for all four cases including February, May, August, and November initial conditions is shown. *Black* for observation, *red* for 10 CGCM multi-model ensemble, *blue* for the Stat-Dyn forecast, and *colored dots* for individual coupled models as shown in the legend, respectively (From [59])

a high-resolution nested regional atmospheric model. While it may provide greater detail of the mean climate by better resolving terrain and coastlines, it has not been robustly demonstrated that dynamical downscaling improves prediction of the climate variability relative to the global model. Dynamical downscaling cannot overcome large-scale errors in the global model driving the nested model, and in many cases will exacerbate those errors. With increases in computing power, global climate models are starting to close the gap by providing fine spatial resolution, and attempting to provide better representation of weather transients that may be of interest to the end user. However, for the next decade or so downscaling techniques, particularly statistical downscaling will continue to add value to seasonal-to-interannual forecasts.

Seasonal-to-Interannual Prediction: Forecast Skill

Forecast skill is a measure of how accurately the prediction system can predict the observed climate variability or how well the probabilities describe the frequency of occurrence of particular outcomes.

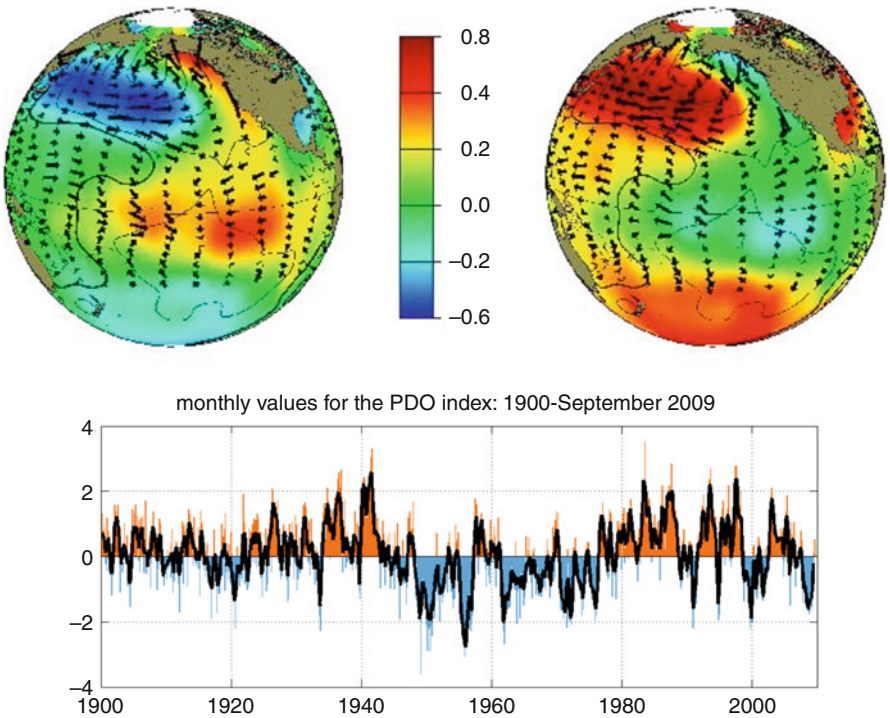

Climate Predictions, Seasonal-to-Decadal. Figure 8
(**a**) The positive (*left*) and negative (*right*) phases of the "Pacific Decadal Oscillation" (PDO), a long-lived El Niño-like pattern of Pacific climate variability, shown in terms of (**a**, *left*) the positive phase in sea surface temperatures (*colors*), sea level pressure anomalies (*contours*), and anomalous low-level winds (*arrows*), and (**b**) the time series of the PDO (Taken from http://jisao.washington.edu/pdo/)

Measures of accuracy between the best guess, or most likely outcome, of the forecasts and what was observed are often referred to as deterministic measures, meaning they are concerned with verifying the prediction for a single specific outcome, such as a prediction for an above-normal temperature or 2°C warmer than average in the coming season. The metrics for deterministic quantitative forecasts include the Brier skill score and its decomposition, which includes anomaly correlations or root-mean squared errors. The quality, or skill, of deterministic categorical forecasts can be assessed using a variety of measures. There is no single measure of forecast performance that can indicate all aspects of forecast quality [68]. Additionally, forecast producers may be interested in different aspects of forecast performance than users of the forecast information. The World Meteorological Organization has compiled a list of recommended deterministic and probabilistic verification measures for seasonal predictions entitled, The Standard Verification System for Long-Range Forecasts [69].

Keeping in mind that there are different, complementary measures of forecast skill, the accuracy of predictions is typically used to estimate the limit of predictability. The limit of predictability is a function of the predictable signal and the unpredictable chaotic, or noise, component in the climate system. With an ensemble of predictions from a single model or a set of models, the signal and noise can be estimated from that set of information. The signal would be the predicted information that the ensemble has in common and the noise is the range of discrepancy about the signal (Fig. 5). When the forecast is initialized, the ensemble contains very little noise, but as the prediction proceeds, the chaotic processes in the climate system lead to divergence of the ensemble members. The limit of temporal predictability is reached once the magnitude of the noise becomes comparable to the signal. This in

part, determines how far into the future the certain aspects of the climate can be predicted. Similarly, the average signal-to-noise ratio for a given region, season, variable, etc. describes the expected climate predictability in that case. Since Nature has only one realization, it is not possible to estimate the inherent limit of predictability of the climate system [9]. Estimates of the limit of predictability can be determined in a given prediction system as described above, but that will be only an estimate, and will be different for different forecast systems. At best, the most accurate prediction system for a given region, season, variable, etc. represents the limit of predictability for that case, and should be considered the lower limit of predictability, as the prediction accuracy is found to be at least that good and may improve further with improved models and data assimilation systems.

Given that real-time predictions have been in production for more than a decade now [1], several properties of forecast skill have emerged for seasonal-to-interannual predictions. First, predictions of seasonal mean temperature are more predictable than those for seasonal precipitation totals. This is related in part to the larger-scale nature of temperature anomalies and the processes behind them. Even the coarse resolution global climate models can represent fairly accurately the changes in seasonal temperatures. Precipitation processes and patterns have much smaller spatial scales and are more affected by local scale features. While the global models may be able to capture large-scale shifts in regions of convection and storm tracks, they may have difficulty with the characteristics of storms or local convective activity. The potential importance of local scale processes on precipitation variability also means that the noise component of seasonal precipitation variability is larger than that for temperature. As a result, more ensemble members are required to estimate the seasonal signal for precipitation than for temperature. The second robust property of seasonal predictions is that the tropics are much more predictable than are the extratropics. In the tropics, the atmospheric circulation is more explicitly tied to the changes in patterns of surface temperatures, and the noise in the resulting atmospheric circulation is relatively small. A third and notable property of the predictions, which actually applies to predictions at all timescales, is that there is conditional skill in the expected accuracy. There are times when the initial and evolving state of the climate system carries a much larger predictable signal than other times. For seasonal-to-interannual forecasts this coincides with El Niño events. For seasonal predictions over the United States most predictability derives from El Niño or La Niña conditions [70]. Similar results hold on a global scale too; the fraction of land area over which skillful forecasts can be made is up to twice as large during El Niño or La Niña conditions than in their absence [71]. Moreover, since these events have an inherent timescale of 6–12 months, or longer, the time horizon into the future that skillful forecasts can be issued is also expanded.

Seasonal-to-Interannual Prediction: Internationally Coordinated Efforts

Several internationally coordinated efforts have led to the understanding of seasonal-to-interannual climate variability and its prediction using dynamical models. One of the earliest was the Atmospheric Model Intercomparison Project (AMIP) [72]. This project was organized by the Working Group on Numerical Experimentation as a contribution to the World Climate Research Programme. Different atmospheric models were run with the same observed sea surface temperatures as boundary conditions for the period 1979–1988. The goal was to identify systematic errors as well as systematic responses to the boundary conditions across models. Without such a coordinated effort there had been questions whether the results from a single model were particular to that model or a more robust response expected of the climate system. Other coordinated activities followed.

In the late 1990s, experiments were carried out using different atmospheric models to test the predictability of seasonal climate relative to the variability of sea surface temperatures. Two important issues addressed in that collection of research were the relative impact of initial atmospheric conditions predictability of the seasonal climate and a suggestion that prediction skill could be improved through a multi-model approach. In the United States five modeling centers participated in this research under the Dynamical Seasonal Prediction (DSP) project. On the other side of the Atlantic, 11 different partners throughout

Europe contributed to the Prediction of Climate Variations on Seasonal to Interannual Timescales (PROVOST) project [73].

Further research on seasonal predictability and the value of multi-model ensembles was conducted with coupled models from seven European modeling centers under the Development of a European Multimodel Ensemble system for seasonal to inTERannual prediction (DEMETER) project [74]. This project also encouraged research to determine the value of seasonal predictions through their use in models that use the climate data to make prediction over a wide range of interests, from agriculture to health. The next generation of DEMETER was ENSEMBLES, which continued to advance methods and application of seasonal predictions from European Earth system models, thus adding complexity to the dynamical prediction models [75]. The ENSEMBLES project also began to extend those predictions to decadal timescales. The Working Group on Seasonal to Interannual Prediction under the World Climate Research Programme is currently coordinating the Climate-system Historical Forecast Project (CHFP), which will provide access to a wide range of hindcasts to evaluate subseasonal-to-decadal predictions of the climate system, which also aims to quantify the predictability added by elements other than sea surface temperatures, for example through initialization and prediction of the land surface, the cryosphere, and the stratosphere [76].

Decadal Prediction (Experiments)

Decadal Prediction: Drivers of Decadal-Scale Climate

Decadal climate predictions sit between the seasonal-to-interannual forecasts of the next months to a year in the future and the climate change projections of 50–100 years in the future. There are many features of the climate system with timescales that vary over decades (decadal variability). The dominant drivers of climate features over decadal timescales are believed to be changing atmospheric composition, mainly increasing greenhouse gases, and slow changes in ocean circulation that lead to slow changes in the pattern of sea surface temperatures. The changing atmospheric composition changes the energy balance of Earth, which leads to warmer temperatures and other associated climate changes that manifest primarily as trends. The temperature trends are not spatially uniform. Ice-albedo feedback in higher latitudes leads to greater rates of warming there than at low latitudes. Land has a lower heat capacity than water, so the continents warm faster than the oceans. Ocean dynamics also play a role in the patterns of climate change warming, particularly in upwelling regions, where the radiative warming is offset by the upward advection of colder ocean water from depth.

What decadal predictions aim to capture that climate change projections do not is the predicted evolution of naturally occurring decadal-scale features. Climate change projections contain these processes and the associated variability, but since the climate system is not initialized with observations, the decadal evolution will not be temporally consistent with the observations. So one first test of a model is to see whether it is capable of simulating the dominant decadal-scale features observed in Nature.

Decadal-scale variability has been identified in Nature in both the Pacific and Atlantic Oceans. In the Pacific Ocean the variability is referred to as the Pacific Decadal Oscillation (PDO), or more correctly Pacific Decadal Variability (PDV). The pattern of PDV (Fig. 8a) has its signature in sea surface temperatures with cooler than normal temperatures in the midlatitudes of the North Pacific Ocean and warmer than normal temperatures in the eastern and central equatorial Pacific Ocean during the positive PDV conditions [22]. The time series associated with the projection of sea surface temperature anomalies on this pattern represents the PDO index (Fig. 8b). This sea surface temperature pattern is reminiscent of El Niño conditions, except that the magnitude of sea surface temperature anomalies is larger in the midlatitudes than in the tropics, and the tropical sea surface temperatures have a broader meridional extent. This pattern of sea surface temperatures is accompanied by sea level pressure anomalies in the North Pacific. A measure of the time series of changes in North Pacific sea level pressures is known as the North Pacific Pressure Index (NPPI). It was later realized that there is symmetry in the Pacific decadal variability such that a similar pattern of cooler than normal sea surface temperatures and anomalous low sea level pressure is also found in the midlatitudes of

the South Pacific Ocean. The full Pacific view of decadal variability has been named the Interdecadal Pacific Oscillation (IPO, [77]). However, the PDO is the more commonly used index outside Australia.

The symmetry of ocean–atmosphere anomalies outside the tropics, and the resemblance to El Niño, suggests a role for El Niño in driving PDV. It is also notable that there is considerable year-to-year fluctuation in the PDO index. It is very difficult to identify in any particular year what phase, positive or negative, the PDV is in because within the protracted periods in which the PDV is preferentially of one sign or the other, there exist excursions of the index of opposite sign that may only last a year or two.

Simple model experiments have shown that El Niño events can affect the positive phase of PDV [41]. Model analysis suggests an atmospheric Rossby wave train emanating from anomalous convective heating in the central Pacific leads to anomalous low sea level pressure in the region of the Aleutian low, thus strengthening the westerly trade winds. The strengthened winds lead to cooling through enhanced evaporation and also drive southward Ekman flow that brings colder water from the north southward. Those changes in the ocean mixed layer can be sequestered from the atmosphere from one winter to the next due to changes in the ocean mixed layer depth and its connection to the surface from winter, when El Niño peaks, the storm track is strongest and the atmosphere can directly affect the upper ocean, to summer when the previous El Niño would have decayed, the storm track is relatively weak, and increased solar radiation stabilizes the upper ocean. The following winter when the westerly winds of the storm track again increase, the sequestered mixed layer temperature anomalies reemerge [78]. This reemergence mechanism is hypothesized to the main way that the year-to-year variability associated with El Niño and La Niña can be rectified into longer timescale variability. However, other processes may also contribute to PDV. Some mechanisms that have been proposed included ocean–atmosphere coupling of a basin gyre mode [25], excitation of midlatitude oceanic Rossby waves [79], and a complementary, possibly independent oscillation driven by the tropics particularly when El Niño events are focused toward the central equatorial Pacific [80].

Associated with the decadal changes in Pacific Ocean conditions, decadal-scale terrestrial climate anomalies have also been identified over the United States [22] and throughout the Pacific sector [81]. Many of these climate anomalies are consistent with El Niño-related teleconnection patterns, such as wetter conditions in the southern tier of the United States and drier conditions over the Pacific Northwest [82]. Although only a few realizations of each phase of PDV exist in the instrumental records, the broad pattern seems to be consistent across these cases. However, because it is likely that El Niño is a dominant driver of PDV, and is associated with similar terrestrial teleconnections, it is difficult to say with confidence that the PDV is somehow independent of the mere existence of extended periods when El Niño events are stronger or more frequent versus when El Niño events are weaker or less frequent.

Decadal-scale variability in the Atlantic is referred to as the Atlantic Multi-decadal Oscillation (AMO), or more correctly Atlantic Multi-decadal Variability (AMV), because there does not seem to be a spectral peak signaling a true oscillation. Because positive AMV conditions are associated with warming throughout the North Atlantic (Fig. 9), the index of AMV is simply the sea surface temperature anomaly averaged over the North Atlantic, and it is often detrended [83]. Other more elaborate means of isolating decadal-scale variability over the Atlantic have been used (e.g., [24]), but result in very similar time series, so the simple index is now the one most widely used.

The hypothesized mechanism driving the AMV is associated with changes in the Atlantic Meridional Overturning Circulation (AMOC). The AMOC brings warm and salty water from the tropical Atlantic poleward. At high latitudes, cold salty water becomes denser than the water below it due to heat fluxes from the westerly storm tracks and brine injection from sea ice formation. The heavy surface water then sinks and flows back equatorward as North Atlantic Deep Water. The sinking water is replaced by the surface flow from tropics to high latitudes. If the rate of sinking increases, the poleward flow of surface water increases, bringing more warm tropical water into the midlatitudes. This represents an increase in the strength of the AMOC, and the AMV index becomes positive. If the North Atlantic water gets too warm or if it freshens the rate

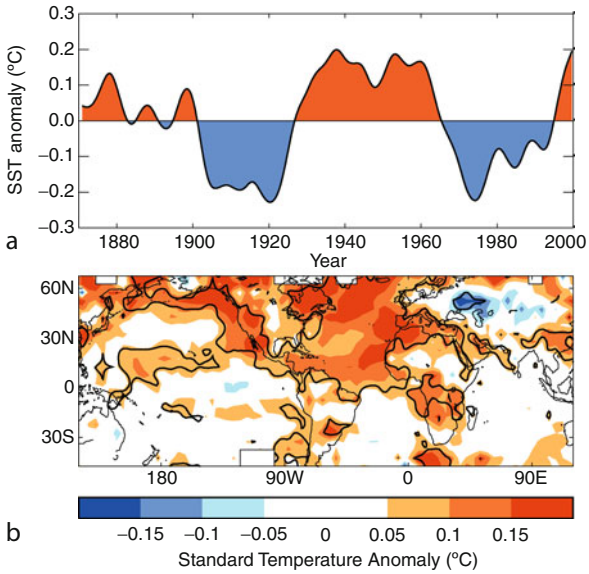

Climate Predictions, Seasonal-to-Decadal. Figure 9 (**a**) AMO index derived from detrended area-weighted mean North Atlantic SST anomalies by using a Chebyshev filter with a half-power period of 13.3 years. (**b**) Surface temperature anomaly associated with one positive standard deviation of the AMO index, calculated by regression of surface temperatures with the index and scaled by its standard deviation. The solid contour bounds regions significant at the 90% limit of a two-sided *t*-test accounting for autocorrelation (Source: From [83])

of sinking water slows down, and the rate of transport of warm tropical water poleward slows down. This represents a decrease in the strength of the AMOC, and the AMV will become negative.

The AMOC is forced on all timescales. Because the Gulf Stream is the western boundary current of the wind-driven ocean gyre as well as contributing to the AMOC, changes in the winds will affect the AMOC as well as ocean temperatures. However, the multi-decadal-scale variability described above is a much slower process related to the inertia of the overturning circulation and the associated impact on the density properties of the Atlantic Ocean. Since observations of the AMOC have become available only since the end of the twentieth century, there is not enough observational evidence to quantitatively link the sea surface temperatures of the AMV with multi-decadal variability of the AMOC. However, the low-frequency variability of AMOC in some models is associated with a pattern of sea surface temperature anomalies that closely resembles the observed AMV pattern [83]. What has not been resolved is what process or collection of processes can influence the AMOC on long timescales. Some studies point to modification of the strength and local of the intertropical convergence zone over the Atlantic as a way to modify the salinity of the water transported from the tropics [84]. Others suggest that the North Atlantic Oscillation (NAO – also called the Arctic Oscillation, AO) plays a dominant role by influencing the strength of the winds, which then influence the rate of convection, or sinking of heavy water, in the Labrador Sea region with an estimated 10-year lag time [85]. Although this would be a fairly white noise process, the suggestion is that the ocean integrates the noise into a longer timescale red noise process, but one that might still carry some predictability due to persistence.

The teleconnections associated with the positive phase of AMV include wetter conditions over the Sahel and India and drier conditions over northeast Brazil, due to the northward shift of the intertropical convergence zone toward the relatively warmer conditions north of the equator [29]. Also the warm tropical North Atlantic provides more fuel for the growth of tropical storms, and empirically it is seen that more tropical storms grow to hurricane intensity during the positive, warm phase of AMV than during the negative or cool phase.

Decadal Prediction: Model Fidelity

The task of judging whether a model captures decadal variability in the Pacific or Atlantic oceans for the right reason is greatly complicated by the limited history of observations compared to the timescale of the variability. Since the measurements of surface temperature and sea level pressure go back to the nineteenth century, most comparisons are made to these fields. In many cases, the question of model fidelity is closely tied to examination of the processes involved in producing the variability in a particular model and to what extent those are observed in Nature. The difficulty with that approach is as described in the previous section: different models may not agree on which process(es) dominates, or is even involved.

Different models also may yield somewhat different spatial patterns or spectra than suggested by the limited observations [86]. A similar situation exists relative to El Niño in coupled dynamical models [87], and this has not prevented the use of those models for El Niño prediction. Thus, the most important factor may be simply whether or not a model is capable of capturing a reasonable representation of decadal variability in sea surface temperatures, as this is how whatever changes are occurring in the ocean will be communicated to the atmosphere.

Exactly how best to validate decadal variability in the models is an area of active research. To date, more work has been focused around Atlantic variability perhaps because of the recognition of the role of the AMOC in the AMV. The idea is that if the AMOC is responsible for the AMV, then it is the AMOC that a model must be able to predict from a given set of initial conditions. The AMOC must then produce a surface temperature of reasonable resemblance to Nature, and the overlying atmosphere must be able to respond to the changes in surface temperature in a way that captures the observed teleconnections. Again, the difficulty is that very few realizations of the variability exist in the observational record, although paleoclimate reconstructions of past temperature or precipitation suggest that, for example, multi-decadal variability consistent with observed AMV has impacted regional climate 400–500 years back [88]. But the few realizations of the spatial pattern of sea surface temperatures makes it difficult to know which parts of the pattern of anomalies are robust across events and which are variable from one positive phase to another.

For PDV, most models capture the response of the midlatitude Pacific Ocean to El Niño variability. However, they often do not demonstrate the same level of multiyear persistence through a reemergence mechanism. Different models are also influenced to differing degrees by other processes hypothesized to contribute to PDV, including the white noise imposed by variability in the storm track. As a result the patterns of PDV, such as where the sea surface temperature anomalies are focused and the magnitude of that temperature variance, also differ among models.

Some modeling studies have shown that at least the atmospheric models can translate the changes in patterns of sea surface temperature into realistic teleconnections. For example, using observed heat fluxes from the positive, warm phase of AMV in the Atlantic Ocean to drive an atmospheric model leads to decadal-scale changes consistent with observed changes in precipitation over the Sahel and India and also in the wind shear over the tropical North Atlantic relevant to hurricane formation (Fig. 10) [30]. Thus as with El Niño, if the sea surface temperatures can be predicted then there may be at least some predictability of the associated terrestrial climate impacts.

Decadal Prediction: Prediction Experiments

Experimental decadal prediction has only recently begun. Decadal prediction differs from climate change projections in the initialization of the climate system, with particular emphasis on initialization of the oceans. The first paper demonstrating actual retrospective, decade-long, initialized forecasts was published in 2007 [3]. They showed improvements in prediction of globally averaged temperatures relative to the uninitialized climate change projections from the same model. However, it was not clear how much predictive information is available at the regional scale from these predictions, and it is not obvious what the main drivers are behind any predictive information they may yield.

The prediction systems for decadal prediction are essentially the same as for seasonal-to-interannual prediction. They require observations, models, and their connection through data assimilation systems. One of the main differences is the requirements on the observations: seasonal-to-interannual predictions mainly need information about the upper several hundred meters of the tropical oceans; decadal predictions require information about the global oceans, including the middle and high latitudes and also to much greater depths to capture information on the lower branch of the AMOC.

Observations needed to produce initial ocean conditions are incomplete. The creation of retrospective forecasts of decadal variability at least several decades into the past requires information on salinity fields that just do not exist. This has tested the limits of ocean state estimation with limited data, and the estimates even for large-scale averages, such as the average salinity anomaly in the upper 700 m of the midlatitudes of the Atlantic Ocean, can vary greatly. The uncertainty

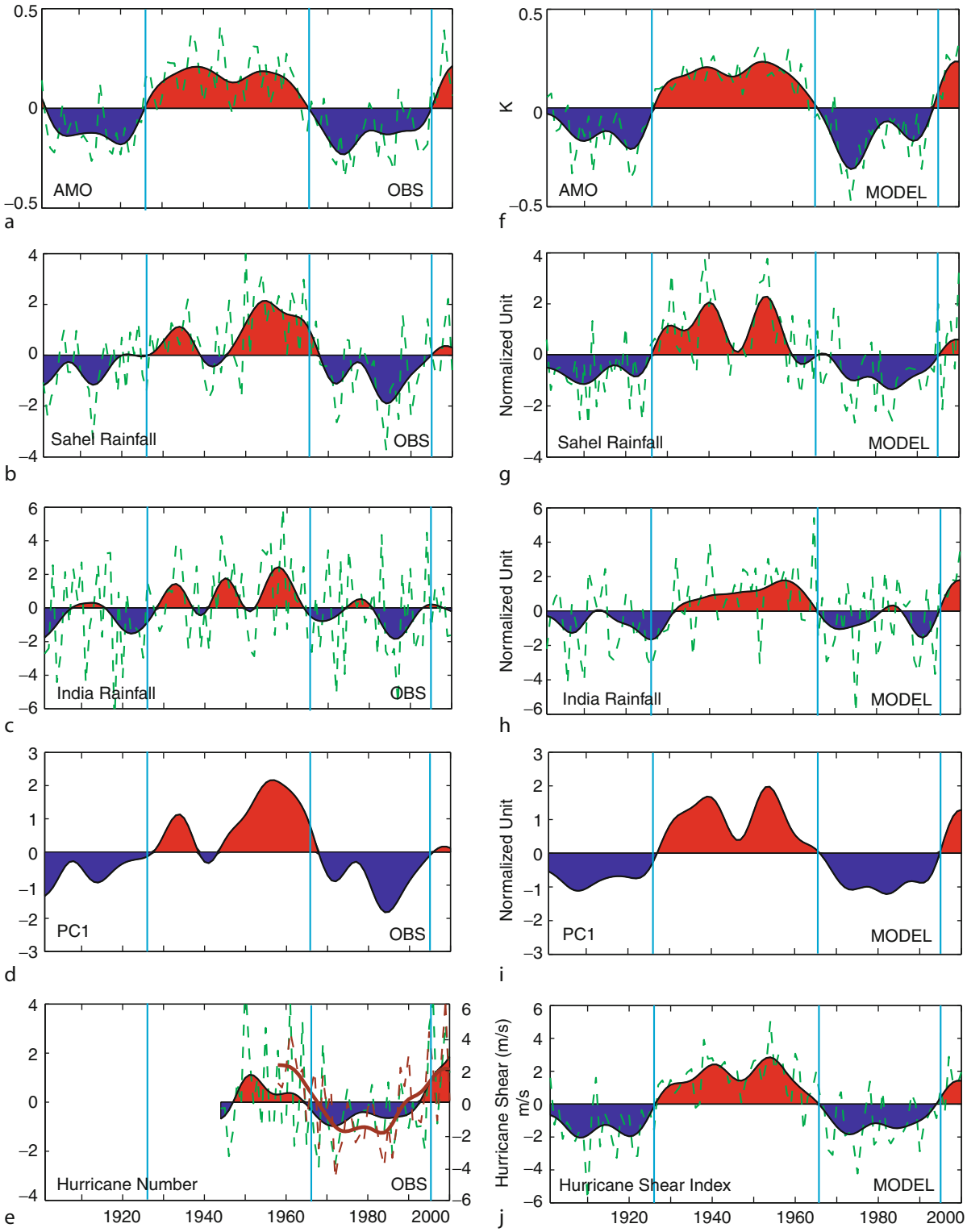

Climate Predictions, Seasonal-to-Decadal. Figure 10 (Continued)

among datasets for upper ocean salinity anomalies on basin scales is larger than the variability within a single dataset [89]. Since the beginning of the twenty-first century, however, the Argo program of drifting buoys has provided unprecedented measurements of the upper 2 km of the global ocean. The floats measure temperature and salinity profiles as they descend and ascend the water column about every 10 days. There are currently over 3,000 floats reporting data through satellites (Fig. 11). Even with good observational data coverage of the global oceans there will still be challenges in merging those data efficiently with models through data assimilation systems to account for both mean biases and biases in space-time variability.

The first step in exploring decadal prediction has been through perfect model studies. In perfect model studies, a free-running integration of the model is taken as truth; this integration assumes the role of the "observations." Ensemble members are set up to start from a particular point in the free-running integration with small perturbations to the initial state, representing the uncertainty in initial conditions. The ensemble members are then integrated forward to see how well they can track the "truth" of the free-running integration. In this experimental setup, the "observations" are perfect because since they are taken from the model they are known everywhere, and the model is perfect, because it is dynamically consistent with the "observations," which are just a snapshot from the model. Similar experiments toward the design of assimilation systems test the insertion of these perfect "observations" but sampled only at locations that the actual observing network could provide data. The idea is to see if in this most idealized of circumstances – perfect observations and perfect model – the model is able to predict the evolution of the "observed" variability taken from the free-running integration. If not, it implies that in the particular model, too much noise exists to extract a predictable signal. The situation will only be worse in a real forecast setting with imperfect observations in the model that is also not perfect.

A number of these perfect model prediction experiments have been carried out since the early part of the twenty-first century. In a coordinated experiment of five European modeling centers, called PREDICATE, two to three experiments were carried out by each group starting their ensemble predictions at different points in time to explore the prediction dependence on the variability of the AMOC. In all cases there was some skill in predicting the evolution of the AMOC (Fig. 12). The experiments also demonstrated conditional predictability much like is seen with El Niño predictions. The perfect model predictions started when the AMOC was stronger than average yielded predictability of the AMOC to about 10–15 years into the future; predictions started with a weak AMOC predicted the future evolution of the AMOC only 2–5 years into the future [90]. The PREDICATE experiments were based on model control runs, meaning that atmospheric composition was held fixed. More recent perfect model studies explore the relative predictive signal due to the initial conditions versus due to radiative forcing from increasing greenhouse gases [91]. Several common lessons are beginning to emerge from these studies. One is that the predictable time horizon, when the signal in the ensemble of predictions is larger than the uncertainty across ensemble

Climate Predictions, Seasonal-to-Decadal. Figure 10
Observed and modeled variability. The *color shading* is the low-pass filtered (*LF*) data and the *green dash line* is the unfiltered data. (**a**) Observed AMO Index (K). (**b**) Observed JJAS Sahel rainfall anomalies (averaged over 20°W–40°E, 10–20°N). (**c**) Observed JJAS west central India rainfall anomalies (averaged over 65–80°E, 15–25°N). (**d**) Observed time series of the dominant pattern (PC 1) of low-frequency JJAS rainfall anomalies. (**e**) Observed anomalous Atlantic major Hurricane number (axis on the *left*, original data from the Atlantic basin hurricane database-HURDAT, with no bias-type corrections from 1944 to 1969, there is no reliable data before 1944) and observed Hurricane Shear Index (1958–2000) (m/s, *brown solid line* for LF data, *brown dash line* for unfiltered data, axis on the *right*). (**f**) Modeled AMO Index (K). (**g**) Modeled JJAS Sahel rainfall anomalies. (**h**) Modeled JJAS west central India rainfall anomalies. (**i**) Modeled PC 1 of LF JJAS rainfall anomalies. (**j**) Modeled Hurricane Shear Index (m/s) (Source: From [30])

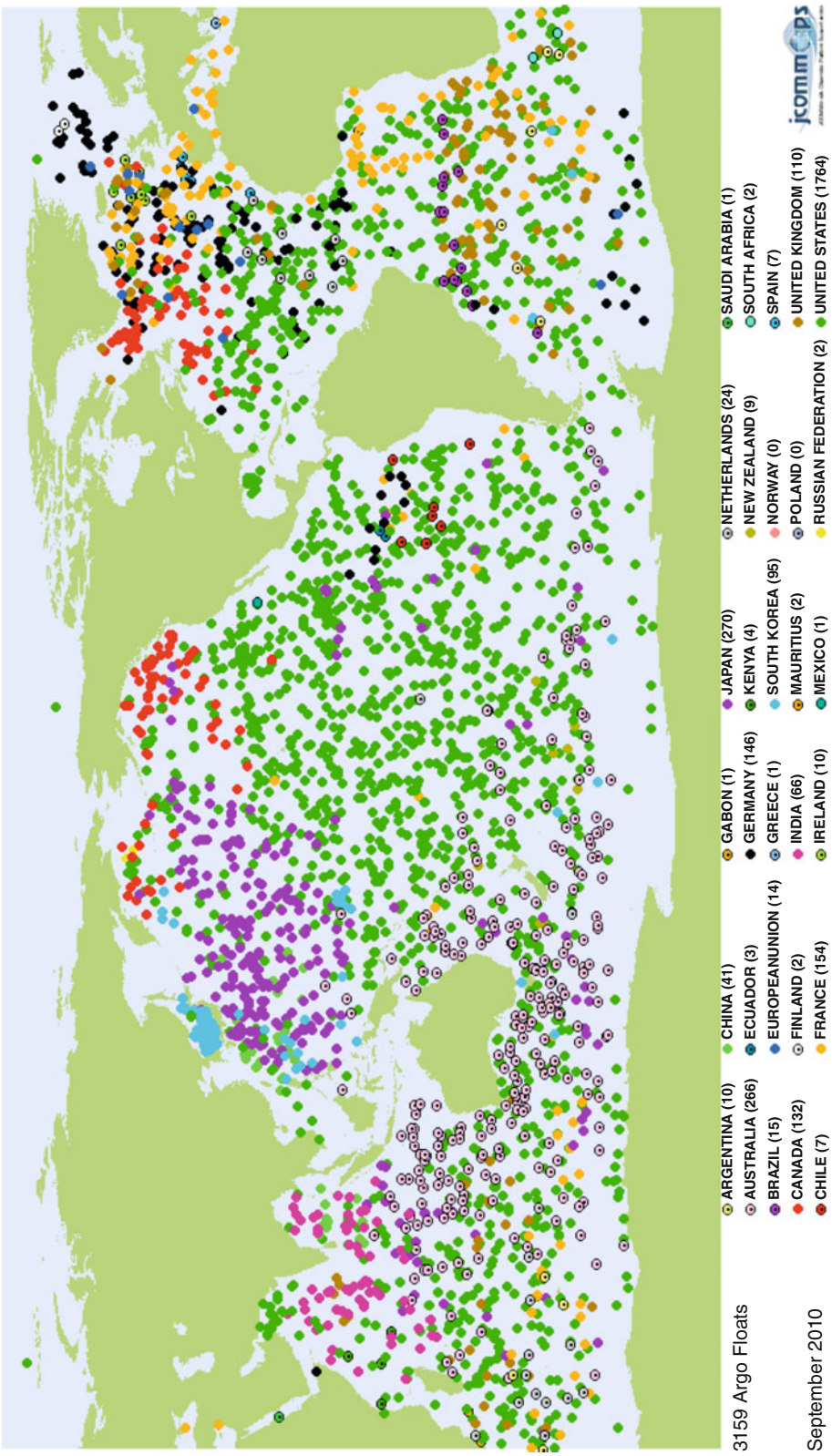

Climate Predictions, Seasonal-to-Decadal. Figure 11
Map of location of Argo floats and the countries that deployed them, as of September 2010. Note that *dot* size is greatly exaggerated relative to size of floats (Source: http://wo.jcommops.org/cgi-bin/WebObjects/Argo.woa)

C

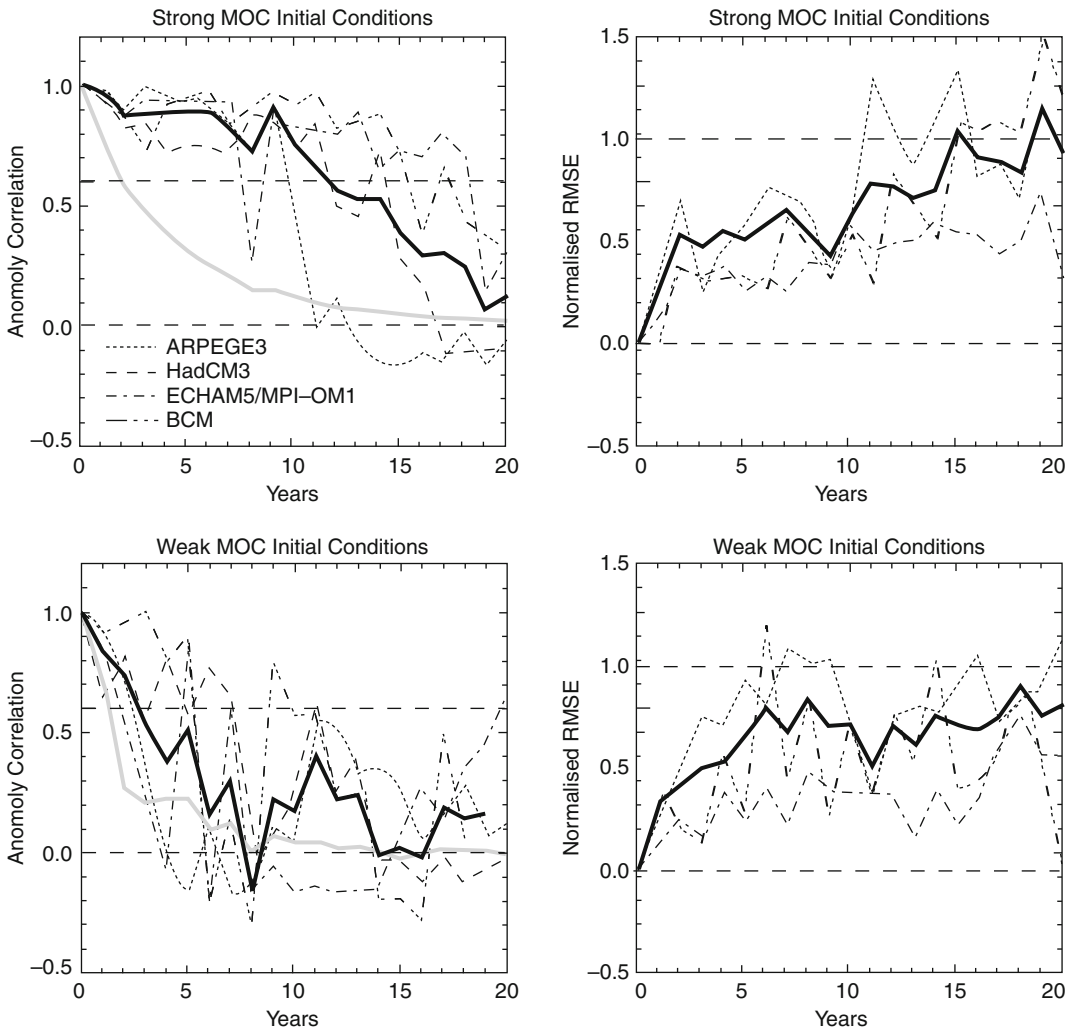

Climate Predictions, Seasonal-to-Decadal. Figure 12

Measures of the potential predictability of variations in the strength of the Atlantic Meridional Overturning Circulation from four of the five coupled models (see legend). (*left*) The anomaly correlation coefficient (ACC: unity for perfect potential predictability; zero for no potential predictability) for (*top*) strong and (*bottom*) weak MOC initial conditions (*right*). The normalized root mean squared error (rmse: zero for perfect potential predictability; unity for no potential predictability) in the same order. Also shown in the figures are the multi-model average ACC and rmse (*thick black line*) and the multi-model average ACC for a simple damped persistence (*thick gray line*) (Source: From [90])

members, is longer for midlatitudes than for the tropics due to the dominance of year-to-year variability in the tropical oceans. Another lesson is that upper ocean heat content is more predictable than sea surface temperature due to the impact of weather noise on surface temperatures, while the upper ocean temperatures are more reflective of the slow changes in the atmospheric circulation. Thus even if the AMOC is predictable, the surface temperatures connected with that feature will be less so, but it is this surface expression that is necessary for predicting the terrestrial climate impacts. Finally, it appears that the external forcing due to increasing greenhouse gases becomes comparable to the information from ocean initial conditions by 10 years out for the midlatitudes and less in the tropics. Again, these are perfect model results. However, such

results only indicate the upper limit of predictability for a particular model, and even though the similar results have been found across several of the current models, it is not to say that different results might be possible from better models.

To date, only a few pioneering attempts have been documented of "retrospective forecasts," which are decadal predictions initialized with real observed initial conditions from some time ago. These prediction experiments not only used different models, they also used very different methods to obtain the initial conditions: one initialized with only sea surface temperatures [4], one initialized the observed data for ocean temperature and salinity anomalies as well as atmospheric anomalies [3], the third nudges their model toward the observational analysis using a different procedure [5].

The results are mixed. All claim to gain benefit from initialization of the climate system compared to the climate change projections that consider only changes in the atmospheric composition. Two of the studies [3, 5] show improvement in global mean temperatures compared to the un-initialized climate change projections; the other study [4] slightly degrades their prediction of global mean temperatures with initialization. All claim, or at least imply, that much of the decadal variability that is captured is due to initialization of the AMOC. Two of the studies [4, 5] demonstrate improved temperature predictions over the eastern North Atlantic region, but for the study that also quantifies the impact of initialization on prediction errors [4] shows larger errors for North Atlantic sea surface temperature in the initialized predictions. The same two studies that show improved correlations for North Atlantic temperature predictions claim that it is due to improved prediction of the AMOC. Since there are no observations of this circulation feature in the twentieth century, the conclusions are based on comparison with the analysis responsible for the initial conditions, which constitutes something like a semi-perfect model result rather than a verified prediction.

Two of the early prediction experiments [3, 4] do show some improvement in regional temperature predictions over land, but how much improvement is not easily discerned, and is difficult to compare across the experiments. There are also some regions where the temperature predictions are less skillful. Maps of skill, or differences in skill, are not provided for precipitation in these studies. These papers are only the beginning of assessment decadal prediction skill.

What these results do or do not show must be viewed with caution though. Several difficulties stand in the way of more conclusive estimates of predictability and prediction skill for decadal climate variability. One difficulty is that the current sets of experiments, and even those that will soon be available (see Decadal Prediction: Internationally Coordinated Efforts) have very few ensemble members. Small ensemble size leads to uncertainty in the predicted signal, and provides very little information about the uncertainty due to uncertain initial conditions in a particular model. Multi-model ensembles will likely be more problematic for decadal predictions given the wide range of approaches to initial conditions; the prediction skill can also be compromised by the data assimilation component, even if the models are of equally high quality. Data assimilation and the development of initialization techniques for current and retrospective decadal predictions require considerable research investment. What experiments do exist and are likely to exist in the next several years will have limited realizations of decadal-scale variability, complicated with the evolution of that variability against a changing background climate due to increasing greenhouse gases. That combined with limited observations, not only of the subsurface ocean but also of terrestrial climate for much of the world, makes verification of retrospective forecasts extremely challenging.

Decadal Prediction: Internationally Coordinated Efforts

Several international efforts have been organized since the beginning of the twenty-first century to ascertain the predictability and prediction skill of decadal climate variability by systematizing the investigation across many models. The PREDICATE project, which was referred to above, provided a systematic comparison of the "perfect model" predictability in five European coupled models. They found potential predictability in the AMOC (Fig. 12), and also to some extent in surface air temperatures, that exceeded damped persistence [90]. The PREDICATE project examined the potential predictability of the response of atmospheric models to prescribed sea surface

temperatures, such as those associated with the AMV, and found good consistency across the models suggesting potential predictability if the pattern of SST was itself predictable [92].

A more recent activity, also drawing on the European modeling and prediction community is ENSEMBLES ([75]; http://ensembles-eu.metoffice.com/). This was a 5-year climate change research project begun in 2004, and involving 66 research partners across Europe. The project generated retrospective climate forecasts from seasonal to multi-decadal scales, provided local interpolation and/or downscaling, and sought to apply that information to sectoral outlooks, such as agriculture, health, and energy, across Europe.

The most extensive collaboration on decadal prediction experiments is the coordinated experiments designed and being run for the IPCC Fifth Assessment Report [93]. Together with the climate change projections for the next IPCC report, these decadal prediction experiments will be part of the Coupled Model Intercomparison Project-5 (CMIP5). There is a minimal set of runs at the core of the experimental design that requires hindcasts initialized for near the end of 1960 and every 5 years after that to 2005, in each case predicting 10 years past the initialization. Of those 10 sets of experimental start dates, a subset – those initialized at 1960, 1980, and 2005 – will be run out for 30 years. These experiments are to be run with a nominal ensemble size of 3. Of the dozen or more international modeling and prediction centers that will participate in the decadal prediction experiments of CMIP5, several will run with larger ensemble sizes and more start dates.

What is not being coordinated for the CMIP5 decadal prediction experiments is the data assimilation or initialization strategy. The guidelines only require that the predictions begin with a state of the climate system representative of the observations at that time. Thus, although there will likely be prediction systems that perform better than others, considerable analyses and further research will be required to assess which part of various prediction systems are responsible for their relative success or failure.

Future Directions

Although seasonal prediction is a relatively mature activity, considerable room for further improvement exists in the production, provision, and application of seasonal climate forecasts [9]. Dynamical models have many recognized biases in their tropical climate, such as tropical upper ocean structure and mixing, a tendency to produce a double intertropical convergence zone in the Pacific, and poor simulation of the stratus clouds that sit near the coasts along the eastern subtropical oceans. These problems are probably not unrelated, but they have proved difficult to solve. These tropical biases impact the realism of predicted El Niño events, which introduces biases into the associated teleconnections. Although much of the discussion in this chapter has focused on the climate predictability that arises from tropical SSTs, and especially El Niño, other factors in the climate system that are not well represented of initialized in models may carry additional prediction skill. Such processes include land characteristics [36] such as soil moisture, snow, and vegetation, as well as sea ice, variability in the stratosphere [94], and intra-seasonal variability such as the Madden–Julian Oscillation [95]. The provision of seasonal forecasts has improved since the 1990s; it has become common practice for operational centers to provide probabilistic information. However, that information is not sufficient for many decision makers if it is not accompanied by information on how the forecast is constructed, the past skill of the system, and more flexible or varied information that would allow sophisticated users to incorporate the data into quantitative decision systems. These types of best practices are much easier to address than model biases. Also, if addressed they would allow for broader use of past forecasts for research to underpin the use of current forecasts for decisions.

Decadal prediction is still in the phase of research and experimentation. Thus, decadal prediction itself should be considered a future direction of climate prediction. Although there have been some pioneering studies that present results from decadal prediction systems, there is no community-wide agreement on how decadal prediction systems should be constructed, what information can be provided, with what accuracy, and even how best to verify the information that is predicted [2]. The internationally coordinated set of experiments under CMIP5 should contribute to a better understanding of these prediction systems and their potential. These experimental predictions

will build on the current limited understanding to illuminate the relative information provided by initial conditions, in a real forecast setting, compared to the radiative forcing from current and future atmospheric greenhouse gas increases. The prediction experiments taken together should also help identify model biases that are of particular concern to decadal variability and set priorities on the future development and maintenance of the ocean observing system. Also, the added complexities of data assimilation for decadal prediction that will encompass longer timescales, greater depths in the ocean, and more need for salinity information, which was not available for most of the ocean prior to the twenty-first century, will lead to innovations in data assimilation systems (e.g., [96]).

The seasonal and decadal prediction systems share many common elements. In particular, they use the same type of dynamical models, and they both rely heavily on ocean initial conditions interpreted through data assimilation systems. They are both potentially impacted by external forcings such as solar variability and volcanoes. The same model biases that affect seasonal prediction skill will impact decadal predictions also. As the research community develops improved dynamical models, that better represent the Earth system in all its complexity, it will benefit climate predictions at all timescales. The additional observational data and more sophisticated data assimilation systems that are required for initialization of decadal predictions will provide more information of the ocean state that could be relevant for seasonal predictions as well. Already, some efforts to create retrospective seasonal predictions are being run farther into the future to investigate the ability of those systems to predict interannual-to-decadal climate variability. On the other side, retrospective decadal predictions that will contribute to the CMIP5 database already predict through the seasonal timescale.

The larger vision for the future direction of seasonal and decadal prediction is the union of the two efforts. This has been called "seamless prediction" [97, 98], which seeks the seasonal predictions to both the longer-term decadal predictions as well as the shorter-term weather forecasts. Initial steps in bridging the weather and seasonal timescales have been made (e.g., [97]), and since the observational and data assimilation systems are in place and have been well tested for these timescales, it is a sensible starting point. The joining of seasonal and decadal prediction scales would appear to be developing naturally as part of the evolving research into climate variability, predictability, and prediction on these timescales.

Bibliography

Primary Literature

1. Stockdale TN, Alves O, Boer G, Deque M, Ding Y, Kumar A, Kumar K, Landman W, Mason S, Nobre P (2010) Understanding and predicting seasonal-to-interannual climate variability – the producer perspective. Procedia Environ Sci 1:55–80
2. Meehl GA, Goddard L, Murphy J, Stouffer RJ, Boer G, Danabasoglu G, Dixon K, Giorgetta MA, Greene AM, Hawkins E, Hegerl G, Karoly D, Keenlyside N, Kimoto M, Kirtman B, Navarra A, Pulwarty RS, Smith D, Stammer D, Stockdale T (2009) Decadal prediction: can it be skillful? Bull Am Meteorol Soc 90:1467–1485
3. Smith D, Cusack S, Colman A, Folland C, Harris G, Murphy J (2007) Improved surface temperature prediction for the coming decade from a global circulation model. Science 317:796–799
4. Keenlyside NS, Latif M, Jungclaus J, Kornblueh L, Roeckner E (2008) Advancing decadal-scale climate prediction in the North Atlantic sector. Nature 453:84–88
5. Pohlmann H, Jungclaus JH, Köhl A, Stammer D, Marotzke J (2009) Initializing decadal climate predictions with the GECCO oceanic synthesis: effects on the North Atlantic. J Clim 22:3926–3938
6. Seager R, Ting M, Held I, Kushnir Y, Lu J, Vecchi G, Huang H-P, Harnik N, Leetmaa A, Lau N-C, Li C, Velez J, Naik N (2007) Model projections of an imminent transition to a more arid climate in southwestern North America. Science 316:1181–1184
7. Stott PA, Stone DA, Allen MR (2004) Human contribution to the European heatwave of 2003. Nature 432:610–614
8. Trenberth KE, Shea DJ (2006) Atlantic hurricanes and natural variability in 2005. Geophys Res Lett 33:L12704
9. NRC (2010) Assessment of intraseasonal to interannual climate prediction and predictability. The National Academies, Washington, DC
10. Orlove B, Chiang J, Cane M (2000) Forecasting Andean rainfall and crop yield from the influence of El Nino on Pleiades visibility. Nature 403:68–71
11. Walker GS (1923) Correlations in seasonal variations of weather, VIII: a preliminary study of world weather. Mem India Meteorol Dep 24:75–131
12. Ropelewski CF, Halpert MS (1987) Global and regional scale precipitation patterns associated with the El Niño/Southern Oscillation. Mon Weather Rev 115:1606–1626
13. Ropelewski CF, Halpert MS (1989) Precipitation patterns associated with the high index phase of the southern oscillation. J Clim 2:268–284

14. Mason SJ, Goddard L (2001) Probabilistic precipitation anomalies associated with ENSO. Bull Am Meteorol Soc 82:619–638
15. Bjerknes J (1969) Atmospheric teleconnections from the equatorial Pacific. Mon Weather Rev 97:163–172
16. Wyrtki K (1975) El Niño – the dynamic response of the equatorial Pacific Ocean to atmospheric forcing. J Phys Oceanogr 5:572–584
17. Zebiak S, Cane MA (1987) A model of El Nino-Southern Oscillation. Mon Weather Rev 115:2262–2278
18. Battisti DS (1988) Dynamics and thermodynamics of a warming event in a coupled tropical atmosphere–ocean model. J Atmos Sci 45:2889–2919
19. Suarez Max J, Schopf Paul S (1988) A delayed action oscillator for ENSO. J Atmos Sci 45:3283–3287
20. Cane MA, Zebiak SE, Dolan SC (1986) Experimental forecasts of El Niño. Nature 321:827–832
21. Graham NE (1994) Decadal-scale climate variability in the tropical and North Pacific during the 1970s and 1980s: observations and model results. Clim Dyn 10:135–162
22. Mantua NJ, Hare SR, Zhang Y, Wallace JM, Francis RC (1997) A Pacific interdecadal climate oscillation with impacts on Salmon production. Bull Am Meteorol Soc 78:1069–1079
23. Hurrell JW, Van Loon H (1997) Decadal variations in climate associated with the North Atlantic Oscillation. Clim Change 36:301–326
24. Goldenberg SB, Landsea CW, Mestas-Nunez AM, Gray WM (2001) The recent increase in Atlantic hurricane activity: causes and implications. Science 293:474–479
25. Latif M, Barnett TP (1994) Causes of decadal climate variability over the North Pacific and North America. Science 266:634–637
26. Griffies SM, Bryan K (1997) Predictability of North Atlantic multidecadal climate variability. Science 275:181–184
27. IPCC (2007) Contribution of working group 1 to the fourth assessment report of the intergovernmental panel on climate change; Solomon S, Qin D, Manning M, Chen Z, Marquis M, Averyt KB, Tignor M, Miller HL (eds). Cambridge University Press, Cambridge
28. Vera C, Barange M, Dube OP, Goddard L, Griggs D, Kobysheva N, Odada E, Parey S, Polovina J, Poveda G (2010) Needs assessment for climate information on decadal timescales and longer. Procedia Environ Sci 1:275–286
29. Knight JR, Folland CK, Scaife AA (2006) Climate impacts of the atlantic multidecadal oscillation. Geophys Res Lett 33: L17706
30. Zhang R, Delworth TL (2006) Impact of Atlantic multidecadal oscillations on India/Sahel rainfall and Atlantic hurricanes. Geophys Res Lett 33:L17712
31. Schubert S, Gutzler D, Wang H, Dai A, Delworth T, Deser C, Findell K, Fu R, Higgins W, Hoerling M, Kirtman B, Koster R, Kumar A, Legler D, Lettenmaier D, Lyon B, Magana V, Mo K, Nigam S, Pegion P, Phillips A, Pulwarty R, Rind D, Ruiz-Barradas A, Schemm J, Seager R, Stewart R, Suarez M, Syktus J, Ting M, Wang C, Weaver S, Zeng N (2009) A U.S. CLIVAR project to assess and compare the responses of global climate models to drought-related sst forcing patterns: overview and results. J Clim 22:5251–5272
32. Lau N-C, Nath MJ (2003) Atmosphere–ocean variations in the Indo-Pacific sector during ENSO episodes. J Clim 16:3–20
33. Xie S-P, Carton JA (2004) Tropical Atlantic variability: patterns, mechanisms, and impacts. Geophys Monogr 147:121–142
34. Giannini A, Chiang JCH, Cane MA, Kushnir Y, Seager R (2001) The ENSO teleconnection to the Tropical Atlantic Ocean: contributions of the remote and local SSTs to rainfall variability in the Tropical Americas. J Clim 14:4530–4544
35. Goddard L, Graham NE (1999) Importance of the Indian Ocean for simulating rainfall anomalies over eastern and southern Africa. J Geophys Res 104:19099–19116
36. Koster RD, Mahanama SPP, Yamada TJ, Balsamo G, Berg AA, Boisserie M, Dirmeyer PA, Doblas-Reyes FJ, Drewitt G, Gordon CT, Guo Z, Jeong J-H, Lawrence DM, Lee W-S, Li Z, Luo L, Malyshev S, Merryfield WJ, Seneviratne SI, Stanelle T, van den Hurk BJJM, Vitart F, Wood EF (2010) Contribution of land surface initialization to subseasonal forecast skill: first results from a multi-model experiment. Geophys Res Lett 37: L02402
37. Fischer EM, Seneviratne SI, Lüthi D, Schär C (2007) Contribution of land-atmosphere coupling to recent European summer heat waves. Geophys Res Lett 34:L06707
38. Cohen J, Fletcher C (2007) Improved skill of northern hemisphere winter surface temperature predictions based on land–atmosphere fall anomalies. J Clim 20:4118–4132
39. Jhun J-G, Lee E-J (2004) A New East Asian Winter Monsoon Index and associated characteristics of the winter monsoon. J Clim 17:711–726
40. Goddard L, Mason S (2002) Sensitivity of seasonal climate forecasts to persisted SST anomalies. Clim Dyn 19:619–632
41. Alexander MA, Bladé I, Newman M, Lanzante JR, Lau N-C, Scott JD (2002) The atmospheric bridge: the influence of ENSO teleconnections on air–sea interaction over the global oceans. J Clim 15:2205–2231
42. Jin F-F (1997) An equatorial ocean recharge paradigm for ENSO. Part I: conceptual model. J Atmos Sci 54:811–829
43. McPhaden MJ, Busalacchi AJ, Cheney R, Donguy J-R, Gage KS, Halpern D, Ji M, Julian P, Meyers G, Mitchum GT, Niiler PP, Picaut J, Reynolds RW, Smith N, Takeuchi K (1998) The tropical ocean-global atmosphere observing system: a decade of progress. J Geophys Res 103:14169–14240
44. Saha S, Nadiga S, Thiaw C, Wang J, Wang W, Zhang Q, Van den Dool HM, Pan H-L, Moorthi S, Behringer D, Stokes D, Peña M, Lord S, White G, Ebisuzaki W, Peng P, Xie P (2006) The NCEP climate forecast system. J Clim 19:3483–3517
45. Barnston AG, Chelliah M, Goldenberg SB (1997) Documentation of a highly ENSO-related SST region in the equatorial pacific. Atmos–Ocean 35:367–383
46. Larkin NK, Harrison DE (2005) On the definition of El Niño and associated seasonal average U.S. weather anomalies. Geophys Res Lett 32:L13705

47. Chen D, Cane MA, Kaplan A, Zebiak SE, Huang D (2004) Predictability of El Niño over the past 148 years. Nature 428:733–736
48. Kirtman Ben P, Shukla J, Huang B, Zhu Z, Schneider Edwin K (1997) Multiseasonal predictions with a coupled tropical ocean global atmosphere system. Mon Weather Rev 125:789–808
49. Barnston AG, He Y, Glantz MH (1999) Predictive skill of statistical and dynamical climate models in SST forecasts during the 1997–98 El Niño Episode and the 1998 La Niña Onset. Bull Am Meteorol Soc 80:217–243
50. Goddard L, DeWitt DG (2005) Seeking progress. In: El Niño Prediction, vol 3. US CLIVAR Variations
51. Davey M, Huddleston M, Sperber K, Braconnot P, Bryan F, Chen D, Colman R, Cooper C, Cubasch U, Delecluse P, DeWitt D, Fairhead L, Flato G, Gordon C, Hogan T, Ji M, Kimoto M, Kitoh A, Knutson T, Latif M, Le Treut H, Li T, Manabe S, Mechoso C, Power S, Roeckner E, Terray L, Vintzileos A, Voss R, Wang B, Washington W, Yoshikawa I, Yu J, Yukimoto S, Zebiak S, Meehl G (2002) STOIC: a study of coupled model climatology and variability in tropical ocean regions. Clim Dyn 18:403–420
52. Zhang S, Harrison MJ, Rosati A, Wittenberg A (2007) System design and evaluation of coupled ensemble data assimilation for global oceanic climate studies. Mon Weather Rev 135:3541–3564
53. Balmaseda MA, Fujii Y, Alves O, Awaji T, Behringer D, Ferry N, Lee T, Rienecker M, Rosati T, Stammer D, Smith D, Molteni F (2009) Initialization for seasonal and decadal forecasts. http://www.oceanobs09.net/blog/?p=57
54. Stockdale T, Anderson DLT, Balmaseda M, Doblas-Reyes FJ, Ferranti L, Mogensen K, Palmer TN, Molteni F, Vitart F (2011) ECMWF System 3 and its prediction of sea surface temperature. Clim Dyn. doi:10.1007/s00382-010-0947-3
55. Toth Z, Kalnay E (1993) Ensemble forecasting at NMC: the generation of perturbations. Bull Am Meteorol Soc 74:2317–2330
56. Molteni F, Buizza R, Palmer TN, Petroliagis T (1996) The ECMWF ensemble prediction system: methodology and validation. Q J R Meteorol Soc 122:73–119
57. Wilks DS (2006) Statistical methods in the atmospheric sciences, vol 59, International geophysics series. Academic, San Diego
58. Goddard L, Hoerling MP (2006) Practices for seasonal-to-interannual climate prediction. US CLIVAR variations, vol 4
59. Jin EK, Kinter JL, Wang B, Park C-K, Kang I-S, Kirtman BP, Kug J-S, Kumar A, Luo J-J, Schemm J, Shukla J, Yamagata T (2008) Current status of ENSO prediction skill in coupled ocean–atmosphere models. Clim Dyn 31:647–664
60. Hagedorn R, Doblas-Reyes FJ, Palmer TN (2005) The rationale behind the success of multi-model ensembles in seasonal forecasting – I. Basic concept. Tellus A 57:219–233
61. Rajagopalan B, Lall U, Zebiak SE (2002) Categorical climate forecasts through regularization and optimal combination of multiple GCM ensembles*. Mon Weather Rev 130:1792–1811
62. Robertson AW, Lall U, Zebiak SE, Goddard L (2004) Improved combination of multiple atmospheric GCM ensembles for seasonal prediction. Mon Weather Rev 132:2732–2744
63. Weigel AP, Liniger MA, Appenzeller C (2009) Seasonal ensemble forecasts: are recalibrated single models better than multimodels? Mon Weather Rev 137:1460–1479
64. NRC (ed) (2008) Review of CCSP draft synthesis and assessment product 5.3: decision-support experiments and evaluations using seasonal to interannual forecasts and observational data. The National Academies, Washington, DC
65. Robertson AW, Moron V, Swarinoto Y (2009) Seasonal predictability of daily rainfall statistics over Indramayu district, Indonesia. Int J Climatol 29:1449–1462
66. Gershunov A, Barnett TP (1998) ENSO influence on intraseasonal extreme rainfall and temperature frequencies in the contiguous United States: observations and model results. J Clim 11:1575–1586
67. Higgins RW, Leetmaa A, Kousky VE (2002) Relationships between climate variability and winter temperature extremes in the United States. J Clim 15:1555–1572
68. Joliffe IT, Stephenson DB (2003) Forecast verification: a practitioner's guide in atmospheric sciences. Wiley, Chicester
69. WMO (2002) World Meteorological Organization (WMO) Standardized verification system (SVS) for long-range forecasts (LRF) In: New attachment II-9 to the manual on the GDPS (WMO-N. 485), vol 1, Geneva
70. Livezey RE, Timofeyeva MM (2008) The first decade of long-lead U.S. seasonal forecasts. Bull Am Meteorol Soc 89:843–854
71. Goddard L, Dilley M (2005) El Niño: catastrophe or opportunity. J Clim 18:651–665
72. Gates WL (1992) AMIP: the atmospheric model intercomparison project. Bull Am Meteorol Soc 73:1962–1970
73. Palmer TN, Shukla J (2000) DSP/PROVOST. Q J R Meteorol Soc 126:1989–2350, Special Issue
74. Palmer TN, Doblas-Reyes FJ, Hagedorn R, Alessandri A, Gualdi S, Andersen U, Feddersen H, Cantelaube P, Terres J-M, Davey M, Graham R, Délécluse P, Lazar A, Déqué M, Guérémy J-F, Díez E, Orfila B, Hoshen M, Morse AP, Keenlyside N, Latif M, Maisonnave E, Rogel P, Marletto V, Thomson MC (2004) Development of a European multimodel ensemble prediction system for seasonal-to-interannual prediction (DEMETER). Bull Am Meteorol Soc 85:853–872
75. Hewitt CD, Griggs DJ (2004) Ensembles-based predictions of climate changes and their impacts. EOS 85:566
76. Kirtman B, Pirani A (2009) The state of the art of seasonal prediction: outcomes and recommendations from the First World Climate Research Program Workshop on seasonal prediction. Bull Am Meteorol Soc 90:455–458
77. Power S, Casey T, Folland C, Colman A, Mehta V (1999) Interdecadal modulation of the impact of ENSO on Australia. Clim Dyn 15:319–324

78. Alexander MA, Deser C, Timlin MS (1999) The reemergence of SST anomalies in the North Pacific Ocean. J Clim 12:2419–2433
79. Schneider N, Miller AJ (2001) Predicting Western North Pacific Ocean Climate. J Clim 14:3997–4002
80. Di Lorenzo E, Schneider N, Cobb KM, Franks PJS, Chhak K, Miller AJ, McWilliams JC, Bograd SJ, Arango H, Curchitser E, Powell TM, Rivière P (2008) North Pacific Gyre oscillation links ocean climate and ecosystem change. Geophys Res Lett 35: L08607
81. Deser C, Phillips AS, Hurrell JW (2004) Pacific Interdecadal climate variability: linkages between the Tropics and the North Pacific during Boreal Winter since 1900. J Clim 17:3109–3124
82. Meehl GA, Hu A (2006) Megadroughts in the Indian Monsoon Region and Southwest North America and a mechanism for associated multidecadal Pacific Sea surface temperature anomalies. J Clim 19:1605–1623
83. Knight JR, Allan RJ, Folland CK, Vellinga M, Mann ME (2005) A signature of persistent natural thermohaline circulation cycles in observed climate. Geophys Res Lett 32:L20708
84. Vellinga M, Wu P (2004) Low-latitude freshwater influence on centennial variability of the Atlantic thermohaline circulation. J Clim 17:4498–4511
85. Latif M, Roeckner E, Botzet M, Esch M, Haak H, Hagemann S, Jungclaus J, Legutke S, Marsland S, Mikolajewicz U, Mitchell J (2004) Reconstructing, monitoring, and predicting multidecadal-scale changes in the North Atlantic thermohaline circulation with sea surface temperature. J Clim 17:1605–1614
86. Stoner AMK, Hayhoe K, Wuebbles DJ (2009) Assessing general circulation model simulations of atmospheric teleconnection patterns. J Clim 22:4348–4372
87. AchutaRao K, Sperber KR (2006) ENSO simulation in coupled ocean–atmosphere models: are the current models better? Clim Dyn 27:1–15
88. Gray ST, Graumlich LJ, Betancourt JL, Pederson GT (2004) A tree-ring based reconstruction of the Atlantic multidecadal oscillation since 1567 A.D. Geophys Res Lett 31: L12205
89. Davey M, and co-authors, 2006. Multi-model multi-method multi-decadal ocean analyses from the ENACT project. CLIVAR Exchanges, Vol 11, No. 3, pgs 22–25. http://eprints.soton.ac.uk/41286/1/Exchanges38.pdf
90. Collins M, Botzet M, Carril AF, Drange H, Jouzeau A, Latif M, Masina S, Otteraa OH, Pohlmann H, Sorteberg A, Sutton R, Terray L (2006) Interannual to decadal climate predictability in the North Atlantic: a multimodel-ensemble study. J Clim 19:1195–1203
91. Branstator G, Teng H (2010) Two limits of initial-value decadal predictability in a CGCM. J Clim 23:6292–6311. doi:10.1175/2010JCLI3678.1
92. Rodwell MJ, Drévillon M, Frankignoul C, Hurrell JW, Pohlmann H, Stendel M, Sutton RT (2004) North Atlantic forcing of climate and its uncertainty from a multi-model experiment. Q J R Meteorol Soc 130:2013–2032
93. Taylor KE, Stouffer RJ, Meehl GA (2011) Bulletin of the American Meteorological Society. http://dx.doi.org/10.1175/BAMS-D-11-00094.1
94. Baldwin MP, Dunkerton TJ (2001) Stratospheric harbingers of anomalous weather regimes. Science 294:581–584
95. Gottschalck J, Wheeler M, Weickmann K, Vitart F, Savage N, Lin H, Hendon H, Waliser D, Sperber K, Nakagawa M, Prestrelo C, Flatau M, Higgins W (2010) A framework for assessing operational Madden–Julian oscillation forecasts: a CLIVAR MJO Working Group Project. Bull Am Meteorol Soc 91:1247–1258
96. Zhang S, Rosati A (2010) An inflated ensemble filter for ocean data assimilation with a biased coupled GCM. Mon Weather Rev 138:3905–3931
97. Vitart F, Buizza R, Balmaseda M, Balsamo G, Bidlot J-R, Bonet A, Fuentes M, Hofstadler A, Molteni F, Palmer TN (2008) The new VarEPS-monthly forecasting system: a first step towards seamless prediction. Q J R Meteorol Soc 134:1789–1799
98. Hazeleger W, Severijns C, Semmler T, Ştefănescu S, Yang S, Wang X, Wyser K, Dutra E, Baldasano J, Bintanja R, Bougeault P, Caballero R, Ekman AML, Christensen JH, van den Hurk B, Jimenez P, Jones C, Kållberg P, Koenigk T, McGrath R, Miranda P, van Noije T, Palmer T, Parodi J, Schmith T, Selten F, Storelvmo T, Sterl A, Tapamo H, Vancoppenolle M, Viterbo P, Willén U (2010) EC-Earth: a seamless earth system prediction approach in action. Bull Am Meteorol Soc 91:1357–1363

Books and Reviews

Hurrell JW, Delworth T, Danabasoglu G, Drange H, Griffies S, Holbrook N, Kirtman B, Keenlyside N, Latif M, Marotzke J, Meehl G A, Palmer T, Pohlmann H, Rosati T, Seager, R, Smith D, Sutton R, Timmermann A, Trenberth KE, and Tribbia J (2010) Decadal climate prediction: opportunities and challenges. In: Hall J, Harrison DE, Stammer D (eds) Proceedings of OceanObs'09: sustained ocean observations and information for society, vol 2. ESA Publication WPP-306: Venice, 21–25 Sep 2009. Available at http://www.oceanobs09.net/blog/?p=97

Latif M, Delworth T, Dommenget D, Drange H, Hazeleger W, Hurrell J, Keenlyside N, Meehl GA, and Sutton R (2010) Dynamics of decadal climate variability and Implications for its prediction. In: Hall J, Harrison DE, Stammer D (eds) Proceedings of OceanObs'09: sustained ocean observations and information for society, vol 2. ESA Publication WPP-306: Venice, 21–25 Sep 2009. Available at http://www.oceanobs09.net/blog/?p=104

Mehta V, Meehl GA, Goddard L, Knight J, Kumar A, Latif M, Lee T, Rosati A, Stammer D (2010) The eighth workshop on decadal climate variability decadal climate predictability and prediction: where are we? Bull Am Meteorol Soc. doi:10.1175/2010BAMS3025.1

Murphy J, Kattsov V, Keenlyside N, Kimoto M, Meehl G, Mehta V, Pohlmann H, Scaife A, Smith D (2010) Towards prediction of decadal climate variability and change. Procedia Environ Sci 1:287–304. doi:10.1016/j.proenv.2010.09.018

CO_2 Capture and Sequestration

S. Julio Friedmann
Lawrence Livermore National Laboratory, Livermore, CA, USA

Article Outline

Glossary
Definition of Subject
Introduction
Carbon Capture
Geological Sequestration
Large-Scale Commercial Deployment
Science and Technology Status
Deployment Challenges
Bibliography

Glossary

Carbon capture and sequestration (CCS) The long-term isolation of carbon dioxide from the atmosphere through physical, chemical, biological, or engineered processes.

CO_2 capture The separation and concentration of CO_2 from mixed, dilute, or flue gas streams, commonly for the purpose of geological sequestration or EOR (which requires 95% concentrations or higher).

CO_2 enhanced oil recovery (EOR) Injection of CO_2 into depleted oil fields for the purpose of increasing production. This typically also results in long-term storage of CO_2.

Geological sequestration The long-term physical or chemical storage of CO_2 in deep geological formations for the purpose of indefinite separation from the atmosphere.

Oxyfired combustion The burning of an hydrocarbon fuel (coal, oil, gas, biofuel) in an oxygen-rich or pure oxygen environment for the purpose of CO_2 concentration or capture.

Precombustion capture Concentration of CO_2 from mixed gas streams that are the products of fuel conversion (e.g., gasification, methanation, or fermentation) before combustion, commonly through physical solvents.

Post-combustion capture Concentration of CO_2 from mixed, dilute, and flue gas streams that are the products of combustion, commonly through chemical solvents, sorbents, or selective membranes.

Definition of Subject

Carbon capture and sequestration (CCS) is the long-term isolation of carbon dioxide from the atmosphere through physical, chemical, biological, or engineered processes. The primary purpose is to reduce the impacts of human-induced climate change associated with increased greenhouse gas concentrations from emissions and land use. CCS can be a major partial solution to climate change, accounting for between 15% and 25% of the needed abatement, and should be considered as part of a portfolio of solutions which include efficiency and conservation, renewable energy, nuclear power, and other options.

Introduction

Carbon capture and sequestration (CCS) is the long-term isolation of carbon dioxide from the atmosphere through physical, chemical, biological, or engineered processes. This includes a range of approaches including soil carbon sequestration (e.g., through no-till farming), terrestrial biomass sequestration (e.g., through planting forests), direct ocean injection of CO_2 either onto the deep seafloor or into the intermediate depths, injection into deep geological formations, or even direct conversion of CO_2 to carbonate minerals. Some of these approaches are considered geoengineering (see the appropriate chapter herein). All are considered in the 2005 special report by the Intergovernmental Panel on Climate Change [1].

Of the range of options available, CCS most commonly entails the capture of CO_2 from power and industrial plants followed by injection into deep geological formation (geological carbon sequestration, or GCS). While the economics are hotly debated, in many ways this form of CCS appears to be a critical option for major greenhouse gas reduction in the next 10–50 years. The basis for this interest includes several factors:

- There is no obvious immediate technical barrier to deployment. Systems to capture and concentrate

CO_2 have been in commercial operation for over 80 years (REF), and the oil and gas industry has injected CO_2 for enhanced oil recovery for over 35 years.

- The initial estimates of potential geological capacities are enormous (Fig. 1). Formal estimates for global storage potential vary substantially, but are likely to be between 800 and 3,300 Gt of C (3,000 and 10,000 Gt of CO_2), with significant capacity located reasonably near large point sources of the CO_2. (REF)
- Testing of large-scale GCS is feasible and has begun (Fig. 1). In many industrialized countries, large CO_2 sources like power plants and refineries lie near prospective storage sites. These plants could be retrofit today and injection begun (while bearing in mind scientific uncertainties and unknowns). Indeed, some have, and five projects described here provide a great deal of information on the operational needs and field implementation of CCS, with more to follow.

Part of this interest comes from several key documents written in the last few years that provide information on the status, economics, technology, and impact of CCS. These are cited throughout this text and identified as key references at the end of this manuscript.

When coupled with improvements in energy efficiency, renewable energy supplies, fuel switching, and nuclear power, CCS helps dramatically reduce current and future emissions [2–4]. If CCS is not available as a carbon management option, it will be much more difficult and much more expensive to stabilize atmospheric CO_2 emissions. Estimates of the cost of carbon abatement without CCS appear 30–80% higher than if CCS were to be available [5].

Carbon Capture

CCS has two separate but coupled steps. The first is the separation and concentration of CO_2 from industrial flue streams, chiefly power plants. This first step is commonly called *carbon capture* and usually includes compression and transportation via pipeline. The second involves the injection of CO_2 as a dense, supercritical (liquid-like) phase into deep geological formations. This step is commonly called *geological carbon sequestration*, or GCS. In short, the cost for CCS lies mostly in the capture stage. The risk lies mostly in the

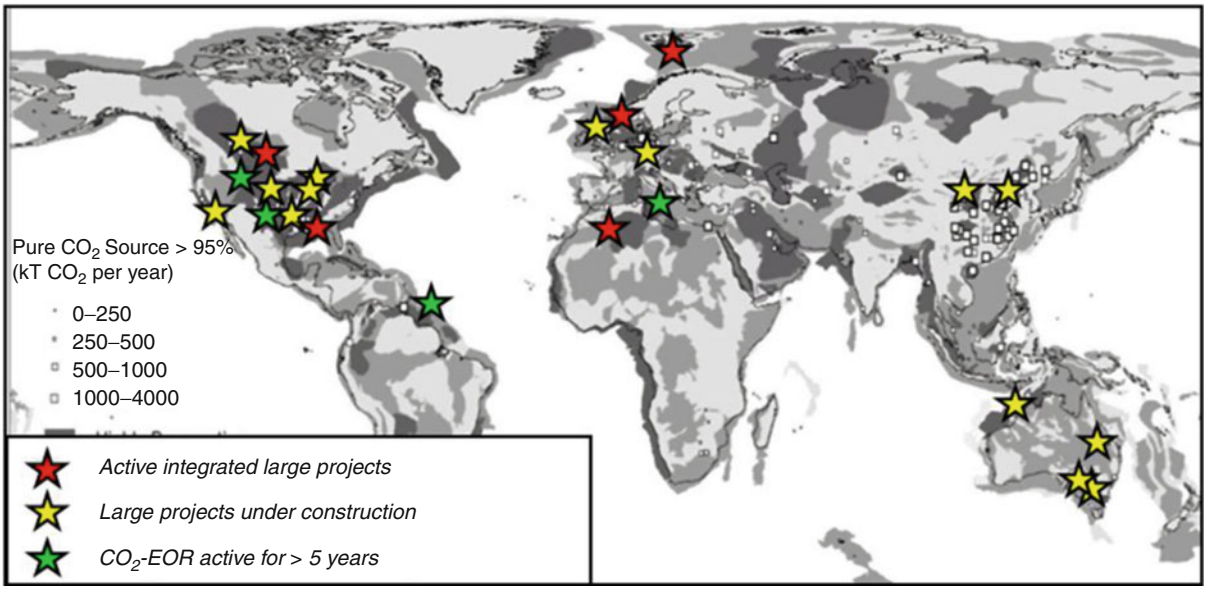

CO_2 Capture and Sequestration. Figure 1
Map of large CCS projects worldwide. Base map shows highly prospective (*dark shaded*) and prospective (*medium shaded*) areas; squares show size of pure CO_2 streams available for sequestration (After Bradford and Dance (2004))

sequestration stage. Both steps are needed for a successful project.

In the first step, CCS requires the separation of CO_2 from industrial flue streams and concentration to CO_2 purities of 95% or greater [2, 6]. This limits compression costs and makes effective and efficient use of available sequestration resource (subsurface pore volume). Currently, four technology pathways exist for commercial CO_2 capture and separation (Fig. 2):

- *Post-combustion capture*: This involves separation of CO_2 from nitrogen, commonly with chemical sorbents (e.g., monoethanolamine (MEA)).
- *Precombustion capture*: This involves conversion of fuel feedstocks (e.g., coal) into syngas via gasification, steam reformation, or partial oxidation and then shifting the syngas chemically to hydrogen and CO_2, and then separating the H_2 from CO_2. Currently, this last step is commonly done with physical or chemical sorbents.
- *Oxyfiring combustion*: This involves combustion of fuels in a pure oxygen or O_2-CO_2 rich environment such that effectively no nitrogen is present in the flue gas. Separation of O_2 from air (N_2) is required and is the main cost element. Chemical looping [7] is considered a variation of this technology.
- *Direct capture of high-purity streams*: In these cases, CO_2 is "pre-captured" and already at or above 95% purity. This requires only compression and transportation before sequestration.
- *Direct air capture*: This involves separation of CO_2 directly from the atmosphere. The very low concentrations of CO_2 in air (~385 ppm) make this approach both expensive and controversial.

Each of these approaches requires substantial power to run the adsorption and air separation units, raising operating expenses and increasing the amount of CO_2 emissions produced simply to drive the sequestration process. They also require more capital in plant construction and have differing operational costs and

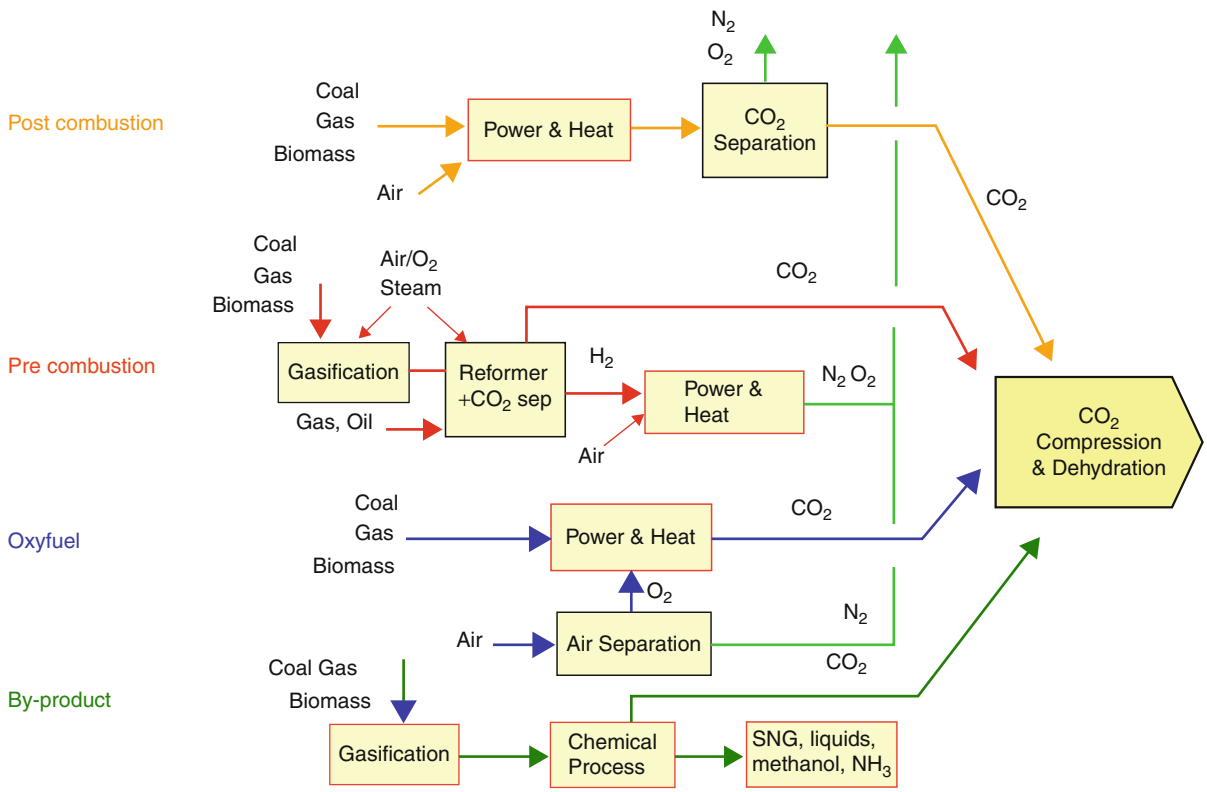

CO_2 Capture and Sequestration. Figure 2
Schematic diagram of the four main CO_2 capture pathways and the main processes involved (After Thambimuthu et al. [6])

energy penalties. At present, each technology pathway appears equally viable from an economic and thermodynamic standpoint [2, 6, 8].

Industry has substantial experience with each of these technology pathways, chiefly from operation of hydrogen plants, fertilizer plants, refineries, and natural gas processing facilities. CO_2 has been separated from industrial flue streams at scales much greater than 1 MMt CO_2/year (270,000 t C/year). Similarly, CO_2 has been separated from small-scale power plants, and the technology to scale these operations to plants of 200 MW or greater exists. Large pipelines transport millions of tons of CO_2 hundreds of kilometers, and millions of tons of CO_2 and other acid gases are compressed and injected into geological formations every year. Thus, a great deal is known about carbon capture, separation, and transportation, and many countries have regulatory frameworks in place to accommodate the permitting of separation facilities and pipelines (in the USA, the Department of Transportation carries this authority).

Cost remains an important barrier to wider commercial deployment [2, 9], especially retrofit costs. However, as the concepts for geological carbon sequestration are proven to be reliable for current power plant technology, improved power plant designs are expected to be able to bring down sequestration costs dramatically. Several large pilot projects are testing pre-, post, and oxyfired combustion tests at the 2–30 MW scale, a necessary precursor to broad commercial deployment. A number of technologies claim to be able to capture and separate CO_2 at \$9–11/t CO_2, less than half the best available technology. As the results from these and future tests are made public, decision makers and investors will be able to plan better for plant economics and design.

Post-combustion Capture

As the name suggests, post-combustion capture (PCC) involves capture and separation of CO_2 from flue gas streams after combustion [2, 6]. It can also apply to capture from high- or low-concentration bag-house streams from industrial applications (e.g., cement manufacturing). Most PCC study has focused on separation from coal plants, both because of their central role in global power production and their high concentration of flue gas CO_2 (14–20%). However, PCC can also be applied to natural gas plants (4–7% concentration) or other post-combustion streams (e.g., biomass fired power generation).

Typically, CO_2 capture involves one of these separation processes:

- *Chemical solvents*: This process operates when flue gas contacts liquid solvents and dissolves into the liquid. The CO_2-rich solvent is typically heated to release the CO_2 and reconstitute the solvent, which is then recirculated.
- *Membranes*: This process separates CO_2 from mixed gases as CO_2 preferentially flows through the membrane, which rejects other gases. Membranes can be made of polymers [10], ceramics [11], or more exotic materials (e.g., [12]). Costs and viability are a function of gas selectivity and permeance.
- *Solid sorbents*: In this process, selective solid materials (e.g., zeolites) adsorb CO_2 from mixed gas streams. These are released under different physical or chemical conditions, typically through heating.
- *Exotic materials*: Other classes of materials have been proposed and remain promising, including ionic liquids [13, 14] and metal-organic frameworks (MOFs; REF).

The cost and performance of different systems varies as a function of loading, energy costs, capital costs, vapor pressure, process efficiency, and other issues (e.g., Abanades et al. 2009). While some processes appear to be highly efficient, they may have cost or volumetric issues which limit deployment. Many prospective processes remain at the bench-scale and have not been tested in large-scale pilots or commercial plants.

Today, most post-combustion capture is performed by liquid solvents, chiefly amines. This is in large part due to the familiarity of the technology (invented in 1930) and the conventional equipment set used, such as gas stripper towers and thermal regeneration. Rochelle [15] argues that the familiarity and performance of amine-based solvents makes them the class of CO_2 capture processes and materials most likely to be widely deployed. Many commercial groups are working to improve the cost and performance of their amine systems today, including Mistubishi, Babcock and Wilcox, Alstom, Aker Clean Carbon, HTC, and Huaneng.

While other capture systems show promise based on bench-scale performance [16], few have been tried. One exception is Alston's chilled ammonia process [17], piloted at the Mountaineer power plant in West Virginia. Work on the pilot project ceased in 2011, and results remain inconclusive.

Precombustion Capture

Precombustion capture involves the removal of CO_2 after the coal is converted into syngas, but before combustion in a turbine or boiler. Typically, the first step involves gasifying the coal. This syngas contains CO_2, which may be separated at this stage for partial capture (typically around 20% of carbon content). To achieve higher fractional capture, a water-gas shift reactor converts carbon monoxide and steam to CO_2 and hydrogen. This increases the concentration of CO_2, improving capture efficiency and increasing the amount of carbon (in the form of CO_2) that can be removed using this process. The CO_2 is then removed using either a chemical or a physical solvent, such as Selexol™ or Rectisol™, and is compressed. This approach is used widely where coal is used for chemical feedstock.

For power production applications, the remnant hydrogen burns in a turbine to generate electricity [2]. The likeliest configuration for these systems is an integrated gasification combined-cycle power plant, or IGCC. While both IGCC and precombustion CO_2 capture technologies are available today, the costs limit commercial deployment. Four gigawatts of IGCC power plants have been built worldwide as of the end of 2007 [1], and no existing IGCC plants have CO_2 capture. In 2003, the US Department of Energy created the FutureGen project [18], aimed at construction of a 275 MW IGCC + CCS plant capturing 1 million tons CO_2/year. FutureGen halted in 2008 [19], and then restarted as an oxyfiring retrofit plant (see below). A similarly scaled project, GreenGen in China [20], is slated for completion in 2012 with CO_2 capture in 2014.

Many companies have proposed specific IGCC designs with CO_2 capture, including GE, Siemens, and Mitsubishi. Overall, IGCC plans with CCS appear to have higher net efficiencies, lower water consumption, and lower energy penalties than other kinds of new plants with carbon capture [21]. The commercial availability of gasifiers, water-gas shift reactors, solvent towers, and gas turbines also provides some commercial advantages. However, the total capital costs for IGCC systems with CCS remain higher than conventional plants.

Other precombustion plant designs show promise. For example, hydrogen and syngas from gasification can also be used to make chemicals such as ammonia, urea, or olefins. Coal-to-chemical plants can use some hydrogen like an IGCC plant and generate power as well. These *polygeneration* plants show some advantages in terms of economic return (e.g., [22]). Several US projects, including the Texas Clean Energy Project [23] and HECA project [20] are attempts to manage costs and create economic return for precombustion plants through polygeneration.

Given the high efficiency of physical solvents for precombustion, little research has focused on solvent-based precombustion technology improvement. Much research has focused on improving efficiency or reducing costs of gasification or on better plant integration to improve overall efficiency and cost. Additional research has focused on alternative separation technologies, including hydrate formation, ceramic membranes, or exotic materials. Alternative gasification technologies such as molten metal gasifiers [24] or underground coal gasification (Friedmann 2009) remain potential avenues to large cost reductions for precombustion capture–based plant designs.

Oxyfired Combustion

The burning of a hydrocarbon fuel (coal, oil, gas, biofuel) in an oxygen-rich or pure oxygen environment for the purpose of CO_2 concentration or capture is called oxyfired combustion (REF). Oxyfiring is premised on this basic chemical reaction:

$$CH_x + O_2 \rightarrow CO_2 + XH_2O$$

where the coefficients x and X vary as a function of fuel type (for methane, x = 4 and X = 2). When oxygen is blended with the fuel stoichiometrically, this reaction balances and water can be separated with compression leaving concentrated, dry CO_2.

One of the potential challenges with oxyfiring combustion is that many hydrocarbon fuels will burn

extremely hot in a pure oxygen environment, making retrofits difficult and new reactors expensive. One common approach to this problem is to mix oxygen with CO_2 at near atmospheric oxygen concentrations (e.g., 25% oxygen and 75% CO_2) creating a "synthetic air." The CO_2 is recirculated after separation, and acts to moderate the temperature and kinetics of the fuel combustion in the reactor (REF). This approach is considered promising for retrofits, both in the power sector (subcritical and supercritical pulverized coal boilers) and in the industrial sector (e.g., in catalytic crackers common in hydrocarbon refining).

A number of commercial projects have made progress on oxyfiring. In Europe, Vattenfall's Schwartzepumpe pilot project successfully ran a 30 MW thermal boiler with synthetic air. Similarly, Total successfully operates a 50 MW oxyfired boiler in association with injection into a depleted natural gas field in Lacq, France. The largest current program in oxyfiring is the revised FutureGen program (FutureGen 2.0; REF). This US project is attempting to retrofit a 250 MW boiler in Meridosia, Illinois for oxyfired combustion. This project plans to capture 1.3 million tons CO_2/year, over 90% of the plant emissions.

The primary cost of oxyfired combustion is the cost of oxygen separation from air (REF). The air separation unit (ASU) requires substantial capital and operating costs. There are also some specific technical considerations associated with the operating pressure of the combustion unit. If the reactor burns its fuel at lower than atmospheric pressure (a common configuration for boilers), then there is a risk of air leaking into the reactor and contaminating the stream with nitrogen.

Chemical looping [7] is considered an oxyfiring variant, although in most ways the technology is radically different from synthetic air combustion. Instead, a metal carrier is oxidized, creating heat which can be used to run a steam cycle. Most commonly, the process is configured with two interconnected fluidized bed reactors: an air reactor and a fuel reactor. The solid oxygen carrier is circulated between the air and fuel reactors, and the metal oxide is reduced in the second stage. This process remains promising, in large part due to the very high theoretical conversion efficiencies (as high as 80%). However, no reactors larger than bench-top have proven viable yet, and questions remain about the operation, longevity, and stability of the metal oxide carriers.

Direct Air Capture (DAC)

Recent carbon cycle research by Solomon et al. [25] and Hansen et al. (2007) has resulted in increased interest in direct capture of carbon dioxide (CO_2) from the air (e.g., [26]). Pielke [27] has described the macro-scale economic playing field for air capture, while others ([28], Lackner 2009, [29]) have begun research into specific technologies capable of removing CO_2 from the air. Several companies have recently formed to develop and commercialize direct air-capture systems, including Kilimanjaro, Carbon Engineering, and Global Thermostat.

The key technical concern is the low partial pressure of CO_2 in air due to its low concentration (<390 ppm). This requires the movement of very large volumes of air through a capture unit, and high expense of energy to execute the separation. The American Physical Society Panel on Public Affairs [30] recently completed a fairly comprehensive assessment of the 2009 state of the art. The key messages of the report include three conclusions:

- DAC is not currently an economically viable approach.
- Generally, low-carbon power and energy is best used directly to minimize losses rather than used for DAC.
- Eventually, DAC could play a role in capture and storage from decentralized sources of CO_2, such as vehicles, ships, or planes.

While the situation may change with CO_2 demand and price, the consensus today is that the economics and engineering of DAC remain formidable and difficult to overcome.

Geological Sequestration

A number of geological reservoirs appear to have the potential to store many hundreds to thousands of Gt of CO_2 [31]. The most promising reservoirs are porous and permeable rock bodies at depth (Figs. 3 and 4).

- *Saline formations* contain brine in their pore volumes, commonly with salinities greater than 10,000 ppm. Because CO_2 is buoyant in most

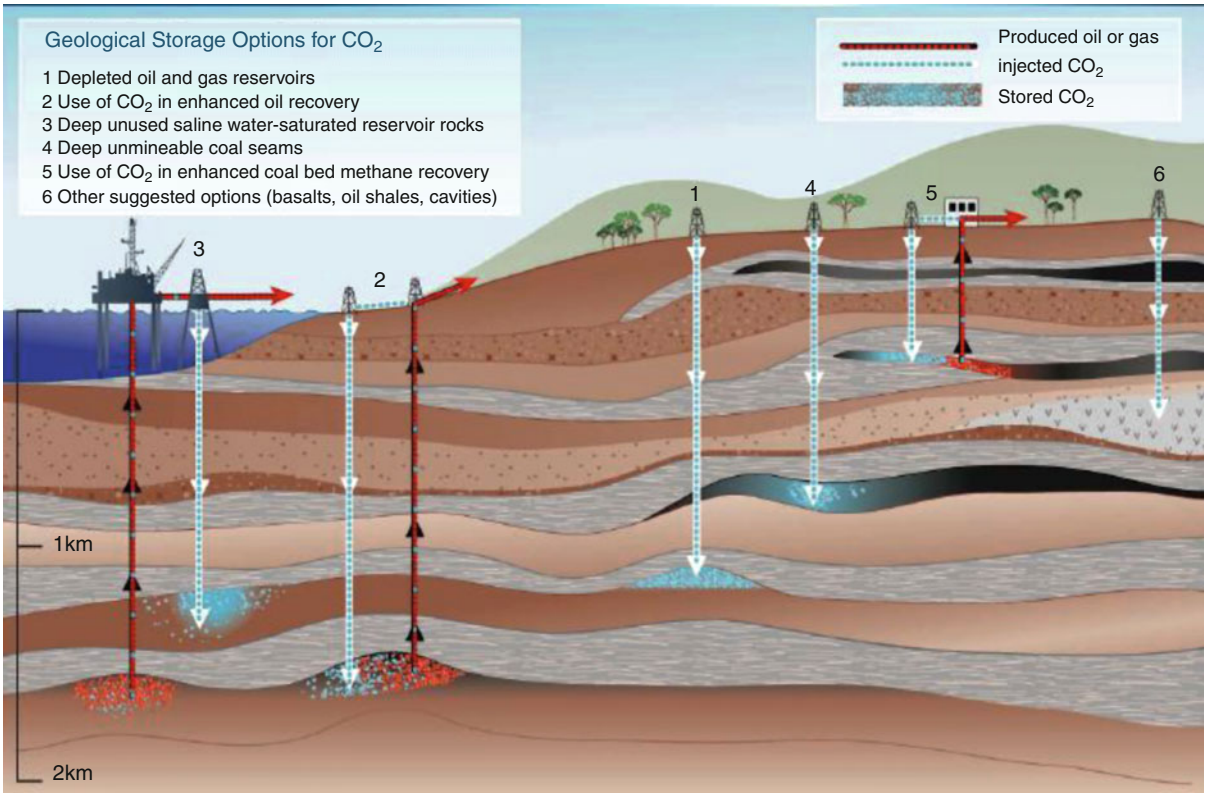

CO_2 Capture and Sequestration. Figure 3
Options for storing CO_2 in underground geological formations (After Benson and Cook [31])

geological settings, target saline formations require a cap rock or sealing unit above the main injection zone.

- *Depleted oil and gas fields* have some combination of water and hydrocarbons in their pore volumes. In some cases, economic gains can be achieved through enhanced oil recovery or enhanced gas recovery [32–34]. Substantial CO_2-enhanced oil recovery already occurs in the USA with both natural and anthropogenic CO_2. These fields provide much of the knowledge base available about the potential issues related to CO_2 sequestration.
- *Deep coal seams*, often called unmineable coal seams, are composed of organic minerals with brines and gases in their pore and fracture volumes that can preferentially adsorb and bind CO_2 as well as store it in pores and minor fractures. These targets present some challenges in that coals are relatively low permeability units, presenting challenges to injection.

Because of their large storage potential and broad distribution, it is likely that most geological sequestration will occur in saline formations. However, initial projects have been proposed for depleted oil and gas fields, accompanying enhanced oil recovery, due to the high density and quality of subsurface data and the potential for economic return. Although there remains some economic potential for enhanced coal bed methane recovery much less is known about this style of sequestration [2, 31, 35, 36]. Even less is known about sequestration in basalts. As such, many workers are not convinced of the economic viability of sequestration projects in coal, basalts, or oil shales given today's technology and understanding [37].

Storage of large CO_2 volumes in geological formations requires that the CO_2 be relatively dense, so that storage capacity is efficiently used. Given typical geothermal gradients and hydrostatic loads, CO_2 is likely to be in a *supercritical* state at most target sites greater than 800 m depth (e.g., [38]). At the likely range of

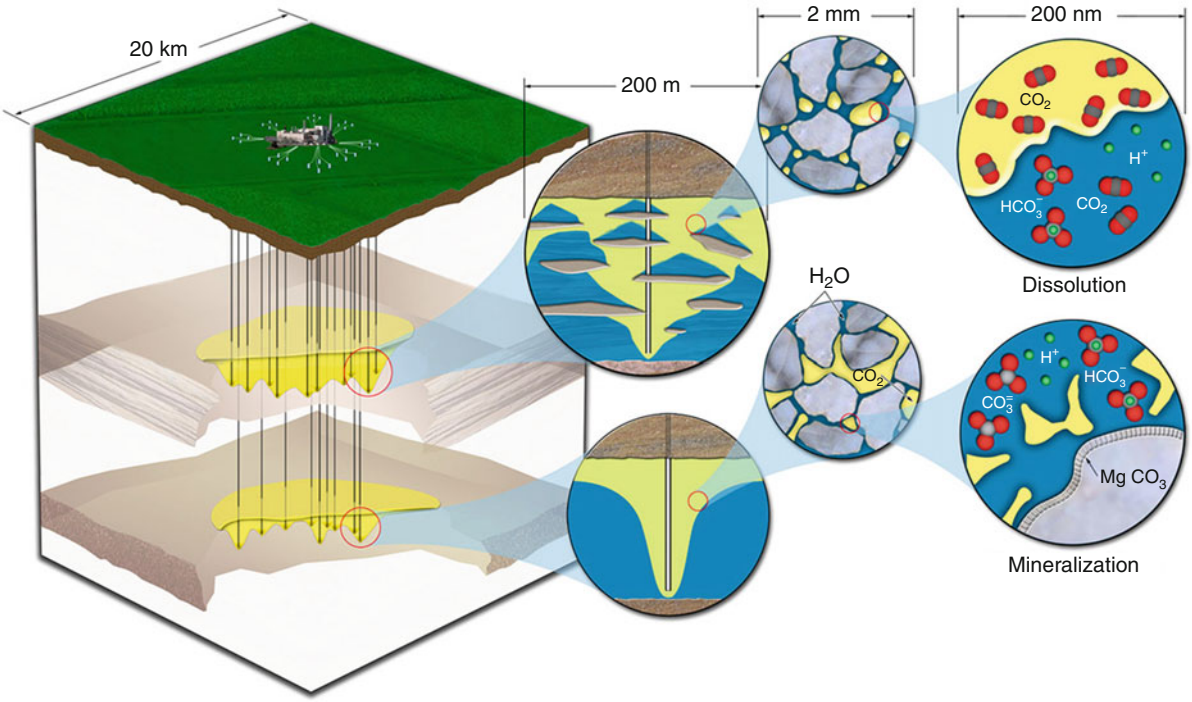

CO_2 Capture and Sequestration. Figure 4

Schematic diagram of large injection at 10 years time illustrating the main storage mechanisms. All CO_2 plumes (*yellow*) are trapped beneath impermeable shales (not shown). The upper unit is heterogeneous with a low net percent usable porosity, whereas the lower unit is homogeneous. Central insets show CO_2 as a mobile phase (*lower*) and as a trapped residual phase (*upper*). Right insets show CO_2 dissolution (*upper*) and CO_2 mineralization (*lower*) (After MIT [2])

injection pressures and temperatures for most projects, CO_2 would be buoyant and gravitational forces would push CO_2 upward from the injection point.

Consequently, trapping mechanisms are needed to store CO_2 effectively. For depleted oil and gas fields or for saline formations, CO_2 storage mechanisms are reasonably well defined and understood (Fig. 4). CO_2 sequestration targets will require *physical barriers* to CO_2 migration out of the crust to the surface. These barriers will commonly take the form of impermeable layers (e.g., shales, evaporites) overlying the sequestration target. This storage mechanism is highly or directly analogous to that of hydrocarbon trapping, natural gas storage, and natural CO_2 accumulations. At the pore scale, *capillary forces* can immobilize a substantial fraction of a dispersed CO_2 bubble, commonly measured to be between 5% and 25% of the CO_2-bearing pore volume. The volume of CO_2 trapped as a residual phase is highly sensitive to pore geometry, and consequently is difficult to predict; however, standard techniques can measure residual phase trapping directly in the laboratory with rock samples.

Once in the pore volume, the CO_2 will *dissolve* into other pore fluids, including hydrocarbon species (oil and gas) or brines. Depending on the fluid composition and reservoir condition, this may occur rapidly (seconds to minutes) or over a period of tens to hundreds of years. Once dissolved, the CO_2-bearing brines are denser than the original brines, and so the strong buoyant forces of free-phase gas are replaced by small downward forces. Over longer time scales (hundreds to thousands of years) the dissolved CO_2 may react with minerals in the rock volume to *dissolve or precipitate* new carbonate minerals. For the majority of the rock volume and major minerals, this process is slow, and may take hundreds to thousands of years to

achieve substantial storage volumes. Precipitation of carbonate minerals permanently binds CO_2 in the subsurface; dissolution of minerals generally traps CO_2 as an ionic species (usually bicarbonate) in the pore fluid.

Although work remains to characterize and quantify these mechanisms, the current level of understanding can be used today to develop estimates of the percentage of CO_2 that can be stored over some period of time. Confidence in these estimates is bolstered by studies of hydrocarbon systems, natural gas storage operations, hazardous waste injection, and CO_2-enhanced oil recovery (CO2-EOR). Current evaluations of CCS effectiveness based on the current understanding of trapping mechanisms estimate that *more than 99.9% of injected CO_2 can be reliably stored over 100 years, and it is likely that 99% of CO_2 can be reliably stored for 1,000 years* [31]. These estimates assume careful siting, due diligence before injection, and appropriate management of injection, and reflect the view that the crust contains many sites that are generally well configured to store CO_2 effectively.

Large-Scale Commercial Deployment

In order to achieve substantial GHG reductions, geological storage deployment has several requirements:

- Projects must be large in scale, roughly in the order of 1 Mt/year CO_2 or more (Friedmann 2006).
- There must be minimal leakage from the underground storage reservoirs back to the atmosphere.
- There must be minimal impact on other uses of the subsurface environment and the resources it contains.

The issue of scale dominates deployment of GCS ([5, 39]; McFarland 2004; [4]). These volumes would have geological carbon sequestration, providing 25–75 Gt C over 50 years, or 15–43% of emissions reduction needed to stabilize atmospheric CO_2 levels at 550 ppm [39].

Today there are five well-established large-scale injection projects with an ambitious scientific program that includes monitoring and verification (Table 1): Sleipner in Norway [40], Weyburn in Canada [41], In Salah in Algeria [42]; Snohvit in northern Norway (REF); and Cranfield, Mississippi (REF). Each project has injected CO_2 at the rate of ~1 MM t/year (~280,000 t C/year). Each project has had a substantial supporting science program or anticipates one. Recently, the Global CCS Institute in Australia compiled a list of active and near active projects, as well as a roster of announced integrated and pilot projects (REFS). A few are listed here.

These projects have sampled a wide array of geology with varying trapping mechanisms, injection depths, reservoir types, and injectivity. Each of these projects appears to have ample injectivity and capacity for success, and none has detected CO_2 leakage of any significance. In addition to the three sequestration projects, many industrial applications have injected large volumes of CO_2 into the subsurface. EOR operations in W. Texas, New Mexico, Colorado, Wyoming, Oklahoma, Mississippi, Trinidad, Canada, and Turkey have individual injection programs as large as 3 MM t CO_2/year (~820,000 t C/year) and cumulative anthropogenic emission injections of ~10 MM t CO_2/year (2.7 MM t C/t) [43]. It should be said that the monitoring and verification program at each site varies substantially [2]. In many EOR projects, there is almost no monitoring beyond that required for CO_2 flood operations [32].

It is worth noting that many of these projects have come online recently in China, which has the potential to ramp up projects very rapidly ([44, 45]; Liu and Gallagher 2009). It should also be noted that all of the first projects do not involve capture from a power plant, but rather from industrial facilities where CO_2 is available at a relatively low cost. While this does improve the knowledge of GCS greatly, some questions will remain about plant integration and economics after these projects which will only be resolved through successive scale-up and demonstration.

Science and Technology Status

As discussed above, the knowledge of trapping mechanisms and the successes of the three large projects provide substantial information. These are augmented by studies of naturally occurring CO_2 systems, [46], natural gas storage facilities, hazardous waste disposal, acid gas injection, and CO_2-EOR [31]. This knowledge provides a firm foundation for commercial action and

CO_2 Capture and Sequestration. Table 1 Some current and pending large CO_2 injection projects

Site	Location	Reservoir class	Plant/capture type	Permeability	Seal type	Start date[a]
Sleipner	Norway	Offshore Saline Fm.	Gas refining	Very high	Thick shale	1996
Weyburn	Canada	Onshore EOR	SNG plant/ precombustion	Moderate	Evaporite	2000
In Salah	Algeria	Onshore Sandstone	Gas refining	Low	Thick shale	2004
Snohvit	Norway	Offshore Saline Fm.	Gas refining	Moderate	Shales	2008
Cranfield	USA (Mississippi)	Onshore Saline Fm. And EOR	Natural CO_2 dome	Very high	Mudstone	2009
FutureGen 2.0	USA (Illinois)	Onshore Saline Fm.	IGCC/precombustion	Moderate to very high	Thick shales	2016
ZeroGen	Australia	Onshore EOR/ Saline	IGCC/precombustion	Low to moderate	Shale	2018
GreenGen	China	Offshore EOR +/− Saline Fm.	IGCC/precombustion	Low to moderate	Shales	2015
HECA	USA (California)	Onshore EOR	IGCC/precombustion	Moderate to high	Thick shale	2016
Gorgon	Australia	Offshore Saline Fm	Gas refining	Moderate	Thick shales	2013
SaskPower Boundary Dam	Canada (Saskatchewan)	Onshore EOR +/− Saline Fm.	SC boiler/Post-combustion	Moderate	Evaporite	2016
Hauneng Shidongkou	China	Onshore saline Fm.	USC boiler/post-combustion	Unclear	Shales	2016
Shenhua DCL/ Majiata	China	Onshore Saline Fm. +/− EOR	Coal liquefaction/ precombustion	Low to moderate	Shales	2013
Archer-Daniels Midland	USA (Illinois)	Onshore Saline Fm.	Ethanol by-product	Moderate to high	Shales	2013
TCEP	USA (Texas)	Onshore EOR	Polygeneration precombustion	Moderate to high	Evaporite	2017

[a] = date of first injection or planned first injection of CO_2

a nascent foundation for the development of regulation, standards, and legal frameworks for sequestration (REFS, including Wilson et al. 2009; CCSREGS project; EPA; EU ruling). GCS itself, however, drives study into specific technical and scientific challenges associated with the central elements of site characterization, selection, operation, and monitoring ([36]; WRI 2009). Forward investigation around these topics will enhance the technical and operational understanding of commercial GCS.

Monitoring and Verification (M&V)

Monitoring and verification must detect and track CO_2 in the deep subsurface near injection targets, in the shallow subsurface, and above ground. Monitoring and verification studies are a chief focus of many applied research efforts. The US Department of Energy has defined M&V technology development, testing, and deployment as a key element to their technology roadmap (US DOE 2010). The European Union

CO_2ReMoVe effort is dedicated to monitoring and verification, and the industry-led CO_2 Capture Project continues to study monitoring in commercial settings [47]. Some form of M&V will be required at commercial sites, but the extent of monitoring required by regulators, operators, or financiers remains uncertain. Many geophysical and geochemical methods are sufficiently well understood for them to be used to make reasonable performance predictions at candidate storage sites ([48]; WRI 2009). Testing which of these approaches will be the most valuable for a given geological environment remains to be determined.

Key Science and Technology Gaps

Despite the tremendous amount of applied and basic knowledge, there remain both cross-cutting-specific and site-specific topics for investigation (e.g., [49]). From an applied perspective, the National Energy Technology Laboratory has written several plans to identify and address key technology gaps (e.g., [36]). Recent new R&D projects aimed at specific components of R&D include the National Risk Assessment Program (NRAP), the Carbon Capture Simulation Initiative (CCSI; REF), Weyburn's Final phase project (REF), and portions of China's project 836 and 927. While these efforts and reports are not meant to be comprehensive, they reflect the current state of knowledge and potential to continue scientific investigations in GCS.

Deployment Challenges

Despite the current gaps in sequestration science and technology, commercial projects have begun and are ready to proceed with confidence in their success. Today, enough is known to safely and effectively execute key tasks around single large-scale injection projects:

- Characterize a site.
- Design and operate the project.
- Monitor the CO_2 injection.
- Mitigate problems that might arise.
- Close and abandon the project.

Although this knowledge is currently being brought to bear on specific injection projects around the world, greater work is needed to codify and develop tools, regulations, and standards for deployment of multiple million ton injections in thousands of wells nationwide and worldwide across a range of geological settings. This affects both sides of the deployment rubric over the project life cycle ([50]; WRI 2009). Potential operators must execute a set of tasks to prepare for and execute injection permitting and operation. Similarly, potential regulators, investors, insurers, and public stakeholders require information to make decisions. Part of the challenge is to provide a technical basis for each set of actors to make decisions concerning the minimal amount of information needed to serve all stakeholders.

While many possible goals and terms may be pursued in site characterization, it is difficult to imagine the success of a large-scale injection project without knowledge of three parameters. These are *injectivity*, *capacity*, and *effectiveness* (Friedmann 2006). In general terms, injectivity and capacity may be estimated by conventional means, such as special core analysis, regional and local structural and stratigraphic mapping, and simple multi-phase fluid flow simulations. However, there are explicit standard measures of effectiveness. Ultimately, characterizations must rely on estimates of geomechanical integrity, hydrodynamic stability, and seal continuity for the rock system, fault system, and well system [51–55].

Given this complexity, it is not broadly accepted today what terms constitute effective storage. The FutureGen project's request for proposals [18] laid out a set of minimum criteria for acceptance. These criteria are based on expert opinion, laboratory experimentation, analog studies, and simulations. Similarly, the World Resources Institute (2009) proposed a set of guidelines to potential operators based on a working group of over 40 experts ranging from geoscientists to lawyers and regulators. However, the few active projects today do not constitute a large empirical data set from multiple geological carbon sequestration deployments to provide a definitive standard for characterization of site effectiveness.

Hazards Assessment and Risk Management

Supercritical CO_2 is buoyant and will seek the Earth's surface; therefore, CO_2 injection carries the possibility of leakage. Importantly, CO_2 leakage risk will not be

uniform across all sites, thus CO_2 storage sites will have to demonstrate minimal risk potential in their site characterization plans [56, 57]. Based on analogous experience in CO_2 injection such as acid gas disposal and enhanced oil recovery, these risks appear to be less than those of current oil and gas operations [31].

The direct hazards associated with geologic sequestration fall into three distinct categories:

- Hazards associated with the release of the carbon dioxide to the Earth surface
- Hazards associated with release into groundwater and subsequent degradation
- Hazards associated with Earth movement caused by the injection process itself

The hazards themselves in turn are associated with failure mechanisms and triggers (Friedmann 2007; [56]). Potential triggering of events associated with these hazards could lead to undesired consequences. As such, it is an important goal to identify and understand these hazards in order to avoid triggering hazard events. Identification and characterization of these hazards is the critical first step to managing the risks at a site. They also serve as the basis for a quantitative probabilistic risk assessment (PRA). A robust PRA cannot be made today due to substantial scientific and technical gaps. However, the hazards associated with a site can be identified, mapped, characterized, and parameterized sufficiently to avoid failure or (alternatively) avoid selecting a bad site.

Water Issues

A number of issues arise from CCS regarding water use and quality. These include additional water use due to process steam and additional hear requirements in the plants; displacement of in situ brines; and potential risks to groundwater quality from unplanned CO_2 leakage [58]. Additional water needs for surface facilities is highly sensitive to capture process and plant type, ranging from 20% to 110% additional water consumption ([59]; b). CO_2 injected into saline formations necessarily interacts with water and brines there. This interaction includes displacement of the brines there, local drying of the reservoir, and dissolution of CO_2 into brine forming carbon acid. Early research focused on the potential risks and impacts of acid brine formation, ultimately concluding that these risks are small.

Injection also creates a pressure transient in the reservoir which increases through time. In the right context, this pressure can drive water co-production (enhanced water recovery) and even drive surface desalination processes [60, 61]. Based on preliminary calculations, it appears that water co-production can cut the water demands for an integrated CCS plant by 50%, or produce freshwater for agricultural or civil use. More work is needed to understand the viability of this technical approach.

Bibliography

1. IPCC (2005) Intergovernmental panel on climate change, IPCC special report on carbon dioxide capture and storage, Interlachen, http://www.ipcc.ch/
2. MIT (2007) Future of coal in a carbon constrained world, MIT Press. http://coal.mit.edu/
3. EPRI REF!! 2007 or 2009
4. US CCTP (2005) US climate change technology program strategic plan, Washington, DC, 256 p. http://www.climatetechnology.gov
5. Edmonds J, Clarke J, Dooley J, Kim SH, Smith SJ (2004) Stabilization of CO_2 in a B2 world: insights on the roles of carbon capture and disposal, hydrogen, and transportation technologies. Energy Econ 26(4):517–537, Special Issue EMF 19 Alternative technology strategies for climate change policy, John P. Weyant, ed
6. Thambimuthu K, Soltanieh M, Abanades JC (2005) Chapter 3: capture, IPCC special report on carbon dioxide capture and storage, intergovernmental panel on climate change, Interlachen. www.ipcc.ch, pp 3–1 to 3–114
7. Hossain MM, de Lasa HI (2008) Chemical-looping combustion (CLC) for inherent CO_2 separations – a review. Chem Eng Sci 63:4433–4451
8. Rao AB, Rubin ES, Keith DW, Morgan MG (2006) Evaluation of potential cost reductions from improved amine-based CO_2 capture systems. Energy Policy 34:3765–3772
9. Al-Juaied M, Whitmore A (2009) Realistic costs of carbon capture, Belfer center discussion paper 2009-08, Harvard University, 73 p. http://belfercenter.ksg.harvard.edu/files/2009_AlJuaied_Whitmore_Realistic_Costs_of_Carbon_Capture_web.pdf
10. Hiroshi M, Hiroshi H (2000) Development of CO_2 separation membranes: (1) Polymer membrane. Sumitomo Electric Tech Rev 157:22–26
11. Meinema HA, Dirrix RWJ, Brinkman HW, Terpstra RA, Jekerle J, Kosters PH (2005) Ceramic membranes for gas separations – recent developments and state of the art. Interceram 54:86–91
12. Holt JK, Park G, Wang Y, Staderman M, Artyukhin AB, Grigoropoulos CP, Noy A, Bakajin O (2006) Fast mass transport through sub-2-nanometer carbon nanotubes. Science 312:1034–1036

13. Blanchard LA, Hancu D, Beckman EJ, Brennecke JF (1999) Green processing using ionic liquids and CO_2. Nature 399:28–29
14. Maiti A (2009) Theoretical screening of ionic liquid solvents for carbon capture. Chem Sus Chem 2:628–631
15. Rochelle G (2009) Amine scrubbing for CO_2 capture. Science 325:1652–1655
16. Herzog H, Hattan A, Meldon J (2009) An R&D "pipeline" for advanced post-combustion CO_2 capture technologies. In: Coal without carbon, Clean Air Task Force. www.coaltransition.org, pp 37–54
17. Kozak F, Petif A, Morris E, Rhudy R, Thimsen D (2009) Chilled ammonia process for CO_2 capture. Energy Procedia 1:1419–1426
18. FutureGen Alliance (2006) Final request for proposals for FutureGen facility host site, 54 p. http://www.futuregen-alliance.org/news/futuregen_siting_final_rfp_3-07-2006.pdf
19. Scientific American (2008) "Clean" coal power plant cancelled – hydrogen economy, too. http://www.scientificamerican.com/article.cfm?id=clean-coal-power-plant-canceled-hydrogen-economy-too
20. MIT (2011a) GreenGen fact sheet: carbon dioxide capture and storage project, MIT Energy Initiative. http://sequestration.mit.edu/tools/projects/greengen.html
21. DOE-NETL (2007b) U.S. Department of Energy, National Energy Technology Laboratory, Cost and performance baseline for fossil energy plants, vol 1. Bituminous coal and natural gas to electricity, Revision 1, Aug 2007
22. Kreutz T, Williams R, Consonni S, Chiesa P (2005) Co-production of hydrogen, electricity, and CO_2 from coal with commercially ready technology, part B: economic analysis. Intl J Hydrogen Energy 30:769–784
23. US DOE (2011) Innovative Texas clean coal project takes major step forward as DOE issues record of decision, press release. http://www.fe.doe.gov/news/techlines/2011/11053-Texas_Clean_Coal_Project_Moves_For.html
24. Redman E, Fennerty K, Fowler M (2009) Mobilizing the next generation coal gasification technology for carbon capture and sequestration. In: Coal without carbon, Clean Air Task Force, www.coaltransition.org, pp 1–16
25. Solomon S et al (2009) Irreversible climate change due to carbon dioxide emissions. Proc Natl Acad Sci 106(6): 1704–1709
26. Keith DW (2009) Why capture CO_2 from the atmosphere? Science 325:1654–1656
27. Pielke RA (2009) An idealized assessment of the economics of air capture of carbon dioxide in mitigation policy. Environ Sci Policy 12(3):216–225
28. Mahmoudkhani M, Keith DW (2009) Low-energy sodium hydroxide recovery for CO_2 capture from atmospheric air–thermodynamic analysis. Int J Greenhouse Gas Control 3(4):376–384
29. Zeman F (2007) Energy and material balance of CO_2 capture from ambient air. Environ Sci Technol 41(21): 7558–7563
30. American Physical Society (2010) Direct air capture of CO_2 with chemicals, APS, 119 p. http://www.aps.org/policy/reports/popa-reports/loader.cfm?csModule=security/getfile&PageID=244407
31. Benson SM, Cook P (2005) Chapter 5: Underground geological storage, IPCC special report on carbon dioxide capture and storage, Intergovernmental Panel on Climate Change, Interlachen, www.ipcc.ch, pp 5–1 to 5–134
32. Jarrell PM, Fox CE, Stein MH, Webb SL (2002) Practical aspects of CO_2 flooding. Monograph 22. Society of Petroleum Engineers, Richardson
33. Oldenburg CM, Stevens SH, Benson SM (2004) Economic feasibility of carbon sequestration with enhanced gas recovery (CSEGR). Energy 29:1413–1422
34. Stevens S (1999) Sequestration of CO_2 in depleted oil and gas fields: barriers to overcome in implementation of CO_2 capture and storage (disused oil and gas fields). IEA Greenhouse Gas R&D Programme, IEA/CON/98/31
35. NPC (2007) Facing hard truths about energy: a comprehensive view to 2030 of global oil and gas, National Petroleum Council, Washington, DC, 442 pp. www.npc.org
36. US DOE (2007a) Carbon sequestration technology roadmap and program plan for 2007, Morgantown, WV, 39 p. www.netl.doe.gov
37. US DOE (2007b) Basic Research needs for geosciences: facilitating 21st century energy systems. Department of Energy Office of Basic Energy Sciences, Washington, DC, 287 p. http://www.sc.doe.gov/bes/reports/list.html
38. Bachu S (2000) Sequestration of CO_2 in geological media: criteria and approach for site selection in response to climate change. Energy Convers Manage 41:953–970
39. Pacala S, Socolow R (2004) Stabilization wedges: Solving the climate problem for the next 50 years using current technologies. Science 305:986–999
40. Arts R, Eiken O, Chadwick A, Zweigel P, van der Meer L, Zinszner B (2004) Monitoring of CO_2 injected at Sleipner using time-lapse seismic data. Energy 29:1383–1392
41. Wilson M, Monea M (eds) (2004) IEA GHG Weyburn CO_2 monitoring & storage project summary report 2000–2004, 273 p
42. Riddiford F, Wright I, Espie T, Torqui A (2004) Monitoring geological storage. In: Salah gas CO_2 storage project, GHGT-7, Vancouver
43. Kuuskraa VA, DiPietro P, Koperna GJ (2006) CO_2 storage capacity in depleted and near-depleted US oil and gas reservoirs. In: NETL 5th annual conference on carbon sequestration. ExchangeMonitor, Alexandria
44. Asia Society (2009) Roadmap for US-China collaboration on carbon capture and sequestration, Asia Society Press, 41 p. http://asiasociety.org/files/pdf/AS_CCS_TaskForceReport.pdf
45. Dalhousie R, Li X, Davidson C, Wei N, Dooley J (2009) Establishing China's potential for large scale, cost effective, deployment of carbon dioxide capture and storage. Pacific Northwest National laboratory report, PNNL-SA-XXXX, 6 p
46. IEA GHG (2005) A review of natural CO_2 emissions and releases and their relevance to CO_2 storage. International Energy

Agency greenhouse gas R&D programme, report 2005/8. http://www.ieagreen.org.uk/
47. CO_2 Capture Project (2009) A technical basis for CO_2 storage. In: Cooper C (ed) CO_2 capture project. CPL Press, ISBN: 978-1-872691-48-0
48. Benson SM, Hoversten M, Gasperikova E, Haines M (2004) Monitoring protocols and life-cycle costs for geological storage of carbon dioxide. In: 7th international greenhouse gas technology conference, Vancouver
49. Friedmann, SJ, Newmark RA (2009) Commercial deployment of geologic carbon sequestration: technical components of an accelerated U.S. program. In: *Coal without carbon*, Clean Air Task Force. www.coaltransition.org, pp 59–76
50. Wilson EJ, Friedmann SJ, Pollak MF (2007) Research for deployment: incorporating risk, regulation, and liability for carbon capture and sequestration. Environ Sci Technol 41:5945–5952
51. Burton EA, Myhre R, Myer LR, Birkinshaw K (2007) Geologic carbon sequestration strategies for California, The assembly bill 1925 report to the California legislature. California Energy Commission, Systems Office. CEC-500-2007-100-SD. http://www.energy.ca.gov/2007_energypolicy/documents/index.html#100107
52. Chiaramonte L, Zoback M, Friedmann S, Stamp V (2006) CO_2 sequestration, fault stability and seal integrity at teapot dome, Wyoming, NETL 5th annual conference on carbon sequestration. ExchangeMonitor Publications, Alexandria
53. Cugini A, DePaolo D, Fox M, Friedmann SJ, Guthrie G, Virden J, 2010, US-DOE's National risk assessment program: bridging the gaps to provide the science base to ensure successful CO_2 storage. Energy Procedia
54. Hovorka SD, Benson SM et al (2006) Measuring permanence of CO_2 storage in saline formations – the Frio experiment. Environ Geosci 13:103–119
55. Streit JE, Hillis RR (2004) Estimating fault stability and sustainable fluid pressures for underground storage of CO_2 in porous rock. Energy 29:1445–1456
56. WRI (2008) Guidelines for carbon capture and sequestration, major contributing author. World Resources Institute, Washington, DC, 103 pp. www.wri.org
57. Bradshaw J, Boreham C, la Pedalina F (2004) Storage retention time of CO_2 in sedimentary basins; examples from petroleum systems. Paper presented at the GHGT-7 conference, Vancouver
58. Newmark RA, Friedmann SJ, Carroll SJ (2010) Water challenges for carbon capture and sequestration. Environ Manage. doi:10.1007/s00267-010-9434-1
59. DOE-NETL (2007a) U.S. Department of Energy, National Energy Technology Laboratory, Power plant water usage and loss study, May 2007 revision
60. Aines RD, Wolery TJ, Bourcier WL, Wolfe T, Hausmann C (2010) Fresh water generation from aquifer-pressured carbon storage: feasibility of treating saline formation waters. Energy Procedia 4:2269–2276
61. Buscheck TA, Sun Y, Hao Y, Aines RD, Wolery TJ, Tompson AFB, Jones ED, Friedmann SJ (2010) Combining brine extraction, desalination, and residual-brine injection with CO_2 storage in saline formations: implications for pressure management, capacity, and risk management. Energy Procedia 4:4283–4290
62. IEA (2011) Carbon capture and storage: legal and regulatory review. International Energy Agency, Paris, 108 p. www.iea.org
63. Abanades JC, Rubin ES, Anthony EJ (2004) Sorbent cost and performance in CO_2 capture systemts. Ind Eng Chem Res 43:3462–3466
64. Bachu S (2003) Screening and ranking of sedimentary basins for sequestration of CO_2 in geological media in response to climate change. Environ Geology 44:277–289
65. Birkholzer JT, Zhou Q (2009) Basin-scale hydrogeologic impacts of CO_2 storage: capacity and regulatory implications. Int J Greenhouse Gas Control 3:745–756
66. Bradshaw J, Dance T (2004) Mapping geological storage prospectivity of CO_2 for the world's sedimentary basins and regional source to sink matching. In: Proceedings of the 7th international conference on greenhouse gas technologies, 2004. Vancouver
67. EPA (2008c) U.S. Environmental Protection Agency, Federal requirements under the Underground Injection Control (UIC) program for carbon dioxide (CO_2) geologic sequestration (GS) wells; proposed rule, 40 CFR Parts 144 and 146, Federal register, vol 73, no. 144, July 2008. http://www.epa.gov/EPA-WATER/2008/July/Day-25/w16626.htm
68. Friedmann SJ (2007a) Operational protocols for geologic carbon storage: facility life-cycle and the new hazard characterization approach. In: 6th annual NETL conference on carbon capture and sequestration. ExchangeMonitor, Pittsburgh, Oral 034
69. Friedmann SJ (2007) Geological carbon dioxide sequestration. Elements 3:179–184
70. Friedmann SJ (2009) Emerging technical challenges of 5-million ton/year CO_2 injection. In: SPE technical proceedings, SPE-126942-MS, 2009 SPE international conference on CO_2 capture, storage, & utilization, San Diego
71. Friedmann SJ (2009) Accelerating development of underground coal gasification: priorities and challenges for U.S. Research and Development. In: Coal without carbon, Clean Air Task Force. www.coaltransition.org, pp 1–16
72. FutureGen Alliance (2011) FutureGen facts, 3p brochure. http://www.futuregenalliance.org/pdf/FutureGenFacts.pdf
73. GCCSI (2011) The global status of CCS, Global Carbon Capture and Storage Institute, Canberra, 204 p. http://www.globalccsinstitute.com/resources/publications/global-status-ccs-2010
74. GCCSI (2011) Status of CCS project database. Global Carbon Capture and Storage Institute, Canberra, http://www.globalccsinstitute.com/resources/data/dataset/status-ccs-project-database
75. Herzog H, Caldeira K, Reilly J (2003) An issue of permanence: assessing the effectiveness of temporary carbon storage. Climatic Change 59(3):293–310

76. IEA GHG (2006) 2nd well bore integrity network meeting, International Energy Agency greenhouse gas R&D, report 2006/12, Sept 2006
77. Ide ST, Friedmann SJ, Herzog, HJ (2006) CO_2 leakage through existing wells: current technology and regulatory basis. In: 8th greenhouse gas technology conference, Trondheim
78. Keith DW, Hassanzadeh H, Pooladi-Darvish M (2004) Reservoir engineering to accelerate dissolution of stored CO_2 in brines. In: 7th international greenhouse gas technology conference, Vancouver
79. Kharaka YK, Cole DR, Hovorka SD, Gunter WD, Knauss KG, Freifield BM (2006) Gas-water-rock interactions in Frio formation following CO_2 injection: Implications for the storage of greenhouse gases in sedimentary basins. Geology 34:577–580
80. Knauss KG, Johnson JW, Steefel CI (2005) Evaluation of the impact of CO_2, contaminant, aqueous fluid and reservoir rock interactions on the geologic sequestration of CO_2. Chem Geology 217:339–350
81. Lackner KS, Wright AB (2009) USA Patent no. 12/265556
82. Liu H, Gallagher K-S (2010) Catalyzing strategic transformation to a low-carbon economy: a CCS roadmap for China. Energy Policy 38:59–74
83. McFarland JR, Reilly JM, Herzog HJ (2004) Representing energy technologies in top-down economic models using bottom-up information. Energy Econ 26(4):685–707. Special Issue EMF 19 Alternative technology strategies for climate change policy, John P. Weyant, ed
84. MIT (2011b) Hydrogen energy California (HECA) project fact sheet: carbon dioxide capture and storage project, MIT Energy Initiative. http://sequestration.mit.edu/tools/projects/heca.html
85. Morris JP, Detwiler RL, Friedmann SJ, Vorobiev OY, Hao Y (2010) The large-scale effects of multiple CO_2 injection sites on caprock and formation stability Intl. J Greenhouse Gas Control 5:69–74
86. Wilson E, Johnson T, Keith D (2003) Regulating the ultimate sink: managing the risks of geologic CO_2 storage. Environ Sci Technol 37:3476–3483

CO_2 Reduction and Coal-Based Electricity Generation

János Beér
MIT, Cambridge, MA, USA

Article Outline

Glossary
Introduction
Pulverized Coal in Ultra-Supercritical Steam Cycle (PC/USC)
Coal Gasification Combined Gas Turbine-Steam Cycle (IGCC)
CO_2 Capture and Compression in PC and IGCC Plant
PC/Oxy/USC
CFBC with Oxy/FGR
Concluding Remarks
Bibliography

Glossary

°C Deg. Celsius
°F Deg. Fahrenheit
AUSC Advanced ultra-supercritical steam
Btu British thermal unit
CCS Carbon capture and storage (sequestration)
CFBC Circulating fluidized bed combustion
CO_2 Carbon dioxide
COE Cost of electricity
DOE U.S. Department of Energy
EIA Energy Information Administration (USDOE)
EPRI Electric Power Research Institute
GW Gigawatt
Hg Mercury
GNP Gross national product
HHV Higher heating value
HRSG Heat recovery steam generator
IEA International Energy Agency
IGCC Integrated gasification combined cycle
MIT Massachusetts Institute of Technology
Mpa Megapascal
MW Megawatt
MWh Megawatt-hour
NETL National Energy Technology Laboratory (USDOE)
NO_x Nitrogen oxides
NRC National Research Council (USA)
OECD Organization for Economic Cooperation and Development
Oxy Oxygen-blown combustion
Oxy/FGR Oxygen-blown combustion with flue gas recirculation
PC Pulverized coal
PC/SC Supercritical steam/pulverized coal
PC/USC Ultra-supercritical steam/pulverized coal

PM Particulate matter
psi Pounds per square inch
R&D Research and development
RD&D Research, development, and demonstration
SO_2 Sulfur dioxide
TCR Total capital requirement

Introduction

The provision of electric power is one of the prerequisites of prosperity; there is strong correlation between electric power-generating capacity and per capita gross domestic product (GDP) (Fig. 1) [8]. Across the world, economic indicators signal that there will be continued growth and increased electricity demand; also, at least 3.6 billion people lack adequate access to electricity and 1.6 billion have no electricity at all.

During the next 15 years, 1,200 GW of new capacity is projected to be added to the world's present electric generation capacity of about 4,000 GW. The EIA projects that by 2030 global demand for electricity will grow by more than 75%.

The U.S. Energy Information Administration (EIA) data for 2008 show that 54% of the electricity supply in the USA was generated by coal, 12% by natural gas (increasing to an estimated 32% by 2020), and about 2% by oil, with the rest produced by nuclear power (21%), hydropower (9%), and by renewable solar or wind (2%).

Electricity generation (billion kilowatt-hours) by fuel type from 1970 to 2020 in the USA is illustrated in Fig. 2 [20]. The increase in the use of coal and, especially, natural gas for power generation projected for the period from 2000 to 2020 is to meet growing demand for electricity and to offset the projected retirement of nuclear power plants.

Because of the large coal reserves in major developing countries such as China, India, and Indonesia, where most of the new power-generating plants are being installed, it can be expected that coal will remain the dominant source of power generation worldwide during the first half of this century. There is also a strongly growing demand for natural gas, a clean fuel capable of being used in power generation with high efficiency.

Coal as an energy source has the attraction of broad availability (there are large reserves in several countries around the world), low cost, and economic utilization by mature technologies.

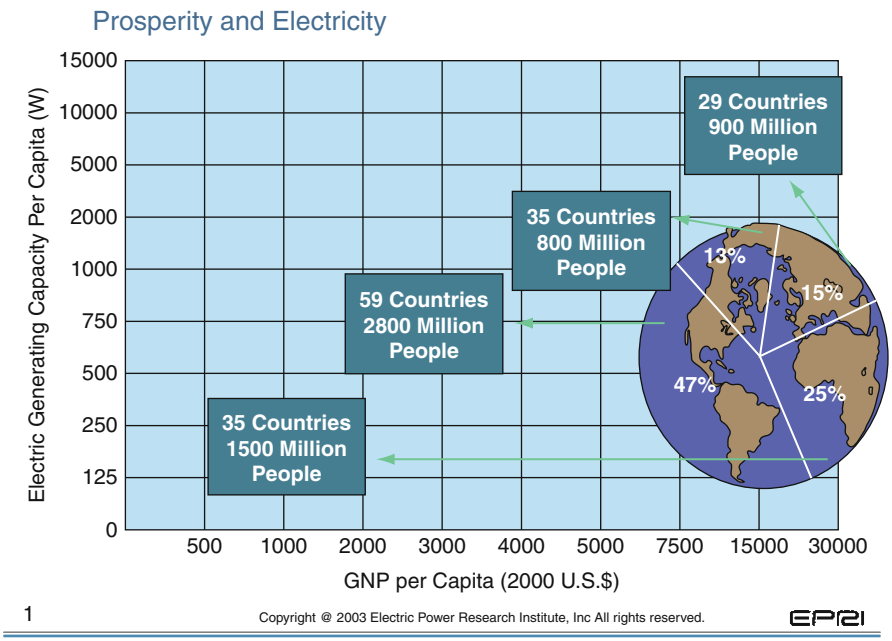

CO_2 Reduction and Coal-Based Electricity Generation. Figure 1
Prosperity and electricity (Source: EPRI [8])

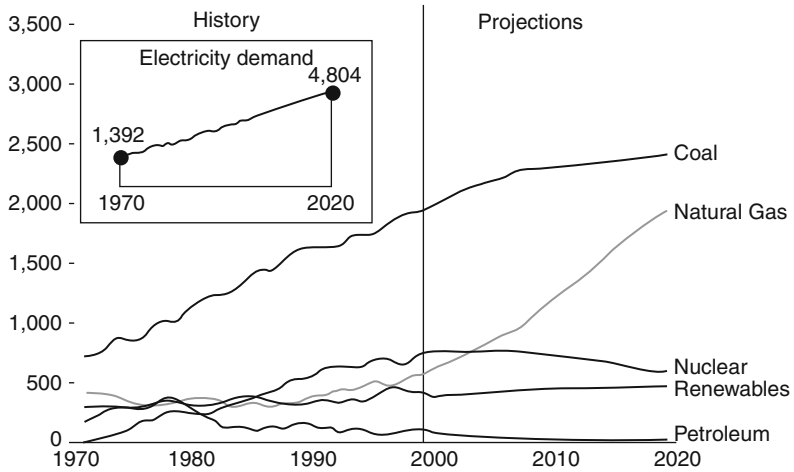

CO_2 Reduction and Coal-Based Electricity Generation. Figure 2
US Electricity generation by fuel, 1970–2020 (billion kilowatt-hours) (Source: US EIA [5])

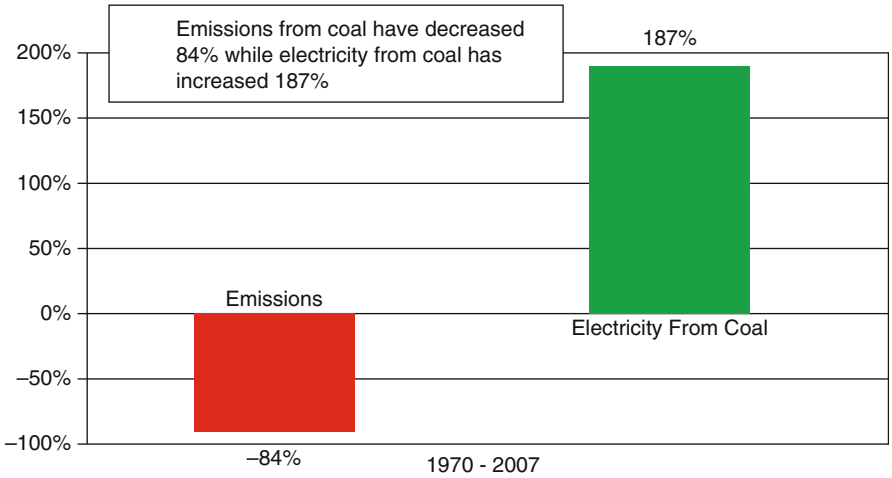

CO_2 Reduction and Coal-Based Electricity Generation. Figure 3
US emissions of criteria pollutants and electricity from coal during 1970–2007 (Source: NCC Report [14])

The disadvantages are due mainly to environmental and health impacts at the mining phase and in the course of coal utilization. Both the mining and the utilization of coal are subject to increasingly tightening standards by governmental regulations.

Because of no acceptable practical alternative to coal and natural gas, industrial research and development programs since the 1970s have been concentrated on methods of reducing the emissions of so-called criteria pollutants (SO_2, NO_x, Hg, and fine particulates). New environmental technologies developed and demonstrated under the Clean Coal Technology Program of the U.S. Department of Energy (DOE) during the past 40 years have become commercial and are being applied worldwide.

US emissions reductions have been significant in the face of increasing output of electricity generation coal (Fig. 3) [14].

The reduction of CO_2 emission remains a challenge. Carbon capture and geological sequestration (CCS) is

the key enabling technology for the long-term significant reduction of CO_2 emissions from coal-based power generation. It is expected that CCS will become commercial (deployed without significant government subsidy) for base load power generation around 2020–2025 following the construction and operation of several demonstration plants during the present and next decade.

Before the advent of commercial CCS, however, higher efficiency technology options are available for coal-based power generation. Improved efficiency will reduce the amount of fuel used for the generation of a given electric energy output and hence reduce the emissions of all pollutants. Also, when the time comes for CCS deployment, higher efficiency will reduce the energy penalty and make new plant or retrofit of existing plant less expensive [1, 2, 6].

Main higher efficiency technology options discussed below are:

- Pulverized Coal Combustion in Ultra-supercritical Steam Cycle
- Integrated Coal Gasification Combined Gas Turbine-Steam Cycle (IGCC)
- PC or CFB/Oxy/Combustion in Supercritical Steam Cycle

Pulverized Coal in Ultra-Supercritical Steam Cycle (PC/USC)

The efficiency of PC/SC power plant can be increased in small steps to 43% (HHV) and beyond, as illustrated in Fig. 4 [18].

The first two steps in the diagram concern the waste gas heat loss, the largest of a boiler's heat losses, about 6–8%. *The air ratio*, usually called excess air factor, represents the mass flow rate of the combustion air as a multiple of the theoretically required air for complete combustion. Excess air increases the boiler exit gas mass flow and, hence, the waste gas heat loss. Improved combustion technology, e.g., finer coal grinding and improved burner design, permit lowering the excess air without sacrificing completeness of combustion. Some of these remedies require additional expenditure in energy, e.g., for finer coal grinding, and for increasing the momentum flux of the combustion air through the burners, but this increase in parasitic energy is usually small compared to the efficiency gain due to the reduced excess air.

The boiler exit gas temperature can be reduced by appropriate boiler design limited only by the dew point of the flue gas. There is a close relationship between the excess air of combustion and the low limit of exit gas

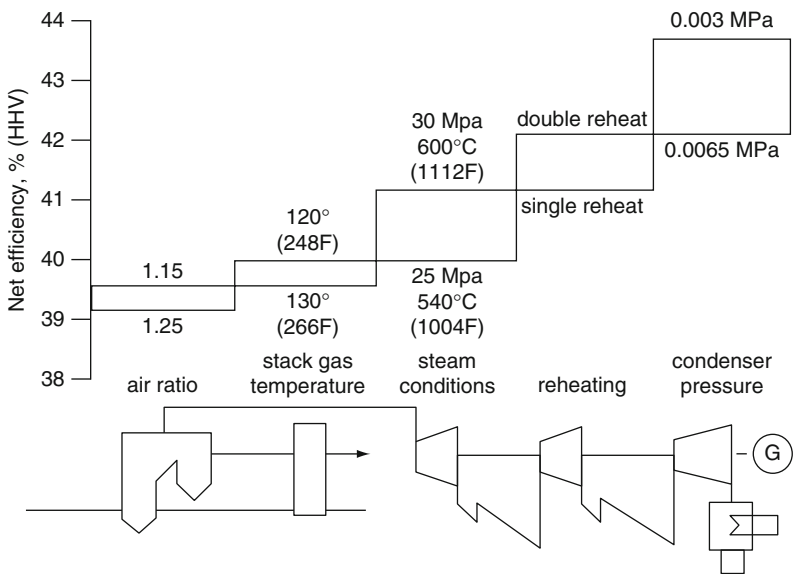

CO_2 Reduction and Coal-Based Electricity Generation. Figure 4
Steps to improve the efficiency in PC/Supercritical Coal Plant (Schilling [18])

temperature from a boiler fired by a sulfur-bearing fuel. Higher excess air leads to an increase in the oxidation of SO_2 to SO_3, with SO_3 promoting sulfuric acid formation in the combustion products. Sulfuric acid vapor increases the dew point of the flue gas and hence raises the permissible minimum exit gas temperature. At an exit gas temperature of 130°C (266°F) a reduction of every 10°C (18°F) in boiler exit temperature increases the plant efficiency by about 0.3%.

The Rankine cycle efficiency is proportional to the pressure and temperature of heat addition to the cycle, and is inversely proportional to the condenser pressure, and therefore to the temperature of the cooling medium. The usual design basis for condenser pressure in the USA is 2.0" Hg abs. (67 mbar). Power plants in Northern Europe with access to lower-temperature cooling water use condenser pressure of 1.0" Hg abs. (30 mbar) pressure. This difference can produce an efficiency gain of more than 2 percentage points [19].

As steam pressure and superheat temperature are increased above 221 bar (3,208 psi) and 374°C (706°F) the steam becomes supercritical (SC); it does not produce a two-phase mixture of water and steam as in subcritical steam, but instead undergoes a gradual transition from water to vapor with corresponding changes in physical properties.

Ultra-supercritical (USC) steam generally refers to supercritical steam at more than 1,100°F temperature. EPRI's terminology for 1,300°F and 1,400°F plants is Advanced Ultra-supercritical (AUSC).

The thermodynamic efficiency of the Rankine steam cycle increases with increasing temperature and pressure of the superheated steam entering the turbine. It is possible to increase further the mean temperature of heat addition by taking back partially expanded and reduced temperature steam from the turbine to the boiler, reheating it, and reintroducing it to the turbine. In the usual designation of steam parameters the second and third temperature refers to single and double reheat, e.g., 309 bar/594°/594°/594°C, respectively.

The average efficiency of the existing US coal-fueled electricity generating fleet is 33%, based on the higher heating value (HHV) of the coal.

Pulverized coal plants with USC parameters of 300 bar and 600/600°C (4,350 psi, 1,112/1,112°F) can be realized today, resulting in efficiencies of 43% (HHV). These plants are 21% more efficient than the mean of today's US fleet of coal-fired plants; i.e., they would use 21% less coal for the same power generation and emit 21% less CO_2. There are several years of experience with these 600°C (1,112°F) plants in service, with excellent availability [4, 11].

Further improvement in efficiency achievable by higher ultra-supercritical steam parameters is dependent on the availability of new, nickel alloys for boilers and steam turbines (Fig. 5) [10, 17].

Two major development programs in progress, the Thermie Project of the European Commission and a US program managed by EPRI for the USDOE's NETL and the Ohio Coal Development Office (OCDO), aim at steam parameters of 375 bar, 700°C/720°C (5,439 psi, 1,292°F/1,328°F), and 379 bar, 760°C/760°C (5,500 psi, 1,346°F/1,400°F), respectively. The plant efficiency increases by about 1 percentage point for every 20°C rise in superheat and reheat temperature. An advanced 700°C (1,293°F) USC plant will likely be constructed during the next 7–10 years constituting a benchmark for 46% efficiency (HHV) coal-fired power plant.

It is estimated that before 2020, the time when CCS technologies may begin to become commercially available, about 13 Gigawatts (GW) new coal-based capacity will be constructed in the USA (EIA 2010). If more efficient presently available (1,112°F) USC technology is utilized instead of subcritical steam plants, CO_2 emissions would be about 570 MMt less during the 30 years' lifetime of those plants, even without installing a CO_2 capture system.

High efficiency coal-based power generation is also important to long-term solutions of reducing CO_2 emissions by using CCS, as it mitigates the significant energy cost of CCS application. Because of the reduced coal use for a given electricity output, the plant has a smaller footprint with respect to size of coal handling and emission control systems. These savings and the use of modern analytical techniques that enable optimal use of Ni alloys can minimize the cost of USPC technology.

Coal consumption and CO_2 emission comparisons for presently available 500 MW PC/SubC, PC/SC and PC/USC plants without CCS are presented below in Table 1 [13].

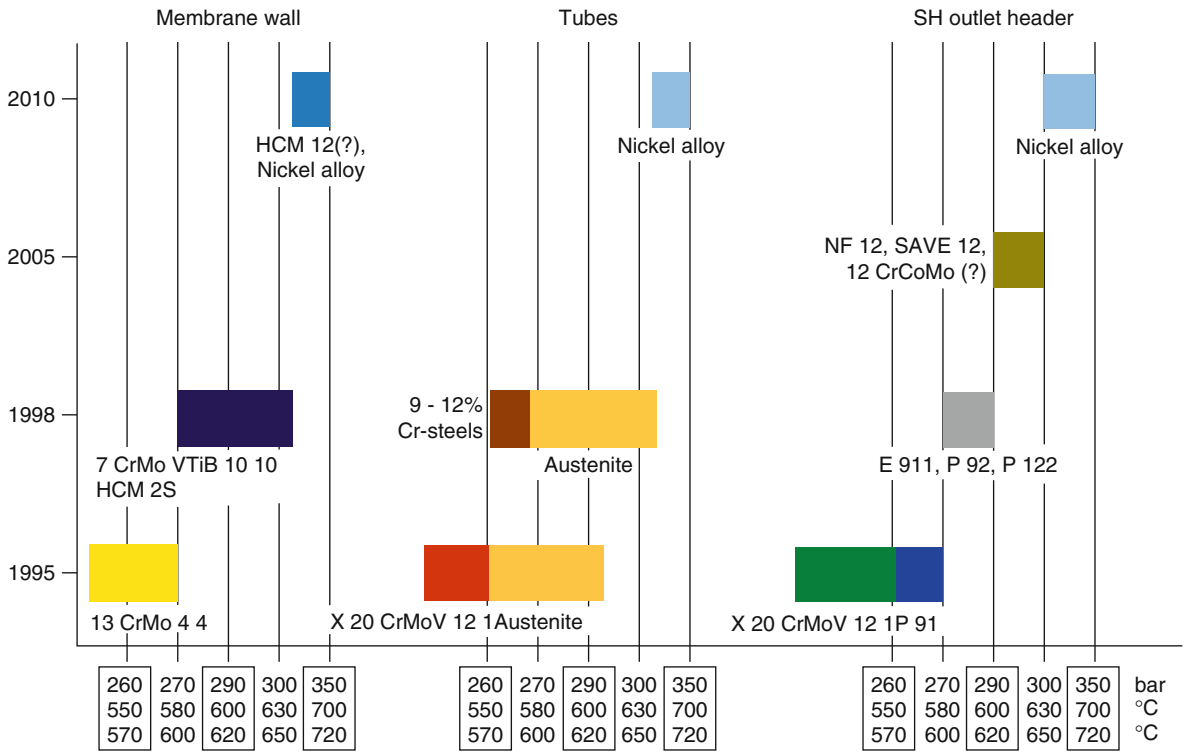

CO_2 Reduction and Coal-Based Electricity Generation. Figure 5
Stages in materials development and related advanced steam parameters (Henry et al. [10])

CO_2 Reduction and Coal-Based Electricity Generation. Table 1 Comparative coal consumptions and emissions of air-blown pulverized coal combustion technologies without CCS (MIT Coal Study [13])

Performance	Subcritical	PC/SC	PC/USC
Heat rate (Btu/kWh)	9,950	8,870	7,880
Gen. efficiency (HHV)	34.3%	38.5%	43.3%
Coal use (MMt/year)	1.54	1.37	1.22
CO_2 emitted (MMt/year)	3.47	3.09	2.74
CO_2 emitted (g/kWh)	931	830	738

Assumptions: 500 MW net plant output; Illinois #6 coal; 85% capacity factor

Coal Gasification Combined Gas Turbine-Steam Cycle (IGCC)

Gasification-based technologies use partial oxidation of coal with oxygen as the oxidant to produce a synthesis gas (syngas) consisting mainly of CO and H_2. The gas is cleaned to remove contaminants before it is used as fuel in a combustion turbine. The exhaust gas of the gas turbine raises steam in a heat recovery steam generator (HRSG) for a steam turbine-electric generator set. The combined cycle efficiency improves through the reduced effect of the steam condenser's heat loss. As with combustion technologies, higher efficiency results in lower emissions per MWh.

While the IGCC concept is being successfully demonstrated in two plants in the USA and two plants in Europe, utility power generation demands introduce new challenges that will require further RD&D to overcome. The gasification process operates best under steady-state conditions. The load change conditions associated with utility electricity generation will burden the technology. The many chemical syngas cleanup processes will have to respond to these changes on a real-time basis. In addition, the gasifier and associated gas cleanup systems will be exposed to a much larger range of fuel quality than experience has demonstrated. Again, this variation introduces conditions that require more RD&D to commercialize.

In the prevalent designs the gasifier operates at high pressure. Bituminous coal is pulverized and fed as coal-water slurry [7]. The temperature in the gasifier is above 1,300°C, so that the coal ash can be removed as liquid slag. The product syngas undergoes rigorous cleanup of particulates, sulfur and nitrogen oxides, and mercury, prior to entering the gas turbine (GT) combustor. Precombustion cleanup of the syngas is economically favorable compared to postcombustion flue gas cleanup because of the lower volume flow rate, undiluted by nitrogen, and elevated pressure. The syngas can be cooled prior to cleanup by radiant and convective heat exchangers which raise steam, and improve plant efficiency. However, because of the additional cost and operational problems due to fouling, the convective heat exchanger is often omitted in recent designs at the detriment of the plant efficiency.

Another element of efficient design is the integration of subsystems with the main generating plant. For example, air can be fed from the main compressor of the GT to the Air Separation Unit that produces oxygen for the gasification process, and the nitrogen can be returned to the gas turbine combustor as a diluent to reduce NO_x formation. The gain in improved efficiency, however, is weighed against operating a more complicated plant of somewhat reduced availability.

The current IGCC units have, and next generation IGCC units are, expected to have electricity generating efficiencies that are less than or comparable to those of supercritical PC generating units [9].

Current units typically gasify high-heating value, high-carbon fuels. Polk IGCC with a Texaco-GE coal-water-slurry gasifier and radiant syngas cooling operates at 35.4% (HHV) generating efficiency. The Wabash River IGCC with a coal-water-slurry fed E-Gas gasifier, radiant and convective syngas cooling, and no integration operates at about 40% generating efficiency. The IGCC in Puertollano Spain with a dry-feed shell-type gasifier, radiant and convective heat exchangers, and combustion turbine-air separation unit integration has a generating efficiency of about 40.5% (HHV). Supercritical PC units operate in the 38–40% efficiency range, and ultra-supercritical PC units in Europe and Japan are achieving 42–46% (HHV) generating efficiency.

A National Research Council Panel reviewing the DOE's Advanced Gasification Research Program estimated the improvements upon successful completion of the research. The research areas and anticipated benefits are listed in Tables 2 and 3 [15].

CO_2 Capture and Compression in PC and IGCC Plant

CO_2 capture from pulverized coal combustion (PC) involves postcombustion cleanup, the separation and recovery of CO_2 that is at low concentration and low partial pressure in the exhaust gas. Chemical absorption with amines is presently the only commercially available technology. The CO_2 is first captured from the exhaust gas stream in an absorption tower. The absorbed CO_2 must then be stripped from the amine solution using a large amount of steam, regenerating the solution for recycle to the absorption tower. The recovered CO_2 is cooled, dried, and compressed to a supercritical fluid. It is then ready to be piped to sequestration.

The use of steam for CO_2 removal reduces the steam available for power generation.

To maintain constant net power generation the coal input, boiler, steam turbine/generator, and emission control equipment must all be increased in size. The thermal energy required to recover CO_2 from the amine solution reduces the efficiency by 5 percentage points. The energy required to compress the CO_2 to a supercritical fluid is the next largest factor, reducing the efficiency by 3.5 percentage points. All other energy requirements amount to less than 1 percentage point.

R&D is in progress pursuing the use of alternative sorbents, such as chilled ammonia to reduce the energy intensity of the CO_2 capture process.

CO_2 Reduction and Coal-Based Electricity Generation. Table 2 Evolutionary improvements due to DOE advanced gasification research

	Change in cost and performance of IGCC system due to R&D					
	Increase in efficiency (%)	Capital cost reduction ($/kW)	O&M reduction ($/year)	Reduction in COE ($/MWh)	Availability improvement (%)	Emissions
DOE gasification project areas						
Warm gas cleanup	1–2	70–100	Minimal	1.8	0	500 ppb sulfur[a]
Instrumentation (temperature measurements)[b]	0.5–1	0	Minimal	Minimal	1–2	–
Materials (refractory)[c]	0	0	2 million	0.5	4–6	–
Non-DOE or non-gasification technical areas						
Heat recovery	3					
Industry learning and evolution	1–2					

Source: National Research Council
COE cost of electricity, *O&M* operation and maintenance, *kW* kilowatt, *MWh* megawatt-hour
[a]Air Products & Chemicals, Inc. analysis
[b]Internal report by Parsons
[c]The DOE turbine program is considered a complementary program to advanced gasification program

CO_2 Reduction and Coal-Based Electricity Generation. Table 3 Evolutionary improvements due to DOE Advanced Gasification Research

	Change in cost and performance of IGCC system due to R&D					
	Increase in efficiency (%)	Capital cost reduction ($/kW)	O&M reduction ($/kWh)	Reduction in COE ($/MWh)	Availability improvement (%)	Emissions
DOE gasification project areas						
Ion transport membrane air separation[a]	1	75	Minimal	1.4	0	–
Stamet pump (from backup material)[b]	0.5	40–100	Minimal	1.4–1.8	0	–
Non-DOE or non-gasification technical areas						
DOE turbine program[c]	2–3 (for combined cycle power island)	60–100				

Source: Gary Stiegel [22], U.S. Department of Energy National Energy Technology Laboratory (for data on DOE gasification project area cost and performance)
COE cost of electricity, *O&M* operation and maintenance, *kW* kilowatt, *kWh* kilowatt-hour, *MWh* megawatt-hour
[a]Air Products & Chemicals, Inc. analysis
[b]Internal report by Parsons
[c]The DOE turbine program is considered a complementary program to advanced gasification program

The stakes are high because a successful solution would be applicable to both new plants and to the retrofit of existing plants with CCS [6].

IGCC lends itself favorably for efficient CO_2 capture and sequestration because CO_2 can be separated from a relatively small volume of fuel gas (syngas) at high pressure. Without CCS, IGCC is more expensive, and has lower efficiency and availability than PC/SC and PC/USC technology but, if CCS were available today, equipped with CCS, IGCC would be cheaper. By recirculating part of the liquid phase supercritical CO_2 the water in the slurry feed can be replaced by CO_2. This could reduce the oxygen required for the vaporization of the water in the slurry and for the attainment of the high temperature necessary for trouble-free liquid slag removal from the gasifier.

For coals of lower heating value such as subbituminous coals or lignite, the COE gap is, however, substantially narrowed or is even reversed.

It is noteworthy that there is significant cost and performance loss attached to the capture and compression of CO_2 from both combustion and gasification plants in preparation of its sequestration [5].

Results of studies presented in Table 4 provide information on CO_2 emitted, efficiency, estimates of total plant cost and cost of electricity for IGCC, PC/USC technologies without and with CO_2 capture and compression, and for SC/PC/Oxy.

PC/Oxy/USC

When oxygen, instead of air is used as oxidant for combustion, the mass flow rate of combustion products is significantly reduced and the flue gas CO_2 concentration is greatly increased. In order to avoid unacceptably high temperatures in the boiler, combustion products, mainly CO_2, are recirculated from the end of the boiler to the combustion chamber. This restores the furnace gas temperature to air combustion levels resulting in an O_2 volume concentration of about 30%, compared to 21% for air-blown combustion. This difference is due to the higher specific heat of CO_2 than that of the replaced nitrogen, and also, to CO_2's high radiative emissivity. Flue gas recirculation (FGR) increases the CO_2 concentration in the flue gas to beyond 90%, the complement being N_2, due to air leakage and about 3% O2 required for complete burn out of coal. This makes the flue gas ready for sequestration after the removal of condensables but without energy-intensive gas separation. If avoidance of corrosion in the compressor and pipeline requires further exhaust gas polishing, the fivefold reduced flue gas volume leads to strongly reduced capital and treatment costs relative to those for an air-blown combustion plant [12].

The presently available Cryogenic Air Separation process consumes a significant fraction of the generating plant's output and reduces its efficiency by 6.4 percentage points. The development of membrane-type oxygen processes with greatly reduced energy requirements are urgent R&D targets

CFBC with Oxy/FGR

CFBC with an external heat exchanger lends itself favorably to oxy/fuel application because the solids circulation provides an effective means, additional to flue gas recycle, for controlling the combustion

CO_2 Reduction and Coal-Based Electricity Generation. Table 4 CO_2 emissions, efficiency, and cost estimates for advanced generation technologies without and with CCS

	PC/SC		PC/USC		IGCC		SCPC/Oxy
	Without	With	Without	With	Without	With	With CCS
CO_2 emitted g/kWh	830	109	738	94	824	101	104
Efficiency, % HHV	38.5	29.3	43.4	34.1	38.4	31.2	30.6
TCR $/kW	2,800	4,524	2,865	4,408	3,016	3,996	4,016
COE c/kWh	6.00	9.64	5.93	9.25	6.44	8.24	8.82

Source: CO_2 and efficiency data from MIT 2007. TCR and COE data modified after Booras [21] to include the effect of the recent increase in construction costs

temperature. Solids, consisting of sorbent, coal ash, and coal char particles, are precipitated from the gas stream exiting the combustor (riser) section of the CFB boiler and are split into two solids streams: one that is recirculated to the riser without cooling, and the other that is cooled in an external heat exchanger before recirculation. The cooling of the combustor by the cold solids permits the reduction of the rate of flue gas recirculation, with the result that the O_2 concentration in the feed stream can rise to above 40% without exceeding a limiting combustor temperature level of about 850°C required by the thermodynamic stability of $CaSO_4$ and by smooth fluidization. The corresponding lower gas mass flow leads to reduced size and cost of the boiler and of the post combustion plan. The advantages also include increased fuel flexibility including the capability of firing biomass, which may allow additional CO_2 credits.

The oxygen-fired CFB concept has been validated in Alstom's 3 MW_{th} pilot scale test facility [16]. The results show that the technology can be developed from that of conventional CFB boilers, so that a 100–350 MW_e oxy-fired demonstration plant could be developed in the short term followed by a commercial size plant in the midterm.

Concluding Remarks

Coal will continue to play a large and indispensable role in electricity generation, in a carbon-constrained world, under any scenario. The key enabling technology for CO_2 emissions mitigation in coal combustion and gasification plants is CO_2 capture and sequestration (CCS).

CCS has to be demonstrated at scale, integrated with power generation, and the legal framework of sequestration has to be developed before CCS becomes commercial, probably by the 2020–2025 period.

Before the advent of CCS there will be about 45 GW new coal-based electricity generating capacity constructed in the USA (about 1,000 GW worldwide) and the question arises of what the technology options are for these new plants.

Increased efficiency of power generation is the most predictable and cost-effective method for CO_2 emissions reduction. In coal plant without CCS it is also the only practical method for mitigating CO_2 emissions now, and it remains important for future plants equipped with CCS to reduce the energy cost of CO_2 capture.

Pulverized coal combustion in Rankine cycle steam plant is the prevailing utilization technology. Compared to average efficiency of the existing coal-based fleet, up to 24% reductions in CO_2 and pollutant emissions can be achieved today in commercial ultra-supercritical new plants.

Coal gasification combined cycle (IGCC) plants are successfully demonstrated in the USA and in Europe. Today, without CCS, IGCC is more expensive, and has lower availability than high efficiency PC/SC and PC/USC plants but, if CCS were available today, equipped with CCS IGCC would be cheaper. Also, IGCC has the capability of less expensively lowering further criteria pollutant emissions.

Use of oxygen instead of air in combustion significantly reduces the mass flow rate of combustion products with the concomitant reduction of flue gas capital and treatment costs. Because of the high concentration of CO_2 in the flue gas it is expected that following the removal of pollutants and agents that could be corrosive in the compressor and the pipeline, the flue gas can be sequestered without the separation of CO_2.

The RD&D challenge is in the development of the membrane oxygen system that is less energy intensive than the presently available cryogenic air separation.

There are important technology developments in progress that can change the performance and economics of advanced technology options by the time CCS will be commercial. A broad portfolio of advanced clean coal technology RD&D should be aggressively pursued to meet the CCS challenge.

Demonstration of CO_2 sequestration at scale and integrated with power generation will give the public more confidence that a practical carbon emission control option exists and maintains opportunities for the lowest cost, widely available energy source to be used to meet the world's pressing energy needs in an environmentally responsible manner.

Bibliography

1. Amor AF, Viswanathan R (2004) EPRI, supercritical fossil steam plants: operational issues and design needs for advanced plants. In: Fourth international conference on advances in materials technology for fossil power plants, Hilton Head Island

2. Beér JM (2007) High efficiency electric power generation, the environmental role. Progr Energy Combust Sci 33:107–134
3. Beér JM (2004) Electric power generation; fossil fuel. In: Cleveland CJ, Ayres RU et al (eds) Encyclopedia of energy, vol 2. Elsevier, Amsterdam, pp 217–227
4. Blum R, Hald J (2002) ELSAM Skaerbaek
5. Booras G, Holt N (2004) Pulverized coal and IGCC plant cost and performance estimates. In: Gasification technologies conference, Washington, DC
6. Dalton St (2007) Efficiency of generation-the role of very efficient/low emission coal. In: International conference on coal utilization and fuel systems, Clearwater
7. Dooher JP (2009) Physio-chemical properties of low rank coal/liquid CO_2 slurries as gasifer feed-stocks. In: The 34th international technical conference of coal utilization and fuel systems, Clearwater
8. EPRI (2003) Electricity technology roadmap. Electric Power Research Institute, PaloAlto, CA
9. EPRI (2006) CoalFleet RD&D augmentation plan for advanced combustion based power plants. EPRI Report 1013221
10. Henry JF, Fishburn JD, Perrin IJ, Scarlin B, Stamatelopoulos GN, Vanstone R (2004) In: Twenty-ninth international conference on coal utilization & fuel systems, US DOE. ASME, Coal and Slurry Technology Association, Washington, DC, pp 1028–1042
11. Kjaer S, Klauke F, Vanstone R, Zeijseink A, Weissinger G, Kristensen P, Meier J, Blum R, Wieghardt K (2001) The thermie project of the EC. Powergen Europe, Brussels
12. Lavasseur AA, Chapman PJ, Nsakala NY, Kluger F (2009) Alstom's oxy-firing technology development and demonstration-near term CO_2 solution. In: The 34th international technical conference on clean coal and fuel systems, Clearwater
13. Deutch J, Moniz J (eds) (2007) MIT the future of coal. MIT Press, Cambridge
14. National Coal Council reports 2008 and 2009. National Coal Council, Washington, DC
15. National Research Council (2005) Report of the panel on DOE's IGCC R&D program. National Academies Press, Washington, DC
16. Nsakala L et al (2003) Greenhouse gas emissions control in circulating fluidized bed boilers. US DOE/NETL [48] Cooperative Agreement, May 2003
17. Palkes M (2003) Boiler materials for ultra supercritical coal power plants. Conceptual Design ALSTOM Approach NETL-DOE, USC T-1
18. Schilling HD (1993) VGB Kraftwerkstechnik 73(8):564–576 (English Edition)
19. Termuehlen H, Empsperger W (2003) Clean and efficient coal fired power plants. ASME Press, NY
20. US Energy Information Administration (2000). Annual energy OUTLOOK
21. Booras G (2008) Economic assessment of advanced coal based power plants with CO_2 capture MIT carbon sequestration forum IX. Cambridge, MA
22. Stiegel G (2005) US DOE Gasification program overview in National Research Council Report. Washington, DC

Coal and Peat: Global Resources and Future Supply

Mikael Höök
Global Energy Systems, Uppsala University, Uppsala, Sweden

C

Article Outline

Glossary
Definition of the Subject
Introduction
Coal and Peat: Global Resources
Future Directions
Bibliography

Glossary

Anthracite Anthracite is the highest rank of coal because it has undergone the greatest degree of metamorphosis away from peat. It features low volatile matter (<10%) and high carbon, giving it the highest energy content of all coals. Semi-anthracite is somewhere in the middle between low volatile bituminous coal and anthracite.

Ash Inorganic residues remaining after combustion. It has less than the initial mineral matter content because of chemical changes during combustion, i.e., the loss of water, carbon dioxide, and sulfurous compounds.

Bituminous coal Bituminous coal lies between subbituminous coal and semi-anthracite in terms of rank. This rank of coal is commonly divided into additional subgroups dependent upon the content of volatile material.

Calorific value Corresponds to the amount of heat per unit mass when combusted. Can be expressed as gross calorific value, which is the amount of heat liberated during combustion under standardized conditions at constant volume so that all of the water in the products remains in liquid form, or as net calorific value, which is the maximum achievable heat release obtainable in a furnace at constant pressure.

Carboniferous A geologic period and system that extends from 360 to 300 million years ago.

Coal preparation Physical and mechanical processes often applied to coal to make it suitable for a particular use.

Coalification The process that transforms vegetation to peat succeeded by the transformation of peat to lignite and later higher coal ranks.

Cretaceous A geologic period and system spanning from 145 to 66 million years ago.

Devonian A geologic period and system spanning from 416 to 360 million years ago.

Exploration The examination of an area by means of surface geological mapping, seismic techniques, geophysical methods, drilling of boreholes and sampling of the underlying sediments and rocks.

Jurassic A geologic period and system extending from 200 to 145 million years ago.

Macerals Microscopic organic constituents of coal that may differ significantly in composition and properties depending on rank and geology.

Ordovician A geologic period and system spanning from 490 to 445 million years ago.

Permian A geologic period and system extending from 300 to 250 million years ago.

Reserves The recoverable volumes that are dependent on certain arbitrary limits in respect of thickness, depth, quality, economics, legal restrictions, and other factors. Reserves are always less than resources.

Resources The amount of coal in place before exploitation; all resources may or may not be economically or technically recoverable; see Reserves.

Silurian A geologic period and system spanning from 445 to 416 million years ago.

Stripping ratio The ratio of the thickness of overburden to that of the total workable coal section.

Tertiary A geologic period and system extending from 66 to 2.6 million years ago.

Triassic A geologic period and system spanning from 250 to 200 million years ago.

Volatile matter Non-moisture component of coal that is liberated at high temperature in the absence of air.

Definition of the Subject

Coal is the second most important fuel currently used by mankind, accounting for over 25% of the world's primary energy supply. It provides 41% of global electricity supplies and is a vital fuel or production input for the steel, cement, and chemical industries. However, coal is a fossil fuel formed from organic material by geological processes over millions of years. Hence, coal is a finite resource in terms of human timescales and its continued availability is important to the world economy.

Peat is a related substance, but is classified somewhere between a fossil fuel and biomass. The energy sector uses peat as a fuel to generate electricity and heat. It also has applications in industrial, residential, and other sectors, but global consumption of peat is insignificant in comparison to coal. Peat shares many similarities with coal, and is increasingly often grouped with coal for resource estimates in reports and assessments by public agencies.

Knowing how coal and peat are created is vital to understanding how deposits are formed and what their basic properties are. Geology provides models and methodologies for describing deposits and where to find them. Exploration, drilling, and surveys provide the data necessary to map deposits and assess the resources they contain. Classification schemes are also central to understanding how the terms relate to the underlying data.

Future production of coal and peat is essential for the development of global energy supplies. It is only the produced volumes that can be used in human activities, and a detailed appreciation of the production process is essential in understanding future supply developments. Factors such as economy, technology, legal, and environmental constraints affect the recoverable share of the available resources, i.e., the reserves. Understanding the complexity and the greater whole of the production mechanism and the limitations that are imposed on it require a wide variety of approaches and conceptual infrastructures.

Introduction

Natural resources are vital in supporting the continued well-being of the world's population. Metals, fossil fuels, minerals, clean water, and many other resources are critical components for many aspects of modern society. Of all available resources, few are as important as energy. In fact, energy has been described as the

ultimate resource by several studies [1–4]. In physics, energy is defined as "the ability to do work." Einstein even showed the equivalence between energy and mass [5], implying that everything in the universe is made from energy in various forms. Naturally, it follows that energy influences everything and cannot be substituted for other resources.

Energy resources take many forms, ranging from fossil fuels and uranium to biomass, human labor, or wind power. Currently, over 80% of all primary energy used by mankind is derived from fossil fuels [6]. Petroleum dominates, with roughly 35% of world primary energy being derived from this particular hydrocarbon, coal at number two (~26%), followed quickly by natural gas (~21%). The contributions from other energy sources range from 2% to 10% (biomass, nuclear, hydropower) to less than 0.1% (wind, solar).

To understand the conceptual importance of coal, one can begin by studying the exceptional expansion of fossil energy in the last 200 years (Fig. 1). The development of modern society, population, and the world economy under this brief period has been remarkable. Nearly all this growth has been powered by fossil energy in various forms, originally coal but later oil and natural gas. The growth soared and mankind both prospered and multiplied in many places, all thanks to cheap and abundant fossil fuels that provided useful energy for a multitude of activities.

The postwar boom also coincides with the green revolution in agriculture and the use of high-yield agricultural techniques based on synthetic fertilizers and high energy use. In fact, fossil energy has been described as the principal raw material of modern agriculture [7–10]. Furthermore, energy is intimately linked to economic growth and development [11, 12]. To summarize, nothing is as important to society as energy and this should never be overlooked when dealing with questions of sustainability.

The rise of the industrial nations in the Western world was chiefly driven by the coal that powered steam engines, transportation, and industry as well as heating homes. Important industrial complexes and cities arose near coal-rich regions, such as the Ruhr or Pennsylvania. In the USA, coal had replaced biomass as the dominant

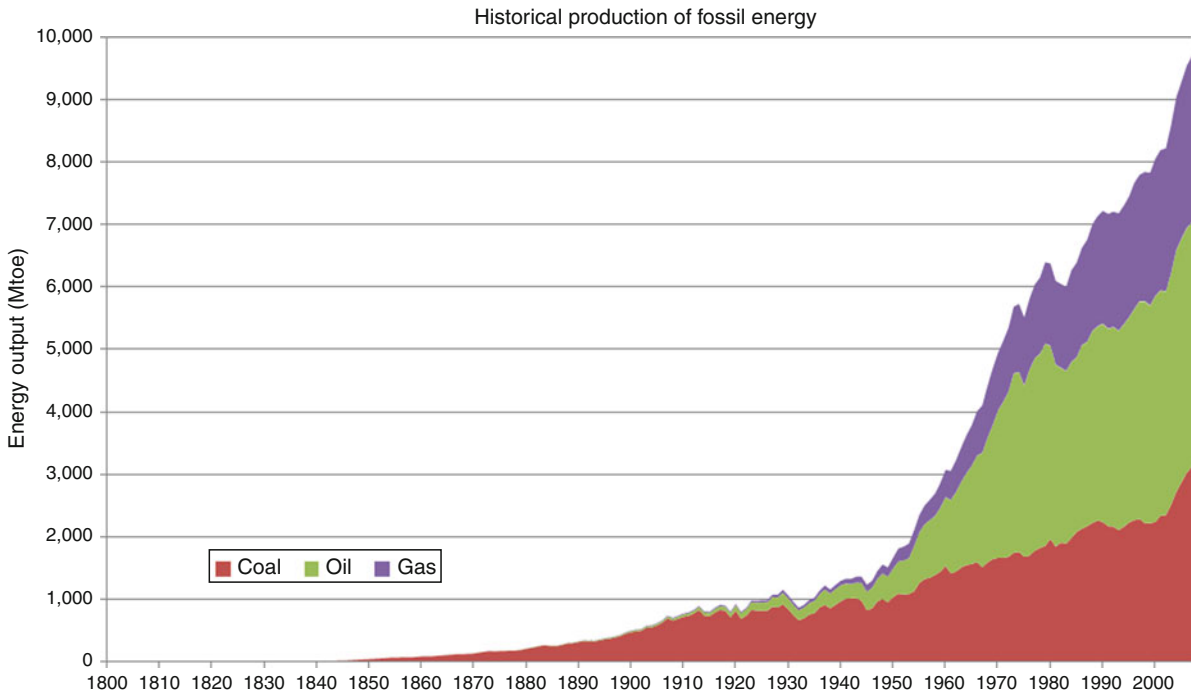

Coal and Peat: Global Resources and Future Supply. Figure 1
World production of fossil energy since 1800 based on the author's compilation and interpolation of historical production statistics

primary energy source by late nineteenth century [13]. Similar events occurred in UK, Germany, and other nations around the early twentieth century. Today, the world is witnessing the rise of China and India as new industrial powers, both countries growth fueled chiefly by coal. However, petroleum eventually surpassed coal as the dominant fuel globally in the 1950s, but coal has remained the second most important energy resource ever since.

Sedimentary layers of coal and peat beds range in age from the Upper Paleozoic to the recent (geologically), and are located all over the world. The layers are a result of the accumulation of vegetable matter in a specialized deposition environment. Local conditions and events can produce different qualities and ranks as well as different degrees of structural complexity.

This chapter provides a fundamental overview of global peat and coal resources, their distribution, and some of the central characteristics in their recovery and utilization. In addition, it presents a brief summary of resource classification schemes and their importance in understanding the amounts that may be available for future supply. Finally, some resource and reserve statistics will be presented with discussion. Estimates of global resources must be dated and can naturally change as more is learnt about their geology. The figures presented here should be seen as a snapshot of the current state of our knowledge. Nevertheless, such estimates indicate where the major deposits and mining activity are currently located and from where future production might originate.

Coal and Peat: Global Resources

Formation of Coal and Peat

Coal and peat derive from vegetable remains that have been deposited in various environments where it has been transformed by geological processes to potentially useful energy resources. The sedimentation of coal and peat has been extensively studied for over a century. This section describes the general mechanism behind the formation of peat and coal.

Mires are the accepted general term for peat-forming ecosystems of all types. The cycling of matter in most ecosystems is relatively fast and complete. In contrast, mires are characterized by an incomplete cycle, resulting in a positive carbon balance. Peat-forming areas are generally wet places where the annual input of dead organic matter from the photosynthetic activity of the plant cover exceeds annual breakdown. Over time organic material accumulates and becomes preserved. Peat deposits typically occur in waterlogged environments where water prevents oxidation of the organic remains. The presence of water limits the diffusion rate of gasses that leads to low oxygen availability. The large heat capacity of water also induces a low temperature, which inhibits decomposing and decomposition-facilitating organisms and leads to reduced rates of decay.

Peat formation is typically initiated by two mechanisms. One is called terrestrialization, which is when bodies of water are replaced by peat-forming mires. The other mechanism is paludification, which is replacement of dry land by mires due to rising groundwater table or some other hydrological change in the local environment. Peat-producing wetlands are divided into ombrogenous peatlands, which are rainfed systems, and topogenous peatlands, which owe their origin to a place and its surface/groundwater regime [14]. Moore defined several important subcategories such as bogs, bog forests, marsh, fens, swamps, floating swamps, and swamp forests [15].

The plant debris undergoes several chemical changes due to bacterial decay, compaction, heat, and time, which eventually leads to formation of peat. Pristine plant parts such as roots, barks, or spores are possible components of peat and can be used to determine the type of plants that originally made up the peatland. The peat harvested in the Northern Hemisphere was chiefly formed during the Holocene epoch just after the retreat of the colossal glaciers that covered most of Europe. Consequently, most of the constituent peat-producing plant species are still thriving and continue to produce peat as of today.

The peat must be buried by additional sediments in order to be transformed to coal. Burial leads to compaction of the peat and squeezes out water during the initial stages. A compaction ratio of 9:1 or more is not uncommon [16]. Continued burial and the addition of heat and time will break down the complex hydrocarbon compounds in the peat through a series of possible reactions. Methane and other gaseous alternation products are typically expelled from the deposit, while other elements disperse. The result is that the deposit

becomes increasingly carbon-rich. The process begins with plant debris and continues through peat, lignite, subbituminous coal, bituminous coal, anthracite coal, to the pure carbon mineral graphite. This process is referred to as coalification.

Some perspectives on the necessary timescales behind the formation of peat and coal resources are indispensable for a better understanding of the whole picture. The surface part of peat below the living ground layer, being less than 300 years old, amounts on average to 10.2% of the total peat carbon volume [17]. Only the deeper and basal parts of the peat are thousands of years old. In comparison, coal requires much longer time periods to form. Analysis of thick bituminous coal bed layers indicates that optimum peat-forming conditions must have been maintained for 5,000–10,000 years for every meter of clean bituminous coal [18]. Other studies have shown that the global consumption of fossil fuel in 1997 was created from ancient plant matter corresponding to over 400 times the net primary production of the world's current biota [19]. Coal cannot be formed at the same rate society uses it and is therefore a nonrenewable fuel. Peat requires shorter time scales, but is still slowly formed in terms of human time scales.

Studies have shown similarities between the extensive coastal plain peat deposits in Southeast Asia and the North American/European carboniferous coal-bearing sequences in terms of sediment accumulation, mineralogy, and geochemistry [20–23]. Several models provide a good understanding of the cyclic nature of coal sequences, the lateral continuity of coal beds as well as physical and chemical properties. However, no single model can provide a comprehensive explanation of all aspects regarding occurrence, development, and types of coal.

There are many books and articles on peat and coal geology that can provide more detailed descriptions of sedimentation, structural changes, and other factors and how they influence the formation process. The formation of coal and peat can be described in a simplified manner (Fig. 2).

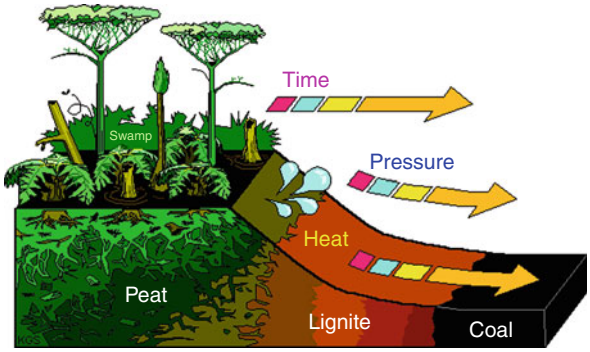

Coal and Peat: Global Resources and Future Supply. Figure 2
Principle mechanism of the formation of coal and peat (From Steve Greb and Kentucky Geological Survey. Reproduced with permission)

Occurrences of Coal and Peat

The oldest known land plant remains have been dated to the Ordovician/Silurian Period [24], but did not produce any noteworthy accumulations. Certain deposits of Devonian age are the oldest known coal accumulations, but it was not until the Carboniferous/Permian Period that the world's plant cover was sufficiently rich to produce and preserve significant amounts of coal. Although coal and peat are continuously being formed, there are a few major episodes of coal accumulation throughout history. In total, three major coal-formation periods have occurred and these coals form the bulk of the world's coal reserves. They occurred during the Carboniferous/Permian Period, Jurassic/Cretaceous Period, and the Tertiary Period.

Plate tectonics and climate have been described as important factors for answering when and where coal is deposited [25]. Places with favorable conditions have changed over time as continental plates have drifted or when climatic properties have been altered over the long time scales involved in the formation process. Changes in vegetation types can also be traced to certain coal components. Geological age distributions of the world's principal black coal and lignite deposits have been compiled by Walker [26].

During the Carboniferous Period, most of what is today the Northern Hemisphere was located near the equator and consisted of tropical peat mires, which later formed the coal basins of western and eastern Europe, the eastern USA, and former Soviet Union. Coals were also formed in the areas that today make up South America, southern Africa, India, Australia, and Antarctica, but this formation occurred under

cooler, more temperate conditions. Coals formed at this time now make up the bulk of the world's black coal reserves. They are generally high in rank, but may have undergone significant structural change.

The climate changed during the Permian Period and the lush vegetation of the northern areas eventually ceased to deposit coal-forming sediments. New, but less abundant coal formation occurred during the Triassic, Jurassic, and Cretaceous Periods. Such coals can chiefly be found in Canada, China, Russia, and the USA. Changes in floral types, such as the onset of angiosperm floras, as well the variety of deposition environments generally lead to the formation of coals that are more complex in their chemical make-up. Analysis of macerals and other constituents in coal provide insight in the specific conditions that were present during their accumulation.

The third major period of coal formation took place during the Tertiary Period, and those coals form the bulk of the world's brown coal reserves as well as important parts of the black coals currently being mined. Tertiary coals are mostly lignite, but in some areas temperature change has resulted in higher-ranking coals.

The age and stratigraphy of all major coal deposits have been studied extensively, in particular those formations that are of economic interest. Meticulous surveys on individual fields are important for development and actual production, but such details for a single field can easily fill an entire bookshelf! More general overviews of the world's most important coal regions have been made by others [26, 27]. Reviews on various pollutants in coal, such as arsenic or metals, can also be found in more specialized literature.

Sometimes it is convenient to express coal deposits in energy terms, especially if they are going to be used as energy sources. Depending on specific properties of the coal in a deposit, the actual energy content may vary significantly. Coal is divided into different ranks depending on the degree of coalification as it matures from peat to anthracite. Coal is broadly divided into these four ranks, namely anthracite, bituminous, subbituminous, and lignite [28, 29], although much more detailed systems can be found.

There are many classification systems used all over the world, each with their own set of definitions. The terms brown coal, black coals, hard coals, stone coals, thermal coal, and steam coal are commonly used, but their meaning may vary from country to country. Lignite and subbituminous coals are commonly seen as low-ranking coals, while bituminous coal and anthracite are considered high-ranking coals. Caution should always be exercised when analyzing global coal data to avoid mixing up different classification schemes.

It should be noted that the ranks tend to overlap in terms of energy and that the calorific value can vary within a rank depending on local geological properties. Relatively high moisture levels and a low carbon content and calorific value characterize low-rank coals, such as lignite and subbituminous coal. Higher-rank coals, such as anthracite and bituminous coal, have a higher carbon and energy content and a lower level of moisture. The following energy contents of coal ranks are common:

Anthracite: 30 MJ/kg
Bituminous coal: 18.8–29.3 MJ/kg
Subbituminous coal: 8.3–25 MJ/kg,
Lignite: 5.5–14.3 MJ/kg

Some of the world's present peat deposits were formed as early as a few hundred thousand years ago, although the main part of the global peat resources was formed during the last 10,000 years [30]. Occurrences of peat are linked to climate, vegetation, local environment, and precipitation that allow peat-forming conditions to arise. There are also less peat occurrences in the Southern Hemisphere, as there is less land there. Present-day peat occurrences can be predicted well by suitable models [31].

Peat is present all over the world and estimates conclude that 2–3% of the global surface is covered by peat-forming areas, equivalent to about 4 million km^2. This figure includes some 200,000 km^2 of tropical peats in Southeast Asia. A major proportion of the world's peatlands are located in North America and the northern parts of Asia, but significant deposits are also found in northern and central Europe. In total, over 90% of the world peatlands are in the temperate and cold belt in the Northern Hemisphere. The remainder is located in tropical and subtropical latitudes and mostly located under forests. Such accumulations have been identified in the tropical regions of Africa, Latin America, as well as Indonesia and southern/eastern Asia.

Estimates of the total area of the world's peatlands vary considerably from study to study. The basic problem is to separate areas where the peat layer is 30 cm thick at minimum, i.e., peatlands, from areas only covered with wetland vegetation, such as floodplains, coastal lagoons, mangroves, and swamps. Hence, only a few countries have performed accurate peatland mappings. More comprehensive discussions on peat and closer description of specific formations are available in reference literature, scholarly journals, and reports from various geological surveys.

Resource and Reserve Classifications

It is first necessary to look closer at classifications and what the terms actually mean in practice before defining and discussing global resources of coal and peat. Far from all coal and peat being available for utilization by society, some formations are technically unfeasible or just too challenging economically to recover or may even prove to be undesirable to consumers, even though they are geologically available. As a result, it is important to use precise terms when talking about future supply of coal and peat. Especially in outlooks related to sustainable utilization as possible energy sources for society.

Concepts such as "endowment" or "potential" are multifaceted and the meaning of such terms is disputed by different schools of thought. One school argues that "resource endowment" is crustal abundance, while another school maintains that the concept is relatively meaningless for supply assessments and should be avoided. As always, the truth is located somewhere in between the two extremes. Crustal abundance is solely determined by geological processes, which are reasonably well understood by geologists. Furthermore, the physical in situ amounts will also be virtually fixed as a result of the slow underlying formation processes, even though in situ estimates might change in reports as a result of new information.

Available coal accumulations can be divided into reserves and resources. Reserves are defined as being proved and recoverable under present technological and economic conditions. Resources include additional discovered, but uneconomic or unavailable amounts together with undiscovered inferred, assumed, and speculative quantities. This distinction is justified by the idea that over time, and perhaps with new technology and higher prices, production and exploration activities will allow a reclassification of some resources into reserves [32]. The terms resources and reserves are often used synonymously by lay people, but it should be absolutely clear that this is a completely erroneous and misleading practice. Being specific and using the right term is essential to paint a realistic picture in any supply assessment or when planning for a sustainable future. Studies have highlighted this problem and the need to include non-geological factors in future supply estimates [13, 33].

It is necessary to investigate and explore any coal or peat deposits to ascertain whether something can be mined economically and that a product can be obtained that is marketable. Two common points of view are typically used to assess resources and reserves:

1. The degree of geologic assurance
2. The degree of economic feasibility

The method of estimation along with the definition and expression of geological assurance is a key factor for the reliance of coal tonnage estimates. Details surrounding the topography, tectonic variability, structural alteration, and postdepositional erosion provide uncertainties and should be taken into account in resource mappings. For example, heavily disturbed coals with great variation in thickness will need many more data points for an accurate and reliable assessment than relatively undisturbed coals of constant thickness. Data point spacing criteria and how far trends are extrapolated from measurement points are essential for the degree of geologic assurance (Fig. 3). Economic feasibility is dependent on the content of sulfur and other unwanted pollutants, thickness, depth, environmental constraints, coal price versus mining costs, and other parameters that affect recovery and consumer desirability.

Sadly there is no international and uniform method for assessment, categorization and designation of coal resources and reserves. Several agencies, countries, and organizations have developed their own sets of definitions and methods to calculate resources and reserves. However, it is possible to roughly convert assessments made within one system to another and form aggregated pictures of the entire world situation. This section will focus on the system used by the United States

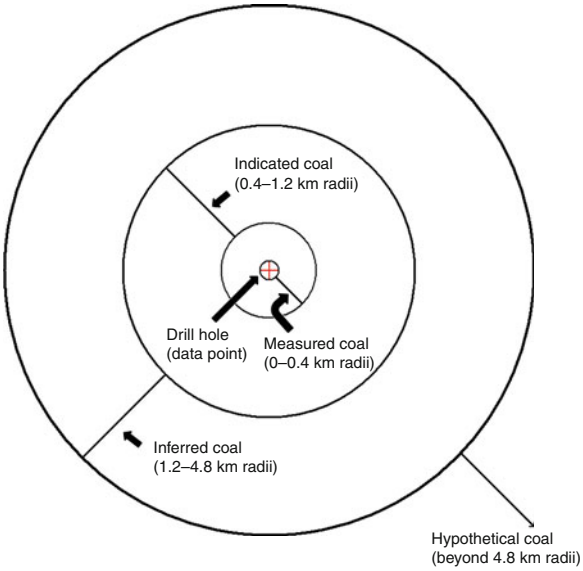

Coal and Peat: Global Resources and Future Supply. Figure 3
Reliability categories based solely on distance from drilling measurement points. Measured and indicated coal together form the demonstrated coal category. Based on USGS resource classification system [34]

Geological Survey (USGS), while closer descriptions on other systems can be found in more specialized literature. For comparison, the Australian and Russian systems are conceptually similar but differ in details. In contrast, the UK system is excellent for mining operation, but not very functional for large areas that may contain coal but are not mined. USGS use the following definition for coal resources [34]:

- Coal resources are naturally occurring concentrations or deposits of coal in the Earth's crust, in such forms and amounts that economic extraction is currently or potentially feasible.

This category is divided into a number of subdivisions, such as inferred, indicated, or measured resources depending on geological certainty, depth, and thickness. Technology and proper investment can, at least in theory, recover all available in situ coal if the required economic conditions exist. However, resource numbers are inadequate as they do not take into account economics, the fundamental utilization properties, or even legal issues surrounding extraction in a geographical region. Recoverability is the crucial property for actual production and this leads to a variety of attempts to express the recoverable volumes of coal that can be extracted from the available resources.

Far from all coal being recovered from a coal bed, some amounts will be unavoidably lost in the recovery process for technical reasons. This includes coal that is (1) left to support underground mine roofs, (2) used as barrier pillars adjacent to the mine or property boundaries, or (3) simply left because for a variety of other reasons [34]. Mining and production practices also place constraints based on thickness, depth, rank, and other properties on the recoverable amount of the in situ resource. USGS has chosen the following definition for the reserve base:

- Reserve base: those parts of the identified resources that meet specified minimum physical and chemical criteria related to current mining and production practices, including those for quality, depth, thickness, rank, and distance from points of measurement. The reserve base is the in-place demonstrated (measured plus indicated) resource from which reserves are estimated. The reserve base may encompass those parts of a resource that have a reasonable potential for becoming economically available within planning horizons beyond those that assume proven technology and current economics. The reserve base includes those resources that are currently economic, marginally economic, some of those that are currently sub-economic, and some of the resources that have been or will be lost-in-mining but whose attributes indicate possible future recovery.

Recoverable volumes are also affected by many other factors that make them dynamic. Higher prices, new exploration, or improved technology yield increased amounts of recoverable coal. In a similar way, increased freight rates, extraction costs, or introduction of various restrictions can decrease recoverable volumes. Likewise, political influences can greatly influence demand patterns or even cause direct physical restrictions for mining. USGS [34] finally uses the following terminology to denote reserves:

- Reserves: Virgin and/or accessed parts of a coal reserve base which could be economically extracted or produced at the time of determination considering environmental, legal, and technologic constraints.

Important restrictions are legal prohibitions on coal mining in certain areas and/or the use of a particular mining methodology, such as strip mining. This can prevent the extraction of coal, despite the fact that the coal might be technically and economically recoverable. For example, land-use regulations and federal laws prevent mining near homes, public buildings, or federally funded highways [30]. Accessibility, availability, and restriction factors are linked to the society and its legal and political climate. This can have a major influence on the volumes practically available for recovery. Detailed discussions of how availability of recoverable coal is estimated by the USGS can be found in other works [35–37]. The Energy Information Administration (EIA), the energy authority of the USA, utilizes the following definition to include restrictions and accessibility in their reports and assessments of American coal commonly used by non-geologists, planners, and policymakers:

- Estimated recoverable reserves: cover the coal in the demonstrated reserve base considered recoverable after excluding coal estimated to be unavailable due to land use restrictions or coal currently economically unattractive for mining (and after applying assumed mining recovery rates).

EIA creates this category by applying economic feasibility criteria factoring downward from the reserve base. The "coal reserve" term used by EIA may better be described as "potential coal reserves," as they are generally not proved by any detailed drilling [38]. A full discussion of coal resources and reserve terminology, as used by EIA, USGS, and US Bureau of Mines, can be obtained from the EIA [39]. The estimated recoverable reserves category corresponds to "proved reserves" discussed in the BP Statistical Review of World Energy [40], "proved recoverable reserves" used by World Energy Council (WEC) [41], or "reserves" as used by the German Federal Institute of Geosciences (BGR) [42].

Coal and Peat Resources in the World

To make accurate coal and peat resource estimates, exploration geologists make detailed studies of relevant accumulations. They take measurements at appropriate intervals and extrapolate using the appropriate classification categories, knowledge of the local geology, and good judgment. In theory, there is no fundamental difference between underground or surface formation maps. However, shallow drilling is cheaper and makes it possible to drill more holes, which makes surface mappings generally more reliable. Because deep boreholes are costly (which means less are drilled, thus making the assessment less reliable) the exploration geologist uses various geophysical methods to supplement the drilling data.

Resources are commonly expressed as in situ tonnage, which is the total amount occurring in place. It can be calculated from the thickness of the deposit, the area of extent, and the relative density. Thickness is commonly determined at each point of measurement, while the area is measured on a map or plan. The relative density is normally taken from the section that will be mined, or alternatively it might be estimated using the known average ash content of a coal or peat seam. The formula for in situ tonnage is:

$$\text{thickness}(\text{m}) \times \text{area}(\text{m}^2) \times \text{relative density}\left(\text{tons}/\text{m}^3\right) = \text{in situ tonnage}$$

At regular intervals, scientists and governmental agencies conduct and publish world coal resource assessments. In particular, since its establishment in 1923, the World Energy Council (WEC) has reviewed all forms of energy resources including coal and peat. Data from the WEC comes from reports by the WEC member committees and constitute a sample that reflects the information available in particular countries. German Federal Institute for Geosciences and Natural Resources (BGR) has also released a number of assessments on global coal resources. These agencies will serve as the main data source for the resource figures presented here.

Peatland resource estimates are commonly quoted on an area basis because initial quantification normally arises through soil survey programs or via remotely sensed data that focuses on geographical extent (Tables 1 and 2). Estimates of the world's peatland area vary considerably. This is partly due to different wetland classification systems and partly due to insufficient survey data. Peat resources have been estimated to be 5,000–6,000 billion cubic meters, but are hard to quantify in any detail [30]. WEC gives an estimate of

Coal and Peat: Global Resources and Future Supply.
Table 1 The distribution of peatlands and other terrestrial wetland ecosystems in the world. Data source: [30]

Region	Peatlands [km^2]	Wetlands [km^2]	Total [km^2]
Africa	58,000	282,000	340,000
Asia	1,119,000	1,149,000	2,268,000
Australia and Oceania	14,000	10,000	24,000
Central and South America	102,000	330,000	432,000
Europe	957,000	n. a.	957,000
North America	1,735,000	657,000	2,392,000
World	3,985,000	2,428,000	6,413,000

3,500–4,000 billion cubic meters [41]. Uncertainties in water and ash content and many other factors influence the result significantly when converting to tonnage. This can be seen as a reason for circumventing tonnage figures and preferring volumetric units in resource assessments. However, it is clear that the world possesses a huge tonnage of peat overall. The important question is: how much of those resources can be realistically recovered in the future?

World coal resource estimates can be traced back to 1936, when the WEC gave a world resource estimate of around 16,000 billion tons (reported as recoverable reserves plus estimated additional in situ amounts). In subsequent assessments, their world coal resources have varied from 10,000 to 14,000 billion tons, with most estimates closer to the lower part of the range. In comparison, BGR estimates of world coal resources have varied from 6,000 to 15,500 billion tons. Using either estimate, it is clear that global coal resources are large and the world production of coal (~6 billion tons) is seemingly insignificant in comparison.

However, there are reasons to doubt these agencies' resource assessments. First, there are large fluctuations in the reported resource amounts as definitions and reporting practices change, coal-bearing areas are added or subtracted and new geological information becomes available.

For instance, total coal resources in the USA decreased by more than 60% between 1913 and 1962.

Coal and Peat: Global Resources and Future Supply.
Table 2 Distribution of peat resources for selected countries and regions. Data source: [41]

Region	Country	Peatlands [km^2]
Africa	Guinea	5,250
	Nigeria	7,000
	South Africa	9,500
	Uganda	14,200
	Zambia	11,060
	Total Africa	58,410
Asia	China	10,440
	Indonesia	270,000
	South Korea	6,300
	Malaysia	25,360
	Burma	9,650
	Total Asia	331,880
Australia and Oceania	Australia	150
	New Zealand	2,600
	Papua New Guinea	6,850
	Total Australia and Oceania	9,640
Central and South America	Brazil	15,000
	Chile	10,470
	Falkland Islands	11,510
	Guyana	8,140
	Venezuela	10,000
	Total South America	62,400
Europe	Belarus	23,970
	Estonia	9,020
	Finland	89,000
	Germany	14,200
	Iceland	10,000
	Ireland	11,800
	Latvia	6,400
	Norway	23,700
	Poland	12,000
	Russia	568,000
	Sweden	64,000
	Ukraine	10,080
	UK	19,260
	Total Europe	876,510

Coal and Peat: Global Resources and Future Supply. Table 2 (Continued)

Region	Country	Peatlands [km^2]
North America	Canada	1,113,280
	Cuba	6,580
	Mexico	10,000
	USA	214,000
	Total North America	1,354,220

In contrast, between 1968 and 1974 coal estimates were revised upward, in part due to improved accuracy in assessing the amount of lower-rank coal [33] and also by including undiscovered resources in the estimates. Further exploration may show that a substantial part of the undiscovered resources do not exist [33]. Similar modifications, as well as some brief reasoning behind the revisions, can be found in recent world coal resource estimates from the BGR (Table 3).

In 2005, BGR reported that they changed coal resource estimates because there was insufficient substantiating information for many countries and many countries had skipped reporting years. In 2006, they incorporated new resources in China and former Soviet Union that lead to a 115% increase in world hard coal resources and a 200% increase in lignite resources. In 2007, BGR made yet another upward revision, increasing world hard coal resources by 68% and lignite resources by 36%. In both cases the majority of the increase came from new resources identified in the USA by a new USGS study [43].

Another important observation and fact of this world is that the peatlands are unevenly distributed with the vast majority concentrated in a few countries (Table 2). This trait can also be seen in the assessment literature of world coal resources (Table 3). This inequality is a sad fact of this world and a function of favorable geology in certain parts of the world, bestowing significant deposits of peat and coal on relatively few countries. However, uncertainties are present and there is a problem with a lack of available data for some countries and regions.

To summarize, resource estimates are important from a geological point of view and are vital for understanding where recoverable amounts may be located.

Coal and Peat: Global Resources and Future Supply. Table 3 Estimated total coal resources (recoverable reserves plus other in situ resources), as published by the BGR. All numbers in million metric tons (Mt). Data source: [42]

Country	2004	2005	2006	2007
USA	1,090,404	1,057,921	1,359,404	6,719,682
China	1,089,787	1,089,789	4,367,000	4,367,000
India	259,217	291,863	252,359	229,867
FSU	2,295,275	2,326,121	2,915,146	2,931,293
Australia	298,400	304,801	193,700	148,200
South Africa	163,851	163,851	48,751	28,559
Germany	87,827	91,497	84,573	83,065
Poland	70,262	101,281	179,459	179,459
UK	5,220	7,220	190,005	187,132
Indonesia	10,581	64,829	26,839	23,948
World	NA	6,038,991	9,553,840	15,510,618

However, it is essential to understand that society does not have economic access to all the reported resources. In situ resources include all amounts, even those located deep or of poor quality, making resource estimates largely an academic figure [33]. Resources must be converted into reserves by a detailed evaluation of the degree of certainty of the size of the particular coal resource, and the economic, legal, and environmental constraints placed on its exploitation. Vast resources do not necessarily mean significant future production, as production is dependent on many more factors than just geological availability. This naturally leads to the next section in which reserves are discussed.

Coal and Peat Reserves in the World

Reserves are usually calculated from resources by applying suitable and relevant constraints. Legal, environmental, and geological factors prohibit the recovery of the entire resource so reserve estimates will always be less than resource estimates. Rather than perform a detailed constraint analysis, it is possible to assume a universal recovery factor based on historic recovery

factors for similar deposits. The US Bureau of Mines performs this type of calculation regularly [33]. However, the most reliable method is a deposit-by-deposit analysis because it can incorporate local economic conditions as well as the technical recoverability of the minable coal.

Coal resources are primarily of academic interest, and unfortunately provide little information about what quantity of the resource can be practically recovered. For example, let us look at the Gillette coal field in Wyoming and USGS' comprehensive investigation of its coal supply. Luppens et al. [44] assessed the Gillette coalfield and its 11 coal beds and estimated the original coal in place to be 182 Gt, with no restrictions applied. Available coal resources, which are a part of the original resource that is accessible for potential mine development after subtracting all restrictions, are about 148 Gt. Recoverable coal, which is the portion of available coal remaining after subtracting mining and processing losses, was determined for a stripping ratio of 10:1 or less and resulted in a total of 70 Gt. Applying current economic constraints and using a discounted cash flow at 8% rate of return, the coal reserve estimate for the Gillette coalfield is only 9.1 Gt. While economic conditions definitely have the largest impact, reductions caused by technical and availability restrictions are also significant.

Extraction of peat and coal is primarily an economic activity that recovers valuable products from certain deposits with a profit. Prevailing and anticipated price, location of the deposit relative to the market, transportation costs, specific use, and the production cost are all important factors for determining the feasibility of exploitation. Forecasting costs, estimating revenues, and handling inflation over long time periods is an uncertain business. Additional uncertainty comes from the regulatory environment, particularly environmental laws, tax policies, and similar. In essence, profitability is a dynamic factor and can quickly change. To obtain an accurate estimate of the recoverable volume of a deposit requires a meticulous economic study in combination with comprehensive physical surveys.

An often overlooked but fundamental factor is the net energy analysis. Hubbert [45] wrote about net energy in relation to oil but the same principle applies to all energy resources: "there is a different and more fundamental cost that is independent of the monetary price. That is the energy cost of exploration and production. So long as oil is used as a source of energy, when the energy cost of recovering a barrel of oil becomes greater than the energy content of the oil, production will cease no matter what the monetary price may be." In the case of coal and peat, a poor net energy return will prevent deposits that are too deep, too complicated, or too thin from being usable as energy sources. Mining companies leave those resources behind because they require more energy to exploit than they can yield in return. Several researchers have used net energy analysis to determine mining boundaries in an objective manner [46].

Rohrbacher et al. developed a methodology for describing recoverability using geological, technical, and economic factors [47]. They concluded that past coal estimates did not address the amount that might realistically be available for production after environmental and technological restraints are considered. They showed how air quality regulations, mine reclamation legislation and regulations, new safety and health standards, and advancements in mining technology had dramatically changed the economic competitiveness of the coal fields they studied. More importantly, they demonstrated that the generous EIA reserve base would be far less than the reported figure using their methodology. The EIA estimate did not include the effects of mined-out prime reserves, environmental, industrial, economic, and social considerations. Nor did it include the technical aspects of the minability and washability of the individual seams. In contrast, second-generation assessments of available coal amounts in the Pittsburgh coal bed were performed and described by Watson et al. [48]. Their assessment was that half of the original coal resource in place had already been extracted leaving only 15 Gt and those resources were increasingly being restricted by new environmental laws, encroaching population, and affected by technological factors.

Several organizations regularly compile peat and coal reserve estimates. Many national energy agencies and geological surveys keep reserve records for their own country. The World Energy Council and the BGR collect country level data and publish global coal reserve estimates. The BP Statistical Review of World Energy [40] is another commonly referenced source of

reserve estimates but it only reproduces the numbers compiled by World Energy Council without backdating the estimates. Table 4 shows the latest reserve figures from these three sources. Several studies have criticized the reserve estimates found in published literature for not adequately accounting for all resource constraints [13, 33, 49–51].

Changes in policy can also cause rapid and significant changes to reserve estimates. For example, when Germany removed their mining subsidy Germany's coal reserves were greatly reduced [52, 53]. In Russia's case, Malyshev [54] shows that according to the best estimates by experienced geologists, mining engineers, and economists around 40% of the Russian coal reserves cannot be regarded as of any practical interest because they are highly unprofitable.

Coal and Peat: Global Resources and Future Supply. Table 4 Estimated coal reserves for selected countries. Note how WEC and BP numbers are identical, except for the fact that BP dates them differently. All numbers in million metric tons (Mt). Data sources: [40–42]

Country or region	WEC Proved at end 2007	BGR Proved at end 2007	BP Proved at end 2008
Australia	76,200	76,900	76,200
Brazil	7,059	6,596	7,059
Canada	6,578	6,578	6,578
China	114,500	192,000	114,500
Germany	6,708	40,936	6,708
India	58,600	73,510	58,600
Indonesia	4,328	6,981	4,328
Japan	355	355	355
Kazakhstan	31,300	18,947	31,300
Poland	7,502	16,329	7,502
Russia	157,010	161,553	157,010
South Africa	30,408	28,559	30,408
Ukraine	33,873	34,375	33,873
UK	155	432	155
USA	238,308	262,971	238,308
World	826,001	989,913	826,001

Highly reliable estimates of coal reserves are rare in part because the factors that influence recoverability change frequently. Changes in classification systems, economics, regulations, and other factors can cause significant changes in reserves over time. In the case of the USA, significant downward revisions of the reserves occurred when mining restrictions and other non-geological factors decreased recoverability [13]. Despite the problems with reserve estimates, they are still the best available estimates of how much of a resource that can be economically and technically recovered.

Regulations can directly affect coal recoverability, such as prohibitions due to land-use conflicts, or indirectly, such as taxation. In the USA, the Surface Mining Control and Reclamation Act of 1977 directly prohibits surface mining in national parks, forests, wildlife refuges, trails, wild and scenic rivers, wilderness, and recreation areas. Many national parks have been established over the years, further limiting land available for coal production. Petsch [55] studied Europe and the Ruhr area and concluded that people have become sensitive to intrusions made on their environment, for instance from mining or colliery spoil. Physical limitations from land-use regulations have generally increased over time in many countries. Historically, air quality regulations have increased the demand for low-sulfur coal [13, 56–58]. Expanded environmental awareness in the 1960s and 1970s had lead to heated debates and stricter regulations.

In 2009, President Obama stated that "at a time of such great challenge for America, no single issue is as fundamental to our future as energy." Part of that challenge is reducing the dependence on imported oil and political pressure to limit greenhouse gas emissions. Governments may very well tighten coal regulations and pursue future efforts for addressing anthropogenic climate change and CO_2 emissions. Generally, the air-quality regulations in the USA have been an environmental success story although it has done little to mitigate CO_2 emissions [59]. Interestingly, tight regulations are not the sole factor in future emissions. Regulatory uncertainty can be significant as businesses delay investments until they can make solid return on investment decisions [60]. Exactly how future CO_2 policies will affect coal reserves remains to be seen but it is likely that such policies will reduce the recoverable proportion of coal resources.

Sustainable development, environmental stewardship, and the importance of natural resources for the continued well-being of mankind are driving forces for future policies, at least in any foreseeable outlook. Historical trends point toward increased restrictions and this implies that future energy policies will result in significantly decreased coal availability. However, politics are constantly shifting and sudden change in any direction cannot be ruled out. To summarize, recoverability is a complex issue and future supply of coal will be dependent on many factors ranging from geological availability and quality to socioeconomic acceptability and energy policies.

Because peat is a small energy source, peat reserve estimates are difficult to find and there is no known comprehensive global study. Volumetric data can be converted to tonnage by using the average bulk density of produced peat. USGS Mineral Commodity Survey on peat [61] contains some reserve estimates (Table 5). Only a small portion of peatlands are available for extraction due to environmental constraints and other factors.

Only a few countries have a peat industry of significant importance, so the global peat reserves should be regarded as highly uncertain. Economics, demand, environmental regulations, and other factors are still uncertain for many regions. The world possesses large amounts of peat, but that should not be seen as guarantee for future production. If demand for peat increases, reserve estimates will in all likelihood become more accurate.

As with coal resources, global peat reserves are very unevenly distributed. A small number of nations control the vast majority of the world's coal reserves. The USA, Russia, China, Australia, India, and South Africa control over 80% of the world's coal reserves (Table 4) – a remarkable concentration of resources. Peat shows a similar distribution with just a few countries as the world's major reserve holders (Table 5).

Coal and Peat: Global Resources and Future Supply.
Table 5 Peat reserves for selected countries. All numbers in million metric tons (Mt). Data source: [61]

Country	Peat reserves as of 2008 [Mt]
Belarus	400
Canada	720
Estonia	60
Finland	6,000
Ireland	NA
Latvia	76
Lithuania	190
Moldova	NA
Russia	1,000
Sweden	NA
Ukraine	NA
USA	150
Other countries	10,000

Global Coal and Peat Production

Production is the activity that actually transforms coal and peat into something useful for consumers and society. Some of the produced volumes are inherently lost in preparation, washing, or transformation to specialized products such as briquettes to meet customer needs. Generally coal and peat are burned to create heat, the heat is transformed into steam, and then the steam into electricity. They are also used in industrial chemical processes, steel-making, and horticulture.

The world produced 6.8 Gt of coal in 2008 [40] and a comparatively tiny amount of peat – only around 25 million tons [61]. Peat's role as an energy source is negligible in the global energy context, while coal is the second most important fuel, second only to oil. As a result, this section will briefly cover peat and coal mining and highlight some important aspects of production.

Currently, just a few countries are the principal producers of peat and all those nations are located in Europe. Finland, Ireland, Belarus, Russia, Sweden, Ukraine, and the Baltic states are the largest producers of peat. Finland is perhaps the most significant peat consumer and derives 6% of its total energy from peat as a way to replace imported fuels [62]. In Finland, over 90% of the total peat production goes to energy production. In contrast, the USA uses most of its peat for horticultural uses [61]. Peat is often used as a practical alternative for smaller heat and/or power plants. There is also significant trade flows of peat among certain

countries, but most of the peat is still being consumed by the same country that produced it.

Wetlands that contain peat have to be drained before they can be exploited. Peat in situ contains roughly 90% water and drainage can reduce this significantly. Additional drying by the wind and sun will further reduce moisture content down to 40–50%. The traditional production method was to hand-cut peat into sods or strips, but this has been replaced by mechanical means. Another production technique yields fine peat granules by using a mechanical miller to disturb and granulate the top layer of the peatland. Some of the produced peat goes to the production of peat briquettes, which is a more practical fuel for households. WEC [41] states that the bulk of peat production is obtained from milling, which is more easily used for electricity and heat plants.

Producing coal requires more complex operations and often underground mining methods. Coal mining can be done from the surface by using draglines and other machines to remove the overburden and expose the coal for recovery. Surface mining methods can generally recover a high percentage of the coal and are relatively cost-effective. However, there are limits to the amount of overburden that can be practically removed to obtain access to the coal. Above certain stripping ratios (the amount of overburden that must be removed divided by the amount of recoverable coal), the surface method becomes unworkable and is replaced by deep mining.

In comparison, underground mining is more complicated and expensive and recovers less coal since certain parts must be left to support the roof. Up to 40% of the total coal in a coal seam may be left as supporting pillars, although this sometimes can be recovered at a later stage. Worldwide, about 40% of the production originates from surface mines, while 60% stems from underground operations. Surface mining dominates in some important producing countries [63]. The chosen production method will have a significant impact on the economic as well as technical restrictions that affect the recoverability of the coal.

Since the 1950s, the six largest coal reserve holders have increased their share of world production (Fig. 4). China in particular has rapidly increased its coal production and now accounts for over 40% of world coal production. The USA is the second largest coal producer, followed by India, Australia, Russia, and South

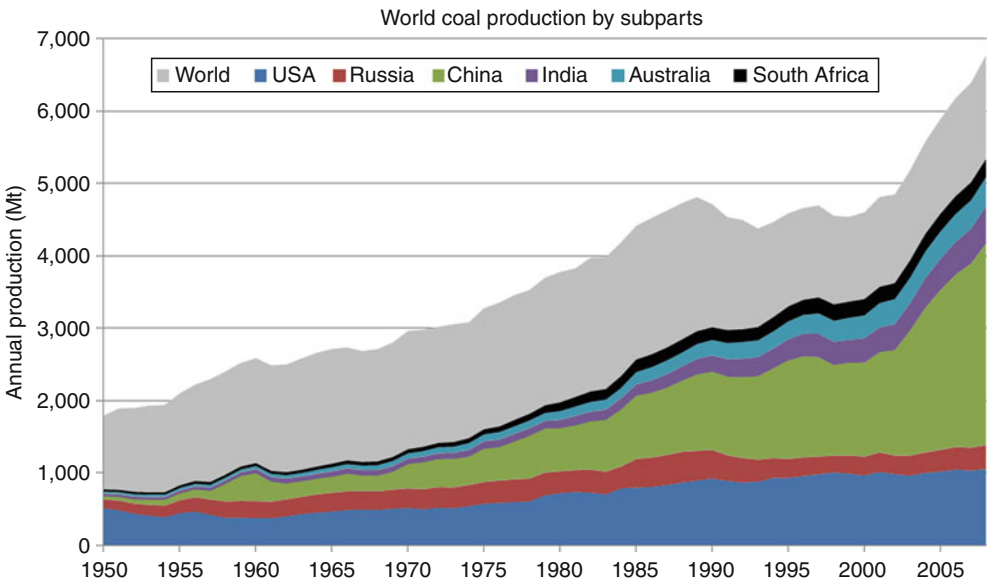

Coal and Peat: Global Resources and Future Supply. Figure 4
Total world production 1950–2008. Prior to 1985, the coal production from the Donetsk basin is not included in Russia. In 2008, just six countries accounted for roughly 80% of the total world coal production. These countries will determine the shape of future global coal production. Data source:[40, 64]

Africa. Even though coal is mined in over 50 different countries [63], the bulk of production comes from these six nations.

It is impossible for coal and peat production to avoid affecting and disturbing the local environment. Measures that restrict or even prevent mining in environmentally sensitive and other protected areas are affecting legal and economic feasibility of new mines. Mine tailings, acid mine drainage, leakage of associated substances like sodium and heavy metals, land subsidence, impact on local wildlife and landscape changes are problems that are intrinsically associated with production. Avoiding addressing these issues will stir up political or legal controversies [13, 55].

In addition, safety regulations are another complicating factor. Mining companies must agree to follow specific safety laws to receive a mining permit. Some major hazards are explosions (caused by methane gas and dust), roof collapse, and machine failure. Surface mining is generally safer since the risk of explosions is lower and the risk of roof collapses is almost completely absent. Since many coal deposits are not reachable by surface mining, the company must resort to underground mining. Closer discussions on safety related issues have been made by others [65, 66]. Good safety brings additional costs, while poor safety will hurt the public acceptance of the mining operations as well as potentially risking the demand for the "unsafe" coal. Poor safety may also result in governmental intervention and the closure of mining operations if required safety regulations are not followed.

New technology and recovery methods can change or potentially even revolutionize production. Improved mechanization, use of long-wall techniques that minimize the coal left behind to support the roof, and other measures have improved productivity and economic competitiveness of mining operations [67, 68]. These new mining methods have made previously unreachable deposits feasible for development, especially when they reduce production costs. New inventions will likely continue to improve production even further as research and development continues.

However, there is a danger in expecting too much from new technology. Increasing depletion of the best and most easily accessible coal seams will force future production to be derived from less favorable deposits. This will increase mining costs, which in turn will make energy more expensive across the whole economy. Some studies even show that technological progress will not meaningfully be able to offset depletion [69–71]. The study authors reason that new technologies and mining methods that boost efficiency and decrease labor requirements will be unable to offset the higher production costs of more complicated and labor-intensive deposits.

Coal has been produced in many countries for many decades, which enables us to perform longitudinal studies of production data. Several countries are currently producing only a small share of what they have produced historically (Fig. 5). Much of the reduced production can be explained by the move to other energy sources like petroleum or uranium, depletion of commercially feasible deposits, energy policy changes, and similar reasons.

Countries such as the UK still have a significant amount of coal resources left (Table 3), but not enough to suggest that coal will be the fuel of choice again. The remaining coal is generally located deeper than the previously mined coal and will be more expensive to mine in terms of labor and capital investment. Given the drawbacks of coal, especially in terms of climate change because of its high carbon content, it is not at all certain that demand for coal will grow again. This naturally leads to the question of future production of coal and peat.

Future Production

Future production of peat and coal is an open and complex question. The resources might be vast, but only a small amount is recoverable once legal, environmental, and economic constraints are accounted for. In particular, it would be a mistake to think that the huge worldwide resource estimates mean that coal and peat will provide a steady energy supply in to the future. In addition to the previous factors, production also depends on social acceptability (i.e., who would want to see mountain-top removal), technical restrictions, the development and competitiveness of alternative energy sources, and expected demand. Although the following overview is unable to discuss all the factors that will affect future production, it will illuminate some of the complexity and leading indicators of future production projections.

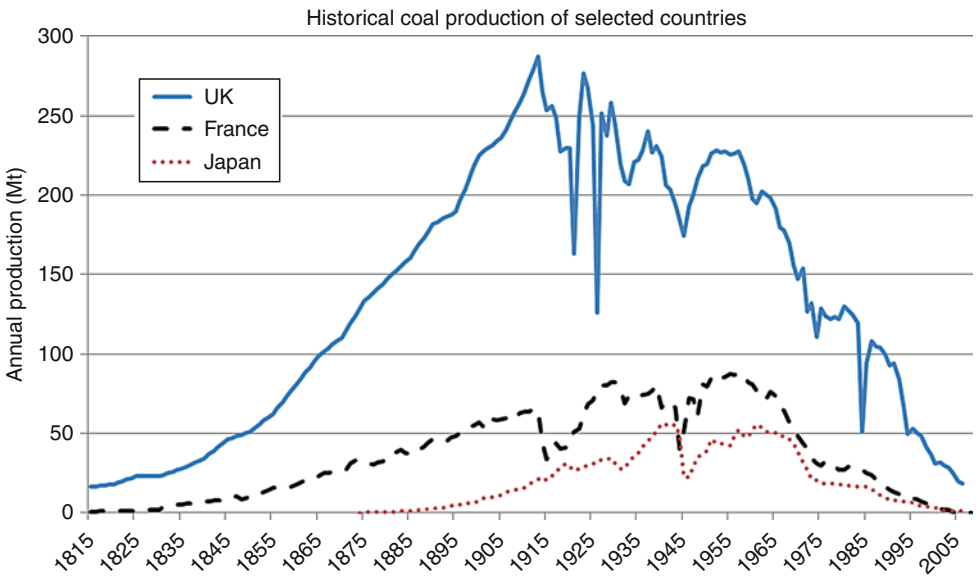

Coal and Peat: Global Resources and Future Supply. Figure 5
Historical coal production of UK, France, and Japan. All countries experienced production disturbances around the two world wars and the great depression. Data source: [40, 64]

There are many methodologies for creating production and supply projections for coal or peat. Some methods are quantitative, and rely on field data, while others are qualitative. Some analysts base their projections on economic theories, others use physical or statistical models derived from natural sciences. The life of the reserves and whether production can match demand are important questions for planning and sustainability.

The economist Adelman [72] has said that the amount of mineral in the earth is an irrelevant, nonbinding constraint to production. He further says that the amount of resource in the ground is probably unknowable but surely is unimportant and of no economic interest. This is correct in the very limited sense that producers will never recover the very last amounts of coal or any other resource from the earth. The ultimate recovery is undefined and governed by nongeological circumstances. However, although the recovery factor might be undefined that does not make it unlimited. It is bound between 0% and 100% of the resource in the earth's crust, which is clearly defined but not known exactly. Thus, the fact that the amount of recoverable coal is undefined and unknown cannot be an argument against the existence of future production limitations. The slow creation of coal and peat in comparison to their rapid extraction from mining imposes an inherent finiteness to the amount of coal and peat available.

Hubbert [73] proposed a model that extrapolates the production curves of finite resources such as petroleum or coal. His model assumes that production begins at zero, just before production has started, and ends at zero, when the resource has been exhausted. In between, the production curve passes through one or more maxima. The actual shape of the production curves may vary, but they are ultimately limited by the amount of resource that was deemed to be recoverable. Hubbert initially proposed a bell-shaped curve for an idealized production behavior, representing various development stages without giving any mathematical description for it. Later, he derived a mathematical framework chiefly based on the logistic function and curve fitting to production and discovery data [74].

Figure 6 shows a simple example of how actual production can be described by mathematical curves. When doing long-term projections, a suitable curve is fitted against historical production and constrained by a reasonable estimate on the recoverable volumes that may be ultimately produced. The total resource in the

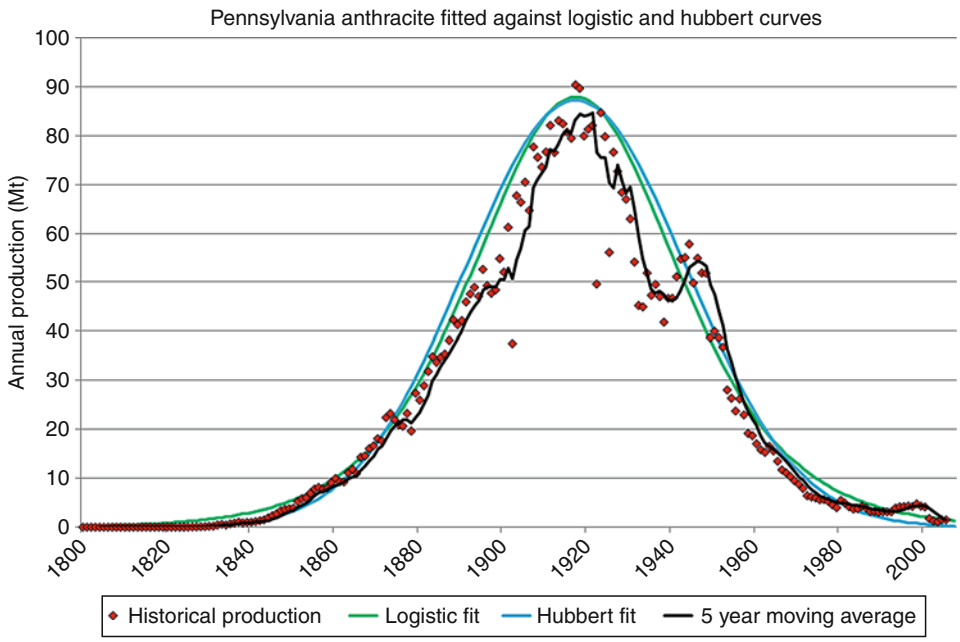

Coal and Peat: Global Resources and Future Supply. Figure 6
Historical production of anthracite in Pennsylvania fitted with both logistic and Hubbert curves. Data source: [13]

earth's crust will ultimately place a limit on future production, but the real limit will be lower since it is unrealistic to assume that all geologically existing volumes can be recovered.

Hubbert himself [73] used 2,500 Gt as the ultimate world coal reserves and placed the production peak around 2,150 at an annual output of 6 Gt. This implies that there are no near-term problems for coal production. However, his simple approach does not consider all aspects of recoverability. It also agrees poorly with actual production history since current production reached 6 Gt per year in 2008 and production is still increasing.

Hubbert's method is sensitive to the assumed ultimate reserve that constrains the curve so it is essential to have the best possible resource estimate. It has been described as a reasonable model provided that it is acknowledged that reserves are dynamic and that other factors also influence production [75]. Growth curve methods can provide insight into the general long-term flow of finite energy resources, but perturbations caused by sudden and unforeseen near-term economic or political changes cannot be predicted. Therefore, long-term life-cycle projections should not be used as a substitute for meticulous economic studies that forecast perturbations in coal production over the upcoming years or decades [76]. Studies have also used the development of regulations, restrictions, and recoverable volume estimates to create production projections [13].

Other quantitative assessments that have relied on reported reserve and resource assessments found that coal output can increase until 2050 or even 2100 [32, 76]. Thielemann et al. [32] assumed that resources will simply be converted into reserves and then produced due the self-regulating price-driven supply cycle. This model gives no foreseeable production limitations within the next century. Mohr and Evans [77] point out that shrinking coal resource and reserve estimates over the last 25 years seem to indicate that factors other than the self-regulating supply mechanism are playing a role. In any case, future production will still be limited to the countries and regions where the resources are located.

Watson et al. [48] concluded that future coal production from the Pittsburgh coal area is dependent on a complex set of factors, including future transportation costs and environmental policies. Without

a holistic view of all factors affecting recoverability and geological availability, no reasonable supply projection can be made. Although predictions of future production will always be uncertain, it is important to remember that production is dependent on much more than just geological existence. Claims that abundant resources will automatically provide future energy supply need to be treated with suspicion – they oversimplify the production situation.

For example, there are significant unexploited coal reserves located in eastern Siberia and far eastern Russia. However, these deposits are far from major population centers and will need major investments in infrastructure before they can be exploited. How fast this can occur is an open question and depends primarily on economic and political factors. Also, Russia might never develop those deposits and may use other energy sources instead. A similar point can be made for the USA and the vast coal resources locked up in Alaska [43]. Underlying assumptions can greatly affect future production projections and one must always remember that production is a complex issue with many factors involved.

Recent concern for the CO_2 emissions that come from burning fossil fuels may turn coal and peat into undesired fuels for the future in some countries. On the other hand, countries that care less about the environment might turn to coal and peat as cheap, but polluting, alternatives to imported oil. Clean coal technologies and carbon capture and storage might alleviate much of the emission problems from combustion, which can improve coal's attractiveness. Cheap and reliable wind and solar energy or improved nuclear power might also deliver cheaper energy to consumers than coal and peat if carbon emissions are taxed. Increasing global competition for the remaining petroleum might cause countries to increase their reliance on domestic energy sources. In summary, there are many factors that can affect future production and without a holistic approach it is difficult to make reliable projections.

The current world dependence on fossil fuels also brings about another problem. Since fossil fuels dominate the existing energy system, they will have to power any possible shift to renewable or other energy sources [78]. The effect this has on fossil fuel reserves will depend largely on the size and speed of the shift, since fossil fuel energy used will be additional to that already in use.

In conclusion, there is a lot of coal and peat available in terms of resources. However, far from all the resources are suitable for production, and future production will largely depend on the choices people make. The model and assumptions about recoverability have a significant impact on future production projections. The key point is that huge worldwide resource estimates for coal and peat do not automatically translate into an assured supply. Vast resources are present if society demands coal and peat and is prepared to pay the price for recovering them.

Future Directions

This section should start with a frank admission that coal will remain one of the most important energy sources for mankind for the foreseeable future. Future development of coal production will be linked to the development of global energy supply, which will affect virtually all aspects of society in some way. However, production is a complex issue that requires a holistic treatment. This chapter has attempted to highlight several of the indicators and parameters that affect future production of coal and peat.

It is also obvious that more work needs to be done in exploration and geology to better understand the occurrence of coal and peat. Better survey data and increased geologic certainty would also help to improve the accuracy of resource estimates – especially in those countries and regions where few assessments have been made or where only old data is available. There is no substitute for a good geological understanding of depositional systems and detailed surveys when making resource estimates.

Estimation of reserves and recoverable volumes involve consideration of numerous economic, technical, legal, and social parameters relative to specific markets and expected demand during a present and period with economic and regulatory uncertainty. Improved understanding and handling of this complex set of factors are required for more accurate and reliable assessments in the future. Recoverability is not a topic that should be taken lightly or oversimplified. Instead it needs holistic treatment to provide reasonable outlooks for future world supply of coal and peat.

Bibliography

Primary Literature

1. Ehrlich PR, Ehrlich AH, Holdren JP (1970) Ecoscience: population, resources, environment. W.H Freeman and Company, San Francisco
2. Cook E (1977) Energy: the ultimate resource? Resource Papers for College Geography, Issue 77–4, 42 p
3. Simon J (1966) The ultimate resource 2. Princeton University Press, Princeton
4. Bromley DA (2002) Science, technology, and politics. Technol Soc 24:9–26
5. Einstein A (1905) Ist die Trägheit eines Körpers von seinem Energieinhalt abhängig? Ann Phys 323:639–641
6. IEA (2008) Key World Energy Statistics 2008. See also: http://www.iea
7. Pimentel D, Hurd LE, Bellotti AC, Forster MJ, Oka IN, Sholes OD, Whitman RJ (1973) Food production and the energy crisis. Science 182(4111):443–449
8. Green MB (1978) Eating oil: energy use in food production. Westview Press, Boulder
9. Pfieffer DA (2006) Eating fossil fuels: oil, food and the coming crisis in agriculture. New Society Publishers, Gabriola Island
10. Pimentel D (2007) Food, energy, and society. CRC Press, Boca Raton
11. Akinlo AE (2002) Energy consumption and economic growth: evidence from 11 Sub-Sahara African countries. Energy Econ 30:2391–2400
12. Hondroyiannis G, Lolos S, Papapetrou E (2002) Energy consumption and economic growth: assessing the evidence from Greece. Energy Econ 24:319–336
13. Höök M, Aleklett K (2009) Historical trends in American coal production and a possible future outlook. Int J Coal Geol 78(3):201–216
14. Diessel CFK (1992) Coal-bearing depositional systems. Springer, Berlin
15. Moore PD (1987) Ecological and hydrological aspects of peat formation. In: Scott AC (ed) Coal and coal-bearing strata: recent advances, vol 32. Geological Society, London, pp 7–15, Special publications
16. Nadon GC (1998) Magnitude and timing of peat-to-coal compaction. Geology 26(8):727–730. doi:10.1130/0091-7613
17. Mäkilä M (2006) Lot of peat deposits under 300 years old in Finland. Geological Survey of Finland, Peat research report 59/2006
18. Ryer TA, Langer AW (1980) Thickness change involved in the peat-to-coal transformation of bituminous coal of Cretaceous age in central Utah. J Sed Petrol 50:987–992
19. Dukes JS (2003) Burning buried sunshine: human consumption of ancient solar energy. Clim Change 61(1–2):31–44. doi:10.1023/A:1026391317686
20. Neuzil SG, Supardi CCB, Kane JS, Soedjono K (1993) Inorganic geochemistry of domed peat in Indonesia and its implication for the origin of mineral matter in coal. Geol Soc Am Spec Pap 286:23–44
21. Cecil CB, Dulong FT, Cobb JC, Supardi K (1993) Allogenic and autogenic controls of sedimentation in the central Sumatra basin as an analogue for Pennsylvanian Coal-bearing strata in the Appalachinan Basin. Geol Soc Am Spec Pap 286:2–22
22. Gastaldo RA, Allen GP, Huc AY (1993) Detrial peat foundation in the tropical Mahakam River Delta, Kalimantan, Eastern Borneo: sedimentation, plant composition and geochemistry. Geol Soc Am Spec Pap 286:107–118
23. Ruppert LF, Neuzil SG, Cecil CB, Kane JS (1993) Inorganic constituents from samples of a domed and lacustrine peat, Sumatra, Indonesia. Geol Soc Am Spec Pap 286:83–96
24. Wellman CH, Osterloff PL, Mohuiddin U (2003) Fragments of the earliest land plants. Nature 425:282–285. doi:10.1038/nature01884
25. Butler J, Marsh H, Goodarzi F (1988) World coals: genesis of the world's major coal fields in relation to plate tectonics. Fuel 67(2):269–274
26. Walker S (2000) Major coalfields of the world. IEA Coal Research, London
27. Saus T, Schiffer HW (1999) Lignite international. Rheinbraun AG, Cologne
28. American Society for Testing and Materials (2005) Standard classification of coals by rank, ASTM D388-05. ASTM International, West Conshohocken
29. Carpenter AM (1988) Coal classification. IEA Coal Research, London
30. Lappalainen E (1996) General review on world peatland and peat resources. In: Lappalainen E (ed) Global peat resources. International Peat Society, Jyskä
31. Lottes AL, Ziegler AM (1994) World peat occurrence and the seasonality of climate and vegetation. Palaeogeogr Palaeoclimatol Palaeoecol 106(1–4):23–37
32. Thielemann T, Schmidt S, Gerling PJ (2007) Lignite and hard coal: energy suppliers for world needs until the year 2100 – an outlook. Int J Coal Geol 72:1–14
33. van Rensburg WCJ (1982) The relationship between resources and reserves estimates for US coal. Resour Policy 8(1):53–58
34. Wood GH, Kehn TM, Carter MD, Culbertson WC (1983) Coal resource classification system of the U.S. geological survey. US Geological Survey Circular 891. http://pubs.usgs.gov/circ/c891/
35. Eggleston JR, Carter MD, Cobb JC (1990) Coal resources available for development – a methodology and pilot study. US Geological Survey Circular 1055. http://pubs.usgs.gov/circ/c1055/
36. Carter MD, Gardner NK (1989) An assessment of coal resources available for development, central Appalachian region. US Geological Survey open-file report 89–362. http://pubs.usgs.gov/of/1989/of89-362/
37. Luppens JA, Rohrbacher TJ, Haacke, JE, Scott DC, Osmonson LM (2006) Status report: USGS coal assessment of the powder river, Wyoming. U.S. Geological Survey open-file report 2006-1072. http://pubs.usgs.gov/of/2006/1072/

38. American Association of Petroleum Geologists (2007) Unconventional energy resources and geospatial information: 2006 review. Nat Resour Res 16:243–261
39. Energy Information Administration (1996) U.S. coal reserves, appendix A, specialized resource and reserve terminology. http://tonto.eia.doe.gov/ftproot/coal/052995.pdf
40. BP (2009) BP statistical review of world energy 2009. http://www.bp.
41. World Energy Council (1924–2007) Survey of energy resources 2007 and previous reports and statistical yearbooks from previous world power conferences, World Energy Council, London. http://www.worldenergy.org/
42. German Federal Institute of Geology and Natural Resources (1980–2008) Reserves, resources and availability of energy resources. Various editions. http://www.bgr.bund.de/. Accessed 11 Nov 2010
43. Flores RM, Stricker GD, Kinney SA (2004) Alaska coal geology, resources, and coalbed methane potential. USGS report. http://pubs.usgs.gov/dds/dds-077/
44. Luppens JA, Scott DC, Haacke JE, Osmonson LM, Rohrbacher TJ, Ellis MS (2008) Assessment of coal geology, resources, and reserves in the Gillette Coalfield, Powder River Basin, Wyoming. U.S. Geological Survey Open-File Report 2008–1202. http://pubs.usgs.gov/of/2008/1202/
45. Hubbert MK (1982) Response to David Nissens remarks. http://www.hubbertpeak.com/Hubbert/to_nissen.htm
46. Kurleyna MV, Tanaino AS (1997) Open-pit and underground mines – energy analysis of open-pit mining. J Min Sci 33(5):453–462
47. Rohrbacher TJ, Teeters DD, Sullivan GL, Osmonson LM (1993) Coal resource recoverability – a methodology. U.S. Bureau of Mines Circular 9368. http://pubs.usgs.gov/usbmic/ic-9368/
48. Watson WD, Ruppert LF, Tewalt SJ, Bragg LJ (2001) The upper Pennsylvanian Pittsburgh coal bed: resources and mine models. Nat Resour Res 10:21–34
49. Blackmore G, Ehrenreich SB (1987) Reserve data base report of the National Coal Council: advisory report to the U.S. Department of Energy. National Coal Council, Arlington
50. National Petroleum Council (2007) Facing hard truths about energy. http://www.npchardtruthsreport.org/
51. U.S. National Academies (2007) Coal: research and development to support national energy policy. National Academies Press, Washington
52. Storchmann K (2005) The rise and fall of German hard coal subsidies. Energy Policy 33(11):1469–1492
53. Frondel M, Kambeck R, Schmidt CM (2007) Hard coal subsidies: a never-ending story? Energy Policy 35(7):3807–3814
54. Malyshev YN (2000) Strategy for the development of the Russian coal industry. J Min Sci 36(1):57–65
55. Petsch G (1982) Environmental problems of coal production in the federal republic of Germany with particular reference to the Ruhr. Environ Geochem Health 4:75–80
56. Tobin RJ (1984) Air quality and coal – the US experience. Energy Policy 12:342–352
57. Yeager KE, Baruch SB (1987) Environmental issues affecting coal technology: a perspective on US trends. Annu Rev Energy 12:471–502
58. O'Brien B (1997) The effects of title IV of the clean air act amendments of 1990 on electric utilities: an Update. EIA report DOE/EIA-058297 distribution category UC-950. ftp://ftp.eia.doe.gov/pub/electricity/ef_caau1.pdf
59. Ackerman F, Biewald B, White D, Woolf T, Moomaw W (1999) Grandfathering and coal plant emissions: the cost of cleaning up the clean air act. Energy Policy 27:929–940
60. Patiño-Echeverri D, Fischbeck P, Kriegler E (2009) Economic and environmental costs of regulatory uncertainty for coal-fired power plants. Environ Sci Technol 43:578–584
61. U.S. Geological Survey (2009) Mineral Commodity data – peat statistics and Information. http://minerals.usgs.gov/minerals/pubs/commodity/peat/
62. Geological Survey of Finland (2009) Peat resources of Finland. http://en.gtk.fi/Resources/peat_resources.html
63. World Coal Institute (2005) The coal resource – a comprehensive overview of coal. http://www.worldcoal.org/
64. Mitchell B (2003) International historical statistics 1750–2000. Palgrave MacMillan, London
65. Kecojevic V, Nor ZD (2008) Hazard identification for equipment-related fatal incidents in the U.S. underground coal mining. J Coal Sci Eng (China) 15(1):1–6
66. Grayson RL (2008) Improving mine safety technology and training in the U.S. recommendations of the mine safety technology and training commission. J Coal Sci Eng (China) 14(3):425–431
67. Szwilski AB (1988) Significance and measurement of coal mine productivity. Min Sci Technol 6(3):221–231
68. Kulshreshtha M, Parikh JK (2002) Study of efficiency and productivity growth in opencast and underground coal mining in India: a DEA analysis. Energy Econ 24(5):439–453
69. Tilton JE (2003) Assessing the threat of mineral depletion. Miner Energy 18:33–42
70. Rodríguez XA, Arias C (2008) The effects of resource depletion on coal mining productivity. Energy Econ 30:397–408
71. Topp V, Soames L, Parham D, Bloch H (2008) Productivity in the mining industry: measurement and interpretation. Productivity Commission, Melbourne
72. Adelman MA (1990) Mineral depletion, with special reference to petroleum. Rev Econ Stat 72:1–10
73. Hubbert MK (1956) Nuclear energy and the fossil fuels. Shell Development Company, Houston
74. Hubbert MK (1959) Techniques of prediction with application to the petroleum industry. Shell Development Company, Dallas
75. van Rensburg WCJ (1975) 'Reserves' as a leading indicator to future mineral production. Resour Policy 1:343–356
76. Milici RC, Campbell EVM (1997) A predictive production rate life-cycle model for Southwestern Virginia Coalfields. Geological Survey Circular 1147. http://pubs.usgs.gov/circular/c1147/
77. Ion DC (1979) World energy supplies. Proc Geologists' Assoc 90:193–202

78. Mohr SH, Evans GM (2009) Forecasting coal production until 2100. Fuel 88:2059–2067
79. Moriatry P, Honnery D (2009) What energy levels can the Earth sustain? Energy Policy 37:2469–2474

Books and Reviews

Cobb CJ (1993) Modern and ancient coal-forming environments. Geological Society of America, Boulder
George H, Meech J, Workman L (1986) Towards reducing the physical environmental impact of North American surface coal mines; a review of potential selective overburden handling techniques. Min Sci Technol 3(2):81–94
Lappalainen E (1996) Global peat resources. International Peat Society, UNESCO, and Geological Survey of Finland, cop, Jyskä, 359 pp
Schilstra AJ, Gerding MAW (2004) Peat resources. In: Cleveland CJ (ed) Encyclopedia of energy. Elsevier Academic, San Diego
Schissler AP (2004) Coal mining, design and methods of. In: Cleveland CJ (ed) Encyclopedia of energy. Elsevier Academic, San Diego
Seredin VV, Finkelman RB (2008) Metalliferous coals: a review of the main genetic and geochemical types. Int J Coal Geol 76(4):253–289, 1 Dec 2008
Suárez-Ruiz I, Crelling JC (2008) Applied coal petrology: the role of petrology in coal utilization. Academic, New York
Thomas L (2002) Coal geology. Wiley, New York
Yudovich YE, Ketris MP (2005) Arsenic in coal: a review. Int J Coal Geol 61(3–4):141–196, 9 Feb 2005

Coal Preparation

Gerald H. Luttrell[1], Rick Q. Honaker[2]
[1]Department of Mining and Minerals Engineering, Holden Hall Virginia Polytechnic Institute & State University, Blacksburg, VA, USA
[2]Department of Mining Engineering, Mining & Mineral Resources Engineering University of Kentucky, Lexington, KY, USA

Article Outline

Glossary
Definition of the Subject
Introduction
Assessment of Cleaning Characteristics
Coal Processing Operations
Beneficial Impacts of Coal Preparation
Challenges for Coal Preparation
Future Directions
Bibliography

Glossary

Ash A measure of coal purity that consists of the noncombustible residue that remains after coal is completely burned.

Cut size The particle size that has an equal probability of reporting to either the oversize or undersize product of a sizing device such as a screen or hydraulic classifier.

Cut point The density corresponding to a particle that has an equal probability of reporting to either the clean coal or reject product of a density-based separator.

Dense medium An aqueous suspension of high-density micron-sized particles (usually magnetite) used to separate coal from rock based on differences in density.

Organic efficiency An indicator of coal cleaning performance calculated by dividing actual clean coal yield by the theoretical maximum yield attainable at the same ash content according to washability analysis.

Washability A laboratory procedure that uses dense liquids (usually organic) to partition particles into various density fractions that represent the ideal separation potential of coal (also called float–sink analysis).

Yield An indicator of separation performance (usually reported as a percentage) that is calculated by dividing the clean coal tonnage by the feed coal tonnage.

Definition of the Subject

Coal preparation, which may also be called washing, cleaning or processing, is the methodology by which coal feedstocks are upgraded in order to reduce freight costs, improve utilization properties and minimize environmental impacts. The upgrading, which occurs after mining and before transport of the cleaned product to market, is achieved using a variety of low-cost solid–solid and solid–liquid separation processes. Examples of processing technologies used by this industry include screening, classification, dense medium separation, gravity concentration, froth flotation, centrifugation, filtration and thickening. Several

of these processes also play an important role in environmental control for the preparation facility.

Introduction

According to the annual census of coal preparation plants conducted by Coal Age [1], the USA operates 286 coal preparation plants in 12 states. This number is relatively small by comparison to the worldwide fleet which is estimated to be 2,283 plants [2]. The capacity of the plants can range from less than 200 t/h for small operations to 6,000 t/h or more for large industrial plants. The need for such facilities can be attributed to the fact that freshly mined coals contain a heterogeneous mixture of both organic (carbonaceous) and inorganic (mineral) matter. The inorganic matter includes noncombustible materials such as shale, slate and clay. These impurities reduce the coal heating value, leave behind an undesirable ash residue, and increase the cost of transporting coal to market. The presence of unwanted surface moisture also reduces the heating value and can lead to handling and freezing issues for consumers. Therefore, essentially all coal supply agreements with electrical power stations impose strict limitations on the specific energy (heat), ash and moisture contents of purchased coal. Moreover, as the first step in the power cycle, coal preparation plants improve the environmental acceptability of coal by removing impurities that may be transformed into harmful gaseous or particulate pollutants when burned. These pollutants typically include particulates (fly ash) and sulfur dioxide (SO_2) as well as toxic trace elements such as mercury. The presence of mineral impurities can also influence the suitability of coal for high-end uses such as the manufacture of metallurgical coke or generation of petrochemicals and synthetic fuels. As such, coal preparation is typically needed to achieve the high levels of coal purity demanded by these secondary markets.

This entry provides a brief overview of some of the technological systems used in coal preparation. In addition, this entry highlights the benefits resulting from coal preparation activities as well as the issues associated with the sustained operation of coal processing facilities. This review suggests that coal preparation will continue to have a significant impact on the cost, recovery and quality of coal supplies. However, future improvements in separation technology and practices are needed to provide further reductions in waste generation and downstream environmental impacts. In many cases, these improvements may also generate incremental revenue due to the recovery of usable coal from waste streams, which could provide a financial incentive for pursuing these activities.

Assessment of Cleaning Characteristics

The capability of coal preparation to improve coal quality varies widely due to inherent differences in the liberation characteristics of mined coals. The degree of liberation is determined by the relative proportion of composite particles (i.e., particles of intermixed coal and rock that are locked together) present in a particular coal. The composite particles make it impossible to physically separate all of the carbonaceous matter from the host inorganic matter. Consequently, plant operators are often forced to sacrifice coal recovery by discarding some composite particles as waste in order to improve clean coal quality to a level that can meet customer specifications.

The theoretical trade-off between coal recovery and quality can be quantified in the laboratory using washability (float–sink) analysis. An example of experimental data collected from a float–sink analysis is shown in Fig. 1. The analysis is performed by sequentially passing a coal sample through containers containing liquids (usually organic) of increasingly higher densities [3]. Pure coal has a relatively low specific gravity (SG < 1.3) and is collected as a float product from the first container, whereas pure rock is much denser (SG > 2.2) and is collected as a sink product from the last container. Composite particles report as float products in the intermediate containers filled with liquids having densities between that of the first and last containers. After density partitioning, the products from this procedure are dried, weighed and analyzed for quality (ash, sulfur, mercury, etc.). Washability data are very useful for predicting and analyzing the performance of coal preparation plants since most cleaning processes separate coal and rock based on differences in density.

Coal washability has a tremendous impact on how effectively a preparation plant can upgrade a particular coal feedstock. However, the types of processes

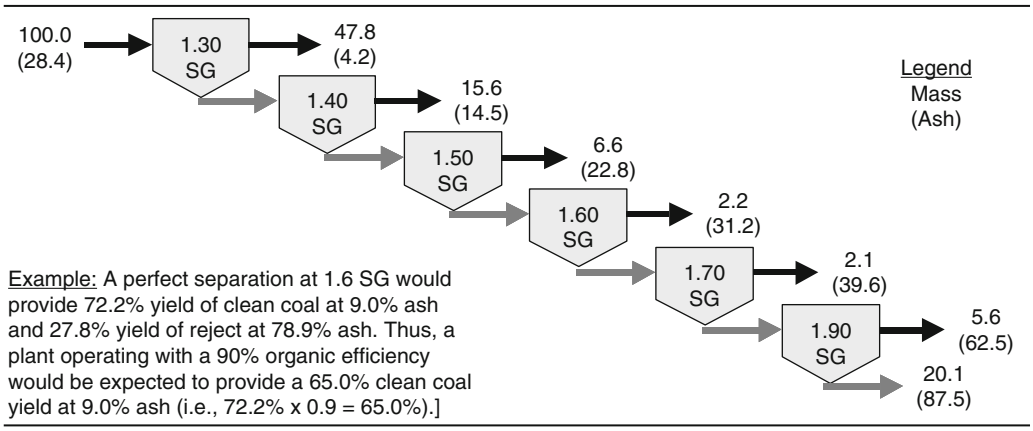

Specific gravity		Mass	Ash	Cumulative float		C Sink	
Sink	Float	(%)	(%)	Mass (%)	Ash (%)	Mass (%)	Ash (%)
	1.30	47.8	4.2	47.8	4.2	100.0	28.4
1.30	1.40	15.6	14.5	63.4	6.7	52.2	50.5
1.40	1.50	6.6	22.8	70.0	8.3	36.6	65.9
1.50	1.60	2.2	31.2	72.2	9.0	30.0	75.4
1.60	1.70	2.1	39.6	74.3	9.8	27.8	78.9
1.70	1.90	5.6	62.5	79.9	13.5	25.7	82.1
1.90		20.1	87.5	100.0	28.4	20.1	87.5
Totals		100.0	28.4				

Coal Preparation. Figure 1
Float–sink (washability) analysis for a 28.4% ash run-of-mine coal

employed and practices used for operation and maintenance (O&M) can also greatly influence the performance of the preparation facility. This effectiveness is typically reported as an organic efficiency, which is defined as the yield of clean coal actually produced by the separation divided by the theoretical maximum yield of clean coal that could be achieved at the same ash content according to washability analysis. Organic efficiencies are often in the high 90 percentiles for well designed and well run operations, although values well below this desired level are not uncommon for problematic plants. Inefficient processes or practices, which misplace significant amounts of clean coal into waste and/or rock into the clean product, have a large negative impact on profitability. For example, a decrease in organic efficiency of just one percentage point can potentially represent a reduction in plant profitability of 20% or more.

Coal Processing Operations

During the early part of the last century, coal mines made use of labor intensive sorting methods such as manual hand-picking to remove unwanted rock from mined coal. This inefficient approach was soon replaced by simple mechanical sorting processes that reduced misplacement and provided higher levels of productivity. These early plants typically cleaned only the coarser particles (usually larger than >5–10 mm) and either recombined the untreated fine particles back into the washed product or discarded the fines as waste. These inefficient systems dumped large tonnages of coal into waste piles, some of which are being re-mined and reprocessed today. These historic periods were followed by many decades of technology development that ultimately led to the design and operation of relatively efficient plants that are capable of complete or

partial upgrading of the entire size range of mined coals. Many modern coal preparation plants operating today are as complex as industrial facilities once employed only by the chemical processing industry.

Figure 2 shows a simplified process flowsheet for a modern plant that includes operations for particle sizing, cleaning and dewatering. This sequence of operations, which is called a circuit, may be repeated for different size fractions since the processes used in coal preparation have a limited range of applicability in terms of particle size (Fig. 3). Modern plants may include as many as four separate processing circuits for treating the coarse (plus 10 mm), small (10 × 1 mm), fine (1 × 0.15 mm), and ultrafine (minus 0.15 mm) feed material. Although many commonalities exist, the final selection of what number of circuits to use, which types of unit operations to employ, and how they should be configured, is highly subjective and dependent on the characteristic properties of the feed coal in terms of size and composition.

Unit Operations for Particle Sizing

Coal produced by mechanized mining operations contains particles as small as fine powder and as large as several hundred millimeters. Particles too large to pass into the plant are crushed to an appropriate upper size, or rejected where insufficient recoverable coal is present in the coarse size fractions. The crushed material is

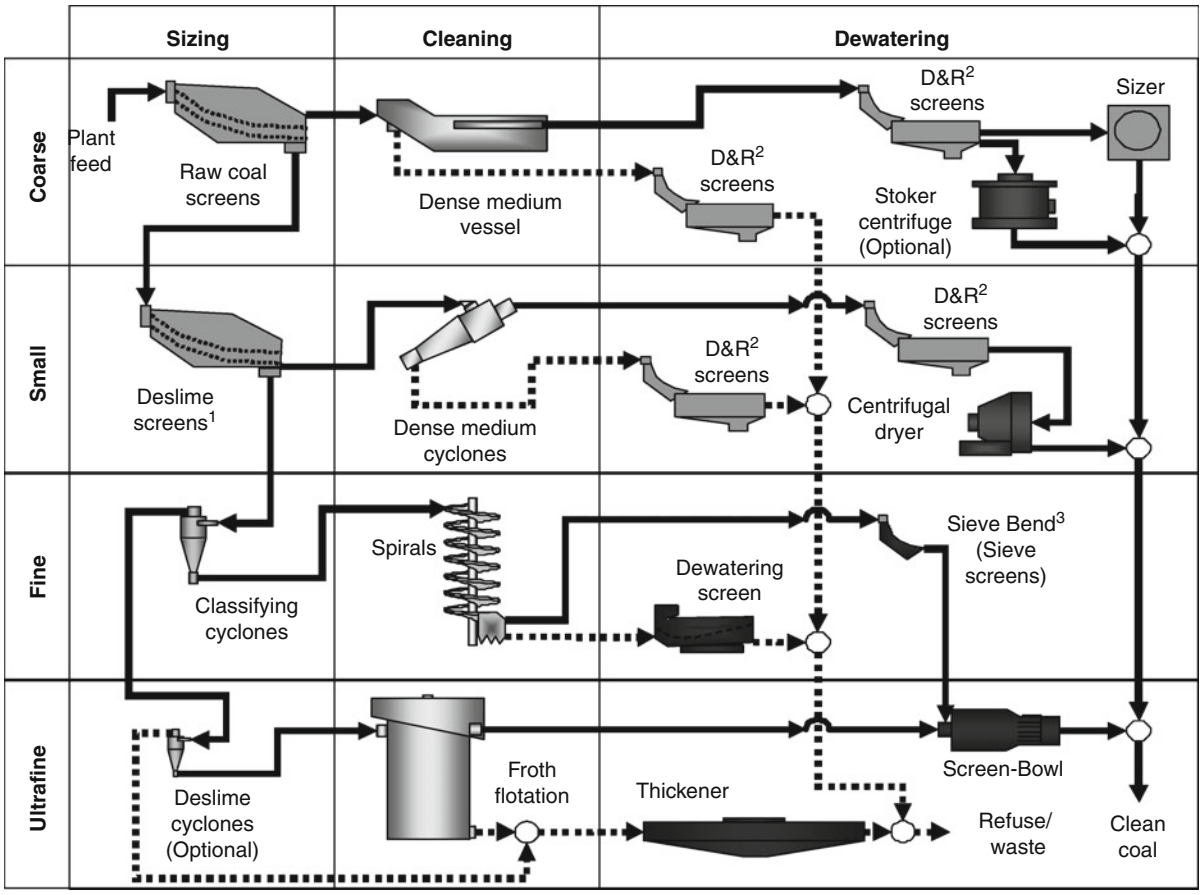

Notes: 1 -Raw coal and deslimescreen decks may be on the same machine, 2 –D&R screens primarily used to recover dense medium, 3 -Sieve bends may also be combined with clean coal classifying cyclones.

Coal Preparation. Figure 2
Simplified flowsheet for a modern coal preparation plant showing unit operations for sizing, cleaning and dewatering of four different size fractions required for efficiency coal upgrading

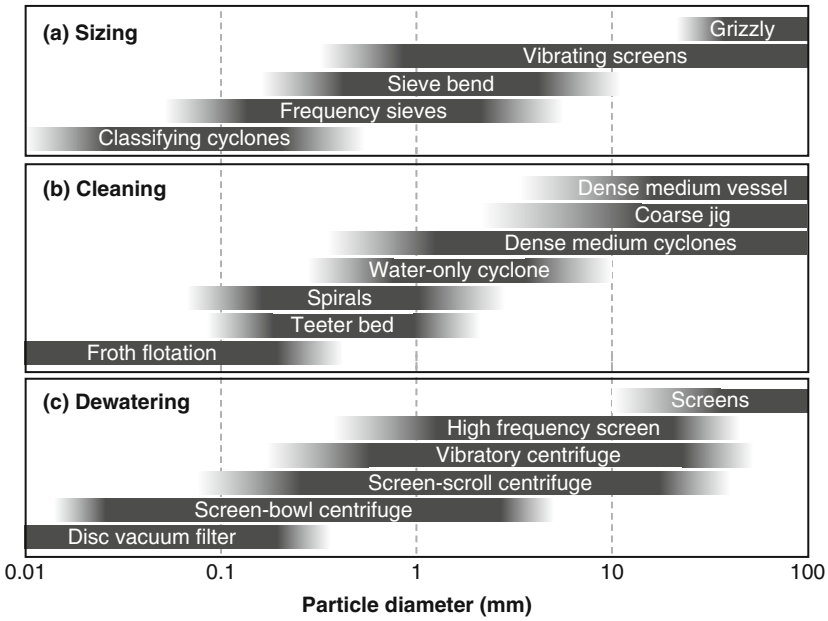

Coal Preparation. Figure 3
Effective range of particle sizes treated by various coal preparation processes

then segregated into groups having well defined maximum and minimum sizes. Screens are typically employed for sizing coarser particles, while combinations of stationary sieves and classifying cyclones are used for sizing finer particles. Figure 3a shows the typical sizes of particles that can be effectively handled by common types of industrial sizing equipment.

Screens and Sieves Screens are mechanical sizing devices that use a mesh or perforated plate to sort particles into fine (particles that pass through the screen openings) and coarse (particles that are retained on the screen surface). Screens are used for a wide range of purposes including the extraction of large rock and trash prior to treatment, the production of optimum size fractions for separation devices and the rinsing/dewatering of products from cleaning operations. The types of screens commonly used in coal preparation include grizzly, vibrating and high-frequency screens. A grizzly is a series of evenly spaced parallel bars that are positioned in the direction of material flow. This simple device is used only for gross sizing of very coarse particles (>50 mm) and is generally applied only for the protection of equipment from large oversize material. Vibrating screens are the most common equipment for sizing particles and are used in almost every aspect of coal preparation. Vibrating screens (Fig. 4) utilize an out-of-balance rotating mechanism to create a vibrating motion to sort particles and to move material along the screen surface. High-frequency screens (Fig. 5) are normally used for dewatering fine coal or rock by retaining slurry between two opposing inclines. As the name implies, this type of screen operates at a high vibrating frequency, which is beneficial for dewatering fine solids.

The sizing of fine coal is particularly difficult due to the increased likelihood of plugging and the large number of particles that must pass through the screen surface. As such, fine sizing is performed in many cases using sieve bends. A sieve bend (Fig. 6) consists of a curved panel constructed from inverted trapezoidal bars (profile or wedge wire) placed at right angles to fluid flow. The capacity of the sieve is relatively high since the leading edge of the trapezoidal bars "slice" material from the flowing stream. However, due to the unique geometry, the particle size retained by the sieve is smaller than the spacing between bars. Sieve bends are commonly used for fine particle dewatering and may also be used ahead of vibrating screens to enhance sizing performance.

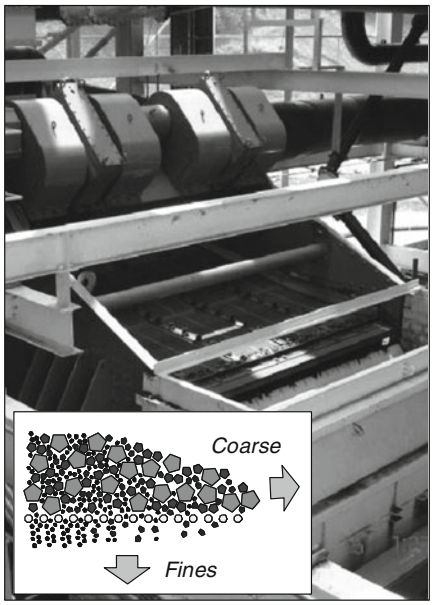

Coal Preparation. Figure 4
Vibrating screen used for feed coal sizing

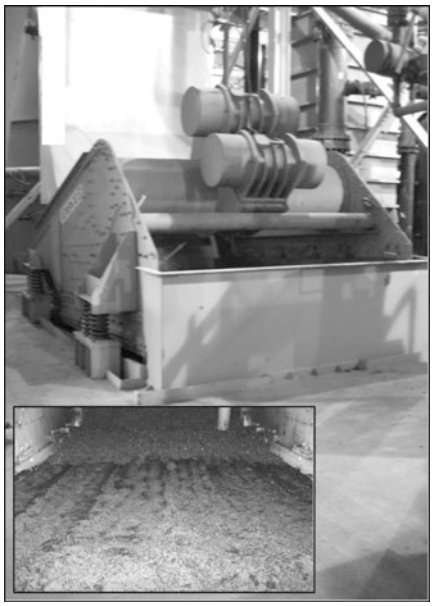

Coal Preparation. Figure 5
High-frequency screen used for dewatering of fine rock

Classifying Cyclones Classification is used in coal preparation for fine sizing where conventional screening and sieving becomes impractical or too expensive. Classification exploits differences in the settling rates of particles of different size (i.e., smaller particles settle slower than larger particles). Classification is usually applied to dilute suspensions of <1 mm diameter particles. This technique is generally less efficient than screening or sieving since the separation can be influenced by particle shape and density as well as particle size. The most common type of classification device used in the coal industry is the classifying cyclone (Fig. 7). In this device, dilute slurry is pumped under pressure to multiple parallel units (banks) of cyclones. The rotating flow field within the cyclone creates a centrifugal force that increases the settling rate of the particles. Larger particles are forced to the wall of the cyclone where they are carried to the discharge port (apex) at the bottom of the cyclone, while finer particles exit out the top of the cyclone (vortex finder). Classifying cyclones are commonly applied to obtain cut sizes of 0.10–0.15 mm and represent the only practical option for sizing ultrafine particles (cut size of 50 μm or less). Smaller cyclones are typically used to size finer particles since these units provide a higher centrifugal force. Classifying cyclones are very popular in the coal industry since they offer a high unit capacity, operational flexibility and low maintenance.

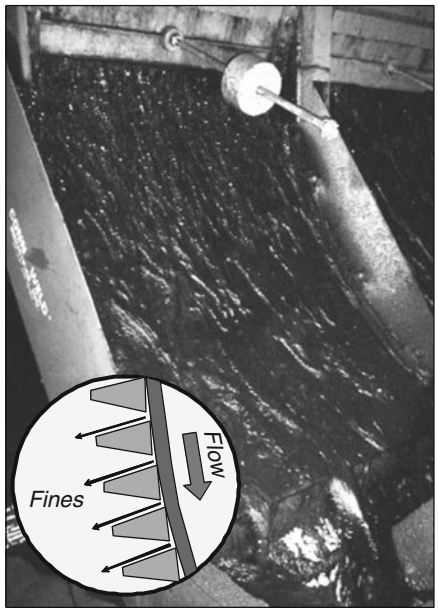

Coal Preparation. Figure 6
Sieve bend used to remove fine "slimes" from coal

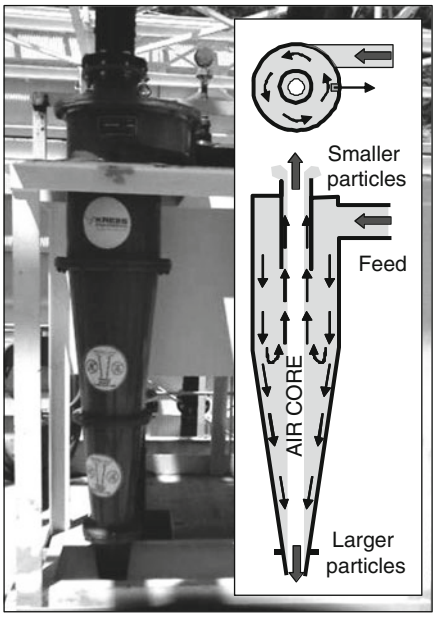

Coal Preparation. Figure 7
Classifying cyclone used to hydraulically size fine coal

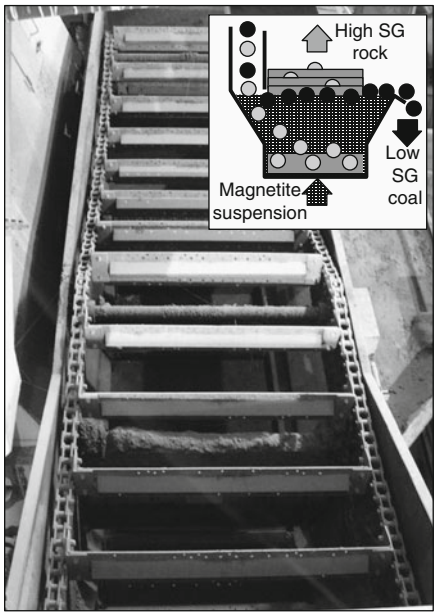

Coal Preparation. Figure 8
Chain-and-flight dense medium vessel used to separate coarse coal and rock

Unit Operations for Coal Cleaning

The primary purpose of coal preparation is to separate valuable carbonaceous material from contaminants in the surrounding host rock. The separation is typically accomplished using low-cost processes that exploit differences in physical properties that vary according to mineralogical composition of individual particles. Some of the common properties that are used to separate coal and rock include size, density and wettability. As shown in Fig. 3b, the effectiveness of different types of separators is limited to a relatively narrow range of particles sizes due to limitations associated with equipment efficiency and geometry.

Dense Medium Separators The most common process for upgrading coarse coal (>12.5 mm) is the dense medium vessel. While a wide variety of different designs exist in industry, one of the most popular is the chain-and-flight vessel (Fig. 8). This density-based separator consists of a large open tank through which an aqueous suspension of finely pulverized magnetite (SG = 5.2) is circulated. The magnetite creates a suspension with an artificial density that is between that of coal and rock. Consequently, lighter coal particles introduced into the medium float to the surface of the vessel where they are transported by the overflowing medium to a collection screen. Waste rock, which is much denser, sinks to the bottom of the vessel where it is collected by a series of mechanical scrapers called flights. The flights travel across the bottom of the vessel and eventually drag the waste rock over a discharge lip at one end of the separator. The unit is highly flexible since the quality of the clean coal product can be readily adjusted by varying the density of the medium from 1.3 to 1.7 SG by controlling the amount of magnetite and water introduced into the suspension.

Particles smaller than about 0.5 mm float or sink too slowly in a static vessel to be effectively separated. Therefore, dense medium cyclones (DMCs) are typically used to clean coal and rock in the size range between 0.5 and 12.5 mm. These high-capacity devices (Fig. 9) make use of the same basic principle as dense medium vessels, i.e., an artificial magnetite-water medium is used to separate low-density coal from high-density rock. In this case, however, the rate of separation is greatly increased by the gravitational effect created by passing medium and coal through one or more cyclones. Dense particles of rock sink in

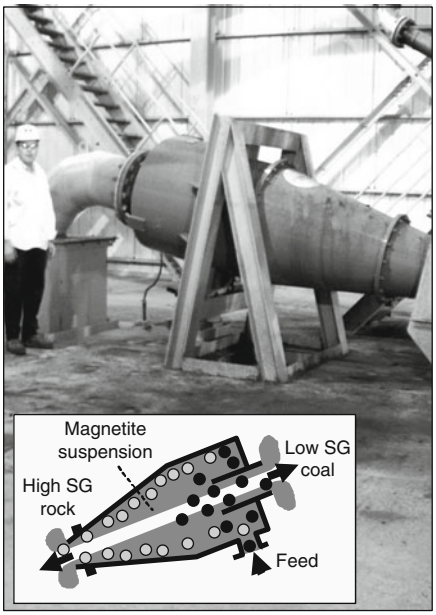

Coal Preparation. Figure 9
Dense medium cyclone used to separate small coal and rock

Coal Preparation. Figure 10
Bank of twin water-only cyclones used to separate fine coal and rock

the rotating medium and are pushed toward the wall of the cyclone where they are eventually rejected out the bottom. Lighter particles of coal rise to the surface of the rotating medium and are carried with the bulk of the medium flow out the top of the cyclone. Recent advances in cyclone technology have allowed the upper particle size limit for DMCs to increase in many current applications to 60–75 mm. This development has made it possible to simplify plant circuitry in some facilities by eliminating the need for a dense medium vessel.

The primary disadvantage of dense medium processes is that they require considerable ancillary equipment to support the operation. A typical circuit requires that the clean coal and rock products pass over drain-and-rinse (D&R) screens to wash the medium from the surfaces of the products and to dewater the particles. The medium recovered from the drain section is circulated back to the separator by a pump, while medium from the rinse section is diluted by spray water and must be concentrated before being fed back. The concentration is achieved using magnetic separations that effectively recover magnetite from nonmagnetic particles that would otherwise contaminate the circulating medium.

Water-Based Separators A wide variety of water-based density separators, which avoid the need to utilize a artificial dense medium, are also available for separating coal and rock in the particle size range between 0.15 and 1 mm. The most common methods include water-only cyclones (WOCs) and spirals. A WOC is similar to a classifying cyclone, but typically has a stubby wide-angled conical bottom (Fig. 10). Separations occur in a WOC due to differences in the settling rates of coal and rock in the centrifugal field within the cyclone. The separation is also enhanced by the formation of autogenous medium created by the natural fines already in the feed slurry. These units are often employed in two stages or in combination with other water-based separators to improve performance.

Another water-based separator for treating fine coal that has grown tremendously in popularity is the spiral concentrator (Fig. 11). A spiral consists of a corkscrew shaped conduit with a modified semicircular cross-section. During operation, feed slurry is introduced to the top of the spiral and is permitted to flow by gravity along the helical path to the bottom of the unit. Particles in the flowing film are stratified such that lighter coal particles are forced to the outer wall of the spiral,

whereas heavier particles are forced inward to the center of the spiral. The segregated bands of heavy to light materials are collected at the bottom of the spiral. Adjustable diverters (called splitters) are used to control the proportions of particles that report to the various products. A three-product split is usually produced, giving rise to three primary products containing clean coal product, refuse and misplaced "middlings." Because of the low unit capacity (2–4 t/h), spirals are usually arranged in groups fed by an overhead radial distributor. To save space, several spirals (two or three) may be intertwined along a single central axis. Spirals have been successfully utilized in combination with WOCs to improve the efficiency of separating fine coal.

Froth Flotation Separators The smallest size fraction of coal (<0.15 mm) cannot be effectively separated using density-based separators. For these particles, a process known as froth flotation must be used. Flotation is a physicochemical process that separates particles based on differences in surface wettability. Flotation takes place by passing finely dispersed air bubbles through an aqueous suspension of particles. A chemical reagent, called a frother, is added to promote the formation of small bubbles. Typical addition rates are in the order of 0.1–0.5 lb of reagent per ton of coal feed. Coal particles, which are naturally hydrophobic, selectively attach to air bubbles and are buoyed to the surface of the pulp where they are collected from a coal-laden froth bed that forms atop the cell. Most of the impurities that associate with coal are hydrophilic and remain suspended until they are discharged as a dilute slurry waste. Another chemical additive, called a collector, may be added to improve the adhesion between air bubbles and coal particles. Collectors are commonly hydrocarbon liquids such as diesel fuel or fuel oil. In some plants, clay slimes (<0.03 mm) are removed ahead of flotation using small diameter classifying cyclones to minimize the carryover of the high ash slimes into the froth product with the process water.

Most industrial installations make use of mechanical flotation machines (Fig. 12). These machines consist of a series of agitated tanks (4–6 cells) through which fine coal slurry is passed. The agitators are used to ensure that larger particles are kept in suspension and to disperse air that enters down through the rotating shaft assembly. The air is either injected into the cell using a blower or drawn into the cell by the negative pressure created by the rotating impeller. Most

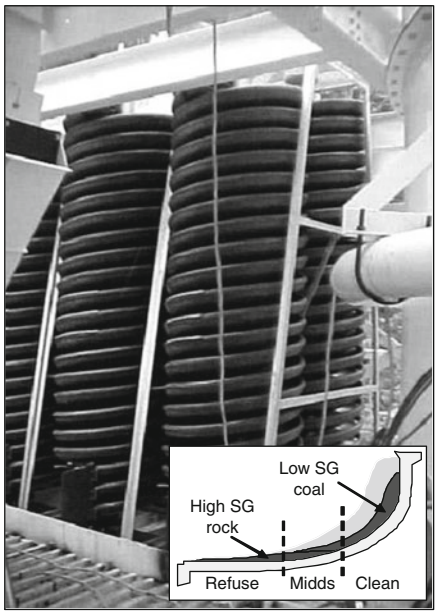

Coal Preparation. Figure 11
Bank of spirals used to separate fine coal and rock

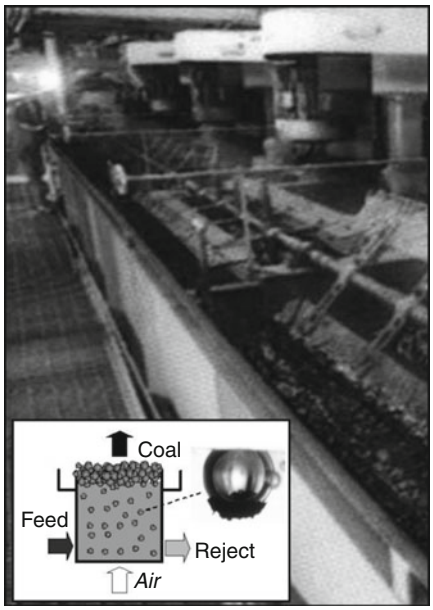

Coal Preparation. Figure 12
Conventional flotation bank used to clean ultrafine coal

commercial units are very similar, although some variations exist in terms of cell geometry and impeller design. A disadvantage of conventional flotation cells is that they allow a small amount of clay slimes to be recovered with the water that reports to the froth product. Therefore, in cases where high clay concentrations are expected, advanced flotation processes such as column cells (Fig. 13) are often used. Column cells virtually eliminate the recovery of clay slimes by washing the froth with a countercurrent flow of water. This feature allows columns to produce a higher purity coal product without sacrificing coal recovery.

Unit Operations for Coal Dewatering

Solid–liquid separators are used downstream of coal cleaning processes to remove unwanted surface moisture from the sorted products. Excess moisture lowers the heating value of the coal, may lead to handling/freezing problems, and increases the overall costs of transporting the coal to customer sites. As shown in Fig. 3c, several different types of mechanical dewatering methods are required depending on the size of particles to be treated. The removal of water from the surfaces of coarser (>5 mm) coal is predominantly carried out using screens, where the prime force involved is gravity. Finer particles have a higher surface area and tend to have correspondingly higher moisture content. There finer particles are typically dewatered using centrifugal methods or filtration systems.

Centrifugal Dewatering Centrifugal dryers, which consist of a rotating screen or basket, use centrifugal force to pull water away from the surfaces of coal particles. These devices operate in much the same fashion as the spin cycle in a washing machine. For coarser fractions, two popular centrifugal dryers are the vibratory centrifuge and the screen-scroll centrifuge. The vibratory centrifuge (Fig. 14) uses a vibrating mechanism to move solids through the unit, while the screen-scroll design uses a screw conveyor to move the solids. For finer particles (<1 mm), both the screen-scroll centrifuge and another popular design, called a screen-bowl centrifuge, may be used. The screen-bowl centrifuge is a horizontal unit that consists of both a solid bowl section and a screen

Coal Preparation. Figure 13
Column-type flotation cell used to clean ultrafine coal

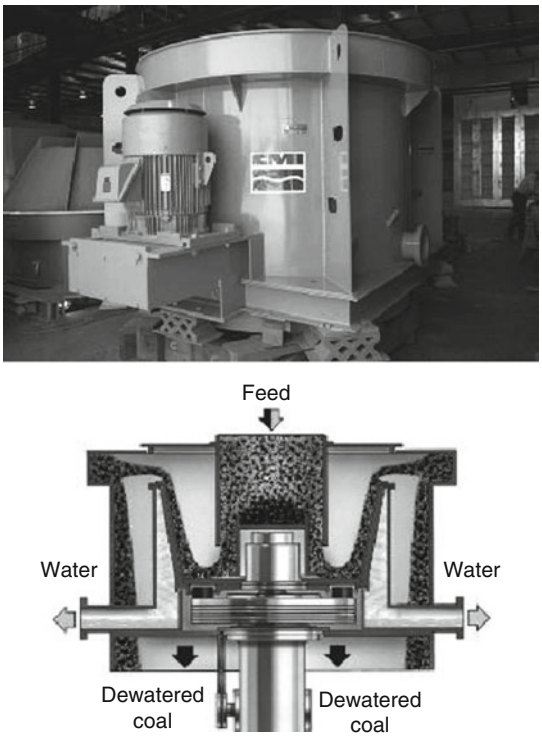

Coal Preparation. Figure 14
Vibratory centrifugal dryer used to dewater small/fine coal

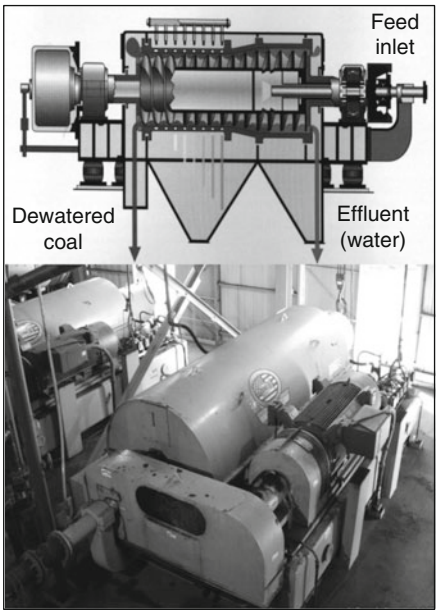

Coal Preparation. Figure 15
Screen-bowl centrifuge used to dewater fine coal

Coal Preparation. Figure 16
Disc vacuum filter used to dewater fine coal

section (Fig. 15). Feed slurry is introduced into the bowl section where most of the solids settle out under the influence of the centrifugal field. A rotating scroll transports the settled solids up a beach and across the screen section where additional dewatering occurs before the solids are discharged. Solids that pass through the screen section are typically added back to the machine with the fresh feed. This unit is capable of providing low product moistures, although some ultrafine solids are lost with the main effluent that is discarded from the solid bowl section.

Filtration Dewatering Filtration processes may be used to dewater fine coal whenever a high coal recovery is desirable. Filtration involves the entrapment of fine solids as a cake against a porous filtering media. Traditionally, flotation concentrates have been dewatered using some form of vacuum filtration. These units are capable of high coal recoveries (>97%) while generating product moisture in the 20–30% range. The most popular type of vacuum filter is the disc filter (Fig. 16). This device consists of a series of circular filtration discs that are constructed from independent wedge shaped segments. At the beginning of a cycle, a segment rotates down into the filter tub filled with fine coal slurry. Vacuum is applied to the segment so that water is drawn through the filter media and a particle cake is formed. The resultant cake continues to dry as the segment rotates out of the slurry and over the top of the machine. The drying cycle ends when the vacuum is removed and the cake is discharged using scrapers and a reverse flow of compressed air.

Thermal Dewatering Thermal dryers have been successfully employed in the coal industry to reduce clean coal moisture to single-digit values whenever mechanical dewatering processes are incapable of meeting contract specifications. The most popular design is the fluidized bed dryer (Fig. 17), which uses coal, oil or gas as the fuel source to heat the incoming air stream. The amount of fuel required depends on the amount of water that must be evaporated which, in turn, depends on the amount of coal fed to the dryer and the percentage of water in the dewatered product [4]. When operating correctly, thermal dryers can reduce the clean coal moisture to less than 6% by weight at a unit cost proportional to the tonnage of water evaporated [5]. Unfortunately, thermal dryers require high capital costs, often in excess of several million or more. Dryers can also suffer from emission problems associated

Coal Preparation. Figure 17
Thermal dryer used to dry coal to low moisture contents

fugitive dust and poor opacity. Emissions of nitrous oxides, sulfur dioxide, volatile organic compounds (VOCs) may also present issues for some sites seeking operating permits. Moreover, thermal drying of combustible particles of coal can present safety hazards resulting from accidental fires or dust/gas explosions.

Thickening and Clarification Another essential solid–liquid separation process used in coal preparation is thickening. Thickening (or clarification) processes are used to treat the process water so that it can be recycled and reused within the plant. A thickener consists of a large tank in which particles are permitted to settle, thereby producing a clarified overflow and thickened underflow (Fig. 18). Thickeners are usually fed dilute slurry (<5–10% solids) that is rejected from the fine coal cleaning circuits. The clarified water that overflows along the circumference of the thickener is recovered and reused as process water. The thickened underflow, which often contains 20–35% solids, is transported to the center of the thickener by a series of rotating rakes. The thickened sludge is then pumped to an appropriate disposal area or is further dewatered prior to disposal. Chemical additives (coagulants and flocculants) are usually introduced ahead of the thickener to promote the aggregation of ultrafine particles

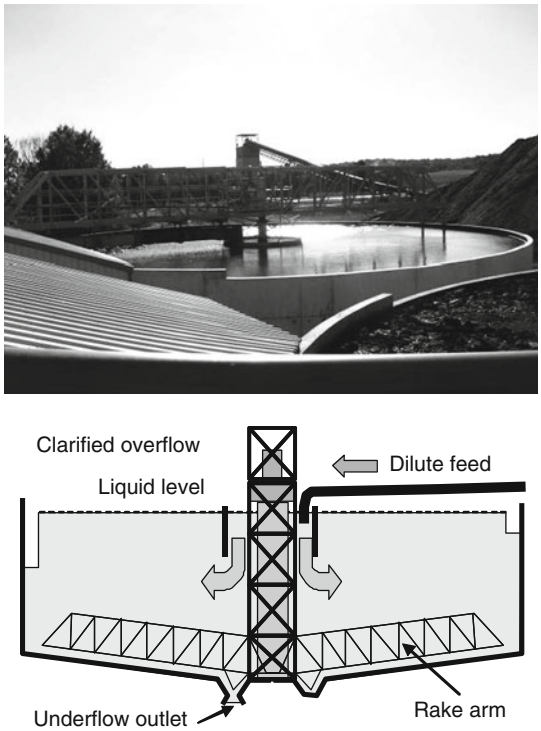

Coal Preparation. Figure 18
Conventional thickener used to clarify process water and thicken solids

so as to enhance water clarity and increase settling rates. The pH levels must also be carefully monitored and controlled. Conventional thickeners, which are typically 50–200 ft diameter, require constant monitoring to ensure that overflow clarity and underflow density is maintained and the rake mechanism is not overloaded. A torque sensor on the central drive is typically used to monitor rake loading, while a nuclear density gauge is often used to monitor underflow density.

Waste Disposal and Storage

The separation processes used in coal preparation often generate large volumes of waste rock and slurry. As a result, the final step in coal preparation involves the disposal and permanent storage of these waste products into various types of surface and/or underground repositories. Although many variations exist, a common approach is to use separate refuse piles and slurry impoundments. Refuse piles are designed to

receive coarse particles of waste rock that can be easily dewatered by screens or sieves. This material is relatively easy to handle and can be transported by truck or belt haulage systems to the disposal area. On the other hand, fine coal wastes are difficult to dewater and are typically discarded in slurry form. The waste slurry contains water, coal fines, silt, clay and other fine mineral particles from the processing plant. In most cases, the slurry is discarded into an impoundment (Fig. 19). An impoundment is an engineered structure consisting of a large volume earthen settling basin formed behind a man-made dam or embankment. The dam or embankment is usually constructed from compacted coarse refuse material. The waste slurry is transferred to the impoundment by pumping thickened underflow from the plant thickener through a pipeline. The volume of the impoundment must be sufficiently large to ensure that fine particles settle by gravity before the clarified water at the surface is recycled back to the plant for reuse.

Beneficial Impacts of Coal Preparation

Coal preparation provides several attractive benefits from both an economic and environmental perspective.

Coal Preparation. Figure 19
Active slurry impoundment used for fine waste disposal (before reclamation)

The most recognized of these include increased coal reserves, lower transportation costs, improved utilization properties and abatement of pollution.

Coal Reserves

Perhaps no other technology has had a greater impact on expanding the reserve base of economically recoverable coal than coal preparation. Preparation plants employ low-cost physical separation processes to convert run-of-mine coal resources into saleable coal reserves. The percentage of clean coal tonnage generated from each ton of run-of-mine coal is commonly referred to as plant yield. This parameter is one of the most difficult to estimate when evaluating the reserve base for a previously undefined coal property. The yield can be influenced by several factors including the quality of the in-place coal, the washability (separating characteristics) of the run-of-mine coal, the efficiency of the separation processes used by the preparation facility and the strictness of the quality demands imposed by the coal consumer. The quality of the in-place can be affected by small changes to mining practices that directly influence out-of-seam dilution. Variations in washability, which reflect the selective liberation of composite particles of intermixed coal and rock, can also make estimations of coal yield unreliable when coal is subjected to size reduction.

The average yield produced by coal preparation plants has steadily declined over the years due to a depletion of lower ash feeds and increased mining mechanization. For example, Fig. 20 shows the yield of clean coal currently obtained from a random survey of several major plants operating in the eastern USA. It is not uncommon for eastern operations to experience yields under 30–35%, thereby producing only 1 t of clean coal from three or more tons of mined product. An estimate complied from production records supplied by coal producers suggests that the average yield is now less than 50% (i.e., 49.8% $\pm$ 3.5%) for the total USA. This situation is expected to worsen as eastern reserves become thinner and more challenging to mine. A study reported by Weisenfluh et al. [6] indicated that nearly 52% of the remaining eastern Kentucky coalfield resources are located in coal seams that are 0.35–0.70 m in thickness, while 31% are in 0.70–1.1 m thick seams. Likewise, a study of the Virginia

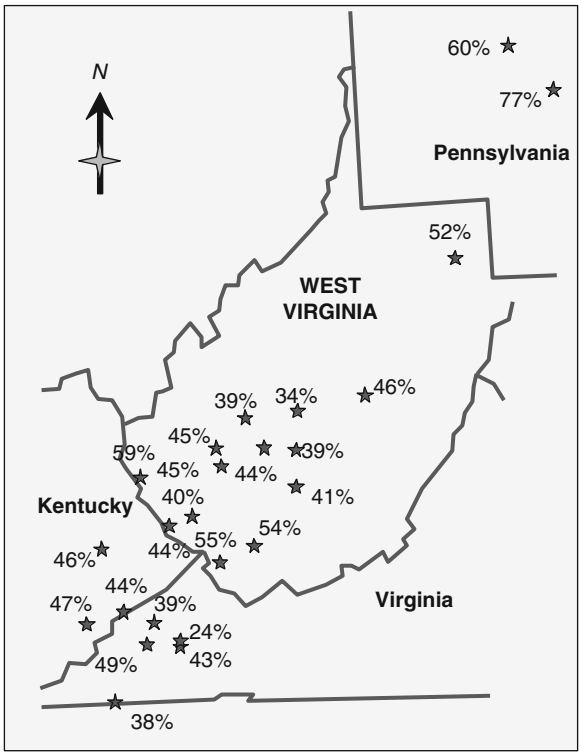

Coal Preparation. Figure 20
Examples of clean coal yield values for a selected sampling of eastern US plants

coalfields found that 30% of the total reserve base (more than 200 million tons) exists in seams with a thickness less than 0.70 m [7]. Consequently, ever increasing amounts of rock from out-of-seam dilution are being mined, loaded and hauled to preparation plants for removal and disposal.

Coal Transportation

Most of the coal consumed in the USA is used for the production of electricity. The cost of transporting the coal to the power station is usually borne by the utility and paid based on the delivered tonnage. The mine operator is also paid by the utility based on tonnage, although the unit price is typically adjusted up or down to account for the actual heat content of the supplied coal fuel. In most cases, this simple pricing structure provides the base economic justification for the operation of coal preparation facilities. The high-ash rock rejected by coal preparation plants contains insufficient heating value to justify the shipment of this material to the utility. The savings in transportation costs are directly proportional to the increase in heating value.

Cost–benefit studies suggest that the economics of coal production are more sensitive to transportation cost than to any other factor. For example, a study by Norton [8] was one of the first to demonstrate how unfavorable changes in the cost of mining, processing and transportation affect profitability. The study concluded that the cost of coal transportation had the greatest overall impact on total revenue. This study also indicated that the clean coal yield was second only to transportation cost in determining revenues. In contrast, increases in the capital and operating costs of the coal preparation plant had only a minor impact on revenue. Therefore, any steps taken to reduce preparation costs (fewer capital improvements, less maintenance, workforce reductions, etc.) usually need to be closely examined to ensure that clean coal yield is not adversely impacted by these cost-cutting measures.

Utility Performance

The thermal efficiency of a power station is very important. A higher efficiency is obviously beneficial from an economic perspective since this provides a proportional improvement in generated revenue for the power station. Moreover, a higher efficiency also reduces the production of greenhouse gases and other pollutants of environmental concern since less coal fuel needs to be burned per unit of electrical power generated.

One method for improving thermal efficiency is to use washed coals of higher quality can significantly improve the thermal efficiency of a boiler [9–12]. Higher quality coals are more reactive and require less excess air for effective combustion, thereby improving efficiency via a reduction in heat lost with the flue gas. Higher quality coals also improve efficiency by avoiding fouling/slagging problems in the boiler, which tend to raise the flue gas temperature and increase heat losses. The extent to which the proper application of coal preparation technology improves thermal efficiency is highly case specific and difficult to predict from purely theoretical considerations. The most reliable data for quantifying efficiency improvements are typically reported based on actual plant

studies. One such classic study [13] monitored improvements to boiler performance resulting from switching from an untreated coal (15% ash and 3.5% sulfur) to washed coal (9% ash and 2.8% sulfur) from the same mine. Despite the modest improvement in coal quality, the boiler efficiency increased from by about 1.5 absolute percentage points as a result burning better quality coal. The capacity factor also rose by almost 10% due to less fouling/slagging problems.

The use of coal preparation technologies to improve boiler efficiency has also been a major benefit reported in other nations. The International Energy Agency (IEA) estimates that coal-fired power plants in India can increase thermal efficiency by up to 10 percentage points by switching from unwashed to washed coal [14]. China also expects to make greater use of coal preparation technology to improve thermal efficiencies and environmental performance [15]. The average thermal efficiency in China has been reported to be less than 29% [16], compared to around 38% in OECD countries. As such, coal preparation is expected to continue to have a large impact on the international community.

Another benefit of coal preparation is that it removes impurities that have a significant influence on the O&M costs for a coal-fired boiler. Studies have demonstrated that the removal of abrasive mineral impurities such as pyrite and quartz can substantially reduce wear rates and increase the throughput capacity of utility pulverizers [17, 18]. The impacts associated with the abrasive wear and slagging/fouling of boiler tubes can also be mitigated to a large extent by utilizing washed coals that have been properly cleaned to remove unwanted mineral matter [19–21]. Vaninetti and Busch [22] have provided a detailed description of these problems and have developed empirical formula that can be used to assist in the evaluation of changes to coal quality in specific types of boilers.

The handling characteristics of solid coal are also an important issue. A poor handling coal may hang in railcars, plug chutes and bins and stick to conveyor belts. These problems may result in unscheduled shutdowns, thereby reducing power station availability. Washed coals from preparation plants typically have superior handling characteristics to run-of-mine coals, especially if all or a portion of the ultrafines have been removed. These coals also typically present fewer problems in terms of unwanted dust generation, solids run-off during precipitation events and freezing problems during colder months [23].

Pollution Abatement

Coal preparation plays an important role in reducing the emissions of pollutants that associate with the mineral matter contained in coal. These emissions normally include solid particulate emissions such as fly ash as well as gaseous emissions of precursors associated with acid-rain and air toxics. These emissions are strictly regulated for coal-fired utilities through various legislative acts such as the 1990 Clean Air Act Amendment (CAAA) and 2005 Clean Air Interstate Rule (CAIR). Moreover, coal preparation has a beneficial impact on reducing greenhouse gas emissions by increasing the thermal efficiencies.

Noncombustible impurities present in the feedstocks supplied to coal power stations generate waste steams as either bottom ash/slag or fly ash. Of these, the finest particles of fly ash emitted to the atmosphere are considered to be of greatest environmental concern due to their potential adverse impact on human respiratory health [24]. Power stations make use of several types of effective control technologies to minimize fine particulate emissions. These postcombustion technologies include efficient processes such as electrostatic precipitators (ESPs), fabric filters (FFs), cyclones and wet scrubbers. Modern control systems typically achieve better than 99.5% removal of all particulates and exceed 99.99% in some cases. However, standards for particulate emissions continue to become increasingly stringent as reflected by expanded regulations by the US EPA to include particles finer than 2.5 μm in new ambient air quality standards [25]. As such, there is continued interest in removing greater amounts of particulates upstream of other emission controls using coal preparation technologies.

The separation processes used in coal preparation plants remove noncombustible minerals that ultimately affect the amount and type of particulate matter (PM) that passes downstream to emission control systems. For these systems, proper levels of coal washing can be identified that effectively reduce ash loading and improve removal efficiencies. A recent presentation by American Electric Power to the Asia Pacific

Partnership [26] concluded that "*Consistent and proper quality coal is best tool to improve plant operating performance and reduce PM and SO_2 emissions. Removal of some of the coal ash (includes rocks) at the mine is more economic than in the pulverizer, boiler, precipitator and scrubber.*" Washing also minimizes the total amount of high-surface-area fly ash that is more hazardous to dispose due to its high reactivity. Even in cases where particulate controls are currently deemed adequate, greater use of coal preparation may be required in the future to compensate for deterioration in feedstock quality as higher quality coal reserves become depleted.

Coal preparation has also played an important role in environmental compliance by reducing the sulfur contained in coal feedstocks prior to combustion [27]. Sulfur occurs in coal as three distinct forms (e.g., sulfate, organic and pyritic). Sulfate sulfur is present in very small quantities and is not considered a serious problem. Organic sulfur, which is part of the basic structure of coal, is not removable by conventional cleaning. The precombustion removal of organic sulfur is possible using chemical cleaning methods; however, these elaborate processes are not economically competitive with flue gas scrubbing. Pyritic sulfur is present as discrete inclusions of iron sulfides distributed within the coal matrix. As such, this form of sulfur has the potential to be removed by physical cleaning processes such as coal preparation [28]. Fortunately, many of the high sulfur coals in the USA also contain a high proportion of pyritic sulfur (Fig. 21).

Coal preparation plants have been reported to remove up to 90% by weight of pyritic sulfur, although rejections are typically in the 30–70% range due to liberation constraints [28–30]. When compared to the postcombustion control of sulfur, coal preparation offers several distinct advantages including improved market flexibility, lower scrubber loading and concurrent removal of other impurities (ash, trace elements, moisture, etc.). Although coal preparation does not directly impact the nitrogen content of coal, washing has been shown to help reduce NO_x emissions by providing a consistent high quality fuel that makes it easier to control the combustion environment [31].

Coal preparation also has a tremendous impact on the amount of air toxics released to the atmosphere. The 1990 CAAA contained provisions that established new emission standards for a variety of air toxics, which

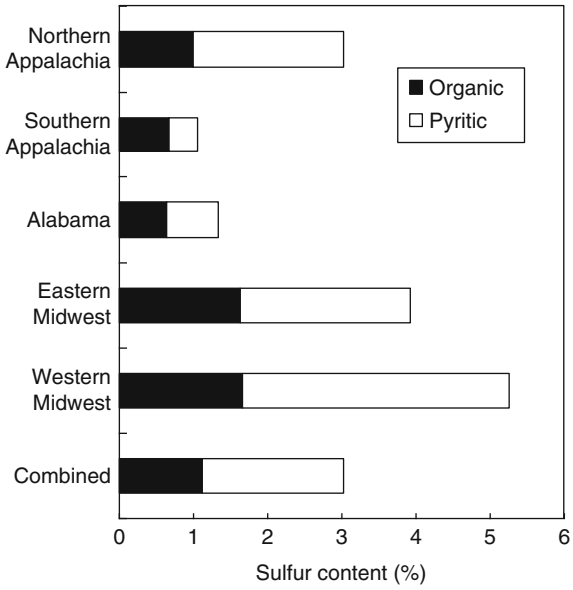

Coal Preparation. Figure 21
Distribution of sulfur types typically in US coals (After Cavallaro et al. [29])

are commonly referred to as hazardous air pollutants (HAPs). Many of the HAPs identified in the CAAA are present as trace elements in coal [32, 33]. Some of the most noteworthy of these are antimony, arsenic, beryllium, cadmium, chlorine, chromium, cobalt, fluorine, lead, manganese, mercury, nickel, selenium and radionuclides. The concentrations of these elements are known to vary considerably from seam to seam, and in some cases within the same seam [34, 35]. During combustion at electrical utilities, these elements may be released to the atmosphere as solid compounds with the fly-ash and in the vapor phase with the flue-gas. Existing post-combustion control technologies, such as electrostatic precipitators, can be reasonably effective in reducing the concentration of trace elements associated with fly-ash. These commonly include elements such as antimony, beryllium, cadmium, cobalt, lead and manganese. Capture efficiencies of >97% have been reported for electrostatic separators [36]. On the other hand, trace elements such as arsenic, chlorine, mercury and selenium have the potential to volatilize and are less effectively controlled by postcombustion methods.

Studies have shown that many of the HAP precursors identified in the CAAA are associated with the

mineral matter commonly rejected by coal preparation plants. This approach to HAPs control is attractive since the waste rock rejected by coal preparation plants is coarser and has a lower reactivity than the high-surface-area ash generated by power stations [37]. In-plant sampling campaigns conducted by various researchers [36, 38] suggest a good correlation between the rejection of mineral matter and the removal of trace elements during physical cleaning. These findings are also supported by laboratory float–sink tests performed using a variety of eastern US coals [39–41]. These data suggest that trace elements are typically rejected at levels of 40–70% by weight using conventional preparation technologies. These values appear to be in good agreement with earlier values reported by Fonseca et al. [36], which showed an average trace element removal by conventional coal preparation of approximately 64% for six different coals (Fig. 22). On the other hand, the large degree of variability observed in the data from these and other studies suggest that the rejections of trace elements by coal preparation are very site specific and need to be quantified on a case by case basis.

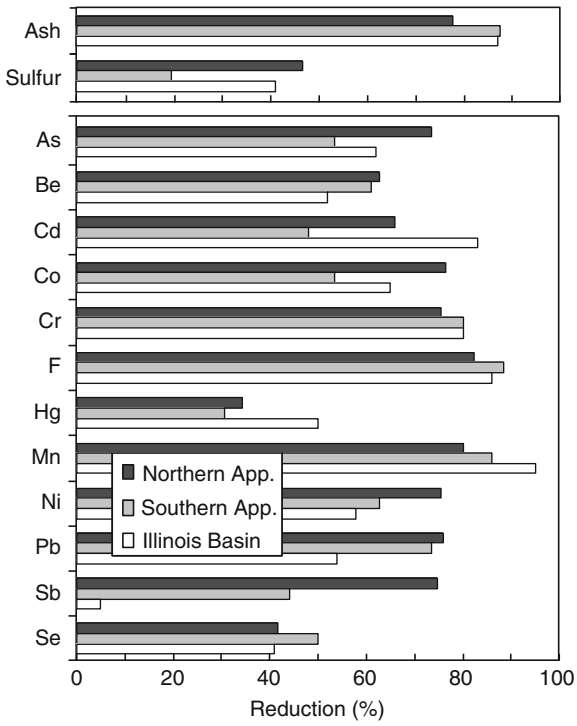

Coal Preparation. Figure 22
Reduction in trace element content after coal preparation (After Fonseca et al. [36])

Of the air toxics reduced by coal preparation, mercury is perhaps the trace element in coal of greatest environmental concern [35]. Mercury can be released during coal combustion and subsequently deposited in the environment. Ecological studies have shown that mercury bio-accumulates in the food chain as higher species consume lower life forms exposed to mercury contamination [42]. Data reported by the US Environmental Protection Agency (EPA) indicate that coal-fired utilities are currently the largest human-generated source of mercury releases in the USA. It is estimated that these plants release approximately 48 t annually [43]. In order to curb these emissions, EPA issued the world's first-ever rule to cap and reduce mercury emissions for coal-fired power plants. Compliance options available to utilities include postcombustion capture of mercury by existing or new flue gas scrubbing technologies as well as precombustion control of mercury by coal preparation and coal switching [44].

A recent study by Quick et al. [45] showed that the mercury content of coal delivered to utilities (based on ICR data) was lower than that of the in-ground coal resources in the USA (based on COALQUAL data). This comparison is shown in Fig. 23 for the primary eastern coal producing states. Based on this study, Quick et al. [45] concluded that "...selective mining and more extensive coal washing may accelerate the current trend toward lower mercury content in coal burned at US electric utilities..." and "...since recent reductions of sulfur emissions from coal-burning electric utilities are largely due to a declining sulfur content of delivered coal, rather than from scrubbing combustion gases, these simple, low-cost approaches to reduce Hg emissions should not be overlooked."

According to Alderman [46], cleaning can reduce mercury by more than 50% in many eastern and western coals and lignites, excluding southern Powder River basin coals. Greater rejections of mercury by coal preparation appear to be limited by inadequate liberation and/or the presence of organically associated mercury. Several studies have suggested that mercury has some degree of association with the iron sulfides present in many run-of-mine coals [47–49]. In fact, the data summarized in Fig. 24 suggest that the concentration of many metallic elements found in coal often correlate

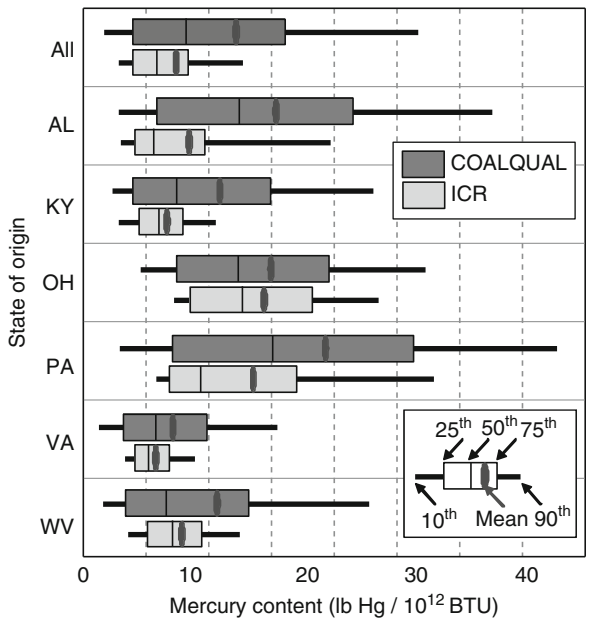

Coal Preparation. Figure 23
Comparison of mercury contents for delivered (ICR) and in-ground (COALQUAL) coals (after Quick et al. [45])

well with the presence of sulfide minerals [50]. As a result, the rejection level for mercury is often in the same range as the pyritic sulfur rejection for coals subjected to coal preparation. While liberation can be improved by reducing the topsize of the feed coal [51], this approach is difficult to justify in today's marketplace due to the high costs associated with the fine grinding of coal [28]. Moreover, fine particles are also difficult and costly to upgrade, dewater and handle in existing coal preparation facilities.

Another important impact of coal preparation is in the reduction of greenhouse gas emissions resulting from improvements in thermal efficiency, i.e., less CO_2 is produced per unit of electricity generated. Calculations indicate that a one percentage point improvement in thermal efficiency provides a two to three percentage point reduction in CO_2 emissions for a typical coal-fired utility. An investigation conducted by Couch [52] indicated that there are more than 4,000 coal-fired boilers (>50 MW capacity) worldwide that could improve thermal efficiencies and reduce CO_2 emissions by using coal preparation to improve coal quality. Moreover, von Hippel and Hayes [53] have noted that coal preparation reduces the amount of energy consumed (and CO_2 generated) during coal transportation by increasing the specific heating value of the delivered coal. Smith [13] also found that freshly mined coals subjected to coal preparation processes tended to display slower releases of methane, another greenhouse gas.

Challenges for Coal Preparation

Coal preparation offers may attractive benefits for coal-fired power generation. These typically include lower transportation costs, improved properties for coal utilization and reduced emissions of particulate and gaseous pollutants. However, the industry also faces several challenges that need to be resolved to ensure that preparation plants can continue to operate at a profit without damage to the environment. These concerns can be generally classified as technical factors that relate to shortcomings in current processing systems, environmental factors that involve improving waste handling and disposal, or health and safety factors that may affect workers or citizens in the surrounding area.

Technical Issues

Cleaning of Fine Particles The freshly mined coals that are fed to coal preparation plants are typically crushed to liberate rock before washing and to limit the largest size of particles that enter the plant. Operators prefer to keep the particles as large as possible (usually >50 mm) since fine coal processes are considerably less efficient and substantially more costly. This is unfortunate since the amount of high quality recoverable coal within a given reserve can theoretically be increased by crushing. The size reduction improves the liberation by reducing the population of intermixed composite particles of coal and rock. A study conducted by DOE [30] indicates that the reserves of compliance coal in central Appalachia could be nearly doubled by efficiently cleaning at a particle size of 1 mm (Fig. 25). Although a systematic assessment has not been performed to date for trace elements, the size reduction would also be expected to substantially improve the removal of coal-related pollutants other than just ash and sulfur.

Unfortunately, the solid–solid separation processes used industrially to treat fine coal represent the single

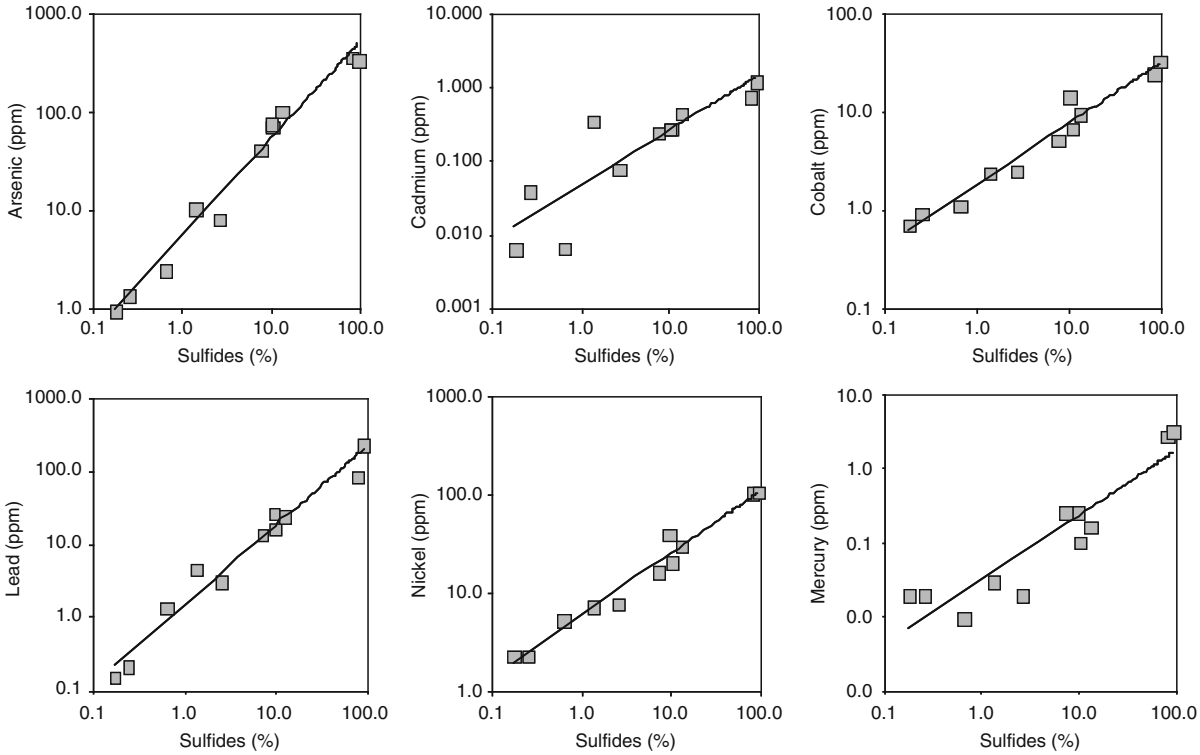

Coal Preparation. Figure 24
Effect of sulfide mineral content on the concentration of trace metals in a sample of Pittsburgh seam coal (After Luttrell et al. [50])

greatest loss of potentially recoverable coal in a preparation facility. Field studies indicate that the froth flotation process, which is normally used to recover <0.2 mm coal, typically recovers only 60–80% of the organic matter in this size range. This surface-based separation is inherently less effective in removing pyritic sulfur than density-based processes used to treat the coarser sizes of coal [54]. As such, the desulfurization of fine particles is also often poor in many operating preparation facilities. Therefore, the development of effective, low-cost processes for treating fine coal is a major need for the preparation industry. Effective solutions need to be found for improving the recovery, selectivity and capacity of froth flotation processes. This goal may be achieved through fundamental and applied studies that seek to understand and improve flotation chemistry, equipment design and process control. In addition, new types of density separators need to be developed for treating fine coal. Centrifugal separators such as enhanced gravity concentrators, which have been successfully applied in the gold industry, may prove useful for this purpose. These devices have the potential to reject significantly greater amounts of pyritic sulfur (and mercury) that is not efficiently removed using surface-based separators such as froth flotation [55, 56]. However, these machines have several limitations including low throughputs and control difficulties.

Dewatering of Fine Particles The solid–solid separation processes employed by modern coal preparation plants require large amounts of process water. After cleaning, the unwanted water must be removed from the surfaces of the particles using mechanical dewatering equipment. Inefficient removal of moisture lowers the heating value, increases transport costs and creates handling/freezing problems for the cleaned coal. Coarse particles can be readily dewatered using simple screening systems, while finer particles require

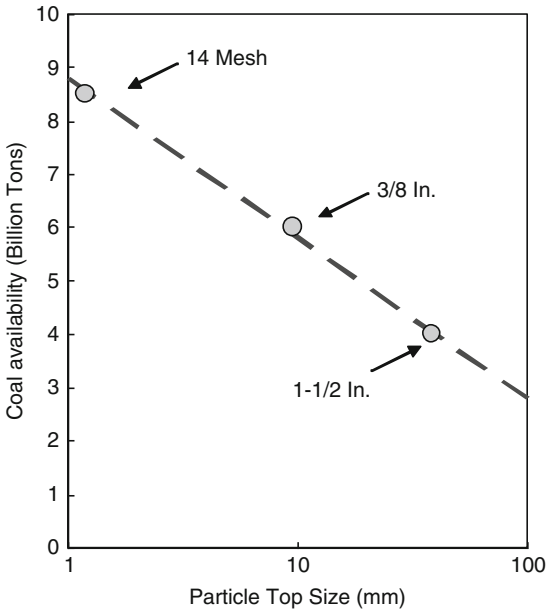

Coal Preparation. Figure 25
Effect of decreasing top size on low-sulfur coal availability (After Cavallero et al. [30])

more complicated unit operations such as centrifuges and filters. Unfortunately, the mechanical systems used to dewater fine coal are inefficient and costly [57]. Fines often represent as little as 10% of the total run-of-mine feed; however, this size fraction may contain one third or more of the total moisture in the delivered product.

The availability of low-cost mechanical dewatering equipment that can efficiently remove moisture from fine coal is widely considered to be an important need for the coal preparation industry. Existing technologies for fine coal dewatering tend to produce unacceptably high moistures exceeding 25–35% by weight or intentionally sacrifice half or more of the ultrafines as a waste in an attempt to lower the product moisture. In addition, these processes are typically the most energy intensive processes used in coal preparation, often consuming 6–12 kW/t/h of dry solids processed [58]. Thermal dryer systems can effectively reduce moisture; however, these massive units require very large capital expenditures that are difficult to justify in the coal industry. Also, indirect thermal drying systems (e.g., Holoflite and Torus Disc) typically require 200–400 kW/t/h of product for drying fine coal solids to single-digit moistures [59]. Moreover, stringent air quality standards make it impossible in many cases to obtain new operating permits for thermal dryers. Therefore, the coal preparation industry needs to develop new mechanical solid–liquid separation processes that are substantially more efficient in terms of removing moisture and less expensive to purchase, operate and maintain. Innovative systems are critically needed, which may require fundamental studies to identify controlling mechanisms that can lead to the development "breakthrough" technologies.

Sizing of Fine Particles There are many technical challenges for the coal preparation industry that directly relate to size–size separations. Size–size separations are required ahead of solid–solid separations since these units are only effective within a narrow particle size range. Vibrating screens are generally efficient and cost effective for sizing and dewatering coarser particles. On the other hand, screening systems for finer particles, particularly those finer than 0.5 mm, tend to blind easily, wear quickly, and suffer from low throughput and low efficiency. The misplacement of incorrectly sized particles into equipment not designed to handle such sizes can have a large adverse impact on both the separating performance and maintenance requirements for a preparation plant. Another important issue with screening is the desliming of coal products to remove ultrafine mineral sediments that are detrimental to quality and moisture. Many in the industry believe that the ability to screen ultrafine particles at sizes of 0.15 mm and smaller is particularly important.

In addition to new screening systems, breakthrough technologies in ultrafine classification are also needed in the coal preparation industry [60]. Classification is the separation of particles due to differences in settling velocities, which depends not only on particle size, but also on particle density and shape. Firth and O'Brian [61] noted that while existing classification systems were adequate for the coal preparation industry of the past, "...it is apparent that further improvements in yield/ash/moisture relationship achieved by coal preparation plants will require increased efficiency in this size separation step." The ability to classify and better utilize ultrafine particles will increase industry productivity and reduce the generation of wastes. Many in the industry believe that currently there is a lack of efficient

ultrafine sizing and desliming technologies for separating at cut sizes of 100 μm and finer.

On-Line Analysis and Control Tremendous strides have been made in the automation and control of coal preparation plants during the past several decades [62]. The application of on-line sensors together with programmable logic controllers (PLCs) has allowed modern plants to operate more efficiently and to improve safety by reducing manpower requirements. On the other hand, the industry continues to struggle with the determination in real-time of the quality of their coal products [63]. Analyzers are commercially available for the on-line analysis of many quality parameters for coal including ash, sulfur and moisture, although the measurement accuracy is often poor due to sampling and calibration issues. On-line analyzers do not currently exist that can be used to determine important data such as particle size distributions and washability in real-time. Therefore, improving automation, control and sensor technologies is a key challenge for the industry to overcome. Advances in on-line analysis would enhance the industry's ability to maximize the recovered energy in a marketable product and minimize the generation of unwanted wastes.

Environmental Issues

Environmental compliance in the coal mining industry is strictly controlled by government regulations. History suggests that these regulations were necessary in many cases to ensure uniform environmental stewardship across the industry as a whole. Today, mining companies accept these environmental standards as good business practice and, in some cases, may go beyond simple compliance to promote goodwill and to set an example for others. Nevertheless, potential environmental issues associated with coal processing still exist. These issues have been generically classified by the World Bank to include air emissions, wastewater, hazardous materials, solid wastes and noise [64].

Coarse Waste Disposal Of the various challenges facing the coal preparation industry, perhaps none are as significant as those which relate to waste handling and disposal. This importance can be attributed to the fact that coal cleaning operations produce large volumes of waste that must be discarded into refuse piles or impoundments. Refuse piles are designed to receive coarse particles of waste rock that can be easily dewatered. This material is relatively easy to handle and can be safely transported by truck or belt haulage systems to the disposal area with little or no potential for environmental damage. On the other hand, the waste contains solid and liquid components that may present long-term disposal problems depending on the sizes, types and quantities of minerals present and the conditions under which the wastes are stored (dry vs wet, loose vs compacted, etc.). The factors play a key role in establishing the structural integrity (slope stability, surface water run-off, sediment containment, seepage, etc.) and chemical nature (acid generation, metal dissolution, etc.) of the wastes. Solid sediments and dissolved may be transported by rainwater where it would pollute streams or groundwater. Many of these issues can be effectively managed via proper disposal practices and monitoring programs. On the other hand, uncertainties related to the intricate biochemistry and complex hydrology of the waste warrant continued investigation to fully assess the potential for negative impacts associated with long-term disposal of coarse waste. Overall, improved waste characterization, including better methods to define the nature of wastes from coal preparation operations, is considered by many to be a high-priority need for the coal preparation industry.

Slurry Disposal and Storage The handling and disposal of fine slurry waste is widely considered to be one of the most difficult challenges facing the coal preparation industry. Fine wastes have historically been discarded into earthen impoundments for permanent disposal. An impoundment is an engineered structure consisting of a large volume settling basin formed behind a man-made dam or embankment. The waste, which is difficult to dewater, is normally pumped from the preparation plant thickener to the impoundment as slurry. The slurry contains water, coal fines, silt, clay and other fine mineral particulates from the processing plant. In most cases, the slurry is retained behind a man-made embankment (earthen dam) constructed from compacted refuse material. The impoundment is designed to have a volume that is sufficiently large to ensure that fine particles settle by gravity before the

clear water at the surface is recycled back to the plant for reuse. In some cases, chemical additives may be used to promote settling and to control pH. According to the National Research Council [65], the coal industry discards 70–90 million tons of fine wastes each year into existing impoundments. There are 713 active impoundments and ponds, most of which are located in central Appalachia. In addition, it has been estimated that more than 2.5 billion tons of fine coal waste has been discarded in the past into existing and abandoned impoundments.

Impoundments, like any body of water contained behind a dam, can pose a safety and environmental risk if not properly constructed, monitored and maintained. Potential problems include structural failures, seepage/piping, overtopping, acid drainage and black water discharges. Since the well-known Buffalo Creek dam failure in 1972, strict engineering standards have been mandated by government agencies to regulate the design and operation of impoundments. A detailed report on the design and evaluation of tailings dams for the mining industry has been published by the EPA [66]. No failures of impoundment dams or overspills have occurred since this legislation was enacted. However, several breakthroughs of slurry into old mine workings beneath impoundments have occurred. The most notable was the Martin County incident, which released about 309 million gallons of slurry into streams and rivers in late 2000. A number of small accidental releases of black water have also been reported at various plant sites.

Several alternatives to impoundments have been employed by the coal industry in an attempt to avoid any future potential for environmental damage. These alternatives have been examined extensively by Gardner et al. [67]. For example, some mines use new modes of slurry disposal such as slurry cells and underground injection wells. Slurry cells have been used successfully in some cases (albeit at higher cost), but limitations associated with maintaining less than 20 acre-ft of settling area make this alternative difficult to apply in all cases. Likewise, the use of injection wells has raised public concerns about groundwater contamination and well water quality [68, 69]. To overcome these problems, various types of mechanical solid–liquid separators have recently been investigated as a means of more fully dewatering the fine solids prior to disposal. Notable examples include deep-cone (paste) thickeners and different types of filters (pressure, vacuum, belt press, plate-and-frame, etc.). Deep-cone thickeners have been shown to be capable of producing a paste of 45–55% solids as underflow in waste coal applications [70]. Ideally, the paste can be discarded as a stacked pile, thereby avoiding the need for impoundments to handle waste slurry. This technology has already been demonstrated projects at two mining sites in the eastern USA [71, 72]. Despite these advancements, the Committee on Coal Waste Impoundments [65] that recently examined the issue of slurry disposal concluded that "*. . .although there are alternatives to disposing of coal waste in impoundments, no specific alternative can be recommended in all cases.*" Therefore, in the absence of a preferred disposal method, continued development of new and improved processes and practices for slurry disposal is critically needed in the coal preparation industry.

Process Water Quality The overwhelming majority of cleaning processes used in coal preparation require large amounts of process water. Nearly all of the process water is supplied by thickening units, which settle out ultrafine suspended solids and recycle clarified water back into the plant. A small amount of fresh make-up water from an external source is usually required to satisfy the balance between moisture contents of solids entering and exiting with the plant. The clarification and recycling of process water provides an effective means of reducing fresh water demands and lowing environmental impacts. On the other hand, plant operators are faced with the difficulty of avoiding the buildup of suspended solids and dissolved substances in the process water. The effects of these components on separating performance and plant maintenance (e.g., rusting and scaling) are not well understood. Deterioration of process water quality is known to reduce sizing efficiency, lower flotation recovery and increase magnetite losses [73]. Evidence also exists suggesting that dissolved ions also adversely impact the performance of dewatering processes [74]. Detailed studies are needed to better understand these problems so that effective solutions can be identified and implemented before they impede preparation plant operations.

There are also growing concerns by the public that chemicals used in the process of coal may be harmful to the environment. The vast majority of coal is upgraded without being contacted with any chemical additives using density-based separation processes. On the other hand, finer coal particles (typically <0.2 mm) are processed using froth flotation circuits, which require small dosages of reagents known as collectors and frothers. Collectors consist of oily hydrocarbons, such as diesel fuel, kerosene and fuel oil, which are insoluble in water and coat fine coal particles. If required, dosages are typically less than 0.3–2 lbs of collector per ton of fine coal processed. Likewise, frothers are added to all flotation systems to promote the formation of small air bubbles and to create a stable froth. Frothers are typically various types of alcohol and/or polyglycol surfactants [75]. Addition rates for frothers are typically less than 10–15 ppm in the process water. In addition, plants add water treatment chemicals into their thickening circuits to enhance settling rates and improve water clarity. These reagents commonly include various types of natural and synthetic coagulants and flocculants. Polymer flocculants, which are added in very small amounts, are diluted in strength to 0.01–0.05% solutions with water to improve performance. These chemical are also widely employed in the purification of drinking water and food as well as in the treatment of sewage, paper-making, oil recovery, storm water run-off and many other types of industrial wastewater [76]. Finally, coal operations may occasionally use small amounts of dust suppressants or freeze inhibitors to address seasonal problems that may arise at the plant site.

Several studies have been carried out in recent years to assess the ecotoxicological impacts of chemicals used by processing plants. For example, several studies have raised concerns that seepage from impoundments containing mine influenced waters (e.g., residual chemicals, particulates, acid drainage) may be impacting the population of fresh water muscles/mollusks in tributaries around coal mining and processing facilities [77]. Many of these issues were addressed in a recent symposium hosted by the Nature Conservancy that addressed the coexistence of coal mining and healthy aquatic ecosystems [78]. Another recent study commissioned by the New Zealand Auckland Regional Council (ARC) examined the effects of residual coagulants and flocculants on natural waters [79]. The study concluded that the negative impacts of these chemicals were "... low level and not likely to be significant in relation to other factors which govern the health of aquatic communities. The benefit of reduced sediment levels in discharges is considered to outweigh the risk of any low level impacts attributable to residual flocculants." However, the study noted that improper application of these chemicals associated with misusage or overdosing may create an environmental risk. Therefore, to avoid these concerns, the development of new technologies that eliminate and/or significantly reduce the additions of process reagents is desirable as a long-term solution to this potential problem. In the near-term, it is likely that chemical manufacturers will continue to develop low-risk "green" reagents for use in coal preparation facilities. Many plants that dispose of waste slurry via underground injection have successfully switched to natural flotation collectors, such as blends of canola oil, vegetable oil, soybean oil, etc., as environmentally friendly replacements for petroleum-based hydrocarbon collectors [80].

Air Quality and Dust The US EPA promulgated standards of performance for air quality for all new and modified coal preparation plants under the 1976 Clean Air Act. These New Source Performance Standards (NSPS) address all types of particulate emissions, including fugitive dust, which may result from producing, handling, transporting and storing coal. Operations impacted by such regulation include crushers and breakers, sizing equipment, cleaning systems, thermal dryers, conveying systems, coal storage areas and coal transfer/loading systems that are directly part of the coal preparation facility. For some processes, such as thermal dryers, opacity less than 10% must be maintained [81]. Dusting problems are not uncommon around material handling transfer points where ultrafine particles have the opportunity to become airborne. These locations may include truck and railcar load-outs as well as conveyor and chute transfer points in and around the preparation plant. Many operations utilize water trucks and water sprays in combination with additions of various chemical and/or crusting agents to lower dusting problems. In addition, some operations make use of enclosures, such as silos and bins, to avoid exposure of coal to the environment.

The use of inflatable structures over coal storage piles have also been attempted with limited success [82]. Despite these efforts, fugitive dust still seems to be an issue for many plant sites, often leading to disputes with the public and creating concerns for worker health. Therefore, work is needed to develop better practices and control technologies for reducing dust emissions. The reconstitution of fines via agglomeration and briquetting technologies would be expected to substantially reduce dust emissions, but these processes are currently too expensive to be practical in the coal industry.

Future Directions

Dry Processing

The low-sulfur coal reserves in the western states have become the most important supply of domestic fossil fuel in the USA during the past few decades. Historically, the majority of coal mined in this region was of sufficient quality to not require any coal preparation except for simple crushing and sizing. More recently, however, increased levels of rock dilution have been noted for coals mined in this region, largely due to the mining of more challenging reserves and the use of larger mining equipment that are less selective [83]. This trend is pushing some coal producers to consider coal washing for the first time. In addition, new federal and state clean air quality requirements are pressuring utilities and coal companies to use precombustion cleaning as a means of reducing SO_x and trace element emissions [84]. One example is the proposed Springerville power plant in New Mexico, which has been tentatively approved contingent upon the use of precombustion cleaning to improve the quality of their coal feedstock.

There are many challenges in using precombustion cleaning to upgrade western coals. The processes traditionally used to wash eastern coals cannot be readily adopted in the west since water resources are lacking and low rank coals often disintegrate in water. As a result, current industry efforts are focusing on the development of dry cleaning processes to upgrade these lower rank reserves. Dry coal separators, such as pneumatic jigs and air tables, are already finding applications at selected mine and utility sites [85–87]. Other developing technologies that may be applicable for this purpose include various types of electrostatic [88, 89] and magnetic separators [90, 91]. The continued development of these low-cost units is believed to be important for upgrading many of the western coal reserves where water is scarce. The development of automated sorters, which use optical, electromagnetic or X-ray detection, to identify and extract rock from coal, also show considerable promise for dry coal concentration [92]. Optical sorters are used for separating particles that are liberated at relatively large sizes (>10 mm). These devices are already being used for separating diamond, gold, uranium and sulfide ores as well as for separating plastic bottles in the recycling industry. Such devices are particularly useful for preconcentration, which can increase throughput and result in energy savings for other types of solid–solid separators. Continued R&D is necessary to improve separation efficiency (particularly for finer sizes), increase reliability and lower costs for this new generation of coal preparation technology.

Conversion Processes

Coal preparation activities have traditionally been limited to include only those processes that involve physical separations. These processes include unit operations for particle sizing, concentration of organic matter and dewatering/disposal of plant products. These processes are generally considered to be inherently benign since they do not alter the chemical structure of the individual particles contained in the coal. Conversion processes, which include carbonization, gasification and liquefaction operations, are by this definition not considered to be part of the coal preparation industry. On the other hand, a new generation of coal preparation technology is being developed and commercialized that bridges the gap between traditional coal cleaning and coal conversion processes. These gateway technologies have the potential to reduce transportation costs and improve utilization properties for many of the low rank coals located in the Powder River basin. Under this expanded definition, conversion processes that are geared to the production of enhanced solid fuels may also be included under the coal preparation umbrella. Perhaps the best known of these processes include the K-Fuel, Encoal and SynCoal

processes [93–95]. Some of these solid fuel production facilities may also produce gaseous or liquid byproducts that are of value in the synthetic fuel market. The upgrading of low rank coals, which are abundant in the USA, is believed to be an attractive means of producing low-emission coals capable of meeting the 2010 CAIR standards. This approach is particularly attractive if the process simultaneously produces syncrude oil as a byproduct [96].

One of the most highly developed and well demonstrated technologies for upgrading low rank coal is the K-Fuel process. This technology is a decarboxylation process that uses heat and pressure to modify the structure of subbituminous coals. By driving off moisture and oxygen, the process has been shown to be capable of reducing emissions of nitrous oxides by 10–20%, carbon dioxide by 8–12% and mercury by as much as 70% [97]. A commercial-size demonstration plant owned by Evergreen Energy is currently being operated in Gillette, Wyoming. Specific concerns associated with this technology include the high cost of thermal processing as well as problems related to disposal of process wastewater and spontaneous combustion of the treated products.

Another widely discussed coal conversion technology is the Encoal Process developed by SMC Mining Company and SGI International. The technology uses a two-step thermal treatment process to produce an enhanced solid coal fuel (char) as well as some derived liquid fuel. In the first processing step, the low rank feed coal is heated until a completely dry solid is produced. The temperature is then increased in a second processing step to promote decomposition and drive off gases via mild gasification. According to published reports [98], the Encoal process generates about one-half ton of solid fuel and one-half barrel of condensed liquids from each ton of feed coal supplied to the thermal reactor. The products, as alternatives to existing fuel sources, are capable of lowering sulfur emissions in coal-fired boilers nationwide [99]. The gaseous products that are not condensed into useful liquid are burned to supply thermal energy for the process. A 1,000 t/day demonstration plant was successfully operated between 1992 and 1998 under DOE sponsorship. However, concerns associated with this process include high treatment costs, excess fines production, dusting problems, wastewater generation and need for coal-char stabilization (to prevent spontaneous combustion).

Another intriguing conversion processes that couples thermal upgrading with physical cleaning to improve the quality of low rank coals is the SynCoal technology. In this process, high moisture coal is processed through vibrating fluidized bed reactors in three sequential stages, two heating stages followed by an inert cooling stage. These reactors remove chemically bound water, carboxyl groups and volatile sulfur compounds. After thermal upgrading, the coal is put through a deep bed stratifier cleaning process to separate the pyrite rich ash from the coal. When fed a typical low rank western coal, the SynCoal process can provide a product with a heating value of up to 12,000 BTU/lb with moisture and ash contents as low as 1% and 0.3%, respectively [100]. A demonstration plant (45 t/h) was successfully operated near Western Energy Company's Rosebud coal mine near Colstrip, Montana. Although the plant closed in 2001, the facility generated more than 2 million tons of products during its lifespan [101]. Similar to the other mild conversion technologies, concerns associated with this process include high treatment costs, dusting problems and product instability.

Bibliography

Primary Literature

1. Fiscor S (2010) U.S. preparation plant census 2010. Coal Age 9:38–46
2. Kempnich RJ (2003) Coal preparation – a world view. In: Proceedings, 20th international coal preparation exhibition and conference, Lexington, pp 17–39
3. ASTM (1994) Standard test method for determining the washability characteristics of coal, Annual Book of ASTM Standards, 5.05, No. D4371. American Society for Testing and Materials, Philadelphia
4. Miller I (1998) Use of coal mine methane in coal dryers. Coalbed Methane Outreach Program Technical Options Series, U.S. EPA, Air and Radiation Draft 6202J, pp 1–4
5. Meenen G (2005) Implications of new dewatering technologies for the coal industry. In: CAST workshop, 26–28 July, Virginia Tech, Blacksburg
6. Weisenfluh GA, Andrews WA, Hiett JK (1998) Availability of coal resources for the development of coal. Kentucky Geological Survey, Report, U.S. Department of Interior Grant 14–08–0001–A0896, pp 1–32

7. Sites RS, Hostettler KK (1991) Available coal resource study of Appalachia 7.5-minute quadrangle Virginia-Kentucky. Virginia Division of Mineral Resources, Publication 118, pp 1–51
8. Norton G (1979) The economic role of coal preparation in the production and utilization of coal for the market. Norton-Hambelton Consultants, Ann Arbor, pp 1–24
9. Harrison CD, Hervol JD (1988) Reducing electricity generation costs by improving coal quality. EPRI Report CS-5713, Electric Power Research Institute, Palo Alto
10. Davidson PG, Galluzzo NG, Stallard GS, Jennison KD, Brown RE, Jonas TS, Pavlish JH, Mitas DW, Lowe DA, Arroyo JA (1990) Development and application of the coal quality impact model: CQIM™. EPRI Report GS-6393, Electric Power Research Institute, Palo Alto
11. Kehoe DB, Parkinson JW, Evans RJ, Levasseur AA (1990) Environmental and economic benefits of using clean coals in utility boilers. In: Joint ASME/IEEE power generation conference, Boston, 21–25 Oct 1990
12. Harrison CD, Kehoe DB, O'Connor DC, Stallard GS (1995) CQE: integrating fuel decisions. In: Fourth annual clean coal technology conference, Denver, 5–8 Sept 1995
13. Smith SR (1988) Tennessee Valley Authority's experience with switching to improved quality coal. In: Proceedings, conference on reducing electricity generation costs by improving coal quality, 5–6 November, Electric Power Research Institute, Palo Alto
14. Bhaskar U (2007) NTPC looking for sites to set up coal washeries. Wall Street Journal December 3, 2007
15. Glomsrod S, Taoyuan W (2005) Coal cleaning: a viable strategy for reduced carbon emissions and improved environment in China? Energy Policy 33:525–542
16. Blackman A, Wu X (1999) Foreign, direct investment in China's power sector: trends, benefits and barriers. Energy Policy 27:695–711
17. Corder WC (1983) For lower power costs, use high quality coal. In: Proceedings, 3rd European coal utilization conference, COALTECH, Amsterdam, 1:221–240
18. Scott DH (1995) Coal pulverisers—performance and safety. IEACR/79, IEA Coal Research, London, pp 1–83
19. Raask E (1983) Ash related problems in coal-fired boilers. In: Proceedings, engineering foundation conference on fouling of heat exchange surfaces, White Haven, Engineering Foundation, New York, 31 Oct–5 Nov 1982, pp 433–460
20. Couch GR (1994) Understanding slagging and fouling during PF combustion. In: International energy agency, clean coal center, Gemini House, London, IEACR/72, pp 1–118
21. Hatt R (1995) Correlating the slagging of a utility boiler with coal characteristics. In: Engineering foundation conference, Waterville Valley, 16–22 July
22. Vaninetti GE, Busch CF (1982) Mineral analysis of ash data: a utility perspective. J Coal Qual 1(2):22–31
23. Jones C (1998) Fuel management: solve common coalhandling problems. Power 142(6):31–32
24. Smith IM, Sloss LL (1998) PM10/PM2.5 – Emissions and effects. CCC/08, International Energy Agency, Coal Research, London, pp 1–75
25. EPA (1997) The benefits and costs of the Clean Air Act, 1970 to 1990. U.S. Environmental Protection Agency (EPA), pp 1–28
26. Doherty M (2006) Coal quality impact on unit availability and emissions. American Electric Power Site Visit, Asia Pacific Partnership on Clean Development and Climate, Columbus, 30 October–4 November, pp 1–10
27. Couch GR (1995) Power from coal: where to remove impurities? International Energy Agency, Coal Research, London, IEACR/82, pp 1–87
28. Kawatra SK, Eisele TC (2001) Coal desulfurization: high efficiency preparation methods. Taylor & Francis, New York, pp 1–376
29. Cavallaro JA, Deurbrouck AW (1977) An overview of coal preparation. In: Proceedings of the coal desulfurization: chemical and physical methods symposium, New Orleans, 23 Mar 1977, pp 35–57
30. Cavallaro JA, Deurbrouck AW, Killmeyer RP, Fuchs W, Jacobsen PS (1991) Sulfur and ash reduction potential and selected chemical and physical properties of United States coals. U.S. Department of Energy, DOE/PETC/TR-91/6, pp 1–309
31. Couch GR (2003) Coal preparation. International Energy Agency, Clean Coal Center, pp 1–181
32. Obermiller EL, Conrad VB, Lengyel J (1993). Trace element contents of commercial coals. In: Chow W, Connors KK (eds) Managing Hazardous air pollutants: state-of-the-art. Electrical Power Research Institute, Washington, DC. CRC Press, Boca Raton, pp 73–92
33. Meij R, te Winkel H (2007) The emissions of heavy metals and persistent organic pollutants from modern coal-fired power stations. Atmos Environ 41(40):9262–9272
34. Zubovic P (1966) Physicochemical properties of certain minor elements as controlling factors in their distribution in coal. In: Coal science, vol 55, Advances in Chemistry. American Chemical Society, Washington, DC, pp 221–231
35. Swaine DJ (1990) Trace elements in coal. Butterworth, London, pp 1–278
36. Fonseca AG, Tumati RP, DeVito MS, Lancet MS, Meenan GF (1993) Trace element partitioning in coal utilization systems. In: SME-AIME annual meeting, Reno, 15–18 February, Preprint No. 93–261, pp 1–25
37. Jacobsen PS, Blinn MB, Wan EI, Nowak MA (1992) Role of coal preparation in the precombustion control of hazardous air pollutants. In: Proceedings, 8th annual coal preparation, utilization, and environmental control contractors conference, PETC, Pittsburg, pp 412–419
38. Ford C, Price A (1982) Evaluation of the effect of coal cleaning on fugitive elements. Final report, Phase III, BCR Report L-1304
39. Akers DJ (1996) Coal cleaning controls HAP emissions. Power Eng 100(6):33–36
40. Akers DJ, Raleigh CE, Lebowitz HE, Ekechukwu K, Aluko ME, Arnold BJ, Palmer CA, Kolker A, Finkelman RB (1997)

HAPs-RxTM: precombustion removal of hazardous air pollutant precursors. Final Report, DOE Contract DE-AC22-95PC95153, U.S. Department of Energy, pp 1–115
41. Palmer CA, Luppens JA, Finkelman RB, Luttrell GH, Bullock JH (2004) The use of washability studies to predict trace-element reductions during coal cleaning. In: Proceedings, 29th international technical conference on coal utilization & fuel systems, Coal Technology Association, Gaithersburg, pp 1365–1376
42. Trasande L, Schechter CB, Haynes KA, Landrigan PJ (2006) Mental retardation and prenatal methylmercury toxicity. Am J Ind Med 49(3):153–158
43. EPA (2001) Results of Part III of information collection request. http://www.epa.gov/ttnatw01/combust/utiltox/utoxpg.html
44. Pavlish JH, Sondreal EA, Mann MD, Olson ES, Galbreath KC, Laudal DL, Benson SA (2003) Status review of mercury control options for coal-fired power plants. Fuel Process Technol 82:89–165
45. Quick JC, Brill TC, Tabet DE (2002) Mercury in U.S. coal: Observations using the COALQUAL and ICR data. Environ Geol 43:247–259
46. Alderman K (2007) Market opportunities for coal preparation. Presentation to the Report Committee of the National Commission on Energy Policy – Coal Study. 17 September, Denver
47. Tkach BI (1975) On the role of organic matter in concentration of mercury. Geochem Int 11:973–975
48. Finkelman RB, Stanton RW, Cecil CB, Minkin JA (1979) Modes of occurrence of selected trace elements in several Appalachian coals. Am Chem Soc Div Fuel Chem 24(1):236–241
49. Minken JA, Finkelman RB, Thompson CL, Chao ET, Ruppert LF, Blank H, Cecil CB (1984) Microcharacterization of arsenic- and selenium-bearing pyrite in Upper Freeport coal. Scan Electron Microsc 4:1515–1524
50. Luttrell GH, Venkatraman P, Yoon R-H (1998) Removal of hazardous air pollutant precursors by advanced coal preparation. Coal Prep 19:243–255
51. Hucko RE (1984) An overview of U.S. Department of Energy coal preparation research. In: SME-AIME annual meeting, Los Angeles, 26 February–1 March, Preprint No. 84–105, pp 1–6
52. Couch GR (2000) Opportunities for coal preparation to lower emissions. International Energy Agency Coal Research, CCC/30, London, pp 1–46
53. von Hippel D, Hayes P (1995) Prospects for energy efficiency improvements in the Democratic People's Republic of Korea: evaluating and exploring the options. Nautilus Institute for Security and Sustainable Development, Berkeley, pp 1–31
54. Adel GT, Wang D (2005) The assessment of fine coal cleanability. Int J Coal Prep Util 25(3):129–140
55. Honaker RQ (1998) High capacity fine coal cleaning using an enhanced gravity concentrator. Miner Eng 11(12):1191–1199
56. Honaker RQ, Wang D, Ho K (1996) Application of the falcon concentrator for fine coal cleaning. Miner Eng 9(11):1143–1156
57. Le Roux M, Campbell QP, Watermeyer MS, de Oliveira S (2005) The optimization of an improved method of fine coal dewatering. Miner Eng 18(9):931–934
58. Yoon R-H, Eraydin M, Keles S, Luttrell GH (2007) Advanced dewatering methods for energy savings in the mineral processing industry. In: SME annual meeting and exhibit, 25–28 February, Denver, Preprint 07–124, pp 1–5
59. van den Broek JJM (1982) From metallurgical coal tailings to thermal feed. AIME Trans 272:49–52
60. Mohanty MK, Palit A, Dube B (2002) A comparative evaluation of new fine particle size separation technologies. Miner Eng 15(10):727–736
61. Firth B, O'Brian M (2003) Hydrocyclones circuits. Coal Prep 23(4):167–183
62. Couch G (1996) Coal preparation: Automation and control. International Energy Agency, London, IEAPER/22, pp 1–64
63. Belbot M, Vaurvopoulos G, Paschal J (2001) A commercial elemental on-line coal analyzer using pulsed neutrons. In: CAARI 2000: 16th international conference on the application of accelerators in research and industry, AIP Conference, Denton, pp 1065–1068. DOI 10.1063/1.1395489
64. Anon (2007) Environmental, health, and safety guidelines for coal processing. International Finance Corporation (IFC), World Bank Group, Good International Industry Practice (GIIP) Technical Reference Document, April 30, pp 1–22
65. NRC (2002) Coal waste impoundments: risks, responses and alternatives. National Academies Press, Washington, DC, pp 1–244
66. EPA (1994) Design and evaluation of tailings dams. Technical Document, EPA 530-R-94-038, 59 pp. http://nepis.epa.gov/EPA/html/Pubs/pubtitleOSWER.htm
67. Gardner JS, Houston KE, Campoli A (2003) Alternatives analysis for coal slurry impoundments. In: SME annual meeting, 24–26 February, Cincinnati, Preprint 03–032, pp 1–5
68. Breen T (2007) Lawmakers want study of coal slurry in drinking water. Charleston Daily Mail, Charleston, 9 January 2007
69. Wilcox L (2007) Coal industry official disputes research about health of people living near mines. The Exponent Telegram, Clarksburg Publishing, Clarksburg, 30 October 2007
70. Parekh BK, Patil D, Honaker RQ, Baczek F (2006) Improving the densification of fine coal refuse slurries to eliminate slurry ponds. In: Proceedings, XV international coal preparation congress, China University of Mining and Technology Press, Beijing, pp 549–554
71. Bethell PJ, Gupta BK, Gross R (2008) Replacement of belt presses with a deep cone thickener at Lone Mountain Processing. In: 25th annual international coal preparation exhibition and conference, Lexington, pp 41–50
72. Henry CD (2008) Fine coal recovery project: Pinnacle mine Smith Branch impoundment. Technical Presentation, Marshall University CBER Summit, pp 1–39. http://www.marshall.edu/cber/summit/S2%20-%201%20Henry%20Beard%20Tech.pdf
73. Osborne DG (1988) Flotation, agglomeration, and selective flocculation. In: Coal preparation technology, vol 1. Graham and Trotman, London, pp 415–477
74. Yoon RH, Luttrell GH (2008) Advanced dewatering systems development. U.S. Department of Energy, Final Report for Contract No. AC26-98FT40153, 31 July, pp 1–225

75. Laskowski JS (2001) Coal flotation and fine coal utilization, vol 14, Developments in mineral processing. Elsevier Science, Amsterdam, pp 1–350
76. Gregory J, Bolto B (2007) Organic polyelectrolytes in water treatment. Water Res 41(11):2301–2324
77. Beaty B (2007) The Nature Conservancy, Clinch Valley Program, Personal Communication
78. Nature Conservancy (2007) Conservation management of the Clinch and Cumberland river systems: a collaborative discussion on coal mining and the aquatic environment. 5–7 September, Abingdon. http://www.cpe.vt.edu/cmrs/agenda.html
79. ARC (2004) Overview of the effects of residual flocculants on aquatic receiving environments. Publication TP226, Auckland Regional Council (ARC), Auckland, pp 1–31
80. Skiles KD (2003) Search for the next generation of coal flotation collectors. In: 20th Annual international coal preparation exhibition and conference, 29 April–1 May, Lexington, pp 187–204
81. EPA (2009) Coal preparation and processing plants new source performance standards (NSPS), US Environmental Protection Agency (EPA), Fact Sheet. http://www.epa.gov/airtoxics/nsps/coal/cpp_nsps_fr_fs_092509.pdf
82. Bowling B (2003) Elk Run may use plant – agreement similar to one made after first dome rupture. Charleston Daily Mail, Charleston, 29 April 2003
83. Bethell PJ (2007) Coal preparation: current status and the way ahead. Presentation to the Report Committee of the National Commission on Energy Policy – Coal Study, Denver, 17 September 2007
84. Honaker RQ, Luttrell GH, Bratton RC, Saracoglu M, Thompson E, Richardson V (2007) Dry coal cleaning using the FGX separator. In: 24th International coal preparation conference, Lexington, pp 61–76
85. Kelley M, Snoby R (2002) Performance and cost of air jigging in the 21st century. In: 19th annual international coal preparation exhibition and conference, 30 April–2 May, Lexington, pp 175–186
86. Lu M, Yang Y, Li G (2003) The application of compound dry separation technology in China. In: 20th Annual international coal preparation exhibition and conference, Lexington, pp 79–95
87. Weinstein R, Snoby R (2007) Advances in dry jigging improves coal quality. Min Eng 59(1):29–34
88. Yoon R-H, Luttrell GH, Adel GT (1995) POC-scale testing of a dry triboelectrostatic separator for fine coal cleaning. In: 11th Annual coal preparation, utilization, and environmental control contractors conference, 12–14 July, U.S. Department of Energy, Pittsburgh, pp 65–72
89. Stencel JM, Schaefer JL, Ban H, Li JB, Neathery JK (2002) Triboelectrostatic coal cleaning: mineral matter rejection in-line between pulverizers and burners at a utility. In: Impact of mineral impurities in solid fuel combustion. Springer, New York, pp 645–651
90. Oder RR (2005) The co-benefits of pre-combustion separation of mercury at coal-fired power plants. In: 98th Annual conference and exhibition, Air & Waste Management Association, Minneapolis, Paper 990
91. Oder RR (2005) The use of magnetic forces to upgrade low rank coals. In: Upgrading low rank coals symposium, coal & aggregate processing exhibition and conference, Lexington, 2–6 May
92. Jong TPR, Mesina MB, Kuilman W (2003) Electromagnetic deshaling of coal. Phys Sep Sci Eng 12(4):223–236
93. Collins KR (2007) EEE: Delivering cleaner coal today. In: 2nd Annual capital one southcoast energy conference, 3–5 December, New Orleans, pp 1–21
94. Federick JP, Knottnerus BA (1997) Role of the liquids from coal process in the world energy picture. In: 5th Annual clean coal technology conference, Tampa
95. Sheldon RW (1997) Rosebud SynCoal partnership: syncoal demonstration technology update. In: 5th Annual clean coal technology conference, Tampa
96. Skov ER, England DC, Henneforth JC, Franklin GR (2007) Syncrude and syncoal production by mild temperature pyrolysis processing of low-rank coals. American Institute of Chemical Engineers, Spring National Meeting, 22–26 April, Houston, Session TB004, pp 1–16
97. Wingfield G (2007) Cleaner coal? Forbes, 17 April 2007. http://www.forbes.com/2007/04/16/clean-coal-congress-biz-wash-cx_bw_0417coal.html
98. DOE (2003) Clean coal technology programs: Completed projects 2003. Clean Coal Technology, U.S. Department of Energy (DOE), National Energy Technology Laboratory (NETL) Clean Coal Technology Compendium, December 2003, 2:1–149
99. DOE (2002) The ENCOAL mild coal gasification project: A DOE assessment. DOE National Energy Technology Laboratory, Technical Report, Clean Energy Document No. 91, March 2002, pp 1–40
100. DOE (1997) Clean coal technology: upgrading of low-rank coals. U.S. Department of Energy, Topical Report No. 10, August 1997, pp 1–28
101. DOE (2006a) Advanced coal conversion process demonstration: Project performance summary – Clean coal demonstration program. Report DOE/FE-0496, March 2006, pp 1–16

Books and Reviews

Arnold BJ, Klima MS, Bethell PJ (2007) Designing the coal preparation plant of the future. Society for Mining Metallurgy and Exploration (SME), Littleton, pp 1–205

Couch GR (2003) Coal preparation. IEA Clean Coal Center, London, pp 1–182

Kawatra KS, Eisele TC (2001) Coal desulfurization: high-efficiency preparation methods. Taylor & Francis, New York, pp 1–360

Kona BB (1997) Coal preparation. Golden Jubilee Monographs. Allied Publishers, Buffalo, pp 1–221
Leonard JW, Hardinge BC (1991) Coal preparation. Society for Mining, Metallurgy and Exploration (SME), Littleton, pp 1–1131
Miller BC (2005) Coal energy systems. Elsevier Academic, Burlington, pp 1–526
Sanders J (2007) Principles of coal preparation, 4th edn. Australian Coal Preparation Society, Dangar, New South Wales, pp 1–560

Coal to Liquids Technologies

Marianna Asaro[1], Ronald M. Smith[2]
[1]SRI International, Menlo Park, CA, USA
[2]SRI Consulting, Menlo Park, CA, USA

Article Outline

Glossary
Definition of the Subject
Introduction
Survey of Specific Coal Liquefaction Technologies
Future Directions
Bibliography

Glossary

Coal-to-liquids (CTL) The conversion of coal to liquid fuels and/or chemicals

Coprocessing (of coal) The simultaneous conversion of coal and waste carbonaceous feedstocks such as petroleum-based residual oil or tar, plastics, or rubbers via once-through direct liquefaction into liquid, solid, and gaseous hydrocarbonaceous materials intended primarily for use as fuel.

Direct coal liquefaction (DCL) The conversion of coal to liquids via dissolution and/or hydroprocessing, without first gasifying the coal.

DOE United States Department of Energy.

Fischer–Tropsch reaction The catalytic conversion of synthesis gas to primarily hydrocarbons, the discovery being credited to Franz Fischer and Hans Tropsch.

Gasification (of coal) The conversion of coal to primarily synthesis gas plus ash at elevated temperature and pressure of oxygen and steam.

Indirect coal liquefaction (ICL) The conversion of coal to liquids via the intermediacy of synthesis gas.

Light distillate A distillation cut of low molecular weight and low boiling range, obtained from refining of hydrocarbonaceous feedstocks, used to produce liquefied petroleum gas (LPG), gasoline, and naphtha.

Middle distillate A distillation cut of mid-range boiling point, obtained from refining hydrocarbonaceous feedstocks, containing hydrocarbons ranging from C_5 through about C_{20} or C_{22}. When further distilled, the portion of middle distillates containing C_5 through about C_{15} is often referred to as naphtha, and the portion containing C_{16} through up to C_{22} is referred to as diesel. The naphtha is often distilled further to produce gasoline and kerosene/jet fuel, or can be used as feed for a naphtha cracker unit to make light olefins. (Less commonly, the gasoline cut is initially collected along with the light distillates).

Pyrolysis (of coal) A mild gasification process wherein coal is heated in the absence of oxygen at sufficiently mildly elevated temperature as to produce a mixture of hydrocarbonaceous gases, liquids, and solids suitable for use as chemical precursors or fuel.

Synthesis gas (syngas) A mixture of primarily hydrogen and carbon monoxide produced by gasification or reforming of hydrocarbonaceous materials, used to synthesize fuels or chemicals.

Water gas shift reaction The chemically reversible, catalyzed conversion of water and carbon monoxide to hydrogen and carbon dioxide.

Definition of the Subject

Like oil and natural gas, coal is a fossil resource and as such is not what first comes to mind when considering sustainable fuel sources. Coal contributes to sustainability as a complement to maintaining continuous availability of sufficient fuel to meet growing global demand [1–3].

As for other fossil sources, conversion of coal to transportation fuel is currently more affordable than conversion of renewable resources such as wind and solar, which are technically far away from availability at even a fraction of the scale required for sustainability over the coming decades. Given that proved coal

reserves in North America alone are currently estimated as capable of producing more than 840,000,000,000 equivalent barrels of oil (the energy equivalent of 32 cubic miles of oil) [4], the abundance of coal is a boon to a sustained global liquid fuel supply if used wisely.

Just as renewable fuel sources will be benchmarked against fossil sources in terms of economics, so also coal will be benchmarked against renewable fuel sources in terms of environmental sustainability. Today, modern coal-to-liquids (CTL) technology can produce synthetic fuels that burn more cleanly than conventionally produced fuels. CTL technology can produce a virtually sulfur-free diesel fuel, much cleaner than conventional diesel – reducing smog and acid rain – and can also produce gasoline, jet fuel, or chemicals.

Most coal used today is for production of power or for steelmaking. Coke plants use coal to produce high purity carbons for use in steel manufacture. Combustion of coal provides heat and power for industrial process operations. Production of liquid fuels and chemicals from coal are lower volume uses; these applications will tend to increase in importance as the ease of oil recovery decreases and its price increases.

Introduction

Coal has been mined and used as a source of energy for centuries. The first recorded use of coal was in China, with indications that the Chinese began using coal for heating and smelting about 2,500 years ago, and most historians believe that coal was used in various parts of the world 3,000–4,000 years ago during the Bronze Age [5]. A system for mining coal was present in England by 1180 [6]. Coal provided heat for homes and industry, fuel gas for town lighting, process gas for industry, coke for the iron industry, and fuel for steam locomotives and shipping during the first quarter of the twentieth century. Although electric power has supplanted coal gas for public lighting (town gas), the electric power industry remains significantly coal based today.

Coal resources have been used to produce liquid transportation fuels by several process routes, collectively referred to as coal liquefaction or, more generally stated, as Coal to Liquids (CTL). Early records of coal conversion to liquid fuel date to 1913 and an extraction process developed by Friedrich Bergius in Germany [7]. Bergius treated a mixture of pulverized bituminous coal and coal-derived heavy oil with hydrogen, at high temperature and pressure, to give a liquid product consisting of heavy oils, middle distillates, gasoline, and gases. Various metal compounds have been used to catalyze the process. This type of CTL technology is called Direct Coal Liquefaction (DCL).

DCL technology involves making a partially refined synthetic crude oil directly from coal, which is then further refined into synthetic gasoline and diesel as well as liquefied petroleum gas (LPG). Raw coal oil is highly aromatic and requires further upgrading. Heavy residues generated in the process, referred to as asphaltenes, also include ash from the coal and are either disposed of or gasified to produce part of the hydrogen required for the upgrading. The hydrocarbon fuel products of DCL are similar to hydrocarbon fuels derived from crude oil. A slate of partially refined gasoline-like and diesel-like products, as well as propane and butane, are recovered from the synthetic crude oil mainly by distillation. Liquid yields in excess of 70% by weight of the dry, mineral matter-free coal feed have been demonstrated under favorable circumstances. Overall thermal efficiencies (% calorific value of the input fuel converted to finished products) for modern processes are in the range of 60–70% if allowance is made for generating losses and other non-coal energy imports. These processes generally have been developed to process development unit (PDU) or pilot plant scale. However, no demonstration or commercial-scale plant had yet been built until very recently, primarily because petroleum fuels had been available at lower overall cost.

Development of the DCL approach in the twentieth century proceeded with ambition and then reserve. DCL was first commercialized in the 1920s (the Pott-Broche/IG Farben Process). In the Second World War, Germany produced more than 4 million tons of fuels by DCL. Plants were also built during this time in the UK, France, and Japan. A Japanese-influenced pilot unit at Fushun Coal Mine was operated by the South Manchurian Railway Company from 1938 [8] until 1943 and processed 20,000 t/year of coal. During this same period, the Korean Artificial Petroleum Company operated a 100 t/day plant at its Agochi factory [9].

DCL underwent a new phase of development in the 1970s in response to oil shocks. Major research

efforts in the USA during the 1970s and 1980s, in particular, involved work by Hydrocarbon Research Inc. (HRI, now Hydrocarbon Technologies Inc, HTI), cosponsored by the US Department of Energy (DOE) and including substantial R&D at a dedicated facility in Wilsonville, Alabama.

Research on DCL in Japan began in 1974 with the Sunshine project and sponsorship by the New Energy and Industrial Technology Development Organization (NEDO) [10]. Early players included Sumitomo Metals and Hasaki, and Nippon Steel and Kimitsu. The program experienced delays in the next decade, presumably resulting from the drop in oil price. A 150 t/day pilot plant was built at Sumitomo Metal Industries Kashima Steelworks and operated during 1997 and 1998, with a longest run of 1,921 h [11]. Research on DCL in Britain included the two-stage Liquid Solvent Extraction (LSE) and the Supercritical Gas Extraction (SGE) processes from British Coal. Research on DCL in Germany has included the single-stage Kohleöl process, as improved with the Integrated Gross Oil Refining (IGOR+) development by Ruhrkohle AG and Veba Öl AG, as well as the single-stage Imhausen High-Pressure Process [12].

The main focus of DCL research and development continues to be making the process more economically competitive with crude oil refining by decreasing the cost of production, particularly the capital cost of the plant, and the related challenge of finding more efficient ways to deal with tar and solid by-products of the liquefaction.

In addition to the price of oil, increasingly stringent environmental limitations on the content of aromatic compounds and sulfur in motor fuels have presented challenge. Fuels generated by DCL are rich in high-octane aromatics, which is an asset to engine performance but also an environmental issue. Coal-based processes also require desulfurization. The challenge of altering the product slate to meet environmental regulations is compounded by the resultant loss of benefits imparted by aromatics: in facilitating the liquefaction chemistry itself and then in promoting engine performance when using the final fuel product. Desulfurization presents its own performance challenges, because sulfur functions as an engine lubricant.

In the 1920s, Franz Fischer and Hans Tropsch of the Kaiser Wilhelm Institute developed a catalyst to convert hydrogen and carbon monoxide obtained from gasification of coal to hydrocarbon liquids. Because the coal is first gasified before conversion to liquid fuels, the Fischer–Tropsch (F-T) process for CTL is known as a type of Indirect Coal Liquefaction (ICL).

Indirect coal liquefaction (ICL) is a completely different approach from DCL for providing liquid fuels from coal. ICL processes first convert coal to a gaseous intermediate, which is then converted to liquid fuel. Coal gasification technologies rely on incomplete combustion, wherein coal is heated with a quantity of air that is insufficient to allow complete combustion (formation of carbon dioxide and water). The products are condensables and tars, flammable gases, and a solid fuel (or waste). Most coal-derived chemicals are made from the tars, although synthesis gas from coal gasification also can be used for the production of chemicals such as BTX (benzene, toluene, and xylenes), hydrogen, sulfur, methanol, and ammonia. Coal-derived fuels are obtained from the condensables, which are distilled and in some cases hydrotreated to give gasoline, diesel, and fuel oil cuts.

Of particular utility is the gasification of coal to provide the process intermediate synthesis gas, or syngas, a mixture of primarily CO (carbon monoxide) and H_2 (hydrogen). The ratio of H_2/CO varies with the source within the range of 0.7–1 for coal. Syngas can be used to generate liquid fuels via the aforementioned Fischer–Tropsch (F-T) technology, which provides hydrocarbon fuels that resemble crude oil derived products. The F-T processes produce synthetic middle distillates that can be used either directly as diesel or in blends with petroleum-derived diesel.

The CTL Fischer–Tropsch process was first taken forward commercially in the 1930s by the German company Ruhrchemie, in conjunction with other partners including Lurgi, to produce gasoline and oil. By 1938 there were nine German plants in operation having a total capacity of 660,000 t/year [13]. Individual reactors yielded about 5,000 L of gasoline/day, with 100 such units used in the first German F-T plants. However, the Bergius process DCL plants were chosen in 1939 when Germany expanded production during World War II, because these were further developed and could be more readily scaled to larger size, eventually processing up to 350 t of coal and yielding 250,000 L of gasoline/day.

By the mid-1940s, natural gas and oil production had become more developed and cost-competitive with coal, and technology for production of synthetic transportation fuels was not considered economic after the Second World War. Since then, research on CTL processes has waxed and waned largely in response to surges and ebbs in the price of oil. However, a perception by some at the time that reserves of crude oil were limited led to continued low-level development of CTL. Sasol purchased rights from the German companies and developed its own CTL process. Construction began in 1950 and an F-T plant came on line in Sasolburg, South Africa during the mid-1950s using Lurgi coal gasifiers and Sasol Synthol reactors to produce gasoline and diesel fuels as well as chemical feedstocks from coal. Even so, in the late 1950s and 1960s the huge oil fields of the Middle East dominated fuel supply chains to the point that further development of CTL technology worldwide essentially disappeared.

Shocks in the price of oil during the 1970s prompted renewed efforts; particularly in South Africa, the USA, Japan, and Britain; to promote an alternative to crude oil: a synthetic crude (syncrude) that would be cost-competitive with oil for refining to transportation fuels. Trade embargoes lasting until the mid-1980s effected large-scale application of F-T ICL in South Africa, at that point up to 60% of the country's transportation fuel requirements being met by coal. With the benchmark price of oil at US $30 per barrel, Sasol brought two F-T ICL plants online, in 1980 and 1983, with the total capacity of the company's three plants at 6,000 t/year [14].

As a result of a drop in the price of crude oil, worldwide developments in indirect coal liquefaction were largely put on hold after the 1980s, with the exception of those in South Africa where Sasol has been using its F-T Advanced Synthol (SAS) reactors since 1989. The ICL approach underwent an R&D resurgence in the 1990s, then in response to an increase in the price of oil [15]. All of these early plants utilized high-temperature Fischer–Tropsch (HTFT) technology with an iron-based catalyst. In 1993, Sasol successfully proved its low temperature Fischer–Tropsch (LTFT) technology with an iron-based catalyst to convert coal-derived syngas to liquid products. The plant is a relatively small scale, 2,500 bpd commercial facility that was recently converted to use natural gas as feed. Sasol's newest generation of LTFT utilizes high performance cobalt based catalysts in the Sasol Slurry Phase Distillate (SSPD) process [14], now used in Qatar to convert natural gas to middle distillates.

Currently, the best option for using coal to produce a high cetane number diesel fuel virtually free of aromatics and of S and N compounds is the F-T process coupled with the applicable downstream work-up of the crude F-T product [16]. Gasification of coal provides syngas, which is converted to a range of hydrocarbons. Alternatively, the syngas can be converted to liquid specialty [17, 18] or commodity chemicals including methanol or dimethylether (DME), either or both of which also can be used as automotive fuels. Methanol can be used alone, or preferably as a bend with conventional gasoline, in a spark ignition internal combustion engine (but not in a diesel engine, because methanol's cetane number is too low). A separate fuel distribution network for methanol also would be required as well as consideration of toxicity (and preventing people from drinking it as a replacement for ethanol). In contrast to methanol, DME can be used as a fuel or fuel additive for automotive transportation in a diesel engine.

DME has an inherent combination of both oxygenate functionality, for antiknock characteristics, and saturated hydrocarbon functionality, for fuel energy content. DME also imparts improved cold-start characteristics as an additive to methanol fuel and has almost twice the fuel content of methanol on a volume basis. DME can be used as a utility fuel or can serve as a blending component or replacement fuel for diesel engines. DME is also an intermediate in production of other fuel, as in ExxonMobil's methane-to-gasoline (MTG) process [19]. DME is a potential feedstock for novel oxygenated fuels [20] and is an alternative source of lower olefins such as propylene [21]. Using low CO content syngas, as derived from coal, a one-step DME process is more efficient and achieves higher syngas conversion than using two or three separate unit operations. DME can be produced with methanol in a dedicated plant, or it can be used as the fuel's production arm of a cogeneration plant to produce power and clean fuels (including even cooking fuel [22]) from coal [23].

ChemSystems Inc., the University of Ohio at Akron and the University of Missouri-Columbia, and Air

Products and Chemicals Inc. (APCI) all performed primary early research toward one-step conversion of syngas to methanol in the liquid phase. This development and demonstration work in the USA was performed predominantly in the 1980s and 1990s. Air Products' work with the Alternative Fuels Program of the US DOE additionally focused on dual catalysts for one-step DME production from coal-derived syngas and led to demonstration of processes for conversion of coal-derived syngas to fuels and chemicals, including demonstration at the DOE's Alternative Fuels Development Unit (AFDU) at LaPorte, Texas [24].

In Japan, work on DME was intensified in the 1990s by NKK Corporation [25]. NKK first researched the one-step slurry DME synthesis at bench scale and then teamed with the Center for Coal Utilization, Taiheiyo Coal Mining, and Sumitomo Metal Industries to pilot a 5 t/day DME plant with funding from METI (the Ministry of Economy, Trade, and Industry). The long-range plan at that time was described as producing DME at the site of coal mining and then transporting it to user sites. In terms of fuel value per unit weight, this would be much more efficient than transporting coal itself.

Substantial research and development efforts have been devoted to optimizing product yields and process efficiencies in conversion of syngas to fuels and chemicals. Mechanistic and kinetic studies have been conducted to interpret the fundamentals of specific conversion processes. Methods and hardware to impart temperature control and stability in conversion reactors are under continuous development because of the large excess heat of reaction. In the case of syngas conversions, this research has included discovery of catalytic systems having optimized formulations containing metals with high activity in combination with cocatalysts or additives that improve activity and selectivity for the desired type of product slate. Reactor design and engineering have proceeded in tandem with the catalyst developments in syngas conversions.

Survey of Specific Coal Liquefaction Technologies

A primary requirement of all coal liquefaction processes is that the fuel value inherent in the coal feedstock must be increased to be more similar to that of conventional liquid fuels. The ratio of elemental hydrogen to carbon, H/C, or even just simply the content of hydrogen itself, is important to determining the fit between feedstock and process options. Coal has a hydrogen content of about 5% whereas that of refined petroleum-based transportation fuel is in the range of 12–15%. Fuel derived from petroleum has an average H/C ratio of about 2 whereas that of coal itself ranges from about 0.7–1.

Table 1 shows the full range of process options that have been studied for converting coal to liquids [26]. These approaches include pyrolysis, direct liquefaction, coprocessing, and indirect liquefaction.

Pyrolysis

In pyrolysis processes, the H/C ratio of coal is raised by rejecting carbon. The liquid products have little value, but pyrolysis is used on a massive scale to turn coal into coke for metallurgy, especially steelmaking. The coking process involves heating coal in closed vessels to very high temperatures (up to 2,000°C) in the absence of oxygen. Without oxygen present to cause combustion, at these high temperatures the coal is broken down into lighter molecular weight substances that leave the vessel in the gaseous state. A hard, porous residue containing mostly carbon and inorganic ash is left behind. The amount of volatiles is typically 25–30 wt% of the coal. Pyrolysis is also used to make chemicals.

In coking, the coal beds are deep and the temperatures are kept very high to promote resolidification of the decomposing coal. When making chemicals, the coal beds are thinner and temperatures are lower than for a more complete gasification near the melting or the decomposition temperature of coal to promote production of liquids and gases. In both of these processes, fuel gas containing carbon and hydrogen is formed in significant quantities and high quality as measured by the gas heating value (BTU/scf). Where possible, this gas has been used for process heat but any excess gas also could be sold.

Chemical products can be obtained from high-temperature coking by-products, synthesis gas, and coal liquids. The by-products of the high-temperature coking process are fuel gas, crude tar, and light oils such as benzene, toluene, and xylene (BTX), naphtha, and ammonia. Most coal- derived chemicals today are obtained from the processing of tars. Coke manufacturers burn crude coal tar in coke ovens, refine it

Coal to Liquids Technologies. Table 1 Coal to liquids processes

Mild gasification/ pyrolysis	Single-stage direct liquefaction	Two-stage direct liquefaction	Coprocessing	Indirect liquefaction, F-T	Indirect liquefaction, other
TOSCOAL – Tosco, USA	H-Coal – HRI, USA	Catalytic Two-Stage Liquefaction, CSTL – HTI/ DOE, USA	MITI Mark I and Mark II – Japan	Sasol – South Africa	Methanol-to Gasoline (MTG) – ExxonMobil, USA
Char-Oil Energy Development, COED – FMC, USA	Kohleöl/IGOR^{+} – Ruhrkohle & Veba Öl, Germany (today BP, UK)	H-coal CSTL – Axens, France	Cherry P – Osaka Gas, Japan	Gasel – Axens, France	Direct DME –JFE, Japan
Liquids from Coal, LFC – Encoal, USA	Solvent Refined Coal, SRC-I and SRC-II – Gulf Oil, USA	Liquid Solvent Extraction, LSE – British Coal, UK	Solvolysis –Mitsubishi, Japan	GTL.F1 (Statoil, PetroSA, Lurgi), Switzerland	Direct DME –NEDO, Japan
EERC/AMAX – Univ. N. Dakota, USA	Exxon Donor Solvent EDS – US	Brown Coal Liquefaction, BCL – NEDO, Japan	Mobil – USA	Syntroleum – USA	LPDME – air products, USA
Lurgi-Ruhrgas – Germany	NEDOL – NEDO, Japan	Chevron Coal Liquefaction, CCLP – USA	Pyrosol –Saabergwerke, Germany	Rentech - USA	Topsøe DME –Haldor Topsøe, Denmark
Pyrolysis of coal – Inst. of Gas Technol., USA	Imhausen High-Pressure – Germany	Lummus Integrated Two-Stage Liquefaction, ITSL – USA	Chevron – USA	Shell Middle Distillates (SMDS) – Royal Dutch Shell, Netherlands	
Twin screw – Coal Technol. Corp., USA	Conoco zinc chloride – USA	Kerr-McGee ITSL –USA	Lummus Crest – USA	BP, UK	
	Suplex – Sasol, South Africa	Amoco CC-TSL – USA	Alberta Research Council, ARC –Canadian Energy Dev., Canada	ExxonMobil, USA	
		Pyrosol – Saabergwerke, Germany	CANMET AOSTRA – Canada	ConocoPhil-lips, USA	
		Mitsubishi Solvolysis – MHI, Japan	Rheinbraun – Germany		
		Consol Synthetic Fuel, CSF – Consolidated Coal, USA	Technical University Clausthal, TUC – Germany		
		Supercritical Gas Extraction, SGE – British Coal, UK	UOP Slurry-Catalyzed – US		
			HTI – US		

C

to tar-based products, or sell it to coal tar distillers. Tar derived products include ammonium sulfate, sulfuric acid, phenols, cresols, BTX, naphthalene, pyridine, phenanthrene, anthracene, creosote, road tars, roofing pitches, and pipeline enamels. Today, synthesis gas from coal gasification also can be used for the production of petrochemicals such as BTX, sulfur, methanol, and ammonia as well as hydrogen.

The Liquids from Coal (LFC^{TM}) process uses mild coal gasification to upgrade low-rank coals to two fuels: a stable, low-sulfur, high-BTU solid fuel similar in composition and handling properties to bituminous coal (referred to as process-derived fuel, PDFTM) and a low-sulfur industrial fuel oil (referred to as coal-derived liquid, or CDL^{TM}) [27, 28]. The process was originally developed by SGI International and then taken further by the ENCOAL Corporation. Development was about 50% financially supported by $90 million from the US DOE.

A PDU was constructed in 1986 and then a 1,000 t/day demonstration unit was constructed and operated for over 4 years near Gillette, WY in the mid-1990s. Later configurations included a vibrating fluidized bed (VFB) as part of a deactivation loop for solid product, where quenched solids are partially fluidized and exposed to oxidative deactivation to reduce the tendency for spontaneous ignition. The residence time, oxygen content, and temperature of the gas stream are selected to deactivate the coal within the VFB unit. Hydration further stabilizes the solid PDF product, and after treatment in the VFB system the solids are cooled and a controlled amount of water is added to rehydrate the PDF to near its equilibrium moisture content. The CDL portion of the product is condensed. The technology appears to be moving forward, with the transformation of ENCOAL into the Saskatchewan-based company NuCoal, which has memos of understanding with several potential partners including Sinopec.

Direct Liquefaction

In DCL, the H/C ratio of coal is raised by adding hydrogen. The objective of hydrogenation is to maximize the yield of distillate fractions that can be subsequently converted into fuels. Distillate materials comprise the naphtha fraction, typically boiling C_5 – 215°C, plus the middle distillate fraction typically boiling between 150°C and 370°C, with the exact cuts depending on product specifications. The liquid products are then refined into diesel, gasoline, and other petroleum products.

The traditional mechanistic view has been that upon heating, inherently weak bonds in coal are broken, and that the resulting and then hydrogen is rapidly transferred from the solvent to cap the resultant free radicals. Rapid hydrogenation is indeed critical to liquid yield; preventing retrogressive reactions leading to formation of solid char. While this picture is largely true, in-depth research showed that it is insufficient. Concurrent with this pathway are solvent-mediated hydrogenolyses of strong C–C bonds – bonds too strong undergo simple thermolysis under reaction conditions – engendered by addition of a free hydrogen atom or a bimolecular H-transfer from solvent species and their radicals [29]. Inclusion of these pathways helps rationalize many otherwise inexplicable phenomena in coal liquefaction, and also helps identify conditions that maximize utilization of hydrogen for liquid production rather than produce the less desirable light gases.

Hydrogen is also critical in the DCL process to reduce oxygen, sulfur, and nitrogen in the coal feedstock. These elements are removed from the crude liquid product as water (H_2O), hydrogen sulfide (H_2S), and ammonia (NH_3), respectively. Oxygenates are reduced to hydrocarbons, because their oxygen content would otherwise lower the fuel value. The nitrogen and sulfur compounds are removed because they would otherwise poison the cracking catalysts in refining operations downstream of the DCL unit. DCL products are only partially refined at the DCL plant. They must be further refined into finished liquid fuel products at conventional refineries, where additional H_2 is added to bring the H/C ratio up to about 2 for the fuel products.

Many factors affect the rate and extent of coal liquefaction, including temperature, hydrogen partial pressure, residence time, coal type and properties, solvent properties, solvent to coal ratio, ash composition, and catalyst. In general, liquefaction is promoted by increasing the temperature, hydrogen partial pressure, and residence time. However, if the temperature is too high, gas yield is increased and coking can occur. Solvent to coal ratio is important. If the ratio is too low, there will be insufficient hydrogen transfer activity. If the ratio is high, a larger reactor will be necessary to

provide the required residence time. Typical operating conditions are listed in Table 2.

For the most highly developed processes, coal conversion can be as high as 90% on a mineral ash free basis, with a C_{5+} distillate yield up to 75% and hydrogen consumption of 5–7% wt. When an external catalyst is used, it is typically some combination of cobalt, nickel, and molybdenum on a solid acid support such as silica-alumina [30]. In slurry hydrogenation processes, catalyst lifetime is fairly short because of the large number of potential poisons present in the system.

DCL process concepts have been based on a variety of operating conditions and catalysts and can be performed in a single stage or two stages. In a typical single-stage process, coal is contacted with hydrogen or with hydrogenated solvent at ca. 450°C. The yield of fuel oil is about 3 barrels of oil/t of coal with bituminous coals. The light oil fraction is recycled. A high yield of light hydrocarbons is obtained and the efficiency of hydrogen utilization is low. The product is difficult to refine because of its high aromaticity and nitrogen content. Single stage liquefaction is not as effective for subbituminous coals as for higher rank coal.

Most current DCL processes have settled on a multistage approach. Multistage DCL typically uses dispersed catalysts in the liquefaction stage followed by use of supported catalysts in subsequent upgrading stages, with different pressures and temperatures for the different stages. The technologies were demonstrated in several laboratory and pilot plants and the products were more easily refined than many crude oils. There are many variations of two-stage DCL processes, including use of catalyst in the two stages (both stages being catalyzed, versus thermal and catalyzed stages), distillation between stages, whether solids are separated between the two stages or only after the second stage, recycle of ashy bottoms, and the operating hydrogen balance.

Coal to Liquids Technologies. Table 2 Typical operating conditions for direct coal liquefaction

Operating parameter	Typical operating conditions
Temperature (°F)	750–850
Pressure (psia)	1,500–3,000
Residence time (h)	0.5
Solvent to coal ratio (lb/lb)	1.5/2

A block flow diagram (BFD) for a typical direct coal liquefaction plant using coal slurry hydrogenation is shown below in Fig. 1. Coal is ground and slurried with a process-derived solvent, mixed with a hydrogen-rich gas stream, preheated, and sent to a two-stage liquefaction reactor system where the organic fraction of the coal dissolves in the solvent and the dissolved fragments react with hydrogen to form liquid and gaseous products. Sulfur in the coal is converted to hydrogen sulfide, nitrogen to ammonia, and oxygen to water. The reactor products go to vapor/liquid separation. The gas is cleaned, and after removal of a purge stream to prevent buildup of inert materials, the gas is mixed with fresh hydrogen and recycled. The liquid is sent to vacuum fractionation for recovery of distillates. Heavy gasoil is recycled as process solvent and vacuum bottoms are gasified for hydrogen production.

Ash from the gasifier is sent to disposal. Heavy direct liquefaction products contain polynuclear aromatics that are carcinogenic. This problem can be solved, however, by recycling to extinction all material boiling above the desired product end point. A recent development, shown in Fig. 1, is to put the ash residue and carbon from recycled solvent directly through the gasifier to produce hydrogen (and power).

The longest experience base with DCL in the USA was a PDU at the R&D facility of Hydrocarbon Technology Inc. (HTI) that consumed 3 metric tons of coal/day. Among the many liquefaction processes developed and tested at pilot plant scale have been Kohleöl (by Ruhrkohle, Germany); Exxon Donor Solvent (by Exxon, now ExxonMobil, USA); Solvent Refined Coal-I (SRC-I) and SRC-II (*by Gulf Oil, USA.*); H-Coal (by HRI, now HTI, and DOE, USA); Catalytic Two-Stage Liquefaction (CTSL, by HRI and DOE, USA); Liquid Solvent Extraction (LSE, by British Coal Corporation, UK); Brown Coal Liquefaction (BCL, by NEDO, Japan) and NEDOL (by NEDO, Japan). Only the CTSL, LSE, BCL, and NEDOL processes continued in development at pilot plant scale beyond the late 1980s. Between 1975 and 2000, the USA alone invested

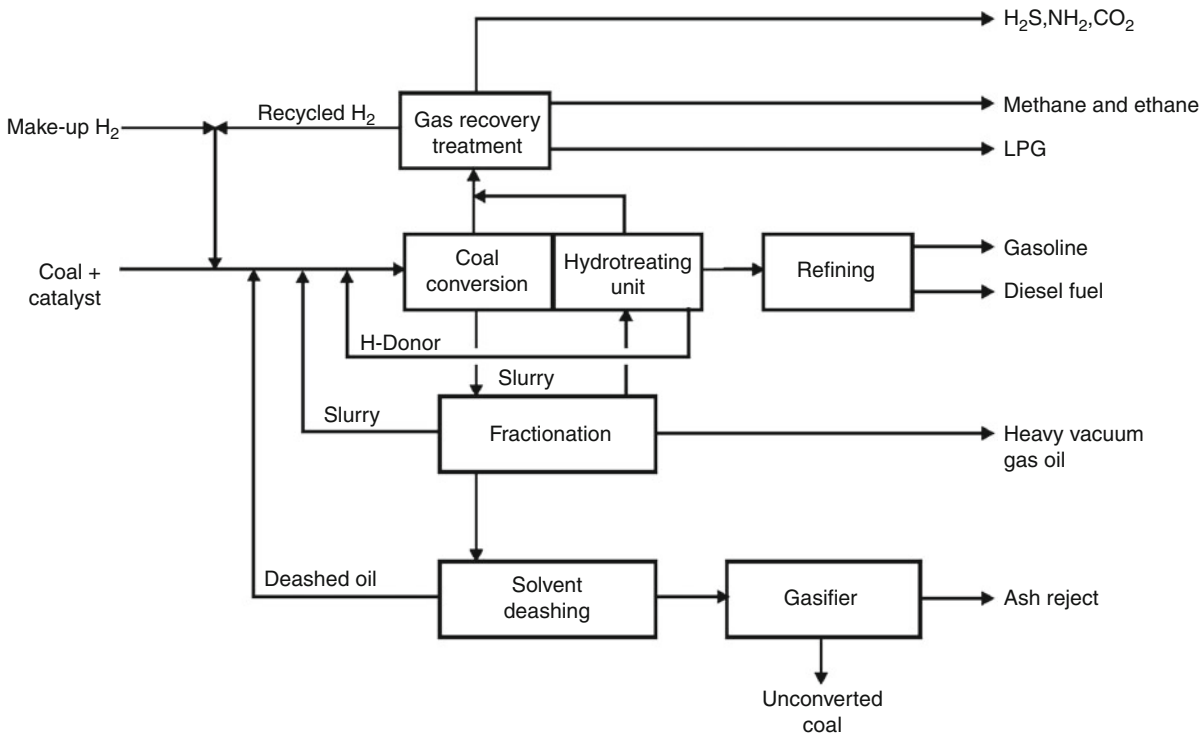

Coal to Liquids Technologies. Figure 1
Block flow diagram of a typical direct coal liquefaction process [31]

$3.6 billion in direct liquefaction technologies; some are now licensed to China [31].

H-Coal was an early single-stage DCL process piloted by HRI and Ashland Synthetic Fuels, Inc. in a 600 t/day pilot plant adjacent to Ashland's refinery in Cattlesburg, Kentucky [32]. The process consists of slurry preparation followed by catalytic hydrogenation/hydrocracking at a single temperature and pressure, 450°C and 2,200 psia respectively, in an ebullating bed reactor. The ebullating bed is a backmixed three-phase isothermal reactor that keeps catalyst in constant motion. It uses the upward flow of liquid to expand the catalyst bed and to distribute liquid, gas, and catalyst evenly across the reactor. The reactor has the characteristics of a uniform temperature similar to continuous stirred tank reactor.

The H-Coal process was a starting basis for subsequent process development sponsored by the US DOE over about 3 decades time. A principal focus of this long-term project was R&D of catalysts that were tolerant of, and would not be rapidly deactivated by, coal-derived mineral matter in the reactor. Typical early catalysts showed rapid deactivation because of coking and metals laydown with loss of surface area. A later process version sought to address this deactivation problem by using two coupled reactor stages, one operating at 400°C and the other operating at 420–425°C. The catalyst was also changed from cobalt/molybdenum/alumina to nickel/molybdenum on bimodal alumina. This Catalytic Two-Stage Liquefaction (CTSL) process is shown in a block flow diagram in Fig. 2. The role of catalyst in the first stage of the CTSL process is to promote hydrogenation of the solvent, stabilization of the primary liquefaction products, and hydrogenation of the primary and recycle resid. In the second stage, the catalyst promotes heteroatom removal and thus product quality improvement, conversion of resid to distillate, and secondary conversion to lighter products. The catalyst also aids in avoiding dehydrogenation.

In the first ebullating bed reactor, coal is dissolved with minimal catalysis at about 400°C for bituminous coal (or 435–460°C for subbituminous coal) and 170 bar. The catalyst for this first reaction is

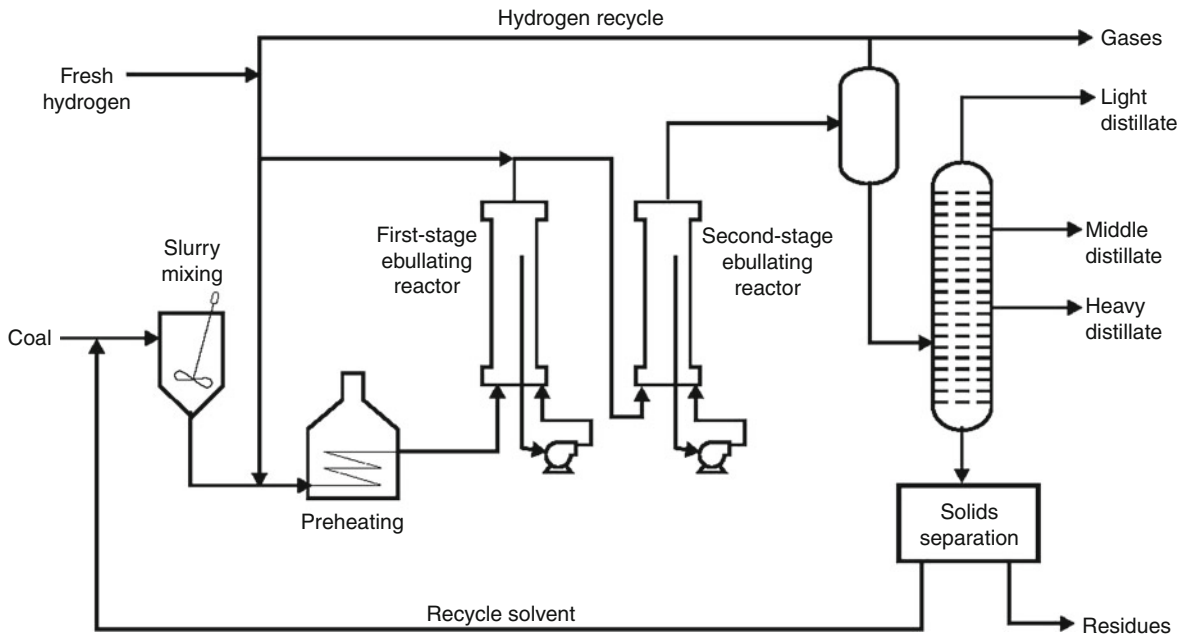

Coal to Liquids Technologies. Figure 2
Process flow schematic of two-stage CTSL direct liquefaction process [33]

typically nickel-molybdenum on alumina and aids in re-hydrogenating the recycled process solvent. The resultant heavy coal liquids are fed to a second ebullating bed reactor and hydrogenated at about 440°C and 170 bar with a catalyst such as that used in the first reactor, or a high-activity iron catalyst. After separation and depressurization, the product of the second reactor is sent to a distillation column at atmospheric pressure, where distillate up to 400°C is removed, with yield from coal of up to 65%. The distillation residue is unconverted coal and asphalt, which are typically gasified for captive fuel value or feed hydrogen.

The CTSL process was further developed over almost 15 years in a pilot plant at the Wilsonville liquefaction test facility. Beginning in 1973, a 6 t/day coal liquefaction plant was built by the Edison Electric Institute (EEI) and Southern Company Services, and the US DOE became the primary sponsor in 1976. Amoco Oil Co. (now BP) joined the project in 1984.

Developments at the Wilsonville Facility in the USA
Because of the role of Wilsonville in consistently demonstrating success or failure of a large number of concepts, particular attention has been paid to the results from this facility. The plant began operation in 1974 in a single-stage mode referred to as Solvent Refined Coal (SRC-II, which made liquid fuel as opposed to SRC-I, which made a solid fuel from coal) but evolved to a two-stage operation utilizing two ebullating bed catalytic reactors. Initial efforts in two-stage liquefaction focused on catalytic upgrading of the thermal products, referred to as Nonintegrated Two-Stage Liquefaction (NTSL). This configuration was termed nonintegrated because the coal-derived resid hydrocracking step did not interact with the primary thermal part of the plant. The NTSL concept proved excessively inefficient because of the high hydrogen consumption associated with the thermal part of the operation.

Coal throughput, expressed as space velocity per unit reactor volume, was substantially improved in going from NTSL to Integrated Two-Stage Liquefaction (ITSL) mode. In ITSL, a short contact time thermal reactor is closely coupled to an ebullating bed catalytic reactor where hydrocracking occurs. The thermal resid produced in the ITSL at short contact times is more reactive toward expanded-bed hydrocracking, which permits operation of the hydrocracker at lower temperature and minimizes gas make. Minimizing formation of light hydrocarbon gases in turn would be

expected to reduce the rate of catalyst coking, improve hydrogen utilization efficiency, and increase selectivity for higher distillate. A 35% increased yield from C_{5+} distillation was observed.

From 1985 to 1992, work at Wilsonville focused on development of the CTSL, utilizing ebullating bed catalytic reactors in both stages. The ebullating bed allows use of the substantial heat of reaction to preheat coal slurry feeds, and this improves process thermal efficiency. The converted and refined products are separated at high pressure and temperature into lighter oils and gases, and heavy oils and solids. Following pressure letdown and heat exchange, the lower boiling oils are fractionated while the heavier oils are separated from the unconverted coal and ash and recycled as the slurry solvent for the coal. Initial work indicated that distillate yields as high as 78% could be obtained by operating the first stage at low severity (399°C) and by using a large pore bimodal Ni-Mo catalyst. Significant improvement in distillate production can be achieved but again at the cost of increased hydrogen consumption.

Also explored were Reconfigured Integrated Two-Stage Liquefaction (RITSL), where solvent de-ashing was practiced after the hydrocracking stem, and Close-Coupled Integrated Two-Stage Liquefaction (CC-ITSL), where two reactors (thermal/catalytic) were linked directly without any intervening processing steps. Incremental improvements in distillate yield and selectivity were realized by changing the process configuration, but at the expense of increased hydrogen consumption.

The Wilsonville facility was closed in 1992 and was decommissioned shortly thereafter, but development work funded by the DOE continued at the Lawrenceville, N.J. facility [34–36]. The process has now evolved into a generic composite of much of the liquefaction development work funded by the DOE in the 1980s and 1990s. Most recently, a close-coupled configuration has been adopted in which both stages use an active supported catalyst, and HTI has included an in-line hydrotreater after the second-stage reactor to improve product quality. In 1997, with support from the DOE, HTI signed a 2-year agreement with the Chinese Coal Research Institute (CCRI) to carry out a feasibility study for a direct coal liquefaction plant using Shenhua coal [37].

The Kerr-McGee critical solvent de-ashing (CSD) technology (also termed the Residual Oil Solvent Extraction, or ROSE, process) was also tested at Wilsonville, resulting in the development of alternative methods for solids removal from primary liquefaction products. Other DCL process developments in the USA have included the single-stage Exxon Donor Solvent (EDS) process, and two-stage processes have included Lummus's Integrated Two-Stage Liquefaction (ITSL), Kerr-McGee's ITSL, Chevron Coal Liquefaction (CCLP), Consol Synthetic Fuel (CSF), and Amoco's (now BP's) Close-Coupled Two-Stage Liquefaction (CC-TSL) process.

In 1996, Sandia National Labs published results of its study on the efficacy of hydrogenation for removing nitrogen and sulfur from the CTSL crude product [38]. The kerosene fraction from HTI's first proof-of-concept run was used and denitrogenation and desulfurization were achieved under relatively mild conditions. Processing at the highest severity condition (388°C, 103 psig H_2, 1.5 g/h/g-cat) decreased nitrogen from 645 ppm in the feed to 7.9 ppm in the hydrotreated product. Sulfur content of 239 ppm in the feed was decreased by hydrotreating to less than 20 ppm.

In the early the 1990s, HTI was engaged in DOE-sponsored research on coprocessing of coal and plastics waste using DCL.

DCL Developments in Europe The Kohleöl DCL process [39] is based on technology used at commercial scale in Germany, until after the Second World War, and then improved with the advent of the Integrated Gross Oil Refining ($IGOR^+$) process [40]. Coal is slurried with a process-derived recycle solvent and a "red mud" disposable iron catalyst. The pressurized and preheated slurry is sent to an up-flow tubular reactor operated at about 470°C and 300 bar H_2. Products from the top of the reactor pass to a hot separator, the overheads from which are hydrotreated at 350–420°C in a fixed-bed reactor maintained at the same pressure as the main reactor. The hydrotreated products are depressurized and cooled in two stages. The liquid product from the first stage is recycled for use as solvent in the slurry step. The liquid product from the second stage is routed to an atmospheric distillation column to give light oil (C_5 – 200°C bp) and a medium oil

(200–325°C bp) product. The bottoms from the original hot separator pass to a vacuum distillation column to recover distillable liquids. These are added to the hydrotreating reactor feed and are subsequently largely recycled as solvent. The vacuum column bottoms consist of pitch, mineral matter, unreacted coal, and catalyst, which in commercial operation would be used as a gasifier feedstock for hydrogen production. Greater than 90% conversion can be obtained with bituminous coals, with liquid yields in the range 50–60% on a dry ash-free coal basis. The product distribution is about 19% C_1–C_4 hydrocarbons, 25% light oil (C_5 through 200°C bp), 33% medium oil (200–325°C bp) and 22% unreacted coal and pitch.

The LSE process was developed more fully than other European DCL processes, by British Coal Corporation between 1973 and 1995 [12]. In the LSE process, coal is slurried with a process-derived recycle solvent, preheated, and passed to a noncatalytic digestion step, which consists of two or more continuous-stirred tank reactors. These reactors operate in series at a temperature of 410–440°C and 10–20 bar. The solvent acts as a hydrogen donor, transferring up to 2% by weight of hydrogen to the coal. The digester product is partially cooled, filtered to remove unreacted coal and ash, and dried. The filtered coal extract is distilled to recover the light oil wash solvent and is then preheated, mixed with H_2, and sent to one or more ebullating bed reactors in series. There is no interstage separation and the reactors operate at 400–440°C and about 200 bar. The cooled, depressurized reactor products are distilled with cut-point adjusted to maintain solvent balance, resulting in a product that typically boils below 300°C. The column bottoms are routed partially to a vacuum distillation column, used to control the level of pitch in the recycle solvent. The overheads from this column are recombined with the main atmospheric column bottoms stream and recycled as the solvent to the slurrying step. The product distribution is about 15% C_1–C_4 hydrocarbons, 50% light oil (C_5 through 300°C bp), 50% solvent surplus (300–450°C bp), 24% filter cake organics, and less than 1% pitch. A 2.5 t/day pilot plant was built and operated for 4 years at Point of Ayr, North Wales but has since been decommissioned.

DCL Developments in Japan The Sunshine project pursued in Japan examined three approaches to direct liquefaction of bituminous coal: solvolysis, solvent extraction, and direct hydrogenation of coal. From these studies, NEDO found that increasing catalyst activity correlated with increased liquid yield; that hydrogenation was most effective for liquefaction at pressures in the 150–250 atm range and temperatures in the 400–450°C range; and that increased solvent viscosity aided production of light oil as fuel. The approaches were consolidated over a time span of 18 years, with demonstration of the resultant NEDOL process completed in 2000. The process uses 170 atm H_2 in the liquefaction reactor at 450°C. A process flow diagram of the NEDOL process is shown in Fig. 3. [11].

Like H-Coal, the NEDOL process is single-stage, meaning that all liquefaction reactors are operated at a single temperature and pressure. The NEDOL process has been further developed, however, and is said to have low severity conditions and high distillate yield comparable to those of the CC-ITSL and IGOR$^+$ processes.

NEDO also developed the BCL process, in the early 1980s, to use brown coal (lower rank, wetter coal), to the scale of 50 t/day in a pilot-plant constructed at Morwell in Victoria, Australia [41]. It was operated during 1985–1990, processing a total of about 60,000 t of coal. Operations ceased in October 1990. In the 1990s, NEDO worked with Indonesia on developing technology for use with that country's brown coal. Also in Japan, Mitsubishi Heavy Industries (MHI) researched a two-stage DCL process referred to as Mitsubishi Solvolysis.

The development of DCL is depicted from a historical process economic perspective in Fig. 4, which shows the cost that the oil product would need to sell for to make specific DCL processes economically competitive. As the process technology advanced the liquids yield from bituminous coals increased from 2.7 to 4.3 bbl/t. The increase in the yield of liquids are partly due to the fact that the later process designs used steam reforming of natural gas to provide hydrogen instead of gasifying a portion of the coal. The costs decreased concomitantly, but today direct coal liquefaction still remains highly capital-intensive.

Overcoming the techno-economic difficulties of DCL could enable a lower cost overall CTL process than ICL, given that DCL does not require the gasification step. Although largely dormant for over a decade

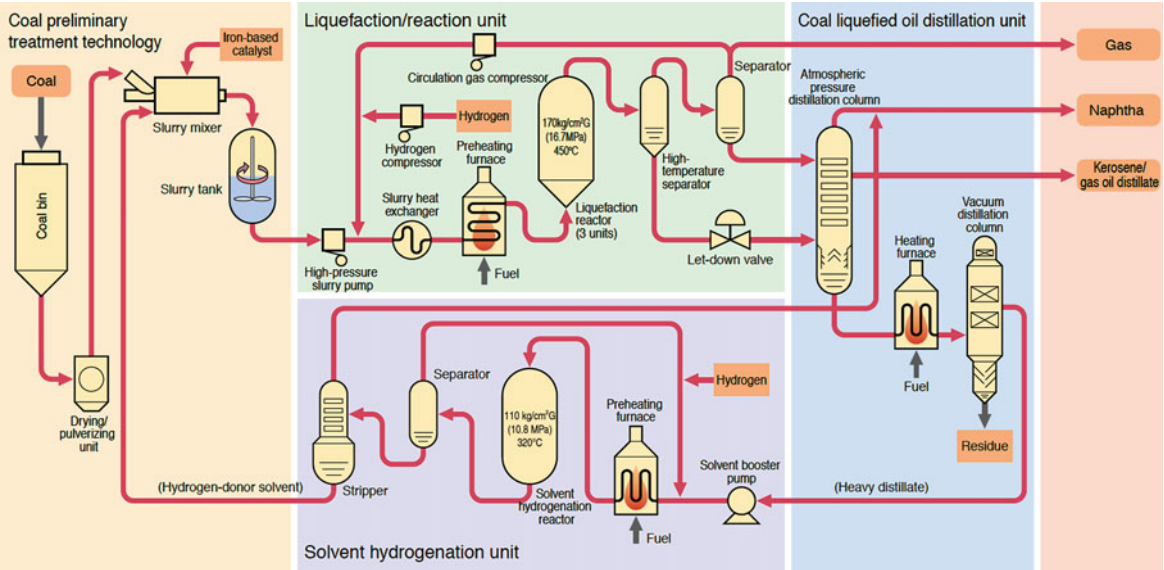

Coal to Liquids Technologies. Figure 3
Flowchart for the NEDOL process for direct liquefaction of bituminous coal

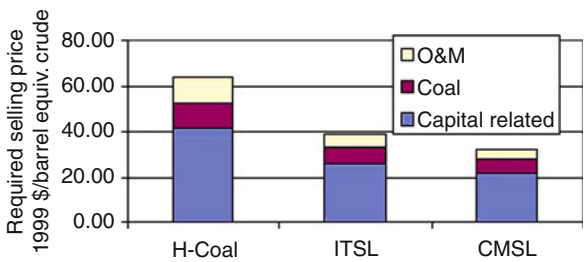

Coal to Liquids Technologies. Figure 4
Relative economics for representative DCL processes [36] (O&M is operations and maintenance)

in the USA, Europe, and Japan; direct liquefaction is undergoing renewed research effort, most actively pursued in the People's Republic of China (PRC).

Recent DCL Developments in China Shenhua has recently constructed the world's first commercial DCL facility, in the Inner Mongolia Autonomous Region. Shenhua's direct liquefaction process combines elements of German, Japanese, and, primarily American technologies with its own innovations. The single-train reactor system and process plant were designed by HTI and licensed from Headwaters Inc. (HTI is currently a subsidiary of Headwaters), and operations of its first production line commenced in 2008. Shenhua has planned expansion in two phases, for a total of ten production lines with projected oil equivalent products of 10 million t/year, including approximately 150,000 barrels/day of middle distillate fuels (naphtha + diesel). The engineering design of the plant, called SH-I, calls for a daily input of 7,000 metric tons of Shenhua's subbituminous coal. Also, Shenhua Group, Shanghai Huayuan Group, and Shanghai Electric Group have set up a coal liquefaction research center in Shanghai. The center will mainly explore and develop direct and indirect coal liquefaction technologies.

In summary, advantages of DCL include:

- High-octane gasoline is produced
- More energy efficient than ICL
- Products have a higher energy density than indirect conversion

Disadvantages of DCL include:

- Processing difficulties associated with solids separation
- High aromatic content
- Low cetane number diesel (45)
- Potential water and air emissions issues
- High capital intensity
- May have higher operation expenses than ICL

- Lower feedstock flexibility than ICL
- High requirements for external hydrogen supply (which has to be provided by, e.g., additional coal gasification or natural gas)

Coprocessing

Coprocessing combines waste materials having high hydrogen content (relative to coal) with coal as feed for conversion to liquid fuel products. Over 44 billion pounds of plastic waste materials, 280 million automotive tires, and about 1.2 billion barrels of waste oil are generated in the USA each year [42]. Coprocessing with coal would allow capture of energy content in these waste materials instead of simply disposing of them. It has frequently been stated that synergistic interactions between coal and heavy oil can result in distillate yields and coal conversion levels greater than expected from individually processing the coal and heavy oil. Several companies researched coprocessing, including Chevron's 6 t/day coprocessing plant run in 1983 at the company's Richmond, California site. The research included synergistic incorporation of pretreated petroleum vacuum resids with coal as feedstocks, and demetallation of resids was also performed [43]. The process was said to have good operability.

The poorer solvent properties of heavy oils detracted from the conceptual simplicity and led to use of forcing conditions and increased hydrogen consumption that have adversely affected economics of coprocessing [44]. Although developments in coprocessing have been essentially on hiatus for over a decade, the topics of energy and reuse of materials remain prominent. Improvements in technologies for gasification, solvation, and CO_2 capture might lead to a resurgence of this CTL approach.

Indirect Liquefaction

Indirect coal liquefaction typically refers to processes that first generate synthesis gas by gasification of coal followed by production of solid, liquid, and gaseous hydrocarbons via catalytic reduction of CO in subsequent stages of the process. Frequently, the term ICL refers to the synthesis of liquid transportation fuels by means of Fischer–Tropsch synthesis catalyst. Other ICL technologies include methanol and/or dimethylether from syngas, or methanol-to-gasoline (MTG). MTG was commercialized in 1986 and uses ZMS-5 zeolite catalyst to convert methanol to gasoline.

A basic block flow diagram of key process steps in F-T ICL is shown below in Fig. 5.

After mining and coal preparation, beneficiated coal (coal that has been subjected to physical grinding and chemical cleaning methods during coal preparation) is first gasified with oxygen and steam to produce syngas. This syngas is cleaned of all impurities and sent to the F-T reactors where most is converted to liquid hydrocarbon fuels. The liquid products from F-T ICL contain zero sulfur and essentially zero aromatic hydrocarbons, and therefore ultra clean diesel or jet fuels can be produced after additional refining. Carbon dioxide is produced mainly during water gas shift (vide infra) and the F-T synthesis reactions, and can be captured for subsequent storage or use. The unconverted synthesis gas can be either recycled back to the F-T reactors, to maximize liquid fuels production, or combusted in a gas turbine combined cycle power plant to generate internal and external power. Thus ICL plants can be configured to produce liquid fuels only, on a freestanding basis, or to produce a combination of liquid fuels and power for export.

The other major ICL approach produces methanol from the syngas, via a different set of chemistries from F-T, and uses the methanol as a chemical or as a fuel, typically as a blend with petroleum derived gasoline. The methanol serves as oxygenate and fuel extender. Dimethylether (DME) also can be produced from syngas, either directly or via dehydration of methanol.

Synthesis of fuels and chemicals from syngas does not occur in the absence of appropriate catalysts.

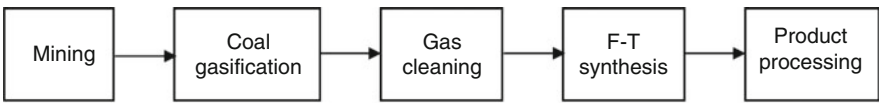

Coal to Liquids Technologies. Figure 5
Key process steps for indirect coal liquefaction [45]

The basic concept of a catalytic reaction is that reactants absorb onto the catalyst surface, rearrange atoms, and combine into products that desorb from the surface. One fundamental functional difference between different syngas conversion catalysts is whether or not the adsorbed CO molecule is cleaved during reaction at the catalyst surface. In Fischer–Tropsch synthesis, C–O bond cleavage is a necessary reaction step. In methanol synthesis, the CO bond remains intact. Hydrogen plays two roles in catalytic syngas conversions, as a reactant needed for hydrogenation of CO to give the hydrocarbon moieties, and as a reductant to activate and regenerate the metal surface.

Much of the research and process development on coal liquefaction after the 1990s was aimed at matching the fuels synthesis conditions with modern, efficient coal gasifiers such as those developed by Uhde, Texaco (now GE), Shell, and ConocoPhillips. A block flow diagram of a typical F-T CTL process to produce naphtha and diesel middle distillate cuts is shown below in Fig. 6, with the liquefaction end of the process indicated within the dash-lined boundary. Coal feed is prepared in the milling and drying section and then sent to the gasifier where it is fully converted to raw synthesis gas (or a coal slurry gasifier may also be employed instead).

In the F-T synthesis step, the syngas is converted to raw product. The lighter ends of the raw F-T product are partially recycled internally and the remainder is sent to the heavy ends recovery unit. Oxygen for coal gasification is supplied by an air separation unit (ASU, not shown). A part of the raw synthesis gas is treated in the water gas CO-shift unit to convert steam and CO to hydrogen and CO_2, after which this treated gas is remixed with the untreated portion. The split between the portions is controlled such that the required H_2/CO ratio of the F-T synthesis is always met. The shifted syngas is then submitted to an acid gas removal (AGR) step, where COS, H_2S, and CO_2 are removed to produce clean syngas feed for the F-T synthesis unit. The Rectisol adsorption process is commercially proven in CTL applications and is typically deployed for AGR, applying methanol at low temperatures as a solvent. However, a more energy efficient system, such as polyethylene glycol (PEG)- or glycol diether-based processes (e.g., Selexol or Genosorb) may be used instead of Rectisol, although in these processes the COS has to be removed in a separate, COS hydrolysis step. A small fraction of the clean syngas is sent to a pressure swing adsorption (PSA) unit for production of pure hydrogen, as H_2 is required in the product workup section, and the major portion of the syngas is routed to the F-T plant.

The tail gas from the heavy ends recovery unit is sent to a combined cycle plant to produce sufficient power for the entire CTL complex. The F-T waxes and

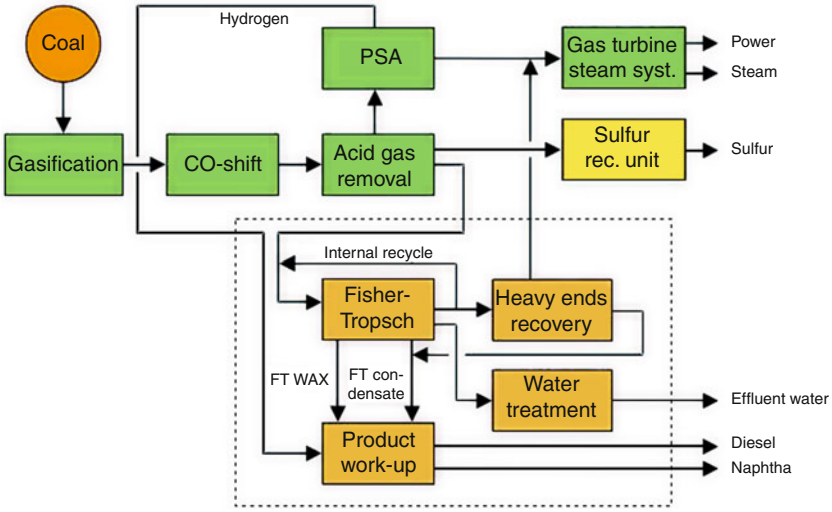

Coal to Liquids Technologies. Figure 6
Fischer–Tropsch coal to liquids process [15] (Figure courtesy Uhde Corporation of America)

FT condensate products are sent to the product upgrade section, where they are hydroprocessed with hydrogen (from the PSA unit) to produce primarily diesel product. A significant amount of water is coproduced with the hydrocarbons during F-T synthesis hydrocarbons. This water fraction contains impurities such as oxygenates, which have to be removed in a water treatment step. Sour gas (H_2S, COS) removed in the AGR unit is sent to a sulfur recovery unit, a Claus plant, where it is converted into elementary sulfur. The tail gas from the Claus plant is hydrogenated and recycled to the acid gas removal unit, or it can be treated in a SCOT (Shell Claus Off-gas Treating) treatment unit. Using the SCOT process, the sulfur components in the Claus tailgas are catalytically converted to hydrogen sulfide, which is removed by solvent extraction and recycled to the Claus plant, and the off gas from the absorber is incinerated. As an alternative to the recovery of elemental sulfur, sulfuric acid can be produced from the sour gas components.

The yield of products in a fully self-sufficient CTL plant based on hard coal gasification is approximately 1,875 barrels per ton of coal. The amount of sulfur produced depends on the concentration of sulfur in the coal.

Gasification Gasification breaks down coal into molecules of much lower molecular weight, CO and H_2, usually using high temperature in the presence of oxygen at high pressure. Gasification technologies introduce air and/or oxygen, often with steam to moderate the temperature in the combustion zone of the gasifier. The product is syngas, a mixture of hydrogen and carbon monoxide. The syngas is subsequently converted to liquid fuels and chemicals in ICL processes. The three main types of gasifiers are the moving bed, fluidized bed, and entrained flow reactors. Gasification technology alternatives are grouped under the three technology types in Table 3. All three types work well and are in commercial use.

Coal to Liquids Technologies. Table 3 Types of coal gasification technology

Gasification type	Technology
Moving bed	Lurgi – Dry Gas (Germany)
	FBDB – Sasol (South Africa)
	British Gas and Lurgi – BGL (UK)
Fluidized bed	High Temperature Winkler (HTW) – RWE, formerly Rheinbraun – marketing byUhde (Germany)
	Kvaerner (Finland)
	Foster-Wheeler (Switzerland)
	GTI/SES – U-gas (USA)
Entrained	SCGP – Shell (USA)
	Koppers-Totzek – Uhde (Germany)
	PRENFLO™ – Uhde (Germany)
	SFG – Siemens (Germany)
	GE (USA)
	ConocoPhillips (USA)

Moving Bed Gasifiers The moving bed may use co-current or counter-current flows and is sometimes referred to as a fixed bed because the coal bed is kept at a fixed, constant height. The moving bed gasifier first provided a convenient means to handle solid residuals (ash) from the gasification. Moving bed gasifiers can accommodate coal with moisture content as high as 35%, as long as the ash content is less than 10%. Depending on the temperature at the base of the bed of coal, the ash is either dry solid or a molten slag. If excess steam is added, the temperature can be kept below the ash fusion point. The coal bed typically rests on a rotating grate through which dry ash residue falls for removal. To reduce steam usage, British Gas and Lurgi developed a slagging bottom gasifier (BGL gasifier) in which the ash is allowed to melt and drain off through a slag tap. This gasifier has over twice the capacity per unit of cross-sectional area compared to the dry bottom gasifier. Allied Syngas, Advantica, and Envirotherm offer the BGL technology commercially.

Fluidized Bed Gasifiers In the fluidized bed gasifier, the feed is fluidized in air, or sometimes oxygen, and steam with upward, turbulent flow for efficient mixing. The temperature is normally below ash melting temperature. The ash is removed as dry particles, which is advantageous if the ash is highly corrosive and would damage the reactor if removed as a molten

slag (a problem when gasifying high-sulfur coal or biomass). Throughput of the fluidized bed gasifier is higher than for the moving bed. The low operating temperature of the circulating fluidized bed reactor technologies of Kvaerner and Foster Wheeler are particularly appropriate for low-rank coal (or other reactive feed such as biomass). The higher pressure of the HTW gasifier technology is suitable for coal (and biomass) [46].GTI developed an agglomerating ash fluidized bed gasifier for its U-Gas process in which crushed limestone for sulfur capture is injected with the coal, and adding the limestone aids in processing ashes having very high fusion temperatures. Char and ash that exit the gasifier with the product gas are recycled to the hot agglomerating and jetting zone, where temperatures are high enough to pyrolyze freshly introduced coal, gasify the char, and soften the ash particles. The ash particles stick together and fall to the base of the gasifier where they are cooled and removed. The agglomerating fluid bed gasifier can be blown by either air or oxygen. The U-Gas technology is licensed by Synthesis Energy Systems (SES).

Alkaline metal compounds, especially chlorides and carbonates, can be used as catalysts for coal gasification in a fluidized bed including such compounds as potassium carbonate, zinc chloride, and sodium carbonate.

Entrained Flow Gasifiers Entrained flow technologies particularly target issues of solids handling in coal gasification. When bituminous coals are heated to 300–350°C, the particles tend to swell and agglomerate in producing a consolidated cake. The handling of this caking char and the heavy tars that accompany it has been critical to the development of gasification processes. The agglomerate that forms can disrupt gas flow patterns and lower thermal efficiency.

In the entrained flow reactor technology, coal is fed as a dry, pulverized solid or as a fine slurry with liquid and is most commonly gasified with oxygen (rather than air) in co-current flow. It is operated above the ash-melting point, which means that the molten ash forms a liquid slag inside the gasifier that runs down the walls of the gasifier and is removed through a bottom hole. The use of oxygen at high pressure and temperature is a source of both high throughput and versatility. Typically a dry-feed gasifier such as SCGP or PRENFLO can process a wide range of coals, from low-grade soft brown coal to top-grade hard anthracite. These dry-fed entrained-flow gasifiers have single-train capacities of about 3,500–4,000 t/day. Most of the ash is removed as slag.

Uhde's PRENFLO entrained gasifier technology has operated successfully for the last 12 years in the world's largest dry-fed IGCC plant, located in the Elcogas plant in Puertollano, Spain. PRENFLO employs dry-feeding, multiple side-fired burners, and a cooled membrane wall for robustness under the slagging conditions inside the gasifier. The raw gas leaving the PRENFLO™ gasifier is first cooled down to approximately 900°C in a gas quench system with a recycle gas stream. The sensible heat of the raw gas is used to produce saturated high pressure steam, and saturated medium pressure steam, both of which are ultimately used in the steam turbine of the power block to produce power. The raw gas is next sent to gas conditioning operations; consisting of filtration to remove particulates, scrubbing with water to remove chlorine and other soluble components, removal of COS and HCN in a hydrolysis reactor, and removal of H_2S using a methyldiethanolamine (MDEA) solution. The H_2S fraction from the desulfurization unit is treated in the Claus unit with tail-gas recycle, where liquid elemental sulfur is produced for sale on the local market. Electrical power is generated by a single combustion turbine and a single steam turbine.

A slurry feed may be used with low rank coals as these can exhibit serious particle decrepitation, dusting, and even spontaneous combustion when exposed to drying conditions upon storage, crushing, and handling. A typical coal water slurry contains about 70% mass of coal, pulverized to minus 200 mesh or finer, and water with about 1% mass of an additive to alter the rheological properties of the liquid mixture and thus allow a larger coal loading [47]. Slurry-fed entrained flow gasifiers include the GE gasifier and the E-Gas gasifier (now owned by ConocoPhillips). The GE gasifier coal slurry is fed through single-burner at the top of the gasifier, which is a refractory lined pressure vessel. Refractory stability under slagging conditions depends largely on the ash content and ash properties. Furthermore the burner lifetime of slurry-fed burners is considerably lower than that of dry-fed burners. Reactor exit gas is cooled either by direct water injection or by a radiative cooler located directly below the

reactor. The E-Gas gasifier differs from other systems in that it uses a two-stage reactor, also involving refractory lined pressure vessels. The bulk of the feed slurry and all the oxygen are sent to the first (horizontal) stage, where the coal is gasified. Hot gas flows into the second (vertical) stage, where the remainder of the coal slurry is injected. Hot fuel gas is cooled in a fire tube boiler gas cooler and then sent to the F-T unit. The process produces no ash and recycles by-products for uses such as road construction materials.

Today, both solid (dry) and slurry-fed gasifiers are likely to be entrained flow gasification systems. The newer entrained flow gasifiers are considerably more efficient, albeit at the price of making product gas having a higher content of syngas, total H_2 and CO, but a lower H_2/CO ratio [48]. A critical aspect of long-term sustainability of any gasification technology is that it be versatile enough to accommodate various ranks of coal as well as other feeds such as biomass.

The first commercial scale and currently longest running coal gasification plant in the USA was put into service in 1983 by Eastman at its Kingsport, Tennessee facility. A schematic of the gasification plant is shown in Fig. 7. The process uses two high-pressure (1,000 psig) GE gasifiers, one being a spare, to convert about 1,250 t/day of bituminous coal into acetyl chemicals via methanol and CO. Over 99.9% of the sulfur (as H_2S) is removed from the syngas via a Rectisol unit designed by Linde AG and is recovered as elemental S by a combination of Claus sulfur recovery units (SRUs) and Shell Claus off-gas treating (SCOT) processes. CO_2 is also removed by the Rectisol process and is currently vented, but could easily be captured for sequestration. A cold box, also designed by Linde AG, is used for cryogenic separation of CO from a portion of the syngas, and some of the syngas itself is used in downstream methanol plants based on technology from Lurgi and Air Products. Mercury

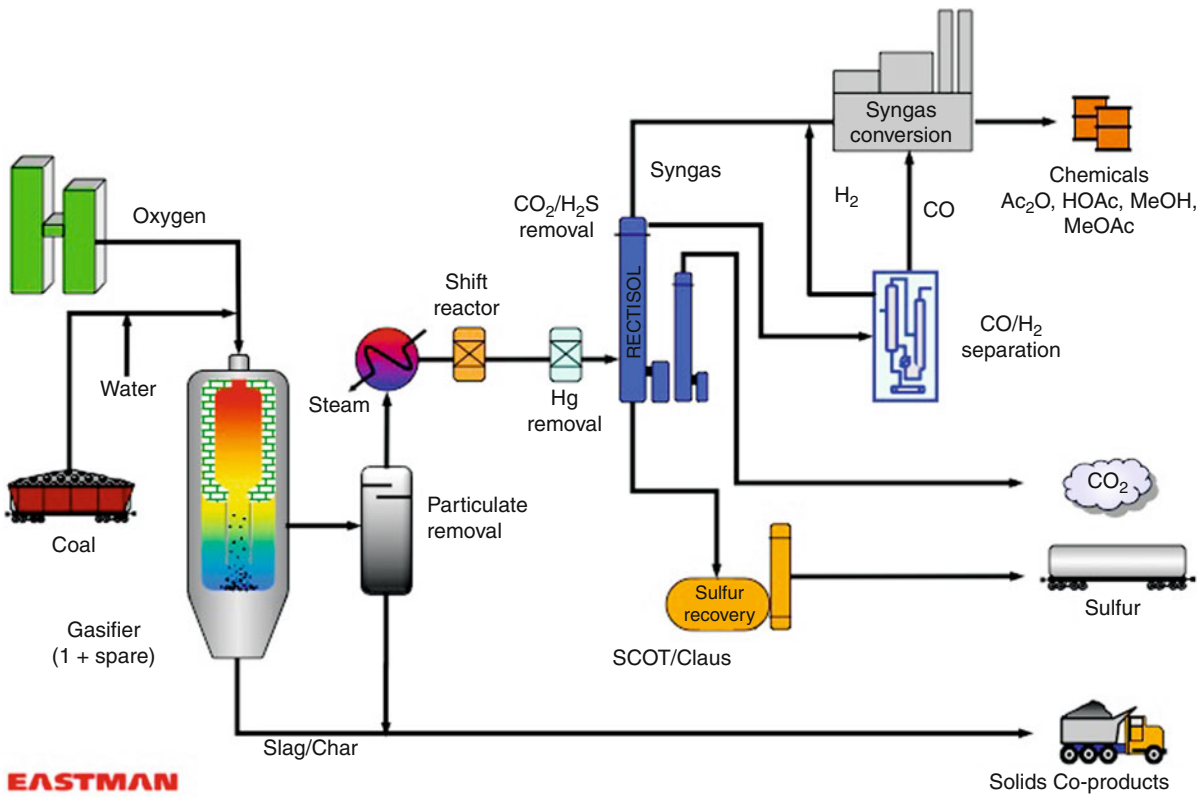

Coal to Liquids Technologies. Figure 7
Flow diagram of Eastman's coal gasification plant (Figure courtesy of Eastman Chemical Company)

contaminant originally present in the coal is removed using a packed bed of sulfur-impregnated activated carbon. Originally built for production of chemicals from coal, the Eastman gasification process and associated learning curve with a variety of coals are representative of what would be used for future production of power and fuels from coal in processes such as integrated combined cycle gasification (IGCC) and industrial gasification.

Disadvantages of entrained-flow gasification include a rather high oxygen requirement and a high waste heat recovery duty. However, the ability to feed coal that is dry reduces the oxygen requirement and increases efficiency compared to a single-stage entrained gasifier using slurry feed.

Fischer–Tropsch The Fischer–Tropsch (F-T) reaction is a polymerization or oligomerization of carbon monoxide performed catalytically under reducing conditions. Chemically F-T is single reaction, with approximate stoichiometry for linear hydrocarbon production as shown in Eq. 1. The greater hydrogen content of methyl groups at the chain termini increase the stoichiometric ratio of H_2:CO slightly beyond 2:1, with the actual F-T stoichiometry for paraffinic hydrocarbon production being about 2.1:1.

$$\begin{aligned} &n\mathrm{CO} + (2n+1)\mathrm{H_2} \leftrightarrow \mathrm{CH_3}-(\mathrm{C_{n-2}H_{2n-4}})-\mathrm{CH_3} \\ &\quad + n\mathrm{H_2O} \\ &\Delta \mathrm{H}_{298} \approx -38\ \mathrm{kcal/molCO} \end{aligned} \tag{1}$$

Mechanistically, the F-T reaction consists of four steps: (1) formation of metal-bound C_1 species from feed CO (or possibly CO_2 if present); (2) chain initiation wherein metal-bound C_2 species form from intramolecular or intermolecular coupling of the metal-bound C_1 species; (3) chain propagation wherein the initial metal-bound C_2 species grows as it couples with newly formed metal-bound C_1 species; and (4) chain termination wherein metal-bound C_n species undergo hydrogen transfer reactions that disable further propagation [49].Mechanistic specifics remain in debate but it is well accepted that hydrogen transfer reactions play key mechanistic roles throughout the reaction, including metal-catalyzed hydrogenation of CO, β-hydride elimination from the growing chain to give terminal olefins, and intramolecular reductive elimination of hydrocarbon (R) and hydrogen (H) fragments from the catalytic center to give products during chain termination. Hydrogenation is not always complete and oxygenation products such as lower alcohols and carbonyl compounds also form. Olefins form throughout the process via β-hydride elimination, and these either re-hydrogenate during propagation or exit from the catalytic cycle during termination.

Performance Variables and Parameters, and Product Distribution The reaction temperature and catalytic metal strongly influence the chemistry and product distribution. The reaction is run in either a high temperature (HTFT) or low temperature (LTFT) regime. The HTFT reaction is always performed with iron as catalyst, at ~340°C, and the LTFT reaction is run at ~220°C when using a Co-based catalyst. The Fe-catalyzed LTFT reaction can be run a little hotter, at 230–270°C. The HTFT reaction is traditionally used to make light syncrude for production of gasoline and diesel. The LTFT reaction produces primarily high molecular weight hydrocarbons, referred to collectively as F-T wax, that are typically hydrocracked to make diesel [50].

Much novel work on stable cobalt catalysts for slurry bed gas to liquids (GTL) applications has been patented in the past 15 years. Although some companies, notably Syntroleum, apparently plan to use cobalt in CTL F-T operations, reports dedicated specifically to the use of Co in F-T CTL are essentially unavailable [51]. This is mainly because unlike iron, cobalt does not undergo the water gas shift reaction (WGSR) at the conditions needed to produce the supplemental hydrogen needed to make saturated hydrocarbons from coal. It is also the case that, while essentially all examples of Co patents use GTL conditions, many of these Co patents state that various feed sources including syngas from coal may be used instead of natural gas [52]. Major research domains of emphasis in F-T CTL catalysis include understanding and fixing problems of catalyst instability and attrition at slurry LTFT conditions [53, 54].

The parameters used to assess and report performance of F-T catalysts are those typically used for catalytic reactions: conversion, selectivity, product distribution, yield, reactor productivity, and catalyst fate

or lifetime. The selectivity of a catalyst with a given feed composition is the main determinant of measured product distribution (although product distribution is also influenced by process design). The yield of a given cut is the product of overall conversion and selectivity for that cut. Yield is usually expressed as a function of time and catalyst quantity in these continuous processes. Catalyst fate relates to the mechanism and time frame of catalyst deactivation and therefore determines its useful lifetime.

The conversion for a F-T process is generally reported as %CO converted to any product, although conversion of total feed ($CO + H_2$) is sometimes used. Coproduction of the undesired by-product methane typically rises directly with conversion. F-T synthesis with Co is typically run at about 60% conversion, and conversions in LTFT are typically in the range of 50–70%.

The reactor productivity is the quantity of product produced per quantity of catalyst per unit time, expressed by weights of product and catalyst (e.g., $kg_{prod}/kg_{cat}/h$) or by volumes ($L_{prod}/L_{cat}/h$). Productivity may be reported for bulk product or for specific cuts, or even as the quantity of CO converted per quantity of catalyst per unit time. Productivity of the LTFT reaction performed in a slurry bed reactor is higher than for a fixed bed, primarily as a result of improved heat management in the slurry system. The continuous motion of the liquid-catalyst matrix allows sufficient heat transfer to achieve commercial slurry reactor productivities of about 200 volumes of CO converted/vol catalyst/h.

The product distribution reflects the selectivity of the catalytic system at the reaction conditions, typically reported as a percentage of the total product or as a percentage of the CO converted (carbon basis). Selectivity data also may be supplied in absolute quantities, as reactor productivities for specific cuts. The weight fractions of various product cuts obtained within the F-T kinetic regime are shown in Fig. 8. The product slate is influenced by many reaction variables; particularly the feed composition, the reaction temperature, the catalytic metal and reaction promoters, and the support material if present.

F-T product slates include gaseous and liquid fractions. The gaseous reaction product includes hydrocarbons boiling below about 650°F (tail gases through middle distillates). The liquid reaction product (the condensate fraction) includes hydrocarbons boiling above about 650°F (vacuum gas oil through heavy paraffins). Commercially, the product boiling below 650°F is typically separated into a tail gas fraction and a condensate fraction of about C_5–C_{20} normal paraffins plus higher boiling, branched hydrocarbons. Branching may be advantageous to a number of end-uses, particularly when increased octane values and/or decreased pour points are desired for lube oil additives. The degree of isomerization is preferably greater than 1,

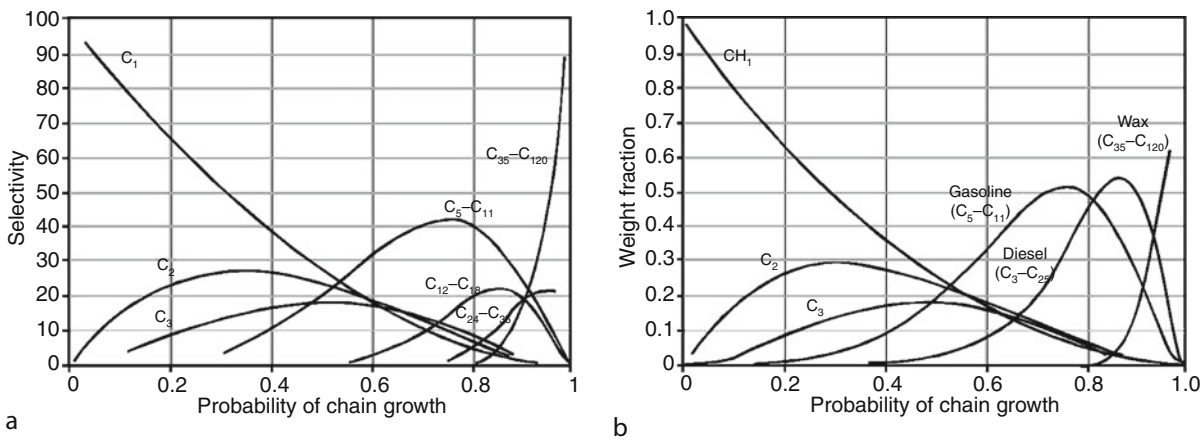

Coal to Liquids Technologies. Figure 8
Product distribution plots for the Fischer–Tropsch reaction [55]. (**a**) General distribution, and (**b**) additional breakdown of the C_{12+} cuts

and more preferably, greater than 3 mol of isoparaffin per mole of *n*-paraffin. If used in a diesel fuel composition, the products preferably have a cetane number of at least 60.

The F-T reaction produces a wide range of saturated and olefinic hydrocarbons. Figure 9 shows the percentage proportions of olefins, alkanes, oxygenates, and aromatics in upgrades syncrude obtained from the F-T reaction at varied conditions of temperature regime and catalytic metal. The HTFT reaction gives aromatics, while the LTFT reaction does not give aromatics with any catalytic metal. Cobalt is a better hydrogenation catalyst than iron, and therefore products of the Co-catalyzed F-T reaction tend to have a lower olefin/paraffin ratio than those of iron. (Not shown in Fig. 9, the high temperature reaction also gives more branched hydrocarbons, and with a higher degree of branching, than the low temperature reaction using either Fe or Co.) The LTFT and HTFT both give oxygenates, typically 10–15% for the HTFT reaction and about half of that for the LTFT reaction with Fe (and much less with Co). Most oxygenates produced in the LTFT reaction are alcohols. The HTFT reaction gives alcohols and ketones, plus a lesser amount of carboxylic acids and aldehydes. The LTFT reaction gives more methanol than the HTFT reaction, and the two temperature regimes give comparable amounts of ethanol.

Product slates for F-T catalysis are controlled by polymerization kinetics, with fairly constant chain growth probabilities that fix the ranges of possible product distributions [56]. The moles of species with carbon number n decrease exponentially with n. The weight fraction of product having carbon number *n*, W_n, is given by the Anderson-Schultz-Flory (ASF) distribution (Eq. 2):

$$W_n = (1-\alpha)^2 n a^{n-1} \tag{2}$$

The parameter "a" is the Schultz-Flory distribution factor and represents the ratio of the rate of chain propagation to the rate of chain propagation plus the rate of chain termination. The parameter "α" is the chain growth probability, and 1−α is the probability of chain termination. In using this equation, a and a are considered as independent of chain length. Either value can be obtained graphically using this equation in log form, with analytical data for W_n as obtained, for example, by gas chromatography. In practice, the parameter α is used most often to characterize product distribution [45].

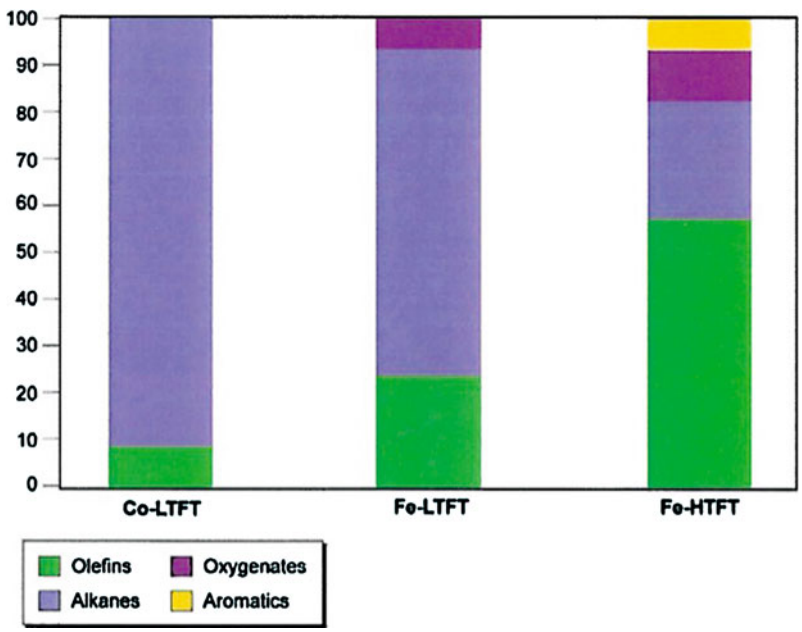

Coal to Liquids Technologies. Figure 9

F-T product slates dependence on temperature and catalytic metal (Figure courtesy of SRI Consulting) [57]

Values of $\alpha > 0.9$ are representative of processes producing high amounts of wax, α values of about 0.8 maximize diesel cuts, and a values of about 0.7 are characteristic of naphtha production. For the intermediate molecular weight cuts of relevance to fuels production, diesel and naphtha, the ASF distribution reveals the limitations on selectivity shown in Fig. 8. Because selectivity for diesel cuts does not exceed about 22% but wax selectivity can reach 90 + %, much industrial research has focused on wax production with downstream hydroprocessing of wax to diesel (or to lube oil base stocks). The α values for oxygenated products appear to be about the same as those for hydrocarbons, which suggests that the products all form by the same or similar chain propagation steps and with similar rates of chain termination, albeit with different chain termination chemistries for the oxygenates, olefins, and paraffins.

In practice, there are several deviations from the ASF product distribution inherent to the F-T process. The amount of methane produced is often higher than would be predicted from this equation, because methane is formed by a chain termination mechanism that is separate from those forming the higher molecular weight products (methane is formed by addition of 2H atoms to a metal-bound C_1). Catalysts that preferentially catalyze hydrogenation over chain initiation, particularly nickel, increase the probability of termination to give methane. A second deviation from the ASF distribution is that the amount of C_2 species formed is often lower than expected based on the ASF equation, although the reason for this is not clear. It has been suggested that an adsorbed ethylene can react with a surface methylene from either side to propagate the chain; whereas higher alkyl adsorbed species would show a lesser rate of chain propagation due to steric constraints.

Some approaches to catalyst design have succeeded in controlling the F-T product distribution by altering the value of alpha. One such approach is the inclusion of alkali metal elements, particularly potassium. Oxides of the alkali metals increase α and promote formation of wax in LTFT catalysis by iron. Use of K_2O helps keep the iron reduced, in the carbide form, which promotes growth of longer chains.

With iron catalysts, alpha can exhibit two regimes of relatively constant value, sometimes referred to as the "two alpha" phenomenon. The value of a can increase with chain length rather than remain constant, and typically changes from about 0.60–0.65 to about 0.90–0.93 at roughly C_{20} [58]. A double α is most evident for low temperature catalyst systems with high wax productivity and is not evident for high temperature systems that make diesel or functionalized hydrocarbons.

HTFT The HTFT reaction has been run in a fixed bed reactor (FBR) or fluidized bed reactor. Traditionally, Sasol used a circulating fluidized bed reactor (CFBR), in its Synthol process. The Synthol CFBR was replaced in 1989 with the Sasol Advanced Synthol (SAS) reactor, based on a conventional fluidized bed and providing superior RAMO (Reliability, cost-effective Availability, Maintainability, and efficient Operability). A block flow diagram of the F-T and downstream portion of Sasol's Secunda plant using the SAS technology is shown in Fig. 10.

The process is employed to produce a range of fuels and also olefins. The fluidized, iron-based catalyst gives primarily C_1–C_{20} raw product. The C_2-rich stream is split into ethylene and ethane. Ethane is cracked in a high-temperature furnace to ethylene, which is then purified. Propylene from the light hydrocarbon gases is purified and used in the production of polypropylene. Large quantities of olefins in the C_5–C_{11} range are produced at these HTFT conditions and the alpha-olefins (straight chain olefins with an ene group in the terminal position) are recovered for use as chemicals (C_5, C_6, and C_8) are recovered or sent into the fuel pool (C_7–C_{11}). Oxygenates in the aqueous stream are separated and purified in the chemical work-up plant to produce alcohols, acetic acid, and ketones including acetone, methyl ethyl ketone (MEK), and methyl isobutyl ketone (MIBK).

LTFT The early German LTFT plants used fixed bed reactor (FBR) technology with Fe catalysts, through World War II. In 1955, Sasol began using a tubular fixed bed reactor (TFBR), consisting of a shell containing 2,050 tubes of 12 m length and 5 cm diameter packed with extruded precipitated iron-based catalyst. A typical catalyst system would be potassium-promoted precipitated iron (such as a Sasol-type catalyst consisting of K = 1.9 wt%, Cu = 2.4 wt%, Si = 5.9 wt%, Fe = 47.3 wt%, O_2 = ~42.5 wt.)

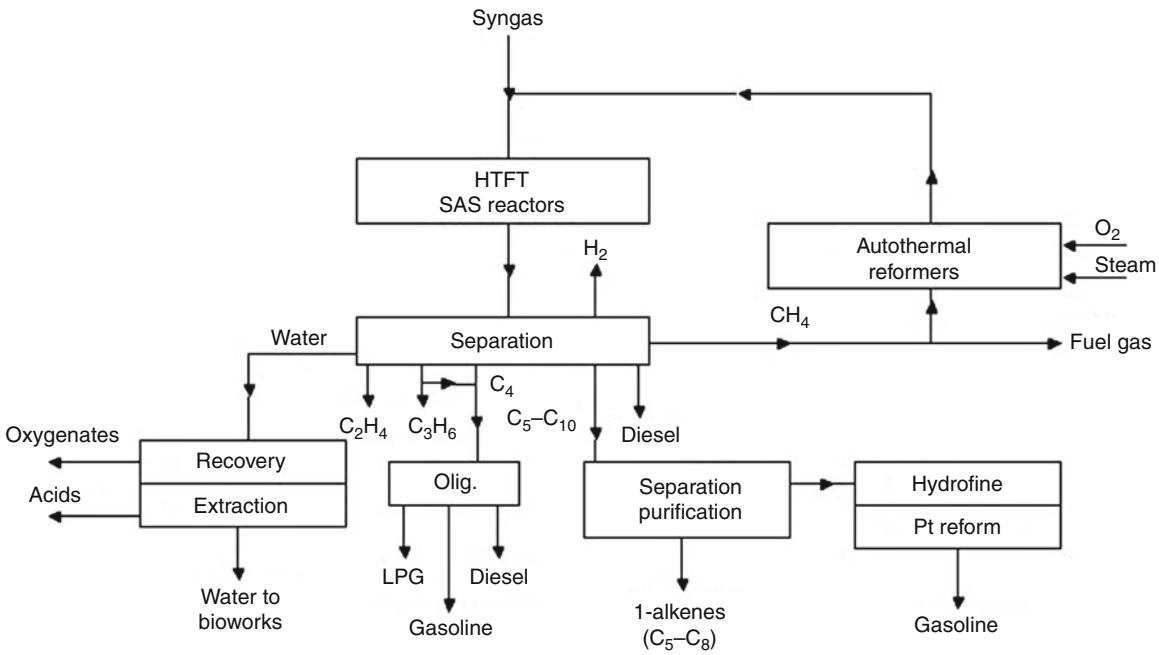

Coal to Liquids Technologies. Figure 10
Secunda plant block flow diagram [59]

This LTFT is referred to as the Arge process and is operated with a shell side temperature of about 220°C and reactor pressure of 25 bar (early Arge) or 45 bar (Arge commissioned in 1987), wherein the heat of reaction is dissipated by generation of steam on the shell side. Further scalability could be achieved by more than doubling the number of tubes, to, for example, 5,000, but the reactor size eventually becomes unwieldy. Sasol found that a slurry phase system is more readily scaled, in part due to engineering design and in part because the Co-based catalysts used are more efficient than the Fe-based catalysts used for the LTFT reaction. Sasol commissioned its first slurry bed reactor (SBR) in 1993.

Table 4 shows typical product slate selectivities for the LTFT, TFBR; the LTFT, SBR; and the HTFT FBR. Both fixed- and slurry-bed LTFT processes give much more paraffin, less olefin, no aromatics, and less oxygenates compared to the HTFT process. LTFT is particularly suited for a modern coal to diesel (CRD) plant.

As indicated in Eq. 1, the F-T reaction is highly exothermic. The reaction heat must be removed rapidly, to avoid temperature increases that would result in undesired formation of high levels of methane, light hydrocarbons, and, in the extreme, catalyst deactivation due to coking, sintering, and disintegration. Deposition of carbon by the Boudouard disproportionation reaction, Eq. 3, is to be avoided, and the heat distribution imparted by the slurry bed is advantageous.

$$2CO \leftrightarrow C + CO_2 \qquad \Delta H_{298} = -20.6 \text{ kcal/molCO} \tag{3}$$

Attrition and breakage of catalyst particles is a more difficult issue to overcome than coking, particularly for slurry bed catalyst systems [61]. Attrition refers to abrasive or erosive removal of surface material that is less than about 50 μm in particle diameter. Breakage refers to a decrease in median particle size caused by fracture of catalyst particles. As the concentration of smaller particles builds up, catalytic activity eventually decreases and also the downstream separation of wax from solid catalyst becomes inefficient. Catalyst particles are subjected to hydrodynamically induced mechanical stress at slurry bubble column conditions that has severely limited the lifetime of LTFT iron catalysts.

Coal to Liquids Technologies. Table 4 Carbon selectivity of selected LTFT and HTFT processes (%) [60]

Product	TFBR (LTFT)	SBR (LTFT)
CH_4 (methane)	4	7
C_2–C_4 olefins	4	24
C_2–C_4 paraffins	4	6
Gasoline	18	36
Middle distillate	19	12
Heavy oil, waxes	48	9
Polar oxygenates	3	6

	TFBR (LTFT)		SBR (LTFT)		SASR FBR (HTFT)	
	C_5–C_{12}	C_{13}–C_{18}	C_5–C_{12}	C_{13}–C_{18}	C_5–C_{12}	C_{13}–C_{18}
n-Paraffins	95	93	96	95	55	60
Paraffins	53	65	29	44	13	15
Olefins	40	28	64	50	70	60
Aromatics	0	0	0	0	5	15
Oxygenates	7	7	7	6	12	10

Precipitated, unsupported iron catalysts are particularly prone to disintegration into smaller particles. Supporting the iron imparts strength to the particle to decrease fracture, but at the expense of decreased volumetric productivity due to dilution of the active catalyst by the support material. Making spherical particles by spray drying [62] can help with fracture or with attrition, but not always with both [63, 64].

The pursuit of mechanically robust iron F-T catalysts remains an area of active research. Traditionally, Fe catalysts have been disposed of rather than regenerated, because iron is inexpensive. However, a few reports of potential use and even regeneration [65] of Fe slurry catalysts have recently appeared, notably from Rentech [66], presumably because management of even low hazard waste volumes is of increasing interest. It is also the case that using a fluidized slurry bed catalyst system allows longer runs, since deactivated catalyst can be removed and fresh catalyst added without taking the reactor off-line as is required for fixed bed reactors. On the other hand, an advantage of fixed bed reactors is that since the wax produced simply trickles down the bed, there is no problem separating the wax from the catalyst. In the slurry system, special internal and/or external devices are required to continuously remove wax from the finely divided catalyst in the slurry.

Water–Gas Shift Reaction The water-gas shift reaction (WGSR), Eq. 4, is important for CTL because the H_2/CO ratio produced by gasification of coal is lower than that produced by steam reforming of methane in GTL (gas to liquids), by about a factor of 3. Without the WGSR, other sources of hydrogen must be provided in CTL, if hydrocarbon fuels are the intended product slate as per Eq. 1, and additional sources of hydrogen in turn typically require additional use of power that itself generates CO_2.

$$\begin{aligned} &CO + H_2O \leftrightarrow CO_2 + H_2 \\ &\Delta H_{298} = -9.8\ \text{kcal/molCO} \end{aligned} \tag{4}$$

The in situ WGSR occurs concurrently during the iron-catalyzed F-T reaction. Cobalt does not catalyze the WGSR under F-T conditions and therefore iron catalysts produce more CO_2 than do cobalt catalysts. In practice the WGSR is one of several factors that affect the overall efficiency of an F-T CTL process when using

Fe versus Co as catalyst, another being the greater efficiency of the smaller reactor used for Co compared to Fe, and each must be taken into account by process engineers when designing CTL plants.

Another key aspect of the WGSR is that it can run in reverse. A potential use for some of the by-product heat typically available in hot outlet gases from high temperature gasifiers is to generate steam heat for an external water gas shift reaction, to be conducted downstream of the gasifier, wherein some H_2 (from recycle or tailgas) consumes the undesirable by-product CO_2.

Downstream Product Upgrading Upgrading technologies for F-T syncrude are modifications of those developed for crude oil refining. Refinery process options for producing fuels from F-T middle distillates include wax hydrocracking, distillate hydrotreating, catalytic reforming, naphtha hydrotreating, alkylation, and isomerization. The many technology licensors for hydroconversion processes include ChevronTexaco, UOP, IFP (Axens), Süd-Chemie Sasol Catalysts, and Haldor-Topsøe. Catalysts can be obtained from these companies as well as from AkzoNobel, Süd-Chemie, and Axens among others.

Reforming and alkylation of gaseous products to produce liquid fuel-range products are appropriate when upgrading synthetic crude from the Fe-catalyzed HTFT reaction. Skeletal modification technologies most important to upgrading synthetic crude from HTFT include isomerization, mild hydrocracking, and even fluidized catalytic cracking. Catalytic oligomerization of olefins is especially applicable to the product from an iron-catalyzed, HTFT process because the bulk of the crude product consists of these olefins, particularly C_3–C_5 olefins (gases). The Sasol Synfuels CTL refinery in Secunda uses an alkene oligomerization process based on solid phosphoric acid (SPA) catalysis to convert most of the light alkene HTFT product into liquid fuels [67].

Currently, the production of a high quality diesel fuel is preferred to the production of gasoline in F-T fuels production. This is because the same factors that count against F-T gasoline, such as product linearity and low aromatic content, serve as very positive factors in favoring high quality, high cetane number in F-T diesel fuel. Straight run F-T diesel makes up about 20% of the total F-T product and has a cetane number of about 75 because it is predominantly linear. For maximum production of high quality diesel, the slurry bed reaction operating in the high wax selectivity mode with cobalt-based catalyst, or the high diesel selectivity mode with iron-based catalyst, is the most efficient approach. Lighter and heavier fractions are usually less desirable due to limited markets and/or lower prices.

The Co-catalyzed process is typically chosen for maximum wax production in LTFT gas to liquid (GTL) processes; however, the use of iron-based catalysts is generally preferred for CTL because coal-derived syngas is deficient in H_2 and cobalt does not catalyze the WGSR that supplements H_2 production during the iron-catalyzed F-T reaction. When operating in the LTFT mode, iron catalyst can produce up to 50–75% linear wax products. LTFT-derived feeds can be hydrocracked under much milder conditions than typical crude oil derived feeds, such as vacuum gas oils, which require pressures as high as 150 bar to prevent coking of the catalyst by aromatic compounds. This is not an issue with paraffinic feeds, and pressures between 35 and 70 bar are used to hydrocrack LTFT products using commercial hydrocracking catalysts. The relatively low levels of oxygenates present in F-T waxes, mainly alcohols and lesser amounts of acids or carbonyls, are easily and completely hydrodeoxygenated.

After hydrotreatment, the straight run diesel fuel cut has a cetane number ranging from 70 to 75. If both hydrotreating and hydrocracking are used, they may be operated at the same pressure using a common hydrogen loop. Alternatively, the hydrotreater can be operated in a once-through mode, at lower pressure, and the hydrogen tail gas then subsequently pressurized and fed to the hydrocracker loop. For a 30,000 bpd equivalent product upgrading system involving both hydrocracking and hydrotreating, the size of the unit is comparable to those used in oil refineries. There are many process configurations possible depending on site-specific factors including plant capacity, available land, and possible integration with other facilities.

When using the slurry phase LTFT reactor, water is removed from overhead gases in a three-phase separator and then the remaining condensate is sent to a low temperature distillation column, in the heavy

ends recovery section, to recover condensate from tail gas in the reactor overheads. The overheads from the low temperature fractionation column are used as fuel gas. Recovered condensates from the column are sent to the product work up section. The waxy reactor product is withdrawn from the side of the F-T reactor and continuously separated from the catalyst. The waxy product is then sent to the first low temperature column, which sends a heavy cut to the hydrocracker and a light cut to the hydrotreater. The wax hydrocracker produces the diesel product, while olefins in the condensate are hydrogenated to paraffins in the hydrotreater. The hydrocracking step typically uses a silica-alumina supported Ni-Mo-based catalyst and can be adjusted to maximize the production of ultraclean diesel product. The products from the hydrotreater and hydrocracker are then combined and fractionated into diesel and naphtha products. Up to approximately 80% of the product is diesel and the remaining portion is naphtha.

Product upgrading schemes center around three fuel products (diesel, LPG, and naphtha), but the upgrading plant is quite amenable to different configurations if market demand so indicates. The ASF distribution means that the F-T process and its associated refinery also produce transportation fuels and products other than diesel and gasoline. Other saleable products may include solvents, kerosene, jet fuel, illuminating paraffins (sold for use in lighting and appliances in South Africa), base oils (for lubricant products), and chemicals. Maximizing recovery of the higher boiling jet fuel while maintaining diesel production will tend to increase economic return.

Major projects planned in F-T ICL include a US $3.3 billion plant in Ningdong with Shenhua Ningxia Coal Group and Sasol Ltd, scheduled to begin construction in 2010 [68].

Methanol and Dimethylether Supplementation of liquid fuel supplies with methanol made from abundant coal reserves has become increasingly attractive in countries that are oil and natural gas resource poor. Methanol has a broad range of applications including:

- Fuel substitute for gasoline
- Gasoline fuel blend to extend conventional fuel supplies
- Energy storage medium in coproduction of power and fuel
- Rapid start combustion turbines to meet peak electricity demand
- Advanced methanol powered and plug-powered vehicles
- Direct methanol fuel cells

Methanol can be synthesized from syngas according to Eq. 5, where the thermodynamics assume gas phase components. The formation of methanol from syngas is highly exothermic.

$$\begin{aligned} &CO + 2H_2 \leftrightarrow CH_3OH \\ &\Delta H_{298} = -21.6\ \text{kcal/molCO} \end{aligned} \tag{5}$$

The feasible operating temperature for methanol synthesis is strongly affected by the temperature sensitivity of the copper-based catalyst, which is prone to deactivation via sintering of copper or coking [69]. Methanol synthesis occurs at significant rate in the temperature range of 210–260°C, optimizing at about 237°C [70]. Modern commercial methanol synthesis catalysts make use of the high reactivity of copper oxides combined with the dispersant function of zinc oxide, supported on alumina. This combination was pioneered by ICI [71] (Imperial Chemical Industries PLC, acquired by AkzoNobel in 2008) and allows methanol synthesis to be performed at low pressure with recycle (35–55 atm) and relatively low temperature (200–300°C, typically 250°C). The component contents are in the range of about 40–80% CuO and 10–40% ZnO, with 5–10% Al_2O_3. For example, the unreduced material RPJ-19, from United Catalysts Inc., has been described as 55 wt% CuO, 36% ZnO, and 8% Al_2O_3, with 1% SiO_2 [70]. Magnesia may be added to control sintering and increase the available surface area of copper.

The methanol synthesis catalysts are also sensitive to catalyst poisons. The contaminants sulfur and halide are typically removed upstream to <100 ppm. Because catalyst lifetime is significantly diminished by excessive temperature, reactor temperature control is very important. Currently, all commercial processes produce methanol from synthesis gas in a vapor phase reactor with a synthesis loop, using packed bed or tubular reactors, and temperature moderation is achieved by recycling large quantities of hydrogen-rich gas.

Typically, a gas phase process is limited to about 16% CO in the reactor inlet, as a means of avoiding excess heating by constraining the activity per pass. Cool, unreacted gas is injected at different stages in the catalyst bed or internal cooling surfaces are used to provide further temperature control.

As a means to improve throughput per pass with temperature control, ChemSystems and Air Products developed a fundamentally different, liquid phase reactor system. In this system, referred to as the LPMeOH^{TM} (Liquid Phase Methanol) process, synthesis gas is bubbled through a slurry, consisting of micrometer-sized catalyst particles and methanol in a suspension of mineral oil. The nonvolatile mineral oil acts as a temperature moderator, transferring the heat of reaction from the catalyst surface via the liquid slurry to boiling water in an internal tubular heat exchanger. As a result of maintaining a constant, highly uniform temperature through the entire length of the reactor, the slurry reactor can achieve a much higher per pass syngas conversion than its gas-phase counterparts and also CO concentrations in excess of 50% have been maintained without adverse effect on catalyst activity. As with slurry F-T systems, the liquid phase methanol process benefits from the ability to withdraw spent catalyst slurry and add fresh catalyst on line periodically, without having to shut the system down.

Typical commercial Cu/Zn/alumina methanol synthesis catalysts are also active for the low temperature water gas shift (LTWGS), which enables use of syngas from lower quality, low-hydrogen feedstocks such as coal to be used in making methanol. Reduction of CO or CO_2 to methanol with H_2 is exothermic, and heat dissipation in fixed bed reactors is inadequate to protect the catalyst or to allow optimal product recovery. While less exothermic than the methanol synthesis reaction, the WGSR also adds heat to the system.

ChemSystems performed pioneering development of the LPMeOH process in the 1970s [72]. The LPMeOH technology was based on early design and demonstration work funded by EPRI (Electric Power Research Institute) in the mid-1970s, wherein methanol is produced in one step using the high-CO content syngas from coal [73]. Air Products then undertook a significant research effort together with ChemSystems and DOE co-funding, to further develop the process in the 1980s and 1990s, as part of the DOE's cogeneration program. While ChemSystems originally used an ebullating bed design with an aromatic (1,2,4-trimethylbenzene) or mineral oil liquid, Air Products used the more stable mineral oil in a slurry bubble reactor to further augment heat and mass transfer.

The LPMeOH process was demonstrated at large pilot scale during 1997–2002, in a collaborative effort between Air Products (technology supplier), Eastman Chemical (syngas supplier, plant operator, and end user of methanol), and Arcadis (fuel and power testing). This facility in Kingsport, TN operated for nearly 6 years, with continuous runs of up to 3 months. The nameplate capacity of 80,000 gpd was exceeded by 15%. Eastman syngas, derived from high-sulfur (3–5%) bituminous coal, was used. Of note is the ability to produce sulfur-free methanol containing less than 1% water, which makes this methanol directly suitable for transportation as well as chemical use. Used as a fuel additive, methanol also showed promise for reducing NOx emissions from gas turbines and diesel engines. Air Products also applied the understanding gained from developing the LPMeOH process in developing the Liquid Phase Dimethyl Ether Process (LPDME^{TM}) process, which was demonstrated in the early 1990s.

Sunggyu Lee and colleagues, at the University of Akron and later at the University of Missouri-Columbia, pioneered the mechanistic understanding of the one-step slurry methanol process and also worked on the MeOH/DME slurry process [74]. The LPMeOH process has three distinctive features and benefits compared to prior art using fixed beds. First, the commercial Cu/Zn/alumina methanol synthesis catalyst is slurried instead of fixed, which greatly improves heat transfer via the inert, liquid medium. Second, the slurried catalyst is a fine powder, which avoids mass transfer limitations involving pore diffusion. Third, the improved mass transfer in the well-agitated slurry allows much higher single-pass conversion of the syngas.

The initial method devised to combine steps in liquid-phase DME production involved combining the methanol dehydration catalyst with the slurry phase methanol synthesis catalyst [75]. For DME, typically, the methanol synthesis catalyst is copper on alumina promoted by zinc oxide. The ratio of $CuO/ZnO/Al_2O_3$ is typically about 2:1:5 with a H_2:CO ratio

of 2:1 but will vary with syngas composition. Alumina is the most common dehydration catalyst. Both CO conversion and selectivity for DME are improved by including 10%wt sulfate in the alumina. Many researchers have reported using zeolites, and recent research with zeolites has been quite active in Asia [76]. Likewise, silicoaluminophosphate (SAPO) molecular sieves have been reported recently for use as dehydration catalysts in direct synthesis of DME. A third catalyst functionality may be included to enhance the water gas shift reaction, although the methanol synthesis catalyst is itself also an effective water gas shift catalyst.

Long-term stability of one-step DME synthesis catalyst systems was noted as a primary difficulty by Mobil in the early 1980s and continued as an issue in Air Products' work. The temperature needs and catalyst stability are considered for three simultaneous reactions in direct synthesis of DME: water gas shift (Eq. 4), methanol synthesis (Eq. 5), and methanol dehydration (Eq. 6) [77]. The methanol synthesis via Eq. 5 can be considered in principle as the combination of water gas shift and the reduction of CO_2 by hydrogen (Eq. 7).

$$2CH_3OH \leftrightarrow CH_3OCH_3 + H_2O \qquad \Delta H_{298} = -5.9 \text{ kcal/molDME} \tag{6}$$

$$CO_2 + 3H_2 \leftrightarrow CH_3OH + H_2O \qquad \Delta H_{298} = -11.7 \text{ kcal/molMeOH} \tag{7}$$

Even so, the mechanism actually in effect during direct synthesis of DME is in some debate and might not involve the explicit intermediacy of methanol as per Eq. 6. Figure 11 shows the results of modeling done by JFE Holdings (formed in 2002 by the merger of NKK and Kawasaki Steel) based on their pilot plant results, which give best conversion at a ratio of 1:1 CO:H_2. Specifically, DME may form directly from coal-derived syngas as per Eq. 8. The stoichiometry of Eq. 8 being noted for coal-derived syngas, it is also the case that catalysts for direct DME synthesis have been based on methanol synthesis catalysis and most processes give some combination of both DME and methanol.

$$3CO + 3H_2 CH_3OCH_3 + CO_2 \qquad \Delta H_{298} = -19.6 \text{ kcal/molCO} \tag{8}$$

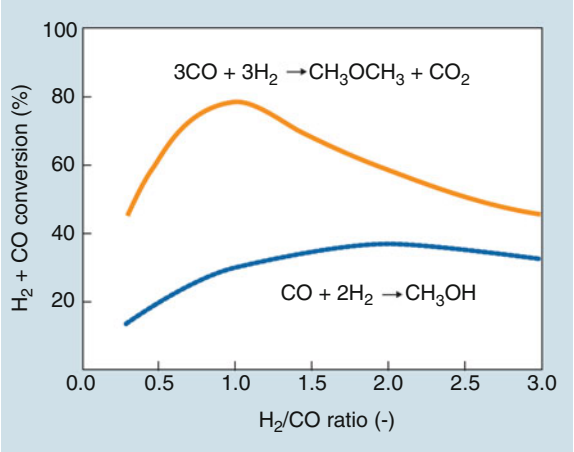

Coal to Liquids Technologies. Figure 11 Equilibrium conversion of CO and H_2 to DME (280°C, 5 MPa) [81]

The WGS reaction used for one-step DME/MeOH production is of the low temperature type (LTWGS) and operates best at about 180–240°C, which overlaps substantially with the methanol synthesis temperature range. The overall chemistry is more easily controlled if the WGS catalyst has little or no F-T activity for hydrocarbon production, which means that the LTWGS catalyst needs to be copper-based instead of iron-based. The typical catalyst used for LTWGS in DME or methanol synthesis has the general formula xCu/yZnO/Al_2O_3 and has no hydrocarbon-producing F-T activity. A typical low temperature shift catalyst contains 30–70% CuO (prior to reduction), 20–50% ZnO, and up to about 40% alumina [78].

The optimal temperature for the methanol dehydration reaction is set not by catalyst stability but by the equilibrium dehydration reaction thermodynamics. The dehydration proceeds best at about 250°C and yield declines as the temperature is raised further. The catalyst function for dehydration of alcohol to ether is a solid acid. Various options are possible, including acidic aluminas, silica-aluminas, zeolites, and various solid or supported inorganic acids. In practice, γ-alumina is preferred to date. The dehydration rate is directly related to the acid strength of the zeolite and the overall rate of DME synthesis can be controlled by the proportion of ion exchange in the dehydration catalyst [79]. Dehydration is relatively fast above

about 240°C and only a few percent of dehydration catalyst is needed in the total catalyst formulation [70]. The LPDME process was demonstrated on a 10 t/day scale for 25 days at Air Products' LaPorte facility using commercially available methanol synthesis and γ-alumina dehydration catalyst in a ratio of 95:5 wt%. The temperature and pressure were approximately 250°C and 50 bar, respectively. Deactivation occurred at a rate of 0.7%/day for both catalyst components [80].

The concern that LPG used heavily in Asia as a fuel and a power source will become increasingly unavailable has sparked significant research to develop DME as a replacement [81]. Properties of DME and LPG are similar in terms of fuel characteristics, low toxicity, and especially handling, distribution, and storage. Some use of DME as an LPG substitute has recently begun in China. To demonstrate the potential replacement of automotive fuel, fleet tests with DME have been performed (the fuel injection system requiring modification to accommodate the lower viscosity of DME compared to diesel, but without modification of the engine itself) [82]. Turbine, boiler, and fuel cell tests with DME have also been performed [83].

JFE in Japan has been a major driver for development and commercialization of one-step slurry DME production. NKK, Taiheiyo Coal Mining, and their partners constructed a 5 t/day direct syngas to DME pilot plant in 1999 at Taiheiyo's site in Hokkaido and operated it intermittently for about 5 years [83]. In 2002, JFE began a 5-year development plan for a 100 t/day pilot plant demonstration in Kushiro, with METI and many collaborators that together formed the DME Development Corp. and the DME International Corp. Interestingly, the feed for syngas production actually used is natural gas; however, JFE opts to bring the 2:1 H_2:CO ratio (produced by reforming natural gas) down to 1:1 (more like the ratio produced from coal) by adding CO_2 during reforming, and the work therefore also relates to advancement of the state of the art in producing DME and methanol by ICL of coal.

JFE reported an impressive purity from their overall process: 99.5 + % DME and <100 ppm combined water and methanol [84]. In this process, shown in Fig. 12, coal is fed to the gasifier and then raw syngas is brought up to a H_2:CO ratio of 1:1 via the WGSR using steam from the gasifier. Sulfur and CO_2 are removed prior to DME synthesis. Unreacted CO and H_2 are separated from liquid products and sent back to the DME synthesis reactor. The DME synthesis makes CO_2 as a by-product, plus some methanol and a slight amount of water. The separation of CO_2, DME, methanol, and water involves a low temperature extraction (−39 °C) [85]. After downstream distillation, methanol is cycled back to the DME reactor.

A different type of ICL process involving methanol is the gasification of coal followed by conversion to methanol and subsequent conversion of methanol to a marketable gasoline product. A $3 billion plant with a production capacity of approximately 700,000 t/year to be built by TransGas is planned in Mingo County, West Virginia. The plant will use Uhde's PRENFLO direct quench gasifier technology to make syngas, which will be converted to methanol and subsequently to gasoline using ExxonMobil's methanol-to-gasoline technology. Methanol conversion is nearly complete and the total liquids yield is higher than in F-T synthesis, including significantly less tail-gas production. The product of the MTG reaction does not require much further upgrading and refining compared to other coal liquefaction routes. A 100,000 t/year MTG process plant was started in China's Jincheng, Shanxi province in 2009, as part of a CTL demonstration complex.

Like DCL, ICL is complex and characterized by heavy investment, but CTL processes, in general, have been recently described as economically competitive at an oil price as low as $25/barrel [86] or, more typically, at an oil price of about $55/barrel [45], with the cost of coal being that incurred at the mine (i.e., without the cost of shipping and handling).

Environmental Factors The overall conversion of coal to liquids not only produces fuel- or chemical-grade products but also consumes water and produces carbon dioxide, as shown in Eq. 9 [87].

Carbon Dioxide The high carbon content of coal combined with the energy use in ICL processes involving gasification means that carbon dioxide emissions on a well-to-wheel basis are about 1.8 times more for coal than for oil. In terms of fuel preparation alone, it has been estimated that an F-T CTL plant without capture would release about 0.78 t of carbon

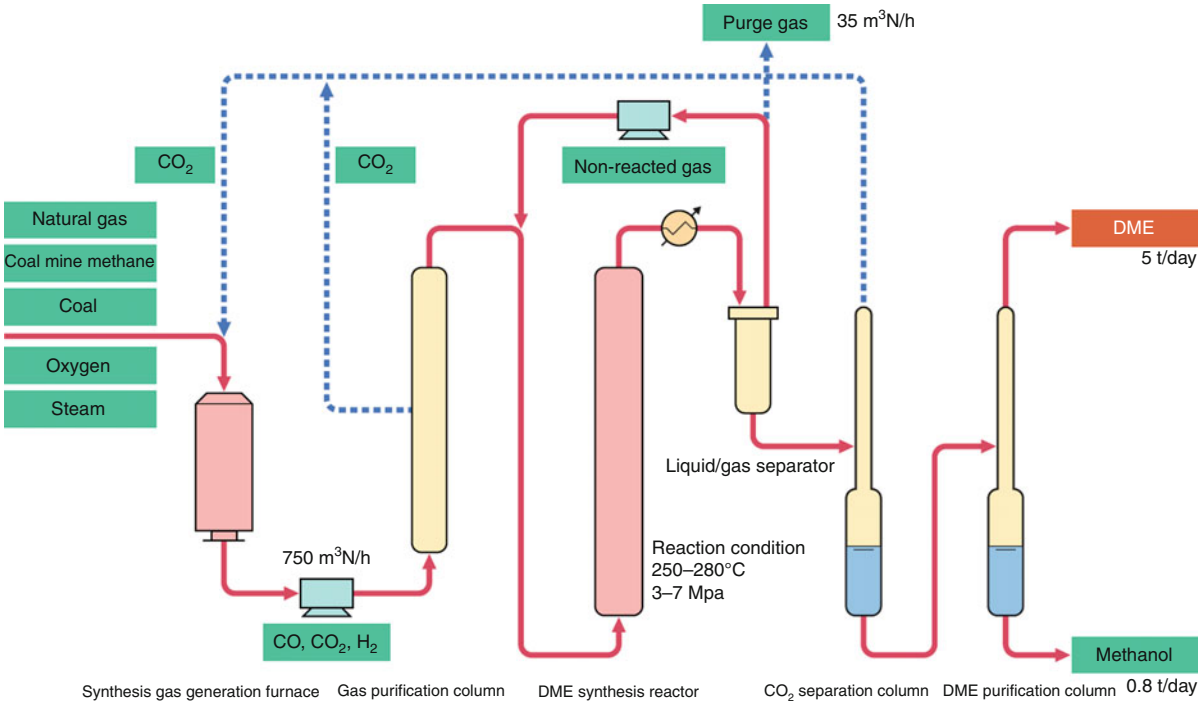

Coal to Liquids Technologies. Figure 12
Process flow diagram of DME direct synthesis from coal (or methane)

dioxide per barrel of product, in comparison to a comparable oil refinery emitting about 0.1 t of carbon dioxide per barrel of product. For a typical bituminous coal, approximately 670 lb of carbon (or 2,450 lb of carbon dioxide) would be emitted for every barrel of F-T liquids produced. This compares to about 250 lb of carbon (or 900 lb of carbon dioxide) emitted for every barrel of petroleum fuels produced by refineries. When carbon sequestration is employed for both facilities (92% captured and stored at the F-T CTL plant and 40% at the refinery), the carbon dioxide emissions become approximately equal.

$$(4+y)\mathrm{CH} + 2(y-x)\mathrm{H_2O} \rightarrow (4+x)\mathrm{CH}_y + (y-x)\mathrm{CO_2} \quad (9)$$

The large quantity of CO_2 produced currently poses a significant challenge to development of the industry. At the time of this writing, no requirements exist in the USA to manage carbon emissions from fossil fuel sources, but should carbon management be required, carbon dioxide produced during the conversion process could be captured for subsequent storage in deep saline aquifers or sold for use in enhanced oil recovery (EOR) operations. A range-finding study done in 2004 by Mitretek Systems (now Noblis) for the US DOE considered production of substitute natural gas (SNG) from coal and assumed that the value of CO_2 for EOR was \$12/t, which would significantly improve the economics of a CTL plant [88]. At present, there are over 2,500 km of dedicated CO_2 pipelines within the US delivering to commercial EOR projects in areas such as the Permian Basin of West Texas, southeastern New Mexico, the Rocky Mountain Region of Utah, Wyoming and Colorado, Louisiana, and the Weyburn Fields in Saskatchewan. With the exception of CO_2 from the Dakota Gasification Plant, all of this CO_2 is naturally occurring.

Total production related emissions from a 2 million barrels/day F-T CTL industry could be as much as a 0.5 Gt/year. There is already a significant knowledge base regarding how to handle CO_2 and inject it into deep geological structures, because injection of CO_2 is already used commercially in the USA to augment natural gas production. The transport of large volumes

of CO_2 via pipeline is also a well-established practice, within segments of the oil and gas industry. Given adequately scaled infrastructure for carbon capture and storage in place, emissions from CTL plants and emissions from use of CTL fuels would be comparable to those associated with the production and consumption of petroleum-based fuels. If sequestration of carbon dioxide becomes mandatory, an additional \$4–\$8/barrel for the price of low-sulfur, light crude oil would be required for profitable operation, depending on specific site logistics [89].

The high sulfur content of most coals is addressed at multiple junctures in the F-T ICL process. Sulfur is removed when the raw synthesis gas is scrubbed to remove CO_2 and sulfur compounds (predominantly H_2S) and again during purification of F-T product streams. The H_2S containing CO_2 streams are treated in a Claus or similar process, where the H_2S is oxidized to elemental sulfur.

Fischer–Tropsch Reaction Product Water Water is a net reactant in CTL processes (Eq. 9) but is a product of the F-T portion of CTL processes (Eq. 1). On a mass basis, approximately 1.3 t of water is produced per ton of hydrocarbon product. After separation of the hydrocarbon product, the F-T reaction water typically contains numerous dissolved oxygenated compounds such as alcohols, aldehydes, acids, ketones, esters, and traces of other hydrocarbons. Purification of F-T reaction water is required in commercial processes, because all water is reused. Distillation removes most of the nonacid oxygenates to leave a bottom stream known as F-T acid water, rich in carboxylic acids. The recovered oxygenated compounds can be purified to chemical products or used as a fuel source. After extraction of the oxygenates, only low concentrations of organic acids remain and these are easily biodegraded by either aerobic or anaerobic digestion to produce water of very high quality, for use as coolant or even for drinking, from the original F-T acid water stream. High purity water suitable for use as boiler feed water can also be produced but requires a third set of treatments, after distillation and digestion, such as adsorption of trace suspended solids, dissolved salts, and organic material on activated carbon.

In addition to distillation-based purification of F-T reaction water, membrane-based, liquid-liquid extraction, and biological operations have been developed to remove and recover carboxylic acids from F-T acid water [90]. The resultant water stream from these processes is generally of a good quality and can be reused or disposed of to the environment.

After physical separation of oil and water streams, plus steam stripping and oil extraction to remove volatiles and aromatics, respectively, sulfur recovery is performed by conversion to elemental sulfur. Tail gas streams are also cleaned for use in recycle or as fuel.

The stream of water from the cooling system (referred to as the blowdown stream) must be cleaned also. This water contains inorganic salts and is treated with coal ash that chemically binds the salts, before the remaining water is collected by evaporation and condensation.

In addition to fuels, chemicals, and purified water, F-T ICL processes generate mineral waste derived from the coal. This non-leachable slag is suitable for sale as aggregate. Other, low-volume solid wastes include spent catalysts, organic sludge from biological wastewater facilities, inorganic sludge from flue gas desulfurization or evaporation ponds, and by-product sulfur if not recovered. These wastes may require specialized treatment to avoid transmission of soluble components if present, such as traces of the elements arsenic, chromium, mercury, molybdenum, and selenium, to local water supplies. However, F-T CTL plants incorporating modern, state-of-the-art gasification plants should accomplish removal of these and other potential pollutants within the normal plant process operations.

Utility Water The CTL process chemistry uses water as a source of hydrogen and oxygen, during gasification of coal, and also produces water during the F-T reaction. The overall chemistry consumes water, but the chemical transformations are not the only use of water during coal liquefaction. The other major uses of water are for cooling, boiler feed water, and in solids handling, including processing of fine coal or dust. Most of the water is recovered after purification, but in a DCL plant, for example, 3–5% of the water being circulated in a cooling tower is lost to evaporation, leaks, and blowdown [91]. Thus, for every 1,000 gal circulated, 30–50 gal of makeup water is needed.

The amount of water needed varies with the process design, choice of gasifier, ambient temperature and

humidity, and type of coal. According to the DOE Idaho National Lab, approximately 12–14 barrels of water are used for every barrel of F-T liquid fuel produced, [92] meaning that 40 million gallons of water/day are needed for an 80,000 barrel/day CTL facility. That is enough water to meet the domestic needs of more than 200,000 people (or 1/5 the population of the state of Montana).

The usage level of water in F-T CTL plants is considered a significant logistic issue in geographical areas of low rainfall or otherwise limited water resources. For example, competing use of water for agriculture would be a problem in the Western USA, and competing use of water for thermal-electric plants would be an issue in the Eastern USA. The availability of water is already an issue in Montana and Wyoming, where most of the inexpensive supplies of coal in the USA are located. Where water is in short supply, this logistic requirement becomes an environmental and/or economic issue and therefore has precluded construction of some planned CTL plants. Use of air, instead of water, as coolant may substantially reduce water usage requirements of the exothermic F-T reaction.

Future Directions

Current commercialization of CTL technology serves the global interest in sustainability of fuel supply. Any additional production of fuels from alternative resources reduces overall world demand for petroleum and benefits all consumers by easing pressure on crude oil prices. As the price of oil increases and its easy availability decreases, countries with large coal reserves and insufficient domestic petroleum to meet increasing transportation fuel demands – particularly the PRC and India – are potential candidates for using CTL technologies to supplement conventional petroleum-based fuel products.

In the case of DCL, contribution to sustained fuel supply requires that the Shenhua project be successful and lead to commissioning of additional units, given estimates of proven coal Shenhua coal reserves in the Shanxi Province/Inner Mongolia Autonomous Region of about 200 billion tons [93]. In this context, it is important to note that parallel efforts are also underway in the PRC and elsewhere to erect commercial scale indirect coal liquefaction plants. Presumably, these plants have lower technical risks because the designs are derived from ICL technology that has already been well proven at full commercial scale, by Sasol. On the other hand, the direct liquefaction project, while supported by a 6 t/day pilot plant constructed in Shanghai, has no precedent on a larger scale. The more than 1,000-fold scale up from pilot plant to commercial unit is an ambitious objective that carries more than the typical amount of technical risk. These plants will also incorporate technologies specific to regional coals and environmental regulations.

If DCL technology is successful in the PRC, it will garner increased global interest, perhaps in combination with indirect liquefaction in a hybrid systems configuration. In this scenario, the low value residue from the direct liquefaction process would be gasified to provide a low cost source for synthesis gas production, rather than incurring a cost penalty for disposal. A recent US National Coal Council (NCC) report suggests that this might be a good time and justification to revisit the direct liquefaction pathway, particularly if the scale-up in the PRC is successful. The NCC report also suggests the speculative possibility of hybrid direct and indirect plants.

In the case of ICL, the F-T technology is already well commercialized but currently has a very limited worldwide aggregate production volume. Computational science is a rapidly expanding area of research that offers the potential to shortcut development time by providing a theoretical basis for subsequent R&D and technology design activities. It provides the opportunity to quickly explore novel processing strategies to guide and accelerate experimental research. The computational work focuses on the complex and critical chemical and physical aspects of converting coal to premium fuels: the fundamentals of catalyst activity/selectivity; hydrodynamics; separation of small catalyst particles from the liquid product; optimum system integration to achieve high process efficiency, minimal pollutant emissions and CO_2 capture; and computational frameworks to enable virtual demonstration of the entire fuel life cycle.

Laboratory research and additional modeling, followed by larger-scale bench and pilot-scale testing, could experimentally verify the computational findings. However, systems engineering is an important component activity needed to evaluate the technical

and economic feasibility of: novel processes resulting from computational research; advanced integrated gasification and F-T processing concepts and cleanup technology; advanced reactor types needed to improve the process efficiency when utilizing specific regional coals; novel in situ reactions/processing; and modeling of the gas-solid–liquid physics of the F-T reactor to help achieve the highest throughput and liquid product quality.

Life cycle analyses performed on a "mine-to-wheels" basis likely will be used to identify those parts of the overall system impacting health and the environment now. Estimates of the impact of CO_2 on global warming, and estimates of the impacts of global warming itself, may also be attempted but these projections appear at present as far too broad in range to aid in resolving issues of energy sustainability. The greatest current push for the future use of coal appears to be in developing sustainable concepts for capturing and then storing or using the CO_2, because doing so obviates a significant portion of the large uncertainty as to potential effects of that CO_2 were it not captured. A related type of research involves combining coal use with chemistries or processes that generate less (or consume some amount of) CO_2, to decrease the overall output of CO_2 per barrel of oil equivalent produced.

In addition to the freestanding F-T CTL process configuration, the basic plant can be reconfigured to capture about 90% of the carbon that otherwise would be released into the atmosphere within the plant boundary. Also, another option, not involving CO_2 recycle, would be to design a polygeneration plant that produces both fuels and power.

More production from existing mines and the opening of new coalmines will be required to accommodate growth in the CTL industries as well as growing global demand for electric power. These facilities will require land for construction and support operations such as roads, railroads, and storage facilities that create changes in land use, alter topography, and impact ecological systems. Mitigation and reclamation strategies would need to be implemented to offset some of these changes to land and ecological resources. Currently, there are very strict reclamation regulations in place and they are being further enhanced to encourage a reforestation initiative to better restore the land, while concurrently improving water quality and providing a source for carbon sequestration. Even if the environmental risks are addressed, there is a very good possibility of public reluctance to accept the need for new facilities, particularly these coal-based plants. Measures would need to be taken to involve the general public and other state, local, and nongovernmental entities to assure them that these plants could effectively protect human health and safety and the environment.

However, F-T CTL plants would be expected to have very low environmental criteria pollutant emissions. They could also be designed to accommodate carbon capture and pressurization for subsequent sequestration in saline aquifers or oil reservoirs for enhanced oil recovery (EOR). Therefore, these plants could remove a good deal of uncertainty associated with possible new environmental regulations. Early plants that would sell or demonstrate CO_2 use for EOR would be encouraged.

Regarding methanol and DME, natural gas is currently the preferred feedstock for methanol production but companies such as Eastman Chemical in particular have rendered the coal-based process commercial, and cost-effective technology for CO_2 mitigation could pave the way for significant increase in commercial production of methanol and DME from coal in Asia and elsewhere.

Future CTL plants will use advanced clean coal gasification technology to produce transportation fuels and optionally electric power. Pollutant emissions will be minimal because coal-derived sulfur will be removed and converted into elemental sulfur. Nitrogen oxides will be minimized using low-NOx burners and selective catalytic reduction (SCR) in the flue gas stream and mercury will be removed, perhaps by some combination of pre- and post-combustion processes. Using air coolers where possible will minimize water use, and solids emissions will consist of nonleachable slag from the gasification process. Because of the sensitivity of the F-T catalyst to poisons, all contaminants must be removed to near-zero levels (ppb levels), thus ensuring that overall plant emissions would be close to zero.

Certainly coal conversion to hydrocarbon liquids and electricity is now economically attractive from a cash cost viewpoint. However, large capital investments are required and small to medium coal conversion plants will not become a reality unless there are

effective forms of state assistance with the initial capital investment. This would be motivated by the desire for independence from imported energy and the more efficient and cleaner utilization of the local energy resource. The Chinese government has accepted this approach, and China is rapidly becoming the pioneer for developing commercial CTL technology options. However, it is the duty of technology providers to ensure that technology is made available to allow coal use to be as efficient as possible.

Site-specific early design studies would provide the ability to obtain information on environmental baselines for CTL plants. These plants would be ready for CO_2 separation and capture and the information obtained would define resource requirements. Site-specific information would also address where the resources, such as coal and water, are coming from, how they are delivered, and how waste products are to be reused or disposed. Additionally, current R&D activities cosponsored by the DOE and industry are being pursued to improve CO_2 separation and capture and define CO_2 storage sinks.

Making fuels from coal via either DCL or ICL processes has the advantage that fuel infrastructures already in place for petroleum crude oil products can be used largely unchanged when a shift is made to coal-derived fuels. The advantage of fuel infrastructure compatibility offered by synthetic hydrocarbon fuels is not so great in the PCR at present, where a liquid hydrocarbon fuel infrastructure for transportation fuels is in a highly developmental state. The challenges are primarily economic, as prospective air pollutant regulatory constraints worldwide give high value to clean synthetic fuels having emission characteristics superior to crude oil derived fuels, whereas coal-based synfuels processes incur significant cleanup costs. Much, although not all, of the contaminants needing to be cleaned up result from the biological origins of coal itself. In that regard, clean coal research might also provide insight on more efficient processing and cleanup in emerging biomass-to-liquids processes.

Bibliography

Primary Literature

1. Appert O (2008) CTL could provide long-term, transport-fuel supply. Syngas Refiner, IV 9:14–18
2. Gray D, White C, Tomlinson G, Ackiewicz M, Schmetz E, Winslow, J (2007) Increasing security and reducing carbon emissions of the US transportation sector: a transformational role for coal with biomass. DOE/NETL-2007/1298, p 61
3. De Klerk A (2009) Overview of coal-to liquids technology. In: De Klerk (ed) Beyond Fischer–Tropsch. Elsevier, Amsterdam, p 1. Arno de Klerk comments, "Coal-to-liquids technology started as an ironic twist of fate seen against the present day drive to move towards renewable sources of energy, since coal replaced whales as feed material for the production of lamp oil (kerosene). Coal is not a renewable energy source, except when viewed on a geological time scale, but whales are, yet, the whaling industry came close to making whales a non-renewable resource by converting all whales into oil." The anecdote illustrates a growing understanding among energy experts, that even with conservation global demand for energy is growing and can best be met by careful use of both renewable and nonrenewable resources. On this point, see also Crane et al
4. Crane H, Kinderman E, Malhotra R (2010) A cubic mile of oil. Oxford University Press, New York
5. Thomson E (2002) The Chinese coal industry: an economic history. Routledge, London
6. Lister G (1944) Chronological records of coal mining, transport etc. In: Northumberland and Durham from A.D. 1180 to 1839. Ramsden Williams, Consett
7. Perry H (1974) Coal conversion technology. Chem Eng 81(15):88–102
8. Murakushi N (1981) The transfer of coal-mining technology from Japan to Manchuria and manpower problems: focusing on the development of the Fushun coal mines. Japanese Experience of the UNU Human and Social Development Programme series, p 47
9. NEDO (2006) Clean coal technology in Japan. 4A1. Coal liquefaction technology development in Japan, pp 57–58. www.nedo.go.jp/kankobutsu/pamphlets/sekitan/cct2006e.pdf. Accessed 10 April 2010
10. Sugawara A, Kurosawa S, Hatori H, Saito K, Yamada, Y, Sugihara M, Wasaka S, Yoshida H, Seo T, Susuki T, Inoguchi M, Sohnai M (1998) Coal conversion technologies on the new sunshine program in Japan. Preprints of symposia – American Chemical Society, Division of Fuel Chemistry 43(2): 330–334
11. NEDO (2006) Clean coal technology in Japan. 4A2. Bituminous coal liquefaction technology (NEDOL), pp 59–60. www.nedo.go.jp/kankobutsu/pamphlets/sekitan/cct2006e.pdf. Accessed 10 April 2010
12. Ghosh TK, Prelas MA (2009) Energy resources and systems: volume 1: Fundamentals and non-renewable resources. Springer Science + Business Media, Berlin
13. Dry ME (2002) The Fischer–Tropsch process: 1950–2000. Catal Today 71:227–241
14. Jager B, Espinoza R (1995) Advances in low temperature Fischer–Tropsch. Catal Today 23(1):17–28
15. Radtke K, Heinritz-Adrian M, Marsico C (2006) New wave of coal-to-liquids. An opportunity to decrease dependency on oil

and gas imports and an appropriate approach to a partial revival of domestic coal industries. VGB PowerTech 86(5):78–84
16. Williams RH, Larson ED (2003) A comparison of direct and indirect liquefaction technologies for making fluid fuels from coal. Energy Sustain Dev VII(4):103–129
17. Grant-Huyser M, Maharaj S, Matheson L, Rowe L, Sones E (2004) Ethoxylations of detergent-range oxo alcohols derived from Fischer–Tropsch alpha-olefins. J Surfactants Deterg 7(4):397–407
18. Price JG (2004) Chemicals from synthesis gas. US 6740683 to Sasol Technology, 25 May 2004
19. Degnan TF Jr, Chen NY, Somorjai GA (2009) Heinz Heinemann's legacy at ExxonMobil: an illustrious career in industrial catalysis. Catal Lett 133(1–2):227–230
20. Brown D, Bhatt B, Hsiung T, Lewnard J, Waller F (1991) Novel technology for the synthesis of dimethyl ether from syngas. Catal Today 8:279–304
21. Sardesai A, Lee S (2005) Alternative source of propylene. Energy Sources 27(6):489–500
22. Larson ED, Yang H (2004) Dimethyl ether (DME) from coal as a household cooking fuel in China. Energy Sustain Dev, VII 3:115–126
23. Jones G, Jr Holm-Larsen H, Romani D, Sillis R (2001) DME for power generation fuel: supplying India's southern region. PETROTECH-2001 January 08–12, New Delhi, India
24. Bhatt B, Schaub E, Heydorn E (1993) Recent developments in slurry reactor technology at the LaPorte alternative fuels development unit. In: International technical conference on coal utilization & fuel systems, Clearwater, April 26–29, pp 197–208
25. Shikada T, Ohno Y, Ogawa T, Ono M, Mizuguchi M, Tomura K, Fujimoto K (1998) Direct synthesis of dimethyl ether from synthesis gas. In: Parmaliana A, Sanfilippo D, Frusteri F, Vaccari A, Arena F (eds) Studies in surface science and catalysis (Natural Gas Conversion V) 119: 515–520
26. Miller CL, Cicero D, Ackiewicz M, Anderson J, Schmetz E, Winslow J (2006) Coal conversion – a rising star? In: 23rd international Pittsburgh coal conference, Pittsburgh, September 25–28
27. White LC, Frederick JP (1995) ENCOAL mild coal gasification project. In: Proceedings of the 12th annual international Pittsburgh coal conference, Pittsburgh, pp 151–156
28. US Department of Energy, National Energy Technology Laboratory (2002) The ENCOAL® mild coal gasification project. A DOE assessment. DOE/NETL-2002/1171
29. McMillen DF, Malhotra M (1989) The role of hydrogen transfer in bond-cleavage and bond-forming processes during coal conversion. In: Schindler HD (ed) Coal liquefaction. A research needs assessment DE-AC01-87ER30110 final report, v2, ch 4, US Department of Energy, pp 30–49
30. Haenel MW (2008) Catalysis in direct coal liquefaction. In: Gerhard E (ed) Handbook of heterogeneous catalysis, vol 6, 2nd edn. Wiley-VCH Verlag, Weinheim, Germany, pp 3023–3036
31. Miller L (2008) Coal conversion technology. Congressional noontime briefing. Rayburn House Office Building, Washington DC, April 24
32. Eccles RM, DeVaux GR (1982) H-coal commercialization: current status. Energy Progress 2(2):111–115
33. Cleaner Coal Technology Programme (1999) (PDF). Technology status report 010: coal liquefaction. Department of Trade and Industry. http://www.dti.gov.uk/files/file18326.pdf. Accessed 10 April 2010
34. Styles GA (1982) The Wilsonville advanced coal liquefaction R&D facility – accomplishments and process evolution. Energy Progress 2(3):160–162
35. Valente AM, Cronauer DC (2003) Progress in coal liquefaction including a discussion of Wilsonville. Preprints of symposia – American Chemical Society, Division of Fuel Chemistry 48(1): 147–148
36. Burke FP, Brandes SD, McCoy DC, Winschel RA, Gray D, Tomlinson G (2001) Summary report of the DOE direct liquefaction process development campaign of the late twentieth century: topical report. DE2002-794281/XAB; DOE/PC-93054-94 Department of Energy, Washington DC
37. Nolan P, Shipman A, Rui H (2004) Coal liquefaction, Shenhua group, and China's energy security. Eur Manage J 22(2):150–164
38. Stohl FV, Lott SE, Diegert KV, Goodnow DC (1996) Results of hydrotreating the kerosene fraction of HTI's first proof of concept run. US DOE, SAND–96-0990C; CONF-960807–2
39. Friedrick F, Strobel BO (1983) The KOHLEOEL experimental plant at Bergbau-Forschung. In: Proceedings of the 3rd European coal utilisation conference, Amsterdam, pp 227–235
40. Strobel BO, Loering R (1992) IGOR – taking the short cut in coal hydrogenation. Preprints of papers – American Chemical Society, Division of Fuel Chemistry 37(1):448–455
41. NEDO (2006) Clean coal technology in Japan. 4A3. Brown coal liquefaction technology (BCL), pp 61–62. www.nedo.go.jp/kankobutsu/pamphlets/sekitan/cct2006e.pdf. Accessed 10 April 2010
42. Ramdoss PK, Tarrer AR (1997) Modeling of two-stage coal coprocessing process. Energy Fuels 11(1):194–201
43. Wender I, Tierney JW (1995) Effect of pretreating of host oil on coprocessing. Final report. DOE/PC/91054–T15, Contract Number AC22-91PC91054, Oct. 1 1995 Oct 01
44. Miller RL, Giacomelli GF, McHugh KJ, Baldwin RM (1989) Coprocessing of coal and residuum under low-severity reaction conditions: effect of basic nitrogen promoters. Energy Fuels 3(2):127–131
45. Smith R, Asaro M, Naqvi S (2008) Fuels of the future: technology intelligence for coal to liquids strategies. SRI Consulting, Menlo Park
46. Koornneef J, Junginger M, Faaij A (2007) Development of fluidized bed combustion – an overview of trends, performance and cost. Prog Energy Combust Sci 33(1):19–55
47. Senapati PK, Das D, Nayak A, Mishra PM (2008) Studies on preparation of coal water slurry using a natural additive. Energy Sources A 30(19):1788–1796

48. SRI Consulting (2006) Coal gasification. Process Economics Program report 154A, ch 4, SRI Consulting, Menlo Park, pp 4–46
49. Davis BH (2001) Fischer–Tropsch synthesis: current mechanism and futuristic needs. Fuel Process Technol 71(1–3):157–166
50. Leckel D (2005) Hydrocracking of iron-catalyzed Fischer–Tropsch waxes. Energy Fuels 19:1795–180
51. Davis BH (2007) Fischer–Tropsch synthesis: comparison of performances of iron and cobalt catalysts. Ind Eng Chem Res 46(26):8938–8945
52. Smith R, Asaro M (2005) Fuels of the future: technology intelligence for gas to liquids strategies. SRI Consulting, Menlo Park
53. Bukur DB (2005) Attrition studies with catalysts and supports for slurry phase Fischer–Tropsch synthesis. Catal Today 106(1–4):275–281
54. Bukur DB, Carreto-Vazquez VD, Pham HN, Datye AK (2004) Attrition properties of precipitated iron Fischer–Tropsch catalysts. Appl Catal, A 266(1):41–48
55. Dry M (2004) Chemical concepts used for engineering purposes. In: Steynberg A, Dry M (eds) Studies in surface science and catalysis 152: Fischer–Tropsch technology. Elsevier, Amsterdam, p 215
56. Donnelly TJ, Yates IC, Satterfield CN (1988) Analysis and prediction of product distributions of the Fischer–Tropsch synthesis. Energy Fuels 2:734–739
57. Smith R (2009) SRI Consulting Coal to gasoline. Process Economics Program report 271, SRI Consulting, Menlo Park. Data for the figure were obtained from reference 58
58. Donnelly TJ, Satterfield CN (1989) Product distributions of the Fischer–Tropsch synthesis on precipitated iron catalysts. Appl Catal 52(1):93–114
59. Dry M (2004) Chemical concepts used for engineering purposes. In: Steynberg A, Dry M (eds) Studies in surface science and catalysis 152: Fischer–Tropsch technology. Elsevier, Amsterdam, pp 196–257
60. Jager B, Kelfkens RC, Steynberg AP (1994) A slurry bed reactor for low temperature Fischer–Tropsch. In: Curry-Hyde HE, Howe RF (eds) Natural gas conversion II. Elsevier, Amsterdam, pp 419–425
61. Adeyiga AA, Bukur DB, Carreto-Vazquez V, Ma W, Nowicki L (2004) Attrition resistance and catalytic performance of spray-dried iron Fischer–Tropsch catalysts in a stirred-tank slurry reactor. Ind Eng Chem Res 43(6):1359–1365
62. Bai L, Chang J, Hao Q, Li Y, Liu F, Wang H, Xiang H, Xu B, Yi F, Zhang C (2007) Effect of reduction temperature on a spray-dried iron-based catalyst for slurry Fischer–Tropsch synthesis. J Mol Catal A: Chem 261(1):104–111
63. Bartholomew C, Bukur DB, Datye AK, Nowicki L, Pham HN, Xu J (2003) Attrition resistance of supports for iron Fischer–Tropsch catalysts. Ind Eng Chem Res 42(17):4001–4008
64. Zhao R, Goodwin JG, Jothimurugesan K, Gangwal K, Spivey JJ (2001) Spray-dried iron Fischer–Tropsch catalysts.1. Effect of structure on the attrition resistance of the catalysts in the calcined state. Ind Eng Chem Res 40(4):1065–1075
65. Demirel B, Bohn MS, Benham CB, Siebarth JE, Ibsen MD (2005) Method and apparatus for regenerating an iron-based Fischer–Tropsch catalyst. US 6838487 to Rentech, 4 January 2005
66. Benham CB, Bohn MS, Yakobson DL (1996) Process for the production of hydrocarbons. US 5504118 to Rentech, 2 April 1996
67. van der Merwe W (2010) Conversion of spent solid phosphoric acid catalyst to environmentally friendly fertilizer. Environ Sci Technol 44(5):1806–1812
68. AsiaPulse News (2009) SHENHUA NINGXIA COAL, SASOL'S COAL LIQUEFACTION PJT BEGINS 2010. Yinchuan, 22 June 2009
69. Peng X, Toseland B, Underwood T (1997) A novel mechanism of catalyst deactivation in liquid phase synthesis gas-to-DME reactions. In: Bartholomew C, Fuentes GH (eds) Catalyst deactivation. Elsevier, Amsterdam
70. Gogate M, Lee S (1991) A single- stage, liquid-phase dimethyl ether synthesis process from syngas. I. Dual catalytic activity and process feasibility. Fuel Sci Technol Int 9(6):653–679
71. Cornthwaite D (1972) British patent 1296212 to Imperial Chemicals Inc. (ICI)
72. Espino RL, Plezke TS (1975) Methanol production. US 3888896 to ChemSystems, 10 June 1975
73. Sherwin M, Blum D (1979) Liquid-phase methanol. Final report. Electric Power Research Institute, EPRI-AF-1291
74. Lee S, Sardesai A (2005) Liquid phase methanol and dimethyl ether synthesis from syngas. Top Catal 32(3–4):197–207
75. Air Products Liquid Phase Conversion Company (2004) Commercial-scale demonstration of the liquid-phase methanol (LPMEOH) process. DOE/FE-0470, US Department of Energy
76. Joo O, Jung K, Han S (2002) Modification of H-ZSM-5 and gamma-alumina with formaldehyde and its application to the synthesis of dimethyl ether from syn-gas. Bull Korean Chem Soc 23:1103–1105
77. Lee S, Parameswaran VR, Wender I, Kulik CJ (1989) Roles of carbon dioxide in methanol synthesis. Fuel Sci Technol Int 7(8):1021–1058
78. Cai Y, Davies S, Wagner J (2003) Water gas shift catalyst. US 6627572 to Süd-Chemie, 30 September 2003
79. Kim J, Park MJ, Kim SJ, Joo O, Jung K (2004) DME synthesis from synthesis gas on the admixed catalysts of $Cu/ZnO/Al_2O_3$ and ZSM-5. Appl Catal, A 264(1):37–41
80. Tijm PJ (2003) Development of alternative fuels and chemicals from synthesis gas. DOE contract number FC22-95PC93052, final report
81. NEDO (2006) Clean coal technology in Japan. 4A4. Dimethyl ether production technology (DME), pp 63–64. www.nedo.go.jp/kankobutsu/pamphlets/sekitan/cct2006e.pdf. Accessed 10 April 2010
82. Hayashi H, Todoroki A, Yasuto A, Ohno Y (2002) NKK DME diesel vehicle development and fleet test in Japan. In: International symposium on alcohol fuels, Sao-Paulo, November 12–15

83. Ohno Y, Tanishima S, Aoki S (2005) Coal conversion into dimethyl ether as an innovative clean fuel. In: International conference on coal science and technology, ICCST, Okinawa, Japan, October 09–14
84. Mogi Y, Ohno Y, Ogawa T, Inoue N, Shikada T (2000) Development of slurry phase dimethyl ether synthesis technology. In: Pittsburgh coal conference, Pittsburgh, September 11–14, pp 398–408
85. Ohno Y, Yagi H, Inoue N, Okuyama K, Aoki S (2007) Slurry phase DME direct synthesis technology – 100 tons/day demonstration plant operation and scale up study. In: Noronha FB, Schmal M, Sousa-Aguiar EF (eds) Studies in surface science and catalysis: natural gas conversion VII. Elsevier, Amsterdam
86. Liu Z (2005) Clean coal technology: direct and indirect coal-to-liquid technologies. InterAcademy Council. http://www.interacademycouncil.net/Object.File/Master/10/335/CleanCoal technology_ coal liquefaction.pdf. Accessed 24 April 2010
87. Probstein RF, Hicks RE (2006) Synthetic fuels. Dover, Mineola
88. Gray D, Salerno S, Tomlinson G, Marano JJ (2004) Polygeneration of SNG, hydrogen, power, and carbon dioxide from Texas lignite. Mitretek technical report for the DOE, MTR-04-2004-18
89. Camm F, Bartis JT, Bushman CJ (2008) Federal financial incentives to induce early experience producing unconventional liquid fuels. Report prepared for the United States Air Force and the National Energy Technology Laboratory of the DOE. http://www.rand.org/pubs/technical_reports/TR586/, RAND corporation. Accessed 10 April 2010
90. Kohler LPFD, Du Plessis GH, Du Toit FJ, Koper EL, Phillips TD, Van Der Walt J (2006) Method of purifying Fischer–Tropsch derived water. US 7153432 to Sasol Technology, 26 December 2006
91. US Department of Energy (2006) Emerging issues for fossil energy and water. DOE/NETL-2006/1233
92. Boardman R (2007) Gasification and water nexus. Presented March 14, 2007 at the GTC workshop on gasification technologies, Denver
93. Wei W (2003) Current issues of China's coal industry: the case of Shanxi. In: Coate B, Brooks R, Fraser I, Xu L (eds) Proceedings of the 15th annual conference of the association for Chinese economics studies Australia (ACESA), RMIT (Royal Melbourne Institute of Technology) Business Research Development Unit, Melbourne

Books and Reviews

Dry ME (2001) High quality diesel via the Fischer–Tropsch process – a review. J Chem Technol Biotechnol 77(1):43–50
Egan CJ (1976) Method of power generation via coal gasification and liquid hydrocarbon synthesis. US 3986349 to Chevron Research Company, 19 October 1976
Furstner AE (1995) Active metals: preparation characterization applications. In: Furstner A (ed) Supported metals. Wiley, New York
Iglesia E, Reyes S, Madon RS (1993) Selectivity control and catalyst design in the Fischer–Tropsch synthesis: sites, pellets, and reactors. Adv Catal 39:221–302
Iglesia E, Reyes S, Soled S (1993) Reaction-transport selectivity models and the design of Fischer–Tropsch catalysts. In: Becker ER, Pereira CJ (eds) Computer-aided design of catalysts and reactors. Marcel Dekker, New York, p 640
Jin Y, Wang J, Wang T (2007) Slurry reactors for gas-to-liquid processes: a review. Ind Eng Chem Res 46(18): 5824–5847
O'Brien R, Xu L, Bao S, Raje A, Davis B (2000) Activity, selectivity and attrition characteristics of supported iron Fischer–Tropsch catalysts. Appl Catal, A 196(2):173–178
Rahmin II (2008) GTL, CTL finding roles in global energy supply. Oil Gas J 24:22–31
Sloane D (2008) Clean coal technologies accelerating commercial and policy drivers for deployment. International Energy Agency/Coal Industry Advisory Board, p 70
Tijm PA, Waller F, Brown D (2001) Methanol technology developments for the new millennium. Appl Catal, A 22(1–2): 275–282
Williams A, Pourkashanian M, Jones JM (2001) Combustion of pulverized coal and biomass. Prog Energy Combust Sci 27:587–610

Coastal Ecosystems, Sustainable Management

Paul A. Sandifer[1], Tracy K. Collier[2], Juli M. Trtanj[2]
[1]National Oceanic and Atmospheric Administration, National Ocean Service, c/o Hollings Marine Laboratory, Charleston, SC, USA
[2]National Oceanic and Atmospheric Administration, National Ocean Service, Oceans and Human Health Initiative, Silver Spring, MD, USA

Article Outline

Glossary
Definition of the Subject and Its Importance
Introduction
History and Evolution of Oceans and Human Health Programs
The "One Health" Paradigm
Ocean Health Early Warning Systems (OHEWS)
Response to Emergency Situations
Future Directions
Bibliography

Glossary

Antibiotic resistance Situation where microorganisms, particularly bacteria, are able to survive exposure to antibiotics. Of major concern when resistant microorganisms are the causative agents of significant human or animal diseases.

Coastal and marine spatial planning "A comprehensive, adaptive, integrated, ecosystem-based, and transparent spatial planning process, based on sound science, for analyzing current and anticipated uses of ocean, coastal, and Great Lakes areas" (Interagency Ocean Policy Task Force (IOPFT) (2010) Final recommendations of the interagency ocean policy task force. The White House Council on Environmental Quality, Washington, DC, 96 pp).

Ecological forecasting Combining environmental and biological information to predict effects that biological, chemical, physical, and human-induced changes will have on ecosystems in general or more typically specific ecological components (e.g., harmful algae, fishery populations, jellyfish).

Epidemiological Pertaining to the study of the incidence, distribution, causes, and prevention of diseases.

Harmful algal blooms Harmful algal blooms (HABs) are proliferations (blooms) of microscopic algae that produce toxins that may cause serious illness or death in both animals and humans. HABs are caused by numerous species of algae and may occur in salt, brackish, and fresh waters.

One health The paradigm that links environmental, human, and animal health.

Pathogens Microorganisms that cause infectious disease.

Zoonotic Referring to diseases of animals that may be transmitted to and cause illness in humans.

Definition of the Subject and Its Importance

Oceans and Human Health is a "meta-discipline" comprising elements of oceanography, marine biology and ecology, biomedical science, environmental health science, medicine, and public health. It focuses principally on water- and food-borne causes of human and animal illness associated with exposure to ocean, coastal and/or Great Lakes waters, habitats, and organisms. It seeks to integrate information across many disciplines to achieve a fuller understanding of health risks and benefits associated with these environments and how they can be managed to protect or enhance public health.

Introduction

That the health of the oceans and humans are tightly and inextricably connected has been recognized by some scientists for many years [1–3]. However, only in the last few decades have these connections – and the implications of human health effects of degraded coastal and ocean environments – come clearly into focus as an important emerging arena for broad scientific investigation and policy development. The developing "meta-discipline" known as Oceans and Human Health (OHH) is a direct manifestation of that clearer focus.

Degradation of ocean and coastal ecosystems and the crucial ecosystem services they provide to humans have negatively impacted tourism; treasured aesthetic and cultural attributes, coastal properties and their values; and have resulted in increasingly evident and serious health threats to humans from *harmful algal blooms* (HABs) and their toxins, chemical pollution, and infectious diseases [2, 4, 5]. Dealing with these complex and interwoven issues to support resilient and sustainable coastal ecosystems and communities requires dedicated, integrated, interdisciplinary, and multi-institutional approaches. OHH brings together not only oceanographers and marine biologists but also physicians, public health professionals, social scientists, coastal managers, planners, and others to work collaboratively on the human health benefits and threats that emanate from ocean, coastal, and Great Lakes environments [2].

History and Evolution of Oceans and Human Health Programs

Named OHH programs have focused predominantly on the deleterious environmental and human health effects of harmful algal blooms and their toxins; sewage- and contamination-mediated, naturally occurring, and *zoonotic* infectious diseases; and chemical contamination in ocean, coastal, and Great Lakes waters. These programs also target beneficial products such as new drugs to combat various diseases and pain,

high-quality seafood with its cardiovascular protective and other healthful qualities, and use of marine organisms and habitats as tools to study disease processes or as sentinels of likely human health risks. In addition to direct focus on the root causes, effects, and ecological processes involved with each of these, OHH programs are utilizing a variety of tools such as warning systems, sensors, cutting edge "omics" and other scientific methods, and sentinel species and habitats to address ocean-related health risks and benefits. As a result of the activities of OHH programs, a new interdisciplinary community of science and practice is developing to concentrate on potential ocean health risks and benefits to humans.

It is fairly easy to identify when named programs in OHH began (e.g., see [6–8]), but it is much more difficult to unravel the evolutionary history and determine when the collaborations that eventually culminated in these programs really got underway (e.g., see [9]). Nonetheless, it is clear that a variety of programs played pivotal roles in this evolution. These include but are not limited to such activities as the National Institute of Environmental Health Sciences' (NIEHS) Marine and Freshwater Biomedical Sciences Centers program initiated in 1978 that focused on seafood safety, harmful algal blooms, and toxicology among other things; the National Institute of Health's (NIH) support of work to grow aquatic organisms for use in research [10]; the National Oceanic and Atmospheric Administration's (NOAA) studies in seafood safety including effects of HAB toxins; the passage of the initial Harmful Algal Bloom Research and Control Act (HABHRCA) in 1998 and resulting further development of HAB programs in NOAA and elsewhere; and the pioneering work by Rita Colwell [11] and subsequently by her, her associates, and others on links between cholera outbreaks and climate.

In addition to the nascent efforts at the federal level, beginning in the late 1980s and through the 1990s, a team initially composed of researchers from NOAA and the South Carolina Department of Natural Resources and later expanded to include other partners (the College of Charleston, Medical University of South Carolina, and the National Institute of Standards and Technology) developed plans for a new partnership laboratory, initially known as the Marine Environmental Health Research Laboratory, to be located in Charleston, SC. By 1994, the planning team had zeroed in on an initial mission statement for the new facility, today known as NOAA's Hollings Marine Laboratory (HML): "[it] will be directed specifically toward achieving a better understanding of the health of marine organisms, populations, and habitats and their relationship to human health" [12, 13]. Today, the HML, also designated as NOAA's Coastal Center for Human Health Risk, conducts research to understand and forecast relationships between coastal ocean ecosystems and human health and communicates findings to ocean, coastal, and public health officials and interested parties.

At about the same time as formal planning got underway for the HML, the first National Harmful Algal Bloom research plan was prepared in response to growing concerns about the occurrence and impacts of such blooms [14]. This plan guided US HAB-related research for well over a decade and led to establishment of an informal national network of HAB researchers in the USA. Then, in 1998, the US Congress passed the HABHRCA, which authorized an interagency task force, required HAB and hypoxia assessments, authorized funding for research in these areas, and established programs that became Ecology and Oceanography of Harmful Algal Blooms (ECOHAB), Monitoring and Event Response for Harmful Algal Blooms (MERHAB), and the Coastal Hypoxia Research Program (CHRP).

More recently, HARNESS (the Harmful Algae Research and Response National Environmental Science Strategy, 2005–2015) [15] was completed to continue to provide broad guidance for HAB-related research in the USA. This major report focused on four broad thematic areas of inquiry: bloom ecology and dynamics, toxins and their effects, food webs and fisheries, and public health and socioeconomic impacts. A part of the HARNESS effort included formal establishment of a National HAB Committee designed to facilitate implementation of the plan and coordination among the numerous interested agencies, academic institutions, other entities, and individuals, along with international cooperation. Because of the increasing frequency, duration, intensity, geographical extent, and number of species and toxins involved [2, 16–18], HAB research has remained one of the primary

foci of oceans and human health programs, both nationally and internationally.

Broader recognition of the multiple roles the ocean (and its coastal environments) may play in human health and well-being followed US sponsorship of an OHH-themed pavilion at the 1998 World's Fair in Lisbon, Portugal, and, as noted above, 1998 also saw passage of the HABHRCA. Shortly thereafter, the National Research Council of the National Academies of Science published the highly influential report "From Monsoons to Microbes: Understanding the Ocean's Role in Human Health" [19] which focused substantial attention on the myriad relationships between ocean and coastal environments and human health and well-being. This report was quickly followed by other NRC reports that further helped shape the OHH landscape, including "Under the Weather: Climate, Ecology, and Infectious Disease" [20] and "Marine Biotechnology in the Twenty-First Century: Problems, Promise, and Products" [21].

Following quickly on the heels of these seminal publications, the National Science Foundation (NSF) and NIEHS joined forces to develop a collaborative OHH program. Their combined effort was initiated through a scientific community workshop held in December 2001, which was followed by a joint Request for Proposals in November 2002 for creation of academic centers of excellence in OHH [6, 8]. NOAA's named OHH program got underway shortly thereafter, with initial Congressionally directed funding appropriated in 2003 for the agency to establish an Ocean and Human Health Initiative (OHHI) to "coordinate and focus agency activities on critical areas of concern and identify critical gaps in coverage, and . . . to be used for critical research and projects aimed at closing identified gaps." The Congressional language directed NOAA to work with NSF and other federal agencies and establish NOAA Centers of Excellence in OHH, a national advisory panel, and competitive external grant, distinguished scholar, and traineeship programs. Like NSF and NIEHS, NOAA utilized a scientific workshop, held in October 2003, as a mechanism to solicit external as well as internal input for development of its OHH Initiative [7]. These actions led to creation of a national network of competitively funded OHH Centers of Excellence, with four awarded in the academic sector in May 2004 by NSF and NIEHS (at the Woods Hole Oceanographic Institution, University of Miami, University of Washington, University of Hawaii) and three selected in NOAA a few months later (at the Great Lakes Environmental Research Laboratory, the Hollings Marine Laboratory, and the Northwest Fisheries Science Center).

In September of 2004, the US Commission on Ocean Policy released its final report [22] which included a full chapter on OHH and recommended the establishment of a national research effort in this area. This report had a major and positive impact on the continued development of OHH programs in the USA. Shortly after its release, the Congress passed the Oceans and Human Health Act (OHHA) of 2004 to ". . .improve understanding of the role of the oceans in human health." The OHHA established the national, interagency OHH program in law and formally authorized the Secretary of Commerce to create the OHHI within NOAA, with its component parts including internal centers of excellence, expert advisory panel, support for grants, distinguished scholars, traineeships in the external scientific community, and requirements to collaborate with other agencies. The USCOP report also resulted in action by the George W. Bush Administration to establish a cabinet-level National Ocean Committee, with subordinate committees and interagency working groups [23]. One of the high-level interagency bodies was the Joint Subcommittee on Ocean Science and Technology (JSOST) which was established by the National Science and Technology Council's Committee on the Environment and Natural Resources and Interagency Committee on Ocean Science and Resource Management Integration. The JSOST produced the first interagency ocean research plan, "Charting the Course for Ocean Science in the United States for the Next Decade: An Ocean Research Priorities Plan and Implementation Strategy" [24], which was organized around six primary themes, including one on "Enhancing Human Health." This was a major step forward for OHH programs because it was the first time that all the federal agencies involved in any kinds of ocean-related research agreed on the importance of including human as well as animal health-oriented studies in a comprehensive ocean research portfolio.

The JSOST also formed a number of interagency working groups under its umbrella. One of these, the

Interagency Working Group on Harmful Algal Blooms, Hypoxia, and Human Health (IWG-4H), was chartered in fall 2005 with a principal focus on responding to the Congressional requirements of the HABHRCA Amendments of 2004 and the OHHA of 2004. Working under the general oversight of the JSOST, the IWG-4H produced a series of major reports related to oceans and human health, including the first ever *Interagency Oceans and Human Health Research Implementation Plan* [2] which expanded upon the "Enhancing Human Health" theme of the JSOST's [24] overarching ocean research plan. The purpose of this OHH Research Plan was to define "the goals and priorities for Federal research which most effectively advance scientific understanding of the connections between the oceans and human health, provide usable information for the prediction of marine-related public health problems, and use the biological potential of the oceans for development of new treatments of human diseases and a greater understanding of human biology" [2]. In addition to the OHH plan, the IWG-4H produced the *National Assessment of Efforts to Predict and Respond to Harmful Algal Blooms in U.S. Waters* [25], *Scientific Assessment of Freshwater Harmful Algal Blooms* [26], *Harmful Algal Bloom Management and Response: Assessment and Plan* [27], *Scientific Assessment of Marine Harmful Algal Blooms* [28], and *Scientific Assessment of Hypoxia in U.S. Coastal Waters* [29], all of which are important resources for OHH research activities. The IWG-4H is continuing to focus on interagency coordination and collaboration among a variety of agencies involved in one or more aspects of OHH work, including the Centers for Disease Control and Prevention (CDC), Environmental Protection Agency (EPA), Food and Drug Administration (FDA), Marine Mammal Commission (MMC), National Aeronautics and Space Administration (NASA), US Department of Agriculture (USDA), and US Geological Survey (USGS), in addition to the NIEHS, NSF, and NOAA.

The years 2007–2008 marked other important developments for OHH as a recognized meta-discipline. NOAA inaugurated its OHH Traineeship Program, with initial awards to five academic consortia specifically focused on providing support for the interdisciplinary education and training of doctoral and post-doctoral scholars in OHH, as part of a long-term strategy to build a new cadre of OHH scientists. Most if not all of the NSF–NIEHS-funded OHH research projects and many of those supported by NOAA, whether internally or externally, also supported students, but the NOAA traineeships have the education and development of the next generation of OHH scientists as the principal focus. Also in 2008, the first textbook devoted specifically to support teaching in the interdisciplinary oceans and human health arena was published [9]. Several academic institutions had already begun offering formal OHH courses, but for the first time there was a strong textbook to support them, leading to further development, refinement, and breadth of OHH-related course offerings. In addition, the first Gordon Research Conference (GRC) and Graduate Research Seminar (GRS) on OHH was held in 2008, and these have followed every 2 years since, with the next GRC/GRS scheduled for summer 2012. Acceptance of OHH as a recurring theme for Gordon Research Conferences marked a broad level of recognition of OHH as a scientific area of ongoing significance, major community interest, and likely important discoveries.

During 2010–2011, the JSOST (now renamed Subcommittee on Ocean Science and Technology or SOST) initiated an update of the "Charting the Course" Ocean Research Priorities Plan [24]. The new version, expected to be released in 2011 and entitled "Science for an Ocean Nation: An Update of the Ocean Research Priorities Plan," [30] is expected to include updates of the previous plan's OHH-oriented theme, "Enhancing Human Health," demonstrating the continuing significance placed on this arena of interdisciplinary and interagency ocean research by US government agencies.

Following a workshop on climate change sponsored by the Institute of Medicine's (National Academies of Science) Roundtable on Environmental Health Sciences, Research and, Medicine in January 2009, senior representatives from four federal agencies (NIEHS, EPA, NOAA, and CDC) formed an ad hoc Interagency Working Group on Climate Change and Health (IWGCCH) to prepare a white paper to "to identify research needs for all aspects of the research-to-decision making pathway that will help us understand and mitigate the health effects of climate change, as well as ensure that we choose the healthiest and most efficient approaches to climate change adaptation."

This effort resulted in the first comprehensive evaluation of research needs related to likely human health effects of climate change, including ocean-associated health risks and benefits [31]. An additional outcome of the work of the ad hoc IWGCCH was the establishment by the US Global Climate Change Research Program of a formal Interagency Working Group on Climate Change and Human Health (IWGCCHH), which includes strong representation of OHH programs and issues.

On June 12, 2009, US President Obama issued a memorandum establishing an Interagency Ocean Policy Task Force (IOPTF) led by the Chair of the White House Council on Environmental Quality (CEQ) and comprised of senior officials representing 24 executive departments, agencies, and other offices across the Federal government. President Obama charged the IOPTF with responsibility for developing recommendations to maintain healthy and resilient ocean, coastal, and Great Lakes ecosystems, resources, and uses. On July 19, 2010, President Obama issued Executive Order 13547 [32] that established the US National Policy for the Stewardship of the Ocean, Our Coasts, and the Great Lakes (National Ocean Policy) including the Final Recommendations of the Interagency Ocean Policy Task Force [33]. The Final Recommendations include 17 mentions of "human health" and specifically reference issues dealing with harmful algal blooms, *pathogens*, disease, and chemical pollution, all primary OHH issues. Most significantly, in its first paragraph the President's Executive Order includes human health among the central foci of the National Ocean Policy, stating that "America's stewardship of the ocean, our coasts, and the Great Lakes is intrinsically linked to environmental sustainability, *human health and well-being* [emphasis added], national prosperity, adaptation to climate and other environmental changes, social justice, international diplomacy, and national and homeland security."

The "One Health" Paradigm

There is a growing worldwide effort to link scientists and practitioners working on human, animal, and environmental health into a single, health-oriented movement aptly named "One Health" [34]. This paradigm recognizes the myriad and important linkages between the condition of the environment and the health of humans and animals and the numerous shared diseases and disease processes in humans and animals. Approximately 61% of known human pathogens are zoonotic, meaning they were originally transmitted from animals to humans, and approximately 75% of emerging infectious diseases are zoonotics [35]. In addition, many diseases are exacerbated by stressful environmental conditions. Thus, the case for connecting human, animal, and environmental health is clear. Co-equal collaborations among environmental and biomedical scientists, medical doctors, veterinarians, and public health workers are expected to lead to rapidly expanding knowledge, new health care approaches and treatments, and synergisms not yet even contemplated.

Considering that the oceans harbor an incredible range of life forms, including representatives of 34 of the 36 phyla of animal life found on Earth compared to 17 occurring on land, there is a high likelihood for increasing interactions leading to transfer of both known and new diseases from marine organisms to humans and from human and domesticated animals to marine organisms. There are numerous instances of zoonotic diseases being detected in marine mammals and seabirds, including avian influenza, and several required reportable pathogens (*Brucella*, *Salmonella*, *Leptospirosis*) (e.g., see [36]). Broad occurrence of antibiotic-resistant bacteria is also being observed in marine organisms, raising additional health risks related to ocean exposures [36–38]. At the same time, because of the high but relatively poorly known biodiversity of much of the ocean [39], there is significant likelihood of discovery of many new drugs and other natural products to treat human diseases [40–43]. There is also a growing body of evidence that connects biodiversity and human health and that implicates declining biodiversity as a factor exacerbating health threats, although many uncertainties remain [44, 45]. Some marine organisms have been used for many years to study human diseases, and this area is likely to increase substantially in the future [2]. And as pointed out in a later chapter, numerous marine organisms and habitats make excellent sentinels or indicators of potential health threats to humans (e.g., [46–49]).

Degradation of ocean and coastal environments is known to lead to increasing health threats to humans,

including those from infectious diseases as well as from chemical contaminants and algal toxins. The OHH meta-discipline is a clear example of a health arena where the One Health approach is particularly applicable (Fig. 1), and application of this interdisciplinary approach will become even more important in unraveling and addressing the expected effects of climate change and variability on humans and marine organisms [50–54]. In the ocean, it is anticipated that climate change may result in increased prevalence, distribution, and virulence of both known as well as emerging zoonotic, vector-, water-, and seafood-borne pathogens; increased distribution, frequency, duration, and intensity of harmful algal blooms [54]; and increased and/or changed mobilization, bioaccumulation, and transfer of chemical contaminants. As the Ocean Heath Working Group of NOAA's Science Advisory Board recently stated: "The concept of the combined health of people and wildlife – one health – when combined with the concept of the ocean as an essential modulator/caregiver of all life on Earth, inexorably leads to the prime tenet that the health of the 'one ocean' is essential to the 'one health' of all life on earth, including that of humans" [55].

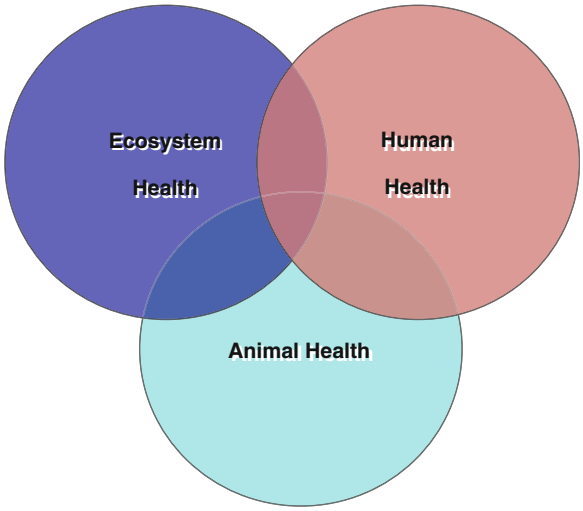

Coastal Ecosystems, Sustainable Management. Figure 1 "One Health" paradigm illustrating areas of intersection among environmental health, veterinary, and medical sciences

Ocean Health Early Warning Systems (OHEWS)

A resilient and secure coastal community depends on a vibrant economy, healthy coastal ecosystems, and healthy people. The security and resilience of ocean and coastal communities are increasingly threatened by health consequences related to natural hazards, changes in climate and land use, anthropogenic contaminants, and naturally occurring and introduced pathogens. In general, ocean health threats to humans and marine animals appear to be increasing [1, 2], resulting in economic losses, illnesses, and a loss of public confidence in the healthful condition and safety of coastal environments and resources, including seafood. For example, news about a contaminated product, such as oysters, can shut down a fishery that will affect local commerce, but such an event may also affect consumers' behavior toward the resource and the use of the environment. The information is rapidly picked up by news media, with the result that consumers – even those far away from the original incident – may be reluctant to eat seafood or go to the beach. An excellent example is the recent resistance to consumption of Gulf of Mexico seafood even after it has been deemed safe by comprehensive government testing for months and over a year after the Deep Water Horizon oil spill (see for example [56]). In addition, researchers are finding growing evidence of *antibiotic resistance* in marine organisms and the presence of MRSA (methicillin-resistant *Staphylococcus aureus*) and other human diseases in coastal animals and waters [36, 38, 57]. Understanding interactions among these environmental stressors is crucial to ensure a safe supply of food from the sea and to protect coastal-associated commerce (e.g., fisheries, aquaculture, tourism) (Fig. 2).

One important concept under development to improve coastal security and resilience and to protect the public at larger from increasing exposures to ocean-related health risks is an "Ocean Health Early Warning System" or OHEWS. Similar early warning systems or forecasts are routinely used for hazardous natural events such as hurricanes, tsunamis, floods, and volcano eruptions. The objective of an OHEWS is to reduce or mitigate threats to marine animal and human health from the oceans through development of a comprehensive oceans and health assessment and forecasting capability that combines new and

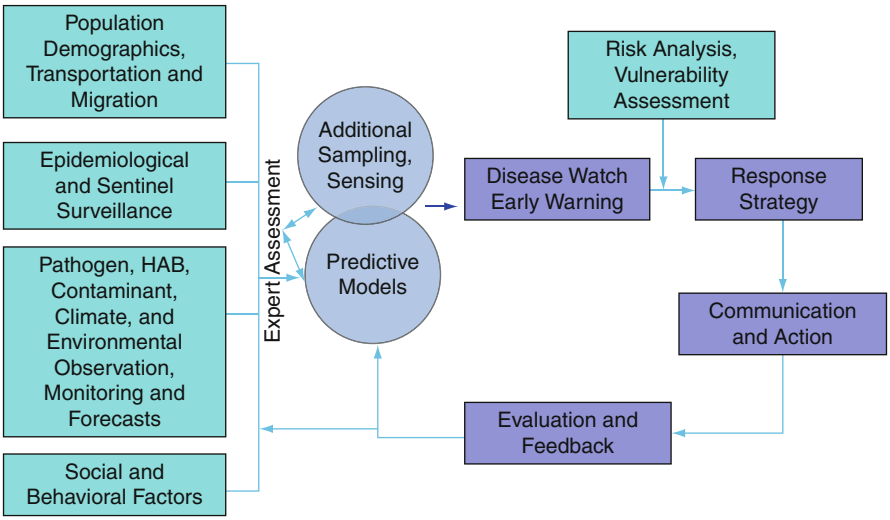

Coastal Ecosystems, Sustainable Management. Figure 2
Schematic diagram of major components of, and information flows in, a hypothetical ocean health early warning system (modified and used with permission from Trtanj JM, Davis JR (2002) Climate variability information as an adaptation tool: the case of public health. Presentation at Energy Modeling Forum Workshop on Adapting to climate change and variability. Snowmass Conference Series: Climate Impacts and Integrated Assessment (CCI-IA) (Stanford University), Snowmass Colorado)

developing diagnostic and detection capabilities, surveillance and monitoring data, sentinel species and habitats, and targeted outreach to public health officials and the public. While this effort is relatively new, it is building on extensive research that connects environmental signatures with a variety of health concerns (e.g., [11, 58–65]) and a growing understanding of the value of sentinel species and habitats as indicators of potential health threats to humans [1, 46–49]. Based on a broad base of previous research, development is well underway for forecasting capability for harmful algal bloom events [66, 67]. A few examples include NOAA's Harmful Algal Bloom Operational Forecast System [68], the Harmful Algae websites maintained by the Woods Hole Oceanographic Institution [18] and the Great Lakes Environmental Research Laboratory [69], the *Vibrio* Remote Sensing Report [70], and Mapping Pathogens in the Chesapeake Bay [71]. The goal of these nascent warning systems is to protect human life, health, and property and provide decision-makers with as much advance notice as possible about the likelihood of a threatening event in a particular location, thus widening the range of feasible response options.

Ongoing surveillance using meaningful indicators of ecosystem health, such as the examples mentioned above, and development of other *ecological forecasting* tools, followed by assimilation of the indicators into an index or suite of indices that could be integrated into an overall OHEWS could provide early warning of environmental changes likely to have measurable impacts on human health and well-being with sufficient lead time to take corrective actions. In addition to providing warnings in time to treat symptoms, an OHEWS may suggest testable hypotheses that, in turn, may lead to a much deeper understanding of cause and effect relationships and opportunities to mitigate, minimize, control, or prevent environmental degradation and the related threats to human, animal, and environmental health.

Response to Emergency Situations

Federal, state, and local agencies regularly respond to natural and human-caused environmental emergencies and disasters, such as hurricanes, tornadoes, floods, tsunamis, oil and chemical spills, etc. Such incidents may involve increased likelihoods of water- or

food-borne health threats, including infectious disease and chemical contamination. On occasion OHH researchers can enhance the capacities of emergency responders by providing additional scientific expertise and laboratory capabilities to address the large volumes of samples that require processing and data that needs analysis and interpretation following environmental emergencies [2], leading to better awareness and communication of factual information. For example, following Hurricane Katrina in late summer of 2005 and the tragic flooding of New Orleans, the dewatering of New Orleans created an unprecedented situation regarding public safety, including the perception of unsafe seafood. The floodwaters that were pumped into nearshore areas of the Gulf of Mexico (GoM) were known to contain oils, metals, and a wide range of pathogens and enteric bacteria, and there was also concern about synthetic chemical contaminants from flooded businesses and homes. OHH scientists were asked to mount an immediate response, both to collect samples of fish and shrimp from the potentially affected area as well as provide a wide range of chemical and microbiological analyses. Scientists from government and academia moved quickly into action. NOAA OHH scientists deployed within 1 week after the floodwater pumping began, and issued the first public report on seafood safety 3 weeks later [72]. Their experience and recommendations for ways to further improve emergency responses involving oceanic conditions were subsequently published as part of a series of papers on mitigating the effects of natural disasters on fishery ecosystems [73]. Similarly, rapid action by academic OHH scientists led to significant improvements in our understanding of risks associated with infectious microbes following hurricane events [74, 75].

More recently, the Deepwater Horizon oil spill led to grave public concern regarding the safety of seafood from the GoM, and again lessons learned in the OHH science community were applied to a large multi-agency effort to assure seafood safety and protect public health. Several thousand seafood samples were analyzed for injurious components of oil, and after developing appropriate methods, for dispersants as well. The results of this massive effort showed that seafood in areas re-opened to harvest after oil was no longer apparent was indeed safe for human consumption [76, 77], although as noted previously, public confidence in the safety of GoM seafood was not restored as readily.

Despite many significant spills over the past few decades, surprisingly little is known about the direct effects of oil spills on human health, such as on those people working in oil spill response and cleanup activities [78–80]. Following the DWH release, the NIEHS is planning a study that will be the largest ever investigation of effects of an oil spill on human health. The NIEHS intends to enroll approximately 55,000 response and cleanup workers in a 10-year-long longitudinal study, with the goal of evaluating both physiological and psychological health that might be affected by the spill [81]. OHH science will assist in this study, for example, by assessing the health of marine mammals in the Gulf of Mexico, partly as sentinels for human health, as well as providing other information about likely human exposures. Finally, as the great Japanese earthquake and tsunami of March 11, 2011, have shown, unanticipated effects of disasters, such as the damages to the Fukushima nuclear reactors that resulted in discharges of radionuclides to coastal waters (e.g., see [82, 83]), will continue to bring OHH-related concerns forward into public consciousness as well as raise questions for policymakers and public health communities around the globe. Ongoing and sustained progress in OHH science should allow us to better address such concerns and better safeguard public health following future emergencies involving our oceans, coasts, and Great Lakes.

Future Directions

Principally because of resource limitations, many if not most of the opportunities for future research and development identified by Refs. [2, 24, 31, 84] remain incompletely addressed, though still valid. Some of the more pressing issues, that we believe are most likely to lead to significant advances in science and in protection of human and animal health, include the following:

1. Continue fundamental research to address known and emerging human and animal pathogens, harmful algal blooms and their toxins, and impacts of chemical pollution in ocean, coastal, and Great Lakes environments, including occurrence, source, transport, fate, physical factors and ecological processes affecting occurrence,

abundance, and virulence, and the development and use of models to provide reliable forecasts of likely exposures and risk of contracting disease.

2. Determine how the prevalence and virulence of pathogens, HABs, and chemical contaminants may be affected by seasonal factors and climate change, including ocean acidification, temperature, sea level rise, and other factors, and develop models and predictive capacity to forecast risks and effects of alternative management and adaptation scenarios.
3. Further develop robust capacity to monitor condition and health of sentinel species, habitats, and sites and to integrate the data derived from such monitoring with other environmental and human health information to provide additional foundation for risk characterization and assessment and development of early warning systems.
4. Establish robust monitoring and investigative capacity for regular evaluation of seafood safety and to identify and characterize ongoing and emerging risks to humans and animals in time to take corrective or preventive action before seafood products reach markets and are consumed.
5. Develop and implement sustained *epidemiological* investigations to characterize and quantify human health risks associated with pathogens, toxins, and chemical contaminants from ocean, coastal, and Great Lakes waters, and ensure that ocean observing systems acquire related environmental data at the appropriate temporal and spatial scales for combination with epidemiological information to present a more complete picture of factors affecting human health.
6. Conduct continuing research on the potential of ocean, coastal, and Great Lakes environments to provide new drugs and other beneficial products derived from marine biota and establish the necessary long-term mechanisms to support ocean product development over the long period between initial discovery and laboratory trials to commercialization.
7. Develop, test, and deploy new and improved sensors capable of detecting and quantifying occurrence of specific ocean-derived health threats (pathogens, HABs and their toxins, chemical contaminants) and incorporate into ocean observing, seafood safety monitoring, and human and marine wildlife disease surveillance.
8. Focus a sustained research effort on understanding the linkages between biodiversity and either reduced or increased human health risks in coastal and ocean environments, with particular focus on increasing knowledge of the health-related values of conservation of natural biodiversity.
9. Acquire and integrate social, economic, and cultural information related to human health risks, impacts, and benefits associated with the sea and incorporate into OHH analyses, models, and forecasts.
10. Develop and implement a variety of ocean health early warning systems, incorporating data from remote sensing; ocean observing systems; new and improved sensors designed specifically to detect marine ocean health threats, sentinel species, sites, and habitats; and socioeconomic and epidemiological studies with physical and ecological models to provide forecasts and evaluate management alternatives.
11. Integrate OHH results into *Coastal and Marine Spatial Planning* (CMSP) as described in the US National Ocean Policy [32, 33] to identify those geographic areas that should not be considered for public and recreational uses due to the likelihood of exposure to health threats and to monitor ongoing conditions in areas heavily used by the public to ensure public safety.

Bibliography

Primary Literature

1. Fleming LE, Broad K, Clement A, Dewailly E, Elmir S, Knap A, Pomponi SA, Smith S, Solo Gabriele H, Walsh P (2006) Oceans and human health: emerging public health risks in the marine environment. Mar Poll Bull 53:545–560
2. Sandifer P, Sotka C, Garrison D, Fay V (2007) Interagency oceans and human health research implementation plan: a prescription for the future. Interagency Working Group on Harmful Algal Blooms, Hypoxia, and Human Health of the Joint Subcommittee on Ocean Science and Technology. Executive Office of the President, Office of Science and Technology Policy, Council on Environmental Quality, Washington, DC, 92 pp
3. Lubchenco J, Sutley N (2010) Proposed US policy for ocean, coast, and Great Lakes stewardship. Science 328:1485–1486

4. Millennium Assessment (MA) (2005) Millennium ecosystem assessment. Synthesis report. Island Press, Washington, DC. www.millenniumassessment.org
5. Worm B, Barbier EB, Beaumont N, Duffy JE, Folke C, Halpern BS, Jackson JBC, Lotze HK, Micheli F, Palumbi SR, Sala E, Selkoe KA, Stachowicz JJ, Watson R (2006) Impacts of biodiversity loss on ocean ecosystem services. Science 314:787–790
6. Rice DL, Dearry A, Garrison DL (2004) Pioneering interdisciplinary research initiatives for oceans and human health. EcoHealth 1:220–225
7. Sandifer PA, Holland AF, Rowles TK, Scott GI (2004) The oceans and human health. Environ Health Persp 112(8): A454–A455
8. Tyson FL, Rice DL, Dearry A (2004) Connecting the oceans and human health. Environ Health Persp 112(8):A455–A456
9. Walsh PJ, Smith SL, Fleming LE, Solo-Gabriele HM, Gerwick WH (eds) (2008) Oceans and human health, risks and remedies from the seas. Elsevier, Amsterdam, 644 pp
10. Baden DG (2005) Oceans and human health: a new era of environmental opportunities. In: Goehl TJ (ed) Essays on the future of environmental health research: a tribute to Dr. Kenneth Olden. Special issue of environmental health perspective. U.S. Department of Health and Human Services, National Institutes of Health, National Institute of Environmental Health Sciences, Research Triangle Park, pp 116–127
11. Colwell RR (1996) Global climate and infectious disease: the cholera paradigm. Science 274:2025–2031
12. Anonymous (1994) Vision statement. Marine Research Laboratory, South Carolina Marine Resources Center, Charleston. Unpublished report, 9 pp
13. Sandifer PA, Becker PR, Burnet LE, Holland AF, Lacy ER, Scott GI, Van Dolah RF (2005) The Hollings Marine Laboratory: a new model for government-academic partnering. In: Proceedings of the 14th biennial coastal zone conference, New Orleans (extended abstract)
14. Anderson DM, Galloway S, Joseph JD (1993) Marine biotoxins and harmful algae: a national plan. Technical Report. Woods Hole Oceanographic Institution, Woods Hole
15. HARRNESS (2005) Harmful algal research and response: a national environmental science strategy 2005–2015. In: Ramsdell JS, Anderson DM, Glibert PM (eds) Ecological society of America, Washington DC, 96 pp
16. Van Dolah FM (2000) Marine algal toxins: origins, health effects, and their increased occurrence. Environ Health Persp 108(1):133–141
17. Brand LE, Compton A (2007) A long-term increase in *Karenia brevis* abundance along the southwest Florida coast. Harmful Algae 6:232–252
18. Harmful Algae. http://www.whoi.edu/redtide/
19. National Research Council (NRC) (1999) From monsoons to microbes: understanding the ocean's role in human health. National Academies Press, Washington, DC, 144 pp
20. NRC (2001) Under the weather: climate, ecosystems, and infectious disease. National Academies Press, Washington, DC, 160 pp
21. NRC (2002) Marine biotechnology in the twenty-first century: problems, promise, and products. National Academies Press, Washington, DC, 132 pp
22. U.S. Commission on Ocean Policy (USCOP) (2004) An ocean blueprint for the 21st century. Final report. U.S. Commission on Ocean Policy, Washington, DC, 676 pp
23. U.S. Ocean Action Plan (2004) The Bush Administration's response to the U.S. Commission on Ocean Policy. Washington, DC, 39 pp
24. Joint Subcommittee on Ocean Science and Technology (JSOST) (2007) Charting the course for ocean science in the United States: research priorities for the next decade. NSTC Joint Subcommittee on Ocean Science and Technology, Washington, DC, 67 p
25. Jewett EB, Lopez CB, Dortch Q, Etheridge SM (2007) National assessment of efforts to predict and respond to harmful algal blooms in U.S. waters. Interim report. Interagency Working Group on Harmful Algal Blooms, Hypoxia, and Human Health of the NSTC Joint Subcommittee on Ocean Science and Technology. Washington, DC
26. Lopez CB, Jewett EB, Dortch Q, Walton BT, Hudnell HK (2008) Scientific assessment of freshwater harmful algal blooms. Interagency Working Group on Harmful Algal Blooms, Hypoxia, and Human Health of the NSTC Joint Subcommittee on Ocean Science and Technology. Washington, DC, 65 pp
27. Jewett EB, Lopez CB, Dortch Q, Etheridge SM, Backer LC (2008) Harmful algal bloom management and response: assessment and plan. Interagency Working Group on Harmful Algal Blooms, Hypoxia, and Human Health of the NSTC Joint Subcommittee on Ocean Science and Technology, Washington, DC, 76 pp
28. Lopez CB, Dortch Q, Jewett EB, Garrison D (2008) Scientific assessment of marine harmful algal blooms. Interagency Working Group on Harmful Algal Blooms, Hypoxia, and Human Health of the NSTC Joint Subcommittee on Ocean Science and Technology. Washington, DC, 62 pp
29. Committee on Environment and Natural Resources (CENR) (2010) Scientific assessment of hypoxia in U.S. coastal waters. Interagency Working Group on Harmful Algal Blooms, Hypoxia, and Human Health of the NSTC Joint Subcommittee on Ocean Science and Technology. Washington, DC, 154 pp
30. Subcommittee on Ocean Science and Technology (SOST) (2011) Science for an ocean nation: an update of the ocean research priorities plan. SOST, Washington, DC (In preparation)
31. Portier CJ, Thigpen Tart K, Carter SR, Dilworth CH, Grambsch AE, Gohlke J, Hess J, Howard SN, Luber G, Lutz JT, Maslak T, Prudent N, Radtke M, Rosenthal JP, Rowles T, Sandifer PA, Scheraga J, Schramm PJ, Strickman D, Trtanj JM, Whung P-Y (2010) A human health perspective on climate change: a report outlining the research needs on the human health effects of climate change. Environmental Health Perspectives/National Institute of Environmental Health Sciences, Research Triangle Park. doi:10.1289/ehp.1002272, www.niehs.nih.gov/climatereport

32. Obama B (2010) Executive order 13547: stewardship of the ocean, our coasts, and the great lakes, Washington, DC
33. Interagency Ocean Policy Task Force (IOPFT) (2010) Final recommendations of the interagency ocean policy task force. The White House Council on Environmental Quality, Washington, DC, 96 pp
34. One Health. www.onehealthinitiative.com
35. Taylor LH, Latham SM, Woolhouse ME (2001) Risk factors for human disease emergence. Phil Trans R Soc Lond B Biol Sci 356(1411):983–989
36. Bogomolni AL, Gast RJ, Ellis JC, Dennett M, Publiares KR, Lentall BJ, Moore MJ (2008) Victims or vectors: a survey of marine vertebrate zoonoses from coastal waters of the Northwest Atlantic. Diseases Aqua Organ 81:13–38
37. Rose JM, Gast RJ, Bogomolni A, Ellis JC, Lentell BJ, Touhey K, Moore M (2009) Occurrence and patterns of antibiotic resistance in vertebrates off the northeastern United States coast. FEMS Microbiol Ecol 67:421–431
38. Schaefer AM, Goldstein JD, Reif JS, Fair PA, Bossart GD (2009) Antibiotic-resistant organisms cultured from Atlantic bottlenose dolphins (*Tursiops truncatus*) inhabiting estuarine waters of Charleston, SC and Indian River Lagoon, FL. EcoHealth. doi:10.1007/s10393-009-0221-5
39. Costello MJ, Coll M, Danovaro R, Halpin P, Ojaveer H, Miloslavich P (2010) A census of marine biodiversity knowledge, resources, and future challenges. PLoS One 5(8):e12110, 15 pp
40. Carter GT (2008) Discovering anti-infectives from the sea. In: Walsh PJ, Smith SL, Fleming LE, Solo-Gabriele HM, Gerwick WH (eds) Oceans and human health, risks and remedies from the seas. Elsevier, Amsterdam, pp 453–468
41. Gerwick W (2008) Marine remedies. In: Walsh PJ, Smith SL, Fleming LE, Solo-Gabriele HM, Gerwick WH (eds) Oceans and human health, risks and remedies from the seas. Elsevier, Amsterdam, pp 425–429
42. Simmons TL, Gerwick W (2008) Anticancer drugs of marine origin. In: Walsh PJ, Smith SL, Fleming LE, Solo-Gabriele HM, Gerwick WH (eds) Oceans and human health, risks and remedies from the seas. Elsevier, Amsterdam, pp 431–452
43. Teichert RW, Olivera BM (2008) Novel pain therapies from marine toxins. In: Walsh PJ, Smith SL, Fleming LE, Solo-Gabriele HM, Gerwick WH (eds) Oceans and human health, risks and remedies from the seas. Elsevier, Amsterdam, pp 497–506
44. Fautin D, Dalton P, Incze L, Leong J-A, Pautzke C, Rosenberg A, Sandifer P, Sedberry G, Tunnel J, Abbott I, Brainard R, Brodeur M, Eldredge L, Feldman M, Moretzsohn F, Vroom P, Wainstein M, Wolff N (2010) An overview of marine biodiversity in United States waters. PLoS One 5(8):e11914. doi:10.1371/journal.pone.0011914
45. Keesing F, Belden LK, Daszak P, Dobson A, Harwell CD, Holt RD, Hudson P, Jolles A, Jones KE, Mitchell CE, Myers SS, Bogich T, Ostfield R (2010) Impacts of biodiversity on the emergence and transmission of infectious diseases. Nature 468:647–652
46. DiDonato GT, Stewart JR, Sanger DM, Robinson BJ, Thompson BC, Holland AF, Van Dolah RF (2009) Effects of changing land use on the microbial water quality of tidal creeks. Mar Poll Bull 58(1):97–106
47. Bossart GD (2010) Marine mammals as sentinel species for oceans and human health. Vet Pathol. doi:10.1177/03009858 1038853=25
48. Schwacke LH, Twiner MJ, De Guise S, Balmer BC, Wells RS, Townsend FI, Rotstein DC, Varela RA, Hansen LJ, Zollman ES, Spradlin TR, Levin Leibrecht MH, Wang S, Rowles TK (2010) Eosinophilia and biotoxin exposure in bottlenose dolphins (*Tursiops truncates*) from a coastal area impacted by repeated mortality events. Environ Res 110:548–555
49. Schwacke LH, Zolman ES, Balmer BC, De Guise S, George RC, Hoguet J, Hohn AA, Kucklick JR, Lamb S, Levin M, Litz JA, McFee WE, Place NJ, Townsend FI, Wells RS, Rowles TK (2011) Anaemia, hypothyroidism and immune suppression associated with polychlorinated biphenyl exposure in bottlenose dolphins (*Tursiops truncatus*). Proc R Soc B Biol Sci. doi:10.1098/rspb.2011.0665
50. Harvell CD, Mitchell CE, Ward JR, Alitzer S, Dobson AP, Ostfield RS, Samuel MD (2002) Climate warming and disease risks for terrestrial and marine biota. Science 296:2158–2162
51. Wilcox BA, Aguirre AA (2004) One ocean, one health. EcoHealth 1:211–212
52. Patz JA, Campbell-Lendrum D, Holloway T, Foley JA (2005) Impact of regional climate change on human health. Nature 438:310–317
53. Moore SK, Trainer VL, Mantua NJ, Parker MS, Laws EA, Backer LC, Fleming LE (2008) Impacts of climate variability and future climate change on harmful algal blooms and human health. Environ Health 7(Suppl 2):S4, 12 pp
54. Moore SK, Mantua NJ, Salathe EP Jr (2011) Past trends and future scenarios for environmental conditions favoring the accumulation of paralytic shellfish toxin in Puget Sound shellfish. Harmful Algae 10:521–529. doi:1016/j/hal.2011.04.004
55. Ocean Health Working Group (OHWG) (2010) One ocean, one health, NOAA in the lead. A report from the NOAA Science Advisory Board, 50 pp
56. USA Today (2011). http://yourlife.usatoday.com/fitness-food/safety/story/2011/05/Gulf-seafood-safety-concerns-consumers/47507778/1
57. Plano LRW, Garza AC, Shibata T, Elmir SM, Kish J, Sinigalliano CD, Gidley ML, Miller G, Withum K, Fleming LE, Solo-Gabriele HM (2011) Shedding of *Staphylococcus aureus* and methicillin-resistant *Staphylococcus aureus* from adult and pediatric bathers in marine waters. BMC Microbiol 11(1):5. http://www.biomedcentral.com/1471-2180/11/5, 10 pp
58. Constantin de Magny G, Murtugudde R, Sapiano MRP, Nizamc A, Brown CW, Busalacchi AJ, Yunus M, Nair GB, Gil AI, Lanata CF, Calkins J, Manna B, Rajendran K, Bhattacharya MK, Huq A, Sack RB, Colwell RR (2008) Environmental signatures associated with cholera epidemics. Proc Nat Acad Sci USA 105(46):17676–17681
59. Ford TE, Colwell RR, Rose JB, Morse SS, Rogers DJ, Yates T (2009) Using satellite images of environmental changes to predict infectious disease outbreaks. Emer Infect Dis 15(9):1341–1346

60. Lane JQ, Raimonid PT, Kudela RM (2009) Development of a logistic regression model for the prediction of toxigenic Pseudo-nitzschia blooms in Monterey Bay, California. Mar Ecol Progr Ser 383:37–51
61. Li Y, He R, McGillicuddy DJ, Anderson DM, Keafer BA (2009) Investigation of the 2006 *Alexandrium fundyense* bloom in the Gulf of Maine: in-situ observations and numerical modeling. Cont Shelf Res 29:2069–2082
62. Jochens AE, Malone TC, Stumpf RP, Hickey BM, Carter M, Morrison R, Dyble J, Jones B, Trainer VL (2010) Integrated ocean observing system in support of forecasting harmful algal blooms. Mar Technol Soc J 44(6):99–121
63. Johnson CN, Flowers AR, Noriea NF III, Zimmerman AM, Bowers JC, DePaola A, Grimes DJ (2010) Relationships between environmental factors and pathogenic *Vibrios* in the Northern Gulf of Mexico. Appl Environ Micro 76(21):7076–7084
64. Moore SK, Mantua NJ, Hickey BM, Trainer VL (2010) The relative influences of El Nino-Southern Oscillation and Pacific Decadal Oscillation on paralytic shellfish toxin accumulation in Pacific Northwest shellfish. Limnol Oceanogr 55(6):2262–2274
65. Wynne TT, Stumpf RP, Tomlinson MC, Dyble J (2010) Characterizing a cyanobacterial bloom in western Lake Erie using satellite imagery and meteorological data. Limnol Oceanogr 55(5):2025–2036
66. Stumpf RP, Tomlinson MC, Calkins JA, Kirkpatrick B, Fisher K, Nierenberg K, Currier R, Wynne TT (2009) Skill assessment for an operational algal bloom forecast system. J Mar Syst 76(1–2): 151–161
67. Constantin de Magny G, Long W, Brown CW, Hood RR, Huq A, Murtugudde R, Colwell RR (2010) Predicting the distribution of *Vibrio* spp. in the Chesapeake Bay: a *Vibrio cholearae* case study. EcoHealth 6(3):378–389
68. NOAA Harmful Algal Bloom Operational Forecast System. http://tidesandcurrents.noaa.gov/hab/
69. http://www.glerl.noaa.gov/res/Centers/HABS/habs.html
70. Vibrio Remote Sensing Report [67]. http://www.eol.ucar.edu/projects/ohhi/vibrio/
71. Mapping Pathogens in the Chesapeake Bay. http://155.206.18.162/pathogens/, http://www.eol.ucar.edu/projects/ohhi/vibrio/
72. Krahn MM, Ylitalo GM, Brown DW, Collier TK (2005) Analysis of edible tissue from white shrimp collected in coastal waters of the Gulf of Mexico potentially affected by Hurricane Katrina to determine recent exposure to persistent organic pollutants (POPs) and polycyclic aromatic compounds (PACs). NOAA Fisheries, Northwest Fisheries Science Center, Seattle
73. Hom T, Collier TK, Krahn MM, Strom MS, Ylitalo GM, Nilsson WB, Paranjpye RN, Varanasi U (2008) Assessing seafood safety in the aftermath of hurricane Katrina. In: McLaughlin KD (ed) Mitigating impacts of natural hazards on fishery ecosystems, vol 64, American fisheries society symposium series. Bethesda, American Fisheries Society, pp 73–94
74. Sinigalliano CD, Gidley ML, Shibata T, Whitman D, Dixon TH, Laws E, Hou A, Bachoon D, Amaral-Zettler L, Gast RJ, Steward GF, Nigro OD, Fujioka R, Betancourt WQ, Vithanage G, Mathews J, Fleming LE, Solo-Gabriele HM (2007) Impacts of hurricanes Katrina and Rita on the microbial landscape of the New Orleans area. Proc Nat Acad Sci USA 104(21):9029–9034
75. Amaral-Zettler LA, Rocca JD, Lamontagne MG, Dennett MR, Gast RJ (2008) Changes in microbial community structure in the wake of hurricanes Katrina and Rita. Environ Sci Technol 42(24):9072–9078
76. FDA. http://www.fda.gov/food/ucm210970.htm
77. NOAA. http://sero.nmfs.noaa.gov/deepwater_horizon_oil_spill.htm
78. Solomon G, Janssen S (2010) Health effects of the gulf oil spill. J Am Med Assoc. doi:10.1001/jama.2010.1254
79. Goldstein BD, Osofsky HJ, Lichtveld MY (2011) The gulf oil spill. N Engl J Med 364:1334–1348
80. National Commission on the BP Deepwater Horizon Oil Spill and Offshore Drilling (2011) Deep water: the gulf oil disaster and the future of offshore drilling. Report to the President. National Commission on the BP Deepwater Horizon Oil Spill and Offshore Drilling, Washington, DC, 381 p
81. GuLFSTUDY. www.nihgulfstudy.org
82. Reardon S (6 Apr 2011) Primer: will radiation lay waste to Japan's fish. Science Insider. http://news.sciencemag.org/scienceinsider/2011/04/primer-will-radiation-lay-waste.html
83. Reardon S (2011) Fukushima radiation creates unique test of marine life's hardiness. Science 332:292
84. Kite-Powell HL, Fleming LE, Backer LC, Faustman EM, Hoagland P, Tsuchiya A, Younglove LR, Wilcox BA, Gast RJ (2008) Linking the oceans to public health: current efforts and future directions. Environ Health 7(Suppl 2):S6, 15 pp

Co-combustion of Wood in Coal-Fired Large-Scale Power Plants

Egbert Broßmann[1], Martin Kaltschmitt[2,3], Marc Koch[1]
[1]Vattenfall Europe Wärme AG, Berlin, Germany
[2]German Biomass Research Centre, Leipzig, Germany
[3]Institute of Environmental Technology and Energy Economics, Hamburg University of Technology, Hamburg, Germany

Article Outline

Glossary
Definition of the Subject
Introduction
Biomass Processing
Co-combustion in Dust-Fired Systems
Co-combustion in Fluidized Bed Systems

Berlin Case Study
Conclusion
Bibliography

Glossary

Ash Residue obtained after combustion of a fuel.

Biomass From a scientific and technical point of view, biomass is defined as material of biological origin, excluding material embedded in geological formations and/or transformed to fossil.

Bioenergy Bioenergy is defined as energy from biomass.

Co-combustion Simultaneous combustion of biomass and fossil fuels within the same combustion device.

Combustion Full oxidation of a fuel.

Solid Biofuel Solid fuel produced directly or indirectly from biomass.

Thermochemical conversion Heat-induced conversion of biofuels into energy carrier and/or energy.

Definition of the Subject

Due to the introduction of the CO_2 emissions trading, the co-combustion of wood in coal-fired large-scale power plants gains more and more importance within the energy industry. Co-combustion of biomass in coal-fired power plants means the utilization of solid biofuels in existing hard coal- or lignite-fired power plants or combined heat and power (CHP) plants for the replacement of fossil fuel energy. (Parts of this paper are retrieved from [1].) For detailed citation see [1].

This option is particularly characterized by the following benefits:

1. Highly efficient electricity provision from biomass compared to a electricity production in small-scale units; this allows conserving natural resources, which can even be improved by additional extraction of heat in combined heat and power generation plants,
2. High greenhouse gas (GHG) reduction efficiency by direct replacement of coal as the fossil energy source with the highest specific greenhouse gas emission,
3. Relatively low investments for the prevalent co-combustion rates of 3–10% of the boiler capacity.

Therefore, the objective of the following explanations is it to provide a comprehensive analysis of the technical effects on the power plant processes by different co-fired solid biofuels. Subsequently, a special focus is put on the experiences with co-combustion of natural wood in three large-scale coal-fired power plants in Berlin/Germany. Finally, appropriate conclusions are drawn.

Introduction

Of all renewable sources of energy, biomass contributes by far most to cover the demand of energy in Germany and globally. In Germany, for instance, approximately 70% of the total primary energy from renewable sources of energy is derived from biomass; for the generation of heat, biomass (mainly wood) takes a share of almost 94%, for the biofuels this is 100%, and for electricity, it ranks second (28%) behind wind (40%).

Approaches of a combined use of fossil and renewable sources of energy particularly apply for biomass, for example, adding a mixture of solid biofuels to fossil fuels or feeding biogas into natural gas distribution systems as well as co-combustion of biomass in large-scale power plants. This combined utilization with a limited share of renewable energies is mainly used for technical reasons so that the high efficiency of the technical installations achieved with fossil standard and regular fuels as well as their life cycle will not be compromised.

The latter particularly applies to biomass co-combustion in large-scale combined heat and power (CHP) plants, where a high efficiency for electricity generation exists due to advanced steam parameters. In addition, hard coal or lignite is directly replaced by the CO_2-neutral biomass. Therefore, co-combustion of solid biofuels in coal-fired power plants is particularly efficient from a climate protection point of view due to direct and immediate replacement of fossil fuel energy with high specific CO_2 emissions (i.e., coal). In contrast to that, pure biomass-fired power plants primarily displace electricity from the local electricity mix and thus electricity provided with a high percentage of low-CO_2 electricity from, e.g., windmills or PV systems. The moderate additional investments and short transport distances for the manageable quantities account for other benefits of biomass co-combustion in a limited

scope of approximately 3–5% of the boiler capacity. Such co-combustion of biomass in conventional coal-fired power plants is influenced by a series of ancillary conditions, which will be briefly discussed below.

The share of solid biofuels in the total thermal performance of a conventional power plant fired with hard coal or lignite is limited by the amount of biomass, which can be used in the combustion system without significant disadvantages to be expected (e.g., corrosion, emissions, flow conditions). For instance, usually a share of 10% of biomass energy referring to the amount of fossil fuel energy resp. the installed thermal capacity should not be exceeded to keep measures of adjusting the existing power plant to such changed conditions as low as possible. However, higher percentages are possible for lignite-fired systems for firing systems converted from lignite to hard coal with flue gas recirculation and for fluidized bed systems. Additionally, the biomass flow, which can be used for co-combustion, is also limited by the quantity of biomass fuels, which can be provided at a certain power plant site for economic reasons. For example, the upper performance limit of biomass provision under Central European conditions would be approximately 50–100 MW of biomass fuel capacity. For higher capacities, the size of the required catchment area will increase so that transport effort, which is mostly handled by road due to infrastructural constraints, will increase too much and thus the procurement costs for biomass will become too high.

Against this background, the coal-fired power plants coming into consideration for co-combustion of solid biomass are on the one hand comparably "small" combined heat and power (CHP) generation plants normally operated by public utility companies in a capacity range below approximately 100 MW of electric power. On the other hand, also the larger block-unit power stations with installed electrical capacities of 500–1,000 MW come into consideration. Facing the comparably large installed electric (and thus also thermal) power in the scope of large-scale power stations, even percentages of co-firing of 5–10% mean truly significant quantities of solid biomass, so that for the large-scale biomass co-firing, there is no need to be worried about higher shares of biomass in the firing heat capacity.

The utilization of biomass in existing large-scale coal-fired power plants for the generation of electricity has a number of advantages compared to the generation of electric energy in smaller plants exclusively fired with biomass.

- The significant power plant capacity available in Central Europe for generating electricity from coal results in a high potential for the utilization of biomass. From a technical point of view, this potential is quickly available; limitations only exist due to the fact that principally not all locations of large-scale power plants are qualified for co-combustion of biomass (e.g., due to logistic limitations). Even with a comparably small share of biomass referring to the overall installed thermal capacity resp. to the overall used fossil fuel energy, a huge amount of solid biomass can be used.
- Compared to smaller plants exclusively fired with biomass, the efficiency of electricity generation in large-scale power plants normally is significantly higher due to a higher technical effort possible in large-scale plants due to economic reasons.
- In case of seasonal nonavailability or in case of supply bottlenecks for solid biofuels due to weather conditions, electricity generation can be ensured by the basic fuel of coal (i.e., high security of supply with high fuel flexibility).
- The additional investment required for the realization of biomass co-combustion is relatively low because only the additional equipment is counted for.

The substitution of the fossil fuel of coal by solid biofuels makes the acquisition of an according quantity of emission permits dispensable, thus creating the financial scope for the co-combustion of biomass.

Principally, besides solid biofuels (like wood) also, other biomass fractions available in a corresponding quantity and homogeneity (e.g., sewage sludge) can (and will) be co-fired in existing coal-fired power plants along with solid biomass such as wood and straw. Thus co-combustion is also suitable for types of biomass which from a combustion point of view are rather problematic and for which revenues for disposal is paid to some extent.

Biomass Processing

The required processing of the solid biofuel for co-combustion in existing power plants depends on the type of biomass and on the firing system technology (see [1–31]).

The solid biofuel co-fired in large-scale power plants should principally be free of foreign substances (e.g., rocks, metal parts) so that downstream conveying equipment, processing units (e.g., shredders for coarse matter), or dosing units will not be affected.

Drying of the biomass may possibly be required. While this, from a combustion point of view, is normally not required for wood and straw, it could however be advantageous from an energetic point of view. This particularly applies if waste heat can be utilized for this purpose, which before that had not been used.

Due to some impurities within some solid biofuels (e.g., chlorine in straw) problems can be expected during the combustion within the power plant (e.g., corrosion). For example, one measure to prevented such problems is the "washing" the fuel if the impurities are water-soluble (which is the case for the chlorine within the straw). In this process, some impurities (e.g., chlorine, alkalines) are washed out of the solid biofuel with water. Because of this, the biofuel can be used within the firing system of the power plant with probably less problems. However, the negative aspect is the high-energy input for the practical realization of such considerations.

The particularities for dust firing and fluidized bed systems with respect to processing of the biofuels to be co-combusted are discussed below.

Processing for Dust-Fired Systems

Dust firing requires extensive milling of the biomass used (e.g., wood-like woodchips, herbaceous biomass like straw bales) to achieve a complete burnout. Cutting mills, hammer mills can be used for this purpose.

The wood particles milled with a cutting mill have a rather cubic shape, while particles from herbaceous biomass (e.g., straw, hay) have the shape of oblong, rectangular platelets. The demand of electric energy needed for such milling is increasing with declining particle size. In average, the energy demand is between approx. 0.8 and 2% of the calorific value of the biomass, when cutting mills are used with screens of a mesh size between 2 and 6 mm. Using a hammer mill, the energy demand can be reduced to 0.5–1% of the calorific value. Increased water content of the fuel principally leads to higher energy consumption; the energy demand is especially increasing with water contents of more than 10–20%. For straw, for example, more than 8% of the calorific value is needed for milling in a cutting mill with a mesh width of 2 mm and a water content of 30%. This energy demand can be reduced by previous torrefaction.

Processing for Fluidized Bed Systems

Wood can be used in fluidized bed systems as woodchips without further milling. For example, maximum piece sizes for wood in circulating fluidized bed systems are around 60 mm and in stationary fluidized bed systems around 100 mm. For herbaceous biomass, the bales have to be opened to get loose stalks and the stalks need to be cut to lengths of around 10–30 cm. Thus, there are virtually no differences to exclusive biomass combustion with regard to fuel dimensions.

Fluidized bed systems therefore require only little processing of the fuel to be fired. In addition, they are resistant to increased water content of fuels and/or low calorific values, as well as fluctuations in water content.

Co-combustion in Dust-Fired Systems

The resulting mass and volume flows and their changes compared to exclusive firing of coal, as design fuel, is of fundamental importance for the possibility of co-combustion of biomass in existing dust fired systems (see [1–31]). Also, the existing facilities for transport and processing of the fuel must be suitable with respect to the changed fuel volume flow. Beside this, they necessarily have the required capacity. In addition, the change of the flue gas volume flow has to be evaluated as this is influenced by the different water content in the solid biofuel resp. the coal and by the different quantities of reaction water from the oxidation of the hydrogen contained in the fuel. This will significantly affect the behavior of heat transfer and retention time inside the steam generator and the function of the downstream flue gas cleaning equipment. Figure 1 outlines the effects of the co-combustion to the

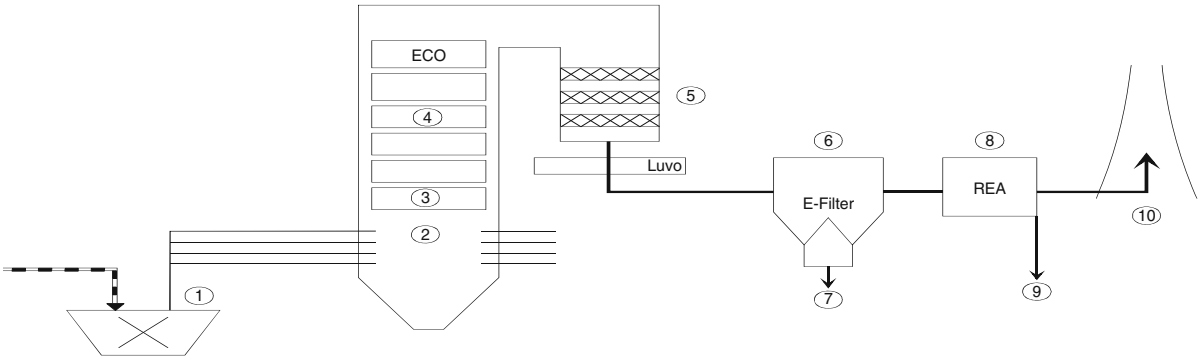

1 Mill: Capacity, attrition
2 Combustion chamber: Slagging
3 Super heater: Corrosion
4 Heat exchanger: Dirtiness, erosion
5 Flue gas denitrification system: Deactivation, capacity, erosion
6 Electrostatic precipitator: Capacity
7 Ash: Utilization
8 Flue gas desulphurisation plant: Capacity
9 Products of the flue gas desulphurisation plant: Utilization
10 Flue gas: Emissions

Co-combustion of Wood in Coal-Fired Large-Scale Power Plants. Figure 1
Possible effects and affected plant components with co-combustion (according to [1])

components of a dust-fired power plant based on hard coal. They are discussed below for the co-combustion of wood and herbaceous biomass. In addition, sewage sludge will be considered as an example because, until now, this fuel of biogenic origin has gained the largest importance in practical realization.

Fuel and Flue Gas Volume Flow

From fuel supply to fuel input, the fuel volume flow is strongly increasing by the addition of wood and herbaceous biomass to the coal (Fig. 2) (see [1–31]). This is due to the significantly lower heating value of the solid biofuels compared to coal and, therefore, relatively larger biomass flow (also compared to coal) to achieve the same energy input. For example, a capacity share of 10% of co-combustion of straw in hard coal dust-fired systems will lead to doubling of the total fuel volume flow. Therefore, both milling of the biomass and conveying of the solid biofuel to the combustion chamber should be carried out separately. In this process, in most cases, the coal-grinding mills cannot be used for the biomass to be co-fired due to the different structure of the solid biofuel and the coal. Therefore, separate grinding mills are usually required for this.

The co-combustion of biomass in coal-fired systems will change the gas flow inside the boiler only to a small extend. Both, the fed combustion air and the flue gas volume remain constant largely. If, for example, dry wood or straw is used in a hard coal–fired system, the moist flue gas volume flow will change by maximum 1% with a share of 10% biomass of the installed thermal capacity, depending on the biomass and its humidity (Fig. 2). Even with very moist biomass (e.g., bark, fresh-cut grass), the increase of flue gas caused by this will remain in the area of a few percent.

By co-combustion of biomass with hard coal, the water content of the sewage sludge will influence the fuel-mass flow as well as the flue gas volume flow. While for a thermally dried sewage sludge with 95% dry matter (TM) with a 10% share of sewage sludge referring to the overall installed thermal capacity, the fuel mass flow will increase by 18%, the increase with mechanically well dehydrated sludge with 45% dry matter (TM) is approx. 70% already with the same percentage of thermal capacity.

This results in a high demand of adaptation for the conveyor technology, the mills and the feeding system for the fuel into the boiler, when disproportionately large quantities of water are entered together with the sewage sludge into the system. A similar situation is also given to the flue gas treatment system. The increased flow speed of the flue gas due to the increased volumes leads to a change of the heat transfer as well as

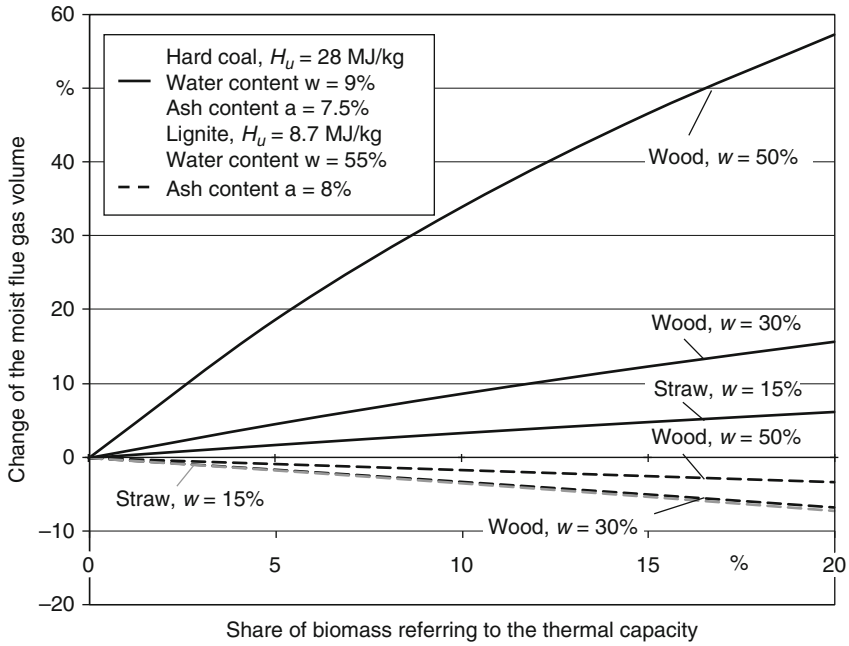

Co-combustion of Wood in Coal-Fired Large-Scale Power Plants. Figure 2
Change of the moist flue gas volume flow with biomass co-combustion [1]

an increase of the pressure losses; furthermore, it also affects the cleaning efficiency of the flue gas–treatment system.

If however the main and the additional fuel have nearly the same content of water, the required changes are low. Therefore, co-combustion of moist biomass (e.g., humid wood, dehydrated sewage sludge) with raw lignite (water content approximately 50%) is a suitable and very promising option. The humid flue gas volume is slightly decreasing in this process. Dry biomass or dried sewage sludge can be fired with hard coal with a water content of approximately 7%. Moist wood would not lead to an acceptable increase of volume flow with higher shares referred to the thermal capacity. For the usually realized low percentages of co-combusted referred to the thermal capacity, however, also mechanically dehydrated sewage sludge can be used in hard coal–fired plants usually without any major problems.

Combustion Process

The biofuel needs to be appropriately milled to ensure complete combustion within dust-fired systems (see [1–31]). The maximum particle size for safe ignition and complete burn-off – for example, in a 0.5 MW pilot plant – is approximately 6 mm for straw and approx. 4 mm for Miscanthus (mesh diameter of mill) due to its woody structure. Grinding of wood is required between 2 and 4 mm for co-combustion in coal dust flames. In plants with a higher thermal capacity of up to several 1,000 MW, also coarser biomass particles can principally be co-fired due to the longer retention times. In a large-scale power plant, for example, straw with stalk lengths up to 10 cm was completely burned up.

In addition, significantly coarser fuel particles can be used in dust-fired systems than for coal due to the high volatile content of the solid biofuels. In this process, herbaceous biomass is more reactive than woody biomass and thus requires less fine grinding. So, there is no need to dry the solid biofuels for water contents of up to 50%.

The significantly coarser grinding of the biomass particles affects the combustion process. This is exemplarily shown in Fig. 3 in a coal dust flame and coal dust/biomass flame, respectively. The delayed ignition of the coarse straw particles can be seen for the run of the medium oxygen concentration along the combustion path. After ignition, the oxygen is used up faster

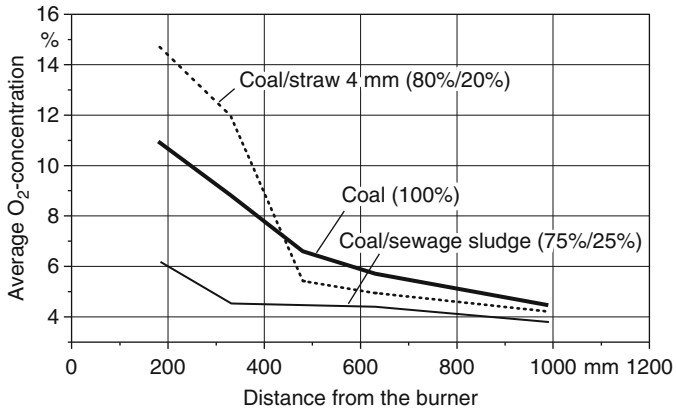

Co-combustion of Wood in Coal-Fired Large-Scale Power Plants. Figure 3
Combustion process of a mixed biomass/coal flame (according to [1])

and the combustion after ignition until burn-off is faster than for coal.

Slagging and Fouling

Due to the lower melting points of the biomass ash particles (especially for straw) compared to coal ash particles, there is a higher risk of slagging in the area of the combustion chamber (see [1–31]). The effects of low melting temperatures are different for dry deashed and molten deashed firing equipment. While low melting temperatures can be absolutely desirable for slag-tap furnaces, a lower melting temperature in dry furnaces can lead to slagging in the combustion chamber and especially in the area of the burner, which will affect operation and does not allow a continuous and safe operation any more.

Fouling and slagging on the convective heating surfaces resulting from the solid biofuel increases with growingly lower melting points of the biofuel used. Examinations at a 0.5 MW research plant however show that the fouling rate for the co-combustion of straw was only insignificantly higher than for firing of coal which is rather less prone to pollution. Furthermore, the dust layer resulting from the combustion can be easily cleaned. The properties of the coal ash therefore dominate the ash behavior of the ash mixture if the share of biomass within the fuel mixture is not too high. If however larger straw particles will deposit, which are incompletely burned off, they lead to corresponding slagging due to their low melting point of straw ash.

Corrosion and Erosion

Herbaceous biomass (e.g., straw) has a significantly higher chlorine content compared to coal and wood (see [1–31]). This can lead to increased high-temperature corrosion with corresponding abrasion of the surfaces of the heat exchanger. The heating surfaces of the superheater with their high steam and flue gas temperatures are affected first and foremost (Fig. 4). All in all, however, the measured corrosion rates at the heating surfaces of the coal dust-fired equipment seem to be acceptable compared to exclusive firing of coal if the percentage of biomass in the total firing heat capacity is limited to small quantities, as shown.

Due to the low share of ash referring to the fuel mass in most biomasses discussed for co-combustion, there will be almost no increase of erosion (i.e., material removal by abrasive flue gas components) to equipment parts, where the dust-loaded flue gas volume flow is passing through.

The chlorine content of sewage sludge is in the range of the chlorine contents of coal. Therefore, increased high-temperature corrosion cannot be expected in case of co-combustion of coal with sewage sludge. However, increased pollution and erosion may result in the area of the convective heating surfaces.

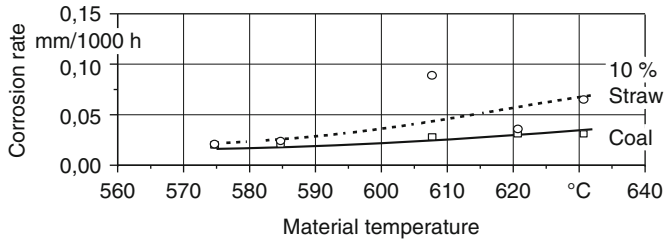

Co-combustion of Wood in Coal-Fired Large-Scale Power Plants. Figure 4
Corrosion rates for co-combustion of straw in a dust-firing system with an electric capacity of 130 MW, exemplary for the material X20CrMoV121 (according to [1])

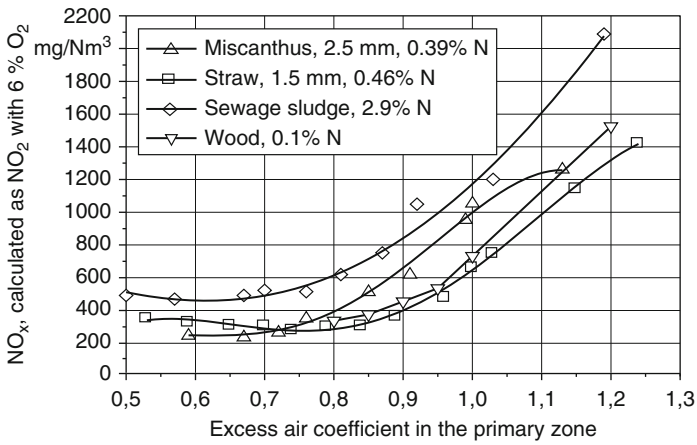

Co-combustion of Wood in Coal-Fired Large-Scale Power Plants. Figure 5
Nitrogen oxide (NO_x) emissions with different excess air coefficients in the primary zone for different types of biomass with fuel mixture of 25% biomass and 75% coal, each time related to the thermal fuel capacity (according to [1])

Emissions

The co-combustion of wood and herbaceous biomass in coal-fired power plants leads to a reduction of the main harmful substances in the raw flue gas prior to flue gas cleaning (see [1–31]). Sulfur dioxide (SO_2) is reduced, on the one hand, by the integration of sulfur into the ash and, on the other hand, by dilution, because the biomass fuels shows in average significant lower sulfur content than coal. Also, nitrogen oxide (NO_x) can reach lower values due to biomass-specific advantages in combustion kinetics even if there is not much change for the total nitrogen content in the fuel. Beside this, the carbon monoxide (CO) emissions do not increase when the biomass is sufficiently milled.

Due to the high content of volatile matter, biomass is particularly suitable for the application of nitrogen oxide (NO_x) reduction processes such as air and fuel grading. Although for straw, the fuel nitrogen related to the calorific value approximately corresponds to the value of coal. Thus, the higher release of products of pyrolytic degradation and volatile nitrogen compounds produce less nitrogen oxide in the process of thermochemical reaction. Figure 5 therefore shows as an example the NO_x emissions identified in a pilot plant for a fuel mixture of 25% of particular biomass and 75% of hard coal (each time related to the total installed thermal capacity). Thus, approximately the same NO_x emissions result independently of the nitrogen content in the biomass.

Therefore, the co-combustion of biomass in dust-fired systems does not place any requirements on the nitrogen content of the biomass. Also, higher nitrogen

concentrations in the biofuel can be managed by measures of firing technology.

The co-combustion of sewage sludge however leads to an increase of the concentration in the raw flue gases for specific substances such as sulfur dioxide, nitrogen oxides, or volatile heavy metals, which may require additional downstream flue gas cleaning stages. The pollutant concentrations within the flue gas depends on the percentage of sewage sludge in the total fuel throughput, the percentage of sulfur or nitrogen relating to the calorific value and the conversion rate. In case of co-combustion of thermally dried sewage sludge with hard coal, for example, the nitrogen input of the sewage sludge relating to the calorific value is approximately 7 times larger than that of coal. For fuel sulfur, the relation is about 3.3.

The conversion rate of sulfur to sulfur oxide (SO_2) is independent of the percentage of sewage sludge and is approximately 90%; this results in an increase of the SO_2 emissions proportional to the percentage of the sewage sludge. The high content of calcium oxide (CaO) of the sewage sludge ash does not lead to a reduction of the SO_2 emissions. This can be explained by an inactivation of the calcium oxide by the surface fusion with the high temperatures in the dust firing.

With corresponding reduction measures of air and fuel grading in the combustion chamber, the nitrogen oxide emissions of the sewage sludge co-combustion are comparable to those with exclusive firing of coal. The high nitrogen percentage in the fuel, however, should be considered for the burner design and the air distribution in the particular combustion chamber.

The chlorine contents related to the calorific value for hard coal and municipal sewage sludge is approximately in the same range; a significant increase is possible only for industrial sludge. Generally, no increased values are measured also for the PCDD/PCDF emissions, which can be formed in the fuel in the absence of chlorine.

Flue Gas Denitrification

By analyzing the effects of biomass co-combustion to the denitrification in DENOX plants, it must be differentiated between high-dust and low-dust configuration (see [1–31]).

Altogether for a low-dust configuration, the possible effects (e.g., catalyst deactivation) to the operation of a DENOX plant are less compared to the high-dust configuration due to the previously realized flue gas cleaning with the electrostatic precipitator and the flue gas desulfurization system (REA); therefore, this configuration offers advantages for the co-combustion compared to the high-dust configuration.

In particular, for a configuration of the DENOX system in the high-dust area as usually realized in hard coal dry-firing systems, the catalyst is endangered by possible deactivation during co-combustion; this particularly applies if straw is used. Different mechanisms can be involved in this deactivation process. For example, the catalyst can react with potassium and sodium. Therefore, limit values of the alkaline percentage are specified by manufacturers of DENOX-catalysts (K_2O and Na_2O below 4% by weight of ash), which however – depending on the coal used – can already be reached with small fractions of straw. Additionally, a blockage of the pores of the active catalyst cells may result due to alkaline and alkaline earths. In addition, phosphor may contribute to a toxification of the catalyst. Such damage can be prevented by arranging the catalyst behind the flue gas desulfurization system (REA) (i.e., low-dust configuration). This problem does not occur in lignite firing systems, where primary measures are used for denitrification. In general, significantly less problems can also be expected for wood due to the considerably lower content of problematic substances.

For the high-dust configuration, the relatively high ash content of sewage sludge can lead to pollution and to erosion on the DENOX-catalyst. Due to the high nitrogen fraction, the NO_x-concentrations in the raw flue gas can increase. Due to this, they need to be subsequently reduced in the DENOX system. Specific substances (e.g., arsenic, phosphor) may lead to a deactivation of the catalyst here.

Flue Gas Desulfurization

The low content of sulfur of most solid biofuels leads to a relief of the flue gas desulfurization plant (REA) (see [1–31]). The input of other flue gas substances however can possibly affect the function of the flue

gas desulfurization plant or additionally burden it; this also may result in a limitation of the biomass share. This particularly applies to the chlorine input into the flue gas desulfurization plant.

Next to sulfur, also a number of other flue gas components are deposited in the flue gas desulfurization plant (REA); these are, e.g., the volatile ash components in the flue gas such as mercury, arsenic, lead, and other heavy metals. They can be found in the REA residuals (e.g., REA gypsum); therefore, their quality has to be inspected prior to marketing. For wood and herbaceous biomass considered here, the concentrations of such substances can be disregarded compared to coal.

The sulfur contained in the sewage sludge however significantly exceeds the sulfur content of coal in most cases. Therefore, the desulfurization plant has to have a sufficient capacity to safely adhere to the legal emission limits. For example, for a 25% co-firing of sewage sludge within a coal-fired power plant, the SO_2 amount to be bonded within the flue gas desulfurization plant will increase by the factor 1.6.

Ash Formation and Utilization

When considering the possible effects of co-combustion of biomass in coal-fired power plants, also the results for ash formation and ash utilization has to be taken into consideration (see [1–31]).

Ash formation. The small ash fractions of the soli biofuels wood and straw relieve the facilities for dust separation. Altogether, less ash accrues in case of co-combustion of wood and herbaceous bioenergy sources.

In contrast, the high ash content of sewage sludge can lead to overcharge of the electrostatic precipitator. When 5–25% thermally dried sewage sludge is co-fired with hard coal (relating to the fuel capacity), an ash quantity multiplied by the factor 1.7–4.7 must be anticipated. For a sewage sludge proportion of 5 resp. 25% for example, already 44 resp. 84% of the ash comes from the sewage sludge. This results in corresponding changes of the ash properties.

Ash utilization. The composition of the fly ash and the bottom ash of coal dust-fired systems determine the possibilities for its utilization. For example, the concentration of alkaline, sulfates, chlorides, and unburned carbon is essential for using the fly ash in the cement and concrete industry.

The co-combustion of wood is least critical due to the very low ash content. For straw, the increase of the alkaline content and of the unburned substances can limit the utilization of ash as soon as a straw fraction of 10% referring to the thermal capacity is exceeded. In addition, an increased amount of unburned straw nodes can remain, which will make the utilization of the fly ash difficult. For lignite-fired systems, however, the ash is mostly used for recultivation in open-hole mining so that appropriate measures shall ensure that specific ash substances should not leach out and enter, e.g., the ground water.

A decrease of the carbon content was observed in the fly ash with an increasing proportion of sewage sludge. Insofar, the higher ash fraction in the sewage sludge improved the fly ash product to be marketed.

Primarily, the other ingredients of the sewage sludge ash need to be considered for further assessment of the ash properties compared to the coal ash. Next to the main ingredients, first of all the substances with toxic behavior and/or accumulation behavior in the biosphere are of special interest. Despite of the given spread, however, it turns out that only very few sludges are more contaminated than this is permitted for agricultural use.

Apart from substances like mercury, selenium, and arsenic, which as elements or in their compounds emit significant fractions via the flue gas flow due to low boiling points, most microelements from sewage sludge can be found in the solid residues of firing or flue gas cleaning. Figure 6 shows a direct comparison between sewage sludge ash and typical hard coal ash. Accordingly, the concentration of microelements in consideration of the different ash contents becomes similar. The co-combustion of sewage sludge with hard coal thus does not lead to a significant change of the pollutant concentration in the ash.

For heavy metals leaving the boiler, where the combustion takes place partly via the flue gas flow, the removal from the flue gas has to be examined in the following cleaning stages. In the wet flue gas desulfurization systems (REA) usually integrated within power plants, heavy metals are only partly removed. The remaining part is emitted via the flue gas flow into

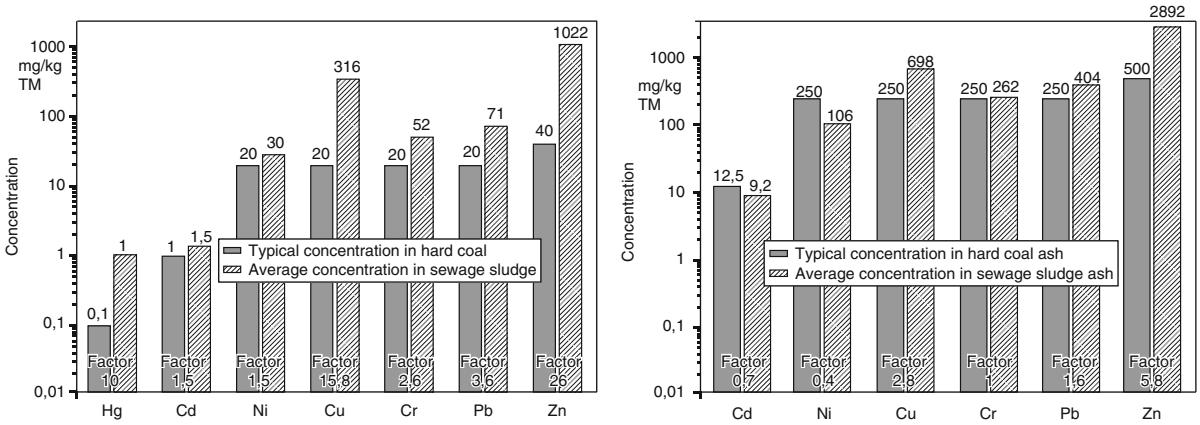

Co-combustion of Wood in Coal-Fired Large-Scale Power Plants. Figure 6
Comparison of trace elements in dry fuels (*left*) and ashes (*right*) (*TM* dry matter; according to [1])

the atmosphere. For mercury, for example, a removal of approximately 50% is achieved; the rest is emitted into the atmosphere. This may require improvement of the flue gas desulfurization systems (REA) customary in power plants, for example, by specifically adapted precipitating agents or an additional downstream filter stage (e.g., activated charcoal filter). It has to be noted in this respect that different regulations apply according to the legal emission limits for coal and for sewage sludge. The latter is basically categorized as waste; in Germany, for example, the requirements of the 17. BlmSchV (17th Federal Control of Pollution Act) has to be met, which are stricter than those of the 13th BImSchV, which apply for exclusive firing of coal in conventional power plants. The European standard EN 450, amended in 2005, which regulates the utilization of fly ash as a concrete additive, now also includes fly ash from the co-combustion of fuels such as wood, straw, sewage sludge, or also paper sludge. This is valid as long as the mass fraction of the co-fired fuels does not exceed 20%, and the ash formation from the additional fuel is not more than 10%. Next to the mentioned quality requirements, further characteristics are specified in the EN 450. Thus, by the amendment of the standard, an essential obstacle was overcome for the propagation of co-combustion.

Co-combustion in Fluidized Bed Systems

Aspects of co-combustion in fluidized bed systems are discussed below (see [1–31]).

Combustion Process

In contrast to coal, biomass with its higher content of volatiles tends to post-combustion in the free space of the fluidized bed firing system (see [1–31]). This is in particular true for stationary fluidized bed systems. Furthermore, smaller, light particles (e.g., straw) can be carried out of the fluidized bed. These light particles combust within the free space and increase due to this post-combustion the temperature inside the free space. A good mixing within a circulating fluidized bed system will evenly distribute the fire-room temperature. However, a temperature shift upward can result also here, if biomass fuels are co-incinerated.

Since fluidized bed systems are particularly suitable for fuels containing ballast, co-firing of mechanically dehydrated sewage sludge makes sense. However, this mainly serves for disposal and less for energy gain due to the low calorific value and the revenues which can be achieved. While the higher content of water of the sewage sludge increases the volume flow of the flue gas compared to hard coal, this effect is low for the co-combustion with lignite. Depending on the calorific value and on the added amount of sewage sludge, however, the thermal capacity and thus the steam production will correspondingly decrease.

On the other hand, synergy effects can result due to the co-combustion of biomass increasing the efficiency of power plant operation. For example, it has been proven in an industrial fluidized bed power plant that by the co-combustion of wood pellets and the thus

resulting fine wood ash, the balance of particle size of the fluidized bed system shifted toward finer particle sizes. This significantly reduced the solid matter inventory inside the combustion chamber, leading to a reduction of the electricity demand of the power plant (i.e., the own consumption has been reduced).

Slagging and Fouling

While no additional operation problems are expected for the co-combustion of wood, solid biofuels based on herbaceous biomass can lead to increased slagging and fouling compared to coal (see [1–31]). This is particularly due to the potassium chloride contained in herbaceous biofuels.

In a circulating fluidized bed system (88 MW thermal capacity), for example, firing of coal with a sulfur content of 3% together with straw (proportion in the thermal capacity each 50%) resulted in heavy slagging within the combustion chamber in the cyclone and in the area of the superheater. After short operations time, the operating parameters could no longer be met. Afterward, only coal was used with sulfur content below 1%. The increasing melting temperatures of the ash deposits with the use of such low-sulfur fuel resulted in less slagging; slagging only occurred in the area of the superheater, where it was facilitated by the design of the superheater with narrow channels (here: 37 mm). However, this problem could be avoided to a large extent by use of suspended superheaters with a channel width of 50 mm (for the prevention of bridging) as well as lowering the flue gas temperature below the melting point of potassium chloride (770°C).

Compared to an exclusive coal firing, the fouling rate on plant components subject to flue gas contamination increases, e.g., for a straw proportion of 50% of the installed thermal capacity, the fouling rate reaches five times the value of exclusive coal firing. However, such pollution is easy to remove.

Corrosion and Erosion

Corrosion problems are not expected when wood is co-combusted in fluidized bed systems (see [1–31]). This however does not apply for biofuels produced from herbaceous biomass, particularly due to the potassium chloride contained in it.

Corrosion examinations of different materials within a circulating fluidized bed system showed significant corrosion to the convective superheater heating surfaces with the co-combustion of straw, although the test results with short test periods of 500–1,000 h are associated with a certain degree of uncertainty. When martensitic steel (X20CrMoV121) was used, the corrosion rates, for example, for co-combustion of straw were approximately 10 times higher than with exclusive firing of coal (Fig. 7). They are thus significantly higher than within a dust-firing system with the same proportion of straw. It is assumed for the reason for the high corrosion rates that the in situ desulfurization in the fluidized bed facilitates the formation of potassium chloride. This potassium chloride will precipitate on the superheater pipes and releases the corrosion-causing chlorine when potassium sulfate is formed. Also, the selection of different high-alloy steels did not result in a significant decrease of the corrosion tendency.

Different measures are taken to reduce the corrosion of the convective heating surfaces. The most important measure turned out to be the reduction of the bed temperature below 860°C. By this and other modifications, it has been achieved that after 7 years, the superheater still was in operation.

Newer concepts therefore aim not to arrange the superheater in the flue gas tract, but as immersion heating surface within a fluidized bed cooler, and thus

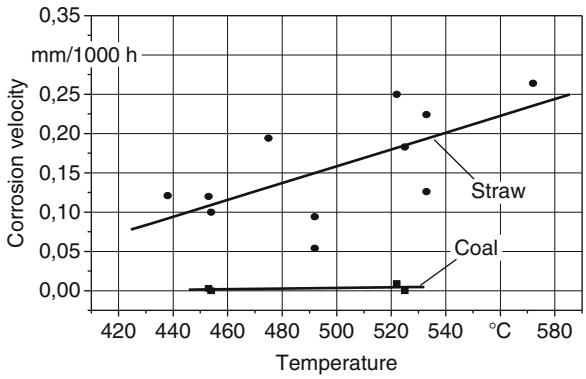

Co-combustion of Wood in Coal-Fired Large-Scale Power Plants. Figure 7
Corrosion rate for co-combustion of 50% straw in a circulating fluidized bed system versus steam temperature (according to [1])

to utilize the characteristic of a circulating fluidized bed system. Since there may be unconsummated straw components in the cyclone return of the circulating fluidized bed, forming potassium chloride during their combustion, comparably high abrasion rates were determined with corrosion sensors arranged inside the return. If corrosion is to be prevented, it is therefore required to connect a non-cooled fluidized bed upstream of the fluidized bed cooler with superheater in order to assure burnout prior to reaching the superheater. This design has proven to be successful; however, the immersion heating surfaces eroded after several years.

Both the corrosion and emission problems as well as the mentioned slagging and fouling problems can be practically prevented best by input of correspondingly less fractions of biomass relating to the firing heat capacity (below 10%).

Emissions

The co-combustion of biomass in coal-fired fluidized bed systems mainly has the effect that emissions are reduced, except for the hydrogen chloride (HCl) emissions when straw is used (see [1–31]).

The sulfur dioxide (SO_2) emissions decrease with increasing biomass proportion in relation to the thermal capacity. This, on the one hand, is due to the lower sulfur content of the biomass compared to coal and, on the other hand, to the encapsulation of the SO_2 in the biomass ash.

For the nitrogen oxide (NO_x) emissions, the possible effects are not uniform. Tests showed that there were only small changes of the NO_x emissions with small proportions of biomass to be co-combusted. Other experiences even revealed a reduction of NO_x with an increasing biomass proportion; this particularly applies to co-combustion of wood. Tests have also shown that the N_2O emissions significantly decrease with the co-combustion of biomass.

Similar as for dust-fired systems, the co-combustion of straw causes an increase of hydrogen chlorine (HCl) emissions. In a fluidized bed system, for example, with a straw proportion of 60% relating to the installed thermal capacity, the chlorine input into the firing system was about 20 times higher than in case of exclusive firing of coal. The entered amount of chlorine can be found almost completely in the flue gas. The co-combustion of wood however leads to a reduction of the HCl emissions.

For the co-combustion of sewage sludge within a circulating fluidized bed system, the emissions of SO_2, NO_x, CO, and dust are within the legal range of fluctuation. For example, in Germany, the limit values for the application of the proportional regulation according to 17th BImSchV are therefore undercut. In order to safely meet the limit value for heavy metals (e.g., mercury) it may be required to add an additional flue gas cleaning system (e.g., fly stream absorber with lignite coke) downstream of the electrostatic precipitator.

Ash Formation and Utilization

Correspondingly, similar conclusions as for dust-fired systems apply to the accruing ash and its possibilities for utilization (see [1–31]).

As, for example, the ash proportion in the introduced sewage sludge is approximately 50% relating to the dry matter (TM), the ash quantity accruing in the fluidized bed system will significantly increase. In this process, the toxic substances contained in the sewage sludge are encapsulated inert within the ash. The only exception is mercury that is released from the boiler with the flue gas. The ash can therefore be used, e.g., for purposes of recultivation in open-top lignite mines, because, for example, in Germany the requirements of the dump category 1 of the TA (Technical Instruction) for municipal waste are met.

Berlin Case Study

A detailed analysis of the options and limits of co-combustion of solid biomass in existing coal-fired power plants was carried out for Berlin/Germany. The prepared technical analysis as well as the existing approvals for the power plants resulted in a clear decision for a co-combustion of virgin wood. On this basis, both the availability of resources and the technical consequences potentially resulting from co-combustion to the existing plants are discussed below.

Fuel Procurement

Germany is a densely wooded country. Approximately 11.1 million hectares, almost one third of the total area

of Germany, is covered with forests. Due to the favorable climate, the average amount of wood produced per hectare is 3 times the amount produced, e.g., in Sweden. The annual felling in Germany steadily remains between 60 and 80 million solid cubic meters. Acting on the assumption of a bulk density of 0.6 t/m^3 and an average calorific value of 3 MWh/t, this is 126 million MW of heat energy for 70 million solid cubic meters. Thus, the heat energy of the total German annual felling would be sufficient for the electricity generation in five 1600 MW state-of-the-art large hard coal–fired power plants (57 million MWh_{el}). This is approximately one tenth of the demand for electric energy in Germany.

This context on the one hand makes clear the limited quantities of wood as a resource. On the other hand, it also required maximum efficiency of wood utilization. In addition, the use of wood as a raw material should be favored because of considerations of climate politics since the carbon will then be bonded in the wood products after the growth phase of the plant and is not immediately released back to the atmosphere in the form of CO_2.

Therefore, mainly rather low-grade wood (including short stubs, rotten knots) is suitable. This will be initially shredded for further processing. Thus, the co-combustion primarily focuses on wood from landscape conservation, scrap wood, rolled lumber, wood affected by bark beetles and thinning material from short rotational plantations, and similar types of wood. Wood, which can be used as a raw material, is out of question often also for reasons of costs.

In addition, it should be observed for the mentioned low-grade types of wood basically suitable for co-combustion that brushwood, leaves, needles, and roots should remain in the forest for the formation of humus, in terms of sustainable forestry. However, there are special cases (e.g., leaves from parks or streets), where energetic utilization may be considered. Subject to the ancillary conditions mentioned here, an approval for the coal-fired power plants in Germany should be assumed according to the legal frame conditions for waste and similar combustible substances.

Due to the relatively low calorific value and partly high water content of the firewood, which basically would be suitable for co-combustion, only short transport distances can be economically reasonably realized. Even if the economic efficiency of firewood for co-combustion is supported by saving of CO_2 certificates, this advantage is in contrast with the high specific transport costs per ton of fuel for overland transportation. One individual lorry with two 38 m^3 containers with approximately 18–20 t of wood cannot compete against the specific costs of large-scale technology, for example of lorries, with 7,000 t of oil or huge conveyor lines from the nearby open-top mining with almost 1,000 t/h of lignite. Long transport distances therefore are generally economically conceivable for energy sources with a high-energy density and good-handling properties (e.g., oil, hard coal). This however also applies to wood pellets.

Technical Solutions

The coal boilers available in Berlin/Germany are designed as dust-firing systems. A fast and fully combustion of the coal dust particles is achieved with the coal grinded to dust. The wood co-combusted within this boiler needs to be of appropriately small size, which places increased requirements to wood processing compared to grate firing.

In order to meet this requirement with respect to the size of the woodchips, a two-stage strategy is pursued for the three coal-fired combined heat and power plants used and/or designed for co-combustion. The wood is initially shredded to approximately 40 mm delivery size, and then there is another grinding process to lengths of several millimeters within the particular hammer mills of the power plants.

For this technology of joint milling of the coal–woodchips mixture, the grinding and feeding into the boiler is the main problem of the co-combustion within these power plants. The reason lies in the different fuel properties of hard coal and wood.

- On the one hand, wood has a significantly larger volume relating to the calorific value compared to hard coal. The result is that the amount of wood is limited which maximally can be conveyed through the coal mills. For a proportion of 5% of the thermal boiler capacity, the total fuel volume increases by up to 30–40%.
- On the other hand, the proportion of moisture and volatile substances in wood is larger than in hard coal. The larger content of moisture requires more

intense drying of the mixture and leads to higher flue gas losses. In addition, for the co-combustion of wood, there is an increased risk that the wood components will already ignite before they enter into the mill due to the higher content of volatile matters. There also is an increased risk of slagging in the combustion chamber due to the lower melting point of the wood ash, which at least in the slag-tap furnace of one of the Berlin power plant is beneficial for the slag removal from the boiler.

These issues shown here were tested in the Reuter C hard-coal power plant in several test series with an electric capacity rating of 132 MW, and technical solutions were found for the co-combustion of wood (e. g., by a reduction of the sifter temperatures in front of the mills).

An addition, the effects of co-combustion of wood of up to 5% of the fuel heat for the efficiency of the boiler in Reuter C has been examined. A maximum loss of efficiency of 0.25% has been measured for wood with a moisture content of 50%. This however can be assessed as very low.

Due to the longer holding times of the fuel in fluidized bed systems, higher co-combustion rates than 5% of wood are possible there. A direct supply of the wood into the boiler, i.e., no longer via the hammer mills, can here open up new dimensions for the co-combustion of wood.

Economic Efficiency

The economic efficiency of the co-combustion of wood is mainly influenced by the price of wood as a fuel, the price of the coal replaced by the wood and the costs for the CO_2 certificates as well as the additional investment costs and operating costs for the co-combustion of wood. The main cost factor of the co-combustion in this process is the costs for the fuel itself. These costs roughly are broken down into the actual price of wood as well as the shredder and transport costs. For preferential use of wood from landscape conservation from the close vicinity, the prices of wood and transport accordingly are moderate, and the highest costs result from the mobile shredder equipment on location. These shredder costs however can be reduced to approximately two thirds with stationary electric shredders; for economic reasons, however, a fixed location and larger quantities of wood is required.

The other important economic parameters such as the market prices for electricity, heat, and the efficiency of the power plant play the important part in the resource planning of the power plant; it is decided here whether it is economically worthwhile to operate of shut off a power plant in a specific market situation. The co-combustion of wood to the amount of 5% of the thermal capacity has only small influence to this. But the economic efficiency of the co-combustion of wood is adversely affected by longer standstill periods of the combined heat and power plants, in particular outside the heating period, because then less wood can be co-combusted.

At the end of 2009, for example, the following circumstance has been observed. The price of hard coal declined to approximately half the price compared to fall 2008. At the same time, the price for CO_2 certificates declined by approxiamtely one quarter compared to the end of 2008. In contrast, the price of wood declined only to a small extent. The forest owners practise retentiveness with felling when the prices for wood are going down and wait for a higher price level. For wood from landscape conservation, however, the price remained stable with slightly reduced shredder and lorry transport costs depending on the oil price. Therefore, the economic situation of the co-combustion of wood in hard-coal fired power plants in Germany changed to the worse in 2009 compared to 2008, but slightly recovered again in the year 2010.

Conclusion

The co-combustion of biomass is an option for a relatively efficient production of electricity out of large quantities of biomass. Against this background, the goal of this paper is it to analyze these options and to examine them by means of a case study. The issues explained can be briefly summarized as follows.

- Basically, a multitude of different types of biomass can be used in existing coal-fired power plants. Recently, quite different technical solutions were realized.
- There should be no basic technical problems as long as the proportion of the biomass used in relation to the coal is small, and this does not significantly change the properties of the coal with regard to combustion.

- Nevertheless, co-combustion of wood in coal-fired power plants requires individual technical solutions depending on the unloading situation, on the type of mill and boiler, as well as on the location of the power plant. Generally, appropriate solutions can be found, as indicated by the development in some European countries in the past years.

All in all, the co-combustion is a technically promising option for the large-scale highly efficient production of electricity from biomass by the substitution of an energy source with relatively high specific greenhouse gas emissions. This efficiency can even be improved by co-combustion in combined heat and power plants.

Bibliography

1. Kaltschmitt M, Hartmann H, Hofbauer H (2009) Energie aus Biomasse, 2. Auflage. Springer, Berlin
2. (June 2009) Bundesministerium für Umwelt, Naturschutz, Reaktorsicherheit. Erneuerbare Energien in Zahlen
3. Spliethoff H (2000) Verbrennung fester Brennstoffe zur Strom und Wärmeerzeugung... Fortschritt-Berichts VDI, Reihe 6, Energietechnik, Nr.443; VDI Verlag
4. Sontow J, Siegle V, Spliethoff H, Kaltschmitt M (1997) Biomassezufeuerung in Kohlekraftwerken. Energiewirtschaftliche Tagesfragen 47 (6):338–344
5. Siegle V, Spliethoff H, Hein KRG (1996) Aufbereitung und Mitverbrennung von Ganzpflanzen mit Steinkohle in einer Staubfeuerung; DGMK-Fachtagung "Energetische und stoffliche Nutzung von Abfällen und nachwachsenden Rohstoffen", Velen/Westfalen
6. Siegle V (2000) Biogene Brennstoffe in Aufbereitung und Verbrennung. Dissertation Universität Stuttgart. Shaker Verlag, Aachen
7. Bauer F (1994) Einsatz von Biobrennstoffen in der Wärmeersatzanlage Lübbenau; DGMK-Fachtagung "Energetische und stoffliche Nutzung von Abfällen und nachwachsenden Rohstoffen", Velen/Westfalen
8. McCann D, Simons HA (1997) Design review of biomass bubbling fluidized bed boilers. 14th International conference on fluidized bed combustion. ASME
9. Spliethoff H, Siegle V, Hein KRG (1996) Erforderliche Eigenschaften holz- und halmgutartiger Biomasse bei einer Zufeuerung in existierenden Kraftwerksanlagen; Tagung "Biomasse als Festbrennstoff – Anforderungen, Einflussmöglichkeiten, Normung", Schriftenreihe "Nachwachsende Rohstoffe" Band 6, Landwirtschaftsverlag, Münster, 155–175
10. Spliethoff H (2000) Verbrennung fester Brennstoffe zur Strom- und Wärmeerzeugung: Verfahren und Stand der Technik – Wirkungsgrad, Betrieb, Emissionen und Reststoffe. VDI Fortschritt-Berichte, Energietechnik, Reihe 6, Nr. 443, VDI-Verlag, Düsseldorf
11. Spliethoff H (1999) Verbrennung fester Brennstoffe zur Strom- und Wärmeerzeugung; Habilitationsschrift, Universität Stuttgart
12. Gerhardt T, Spliethoff H, Hein KRG (1996) Thermische Nutzung von Klärschlämmen in Kraftwerksfeuerungen – Untersuchungen an einer Staubfeuerung im Pilotmaßstab; Entsorgungspraxis 3/1996
13. Bemtgen JM, Hein KRG, Minchener A (1998) Combined combustion of biomass/sewage sludge and coals. Volume II: Final reports, APAS clean coal technology programme, EC, Brüssel
14. Spliethoff H, Hein KRG (1995) Eignung von Kohlenstaubfeuerungen zur Mitverbrennung von Biomasse und Klärschlamm; VDI-Berichte 1193; VDI, Düsseldorf S. 125–133
15. Wieck-Hansen K, Overgaard P et al (2000) Cofiring coal and straw in a 150 MWe power boiler experiences. Biomass Bioenergy 19(6):395–409
16. Wieck-Hansen K, Sander B (2003) 10 Years experience with co-firing straw and coal as main fuels with different types of biomasses in A CFB boiler in Grena, Den-mark. VGB PowerTech 83(10):64–67
17. Zheng Y, Jensen PA et al (2007) Ash transformation during co-firing coal and straw. Fuel 86(7–8):1008–1020
18. Kicherer A (1996) Biomassemitverbrennung in Staubfeuerungen, Technische Möglichkeiten und Schadstoffemissionen; Dissertation, Universität Stuttgart; VDI-Fortschrittsberichte Reihe 6 "Energietechnik", Nr. 344; VDI, Düsseldorf
19. Spliethoff H, Hein KRG (1996) Effect of Co-combustion of biomass on emissions in pulverized fuel furnaces. Conference Biomass usage for utility and industrial Power, Snowbird, USA
20. Gerhardt T, Rebmann M, Spliethoff H, Hein KRG (1995) Untersuchungen zur Mitverbrennung von kommunalen Klärschlämmen in der Kohlenstaubfeuerung; 9. Internationale VGB Konferenz "Forschung in der Kraftwerkstechnik", Essen
21. Hartmann H, Böhm T, Maier L (2000) Naturbelassene biogene Festbrennstoffe – Umweltrelevante Eigenschaften und Einflussmöglichkeiten. Bayerisches Staatsministerium für Landesentwicklung und Umweltfragen (Hrsg.), München, Reihe "Materialien", Nr. 154
22. Tauber C, Klemm J, Schönrok M (1996) Mitverbrennung kommunaler Klärschlämme in Steinkohlekraftwerken - Erfahrungen der PreussenElektra aus einem Langzeitversuch; VDI-Seminar Klärschlammentsorgung II; VDI, Düsseldorf
23. Fahlke J (1996) Spurenelementbilanzierungen bei Steinkohlefeuerungen am Beispiel einer Trocken- und einer Schmelzkammerfeuerung unter Berücksichtigung der Rauchgasreinigungsanlagen; VDI-Fortschrittsberichte Reihe 15 "Umwelttechnik", Nr. 120; VDI, Düsseldorf
24. Wiens U (2005) Neues aus den Regelwerken zur Verwendung von Flugasche in Beton. VGB PowerTech 5(10):73–79
25. Wischnewski R, Werther J, Heidenhof N (2006) Synergy effects of the co-combustion of biomass and sewage sludge with coal

in the CFB combustor of Stadtwerke Duisburg AG. VGB PowerTech 12:63–70
26. Binderup Hansen PF, Lin W, Dam-Johansen K (1997) Chemical reaction conditions in a Danish 80 MWth CFB-Boiler co-firing straw and coal. 14th International conference on fluidized bed combustion, ASME
27. Clausen C, Sorensen M (1997) Anlagen- und Betriebserfahrungen mit strohgefeuerten Kesseln in Heizkraftwerken. VGB Kraftwerkstechnik 77(10):802–806
28. Bemtgen JM, Hein KRG, Minchener A (1998) Combined combustion of biomasssewage sludge and coals. Volume II: Final reports, APAS clean coal technology programme, EC, Brüssel
29. Henriksen N, Larsen OH, Blum R, Inselmann S (1995) High-temperature Corrosion When Co-Firing Coal and Straw in Pulverized Coal Boilers and Circulating Fluidized Bed Boilers; VGB-Konferenz "Korrosion und Korrosionsschutz in der Kraftwerkstechnik", Essen
30. Bierbaum K, Lambertz J, Thomas G (1996) Klärschlamm-Mitverbrennung in einem braunkohlegefeuerten Industriekraftwerk; VDI-Seminar Klärschlammentsorgung II, Bamberg
31. Becker A (2009) "Untersuchung der Auswirkung der Holzmitverbrennung auf den Kesselwirkungsgrad im Heizkraftwerk Reuter" Diploma thesis FH Stralsund

Commercialisation of GM Crops: Comparison of Regulatory Frameworks

Wendy Craig[1], Siva Reddy Vanga[2], Jorge Cabrera Medaglia[3]
[1]Biosafety Unit, International Centre for Genetic Engineering and Biotechnology (ICGEB), Trieste, Italy
[2]ICGEB, Plant Biology: Plant Transformation Group, New Delhi, India
[3]Centre for International Sustainable Development Law, Lead Counsel on Biodiversity and Biosafety, Montreal Canada, University of Costa Rica, San Rafael de Heredia, Costa Rica

Article Outline

Glossary
Definition of the Subject
Introduction
Argentina
Canada
China
India
The Philippines
South Africa
United States of America (USA)
International Obligations Relevant to the Biosafety Frameworks
A Comparative Analysis of Regulatory Processes in All Study Countries
Conclusion and Future Directions
Disclaimer
Bibliography

Glossary

Cartagena protocol on biosafety (CPB) The Cartagena Protocol on Biosafety to the Convention on Biological Diversity is an international agreement which aims to ensure the safe handling, transport, and use of living modified organisms resulting from modern biotechnology that may have adverse effects on biological diversity, taking also into account risks to human health. It was adopted on 29 January 2000 and entered into force on 11 September 2003 (for full text, see http://bch.cbd.int/protocol/text/).

Convention on biological diversity (CBD) The objectives of this Convention are the conservation of biological diversity, the sustainable use of its components, and the fair and equitable sharing of the benefits arising out of the utilization of genetic resources, including by appropriate access to genetic resources and by appropriate transfer of relevant technologies, taking into account all rights over those resources and to technologies, and by appropriate funding (for full text, see http://www.cbd.int/convention/text/).

Convention/protocol/treaty A treaty is an agreement in written form between nation-states (or international agencies, such as the United Nations, that have been given treaty-making capacity by the states that created them) that is intended to establish a relationship governed by International Law. It may be contained in a single instrument or in two or more related instruments such as an exchange of diplomatic notes. Various terms have been used for such an agreement, including treaty, convention, protocol, declaration, charter, covenant, pact, act, statute, exchange of notes, agreement, modus

vivendi ("manner of living" or practical compromise), and understanding. The particular designation does not affect the agreement's legal character.

Genetically modified/genetically engineered/transgenic organisms Organisms, such as plants, animals, and microorganisms (with the exception of human beings), in which the genetic material (DNA) has been altered in such a way that does not occur naturally by mating and/or natural recombination (The terms "genetically modified" (GM), "transgenic," "genetically engineered" (GE), and "living modified" (LM) are used in different legal instruments around the world. It is useful (and deliberate) in this document to essentially use them interchangeably).

Living modified organism (LMO) Any living organism that possesses a novel combination of genetic material obtained through the use of modern biotechnology (according to the CPB).

Modern biotechnology The application of [1] in vitro nucleic acid techniques, including recombinant deoxyribonucleic acid (DNA) and direct introduction of nucleic acid into cells or organelles, or [2] fusion of cells beyond the taxonomic family, that overcome natural physiological reproductive or recombination barriers and that are not techniques used in traditional breeding and selection (according to the CPB).

Definition of the Subject

This contribution describes and compares the regulation of GMOs and the underpinning legislative frameworks in selected countries from around the world. It also includes a description of the relevant international agreements related to biosafety and a description of the main characteristics and attributes of a modern biosafety regulatory framework in this area.

Introduction

The rapid development and deployment of modern biotechnology in the last decades have made biosafety a critical issue. Although modern biotechnology has the potential of benefiting agricultural interests in developing countries as well as overall human welfare, living modified organisms (LMOs) resulting from modern biotechnology or genetically modified organisms (GMOs) remain a source of concern with regard to the conservation and sustainable use of biodiversity, as well as to human health. The perceived risks, which relate to the release of GMOs into the environment as well as the placement of GMOs onto the market, have as much to do with social values as scientific concerns. For example, social concerns may require the labeling of genetically modified (GM) food and feed, the mitigation of socioeconomic impacts, and the demonstrated potential for the co-existence of organic, conventional, and GM farming [1].

Global use of GM crops is growing rapidly, increasing approximately 87-fold from 1996 to 2010 to 148 million hectares under cultivation by 15.4 million farmers in 29 different countries [2]. Furthermore, the estimated value of the global GM crop market in 2010 grew to US$11.2 billion, while the value of harvested products was estimated at US$150 billion [2]. Although the majority (52%) of GM crops are still grown in industrialized countries, developing countries are rapidly approaching parity and, due to their high rates of adoption, are soon expected to grow the majority of GM crops [2]. By 2009, the major biotech crops had achieved high levels of market penetration: 77% of soybean, 49% of cotton, 26% of maize, and 21% of oilseed rape grown globally in 2009 were GM varieties [3].

Despite expected high benefit-cost ratios from biotechnology, only a few developing countries, such as Brazil and Argentina, have had high uptake rates (over 20 million hectares) [2] of GM crops, with uptake typically concentrated in crops that are exported to developed country markets. Few others (mainly India and China) have started exploring their own national research capability in biotechnology. In the vast majority of developing countries, both investment in biotechnology research and development and the transfer to farmers of transgenic crops already being marketed have been generally low. This in part reflects a lack of transparent regulatory capacity necessary in dealing with risks associated with biotechnology as well as in addressing the issues of property rights development and protection that are essential to promoting innovative research. This is particularly important because of the high cost of undertaking the initial research and development in biotechnology [4].

As GM technologies are very recent and fast developing, most governments are trying to keep pace by developing regulatory policies that reflect consumer demands and preferences affecting GM agricultural products. Almost all developed countries require products derived from GM sources to be assessed both for their safety as foods and for their environmental impacts. However, there are considerable differences in the approaches taken by different countries. In the United States, analysis and approval mechanisms for GM foods have been subsumed into existing regulations governing the release of new foods, plants, and pesticides, whereas in the European Union, regulation of GM products requires considerable separate scrutiny (see chapter "► Commercialisation of GM Crops: Comparison of Regulatory Frameworks" by Devos et al.). Countries worldwide are in different stages of policy development, with the majority of the developing countries still in the infant stage [4]. In setting up domestic legislation, developing countries seem to be paying increasing attention to international trade concerns [5].

India along with Argentina, South Africa, and others constitute a group of developing countries that aspire to develop domestic biotechnology through national public R&D and/or by creating incentives for the participation of multinationals as sources of technology. They each have relatively liberal regulations as well as more explicit regulatory institutional arrangements [6]. Those developing countries with well-developed public agricultural research and extension systems (such as India) are well placed to benefit promptly from the new biotechnology by working in partnership or in parallel with private biotechnology and seed companies. Approving investments in those activities by the private sector – and the overall investment climate – will allow the process of adaptation and adoption to move forward. The experiences in India, China, and South Africa all indicate that rapid and widespread adoption is then possible, including by small farmers [7].

The biosafety frameworks of the described countries were selected based, primarily, on considering the following criteria: level of production and commercialization of GMOs, investments made and political commitment with the research and development particularly in the field of GMOs, regional leadership in the adoption of GMOs and in the elaboration and implementation of biosafety legal frameworks, and the existence of a functional biosafety framework in place.

Argentina

Argentina is a major producer of agricultural products and the third largest producer of soybeans. Initially, the harvested area of soybean was 36,000 ha (59,000 mt) in 1970, increasing to 5.98 million hectares in 1995/1996 (12.43 mmt). The country has historically been the earliest and most aggressive adopter of GM crops in Latin America, first planting glyphosate-tolerant soybeans in 1996, which sparked a further expansion of soy production and which is now in excess of 14 million hectares, of which at least 98% is GM [8]. This rate of adoption is far higher, and much faster, than that in the USA, which was the first country to introduce this technology [9]. In addition, Argentina also grows significant quantities of GM corn (Bt and glufosinate ammonium tolerant) and Bt cotton, comprising 40% and 20% of overall production in 2009 for these two crops, respectively [3, 10]. Available estimates place accumulated benefits (extra income which would have not been generated in the absence of the technology) until the year 2001/2002 at approximately US$5.2 billion in the case of soybeans, about US$400 million for Bt maize, and approximately US$40 million for Bt cotton [7]. Argentina is now third only to the United States and Brazil in terms of the area planted with transgenic crops (22.9 million hectares) [2] and is thus a very important player in the international arena. Notably, Argentina signed, but has yet to ratify, the Cartagena Protocol on Biosafety (CPB, hereinafter referred to as "the Protocol") of the Convention of Biological Diversity in May 2000. Argentina is currently undergoing a consultation process, analyzing and debating with all the involved sectors the position the country will take in this respect [8].

Regulatory Oversight in Argentina

Argentina was one of the first countries to establish a system of regulatory oversight for GMOs [11]. It has instituted regulatory measures for the safe development and application of biotechnology in general and GMOs in particular. It chose to develop the policy on biosafety within the context of trade-related

issues [12] and as such has policies, procedures, and institutional arrangements to regulate the development, importation, and export of GMO products. The Argentine biosafety system is based on guidelines, not on legislation. Argentina's legislative framework for regulating GMOs is based on the existing agricultural regulatory system (e.g., for plant protection chemicals) supplemented with GM crop-specific regulations established to specify conditions for environmental release or to assess food safety. The non-statutory guidelines include standards for facilities and practices designed to prevent the unintended release of a GMO, conditions of isolation, monitoring field trials, and standards for risk assessment for conducting the environmental release. This approach gives the system flexibility and allows for changes needed to keep up with scientific advances. One disadvantage, however, is that compliance with guidelines is not legally enforceable; there is no way to prosecute offenders in the rare cases of non-compliance that have occurred [13].

Similar to the USA and Canada (see below), Argentine biosafety regulation follows a product-based approach which results in several agencies, all within the Agriculture Directorate of the Secretariat of Agriculture, Livestock, Fisheries and Food (SAGPyA), mandated to regulate GM crops and products. The National Advisory Commission on Agricultural Biotechnology (CONABIA) is the lead agency in charge of regulating GM crops and was established in 1991 by Resolution 124/91 (later expanded by Resolution 669/93) of the SAGPyA to provide advice and oversee the implementation of biosafety regulations [14]. CONABIA's jurisdiction and procedures were established in Resolutions 656/92, 837/93, and 289/97 (later replaced with 39/03) [13]. Resolution 39/03 is part of the general regulatory system governing the existing agricultural regulations in Argentina related to plant protection (Decree-Law of Agricultural Production Health Defense 6704/66 and its amendments), seed and phytogenetic creations (Seed and Phytogenetic Creations Law 20.247/73 and its regulatory decree), and animal health (Law of Veterinarian Products, and Supervision of Creation and Commercialisation 13.636/49).

CONABIA is a multidisciplinary and inter-institutional organization with advisory duties and comprises representatives from the public sector, academia, and private sector organizations related to agricultural biotechnology. Its main responsibility is to assess the potential environmental impact of the introduction of GMOs in Argentine agriculture [8]. The Commission handles applications for laboratory and greenhouse testing, field trials, and governs the "flexibility status" of release conditions (unconfined release, usually large-scale, for regulatory purposes or off-season seed multiplication) of GM plants [13]. Resolution 60/2007 provides a differentiated treatment for the authorization of the breeding of parental material which contains transgenic events already approved for commercialization. Furthermore, it advises SAGPyA on the issuance of necessary licenses and authorizations for experimentation and/or environmental release of GM microorganisms, as well as GMO-derived or GMO-containing products (although the final decision is made by SAGPyA) [6]. In order to obtain the appropriate marketing license, varieties must also comply with requirements stipulated by the National Service of Health and Agrofood Quality (SENASA) [15]. SENASA's jurisdiction concerning the oversight of GMO-derived food was established in Resolution 289/87, while Resolution 511/98 including Annexes established the food-safety review criteria [13]. The latter was based on FAO and WHO documents, as well as on relevant regulations from Australia, Canada, the EU, Japan, and the US, but has since been replaced by Resolution 412/2002.

A key part of the GMO regulatory process consists of verifying that the commercial approval will not have a negative impact on Argentina's foreign trade. This specific assessment is carried out under Resolution 39/03 by the National Bureau of Agrifood Markets (NBMA), and it includes an analysis of the current status of regulatory systems and public acceptance in the importing countries. The National Seed Institute (ex-INASE) is responsible for ensuring that all the necessary requirements for registration in the National Registry of Cultivars have been established. Ex-INASE plays a further role in the biosafety system by receiving and logging applications for GMO field trials. Applications containing confidential business information are kept secure at INASE's offices. Agency personnel perform field test site inspections, checking for compliance with the biosafety requirements set by CONABIA [13].

During 2001, the SAGPyA actively cooperated with members of the Argentine Congress in drafting

a biosafety law. This draft represented a major improvement on the current situation, since it clearly set forth a conceptual framework, as well as issues and instances to be considered as participants in risk analysis procedures. But due to the institutional and economic crisis that broke out on December 2001, the draft was never discussed in Congress, and there is no evidence that it will be discussed in the near future [8].

Commercialization of GM Crops: Argentine Approval Process

When an organization intends to obtain an authorization for commercialization of a GM crop in Argentina, it has to pass reviews by the three regulatory agencies. Briefly, CONABIA should determine that the environmental impact of the large-scale release of the GM crop will not significantly differ from that of its non-modified counterpart; SENASA's Technical Advisory Committee on the Use of GMOs should determine that the derived foods are safe for human and animal consumption, and the DNMA should determine that the release will not have an undesired impact on the country's international trade [16].

The prerequisite for entering the commercial evaluation process is that authorizations for experimentation and/or release into the environment of the specific GM crop have been previously granted [16]. After at least one release into the environment has been approved and the safety of the GM crop has been demonstrated, the applicant can apply for a "flexibilization" permit which allows future releases by simply providing notification of the location, area, sowing date, and intended harvest date [11]. Flexibility status conditions are granted for the following purposes [13]:

- For providing testing material
- For export
- For off-season seed multiplication (not for use in Argentina)
- For tests, which need to be presented at later stage (e.g., variety registration)
- For pre-commercial seed multiplication for a pending variety registration

The deregulation of field testing conditions is dependent on the results of the biosafety assessment conducted by CONABIA with regard to the criteria laid down in Resolution 131/98. These include the characterization of the GMO (recipient organism, genetic modification, insert, donor organisms, phenotypic characterization, potential environmental interactions of GMO) and the impacts expected from the production of the GM crop at commercial scale (environmental effects and impact on human health) [16]. If SAGPyA, on the recommendation of CONABIA, authorizes "flexibility status" release conditions for the GM crop in question, the applicant only needs to submit information on the area to be sown, the date of sowing, the site of release and the harvest date [16]. The flexibility status of a GM crop allows large-scale planting, but not planting for commercial purpose.

The second step to commercialization is the evaluation of the safety of the GM crop for human consumption and feed. This evaluation is carried out by SENASA under Resolution 412/2002 [17]. In the third step of the commercialization process, the NBMA assesses the impact of the GM crop in question on export market security. It does this by analyzing the status (if any) of the specific event in the destination markets and, as a result, whether the addition of this event to Argentina's export supply might represent a potential barrier to the access to these markets.

After completion of all of the steps mentioned above, CONABIA's Office of Technical Coordination compiles all pertinent information and prepares a "Project of Resolution" on the basis of its own, SENASA's, and DNMA's assessments and submits it to the SAGPyA, which takes the final decision on approval or denial of the commercialization request [13]. Should the GM crop be authorized for open cultivation, it must also be registered in the National Registry of Cultivars, a process overseen by ex-INASE. For those GM crops expressing either herbicide tolerance or insect resistance, they require a pesticide approval from SENASA prior to their commercial use [13].

Canada

Regulatory Oversight in Canada

In line with a similar approach adopted in the United States (see below), the regulatory framework established in Canada is based on the extension of the existing regulations to GMOs [18]. However, in

contrast to all other countries, Canada relies on the concept of novelty to trigger regulatory oversight, thereby enabling the regulation of a wider array of novel seeds or food [19], and includes those produced by conventional breeding, mutagenesis, or rDNA techniques. Directive 94–08, first published in 1994, defines these as "plants containing traits not present in plants of the same species already existing as a stable population" [20].

The Canadian Environmental Protection Act (CEPA) of 1988 formally recognizes biotechnology as a manufacturing process for products potentially posing environmental risks, and therefore, the act requires environmental assessments. CEPA, however, embraces a product-based approach to biotechnology, an approach explicitly defined in the 1993 Regulatory Framework for Biotechnology [21]. In accordance with this framework, policy-makers proceeded to the amendment of a series of regulations (below) contiguous to the laws governing the products of biotechnology. These amendments were mostly aimed at inscribing a trigger (the novelty of the trait) launching the risk evaluation process for the products of biotechnology.

The Canadian approach is based on an agreement between the Canadian Federal agencies in 1993 that was renewed in 1998. The responsibility for regulating plants with novel traits (PNTs), including GM plants, is shared between the Canadian Food Inspection Agency (CFIA) and Health Canada [18]. The CFIA operates under the authority of the Seed Act, the Plant Protection Act, the Feeds Act, the Fertilizer Act, and the Health of Animals Act. It also shares some responsibilities with Environment Canada under the Canadian Environmental Protection Act, and with Health Canada under the Pest Control Products Act, and the Food and Drugs Act. The Canadian Environmental Protection Act is an umbrella legislation intended to serve as a regulatory "safety net" for any biotechnological products not currently regulated by another federal act. The Department of Fisheries and Oceans regulates aquatic organisms under the Fisheries Act.

In 1997, the CFIA took over the risk management of novel seeds and feeds from Agriculture and Agri-food Canada. The agency regulates novel plants following assessment criteria provided by Directive 94–08. In particular, the CFIA is responsible for the regulations and guidelines dealing with cultivating PNTs, assessing their impact on the environment and biodiversity. Canadian authorities state that "all plants derived through genetic engineering have been considered novel, and as such have undergone a full, comprehensive, and rigorous safety assessment prior to release into the environment" [22]. In addition, the agency is also in charge of ensuring livestock feed safety, along with the responsibility for the regulation of seeds, veterinary biologics, and fertilizers. Furthermore, the CFIA develops standards related to the packaging, labeling, and advertising of foods and handles all inspection and enforcement duties [23].

Many GM crops are destined, in whole or in specific parts, for the human food supply system. For this reason, they must not only obtain CFIA approval but must also be assessed by Health Canada. It is within the jurisdiction of Health Canada to regulate GM foods according to the Food and Drugs Act under Division 28 of Part B of Food and Drug Regulations (Novel Food). As with seeds, the trigger for pre-market safety assessments is novelty, and as such, Health Canada treats as novel food all those derived from GMOs "whether it is a micro-organism, a plant or an animal, such that it exhibits characteristics that were not previously observed, no longer fall within the anticipated range or no longer exhibits characteristics that were previously observed, for that plant, animal or micro-organism" [23].

Environment Canada is only responsible for the environmental assessment of GMOs used in industrial processes. Although the Canadian Environmental Act requires environmental risk assessments for GMOs, the responsibility for conducting assessments relevant to novel plants, feeds, and food rests with the CFIA, PMRA, and Health Canada. Notably, CFIA, as the agency most involved in the environmental risk assessment of GMOs, is the responsibility of the agriculture minister whose mandate is to promote agricultural development.

Commercialization of GM Crops: Canadian Approval Process

Before crops with novel traits may be authorized for unconfined release, they must be fully assessed for environmental safety by the CFIA. In meeting the

extensive information requirements for these applications to the CFIA, applicants will have conducted experiments at the earlier confined release stage. These experiments are expected to contribute scientifically robust data to address the key criteria of environmental safety assessments. The applicant is required to provide the Plant Biosafety Office (PBO) at the CFIA with extensive high-quality, statistically sound data and/or valid scientific rationale to demonstrate the environmental safety of the PNT. This information initiates a review and decision for authorization of the release. CFIA officials also use pertinent information generated from the Agency's own research, either conducted in-house or contracted out, on specific key environmental areas [18].

The unconfined release assessment by the PBO focuses on real or potential interactions of the PNTs with the wider agricultural and ecological environment, using "substantial equivalence" as the basis for these assessments. Evaluations consider the unique combination of species and traits, using standard descriptions of each species known as biology documents as a baseline for comparison. If the PBO concludes that there is minimal potential for significant negative environmental impact of the PNT relative to its unmodified counterpart, an unconfined environmental release may be authorized. In some cases, the PBO may authorize an unconfined release with conditions, such as a requirement that the applicant ensures that users of an insect-resistant PNT deploy methods to delay development of resistance among insect populations. Note that for species that may be used for food or feed, developers of PNTs must also seek approvals from Health Canada for human food use and from the CFIA Feed Section for livestock feed use [19]. The starting point for the safety assessment of novel foods is also based on "substantial equivalence," where the novel food is evaluated relative to conventional counterparts that have a history of safe use [23]. Health Canada has 45 days to decide whether the product is safe or to request additional information to pursue the risk analysis, even to the extent of involving experiments [23].

All imported PNTs (or products derived from them) require a prior import permit, being subject to the CFIA regulatory review under the Plant Protection Act and Regulations. Pest risk assessments (PRAs) are conducted by the Plant Health Division in order to evaluate the potential capability of PNTs to pose a pest risk to the agricultural and forestry environment. Those commodities determined not to pose a plant pest risk are now no longer required to have an import permit. Additional exempted commodities include: PNTs with prior approval; PNTs (or products derived from them) that are incapable of sexual or asexual propagation, i.e., have been processed in some way to render them non-viable, such as by grinding or freezing; and plants further developed from exempted PNTs, or considered substantially equivalent to them provided that the intended use is similar, and that the plants do not display any additional novel traits, do not contain novel genetic elements, and have not been subject to inter-specific breeding [24].

China

China has become one of the Asian leaders in biotechnology and has dedicated substantial economic, scientific, and technological resources to R&D. Since the 1980s, ministries and relevant government agencies in China have been investing significantly in agro-biotechnology research and have established more than 150 laboratories, resulting in the largest plant biotechnology capacity outside of North America [25]. The government has allocated research budgets to biosafety and management, and nearly all biotechnology research programs have expanded their scope into biosafety issues [5]. The commitment to sustain biosafety after project closure is demonstrated by its growing budget to support agricultural research in biosafety over the last few years. From an initial budget of slightly over US$ 80,000 in 1999, China now spends about US$ 3 million annually on agricultural biosafety-related activities [10].

A wide variety of crops and traits has passed through China's biosafety system and are now planted commercially, while many others remain at the field trial stage, including many varieties with adaptation-related traits developed by Chinese institutes and companies [26]. In contrast to the other countries described in this chapter, most of these crops have been developed predominantly by public sector laboratories in China. The biosafety regulatory system in China has also reviewed a large number of applications since it

was formally set up in the late 1990s. The government received 1,044 applications for field trials or commercial release, and 777 of these were approved [27, 28]. These applications predominantly covered 60 crops, as well as several animals and a large number of microorganisms [28]. Varieties of cotton, tomatoes, phytase maize, insect-resistant rice, and sweet and chili peppers have all been approved for commercial planting [3].

Regulatory Oversight in China

China has adopted a policy that promotes research and development of biotechnology, while at the same time, retaining control over research in genetic engineering. In the early 1990s, China had already implemented a very pragmatic approach to GM crop regulation. Regulations were basically product-based with special attention given to the economic interest of a given application. By 1993, China had already established its first biosafety regulation, namely the "Safety Administration Regulation on Genetic Engineering" issued by the Ministry of Science and Technology (MOST). This instrument required relevant ministries to draft and issue corresponding biosafety regulations on biological engineering (i.e., the Ministry of Agriculture (MOA) for agriculture and the Ministry of Public Health for food safety) and established general principles, safety categories, risk assessment and risk management procedures, application and approval mechanisms, and legal responsibilities [29]. It was followed in 1996 with the "Safety Administration Implementation Regulation on Agricultural Biological Genetic Engineering" by the MOA [12]. This was an explicit regulatory regime for the risk assessment and management of agricultural products of genetic engineering. Labeling was not part of this regulation, nor was any restriction imposed on imports or exports of GM products. The regulation did control GMOs for research and commercial production, as well as establishing the National Agricultural GMO Biosafety Committee (Biosafety Committee) to provide the MOA with expert advice on biosafety regulations.

Criticism of GM crops on environmental, food-safety, and ethical grounds, however, led to some significant changes in the Chinese legal framework on agro-biotechnology [5]. In 2001, the State Council decreed a new and general rule on biosafety, with the aim of protecting human, animal, and plant health and the environment. This new "Regulations on Safety of Agricultural Genetically Modified Organisms" replaced the 1993 Regulation issued by MOST. The 2001 regulations provide the MOA with overall national authority to oversee the use of GM crops, whereas the 31 provincial biosafety management offices are responsible for the supervision and administration of biosafety in their respective areas [30]. The 2001 regulations meet the generally accepted risk assessment procedures outlined in the relevant international instruments and also stipulate a comparative risk assessment approach, in which a GM crop is compared with the corresponding non-transgenic crop for environmental/ecological safety and food safety.

To implement this Regulation, the MOA issued three implementation regulations including Implementation Regulations on Safety Assessment of Agricultural Genetically Modified Organisms, which provided the legal basis and technical guidelines in GM crops risk assessment in China [31]. These new regulations primarily concerned Biosafety Evaluation, Import Safety, and Labeling and included several important changes to existing procedures and details of regulatory responsibilities after commercialization. The changes included an extra pre-production trial stage prior to commercial approval, new processing regulations for GM products, labeling requirements for marketing, new export and import regulations for GMOs and GMO products, and local and provincial-level GMO monitoring guidelines [29]. Specifically, the Regulation on Biosafety Evaluation establishes procedures for handling applications for GM cultivation and sets up an advisory body, the National Biosafety Committee (NBC), and a decision-making body, the Office of Agricultural Genetic Engineering Biosafety Administration (OGEBA), under the MOA to handle applications. Applicants must provide information on risk assessment, and GMOs are classified into four classes depending on their potential danger to human and animal health and to the environment. The Regulation establishes the requirements that should be met to obtain authorization to import GMOs and will vary according to the intended purposes of the imports, i.e., research, release into the environment, or processing. In response to representations from GM-producing countries, China agreed to allow trade to continue as

normal until the new Regulation on Safety of Imports entered into force on 20 April 2004 [32, 34]. The Ministry of Public Health (MPH) is responsible for food-safety management of biotechnology products (processed products based on GMOs) and promulgated its first regulation on GMO food safety in April 2002, to take effect after July 2002.

China's policy on GM regulation is now under the responsibility of an agency which was established by the State Council, the name of which has been variously reported as either the Joint Monitoring and Management Commission [12] or the Allied Ministerial Meeting [29]. It has a multi-stakeholder membership comprising the highest representatives from ministries like Agriculture, Health, Commerce, Science and Technology, the National Development and Reform Commission, the National Inspection and Quarantine Agency, and the State Environmental Protection Administration. It is responsible for the coordination of key issues related to the biosafety of agricultural GMOs, the examination and approval of the applications for GMO commercialization, determining the list of GMOs for labeling, and establishing import or export policies for agricultural GMOs and their products. In addition, under the new regulation, foreign investment in biotechnology has been prohibited [5].

The NBC remains the major player in the process of biosafety management. Currently, the NBC is composed of 56 members who come from different administrative departments, academic institutions, etc. They are experts in biological research, production, processing, inspection and quarantine, public health, and environmental protection with respect to agricultural GMOs [31]. The committee meets twice each year to evaluate all biosafety assessment applications related to experimental research, field trials, environmental release, pre-production trials, and commercialization of agricultural GMOs. It makes recommendations to the OGEBA based on the results of its biosafety assessments. OGEBA is responsible for the final approval of decisions, as well as handling routine work and daily operations [29]. In 2005, all 31 provinces in China established biosafety management offices. These biosafety management offices collect local statistics on and monitor the performance of research and commercialization of agricultural biotechnology in their provinces and assess and approve (or disapprove) all applications of GM-related research, field trials, and commercialization in their provinces. Only those cases that are approved by provincial biosafety management offices are submitted to the NBC for further assessment [29].

In May 2007, the National Development and Reform Commission in China announced that it had approved the establishment of a National Biosafety Research Centre. To be completed by 2009, the Centre will manage agricultural and biological-related issues. It is to house several research departments, including laboratories for high-risk plant pathogens, insects, and plants, as well as units for agriculture-related information analysis and quarantine facilities. The Centre will be supervised by the Plant Protection Institute of the Chinese Academy of Agricultural Sciences.

In 2009, a major development in China was the commercialization of transgenic Bt rice, which reached pre-production trials but was still pending final commercialization approval for several years. Influenced in part by opposition to the technology in Europe and to some extent Japan, the final approval of many crops stalled at the level of China's inter-ministerial committee even as research and field trials continued apace. The discovery by Greenpeace that some transgenic seed was planted by farmers without authorization caused international debates about China's biosafety system and may have contributed to regulatory approval delays [33].

Commercialization of GM Crops: Chinese Approval System

If the product is for cultivation, applications must be authorized before the first import of a specific GMO can take place and must be accompanied by a safety assessment carried out in the country of origin of the GM material [5]. For permanent approval of each imported GM product, compulsory field trials are carried out in China in order to re-assess safety within the Chinese context [35]. Generally, the practice in China is to use a comparative risk assessment approach, in which the transgenic crop is compared with the corresponding non-transgenic crop in ecological risk assessment and hazard identification in transgenic foods [36, 37]. Although there are no official guidelines in China for risk assessment on food derived from transgenic crops, the assessments carried out so far on

nutrition, toxicity, and allergenicity generally followed the relevant Codex principles and guidelines [31].

In China, agricultural GMOs also need to satisfy the procedures governing the release of new seed varieties. These procedures are governed by the Seed Law in China. Only agricultural GMOs that have previously obtained a biosafety certificate are eligible to be classified as a new seed variety in accordance with the Seed Law and relevant regulations. After the GMO has passed seed variety testing and received the permission for production, it is eligible to enter into the chain of production and marketing [31].

India

In India, a wide variety of crops have been field trialed, but most have not yet been commercialized. The first approval for the commercial production of any GM crop in India occurred in March 2002 when the Indian competent authority approved three varieties of *Bacillus thuringiensis* (Bt) cotton (MECH 12, MECH 162, and MECH 184 expressing the *cry1Ac* gene for insect resistance) amid widespread protests by anti-GM activists. This was followed by a significant increase in the availability of Bt cotton (currently 809 hybrid varieties) [38] better suited to Indian cultivation. By 2003, more than 34 genes were being tested in a wide variety of crops, including cotton, rice, mustard, maize, potatoes, eggplant, tomatoes, pigeon pea, and cabbage [29]. Most of the varieties initially introduced included insect-resistant cotton varieties as well as some crops modified with herbicide tolerance. Several Bt crop varieties have passed through the field trial stage and have received approval for commercial planting. The primary technology used in India originated in the Monsanto Company, which partnered with Maharashtra Hybrids Company (MAHYCO) to develop transgenic hybrid Bt cotton for sale in India. Once some Bt varieties had been approved for commercial planting, it was discovered that 800,000 ha of unapproved BT cotton had been planted, weakening confidence in the biosafety system [29]. The latest GM crop awaiting regulatory approval for commercial release is Bt brinjal (known also as aubergine or eggplant), which received positive assessments by the regulatory bodies based on years of field trials [3] but was refused authorization by the Environment Minister at the last stage of the commercialization process.

Regulatory Oversight in India

With the signing of the CPB in 2001, India became committed to introducing structures and procedures commensurate with the conditions laid down in the CPB agreement – one of the main guiding principles for India when dealing with products derived from agricultural biotechnology. This commitment provided India with the incentive to strengthen its biosafety capacity and have relevant institutional mechanisms at hand to enable the proficient dealing of GMOs. As the CPB places due importance to national legislations, provided it is developed in accordance with the former, the existing domestic policy on GMOs was required to be fine-tuned and amended wherever necessary. The goal of the Indian regulatory system is therefore to ensure that their GM crops pose no major risk to food safety, environmental safety, or agricultural production and that there are no adverse economic impacts on farmers [29]. As such, the Government of India has adopted a policy of careful assessment of the benefits and risks of GMOs at various stages of their development and field release to ensure biosafety [39].

The existing regulatory framework takes the form of rules and guidelines and is based upon three specific provisions of the Environment Protection Act of 1986 (EPA). These are sections 6, 8, and 25. While Section 6 of the Act empowers the Central Government to make rules on procedures, safeguards, prohibition, and restrictions for handling of hazardous substances, Section 8 of the Act prohibits a person from handling hazardous substances, except in accordance with procedures and after complying with safeguards. Section 25 of the EPA empowers the Central Government to lay down rules regarding procedures and safeguards for handling hazardous substances. Thus, the biosafety rules in India are statutory in nature as they originate from the EPA. These provisions of the EPA led to the adoption of the 1989 Rules for the Manufacture, Use, Import, Export and Storage of Hazardous Micro organisms Genetically Engineered Organisms or Cells ("1989 Rules") [39, 40].

In 1994, the Department of Biotechnology revised its earlier guidelines of 1990, entitled "Revised Guidelines for Safety in Biotechnology." These revised guidelines aimed at regulating large-scale production and the

deliberate release of GMOs, plants, animals, and products into the environment and shipment and importation of GMOs for laboratory research [6]. By 2002, an array of legislation likely to impact biosafety regulations had come into existence. This included the National Biodiversity Act 2002 (NBA) and the Protection of Plant Varieties and Farmers' Rights Act 2001 (PPVFR), the latter of which derived from a broad-based consultation with a view to incorporate a form of farmers' rights into the national plant variety rights legislation. The biosafety rules have since been supplemented by the Biotechnology Safety Guidelines issued by the Department of Biotechnology (DBT). These guidelines have been issued in pursuance of Rule 4[2] of the Biosafety Rules, which require manuals of guidelines to be brought out by the Review Committee on Genetic Manipulation [40].

Therefore, the Indian biosafety regulatory framework, comprising the 1989 Rules and the 1990, 1994, and 1998 DBT guidelines, covers the entire spectrum of activities relating to GMOs. This includes "research involving GMOs, as well as genetic transformations of green plants, recombinant DNA (rDNA) technology in vaccine development, and large-scale production and deliberate/accidental release into the environment of organisms, plants, animals and products derived from rDNA technology." Production facilities such as distilleries and tanneries that use GMOs are also covered. In India, the risk assessment and regulatory approval for releases of GMOs and GM products are mandatory. The concept of "biosafety" used in the regulations is a broad one, covering the health safety of humans and livestock, environmental safety (ecology and biodiversity), and economic impact. The first two safety aspects dominate the regulations, while economic impact is given less prominence.

Two nodal agencies, the Ministry of Environment and Forests (MoEF) and the DBT at the Ministry of Science and Technology, are responsible for the implementation of the regulations [39]. The life cycle of a GM product features four domains, pre-research, research, release, and post-release, and is characterized by the presence of six competent authorities [41, 42]. The Recombinant DNA Advisory Committee (RDAC) is in the pre-research domain as it triggers research through its initial approval mechanisms. The Review Committee on Genetic Manipulation (RCGM) resides in the DBT and functions in the research domain, closely monitoring the process of research and experimental releases. It requests food biosafety, environmental impact, and agronomic data from applicants who wish to do research or conduct field trials and will give permits to import GM material for research. Pursuant to Rule 4 [2] of the 1989 "Rules," the RCGM is also required to produce manuals of guidelines. The RCGM is primarily made up of scientists (including agricultural scientists) and can request people with specialized knowledge to review cases. It has a Monitoring cum Evaluation Committee (MEC) that monitors limited and large-scale field trials of GM crops and is primarily made up of agricultural scientists. Commercial production of GM crops, large-scale field trials of GM crops, and the imports of GM commercial products and GM-derived products (e.g., foodstuffs, ingredients in foodstuffs, and additives including processing aids containing or consisting of GMOs) come under the authority of the Genetic Engineering Approval Committee (GEAC) at the MoEF. The committee members are primarily bureaucrats representing different ministries, and they draw on the scientific expertise of each ministry. Additional to these national committees are the State Biotechnology Coordination Committee (SBCC) and the District Level Biotechnology Committee (DLC), who, along with the MEC, basically occupy the post-release domain, although they also contribute to the research domain activities through data provisioning to the RCGM. Completing the regulatory apparatus are the Institutional Biosafety Committees (IBSC) which undertake the monitoring and implementation of safeguards at the R&D sites, under the close supervision of the RCGM, the SBCC, and the DLC. IBSCs must be established in any public or private institute using rDNA in their research and comprise scientists from their respective institutes and a member from the DBT. There are more than 230 IBCs in India, of which 70 deal with agricultural biotechnology. They can approve contained research at institutes unless the research uses a particularly hazardous gene or technique which will require specific approval from the RCGM [29]. In general, these authorities are vested with non-overlapping responsibilities [39, 43].

Under the Constitution of India, it is not the central Government of India but the state governments that

exercise formal authority over agriculture. Thus, while the national government may take the initiative in the policy arena and formulate policies concerning agricultural biotechnology and GM crops (in R&D as well as commercialization), as well as being where the decision-making process resides, the agreement and active cooperation of state governments are indispensable for their implementation [44].

The multitude of rules and regulations underline the complexities involved in biosafety as it cuts across ministries and agencies and does not merely govern environmental issues. Most of these regulations deal with GMOs in seclusion without referring to a common agency or secretariat to deal with the risks that are associated with the organism [46], resulting in the biosafety regulations being subjected to criticism both by industry and civil society groups. While industry associations consider these regulations as affecting their growth, civil society groups consider biosafety regulations as not being strong enough to check the introduction of potentially harmful biotechnology products. Since 2004, there have been serious discussions in India on re-engineering the structure of biosafety regulations. The primary objective of the exercise is to cut down red tape and ensure greater transparency in decision-making. Calls have come for the replacement of the present regulatory system (with its dispersed, unclear, and confusing mandates; responsibilities; and powers) by a new, single, integrated, and professionally led authority, the National Biotechnology Regulatory Authority (NBRA), with a comprehensive mandate and a wide range of responsibilities, with the power to implement the regulatory regime with speed and efficiency [40, 44] and to help the assessment of risks and benefits associated with GM crops in a credible and transparent manner [47]. In May 2007, it was announced that the NBRA will be fully functional in 2 years time and will be administered by the DBT to expedite the application of biotechnology in the agriculture, veterinary, and medicine sectors [48].

The current amendments or changes that have favored the industry relate to changes in the 1998 revised guidelines for research in transgenic plants, whereupon a relaxation was permitted regarding the concept of deliberate release. This amendment, by conferring powers to the RCGM to permit limited conduct of field trials in multi-locations, was at variance with the 1989 Rules that prohibited deliberate or unintentional release for experimental purposes, except where the GEAC approved it as a special case. The distinction between small-scale and large-scale releases brought about by the changed guidelines was unusual and was designed to ensure the control of the DBT and the RCGM over initial field testing of transgenic crops. An amendment was made by the DBT in September 1999 conferring rights to the RCGM to approve small experimental field trials for research, limited to a total area of 20 acres in multi-locations with any one location not exceeding 1 acre. Through this amendment, the DBT removed small experimental trials for research from the deliberate release clause of the 1989 Rules [40].

The changes that have been made to accommodate civil society concerns are basically twofold. The first relates to the formation of the MEC by the DBT in 1998 in order to closely and objectively monitor private sector biosafety data and through the mandatory involvement of state-level agricultural university scientists. The second change, which was induced by the Bt cotton controversy in India, has been the introduction of allergenicity tests of transgenic seeds, leaves, and vegetables on rodents, rabbits, guinea pigs, and goats in the 1998 version of the Biotechnology Safety Guidelines [42]. This precautionary step is viewed by the industry as having contributed to the delay in the regulatory approval for Bt cotton [40]. Additional regulations have recently been added to the PPVFR Act of 2001, requiring applicants to provide relevant GEAC clearances and approvals for registering transgenic varieties, as well as an affidavit stating that the "Terminator" Technology or the Genetic Use Restriction Technology is not involved [52]. Notably, the decision-making circle does not include the participation of industry, civil society, or consumer groups. While the 1989 Rules explicitly say that the RCGM, the GEAC, the SBCCs, and the DLCs may co-opt other members/experts as necessary, they neither include nor exclude representatives of NGOs and the private sector. In practice, however, these non-governmental stakeholders have been excluded [44]. However, following the "Terminator" controversy, the National Bureau of Plant Genetic Resources is now mandated by the government of India to develop probes to detect the presence of terminator genes in imported material,

highlighting how the force of public opinion can still shape biosafety rules in India.

To keep up with the rapid pace of developments in plant biotechnology, especially GMOs, the Indian regulatory system revised its existing guidelines in 2008. These were to provide greater clarity on data requirements and include: Standard Operating Procedures (SOPs) for Confined Field Trials of Regulated, Genetically Engineered (GE) Plants [49], Guidelines for the Safety Assessment of Foods Derived from Genetically Engineered Plants [50], and Protocols for Food and Feed Safety Assessment of GE crops [51]. Guidelines for Institutional Biosafety Committees (IBSCs) are also currently under review.

While the overall regulatory system remains unchanged, a notable difference is the classification of all GM field trials into two categories, based on size. The RCGM, operating in the DBT, is now the regulatory authority for Biosafety Research Level I (BRLI) trials. BRLI trials are limited in size to no more than 1 acre (0.4 ha) per location and a maximum cumulative total of 20 acres (8.1 ha) for all locations for each plant species/construct combination (e.g., one or more events originating from the transformation of a plant species with the same genetic construct), per applicant, per crop season. The GEAC, operating in the MoEF, is now the regulatory authority for Biosafety Research Level II (BRLII) trials. BRLII trials are limited in size to no more than 2.5 acres (1 ha) per location, and the number of locations is decided on a case-by-case basis for each plant species/construct combination, per applicant, per crop season.

Members of the MEC, SBCCs, and DLCs and monitoring teams of SAUs have the authority to inspect and monitor confined field trials at the time of planting, during the growing and harvesting season, and during the period of post-harvest land-use restriction for compliance with the terms and conditions of authorization.

Commercialization of GM Crops: Indian Approval Process

The approval process in India begins with the submission of an application regarding a new LMO event with potential benefits over the conventional variety/hybrid in terms of economic benefit to the farmer and/or the environment. The developer is required to follow a set procedure that involves providing all the necessary information specified by the regulatory body. Such an application is reviewed by the RCGM which, in the first instance, may recommend various limited contained or open field trials to be undertaken in order to generate specific biosafety data which may be lacking in the original submission. Once the full dossier of information from experiments undertaken under confined conditions is submitted, the RCGM will then ascertain as to whether the LMO presents any immediate adverse effects, either to humans, animals, and the environment (including the likely impact of large-scale cultivation on biodiversity). If considered as presenting minimal risk, the RCGM may permit large-scale open field trials to be conducted to generate data concerned with the agronomic performance of the LMO. Once more, possible adverse impacts on the environment, including on non-target organisms, are evaluated. The unconfined, open field trials are conducted either by the applicant or by the ICAR, involving their institutes/State Agriculture Universities, and are monitored by the MEC. The MEC reports their observations directly to the RCGM and the GEAC. Based on the biosafety data and the field performance, the RCGM may recommend the case to the GEAC for further evaluation. The GEAC will consider all the data provided and may ask the company to furnish additional data or repeat the trials in multi-locations during the next season. Based on the overall recorded benefits, the GEAC can approve the commercialization of the GM crop for a limited period and in a specified geographical zone. Data collected during this period will form the basis of the review undertaken by the GEAC for any extension or expansion to the set conditions of commercialization. Any adverse impact on human, animals, and environment derived from such large-scale cultivation is required to be immediately notified by any individual or organization directly to the GEAC.

All commercial authorizations are for a limited period, requiring renewal after the expiry period. Furthermore, approval is conditional upon the observing and collecting of relevant information on the risks, if any, arising from the commercial use of the GMOs and products thereof [42]. A key addition in the 1998 guidelines is the requirement to generate data on comparative economic benefits of a modified plant. Thus, the 1998 guidelines call for a demonstration that

a transgenic crop is both "environmentally safe and economically viable." An agronomic evaluation of the transgenic crop to determine economic advantage to farmers is seen as an integral component of the transgenic crop approval process, along with the biosafety evaluation [42]. Thus, when the government granted permission for large-scale field testing of transgenic cotton in India in July 2000 (the first crop to receive such approval), mandatory data to be generated by the applicant included "cost of transgenic seed, projected demand, and the area to be covered under transgenic cotton cultivation" [45].

The Philippines

The Philippines' National Agenda for Sustainable Development for the twenty-first Century (PA 21) provides the policy framework of the country's strategy for sustainable development. In 2001, the Presidential Policy Statement on Modern Biotechnology [53] reiterated the government policy of promoting the safe and responsible use of modern biotechnology and its products as one of several means to achieve and sustain food security, equitable access to health services, sustainable and safe environment, and industry development. The Philippine government formally funds biotechnology as part of the annual budget for agricultural R&D through legislation [54]. In December 2002, the Philippines became the first country in Asia to commercialize a GM crop for use as food, feed, or for processing [55] when the Department of Agriculture (DA) approved the Bt corn MON810 for import and propagation [56]. By summer 2005, the Philippines had approved 19 different LMOs for direct use as food, feed, or propagation [57], while in 2010, this had increased to 53 (when stacked events are also included).

Regulatory Oversight in the Philippines

The Filipino biotechnology regulatory system was established as a result of the recommendations from the scientists asking the national government to formulate a national policy on biosafety and create a technical body to draft guidelines to ensure that experiments using GMOs do not pose unacceptable risks to human health and the environment [12]. The Philippines has a body of policies aimed at regulating the development, importation, transfer, and use of GMOs. The first guidelines for biosafety were promulgated in October 1990 as Executive Order (EO) 430, which established the National Committee on Biosafety of the Philippines (NCBP). The NCBP was established to "oversee the compliance with policies and guidelines in all institutions, public or private, as well as to coordinate with the appropriate national bodies that have regulatory powers over any violations" [58]. At present, the NCBP is concerned with contained use (confined laboratory and greenhouse experiments on the regulated article), and its primary function is to identify and evaluate potential hazards involved in initiating genetic modification experiments and recommend measures to minimize risks [59]. Additional guidelines were developed and published by the NCBP and the Department of Science and Technology in 1991, 1998, and 2002 before being incorporated into the National Biosafety Framework, which was finalized in 2004 and issued as EO 514 in April 2006 [5, 12]. The rules and regulations for the import and release into the environment of plants and plant products derived from the use of modern biotechnology are set out in Administrative Order no. 8, Series of 2002 of the Philippine Department of Agriculture (AO 8) [35, 55]. The following year, the DA issued Memorandum Circular No. 8, which outlined the import requirements for biotech products. This was quickly followed by the issuance of Memorandum Circulars 11 and 12 in August 2003, which further clarified the import rules for biotech products for direct use as seed, food, feed, or for further processing [57]. Importers of GM plants for contained use, field testing, and propagation (or commercial planting), as well as GMOs for direct use as food, feed, and processing, are required to obtain an approval permit [15, 55] which stipulates that the performance of the GM crop and its effect on the environment as well as human and animal health have been positively assessed [11].

The decision-making process is vested in multiple national competent authorities (NCAs) after consultation with other agencies and/or with a multi-stakeholder advisory body. The Department of Agriculture (DA) is the competent national authority responsible for biosafety decisions concerning plants and plant products derived from modern biotechnology, fisheries and other aquatic resources, domesticated

animals and biological products used for animal husbandry or veterinary purposes, and biological agents used for biocontrol. It is the government institution with mandatory responsibility for GM crop field releases and commercialization. Likewise, the Department of Science and Technology is responsible for research and development, the Department of Health for pharmaceuticals which are not addressed by other relevant international agreements or organizations, and the Department of Environment and Natural Resources concerning regulated organisms intended for bioremediation, the improvement of forest genetic resources, and wildlife genetic resources, and applications of modern biotechnology with potential impact on the conservation and sustainable use of biodiversity [12].

Commercialization of GM Crops: Filipino Approval Process

In consultation with the NCBP, the Bureau of Plant and Industry (BPI) of the DA is responsible for the granting of permits issued under AO 8 and are classified according to the intended use of the regulated article: (a) importation for contained use, (b) field testing, (c) release for propagation, and (d) importation for direct use as food or feed or for processing [61]. Applications for import must be accompanied by a certificate from the competent authority in the country of origin stating that the regulated article has been locally approved and a notification in accordance with international obligations. Local applications must be supported with the necessary technical and scientific dossiers, a public information sheet (PIS), and a certificate from the BPI stating that the regulated article has undergone satisfactory field testing in the Philippines. The AO 8 policy for commercial propagation stipulates that no regulated article will be released unless (a) field testing showed that the GM crop will not pose any significant risks to the environment, (b) food and/or feed safety studies showed that the GM crop will not pose any significant risks to human and animal health, and (c) a permit for propagation has been secured from the DA. If the GM crop has transgene-derived pesticidal properties, it must also be duly registered with the Fertilizer and Pesticide Authority (FPA) [61]. Upon receipt of an application, the BPI has 5 days to process and evaluate all of the documentation to ensure that it is sufficient in form and substance. If it is found to be defective, then the applicant is given a 60-day grace period to correct or provide further necessary information. Only a complete application will be accepted for evaluation by a multi-stakeholder advisory body, the results of which must be reported to the BPI within 30 days of acceptance. For the duration of the evaluation process, the reviewers remain anonymous to both the public and the BPI. The Scientific and Technical Review Panel (STRP) and the Bureau of Agriculture and Fisheries Products Standards (BAFPS) evaluate all applications; the STRP comprises of at least three experts from a roster of independent scientists and particularly evaluates the risk assessment and risk management strategies outlined by the applicant, whereas the BAFPS will make a determination of compliance with food-safety standards. Additionally, the Fertilizer and Pesticide Authority (FPA) and the Bureau of Animal Industry (BAI) will also evaluate applications of those regulated articles which are also pest-resistant plants or to be used as feed, respectively. Concurrently, the applicant must carry out a public consultation by publishing the PIS in two newspapers of general circulation and inviting the public to make comments directly to the BPI within 60 days of posting the notice. A decision, together with any agreed permit conditions, is made within 120 days of publication of the notice [62]. Approved products are then included in the registry for direct use maintained by the BPI. Once in the registry, for imported articles, the applicant is no longer required to secure an import permit for succeeding shipments. However, a notification of shipment to BPI is required within 15 days before its arrival at a Philippine port [57].

South Africa

South Africa is a biotechnology leader in Africa and is involved in sophisticated biotechnology activities, including those pertaining to the development and commercialization of GMOs [6, 63]. In 2000, the South African government began to focus on, and substantially increased, its research support for biotechnology. This led to the adoption of the 2001 National Biotechnology Strategy (NBS), a policy framework to create incentives for the biotechnology

sector [63], involving several government departments [64]. The NBS commits more than US$300 million per year from government to finance a variety of biotechnology initiatives [6].

South Africa is among only three African countries in which GM crops are commercially grown [2]. In 2006, the commercial release of insect-resistant (Bt) cotton and maize; herbicide-tolerant (RR) soybeans, cotton, and maize; and cotton with the "stacked gene" (Bt and RR) had been approved. At the time, it was estimated that these GM crops accounted for the cultivation of 30.5% of yellow maize, 28.8% of white maize, 59% of soybean, and 90% of cotton in South Africa [65]. The total area of commercialized transgenic crops increased in 2010 to 2.2 million hectares [2], which is mostly due to white and yellow maize, followed by RR soybeans and insect-resistant cotton. Giving an insight into potential future commercial releases, several varieties of these crops were also in field trials as of 2009, along with additional new crops. Between January and September 2009, the number of field trial permits issued totaled 267 [3]. Maize topped the list with 222 approvals, followed by 24 permits for cotton, 15 for vaccines, 3 for soybeans, and one each for sugar cane, sorghum, and table grapes. The traits associated in these approvals included drought tolerance and herbicide tolerance in maize, herbicide tolerance in cotton, biofortified sorghum, fungus resistance in table grape, alternative sugar production pathways in sugar cane, and cassava with altered starch content.

Regulatory Oversight in South Africa

Concerns regarding the commercial release of GMOs led to South Africa enacting legislation to regulate the development, importation, and application of GMOs. The Genetically Modified Organism Act 1997 (GMO Act) was passed in 1997, and it was subsequently modified in 2006 to bring it in line with the CPB [66]. Regulations for its implementation were initially adopted in 1999, and then, amended regulations took effect in February 2010. The formal structures for the implementation of this act include an Executive Council, which reviews applications for GMO work; a scientific advisory committee (South African Committee for Genetic Experimentation [SAGENE]); a registrar to administer the GMO Act; and an inspectorate to monitor function. According to the legislation, no person may import or export from South Africa, or develop, produce, use, release, or distribute any GMO in South Africa, other than under a permit for undertaking such an activity [67]. Such a permit is to be issued after a technical assessment and risk analysis report has been submitted by the applicant and has been approved by the Executive Council. This Council is responsible for making regulatory decisions and is comprised of ten members: one representative from each of eight government ministries (Agriculture, Science and Technology, Health, Environmental Affairs and Tourism, Trade and Industry, Labour, Water Affairs and Forestry, and the Department of Arts and Culture), the chair of SAGENE who provides scientific and technical analysis of risk assessment data, and the GMO Registrar [68]. The GMO Regulations provide that an applicant shall notify the public of any proposed release of GMOs prior to the application for a permit for such release. Public notifications shall be in the form of a standard notice published in the printed media informing the public of the intended release. It is worth noting, however, that the first field trials were allowed in 1994, and since 1997, several multinational companies have been permitted to grow and import GMOs even before the GMO Act was belatedly implemented in November 1999 [63, 69].

Commercialization of GM Crops: South African Approval Process

Commercial activities concerning GMOs all require a permit, including those for: import, export, contained use (including development, production, distribution, transport, but not those under containment levels 1 & 2, i.e., in the laboratory or growth chamber), deliberate release of GMOs into the environment (trial and general release), and commodity clearance [70]. All applications must be submitted to the GMO Registrar at the DA, along with a copy of the public notice and proof (newspaper clippings) in order for the application to be processed. The public notice allows interested parties to submit comments or objections in connection with the intended release to the Registrar within 30 days after the date of the notification [71]. The Registrar then undertakes an initial review of the application to determine compliance

with the provisions of the GMO Act. If the application is not compliant, the application is referred back to the applicant. Once compliant, the application is forwarded to a committee (expertise nominated by SAGENE chairperson) formed under SAGENE to conduct a review of the proposed activity. The review includes an evaluation of the risk assessment data, including food safety (if applicable), submitted in the application. Conclusions of the assessment are detailed in a recommendation report, which is sent to the Registrar on completion of the review. At this stage, the application can be referred back to the applicant to address any concerns raised or to supply additional information, and the response returned to the committee. Once all concerns have been addressed, the committee makes a recommendation on the application. The recommendation document, public input, and a copy of the application is forwarded to the Executive Council for consideration, who will also take into account the socioeconomical impact that the GMO may have. The Council then submits its decision in writing to the Registrar. Should the Council raise any concerns, the Registrar will once again refer the application back to the applicant for clarification. Based on the information received from the applicant and the assessment done by the Council, the application will be approved or rejected. If the application is approved, the Council authorizes the Registrar to issue a permit to the applicant. This permit will be accompanied by specific containment conditions as prescribed by the Council. If the application was rejected, the Registrar will communicate the decision back to the applicant with reasons for the rejection [70]. Regulations of the Department of Health of 2004 provides for the labeling of foodstuff with genetically modified ingredients that are significantly different to the non-GMO ingredients. The Consumer Protection Act of 2008 also addresses this issue.

United States of America (USA)

In the USA, GM crops have been sold since 1994 and in 2006 were already planted on 54.6 million hectares (soybean, maize, cotton, canola, squash, papaya, and alfalfa), confirming the USA's role as the world leader in agro-biotechnology [10]. The regulatory system in the USA relative to biotechnology products is rather different from the one put in place in the EU, and the discrepancies mainly reflecting the different approaches taken by the governmental authorities, citizens, and firms toward GMOs and GM food, especially in the initial years of the biotechnology revolution.

In the USA, agricultural biotechnology politics has been dominated by a strong and cohesive coalition of pro-biotechnology upstream and downstream producers and farmers. Lower public outrage has made mobilization of NGOs in the United States difficult and, in combination with a less-favorable institutional environment (notably, centralized regulatory policy-making), has resulted largely in their exclusion from agri-biotech policy-making [72].

Regulatory Oversight in the USA

Taking the approach that GM products are essentially an extension of conventional products, the US Government has made use of existing laws to ensure the safety of GM products [15]. US regulatory authorities operate under the assumption that the fact that a plant has been genetically modified is less important than the specific effects of the modification [4]; therefore, the regulation focuses on the characteristics of the products rather than the way in which the product was produced [35]. The current system was delineated by the White House Office of Science and Technology Policy under the 1986 Coordinated Framework for Regulation of Biotechnology [73]. It is still the key document for regulating gene technology in the United States and provides the basis for the regulation of crop varieties produced by rDNA techniques. Under the Framework, the US Department of Agriculture (USDA), the Food and Drug Agency (USFDA), and the Environmental Protection Agency (USEPA) that were responsible for regulatory oversight of certain product categories or for certain product uses are also responsible for evaluating those same kinds of products developed using genetic engineering techniques. Transportation, growing (including field testing), and propagation of GM crops are governed by the USDA's Animal and Plant Health Inspection Service (APHIS) under the Federal Plant Pest Act 1996 (FPPA) and the National Environmental Policy Act 1969. Specifically, the APHIS has two responsibilities: deciding on which GM seeds to oversee, so-called regulated articles, and which GM seeds

are safe enough to be free from the agency's oversight, so-called deregulated articles. Deciding on GM seeds to be regulated depends on "familiarity," gained from direct experience through field testing under regulated conditions. Any eventual deregulation, that is, exempting a GMO from the oversight of APHIS, involves a petition process whereby an advertisement is published in the US Federal Register, and a period to comment is provided to the public [74].

If a GM plant is not intended for human consumption and is not modified to contain a pesticide, the USDA is the leading agency. For plants genetically modified to produce their own pest protection, APHIS coordinates its evaluation with the USEPA. Pest-resistant GM crops fall under the authority of the USEPA under the Federal Insecticide, Fungicide, and Rodenticide Act 1996 (FIFRA) and the Toxic Substances Control Act 1976. They are subject to a strict testing regime, where producers must submit testing data to the USEPA who determines the quantity of pesticidal substances that may be present in food [75]. In fact, industry is required to obtain an Experimental Use Permit (EUP) from the USEPA to test any pest-resistant plant in a field larger than 10 acres. Once the permit is granted, firms are expected to consult the USEPA on the details of the field experiment. While the APHIS analyzes data on the source of the new gene, the nature of the pesticidal substance produced, differences with its natural equivalent, effects on non-target organisms, and environmental fate, the USEPA focuses on the toxicology, the digestive fate, and the potential allergenicity of the toxin. In line with the product-based approach, the USEPA does not assess the GM plant per se but the toxin produced by the plant. As for any pesticides, the USEPA subjects these toxins to a registration process. Pest-resistant plants whose toxin falls under this process are mostly of the Bt variety. Following this registration logic, if the toxin produced by a GM plant has been approved previously as a regular pesticide, a new registration is not required. The USEPA has been requesting for years new regulations to obtain a wider role in the assessment and the management of GM plants, but thus far with only limited success [11, 72, 74]. The US Food and Drug Administration (USFDA) regulates food applications of GM crops and relies on existing laws that hold food manufacturers responsible for food safety. Of the three agencies, the USFDA has had the most influence on biotechnology policy because most biotechnology products on the American market are health care or food products [72]. In 1999, public meetings were held by the agency with the aim of sharing its experience regarding GM foods and soliciting views on whether its policies and procedures should be modified. Public comments indicated considerable public support for a mandatory and more transparent process [4].

Commercialization of GM Crops: US Approval Process

The APHIS oversees the confined and unconfined release of transgenic plants as well as any importation and interstate movement under the FPPA. In addition to the FPPA, the USDA issued rules in 1987 for the "introduction of organisms and products altered or produced through genetic engineering which are plant pests or which there is reason to believe are plant pests" [76]. By these rules, the introduction of a crop produced by rDNA techniques into the environment is only legal with an authorization by the APHIS. The APHIS grants a release permit after preparing an environmental impact assessment and "Finding Of No Significant Impact" ("FONSI"). Exempt from these rules are experiments with plants produced by rDNA technology in a contained environment (e.g., laboratory, green house).

In 1997, the USDA simplified the procedure for the unconfined release of GM crops into the environment by allowing the applicant to petition the APHIS for a "determination of non-regulated status" [77]. When receiving a petition, the APHIS prepares an environmental impact assessment taking into account the following eligibility criteria:

- The crop must not be listed as noxious weed or weed.
- The introduced genetic material must be stable and characterized.
- The introduced genetic materials must not
  - Result in any plant disease
  - Confer an infectious entity or encode toxic substances to non-target organisms
  - Encode products intended for pharmaceutical use

- Any plant virus-derived sequences must not pose a significant risk for new plant virus creation.
- The GM crop must be free of known human and animal pathogens or allergens.

After a complete petition is filed, it is published in the Federal Register to solicit comments from the public. Thereafter, the APHIS reviews the data, taking into account public comments and takes a final decision, which is again announced in the Federal Register. The issuance of a "non-regulated" status for a transgenic crop means that it is deregulated and can be freely commercialized in the US (unconfined release, import, interstate movement), except if it contains a pesticidal substance. In that case, an additional "plant pesticide" approval by the USEPA is required.

The responsibility of the USEPA is to evaluate the risks of GM crops "producing their own pesticide" for human consumption under the FIFRA. The evaluation process is held to the same standards as those for pesticides applied to plants. To be registered under the FIFRA, a pesticide must not cause "unreasonable adverse effects" on the environment and on human health [78]. Transgenic insect- and virus-resistant plants fall under the jurisdiction of the USEPA; however, viral coat proteins are normally exempted from the requirements as the USEPA considers these proteins as "low-risk applications" based on the principle of familiarity and their ubiquitous presence in the food supply. Today, Bt toxins, one viral coat protein, and the potato leaf roll virus protein are registered as pesticides and supervised by the USEPA. The agency evaluates the risks of these "plant-incorporated protectants" by taking into account the following criteria: toxicological effects, effects on non-target organisms, insect resistance management, and persistence of the substance in the environment. The evaluation process lasts approximately 1 year. If adverse effects of insect- or virus-resistant plants are observed after commercialization, the USEPA has the legal power to amend existing registrations. Moreover, the USEPA may impose new measures such as new pest resistance schemes [79].

Besides the pesticide registration under FIFRA, Section 408 of the FFDCA requires the USEPA to determine tolerance limits for substances used as pesticides on and in food and feed [78, 80]. "Nucleic acids that are part of a plant-incorporated protectant" are exempted from this requirement because the USEPA considers them as "safe" [80]. Once approvals from the APHIS, and from the USEPA when pesticidal substances are used, have been granted, it is legal to commercialize the GM plant or derived product in the USA. However, applicants normally engage in a voluntary consultation process with the USFDA before marketing of the GM plant or derived products. This policy is now under review.

International Obligations Relevant to the Biosafety Frameworks

Countries do not have complete discretion when deciding how to set up their biosafety regulatory system as there are several international treaties and agreements that relate to biosafety. If a country is bound by any or all of those international agreements, then their biosafety regulatory system must be compliant with those obligations [81].

Cartagena Protocol on Biosafety

The conclusion of the CPB was broadly recognized as a step forward in providing an international regulatory framework to reconcile trade with environmental protection by creating an enabling environment for the environmentally sound application of biotechnology [82]. The Convention on Biological Diversity (CBD) [83] in Article 19 [3] states that:

> The Parties shall consider the need for and modalities of a protocol setting out appropriate procedures, including, in particular, advance informed agreement, in the field of the safe transfer, handling and use of and living modified organism resulting from biotechnology that may have adverse effect on the conservation and sustainable use of biological diversity.

In 1995, the second Conference of the Parties (COP) to the CBD began the consideration of the need for and modalities of such a protocol. COP Decision II/5 commenced the negotiations for the protocol by launching an open-ended ad hoc Working Group on Biosafety [1]. Meeting six times between 1996 and 1999, the Working Group concluded its work with the submission of a draft protocol for consideration by the first extraordinary meeting of the COP, convened with

the purpose of adopting a protocol on biosafety to the CBD. The result of this first extraordinary meeting, which took place in two separate meetings in 1999 and 2000, was the adoption of the Protocol [84]. In accordance with its Article 36, the Protocol was opened for signature by States and regional economic integration organizations from 15 to 26 May 2000 and remained open for signature from 5 June 2000 to 4 June 2001. By that date, the Protocol had received 103 signatures. The Protocol entered into force on 11 September 2003, 90 days after receipt of the 50th instrument of ratification [85]. There are presently 160 parties to the Protocol [86], with the COP to the CBD serving as the meeting of the Parties to the Protocol (COP-MOP), the Protocol's governing body. Since the coming into force of the Protocol, the COP-MOP has met five times. The fifth meeting of the COP-MOP took place from 11 to 15 October 2010 in Nagoya, Japan, and it approved a Supplementary Protocol on Liability and Redress to the Cartagena Protocol on Biosafety [87].

The Protocol's scope is the "transboundary movement, transit, handling, and use of all living modified organisms that may have adverse effects on the conservation and sustainable use of biological diversity, taking also into account risks to human health" [82]. To ensure the safe transfer, handling, and use of GMOs, the Protocol sets up two separate procedures. The first time that a GMO is to be intentionally introduced into the environment, the Protocol sets up an Advance Informed Agreement (AIA) procedure. That procedure requires that the exporter of the GMO provides a notice with detailed information about the GMO to the importing country. The importing country then reviews the information, conducts a risk assessment, and decides, based on the risk assessment results, whether to approve or reject the GMO. The second procedure set up by the Protocol is for GMOs to be used for food or feed or for processing (such as corn, soybeans, wheat, or other grains that will be fed directly to humans or animals or used for processing). For those GMOs, the AIA procedure is not required. Instead, the Protocol establishes a simpler system that reflects the decreased likelihood that those GMOs will affect the importing country's biodiversity. Before the GMO can be exported to another country, the only requirement is that the safety decision in the exporting country is communicated to other countries through the Biosafety Clearing-House. For LMOs used for other purposes, such as LMOs used in the laboratory, the Protocol leaves any regulation to the discretion of the individual country. The Protocol also does not cover products derived from LMOs, such as processed foods that have ingredients that came from LMOs. Although the Protocol comprehensively covers many issues, there are a few remaining to be addressed by the individual Party when establishing their biosafety regulatory regime [81].

In addition to the CPB, other relevant international agreements exist. Under international law, countries shall comply with all treaties to which they are parties, provided that the provisions of these treaties are not contradictory (principle of accumulation of international obligations). According to the principle of integration contained in the Rio Declaration on Environment and Development (Principle 4) and the 2002 Plan of Implementation of the World Summit on Sustainable Development (Paragraph 92), environmental treaties and trade goals shall mutually support each other. In fact, the various agreements and instruments on the topic of the development and use of agrobiotechnology are all closely interrelated and need to be carefully considered in the decision-making process, both individually and collectively. This regulatory and public policy background consists of relevant international instruments and processes, such as: the entry into force of the CPB, the Codex Alimentarius Guidelines on Food Safety and Labelling of GMOs, and the World Trade Organization (WTO) Agreements on Sanitary and Phytosanitary Measures and Technical Barriers to Trade. Table 1 presents a summary of the main international instruments and processes of relevance for biosafety.

A Comparative Analysis of Regulatory Processes in All Study Countries

Attributes of a Modern Regulatory Biosafety System

Although the development of regulatory regimes is essentially based on national specific practices, legal systems, public management strategies, and local socioeconomic considerations, national regulatory biosafety frameworks will generally always consider the following elements [110–112]:

Commercialisation of GM Crops: Comparison of Regulatory Frameworks. Table 1 Relevant international instruments and processes (Taken from [88])

Agreement, declaration, or process	Content
Rio Declaration on Environment and Development	The precautionary principle is a fundamental instrument for the safe use of biotechnology. This principle is contained in Principle 15, which sets forth that: "*In order to protect the environment, the precautionary approach shall be widely applied by States according to their capabilities. Where there are threats of serious or irreversible damage, lack of full scientific certainty shall not be used as a reason for postponing cost-effective measures to prevent environmental degradation*".
United Nations Environment Program – International Technical Guidelines for Safety in Biotechnology	Enacted in Cairo in 1995, these guidelines may assist governments, intergovernmental organizations, private organizations, and others to strengthen capacities and exchange biosafety information.
	The guidelines are based on the following principles: (a) identification of hazards; (b) risk assessment, taking into account the probability of any hazards arising and the potential consequences of such hazards; and (c) risk management, applying adequate management strategies which include developing procedures and methods to minimize risks and their consequences, or making decisions not to proceed. Such management strategies shall be proportional to the risk assessment results.
World Trade Organization (WTO) Agreement	The WTO Agreement recognizes the goal of sustainable development, considering that free trade shall protect and preserve the environment [89]. There are three WTO Agreements which can be associated with GMOs: The Agreement on the Application of Sanitary and Phytosanitary Measures (SPS; [90]), the Agreement on Technical Barriers to Trade (TBT; [91]), and the Agreement on Trade-Related Aspects of Intellectual Property Rights (TRIPS; [92]). It is also important to understand the regulations and procedures that govern Dispute Settlement Understanding (DSU) in the WTO context [93].
Agreement on Technical Barriers to Trade (TBT)	The TBT Agreement is relevant to biotechnological products as it applies to technical regulations and rules, including requirements for packaging and labeling [91]. The TBT Agreement recognizes that no country shall be prevented from taking necessary measures to ensure the quality of its exports, the prevention of deceptive practices, and the protection of the environment and human, animal, and plant life or health. However, such measures shall not be taken as means of arbitrary or unjustifiable discrimination between countries, where the same conditions prevail, or as disguised restrictions on international trade. Furthermore, such measures must otherwise comply with the provisions of the Agreement [91].
The Agreement on the Application of Sanitary and Phytosanitary Measures (SPS)	SPS rules are summarized in the following manner [90]: 1. Members have the right to take necessary sanitary and phytosanitary measures to protect human, animal, and plant life or health, provided that such measures are not inconsistent with the provisions of the Agreement. 2. Any sanitary or phytosanitary measures are applied only to the extent that is necessary to protect human, animal, and plant life or health, based on scientific principles. Furthermore, such measures cannot be maintained in the absence of sufficient scientific evidence of their necessity. 3. Members shall ensure that their sanitary and phytosanitary measures do not arbitrarily or unjustifiably discriminate between members among whom identical or similar conditions prevail. Moreover, sanitary and phytosanitary measures shall not be applied in a manner that would constitute a disguised restriction on international trade.

Commercialisation of GM Crops: Comparison of Regulatory Frameworks. Table 1 (Continued)

Agreement, declaration, or process	Content
	4. Sanitary or phytosanitary measures, which are taken in accordance with the relevant provisions of the Agreement, are presumed to comply with the members' obligations under GATT 1994, which relate to the use of sanitary or phytosanitary measures, in particular, the provisions of Article XX(b) [94]. 5. In principle, members shall base their sanitary or phytosanitary measures on international standards, guidelines, or recommendations, where these exist. 6. Sanitary or phytosanitary measures which comply with international standards, guidelines, or recommendations are deemed necessary to protect human, animal, and plant life or health and are presumed to be consistent with the relevant provisions of GATT 1994 [94] and the SPS Agreement [90]. 7. Members may introduce or maintain sanitary or phytosanitary measures which result in a higher level of sanitary or phytosanitary protection than the level that is required by the relevant international standards, guidelines, or recommendations, provided that there is a scientific justification to this heightened level of protection or that this level of protection is determined by a member country to be appropriate according to Article 5 of the SPS Agreement regarding risk assessment and adequate protection levels [90]. However, measures which result in a heightened level of sanitary or phytosanitary protection need not go against any other provisions in the Agreement. The above-mentioned standards, guidelines, and recommendations are defined as those established by international organizations, such as the Codex Alimentarius Commission, the Office International des Epizooties, and the Secretariat of the International Plant Protection Convention. As for other subjects that are not within the scope of the aforementioned organizations, they shall be regulated by "other international organizations" identified by the WTO Committee on Sanitary and Phytosanitary Measures as being open to the Parties' membership.
The Codex Alimentarius	Created by the World Health Organization (WHO) and the Food and Agriculture Organization (FAO) of the United Nations, the Codex Alimentarius (http://www.codexalimentarius.net) is the organization which is in charge of establishing regulations related to food safety. Codex Alimentarius standards need to ensure fair trade practices in food trade, according to WTO rules. The Codex Alimentarius Commission established an Ad Hoc Intergovernmental Task Force on Food Derived from Biotechnology [95] to handle issues associated with food obtained through biotechnological processes, particularly food used for health and nutrition purposes. In July 2003, the Codex Alimentarius Commission held a meeting during which three risk assessment standards for food resulting from biotechnology were approved [96]. These standards establish risk assessment principles for food derived from modern biotechnology. The principles refer to the concept of "tracing," which is a risk assessment tool whose meaning is the subject of an important debate. In fact, the United States of America consider this concept to be different from traceability and limit themselves to following only the previous and subsequent link in the LMO movement chain. The approved standards are the following: – Principles for the Risk Analysis of Foods Derived from Modern Biotechnology [97] – Guideline for the Conduct of Food Safety Assessment of Foods Derived from – Recombinant-DNA Plants [98] – Guideline for the Conduct of Food Safety Assessment of Foods Produced Using Recombinant-DNA Micro-organisms [99]

Commercialisation of GM Crops: Comparison of Regulatory Frameworks. Table 1 (Continued)

Agreement, declaration, or process	Content
	In 2008, the Ad Hoc Intergovernmental Task Force on Food Derived from Biotechnology completed a Guideline for the Conduct of Food Safety Assessment of Foods Derived from Recombinant-DNA Animals [100]. At its 31st session, the Commission noted that the Task Force had completed its work, one year ahead of schedule, and agreed to its dissolution [101]. Likewise, the Codex Committee on Food Labelling is working on draft guidelines for the Labelling of Food and Food Ingredients Obtained through Certain Techniques of Genetic Modification/Genetic Engineering, as well as on a Draft Amendment to the General Standard for the Labelling of Pre-packaged Foods (in order to address the issue of genetically modified foods) [102]. Finally, in 2007, the Codex Alimentarius Commission adopted the "Working Principles for Risk Analysis for Food Safety for Application by Governments" that were proposed by the Codex Committee on General Principles [103]. These principles allude to the precautionary approach. For more information on Codex activities, see www.codexalimentarius.net.
International Plant Protection Convention (IPPC)	The IPPC (https://www.ippc.int/) aims to prevent the international spread and introduction of pests of plants and plant products and to promote appropriate measures for their control. The Convention was reviewed in 1997 and entered into force in 2005 [104]. A Commission Working Group studied plant pest risks associated to LMO issues and an international standard (ISPM No.11 pest risk analysis for quarantine pests, including analysis of environmental risk and LMOs) [105]. This text intends to protect plants and ecosystems from LMO-related risks. According to the text, such protection measures should be cost effective, nondiscriminatory, and feasible and should not limit basic trade needs.
World Organization for Animal Health (OIE)	The World Organization for Animal Health, also known as the Office International des Epizooties (OIE; http://www.oie.int/), is an intergovernmental organization created by the International Agreement signed on 25 January 1924. OIE's mission is to ensure the transparency of animal health conditions worldwide. Member countries promise to declare animal diseases detected on their territory. In addition, the OIE is in charge of safeguarding international trade through the elaboration of health regulations destined to be applied to international transboundary movements of animals and animal products. The WTO recognizes such regulations as international reference rules.
Regional International Organization for Plant Protection and Animal Health (OIRSA)	In 2000, the Regional International Organization for Plant Protection and Animal Health (OIRSA; http://www.oirsa.org) produced a Regional Guideline on the Safety of Plant Biotechnology [106]. In fact, the Guideline is based on the CPB and essentially regulates the same issues as the Protocol. However, in view of its nature, the guideline also aims to harmonize the various regional laws and practices pertaining to the issue of biosafety.
Central American Commission for Environment and Development (CCAD)	The Central American Commission for Environment and Development (CCAD), which is the environmental authority of the Central American Integration System (SICA), through its biodiversity program and territorial legal system, prepared a Central American Protocol on the Safety of Modern Biotechnology. A series of technical consultations was undertaken and led to the adoption of a draft Protocol, which was then approved by the Central American Ministries of Environment in 2002. Although the Central American Protocol is based on the CPB, some of its provisions go beyond the scope of the CPB. In fact, provisions regarding labeling, documentation, liability, contained use, and transit, as well as various biosafety principles, have been included in the Central American Protocol in an attempt to avoid the inconsistencies and ambiguities which resulted from the multilateral negotiations that lead up to the adoption of the CPB.

Commercialisation of GM Crops: Comparison of Regulatory Frameworks. Table 1 (Continued)

Agreement, declaration, or process	Content
The Inter-American Institute for Cooperation in Agriculture (IICA)	As requested by the Ministries of Agriculture in 2002, IICA, in collaboration with the OIRSA and the Tropical Agricultural Research and Higher Education Centre (CATIE), was put in charge of preparing a regional biosafety regulatory framework, in response to the lack of regulations in certain countries that are receiving, or may potentially receive, requests for field trials or trade in LMOs. A group comprising of various agencies was formed, along with a consultative process, which led to the preparation of a Regulatory Framework Draft for Living Modified Organisms for Agricultural and Livestock Use in Central American Countries. This initiative intends to promote a model regulation on agricultural biotechnology that is to be adapted by each country, according to its particular needs and situation. There is hope that this regulation will be enacted in a similar fashion by the various nations, thereby triggering a process of harmonization of regulatory frameworks in the region.
Other relevant agreements and declarations	– CGRFA draft Code of Conduct on Biotechnology [107] – United Nations Model Regulations on the Transport of Dangerous Goods (UN Recommendations) [108] – The Aarhus Convention on Access to Information, Public Participation in Decision-making and Access to Justice in Environmental Matters, which contains specific guidelines on public participation in LMO-related decision-making processes [109]. The Convention entered into force in 2001. Although it was enacted by the United Nations Economic Commission for Europe, the convention is open to other nations. The Convention was amended in 2005 in order to set out more precise provisions on the deliberate release of genetically modified organisms, but the amendment has not yet entered into force. The amendment will enter into force once it has been ratified by at least three-quarters of the Parties. In September 2007, the amendment had only been ratified by four countries. The third meeting of the Parties was held in Riga, Latvia, on 11–13 June 2008. The meeting adopted the Riga Declaration and a strategic plan for the Convention, resolved the issue of how to calculate ratification of amendments, and renewed the mandates of task forces dealing with access to justice, electronic information tools, and public participation in international forums.

- Biosafety policy, occasionally as part of a broader biotechnology or biodiversity policy
- Regulatory policy
- A mechanism to handle requests and permits related to LMO use, in particular, notifications required by the CPB (i.e., an administrative system)
- A mechanism for monitoring and inspections
- A system that allows public participation and information

According to Jaffe [113]:

- The purposes of a national biosafety regulatory system are to scientifically assess the safety of genetically engineered (GE) organisms to humans and the environment, manage any potential risks, and authorize the development and marketing of safe GE organisms and their products. To develop such a regulatory system, a government can use existing laws or develop new laws. Any national biosafety regulatory system that is proposed, however, must be functional, protective, and also comply with international trade standards that are evolving in recognition of the growing importance of GE organisms in world affairs.

A national biosafety regulatory system is a regulatory regime responsible for assessing and managing the full range of potential risks that might be posed by a GMO and its products. It addresses potential risks to the environment and biological diversity as well as any food/feed risks or other safety-related issues

involving GMOs (e.g., worker health, drug safety, etc.). A protective biosafety regulatory system ensures that any risks from GMOs are managed and allows safe GMOs to be developed, marketed, and utilized for their intended purpose. Such a system, however, must also be functional, which means that it should be understandable, workable, equitable, fair, adaptive, and enforceable [114].

Existing biosafety regulatory systems from around the world reflect, among other things, the type of government in the country, the politics of the country, the country's view on the relative safety of GMOs, and the country's regulation of food, agriculture, and environmental issues. Establishing those systems required balancing numerous goals and trading off different interests. Through an analysis and comparison of different existing biosafety regulatory systems, however, one can identify key characteristics and components that are generally important to a functional and protective biosafety regulatory system [113]. Incorporating each of those characteristics and components in a functional and protective biosafety regulatory system involves problem solving because there can be tensions between the different characteristics.

Jaffe [113] indicates the following attributes of a system:

- Comprehensive.
- Adequate legal authority to subject each GMO to a food-safety and environmental risk assessment approval.
- A clear safety standard.
- Proportionate risk-based reviews.
- Transparent and understandable.
- Participatory.
- Post-approval oversight. A biosafety regulatory system does not stop its oversight once a GMO has been approved for a confined field trial or for a commercial release.
- Flexible and adaptable.
- Efficient, workable, and fair.

Decision-makers are facing an important challenge because biotechnology and biosafety fields are ever evolving at a dramatic pace. In this context, overly precise and detailed regulatory frameworks can easily become obsolete in a short period of time. In order to avoid forever having to enact new legislation and policies, it is preferable to develop a regulatory framework that takes on the form of a general guide, thus regulating more specific biosafety aspects by way of by-laws and other regulations. In fact, this alternative allows more efficient regulation of future situations but has the effect of conferring the power of regulating specific aspects of biotechnology to the executive branch of government and other administrative institutions, instead of to the Parliament [115].

General Comments on Evolution of Biosafety Regulatory Systems

The nature of GM crop regulations around the world has as much to do with social and political values as with concerns about health and safety. Consumers' growing awareness of their rights and farmers' increasing fear of dependence on multinational companies are symptoms of a deeper concern about values and priorities, the type of environment that people want, the role of biodiversity, their tolerance to risk, and the price that people are prepared to pay for regulation. Therefore, the regulations in the study countries were formed, or amended, during this period of heightened public awareness and are a reflection of how the various governments have attempted, or not, to address these concerns. A comprehensive discussion of regulatory requirements for GM crops at the national and international levels is a broader topic than can be covered here, and previous studies have addressed them in detail [5, 116].

In general terms of regulatory systems, several approaches have been considered worldwide with respect to the safe use of modern biotechnology: (a) certain countries decided to apply preexistent plant or animal health regulations to GMO-related issues or to incorporate biosafety provisions into plant and animal health protection laws; (b) other countries decided to adopt specific biosafety regulations that need to be enacted by the Parliament, the executive power (through agreements or resolutions), or public sector institutions; (c) certain countries decided to mention biosafety in their environmental regulations; (d) some countries decided to apply seeds, pest control, and plant or animal regulations to

modern biotechnology, enacting but a few coordination rules and specific provisions associated to biosafety.

The original trend of agricultural biosafety regulations focusing on transgenic plants continues to exist in some countries but is in the process of being replaced by a broader focus that comprises biosafety regulation of animals, microorganisms, fish, and forest species. This progressive expansion of biosafety toward new areas results from the need to regulate research and eventual trade of other types of organisms created through genetic engineering. The CPB, whose scope extends beyond the issue of plants, and the subsequently developed regulatory frameworks implementing its provisions, brought on a gradual increase in the number and variety of organisms and activities being regulated. In addition, health authorities have increased participation in biosafety advisory commissions and committees.

In view of the complexity of biosafety issues, particularly issues of risk assessment and risk management, and several other issues associated to the introduction of GMOs into the environment, almost all of the countries have established a committee or a national commission to assist decision-makers in the development of biosafety regulations. The composition of these committees and commissions varies considerably in the region, mainly with respect to the inclusion of the productive sector, consumers, and non-governmental organizations. However, the trend points toward the inclusion of these organizations, even though such an inclusion can potentially lead to conflicts of interest. Currently, these committees or commissions are for the most part directly connected to the regulatory authorities in place. Nevertheless, independent national commissions (commissions that are not connected to the regulatory authorities) were created in some countries and were assigned political and coordinative functions, leaving the issue of technical recommendations to be dealt with by other sector-based authorities established by each country's competent Ministry or Secretariat.

The entry into force of the CPB had the effect of introducing the Ministries of Environment to the biosafety debate. For the reasons mentioned in the previous paragraph, the Ministries of Agriculture have traditionally been the authorities involved in the decision-making process regarding GMOs. Gradually, environmental authorities started demanding and assuming an active role in the regulation of GMOs in view of their mandate to protect the environment. This trend has been strengthened by the incorporation of biosafety provisions into environmental laws and regulations. In some cases, GMOs are even subject to environmental impact assessments (at least based on a literal interpretation of the pertinent legal provisions).

Comparison of Approval Systems

In Asia, the only major GM crops approved for commercial release are Bt cotton, which is grown commercially in China, India, and Indonesia, and GM corn recently approved in the Philippines. To date, no Asian government has given official permission to plant GM soybeans or rice.

In the context of GM crops, the concept of "biosafety" is, in principle, a broad one, covering three areas: the health safety of humans and livestock, the safety of the environment (i.e., ecology and biodiversity), and socioeconomic safety (i.e., the economic and social impact on farmers, consumers, and different social classes, as well as on trade and economy in general) [44]. While the biosafety regulations in force in industrialized countries (e.g., Canada, the European Union, and the USA) address only the health and environmental risks and exclude socioeconomic considerations, the regulations in developing countries (e.g., India, Argentina, SA, and the Philippines) tend to include all three areas.

Countries have responded differently to the opportunities presented by GM crops and the potential risks associated with them (Table 2). The composition of the "trade off" between potential benefits and risks in each case depends upon whether a government adopts a permissive, precautionary, or prohibitive policy approach to GM crops. Three basic conditions may thus trigger application of protective measures: uncertainty, risk, and lack of proof of direct causal link [5]. As major agricultural exporters, Argentina, Canada, and the USA have each adopted a permissive attitude very early on, widely authorizing most GM products for production and consumption, thereby benefiting from lower production costs and greater export profits.

Commercialisation of GM Crops: Comparison of Regulatory Frameworks. Table 2 Main characteristics of commercialization approval systems in study countries

Element of approval system	Country/region							
	Argentina	Canada	China	Europe	India	Philippines	S. Africa	USA
Biosafety/GMO-specific law/act	X	X	X	✓	X	X	✓	X
Regulatory trigger: process (A) or product (B)	B	B[a]	B	A	A	A	A	B
Responsible ministry or government department: agriculture (A), environment (E), or health (H)	A	A,H	A	A or E[b]	E	A		A, E[c]
ERA committee composition: academia (A), commercial (C), government (G), or public (P) representatives	A,C, G,P	G	A,G	A	G	A,G	A,G	G
Obligatory domestic field testing	✓	X[d]	✓	X[d]	✓	✓[e]		
Obligatory prior approval in export country		X	✓	X		✓	✓	
Compulsory compliance with food-safety requirements	✓	✓	✓	✓	✓	✓	✓	X[f]
Socioeconomic impacts considered	✓	X	X[g]	X	✓		✓	X
Compulsory variety registration	✓	✓	✓		✓			
Mandatory post-market monitoring[h]		X		✓	✓			X
Time- or spatially restricted authorization		✓		✓	✓			X
Public consultation (days)				30	30[i]	60	30	✓

[a]In contrast to all other countries, Canada relies on the concept of novelty to trigger regulatory oversight and has declared that all plants derived through genetic modification are considered novel

[b]The European Commission sends its draft approval to the Council of Ministers (agricultural or environmental ministers), which has three months to reject or adopt it. If they do not act within this time, the Commission may adopt its own decision and authorize the new GM product

[c]For those GM plants producing their own pesticide, the evaluation is coordinated between APHIS and the USEPA

[d]Where data from field studies on other continents are supplied, the applicant should submit a reasoned argument that the data is applicable to domestic conditions

[e]For local applications only, not for applications for import

[f]Developers of GM crops engage in a voluntary, but recommended, consultation process with the USFDA (voluntary pre-market review). This process is currently under review

[g]Taking socioeconomic considerations into account during the risk assessment process is not legally required in China [30]

[h]✓ – Mandatory requirement for approved post-marketing monitoring plans and reporting. X – No specific approval requirement, but the developer is expected to monitor for existing and emerging risks that may be associated with its product and notify the regulatory authorities whenever new information is uncovered

[i]Thirty-day time period is provided for public consultation after the formal approval

Regulators in India, Europe, and the Philippines, on the other hand, have taken a more cautious approach based on guaranteeing a very low level of risk to human health and the environment. They have therefore imposed strict control measures on approval and marketing of GMOs and GM products [5]. While China had initially moved quickly on the approval of GM crops for environmental and commercial releases, the approval process has slowed considerably since 2000, and strict regulations have been implemented for GMO imports [15].

Further differences are obvious. Process-based regulation is the rule in almost all countries that have developed national biosafety regulatory systems. Even in countries employing a product-focused RA process, the scope of regulatory oversight is defined by the process of genetic modification. Canada is the only country in which regulatory oversight is triggered solely by the novelty of the trait(s) expressed by plants, irrespective of the means by which the novel traits were introduced – an approach that is most consistent with the scientific principle that the risks associated with GM crops are not inherently different than those posed by more conventional crops [117, 118]. Indeed, the US National Research Council has explicitly recommended using objective compositional changes, not breeding method, as the basis for regulatory scrutiny and even then, only "when warranted" [119]. India, Argentina, Canada, most EU countries, and South Africa have all used non-statutory guidelines to manage the environmental impact of GM crops before promulgating new acts or regulations. There is no evidence that this approach has ever compromised environmental safety. India is the exception among the study countries in locating its biosafety decision-making authority solely within the ministry responsible for the environment, while the Ministry of Agriculture predominates among the remaining study countries. As a rule, environment ministries have a more precautious or preventative approach to introducing new technologies, as compared to those with the responsibility for agriculture. Different structural approaches are used to secure the necessary scientific advice for the decision-making process. The EU has implemented a system of expert advisory committees, while others, such as India, Canada, and the USA, rely primarily on scientists and professionals working within government departments and agencies. Other countries, e.g., Argentina, China, and South Africa, have a combination of both. Only India and the EU mandate post-market monitoring in attempts to gauge the impacts of the introduction of GM crops over the long-term as well as larger spatial scales. Other countries may address this indirectly by authorizing time-limited or geographically limited introductions (e.g., Canada), whereas the USA does neither.

Conclusion and Future Directions

Governments have an important role in ensuring that novel foods are safe for human consumption and that novel agricultural inputs do not cause major negative impacts on the environment and long-term agricultural production. The adoption of biosafety regulatory frameworks is a challenging task since decision-makers are faced with numerous difficulties, such as ever-evolving technology, which can quickly render specific regulations obsolete. Countries and policy-makers are responding to these various problems with different legislative and policy-based strategies. As seen above, most countries, with the notable exception of the USA, consider GM crops to be novel foods, regardless of the characteristics of their final product. Hence, new laws and institutions to regulate potential biosafety and food-safety issues have and continue to be established, requiring that GM products be approved before they may be grown in, consumed in, or imported into a country. Concurrently, public opinion in many parts of the world still regards the use of GM crops as controversial. Concerns about new risks have led biosafety, food-safety, and labeling regulations to become complex and costly, with no tiered mechanisms in place to regulate the various and different GMOs based upon the level of risk presented and the amount of regulatory experience gained with similar products. As a result, regulation has evolved which implicitly assumes that all GMOs have the ability to present the same (high) risk unless proven otherwise, requiring the over-production of data of questionable value to decision-making. This regulatory position has become a real threat to the future development of GM crops in the non-corporate and public sectors,

especially for those subsistence crops involving tolerance to abiotic stress and higher nutrient contents being specifically developed for the benefit of farmers and consumers in the developing world. Should regulatory safety standards be set to an impossibly high threshold (e.g., at zero risk), these GM crops are unlikely to be approved in those countries who stand to gain most from their potential benefits.

The requirements of setting up effective and efficient regulations and legislative systems pertaining to products of rDNA technology inevitably involve additional costs, e.g., the development and maintenance of institutions, procedures, and management tools, costs which many developing countries cannot afford. Even should developing countries decide to form their regulatory frameworks by adapting regulatory guidance already implemented elsewhere, cost sharing still carries a financial burden. Once a system is in place, other relevant costs include the cost of compliance with biosafety regulations and risk management conditions, as well as the economic, environmental, and health costs related to delayed access to new technologies and products and their associated benefits. The variety and disparity of potential frameworks call for a normalization of information requirements and, wherever synergies and cooperation mechanisms are promoted, a harmonization of the scientific and technical aspects of regulatory oversight at the national and subregional level. As such, an expanded use of internationally accepted consensus can promote the acceptance of regional approaches to regulation. Examples include OECD documents on scientific aspects of risk assessment, as well as guidelines issued by international standard-setting bodies such as the International Plant Protection Convention and the Codex Alimentarius. Programs that create networks on regional and subregional levels may also facilitate the acquisition and dissemination of biosafety expertise at reduced costs. Providing useful, relevant information is a worthwhile task, but it can also prove expensive to provide training on how best to utilize such information in decision-making. It is therefore imperative that external funding streams continue to be directed toward supporting the establishment of effective regulatory systems in developing countries that respond to national needs and policies, until such time that they become self-sustainable.

Disclaimer

Opinions and views expressed in this chapter are strictly those of the authors and may not necessarily represent those of the organizations where the authors are currently employed.

Bibliography

1. Cordonier Segger M-C, Perron-Welch F, Frison (eds) (2012) Introduction. In: Legal aspects of implementing the Cartagena protocol: Biosafety becomes binding. Cambridge University Press, UK
2. James C (2010) Global status of commercialized biotech/GM crops: 2010. ISAAA Brief No. 42. International service for the acquisition of agri-biotech applications (ISAAA), New York, USA. http://www.isaaa.org/resources/publications/briefs/42/executivesummary/pdf/Brief42-ExecutiveSummary-English.pdf
3. James C (2009) Global status of commercialized biotech/GM crops: 2009. The first fourteen years, 1996 to 2009. ISAAA Brief No. 41. International service for the acquisition of agri-biotech applications (ISAAA), New York, USA. http://www.isaaa.org/resources/publications/briefs/41/executivesummary/pdf/Brief41-ExecutiveSummary-English.pdf
4. Falck-Zepeda J, Cavalieri A, Zambrano P (2008) Delivering genetically engineered crops to poor farmers. Recommendations for improved biosafety regulations in developing countries. IFPRI Policy Brief 14. Washington DC, USA. http://www.ifpri.org/sites/default/files/publications/bp014.pdf
5. Zarrilli S (2005) International trade in GMOs and GM products: National and multilateral legal frameworks. Policy issues in international trade and commodities study series, 29. United Nations conference on trade and development, New York, USA and Geneva, Switzerland. http://www.eldis.org/static/DOC18565.htm
6. Mugabe J (2003) International trends in modern biotechnology: Entry by and implications for African countries. ATPS special paper series No. 15, African technology policy studies network (ATPS), Nairobi, Kenya. http://www.atpsnet.org/content/files/documents/SpecialPaperSeries15.pdf
7. Anderson K, Valenzuela E, Jackson LA (2006) Recent and prospective adoption of genetically modified cotton: a global CGE analysis of economic impacts. World Bank policy research working paper 3917. http://www-wds.worldbank.org/external/default/WDSContentServer/IW3P/IB/2006/05/10/000016406_20060510092736/Rendered/PDF/wps3917.pdf
8. US Department of Agriculture (2006) Argentina. Biotechnology Annual Report 2006. Foreign agricultural service GAIN Report AR6027, Washington DC, USA. http://www.fas.usda.gov/gainfiles/200610/146249372.pdf
9. Trigo EJ, Cap EJ (2003) The impact of the introduction of transgenic crops in Argentinean agriculture. J Agrobiotechnol Manage Econ (AgBioForum) 6(3):87–94, http://www.agbioforum.org/v6n3/v6n3a01-trigo.pdf

10. James C (2006) Global Status of Commercialized Biotech/GM Crops: 2006. ISAAA Brief No. 35. ISAAA, New York, USA. http://www.isaaa.org/resources/publications/briefs/35/executivesummary/pdf/Brief35-ExecutiveSummary-English.pdf
11. Nap J, Metz P, Escaler M, Conner A (2003) The release of genetically modified crops into the environment. Part 1. Overview of current status and regulations. Plant J 33(1):1–18
12. UNEP-GEF Biosafety Unit (2006) A comparative analysis of experiences and lessons from the UNEP-GEF biosafety projects. United Nations Environment Programme (UNEP)-Global Environment Facility (GEF), Geneva, Switzerland. http://www.unep.ch/biosafety/development/devdocuments/UNEPGEFBiosafety_comp_analysisDec2006.pdf
13. Burachik M, Traynor P (2002) Analysis of a national biosafety system: regulatory policies and procedures in Argentina. ISNAR Country Report no. 63, International Service for National Agricultural Research, The Hague, The Netherlands. ftp://ftp.cgiar.org/isnar/Publicat/cr63.pdf
14. BATS (2003) Genetically modified (GM) crops: molecular and regulatory details. Version 2. http://www.bats.ch/gmo-watch/GVO-report140703.pdf
15. Baumüller H (2004) Domestic import regulations for genetically modified organisms and their compatibility with WTO rules. Asian Biotechnol Dev Review 6(3):33–42. http://www.ris.org.in/images/RIS_images/pdf/abdr_July044.pdf
16. SAGPyA (2003) Resolution No. 39/03. Annex. Application for permit to release genetically modified plant organisms into the environment. Secretariat of agriculture, livestock, fisheries and food (SAGPyA), Argentina. http://www.sagpya.mecon.gov.ar/new/0-0/programas/biotecnologia/resolutionn39annex.pdf
17. SAGPyA (2002) Resolution No. 412/02. Requisitos para la evaluación de la aptitud alimentaria de los de organismos genéticamente modificados. Secretariat of agriculture, livestock, fisheries and food (SAGPyA), Argentina. http://www.sagpya.mecon.gov.ar/new/0-0/programas/biotecnologia/marco_regulatorio/028_412.php
18. Macdonald P, Yarrow S (2003) Regulation of Bt crops in Canada. J Invertebr Pathol 83:93–99
19. Finstad K, Bonfils A-C, Shearer W, Macdonald P (2007) Trees with novel traits in Canada: regulations and related scientific issues. Tree Genet Genomes 3:135–139
20. Agriculture and Agri-Food Canada (1994) Regulatory directive Dir94-08: Assessment criteria for determining environmental safety of plants with novel traits. Ottawa, Canada. http://www.inspection.gc.ca/english/plaveg/bio/dir/dir9408e.shtml#ch1
21. Industry Canada (1998) The federal regulatory framework for biotechnology (1993), Annex C of the 1998 Canadian biotechnology strategy: an ongoing renewal process. http://www.biostrategy.gc.ca/CMFiles/1998strategyE49RAI-8312004-5365.pdf
22. CFIA (2005) Long term testing/substantial equivalence. http://www.inspection.gc.ca/english/sci/biotech/reg/equive.shtml
23. Health Canada (2006) Guidelines for the safety assessment of novel foods. Ottawa, Canada. http://www.hc-sc.gc.ca/fn-an/alt_formats/hpfb-dgpsa/pdf/gmf-agm/guidelines-lignes directrices_e.pdf
24. CFIA (2006) Directive 96–13: import permit requirements for plants with novel traits (including transgenic plants), and their products. http://www.inspection.gc.ca/english/plaveg/protect/dir/d-96-13e.pdf
25. Huang J, Wang Q (2002) Agricultural biotechnology development and policy in China. J Agro-biotechnol Manag Econ (AgBioForum) 5(4):122–135, http://www.agbioforum.org/v5n4/v5n4a01-huang.htm
26. Karplus V, Deng XW (2008) Agricultural biotechnology in China: origins and prospects. Springer, New York
27. Chen ZL (2006) Chinese agricultural biotechnology in the field. In: Agricultural biotechnology: economic growth through new products, partnerships and workforce development, NABC Report 18. National agricultural biotechnology council (NABC), Ithaca, USA. http://nabc.cals.cornell.edu/pubs/nabc_18/NABC18_Chen.pdf
28. Pray CE, Naseem A (2007) Supplying crop biotechnology to the poor: opportunities and constraints. J Dev Stud 43(1):192–217
29. Pray C, Ramaswami B, Huang J, Hu R, Bengali P, Zhang H (2006) Costs and enforcement of biosafety regulations in India and China. Int J Technol Globalisation 2(1/2):137–157
30. Wang Y, Johnston S (2007) The status of GM rice R&D in China. Nat Biotechnol 25(7):717–718
31. Wang Y, Johnston S (2007) Review on GM rice risk assessment in China. UNU-IAS Working Paper No. 152. United Nations University-Institute of Advanced Studies, Yokohama, Japan. http://www.ias.unu.edu/resource_centre/152YanqingWang.pdf
32. US Department of Agriculture (2004) China, Peoples republic of: food and agricultural import regulations and standards (FAIRS) Country Report 2004. Foreign Agricultural Service GAIN Report CH4028, Washington DC, USA. http://www.fas.usda.gov/gainfiles/200408/146107026.doc
33. OECD (2011) Adapting agriculture to climate change: what role for biotechnology? ENV/EPOC/WPCID(2011)2, Working party on climate, Investment and Development, Environment Policy Committee, Environment Directorate, Organisation for Economic Co-operation and Development (OECD), Paris, France
34. US Department of Agriculture (2005) China, Peoples Republic of: Biotechnology Annual Report 2005. Foreign Agricultural Service GAIN Report CH5069, Washington DC, USA. http://www.fas.usda.gov/gainfiles/200601/146176661.pdf
35. Foster M, Berry P, Hogan J (2003) Market access issues for GM products. Australian bureau of agricultural and resource economics (ABARE) eReport 03.13, Canberra, Australia. http://abareonlineshop.com/PdfFiles/PC12559.pdf
36. Conner A, Glare T, Nap J (2003) The release of genetically modified crops into the environment. Part II. Overview of ecological risk assessment. Plant J 33:19–46
37. König A, Cockburn A, Crevel RWR, Debruyne E, Grafstroem R, Hammerling U, Kimber I, Knudsen I, Kuiper HA, Peijnenburg AACM, Penninks AH, Poulsen M, Schauzu M, Wal JM (2004)

Assessment of the safety of foods derived from genetically modified (GM) crops. Food Chem Toxicol 42:1047–1088
38. GEAC (2010) Yearwise list of commercially released varieties of Bt cotton hybrids by GEAC. Genetic engineering approval committee (GEAC), Ministry of Environment and Forests, Government of India. http://igmoris.nic.in/files/Final_commercially_approved.pdf
39. APCoAB (2006) Bt cotton in India – a status report. Asia-Pacific consortium on agricultural biotechnology (APCoAB), New Delhi, India. p 34. http://www.apcoab.org/documents/bt_cotton.pdf
40. Damodaran A (2005) Re-engineering biosafety regulations in India: towards a critique of policy, law and prescriptions. Law Environ Develop J 1(1):1–16, http://www.lead-journal.org/content/05001.pdf
41. Government of India (1989) Rules for the manufacture, use, import, export and storage of hazardous micro organisms genetically engineered organisms or cells. Ministry of Environment and Forests, Government of India. http://www.envfor.nic.in/legis/hsm/hsm3.html
42. Government of India (1998) Revised guidelines for research in transgenic plants & guidelines for toxicity and allergenicity evaluation of transgenic seeds, plants and plant parts. Department of Biotechnology, Ministry of Science and Technology, Government of India. August 1998. http://dbtindia.nic.in/policy/guidelines_98.pdf
43. US Department of Agriculture (2005) India biotechnology annual 2005. Foreign Agricultural Service GAIN Report IN5078, Washington DC, USA. http://www.fas.usda.gov/gainfiles/200507/146130314.pdf
44. Indira A, Bhagavan MR, Virgin I (2005) Agricultural biotechnology and biosafety in India: expectations, outcomes and lessons. Stockholm Environment Institute, Sweden. http://www.agbios.com/docroot/articles/05-268-001.pdf
45. Gupta A (2002) Ensuring "Safe use" of biotechnology: key challenges. Economic and Political Weekly, 6 July 2002, pp 2762–2769. http://www.epw.org.in/epw/uploads/articles/9705.pdf
46. Chaturvedi S, Chawii L (2005) RIS-DP # 99. Research and information system for developing countries, New Delhi, India
47. National Commission on Farmers (2006) Fifth and final report. Ministry of Agriculture, Government of India. http://krishakayog.gov.in/revdraft.pdf
48. Bhan MK (2007) BIO 2007, Boston, 9 May 2007. http://www.ciionline.org/news_new/newsMain09-05-2007_2.asp
49. Department of Biotechnology and the Ministry of Environment and Forests (2008) Guidelines & standard operating procedures (SOP) for confined field trials of genetically engineered (GE) plants. Government of India. http://igmoris.nic.in/Guideline_index.htm
50. Indian Council of Medical Research (2008) Guidelines for the safety assessment of foods derived from genetically engineered plants. New Dehli, India. http://igmoris.nic.in/files%5CCoverpage.pdf
51. Department of Biotechnology (2008) Protocols for food and feed safety assessment of GE crops. Ministry of Science and Technology, Government of India. http://igmoris.nic.in/files%5CCoverpage1.pdf
52. Indian Ministry of Agriculture (2006) Protection of plant varieties and farmers' rights regulations, 2006. The Gazette of India: Extraordinary (Part II Sec. 3(i)), 7th December 2006, New Delhi, India. http://www.plantauthority.in/PDFile/Indgazette.pdf
53. Secretary of Agriculture, the Republic of the Philippines (2001) Policy statement on modern biotechnology. http://www.ncbp.dost.gov.ph/downloads/PSMB.pdf
54. Republic of the Philippines (1998) Republic Act No. 8435, Agriculture and Fisheries Modernization Act, 10 June 1998. http://www.da.gov.ph/agrilaws/ra/afma.pdf
55. APCoAB (2005) Commercialization of Bt corn in the Philippines. A status report. Asia-Pacific consortium on agricultural biotechnology (APCoAB), New Dehli, India. p 41. http://www.apcoab.org/documents/bt_corn.pdf
56. Yorobe JM Jr, Quicoy CB (2006) Economic impact of Bt corn in the Philippines. The Philippine Agric Sci 89(3):258–267
57. US Department of Agriculture (2005) Philippines Biotechnology Annual Report 2005. Foreign Agricultural Service GAIN Report RP5027, Washington DC, USA. http://www.fas.usda.gov/gainfiles/200507/146130361.pdf
58. Republic of the Philippines (1990) Executive Order 430 Constituting the NCBP, 1990. Government of Republic of the Philippines. http://www.ncbp.dost.gov.ph/index.php?option=$com_remository&Itemid=55&func=download&filecatid=25
59. Manalo AJ, Ramon GP (2007) The cost of product development of Bt corn event MON810 in the Philippines. J Agrobiotechnol Manag Econ (AgBioForum) 10(1):19–32, http://www.agbioforum.org/v10n1/v10n1a03-manalo.pdf
60. de Leon A, Manalo A, Cielo Guilatco F (2004) The cost implications of GM food labeling in the Philippines. http://www.bcp.org.ph/downloads/CostImplicationsofGMFoodLabelinginthePhilippines.pdf
61. Department of Agriculture's Administrative Order No. 8, s. 2002. Government of Republic of the Philippines. http://www.ncbp.dost.gov.ph/downloads/commercialization.pdf.
62. Andanda AP (2006) Developing legal regulatory frameworks for modern biotechnology: the possibilities and limits in the case of GMOs. Afr J Biotechnol 5(15):1360–1369, http://academicjournals.org/ajb/PDF/pdf2006/3Aug/Andanda.pdf
63. Department of Science and Technology (2001) National biotechnology strategy for South Africa. Government of the Republic of South Africa. http://www.dst.gov.za/publications/reports/dst_biotechnology_strategy.PDF
64. Cloete TE, Nel LH, Theron J (2006) Biotechnology in South Africa. Trends Biotechnol 24(12):557–552
65. van der Walt WJ (2006) South African GM crop adoption in 2006. African Crops News Service. Newsletter May 2006. http://www.africancrops.net/news/may06/gm-southafrica.htm

66. US Department of Agriculture (2005) Republic of South Africa. Biotechnology Annual Report 2005. Foreign Agricultural Service GAIN Report SF5024, Washington DC, USA. http://www.fas.usda.gov/gainfiles/200512/146131662.pdf
67. Government of the Republic of South Africa (1997) Genetically Modified Organisms Act (No. 15 of 1997), Government Gazette, vol 383, no. 18029. 23 May 1997. http://www.info.gov.za/acts/1997/act15.htm
68. Government of the Republic of South Africa (2005) The GMO Amendment Bill. Government Gazette 27913, 26 August 2005. http://www.info.gov.za/gazette/bills/2005/b34-05.pdf
69. Gouse M, Pray CE, Kirsten J, Schimmelpfennig D (2005) A GM subsistence crop in Africa: the case of Bt white maize in South Africa. Int J Biotechnol 7(1/2/3):84–94, http://inderscience.metapress.com/media/7hxdqlmumk0y0qgunm13/contributions/j/d/2/p/jd2pphettplpyg50.pdf
70. RSA Department of Agriculture (2004) Guideline document for use by the advisory committee when considering proposals/applications for activities with genetically modified organisms. Government of the Republic of South Africa (RSA). http://www.nda.agric.za/docs/geneticresources/GuidelinesforAC-May2004.pdf
71. RSA Guidelines. Public notification in terms of the Genetically Modified Organisms Act, 1997 (Regulation 6). Republic of South Africa (RSA). http://www.nda.agric.za/docs/geneticresources/publicnotice.pdf
72. Bernauer T, Meins E (2003) Technological revolution meets policy and the market: explaining cross-national differences in agricultural biotechnology regulation. Eur J Polit Res 42:643–683
73. US Office of Science and Technology Policy (1986) Coordinated framework for regulation of biotechnology, United States Federal Register, 51:23302, June 26, 1986. http://usbiotechreg.nbii.gov/Coordinated_Framework_1986_Federal_Register.html
74. MacKenzie DJ (2000) International comparison of regulatory frameworks for food products of biotechnology. Prepared for the Canadian Biotechnology Advisory Committee Project Steering Committee on the Regulation of Genetically Modified Foods. http://www.cbac-cccb.ca/epic/internet/incbac-cccb.nsf/vwapj/InternatComparisons_MacKenzie.pdf/$FILE/InternatComparisons_MacKenzie.pdf
75. US Department of Agriculture (2001) Economic issues in biotechnology. economic research service, Agriculture Information Bulletin no. 762, Washington DC, USA. http://www.ers.usda.gov/Publications/aib762/
76. US Department of Agriculture (1987) Introduction of organisms and products altered or produced through genetic engineering which are plant pests or which there is reason to believe are plant pests, 7 CFR Parts 330 and 340. United States Federal Register 52(115), June 16 1987. http://www.aphis.usda.gov/brs/687rule.txt
77. US Department of Agriculture (1997) Simplification of requirements and procedures for genetically engineered organisms and products, 7 CFR Part 340. United States Federal Register 62(85), May 2 1997. http://www.aphis.usda.gov/brs/pdf/r597rule.pdf
78. US National Research Council (2000) Genetically modified pest-protected plants, science and regulations. National Research Council, National Academy, Washington DC, USA, pp 104–207. http://newton.nap.edu/catalog/9795.html#toc
79. US Environmental Protection Agency (2001) Plant incorporated protectants. US Environmental Protection Agency, Washington DC, USA. http://www.epa.gov/pesticides/biopesticides/pips/index.htm
80. US Environmental Protection Agency (2001) Plant-incorporated protectants, final rules and proposed rule, 40 CFR Parts 152 and 174. United States federal register 66(139), 19 July 2001. http://www.epa.gov/pesticides/biopesticides/pips/pip_rule.pdf
81. Jaffe G (2012) Crafting national biosafety regulatory systems. In: Cordonier Segger M-C, Perron-Welch F, Frison (eds) Legal aspects of implementing the Cartagena protocol: Biosafety becomes binding. Cambridge University Press, UK
82. Secretariat of the Convention on Biological Diversity (2000) Cartagena Protocol on Biosafety to the Convention on Biological Diversity. Montreal, Canada. http://www.cbd.int/biosafety/protocol.shtml.
83. Secretariat of the Convention on Biological Diversity (1992) Convention on biological diversity. Montreal, Canada. http://www.cbd.int/doc/legal/cbd-en.pdf
84. Secretariat of the Convention on Biological Diversity (2000) Decision EMI/3. Adoption of the Cartagena protocol and interim arrangements. First extraordinary meeting (ExCOP 1), 22–23 Feb 1999, Cartagena, Colombia 1999, and Montreal, 24–29 Jan 2000. http://www.cbd.int/doc/meetings/cop/excop-01/official/excop-01-03-en.pdf
85. Secretariat of the Convention on Biological Diversity (2003) The Cartagena protocol on biosafety: a record of the negotiations. Montreal, Canada. http://bch.cbd.int/database/attachment/?id=10886
86. Secretariat of the Convention on Biological Diversity (2011) Cartagena protocol on biosafety ratification list. Montreal, Canada. http://www.cbd.int/doc/lists/cpb-ratifications.pdf
87. Secretariat of the Convention on Biological Diversity (2011) Nagoya – Kuala lumpur supplementary protocol on liability and redress to the cartagena protocol on biosafety. Montreal, Canada. http://bch.cbd.int/database/attachment/?id=10898
88. Cabrera Medaglia J (in press) Biosafety regulatory frameworks in the Americas. In: Cordonier Segger M-C, Perron-Welch F, Frison (eds) Legal aspects of implementing the Cartagena protocol: Biosafety becomes binding. Cambridge University Press, UK
89. WTO (1994) Marrakesh agreement establishing the world trade organization. Final Act of the 1986–1994 uruguay round of trade negotiations. World Trade Organization (WTO), Geneva, Switzerland. http://www.wto.org/english/docs_e/legal_e/04-wto_e.htm

90. WTO (1994) Agreement on the application of sanitary and phytosanitary measures (SPS Agreement) (Article 1 – 14). Final Act of the 1986 –1994 uruguay round of trade negotiations. Annex 1a, Multilateral agreements on trade in goods. World Trade Organization (WTO), Geneva, Switzerland. http://www.wto.org/english/docs_e/legal_e/15sps_01_e.htm
91. WTO (1994) Agreement on technical barriers to trade (TBT Agreement) (Article 1 – 15). Final Act of the 1986 – 1994 Uruguay round of trade negotiations. Annex 1a, multilateral agreements on trade in goods. World Trade Organization (WTO), Geneva, Switzerland. http://www.wto.org/english/docs_e/legal_e/17-tbt_e.htm
92. WTO (1994) Agreement on trade-related aspects of intellectual property rights (TRIPS Agreement). Final Act of the 1986 –1994 uruguay round of trade negotiations. Annex 1, Multilateral agreements on trade in goods. World Trade Organization (WTO), Geneva, Switzerland. http://www.wto.org/english/docs_e/legal_e/27-trips_01_e.htm
93. WTO (1994) Understanding on rules and procedures governing the settlement of disputes. Final Act of the 1986 – 1994 uruguay round of trade negotiations. Annex 2, multilateral agreements on trade in goods. World Trade Organization (WTO), Geneva, Switzerland. http://www.wto.org/english/docs_e/legal_e/28-dsu_e.htm
94. WTO (1994) General agreement on tariffs and trade. Final act of the 1986 –1994 uruguay round of trade negotiations. Annex 1A, multilateral agreements on trade in goods. World Trade Organization (WTO), Geneva, Switzerland. http://www.wto.org/english/docs_e/legal_e/06-gatt_e.htm
95. CAC (1999) Summary and conclusions. Report of the twenty-third session, FAO headquarters, Rome, Italy, 28 June–3 July 1999. Codex Alimentarius Commission (CAC) of the World Health Organisation (WHO), Geneva, Switzerland, pp 124. www.codexalimentarius.net/download/report/518/Al99_37e.pdf
96. CAC (2003) Alinorm 03/41. Report of the twenty-sixth session, FAO headquarters, Rome, Italy, 30 June–7 July 2003. Codex Alimentarius Commission (CAC) of the World Health Organisation (WHO), Geneva, Switzerland. ftp://ftp.fao.org/codex/alinorm03/al03_41e.pdf
97. CAC (2003) Principles for the risk analysis of foods derived from modern biotechnology. CAC/GL 44–2003. Amended in 2008. Codex Alimentarius Commission (CAC) of the World Health Organisation (WHO), Geneva, Switzerland. http://www.codexalimentarius.net/download/standards/10007/CXG_044e.pdf
98. CAC (2003) Guideline for the conduct of food safety assessment of foods derived from recombinant-DNA plants. CAC/GL 45–2003. Codex Alimentarius Commission (CAC) of the World Health Organisation (WHO), Geneva, Switzerland. http://www.codexalimentarius.net/download/standards/10021/CXG_045e.pdf
99. CAC (2003) Guideline for the conduct of food safety assessment of foods produced using recombinant DNA microorganisms. CAC/GL 46–2003. Amended in 2008. Codex Alimentarius Commission (CAC) of the World Health Organisation (WHO), Geneva, Switzerland. http://www.codexalimentarius.net/download/standards/10025/CXG_046e.pdf
100. CAC (2008) Guideline for the conduct of food safety assessment of foods derived from recombinant-DNA animals. CAC/GL 68–2008. Codex Alimentarius Commission (CAC) of the World Health Organisation (WHO), Geneva, Switzerland. http://www.codexalimentarius.net/download/standards/11023/CXG_068e.pdf
101. CAC (2008) Alinorm 08/31/REP. Report of the thirty-first session, FAO headquarters, Rome, Italy, 30 June–4 July 2008. Codex Alimentarius Commission (CAC) of the World Health Organisation (WHO), Geneva, Switzerland. http://www.codexalimentarius.net/download/report/698/al31REPe.pdf
102. CAC (2007) Alinorm 07/30/22. Report of the thirty-fifth session of the Codex committee on food labelling, Ottawa, Canada, 30 April–4 May 2007. Codex Alimentarius Commission (CAC) of the World Health Organisation (WHO), Geneva, Switzerland. http://www.codexalimentarius.net/download/report/682/al30_22e.pdf
103. CAC (2007) Working principles for risk analysis for food safety for application by governments. CAC/GL 62–2007. Codex Alimentarius Commission (CAC) of the World Health Organisation (WHO), Geneva, Switzerland. http://www.codexalimentarius.net/download/standards/10751/CXG_062e.pdf
104. FAO (1997) International plant protection convention. New revised text approved by the FAO conference at its 29th session, November 1997. Food and Agriculture Organization of the United Nations (FAO), Rome, Italy. https://www.ippc.int/file_uploaded//publications/13742.New_Revised_Text_of_the_International_Plant_Protectio.pdf
105. Secretariat of the IPPC (2004) Pest risk analysis for quarantine pests including analysis of environmental risks and living modified organisms. International plant protection convention (IPPC), Food and Agriculture Organization of the United Nations, Rome, Italy. https://www.ippc.int/file_uploaded/1146658377367_ISPM11.pdf
106. OIRSA (2000) Eighth meeting of the executive committee, 31 March 2000. Organismo Internacional Regional de Sanidad Agropecuaria (OIRSA), San Salvador, El Salvador. http://www.oirsa.org/documentos/actasyresoluciones/resoluciones/xiii-31-mar.-2000-recomendaciones.pdf
107. CGRFA (2007) Code of conduct on biotechnology as it relates to genetic resources for food and agriculture. Commission on Genetic Resources for Food and Agriculture (CGRFA), Food and Agriculture Organization of the United Nations, Rome, Italy. http://www.fao.org/ag//CGRFA/biocode.htm
108. UNECE (2001) UN recommendations on the transport of dangerous Goods – model regulations. Twelfth revised edition. United Nations Economic Commission for Europe (UNECE), Geneva, Switzerland. http://www.unece.org/trans/danger/publi/unrec/12_e.html

109. UNECE (1998) Convention on access to information, public participation in decision-making and access to justice in environmental matters (Aarhus Convention), United Nations Economic Commission for Europe (UNECE), Geneva, Switzerland. http://www.unece.org/env/pp/welcome.html
110. UNEP-GEF Biosafety Unit (2003) Guide for the implementation of national biosafety frameworks. United Nations Environment Programme (UNEP)-Global Environment Facility (GEF) Projects on Implementation of national biosafety frameworks, Geneva, Switzerland. http://www.unep.org/biosafety/Documents/Impl.Guide-RegReg.pdf
111. McLean MA, Frederick RJ, Traynor P, Cohen JI, Komen J (2002) A conceptual framework for implementing biosafety: linking policy, capacity and regulation. Briefing paper No. 47, Program for biosafety systems, International Food Policy Research Institute, Washington DC, USA. http://programs.ifpri.org/isnararchive/publications/pdf/bp-47.pdf
112. Burachik M, Traynor P (2002) An analysis of a national biosafety system: regulatory policies and procedures in Argentina. Country Report No. 63, Program for biosafety systems, International Food Policy Research Institute, Washington DC, USA. http://programs.ifpri.org/isnararchive/publications/pdf/ cr63.pdf
113. Jaffe G (2004) Regulating transgenic crops: a comparative analysis of different regulatory processes. Transgenic Res 13(1):5–19
114. UNEP-GEF Biosafety Unit (2005) Toolkit for the development project, phase 3 – Drafting the NBF. Part I: Formulation of the regulatory regime, project on development of national biosafety frameworks. United Nations Environment Programme (UNEP) – Global Environment Facility (GEF), Geneva, Switzerland. http://www.unep.org/biosafety/Documents/Drafting_the_NBF_Formulation_of_the_regulatory_regime.pdf
115. Garforth K (2005) When biosafety becomes binding. In: Cordonier Segger M-C, Weeramantry CG (eds) Sustainable justice: reconciling economic, social and environmental law. Martinus Nijhoff, Boston
116. Pew Initiative on Food and Biotechnology (2004) Issues in the regulation of genetically engineered plants and animals. Washington, DC, USA. http://www.pewtrusts.org/uploadedFiles/wwwpewtrustsorg/Reports/Food_and_Biotechnology/food_biotech_regulation_0404.pdf
117. OECD (1986) Recombinant DNA safety considerations: safety considerations for industrial, agricultural and environmental applications of organisms derived by recombinant DNA techniques. Organisation for Economic Co-operation and Development (OECD), Paris, France. http://www.oecd.org/dataoecd/45/54/1943773.pdf
118. US National Research Council (1987) Introduction of recombinant DNA-engineered organisms into the environment, Key Issues. White Paper. National Academies Press, Washington DC, USA
119. US National Research Council (2004) Safety of genetically engineered foods. National Academies Press, Washington DC, http://www.nap.edu/books/0309092094/html/

Community-Owned Water Resource and Climate Change, Quality Management

G. G. Tushara Chaminda[1], Michio Murakami[1], Hiroaki Furumai[2]
[1]The University of Tokyo, Bunkyo-ku, Tokyo, Japan
[2]Department of Urban Engineering,
The University of Tokyo, Bunkyo-ku, Tokyo, Japan

Article Outline

Glossary
Definition of the Subject and Its Importance
Introduction
Importance of Community-Owned Water Resources
Evaluation of Water Quality in Community-Owned Water Resources
Characterizing and Ranking of Different Water Resources – A Case Study on WQ Information Platform in Japan
Future Direction
Acknowledgment
Bibliography

Glossary

Community-owned water resources Water sources that can be easily found within the boundaries of a community such as rainwater or reclaimed water.

Non-potable water Water use for all applications except a direct potable application such as drinking.

Potable water Water that is suitable for any kind human consumption. Simply, the term can be defined as drinking water.

Public perception As applied to water aggregate of individual attitudes or beliefs held by general public on water or wastewater.

Rainwater harvesting Collection, storage, and use of rainwater for various water applications.

Reclaimed water Already used water that has been recovered by various treatment processes to meet specific water quality criteria.

Reuse As applied to water, the use of treated water for a beneficial use including domestic, urban, industrial, or agricultural application.

Runoff water Part of the precipitation that appears in surface and does not soak into the ground where it falls.

Sustainable water use Optimizing the benefits of present water use without diminishing the ability of future generation to meet their water needs.

Definition of the Subject and Its Importance

Observational records and climate projections provide abundant evidence that climate change affects the hydrological systems such as changing precipitation patterns, intensity and extremes, increasing evaporation, changes in soil moisture and runoff, etc. Thus, global freshwater resources are being under growing pressure owing to climate change effect on hydrological cycle. Population growth, rapid economic development, and land use change along with climate change bring water issues to the forefront. The insufficient water availability may cause the degradation in human health, ecosystems, agricultural and industrial output, and increase the potential of water-related conflict. Adaptation measures have to be pursued to deal with the water scarcity problem and to manage water resources sustainably. It is better to explore more stable, economical, and environmental friendly ways to meet water demand through the proper evaluation. Rainwater and reclaimed water have been receiving growing interests as complementary water sources for urban communities.

Water quality (WQ) is the most important issue in such complementary waters that determines the acceptable and safety use for a given application. However, general public often does not understand the quality difference among different types of possible water resources and hence many communities do not have a positive image on alternative water sources such as reclaimed water and rainwater. Complexity of understanding the WQ causes people to hesitate use of reclaimed water or rainwater. Therefore, it is important to provide WQ information from trusted scientific and regulatory sources in a simple manner so that general public can easily understand the quality characteristics of water resources for different water use. The proposed WQ information platform integrates the multivariate nature of WQ data by providing scoring system that will logically combine all WQ parameters and provide a simple and easily understood description of community-owned water resources.

Introduction

Impact of Climate Change on Freshwater Resources

The United Nation Framework Convention on Climate Change (UNFCCC), in its Article 1, defines "climate change" as a change of climate which is attributed directly or indirectly to human activity that alters the composition of the global atmosphere and which is in addition to natural climate variability observed over comparable time periods [1]. The scientific panel of International Panel on Climate Change (IPCC) revealed that the global average surface temperature has increased since 1861 and over the twentieth century, the increase has been $0.6°C \pm 0.2°C$ [2]. Knowing the future global threat, at the United Nations Climate Change Conference in Copenhagen in the end of year 2009, world leaders agreed to cap the global temperature rise by committing to significant emission reductions, and to raise finance to kick-start action in the developing world to deal with climate change [3]. Therefore, it is now well evident that climate change is already happening and going to be one of the greatest environmental, social, and economic threats facing the whole world.

While many factors continue to influence climate, scientists have shown that human activities are the most dominant force, and responsible for most of the climate change observed over the past 50 years [4]. Human activities contribute to climate change by causing changes in Earth's atmosphere in the amounts of greenhouse gases, aerosols, and cloudiness [5]. Increases in the concentrations of greenhouse gases and aerosols will affect climate by altering incoming solar radiation and outgoing infrared radiation that are parts of Earth's energy balance [6]. The overall effect has caused to warm the lower atmosphere and earth surface and is likely to continue to increase the mean temperature about 1°C by 2025 and 3°C by the end of the next century [7]. The impacts of climate change are across many sectors including health, ecosystem, agriculture, and water. The Second Climate Conference, which was held in 1990, in Geneva, recognized that among the most important impacts of climate change were its effects on the hydrological cycle and on water

management systems [8]. Thus, climate change and its potential impacts on water resources have become an increasingly common topic among the general public, engineers, water managers, as well as scientists.

Since the water is involved in all components of the climate system including atmosphere, hydrosphere, cryosphere, land surface, and biosphere, climate change affects water through many ways. Climate change observed over the past several decades is potentially associated with changes in several processes of the hydrological cycle and systems such as changing precipitation patterns, intensity and extremes, widespread melting of snow and ice, increasing atmospheric water vapor, increasing evaporation. It leads to changes in soil moisture and runoff [9–11].

Quantity The Earth's surface radiates part of the solar energy back to the atmosphere in the form of infrared radiation. Most of this infrared radiation is trapped in the atmosphere by greenhouse gases, such as carbon dioxide, methane, and nitrous oxide and directed back toward the Earth's surface. This process causes warming the planet and ultimately will lead to change in hydrological cycle. As suggested by some research, warmer temperature will cause more water to escape from earth surface and return to atmosphere through evaporation and transpiration. Thus, precipitation changes are expected and will be highly complex and variable than the usual pattern.

Figure 1 shows the unstable precipitation patterns in Japan and it seems that the fluctuations have gradually become larger in last 50 years. The consequent change in the hydrological cycle adversely affects the stability of groundwater and surface water sources, accounting for nearly 31% of total fresh water budget in the world. As a result of the overall effects, some regions will receive more precipitation, while other regions receive less. Therefore, depending on the fluctuating precipitation, severe droughts and floods may occur more frequently. The flood frequency was projected to increase over many regions except those including North America and central to western Eurasia, whereas the drought frequency was projected to increase globally except northern high latitude, eastern Australia, and eastern Eurasia. Both flood frequency and drought frequency are projected to increase even in the same region of the world. Such regions show a decrease in the number of precipitation days, but an increase in days with heavy rainfalls [13]. At the end of the twenty-first century, the annual mean

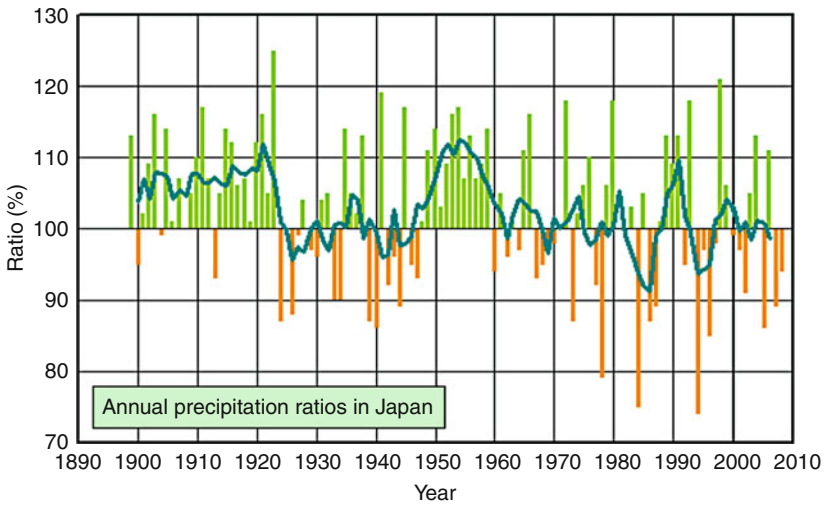

Community-Owned Water Resource and Climate Change, Quality Management. Figure 1
Annual precipitation ratios from 1898 to 2008 in Japan (The Japan Meteorological Agency [12]). Note: The *bars* indicate annual precipitation ratios to normal (1971–2000 average) averaged of the 51 stations. The *green line* indicates 5-year running mean

precipitation, evaporation, and runoff increase in high latitudes of the Northern Hemisphere, southern to eastern Asia, and central Africa, whereas they decrease in the Mediterranean region, southern Africa, southern North America, and Central America [14]. Changes in precipitation patterns and evapotranspiration will also directly affect the soil moisture condition. In a summer season, high evaporation may exceed the precipitation and hence subsurface water storage would act as a moisture source to the atmosphere. This may cause the upward movement of water from shallow aquifers, resulting in a steep decline of the water table.

As climate change increases ocean temperatures, the seawater will expand, contributing to sea level rise due to thermal expansion. The IPCC has found that the global mean sea level has risen at an average rate of about 1.7 ± 0.5 mm/year during the twentieth century [15]. Changes in sea level will increase coastal erosion, and flooding of wetlands and lowlands, leading to significant impacts on the availability of freshwater. Climate changes will also have impact on saltwater instruction into aquifers due to the sea level rise, and thus adversely affect the groundwater in coastal aquifers [16].

Quality In addition to the water availability, changes in climate could lead to important changes in water quality as well. Current changes in climate possibly influence water quality by altering the balance between atmospheric, terrestrial, and aquatic processes in a watershed in a variety of ways. Frequent heavy precipitation in some regions may cause wash-off of more nonpoint pollutants and soil erosion into water bodies further deteriorating the water quality.

Increasing water temperature caused by increased air temperatures may affect the reaction rate in biogeochemical processes and the chemical properties of water [11, 16, 17]. Among water quality parameters, dissolved organic matter, nutrients, micropollutants, and pathogens are susceptible to rise in concentration because of temperature increase [18]. Since warmer water can hold less oxygen, global warming would lead to lower dissolved oxygen contents in surface waters [19]. The warmer temperature will also foster algal blooms [20] in water bodies. In addition, evaporative water losses could increase the salinity of surface waters, especially in lakes and reservoirs. Warmer water combines with excess nutrients washed by heavy rainfalls and increase of algae, bacteria, and fungi content will ultimately deteriorate the ecosystem of lakes, streams, and their biological communities. Water quality impairment has been also observed in rivers, such as increased BOD and NH_4, because of the loss of stream dilution capacity and low water velocities derived from the reduced stream flows [21]. Increased salinity is another potential problem in rivers and estuaries, where streamflows are reduced. Figure 2 is a simple illustration showing the influence of climate change on water quality of freshwater resources.

Adaptive Measures Against Climate Change Effect on Water Resources

There is absolutely no doubt that climate change is possibly the major environmental challenge for the coming decades. It is also well evident that climate change has the potential to be affecting the quantitative and qualitative status of freshwater resources by altering hydrological cycles with wide-ranging consequences for human societies and ecosystems. Therefore, in order to cope with the climate change effect on water resources, there have been two main responses: mitigation and adaptation. Mitigation is needed in order to prevent future anthropogenic interference with the climate system that can influence water resources and their management. On the other hand, adaptation is an adjustment in natural or human systems to a new or changing environment, including water resources. Adapting or coping with climate change will therefore become necessary in sustainable water use. Adaptation measures may differ across and within local, national, regional, or global level and must be addressed under complex and uncertain conditions. These measures can be undertaken at different scales and may vary from individual households and local communities to a range of public and private sectors through policies, investments in infrastructure and technologies, and behavioral change.

As the impacts of climate change on water resources begin to be realized, attention on adaptation technologies is also becoming increasingly important and must be increased as a matter of urgency. The report of Working Group II, Fourth Assessment of IPCC (2007), addresses the future impacts of climate change

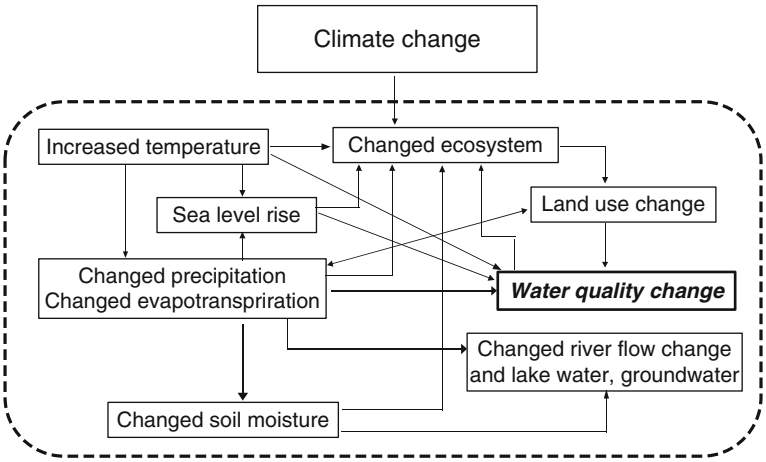

Community-Owned Water Resource and Climate Change, Quality Management. Figure 2
Influence of climate change on water quality of freshwater resources

on various sectors including water resources and the potential for adaptation and the implications for sustainability [22]. Adaptation to climate change impact on water resources can adopt a variety of forms, such as water demand control through better education, training, and awareness of climate change as well as more technical measures for water resource management, water withdrawal, transportation, treatment, supply, water uses, etc. Some possible adaptation initiatives that take into account the potential impacts of climate change on water resources can be listed as follows.

1. Water demand and supply management
   (a) Water demand management through metering and pricing
   (b) Water leakage reduction
   (c) Efficient water usage in agriculture
2. Water resource conservation
   (a) Soil moisture conservation
   (b) Coastal defense design and implementation to protect water supply against contamination
   (c) Eutrophication control
   (d) Conservation of groundwater through artificial recharge
   (e) Conservation of upstream forest
3. Enhancement and development of new water resources
   (a) Stimulate artificial rainfall
   (b) Seawater desalination
   (c) Reclaimed water usage and rainwater harvesting
4. Other measures
   (a) Public participation in water-saving activities
   (b) Education for sustainable water use
   (c) Continuous water quality monitoring

Climate change effect, coupled with current water use patterns and increased freshwater demands with increased population, will worsen the water challenges already existent. Therefore, coping with the effects of climate change on water will require better demand management measures to enhance efficiency of water use. There are ranges of demand management techniques that may be engaged to reduce water use and encourage greater productivity of water usage. Reducing the quantity of water required to accomplish a specific water application is one of effective way to mange water demand. For example, toilet flushing or landscaping does not require high-quality water, used for potable purpose. Water metering and pricing assures the optimal allocation of water as it provides a clue to both water producers and consumers, hence indirectly reducing the water consumption. Public participation in water-saving activity plays a major role in adaptation measures. Significant water savings can be achieved by introducing a dual water supply system such as toilet flushing by reclaimed water. It is required that communities, scientists, and policy makers work

together to implement adaptation activities. Therefore, better information, communication, and public awareness are necessary to produce changes in the behavior of water users to complement sustainable water use. Moreover, the development of public understanding on the links between climate change and its impacts on water resources is vital in order to promote adaptive behavior to climate change, which are happening now, and potential future impacts.

Reducing the water loss in distribution system is an important adaptation practice. Control of water leakage is one of the most critical aspects in sustainable water use. On the other hand, leakage is an energy loss that results in unnecessary carbon dioxide emission, ultimately contributing to global climate change. Detecting and repairing water leaks in Tokyo metropolitan area has reduced the amount of water wastage from 8.0% (1998) to 3.1% (2008) [23].

The water available for agriculture becomes limiting due to competition with other water users, precipitation changes, and water quality degradation. Since the agricultural sector is the largest water user, efficient water usage in agriculture will be essential. Educating efficient water use within farming communities is also an important factor so that they could adapt to climate change. In addition, better information on challenges and solutions should be provided toward improvement in the agricultural irrigation systems through better maintenance and adapting the scheduling of plant watering.

Groundwater resources are vulnerable and have the potential to be strongly impacted by climate change effect in terms of quantity as well as quality. Moreover, rapid urbanization with land use changes has decreased significantly the infiltration rates of rainfall into the soil, which causes to diminish the natural recharging of aquifers. One of adaptive methods of sustaining groundwater resources is recharge of aquifers naturally as well as artificially. Rainwater or reclaimed water have been successfully used for augmentation of groundwater in many regions. In Tokyo metropolitan area, infiltration facilities have been constructed with the objective of groundwater recharge as well as storm water runoff control [24]. Artificial groundwater recharge with reclaimed water has been effectively practiced in Orange County, California and contributed to the prevention of water shortages in the area [25].

Seawater desalination can produce good quality water, which can be used as even potable water. One of the leading desalination methods is reverse osmosis technique using membranes that filter out the salt, but the main drawback is high-energy consumption as well as the conventional desalination by distillation method. The high-energy need ultimately will result in acceleration of greenhouse effect. However, it is being discussed now the possibility of coupling the desalination technology with renewable energy such as solar, wind, etc. [26].

Domestic and municipal applications of rainwater harvesting and water recycling and reuse for non-potable usage have been receiving increased interests as a reliable solution to cope with climate change and rapid urbanization issues. Reclaimed water use has been successfully implemented in several countries such as US and Japan for a number of years (see section "Reclaimed Water Use" in this article). Thus, wastewater reclamation and reuse can be used as economically promising adaptation measure for water scarcity and it plays a significant role to achieve a sustainable development, especially in arid regions. Rainwater harvesting as a method of utilizing rainwater for both potable and non-potable use is widely used throughout the world. It is a technique that has been used since ancient times and is increasingly being accepted as a practical method in urban and peri-urban areas, where water supply service is still limited (see section "Rainwater Use"). One of the advantages of rainwater harvesting is very simple to use and consumes less energy. In a feasibility study in Tokyo, it has been estimated that rainwater usage for non-potable water application could reduce the demand for traditional potable water supply by 77% while cutting down the emission of greenhouse gas CO_2 by as much as 36% [27].

As part of adaptation against climate change effect on water resources, the potential use of supplementary water resources such as rainwater, brackish water, gray water, even reclaimed water for the purposes of non-potable application will need to be assessed. This paper discusses how to assess rainwater and reclaimed water, available for urban communities. These alternative water resources in this paper are defined as

"community-owned water resources" and it is important to evaluate their water quality from the viewpoint of sustainable water use. A water quality labeling approach is explained focusing on a case study in Japan, where they are deeply dependent on surface water resources.

Water Availability in the Future

Climate change is regarded as one of many processes affecting water availability. Population growth, economic development, land use change, aging infrastructure, and changing social values along with climate change bring water scarcity to the top problem. As depicted in Fig. 3, it is also anticipated that the future increase in world populations is expected in developing countries, especially in Asia and Africa. With the urban population increases, remarkable increase of water demand by population growth and elevated water consumption per capita for these regions can be expected. This may also lead to increased competition for water, and conflicts between water uses and users [19].

The second assessment report of the IPCC (1995) discussed the uncertainties on water availability as to the impacts of population and economical growth, and climate change and Fig. 4 depicts the water availability per capita in 21 countries as of 1990 and forecasts for 2050 [29].

According to Falkenmark's water crowding indicator Aw (= Q/C; where Q and C are renewable freshwater resources and population) [30], regions with more than 1,700 m^3/capita/year were categorized as "no water stress," which means that only local water management problems occur. Below this threshold limit, countries may begin to experience frequent water stress issues. The range of 1,000–1,700 m^3/capita/year indicates "water stress," while 500–1,000 m^3/capita/year means "water scarcity" and less than 500 m^3/capita/year "absolute water scarcity." As in the Fig. 4, some countries, particularly in Africa, Asia, and the Middle East, will shift from "no water stress" toward "water stress" or "water scarcity" as combination results of population and economic growth and climate change effects. It is noticeable that if the current consumption trends continue, several countries will face water availability limitations by the middle of this century.

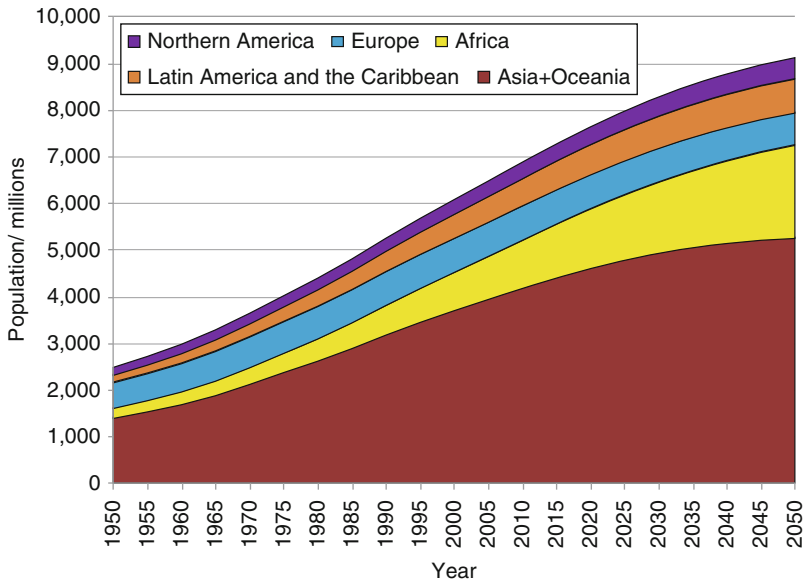

Community-Owned Water Resource and Climate Change, Quality Management. Figure 3
Projected world population (Adapted from population data from population division of the department of economic and social affairs of the United Nations, 2009 [28])

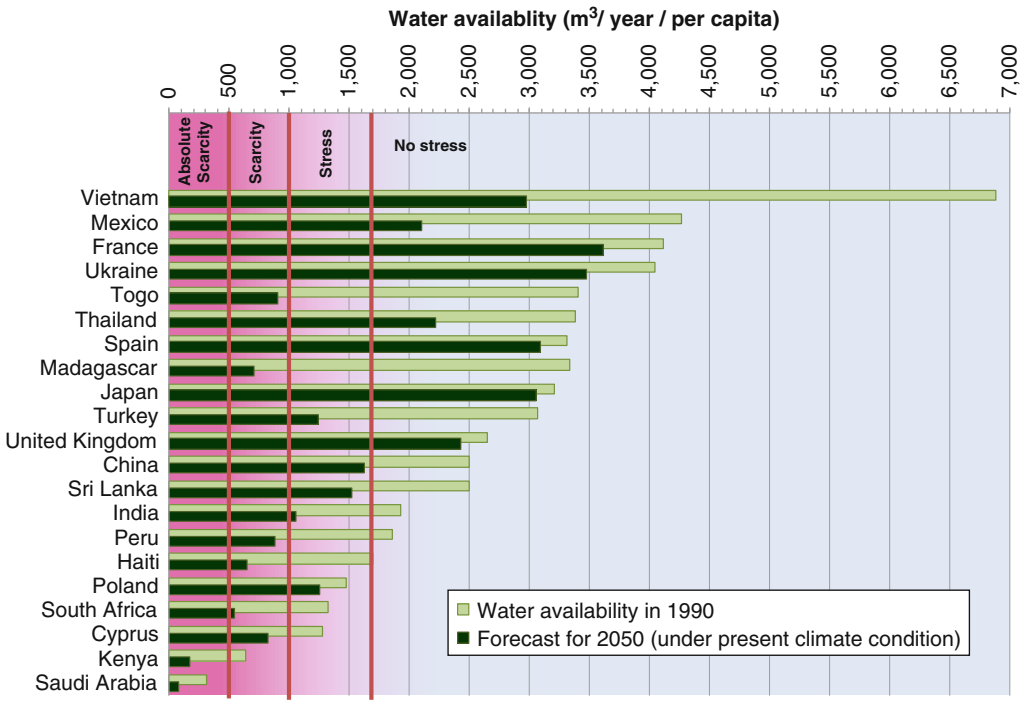

Community-Owned Water Resource and Climate Change, Quality Management. Figure 4
Forecast for water availability (m^3/year/capita) in 2050 for the present climatic conditions (Adapted from the second assessment report of the IPCC (1995) cited in [29])

Climate change is expected to accelerate water cycles and thereby increase available renewable freshwater resources. As a result, the available renewable freshwater resources are expected to increase at a higher rate than water demand, calculated from population and economic growth. Because of this, two conventional water stress indexes, Falkenmark's water crowding indicator *Aw* (<1,000 m^3/year/capita) and water scarcity index *Rws* ($= [W - S]/Q > 0.4$; *W* and *S*, are water withdrawal and water generated by desalination) showed that climate change contributes to slow down increase of the number of people living under water stress on a macro scale [31]. It is, however, important to note that these indexes are based on estimates of annual average volume. As described above, precipitation will become more intense and intermittent, and the risks of both floods and droughts will increase even in the same region owing to climate change. Oki and Kanae pointed out that several anticipated impacts of climate change on water resources, such as seasonal variation, degradation of water quality, and associated changes in water resource management, are not taken into account and that these changes in risks are not well considered in current global assessments on future water resource management [31].

Future challenges are required to respond to such anticipated impacts of climate changes and changes in risks. Water engineers and managers as well as different water users have to deal with those challenges in the development of sustainable water resource management. The achievement of the sustainability is required ensuring a long-term supply of water with adequate quality for all designated purposes minimizing adverse economic, social, and ecological impacts [32]. It is very clear now that merely dependence on a single water resource and centralized piped system cannot cope with these challenges for sustainable water use. These uncertainties stimulate research on alternative ways of providing water for a community. Reclaimed water and

runoff water are two types of promising water resources that can be adapted as complementary sources.

Importance of Community-Owned Water Resources

General Status of Rainwater and Reclaimed Water Use in Water Balance

Understanding of water balance is essential for effective water management including water supply and sewerage systems. The water balance approach helps us to evaluate the significance of rainwater and reclaimed water.

As an example of increase of water demand by population increases, water balance in Tokyo 23 wards and Japan are shown in Fig. 5. The district of Tokyo 23 wards is the most populated metropolitan city, and the population density is 14,000 persons/km^2. Amount of water use (m^3/year) is divided by the city area (km^2) and illustrated at the unit of mm/year. It is hence easy to compare the amount of water use with that of precipitation. The average annual precipitation in Tokyo 23 wards is 1,467 mm, and is distributed to 906 mm (62%) of runoff, 438 mm (30%) of evapotranspiration, and only 123 mm (8%) of infiltration. Since the imperviousness is estimated to be greater than 80% in Tokyo 23 wards, the infiltration volume (123 mm) is remarkably lower in Tokyo 23 wards than the nationwide average (361–542 mm), which is approximately 20–30% of the precipitation. On the other hand, total water demand in Tokyo 23 wards is 1,811 mm and larger than precipitation (1,467 mm). Large amount of water is supplied from outside of Tokyo 23 wards to meet the water demand. In response, water recycling has been much higher in the field of domestic water in Tokyo, while the recycling level is similar for Tokyo and nationwide average.

Figure 6 shows temporal trends of three types of reused water in Tokyo; building-scale, community-scale, and large-scale. All types of reused water have been increasing, especially within a recent decade. Reuse rates of domestic water (building-scale + community-scale), and reclaimed water and rainwater are 2.4% (43/1,811 mm), 2.0% (56/2,816 mm), and 0.05% (0.8/1,467 mm) in Tokyo 23 wards, respectively and much higher than nationwide averages (0.044%, 1.4%, 0.001%), as shown in Fig. 5. Nonetheless, the reuse rates are not high enough to cover the large amount of the water demand in Tokyo 23 wards. To minimize the risks of droughts, it is now expected to increase community-owned water resources such as reclaimed water and rainwater as well as groundwater.

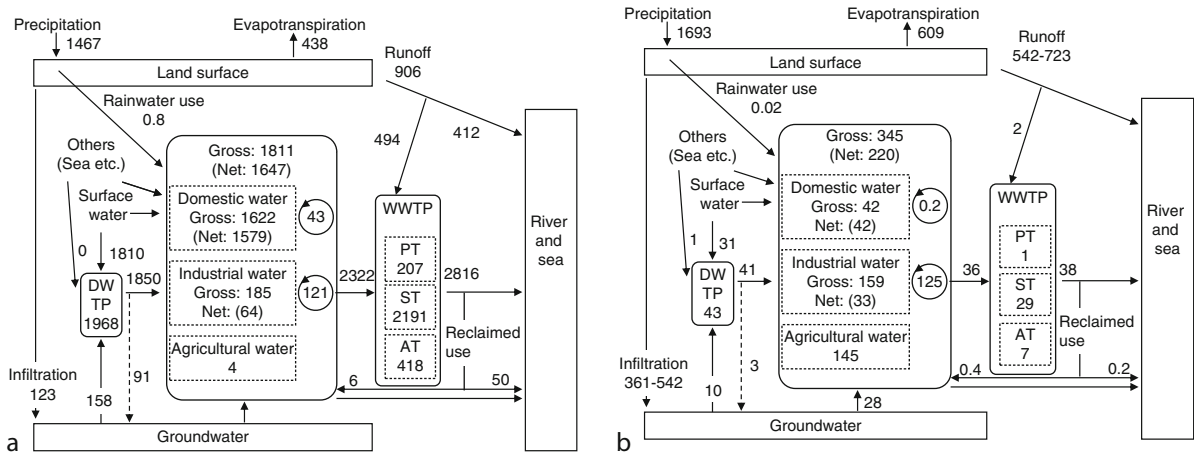

Community-Owned Water Resource and Climate Change, Quality Management. Figure 5
Water balance in (**a**) Tokyo (23 Wards) and (**b**) Japan [unit: mm/year]. *DWTP* drinking water treatment plant, *WWTP* wastewater treatment plant, *PT* primary treatment, *ST* secondary treatment, *AT* advanced treatment (Data were quoted with modifications from [32–34])

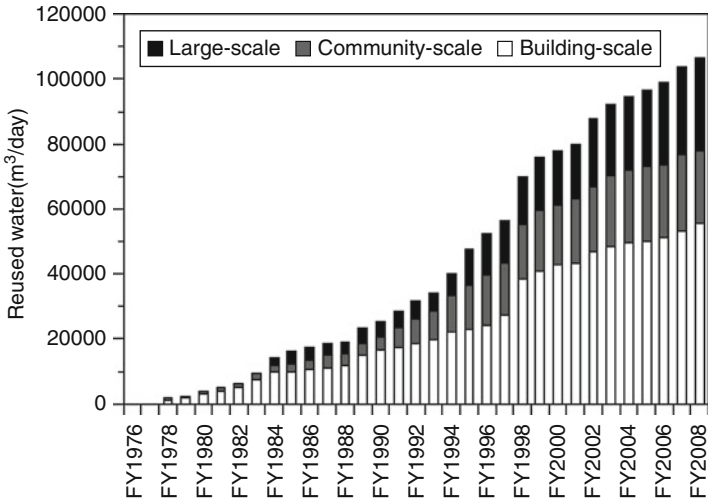

Community-Owned Water Resource and Climate Change, Quality Management. Figure 6
Temporal trends of reused water in Tokyo (Adapted from [35])

Reclaimed Water Use

It is better to explore more stable, economical, and environmental friendly ways to meet water demand through the proper evaluation. Reclaimed water use has been practiced in various ways for decades in several countries. The rapid development of new technology in wastewater treatment, such as membrane technology, makes it possible to deal with various contaminants including pathogenic organisms and viruses present in wastewater, gaining more attention toward the reclaimed water.

As shown in the Fig. 7, reclaimed water has been identified as a readily available source that covers a wide range, including industrial, residential, recreational, and environmental enhancement purposes. Reclaimed water use has several advantages; it reduces demand for higher quality water; it reduces wastewater discharge, subsequently reducing water pollution; and it is economically efficient since it minimizes the water transporting cost from distant sources [36, 37].

However, reclaimed water or reuse water systems may also link with some drawbacks. Additional costs and energies are needed for advanced treatment and if not well managed, reclaimed water may generate number of risks associated with public health.

Geographic, climate, and economical factors dictate the degree and form of water reclamation and reuse in different regions or countries [38]. Table 1 demonstrates the water reuse quantity in Israel, Italy, Japan, South Korea, Spain, and USA. As in the Table 1, the water reuse in Israel is considered as one of the highest rates and water reuse per capita in the world [39, 40]. Spain shows by far the highest water reuse rate in European Union (EU) followed by Italy [41]. In terms of quantity, USA is the largest producer, with a volume of reused water estimated as 3,650 million cubic meters per year [42].

Figure 8 shows breakdown of reclaimed water use in Japan, South Korea, and California. Although the water use category is different among three countries, reclaimed water can be applied in agriculture, industry, maintenance of river water level, groundwater recharge, and municipal use including toilet flushing, and landscape irrigation. In Japan, reclaimed water is mainly used for maintenance of water levels of rivers, landscaping, and snow melting. The total amount of wastewater treated in wastewater treatment plant (WWTP) is 14.1 billion cubic meters per year in Japan. However, reuse rate is only 1.4% (0.19 billion cubic meters). In Korea, total amount of wastewater treated is 6.6 billion cubic meters per year. Reuse rate is 4.7% (0.31 billion cubic meters). Reclaimed water is mainly used to maintain water level of rivers, similar to Japan. However, the rate of reclaimed water used for agriculture is higher in South Korea than in Japan.

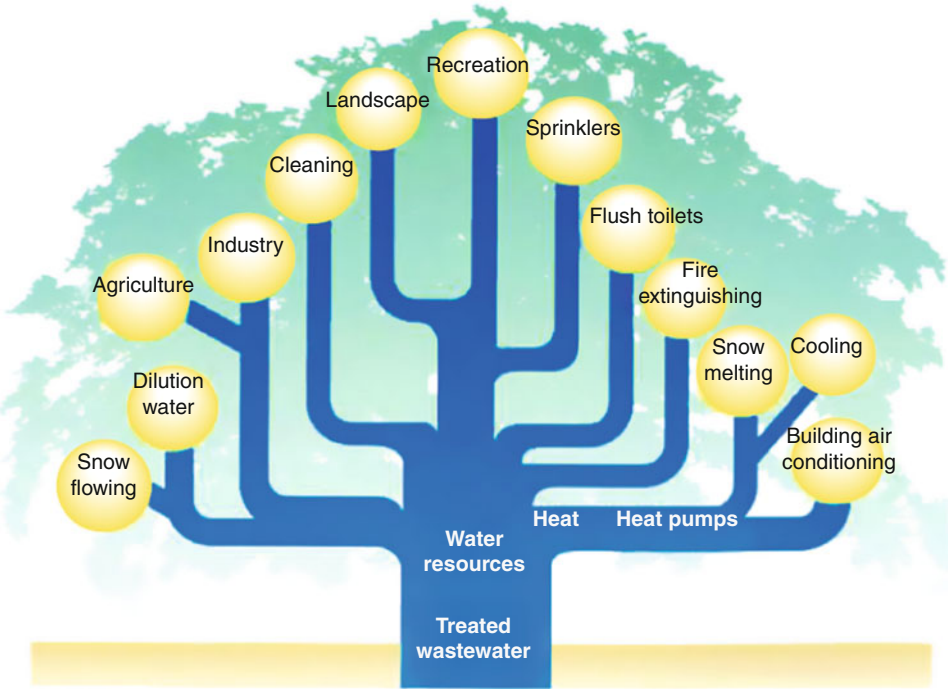

Community-Owned Water Resource and Climate Change, Quality Management. Figure 7 Tree of water resources recycling [43]

Community-Owned Water Resource and Climate Change, Quality Management. Table 1 Water reuse status in some countries [42, 44, 45]

Country	Water reuse quantity		Reuse water amount per capita (L/day)[a]
	Percentage (%)	Total quantity (million m^3/year)	
Israel	83	280	107
Italy	7	230	11
Japan	1.4	200	4
South Korea	4.7	310	18
Spain	12	350	21
US	6	3,650	32

[a]Based on population data from population division of the department of economic and social affairs of the United Nations, 2009 [28]

It is known that reclaimed water use for agriculture is remarkably high in the State of California as shown in Fig. 8. By the end of 2001, reclaimed water use in California had reached over 0.65 billion cubic meters per year [46]. Compared to Japan and Korea, agricultural and landscape irrigation is the dominant use of reclaimed water in California, which accounts for more than two third of the total water reuse by volume. Artificial groundwater recharge is also practiced successfully in California. Groundwater replenishment system at the Orange County, California is a frontier region where the largest water reclamation facilities have been operated with advanced treatment process that includes reverse osmosis, and treatment by ultraviolet light and hydrogen peroxide [25, 46].

Reclaimed water is also being used to maintain constructed wetlands, to enhance natural and artificial wetlands, and to sustain or augment stream flows. Reclaimed water has been successfully used in Tokyo for regeneration and restoration of the dried-up rivers and waterways. This gives multiple benefits such as restoring ecological habitats, enhancing landscape, and providing opportunity for citizens for environmental education (Fig. 9).

Another new type of water reuse application is practiced in Tokyo. Extensive built-up of subways and underground structures have occupied large

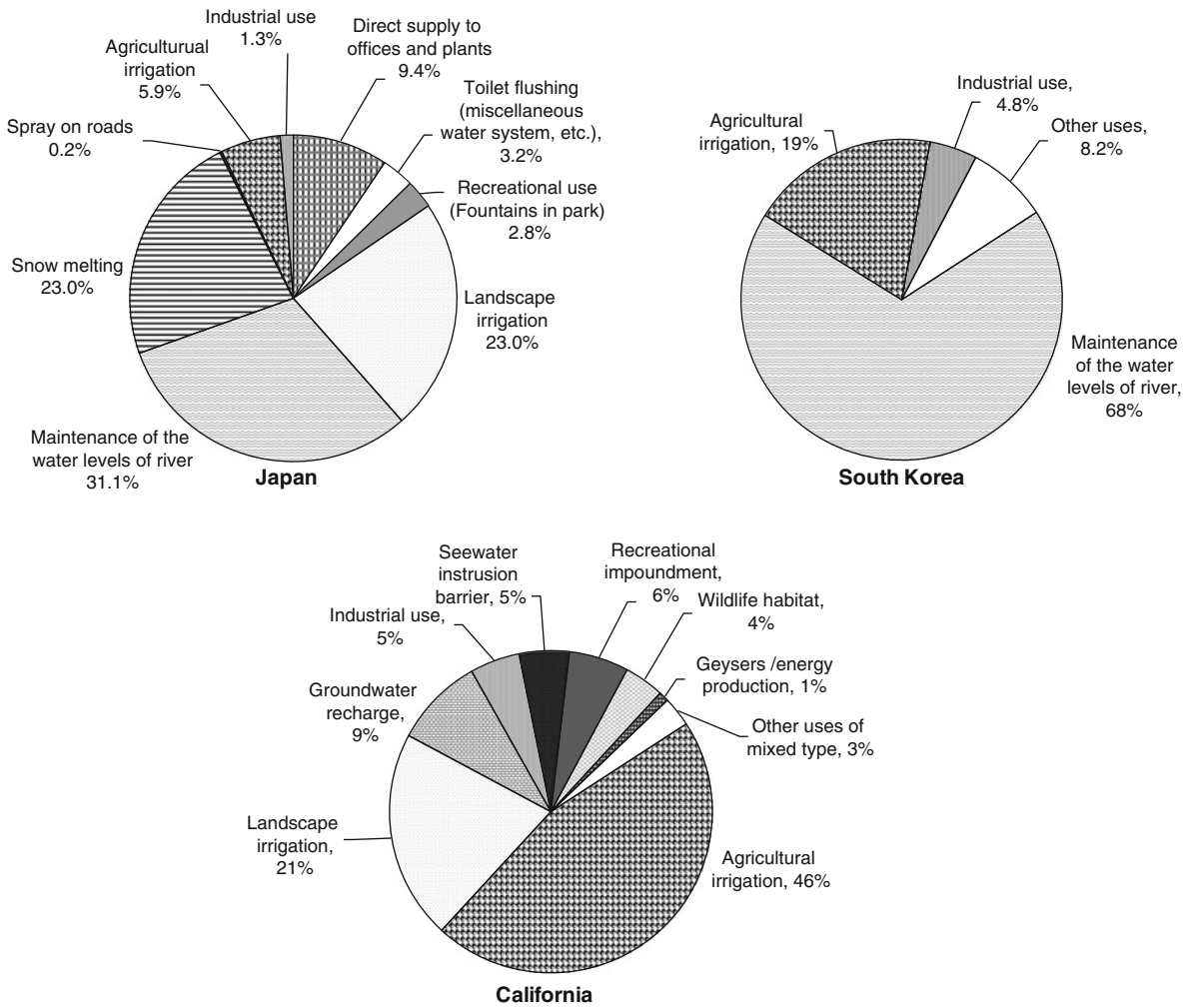

Community-Owned Water Resource and Climate Change, Quality Management. Figure 8
Percentage and purpose of reclaimed water use in Japan, South Korea, and California [44–46]

surface volume in Tokyo and hence raise the groundwater level causing seepage. Railway companies collect this seepage water in tunnels and drain into sewerage system with payment. This was considered as waste of good quality water and additional financial burden for the railway companies and extra water to treatment system. Recently, collected seepage water began to be introduced into neighboring recreational ponds and waterways for their restoration.

Rainwater Use

Rainwater is widely recognized as a valuable water resource and it can provide a readily accessible water supply. Rainwater harvesting systems vary from the small and simple to the large and complex ones. Where a suitable harvesting surface exists, such as roof or even road, rainwater collection can provide sufficient and low-cost source of water for non-potable usage. Effective use of rainwater as a supplementary water supply can indirectly be beneficial for flood control too. Generally, rainwater can be regard as better quality water than treated wastewater and is likely to be suitable for wide range of potable and non-potable applications, including cooking, laundry use, toilet flushing, car and equipment washing, garden irrigation, cooling and heating, and many industrial processes. Rainwater usually gets better public acceptance

Community-Owned Water Resource and Climate Change, Quality Management. Figure 9
Created waterways using reclaimed water in urban zones, which function as amenity and community activity places

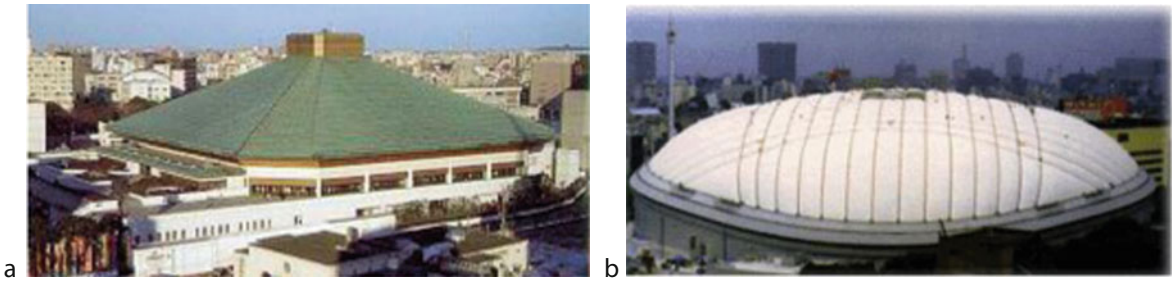

Community-Owned Water Resource and Climate Change, Quality Management. Figure 10
Rainwater harvesting at (**a**) Kokugikan for Sumo wrestling and (**b**) Tokyo Dome Stadium

for domestic use than reclaimed water. However, it is important to realize that air pollutants, particularly in urban areas, from industrial discharges, vehicle exhaust fumes, and agricultural chemicals used at farms or in-home gardens may wash off with rainwater. Moreover, dust, leaf debris, animal feces, and leaching from roofing, guttering and plumbing materials, or materials of storage tank may further degrade the quality of rainwater.

Roof runoff for miscellaneous use such as toilet flushing and water cooling is successfully employed in various regions in the world, in an individual scale as well as in a large scale. Although road runoff generally has higher pollutant concentrations than roof runoffs, there is a trend to use the relatively polluted rainwater draining from streets and courtyard surfaces as service water in some countries [47]. Roof runoff water collection can be successfully practiced under different scales in both urban and rural areas. A frontier attempt of the large-scale harvesting in Japan can be seen at Kokugikan (indoor Sumo stadium in Tokyo's Ryogoku area) for Sumo wrestling as shown in on Fig. 10a. This system was introduced in 1984 and utilizes a tank with effective capacity of 750 m^3 to store the rainwater collected from the roof with an area of 8,400 m^2. The collected water is used for cooling system and toilet flushing. Other early examples are City Office Building in Sumida ward, Tokyo in 1988, and Tokyo Dome Stadium in 1988. Figure 10b shows the system at the Tokyo Dome Stadium having a storage tank with a capacity of 3,000 m^3. The maximum capacity for storage is controlled at 2,000 m^3. It means that one third of its capacity is used for flood control (this capacity is left empty for the case), another 1,000 m^3 for miscellaneous water use, and the remaining 1,000 m^3 for urgent water use in earthquake and fire events.

Water retention pavement as a countermeasure against heat island phenomena is one of the new types of rainwater use adopted in Tokyo. Rainwater falling on square block flows into side ditch and is stored in an underground tank as shown in Fig. 11. Water from the tank is then supplied to paving blocks via sprinkling pipes.

Another application of rainwater is groundwater recharge via infiltration-type sewerage system. Tokyo Metropolitan Sewerage Bureau constructed infiltration facilities over 1,400 ha area [24, 48, 49] to cope with a heavy rainfall of 50 mm/h and hence provide benefits such as groundwater recharge and reduction of non-point pollution loads from urban surfaces.

However, rainwater has a limitation as a stable water source because the amount largely is dependent on the variability of weather and climate. It is also expected to greatly vary in precipitation in future due to the effect of climate change. Thus, during a long drought season, the storage tank may dry up. As rainfall is typically unevenly distributed throughout the year, rainwater collection can serve as a supplementary method to support household and municipal water use. Therefore, rainwater may be used along with other stable water supply from surface water or/and groundwater at household or community-scale level from the viewpoint of sustainable water use.

Standards and Guidelines for Reclaimed Water and Rainwater

It is well evident that global freshwater resources are being under growing pressure as a result of rapid urbanization, industrial development, and climate change effect. As a result, supplementary water resources such as reclaimed water can no longer be neglected. As discussed in the previous section, reclaimed water has been used successfully in many regions, where wastewater collection and treatment have been the common practice. However, water reclamation and reuse activities should be in practice with proper attention to the environment, public health, and esthetic consideration. Therefore, it is necessary to consider use of reclaimed water in terms of not only quantity aspect but also quality aspect. The water quality should be characterized and evaluated in terms of its intended application and practice.

Standards and guidelines for reclaimed water applications have been established in various localities and countries, for example, by the World Health Organization (WHO), US Environmental Protection Agency (USEPA), Australia, and Japan. In general, the implementation of standards and guidelines for reclaimed water is based on local environmental and socioeconomic conditions in each country. However,

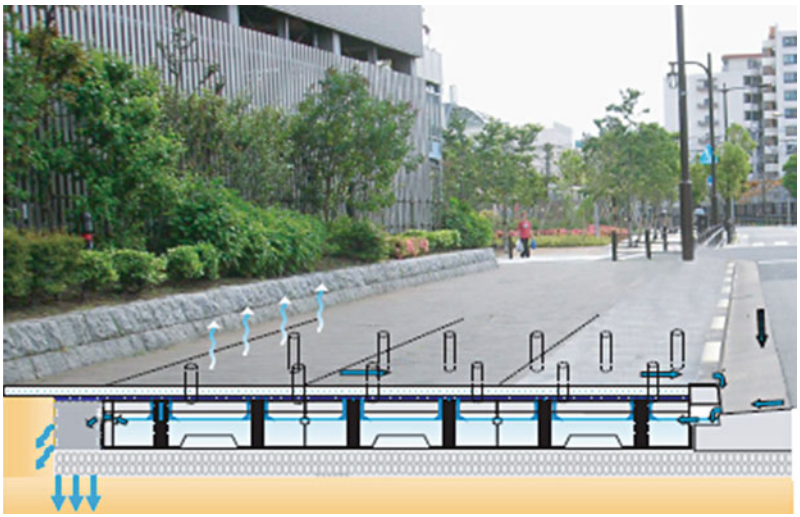

Community-Owned Water Resource and Climate Change, Quality Management. Figure 11
Rainwater use for water retention block pavement in Tokyo

these guidelines may also provide insight for other countries or localities. In 1973, WHO first developed guidelines for the reuse of effluents, considering methods of wastewater treatment and health safeguard This guideline provided direction on how to protect public health and how to facilitate the rational use of wastewater and excreta for agriculture and aquaculture purposes [50]. When this criterion was revised in 1989 and most recently in 2006, more epidemiological and microbiological evidence concerning health risks had been taken into account [51, 52].

In 1992, USEPA together with USAID (United States Agency for International Development) published guidelines for reclaimed water and these guidelines were updated in 2004, including many new and updated research activities and results, new information on treatment and disinfection technologies, emerging chemicals and pathogens of concern [53, 54]. This new regulation and guideline in 2004 also summarized the water reuse regulations of various states throughout the USA. In general, USEPA suggests guidelines on reuse of wastewater for urban, industrial, agricultural, recreational and habitat restoration usage, groundwater recharge, and augmentation of potable supplies [54].

Comprehensive national guideline was established in Australia in 2006. It was designed for how water recycling can be safely and sustainably achieved for agriculture, fire control, municipal, residential and commercial property, and industry usage. The guidelines consider management of risks to human health and environmental health and focus on two specific situations; water recycled from a centralized sewage treatment plant and from gray water [55]. This guideline was extended later in 2008, considering the use of treated wastewater and storm water to augment water resources for potable purpose. The guideline also focuses on the source of water, initial treatment processes, and blending of recycled water with drinking water sources [56].

At the moment, there are no guidelines or regulations of water reuse at European Union (EU) level. Despite the fact that no guidelines or regulations yet exist, several member states or autonomy regions in EU have now published their own standards or regulations [57].

The water quality criteria and guidelines on the reclaimed water use for miscellaneous purposes in Japan were established by the Ministry of Land, Infrastructure and Transportation since 1981. Any guideline or standard should be dynamic in nature and subjected to revision as new scientific information becomes available. The standard and guideline for reclaimed water quality in Japan were established for four respective miscellaneous applications in 2005 [58]. Water quality standard for rainwater and treated gray water under the Building Sanitization Law were amended in 2004. The latest values for water quality of reclaimed water, used for miscellaneous purposes, and water quality of rainwater and treated gray water are summarized in Table 2. These standards help to enforce the water quality standards for reclaimed water and also help to ensure the restrictions for its safe use. Primarily, the reclaimed water should be utilized securing hygienic safety to protect the public health. The usual practice is that the greater the contact or potential for contact with humans, the greater the risk and hence the more exacting the water quality requirements. Therefore, where there is likely to be more human contact with reclaimed water, advanced treatment and high level of disinfection are needed to minimize health risks [46]. In the case of human-related uses, pathogens including virus should be considered as quality guideline parameters. The introduction of virus parameter in the reclaimed water quality standard in Japan has been discussed in the Explorer Committee for the standard establishment, but has not been included because of absence of commonly available detection method of viruses [37].

These guidelines and standards propose on minimum standards for reclaimed water and draw risk management protocols to protect the public health and environment. Implementation of sustainable water use will likely require combination of policy/regulation and technology and participation of general public. However, general public's perception on alternative water sources such as reclaimed water or rainwater is influenced by attitudes, emotions, and their accepted practice. Therefore, it is important to provide water quality information from trusted scientific and regulatory sources in a simple manner so that general public can easily understand the quality of different water resources.

Community-Owned Water Resource and Climate Change, Quality Management. Table 2 Water quality standards and guidelines for reclaimed water, rainwater, and treated gray water for miscellaneous use in Japan

	Guidelines for reclaimed water quality				Standards for rainwater and treated gray water quality[a]	
	Toilet flushing	Sprinkling water	Landscaping water	Amenity water	Toilet flushing	Sprinkling/ landscaping/ cleaning water[b]
Escherichia coli	Not detectable	Not detectable	<1,000 CFU/100 mL (tentative value)	Not detectable	Not detectable	Not detectable
pH	5.8–8.6	5.8–8.6	5.8–8.6	5.8–8.6	5.8–8.6	5.8–8.6
Appearance	Not be distasteful	Not be distasteful	Not be distasteful	Not be distasteful	Almost clear and colorless	Almost clear and colorless
Turbidity (degree)	(Control target) ≤2	(Control target) ≤2	(Control target) ≤2	≤2	–	≤2
Chromaticity (degree)	–[c]	–[c]	≤40[d]	≤10[d]	–	–
Odor	Not be distasteful[c]	Not be distasteful[c]	Not be distasteful[c]	Not be distasteful[c]	Not be abnormal	Not be abnormal
Residual chlorine (mg/L)	(Control target) free: ≥0.1 or combined: ≥0.4	(Control target)[e] free: ≥0.1 or combined: ≥0.4	Not be stipulated	(Control target)[e] free: ≥0.1 or combined ≥0.4	Free: ≥0.1 or combined: ≥0.4	Free ≥0.1 or combined: ≥0.4
Facility standards	Sand filtration or its equivalent	Sand filtration or its equivalent	Sand filtration or its equivalent	Coagulation and sedimentation + sand filtration or its equivalent	–	–

[a]The standard values stated by the Building Sanitation Laws.
[b]For this purpose, raw water should not include human wastes.
[c]Based on the intent of the users, standard values shall be set as required.
[d]Based on the intent of the users, more stringent value shall be set as required.
[e]This guideline value is not applied if disinfection is not required.

Evaluation of Water Quality in Community-Owned Water Resources

Community-owned water resources can be an attractive solution for many regions as a competitive option to increase water availability and adapt to water shortage due to climate change. Reclaimed water and rainwater have been receiving growing interests as community-owned water resources as a substitution for conventional water resources. Water quality is the most important issue in such a community-owned water system that determines the acceptable and safety use for a given application. However, general public still fears or hesitates to use this kind of alternative water sources as they usually do not understand the quality difference among different types of waters.

Public Perception to Reclaimed Water and Rainwater

Successful execution of a reclaimed water project depends on several aspects such as economical environmental feasibility and as well as the social aspects

related to using reclaimed water. In addition to the scientific and engineering-based factors, public acceptance can be considered as the key to cause a reclaimed water system in a community to fail or succeed, because general public has to be willing to pay for such a reclaimed system [59]. Reclaimed water or runoff water system may face public opposition resulting from a combination of prejudiced beliefs, fear, attitudes, lack of knowledge, and distrust.

The main public objection is related to the quality of the reclaimed water. Because the primary source of recycled water is municipal wastewater that carries what humans excrete and discharge to the drain from sources such as toilet, bathroom, kitchen, and laundry, or miscellaneous dumps of household, a psychological objection to close contact frequently occurs [38, 61]. This has prompted the community to always be concerned about water quality. However, general public often does not understand the quality difference among different types of possible water resources and hence many communities do not have a positive image on alternative water sources such as reclaimed water. Lack of knowledge on the water quality of water sources causes people to hesitate to use water sources such as reclaimed water or rainwater. Figure 12 shows a survey result of public opinion toward reclaimed water and rainwater harvesting in Tokyo. The survey was conducted in 2008 with 1,839 randomly selected Tokyo residents. In general, results revealed that 86% of Tokyo residents are positive to use reclaimed water or rainwater. However, majority of them (59%) are ready to use reclaimed water or rainwater if only water quality is good enough for the intended application [60]. Therefore, public awareness of water quality information of these alternative water sources plays a key role in sustainable water use project.

Kantanoleon et al. also emphasized that there is a major knowledge gap affecting the public perception of wastewater nature, treatment, and reuse [62]. This public's fears related to water quality can be overcome with clear and adequate scientific explanations in terms of benefits on the use of reclaimed water from wastewater or rainwater. The challenge is how to share scientific knowledge such as water quality information with public and communicate with them in simple manner.

Development Method of Water Quality Information Platform

One of the difficult tasks that environmental engineers are facing is how to transfer complex water quality (WQ) data into information that is understandable and useful to technical and policy persons as well as the general public. Therefore, it is important to develop a simple way to represent the difference of WQ among various water resources available in a community, including reclaimed water. The objective of this section is to propose a methodology to develop a WQ information platform. The WQ information platform provides WQ criteria reference to be compared among different waters using WQ labeling and ranking. The WQ labeling and ranking is a better tool to evaluate WQ level of possible water resources available in a community including reclaimed waters.

The general practice is to describe WQ of water sources along with official guidelines on the basis of different WQ parameters. Although these traditional practices consist of bunch data and information, the

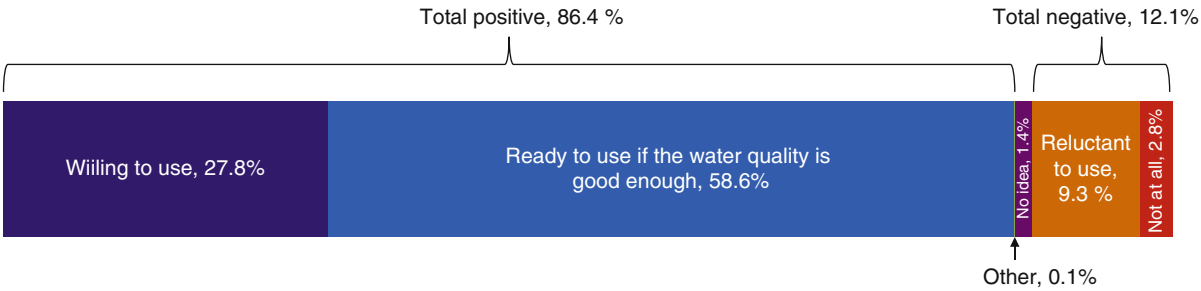

Community-Owned Water Resource and Climate Change, Quality Management. Figure 12
Public opinion on reclaimed water and rainwater in Tokyo [60]

general public has neither the inclination nor the training to study these details. The new proposed WQ information platform reduce the multivariate nature of WQ data by providing scoring system that will logically combine all WQ measures and provide a simple and easily understood description of different waters [27]. The proposed WQ evaluation method is based on five steps:

1. Data Gathering: Selecting WQ parameters of water sources and collecting WQ standard values
2. WQ Scoring: Determining five-level scores based on scientific evidences such as drinking and ambient WQ standards
3. WQ Characterization: Characterizing WQ using multiple scores based on scientific evidence
4. Water Use Ranking: Ranking by water availability and WQ characterizing information for several water usage
5. WQ Labeling and User judgment: Judging the type of water usage such as gardening, toilet flushing, car washing, landscape, etc.

This framework can accurately evaluate and summarize WQ data in a way that should be scientifically accepted and easily understood by both professionals and the public. Relative evaluation of WQ of different water sources is beneficial rather than absolute values of WQ parameter. If the relative evaluation is conducted on familiar water sources to community such as well-known river waters, it is easy for citizens to understand the WQ levels of community-owned water resources. Thus, this kind of WQ information platform will be useful for general public to change their attitude and behavior toward the quality of reclaimed water system. The evaluation is also a useful tool for describing the WQ state of the different water sources and for ranking the suitability of waters for different usage. The next entry will provide details of WQ information platform development using a case study in Japan.

Characterizing and Ranking of Different Water Resources – A Case Study on WQ Information Platform in Japan

The ultimate aim of developing WQ information platform is to develop effective management and monitoring system for community-based water reuse system. The WQ information platform provides a WQ reference for a community to evaluate reclaimed waters or any alternative water sources. Therefore, WQ information platform should integrate the significant physicochemical and biological constituents of different water resources available for a community and present them in a simple and scientifically defensible way. The case study in Japan explains five steps to develop a nationwide WQ information platform that indicates the ranking and labeling of water resources. The steps contained in this case study can be used as a guide for a process of evaluation of WQ in any community or a region, depending on the needs or objectives of that particular community. In this case study, WQ of advanced treated wastewater, runoff waters, and groundwater was evaluated and compared with the first-class rivers in Japan, in terms of their usage.

Data Gathering

Appropriate assessment of several WQ data is essential to develop WQ information platform. The first important step is to make WQ reference to be compared with WQ level of different water sources. In this study, river waters were selected as reference water resource, because surface water is the major source of water supply in Japan. Out of 109 rivers throughout Japan that are designated as "the first-class" by the River Bureau Ministry of Land Infrastructure Transport and Tourism, 37 rivers were selected to develop the reference profile [63]. Figure 13 shows the selected rivers and sample locations, which represent nine administered regions in Japan. Water samples were collected during dry season from the most downstream section.

To confirm the representativeness of the selected rivers, catchment areas, population density, concentrations of total nitrogen (T-N) and total phosphorus (T-P) of the selected 37 rivers of this study and the annual average of 109 rivers based on monthly monitoring were compared [64]. Figure 14 shows that the distributions of catchment areas, population density, T-N and T-P concentrations in this study agreed well with their annual averages. Therefore, the selected rivers could be regarded as being representative, and hence can be used as WQ criteria reference.

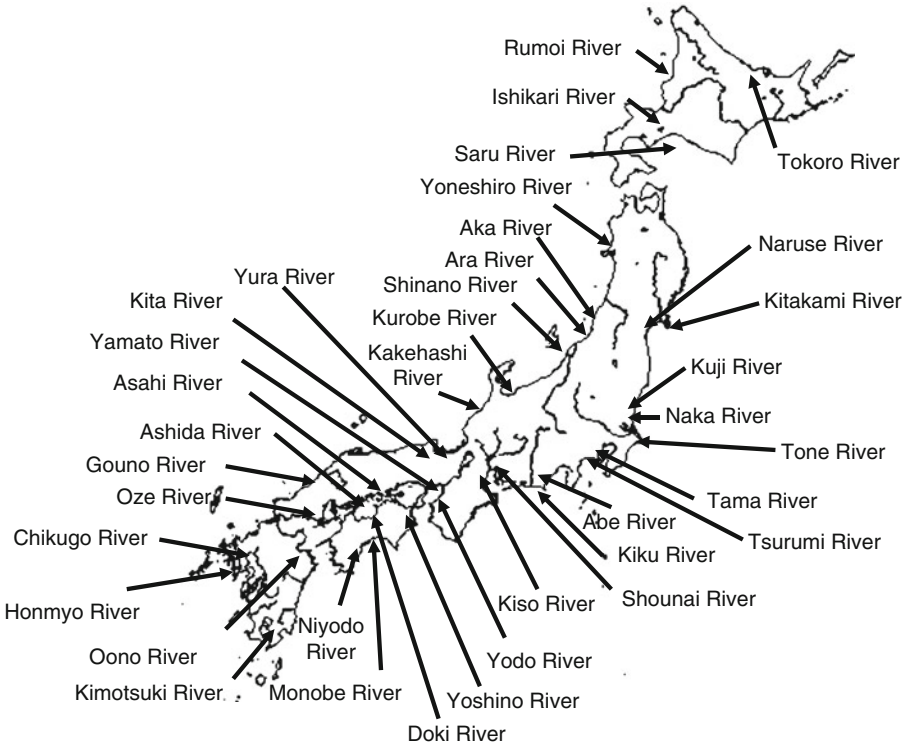

Community-Owned Water Resource and Climate Change, Quality Management. Figure 13
Selected rivers in Japan for sampling in this study

The first stage was to select WQ parameters that will be used to evaluate the water resources. In order to develop the WQ information platform in this study, the data related to several chemical analysis and estrogenic activity (bioassay) as shown below were used. It is better to use assessment using multiple bioassay tests in more advanced study. However, in this case study, estrogenic activity alone was used as bioassay.

Chemical analysis:

- Organic matter (TOC, COD, BOD)
- Nitrogen (TN, NO_2, NO_3, NH_4)
- Phosphorus (TP, PO_4)
- Metals (Zn, Cu, Mn, Ni, Pb, Cd, As, etc.)
- Endocrine disrupting chemicals (E1, α-E2, β-E2, E3, BPA, NP, OP)
- Polycyclic aromatic hydrocarbons (benzo(a) pyrene, etc.)
- Perfluorinated surfactants (PFOS, PFOA, etc.)
- Pharmaceuticals and personal care products (ibuprofen, carbamazepine, triclosan, etc.)
- Synthetic detergents (LAS, SPC, etc.)

Bioassays:

- Estrogenic activities

Only use of traditional chemical parameters is not sufficient for WQ assessments, since reclaimed water contains complex mixtures of trace contaminants. Emerging organic and microbial contaminants usually represent major concerns in water reclamation as they pose either acute or chronic health impacts to the consumers. Therefore, apart from the typical chemical WQ parameters of organic matters, nitrogen and phosphorus, other micropollutants such as heavy metals, endocrine disrupting chemicals (EDCs), polycyclic aromatic hydrocarbons (PAHs), perfluorinated surfactants (PFSs), pharmaceuticals and personal care products (PPCPs), and synthetic detergents were also taken into account for developing WQ information platform [63, 65–68]. It is always better to use multiple bioassay data along with chemical data, in more advanced assessment study. Bioassays are important for effective integrated assessment of WQ. Because chemical

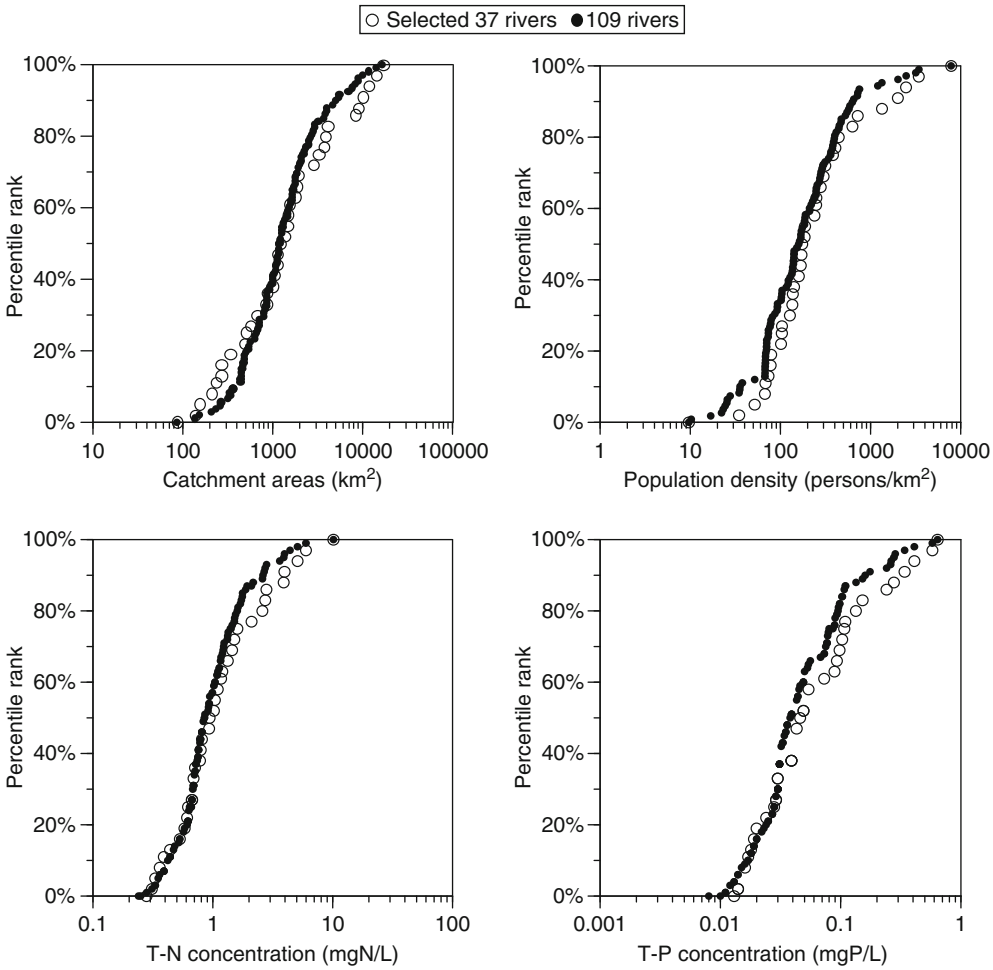

Community-Owned Water Resource and Climate Change, Quality Management. Figure 14
Comparison of catchment areas, population density, T-N concentrations, and T-P concentrations between 109 rivers and selected 37 rivers

analysis gives only quantitative statements for a limited number of chemicals, bioassays such as estrogenic activities, algal growth inhibition, algal growth potential, Microtox, and mutagen formation potential (MFP) are required for an integrated assessment of effects or toxic potentials of chemical substances. However, this case study will be explained only with the data of estrogenic activities along with chemical data, because bioassay data are not so easily available in most cases.

The selection of parameters to evaluate the water resources depends on the usage that is intended. If the water usage is only limited for purposes such as toilet flushing, the coloring and appearance are also focused on to develop the WQ information platform. However, additional parameters are recommended when the WQ information platform is being used as a decision tool for more advanced water usage such as amenity purpose with human contact.

Subsequently, WQ references of each parameter were represented as percentile distributions. Percentiles are values that divide a set of observations into 100 equal parts. The percentile rank is the proportion of values in a distribution that a specific value is greater than or equal to. Therefore, the lower percentile rankings here indicate the better WQ while higher percentile

rankings indicate poorer WQ. Thus, the 0th and 100th percentiles describe the best and worst of the WQ distribution, respectively, while the median or 50th percentile describes the WQ value at the middle of the distribution. These percentile distributions can be used for WQ criteria reference to be compared with different water resources such as reclaimed waters. In this study, different types of water resources; infiltrated water of road runoff [69] secondary treated effluent [70], advanced treated wastewater by sand filtration [70], infiltrated water of secondary treated effluent [71, 72], advanced treated wastewater by ozonation [70], and groundwater [68, 73] were compared with the river WQ references.

Figure 15 shows the example of percentile distribution of TN and two PPCP parameters (ibuprofen and carbamazepine) of 37 rivers in Japan. The figure also compares the secondary effluents, sand filtered effluents, and ozonated effluent of WWTP with the reference river WQ. As in this example of Fig. 15, there is no significant difference in TN among three types of treated wastewater effluents and value is equal to 100th percentile rank of the selected rivers. Ibuprofen concentration in ozonated effluent is equal to 35% of the percentile distribution. The 35th percentile describes a value (or 0.5 ng/L of ibuprofen) for which around 35% of selected rivers in the distribution are equal to, or lower than, ibuprofen concentration in the ozonated effluent. In the case of carbamazepine, the percentile rank of the ozonated effluent is 20%, indicating 80% of the river water contains higher concentration of carbamazepine than the ozonated effluent. Since no WQ standards are set so far for emerging contaminants such as PPCP, this kind of comparison with known river waters can be used to reflect the WQ condition of the relevant water source.

Water Quality Scoring

Once the WQ references have been developed as the percentile distribution, the next step is the scoring process. The first stage of this step is to divide the WQ percentile distribution of rivers into six factors according to the criteria of each WQ parameters, which describe the state of WQ based on scientific evidence such as drinking and ambient WQ standards. Then, the other water resources were compared with reference scale to determine their scores.

All the WQ parameters available for chemical analysis and bioassay were classified into six different WQ factors, such as:

WQ factors based on chemical analysis:

1. Coloring and appearance
2. Eutrophication
3. Conservation of aquatic ecosystem
4. Chronic toxicity to human
5. Acute toxicity to human

WQ factors based on bioassay:

6. Estrogenic activity

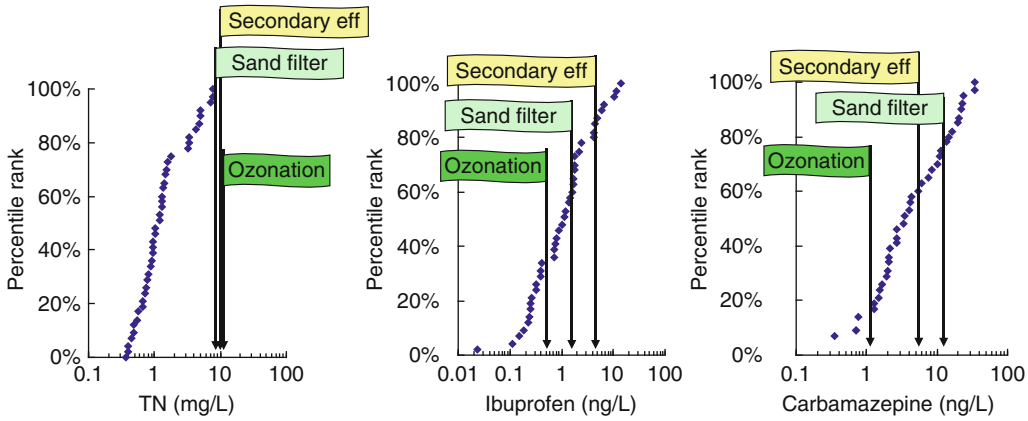

Community-Owned Water Resource and Climate Change, Quality Management. Figure 15
Comparison of the TN, PPCP (ibuprofen and carbamazepine) of secondary effluents, sand filtered effluents, and ozonated effluent with those of percentile distribution of reference river waters

These six factors are combined to form the score matrix, which can fall into one of the five level score index. Although six different factors were used in this study, the number of factors may depend on the availability of data and purpose of WQ evaluation. The factors based on chemical analysis were scored according to the WQ standard or guideline, while the factors based on bioassays were scored according to the potential effect of biological and on ecosystems. The five level scores index, which gives a number between 0 and 4, was used, with 0 being the best and 4 indicating the poorest WQ within the distribution. The score "0" implies the water is safe with a virtual absence of threat or impairment. The score "1" implies there is a minor degree of threat or impairment and continuous monitoring is needed for that particular water. The score "2" to "4" means the water is threatened or impaired in terms of particular WQ parameter and some action is needed to improve the WQ. Depending on the degree of action level, scores were given as 2, 3, or 4.

The example of the Fig. 16 shows the score distribution for Zn concentration considering the WQ factor for "conserving of aquatic ecosystem" within the same percentile ranking in the first-class rivers in Japan. Since 0.03 mg/L is the guideline value in the rivers for conservation of aquatic ecosystem in Japan, less than 0.003 mg/L of Zn in waters is regarded as score 0, 0.003–0.03 mg/L as score 1, 0.03–0.3 mg/L as score 2, 0.3–3 mg/L as score 3, and more than 3 mg/L as score 4. The waters of score 3 represent the water even after ten times dilution is threatened from the view point of conservation of aquatic ecosystem. Similarly, scores can be given to all other parameters related to each WQ factors.

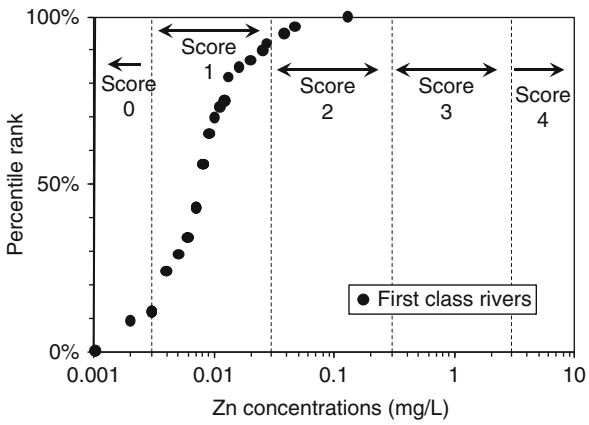

Community-Owned Water Resource and Climate Change, Quality Management. Figure 16
Distribution of Zn concentrations and their scores in the first-class rivers based on the WQ factors for conservation of aquatic ecosystem

Table 3 summarizes the example of WQ thresholds value for WQ factors and their scores with respect to the relevant WQ parameters. In this way, once all the six factors have been divided into five levels index in the reference distributions, scores of different types of water resources could be determined. Table 4 shows the example of final score matrix of different water resources.

Water Quality Characterization

This is the step to summarize the scores given to the each water resource in the previous step. Characterization can be considered as similar to a WQ label in a drinking or mineral water bottle. As several WQ parameters (nitrogen, fluoride, etc.) are seen in a water bottle to show the quality of water, five WQ factors (coloring, eutrophication, acute toxicity, etc.) were used in this study to characterize the different water resources including reclaimed waters. Based on scores in Table 4, characterizing indexes were calculated. In the case of the WQ factor of "Acute toxicity to human," the characterizing indexes were determined by taking the maximum score value, while the index values of all the other five factors might be determined by taking the average of each score under a particular WQ factor. It is also possible to give weighting coefficients to WQ parameters of each factor.

In order to understand the WQ characterizing indexes easily, radar charts (also known as spider charts) were developed to express characterizing WQ graphically. In the radar charts, each axis represents the WQ factor developed at the step 2 of WQ Scoring. The six factors are plotted along the chart axes from the center of the chart. For a given WQ factor, score of "4" is located in the center and "0" at the edge. Lines connect the axes at the position of

Community-Owned Water Resource and Climate Change, Quality Management. Table 3 Example of water quality thresholds value for scoring

	Unit	Score 0	Score 1	Score 2	Score 3	Score 4
Coloring and appearance						
pH	–	5.8–8.6	4.8–5.8, 8.6–9.6	3.8–4.8, 9.6–10.6	2.8–3.8, 10.6–11.6	≤2.8, ≥11.6
TOC	mg/L	<0.5	0.5–5	5–50	50–500	≥500
Cu	mg/L	<0.1	0.1–1	1–10	10–100	≥100
Zn	mg/L	<0.1	0.1–1	1–10	10–100	≥100
. . .						
Conservation of aquatic ecosystem						
NH_4	mgN/L	<0.02	0.02–0.2	0.2–2	2–20	≥20
Zn	mg/L	<0.003	0.003–0.03	0.03–0.3	0.3–3	≥3
Triclosan	ng/L	<6.3	6.3–63	63–630	630–6,300	≥6,300
. . .						
Estrogenic activity						
Yeast estrogen screen assay	ng-E2/L[a]	<1	1–10	10–100	100–1,000	≥1,000

[a]E2 (17β-estradiol) equivalent concentration.

Community-Owned Water Resource and Climate Change, Quality Management. Table 4 Example of scores in several water resources

	100% percentile rank river	50% percentile rank river	0% percentile rank river	Groundwater	Wastewater treated by sand filtration	Wastewater treated by ozonation	Infiltrated water of secondary wastewater	Infiltrated water of road runoff
Coloring and appearance								
pH	1	0	0	0	0	0	0	0
TOC	2	2	1	2	1	1	1	1
Cu	0	0	0	0	0	0	0	0
Zn	1	0	0	0	0	0	0	0
. . .								
Conservation of aquatic ecosystem								
NH_4	2	1	0	0	1	1	1	0
Zn	2	1	0	0	2	2	1	1
Triclosan	1	1	0	0	2	1	1	0
. . .								
Estrogenic activity								
Yeast estrogen screen assay	2	0	0	0	1	0	0	0

each data object, forming a spiral around the center. The larger the area of the spiral, better the WQ of a particular water source.

Figure 17 shows the radar chart related to 0th, 50th, and 100th percentile rank of the first-class rivers in Japan as well as groundwater, ozonated wastewater effluent, and infiltrated water of road runoff. According to the graphical representation, overall WQ of groundwater is roughly equal to 50th percentile rank of the first-class rivers. Radar charts of ozonated wastewater effluent and infiltrated water of road runoff depict that their overall WQ is between 50th and 100th percentile rank of the first-class rivers.

However, each WQ factor should be carefully evaluated in the viewpoint of the water usage purpose. For example, ozonated wastewater effluent shows poorer WQ for eutrophication than the 100% percentile rank river. This indicates that the ozonated wastewater effluent in this case is not suitable to apply to water usage such as landscaping pond water, in which the eutrophication would be a possible impairment factor.

Water Use Ranking

The aim of this step is to integrate the characterized water resources with the objectives of water usage. Since water for amenity, landscaping, toilet flushing, and fire protection has different WQ requirements, suitability of water resources depends on the usage for which it is intended. Under this step, the characterized values of WQ factors were used to provide a water use ranking as "good," "fair," or "not applicable" for different water usages. Table 5 describes an example of criteria to judge the ranking for water usage. It is not necessary to consider all the factors for each water usage. As in the Table 5, for amenity water usage only, four factors were considered, while six factors were considered in water for landscaping usage.

Table 6 shows an example for ranking of different water usage of ozonated wastewater effluent in terms of considered WQ factors. Regarding the WQ factor of "acute toxicity to human," ozonated wastewater effluent can be ranked as "good" for most of water usage, but "fair" for water for emergency usage, in which

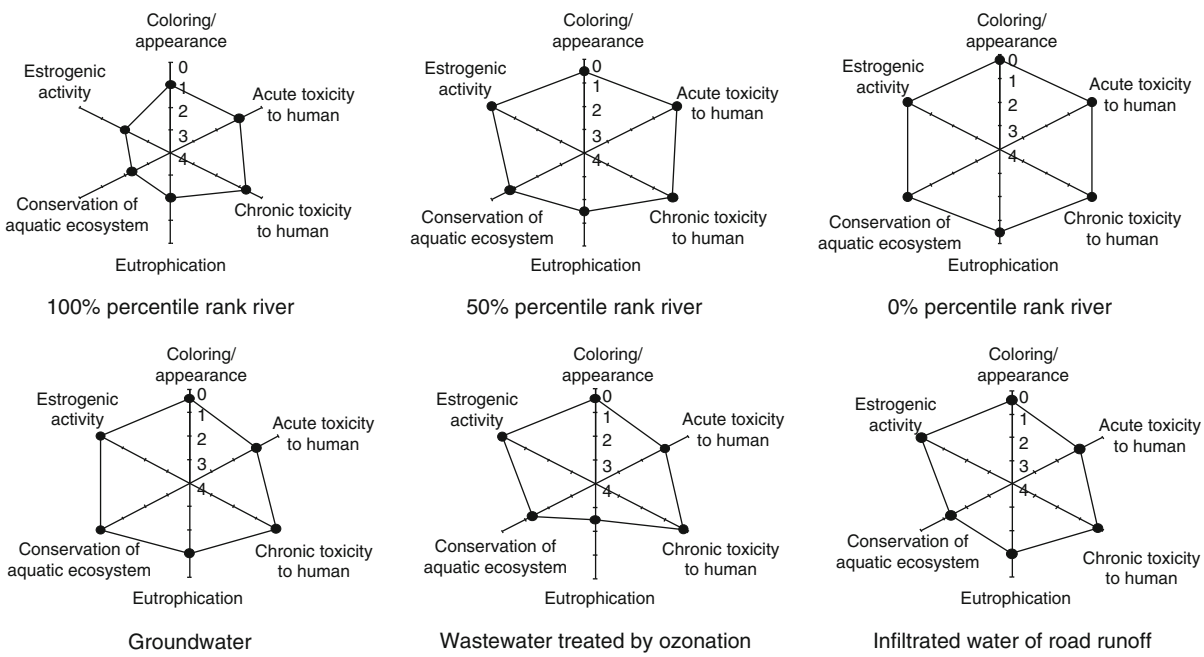

Community-Owned Water Resource and Climate Change, Quality Management. Figure 17
Example of WQ characterization of several water resources

Community-Owned Water Resource and Climate Change, Quality Management. Table 5 Example of criteria for several water applications

	Coloration/ appearance	Acute toxicity to human	Chronic toxicity to human	Eutrophication	Conservation of aquatic ecosystem	Estrogenic activity	...
Amenity water	≥2: n.a.	≥4: n.a.	≥3: n.a.	≥3: n.a.	–	–	
	1–2: fair	3–4: fair	2–3: fair	2–3: fair			
	<1: good	<3: good	<2: good	<2: good			
Water sprinkling and car wash	≥3: n.a.	≥4: n.a.	≥4: n.a.	–	–	–	
	2–3: fair	3–4: fair	3–4: fair				
	<2: good	<3: good	<3: good				
Toilet water	≥3: n.a.	≥4: n.a.	≥4: n.a.	–	–	–	
	2–3: fair	3–4: fair	3–4: fair				
	<2: good	<3: good	<3: good				
Landscaping water	≥3: n.a.	≥4: n.a.	≥4: n.a.	≥3: n.a.	≥3: n.a.	≥3: n.a.	
	2–3: fair	3–4: fair	3–4: fair	2–3: fair	2–3: fair	2–3: fair	
	<2: good	<3: good	<3: good	<2: good	<2: good	<2: good	
Water for emergency use	≥2: n.a.	≥2: n.a.	≥3: n.a.	–	–	–	
	1–2: fair	1–2: fair	2–3: fair				
	<1: good	<1: good	<2: good				
Water for fire protection	≥4: n.a.	≥4: n.a.	≥4: n.a.	–	–	–	
	3–4: fair	3–4: fair	3–4: fair				
	<3: good	<3: good	<3: good				

n.a. not applicable, - not considered

household water use is expected, including toilet flushing, washing, and bathing.

Water Quality Labeling and User Judgment

The last but the most important step is the judgment of water usage by users using WQ labeling information. In the previous step, each water resource was ranked with respect to the each factor such as "coloration," "acute toxicity," etc. The aim of this step is to decide the overall judgment for water usage of each water resources. As shown in Table 6, use of ozonated wastewater effluent for amenity purpose has been ranked as "good" for WQ factors of coloration, acute toxicity to human, chronic toxicity to human, but been ranked as "fair" for WQ factor of eutrophication. Therefore, overall WQ rank of ozonated wastewater effluent for amenity purpose was labeled as "fair" taking the lowest rank in each factor. Similarly, all the water resources subjected to evaluation were ranked and labeled in Table 7.

As summarized in Table 7, water usage labeling evaluates each water source and simply describes "how good or how bad" water sources are for different water applications. The outcome of this labeling information provides easy expression to compare WQ of different water resources directly with those of river WQ reference. Hence, it leads to overcome public

Community-Owned Water Resource and Climate Change, Quality Management. Table 6 Example for ranking of wastewater treated by ozonation for several water applications

	Coloration/ appearance	Acute toxicity to human	Chronic toxicity to human	Eutrophication	Conservation of aquatic ecosystem	Estrogenic activity	. . .	Example of user judgment
Amenity water	Good	Good	Good	Fair	–	–		Fair
Water sprinkling and car wash	Good	Good	Good	–	–	–		Good
Toilet water	Good	Good	Good	–	–	–		Good
Landscaping water	Good	Good	Good	Fair	Good	Good		Fair
Water for emergency use	Good	Fair	Good	–	–	–		Fair
Water for fire protection	Good	Good	Good	–	–	–		Good

–: not considered.

Community-Owned Water Resource and Climate Change, Quality Management. Table 7 Example of labeling of several water resources

	Amenity water	Water sprinkling and car wash	Toilet water	Landscaping water	Water for emergency use	Water for fire protection
100% percentile rank river	Fair	Good	Good	Not applicable	Not applicable	Good
50% percentile rank river	Good	Good	Good	Fair	Fair	Good
0% percentile rank river	Good	Good	Good	Good	Good	Good
Groundwater	Good	Good	Good	Good	Fair	Good
Wastewater treated by sand filtration	Fair	Good	Good	Fair	Fair	Good
Wastewater treated by ozonation	Fair	Good	Good	Fair	Fair	Good
Infiltrated water of road runoff	Good	Good	Good	Fair	Fair	Good
Infiltrated water of wastewater	Fair	Good	Good	Fair	Not applicable	Good

uncertainty in the use of alternative water sources (reclaimed water, runoff, etc.). The concept and process described in this case study can be used as a guide for WQ evaluation of community-based water resources. It should be mindful that required WQ might depend on the needs or objectives of that particular community and should be combined with effective management and monitoring system.

Although the WQ labeling framework indicates the relative WQ of a particular water source and can be used to compare and rank the water sources, the WQ labeling should never stand alone for the full interpretation of the feasibility of a water source. Therefore, in order to optimize the community-owned water use, it is beneficial to analyze both the quality and the quantity of water resources against potential reuse applications and WQ requirements. Moreover, energy consumption for water intake, purification, and distribution should be further considered to compare an existing water supply system and community-owned water resources [27].

Future Directions

It is apparent that climate change is already happening and going to be one of the greatest environmental, social, and economic threats facing the whole world. Since the water is involved in all components of the climate system, including atmosphere, hydrosphere, cryosphere, land surface, and biosphere, climate change affects water through many ways. Therefore, the climate change has the potential to be affecting the quantitative and qualitative status of global freshwater resources by altering hydrological cycles with wide-ranging effects on human societies and ecosystems. It is also anticipated that growing pressure on water resources will stimulate by the population growth, urbanization, land use changes, and some other drivers.

Various proposals have already been made to help for mitigation and adaptation measures focusing particularly on impacts of climate change on water resources. As part of adaptation against climate change effect on water resources, the potential use of rainwater and reclaimed water, which can be found within a community, is an attractive solution for many regions to meet the increase in water demand. However, public's perception on the community-owned water resources is influenced by attitudes, emotions, and accepted practice, and hence makes general public to hesitate to use them due to the lack of knowledge or complexity of understanding the WQ.

Therefore, it is important to provide WQ information from trusted scientific and regulatory sources in a simple manner so that general public can easily understand the quality of different water resources. The proposed WQ information platform in the last section reduces the multivariate nature of WQ data by providing scoring system that will logically combine all WQ information and provide a simple and easily understood description of different waters. The concept and process in this evaluation will assess each water resource and simply describes "how good or how bad" water resources are for different water applications. However, it should be mindful that required WQ might depend on the needs or objectives of a particular community and should be combined with effective management and monitoring system. Moreover, quantitative analysis of water resources and energy consumption for water intake, purification, and distribution should be further considered to compare an existing water supply system and community-owned water resources.

Acknowledgment

The authors acknowledge the CREST project, "Risk-Based Management of Self-Regulated Urban Water Recycle and Reuse System" (granted by JST), for the concept of WQ ranking and labeling.

Bibliography

Primary Literature

1. United Nations Framework Convention on Climate Change, Article 1: Definitions. http://unfccc.int/essential_background/convention/background/items/2536.php
2. Folland CK, Karl TR, Christy JR, Clarke RA, Gruza GV, Jouzel J, Mann ME, Oerlemans J, Salinger MJ, Wang SW (2001) Observed climate variability and change. In: Houghton JT, Ding Y, Griggs DJ, Noguer M, van der Linden PJ, Dai X, Maskell K, Johnson CA (eds) Climate change 2001: the scientific basis. Contribution of Working Group I to the Third Assessment Report of the Intergovernmental Panel on Climate Change. Cambridge university press, Cambridge/New York, 881 pp
3. The United Nations Climate Change Conference in Copenhagen, 7–19 Dec 2009. http://unfccc.int/meetings/cop_15/items/5257.php
4. Le Treut H, Somerville R, Cubasch U, Ding Y, Mauritzen C, Mokssit A, Peterson T, Prather M (2007) Historical overview of climate change. In: Solomon S, Qin D, Manning M, Chen Z, Marquis M, Averyt KB, Tignor M, Miller HL (eds) Climate change 2007: the physical science basis. Contribution of Working Group I to the Fourth Assessment Report of the

Intergovernmental Panel on Climate Change. Cambridge University Press, Cambridge/New York
5. Forster P, Ramaswamy V, Artaxo P, Berntsen T, Betts R, Fahey DW, Haywood J, Lean J, Lowe DC, Myhre G, Nganga J, Prinn R, Raga G, Schulz M, Van Dorland R (2007) Changes in atmospheric constituents and in radiative forcing. In: Solomon S, Qin D, Manning M, Chen Z, Marquis M, Averyt KB, Tignor M, Miller HL (eds) Climate change 2007: the physical science basis. Contribution of Working Group I to the Fourth Assessment Report of the Intergovernmental Panel on Climate Change. Cambridge University Press, Cambridge/New York
6. IPCC (2001) In: Houghton JT, Ding Y, Griggs DJ, Noguer M, van der Linden PJ, Dai X, Maskell K, Johnson CA (eds) Climate change 2001: the scientific basis. Contribution of Working Group I to the Third Assessment Report of the Intergovernmental Panel on Climate Change. Cambridge University Press, Cambridge/New York, 881 pp
7. Tickell C (1993) Global warming and its effects, engineering for climate change. Institute of Civil Engineers, UK, pp 9–16
8. Haman DZ, Brown DA (1994) AE250. Agricultural and Biological Engineering Department, Florida Cooperative Extension Service, Institute of Food and Agricultural Sciences, University of Florida. http://edis.ifas.ufl.edu
9. Bates BC, Kundzewicz ZW, Wu S, Palutikof JP (2008) Climate change and water. Technical paper of the Intergovernmental Panel on Climate Change, IPCC Secretariat, Geneva
10. Trenberth KE, Jones PD, Ambenje P, Bojariu R, Easterling D, Klein Tank A, Parker D, Rahimzadeh F, Renwick JA, Rusticucci M, Soden B, Zhai P (2007) Observations: surface and atmospheric climate change. In: Solomon S, Qin D, Manning M, Chen Z, Marquis M, Averyt KB, Tignor M, Miller HL (eds) Climate change 2007: the physical science basis. Contribution of Working Group I to the Fourth Assessment Report of the Intergovernmental Panel on Climate Change. Cambridge University Press, Cambridge/New York
11. Brekke LD, Kiang JE, Olsen JR, Pulwarty RS, Raff DA, Turnipseed DP, Webb RS, White KD (2009) Climate change and water resources management – a federal perspective. US Geol Surv Circ 1331:65 http://pubs.usgs.gov/circ/1331/
12. Climate change monitoring report – 2008 (2009) Japan Meteorological Agency, Tokyo, Japan. http://ds.data.jma.go.jp/tcc/tcc/products/gwp/gwp.html
13. Hirabayashi Y, Kanae S, Emori S, Oki T, Kimoto M (2008) Global projections of changing risks of floods and droughts in a changing climate. Hydrol Sci J 53(4):754–772
14. Nohara D, Kitoh A, Hosaka M, Oki T (2006) Impact of climate change on river discharge projected by multimodel ensemble. J Hydrometeorol 7:1076–1089
15. Bindoff NL, Willebrand J, Artale V, Cazenave A, Gregory J, Gulev S, Hanawa K, Le Quéré C, Levitus S, Nojiri Y, Shum CK, Talley LD, Unnikrishnan A (2007) Observations – oceanic climate change and sea level. In: Solomon S, Qin D, Manning M, Chen Z, Marquis M, Averyt KB, Tignor M, Miller HL (eds) Climate change 2007 – the physical science basis. Contribution of Working Group I to the Fourth Assessment Report of the Intergovernmental Panel on Climate Change. Cambridge University Press, New York. http://ipccwg1.ucar.edu/wg1/Report/AR4WG1_Print_Ch05.pdf
16. Kundzewicz ZW, Mata LJ, Arnell NW, Döll P, Kabat P, Jiménez B, Miller KA, Oki T, Sen Z, Shiklomanov IA (2007) Freshwater resources and their management. In: Parry ML, Canziani OF, Palutikof JP, Van der Linden PJ, Hanson CE (eds) Climate change 2007: impacts, adaptation and vulnerability. Contribution of Working Group II to the Fourth Assessment Report of the Intergovernmental Panel on Climate Change. Cambridge University Press, Cambridge, pp 173–210
17. Arheimer B, Andréasson J, Fogelberg S, Johnsson H, Pers CB, Persson K (2005) Climate change impact on water quality: model results from Southern Sweden. Ambio 34(7):559–566
18. Delpla I, Jung A-V, Baures E, Clement M, Thomas O (2009) Impacts of climate change on surface water quality in relation to drinking water production. Environ Int 35: 1225–1233
19. Arnell N (1998) Climate change and water resources in Britain. Clim Change 39:83–110
20. Kumagai M, Ishikawa K, Chunmeng J (2003) Dynamics and biogeochemical significance of the physical environment in Lake Biwa. Lakes Reserv Res Manage 7:345–348
21. Mimikou MA, Baltas E, Varanou E, Pantazis K (2000) Regional impacts of climate change on water resources quantity and quality indicators. J Hydrol 234:95–109
22. Parry ML, Canziani OF, Palutikof JP, van der Linden PJ, Hanson CE (eds) Contribution of Working Group II to the Fourth Assessment Report of the Intergovernmental Panel on Climate Change. Cambridge University Press, Cambridge, p 976
23. Leakage prevention guidebook, 2009, Bureau of Waterworks, Tokyo Metropolitan Government, Japan. http://www.waterprofessionals.metro.tokyo.jp/pdf/leakage_prevention_guidebook_2009.pdf
24. Fujita S (1997) Measures to promote stormwater infiltration. Water Sci Technol 36(8–9):289–293
25. Orange County, 2010, Groundwater replenishment system, Orange County Water District, California. http://www.gwrsystem.com/about/contact.html
26. Lucio R, Hisham ME, Andrea C (eds) (2007) Solar desalination for the 21st century; a review of modern technologies and researches on desalination coupled to renewable energies. In: Proceedings of the NATO advanced research workshop on solar desalination for the 21st century, Hammamet, Tunisia, 23–25 Feb 2006
27. Furumai H, Murakami M, Chaminda GGT (2010) Evaluation of community-owned water resources based on water quality labeling system. In: Hao X, Novotny V, Nelson V (eds) Water infrastructure for sustainable communities: China and the world. IWA Publishing, London, pp 89–116
28. Population Division of the Department of Economic and Social Affairs of the United Nations Secretariat, World Population Prospects: The 2008 Revision and World Urbanization

Prospects: The 2009 Revision. http://esa.un.org/wup2009/unup/index.asp
29. Frederick KD, Major DC (1997) Climatic change and water resources. Clim Change 37:7–23 (Kluwer, Dordrecht)
30. Falkenmark M (1989) The massive water scarcity now threatening Africa: Why isn't it being addressed. Ambio 18(2):112–118
31. Oki T, Kanae S (2006) Global hydrological cycles and world water resources. Science 313(5790):068–1072
32. Furumai H (2008) Rainwater and reclaimed wastewater for sustainable urban water use. Phys Chem Earth 33: 340–346
33. Watanabe H, Murakami M, Komura T, Moroizumi T, Furumai H (2009) Evaluation of water balance and water use stress in principal cities in Japan. J Water Waste 51(2):137–148 (in Japanese)
34. Ministry of Land, Infrastructure, Transport and Tourism, Japan (2009) Water resources in Japan (in Japanese)
35. Bureau of Waterworks Tokyo Metropolitan Government Website (2010). https://www.waterworks.metro.tokyo.jp/water/pp/kh21/kh21_05.pdf
36. UNEP (2005) Water and wastewater reuse, an environmentally sound approach for sustainable urban water management. United Nations Environment Programme (UNEP), Division of Technology, Industry and Economics-International Environmental Technology Centre. http://www.unep.or.jp/
37. Furumai H (2007) Reclaimed stormwater and wastewater and factors affecting their reuse. In: Novotny V, Brown P (eds) Cities of the future towards integrated sustainable water and landscape. IWA publishing, UK, pp 219–235
38. Asano T (ed) (1998) Wastewater reclamation and reuse, vol 10, 1st edn. Technomic Publishing Company, Lancaster
39. Alon T (2006) Seeking sustainability: Israel's evolving water management strategy. Science 313:1081–1084
40. UNEP (2004) Israel's experience in the management of water and wastewater. In: Proceedings of the 8th special session of the governing council/global ministerial environment forum, Jeju, Republic of Korea, 29–31 Mar 2004. http://www.unep.org/gc/gcss-viii/Ministerial_level.asp
41. Angelakis AN, Durham B (2008) Water recycling and reuse in EUREAU countries: trends and challenges. Desalination 218:3–12
42. Ministry of Land, Infrastructure and Transport (MLIT) (2008) Tokyo, Japan. http://www.mlit.go.jp/common/000015573.pdf
43. Ministry of Land, Infrastructure and Transport, Japan (MLIT) (2001) Sewage works in Japan 2001. Tokyo, Japan
44. Kim KS (2009) The present state and policy plan of sewerage in Korea, Special seminar at Department of Urban Engineering, The University of Tokyo
45. Japan Sewage Works Association (2004) Tokyo, Japan. http://www.jswa.jp/05_arekore/data-room/05/riyou/shorisui.html
46. Asano T, Burton FL, Leverenz HL, Tsuchihashi R, Tchobanoglous G (2007) Water reuse: issues, technologies and applications. Metcalf & Eddy, New York
47. Nolde E (2007) Possibilities of rainwater utilisation in densely populated areas including precipitation runoffs from traffic surfaces. Desalination 215:1–11
48. Furumai H, Jinadasa HKPK, Murakami M, Nakajima F, Aryal RK (2005) Model description of storage and infiltration functions of infiltration facilities for urban runoff analysis by a distributed model. Water Sci Technol 52(5):53–60
49. Murakami M, Nakajima F, Furumai H, Tomiyasu B, Owari M (2007) Identification of particles containing chromium and lead in road dust and soakaway sediment by electron probe microanalyser. Chemosphere 67:2000–2010
50. WHO (1973) Reuse of effluents: methods of wastewater treatment and health safeguards. Report of a WHO Meeting of Experts, Geneva, 1973. Technical Report Series No. 517, World Health Organization, Geneva, Switzerland
51. WHO Scientific Group (1989) Health guidelines for the use of wastewater in agriculture and aquaculture. Technical Report Series 778, World Health Organization, Geneva, Switzerland
52. WHO (2006) WHO guidelines for the safe use of wastewater, excreta and greywater. World Health Organization, Geneva, Switzerland
53. USEPA (1992) Guidelines for water reuse. Technical Report No. EPA/625/R-92/004. U.S. Environmental Protection Agency, Washington, DC
54. USEPA (2004) Guidelines for water reuse. Technical Report No. EPA/625/R004/108. U.S. Environmental Protection Agency, Washington, DC
55. Australian guidelines for water recycling: Managing health and environmental risks (Phase 1) (2006) Publication of the Environment Protection and Heritage Council, the National Health and Medical Research Council and the Natural Resource Management Ministerial Council, Australia
56. Australian guidelines for water recycling: Managing health and environmental risks (Phase 2); augmentation of drinking water supplies (2008) Publication of the Environment Protection and Heritage Council, the National Health and Medical Research Council and the Natural Resource Management Ministerial Council, Australia
57. Bixioa D, Thoeyea C, Koningb J, De JD, Savicc D, Wintgensd T, Melind T (2008) Wastewater reuse in Europe. Desalination 187:89–101
58. Tajima A (2006) Establishment of guidelines for the reuse of treated wastewater. Wastewater and Sludge Management Division, Water Quality Control Department, National Institute for Land and Infrastructure Management, Ministry of Land, Infrastructure, Transport and Tourism, Tokyo, Japan. http://www.nilim.go.jp/lab/ecg/eindex.htm
59. Abu-Madi M, Mimi Z, Abu-Rmeileh N (2008) Public perceptions and knowledge towards wastewater reuse in agriculture in Deir Debwan. In: First symposium on wastewater reclamation and reuse for water demand management in Palestine, Birzeit University, Palestine, 2–3 Apr 2008
60. Cabinet Office, Government of Japan (2008) Public opinion research on water, August, 2008. http://www8.cao.go.jp/survey/index.html

61. Baumann DD (1983) Social acceptance of water reuse. Appl Geogr 3:79–84
62. Kantanoleon N, Zampetakis L, Manios T (2007) Public perspective towards wastewater reuse in a medium size, seaside, Mediterranean city: a pilot survey. Resources Conserv Recycling 50:282–292
63. Harada A, Nakada N, Yamashita N, Sato N, Ito M, Suzuki Y, Tanaka H, Furumai H (2006) Relative evaluation of reclaimed wastewater in urban area in comparison with the distribution of river water quality. Environ Eng Res 43:501–508 (in Japanese)
64. The River Bureau Ministry of Land Infrastructure Transport and Tourism Japan (2004) River water quality yearbook 2002 (Kasen suishitsu nenkan 2002). River Association Japan, Tokyo (in Japanese)
65. Managaki S, Kojima S, Harada A, Nakada N, Tanaka H, Takada H (2005) Development of analytical method of linear alkylbenzenesulfonates and their degradation intermediates by high performance liquid chromatography equipped with tandem mass spectrometry and its application to major Japanese rivers. J Jpn Soc Water Environ 28(10): 621–628 (in Japanese)
66. Komatsu T, Manabe Y, Himeno S, Harada A, Murakami M, Furumai H (2007) Distribution of mutagen formation potential in nationwide river waters in Japan and relationship with general water quality or river basin characteristics. J Jpn Soc Water Environ 30(8):433–440
67. Murakami M, Imamura E, Shinohara H, Kiri K, Muramatsu Y, Harada A, Takada H (2008) Occurrence and sources of perfluorinated surfactants in rivers in Japan. Environ Sci Technol 42(17):6566–6572
68. Nakada N, Kiri K, Shinohara H, Harada A, Kuroda K, Takizawa S, Takada H (2008) Evaluation of pharmaceuticals and personal care products as water-soluble molecular markers of sewage. Environ Sci Technol 42(17):6347–6353
69. Murakami M, Sato N, Anegawa A, Nakada N, Harada A, Komatsu T, Takada H, Tanaka H, Ono Y, Furumai H (2008) Multiple evaluations of the removal of pollutants in road runoff by soil infiltration. Water Res 42(10–11): 2745–2755
70. Nakada N, Shinohara H, Murata A, Kiri K, Managaki S, Sato N, Takada H (2007) Removal of selected pharmaceuticals and personal care products (PPCPs) and endocrine-disrupting chemicals (EDCs) during sand filtration and ozonation at a municipal sewage treatment plant. Water Res 41(19): 4373–4382
71. Shinohara H, Murakami M, Managaki S, Kojima S, Takada H, Sato N, Suzuki Y, Nakada N (2006) Removal of water-soluble organic micro-pollutants by soil infiltration. Soc Environ Sci Jpn 19(5):435–444 (in Japanese)
72. Nakada N, Yamashita N, Miyajima K, Suzuki Y, Tanaka H, Shinohara H, Takada H, Sato N, Suzuki M, Ito M, Nakajima F, Furumai H (2007) Multiple evaluation of soil aquifer treatment for water reclamation using instrumental analysis and bioassay. In: Furumai H, Kurisu F, Katayama H, Satoh H, Ohgaki S, Thanh NC (eds) Southeast Asian water environment, vol 2. IWA Publishing, UK, pp 303–310
73. Murakami M, Kuroda K, Sato N, Fukushi T, Takizawa S, Takada H (2009) Groundwater pollution by perfluorinated surfactants in Tokyo. Environ Sci Technol 43(10):3480–3486

Books and Reviews

Al-Hoti BA, Abdullah R (1989) Reuse of collected storm water runoff for irrigation in Kuwait. Desalination 75:329–340

Arnell NW (1999) Climate change and global water resources. Glob Environ Change 9:S31–S49

Asano T (2009) Milestones in wastewater reclamation, recycle and reuse, Water reuse and sea water utilization workshop, In: ASPIRE-2009, Taipei International Conference Center, Taipei, Taiwan, Oct 2009

Begum S, Rasul MG (2009) Reuse of storm water for watering gardens and plants using green gully: a new storm water quality improvement device (SQID). Water Air Soil Pollut Focus 9:371–380

Blumenthal UJ, Peasey A, Ruiz-Palacios G, Mara DD (2000) Guidelines for wastewater reuse in agriculture and aquaculture: recommended revisions based on new research evidence, WELL study, Task No: 68 Part 1, London School of Hygiene & Tropical Medicine, Loughborough University, UK. http://www.lboro.ac.uk/well/resources/well-studies/full-reports-pdf/task0068i.pdf

Dolnicar S, Schafer AI (2009) Desalinated versus recycled water: public perceptions and profiles of the accepters. J Environ Manage 90:888–900

Hatt BE, Deletic A, Fletcher TD (2006) Integrated treatment and recycling of stormwater: a review of Australian practice. J Environ Manage 79:102–113

Kabat P, Schulze RE, Hellmuth ME, Veraart JA (eds) (2002) Coping with impacts of climate variability and climate change in water management: a scoping paper. DWC-Report No. DWCSSO-01(2002), International Secretariat of the Dialogue on Water and Climate, Wageningen

Kazmi A, Furumai H (2005) Sustainable urban wastewater management and reuse in Asia. Int Rev Environ Strat 5(2): 425–448

Radcliffe JC (2006) Future directions for water recycling in Australia. Desalination 187:77–87

Ragab R, Prudhomme C (2002) Climate change and water resources management in arid and semi-arid regions: prospective and challenges for the 21st century. Biosystems Eng 81(1):3–34

Takizawa S (2008) Groundwater management in asian cities: technology and policy for sustainability. Springer, Japan

Vairavamoorthy K, Gorantiwar SD, Pathirana A (2008) Managing urban water supplies in developing countries: climate change and water scarcity scenarios. Phys Chem Earth 33:330–339

Concentrating Receiver Systems (Solar Power Tower)

Spiros Alexopoulos, Bernhard Hoffschmidt
Solar-Institut Jülich (SIJ), FH Aachen, Aachen University of Applied Sciences, Jülich, Germany

Article Outline

Glossary
Definition of the Subject and Its Importance
Introduction
Advantages of the Use of CRS for Supply of Energy
Concentrating Receiver Systems for Power Production
Providing Firm and Dispatchable Power
Characteristics of Different Heat Transfer Fluids
Increase of Operation Hours of CRS by Storage and Hybridization
Examples of CRS Plants
Secondary Uses of CRS
Economical Considerations
Future Directions
Bibliography

Glossary

Absorber Device which absorbs concentrated solar radiation and produces heat.

Black body Ideal body which would absorb all of the radiation falling upon it.

Blocking, blocking losses Power which is lost due to interception of part of reflected sunlight from one heliostat by the backside of another heliostat.

Capacity factor Energy produced over a specified time interval.

Central receiver system, concentrating receiver system (CRS) Solar power plant system in which solar radiation is converted by a heliostat field onto a tower-mounted solar receiver.

Concentration ratio Ratio of radiant flux density output to radiant flux density input.

Direct normal irradiation (DNI) Direct part of energy carried by sun rays on a given area.

Dispatchability, dispatchable Ability to dispatch on-demand produced electricity to the grid.

Heat recovery steam generator (HRSG) A conventional power plant component which produces steam.

Heat transfer fluid (HTF) in a CRS Fluid used to absorb heat in the solar central receiver and to transport and to deliver it to another component of a power plant (e.g., Heat recovery steam generator, storage)

Heliostat Device consisting of an assembly of mirrors, support structure, drive mechanism, and mounting foundation, which follows continuously the sun in two dimensions and reflects the sun rays to a fixed direction.

Heliostat field Sum of all heliostats of a CRS.

Hybrid system Any energy system which operates on two or more energy input sources, or which provides more than one form of energy output.

Parasitic power, parasitic losses Power required to operate an energy conversion system (e.g., pumps, buildings, blowers, electric devices).

Radiation Emission and propagation of electromagnetic energy through space or material.

Receiver efficiency Ratio of the thermal output delivered by the receiver HTF to the incident solar radiant flux under reference conditions.

Receiver, solar receiver Radiation absorbing system that works like a heat exchanger as it accepts solar radiation and delivers heat to a HTF.

Spillage, spillage losses Fraction of concentrated solar radiation which misses the absorber of the solar receiver.

Thermocline Zone or layer in a thermal storage volume in which the vertical temperature profile changes rapidly.

Definition of the Subject and Its Importance

This contribution is an attempt to write an original comprehensive yet concise introduction to concentrated solar receiver technologies, with the specific aim to find ways to solve the rising energy demand with using clean energy.

Among others in the world today there are two huge problems: climate change and rising energy demand. Solar-thermal power plants constitute a significant technological option for a sustainable future energy-mix. Solar-thermal energy is booming all around the world as many power plants are being built or planned.

Since the decade of the 1980s power production with concentrated solar tower power plants, as for example solar towers, has been a way to substitute fossil fuels.

From the beginning of the 1980s until the end of the 1990s many research activities in the field of solar tower technology took place in North America and Europe. The experience gained from these activities provided the necessary conditions for commercialization and creation of the first solar tower power plants. Pioneers in establishment and development of this technology in Europe are Germany and Spain. Different solar tower technologies concerning the concentrator, heat transfer media, and power cycle are competing.

In order to raise the operation hours of a central receiver system (CSR) a combination with a storage system or an upgrade to a hybrid system by combining the solar operation with different components is possible. This is a significant advantage over many other renewable energy technologies because heat is used as an intermediate energy carrier. In order to achieve 'round-the-clock, 100% renewable energy, CSP can be hybridized with biomass energy. For finding ways to solve a further important problem of the water shortage, desalination systems using the heat and the electricity from solar power plants can be applied.

The introduction depicts the huge solar thermal potential of the world's Sunbelt. In the next section the advantages of solar tower technology are analytically described. The third section of this article presents, in a technical but reader-friendly way, the different components of CRS technologies. Although the main focus of this article is to describe this technology and to present the installed solar plants (section "Examples of CRS Plants"), there is a diverse coverage from solar only operation (section "Providing Firm and Dispatchable Power") to combination with storage systems and hybrid solar tower power systems (section "Increase of Operation Hours of CRS by Storage and Hybridization").

Section "Characteristics of Different Heat Transfer Fluids" emphasizes the characteristics of different heat transport fluids which are used in CRS. Section "Secondary Uses of CRS" presents ways to use the heat provided by solar central receivers for other applications.

The chapter closes with a short economical consideration and an overview of the future perspectives, emphasizing the potential of future technology and the cost estimations.

The most immediate value of this contribution resides in providing important and up-to-date information for all readers who may be interested in the growing field of concentrated solar power (CSP) and especially CRS technology. The article fills the need for a wide-coverage systematic description of the different systems as well as of different power plant configurations which enable firm and dispatchable energy production, thus helping the reader to understand the key technological advantages and disadvantages of the central receiver technologies.

It is addressed to experts in engineering professionals, academics and scientists, technicians, managers, private and public institutions, students, and common citizens. The article may even be adopted as a text contribution for college courses that deal with renewable energy focusing on solar thermal energy and/or sustainability.

It includes tables and colored figures as well as equations which describe the thermodynamic behavior as well as the efficiencies of CRS technologies and applications. Especially, many colored pictures are selected in order to show almost all installed solar thermal power plants and test facilities worldwide. Complete literature is included at the end of the article to direct the curious and interested reader to further information.

The main aim of the contribution is to find solutions for main global environmental problems, so that the energy future mix may be made more efficient, clean, and sustainable.

Introduction

In spring 1931, about half a year before his death, Thomas Alva Edison, US American inventor, had a conversation with Henry Ford and Harvey Firestone, in which he apparently said: "I'd put my money on the sun and solar energy. What a source of power! I hope we don't have to wait till oil and coal run out before we tackle that."

This is not surprising since only about 1% of the Sahara (used for solar thermal power plants) is sufficient to cover the total current electricity demand of the earth (Fig. 1).

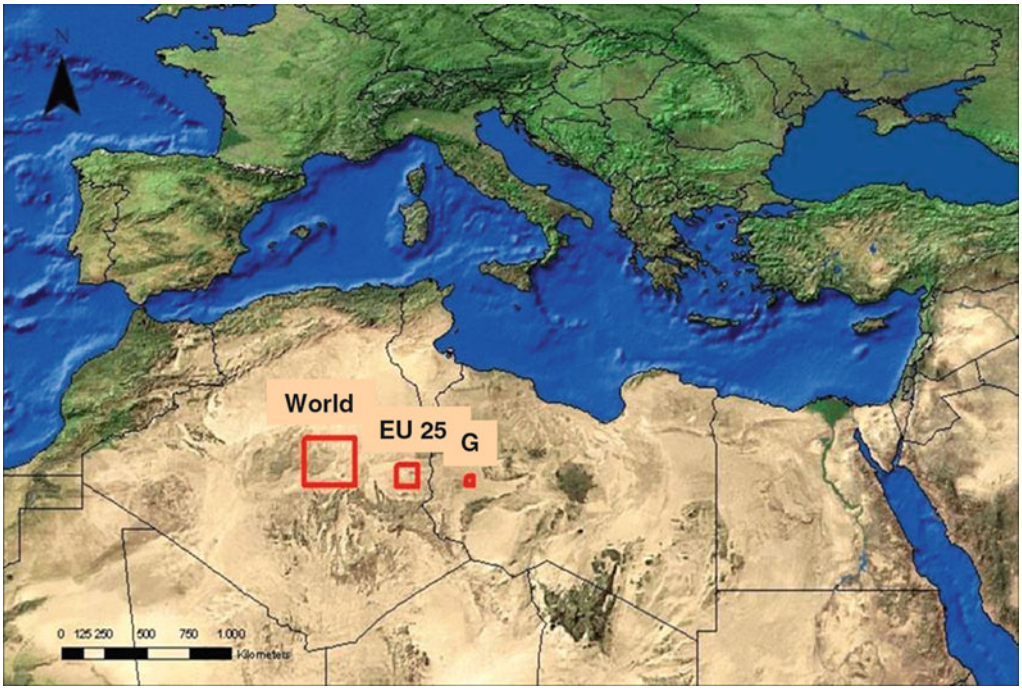

Concentrating Receiver Systems (Solar Power Tower). Figure 1
Potential of solar thermal power plants (Source: DLR)

According to the International Energy Agency, solar thermal power stations are the cheapest option in MW-scale for generating electricity from direct solar radiation commercially and constitute a pillar for the long-term worldwide electricity supply. Contrary to other renewable energy technologies the application of large thermal storages or, as advised in this project, the combination with additional conventional components for the hybridization, enable the decoupling of solar input. Thus, solar thermal power stations can also be used for grid stabilization and a need-based power production.

The parabolic trough, the solar dish, the Fresnel collector, and the solar tower belong to the group of solar thermal power systems. Parabolic trough and the solar tower are already competitive and economically feasible.

In solar thermal tower power plants with nearly planar mirrors focus solar radiation and direct it onto a receiver, which is located on the top of a tower. Very high temperatures in the receiver, resulting from this concentrated solar radiation enable generation of power plant process steam. The steam can be expanded in a steam turbine and generate power. Replacing fossil fuels, this clean power generation technology solely makes use of highly concentrated sunlight to produce electricity.

Advantages of the Use of CRS for Supply of Energy

The development of solar tower power plants aims to use higher concentrating solar radiation compared to parabolic trough as the power plant process at higher temperature and therefore operates with better efficiency. Higher temperature is also an advantage for storage of thermal energy, as storage volume per unit of energy can be reduced. Short-term developments aim to couple the heat from the solar towers in steam power plants.

Life cycle assessment of the emissions produced, together with the land surface impacts of CRS systems, shows that they are ideally suited to the task of reducing greenhouse gases and other pollutants, and without creating other environmental risks or contamination (Power 2020). Its low adverse environmental impact, with none of the polluting emissions or safety concerns

associated with conventional generation technologies is a major benefit of solar thermal tower power. Like all solar technologies CRS have an inexhaustible fuel source and the entire process is not polluting and no emissions or greenhouse gases are produced. There is hardly any pollution in the form of noise during operation, and decommissioning a system is not problematic [1]. Even considering the live cycle of the emission of carbon dioxide in the atmosphere during the production of the plant components, in the dismantling and installation of the power plant it has been found that comparatively the solar thermal systems emit only 12 kg of carbon dioxide per MWh, the hydropower plants 14 kg/MWh, the wind turbines 17 kg/MWh, and the photovoltaic systems 110 kg/MWh.

CRS plants have a very good ecological balance. All materials used are fully recyclable and most used materials like glass and steel are available worldwide. Solar tower power can therefore make a substantial contribution toward international commitments to reduce the steady increase in the level of greenhouse gases and their contribution to climate change.

The use of tower technology is not restricted to level surfaces. It can also be installed in hilly landscapes. Tower plants can adapt to land diverse in orography, ranging from certain undulations in the area for implementation, to include land characterized by more complex orography, which may involve valley slopes for positioning solar fields. An important requirement is that the heliostat field should face the south in latitudes in the Northern Hemisphere or the north in the Southern Hemisphere. In the end, considerable additional area can be exploited for solar technology worldwide.

A central receiver plant is made up of proven components. Operational safety and reliability as well as easy maintenance and cutting edge technology can be guaranteed. Parasitic pumping losses are smaller due to reduced pipe lengths, and the heat transfer fluid can also serve as the storage fluid, eliminating the need for heat exchangers that increase costs and decrease efficiency [2].

A cost-effective series production is possible for middle- to large-scale solar tower plants. This feature is not only applicable for solar parts like heliostats or receiver components but also for conventional parts like tubes. Furthermore the solar tower technology creates new jobs and contributes to the development of a new market.

Another important advantage is the capability for storage at high temperatures and the possibility of hybrid operation (see Increase of Operation Hours of CRS by Storage and Hybridization). In the future, further applications are possible in the fields of solar chemistry by the production of fuels and in industrial processing, for example, by the melting of metals.

Concentrating Receiver Systems for Power Production

Main components of a solar tower are the heliostat field, the receiver, and the tower itself.

Heliostat Field

A heliostat field is the sum of all heliostats of a solar tower.

Heliostats are mirrors which are equipped with a two-axes tracking system in order to track the sun's path. A heliostat field provides thermal energy for a solar tower power plant (also referred to as a central receiver system). Heliostats are named after the Greek words helio meaning "sun" and stat meaning stationary, because it describes the heliostat's function which is to reflect the solar image and to focus it on a fixed position on a tower-mounted absorber, called receiver. In order to do so, the heliostat must track the sun's position over the course of the day. As many hundreds or thousands of heliostats with a lot of mirror area reflect the solar image onto a comparatively small area of the receiver, high sunlight concentrations are reached. The furthest distance that a heliostat can be located away from the tower is approximately 1 km [3].

A heliostat has to satisfy criteria like the precision of the device and local conditions at the heliostat field site. The list of these criteria has a major influence on the design and the costs. They include the optical quality required, all the extraneous loads to be sustained, the required performance of the tracking system, protective measures for the heliostat and the receiver, and the life of individual components, and the heliostat whole system [4].

Wind loads, temperature, and hail impacts have a major impact on the supporting structure of a heliostat.

Heliostat Components Classical heliostat design is dominated by mirrors brought into position by steel structures and drives that guarantee high accuracies under wind loads and thermal stress situations. Figure 2 shows the typical parts of a heliostat (shown from the back).

To the structures that hold the mirrors include struts, beams, the pylon, and the foundation. The linear actuators enable moving of the heliostat in two dimensions (Fig. 3). There exists a zenith and an azimuth actuator together with their step motors.

Heliostat Types Several different types of heliostat mirrors exist, which can be differentiated according to size, shape, basic design concept, or even according to their tracking systems. Each type has its own characteristics in terms of wind-performance (and tracking during windy conditions), costs, and complexity of control. A field made up of more small heliostats will require a more complex control system than a field of fewer heliostats. Thus, large heliostats are more cost-efficient than small ones (on a $/m^2 basis). Improvements in controllability may cause this to change, however, and several companies are attempting the strategy of many small heliostats as opposed to fewer large heliostats [6].

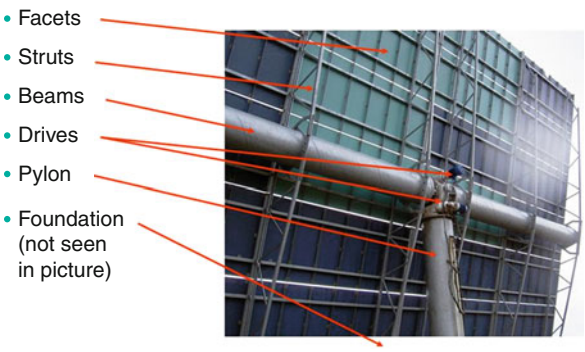

Concentrating Receiver Systems (Solar Power Tower). Figure 2
Parts of a heliostat [5]

Heliostat Shapes

Canted-Glass Mirror Heliostat A canted-glass mirror heliostat is often a single large heliostat that is divided into a number of sub-mirrors (it may also be a single, large mirror). Each sub-mirror is displaced relative to the others so that rays from the center of the sun are reflected from analogous points of the sub-mirrors and all converge to the same point on the receiver. Thus, perfect focusing results in the minimum image size by eliminating the contribution of the heliostat size to the size of the reflected image. Perfect canting also approximates perfect focusing by reducing the total heliostat size to that of a single sub-mirror. The greater the number of canted sub-mirrors a given sized heliostat has, the smaller the contribution of the size of the heliostat to the image will be. In other words, canting is a Fresnel approximation to focusing (note also that the sub-mirrors of a canted heliostat can each

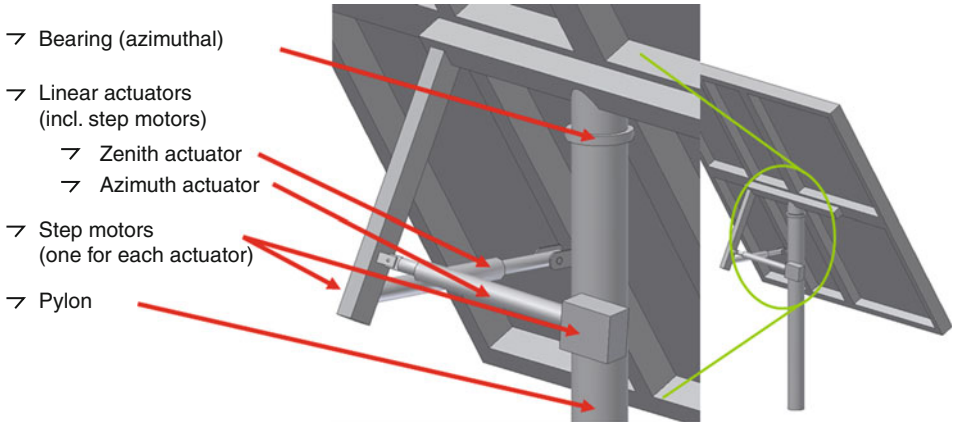

Concentrating Receiver Systems (Solar Power Tower). Figure 3
View of the main heliostat components (Source: SIJ)

be focused in 0–2 dimensions). The curvature or displacement required for focusing or canting is time dependent, since it depends on the angles between the heliostat, sun, and receiver. For most heliostat designs the curvature cannot be varied, and the heliostat will be perfectly focused or canted for only the one or two times of the year when the sun is in the correct position. At all other times, the heliostat will produce "off-axis aberration" of the image: distortions of the ideal image due to operation when the sun is not in the design position for the heliostat to be perfectly focused [7] (Fig. 4).

Stretched-Membrane Focused and Non-focused Heliostat The reflector of a stretched-membrane (SM) focused heliostats is made of either stretched polymer (plastic) or metallic foil. Figure 5 shows how the image from a SM heliostat is focused.

The SM design concept has not been very widely developed. It uses a thin reflective plastic membrane stretched over a hoop. Wind and temperature have a direct impact on the supporting structure of a SM heliostat. This design must be protected from the weather but requires considerably less expenditure in support structure and the mechanical drive mechanism because of its light weight. Membrane renewal and cleaning are important considerations with this design.

McDonnell Douglas, a former major American aerospace manufacturer and defense contractor, calculated that a 20% cost reduction could be achieved with developing heliostats with a mirror area of at least 100 m^2. In order to further reduce the heliostat costs, Sandia National Laboratories (USA) proposed a circular SM heliostat with a size of 150 m^2.

The proposed SM heliostat was lighter and simpler (i.e., requiring fewer parts) than a heliostat constructed of glass and metal.

Moreover, predictions showed that larger sized heliostats are more cost-effective [7]. Figure 6 below shows an SM heliostat design.

Flat Type Single Mirror Heliostats The Solar Tower Jülich concentrator field consists of 2,150 heliostats with about 8 m^2 of reflective surface densely packed in rows on an area of about 18,000 m^2. The heliostats are designed with a single glass facet fixed to a metal frame. The small size allows the use of simple linear drive units to track the sun's position (Fig. 7).

Heliostat Size The reflective mirror area of heliostats varies between 1 and 150 m^2. The advantage of having larger sized heliostats is that since fewer heliostats are installed, fewer step motors are required and fewer units need to be maintained. The disadvantage however, is the more difficult installation and maintenance of large heliostats, for example, replacement of actuators or broken mirrors. In order to withstand the high wind loads, the pylon, foundation, crossbeam and the cantilever arm must be designed a lot larger than for small heliostats (Fig. 8).

In the 1980s, it was believed that the way to reduce area-specific costs was to build larger heliostats. A more recent analysis by Sandia National Laboratories in the USA has reconfirmed this; however it does not apply to all power tower technologies.

Several research organizations have predicted that much smaller (10–20 m^2) heliostats could be cheaper. However, these organizations are generally using heliostats within an ultra-high concentration power tower system. Such systems require small beam sizes, which can be more easily achieved with small heliostats [6].

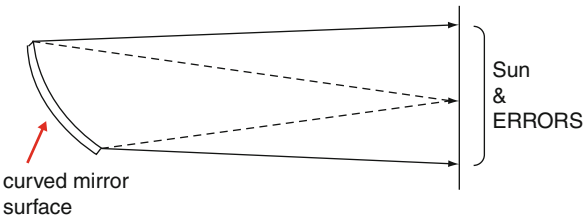

Concentrating Receiver Systems (Solar Power Tower). Figure 4
Canted heliostat [7]

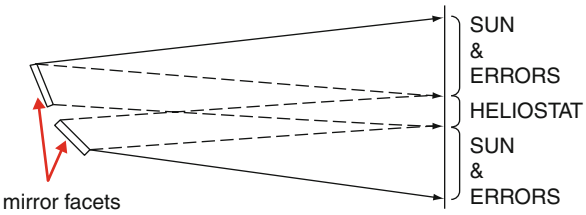

Concentrating Receiver Systems (Solar Power Tower). Figure 5
Focused heliostat [7]

Concentrating Receiver Systems (Solar Power Tower). Figure 6
ASM-150 SM heliostat built by Babcock Borsig Power Environment [3]

Concentrating Receiver Systems (Solar Power Tower). Figure 7
Flat type heliostat (Source: SIJ)

The research and demonstration power tower in Jülich, Germany, is a good example of this. The concentration factor is more than 750 times, on an ambient-air-pressure volumetric receiver. For the lower concentration power towers utilizing molten-salt or solid-particle receivers, the analysis predicts that low-cost heliostats are most likely to be $\geq$150 m^2.

The 148 m^2 Advanced Thermal Systems (ATS) heliostat has successfully operated for the last 20 years at the NSTTF (National Solar Thermal Test Facility) in Albuquerque, USA. It has survived multiple high-wind events, some in excess of 144 km/h, and the quality of the beam has not degraded significantly [6].

The SM heliostats (ranging between 120 and 150 m^2) proved to be good mechanically, although the polymer mirror glued to the metal membrane quickly suffered ultraviolet (UV) damage and the face-up stow position led to hail-induced membrane damage. As a result, Sandia recommended the use of thin glass rather than a polymer film. SM heliostats employing glass were built and tested at Solar Two and in Spain in the mid 1990s [6].

In 2006 and 2007, in Spain, more than 200,000 m^2 of heliostats were installed at the PS10 and PS20 solar tower plants. A large-area (121 m^2) pedestal-mounted heliostat similar to the ATS was selected after an evaluation of alternate concepts indicated it was the lowest-cost option.

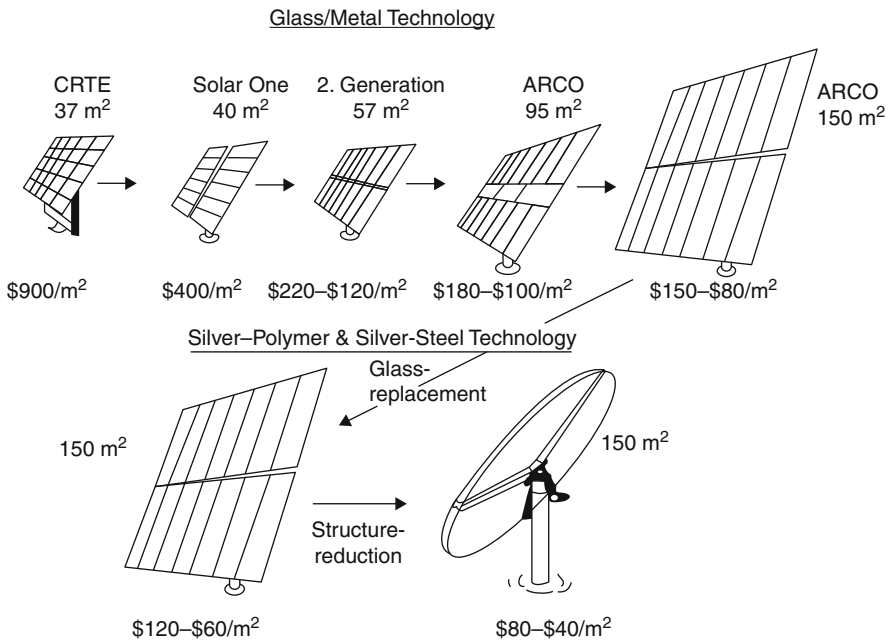

Concentrating Receiver Systems (Solar Power Tower). Figure 8
Heliostats used in solar power plants and their costs (Source: Sandia)

A recent development toward using small heliostat sizes was realized by the company eSolar, which built the Sierra SunTower. The advantage of using such small mirrors is that they are easily and quickly mountable (no cranes are required, see Fig. 9) and the heliostats can be mass manufactured. The mirror and 2-axes tracking system is deployed on a frame.

Current research on innovative small-mirror systems is also being conducted by the Solar-Institut Jülich (SIJ) and German Aerospace Center (DLR) in Germany. A possible option to reduce costs lies in a heliostat design where all moving parts are protected from wind loads. In this way, drives and mechanical layout may be kept less robust thereby reducing material input and costs. In order to keep the heliostat at an appropriate size, small mirrors are used. These are placed in a box with a transparent cover. Several designs have been examined concerning the drive system and the mechanical structures of the mirror array in order to develop a cost-effective design.

Heliostat Field Design The layout of the heliostat field is a complex topic. Decisions regarding the best position for locating heliostats relative to the receiver and how high to place the receiver above the field constitute a multifaceted problem, in which costs and heliostat loss mechanisms are among the variables, and which is solved by an iterative process [8].

Figure 10 shows the various basic field positions according to the location of the power plant on the earth. In the Northern Hemisphere, the sun's position is to the south of the plant and the field must be placed to the north of the tower. In the Southern Hemisphere the opposite is true. The general terminology for this position would be the "polar side" of the tower, which can be applied to towers in both the Northern and Southern Hemispheres. The opposite side of the tower is the "equatorial side." With a field on only one side of the tower, a cavity receiver is usually used. Close to the equator, where the sun passes directly overhead, a surrounding-field can be used in combination with an open receiver. Another possibility is the use of two fields – one on either side of the tower, in combination with a cavity receiver for each. In a system using secondary concentrators, an elliptical field should be used, since light reflected from wider-angled positions in the field would not enter the secondary concentrators.

Concentrating Receiver Systems (Solar Power Tower). Figure 9
Deployment of mirror field (Source: eSolar)

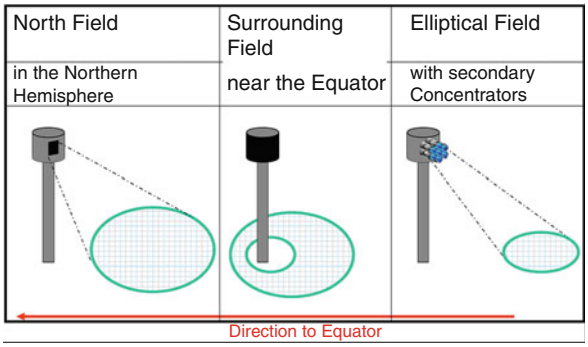

Concentrating Receiver Systems (Solar Power Tower). Figure 10
Heliostat field design in dependence of the location [5]

The aim in the designing of a heliostat field is to reliably produce the power required by the power block whilst keeping land usage and total costs to a minimum. As previously mentioned, the calculation of the losses, laying out and optimization of the field is an iterative process and there are many computer programs which have been designed over the last 30 years to perform this task. A detailed analysis of these computer programs is beyond the scope of this article.

Theoretical Considerations When laying out a heliostat field there are several types of losses that must be considered. These are not only the optical losses, namely, the cosine losses and losses due to shadowing, blocking, spillage, and atmospheric attenuation, but also technical considerations, that is, the mirror reflectivity, mirror surface defects, tracking accuracy, wind load, and tower oscillations (due to wind load) as well as the heliostat fault rate. The normal to the heliostat mirror surface is practically never facing the sun, except at the day in the year when at solar noon the sun's position is directly behind the receiver (in that case the particular heliostat would be covered in shade from the tower shadow). Over the course of any day the heliostat's azimuth and zenith angle orientation is changed every few seconds in order to guarantee accurate tracking of the sun's path. Hence, mathematically, the effective mirror area is less than the actual mirror area. The reduction in effective mirror area is proportional to the cosine angle of the angle of incidence [9].

The equation for the loss due to the cosine is given by:

$$Q_{cos,los} = 1 - cos\beta \quad (1)$$

The radiant power is calculated with the equation:

$$P_{rad} = I_{dir} \cdot A_{eff} \quad (2)$$

Figure 11 shows the effect that the cosine loss has on the radiant power, which is reflected by a heliostat. The cosine loss is the most significant loss of the heliostat field.

In the illustration, the example heliostat is positioned directly north of a solar tower. The equation for the cosine loss, however, is valid for heliostats in any location in a heliostat field.

Blocking is an effect which occurs for any heliostat which has neighboring heliostats in front and front sideways of it. Blocking means that a rear heliostat cannot reflect a portion of the light rays onto the receiver surface because a front heliostat blocks some of it, that is, some of the backside of the heliostat is illuminated. The lower the sun elevation angle and the further a heliostat is located away from the tower, the more blocking will occur.

The following graph illustrates the mechanism of blocking (Fig. 12):

Blocking can be avoided as much as possible by increasing the distance between the heliostats Δx as shown in Fig. 13.

To eliminate blocking completely, Δx has to take a value such that a line (here illustrated in orange color) can be drawn from the center of the receiver to the upper tangent of the mirror's swivel circle of heliostat and in continuation to the lower tangent of the mirror swivel circle of heliostat$_{i+1}$.

As an approximation, Δx can be calculated as follows:

$$\frac{z_s}{\Delta x} \approx \frac{z_T}{x} \tag{3}$$

Rearranging for Δx:

$$\Delta x \approx x \cdot \frac{z_s}{z_T} \tag{4}$$

where x is the horizontal distance of the heliostat pivot point to the center of the surface of the receiver. With growing distance x from the tower and with increasing ratio of z_s/z_T the distance between the consequent heliostats must be increased. The distance between the heliostats must not be chosen bigger than necessary because otherwise the tracking of the sun becomes too complex and the land requirement too much [9].

Shadowing is similar to blocking except that here the light rays, incident on a mirror surface, cast a shadow on the heliostat behind or sideways behind it. Figure 14 shows the partial shadowing of a mirror.

The heliostat field reflects and directs the direct normal irradiance on the receiver surface. Depending on factors such as the mirror quality and tracking

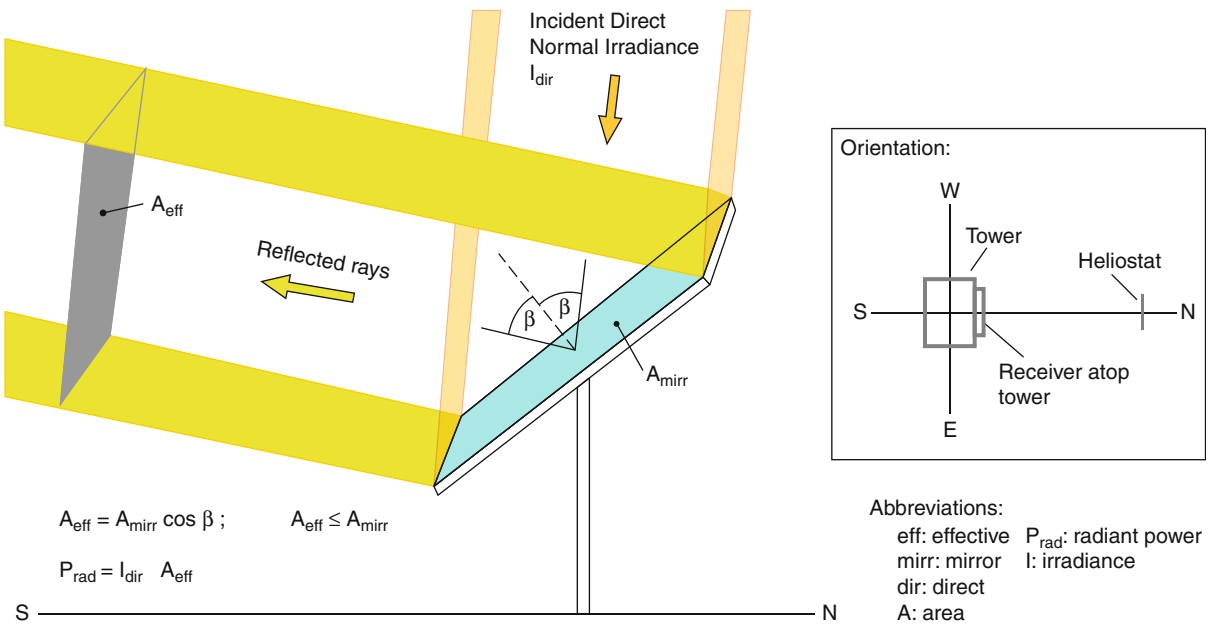

Concentrating Receiver Systems (Solar Power Tower). Figure 11
Effect of cosine loss on radiant power reflected by heliostat (Source: SIJ)

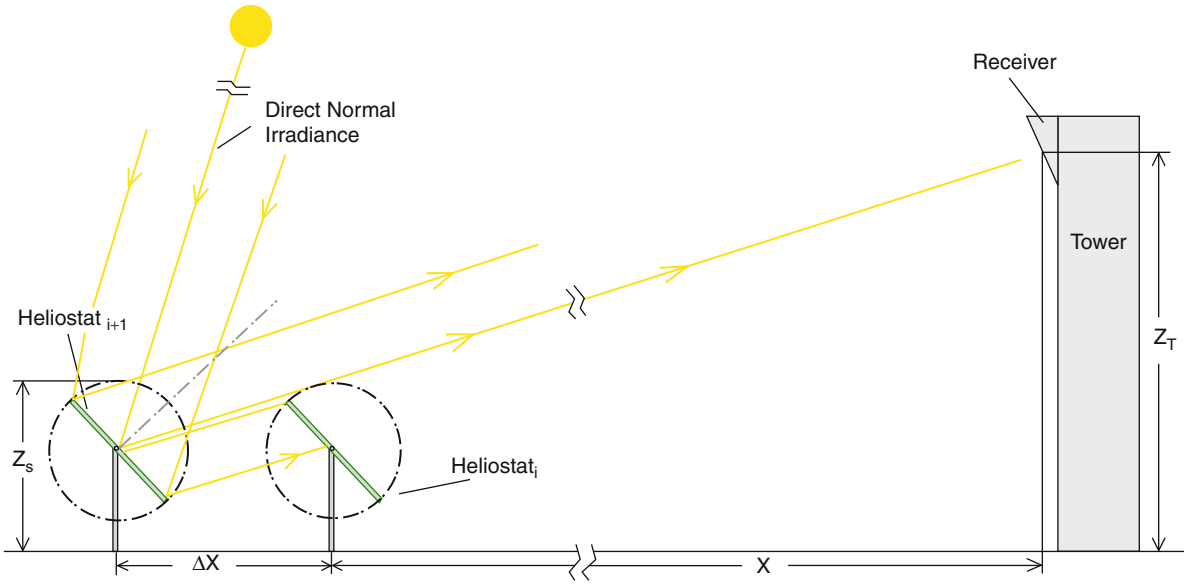

Concentrating Receiver Systems (Solar Power Tower). Figure 12
Heliostat blocking (Adapted from [9])

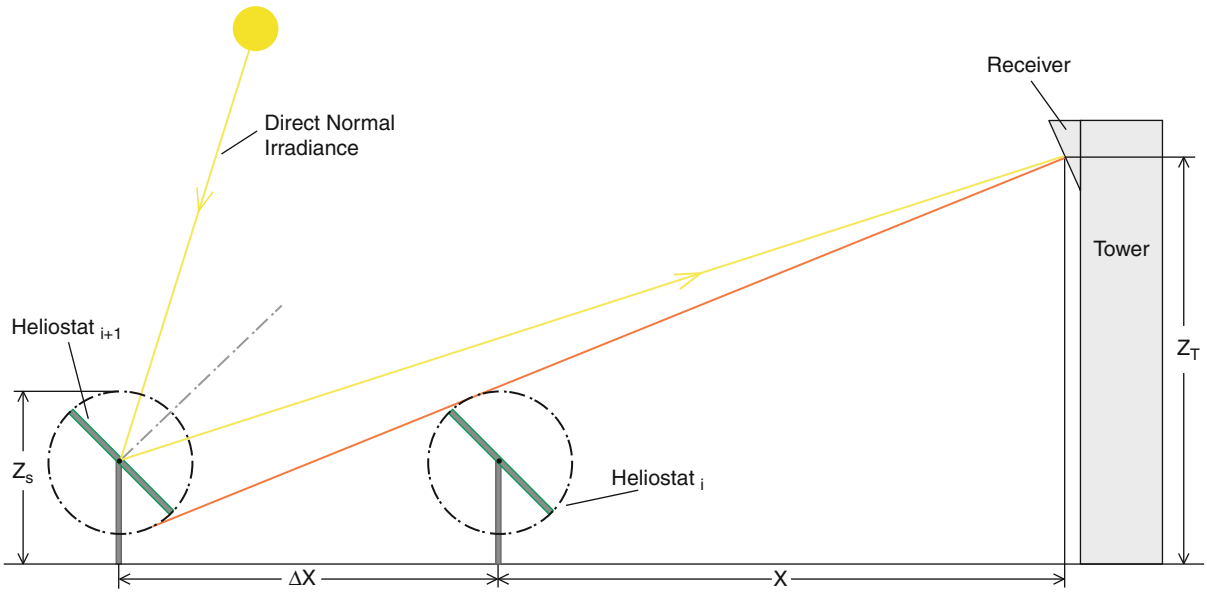

Concentrating Receiver Systems (Solar Power Tower). Figure 13
Blocking of neighboring heliostats according to [9]

system accuracy, a portion of radiation may miss the receiver surface – this is called spillage.

These factors contribute to a reflected image at the receiver surface that is errant from its intended path to the receiver and distorted from its shape as it originates from an individual heliostat.

Figure 15 illustrates the spillage loss for a solar tower with north-only field. Spilled radiation is the radiation which does not hit the receiver surface (rectangular gray area).

Another field loss is due to atmospheric attenuation, or scattering of beam radiation as the reflected

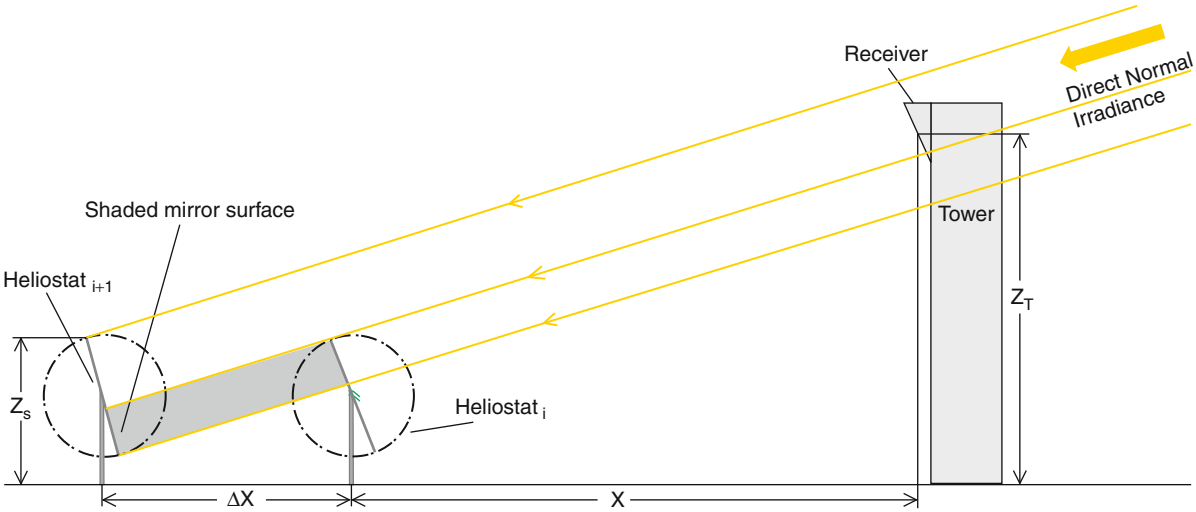

Concentrating Receiver Systems (Solar Power Tower). Figure 14
Shadowing loss (Source: SIJ)

heliostat image passes through air toward the receiver. The overall loss due to the atmospheric attenuation depends on the distances of the heliostats to receiver. The attenuation on the other hand is a function of the visibility, which, of course, can vary during the course of the day. As an example for the test location Barstow (USA), the visibility of a clear day is defined to be 23 km and for a hazy day 5 km [7].

How good a mirror reflects depends not only on the quality of the reflective surface, but also on the degree of mirror soiling (in certain time intervals the heliostat mirrors need to be washed to increase reflectivity) [7].

The overall optical loss is the product of the individual optical losses, according the following equation:

$$\eta_{SF,i} = \eta_{B,S} \cdot \eta_C \cdot \eta_F \cdot \eta_{W,T} \cdot \eta_R \cdot \eta_{Fail} \tag{5}$$

For computing the overall efficiency of the heliostat field $\eta_{S,F}$, the following weighted equation is valid:

$$\eta_{SF} = \frac{\sum_{i=1}^{n} \eta_{SF,i} \cdot A_{SF,i}}{A_{SF}} \tag{6}$$

Where n is the number of mirrors, $A_{SF,i}$ the area of a single heliostat in m^2, and ASF the area of the entire heliostat field.

The heliostat field reflects and directs a usable thermal power $\dot{Q}_{use,SF}$ to the receiver according to the following equation:

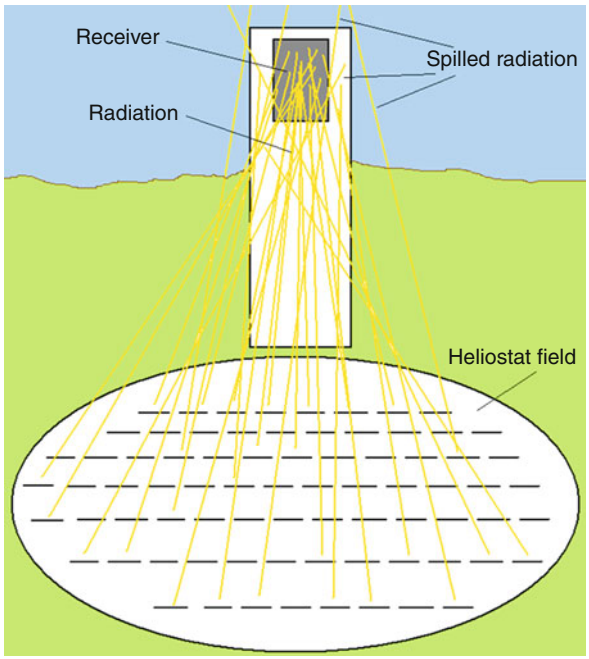

Concentrating Receiver Systems (Solar Power Tower). Figure 15
Spillage loss (Source: SIJ)

$$\dot{Q}_{use,SF} = A_{SF} \cdot \eta_{SF} \cdot I_{dir} \tag{7}$$

where I_{dir} is the direct normal irradiance.

Heliostat Aiming Strategies Aiming strategies serve the purpose of distributing the irradiation as evenly as possible on the receiver. There are several reasons for this:

- Absorbed radiation is transformed into heat and must be removed by a heat transfer medium
- Resulting temperature of the absorber material of the receiver depends on the mass flow of the heat transferring fluid
- If the temperature of the fluid is to be kept as high as possible, the mass flow cannot be increased arbitrarily
- Allowable flux density is fixed indirectly by the allowable temperature of the absorber material of the receiver
- One (central) aim point in the receiver plane cannot be used in most cases. Along with this, high temperatures result in higher-than-average radiation losses

There are several options for aiming the heliostats at different points. Many of the computer programs used to lay out the heliostat field are also designed to control the aiming strategies of the heliostat field as well as measure and control the flux density distribution on the receiver. This makes perfect sense, since the flux density incident upon the receiver is a direct result of the layout and aiming strategies of the heliostat field. As with the heliostat field layout programs, a detailed analysis of these programs is also beyond the scope of this text and mathematical details can again be found in each of the quoted sources [7, 10, 11].

The flux density on the receiver depends on several factors:

- Sun position, sun shape (daytime and season)
- Number, size, and optical quality of the heliostats
- Focal length and the canting of the heliostats
- Most important influence: distribution of the individual aim points of the heliostats

The aiming options described below (A to F, in Fig. 16) are quoted from the handbook of "Delsol 3" [7], which is an early computer code for calculating the optical performance and optimal system design for solar thermal central receiver plants. The five different strategies are generally required for the design of flux-limited liquid-(or steam)-carrying receivers. Different aiming strategies are also applicable to various types of receivers. The receiver types which will be mentioned here are:

- External (cylindrical)
- Cavity with Single Aperture
- Single Flat Plate
- Rectangular Aperture or Flat Plate
- Elliptical Aperture or Flat Plate

The aiming options are time dependent; that is, the number of aim-points can change over the year if the image changes.

(A) Single Aim Point: This is the simplest of all aiming options. All heliostats are pointed at the center of the receiver (when viewed from the heliostat surface). This option produces the maximum flux on the receiver.

(B) One-Dimensional Aiming: The heliostat images are spread out along the "height" of the receiver or aperture until the spillage starts to increase. As seen in the figure, the smaller images of the inner (or best focused) heliostats can be spread out over more aim points than the larger images of the outer (or less well focused) heliostats. This option reduces both the peak flux and the flux gradients on the receiver. This is the aiming option to use with external receivers and with cavity or flat plate receivers of elliptical shape. Since the size of the images from the heliostats can change with time, the one-dimensional aiming also changes with time, so that both the number and position of the aim-points may change.

(C) Two-Dimensional Aiming: This option is similar to (B) except that the images are spread out in two dimensions as shown in the figure. This results in even smaller peak fluxes than (B). However, this option should only be used with rectangular cavity apertures or rectangular flat plates. If used with elliptical receivers the spillage will increase. Furthermore, if used with external cylinders much of the flux will be incident on the receiver at very fine incidence angles where the absorption is poor.

(D) Single Aim Point at the Lower Part of the Receiver: The heliostats are aimed as close to the bottom of the receiver as is possible without increasing spillage significantly, as shown in the figure.

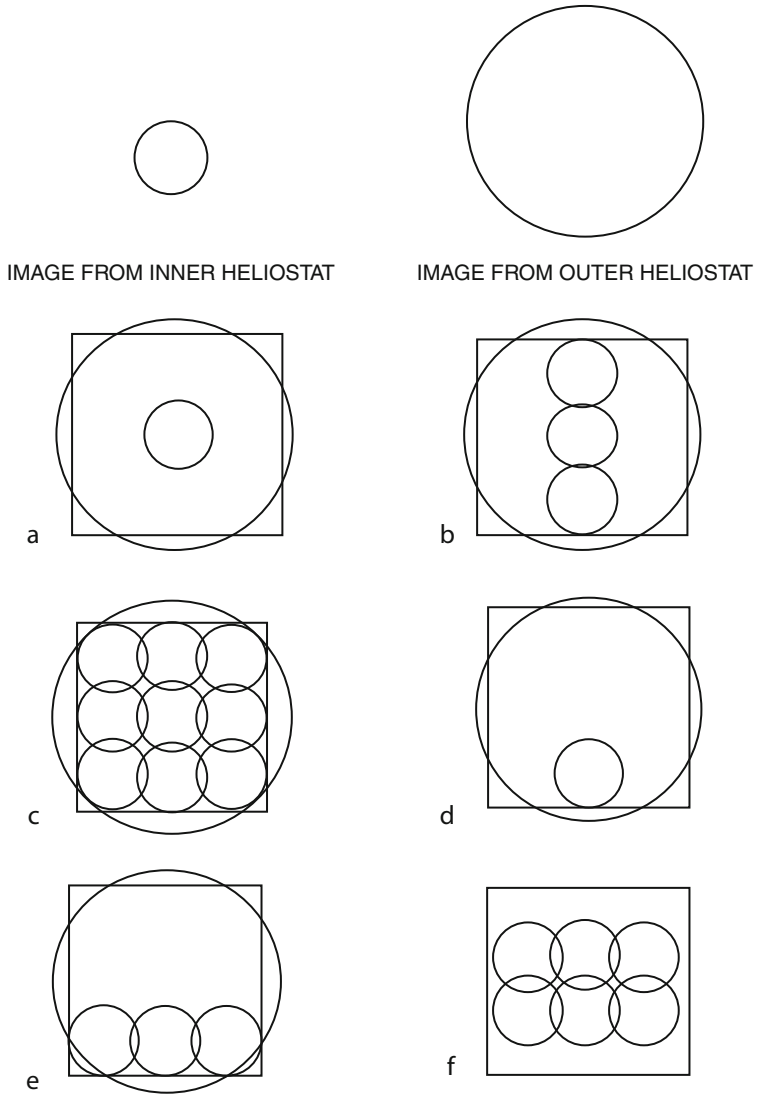

Concentrating Receiver Systems (Solar Power Tower). Figure 16
Basic heliostat aiming strategies of computer code "Delsol 3" [6]

The aim-points will vary somewhat with time as the heliostat image sizes vary, so that spillage remains relatively constant. There are several reasons for considering this strategy. First, if the fluid enters from the bottom of the receiver the peak fluxes will occur near the colder (and presumably stronger) end of the piping. In reality, the penalty is increased radiation and convection losses, since the average receiver temperature is increased. However, if the fluid enters from the top of the receiver, the radiation and convection losses are minimized, but the peak flux occurs near the hot end of the tube. Typically, peak fluxes will be close to those levels resulting from the single aim-point strategy (A).

(E) One-Dimensional Aiming at the Lower Part of the Receiver: Similar to (D), except that the images are spread out along the bottom of the receiver, as shown in the figure. This option should only be used with rectangular cavity apertures or rectangular flat plates, for the same reasons as described in Section (C).

(F) User Defined Aiming Strategy: A user defined aiming strategy can be defined for each zone. Each zone can be assigned a rectangular grid of points. This aiming strategy is not time dependent; that is, the aim-points are the same no matter what time of day or year it is, even though image size and thus spillage might change with time.

A combination of the aiming strategies (C) and (E) is also possible. For this aiming strategy, inner heliostats will be aimed at the bottom of the aperture or flat plate receiver. However, starting at zones farther out, aim-points are spread out over the entire aperture or flat plate. This option is one method of reducing the internal spillage (flux impinging on un-cooled parts of the receiver, such as the roof) in a cavity receiver without exceeding flux limits at the bottom of the heat absorbing area.

Examples of systems which have been applied in real power plants are [11]:

- Solar-Two Plant at Barstow, California:
  Full-System-Experiment with cylindrical salt-receiver required a 3-level aim point strategy to avoid receiver damage.
  Excess Flux Density Protection System:
  SAPS (Static Aim Processing System). Every 10 min a new aim point distribution for all 1926 heliostats is calculated for optimal flux density distribution. New aim points are transmitted to the heliostat field control system.
  DAPS (Dynamic Aim Processing System). Flux density distribution is re-calculated under current operation conditions. Currently, allowable flux density distribution is calculated in dependence of the current salt temperature at each measuring point. If local flux exceeds allowable local flux due to abnormal operating conditions, the responsible heliostat will be driven to a stand-by position.
- PHOEBUS-Receiver system on CESA-1-Tower at Almería, Spain:
  Full-System-Experiment required an aim point strategy to avoid deterioration of the receiver due to excessive temperatures. Open Volumetric Receiver with metal-wire-mesh-absorber.
  Heuristic knowledge-based heliostat field control to control the temperature distribution of the receiver. 36 thermocouples were used for the measurement of the current temperature distribution on the receiver.
  The system used a five-point aiming strategy, with displacement of the five aim points on the receiver plane to adjust the temperature distribution.

Receiver

The function of a receiver is to absorb the concentrated solar irradiation energy impinging from the heliostat field and transfer it to the working fluid. Requirements to a solar receiver include high thermal conductivity, dark color of the body for high absorptivity, and temperature resistance. Four concepts for receivers are described in this section.

Direct Absorption Receiver: Falling Particle or Molten Salt Liquid Film Falling particle or molten salt liquid film receivers fall in the category of direct absorption receivers, which is a concept where the heat transfer medium is directly exposed to and heated by concentrated solar irradiation. This concept is a very interesting and promising option as the medium of either of the two technologies has the ability to handle high temperatures up to 2,000°C as well as high fluxes up to 2 MW/m^2, or more. Moreover, no walls, but merely containment is required. The design with particles as a heat transfer fluid has the advantage that particles have a selective behavior [12].

A concept for a molten salt liquid film receiver was worked out by researchers who developed a beam-down receiver design. The receiver is designed cone shaped and is located near the ground. The incident concentrated solar irradiation from the heliostat field is reflected by a central reflector and directed onto the receiver. The design includes a hot and a cold heat storage system. When the plant is in operation, molten salt is pumped from the cold storage and fed to the receiver's salt distribution system. After the molten salt is heated by the receiver it is passed to the hot storage and, when the design temperature has been reached, from there is passed to a steam generator (not shown in diagram). The molten salt transfers its heat to the steam cycle and is pumped to the cold storage.

The advantage of this receiver design is that all components but the central reflector are located on the ground, hence the pumping power requirement is lower as no media are pumped to high altitudes. The disadvantages are the optical losses associated with the central reflector. These are beam dilution due to a longer beam path and the increased number of reflections [13].

To date, studies on the concept of falling particle or molten salt liquid film receivers exist. Such studies were conducted in Germany (German Aerospace Center – DLR) and in the USA (Sandia National Laboratories, SERI, LBL). Further prototypes for direct absorption central receiver have been build and tested. A solid particle receiver was built and tested on-sun at Sandia National Laboratories. It consists of a 6 m tall cavity through which a 1 m wide curtain of spherical ceramic particles is dropped and directly heated with concentrated solar energy [14]. The receiver was tested on top pf Sandia's 61 m tall central receiver located at the National Solar Test Facility in Albuquerque, NM.

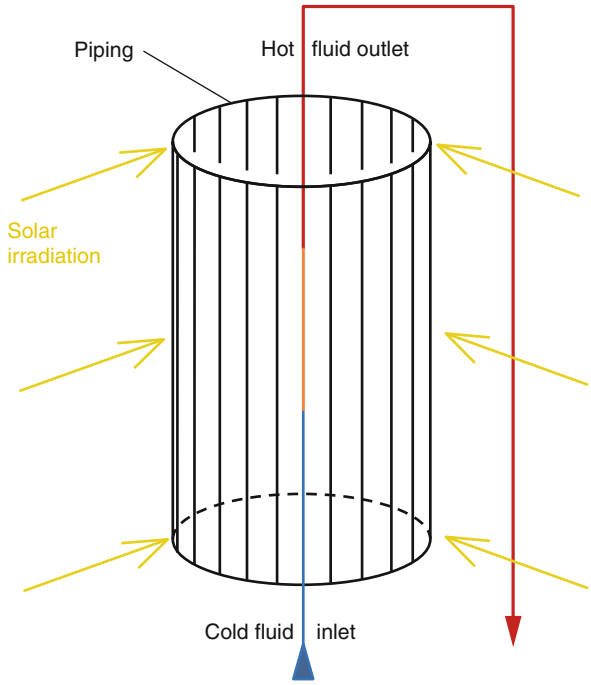

Concentrating Receiver Systems (Solar Power Tower). Figure 17
Tube receiver concept and HTF flow direction (Adapted from [15])

Tube Receiver A tube receiver consists of a large number of vertically arranged pipes through which the HTF is pumped in upward direction as shown in the following illustration (Fig. 17).

The heat transfer fluids that have been deployed in the past years are molten salt, H_2O for direct steam generation, and sodium.

An example of such a tube receiver is the solar tower power plant Solar Two near Barstow, California that used molten salt as HTF. The receiver consists of a great number of HTF pipes. The pipes are fixed vertically whereby the salt smelt is pumped in upward direction. On leaving the receiver, the molten salt is pumped into a hot-salt storage tank where it has a temperature of approximately 565°C.

A disadvantage for using the pipe receiver is the high reflection loss which is higher than for other receiver types, especially the receiver with porous absorbers.

Cavity Receiver A cavity receiver consists of a cavity with a small opening (inlet aperture). The concentrated solar irradiation is directed into the small opening where it impinges on tubes carrying the working fluid. Cavity receivers can have the same working fluids as external tube receivers, but also work with a gas. The idea behind the cavity receiver is to minimize the radiation losses. From the radiation entering the inlet aperture, only small amounts are reflected back into the atmosphere through the inlet aperture (Fig. 18).

In the 20 MW_e industrial Gas Cooled Solar Tower project GAST, which the German Aerospace Center (DLR) participated in, air was used as heat transfer fluid (HTF). The dual cavity receiver atop the 80 m high CESA-1 tower at the Plataforma Solar de Almería (PSA), Spain, had a design thermal power of 28 MW_{th} each, which was provided to the subsequent Brayton cycle [15].

Another cavity receiver concept is implemented in the PS10 solar tower plant in Spain. The tube receiver is basically a forced circulation radiant boiler with low ratio of steam at the panels output, in order to ensure wet inner walls in the tubes. Special steel alloys have been used for its construction so that it can operate under significant heat fluxes and possible high temperatures [16].

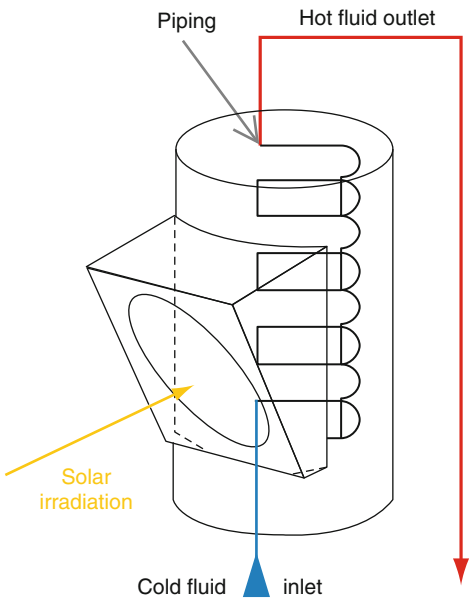

Concentrating Receiver Systems (Solar Power Tower). Figure 18
Basic cavity receiver concept (Adapted from [15])

Air Receiver There are two types of air receivers, the open volumetric and pressurized volumetric receiver.

Open Volumetric Receiver The class of volumetric receivers may be summarized according to two criteria [17]. Firstly, with regard to materials used there exist metal or ceramic types. Secondly, with regard to geometry design there exist a great variety of designs which seek to achieve an acceptable compromise between good optical properties and high heat transfer properties. Volumetric receivers of different designs have been developed in the last three decades and nowadays several design concepts of absorbers have been tested and will be developed further in future. The current available types are grouped into three categories: Absorbers with channel geometry, ceramic or metal wire-mesh absorbers, and ceramic foam absorbers [18].

For all these absorber types there are two characteristic dimensions that play an important role in their design [18]:

Open porosity: The open porosity describes how much open cross-sectional area the porous structure has for the inflow air. The higher the porosity, the thinner the walls of the channels, and hence the more prone to breaking of the structure becomes due to thermal stresses.

Volume-related heat transfer cross-sectional area: This characteristic dimension is calculated via the porosity and the distance between the inner walls of a channel. Generally, it is desired that the volume-related heat transfer cross-sectional area is as large as possible such that more irradiation can be absorbed. However, it has to be taken into account that the thickness of the channel walls cannot be designed too thin or the structure would becomes prone to breaking, hence there is a limit to increasing the volume-related heat transfer cross-sectional area.

In this receiver type, the absorption of concentrated solar radiation takes place in a spatial volume and not, as usual, on a surface. Because of the enlargement of the heat transfer surface, gases like air which are easy to handle can be used as HTF [19].

Three main conditions must be posed to the development of the volumetric receiver:

- Receiver material must consist of small substructures to ensure an acceptable heat transfer
- Receiver material must stand high temperatures and temperature gradients
- Receiver geometry must support a temperature distribution within the receiver that increases toward the inner region

The main advantage of volumetric structures on the one hand is that the absorption does no longer take place on just one level, but within a volume, which results in a lower radiation ratio per aperture unit. On the other hand, spatial structures alter the development of the temperature profile within the receiver, leading to a more favorable efficiency [20]. Because of the spatial absorption, the temperature maximum is shifted from the aperture plane into the receiver core, causing a reduction of the emissive losses, which are the major source of loss in any receiver.

The open volumetric receiver technology is best described taking the Solar Tower Jülich (STJ), Germany, as an example as it is the first tower using this technology:

The Solar Tower Jülich (STJ) is a research and demonstration plant for central receiver systems and has been built to demonstrate the high temperature air receiver technology as a complete system [21].

The receiver of the Solar Tower Jülich has been fitted with open volumetric absorber type, which is an absorber with channel geometry, because it best meets the high demand in the application of a solar tower power plant that is, withstand high temperatures and offering high stability. This technology works with a porous absorber material that absorbs concentrated radiation inside the volume of the structure and transfers the absorbed heat to a fluid passing through the structure. This allows the use of air as heat transfer medium despite its low heat transfer coefficient. This volumetric receiver technology has been developed since the early 1990s in various R&D projects with major contribution of the German Aerospace Center (DLR).

Pressured Volumetric Receiver The pressurized volumetric receiver was developed within the project REFOS and offers new opportunities for solar towers.

The closed volumetric receiver has a quartz window in front of the absorber modules separating them from the ambience. An air compressor sucks in ambient air and builds up the air pressure to 15 bar, the pressure at which the air enters the receiver (see Fig. 19).

The high operating pressure enables a hot air temperature of approximately 800°C.

The advantage of the closed to the open volumetric receiver lies in the higher efficiency that can be reached as combined gas and steam turbine processes can reach efficiency beyond 50% compared to only 35% of that of a conventional steam turbine process. This type solar tower with closed volumetric receiver therefore makes possible solar system efficiencies of over 20% [23].

Tower

The choice of tower constructions depends primarily on the required height of the tower. Towers are mainly constructed of steel or reinforced concrete. Steel towers are similar to guy-wire supported television transmission towers or free-standing microwave relay towers. Several central receiver design studies have considered guyed towers, but the presence of guy wires and their attachments to the tower in concentrated solar flux proved unworkable [24]. Concrete towers are similar to tall chimneys at conventional fossil power plants.

Factory-made monopoles commonly used for wind turbines may also be a possible solution for tower constructions. The shape of a tower differs from cylindrical to quadratic.

Providing Firm and Dispatchable Power

CRS main application is the production of electricity. For this reason the heat produced at the solar receiver is fed to a heat recovery steam generator. The steam is then expanded in a steam turbine producing electricity. Three main systems for providing firm and dispatchable power with a CSR exist nowadays depending on the heat transfer fluid that is used.

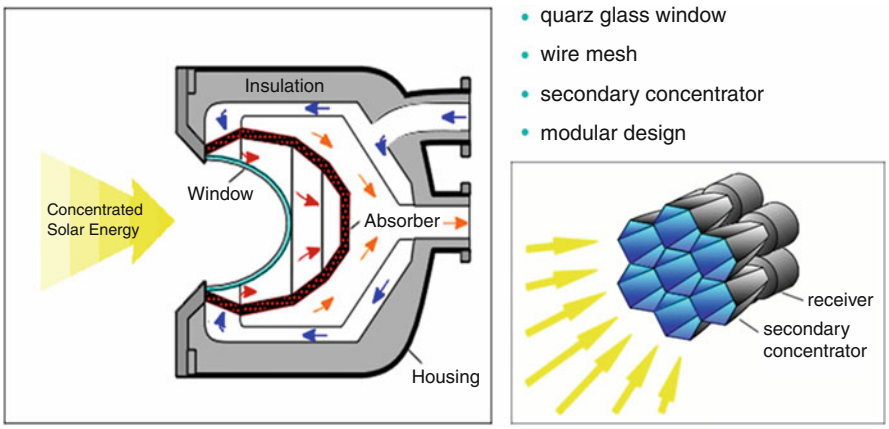

Concentrating Receiver Systems (Solar Power Tower). Figure 19
Concept REFOS [22]

In the first system, molten salt is pumped and passed through the receiver till the receiver temperature reaches the operating temperatures, being ready for normal operation (see Fig. 20). Once the receiver has reached a sufficient temperature and the circuit has been adequately heated, the receiver bypass is closed, the receiver is loaded, and the salt outlet tank is filled at 565°C [25].

While the salts are circulating through the receiver, the heliostat field focuses on the receiver to transmit the thermal power to the salt. From the receiver's output tank, the hot salt descends to the hot salt storage tank, where the molten salts are pumped with the required flow from the hot salt tank to the steam generator system (SGS).

Molten salt is passed through a steam generator where the heat is transferred onto the water-steam circuit. When this salt flow has been cooled at the outlet from the SGS, it returns to the cold salt storage tank. When leaving the steam generator the molten salt still has a temperature of at least 290°C and is pumped into a cold-salt storage tank.

Such a system is implemented additionally to the Solar Two plant in the Gemasolar central receiver power plant in Spain.

The second system uses water/steam as a HTF in the PS 10 receiver system (Fig. 21).

The solar receiver on top of the tower produces saturated steam and circulates it to a conventional steam turbine. In the turbine, it expands to produce mechanical work and electricity.

For cloudy periods, the plant has a saturated water thermal storage system. During full load operation of the plant, part of the steam produced by the receiver is used to load the thermal storage system. When energy is needed to cover a transient period, energy from saturated water is recovered at 20 bar to run the turbine at a 50% partial load [16]. Such a system is implemented in the PS10 and PS20 central receiver power plants in Spain and in the Sierra SunTower in the USA.

The third system uses air as a HTF. Figure 22 shows the schematic diagram of such a solar tower system. The heat is transferred to air, which is sucked through the receiver structure. The hot air is transported to the storage system or the heat recovery steam generator (HRSG).

In the conventional cycle, steam is produced in the boiler and thermal energy is transported to a steam turbine. The steam expands in the turbine producing mechanical work which is then converted into electrical energy by a generator. The exhaust steam from the turbine is then condensed in a condenser, and the condensate thereafter is pumped to the boiler where it receives heat from the solar receiver again, and the cycle is repeated.

Part of the received energy is used for direct electric generation with the HRSG and the rest energy is stored at the storage system to generate electricity when there is no solar radiation during day or at night. The thermal storage unit is integrated into the air cycle, through which the operation of the power plant can be held for a certain time at constant power, depending on the

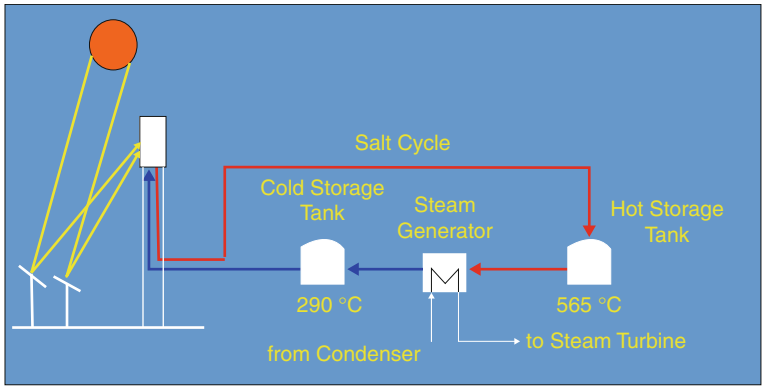

Concentrating Receiver Systems (Solar Power Tower). Figure 20
Schematic diagram of a solar tower power plant (Solar Two) using salt as a HTF [3]

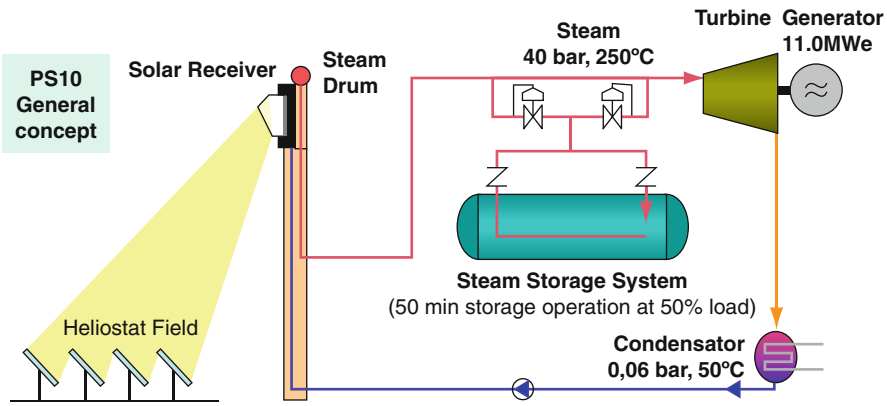

Concentrating Receiver Systems (Solar Power Tower). Figure 21
Schematic diagram of the PS10 solar tower using water/steam as HTF (Source: Abengoa Solar)

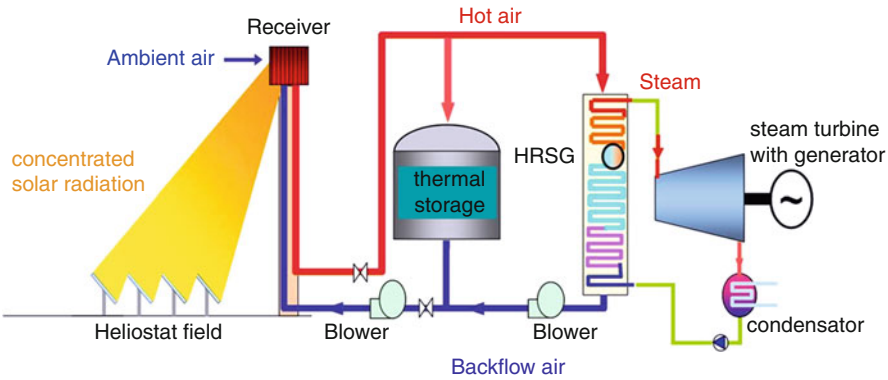

Concentrating Receiver Systems (Solar Power Tower). Figure 22
Schematic diagram of the test and demonstration power plant Jülich using air as a HTF (Source: SIJ)

storage dimensions. In principle, this thermal storage can be designed with an unlimited capacity, securing a continuous power plant operation. It is used as a buffer that stores energy in times of high irradiation and enables operation of the plant after sunset or during periods of reduced solar input.

This third system finds application in the Solar Tower Jülich located in Germany.

Characteristics of Different Heat Transfer Fluids

A heat-transfer fluid medium (HTF) in a central receiver absorbs the highly concentrated radiation reflected by the heliostats and converts it into thermal energy to be used for the subsequent generation of superheated steam for turbine operation. Different heat transfer can be used. To date, the heat transfer media demonstrated include water/steam, molten salts, liquid sodium, and air. While the US industry uses molten salt as heat transfer and storage device the European industrial sector provides air or water/steam, preferably as a heat carrier, and uses fixed-beds for storage of thermal energy. If pressurized gas or air is used at very high temperatures of about 1,000°C or more as the heat transfer medium, it can even be used to directly replace natural gas in a gas turbine, thus making use of the excellent cycle efficiency (60% and more) of modern gas and steam combined cycles [26].

Salt

In general, salt can be stored easily because of its promising heat transport capability. For this purpose it can be stored in a hot tank and recirculated to a cold tank.

Molten salt is mainly based on sodium and potassium nitrates. A further advantage of molten salt as a HTF includes a lower operating pressure and better heat transfer than a water/steam receiver. Better heat transfer results in a higher allowable incident solar flux at the receiver. That means that a smaller receiver can be implemented in the solar tower system.

On the other hand, the working fluid molten salt requires special handling because of its low viscosity (similar to water) and due to the problem of solidification at temperatures of approximately 220°C. The molten salt is kept at a minimum temperature of approximately 290°C. Due to the low viscosity, storage and transport of the molten salt is difficult [27]. As the salt must always be kept in a molten state, special heating is required whenever the plant is not in operation. As a result, additional heating requirements contribute to the operating costs.

An electric heating system is also necessary in order to avoid corrosion. Additionally, its accident sensitivity is a further disadvantage.

Water/Steam

When using water/steam as a HTF no heat exchanger is needed because the steam production results directly in the central solar receiver at the top of the tower. Then a direct link-up to the steam turbine is achieved.

Fluctuating solar radiation leads to rapidly fluctuating parameters and phase change and therefore the operation control turns out to be complicated. Further, the heat transport is not optimal and the thermal storage becomes difficult.

Air

Air as a HTF is freely available, easy to handle, nontoxic and ambient friendly. No hazardous substances are used. The air receiver offers the highest level of safety and protection from view of environmental impact and less costs.

In contrast to molten salt, air does not require freeze protection during times of nonoperation and allows working with very high process temperatures and no limitation of temperature. This enables the operation with high steam parameters and therefore high efficiencies in combination with modern conventional steam power technology.

On the other hand, air does not provide good heat transfer, has a lower heat capacity, and the storage capability is not optimal.

Solar central receiver power plants based on air-cooled receivers are a promising technology offering both operational advantages due to the simplicity of the hot air loop and the potential for high conversion efficiencies.

Others

Different gases too, like CO_2, helium, organic fluids, and sodium may be used as HTF.

The use of sodium was realized only once. Only once sodium was used as a HTF in the Small Solar Power System (SSPS) plant in Spain. The SSPS plant was the first central receiver plant in Europe and was built on the Plataforma Solar de Almeria (PSA) in Almeria, southern Spain, by the International Energy Agency (IEA). This solar tower producing 0.5 MW started operation in 1981. This CRS was destroyed in the year 1986 by a sodium fire. Due to this experience, sodium as a HTF was never used again in solar tower power plants.

Increase of Operation Hours of CRS by Storage and Hybridization

A solar thermal power station consists of a conventional block-unit power station and a solar component which replaces the combustion chamber of a conventional power station. Such power stations reach annual nominal loads of up to 3,000 h in locations of high irradiation (e.g., North Africa).

In order to increase the operation hours of a central receiver plant, storage or hybridization may be implemented. By both systems, an increase of the capacity factor of the conventional power block of the solar tower power plant can be achieved.

Through the integration of solar thermal storage or supplemental fossil or biomass firing, solar tower power plants produce dispatchable electricity to match peak demands at any time.

Storage

Storage represents one approach for achieving a high capacity factor for a central receiver system. Finding efficient ways of storing energy is one option to deal

with the lack of year-round sunshine. By using thermal storages nominal loads of 4,000 h can be reached. For solar technologies it is necessary to include an energy storage system due to the variation of the solar irradiation onto the earth's surface with time (e.g., night and day, seasonal changes, diurnal variation, and weather). Using storage units increases secure and permanent energy supply, and as a result the solar fraction is enlarged when the energy is provided by solar irradiation.

The current heat storage types for CRS may be sensible heat storage system, latent-heat storage system, steam accumulator, and thermochemical storage system.

The term "sensible heat" describes the heat which is absorbed or released by a material as a result of a change in temperature, whereupon the material does not undergo a change of aggregate state. Two sensible heat storage systems can be distinguished: indirect storage and direct storage [28].

An example of indirect storage is a regenerator. Regenerators are the "natural" technology choice for heat storage in air-cooled central solar power plants. The technology offers considerable design freedom that needs to be exploited to come to well-adapted solutions for market-scale implementations.

Heat storage regenerators represent a self-evident choice for the combination with air-cooled solar central receiver systems: The solar-heated air-stream passes along a solid storage medium taking up the heat to be stored. Reversing the flow direction allows to supply the steam generator at times of insufficient solar radiation. In principle, this technology is applicable to both atmospheric and pressurized systems [29]. The STJ solar tower in Jülich, Germany, uses a regenerator as a storage system.

In direct storage systems, the HFT which is heated by a receiver is used directly as a storage medium. The solar tower power plant Solar Two, for example, uses a 2-tank direct storage system consisting of a hot-salt and a cold-salt storage tank.

The storage fluid consists of a eutectic salt mix of sodium nitrate ($NaNO_3$) and potassium nitrate (KNO_3) in the proportion 60% $NaNO_3$ + 40% KNO_3, with a total weight of 1,500 t. Eutectic means that mixed in this specific ratio, the salt mixture has the lowest possible melting temperature that can be achieved, which in this case is 221°C. It is important to keep the salt temperature above the solidification temperature permanently, even if the plant is not in operation [28].

Latent-heat storage systems utilize the material property of absorbing or releasing heat energy during a phase change. In principle, there are three possible phase changes: solid–solid, solid–liquid, and liquid–vapor.

Only during the phase change from solid to liquid, storage capacity and storage volume are in a realistic ratio to one another. For latent-heat storage systems used in medium and high temperature applications, materials are chosen whose melting temperatures lie within the temperature range of the process. Based on the mass or the volume of the storage medium, it is possible to store considerably more energy with such a phase change material than, for example, with concrete. An advantage of latent-heat is that the temperature stays constant during melting and solidification, which is important for stable power plant operation. Latent-heat storage systems can have a compact design and are, for example, under development for dish power stations. Moreover, latent-heat storage systems are also under development for parabolic trough and solar tower power plants [28].

Steam accumulators are pressure vessels in which a charging system feeds steam in the hot water (well distributed). Through the input of heat of condensation, the temperature of the hot water in the storage vessel rises. Steam accumulators utilize the ecologically most worthwhile and cheapest HTF available. The necessary pressure vessels, however, dominate the investment costs. The PS10 solar tower in Seville, Spain, uses a steam accumulator as a storage system.

In thermochemical energy storage systems, reversible reactions are used to store energy, which are endothermic when charging and exothermic when discharging. The useful specific reaction enthalpy of such reactions is merely one order of magnitude smaller than that in the combustion of fossil fuels and hence considerably larger than that in the storage of sensible or latent heat. Moreover, after separating the reaction products the energy can practically be stored loss-free over a longer period of time [28].

In regions with very high radiation, solar thermal power plants with heat storage facilities can reach

a maximum of 3,000–4,000 nominal load hours per year. Modern storage technology using molten salt enables solar tower power plants to bridge more than 6 h of nonsolar periods depending on the chosen storage capacity.

Hybridization

One major option for accelerating the market introduction of solar thermal power technology is the concept of solar-fossil hybrid power plants. Their advantage compared to solar-only systems lies in low additional investment costs due to an adaptable solar share, high operation time, dispatchable power production, and reduced technical and economical risks [30]. Dispatchability implies that power production can be shifted to the period when it is needed. At times of low or no solar irradiation, a hybrid operation of the power station would decrease the specific electricity generation costs and increase the plant availability for the potential customer. Hybridization of a power tower with a fossil fuel holds further several additional distinct advantages, including power ride-through for solar intermittency, increased capacity factor, and potentially enhanced acceptance among utilities [31].

In order to demonstrate the hybridization of a solar tower system, an open central receiver system with air as HTF is considered.

For the hybridization, one main option is to place a gas turbine or a burner in the solar cycle before the heat recovery steam generator (HRSG) [32]. As has been pointed out, in [30] burning fuel might be natural gas or biogas and after the HRSG the exhaust gas is recirculated to the receiver or can be passed to a stack. In order to achieve round-the-clock, 100% renewable energy CRS can be hybridized with biomass energy.

The idea of hybridization is to combine fuel such as biogas or gas with low-carbon solar power during daylight to generate uninterrupted electricity. The power plant can then shift seamlessly between using the sun as fuel and a conventional or another renewable fuel [33].

Figure 23 shows the realization for such a hybrid system with a gas turbine.

At days of low solar radiation, the gas turbine or the burner adds partly or entirely heat to achieve nominal load of the boiler [34].

Through hybridization, for example, by combustion of biofuels, the production of electricity can be increased up to 8,600 h [33]. It is expected that such hybrid power plants will have a high potential for the market introduction in the next decade. Due to the high electricity demand, especially in countries of the sunbelt, it is expected that the hybrid system has a considerable market potential and will facilitate the market penetration.

Another hybridization option is to combine solar energy with a pressurized solar receiver with a gas turbine at high temperatures. As outlined in [35] using solar energy into the gas turbine of combined cycle systems (CCS) is a very promising way as it is used to preheat the compressor discharge air before it enters the combustor or the gas turbine. Solar air preheating

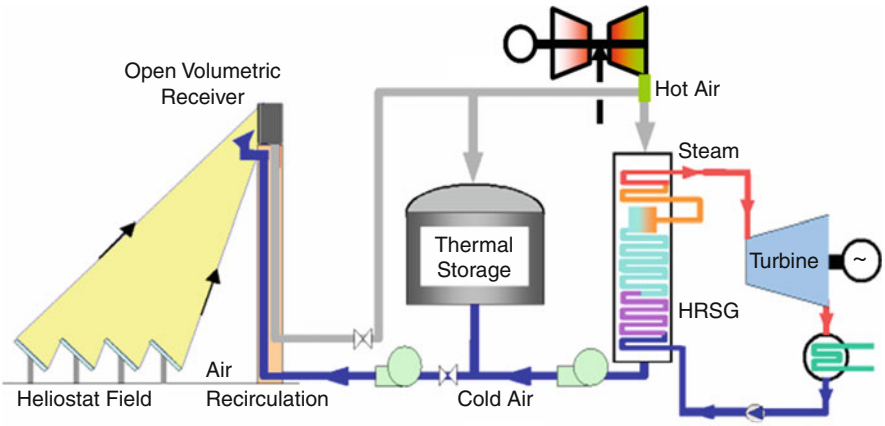

Concentrating Receiver Systems (Solar Power Tower). Figure 23
Schematic diagram of the Jülich demonstration plant with a gas turbine (Source: SIJ)

offers superior performance, as the solar energy absorbed in the heated air is directly converted with the high efficiency of the CCS [36]. It can be realized by molten salt receivers up to 560°C [37] or with pressurized volumetric receivers [38]. Figure 24 shows the concept of a solar-hybrid gas turbine system, which was investigated by the DLR.

Concentrated solar radiation enters the receiver which is heated up. Air from the gas turbine is passing through the closed pressurized receiver and is heated up by forces convection [39]. Then the hot air is passed through a gas turbine which expands it. The exhaust gas is then passed through a steam generator and afterward leaves the system through a chimney. In the steam generator, steam that drives a steam-cycle process is produced.

Different projects run in this research field. EU, for example, funded in the last decade research on hybrid solar technology in the modifying of the combustion chamber of a gas turbine to allow dual use of solar heat and fossil fuel (Solgate) and in the developing of an efficient solar-hybrid micro turbine (Solhyco).

The project objective of Solgate was the development of a solar-hybrid power system with direct solar heating of a gas turbine's pressurized air. A pressurized receiver module for 1,000°C was developed and built. The high temperatures were achieved using ceramic absorbers in combination with active cooling measures on the receiver window. To reduce receiver cost, a low temperature tubular receiver module was designed and built, with emphasis on low-pressure drop. The test setup consisted of three modules and a gas turbine system with modified combustion system, air ducts and control system coupled to a generator. The components were integrated to a complete solar-hybrid power system and installed in the PSA solar tower facility in Almeria, Spain. Within the Solgate project, for the first time a gas turbine was operated with solar energy from a volumetric pressurized receiver [40].

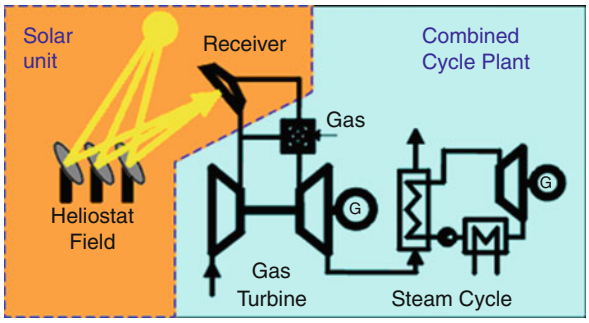

Concentrating Receiver Systems (Solar Power Tower). Figure 24
Scheme of solar-hybrid gas turbine system (Source: DLR)

According to the approach taken by Solgate, the gas turbine receives hot air from the outlet of the high temperature receiver module. This hot air enters the modified gas turbine combustor through a cooling bypass system [16]. The development of a gas turbine able to operate at higher temperatures allows the use of this solar technology without changes.

The main aim of the Solhyco project was to develop a highly efficient solar-hybrid micro-turbine (SHM) system for power and heat generation with dual solar power and fuel input. A reliable and cost-effective receiver system is being designed to reduce the generation cost. And a new combustion system was developed to allow the use of biofuels.

In the last years another interesting project (Solugas) aims in the further development of solar-hybrid gas turbine. For this demonstration project, a solar tower was planed to be designed and implemented to house the receiver, hot gas piping and gas turbine package [41]. The hot, pressurized air from the solar receiver is directly fed into the combustion chamber of a gas turbine where natural gas is added to further heat the air to the turbine firing temperature design point.

Examples of CRS Plants

Typical optical concentration factor ranges in CRS plants from 200 to 1,000 and plant sizes of 10–200 MW are chosen because of economy-of-scale constraints, even though advanced integration schemes are claiming economic sense for smaller units as well [42].

Research Facilities

Solar One The Solar One plant near Barstow, California was a 10 MW_e water-steam solar power tower facility. It operated from 1982 to 1988 and ultimately achieved 96% availability during hours of sunshine [43]. During its power production years Solar One delivered over 37,000 MWh to the utility grid [44].

Figure 25 shows an aerial view of the Solar One solar tower power plant at operation.

Concentrating Receiver Systems (Solar Power Tower). Figure 25
Solar One power plant aerial (Source: Sandia)

The heliostat field included 11,318 heliostats positioned 360° around the tower. The total reflective area of each heliostat was 40 m^2.

Solar One used a water/steam solar receiver coupled directly to the turbine-generator. The receiver system used the reflected sunlight to heat water directly, creating superheated steam.

A thermocline oil/rock system provided thermal storage [45]. This storage had the disadvantage of having high thermodynamic losses. Additionally, as mentioned in [45], the coupling of the solar receiver with the turbine caused the turbine to drop off-line each time a cloud came by. These two disadvantages initiative the US Department of Energy to start supporting a new project: Solar Two.

Solar Two Solar Two (Fig. 26) employed a molten-salt heat transfer system. Solar Two operated from 1996 to 1999 and helped validate nitrate salt technology, reduce the technical and economic risks of power towers, and stimulate the commercialization of solar power tower technology [43].

During operation, cold molten salt is pumped from a cold salt tank through a receiver. With the high solar concentration reaching the receiver the salt is heated up to 565°C. Then it is stored in a hot salt tank and used to produce steam to power a steam turbine.

The molten salt is kept to a minimal temperature of 290°C at all times to avoid solidification. The figure below shows the power plant of Solar Two.

The plant demonstrated an energy storage design with a two-tank molten-salt system. With the aid of heat storage tanks, the capacity factor of power plants can be raised from near 25% without storage operation to potentially 65% of the year operation in solar-storage operation [46].

The Solar Two power plant can generate up to 10 MW_e. Its storage tank has a capacity of 3 h and the capacity of the storage system is approximately 115 MWh_{th}. The efficiency of charging, storing, and discharging of this storage system is approximately 97%.

The heliostat field used the Solar One heliostats of 72,500 m^2 as well as 108 new heliostats of 95 m^2 each. The additional heliostats provided a flux distribution representative of a commercial receiver, eliminated the excessive morning start times common to Solar One, and provided additional energy for charging the thermal storage system.

Concentrating Receiver Systems (Solar Power Tower). Figure 26
Solar Two receiver and tower, Dagett, CA (Source: Sandia)

National Solar Thermal Test Facility The National Solar Thermal Test Facility at Sandia National Laboratories, is located in Albuquerque, New Mexico.

Figure 27 shows an aerial view of Sandia National Laboratories 5-MW_t Central Receiver Test Facility, including 222 heliostats. The facility is used for testing of advanced Concentrating Solar Power systems for a variety of applications.

CESA-1 CESA 1 is a test plant for solar power plants components as well as a flexible testing facility for large pieces of advances materials, as demonstrated since 1988 in various test campaigns. Figure 28 shows a CESA-1 Tower distant view.

The heliostat field focuses on the receiver at the top the CESA-1 tower.

It consists of a field of 300 heliostat mirrors, able to generate up to 7 MW_t on the receiver with energy densities of up to 3.5 MW/m^2 [47]. The main test piece is the receiver which is installed at any of the several levels of the 80-m tower prepared as test beds.

Themis The 2.5 MW Themis prototype of solar tower and molten salt power plant technology was designed and erected in France in the early 1980s. This solar plant, as shown in Fig. 29, was successfully operated until 1986 [48].

In the last years, a completely new control system as well as a heliostat prototype has been implemented and tested on site.

CSIRO A heliostat field of more than 800 m^2 reflector area has been installed in 2006 at the CSIRO solar tower in Newcastle, Australia (Fig. 30).

In late 2010, a second heliostat field was commissioned adjacent to the existing field. It includes 450 heliostats and has a thermal capacity of 1.2 MW_t and will be used to demonstrate a 200 kW Brayton cycle gas turbine [49].

Solar Research Facility Unit The Solar Research Facility of the Weizmann Institute of Science (WIS), shown in Fig. 31, is located in Israel.

Its major feature is a solar power tower containing a heliostat field of 64 large, multifaceted mirrors. Each heliostat has an aperture area of 56 m^2. As can be seen in the figure, it has several levels where different receiver systems can be tested.

Solar Tower Plant Jülich (STJ) The Solar Tower Plant of Jülich aims on the one hand in the production of electricity and in the other hand on research and development. The main principle of the STJ is analyzed in section "Solar Tower Plant Jülich (STJ)."

Regarding research, it is focused on two main branches: One is ensuring quality of existing technologies by developing new test procedures and setting up a framework of norms. The second is the technical improvement of components and the development of new technical features. Examples of technical questions under research by the Solar-Institut Jülich and the German Aerospace Center are [50]:

- Improvements of solar-specific components, such as heliostat, heat storage, and absorber

Concentrating Receiver Systems (Solar Power Tower). Figure 27
National solar thermal test facility, Albuquerque, New Mexiko (Source: Sandia)

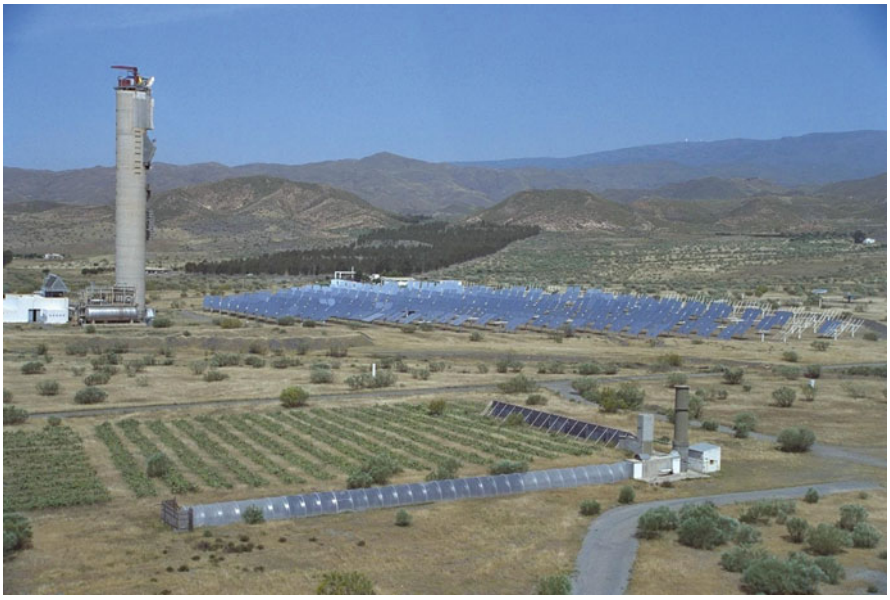

Concentrating Receiver Systems (Solar Power Tower). Figure 28
CESA-1, Plataforma Solar de Almeria, Spain (Source: Sandia)

Concentrating Receiver Systems (Solar Power Tower). Figure 29
The Thémis solar tower power plant in the Eastern Pyrenees of southern France, showing the field sloping from right to left (Source: Centrale solaire Thémis)

Concentrating Receiver Systems (Solar Power Tower). Figure 30
CSIRO test facility in Australia (Source: CSIRO)

- Optimization of operation and control.
- Adaptations of conventional components especially for CRS, for example, heat recovery boilers specially designed for the heat input from solar and fossil fuels or highly efficient steam turbines.
- Hybridization of solar tower power plants with fossil fuels.

Concentrating Receiver Systems (Solar Power Tower). Figure 31
Solar tower at the Solar Research Facility in Rehovot, Israel (Source: Weizmann Institute of Science (WIS))

Commercial

Sierra SunTower Sierra SunTower, which is shown in Fig. 32, supplies 5 MW of clean, renewable energy to the grid. The full-scale power plant, the only commercial CSP tower in the USA, supplies electricity to Southern California Edison (SCE) and power up to 4,000 homes. It is operational since 2009 [51].

A field of 24,000 mirrors reflects solar heat to a thermal receiver mounted atop a central power tower. Each small heliostat has an aperture area of about 1.14 m^2. The Sierra plant has two different types of direct-steam, natural-circulation solar receivers in operation – a dual-cavity receiver and an external receiver [52]. The focused heat boils water within the thermal receiver and produces steam at 440°C and 60 bar. The plant pipes the steam from each thermal receiver and aggregates it at the turbine, powering a power generator. The steam then reverts back to water through cooling, and the process repeats [53].

The project created over 250 construction jobs and 21 permanent jobs. The 5 MW output of Sierra SunTower will reduce CO_2 emissions by 7,000 t/year [54].

PS10 A land with a high number of installed solar power plants is Spain. The PS10 solar tower was the first commercial solar tower in Europe (Fig. 33) and is located in Sanlúcar la Mayor, 15 km west of the city of Seville. It is promoted by Solúcar Energía, S.A., an Abengoa Group company. The project makes use of glass-metal heliostats, a pressurized water thermal storage system, and a saturated steam receiver and turbine. These technologies have been developed by European companies, and already tested and qualified at the solar test facility located at the Plataforma Solar de Almería.

The PS10 plant has a solar field composed of 624,120 m^2 heliostats with a mobile curved reflective surface that concentrate solar radiation on a receiver at the top of a 100 m tower [55]. The receiver, which produces 40 bar 250°C saturated steam from thermal energy supplied by the concentrated solar radiation flux, has a cavity design to reduce radiation and convection losses.

It is formed by four vertical panels of 5.40 m wide by 12 m high, each one making up an overall heat exchange surface of about 260 m^2. These panels are arranged into a semi-cylinder of 7 m radius. During operation at full load, the receiver receives a thermal power of about 55 MW of concentrated solar radiation with peaks of 650 kW/m^2 [16].

The steam is sent to the turbine, where it expands, producing mechanical work and electricity. The turbo

Concentrating Receiver Systems (Solar Power Tower). Figure 32
eSolar tower power plant (Source: eSolar)

Concentrating Receiver Systems (Solar Power Tower). Figure 33
Bird's eye view of the PS10 (Source: NREL)

generator output goes to a water-cooled 0.06-bar pressurized condenser. The condenser output is preheated by 0.8 and 16 bar turbine extractions. The output of first preheater is sent to a deaerator fed with steam from another turbine extraction. A third and last preheater is fed with steam coming from the receiver. This preheater increases the water temperature to 245°C. This flow is mixed with the flow of water returning from the drum, raising the temperature of water fed to the receiver to 247°C [53].

For cloud transients, the plant has a 20-MWh thermal capacity saturated water thermal storage in form of four storage tanks. During full-load plant operation, part of the steam produced by the receiver is employed to load the thermal storage system. When energy is needed to cover a transient period, the energy is recovered from the saturated water at 20 bar to run the turbine at 50% load.

PS20 PS20 solar power tower plant is also located at the Solúcar Platform, near Seville (Spain) near to the PS10 plant (Fig. 34).

With a power capacity of 20 MW, the solar power plant will produce enough clean energy to supply 10,000 homes, and will avoid the emission of approximately 12,000 t of CO_2 into the atmosphere.

The plant with a Heliostat Solar-Field Aperture Area of 150,000 m^2 has the capacity to generate more than 40 GWh of energy each year.

PS20 consists of a solar field made up of 1,255 heliostats designed by Abengoa Solar [56]. Each heliostat, with a surface area of 120 m^2, reflects the solar radiation onto the receiver, located on the top of a 165 m high tower, producing steam which is converted into electricity generation by a steam turbine [53].

The storage capacity is 1 h and a wet cooling is used. These enhancements include a higher-efficiency receiver, various improvements in the control and operational systems, and a better thermal energy storage system compared to PS10.

Gemasolar Gemasolar, as shown in Fig. 35, is the first commercial-scale plant in the world to apply central tower receiver and molten salt heat storage technology.

The tower power plant is located in Fuentes de Andalucía, Seville, Spain and the expected net electrical annual production is 110 GWh. The 17 MW_e plant will supply power to 25,000 homes and reduce atmospheric CO_2 emissions by more than 30,000 t a year.

The surrounding heliostat field concentrates the solar radiation at the receiver placed at the top of a tower located in the center of the solar field. As mentioned in [57] each heliostat with a total reflective surface of 115.7 m^2 has a galvanized steel structure with 35 mirror elements. The heliostat field consists of 2,650 heliostats and takes an area of 185 ha [58]. The tower has a height of 140 m and the total mirror surface is about 300,000 m^2. The estimated annual operation hours will be 6,500 h with an amount of 15%

Concentrating Receiver Systems (Solar Power Tower). Figure 34
Aerial view of PS10 (at the *back*) and PS20 (at the *front*) solar tower power plants in Sevilla, Spain (Source: Abengoa Solar)

Concentrating Receiver Systems (Solar Power Tower). Figure 35
Gemasolar, tower view, Stand 2010 (Source: Gemasolar)

hybridized with burning of natural gas. The reached capacity factor may exceed 70%.

Through this receiver circulates a mixture of molten salts, which is heated by this radiation input and stored inside a tempered tank [57]. From there, hot salts are pumped to the steam generator system, where superheated steam is produced to drive a conventional turbine-generator set, producing electricity that is fed to the net.

The molten salt storage tank permits independent electrical generation for up to 15 h without any solar feed. The turbine can be operated at normal capacity when there is loss of or a reduction in solar radiation due to clouds.

The salts are impelled from a "cold tank" to a receiver located at the top of a tower where they are heated to 565°C. The hot salts then descend to the heat exchanger and generate water steam [52].

Solar Tower Plant Jülich (STJ) Germany's first solar tower power plant for experimental and demonstration purposes has been constructed and is now in operation in the town of Juelich. The central receiver plant, with an open volumetric receiver, supplies the grid with a nominal power of 1.5 MW_e. It is operational since December 2008 and started the production of electricity in spring of 2009.

The construction of the facility was funded by the BMU and the Ministry of Economics of the federal states of NRW and Bavaria. Kraftanlagen München built the facility as prime contractor. The subsequent operation was carried out by the local utility Stadtwerke Jülich. Scientific project partners are the Solar-Institut Jülich (SIJ) and the German Aerospace Centre (DLR). Since Summer 2011 the STJ belongs to the DLR.

The objective of the solar power tower project in Jülich is to demonstrate the entire system. Figure 36 shows a bird's eye view of the STJ. The concentrator system consists of about 2,150 sun-tracking heliostats of about 8 m^2 reflective surface each. They follow the path of the sun and concentrate the solar radiation on a receiver that is installed at the top of a 60 m tower. The absorber is made of porous ceramic elements through which incoming ambient air flows.

The applied open volumetric receiver technology is used to heat up ambient air to high temperatures of around 700°C and this heat is delivered for steam generation in a boiler of a conventional steam turbine cycle. The steam generated there drives a steam turbine, which produces power via a generator.

The porous absorber located at the top of the tower traps the highly concentrated solar radiation inside the structure allowing the heat to be transferred to air very effectively. The receiver is made up from identical sub-receivers, in which the absorber modules can easily be exchanged in case of failure or to test innovative modules [12].

The advantages of this technology are simplicity and scalability, the ability to include a thermal storage, the low thermal capacity (quick start-up), and a high efficiency potential due to high achievable temperatures.

Concentrating Receiver Systems (Solar Power Tower). Figure 36
Bird's eye view of the STJ (Source: SIJ)

Under Construction or Under Development

A lot of solar tower power plants are under construction or under development in the world, mainly in the USA.

Ivanpah Solar Electric Generating Station (ISEGS) will be located in Primm, NV, California. The steam turbine will have a capacity of 370.0 MW. The tower will have a height of 140 m and the heliostat field will consist of 214,000 heliostats, each with a mirror area of 14.08 m^2. As HTF water/steam will be used and a solar receiver steam generator will be implemented [56].

Crescent Dunes Solar Energy Project (Tonopah) will be installed in Tonopah, Nevada and start operation in 2013. The receiver will be cylindrical and molten salt will be heated up by concentrated solar radiation. The steam turbine has a nominal power of 110 MW.

As mentioned in [56] Gaskell Sun Tower (Gaskell), a 245 MW solar tower plant will be located in Lancaster, California and will start production in 2012.

Rice Solar Energy Project (RSEP) is another CRS project in the USA. It will be installed in the Mojave Desert and shall use molten salt as a HTF. The total power capacity is planned to be 150 MW and it will have a total heliostat area of more than 1 million m^2. The system will include a storage system and will start producing power by the year 2013.

Additionally, two solar tower plants of 400 MW are under development in Nevada and three plants of 600 MW in California. Further, some solar tower power plants are announced in Spain and in the rest of the world.

Secondary Uses of CRS

There exist many ways in which solar concentrated sunlight from a central receiver system may be used for the delivering of clean sustainable energy services.

To these services belong solar chemical technologies, desalination, and absorption cooling.

Solar chemical technologies include the solar thermal production of fuels and the use of the solar thermal heat for chemical processes.

Chemical processes include the melting of metals and the processing of cement and the recycling of hazardous solid waste materials. Recycling of hazardous wastes enables the reduction of exhaust gas streams and avoids additional generation of greenhouse gases and other pollutants.

Solar energy can be converted into storable and transportable chemical fuels such as hydrogen and methanol.

Today's production of hydrogen, its distribution, storage, and utilization are dependent upon conventional technologies, which are not commercially feasible at this time. At the moment, more than 90% of hydrogen is produced using heat from fossil-fuels, mainly natural gas [59]. Today, the production of hydrogen by using of different renewable energies is investigated. If hydrogen is generated from concentrated solar energy, it is a completely clean technology with no hazardous wastes. This is the vision outlined in the European Commission's "European hydrogen and fuel cell roadmap," which runs up to 2050. Solar towers are most appropriate for future large-scale production of solar fuels, because they can achieve the necessary high temperatures (>1,000°C) due to their high concentration ratio.

One solution of the direct concentrated solar production of hydrogen is accomplished at the "Plataforma Solar de Almeria"(PSA) in Southern Spain. The German Aerospace Center is also working on iron-based thermochemical cycle processes. Here, the reactive material – based on iron oxide – is rotatory oxidized and reduced again. Such a ceramic cylinder, which features many parallel channels and bears resemblance to an auto exhaust catalyst, is heated in a solar receiver-reactor with concentrated solar radiation to about 800°C [60]. The water steam reacts with the coating, whereupon oxygen is bounded and hydrogen is released. In a second reaction step, the water vapor is turned off and the receiver-reactor is heated up to about 1,200°C. Thereby, the oxygen on the reactive coating escapes and the cycle begins again.

This procedure has had, after initial pilot tests of the Institute of Technical Thermodynamics at the DLR in Germany, its successful dress rehearsal in November 2008 on the Spanish Plataforma Solar de Almeria.

Solar fuels such as hydrogen can be used in several ways; "upgrading" fossil fuels burned to generate heat, fed into turbines or engines to produce electricity or motion, or used to generate electricity in fuel cells and batteries. By storing energy in a fuel like hydrogen, it can be retrieved when needed, and is available even when the sun is not shining.

One further chemical application of CRS is the reforming process. Research on solar steam reforming of natural gas has been conducted in the EU projects SCR, SOLASYS and the recent study SOLREF, all in which the German Aerospace Center participated. Further, solar concentrated radiation from a heliostat field may be used for the production of methanol or synthesis gas in solar reactors. Additionally, solid waste material may be treated by the use of concentrated sunlight. Waste materials containing carbonaceous compounds can be converted by solar concentrated energy into syngas and hydrocarbons that can be further processed into other valuable synthetic chemicals [61].

The solar tower technology can be used for desalination as well. There are different ways for the exploitation of the heliostat field for producing clean water (Fig. 37).

Desalination systems can be powered from solar tower energy systems, either by producing the electricity for the supply of existing or planned RO systems or by using the produced heat for the distillation evaporators (MED) [63].

Figure 37 shows three different desalination systems combined with a CSP. The first desalination system, in combination with a solar tower (see Fig. 37, left), uses only the heat from the solar cycle for the supply of the MED system with heat and the electricity is provided by the grid. The MED process usually operates as a once through system without a large mass of brine recirculating around the plant. This design reduces both pumping requirements and scaling tendencies [64].

In the second system, the solar tower provides only the necessary electricity for the reverse osmosis (RO) unit (see Fig. 37, middle). The RO plant uses electricity generated by a solar thermal power block to work the pumps. Theoretically, the only energy requirement is to pump the feed water at a pressure above the osmotic pressure. In practice, higher pressures must be used, typically 50–80 atm., in order to have a sufficient amount of water pass through a unit area of membrane [65].

Finally, the last MED system (see Fig. 37, right) includes the conventional cycle for the supply of the desalination system with heat and electricity.

These three systems may find application in islands and coastal areas which face water shortage problems. Cogeneration of electricity and fresh water would probably work best with higher temperature levels provided by a solar tower system.

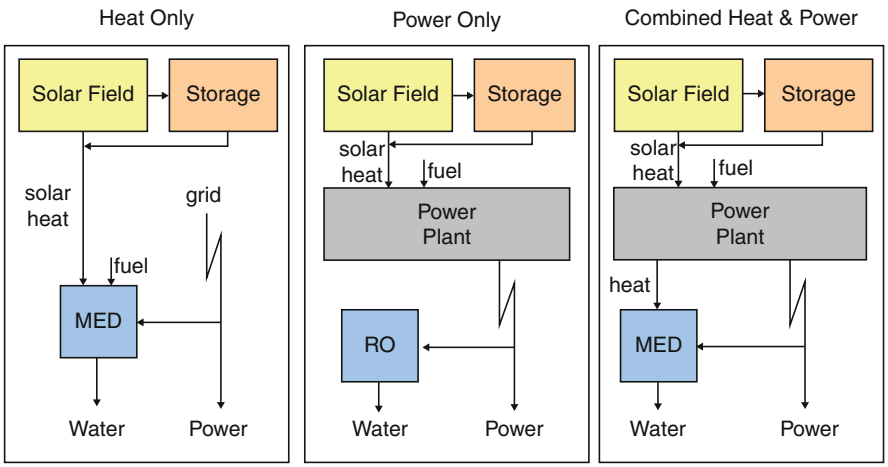

Concentrating Receiver Systems (Solar Power Tower). Figure 37
Desalination systems combined with solar tower plant (Source: [62])

Desalination plants have to be operated continuously. Therefore, a solar tower power plant should be in operation day and night. This is only possible with an additional storage unit or with the hybridization of the plant [66]. The choice of which system is to apply for a particular case should depend on the requirements of each commodity and the characteristics of the load and water demand [67].

Well-proofed thermally driven cooling technologies that can use the heat provided by a solar tower for cold production are absorption and adsorption chillers. Absorption cooling uses a liquid sorption material or a solid material. Solar thermal energy from a CRS may change the refrigerant into a vapor. A solar tower may also be combined with an adsorption chiller in order to provide heat for cooling.

An adsorption chiller uses a solid sorbent material, such as silica gel or zeolith, to adsorb the cooling medium water on its surface, which is a process that releases latent heat. Adsorption chillers consist of two chambers filled with sorbent, an evaporator, and a condenser (Fig. 38).

The two chambers work simultaneously, accomplishing their individual tasks. In the first chamber, the water, bounded to the silica gel, is driven out under heat supply, for example, provided by the heat from the steam cycle of a solar tower plant. Water is liquefied in the condenser and the heat is removed by the cooling water. The condensed water is injected into the evaporator and evaporated. The water vapor is then passed to the other chamber, where the sorbent adsorbs it. Heat resulting from the adsorption processes in dissipated to the cooling water of the second chamber. The evaporator works at a low pressure and the refrigerant is evaporated as it is absorbing the evaporation heat from the chilled water loop. This leads to the production of useful chilled water [28].

Economical Considerations

Investment Costs

Of the current CSP technologies, central receiver (power tower) systems have been recognized as having the highest potential for producing baseload power with a capacity factor above 75% at a lower levelized cost of energy.

The solar field, electric power block, and receiver encompass in general, as depicted also by [68], approximately three fourth of the total direct costs.

The heliostat field (materials plus labor) represents the largest single capital investment in a power tower plant, and thus represents the greatest potential for cost reductions [31]. The heliostat field of a solar tower power plant makes up roughly 50% of the investment costs. For installing the heliostat field, expected costs range from 180 to 250 €/m^2 for small production runs in the USA, and from 140 to 220 €/m^2 in Europe [69]. As a result, it is important to press on reducing the cost

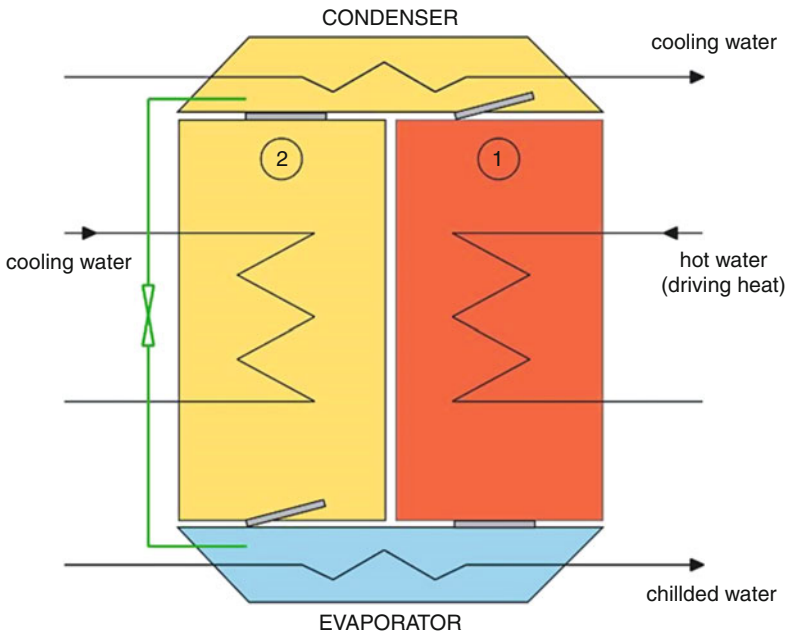

Concentrating Receiver Systems (Solar Power Tower). Figure 38
Adsorption chiller principle (Source: Solair)

of heliostats as far as accomplishable in order to improve and strengthen the economic viability of the solar power tower technology [6].

Operation and maintenance costs include plant operation, fuel expenses in the case of hybridization or backup, feed and cooling water, and field maintenance costs. Investment and operating costs need wider scale proof in commercial operation.

LEC

The project's analysis of different solar-hybrid gas turbine systems found that for a 16 MW (electrical) installation operating at 800°C, the investment cost would be 1,440 €/kW, with an electricity generation cost of 0.057 €/kWh at 16% annual solar share. With an operating temperature of 1,000°C, a solar share above 50% was found to be achievable, although the electricity generation cost would then rise to €0.086/kWh [16].

As estimated in [70], hybrid systems offered at the beginning of this century estimated costs of electricity production from the solar portion of $0.08–$0.15/kWh, whereas solar-only plants were expected to have costs in the range of $0.15–$0.20/kWh.

The other technologies analyzed are currently planned in significantly smaller pilot scale of up to 15 MW_e. The LEC is significantly higher for these small systems ranging from 19 to 28 cents/kWh. Assuming that several of the smaller systems are built at the same site to achieve a power level of 50 MW and take benefit of a similar O&M effort as the larger plants, LEC estimates of all of the systems also range between 15 and 20 cents/kWh. In [71] similar values were obtained. The systems achieve a solar capacity factor of up to 30% under these conditions.

Estimates range from €0.135–€0.218/kWh depending on design and location and it is expected that these costs will fall relatively quickly [72].

To nearly similar results comes an estimation presented in [59]. The cost of generating electricity from concentrated solar power currently ranges from approximately 15 €cents/kWh (USD 0.19) at high solar irradiation (DNI) sites up to approximately 23 €cents/kWh (USD 0.29) at sites with low average solar resource.

Future Cost Development

In combination with highly efficient combined cycle systems or recuperated gas turbines, significant cost reductions for solar electric power generation can be

achieved (predicted LEC of 0.069 €/kWh at 50% solar share, specific investment cost of 1,410 €/kW).

Scenario studies suggest that CSP and therefore also CRS could achieve cost competitiveness with coal and gas between 2030 and 2045 [73].

The German Advisory Council on Global Change of the government (Wissenschaftlicher Beirat der Bundesregierung für Globale Umweltveränderungen, WBGU) presented a large study in 2007 [74] and Table 1 shows the foreseen development of CRS from this study.

Regarding to the results of the WBGU study, cost of CRS may be around 10 cents by 2020 and drop under 0.10 €/kWh by 2050.

With increased plant sizes, better component production capacities, and more suppliers and improvements from R&D, costs are expected to fall between 10 and 14 €cents/kWh (USD 0.15–0.20) by 2020 [59].

Besides the estimation of further price drops, the gap with generation costs from conventional fuels is expected to decrease rapidly due to increased prices of conventional fuels at world markets. The competitiveness with mid-load, for example, gas-fired plants, might be achieved by the year 2020.

In the future, central receiver plant projects will benefit from similar cost reductions to those expected from parabolic trough plants. The expected evolution of total electricity costs, according to the World Bank, is that they will drop to 8–7 €cents/kWh in the medium term (100 MW_e Rankine-cycle plant or 100 MW_e ISCC, both with storage) and to 5 €cents/kWh in the long-term period (200 MW_e Rankine-cycle plant with storage) for high insulation sites with an annual DNI of more than 2,700 kWh/m^2 [69].

Increases in installed capacity along with ongoing technology enhancements will result in lower LCOEs and useful operational information that can be used to guide future R&D activities [72].

Regarding secondary applications of CRS, for example, the projected costs of hydrogen produced by solar tower and electrolysis range from 15 to 20 US cents/kWh, or USD 5.90–7.90/kg H_2 (assuming solar thermal electricity costs of 8 US cents/kWh_e). Both the US Department of Energy and the European Commission have a clear vision of the future hydrogen economy, with firm targets for hydrogen production costs. The US target for 2017 is USD 3/gge (gasoline gallon equivalent; 1 gge is about 1 kg H_2), and the EU target for 2020 is €3.50/kg [75].

Concentrating Receiver Systems (Solar Power Tower).
Table 1 Foreseen development of CRS according to [74]

	2020	2050
Efficiency (electric)	20–25%	25–30%
Costs (€/kWh)	0.07–0.14	Ca. 0.06
Power level per unit	Many 10–100 MW	Many 10–100 MW

Future Directions

Many studies dealing with the composition of future energy mixes come to the conclusion that solar concentrated thermal power will be increasingly important.

In 2008, the German Ministry for the Environment, Protection of Nature and Nuclear Safety (BMU) published a guiding study on the "Continued development of the strategy for the expansion of renewable energies." This study focuses on the German energy market and on how to reach the government's goal to reduce greenhouse gases to 20% of the 1990 level by 2050. Solar thermal power plants like solar tower are considered as one significant contributor to this aim [76].

A study for Greenpeace in [77] comes to the conclusion that in the next 5 years (2015), in the conservative model, the annual commissioning of solar thermal power plants may reach a capacity of 566 MW and in the ambitious scenario 6,814 MW/year. In these installed capacity, solar towers play a significant role.

A further study prepared by Greenpeace International and the European Solar Thermal Power Industry Association comes to the result that by 2015 the total installed capacity of solar thermal power plants will have passed 5,000 MW. By 2020, additional capacity would be rising at a level of almost 4,500 MW each year where solar tower plants are included. At the end of the scenario period, the total installed capacity around the world will have reached 21,540 MW. This Greenpeace-ESTIA scenario considers that in 2040, CSP plants could total 630 GW_e. The scenario of the study

presented in [69] also shows how much electricity would be produced by solar thermal power plants. This is based on the assumption that 1 MW of capacity produces 2,500 MW hours of electricity per annum. By 2020, solar thermal power will have achieved an annual output of more than 54 TWh [69].

According to the IEA [78], before 2030 some 4,700 GW_e of total power capacity is expected to be built worldwide, either as additional capacity or in replacement of existing capacity.

Cheap, safe, and environmentally friendly electricity from concentrating solar power systems could meet about 15% of European power needs by 2050. This was confirmed by a study prepared by the German Aerospace Center on behalf of the German Federal Environment Ministry [79].

The Desertec concept (Fig. 39), by considering the results of this study envisions solar power stations in North Africa and the Middle East providing electricity to those regions and to Europe in a way that is sustainable and cost-effective.

A variety of international companies participate in this Desertec Initiative. They have set themselves the goal of 2012 to the smallest detail to clarify whether the project is feasible. A long-term objective is to be able to meet a considerable part of the increasing electricity demand of MENA countries and, in addition to that, to cover about 15% of Europe's energy demand with clean like solar thermal power from deserts by the year 2050.

The potential for improvements is probably great for solar tower technologies. With two dimensions of concentration, such a technology can reach higher

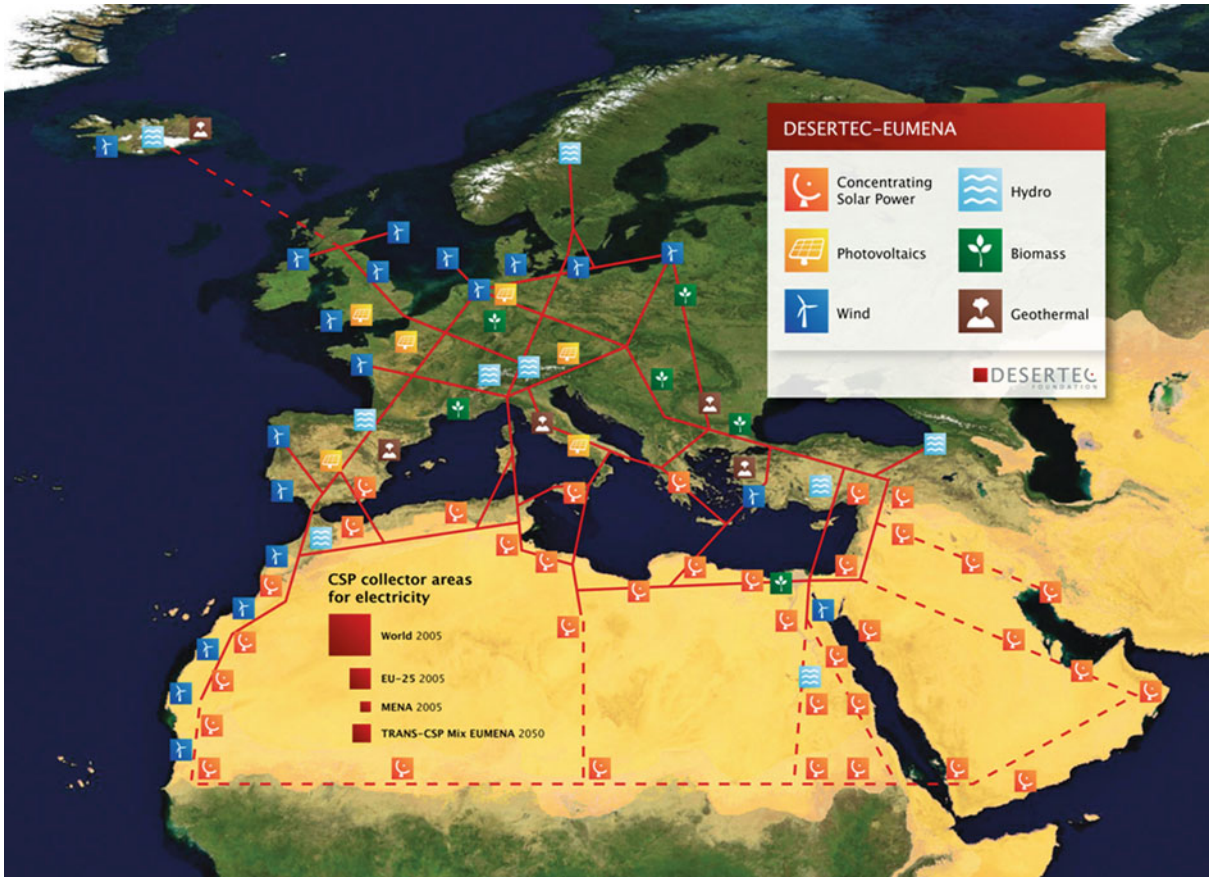

Concentrating Receiver Systems (Solar Power Tower). Figure 39
The Desertec concept (Source: Desertec Foundation)

temperature and offer higher conversion efficiencies. Concentrating solar power technologies would become competitive in the world's solar belt when a concerted effort for building about 5 GW_e worldwide has been made.

Improvements include all major components of a solar tower: heliostat, receiver, storage, and conventional cycle components.

Regarding the size of the heliostats, different approaches will continue: whether in large scale (around 100–120 m^2), medium size (30–50 m^2), small scale (1–10 m^2), or micro scale (less than 1 m^2). An increase of the size of a heliostat yields to a decrease of the control requirements. Small heliostats enable lower foundation and installation costs as well as low cost of the tracking system. On the other hand, such a development toward small scale should consider possible higher operation and maintenance costs resulting for many heliostat components.

Also the chemical composition of new steel products with different percentage of carbon and stainless steel may lead to better material for tower and heliostat optimization design.

At the receiver development, it is sure that the future development will be toward higher operating temperatures in order to achieve better thermal efficiencies. Main alternatives for solar tower receivers currently under development include the use of the following HTF: superheated steam, molten salt, and air. Due to the higher operating temperatures, materials with better thermal and mechanical properties will be tested in order to be applicable in the future receiver layouts.

In a high flux receiver, radiated materials of the absorber are exposed to extreme working conditions. These include high temperature, hot spots, and high temperature gradients. Material selection through laboratory and field studies is a critical issue to guarantee receiver integrity during their whole design life. Possible degradation expected in CRS occurs related to the thermal cycle, high temperature operation, and/or severe temperature changes and those due to the HTF exposure. The primary consequence of the thermal cycling is the occurring of degradation due to low cycle fatigue and thermal fatigue. In addition, thermal aging during the receiver life time modifies microstructure. Such modifications have direct impact on the mechanical properties of the receiver. In the future, an increase of scientific work and of investment in these optimization fields is expected.

Molten Salt is used as a HTF in a solar tower. Further research in new chemical composition of the salts like different qualities of mix binary and tertiary salts may enable higher working temperature.

High-temperature tower concepts also include atmospheric air as the heat transfer fluid (tested in Germany with the Jülich solar tower project) with solid material storage. Solar-to-electricity efficiencies of up to about 25% can be delivered by such towers [80].

Multi-tower configuration appears to present a further promising alternative. Such a concept consists of installing more than one tower for the same steam turbine and for the same heliostat field. This results in an increase of tower efficiency by the reduced distance between heliostats and towers [81]. However, such systems may be correlated to higher pressure drops and thermal losses of the piping system.

Another future step will be the path toward construction of large CSR units. Scaling reduces unit investment cost, unit operation, and maintenance costs, and increases performance [82].

Currently, there exist projects, mainly in the USA, for large-scale solar thermal tower power plants. Such large units have unique requirements and a special feature is the long-term test run, which includes some functional tests but also a 4-seasons-test run. This testing is not typical for conventional power plants and requires new models to formulate warranty conditions. During this phase, electrical power is produced but the contractor is still on site in order to witness the test run and to reach final acceptance of the plant [83].

Even if the early deployment of solar tower systems now has higher costs of immediate emission reductions than other options, this deployment must be undertaken if the cost reductions it drives are key to future large-scale deployment. As mentioned in [84], the early deployment of renewable energy technologies like CRS is a cost-effective measure for long-term climate change mitigation, even if it looks too costly when only short-term reductions are considered.

The increase in annually installed power plant capacity means entry into a period of distinctly more cost-efficient mass production of components [85].

Future aims will be to improve the manufacturability, focusing on mass production, assembly, and cost reduction, ensuring that the heliostat has optical, mechanical, and thermal properties, equal to or better than already existing structure designs.

Advanced technologies, mass production, economies of scale, and improved operation will together enable a reduction in the cost of solar electricity to a level competitive with other power sources within the next 10–15 years. This will, as outlined in [69], reduce dependency on fossil fuels and avoid the risk of future electricity cost escalation.

CRS industry has to realize the cost reduction potentials in component manufacturing (mirrors and absorbers), collector and plant assembly, system integration and design.

According to the ECOSTAR study, cost reductions of 25–35% due to technical innovations and scaling up to 50 MW_e are feasible for most of the technologies. These figures do not include effects of volume production or scaling of the power size of the plants beyond 50 MW unit size, which would result in further cost reductions [82].

Solar tower power plants need to be built in areas of high direct solar radiation, which generally translates into arid, desert areas where water is a scarce resource. In[86], it was verified that a typical power tower power block that employs wet cooling requires approximately 2,500 L of water to produce 1 MWh of solar electricity. Although plants in the near future will probably be able to secure the necessary water rights for wet cooling, the issue of water use will likely require CRS to transition to dry cooling. Thus, it is possible that dry cooling technology of the power block will be a necessity for power towers to become a major provider of solar electricity in the future. In these fields, in the future, the demand for investments and research activities will rise for many companies.

Major future goals of the future development of CRS are to try to find the right balance between high thermal efficiency, low pressure drop, high durability, and low cost of the components of a solar tower. Improved operating procedures will be developed to provide more reliable operation and to raise the capacity factor of a solar tower plant. Use of efficient Rankine cycles and construction of new steam generator, which are extra developed for solar application, enable the rising of the efficiency of a CRS. Given a fixed plant size and capacity factor, the net annual solar-electric efficiency sets the required heliostat field area. As the efficiency increases, the collector area and cost decrease in proportion [56].

Future solar-only solar tower plants have good long-term perspective for high conversion efficiencies and for use of very efficient energy storage systems by utilization of high temperatures in order to enlarge the solar capacity or solar share.

Storage Systems are a second key factor for cost reduction of solar power plants.

Development needs are very much linked to the specific requirements of the systems in terms of the used heat transfer medium and the required temperature. In general, storage development needs several scale-up steps generally linked to an extended development time before a market acceptance can be reached [82].

Another significant key issue is the ability to be combined with hybrid systems by firing of conventional fuels or even biofuels like biogas. In addition, they have the potential to be applied to other high-temperature heat processes like process heat, solar chemical processes, and desalination.

As modified in [70], already at the beginning of this century, implementation of hybridized systems is one of the paths to break the nontechnological financial barriers to deploy solar electric technologies, which enable the reduction of the initial investment. Hybrid solar-fossil fuel plants making use of special finance schemes at favorable sites can, according to [69], already deliver competitively priced electricity.

The commercial confidence in this technology is growing as more operational plants are being built and consequently it will improve in the near future. With a concentration factor of up to 1,000 suns, power towers have much greater development potential in terms of cost-effectiveness [87]. In this new century, concentrated solar technologies like CRS will play a significant role in providing sustainable energy and heat for different applications. But always economical and environmental considerations will play a key factor when the appropriate technology, which covers the permanent rising demands for energy and water availability, has to be chosen.

Bibliography

Primary Literature

1. ESTIA, SolarPACES, Greenpeace (2005) Concentrated solar thermal power now
2. Gary J (2010) Overview of power towers within the CSP subprogram. Presentation to the tower roadmap meeting, Sandia National Laboratories, Albuquerque
3. SolarPACES Technical Report No. III (2000) 1/00 Catalogue of solar Heliostats, June 2000. IEA-solar power and chemical energy systems Task III: solar technology and applications
4. DLR (1991) Solar thermal energy utilization, vol 4, Final reports. Springer, Berlin
5. Hoffschmidt B, Schmitz M (2009) Energy conversion processes for the different energy carriers – high- temperature solar systems. Lecture notes Aachen University of Applied Sciences
6. Kolb G, Jones S, Donnelly M, Gorman D, Davenport RTR, Lumia R (2007) Heliostat cost reduction: report, Sandia National Laboratories
7. Kistler BL (1986) A user's manual for DELSOL3: a computer code for calculating the optical performance and optimal system design for solar thermal central receiver plants. Sandia National Laboratories, Livermore
8. Stine WB, Geyer M (2001) Power from the Sun. www.powerfromthesun.net
9. Kleemann M, Meliß M (1993) Regenerative Energiequellen. Springer, Berlin
10. Belhomme B (2010) Development of optimized aim point strategies for central receiver systems. SOLLAB Doctoral – Colloquium. German Aerospace Center, Institute of Technical Thermodynamics, Cologne, Germany
11. Ahlbrink N, Belhomme B, Pitz-Paal R (2010) Modelling and simulation of a solar tower power plant with open volumetric air receiver. German Aerospace Center, Institute of Technical Thermodynamics, Cologne
12. Winter C-J, Sizmann RL, Vant-Hull LL (1991) Solar power plants – fundamentals, technology, systems, economics. Springer, Berlin
13. Tamaura Y, Utamura M, Kaneko H, Hasuike H, Domingo M, Relloso S (2006) A novel beam-down system for solar power generation with multi-ring central reflectos and molten salt thermal storage. In: Proceedings of the 13th SolarPACES international symposium, Seville, Spain
14. Siegel N, Kolb G (2008) Design and on-sun testing of a solid particle receiver prototype. In: Proceedings of Energy Sustainability 2008 (ES2008), Jacksonville, 10–14 Aug 2008
15. Winter C-J, Silzmann RL, Vant-Hull LL (1991) Solar power plants fundamentals technology systems economics. Springer, Berlin
16. EU (2007) Concentrating solar power: from research to implementation. European Communities, Luxembourg, Luxembourg 2007
17. Pitz-Paal R, Morhenne J, Friebig M (1988) Investigation on the development of a volumetric receiver with a staggered structure. In: DLR (ed) Solar thermal energy utilization, vol 5, Final reports. Springer, Berlin
18. Hoffschmidt B (1997) Comparison and evaluation of different concepts of volumetric radiation receivers. Dissertation, German Aerospace Centre, Colgne
19. Pitz-Paal R, Morhenne J, Friebig M (1989) The construction of a volumetric receiver with a staggered structure. In: DLR (ed) Solar thermal energy utilization, vol 5, Final reports. Springer, Berlin
20. Morhenne J, Pitz-Paal R (1989) Analysis of convective heat transfer in volumetric receivers built of porous media. In: DLR (ed) Solar thermal energy utilization, vol 5, Final reports. Springer, Berlin
21. Koll G, Schwarzbözl P, Hennecke K, Hartz T, Schmitz M, Hoffschmidt B (2009) The solar tower Jülich: a research and demonstration plant for central receiver systems. In: Proceedings of SolarPACES 2009, Berlin
22. Buck R, Lüpfert E, Telez F (2010) Receiver for solar hybrid gas turbine and CC systems (REFOS). In: Proceedings of 10th international symposium on solar thermal, Sydney
23. Quaschning V (2009) Regenerative Energiesysteme: Technologie – Berechnung – Simulation. Hanser, München
24. Falcone PK (1986) A handbook for solar central receiver design, SAND 86–8009. Sandia National Laboratories, Albuquerque, Sandia, United States
25. Álvarez-Lara M, Perosanz F (2009) Alloys selection of molten salts central receivers for solar power plants. In: Proceedings of SolarPACES 2009, Berlin
26. Giuliano S, Buck R, Schillings C, Al Nuaimi S, Al Obaidli A (2009) Analysis of solar-hybrid gas turbine cogeneration systems with absorption chillers in hot and dry climates. In: Proceedings of SolarPACES 2009, Berlin
27. SolarPACES (2011) Information about solar tower. www.solarpaces.org
28. Sattler J, Hoffschmidt B, Trieb F, O'Connell (2011) Towards a sustainable implementation of solar thermal power plant technology in the MENA region, Jülich (in preparation)
29. Zunft S, Hänel M, Krüger M, Dreißigacker V (2009) High temperature heat storage for air-cooled solar central receiver plants: a design study. In: Proceedings of SolarPACES 2009, Berlin
30. Alexopoulos S, Göttsche J, Hoffschmidt B, Rau C, Schwarzbözl P (2008) First simulation results for the hybridization of small solar power tower plants. In: EUROSUN 2008, Lissabon
31. Gary JA, Ho CK, Mancini TR, Kolb GJ, Siegel NP, Iverson BD (2010) Development of a power tower technology roadmap for DOE. In: Proceedings of SolarPACES 2010, Perpignan, France
32. Alexopoulos S, Helsper C, Hoffschmidt B, Rau C (2009) Simulation tool including a transient smoke tube boiler model for the calculation of small hybrid solar power tower plants. In: Proceedings of twentieth international conference on systems engineering, ICSE2009, Coventry University, Coventry, pp 28–33
33. Alexopoulos S, Hoffschmidt B, Rau C, Schwarzbözl P (2009) Simulation results for a hybridization concept of a small solar tower power plant. In: SolarPACES symposium, Berlin

34. Alexopoulos S, Hoffschmidt B, Rau C, Schmitz M, Schwarzbözl P, Pomp S (2010) Simulation results for a hybridized operation of a gas turbine or a burner for a small solar tower power plant. In: SolarPACES symposium, Perpignan
35. Romero M, Buck R, Pacheco JE (2002) An update on solar central receiver systems, projects and technologies. Trans ASME 124:98–108
36. Schwarzboezl P, Buck R, Pfänder M, Tellez F (2001) Solar-hybrid gas turbine systems using pressurized volumetric air receiver technology (REFOS). In: Solar thermal power plants and solar chemical processes: advances and perspectives for international cooperation, 5th Cologne solar symposium, Cologne, pp 68–70
37. Price HW, Whitney DD, Beele HI (1996) SMUD Kokhala power tower study. In: Proceedings of 1996 international solar energy conference, San Antonio
38. Kribus A, Zaibel R, Carrey D, Segal A, Karni J (1997) A solar-driven combined cycle power plant. Sol Energy 62:121–129
39. Buck R (2001) Volumetric Receivers for solar-hybrid gas turbine power systems. In: Solar thermal power plants and solar chemical processes: advances and perpectives for international cooperation, 5th Cologne solar symposium, Cologne, pp 68–70
40. Heller P, Pfänder M, Denk T, Tellez F, Valverde A, Fernandez J, Ring A (2006) Test and evaluation of a solar powered gas turbine system. Sol Energy 80:1225–1230
41. Solugas (2009) Project information. www.solugas.com
42. Romero M, Marcos MJ, Telez FM, Blanco M, Fernandez V, Baonza F, Berger S (2000) Distributed power from the solar tower systems: a MIUS approach. Sol Energy 67(4–6):249–264
43. Mancini T (2010) An evaluation of trough and power tower systems for near- and long-term markets. Presentation to the U.S. DOE SETP, Washington, DC
44. Kolb GJ (1990) The design of future central receiver power plants based on lessons learned from the Solar One pilot plan. Sandia National Laboratories, Albuquerque, United States, 1990
45. Tyner CE, Sutherland JP, Gould WR (1995) Solar-two: a molten salt power tower demonstration. Solarthermische Kraftwerke II. VDI Berichte Nr. 1200
46. Information provided by Flagsol company (2009)
47. PSA (1996) Annual technical report 1996
48. Ferriere A, Perez A, Pruvost A, Albert R, Boutonet C (2010) Development of a heliostat control system and experimental evaluation on a small field at Themis solar site In: Proceedings of SolarPACES 2010, Perpignan, France
49. Stein W, Kim J-S, Burton A, McNaughton R, Soo Too YC, McGregor J, Nakatani H, Tagawa M, Osada T, Okubo T, Kobayashi K (2010) Design and construction of a 200 kWe Tower Brayton Cycle pilot plant. In: Proceedings of 16th concentrating solar power, SolarPACES symposium 2010, Perpignan
50. Alexopoulos S, Göttsche J, Hoffschmidt B, Rau C, Schmitz M, Warerkar S, Hennecke K, Schwarzbözl P, Beuter M, Koll G, Hartz T (2009) Solar tower power plant Jülich first experience with an open volumetric receiver plant and presentation of future enhancements. In: Conference Renewable World Europe, Cologne, 26–28 May 2009
51. eSolar (2011) Utility-scale solar power brochure 2011. www.esolar.com
52. Meduri PK, Hannemann CR, Pacheco JE (2010) Performance characterization and operation of eSolar's Sierra Sun Tower power tower plant. In: Proceedings of SolarPACES 2010, Perpignan
53. Alexopoulos S, Hoffschmidt B (2011) Recent commercial and demonstration solar tower power plants around the world. In: Proceedings of MSE, Nicosia, Cyprus. www.abengoasolar.es
54. Sierra fact sheet, Sierra SunTower: a new blueprint for solar energy. www.esolar.com
55. SolarPACES (2011) PS10
56. NREL (2011) Concentrated solar power projects. www.nrel.gov
57. Lata J, Alcalde S, Fernández D, Lekub X (2010) First surrounding field of heliostats in the world for commercial solar power plants, Gemasolar. In: Proceedings of SolarPACES 2010, Perpignan
58. Gemasolar (2010) Project information torresol energy. www.torresolaenergy.com
59. Concentrated solar power (2009) Global Outlook 09, Greenpeace 2009
60. Evers AA (2009) Direkt solar hydrogen: the next steps. In: Proceeding of SolarPACES 2009, Berlin
61. Meier A, Palumbo R, Steinfeld A (2001) Chemical fuels and materials from sunlight. In: Solar thermal power plants and solar chemical processes: advances and perpectives for international cooperation, 5th Cologne solar symposium, Cologne, pp 107–116
62. DLR (2007) AQUA-CSP concentrating solar power for desalination, final report. German Aerospace Center, Stuttgart, Nov 2007
63. Alexopoulos S, Hoffschmidt B (2009) Solar tower plant of Jülich and perspectives to combine this technology with desalination in the future for Cyprus. In: 2nd international conference on renewable energy sources & energy efficiency, Nicosia, Cyprus, 23–24 Oct 2009
64. Kalogirou SA (1997) Survey of solar desalination systems and system selection. Energy Int J 22(1):69–81
65. Kalogirou SA (2005) Seawater desalination using renewable energy sources. Prog Energy Combustion Sci 31(3):242–281
66. Alexopoulos S, Hoffschmidt B (2010) Solar tower power plant in Germany and future perspectives of the development of the technology in Greece and Cyprus. Renewable Energy 35:1352–1356
67. Kalogirou SA (2011) Concentrated solar power plants for electricity and desalinated water production. In: Proceeding World Renewable Energy Congress 2011, Linköpping, Schweden
68. NREL (2003) Assessment of parabolic trough and power tower solar technology cost and performance forecasts
69. Solar thermal power (2020) Greenpeace
70. Kolb GJ (1998) Economic evaluation of solar-only and hybrid power towers using molten-salt technology. Sol Energy 62(1):51–61

71. Quaschning V, Ortmanns W (2003) Specific cost development of photovoltaic and concentrated solar thermal systems depending on the global irradiation: a study performed with the simulation environment Greenius. In: ISES Solar World Congress 2003, Göteborg, Sweden, 14–19 June 2003
72. PriceWaterhouseCoopers 100% renewable electricity: a roadmap to 2050 for Europe and North Africa
73. Williges K, Lilliestam J, Patt AG (2010) Making concentrated solar power competitive with coal: the costs of a European feed-in tariff. Journal Energy Policy 38(6):3089–3097
74. WBGU (2003) Welt im Wandel: Energiewende zur Nachhaltigkeit. Springer, Berlin/Heidelberg/New York
75. Meier A, Sattler C (2008) Solar fuels from concentrated sunlight. SolarPACES. www.solarpaces.org
76. Nitsch J (2008) Weiterentwicklung der Ausbaustrategie Erneuerbare Energien Leitstudie 2008. BMU, Berlin
77. Richter C (2009) Sauberer Strom aus den Wüsten – Globaler Ausblick auf die Entwicklung solarthermischer Kraftwerke
78. Philibert C (2005) The present and future use of solar thermal energy as a primary source of energy. International Energy Agency, Paris
79. DLR Study (2006) TRANS-CSP Trans-Mediterranean interconnection for concentrating solar power, Stuttgart, June 2006
80. IEA (2010) Technology roadmap: concentrated solar power. OECD/IEA, Paris, France, 2010
81. Kearney AT (2010) Solar thermal electricity 2025, June 2010
82. Pitz-Paal R, Dersch J, Milow B (2005) European concentrated solar thermal road-mapping. DLR, Cologne
83. Funke A (2009) Challenges for EPC projects of large scale solar thermal power plants. In: Proceedings of SolarPACES 2009, Berlin
84. IEA (2011) Interactions of policies for renewable energies and climate. OECD/IEA, Paris
85. Schott Solar Memorandum on concentrated solar power plant Technology Schott solar. www.schottsolar.com
86. U.S. Department of Energy (2008) Concentrating solar power commercial application study: reducing water consumption of concentrating solar power electricity generation, report to Congress
87. (2008) Extracting ourselves from oil, April 2008. Journal Research EU, Special issue, pp 23–25

Books and Reviews

Kalogirou S (2009) Solar energy engineering: processes and systems. Academic, Burlington
Mohr M, Svoboda P, Unger H (1999) Praxis solarthermischer Kraftwerke. Springer, Berlin
Newton CC (2008) Concentrated solar thermal energy. VDM, Saarbrücken
Quasching V (2009) Regenerative Energiesysteme: Technologie-Berechnen-Simulation. Hanser, München
Vogel K (2010) Large scale solar thermal power. Wiley-VCH, Weinheim

Construction and Demolition Wastes

Thomas Dyer
Division of Civil Engineering, University of Dundee, Dundee, UK

C

Article Outline

Glossary
Definition of the Subject and Its Importance
Introduction
Construction and Demolition Waste
Composition of Construction and Demolition Waste
Managing Construction and Demolition Waste
Environmental and Sustainability Issues
Future Directions
Bibliography

Glossary

Deconstruction Systematic dismantling of a structure for reuse and recycling.

Embodied energy Energy employed in the manufacture of a product. Sometimes referred to as "emergy."

Recycled aggregate (RA) Construction and demolition waste containing a range of different inorganicnonmetallic constituents processed for use as aggregate.

Recycled concrete aggregate (RCA) *a*ggregate derived from processing end- of-life concrete.

Reclaimed asphalt pavement (RAP) Also known as recycled asphalt planings, is an asphalt material reclaimed by planing or milling asphalt from road surfaces. The material can be recycled in hot or cold mix asphalt.

Definition of the Subject and Its Importance

Construction and demolition waste comprises a wide variety of materials including concrete, metals, timber, ceramics, soil, plaster, asphalt, and polymers which arise either during construction, renovation, or demolition activities.

National arisings of construction and demolition waste typically make up a large proportion of most countries' total waste – typically between 15% and 30%,

but sometimes higher. As a result, it is often identified as an area in which great potential exists for enhancing sustainability through reduction, reuse, and recycling. The past 20 years have seen significant growth in the recycling and reuse of construction and demolition waste, partly driven by legislation, taxation, and increasing scarcity of landfill space. As such activities grow, the importance of adopting the most sustainable approaches to managing this waste has started to be recognized as the key to moving toward a wholly sustainable construction industry.

Introduction

The construction process involves manipulating materials to form structures, coupled with the excavation and removal of soil and other materials. As a result, it will frequently produce material which is surplus to requirement. Moreover, once a structure reaches the end of its useful life, it must eventually be demolished, creating a quantity of waste.

The magnitude of arisings of construction and demolition is often disproportionately large in comparison to the extent to which the sector contributes toward economic growth, and there is a strong argument for concluding that this situation is unsustainable in both economic and environmental terms. The recognition of this has grown over the last 30 years, with developments both in terms of legislation and policy to reduce construction and demolition waste and also in terms of the development of procedures and technology which make recycling of end-of-life construction materials more viable.

This chapter examines the nature of construction and demolition waste and the mechanisms which cause it to arise. It then explores some of the options available (both established and developing) for reducing the amounts of waste deposited in landfill before discussing some of the environmental hazards that must be addressed when processing and using such materials.

Construction and Demolition Waste

Estimates of quantities of construction and demolition waste arising globally are, by their nature, likely to be imprecise. One attempt to do this arrives at a value of around 1.42 billion tonnes of material [1]. This is likely to be an underestimate, given that the total estimated amount of construction and demolition waste deriving from a limited range of countries in Table 1 yields a value close to this. However, the actual total is likely to be of such an order of magnitude.

The manner in which this is distributed around the world is partly dependent on economic activity, but while there is certainly some correlation between economic activity and the rate of production of construction and demolition waste, other factors also have a strong influence. This is illustrated in Fig. 1, which plots construction and demolition arisings versus the economic activity of the construction sector for 27 European Union member states (plus Norway) and indicates a far-from-strong correlation. Nonetheless, it is generally the case that the bulk of construction and demolition waste arises in the more economically developed world [15].

More insight into economic influences can be obtained by plotting the proportion of construction and demolition waste as a percentage of total waste against the percentage contribution of the construction sector to gross domestic product for member states of the European Union. This is shown in Fig. 2, which indicates that many member states produce construction and demolition waste at disproportionately higher rates than their construction sector contributes toward GDP. Such an outcome hints at a highly unsustainable situation.

It is also worth noting the countries where the percentage of construction and demolition waste is proportionately lower than the sector contribution to GDP: Bulgaria, Estonia, Latvia, Lithuania, Poland, Romania, Slovakia – the seven member states with the lowest GDP in the studied group. The implication of this is significant – it is not so much the case that a high GDP equates to high levels of construction and demolition waste. Rather, high GDP offers the opportunity to be wasteful, or possibly more accurately, low GDP restricts it.

Thus, it is evident that high arisings of construction and demolition waste are by no means an inevitable side effect of an active economy. For instance, Sweden, whose GDP per capita is in the top six of EU member states, makes a construction and demolition waste contribution to total waste which is nearly at parity with its construction sector's contribution to GDP.

Construction and Demolition Wastes. Table 1 Estimated annual arisings of construction and demolition waste from a range of countries

Country	Annual arisings, tonnes	Year	Reference
Australia	12,345,178	2006	[2]
Austria	31,321,626	2006	[3]
Belgium	13,089,649	2006	[3]
Brazil	62,143,200	2004	[4]
Bulgaria	1,023,303	2006	[3]
Canada	2,816,528	2002	[5]
China	2,185,445	2004	[6]
Cyprus	306,846	2006	[3]
Czech Republic	8,379,851	2006	[3]
Denmark	5,802,367	2006	[3]
Estonia	717,105	2006	[3]
Finland	23,145,713	2006	[3]
France	358,878,312	2006	[3]
Germany	196,536,165	2006	[3]
Greece	6,829,161	2006	[3]
Hungary	3,045,335	2006	[3]
India	13,154,400	2005	[7]
Ireland	16,599,467	2006	[3]
Italy	52,315,620	2006	[3]
Japan	680,400	2006	[2]
Latvia	19,340	2006	[3]
Lithuania	348,967	2006	[3]
Luxembourg	6,774,547	2006	[3]
Malaysia[a]	<1,807,525	1998,2001	[8, 9]
Malta	2,492,522	2006	[3]
Netherlands	56,609,820	2006	[3]
New Zealand	572,400	1997	[10]
Norway	1,247,936	2006	[3]
Poland	14,141,031	2006	[3]
Portugal	3,607,232	2006	[3]
Romania	33,870	2006	[3]
Slovakia	916,227	2006	[3]
Slovenia	994,887	2006	[3]
Spain	47,323,392	2006	[3]
Sweden	8,943,362	2006	[3]

Construction and Demolition Wastes. Table 1 (Continued)

Country	Annual arisings, tonnes	Year	Reference
Taiwan[b]	2,400,000	2001	[11]
Thailand	997,920	2002–2005	[12]
UK	109,545,988	2006	[3]
USA	123,000,000	1996	[13]
Vietnam	773,515	1997–1999	[14]
TOTAL	**1,192,058,626**		

[a]Construction and demolition waste + industrial waste
[b]Concrete only

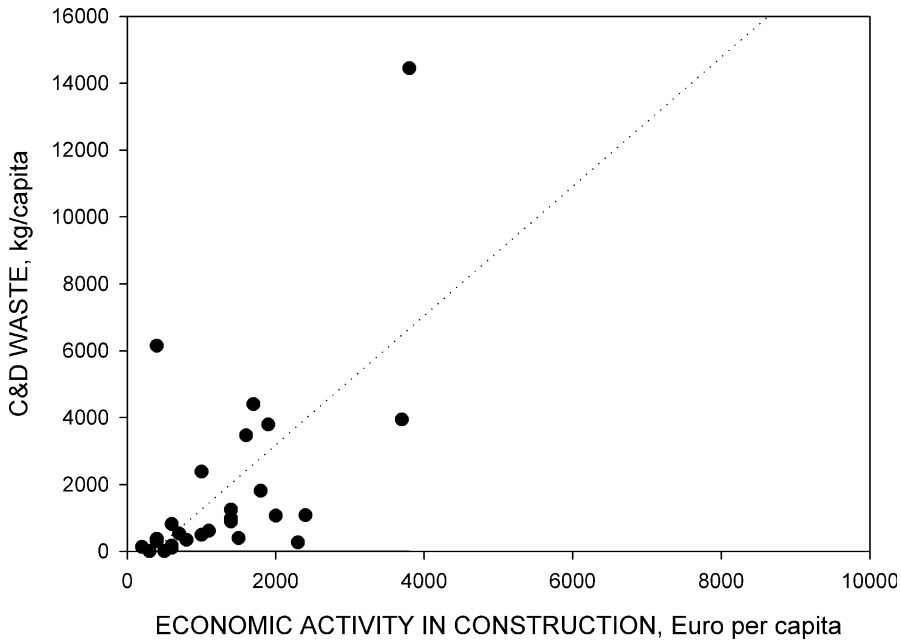

Construction and Demolition Wastes. Figure 1
Mass of construction and demolition waste per capita versus economic activity in construction for 27 European Union member states plus Norway (Derived from Eurostat data for 2006 [3])

This efficient performance has partly been attributed to the implementation of taxation and legislation in Sweden, including a landfill tax and the introduction of a stringent Environmental Code whose aim was to promote sustainable development. However, it should be stressed that social and cultural aspects may also play a role – the UK operates a landfill tax at a comparable level, and yet performs much less impressively.

Production of waste on the scale seen for the construction sector clearly presents a significant obstacle in moving toward sustainable development. Materials leaving construction sites and sites of demolished structures for landfill were once primary raw materials, and extraction of further raw material is required to replace material lost from the system. This, in turn, requires additional energy and resources for processing, manufacture and transport, which generates pollutants and further waste. Furthermore, the disposal of waste in landfill or through combustion reduces the quality of land resources and presents additional pollution problems.

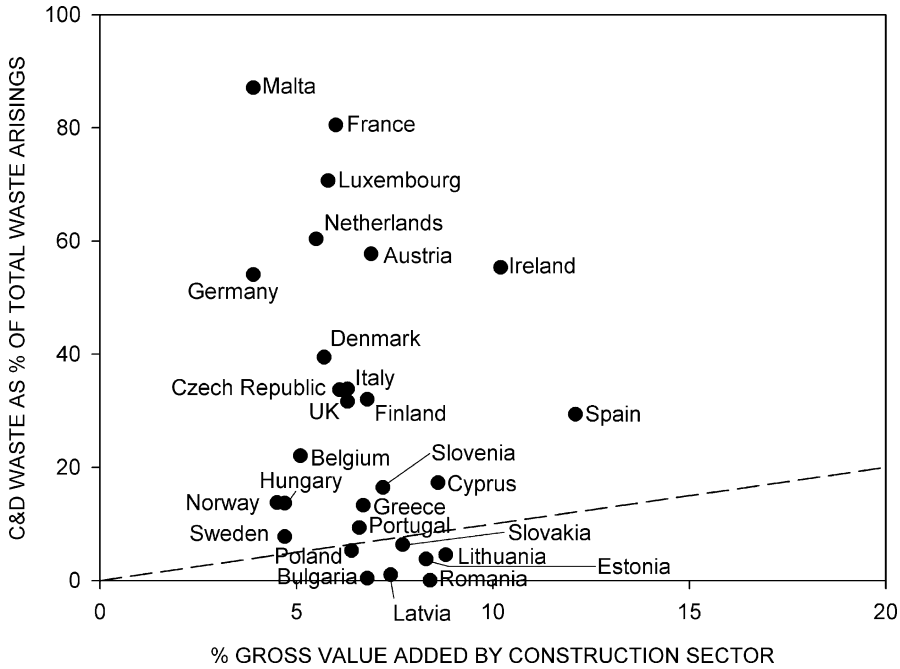

Construction and Demolition Wastes. Figure 2
Construction and demolition waste expressed as a percentage of total waste versus the percentage contribution to GDP from the construction sector for 27 European Union member states plus Norway (Derived from Eurostat data for 2006 [3]). *Dashed line* is the line of equivalence

Construction Waste

Construction waste is waste derived from the construction process itself. It has been proposed that this waste can be divided into two categories based on the types of events that generate it: accidental and predictable wastes [16].

Accidental waste is produced unintentionally on-site as a result of accidents and poor management of materials. It can include breakages, materials exposed to the elements in a way which degrades them and spoiled materials arising from inadequate supervision and training of operatives.

Predictable waste is the inevitable product of a specific construction project which can be anticipated from the construction procedures devised during the design and planning stages. This can include excavated soil, cutoffs, and concrete residues washed out of mixers.

Due to the manner in which construction waste arises, there is usually more scope for allowing the sorting of wastes. The presence of skips for individual material types on construction sites is now a common site in many countries. In many cases, skips are provided by recycling companies.

Demolition Waste

By its nature, the vast majority of construction and demolition waste derives from demolition. The demolition of a structure is typically a relatively destructive process, regardless of what technique is employed, meaning that the resulting rubble consists of a complex mixture of a range of different materials. This presents problems when reuse or recycling of demolition waste is an objective, although, as will be discussed, sorting of the material is possible, albeit with some compromise in terms of the efficiency of isolation of individual material components.

The problems related to conventional demolition have led to attempts to promote the "deconstruction" of structures – the careful, systematic disassembly of structures with as little damage as possible [17]. Partial deconstruction of buildings is encountered relatively frequently, but is usually limited to high-value

materials such as copper. For such an approach to be successful on a much wider scale, design of structures with future disassembly in mind is necessary. Thus, while it is likely that the deconstruction is likely to become increasingly common, it is likely to be some time before the process becomes commonplace.

Another source of waste other than from construction and demolition is during renovation of structures. Since renovation involves the removal of existing material and replacement with new materials, the nature of the resulting material shares characteristics of both demolition and construction waste. However, because the removal of material is likely to be conducted in a very controlled manner, in many cases the opportunity for sorting of waste is high.

Composition of Construction and Demolition Waste

The materials that make up construction and demolition waste can be divided up into many different classifications based on composition, physical properties, and original use. Here, three classifications are used – "metallic," "organic," and "mineral" – since the waste management options available for different materials within each classification are often, but not always, similar. These classifications are discussed below. Estimates and measured quantities of each type of material classification from selected literature are shown in Table 2.

It should be stressed that the composition of construction and demolition waste will vary from location to location depending on the nature of the building stock in a region and local traditions and trends with respect to the use of materials for construction. This also means that the nature of construction and demolition waste will change with time. An analysis of the changing nature of materials used in construction in the US identified essentially parallel increases in the use of most materials over the last 100 years. However, the rate of growth in the use of plastics and aluminum, which only started being used for construction in the twentieth century, has been higher than all other materials [26].

The Metallic Fraction

Metallic materials encountered in construction and demolition waste depend on the nature of the source and, in the case of demolition waste, the age of the structure. They are likely to include ferrous metals, copper, lead, aluminum, and zinc [18]. Table 2 shows

Construction and Demolition Wastes. Table 2 Composition of construction and demolition waste from a range of locations

Data type	Location	Material type (mass%)			
		Metallic	Organic	Mineral	Others
Measured	Switzerland, 1991 [18]	0.2	11	56	32.8
	Switzerland, 1993 [18]	3.1	24.7	72.1	0.1
	USA, 1995 (construction, residential) [12]	2	44	39	15
	USA, 1997 (demolition, residential) [12]	2	42	24	32
	USA, 1997 (demolition, nonresidential) [12]	5	16	79	0
	Austria, 2000 [19]	0.2	2.8	79	18
	Taiwan, 2001 [20]	5.5	13.4	81.1	–
	San Francisco, USA, 2004 [21]	15.5	20.6	33.4	30.5
Estimated	UK, 2000 [22]	7	20.3	71.8	0.9
	USA, 2003 [23]	1–5	21–35	46–70	–
	Florida, USA, 2007 [24]	2.6	21.6	65.9	9.9
	Massachusetts, USA, 2008 [25]	5	36	30	29

that the metallic fraction normally makes up the smallest proportion of construction and demolition waste – usually below 10% by mass.

The Organic Fraction

Here "organic" refers to the chemistry of the materials, and thus includes any materials whose major constituents are organic compounds.

Organic materials likely to occur in construction and demolition waste include timber, paper, organic polymers, and bituminous roofing.

During the construction process, much of the organic fraction is likely to be packaging waste in the form of plastic and paper packaging and timber pallets. Table 2 shows that, while the proportion of organic fraction varies from source to source, in the majority of cases, it is usually present in construction and demolition waste at between 20% and 30% by mass.

The use of plastics in construction is dominated by polyvinyl chloride (PVC), which is used in pipes and ducts, window frames, and flooring. Additionally, high- and low-density polyethylene (HDPE and LDPE), polypropylene, polystyrene, polyurethanes, and acrylonitrile butadiene styrene are all encountered in construction products (Table 3).

Construction and Demolition Wastes. Table 3 Polymers typically encountered in construction and demolition waste

Polymer	Acronym	Application
Polyvinyl chloride	PVC	Pipes/ducts
		Window frames
		Flooring
High-density polyethylene	HDPE	Pipes/ducts
Low-density polyethylene	LDPE	Pipes/ducts
		Sheeting
		Packaging
Polypropylene	PP	Pipes/ducts
Polystyrene	PS	Insulation
		Packaging
Polyurethane	PU	Insulation
Acrylonitrile butadiene styrene	ABS	Pipes/ducts

The Mineral Fraction

The mineral fraction includes concrete, fired-clay ceramics, soil, gypsum plaster, glass, and masonry – the nonmetallic, inorganic constituents of construction and demolition waste.

In terms of mineralogy, the mineral fraction commonly contains large quantities of quartz, along with calcite, dolomite, and phyllosilicates such as chlorite, muscovite, and illite [27]. As a result, the main elemental constituents, other than oxygen, are calcium, silicon, and aluminum. Figure 3 shows the chemical composition of a selection of mineral fractions from a UK-wide sampling of demolition waste plotted in the form of a $CaO–SiO_2–Al_2O_3$ ternary diagram. The material is generally limited to a narrow compositional "corridor" that runs from the CaO-rich corner of the plot to the $SiO_2–Al_2O_3$ axis. These limits to composition are not particularly surprising – aggregates and stone masonry will typically occupy the top SiO_2-rich corner of the diagram, while the composition of clay soil, slate, and most brick will be limited to a region on the $SiO_2–Al_2O_3$ axis, richer in SiO_2 than Al_2O_3. Limestone aggregate and masonry occupy the CaO-rich corner of the system, while Portland cement, deriving from a raw material feedstock of limestone and clay (or similar), occupies a position between the SiO_2 and CaO-rich regions on the diagram.

One group of materials that sits between the organic and mineral categories is that of asphalt deriving from highways. These materials will typically consist largely of inorganic mineral constituents bound together with a smaller volume of organic bitumen. However, where mixed waste is being handled, because the inorganic and organic components are extremely difficult to separate, and because their density usually lies closer to the range of the mineral fraction, it is normally the case that these materials end up as part of this fraction.

Managing Construction and Demolition Waste

Over the last 30 years, the application of integrated waste management strategies to wastes deriving from most industrial activities has become the favored approach. Such strategies adopt a collection of management options whereby waste arisings from a given activity are dealt with comprehensively and in

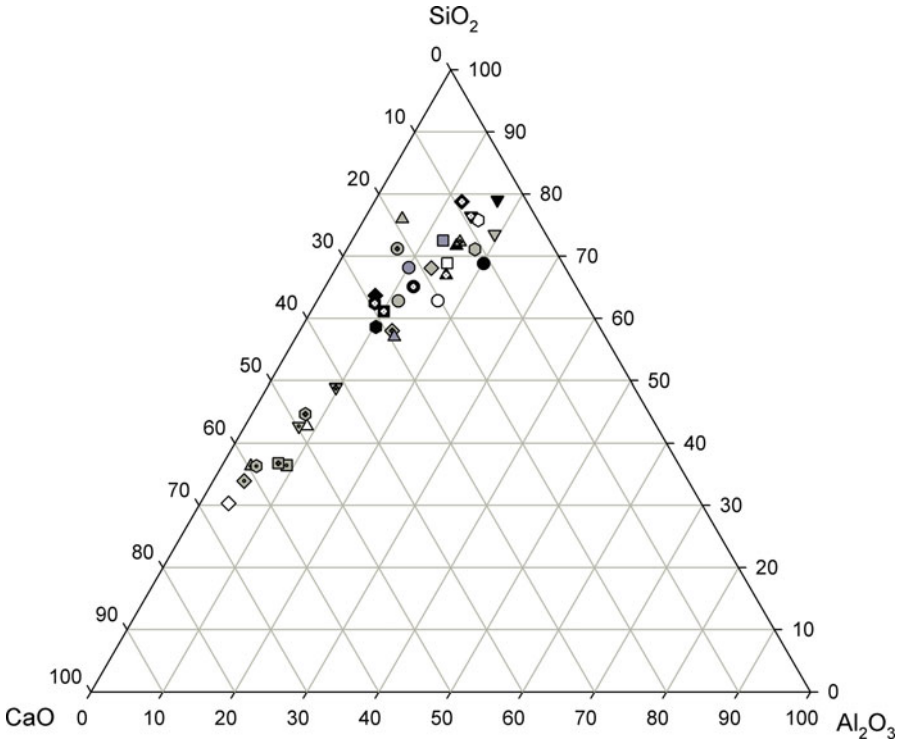

Construction and Demolition Wastes. Figure 3
$CaO–SiO_2–Al_2O_3$ ternary diagram for demolition waste sampled from sites in the UK [28]

a manner which satisfies a series of objectives, including safety and sustainability.

Where sustainability is an objective, it is common for an integrated waste management strategy to strive to select options at as high a level as possible within a "waste hierarchy." The detail of waste hierarchies varies from source to source, but the general form taken is usually that shown in Fig. 4, with reduction of waste being the most desirable management option and disposal being the least. In between these options are reuse: the return of material back to its previous application with minimal reprocessing; recycling, where return is only possible with reprocessing; composting; and energy recovery, which normally refers to waste-to-energy combustion, but may also include the production of fuels through pyrolysis or anaerobic digestion.

Recycling can take either a closed- or open-loop form, with the former referring to the return of material back to its original mode of use and the latter referring to recycling into an alternative application.

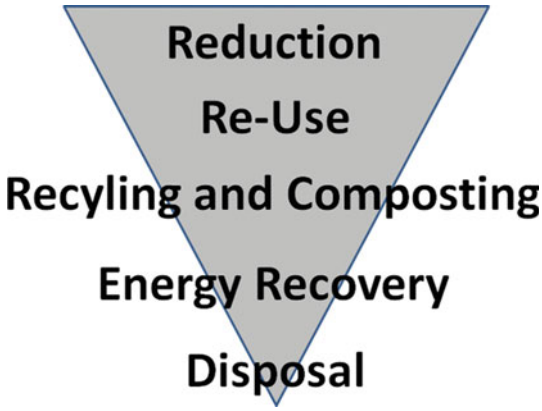

Construction and Demolition Wastes. Figure 4
The waste hierarchy

The fact that construction and particularly demolition waste frequently arises in mixed form often prevents closed-loop recycling on the grounds that separation of many constituents is impossible, and so return to original use is no longer an option.

Open-loop recycling tends to be viewed as being a slightly less desirable route, since there is sometimes, but not always, a compromise in quality of the resulting product leading to a loss of value. Recycling to lower-value products is sometimes referred to as "down-cycling." Another potential problem with open-loop recycling is that the "recyclability" of the resulting product may be progressively compromised at each cycle, which clearly reduces the sustainability of the process.

The Delft ladder is an attempt at applying the waste hierarchy specifically to demolition waste [29]. This is a hierarchy which attempts to prioritize different options for end-of-life structures and the structural elements and components which make up structures. The hierarchy is as follows:

1. Prevention: devise building systems that allow dismantling and reassembling for full recycling
2. Object renovation: renovating a structure for continued use
3. Element reuse: remove elements and refurbish for reuse
4. Material reuse (recycling): waste materials processed for return to production process
5. Useful new application: material, element, or component used in a different situation
6. Immobilization with useful application: potentially harmful material rendered benign when used as a raw material for a new component
7. Immobilization: potentially harmful material rendered benign and sent to landfill
8. Incineration with energy recovery: heat from combustion of waste used to heat water and generate electricity
9. Incineration
10. Landfill

As shall be seen, this chapter takes a slightly modified approach to that proposed by the Delft ladder. Nonetheless, the basic philosophy of this and the more generic waste hierarchy are adopted in subsequent sections.

Various options available for using construction and demolition waste are discussed below, using the waste hierarchy as a means of structuring the discussion. The options examined include both established technologies and technologies whose feasibility has been demonstrated, but whose large-scale adoption has not yet been realized. The options examined are summarized in Fig. 5.

Reduction

During construction, reduction of both accidental and predictable construction wastes requires different approaches. The nature of predictable waste means that there is potentially scope at the planning stages of a project to "design-out" many occurrences of waste. This can include planning to allow offcuts and other inevitable arisings to be used elsewhere, ordering sizes which minimize offcuts, providing suitable storage facilities on-site for materials, and coordinating deliveries to reduce storage times.

Accidental waste, being caused by accidents, is best reduced through ensuring good health and safety practices on-site and employing good materials acceptance procedures to minimize the extent to which damaged materials enter a site.

Demolition waste is, ultimately, impossible to reduce in the sense that the eventual demolition of a structure will yield a fixed volume of material. One interpretation of what waste reduction means in this context is simply the avoidance of demolition via the refurbishment of existing structures for new purposes. Such activities have been established practice in many parts of the world for some time, but have become increasingly popular.

Some caution is required in terms of recommending refurbishment over other options in the waste hierarchy. A recent life-cycle assessment study found that refurbishment of a particular structure (a bank headquarters) had larger levels of associated carbon dioxide emissions compared to demolition and construction of a new building [30]. The main reason for this was that projected emissions associated with service and maintenance of the refurbished structure were higher. This does not necessarily mean that refurbishment is not a sustainable option, but does stress the importance of establishing the appropriateness of an existing structure and making sure that refurbishment addresses issues relating to energy efficiency as thoroughly as possible.

Reuse

Reuse refers to the removal and possible refurbishment of structural elements or components from buildings for use in a similar application. Generally, the

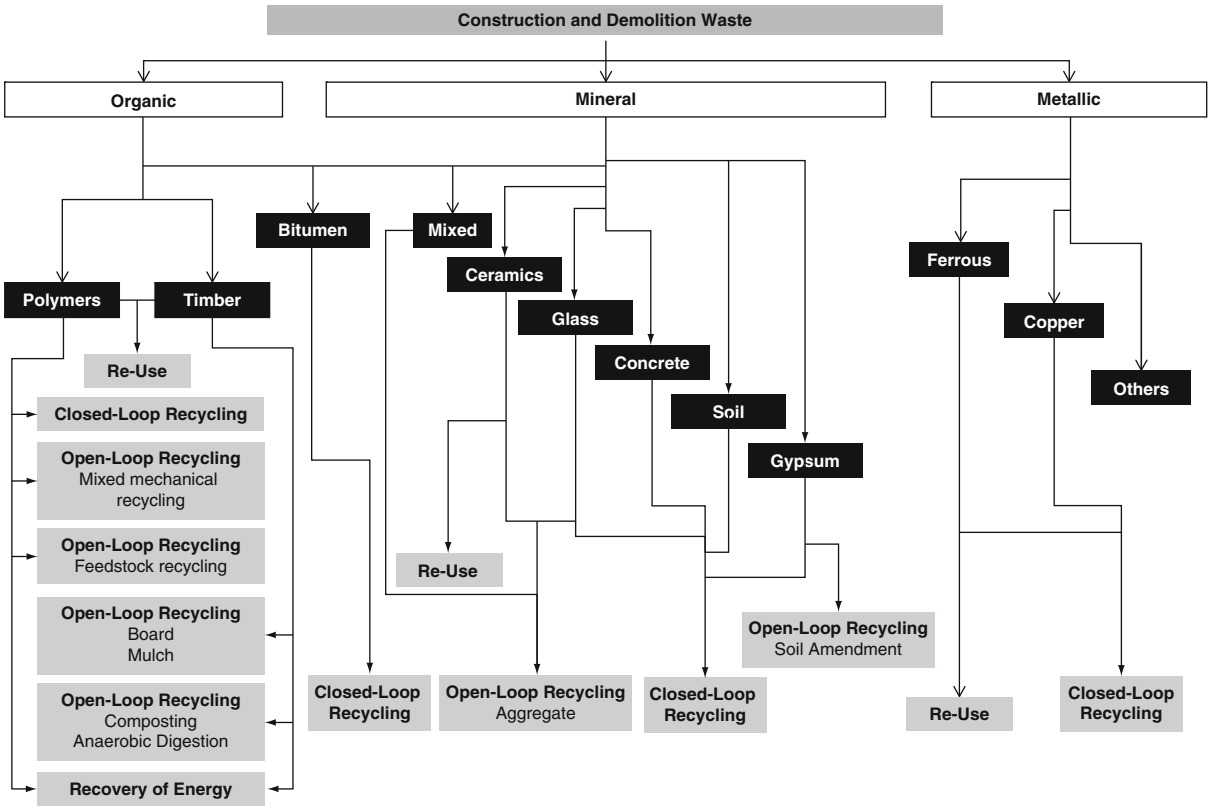

Construction and Demolition Wastes. Figure 5
Options for the various constituents of construction and demolition waste

reusability of an article will depend on the ease with which it can be removed, and the extent to which service has affected its aesthetic and engineering qualities. Currently the main markets for reclaimed materials are fired-clay bricks (usually from structures in which lime mortar was used) and timber flooring. Both types of article are modular, thus allowing removal of individual items with relative ease, and have agreeable aesthetic qualities, sometimes improved by age.

A UK study has appraised various construction systems in terms of their reusability [17]. The results of the appraisal are summarized in Table 4.

Recycling

The nature of recycling of wastes deriving either from construction, renovation, or demolition is very dependent on the form in which the material is obtained. Where the material has been separated into individual material types, there is usually more scope for recycling, and closed-loop recycling is likely to be one of these options. However, where waste is mixed, it is much more likely that lower-value recycling options will be the only ones available.

The following section examines the most obvious options for recycling, but makes no claim to be comprehensive. Where materials have been separated, the options for recycling, whether wastes derive from construction or demolition, are in most cases the same. However, the section will start by examining the processing of mixed demolition waste for recycling, the main product of which is recycled aggregate.

Processing Mixed Demolition Waste for Recycling

The processing of concrete or mixed demolition waste requires two basic operations – size reduction and screening – to obtain the required grading of particles. However, depending on the nature of the source material, there is likely to be a need to remove undesirable

Construction and Demolition Wastes. Table 4 Results of evaluation of various construction systems for their suitability for subsequent reuse [17]

Category	Suitability for reuse	
	Lower	Higher
Wall finishes	• Plaster on substrate • Ceramic wall tiles • Metal wall sheeting • Synthetic flexible wall tiles • Wallpaper	• Mirror finishes • Timber boarding system • Textile fixed to timber support • Waterproof wall panels • Polished plaster panels
Internal partitioning systems	• Metal stud walling system with plaster skim coat	• Metal stud walling system with removable wallpaper • Glass partitioning system • Solid straw internal partition with plaster finish
Ceiling finishes	• Plasterboard screwed to timber joists with plaster skim coat	• Plasterboard ceiling on support system • Resin-bonded glass wool tiles on support system • Suspended metal tiles on support system • Timber decorative boarding fixed to timber joists
Floor finishes	• Ceramic tiles fixed with adhesive/grout • Wool carpet fixed with adhesive • Terrazzo floor fixed with adhesive	• High-density fiberboard with loose laid carpet tiles • Loose laid carpet tiles • Wool carpet with carpet grippers • Solid wooden floor • Floating laminate flooring • Terrazzo floor on vinyl release system • Loose laid rubber tiles
External wall systems	• Render finish on solid cavity block construction • Brick and block cavity wall system with cement mortar • Planar structural glazing	• Stone cladding or terracotta rainscreen • Curtain walling – metal sections with solid/glass infill panels • Metal cladding • Brick and block cavity wall system with lime mortar • Timber cladding
Roofing finishes	• Single-ply membrane fixed with adhesive • Asphalt applied as hot fluid • Plastic finish applied as liquid	• Single-ply membrane fixed mechanically • Thatch roofing • Lead/copper/aluminum roofing • Clay tiles • Bitumen impregnated fiberboard
Structural elements	• Permanent formwork walling • Prefabricated concrete wall and floor panels • Concrete beam and insulation block floor • Concrete beam and block floor with screed finish • Structural insulated wall/roof • Panels with external render and internal plasterboard on plaster dabs	• Studs, insulation, and panels with external timber boarding and internal screw-fixed plasterboard • Structural insulated wall/roof panels with external timber boarding and internal plasterboard on battens • Timber floor joists on joist hangers with timber boarding and plasterboard • 2Concrete beam and block floor with dry finish • Exposed steel roof construction with Z-purlins and C-sections

constituents to ensure that the product of processing satisfies the required standards for end-use. Additionally, there may be constituents present whose market value makes separation desirable.

Equipment for processing demolition materials is available in both mobile and static forms. In many cases, mobile equipment is favored on the grounds that processing can be carried out on-site, removing

the need for transportation to a processing center, a particularly useful arrangement when the processed material is to be used on the site of origin. The variable processing requirements for demolition waste mean that equipment on the market is often modular, allowing a range of plant units to be selected and arranged in sequence to tailor a processing scheme to a given material source and product type. Examples of three such sequences are shown in Fig. 6.

Equipment for crushing and screening will usually be identical to that used for quarrying activities, although some of the plant used to remove undesirable components is often designed specifically for demolition waste processing.

Modular processing systems require the movement of material from one process to another, and this is normally achieved through the use of belt and radial conveyors and apron, plate, and reciprocating feeders.

In most cases, demolition waste will undergo some degree of pre-sorting prior to processing. This normally involves the identification and removal of large components either for disposal or recycling. Such components may include steel sections and reinforcement bars, plastic components and oversized pieces of timber.

The material entering the process sequence is then usually crushed using impact, jaw (see Fig. 7), or cone crushers [18]. In some cases, a screen will be located immediately prior to crushing to ensure oversize material does not jam or damage machinery. It is often the case that a concrete crusher mounted on an excavator will be located directly after this screen to break down the material to crushable size and to remove steel reinforcement, etc.

After crushing, the resulting material is screened, often using a sequence of screens which might include grizzly screens, finger screens, trommel screens, and vibrating screens. A screen sequence can be achieved either through placing screens in series or by stacking screens in decks with different size fractions being directed into different process streams. By selecting appropriate screen configurations, sorting for shape as well as size is possible, which potentially has benefits. For instance, long, narrow objects such as metal pipes and rods can be removed by including bar screens or similar in the screening sequence.

Either before or after screening, the removal of various nonmineral constituents can be conducted. This may involve processes which differentiate between organic or metallic constituents and mineral constituents based on their physical properties. However, it is not uncommon for hand sorting to be carried out, where operatives identify and remove metals, plastics, timber, and paper from material passing on a conveyor.

The removal of ferrous metals can be achieved through the use of magnets (either permanent or electromagnets) which can be suspended over conveyors or mounted in revolving drums or belt configurations.

Where significant quantities of non-ferrous and, hence, nonmagnetic metal is present, eddy current devices can be used. Eddy current devices expose metal particles to a changing magnetic field which induces eddies of electrical current within them, in turn inducing magnetic fields which oppose the original magnetic field and cause the metal particles to be repelled [32]. During the processing of construction and demolition waste, the repulsive force is used to drive metallic particles off a conveyor.

The density of the various constituents of construction and demolition waste is also a physical characteristic which can be exploited in the separation process. Because most polymers and timber have specific gravities below one, the use of water as a medium for separation is an option. Separation in this way can involve settling tanks or revolving, water-filled drums [33]. Air classification can also be used, which involves passing the material over a vertical stream of air which will remove less dense constituents. Air classification has the additional benefit of removing fines having terminal velocities lower than the velocity of the air stream. Because of this, however, it is usually necessary for the exhaust from air classification to subsequently pass through pollution control devices capable of removing particulates [18].

Other devices with origins in minerals processing that separate on the basis of differences in density, and which can potentially be used on construction and demolition waste, include jigs and shaking tables [34].

The removal of fines can also be achieved through washing, which can be carried out using barrel or log washers, in the same way as for conventional aggregates.

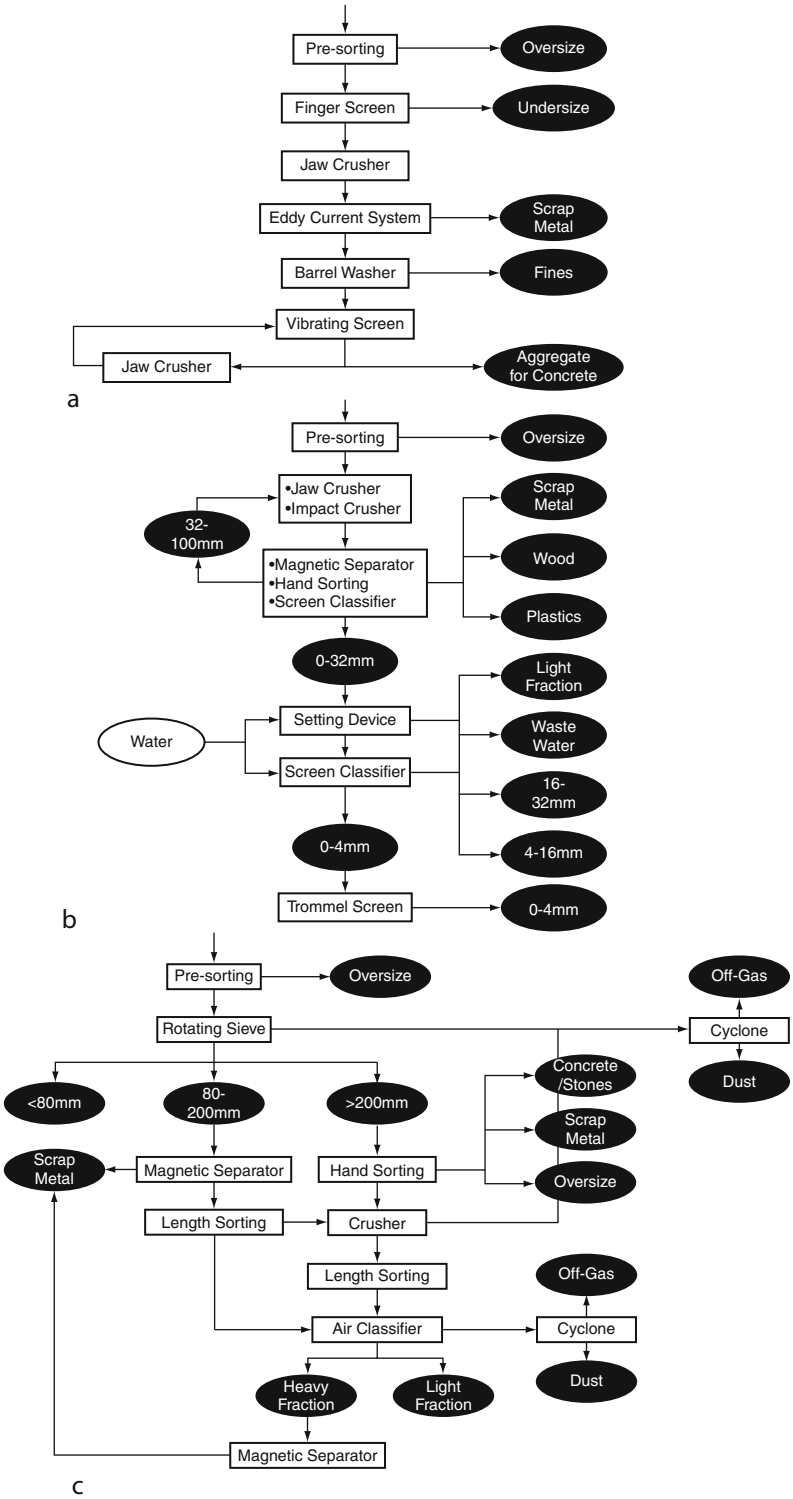

Construction and Demolition Wastes. Figure 6

Three configurations for recycling of mixed demolition waste. (**a**) Basic process [31]; (**b**) wet process with hand sorting [19]; (**c**) dry process with air classification, hand sorting, and length sorting [18]

Construction and Demolition Wastes. Figure 7
Mobile jaw crusher being used to crush demolition waste (Photograph courtesy of tayside contracts)

Recycling Mineral Waste The use of mineral fractions derived from the processing of construction and demolition waste as aggregate is an obvious option. Both coarse and fine aggregates can be produced, with applications as granular fill, aggregate for hydraulically bound and unbound roadbase and pipe-bedding materials. The material can also be used as an aggregate in concrete.

Usually, a distinction is made between aggregate obtained from the reprocessing of what is essentially waste containing only concrete and waste containing a range of different constituents of the mineral fraction. The former is usually referred to as recycled concrete aggregate (RCA), while the latter is recycled aggregate (RA). This distinction has most significance where the recycled material is used in concrete.

RCA and RA in Concrete The use of RCA and RA in concrete is an approach that has been extensively explored, and it is generally agreed that, with adequate quality control and the use of suitable mix design methods, good quality material can be produced.

Particles of RCA typically have a thin layer of hardened mortar at their surface, retained during the crushing process. This layer usually has a strong influence on the subsequent performance of the material in concrete. Because the porosity of the layer is usually higher than that of the aggregate within, water absorption of the recycled material is higher than that of the aggregate in its virgin state. The extent to which water absorption is increased is partially influenced by the nature of the concrete from which the aggregate was obtained, although the effect is slight [35].

Higher water absorption has the effect of reducing workability of fresh concrete, and this means that to achieve a given workability, a higher level of mixed water is required [36].

The presence of mortar also influences the compressive strength of the hardened concrete, with recycled aggregate reducing compressive strength relative to a natural aggregate mix with the same water–cement ratio. This effect is more pronounced when RCA is used as a fine aggregate, resulting from the higher surface to volume ratio giving the material a higher mortar content. Where recycled aggregate is used as a partial replacement for virgin aggregate, the effect is minor at low levels of replacement, but becomes more pronounced at higher levels [37].

Drying shrinkage and creep are also typically more pronounced in concrete mixes containing RCA [38] as are durability properties relating to the permeation properties of concrete [39].

The solution to the reduction in strength and compromise of other properties is usually simply to reduce the water–cement ratio of a concrete mix. However, the

higher levels of water required to maintain workability mean that potentially uneconomic quantities of cement may be required through conventional mix proportioning. This makes the use of superplasticizing admixtures an attractive option. Appropriate modification of mix proportions has been shown to produce concrete whose structural performance in reinforced concrete elements in terms of shear capacity and flexural behavior has been demonstrated to be comparable to concrete of equivalent strength made with natural aggregate [40, 41].

The performance of recycled aggregate in concrete is very much dependent on what constituent materials are present, although similar effects are typically encountered in terms of water absorption. The main concern with RA is its greater potential for the contamination with undesirable components, as discussed below.

Good quality control in the production of RCA and RA is necessary, mainly to avoid problems relating to the presence of detrimental substances. Contamination with chlorides is one of the major concerns.

Chlorides may arise in RA and RCA as a result of contamination during service from chloride-bearing environments such as those experienced by coastal and highway structures. In addition, chlorides may have been introduced into concrete at the construction stage through contaminated materials, the use of seawater as a mix constituent, or via the use of calcium chloride as an accelerating agent. Chlorides are capable of significantly accelerating the rate of corrosion of steel reinforcement. As a result, chloride levels in concrete are strictly limited in concrete standards.

Additional potential problems presented by the use of RA in concrete include the presence of sulfates, aluminum metal, and materials capable of undergoing alkali–silica reaction (ASR).

In the case of sulfates, contamination may arise from gypsum plaster from the original structure, or possibly as a result of ingress from an external source. Soluble sulfate has the potential to cause delayed ettringite formation, where concrete containing relatively high levels of concrete aggregate and cured at elevated temperatures expands and cracks as a result of the decomposition and subsequent reformation of ettringite.

Aluminum will, in the alkaline conditions created by hydrating Portland cement, react to evolve hydrogen gas [42]. When evolved within concrete, bubbles form, which can lead to significant expansion of the fresh material and compromise strength. Additionally, the presence of hydrogen gas presents an explosion hazard.

The presence of glass in RA may be capable of undergoing harmful ASR in contact with hydrating cement, which causes expansion and cracking of concrete [43].

While the implications of chloride contamination are serious, screening of aggregate is relatively straightforward, since chlorides can be readily determined through chemical analysis. Analysis for sulfates is also easily conducted, but much of the problems of delayed ettringite formation from recycled aggregate stems from localized agglomerations of gypsum plaster. Such features are potentially missed by chemical analysis of bulk samples.

Aluminum metal can be identified through powder x-ray diffraction, although analysis tends to be qualitative rather than quantitative and low levels of aluminum, which may not be detected by this technique, are still capable of damaging concrete. Most ASR-susceptible materials elude detection by chemical and mineralogical analysis methods, meaning that screening for these components requires the use of accelerated ASR test methods. These issues are one of the main reasons that the growth in the use of recycled concrete aggregate in concrete has exceeded that of recycled aggregate.

It should be pointed out, however, that the presence of aluminum particles is likely to be limited in processed construction and demolition waste, due to the fact that ductile metals will tend not to fragment to any great extent during processing, and thus will end up in the oversize fraction. Where handpicking and eddy current devices are employed, the risk of aluminum being present is still lower. Furthermore, a recent study of the propensity for recycled aggregate from a range of sources to undergo ASR found that the materials presented very little risk [44].

Pozzolanic Components in the Mineral Fraction One interesting potential future option for the recycling of the mineral fraction is in exploiting the pozzolanic properties of certain constituents. Certain silica-rich materials undergo pozzolanic reactions with lime in the presence of water to form cementitious products which provide compressive strength. This is exploited

in concrete production by combining industrial by-products such as fly ash from coal-fired power generation with Portland cement. In construction and demolition waste, both fired-clay ceramics and glass possess pozzolanic characteristics [45, 46], and the mineralogy of many fired-clay ceramics is frequently very similar to that of fly ash.

To exploit this chemical characteristic, it is necessary to grind the materials to very fine particle sizes, or at least to utilize the fines derived from processing. However, the main barrier to adopting such an approach is the mixed nature of the mineral fraction. Research examining the possibility of thermally processing mixed mineral demolition waste to render more of the mixture cementitious [28], while partially successful, found that variation in performance of the various materials made the viability of such an approach questionable. The most promising route toward utilizing materials in this way is via the deconstruction of structures.

RCA and RA in Asphalt RCA and RA can also potentially be used as aggregate in asphalt mixtures, although research in this area has largely concentrated on RCA. In asphaltic mixtures, the higher porosity of the RCA particle surfaces is thought to absorb asphalt, which has the effect of reducing the effective asphalt content and increasing air voids [47].

The increase in air voids usually has the effect of reducing stiffness [48]. The decline in stiffness has implications in terms of load-bearing capacity during service. Deterioration in integrity of asphaltic mixtures resulting from contact with water is more marked with increasing RCA content, although this only becomes problematic at relatively high RCA levels. Creep rates and rutting depth also increase with RCA content.

Unlike concrete, there is limited scope for adjusting asphalt proportions to accommodate RCA – reduction of bitumen content can improve properties such as resilient modulus, but has undesirable implications for the behavior of the material during placing and compacting.

It should be stressed that performance is very much dependent on the source material. For instance, one study has observed wholly acceptable behavior from asphalt mixtures containing only RA [49].

Reclaimed Asphalt Pavement The recycling of reclaimed asphalt pavement or recycled asphalt planings (RAP) is now a well-established practice in many areas of the world. Due to the fact that asphalt surfaces are isolated from other structures, the problem of contamination is much less of an issue. As a result, the process of reclamation and recycling is relatively straightforward in comparison to other end-of-life construction materials. Reclamation is conducted by planing or milling asphalt from a road surface (Fig. 8).

Construction and Demolition Wastes. Figure 8
Planing of asphalt (Photograph courtesy of tayside contracts)

Recycling then involves reducing the particle size of the RAP and introducing it into the manufacture of hot or cold mix asphalt.

Recycling in hot mix asphalt involves introducing a proportion of RAP into a conventional hot mix manufacturing process. This involves combining bitumen with aggregate which has been heated using a burner. Recycling as part of the hot mix process can either be done at a manufacturing plant or in situ using mobile plant in which the planing, crushing, and hot mix production processes are carried out sequentially.

During service of an asphalt road surface, bitumen undergoes oxidation reactions which lead to an increase in the proportion of larger molecules of hydrocarbons. This degradation leads to a reduction in the viscosity of mixes containing RAP [50]. To overcome this problem, the introduction of new bitumen and sometimes a "recycling agent" during hot mix recycling is employed to "rejuvenate" the mix [51]. The recycling agent is normally either a hydrocarbon wax or an inorganic zeolite and has the effect of reducing the required mixing temperature, which would otherwise need to be high to sufficiently reduce the viscosity of the bitumen present in RAP to allow adequate mixing and compaction. Such high temperatures are both costly in terms of energy consumption and present a safety risk.

Most studies which have characterized hot mix asphalt mixtures containing RAP have found that stiffness (and, hence, the ability of the material to spread load) is increased as a result of the presence of stiffer oxidized bitumen [52]. However, where milling processes lead to significant reduction in particle size, a decline in stiffness is possible with increasing RAP content [53]. Typically, the inclusion of RAP in hot mix asphalt has the effect of compromising performance under cyclical loading, although it has been suggested that durability properties are enhanced.

Technical requirements for the use of RAP in asphalt have typically placed stricter limits on materials in the pavement surface layer, compared to base and binder courses. This has certainly been the case for the Specification for Highway Works in the UK and the requirements of State Highway Administrations in the USA [53]. However, there is a growing recognition that this approach is excessively cautious, and the UK requirement now places emphasis on demonstrating that performance is appropriate at high RAP levels [54].

Another concern with hot mix recycling is that the presence of RAP leads to the emission of greater quantities of fumes during production and placing [55]. Furthermore, there is evidence that the toxicity of the hydrocarbons released is higher where RAP is used [56].

Even with the use of recycling agents, the required temperatures for mixing and compacting limit levels of RAP to around 50% [57]. Cold mix recycling permits higher levels of usage.

Cold mix production involves mixing aggregate with an emulsion of bitumen droplets dispersed in water and stabilized with an emulsifying agent. The viscosity of such emulsions is sufficiently low to allow mixing and placing at ambient temperatures (Fig. 9), thus offering a route for utilizing RAP at levels up to 100% of the total aggregate. Once placed, the emulsion breaks and the pavement stiffens.

Another way of overcoming problems of high viscosity in asphalt mixtures through the use of cold mix technology is to employ foamed bitumen. Foam is created by injecting fine, cold water droplets into hot bitumen causing their conversion to steam and consequent expansion. The foamed bitumen's viscosity is temporarily reduced, making mixing with RAP possible at ambient temperatures [58]. After a few seconds, the foam breaks down, but the presence of moisture maintains a low viscosity, and this allows the mix to also be compacted at ambient temperatures.

Fresh Concrete Recycling options also exist for excess fresh concrete from construction. Residue remaining in ready-mixed concrete trucks has, in the past, been disposed of by washing out the mixer and disposing of the resulting material by settling out the aggregates and discharging the remaining sludge ("wash water") which consists of water and particles of cement and fines into sewers. This approach has gradually evolved toward less wasteful procedures as a result of the increasing economic burden of landfill disposal and restrictions in many parts of the world on wastewater disposal. The most obvious way in which the mixer residue can be recycled is by recycling both the settled aggregates and the clarified water (which has been allowed to undergo sedimentation) in concrete production and disposing of the sedimented fines. However, a more sustainable solution is to recycle the

Construction and Demolition Wastes. Figure 9
Asphalt paver laying cold mix asphalt (Photograph courtesy of tayside contracts)

wash water without sedimentation. The affect of this approach on concrete performance has been demonstrated to be minimal [59].

An alternative means of achieving the same objective is through the use of stabilizer/activator systems for halting and restarting the cement hydration process [60]. This technique involves concrete returned to the ready-mixed concrete plant being dosed with a retarding admixture referred to as a "stabilizer." The retarder is usually a phosphate or phosphonic acid. An appropriate dosage is used to ensure a sufficient level of retardation, and the stabilized mix is either stored in the truck or in separate containers. When concrete production resumes, an accelerating admixture (the "activator") is added at a dosage sufficient to counteract the effect of the stabilizer. It is then combined with fresh concrete to produce mixes containing up to 35% recycled concrete. The impact on hardened concrete performance is minimal.

Soil Conditioning The use of mineral constituents of construction and demolition waste as a means of ameliorating soils is an application which has been given some consideration in recent years. The mineral fraction of mixed construction and demolition waste typically contains relatively high levels of soluble calcium, sulfate, and potassium [61], which are valuable nutrients to all plants [62]. Additionally, in "sodic" soils, where sodium accumulation compromises soil structure in arid environments, calcium can be used to mobilize sodium ions fixed in clays, allowing them to be washed away [63]. Also, calcium additions can be used to tackle problems such as subsoil acidity syndrome [64] and crust formation [65] in soils.

Typically the application of calcium to soils to realize these benefits is achieved using gypsum, meaning that the use of waste plaster from either construction or demolition activities has also been considered for such a role [66].

Gypsum Regardless of the unsustainability of disposing of any construction and demolition waste component to landfill, there is a very strong environmental argument for removing gypsum waste from waste streams destined for such a fate. This is because leaching of sulfate can present environmental problems, and the presence of gypsum promotes the formation of hydrogen sulfide gas which has an unpleasant odor and can lead to health problems [67, 68].

Closed-loop recycling of gypsum in the form of plasterboard (drywall) is an established practice in many parts of the world [69–71]. Reprocessing for recycling involves grinding up the recovered material using grinding apparatus, usually in combination with trommel screens which act to remove the paper-backing material which would otherwise render the

material unusable [71]. In some cases, magnetic separation is used to remove metallic contaminants, such as nails. New plasterboard can tolerate levels of around 25% by mass of recovered gypsum [70]. The separated paper is also suitable for recycling.

The tolerance of the process to contaminants is extremely low (less than 3% contamination can be accommodated) [69]. As a result, removal of plasterboard prior to demolition or, at the very least, well-managed pre-sorting of demolition rubble prior to processing for other purposes is necessary. In the case of plasterboard deriving from construction, uncontaminated material can be obtained by locating skips at construction sites into which waste board can be deposited for collection by reprocessors [69, 71]. Additionally, contamination with moisture renders plasterboard potentially unrecyclable, although processes have been developed more recently which have overcome this problem [70].

Recovered material can also be used as the gypsum component of Portland cement [71].

Glass Infrastructure for the recycling of glass is well established globally, and recycling of flat glass from structures is, in theory, a relatively straightforward process. Furthermore, glass recycling has favorable sustainability credentials, since its return to the glass furnace reduces the overall energy requirement of the manufacturing process. The saving in energy is dependent on the production rate, but at high production rates, a saving of around 19% is possible by using 50% recycled glass (or "cullet") [72].

In reality, the physical characteristics of glass make it indistinguishable from the bulk of the mineral fraction of demolition waste, making separation after demolition impossible. This means that glazing must be removed from structures prior to demolition. Presently, therefore, the majority of glass arising from construction for recycling tends to come from the replacement of glazing as a result of maintenance and refurbishment activities. Additionally, problems with contamination of glass with putty and other materials have acted as an obstacle to recycling. Nonetheless, some progress is being made, with recycling rates increasing, particularly for the manufacture of container glass and glass fiber, whose cullet quality criteria are slightly more tolerant [73].

The possibility of using glass as aggregate has also been explored. When employed as an unbound material, for instance as a pipe-bedding material, the use of glass is relatively straightforward. The use of glass as a bound material in asphalt mixtures is an established practice, albeit normally using material from the recycling of container glass. Although successful use of glass in asphalt pavement surfaces has been demonstrated at aggregate replacement levels of up to 15%, low bonding strengths and reduced friction mean that use in non-wearing courses is favored [74]. Glass aggregate in concrete functions well physically, but can potentially undergo expansive alkali–silica reaction (ASR) [75]. However, the inclusion of materials such as ground granulated blast furnace slag in concrete mixes containing glass appears to control expansion effectively [43].

Recycling Organic Waste

Timber There are many potential means of recycling waste timber in the manufacture of construction materials. These include particleboard (or chipboard), wet-processed fiberboard, dry-processed fiberboard (MDF), oriented strand board (OSB), and cement-bonded particleboard [76]. Currently, only particleboard manufacture employs significant quantities of recycled timber.

All of the products involve timber-derived material held together by some form of binder. In every case, reprocessing of the timber is required, firstly through size reduction. The least amount of size reduction is required in the manufacture of OSB, where timber strands up to 75 mm in length are cut and then sprayed with a layer of adhesive. The strands are then laid into mats, usually of three layers in which the grain of the strands may be aligned. The mats are then pressed between platens to form the boards and heat applied to cure the resin.

Smaller particle sizes are used for particleboard and cement-bonded particleboard. The former is bound with an organic resin, while the latter is bound with Portland cement. Like OSB, particle board is manufactured by first producing a mat of particles which have been sprayed with resin and then pressing the mat between heated platens, passing the mat through heated rollers or extrusion of particles through a heated die. Cement-bonded particle board is

produced by combining Portland cement and wood particles in ratios of approximately 75:25 by mass.

The manufacture of fiberboard requires further processing prior to manufacture, in the form of exposure to steam at high pressure. This allows a subsequent mechanical defibration process to separate the fibers.

Wet-processed fiberboard is produced by forming a mat of wetted fibers which is then pressed between heated platens. No application of resin is required, as the heat softens the lignin on the surface of the fibers, binding them. In the manufacture of MDF, resin is sprayed onto dry fibers, which are then formed into boards in a similar manner to particleboard.

Uses for chipped timber include animal bedding, surfacing material for bridleways, footpaths, and children's playgrounds. Additionally, chipped timber mulches have been found to be highly effective, with good capabilities in suppressing the growth of weeds, maintaining surface soil temperatures and retaining soil moisture [77].

However, concern has been expressed regarding the use of treated timber in many of these applications. Timber treatments are principally used as a means of preserving wood from biological degradation. Timber treatments include waterborne preservatives such as copper–chromium–arsenic (CCA) compounds, tar oil preservatives (such as creosote), copper and zinc organics delivered via organic solvents, as well as paints or varnishes [76]. It has been found that arsenic deriving from CCA treatments can leach from mulches (see section Environmental and Sustainability Issues). Furthermore, a risk assessment carried out in the UK concluded that the use of treated wood chippings for animal bedding, mulches, and compost was, in most cases, inappropriate [77]. In many countries, limits are now set for levels of preservatives in board materials, and this is likely to improve mattes in the future.

Composting The composting of timber and other biodegradable components of construction and demolition waste is also an available option. Composting involves the aerobic digestion of biodegradable waste by microorganisms to produce humus for agricultural purposes. The success of composting is dependent on factors such as moisture content, oxygen levels, temperature, pH, and the texture and biochemical composition of the waste.

The key factor relating to chemical composition is the carbon–nitrogen (C/N) ratio, which should ideally be around 30 [78]. Because the main chemical constituents of timber are based around carbon, oxygen, and hydrogen, the C/N ratio of timber is typically around 700. Thus, composting involving timber is best conducted in combination with wastes richer in nitrogen, such as agricultural manure or green plant wastes [79].

Biochemical composition is also relevant in the case of timber, as a major constituent of timber is lignin, which is usually broken down at a relatively slow rate by microorganisms.

The issue of texture is also important. Texture in this context refers to the structure of the waste, with a high surface area and open structure allowing access to microorganisms and retention of oxygen and moisture. To obtain a suitable texture, timber requires chipping prior to composting.

As before, the presence of CCA preservatives is likely to compromise the extent to which certain sources of wood can be used in this way. However, it should be stressed that the fungal and microbial decomposition of timber during composting appears to have the effect of reducing the plant toxicity of timber (albeit in timber containing no CCA) [80]. The presence of CCA seems to have little effect on the populations of microorganisms present during composting, and there is little evidence of release of the metals used in CCA [81]. However, the longer-term consequences of their presence are likely to be detrimental and should be avoided.

Recycling Plastics Recycling plastics can be conducted in two ways – mechanical recycling and feedstock recycling. Mechanical recycling refers to the reforming of plastics into new articles. When the plastics involved are thermoplastics, mechanical recycling normally involves the application of heat to produce a melt which is then extruded. Elevation of temperatures can potentially cause the polymers to undergo thermal degradation leading to deterioration of mechanical and durability properties.

Plastics derived from construction and demolition waste are currently most commonly encountered in mixed form. Recycling of such material presents problems, mainly as a result of the immiscibility of different

polymers. This immiscibility leads to a lack of homogeneity in the melt which ultimately yields poor mechanical properties.

Despite this, some success has been achieved in the extrusion of articles using blends of incompatible polymers at temperatures at which one polymer melts and the other remains solid, but above the glass transition temperature. Extrusion causes the solid polymer to be drawn out into fibers held within a matrix of the molten polymer. This approach has been successfully used to manufacture items such as ties for rail tracks. However, the approach is limited to a specific pair of polymers (HDPE and PS) and would likely be unsuitable for the PVC-rich plastics fraction deriving from construction and demolition waste [82]. Other similar techniques have been developed for the manufacture of board, pallets, stadium seating, benches, cable drums, perforated paving blocks, and underground chambers for water distribution applications [83].

Laboratory studies have examined the possibility of overcoming the issue of immiscibility. One approach is through the use of compatibilizers – compounds which are capable of producing a more uniform melt. While compatibilization is well established for binary polymer blends, the situation is more complex for the combinations of multiple polymer blends. However, some success has been achieved with mixtures of polyolefins (PE and PP) and mixtures of polyethylenes and PS [84, 85]. Examples of compatibilization of multiple polymer blends containing PVC are not documented, although the improved properties of PVC/LDPE blends observed after the addition of a chlorinated polyethylene compatibilizer indicate one potential route [86].

Another means of improving the properties of materials derived from mixed plastic melts is by milling the waste into a powder prior to melting and extrusion. Many polymers used in construction are above their glass transition temperature under ambient conditions and are consequently sufficiently tough to resist milling processes (Table 5). For this reason, successful reduction of waste plastics to very small particle sizes is best achieved by milling at low temperatures. At laboratory scale, the injection of liquid CO_2 into the chamber of a ball mill has been demonstrated to produce PE–PP mixtures which display evidence of greater compatibility and possible copolymerization [88]. Similarly, cryogenic impact milling – in which liquid N_2 is used to reduce the temperature to below −150°C – has been shown to produce enhanced tensile strength in mixtures of post-consumer polymer waste comprising PE, PP, and PS compared to the unmilled mixture [89]. Comparable results can be achieved through the extrusion of polymer mixtures at cryogenic temperatures [90]. It should be stressed that the energy required to produce liquid CO_2 and N_2 is likely to significantly compromise the viability of such techniques in both economic and sustainability terms.

The problems associated with using mixed polymer wastes have lead to much research and development activity focusing on the separation of such wastes. One of the characteristics of the polymers which can be exploited to effect separation is density. Separation of

Construction and Demolition Wastes. Table 5 Properties of polymers in construction and demolition waste

Polymer	Density, kg/m^3	Typical glass transition temperature, °C	Charge from triboelectric effect, pC after contact with gold or brass [87]
PVC	1,400	80	−1.6
HDPE	960	25	0 (Brass)
LDPE	920	−5	0 (Brass)
PP	900	−20	0
PS	1, 050 (High impact PS)	100	0
PU	1,120	−30	+0.1
ABS	1,060	110	+0.1

high- and low-density polymers is possible using technologies such as air tables, cylinder cyclones, and flotation [91, 92]. All these techniques permit the separation density to be controlled to permit specific fractions to be isolated.

In the case of air tabling, plastics waste is passed over a vibrating porous deck through which air is passed – the velocity of the air controls the separation density. The technique has been found to be most efficient when the difference between the densities of the components to be separated exceeds around 400 kg/m^3. Table 5 shows that air tabling is most appropriate for the separation of PVC from other polymers deriving from construction and demolition wastes.

Cylinder cyclones create a cyclone of liquid with an air core within a cylinder such that material less dense than liquid floats on the cyclone surface, while denser material is forced out through exit port in the cylinder's side. The separation density in this case is controlled by adjusting the density of the liquid medium. The liquid is normally water, and its density can be increased by the addition of fine mineral particles.

The use of flotation in liquid is also an effective means of separating certain polymers from others. The use of water is the most straightforward technique, and Table 5 shows that the densities of polymers commonly encountered in construction and demolition waste fall either side of that of water. Furthermore, solutions can be tailored to a required density through the addition of salts or organic solvents.

Exploitation of density is, however, not usually sufficient to fully isolate individual polymer components in construction and demolition waste streams, since there is little difference in the densities of many polymers. A flotation technique that does not rely on differences in density is froth flotation [93]. This involves introducing mixed polymer waste in particle form into a cell containing a solution of frothing agent through which air is passed in a manner which allows froth formation. The solution also contains a collector compound which is preferentially adsorbed onto the surface of certain polymers, rendering them hydrophobic. This preferential absorption can be promoted by adjusting the solution pH to within a specific range. Air bubbles attach themselves to the surfaces of polymer particles which have been rendered hydrophobic, causing them to float to the surface of the cell. Of particular relevance to construction and demolition waste is the successful separation of ABS and high impact PS (two polymers with very similar densities) using this technique [94].

Triboelectric separation is another technique suited to separating plastics of similar density. It exploits the triboelectric effect, where particles of different materials acquire charges of differing polarity and magnitude after being brought into contact with another material, usually with friction acting between the two. Electrostatic charges acquired by polymers are given in Table 5, indicating that, again, PVC is distinct from the other materials. By allowing the particles to then fall through space containing an electric field created by establishing a high potential difference between two electrodes, the differently charged particles are directed by electrostatic deflection either toward one or other of the electrodes. Contact between polymer particles and other materials to induce charging can be achieved in a number of ways including the use of cyclones, fluidized beds, and rotating drums [95].

Most of the commonly encountered polymers in waste streams have very distinct infrared spectra. Since the 1990s, there have been significant advances in the development of infrared spectrometers capable of rapidly distinguishing between different types of plastics. This has, in turn, lead to the appearance of a wide range of plastics separation systems on the market. Such devices are able to identify the constituent polymer in individual plastic articles passing a spectrometer via a conveyor. Articles can be accepted or rejected usually through the application of an air blast. Such systems are highly effective when dealing with packaging waste in municipal waste streams. However, application to polymer mixtures deriving from construction and demolition waste, where individual articles are potentially bulky and thick, is much less viable.

Separation of polymers opens up new possibilities for recycling, although the mechanical recycling of recovered polymers is not without problems. This is principally the result of peroxidation, which results from reactions involving organic hydroperoxide compounds at ambient temperatures initiated by sunlight in external exposure conditions [83]. Peroxidation is partly responsible for deterioration of polymer properties during service. However, it presents an

additional problem during recycling, since partially peroxidated polymers are particularly prone to undergo thermal degradation when exposed to elevated temperatures.

PVC will normally contain stabilizing additives which prevent degradation during melting and extrusion. The stabilizing effect of these additives persists during mechanical recycling, and it has been demonstrated that PVC can be mechanically recycled up to five times between periods of accelerated aging to promote peroxidation [96]. Furthermore, additional stabilizers can be added prior to recycling to ensure stability. However, the situation is less straightforward where PVC from a range of sources is being recycled. Problems can arise from the presents of contaminants in recovered PVC. For instance, it has been shown that very small quantities of PE accelerate the degradation of PVC during mechanical recycling [97]. This problem can be resolved by combining recycled PVC with virgin material.

Combining sources of PVC containing different additives can cause problems. For instance, the combination of lead-based additives with sulfur-bearing additives causes discoloration [98]. Of most concern, however, is the formation of transformation products from stabilizers during the processing of PVC. These products are usually metal chlorides, which are potentially highly toxic. The issue is of greater importance where recycling is involved, since these products will accumulate with each cycle of reprocessing [83].

The problems associated with PVC tend to mean that the material is usually recycled in products where release of metals does not pose a significant risk. Recently, research has shown that PVC waste can be utilized in the manufacture of lightweight aggregate for concrete [99].

The recycling of plastics in asphalt mixtures has been demonstrated to be feasible, with some benefits in terms of modification of properties. Most research into this area has concentrated on polyethylene, which has been shown to enhance stability with respect to degradation resulting from exposure to water [100]. The inclusion of PVC in hot mix asphalt has been shown to improve flexural strength and wear resistance [101]. Incorporation of PVC in asphalt for waterproofing improves mechanical performance as well as resistance to chemical attack [102].

Recycling Metallic Waste A study of the economics of recycling materials has concluded that only the recycling of ferrous metals and copper from construction and demolition waste are currently viable economically [103]. This is partly because these two metals are easily removed from this stream.

Ferrous metals are likely to largely take the form of steel structural components such as sections and reinforcement bars and are, hence, easily identified and removed. Moreover, they are magnetic. Copper is mainly present as piping and cable, which is readily recovered from construction sites and will usually be stripped from a structure prior to demolition. It is, however, important to remember that this conclusion is potentially dependent on the techniques and technology used for separation and the market value of metals, with future increases in price potentially converting construction and demolition waste into resources for more extensive metals recovery. For instance, construction and demolition waste is one of the largest zinc-bearing waste streams in existence [104].

The benefits of recycling metals from a sustainability perspective are significant, since recycling usually requires significantly less energy than production of virgin metal from ore. This is shown in Table 6, which indicates embodied energy values associated with the production of recycled steel, copper, aluminum, lead, and zinc are considerably less than the virgin metal. While it should be stressed that embodied energy values will be dependent on local conditions such as

Construction and Demolition Wastes. Table 6
Embodied energy of virgin and recycled metals commonly encountered in construction and demolition waste [105]

Metal	Embodied energy, MJ/kg		Saving
	Virgin	Recycled	
Steel	35.3	9.5	73%
Copper	70.0	17.5 (High-grade scrap)	75%
Aluminum	218.0	28.0	87%
Lead	49.0	10.0	81%
Zinc	72.0	9.0	88%

transport distances, ore purity, and local manufacturing practice, the overall result is likely to be similar regardless of location.

Energy Recovery

The organic fraction of construction and demolition waste is combustible, and the generation of heat and power from the combustion of wood, plastics, and paper is an obvious means by which energy can be recovered [20]. However, problems associated with this approach have led to the development and growth of other means of energy recovery.

Combustion Combustion can be carried out in combined heat and power incineration plants where heat is used both to generate electricity through a steam turbine and also to heat water for local homes and industries.

The calorific value of plastic is relatively high, with higher heating values for construction plastics varying between 18.0 and 46.6 MJ/kg (Table 7) [106]. This compares favorably with many conventional oil-derived fuels such as fuel oil whose higher heating value is around 46 MJ/kg. However, it should be noted that the higher heating value of PVC, which is usually present to the largest extent in construction and demolition waste, is much lower than many other polymers. The higher heating value of timber lies between 19 and 28 MJ/kg of dry wood (Table 8), although this is compromised by the presence of water [107].

Construction and Demolition Wastes. Table 7 Higher heating values of a range of polymers [106]

Polymer	Higher heating value, MJ/kg
Polyvinyl chloride	18.0
High-density polyethylene	46.6
Low-density polyethylene	46.6
Polypropylene, isotactic, or syndiotactic	46.6
Polypropylene, isotactic	46.5
Polystyrene, isotactic	41.5
Polystyrene, atactic	41.6
Polyurethanes	23.7
Acrylonitrile butadiene styrene	40.0

Separation of the organic fraction from the noncombustible materials is the only viable option, since the specific heat capacities of many noncombustible construction and demolition waste constituents is relatively high, meaning that efficiency would be compromised considerably by using mixed waste.

In both cases, the combustion of these materials is not without detrimental consequences. The combustion process will contribute toward climate change via the emission of carbon dioxide, although it has been demonstrated that where combustion is carried out using only plastics (and taking into account avoided emissions from conventional power generation and heating, emissions from treatment of waste and emissions from conventional incineration fuel), net CO_2 emissions can be negative where efficiencies are high and electricity generation takes precedence over water heating.

Plastics used in construction can contain additives comprising trace metals with detrimental effects on the environment. For instance, PVC window frames have historically contained lead stabilizers [108], although their use is being phased out in many countries. Additionally, the combustion of plastic waste containing PVC has been partly blamed for the formation of dioxins and furans in the exhaust gases of incinerators [109]. These substances are condensed onto particulates which are collected by the pollution control equipment of incinerators and which must be disposed of with great care.

However, probably the main objection to combustion as a waste management option is simply that there are arguably more sustainable uses that plastics and timber can be put to, which do not involve their destruction.

Some of the problems of recovering energy from organic wastes are potentially avoided by thermally processing the material to produce solid, liquid, or gaseous fuels. This can be done either via biological processes, in the form of anaerobic digestion, or using pyrolysis-based techniques.

Pyrolysis Pyrolysis is the thermal decomposition of organic substances in the absence of oxygen. Temperatures between 350°C and 900°C are required to effect

Construction and Demolition Wastes. Table 8 Higher heating values of a range of timber species in an oven-dry condition [107]

Species	Higher heating value, MJ/kg	Species	Higher heating value, MJ/kg
Bigleaf maple	19.5–19.6	Red oak	21.8
Black cottonwood	20.5	Redwood	21.4
Cypress	24.8	Sitka spruce	18.8
Douglas-fir	20.5–21.4	Western hemlock	18.6–20.1
Hickory	21.8	Western red cedar	22.6
Lodgepole pine	20.0	White ash	22.4
Oregon ash	19.1	White birch	21.7
Oregon white oak	18.9	White cedar	21.1
Pitch pine	28.4	White fir	18.6–19.3
Ponderosa pine	21.2–21.3	White oak	22.1
Poplar	22.4	White pine	22.4
Red alder	18.6	Yellow pine	24.1

decomposition [110], although temperatures at the lower end of this range are more typical. The products of pyrolysis of polymers are smaller molecules (in both gas and liquid form) deriving from the decomposition of polymer chains and a quantity of char – solid carbon-rich residue. Table 9 shows the products of pyrolysis of a range of individual polymers used in construction.

The gases formed are largely mixtures of carbon dioxide (CO_2), carbon monoxide (CO), methane (CH_4), ethane (C_2H_6), ethene (C_2H_4), propane (C_3H_8), and propene (C_3H_6), which require further refinement to produce gas which can be employed as fuel. As a result, it is the liquid or solid fractions which are more typically used as fuels.

When pyrolysis is carried out for recovery of energy, it is desirable for the majority of liquid hydrocarbon products to consist of compounds in the gasoline range – molecules containing between 5 and 12 carbon atoms. A bias toward such a range can often be achieved through the use of catalysts, which also permit reductions in pyrolysis temperatures and times [110]. Additionally, where mixtures of polymers are present (which is the most likely scenario in the case of plastics deriving from construction and demolition waste), a significant amount of chemical interaction between polymers leads to the formation of lower molecular weight liquid fractions, albeit at lower yields [111].

Construction and Demolition Wastes. Table 9 Products of pyrolysis of polymers commonly used in construction [110]

Polymer	Pyrolysis products: Low temperature (<500°C)	Pyrolysis products: High temperature (>500°C)
Polyethylene	• Waxes	• Gases
	• Paraffin oil	• Light oils
	• α-olefins	
Polypropylene	• Soft paraffin	• Gases
	• Olefins	• Light oils
Polyvinyl chloride	• HCl (<300°C)	• Toluene
	• Benzene	
Polystyrene	• Styrene	• Styrene
	• Styrene oligomers	• Styrene oligomers

In the case of processed demolition waste, it is often the case that plastics and timber waste will be present together due to their similar density. Co-pyrolysis of timber and plastics is an option in this case, although it

has both advantages and disadvantages. Co-pyrolysis of timber with mixed plastics typically has a negative influence on the yield of liquid hydrocarbons relative to the products obtained from plastics alone and appears to promote a shift toward gases richer in CO_2 and CO [112, 113]. However, the presence of plastics alongside timber provides the advantage of reducing the oxygen content of the resulting compounds relative to the products of wood pyrolysis alone [113]. This is beneficial, since the presence of oxygen reduces the heating value of the liquid fraction and renders it corrosive.

Examination of chemical interactions between cellulose in wood and individual polymers indicates that there is little reaction between most polymers and wood during pyrolysis [114]. The main exception to this is PVC, whose presence reduces the temperatures at which cellulose decomposes, and promotes the formation of char, possibly as a result of acid catalysis by HCl released during pyrolysis.

The high carbon content of char means that it is possible to employ it as a solid fuel in power generation [115]. Where pyrolysis is carried with the express aim of producing char for fuel, the process is referred to as "carbonization." The successful carbonization of the combustible fraction of construction and demolition wastes has been demonstrated and the resulting char possessed a higher heating value of up to around 23 MJ/kg. When compared with wastes from other sources, this was only exceeded by materials derived from shredded bulky wastes from a source of municipal waste and wastes from the food-processing industry [116].

Another related technique to extract fuels from organic wastes is *gasification* which involves heating wastes in the presence of oxygen and steam. The process starts with pyrolysis, but the presence of oxygen causes the hydrocarbons and some of the char to undergo partial combustion to form CO and CO_2. Further CO and CO_2 are formed by the *gasification* reaction of the char, during which carbon reacts with water, also causing the formation of hydrogen gas (H_2). *Methanation* follows, during which carbon in the char reacts with hydrogen to form methane (CH_4). The carbon monoxide subsequently undergoes *water–gas shift* with water to form more hydrogen and CO_2. *Reforming* reactions involve a reaction between CH_4 and both water and CO_2 to yield further H_2 and CO. Thus, a gas is produced which is rich in H_2 and CO [117]. This synthetic gas, or "syngas," can be burnt as fuel, with higher efficiency than combustion of the raw waste, or used as a raw material in the manufacture of other petrochemical products. From a sustainability perspective, the latter option is likely to be viewed in more favorable terms. Additional products in the form of char and tar (higher molecular weight hydrocarbons) are also formed.

Co-gasification of plastics and wood (conducted in combination with coal, which assists in stabilizing the process) has been examined, with the conclusion that where utilization as fuel is the overall aim, high temperatures are required, compromising efficiency.

The formation of HCl during both pyrolysis and gasification of mixed plastic waste containing PVC is potentially a problem, since pollution control requirements will be heavier. However, a gasification process has been proposed in which separation of HCl is conducted and revenue generated from its sale for use as a raw material in other chemical manufacturing processes [118].

Anaerobic Digestion Anaerobic digestion, like composting, relies on microorganisms to break down wastes into gas, liquid, and solid products. Unlike composting, anaerobic digestion is carried out in the absence of gaseous oxygen, which is achieved by allowing digestion to occur within a sealed tank. The microorganisms involved still require oxygen, and so in this environment, this must be obtained from compounds present in the waste.

The digestion process produces gas comprising CO_2, ammonia (NH_3), hydrogen sulfide (H_2S), and a relatively large quantity of CH_4, the latter giving this product value as fuel. It is frequently the case that the gas is treated prior to use to remove H_2S, which would otherwise contribute toward acid rain. Additionally, liquid and solid digestates are produced, both of which can be employed as fertilizer.

This option is clearly only applicable to organic construction and demolition wastes, and the lack of biodegradability of construction polymers excludes them from such a technique [119]. While there has been growth in the use of biodegradable plastics in many areas, this has not been the case in construction,

where durability is an essential requirement, and usually one of the main reasons for using plastics in the first place.

Anaerobic digestion of timber alone is not an option – the process requires nutrients in the form of nitrogen and potassium, and these are present in very low concentrations. However, the option of co-digestion exists, where multiple-source wastes are blended to achieve higher yields of methane than would be obtained with single sources [120].

Two of the most common feedstocks for anaerobic digestion are municipal biosolids and manure from livestock. Both of these wastes have previously undergone digestion and, consequently, contain a relatively little carbon, yielding low methane levels. As for aerobic composting, an optimum C/N ratio of between 20 and 30 is necessary for optimum digestion, which can be achieved by co-digesting biosolids or manure with materials with higher carbon content, such as timber.

The high levels of lignin present in timber mean that a large proportion remains undigested. The potential to use this solid digestate as fertilizer may be compromised by the presence of metals, particularly those deriving from preservatives. Recently, a two-stage anaerobic digestion process starting with a stage in which the feedstock is acidified and liquefied to remove a large proportion of these metals has been proposed [121].

Environmental and Sustainability Issues

Environmental Hazards of Construction and Demolition Waste

Despite the environmental benefits of recycling construction and demolition waste, the composition of such material can potentially present hazards to both human health and the environment. Key concerns include general dust, asbestos, and the leaching of constituents into the surrounding environment.

Dust Construction and demolition activities can have the effect of raising atmospheric particulate levels which threaten public health [122], and links between airborne demolition particulates and exacerbation of conditions such as asthma have been established [123]. Additionally, levels of fungi particles in the air increase during demolition activities, potentially increasing the rate of occurrence of lung infections [124]. It can therefore be concluded that processing of construction and demolition waste can potentially have similar implications. In practice, however, it has been found that control of particulates is wholly feasible through the application of water using bowsers, sprays, and wheel washers and through the use of sweepers, hoods, extractor fans, and balanced air systems where processing is carried out indoors [125]. Demolition waste processing facilities employing air classification will often control particulate emissions downstream using pollution control devices such as cyclones [18].

Asbestos The use of asbestos in structures began on a large scale in the late nineteenth century. The material was used in construction in cements, plasters, boards, and reinforcement in plastic components, such as flooring tiles, principally for its good resistance to heat and chemical attack. Relatively soon after asbestos use started on a large scale, respiratory health problems in people working with the material began to be identified. Inhalation of fibers of asbestos leads to asbestosis as well as various forms of cancer. The brown and blue forms of asbestos are the most hazardous, although all forms are now known to be harmful to health [126].

Asbestos in construction is now prohibited in most parts of the world. However, many structures built or refurbished before the 1980s can potentially contain the material in various forms. Demolition of structures containing asbestos clearly presents a risk of releasing this substance into the environment. While atmospheric release of fibers can be controlled by spraying with water [127], the dispersal of asbestos into the wider environment is clearly not desirable. Thus, in many countries, it is a legal requirement that asbestos is removed from structures prior to demolition.

Asbestos cannot be readily isolated from other components in the mineral fraction of demolition waste. Moreover, removal of asbestos after size reduction would potentially permit quantities of fibers to be released. For this reason, the only practical means of guaranteeing the absence of asbestos is to ensure thorough removal prior to demolition, and this, in turn, requires a comprehensive survey of the fabric of the structure to identify occurrences of this material.

Leaching Most research carried out into the leaching of chemical constituents from construction and demolition waste has concentrated on leaching occurring in landfill facilities. However, much of the general findings of this work can be applied to situations in which the material is employed in an application, with the qualification that the chemical conditions within landfill may differ considerably from those elsewhere.

While the majority of inorganic ions typically found to leach from construction and demolition waste are not toxic, their concentrations in leachate can be of such a magnitude as to exceed regulatory drinking water limits [128]. Cations released in large quantities can include calcium, potassium, sodium, magnesium, manganese, and iron, while anions are mainly sulfate, chloride, carbonate, and hydroxide [128–130].

The types of trace metal found to leach from construction and demolition waste are very much dependent on the types of material present. Trace metals found to leach from construction and demolition waste have included arsenic, barium, cadmium, chromium, copper, lead, nickel, and zinc [128–130]. Of these, arsenic, chromium, and lead are of greatest concern due to their toxicity [131].

Much of the arsenic and chromium derives from waste timber which has been treated with CCA wood preservative [128]. Of these two elements, the greatest hazard is usually considered to be presented by arsenic on the grounds that it is more toxic. Moreover, chromium in treated timber will typically be in the trivalent (Cr(III)) form, which is significantly less toxic than the hexavalent (Cr(VI)) form [132, 133]. However, leaching of chromium in high pH environments could potentially oxidize chromium to its hexavalent state [134].

The source of manganese has been speculated as also being from timber [135], while one possible source of lead is lead-based paint [136].

The leaching of organic compounds has been examined in research aimed at establishing potential risks presented by fines from processed construction and demolition waste [137]. The conclusion drawn from this work is that, while organic compounds are detected in leachate from such wastes (deriving from sources such as asphalt, paints, varnishes, and fuel), they are normally found well below regulatory limits.

Wastewater Where wet processes are used during the processing of construction and demolition waste, appropriate measures need to be taken to ensure that waste water is disposed of correctly and in a form which is compatible with local environmental requirements. Most commonly, the use of settlement tanks and filters is employed to ensure particulate levels in waste water are reduced to acceptable levels.

Evaluating Impact

Sustainable management of construction and demolition wastes using the waste hierarchy as a general guide is largely a sound approach. However, it should be stressed that there are likely to be exceptions to this. A good example of such a grey area is the production of RA and RCA.

The processing of demolition waste to produce RCA and RA involves operations not dissimilar to the production of virgin crushed rock aggregate. For this reason, the embodied energy of the material is likely to be only slightly less than that of virgin aggregate, with any energy advantage coming from the potential reduction in transportation distances (particularly if the aggregate can be used on the site on which it is being processed). Since emission rates of pollution from such processing are likely to closely correlate with embodied energy, these will also be close to that of virgin aggregate.

Where the sustainability of a waste management option is in question, it is clearly of great value to conduct an analysis of the environmental impact of using construction and demolition waste in a particular application against an equivalent product derived from virgin material. A useful tool in carrying out such an analysis is environmental life-cycle assessment (LCA), which is a systematic methodology for compiling an inventory of the inputs (resources and energy) and outputs (pollution and waste) associated with the unit processes that make up the entire life cycle of a material and then assigning quantitative measures of environmental impact to each of these [138].

This type of analysis can also be extremely useful in making larger-scale decisions about waste management strategies for construction and demolition waste. A study carried out in Sweden examined two scenarios – one in which the maximum level of recycling of construction and demolition waste was achieved, and one

in which the maximum level of reuse was achieved [139]. Recycling in this case included combustion of certain materials with the recovery of energy. The benefits of the two different approaches were measured in terms of the amount of mineral resources and energy saved. The main energy savings from both scenarios were in the recycling or reuse of metals and masonry, and the combustion or reuse of timber. The most significant conservation of mineral resource in both cases was gravel. The study also examined projected future scenarios, potentially providing useful information to those making planning decisions.

It should be stressed that levels of resource use and environmental impact will not be the only factors which decide the extent to which an option for utilizing construction and demolition waste is sustainable. As well as the need for a utilization option to have reduced embodied energy and associated pollution emissions when compared to a conventional product, the processing requirements must have a lower cost and the material must have at least an equal market value [140]. Moreover, consideration of the renewability of the primary resource from which a material is derived should also be given consideration. For instance, taking into account renewability, the finite nature of metal ores in the Earth means that there is potentially a stronger argument for recycling metals than for recycling timber deriving from well-managed sources.

Future Directions

The drivers for growth in the recycling and reuse of construction and demolition waste include scarcity of landfill space, legislation, and taxation. It is likely that these incentives toward more sustainable approaches to managing this material will increase in the future, with additional pressures potentially coming from increasing energy prices and resource scarcity – particularly for metals and polymers.

Another future development is likely to be the placing of greater emphasis on "producer responsibility" in the field of construction and demolition waste. The philosophy behind producer responsibility is essentially an extension of the "polluter pays" principle – the responsibility for managing waste is placed with the sector which produces it. In Europe, one way in which this is achieved is by requiring waste producers in certain sectors to satisfy quotas for the collection and processing of waste for recycling or reuse. This is, in fact, frequently carried out by other parties who are then able to sell credits to the industry in question which contribute toward satisfying the quota. However, this is by no means the only way in which producer responsibility can be implemented. For instance, by placing taxation on a product which reflects the cost of disposal, an incentive for waste reduction is created for the producer.

These increasing demands for sustainable management of construction and demolition waste are likely to have two major influences on the future direction of development in this area – a drive toward more appropriate use of waste materials and increased emphasis on deconstruction over demolition.

Currently, much of the material deriving from the processing of demolition waste is being employed at its lowest engineering value – as a general fill material where the main property being utilized is simply the material's volume. Application of sustainable philosophies and the increasing economic burdens placed on those responsible for utilizing construction and demolition waste are both likely to drive management strategies to higher levels of the waste hierarchy. This would mean materials being elevated to their most appropriate point on the waste hierarchy where their performance as a recycled or reused item is comparable to that of a conventional product at comparable or lesser cost.

The key to obtaining the largest amount of value from a waste material, in both engineering and economic terms, lies in efficient separation. For this reason, it is highly likely that future developments will include shifts toward both deconstruction and design of structures with deconstruction in mind. It is also likely to mean a growth in infrastructure for the collection and processing of individual construction and demolition waste components and further development of technologies for separation.

Bibliography

1. Marxsen CS (2001) Potential world garbage and waste carbon sequestration. Environ Sci Policy 4:293–300
2. Tam VWY (2009) Comparing the implementation of concrete recycling in the Australian and Japanese construction industries. J Clean Prod 17:688–702

3. Eurostat statistics database (2010) http://epp.eurostat.ec.europa.eu/portal/page/portal/eurostat/home. Accessed Jan 2010
4. John VM, Angulo SC, Miranda LFR, Agopyan V, Vasconcellos F (2004) Strategies for innovation in construction demolition waste management in Brazil. CIB World Building Congress, Toronto
5. Statistics Canada (2004) Waste management industry survey: business and government sectors 2002. Statistics Canada, Ottawa
6. National Bureau of Statistics of the People's Republic of China (2006) http://www.allcountries.org/china_statistics/24_5_daily_average_solid_waste_generation.html. Accessed Jan 2010
7. Pappu A, Saxena M, Asolekar SR (2007) Solid wastes generation in India and their recycling potential in building materials. Build Environ 42:2311–2320
8. World Health Organization (2005) Malaysia – environmental health country profile. World Health Organization, Geneva
9. Begum RA, Siwar C, Pereira JJ, Jaafar AH (2006) A benefit-cost analysis on the economic feasibility of construction waste minimisation: the case of Malaysia. Resour Conserv Recy 48:86–98
10. Ministry for the Environment (New Zealand) (1997) National waste data report. Ministry for the Environment, Wellington, New Zealand
11. Hsiao TY, Huang YT, Yu YH, Wernick IK (2002) Modelling materials flow of waste concrete from construction and demolition wastes in Taiwan. Resour Policy 28:39–47
12. Kofoworola OF, Gheewala SH (2009) Estimation of construction waste generation and management in Thailand. Waste Manage 29:731–738
13. US Environmental Protection Agency/Franklin Associates (1998) Characterization of building-related construction and demolition debris in the United States, US Environmental Protection Agency, Washington
14. World Bank (2002) Vietnam environment monitor 2002. World Bank, Washington, DC
15. Lauritzen EK, Hahn NJ (1992) Building waste: generation and recycling. International Solid Waste Association, Vienna
16. Lowton RM (1997) Construction and the natural environment. Butterworth-Heinemann, Oxford
17. Addis W, Schouten J (2004) Principles of design for deconstruction to facilitate reuse and recycling. CIRIA, London
18. Brunner PH, Stämpfli D (1993) Material balance of a construction waste sorting plant. Waste Manage Res 11:27–48
19. Schachermayer E, Lahner T, Brunner PH (2000) Assessment of two different separation techniques for building wastes. Waste Manage Res 18:16–24
20. Chang N-B, Lin KS, Sun Y-P, Wang HP (2001) Oxidation kinetics of the combustible fraction of construction and demolition wastes. J Environ Qual 30:1392–1401
21. Quillen MB, Reed R (2004) Mixed C&D recycling on-line in San Francisco. Biocycle 45:22–25
22. Howard N (2000) Sustainable construction – the data. Building Research Establishment, Watford
23. Sandler K (2003) Analyzing what's recyclable in C&D debris. Biocycle 44:51–54
24. Cochran K, Townsend T, Reinhart D, Heck H (2007) Estimation of regional building-related C&D debris generation and composition: case study for Florida. Waste Manage 27:921–931
25. DSM Environmental Services Incorporated (2008) 2007 Massachusetts construction and demolition debris industry study - final report, DSM Environmental Services Incorporated, Windsor, Vermont
26. Wilson DG (1990) Recycling of demolition wastes. In: Moavenzadeh F (ed) Concise encyclopedia of building and construction materials. Pergamon, Oxford, pp 517–518
27. Bianchini G, Marrocchino E, Tassinari R, Vaccaro C (2005) Recycling of construction and demolition waste materials: a chemical-mineralogical appraisal. Waste Manage 25:149–159
28. Dhir RK, Halliday JE, Dyer TD, Dick RS (2005) A feasibility study: opportunities for creating medium-value construction projects via demolition waste reconstitution, Technical Report CTU/3705, Department of Trade and Industry, London
29. Kristinsson J, Hendriks CF, Kowalczyk T, Dorsthorst BJH (2001) Reuse of secondary elements: utopia or reality CIB World Building Congress, Wellington, New Zealand, Paper 230
30. Rønning A, Vold M, Nereng G (2009) Refurbishment or replacement of buildings – what is best for the climate? Joint Actions on Climate Change, Aalborg
31. Waste and Resources Action Programme (2010) Aggregain website http://aggregain.wrap.org.uk/. Accessed Dec 2009
32. Rudy S (1978) New metal recycling system. JOM-J Min Met Mat S 30:21–23
33. Rothery K, Mellor S (2007) Crushing and screening. Institute of Quarrying, Nottingham
34. Xing W, Hendriks C (2006) Decontamination of granular wastes by mining separation techniques. J Clean Prod 14:748–753
35. Zega CJ, Villagrán-Zaccardi YA, Di Maio AA (2010) Effect of natural coarse aggregate type on the physical and mechanical properties of recycled coarse aggregates. Mater Struct 43: 195–202
36. Poon CS, Shui ZH, Lam L, Fok H, Kou SC (2004) Influence of moisture states of natural and recycled aggregates on the slump and compressive strength of concrete. Cement Concrete Res 34:31–36
37. Dhir RK, Limbachiya MC, Leelawat T (1999) Suitability of recycled concrete aggregate for use in BS 5328 designated mixes. P I Civil Eng-Str B 134:257–274
38. Domingo-Cabo A, Lázaro C, López-Gayarre F, Serrano-López MA, Serna P, Casaño-Tabares JO (2009) Creep and shrinkage of recycled aggregate concrete. Constr Build Mater 23:2545–2553
39. Sagoe-Crentsil KK, Brown TT, Taylor AH (2001) Performance of concrete made with commercially produced coarse recycled concrete aggregate. Cement Concrete Res 31:707–712
40. Fathifazl G, Razaqpur AG, Isgor OB, Abbas A, Fournier B, Foo S (2009) Flexural performance of steel-reinforced recycled concrete beams. ACI Struct J 106:858–867

41. Etxeberria M, Marí AR, Vázquez E (2007) Recycled aggregate concrete as structural material. Mater Struct 40:529–541
42. Alwitt, RS (1976) The aluminium-water system. In: Diggle JW, Vijh AK (eds) Oxides and oxide films, Marcel Dekker, New York, 1976, pp169–254
43. Dhir RK, Dyer TD, Tang MC (2009) Alkali-silica reaction in concrete containing glass. Mater Struct 42:1451–1462
44. McCarthy MJ, Halliday JE, Csetenyi LJ, Dhir RK (2009) Alkali-silica reaction guidance for recycled aggregates in concrete, Report CTU/4909 Waste and Resources Action Programme, Banbury
45. Wild S (1996) Observations on the use of ground waste clay brick as a cement replacement material. Build Res Inf 24:35–40
46. Dyer TD, Dhir RK (2001) Chemical reactions of glass cullet used as cement component. J Mater Civil Eng 13:412–417
47. Paranavithana S, Mohajerani A (2006) Effects of recycled concrete aggregates on properties of asphalt concrete. Resour Conserv Recy 48:1–12
48. Mills-Beale J, You Z (2010) The mechanical properties of asphalt mixtures with recycled aggregates. Constr Build Mater 24:230–235
49. Aljassar AH, Al-Fadala KB, Ali MA (2005) Recycling building demolition waste in hot-mix asphalt concrete: a case study in Kuwait. J Mater Cycles Waste 7:112–115
50. Doh YS, Amirkhanian SN, Kim KW (2008) Analysis of unbalanced binder oxidation level in recycled asphalt mixture using GPC. Constr Build Mater 22:1253–1260
51. Romera R, Santamaría A, Peña JJ, Muñoz ME, Barral M, García E, Jañez V (2006) Rheological aspects of the rejuvenation of aged bitumen. Rheol Acta 45:474–478
52. Shu X, Huang B, Vukosavljevic D (2008) Laboratory evaluation of fatigue characteristics of recycled asphalt mixture. Constr Build Mater 22:1323–1330
53. Robinson GR, Menzie WD, Hyun H (2004) Recycling of construction debris as aggregate in the Mid-Atlantic region, USA. Resour Conserv Recy 42:275–294
54. Highways Agency (2006) Manual of contract documents for highway works – Volume 1 specification for highway works, Series 900 – Road pavements – Bituminous bound materials. Highways Agency, London
55. Jullien A, Monéron P, Quaranta G, Gaillard D (2006) Air emissions from pavement layers composed of varying rates of reclaimed asphalt. Resour Conserv Recy 47:356–374
56. Heikkilä PR, Monéron P, Hämmeilä M, Linnainmaa K (2003) Mutagenicity of bitumen and asphalt fumes. Toxicol in Vitro 17:403–412
57. Woodside AR, Woodward WDH, Phillips P (2000) Sustainable reuse of highway materials in hot and cold bituminous mixtures. P I Civil Eng-Munic 139:181–186
58. Jenkins KJ, Molenaar AAA, de Groot JLA, van de Ven MFC (2000) Developments in the uses of foamed bitumen in road pavements. HERON 45:167–176
59. Sandrolini F, Franzoni E (2001) Waste wash water recycling in ready-mixed concrete plants. Cement Concrete Res 31: 485–489
60. Rixom R, Mailvaganam N (1999) Chemical admixtures for concrete, 3rd edn. Spon, London
61. Townsend TG, Jang Y-C, Weber X (2000) Continued research into the characteristics of leachate from construction and demolition waste landfills. Florida Centre for Solid and Hazardous Waste Management, Gainesville
62. Hewitt EJ, Smith TA (1975) Plant mineral nutrition. The English Universities Press, London
63. Shainberg I, Sumner ME, Miller WP, Farina MPW, Pavan MA, Fey MV (1989) Use of gypsum on soils: a review. Adv Soil S 9:1–111
64. Reeve NG, Sumner ME (1972) Amelioration of subsoil acidity in Natal oxisols by leaching of surface-applied amendments. Agrochemophysica 4:1–6
65. Miller WP (1987) Infiltration and soil loss of three gypsum-amended ultisols under simulated rainfall. Soil Sci Soc Am J 51:1314–1320
66. Waste and Resources Action Programme (2007) Recycled gypsum as a soil treatment in potato production. Waste and Resources Action Programme, Banbury, UK
67. Jang Y, Townsend TG (2001) Sulfate leaching from recovered construction and demolition debris fines. Adv Environ Res 5:203–217
68. Musson SE, Xu Q, Townsend TG (2008) Measuring the gypsum content of C&D debris fines. Waste Manage 28:2091–2096
69. Waste and Resources Action Programme (2006) International practice in plasterboard recycling: Denmark – Gypsum Recycling International A/S', Waste and Resources Action Programme, Banbury, UK
70. Anon. (2003) Stop landfilling drywall. Pollut Eng 35: 24–29
71. Cochran K (2003) Florida phenomenon. Waste Age 34:24–25
72. United Nations Industrial Development Organization (1993) Output of a seminar on energy conservation in glass industry. United Nations Industrial Development Organization, Vienna
73. Tandy BC, Way AGJ (2004) R&D to improve site practices for collection and clean separation of composite (glass) materials in the construction and demolition industry. Waste and Resources Action Programme, Banbury, UK
74. Huang Y, Bird RN, Heidrich O (2007) A review of the use of recycled solid waste materials in asphalt pavements. Resour Conserv Recy 52:58–73
75. Jin W, Meyer C, Baxter S (2000) "Glascrete" – concrete with glass aggregate. ACI Struct J 97:208–213
76. Dinwoodie JM (2000) Timber: its nature and behaviour. Spon, London
77. Buckinghamshire Chilterns University College Forest Products Research Centre (2007) Assessment of the mechanical and physical properties of recycled wood products: field tests – final report. Waste and Resources Action Programme, Banbury, UK
78. Kiely G (1996) Environmental engineering. McGraw-Hill, Boston
79. McMahon V, Garg A, Aldred D, Hobbs G, Smith R, Tothill IE (2008) Composting and bioremediation process evaluation of

wood waste materials generated from the construction and demolition industry. Chemosphere 71:1617–1628
80. Beauchemin S, N'dayegamiye A, Laverdiere MR (1992) Phytotoxicity of fresh and composted wood wastes applied as organic amendments in soil. Can J Soil Sci 72:177–181
81. McMahon V, Garg A, Aldred D, Hobbs G, Smith R, Tothill IE (2009) Evaluation of the potential of applying composting/bioremediation techniques to wastes generated within the construction industry. Waste Manage 29:186–196
82. Schut JH (2003) Entrepreneur puts mixed-polymer recycling on track to success. Plast Technol 49:128
83. Scott G (1999) Polymers and the environment. Royal Society of Chemistry, Cambridge
84. Tall S, Albertsson A-C, Karlsson S (1998) Recycling of mixed plastic fractions: mechanical properties of multicomponent extruded polyolefin blends using response surface methodology. J Appl Polym Sci 70:2381–2390
85. Fortelný I, Michálková D, Kruliš Z (2004) An efficient method of material recycling of municipal plastic waste. Polym Degrad Stabil 85:975–979
86. Kabdi S-A, Belhaneche-Bensemra N (2008) Compatibilization of regenerated low density polyethylene/poly(vinyl chloride) blends. J Appl Polym Sci 110:1750–1755
87. Diaz AF, Felix-Navarro RM (2004) A semi-quantitative triboelectric series for polymeric materials: the influence of chemical structure and properties. J Electrostat 62:277–290
88. Cavalieri F, Padella F (2002) Development of composite materials by mechanochemical treatment of post-consumer plastic waste. Waste Manage 22:913–916
89. Jonna S, Lyons J (2005) Processing and properties of cryogenically milled post-consumer mixed plastic waste. Polym Test 24:428–434
90. Nesarikar AR, Carr SH, Khait K, Mirabella FM (1997) Self-compatibilization of polymer blends via novel solid-state shear extrusion pulverization. J Appl Polym Sci 63:1179–1187
91. Dodbiba G, Sadaki J, Okaya K, Shibayama A, Fujita T (2005) The use of air tabling and triboelectric separation for separating a mixture of three plastics. Miner Eng 18: 1350–1360
92. Gent MR, Menendez M, Toraño J, Isidro D, Torno S (2009) Cylinder cyclone (LARCODEMS) density media separation of plastic wastes. Waste Manage 29:1819–1827
93. Burat F, Guney A, Kangal MO (2009) Selective separation of virgin and post-consumer polymers (PET and PVC) by flotation method. Waste Manage 29:1807–1813
94. Pascoe RD (2005) The use of selective depressants for the separation of ABS and HIPS by froth flotation. Miner Eng 18:233–237
95. Park C-H, Jeon H-S, Yu H-S, Han O-H, Park J-K (2008) Application of electrostatic separation to the recycling of plastic wastes: separation of PVC, PET, and ABS. Environ Sci Technol 42:249–255
96. Yarahmadi N, Jakubowicz I, Gevert T (2001) Effects of repeated extrusion on the properties and durability of rigid PVC scrap. Polym Degrad Stabil 73:93–99
97. Arnold JC, Maund B (1999) The properties of recycled PVC bottle compounds. 2: reprocessing stability. Polym Eng Sci 39:1242–1250
98. Braun D (2002) Recycling of PVC. Prog Polym Sci 27:2171–2195
99. Kou SC, Lee G, Poon CS, Lai WL (2009) Properties of lightweight aggregate concrete prepared with PVC granules derived from scraped PVC pipes. Waste Manage 29:621–628
100. Zoorob SE, Suparma LB (2000) Laboratory design and investigation of the properties of continuously graded asphaltic concrete containing recycled plastics aggregate replacement (Plastiphalt). Cement Concrete Comp 22:233–242
101. Ergun M, Iyinam S, Iyinam AF (2005) Flexural behaviour of waste plastic added asphalt concrete mixture. In: Proceedings of the international symposium on pavement recycling, Sao Paulo, Brazil
102. Fang C, Zhou S, Zhang M, Zhao S (2009) Modification of waterproofing asphalt by PVC packaging waste. J Vinyl Addit Techn 15:229–233
103. Johnson J, Harper EM, Lifset R, Graedel TE (2007) Dining at the periodic table: metals concentrations as they relate to recycling. Environ Sci Technol 41:1759–1765
104. Spartari S, Bertram M, Fuse K, Graedel TE, Shelov E (2003) The contemporary European zinc cycle: 1-year stocks and flows. Resour Conserv Recy 39:137–160
105. Hammond G, Jones C (2008) Inventory of carbon and energy (ICE). University of Bath, Bath
106. Throne JL, Griskey RG (1972) Heating values and thermochemical properties of plastics. Mod Plast 49:96–100
107. Ince PJ (1979) How to estimate recoverable heat energy in wood or bark fuels. Forest Products Laboratory Report FPL 29, US Department of Agriculture Forest Service, Madison, Wisconsin
108. Delgado C, Barruetabeña L, Salas O (2007) Assessment of the environmental advantages and drawbacks of existing and emerging polymers recovery processes. European Commission Joint Research Centre, Institute for Prospective Technological Studies, Seville
109. Wikstrom E, Lofvenius G, Rappe C, Marklund S (1996) Influence of level and form of chlorine on the formation of chlorinated dioxins, dibenzofurans, and benzenes during combustion of an artificial fuel in a laboratory reactor. Environ Sci Technol 30:1637–1644
110. Panda AK, Singh RK, Mishra DK (2010) Thermolysis of waste plastics to liquid fuel. A suitable method for plastic waste management and manufacture of value added products – a world perspective. Renew Sust Energ Rev 14:233–248
111. Williams PT, Williams EA (1999) Interaction of plastics in mixed-plastics pyrolysis. Energ Fuel 13:188–196
112. Paradela F, Pinto F, Gulyurtlu I, Cabrita I, Lapa N (2009) Study of the co-pyrolysis of biomass and plastic wastes. Clean Technol Envir 11:115–122
113. Bhattacharya P, Steele PH, Hassan EBM, Mitchell B, Ingram L, Pittman CU (2009) Wood/plastic copyrolysis in an auger reactor: chemical and physical analysis of the products. Fuel 88:1251–1260

114. Matsuzawa Y, Ayabe M, Nishino J (2001) Acceleration of cellulose co-pyrolysis with polymer. Polym Degrad Stabil 71:435–444
115. Ryu C, Sharifi VN, Swithenbank J (2007) Thermal waste treatment for sustainable energy. P I Civil Eng–Eng Sustain 160:133–140
116. Hwang IH, Matsuto T, Tanaka N, Sasaki Y, Tanaami K (2007) Characterization of char derived from various types of solid wastes from the standpoint of fuel recovery and pretreatment before landfilling. Waste Manage 27:1155–1166
117. Pinto F, Franco C, André RN, Tavares C, Dias M, Gulyurtlu I, Cabrita I (2003) Effect of experimental conditions on co-gasification of coal biomass and plastics wastes with air/steam mixtures in a fluidized bed system. Fuel 82:1967–1976
118. Slapak MJP, van Kasteren JMN, Drinkenburg AAH (2000) Design of a process for steam gasification of PVC waste. Resour Conserv Recy 30:81–93
119. Jayasekara R, Harding I, Bowater I, Lonergan G (2005) Biodegradability of a selected range of polymers and polymer blends and standard methods for assessment of biodegradation. J Polym Environ 13:231–251
120. Totzke D (2009) Tapping the potential of codigestion. Biocycle 50:32–35
121. Selling R, Håkansson T, Björnsson L (2008) Two-stage anaerobic digestion enables heavy metal removal. Water Sci Technol 57:553–558
122. Haynes R, Savage A (2007) Assessment of the health impacts of particulates from the redevelopment of Kings Cross. Environ Monit Assess 130:47–56
123. Dorevitch S, Demirtas H, Perksy VW, Erdal S, Conroy L, Schoonover T, Scheff PA (2006) Demolition of high-rise public housing increases particulate matter air pollution in communities of high-risk asthmatics. J Air Waste Manage 56:1022–1032
124. Bouza E, Peláez T, Pérez-Molina J, Marín M, Alcalá L, Padilla B, Muñoz P (2002) Aspergillus study team, Demolition of a hospital building by controlled explosion: the impact on filamentous fungal load in internal and external air. J Hosp Infect 52:234–242
125. Quillen MB, Reed R (2004) Mixed C&D recycling on-line in San Francisco. Biocycle 45:22–25
126. Construction Industry Publications (2009) Construction health and safety manual – section 24 – asbestos. Construction Industry, Bedford
127. Perkins RA, Hargesheimer J, Fourie W (2007) Asbestos release from whole-building demolition of buildings with asbestos-containing material. J Occup Environ Hyg 4:889–894
128. Townsend TG, Jang Y, Thurn LG (1999) Simulation of construction and demolition waste leachate. J Environ Eng 125:1071–1081
129. Weber WJ, Jang Y-C, Townsend TG, Laux S (2002) Leachate from land disposed residential construction waste. J Environ Eng 128:237–245
130. US Environmental Protection Agency/ICF Incorporated (1995) Construction and demolition waste landfills, US Environmental Protection Agency, Washington, USA
131. Agency for Toxic Substances and Disease Registry (2007) 2007 CERCLA priority list of hazardous substances that will be the subject of toxicological profiles and support document. Agency for Toxic Substances and Disease Registry, Atlanta
132. Song J, Dubey B, Jang Y-C, Townsend T, Solo-Gabriele H (2006) Implication of chromium speciation on disposal of discarded CCA-treated wood. J Hazard Mat B128:280–288
133. Katz S, Salem H (1993) The toxicology of chromium with respect to its chemical speciation: a review. J App Toxicol 13:217–224
134. Cooper PA (1991) Leaching of CCA from treated wood: pH effects. Forest Prod J 41:30–32
135. Ferguson DW, Male JW (1980) The water pollution potential from demolition waste disposal. J Environ Sci Heal A 15: 549–559
136. Wadanambi L, Dubey B, Townsend T (2008) The leaching of lead from lead-based paint in landfill environments. J Hazard Mat 157:194–200
137. Jang Y-C, Townsend TG (2001) Occurrence of organic pollutants in recovered soil fines from construction and demolition waste. Waste Manage 21:703–715
138. International Organization for Standardization (2006) ISO 14040:2006 - Environmental management – life-cycle assessment – Principles and framework. International Organization for Standardization, Geneva
139. Thormark C (2001) Conservation of energy and natural resources by recycling building waste. Resour Conserv Recy 33:113–130
140. Winter MG (2002) A conceptual framework for the recycling of aggregates and other wastes. P I Civil Eng-Munic 151:177–187

Construction Planning, Environmental Impact of Foundation Studies and Earthquake Issues

Asadullah Kazi[1], Bashir Memon[2]
[1]Isra University, Hyderabad, Pakistan
[2]P.E. LaMoreaux & Associates, Tuscaloosa, AL, USA

Article Outline

Glossary
Definition of the Subject
Introduction
Ground Motion Considerations
Ground Condition Considerations

Ground and Structure Interaction
Mitigation and Construction Planning
Future Directions
Bibliography

Glossary

After shocks Smaller earthquakes following the largest one (the main shock).

Amplification Increase in the amplitude of earthquake wave depending on the nature of ground.

Amplitude The maximum height of a wave crest or depth of a trough.

Attenuation Decrease in the amplitude of earthquake waves.

Earthquake The vibration of the Earth caused by the passage of seismic waves.

Epicenter The point on ground surface directly above the focus (hypocenter) of an earthquake.

Focus The place at which an earthquake is initiated.

Frequency Number of vibrations per unit time.

Fundamental period It is the period of an oscillating structure when subjected to shaking.

Ground motion Movements of ground caused by the vibrations of earthquake.

Intensity A measure of ground shaking obtained from damage to man-made structures (Modified Mercalli Scale).

Isoseismal map Contour lines drawn to separate one level of seismic intensity from another for a given earthquake or maximum intensity expected of earthquakes in a given area.

Magnitude A measure of energy released by an earthquake (Richter Scale).

Main shock The main earthquake event, which may be followed by aftershocks.

Mitigation To lessen or alleviate the damage likely to be caused by an earthquake.

Period The time interval between successive crests or troughs of an earthquake wave.

Resonance Increase in the amplitude of an earthquake caused by an overlap between the frequency of ground and that of the structure resting on it.

Retrofit To bring back to stable condition after having been damaged by an earthquake.

Return period Recurring period of an earthquake of a given magnitude or intensity.

Seismic wave An elastic wave generated by natural or man-made causes.

Seismic zoning A map based on the distribution of earthquakes, classified according to expected intensity translated into acceleration as the percentage of gravity.

Seismicity The occurrence of earthquakes in space and time.

Seismology The study of earthquakes.

Tectonic plates Major regions of the Earth separated by geological faults along which these regions (plates) move relative to each other.

Definition of the Subject

Earthquakes are simply the shaking of the ground initiated by natural or man-made causes. The waves generated by earthquakes are called seismic waves, and they are broadly classified into body waves and surface waves. A point from which the earthquake waves first emanate is called the earthquake focus. Moreover, the point directly above the focus is called the epicenter of an earthquake. Natural earthquakes can be caused by tectonic, volcanic (related to movement of tectonic plates), or collapse-related behavior of rock/soil. Man-made shaking, on the other hand, can be initiated by a variety of activities such as blasting, underground nuclear explosions, movement of heavy vehicles, and so forth.

Natural earthquakes are known to have occurred throughout history [1, 2]. They have left their traces as manifestations of geological processes at work on the geological time scale. These traces are generally evident in places where people lived, and no such records are available for places which were uninhabited. Most of these earthquakes are located along tectonic plate boundaries, while some are located in the intraplate regions of the world [3], as reflected in global hazards maps published by the United States Geological Survey.

Many lessons were learned from the damage caused by the Great California earthquake of 1857 and subsequent earthquakes associated with movements along the San Andeas fault [4]. The great Alaskan earthquake of 1964 [5] and a history of earthquakes in Lima, Peru, and elsewhere have helped in developing guidelines for the design of earthquake-resistant small and higher rise buildings, under different ground conditions [6].

The Engineering Research Institute in California has recently prepared a report dealing with contributions of earthquake engineering to protecting communities and critical infrastructure from multi-hazards. Both, the 2009 International Building Code in general and the Seismic Design Maps and Tools for engineering in particular give guidance to these questions.

Introduction

Earthquakes are one of the most destructive environmental hazards. The power of an earthquake is expressed according to its intensity or magnitude. The effect of both the parameters generally decreases as the distance of the affected place increases from the epicenter of the earthquake.

The Modified Mercalli Intensity Scale [7], as shown in Table 1, ranges from the lowest of 1 (not felt except by a few) to a maximum of 12 (total damage, where objects are thrown into the air). The intensity is a noninstrumental quantity assigned according to observed geological effects, damage to structures, and the perception of shaking by people and animals at a given place. It is not a fixed quantity, but varies from place to place. The magnitude of an earthquake, on the other hand, as shown in Table 2, is a fixed instrumental quantity. It is a measure of the energy released by an earthquake [8]. For example, the magnitude of six is approximately equal to the energy released by the atomic bomb used at Hiroshima during the Second World War.

Ground Motion Considerations

The outcome of earthquakes on buildings depends generally more on the severity of ground shaking than on any other single factor. Two earthquakes of the same magnitude, but located in two different areas, may produce quite different effects on buildings. The depth of an earthquake from its focus is an important factor in this regard. Generally, the shallower the earthquake, the more severe the effect. The energy of deeper earthquakes is dissipated over a larger volume of rock, while that of the shallower earthquake is spread over a smaller volume of rock.

Engineers use strong-motion seismographs to record how the ground shakes during an earthquake. The most important parameters of ground motion (free-field motion) obtained from these instruments are the peak velocity, the peak acceleration, the frequency or period of waves, and the duration of strong motion. The peak velocity determines how fast the ground is shaking, whereas the peak acceleration indicates how quickly the velocity is changing, and the latter is more often used in the engineering design of structures. It may be borne in mind that the force generated by an earthquake is a product of the mass of a structure and the ground acceleration.

Ground Condition Considerations

Earthquake shaking is attenuated or reduced with distance from the epicenter. Nevertheless, for a fixed distance, the type of geological material has also a strong influence on the nature and magnitude of ground motion. It may be emphasized that the high-frequency (short-period) earthquake waves, transmitted by strong rocks, attenuate more rapidly with distance than the low-frequency (long-period) waves transmitted by soils (Fig. 1). Furthermore, earthquake waves change their characteristics as they encounter a material different from the one through which they were initially propagating. For instance, the high-frequency waves, while passing through rocks, are slowed down as they enter the overlying soil cover, but their period is increased instead. A clear distinction must, however, be made between attenuation described above and amplification. Although the ground motion of soils is attenuated more than that of rocks, the reverse is true as far as amplification of ground motions in soil. For the same epicenter distance, the thicker the soil cover, the greater the amplification factor, and the longer the duration of ground shaking. Topographic variations can also cause amplification of seismic waves. Summits of isolated hills and edges of plateaus and cliffs are sites of large amplification within a fairly wide frequency range.

Ground and Structure Interaction

Fundamental periods or frequencies of buildings vary according to the height and nature of buildings. When such structures are subjected to free-field ground motions, they respond differently to different frequencies or periods of ground motion. For the same amplitude of ground motion, it is the resonance of

Construction Planning, Environmental Impact of Foundation Studies and Earthquake Issues. Table 1 Abridged modified Mercalli Intensity Scale [1] (1956 version)

	Description
I.	Not felt except by very few under-favorable circumstances (I Rossi–Forel scale)
II.	Felt only by a few people at rest, especially on upper floors of buildings
	Delicately suspended objects may swing (I–II on Rossi–Forel scale)
III.	Felt quite noticeably indoors, especially on upper floors of buildings, but many people do not recognize it as an earthquake. Standing automobiles may rock. Vibration like passing of truck (3 on Rossi–Forel scale)
IV.	During the day felt indoors by many, outdoors by few. At night, some awakened. Dishes, windows, doors disturbed; walls make creaking sound. Sensation like heavy truck striking building. Standing automobiles rocked noticeably (IV–V or Rossi–Forel scale)
V.	Felt by nearly everyone, many awakened. Some dishes, windows, and so on broken; cracked plaster in a few places; unstable objects overturned. Disturbance of trees, poles, and other tall objects sometimes noticed. Pendulum clocks may stop (V–VI Rossi–Forel scale)
VI.	Felt by all, many frightened and run outdoors. Some heavy furniture moved; a few instances of falling plaster and damaged chimneys. Damage slight (VI–VII Rossi–Forel scale)
VII.	Everybody runs outdoors. Damage negligible in buildings of good design and construction; slight to moderate in well-built ordinary structures; considerable in poorly built or badly designed structures; some chimneys broken. Noticed by people driving cars (VIII Rossi–Forel scale)
VIII.	Damage slight in specially designed structures; considerable in ordinary substantial buildings, with partial collapse; great in poorly built structures. Panel walls thrown out of frame structures. Fall of chimneys, factory stacks, columns, monuments, and walls. Heavy furniture overturned. Sand and mud ejected in small amounts. Changes in well water. People driving cars disturbed (VIII + to IX Rossi–Forel scale)
IX.	Damage considerable in specially designed structures; well-designed frame structures thrown out of plumb; great in substantial buildings, with partial collapse. Buildings shifted off foundations. Ground cracked conspicuously. Underground pipes broken (IX+ Rossi–Forel scale)
X.	Some well-built wooden structures destroyed; most masonry and frame structures destroyed with foundations; ground badly cracked. Rails bent. Landslides considerable from river banks and steep slopes. Shifted sand and mud. Water splashed, slopped over banks (X Rossi–Forel scale)
XI.	Few, if any, (masonry) structures remain standing. Bridges destroyed. Broad fissures in ground. Underground pipelines completely out of service. Earth slumps and land slips in soft ground. Rails bent greatly
XII.	Damage total. Waves seen on ground surface. Lines of sight and level distorted. Objects thrown into the air

Masonry A, B, C, D. To avoid ambiguity of language, the quality of masonry, brick, or otherwise is specified by the following lettering

Masonry A. Good workmanship, mortar, and design; reinforced, especially laterally, and bound together by using steel, concrete, etc.; designed to resist lateral forces

Masonry B. Good workmanship and mortar; reinforced, but not designed in detail to resist lateral forces

Masonry C. Ordinary workmanship and mortar; no extreme weaknesses like failing to tie in at corners, but neither reinforced nor designed against horizontal forces

Masonry D. Weak materials, such as adobe; poor mortar; low standards of workmanship; weak horizontally

frequencies (or periods) of ground motion and that of the building which is the cause of maximum damage. Thus, in terms of the frequency content of an earthquake wave, low-rise buildings (such as ordinary one- or two-story dwellings and similar structures) are more affected by high-frequency or short-period ground motions, as compared to low-frequency or long-period motions of the ground. The reverse is true for the high-rise buildings, which are less affected by high-frequency or short-period motions of the ground. This change in

Construction Planning, Environmental Impact of Foundation Studies and Earthquake Issues. Table 2 Energy release of an earthquake. Magnitude (M) – energy (E) relation can be given the following formula:

$$\text{Log E} = 11.8 + 1.5\ \text{M}.$$

If M is increased by 1.0, E is magnified by a factor of $10^{1.5}$, i.e., approximately 32. Therefore, the seismic energy of an M = 6 earthquake is about 32 times as large as that of an earthquake M = 5 earthquake, and is about 1,000 times that of an M = 4 earthquake.

Magnitude and energy of earthquakes (Modified from Earthquake Mechanics, [8]

Magnitude (M)	Energy (tons of TNT)	Nuclear bomb equivalence
4.0	15	0.001 × Hiroshima
		0.0008 × Nagasaki
4.5	86	0.006 × Hiroshima
		0.004 × Nagasaki
5.0	478	0.03 × Hiroshima
		0.02 × Nagasaki
5.5	2,629	0.17 × Hiroshima
		0.13 × Nagasaki
6.0	15,057	1 × Hiroshima
		0.75 × Nagasaki
6.5	86,042	5.7 × Hiroshima
		4.3 × Nagasaki
7.0	478,011	31.7 × Hiroshima
		23.8 × Nagasaki
7.5	2,639,063	175 × Hiroshima
		131 × Nagasaki
8.0	15,057,361	1,000 × Hiroshima
		750 × Nagasaki
8.5	860,420,065	57,514 × Hiroshima
		4,285 × Nagasaki

TNT (Trinitrotoluene) is a chemical compound
Dynamite has 60% greater energy than TNT of the same weight
Hiroshima atom bomb ~ 15,000 t TNT
Nagasaki atom bomb ~ 20,000 t TNT

behavior of buildings is mainly attributed to resonance of soil–structure interaction, which can cause more damage when the ground motion frequency of earthquake waves and that of the building structure are the same. It is, therefore, advisable to avoid high-rise buildings (low-frequency) on low-frequency soils, and, similarly avoid low-rise buildings (high-frequency) on high-frequency grounds.

It must also be remembered that the frequency of earthquake waves decreases as the distance of the site in question increases. Therefore, it is not surprising to note that sometimes high-rise buildings located farther from the epicenter suffer more than high-rise buildings located closer to the epicenter. This is particularly noticeable in situations where the buildings are underlain by rock. Low-rise buildings, founded on rock and close to the epicenter, are more vulnerable to damage than the high-rise buildings situated in the same area.

It has been shown from the foregoing that the damage to structures in earthquake-prone areas is largely dependent on ground acceleration; depth of earthquake focus; distance of the epicenter from the structure; site conditions including the nature of the ground, its thickness, and topography of the site; duration of ground shaking; and last but not the least, the type of structure. It must be emphasized that for engineering purposes, it is the intensity or resulting acceleration of the ground motion that is important and not the magnitude of the earthquake.

Mitigation and Construction Planning

Earthquake risk varies from location to location, from structure to structure, and from person to person. Damage due to earthquakes is particularly great in certain locations, and it is very difficult to prevent the earthquakes from occurring. Nevertheless, precautions must be taken to mitigate the impacts of earthquake in the vulnerable area. Earthquakes are often followed by aftershocks, which can be more detrimental to the main earthquake shock, because the structures may have weakened by the main shock. The magnitude of the main shock is generally greater than the aftershocks, the magnitude of which generally decreases with time and can be empirically determined as to how long the aftershocks will continue.

Earthquakes are inevitable, but the damage from earthquakes is not. Safety and survival in an earthquake is very important. It is important to be prepared and take necessary precaution to reduce losses; in the event

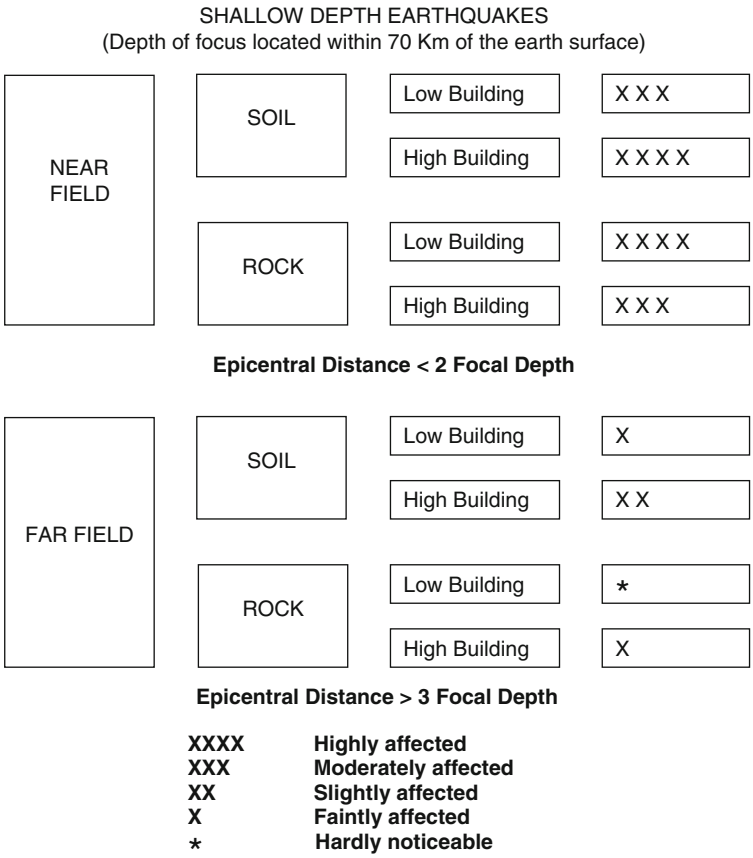

Construction Planning, Environmental Impact of Foundation Studies and Earthquake Issues. Figure 1
Effect of earthquakes on low- and high-rise buildings founded on soil and rock

of an earthquake, it is advisable to protect belongings and persons from falling objects. The instructions published by the United States Geological Survey, Department of the Interior, are very helpful in this regard.

If need be, vacate or demolish hazardous old buildings, and retrofit by strengthening the newly built structure, as well as regulating the construction of new buildings by adopting methods that cater to ground–structure interaction principles. Instances of fire, breaking of pipelines, disruption of electricity and water supply, and outbreak of disease are common following earthquakes, and among other things, they call for rescue, relief, rehabilitation of displaced people, relocation, and reconstruction of structures at safer places. The migration of displaced people from one area to another creates problems of adaptability, and issues raised by the native community in accepting people from different social backgrounds. The burden on the native community can be reduced by the construction of additional infrastructure such as hospitals, schools, community centers, market places, and so on.

In an attempt to avoid adverse environmental impact to buildings, it is important to prepare isoseismic maps of major earthquakes, which may have occurred in the area [10, 11]. These maps delineate areas of equal damage or of equal intensity of the earthquake in the past. A similar exercise can be initiated to delineate areas in terms of return periods of earthquakes of the same intensity. Furthermore, seismic zoning maps can be prepared to define areas which are extremely, highly, moderately, and slightly susceptible to the likely damage, which may be caused by an

earthquake of a specified return period. Building codes should be prepared and enforced to avoid damage to high-risk installation as well as buildings in different seismic zones.

Future Directions

Natural earthquakes are a major threat to society. Therefore, monitoring earthquakes is essential for providing scientific data to investigate complex earthquake phenomena, and to mitigate seismic hazards [12].

The earthquake early warning systems offer practical information for reducing seismic hazards in earthquake-prone regions. Attempts will be made here to mention about some recent developments followed by suggestions for future work, in this direction.

Over the past few decades, notable progress has been made in the understanding of some of the factors and processes that govern the occurrence of earthquakes. For instance, it is known [13] that the amount of damage caused by an earthquake is not only related to its magnitude, depth, and geographical location of the site, but also factors such as the type and quality of affected buildings, as well as the nature of the ground on which such buildings are constructed.

Building codes, relevant to different regions of the world, defined by earthquake zoning, earthquake recurrence interval, and isoseismic maps help in providing guidelines for the design, evaluation, and in some instances rehabilitation or retrofitting of building structures, in a given area.

The advent of Global Positioning Systems (GPS) opened a new avenue of opportunity to seismologists for monitoring movements in geographical positions of marked stations, and allows better long-term forecasts of areas likely to be affected by earthquakes. This development together with advances in telemetry and invention of earthquake early warning systems linked with real-time seismology offer practical information for reducing seismic hazards in earthquake-prone regions. Such systems are already successfully deployed in Mexico, Japan, and Taiwan [14]. However, there is no general method for predicting earthquakes in the actual time domain, and only probable estimates of recurrence of earthquakes of a given magnitude are available. Moreover, as described above, there are techniques that can detect an earthquake in progress and provide notice of seconds to tens of seconds, prior to actual ground shaking.

Real-time seismology refers to a practice in which seismic data are collected and analyzed quickly after a significant seismic event. The results thus obtained can be effectively used for post-earthquake emergency response and early warning. Such systems, on their own, can generally detect strong shaking at an earthquake's epicenter, and transmit alerts ahead of the damaging earthquake waves. The speed of an electronic warning signal, in time domain, is faster than the speed of earthquake waves traveling through the earth.

Unfortunately, there is no worldwide public early warning system for earthquakes. It is important to use this relatively new science and modern technology to rapidly detect the beginning of an earthquake, assess the hazard that the earthquake poses, and then provide a warning to people if they are in any harmful situation. Such early information about past earthquake occurrences is particularly useful in the discipline of disaster management. It calls for hazard mitigation plans from on-site and regional bases to consider post-earthquake emergency response and early warning.

There is a real need for a radically different design of seismographic networks employing earthquake early warning system. The importance of actively exploring the potential of wireless sensor networks cannot be overemphasized. However, building a radically different design of high-density seismic networks at national and international levels is not economical using existing seismic technology. Innovative approaches must be developed and perseverance is needed.

Bibliography

Primary Literature

1. Ambraseys NN (1971) Value of historical records of earthquakes. Nature 232:375–379
2. Poirier JP, Taher MA (1980) Historical seismicity in the near and Middle East, North Africa, and Spain from Arabic documents (VIIth–XVIIIth century). Bull Seismol Soc Am 70(6):2185–2201
3. Press F, Sielver R (1982) Earth. W. H. Freeman, New York
4. Wesson RL, Wallace RE (1985) Predicting the next great earthquake in California. Sci Am 252:23–31

5. Mavroeidis GP (2008) Estimation of strong ground motion from the great 1964 Mw 9.2 Prince William Sound, Alaska earthquake. Bull Seismol Soc Am 98:2303–2324
6. Chopra AK (1995) Dynamics of structures. Prentice Hall, Englewood Cliff
7. Richter CF (1958) Elementary seismology. W. H. Freeman, San Francisco
8. Kasahara K (1981) Earthquake mechanics. Cambridge University Press, Cambridge
9. Newmark NM (1970) Current trends in seismic analysis and design of high-risk structure. In: Weigel RL (ed) Earthquake engineering. Prentice Hall, Englewood Cliffs
10. Deputy Ministry for Mineral Resources (1996) Gulf of Aqba earthquake of November 22, 1995 with emphasis on its effects in Saudi Arabia. Special report: Ministry of Petroleum and Mineral Resources, Jeddah
11. Shehata WM, Kazi A, Zakir FA, Allam AM, Sabtan AA (1983) Preliminary investigations on Dhamar earthquake, North Yemen of December 13, 1982, King Abdulaziz University, Jeddah. Bull Fac Earth Sci 5:23–52
12. Kanamori H (2005) Real-time seismology and earthquake damage mitigation. Annu Rev Earth Planet Sci 5: 195–214
13. Green AG (1999) Mitigating the effects of earthquakes: problems, progress and future trends. In: Proceedings of the WMO/UNESCO sub-forum on science and technology in support of natural disaster reduction, WMO-914, pp 74–82
14. Nishenko SP, Savage WU, Johnson T (2009) Earthquake early warning: a prospective user's perspective (Invited), abstract #S21C-04, American Geophysical Union, Fall Meeting 2009

Books and Reviews

Anon (1978) Joint conference on predicting and designing for natural and manmade hazards. In: Proceedings of ASCE-ICE-CSE, American Society of Civil Engineers, New York

Bolt AB (1998) Earthquakes. W. H. Freeman, New York

Dowrick DJ (1987) Earthquake persistent design. Wiley, Singapore

Elnashai AS, Sarno LD (2008) Fundamentals of earthquake engineering. Wiley, England

Isenberg J (1981) Proceedings of social and economic impact of earthquakes on utility lifelines: seismic consideration in lifelines, planning, siting and design. American Society of Civil Engineers, New York

Johnson RB, Degraff JV (1988) Principles of engineering geology. Wiley, New York

Kokusho T, Yoshimichi Y, Yoshimine M (2009) Performance based design in earthquake geotechnical engineering: from case history to practice. Taylor and Francis, Singapore

Smith K, Petley DN (2007) Environmental hazards. Rutledge, New York

United Nations Educational Scientific and Cultural Organization (1978) The assessment and mitigation of earthquake risk. UNESCO, Paris

Contaminated Soil, Remediation of

Dimitris Dermatas[1], Iraklis Panagiotakis[2]
[1]Department of Water Resources and Environmental Engineering, School of Civil Engineering, National Technical University of Athens, Zografou, Greece
[2]ENYDRON - Environmental Protection Services, Athens, Greece

Article Outline

Glossary
Definition of the Subject and Its Importance
Introduction
Soil Contamination
Remedial Approach
Remediation Technologies
Future Directions
Bibliography

Glossary

Contaminant Any substance which, in sufficient concentration, can adversely affect living organisms.

Contaminated soil The soil containing substances at levels where they would not normally be present.

Ex situ treatment technologies Technologies that require excavation or removal of the contaminated source media.

Groundwater The subsurface water that lies beneath the water table in soils and geologic formations which are fully saturated.

Groundwater treatment technologies Technologies that address the contaminated groundwater directly.

In situ treatment technologies Technologies that treat or remove the contaminant without excavation or removal of the source media.

Nonaqueous phase liquids (NAPLs) Refer to liquids that are immiscible with water, which can be further classified to less dense (light NAPLs or LNAPLs) or more dense (dense NAPLs or DNAPLs) than water.

Soil The three-phase system of the earth, including a solid, a gas, and a liquid phase, which might range from very soft organic deposits through less compressible clays and sand to soft rock.

Soil remediation The collective term for various strategies that are used to purify and revitalize soil.

Source treatment technologies Technologies that address only the source of contamination, namely, soil, sediment, sludge, solid-matrix wastes, or NAPL, but do not address groundwater directly.

Definition of the Subject and Its Importance

"Contaminated soil," "contaminated site," "contaminated land" are different terms for the same environmental problem, which is encountered in millions of sites across the world. Soil becomes contaminated when a single or a mixture of contaminants reaches the soil surface, the vadose zone, or the aquifer. Soil is a limited and valuable natural resource, since it controls the element and energy cycles within the ecosystems, it is the habitat to countless organisms and plants, but, mainly, because it accommodates the groundwater, which makes up 97% of global freshwater, and the most important source of drinking water across the world [1]. However, at the same time, soil is the field that accommodates numerous essential socioeconomic and inevitably contaminating human activities. As a result, the extended production of a high number of chemicals and their wide use for domestic, industrial, and military reasons, combined with the common practice of its improper storage and neglectful disposal, has resulted in millions of contaminated sites across the world [2]. Soil contamination is an old problem dating back to the Industrial Revolution. However, this crucial environmental problem failed to receive prompt attention, and it was only recognized when incidents such as the Love Canal site in New York and the Lekkerkerk site in the Netherlands were published in 1970s, increasing the public concern about this serious environmental issue. The extent of the above environmental disorder is vividly portrayed if one bears in mind that the estimated cost of the potential remediation actions exceeds hundreds of billions of US dollars and the estimated number of contaminated sites today exceeds 500,000 in the USA, 30,000 in Canada, and 500,000 in Japan, while there are no available data for Eastern Europe, Africa, South America, and for key countries such as China and India [2]. Additionally, in European Union (EU), the number of contaminated sites requiring cleanup has been estimated as approximately 250,000 and the potential polluting activities have been expected to have occurred at nearly three million sites [3]. These numbers underline the significant lack of data for the EU and underscore the apparent differences in reporting among different geographical and other entities, where "apples" do not always mean "apples" depending on which country or organization does the reporting. It is, thus, imperative that a common language of data on environmental damage and solutions should be developed and implemented.

Furthermore, taking into account the large numbers of known or estimated contaminated sites across the world and the huge budget for soil remediation, the focus should be on those contaminated sites that potentially pose the highest risks to humans and the environment. Therefore, appropriate decision-making tools have been developed and applied to prioritize contaminated sites, thereby saving valuable resources for the most significant of them [4].

Contaminated soil remediation is one of the most rapidly developing environmental protection subjects. However, the high cost that soil remediation requires along with the complexity of the problem renders contaminated soil remediation a real challenge for environmental professionals and society altogether.

Introduction

Soil is usually defined as the three-phase system of the earth, including a solid, a gas, and a liquid phase, which might range from very soft organic deposits through less compressible clays and sand to soft rock [5]. Therefore, soil contamination is by definition a very complex problem to solve, since a three-phase medium is contaminated by chemicals, commonly as mixtures, which not only interact together but also with each phase of the soil concurrently. As a result, the way in which this system is changing both in place and in time depends on a series of different and interacting parameters relating both to the soil and the contaminants. Contaminated soil remediation is usually approached using a phased methodology, during which the contaminated soil is investigated, the remedial goals are determined and the most appropriate remediation technology is selected. The most commonly employed remediation technologies include solidification/stabilization, enhanced in situ bioremediation, monitored natural attenuation, soil vapor

extraction, in situ chemical oxidation, multiphase extraction, incineration, pump-and-treat, and others [6].

Today, the leading country in contaminated soil remediation is definitely the USA, where regulations for soil contamination have been in force as early as the 1980s. Sites with contaminated soil in the USA have been divided into several different categories, the most important of which is the Superfund sites, which are uncontrolled or abandoned places, where hazardous waste is located and can potentially affect local ecosystems or people. Other site categories are the Resource Conservation and Recovery Act (RCRA) Corrective Action sites, the Underground Storage Tanks (USTs) sites, the Department of Energy (DOE) sites, the Department of Defense (DOD) sites, various Civilian Federal Agencies sites, and State and private parties, including brownfields sites [7]. In the EU, there still does not exist a dedicated legislation for soil contamination on the grounds that the Soil Directive is still pending since 2006. Therefore, soil remediation policy in the EU is presently based solely on the "polluter pays" principle which is mainly applied via the environmental liability Directive (Directive 2004/35/EC) [3]. In other words, EU has a long way to go before it provides a safer and more sustainable context for its citizens with reference to contaminated soil remediation.

This entry aims to summarize and present the key and updated information on contaminated soil remediation and is divided into four parts. In the first part, the main key concepts, such as the soil properties, the main pollutants, and their fate and transport, are initially developed, while, in the second part, the remedial approach that should be followed by scientists and engineers is described. In the third part of this entry, the main remediation technologies are analyzed, while in the fourth and the last part, the future directions of contaminated soil remediation are outlined.

Soil Contamination

Soil Origin, Constituents, and Properties

Soil is mainly derived from solid materials of the earth's crust, the so-called rocks, by a series of physical, chemical, and biological mechanisms, collectively called weathering. Once the soil is formed, it may either remain in place as weathered soil material or be transported to new locations by various potential agents, such as wind and water or by glacial and anthropogenic activity [5, 8]. The soil that remains in place is termed residual soil, while the soil that is transported is termed alluvial, aeolian, or glacial soil, if water, wind, or ice was the transfer agent, respectively [9]. Generally speaking, soil consists of solid particles with pores in between, where water potentially flows replacing air and gradually turning dry soil, where pores have no water, to unsaturated soil, where pores are filled with air and water, and, finally, to saturated soil, where water completely replaces air and pores are totally filled with water. Unsaturated soils are typically near the ground surface, while saturated soils lie beneath the water table. Therefore, regarding its saturation state and overall environmental and physicochemical behavior, soil potentially consists of three different phases which are the solid, the liquid, and/or the gaseous phase, commonly referred to as geoenvironment, which are further described below.

The solid phase component consists of solid particles with size ranges from colloids (<0.001 mm) to boulders (>300 mm), which typically have an inorganic and an organic fraction. Inorganic fraction mostly consists of soil minerals and free oxides and hydroxides. Soil minerals are usually divided into two categories, carbonates and silicates. The most common carbonate minerals are calcite and dolomite, and the most common silicate minerals are quartz, feldspar, and mica in coarse-grained soils and the clay minerals kaolinite, illite, and montmorillonite in fine-grained soils. Furthermore, another very important constituent of the inorganic fraction of soil is free oxides and hydroxides, which exist in soil either as coating of soil particles, discrete particles, or cementing agents between soil particles and organic matter. Finally, the organic fraction of the solid phase includes nonhumified compounds, such as proteins and carbohydrates, and humified compounds, such as humic and fulvic acids [10]. All of these constituents, especially when they exist in finer grade (i.e., higher surface area) or amorphous state, are the main culprits of what is called geochemical attenuation of contaminants (explained in section "Fate and Transport of Contaminants in the Geoenvironment") as they strongly react with contamination in the geoenvironment.

The liquid phase component typically comprises only groundwater in pristine aquifers, while a mixture of groundwater, dissolved chemicals, chemicals in free phases, and dissolved gases might be the liquid phase in contaminated aquifers. Groundwater may exist in pores either as absorbed water on solid phase surfaces, as double-layer water close to a clay surface, or as free water surrounding the diffuse double layer [5, 10]. Due to its chemical properties, groundwater contains a variety of inorganic constituents in various concentrations, which are typically classified into major constituents, such as calcium and sulfate, into minor constituents, such as boron and iron, and into trace constituents, such as arsenic and nickel. On the other hand, groundwater contains also organic constituents, such as humic and fulvic acids, and dissolved gases, such as N_2, O_2, CO_2, CH_4, H_2S, and N_2O [11].

The gaseous phase exists in unsaturated soils or, in other words, in the vadose zone, where the liquid phase does not occupy the total volume of pores. However, as soon as the liquid phase enters the pores, gaseous phase is pushed out, while the procedure is reversed when the pores are drained out. Gaseous phase quality of surfacial soils is similar to the atmospheric air, despite the fact that oxygen concentration decreases and carbon dioxide increases with soil depth [10, 12]. Additionally, gaseous phase quality might also be affected by contaminants vapors, which could be further generated through several remediation activities.

Physical properties of soil (e.g., hydraulic conductivity, particle size, and surface area), along with chemical properties (e.g., mineralogy, pH, and oxidation-reduction status) and biological properties (e.g., particular bacteria species existence) are significant parameters that control both soil contamination and remediation. In particular, hydraulic conductivity, namely, the ease with which water can flow through the soil, controls groundwater flow and contaminant plume propagation and is the determining parameter in coarse-grained contaminated soils. However, particle size and surface area are more significant parameters in fine-grained soils. A typical example that is commonly employed to outline these concepts is the striking surface area of the clay mineral montmorillonite (800 m^2/g), 12 g of which would be sufficient to cover an entire football field [13]. Thus, particle size and surface typically appear as the key parameters affecting sorption processes of organic and inorganic contaminants and, therefore, geochemical attenuation and adopted remediation strategies [14]. Mineralogy and pH also play key roles in the fate and transport of contaminants in geoenvironment. For instance, it has been found that Pb release in soil which has been used as firing range can affect its pH and buffering capacity, while mineralogy and the presence of organic matter and ferromanganese in particular have been reported as responsible for Pb retention in several studies [14–19]. On the other hand, the oxidation-reduction conditions, usually called redox conditions, is another key factor that also affects a series of critical parameters, such as chemical speciation, bioavailability, toxicity and mobility of metals and metalloids, and the efficiency of remediation processes [20]. A typical example is the biodegradation of vinyl chloride (VC), which might behave either as electron acceptor or electron donor depending on the redox conditions [21]. Finally, since contaminant detoxification is sometimes accomplished only by very specific microorganisms (e.g., *Dehalococcoides* spp.), the presence of these microorganisms is a prerequisite for a successful soil remediation effort [22].

Major Soil Contaminants and Their Sources

Soil contaminants can be classified into several different ways. First of all, they can be roughly classified as organic and inorganic compounds, according to the presence or the absence of carbon atoms in their molecules, respectively. Organic contaminants can be further classified by the presence of halogens atoms in their molecules as halogenated or nonhalogenated compounds, by their carbon backbone shape as aliphatic or aromatic, or by their vapor pressure as volatilized (VOCs), semivolatilized (SVOCs), or nonvolatilized compounds. Additionally, organic contaminants, which are immiscible with water and may form a separate phase, are referred to as nonaqueous phase liquids (NAPLs) and are further classified according to whether they are less dense (light NAPLs or LNAPLs) or more dense (dense NAPLs or DNAPLs) than water. Most chlorinated VOCs, such as tetrachloroethene (PCE) and trichloroethene (TCE), are DNAPLs, and most nonchlorinated VOCs, such as benzene, are LNAPLs. Less complicated is the

classification of inorganic pollutants, which are usually classified as metals and metalloids and radionuclides. The most significant categories of soil contaminants are (a) petroleum hydrocarbons, (b) halogenated organic compounds, (c) metals and metalloids, (d) radionuclides, and (e) explosives. The most significant contaminants of these categories and their typical sources are presented in Table 1 and further discussed below.

However, although the most commonly detected contaminants were classified above as pure materials, in real life, they typically occur as mixtures, since many chemicals used in commerce and industry are mixtures and disposal sites receive a large variety of chemicals that can leach into soil. For example, gasoline contains numerous hydrocarbons as well as a range of organic and inorganic additives and waste generated from cleaning operations containing the cleaning agents and the chemical removed during cleaning, while waste from nuclear weapons manufacturing activity contains mixtures of several chemicals, such as radionuclides, metals, solvents, and organic chelating agents [23]. Therefore, soil contamination is usually a complicated phenomenon where several contaminants coexist under a wide variety of conditions.

Soil contamination might be caused either by point sources, such as damaged storage tanks and defectively designed waste disposal sites, or nonpoint sources, such as transport activity, intensive agricultural activities, organized or nonorganized military activities, and extreme natural phenomena, such as floods and hurricanes. In particular, sites where petroleum hydrocarbons, halogenated organic compounds, and metals and metalloids may be found include burn pits, chemical manufacturing plants or disposal areas, disposal wells and leach fields, electroplating/metal finishing shops, firefighting training areas, hangars/aircraft maintenance areas, landfills and burial pits, leaking collection and system sanitary lines, etc. Additionally, metals and metalloids may also be found in artillery and small-arms impact areas, battery disposal areas, and sandblasting areas. Sites where radionuclides are usually found include radioactive and mixed waste disposal areas, while the most common sites where explosives are usually found include artillery/impact areas, contaminated marine sediments, disposal wells, leach fields, landfills, burial pits, and TNT washout lagoons [24].

Petroleum Hydrocarbons Petroleum hydrocarbons are aliphatic or aromatic, linear or branched, saturated or unsaturated, simple or complex natural compounds, which are composed solely of carbon and hydrogen atoms and are mainly used as combustible fuels [25]. Among the most environmentally significant petroleum hydrocarbons are the monoaromatic benzene, toluene, ethylbenzene, and xylene, collectively called BTEX, and the polycyclic aromatic hydrocarbons (PAHs). Gasoline additive such as methyl tertiary butyl ether (MTBE), which are used to make gasoline burn cleaner, are common cocontaminants with BTEX

Contaminated Soil, Remediation of. Table 1 Main soil contaminants

Type of contaminants	Typical contaminants	Typical sources
Petroleum hydrocarbons	BTEX, alkanes, PAHs	Aircraft areas, leaking storage tanks, vehicle maintenance areas
Halogenated organic compounds	TCE, PCE, PCBs, Aldrin, Dieldrin, DDT	Electroplating/metal finishing shops, solvent degreasing areas
Metals and metalloids	Pb, Cr, As, Cd, Ni, Zn, Hg, Se, Cu	Shooting ranges, battery disposal areas, electroplating/metal finishing shops
Radionuclides	Uranium, Tritium, Plutonium	Radioactive and mixed waste disposal areas, areas affected by nuclear power plant accidents
Explosives	TNT, DNT, RDX, Nitroaromatics	Shooting ranges, TNT washout lagoons

in a large number of contaminated sites. BTEX might be found in soil due releases associated with fuels but also due effluents associated with industrial activities, wood processing, and manufacturing of pesticides, detergents, chemicals, paints, and varnishes [26]. Typically, the presence of BTEX in soil is accompanied by the presence of additives such as MTBE, whose high solubility hinders the remediation activity. PAHs are produced either by incomplete combustion and pyrolysis, natural or anthropogenic, of organic matter and easily adsorb onto the organic matter of soil. Several different physical, chemical, and biological remediation technologies have been used for soil contaminated with petroleum hydrocarbons so far, some of which are aerobic or anaerobic Enhanced In Situ Bioremediation, Monitored Natural Attenuation, in situ chemical oxidation (section "Chemical Treatment"), Pump-and-Treat, Phytoremediation, Thermal Treatment, Air Sparging), and Incineration [27, 28].

Halogenated Organic Compounds Another group of very common soil contaminants are the halogenated organic compounds, which are mainly anthropogenic and have been used in a wide variety of applications, such as solvents, degreasing agents, biocides, pharmaceuticals, plasticizers, hydraulic and heat transfer fluids, intermediates for chemical synthesis and in many other activities. The majority of them are chlorinated, although brominated, fluorinated, and iodinated compounds are also used in various industrial activities [29]. Among them, chloroethenes, mainly PCE and TCE, are some of the most commonly detected pollutants in the contaminated sites [30]. Chloroethenes belong to DNAPL group and the technologies selected for chloroethene-contaminated soil used to involve mainly extraction technologies such as Soil Vapor Extraction, Pump-and-Treat, or Air Sparging. However, there has currently been a clear trend in favor of in situ destruction mechanisms employing either biotic, such as Enhanced In Situ Bioremediation, Monitored Natural Attenuation, or abiotic processes, such as in situ chemical oxidation (section "Chemical Treatment") or Thermal Treatment [31].

Metals and Metalloids Metals and metalloids, such as lead, chromium, cadmium, nickel, zinc, copper, mercury, silver, and arsenic, are another group of contaminants that is usually detected in contaminated soils [12]. Typical sources of soil contamination include land disposal of solid wastes, liquid sewage or sewage sludge, leachate from mine tailings and other mining wastes, deep-well disposal of liquid wastes, seepage from industrial waste lagoons, or from other spills and leaks from industrial metal processing facilities [32]. However, since all soils naturally contain trace levels of metals and metalloids, only the difference between their ambient and their background concentrations could be a reliable criterion for diagnosing soil contamination by those contaminants. As opposed to organic contaminants, metals and metalloids cannot be degraded and completely destroyed. Nevertheless, contaminated soil might be remediated by contaminant transformation in less mobile and/or less toxic forms by changing its speciation. The most applicable remediation technologies for soil contaminated with metals and metalloids include Solidification/Stabilization, Permeable Reactive Barriers, Soil Flushing, Phytoremediation, and Soil Washing [33].

Radionuclides Radionuclides, such as uranium-238, thorium-228, and plutonium-238, are elements with unstable nuclei that spontaneously alter their composition through radioactive decay in a series of successive nuclear reactions, ultimately leading to a stable configuration. Radionuclides can be found in soil either due to natural processes or due to man-made activities, such as nuclear weapon tests and nuclear power plant accident [12, 34]. Radionuclides are a widely spread group of contaminants across the world, since in the USA, only they were detected in 120 contaminated sites [20]. The most applicable remediation technology for soil contaminated with radionuclides is the Solidification/Stabilization, while other remediation methods, such as the enhanced in situ Bioremediation and Electrokinetic Separation, have started to be used as well [33, 35].

Explosives Finally explosives, such as TNT (2,4,6-trinitrotoluene), RDX (1,3,5-trinitro-1,3,5-triazine), and HMX (1,3,5,7-tetranitro-1,3,5,7-tetrazocane), are mainly nitrogen-containing organic compounds with the potential of self-oxidation to small gaseous molecules (N_2, H_2O, and CO_2). It has been estimated that there are hundreds of explosives-contaminated sites

within the USA, and the number significantly increases in Europe and Asia. Several different technologies have been used so far to remediate explosives-contaminated soil, but the most widely applied one is Incineration. However, the high cost of incineration and the wide environmental concerns that this technology brought about have triggered the development of more sustainable alternatives, such as in situ chemical oxidation (section "Chemical Treatment") and Phytoremediation [36].

Fate and Transport of Contaminants in the Geoenvironment

As soon as a single pollutant or, most commonly, a mixture of pollutants encounters soil, it tends to travel via the unsaturated pores of the vadose zone toward the aquifer, creating a plume which is transported with groundwater. During this journey, a number of physical, chemical, and biological processes, collectively called natural attenuation, might take place which can lead to dilution, immobilization, or degradation of a soil contaminant, alter its chemical and biological identity, and usually decrease its environmental footprint. These processes, which are further discussed below, are generally grouped into three categories: (a) the transport processes, (b) the geochemical attenuation processes, and (c) the intrinsic bioremediation processes.

Transport of a contaminant is generally accomplished via a threefold mechanism comprising (a) advection, (b) diffusion, and (c) mechanical dispersion [37]. The first process, advection, refers to the macroscopic contaminant movement by flowing water as a result of a hydraulic gradient. However, contaminant transport also occurs in the microscopic level either due to a chemical concentration gradient resulting in diffusion or due to the heterogeneous subsurface pore geometry resulting in both longitudinal and transverse mechanical dispersion. Additionally, contaminant transport also depends on its immiscibility, namely, on whether it belongs or not to the NAPL group and, if it does, whether it is LNAPL or DNAPL. In particular, in incidents of LNAPL spills, contaminants are retained on grain surfaces within the vadose zone, when spills are small, or they are accumulated on the water table in the case of larger scale spills. On the contrary, in cases of DNAPL, contaminants reach a larger depth of the vadose zone when the spills are small, while contaminants can either be dispersed around or near the water table or penetrate the water table and be accumulated on deeper impermeable layers, when the spills are large enough [12].

As it has already been stated, apart from transportation through its pores, contaminants also interact with soil, usually resulting to the partial or total immobilization of soil contaminants, a process called geochemical attenuation. The ability of soil to trap contaminants and geochemically attenuate their movement in soil depends on (a) the chemical composition of seepage or groundwater, (b) the geochemical and mineralogical properties of the soil, and (c) the pH and Eh conditions that are established in the soil–water interface and overall matrix [38]. In particular, geochemical attenuation of contaminants depends on a series of geochemical reactions, the most important of which are (a) the acid–base reactions, (b) oxidation-reduction, (c) precipitation, (d) aqueous complexation, (e) sorption, (f) hydrolysis, and (g) radioactive decay [23]. Acid–base reactions determine the pH of groundwater and, therefore, affect almost all geochemical and biological reactions in the subsurface. As a general rule, geochemical attenuation mechanisms are most active in a pH range from 5 to 8 [38, 39]. Oxidation-reduction reactions are usually catalyzed by microorganisms, although some of them can occur abiotically, where electrons are transformed from the electron donor (reductant) to the electron acceptor (oxidant), without the mediation of microorganisms. Typical electron donors for abiotic oxidation-reduction processes are ferrous iron (Fe^{2+}), sulfides (S^{2-}, HS^{-}, H_2S), and humic substances [23]. Another important geochemical reaction is the precipitation, in which cationic dissolved metals react with anions, such as carbonate, hydroxide, and sulfide, to form a solid or precipitate. This process, which is promoted with increasing pH values, can be further enhanced via the processes of coprecipitation, where metals precipitate along with or are trapped within the solid formed by major ions, such as Ca, Al, and Fe [23]. Dissolved metal cations can also react with anions to form complexes. Complexation prevents the metal from precipitating and changes the sorption to solids regime in comparison to free metal ions. Sorption is another process that

plays a pivotal role in contaminant attenuation by slowing the contaminant transport in groundwater. To make matters more tangible, sorption reactions concentrate dissolved chemicals on the soil particles. This process might occur by two different mechanisms, which are (a) adsorption and (b) absorption. Adsorption occurs when chemicals cling to the surface of the soil particles, while absorption takes place when chemicals are diffused into the particle. Another significant process in soil is hydrolysis, in which an electron-withdrawing group, such chlorine, is replaced either by OH^- or H_2O. Finally, radioactive decay is the process in which radioactive elements are spontaneously decayed to daughter products. Geochemical attenuation is exemplified in the process of the Cr^{3+} immobilization via the mechanisms of adsorption when pH values are lower than 4, via adsorption precipitation when pH values range between 4 and 6, and via precipitation when pH values are higher than 6 [38, 39].

The strong presence of microorganisms in the soil and their remarkable ability to degrade contaminants through a plethora of enzyme systems placed biodegradation among the most important attenuation mechanisms. The biodegradation of contaminants is carried out mainly by oxidation-reduction reactions, where microorganisms generate the required energy through the transfer of electrons from the electron donor to the electron acceptor. Biodegradation is a vital mechanism of natural attenuation, since it is possible to completely detoxify organic contaminants to CO_2 and water and immobilize inorganic compounds, transforming them to less mobile and less toxic species. During this process, microorganisms can use a wide variety of organic or inorganic compounds as electron donors but relatively limited electron acceptors. Common electron acceptors include O_2 in aerobic conditions and NO_3^-, SO_4^{2-}, Mn_4^+, Fe^{2+}, or CO_2 in anaerobic conditions. However, there are also microorganisms which are able to use contaminants as electron acceptor, when the appropriate electron donor is sufficient. A typical example of these microorganisms is the bacteria of the genus *Dehalococcoides*, which are capable of completely reducing PCE or TCE to ethene, in the presence of a sufficient electron donor, which in their case would be H_2 [40]. However, the aforementioned example also indicates that natural attenuation does not always reduce the environmental footprint of the contaminants, since if H_2 is not sufficient or other environmental conditions are not the appropriate ones, PCE or TCE dechlorination would never be complete and intermediate dechlorination products, such as VC, which is more toxic than the parent compounds, are usually produced [41]. Finally, microorganisms can also degrade contaminants without gaining energy, by a process known as cometabilism, which is the fortuitous degradation of a contaminant when other compounds are available to serve as the energy source [42].

Remedial Approach

During the last 30 years, the perspective of contaminated soil remedial approaches has changed significantly from the cost-driven approach of the mid-1970s, through the feasibility-driven approach of the mid-1980s, the risk-based approach of the mid-1990s, to the recently emergent sustainable remediation [43]. Sustainable remediation can be broadly defined as a remedy or combination of remedies whose net benefit on human health and the environment is maximized through the judicious use of limited resources [44]. In particular, when a sustainable remediation approach is adopted (a) the energy consumption or the consumption of other natural sources and the associated costs of the remediation application approach should be minimized, (b) the contaminant releases to the environment should be reduced or eliminated, (c) the process should harness or mimic the natural attenuation processes, and (d) the contaminated land and undesirable materials should be reused or recycled. Generally speaking, the remedial approach consists of three successive actions, which are described in detail below and are the following: (a) site characterization, (b) risk assessment, and (c) remediation technology selection.

Site Characterization

Site characterization is always the first action of a remedial approach. During this action, all the appropriate data should be gathered, in order to determine the type, the extent, and the fate and transport of the contamination, while constructing a conceptual site model based on the site geoenvironmental properties acquired. Since site characterization is usually an expensive and a time-consuming process and the nature of the

contaminated site is at the beginning unknown, a phased approach is commonly adopted, which usually comprises two parts typically called the Phase I and the Phase II environmental site assessments (ESA).

The Phase I ESA, or the so-called preliminary site assessment, aims at identifying the presence or likely presence of contamination in a site. In particular, during the Phase I ESA, information is gathered on the background environmental conditions, the current and the historical uses of the site, and the permitting regulations, rendering the first picture of the contamination problem being as comprehensive as possible. A Phase I ESA typically consists of four components, which are [45] (a) the records review, (b) the site reconnaissance, (c) the interviews, and (d) the reporting. Records review includes information sources such as maps, photographs, soil and mineral resource surveys, and previous reports, while site reconnaissance is a tool for verifying the collected information and collecting new data pertaining to information such as unrecorded pollution sources or receptors. Interviewing of people being involved, such as past and present owners and occupants, is another significant step of the Phase I ESA process, via which additional valuable information for the site is typically gathered, while reporting is the final step of the Phase I ESA. Reporting encompasses all relevant information pertaining to the contamination problem at hand, where existing data gaps are clearly identified and an action plan is devised so as to obtain the missing information in order to enable remediation of the contaminated site and a comprehensive solution to the contamination problem.

The next step of site characterization is the Phase II ESA, which aims to evaluate those environmental conditions that were identified by the previous site characterization phase and link them to possible remediation approaches and their associated costs. Phase II ESA is an iterative process typically comprising four components [46]: (a) the scope of work development, (b) the assessment activities, (c) the evaluation and interpretation of the data, and (d) the reporting. A typical Phase II ESA starts with the description of the work that will be performed. As soon as the rationale of the sampling locations and the measured parameters is determined, the appropriate assessment activities, ranging from simple field screening methods to complicated intrusive multimedia sampling and laboratory analyses, should be properly chosen and conducted. When data gathering has been completed, the assumptions, such as the groundwater direction and the depth to the water table, where the assessment was based, should be verified and the results should be interpreted and evaluated. During this stage of assessment, issues such as the existence of nearby contamination sources and naturally occurring contaminants should be addressed and properly evaluated. Finally, site characterization is completed with a report where the work that was performed and the conclusions that were drawn should be summarized and presented properly.

Today a consensus has been reached that the most important factor of site characterization is the contaminant speciation, namely, the determination of the chemical form of contaminant (formula, valence, and crystalline structure or amorphicity) as well as the physicochemical association between soil and contaminants (sorption and crystal or amorphous inclusion). Contaminant speciation is considered as the cornerstone of the decision-making process, since among others it (a) explains the mechanisms of contaminants' attenuation and possible degradation, (b) evaluates public health risk associated with contamination, (c) delineates mechanisms of contaminant release and their ultimate fate under specific exposure environments, and (d) determines the release potential and the contaminant bioavailability.

Although the water quality analysis methods can be considered to implement cutting edge technology, this does not apply for the analysis of contaminated soil, since the discovery of reliable, simple, and cost-effective lab and field investigatory tools using readily accessible equipment is still among the greatest challenges of this scientific area. The main field methods that are currently used for site characterization of contaminated soils are the penetrating tests and the geophysical methods, each of which has its own advantages and drawbacks. Therefore, although penetration tests are relatively inexpensive and capable of providing continuous records, they cause mechanical disturbance of contaminated soils. On the other hand, although geophysical methods are nondestructive and less expensive, they cannot be used alone, but only in conjunction with limited traditional characterization

methods, where actual samples are obtained and evaluated, which, in turn, should verify the geophysical methods' results. Despite the fact that it is clear that the nondestructive methods constitute the future trend in site characterization, it is expected that it will take time and further research to develop the appropriate nondestructive methods that could be reliably applied on their own. In addition, laboratory methods for site characterization also need further research so as to provide reliable information mainly in relation to contaminant speciation. In particular, traditional batch, leach/extraction tests, such as Toxicity Characteristic Leaching Procedure (TCLP) and Sequential Extraction Test (SET), can be viewed as problematic so long as contaminant speciation is altered during the test, while methods such as X-ray Powder Diffraction (XRPD) and Electron Microprobe Analysis (EPMA) need to become more standardized. Finally, state-of-the-art site characterization methods such as X-ray Absorption Near-Edge Spectroscopy (XANES) and X-ray Fluorescence Spectroscopy (XFS) are very expensive, difficult to gain access to, and also formidable in terms of results interpretation. Overall, there are still numerous unresolved issues in field and laboratory site characterization methods, and additional research and development are regarded as mandatory, in order to further improve this very crucial subject.

Risk Assessment

If site characterization confirms the existence of contamination, a risk assessment should follow to evaluate the risk posed to potential receptors, which are usually the humans and the neighboring ecosystems. Therefore, a comprehensive risk assessment typically comprises the human health risk assessment and, the much more complex, ecological risk assessment. Although these two procedures have much in common, the main difference between them is that, while human health risk assessment is limited to how humans can be affected, ecological risk assessment should also take into account the complexity of factors affecting the whole ecosystem.

Risk assessment comprises four successive stages which are [47] (a) hazard identification, (b) hazard assessment, (c) risk estimation, and (d) risk evaluation. In particular, during the hazard identification stage, site characterization data are further analyzed in a more systematic way in order to identify the contaminants of potential concern, their sources, the environmental media that they could affect, their fate and transport in the geoenvironment, and, finally, their potential receptors. As soon as the hazard has been identified, the potential pathways by which pollutants of concern could reach receptors and the characteristics of the receptors should be determined during the hazard assessment stage. If the hazard assessment indicates a possible and significant exposure, a risk estimation stage is further required, during which the potential exposures and effects are assessed. More specifically, during the risk estimation stage, the intensity, the frequency, and the duration of the exposure are measured or estimated, while potential human health and environmental effects are determined and quantified. Finally, based on the information gathered during the previous stages, risk is evaluated using appropriate indicators of acceptability of the risk in human health or in the environment. If the risk assessment concludes that the risk of contamination is unacceptable, the site should be remediated and the appropriate remediation technology should be selected. However, political reasons and social pressures may very well supersede all of the above and render that a site should be remediated without following all the aforementioned risk assessment steps. Nevertheless, some limited risk assessment is still applied in order to set the specific goals (e.g., target concentration levels) of remediation.

Remediation Technology Selection

As soon as site characterization and risk assessment have been completed and the remedial goals for soil and water have been determined, decision-makers should select the appropriate remediation scheme. However, although soil remediation is a point-in-time process, it should be capable of permanently solving a very complex and dynamic phenomenon, which is variously affected by a series of interactive parameters, such as

- Type of soil
- Type of contaminants
- Sources of contaminants
- Age of contamination (aging)
- Depth of contamination

- Type of receptors
- How contaminants are introduced into soil

Taking into account that soil contamination is a highly costly and complex problem, it is evident that selection of the appropriate remediation technology is more of an "art" rather than a standard practice yet. The decisive parameters are the experience of decision-makers coupled with the overall quality of site characterization, which will highly affect the ultimate success of any remediation effort.

Remediation Technologies Classification Remediation technologies are generally classified in several useful ways. First of all, they are divided, based on the medium that they address, into two classes and particularly in (a) source treatment technologies, which address only the source of contamination, namely, soil, sediment, sludge, solid-matrix wastes, or NAPL, but do not address groundwater directly and (b) groundwater treatment technologies, which address the groundwater directly. Other interesting classifications of remediation technologies are based either on the depth of contamination or where remediation takes place or, finally, on the predominant remediation process employed. In particular, given that different technologies should be used for shallow soil contamination and others for deep soil contamination, remediation technologies can be classified as (a) shallow remediation technologies, which are appropriate for vadose zone and shallow aquifers and (b) deep remediation technologies, when soil contamination has reached deeper aquifers. Additionally, they are typically classified also into (a) in situ technologies or (b) ex situ technologies, based on whether contaminated soil or groundwater is treated in place or after removal, respectively, or according to the primary mechanisms by which treatment is achieved in (a) biological, (b) physical/chemical, and (c) thermal technologies. Finally, a rougher but very useful classification is based on the fate of the contaminant during remediation, and consequently, technologies are divided into

- Removal technologies
- Immobilization technologies
- Extraction technologies
- Destruction technologies

Removal technologies, such as the Dig-and-Dump and the Pump-and-Treat, intend to completely remove soil and groundwater contamination in order to restore the contaminated soil to "pristine" conditions. Although this seemed possible in the past, nowadays it has become clear that return to pristine conditions is an extremely difficult and expensive practice, which is very rarely successful. Therefore, during the last decade, the accumulated experience and the adoption of the risk-based approach led to broader application of more sober management practices, including immobilization and destruction technologies. The main representative of immobilization and destruction technologies is Solidification/Stabilization and Bioremediation, respectively, which, although they do not restore "pristine" conditions, can efficiently reduce the groundwater contaminants' concentrations to accepted levels. Another approach, which is usually adopted, is based on extraction technologies, such as Phytoremediation and Soil Washing, which are capable of extracting contaminants from the soil and the groundwater-reducing contaminants' concentrations to an acceptable level. However, the major drawback of extraction technologies is the generation of another waste stream, which, in the case of Soil Washing, amounts to large volumes of wastewater and sludges, while in the case of phytoremediation, large volumes of harvested plants or even worse plant parts. Finally, Containment Technologies such as Vertical Engineered Barriers (section "Containment Technologies") can also be used mainly to protect sensitive receptors by effectively controlling contaminant migration. Table 2 illustrates the diverse classifications of remediation technologies along with their frequency of application and the cost. However, it should be noted that combinations of remediation technologies are usually required, either in sequence or as cotreatment procedures, mainly due to the contamination complexity and the different efficiency that different technologies are capable of achieving.

Selection Process and Criteria Generally speaking, a remediation technology selection process can be divided into three successive stages, which are

- Development of remediation alternative scenarios
- Screening of alternatives
- Treatability and pilot studies

Contaminated Soil, Remediation of. Table 2 Main contaminated soil remediation technologies

Remediation technology	Depth	Place	Fate of contaminant	Typical contaminants	Application frequency[a]	Application trend[a]	Cost
Source treatment technologies							
Solidification/ stabilization	Shallow/ deep	In situ/ ex situ	P/C-I	Metals, radionuclides, organic	VF	↑	Low
Soil vapor extraction	Shallow	In situ	P/C-E	BTEX, solvents	VF	–	Medium
Bioremediation	Shallow/ deep	In situ/ ex situ	B-D	PAHs, BTEX, pesticides, solvents	F	–	Low–Medium
Incineration	Shallow	Ex situ	P/C-D	PCBs, solvents, explosives	F	↓	High
Chemical treatment	Shallow	In situ	P/C-D	BTEX, pesticides, solvents	NF	↑	Medium
Multiphase extraction	Shallow	In situ	P/C-E	BTEX, solvents	NF	–	Medium–High
Phytoremediation	Shallow	In situ	P/C-E	Metals, solvents	NF	–	Low–Medium
Thermal treatment	Shallow	In situ/ ex situ	P/C-D	BTEX, pesticides	NF	–	High
Flushing	Shallow	In situ	P/C-E	BTEX, metals, radionuclides	NF	–	Medium–High
Bioventing	Shallow	In situ	B-D	BTEX, pesticides	NF	–	Low–Medium
Soil washing	Shallow	Ex situ	P/C-E	Metals, PAHs, PCBs, pesticides	NF	↓	High
Electrokinetic separation	Shallow	In Situ	P/C-E, P/C-I	Metals, radionuclides	NF	–	High
Groundwater treatment technologies							
Monitored natural attenuation	Shallow/ deep	In situ	P/C/B-I-D	BTEX, pesticides, solvents	VF	↑	Low
Pump-and-treat	Shallow/ deep	Ex situ	P/C-E	TCE, BTEX	VF	↓	High
Bioremediation	Shallow/ deep	In situ/ ex situ	B-D	BTEX, pesticides, solvents	F	↑	Low–Medium
Chemical treatment	Shallow/ deep	In situ	P/C-D	BTEX, pesticides, solvents	NF	↑	Medium–High
Phytoremediation	Shallow	In situ	P/C-E	Metals, solvents	NF	–	Low–Medium
Flushing	Shallow	In situ	P/C-E	BTEX, metals, radionuclides	NF	–	Medium–High
Multiphase extraction	Shallow	In situ	P/C-E	BTEX, solvents	NF	–	Medium–High

Contaminated Soil, Remediation of. Table 2 (Continued)

Remediation technology	Depth	Place	Fate of contaminant	Typical contaminants	Application frequency[a]	Application trend[a]	Cost
Permeable reactive barriers	Shallow/ deep	In situ	P/C-B-D	Metals, solvents, radionuclides	NF	↑	Medium–High
Air sparging	Shallow	In situ	P/C-E	BTEX, solvents	NF	↓	Medium

B biological process, *P/C* physical/chemical process, *D* destruction, *I* immobilization, *R* removal, *C* containment
[a]Application frequency and trend at Superfund sites where the treatment option or MNA was selected in the USA [6], *VF* very frequent (>20% of the Superfund sites), *F* frequent (10–20% of the Superfund sites), *NF* not frequent (<10% of the Superfund sites)

During the first stage, a series of scenarios should be created which should be applicable to the specific contamination problem, site-specific hydrogeological and other geoenvironmental conditions, and the feasibility of the remediation goal. Thus, the remediation scenarios created ought to cater for the respective differences between organic and inorganic contaminants, mixtures and single contaminants, coarse and fine soils, point and nonpoint sources, vadose zones and aquifers, shallow and deep contamination, etc. As soon as remediation scenarios have been created, the alternative scenarios should be further screened on the basis of several technical, environmental, health and safety, and socioeconomic criteria.

The most important of these criteria are the following [48]:

- Short-term and long-term effectiveness
- Reduction in toxicity, mobility, or volume of contamination
- Implementability and cost
- Compliance with applicable or relevant and appropriate requirements
- Overall protection of human health and the environment
- Regulatory acceptance
- Sustainability

The remediation technology that will be screened from the second stage should ensure the long-term effectiveness of the remediation effort but with an affordable cost for construction and operation that would not cause the remediation effort termination before the remedial goal has been achieved. Additionally, a remediation technology that fails to gain the community support is difficult to be implemented and operated over the extended period of time that a remediation effort usually requires.

Finally, the most prevailing remediation scenarios, which have successfully passed through the first and the second stage of the selection process, should be further examined with treatability studies and pilot tests. Treatability studies are laboratory tools which are used to determine the treatability of specific contaminants under conditions similar to those prevailing in the field. Typical examples of treatability studies are

- TCLP or synthetic precipitation leaching procedure (SPLP) for solidification/stabilization performance evaluation
- Microcosm studies, which are employed to examine the efficiency of enhanced in situ bioremediations

Solidification/stabilization performance and overall sustainability are usually evaluated solely on the basis of regulatory leaching tests and typically the TCLP. Interestingly, these tests and other similar leaching tests, used in Europe and elsewhere, provide point-in-time performance data and cannot provide a solid foundation for a reliable assessment of long-term performance and treatment overall sustainability. In particular, Dermatas et al. [49] have pointed out the inadequacy of TCLP and sequential extraction procedures in evaluating Pb release, while Sheckel et al. [50] found that in phosphate-treated Pb-contaminated soils, a significant shift of extractable Pb to the residual phase occurred due to the formation of pyromorphite during the extraction process, artificially overestimating the presence of pyromorphite. Additionally, Cao and Dermatas [51] concluded that the standard one-point TCLP test would either over- or underestimate Pb leachability in firing range soils and that the SPLP is a more appropriate alternative than TCLP for assessing Pb leachability. Similarly, Kosson et al. [52] and van der Sloot et al. [53] point out to the inadequacies of regulatory

leaching tests to explain the fact that the European regulatory framework is still under development. Thus, it appears that treatability bench scale screening studies, which are mainly based on regulatory testing, may lead to the wrong treatment alternative selection. Even worse, there have been many cases where solidification/stabilization treatment that appeared to be initially successful, ended up failing in the near or long term [39]. Moreover, this approach often leads to solidification/stabilization overtreatment along with the associated waste of energy and resources. Therefore, a multiple line of evidence strategy should be adopted to understand the actual phenomena given the limitations of the individual investigation techniques [49]. This involves at least a combination of traditional geotechnical analyses (particle size distribution, unit weight, water content), physicochemical analyses (pH, total metal contents), and a subset of controlled pH extraction tests (TCLP, SPLP, etc.) coupled with non-destructive mineralogical quantitative analyses (XRPD combined with Rietveld Quantitative Analysis, RQA). Following these analyses, micromorphological (Scanning Electron Microscopy-Energy Dispersive Spectroscopy, SEM-EDS and/or EPMA) and contaminant speciation analyses (XANES and/or Extended X-ray Absorption Fine Structure, EXAFS or other newly developed techniques) should be used once a more in-depth assessment is required [49, 54].

On the other hand, microcosm studies provide evidence of the potential response of the indigenous microbial community to several different electron donor additions (e.g., butyrate, lactate) while, at the same time, they allow for mass balance calculations regarding the chloroethenes that were dechlorinated and the electron donor that was consumed either by dechlorination or by other competing final-accepting processes (e.g., methanogenesis, sulfate reduction) [55]. Microcosm studies evaluating enhanced remediation of sites contaminated with chloroethenes should be prepared under aseptic and anaerobic conditions. A focal point in microcosm studies is samples representative preparation, which, more often than not, is a difficult task, since microcosm conditions should mimic the site-specific conditions as much as possible and laboratory cross-contamination phenomena, which could violate the study results, should be avoided. Microcosm studies are usually coupled with molecular techniques, such as fluorescence in situ hybridization (FISH) or polymerase chain reaction (PCR), which by studying the microbial community structure and the functional relationships between community members provide valuable information for the potential behavior of the microbial community.

Finally, as soon as treatability studies indicate the potential applicability of a remediation technology, a field pilot test is usually employed to further prove the treatability study results under real-life conditions and to obtain critical information so as to make the final decision or to optimize implementation of the selected option. If the results of the pilot test agree with the results of treatability test, a full-scale scheme of the selected remediation technology should be designed and implemented properly, otherwise alternative scenarios should be considered and the most appropriate technology should be tested again.

Remediation Technologies

According to the latest USEPAs Superfund Remedy Report [6], solidification/stabilization, soil vapor extraction, bioremediation, and incineration were selected for approximately 80% of the applied source treatment technologies. Other technologies, such as chemical treatment, soil washing, and phytoremediation, have also been applied in a limited number of Superfund sites, though [6]. On the other hand, pump-and-treat, monitored natural attenuation, and vertical engineered barriers are the most frequently applied groundwater treatment technologies for Superfund sites [6]. These technologies have demonstrated different trends during the last three decades, since, although the selection of pump-and-treat, soil washing, incineration, and air sparging have leveled off, the use of solidification/stabilization, chemical treatment, monitored natural attenuation, bioremediation, and permeable reactive barriers has increased. The most significant source and groundwater treatment technologies are discussed in detail below, while a brief description of the remaining treatment and containment technologies is limited only to the key points.

Solidification/Stabilization

Solidification/stabilization refers to a group of in situ or ex situ source treatment technologies which, using

the appropriate binder agents, prevent or minimize the migration of contaminants in the environment rather than degrade them [56, 57]. According to USEPAs Superfund Remedy Report [6], solidification/stabilization is the most frequently selected ex situ and among the most frequently selected in situ source treatment technologies for Superfund sites, being used in 203 and 56 projects, respectively. The widespread acceptance of this technology stems from the lower cost incurred in comparison to much more expensive alternatives and the better understanding of the prevailing mechanisms which render possible the reliable evaluation of the technology performance. Solidification/stabilization has been applied so far to contain or treat soils contaminated with various hazardous contaminants, such as metals, radionuclides, and organic contaminants [57]. In particular, solidification/stabilization technologies, using a binder agent, encapsulate soil contaminants in a nontoxic or less toxic material, which may be either a monolithic block, a clay-like material, a granular particulate, or some other physical form commonly considered "solid" (Solidification) while, at the same time, chemically transform soil contaminants in less soluble, immobile and less toxic forms (Stabilization) [56–58]. Moreover, the stabilized wastes may attain adequate stress–strain properties to enable their utilization in construction applications, such as engineering fill, road or pavement subgrade, backfill, and base material [39, 59, 60]. Binder agents that have been used so far are mainly inorganic materials, such as cement [61], lime [39], and phosphate [62, 63]. However, other binders that could be used in the context of the waste combination approach include fly ash [39], fish cannery wastes [64], and a plethora of other waste materials. Lately, sorbents such as zero-valent iron (ZVI), titanium dioxide, zeolites, and other nonwaste materials have also been employed, increasingly so in nanosize forms.

The most costly version of solidification/stabilization is the in situ or ex situ Vitrification, which immobilizes inorganics and destroys organic contaminants by heating the soil at extremely high temperatures (1,600–2,000°C), using a powerful source of energy, such as electric current, direct-fired kiln, or other heat sources. By this method, most inorganics are immobilized and incorporated within the vitrified glass and crystalline mass, while organic pollutants are destroyed by pyrolysis and the water vapors and organic by-products are captured by an off-gas treatment system prior to discharge.

Bioremediation

Bioremediation comprises a group of in situ or ex situ technologies, which achieve either source or groundwater remediation using microorganisms' metabolism. The most promising among them is the enhanced in situ bioremediation (EISB). EISB is a source and a groundwater remediation technology, in which additives, such as nutrients, electron donors or acceptors, stimulate the biodegradative activity of native (biostimulation) or added microorganisms (bioaugmentation) [58]. This technology has been successfully used for soil contaminated with petroleum hydrocarbons, solvents, pesticides, wood preservatives, and other organic chemicals [24]. The most frequently used versions of this technology include landfarming, reductive dechlorination, and biosparging, the analysis of which will follow.

Landfarming is an ex situ source treatment technology, in which excavated soil, being contaminated with petroleum hydrocarbons, is spread in a layer with a width of less than 1.5 m where aerobic biodegradation mechanisms are stimulated by aeration and/or addition of required bacteria, nutrients, minerals, and water. However, among the most significant drawbacks of Landfarming are the large amount of land requirement, the air pollution induced by contaminants' volatilization, the low efficiency regarding heavy petroleum components, its potential of accidentally contaminating uncontaminated sites, the high optimum temperature that is required, and the difficulty involved both in achieving efficiency higher than 95% and in remediating very contaminated soil [65].

Reductive Dechlorination (RD) is among the most commonly used groundwater treatment technologies for soil contaminated mainly with PCE or TCE, which, being in an oxidized state, are susceptible to anaerobic reduction rather than to aerobic oxidation processes [66, 67]. Two decades of intense research efforts have proved that under strictly anaerobic conditions, PCE and TCE can be detoxified, via a process of the so-called chlororespiration, consecutively producing *cis*-dichloroethene (cDCE), VC, and finally innocuous ethylene (ETH), when sufficient H_2-releasing electron

donor and dechlorinating bacteria coexist [68]. Although a large number of dechlorinating bacteria has already been isolated [41], only members of the genus *Dehalococcoides* have been shown to be capable of completely dechlorinating TCE to ETH [40, 69–72]. However, since normally electron donors are not sufficient for the complete PCE or TCE to ETH dechlorination [73], H_2-producing simple substrates, such as lactate, butyrate, and methanol, or more complex substrates, such as molasses, vegetable oils, mulch, or compost, should be added, which stimulate the native biological mechanisms [66, 74]. Furthermore, the lack of electron donor can be intensified due to the competition that is mainly developed between dechlorinators and methanogens or sulfate-reducing bacteria (SRB) [55]. Nevertheless, research studies conducted during the last 15 years have proved that dechlorinators can easily outcompete methanogens for H_2, if electron donor is slowly and consistently degraded producing low H_2 concentration [75–78]. Unfortunately, sulfate appears to delay RD under sulfate-reducing conditions, although *Dehalococcoides* population seems not to be affected by sulfate concentration [79]. Although RD is today a widely accepted and relatively low-cost in situ groundwater treatment technology, it cannot be applied indiscriminately to all contaminated sites with chlorinated solvents due to a series of limitations. The most important of them are the site-specific limitations, such as the low permeability or heterogeneity of the aquifer, the slow and incomplete dechlorination, due to microbial competition, unfavorable redox conditions or lack of the appropriate microbial consortia, and the secondary degradation effects, such as solubilization of metals or production of other undesirable fermentation products, due to the electron donor addition.

Biosparging is a remediation technology which, generally, stimulates the indigenous aerobic microorganisms of aquifers by injecting air or oxygen and nutrients, if needed [67, 80]. By and large, Biosparging is a technology that is recommended for sites where lightweight (e.g., gasoline) or midweight (e.g., diesel, jet fuel) petroleum hydrocarbons are dissolved in groundwater and adsorbed to soil below the water table and/or within the capillary fringe [67, 80]. However, Biosparging is not the appropriate remediation technology when free product is present, when basements, sewers, or other subsurface confined spaces are located near the site, and when the aquifer is confined [80]. The efficiency of Biosparging primarily depends on soil permeability, since this parameter controls how well oxygen can be delivered to the subsurface microorganisms and contaminant biodegradability, which determine the rate of remedy action. Other parameters such as soil stratification, groundwater temperature, pH level, microbial population density, nutrient concentration, and contaminants concentration and properties should also be taken into account to appropriately evaluate and design a Biosparging system [80]. Since soil gas and vapors produced commonly require further treatment, Biosparging may be implemented in conjunction with source treatments technologies, such as SVE or bioventing [67].

Despite the fact that the appropriate microorganisms, capable to degrade the target contaminants, can be widely distributed in contaminated soils, this is not always the case [81]. This seems even more likely it is considered that most of times, soil is contaminated by complex contaminants, and often mixture of them, that can only be degradated by a very specific microbial consortium. In cases like these, Bioaugmentation, namely, the inoculation of the contaminated soil with specific competent strain or consortia of microorganisms, could be the solution, if the site conditions have been thoroughly studied and understood [82]. However, today, bioaugmentation is still a limited-applied technology, and further research is needed to build a robust knowledge base of this technology.

Monitored Natural Attenuation

As it has been determined by USEPA, monitored natural attenuation or MNA is the remediation technology, which relies on natural chemical, physical, or biological attenuation processes and, as such, it is suitable to achieve site-specific remediation objectives without human intervention within a more reasonable time frame compared to that offered by other more active remediation technologies. These in situ processes include biodegradation, dispersion, dilution, sorption, volatilization, radioactive decay, and chemical or biological stabilization, transformation, or destruction of contaminants [83]. Monitored natural attenuation has been successfully implemented to date at sites

contaminated with petroleum hydrocarbons, alcohols, ketones, esters, ethers, iron, and manganese, while MNA could also be applicable, under a narrow range of conditions, to chlorinated solvents, lightly halogenated aromatics, PCBs, nitroaromatics, some pesticides, chromium, copper, cadmium, lead, zinc, and nickel [67]. However, prior to selecting MNA as the appropriate treatment technology for a contaminated site, it must be verified that natural processes are efficient enough to consistently ensure the protection of the environment. For this reason, a number of protocols have been published so far that allow proponents of this technology to show that natural degradation processes will reduce the concentrations of corresponding contaminants below regulatory standards before potential receptor exposure pathways are completed [84, 85]. MNA is frequently used in conjunction with EISB.

Soil Vapor Extraction

Soil vapor extraction (SVE), also known as Soil Venting or Vacuum Extraction, is a mature and widely used in situ physical/chemical technology usually applied to remediate well-drained, high permeability unsaturated soils with low organic carbon content mainly contaminated with VOCs or SVOCs [58]. Examples of contaminants that can be removed by SVE include common chemical mixtures, such as gasoline, kerosene, jet fuels, BTEX, styrene, chlorobenzene, chloroform, carbon tetrachloride, PCE, TCE, DCEs, VC, trichloroethane (TCA), dichloroethane (DCA), ethylene dibromide, methylene chloride, acetone, methyl ethyl ketone (MEK), and methyl isobutyl ketone (MIBK) [86]. The general idea behind this technology is to induce a controlled subsurface airflow, in order to remove the soil vapors directly from the subsurface and vaporize contaminants, which are either adsorbed on soil particles, dissolved in pore water or in the form of free-product phase [58]. A typical SVE system usually consists of the extraction wells, equipped with vacuum blower, the injection wells or the air vents, the vapor/liquid separator system, the liquid treatment system, and the off-gas treatment system, which commonly employs an adsorption system, such as Granular Activated Carbon (GAC) or a thermal oxidation system, when a more concentrated waste streams should be treated [86]. As soon as vacuums are applied through the extraction wells to the vadose zone near the source of contamination, a stream of vapors is generated, due to the concurrent accomplished of volatilization, dissolution, and desorption of the free-phase, of the dissolved-phase, and of the sorbed-phase contaminant, respectively. These processes can be promoted through high contaminant vapor pressures, high contaminant Henry's law constants, low contaminant solubilities, high soil intrinsic permeability, and low water and organic carbon soil content [58, 87, 88].

As it has become evident, SVE may achieve more than 90% removal of the contaminants, and generally, its effluent contaminant concentrations become asymptotic after a period of operation [58]. Although this asymptotic performance is usually interpreted as successful completion of the remediation effort, a series of reasons, such as the water table rise and the overdryness of soil, can potentially account for inducing the effluent contaminant concentration [58]. According to USEPAs Superfund Remedy Report [6], SVE has been used in 276 Superfund sites so far, and it is the most frequently used source treatment technology in the USA.

Chemical Treatment

Chemical Treatment comprises a group of in situ or ex situ technologies, which treat either the source or the groundwater employing chemical reactions. The typical representative of this group is the in situ chemical oxidation (ISCO).

ISCO is among the most frequently selected in situ soil remediation technologies either for source or groundwater treatment, mainly due to the wide range of organic contaminants (BTEX, MTBE, petroleum hydrocarbons, chlorinated solvents, PAHs, PCBs, chlorinate benzenes, phenols, organic pesticides, and explosives) that are amenable to chemical oxidation treatment [6, 89]. Generally speaking, ISCO is based on the oxidation of groundwater contaminants into carbon dioxide, water, and chloride ions (in the presence of chlorinated compounds), brought about by the oxidative power of mainly six classes of oxidants, which include permanganate, catalyzed hydrogen peroxide, ozone, persulfate, ozone activated with hydrogen peroxide (peroxone), and percarbonate. Among these, permangnate is the most frequently used [90, 91].

The most common forms of permanganate are the potassium permanganate ($KMnO_4$) and the sodium permanganate ($NaMnO_4$), which are both very strong oxidizing agents and present a remarkable affinity for organic compounds containing carbon–carbon double bonds, aldehyde groups, or hydroxyl groups [89]. However, each kind of permanganate has its own advantages and disadvantages. In particular, since $KMnO_4$ is provided as a solid product transportation hazards are minimized, while the concentrated liquid form of $NaMnO_4$ permits more flexibility in the design of the injection volume. Since manganate can have several different mineral forms and exists in multiple valence states, it can participate into a complex system of different pH-dependent chemical reactions, producing Mn^{2+}, $MnO_2(s)$, or MnO_4^-. In addition to being nonselective, permanganate can be readily consumed, oxidizing in this way other reduced species present in contaminated soil as well, such as natural organic matter or reduced minerals, which could severely affect ISCO performance [89].

Multiphase Extraction

Multiphase extraction (MPE) is a technology employed to remediate both the groundwater and the vadose zone that involves simultaneous extraction of soil vapor and groundwater, which are further treated on site [92]. MPE is usually combined with other remediation technologies, such as bioremediation, air sparging, or bioventing, when the target contaminants include long-chained hydrocarbons, in order to shorten the cleanup time at a site [24]. Although MPE is more effective than SVE for heterogeneous clays and fine sands, it is not recommended for lower permeability formations due to its tendency of leaving isolated lenses of undissolved product in the formation [24]. MPE is usually selected to remediate sites contaminated by VOCs and petroleum hydrocarbons [24], since, according to the recent USEPAs Superfund Remedy Report, it has been implemented in 54 Superfund sites [6]. MPE can be designed and implemented either as a system of a single or two pumps configuration or as the so-called technology of bioslurping, which is applied in order to recover the free-product phase of pollutants. In the single-pump configuration, which can be used only for shallow aquifers, a single vacuum pump is employed to extract both liquid and vapor from a single well. The depth limitation can be overcome by using the two-pump configuration, where a submersible pump for groundwater recovery is used in conjunction with a separate vacuum applied at the sealed wellhead. In this configuration, liquid and vapor streams are separated from one another [92]. Finally, the third configuration, the so-called bioslurping, combines the vacuum-enhanced free-product recovery, which extracts LNAPLs from the capillary fringe and the water table, with bioventing, which stimulates the aerobic bioremediation of hydrocarbon-contaminated soils [24, 92].

Permeable Reactive Barriers

Permeable reactive barriers (PRBs) is a shallow or deep groundwater in situ remediation technology, in which contaminants are treated by means of physical, chemical, or biological processes. In particular, PRBs are continuously permeable treatment zones designed to remediate a contaminant plume, so that the groundwater quality will be acceptable downgradient of the barrier. Generally speaking, PRBs might be divided into conventional and advanced systems. Typical representatives of conventional systems are the continuous PRBs, consisting of a single reactive zone, and the Funnel-and-Gate PRBs, consisting of a reactive placed between two impermeable walls, while advanced systems employ other techniques such as injection systems, hydraulic/pneumatic fracturing, and passive groundwater capture and treatment by reactor cells [93]. PRBs are usually applied to remediation groundwater plumes contaminated with organic compounds, such as chlorinated solvents, BTEX, metals and metalloids, and radionuclides [33, 94, 95]. Today the most widely applied reactive material is by far the zero-valent iron (ZVI), while other materials such as red mud, zeolites, activated carbon, and TiO_2 appear to be among the emerging trends of the subject [33, 93].

Pump-and-Treat

A pump-and-treat system consists of a groundwater extraction system and an aboveground treatment/disposal system, where the pumped groundwater is treated properly and the treated water is either reinjected into the subsurface or discharged into

surface water bodies or to municipal sewer systems [96]. Generally speaking, the purpose of a pump-and-treat system is typically to combine the groundwater treatment with its hydraulic containment [96]. Pump-and-treat has been the dominant treatment technology for groundwater until recently, although its low efficiency and the emergence of more innovative technologies, such as the EISB and the ISCO, have leveled off its application during the last 15 years [6]. The failure of the pump-and-treat was identified as its inability to achieve the remedial goal within a reasonable time period. The most significant factors that contribute to this shortcoming are, on the one hand, the progressively slower rate of decline in dissolved contaminant concentration, referred to as tailing, and, on the other hand, the fairly rapid increase in contaminant concentration that can occur after pumping has been discontinued, referred to as rebound, which usually results in longer treatment times and higher residual concentrations than the cleanup standards. Today it is generally accepted that, although a stand-alone pump-and-treat system is not as efficient as it was expected in the past, the combination of pump-and-treat system with other remediation technologies, such as EISB, may improve the groundwater cleanup efforts [96].

Soil Flushing

Soil flushing is an in situ source treatment technology, in which an aqueous solution is injected or infiltrated into a moderate-to-highly permeable contaminated soil, and the produced elutriate (flushing solution mixed with contaminants) is extracted and treated by the appropriate aboveground processes. Soil flushing can be used to remediate soils contaminated either with inorganics, such as volatile and nonvolatile metals, corrosive, cyanides and radioactive contaminants, or organics, such as NAPLs, VOCs, SVOCs, PCBs, halogenated pesticides [97], where it has been proven that a strong function of interfacial tension is existent [98].

Bioventing

Bioventing is an in situ source treatment technology that, enhancing indigenous microorganism activity, biodegrades organic constituents adsorbed in soils of the unsaturated zone or capillary fringe [67]. More specifically, when bioventing is applied, oxygen is introduced into the unsaturated zone either by injection of either oxygen or air or by the atmosphere due to pressure difference, when soil gas is extracted. In this case, the principle of bioventing is similar to SVE, although biodegradation is the principle mechanism in the former technology and volatilization in the latter. Bioventing is usually applied in sites contaminated with petroleum hydrocarbons, nonchlorinated solvents, some pesticides, wood preservatives, and other organic chemicals [24].

Phytoremediation

Phytoremediation is a shallow in situ technology mainly employed to contain and extract metals, pesticides, explosives, or oil for contaminated soil [99]. Basic mechanisms being involved in phytoremediation technology are phytosequestration, rhizodegradation, phytohydraulics, phytoextraction, phytodegradation, and phytovolatilization. Recently, this technology has been into the spotlight thanks to its numerous benefits, the most important of which are the low construction and operating cost, its ability to remediate soil with organic and inorganic contaminants, its solar-powered nature, the improvement of aesthetics that causes and its applicability as a polishing step in conjunction with another remediation technology, as well [100]. However, the slow removal of contaminants from soil and the absence of significant detoxification, which possibly leads to toxic metabolites accumulation inside plant tissues, result in the generation of large volumes of harvested contaminated plants, which are difficult to dispose, along with the possibility of contaminants being transferred from soil to the food chain via animals and insects' activities. These significant limitations are mainly responsible for the limited application of phytoremediation in real sites so far and for intensive research on engineered plants, which could more efficiently remediate contaminated soil [101–103].

Thermal Treatment

Thermal treatment is an ex situ or an in situ technology, which might achieve contaminated soil remediation by enhancing contaminant vapors and liquids removal as soil temperature is increased. In particular, increasing soil temperature contaminant liquid

viscosity will result in a decrease in interfacial tension as well, while biodegradation rates, solubility, and/or volatility might be increased. The most commonly used thermal technologies include steam-based heating, conductive heating, electrical resistance heating, radio frequency heating, and in situ soil mixing with large diameter augers combined with steam and hot air injection. Thermal treatment presents some noteworthy advantages in comparison with other treatment alternatives, the most significant of which are the reduced operation time, the high variability of the chemical that could be treated, and the low sensitivity to subsurface heterogeneities. However, thermal treatment bears several drawbacks, on the grounds that it is not applicable to occupied sites, is very costly, demands more sophisticated design and operation, has the potential of transferring contaminants to uncontaminated sites, and, finally, elevating temperature after treatment which could remain in that state for months or years [104, 105].

Air Sparging

Air sparging is an in situ remediation technology by which clean pressurized air is injected directly to aquifers mainly contaminated with fuels and VOCs. Air sparging is mainly an extraction technology, since the main remediation mechanism is the volatilization of dissolved, trapped, or sorbed contaminants. Additionally, oxygen introduced into the aquifer via aeration also promotes contaminants' biodegradation, which further increases technology's performance. However, since vapors of contaminants are the technology end-product, air sparging is usually applied in conjunction either with the SVE or with the EISB, which undertake contaminant vapor treatment in the vadose zone [24, 65].

Electrokinetic Separation

The electrokinetic separation is an in situ remediation technology with very limited application so far [6]. The principle behind this technology is the mobilization of contaminants and contaminated water due to an imposed electric field formed by the application of a low-voltage direct current through the soil [106]. The basic mechanisms of contaminants transport are the electroosmosis and electromigration. Electroosmosis induces the movement of contaminated groundwater from the anode to the cathode, through a treatment zone, while electromigration induces the movement of charged particles to the electrode with opposite charge, where contaminants are removed for ex situ treatment. Typical contaminants that could be treated with electrokinetic separation include heavy metals, anions, and polar organics, with concentrations ranging from a few parts per million (ppm) to tens of thousands ppm [24]. Among the main limitations of this technology are the high energy amount required, the close dependence on the local geology, and the production of undesirable end-products.

Soil Washing

Soil washing is an ex situ technology by which contaminants, such as SVOCs, heavy metals, petroleum and fuel residuals, PAHs, PCBs, and pesticides, are removed from excavated soil by physical and/or chemical separation processes [65, 107]. Some physical separation processes commonly used include mechanical screening, hydrodynamic classification, gravity concentration, froth flotation, magnetic separation, electrostatic separation, and attrition scrubbing. Since further treatment might be necessary to efficiently remediate excavated contaminated soil, appropriate reagents might be used to extract contaminants from soil [107]. These reagents are selected based on their ability to react with specific contaminants and typically include acids, chloride solutions, chelating agents, surfactants, or reducing and oxidizing agents [108]. A major drawback of soil washing is the generation of a heavily contaminated stream of waste, which should be further and properly treated usually by another remediation technology such as incineration or bioremediation [65].

Incineration

Another widely used source treatment technology is the incineration via which harmful chemicals, such as PCBs and dioxins, are volatilized, combusted in 870–1,200°C, and, finally, destroyed and removed by as much as 99.9999%, while off gases and combustion residuals are further treated and properly disposed [24, 109]. The economics of incineration, however, are generally questionable, even more so in the treatment of contaminated soils.

Containment Technologies

Containment Technologies might be used either independently or in conjunction with treatment technologies, such as EISB, MNA, ISCO, etc. Typical Containment Technologies that are widely used today are the cover systems, the bottom liner, and the vertical engineered barriers [6]. Cover systems are surface barriers used to contain source material to minimize leachate creation and direct contact with receptors, while bottom liner is a subsurface barrier that prevents the leachate from contaminated source to migrate to groundwater. Finally, vertical engineered barriers are usually designed either to contain source material and groundwater or to divert contaminated groundwater from receptors [6].

Emerging Trends

Since the need for more sustainable and more efficient contaminated soil remediation is continuously growing, new trends have emerged to these directions. Among them, the waste combination approach, remediation with nanoparticles and phytoremediation with engineered plants are probably the most important ones.

In particular, the waste combination approach appears to be an attractive alternative to traditional technologies, since waste disposal and contaminated soil remediation are combined. Typical examples of the waste combination approach are the use of fly-ash waste materials [39], fish cannery wastes [64], barium wastes [110], and red mud [111] to remediate heavy-metals-contaminated sites.

The use of nanoparticles is another very promising emerging trend in contaminated soil remediation, called nanoremediation [112]. Many different nanoparticles have been studied so far for contaminated soil remediation such as nanoscale zeolites, metal oxides, carbon nanotubes and fibers, enzymes, various noble metals, titanium dioxide, and nanoscale zero-valent iron (nZVI). However, the most important of these materials are the nZVI, commonly being modified to improve their deliverability in porous media [112, 113]. Extensive research studies have demonstrated that nZVI can effectively treat a series of commonly detected soil contaminants such as PCE, TCE, carbon tetrachloride, nitrate, explosives, pesticides, and heavy metals [114]. Although nZVI holds great potential becoming an efficient remediation perspective, there still remain open questions concerning the fate, transport, and toxicity of nZVI and nanomaterials in general, awaiting convincing answers [115].

The last of the aforementioned emerging trends regards the use of transgenic plants to improve phytoremediation efficiency in soil contaminated with organic compounds. In particular, plants usually lack the catabolic enzymes which are necessary for the complete detoxification of organic compounds [101, 102]. Therefore, during the last decade, intensive research has been conducted in order to produce and test new transgenic plants, such as *Nicotiana tabaccum* and *Oryza sativa*, which are able to completely detoxify organic pollutants, such as solvents, pesticides, and explosives [101–103].

Future Directions

Contaminated soil remediation is a costly and technically challenging activity, but it can be viewed as imperative for human health and the environment's protection worldwide. Since our scientific knowledge is continuously expanding and our analytical capabilities are rapidly improving, requirements for cleaner drinking water, increased reliance on groundwater resources, and a drive for more extensively restored contaminated land will be intensified during the coming years. However, the high complexity of contaminated soil problems along with the very high cost that soil remediation requires render appropriate contaminated site characterization, effective design of remediation schemes, and affordable implementation of the selected technologies great challenges for scientists, engineers, and practitioners. Since the cost investment required for remediation of all the known contaminated sites is currently out of reach, the most significant contaminated site problems in terms of risk for potential receptors should be prioritized and addressed first. Thus, sites currently posing the most significant risk to human health and the environment should be high in the list, while remediation of contaminated sites that pose no significant risk could be delayed. On the other hand, as the high cost of remediation allows practitioners to test merely one or two different alternatives in practice, the whole decision-making process should

be further improved. In particular, regarding site characterization, procedures such as the determination of contaminant speciation ought to be mandated as well as improved, in order to become standard practice while been more informative, widely available, and less expensive. In addition, as far as laboratory techniques are concerned, treatability studies and molecular techniques should be simplified and be more representative of the field conditions. Furthermore, the rationale of waste combination should be adopted whenever possible, in order to achieve a twofold goal, namely, waste minimization and soil remediation. Taking into account the high value of soil and water for mankind and the environment and the collectively unaffordable remediation costs, it can be safely concluded that there will be a future shift of focus in this subject aiming both in pollution prevention at or near the source and overall sustainability of remediation activities.

Bibliography

Primary Literature

1. Howard G, Bartram J, Pedley S, Schmoll O, Chorus I, Berger P (2006) Groundwater and public health. In: Schmoll O, Howard G, Chilton J, Chorus I (eds) Protecting groundwater for health. World Health Organization, Geneva
2. Singh A, Kuhad RC, Ward OP (2009) Biological remediation of soil: an overview of global market and available technologies. In: Singh A, Kuhad RC, Ward OP (eds) Advances in applied bioremediation. Springer, Berlin, pp 1–19
3. European Environment Agency (2007) Progress in management of contaminated sites (CSI 015). http://www.eea.europa.eu/data-and-maps/indicators/progress-in-management-of-contaminated-sites/progress-in-management-of-contaminated-1
4. Vatseris C, Tsatsarelis T, Karteris A, Papadopoulos S, Dermatas D (2010) Environmental risk assessment model for potentially contaminated sites. In: Protection and restoration of the environment X, 5–9 July, Corfu (CD-ROM edition)
5. Mitchell JK (1993) Fundamentals of soil behavior. Wiley, New York
6. USEPA (2010) Superfund remedy report, 13th edn. Office of Solid Waste and Emergency Response, Washington, DC, EPA 542-R-10-004
7. Reddy KR (2008) Physical and chemical groundwater remediation technologies. In: Darnault CJG (ed) Overexploitation and contamination of shared groundwater resources. Springer, Dordrecht, pp 257–274
8. Yong RN (2001) Geoenvironmental engineering, contaminated soils, pollutant fate, and mitigation. CRC Press, Boca Raton
9. Reddi L, Inyang HI (2000) Geoenvironmental engineering. Marcel Dekker, New York
10. Sharma HD, Reddy KR (2004) Geoenvironmental engineering, soil remediation, waste containment and emerging waste management technologies. John Wiley & Sons Inc, Hoboken, New Jersey
11. Freeze RA, Cherry JA (1979) Groundwater. Prentice Hall, Englewood Cliffs, New Jersey
12. Mirsal IA (2010) Soil pollution, origin, monitoring and remediation. Springer, Berlin
13. Lambe TW, Whitman RV (1969) Soil mechanics. Wiley, New York
14. Dermatas D, Menounou N, Dadachov M, Dutko P, Shen G, Xu X, Tsaneva V (2006) Lead leachability in firing range soils. Environ Eng Sci 23:86–99
15. Tessier A, Campbell PGC, Bisson M (1982) Particulate trace metal speciation in stream sediments and relationship with grain size: implication for geochemical exploration. J Geochem Explor 6:77–104
16. Yong RN, Warkentin BP, Phadungchewit Y, Galvez R (1990) Buffer capacity and lead retention in some clay materials. Water Air Soil Pollut 53:53–67
17. Yong RN, Phadungchewit Y (1993) pH Influence on selectivity and retention of heavy metals in some clay soil. Can Geotech J 30:821–833
18. Cao X, Ma LQ, Chen M, Hardison DW, Harris WG (2003) Lead transformation and distribution in the soils of shooting ranges in Florida, USA. Sci Total Environ 307:179–189
19. Dermatas D, Menounou N, Meng XG (2006) Mechanisms of lead immobilization in treated soils. Land Contam Recl 14:43–56
20. Borch T, Kretzschmar R, Kappler A, Van Cappellen P, Ginder-Vogel M, Voegelin A, Campbell K (2010) Biogeochemical redox processes and their impact on contaminant dynamics. Environ Sci Technol 44:15–23
21. Chapelle FH, Bradley PM (2003) Redox conditions and the reductive/oxidative biodegradation of chlorinated ethenes in groundwater systems. In: Häggblom MM, Bossert ID (eds) Dehalogenation, microbial processes and environmental applications. Kluwer Academic, Boston, pp 373–384
22. Major D, Edwards E, McCarty P, Gossett J, Hendrickson E, Löffler F, Zinder S, Ellis D, Vidumsky J, Harkness M, Klecka G, Cox E (2003) Discussion of environment vs. bacteria or let's play, name that bacteria. Ground Water Monit R 23:32–48
23. NRC (2000) Natural attenuation for groundwater remediation. National Academic Press, Washington, DC
24. FRTR (2007) Remediation technologies screening matrix and reference guide, version 4.0. http://www.frtr.gov/matrix2/top_page.html
25. Kostecki P, Morrison R, Dragun J (2005) Hydrocarbons. In: Hillel D (ed) Encyclopedia of soils in the environment. Elsevier, Oxford, pp 217–226
26. Andreoni V, Gianfreda L (2007) Bioremediation and monitoring of aromatic-polluted habitats. Appl Microbiol Biotechnol 76:287–308

27. Farhadian M, Vachelard C, Duchez D, Larroche C (2008) In situ bioremediation of monoaromatic pollutants in groundwater: a review. Bioresour Technol 99:5296–5308
28. Gan S, Lau EV, Ng HK (2009) Remediation of soils contaminated with polycyclic aromatic hydrocarbons (PAHs). J Hazard Mater 172:532–549
29. Häggblom MM, Bossert ID (2003) Halogenated organic compounds – a global perspective. In: Häggblom MM, Bossert ID (eds) Dehalogenation, microbial processes and environmental applications. Kluwer Academic, Boston, pp 3–29
30. Moran JM, Zogorski JS, Squillace PJ (2007) Chlorinated solvents in groundwater of the United States. Environ Sci Technol 41:74–81
31. McCarty PL (2010) Groundwater contamination by chlorinated solvents: history, remediation technologies and strategies. In: Stroo HF, Ward CH (eds) In situ remediation of chlorinated solvent plumes. Springer, New York, pp 1–28
32. Evanko CR, Dzombak DA (1997) Remediation of metals – contaminated soils and groundwater. Technology Evaluation Report, TE-97-01. Ground-Water Remediation Technologies Analysis Center (GWRTAC), Pittsburg
33. Hashim MA, Mukhopadhyay S, Sahu JN, Sengupta B (2011) Remediation technologies for heavy metal contaminated groundwater. J Environ Manage 92:2355–2388
34. USEPA (2006) Radionuclides in soil. RadTownUSA, United States Environmental Protection Agency Office of Radiation and Indoor Air, Washington, DC, EPA 402-F-06-051
35. Gavrilescu M, Pavel LV, Cretescu I (2009) Characterization and remediation of soils contaminated with uranium, review. J Hazard Mater 163:475–510
36. Kalderis D, Juhasz AL, Boopathy R, Comfort S (2011) Soil contaminated with explosives: environmental fate and evaluation of state-of-the-art remediation processes (IUPAC technical report). Pure Appl Chem 83:1407–1484
37. Shackelford CD (1993) Contaminant transport. In: Daniel DE (ed) Geotechnical practice for waste disposal. Chapman and Hall, London, pp 33–65
38. Rouse JV, Pyrih RZ (1993) Geochemistry. In: Daniel DE (ed) Geotechnical practice for waste disposal. Chapman and Hall, London, pp 15–32
39. Dermatas D, Meng X (2003) Utilization of fly-ash for stabilization/solidification of heavy metal contaminated soils. Eng Geol 70:377–394
40. Maymó-Gatell X, Chien YT, Gossett JM, Zinder SH (1997) Isolation of a bacterium that reductively dechlorinates tetrachloroethene to ethene. Science 276:1568–1571
41. Aulenta F, Majone M, Tandoi V (2006) Review: enhanced anaerobic bioremediation of chlorinated solvents: environmental factors influencing microbial activity and their relevance under field conditions. J Chem Technol Biot 81:1463–1474
42. Bhatt P, Kumar MS, Mudliar S, Chalrabarti T (2007) Biodegradation of chlorinated compounds – a review. Crit Rev Environ Sci Technol 37:165–198
43. Pollard SJT, Brookes A, Earl N, Lowe J, Kearney T, Nathanail CP (2004) Integrating decision tools for the sustainable management of land contamination. Sci Total Environ 325:15–28
44. Ellis DE, Hadley PW (2009) Sustainable remediation white paper – integrating sustainable principles, practices, and metrics into remediation projects. Remediation 19:5–10
45. ASTM E1527-05 (2005) Standard practice for environmental site assessment: phase I environmental site assessment process. ASTM, West Conshohoken, Pennsylvania
46. ASTM E1903–97 (2002) Standard guide for environmental site assessment: phase II environmental site assessment process. ASTM, West Conshohoken, Pennsylvania
47. Petts J, Cairney T, Smith M (1997) Risk-based contaminated land investigation and assessment. John Wiley & Sons Ltd, Chichester
48. Caliman FA, Robu BM, Smaranda C, Pavel VL, Gavrilescu M (2011) Soil and groundwater cleanup: benefits and limits of emerging technologies. Clean Technol Environ Policy 13:241–268
49. Dermatas D, Shen G, Chrysochoou M, Grubb DG, Menounou N, Dutko P (2006) Pb speciation versus TCLP release in army firing range soils. J Hazard Mater 136:34–46
50. Scheckel KG, Impellitteri CA, Ryan JA, Mcevoy T (2004) Assessment of a sequential extraction procedure for perturbed lead-contaminated samples with and without phosphorus amendments. Environ Sci Technol 37:5296–5304
51. Cao X, Dermatas D (2007) Evaluating the applicability of regulatory leaching tests for assessing lead leachability in contaminated shooting range soils. Environ Monit Assess 139:1–13
52. Kosson DS, van der Sloot HA, Sanchez F, Garrabrants AC (2002) An integrated framework for evaluating leaching in waste management and utilization of secondary materials. Environ Eng Sci 19:159–204
53. van der Sloot HA, van Zomeren A, Meeuwsen HCL, Seignette P, Bleyerveld R (2007) Test method selection, validation against field data, and predictive modelling for impact evaluation of stabilized waste disposal. J Hazard Mater 141:354–369
54. Dermatas D, Chrysochoou M, Moon DH (2008) Geoenvironmental characterization to assess waste stabilization/solidification treatment performance and sustainability. GeoCongress 2008: Geotechnics of Waste Management and Remediation, pp 660–667
55. Fennell DE, Gossett JM (2003) Microcosms for site-specific evaluation of enhanced biological reductive dehalogenation. In: Häggblom MM, Bossert ID (eds) Dehalogenation, microbial processes and environmental applications. Kluwer Academic, Boston, pp 385–420
56. USEPA (2001) A citizen's guide to solidification/stabilization. Office of Solid Waste and Emergency Response, Washington, DC, EPA 542-F-01-024
57. USEPA (2009) Technology performance review: selecting and using solidification/stabilization treatment for site remediation. National Risk Management Research Laboratory, Washington, DC, EPA 600-R-09-148

58. USEPA (2006) In situ treatment technologies for contaminated soil. Office of Solid Waste and Emergency Response, Washington, DC, EPA 542/F-06/013
59. Mitchell JK, Dermatas D (1992) Clay soil heave caused by lime-sulfate reactions. Innovations in uses for lime, ASTM STP 1135. American Society for Testing and Materials (ASTM), Philadelphia, pp 41–64
60. USEPA (1999) Solidification/stabilization resource guide. Office of Solid Waste and Emergency Response, Washington, DC, EPA 549-B-99-002
61. Conner JR (1990) Chemical fixation and solidification of hazardous wastes. VNR, New York
62. USEPA (2001) Best management practices for lead at outdoor shooting ranges. Division of Enforcement and Compliance Assistance, New York, EPA-902-B-01-001
63. Chrysochoou M, Dermatas D, Grubb DG (2007) Phosphate application to firing range soils for Pb immobilization: the unclear role of phosphate. J Hazard Mater 144:1–14
64. ESTCP (2006) PIMS^{MT}: remediation of soil and groundwater contaminated with metals, cost and performance report (ER-0020)
65. Khan FI, Hussain T, Hejazi R (2004) An overview and analysis of site remediation technologies. Environ Manage 71:95–122
66. Parsons Corporation (2004) Principles and practices of enhanced anaerobic bioremediation of chlorinated solvents Prepared for AFCEE (Air Force Center for Environmental Excellence), NFESC (Naval Facilities Engineering Service Center) and ESTCP (Environmental Security Technology Certification Program)
67. USEPA (2006) In situ and ex situ biodegradation technologies for remediation of contaminated sites. Office of Research and Development National Risk Management, Cincinnati, EPA 625-R-06-015
68. Bradley PM, Chapelle FH (2010) Biodegradation of chlorinated ethenes. In: Stroo HF, Ward CH (eds) In situ remediation of chlorinated solvent plumes. Springer, New York, pp 39–67
69. Cupples AM, Spormann AM, McCarty PL (2003) Growth of a *Dehalococcoides*-like microorganism on vinyl chloride and *cis*-dichloroethene as electron acceptors as determined by competitive PCR. Appl Environ Microbiol 69:953–959
70. He J, Ritalahti KM, Yang KL, Koenigsberg SS, Löffler FE (2003) Detoxification of vinyl chloride to ethene coupled to growth of an anaerobic bacterium. Nature 424:62–65
71. He J, Sung Y, Krajmalnik-Brown R, Ritalahti KM, Löffler FE (2005) Isolation and characterization of *Dehalococcoides* sp. strain FL2, a trichloroethene (TCE)- and 1,2-dichloroethene-respiring anaerobe. Environ Microbiol 7:1442–1450
72. Sung Y, Ritalahti KM, Apkarian RP, Löffler FE (2006) Quantitative PCR confirms purity of strain GT, a novel trichloroethene-to-ethene-respiring *Dehalococcoides* isolate. Appl Environ Microbiol 72:1980–1987
73. Wiedemeier TH, Swanson MA, Moutoux DE, Gordon EK, Wilson JT, Wilson BH, Kampbell DH, Hansen JE, Haas P, Chapelle FH (1998) Technical protocol for evaluating natural attenuation of chlorinated solvents in groundwater. Office of Research and Development, Cincinnati, EPA 600-R-98-128
74. Panagiotakis I, Mamais D, Pantazidou M, Marneri M, Parapouli M, Hatziloukas E, Tandoi V (2007) Dechlorinating ability of TCE-fed microcosms with different electron donors. J Hazard Mater 149:582–589
75. Smatlak CR, Gossett JM, Zinder SH (1996) Comparison kinetics of hydrogen utilization for reductive dechlorination of tetrachloroethene and methanogenesis in an anaerobic enrichment culture. Environ Sci Technol 30:2850–2858
76. Ballapragada BS, Stensel HD, Puhakka JA, Ferguson JF (1997) Effect of hydrogen on reductive dechlorination of chlorinated ethenes. Environ Sci Technol 31:1728–1734
77. Fennell DE, Gossett JM, Zinder SH (1997) Comparison of butyric acid, ethanol, lactic acid, and propionic acid as hydrogen donors for the reductive dechlorination of tetrachloroethene. Environ Sci Technol 31:918–926
78. Yang Y, McCarty PL (1998) Competition for hydrogen within a chlorinated solvent dechlorinating anaerobic mixed culture. Environ Sci Technol 32:3591–3597
79. Pantazidou M, Panagiotakis I, Mamais D, Zikidi V (2011) Chloroethene biotransformation in the presence of varying sulfate concentrations. Ground Water Monit R (to appear) doi:10.1111/j1745-6592.2011.01372.x
80. USEPA (2004) How to evaluate alternative cleanup technologies for underground storage tank sites: a guide for corrective action plan reviewers. Office of Solid Waste and Emergency Response, Washington, DC, EPA/510/R-04-002
81. Hendrickson ER, Payne JA, Young RM, Starr MG, Perry MP, Fahnestock S, Ellis DE, Ebersole RC (2002) Molecular analysis of *Dehalococcoides* 16S ribosomal DNA from chloroethene-contaminated sites throughout North America and Europe. Appl Environ Microbiol 68:485–495
82. El Fantroussi S, Agathos SN (2005) Is bioaugmentation a feasible strategy for pollutant removal and site remediation? Curr Opin Microbiol 8:268–275
83. USEPA (1999) Monitored natural attenuation of petroleum hydrocarbons. Office of Research and Development, Washington, DC, EPA 600-F-98-021
84. Stiber NA, Pantazidou M, Small MJ (1999) Expert system methodology for evaluating reductive dechlorination at TCE sites. Environ Sci Technol 33:3012–3020
85. Wiedemeier TH, Swanson M, Moutoux DE, Gordon EK, Wilson JT, Wilson BH, Kampbell DH, Hansen JE, Haas P, Chapelle FH (1998) Technical protocol for evaluating natural attenuation of chlorinated solvents in groundwater. U.S. Government Printing Office, Cincinnati, EPA 600-R-98-128
86. USEPA (2006) Off-gas treatment technologies for soil vapor extraction systems: state of the practice. Office of Solid Waste and Emergency Response, Washington, DC, EPA 542-R-05-028
87. Albergaria JT, Alvim-Ferraz MCM, Delerue-Matos C (2006) Remediation efficiency of vapour extraction of sandy soils contaminated with cyclohexane: influence of air flow rate, water and natural organic matter content. Environ Pollut 143:146–152

88. Soares AA, Albergaria JT, Domingues VF, Alvim-Ferraz MCM, Delerue-Matos C (2010) Remediation of soils combining soil vapor extraction and bioremediation: benzene. Chemosphere 80:823–828
89. ITRC (2005) Technical and regulatory guidance for in situ chemical oxidation of contaminated soil and groundwater, 2nd edn. In Situ Chemical Oxidation Team, Washington, DC
90. Krembs FJ, Siegrist RL, Crimi ML, Furrer RF, Petri BG (2010) ISCO for groundwater remediation: analysis of field applications and performance. Ground Water Monit R 30:42–53
91. USEPA (2006) In situ chemical oxidation. Office of Research and Development National Risk Management Research Laboratory, Washington, DC, EPA 600-R-06-072
92. USEPA (1999) Multi-phase extraction: state-of-the-practice. Solid Waste and Emergency Response, Washington, DC, EPA 542-R-99-004
93. Thiruvenkatachari R, Vigneswaran S, Naidu R (2008) Permeable reactive barrier for groundwater remediation, review. J Ind Eng Chem 14:145–156
94. USEPA (1998) Permeable reactive barrier technologies for contaminant remediation. Office of Research and Development, Office of Solid Waste and Emergency Response, Washington, DC, Report number EPA 600-R-98-125
95. Gillham RW, Vogan J, Gui L, Duchene M, Son J (2010) Iron barrier walls for chlorinated solvent remediation. In: Stroo HF, Ward CH (eds) In situ remediation of chlorinated solvent plumes. Springer, New York, pp 537–571
96. USEPA (1996) Pump-and-treat ground-water remediation a guide for decision makers and practitioners. Office of Research and Development, Cincinnati, EPA 625-R-95-005
97. Roote DS (1997) In situ flushing. GWRTAC, Technology overview report, TO-97-02
98. Dermatas D, Korfiatis GP, Kostarellos D (1993) Soil column study of DNAPL recovery using surfactant flushing. In: National conference on environmental engineering, July, 1993, Montreal, vol 2, pp 1411–1418
99. USEPA (2001) A citizen's guide to phytoremediation. Office of Solid Waste and Emergency Response, Washington, DC, EPA 542-F-01-002
100. ITRC (2009) Phytotechnology technical and regulatory guidance and decision trees, revised. ITRC, Washington, DC
101. Van Aken B (2008) Transgenic plants for phytoremediation: helping nature to clean up environmental pollution. Trend Biotechnol 26:225–227
102. Van Aken B (2009) Transgenic plants for enhanced phytoremediation of toxic explosives. Curr Opin Biotechnol 20:231–236
103. Abhilash PC, Jamil S, Singh N (2009) Transgenic plants for enhanced biodegradation and phytoremediation of organic xenobiotics. Biotechnol Adv 27:474–488
104. USEPA (2004) In situ thermal treatment of chlorinated solvents fundamentals and field applications. Office of Solid Waste and Emergency Response, Washington, DC, EPA 542-R-04-010
105. Kingston JT, Dahlen PR, Johnson PC, Foote E, Williams S (2010) Critical evaluation of state-of-the-art in situ thermal treatment technologies for DNAPL source zone treatment. ESTCP project final report
106. Virkutytea J, Sillanpää M, Latostenmaa P (2002) Electrokinetic soil remediation – critical overview. Sci Total Environ 289:97–121
107. Dermont G, Bergeron M, Mercier G, Richer-Laflèche M (2008) Soil washing for metal removal: a review of physical/chemical technologies and field applications. J Hazard Mater 152:1–31
108. Chu W, Chan KH (2003) The mechanism of the surfactant-aided soil washing system for hydrophobic and partial hydrophobic organics. Sci Total Environ 307:83–92
109. USEPA (2002) A citizen's guide to incineration. Office of Solid Waste and Emergency Response, Washington, DC, EPA 542-F-01-018
110. Chrysochoou M, Dermatas D, Moon DH, Christodoulatos C, Wazne M, French C, Morris J, Kaouris M (2006) Investigation of barium treatment of chromite ore processing residue (COPR). In: Fukue M, Kita K, Ohtsubo M, Chaney R (eds) Contaminated sediments, evaluation and remediation techniques. ASTM, West Conshohocken, pp 165–175
111. Lombi E, Zhao F-J, Zhang G, Sun B, Fitz W, Zhang H, McGrath SP (2002) In situ fixation of metals in soils using bauxite residue: chemical assessment. Environ Pollut 118:435–443
112. Karn B, Kuiken T, Otto M (2009) Nanotechnolgy and in situ remediation: a review of the benefits and potential risks. Environ Health Persp 117:1823–1831
113. Phenrat T, Saleh N, Sirk K, Tilton RD, Lowry GV (2007) Aggregation and sedimentation of aqueous nanoscale zerovalent iron dispersions. Environ Sci Technol 41:284–290
114. X-Q Li, Elliott DW, Zang W-X (2006) Zero-valent iron nanoparticles for abatement of environmental pollutants: materials and engineering aspects. Crit Rev Solid State 31:111–122
115. Keane E (2009) Fate, transport, and toxicity of nanoscale zero-valent iron (nZVI) used during superfund remediation. USEPA, Office of Solid Waste and Emergency Response, Office of Superfund Remediation and Technology Innovation, Washington, DC

Books and Reviews

NRC (2004) Contaminants in the subsurface, source zone assessment and remediation. The National Academic Press, Washington, DC

Nielsen DM (2006) Environmental site characterization and ground-water monitoring. Taylor & Francis, Boca Raton

Pankow JF, Cherry JA (1996) Dense chlorinated solvents and other DNAPLs in groundwater history, behavior, and remediation. Waterloo Press, Portland

Sara MN (2003) Site assessment and remediation handbook. Lewis Publishers, Boca Raton

Siegrist RL, Crimi M, Simpkin TJ (2011) In situ chemical oxidation for groundwater remediation. Springer, New York

Stroo HF, Ward CH (2010) In situ remediation of chlorinated solvent plumes. Springer, New York

Contemporary Sea Level Variations, Observations and Causes

Anny Cazenave
LEGOS, Laboratoire d'Etudes en Geophysique et Oceanographie Spatiales, Toulouse, France

Article Outline

Glossary
Definition of the Subject
Introduction
Observations of Sea Level Change and Variability (Twentieth Century and Last Two Decades)
Causes of Present-Day Sea Level Changes (Global Mean and Regional Variability)
Future Sea Level Rise
Impacts of Sea Level Rise
Future Directions
Bibliography

Glossary

Glacier Large persistent ice body, generally formed in mountain areas by snow accumulation during winter and further compaction into ice.

Ice sheets Ice bodies covering the Greenland and Antarctica continents.

Mean sea level A measure of the average height of the ocean's surface with respect to a fixed reference surface.

Satellite altimetry Space technique dedicated to the measurement of the height of the sea surface from a satellite-borne radar altimeter.

Sea level rise Sea level rises in response to global warming. The components that cause sea level rise are ocean thermal expansion and freshwater mass addition to the oceans due to land ice melt and land water-storage decrease.

Steric sea level Contribution to observed sea level due to temperature and salinity variations.

Thermal expansion Volume change of ocean water response to a change in temperature.

Definition of the Subject

Sea level change is a very sensitive index of climate change and variability. For example, as the ocean warms in response to global warming, seawaters expand, and thus sea level rises. When mountain glaciers melt in response to increasing air temperature, sea level rises because of freshwater mass input to the oceans. Similarly, ice mass loss from the ice sheets causes sea level rise. Corresponding increase of freshwater into the oceans changes water salinity, hence seawater density as well as ocean circulation that in turn affects sea level and its spatial variability. Modification of the land hydrological cycle due to climate variability and direct anthropogenic forcing leads to increased or decreased runoff, hence ultimately to sea level change. Hence local and regional climate changes may affect the sea level.

Introduction

Sea level variations spread over a very broad spectrum. The largest global-scale sea level changes (100–200 m in amplitude) occurred on geological timescales (~100 myr) and depended primarily on tectonics processes (e.g., large-scale change in the shape of ocean basins associated with seafloor spreading and mid-ocean ridges expansion). With the formation of long-live ice sheets (e.g., formation of the Antarctica ice sheet about 35 myr ago) global mean sea level dropped by about 60 m. Cooling of the Earth since about 3 myr ago has led to glacial/interglacial cycles driven by changes of the Earth's orbit and obliquity. Quasi-periodic growth and decay of the northern hemisphere ice caps on a timescale of tens of thousands of years have produced large oscillations of the global mean sea level, on the order of 100 m. On shorter (decadal to multi-centennial) timescales sea level fluctuations are mainly driven by natural forcing factors (e.g., solar radiation, volcanic eruptions) and internal variability the climate system (e.g., atmosphere-ocean perturbations such as El Nino-Southern Oscillation (ENSO), North Atlantic Oscillation (NAO), and Pacific Decadal Oscillation (PDO)). Since the beginning of the industrial era, sea level is also responding to anthropogenic global warming. In this chapter, only recent (last few decades) sea level variations and their causes are discussed.

Observations of Sea Level Change and Variability (Twentieth Century and Last Two Decades)

Twentieth Century

Our knowledge of the past century sea level change comes from tide gauge measurements located along

continental coastlines and islands. The largest tide gauge data base of monthly and annual mean sea level records is the Permanent Service for Mean Sea Level (PSMSL, www.psmsl.org) which contains data for the twentieth century from ~2,000 sites maintained by about 200 nations. The records are somewhat inhomogeneous in terms of data length and quality. For long-term sea level studies, only ~10% of this data set is useable because of data gaps. Tide gauges measure sea level relatively to the ground, hence monitor also ground motions. In active tectonic and volcanic regions, or in areas subject to strong ground subsidence due to natural causes (e.g., sediment loading in river deltas) or human activities (groundwater pumping and oil/gas extraction), tide gauge data are directly affected by the corresponding ground motions. Postglacial rebound, the visco-elastic response of the Earth to last deglaciation (also called Glacial Isostatic Adjustment (GIA)) is another process that gives rise to vertical land movement.

After the ~130 m sea level rise associated with the deglaciation that followed the Last Glacial Maximum ~20,000 years ago, geological, geochemical and archeological observations indicate that the mean sea level remained almost stable during the last 2–3 millennia [1, 2]. However, since the late nineteenth century tide gauge records have shown significant sea level rise. During the twentieth century, a mean rate of ~1.8 mm/year is reported [3–5]. Figure 1 shows tide gauge-based sea level evolution for the twentieth century.

Satellite Altimetry Era

Since the early 1990s, satellite altimetry has become the main tool for precisely and continuously measuring sea level with quasi-global coverage and a few days revisit time. Compared to tide gauges which provide sea level relative to the ground, satellite altimetry measures "absolute" sea level variations. The concept of the satellite altimetry measurement is simple: the onboard radar altimeter transmits microwave radiation toward the sea surface which partly reflects back to the satellite. Measurement of the round-trip travel time provides the height of the satellite above the instantaneous sea

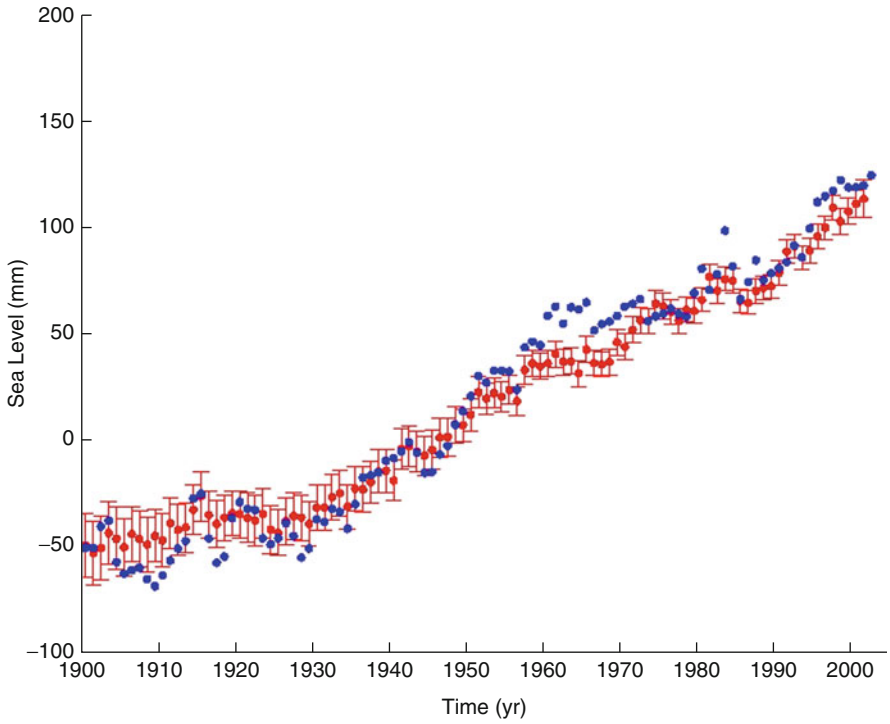

Contemporary Sea Level Variations, Observations and Causes. Figure 1
Global mean sea level evolution (1900–2000) during the twentieth century (Data based on tide gauges; *red points* from Ref. [3]; *blue points* from Ref. [5])

surface (called "range"). The quantity of interest in oceanography is the sea surface height above a fixed reference surface (typically a conventional reference ellipsoid). It is obtained by the difference between the altitude of the satellite above the reference (deduced from precise orbitography) and the range measurement. The estimated sea surface height needs be corrected for various factors due to ionospheric and atmospheric delay, and of biases between the mean electromagnetic scattering surface and sea at the air-sea interface. Other corrections due geophysical effects, such as solid Earth, and pole and ocean tides, are also applied. High-precision satellite altimetry started with the launch of Topex/Poseidon in 1992 and its successors Jason-1 and Jason-2 launched in 2001 and 2008, respectively. The precision of an individual sea surface height measurement based on these missions has reached the 1–2 cm level. Precision on the global mean rate of rise is currently of $\sim$ 0.4–0.5 mm/year. This value is based on error budget analyses of all sources of errors affecting the altimetry system or on comparisons with tide gauge-based sea level measurements (e.g., [6–10]). The temporal evolution of the global mean sea level from satellite altimetry since early 1993 is shown in Fig. 2. It is characterized by an almost linear increase (except for temporary anomalies associated with the 1997–1998 El Nino and the 2007–2008 and 2010–2011 La Ninas). Over this 18-year-long period, global mean sea level has been rising at a rate of $\sim 3.2 \pm 0.4$ mm/year. This rate is significantly higher than the mean rate recorded by tide gauges over the past decades.

Satellite altimetry has also revealed that sea level is not rising uniformly (Fig. 3). In some regions (e.g., Western Pacific), the rates of sea level rise have been faster than the global mean rate by a factor of up to 3 over the past two decades. In other regions rates have been slower than the global mean (e.g., Eastern Pacific).

Causes of Present-Day Sea Level Changes (Global Mean and Regional Variability)

Global Scale

The main factors causing current global mean sea level rise are thermal expansion of seawaters, land ice loss, and freshwater mass exchange between oceans and land water reservoirs. These contributions vary in response

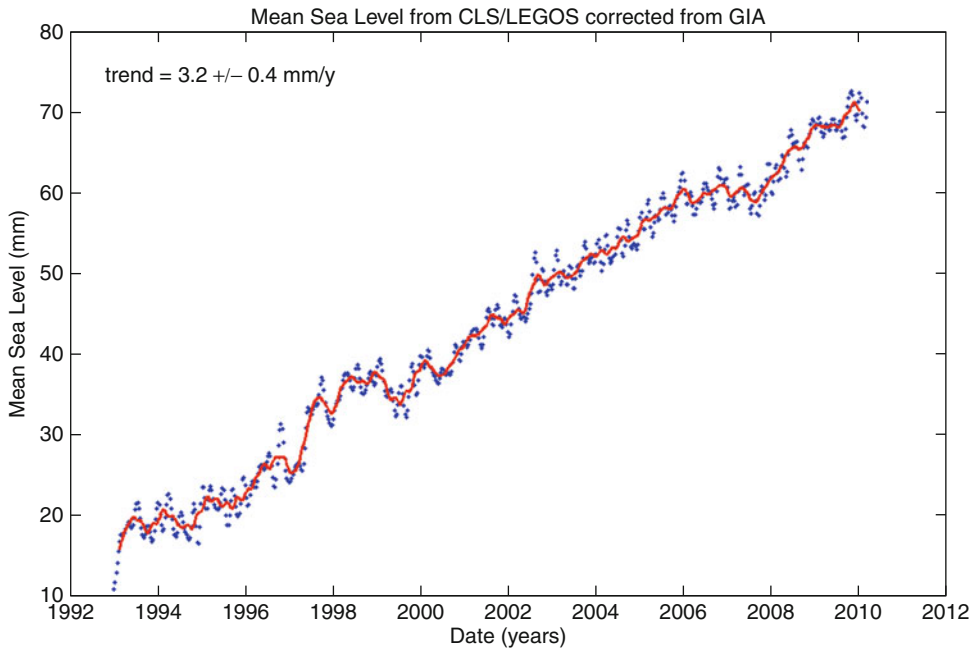

Contemporary Sea Level Variations, Observations and Causes. Figure 2
Global mean sea level evolution from satellite altimetry (1993–2010) (Updated from Ref. [19])

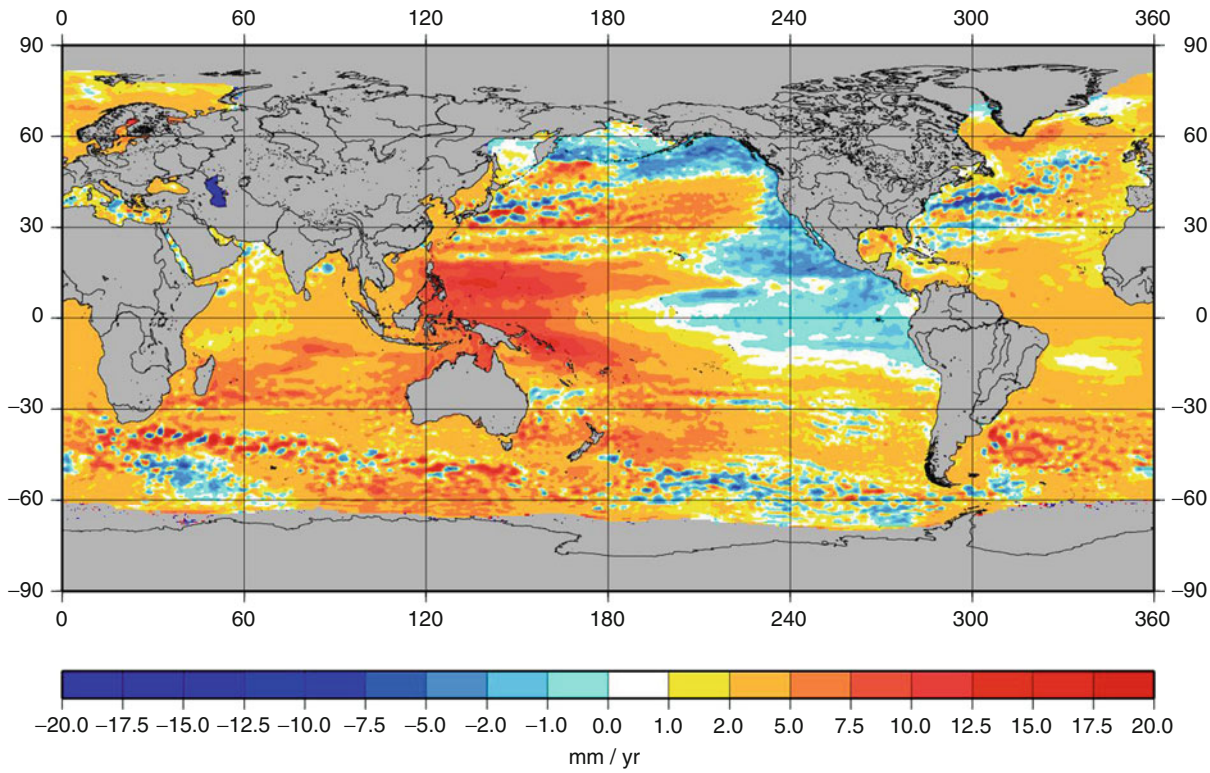

Contemporary Sea Level Variations, Observations and Causes. Figure 3
Observed spatial trend patterns in sea level over the altimetry era (1993–2010) (Updated from Ref. [19])

to natural climate variability and to global climate change induced by anthropogenic greenhouse gases emissions.

Ocean Warming Analyses of in situ ocean temperature data collected over the past 50 years by ships and recently by Argo profiling floats [11] indicate that ocean heat content, and hence ocean thermal expansion, has significantly increased since 1950 (e.g., [12–14]). Ocean warming explains about 25% of the observed sea level rise of the last few decades (e.g., [15]). However, this value is likely a lower bound, due to the lack of hydrographic data in remote regions of the southern hemisphere and in the deep ocean (below 1,000 m). Recent reevaluation of ocean warming estimates to >40% this contribution to past decades sea level rise [16]. A steep increase was observed in thermal expansion over the decade 1993–2003 (e.g., [15, 17]), but since about 2003, thermal expansion has increased less rapidly [14, 18]. The recent slower rate of steric rise likely reflects short-term variability rather than a new long-term trend. On average, over the satellite altimetry era (1993–2010), the contribution of ocean warming to sea rise accounts for ∼ 30–40% [19, 20].

Glaciers Melting Being very sensitive to global warming, mountain glaciers and small ice caps have retreated worldwide during the recent decades, with significant acceleration during the 1990s. From mass balance studies of a large number of glaciers, estimates have been made of the contribution of glacier's ice melt to sea level [21–24]. For the period 1993–2010, glaciers and ice caps have accounted for ∼ 30% to the observed sea level rise [19, 20].

Ice Sheets If totally melted, Greenland and West Antarctica would raise sea level by about 7 m and 3–5 m, respectively. Thus even a small amount of ice mass loss from the ice sheets would produce substantial sea level rise, with adverse societal and economical impacts on vulnerable low-lying coastal regions.

Since the early 1990s, different remote sensing observations (airborne and satellite radar and laser altimetry, Synthetic Aperture Radar Interferometry (InSAR), and since 2002, space gravimetry from the GRACE mission) have provided important observations of the mass balance of the ice sheets. These data indicate that Greenland and West Antarctica are loosing mass at an accelerated rate (e.g., [25, 26]). Most recent mass balance estimates from GRACE space gravimetry suggest for the 2002–2009 time span, averaged rates of ice mass loss of 240 Gt/year for Greenland and 150–200 Gt/year for Antarctica (e.g., [27, 28]), in rather good agreement with INSAR (e.g., [29, 30]) and radar and laser altimetry results (e.g., [31]). The space-based observations unambiguously show ice mass loss acceleration in the recent years. For the period 1993–2003, <15% of the rate of global sea level rise was due to the ice sheets [21]. But their contribution has increased up to ~75% since 2003–2004, about equally split between Greenland and Antarctica (e.g., [29, 30]). Accelerated polar ice loss over the past few years has more than compensated recent slower rate of ocean thermal expansion, and as a result, sea level has continued to rise at almost the same rate (e.g., [32]). Although not constant through time, on average over 2003–2010, ice sheets mass loss explains ~25% of the rate of sea level rise [19, 20].

There is more and more evidence that recent negative ice sheet mass balance mainly results from rapid outlet glacier flow along some margins of Greenland and West Antarctica, and further iceberg discharge into the surrounding ocean (e.g., [33–38]). This process, known as dynamic thinning, is often observed in regions where glaciers are grounded below sea level (e.g., in the Amundsen Sea sector, West Antarctica). Thinning and subsequent breakup of floating ice tongues or ice shelves that buttressed the glaciers result in rapid grounding line retreat and accelerated glacier flow. Several recent observations have suggested that warming of subsurface ocean waters may trigger these dynamical instabilities [34–38].

Land Water Storage Change in land water storage, due to natural climate variability and human activities (i.e., anthropogenic changes in the amount of water stored in soils, reservoirs and aquifers as a result of dam building, underground water mining, irrigation, urbanization, deforestation, etc.) is another potential contribution to sea level change. Model-based estimates of land water-storage change caused by natural climate variability suggest no long-term contribution to sea level for the past few decades, although interannual/decadal fluctuations have been significant. Since 2002, space gravimetry observations from the GRACE space mission now allow determination of the total (i.e., due to climate variability and human activities) land water contribution to sea level. GRACE data confirm that the land water signal is dominated by interannual variability with only a modest contribution (<10%) to the trend [39, 40]. On the other hand, intensive dam building along rivers during the second half of the twentieth century may have lowered sea level by ~ −0.5 mm/year [41], but groundwater pumping, in particular for irrigation, may have more or less counterbalanced this effect.

Sea Level Budget over 1993–2010 Although none of the climate factors discussed above evolve linearly with time, on average over the 1993–2010 time span, ocean warming, glaciers melting, and ice sheet mass loss have each contributed by roughly 30% to global mean sea level rise [19, 20].

Regional Scale

The regional variability in sea level trends is mainly due large-scale changes in the density structure of the oceans in response to forcing factors (e.g., heat and freshwater exchange at the sea-air interface) and changes of the ocean circulation [15]. The largest regional changes in sea level trends result from ocean temperature change (i.e., from nonuniform thermal expansion) but in some regions, change in water salinity is also important (e.g., [42, 43]).

Observations of ocean temperature over the past few decades show that trend patterns in thermal expansion are not stationary but fluctuate both in space and time in response to internal perturbations of the climate system such as ENSO, NAO, and PDO [15]. As a result, sea level trend patterns observed by satellite altimetry over the last 18 years are expected to be different from those of the last 50 years, as confirmed by past sea level reconstructions (e.g., [44, 45]).

Processes other than thermal expansion may also give rise to regional sea level variations. This is the case for the response of the solid Earth to the last deglaciation (GIA). The meltwater from the former ice sheets does not redistribute uniformly over the oceans because of several processes: self-gravitation between ice and water masses, ocean basin deformations associated with the viscoelastic response of the Earth to the changing load, and changes of the Earth's rotation due to water and ice mass redistribution [46, 47]. On-going ice mass loss of the Greenland and Antarctica ice sheets also leads to nonuniform sea level rise because of about the same processes [48, 49]. These regional sea level changes are broadscale but their regional fingerprint is different for each melting source (Greenland, Antarctica, glaciers). Amplification by up to 30% are expected far from the melting source while significant sea level drop should occur around the region which is losing ice.

Future Sea Level Rise

IPCC AR4 projections based on coupled climate models indicate that sea level should be higher than today's value by $\sim$ 40 cm by 2100 (within a range of $\pm$ 20 cm due to model results dispersion and uncertainty on future greenhouse gases emissions) [50]. However this value is possibly a lower bound because it only accounts for future ocean warming, glaciers melting and changes in ice sheet surface mass balance. As discussed above, a large proportion of Greenland and West Antarctica ice mass loss results from coastal glacier flow into the ocean through complex dynamical instabilities. Such processes have begun to be understood only recently and thus were not taken into account in the IPCC AR4 sea level projections. Recent studies suggest that account of ice sheet fast dynamics will increase future sea level rise (e.g., [51]). But the exact global mean sea level elevation by the end of the 21st century remains quite uncertain. Present-day sea level rise is not uniform; this is also expected for the future. The regional sea level map for 2090–2100 provided by IPCC AR4 (average of 16 models for one emission scenario; Ref. [50]) shows higher than average sea level rise in the Arctic Ocean due to decrease in salinity in response to fresh water input and along a narrow band in the south Atlantic and south Indian oceans. Recent studies confirm this general behaviour (e.g., [52]).

Impacts of Sea Level Rise

Sea level rise is a major concern for populations living in low-lying coastal regions (about 25% of human beings) because it will give rise to inundation, wetland loss, shoreline erosion, and saltwater intrusion in surface water bodies and aquifers, and will raise water tables [53]. Moreover, in many coastal regions of the world, the effects of rising sea level act in combination with other natural and/or anthropogenic factors, such as decreased rate of fluvial sediment deposition in deltaic areas, ground subsidence due to tectonic activity or groundwater pumping, and hydrocarbon extraction [54].

Besides factors that modify shoreline morphology (e.g., sediment deposition in river deltas, change in coastal waves and currents), what does matter in coastal regions is relative sea level rise, i.e., the combination of sea level rise and vertical ground motions. In many coastal regions of the world, these two factors are currently of the same order of magnitude and most often of opposite sign (sea level rises and ground subsides). Accelerated ground subsidence is reported in many regions, either because of local groundwater withdrawal (Tokyo subsided by 5 m, Shanghai by 3 m, and Bangkok by 2 m during the last decades; Ref. [53]) or hydrocarbon extraction (e.g., Gulf Coast where ground subsidence in the range 5–10 mm/year is observed; Ref. [55]). Whatever the causes, ground subsidence directly interacts with and amplifies climate-related sea level rise (long-term trend plus regional variability). However, if sea level continues to rise at current rates and more likely accelerates, the climate factors (sea level rise) will become dominant. However, it remains difficult to quantify future sea level rise in specific regions where various factors interfere in a complex way.

Future Directions

Most recent developments indicate that sea level is currently rising slightly faster since the early 1990s than during the previous decades. Owing to the recent progress in understanding the causes of present-day sea level rise, the sea level budget for the period 1993–2010 can be nearly closed. Approximately 30–40% of the rate of sea level rise is due to ocean thermal expansion in response to ocean warming. Mass loss in mountain glaciers and ice sheets accounts for the remaining 60–70%. Sea level will continue to rise in the future

decades because of expected increased global warming. However, the exact amount of sea level rise in the coming decades is still an open question. The main source of uncertainty is the future behavior of the Greenland and Antarctica ice sheets in a warming climate. Improved understanding and modeling of the complex dynamical response of the ice sheets to global warming is among the priorities of the international climate research community. In parallel, observing change and variability of sea level and its different components using in synergy various in situ and space-based observing systems is another important goal.

The recently launched high-precision altimeter satellites of the Topex/Jason series and their expected successors will provide continuity in the monitoring of sea level variations from space on multidecadal timescale. In addition to ocean temperature and salinity measurements from the international Argo project, mass balance of the ice sheets from GRACE and other remote sensing techniques, GRACE-based land water-storage change and in situ and remote observations of mountain glaciers will provide invaluable observations for understanding the causes of sea level variations.

Sea level changes involve interactions of all components of the climate system (oceans, ice sheets and glaciers, atmosphere, land water reservoirs) on a wide range of spatial and temporal scales. Even the solid Earth through its visco-elastic response to water mass redistribution affects sea level. Systematic monitoring of oceans, cryosphere, and land waters from in situ and space-observation systems are thus crucial to validate climate models, and hence improve future sea level projections. Considering the highly negative impact of future sea level rise for society, the multidisciplinary aspects of sea level rise (observations, modeling, coastal impact studies) should remain a major area of future climate research.

Bibliography

Primary Literature

1. Lambeck K, Yokoyama Y, Purcell T (2002) Into and out of the last glacial maximum: sea level change during oxygen isotope stages 3 and 2. Quater Sci Rev 21:343–360
2. Kemp AC, Horton B, Donnelly JP, Mann ME, Vermeer M, Rahmstorf S (2011) Climate related sea level variations over the past two millennia. Proc Natl Acad Sci USA 108: 11017–11022
3. Church JA, White NJ (2006) A 20th century acceleration in global sea-level rise. Geophys Res Lett 33:L01602. doi:10.1029/2005GL024826
4. Holgate SJ, Woodworth PL (2004) Evidence for enhanced coastal sea level rise during the 1990s. Geophys Res Lett 31:L07305. doi:10.1029/2004GL019626
5. Jevrejeva S, Grinsted A, Moore JC, Holgate S (2006) Non linear trends and multiyear cycles in sea level records. J Geophys Res C09012. doi:1.1029/2005JC003229, 2006
6. Ablain M, Cazenave A, Valladeau G, Guinehut S (2009) A new assessment of the error budget of global mean sea level rate estimated by satellite altimetry over 1993—2008. Ocean Sci 5:193–201
7. Leuliette EW, Nerem RS, Mitchum GT (2004) Results of TOPEX/Poseidon and Jason-1 calibration to construct a continuous record of mean sea level. Mar Geod 27:79–94
8. Leutiette EW, Scharroo R (2010) Integrating Jason-2 into a multiple-altimeter climate data record. Mar Geod 33:504–517
9. Beckley BD, Lemoine FG, Lutchke SB, Ray RD, Zelensky NP (2007) A reassessment of global rise and regional mean sea level trends from TOPEX and Jason-1 altimetry based on revised reference frame and orbits. Geophys Res Lett 34:L14608. doi:10.1029/2007GL030002
10. Nerem RS, Chambers DP, Choe C, Mitchum GT (2010) Estimating mean sea level change from the TOPEX and Jason altimetermissions. Mar Geod 33(1):435–446
11. Roemmich D, Owens WB (2000) The ARGO project: global ocean observations for understanding and prediction of climate variability. Oceanography 13:45–50
12. Levitus S, Antonov JL, Boyer TP, Locarnini RA, Garcia HE, Mishonov AV (2009) Global ocean heat content 1955–2008 in light of recently revealed instrumentation. Geophys Res Lett 36:L07608. doi:10.1029/2008GL037155
13. Ishii M, Kimoto M (2009) Reevaluation of historical ocean heat content variations with varying XBT and MBT depth bias corrections. J Oceanogr 65:287–299
14. Lyman JM, Godd SA, Gouretski VV, Ishii M, Johnson GC, Palmer MD, Smith DM, Willis JK (2010) Robust warming of the global upper ocean. Nature 465:334–337. doi:10.1038/nature09043
15. Bindoff N, Willebrand J, Artale V, Cazenave A, Gregory J, Gulev S, Hanawa K, Le Quéré C, Levitus S, Nojiri Y, Shum CK, Talley L, Unnikrishnan A (2007) Observations: oceanic climate and sea level. In: Solomon S, Qin D, Manning M, Chen Z, Marquis M, Averyt KB, Tignor M, Miller HL (eds) Climate change 2007: the physical science basis. Contribution of working group I to the fourth assessment report of the intergovernmental panel on climate change. Cambridge University Press, Cambridge/New York
16. Domingues C, Church J, White N, Gleckler PJ, Wijffels SE et al (2008) Improved estimates of upper ocean warming and multidecadal sea level rise. Nature 453:1090–1093. doi:10.1038/nature07080

17. Lombard A, Cazenave A, Le Traon PY, Ishii M (2005) Contribution of thermal expansion to present-day sea level rise revisited. Global Planet Change 47:1–16
18. Llovel W, Guinehut S, Cazenave A (2010) Regional and interannual variability in sea level over 2002–2009 based on satellite altimetry, Argo float data and GRACE ocean mass. Ocean Dyn 60:1193–1204. doi:10.1007/s10236-010-0324-0
19. Cazenave A, Llovel W (2010) Contemporary sea level rise. Annu Rev Mar Sci 2:145–173
20. Church J et al (2011) The Earth's sea level and energy budgets from 1961 and 2008. Geophys Res Lett 38:L18601
21. Lemke P et al (2007) Observations: changes in snow, ice and frozen ground. In: Solomon S, Qin D, Manning M, Chen Z, Marquis M, Averyt KB, Tignor M, Miller HL (eds) Climate change 2007: the physical science basis. Contribution of working group I to the fourth assessment report of the intergovernmental panel on climate change. Cambridge University Press, Cambridge/New York
22. Kaser G, Cogley JG, Dyurgerov MB, Meier MF, Ohmura A (2006) Mass balance of glaciers and ice caps: consensus estimates for 1961–2004. Geophys Res Lett 33:L19501. doi:10.1029/2006GL027511
23. Meier MF, Dyurgerov MB, Rick UK, O'Neel S, Pfeffer WT, Anderson RS, Anderson SP, Glazovsky AF (2007) Glaciers dominate Eustatic sea-level rise in the 21st century. Science 317(5841):1064–1067
24. Cogley JC (2009) Geodetic and direct mass balance measurements: comparison and joint analysis. Ann Glaciol 50: 96–100
25. Alley R, Spencer M, Anandakrishnan S (2007) Ice sheet mass balance, assessment, attribution and prognosis. Ann Glaciol 46:1–7
26. Allison I, Alley RB, Fricker HA, Thomas RH, Warner RC (2009) Ice sheet mass balance and sea level. Antarct Sci 21:413–426
27. Velicogna I (2009) Increasing rates of ice mass loss from the Greenland and Antarctica ice sheets revealed by GRACE. Geophys Res Lett 36:L19503
28. Chen JL, Wilson CR, Blankenship DD, Tapley BD (2009) Accelerated Antarctic ice loss from satellite gravity measurements. Nat Geosci. doi:10.1038/ngeo694, 2009
29. Rignot E, Bamber JL, Van Den Broecke MR, Davis C, Li Y et al (2008) Recent Antarctic ice mass loss from radar interferometry and regional climate modeling. Nat Geosci 1:106–110
30. Rignot E, Box JE, Burgess E, Hanna E (2008) Mass balance of the Greenland ice sheet from 1958 to 2007. Geophys Res Lett 35:L20502. doi:10.1029/2008GL035417
31. Zwally HJ et al (2011) Greenland ice sheet mass balance: distribution of increased mass loss with climate warming; 2003–07 versus 1992–2002. J Glaciol 57(201):88–102
32. Cazenave A, Dominh K, Guinehut S, Berthier E, llovel W, Ramillien G, Ablain M, Larnicol G (2009) Sea level budget over 2003–2008: a reevaluation from GRACE space gravimetry, satellite altimetry and Argo. Global Planet Change 65:83–88. doi:10.1016/j/gloplacha.2008.10.004
33. Howat IM, Joughin IR, Scambos TA (2007) Rapid changes in ice discharge from Greenland outlet glaciers. Science 315:1559–1561. doi:10.1126/science.1138478
34. Holland D, Thomas RH, De Young B, Ribergaard MH, Lyberth B (2008) Acceleration of Jakobshawn Isbrae triggered by warm subsurface ocean waters. Nat Geosci 1:659–664. doi:10.1038/ngeo316
35. Straneo F et al (2010) Rapid circulation of warm subtropical waters in a major glacial fjord in East Greenland. Nat Geosci 3:182–186
36. Joughin I, Das SB, King M, Smith BE, Howat IM, Moon T (2008) Seasonal speedup along the western flank of the Greenland ice sheet. Science 320:781–783
37. Pritchard HM, Arthern RJ, Vaughan DG, Edwards L (2010) Extensive dynamic thinning on the margins of the Greenland and Antarctic ice sheets. Nature. doi:10.1038/nature08471
38. Rignot EK, And KM, Velicogna I (2010) Rapid submarine melting of the calving faces of West Greenland glaciers. Nat Geosci 3:187–191
39. Ramillien G, Bouhours S, Lombard A, Cazenave A, Flechtner F, Schmidt R (2008) Land water contributions from GRACE to sea level rise over 2002–2006. Global Planet Change 60:381–392
40. Llovel W, Becker M, Cazenave A, Jevrejeva S, Alkama R, Decharme B, Douville H, Ablain M, Beckley B (2011) Terrestrial waters and sea level variations on interannual time scale. Global Planet Change 75:76–82. doi:10.1016/j.gloplacha.2010.10.008
41. Chao BF, Wu YH, Li YS (2008) Impact of artificial reservoir water impoundment on global sea level. Science 320:212–214. doi:10.1126/science.1154580
42. Lombard A, Garric G, Penduff T, Molines JM (2009) Regional variability of sea level change using a global ocean model at ¼ resolution. Ocean Dyn. doi:10.1007/s10236-009-0161-6
43. Wunsch C, Ponte RM, Heimbach P (2007) Decadal trends in sea level patterns: 1993–2004. J Clim 20(24). doi:10.1175/2007JCLI1840.1
44. Church JA, White NJ, Coleman R, Lambeck K, Mitrovica JX (2004) Estimates of the regional distribution of sea-level rise over the 1950 to 2000 period. J Clim 17(13): 2609–2625
45. Llovel W, Cazenave A, Rogel P, Berge-Nguyen M (2009) 2-D reconstruction of past sea level (1950–2003) using tide gauge records and spatial patterns from a general ocean circulation model. Clim Past 5:1–11
46. Mitrovica JX, Tamisiea ME, Davis JL, Milne GA (2001) Recent mass balance of polar ice sheets inferred from patterns of global sea-level change. Nature 409:1026–1029
47. Peltier WR (2004) Global glacial isostasy and the surface of the ice-age Earth: the ICE-5 G (VM2) model and GRACE. Annu Rev Earth Planet Sci 32:111–149
48. Mitrovica JX, Gomez N, Clark PU (2009) The sea-level fingerprint of West Antarctic collapse. Science 323:753

49. Milne G, Gehrels WR, Hughes C, Tamisiea M (2009) Identifying the causes of sea level changes. Nat Geosci 2: 471–478
50. Meehl GA et al (2007) Global climate projections. In: Solomon S, Qin D, Manning M, Chen Z, Marquis M, Averyt KB, Tignor M, Miller HL (eds) Climate change 2007: the physical science basis. Contribution of working group I to the fourth assessment report of the intergovernmental panel on climate change. Cambridge University Press, Cambridge/New York
51. Pfeffer WT, Harper JT, O'Neels S (2008) Kinematic constraints on glacier contributions to 21st century sea level rise. Science 321:1340–1343
52. Slangen AB, Katsman CA, van de Wal RSW, Vermeersen LLA, Riva REM (2011) Towards regional projections of twenty-first century sea level change based on IPCC SRES scenarios. Clim Dyn. doi:10.1007/s00382-011-1057-6
53. Nicholls RJ (2007) The impacts of sea level rise. Ocean Challenge 15(1):13–17
54. Nicholls RJ, Cazenave A (2010) Sea-level rise and its impact on coastal zones. Science 328:1517–1520
55. Ericson JP, Vorosmarty CJ, Dingman SL, Ward LG, Meybeck L (2006) Effective sea level rise and deltas: causes of change and human dimension implications. Global Planet Change 50:63–82

Books and Reviews

Bigg G (2003) The oceans and climate. Cambridge University Press, Cambridge, MA

Church JA, Woodworth PL, Aarup T, Wilson WS (Eds) (2010) Understanding sea level rise and variability. Wiley-Blackwell

Cazenave A, Nerem S (2004) Present-day sea level change: observations and causes. Rev Geophys 42:RG3001. doi:8755-1209/04/2003RG000139

Cazenave A, Remy F (2011) Sea level and climate: measurements and cause of changes. Wiley Interdiscip Rev Clim Change 2:647–662

Church JA, White NJ, Aarup TG, Wilson WS, Woodworth PL, Domingues CM, Hunter JR, Lambeck K (2008) Understanding global sea levels: past, present and future. Sustain Sci. doi:10.1007/s11625-008-0042-4

Church JA, Woodworth PL, Aarup T, Wilson WS (eds) (2010) Understanding sea level rise and variability. Wiley-Blackwell, Chichester

Nerem S, Leuliette E, Cazenave A (2006) Present-day sea level change. C R Geosciences 338(14–15):1077–1083

Solomon S, Qin D, Manning M, Chen Z, Marquis M, Averyt KB, Tignor M, Miller HL (eds) IPCC 4th assessment report, 2007. Climate change 2007: the physical science basis. Contribution of working group I to the fourth assessment report of the intergovernmental panel on climate change. Cambridge University Press, Cambridge/New York

Cooperative Group of Vehicles and Dangerous Situations, Recognition of

Kym Watson[1], Christian Frese[2], Thomas Batz[1], Jürgen Beyerer[2,3]
[1]Department Information Management, Fraunhofer Institute of Optronics, System Technologies and Image Exploitation IOSB, Karlsruhe, Germany
[2]Institute for Anthropomatics, Vision and Fusion Laboratory, Karlsruhe Institute of Technology, Karlsruhe, Germany
[3]Fraunhofer Institute of Optronics, System Technologies and Image Exploitation IOSB, Karlsruhe, Germany

Article Outline

Glossary
Definition of the Subject
Introduction
Cooperative Groups
Recognition of Dangerous Situations
Cooperative Decision Making
Future Directions
Acknowledgments
Bibliography

Glossary

Cognitive vehicle A road vehicle equipped with sensors like video, radar, or lidar and information processing resources for environment perception. Furthermore, cognitive vehicles may have human–machine interfaces, actuators for automatic intervention or fully autonomous operation, and wireless communication devices.

Common relevant picture Data structure containing the information necessary for situation analysis and decision making within a cooperative group. The information originates from the sensors of the vehicles, is enhanced by fusion algorithms, and is communicated to all vehicles of the group.

Cooperative group (CG) A set of cognitive vehicles which cooperate in order to mitigate dangerous traffic situations.

Dangerous situation Traffic situation with immediate threat of an accident.

Driver assistance system Technical system supporting human drivers in performing certain driving tasks. Driver assistance systems can be classified into comfort systems (not subject of this entry) and safety systems.

Motion planning Algorithmic planning of feasible, collision-free vehicle trajectories.

Prediction Projection of system states into the near future. Specifically, in this context, model-based prognosis of vehicle position.

Wireless vehicular communication Networking of multiple vehicles using wireless local area network or cellular communication technologies.

Definition of the Subject

The subject of this entry is cooperation among cognitive vehicles with the aim of increasing traffic safety. This includes the formation of cooperative groups, the recognition of dangerous situations using stochastic prediction methods, and the planning of cooperative maneuvers to avoid collisions (see Fig. 1).

Introduction

Intelligent vehicle technologies have been a topic of extensive research for the last decades. Important research areas include perception of roads, obstacles and environment, situation recognition, vehicle control, and behavior planning. Most of the developed technologies can be used both for driver assistance systems and for fully autonomous vehicles. Regarding driver assistance, some comfort and safety systems have been released to market, e.g., adaptive cruise control, antilock braking, and emergency brake assist systems [1, 2]. State-of-the-art autonomous road vehicles have been demonstrated at the DARPA Urban Challenge 2007, where several automated vehicles completed driving missions lasting for hours in a restricted traffic environment [3].

Cooperative systems offer even more potential for increasing safety and improving traffic flow. In recent years, there has been a lot of research on wireless vehicle-to-vehicle communication, see [4] for an overview. Applications of vehicular communication technology include wireless local danger warning [5, 6], distributed sensor fusion [7–9], and improvement of traffic efficiency (e.g., platooning [10–12], intersection control [13, 14]). However, this entry focuses on the safety applications of recognizing dangerous situations and avoiding or mitigating collisions by automated cooperative maneuvers.

The benefits of cooperative behavior compared to selfish actions of each driver have been shown for other

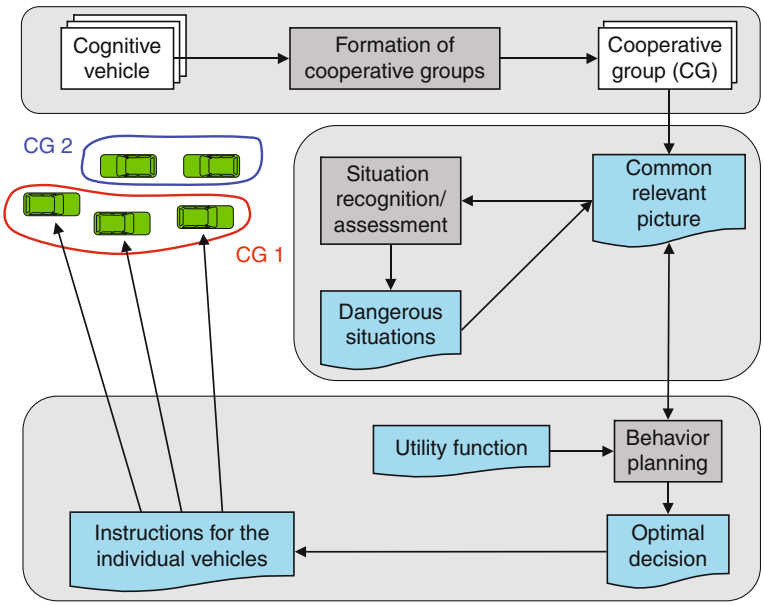

Cooperative Group of Vehicles and Dangerous Situations, Recognition of. Figure 1
Architecture of a cooperative collision warning and avoidance system

problems [15], and it is worthwhile to exploit the potential of cooperation also for the improvement of traffic safety.

Cooperative Groups

Before methods for cooperative collision warning and avoidance systems can be designed, the set of vehicles which can cooperate reasonably has to be determined. A predefined, but not static, group structure enables an efficient and unambiguous decision making in case of a dangerous situation. Limiting the size of cooperative groups is important because cooperative reasoning entails significant computation and communication complexity.

A suitable distance measure for group formation has to take into account the road topology [16]. Based on this notion of spatiotemporal distance, a criterion for the distributed formation of cooperative groups is developed [17].

These concepts will be presented in detail, and related work will be reviewed.

Motivation and Definition

In dangerous situations, fast and unambiguous cooperative decision making is essential. Therefore, it is beneficial to know the possible cooperation partners in advance and to establish a decision structure. This is achieved by the concept of dynamic cooperative groups. A cooperative group consists of cognitive vehicles which might encounter a dangerous situation requiring cooperative actions in the near future. Vehicles are partitioned into groups, i.e., each vehicle belongs to exactly one group at any point in time. The set of possible cooperation partners is restricted to the vehicles within the group. Each group has a designated coordinator vehicle which handles the necessary communication (see section "Distributed Negotiation Protocol" below). A cooperative decision may only be selected and communicated by the coordinator. Otherwise, ambiguous decisions might arise if two or more vehicles recognize a dangerous situation at the same time.

Computation and communication efforts increase rapidly with the number of vehicles involved. To enable real-time cooperative reasoning, cooperative groups are limited in size. This requires a reliable grouping criterion which assigns all vehicles within one dangerous traffic situation to the same group. This cannot always be achieved with a limited group size, but the results will never become worse than without cooperation.

Distance

Intuitively, it is clear that vehicles "near" to each other should be in one group. However, it is not so clear what a suitable notion of distance for vehicles within a road network should be. For example, cars driving in different directions on a dual carriageway are not able to perform cooperative maneuvers when they are separated by a guard rail or concrete barriers. This means that sometimes cars which are very near to each other in terms of Euclidean distance should nevertheless belong to different cooperative groups (Fig. 2). Therefore, an appropriate distance measure has to incorporate knowledge of the road network.

For navigation applications, it is common to represent the road network as a graph [18]. For the purpose

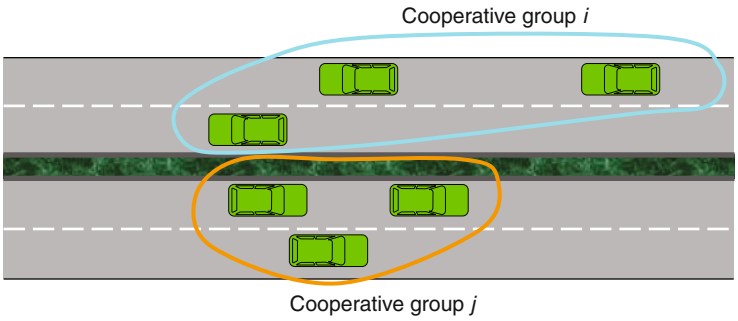

Cooperative Group of Vehicles and Dangerous Situations, Recognition of. Figure 2
Even though all six cars in this highway example are close enough to communicate, only the two indicated sets of vehicles constitute suitable cooperative groups because of the barrier between the lanes

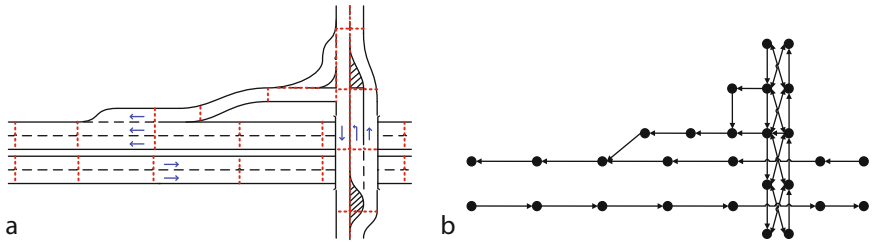

Cooperative Group of Vehicles and Dangerous Situations, Recognition of. Figure 3
(**a**) Example of a road network, in which the partition into disjoint vertices is indicated with *dotted lines*. (**b**) The graph $\mathcal{R}$ corresponding to (**a**)

of defining a distance measure, a graph $\mathcal{R}$ is created by partitioning the road area into polygons and identifying each polygon with a vertex v of the graph (see Fig. 3). Edges between neighboring polygons are inserted according to the allowed driving directions and lane change possibilities. The weight $w(e)$ of an edge $e = (v_1, v_2)$ models the minimal time required for driving from vertex v_1 to the v_2,

$$w((v_1, v_2)) := \frac{d_2(v_1, v_2)}{vel_{\max}(v_1, v_2)}, \tag{1}$$

where $d_2(v_1, v_2)$ is the Euclidean distance between the centroids of the polygons associated with v_1 and v_2, respectively, and $vel_{\max}(v_1, v_2)$ is the maximal velocity possible when driving from v_1 to v_2, determined by speed limits and road curvature. Some simplifying assumptions are made in order to obtain a conceptually elegant formalism: maximum speeds varying with the vehicle type are not considered in favor of a conservative approximation. Distances within one road polygon are neglected. This does not cause any problems if the discretization is fine enough.

The shortest-path distance $p_{\mathcal{R}}(v_1, v_2)$ between arbitrary vertices v_1, v_2 of $\mathcal{R}$ corresponds to the minimal time required for driving from v_1 to v_2. However, this does not exactly capture the distance between two cars c_1, c_2 positioned at v_1 and v_2, respectively, as the cars could drive toward each other and meet much earlier at a vertex v_m in the middle of v_1 and v_2 (see Fig. 4). In this case, a time span of $\max\{p_{\mathcal{R}}(v_1, v_m), p_{\mathcal{R}}(v_2, v_m)\}$ elapses until both cars have reached the meeting point v_m. Using this notion of virtual meeting points, the distance between two vehicles c_1, c_2 can be defined as follows:

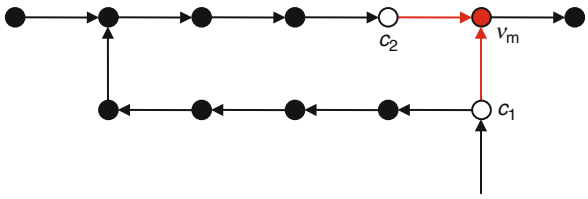

Cooperative Group of Vehicles and Dangerous Situations, Recognition of. Figure 4
The cars c_1 and c_2 can meet each other at vertex v_m

$$d(c_1, c_2) := \min_{v_m} \max\{p_{\mathcal{R}}(v(c_1), v_m), p_{\mathcal{R}}(v(c_2), v_m)\} \tag{2}$$

This distance corresponds to the minimal time within which both vehicles can reach a common meeting point v_m (see Fig. 5). It thus incorporates both spatial and temporal aspects. The function $v(c)$ determines the unique vertex v of $\mathcal{R}$ so that the polygon associated to v contains the geometric centroid of the vehicle c. The vehicles' positions of course depend on time; however, this is not expressed explicitly here for the sake of notational brevity. Obviously, $d(\cdot,\cdot)$ is symmetric and nonnegative.

The distance measure d can be computed efficiently by an appropriate modification of Dijkstra's shortest-path algorithm [19], Chap. 24.3. Search frontiers are expanded simultaneously starting from both $v(c_1)$ and $v(c_2)$. In each step, the vertex v having the minimal value of $\min\{p_{\mathcal{R}}(v(c_1), v), p_{\mathcal{R}}(v(c_2), v)\}$ among the vertices not yet visited by the respective search tree is chosen for processing. Once the two search trees reach a common vertex, this must be the nearest meeting point v_m, and the distance can be computed as

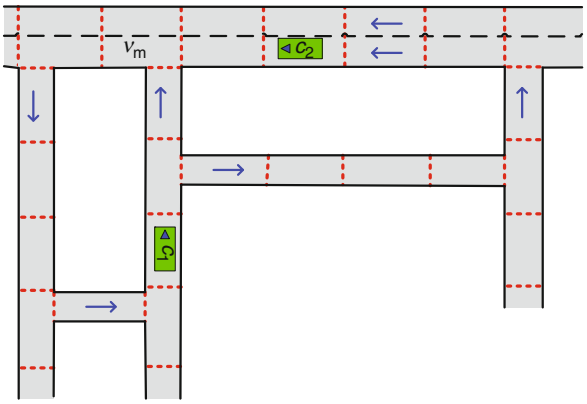

Cooperative Group of Vehicles and Dangerous Situations, Recognition of. Figure 5
Example of a situation in which the path length $p_{\mathcal{R}}$ is not a suitable distance. Assuming unit edge weights, we have $p_{\mathcal{R}}(c_1, c_2) = 11$ and $p_{\mathcal{R}}(c_2, c_1) = 10$, while both cars can meet each other at v_m within three time steps: $p_{\mathcal{R}}(c_1, v_m) = 3$, $p_{\mathcal{R}}(c_2, v_m) = 2$. Accordingly, $d(c_1, c_2) = d(c_2, c_1) = 3$

$d(c_1, c_2) = \max\{p_{\mathcal{R}}(v(c_1), v_m), p_{\mathcal{R}}(v(c_2), v_m)\}$. The pseudocode of the method is shown in Algorithm 1.

Algorithm 1 Computation of the distance $d(c_1, c_2)$

```
procedure ComputeDistance (R, c1, c2)
    Insert (heap, c1, v(c1),0)
    Insert (heap, c1, v(c1),0)
    for all vertices v of R do                ▷ Initialization
        for c = c1,c2 do
            p_R(c, v) ← ∞
        end for
    end for
    while not isEmpty(heap) do
        (c,v,w) ← RemoveMinimum(heap)
        p_R(c, v) ← w
        if p_R(c1, v) < ∞ ∧ p_R(c2, v) < ∞ then
            return max{p_R(c1, v), p_R(c2, v)}
        end if
        for all edges e = (v,v') of R do
            if p_R(c, v) = ∞ then
                Insert(heap,c, v', w + w(e))
            else if p_R(c, v') > w + w(e) then
                DecreaseKey(heap,c,v',w+w(e))
            end if
        end for
    end while
    return ∞                                  ▷ No meeting point of c1
    and c2 is reachable within R.
end procedure
```

The computational complexity of the algorithm is in $\mathcal{O}(n \log n)$, where n is the number of explored edges. This number can be restricted in two ways. First, a graph $\mathcal{R}$ is chosen that is restricted to the surrounding of the vehicle (electronic horizon method). Second, the algorithm can be stopped when the searched distance exceeds a threshold beyond which no suitable cooperation is possible. Altogether, the real-time computation of the distance measure is possible without any difficulty using the described algorithm.

Objective Function

Based on the distance measure d, an objective function rating a cooperative group $\mathcal{G} = \{c_1, c_2, \ldots, c_m\}$ of m cognitive vehicles can be defined. Several terms have been designed in order to capture certain criteria for the formation of cooperative groups. Besides distance, these are group size, relative velocity, and temporal consistency.

The minimum spanning tree has proven to be a good indicator for the inter-vehicle distances within a group. A group can be represented as a complete graph with vertices c_i and edge weights $d(c_i, c_j)$. The weights of the edges in the minimum spanning tree $MST(\mathcal{G})$ of the group graph $\mathcal{G}$ are summed up to yield the distance term s_D of the objective function:

$$s_D(\mathcal{G}) := \frac{m}{m-1} \sum_{(c_i,c_j) \in MST(\mathcal{G})} d(c_i, c_j) \quad (m > 1) \tag{3}$$

The prefactor $\frac{m}{m-1}$ accounts for the fact that a graph with m vertices has a minimum spanning tree consisting of $m - 1$ edges.

As mentioned above, cooperative groups should be limited to a reasonable number of vehicles. On the other hand, groups should not be too small either because this would narrow the possibilities of cooperation. Especially, groups consisting of a single vehicle have to be penalized because the distance function cannot be defined for these groups. Accordingly, a desired group size of m_0 vehicles is chosen, and the term s_S of the objective function rates the deviation from this value:

$$s_S(\mathcal{G}) := (m - m_0)^2 \tag{4}$$

These two terms already enable the formation of reasonable cooperative groups. However, two additional terms will be defined in order to select among

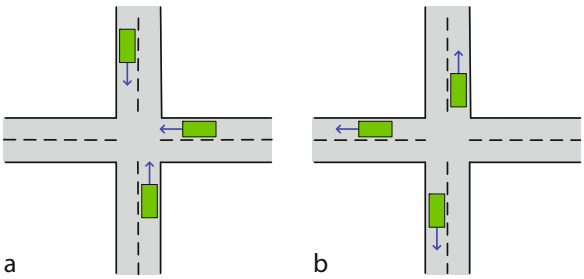

Cooperative Group of Vehicles and Dangerous Situations, Recognition of. Figure 6
Motivation for the velocity term. (**a**) Vehicles approaching each other are more likely to encounter a common dangerous situation. (**b**) Cooperative groups of vehicles driving away from each other are less desirable

alternative group structures having almost equal distance and size values. Obviously, a dangerous situation is more likely to occur within a cooperative group if its vehicles are driving toward each other, i.e., if the distances are decreasing. By contrast, vehicles moving away from each other are less desirable to be assigned to the same group (see Fig. 6). These criteria are captured by the change rate of the distance measure d. The relative velocity term s_V of the objective function can therefore be formulated using the derivative of d with respect to time:

$$s_V(\mathcal{G}) := \sum_{i=1}^{m} \frac{1}{m-1} \sum_{j \neq i} \frac{\partial}{\partial t} d(c_i, c_j) \quad (m > 1) \tag{5}$$

From the perspective of the cooperative group, s_V can be interpreted as the rate of contraction or expansion, respectively, of the group. Contracting groups are more desirable and hence have a lower (possibly negative) value of s_V.

Finally, a temporal consistency term s_T is defined in order to avoid frequent changes of the group structure, especially oscillations of vehicles between two neighboring groups. Such oscillations could be caused by small fluctuations of the distances, or by discretization artifacts. A countermeasure is to improve (i.e., decrease) the objective value of a vehicle that has just joined a new group,

$$s_T(\mathcal{G}) := \sum_{i=1}^{m} \begin{cases} t_i & \text{if } 0 < t_i < t_T \\ t_T & \text{if } t_i = 0 \text{ or } t_i \geq t_T \end{cases}, \tag{6}$$

where t_i is the time elapsed since vehicle c_i has joined group $\mathcal{G}$, and t_T is a threshold value. The temporal consistency term penalizes vehicles changing groups ($t_i = 0$) but rewards newly established groups ($0 < t_i < t_T$) in order to increase their stability.

The different terms introduced above can be combined in a weighted sum to yield the objective function

$$s(\mathcal{G}) := \begin{cases} \max\{0, \lambda_D s_D(\mathcal{G}) + \lambda_S s_S(\mathcal{G}) + \lambda_V s_V(\mathcal{G}) + \lambda_T s_T(\mathcal{G})\} & m > 1 \\ \lambda_S s_S(\mathcal{G}) + \lambda_T s_T(\mathcal{G}) & m = 1 \end{cases} \tag{7}$$

rating a cooperative group $\mathcal{G}$ of m vehicles, where $\lambda_k \geq 0$ are weighting factors. The objective function s can be used to compare an existing cooperative group with hypothetical alternative groups.

Computing Optimal Partitions

The objective function $s(\mathcal{G})$ can be extended to a set $P = \{\mathcal{G}_1, \ldots, \mathcal{G}_k\}$ of mutually disjoint cooperative groups as follows:

$$s(P) := \sum_{\mathcal{G} \in \mathcal{P}} s(\mathcal{G}) \tag{8}$$

Given a set $C = \{c_1, \ldots, c_n\}$ of cognitive vehicles, the optimal group structure P^* according to the objective function is obtained as

$$P^* = \underset{P \in \mathcal{P}(C)}{\arg\min}\, s(P), \tag{9}$$

where $\mathcal{P}(C)$ is the set of all partitions of C. The exact minimization of (9) is possible using, e.g., depth-first branch and bound search. However, the set of partitions grows rapidly as the number of vehicles increases. To enable real-time computation, strict optimality is abandoned. A suboptimal anytime algorithm is designed starting from the greedy clustering method. The greedy algorithm is initialized with each vehicle being in its own single-vehicle group. In each stage of the algorithm, every possible merging of two groups is evaluated by the objective function. The merging having the largest improvement is carried out before the next stage starts. The greedy algorithm halts if no merging remains which yields an improvement of the total objective value.

An anytime algorithm is obtained by inserting every evaluated merging step into a priority queue and processing the merging with the totally maximum

improvement in each stage as long as execution time is left (Algorithm 2). Experiments have shown that the group structure resulting from this algorithm is identical to the optimal partition with a probability of more than 99%, and that the increase in the objective function is less than 1% in the remaining cases.

Algorithm 2 Any-time group partitioning algorithm

```
procedure ComputePartition (C = {c_1, ..., c_n})
    P_0 ← {{c_1}, ..., {c_n}}
    Insert(heap,P_0,s(P_0))
    P* ← P_0
    while time left do
        (P,s) ← RemoveMinimum(heap)
        for all G_i ∈ P do
            for all G_j ∈ P, G_j ≠ G_i do
                P ← P\{G_i, G_j} ∪ {G_i ∪ G_j}
                if P' ∉ closed then
                    Insert(heap,P',s(P'))
                    Insert(closed,P')
                    if s(P') < s(P*) then
                        P* ← P'
                    end if
                end if
            end for
        end for
    end while
    return P*
end procedure
```

Distributed Negotiation Protocol

To realize the group formation in a distributed vehicular environment, the cognitive vehicles have to negotiate the group structure without any centralized instance. This implies that a mechanism is required which performs reliably with incomplete and local knowledge. The negotiation method chosen for group formation is based on coordinator vehicles communicating with neighboring groups.

The notion of neighborhood can be formalized by means of the distance measure d introduced above. Two groups $\mathcal{G}_1$ and $\mathcal{G}_2$ are neighbored, $N(\mathcal{G}_1, \mathcal{G}_2)$, if

$$\forall \mathcal{G} \quad \forall c \in \mathcal{G} \quad \exists c_1 \in \mathcal{G}_1 \quad \exists c_2 \in \mathcal{G}_2 \quad \max\{d(c, c_1), d(c, c_2)\} > d(c_1, c_2). \tag{10}$$

Informally, this means that there does not exist any group $\mathcal{G}$ in between $\mathcal{G}_1$ and $\mathcal{G}_2$. The resulting set of vehicles from neighboring groups is

$$C(\mathcal{G}_0) := \mathcal{G}_0 \cup \bigcup_{N(\mathcal{G}_0, \mathcal{G}_j)} \mathcal{G}_j \tag{11}$$

The optimal group structure for the local neighborhood of $\mathcal{G}_0$ is obtained by evaluating (9) for $C(\mathcal{G}_0)$. The coordinator of group $\mathcal{G}_0$ can perform this computation approximately using the anytime algorithm presented above.

With this notion of neighborhood, a negotiation protocol can be designed as follows (see Fig. 7). Each vehicle periodically sends its position information to its group coordinator. Group coordinators exchange their information with neighboring coordinators and compute the optimal partition. If it differs from the current group assignment, a change of group structure is initiated. The change of group assignment is performed after the involved coordinators have agreed.

Whenever possible, a change of the group coordinator is avoided in order to minimize communication and initialization costs. However, it is sometimes inevitable to choose a new coordinator, e.g., when the previous coordinator has left the group, or when a new group is established. In these cases, group coordinators may be selected arbitrary, e.g., based on the identification numbers of the vehicles, or according to certain criteria. For example, it may be preferable to choose the central vehicle of the group, given by

$$\arg\min_{c \in \mathcal{G}} \sum_{c' \in \mathcal{G}} \left(\lambda_{\mathrm{D}} d(c, c') + \lambda_{\mathrm{V}} \frac{\partial}{\partial t} d(c, c') \right). \tag{12}$$

Results

The described group formation method has been implemented and integrated with a traffic simulator [20]. Various highway, country road, and inner city scenarios have been simulated successfully with real-time performance. Figure 8 shows an example of the results.

The approach has been evaluated with regard to the application of cooperative collision avoidance. The traffic simulator has been modified in order to provoke accidents. In all considered scenarios, the vehicles involved in the accidents have been assigned to the

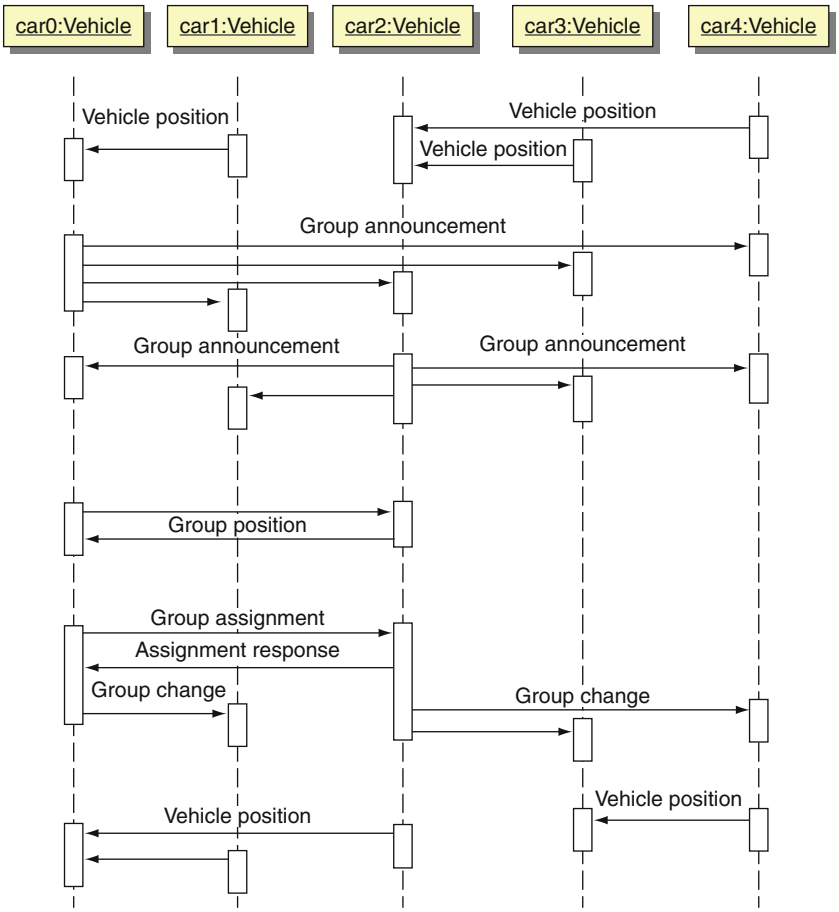

Cooperative Group of Vehicles and Dangerous Situations, Recognition of. Figure 7
Sequence diagram of the proposed negotiation protocol. At the beginning of this example, $\mathcal{G}_1 = \{\text{car0}, \text{car1}\}$ and $\mathcal{G}_2 = \{\text{car2}, \text{car3}, \text{car4}\}$ with car0, car2 being the group coordinators. Then car0 initiates a new group assignment that is agreed by car2, resulting in $\mathcal{G}_1 = \{\text{car0}, \text{car1}, \text{car2}\}$ and $\mathcal{G}_2 = \{\text{car3}, \text{car4}\}$

same group in more than 90% of the cases, implying that the accidents can potentially be prevented by cooperative maneuvers.

Related Work

Related vehicle grouping approaches can be classified according to the purpose of the groups. Often, groups are used to structure the communication network [21–26]. However, communication groups have to be distinguished from application-specific groups [27]. The method described above is designed to be applied to cooperative collision avoidance. Other conceivable applications include cooperative local danger warning, cooperative perception, intersection management, and platooning. Different, but possibly similar group formation criteria may be needed for these applications. For example, warning messages may be propagated by oncoming traffic on a dual carriageway, while cooperative maneuvering is not possible across the central barrier.

Many researchers neglect the issue of grouping and assume that all vehicles within communication range can cooperate [28]. Thus, the simplest approach is to consider groups identical to the connected components of the communication network [29]. Formation of groups based on a threshold for the Euclidean distance between vehicles has been evaluated in robotics [30], in road traffic applications [31], and in air traffic control [32, 33]. A more elaborated method incorporating road topology information is described in [34].

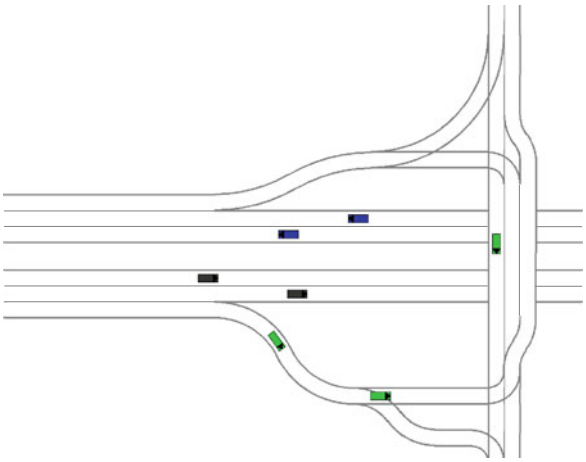

Cooperative Group of Vehicles and Dangerous Situations, Recognition of. Figure 8
Example of resulting cooperative groups. Cars belonging to one group are depicted in the same color. Note that vehicles physically separated – by the central barrier of the highway or by the bridge – are assigned to different groups, while the vehicles approaching the intersection form one group, shown in *green*

For traffic efficiency applications, groups consisting of all vehicles within a fixed area have been considered, e.g., all vehicles near to an intersection [13, 35, 36] or on a specific highway section [37–39]. Regarding collision avoidance, it is also possible to group all vehicles whose probability of mutual collision exceeds a predefined threshold [40–42]. However, this requires to compute the collision probabilities for all vehicles within communication range.

Platoons consist of vehicles having common goals [10, 43]. Therefore, criteria evaluating destinations and, e.g., desired speed of vehicles are appropriate for platoon formation [44, 45]. By contrast, cooperative groups encompass possibly conflicting vehicles, independent of their destinations.

Recognition of Dangerous Situations

An important target for a cooperative group (CG) $\mathcal{G} = \{c_1, \ldots, c_m\}$ of vehicles c_i is the automatic detection of short-term dangerous situations [46]. Short-term means within a forecasting horizon Δt that is shorter than the reaction time of human drivers. Such situations require an automatic reaction of the cooperative group as they cannot be handled safely by the drivers themselves. A typical value for the short-term prediction horizon Δt is about 1 s for moderate speeds of 20 m/s in curves.

With this objective, the likely path of each vehicle c_i in the time interval $[t_0, t_0 + \Delta t]$ starting at the current time t_0 is predicted with an appropriate dynamic model. Then, for each vehicle pair $\{c_i, c_j\}$, $i \neq j$ the progression of its mutual Euclidean distance $e_{i,j}(t)$ is computed for $t \in [t_0, t_0 + \Delta t]$. Here the Euclidean distance between two cars is the smallest distance $\|p_i - p_j\|$ between points p_i and p_j of vehicles c_i and c_j at the given time t, respectively. Thus this distance concept differs from the definition of distance d for the formation of cooperative groups. The distance e depends on the vehicle geometry and will be further refined below to take the uncertainty of the predicted vehicle position into account.

If at least one of the $e_{i,j}(t)$ falls below a distance threshold ε with $t \in [t_0, t_0 + \Delta t]$, then a dangerous situation for the CG $\mathcal{G}$ arises, i.e., when

$$\min_{\substack{c_i, c_j \in \mathcal{G} \\ i \neq j}} \left\{ \min_{\tau \in [0, \Delta t]} \left\{ e_{i,j}(t+\tau) \right\} \right\} < \varepsilon \Rightarrow Danger \tag{13}$$

Figure 9 illustrates the detection strategy within the time distance plane.

Vehicle Model and State Description

For an overview of vehicle models, associated sensors, and state equations, see for example, the results of Tan and Huang in [47], where preprocessing of the GPS signals and measurement of yaw are also discussed. The authors propose a system design for a vehicle to vehicle cooperative warning system in [48]. The vehicle state model and equations for vehicle tracking are as follows:

$$\mathbf{x}(t) = \begin{bmatrix} x(t) & y(t) & \phi(t) & \omega_b(t) \end{bmatrix}^{\mathrm{T}} \tag{14}$$

$$\dot{\mathbf{x}}(t) = \begin{bmatrix} v(t)\cos\phi(t) \\ v(t)\sin\phi(t) \\ \omega_z(t) - \omega_b(t) \\ n_{wb}(t) \end{bmatrix} \tag{15}$$

where x and y are the east and north distances in the earth-fixed coordinate frame respectively, ϕ is the vehicle heading angle (measured positive anticlockwise

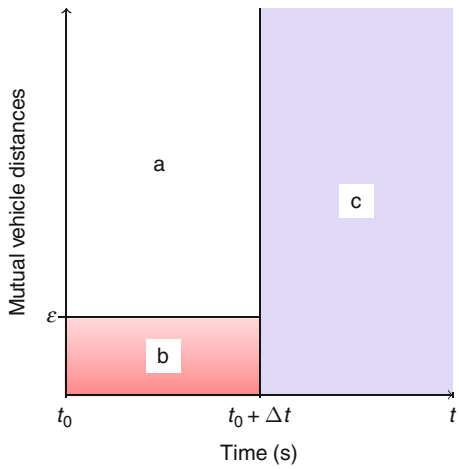

Cooperative Group of Vehicles and Dangerous Situations, Recognition of. Figure 9
(**a**) Predicted mutual distances within a forecast horizon of Δt are above a critical level ε. (**b**) Distances too small and time too short to manually master the situation ⇒ danger. (**c**) Enough time ahead for the drivers to manage the situation safely

from the x axis), v is the longitudinal velocity of the vehicle, ω_z is the vehicle's yaw rate, ω_b is the bias in the yaw rate measurement, and n_{wb} is a Gaussian white noise.

The nonlinear differential equation (15) is solved approximately using an Extended Kalman Filter (EKF [49]) to track the vehicle position. The input values to the EKF are v from a wheel speed sensor, $\omega_z(t)$ from a yaw gyro and the Gaussian noise n_{wb}. The observation vector $[x(t)\ y(t)\ \phi(t)]^{\mathrm{T}}$ comprises preprocessed DGPS (Differential Global Positioning System) measurements. The measurement and observation values are transferred by the group members to the group coordinator in order to update the information in the Common Relevant Picture. The group coordinator executes the EKF algorithm to track the vehicle positions.

Path Prediction

Using the information of the Common Relevant Picture, the group coordinator predicts the paths of the vehicles in its neighborhood based on their state information.

The reference position of the vehicle is taken to be at the center of the rear axle. The vehicle shape is modeled as a rectangle with the parameters shown in Table 1.

Cooperative Group of Vehicles and Dangerous Situations, Recognition of. Table 1 Vehicle parameters with values as used in the example

Length	R_l	5.0 m
Width	R_w	1.8 m
Distance of rear axle from back	R_d	1.0 m

These parameters depend on the vehicle type. The rectangle at vehicle position (0, 0) and heading angle 0 is called the Reference Rectangle of the vehicle and has vertices $\mathbf{r}_1 = (-R_d, 0.5R_w)^{\mathrm{T}}$, $\mathbf{r}_2 = (R_l - R_d, 0.5R_w)^{\mathrm{T}}$, $\mathbf{r}_3 = (R_l - R_d, -0.5R_w)^{\mathrm{T}}$ and $\mathbf{r}_4 = (-R_d, -0.5R_w)^{\mathrm{T}}$.

Assuming that the current time is t_0, the vehicle paths are to be predicted for a time interval $[t_0, t_0 + \Delta t]$. It is assumed that there are no changes of the driver actions in this interval and that vehicle paths are independent of each other. This assumption can be justified by taking a prediction horizon shorter than the time necessary for a specific human reaction. The path of a given vehicle is described with the equations

$$\mathbf{x}(t) = [\,x(t) \quad y(t) \quad \phi(t) \quad v(t)\,]^{\mathrm{T}} \tag{16}$$

$$\dot{\mathbf{x}}(t) = \begin{bmatrix} v(t)\cos\phi(t) \\ v(t)\sin\phi(t) \\ \omega_z(t_0) - \omega_b(t_0) \\ a_x(t_0) - a_b(t_0) \end{bmatrix} \tag{17}$$

where it is assumed that the unbiased yaw rate $\omega_z(t_0) - \omega_b(t_0)$ and the unbiased acceleration $a_x(t_0) - a_b(t_0)$ are constant in the time interval. x, y, ϕ and v are as above. The lateral velocity is ignored as it is normally small. The model does not use any vehicle specific parameters in contrast to the more detailed bicycle model, cf. [47].

The state-space equations are nonlinear differential equations. An EKF can be used to solve them approximately, for example, as in [48]. Better solutions are achieved with the Unscented Kalman Filter as described in [50] and also applied in [46].

The propagation of sigma particles representing the initial state distribution is calculated using numerical integration. The path of each sigma particle is weighted with an outcome probability. Following [50], the sigma particles of the unscented Kalman filter may be selected as

$$\mathbf{x}(t_0, 0) = \overline{\mathbf{x}}(t_0, 0) \tag{18}$$

$$\mathbf{x}(t_0, i) = \overline{\mathbf{x}}(t_0, 0) + \mathbf{Q}_i \text{ for } i = 1, \ldots, L \tag{19}$$

$$\mathbf{x}(t_0, i) = \overline{\mathbf{x}}(t_0, 0) - \mathbf{Q}_{i-L} \text{ for } i = L+1, \ldots, 2L \tag{20}$$

where $\overline{\mathbf{x}}$ is the mean of $\mathbf{x}$, L is the dimension of $\mathbf{x}$, i.e., 4, and $\mathbf{Q}_i$ is the ith row of the matrix square root (upper triangular Cholesky factorization):

$$\mathbf{Q} = \sqrt{(L+\lambda)\mathbf{P}_\mathbf{x}} \tag{21}$$

$\mathbf{P}_\mathbf{x}$ is the covariance matrix of $\mathbf{x}$ at the current time t_0. The scaling parameter $\lambda = \alpha^2(L + k) - L$ with $\alpha = 0.001$ and $k = 0$.

Let $\mathbf{x}(t,i)$ be the propagation of $\mathbf{x}(t_0,i)$ through the differential equation (17) till time t for $i = 0, \ldots, 2L$. The differential equation can be solved in MATLAB with the ode45 function for non-stiff ODEs.

The mean of the predicted $\mathbf{x}(t)$ is the weighted mean of the $\mathbf{x}(t,i)$:

$$\overline{\mathbf{x}}(t) = \sum_{i=0}^{2L} W_i^{(m)} \mathbf{x}(t, i) \tag{22}$$

with the weights defined as follows:

$$W_0^{(m)} = \lambda/(L+\lambda) \tag{23}$$

$$W_i^{(m)} = 1/(2(L+\lambda)) \text{ for } i = 1, \ldots, 2L \tag{24}$$

The covariance matrix of $\mathbf{x}(t)$ is the weighted sum

$$\hat{\mathbf{P}}_\mathbf{x}(t) = \sum_{i=0}^{2L} W_i^{(c)} \{\mathbf{x}(t, i) - \overline{\mathbf{x}}(t)\}\{\mathbf{x}(t, i) - \overline{\mathbf{x}}(t)\}^\mathrm{T} \tag{25}$$

with the weights defined as follows (with $\beta = 2$):

$$W_0^{(c)} = \lambda/(L+\lambda) + 1 - \alpha^2 + \beta \tag{26}$$

$$W_i^{(c)} = W_i^{(m)} \text{ for } i = 1, \ldots, 2L \tag{27}$$

For $t \in [t_0, t_0 + \Delta t]$, let $A(t)$ be the point set of the likely area occupied by the vehicle at time t given its state as described by the mean $\overline{\mathbf{x}}(t)$ and covariance matrix $\hat{\mathbf{P}}_\mathbf{x}(t)$. $A(t)$ is estimated by firstly using the covariance ellipse as an estimate of the uncertainty of the vehicle reference position:

$$E(t) = \left\{\mathbf{v} \in \mathbf{R}^2 : \mathbf{v}^\mathrm{T} Q(t)^{-1} \mathbf{v} \le \gamma\right\} \tag{28}$$

where $Q(t)_{ij} = \hat{\mathbf{P}}_\mathbf{x}(t)_{ij}$ for $i, j = 1,2$ and parameter $\gamma = 1$, and secondly by considering the rotational uncertainty of the vehicle about its reference position (heading angle):

$$\sigma_\phi = \sqrt{\hat{\mathbf{P}}_\mathbf{x}(t)_{33}} \tag{29}$$

$$I_\phi = [\overline{\mathbf{x}}(t)_3 - b\sigma_\phi, \overline{\mathbf{x}}(t)_3 + b\sigma_\phi] \tag{30}$$

$$F(t) = \mathcal{H}\left(\{R(\psi, \mathbf{r}_i) : \psi \in I_\phi, i \in \{1, \cdots, 4\}\}\right) \tag{31}$$

where σ_ϕ is the standard deviation of the heading angle, parameter $b = 1$, $R(\psi, \mathbf{u})$ is the counterclockwise rotation of vector $\mathbf{u}$ by ψ, $\mathbf{r}_i$ are the vertices of the Reference Rectangle of the vehicle, and $\mathcal{H}$ is the convex hull set operator.

Finally, we set $A(t)$ as

$$A(t) = E(t) \oplus F(t) \oplus (\overline{\mathbf{x}}(t)_1, \overline{\mathbf{x}}(t)_2)^\mathrm{T} \tag{32}$$

where the $\oplus$ denotes the vector (Minkowski) sum of the sets.

Now consider a group of m vehicles c_i for $i = 1, \ldots, m$. An obstacle on the road can be modeled as a stationary vehicle. The path prediction is performed as above for each vehicle separately, assuming that there are no dependencies in the interval $[t_0, t_0 + \Delta t]$.

Let $A_i(t)$ denote the likely area occupied by c_i at time t for $i = 1, \ldots, m$.

For the assessment of collision danger, we compute the Euclidean distance between the vehicles:

$$e_{ij}(t) = \mathrm{dist}(A_i(t), A_j(t)) \tag{33}$$

$$= \min\left\{\| p_i - p_j \| : p_i \in A_i(t), p_j \in A_j(t)\right\} \tag{34}$$

and consider the minimum in the prediction interval $[t_0, t_0 + \Delta t]$:

$$e_{ij}^m = \min\{e_{ij}(t) : t \in [t_0, t_0 + \Delta t]\} \tag{35}$$

A dangerous state is detected if $e_{ij}^m < \varepsilon$ for at least one vehicle pair c_i, c_j, where ε is a distance threshold (in the example set to 1 m).

The geometric computations in (28), (32), and (33) may be executed efficiently with packages for polytope calculus such as the Multi-Parametric Toolbox (MPT, [51]) with the optimization toolbox YALMIP [52]. Distances below 5 m as considered here require an accurate polytope approximation of the vehicle and covariance ellipse. For vehicles whose predicted trajectories are sufficiently distant, say at least 30 m, only the positions of the Reference Points need be computed.

For intermediate distances above 5 m, the polytopes can be replaced by bounding rectangles.

Example

Figure 10 shows the scenario under discussion. Two vehicles c_1 and c_2 (vehicle sizes as in Table 1) are approaching each other in a 45° curve on a country road. The center line of the road is composed of two clothoids, each of arc length $l = 100$ m. The curvature κ of the center line as a function of the arc length from the bottom left is

$$\kappa(s) = \begin{cases} s/a^2 & \text{for } 0 \le s \le l \\ (2l - s)/a^2 & \text{for } l \le s \le 2l \end{cases}$$

where $a = 2l/\sqrt{\pi}$. The smallest radius of curvature is $\kappa(\mathrm{l})^{-1} = 4\,\mathrm{l}/\pi \simeq 127$ m. We assume that each lane of the road is 4 m wide and that the vehicles travel in the center of their lane. The longitudinal velocity of both vehicles is a constant 20 m/s = 72 km/h. At time $t = 0$, c_1 and c_2 are at the top right and bottom left corners, respectively.

In addition, a stationary, broken down vehicle c_3 of the same size is located at 110 m from the bottom left in the middle of the right lane. So c_2 will hit c_3 in about 5.2 s if no action is taken and we, therefore, consider the prediction time interval [3.2 s, 5.2 s] in detail in this example.

The state transition equations (17) assume that the unbiased yaw rate is constant in the time prediction interval. This is only an approximation in the curve where the yaw rate must change continually to follow the curve precisely. An improved prediction must either use information about the change of yaw rate derived from a presumed vehicle-driver behavior or the period without measurement feedback must be reduced. This assumption is reasonable if we restrict the prediction horizon to be below human reactivity.

The future trajectories of the vehicles are predicted for the next 2 s given the uncertain information on their positions, heading angle, and velocity (units: m, radian, m/s). The covariance matrix of the state information is assumed to be the same for all vehicles:

$$diag(0.04, 0.04, 0.001, 0.1) \tag{36}$$

The standard deviations of the state are, therefore, for the x or y position: 0.2 m, heading angle: 0.0316 rad and velocity: 0.316 m/s.

Figure 11 shows the pairwise distances between the three vehicles as calculated from (33) for the prediction time interval [3.2 s, 5.2 s]. c_1 passes the stationary c_3 without danger, but the distance between c_1 and c_2 is predicted to enter the danger zone at 4.8 s. As shown in Fig. 12, this dangerous situation is due to the predicted understeering of c_1 and c_2 in the curve. As expected, this problem becomes more serious when the velocities or curvature increase. In addition, the predicted distance between c_2 and c_3 becomes dangerous at 5.1 s.

The next step for the cooperative group would be to calculate and evaluate possible joint reactions and new

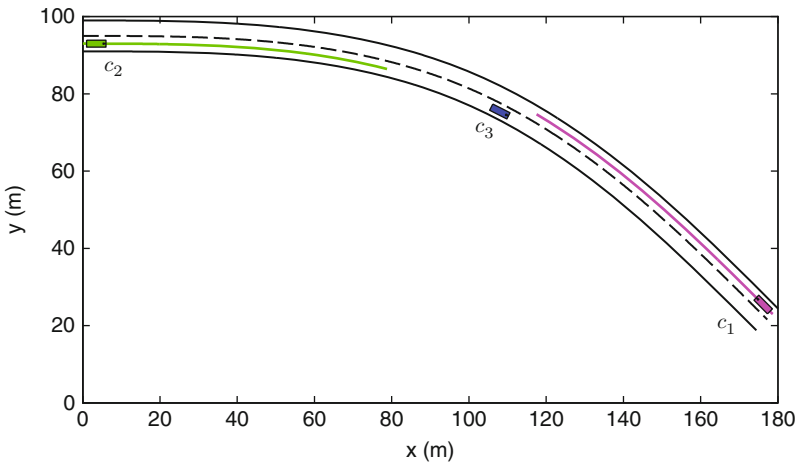

Cooperative Group of Vehicles and Dangerous Situations, Recognition of. Figure 10
Initial positions of vehicles c_i for $i = 1, \ldots, 3$ and the planned trajectories of c_1 and c_2

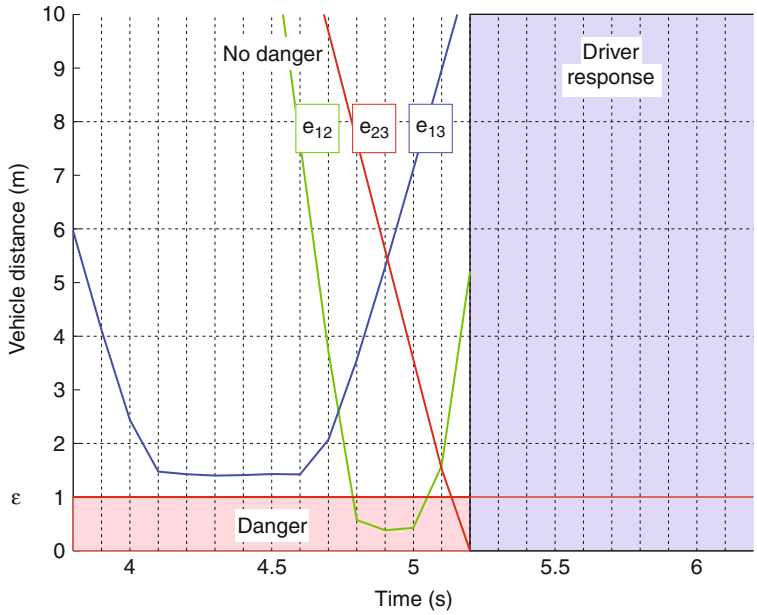

Cooperative Group of Vehicles and Dangerous Situations, Recognition of. Figure 11
Predicted distances e_{ij} between the vehicles considering the uncertainty of their state. If uncertainty is not considered, then min(e_{12}) and min(e_{13}) are both approx. 2.14 m

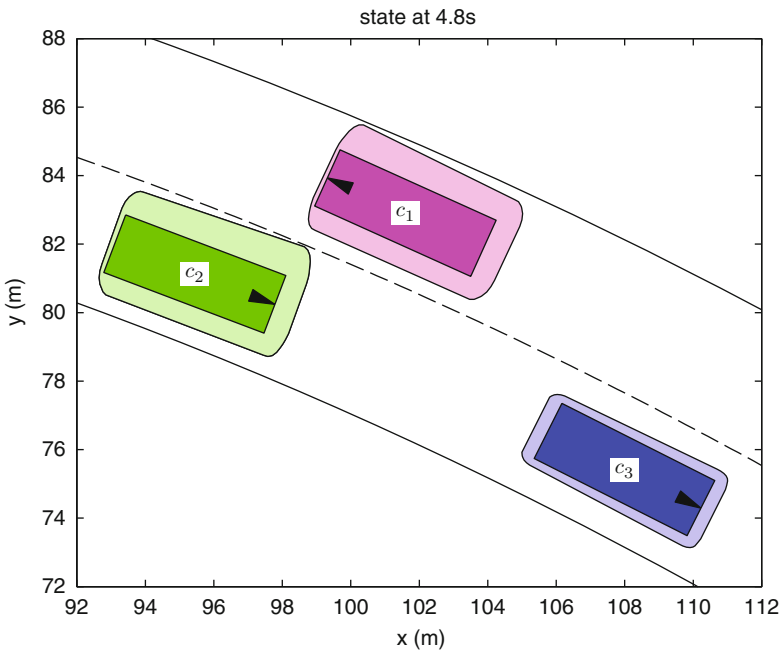

Cooperative Group of Vehicles and Dangerous Situations, Recognition of. Figure 12
Likely positions of vehicles at 4.8 s with *solid rectangles* for the actual positions and surrounding *polytopes* for the uncertainty area. Prediction calculated at 3.2 s

trajectories. In the example, c_1 and c_2 should move closer to the road borders, and c_2 should decrease its velocity to avoid both dangers. However, depending on the parameter constellations, additional reactions are feasible, such as c_1 changing its velocity to allow c_2 to overtake c_3. The development of cooperative maneuvers will be explored in more detail in the next section.

Cooperative Decision Making

Once a dangerous situation has been detected, the system can either issue a warning and leave the conflict resolution to the driver or it can intervene autonomously by executing a cooperative maneuver.

Warning Systems

The following two questions are of particular importance for the design of collision warning systems:

1. Which is the criterion to issue a warning? Typically, thresholds in terms of collision probability or time to collision are defined [28, 53, 54]. It is important to minimize false alarms because drivers tend to ignore warnings if there are frequent false alarms.
2. How is the warning presented to the driver? Possibilities include optic, acoustic, and haptic warnings, or combinations of these [55–57]. Ideally, the warning should induce the driver to perform an adequate collision avoidance maneuver. For example, vibrations of the steering wheel could indicate a necessary steering maneuver to the driver. This technique is used in lane departure warning systems [58, 59].

Monitoring driver behavior is also of interest. For example, a driver who has already initiated a collision avoidance maneuver should not be distracted by an alarm [53, 60]. Some of the systems specifically address certain traffic scenarios, e.g., intersections, left-turning, lane changes, or rear-end collisions [61, 62].

Cooperative Driving

Various approaches to realize cooperative driving are conceivable, many of them tailored to specific traffic situations or types of accidents. For example, a cooperative variant of adaptive cruise control has been developed, which increases the foresight horizon in order to reduce the amount of necessary accelerations and decelerations [11, 63]. A similar system is an emergency braking assistant preventing rear-end collisions based on cooperative information exchange [64]. Both systems only affect the longitudinal control of the vehicle. Platooning systems additionally address the task of lane keeping and the execution of some maneuvers like merging into a platoon [10, 65]. Lane assignment for platoons with the aim of optimizing traffic flow is another topic of research [12]. Collision avoidance with obstacles or vehicles outside the platoon is usually not covered by these approaches. A method specialized on merging maneuvers is described in [38].

Cooperative intersection control systems can have two different goals: the focus is either on collision warning, as described in the previous section, or on optimizing traffic flow. Systems of the latter type usually assume fixed paths of the vehicles and optimize order of precedence and velocity profiles [13, 14, 66], see also section "Decoupled Planning" below.

Cooperative control approaches keep formations of aerial, underwater, or land vehicles, usually in off-road exploration scenarios [67]. Few of these works address collision avoidance among cooperative vehicles [68].

Other systems specialize on obstacle avoidance from a single-vehicle perspective. Typically, prespecified evasive trajectories are parameterized to fit the encountered situation [69, 70]. A system that can handle more general situations, such as multiple obstacles, has to use motion planning techniques [71]. Another approach applies differential game theory to avoid the collision of a single vehicle with a driver going the wrong way [72].

Altogether, motion planning techniques seem to be the most general approach to cooperative driving in dangerous situations as they can handle arbitrary obstacles and road geometries. Therefore, motion planning is covered in more detail in the following section.

Multi-vehicle Motion Planning

In this section, methods are described which compute a cooperative motion plan for given initial positions of vehicles and obstacles. The plan must be feasible with regard to the kinematic and dynamic capabilities of the involved vehicles. Therefore, a level of abstraction

appropriate for cooperative motion planning has to represent vehicle dynamics and geometry. Once a feasible cooperative plan has been computed by the group coordinator, it can be communicated to the vehicles of the cooperative group. Within the tolerances of the cooperative plan, each vehicle can perform a finer planning of its own trajectory, e.g., optimizing comfort criteria, before executing the maneuver (cf. Fig. 1).

This section starts with a formalization of the motion planning problem, especially introducing the concept of configuration spaces. Afterward, some motion-planning algorithms are described. The methods can be distinguished by the criterion if they do or do not make decoupling assumptions in order to reduce the computational complexity.

Configuration Space Path planning and motion planning originate from robotics, and car-like vehicles may be regarded to be specializations of robots. An important concept from robot motion planning is the configuration space.

The configuration of a robot is a parametric specification of the geometric position of every point of the robot [73]. The manifold of all possible configurations is called the configuration space $\mathcal{Q}$ of the robot [74, 75]. A path is a parametric curve in the configuration space, i.e., a continuous mapping $[0, 1] \to \mathcal{Q}$.

The relevant configuration parameters of a car-like vehicle c_i are its position x_i, y_i in the road plane and its orientation (yaw angle) ϕ_i. It is common to assume a sufficiently planar road so that vertical position, roll, and pitch angle can be neglected. This results in the three-dimensional configuration space $\mathcal{Q}_i = \mathbb{R}^2 \times \mathbb{S}$, where $\mathbb{S}$ is the unit circle parameterized by $[0,2\pi)$. Note that the angles 0 and 2π describe the same orientation, which causes $\mathcal{Q}_i$ to be a cylindrical manifold [75].

The motions of a car are restricted by the orientation of its wheels, it cannot move in arbitrary directions. This is expressed by the following constraint on incremental position changes $\mathrm{d}x_i$, $\mathrm{d}y_i$:

$$\mathrm{d}x_i \sin\phi_i = \mathrm{d}y_i \cos\phi_i \tag{37}$$

Despite this constraint, all configurations in $\mathcal{Q}_i$ can be reached if no obstacles are present. Such constraints which do not reduce the dimensionality of the configuration space are called nonholonomic [75]. The nonholomic properties of a car are of special importance when parking maneuvers are considered. It is possible to plan a path without considering the nonholonomic constraint and to subsequently transform it to enforce conformity with the constraint [76].

The motion of a car is not only restricted by its nonholonomic kinematics, but also by its dynamics. Instantaneous accelerations or decelerations are impossible due to inertia. A state space model can be used to describe the vehicle kinematics and dynamics. A simple state space model for a car-like vehicle is given as follows,

$$\begin{pmatrix} \dot{x}_i \\ \dot{y}_i \\ \dot{\phi}_i \\ \dot{v}_i \end{pmatrix} = \begin{pmatrix} v_i \cos\phi_i \\ v_i \sin\phi_i \\ 0 \\ 0 \end{pmatrix} + \begin{pmatrix} 0 \\ 0 \\ v_i \frac{\tan\alpha_i}{l_i} \\ a_i \end{pmatrix}, \tag{38}$$

where v_i denotes the longitudinal velocity, a_i the acceleration, α_i the steering angle, and l_i the wheelbase of the car (cf. Fig. 13). The first summand on the right-hand side of the equation models the state evolution, while the second one characterizes the actuator behavior. Acceleration and steering angle are the control inputs of the system. They are bounded by the capabilities of the vehicle, which depend on brakes, engine power, steering geometry, tires, and the friction of the road surface. A simplified model for the dynamic limits is Kamm's circle stating that longitudinal and lateral acceleration $a_{i,\mathrm{lon}}$ and $a_{i,\mathrm{lat}}$ are limited by

$$\sqrt{a_{i,\mathrm{lon}}^2 + a_{i,\mathrm{lat}}^2} \le \mu_i g, \tag{39}$$

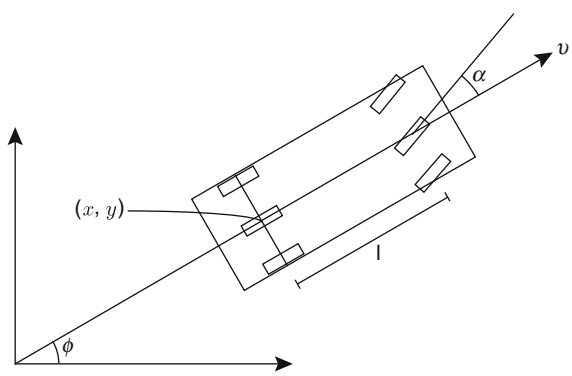

Cooperative Group of Vehicles and Dangerous Situations, Recognition of. Figure 13
Notation used in the vehicle model (38)

where $g \approx 9.8$ m/s^2 is Earth's gravitational acceleration and $\mu_i \approx 1$ is the road-tire friction coefficient [71]. Additional bounds may be imposed on acceleration and steering angle, e.g., $a_{i,\text{lon,min}} \leq a_{i,\text{lon}} \leq a_{i,\text{lon,max}}$ and $|\alpha_i| \leq \alpha_{i,\max}$.

When vehicle dynamics have to be considered, it is usually necessary to solve a motion planning problem, i.e., to compute a continuous mapping $[0, t_{\max}] \to \mathcal{Q}_i$. This mapping is sometimes called a trajectory. Unlike a path, it is explicitly parameterized by time. Methods for vehicle motion planning include sampling-based approaches [75], especially rapidly exploring random trees [77, 78], and elastic-band planning [79]. Vehicles with different configuration spaces, e.g., trucks pulling trailers, have also been considered [76].

Obstacles divide the configuration space into free space and obstacle regions. A configuration $\mathbf{q}_i \in \mathcal{Q}_i$ belongs to free space if every point of the robot in configuration $\mathbf{q}_i$ is collision-free with every obstacle. For collision checking, both robot and obstacle geometry have to be considered. The explicit construction of the free space is avoided by most practical planning algorithms due to its algorithmic complexity [75].

Path planning for multiple vehicles can be performed in the composite configuration space, which is the Cartesian product of the individual configuration spaces [80]: $\mathcal{Q} = \mathcal{Q}_1 \times \ldots \times \mathcal{Q}_m$. The possibility of motion planning in the composite configuration space is well known from robotics textbooks [74, 75]. However, the computational complexity of motion planning algorithms usually increases exponentially with the dimensionality of the configuration space [80]. If each individual configuration space $\mathcal{Q}_i$ is of dimension d_i, the composite configuration space has dimension $d = \sum_{i=1}^{m} d_i$. Therefore, cooperative motion planning in the composite configuration space has rarely been used in practice. See [81, 82] for some robotics examples. More common are decoupling approaches which make simplifying assumptions in order to lower the computational complexity. However, these assumptions also restrict the space of solutions, which might be particularly critical in dangerous situations. Therefore, both decoupling and cooperative planning methods are presented in the following sections.

Altogether, the motion planning task for m vehicles can be formalized as follows: compute a continuous trajectory $[0, t_{\max}] \to \mathcal{Q} = \mathcal{Q}_1 \times \ldots \times \mathcal{Q}_m$ which

1. Starts at the initial states of the vehicles
2. Avoids collisions among the m cooperative vehicles, considering their geometric models
3. Avoids collisions with both static and moving obstacles
4. Keeps the vehicles on the road area
5. Respects the kinematic and dynamic constraints of the vehicles

Additionally, a goal region is specified usually. This has been omitted here because collision avoidance is the main objective in dangerous situations.

When moving obstacles are considered, the obstacle-free regions of the configuration space become time-dependent. This can be incorporated by adding a time axis, resulting in the configuration space-time [75, 80]. The trajectories of moving obstacles may be derived from prediction methods as described above in section "Path Prediction." The road constraint may be dealt with by declaring all off-road areas as obstacles.

The resulting trajectory in composite configuration space is communicated to the vehicles of the cooperative group (cf. Fig. 1). Before execution, each vehicle can perform a refinement of its individual trajectory within the tolerances of the cooperative plan according to more detailed models and specific criteria. In fact, the main purpose of cooperative planning is not to find an optimal trajectory, but to construct and select a homotopy class of solutions in the composite configuration space [75]. Optimizations within the tolerances of the correct homotopy class, such as smoothing, can be performed by the individual vehicles.

Decoupled Planning Decoupling methods reduce the computational complexity of multi-vehicle motion planning by considering lower-dimensional subspaces of the composite configuration space. Usually, a subspace corresponding to a single vehicle is chosen.

The path-velocity decomposition is a well-known method which decouples the composite problem into m path planning problems and a velocity coordination problem [83]. It uses path planning algorithms to find individual paths in $\mathcal{Q}_i$ for each vehicle. Each path circumvents the static obstacles but ignores the

existence of the other vehicles. In a second stage of the algorithm, the relative velocities along the individual paths are coordinated in order to avoid inter-vehicle collisions [84]. This corresponds to a one-dimensional reparameterization of each path. It is a path planning problem in the m-dimensional coordination space. Alternatively, paths may be coordinated incrementally, resulting in $m - 1$ two-dimensional coordination problems. In the last stage of the algorithm, the time scaling of the path is performed to obtain a motion respecting the dynamic constraints. It is also possible to perform the time scaling during the coordination stage, which requires increasing the dimensionality of the coordination space by one.

The path-velocity decomposition is an adequate approximation in many robotic scenarios [85–87] and has also been applied to road traffic problems [40]. It shows certain parallels to resource allocation methods which consider regions such as intersections to be mutual exclusive resources and apply scheduling mechanisms to resolve conflicts [66, 88]. Other methods weaken the restriction to a single path and allow the coordination procedure to select a path within a probabilistic roadmap [89, 90].

The second approach to decouple multi-robot motion planning assigns priorities to the robots [91–95]. The robots are processed in the order of priorities, which means that lower-priority robots already know the planning results of the higher-priority ones. The ith robot plans a motion in its configuration space-time which considers the planned motions of the higher-priority robots $1, \ldots, i - 1$ as moving obstacles but completely ignores the lower-priority robots $i + 1, \ldots, m$. This replaces the d-dimensional planning problem in the composite configuration space with m planning steps in configuration space-times of dimension $d_i + 1$. Of course, the results depend on the selected order of priority. Therefore, methods for constructing somewhat optimal priorities are of interest [96, 97]. However, prioritized planning may be suboptimal even with the best priorities. The approach has been applied to manipulators, mobile robots, and vehicle-parking scenarios.

In dangerous situations involving multiple vehicles, decoupled planners may fail to find an existing collision-free solution. This can already happen in very simple scenarios (Fig. 14). Additionally, it is difficult to consider vehicle dynamics in the path-velocity decomposition and in the roadmap coordination approach. Therefore, three recent methods for cooperative planning in the composite configuration space are presented in the following sections (Fig. 15).

Tree Search The current action of a vehicle can be characterized by its acceleration and its steering angle, see (38). The continuum of actions can be discretized by choosing a finite set of representatives. When an action is applied for a certain interval of time Δt before the next action is selected, a tree structure of decisions results. The discrete action set should contain extreme actions like maximum braking and maximum steering admissible by the dynamics of the vehicle, given by (39). These extreme actions are known to be optimal for a single vehicle evading an obstacle [69, 71]. In the automobile domain, time discretization is justified because actuator limits prohibit a quick change of actions.

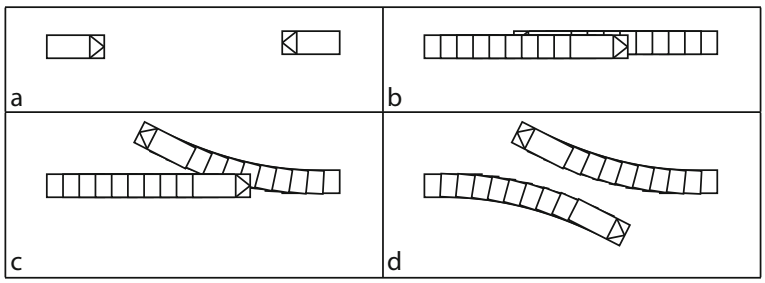

Cooperative Group of Vehicles and Dangerous Situations, Recognition of. Figure 14
Comparison of cooperative and decoupled motion planning. (**a**) Oncoming traffic scenario, (**b**) path-velocity decoupling, (**c**) prioritized motion planning, (**d**) cooperative motion planning in the composite configuration space

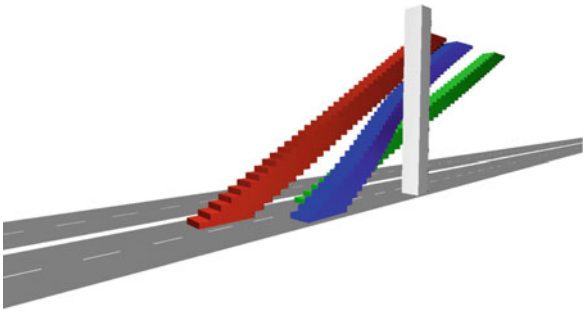

Cooperative Group of Vehicles and Dangerous Situations, Recognition of. Figure 15
Space-time visualization of a cooperative merging maneuver. In this 3D illustration, *x* and *y* directions of the road plane are depicted together with the time axis pointing upward vertically. Motion sequences of three vehicles can be seen, and a static obstacle appears as a *pillar*

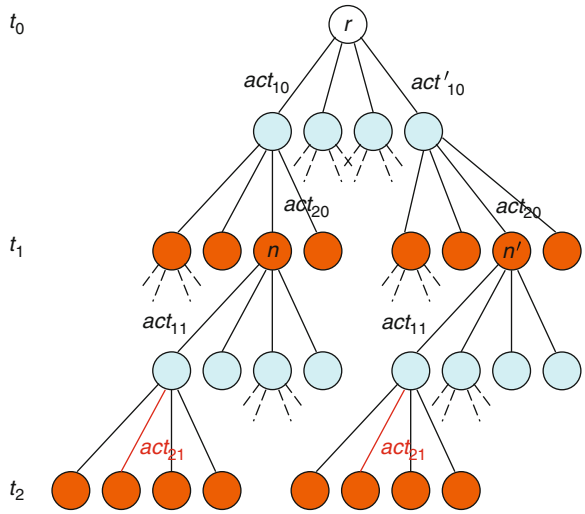

Cooperative Group of Vehicles and Dangerous Situations, Recognition of. Figure 16
Tree $\mathcal{T}$ of cooperative actions for $m = 2$ vehicles

Each node n_i of the tree $\mathcal{T}_i$ corresponds to a state $\mathbf{x}_i = (x_i, y_i, \phi_i, v_i)^{\mathrm{T}}$ of the ith vehicle. Applying an action $act_i = (a_i, \alpha_i)^{\mathrm{T}}$ results in a successor state which can be computed by integrating (38) (cf. [80]):

$$
\begin{aligned}
v_i(t+\Delta t) &= v_i(t) + a_i(t)\Delta t \\
\phi_i(t+\Delta t) &= \phi_i(t) + \frac{\tan\alpha_i(t)}{l_i}\left(v_i(t) + \tfrac{1}{2}a_i(t)\Delta t\right)\cdot\Delta t \\
x_i(t+\Delta t) &= \begin{cases} x_i(t) + \left(v_i(t) + \frac{1}{2}a_i(t)\Delta t\right)\cdot\Delta t\cdot\cos\phi_i(t) & \text{if } \alpha_i(t) = 0 \\ x_i(t) + \frac{l_i}{\tan\alpha_i(t)}\left(\sin\phi_i(t+\Delta t) - \sin\phi_i(t)\right) & \text{if } \alpha_i(t) \neq 0 \end{cases} \\
y_i(t+\Delta t) &= \begin{cases} y_i(t) + \left(v_i(t) + \frac{1}{2}a_i(t)\Delta t\right)\cdot\Delta t\cdot\sin\phi_i(t) & \text{if } \alpha_i(t) = 0 \\ y_i(t) + \frac{l_i}{\tan\alpha_i(t)}\left(\cos\phi_i(t+\Delta t) - \cos\phi_i(t)\right) & \text{if } \alpha_i(t) \neq 0 \end{cases}
\end{aligned}
\tag{40}
$$

The tree $\mathcal{T}_i$ consists of $T + 1$ levels, resulting in a planning horizon of $t_{\max} = T \cdot \Delta t$. It has A_i^T leaf nodes, where A_i denotes the number of actions. With each action act_i leading to tree node n_i, a loss $L(n_i)$ is incurred for the violation of constraints listed in section "Configuration Space." Loss is a notion used in utility theory to determine preferences between alternative actions [98]. The loss is composed additively of a term $L_{\mathrm{road}}(n_i)$ penalizing road departure, $L_{\mathrm{obst}}(n_i)$ for collisions with obstacles, $L_{\mathrm{coll}}(n_i)$ for collisions among cooperative vehicles, and $L_{\mathrm{control}}(n_i)$ rating control effort with the aim of avoiding unnecessary braking and steering. The optimal action sequence corresponds to a path from the root r_i to a leaf node n_i^* having minimum accumulated loss L_i^*.

For cooperative motion planning, every action of one vehicle can be combined with every action of all other vehicles, resulting in a set of $A = A_1 \cdot \ldots \cdot A_m$ composite actions and a tree $\mathcal{T}$ having A^T leaf nodes (Fig. 16). Even for moderate values of A and T, explicit construction of this tree exceeds memory and computational resources. Therefore, pruning techniques are required which allow the optimal solution to be found without searching the whole tree.

An important observation is that many computations during traversal of $\mathcal{T}$ depend only on the action sequences of a single vehicle. This holds for vehicle states and for some loss components, namely L_{obst}, L_{control}, and L_{road}. As a consequence, this information occurs redundantly in $\mathcal{T}$, for example, at the edges highlighted in Fig. 16. It is possible to store these values in the single vehicle trees $\mathcal{T}_i$ and look them up if they are needed several times. This can avoid many redundant computations.

The single vehicle trees can also be precomputed completely as they are much smaller than $\mathcal{T}$. This allows

the establishment of lower bounds for the loss within a subtree. A lower bound $h(n_i)$ for a subtree of $\mathcal{T}_i$ rooted at n_i is obtained by recursively taking the minimum values of the children of n_i:

$$h(n_i) := \begin{cases} 0 & \text{if } n_i \text{ is a leaf} \\ \min\limits_{n_i' \text{: child of } n_i} \{L(n_i) + h(n_i)\} & \text{otherwise} \end{cases} \tag{41}$$

A lower bound $h(n)$ for a node n of the cooperative tree $\mathcal{T}$ is given by the sum of the values from the corresponding nodes $n_i(n)$ of the single-vehicle trees $\mathcal{T}_i$:

$$h(n) := \sum_{i=1}^{m} h(n_i(n)) \tag{42}$$

These lower bounds can be used for an efficient branch and bound search in $\mathcal{T}$. It explores the tree in depth-first order, remembering the best solution found so far and its loss value L^*. Subtrees are excluded from the search if it can be proven that they cannot contain any part of the optimal solution. To this end, the sum $g(n) := L(r,n) + h(n)$ is computed for the root node n of the subtree, where $L(r,n)$ is the loss accumulated on the path from the root r of $\mathcal{T}$ to n. If $g(n) > L^*$, the total loss of any path passing through the subtree must be greater than L^*. In this case, the subtree can be excluded from the search without losing the guarantee to find the optimum (Fig. 17). The resulting branch and bound search method is shown in Algorithm 3. Alternatively, it is possible to search $\mathcal{T}$ using the A* algorithm, which also relies on the lower bounds $h(n)$ to improve efficiency [99, 100].

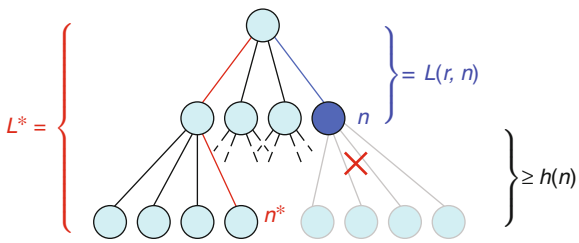

Cooperative Group of Vehicles and Dangerous Situations, Recognition of. Figure 17
Criterion to prune a subtree

Algorithm 3 General branch and bound method for cooperative motion planning

```
procedure SEARCH (t, n, L)
    for all act ∈ 𝒜 do
        Compute child node n_c, x(n_c) and L(n_c)
        if L + L(n_c) + h(n_c) < L* then
            if t + Δt < t_max then
                SEARCH (t + Δt, n_c, L + L(n_c))
            else
                L* ← L + L(n_c)
                n* ← n_c
            end if
        end if
    end for
end procedure
procedure PLAN(x_start)
    Perform precomputation
    L* ← ∞
    x(r) ← x_start
    SEARCH (0, r, 0)
    return n*
end procedure
```

The only remaining loss component is L_{coll}, which does not depend on the full cooperative action sequence either but only on the actions of pairs of vehicles [90]. Therefore, similar techniques can be applied in order to avoid redundant computations and to obtain lower bounds. The collision information can be stored in two-vehicle trees $\mathcal{T}_{ij}$ for every pair of vehicles. There is, however, a trade-off between precomputation effort and savings during branch and bound search, and experiments show that precomputation of collision loss does not improve overall performance in most cases [101].

An important advantage of the tree search formulation is the use of explicit vehicle, loss, and action models, which can be chosen in the level of detail appropriate for the task under consideration. Precomputation of lower bounds significantly improves computational performance of the method. By shifting most of the computational effort into the precomputation stage, running times become more predictable, increasing the real-time capability of the algorithm [101]. Figures 18 and 19 show collision avoidance maneuvers planned with the tree search method.

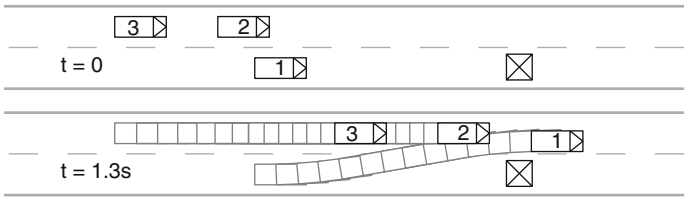

Cooperative Group of Vehicles and Dangerous Situations, Recognition of. Figure 18
Example of a cooperative merging maneuver planned by the tree search algorithm. While vehicle 1 changes to the left lane due to the obstacle, vehicles 2 and 3 brake in order to allow the merging. The full planning horizon has been 2.5 s

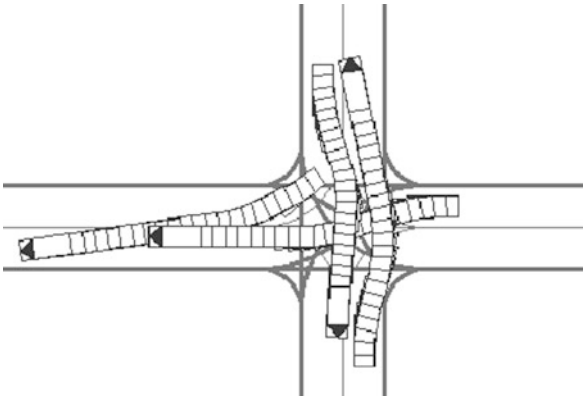

Cooperative Group of Vehicles and Dangerous Situations, Recognition of. Figure 19
A cooperative collision avoidance maneuver in an intersection scenario

Mixed-Integer Linear Programming The linear programming framework allows large systems of linear inequalities to be optimized efficiently. A linear program consists of an objective function, equality and inequality constraints, all of them being linear in the real-valued variables. An extension is mixed-integer linear programming (MILP) which constrains some of the variables to be integer, or – as a special case – binary. This makes the problem much harder.

As efficient standard software exists for solving MILPs, cooperative motion planning has been formulated in this framework in recent years, with focus on the air traffic domain [102–104]. Variables x_{ik}, y_{ik} denote the position of the ith vehicle at time $t = k \cdot \Delta t$ within a planning horizon $k = 0, \ldots, T$. Further variables are introduced for velocities and control inputs, with appropriate inequality constraints based on vehicle dynamics. They are coupled by equations describing a linearized version of a vehicle model like (38). Binary variables b_{ijkl} are required for the collision avoidance constraints:

$$\begin{aligned} x_{ik} - x_{jk} + b_{ijk1}M &> r_{ij} \\ y_{ik} - y_{jk} + b_{ijk2}M &> r_{ij} \\ -x_{ik} + x_{jk} + b_{ijk3}M &> r_{ij} \\ -y_{ik} + y_{jk} + b_{ijk4}M &> r_{ij} \\ \sum_{l=1}^{4} b_{ijkl} &\leq 3 \\ b_{ijkl} \in \{0,1\} \qquad k &= 1, \ldots, T \end{aligned} \tag{43}$$

Therein, r_{ij} is the minimum distance to be enforced between the vehicle reference points $(x_{ik}, y_{ik})^{\mathrm{T}}$ and $(x_{jk}, y_{jk})^{\mathrm{T}}$ at time $k \cdot \Delta t$, and $M \gg 0$ is a large constant. This formulations makes use of a well-known modeling technique to transform a disjunction of inequalities into a conjunction, which is the standard semantics of MILP constraints [105]. Only one of the first four inequalities has to be active, while the others can be trivially satisfied with $b_{ijkl} = 1$. The binary variables thus describe on which side the vehicles pass each other. It may be necessary to discretize the space of directions into more than the four paraxial directions of (43). This can be accomplished by additional separating half-planes [106]. Obstacle avoidance is modeled in the same way, the only difference being that the position of the second object is no longer variable. Complex objects may be represented by a covering of several geometric primitives.

Paralleling the tree search approach of the previous section, MILP solvers often employ branch and bound methods. However, in the tree search formulation, the branching occurs over the vehicle actions and collisions are tested depending on the selected actions, whereas in the MILP formulation, the binary decision variables

describe collision avoidance constraints and the vehicle actions are optimized dependent on the collision avoidance decisions. As a consequence, time discretization is tightly coupled with passing distances and cannot be coarsened without impairing collision avoidance. By contrast, in the tree search method, the number of decision points can be reduced without any difficulty in order to improve computational efficiency. This may be an explanation for the observed running times of the MILP approach, which seem to question a real-time usage at present [107]. Another drawback of the MILP method is the restriction to linear models and objective functions. An important advantage is the utilization of an established framework with available tool support, which facilitates modeling and implementation. Related work includes pure linear programming applied to air traffic control [108] and nonlinear optimization [109].

Elastic Bands Different variants of the elastic-band method have been applied to path adaptation for mobile robots [110–112] and to path planning for cars [79, 113–115]. Recently, the method has been extended to cooperative motion planning in dangerous situations [116].

Once again, nodes $\mathbf{x}_{i,k} = (x_{i,k}, y_{i,k})^{\mathrm{T}}$ describe the vehicle positions at discrete points in time. Consecutive nodes of one vehicle are connected to form an elastic band. Orientation and velocity of the vehicle are implicitly represented by the sequence of nodes.

Virtual forces are designed to represent the constraints described above in section "Configuration Space." The resulting elastic band can be interpreted as a combination of point masses and springs [114]. The virtual forces show some similarities with potential field path planners as forces can be interpreted as derivatives of potential fields. However, potential field planners only have a local view of the environment [80], while elastic bands allow collision avoidance forces to propagate along the band. Internal forces can be designed to represent the dynamic and kinematic constraints of the vehicle.

The total force vector applied to node $\mathbf{x}_{i,k}$ is denoted by $\mathbf{f}_{i,k}$. It is additively composed of several force terms. The internal forces $\mathbf{f}^{\mathrm{dist}}$ and $\mathbf{f}^{\mathrm{ang}}$ implement the dynamic and kinematic constraints of the vehicle in longitudinal and lateral direction, respectively. They correspond to springs between consecutive nodes of one band, $\mathbf{x}_{i,k}$ and $\mathbf{x}_{i,k+1}$.

External forces repel the band from obstacles, other vehicles, and the road boundary. For example, the force $\mathbf{f}^{\mathrm{coop}}$ acts between nodes of different bands having the same time index, $\mathbf{x}_{i,k}$ and $\mathbf{x}_{j,k}$. The elastic-band framework uses a circular object model. Other object shapes are approximated by a covering of circles [113]. A visualization of elastic bands and virtual forces is shown in Fig. 20.

The nodes of an elastic band have to be initialized in a meaningful way, e.g., corresponding to a lane-keeping behavior of the vehicle. The virtual forces are applied to the band iteratively until an equilibrium is reached in which the resulting forces vanish for every node: $\forall i\, \forall k\, \mathbf{f}_{i,k} \approx 0$. A continuous state and control trajectory is obtained from the discrete sequence of nodes using, e.g., cubic spline interpolation [113].

The elastic-band method has been successfully applied to obstacle avoidance, merging, overtaking,

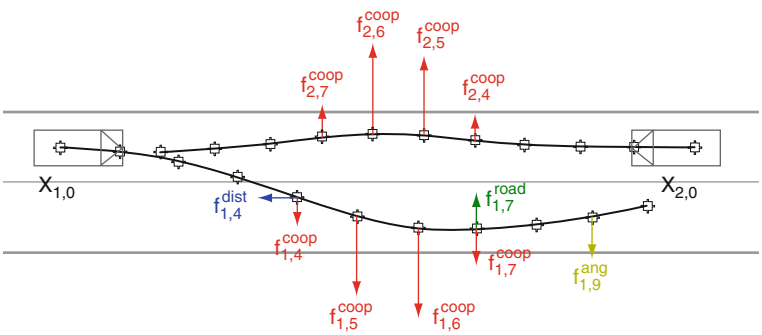

Cooperative Group of Vehicles and Dangerous Situations, Recognition of. Figure 20
Visualization of the elastic bands of two oncoming vehicles. *Arrows* indicate some selected force components

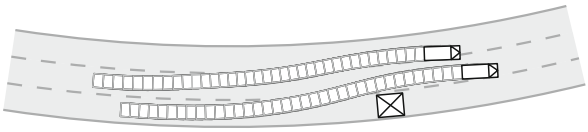

Cooperative Group of Vehicles and Dangerous Situations, Recognition of. Figure 21
Cooperative obstacle avoidance maneuver planned by the elastic-band method

and intersection scenarios. Figure 21 shows a cooperative maneuver planned by the elastic-band method, and Fig. 15 shows a space-time visualization of a merging scenario. Elastic bands exhibit potential for real-time implementation and a good scalability with the number of cooperative vehicles, even when a comparatively fine time discretization is chosen. However, the method can only find a local optimum, unlike the tree search and MILP approaches. This means that the result depends on the initialization of the elastic bands.

Future Directions

Many of the methods described in this entry are still at the research stage. They have been verified in simulations or experiments but are not yet ready for market deployment. The time to market may be quite long, e.g., as shown by platooning technologies that were demonstrated back in 1997 [117], but a commercial implementation of such systems is still pending.

A major unsolved problem is how to deal with the inevitable uncertainty in the environment information caused by sensor-based perception. On the one hand, this can be alleviated by improving sensor technology, processing algorithms, and multi-sensor fusion. In the context of cooperating vehicles, the integration of perceptions made by multiple vehicles is of particular interest. Research on appropriate fusion architectures is in progress [8, 118]; however, to the best of the authors' knowledge, cooperative perception has not yet been implemented in a real-world scenario. On the other hand, situation recognition and planning algorithms can be designed which take the uncertainties into account. For situation recognition and prediction, the methods described in this entry can already cope with uncertain information to a certain degree. Planning under uncertainty is a very difficult problem that is only partially solved. Statistical decision theory offers a framework to determine the best action under uncertain information [98]. In principle, this approach is equivalent to Bayesian decision networks, which establish a connection between situation assessment and decision making [119, 120]. However, its application to cooperative motion planning causes a dramatic increase in computational complexity. For single vehicles and robots, there are several approaches to considering model based probabilistic uncertainties [121–124]. A related, but different objective in motion planning is to reduce the uncertainty of vehicle localization [125, 126]. Cooperative motion planning with uncertain environment information is still an unsolved problem. The problem complexity may require a hierarchical planning, increasing the level of detail step-wise.

Regarding prediction methods, a comparative evaluation of the numerous approaches would be a topic for useful future work. [127] describes a prediction method that considers the interaction of several vehicles. The evaluation of cooperative maneuvers is treated in [128].

In the field of automatic maneuvers, a promising approach to guarantee the safety of a planned motion is the concept of inevitable collision states and the partial motion planner [78]. This is a scheme of iterated planning and execution. The plans selected are guaranteed not to induce a state in which a collision becomes inevitable. At least a collision-free contingency maneuver remains possible [129]. This principle has been extended to cooperative motion planning [130]. However, it is not directly applicable to dangerous situations because the assumption of an initial safe state does not hold there.

The group formation and decision algorithms described in this entry rely on a designated group coordinator vehicle. Future research should investigate to what extent decision making can be distributed. This could result in a better reliability and better distribution of the computational load. Consensus algorithms or game theoretic methods might possibly be extended to handle distributed decision making in dangerous traffic situations [67, 131–133].

Regarding wireless vehicular communication, standardization of protocols and bandwidth allocation are important prerequisites [134]. Field tests of wireless vehicular communication and cooperative local danger

warning are currently under way [135]. The US Department of Transportation is soliciting new ideas on this subject [136]. In Europe, a cooperative driving challenge has been initiated [137]. Several teams want to show improved driving capabilities based on cooperative information exchange. This could initiate further research and development in this area, similar to the impulse generated by the DARPA Grand Challenges and Urban Challenge for autonomous vehicles [3].

As real-world testing of cooperative maneuvers is a safety-critical task, suitable testing methodologies have to be found. Urmson et al. [138] gives a general overview of testing. For single-vehicle driver assistance, hardware-in-the-loop simulation and driving tests with mock-up obstacles have been applied [139, 140]. Cooperative maneuvers could be tested by starting with only one real vehicle and several simulated vehicles, but including real communication. In order to ensure the safety of a system in real use, an enormous number of experiments under a wide range of conditions is required. Since particular dangerous situations may be rare in real traffic, it is difficult to collect sufficient data. The rate and handling of false alarms is another key issue. A major related difficulty is the development of appropriate certification procedures for vehicles and their systems [141]. Aspects such as user acceptance and legal regulations are still to be addressed [142].

These issues will have to be resolved before cooperative technologies may develop their potential to increase traffic safety and efficiency.

Acknowledgments

The authors' research has been partially supported by Deutsche Forschungsgemeinschaft (German Research Foundation) within the Transregional Collaborative Research Center 28 "Cognitive Automobiles."

Bibliography

1. Vahidi A, Eskandarian A (2003) Research advances in intelligent collision avoidance and adaptive cruise control. IEEE Trans Intell Transp Syst 4(3):143–153
2. Tideman M, van der Voort MC, van Arem B, Tillema F (2007) A review of lateral driver support systems. In: Proceedings of the IEEE intelligent transportation systems conference, Seattle, Washington, pp 992–999
3. Buehler M, Iagnemma K, Singh S (eds) (2009) The DARPA urban challenge – autonomous vehicles in city traffic. In: Springer tracts in advanced robotics, vol 56. Springer, Berlin
4. Hartenstein H, Laberteaux K (2008) A tutorial survey on vehicular ad hoc networks. IEEE Commun Mag 46(6): 164–171
5. Schulze M, Nöcker G, Böhm K (2005) PReVENT: a European program to improve active safety. In: Proceedings of the 5th international conference on intelligent transportation systems telecommunications, Brest
6. Adler C, Straßberger M (2006) Putting together the pieces – a comprehensive view on cooperative local danger warning. In: Proceedings of the world congress on intelligent transport systems and services, London
7. Dao T-S, Ng L, Clark C, Huissoon JP (2008) Realtime experiments in Markov-based lane position estimation using wireless ad-hoc network. In: Proceedings of the IEEE intelligent vehicles symposium, Eindhoven, pp 901–906
8. Tischler K, Vogt H (2007) A sensor data fusion approach for the integration of negative information. In: Proceedings of conference on information fusion, Quebec
9. Huang D, Leung H (2005) An expectation-maximization-based interacting multiple model approach for cooperative driving systems. IEEE Trans Intell Transp Syst 6(2):206–228
10. Varaiya P (1993) Smart cars on smart roads: problems of control. IEEE Trans Autom Control 38(2):195–207
11. Zambou N, Enning M, Abel D (2004) Nonlinear spacing control of following vehicles within platoon – a controlled Lagrangian approach. In: IFAC symposium on nonlinear control systems, Stuttgart, pp 931–936
12. Dao T-S, Clark C, Huissoon JP (2008) Distributed platoon assignment and lane selection for traffic flow optimization. In: Proceedings of the IEEE intelligent vehicles symposium, Eindhoven, pp 739–744
13. Li L, Wang F-Y (2006) Cooperative driving at blind crossings using intervehicle communication. IEEE Trans Veh Technol 55(6):1712–1724
14. Schepperle H, Böhm K, Forster S (2007) Traffic management based on negotiations between vehicles – a feasibility demonstration using agents. In: Workshop on agent mediated electronic commerce, Honolulu
15. Roughgarden T (2005) Selfish routing and the price of anarchy. MIT Press, Cambridge, MA
16. Frese C, Beyerer J, Zimmer P (2007) Cooperation of cars and formation of cooperative groups. In: Proceedings of the IEEE intelligent vehicles symposium, Istanbul, pp 227–232
17. Frese C, Batz T, Wieser M, Beyerer J (2008) Life cycle management for cooperative groups of cognitive automobiles in a distributed environment. In: Proceedings of the IEEE intelligent vehicles symposium, Eindhoven
18. Schultes D (2008) Route planning in road networks. PhD thesis, Universität Karlsruhe (TH)
19. Cormen T, Leiserson C, Rivest R (2001) Introduction to algorithms, 2nd edn. MIT Press, Cambridge, MA
20. Vacek S, Nagel R, Batz T, Moosmann F, Dillmann R (2007) An integrated simulation framework for cognitive automobiles. In: Proceedings of the IEEE intelligent vehicles symposium, Istanbul, Türkei, pp 221–226

21. Munaka T, Yamamoto T, Watanabe T (2005) A reliable advanced-join system for data multicasting in ITS networks. IEEE Trans Intell Transp Syst 6(4):424–438
22. Chen W, Lee J, Hikita T, Onishi R (2007) Embedded multicasting with vehicle local peer group for efficient vehicle communications. In: Proceedings of the IEEE workshop on vehicle-to-vehicle communications, Istanbul
23. Mocito J, Rodrigues L (2006) Reconfigurable architecture for group communication support in hybrid networks. In: Koldehofe B (ed) Proceedings of the 4th MiNEMA workshop, Sintra
24. Miller J (2008) Vehicle-to-vehicle-to-infrastructure (V2V2I) intelligent transportation system architecture. In: Proceedings of the IEEE intelligent vehicles symposium, Eindhoven, pp 715–720
25. Huang Q, Julien C, Roman G-C (2004) Relying on safe distance to achieve strong partitionable group membership in ad hoc networks. IEEE Trans Mob Comput 3(2):192–205
26. Shimura A, Sakaibara T, Hiraiwa M, Aizono T (2003) Proposal of an autonomous group-management model and its application to intelligent transport system. In: Proceedings of the 6th international symposium on autonomous decentralized systems, Pisa
27. Fujii H, Akiyama M, Tokuda K (1999) Inter-vehicle communications protocol for group cooperative driving. In: Proceedings of the IEEE vehicular technology conference, Amsterdam, The Netherlands
28. Huang J, Tan H-S (2006) Design and implementation of a cooperative collision warning system. In: Proceedings of the IEEE intelligent transportation systems conference, Toronto
29. Clark C (2004) Dynamic robot networks: a coordination platform for multi-robot systems. PhD thesis, Stanford University
30. Premvuti S, Yuta S (1990) Consideration on the cooperation of multiple autonomous mobile robots. In: Proceedings of the IEEE/RSJ conference on intelligent robots and systems, Ibaraki
31. Briesemeister L (2001) Group membership and communication in highly mobile ad hoc networks. Dissertation, Technische Universität Berlin
32. Pallottino L, Scordio V, Bicchi A (2004) Decentralized cooperative conflict resolution among multiple autonomous mobile agents. In: Proceedings of the IEEE conference on decision and control, Atlantis, Paradise Island
33. Ragothaman V, Baloch F, Pendse R (2006) Unassisted aircraft landing via co-operative data exchange. In: Digital avionics systems conference, Portland
34. Chisalita I, Shahmehri N (2004) A context-based vehicular communication protocol. In: Proceedings of the IEEE symposium on personal, indoor and mobile radio communications, Barcelona
35. Nett E, Schemmer S (2003) Reliable real-time communication in cooperative mobile applications. IEEE Trans Comput 52(2):166–180
36. Meier R, Killijian M-O, Cunningham R, Cahill V (2001) Towards proximity group communication. In: Middleware for mobile computing, Heidelberg
37. Dao T-S, Clark C, Huissoon JP (2007) Optimized lane assignment using inter-vehicle communication. In: Proceedings of the IEEE intelligent vehicles symposium, Istanbul
38. Li L, Wang F-Y, Zhang Y (2007) Cooperative driving at lane closures. In: Proceedings of the IEEE intelligent vehicles symposium, Istanbul
39. Haruna T, Okada Y, Shigeno H (2007) A construction method of road-static network with vehicular ad-hoc networks. In: Proceedings of the IEEE workshop on vehicle-to-vehicle communications, Istanbul
40. Sheng W, Yang Q, Guo Y (2006) Experimental testbed and distributed algorithm for cooperative driving in VII simulation. In: Proceedings of the IEEE intelligent transportation systems conference, Toronto
41. Judaschke U (1994) Verfahren zur kollisionsfreien Führung und Koordination mobiler Transportsysteme. PhD thesis, Universität Dortmund
42. Chiang Y-J, Klosowski J, Lee C, Mitchell J (1997) Geometric algorithms for conflict detection/resolution in air traffic management. In: Proceedings of the IEEE conference on decision and control, San Diego
43. Zhou M (2007) A traffic data exchange protocol in vehicular ad-hoc network. In: Proceedings of the international workshop on intelligent transportation, Hamburg
44. Khan MA, Bölöni L (2005) Convoy driving through ad-hoc coalition formation. In: Proceedings of the IEEE real time and embedded technology and applications symposium, San Francisco, pp 98–105
45. Hallé S, Chaib-draa B (2004) Collaborative driving system using teamwork for platoon formations. In: Proceedings of workshop on agents in traffic and transportation, New York
46. Batz T, Watson K, Beyerer J (2009) Recognition of dangerous situations within a cooperative group of vehicles. In: Proceedings of IEEE intelligent vehicles symposium, Xi'an, China, pp 907–912
47. Tan H-S, Huang J (2006) A low-order DGPS-based vehicle positioning system under urban environment. IEEE ASME Trans Mechatron 11(5):567–575
48. Tan H-S, Huang J (2006) DGPS-based vehicle-to-vehicle cooperative collision warning: engineering feasibility viewpoints. IEEE Trans Intell Transp Syst 7(4):415–428
49. Wan EA, Van Der Merwe R (2001) Chapter 7: the unscented kalman filter. In: Kalman filtering and neural networks. Wiley, New York, pp 221–280
50. Caveney D (2007) Stochastic path prediction using the unscented transform with numerical integration. In: Proceedings of the 2007 IEEE intelligent transportation systems conference, Seattle, 30 Sept–3 Oct 2007
51. Kvasnica M, Grieder P, Baotić M (2004) Multi-parametric toolbox (MPT). http://control.ee.ethz.ch/~mpt/
52. Löfberg J (2004) YALMIP: a toolbox for modeling and optimization in MATLAB, http://control.ee.ethz.ch/~joloef/yalmip.php. In: Proceedings of the CACSD conference, Taipei, Taiwan

53. Miller R, Huang Q (2002) An adaptive peer-to-peer collision warning system. In: Proceedings of the IEEE vehicular technology conference, Birmingham, pp 317–321
54. van den Broek T, Ploeg J (2010) Collision warning system based on probability density functions. In: Proceedings of the International workshop on intelligent transportation, Hamburg, pp 141–147
55. Misener JA, Sengupta R, Krishnan H (2005) Cooperative collision warning: enabling crash avoidance with wireless technology. In: Proceedings of the world congress on intelligent transport systems and services, San Francisco
56. Benmimoun A, Chen J, Suzuki T (2007) Design and practical evaluation of an intersection assistant in real world tests. In: Proceedings of the IEEE intelligent vehicles symposium, Istanbul
57. Chen J, Deutschle S, Fuerstenberg K (2007) Evaluation methods and results of the INTERSAFE intersection assistants. In: Proceedings of the IEEE intelligent vehicles symposium, Istanbul, pp 142–147
58. Onken R (1994) DAISY, an adaptive, knowledge-based driver monitoring and warning system. In: Proceedings of the vehicle navigation & information systems conference, Yokohama, pp 3–10
59. Ishida S, Gayko J (2004) Development, evaluation and introduction of a lane keeping assistance system. In: Proceedings of the IEEE intelligent vehicles symposium, Parma, pp 943–944
60. McCall J, Wipf D, Trivedi M, Rao B (2005) Lane change intent analysis using robust operators and sparse bayesian learning. In: IEEE/CVPR workshop on machine vision for intelligent vehicles, San Diego
61. Zhang J, Roessler B (2009) Situation analysis and adaptive risk assessment for intersection safety systems in advanced assisted driving. In: Autonome mobile system, Karlsruhe, pp 249–258
62. ElBatt T, Goel S, Holland G, Krishnan H, Parikh J (2006) Cooperative collision warning using dedicated short range wireless communications. In: ACM VANET, Los Angeles
63. Morsink P, Hallouzi R, Dagli I, Cseh C, Schäfers L, Nelisse M, de Bruin D (2003) CarTALK 2000: development of a cooperative ADAS based on vehicle-to-vehicle communication. In: Proceedings of the world congress on intelligent transport systems and services, Madrid
64. Girard AR, de Sousa JB, Misener JA, Hedrick JK (2001) A control architecture for integrated cooperative cruise control and collision warning systems. In: Proceedings of the IEEE conference on decision and control, Orlando
65. Uno A, Sakaguchi T, Tsugawa S (1999) A merging control algorithm based on inter-vehicle communication. In: Proceedings of the IEEE intelligent transportation systems conference, Tokyo, pp 783–787
66. Bruns T, Trächtler A (2009) Intersection management: trajectory planning by means of dynamic programming. Automatisierungstechnik 57(5):253–261
67. Murray R (2007) Recent research in cooperative control of multivehicle systems. ASME J Dyn Syst Meas Control 129:571–583
68. Dimarogonas D, Kyriakopoulos K (2005) A feedback stabilization and collision avoidance scheme for multiple independent nonholonomic non-point agents. In: Proceedings of the 2005 IEEE international symposium on intelligent control limassol, Cyprus, pp 820–825
69. Hillenbrand J, Spieker A, Kroschel K (2006) A multilevel collision mitigation approach – its situation assessment, decision making, and performance tradeoffs. IEEE Trans Intell Transp Syst 7(4):528–540
70. Isermann R, Schorn M, Stählin U (2008) Anticollision system PRORETA with automatic braking and steering. Veh Syst Dyn 46:683–694
71. Schmidt C, Oechsle F, Branz W (2006) Research on trajectory planning in emergency situations with multiple objects. In: Proceedings of the IEEE intelligent transportation systems conference, Toronto, pp 988–992
72. Lachner R, Breitner M, Pesch HJ (2000) Real-time collision avoidance: differential game, numerical solution, and synthesis of strategies. In: Filar J, Gaitsgory V, Mizukami K (eds) Advances in dynamic games and applications. Birkhäuser, Boston
73. Lozano-Pérez T (1983) Spatial planning: a configuration space approach. IEEE Trans Comput 32(2):108–120
74. Choset H, Lynch K, Hutchinson S, Kantor G, Burgard W, Kavraki L, Thrun S (2005) Principles of robot motion. MIT Press, Cambridge
75. LaValle S (2006) Planning algorithms. Cambridge University Press, Cambridge, UK
76. Laumond J-P, Sekhavat S, Lamiraux F (1998) Guidelines in nonholonomic motion planning for mobile robots. In: Laumond J-P (ed) Robot motion planning and control. Springer, New York
77. LaValle S, Kuffner J (1999) Randomized kinodynamic planning. In: Proceedings of the IEEE conference on robotics and automation, Detroit, pp 473–479
78. Petti S, Fraichard T (2005) Safe motion planning in dynamic environments. In: Proceedings of the IEEE/RSJ conference on intelligent robots and systems, Edmonton, pp 3726–3731
79. Hesse T, Sattel T (2007) An approach to integrate vehicle dynamics in motion planning for advanced driver assistance systems. In: Proceedings of the IEEE intelligent vehicles symposium, Istanbul
80. Latombe J-C (1991) Robot motion planning. Kluwer, Boston, MA
81. Sánchez G, Latombe J-C (2002) On delaying collision checking in PRM planning: application to multi-robot coordination. Int J Robot Res 21(1):5–26
82. Clark C, Rock S, Latombe J-C (2003) Motion planning for multiple mobile robots using dynamic networks. In: Proceedings of the IEEE conference on robotics and automation, Taipei, pp 4222–4227
83. Kant K, Zucker S (1986) Toward efficient trajectory planning: the path-velocity decomposition. Int J Robot Res 5(3):72–89
84. O´Donnell P, Lozano-Pérez T (1989) Deadlock-free and collision-free coordination of two robot manipulators. In: Proceedings of the IEEE conference on robotics and automation, Scottsdale
85. Leroy S, Laumond J-P, Siméon T (1999) Multiple path coordination for mobile robots: a geometric algorithm. In: Proceedings of the international joint conference on artificial intelligence, Stockholm

86. Ghrist R, LaValle S (2006) Nonpositive curvature and pareto optimal coordination of robots. SIAM J Control Optim 45(5):1697–1713
87. Peng J, Akella S (2005) Coordinating multiple robots with kinodynamic constraints along specified paths. Int J Robot Res 24(4):295–310
88. Alami R, Fleury S, Herrb M, Ingrand F, Robert F (1998) Multi-robot cooperation in the MARTHA project. IEEE Rob Autom Mag 5(1):36–47
89. Švestka P, Overmars M (1998) Coordinated path planning for multiple robots. Rob Autom Syst 23:125–152
90. LaValle S, Hutchinson S (1998) Optimal motion planning for multiple robots having independent goals. IEEE Trans Robot Automation 14(6):912–925
91. Erdmann M, Lozano-Pérez T (1987) On multiple moving objects. Algorithmica 2:477–521
92. Freund E, Hoyer H (1988) Real-time pathfinding in multirobot systems including obstacle avoidance. Int J Robot Res 7(1):42–70
93. Warren CW (1990) Multiple robot path coordination using artificial potential fields. In: Proceedings of the IEEE conference on robotics and automation, Cincinnati
94. Azarm K, Schmidt G (1996) A decentralized approach for the conflict-free motion of multiple mobile robots. In: Proceedings of the IEEE/RSJ conference on intelligent robots and systems, Osaka
95. Bekris K, Tsianos K, Kavraki L (2007) A decentralized planner that guarantees the safety of communicating vehicles with complex dynamics that replan online. In: Proceedings of the IEEE/RSJ conference on intelligent robots and systems, San Diego, pp 3784–3790
96. Bennewitz M, Burgard W, Thrun S (2001) Optimizing schedules for prioritized path planning of multi-robot systems. In: Proceedings of the IEEE conference on robotics and automation, Seoul
97. van den Berg J, Overmars M (2005) Prioritized motion planning for multiple robots. In: Proceedings of the IEEE/RSJ conference on intelligent robots and systems, Edmonton
98. Berger JO (1993) Statistical decision theory and Bayesian analysis, Springer series in statistics. Springer, New York
99. Hart P, Nilsson N, Raphael B (1968) A formal basis for the heuristic determination of minimum cost paths. IEEE Trans Syst Sci Cybern 4(2):100–107
100. Russell S, Norvig P (2003) Artificial intelligence: a modern approach. Prentice Hall, New York
101. Frese C, Beyerer J (2010) Planning cooperative motions of cognitive automobiles using tree search algorithms. In: Dillmann R, Beyerer J, Hanebeck UD, Schultz T (eds) KI 2010: advances in artificial intelligence. Lecture notes in artificial intelligence, vol 6359. Springer, Heidelberg, pp 91–98
102. Schouwenaars T, De Moor B, Feron E, How J (2001) Mixed integer programming for multi-vehicle path planning. In: Proceedings of the European control conference, Porto, pp 2603–2608
103. Borrelli F, Subramanian D, Raghunathan A, Biegler L (2006) MILP and NLP techniques for centralized trajectory planning of multiple unmanned air vehicles. In: Proceedings of the American control conference, Minneapolis
104. Richards A, How J (2002) Aircraft trajectory planning with collision avoidance using mixed integer linear programming. In: Proceedings American control conference, Anchorage
105. Sierksma G (1996) Linear and integer programming: theory and practice. Dekker, New York
106. Earl M, D'Andrea R (2007) Multi-vehicle cooperative control using mixed integer linear programming. In: Shamma J (ed) Cooperative control of distributed multi-agent systems. Wiley, New York, pp 233–259
107. Richards A, How J (2004) Decentralized model predictive control of cooperating UAVs. In: Proceedings of the IEEE conference on decision and control, Atlantis
108. Niedringhaus W (1995) Stream option manager (SOM): automated integration of aircraft separation, merging, stream management, and other air traffic control functions. IEEE Trans Syst Man Cybern 25(9):1269–1280
109. İnalhan G, Stipanović D, Tomlin C (2002) Decentralized optimization, with application to multiple aircraft coordination. In: Proceedings of the IEEE conference on decision and control, Las Vegas
110. Quinlan S, Khatib O (1993) Elastic bands: connecting path planning and control. In: Proceedings of the IEEE conference on robotics and automation, Atlanta
111. Brock O (1999) Generating robot motion: the integration of planning and execution. PhD thesis, Stanford University
112. Khatib M, Jaouni H, Chatila R, Laumond J-P (1997) Dynamic path modification for car-like nonholonomic mobile robots. In: Proceedings of the IEEE conference on robotics and automation, Albuquerque, pp 2920–2925
113. Hilgert J, Hirsch K, Bertram T, Hiller M (2003) Emergency path planning for autonomous vehicles using elastic band theory. In: Proceedings of the IEEE/ASME conference on advanced intelligent mechatronics, Kobe
114. Brandt T, Sattel T, Wallaschek J (2005) On automatic collision avoidance systems. In: Proceedings of SAE world congress, Detroit
115. Gehrig S, Stein F (2007) Collision avoidance for vehicle-following systems. IEEE Trans Intell Transp Syst 8(2):233–244
116. Frese C, Batz T, Beyerer J (2008) Cooperative behavior of groups of cognitive automobiles based on a common relevant picture. Automatisierungstechnik 56(12):644–652
117. Thorpe C, Jochem T, Pomerleau D (1997) The 1997 automated highway free agent demonstration. In: Proceedings of the IEEE intelligent transportation systems conference, Pittsburgh, pp 496–501
118. Demmel S, Gruyer D, Rakotonirainy A (2010) V2V/V2I augmented maps: state-of-the-art and contribution to real-time crash risk assessment. In: Proceedings of the 20th Canadian multidisciplinary road safety conference, Niagara Falls, Ontario
119. Jensen FV (2001) Bayesian networks and decision graphs. Springer, New York

120. Forbes J, Huang T, Kanazawa K, Russell S (1995) The BATmobile: towards a bayesian automated taxi. In: Proceedings of the international joint conference on artificial intelligence, Montreal, pp 1878–1885
121. Fraichard T, Mermond R (1998) Path planning with uncertainty for car-like robots. In: Proceedings IEEE conference on robotics and automation, Leuven, pp 27–32
122. Gonzalez JP, Stentz A (2005) Planning with uncertainty in position: an optimal and efficient planner. In: Proceedings of the IEEE/RSJ conference on intelligent robots and systems, Edmonton, pp 2435–2442
123. Melchior N, Simmons R (2007) Particle RRT for path planning with uncertainty. In: Proceedings of the IEEE conference on robotics and automation, Roma, pp 1617–1624
124. Toussaint M, Goerick C (2007) Probabilistic inference for structured planning in robotics. In: Proceedings of the IEEE/RSJ conference on intelligent robots and systems, San Diego
125. Lambert A, Bouaziz S, Reynaud R (2003) Shortest safe path planning for vehicles. In: Proceedings of the IEEE intelligent vehicles symposium, Columbus, OH
126. Gonzalez JP, Stentz A (2007) Planning with uncertainty in position using high-resolution maps. In: Proceedings of the IEEE conference on robotics and automation, Roma, pp 1015–1022
127. Broadhurst A, Baker S, Kanade T (2005) Monte Carlo road safety reasoning. In: Proceedings of the IEEE intelligent vehicles symposium, Las Vegas, pp 319–324
128. Althoff M, Althoff D, Wollherr D, Buss M (2010) Safety verification of autonomous vehicles for coordinated evasive maneuvers. In: Proceedings of the IEEE intelligent vehicles symposium, San Diego, pp 1078–1083
129. Bekris K, Kavraki L (2007) Greedy but safe replanning under kinodynamic constraints. In: Proceedings of the IEEE conference on robotics and automation, Rome, pp 704–710
130. Bekris K, Tsianos K, Kavraki L (2007) A distributed protocol for safe real-time planning of communicating vehicles with second-order dynamics. In: Proceedings of the conference on robot communication and coordination, Athens
131. Olfati-Saber R, Fax JA, Murray RM (2007) Consensus and cooperation in networked multi-agent systems. Proc IEEE 95(1):215–233
132. Georgiev D, Kabamba P, Tilbury D (2008) A new model for team optimization: the effects of uncertainty on interaction. IEEE Trans Syst Man Cybern A 38(6):1234–1247
133. Garg D, Narahari Y (2008) Mechanism design for single leader Stackelberg problems and application to procurement auction design. IEEE Trans Autom Sci Eng 5(3):377
134. Kenney J (2010) Standards and regulations. In: Hartenstein H, Laberteaux K (eds) VANET: vehicular applications and internetworking technologies, Intelligent transportation systems. Wiley, Chichester, pp 365–429
135. Stübing H, Bechler M, Heussner D, May T, Radusch I, Rechner H, Vogel P (2010) simTD: a car-to-X system architecture for field operational tests. IEEE Commun Mag 48(5):148–154
136. US Department of Transportation (2011) Connected vehicle technology challenge. http://connectedvehicle.challenge.gov/
137. Grand cooperative driving challenge. http://www.gcdc.net/
138. Urmson C, Whittaker WR, Harbaugh S, Clark M, Koon P (2006) Testing driver skill for high-speed autonomous vehicles. Computer 39(12):48–51
139. Christen F, Sandkühler D, Benmimoun A, Breuer K (2004) Verwendung des Verkehrsflusssimulationswerkzeugs PELOPS mit HiL-Funktionalität bei der Entwicklung von Fahrerassistenzsystemen. In: VDI Kongress Berechnung und Simulation im Fahrzeugbau
140. Jansson J, Johansson J, Gustafsson F (2002) Decision making for collision avoidance systems. In: Society of automotive engineers technical paper
141. Winner H, Wolf G (2009) Quo vadis, FAS? In: Winner H, Hakuli S, Wolf G (eds) Handbuch Fahrerassistenzsysteme – Grundlagen, Komponenten und Systeme für aktive Sicherheit und Komfort, Vieweg + Teubner, pp 664–673
142. Wahl R, Tørset T, Vaa T (2007) Large scale introduction of automated transport: which legal and administrative barriers are present? In: Proceedings of the world congress on intelligent transport systems and services, Beijing

Coral Reef Ecosystems

Helen T. Yap
The Marine Science Institute, University of the Philippines, Quezon City, Philippines

Article Outline

Glossary
Definition of the Subject and Its Importance
Introduction
Geology and Distribution
Biology and Ecology
Ecological Goods and Services from Coral Reefs
Threats to Coral Reefs
Management
Future Directions
Bibliography

Glossary

Coral reef A geological structure of significant topographic relief above the sea floor, made of calcium carbonate and constructed by living organisms (mainly corals belonging to the order Scleractinia, phylum Cnidaria, and coralline algae).

Hermatypic Refers to corals that are able to build reefs.

Holocene A geologic age that corresponds to 10,000 years before the present, or "B.P."

Scleractinia The order of hard or stony corals to which the reef builders belong, under the phylum Cnidaria.

Zooxanthellae Golden brown single-celled algae that inhabit the gastrodermal cells of reef-building corals (belonging to the phylum Dinophyta, order Gymnodiniales).

Definition of the Subject and Its Importance

Coral reefs are geological structures of significant dimensions, constructed over millions of years by calcifying organisms. The present day reef-builders are hard corals belonging to the order Scleractinia, phylum Cnidaria. The greatest concentrations of coral reefs are in the tropics, with highest levels of biodiversity situated in reefs of the Indo-West Pacific region. These ecosystems have provided coastal protection and livelihood to human populations over the millennia. Human activities have caused destruction of these habitats, the intensity of which has increased alarmingly since the latter decades of the twentieth century. The severity of this impact is directly related to exponential growth rates of human populations especially in the coastal areas of the developing world. However, a more recently recognized phenomenon concerns disturbances brought about by the changing climate, manifested mainly as rising sea surface temperatures, and increasing acidification of ocean waters due to greater drawdown of higher concentrations of atmospheric carbon dioxide. Management efforts have so far not kept pace with the rates of degradation, so that the spatial extent of damaged reefs and the incidences of localized extinction of reef species are increasing year after year. The major management efforts to date consist of establishing marine protected areas and promoting the active restoration of coral habitats.

Introduction

Over the millennia, coral reef ecosystems have served as the basis of human survival and sustenance in many coastal areas in the tropics and subtropics. They are significant geologic formations that provide crucial protection from destructive forces of the sea. They also harbor the greatest diversity of animal phyla than any other habitat on the planet. But because of the finely tuned balance between primary production and energy consumption within the ecosystem, coral reefs are unable to sustain high levels of biomass extraction. Added to this, a range of human impacts from overfishing to pollution and direct destruction of the habitat has caused extensive degradation of these ecosystems since the latter decades of the twentieth century. This trend has been exacerbated by recently recognized effects of climate change. The main culprits are rising sea surface temperatures and increasing acidification of ocean waters, both of which exert adverse impacts on the physiology of the coral-zooxanthellae complex, thus hampering its ability to effectively recover from various environmental disturbances. The best management option at the present time is to put as many reefs as possible under protection, while providing for alternative means of livelihood to displaced fishers. The field of active coral restoration is still at an early stage and warrants further research.

Geology and Distribution

A reef is a "discrete carbonate structure formed by in situ or bound organic components that develops topographic relief upon the sea floor" [1]. The majority of coral reefs are located in the tropics [2, 3] (Fig. 1). The limit of their distribution is represented by Midway and Kure, for example, which are well-developed algal-coral atolls that lie north of 28°N latitude at the northwestern end of the Hawaiian chain. As summarized by Moberg and Folke [4], coral reefs are estimated to constitute from 0.1% to 0.5% of the ocean floor, with actual areal estimates ranging between 255,000 and 1,500,000 km^2. The coastlines of more than 100 countries are lined by coral reefs. Advances in methodology, particularly remote sensing, are helping to delineate more accurately the distribution and extent of coral reefs, and the proportions of the different components that constitute the bottom substrate (live coral, vegetation, nonliving cover such as rock and sand) [5]. However, remote sensing is still limited by the fact that only the visible range of the electromagnetic spectrum can penetrate the water column sufficiently down to depths occupied by coral reefs which are shallow-water ecosystems. Hence, this tool should be complemented by actual ground-truth surveys whenever possible [5].

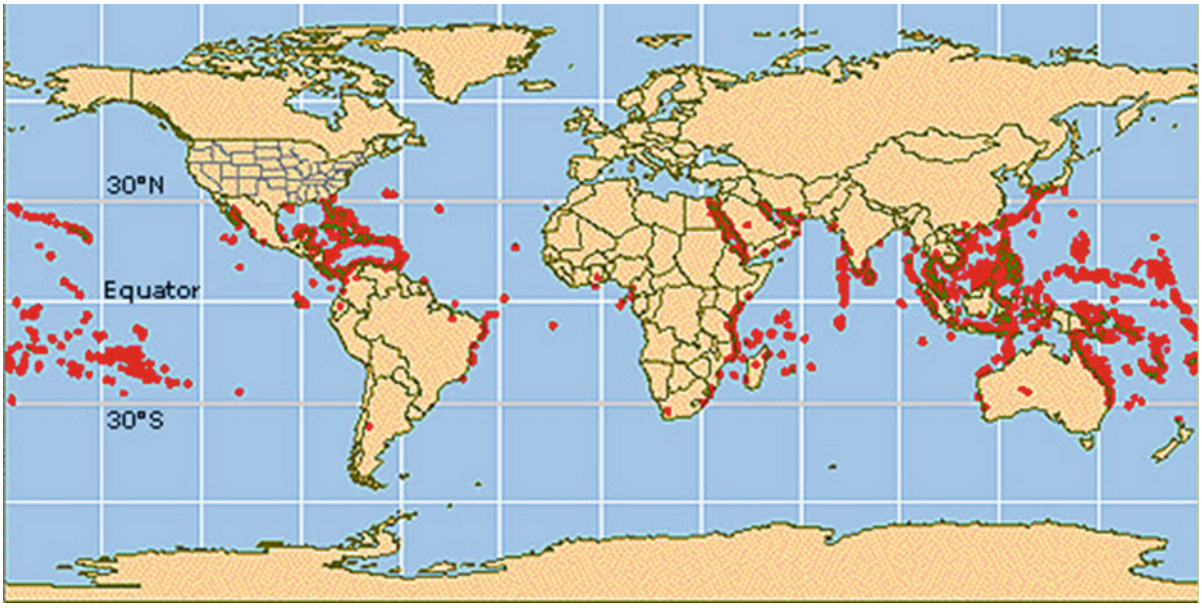

Coral Reef Ecosystems. Figure 1
Global distribution of coral reefs (Source: NOAA National Ocean Service Education Web Site, revised 25 March 2008, http://oceanservice.noaa.gov/education/, NOAA National Ocean Service, Communications and Education Division)

The three main types of coral reefs are fringing reefs, barrier reefs, and atolls [2–4]. Other than these major categories, there are minor reef forms of various sizes and shapes, and situated at different depths of the ocean floor. For example, Moberg and Folke [4] mention platform reefs as a fourth category (Table 1). Fringing reefs develop close to the shore in relatively shallow waters. Among the longest expanses of reefs in the world is the fringing reef that lines the shores of the Red Sea [2], with a length, if stretched out, exceeding 2,500 miles (4,000 km). Barrier reefs are composed of a series of reef structures arranged roughly parallel to the coast, and separated from it by a fairly deep lagoon. The largest such aggregation of reefs in the world is the renowned Great Barrier Reef off the Queensland coast of Australia [2] with a length of more than 1,200 miles (almost 2,000 km). It varies in width from about 10 miles (16 km) to almost 200 miles (320 km). The total area of reef habitat that it encompasses is about 25,000 km^2 [6]. The various reef structures within the barrier reef are separated from each other by lagoons of different sizes. Atolls are annular reefs that encircle a lagoon. They may arise from the deep sea, or from the shallower depth of the continental shelf [2]. Platform reefs are carbonate structures

Coral Reef Ecosystems. Table 1 The four main reef types

Platform reefs	Fringing reefs	Barrier reefs	Atolls
Frequently found in the lagoons created by atolls and barrier reefs	Closely follow shorelines, narrow shallow lagoon	Separated from land by a relatively wide, deep lagoon	Horseshoe shaped or circular reef surrounding a central lagoon (often far from land in the open ocean)
In the Great Barrier Reef lagoon, Belize, Red Sea, Bahamas	Red sea, East Africa, Seychelles, and other Indo-Pacific islands, most Caribbean reefs	The Great Barrier Reef in Australia, Belize Barrier Reef, off Mayotte in the Western Indian Ocean	>95% of the atolls are in the Indo-Pacific, others are found outside Belize and in Western Atlantic

Source: From [4]

of various shapes and sizes usually situated inside lagoons.

A major factor controlling reef growth is sea level rise [1]. It is to be noted, however, that the more relevant metric is *relative* sea level change, because the actual sea level in an area is a net result of both sea level change and tectonic movement of the land due to the presence of active faults [7, 8]. Thermal expansion of the ocean due to increasing heat content caused by climate change also contributes to sea level rise [9]. In terms of the effects of sea level changes on reef growth, more information exists for tropical Atlantic reefs compared to their counterparts in the Pacific [10]. Much geological research has focused on Holocene reefs. These are considered analogues of ancient reefs, and preserve records of eustatic changes in sea level and neotectonics. The measured vertical accretion rates during the Holocene display some variability (reviewed in [10]). Caribbean reefs had higher average rates, on the order of 6 m/ky, compared with Indo-Pacific reefs which have grown at an average rate of 4.4 m/ky. Reasons for this difference still remain unknown. In the Pacific, the Philippines, though it lies in the acknowledged center of shallow-water marine biodiversity, has been little studied compared to the Great Barrier Reef, the Ryukyus, and the islands of Hawaii and Polynesia. The study of Shen et al. [10] represents the first coral-based sea level record from the South China Sea. Reef accretion rate is estimated to have reached as high as 10–13 m/ky during the period 9.2–8.2 ka.

Amphitropical distributions are disjunct distributions where the population or species occurs subtropically on both sides of the equator [11]. Such patterns have been most commonly observed in fish. In the case of corals, however, disjunct distributions in central Indo-Pacific species are observed by Veron [11] to display no significant amphitropical component. Veron [11] also claims similarities between corals of Hawaii and those in the southeast Pacific on a larger scale. Dispersal is believed to play a key role in the speciation and distribution of coral species.

The tropical oceans consist of four major biogeographic regions [4]: the Indo-West Pacific (IWP), the Eastern Pacific, the Western Atlantic, and the Eastern Atlantic.

Knowledge about coral distributions is summarized as follows (quoted from [11]):

- There are areas of high diversity in the tropical western margins of the world's three great ocean basins, that of the Indian Ocean being relatively ill-defined.
- Within the Indo-Pacific, there is little generic variation within the center of high diversity.
- There is attenuation of species diversity latitudinally and longitudinally from these centers.
- Regions distant from centers of species diversity tend to have similar genera.
- Latitudinal attenuation occurs in the same or similar "drop-out" sequence in the northern and southern hemispheres.
- Latitudinal attenuation is highly correlated with sea surface temperature.
- The mean generic age of Caribbean corals is twice that of Indo-Pacific corals and centers of diversity have relatively young generic ages.

In a recent analysis of biogeographic patterns of corals and reef fish across the Pacific and Indian Oceans, Bellwood and Hughes [12] established a "remarkable congruence" between the two groups in terms of gradients in diversity. The peak in diversity for both corals and fish was observed in the Indo-Australian region, between 120°E and 170°E longitude. There was a steep decline across the Pacific toward its eastern boundary, where assemblages are notably more depauperate. There also was a decline westward across the Indian Ocean, though not as steep. A similar congruence for corals and fish was observed in terms of biodiversity patterns along latitudinal gradients. The peak in diversity was near the equator, with declines on either side at higher latitudes.

Biology and Ecology

The main builders of modern-day reefs are the hard or stony corals belonging to the order Scleractinia of the phylum Cnidaria [13]. They constitute the main framework structure, as well as act as fillers and cementers of the reef matrix together with the coralline algae. The basic unit of the coral is an anemone-like structure called the coral polyp. Large coral forms are often colonial, consisting of numerous polyps that

have reproduced asexually by budding. However, there are a few solitary forms such as members of the genus *Fungia*, commonly known as "mushroom corals." Recent phylogenetic evidence indicates that deep-water coral species arose from shallow-water ancestors, following a long established process of diversification of marine taxa along a gradient from shallow to deeper habitats [14].

The majority of reef corals are in a symbiotic relationship with a dinoflagellate of the genus *Symbiodinium*. Dinoflagellates are golden brown single-celled algae belonging to the phylum Dinophyta, order Gymnodiniales [13]. They have been given the name "zooxanthellae" [15]. They inhabit the gastrodermal cells of the coral polyp where they perform the basic function of photosynthesis. The products of photosynthesis are used primarily by the algae for their own metabolic maintenance and for reproduction. However, under favorable conditions the zooxanthellae produce an excess of photosynthetic products such as simple sugars, lipids and amino acids which are then translocated to the coral host cell [15]. The photosynthate is utilized by the coral to supply its own nutritional needs. In addition, this supplementary energy source fuels the all-important mechanism of calcification which is the basis of reef building [16]. The symbiotic algae also provide oxygen, a by-product of photosynthesis, which helps support the metabolism of the coral host. Because of a finely tuned balance between primary production and energy consumption of all species within the ecosystem, coral reefs have relatively low rates of net primary production [17]. Hence, they are unable to sustain high levels of biomass extraction.

Not all coral species harbor symbiotic algae, and are termed "azooxanthellate" [3]. It is the zooxanthellate forms that possess the in-house power unit, so to speak, which helps support calcification on a large scale. Hence, the majority of these are so-called hermatypic or reef-building corals. They are colonial in form, and this trait together with their symbiosis with algae is believed to confer on them a competitive advantage over other benthic invertebrates, and helps explain their dominance in tropical reefs [14].

The extant members of the order Scleractinia are evenly divided between zooxanthellate and azooxanthellate species [14]. Most azooxanthellate species are solitary (as opposed to colonial) and are nearly absent from reefs. However, they have wider geographic and bathymetric distributions than reef corals, extending up to aphotic depths in the ocean. Recent phylogenetic analyses indicate that they originated from ancestors that were symbiotic [14].

With respect to the zooxanthellate coral taxa, it is, ironically, the possession of this singular advantageous feature that has rendered them extremely susceptible to a relatively recent stress in the form of increasing ocean temperatures. This phenomenon is part of what has been recognized as global climate change [18]. Temperature stress, that is, water temperatures significantly above normal for prolonged periods, causes zooxanthellae to lose their pigment, or to be expelled by the host polyp. In both instances, there is a loss of photosynthetic capability of the coral-algae symbiotic complex with a resulting impairment in the ability to meet nutritional needs of both coral host and symbiont.

Scientific findings over the last few decades have established that there are a number of clades of zooxanthellae, originally thought to belong only to one species of the genus *Symbiodinium*. These clades are genetically distinct from one another. To date, there are eight known phylogenetic clades, with each clade containing multiple subclades or types [19, 20]. Scleractinian corals establish functional symbioses primarily with clades A-D. Their genetic distinction imparts different physiological properties to the various clades, properties that are manifested at the level of the host-zooxanthellae complex or "holobiont" [19–21], notably the ability to adapt to various ambient temperature regimes. Hence, some zooxanthellate corals are able to tolerate increases in water temperature better than others. In some instances, the algae are not expelled by the host coral and are able to continue photosynthesizing, providing the latter with vital nourishment during stressful thermal conditions.

Reef accretion is due to a net positive balance of calcium carbonate production over calcium carbonate loss (Fig. 2, [22]). The major producers of calcium carbonate are the hard corals. Their skeletons constitute the main framework of the reef, which is a geological structure in three dimensions and which

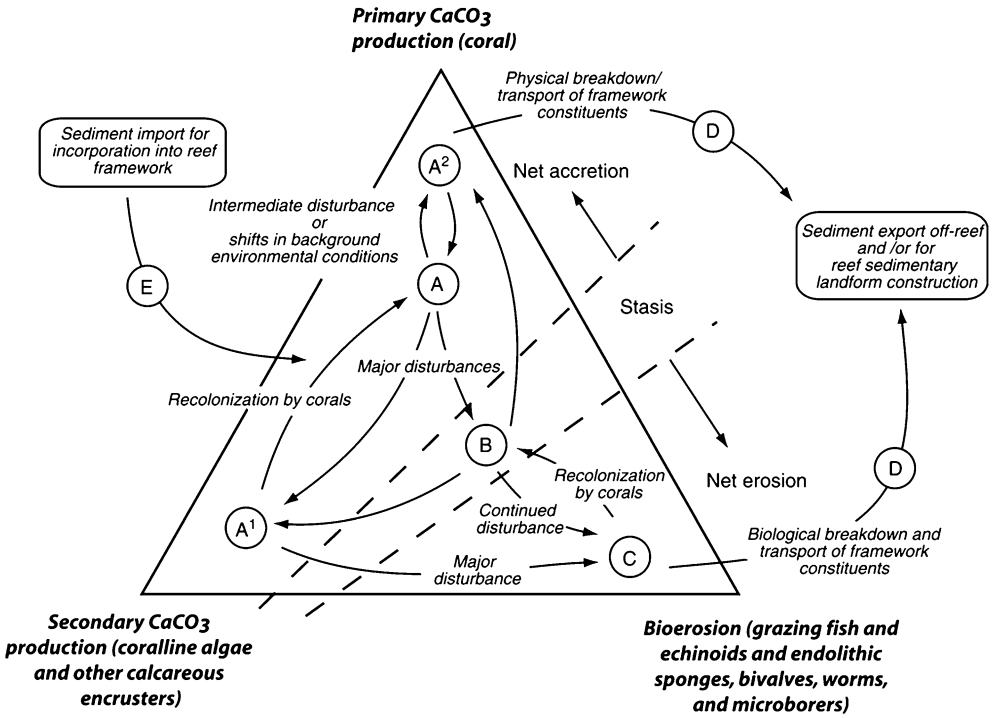

Coral Reef Ecosystems. Figure 2
Conceptual model depicting processes contributing to coral reef carbonate accretion or erosion, and the effects of environmental change (From [22])

can measure thousands of meters across. There are other important calcifying organisms as well, notably the coralline algae. The remains of these and other calcifiers such as molluscs and foraminiferans serve to fill in the reef matrix over geologic time. Another source of calcium carbonate on the reef is the import of sediment from outside sources via water currents. The loss of calcium carbonate is due to erosion, dissolution, or export of sediment out of the reef. Erosion can be due to physical or biological processes. Important bioeroders are fish that graze on coral (notably parrotfish), sea urchins that scrape hard substrates in the process of feeding, sponges, molluscs, and worms that bore into coral skeletons, plus a variety of microborers.

Optimal Environmental Requirements

Because of the intimate symbiosis with algae, reef-building corals will survive and grow down to particular depth limits in the ocean due to specific light requirements for algal photosynthesis [15]. Most extensive reef structures occur in relatively shallow waters, typically down to depths of thirty (30) meters [15]. Hermatypic corals require high levels of aragonite supersaturation in order to maintain sufficient rates of calcification. Coral reef communities also thrive best in nutrient-poor waters [1].

Another critical environmental factor is temperature. The physiology of the coral-alga symbiotic complex functions optimally within specific temperature ranges, typically not lower than 18°C, with the limiting high temperatures believed to be sustained maxima of 30–34°C [1]. Although coral reefs achieve maximal development in the tropics, recent trends indicate that the highest summer temperatures in many tropical areas are probably exceeding the upper thermal tolerance limits of many coral species. The phenomenon of coral bleaching, whereby a coral colony becomes white because the symbiotic zooxanthellae either lose their pigments or are altogether expelled [23], is becoming more frequent [18].

Different coral species are adapted to a wide range of hydrodynamic regimes, from calm to turbulent. They may be found in a corresponding range of habitats from sheltered lagoons to reef slopes exposed to the open sea. However, they require a minimum of water circulation around the coral colony to ensure that wastes are carried away, and that a sufficient amount of oxygen is made available for respiration. A microscopic boundary layer exists around the surface of the coral colony that controls the diffusion of nutrients and gases between the external environment and the internal environment of the coral-alga symbiotic complex.

Because of their metabolic requirements, corals, just like all other organisms with aerobic respiration, need a minimum amount of dissolved oxygen in the water in order to survive. Hypoxic conditions that are generated by excessive microbial decay of organic matter, or by abnormally high water temperatures, can impair coral survival and health. Similarly, salinity, because of its effects on coral-algal physiology, must also be maintained within certain ranges (34–36 ppt) for optimal survival and growth of coral colonies [13]. If levels of salinity drop precipitously, as in periods of heavy rainfall coinciding with low tides, for example, corals in shallow areas can experience osmotic stress. If the period of immersion in low salinity water is protracted, then some colonies can experience mortality. Abnormally high salinity, above typical oceanic values of 35 ppt, can also inflict metabolic stress on corals. Exceptions, however, are coral populations in normally high salinity areas like the Red Sea [13] which have adapted over the millennia to such extreme conditions.

Waters around flourishing reef areas are characteristically oligotrophic, with relatively low nutrient concentrations. The coral-alga symbiotic complex is efficient in taking up nutrients from surrounding waters, utilizing them for photosynthesis, and recycling them back into the external medium through metabolism. Important nutrients in reef areas are nitrate, ammonium, and phosphate. They exist in a fine balance with the living community, a balance that is easily disrupted by excessive influx of nutrients from external sources. An increased supply of nutrients favors the primary producers over the coral. Thus, depending on a particular situation, there would be increased abundances of zooxanthellae residing within coral colonies, of phytoplankton in the water column, or of algae inhabiting the bottom substrate. Algae compete with corals for space and light.

Biodiversity

Coral reefs are among the richest marine habitats in terms of species diversity [3, 11]. They are often alluded to as the "rainforests of the sea." The high species diversity is attributable to known factors, namely, the location of coral reefs in the tropical and subtropical latitudes with their attendant climatic regimes, and the complex topography afforded by the three-dimensional geological structure. The relatively high light intensities close to the equator support the levels of primary production that are needed to drive the multitude of trophic pathways in a typical coral reef ecosystem. The relatively small ranges of temperature fluctuations, as compared to temperate and higher latitudes, enable a sustained level of metabolism throughout the entire year for many species, including several reproductive episodes.

Recent analyses of the fossil record indicate that reefs were probably cradles of evolution during the Phanerozoic era (which covers about 500 million years from the present), with approximately 22% of examined genera originating in reef environments [24]. The class Anthozoa, which contains the reef-building scleractinian corals, contains the largest number of genera originating in reef environments. In addition to being sites of the appearance of new species, coral reefs are seen to have exported various taxa to other environments. The most likely explanation as to why reefs have played this role over their geologic history is their habitat complexity [24].

The complex three-dimensional structure of a typical reef provides a plethora of habitable space for a wide variety of organism types with a corresponding wide range of behaviors. In an analysis of a large contemporary data set, Bellwood and Hughes [12] determined that patterns in the diversity of corals and reef fish on a biogeographic scale were best explained by the availability of habitat area, a key feature of topographic complexity. The various species interact primarily via feeding or trophic pathways, although the picture has sadly been drastically altered by excessive human exploitation, in addition to other natural and anthropogenic impacts [25].

Coral reefs contain the greatest number of phyla of any habitat on earth, including 32 of the estimated total of 34 animal phyla [13]. The stony corals which build up the reef framework belong to the phylum Cnidaria, which also includes the hydroids and jellyfish, and the non-reef building soft corals. Another dominant component of the benthic community are the sponges belonging to the phylum Porifera. Other conspicuous invertebrates are represented by the phylum Echinodermata which includes the starfish, sea urchins, sea cucumbers, and crinoids and the phylum Mollusca covering a huge variety of clams and shells, not to mention squid and octopus. The phylum Arthropoda includes the class Crustacea, a very large one that includes crabs, lobsters, and shrimps. It is a member of the subphylum Vertebrata, however (apart from the hard corals themselves), that captures the most attention from coral reef enthusiasts. The most renowned vertebrate group is the fishes which comprise thousands of species on a pristine reef. Other vertebrates that used to dominate coral reef habitats in different parts of the globe, but that are sadly depleted now [25] include the sea cows, turtles, and crocodiles. Even sea birds that were once plentiful around reef ecosystems are now dwindling in numbers.

Among reef habitats, the most diverse are found in the Indo-West Pacific region, particular around the islands of the Philippines, Indonesia, and Papua New Guinea [26–28]. These islands combined harbor more than 2,500 species of fish belonging in 165 families, more than 3,200 species of mollusc, and about 500 species of coral in almost 80 genera. A recent study involved mapping of the geographic ranges of 1,700 species of reef fish, 804 species of coral, 662 species of snail, and 69 species of lobster [27]. For all taxa, the peak in species richness was determined to be in what has come to be known as the "coral triangle" of Southeast Asia, namely, the islands mentioned above. Species richness then falls off rapidly toward the east across the Pacific, and less rapidly toward the west, across the Indian Ocean. Sites in the southern Philippines and central Indonesia were found to be in the top 10% richest locations.

In the analysis of Roberts et al. [27], 58 species of corals, or 7.2% of the total studied, had restricted geographic ranges. The values for fish, snails, and lobsters were 26.5%, 28.7%, and 53.6%, respectively. The implication of this finding is that many species may be vulnerable to localized extinctions, particularly if they are restricted to geographic locations receiving high levels of human impact. Areas with high degrees of endemism combined with significant levels of impact have been termed marine biodiversity "hotspots." A renowned example of a place which has a high degree of biodiversity but whose reefs are among the most threatened (and degraded) in the world is the Philippines [27, 28].

A recent study has shown that the Philippines harbors a higher concentration of species per unit area than Indonesia, with a rigorous pattern emerging for marine shore fishes [29]. The authors hypothesize a center of origin on the Eurasian plate, with geological events being responsible for allopatric speciation, in addition to island integration. The Philippine center of diversity has significant abundance of both widespread Indo-Pacific species as well as species whose distribution is limited to coral reefs.

Fisheries

Over the millennia, the greatest benefit provided to mankind by coral reef ecosystems has been in the form of harvest, primarily of finfish, in addition to other vertebrates and invertebrates [25]. Human populations along the coast made extensive use of nearby reef areas that were situated typically in shallow water and often in sheltered lagoons or embayments, a fact that rendered them eminently accessible by even the most primitive means of transport such as rafts and hand-paddled canoes. Traditional methods involved the use of various kinds of nets, or of hook-and-line fishing.

There are over 4,000 species of teleost fishes known to be associated with coral reefs [30]. Approximately 10% of these are directly dependent on corals. They are either obligate coral dwellers, corallivores (i.e., they feed on coral tissue), or possess juvenile stages that always settle into live coral in the process of recruitment. The total global fisheries yield from coral reefs is estimated to be USD five billion annually [30].

In the central Philippines, which was recognized recently as among the richest in the world in terms of species diversity [29], the following fish

families contribute substantially to fish catch [31]: Acanthuridae, Siganidae, Scaridae, Labridae, Haemulidae, Lethrinidae, Lutjanidae, Mullidae, Serranidae, Carangidae, Scombridae, Sphyraenidae, Belonidae, and Caesionidae. In terms of total potential fish yield, Alcala and Russ [31] suggest a figure of 350,000 metric tons annually for the entire country, based on an aerial estimate of 25,000 km^2 of reef area.

Physical Connectivity

Marine habitats such as coral reefs have the key distinguishing feature (when compared to terrestrial habitats) of being situated within a water medium, as opposed to air. The physical differences between water and air impart fundamental properties in terms of how the respective communities function, and how they are structured. One obvious difference is that water is considerably denser than air, and is capable of carrying a much larger quantity of material. Because of this, there is significant transport by water currents between habitats over a large range of distances, from microscopic (at the scale of molecular motion) to the macroscopic scale (up to hundreds of kilometers) [32].

Oceanic currents convey a whole spectrum of materials, from dissolved compounds, to particles (living and nonliving) to organisms of various sizes, from microscopic plankton to mammals weighing several tons. The relevant aspect for marine conservation and sustainability is the ecological process of recruitment, whereby gametes or larvae are carried away from particular habitats and transported to other areas at varying distances from the point of origin. Recruitment is a vital process for the maintenance and renewal of populations. Communities that suffer significant decreases in recruitment over appreciable amounts of time are in danger of diminishing or even disappearing altogether.

One of the first papers that advocated a study of surface oceanic currents in order to predict possible recruitment trajectories is that of Roberts [33]. The author, using the Caribbean as an example, proposed that if larvae can be regarded as passively dispersing particles, then upstream reefs, if harboring healthy populations of reef species, may be considered sources supplying downstream areas. The effective distance by which recruitment can occur successfully would, theoretically, be dictated by the length of time during which a larva remains viable in the water column, or the duration of the pelagic larval phase [34]. In an extension of this perspective to management applications, downstream reefs receiving viable recruits in sufficient amounts would be less at risk of decimation even if exploitation rates were high. Upstream reefs, on the other hand, would be in greater need of protection. These ideas helped to inspire the vigorous movement that emerged in a number of countries that have coral reefs in their territorial waters to establish networks of marine reserves or protected areas premised, among other criteria, on the possible existence of connectivity based on oceanographic patterns. Marine protected areas (MPA's) are discussed in section "Marine Protected Areas".

Subsequently, a large number of studies have been conducted to confirm or refute these ideas [6]. One limitation is that the only means of directly determining the actual fate of individual larvae is by tagging and parentage techniques [6]. Other approaches are indirect, and include genetic analysis, the description of local population structure, and the application of biophysical modeling which combines the characterization of current patterns and hydrographic regimes with larval behavior of particular species.

Recent research indicates that the degree of larval retention within a natal reef, as well as the spatial extent of connectivity in both corals and fish appear to be independent of larval duration [6], contrary to previous expectations. In the case of corals, for both broadcast spawners as well as brooding species, both self-recruitment and inter-reef dispersal have been found to be significant. Dispersal can occur over distances as long as tens of kilometers. Broadcast spawners are corals that release gametes into the water column. The eggs and sperm may come from the same colony (hermaphroditic), or from colonies with separate sexes (gonochoric). Fertilization takes place in the water column. The entire series of developmental stages from cleavage, to formation of the embryo and then of the fully-formed larva all occur as part of the pelagic phase. Brooding species are corals where the egg remains inside the polyp, and is fertilized by sperm that find their way into the cavity. The larva develops inside the polyp and emerges after a period of time, fully formed, into the surrounding water.

In the case of reef fish, a number of methods indicate that, for a range of species, there are ecologically significant levels of self-recruitment at the scale of individual reefs or reef clusters [6]. Results have yielded an average of as high as 45–50% self-recruitment. The amount of self-recruitment does not seem to be related to the mode of spawning nor pelagic larval duration. For both corals and fish, the patterns of dispersal may be influenced more by the geographic setting, size, and location of reefs rather than by the biological characteristics or individual life histories of particular species. This finding, again, has implications for the design of networks of marine reserves, including their size, spatial arrangement, and the distances between them.

Ecological Goods and Services from Coral Reefs

Coral reefs have provided benefits to coastal human populations for thousands of years. Perhaps the greatest value that these ecosystems have is as a source of food. A variety of organisms continue to be harvested, notably the finfish which still possess considerable economic value, in addition to their contribution to basic sustenance of populations, particularly in developing countries. Despite their limited cover in proportion to the entire ocean floor (0.1–0.5%), almost a third of marine fish species in the entire world are found on coral reefs, and about 10% of fish consumed by humans are caught from reef areas [4].

Other vertebrate groups that have been the object of traditional fishing are the dugongs (Order Sirenia) and turtles [25]. Invertebrates that have been traditionally harvested from reefs for human consumption include sea urchins, sea cucumbers, molluscs, and crustaceans. A variety of species of seaweed are also used for food.

Coastlines that are lined by coral reefs are afforded natural protection from the destructive forces of the sea. The natural erosion that occurs within reef habitats due to physical abrasion by waves and currents produces sand which accumulates on beaches. Typically white sand is composed of pulverized coral, shells, coralline algae, and foraminiferans in varying proportions.

In some localities, corals are collected for building material in the construction of houses, roads, and other infrastructure. Other less common uses of reef organisms are as sources of pharmaceuticals.

Coral reefs have always been valued for their aesthetic beauty. In recent decades, they have supported a vigorous tourism and leisure industry that has extended its reach globally. Tourists would travel hundreds to thousands of kilometers to visit pristine reefs. The traffic usually emanates from the more affluent societies in Europe and North America, and heads in the direction of the Caribbean, the Red Sea, the Indian Ocean, and all the way to the high diversity reefs of the Indo-West Pacific.

Table 2 presents a general listing of goods and services derived from coral reefs [4].

Threats to Coral Reefs

Unfortunately, the degradation of coral reef habitats has become a worldwide trend [35, 36]. The current concern from the ecological and conservation perspective is how to prevent this trend from becoming irreversible. In the Indo-Pacific region, for example, which is the cradle of coral reef diversity, coral cover is estimated to already lie at least 20% below the best historical reference points [37]. The average loss of coral cover annually is estimated at 1%. This represents a figure of 1,500 km^2 of coral cover lost from the early 1980s to around 2003.

In a recent study, Carpenter et al. [38] compiled data on the status of all known zooxanthellate reef-building corals. These include 845 species from the order Scleractinia, plus reef-building species from other groups of the phylum Cnidaria, the octocorals and hydrocorals. There were sufficient data for 704 species so that conservation status could be assigned. Of these, 32.8%, or roughly one third, were in categories with elevated risk of extinction (Table 3). Following criteria from the International Union for Conservation of Nature (IUCN), these species were considered to be under serious threat of population declines within their established geographic ranges. A combination of natural and anthropogenic factors are responsible for the losses in coral cover in different parts of the world.

Since corals are the natural framework builders for the habitat of other reef species, notably fish, declines in coral cover and abundance are usually accompanied by similar decreases in the other biota as well. A study in the Indian Ocean, for example, documented changes in size structure, diversity, and trophic composition of

Coral Reef Ecosystems. Table 2 Ecological goods and services derived from coral reef ecosystems

Goods		Ecological services					
			Biotic services				
Renewable resources	Mining of reefs	Physical structure services	Within ecosystems	Between ecosystems	Biogeochemical services	Information services	Social and cultural services
Sea food products	Coral blocks, rubble and sand for building	Shoreline protection	Maintenance of habitats	Biological support through "mobile links"	Nitrogen fixation	Monitoring and pollution record	Support recreation
Raw materials for medicines	Raw materials for production of lime and cement	Build up of land	Maintenance of biodiversity and a genetic library	Export of organic production, and plankton to pelagic food webs	CO_2/Ca budget control	Climate record	Aesthetic values and artistic inspiration
Other raw materials (seaweed and algae for agar, manure, etc.)	Mineral oil and gas	Promoting growth of mangroves and sea grass beds	Regulation of ecosystem processes and functions	–	Waste assimilation	–	Sustaining the livelihood of communities
Curio and jewelery	–	Generation of coral sand	Biological maintenance of resilience		–	–	Support of cultural, religious and spiritual values
Live fish and coral collected for the aquarium trade	–	–	–	–	–	–	–

Source: From [4]

reef fish communities following decreases in coral cover as a result of climate change [39].

Natural Threats

The recent literature highlights the phenomenon of global change, particularly change in the climate, as posing an increasing threat to the health of natural ecosystems, both terrestrial and aquatic [40]. The main culprit is commonly believed to be the large-scale release of carbon dioxide into the atmosphere due to the burning of fossil fuel which reached unprecedented levels since the beginning of the industrial revolution [41, 42]. Another cause for the release of large quantities of this gas is land use practices such as deforestation [42]. The presence of large amounts of carbon dioxide in the atmosphere has created the so-called greenhouse effect, whereby long-wave radiation emitted by the earth system is trapped instead of being released into outer space. The result is a net warming of the planet over time. Temperature has been determined to follow a significant upward trend since the start of the industrial era in the 1800s. Thus, although variations in

Coral Reef Ecosystems. Table 3 Families of reef-building coral species that are near threatened (NT) and/or threatened (Thr) according to Red List categories of the International Union for the Conservation of Nature (IUCN). Criteria are defined by population size reduction and changes in geographic range

Family	Total species	NT + Thr	Thr
Acroporidae	271	71.6%	49.5%
Agariciidae	45	38.1%	26.2%
Astrocoeniidae	15	18.2%	9.1%
Caryophylliidae	3	0.0%	0.0%
Dendrophylliidae	15	71.4%	50.0%
Euphylliidae	17	100.0%	64.3%
Faviidae	130	65.6%	20.0%
Fungiidae	46	27.3%	15.9%
Helioporidae	1	100.0%	100.0%
Meandrinidae	10	42.9%	42.9%
Merulinidae	12	36.4%	9.1%
Milleporidae	16	42.9%	35.7%
Mussidae	52	53.3%	26.7%
Oculinidae	16	70.0%	40.0%
Pectiniidae	29	50.0%	25.0%
Pocilloporidae	31	48.3%	31.0%
Poritidae	101	56.0%	34.1%
Rhizangiidae	1	0.0%	0.0%
Siderastreidae	32	42.3%	19.2%
Trachyphyliidae	1	100.0%	0.0%
Tubiporidae	1	100.0%	0.0%
Total	845		

Source: Modified from [38]

temperature are a natural feature of the environment, and occur on a range of time scales ranging from diurnal and seasonal all the way to millions of years (corresponding to the geological epochs), the specific causes as to why it is now perceived to be a problem are human-related.

Monitoring long-term trends in sea surface temperature (SST) has been aided greatly by advances in technology, as exemplified by the suite of satellite products developed by the National Oceanic and Atmospheric Administration's (NOOA)- Coral Reef Watch [26]. Specifically, services have been derived from the 0.5°C (approximately 50 km) resolution twice-weekly product delivered by the Advanced Very High Resolution Radiometer (AVHRR). This product has been effective in detecting large-scale thermal stress in the ocean, and in relating this to coral bleaching events, for example. In the Indo-Pacific region, particularly the islands of the Philippines, Indonesia, and Papua New Guinea also known as the "Coral Triangle," an upward trend in SST has been established for the period 1985–2006, with an average rate of increase of 0.2°C per decade [26]. However, it should be noted that satellites detect the temperature of what is essentially the ocean's "skin," so that satellite-derived data should, wherever possible, be complemented by actual temperature measurements made on site at different depths of the reef [43].

With respect to estimates of warming of the entire global ocean, reliable data exist for the upper 300 m [44]. The majority of in situ measurements have been contributed by expendable bathythermograph (XBT) data. After accounting for multiple sources of uncertainty, a statistically significant linear warming trend has been obtained for the period 1993–2008 amounting to 0.64 Wm^{-2} (reflecting the entire surface area of the Earth) with a 90% confidence interval of 0.53–0.75 Wm^{-2} [44].

The increased levels of carbon dioxide in the atmosphere have resulted in another phenomenon that is detrimental to coral reefs. Because of increased partial pressure of the gas (PCO_2) which results in steeper diffusion gradients, there is greater drawdown into the ocean from the atmosphere. An international survey effort consisting of two research programs, the World Ocean Circulation Experiment and the Joint Global Ocean Flux Study, yielded an estimated oceanic uptake of anthropogenically produced CO_2 for the period 1800–1994 of 118 ± 19 petagrams of carbon [42]. This amount represents about 48% of the total emissions from fossil fuel burning and cement manufacturing, indicating the magnitude of the oceanic sink. Furthermore, this value is projected to be about one third of the long-term potential of the ocean for carbon storage. A more recent estimate made in 2008 puts the value at 140 ± 25 petagrams of carbon,

with the Southern Ocean being the primary conduit for entry [41].

Carbon dioxide reacts with seawater to form carbonic acid, decreasing oceanic pH [45]. If the PCO_2 concentrations in the ocean surface continue to increase in proportion to the increase in atmospheric concentrations of this gas, it is estimated that a doubling of the latter from preindustrial levels will result in a 30% decrease in carbonate ion concentration and a 60% increase in hydrogen ion concentration [42]. The result is increasing acidification of the oceans which is believed to pose a threat to calcifying organisms, including the hard corals [46]. The higher acidity values depress aragonite saturation state which is crucial in the net carbonate balance, and which can spell the difference between net accretion and net dissolution of calcium carbonate. Not only corals but other calcifying organisms such as shellfish, foraminiferans, and echinoderms are at risk [47], with significant consequences for the rest of the ecosystem. For example, trophic pathways will be altered if certain species decrease in abundance as a result of reduction in calcification rates, which imply diminution or weakening of protective shells or armor, thus compromising growth, reproduction and survival from predation.

A long-term study of growth rates of juvenile coral in the Caribbean suggests that corals $\leq$40 mm have actually grown more slowly than previously thought [48]. The period of decline in growth rate corresponds with observations of rising seawater temperature and depressed aragonite saturation state, implying effects of climate change. This finding does not bode well for the future viability of coral communities in the region because juvenile stages are critical for the successful establishment of populations of any species. On the other side of the world, in the Great Barrier Reef, experimental manipulations of temperature directly affected the metabolism of coral larvae, with higher temperatures increasing rates of development, and thus the onset of competency [49]. Thus, expected increases in sea surface temperatures will likely cause changes in larval dispersal ranges.

Another natural phenomenon that is perceived to be growing in severity is the occurrence of diseases in corals and other marine species [50, 51]. Although diverse communities of microbes normally inhabit the surfaces of coral colonies and all other types of surfaces on a reef [13] increasing experimental evidence combined with modeling indicates that environmental factors such as increasing water temperatures might promote a shift in dominance from antibiotic-producing beneficial microbes to pathogenic forms such as certain species of *Vibrio*. The loss of antibiotic protection would render corals more susceptible to disease and increase their risk of mortality [52]. Other causative agents of coral disease that have been identified include *Aspergillus sydowii* (that attacks sea fans) and *Sphingomonas* sp. [51].

Predation on corals has long been considered an important natural threat to the survival of corals [1]. Two notable examples of this phenomenon involve the crown-of-thorns (COT) starfish, *Acanthaster planci*, and the gastropod *Drupella*. Damage on a fairly large scale, up to hundreds of square meters on a number of reefs, has been documented due to active grazing by these two invertebrate predators. Cyclic fluctuations in populations of many species are considered natural, and are connected with changes in climate, food supply or a combination of these. With respect to COT outbreaks, however, the causes are presumed to relate to unnatural factors such as human overharvesting of natural predators and increases in planktonic food supply of the larvae [18, 53]. Recent evidence from the Great Barrier Reef, for example, suggests that nutrient enrichment of the waters (probably due to land-derived pollution) has triggered blooms of phytoplankton that serve as food for COT larvae, thus enhancing their survival and growth to adulthood [53].

Anthropogenic Threats

Up till recent times, the most severe impacts inflicted on coral reefs have been due to human activities, directly or indirectly [22, 54]. A recent review of anthropogenic threats to coral reefs worldwide is that of Wilkinson [36].

Water quality is generally influenced by levels of nutrients such as nitrogen and phosphorus, concentrations of total organic carbon, turbidity, and light attenuation [55]. Water quality, in general, has been documented to correlate directly with species richness of hard corals and of phototrophic octocorals [56]. Clarity of the water, as commonly measured in terms of Secchi depth for example, is a good indicator of

water quality. Low water quality has been observed to be associated with proliferation of macroalgae. The most common cause of diminution in water quality is effluent from the land.

Land-derived impacts have been in existence ever since humans started to modify the land extensively for their use. In terms of documented effects on reefs, the most important activities are agriculture and deforestation. These activities involve the release of huge amounts of sediment which eventually find their way into coastal waters via run-off. Rivers, for instance, transport large amounts of sediment into the ocean. The sediment settles directly on the bottom, physically smothering benthic life-forms.

Another land-derived impact is pollution from both point and nonpoint sources. It can take the form of organic pollution, such as from sewage, and inorganic pollution – for example, heavy metals. Sewage in the water is ultimately degraded by bacteria to yield inorganic nutrients, primarily nitrogen and phosphorus. These elements fuel photosynthesis by both phytoplankton and benthic plants, resulting in high rates of primary production and an increase in biomass of the primary producers. The latter are effective competitors with hard corals for space and light.

In coral reef habitats, the nutrients of interest are nitrate, ammonium, and soluble reactive phosphate assimilated by plants [57]. In addition, dissolved organic forms of nitrogen and phosphorus are significant as well. They are remineralized into the inorganic forms that are utilized by primary producers. Coral reefs that are close to sites of dense human habitation are susceptible to detrimental effects of nutrient pollution. The effects are aggravated if there is limited flushing, such as within embayments and lagoons.

Destructive fishing practices are another cause of major disturbances to coral reef communities [58]. In many parts of the developing world, the use of explosives to catch fish is still a significant problem. The use of the metabolic poison, sodium cyanide, to catch ornamental fish for the aquarium trade, also continues to be widespread [28]. Both categories of disturbance inflict direct harm on the habitat. Explosives cause catastrophic destruction of the reef substrate and all living organisms within the effective radius of the explosion. They leave behind telltale craters of varying size, depending on the blast, and expanses of rubble and broken coral.

Cyanide is usually dissolved in sea water and squirted directly into crevices and other places where the target fish shelter. It kills virtually all living organisms with which it comes into contact, including coral colonies which are common hiding places for fish. The dose of the poison applied is meant to merely stun the fish for ease of capture, because these are intended to be shipped live to prospective customers.

Another major impact is simply the excessive harvest or overfishing of organisms, be they finfish, invertebrates, or economically important species of algae. For coastal ecosystems in general, the ecological extinction of species due to excessive exploitation precedes the effects of other human-related impacts such as pollution and anthropogenic-related climate change [25]. Jackson et al. [25] hypothesize that it is the depletion of entire species groups, or even trophic levels, that paved the way for the occurrence of subsequent disturbances such as eutrophication, outbreaks of disease and the invasion of species.

Impacts on Reef-Associated Organisms

Decreases in diversity and/or abundance of hard corals have been accompanied by declines in other reef-associated species, notably the fish [30]. The families that are directly dependent on corals are most at risk. These include the butterflyfish (Chaetodontidae), the cardinalfish (Apogonidae), and the gobiids (Gobiidae). A recent empirical study demonstrated that live coral provides effective shelter to both adult and juvenile stages of the damselfish *Pomacentrus amboinensis* [59]. In contrast, juveniles attempting to shelter in bleached and dead coral were driven away by larger fish, thus exposing them to greater predation. They subsequently suffered higher mortality rates. In addition, factors associated with climate change and various human impacts will affect the biology and ecology of the fishes themselves. Temperature, for example, exerts a direct effect on fish physiology, and abnormally high levels can impair reproduction. The aggregate effects of perturbations to the coral reef ecosystem will be manifested in changes in the diversity, abundance, and distribution of fish. Climate change per se can exert a direct influence by causing shifts in the geographic ranges of various fish species.

One of the most widely discussed phenomena in the scientific literature is that of the coral-algal phase transition or "shift," meaning that reef communities once dominated by scleractinian corals are now largely populated by macroalgae or turf algae [22, 60] or some other reef-associated species [61]. This phenomenon gained widespread attention in the Caribbean [25, 62] with the occurrence of mass mortalities of animals that normally graze on algae. Such grazers include sea urchins and herbivorous reef fish (scarids and acanthurids), and incidents of mortality have been attributed to disease or overfishing of these functional groups. The resulting depletion in populations of herbivores has been observed to correlate with explosions in abundance of macroalgae, which are competitors of hard corals for light and space. A recent study appears to confirm this belief for some Caribbean locations, where recovery of the sea urchin *Diadema antillarum* has occurred [63]. In sea urchin zones where there is significant grazing on algae, the survival of juvenile scleractinian corals was observed to be higher.

For coral reefs in other parts of the world, however, the shift from coral to macroalgal dominance does not appear to be as widespread as previously assumed [64]. Bruno et al. [64] compiled empirical data from reef surveys in the Indo-Pacific, the Great Barrier Reef, the Caribbean, and the Florida Keys. The results of their analysis indicate that the replacement of corals by macroalgae as the dominant benthic component on reefs is neither common nor geographically extensive as previously thought. Apart from a depletion of populations of grazers, nutrient pollution also contributes to algal blooms [65, 66]. Some evidence suggests that the effects of nutrient enrichment tend to be localized to reefs located near centers of dense human populations, and in areas where there is limited flushing of water, such as lagoons and embayments [57].

Management

Given the problems facing coral reefs enumerated above, it is clear that management action should operate on a range of scales, from highly localized to regional and global. It will have to encompass the whole gamut from reducing destructive fishing practices, to implementation of land use schemes that control sedimentation and pollution, and to activities such as restoring herbivore populations [37]. The global policy arena will also need to be involved as this is the effective scale at which global climate change can be addressed.

The field of coral reef management has seen uneven progress over the past decades [54, 62, 67]. Like in most other areas involving natural resources, the effectiveness of management has been diminished by the fact that responsibility for what is essentially a common domain has been fragmented and distributed over a number of sectors, such as agriculture, fisheries, tourism, human settlements, and industry. The result of this is the often conflicting mandates of different government departments and agencies.

An emerging consensus is that human population growth has begun to far outstrip the capacity of the natural resource base to provide goods and services, and to absorb wastes [67]. This reality manifests itself more clearly in developing countries, where the inability of many citizens to maintain an adequate livelihood results in chronic want, hunger, and disease. In the case of developed countries, the better managed economic sectors (including manufacturing and trade), the superior infrastructure, and the more efficient social delivery system tend to compensate for the diminishing returns from natural resources. Nevertheless, the heavy burden of human demands on natural resources is true for coral reefs in both the developed and developing world.

For coral reef ecosystems, the most pressing goal of management action should be the protection of whatever levels of biodiversity are remaining. Ecological science has demonstrated the advantages of maintaining high species numbers in any natural habitat [61]. One benefit of high species diversity is that a number of different species can play similar ecological roles, a prime example in coral reefs being herbivory or grazing. This aspect is sometimes referred to as "redundancy." If one species becomes locally extirpated because of overfishing, for example, another species can continue its ecological function, thus maintaining the overall balance in the system in terms of fluxes of matter and energy. Examples of reef organisms with similar grazing functions are sea urchins (belonging to the genera *Diadema*, *Tripneustes* and *Salmacis*) and fish belonging to the families Acanthuridae, Chaetodontidae and Scaridae.

Protecting, and then enhancing, existing levels of diversity would necessarily require limits on the extraction of living resources. This would require strict regulation of fishing. If at all possible, fishing for subsistence should be discouraged, and alternative livelihoods developed for traditional fishers. All manner of destructive fishing should be banned, with the imposition of severe penalties.

Marine Protected Areas

The designation of marine protected areas (MPA's), where no extractive activity whatsoever is allowed, is by far the most widely advocated management tool for coral reefs [54, 67, 68]. The core argument for this type of intervention is compelling: If carefully selected areas are protected from human activities, particularly resource extraction, then natural ecological processes will be allowed to proceed without interruption. The expected result is a healthy, thriving community with increased abundance and diversity of many reef-associated species [69].

The natural behavior of the motile species, particularly the finfish, would cause them to move beyond the boundaries of an MPA into areas that are open for fishing. This so-called spillover should be of benefit to subsistence and, where applicable, commercial fishers. An additional benefit of functioning MPA's is in the form of "recruitment subsidy" whereby spawning populations of reef species that are under protection produce adequate quantities of gametes or larvae which are then carried beyond the MPA boundaries to replenish depleted stocks in openly exploited areas.

These two expected benefits of MPA's require further research and experimental testing [70], with available supporting evidence still somewhat sparse and ambiguous [68]. One study providing possible evidence of export of fish from a coral reef reserve is that of Abesamis and Russ [71] in the Philippines. The reserve has been maintained for over two decades, and the observed movement into surrounding areas was attributed to behavior of adult fish as they increased in size and density.

One documented effect of MPA's is increase in the populations of herbivores as a result of protection from fishing [72, 73]. Herbivores include invertebrates such as sea urchins, and fish such as parrotfish (family Scaridae) and surgeonfish (family Acanthuridae). In studies in the Philippines and the Bahamas, adequate populations of herbivores were found to be effective in keeping macroalgal cover in check [72, 73]. It is strongly advocated that the maintenance or restoration of herbivore populations within reef areas should be part of management, in addition to controlling nutrient pollution (see section "Improving Water Quality"). A recent study of a Caribbean marine reserve focused on coral population dynamics after the occurrence of two types of major disturbances, namely, bleaching and hurricane impacts. There was more effective recovery of corals within as compared to outside the reserve [72]. Coral cover increased significantly along with a corresponding reduction in macroalgal cover brought about by grazing of herbivorous parrotfishes. The latter had presumably increased in abundance due to effective protection.

The effects of marine reserves have not always been consistent, however, particularly in the face of large-scale disturbances such as those related to climate change. In a large-scale study of no-take areas (NTA's) spanning several countries across the Indian Ocean, there was little difference in the decline in coral cover between NTA's and areas open to fishing [39]. This finding suggests that management efforts should encompass spatial scales larger than the patchwork of MPA's along with their intervening, openly exploited areas. More attention should be given to reef areas that serve as regional refugia, and which act as viable sources of recruits even in the face of large-scale impacts.

To be effective in the long run, fisheries management must take a comprehensive approach, and combine the designation of MPA's with other interventions such as restrictions on gear types and catch size, as well as the provision of alternative forms of livelihood to fishers [74].

Improving Water Quality

Effective management action to maintain the health and diversity of coral reef communities must include the maintenance of good water quality [56]. Coral reef communities are known to thrive best under conditions of clear water, low nutrient levels, adequate sunlight, and moderate temperatures. The key

intervention in this regard is the strict control of pollutant loading in coastal waters known to harbor sensitive ecosystems such as coral reefs, sea grass beds, and mangrove forests. Thus, all countries that possess these ecosystems in their territorial waters should enforce strict antipollution legislation.

Since another major land-derived stress is sediment loading, management must also address land-based activities that cause the mobilization of significant quantities of sediment and their release into coastal waters. The main sectors of concern would be agriculture (which also employs the use of chemicals in the form of fertilizers and pesticides), deforestation, and the building of coastal infrastructure (for urbanization and industry).

Restoration

The field of coral restoration has, as its current focus, the hard corals themselves, belonging to the order *Scleractinia*. These are the main structural components of present-day reefs, both as framework-builders and as fillers of the reef matrix (section "Biology and Ecology"). The science of coral restoration is still fairly young and very much at an experimental stage [75, 76]. Perhaps one of the earliest works alluding to the possibility of restoring damaged reef habitats by means of the transplantation of either branches or whole colonies of hard corals is that of Maragos [77] in Hawaii. Examples after that include investigations conducted in the Philippines on the survival and growth of transplanted coral fragments [78]. At the present time, the field has seen the entry of new experimental techniques geared toward augmenting live coral cover by increasing the abundance of either adults or recruits [75].

The main rationale for intervention in the form of restoration is if a damaged reef community has not recovered naturally over appreciable amounts of time. The causes of reef degradation are enumerated in section "Threats to Coral Reefs." Unfortunately, many reefs throughout the world are presently in a degraded state, showing little signs of natural recovery. The dominant cover in such reefs typically consists of macroalgae, turf algae, sponges, soft corals, hydroids, or any combination of these in various proportions. Coral restoration, by definition, is the attempt to bring a reef community back to a dominance by scleractinian corals within a relatively short period of time (as opposed to the decades it would take for a reef to recover naturally, if at all). Some experimental evidence indicates that the establishment of live coral cover can increase the local diversity of reef-associated species [79].

Before any attempt at restoration is initiated, a thorough assessment of the candidate site should be made. The causes of damage, both proximal and long term, should be identified and their current degrees of severity evaluated. It would be ideal if the causes of destruction are mitigated prior to intervention. For example, if causes of reef degradation involve poor water quality due to land-based pollution or sedimentation, then these issues should be resolved first. Similarly, if damage is caused by harmful fishing practices, then these should be controlled or eliminated. A further assessment of the candidate site for restoration should consider the prevailing environmental conditions such as suitability of the substrate, water clarity, salinity, and nutrient levels. These are factors that directly affect coral physiology and should be determined to be suitable for coral survival and growth before juveniles or transplants are introduced.

The most common approach in the past has been to transfer live whole colonies, or fragments of colonies from healthy coral populations to degraded sites within the same reef [76]. It is necessary to source material from within the same general area because long periods of transportation would inflict significant stress on the coral. This would potentially lead to unacceptable mortality rates of the transplants. The whole coral colony or transplant is translocated to what is essentially a new environment. One essential criterion for site selection is that the recipient site should show evidence of the existence of coral communities in the past, usually in the form of dead skeletons. This is an indication that the area could possibly support a new coral-dominated community again, provided that environmental conditions are not permanently inimical to the survival and growth of introduced corals.

Since the use of whole colonies or fragments of colonies usually causes some collateral damage to the source population, other strategies have been developed in recent years to avoid this. One strategy is to collect fragments found on the reef substrate and "rear"

these under special conditions of high maintenance ("nurseries") until they reach a size suitable for reestablishment on the natural substrate. Another strategy being tested is to induce spawning of coral colonies under laboratory or hatchery conditions and collect the resulting larvae which can number in the tens of thousands. The larvae are induced to settle on material of a convenient size, such as plastic pins or concrete tiles. When the larvae metamorphose into juveniles, the latter are reared up to a size considered suitable for "outplanting" to the natural reef.

A major problem of coral restoration efforts is the relatively high mortality suffered by either recruits or transplants introduced into a degraded reef [80]. As mentioned above, a degraded reef surface is typically covered by a variety of organisms including turf algae, macroalgae, soft corals, sponges, and hydroids. These are forms that have proven to be able to adapt and thrive under the altered conditions that probably have led to the demise of the original hard coral inhabitants in the first place. Examples of such environmental conditions are increased turbidity and nutrient loading in the water. In addition to being tolerant of the new conditions, these organisms effectively compete with the hard coral recruits and transplants for space.

Coral transplants and recruits introduced into degraded reef environments have also been observed to suffer from predation (pers. obs.). Common predators that occur in the reefs of the Philippines and other similar geographic areas are the crown-of-thorns starfish, *Acanthaster planci*, and the gastropod *Drupella*. There are possibly other causes of coral mortality that are as yet undiscovered, and that have hampered progress in restoration.

Efforts at the present time are focused on developing cost-effective techniques that would minimize expenditure in terms of finances, manpower, and resources, and maximize output in terms of live coral material (juveniles or adults) that can be used in restoration interventions.

A parallel activity to restoration of the hard corals is restocking of other important reef invertebrates. A notable example is the giant clam (Family Tridacnidae) which is a major inhabitant of coral reefs, can grow to appreciable sizes, and can contribute to the carbonate budget of a reef by accreting fairly massive shells. Many species of giant clams have become rare or locally extinct in many reef areas throughout the world, primarily due to overharvesting. Scientific efforts have yielded a fair degree of success in terms of producing large numbers of juveniles under hatchery conditions and then reintroducing these into suitable reef sites [81]. Such established populations have been thriving for several decades in the Philippines, for example. A recent experiment has demonstrated that restocking denuded reef areas with live coral together with giant clams can significantly enhance fish abundance and diversity [82].

Future Directions

Coral reef ecosystems, particularly in the developing world, are clearly no longer able to support major extractive activities, including fishing, on a sustained basis. They are confronted with the twin challenges of limited biological productivity and demands from a relentlessly increasing human population. It is imperative that, as far as possible, coral reef areas all over the world be put under protection to conserve whatever is remaining of their biodiversity and ecological function. However, equally urgent attention should be paid to providing alternative livelihood to the numerous populations of coastal fishers who will be displaced once their traditional fishing grounds are declared off limits for protection. In addition to protecting nature, the fundamental obligation of resource management is to help ensure a decent quality of life for the human inhabitants.

A scrutiny of the existing global economic order would not be unwarranted in this respect, since many coastal populations in developing countries have been reduced to economic desperation. In the management of the use of coastal resources, the perspective should be extended beyond the limited confines of the coastal zone to the national, regional, and even global arenas. For example, it is about time that, in the spirit of interdisciplinary research, fiscal and trade policies also be examined along with traditional ecological investigations. An inherent injustice may still be embedded in legal international structures that tend to disenfranchise the poor of the control over their own natural resources (not just fisheries) and over the generation of economic wealth from the proper use of these resources (including forest, agriculture,

and mineral assets). Unless this aspect is properly addressed, impoverished populations all over the world will continue to deplete natural resources at unsustainable levels simply to ensure their own survival. The related issue of controlling human population growth rate would be a crucial consideration.

Alongside this basic initiative, vigorous efforts should be put in place to control or abate pollution, and to improve water quality. Coral reef communities are extremely sensitive to factors that diminish light availability, such as turbidity, and to abnormally high nutrient levels that promote the proliferation of weedy species such as phytoplankton and benthic algae.

The field of coral restoration is still very much at an experimental stage, with relatively few documented reports of success. It is worthwhile to continue research in this area, as certain coral species have proven to be resilient to variations in climatic factors such as light and temperature, and the enhancement of topographic complexity by coral transplantation has been demonstrated to increase species diversity on local scales.

Bibliography

Primary Literature

1. Wood R (1999) Reef evolution. Oxford University Press, Oxford
2. Ladd HS (1977) Types of coral reefs and their distribution. In: Jones OA, Endean R (eds) Biology and geology of coral reefs, vol IV, Geology 2. Academic, New York, pp 1–18
3. Veron JEN (2000) Corals of the world, vol 1–3. Australian Institute of Marine Science, Townsville
4. Moberg F, Folke C (1999) Ecological goods and services of coral reef ecosystems. Ecol Econ 29:215–233
5. Guild L, Lobitz B, Armstrong R, Gilbes F, Goodman J, Detres Y, Berthold R, Kerr J (2008) NASA airborne AVIRIS and DCS remote sensing of coral reefs. In: Proceedings of 11th International Coral Reef Symposium Session 17, Fort Lauderdale, pp 616–620
6. Jones GP, Almany GR, Russ GR, Sale PF, Steneck RS, van Oppen MJH, Willis BL (2009) Larval retention and connectivity among populations of corals and reef fishes: history, advances and challenges. Coral Reefs 28:307–325
7. Berdin RD, Siringan FP, Maeda Y (2004) Holocene sea-level highstand and its implications for the vertical stability of Panglao Island, southwest Bohol, Philippines. Quat Int 115–116:27–37
8. Maeda Y, Siringan F, Omura A, Berdin R, Hosono Y, Atsumi S, Nakamura T (2004) Higher-than present Holocene mean sea levels in Ilocos, Palawan and Samar, Philippines. Quat Int 115–116:15–26
9. Domingues CM, Church JA, White NJ, Gleckler PJ, Wijffels SE, Barker PM, Dunn JR (2008) Improved estimates of upper-ocean warming and multi-decadal sea-level rise. Nature 453:1090–1093
10. Shen C-C, Siringan FP, Lin K, Dai C-F, Gong S-Y (2010) Sea-level rise and coral reef development of northwestern Luzon since 9.9 ka. Palaeogeogr Palaeoclimatol Palaeoecol 292(3–4):465–473
11. Veron JEN (1995) Corals in space and time: biogeography and evolution of the Scleractinia. Comstock/Cornell, Ithaca
12. Bellwood DR, Hughes TP (2001) Regional-scale assembly rules and biodiversity of coral reefs. Science 292:1532–1534
13. Sheppard CRC, Davy SK, Pilling GM (2009) The biology of coral reefs. Oxford University Press, Oxford
14. Barbeitos MS, Romano SL, Lasker HR (2010) Repeated loss of coloniality and symbiosis in scleractinian corals. Proc Nat Acad Sci. doi:10.1073/pnas.0914380107
15. Muscatine L (1971) Endosymbiosis of algae and coelenterates. In: Lenhoff HM, Muscatine L, Davis LV (eds) Experimental coelenterate biology. University of Hawaii Press, Honolulu, pp 179–191
16. Muscatine L (1971) Calcification in corals. In: Lenhoff HM, Muscatine L, Davis LV (eds) Experimental coelenterate biology. University of Hawaii Press, Honolulu, pp 227–238
17. Yap HT, Montebon ARF, Dizon RM (1994) Energy flow and seasonality in a tropical coral reef flat. Mar Ecol Prog Ser 103:35–43
18. Veron JEN (2008) A reef in time. Belknap Press of Harvard University Press, Cambridge, MA/London
19. Berkelmans R, van Oppen MJH (2006) The role of zooxanthellae in the thermal tolerance of corals: a 'nugget of hope' for coral reefs in an era of climate change. Proc R Soc B 273:2305–2312
20. Mieog JC, Olsen JL, Berkelmans R, Bleuler-Martinez SA, Willis BL, van Oppen MJH (2009) The roles and interactions of symbiont, host and environment in defining coral fitness. PLoS One 4:e6364
21. LaJeunesse TC, Smith R, Walther M, Pinzon J, Pettay DT, McGinley M, Aschaffenburg M, Medina-Rosas P, Cupul-Magaña AL, Perez AL, Reyes-Bonilla H, Warner ME (2010) Host-symbiont recombination versus natural selection in the response of coral-dinoflagellate symbioses to environmental disturbance. Proc R Soc B. doi:10.1098/rspb.2010.0385
22. Perry CT, Spencer T, Kench PS (2008) Carbonate budgets and reef production states: a geomorphic perspective on the ecological phase-shift concept. Coral Reefs 27:853–866
23. Douglas AE (2003) Coral bleaching–how and why? Mar Pollut Bull 46:385–392
24. Kiessling W, Simpson C, Foote M (2010) Reefs as cradles of evolution and sources of biodiversity in the Phanerozoic. Science 327:196–198
25. Jackson JBC, Kirby MX, Berger WH, Bjorndal KA, Botsford LW, Bourque BJ, Bradbury RH, Cooke R, Erlandson J, Estes JA, Hughes TP, Kidwell S, Lange CB, Lenihan HS, Pandolfi JM, Peterson CH, Steneck RS, Tegner MJ, Warner RR (2001)

Historical overfishing and the recent collapse of coastal ecosystems. Science 293:629–638
26. Peñaflor EL, Skirving WJ, Strong AE, Heron SF, David LT (2009) Sea-surface temperature and thermal stress in the Coral Triangle over the past two decades. Coral Reefs 28:841–850
27. Roberts CM, McClean CJ, Veron JEN, Hawkins JP, Allen GR, McAllister DE, Mittermeier CG, Schueler FW, Spalding M, Wells F, Vynne C, Werner TB (2002) Marine biodiversity hotspots and conservation priorities for tropical reefs. Science 295:1280–1284
28. Safina C (1997) Song for the blue ocean. Henry Holt, New York
29. Carpenter KE, Springer VG (2005) The center of the center of marine shore fish biodiversity: the Philippine Islands. Environ Biol Fish 72:467–480
30. Munday PL, Jones GP, Pratchett MS, Williams AJ (2008) Climate change and the future for coral reef fishes. Fish Fish 9:261–285
31. Alcala AC, Russ GR (2002) Status of Philippine coral reef fisheries. Asian Fish Sci 15:177–192
32. Soto I, Andréfouët S, Hu C, Muller-Karger FE, Wall CC, Sheng J, Hatcher BG (2009) Physical connectivity in the Mesoamerican Barrier Reef System inferred from 9 years of ocean color observations. Coral Reefs 28:415–425
33. Roberts CM (1997) Connectivity and management of Caribbean coral reefs. Science 278:1454–1457
34. Grahame J, Branch GM (1985) Reproductive patterns of marine invertebrates. Oceanogr Mar Biol Ann Rev 23:373–398
35. Nyström M, Folke C, Moberg F (2000) Coral reef disturbance and resilience in a human-dominated environment. Trends Ecol Evol 15:413–418
36. Wilkinson C (2008) Status of coral reefs of the world: 2008. Global Coral Reef Monitoring Network and Reef and Rainforest Research Center, Townsville
37. Bruno JF, Selig ER (2007) Regional decline of coral cover in the Indo-Pacific: timing, extent and subregional comparisons. PLoS One 2007(8):e711
38. Carpenter KE, Abrar M, Aeby G, Aronson RB, Banks S, Bruckner A, Chiriboga A, Cortes J, Delbeek JC, DeVantier L, Edgar GJ, Edwards AJ, Fenner D, Guzman HM, Hoeksema BW, Hodgson G, Johan O, Licuanan WY, Livingstone SR, Lovell ER, Moore JA, Obura DO, Ochavillo D, Polidoro B, Precht WF, Quibilan MC, Reboton C, Richards ZT, Rogers AD, Sanciangco J, Sheppard A, Sheppard C, Smith J, Stuart S, Turak E, Veron JEN, Wallace C, Weil E, Wood E (2008) One-third of reef-building corals face elevated extinction risk from climate change and local impacts. Science 321:560–563
39. Graham NAJ, McClanahan TR, MacNeil MA, Wilson SK, Polunin NVC, Jennings S, Chabanet P, Clark S, Spalding MD, Letourneur Y, Bigot L, Galzin R, Öhman MC, Garpe KC, Edwards AJ, Sheppard CRC (2008) Climate warming, marine protected areas and the ocean-scale integrity of coral reef ecosystems. PLoS One 3:e3039
40. Hughes TP, Baird AH, Bellwood DR, Card M, Connolly SR, Folke C, Grosberg R, Hoegh-Guldberg O, Jackson JBC, Kleypas J, Lough JM, Marshall P, Nyström M, Palumbi SR, Pandolfi JM, Rosen B, Roughgarden J (2003) Climate change, human impacts, and the resilience of coral reefs. Science 301:929–933
41. Khatiwala S, Primeau F, Hall T (2009) Reconstruction of the history of anthropogenic CO_2 concentrations in the ocean. Nature 462:346–349
42. Sabine CL, Feely RA, Gruber N, Key RM, Lee K, Bullister JL, Wanninkhof R, Wong CS, Wallace DWR, Tilbrook B, Millero FJ, Peng T-H, Kozyr A, Ono T, Rios AF (2004) The oceanic sink for anthropogenic CO_2. Science 305:367–371
43. Sheppard C (2009) Large temperature plunges recorded by data loggers at different depths on an Indian Ocean atoll: comparison with satellite data and relevance to coral refuges. Coral Reefs 28:399–403
44. Lyman JM, Good SA, Gouretski VV, Ishii M, Johnson GC, Palmer MD, Smith DM, Willis JK (2010) Robust warming of the global upper ocean. Nature 465:334–337
45. Feely RA, Sabine CL, Hernandez-Ayon JM, Ianson D, Hales B (2008) Evidence for upwelling of corrosive "acidified" water onto the continental shelf. Science. doi:10.1126/science.1155676
46. Hoegh-Guldberg O, Mumby PJ, Hooten AJ, Steneck RS, Greenfield P, Gomez E, Harvell CD, Sale PF, Edwards AJ, Caldeira K, Knowlton N, Eakin CM, Iglesias-Prieto R, Muthiga N, Bradbury RH, Dubi A, Hatziolos ME (2007) Coral reefs under rapid climate change and ocean acidification. Science 318:1737–1742
47. Brennand HS, Soars N, Dworjanyn SA, Davis AR, Byrne M (2010) Impact of ocean warming and ocean acidification on larval development and calcification in the sea urchin *Tripneustes gratilla*. PLoS One 5:e11372
48. Edmunds PJ (2007) Evidence for a decadal-scale decline in the growth rates of juvenile scleractinian corals. Mar Ecol Progr Ser 341:1–13
49. Heyward AJ, Negri AP (2010) Plasticity of larval pre-competency in response to temperature: observations on multiple broadcast spawning coral species. Coral Reefs. doi:10.1007/s00338-009-0578-5
50. Harvell CD, Kim K, Burkholder JM, Colwell RR, Epstein PR, Grimes DJ, Hofmann EE, Lipp EK, Osterhaus ADME, Overstreet RM, Porter JW, Smith GW, Vasta GR (1999) Emerging marine diseases – climate links and anthropogenic factors. Science 285:1505–1510
51. Rosenberg E, Ben-Haim Y (2002) Microbial diseases of corals and global warming. Environ Microbiol 4:318–326
52. Mao-Jones J, Ritchie KB, Jones LE, Ellner SP (2010) How microbial community composition regulates coral disease development. PLoS Biol 8(3):e1000345
53. Fabricius KE, Okaji K, De'ath G (2010) Three lines of evidence to link outbreaks of the crown-of-thorns seastar *Acanthaster planci* to the release of larval food limitation. Coral Reefs. doi:10.1007/s00338-010-0628-z
54. Bellwood DR, Hughes TP, Folke C, Nyström M (2004) Confronting the coral reef crisis. Nature 429:827–833
55. Lirman D, Fong P (2007) Is proximity to land-based sources of coral stressors an appropriate measure of risk to coral reefs? An example from the Florida Reef Tract. Mar Pollut Bull 54:779–791

56. De'ath G, Fabricius K (2010) Water quality as a regional driver of coral biodiversity and macroalgae on the Great Barrier Reef. Ecol Appl 20:840–850
57. Szmant AM (2002) Nutrient enrichment on coral reefs: is it a major cause of coral reef decline? Estuaries 25:743–766
58. Salvat B (ed) (1987) Human impacts on coral reefs: facts and recommendations. Antenne Museum E.P.H.E, French Polynesia
59. McCormick MI (2009) Behaviourally mediated phenotypic selection in a disturbed coral reef environment. PLoS One 4:e7096
60. Bahartan K, Zibdah M, Ahmed Y, Israel A, Brickner I, Abelson A (2010) Macroalgae in the coral reefs of Eilat (Gulf of Aqaba, Red Sea) as a possible indicator of reef degradation. Mar Pollut Bull. doi:10.1016/j.marpolbul.2009.11.017
61. Nyström M, Graham NAJ, Lokrantz J, Norström AV (2008) Capturing the cornerstones of coral reef resilience: linking theory to practice. Coral Reefs 27:795–809
62. Mumby PJ, Steneck RS (2008) Coral reef management and conservation in light of rapidly evolving ecological paradigms. Trends Ecol Evol 23:555–563
63. Idjadi JA, Haring RN, Precht WF (2010) Recovery of the sea urchin *Diadema antillarum* promotes scleractinian coral growth and survivorship on shallow Jamaican reefs. Mar Ecol Prog Ser 403:91–100
64. Bruno JF, Sweatman H, Precht WF, Selig ER, Schutte VGW (2009) Assessing evidence of phase shifts from coral to macroalgal dominance on coral reefs. Ecology 90:1478–1484
65. Burkepile DE, Hay ME (2009) Nutrient versus herbivore control of macroalgal community development and coral growth on a Caribbean reef. Mar Ecol Prog Ser 389:71–84
66. Smith JE, Hunter CL, Smith CM (2010) The effects of top-down versus bottom-up control on benthic coral reef community structure. Oecologia. doi:10.1007/s00442-009-1546-z
67. Sale PF (2008) Management of coral reefs: where we have gone wrong and what we can do about it. Mar Pollut Bull 56:805–809
68. Russ GR (2006) Yet another review of marine reserves as reef fishery management tools. In: Sale PF (ed) Coral reef fishes; dynamics and diversity in a complex ecosystem. Elsevier, Amsterdam, pp 421–443
69. Worm B, Barbier EB, Beaumont N, Duffy JE, Folke C, Halpern BS, Jackson JBC, Lotze HK, Micheli F, Palumbi SR, Sala E, Selkoe KA, Stachowicz JJ, Watson R (2006) Impacts of biodiversity loss on ocean ecosystem services. Science 314:787–790
70. Sale PF, Cowen RK, Danilowicz BS, Jones GP, Kritzer JP, Lindeman KC, Planes S, Polunin NVC, Russ GR, Sadovy YJ, Steneck RS (2005) Critical science gaps impede use of no-take fishery reserves. Trends Ecol Evol 20:74–80
71. Abesamis RA, Russ GR (2005) Density-dependent spillover from a marine reserve: long-term evidence. Ecol Appl 15:1798–1812
72. Mumby PJ, Harborne AR (2010) Marine reserves enhance the recovery of corals on Caribbean reefs. PLoS One 5:e8657
73. Stockwell B, Jadloc CRL, Abesamis RA, Alcala AC, Russ GR (2009) Trophic and benthic responses to no-take marine reserve protection in the Philippines. Mar Ecol Prog Ser 389:1–15
74. Worm B, Hilborn R, Baum JK, Branch TA, Collie JS, Costello C, Fogarty MJ, Fulton EA, Hutchings JA, Jennings S, Jensen OP, Lotze HK, Mace PM, McClanahan TR, Minto C, Palumbi SR, Parma AM, Ricard D, Rosenberg AA, Watson R, Zeller D (2009) Rebuilding global fisheries. Science 325:578–585
75. Edwards AJ, Gomez ED (2007) Reef restoration concepts and guidelines. Global Environment Facility (GEF) Coral Reef Targeted Research and Capacity Building for Management Programme, St. Lucia
76. Yap HT (2000) The case for restoration of tropical coastal ecosystems. Ocean Coast Manag 43:841–851
77. Maragos JE (1974) Coral transplantation: a method to create, preserve and manage coral reefs. Seagrant advisory report, UNIHI-SEAGRANT-AR-74-03 CORMAR-14
78. Alcala AC, Gomez ED, Alcala LC (1982) Survival and growth of coral transplants in Central Philippines. Kalikasan Philipp J Biol 11:136–147
79. Yap HT (2009) Local changes in community diversity following coral transplantation. Mar Ecol Progr Ser 374:33–41
80. Shaish L, Levy G, Katzir G, Rinkevich B (2010) Coral reef restoration (Bolinao, Philippines) in the face of frequent natural catastrophes. Restor Ecol. doi:10.1111/j.1526-100X.2009.00647.x
81. Gomez ED, Mingoa-Licuanan SS (2006) Achievements and lessons learned in restocking giant clams in the Philippines. Fish Res 80:46–52
82. Cabaitan PC, Gomez ED, Aliño PM (2008) Effects of coral transplantation and giant clam restocking on the structure of fish communities on degraded patch reefs. J Exp Mar Biol Ecol 357:85–98

Books and Reviews

Bradbury RH, Seymour RM (2009) Coral reef science and the new commons. Coral Reefs. doi:10.1007/s00338-009-0540-6

Coupled Climate and Earth System Models

Peter R. Gent
Oceanography Section, National Center for Atmospheric Research, Boulder, CO, USA

Article Outline

Glossary
Definition of the Subject
Introduction
Earth System Models
Climate Model Simulations

Model Validation
Climate Forecasts
Future Directions
Bibliography

Glossary

Climate model A numerical model consisting of four components: atmosphere, ocean, land, and sea ice.

Earth system model A climate model with additional components, which must include a carbon cycle in the land, atmosphere, and ocean components.

Troposphere The lower part of the atmosphere where most of the weather occurs.

Stratosphere The region of the atmosphere above the troposphere, and is the location of the ozone layer.

Carbon cycle The processes by which carbon in all its forms interacts and moves around in the land, atmosphere, and ocean components of the climate system.

Positive feedback A set of processes whereby a small perturbation in the climate system amplifies and increases in size.

Negative feedback A set of processes whereby a small perturbation in the climate system decays and reduces in size.

Control simulation A run of a climate model or earth system model where the forcing is kept constant in time.

Ensemble simulations A set of runs which have the identical forcing, but start from slightly different initial conditions.

Chaotic system A system of equations with the property that two runs starting from slightly different initial conditions diverge from each other, often quite quickly.

Climate projection A simulation of the climate system into the future with prescribed forcing, where the model has not been initialized to the observed climate.

Climate forecast A simulation of the climate system into the future with prescribed forcing, where the model has been initialized to the observed climate.

Equilibrium climate sensitivity The increase in the globally averaged surface temperature in a model when the atmosphere concentration of carbon dioxide is doubled.

Atmosphere Model Intercomparison Project A standard simulation of the atmosphere component of a climate or earth system model, which allows different models to be compared to each other.

El Nino-Southern Oscillation The largest interannual signal in the climate system, which occurs primarily in the tropical region of the Pacific Ocean.

Thermohaline circulation The overturning circulation in the global oceans where water sinks at very high latitudes, spreads very slowly horizontally to all the ocean basins, and then slowly returns toward the surface.

Conveyor belt Another popular name for the thermohaline circulation.

Deep water formation The process by which very dense water near the surface sinks to near the ocean bottom at high latitudes, which forms the sinking part of the thermohaline circulation.

Definition of the Subject

We are all familiar with weather forecasts that predict the local weather for the next few days. These are made using a high-resolution numerical model of the atmosphere, and sometimes extend out as far as 10 days. Most meteorological centers also produce seasonal outlooks, which give probabilities of the average temperature and precipitation being above, near, or below normal. These outlooks do not forecast the weather for a particular day, but give predictions of the seasonal averages. Seasonal outlooks are also made with an atmosphere model, but use climatological observed values for the evolving state of the surface ocean, land, and sea ice conditions. However, if forecasts are to be made more than a season ahead, then using just an atmosphere model is not sufficient, and the evolution of the ocean, land, and sea ice states must also be made using numerical models for these components of the climate system. The reason is that the surface ocean, land, and sea ice states interact strongly with the atmosphere and influence its future evolution because they change on a much slower timescale than the atmosphere.

A climate model is used to understand how the climate system works, and how the various components interact with each other. It is used to simulate

the present day climate, the recent past climate, and the climates of different paleoclimatic epochs. It can also be used to simulate the future statistical state of the atmosphere a decade or a century into the future, but does not predict the local weather on particular days. The atmosphere resolution of a climate model is much reduced compared to that used in a weather forecast, so that climate information is given on regional to global scales, and not on local scales. The climate state a long time ahead depends on the future levels of quantities that force the climate system, such as the concentrations of carbon dioxide and other greenhouse gases, several different atmospheric aerosols, and the levels of solar and volcanic activity. Therefore, these climate projections depend on many future choices to be made by mankind, which will determine the concentrations of greenhouse gases and aerosols over the next century. Each climate projection needs a scenario for the future concentrations of greenhouse gases and aerosols before it can be carried out.

Thus, a physical climate model consists of four components; atmosphere, ocean, land, and sea ice. These components are used to calculate the future state of the component given an initial state and the various quantities that force the component. These four basic components have to interact with each other, so that most climate models have a fifth component, often called the coupler, see Fig. 1, which has two main functions. The first function is to start, oversee the time evolution, and finish each model simulation. The second is to receive all the information from each component that is required by the other components and to send back to each component all the information that it requires to continue its simulation forward in time. For example, the ocean component needs the atmosphere-ocean wind stress that drives the ocean currents, the net heat flux and net fresh water flux (precipitation plus river runoff and sea ice melt minus evaporation) going from the atmosphere, ice, and land into the ocean. These are most often calculated in the coupler, and depend on the atmosphere surface wind, temperature, and humidity, etc., and the ocean sea surface temperature and currents, which are fields that are sent to the coupler.

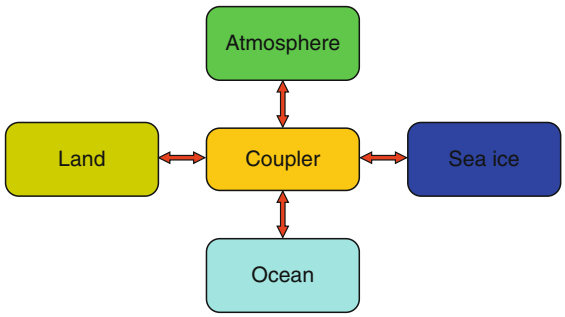

Coupled Climate and Earth System Models. Figure 1 Configuration of a climate model

There is another reason why the set up using a coupler shown in Fig. 1 is extremely useful. Only a relatively small fraction of climate model runs are in fully coupled mode, and there is a large number of different ways to run the model components. In runs described in more detail later, one or more of the components is replaced by its data equivalent, which provides the observed data required by the coupler to force the active components. For example, in an Atmosphere Model Intercomparison Project (AMIP) run, the numerical ocean and sea ice components are turned off and replaced by simple data components that provide observed time series of surface ocean and sea ice temperatures to the coupler. The coupler framework shown in Fig. 1 then ensures that the fluxes exchanged between various components are always calculated consistently, whether using observations or predicted model fields.

There is no universally accepted definition of an Earth System Model (ESM), but it must have more components than the four in a climate model. The usual additional components are a model for the distribution of carbon on the land surface, and an ocean ecosystem component, which are required if the ESM is to simulate the earth's carbon cycle. However, an ESM will often have additional components as well. The commonest of these is an atmospheric chemistry component, but some ESMs have an atmosphere component that simulates the upper levels of the atmosphere, including the stratosphere, not just the troposphere, which is the lowest layer of the atmosphere where most of the weather takes place. Finally, several ESMs will soon include a component that simulates the Greenland and Antarctic ice sheets, in order to estimate the future rate of ice loss that will raise the level of the earth's oceans.

Introduction

Numerical model simulation of the atmosphere has a long history that goes back over 60 years. The first integrations were done on the ENIAC machine at the Advanced Study Institute in Princeton by 1950 [1]. It took another 10 years for this to develop into weather forecasts that used models that had vertical structure and could be initialized using atmospheric observations. The first numerical ocean models were developed in the mid 1960s by Kirk Bryan at the Geophysical Fluid Dynamics Laboratory (GFDL) in Princeton [2], which used simplified sector geometry for the ocean basins. The first coupled atmosphere/ocean model was developed at GFDL when the global atmosphere model of Syukuro Manabe was coupled to Bryan's ocean model, and the results were published in 1969 [3]. However, the first real coupled climate model that had realistic geometry for the ocean basins and very elementary components for the land and sea ice was developed over the first half of the 1970s. The first results were published in two landmark papers by Manabe, Bryan, and coworkers in 1975 [4, 5]. The horizontal grid-spacing of this model was $5^\circ \times 5^\circ$, and there were nine vertical levels in the atmosphere component, and five levels in the ocean component. Even this coarse resolution was sufficient that the climate model ran slowly on GFDL's supercomputer of the early 1970s. Other meteorological and weather centers in several countries followed the GFDL lead and produced similar climate models of their own over the 1980s. As supercomputers became faster and larger, so the four components became more sophisticated, and the resolution of climate models improved.

However, there was a serious problem with all climate models when trying to obtain a control run for the present day climate. All the components would be initialized using the best set of observations available. It is most important to initialize the ocean component because it has by far the largest heat capacity, and its evolution is governed by much longer time scales than the other components. The problem was that, as the control run continued in time, the ocean and sea ice solutions would drift away from the realistic initial conditions. The drift was fast enough that rather quickly the model climate became significantly different than that of the present day earth.

The cause of this problem was diagnosed as follows. When the atmosphere and ocean components were run in standalone mode with the other component replaced by a data component that provides observations, the fluxes of heat and fresh water at the air–sea interface can be calculated. These fluxes from the atmosphere and ocean were very different, so that they were incompatible when coupled together. The problem was overcome by a very unphysical fix called flux correction [6]. The diagnosed heat and fresh water fluxes from atmosphere and ocean stand alone runs were differenced, and this difference was added to the fluxes exchanged between the atmosphere and ocean every time step of the coupled run. This enabled a climate model to maintain a non-drifting solution in a present day control run. However, it disguised the fact that the climate model components needed further development work to improve the simulations and make their fluxes of heat and fresh water across the air–sea interface compatible with each other. Use of flux corrections in climate models remained the standard method of running until the late 1990s.

The first model that could maintain the present day climate in a control run without the use of flux corrections was the first version of the Community Climate System Model (CCSM) developed at the National Center for Atmospheric Research (NCAR). A 300 year present day control simulation that showed virtually zero drift was run during the second half of 1996 and documented in 1998 [7]. The reason for this success was further refinement of the atmosphere, and especially the ocean [8] components, so that the surface heat and fresh water fluxes produced by the two components were compatible. Quite quickly, the climate centers in Australia and the UK implemented two of the new ocean parameterization improvements from the CCSM and were also able to run their models without flux corrections [9, 10]. Now, a large majority of climate models run without flux corrections, although some of the coarser resolution models still use this technique. Coarse horizontal resolution now means a grid-spacing of about $3^\circ \times 3^\circ$, whereas many climate models currently use about $1^\circ \times 1^\circ$ grid-spacing, or slightly higher, for their standard runs.

The number of climate models maintained around the world has steadily increased over the last decade, so that results from 18 different models were submitted to

the 4th Assessment Report of the Intergovernmental Panel on Climate Change (IPCC), which was published in February 2007. This 4th Assessment Report [11] was the joint recipient of the 2007 Nobel Peace Prize.

Earth System Models

All ESMs contain components that enable the carbon cycle in the land, ocean, and atmosphere to be predicted, rather than being passive in simulations of the earth's climate, for the following reason. Only about half the carbon dioxide (CO_2) emitted into the atmosphere over the past 150 years has stayed in the atmosphere; the other half has been taken up by the land and oceans in about equal measure. Climate models need past and future concentrations of CO_2 and other greenhouse gases in order to simulate the past and future climates. For future climate projections, it is currently assumed that the land and oceans sinks will continue to be as effective as in the past in taking up CO_2, so that future atmosphere concentrations will be based on about half of the future emissions staying in the atmosphere. However, there are real concerns that in the future, the ocean especially will not be able to take up the same fraction of CO_2 emissions because it is becoming warmer and more saturated with CO_2 [12]. Whether the land will continue to take up the same fraction of CO_2 is also not obvious and strongly depends on future land use practices. Over the last 30 years, deforestation of tropical forests has rapidly increased, which results in less CO_2 taken up by the land and more emitted into the atmosphere if the wood is burnt. This is now the cause of a substantial fraction of the recent increase in atmospheric CO_2 concentration. In contrast, there has been reforestation at some locations in the northern hemisphere mid-latitudes, such as the eastern part of the USA. Rather than assuming how much of the emitted CO_2 stays in the atmosphere, this fraction is predicted by an ESM with a carbon cycle. Thus, if the model predicts that the ocean will take up less CO_2 in the future, then a larger fraction will stay in the atmosphere to act as a greenhouse gas. This is a positive feedback in the climate system that is in ESMs, but not in climate models. Interactive carbon cycles have been put into a number of climate models around the world, and there has been an intercomparison project that compares their results [13]. The strength of the positive feedback from the carbon cycle is quite different in these various models, so the strength of this positive feedback is presently quite uncertain and needs to be constrained better.

There is some evidence that the stratospheric circulation can affect phenomena such as the Arctic and Antarctic Oscillations [14, 15] and will be important in how quickly the observed "ozone hole" in the southern hemisphere stratosphere will recover over the first half of the twenty-first century. If these processes are to be included in an ESM, then the atmosphere component needs to include all of the stratosphere, which is located above the troposphere. The region usually modeled by the atmosphere component of a climate model is the troposphere and just the lower part of the stratosphere. How important these processes are to the future trajectory of climate change has not been fully evaluated at present. In addition, an atmospheric chemistry component may be important to model the future levels of atmospheric aerosols. These are important in reflecting incoming solar radiation and in the formation of clouds, which are extremely important in the radiation budget of the atmosphere. A chemistry component is also needed if an ESM is to evaluate future levels of natural and man-made pollution in the very large cities of the future.

Another component of the earth system that has recently taken on more importance is the role of the Greenland and Antarctic ice sheets. There is growing evidence that the Greenland ice sheet has lost mass more quickly in the first decade of the twenty-first century than previously [16, 17], and there are changes in how quickly it is moving [18]. There are also observations of accelerations in Antarctic glaciers, especially after small ice shelves have collapsed [19, 20]. This has two important effects. The first is that the fresh water input to the ocean from these ice sheets increases the mean sea level [21], although it is important to note that this increase is not uniform over the ocean. The second is that fresh water input from the Greenland ice sheet can possibly cause a future weakening of the so-called thermohaline circulation in the North Atlantic Ocean [22, 23]. This circulation carries a lot of heat northward and certainly affects the climate of Western Europe, and is discussed in more detail in the next section. These possible future effects are not included

in climate models at present. A new ice sheet component to evaluate these future climate change possibilities will be a vital component of ESMs over the next few years.

Climate Model Simulations

One or Two Active Components

As a climate model is being built and assembled, the first type of simulation that is performed and analyzed is runs using either one or two of the components in active mode, with the other components being replaced by simple data components that provide observed time series of the required fields. The best known of this type of run is when the atmosphere and land components are active, and the ocean and sea ice are replaced by observations of sea and sea ice surface temperature. When the observations are over the period 1960–2005, this is called an AMIP run, which is named after the Atmosphere Model Intercomparison Project, which first formalized this type of run. Results from AMIP runs made with the atmosphere and land components of many different climate models have been compared in this type of intercomparison for 20 years or more [24]. These comparisons have given, and continue to give, insight into the validity of the parameterizations used to simulate the many important processes in the atmosphere component of different climate models.

Scientists developing the land component of a climate model use these AMIP runs to validate their component. However, in order to isolate parameterizations in the land component, they frequently make simulations with just the land component active. In this type of run, the land is forced by a time series of observations from 1960 to 2005 of all the surface atmosphere variables that are required to force the land component.

This same time series of surface atmosphere variables, but over the oceans, is very frequently used to force the ocean component of climate models run in standalone mode. This type of run is done to validate the ocean component because the ocean observations available for comparison are mainly from the period 1960–2005. One of the difficulties in setting up this type of run is how to force the ocean under sea ice. The interaction between the ocean and sea ice is very important, especially when ice is being formed. Sea ice is formed with a salinity of about 5 parts per 1000 from sea water with a salinity of about 35 parts per 1000. Therefore, this process rejects brine into the surface water, and at cold temperatures, the ocean salinity is more important than temperature in determining its density. Thus, sea ice formation produces very dense surface water, and when this is denser than the water below, the water column overturns down to a depth of 2 km or more, resulting in what is called "deep water formation." This only occurs in winter in a very few locations in the world oceans. Off Antarctica, it occurs in the Weddell and Ross Seas, producing Antarctic Bottom Water, which is the densest water mass in the oceans. It also occurs in the North Atlantic Ocean in the Greenland–Iceland–Norwegian Seas north of Iceland and in the Labrador Sea between Canada and western Greenland. This forms North Atlantic Deep Water, which flows south at 2–3 km depth, and is the return flow of the North Atlantic thermohaline circulation. This overturning circulation is often called the "Conveyor Belt," following Broecker [25], and a schematic is shown in Fig. 2. The deep water formation regions in the North Atlantic and off Antarctica are the sinking branches of the Conveyor Belt. The dense water near the bottom of the ocean very slowly makes its way into the Indian and Pacific Oceans, and then slowly rises toward the surface in all the oceans. It has been estimated from ocean observations and models that deep water formed near Antarctica, which then goes into the Pacific Ocean, will take between 800 and 1,000 years before it returns to the ocean surface. It is also interesting to note that deep water formation does not occur in the North Pacific Ocean. The main reason is that the salinity there is much less than in the North Atlantic, and the surface water is never dense enough to overturn.

In order to overcome the difficulty of how to force the ocean under ice, the ocean and sea ice components are sometimes run together in active mode, forced by the time series of atmospheric surface observations. Often the scientists developing the sea ice component wish to isolate that component, and make stand alone sea ice runs forced by atmospheric observations, and allowing the sea ice to interact with a much simpler ocean component called a slab ocean. A slab ocean component only models the upper mixed layer near the ocean surface. This is needed because there are no

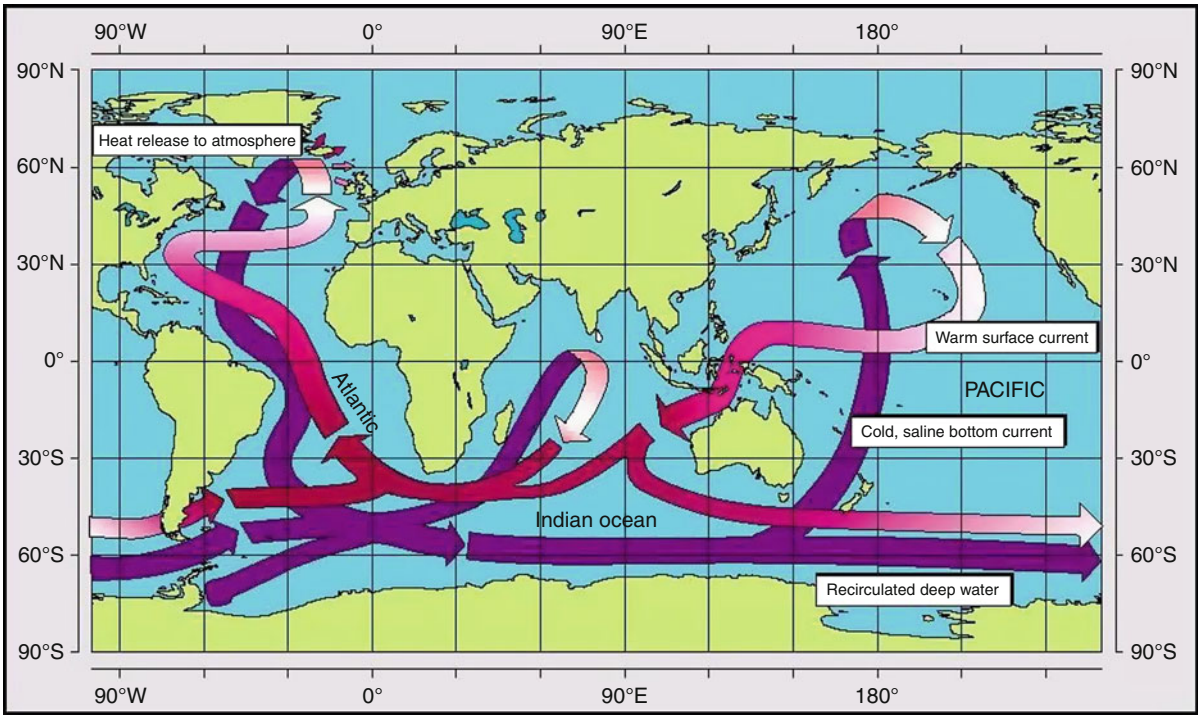

Coupled Climate and Earth System Models. Figure 2
Schematic of the thermohaline circulation, or the "Conveyor Belt," after Broecker [25]

observations of the surface ocean under ice, so that a slab ocean component is used which exchanges heat and salt with the sea ice above. As stated earlier, given this very large variety of ways required to run the climate model components, it becomes obvious why the setup using a coupler shown in Fig. 1 is extremely useful.

Fully Coupled Simulations

The first fully coupled simulation performed with a new version of a climate model is a present day control run. The model is given the year 2000 values of CO_2 and other greenhouse gases, the observed levels of natural and man-made aerosols, and the level of solar radiation. As discussed in the Introduction, the first requirement of the model is that the drift in this control run is small, so that the model does not drift very far from the present day initial conditions. Once that is established by a run of at least 100 years, then the simulation is continued for a longer period, sometimes for as long as 1,000 years, and carefully examined for its variability. There is variability on all time scales, such as the diurnal cycle, seasonal variability, the annual cycle, interannual variability, for example, the El Nino-Southern Oscillation (ENSO), and decadal variability. There is also plenty of data for comparison, see the next section. However, this control run assumes that the climate forcings are fixed, and the earth's present day climate is in a statistical equilibrium, which means that the climate is not in a truly steady equilibrium state, but has variability on all time scales around a steady state climate. This is clearly not the case in 2000, as the levels of CO_2 and other greenhouse gases have been increasing substantially over the twentieth century.

The last time the earth's climate was essentially in a statistically steady state was before mankind had started making large changes to the planet. This date can be argued over because man's changes to how land was used and trees felled changed the earth's climate somewhat. However, the date is usually taken to be before the atmospheric CO_2 level had increased significantly over the level at the Industrial Revolution. In simulations to be submitted to the 5th IPCC

Assessment Report, this date has been chosen to be 1850. Therefore, most climate models will run another control for 1850 conditions, forced by the CO_2, aerosol, and solar values of that year. A very desirable outcome of this control run is that the simulated climate system does not lose or gain heat and fresh water over the duration of the control run. In practice, it is extremely difficult to balance these budgets precisely to zero, especially for heat, and all climate models lose or gain some heat from the ocean during any control run. However, in modern climate models this drift is very small, and is not a substantial problem. The real problem is that we do not have observations of the climate system in 1850 to compare with the model results. For example, we do not know the extent or thickness of Arctic and Antarctic sea ice in 1850.

The real purpose of an 1850 control run is to provide initial conditions for runs that simulate the period from 1850 to 2005, which are often called twentieth century runs. Time series over this period of four quantities are needed to force this type of run. They are the atmospheric concentrations of CO_2 and other greenhouse gases, the levels of natural and man-made aerosols, the level of solar output, and the level of aerosols in the atmosphere from volcanic eruptions. The last quantity is determined from the observed levels of aerosols from recent eruptions, such as El Chichon in 1982 and Pinatubo in 1991, and then scaled by the size of significant eruptions earlier in the 1850–2005 period. Very often an ensemble of these twentieth century simulations is run, where the initial conditions are taken from different times in the 1850 control run. If a climate model is to be useful, then its twentieth century runs must reproduce well many of the observed changes in the earth's climate over the last 150 years. Most of the comparisons with observations will use the last 50 years of these runs, which is when virtually all of the observations were made.

Note that for ESMs, which have an active carbon cycle, the twentieth century runs will be forced by CO_2 emissions, rather than atmospheric concentrations. A severe test for twentieth century ESM simulations will be to reproduce the time history of atmospheric CO_2 concentration over the time period 1850–2005. The reason is that to accomplish this, the ocean and land components of the ESM will have to take up the correct fraction of CO_2 emitted into the atmosphere. This nicely illustrates the fact that as a climate model or ESM becomes more complicated with more components, then it is required to perform at a higher level. The reason is that very important quantities, such as the atmospheric CO_2 concentration, are now being predicted by the model, instead of being prescribed from observations.

The ensemble of twentieth century runs will then be continued to make projections of future climate changes over the rest of the twenty-first century. In order to make a future climate projection, time series of two quantities are required: the atmospheric CO_2 concentrations (for climate models) or emissions (for ESMs) and other greenhouse gases, and the levels of natural and man-made aerosols. In these projections, the solar output is kept constant at its 2005 level, and only a background level of volcanic aerosols is used to account for future small volcanic eruptions. In all climate models, the magnitude of future climate change depends crucially on the concentrations of CO_2 and other greenhouse gases in the future, and to a smaller extent on the future levels of man-made aerosols, which are expected to keep reducing, as they have done over the last 30 years. For the 4th IPCC Assessment Report, three scenarios for the future concentrations of CO_2 were used, which all had CO_2 levels strongly increasing until 2100. For the 5th Assessment Report, scenarios will be used where the CO_2 concentrations increase at a much slower rate during the second half of the twenty-first century because it has been assumed that emissions will be much reduced over that period.

The second crucial factor that determines the magnitude of a model's future climate change over the twenty-first century is its climate sensitivity. Equilibrium climate sensitivity (ECS) is defined as the increase in the globally averaged surface temperature that results from a doubling of CO_2 in the atmosphere component when it is coupled to a slab ocean model. This setup of a climate model only takes about 30 years to come into equilibrium, whereas the full depth ocean component takes about 3,000 years. However, it has recently been shown [26] that the ECS using a full depth ocean is not very different than that obtained using a slab ocean model. Transient climate sensitivity (TCS) is defined as the increase in globally averaged surface temperature that occurs when CO_2 has doubled

after 70 years of a transient simulation where CO_2 concentration increases at the rate of 1% per year. In general, a model with a small (large) ECS will also have a small (large) TCS, but the relationship is not one-to-one because models differ in the rate of heat uptake into the ocean and the timescales of other feedbacks. It is interesting to note that the ECS of every climate model ever developed has been positive, which is a very strong indication that the equilibrium climate is warmer when there is an increased concentration of atmospheric CO_2. Almost all models used in the IPCC 4th Assessment Report have an ECS in the range of 2°C–4.5°C. Despite dramatic improvements in climate models over the last 20 years, this range of ECS is the same as in the IPCC 1st Assessment Report [27]. It can be viewed as a disappointment that the range of ECS in climate models has not been reduced over this time period, but it reflects the fact that climate models still have to parameterize several important processes that affect climate sensitivity, the most important of which is clouds. The earth's climate sensitivity has also been estimated using observations [28], but this estimate has also not reduced the possible spread in its value. This brings up the subject of how climate models are validated.

Model Validation

The atmosphere component is the easiest to validate because there is a whole host of observations to compare its results against. These include observations taken by instruments, including satellites, and the so-called atmospheric reanalyses, which use a numerical model to assimilate many different observations to provide a time history of the state of the global atmosphere. These observations and reanalyses are compared with the results from AMIP simulations, which are described in the previous section. AMIP runs use a time history of observed sea surface temperature (SST), which is a relatively accurately observed quantity, especially since the start of the satellite era. There are a large number of variables that can be compared, which include temperature, winds, pressure, cloud amount, precipitation, shortwave solar radiation, and long-wave radiation emitted by the earth. These quantities can also be compared on many timescales from diurnal, seasonal, annual to interannual variability. In general, most of these comparisons are quite good, with cloud amount and precipitation being two of the more difficult variables for the atmosphere component to simulate well. As an example, Fig. 3a shows the mean annual cycle of precipitation from an AMIP simulation using the CCSM4 atmosphere component compared to long-term observations made at the Southern Great Plains site in Oklahoma. The difference between the model and observations is plotted in Fig. 3b, and shows that the model has too little precipitation during the fall and winter, but has too much precipitation in the late summer. Overall, the comparison is reasonable because the annual mean values from the model and observations are quite close. Literally hundreds of such comparisons can be made, but what is a lot more difficult is how to synthesize and interpret the comparison results in order to produce better parameterizations for the clouds and precipitation in the atmosphere component.

It is a different story for the ocean component because there are far fewer observations to compare to ocean alone simulations. There is a compendium of temperature and salinity observations at prescribed depths [29] that can be used to compare to average conditions in the late twentieth century. In the best observed oceans, these observations can be split into the four seasons, so that the annual cycle in the upper ocean can be verified. It should be pointed out that satellites can only measure surface ocean quantities, so that their observations do not give information about the ocean vertical structure, unlike the atmosphere. However, there are direct observations in a few regions of the ocean, such as the upper, tropical Pacific Ocean, which can be used to make comparisons. Figure 4 shows the zonal current along the equator in the upper 400 m of the Pacific Ocean from an ocean alone simulation of the CCSM4 and observations [30]. It shows that the component does quite a good job in reproducing the westward surface current, and the very strong eastward equatorial undercurrent, which is one of the fastest ocean currents with a maximum speed of about 100 cm/s. The model simulation depends on the atmosphere winds used to force it, as well as some of the model parameterizations, and it is frequently difficult to decide whether a poor comparison with observations is the result of poor forcing fields or a problem with the model parameterizations.

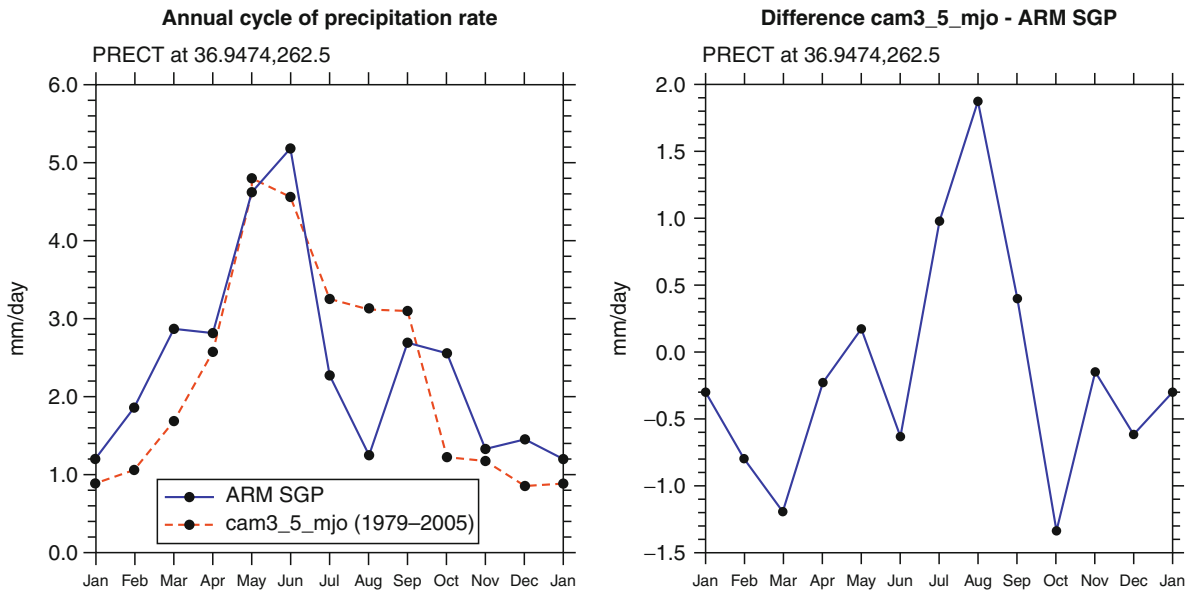

Coupled Climate and Earth System Models. Figure 3
Mean annual cycle of precipitation from an AMIP run of the CCSM4 atmosphere component and observations in the Southern Great Plains of the USA

The situation is worse for sea ice because there are even fewer observations. Sea ice extent and concentration were not well known until they began to be observed from satellites in 1979. Sea ice thickness is still not well observed, although the general spatial patterns are known from accumulating point measurements over the years. However, there are many processes that affect sea ice, such as ridging, the formation of polynas, and melt ponds, and how snow aging affects the albedo that have to be parameterized, although there are few observations of them. There are also not too many measurements to compare with the variables in the land component, although more than for sea ice. The measurements of quantities such as soil temperature and moisture, albedo, and the leaf area amount have to be taken in areas with natural vegetation, as well as in man-made areas such as croplands. Again, there has been a large increase in observations over the past 20 years or so during the satellite era, and from land based observations at several specific sites.

As mentioned in the previous section, there are difficulties comparing both present day and 1850 control simulations with observations because the present climate is not in equilibrium, and there are not many observations from 1850. The only quantity from that time that can be estimated directly from observations is the globally averaged surface temperature. Also, the global SST pattern from 1850 to the present has been estimated in the HadISST dataset [31] by determining the principle variation patterns from the period when SST has been well measured and using these patterns to produce global data in the early part of the period when there were only a few measurements. However, the best simulations to compare with observations are the ensemble of twentieth century runs from 1850 to 2005.

There are a very large number of variables that can be compared to observations from the second half of the twentieth century, but some of the most important are large-scale patterns of interannual variability, such as ENSO and the North Atlantic Oscillation [32]. ENSO is the largest interannual signal in the earth's climate and much about it has been learned from observations over the last 25 years. The variable that is most often used to characterize ENSO is called the nino3 SST, which is the SST averaged over the area 90°W–150°W, 5°S–5°N in the central Pacific Ocean. Figure 5 shows the nino3 monthly SST anomalies, and a wavelet analysis, which is a method to plot the time variation of the amplitude of the anomalies as a function of the frequency content. The three smaller

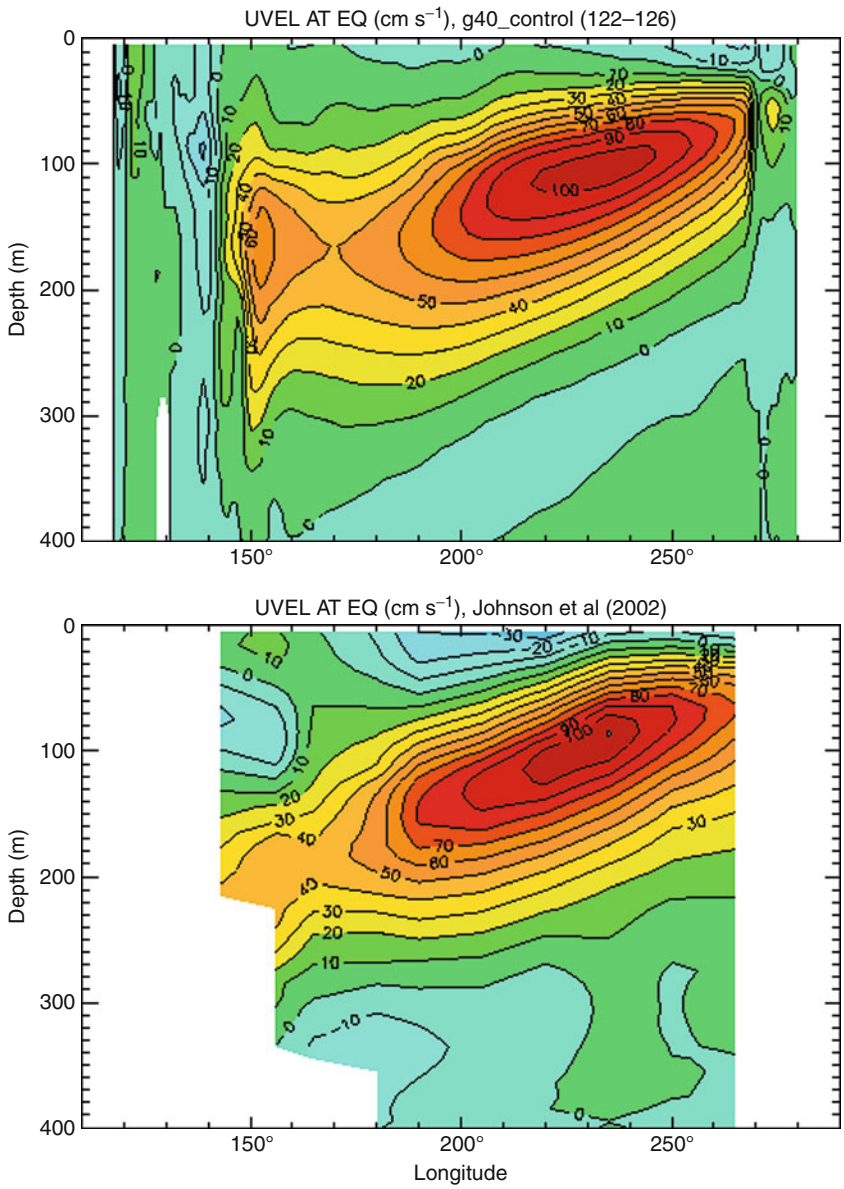

Coupled Climate and Earth System Models. Figure 4
Comparison of zonal velocity along the equator in the upper Pacific Ocean between the ocean component of the CCSM4 and the observations in [30]

boxes show the power spectrum (variance against period in years), the autocorrelation against lag time in months, and the annual cycle of the variance amplitude.

Figure 5 shows that the amplitude of nino3 SST anomalies in the CCSM4 is a little smaller than in the HadISST observations, especially the warm events which have a maximum amplitude of just over 3°C in the data, but are only 2.5°C in the model. This means that the wavelet and power spectrum are also a little weak in the CCSM4. However, the amplitude of nino3 SST anomalies from earlier periods of the twentieth century run is larger than the HadISST data, which shows there is strong decadal variability in the CCSM4 ENSO amplitude. The CCSM4 power spectrum peaks at a period of 3–4 years compared to

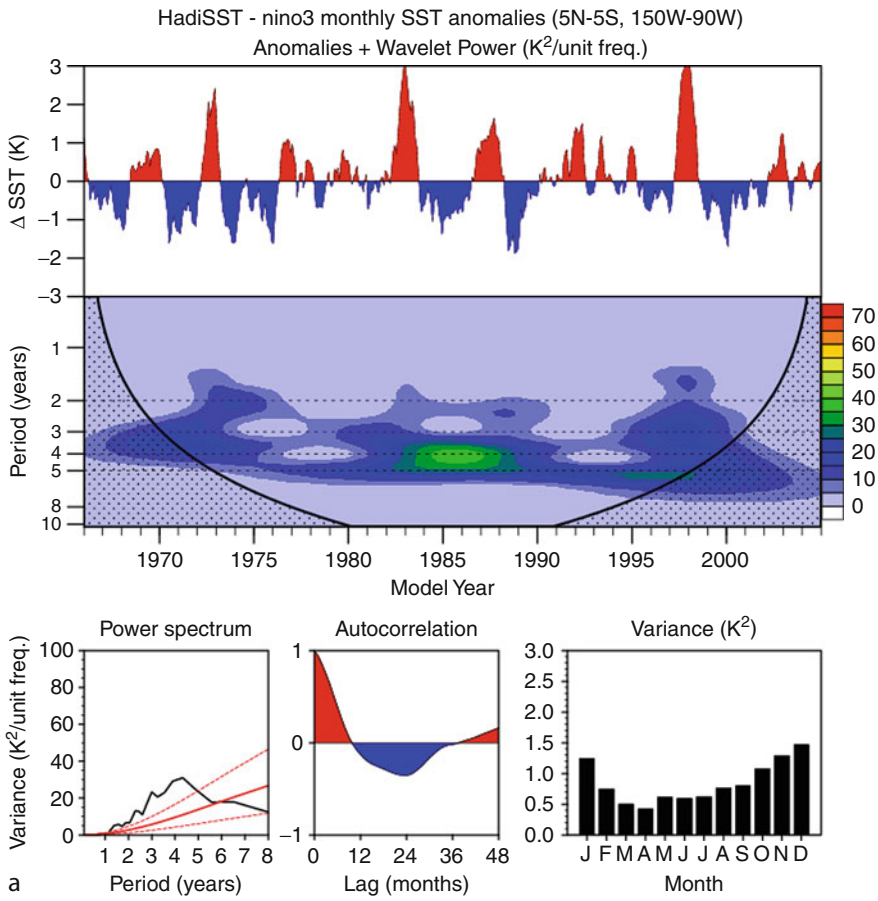

Coupled Climate and Earth System Models. Figure 5 (Continued)

4–5 years in the data, the autocorrelation compares quite well, and the annual cycle of variance is quite good with a minimum in May compared to April in the HadISST data. This good comparison is independent of the period of the run examined and is a very important improvement over all the previous versions of the CCSM, which had ENSO spectra that had a dominant peak at 2 years. This improvement was due to two changes made to the convection parameterization scheme in the atmosphere component [33]. The CCSM was one of many climate models that had a poor ENSO simulation for a long time [34], which was not a good situation given that ENSO is the largest interannual signal in the earth's climate.

Probably the only well-measured variable that can be compared to the model over the whole period of a twentieth century run is the globally averaged surface temperature. Figure 6 shows this comparison over 1890–2000 between the HadISST data and an ensemble of twentieth century runs using the CCSM version 3. The red line is the mean value from the ensemble, and the shading indicates the standard deviation across the eight member ensemble. This comparison is not perfect, but the data is not too often outside the shading. The model was then integrated forward to make an ensemble of projections for the twenty-first century [35] that were submitted to the IPCC 4th Assessment Report.

Another quantity that has been given a lot more attention in recent years is the sea ice extent in the Arctic Ocean. In order to give realistic projections of the future state of Arctic sea ice, a climate model must

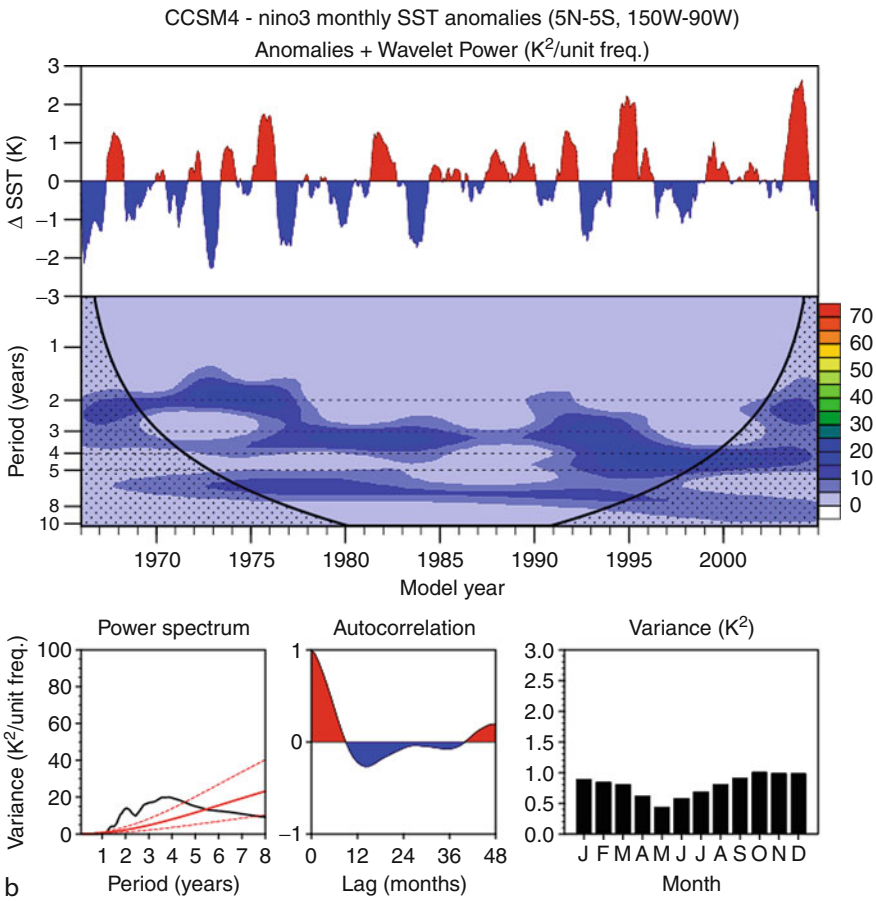

Coupled Climate and Earth System Models. Figure 5
Nino3 monthly SST anomalies between 1966 and 2005, wavelet power, power spectrum, autocorrelation, and variance from (**a**) HadISST observations, and (**b**) a twentieth century simulation using the CCSM4

simulate it well at the end of the twentieth century. Arctic sea ice has a minimum extent in September, and this has been well measured by satellite since 1979. Figure 7 shows the observed September Arctic sea ice extent from observations and the latest two versions of the CCSM. For the CCSM3, the twentieth century run forced by observed concentrations of CO_2 ends in 2000, and the model then used a scenario for the future levels of CO_2. The projected decline in the CCSM3 ice extent between 2000 and 2009 is not quite as large as has been observed. However, the actual rise in CO_2 concentration in the earth's atmosphere in the decade since 2000 has been somewhat larger than in the forcing scenario used in the CCSM3 projection shown in Fig. 7. It is important to remember that results from future projections strongly depend on the forcing scenario used. This same projection suggests that the Arctic Ocean will become virtually ice free in September by 2040 [36], but again the actual year when this might occur will depend on the concentrations of CO_2 and other greenhouse gases over the next 30 years. The result from the CCSM4 shown in Fig. 7 is just from a twentieth century run, which goes to the beginning of 2005. Again the comparison is good, and the CCSM4 will be used to make future projections for the IPCC 5th Assessment Report.

Other comparisons to validate the ability of a climate model to simulate the historical evolution of the earth's climate can be made, but the observations are probably not as accurate as for surface temperature and sea ice

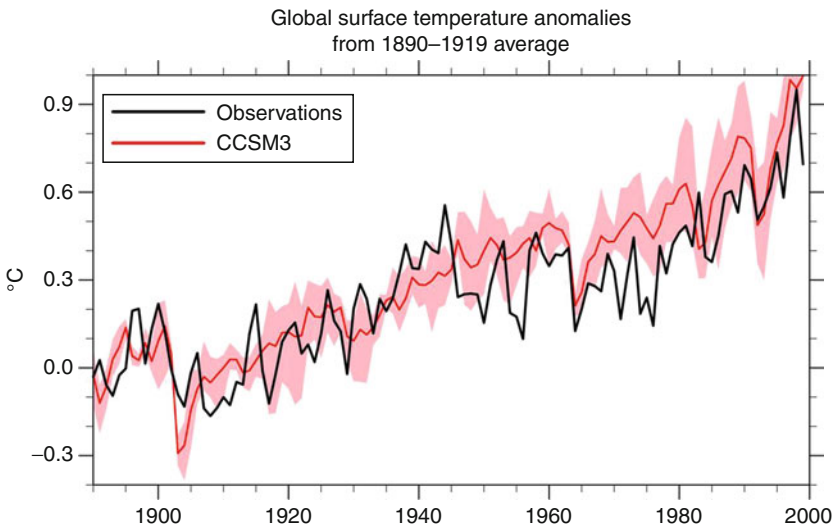

Coupled Climate and Earth System Models. Figure 6
Globally averaged surface temperature anomalies from HadISST data plotted against the results of an ensemble of twentieth century runs using the CCSM3

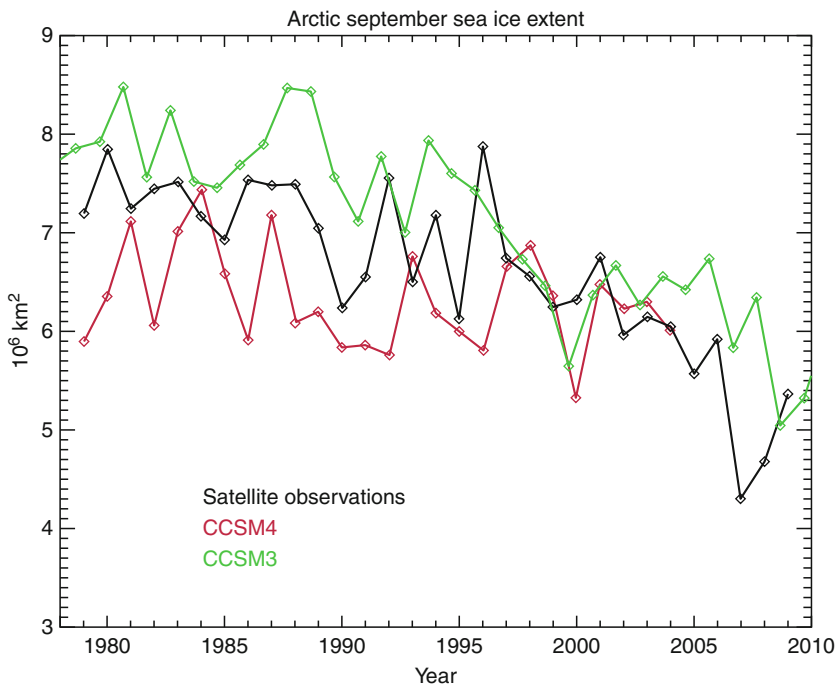

Coupled Climate and Earth System Models. Figure 7
Arctic September sea ice extent from observations, CCSM3, and CCSM4

extent. Two examples are ocean heat content and the distribution of chlorofluorocarbon-11 (CFC-11) in the ocean. The time history of CFC-11 concentration in the atmosphere is well known, so this can be used as an input to the ocean component during a twentieth century simulation. Observations of both ocean heat content and CFC-11 are sparse in both time and space, but estimates of their changes can be made and compared to model results [37]. This comparison helps to determine whether the ocean component is taking up quantities at the correct rate. It is very important in an ESM that the ocean takes up the correct fraction of the CO_2 that is emitted into the atmosphere. It is more difficult to make comparisons of changes in the land component because the largest changes in land use over the twentieth century are man-made and not changes in the natural vegetation. Changes in how land has been, and might be, used are often imposed in the land component during twentieth and twenty-first century simulations, which allows an assessment of how these changes have affected the past climate and might affect future climate changes [38]. On the global scale, these changes are much smaller than changes due to increases in CO_2 and other greenhouse gases, but they can be important in affecting the climate locally.

Climate Forecasts

First, the difference between a forecast and a projection needs to be explained. When a weather forecast is made, there are two separate factors that determine the quality of the forecast. The first is the quality of the atmosphere model used; all models are not perfect, but some are better than others. However, just as important is the quality of the analysis of the current state of the atmosphere that is used as the initial condition for the forecast. Even if the model were perfect, if the initial condition is slightly incorrect, then the model forecast and the real evolution of the atmosphere will diverge. The reason is that both the real atmosphere and the forecast model are examples of a chaotic system. What defines a chaotic system of equations is that, if they are integrated forward from two very slightly different initial conditions, then the two future solutions will diverge from each other, often quite quickly. Chaos theory was founded by a famous meteorologist, Edward Lorenz, who published a classic paper in 1963 [39]. He made drastic approximations to the equations that represent the atmosphere to produce a set of three, quite simple ordinary differential equations. When he integrated them forward in time from two slightly different initial states, the solutions diverged, which is the characteristic of what came to be called a chaotic system. In practice, it is very difficult to separate these two sources of error in a weather forecast because the model is also used to create the initial conditions on the model grid using all the latest meteorological observations from around the world. In order to reduce the likelihood of a bad weather forecast, an ensemble of forecasts is made using a set of slightly different initial conditions. If all the ensemble forecasts predict that something will occur, then it is forecast with a high probability; whereas if the ensemble forecasts differ markedly, then it is forecast with a low probability.

Virtually all long climate model simulations of the future done so far are projections, not forecasts. The reason is that most twenty-first century runs are just a continuation of a twentieth century run of the model, and no attempt is made to initialize the climate model to the observed climate in 2005, or whatever year the twenty-first century run starts. All results submitted to the IPCC 4th Assessment Report were from future climate projections. If something, such as a large ENSO event or a sudden reduction in the September extent of Arctic sea ice for example, occurs in 2015 in a projection, then this is not a forecast that it will actually happen in 2015, but a strong indication that this type of event might very well occur in the years around 2015. The case of ENSO events is interesting and instructive because ENSO forecasts up to a year in advance are now regularly made by a number of centers around the world using climate models [40].

For a weather forecast using an atmosphere model, it is important to start with the correct initial state of the atmosphere. However, for a seasonal or ENSO forecast, a full climate model must be used because the land, ocean, and sea ice evolve on these time scales. For these forecasts, therefore, initial conditions for the climate model are needed, and the most important component to initialize correctly is the ocean because it has the slowest time scales and by far the largest heat capacity. For an ENSO forecast, what is needed is the correct thermal state of the upper 300–400 m of the

tropical Pacific Ocean between about 15° north and south. ENSO forecasts could not become a reality until there was an observing system in the tropical Pacific to continuously measure and report upper ocean temperatures [41]. An analysis is performed on these observations to produce a temperature field on the model grid, and this is used as the ocean component initial condition. As the forward integration starts, the tropical atmospheric circulation comes into balance with the sea surface temperature field in about a week, which is why it is not necessary to initialize the atmosphere component. As always, an ensemble of ENSO forecasts is made by slightly changing the initial conditions used in the ocean component. For an ENSO forecast, it is important to initialize correctly the upper tropical Pacific Ocean, but for a climate forecast over a decade, there are many more aspects of the climate model that need to be initialized correctly: the ocean deeper than the upper 400 m, especially in the North Atlantic Ocean where the thermohaline circulation occurs, the sea ice distribution in both the Arctic and Antarctic, and some aspects of the land component, such as where the soil moisture content is above or below normal. We do not know precisely all the quantities that need to be initialized correctly, but we are absolutely certain that there are not adequate observations of all these quantities.

Forecasts of climate changes over the next decade on a regional basis are what would be most helpful in planning for the future. A few preliminary decadal forecasts have been made by centers in the UK and Germany [42, 43], and many centers will submit a suite of decadal forecasts to the IPCC 5th Assessment Report. However, the science of decadal climate forecasts is in its infancy [44], and there is a very large amount of research to be done before they will become reliable. Decadal forecasts are now where weather forecasts were 50 years ago, but they have another disadvantage. Weather forecasts are made and verified every day, so that there is a very large number of realizations that can be used to make improvements. By their very nature, decadal forecasts are only verified after 10 years, so that the number of opportunities to compare model predictions to observations is reduced enormously. However, the outlook for decadal forecasts has improved over the last few years. First, there is now an ocean observing system called ARGO floats (named after the mythical Greek ship used by Jason and the Argonauts to seek the Golden Fleece), that since about 2003 has been giving nearly global coverage of temperature and salinity down to a depth of 2 km, which has improved enormously our ability to correctly initialize the ocean component [45]. However, no decadal forecast initialized using ARGO data, which can start at the beginning of 2005 at the earliest, has yet had enough time to be verified. There are also satellite observations of Arctic and Antarctic sea ice extent and the soil moisture content over the continents, which could potentially be used in the initialization. Second, as the computing capacity continues to increase, then the resolution of climate models used for predictions will continue to improve, which will enable decadal forecasts to be more accurate on the regional scales that are required for future planning.

Future Directions

The computational power available to climate modelers will continue to increase in the future, so how should it be used? Should it be used to increase the resolution of present day climate models or used to increase the range of components in ESMs? This is an extremely difficult question to answer definitively. Increased resolution will undoubtedly improve some aspects of climate model simulations, but omitting an additional component may well leave out feedbacks that are potentially important. The answer will almost certainly be to push forward in both directions because scientists with different interests will lead the work in the two different directions. Another possibility is to increase the ensemble size used in future projections and predictions, which will give more reliability to simulated changes in extreme events [46], for example, which is a very important factor in planning for the future.

As mentioned above, clouds have to be parameterized in the atmosphere, and the way this is done can change the ECS of a climate model. Clouds also have to be parameterized in weather forecast models, but are often done so in a different way because the weather forecast model is run at a much higher resolution than the climate model. Over the last few years, there has been the suggestion, called Seamless Prediction, that the same atmosphere component should be used in both weather and climate prediction. In this situation,

the cloud parameterization used would have to work well across all the scales involved in both weather and climate predictions. This is not as easy as it sounds because both groups have developed their own parameterizations over past years, which make rather different assumptions. There have even been suggestions that both models should use extremely fine resolution on the order of 1 km, so that clouds can be resolved rather than parameterized, but running climate models at this resolution is still many years away. Seamless Prediction is a long-term goal, but it will probably not be realized over the next few years.

Another example of a phenomenon that is not resolved in present day climate models is mesoscale eddies in the ocean. These are the equivalent of atmospheric highs and lows, but occur at a range of scales from 200 to 300 km near the equator to 20–30 km in the very high latitude oceans. Only the equatorial eddies are partially resolved if the ocean component has a grid-spacing of about 1°. So, the effect of these energetic eddies on the large-scale mean flow has to be parameterized in present day climate models. However, it has been shown that a majority of these eddies can be resolved when using a grid-spacing of 1/10° in the ocean component [47, 48]. Diagnosis of these simulations has shown that the eddy parameterization used in the 1° simulations works quite well, but still the question remains: will future climate change projections in models that resolve the mesoscale eddies give very similar answers to future projections where they are parameterized? The answer to this important question should be found in the next few years because some climate change runs with resolved eddies are now possible with the available computer time.

Examples of new components that are currently being incorporated into ESMs have been discussed earlier, and include chemistry-air quality, hydrological, dynamic vegetation, and crop model components. The new component to simulate the Greenland and Antarctic ice caps is a very nice example of an important new component. However, there is a long list of possible feedbacks that have not been included in any ESM so far. Good examples are the increased release of methane, which is a very potent greenhouse gas, from Arctic tundra as the Arctic region warms [49], the possible release of methane from ocean clathrates [50, 51], and the possible fast breakup of the West Antarctic Ice Sheet [52]. All these are examples of possible abrupt climate changes that could result in large future changes that would have very far reaching consequences. However, all are very difficult to simulate accurately in an ESM and to assess quantitatively the possibilities that they will occur.

The science of decadal forecasts will also be advanced in the near future, both by new ideas and experience in how they should be initialized, and by increasing the resolution of the components used that will give more regional information. As explained in the previous section, there is a lot to learn and much experience needs to be gained before decadal forecasts become reliable. However, they will produce the most useful kind of information that is required by people planning for the future.

Finally, what motivates the scientists working to develop climate models and ESMs? First, it is a very stimulating intellectual challenge to understand what controls the earth's past, present and future climates, and to build an ESM that gives a faithful representation of this. This requires the expertise of many scientists across a large and diverse set of sciences ranging from several earth sciences to computer science. It is a real challenge to make these models run correctly and efficiently on several of today's massively parallel supercomputers. I also know from experience, that managing an ESM project is very challenging because it is such a diverse scientific enterprise. A second motivating factor is also very important to many scientists working on ESMs. It is that they believe these models are the best means we have available to anticipate possible future changes to the earth's climate, and that their results should be made freely and widely available to anyone who wants to see them.

Bibliography

Primary Literature

1. Charney JG, Fjortoft R, von Neumann J (1950) Numerical integration of the barotropic vorticity equation. Tellus 2:237–254
2. Bryan K, Cox MD (1967) A numerical investigation of the oceanic general circulation. Tellus 19:54–80
3. Manabe S, Bryan K (1969) Climate calculations with a combined ocean- atmosphere model. J Atmos Sci 26:786–789
4. Manabe S, Bryan K, Spelman MJ (1975) A global ocean-atmosphere climate model. Part I. The atmospheric circulation. J Phys Oceanogr 5:3–29

5. Bryan K, Manabe S, Pacanowski RC (1975) A global ocean-atmosphere climate model. Part II. The oceanic circulation. J Phys Oceanogr 5:30–46
6. Sausen R, Barthels RK, Hasselmann K (1988) Coupled ocean-atmosphere models with flux correction. Clim Dyn 2:154–163
7. Boville BA, Gent PR (1998) The NCAR climate system model, version one. J Clim 11:1115–1130
8. Gent PR, Bryan FO, Danabasoglu G, Doney SC, Holland WR, Large WG, McWilliams JC (1998) The NCAR climate system model global ocean component. J Clim 11:1287–1306
9. Hirst AC, McDougall TJ (1996) Deep-water properties and surface buoyancy flux as simulated by a z-coordinate model including eddy-induced advection. J Phys Oceanogr 26:1320–1343
10. Gordon C, Cooper C, Senior CA, Banks H, Gregory JM, Johns TC, Mitchell JF, Wood RA (2000) The simulation of SST, sea ice extents and ocean heat transports in a version of the Hadley Centre coupled model without flux adjustments. Clim Dyn 16:147–168
11. IPCC (2007) The physical science basis. In: Solomon S, Qin D, Manning M, Chen Z, Marquis M, Averyt K, Tignor M, Miller H (eds) Contribution of working group 1 to the 4th assessment report of the Intergovernmental Panel on Climate Change, Cambridge University Press, Cambridge
12. Fung IY, Doney SC, Lindsay K, John J (2005) Evolution of carbon sinks in a changing climate. Proc Natl Acad Sci 102:11201–11206
13. Friedlingstein P, Cox P, Betts R, Bopp L, von Bloh W, Brovkin V, Cadule P, Doney S, Eby M, Fung I, Bala G, John J, Jones C, Joos F, Kato T, Kawamiya M, Knorr W, Lindsay K, Matthews H, Raddatz T, Rayner P, Reick C, Roeckner E, Schnitzler K, Schnur R, Strassmann K, Weaver A, Yoshikawa C, Zeng N (2006) Climate-carbon cycle feedback analysis: Results from the C^4MIP model inter-comparison. J Clim 19:3337–3353
14. Thompson DW, Baldwin MP, Solomon S (2005) Stratosphere-troposphere coupling in the southern hemisphere. J Atmos Sci 62:708–715
15. Son SW, Polvani LM, Waugh DW, Akiyoshi H, Garcia RR, Kinnison D, Pawson S, Rozanov E, Shepherd TG, Shibata K (2008) The impact of stratospheric ozone recovery on the southern hemisphere westerly jet. Science 320:1486–1489
16. Steffen K, Nghiem SV, Huff R, Neumann G (2004) The melt anomaly of 2002 on the Greenland Ice Sheet from active and passive microwave satellite observations. Geophys Res Lett 31:L20402. doi:10.1029/2004GL02044
17. Hanna E, Huybrechts P, Steffen K, Cappelen J, Huff R, Shuman C, Irvine-Fynn T, Wise S, Griffiths M (2008) Increased runoff from melt from the Greenland Ice Sheet: A response to global warming. J Clim 21:331–341
18. Rignot E, Kanagaratnam P (2006) Changes in the velocity structure of the Greenland Ice Sheet. Science 311:986–990
19. Joughin I, Rignot E, Rosanova CE, Lucchitta BK, Bohlander J (2003) Timing of recent accelerations of Pine Island Glacier, Antarctica. Geophys Res Lett 30:1706. doi:110.1029/2003GL017609
20. Scambos TA, Bohlander JA, Shuman CA, Skvarca P (2004) Glacier acceleration and thinning after ice shelf collapse in the Larsen B embayment, Antarctica. Geophys Res Lett 31:L18402. doi:10.1029/2004GL020670
21. Shepherd A, Wingham D (2007) Recent sea-level contributions of the Antarctic and Greenland Ice Sheets. Science 315:1529–1532
22. Gerdes R, Hurlin W, Griffies SM (2006) Sensitivity of a global ocean model to increased run-off from Greenland. Ocean Model 12:416–435
23. Hu A, Meehl GA, Han W, Yin J (2009) Transient response of the MOC and climate to potential melting of the Greenland ice sheet in the 21st century. Geophys Res Lett 36:L10707. doi:10.1029/2009GL037998
24. Gates WL, Rowntree PR, Zeng QC (1990) Validation of climate models. In: Houghton JT, Jenkins GJ, Ephraums JJ (eds) Climate change: the IPCC scientific assessment, Cambridge University Press, Cambridge, pp 93–130
25. Broecker WS (1991) The great ocean 'conveyor'. Oceanography 4:79–89
26. Danabasoglu G, Gent PR (2009) Equilibrium climate sensitivity: Is it accurate to use a slab ocean model? J Clim 22:2494–2499
27. Houghton JT, Jenkins GJ, Ephramus JJ (eds) (1990) Scientific assessment of climate change. Report of working group 1 to the 1st assessment report of the Intergovernmental Panel on Climate Change, Cambridge University Press, Cambridge
28. Gregory JM, Stouffer RJ, Raper SC, Stott PA, Rayner NA (2002) An observationally based estimate of the climate sensitivity. J Clim 15:3117–3121
29. Locarnini RA, Mishonov AV, Antonov JI, Boyer TP, Garcia HE (2006) In: Levitus S (ed) World ocean atlas 2005, volume 1: Temperature, NOAA Atlas NESDIS 61. U.S. Government Printing Office, Washington, DC
30. Johnson GC, Sloyan BM, Kessler WS, McTaggart KE (2002) Direct measurements of upper ocean currents and water properties across the tropical Pacific Ocean during the 1990's. Prog Ocean 52:31–61
31. Rayner NA, Parker DE, Horton EB, Folland CK, Alexander LV, Rowell DP, Kent EC, Kaplan A (2003) Global analyses of sea surface temperature, sea ice, and night marine air temperature since the late nineteenth century. J Geophys Res 108:D14, 4407. doi:10.1029/2002JD002670
32. Hurrell JW (1995) Decadal trends in the North Atlantic Oscillation: Regional temperature and precipitation. Science 269:676–679
33. Neale RB, Richter JH, Jochum M (2008) The impact of convection on ENSO: From a delayed oscillator to a series of events. J Clim 21:5904–5924
34. Guilyardi E, Wittenberg A, Fedorov A, Collins M, Wang C, Capotondi A, van Oldenborgh GJ, Stockdale T (2009) Understanding El Nino in ocean-atmosphere general circulation models: progress and challenges. Bull Am Met Soc 90:325–340
35. Meehl GA, Washington WM, Santer BD, Collins WD, Arblaster JM, Hu A, Lawrence DM, Teng H, Buja LE, Strand WG (2006) Climate change projections for the twenty-first century and climate change commitment in the CCSM3. J Clim 19:2597–2616

36. Holland MM, Bitz CM, Tremblay B (2006) Future abrupt reductions in the summer Arctic sea ice. Geophys Res Lett 33: L23503. doi:10.1029/2006GL028024
37. Gent PR, Bryan FO, Danabasoglu G, Lindsay K, Tsumune D, Hecht MW, Doney SC (2006) Ocean chlorofluorocarbon and heat uptake during the twentieth century in the CCSM3. J Clim 19:2366–2381
38. Feddema JJ, Oleson KW, Bonan GB, Mearns LO, Buja LE, Meehl GA, Washington WM (2005) The importance of land-cover change in simulating future climates. Science 310:1674–1678
39. Lorenz EN (1963) Deterministic nonperiodic flow. J Atmos Sci 20:130–141
40. See the web site: iri.columbia.edu/climate/ENSO/currentinfo/SST_table.html
41. McPhaden MJ, Busalacchi AJ, Cheney R, Donguy JR, Gage KS, Halpern D, Ji M, Julian P, Meyers G, Mitchum GT, Niiler PP, Picaut J, Reynolds RW, Smith N, Takeuchi K (1998) The Tropical Ocean-Global Atmosphere observing system: A decade of progress. J Geophys Res 103:14169–14240
42. Smith DM, Cusack S, Colman AW, Folland CK, Harris GR, Murphy JM (2007) Improved surface temperature prediction for the coming decade from a global climate model. Science 317:796–799
43. Keenlyside N, Latif M, Junclaus J, Kornblueh L, Roeckner E (2008) Advancing decadal climate scale prediction in the North Atlantic. Nature 453:84–88
44. Meehl GA, Goddard L, Murphy J, Stouffer RJ, Boer G, Danabasoglu G, Dixon K, Giorgetta MA, Greene A, Hawkins E, Hegerl G, Karoly D, Keenlyside N, Kimoto M, Navarra A, Pulwarty R, Smith D, Stammer D, Stockdale T (2009) Decadal prediction: Can it be skillful? Bull Am Meteorol Soc 90:1467–1485
45. Balmaseda M, Anderson D, Vidard A (2007) Impact of Argo on analyses of the global ocean. Geophys Res Lett 34:L16605. doi:10.1029/2007/GL030452
46. Meehl GA, Tebaldi C, Teng H, Peterson TC (2007) Current and future U.S. weather extremes and El Niño. Geophys Res Lett 34: L20704. doi:10.1029/2007GL031027
47. Maltrud ME, McClean JL (2005) An eddy resolving global $1/10^0$ ocean simulation. Ocean Model 8:31–54
48. Bryan FO, Hecht MW, Smith RD (2007) Resolution convergence and sensitivity studies with North Atlantic circulation models. Part 1: The western boundary current system. Ocean Model 16:141–159
49. Brook E, Archer D, Dlugokencky E, Frolking S, Lawrence D (2008) Potential for abrupt changes in atmospheric methane. In: Abrupt climate change. US Climate Change Science Program. US Geological Survey, Reston, pp 163–201
50. Dickens GR (2003) A methane trigger for rapid warming. Science 299:1017
51. Archer D (2007) Methane hydrate stability and anthropogenic climate change. J Geophys Res Biogeo 4:521–544
52. Bamber GL, Riva RE, Vermeersen BL, LeBrocq AM (2009) Reassessment of the potential sea-level rise from a collapse of the West Antarctic ice sheet. Science 324: 901–903

Books and Reviews

Griffies SM (2004) Fundamentals of ocean climate models. Princeton University Press, Princeton
Lorenz EN (1993) The essence of chaos. University of Washington Press, Seattle
Philander SG (1990) El Nino, La Nina, and the southern oscillation. Academic, San Diego
Randall DA (ed) (2000) General circulation model development: Past, present and future. Academic, San Diego
Sarachik ES, Cane MA (2010) The El-Nino-southern oscillation phenomenon. Cambridge University Press, Cambridge
Siedler G, Church J, Gould J (eds) (2001) Ocean circulation and climate: observing and modeling the global ocean. Academic, San Diego
Trenberth KE (ed) (1992) Climate system modeling. Cambridge University Press, Cambridge
Washington WM, Parkinson CL (2005) An introduction to three-dimensional climate modeling, 2nd edn. University Science Books, Sausalito
Wigley TM, Schimel DS (eds) (2000) The carbon cycle. Cambridge University Press, Cambridge

Crop Breeding for Sustainable Agriculture, Genomics Interventions in

Pawan L. Kulwal[1], Mahendar Thudi[2]
Rajeev K. Varshney[2,3,4]
[1]State Level Biotechnology Centre, Mahatma Phule Agricultural University, Rahuri, Maharashtra, India
[2]Centre of Excellence in Genomics (CEG), International Crops Research Institute for the Semi-Arid Tropics (ICRISAT), Patancheru, Hyderabad, AP, India
[3]Genomics Towards Gene Discovery Sub programme, Generation Challenge Programme (GCP), Generation Challenge Programme (GCP) c/o CIMMYT, Mexico, DF, Mexico
[4]School of Plant Biology, Faculty of Natural and Agricultural Sciences, The University of Western Australia, Crawley, WA, Australia

Article Outline

Glossary
Definition of the Subject
Introduction and Importance of Sustainable Agriculture

Contribution of Plant Genomics Technologies to Crop Breeding
Some Modern Breeding Approaches
Challenges in Adoption of Genomics Technologies
Future Directions
Acknowledgments
Bibliography

Glossary

Association mapping Association mapping is a high-resolution method for mapping quantitative trait loci (QTLs) or gene(s) for traits of interest based on linkage disequilibrium (LD) and holds great promise for the dissection of complex genetic traits.

Back cross (BC) Back cross is a cross of the F_1 with either of the parental genotype and the resultant progeny is called BC_1. The progeny of the cross between BC_1 and the recurrent parent is called as BC_2.

Gene pyramiding Gene pyramiding is a process of accumulating the favorable genes/alleles from different genotypes into an elite/commercial cultivar. Gene pyramiding is often performed through marker-assisted selection (MAS).

Genome-wide selection or genomic selection (GS) Genome-wide selection or genomic selection is a concept for accelerating genetic gain especially for complex traits in elite genotypes by utilizing genomic information and estimating their breeding values in breeding strategies. GS is becoming very popular over marker-assisted selection that was focused on few individual genes or few QTLs to improve genotypes, especially when recent advances in genomic technologies have drastically reduced the cost on marker genotyping.

Genomics-assisted breeding (GAB) Genomics-assisted breeding is a holistic approach, where genomics technologies including molecular markers, trasncriptomics, metabolomics, proteomics, bioinformatics, and phenomics are integrated with conventional breeding strategies for breeding crop plants resistant/tolerant to biotic and abiotic stresses or improved for quality and yield.

Haplotype Haplotype is a set of alleles of closely linked loci on a chromosome that tend to be inherited together.

Linkage disequilibrium (LD) Linkage disequilibrium is a nonrandom association of alleles at different loci, describing the condition with non-equal (increased or reduced) frequency of the haplotypes in a population at random combination of alleles at different loci. LD is not the same as linkage, although tight linkage may generate high levels of LD between alleles.

Marker-assisted selection (MAS) Marker-assisted selection is a process of indirect selection for improving the traits of interest by employing morphological, biochemical, or DNA-based markers. DNA-based markers/molecular markers, in the recent past, were proven to be the markers of choice for MAS.

Narrow genetic base Narrow genetic base does frequently exists in modern crop cultivars or breeding lines due to the continuous use of small number of elite genotypes in breeding programs. In fact, it is a serious obstacle to sustain and improve crop productivity due to rapid vulnerability of genetically uniform cultivars to emerging biotic and abiotic stresses.

Next-generation sequencing (NGS) technologies Next-generation sequencing (NGS) technologies include various novel sequencing technologies for example 454/FLX (Roche Inc.), ABI SOLiD (Applied Biosystems), Solexa (Illumina Inc.), etc., that have surpassed traditional Sanger sequencing in through-put and in cost-effectiveness for generating large-scale sequence data.

Polygenes Polygenes are a group of non-allelic genes, each having a small quantitative effect, that together produce a wide range of phenotypic variation.

Quantitative trait loci (QTLs) Quantitative trait loci are the loci or regions in the genome that contribute towards conferring tolerance to abiotic stresses (e.g., drought, salinity) or resistance to biotic stresses (e.g., fungal, bacterial, viral diseases) or improving agronomic traits (e.g., yield, quality) which are generally controlled by polygenes and greatly depend on gene $\times$ environmental ($G \times E$) interactions.

Sustainable agriculture Sustainable agriculture refers to efficient agricultural production while maintaining the environment, farm profitability, and prosperity of farming communities.

Sustainable development Sustainable development is defined as balancing the fulfillment of human needs with the protection of the environment so that these needs can be met not only at the present time, but also in the future.

Definition of the Subject

There has been significant improvement in production and productivity of important cereal crops globally as a consequence of the "Green Revolution" and other initiatives [1]. However, today the stage has reached that the available traditional methods of crop improvement are not sufficient to provide enough and staple food grains to the constantly growing world population [2]. This situation is projected to be worse by the year 2050, especially in context of climate change [3]. In other words, the conventional plant breeding practices may not be able to achieve the sustainability in today's agriculture.

It is under such circumstances that advances in plant genomics research are opening up a new era in plant breeding, where the linkage of genes to specific traits will lead to more efficient and predictable breeding programs in future. Several initiatives have been started towards use of genomics technologies in number of crop plants to ensure the sustainable production of healthy and safe crops and the results are encouraging. It is therefore expected that the genomics will be the integral part of the agricultural/plant breeding practices in future for improving crop productivity leading to achieve food security and sustainable production.

Introduction and Importance of Sustainable Agriculture

The goal of agricultural science is to increase crop productivity coupled with the quality of the products, and maintain the environment [1]. Food security is a growing concern worldwide, and more than 1 billion people are estimated to lack sufficient dietary energy availability [2]. The issue of "food security" has become so important that prominent scientific journals, including Science, have also published a special issue on this subject recently (February 12, 2010 issue). With the current rate of growth, the global population is likely to plateau at some 9 billion people by roughly the middle of this century [3]. With this ever-increasing human population and amidst the fear of shrinking resources in terms of cultivable area, irrigation resources, newly emerging insect pests, stagnated yields, etc., it has become difficult to maintain agricultural sustainability. In order to make today's agriculture sustainable, it is necessary that plant breeders adopt innovative technologies that can increase the efficiency of selection with more precision [4]. Under such circumstances, molecular approaches including modern genomics and genetic engineering technologies have emerged as powerful tools to assure rapid and precise selection for the trait(s) of interest. Maintaining effective and environmentally friendly agricultural practices is a necessary prerequisite for maintaining sustainability.

Plant genomics is a rapidly developing field, which is radically improving our understanding of plant biology by making available novel tools for the improvement of plant properties relevant to sustainable agricultural production. Recent advances in high-throughput genomics technologies, including that of next-generation sequencing and high-throughput genotyping, have helped immensely in understanding the functions and regulation of genes in crop plants [5]. The ever-increasing availability of genome sequences in crop plants have facilitated greatly the development of genomic resources that will allow us to address biological functions and a number of basic processes relevant to crop production leading to sustainable agriculture.

One of the myths linked to sustainable agriculture means going back to past techniques/farm practices, which were followed by our ancestors. In fact, sustainable agriculture can be achieved by combining some of the wisdom of past practices with careful use of current technology, including the vast array of information technologies now available. Sustainable agriculture is a key element of sustainable development and is essential to the future well-being of the human race and the planet. A compelling need exists for restorative and sustainable agriculture to help address the pressing trends of population, climate, energy, water, soil, and food. Sustainable agriculture needs to be economically viable, environmentally sound, and socially acceptable. In other words, it is a system of agricultural production that, over the long term, will: (1) satisfy human food, feed, and fiber needs; (2) enhance the environmental

quality and the natural resource base upon which the agricultural economy depends; (3) make the most efficient use of available technologies, nonrenewable resources, and on-farm resources, and integrate, where appropriate, natural biological cycles and controls; (4) sustain the economic viability of farm operations; and (5) enhance the quality of life for farmers and society as a whole.

There are various components of sustainable agriculture, which include technological interventions, and environmental and socio-economic factors. As the factors related to socio-economics and environments have been discussed in a number of reviews earlier, in this article, we focus on the interventions of plant genomics technologies in crop breeding.

Contribution of Plant Genomics Technologies to Crop Breeding

Plant genomics technologies have contributed immensely in today's agriculture which has led to better understanding of how plants function, and how they respond to the environment. This has also helped in achieving targeted objectives in breeding programs to improve the performance and productivity of crops. The DNA-based molecular markers have facilitated smarter and knowledge-based breeding, by enabling early-generation selection for key traits, thus reducing the need for extensive field selection. Besides this, the molecular tools can effectively be used for the characterization, conservation, and use of genetic resources.

Recent advances made in the area of molecular biology and bioinformatics offer substantial opportunities for enhancing the effectiveness of classical plant breeding programs. These tools can be integrated into breeding work in order to analyze efficiently high numbers of crosses at the early seedling stage. This approach is known as "genomics-assisted breeding" [6]. Through this approach, both the phenotype and the genotype of new varieties can be analyzed and the performance of new specific introgressed traits can be predicted. The goals of the integration of these technologies in classical breeding are to create genotype-to-phenotype trait knowledge for breeding objectives and to use this knowledge in product development and deployment for the resource poor farmer.

For successful utilization of genomics-assisted breeding approach in a crop, availability of basic molecular tools, such as molecular markers, genetic maps, etc., is a prerequisite. Among molecular markers, though a variety of molecular markers such as restriction fragment length polymorphism (RFLP), randomly amplified polymorphic DNA (RAPD), microsatellite or simple sequence repeat (SSR), amplified fragment length polymorphism (AFLP), and single nucleotide polymorphism (SNP) markers have been developed in a range of crops, SSR and SNP markers have emerged as the markers of choice [7, 8]. Because of advent of NGS technologies [5] and high-throughput genotyping platforms, SNP marker system and array-based genotyping platforms are becoming more popular [9, 10]. An overview on availability of genomic resources in some selected important crop species is shown in Table 1. It is evident that cereal crops, especially rice, maize, wheat, barley, etc., are on top in terms of availability of genomic resources (see [11]). Genome sequences have already become available for several crop species, including rice (http://rgp.dna.affrc.go.jp/IRGSP/), sorghum [12], and maize (http://gbrowse.maizegdb.org/cgi-bin/gbrowse/maize/). Recent investments coupled with advances in genomics technologies have contributed towards developing a good resource of genomics tools in legumes as well [13, 14].

Some Modern Breeding Approaches

The availability of genomic resources in almost all important crops combined with information on pedigrees as well as optimized methods of precise phenotyping make it possible to undertake genomics-assisted breeding approaches for crop improvement. In fact, some molecular breeding approaches like advanced backcross QTL (AB-QTL) analysis and marker-assisted selection (MAS) have been successfully employed in several crops, leading to improved cultivars, some other approaches such as marker-assisted recurrent selection (MARS) or genomics selection (GS) are being used in several crops [15, 16].

Marker-Assisted Selection (MAS)

There are three major steps involved in MAS: (1) identification of molecular marker(s) associated with trait(s) of interest to breeders, (2) validation of identified

Crop Breeding for Sustainable Agriculture, Genomics Interventions in. Table 1 Genomic resources among selected cereals and legumes

Crop plant	Molecular markers (SSRs and SNPs)	Molecular maps (Genetic/QTL map/ comparative/physical maps)	Transcript data and expression profiling	Genome sequence data
Rice	++++[a]	++++[b,c]	++++[d]	++++[e]
Maize	++++[f]	++++[b,g,h]	++++[d]	++++[i]
Wheat	+++[j]	+++[b,k,l]	+++[d]	++[m]
Sorghum	+++[n]	++++[b,o]	+++[d]	++++[p]
Barley	+++[q]	+++[r]	+++[d,s]	+++[t]
Soybean	++++[u,v]	+++[w,x,y]	+++[z]	++++[aa]
Groundnut	++[bb]	+[cc]	+[z]	
Cowpea	+++[bb]	++[cc]	+[z]	
Common bean	++[bb]	++[cc]	+[z]	
Chickpea	+++[bb]	++[cc]	+[z]	
Pigeonpea	+++[bb]			

+, Very few; ++, Few; +++, Moderate; ++++, Abundant

[a]http://www.gramene.org/markers/index.html
[b]http://www.gramene.org/cmap/
[c]http://www.gramene.org/db/qtl/qtl_display?query=&search_field=&species=Oryza+sativa&submit=Submit
[d]http://www.ncbi.nlm.nih.gov/dbEST/dbEST_summary.html; http://compbio.dfci.harvard.edu/tgi/plant.html
[e]http://www.gramene.org/Oryza_sativa/Info/Index
[f]http://www.maizegdb.org/probe.php
[g]http://www.maizegdb.org/map.php
[h]http://www.gramene.org/db/qtl/qtl_display?query=*&search_field=trait_name&species=Zea+mays+subsp.+mays&submit=Submit
[i]http://www.maizesequence.org/Zea_mays/Info/Index
[j]http://wheat.pw.usda.gov/cgi-bin/graingenes/browse.cgi?class=marker
[k]http://wheat.pw.usda.gov/GG2/maps.shtml#wheat
[l]http://wheat.pw.usda.gov/cgi-bin/graingenes/quickquery.cgi?query=qtls&arg1=*
[m]http://wheat.pw.usda.gov/cgi-bin/graingenes/search.cgi?class=sequence
[n]http://www.gramene.org/db/markers/marker_view?
marker_name=*&marker_type_id=&taxonomy=sorghum&action=marker_search&x=0&y=0
[o]http://www.gramene.org/db/cmap/map_set_info?species_acc=sorghum&map_type_acc=-1
[p]Paterson et al. [12]
[q]http://wheat.pw.usda.gov/GG2/Barley/
[r]http://wheat.pw.usda.gov/GG2/maps.shtml#barley
[s]http://wheat.pw.usda.gov/cgi-bin/graingenes/browse.cgi?class=sequence&query=barley1_*
[t]http://www.public.iastate.edu/~imagefpc/IBSC%20Webpage/IBSC%20Template-home.html
[u]http://soybeanbreederstoolbox.org/
[v]http://soybase.org/BARCSOYSSR/index.php
[w]http://lis.comparative-legumes.org/cgi-bin/cmap/viewer?changeMenu=1
[x]http://soybeanbreederstoolbox.org/search/search_results.php?category=QTLName&search_term=
[y]http://soybeanphysicalmap.org/
[z]http://lis.comparative-legumes.org/lis/lis_summary.html?page_type=transcript
[aa]http://www.phytozome.net/cgi-bin/gbrowse/soybean/?name=Gm09
[bb]See Varshney et al. [13]
[cc]See Varshney et al. [14] marker assisted recurrent selection (MARS) or genomic selection (GS) are being used in several crops [15, 16].

marker(s) in the genetic background of the targeted genotypes to be improved, and (3) marker-assisted backcrossing (MABC) to transfer the QTL/gene from the donor genotype into the targeted genotype. In context of marker-trait association, linkage mapping has been extensively used for identifying the markers associated with a trait of interest in a range of crops including cereals, legumes, horticultural crops, etc. These studies have been reviewed in detail in several reviews [14, 17] and books [18]. Although hundreds of studies have been undertaken, only a few studies were taken further to marker validation and MABC. This may be attributed to (1) identification of few markers associated with small-effect QTLs, (2) non-validation of markers in elite genotypes, and (3) slow adoption of markers by breeders in their breeding programs. Recent advances in association genetics, however, offer opportunities to overcome the first two constraints.

Association mapping (AM) is considered an alternative strategy to linkage mapping for identifying marker-trait associations and has been used extensively in human and animal systems. AM has a number of advantages over linkage mapping, including the potential for increased QTL resolution and an increased sampling of molecular variation (for reviews see [19, 20]). AM involves studying a natural population rather than the offspring of crosses, and associations in natural populations are typically on a much finer scale because they reflect historical recombination events. Several examples on marker-trait association using AM are available [21]; however, there is a need for optimization of more advanced analytical tools in the area of association genetics [22]. It is anticipated that because of reduction in costs on marker genotyping [10], AM will be extensively used for trait mapping in the future.

Once the markers associated with a trait of interest are identified through linkage mapping or AM, the next step is to use these markers in the breeding programs. In this context, the selection of one or a few genes (QTLs) through molecular markers using backcrossing is a very efficient technique [23, 24]. Important advantages of MAS are that it can be effectively utilized for traits with low heritability; for gene pyramiding, selection can be made at seedling stage; and, above all, there are no issues involving GE crops [25]. Although use of markers in breeding programs through MABC is a common practice in the private sector [26], MAS is in routine use in wheat and barley breeding programs in Australia [8, 27–29] and USA (www.maswheat.ucdavis.edu; http://barleycap.cfans.umn.edu/). Nevertheless, there are several success stories in many crops including wheat, rice, barley, maize, soybean, etc., where MAS has successfully been utilized to develop superior lines/varieties/hybrids for improving quality, resistance to diseases or tolerance to abiotic stresses. For example, Gupta et al. [17] has recently summarized success stories of molecular breeding in wheat.

A widely discussed success story of molecular breeding is the introgression of the FR13A *Sub1* locus conferring resistance against submergence in an Asian rice cultivar, Swarna [30, 31] that can confer tolerance up to 2 weeks of complete submergence. This has offered great relief to the large number of Asian farmers whose rice land is located in deltas and low-lying areas that are at risk from flooding during the monsoon season every year. Some selected examples of molecular breeding in rice and wheat (adopted from [17]) are summarized in Table 2.

Advanced Backcross QTL (AB-QTL) Analysis

Although MAS has been quite successful, it has always been a difficult task to tackle linkage drag, especially when a QTL or a gene is to be introgressed from wild/exotic species. Furthermore, in MAS, QTL/gene discovery and variety development are two separate processes. To deal with this problem and to harness the potential of the wild/unadapted germplasm in breeding programs, a new approach referred as advanced backcross QTL (AB-QTL) analysis was proposed by Tanksley and Nelson [32]. AB-QTL aims at simultaneous detection and transfer of useful QTLs from the wild/unadapted relatives to a popular cultivar for improvement of a trait. In this context, a superior cultivar/variety is crossed with a wild species leading to the production of a backcross population (BC_2, BC_3), and molecular markers are used to monitor the transfer of QTLs by conventional backcrossing. The advanced backcross approach has already been successfully utilized in different crops, including tomato [59], rice [60, 61], barley [62], and wheat [63]. It is anticipated that the use of AB-QTL will be accelerated in a range of crops for improving important traits such as disease resistance as well as yield traits.

Crop Breeding for Sustainable Agriculture, Genomics Interventions in. Table 2 Some examples of improved cultivars or varieties developed through marker-assisted introgression of important genes/QTLs in rice and wheat

Crop	Genes/QTL introgressed	Function	Variety developed/ released	Reference
Rice	*GBSS*	Unique cooking and processing quality traits including amylose content	Cadet and Jacinto	[33]
	Xa33t	Bacterial blight resistance	BC_3F_2	[34]
	Xa21	Bacterial blight resistance	Zhongyou 6 and Zhongyou 1176	[35]
	Sub1	Submergence tolerance	BC_3F_2	[30]
	Sub1	Submergence tolerance	Samba Mashuri-*Sub1*	[36]
			IR64-*Sub1*	
			TDK1-*Sub1*	
			CR1009-*Sub1*	
			BR11-*Sub1*	
	SUB1QTL	Submergence tolerance	*Sub1* introgression lines	[37]
	Piz-5+Xa21	Blast and bacterial blight resistance	BC_4F_2	[38]
	Xa4+xa5 and *Xa4+Xa7*	Bacterial blight resistance	Angke and Conde	[39]
	xa7 and *Xa21*	Bacterial blight resistance	Zhenshan97 × Minghui 63	[40]
	xa13 and *xa21*	Bacterial blight resistance, strong aroma	Pusa1460, IET18990	[41]
	xa13 and *Xa21*	Bacterial blight resistance	Improved Pusa RH1	[42]
	xa5, *xa13* and *Xa21*	Bacterial blight resistance	Improved PR106	[43]
	Xa5, xa13 and xa21	Bacterial blight resistance	BC_3F_2	[44]
	Xa5, *Xa13 and Xa21*	Bacterial blight resistance	IET19046	http://www.drricar.org/four_varieites.htm
	Xa4, xa8, xa13 and *Xa21*	Bacterial blight resistance	BC_1F_3	[45]
	Xa4, *Xa5*, *Xa13* and *Xa21*	Improved bacterial blight resistance	Pusa1526–04–25	http://www.iari.res.in/?q = node/233

Crop Breeding for Sustainable Agriculture, Genomics Interventions in. Table 2 (Continued)

Crop	Genes/QTL introgressed	Function	Variety developed/ released	Reference
	–	Bacterial blight resistance	Xieyou218	[46]
	QTL	Drought-tolerant aerobic rice	MAS946–1	www.hindu.com/2007/11/17/stories/2007111752560500.htm
	q*SALTOL* and q*SUB1*	Enhanced salt and submergence tolerance	F_6	http://open.irri.org/sabrao/images/stories/conference/site/papers/apb09final00098.pdf
	QTL	Improved performance under drought	Birsa VikasDhan111 (PY 84)	http://claria13.securesites.net/News/releases/2009/may/26018.htm
Wheat	*QPhs.ccsu-3A.1* and *Lr24 +Lr28*	Preharvest sprouting tolerance and leaf rust resistance	BC_3F_3	[47]
	Lr47	Resistance to leaf rust	BIOINTA2004	[48]
	*Gpc-B*1	High grain protein content	Lillian	[49]
	Qfhs.ndsu-3AS	Resistance to fusarium head blight	Bena	[50]
	Sm1	Resistance to the insect orange blossom wheat midge	Goodeve	[51]
	Stb4	Resistance to *Septoria*	Kern	Cited from [17]
	Wsm-1	Resistance to wheat streak mosaic virus (WSMV)	Mace	[52]
	Yr15	Seedling stripe rust	$BC_3F_{2:3}$	[53]
	Qss.msub-3BL	Resistance to wheat stem sawfly	McNeal, Reeder, Hank	http://www.wheatworld.org/pdf/dubcovsky.pdf
	Bdv2	Resistance to yellow dwarf virus	Above, Avalanche, Ankor	http://www.wheatworld.org/pdf/dubcovsky.pdf
	Yr17 and Lr37	Stripe rust and leaf rust resistance	Patwin	[54]
	CreX and *CreY*	Cyst nematode resistance	F_3 progenies	[55]
	Yr36 and *Gpc-B*1	Resistant to stripe rust and high grain protein content	Westmore	[56]
	Yr17 and *Yr36*	Resistance to stripe rust	Lassik	Cited from [17]
	Lr19 and *Sr*25	Resistant to stem rust race UG99	UC1113 (PI638741)	[57]
	Yr36 and Gpc-B1	Resistance to stripe rust, high grain protein content	Farnum (WA7975)	http://www.ars-grin.gov/cgi-bin/npgs/acc/display.pl?1671746
	Yr15 and *Gpc-B*1	Resistance to stripe rust and high grain protein content	Scarlet (WA7994)	http://css.wsu.edu/Proceedings/2005/2005_Proceedings.pdf
	Lr1, Lr9, Lr24, Lr47	Leaf rust resistance	BC_1F_2	[58]

Marker-Assisted Recurrent Selection (MARS)

In the majority of traits of interest, quantitative variation is controlled by many QTLs, each with minor effect. Moreover, minor QTLs show an inconsistent QTL effect in different environments and over different seasons. Even when the effect of these minor QTLs is consistent, their introgression into the desired genotype through MABC becomes extremely difficult as a larger number of progenies are required to select appropriate lines. In such cases, MARS has been proposed for pyramiding of superior alleles at different loci/QTLs in a single genotype [64, 65].

It was demonstrated in recent studies that the response of MARS is larger when prior knowledge of the QTLs exists and the response decreases as the knowledge of the number of minor QTL associated with the trait decreases [66]. In sweet corn, MARS was employed to fix six marker loci in two different F_2 populations which showed an increase in the frequency of marker allele from 0.50 to 0.80 [64]. Similarly, in a separate study, enrichment of rust resistance gene (*Lr34/Yr18*) with an increase in frequency from 0.25 to 0.60 was reported in wheat BC_1 through MARS [28]. MARS can be utilized effectively for selection of traits associated with multiple QTLs by increasing the frequency of favorable QTLs or marker alleles. Several companies are using MARS in their maize, soybean, etc., breeding programs [66, 67]. Recently, some institutes like International Crops Research Institute for the Semi-Arid Tropics (ICRISAT), the French Centre for International Agricultural Research (CIRAD), and the University of California-Riverside, USA, have also initiated MARS programs in chickpea (PM Gaur, personal communication 2010), sorghum (J-F Rami, personal communication 2010), cowpea (J Ehlers, personal communication 2010), etc., for pyramiding favorable drought-tolerant alleles.

Genome-Wide or Genomic Selection (GS)

Although MAS has been practiced for the improvement of quantitative traits, it has its own limitations. Therefore, in addition to MARS, Genomic Selection can be used to pyramid favorable alleles for minor effect QTLs at the whole genome level [68, 69]. Genomic selection predicts the breeding values of lines in a population by analyzing their phenotypes and high-density marker scores. A key to the success of GS is that, unlike MABC or MARS, it calculates the marker effects across the entire genome that explains the entire phenotypic variation. In simple terms, genome-wide selection refers to marker-based selection without significance testing and without identifying of a subset of markers associated with the trait [68]. The genome-wide marker data (marker loci or haplotypes) available or generated on the progeny lines, therefore, are used to calculate genomic estimated breeding values (GEBV) as the sum of the effects of all QTLs across the genome, thereby potentially exploiting all the genetic variance for a trait [68, 69]. The GEBVs are calculated for every individual of the progeny based on genotyping data using a model that was "trained" from the individuals of another training populations having both phenotyping and genotyping data. These GEBVs are then used to select the progeny lines for advancement in the breeding cycle. Thus GS provides a strategy for selection of an individual without phenotypic data by using a model to predict the individual's breeding value [69].

Recently, Wong and Bernardo [70] simulated the comparative responses of phenotypic selection (PS), MARS, and GS with small population sizes in oil palm, and assessed the efficiency of each method in terms of years and cost per unit gain (i.e., the time and cost saved by these different methods over each other for making selection). They used markers significantly associated with the trait to calculate the marker scores in MARS, whereas all markers (without significance tests) to calculate the marker scores in GS. Responses to PS and GS were consistently greater than the response to MARS. Furthermore, with population sizes of $N = 50$ or 70, responses to GS were 4–25% larger than the corresponding responses to PS, depending on the heritability and number of QTLs. In terms of economics, cost per unit gain was 26–57% lower with GS than with PS when markers cost US \$1.50 per data point, and 35–65% lower when markers cost \$0.15 per data point. Reduction in costs in sequencing and high-throughput marker genotyping may enhance uptake of GS for crop improvement in the future.

Challenges in Adoption of Genomics Technologies

Developing sustainable approaches to agriculture is one of the most difficult challenges facing growers and scientists today. Agricultural sustainability involves

successful management of resources for agriculture to satisfy changing human needs, while maintaining or enhancing the quality of the environment and conserving natural resources [71]. However, sustainable production is hampered by the decline in land and soil productivity as a result of inappropriate soil and water management and other agricultural practices, as well as misguided policies and frequent opposition to technological advances that have the potential to improve the quality of life of billions of people worldwide. This is in addition to the postulated challenges of climate change, the number of hazardous chemicals (pesticides and fungicides) that are constantly being released into the environment and are becoming increasingly toxic to human and animal life [71]. In recent years, the use of promising biotechnology tools like genetic engineering (GE) has offered potential solutions to the above problems. However, the adoption of any new technique, particularly related to genetic engineering, remains a policy matter and as mentioned above faces stiff opposition many a times. In a recent review, Farre et al. [25] addressed several of these issues and advocated to overcome on the major barriers to adoption, which are political rather than technical, for realization of the potential of GE crops in developing countries.

It is thus obvious that the challenges facing agriculture are massive, particularly with the controversies over GE crops world over. It is clear that current methods of food production, in both the developing as well as the developed countries, are neither sufficient nor sustainable [72]. Under these circumstances, genomics interventions have great role to contribute to sustainable agriculture. As mentioned in this article, genomics approaches are very powerful to predict the phenotype, with higher precision and efficiency, based on the genotype. A variety of approaches ranging from MAS to GS are available to become integral part of plant breeding. While in the past, plant breeders were hesitant to use genetic variation existing in wild relatives of crop species in commercial breeding programs due to the long time it takes to recover desired phenotypes because of linkage drag, approaches like AB-QTL, in addition to MAS, can be successfully utilized. Availability of NGS technologies, associated with low costs and high-throughput, offers the opportunity to sequence either entire or major proportion of the germplasm collection for a species present in the gene banks around the word to understand genome variation. In case, the genome variation can be associated with the phenotype, which is not trivial, it will be possible to develop the ideotype, based on haplotype, of the variety to be developed.

Future Directions

While success stories of genomics-assisted breeding are available in several crops, it must also be recognized that much of the genome information generated is not being routinely used by plant breeders, especially in public breeding programs [26]. This may be due to shortage of trained personnel, inadequate access to genotyping, inappropriate phenotyping infrastructure, unaffordable bioinformatics systems, and a lack of experience of integrating these new technologies with traditional breeding [4, 26]. However, recently, several international initiatives such as the Integrated Breeding Platform (formerly Molecular Breeding Platform, www.mbp.genertaioncp.org), a joint initiative of The Bill and Melinda Gates Foundation and The Generation Challenge Program, have been started so that plant breeders especially from developing countries can have access to many genotyping, phenotyping, as well as information technologies to integrate their breeding programs with modern genomics approaches.

We believe that integration of modern genomics in combination with other cutting edge technologies in breeding programs is invaluable for crop improvement (Fig. 1) and will lead to sustainable agriculture for food security, especially in developing countries.

A vital task facing the plant breeding community today is to enhance food security in an environmentally friendly and sustainable manner. Though genomics interventions will not solve all the problems associated with agricultural production leading to sustainability, they have the potential, especially when they are used in an integrated manner as described in Fig. 1, to improve the breeding efficiency to address specific problems. These include increasing crop productivity, diversification of crops, enhancing nutritional value of food (biofortification), and reducing environmental impacts of agricultural production. However, only through judicious, rational, and science- and need-based exploitation of genetic resources through genomic technologies coupled with conventional plant breeding and genetic engineering will lead to sustainable agriculture.

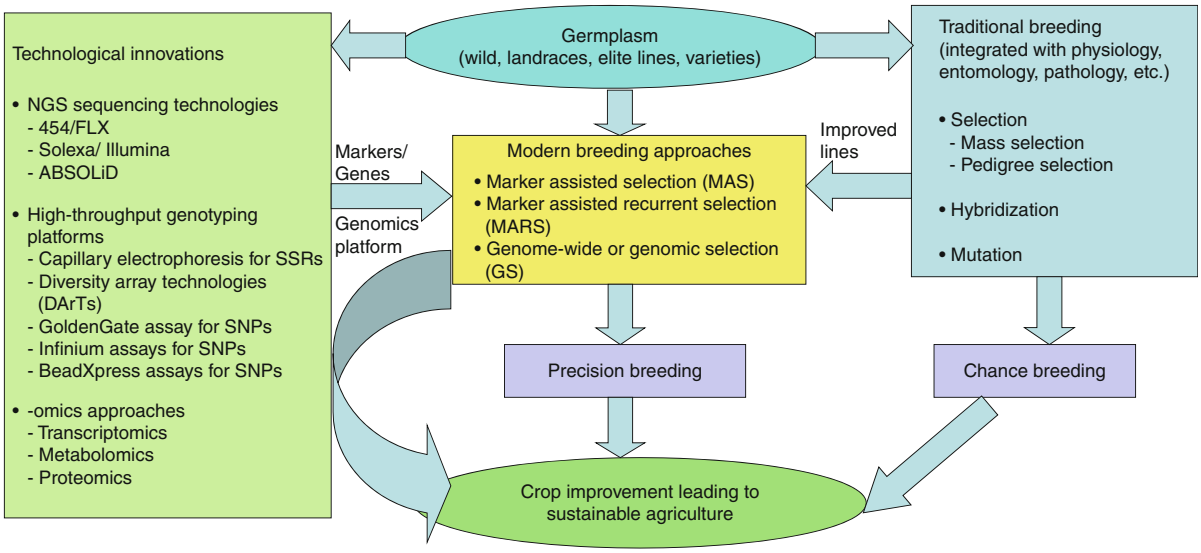

Crop Breeding for Sustainable Agriculture, Genomics Interventions in. Figure 1
Schematic representation of genomics technologies for crop improvement and sustainable agriculture
In general, traditional crop improvement programs (shown in the box on the right hand side in Fig. 1) employ different breeding strategies integrated with physiology, pathology, entomology, etc., and generate superior lines or improved crop varieties. These approaches, however, take more time, and sometimes such breeding is referred as "chance breeding" due to uncertainty in successes predicted in these approaches. On the other hand, genomics technologies (shown in the box on the left hand side) such as a number of next-generation sequencing (NGS) technologies, availability of high-throughput genotyping such as capillary electrophoresis for large-scale SSR genotyping, microarray-based DArTs, GoldenGate/Infinium/BeadXpress assays for large-scale SNP genotyping, and a range of -omics technologies provide candidate markers, gene(s), and QTLs to be integrated into the breeding programs by using high-throughput genomics platforms. Integrated breeding approaches (shown in the box in the middle) such as marker-assisted selection (MAS), marker-assisted recurrent selection (MARS), and genome-wide selection (GS) offer "precision breeding" with a great potential, versus "chance breeding" to contribute to sustainable crop improvement.

Acknowledgments

We thank the Generation Challenge Program (www.generationcp.org), the Indian Council of Agriculture Research (ICAR) and the Department of Biotechnology (DBT) of Government of India for funding various research projects (RKV) on genomics applications in breeding.

Bibliography

Primary literature

1. Briggs SP (1998) Plant genomics: more than food for thought. Proc Natl Acad Sci USA 95:1986–1988
2. Barrett CB (2010) Measuring food insecurity. Science 327: 825–828
3. Godfray HCJ, Beddington JR, Crute IR, Haddad L, Lawrence D, Muir JF, Pretty J, Robinson S, Thomas SM, Toulmin C (2010) Food security: the challenge of feeding 9 billion people. Science 327:812–818
4. Tester M, Langridge P (2010) Breeding technologies to increase crop production in a changing world. Science 327:818–822
5. Varshney RK, Nayak SN, May GD, Jackson SA (2009) Next generation sequencing technologies and their application for crop genetics and breeding. Trends Biotechnol 27:522–530
6. Varshney RK, Graner A, Sorrells ME (2005) Genomics-assisted breeding for crop improvement. Trends Plant Sci 10:621–630
7. Gupta PK, Varshney RK (2000) The development and use of microsatellite markers for genetics and plant breeding with emphasis on bread wheat. Euphytica 113:163–185
8. Varshney RK, Langridge P, Graner A (2007) Application of genomics to molecular breeding of wheat and barley. Adv Genet 58:121–155

9. Gupta PK, Rustgi S, Mir RR (2008) Array-based high-throughput DNA markers for crop improvement. Heredity 101:5–18
10. Varshney RK (2009) Gene-based marker systems in plants: high throughput approaches for discovery and genotyping. In: Jain SM, Brar DS (eds) Molecular techniques in crop improvement, vol II. Springer, The Netherlands, pp 119–140
11. Varshney RK, Hoisington DA, Tyagi AK (2006) Advances in cereal genomics and applications in crop breeding. Trends Biotechnol 24:490–499
12. Paterson AH, Bowers JE, Bruggmann R, Dubchak I, Grimwood J, Gundlach H, Haberer G, Hellsten U, Mitros T, Al P et al (2009) The *Sorghum bicolor* genome and the diversification of grasses. Nature 457:551–556
13. Varshney RK, Close TJ, Singh NK, Hoisington DA, Cook DR (2009) Orphan legume crops enter the genomics era! Curr Opin Plant Biol 12:202–210
14. Varshney RK, Thudi M, May GD, Jackson SA (2010) Legume genomics and breeding. Plant Breed Rev 33:257–304
15. Varshney RK, Dubey A (2009) Novel genomic tools and modern genetic and breeding approaches for crop improvement. J Plant Biochem Biotechnol 18:127–138
16. Phillips RL (2010) Mobilizing science to break yield barriers. Crop Sci 50:S99–S108
17. Gupta PK, Kumar J, Mir RR, Kumar A (2009) Marker-assisted selection as a component of conventional plant breeding. Plant Breed Rev 33:145–217
18. Kole C (2007) Genome mapping and molecular breeding in plants, a series of seven volumes: cereals and millets; oilseeds; pulses, sugar and tuber crops; fruits and nuts; vegetables; technical crops; and forest trees. Springer, Berlin/Heidelberg
19. Flint-Garcia SA, Thornsberry JM, Buckler ES IV (2003) Structure of linkage disequilibrium in plants. Ann Rev Plant Biol 54:357–374
20. Gupta PK, Rustgi S, Kulwal PL (2005) Linkage disequilibrium and association studies in higher plants: present status and future prospects. Plant Mol Biol 57:461–485
21. Buckler ES IV, Ersoz E, Yu J (2007) Applications of linkage disequilibrium and association mapping in crop plants. In: Varshney RK, Tuberosa R (eds) Genomics assisted crop improvement, vol I, Genomics approaches and platforms. Springer, Dordrecht, pp 97–119
22. Rafalski JA (2010) Association genetics in crop improvement. Curr Opin Plant Biol 13:174–180
23. Collard BCY, Mackill DJ (2008) Marker-assisted selection: an approach for precision plant breeding in the twenty-first century. Phil Trans R Soc B 363:557–572
24. Varshney RK, Hoisington DA, Nayak SN, Graner A (2009) Molecular plant breeding: methodology and achievements. In: Somers D, Langridge P, Gustafson PJ (eds) Methods in molecular biology: plant genomics. Humana, Totowa, pp 283–304
25. Farre G, Ramessar K, Twyman RM, Capell T, Christou P (2010) The humanitarian impact of plant biotechnology: recent breakthroughs *vs* bottlenecks for adoption. Curr Opin Plant Biol 13:219–225
26. Ribaut J-M, de Vicente MC, Delannay X (2010) Molecular breeding in developing countries. Curr Opin Plant Biol 13:213–218
27. Langridge P (2003) Molecular breeding of wheat and barley In: Tuberosa R, Phillips RL, Gale M (eds) Proceedings of the international congress "In the wake of the double helix: from the green revolution to the gene revolution," Bologna, Italy, 27–31 May 2003, pp 279–286
28. Kuchel H, Fox R, Reinheimer J, Mosionek L, Willey N, Bariana H, Jefferies S (2007) The successful application of a marker-assisted wheat breeding strategy. Mol Breed 20:295–308
29. Cakir M, McLean R, Wilson R, Barclay I, Moore C, Loughman R, Haley S, Kidwell K, Anderson J, Sorrells M, Manes Y, Hayden M, Feuille C, William M (2007) Genome level targeted breeding in wheat. In: Plant and Animal Genomes conference XV, San Diego, 13–17 Jan 2007 (http://www.intl-pag.org/15/abstracts/PAG15_W40_265.html)
30. Neeraja CN, Maghirang-Rodriguez R, Pamplona A, Heuer S, Collard BCY, Septiningsih EM, Vergara G, Sanchez D, Xu K, Ismail AM, Mackill DJ (2007) A marker-assisted backcross approach for developing submergence-tolerant rice cultivars. Theor Appl Genet 115:767–776
31. Xu K, Xu X, Fukao T, Canlas P, Maghirang-Rodriguez R, Heuer S, Ismail AM et al (2006) *Sub1A* is an ethylene-response-factor-like gene that confers submergence tolerance to rice. Nature 442:705–708
32. Tanksley SD, Nelson JC (1996) Advanced backcross QTL analysis: a method for simultaneous discovery and transfer of valuable QTL from unadapted germplasm into elite breeding lines. Theor Appl Genet 92:191–203
33. Hardin B (2000) Rice breeding gets marker assists. Agricultural Research Magazine 48:12, USDA-ARS, USA (www.ars.usda.gov/is/AR/archive/dec00/rice1200.pdf)
34. Natarajkumar P, Sujatha K, Laha GS, Viraktamath BC, Reddy CS, Mishra B, Balachandran SM, Ram T, Srinivasarao K, Hari Y, Sundaram RM (2010) Identification of a dominant bacterial blight resistance gene from *Oryza nivara* and its molecular mapping. Rice Genetics Newsletters 25:54–56
35. Cao L, Zhuang J, Zhan X, Zeng K, Cheng S, Cao LY, Zhuang JY, Zhan D, Zheng KL, Cheng SH (2003) Hybrid rice resistance to bacterial blight developed by marker assisted selection. Chin J Rice Sci 17:184–186
36. Septiningsih EM, Pamplona AM, Sanchez DL, Neeraja CN, Vergara GV, Heuer S, Ismail AM, Mackill DJ (2009) Development of submergence-tolerant rice cultivars: the *Sub1* locus and beyond. Ann Bot 103:151–160
37. Singh S, Mackill DJ, Ismail AM (2009) Responses of *SUB1* rice introgression lines to submergence in the field: Yield and grain quality. Field Crops Res 113:12–23
38. Narayanan NN, Baisakh N, Vera Cruz CM, Gnanamanickam SS, Datta K, Datta SK (2002) Molecular breeding for the development of blast and bacterial blight resistance in rice cv. IR50. Crop Sci 42:2072–2079
39. Toennissen GH, Toole JCO, DeVries J (2003) Advances in plant biotechnology and its adoption in developing countries. Curr Opin Plant Biol 6:191–198

40. He Y, Li X, Zhang J, Jiang G, LiuS, Chen S, TuJ, Xu C, Zhang Q (2004) Gene pyramiding to improve hybrid rice by molecular-marker techniques. In: New directions for a diverse planet: proceedings 4th international crop science congress, Brisbane, Australia (http://www.cropscience.org.au/icsc2004/)
41. Gopalakrishnan S, Sharma RK, Anand Rajkumar K, Joseph M, Singh VP, Singh AK, Bhat KV, Singh NK, Mohapatra T (2008) Integrating marker assisted background analysis with foreground selection for identification of superior bacterial blight resistant recombinants in Basmati rice. Plant Breed 127:131–139
42. Basavaraj SH, Singh VK, Singh A, Singh A, Singh A, Anand D, Yadav S, Ellur RK, Singh D, Gopalakrishnan S, Nagarajan M, Mohapatra T, Prabhu KV, Singh AK (2010) Marker-assisted improvement of bacterial blight resistance in parental lines of Pusa RH10, a superfine grain aromatic rice hybrid. Mol Breed 26:293–305
43. Singh S, Sidhu S, Huang N, Vikal Y, Li Z, Brar DS, Dhaliwal HS, Khush GS (2001) Pyramiding three bacterial blight resistance genes (*xa5, xa13 and Xa21*) using marker assisted selection into *indica* rice cultivar PR106. Theor Appl Genet 102:1011–1015
44. Sundaram RM, Vishnupriya MR, Laha GS, Rani NS, Rao PS, Balachandran SM, Reddy GA, Sarma NP, Sonti RV (2009) Introduction of bacterial blight resistance into Triguna a high yielding, mid-early duration rice variety. Biotechnol J 4:400–407
45. Joseph M, Gopalakrishnan S, Sharma RK, Singh VP, Singh AK, Singh NK, Mohapatra T (2004) Combining bacterial blight resistance and Basmati quality characteristics by phenotypic and molecular-marker assisted selection in rice. Mol Breed 13:377–387
46. Cheng S-H, Zhuang J-Y, Cao L-Y, Chen S-G, Peng Y-C, Fan Y-Y, Zhan XD, Zheng KL (2004) Molecular breeding for super rice. Chinese J Rice Sci 18:377–383
47. Kumar J, Mir RR, Kumar N, Kumar A, Mohan A, Prabhu KV, Balyan HS, Gupta PK (2009) Marker assisted selection for preharvest sprouting tolerance and leaf rust resistance in bread wheat. Plant Breed doi:10.1111/j.1439-0523.2009.01758.x
48. Bainotti C, Fraschina J, Salines JH, Nisi JE, Dubcovsky J, Lewis SM, Bullrich L, Vanzetti L, Cuniberti M, Campos P, Formica MB, Masiero B, Alberione E, Helguera M (2009) Registration of 'BIOINTA2004' wheat. J Plant Registr 3:165–169
49. DePauw RM, Townley-Smith TF, Humphreys G, Knox RE, Clarke FR, Clarke JM (2005) Lillian hard red spring wheat. Can J Plant Sci 85:397–401
50. Elias EM (2005) Fusarium resistant tetraploid wheat. United States Patent Application 20050273875
51. DePauw RM, Knox RE, Thomas JB, Smith M, Clarke JM, Clarke FR, McCaig TN, Fernandez MR (2009) Goodeve hard red spring wheat. Can J Plant Sci 89:937–944
52. Graybosch RA, Peterson CJ, Baenziger PS, Baltensperger DD, Nelson LA, Jin Y, Kolmer J, Seabourn B, French R, Hein G, Martin TJ, Beecher B, Schwarzacher T, Heslop-Harrison P (2009) Registration of 'Mace' hard red winter wheat. J Plant Registr 3:51–56
53. Randhawa HS, Mutti JS, Kidwell K, Morris CF, Chen X, Gill KS (2009) Rapid and targeted introgression of genes into popular wheat cultivars using marker-assisted background selection. PLoS ONE 4:e5752
54. Helguera M, Khan IA, Kolmer J, Lijavetzky D, Zhong-Qi L, Dubcovsky J (2003) PCR assays for the *Lr37-Yr17-Sr38* cluster of rust resistance genes and their use to develop isogenic hard red spring wheat lines. Crop Sci 43:1839–1847
55. Barloy D, Lemoine J, Abelard P, Tanguy AM, Rivoal R, Jahier J (2007) Marker-assisted pyramiding of two cereal cyst nematode resistance genes from *Aegilops variabilis* in wheat. Mol Breed 20:31–40
56. Brevis JC, Dubcovsky J (2008) Effect of the Gpc-B1 region from *Triticum turgidum* ssp. *dicoccoides* on grain yield, thousand grain weight and protein yield. In: Appels R, Eastwood R, Lagudah E, Langridge P, Mackay M, McIntyre L, Sharp P (eds) Proceedings of 11th international wheat genet symposium, Brisbane, Australia, 24–29 Aug 2008. Sydney University Press, pp 1–3 (http://hdl.handle.net/2123/3179)
57. Yu L-X, Abate Z, Anderson JA, Bansal UK, Bariana HS, Bhavani S, Dubcovsky J, Lagudah ES, Liu S, Sambasivam PK, Singh RP, Sorrells ME (2009) Developing and optimizing markers for stem rust resistance in wheat. The Borlaug Global Rust Initiative 2009 Technical Workshop, 17–20 March 2009, Ciudad Obregon, Mexico
58. Nocente F, Gazza L, Pasquini M (2007) Evaluation of leaf rust resistance genes *Lr1, Lr9, Lr24, Lr47* and their introgression into common wheat cultivars by marker-assisted selection. Euphytica 155:329–336
59. Tanksley SD, Grandillo S, Fulton TM, Zamir D, Eshed Y, Petiard V, Lopez J, Beck-Bunn T (1996) Advanced backcross QTL analysis in a cross between an elite processing line of tomato and its wild relative *L. pimpinellifolium*. Theor Appl Genet 92:213–224
60. Xiao J, Li J, Grandillo S, Ahn S, Yuan L, Tanksley SD, McCouch SR (1998) Identification of trait-improving quantitative trait loci alleles from a wild rice relative, *Oryza rufipogon*. Genetics 150:899–909
61. Moncada P, Martínez CP, Borrero J, Chatel M, Gauch H Jr, Guimaraes E, Tohme J, McCouch SR (2001) Quantitative trait loci for yield and yield components in an *Oryza sativa* × *O. rufipogon* BC_2F_2 population evaluated in an upland environment. Theor Appl Genet 102:41–52
62. Pillen K, Zacharias A, Léon J (2003) Advanced backcross QTL analysis in barley (*Hordeum vulgare* L.). Theor Appl Genet 107:340–352
63. Huang XQ, Cöster H, Ganal MW, Röder MS (2003) Advanced backcross QTL analysis for the identification of quantitative trait loci alleles from wild relatives of wheat (*Triticum aestivum* L.). Theor Appl Genet 106:1379–1389
64. Edwards M, Johnson L (1994) RFLPs for rapid recurrent selection. In: Analysis of molecular marker data. Joint plant breeding symposia series, ASA, Madison, pp 33–40
65. Bernardo R, Charcosset A (2006) Usefulness of gene information in marker-assisted recurrent selection: a simulation appraisal. Crop Sci 46:614–621
66. Ragot M, Gay G, Muller J-P, Durovray J (2000) Efficient selection for the adaptation to the environment through QTL

mapping and manipulation in maize. In: Ribaut J-M, Poland D (eds) Molecular approaches for the genetic improvement of cereals for stable production in water-limited environments. CIMMYT, México DF, pp 128–130
67. Ribaut J-M, Ragot M (2007) Marker-assisted selection to improve drought adaptation in maize: the backcross approach, perspectives, limitations, and alternative. J Exp Bot 58:351–360
68. Meuwissen THE, Hayes BJ, Goddard ME (2001) Prediction of total genetic value using dense marker maps. Genetics 157:1819–1829
69. Heffner EL, Sorrells ME, Jannink J-L (2009) Genomic selection for crop improvement. Crop Sci 49:1–12
70. Wong CK, Bernardo R (2008) Genome-wide selection in oil palm: increasing selection gain per unit time and cost with small populations. Theor Appl Genet 116:815–824
71. Gregory P (1989) Sustainability and CIP's research. CIP Circular 17,2: 8–11, CIP, Lima, Peru
72. Charlafti I (2003) Science and sustainability. EMBO Rep 4: 454–456

Books and Reviews

Bradford KJ, Van Deynze A, Gutterson N, Parrott W, Strauss SH (2005) Regulating transgenic crops sensibly: lessons from plant breeding, biotechnology and genomics. Nat Biotech 23:439–444

Gupta PK, Varshney RK (2004) Cereal genomics. Kluwer, The Netherlands

Hall D, Tegström C, Ingvarsson PK (2010) Using association mapping to dissect the genetic basis of complex traits in plants. Brief Funct Genom Pro 9:157–165

Innes NL (2008) A plant breeding contribution to sustainable agriculture. Ann Appl Biol 126:1–18

Moose SP, Mumm RH (2008) Molecular plant breeding as the foundation for 21st century crop improvement. Plant Physiol 147:969–977

Persley GJ, Peacock J, van Montagu M (2002) Biotechnology and sustainable agriculture. ICSU series on science for sustainable development No. 6, ICSU

Reganold JP, Papendick RI, Parr JF (1990) Sustainable agriculture. Sci Am 262:112–120

Ribaut J-M (2007) Drought adaptation in cereals. Food Products Press, Binghamton

Salmeron J, Herrera-Estrella LR (2006) Plant biotechnology: fast-forward genomics for improved crop production. Curr Opin Plant Biol 9:177–179

Serageldin I (1999) Biotechnology and food security in the 21st century. Science 285:387–389

Varshney RK, Tuberosa R (2007) Genomics-assisted crop improvement, vol I, Genomics approaches and platforms. Springer, The Netherlands

Varshney RK, Tuberosa R (2007) Genomics-assisted crop improvement, vol II, Genomics Applications in Crops. Springer, The Netherlands

Crop Development Related to Temperature and Photoperiod

Marc Moragues[1], Gregory S. McMaster[2]
[1]Department of Soil and Crop Sciences, Colorado State University, Fort Collins, CO, USA
[2]USDA-ARS, Agricultural Systems Research Unit, Fort Collins, CO, USA

Article Outline

Glossary
Definition of the Subject
Introduction
Canopy Structure: Phytomers, Phyllochron, and Plastochron
Regulation of Crop Development
Modeling Approaches
Future Directions
Bibliography

Glossary

Base temperature Lower temperature threshold below which development ceases.

Epigenetics Genetic information other than DNA sequence information.

Phenology Study of the sequence of developmental stages of a plant and how it relates to climate.

Photoperiod sensitivity Requirement for a minimum (or maximum) day length for reproductive phase induction.

Phytomer Fundamental building block of plant canopies. A vegetative phytomer is comprised of leaf, node, internode, and axillary bud.

Phyllochron Rate of appearance of leaves on a shoot.

Shoot apex The tip of the shoot where usually there is meristematic tissue producing new organs.

Thermal time Temperature response curve used to estimate development rate.

Vernalization sensitivity Requirement for a period of low temperatures for reproductive induction.

Definition of the Subject

Plant development, or the progression of plants through their life cycle, has been of great interest in human history because of the need to know and predict

when the harvested part of the plant was at the optimum stage. This knowledge was especially important (even vital) in medicinal plants, where the timing of harvesting defines the medicinal value of the product. This interest increased as groups moved from hunting and gathering to agrarian societies.

Crop development can be defined with the number and rate of appearance, growth, and senescence of phytomers. However, that definition lacks information about when the switch of vegetative to reproductive phytomers occurs, which is defined by the phenology of the crop. Crop development is of great importance in agriculture because it is the main mechanism for plants to escape both biotic and abiotic stresses, and adapt to the environment. At a more practical level, it affects the management of the crop because cultural practices are more effective at specific stages of crop development.

Introduction

Major food, feed, and industrial crops were domesticated in a few centers of origin, including the "Fertile Crescent," the Americas, and China. The wild relatives of modern crops were adapted to survival in the environment prevalent in the center of origin. Those original crops were locally grown in the region of origin, but some species showed a significant ability to adapt to new environments and were spread globally with human migrations and trade. For instance, wheat was domesticated in the Middle East (the "Fertile Crescent") [1, 2], around 32°N and is currently cultivated from between 30°N and 60°N and from 27°S to 40°S. However, it can grow beyond those limits, in lower latitudes, in high altitudes, or even in the arctic circle. This range of environments where wheat can grow makes wheat one of the most plastic crops currently grown. It requires a large range of developmental mechanisms to adapt to such different environments, where photoperiods vary from 13–14 h to nearly 20 h. One of the major accomplishments of the "Green Revolution" was the discovery of photoperiod insensitive mutants in wheat that could be grown at lower latitudes.

Plasticity in development is key for the adoption of crops in a wide range of environments. Although growth and development are related, they are different processes. Development is the initiation and differentiation of organs and the progression of stages through which cells, organs, and plants go during their life cycle, whereas growth is the change in size or weight of the initiated organs. Biotic (e.g., genetics, weeds, and diseases) and abiotic (e.g., temperature, light, water, and nutrients) factors influence the initiation, growth, and senescence of plant organs.

Since the "The Metamorphosis of Plants" by Johann Wolfgang von Goethe, originally published in 1790 [3], there has been extensive research on how plants proceed from germination to maturity in an orderly and predictable manner. This research has led to an extensive conceptual framework of plant development resulting in many tools to predict plant development. Plant shoots develop by forming a series of nearly identical building blocks, called phytomers [4, 5]. The vegetative phytomer is associated to a leaf, and phytomers are produced in an orderly manner on a shoot; for example, the phytomer of leaf 2 is formed after the phytomer of leaf 1.

Phenology is the study of the plant (or animal) life cycle and how it is influenced by seasonal and interannual variations in climate. The phenology of a crop is defined by the sequence of stages, which, in turn, define phases. Identification of certain stages may require examination of the shoot apex. For example, after germination, the apical meristem produces vegetative structures such as leaf primordia. When temperature and photoperiod requirements are met, the shoot apex will start initiating reproductive structures (e.g., spikelet and floret primordia).

The rate of appearance of phytomers and changes at the shoot apex are regulated by the genetics of the plant, the environment, and often an interaction of both. The main environmental drivers of plant development are temperature and photoperiod; their effects on phenology interact with the genetics of the plant responses by photoperiod sensitivity genes, vernalization genes, and earliness *per se*.

This entry covers how plant development is regulated by temperature and photoperiod. Temperate cereals are emphasized because they are adapted to a wide array of environments and show a diverse set of adaptive mechanisms regulating their development. However, defining plant parts and how canopies are built as well as the sequence of events throughout the crop cycle is required before their regulation can be explained. This entry starts by defining the canopy

structure and the sequence of events that define the developmental processes of a crop, followed by the current knowledge on how temperature (including vernalization) and photoperiod regulate crop development. This entry finalizes with two important parts: modeling crop development and future directions. Modeling crop development is twofold important; first to understand the physiology and genetic basis of crop development, and second to predict when key developmental events are likely to happen as accurately as possible.

Canopy Structure: Phytomers, Phyllochron, and Plastochron

The phytomer is considered the basic building block of plant canopies and is most commonly defined as the leaf, node, internode above the node, and the axillary bud [6]. Therefore, canopy architecture and development is determined by the dynamic appearance, growth, and abortion/senescence of phytomers (and components of the phytomer). Phytomers originate at the shoot apex with the initiation of a leaf, and the potential for a new shoot is formed with the presence of the axillary bud. The growth and differentiation of each component of a phytomer will lead to their visual appearance. For example, the internode can continue differentiating and growing, resulting in its appearance from the leaf sheath. Tillers may appear when the axillary bud differentiates and grows.

Naming Plant Parts

Because plant development is an orderly process, accurately identifying plant parts aids in describing the process and quantifying the developmental rate.

Several naming systems of plant parts have been proposed, but most are quite similar. For example, true leaves can be numbered acropetally for each shoot with an *L* [7–9] (Fig. 1) beginning with the first foliar leaf, L1 [9]. Similarly, Jewiss [7] proposed a system for naming tillers that has been modified and extended by many, but the modified system proposed by Klepper et al. [8, 9] is increasingly being adopted. This system uses the leaf axil number of the parent shoot to name the tiller. The first shoot to appear from the seed is the main stem (MS). Tillers appearing from the axils of leaves on the main stem are primary tillers and are named with a T and a digit corresponding to the leaf number. For example, the tiller appearing from the first leaf (L1) on the main stem is called T1. This system is however limited by the potential production of tillers from the axil of leaf 10 and above, which rarely happens. Primary tillers can produce tillers that are called secondary tillers. Secondary tillers can arise from the axil of the prophyll of primary tillers and their second digit is a zero (Fig. 1).

Haun [10] proposed a numerical leaf staging system to quantify the number of leaves appearing on the main stem (which can be extended to any shoot):

$$\text{Haunstage} = (n-1) + \frac{L_n}{L_{n-1}}, \left(0 < \frac{L_n}{L_{n-1}} \leq 1\right) \quad (1)$$

where n is the number of leaves that have appeared on a shoot, L_{n-1} is the blade length of the penultimate leaf, and L_n is the blade length of the youngest visible leaf extending from the sheath of the penultimate leaf. Therefore, when a shoot is identified, it can be further characterized using the Haun system. For example, the Haun stage for shoots on the plant shown in Fig. 1 is: MS (5.3), T0 (1.5), T1 (2.4), T2 (1.4), and T3 (0.7). The Haun stage of a tiller with one leaf not fully unfolded is arbitrarily assigned as 0.1 or 0.9 when only the tip of the leaf is visible or most of the leaf blade has appeared, respectively.

Similarly, the leaf and tiller naming scheme has been extended to the wheat inflorescence. Klepper et al. [11] defined a numerical index for the development of the inflorescence and Wilhelm and McMaster [12] extended it to uniquely identify each plant part. Spikelets are named with an S followed by the position from the base of the spike. Then, S1 is the basal spikelet and S2 is the second spikelet from the peduncle (Fig. 2). Florets are designated with an F and numbered acropetally from the base of the rachilla. After fertilization, the letter F designating a floret is changed to a C for caryopsis. This system allows naming reproductive structures in grasses with one spikelet per rachis node such as wheat.

These naming systems of leaves, tillers, spikelets, and florets or caryopsis allow the accurate identification of each plant part. For example, the second caryopsis on the third spikelet on the primary tiller from the axil of the second leaf of a wheat plant would be T2S3C2.

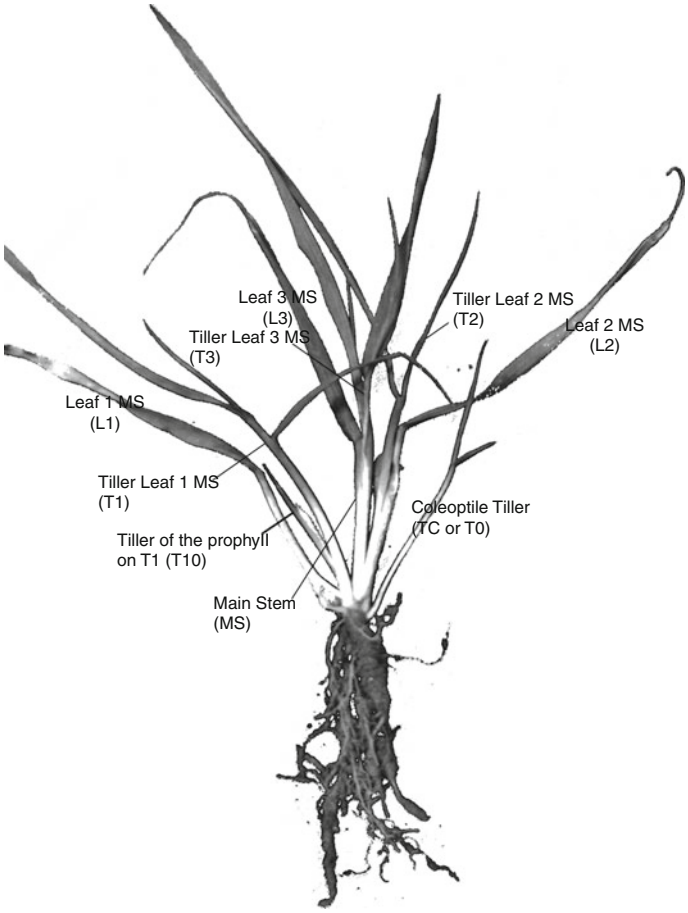

Crop Development Related to Temperature and Photoperiod. Figure 1
Naming leaves and tillers of a winter wheat plant

The systems for naming individual plant organs can be easily extended to name vegetative and reproductive wheat phytomers [13]. A phytomer would be denoted with a "P" followed by an "L," if it is a phytomer associated with a leaf or an "S," if it is a reproductive phytomer and the leaf or spikelet number. The name of the shoot can be added to identify the tiller being described. For example, MS PL2 is the second phytomer on the main stem and T1 PS1 is the basal spikelet phytomer in the spike of the first tiller.

Dynamic Appearance of Plant Organs: The Plastochron and Phyllochron

The naming systems of plant parts described earlier are the landmarks to describe the development and structure of a wheat plant. However, plant development is a dynamic process that follows the formation, growth, and senescence of phytomers and their components resulting in a continually changing architecture. The creation of the vegetative phytomer is dependent on the initiation of the leaf primordium. Therefore, the rate of leaf primordia initiation controls the timing of phytomer formation. The plastochron was first defined as the interval between the formation of two successive internode cells of the green alga *Nitella flexilis* [14], as cited in [15]. Milthorpe [16] and Esau [17] defined the plastochron as the interval between the formations of successive leaf primordia at the shoot apex, which is now commonly accepted. Similarly, the phyllochron was defined as the interval between appearances of consecutive leaves on a shoot [18] as cited in [6]. Wilhelm and McMaster [6] further refine the definition of phyllochron by defining appearance as "visible

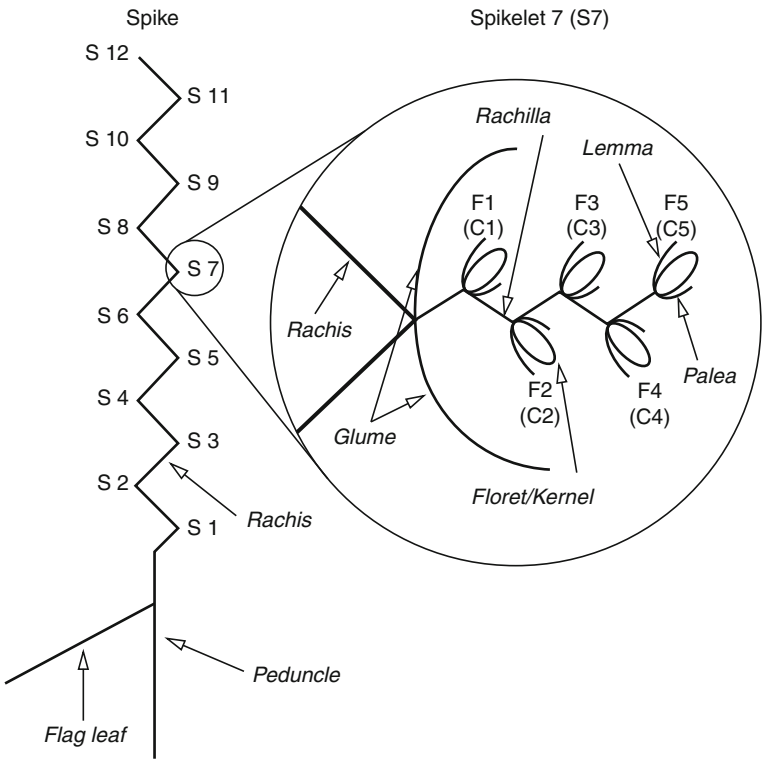

Crop Development Related to Temperature and Photoperiod. Figure 2
Naming scheme for reproductive organs of spike inflorescence. Spikelet positions are denoted by the letter S and numbered acropetally along the rachis. Florets/caryopsis positions are denoted by the letters F/C and numbered acropetally along the rachilla (From Wilhelm and McMaster [12])

without magnification, dissection or changing leaf display." The inverse of the phyllochron is termed development rate (DR), which can be generalized as the inverse of the time interval between two developmental events. The relationship between the plastochron and the phyllochron depends on the species. In wheat, leaf primordia are produced more rapidly than they appear, suggesting that different mechanisms are involved in regulating each process. Leaf primordia are initiated at the meristem on the shoot apex, where new cells are produced very quickly. After a leaf primordium is formed, it continues to grow in cell number and cell size, but this growth does not happen at the shoot apex meristem, rather at the intercalary meristem at the base of the leaf. The amount a leaf grows until it appears through the curl of leaves is much larger than the growth involved in forming a leaf primordia, therefore it is more dependent on the available resources (e.g., water, carbohydrates, and nutrients).

Developmental Stages and Phases: Phenology

Plants develop by the repetition of elementary building blocks (i.e., phytomers), whose morphological, dimensional, functional, and anatomical features change during ontogeny and according to several processes called heteroblasty, phase change, life stages, maturation, aging, age states, or morphogenetic progression [19]. In this entry, those changes will be referred as *developmental stages* (or simply *stages*) and the time between stages will be referred as *developmental phases* (or *phases*). It is common in the literature referring to these stages as "growth stages." However, there is little growth in some developmental events such as anthesis. The phenology of a crop is the ordered succession of stages and phases that can have different lengths determined by internal factors (e.g., the genetics of a variety or species) or biotic and abiotic external factors (e.g., diseases, temperature, light, and nutrients).

Plant development can broadly be divided into vegetative and reproductive phases that often overlap. The switch from vegetative to reproductive phase happens at the meristem level, which stops producing vegetative phytomers (i.e., leaves, nodes, and internodes) to start producing reproductive phytomers (rachis, spikelets, and florets).

Phenological Scales

Developmental stages occur in a consistent pattern in a crop each year and numerous approaches exist that characterize crop phenology. The most widely used phenological scales for temperate cereals are Feekes [20], Zadoks [21], Haun [10], and BBCH [22]. The Feekes scale is shown in Fig. 3 and described, jointly with the Zadoks' decimal code, in Table 1. The BBCH scale for cereals is mainly based on the Zadoks scale, and the Haun scale primarily describes the development of shoots until the last leaf is fully expanded.

Phenological scales consider basic developmental stages like germination, emergence, tillering, stem elongation, heading, flowering, grain filling, and physiological maturity, with differences among scales primarily in how much detail each stage is characterized. Some developmental stages are not well defined, leading to confusion in measuring and reporting these stages. For example, the beginning of stem elongation is usually recorded as the jointing date or when the first node is visible above ground; however, the first node is formed when the apex is underground and is only visible after the stem has elongated sufficiently to elevate the apex and the node above ground. Likewise, physiological maturity is defined as when the

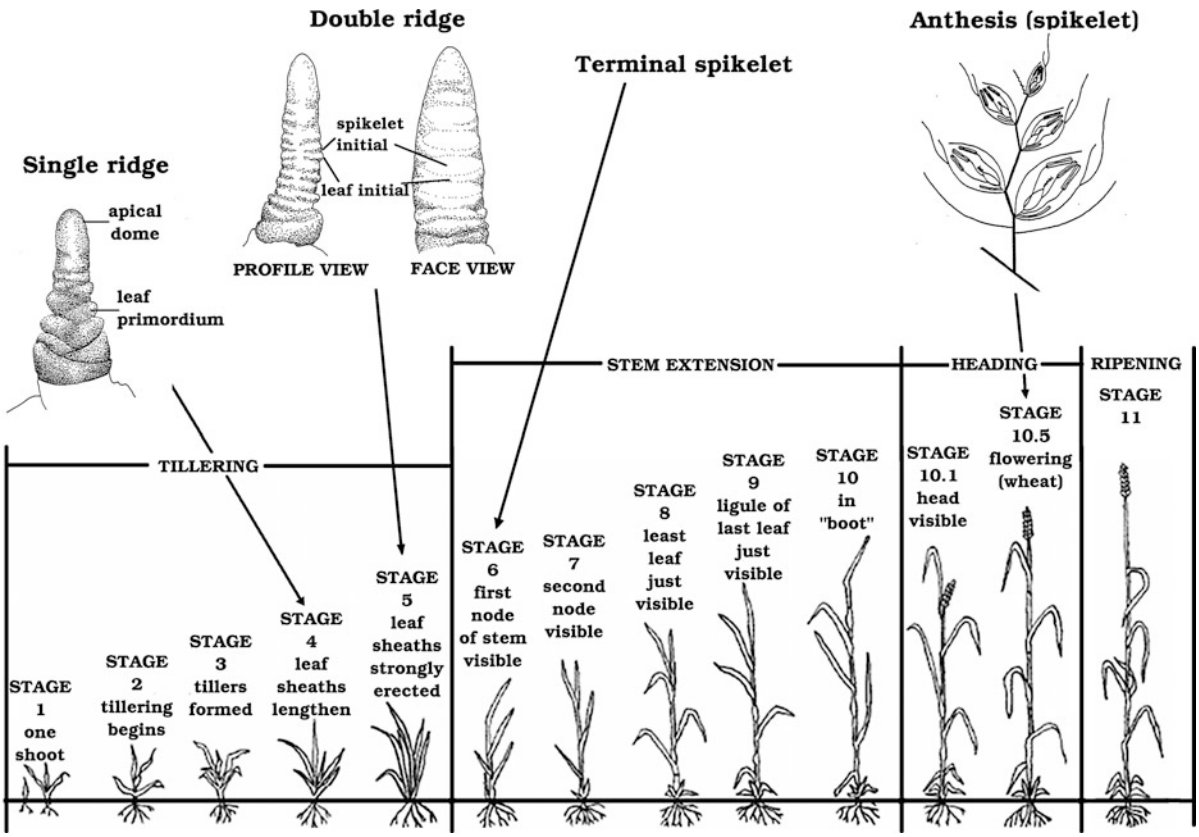

Crop Development Related to Temperature and Photoperiod. Figure 3
Feekes developmental scale with the approximate timing of some shoot apex developmental events (From [13])

Crop Development Related to Temperature and Photoperiod. Table 1 Description of the main developmental stages according to Feekes [20] and Zadoks [21], and suggested measurements characteristics (Modified from [23])

Stage or phase	Description		Measurement characteristics
	Feekes	Zadoks	
Germination	No stage	Stages: 00 – dry seed, 01 – beginning of imbibition, 03 – imbibition complete, 05 – radicle emerged from caryopsis, 07 – coleoptile emerged from caryopsis	Beginning of imbibition: Seed begins to swell
Emergence	Stage 1 – main shoot only	Stage 09 – leaf at the tip of the coleoptile	Beginning of emergence: First true leaf emerges through the coleoptile and the tip is visible above the soil surface
Tillering	Stage 2 – beginning of tillering	Stages 21–29 – main stem plus 1 to 9 tillers	Beginning of tillering: The first tiller is visible
Single ridge	No stage	No stage	Shoot apex shape changes from dome to more elongated and leaf primordia begin to form a ridge around the apex
Double ridge	No stage	No stage	Formation of double ridges around the apex. Bottom ridge is leaf primordia and top ridge is spikelet primordia
Terminal spikelet	No stage	No stage	Apical spikelet primordium appears and noted by a 90° rotation from the plane of previous spikelets
Jointing	Stage 6 – first node visible	Implicit in stage 31 – first node detectable and change of plant habit from prostrate to erect	First node visible above the soil surface
Stem elongation	Stages: 4 – change of plant habit from prostrate to erect, 5 – pseudo-stem clearly erect, 6 – first node visible, 7 – second node visible, 8 – last leaf appearance, 9 – last leaf ligule visible, 10 – last leaf sheath swelling	Stages: 30 – pseudo-stem erect, 31 to 36 first to sixth node detectable, 39 – flag leaf ligule visible, 43 to 49 – flag leaf sheath swelling	Beginning when the first node is formed, usually below soil surface, and pushed above the soil surface
Flag leaf	Stage 9 – last leaf ligule visible	Stage 39 – Flag leaf ligule visible	Ligule of last leaf is visible and no new leaf is emerging

Crop Development Related to Temperature and Photoperiod. Table 1 (Continued)

Stage or phase	Description		Measurement characteristics
	Feekes	Zadoks	
Booting	Stage 10 – last leaf sheath visible	Stages 43–49 – flag leaf sheath swelling	Begins at flag leaf and ends at heading
Heading	Stages: 10.1 – first ears just visible, 10.2 – ¼ of heading completed, 10.3 – ½ of heading completed, 10.4 – ¾ of heading completed, 10.5 – all ears out of the sheath	Stages: 51 – first spikelet just visible, 53 – ¼ of the inflorescence visible, 55 – ½ of the inflorescence visible, 57 – ¾ of the inflorescence visible, and 59 – inflorescence completely emerged	Begins when first spikelet is visible and ends when the inflorescence is fully emerged
Anthesis	Stages: 10.5.1 – anthesis starts, 10.5.2 – flowering completed to the top of the ear, 10.5.3 – flowering completed to the bottom of the ear, 10.5.4 – flowering over/kernel watery ripe	Stages: 61 – beginning of anthesis, 65 – mid-anthesis, 69 – anthesis completed	Starts when the first anther is visible on an inflorescence and ends when no more anthers appear on the inflorescence
Grain filling	Stages: 10.5.4, 11.1 – milky ripe, 11.2 – mealy ripe	Stages: 71 to 77 – milk grain, 83–87 – dough grain	Begins at fertilization, usually considered anthesis and ends at physiological maturity
Physiological maturity		No Stage	When all spike components, internodes, and leaves lose green color
Ripening	Stages: 11.3 – kernel hard, 11.4 – ripe for cutting	Stages 91–99	Ripening and dormancy

maximum dry weight is reached. In wheat, determining physiological maturity is somewhat difficult because there is not a clear morphological change in the plant morphology as it happens in maize (and sunflower). In maize, a black layer near the base of the kernel appears when the maximum dry weight is reached. The Feekes scale defines harvest maturity as when the grain is difficult to divide along the crease and Zadoks [21] defines the 90% of ripeness of rice (*Oryza sativa* L.) when the kernel cannot be dented with the fingernail. These definitions likely are not precisely correlated with maximum seed biomass. Therefore, it is now commonly accepted practice to assume physiological maturity for temperate cereals occurs when all green color has disappeared from the spike. This definition seems reasonable as leaves and internodes have long since lost all green color so that no photosynthesis occurs, and there is no report showing retranslocation from carbohydrate reserves to the grain at this time.

Regulation of Crop Development

Plant development is highly dependent on temperature, which controls the rate of development and the switch from vegetative to reproductive states. Both high and low temperatures may have a major effect on plant development, especially controlling the switch to the reproductive state. For example, winter wheat requires a period of low temperatures to start producing reproductive structures (vernalization). The length of the cold period varies with genotype.

Besides vernalization, day length (or photoperiod) modifies the temperature-controlled rate of development. Photoperiod refers to the number of daylight hours, which changes through the seasons and with latitude. Photoperiod increases after the winter solstice (December 21 in the northern hemisphere or June 21 in the southern hemisphere) and decreases after the summer solstice. Crops and genotypes vary in their sensitivity to photoperiod and the minimum amount of daylight required to switch from vegetative to reproductive phases.

Developmental Response to Temperature

The relationship between temperature and phenology has been long recognized. Temperature is a better predictor of many developmental processes than calendar time. Reamur [24] formalized this relationship by creating the concept of heat units, now referred to as thermal time. The relationship between temperature and developmental rate is a curve with a maximum development rate at the optimum temperature (T_o) and developmental rate reaching zero at temperatures below the base temperature (T_b) or above the maximum temperature (T_m; Fig. 4). This nonlinear relationship is shown in several studies [25, 26].

Thermal time has two components: (1) the average temperature (T_a) over some time interval (e.g., hourly, daily), and (2) a temperature response curve describing the effectiveness of T_a on the development rate for the process (e.g., phyllochron, phenology). T_a is the integral of temperature over the time period of interest;

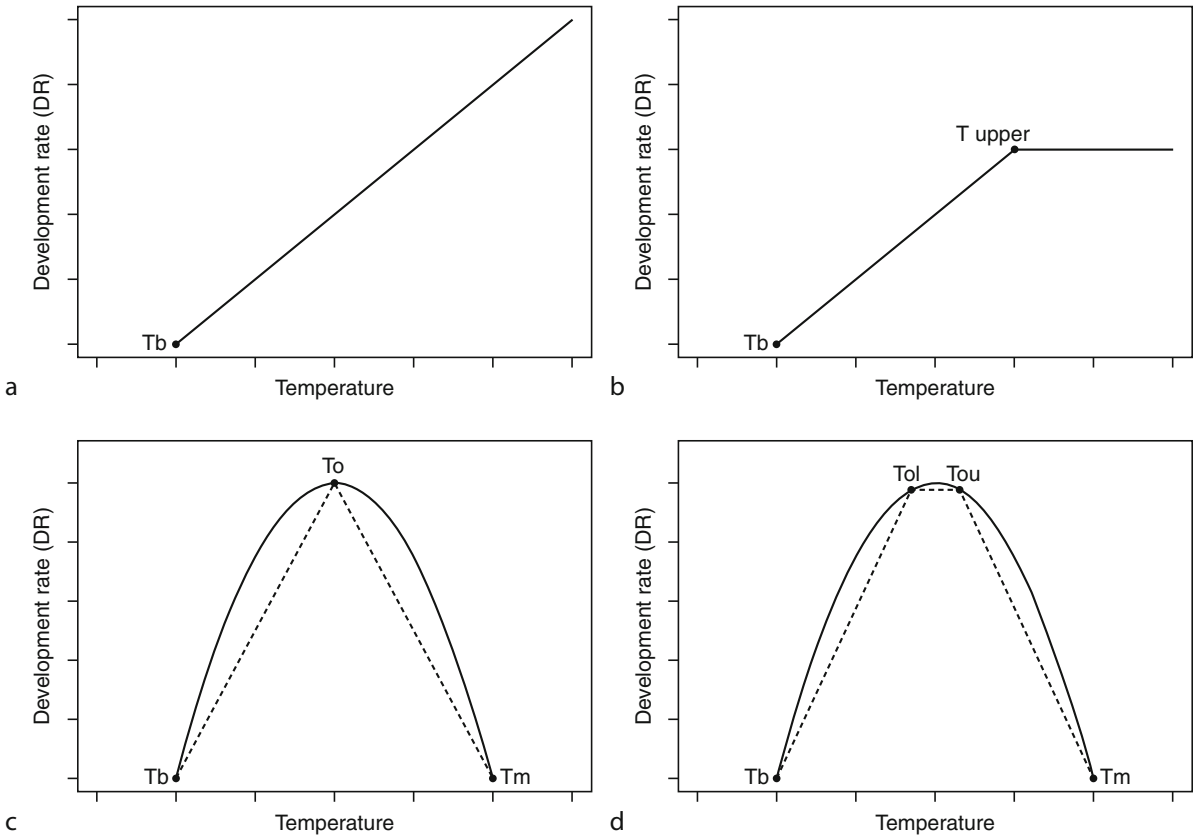

Crop Development Related to Temperature and Photoperiod. Figure 4
Development rate as a function of temperature. Temperature response curves: (**a**) linear response, (**b**) extended linear response with an upper temperature threshold, (**c**) bilinear model with two zero development temperatures (base temperature, T_b, and maximum temperature, T_m) and an optimal temperature (T_o), and (**d**) trilinear model with two zero development temperatures (T_b and T_m) and a range of optimal temperatures defined by optimal lower temperature (T_{ol}) and optimal upper temperature (T_{ou})

however, in practice the average of the maximum and minimum temperatures in the time interval is often used:

$$T_a = \frac{T_{max} + T_{min}}{2} \quad (2)$$

This approximation is fairly accurate, but its error increases with deviations of from 12 h photoperiods and if sudden changes in temperature happen within the time interval. The time interval mostly depends on data availability, but common intervals range from daily to hourly time intervals, with daily the most commonly used. There are many temperature–response curves, which greatly diversifies the calculation of thermal time (Tt). The most simple form is a linear relationship with the temperature at which there is some plant development (Fig. 4a), i.e., the difference between T_a and the temperature at which development is zero or base temperature (T_b):

$$Tt = T_a - T_b, (Tt \geq 0) \quad (3)$$

where thermal time is expressed as growing degree-days (GGD, °C·days). Modifying Eq. 2 to include a maximum development rate (Fig. 4b) is useful if plants are grown at higher temperatures. Given that the relationship between temperature and development rate is not linear [25–27], further refinements to the accumulation of thermal time can include changing the development rate based on certain cardinal temperatures (Fig. 4c, d). These approaches assume development rate increases with temperatures above T_b until an optimum temperature (T_o, or a range of optimal temperatures, T_{ol} to T_{ou}) is reached, and then decreases until development stops at a maximum temperature (T_m). This can be approximated by two- or three-segmented linear models, or curvilinear models such as a quadratic curve [25] or beta distribution [27, 28].

Vernalization

The term vernalization was first used by Lysenko in 1928, but research on the need of a cold period for winter cereals to flower started as early as 1857 [29]. Vernalization can be viewed as an adaptive mechanism to avoid unfavorable periods for development (e.g., winter) and ensure flower development and subsequent seed growth occurs under favorable conditions (e.g., spring and summer). Hence, vernalization synchronizes plant development with seasonal climate changes.

Commonly, genotypes requiring vernalization are referred to as "winter" wheat (or "winter" barley) and are normally planted late summer or early fall with vernalization occurring during the late fall or early winter. Conversely, "spring" genotypes are commonly viewed as not requiring vernalization, and normally are planted in the spring or in regions where temperatures are often above effective vernalizing temperatures. This well-entrenched distinction between "winter" and "spring" genotypes does not reflect that "spring" genotypes (1) often have at least some vernalization requirements, (2) reach flowering faster if experiencing vernalizing temperatures, and (3) mask the continuum of vernalization requirements present among all wheat genotypes.

Effective vernalizing temperatures range from 0° C to 10° C [30], and a few weeks of cold are usually sufficient to promote the switch from vegetative to reproductive phases and longer periods of cold temperatures can shorten the time to flowering until the vernalization response is saturated [30]. Genotypes vary in the length of the cold period required to saturate the vernalization response. For instance, time to flowering in wheat was reduced in response to longer cold periods [31, 32], and interestingly, genotypes thought to require vernalization to flower eventually flowered without undergoing vernalization treatment [32]. Quantifying responses to varying periods of vernalizing temperatures in calendar time or thermal time does not reflect the biology of the response. A better method to quantify the effects of vernalization would be by counting the number of leaves produced at flowering time [33]. Using this quantification method, vernalization reduces the time to flowering by reducing the number of leaves being produced rather than the phyllochron [31, 33]. That is, the number of leaves produced at flowering increases with shorter vernalization periods, while the phyllochron is not affected by the duration of the vernalization period.

Genetic Regulation of Vernalization Although the mechanisms by which plants sense cold and initiate the cellular signaling to induce flowering are not known, the genetic regulation of vernalization is fairly well

known in cereals like wheat and barley, which benefited of the research done on the model plant *Arabidopsis thaliana*. Four major genes are involved in the expression of vernalization sensitivity in wheat and barley, *VRN-1*, *VRN-2*, *VRN-3*, and *VRN-4*. The first three genes have been cloned and identified [34–36]. However, these three genes do not explain the spring habit of all varieties [35], suggesting that other genetic mechanisms may be involved.

The *VRN-1* gene encodes the MADS box transcription factor similar to *APETALA-1*, which is responsible for meristem identity in several plants [34]. This gene is up-regulated by vernalizing temperatures and the degree at which it is up-regulated depends on the length of the vernalization period. However, spring varieties also show an up-regulation of *VRN-1* during the initiation of the reproductive phase and remain high throughout the reproductive phase, suggesting an involvement of *VRN-1* in meristem identity but not limited to vernalization response.

The *VRN-2* gene encodes the *ZCCT1* protein, which shows high similarity to the CCT domain of the *Arabidopsis CONSTANS* and *CONSTANS*-like genes. *VRN-2* represses flowering and is down-regulated by vernalization [35]. The spring allele *vrn-2* in wheat has a point mutation at the CCT domain that replaces an arginine with a tryptophan. It has been suggested that the CCT domain may be involved in protein–protein interactions [37], so a mutation in this domain can alter these interactions.

The *VRN-3* gene is a RAF kinase inhibitor like protein with high homology to the *Arabidopsis FLOWERING LOCUS T* (*FT*) gene [36], which induces flowering when expressed. *FT* is a flowering signal that moves from leaves to stem apices.

VRN-1, *VRN-2*, and *VRN-3* interact with each other regulating flowering under the vernalization pathway (Fig. 5). Before vernalization occurs, *VRN-2* is expressed and represses the expression of *VRN-3*. When plants are vernalized, *VRN-1* is induced and it represses the expression of *VRN-2*, allowing *VRN-3* to express and promote flowering. At the same time, there is a feedback mechanism by which *VRN-3* up-regulates *VRN-1*. It seems that *VRN-1* is the primary target of vernalization and is essential for flowering.

VRN-4 has been recently fine mapped and its cloning is underway [38]. Identifying and including this gene in the vernalization pathway may increase the understanding of vernalization responses in wheat.

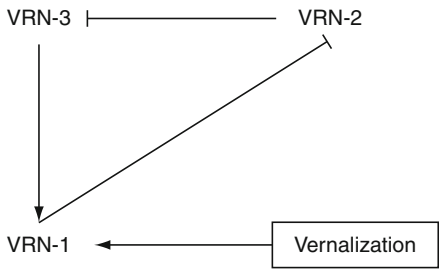

Crop Development Related to Temperature and Photoperiod. Figure 5
Model of the vernalization pathway in temperate cereals. Arrows mean induction (or up-regulation) of gene expression; for example, vernalization induces the expression of VRN-1. Bar-headed lines mean repression (or down-regulation) of gene expression; for example, VRN-2 represses the expression of VRN-3

Photoperiod

Photoperiod can be defined as the number of hours of light in a 24-h period, which changes throughout the season depending on the latitude. It has been long recognized that plants, including crops, normally flower only when the length of the day was favorable [39]. Crops sense the amount of light they receive daily and respond to it by accelerating or slowing their development. There is, however, genetic variation of a quantitative nature in the response to photoperiod within a crop, meaning that different varieties respond differently to changes in the photoperiod, and some show no response to photoperiod (or are photoperiod insensitive). Photoperiod sensitivity is thought to be the wild type phenotype because it is wide spread in wild barley (*Hordeum spontaneum* L.) and confers strong adaptive features in the center of origin of barley, where there might be late spring frosts. Photoperiod insensitivity, however, brings wide geographical adaptability because plants do not require long days to flower, and, hence, they are suitable for environments with short seasons or latitudes where long days do not occur. For example, in wheat, day length neutrality, jointly with semi-dwarfism and rust resistance traits, were used to develop the high yielding varieties of the "green revolution" [40]. Photoperiod insensitivity

promotes earliness thought to be a desirable adaptive trait for environments closer to the equator where high temperatures and drought can be expected at the end of the season. Therefore, earliness allows wheat and barley varieties to escape this terminal stress.

Although the rate of development mainly responds to temperature, when temperature is fixed, longer photoperiod alters the development rate by shortening the phyllochron [41, 42]. In Fig. 6, the appearance of leaves over time follows a linear model when plants are grown at a constant temperature, and the rate of appearance (slope of the curve) increases with the photoperiod; however, as day length increases, fewer leaves are formed per hour of light, hence there is a reduction in photoperiod efficiency for leaf emergence.

Different crops respond differently to photoperiod; crops can be classified as long day (LD) and short day (SD) depending on which photoperiod accelerates development (promotes flowering). Temperate cereals are long-day crops because flowering is promoted by photoperiod longer than 12–14 h, while maize and rice are short-day crops, meaning that short days induce the switch to reproductive phase. In wheat and barley, increased photoperiod shortens the time to flowering by modifying the length from emergence to terminal spikelet initiation. The effects of photoperiod on the duration from terminal spikelet initiation to flowering depend on what environments they are measured (field versus controlled environments). This reduction of time to flowering is not only due to an accelerated phyllochron, but also by the production of fewer leaves.

Genetic Regulation of Photoperiod Sensitivity In temperate cereals, such as wheat and barley, sensitivity to photoperiod is mainly regulated by *Ppd* genes. Homologous genes have been identified in wheat and barley and have the function of a pseudo response regulator (*PRR*), most similar to the *Arabidopsis PRR7* [43]. The *PPR* proteins are characterized by a pseudo receiver domain near the amino-terminus and a CCT domain near the carboxy-terminus [44], which makes them distantly related to other CCT domains important in regulation of flowering such as *CONSTANS* [45] and *VRN-2* [35].

The photoperiod insensitive allele (*ppd-H1*) in barley slightly delays the gene expression of *CONSTANS* (*HvCO1*) that follows a circadian pattern [43] and is a transcriptional regulator of the *FT* gene [46]. In contrast, photoperiod insensitivity in wheat is regulated by a series of three homoeologous genes located in the colinear region on chromosome 2 group, which

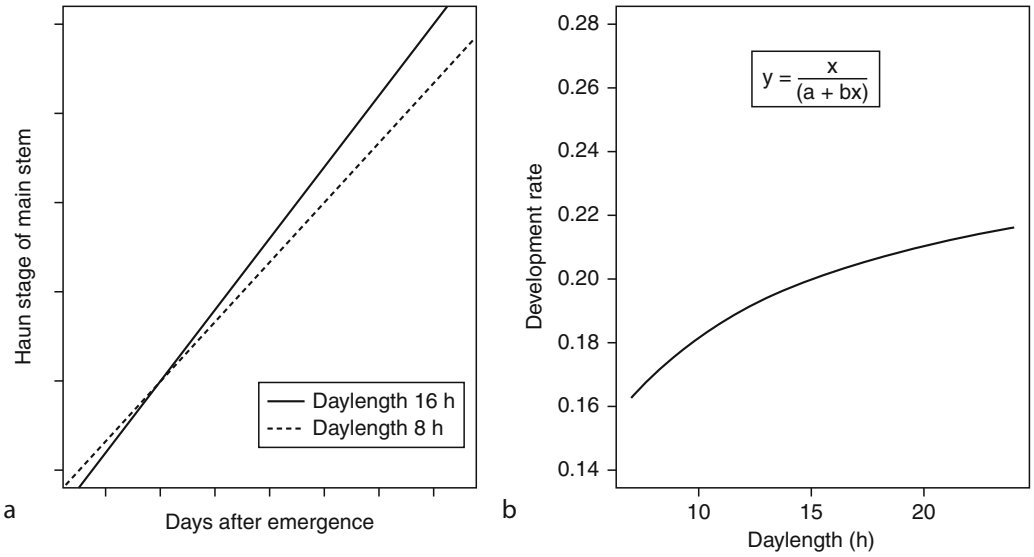

Crop Development Related to Temperature and Photoperiod. Figure 6
Development rate responses to changes in day length at constant temperature. (**a**) Leaf appearance of plants grown in different day lengths and (**b**) development rate as a function of day length (Based on [41])

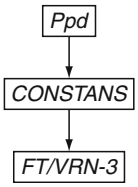

Crop Development Related to Temperature and Photoperiod. Figure 7
Model of the photoperiod pathway of flowering time. Arrows mean induction (or up-regulation) of gene expression; for example, CONSTANS is induced by the expression of *Ppd* genes

seem to be upstream of the *CONSTANS* gene in the photoperiod pathway (Fig. 7). The *Ppd-1 Da* allele confers insensitivity to photoperiod in a semidominant fashion, allowing wheat plants to flower regardless of the photoperiod [47]. Sequence analysis of wheat varieties known to have this mutation shows that there is a 2,089 bp deletion upstream of the coding region responsible for the photoperiod insensitivity phenotype. Other sequence variations producing nonfunctional proteins (*null* alleles) at the 2A and 2D genes in wheat have been observed; however their effects on photoperiod sensitivity are difficult to assess because they might be masked by functional proteins from other homoeologous genes. These, and other mutations, however, may have a quantitative effect in photoperiod sensitivity and flowering time [47].

Coordinated Temperature and Photoperiod Regulation of Crop Development

The temperature and photoperiod regulation of crop development has been described in previous parts of this article, but both environmental factors act in coordination. It is clear that the phyllochron varies with planting date in temperate cereals and it has been suggested that the phyllochron is fixed by the rate of change of the photoperiod at crop emergence [48]. However, in general, temperature and photoperiod change together in the field. Results from experiments in controlled environments show an effect of photoperiod on the temperature–response curve [49, 50]. The term "thermo–photo ratio" (the degree-days divided by day length in hours) has been used to study the coordinated effect of temperature and photoperiod on the phyllochron [49]. A linear relationship was found between the phyllochron and the thermo–photo ratio under both controlled environments and field conditions [49]. Slafer and Rawson [51] partitioned the photoperiod sensitivity of wheat phenophases into different parameters, which were affected by temperature, describing an interaction between genotype, photoperiod, and temperature. The effect of planting date on crop development has been studied extensively, yet it is difficult to draw conclusions of the coordinated effect of photoperiod and temperature on crop development. This is because when planting date is changed, both photoperiod and temperature are changed and their effects are difficult to separate.

Genetic Framework of Flowering Time Several pathways regulate time to flowering in crops, namely, vernalization, photoperiod, autonomous, and gibberellic acid. The vernalization and photoperiod pathways have been described in parts 5.2 and 5.3 and *FT/VRN-3* gene is in both pathways, thus integrating the response to both vernalization and photoperiod factors (Figs. 5, 7, 8).

In the ancestral form of wheat and barley, after germination in the fall *VRN-2* is highly expressed by the long days and represses the expression of *FT/VRN-3*. As winter progresses, the photoperiod decreases and low temperatures induce the expression of *VRN-1* in the leaves, which represses the expression of *VRN-2*, allowing *FT* to be expressed by long days in the spring, a process regulated by photoperiod genes *Ppd* and *CO*. Then, the protein encoded by *FT/VRN-3* is translocated to the shoot apex, where it up-regulates *VRN-1*, which will induce the switch to reproductive phase. The HAP (HEME ACTIVATOR PROTEINS) complexes may mediate the transcriptional regulation of the CCT domain of *CO* and *VRN-2*. In plants, HAP subunits are encoded by multiple genes that, together with CCT domain proteins that can interact with HAP complexes, generate a large number of molecular combinations. These combinations provide a flexible signaling system that can integrate responses to environmental cues as photoperiod, vernalization, or stress (reviewed in [52]).

In environments where temperate cereals usually grow and were domesticated, vernalization requirements

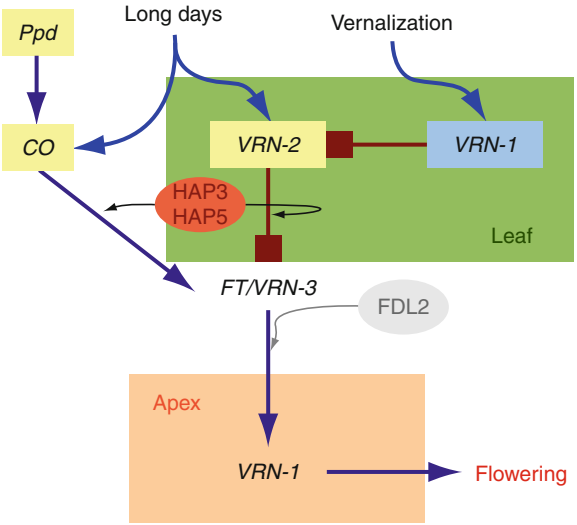

Crop Development Related to Temperature and Photoperiod. Figure 8
Model of flowering related to photoperiod and vernalization. *Thick blue arrows* mean induction (or up-regulation) of gene expression or developmental process; for instance, photoperiod induces the expression of *VRN-2*. Square headed lines indicate repression (or down-regulation) of gene expression; for instance, VRN-3 up-regulates *VRN-1* at the apex

are met long before the photoperiod is inductive of the reproduction phase. This requires plants to "remember" they had been vernalized. The mechanism by which temperate crops "remember" vernalization is not known, but it has been studied in the model plant *Arabidopsis*. In addition to the genetic information carried on the DNA sequence (genes and alleles), chromatin structure is recognized as another source of genetic information. The chromatin can be highly condensed (heterochromatin) or more relaxed (euchromatin). The DNA is combined with proteins called histones and specific covalent histone modifications of histones favor the formation of chromatin structure that influences the level of gene expression. Other nongenetic mechanisms of gene expression are related to DNA methylation. The DNA methylation at the promoter region of genes is generally related to lower levels of gene expression, and even gene silencing. Of the two mechanisms, it seems that histone modifications are involved in regulating the memory of vernalization (reviewed in [53]) in *Arabidopsis*. In *Arabidopsis*, the *FT* gene is repressed by *FLC*, which is down-regulated by vernalization. The stable repression of *FLC* involves de-acetylation of histone 3 (H3) upstream of *FLC*, methylation of H3 Lys9 and Lys27, which allows the binding of HP1 inducing the stable silencing of *FLC*.

Less known is the genetic basis of the quantitative response to temperature (thermal–response curve). The *Earliness* per se *A1* ($Eps^{m}A1$) gene affects time to flowering by reducing the vegetative phase and it has been associated with responses to temperature, probably by modifying the optimum temperature [54]. Two candidate genes for $Eps^{m}A1$ are located in the genomic region where this gene has been located, *Mot1* and *FtsH4* [55]. The *Mot1* gene has features of the SNF2 family of transcriptional regulators. Other members of this family have been related to regulation of flowering in *Arabidopsis*, but the gene expression data do not show differences between the two alternative alleles [55]. The *FstH4* is a member of the FstH family of proteases and is homologous to the *Arabidopsis FstH4*, which has been found highly expressed in seed, and mutants in this gene show delayed germination that is carried over the growth cycle [55].

Modeling Approaches

For centuries, people have wanted to understand and predict aspects of crop development, particularly phenology. To do this, different conceptual, statistical, and mathematical models have been developed. Beginning in the 1970s, a variety of digital technologies began to emerge, one of which was crop simulation models for predicting growth, development, and yield. This section presents a broad overview of these crop simulation models, emphasizing wheat.

Many crop simulation models exist for simulating growth, development, and yield, and they cover scales from specific processes to the agroecosystem. Crop simulation models are a simplified mathematical representation of the plant. At the most fundamental level [56], crop simulation models generally simulate a trait, for example, yield (Y), as the function of daily growth rate (GR) that is partitioned to the yield component (P) and integrated over a daily time

step from emergence (*emerge*) through physiological maturity (*maturity*):

$$Y = \int GR * P \tag{4}$$

Implementing Eq. 3 in a model usually begins assuming non-limiting conditions, thereby allowing for potential production to be estimated. The parameters can either be generic for a crop or adjusted to a specific genotype. By incorporating environmental variables (e.g., temperature, water, light, CO_2, and nutrients), crop simulation models can examine crop or genotype responses across a broad environmental range of limiting conditions, avoiding a common limitation of statistical (or regression) models. Depending on the purposes, including the role of biotic factors or management practices may also be important.

How a model implements Eq. 3 depends on model objectives and interests of the model developers. The earliest crop simulation models tended to focus on the scale of whole-plant growth and development, with little detail on processes at lower scales. These models use an energy- or light-driven approach to determine the growth rate, and this approach remains popular today. The basic approach simulates leaf area index on a daily time step, which is used to capture energy/sunlight and produce biomass that is then distributed to basic plant components of leaves (providing the feedback to the cycle), stems, roots, and seeds. Partitioning coefficients are often used to allocate the biomass produced, and phenology sub-models are essential in accurately predicting the timing when sources and sinks are present, and changing partitioning coefficients based on developmental stage.

As crop simulation modeling progressed, certain trends emerged. First, greater attention focused on representing plant processes below the whole-plant level. In general, energy- or light-driven modeling emphasized functional physiology, particularly for assessing energy balance and leaf functioning at the individual organ level (e.g., [57, 58]). Second, considerable research on crop development during the 1970s and 1980s undoubtedly spurred interest in including this new knowledge in the models. This led to alternative modeling approaches based on more developmentally driven approaches that recognized that plant development is orderly and predictable based on basic units (i.e., the phytomer) that dynamically appear, grow, and senesce over time as discussed earlier in this entry and shown in Fig. 9.

Early efforts beginning in the mid-1980s focused on developmental concepts such as leaf appearance (the phyllochron) and tillering that led to more accurate representation of canopy architecture. For instance, the AFRCWHEAT1/2 model developed in Europe [60–62] contained detailed tillering and leaf dynamics sub-models (e.g., appearance, growth, and senescence/abortion), and the resulting effect on canopy LAI was simulated and then used to estimate biomass. Simultaneously and independently, another effort was underway in the USA that resulted in the developmentally driven MODWht3 [63] and SHOOTGRO [http://arsagsoftware.ars.usda.gov, [59, 64–67]] models. SHOOTGRO is slightly more developmentally detailed for canopy processes than MODWht3, but less detailed in the root system and simulating biomass production. SHOOTGRO provides the foundation to simulate the development and growth of individual phytomers (and phytomer components as shown in Fig. 9) on each morphologically identified shoot (main stem and tillers) on the median plant of up to six age classes, or cohorts, based on time of seedling emergence.

The Sirius model has one of the most developed and robust leaf appearance sub-models of any wheat simulation model [68]. As with the MODWht3 and SHOOTGRO models, the assumption used is that the developmental "clock" from emergence to anthesis is best represented by the rate of leaf appearance and final number of leaves, rather than thermal time. Based on vernalization requirement and photoperiod sensitivity of the variety being simulated and leaf ontogeny, the final leaf number is determined [69, 70]. This allows for an elegant quantitative description of both spring and winter wheat leaf appearance and integration with developmental events.

Regardless of modeling approach and goals, the ability to simulate genotype phenology across a broad range of environments for major crops such as wheat has been quite reliable. Many alternative approaches exist for predicting phenology, and approaches differ in input requirements and number of developmental stages simulated. Essentially all models are based on the thermal time approach, reflecting the importance of temperature discussed in Section Developmental

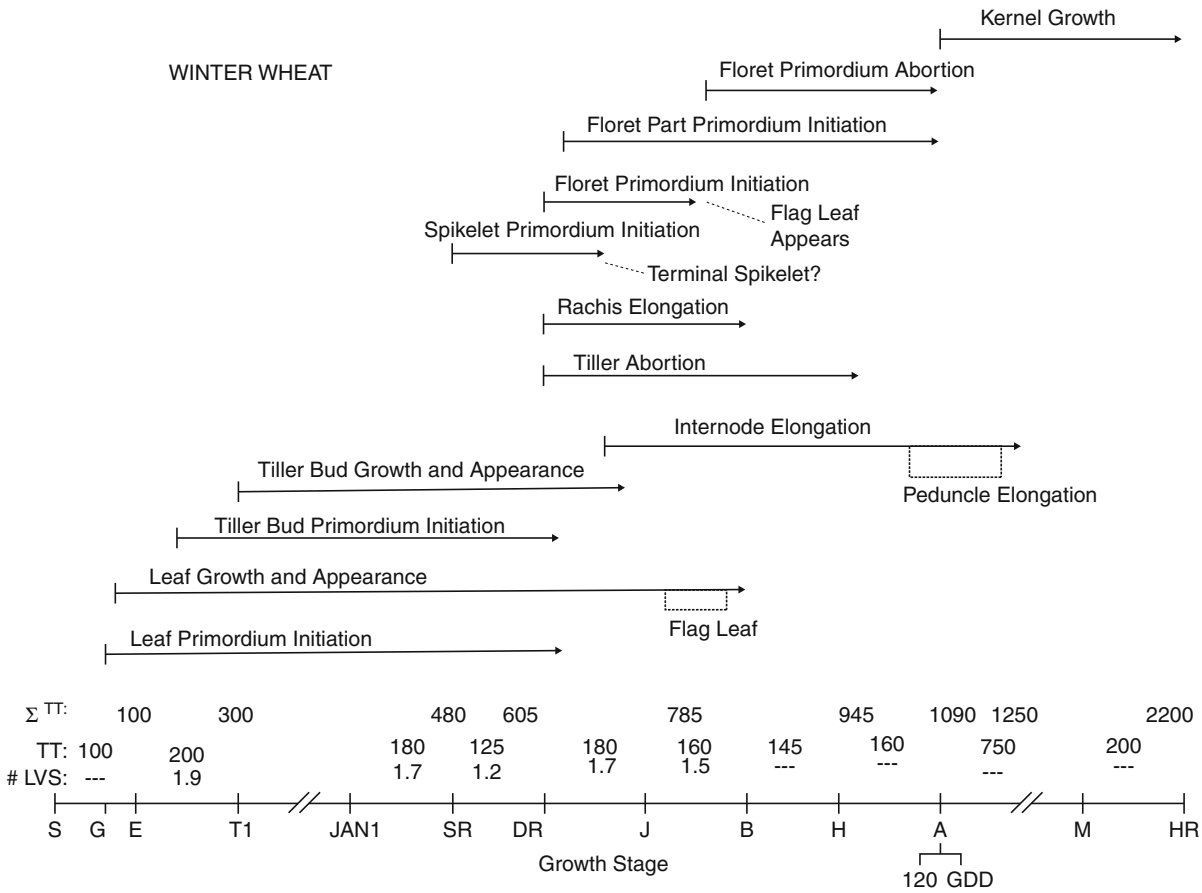

Crop Development Related to Temperature and Photoperiod. Figure 9
Developmental sequence diagram of a generic winter wheat for optimal conditions. Question marks refer to uncertainty, important cultivar variation, or conflicting reports in the literature. Time line legend is TT is the thermal time for the interval; #LVS is number of leaves for the interval; S, sowing date; G, germination; E, seedling emergence; TI, tiller initiation/appearance; SR, single ridge stage; DR, double ridge stage; J, jointing; B, booting; H, heading; A, anthesis; and M, physiological maturity (From [59])

Response to Temperature. An alternative to a strict thermal time approach, particularly for small-grain cereals, has been to use leaf numbers to estimate the time interval between developmental stages. In phenology sub-models, temperature effects are well considered, but rarely are the effects of water deficits (or nutrient availability) considered [71]. Exceptions include the SHOOTGRO model and PhenologyMMS (http://arsagsoftware/ars.usda.gov).

Determining plant parameters and how to address the genotype by environment interaction are common concerns for all models. With the explosion of genome mapping and molecular biology research, opportunities for understanding and resolving these issues are emerging [72–74]. For example, the presence or absence of known alleles influencing a trait can be used to determine the parameters used in the algorithm representing the process [75] or the response to environmental factors [76]. Clarification of gene networks controlling processes such as time of flowering has considerably advanced the understanding and simulation of these processes [77].

Crop simulation modeling is increasingly benefiting from the advent of object-oriented design and programming languages such as C++, C#, and Java, both in terms of developing and maintaining models as

well as providing greater flexibility in representing plant processes within models. Initial object-oriented designs tended to view the plant as a collection of objects that equate to leaf, stem, root, and seed components. Recent attempts have begun to incorporate the phytomer approach of building plant canopies into the object-oriented design that can also be scaled up, or aggregated, into lower levels of resolution, such as the seed component of earlier designs [78–80].

Future Directions

Crop development is regulated by environmental factors that interact with the genetics of the plant. Many developmental responses related to temperature and photoperiod are well known and it is possible to predict them reasonably well at the crop level. Similarly, rapidly emerging knowledge from genomics research is helping to provide understanding of the genetic basis of certain aspects of crop development. Unfortunately, the quantitative integration of genetic and physiological knowledge is largely unknown, and both genetic and physiological models would benefit from better integration of knowledge. For example, the genetic basis of photoperiod and vernalization pathways is fairly well known and as new genomic studies are carried out, more complex models are being built [81] showing the complexity of flowering time. However, the genetic mechanisms described in this entry interact with responses to other environmental factors defining a network of signaling a highly complex response that is not fully understood.

Knowledge in crop development has greatly benefited from research in model organisms; however there are key differences, like the lack of the vernalization gene *FLC* in temperate cereals. For example, four vernalization genes have been described in wheat, but only three have been cloned and located in the vernalization pathway. Completing this pathway would greatly increase the understanding of how temperate crops respond to nonfreezing cold temperatures. At the same time, the physiological response to temperature has been extensively studied, and genetic differences are well documented; however, the basis of genetic effects is not known. It is encouraging that new genes (e.g., *Eps-1*) are being identified, but the quantitative variation of crop development, once major processes (photoperiod and vernalization requirements) are solved, requires the identification of new genes, probably of small effect. For example, a recent study in maize found no large effect QTL for flowering time in a nested mapping population [82]. Although no major epistatic or environmental interactions were found, the individual QTL effect varied across founder lines of the population [82]. QTL or gene effects need to be accurately determined to build quantitative genetic models.

Bibliography

1. Heun M, Schafer-Pregl R, Klawan D, Castagna R, Accerbi M, Borghi B, Salamini F (1997) Site of einkorn wheat domestication identified by DNA fingerprinting. Science 278(80):1312–1314
2. Zohary D, Hopf M (2000) Domestication of plants in the old world. Oxford University Press, Oxford
3. Goethe JWV (2009) The metamorphosis of plants (re-print). MIT Press, Cambidge, MA, 123
4. Gray A (1879) Structural botany: or organography on the basis of morphology. Ivison Blakeman Taylor, New York/Chicago
5. Bateson W (1894) Materials for the study of variation treated with special regard to discontinuity in the origin of species. Macmillan, London
6. Wilhelm WW, McMaster GS (1995) Importance of the phyllochron in studying development and growth in grasses. Crop Sci 35:1–3
7. Jewiss O (1972) Tillering in grasses – its significance and control. J Br Grassl Soc 27:65–82
8. Klepper B, Rickman R, Belford R (1983) Leaf and tiller identification on wheat plants. Crop Sci 23:1002–1004
9. Klepper B, Rickman R, Peterson C (1982) Quantitative characterization of vegetative development in small cereal grains. Agron J 74:789–792
10. Haun JR (1973) Visual quantification of wheat development. Agron J 65:116–119
11. Klepper B, Tucker T, Dunbar B (1983) A numerical index to assess early inflorescence development in wheat. Crop Sci 23:206–208
12. Wilhem W, McMaster G (1996) Spikelet and floret naming scheme for grasses with spike inflorescence. Crop Sci 36:1071–1073
13. McMaster G (2005) Phytomers, phyllochrons, phenology and temperate cereal development. J Agric Sci 143:137–150
14. Askenasy E (1888) Über eine neue methode, um die vertheilung der wachstumsintensität in wachsenden theilen zu bestintaien. Verh Naturh Med Verl Heidelberg 2:70–153
15. Tesarová J, Nátr L (1990) Phyllochron and winter barley leaf growth rate. Biol Plant 32:450–459
16. Milthorpe F (1956) The relative importance of the different stages of leaf growth in determining the resultant area. In: Milthorpe F (ed) The Growth of Leaves. Proceedings of the 3rd Easter School in Agricultural Science, University of Nottingham, Nottingham, Butterwoths, London, pp 20–38

17. Esau K (1965) Plant anatomy. Wiley, New York
18. Bunting A, Drennan D (1966) Some aspects of the morphology and physiology of careal in the vegetative phase. In: Milthorpe F, Ivins J (eds) The Growth of Cereal and Grasses, Proceedings of 12th Easter School of Agricultural Science, University of Nottingham, Nottingham, Butterwoths, London, pp 20–38
19. Barthélémy D, Caraglio Y (2007) Plant architecture: a dynamic, multilevel and comprehensive approach to plant form, structure and ontogeny. Ann Bot 99:375–407
20. Large EC (1954) Growth stages in cereals illustration of the feekes scale. Plant Pathol 3:128–129
21. Zadoks J, Chang T, Konzak C (1974) A decimal code for the growth stages of cereals. Weed Res 14:415–421
22. Lancashire P, Bleiholder H, Boom T, Langelüddeke P, Strauss R, Weber E, Witzenberger A (1991) A uniform decimal code for growth stages of crops and weeds. Ann Appl Biol 119:561–601
23. McMaster G (2009) The development of the wheat plant. In: Carver B (ed) Wheat science and trade. Willey-Blackwell, Ames, pp 31–55
24. Reamur R (1735) Observations du thermomètre, faites è paris l'année 1735, comparées à celles qui ont été faites sous la ligne à l'Isle de france, à alger et en quelques-unes de nos isles de l'amérique. Mem Acad Roy Sci, Paris, France
25. Cao W, Moss DN (1989) Temperature effect on leaf emergence and phyllochron in wheat and barley. Crop Sci 29:1018–1021
26. Friend D, Helson V, Fisher J (1962) Leaf growth in marquis wheat, as regulated by temperature, light intensity, and daylength. Can J Bot 40:1299–1311
27. Jame YW, Cutforth HW, Ritchie JT (1998) Interaction of temperature and daylength on leaf appearance rate in wheat and barley. Agric For Meteorol 92:241–249
28. Yan W, Hunt L (1999) An equation for modelling the temperature response of plants using only the cardinal temperatures. Ann Bot 84:607–614
29. Chouard P (1960) Vernalization and its relations to dormancy. Ann Rev Plant Physiol 11:191–238
30. Flood R, Halloran G (1984) The nature and duration of gene action for vernalization response in wheat. Ann Bot 53:363–368
31. Ahrens J, Loomis W (1963) Floral induction and development in winter wheat. Crop Sci 3:463–466
32. Miao G, Zhang Y, Hou Y, Yin J, Wang S (1992) Effects of vernalization and photoperiod on leaf number of main stem in wheat. Acta Agron Sin 16:321–330
33. Wang S, Ward R, Ritchie J, Fischer R, Schulthess U (1995) Vernalization in wheat. I. A model based on the interchangeability of plant age and vernalization duration. Field Crop Res 41:91–100
34. Yan L, Loukoianov A, Tranquilli G, Helgera M, Fahima T, Dubkovsky J (2003) Positional cloning of the wheat vernalization gene VRN1. Proc Natl Acad Sci USA 100:6263–6268
35. Yan L, Loukoianov A, Blechl A, Tranquilli G, Ramakrishna W, SanMiguel P, Bennetzen JL, Echenique V, Dubcovsky J (2004) The wheat VRN2 gene is a flowering repressor down-regulated by vernalization. Science 303(80):1640–1644
36. Yan L, Fu D, Li C, Blechl A, Tranquilli G, Bonafede M, Sanchez A, Valarik M, Yasuda S, Dubcovsky J (2006) The wheat and barley vernalization gene VRN3 is an orthologue of ft. Proc Natl Acad Sci USA 103:19581–19586
37. Kurup S, Jones HD, Holdsworth MJ (2000) Interactions of the developmental regulator abi3 with proteins identified from developing *Arabidopsis* seeds. Plant J 21:143–155
38. Yoshida T, Nishida H, Zhu J, Nitcher R, Distelfeld A, Akashi Y, Kato K, Dubcovsky J (2010) VRN-D4 is a vernalization gene located on the centromeric region of chromosome 5D in hexaploid wheat. Theor Appl Genet 120:543–552
39. Garner W, Allard H (1920) Effect of the relative length of day and night and other factors of the environment on growth and reproduction in plants. J Agric Res 18:553–606
40. Borlaug NE (1983) Contributions of conventional plant breeding to food production. Science 219(80):689–693
41. Cao W, Moss DN (1989) Daylength effect on leaf emergence and phyllochron in wheat and barley. Crop Sci 29:1021–1025
42. Warrington IJ, Kanemasu ET (1983) Corn growth response to temperature and photoperiod. II. Leaf-initiation and leaf-appearance rates1. Agron J 75:755–761
43. Turner A, Beales J, Faure S, Dunford R, Laurie D (2005) The pseudo-response regulator ppd-h1 provides adaptation to photoperiod in barley. Science 310(80):1031–1034
44. Mizuno T, Nakamichi N (2005) Pseudo-response regulators (prrs) or true oscillator components (tocs). Plant Cell Physiol 46:677–685
45. Griffiths S, Dunford RP, Coupland G, Laurie DA (2003) The evolution of constans-like gene families in barley, rice, and *Arabidopsis*. Plant Physiol 131:1855–1867
46. Song YH, Ito S, Imaizumi T (2010) Similarities in the circadian clock and photoperiodism in plants. Curr Opin Plant Biol 13(5):594–603
47. Beales J, Turner A, Griffiths S, Snape JW, Laurie DA (2007) A pseudo-response regulator is misexpressed in the photoperiod insensitive Ppd-D1a mutant of wheat (triticum aestivum l.). Theor Appl Genet 115:721–733
48. Baker C, Gallagher J, Monteith J (1980) Daylength and leaf appearance in winter wheat. Plant Cell Environ 3:285–287
49. Cao W, Moss DN (1989) Temperature and daylength interaction on phyllochron in wheat and barley. Crop Sci 29:1046–1048
50. Ellis R, Roberts E, Summerfield R, Cooper J (1988) Environmental control of flowering in barley (Hordeum vulgare l). II. Rate of development as a function of temperature and photoperiod and its modification by low-temprateure vernalization. Ann Bot (Lond) 62:156–158
51. Slafer GA, Rawson HM (1996) Responses to photoperiod change with phenophase and temperature during wheat development. Field Crop Res 46:1–13
52. Distelfeld A, Li C, Dubcovsky J (2009) Regulation of flowering in temperate cereals. Curr Opin Plant Biol 12:178–184
53. Sung S, Amasino RM (2004) Vernalization and epigenetics: how plants remember winter. Curr Opin Plant Biol 7:4–10

54. Appendino ML, Slafer GA (2003) Earliness per se and its dependence upon temperature in diploid wheat lines differing in the major gene eps-A^m1 alleles. J Agric Sci 141:149–154
55. Faricelli M, Valárik M, Dubcovsky J (2010) Control of flowering time and spike development in cereals: the earliness per se eps-1 region in wheat, rice, and brachypodium. Funct Integr Gen 10:293–306
56. McMaster G, Ascough II J (2010) Crop management to cope with global change: a systems perspective aided by information technologies. In: Araus J, Slafer G (eds) Crop Stress Management & Climate Change. CAB International, Wallingford
57. Norman J (1979) Modeling complete crop canopy. In: Barfield B, Gerber J (eds) Modification of the aerial environment of plants. American Society of Agricultural Engineers, St. Joseph, pp 249–277
58. Grant R (2001) A review of the Canadian ecosystem model – ecosys. In: Shaffer M, Ma L, Hansen S (eds) Modeling carbon and nitrogen dynamics for soil management. Lewis, Boca Raton, pp 173–263
59. McMaster G, Wilhelm W, Morgan J (1992) Simulating winter wheat shoot apex phenology. J Agric Sci Cam 119:1–12
60. Weir A, Bragg P, Porter J, Rayner J (1984) A winter wheat crop simulation model without water or nutrient limitations. J Agric Sci Cam 102:371–382
61. Porter J (1984) A model of canopy development in winter wheat. J Agric Sci 102:383–392
62. Porter J (1993) Afrgwheat2: a model of the growth and development of wheat incorporating responses to water and nitrogen. Eur J Agron 2:69–82
63. Rickman R, Waldman S, Klepper B (1996) Modwht3: a development-driven wheat growth simulation. Agron J 88:176–185
64. Zalud Z, McMaster G, Wilhelm W (2003) Evaluating SHOOTGRO 4.0 as a potential winter wheat management tool in the Czech Republic. Eur J Agron 19:495–507
65. McMaster G, Klepper B, Rickman R, Wilhelm W, Willis W (1991) Simulation of shoot vegetative development and growth of unstressed winter wheat. Ecol Mod 53:189–204
66. Wilhelm W, McMaster G, Rickman R, Klepper B (1993) Aboveground vegetative development and growth as influenced by nitrogen and water availability. Ecol Mod 68:183–203
67. McMaster G, Morgan J, Wilhelm W (1992) Simulating winter wheat spike development and growth. Agric For Meteor 60:193–220
68. Jamieson P, Brooking I, Semenov M, McMaster G, White J, Porter J (2007) Reconciling alternative models of phenological development in winter wheat. Field Crop Res 103:36–41
69. Brooking I, Jamieson P, Porter J (1995) The influence of daylength on the final leaf number in spring wheat. Field Crop Res 41:155–165
70. Brooking I (1996) The temperature response of vernalization in wheat – a developmental analysis. Ann Bot 78:507–512
71. McMaster G, Wilhelm W (2003) Simulating wheat and barley phenological responses to water and temperature stress. J Agric Sci Cam 141:129–147
72. White J, Hoogenboom G (2003) Gene-based approaches to crop simulation: past experiences and future opportunities. Agron J 95:52–64
73. Edmeades G, McMaster G, White J, Campos H (2004) Genomics and the physiologist: bridging the gap between genes and crop response. Field Crop Res 90:5–18
74. White J (2006) From genome to wheat: emerging opportunities for modeling wheat growth and development. Eur J Agron 25:79–88
75. White J, McMaster G, Edmeades G (2004) Physiology, genomics and crop response to global change. Field Crop Res 90:1–3
76. Weiss A, Baenziger P, McMaster G, Wilhelm W, Al Ajlouni Z (2009) Quantifying phenotypic plasticity using genetic information for simulating plant height in winter wheat. Wagen J Life Sci 57:59–64
77. Welch S, Roe J, Dong Z (2003) A genetic neural network model of flowering time control in *Arabidopsis thaliana*. Agron J 95:71–81
78. Dingkuhn M, Luquer D, Quilot B, Reffye P (2005) Environmental and genetic control of morphogenesis in crops: towards models simulating phenotypic plasticity. Aus J Agric Res 56:1289–1302
79. Vos J, Marcelis L, de Visser P, Struik P, Evers J (2007) Functional-structural plant modelling in crop production. Springer, The Netherlands
80. McMaster G, Hargreaves J (2009) Canon in design: composing scales of plant canopies from phytomers to whole-plants using the composite design pattern. Wagen J Life Sci 57:39–51
81. Higgins JA, Bailey PC, Laurie DA (2010) Comparative genomics of flowering time pathways using *Brachypodium distachyon* as a model for the temperate grasses. PLoS ONE 5:e10065
82. Buckler ES, Holland JB, Bradbury PJ, Acharya CB, Brown PJ, Browne C, Ersoz E, Flint-Garcia S, Garcia A, Glaubitz JC et al (2009) The genetic architecture of maize flowering time. Science 325(80):714–718

Crop Diseases, Management and Control of

Dale R. Walters
Crop & Soil Systems Research Group, Scottish Agricultural College, Edinburgh, UK

Article Outline

Glossary
Definition of the Subject
Introduction: The Need for Disease Control in Crops
Controlling Crop Diseases
Future Directions
Bibliography

Glossary

Biotroph A plant pathogenic microorganism which requires living host tissue in order to complete its life cycle. Rust and powdery mildew fungi are examples of biotrophs, as are viruses.

Oomycetes Also known as water molds, the Oomycetes are a large group of terrestrial and aquatic organisms. They superficially resemble fungi in mycelial growth and mode of nutrition, but molecular studies and distinct morphological characteristics place them in the kingdom Stramenopila (or Chromista) with brown and golden algae and diatoms.

Phytoalexin Antimicrobial substances synthesized de novo by plants and which accumulate rapidly at areas of infection by an incompatible pathogen. Phytoalexins are broad spectrum in action and are chemically diverse with different types characteristic of particular plant species. They can be grouped into several classes including terpenoids, alkaloids, phenolics.

Saprophyte An organism, e.g., a fungus or bacterium, that grows on and derives its nourishment from dead or decaying organic matter.

Virulence Refers to the relative ability of a pathogenic organism to cause disease.

Definition of the Subject

Plant diseases cause substantial crop losses every year and, historically, have led to considerable economic damage and human suffering. Controlling plant diseases is therefore vital to maintaining crop productivity and feeding the ever expanding human population. Crop diseases can be controlled using a variety of methods, notably cultural approaches, the use of resistance in the plant, and the application of chemicals (fungicides). However, the organisms that cause plant disease (plant pathogens) are genetically adaptable and can overcome plant resistance, and the toxic effects of fungicides. Ensuring that crops are adequately protected depends therefore on continually keeping one step ahead of the pathogens by improving existing control measures and developing new approaches. This article provides an overview of the various methods, traditional and novel, used to control crop diseases.

Introduction: The Need for Disease Control in Crops

Plant disease has plagued mankind ever since the beginnings of agriculture. Today, despite the many advances in crop protection technology, crop diseases continue to wreck havoc on crops, because of the genetic adaptability of the pathogens which cause plant disease. Crop losses at farm level can have serious implications for growers, but crop disease can inflict much more serious damage on a larger scale. A good example of just how devastating crop disease can be is the potato blight epidemic of the 1840s in Europe. This disease, caused by the Oomycete pathogen *Phytophthora infestans*, decimated crops across Europe and in Ireland, led to the death of some one million people and the emigration of several million more [1, 2]. Astonishingly, today, more than 170 years later, potato blight still poses a major problem for potato growers across the globe.

Crop losses as a result of disease can be expressed in various ways, such as potential losses and actual losses. Potential loss compares yields in a system without any form of crop protection treatment, with yields from a system with a similar intensity of crop production, but receiving crop protection treatments. Actual losses are those sustained despite the use of crop protection [3]. The efficacy of crop protection can be calculated as the percentage of potential losses prevented. Potential losses range from 8.5% for cotton to 21.2% for potatoes, while actual losses range from 7.2% for cotton to 14.5% for potatoes, highlighting the importance of crop protection in reducing potential losses in all of these crops (Table 1).

Globally, agricultural production has grown faster than the human population over the past few decades [4]. In most parts of the world, this has been the result, not of increased area of cropped land, but of increased inputs, including pesticides [4]. In the period from 1963 to 2002, cereal yields increased by 114% globally, although the annual rate of growth fell from 3.14% in the period 1963–1976 to 0.84% in the period 1989–2002 [4]. In the period from 1960 to 2004, pesticide sales worldwide increased more than ten-fold to some $30 billion [3]. However, despite this increased pesticide use, crop losses as a result of pests, diseases, and weeds have not fallen significantly in the past 40 years.

Crop Diseases, Management and Control of. Table 1 Estimated loss potential and actual losses due to pathogens (fungi and bacteria) in six major crops worldwide in 2001–2003 (Adapted from [3])

Crop	Crop losses (%) due to pathogens	
	Potential	Actual
Wheat	15.6 [12–20]	10.2 [5–14]
Rice	13.5 [10–15]	10.8 [7–16]
Maize	9.4 [8–13]	8.5 [4–14]
Potatoes	21.2 [20–23]	14.5 [7–24]
Soybeans	11.0 [7–16]	8.9 [3–16]
Cotton	8.5 [7–10]	7.2 [5–13]

Controlling Crop Diseases

Crop disease can be controlled using a variety of approaches. The first line of defense is the exclusion of the pathogen through plant quarantine and, for example, the use of pathogen-free propagating material. The next line of defense is to exclude, eliminate, or reduce pathogen inoculum. This can be achieved in various ways, including cultural control, use of host plant resistance, and chemical control. Finally, several of these approaches might be used together in an integrated program of disease control. In the sections below, these disease control options will be examined in more detail.

Cultural Control

Cultural control aims to prevent contact with the pathogen, to create environmental conditions unfavorable to the pathogen or at least to avoid favorable conditions, or to reduce the amount of pathogen inoculum available to infect crop plants. Methods used include host eradication, crop rotation, sanitation, irrigation, tillage, and improving crop growth conditions, for example, through appropriate fertilizer use. Cultural control provides the foundation for disease control in crops, and yet its important is often overlooked.

Host Eradication Host eradication refers to the removal and disposal of whole infected plants. This method is used routinely in nurseries, greenhouses, and fields to prevent the spread of pathogens, since it eliminates the infected plants that act as a source of inoculum. In potato cultivation, pathogens can overwinter in infected tubers left in the field and give rise to infected plants (known as volunteers) in the spring. These volunteers can acts as sources of inoculum, and their removal from the field and subsequent destruction will reduce levels of pathogen inoculum.

If a pathogen requires two hosts to complete its life cycle, control is possible by eradication of the less important host. The wheat stem rust fungus, *Puccinia graminis* f.sp. *tritici*, is a case in point. It requires two hosts, wheat and barberry, to complete its life cycle and until the 1950s was the most important pathogen of wheat in the United States [5]. Since the 1950s, however, stem rust has declined in importance in the United States, due in part to successful eradication of its alternate host, common barberry [6].

Sanitation Sanitation refers to eliminating or reducing the amount of inoculum present by various means, including removal of infected plant parts and plant debris. Destroying crop residues is an important practice, but how it is performed depends upon the type of crop and the type of pathogen. For example, burying crop debris can destroy certain pathogens, particularly if the residues are plowed in deeply enough, while burning crop residue is common practice for cereal crops in some parts of the world and will destroy many pathogens. However, burning has some drawbacks, particularly loss of nutrients and increased soil erosion.

Crop Rotation Crop rotation is an ancient cultural practice and its benefits include maintenance of soil structure and organic matter, and a reduction in soil erosion that is often associated with continuous row crops [7]. The main purpose of rotating crops in conventional arable rotations is to reduce the incidence of diseases, pests, or weeds that are difficult to control with pesticides, and for this reason, short rotations of two to three crops are usually employed. In the United States, for example, the majority of the maize crop is grown on a 2–3 year rotation, while in the UK, barley and wheat usually form the main part of the rotation, with breaks of oilseed rape, beans, peas, or potatoes [8].

Continuous cropping with the same susceptible host plant will result in the establishment of a soil

population of pathogenic microbes. Crop rotation avoids this and is often associated with a reduction in crop diseases caused by soilborne pathogens [7]. Using nonhost or less susceptible crop plants in the rotation can lead to a decline in specific populations of plant pathogens in the soil and is best suited for biotrophs, since they require the presence of the specific living host for survival, or pathogens with low saprophytic ability [9, 10]. Crop rotation is less suitable for controlling root-inhabiting pathogens that survive saprophytically or can exist for long periods in soil, e.g., pathogens with tough survival structures such as *Rhizoctonia solani*, *Sclerotinia sclerotiorum,* and *Pythium* spp. [11, 12].

Tillage Tillage has indirect effects on pathogen spread and can also be used to reduce pathogen inoculum in the soil. Conventional tillage uses primary and secondary cultivation to prepare a seed-bed for planting and results in considerable soil disturbance, while reduced tillage uses a single cultivation, or even no cultivation (no-tillage, zero tillage, direct drilling), and as a result leads to minimal soil disturbance. Minimum tillage and no-tillage practices can be grouped together under the generic term: conservation tillage [13].

Tillage can bury pathogens deeper in the soil where they are less likely to become a problem. It can alter soil texture, aeration, temperature, moisture, and density, and can also influence nutrient release in the soil, with benefits to the crop [8]. Tillage also leads to clear fluctuations in microbial activity and biomass in the soil [14]. Reduced tillage or no-till is often associated with higher microbial biomass and activity in upper soil layers compared to regular tillage (plowing) [15]. This concentration of crop debris in the top layers of the soil can promote the overwintering and survival of numerous pathogens and has prompted concern that increased disease and decreased yields will be the inevitable result of using conservation tillage practices. Although this has proved to be the case under some conditions, there have also been reports of decreases in the incidence of soilborne diseases. As suggested by Sturz et al. [13], such contradictory reports may reflect differences in root development and soil microbial biomass and activity under the different regimes. Thus, conservation tillage practices can lead to pathogen inoculum concentrations several orders of magnitude greater than those found under conventional tillage [16, 17] and, as a result, plant roots growing in the upper soil layers might be more prone to pathogen infection [13]. In contrast, increased microbial biomass and activity in the top soil layers can give rise to greater root density and root activity [18, 19], which may offset the damaging effects of disease on yield, and might also provide a highly competitive soil environment with resulting disease suppressive effects [20].

Severity of tan spot in wheat was found to increase under no-till conditions, but was reduced following reduced tillage [21]. To control blackleg (*Leptosphaeria maculans*) on canola (oilseed rape), it is recommended that crop debris is buried in the autumn and a nonhost crop be direct seeded the following spring to avoid reexposing the buried residue [22, 23]. Recent research suggests that inoculum production by *L. maculans* decreased with increasing duration of stubble burial in the field over 10 months before stopping completely [24]. This effect may be due to the mycobiota associated with the buried stubble, and these workers suggest that it might be possible to manipulate the population of saprophytic microbiota present on oilseed rape stubble to facilitate the decline of *L. maculans* [24].

Sowing Practices

Time of Sowing Altering the time of sowing to avoid high levels of pathogen inoculum or conditions conducive for development of a particular disease can lead to reduced severity of several crop diseases. For example, in the UK, sowing winter oilseed rape in August rather than September exposes the earlier sown crop to inoculum from stubble of the previous crop, resulting in more severe *Alternaria* infection on pods. In contrast, the risk of infection is reduced in the later sown crop because the stubble is buried by tillage [25]. Late sowing may also be recommended for autumn-sown barley crops, in order to decrease exposure of newly emerging seedlings to inoculum of *Rhynchosporium secalis* produced on previous barley crops in the area [26].

Depth of Sowing Sowing depth can influence the risk of infection, since the preemergence stage of the seedling, which is usually more susceptible to pathogen

infection, is longer when seeds are sown deeper. In *Brassica rapa*, for example, rapid emergence of seedlings reduces preemergence damping-off because the period of contact between the emerging seedlings and *R. solani* in the soil is reduced [27]. Thus, significantly higher seedling emergence was reported for several cultivars of *B. rapa* sown at a depth of 1.5 cm compared to 3.0 cm [27].

Crop Density Crop density can exert considerable influence over disease incidence due to the ease with which pathogen inoculum can be transferred between closely spaced plants and alterations in crop microclimate. In densely planted crops, temperatures are more uniform, humidity is increased, and leaves are wet for longer, all of which provides favorable conditions for pathogen infection and subsequent development. Crop density can be manipulated in various ways, e.g., sowing, pruning, and fertilization.

Soil Amendments: Mulching, Fertilizers, and Organic Amendments

Mulches Mulches are used to conserve organic matter and moisture and to reduce soil erosion. A variety of materials can be used as mulches, including straw, manure, plastics, and paper. Mulching can lead to water retention and nutrient enrichment in the soil and can decrease soil temperature, all of which can influence pathogen infection and disease development in plants. Although mulching can reduce the spread of splash dispersed pathogens, by altering the environment, it could lead to increased severity of some diseases. Further, if crop residues are used in mulching, disease incidence could increase since the residues could be used as a food source by a range of pathogens.

Fertilizers Adequate mineral nutrition is central to crop production, and can also exert considerable influence on disease development [28, 29]. Below, the influence of nitrogen, phosphorus, potassium, calcium, and silicon on plant disease will be dealt with briefly.

Nitrogen Using nitrogen fertilizer above recommended rates can lead to increased disease incidence and lesion area. This has been shown for biotrophic fungal pathogens such as powdery mildews and rusts [30, 31] and necrotrophic pathogens such as *Magnaporthe grisea*, the cause of rice blast [32]. It is commonly thought that application of nitrogen fertilizer can increase disease severity via effects on crop canopy development. Thus, large canopies with high shoot densities may be more conducive to spore transfer and pathogen infection than sparse canopies. For example, nitrogen has been shown to increase the severity of *Fusarium* head blight in wheat, and it has been suggested that this might be the result of a nitrogen-induced increase in canopy size, leading to an altered microclimate [33]. In contrast, work on yellow rust on winter wheat suggested that the impact of nitrogen on disease was the result of effects of nitrogenous substances in wheat leaves on pathogen growth, rather than effects on canopy growth and microclimate [34].

But nitrogen is not always associated with increased crop disease. Indeed, various studies have reported no effect of nitrogen on disease severity (e.g., [35, 36]), while Hoffland et al. [31] found that the effect of nitrogen depended on the type of pathogen. Thus, nitrogen increased susceptibility of tomato to the powdery mildew pathogen *Oidium lycopersicum* and the bacterial pathogen *Pseudomonas syringae* pv. *tomato,* while it had no effect on susceptibility to the vascular wilt pathogen *Fusarium oxysporum* f.sp. *lycopersici* [31]. In contrast, tomato plants were more susceptible to *Botrytis cinerea* when grown under low nitrogen conditions [37]. These results do not support the view that nutrient-limited plants are better defended [38, 39]. It seems that generalizing about the effects of nitrogen on plant disease is unwise, and practically, although manipulation or assessment of crop nitrogen status might be used as part of disease control strategies, the approach adopted will depend on the crop and the pathogens from which it is most at risk [29].

Phosphorus In general, phosphorus fertilization tended to improve plant health, with reductions in disease recorded in 65% of cases studied by Perrenoud [40]. Nevertheless, phosphorus fertilization increased disease and pest problems in 28% of the cases examined [40]. As with nitrogen, the effects of phosphorus on plant disease might be the result of direct effects on the pathogen, host plant metabolism, leading to effects on pathogen food supply, and effects on plant defenses [29]. Indeed, foliar application of phosphate salts has been shown to induce resistance to pathogens in

a range of crop plants, including cucumber [41], broad bean [42], grapevine [43], maize [44] and rice [45].

Clearly, an adequate phosphorus supply is important for crop growth and in turn, may well help to reduce disease. However, the regime of phosphorus fertilizer used will depend on a range of factors, including the crop and the pathogens likely to be important. Reuveni and Reuveni [46] suggested that foliar-applied phosphate might be used as part of an integrated disease control program. However, grower adoption of such an approach will depend on the existence of other, effective disease control measures and the economics of disease control in the particular crop.

Potassium There are many reports that potassium is associated with disease reductions [47]. However, as these authors point out, inadequate consideration has been given to the effects of associated anions, nutrient balance, and nutrient status, to allow the definitive role of potassium to be determined. Thus, it has been suggested that in some cases, the effects of potassium, applied as potassium chloride fertilizer, might be due to the chloride ion rather than potassium [48]. Further, chloride fertilization has been shown to suppress disease in cereal crops [49].

There has been much interest in the application of fertilizers to crop foliage, including the effects of foliar fertilizer application for crop disease control [46, 50]. Foliar-applied potassium chloride has been shown to control *Blumeria graminis* and *Septoria tritici* on wheat in field studies [51, 52], probably due to osmotic effects on the fungal pathogens, disrupting pathogen development and subsequent infection [52, 53].

Application of potassium to deficient soils usually increases plant resistance to diseases [47]. This might be partly related to the effect of potassium in increasing epidermal cell wall thickness or disease escape as a result of vigorous crop growth [47], although the mechanisms by which potassium affects plant disease are not well understood.

Calcium There are many reports that application of calcium to soils, foliage, and fruit reduces the incidence and severity of a range of diseases of crops, including cereals, vegetable crops, legumes, fruit trees, as well as postharvest diseases of tubers and fruits [54]. For example, calcium has been shown to inhibit anthracnose (caused by *Colletotrichum gloeosporiodes* or *C. acutatum*) in apples [55] and to decrease postharvest disease development on strawberry [56], while treatment of tomato with calcium carbonate reduced fusarium crown rot disease [57]. In contrast, Nam et al. [58] could find no effect of calcium on anthracnose on strawberry. Because calcium increases resistance of plant cell membranes and cell walls to microbial enzymes, increasing calcium concentrations in storage organs could lead to enhanced resistance to pathogens [59, 60]. However, the form in which the calcium is applied can influence the mechanism by which calcium affects disease. For example, the addition of lime can affect disease by altering pH, while calcium salts (e.g., propionate) can be directly inhibitory to pathogens [54]. Making general recommendations for the use of calcium in plant disease control would be unwise, due to the range of crops and pathogens affected by calcium application. Instead, the appropriate amount and form of calcium to apply need to be determined for individual crop–pathogen interactions. The dwindling availability of fungicides, together with increasing public concern for the environment means that the use of calcium to control plant disease, especially postharvest, is attracting increased attention.

Silicon The effects of silicon in reducing disease severity have been known since 1940 [61]. However, it was not until the 1980s that more detailed work was carried out in this area. Thus, cucumbers grown in nutrient solutions supplemented with silicon were found to have significantly less powdery mildew infection than plants not receiving silicon supplementation [62, 63]. Indeed, silicon has been shown to suppress both foliar and soilborne pathogens in cucurbits [64] and to reduce susceptibility of rice to various pathogens [65]. Wheat grown in soil amended with silicon showed reduced infection by several pathogens, including *B. graminis* f.sp. *tritici, S. tritici,* and *Oculimacula yallundae* (Fig. 1) [66, 67].

It has been suggested that the effects of silicon in providing disease control are due to the creation of a mechanical barrier to penetration [68]. However, this has been disputed by studies which could find no evidence for the creation of a physical barrier following silicon treatment in wheat inoculated with powdery mildew and bitter gourd and tomato inoculated with *Pythium aphanidermatum* [69, 70]. Rather, several

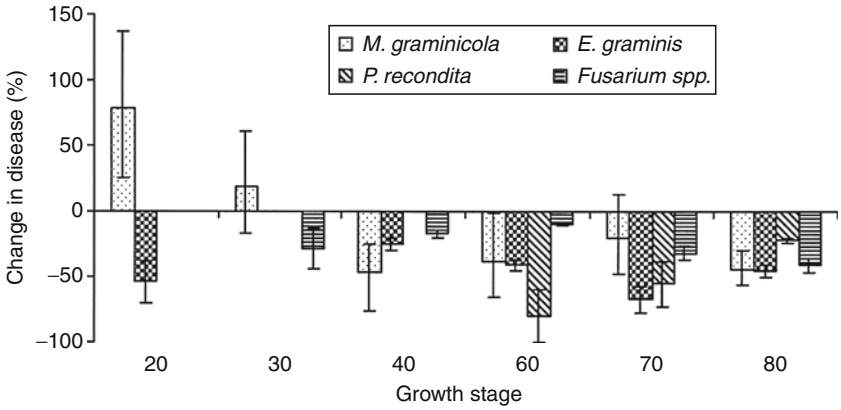

Crop Diseases, Management and Control of. Figure 1
Changes in disease in plots with incorporated straw. Bars show the difference between straw-treated and control plots as a percentage of the average in the control plots. For *Mycosphaerella graminicola,* the data are for severity on the top three living leaves; for other diseases, they refer to incidence. For *M.graminicola*, errors bars were calculated on the transformed scale and back-transformed; for other diseases, no transformation was needed (From [66])

studies have suggested that silicon activates defenses in plants. For example, in wheat inoculated with *B. graminis* f.sp. *tritici*, epidermal cells of silicon-treated plants were shown to react to attempted infection with specific defenses, including papilla formation and callose production [71]. In the rice–*M. grisea* pathosystem – silicon-mediated resistance was found to be associated with accumulation of antimicrobial compounds at infection sites, including diterpenoid phytoalexins [72]. In fact, phytoalexin accumulation occurs in silicon-mediated resistance in both dicots and monocots and since phytoalexins are highly specific to plant species, it has been suggested that silicon might be acting on mechanisms shared by all plant species, e.g., those resulting in activation of plant stress genes [73].

Organic amendments Organic amendments include animal manure, solid wastes, and composts. Such amendments are often used to improve soil quality, usually by contributing to general suppressiveness through enhanced microbial biomass and activity [7]. Organic amendments are rich in labile carbon fractions which are an energy source for microorganisms, and moreover, they can themselves contain antagonistic microbes. A substantial body of data indicates that organic materials can reduce incidence of diseases caused by a range of plant pathogens [74, 75].

Irrigation Although an adequate water supply is vital to crop production, irrigation can play a detrimental rather than a beneficial role in managing plant diseases. For example, irrigation water can spread pathogen propagules and under dry conditions, can prevent desiccation of such propagules, thereby effectively increasing the level of inoculum in soil. Watering from overhead prolongs leaf wetness, thereby providing favorable conditions for germination and infection by fungal spores. Overhead watering also increases the risk of splash-dispersal of spores, thus increasing pathogen spread. However, irrigation can be used to reduce the level of pathogen inoculum. Thus, the activity of microbes that destroy fungal sclerotia can be increased by alternate wetting and drying of the soil. Generally, drip or trickle irrigation, which delivers water directly to the root zone at a rate insufficient to lead to pathogen spread, is least likely to encourage disease development.

Use of Host Resistance

Most plants are resistant to most microbes. Thus, wheat plants are not affected by pathogens of tomato, and vice versa. This is known as nonhost resistance. However, every plant is attacked by its own pathogens, e.g., barley is attacked by the barley powdery mildew fungus, *B. graminis* f.sp. *hordei*, although it might not

be able to defend itself equally well against all pathogens that are able to attack it. This ability of plants to resist attack by pathogens is genetically determined, but the diversity of types of genetic control of this resistance, and of conditions required for their expression, has led to a bewildering number of classifications of resistance types in plants. To complicate matters further, in some cases, different terms used by different authors are synonymous, while in other cases, the terms might be based on different criteria.

Types of Resistance

Seedling and Adult Plant Resistance Seedling resistance operates from the onset of plant growth and is effective throughout the life of the plant. It is generally controlled by single genes and is effective in the absence of matching virulence in the pathogen. In contrast, adult plant resistance (APR) covers a broad range of resistance types all of which are not effective at the plant's seedling stage. APR tends to be controlled by a number of genes, which might operate through a wide variety of mechanisms.

Polygenic and Oligogenic Resistance Resistance controlled by one, or at most two or three genes, is known as oligogenic. Here, a single gene can confer complete resistance. A gene conferring such resistance is often referred to as a major gene. Where resistance is controlled by a larger number of genes, it is known as polygenic. Genes conferring polygenic resistance are often referred to as minor genes.

Race-specific and Race-nonspecific Resistance The terms race-specific and race-nonspecific sought to differentiate between resistance that was subject to loss of effectiveness with the appearance of new virulent strains of a pathogen and resistance that was thought would never be lost because the pathogen was not capable of developing virulence to it. A major problem with these terms has been a lack of evidence to suggest that any particular resistance was race-nonspecific. The assumption was generally made that genes of large effect (major or seedling genes) were race-specific and genes of small effect (minor genes or APR) were race-nonspecific. This has subsequently and comprehensively been shown not to be the case in many host–parasite systems.

Vertical and Horizontal Resistance These terms were introduced to convey the difference between race-specific and race-nonspecific resistance [76]. In vertical resistance, there tends to be a high level of resistance by the host to some races of the pathogen and a low level of resistance to others, while in horizontal resistance, resistance tends to be exhibited equally to all races of the pathogen. Vertical resistance has also been denoted as specific resistance and horizontal resistance as general resistance. However, although the specific nature of some types of resistance can usually be established fairly easily, it is much more difficult to prove that resistance is truly general, since there is always the chance of a new pathogen race appearing with the ability to overcome the resistance.

Qualitative and Quantitative Resistance These terms are a rough match for seedling/APR and vertical/horizontal resistance, with qualitative resistance referring to a high level of resistance controlled by a single gene and quantitative resistance being controlled by several genes of smaller effect. The term "quantitative" subsequently came to be used to describe locations on chromosomes where genes of small effect were identified through mapping studies, hence "quantitative trait locus" or QTL. More recently the use of the term QTL has come to be used for major gene loci as well.

Partial Resistance Partial resistance was originally used in studies of the resistance in barley to leaf rust caused by *Puccinia hordei*. It describes resistance that reduced the rate of epidemic development despite having a susceptible reaction type [77]. Resistance to leaf rust was found to be governed by up to 6–7 minor genes with additive effects and was correlated with increased latency period and reduced infection frequency, pustule size, infectious period, and spore production. The term is now used more generally to describe any resistance that is only partially effective in reducing disease expression and is usually synonymous with minor gene resistance.

Durable Resistance Durable resistance was suggested for use by Johnson and Law [78] to refer to rust resistance in wheat that in practice had provided stable resistance in varieties that had been grown over

a large area for many years. The term specifically avoided identifying the resistance with particular phenotypes or suggesting that the resistance would never be lost to a change in pathogen virulence. Specific well-studied examples are the *Sr2* and *Rpg1* genes for partial stem rust in wheat and barley, respectively, the genes *Lr34* and *Yr18* which provide partial resistance to leaf and stripe rust in wheat and which may in fact be the same gene and the *mlo* locus which provides resistance to powdery mildew in barley.

Genetic Engineering for Disease Resistance Using the techniques of genetic manipulation (GM), it is now possible to sequence and clone resistance genes from distantly related species. These genes could then be transferred into crop species, providing varieties with enhanced disease resistance. For example, the gene for resistance to bacterial blight of rice, *Xa21,* was sequenced, cloned, and transformed into rice, providing resistance against a range of pathogens [79]. This is a good example of how transgenic technologies could be used in a major crop and indeed, transgenic rice lines expressing *Xa21* are currently being tested in the field. The vision is to use GM technology to pyramid several different resistance genes in a rice variety, providing what is hoped will be durable resistance. However, unless there is coordination among plant breeders and the industry to prevent varieties being grown together, thereby allowing the pathogen to mutate one gene at a time, this strategy is unlikely to be successful.

One option for improving resistance to virus infection is to transform the gene that expresses the viral coat protein into the host plant. This approach was used to develop a line of papaya resistant to the very damaging papaya ringspot virus (PRSV). As a result of this work, two papaya varieties, Rainbow and SunUp, were commercialized. Rainbow was widely planted in Hawaii and was important in preventing the complete destruction of the papaya industry by PRSV [80].

Deployment of Resistance in Practice Many new crop varieties have been bred where resistance to a particular pathogen is based on the introduction of one gene. All too often history has shown that the introduction of such varieties is followed, within just a few years, by the appearance of a new race of the pathogen, able to overcome the "new" resistance. Such rapid breakdown of host resistance is favored by modern intensive agriculture, where crops are planted in monoculture covering huge areas. This favors any genetic variants of the pathogen with the ability to infect these new varieties. Breaking this "boom-and-bust" cycle of introducing a new resistant variety, followed by the rapid breakdown of resistance, can be achieved in various ways. One approach is to find durable sources of resistance. Another is to breed for combinations of race-specific genes in one crop variety. This is known as pyramiding and should be quite durable. However, it is controversial, since it might select for complex races of the pathogen possessing several matching virulences. Another approach is to diversify the deployment of resistance genes. This could involve spatial diversity across regions or fields, or the use of multilines or mixtures of cultivars.

A multiline is a series of near-isogenic (genetically identical) plant lines each differing in a single character, e.g., disease resistance. The plant lines can be grown together like a conventional crop, thereby retaining agronomic advantages such as crop uniformity, while confronting the pathogen with the problem of overcoming several different genes for resistance. A number of mechanisms have been proposed to account for disease control in multilines: (1) The high proportion of resistant plants in the multiline grown in the field reduces the amount of pathogen inoculums per unit area of crop, thereby reducing the amount of infection in the succeeding generation and the amount of inoculums produced by that generation. (2) Movement of pathogen inoculums between susceptible plants might be hampered by the presence of intervening resistant plants. (3) The average distance which the pathogen inoculums must travel in order to reach another susceptible plant is increased. (4) There might be induction of resistance, i.e., pre-inoculation with a race of the pathogen to which the line is resistant might protect it from a race to which it is normally susceptible [81]. However, the breeding program required for the development of a multiline is extensive. Similar in concept, but easier to put into practice, is the use of variety mixtures. Here, seed of a number of genetically distinct varieties of the crop are mixed and grown together as a single crop. Each variety possesses a different resistance gene(s), again presenting the pathogen with

a genetic puzzle. But the use of mixtures requires careful choice of varieties, since they must possess similar characteristics, such as crop height and time to flowering. Nevertheless, mixtures have been shown to develop less disease than would be expected in component varieties grown alone. Mixtures can also provide yield increases, and the magnitude of disease control and effects on yield are dependent on the number of components in the mixture (Fig. 2). The mechanisms proposed to account for reductions in disease in mixtures include less efficient spread between plants and the induction of plant resistance by incompatible strains of the pathogen attempting to infect different hosts in the mixture [82].

Use of Chemicals to Control Crop Disease

Chemicals continue to play an important role in crop disease control. These chemicals act either by inhibiting germination, growth, and multiplication of the pathogen, or by killing the pathogen. Although chemicals can be used to control bacterial pathogens (bactericides) and nematodes (nematicides), this section will concentrate on chemicals with activity against fungal pathogens (fungicides).

Fungicides can be divided into several groups according to their mode of action. Protectant fungicides protect the plant against fungal propagules (e.g., spores) landing on the surface of leaves, stems, or fruit, but tend to be ineffective against established infections, since they do not enter the plant to any extent. To be effective therefore, protectant fungicides need to be applied before the fungal pathogen enters the plant. In contrast, systemic fungicides enter the plant, and can become generally distributed within its tissues, thereby offering protection against fungal pathogens. Eradicant fungicides can enter plant tissues and can kill established infections. A number of protectant and systemic fungicides possess eradicant properties, while some systemic fungicides also have protectant activity.

Protectant Fungicides Protectant fungicides can be applied to the crop as high-volume or low-volume sprays, or occasionally as dusts. These fungicides tend to be broad spectrum, with activity against a range of different fungal pathogens. As a result, it is unlikely that pathogens would develop resistance to these chemicals. However, because they must

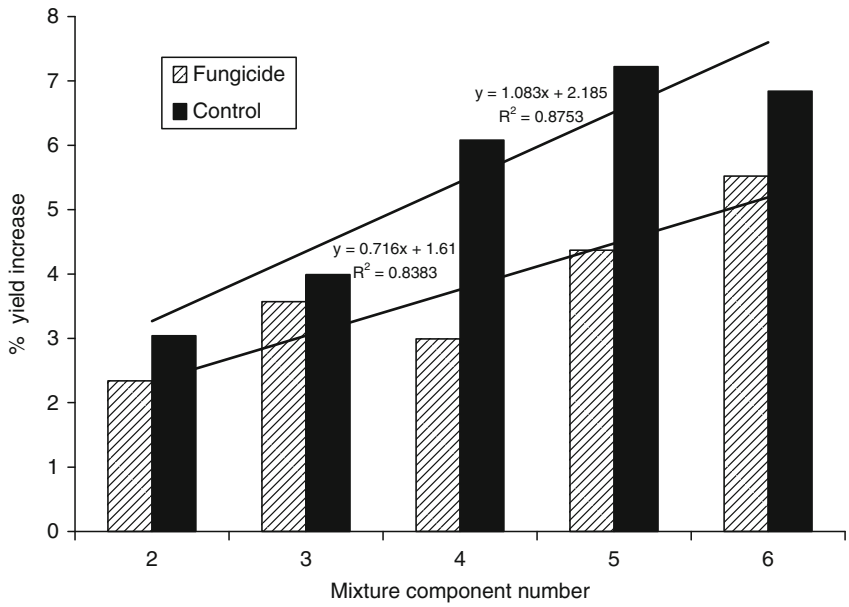

Crop Diseases, Management and Control of. Figure 2
Change in *R. secalis* infection of mixtures of winter barley cultivars compared with the mean of their components with different numbers of component cultivars (From [82])

be applied before the pathogen attempts to penetrate the plant, there is the need for reliable forecasting of infection risk. Protectant fungicides include the oldest and still widely used inorganic sulfur and copper compounds. Sulfur, applied as a dust, wettable powder, paste, or liquid, is used to control powdery mildews, some rusts, leaf blights, and fruit rots. Bordeaux mixture, made by mixing copper sulfate solution with calcium oxide or calcium hydroxide, consists mainly of colloidal hydrated cupric hydroxide stabilized by calcium sulfate. It has been replaced by copper oxychloride, which can be formulated by the manufacturer and simply diluted by the grower.

Organic sulfur compounds are an important and versatile group of fungicides and include thiram, ferbam, maneb, zineb, and mancozeb. These fungicides are all derivatives of dithiocarbamic acid, and because they are metabolized to isothiocyanate, they inactivate the sulfhydryl groups (-SH) in amino acids and enzymes. Thiram is used mostly for seed and bulb treatment for vegetables, flowers, and grasses, while ferbam is used to control foliage diseases, ornamentals, and fruit on trees. Maneb and mancozeb belong to a group of dithiocarbamic acid derivatives known as the ethylenebisdithiocarbamates. Maneb is a broad-spectrum fungicide for the control of foliage and fruit diseases of vegetables such as tomato, potato, and vine crops, as well as flowers, turf, and some fruit crops. Mancozeb is formed by the addition of zinc ion to maneb and a secondary effect of using mancozeb is the provision of manganese and zinc to plants deficient in these elements.

Various aromatic compounds have been developed as fungicides and include dichloran, used as a foliar or fruit fungicide, or as a postharvest spray for vegetables and flowers, and chlorothalonil, which is a broad-spectrum fungicide used on vegetables, field crops, ornamentals, and turf.

A number of very effective protectant fungicides belong to the rather heterogeneous group of heterocyclic compounds and include captan, iprodione, and vinclozolin. Captan is used for the control of leaf spots, blights, and fruit rots on various crops, as well as a seed treatment. It works by inhibiting thiol-containing enzymes in the fungal cell, and may also react with sulfhydryl groups.

Systemic Fungicides For a systemic fungicide to be effective, it must enter the plant and, to be translocated, it must be reasonably water-soluble. It must also be selective, possessing toxicity against the pathogen but not the host plant. Most systemic fungicides are xylem-mobile and as a result, tend to move from the base to the top of the plant, accumulating in leaves and shoot apices. As a result, such fungicides possess no activity against soilborne pathogens affecting roots. Phosphonate fungicides such as fosetyl-Al are also phloem-mobile and so can move down the plant to the roots, providing protection against, for example, root rots caused by *Phytophthora* species.

A wide range of systemic fungicides are now used to control plant pathogens. Unlike protectant fungicides, most systemic fungicides are site specific, and target only one, or just a few, specific steps in fungal metabolism. Although this was seen initially as a strength of systemic fungicides, it soon proved to be a weakness, since fungal pathogens were able to develop resistance to the chemicals, in some cases with alarming rapidity.

Acylalanine fungicides are effective against Oomycete pathogens such as *Phytophthora* and *Pythium* and include the widely used fungicide, metalaxyl. This is used as a soil or seed treatment and also possesses some curative activity. It moves readily from roots to shoots, although its lateral movement is slight. Some fungal pathogens have developed resistance to metalaxyl, and its use tends to be recommended in conjunction with a broad-spectrum fungicide.

Benzimidazole fungicides include some well-established and important chemicals, including benomyl, carbendazim, and thiabendazole. They are converted to methyl benzimidazole carbamate (MBC, carbendazim), which interferes with cell division. Benzimidazoles are broad spectrum in activity. Thus, benomyl is effective against a wide range of leaf spots, blights, rots, scabs, seedborne, and soilborne diseases. It can be applied to plants as a seed treatment, foliar spray, trunk injection, root dip, or fruit dip.

Oxanthiins, such as carboxin and oxycarboxin, possess the distinction of being the first chemicals with demonstrated systemic activity. They are active against some smut and rust pathogens, and also against *Rhizoctonia*. By inhibiting succinate dehydrogenase in fungal mitochondria, they affect respiration.

Organophosphate fungicides, such as foestyl-Al and phosphorous acid, are effective against Oomycete pathogens on a range of crops. Interestingly, fosetyl-Al has been reported to trigger plant defense mechanisms, e.g., phytoalexin biosynthesis and accumulation.

Other systemic fungicides include the pyrimidines, such as ethirimol and bupirimate, with activity against powdery mildews, and the triazoles, such as triadimefon, propiconazole, cyprodinil, and tebuconazole. The triazoles exhibit long-acting protective and curative activities against a broad spectrum of pathogens.

The most recently developed group of fungicides is the strobilurins. They are based on chemicals extracted from the wood rotting fungus *Strobilurus tenacelus*, and a range of highly effective strobilurins have been developed over the years. They work by blocking electron transfer at the site of quinol oxidation (Qo site, hence their description as QoI fungicides), thereby preventing ATP formation in respiration. These fungicides move trans-laminarly within leaves and some also move systemically through the vascular system. Important strobilurins include azoxystrobin, pyraclostrobin, and kresoxim methyl. They have broad-spectrum activity, and some also possess growth-promoting activity on treated plants, apparently by delaying senescence and altering plant–water relations.

Development of Resistance to Fungicides Until the advent of systemic fungicides, fungicide resistance was rare. The development of resistance in *Pyrenophora* to mercury used as a seed dressing, in the apple scab fungus *Venturia inaequalis* to dodine, and in *Penicillium* species to diphenyl compounds are exceptions. In contrast, the use of systemic fungicides soon led to the appearance of fungicide resistance. Thus, the pyrimidine fungicide dimethirimol was introduced in 1968, and by 1971, strains of the powdery mildew fungus *Sphaerotheca fuligenea* were detected on glasshouse cucumbers in the Netherlands. Similarly, following the introduction of QoI fungicides in the UK in 1996, resistance to powdery mildew in wheat was first recorded in 1998.

It seems that where a single site systemic fungicide is used intensively, there is the risk of fungal pathogens developing resistance to it. With single site fungicides, only a single mutation in the fungus might be required for resistance to develop. Some of the mechanisms by which a fungus might develop resistance following such a mutation include: (1) detoxification of the chemical, (2) decreased permeability of fungal cell membranes to the fungicide, (3) reduced affinity of the fungicide to the reactive site within the fungal cell, and (4) bypassing a blocked reaction via an alteration in fungal metabolism.

Given that fungicide resistance is now an accepted fact of life in crop protection, how can it be managed effectively? The first point to remember is that fungicides to which resistance has developed can still be useful in disease control if deployed sensibly. Strategies to minimize the risk of fungicide resistance developing include:

1. Reducing fungicide use
   - Applying fungicides only when necessary
   - Using fungicides as part of an integrated disease control program, including, for example, appropriate cultural control, and if available, resistant varieties
2. Diversifying fungicide treatments
   - Avoiding the repeated use of fungicides with the same mode of action
   - Instead, use mixtures of fungicides with different modes of action
   - During the growing season, alternating fungicides with different modes of action
   - Including a multisite fungicide in any fungicide mixture or spray program

Pesticides and Nontarget Organisms Pesticide use has greatly increased the quantity and improved the quality of food for the increasing world population. However, as pesticide use increased, so did concern about their adverse effects on nontarget organisms, including humans. Increasing public concern about the accumulation of pesticides in the environment and the impact on nontarget organisms has led to the introduction of rigorous regulatory processes [83, 84]. Nevertheless, there is continued concern over the impacts of pesticides on wildlife, including invertebrate populations, wild plants, and farmland birds [85]. These concerns have led to reviews of active substances used in plant protection, with the resulting withdrawal of an increasing number of crop protection

products from the market [86]. This has created problems, and in some situations, effective control measures are no longer available to meet all the challenges posed by pathogens, pests, and weeds [86].

Biological Control of Plant Diseases Using Antagonistic Microorganisms

Biological control can be defined as the control of a plant pathogen using another living organism or organisms. This definition includes direct and indirect effects, as a result of either the introduction of antagonists, or manipulation of existing microbial populations to reduce disease. This section will deal with biological control using antagonistic microorganisms.

Antagonistic microorganisms control plant disease because they weaken or destroy the pathogen. They achieve this by various mechanisms, including: (1) directly parasitizing the pathogen, (2) producing antibiotics or toxins that exert an effect on the pathogen, (3) competing for space and nutrients with the pathogen, and (4) producing hydrolytic enzymes that destroy components of pathogen cells.

To be effective in disease control, a biological control agent (BCA) must be able to colonize a particular habitat or occupy a niche in sufficient numbers to disrupt the growth and survival of the target pathogen. For this reason, the most effective BCAs are likely to be found in the environment in which they are to be used. Thus, if the pathogen to be controlled infects plant roots, the best place to look for a potential BCA would be the rhizosphere. Finding appropriate BCAs is one thing, but using them in practice is quite another. For a start, as a living organism, the BCA must be formulated in such a way as to allow it to remain viable and survive following application [87]. Great advances have been made in the production and formulation of BCAs over the years, but despite the fact that 1,000 of microorganisms have been shown to interfere with growth and survival of plant pathogens under controlled and field conditions, relatively few have been registered and used in commercial practice. Currently, there are more than 50 bacterial products and 50 fungal products available commercially. The majority of both bacterial and fungal products are sold for control of seedborne or soilborne pathogens (Table 2), with fewer for foliar pathogens and timber decay fungi and even fewer for postharvest pathogens. Most contain individual microorganisms although there are some products that contain microorganism mixtures, and some individual microorganism strains are marketed in several different products expanding the potential market of a single active ingredient. Bacterial products are dominated by *Bacillus* species reflecting their ease of growth and production of long-lived spores mentioned earlier. Fungal products are dominated by *Trichoderma* spp. which are also easy to produce, generally have a low toxicity, and can sporulate well.

America's first biological fungicide seed treatment, Kodiak (marketed by Bayer), contains spores of *Bacillus subtilis* GB03 for control of *Alternaria*, *Aspergillus*, *Fusarium*, and *Rhizoctonia* spp. that attack root systems of a number of plants, including seed and pod vegetables, cotton, peanut, soybean, wheat, barley, and maize. The spore concentrate can be applied through standard slurry or mist seed treatment equipment, with fungicides if required, and the bacterium colonizes the root system providing control over the whole growing season.

Numerous products contain strains of *Trichoderma harzianum*, but one isolate, KRL-AG2 (T-22), sold by BioWorks Inc., USA, has been used and developed for several markets in US horticulture and agriculture in a number of different forms. When applied to soil, planting mixes, or turf, this BCA colonizes plant roots and provides protection against root pathogens such as *Cylindrocarpon*, *Fusarium*, *Pythium*, *Rhizoctonia*, and *Thielaviopsis*. RootShield granules are largely targeted at glasshouse and nursery use, and can be incorporated, top-dressed, broadcast, or applied in-furrow or to planting holes for use on flowers, bedding plants, ornamentals, vegetables, pome and stone fruit, trees, and tree nuts. For agriculture, T-22 Planter Box is applied as a coating on seeds and seed pieces, an in-furrow spray, and as a transplant starter and T-22 HC as a broadcast or in-furrow treatment, both for use on field and row crops, hay and forage crops, bulbs and vegetables. In Europe, T-22 (Koppert, the Netherlands) is available as TRIANUM-G and TRIANUM-P, wettable granule and wettable powder formulations. Much of the scientific background concerning the use of this isolate has been extensively reviewed [88].

In terms of the future, advances that can improve quantity, quality, and shelf life of inocula would be

Crop Diseases, Management and Control of. Table 2 Examples of bacteria and fungi registered or commercially marketed as biological control agents for control of soilborne and seedborne plant pathogens (from [87])

Antagonist	Target pathogen(s)/ activity	Disease/host	Product name and source
BACTERIA			
Agrobacterium radiobacter	*Agrobacterium tumefaciens* causing root galls	Ornamentals and other plants sensitive to *A. tumefaciens* root galls	Norback 84-C, Galltrol-A, Nogall, Diegall, Dygall (Becker Underwood Pty Ltd, Australia; Bio-Care Technology Pty Ltd. Australia; New BiProducts, Inc. USA; AgBiChem Inc., USA; Agbioresearch Ltd. New Zealand)
Bacillus cereus BP01	Plant growth promotion	Cotton	Mepplus (MicroFlo Co. LLC, USA)
B. pumilus GB34	*Fusarium* spp., *R. solani*	Soybean	YieldShield concentrate; GB34 Biological Fungicide (Gustafson LLC, USA)
Bacillus licheniformis SB3086	Numerous pathogens, especially *Sclerotinia homeocarpa*	Ornamentals, turf	EcoGuard, Green Releaf (Novozymes Biologicals Inc., USA)
B. subtilis	*Pythium* damping-off	Tomato	Cillus, Green-all G (Greenbiotech Co, Korea)
	R. solani, Fusarium spp., *Alternaria* spp., and *Aspergillus* spp. pathogens	Root rots and seedling diseases generally	Kodiak, Epic, Concentrate, Kodiak HB, Quantum 4,000, System 3 (Gustafson LLC, USA)
	Fusarium spp., *Verticillium* spp., *R. solani,* and *Pythium* spp. pathogens	Various vegetable and field crops	PHYTOVIT WG (Prophyta Biologischer Pflanzenschutz GmbH, Germany)
B. subtilis GB03	*Fusarium* spp., *Phytophthora* spp., *Pythium* spp., *R. solani*	Ornamentals, turf, dry and snap bean, cotton, peanut, soybean, wheat, and barley	Companion, Kodiak (Growth Products Ltd, USA; Gustafson LLC, USA; Bayer CropScience LP, USA)
B. subtilis MBI600	*Alternaria* spp., *Aspergillus* spp., *Fusarium* spp., *Pythium* spp., *R. solani*	*Alfalfa*, dry/snap beans, peanut, soybean, field crops, turf, cotton	HiStick N/T, Pro-mix, Subtilex; Subtilex HB (Becker Underwood Inc., USA; Premier Horticulture Inc, Mexico)
B. subtilis subsp. *amyloliquefaciens* FZB24	*Fusarium* spp., *R. solani*	Various vegetables and ornamentals	Taegro, Tae-Technical (Earth Biosciences Inc. USA)
B. subtilis, *Bacillus circulans*, *Bacillus amyloliquefaciens*, *Paenibacillus polymyxa* (Mixture)	Damping-off (bacterial) diseases	All crops	Hydroguard (American Agritech, USA)
Burkholderia cepacia[a]	*Pythium* spp., *Fusarium* spp., *R. solani,* nematodes	*Alfalfa*, beans, clover, cotton, peas, wheat, vegetables, and others	Deny, Blue Circle (Stine Microbial Products, USA)
	Pythium spp., *Fusarium* spp., *R. solani,*	Maize, vegetables, cotton	Intercept (Soil Technologies Corp., USA)

Crop Diseases, Management and Control of. Table 2 (Continued)

Antagonist	Target pathogen(s)/ activity	Disease/host	Product name and source
Erwinia carotovora, nonpathogenic	Bacterial soft rots	Vegetables, cruciferous plants, rice	Biokeeper (Central Glass Co. Ltd., Japan)
P. polymyxa AC-1	Damping-off	Cucumber	NH, Topseed (Greenbiotech Co., Korea)
Pseudomonas sp.	Growth promotion, various seedborne and soilborne diseases	Vegetables, potato, cereals, etc.	Proradix (Sourcon-Padena, Germany)
Pseudomonas aureofaciens TX-1	Various turf grass pathogens	Turf grass diseases	Spotless (Turf Science laboratories Inc, USA)
Pseudomonas chlororaphis MA 342	*Drechslera* spp., *Septoria* spp., *Fusarium* spp.	Cereal seedborne diseases	Cedomon (BioAgri AB, Sweden)
P. chlororaphis 63-28	*Pythium* spp. *R. solani, F. oxysporum*	Stem and root rots, and wilt disease in various crop plants	AtEze (Eco Soil Systems Inc., USA)
Pseudomonas fluorescens	Frost damage, *E. amylovora*	Fruit, potato, tomato, berries	BlightBan A506 (NuFarm Inc., USA)
Pseudomonas solanacearum, nonpathogenic	*P. solanacearum*	*P. solanacearum* rots in vegetables	PSSOL (Natural Plant Protection, France)
P. syringae	*Botrytis* spp., *Penicillium* spp., *Mucor* spp.	Fruit, potato	Bio-save (EcoScience Corp., USA)
Streptomyces colombiensis WYE20	*R. solani*	Turf	Mycocide (KIBC Co., Korea)
Streptomyces goshikiensis WYE324	*R. solani*	Rice, turf	Safegrow (KIBC Co, Korea)
Streptomyces griseoviridis K61	Various soilborne pathogens	Vegetable and ornamental soilborne diseases	Mycostop (Verdera Oy, Finland)
Streptomyces lydicus WYCD108	Various soilborne pathogens	Root rots in many crops, turf, and ornamentals	Acinovate (Natural Industries Inc. USA)
FUNGI			
Aspergillus flavus AF36	*A. flavus* (aflatoxin +)	Cotton	AF36 (Arizona Cotton Research and Protection Council, USA)
A. flavus NRRL 21882	*A. flavus* (aflatoxin +)	Peanut	Afla-guard (Circle One Global Inc, USA)
Coniothyrium minitans CON/M/91-08	*Sclerotinia minor, S. sclerotiorum*	Protected vegetable and field crops	Contans WG (Prophyta Biologischer Pflanzenschutz GmbH, Germany; Sylvan Bio Products Inc, USA) and Intercept WG (Encore Technologies, MN, USA)
C. minitans KONI	*S. minor, S. sclerotiorum*	Glasshouse crops and amenity areas	KONI (Bioved Ltd., Szigetszentmiklos, Hungary)

Crop Diseases, Management and Control of. Table 2 (Continued)

Antagonist	Target pathogen(s)/ activity	Disease/host	Product name and source
F. oxysporum Fo47	*F. oxysporum*	Asparagus, basil, carnation, cyclamen, gerbera, tomato	Fusaclean (Natural Plant Protection, France)
Gliocladium catenulatum J1446	*Pythium* spp., *R. solani*, and numerous other pathogens	Damping-off of vegetables, herbs, ornamentals, and numerous other plants	Prestop Mix, Prestop WP, Primastop (Verdera Oy, Finland)
Gliocladium (*Trichoderma*) *virens* G-21	*Pythium ultimum, R. solani*	Damping-off of bedding plants, greenhouse crops, and ornamentals	SoilGard 12 G formerly GlioGard (Certis Inc, Columbia, MD, USA)
Pythium oligandrum	Numerous diseases	Numerous crops	Polyversum (Biopreparaty Ltd, Czech Republic)
Trichoderma spp.	Soilborne fungal pathogens	Turf, glasshouse crops, and field crops	Trich-A-Soil (Becker Underwood Pty Ltd, Australia)
	Sclerotium cepivorum, Pyrenochaeta	Onion	Tenet (Agrimm Tecnologies, New Zealand)
	Soilborne plant pathogens	Ornamentals, fruit, turf, olive, vine	Trichomic (AMC Chemical, Spain)
	Armillaria	Tree seedlings	Arborguard (Biodiscovery Ltd, New Zealand)
T. harzianum T-22 (KRL-AG2)	*Fusarium* spp., *Pythium* spp., *Cylindrocarpon* spp., *Thielaviopsis* spp., *R. solani, S. homeocarpa*	Range of crops, ornamentals, and turf	T-22 HC, T-22 Planter Box, T-22 Granules PlantShield HC, RootShield drench and granules, TurfShield, TRIANUM-P, TRIANUM-G (Bio-Works Inc, Fairport, NY, USA; Koppert, the Netherlands)
T. harzianum	Various fungi	Legumes and leaf vegetables	Supresivit (Borregaard and Reitzel, Denmark or Fytovita, Czech Republic)
	Pythium spp., *R. solani* seedling diseases	Numerous crops	Eco-T (Plant health Products, South Africa)
T. harzianum GBF-0208	Numerous pathogens	Vegetables, bulbs, turf	Green-all T WP (Green Biotech Co. Ltd., Korea)
T. harzianum + *Trichoderma viride*	*Fusarium* spp., *Phytophthora* spp., *Pythium* spp., and *R. solani*	Field crops, vegetables, ornamental and turf	Trichodry, Trichoflow, Trichogrow, Trichopel R Trichopel (Agrimm Technologies, New Zealand)
T. harzianum T 35 + *T. harzianum* TH315	*Fusarium* spp., *Pythium* spp., *R. solani, S. rolfsii*	Seedlings diseases on a range of crops and potato	Root Pro and Root-Protato (Mycontrol, Hamovil, Israel)

Crop Diseases, Management and Control of. Table 2 (Continued)

Antagonist	Target pathogen(s)/ activity	Disease/host	Product name and source
T. harzianum + *T. polysporum*	Various root-infecting fungi	Glasshouse crops	BINAB-T W P(Bio-Innovation Eftr AB, Bredholmen, Sweden; or Svenska Predator AB, Sweden; or Bayer, Sweden)
T. viride	*Fusarium* spp., *Pythium* spp., *R. solani*	Damping-off, foot rots and collar rots of several plants	Ecoderma (Margo Biocontrols Private Ltd., Bangalore, India)

[a]*B. cepacia* is no longer available in North America because of concerns over the potential for human pathogenicity of some strains of this species

welcome, particularly for bacteria such as *Pseudomonas* that do not form spores. In recent work, both *Pseudomonas* and *Trichoderma* isolates have been simultaneously applied to seed via drum priming and found to survive and proliferate on roots similarly to when applied individually [89]. This procedure may be a way to apply and maintain multiple BCAs in a commercially relevant process. Further approaches include integration with other control strategies such as cultural methods and chemical treatments [87]. A better understanding of the natural ecology of any potential BCA might facilitate a more rational approach to production and use.

Induced Resistance to Control Crop Diseases

Following infection by a microbial pathogen, susceptible plants can develop an enhanced resistance to further infection [90]. This is known as induced resistance and can be split broadly into two types: systemic acquired resistance (SAR) and induced systemic resistance (ISR).

In SAR plants, develop a broad-spectrum systemic resistance to pathogen infection following a localized infection by a necrotizing pathogen or treatment with various agents, e.g., acibenzolar-S-methyl (ASM) or Probenazole (Oryzemate®). SAR is associated with increased levels of salicylic acid (SA) and with the coordinate expression of a specific set of genes encoding PR proteins ([91]; Fig. 3). Moreover, application of SA or one of its functional analogues, such as ASM, induces SAR and activates the same set of PR genes [92]. Indeed, expression of a set of PR genes, and PR-1 in particular, is used as a marker for SAR induction, although it is important to note that the induction of resistance is not always accompanied by PR-1 expression [93, 94].

In contrast to SAR, ISR develops as a result of colonization of plant roots by certain strains of plant growth–promoting rhizobacteria (PGPR) and is mediated by jasmonic acid– (JA) and ethylene (ET)-sensitive pathways ([91]; Fig. 3). Phenotypically, ISR is similar to SAR in that it acts unspecifically against taxonomically different pathogens [91, 95].

The resistance responses described above can be associated with direct activation of defenses. However, such responses can also be associated with an ability to "recall" previous infection, root colonization, or chemical treatment. This phenomenon is known as priming and results in plants responding more rapidly and effectively when exposed to subsequent pathogen attack ([96]; Fig. 3). Usually, no changes in gene expression or in the levels of resistance traits are detectable in response to the priming agent alone, which might be a chemical elicitor such as ASM or a challenging pathogen. Interestingly, priming of resistance is usually caused by agents that fully induce resistance when applied at higher doses [97, 98] and suggests that direct resistance induction and priming might differ from one another quantitatively rather than qualitatively.

A wide range of microbes and chemicals are known to induce resistance and it seems likely that other forms of induced resistance exist. Thus, it is well known that the nonprotein amino acid, β-aminobutyric acid (BABA), can induce resistance in a variety of crop plants [99]. BABA-induced resistance (BABA-IR) has been used as a model for the study of priming

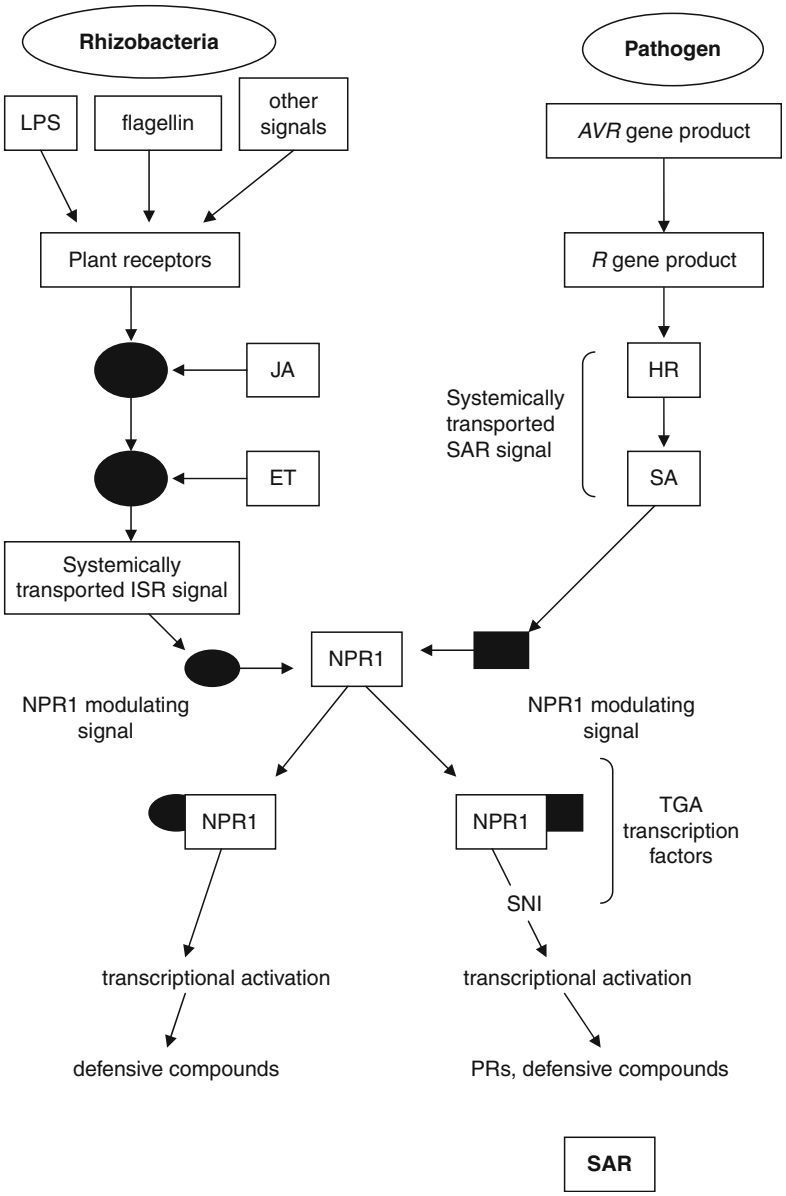

Crop Diseases, Management and Control of. Figure 3
A model for the signal transduction network controlling induced systemic resistance (ISR) mediated by plant growth–promoting rhizobacteria and pathogen-induced systemic acquired resistance (SAR) in *Arabidopsis thaliana*. LPS, lipopolysaccharide; PRs, pathogenesis-related proteins; *AVR*, avirulence gene product; *R*, resistance gene product; HR, hypersensitive response; SA, salicylic acid; JA, jasmonic acid; ET, ethylene; NPR1, a regulatory protein involved in signaling in SAR and ISR in *A. thaliana*; SNI, transcriptional repressor of SAR genes; TGA transcription factors, family of transcription factors interacting with SA-induced NPR1 (From [91])

and in *Arabidopsis*, it is based on various mechanisms. Thus, BABA-IR against *P. syringae* and *B. cinerea* functions via priming for SA-inducible defenses, while against a different set of pathogens (*Hyaloperonospora parasitica*, *Plectosphaerella cucumerina* and *Alternaria brassicicola*), it is based on priming for resistance through the formation of callose-rich papillae [100–102].

Since the introduction of the first chemical resistance activator Probenazole (registered in Japan as Oryzemate®, Meiji Seika Kaisha Ltd) in 1975, a number of other chemical and microbial activators have been developed, including ASM, registered as Bion® and Actigard® (Syngenta), Milsana® (*Reynoutria sacalinensis* extract, KHH BioScience Inc. USA), Elexa® (chitosan, SafeScience, USA), and Messenger® (harpin protein, Eden Bioscience, USA). However, although high levels of disease control can be achieved with plant activators in controlled environments, their performance under field conditions has been less impressive. In fact, the moderate levels of disease control and high levels of variability exhibited by plant activators in the field have been instrumental in the very slow uptake of induced resistance in crop production systems. In the following paragraphs, the performance of selected plant activators under field conditions will be discussed.

Probenazole (3-allyloxy-1,2-benziothiazole-1,1-oxide) was first introduced for the control of rice blast disease (*Pyricularia oryzae*) and bacterial blight (*Xanthomonas oryzae*). It is widely used in Asia where it is applied as a granular treatment either to paddy fields or as a seedling box treatment. Following application, the compound is absorbed by the roots, then systemically transferred to the rest of the plant and can control rice blast disease for between 40 and 70 days post application [103]. However, despite continuous use since its introduction, there have been no reports of pathogen insensitivity to probenzole and indeed, it still accounted for 53% of the chemicals used for seedling box treatments on rice in 2005 [103]. It is believed this is because the compound is only weakly toxic to fungi and activates disease defense systems in rice [104, 105].

A large body of data has accumulated on the efficacy of ASM against a range of diseases under field conditions [106, 107]. Most studies report disease control, although the level of control ranges from 4% to 99%. High levels of disease control were achieved on tobacco, where infections by *P. syringae* pv. *tabaci, Cercospora nicotianae,* and *Alternaria alternata* were reduced by 99%, 91%, and 89%, respectively [108, 109]. In wheat, the crop that ASM was originally aimed at, disease control was not so impressive, ranging from 35% for *Puccinia recondita* and *Septoria* spp., to 77% for *B. graminis* f.sp. *hordei* [110, 111]. ASM even increased disease levels in peanut, where infection by *Cercosporidium personatum* was greater than untreated controls by 52% [112]. Working on oilseed rape, Liu et al. [113] found that pretreatment with ASM in October/November decreased the number of leaf lesions caused by the Phoma stem canker pathogen *L. maculans* in the autumn/winter, as well as the severity of stem canker in the subsequent spring/summer. In this work, reductions in numbers of leaves with lesions were between 25% and 55% [113]. More recently, ASM was shown to reduce infection of barley by the leaf scald pathogen *R. secalis* by 45% [114].

Chitosan is a common polymer in shells of crustaceans, exoskeletons of insects, and cell walls of fungi [115]. A commercial formulation, Elexa®, contains 4% chitosan as its active ingredient and has been shown to protect a range of crops against pathogens. For example, when used as a seed treatment, it reduced downy mildew severity on pearl millet by 58%, and when used as a foliar spray, it reduced infection by 75% [116]. When used on grapevines, eight applications of Elexa® applied over the season reduced the incidence of downy mildew by 50% and powdery mildew by 75% compared to untreated controls [117].

A number commercially available products are based on microbial proteins. One such is Messenger®, which is based on the protein harpin obtained from *Erwinia amylovora* [118]. Used as a crop protectant, Messenger® has had mixed success. For example, although it possessed good efficacy against blue mold in apples [119], its efficacy against gray mold in strawberry [120] and target spot of tomato [121] was poor. In some interesting recent work, Chen et al. [122] generated specific fragments of $HpaG_{Xooc}$, a harpin from *X. oryzae* pv. *oryzicola*, and found that one of these fragments, $HpaG_{10–42}$, stimulated growth of rice plants and provided enhanced resistance to *X. oryzae* pv. *oryzae* and *M. grisea*. $HpaG_{10–42}$ was also shown to control bacterial blight, rice blast, and sheath blight, and to increase grain yields, under field conditions [123]. Here the level of disease control depended on the cultivar, with greater control obtained with *indica* compared to *japonica* cultivars.

ISR was first shown to be effective under field conditions in the mid-1990s, when application of PGPR as a seed treatment followed by soil drench application led to a reduction in severity of bacterial wilt [124], and control of bacterial angular leaf spot and anthracnose

[125]. Subsequent research by Raupach and Kloepper [126] showed that treatment of cucumber seed with PGPR led to increased plant growth and control of angular leaf spot and anthracnose. Field experiments in Thailand in 2001 and 2002 studied the effects of PGPR, used alone or as mixtures, on control of southern blight of tomato caused by *Sclerotium rolfsii*, anthracnose of long cayenne pepper caused by *Colletotrichum gloeospoiroides*, and mosaic disease of cucumber caused by cucumber mosaic virus (CMV) [127]. Mixtures of PGPR (all *Bacillus* spp.) were found to suppress disease more consistently than the PGPR strain *Bacillus pumilus* IN937b, used alone.

Induced resistance offers the prospect of durable, broad-spectrum disease control using the plants own resistance. However, it is plagued by inconsistency and relatively poor disease control compared with fungicides. These problems relate to the fact that induced resistance is a host response and as such is greatly influenced by genotype and environment. Unfortunately, the understanding of the impact of these influences on induced resistance is poor, as is the understanding of how best to use induced resistance in crop protection practice. Understanding in these areas needs to improve, and answers to several important, practical questions are required, for example: (1) Should resistance inducing agents be applied early or late in the season? (2) Is induced resistance effective against pathogens with long periods of asymptomatic growth in plant tissue, e.g., *R. secalis* on barley? (3) Can resistance inducers be used as a means of reducing fungicide applications to crops, e.g., can resistance inducers be applied early to reduce pathogen infection and colonization, thereby allowing less fungicide to be used? What is required is research related to specific crops aimed at trying to determine how best to fit induced resistance into disease control programs. Farmers and crop protectionists have grown accustomed to high levels, or even complete, disease control. Ultimately, for induced resistance to gain more widespread acceptance in crop protection, there will need to be a lowering of expectation in terms of levels of disease control.

Other Approaches to Controlling Crop Diseases

Biofumigation Biofumigation involves the suppression of plant pests and diseases by biocidal hydrolysis products, most notably the isothiocyanates released by glucosinolate (GSL)-containing plants in soil. It can involve GSL-containing plants as rotation crops, or intercrops by incorporating fresh plant material as green manure, or by utilizing processed plant products high in GSLs, e.g., seed meals. Strategies for the field implementation of biofumigation are described in detail by Kirkegaard [128].

Soil Solarization Soil solarization, or soil heating, harnesses solar energy in order to increase soil temperature. This is commonly achieved by mulching (covering, tarping) the soil with transparent polyethylene or other transparent plastic sheets. The following are a few of the important principles of soil solarization: (1) It should be carried out during periods of high temperature and intense solar radiation, with low levels, or no precipitation. (2) Soil needs to be moist in order to increase the thermal sensitivity of resting structures and improve heat conduction. (3) The mulching period needs to be sufficiently long (~4 weeks or greater) in order to achieve disease control at all desired depths. The efficacy of soil solarization in controlling crop diseases and the mechanisms involved are discussed in detail by Gamliel and Katan [129].

Integrated Control of Plant Diseases

As pointed out by Agrios [130], plant disease control is most effective when all of the relevant information regarding the crop, potential pathogens, previous disease history, availability of host resistance, environmental conditions, etc., are taken into account in devising the disease control program. An integrated program of disease control aims to (1) eliminate or reduce the initial pathogen inoculum, (2) reduce the effectiveness of the initial pathogen inoculum, (3) maximize host plant resistance, (4) delay the onset of disease in the plant/crop, and (5) slow down the development and progression of secondary cycles [130].

The precise approach adopted will depend on the crop and its disease spectrum, but would probably include several of the following: (1) appropriate hygiene/sanitation, e.g., using disease-free seed/planting material, (2) using appropriate cultural measures, (3) using resistant plant varieties, (4) using appropriate fungicides, and (5) using biologically based methods, if

available and appropriate, e.g., biological control, induced resistance.

Control of late blight (*P. infestans*) on potato provides a good example of an integrated approach to disease control (see www.endure-network.eu). For late blight, the first step in an integrated strategy is reducing primary sources of inoculum, such as avoiding infected seed tubers, using certified potato seed, preventing or reducing oospore production by controlling volunteer potatoes, for example. The next step is variety choice, since use of a variety expressing some resistance to late blight offers the potential to reduce fungicide inputs as part of an integrated strategy. Nevertheless, fungicides play a crucial role in integrated control of late blight. Although control measures are aimed mainly at preventing infection, if late blight appears in a crop, the control strategy switches to stopping or reducing the epidemic. Effective control of late blight depends on access to information such as phase of crop growth, fungicide products available, dose rates, timings, weather conditions, as well as access to tools, such as an appropriate decision support system (DSS). The DSS can integrate all relevant information to generate spray recommendations, thereby increasing the efficacy of the control strategy without increasing risk.

Future Directions

High crop yields are maintained in most developed countries through the use of improved varieties, together with fertilizers and pesticides. In these countries, farmers and growers are accustomed to achieving high levels of disease control with fungicides, although, as discussed above, the development of fungicide resistance can erode fungicide efficacy. Levels of disease control obtained with many biologically based control methods are lower than those achieved using fungicides, and moreover, many biologically based methods tend to provide inconsistent disease control. Thus, although induced resistance can provide high levels of disease control on some crops, with many crops, disease control is less impressive. Expression of induced resistance in crop plants can also be variable, depending, for example, on genotype and environment. Problems also exist with variability and inconsistency of disease control provided by some BCAs. Farmer perceptions of inadequate and inconsistent disease control will not persuade them to adopt biologically based approaches. Minimizing the effects of these problems clearly requires further research.

In spite of the huge effort by researchers to develop novel biologically based solutions for disease control (such as BCAs, plant-derived substances, induced resistance agents), few products have reached the marketplace. The relatively high cost of registration, together with the limited market size for some products, has been identified as a major barrier. However, this problem has been recognized by regulatory authorities, and in the UK, for example, the Chemicals Regulation Directorate (Pesticides) has launched a scheme that encourages applicants to register their products. Under this scheme, the requirements for registration can be tailored to the product type and importantly, the application fee can be reduced [86].

The continued ability of pathogens to overcome host resistance genes and to develop resistance to fungicides seriously erodes the ability to provide effective, lasting disease control on important crops. These problems combined with the withdrawal of active substances from the market and increasing public concern with the effects of pesticides on the environment create a huge challenge for plant pathology in the future. Plant disease control has an important role to play in efforts to feed the world's increasing population. However, providing effective and lasting disease control, without harming the environment, will require not just a sensible approach to the use of host resistance and fungicides, but also a range of innovative approaches. In some situations, innovative control methods might be used to complement existing approaches. In other cases, for example for those diseases for which no adequate control measures exist, innovative control options might provide the only solution.

Bibliography

Primary Literature

1. Large EC (1940) The advance of the fungi. Jonathan Cape, London
2. Strange RN (2003) Introduction to plant pathology. Wiley, Chichester
3. Oerke E-C (2006) Crop losses to pests. J Agric Sci 144:31–43
4. Hazell P, Wood S (2008) Drivers of change in global agriculture. Philos Trans R Soc B 363:495–515
5. Leonard KJ (2001) Stem rust – future enemy? In: Peterson P (ed) Stem rust of wheat: from ancient enemy to modern foe. APS, St. Paul, pp 119–146

6. Campbell CL, Long DL (2001) The campaign to eradicate the common barberry in the United States. In: Peterson P (ed) Stem rust of wheat: from ancient enemy to modern foe. APS, St. Paul, pp 16–50
7. Janvier C, Villeneuve F, Alabouvette C, Edel-Hermann V, Mateille T, Steinberg C (2007) Soil health through soil disease suppression: which strategy descriptors to indicators? Soil Biol Biochem 39:1–23
8. Ball BC, Bingham I, Rees RM, Watson CA, Litterick A (2005) The role of crop rotations in determining soil structure and crop growth conditions. Can J Soil Sci 85:557–577
9. Bailey DJ, Duczek LJ (1996) Managing cereal diseases under reduced tillage. Can J Plant Pathol 18:159–167
10. Peters RD, Sturz AV, Carter MR, Sanderson JB (2003) Developing disease suppressive soils through crop rotation and tillage management practices. Soil Tillage Res 72:181–182
11. Sumner DR (1982) Crop rotation and plant productivity. In: Rechcigl J (ed) Handbook of agricultural productivity, vol I. CRC, Boca Raton, pp 273–315
12. Umaerus VR, Scholte K, Turkensteen LJ (1989) Crop rotation and the occurrence of fungal diseases in potatoes. In: Vos J, Van Loon CD, Bollen GJ (eds) Effects of crop rotation on potato productions in the temperate zones. Academic, Dordrecht, pp 171–189
13. Sturz AV, Carter MR, Johnston HW (1997) A review of plant disease, pathogen interactions and microbial antagonism under conservation tillage in temperate humid agriculture. Soil Tillage Res 41:169–189
14. Van Bruggen AHC, Semenov AM, van Diepeningen AD, de Vos OJ, Blok WJ (2006) Relation between soil health, wave-like fluctuations in microbial populations, and soil-borne plant disease management. Eur J Plant Pathol 115: 105–122
15. Van Diepeningen AD, de Vos OJ, Zelenev VV, Semenov AM, van Bruggen AHC (2005) DGGE fragments oscillate with or counter to fluctuations of cultivable bacteria along wheat roots. Microb Ecol 50:506–517
16. Khan AG (1975) The effect of vesicular arbuscular mycorrhizal associations on growth of cereals II. Effects on wheat growth. Ann Appl Biol 80:27–36
17. McFadden AG, Sutton JC (1975) Relationships of populations of *Trichoderma* spp. in soil to disease in maize. Can J Plant Sci 55:579–586
18. Lynch JM, Panting LM (1980) Cultivation and the soil biomass. Soil Biol Biochem 12:29–33
19. Carter MR, Rennie DA (1984) Nitrogen transformations under zero and shallow tillage. Soil Sci Soc Am J 48:1077–1081
20. Chen W, Hoitink HAJ, Madden LV (1988) Microbial activity and biomass in container media for predicting suppressiveness to damping-off caused by *Pythium ultimum*. Phytopathology 78:1447–1450
21. Carignano M, Staggenborg SA, Shroyer JP (2008) Management practices to minimize tan spot in a continuous wheat rotation. Agron J 100:145–153
22. Gladders P, Musa TM (1980) Observations of the epidemiology of *Leptosphaeria maculans* stem canker in winter oilseed rape. Plant Pathol 29:28–37
23. Kolte SJ (1985) Diseases of annual edible oilseed crops, vol II, Rapeseed-mustard and sesame diseases. CRC, Boca Raton
24. Naseri B, Davidson JA, Scott ES (2008) Survival of *Leptosphaeria maculans* and associated mycobiota on oilseed rape stubble buried in soil. Plant Pathol 57:280–289
25. Humpherson-Jones FM (1992) Epidemiology and control of dark leaf spot of Brassicas. In: Chelkowski J, Visconti A (eds) Alternaria: biology, plant diseases and metabolites. Elsevier, Amsterdam, pp 267–288
26. Zhan J, Fitt BDL, Pinnschmidt HO, Oxley SJP, Newton AC (2008) Resistance, epidemiology and sustainable management of *Rhynchosporium secalis* populations on barley. Plant Pathol 57:1–14
27. Nuttall WF (1982) The effect of seeding depth, soil moisture regime, and crust strength on emergence of rape cultivars. Agron J 74:1018–1022
28. Datnoff LE, Elmer WH, Huber DM (2007) Mineral nutrition and plant disease. APS, St. Paul
29. Walters DR, Bingham IJ (2007) Influence of nutrition on disease development caused by fungal pathogens: implications for plant disease control. Ann Appl Biol 151:307–324
30. Mascagni HJ Jr, Harrison SA, Russin JS, Desta HM, Colyer PD, Habetz RJ, Hallmark WB, Moore SH, Rabb JL, Hutchinson RL, Boquet DJ (1997) Nitrogen and fungicide effects on winter wheat produced in the Louisiana Gulf Coast region. J Plant Nutr 20:1375–1390
31. Hoffland E, Jeger MJ, van Beusichem ML (2000) Effect of nitrogen supply rate on disease resistance in tomato depends on the pathogen. Plant Soil 218:239–247
32. Talukder ZI, McDonald AJS, Price AH (2005) Loci controlling partial resistance to rice blast do not show marked QTL X environment interaction when plant nitrogen status alters disease severity. New Phytol 168:455–464
33. Lemmens M, Buerstmayr H, Krska R, Schumacher R, Grausgruber H, Rackenbauer P (2004) The effect of inoculation treatment and long term application of moisture on Fusarium head blight symptoms and deoxynivalenol contamination in wheat grains. Eur J Plant Pathol 110:299–308
34. Neumann S, Paveley ND, Beed FD, Sylvester-Bradley R (2004) Nitrogen per unit area affects the upper asymptote of *Puccinia striiformis* f.sp. *tritici* epidemics in winter wheat. Plant Pathol 53:725–732
35. Buschbell T, Hoffmann GM (1992) The effects of different nitrogen regimes on the epidemiologic development of pathogens on winter-wheat and their control. J Plant Dis Prot 99:381–403
36. Olesen JE, Mortensen JV, Jorgensen LN, Andersen MN (2000) Irrigation strategy, nitrogen application and fungicide control in winter wheat on a sandy soil. I. Yield, yield components and nitrogen uptake. J Agric Sci (Cambridge) 134:1–11

37. Hoffland E, van Beusichem ML, Jeger MJ (1999) Nitrogen availability and susceptibility of tomato leaves to *Botrytis cinerea*. Plant Soil 210:263–272
38. Bryant JP, Chapin FS III, Klein DR (1983) Carbon/nutrient balance of boreal plants in relation to vertebrate herbivory. Oikos 40:357–368
39. Herms DA, Mattson WJ (1992) The dilemma of plants: to grow or to defend. Q Rev Biol 67:283–335
40. Perrenoud S (1990) Potassium and plant health, 2nd edn. International Potash Institute, Bern
41. Mucharromah E, Kuc J (1991) Oxalates and phosphates induce systemic resistance against disease caused by fungi, bacteria and viruses in cucumber. Crop Prot 10:265–270
42. Walters DR, Murray DC (1992) Induction of systemic resistance to rust in *Vicia faba* by phosphate and EDTA: effects of calcium. Plant Pathol 41:444–448
43. Reuveni M, Reuveni R (1995) Efficacy of foliar application of phosphates in controlling powdery mildew fungus on field-grown winegrapes: effects on cluster yield and peroxidase activity. J Phytopathol 143:21–25
44. Reuveni R, Agapov V, Reuveni M (1994) Foliar spray of phosphates induces growth increase and systemic resistance to *Puccinia sorghi* in maize. Plant Pathol 43:245–250
45. Mandahar HK, Lyngs Jorgensen HJ, Mathur SB, Smedegaard-Petersen V (1998) Resistance to rice blast induced by ferric chloride, di-potassium hydrogen phosphate and salicylic acid. Crop Prot 17:323–329
46. Reuveni R, Reuveni M (1998) Foliar fertilizer therapy – a concept in integrated pest management. Crop Prot 17:111–118
47. Prabhu AS, Fageria NK, Huber DM, Rodrigues FA (2007) Potassium and plant disease. In: Datnoff LE, Elmer WH, Huber DM (eds) Mineral nutrition and plant disease. APS, St. Paul, pp 57–78
48. Fixen PE, Gelderman RH, Gerwing J, Cholick FA (1986) Response of spring wheat, barley and oats to chloride in potassium chloride fertilizers. Agron J 78:664–668
49. Engel RE, Eckhoff J, Berg RK (1994) Grain yield, kernel weight and diseases responses of winter wheat cultivars to chloride fertilization. Agron J 86:891–896
50. Ehret DL, Menzies JG, Bogdanoff C, Utkhede RS, Frey B (2002) Foliar applications of fertiliser salts inhibit powdery mildew on tomato. Can J Plant Pathol 24:437–444
51. Cook JW, Kettlewell PS, Parry DW (1993) Control of *Erysiphe graminis* and *Septoria tritici* on wheat with foliar-applied potassium chloride. J Sci Food Agric 63:126
52. Mann RL, Kettlewell PS, Jenkinson P (2004) Effect of foliar-applied potassium chloride on septoria leaf blotch of winter wheat. Plant Pathol 53:653–659
53. Kettlewell PS, Cook JW, Parry DW (2000) Evidence for an osmotic mechanism in the control of powdery mildew disease of wheat by foliar-applied potassium chloride. Eur J Plant Pathol 106:297–300
54. Rahman M, Punja ZK (2007) Calcium and plant disease. In: Datnoff LE, Elmer WH, Huber DM (eds) Mineral nutrition and plant disease. APS, St. Paul, pp 79–94
55. Biggs AR (1999) Effects of calcium salts on apple bitter rot caused by two *Colletotrichum* spp. Plant Dis 83:1001–1005
56. Cheour F, Willemot C, Arul J, Desjardins Y, Makhlouf J, Charest PM, Gosselin A (1990) Foliar application of calcium chloride delays postharvest ripening of strawberry. J Am Soc Hortic Sci 115:89–792
57. Woltz SS, Jones JP, Scott JW (1992) Sodium chloride, nitrogen source and lime influence Fusarium crown rot severity in tomato. HortScience 27:1087–1088
58. Nam MH, Jeong SK, Lee YS, Choi JM, Kim HG (2006) Effects of nitrogen, phosphorus, potassium and calcium nutrition on strawberry anthracnose. Plant Pathol 55:246–249
59. Conway WS, Sams CE (1984) Possible mechanisms by which postharvest calcium treatment reduces decay in apples. Phytopathology 74:208–210
60. Biggs AR, Peterson CA (1990) Effect of chemical applications to peach bark wounds on accumulation of lignin and suberin and susceptibility to *Leucostoma persoonii*. Phytopathology 80:861–865
61. Wagner F (1940) Die bedeutung der kieselsnure far das wachstum einiger kulturpflanzen, ihren nnhrstoffhaushalt und ihre anfnlligkeit gegen echte mehltaupilze. Phytopathol Z 12:427–479
62. Miyake Y, Takahashi E (1983) Effect of silicon on the growth of solution cultured cucumber plant. Soil Sci Plant Nutr 29:71–83
63. Adatia MH, Besford RT (1986) The effects of silicon on cucumber plants grown in recirculating nutrient solution. Ann Bot 58:343–351
64. Belanger RR, Bowen P, Ehret DL, Menzies JG (1995) Soluble silicon: its role incrop and disease management of greenhouse crops. Plant Dis 79:329–336
65. Datnoff LE, Rodrigues FA, Seebold KW (2007) Silicon and plant disease. In: Datnoff LE, Elmer WH, Huber DM (eds) Mineral nutrition and plant disease. APS, St. Paul, pp 233–246
66. Rodgers-Gray BS, Shaw MW (2000) Substantial reductions in winter wheat diseases caused by addition of rice straw but not manure to soil. Plant Pathol 49:590–599
67. Rodgers-Gray BS, Shaw MW (2004) Effects of straw and silicon soil amendments on some foliar and stem base diseases in pot-grown winter wheat. Plant Pathol 53:733–740
68. Kim SG, Kim KW, Park EW, Choi D (2002) Silicon-induced cell wall fortification of rice leaves: a possible cellular mechanism of enhanced host resistance to blast. Phytopathology 92:1095–1103
69. Samuels AL, Glass ADM, Ehret DL, Menzies JG (1991) Mobility and deposition of silicon in cucumber plants. Plant Cell Environ 14:485–492
70. Heine G, Tikum G, Horst WJ (2007) The effect of silicon on the infection by and spread of *Pythium aphanidermatum* in single roots of tomato and bitter gourd. J Exp Bot 58:569–577
71. Belanger RR, Benhamou N, Menzies JG (2003) Cytological evidence of an active role of silicon in wheat resistance to powdery mildew (*Blumeria graminis* f.sp. *tritici*). Phytopathology 93:402–412

72. Rodrigues FA, McNally DJ, Datnoff LE, Jones JB, Labbe C, Benhamou N, Menzies JG, Belanger RR (2004) Silicon enhances the accumulation of diterpenoid phytoalexins in rice: a potential mechanism for blast resistance. Phytopathology 94:177–183
73. Fauteux F, Remus-Borel W, Menzies JG, Belanger RR (2005) Silicon and plant disease resistance against pathogenic fungi. FEMS Microbiol Lett 249:1–6
74. Bailey KL, Lazarovits G (2003) Suppressing soil-borne diseases with residue management and organic amendments. Soil Tillage Res 72:169–180
75. Litterick A, Wood M (2009) The use of composts and compost extracts in plant disease control. In: Walters D (ed) Disease control in crops: biological and environmentally-friendly approaches. Wiley, Oxford, pp 93–121
76. Vanderplank JE (1968) Disease resistance in plants. Academic, New York
77. Parlevliet JE, Van Ommeren A (1975) Partial resistance of barley to leaf rust, *Puccinia hordei*. II. Relationship between field trials, micro plot test and latent period. Euphytica 24:293–303
78. Johnson R, Law CN (1975) Genetic control of durable resistance to yellow rust (*Puccinia striiformis*) in the wheat cultivar Hybride de Bersée. Ann Appl Biol 81:385–391
79. Wang GL, Song WY, Ruan DL, Sideris S, Ronald PC (1996) The cloned gene, *Xa21*, confers resistance to multiple *Xanthomonas oryzae* pv. *oryzae* isolates in transgenic plants. Mol Plant Microbe Interact 9:850–855
80. Gonsalves D (2004) Transgenic papaya in Hawaii and beyond. AgBioForum 7(1/2):36–40, http://www.agbioforum.org
81. Burdon JJ (1978) Mechanisms of disease control in heterogeneous plant populations: an ecologist's view. In: Scott PR, Bainbridge A (eds) Plant disease epidemiology. Blackwell, Oxford, pp 193–200
82. Newton A (2009) Plant disease control through the use of variety mixtures. In: Walters D (ed) Disease control in crops: biological and environmentally friendly approaches. Wiley, Oxford, pp 162–171
83. Holm RE, Baron JJ, Kunkel D (2005) The IR-4 programme and its cooperation with the crop protection industry to provide new pest control solutions to US specialty crop growers. Proc BCPC Int Congr Crop Sci Technol 1:239–250
84. Stark G (2008) The EU thematic strategy for pesticides and the UK national pesticides strategy. In: Proceedings crop protection in northern Britain 2008, Dundee, pp 23–26
85. Best J, Burn A (2005) 'Polluter pays' or 'public good': tackling indirect effects of pesticides. Proc BCPC Int Congr Crop Sci Technol 2:1097–1102
86. Richardson DM (2005) The registration process, its effect on active substance availability, and initiatives to reduce the impact on minor crops at both UK and EU level. Proc BCPC Int Congr Crop Sci Technol 1:231–238
87. Whipps JM, McQuilken MP (2009) Biological control agents in plant disease control. In: Walters D (ed) Disease control in crops: biological and environmentally friendly approaches. Wiley, Oxford, pp 27–61
88. Harman GE (2006) Overview of mechanisms and uses of *Trichoderma* spp. Phytopathology 96:190–194
89. Bennett AJ, Whipps JM (2007) Dual application of beneficial microorganisms to seed during drum priming. Appl Soil Ecol 38:83–89
90. Hammerschmidt R (2007) Introduction: definitions and some history. In: Walters D, Newton A, Lyon G (eds) Induced resistance for plant disease control: a sustainable approach to crop protection. Blackwell, Oxford, pp 1–8
91. Pieterse CMJ, Van Loon LC (2007) Signalling cascades involved in induced resistance. In: Walters D, Newton A, Lyon G (eds) Induced resistance for plant disease control: a sustainable approach to crop protection. Blackwell, Oxford, pp 65–88
92. Ryals JA, Neuenschwander UH, Willits MG, Molina A, Steiner H (1996) Systemic acquired resistance. Plant Cell 8:1809–1819
93. Durrant WE, Dong X (2004) Systemic acquired resistance. Annu Rev Phytopathol 42:185–209
94. Sparla F, Rotino L, Valgimigli MC, Pupillo P, Trost P (2004) Systemic resistance induced by benzothiadiazole in pear inoculated with the agent of fire blight (*Erwinia amylovora*). Sci Hortic 101:269–79
95. Zehnder GW, Murphy JF, Sikora EJ, Kloepper JW (2001) Application of rhizobacteria for induced resistance. Eur J Plant Pathol 107:39–50
96. Goellner K, Conrath U (2008) Priming: it's all the world to induced resistance. Eur J Plant Pathol 121:233–242
97. Kohler A, Schwindling S, Conrath U (2002) Benzothiadiazole-induced priming for potentiated responses to pathogen infection, wounding, and infiltration of water into leaves requires the *NPR1/NIM1* gene in *Arabidopsis*. Plant Physiol 128:1046–1056
98. van Hulten M, Pelser M, Van Loon LC, Pieterse CMJ, Ton J (2006) Costs and benefits of priming for defense in *Arabidopsis*. Proc Natl Acad Sci USA 103:5602–5607
99. Jakab G, Cottier V, Toquin V, Rigoli G, Zimmerli L, Metraux J-P, Mauch-Mani B (2001) β-aminobutyric acid-induced resistance in plants. Eur J Plant Pathol 107:29–37
100. Zimmerli L, Jakab G, Métraux J-P, Mauch-Mani B (2000) Potentiation of pathogen-specific defense mechanisms in *Arabidopsis* by beta-aminobutyric acid. Proc Natl Acad Sci USA 97:12920–12925
101. Zimmerli L, Metraux J-P, Mauch-Mani B (2001) β-aminobutyric acid-induced protection of *Arabidopsis* against the necrotrophic pathogen *Botrytis cinerea*. Plant Physiol 126:517–523
102. Ton J, Mauch-Mani B (2004) β-aminobutyric acid-induced resistance against necrotrophic pathogens is based on ABA-dependent priming for callose. Plant J 38:119–130
103. Iwata M (2001) Probenazole – a plant defence activator. Pestic Outlook 12:28–31
104. Watanabe T, Igarashi H, Matsumoto K, Seki S, Mase S, Sekizawa Y (1977) The characteristics of probenazole (oryzemate) for the control of rice blast. J Pesticide Sci 2:291–296

105. Watanabe T (1997) Effect of probenazole (Oryzemate) on each stage of rice blast fungus (*Pyricularia oryzae Cavara*) in its life cycle. J Pesticide Sci 2:395–404
106. Vallad GE, Goodman RM (2004) Systemic acquired resistance and induced systemic resistance in conventional agriculture. Crop Sci 44:1920–1934
107. Walters D, Walsh D, Newton A, Lyon G (2005) Induced resistance for plant disease control: maximizing the efficacy of resistance elicitors. Phytopathology 95:1368–1373
108. Cole DL (1999) The efficacy of acibenzolar-S-methyl, an inducer of systemic acquired resistance, against bacterial and fungal diseases of tobacco. Crop Prot 18:267–273
109. Perez L, Rodriguez ME, Rodriguez F, Roson C (2003) Efficacy of acibenzolar-S-methyl, an inducer of systemic acquired resistance, against tobacco blue mold caused by *Peronospora hyoscyami* f.sp. *tabacina*. Crop Prot 22:405–413
110. Gorlach J, Volrath S, Knauf-Belter G, Hengy G, Beckhove U, Kogel K-H, Oostendorp M, Staub T, Ward E, Kessmann H, Ryals J (1996) Benzothiadiazole, a novel class of inducers of systemic acquired resistance, activates gene expression and disease resistance in wheat. Plant Cell 8:629–643
111. Stadnik MJ, Buchenauer H (1999) Control of wheat diseases by a benzothiadiazole-derivative and modern fungicides. J Plant Dis Prot 106:466–475
112. Zhang S, Reddy MS, Kokalis-Burelle N, Wells LW, Nightengale SP, Kloepper JW (2001) Lack of induced systemic resistance in peanut to late leaf spot disease by plant growth-promoting rhizobacteria and chemical elicitors. Plant Dis 85:879–884
113. Liu SY, Liu Z, Fitt BDL, Evans N, Foster SJ, Huang YJ, Latunde-Dada AO, Lucas JA (2006) Resistance to *Leptosphaeria maculans* (phoma stem canker) in *Brassica napus* (oilseed rape) induced by *L. biglobosa* and chemical defence activators in field and controlled environments. Plant Pathol 55:401–412
114. Paterson L, Walsh DJ, Walters DR (2008) Effect of resistance elicitors on *Rhynchosporium secalis* infection of barley. In: Proceedings crop protection in northern Britain 2008, Dundee, pp 163–168
115. Hadwiger LA (1999) Host-parasite interactions: elicitation of defence responses in plants with chitosan. In: Jolles P, Muzzarelli RAA (eds) Chitin and chitinases. Birkhauser, Switzerland, pp 185–200
116. Sharathchandra RG, Niranjan Raj S, Shetty NP, Amruthesh KN, Shekar Shetty H (2004) A chitosan formulation Elexa™ induces downy mildew disease resistance and growth promotion in pearl millet. Crop Prot 23:881–888
117. Schilder A, Gillet J, Sysak R, Wise J (2002) Evaluation of environmentally friendly products for control of fungal diseases of grapes. In: Proceedings of the 10th International Conference on Cultivation Technique and Phytopathological Problems in Organic Fruit-Growing and Viticulture. Weinsberg, Germany, pp 163–167
118. Wei ZM, Laby RJ, Zumoff CH, Bauer DW, He SY, Collmer A, Beer SV (1992) Harpin, elicitor of the hypersensitive response produced by the plant pathogen *Erwinia amylovora*. Science 257:85–88
119. de Capdeville G, Beer SV, Watkins CB, Wilson CL, Tedeschi LO, Aist JR (2003) Pre- and post-harvest harpin treatments of apples induce resistance to blue mold. Plant Dis 87:39–44
120. Meszka B, Bielenin A (2004) Possibilities of integrated grey mold control on strawberry plantations in Poland. Bull OILB SROP 27:41–45
121. Pernezny K, Stoffella P, Collins J, Carroll A, Beaney A (2002) Control of target spot of tomato with fungicides, systemic acquired resistance activators, and a biocontrol agent. Plant Prot Sci 38:81–88
122. Chen L, Qian J, Qu S, Long J, Yin Q, Zhang C, Wu X, Sun F, Wu T, Hayes M, Beer SV, Dong H (2008) Identification of specific fragments of $HpaG_{Xooc}$, a harpin from *Xanthomonas oryzae* pv. *oryzicola,* that induce disease resistance and enhance growth in plants. Phytopathology 98:781–791
123. Chen L, Zhang S-J, Zhang S-S, Qu S, Ren X, Long J, Yin Q, Qian J, Sun F, Zhang C, Wang L, Wu X, Wu T, Zhang Z, Cheng Z, Hayes M, Beer SV, Dong H (2008) A fragment of *Xanthomonas oryzae* pv. *oryzicola* Harpin $HpaG_{Xooc}$ reduces disease and increases yield of rice in extensive grower plantings. Phytopathology 98:792–802
124. Wei G, Yao GW, Zehnder S, Tuzun S, Kloepper JW (1995) Induced systemic resistance by select plant growth promoting rhizobacteria against bacterial wilt of cucumber and the beetle vectors. Phytopathology 85:1154
125. Wei G, Kloepper JW, Tuzun S (1996) Induced systemic resistance to cucumber diseases and increased plant growth by plant growth promoting rhizobacteria under field conditions. Phytopathology 86:221–224
126. Raupach GS, Kloepper JW (2000) Biocontrol of cucumber diseases in the field by plant growth promoting rhizobacteria with and without methyl bromide fumigation. Plant Dis 84:1073–1075
127. Jetiyanon K, Fowler WD, Kloepper JW (2003) Broad-spectrum protection against several pathogens by PGPR mixtures under field conditions in Thailand. Plant Dis 87:1390–1394
128. Kirkegaard J (2009) Biofumigation for plant disease control – from the fundamentals to the farming system. In: Walters D (ed) Disease control in crops: biological and environmentally friendly approaches. Wiley, Oxford, pp 172–195
129. Gamliel A, Katan J (2009) Control of plant disease through soil solarisation. In: Walters D (ed) Disease control in crops: biological and environmentally friendly approaches. Wiley, Oxford, pp 196–220
130. Agrios GN (2005) Plant pathology, 5th edn. Elsevier, Burlington

Books and Reviews

Cheatham MR, Rouse MN, Esker PD, Ignacio S, Pradel W et al (2009) Beyond yield: plant disease in the context of ecosystem services. Phytopathology 99:1228–1236

Lucas JA (1998) Plant pathology and plant pathogens. Blackwell, Oxford

Pollock C, Pretty J, Crute I, Leaver C, Dalton H (2008) Sustainable agriculture I. Philos Trans R Soc B 363:443–680
Pollock C, Pretty J, Crute I, Leaver C, Dalton H (2008) Sustainable agriculture II. Philos Trans R Soc B 363:681–913
Strange RN (1993) Plant disease control: towards environmentally acceptable methods. Chapman & Hall, London
Walters D, Newton A, Lyon G (2007) Induced resistance for plant defence: a sustainable approach to crop protection. Blackwell, Oxford
Walters D (2009) Disease control in crops: biological and environmentally friendly approaches. Wiley, Oxford

Crop Plants Transformation Methods

Dawei Yuan[1], Svetlana Dashevskaya[1], Richard M. Twyman[2], Teresa Capell[1], Paul Christou[3,4]
[1]Department of Vegetal Production and Forestry Science, ETSEA, University of Lleida, Lleida, Spain
[2]Department of Biological Sciences, University of Warwick, Coventry, UK
[3]Department de Produccio Vegetal i Ciencia Forestal, Universitat de Lleida/ICREA, Lleida, Spain
[4]Institució Catalana de Recerca i Estudis Avançats (ICREA), Barcelona, Spain

Article Outline

Glossary
Definition of the Subject and Its Importance
Introduction
Principles and Methods of Plant Transformation
Vectors for Plant Transformation
Consequences of Nuclear Transformation
Plastid Transformation Methods
Future Directions
Bibliography

Glossary

Acetosyringone A phenolic compound that activates the *Agrobacterium tumefaciens vir* genes and thus initiates DNA transfer.

Agrobacterium-mediated transformation The introduction of DNA into plants by the bacterium *Agrobacterium tumefaciens*.

Bactofection Gene transfer to animal cells mediated by bacteria.

BIBAC A binary vector for plant transformation based on the high-capacity bacterial artificial chromosome (BAC).

Binary vector A plant transformation vector in two parts, one carrying the T-DNA and one carrying the *vir* genes.

Cassette A modular DNA sequence designed for portability between different vectors.

Chimeric (transformed plants) Comprising cells with different genotypes, usually a first-generation transformant (T_0) where some cells are transgenic and others are not.

Concatemer A DNA molecule containing multiple contiguous copies of the same sequence.

Conjugation DNA transfer between cells through a specialized conduit known as a pilus.

Counterselectable marker A selectable marker gene whose absence is required for cells to survive.

Destination vector The vector designated to receive a DNA cassette during LR recombination in the Gateway system.

Direct DNA transfer DNA transfer mediated by physical or chemical means rather than by bacteria or viruses.

Entry clone The vector holding the DNA cassette that needs to be transferred to the Destination vector during LR recombination in the Gateway system.

Episomal A genetic entity that replicates independently of the host chromosome, such as a plasmid or nonintegrating virus.

Explant A piece of plant tissue transferred to culture and propagated independently.

Filler DNA Extra DNA added at junctions during illegitimate recombination, either by synthesis across a template or random addition of nucleotides.

Gateway A proprietary cloning system based on LR recombination, a form of site-specific recombination using the *att*B and *att*P sites of *Escherichia coli* and bacteriophage λ.

Gene targeting Disruption of a preselected gene by homologous recombination with a DNA cassette.

Helper plasmid A plasmid that is not used as a cloning vehicle, but which supplies necessary functions in *trans*.

Homing endonuclease A specialized type of restriction enzyme encoded by introns and inteins with a long asymmetric recognition sequence.

Homologous recombination Recombination requiring long regions of homology but no sequence specificity.

Illegitimate recombination Recombination requiring neither long regions of homology nor specific sequences; it can occur by direct nonhomologous end-joining (all sequences conserved, sometimes with added filler DNA) or at regions of microhomology.

***In planta* transformation** Transformation methods that can be used with intact plants rather than tissue explants, and which therefore require no regeneration.

Integration The insertion of one DNA sequence in the midst of another.

Minichromosome A vector comprising the minimal elements that allow it to function as a chromosome.

Minimal cassette The minimal sequences required to achieve transformation and transgene expression, typically a promoter, gene, and terminator.

Multigene transfer The simultaneous transfer of more than one gene into a plant.

Particle bombardment A physical transformation method based on the acceleration of DNA-coated metal particles into intact plant cells.

Promoter The DNA sequence in front of a gene which controls its spatiotemporal expression profiles and whether its expression is sensitive to external stimuli.

Reporter gene A gene whose function is to yield an easily detectable product that can be used to measure or delimit the activity of a regulatory element such as a promoter.

Screenable marker Another name for a reporter gene.

Selectable marker A gene whose function is to confer on transformed cells some property that allows them to be propagated in conditions under which nontransformed cells either die or cannot grow efficiently.

Southern blot (DNA blot) A method for the detection of DNA sequences using specific labeled complementary probes.

Stable transformation Transformation followed by integration of DNA into the host genome such that the transgene becomes a permanent new genomic locus.

Superbinary vector A binary vector in which the *vir* gene functions are enhanced.

Supervirulent An *Agrobacterium tumefaciens* strain with a broader host range or more efficient DNA transfer ability than normal strains.

T-DNA The section of DNA within a binary vector which is transferred to the host plant.

Transactivation domain The part of a transcription factor that activates transcription.

Transient expression The expression of introduced DNA for a short time before the DNA is diluted and degraded.

Transfection (a) In bacteria, the transfer of phage DNA into bacterial cells by chemical or physical means; (b) in animals and plants, the transfer of any DNA into cultured cells by chemical or physical means.

Transformant A plant that has been transformed with exogenous DNA.

Transformation (a) In bacteria, the transfer of plasmid or genomic DNA into bacterial cells by chemical or physical means; (b) in animal cells, the spontaneous or induced change from a normal to an oncogenic phenotype; (c) in plants, any means of DNA transfer that does not involve the use of a virus.

Transgenic Containing integrated exogenous DNA in the nuclear genome.

Transplastomic Containing integrated exogenous DNA in the plastid genome.

Terminator The sequence following the gene that is required to terminate transcription.

***vir* Gene** One of several genes on binary vectors that are required in *trans* to mediate T-DNA transfer.

Zinc finger A zinc-coordinating protein motif usually associated with DNA binding, often found in sequence-specific DNA binding proteins such as transcription factors.

Definition of the Subject and Its Importance

The term **transformation** (or more properly "genetic transformation") was first coined to describe the natural process by which bacteria take up free DNA from their surroundings. The term was required to distinguish this process from two other ubiquitous natural gene transfer mechanisms in bacteria: **conjugation** (direct transfer of DNA from cell to cell through a connecting tube called a pilus) and **transduction** (transfer of DNA between cells carried by the capsid of a virus). All three of these natural processes have been exploited in the laboratory as ways to introduce

exogenous DNA into bacterial cells, and in this context the definition of transformation was later refined to take into account the different consequences of gene transfer depending on the origins of the transforming DNA. The meaning of **transformation** was thus restricted to the uptake of naked plasmids or genomic DNA fragments, whereas an alternative term – **transfection** – was coined to describe the uptake of naked phage DNA, the distinction required because only the latter can initiate a phage infection.

Unsurprisingly, the same terms have been adopted to describe analogous processes in other organisms, but the precise definitions vary due to preexisting conventions. Cultured animal cells are said to undergo transformation when they change from the normal phenotype (cessation of growth when confluence is achieved) to an oncogenic phenotype (continued growth, formation of foci) so "transformation" is usually avoided in the context of gene transfer to prevent ambiguity. Therefore, transfection is used to describe the introduction of any naked DNA into animal cells regardless of its origin. The transfer of DNA from bacteria to animal cells (including the use of conjugation-like mechanisms) is unusual and has only recently been adopted as a gene transfer procedure in the laboratory, so a new term has been coined for this process – **bactofection**. The introduction of DNA into animal cells using a virus as a carrier is known as transduction, just as it is in bacteria.

The terminology for plants is a hybrid of the conventions used for bacteria and animal cells. Transformation refers to any gene transfer process where a virus is not used as a carrier (otherwise transduction is the correct term, as in bacteria and animal cells). This means that **plant transformation** includes both the uptake of naked DNA (**direct DNA transfer**) and the transfer of DNA by the conjugation-like method adopted by *Agrobacterium tumefaciens* and *Agrobacterium rhizogenes* (***Agrobacterium*-mediated transformation**). However, due to operational analogies with cultured animal cells, the introduction of DNA into cultured plant protoplasts is also termed transfection, so in this specific context the terms transformation and transfection are synonymous.

The fate of the introduced DNA depends on many factors. If it does not contain an origin of replication that is active in plant cells it is usually maintained in the nucleus for a short period of time (hours to days), eventually being diluted and degraded. If the introduced DNA contains an active expression cassette, then a product may be expressed during this time, a process known as **transient expression**. In a very small number of cells, the DNA integrates into the genome and becomes a permanent new locus. This is known as **stable transformation**. It is a rare event (approximately one in every 10,000 cells that takes up exogenous DNA integrates it into the genome) and selectable marker genes are usually employed to ensure that the small number of transformed cells can grow at the expense of their nontransformed peers, allowing the recovery of transgenic tissues and whole plants. Cells, tissues, and whole plants that are stably transformed with a particular fragment of exogenous DNA are termed **transgenic** if the DNA integrates into the nuclear genome or **transplastomic** if it integrates into the plastid genome. The integrated DNA is known as the **transgene** (depending on context this term can refer to a single gene or to the integrated segment of exogenous DNA which may contain one or more genes).

If the introduced DNA does have an origin of replication that functions in plants, then it may be maintained **episomally** (as an extrachromosomal replicon). This occurs when the introduced genetic material is part of a replication-competent recombinant plant virus, or when it includes the components of a plant centromere, allowing it to function as a minichromosome. Viral vectors are generally short-lived, so they are also used for transient expression. However, the ability of viruses to spread systemically means that the transgene may be expressed at very high levels throughout the plant, and the infection may last days or weeks. Minichromosome vectors are a relatively new development in plants but as with equivalent "artificial chromosome" vectors in yeast and animal cells, the idea is that they should facilitate stable transformation without the need for integration into the genome.

Plant transformation is a fundamental component of both basic and applied plant biology. For basic research, transformation allows scientists to study how genes function and allows the expression of both endogenous genes and transgenes to be controlled.

This has increased our understanding of how plants grow, develop, and defend themselves against pests, diseases, and harsh environments, how photosynthesis is controlled, and the basis of primary and secondary metabolism. For applied research, transformation can be used to improve the agronomic performance of crops, making them hardier, more nutritious, more productive, or converting them from conventional crops into green factories producing chemical precursors, novel oils, industrial enzymes, and pharmaceuticals. Plants provide human beings with all types of useful products: food and animal feed, fibers and structural materials, and small molecules that can be used as dyes, scents, and medicines. Plants have been cultivated for these products since the dawn of history, and for the same length of time people have sought to improve plants by breeding them and selecting the better-performing and most useful varieties. The limitations of this approach, i.e., the fact that breeders are restricted to the existing gene pool in each group of sexually compatible species, and that breeding takes a long time to achieve its goals, can be overcome by plant transformation, thus accelerating the development of plants with novel, beneficial traits.

Introduction

Plant transformation became a routine process in the 1980s but several attempts to transfer DNA into plant tissues were reported in the previous 2 decades, although stable transformation was never confirmed. The first deliberate transformation of plant tissue with laboratory-created recombinant DNA was achieved in 1983 when several researchers reported the introduction of recombinant plasmids, including backbone sequences from cloning vectors and selectable marker genes [1–3]. This marked the first creation of transgenic plant cells in the currently accepted meaning of the word. In the intervening 30 years, heterologous genes have been introduced into well over 100 different plant species either through the use of the soil bacterium *A. tumefaciens* or alternative strategies involving direct DNA transfer to plant cells and tissues. In addition, many plant viruses have been developed as episomal vectors, allowing high-level transient gene expression, although because of their inability to achieve stable transformation they are not considered further in this article.

Principles and Methods of Plant Transformation

A fundamental difference between animals and plants is that differentiated plant tissue shows a high degree of developmental plasticity. Depending on the species, isolated stem segments, leaf disks, and seed-derived callus tissue may be able to regenerate an entire new plant under appropriate culture conditions. For most plant species, some form of tissue culture step is therefore used for the successful production of transgenic plants after cells or small tissue explants have been subjected to the actual transformation procedure. However, it should be noted that whole-plant (*in planta*) transformation strategies are also available in some species, in which the need for tissue culture is minimized or eliminated.

The ease with which plant material is manipulated and interconverted in culture provides many opportunities for the development of techniques for gene transfer and the recovery of transgenic plants (Fig. 1). DNA can be introduced into most types of plant material – protoplasts, cell suspensions, callus, vegetative tissue explants, gametes, seeds, zygotes, embryos, organs, and whole plants; so, the ability to recover fertile plants from such material is often the limiting step in plant genetic engineering rather than the DNA transfer process itself. It is also possible to maintain transformed plant cell lines or tissues (e.g., root cultures) rather than regenerating whole plants as these can often be sustained indefinitely in culture.

Gene transfer to plants can be achieved through three types of mechanism – viral transduction, bacterial gene delivery, and chemical/physical direct DNA transfer. Bacterial gene delivery using the soil pathogen *A. tumefaciens* is the most widely used method for dicotyledonous plants, but increasingly also for monocots. Physical methods are the next most popular, especially particle bombardment for the transformation of more recalcitrant monocots such as cereals. Chemical transfection methods are little used these days, and are only suitable for protoplasts. Each of the above methods can be used to achieve either transient expression or stable transformation of the nuclear genome,

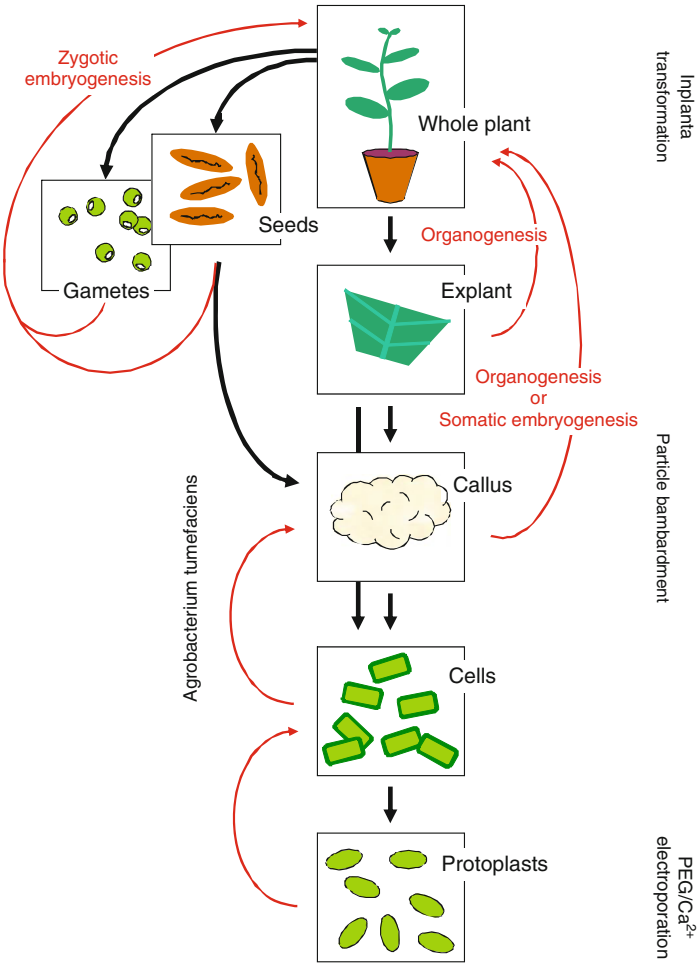

Crop Plants Transformation Methods. Figure 1
Strategies for the transformation of higher plants [4]. *The boxes* show the various different targets for transformation and how they are obtained from whole plants (*black arrows*). The methods used to transform each of these targets are shown in *black text*. *The red arrows* show the routes used to obtain whole transgenic plants

while direct gene transfer can also be used to achieve chloroplast transformation. As stated earlier, viral transduction does not lead to stable transformation and virus vectors are not discussed in this article.

Principles of *Agrobacterium*-Mediated Transformation

Gene transfer from bacteria to plants occurs naturally and is responsible for crown gall disease. This is a plant tumor that can be induced in a wide variety of gymnosperms and dicotyledonous angiosperms by inoculating wound sites with the Gram-negative soil bacterium *A. tumefaciens*. The tumor produces plant hormones responsible for the proliferation of undifferentiated plant tissue, and specialized amino acid derivatives known as opines that the bacteria use as a carbon source. The entire system has therefore evolved as a way for the bacteria to exploit plants for accommodation and food.

Even so, the continued presence of the bacteria is not required to maintain the tumor, indicating that some "tumor-inducing principle" is transferred from the bacterium to the plant at the wound site. Research

in the late 1970s identified the principle as a small segment of DNA that is transferred to the plant genome (hence T-DNA, for transferred DNA). The source of the T-DNA is a large plasmid, the tumor-inducing (Ti) plasmid, resident in the bacterium.

Agrobacterium-mediated transformation was developed as a platform technology following the dissection and functional analysis of two key components of natural Ti-plasmids: the T-DNA, which contains DNA sequences required in *cis* for DNA transfer, and the *vir* (virulence) region, which contains genes whose products are required in *trans* for DNA transfer. The resulting transformation system is known as a binary vector system because the T-DNA and *vir* genes do not need to be present on the same vector. This means that the T-DNA can be housed on a small shuttle vector suitable for cloning in bacteria, while the *vir* genes are provided on a second "helper" plasmid.

Natural T-DNA carries genes encoding enzymes for plant hormone synthesis and enzymes for opine synthesis, and these are the factors that drive the formation of the crown gall tumor. The hormone genes are often called oncogenes because they lead to tumor formation. However, neither the oncogenes nor the opine genes are necessary for DNA transfer. If these genes are removed, leaving an "empty" T-DNA cassette, the "disarmed" T-DNA can still be transferred to the plant genome, but the transformed cells at the wound site no longer proliferate and form a tumor. All that is required for transfer is the *vir* region, the T-DNA border sequences which are targets for excision from the Ti-plasmid, and a small number of loci on the *A. tumefaciens* genome. The T-DNA border sequences are 25-bp imperfect direct repeats which define the boundaries of the T-DNA. An enhancer, sometimes called the *overdrive* sequence, is located external to the right-hand repeat and is also required for high-efficiency transfer [5, 6]. Disarming the T-DNA does not improve the efficiency of transformation but it does improve the efficiency of regeneration, since the oncogenes produce phytohormones that interfere with normal plant development. At the same time, however, this removes any visual confirmation that transformation has taken place, and selectable or screenable marker genes must be included in the T-DNA to allow the identification of transformants.

The *vir* genes are organized into several operons. Two of these genes, *vir*A and *vir*G, are constitutively expressed at a low level and control the plant-induced activation of the other *vir* genes. The VirA protein is a kinase that spans the inner bacterial membrane, and acts as the receptor for certain phenolic molecules that are released by wounded plant cells. Many such compounds have been characterized, but acetosyringone is the most widely used in the laboratory to induce *vir* gene expression [7]. These phenolic compounds do not actually attract bacteria to wounded plant cells (the bacteria are attracted by simple molecules such as sugars and amino acids) but the *vir* genes are induced after bacterial attachment. Activated VirA transphosphorylates the VirG protein, which is a transcriptional activator of the other *vir* genes. Further genes on the bacterial chromosome also encode transcription factors that regulate *vir* gene expression (reviewed in [8, 9]). The induction of *vir* gene expression results in the synthesis of proteins that form a conjugative pilus through which the T-DNA is transferred to the plant cell. The components of the pilus are encoded by genes in the *vir*B operon (reviewed in [10]). DNA transfer itself is initiated by an endonuclease formed by the products of the *virD1* and *virD2* genes. This introduces either single-strand nicks or a double-strand break at the 25-bp borders of the T-DNA, a process enhanced by the VirC12 and VirC2 proteins, which recognize and bind to the overdrive enhancer element. The VirD2 protein remains covalently attached to the processed T-DNA. Recent studies have suggested that the type of T-DNA intermediate produced (single- or double-stranded) depends on the type of Ti-plasmid, with double-stranded T-DNA favored by nopaline plasmids (where the T-DNA is a single element) and single "T-strands" favored by octopine and succinopine plasmids, where the T-DNA is split into noncontiguous sections. T-strands are coated with VirE2, a single-stranded DNA-binding protein. The whole complex, sometimes dubbed the firecracker complex because of its proposed shape, is then transferred through the pilus and into the plant cell. The VirD2 protein may protect the T-DNA against nucleases, target the DNA to the plant cell nucleus, and help integrate it into the plant genome. The protein has two distinct nuclear localization signals, with the C-terminal signal thought to play the major role in targeting the T-DNA [11]. Once in the nucleus, the T-DNA is thought to integrate through a process of illegitimate recombination,

perhaps exploiting naturally occurring chromosome breaks [12–14].

Contemporary binary vectors have all the conveniences of bacterial cloning vectors such as multiple unique restriction sites in the T-DNA region to facilitate subcloning, the *lac*Z gene for blue-white screening and a λ *cos* site for preparing cosmid libraries. A popular binary vector in current use is pGreen, which is <5 kbp in size, has 18 unique restriction sites in the T-DNA, a *lac*Z gene for blue-white screening of recombinants, and a selectable marker that can be used both in bacteria and in transformed plants [15]. The progressive reduction in size has been made possible by removing essential genes required for replication in *A. tumefaciens* and transferring those genes to the bacterium's genome, or onto a helper plasmid. The pGreen plasmid, for example, contains the Sa origin of replication, which is much smaller than the more traditional Ri and RK2 regions. Furthermore, an essential replicase gene is housed on a second plasmid called pSoup resident within the bacterium. All conjugation functions have also been removed [15].

More recent innovations have also been incorporated into binary vectors, such as the inclusion of Gateway technology, a proprietary technology developed by Invitrogen (now part of Life Sciences, Carlsbad, California, USA) which is based on the *att*B and *att*P site-specific recombination sites and associated enzymes employed by bacteriophage λ to integrate into the *Escherichia coli* chromosome during lysogeny (the process by which the bacteriophage genome integrates into the bacterial chromosome and becomes dormant). Under normal circumstances, the *att*P site in the phage genome and the *E. coli att*B site undergoes site-specific recombination catalyzed by a phage enzyme, resulting in integration and the formation of two hybrid sites flanking the prophage, *att*L, and *att*R. To develop this as a cloning system, sequences are prepared with flanking *att*B sites (typically generated using extended PCR primers) and these undergo recombination with *att*P sites in a Gateway vector to generate an Entry Clone in which the sequence is flanked by *att*L sites. The Entry Clone can then be mixed with a plant-specific Destination Vector, which contains *att*R sites flanking a marker gene, such that the cloned gene is transferred into the destination vector to replace the marker (LR recombination). A large number of Gateway-compatible binary vectors have been developed [16] allowing universal cloning independent of the presence of restriction endonuclease sites and the assembly of multiple genes on one plasmid, a modification known as MultiRound Gateway [17].

Methods of *Agrobacterium*-Mediated Transformation

Many dicotyledonous plants can be transformed using variations of the simple protocol developed by Horsch et al. [18] in which small disks punched from leaves are surface-sterilized and inoculated in a medium containing *A. tumefaciens* harboring the recombinant binary vector. The disks are cultured for 2 days, during which T-DNA transfer takes place, and are then transferred to a medium containing the selection agent and carbenicillin to kill the bacteria. After 2–4 weeks, developing shoots are excised from the callus and transplanted to root-inducing medium, and thereafter into soil.

This leaf disk method is unsuitable for most monocotyledonous plants because they lie outside the *Agrobacterium* host range, and do not respond to wounding in the same way as dicots. In order to transform staple crops such as cereals, modified culture conditions were developed involving explants containing a high proportion of actively dividing cells, such as embryos or apical meristems. In dicots, cell division is often induced by wounding, whereas wound sites in monocots tend to become lignified. This probably explains why traditional procedures such as the leaf disk method are inefficient in monocots. Hiei et al. [19] showed that the cocultivation of *Agrobacterium* and rice embryos in the presence of 100 mM acetosyringone was a critical factor for successful transformation. Efficiency could be improved further by using so-called "supervirulent" strains like AGL-1, which incorporate modifications to boost gene transfer activity, such as overexpressed *vir*G (switching on the expression of the other *vir* genes) and/or *vir*E1, which is a major limiting factor in T-DNA transfer (reviewed in [20]). Komari et al. [21] used a different strategy, in which a portion of the virulence region from the Ti-plasmid of supervirulent strain A281 was transferred to the T-DNA-carrying plasmid to generate

a so-called superbinary vector. The advantage of the latter technique is that the superbinary vector can be used in any *Agrobacterium* strain.

Principles of Direct DNA Transfer

Direct DNA transfer, as the name suggests, involves the introduction of DNA directly into the cell without using a biological carrier. This has two important advantages over *Agrobacterium*-mediated transformation. First, there is no dependency on the biological properties of the carrier, so any species and variety is suitable for transformation. Second, there is no need to use specialized vectors for transformation – indeed transformation is possible without any vectors at all. The principles of direct DNA transfer are therefore much more straightforward than those for *Agrobacterium*-mediated transformation. All that is required is a mechanism for getting DNA into the plant cell, and ensuring it reaches the nucleus. This can be achieved using physical or chemical means.

Chemical Methods for Direct DNA Transfer Historically, the first direct transfer methods were chemical, and were closely related to the (at the time) newly devised methods for gene transfer to animal cells. Animal cells lack a cellulose wall and are protected by a simple plasma membrane. Therefore, the methods devised for animal cells would not work directly on plant cells, but were suitable for protoplasts. Gene transfer across the protoplast membrane is promoted by a number of chemicals, of which polyethylene glycol has become the most widely used due to the availability of simple transformation protocols [22]. Alternatively, DNA uptake may be induced by electroporation [23]. Putative transformants are transferred to selective medium, where surviving protoplasts regenerate their cell walls and commence cell division, producing a callus. Subsequent manipulation of the culture conditions then makes it possible to induce shoot and root development, culminating in the recovery of fertile transgenic plants. The major limitation of protoplast transformation is not the gene transfer process itself, but the ability of the host species to regenerate from protoplasts. Protoplast transformation was also the first method developed for gene transfer to the chloroplast genome of higher plants (see below).

Physical Methods for Direct DNA Transfer There is a great diversity of physical approaches for gene transfer to plants, including electroporation of walled plant cells, perforation of the cell with silicon carbide whiskers, microinjection, and poration with a finely focused laser beam. In most of these cases, only transient expression of the introduced DNA has been achieved, although transgenic corn plants have been recovered following whisker-mediated transformation [24]. Particle bombardment (microprojectile bombardment, biolistics) is a more robust and reliable method for stable transformation which has been successful for the transformation of cereals, soybean, cotton, phaseolus, and other recalcitrant crops. Initially, a modified shotgun was used to accelerate small (1–4 μm) metal particles into plant cells at a velocity sufficient to penetrate the cell wall (~250 m/s). In the initial test system, intact onion epidermis was bombarded with tungsten particles coated in tobacco mosaic virus (TMV) RNA. Three days after bombardment, approximately 40% of the onion cells that contained particles also showed evidence of TMV replication [25]. A plasmid containing the *cat* (chloramphenicol acetyltransferase) reporter gene driven by the CaMV35S promoter was then tested to determine whether DNA could be delivered by the same method. Analysis of the epidermal tissue 3 days after bombardment revealed high levels of transient CAT activity [26]. The stable transformation of explants from several plant species was achieved soon after these initial experiments. Early reports included the transformation of soybean [27], and corn [28, 29]. The ability to stably transform plant cells by this method offered the exciting possibility of generating transgenic plants representing species that were, at the time, intractable to other transformation procedures. Early successes included soybean, cotton, papaya, and tobacco (reviewed in [30]). Particle bombardment has also been pivotal in the development of chloroplast transformation technology (see below).

There is no intrinsic limitation to the potential of particle bombardment since DNA delivery is governed entirely by physical parameters [31]. Many different types of plant material have been used as transformation targets, including callus, cell suspension cultures, and organized tissues such as immature embryos, meristems, and leaves. The number of species in which

transgenic plants can be produced using variants of particle bombardment has therefore increased dramatically over the last 20 years including rice [32], wheat [33], and oat [34], as well as many other crops (reviewed in [30]). The original gunpowder-driven device has been improved and modified resulting in greater control over particle velocity and hence greater reproducibility of transformation conditions. An apparatus based on electric discharge has been used for the development of variety-independent gene transfer methods for the more recalcitrant cereals and legumes [35], while several instruments have been developed where particle acceleration is controlled by pressurized gas (reviewed in [36]). Physical parameters such as particle size and acceleration (which affect the depth of penetration and the amount of tissue damage) as well as the amount and conformation of the DNA used to coat the particles must be optimized for each species and type of explant [30, 37]. However, the nature of the transformation target is probably the most important single variable in the success of gene transfer.

In Planta Transformation Methods

Most transformation methods for plants require some form of tissue culture step. This is because the fundamental principle of most transformation methods is that plants are regenerated from a small number of transformed cells that can survive under selection. Experiments using the model dicot *Arabidopsis thaliana* have led the way in the development of so-called *in planta* transformation techniques, where the need for tissue culture is minimized or eliminated altogether. Such methods involve the introduction of DNA, either using *A. tumefaciens* or direct transfer, into intact plants [38, 39].

The procedure is carried out at an appropriate time in the plant's life cycle so that the DNA becomes incorporated into cells that will contribute to the germ line, directly into the germ cells themselves (often at around the time of fertilization), or into the very early plant embryo. Generally, *in planta* transformation methods have a very low efficiency, so the small size of Arabidopsis and its ability to produce over 10,000 seeds per plant is advantageous. This limitation has so far prevented *in planta* techniques from being widely adopted for crop species, although radish, pak choi, and *Medicago truncatula* are exceptions [40–42]. The first *in planta* transformation system involved imbibing Arabidopsis seeds overnight in an *A. tumefaciens* culture, followed by germination [43]. A large number of transgenic plants containing T-DNA insertions were recovered but in general this technique has a low reproducibility. A more reliable method has been described by Bechtold et al. [38] in which the bacteria are vacuum infiltrated into Arabidopsis flowers. An even simpler technique called floral dip has become widely used [39]. This involves simply dipping Arabidopsis flowers into a bacterial suspension at the time of fertilization. In both these methods, the transformed plants are chimeric, but give rise to a small number of transgenic progeny. It has been established that T-DNA is transferred into the ovule during the transformation procedure [44].

An alternative to the direct transformation of germ line tissue is the introduction of DNA into meristems *in planta* followed by the growth of transgenic shoots. In Arabidopsis, this has been achieved simply by severing apical shoots at their bases and inoculating the cut tissue with *A. tumefaciens* suspension [45]. Using this procedure, transgenic plants were recovered from the transformed shoots at a frequency of about 5%. In rice, explanted meristem tissue has been transformed using *A. tumefaciens* and particle bombardment, resulting in the proliferation of shoots that can be regenerated into transgenic plants. Such procedures require only a limited amount of tissue culture.

Vectors for Plant Transformation

Components of Plant Transformation Vectors

The vectors used for plant transformation are usually designed with four purposes in mind – the ability to replicate in both *E. coli* and *A. tumefaciens* (i.e., shuttle vector capability), suitability for subcloning (multiple restriction enzyme sites and/or Gateway compatibility), the ability to confer a selectable phenotype on transformed cells (selectable marker genes), and the ability to drive transgene expression (an expression cassette, consisting minimally of a promoter, site for transgene insertion and a terminator/polyadenylation site).

For *Agrobacterium*-mediated transformation, the binary vector system comprises one transformation

vector and one helper plasmid containing the *vir* genes (see above). The transformation vector contains the T-DNA, with the selectable marker gene and expression cassette housed within (reviewed in [46]). The replication functions are not required for DNA transfer and are found on the plasmid backbone, but they are required for maintenance in *A. tumefaciens* and cannot be dispensed with entirely, nor moved to the helper plasmid because the replication functions are required in *cis*. The *E. coli* replication functions (generally the ColE1 origin) are not required in *A. tumefaciens* but are needed for basic cloning operations prior to transformation (reviewed in [47]) and these are also found on the plasmid backbone.

In contrast to *Agrobacterium*-mediated transformation, direct transfer (e.g., particle bombardment) is an entirely physical process with no dependence on biological functions. Therefore, replication functions on vectors used for direct DNA transfer are solely present to facilitate cloning in *E. coli*. They are entirely dispensable for the transformation process and can indeed be a nuisance if integrated into the plant genome since they encourage recombination and may in some cases promote transgene silencing. Only the expression cassette and selectable marker are required *in planta*, and therefore the plasmid backbones can be removed prior to transformation, leaving the small, linear cassettes as the substrate (reviewed in [31]). Although this is functionally equivalent to the linear T-DNA which is excised from the binary vector during *Agrobacterium*-mediated transformation, it should be noted that the T-DNA excision process is often imprecise, resulting in varying amounts of backbone sequences being cotransferred to the plant genome.

The Development of Binary Vectors

One of the first binary vectors for *Agrobacterium*-mediated transformation was pBIN19 [48] although this has fallen out of favor because of its low copy number in *E. coli*, which makes it difficult to obtain large amounts of DNA for cloning (Table 1). Another disadvantage of pBIN19 is that the selectable marker is next to the right border. Because T-DNA transfer is directional, with the right border being transferred first, it is better to have the marker next to the left border to ensure that resistant plants have received a complete (or nearly complete) copy of the T-DNA. These two disadvantages were addressed in more recent vectors such as pPZP and pBINPLUS, which contained a high-copy-number origin of replication for *E. coli* and

Crop Plants Transformation Methods. Table 1 Development of binary vectors for *Agrobacterium*-mediated transformation

Vector	Category	Details	References
pBIN19	Binary vector	Low copy number in *Escherichia coli*, plant resistance marker is next to the right border	[48]
pPZP	Binary vector	ColE1 origin of replication, plant marker is adjacent to the left border of T-DNA	[49]
pCAMBIA	Binary vector	Modification of pPZP	[49]
pBINPLUS	Binary vector	Selectable marker gene at the left T-DNA border, a higher copy number in *E. coli*, and two rare restriction sites for easier cloning	[50]
pIG121Hm	Binary vector	A derivative of pBIN19	[19]
pTOK233	Superbinary vector	Contains *vir*B, *vir*C, and *vir*G genes from pTiBo542	[19, 51]
pTiBo542	Ti-plasmid	Has *virB, virC,* and *virG*	[52, 53]
pSB11	Intermediate vector of superbinary system	ColE1 origin of replication, multiple cloning sites within T-DNA, replicates only in *E. coli*, has a fragment homologous to the acceptor vector pSB1	[21]
pSB1	Acceptor vector of pSB11 of superbinary system	Replicates in *E. coli* and *Agrobacterium*	[21]

a selectable marker gene at the left T-DNA border [49, 50]. Two rare restriction sites were also provided for cloning convenience.

As discussed above, the successful *Agrobacterium*-mediated transformation of monocots rested on the development of superbinary vectors with extra copies of some of the *vir* genes to enhance transformation efficiency. In the first instance, the *vir*B, *vir*C, and *vir*G genes were transferred from Ti-plasmid pTiBo542 [52, 53] carried by supervirulent strains of the bacterium, such as A281 or EHA101. Hiei et al. [19] constructed a new superbinary vector called pTOK233 by adding the *vir*B, *vir*G, and *vir*C genes of pTiBo542 to achieve rice transformation. The T-DNA in this case carried the *npt*II selectable marker under the control of the *nos* promoter, the *hpt* selectable marker driven by the CaMV 35S promoter and an intron-*gusA* fusion gene also driven by the CaMV 35S promoter. A comparison between the binary vector pIG121Hm in the supervirulent strain EHA101 and the superbinary vector pTOK233 in the regular strain LBA4404 showed that pTOK233 was slightly more efficient [19]. Similar combinations have been used to achieve the transformation of many monocot species (reviewed in [54, 55]). In corn and sorghum, efficient transformation systems were established only with superbinary vectors in LBA4404, whereas a standard binary vector in a supervirulent strain was inefficient even with improved co-culture conditions [56].

One disadvantage of the superbinary system is the large size of all the vector components, reducing the convenience of cloning by standard methods. Therefore, the final construction step of a superbinary vector involves the cointegration of an intermediate vector such as pSB11 and an acceptor vector such as pSB1 via homologous recombination between the shared DNA segments [21]. The intermediate vector is a small plasmid containing the T-DNA and ColE1 origin for replication in *E. coli*. The acceptor vector is an IncP plasmid, which can be replicated in *E. coli* and *A. tumefaciens*, and carries the 14.8-kb *KpnI* fragment. If a gene of interest is to be introduced into plants in tandem with a marker gene, the two genes are first inserted into an intermediate vector, which is introduced into a strain of *A. tumefaciens* that carries an acceptor vector so that the cassette is integrated into the acceptor to generate the final superbinary vector. This approach also facilitates the transfer of large segments of DNA with minimal rearrangement and favors a low number of integrated copies [46].

Other improvements have been made to reduce the frequency of vector backbone transfer. For example, Hanson et al. [57] placed the lethal *barnase* gene outside the left T-DNA border so that any transgenic plants containing sequences beyond the left border were counterselected. Another way to reduce backbone cotransfer is to insert additional left border sequences, increasing the likelihood of recognition by the corresponding Vir proteins and thus suppressing transfer, as has been demonstrated in rice [58] and Arabidopsis [59]. Improvements have also been made to facilitate rapid and efficient subcloning. The zero background TA cloning system [60] was developed for *Agrobacterium*-mediated transformation and uses restriction enzyme *XcmI* to generate 3′-T overhangs in the linearized vector within the counterselectable marker gene *ccd*B, which ensures that self-ligated vectors are not propagated after transformation, but that PCR products with 3′-A overhangs can be inserted without further modification.

Multiple Gene Transfer (MGT)

In the early years of plant biotechnology, most transgenic plants contained two transgenes – one selectable marker under the control of a constitutive promoter to facilitate the selective propagation of transformed cells, and a "primary transgene" or "gene of interest" which could be under the control of any sort of promoter and was intended to alter the plant's phenotype in a specific manner. MGT is now being embraced as an approach to generate plants with more ambitious phenotypes [61]. MGT allows goals that were once impossible to be achieved, e.g., the import of complex metabolic pathways, the expression of entire protein complexes, and the development of transgenic crops simultaneously engineered to produce a spectrum of added-value compounds [61, 62].

Essentially there are two MGT methods known as the linked and unlinked cotransformation strategies. In the linked strategy, all the different genes are linked on the same piece of transforming DNA. This is the normal approach chosen with *Agrobacterium*-mediated transformation where several genes are carried within the same T-DNA borders. However, it is quite

possible to transform plants efficiency with (a) an *Agrobacterium* strain carrying a binary vector that has two separate T-DNAs, and (b) different *Agrobacterium* strains carrying different T-DNAs, although this becomes increasingly complex as the number of genes increases. There are several reports of a mixed strategy where two *Agrobacterium* strains carrying different T-DNAs each with multiple genes has been used to achieve MGT (reviewed in [63]).

MGT is more easily achieved by direct gene transfer because there is no need to combine multiple genes on the same length of DNA. When the genes are supplied separately as a mixed preparation of plasmids, there appears to be no bias in the process of integration. Tandem cotransformation can be undertaken, although it becomes more cumbersome as larger numbers of genes are required, but cotransformation with discrete, unlinked genes is just as efficient, and the genes tend to cointegrate at the same locus. As many as 12 transgenes have been integrated using this unlinked cotransformation approach [64].

The main issue with linked MGT is the inconvenience of serial cloning. Very rare restriction sites can help to address this challenge, as shown by Goderis et al. [65] who developed a binary vector for MGT incorporating 13 hexanucleotide restriction sites, six octanucleotide restriction sites, and five sites for homing endonucleases, which are extremely rare in natural sequences and allow unidirectional cloning. Six different expression cassettes in auxiliary vectors with different promoter and terminator sequences were cut with the five different homing endonucleases plus an additional octanucleotide restriction endonuclease and transferred into the homing endonuclease sites of the binary vector. Modified auxiliary vectors also facilitate N- or C-terminal fusions to five different autofluorescent tags (EGFP, EYFP, Citrine-YFP, ECFP, and DsRed2) expressed from the tandem CaMV 35S constitutive promoter [66]. Similar systems have been developed by Thomson et al. [67], with the pUGA vectors for direct transfer and the pUGA2 vectors for *Agrobacterium*-mediated transformation. A series of unidirectional shuttle vectors containing various combinations of homing endonuclease sites was constructed and used to create artificial gene clusters in the pUGA or pUGA2 vectors, allowing the simultaneous transfer of up to six genes. Versatile systems now exist that offer a large number of promoters, terminators, and autofluorescent tags (reviewed in [68]).

A further strategy for linked MGT is to use the Cre/*lox*P recombination system together with homing endonucleases. In this method, two donor vectors are needed to introduce the expression cassettes into the acceptor vector using Cre recombinase [69]. After each round of recombination, the unnecessary backbone sequence from the donor vector is cleaved out using the homing endonucleases leaving just one *lox*P site for the next step. In this manner, ten transgenes were inserted in the acceptor vector and introduced into rice by *Agrobacterium*-mediated transformation.

The most recent generation of vectors are modular and multifunctional, such as the pCLEAN-G/pCLEAN-S dual binary vectors for *Agrobacterium*-mediated transformation [70] and the pORE vector system that can be adapted for both *Agrobacterium*-mediated transformation and direct DNA transfer [71]. The pORE vector series consists of "open" vectors for general plant transformation, "reporter" vectors for promoter analysis, and "expression" vectors for transgene expression. The sets comprise various combinations of promoters (PHPL, PENTCUP2, and PTAPADH), selectable markers (*npt*II and *pat*), and reporter genes (*gusA* and *smgfp*), and any element can be modified independently.

Direct DNA Transfer Using Minimal Expression Cassettes

As discussed above, vector backbone sequences are not required for direct DNA transfer and they may also promote recombination within the transgenic locus and/or act as triggers for de novo DNA methylation. To determine whether minimal linear cassettes (promoter, transgene, and terminator) could be used for direct DNA transfer, Fu et al. [72] separated the expression cassettes for the marker genes *gusA* and *hpt* from the parent vector, and used these as substrates for coating the microprojectiles used in particle bombardment, with the intact plasmids as a control. They found not only that the linear cassettes were equally efficient for transformation, but also that the elimination of the plasmid backbone had a remarkable positive effect on the resulting transgenic rice plants (Fig. 2). The cassette transformants generally contained fewer transgene

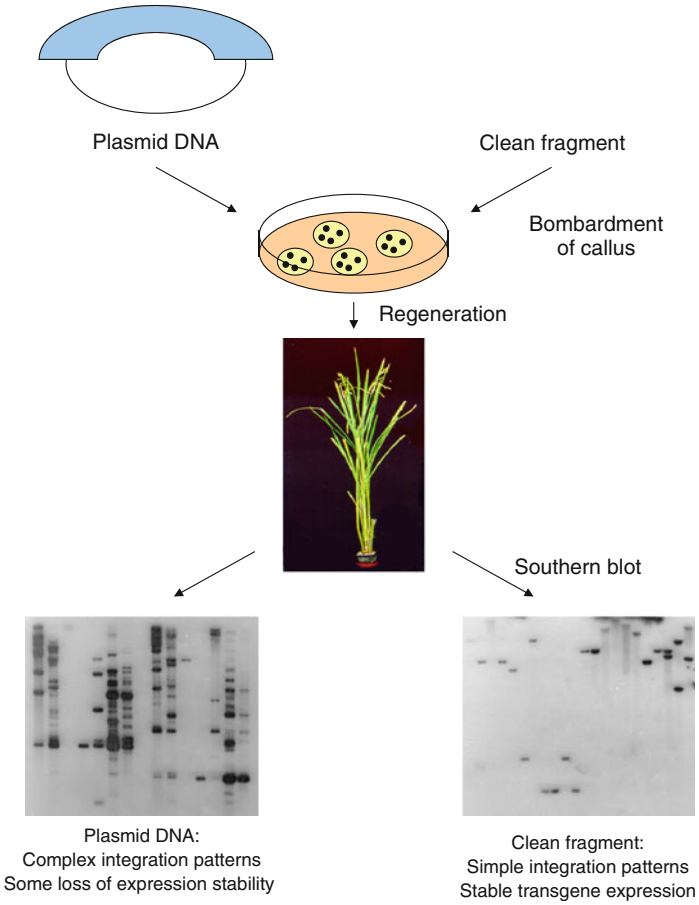

Crop Plants Transformation Methods. Figure 2
The clean DNA transformation system compared to particle bombardment with whole plasmid DNA [4]. The transformation strategy is shown, and two representative DNA blots are compared to demonstrate the simpler integration patterns resulting from transformation with linear minimal cassettes

copies than those transformed with intact plasmids, and they showed stronger and more stable expression. Further analysis of the minimal cassette population showed that the transgenes were expressed in most of the transgenic plants and that, for all the transgenes, overall expression levels and coexpression frequencies were higher than previously reported for whole plasmid transformants. These results were confirmed using the *yfp* (yellow fluorescent protein) and *hpt* markers, with concatemers forming only rarely in such plants [73].

Promoters Used for Plant Transformation

The promoters used in plant biotechnology are traditionally divided into three categories – constitutive (active continuously in most or all tissues), spatiotemporal (tissue-specific or stage-specific activity), and inducible (regulated by the application of an external chemical or physical signal) [74]. Most basic transformation vectors incorporate strong constitutive promoters because it is assumed that the objective is to express the transgene(s) at the highest possible level. Initially, the *A. tumefaciens nos* (nopaline synthase), *ocs* (octopine synthase), and *mas* (mannopine synthase) promoters were popular because they were already present in the natural T-DNA sequences from which the early binary vectors were developed, and had evolved to be active in many plant species (at least those within the *A. tumefaciens* host range). However, the CaMV 35S promoter was found to be stronger and

unaffected by wounding, and its modular nature made it easy to modify [75, 76]. The activity of the CaMV 35S promoter can be increased by duplicating the enhancer up to four times [77] and the enhancer can also increase the activity of heterologous promoters to which it is attached [78].

Although widely used, the CaMV 35S promoter has certain limitations such as its poor performance in monocots, its suppression by feeding nematodes, and the intellectual property issues affecting its commercial deployment (reviewed in [79]). For this reason, alternative virus promoters with similar or improved properties have been sought. Thus far, however, the only virus promoters that have been developed into established expression vectors are those from *Cestrum yellow leaf curling virus* (CmYLCV) [80], which can be licensed from Syngenta Biotechnology, Inc. for limited research purposes, and from *Subterranean clover stunt virus* (SCSV), which has been used to construct the pPLEX series of expression vectors for use in both dicots and monocots [81, 82].

Constitutive expression in monocots is usually achieved with housekeeping promoters, particularly those from the rice *actin1* and corn *ubiquitin1* genes (reviewed in [83, 84]). In both cases, the presence of the first intron of the gene is required for high-level expression [83, 84], and the addition of this intron to the CaMV 35S promoter also enhances its activity in monocots, e.g., 40-fold in corn [85]. In contrast, the first intron of the recently characterized rice *actin2* gene contains a negative regulatory element whose removal is required for high-level promoter activity [86].

Many different plant promoters have been described that restrict expression to particular cells, tissues, organs, or developmental stages, and seed-specific promoters are probably the most diverse. Seeds are a frequent target for genetic engineering in plants because they can accumulate recombinant proteins to levels that would be lethal in vegetative tissues but can do so without compromising plant growth and development; they are also a harvestable product and thus the target for nutritional improvement. Many promoters have been identified that target gene expression specifically to the seed, or to a particular region of the seed such as the endosperm, embryo, or aleurone [74, 79, 87]. Anther-specific promoters are also very useful because they can be used to control male fertility, an important trait in crop breeding, while fruit- and tuber/root-specific promoters are valuable for the nutritional improvement of fruit and root vegetable crops, pest/disease resistance, and the use of staple crops as factories for the production of novel proteins and metabolites.

Inducible promoters are also highly valued in plants because they allow transgenes to be controlled by internal and external physical or chemical cues. Many different inducible promoters have been identified in plants and these generally fall into three categories – (1) those responsive to endogenous signals (plant hormones); (2) those responsive to external physical stimuli (abiotic and biotic stresses); and (3) those responsive to external chemical stimuli. Such promoters provide immense scope for the precise regulation of transgene expression through external control, ranging from the precise control of transgene activation/inactivation in experimental settings to the ability to activate transgenes on an agricultural scale by the application of chemical sprays. Examples of commonly used promoters include those responsive to phytohormones (particularly auxin, abscisic acid, gibberellin, and ethylene), heat-shock promoters responsive to raised temperatures, light-inducible promoters, promoters induced by wounding or by exposure to elicitors produced by pathogens, and promoters that respond to specific metabolites [74, 79]. Sugar responsive promoters fall into the latter category and the *cis*-acting elements that confer sensitivity to sugar are particularly useful for controlling gene expression in cultured plant cells. For example, elements from sporamin and amylase promoters have been studied in detail and the minimal α-amylase 3 promoter makes the normally constitutive rice *actin1* promoter sensitive to the presence of sugar [88]. Inducible promoters that respond to xenobiotic signals are also valuable because transgenes can be activated without affecting endogenous genes. Martinez et al. [89] developed a hybrid system consisting of the tobacco budworm ecdysone receptor ligand-binding domain fused to the mammalian glucocorticoid receptor DNA-binding domain and the VP16 transactivation domain. The receptor responds to tebufenozide (an insecticide better known by its trade name CONFIRM). Similarly, Padidam et al. [90] have developed a system that is based on the spruce budworm ecdysone receptor

ligand-binding domain, and responds to another common insecticide, methoxyfenozide (INTREPID).

Selectable and Screenable Markers

As stated above, selectable marker genes provide a phenotype that allows transformed cells to be propagated under conditions where nontransformed cells cannot survive, such as in the presence of an otherwise toxic or growth-disrupting reagent (positive selection) or in the absence of an otherwise essential nutrient (negative selection). This is necessary to isolate the small number of transformed cells from the overwhelming majority of their nontransformed peers which, without selection, would quickly outcompete them. Although a wide range of selectable markers has been tested in plants, only a few are used routinely (reviewed in [47, 91]). The broadest markers are suitable in most plants and are expressed using the most active constitutive promoters to ensure that all cell types are protected under selection (the CaMV35S promoter in dicots and the actin or ubiquitin promoters in monocots, as discussed earlier). Most selectable markers are described as conditional because an external reagent must be applied to facilitate selection, whereas others are nonconditional, i.e., they work without any external selection reagent. The typical selectable markers used in plant transformation are positive and conditional, and work by conferring resistance to a toxic substance such as an antibiotic or herbicide that has a very specific intracellular target (Table 2).

Marker genes that confer antibiotic resistance originate from bacteria but have been modified to function well in plants. The first marker to be used in plants was neomycin phosphotransferase (*npt*II, *aph*II), which confers resistance to the aminoglycoside antibiotics neomycin, kanamycin, and geneticin (G148) [94]. This is probably still the most widely used marker in the laboratory but some plants are naturally resistant to kanamycin, and the antibiotic can also interfere with normal development in some species. An alternative is hygromycin phosphotransferase (*hph*, *hpt*, *aph*IV), providing resistance to the antibiotic hygromycin through the ATP-dependent phosphorylation of a 7-hydroxyl group [95]. Other antibiotic-resistance markers used less frequently include those conferring

Crop Plants Transformation Methods. Table 2 Selectable markers used for plant transformation (Data compiled and updated from [91–93])

Gene (Product)	Source	Phenotype and other comments
aad (aminoglycoside adenyltransferase)	*Shigella flexneri*	Provides resistance to trimethoprim, streptomycin, spectinomycin, and sulphonamides. Used mainly for chloroplast transformation
bar (phosphinothricin acetyltransferase)	*Streptomyces hygroscopicus*	Resistance to phosphinothricin (PPT), which is a component of the herbicides bialophos, Basta, and glufosinate
ble (glycopeptide-binding protein)	*Streptalloteichus hindustantus*	Resistance to the glycopeptide antibiotics bleomycin and pheomycin (and the derivative Zeocin)
dhfr (dihydrofolate reductase)	Mouse	Resistance to methotrexate
sul1 (dihydropteroate synthase)	*Escherichia coli*	Resistance to sulfonamides (Asulam)
epsps (enolpyruvylshikimate phosphate synthase)	*Petunia hybrida*	Resistance to the herbicide glyphosate
hpt (hygromycin phosphotransferase)	*Klebsiella* spp.	Resistance to the aminoglycoside antibiotic hygromycin B
manA (mannose-6-phosphate isomerase, MIP)	*E. coli*	Ability to grow on mannose as sole carbon source
neo/nptII/aphII (neomycin phosphotransferase)	*E. coli*	Resistance to the aminoglycoside antibiotics neomycin, kanamycin, and geneticin (G148)

resistance to bleomycin [96], gentamycin [97], and methotrexate [98].

Marker genes that confer herbicide resistance may originate from bacteria or plants, and those conferring resistance to the broad-spectrum herbicides phosphinothricin (PPT)/glufosinate and glyphosate are used the most widely. PPT/glufosinate is a competitive inhibitor of glutamine synthetase (GS), the only enzyme that can catalyze the assimilation of ammonia into glutamic acid in plants. Inhibition of GS therefore results in the accumulation of toxic levels of ammonia. The enzyme phosphinothricin *N*-acetyltransferase (PAT) encoded by either the *bar* or *pat* genes (these are genes from different microbial species) can be used to provide PPT/glufosinate resistance in transformed plant cells [99]. Glyphosate, the active ingredient of Roundup, inhibits the enzyme 5-enolpyruvylshikimate-3-phosphate synthase (EPSPS), which is required for the synthesis of aromatic amino acids. Glyphosate resistance can be conferred by markers encoding a modified EPSPS that is not affected by the herbicide, or those encoding a bacterial enzyme that breaks down the herbicide (glyphosate oxidoreductase, GOX) [100]. Markers providing resistance against sulfonamindes such as Asualam [101] and chlorsulfuron [102] are also used occasionally.

Negative selectable markers are useful because they allow transformed cells to be selected based on the absence of something that is necessary for nontransformed cells to grow or regenerate efficiently. The *E. coli manA/pmi* gene confers the ability to use mannose as a sole carbon source so that only transformed cells survive on media containing mannose but lacking sucrose [103]. The gene is a negative conditional marker because mannose itself is not toxic to nontransformed plants, but rather the absence of sucrose (nontransformed plants grow perfectly well in the presence of both sugars). Another example is the *A. tumefaciens ipt* gene, which promotes the synthesis of cytokinins [104]. This is a nonconditional marker because it confers the ability to produce shoots in growth medium lacking exogenous cytokinins, i.e., nothing has to be added to the medium to facilitate selection. Simply, transformed tissues are placed on medium lacking cytokinins and only those tissues that produce shoots are transgenic.

The other major class of marker genes are known as screenable, scorable, or visible markers (or reporter genes) because rather than providing cells with a selective advantage they confer a phenotype that can easily be detected without interfering with other cellular processes, allowing transformed cells to be identified and studied (Table 3). Although screenable markers have been used for the prosaic purpose of identifying transformed cells and manually separating them from nontransformed cells, they tend to be used for more sophisticated purposes, such as reporter assays and tracing experiments. Some screenable marker genes only provide their visual signal when provided with a particular substrate, i.e., they are conditional (e.g., *gusA*, *luc*). Others have an intrinsic ability to yield a visible signal, i.e., they are nonconditional (e.g., *gfp*, *DsRed*), and these are the most useful since they can be used in living organisms.

The *E. coli gusA* (*uid*A) gene encodes the enzyme β-glucuronidase (GUS), the most widely used conditional screenable marker in plants. As well as its endogenous substrates, GUS can process a range of chromogenic and fluorescent derivatives in a range of assays that allow the quantification or in situ localization of reporter gene activity. The most common substrate for GUS histochemical staining is 5-bromo-4-chloro-3-indolyl glucuronide (X-gluc), a clear substrate that yields a blue product. Other common substrates include p-nitrophenyl β-D-glucuronide, which is used for spectrophotometric quantitative assays, and 4-methylumbelliferyl-beta-D-glucuronide (MUG), which produces a quantitative fluorescent signal. GUS is preferred in plants over the very similar reporter GAL (encoded by *lacZ* and widely used in microbes and animals) because of its stability in plants and its lack of toxicity and background activity. The main disadvantage of GUS is that it cannot be conveniently used for in vivo imaging because plant cells must be fixed or destroyed to visualize the reaction. Its stability can also be problematic if the aim of an experiment is to study fluctuations, since the longevity of the protein can mask transient decreases in expression.

Both the disadvantages of GUS are addressed by luciferase (LUC) an enzyme from the firefly (*Photinus pyralis*) which catalyzes the ATP-dependent oxidative decarboxylation of luciferin, producing light in the process. LUC allows nondestructive qualitative and

Crop Plants Transformation Methods. Table 3 Screenable markers (reporter genes) used in plants (Data compiled and updated from [83, 105])

Gene (product)	Comments
gusA (β-glucuronidase)	Source: *Escherichia coli gusA/uid*A gene
	Activity: catalyzes the hydrolysis of β-glucuronides
	Assays: nonisotropic; in vitro assays are colorimetric or fluorometric; also histochemical assay format using X-gluc
	Advantages: simple, sensitive, quantitative, many assay formats available, inexpensive
	Disadvantages: assays are destructive; enzyme is stable so unsuitable for studies of downregulation
cat (chloramphenicol acetyltransferase)	Source: *E. coli* Tn*9*
	Activity: catalyzes the transfer of acetyl groups from acetyl coenzyme A to chloramphenicol
	Assays: in vitro assays only, isotropic
	Advantages: simple to perform
	Disadvantages: low sensitivity, expensive, low resolution in vivo, reliance on isotopic assay format
luc (luciferase)	Source: The firefly *Photinus pyralis*
	Activity: light produced in the presence of luciferase, its substrate luciferin, oxygen, Mg^{2+}, and ATP
	Assays: nonisotopic bioluminescent assays in vitro and in vivo
	Advantages: sensitive, rapid turnover, quantitative
	Disadvantages: Expensive detection equipment, limited reproducibility of some assay formats
Anthocyanin regulators	Source: corn (*Zea mays*)
	Activity: induces pigmentation
	Assays: visual screening for pigmented cells in vivo
	Advantages: simple, inexpensive, nondestructive
	Disadvantages: low sensitivity, not quantitative, background expression, adverse effects on transgenic plants
GFP (green fluorescent protein)	Source: the jellyfish *Aequorea victoria*
	Activity: intrinsic fluorescence under blue/UV light
	Assays: nonisotopic, in vivo assays in live plants
	Advantages: intrinsic activity (no substrate requirements), sensitivity, use in live plants; many variants with modified absorption and emission spectra available, and different subcellular targeting signals; several variants can be used simultaneously
	Disadvantages: weak signal in some systems (this is being addressed through the use of modified GFPs with stronger emission and reduced photobleaching); no variants that emit in the orange-red part of the spectrum

Crop Plants Transformation Methods. Table 3 (Continued)

Gene (product)	Comments
DsRed (red fluorescent protein)	Source: coral reef *Discosoma* spp.
	Activity: intrinsic fluorescence under blue/UV light
	Assays: nonisotopic, in vivo assays in live plants
	Advantages: intrinsic activity (no substrate requirements), sensitivity, use in live plants; many variants with modified absorption and emission spectra available, and different subcellular targeting signals; several variants can be used simultaneously
	Disadvantages: weak signal in some systems, no variants that emit in the violet-blue-green part of the spectrum

quantitative assays to be carried out both in vitro and in vivo, and because the reaction has a short half-life, it can be used to monitor fluctuating activity. A series of vectors that incorporate the *luc* gene have been developed for plants, including the LucTrap series that allow targeted and random transcriptional and translational fusions of a transgene with a *luc* gene optimized for plant cells [106]. One drawback of *luc* is that it is still a conditional reporter, requiring the substrate luciferin and the presence of oxygen, ATP, and magnesium ions. In contrast, the green fluorescent protein (GFP) from the jellyfish *Aequorea victoria* is a nonconditional reporter allowing the direct, noninvasive visualization of fluorescence in vivo in real time merely by exposure to blue/UV light. The original *gfp* gene was nonfunctional in plants because of a cryptic splice site, but this has been corrected and the protein has been widely deployed as a vital marker [107]. One of the major advantages of GFP is that its spectral qualities can be modified by mutation, giving rise to a whole family of derivatives with enhanced brightness, less susceptibility to quenching, and a range of excitation/emission wavelengths allowing different reporters to be used in vivo simultaneously. In combination with variants that allow targeting to different compartments within the plant cell, many sophisticated forms of analysis become straightforward to implement, e.g., allowing the real-time monitoring of protein processing, trafficking and protein–protein interactions [108]. As well as GFP and its derivatives, other bioluminescent proteins have also been identified, including DsRed from *Discosoma* spp. This is similar to GFP but covers a different spectral range (red GFP is not available) but there is little background fluorescence and it can be visible under white light [109].

The useful properties of selectable and screenable markers can also be combined into one protein. For example, Ochiai-Fukuda et al. [110] developed a fusion marker incorporating enhanced green fluorescent protein and blasticidin deaminase, conferring resistance to the aminoacylnucleoside antibiotic blasticidin S. The *gfbsd* marker was introduced into rice callus and allowed the rapid and efficient selection and visual confirmation of transformed cells.

Consequences of Nuclear Transformation

Integration of Nuclear Transgenes

As discussed above, plant transformation is a multistep process, the first step involving the transfer of DNA into the plant cell, which can be achieved either by direct transfer or by *Agrobacterium*-mediated transformation. Once the DNA reaches the nucleus, the next step (transgene integration) is dependent predominantly on that DNA and on factors provided by the plant cell, although in the case of *Agrobacterium*-mediated transformation it is possible that the Vir proteins complexed with the T-strand may facilitate the integration process (see below). A number of groups have investigated the structure of genomic/T-DNA and T-DNA/T-DNA junctions in plants and have concluded that integration occurs by illegitimate recombination (see [111, 112]). A strand invasion mechanism has been proposed (reviewed in [12]), in which the 3′ end of the T-strand initiates the integration process by hybridizing to a short region of homology in the plant

genome, the second strand being completed by primer extension of the plant DNA. Other models suggest conversion of the T-strand into a double-stranded intermediate, which integrates at the site of naturally occurring chromosome breaks via double-strand DNA break repair. This is supported by experiments that show transformation efficiency increases following UV irradiation, which generates nicks and breaks in genomic DNA. However, since T-DNA integration still occurs in DNA repair mutants, it is possible both mechanisms occur simultaneously albeit with different efficiencies.

DNA repair models argue that proteins encoded by the host plant have a much more important role in T-DNA integration than *Agrobacterium* proteins, such as VirD2, which are imported into the plant with the T-DNA. However, since the VirD2 protein remains covalently attached to the 5′ end of the T-strand during transfer it is also likely to influence integration [113]. In an in vitro assay, VirD2 can ligate together a cleaved T-DNA border sequence but cannot ligate T-DNA to other genomic targets unless plant cell extracts are also present [114], a phenomenon supported by the identification of Arabidopsis mutants impaired for T-DNA integration [115].

Much can be learned about the T-DNA integration mechanism by the inspection of borders, especially the borders between adjacent T-DNA sequences in multicopy insertions. The formation of heterodimers during cotransformation argues in favor of T-DNA concatemerization prior to integration. Although inverted repeats around the right border are often precise, those around the left border and those separating direct T-DNA repeats are often characterized by the insertion of variable-sized regions of filler DNA, which may be derived from the T-DNA sequence or from plant genomic DNA [116]. This suggests either the simultaneous integration of multiple T-DNAs at a single locus, or a two-phase mechanism, in which a primary T-DNA integration event stimulates further secondary integrations in the same area, similar to those proposed for particle bombardment (see below). Zhu et al. [117] carried out a comprehensive study of T-DNA border characteristics in a population of transgenic rice plants including 156 T-DNA/genomic DNA junctions, 69 T-DNA/T-DNA junctions, and 11 T-DNA/vector backbone junctions, which included 171 left borders and 134 right borders. Conserved cleavage was observed in 6% of left and 43% of right borders, microhomology was observed in 58% of T-DNA/genomic DNA, 43% of T-DNA/T-DNA, and 82% of T-DNA/vector junctions, mostly at left borders, and about one third of the T-DNA/genomic DNA and T-DNA/T-DNA junctions showed evidence of filler DNA (up to 344 bp). This was derived mainly from the T-DNA region adjacent to the breakpoint and/or from the rice genomic DNA flanking the T-DNA integration site, with T-DNA/T-DNA filler DNA showing the greatest complexity. Interestingly, when two T-DNAs were integrated in the inverted repeat configuration, significant truncation was always observed in one of the two T-DNAs whereas with the direct repeat configuration, large truncations were rare. These data suggest that no single integration mechanism can account for all observations but the presence of filler DNA at many of the junctions argues that a template-driven DNA synthesis mechanism must be involved.

The analysis of plasmid/plasmid and plasmid/genomic junctions in transgenic plants generated by particle bombardment reveals features characteristic of illegitimate recombination similar to those seen for T-DNA junctions, suggesting that the same overall integration mechanisms may be involved [118]. For example, such junctions are characterized by regions of microhomology, filler DNA, trimming of the DNA ends so sequences are lost, and AT-rich elements surrounding the junction site, with similarity to topoisomerase I binding/cleavage sites (Fig. 3). In the analysis of multiple plasmid/plasmid junctions in 12 transgenic rice lines, Kohli et al. [120] observed 10 plants with microhomology at the junctions and 2 plants where junctions appeared to be generated by blunt ligation, with no overlap. A similar ratio of conserved end-joining to microhomology-mediated recombination was observed by Gorbunova and Levy [121] and Salomon and Puchta [111]. Topoisomerase I sites were also observed adjacent to 10 out of 12 junctions characterized in transgenic Arabidopsis plants generated by particle bombardment [122] and in four of the six junctions in the commercial SUNUP variety of papaya [123]. Illegitimate recombination therefore appears to be responsible both for the integration of foreign DNA into the plant genome, and the linking of multiple plasmid copies, which is similar to

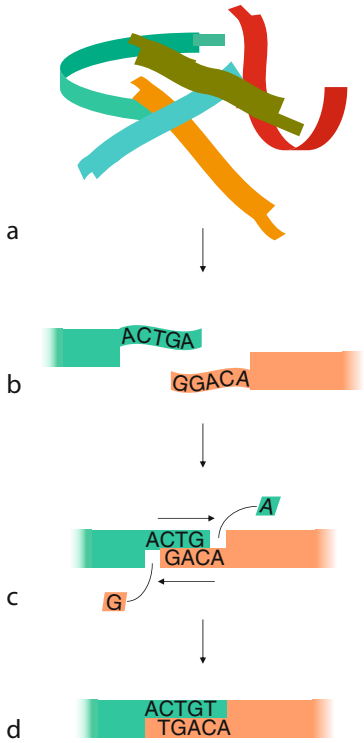

Crop Plants Transformation Methods. Figure 3 Mechanism for transgene integration at regions of microhomology [119]. A mixture of DNA fragments with ragged ends (**a**) interacts with a double-stranded DNA break with partially complementary ragged ends (**b**). Repair synthesis across the gap (**c**) generates a recombination junction (**d**) which may be completely conserved if the homology is precise, or may involve either the loss of terminal sequences or the insertion of filler DNA if the homology is partial

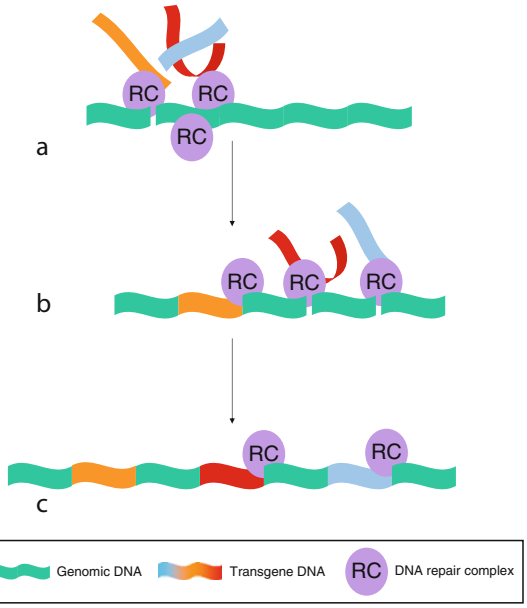

Crop Plants Transformation Methods. Figure 4 Explanation for the formation of transgene arrays and transgene clusters interspersed with genomic DNA [119]. A mixture of DNA fragments interacts with a double-stranded DNA break where a repair complex has already assembled (**a**). The repair complex may stitch together DNA fragments to form concatemers prior to integration, or may integrate single copies. The first integration event stimulates further repair complex activity nearby, resulting in additional nicks and breaks in the genomic DNA that act as further integration sites (**b**). This results in a cluster of transgenes (single copies and concatemers) interspersed with short regions of genomic DNA (**c**)

the mechanism proposed for T-DNA integration (see above).

When nuclei from the cells of transgenic cereal plants generated by particle bombardment are analyzed by fluorescence in situ hybridization (FISH) using a transgene-specific probe, a curious phenomenon in often observed in which a single fluorescent spot in the interphase nucleus separates into multiple signals along a metaphase chromosome [124]. Any model for transgene integration following particle bombardment must take into account some form of three-tier organization, consisting of contiguous transgene arrays, interspersed with short regions of genomic DNA to generate local clusters, and the appearance of widely dispersed signals at metaphase. Two-phase transgene integration mechanisms have been proposed to explain the first two levels of organization, and in such models concatemerization is proposed to occur prior to integration, while interspersion occurs during the integration process [118, 120, 125] (Fig. 4). In each model, penetration of the cell is proposed to elicit a wound response, which would include the induction of DNA repair enzymes, such as nucleases and ligases. The presence of these enzymes and an excess of foreign DNA would result in the linking together of several copies to form concatemers, which would be the substrates for integration. This might be stimulated by homology between individual copies of transforming

plasmids, and "backbone" homology might also result in the concatemerization of plasmids carrying different transgenes in cotransformation experiments. However, as stated above, cotransformation and cointegration also occur when two nonhomologous minimal cassettes are used for transformation, so homology might not be as important as the presence of free DNA ends [72]. Kohli et al. [120] suggested that transgene clusters arise in a second phase where a primary integration event occurring by illegitimate recombination at a chromosome break generates a "hot-spot" for further integration events in the same area. This might be due, for example, to the presence of local repair complexes that can slide along the DNA and introduce nicks which can be exploited by more foreign DNA. Pawlowski and Somers [125] suggested an alternative second phase where a number of discrete transgene concatemers integrate simultaneously at a site containing multiple replication forks. Although there is no direct evidence for either mechanism, it is interesting to note that DNA integration is stimulated in rapidly dividing cells, and is blocked in Arabidopsis mutants lacking essential components of the DNA recombination machinery.

The higher-order organization of transgenic loci observed by FISH is thus far unique to particle bombardment and demands a model which takes into account the three-dimensional structure of the nucleus. It is possible that the transformation event affects a local region of the interphase nucleus, e.g., a metal particle may cause damage to a particular area of chromatin arranged in loops attached to the nuclear matrix, or to a localized transcription factory. If the particle "skims" several loops or several transcription units, there will be regions of DNA damage close together in *trans*, but widely separated in the *cis* configuration were the DNA to be stretched out (Fig. 5). Each of these sites could act as a nucleation point where foreign DNA diffusing from the metal particle is used to patch up double-strand breaks, generating widely separated arrays and/or clusters [124, 126]. In support of this induced break and repair model, Svitashev et al. [127] have shown that in 6 of 25 transgenic oat plants generated by particle bombardment, transgene integration sites were associated with rearranged chromosomes. This suggests that DNA breaks caused by incoming particles are repaired with foreign DNA and may also result in deletions, inversions, and translocations involving genomic DNA.

Transgene Structure and Integrity

Transgene rearrangements following particle bombardment have been widely reported in the literature and many publications repeat the "lore" that direct DNA transfer is more likely than T-DNA transfer to generate complex rearranged loci. The number of rearrangements that can be detected depends entirely on the resolution of the method being used. Thus, careful analysis of locus structure by Southern blot hybridization, PCR, and DNA sequencing has shown that rearrangements may be more widespread than first envisaged in both transformation methods.

In the case of direct DNA transfer, the analysis of transgenic oat loci by Somers et al. has shown that transgene rearrangements can be extensive and extremely complex, with multiple small insertions, inversions, and deletions within any transgene, plus the presence of filler DNA [127]. In corn, Mehlo et al. [128] noted that every single plant among the population they analyzed showed some form of rearrangement, and they speculated that undetected "minor" rearrangements could be responsible for many instances of transgene silencing otherwise attributed to epigenetic processes. In particular, certain transgene rearrangements were not detectable by Southern blot hybridization because they were too subtle, but they could be picked up by long-range PCR and sequencing. Because Southern blot hybridization is normally the sole method used to determine whether a given locus is intact or rearranged, this suggests caution should be used in relying on such results, since only "major" rearrangements can be detected in this manner.

In the case of *Agrobacterium*-mediated transformation, Afolabi et al. [129] and Zhu et al. [117] found that nonintact T-DNAs were present in >70% of transgenic rice lines, in most cases reflecting loss of the mid to right border portion of the T-DNA. Similarly, Rai et al. [130] found that about 50% of rice plants transformed with a T-DNA containing the phytoene synthase (*psy*) and phytoene desaturase (*crtI*) genes showed evidence of rearrangements, and in the majority of cases the rearrangements occurred in the *crtI* expression cassette,

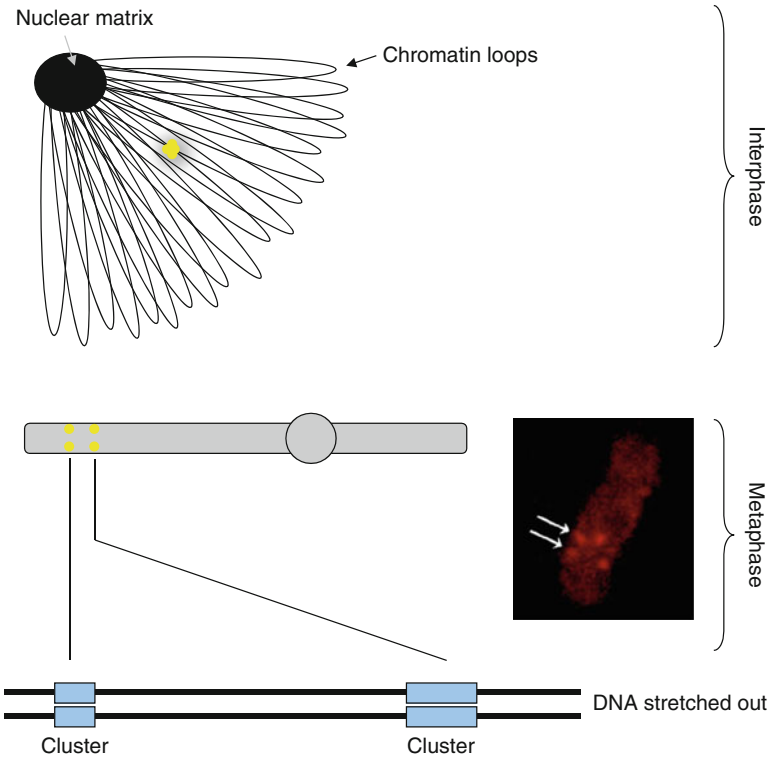

Crop Plants Transformation Methods. Figure 5
Higher-order transgene locus organization in cereals transformed by particle bombardment [124]. Transformation occurs during interphase, when the chromatin is distributed into specific nuclear zones and territories. If a metal particle causes localized damage, DNA repair complexes will form at these sites and initiate transgene integration (**a**). During metaphase, when FISH analysis is generally carried out, loci that are brought together in interphase may be separated, resulting in multiple signals from the same transformation event (**b**). If the DNA were stretched out, this would reveal large (megabase) interspersed sequences, which have also been observed in fiber-FISH experiments

which was adjacent to the right T-DNA border. Rearrangements involving the left border are often characterized by the insertion of variable-size regions of filler DNA, possibly derived from the T-DNA sequence or from plant genomic DNA [116, 131].

Few researchers have characterized transgene rearrangements in detail, but work by Kohli et al. [132] has shown that rearrangements may involve palindromic sequences in the transforming plasmid, which tend to form secondary structures such as hairpins and cruciforms. These investigators characterized 12 transgenic rice lines created by particle bombardment, which had been shown to contain rearranged transgenes. Interestingly, they found that an imperfect palindrome in the CaMV 35S promoter was involved in one third of all rearrangements, i.e., the sequence of this palindrome was adjacent to the rearrangement junction. Similar phenomena have been noted in T-DNA transformants containing the same promoter. This sequence has the ability to adopt a cruciform structure that may stimulate recombination events. Many other promoters contain palindromic sequences of variable length within 100 bp of the transcription start site. The secondary structures formed at these sites enable DNA–protein interactions for transcription under normal circumstances, but may also participate in aberrant recombination events. The fully sequenced papaya genome [123] also revealed a number of previously unidentified transgene rearrangements, i.e., a 1,533-bp fragment comprising a truncated, nonfunctional *tet*A gene and flanking vector backbone sequence, and a 290-bp nonfunctional fragment of the

*npt*II gene, in addition to the intact, primary transgene conferring virus resistance.

Transgene Silencing

A common issue raised in association with nuclear transformation in plants is the phenomenon of transgene silencing, where the phenotype corresponding to the introduced transgene is not expressed. In the absence of a genetic explanation (e.g., an undetected mutation or rearrangement), silencing is an epigenetic phenomenon that can occur at either the transcriptional or posttranscriptional levels. Transcriptional silencing involves the absence of transgene mRNA, and often occurs due to the integration of the transgene at a genomic position that is already repressed (position-dependent silencing). However, transgenes in active regions of the genome may also be silenced if the promoter region is inactivated by hypermethylation, which can occur in response to unusual DNA structures and compositions that attract de novo methylation, or DNA sequences that allow the synthesis of short double-stranded RNA (dsRNA) molecules. In contrast, posttranscriptional silencing actually requires transcription to take place, but the mRNA is rapidly degraded. This is confirmed by nuclear run-on assays, which measure the amount of pre-mRNA in the nucleus. Like transcriptional silencing, posttranscriptional silencing appears to have evolved as a defense against invasive nucleic acids and is also triggered by dsRNA, in this case matching the transcribed region. There is considerable cross talk between the transcriptional and posttranscriptional silencing pathways and if a transgene is homologous to an endogenous gene, the silencing effect can spread to that gene resulting in a phenomenon known as cosuppression.

Transcriptional silencing may be encountered in plants where several copies of the same transgene or part thereof are present in the transgenic locus, or when the same promoter is used to control several transgenes. However, the context is very important. There have been plenty of reports describing transgenic plants carrying multiple transgenes under the control of the same promoter yet showing strong and stable expression. For example, although Zhu et al. [133] used five different endosperm-specific promoters in corn to achieve the high-level expression of carotenogenic genes, Naqvi et al. [134] achieved strong expression of four genes in the same system using the barley D-hordein promoter to control each transgene, with no adverse effects. Transcriptional gene silencing resulting from repetitive promoter regions is correlated with increased promoter methylation [135] and appears to be driven by the production of dsRNA matching the promoter sequence [136]. This has been demonstrated by deliberately expressing dsRNA corresponding to the *nos* promoter in transgenic plants carrying a second transgene driven by the *nos* promoter [137] and by creating transgenic plants with a transgene locus that triggers both transcriptional and posttranscriptional silencing simultaneously, by producing dsRNA corresponding to promoter and transcribed sequences of different target genes [138]. In the absence of deliberately created promoter dsRNA, the transcriptional silencing seen in some transgenic plants carrying multiple copies of the same promoter appears to arise from dsRNA produced either by unfortunate transgene positioning or rearrangements that create hairpin structures, or by transgenes with such high levels of expression that the polyadenylation machinery is saturated. Evidence from many transformation experiments indicates that there is no simple correlation between transgene copy number and expression level, with the exception of certain carefully controlled experiments using boundary elements. In some cases, higher copy numbers have suppressed overall expression levels whereas in others higher copy numbers have enhanced expression. Where suppression effects have occurred, it has been suggested that "runaway expression" resulting in the generation of aberrant RNAs lacking polyadenylate tails has triggered potent silencing through the posttranscriptional silencing pathway [139].

The organization of a transgenic locus is difficult to control, and it is therefore a common occurrence in both *Agrobacterium*-mediated transformation and direct DNA transfer that the juxtaposition of transgenes or fragments thereof can result in the creation of hairpin promoter structures at the DNA level that are transcribed into aberrant dsRNA species. Such arrangements can be obvious and easy to detect, but even where gross rearrangements are absent it is possible that undetected "micro-rearrangements" are

present in the transgenic locus, as observed by Mehlo et al. [128] when investigating the structure of a transgenic locus in corn generated by direct DNA transfer. The siRNAs that trigger RNA-dependent DNA methylation are just 24 bp in length, so it is conceivable that inverted repeats of <50 bp could be sufficient for transgene silencing, and such structures would be undetectable using the coarse analysis methods typically employed to study transgenic plants, such as Southern blot hybridization. The likelihood of dsRNA production depends not only on the presence of damaged or rearranged transgenes, but also on the relative position of intact transgenes, which is itself a reflection of the mechanism of transgene integration. The organization of integrated T-DNA sequences differs among *Agrobacterium* strains, but a common feature of nopaline-type derivatives such as C58 is the preferential integration of T-DNA as dimers with an inverted repeat configuration, linked either at the left or right borders [140]. Where cotransformation is carried out with two T-DNAs containing different genes, the different T-DNAs often integrate as heterodimeric inverted repeats, preferentially around the right border [141]. If the same promoter is used for both genes, this would favor the formation of hairpin structures that could be transcribed from the opposite strand. The structure of loci generated by direct DNA transfer is more variable, but inverted repeat structures involving promoter sequences are not uncommon, allowing the same silencing mechanism to operate [126].

Plastid Transformation Methods

The introduction of DNA directly into the chloroplast genome is considered beneficial for a number of reasons including the high level of gene expression that can be achieved, reflecting the presence of thousands of chloroplasts in photosynthetic cells and the absence of gene silencing. Chloroplast transformation also provides a natural containment method for transgenic plants, since in most crops the transgene cannot be transmitted through pollen (reviewed in [142]).

The first reports of chloroplast transformation were serendipitous, and the integration events were found to be unstable. For example, an early experiment in which tobacco protoplasts were cocultivated with *Agrobacterium* resulted in the recovery of one transgenic plant line in which the transgene was transmitted maternally. Southern blot analysis of chloroplast DNA showed directly that the foreign DNA had become integrated into the chloroplast genome [143]. However, *Agrobacterium* is not an optimal system for chloroplast transformation because the T-DNA complex is targeted to the nucleus. Therefore, direct DNA transfer has been explored as an alternative strategy and efficient chloroplast transformation has been achieved both through particle bombardment and PEG-mediated transformation (reviewed in [144]).

Stable chloroplast transformation was first achieved in the alga *Chlamydomonas reinhardtii*, which has a single large chloroplast occupying most of the volume of the cell [145]. Particle bombardment was used in this experiment and the principles established using this simple organism were extended to tobacco, allowing the recovery of stable transplastomic tobacco plants [146]. These principles included the use of vectors containing chloroplast homology regions, allowing targeted integration into the chloroplast genome, and use of the selectable marker gene *aad*A (encoding aminoglycoside adenyltransferase) which confers resistance to streptomycin and spectinomycin [147]. Basic vectors for plastid transformation include flanking sequences and chloroplast-specific expression cassettes. Species-specific chloroplast flanking sequences are generated by PCR using primers designed from the available chloroplast genomes. The chloroplast expression cassette is composed of a promoter, the selectable marker, and 5′/3′ regulatory sequences to enhance the efficiency of transcription and translation. The most frequently used integration site is the transcriptionally active intergenic region between the *trn*I and *trn*A genes, within the *rrn* operon. The first-generation plastid transformation vectors included the pPRV series and plasmids pRB94/95, in which both the marker gene and the primary transgene have their own 5′ and 3′ regulatory sequences (reviewed in [144]). More recent vectors include modified restriction sites, *lox*P sequences for posttransformation marker excision, and homology regions targeting insertions to the *rbc*L-*acc*D intergenic region [148]. Thus far, chloroplast transformation by particle bombardment has been achieved only in crops that allow direct organogenesis, and this does not include any monocots (reviewed in [142]).

Future Directions

The vast majority of the transgenic plants generated thus far carry a single primary transgene plus a selectable marker. The transgene integrates randomly into the genome, which means it is subject to unpredictable position effects that may result in silencing; the locus structure is also very difficult to control. In the future, there will be a stronger emphasis on strategies to increase the scope of gene transfer and the predictability and preciseness of DNA integration, and consequently the likelihood of stable and predictable transgene expression.

Transfer of Large DNA Molecules Using Modified Conventional Vectors

A precise upper limit for T-DNA transfer has not been established. It is greater than 50 kbp [2, 3], but using standard vectors it is difficult to transfer inserts larger than 30 kbp routinely due to instability in the bacterial host. However, the analysis of very large genes or the transfer of multiple genes linked in series can now be achieved thanks to the development of high-capacity binary vectors based on the artificial chromosome type vectors used in *E. coli*.

The first to be described was BIBAC2 [149]. This contains an F-plasmid origin of replication and is modeled on the bacterial artificial chromosome. The basic vector transforms tobacco with high efficiency, but the efficiency of transformation drops substantially when large inserts are used. This vector has been used to introduce 150 kbp of human DNA flanked by T-DNA borders into the tobacco genome, although virulence helper plasmids supplying high levels of VirG and VirE in *trans* were critical for successful DNA transfer. An alternative vector carrying a P1 origin of replication and modeled on the P1 artificial chromosome was constructed by Liu et al. [150]. This transformation-competent bacterial artificial chromosome (TAC) vector was used to introduce up to 80 kbp of genomic DNA into Arabidopsis, and while there was some loss of efficiency with the larger inserts, it was still possible to produce many transgenic plants. Both vectors contain a kanamycin resistance marker for selection in bacteria and *hpt* for hygromycin selection in transgenic plants. Both vectors also contain the Ri origin for maintenance in *Agrobacterium*, and within the T-DNA region, the *sac*B marker for negative selection, interrupted by a multiple cloning site for transgene insertion. One of the most attractive uses of high-capacity binary vectors is for the positional cloning of genes identified by mutation. The ability to introduce large segments of DNA into the plant genome effectively bridges the gap between genetic mapping and sequencing, allowing the position of mutant genes to be narrowed down by complementation. Genomic libraries have been established for several plant species in BIBAC2 and TAC vectors [151, 152] and cloning in high-capacity vectors has been simplified by the inclusion of Cre/*lox*P and Gateway site-specific recombination technology [153, 154].

Large (80–150 kbp) DNA molecules have also been transferred to plants by direct DNA transfer [155], and although this is not a routine procedure a novel transformation method has been developed recently, based on bombardment with DNA-coated "bioactive beads" to deliver up to 150 kbp of DNA into rice protoplasts [156].

Plant Minichromosomes

In bacteria, plasmid vectors are maintained as episomal replicons to make cloning and isolating recombinant DNA a simple procedure. When it comes to expressing heterologous genes in eukaryotic cells, episomal vectors are widely used to avoid position effects, hence the development of yeast episomal vectors, yeast artificial chromosomes, mammalian plasmid vectors carrying virus origins of replication (e.g., SV40-based vectors, herpes virus-based vectors), and plant expression vectors based on plant viruses (all of which replicate episomally). The yeast artificial chromosome (YAC) system is the most relevant in this context because it allows genes of any size to be introduced into the yeast genome as an independent replicating unit that is treated by the cell as an additional chromosome. YACs comprise a yeast centromere and telomeres, the origin of replication (autonomous replicating sequence), and selectable markers.

More recently, analogous systems have been developed to maintain genes as episomal minichromosomes in plants. These have many advantages for plant genetic engineering including the ability to express large transgenes or groups of transgenes, and the ability to rapidly introduce new linkage groups into diverse

germplasm. Carlson et al. [157] created plant minichromosomes by combining the DsRed and *npt*II marker genes with 7–190 kb of corn genomic DNA fragments containing satellites, retroelements, and other repeat sequences commonly found in centromeres. The circular constructs were introduced into embryogenic corn tissue by particle bombardment and transformed cells were regenerated and propagated for several generations without selection. The minichromosomes were maintained as extrachromosomal replicons through mitosis and meiosis, and showed roughly Mendelian segregation ratios (93% transmission as a disome with 100% expected, 39% transmission as a monosome crossed to wild type with 50% expected, and 59% transmission in self crosses with 75% expected). The *DsRed* reporter gene was expressed over four generations, and DNA blot analysis indicated the genes were intact.

Gene Targeting (Homologous Recombination)

Gene targeting is the directed modification of an endogenous DNA sequence by homologous recombination, an efficient procedure in bacteria, yeast, certain animal cells, and in the plastid genomes of plants, but typically not in the nuclear genome. Only one plant species has been shown to undergo efficient nuclear homologous recombination and that is the moss *Physcomitrella patens* [158]. Among higher plants, low-level gene targeting has been achieved in certain dicots with frequencies ranging from 10^{-3} to 10^{-6} [159]. However, targeting frequencies of up to 1% have been achieved using a T-DNA-mediated gene targeting strategy involving a long homology region in combination with a strong counterselectable marker in rice [160, 161].

There has also been interest in the use of zinc-finger endonucleases to make targeted double-strand breaks in the plant genome, so that homologous recombination is favored at such sites [162]. The modular nature of zinc-finger transcription factors means that recombinant DNA technology can be used to "mix and match" these DNA-binding domains to create recombinant proteins with unique sequence specificities. Zinc-fingers are motifs approximately 30 amino acids in length which coordinate a Zn^{2+} ion and bind to DNA sequences 3-bp long. Combining different zinc fingers in series allows proteins to be tailor made to bind longer DNA sequences. When a nonspecific DNA endonuclease is incorporated into such a protein, it becomes a targeted DNA cutting tool [163, 164]. The recent achievement of targeted transgene integration and endogenous gene disruption in corn [165] and tobacco [166] using zinc-finger endonucleases provides a tantalizing glimpse of the future of plant biotechnology in which precise changes can be made to the genome of any plant genome that is amenable to DNA transfer.

Site-Specific Recombination

Although site-specific recombination has already been described as a cloning tool, particularly the Cre/*lox*P and Gateway systems for rapid vector assembly, it can also be used in transgenic plants to introduce DNA at a specific, favorable locus, or remove DNA sequences *in vivo*. The Cre/*lox*P system has been most widely used in plants for the controlled excision of selectable marker genes after transformation (e.g., [153]), but also for controlled transgene insertion (e.g., [167]). Controlled integration has been studied in transgenic plants already engineered to contain recipient *lox*P sites [168]. In this study, three different recipient wheat lines were generated by bombarding plants with the *lox*P sequence, and these were subsequently bombarded with a *gusA* construct also containing flanking *lox*P sequences, and a *cre* gene. Following transformation, about 80% of lines contained *gusA* at the recipient site, many with single-copy transgenes and others with concatemers. Both types of locus were stably inherited. There was much less variation in expression among the single-copy lines [168]. Chawla et al. [169] generated 18 different transgenic rice lines containing a precise single copy of *gusA* at a designated site. In seven of these lines, additional copies of the transgene integrated at random sites by illegitimate recombination while 11 showed "clean" integration by site-specific recombination only. The single-copy lines were stable over at least four generations and showed consistent levels of expression, which doubled in homozygous plants. In contrast, the multicopy lines showed variable expression and some fell victim to transgene silencing. Interestingly, where the site-specific and illegitimate integration loci segregated in later generations,

transgene expression was reactivated in the plants carrying the site-specific integration site alone, whereas close linkage between the site-specific and random integration prevented segregation in other lines and the silencing persisted.

An exciting recent development is the GENE DELETOR system, which is a hybrid of the Cre-*lox*P and FLP-*FRT* systems. The GENE DELETOR is based on a fusion recognition site (*lox*P-*FRT*), which is inefficient when both recombinases are expressed but highly efficient when either one of the recombinases is expressed alone, giving up to 100% efficiency in populations of up to 25,000 T1 transgenic tobacco plants [170].

Another use for Cre-*lox*P is the simplification of locus structure by resolving multicopy loci to a single transgene copy [171]. A strategy was developed in which the transformation vector contained a transgene flanked by *lox*P sites in an inverted orientation. Regardless of the number of copies integrated between the outermost transgenes, recombination between the outermost sites resolved the integrated molecules into a single copy. The principle was proven by resolving four multicopy loci successfully into single-copy transgenes.

Bibliography

Primary Literature

1. Bevan M, Flavell RB, Chilton MD (1983) A chimaeric antibiotic resistance gene as a selectable marker for plant cell transformation. Nature 304:184–187
2. Herrera-Estrella L, DeBlock M, Messens E, Hernalsteens JP, Montagu MV, Schell J (1983) Chimeric genes as dominant selectable markers in plant cells. EMBO J 2:987–995
3. Herrera-Estrella L, Depicker A, Van Montagu M, Schell J (1983) Expression of chimaeric genes transferred into plant cells using a Ti-plasmid-derived vector. Nature 303:209–213
4. Twyman RM, Christou P, Stoger E (2002) Genetic transformation of plants and their cells. In: Oksman-Caldentey KM, Barz W (eds) Plant biotechnology and transgenic plants. Marcel Dekker, New York, pp 111–141
5. Shaw CH, Watson MD, Carter GH, Shaw CH (1984) The right hand copy of the nopaline Ti-plasmid 25 bp repeat is required for tumour formation. Nucleic Acids Res 12:6031–6041
6. Peralta EG, Hellmiss R, Ream W (1986) Overdrive, a T-DNA transmission enhancer on the *A. tumefaciens* tumour-inducing plasmid. EMBO J 5:1137–1142
7. Stachel SE, Messens E, Van Montagu M, Zambryski P (1985) Identification of the signal molecules produced by wounded plant cells that activate T-DNA transfer in *Agrobacterium tumefaciens*. Nature 318:624–629
8. Gelvin SB (2000) *Agrobacterium* and plant genes involved in T-DNA transfer and integration. Annu Rev Plant Physiol Plant Mol Biol 51:223–256
9. Gelvin SB (2003) *Agrobacterium*-mediated plant transformation: the biology behind the gene jockeying tool. Microbiol Mol Biol Rev 67:16–37
10. Lai EM, Kado CI (2000) The T-pilus of *Agrobacterium tumefaciens*. Trends Microbiol 8:361–369
11. Tinland B, Koukolikova-Nicola Z, Hall MN, Hohn B (1992) The T-DNA-linked *virD2* protein contains two distinct functional nuclear localization signals. Proc Natl Acad Sci USA 89:7442–7446
12. Tinland B (1996) The integration of T-DNA into plant genomes. Trends Plant Sci 1:179–184
13. Tzfira T, Citovsky V (2002) Partners-in-infection: host proteins involved in the transformation of plant cells by *Agrobacterium*. Trends Cell Biol 12:121–129
14. Tzfira T, Li J, Lacroix B, Citovsky V (2004) *Agrobacterium* T-DNA integration: molecules and models. Trends Genet 20:375–383
15. Hellens RP, Edwards EA, Leyland NR, Bean S, Mullineaux PM (2000) pGreen: a versatile and flexible binary Ti vector for *Agrobacterium*-mediated plant transformation. Plant Mol Biol 42:819–832
16. Karimi M, Depicker A, Hilson P (2007) Recombinational cloning with plant gateway vectors. Plant Physiol 145:1144–1154
17. Chen QJ, Zhou HM, Chen J, Wang XC (2006) A Gateway-based platform for multigene plant transformation. Plant Mol Biol 62:927–936
18. Horsch RB, Fry JE, Hoffmann NL, Eichholtz D, Rogers SG, Fraley RT (1985) A simple and general method for transferring genes into plants. Science 227:1229–1231
19. Hiei Y, Ohta S, Komari T, Kumashiro T (1994) Efficient transformation of rice (*Oryza sativa* L.) mediated by *Agrobacterium* and sequence analysis of the boundaries of the T-DNA. Plant J 6:271–282
20. Sheng OJ, Citovsky V (1996) *Agrobacterium* plant cell DNA transport: have virulence proteins will travel. Plant Cell 8:1699–1710
21. Komari T, Hiei Y, Saito Y, Murai N, Kumashiro T (1996) Vectors carrying two separate T-DNAs for co-transformation of higher plants mediated by *Agrobacterium tumefaciens* and segregation of transformants free from selection markers. Plant J 10:165–174
22. Negrutiu I, Shillito R, Potrykus I, Biasini G, Sala F (1987) Hybrid genes in the analysis of transformation conditions. I. Setting up a simple method for direct gene transfer in plant protoplasts. Plant Mol Biol 8:363–373
23. Shillito RD, Saul MW, Pazkowski J, Muller M, Potrykus I (1985) High efficiency direct gene transfer to plants. Biotechnology (N Y) 3:1099–1103
24. Frame BR, Drayton PR, Bagnall SV, Lewnau CJ, Bullock WP, Wilson HM, Dunwell JM, Thompson JA, Wang K (1994) Production of fertile transgenic maize plants by silicon-carbide whisker-mediated transformation. Plant J 6:941–948

25. Sanford JC, Klein TM, Wolf ED, Allen N (1987) Delivery of substances into cells and tissues using a particle bombardment process. J Particulate Sci Technol 6:559–563
26. Klein TM, Wolf ED, Wu R, Sanford JC (1987) High-velocity micro-projectiles for delivering nucleic acids into living cells. Nature 327:70–73
27. Christou P, McCabe DE, Swain WF (1988) Stable transformation of soybean callus by DNA-coated gold particles. Plant Physiol 87:671–674
28. Gordon-Kamm WJ, Spencer TM, Mngano ML, Adams TR, Daines RJ, Start WG, O'Brian JV, Chambers SA, Adams WR Jr, Willets NG, Rice TB, Mackey CJ, Krueger RW, Kausch AP, Lemaux PG (1990) Transformation of maize cells and regeneration of fertile transgenic plants. Plant Cell 2:603–618
29. Fromm ME, Morrish F, Armstrong C, Williams R, Thomas J, Klein TM (1990) Inheritance and expression of chimeric genes in the progeny of transgenic maize plants. Biotechnology (N Y) 8:833–839
30. Twyman RM, Christou P (2004) Plant transformation technology – particle bombardment. In: Christou P, Klee H (eds) Handbook of plant biotechnology. Wiley, New York, pp 263–289
31. Altpeter F, Baisakh N, Beachy R, Bock R, Capell T, Christou P, Daniell H, Datta K, Datta S, Dix PJ, Fauquet C, Huang N, Kohli A, Mooibroek H, Nicholson L, Nguyen TT, Nugent G, Raemakers K, Romano A, Somers DA, Stoger E, Taylor N, Visser R (2005) Particle bombardment and the genetic enhancement of crops: myths and realities. Mol Breed 15:305–327
32. Christou P, Ford TL, Kofron M (1991) Production of transgenic rice (*Oryza sativa* L.) plants from agronomically important Indica and Japonica varieties via electric discharge particle acceleration of exogenous DNA into immature zygotic embryos. Nat Biotechnol 9:957–962
33. Vasil V, Castillo AM, Fromm ME, Vasil IK (1992) Herbicide resistant fertile transgenic wheat plants obtained by microprojectile bombardment of regenerable embryogenic callus. Biotechnology (N Y) 10:667–674
34. Somers DA, Rines HW, Gu W, Kaeppler HF, Bushnell WR (1992) Fertile, transgenic oat plants. Biotechnology (N Y) 10:1589–1594
35. McCabe D, Christou P (1993) Direct DNA transfer using electric discharge particle acceleration (Accell® technology). Plant Cell Tissue Organ Cult 33:227–236
36. Christou P (1996) Particle bombardment for genetic engineering of plants. RG Landes Co, Austin
37. Finer JJ, Finer KR, Ponappa T (1999) Particle bombardment mediated transformation. Curr Top Microbiol Immunol 240:59–80
38. Bechtold N, Ellis J, Pelletier G (1993) In *planta Agrobacterium*-mediated gene transfer by infiltration of adult *Arabidopsis thaliana* plants. C R Acad Sci Paris Life Sci 316:1194–1199
39. Clough SJ, Bent A (1998) Floral dip: a simplified method for *Agrobacterium*-mediated transformation of *Arabidopsis thaliana*. Plant J 16:735–743
40. Qing CM, Fan L, Lei Y, Bouchez D, Tourneur C, Yan L, Robaglia C (2000) Transformation of Pakchoi (*Brassica rapa* L. ssp. *chinensis*) by *Agrobacterium* infiltration. Mol Breed 6:67–72
41. Trieu AT, Burleigh SH, Kardailsky IV, Maldonado-Mendoza IE, Versaw WK, Blaylock LA, Shin H, Chiou TJ, Katagi H, Dewbre GR, Weigel D, Harrison MJ (2000) Transformation of *Medicago truncatula* via infiltration of seedlings or flowering plants with *Agrobacterium*. Plant J 22:531–541
42. Curtis IS, Nam HG (2001) Transgenic radish (*Raphanus sativus* L. var. *longipinnatus* Bailey) by floral-dip method – plant development and surfactant are important in optimizing transformation efficiency. Transgenic Res 10:363–371
43. Feldmann KA, Marks MD (1987) *Agrobacterium*-mediated transformation of germinating seeds of *Arabidopsis thaliana* – a non-tissue culture approach. Mol Gen Genet 208:1–9
44. Bechtold N, Jaudeau B, Jolivet S, Maba B, Vezon D, Voisin R, Pelletier G (2000) The maternal chromosome set is the target of the T-DNA in the *in planta* transformation of *Arabidopsis thaliana*. Genetics 155:1875–1887
45. Chang SS, Park SK, Kim BC, Kang BJ, Kim DU, Nam HG (1994) Stable genetic transformation of *Arabidopsis thaliana* by *Agrobacterium* inoculation *in planta*. Plant J 5:551–558
46. Dafny-Yelin M, Tzfira T (2007) Delivery of multiple transgenes to plant cells. Plant Physiol 145:1118–1128
47. Komori T, Imayama T, Kato N, Ishida Y, Ueki J, Komari T (2007) Current status of binary vectors and superbinary vectors. Plant Physiol 145:1155–1160
48. Bevan M (1984) Binary *Agrobacterium* vectors for plant transformation. Nucleic Acids Res 12:8711–8721
49. Hajdukiewicz P, Svab Z, Maliga P (1994) The small, versatile pPZP family of *Agrobacterium* binary vectors for plant transformation. Plant Mol Biol 25:989–994
50. van Engelen FA, Molthoff JW, Conner AJ, Nap J-P, Pereira A, Stiekema WJ (1995) pBINPLUS: an improved plant transformation vector based on pBIN19. Transgenic Res 4:288–290
51. Ishida Y, Saito H, Ohta S, Hiei Y, Komari T, Kumashiro T (1996) High efficiency transformation of maize (*Zea mays* L.) mediated by *Agrobacterium tumefaciens*. Nat Biotechnol 14:745–750
52. Jin S, Komari T, Gordon MP, Nester EW (1987) Genes responsible for the supervirulence phenotype of *Agrobacterium tumefaciens* A281. J Bacteriol 169:4417–4425
53. Komari T (1990) Transformation of cultured cells of *Chenopodium quinoa* by binary vectors that carry a fragment of DNA from the virulence region of pTiBo542. Plant Cell Rep 9:303–306
54. Veluthambi K, Gupta AK, Sharma A (2003) The current status of plant transformation technologies. Curr Sci 84:368–378
55. Cheng M, Lowe BA, Spencer TM, Ye X, Armstrong CL (2004) Factors influencing *Agrobacterium*-mediated transformation of monocotyledonous species. In Vitro Cell Dev Biol Plant 40:31–45
56. Frame BR, Shou H, Chikwamba RK, Zhang Z, Xiang C, Fonger TM, Pegg SEK, Li B, Nettleton DS, Pei D, Wang K (2002) *Agrobacterium tumefaciens*-mediated transformation of

maize embryos using a standard binary vector system. Plant Physiol 129:13–22
57. Hanson B, Engler D, Moy Y, Newman B, Ralston E, Gutterson N (1999) A simple method to enrich an *Agrobacterium*-transformed population for plants containing only T-DNA sequences. Plant J 19:727–734
58. Kuraya Y, Ohta S, Fukuda M, Hiei Y, Murai N, Hamada K, Ueki J, Imaseki H, Komari T (2004) Suppression of transfer of non-T-DNA "vector backbone" sequences by multiple left border repeats in vectors for transformation of higher plants mediated by *Agrobacterium tumefaciens*. Mol Breed 14:309–320
59. Podevin N, De Buck S, De Wilde C, Depicker A (2006) Insights into recognition of the T-DNA border repeats as termination sites for T-strand synthesis by *Agrobacterium tumefaciens*. Transgenic Res 15:557–571
60. Chen S, Songkumarn P, Liu J, Wang G-L (2009) A versatile zero background T-vector system for gene cloning and functional genomics. Plant Physiol 150:1111–1121
61. Naqvi S, Farre G, Sanahuja G, Capell T, Zhu C, Christou P (2009) When more is better: multigene engineering in plants. Trends Plant Sci 15:48–56
62. Zhu C, Naqvi S, Gomez-Galera S, Pelacho AM, Capell T, Christou P (2007) Transgenic strategies for the nutritional enhancement of plants. Trends Plant Sci 12:548–555
63. Halpin C (2005) Gene stacking in transgenic plants – the challenge for 21st century plant biotechnology. Plant Biotechnol J 3:141–155
64. Chen L, Marmey P, Taylor NJ, Brizard JP, Espinoza C, D'Cruz P, Huet H, Zhang S, de Kochko A, Beachy RN, Fauquet CM (1998) Expression and inheritance of multiple transgenes in rice plants. Nat Biotechnol 16:1060–1064
65. Goderis IJWM, De Bolle MFC, François IEJA, Wouters PFJ, Broekaert WF, Cammue BPA (2002) A set of modular plant transformation vectors allowing flexible insertion of up to six expression units. Plant Mol Biol 50:17–27
66. Tzfira T, Tian GW, Lacroix B, Vyas S, Li J, Leitner-Dagan Y, Krichevsky A, Taylor T, Vainstein A, Citovsky V (2005) pSAT vectors: a modular series of plasmids for autofluorescent protein tagging and expression of multiple genes in plants. Plant Mol Biol 57:503–516
67. Thomson JM, Lafayette PR, Schmidt MA, Parrott WA (2002) Artificial gene-clusters engineered into plants using a vector system based on intron-and intein-encoded endonucleases. In Vitro Cell Dev Biol Plant 38:537–542
68. Chung S-M, Frankman EL, Tzfira T (2005) A versatile vector system for multiple gene expression in plants. Trends Plant Sci 10:357–361
69. Lin L, Liu Y-G, Xu X, Li B (2003) Efficient linking and transfer of multiple genes by a multigene assembly and transformation vector system. Proc Natl Acad Sci USA 100:5962–5967
70. Thole V, Worland B, Snape JW, Vain P (2007) The pCLEAN dual binary vector system for *Agrobacterium*-mediated plant transformation. Plant Physiol 145:1211–1219
71. Coutu C, Brandle J, Brown D, Brown K, Miki B, Simmonds J, Hegedus DD (2007) pORE: a modular binary vector series suited for both monocot and dicot plant transformation. Transgenic Res 16:771–781
72. Fu X, Duc LT, Fontana S, Bong BB, Tinjuangjun P, Sudhakar D, Twyman RM, Christou P, Kohli A (2000) Linear transgene constructs lacking vector backbone sequences generate low-copy-number transgenic plants with simple integration patterns. Transgenic Res 9:11–19
73. Breitler JC, Labeyrie A, Meynard D, Legavre T, Guiderdoni E (2002) Efficient microprojectile bombardment-mediated transformation of rice using gene cassettes. Theor Appl Genet 104:709–719
74. Potenza C, Aleman L, Sengupta-Gopalan C (2004) Targeting transgene expression in research, agricultural, and environmental applications: promoters used in plant transformation. In Vitro Cell Dev Biol Plant 40:1–22
75. Odell JT, Nagy F, Chua NH (1985) Identification of DNA sequences required for activity of the Cauliflower mosaic virus 35S promoter. Nature 313:810–812
76. Fang RX, Nagy F, Sivasubramaniam S, Chua NH (1989) Multiple *cis*-regulatory elements for maximal expression of the Cauliflower mosaic virus 35S promoter in transgenic plants. Plant Cell 1:141–150
77. Kay R, Chan A, Daly M, McPherson J (1987) Duplication of CaMV 35S promoter sequences creates a strong enhancer for plant genes. Science 236:1299–1302
78. Zheng X, Deng W, Luo K, Duan H, Chen Y, McAvoy R, Song S, Pei Y, Li Y (2007) The Cauliflower mosaic virus (CaMV) 35S promoter sequence alters the level and patterns of activity of adjacent tissue- and organ-specific gene promoters. Plant Cell Rep 26:1195–1203
79. Peremarti A, Twyman RM, Gómez-Galera S, Naqvi S, Farré G, Sabalza M, Miralpeix B, Dashevskaya S, Yuan D, Ramessar K, Christou P, Zhu C, Bassie L, Capell T (2010) Promoter diversity in multigene transformation. Plant Mol Biol 73(4–5):363–378
80. Stavolone L, Ragozzino A, Hohn T (2003) Characterization of Cestrum yellow leaf curling virus: a new member of the caulimoviridae family. J Gen Virol 84:3459–3464
81. Schünmann PHD, Llewellyn DJ, Surin B, Boevink P, Feyter RCD, Waterhouse PM (2003) A suite of novel promoters and terminators for plant biotechnology. Funct Plant Biol 30:443–452
82. Schünmann PHD, Surin B, Waterhouse PM (2003) A suite of novel promoters and terminators for plant biotechnology II. The pPLEX series for use in monocots. Funct Plant Biol 30:453–460
83. McElroy D, Brettell RIS (1994) Foreign gene expression in transgenic cereals. Trends Biotechnol 12:62–68
84. Christensen AH, Quail PH (1996) Ubiquitin promoter-based vectors for high-level expression of selectable and/or screenable marker genes in monocotyledonous plants. Transgenic Res 5:213–218
85. McElroy D, Blowers AD, Jenes B, Wu R (1991) Construction of expression vectors based on the rice actin 1 (Act1) 50 region for use in monocot transformation. Mol Gen Genet 231:150–160
86. He C, Lin Z, McElroy D, Wu R (2009) Identification of a rice *actin2* gene regulatory region for high-level expression of transgenes in monocots. Plant Biotechnol J 7:227–239

87. Wobus U, Borisjuk L, Panitz R, Manteuffel R, Baumlein H, Wohlfart T, Heim U, Weber H, Misera S, Weschke W (1995) Control of seed storage protein gene expression: new aspects on an old story. J Plant Physiol 145:592–599
88. Lu CA, Lim EK, Yu SM (1998) Sugar response sequence in the promoter of a rice alpha-amylase gene serves as a transcriptional enhancer. J Biol Chem 273:10120–10131
89. Martinez A, Sparks C, Hart CA, Thompson J, Jepson I (1999) Ecdysone agonist inducible transcription in transgenic tobacco plants. Plant J 19:97–106
90. Padidam M, Gore M, Lu DL, Smirnova O (2003) Chemical-inducible, ecdysone receptor-based gene expression system for plants. Transgenic Res 12:101–109
91. Miki B, McHugh S (2004) Selectable marker genes in transgenic plants: applications, alternatives and biosafety. J Biotechnol 107:193–232
92. Angenon G, Dillen W, van Montagu M (1994) Antibiotic resistance markers for plant transformation. In: Gelvin SB, Schilperoort RA (eds) Plant molecular biology manual, 2nd edn. Kluwer, Dordrecht, pp 1–13, Section C1
93. Wilmink A, Dons JJM (1993) Selective agents and marker genes for use in transformation of monocotyledonous plants. Plant Mol Biol Rep 11:165–185
94. Battraw M, Hall TC (1992) Expression of a chimeric neomycin phosphotransferase II gene in first and second generation transgenic rice plants. Plant Sci 86:191–202
95. Shimamoto K, Terada R, Izawa T, Fujimoto H (1989) Fertile transgenic rice plants regenerated from transformed protoplasts. Nature 338:274–276
96. Hille J, Verhweggen F, Roelvink P, Franssen H, van Kammen A, Zabel P (1986) Bleomycin resistance: a new dominant selectable marker for plant cell transformation. Plant Mol Biol 7:171–176
97. Hayford MB, Medford JI, Hoffmann NL, Rogers SG, Klee HJ (1988) Development of a plant transformation selection system based on expression of genes encoding gentamicin acetyltransferases. Plant Physiol 86:1216–1222
98. Eichholtz DA, Rogers SG, Horsch RB, Klee HJ, Hayford M, Hoffmann NL, Braford SB, Fink C, Flick J, O'Connell KM, Fraley RT (1987) Expression of mouse dihydrofolate reductase gene confers methotrexate resistance in transgenic petunia plants. Somat Cell Mol Genet 13:67–76
99. Rathore KS, Chowdhury VK, Hodges TK (1993) Use of *bar* as a selectable marker gene and for the production of herbicide resistant rice plants from protoplasts. Plant Mol Biol 21: 871–884
100. Shah DM, Horsch RB, Klee HJ, Kishore GM, Winter JA, Tumer NE, Hironaka CM, Sanders PR, Gasser CS, Aykent S, Siegel NR, Rogers SG, Fraley RT (1986) Engineering herbicide tolerance in transgenic plants. Science 233:478–481
101. Guerineau F, Mullineaux P (1989) Nucleotide sequence of the sulfonamide resistance plasmid R46. Nucleic Acids Res 14:4370
102. Haughn GW, Smith J, Mazur B, Somerville C (1988) Transformation with mutant *Arabidopsis* acetolactate synthase gene renders tobacco resistant to sulfonylurea herbicides. Mol Gen Genet 211:266–271
103. Negrotto D, Jolley M, Beer S, Wenck AR, Hansen G (2000) The use of phosphomannose isomerase as a selectable marker to recover transgenic maize plants (*Zea mays* L.) via *Agrobacterium* transformation. Plant Cell Rep 19:798–803
104. Kunkel T, Niu QW, Chan YS, Chua NH (1999) Inducible isopentenyl transferase as a high-efficiency marker for plant transformation. Nat Biotechnol 17:916–919
105. Stepanenko OV, Verkhusha VV, Kuznetsova IM, Uversky VN, Turoverov KK (2008) Fluorescent proteins as biomarkers and biosensors: throwing color lights on molecular and cellular processes. Curr Protein Pept Sci 9:338–369
106. Calderon-Villalobos LIA, Kuhnle C, Li H, Rosso M, Weisshaar B, Schwechheimer C (2006) LucTrap vectors are tools to generate luciferase fusions for the quantification of transcript and protein abundance *in vivo*. Plant Physiol 141:3–14
107. Haseloff J, Siemering KR, Prasher DC, Hodge S (1997) Removal of a cryptic intron and subcellular localization of green fluorescent protein are required to mark transgenic Arabidopsis plants brightly. Proc Natl Acad Sci USA 94:2122–2127
108. Zhong S, Lin Z, Fray RG, Grierson D (2008) Improved plant transformation vectors for fluorescent protein tagging. Transgenic Res 17:985–989
109. Nishizawa K, Kita Y, Kitayama M, Ishimoto M (2006) A red fluorescent protein, DsRed2, as a visual reporter for transient expression and stable transformation in soybean. Plant Cell Rep 25:1355–1361
110. Ochiai-Fukuda T, Takahashi-Ando N, Ohsato S, Igawa T, Kadokura K, Hamamoto H, Nakasako M, Kudo T, Shibata T, Yamaguchi I, Kimura M (2006) A fluorescent antibiotic resistance marker for rapid production of transgenic rice plants. J Biotechnol 122:521–527
111. Salomon S, Puchta H (1998) Capture of genomic and T-DNA sequences during double-strand break repair in somatic plant cells. EMBO J 17:6086–6095
112. Somers DA, Makarevistch I (2004) Transgene integration in plants: poking or patching holes in promiscuous genomes? Curr Opin Biotechnol 15:126–131
113. Ward ER, Barnes WM (1988) VirD2 protein of *Agrobacterium tumefaciens* very tightly linked to 5′ end of T-strand DNA. Science 242:927–930
114. Ziemienowicz A, Tinland B, Bryant J, Gloeckler V, Hohn B (2000) Plant enzymes but not *Agrobacterium* VirD2 mediate T-DNA ligation *in vitro*. Mol Cell Biol 20:6317–6322
115. Nam J, Mysore KS, Zheng C, Knue MK, Matthysse AG, Gelvin SB (1999) Identification of T-DNA tagged *Arabidopsis* mutants that are resistant to transformation by Agrobacterium. Mol Gen Genet 261:429–438
116. Kumar S, Fladung M (2002) Transgene integration in aspen: structures of integration sites and mechanism of T-DNA integration. Plant J 31:543–551
117. Zhu QH, Ramm K, Eamens AL, Dennis ES, Upadhyaya NM (2006) Transgene structures suggest that multiple mechanisms are involved in T-DNA integration in plants. Plant Sci 171:308–322

118. Svitashev SK, Pawlowski WF, Makarevitch I, Plank DW, Somers DA (2002) Complex transgene locus structures implicate multiple mechanisms for plant transgene rearrangement. Plant J 32:433–445
119. Kohli A, Miro B, Twyman RM (2009) Transgene integration, expression and stability in plants: strategies for improvements. In: Kole C, Michler CH, Abbott AG, Hall TC (eds) Biotech plants, vol 1, Concepts & Development. Springer-Verlag, Berlin
120. Kohli A, Leech M, Vain P, Laurie DA, Christou P (1998) Transgene organization in rice engineered through direct DNA transfer supports a two-phase integration mechanism mediated by the establishment of integration hot spots. Proc Natl Acad Sci USA 95:7203–7208
121. Gorbunova V, Levy AA (1997) Non-homologous DNA end joining in plant cells is associated with deletions and filler DNA insertions. Nucleic Acids Res 25:4650–4657
122. Sawasaki T, Takahashi M, Goshima N, Morikawa H (1998) Structures of transgene loci in transgenic *Arabidopsis* plants obtained by particle bombardment: junction regions can bind to nuclear matrices. Gene 218:27–35
123. Ming R, Hou S, Feng Y, Yu Q, Dionne-Laporte A, Saw JH, Senin P, Wang W, Ly BV, Lewis KL, Salzberg SL, Feng L, Jones MR, Skelton RL, Murray JE, Chen C, Qian W, Shen J, Du P, Eustice M, Tong E, Tang H, Lyons E, Paull RE, Michael TP, Wall K, Rice DW, Albert H, Wang ML, Zhu YJ, Schatz M, Nagarajan N, Acob RA, Guan P, Blas A, Wai CM, Ackerman CM, Ren Y, Liu C, Wang J, Wang J, Na JK, Shakirov EV, Haas B, Thimmapuram J, Nelson D, Wang X, Bowers JE, Gschwend AR, Delcher AL, Singh R, Suzuki JY, Tripathi S, Neupane K, Wei H, Irikura B, Paidi M, Jiang N, Zhang W, Presting G, Windsor A, Navajas-Pérez R, Torres MJ, Feltus FA, Porter B, Li Y, Burroughs AM, Luo MC, Liu L, Christopher DA, Mount SM, Moore PH, Sugimura T, Jiang J, Schuler MA, Friedman V, Mitchell-Olds T, Shippen DE, dePamphilis CW, Palmer JD, Freeling M, Paterson AH, Gonsalves D, Wang L, Alam M (2008) The draft genome of the transgenic tropical fruit tree papaya (*Carica papaya* Linnaeus). Nature 452:991–997
124. Abranches R, Santos AP, Wegel E, Williams S, Castilho A, Christou P, Shaw P, Stoger E (2000) Widely separated multiple transgene integration sites in wheat chromosomes are brought together at interphase. Plant J 24:713–723
125. Pawlowski WP, Somers DA (1998) Transgenic DNA integrated into the oat genome is frequently interspersed by host DNA. Proc Natl Acad Sci USA 95:12106–12110
126. Kohli A, Twyman RM, Abranches A, Wegel E, Shaw P, Christou P, Stoger E (2003) Transgene integration, organization and interaction in plants. Plant Mol Biol 52:247–258
127. Svitashev SK, Ananiev E, Pawlonski WP, Somers DA (2000) Association of transgene integration sites with chromosome rearrangements in hexaploid oat. Theor Appl Genet 100:872–880
128. Mehlo L, Mazithulela G, Twyman RM, Boulton MI, Davies JW, Christou P (2000) Structural analysis of transgene rearrangements and effects on expression in transgenic maize plants generated by particle bombardment. Maydica 45:277–287
129. Afolabi AS, Worland B, Snape JW, Vain P (2004) A large-scale study of rice plants transformed with different T-DNAs provides new insights into locus composition and T-DNA linkage configurations. Theor Appl Genet 109:815–826
130. Rai M, Datta K, Parkhi V, Tan J, Oliva N, Chawla HS, Datta SK (2007) Variable T-DNA linkage configuration affects inheritance of carotenogenic transgenes and carotenoid accumulation in transgenic indica rice. Plant Cell Rep 26:1221–1231
131. De Buck S, Jacobs A, Van Montagu M, Depicker A (1999) The DNA sequences of T-DNA junctions suggest that complex T-DNA loci are formed by a recombination process resembling T-DNA integration. Plant J 20:295–304
132. Kohli A, Griffiths S, Palacios N, Twyman RM, Vain P, Laurie DA, Christou P (1999) Molecular characterization of transforming plasmid rearrangements in transgenic rice reveals a recombination hotspot in the CaMV 35S promoter and confirms the predominance of microhomology-mediated recombination. Plant J 17:591–601
133. Zhu C, Naqvi S, Breitenbach J, Sandmann G, Christou P, Capell T (2008) Combinatorial genetic transformation generates a library of metabolic phenotypes for the carotenoid pathway in maize. Proc Natl Acad Sci USA 105:18232–18237
134. Naqvi S, Zhu C, Farre G, Ramessar K, Bassie L, Breitenbach J, Perez Conesa D, Ros G, Sandmann G, Capell T, Christou P (2009) Transgenic multivitamin corn through biofortification of endosperm with three vitamins representing three distinct metabolic pathways. Proc Natl Acad Sci USA 106:7762–7767
135. Kooter J, Matzke MA, Meyer P (1999) Listening to the silent genes: transgene silencing, gene regulation and pathogen control. Trends Plant Sci 4:340–346
136. Mette MF, Aufsatz W, van der Winden J, Matzke MA, Matzke AJM (2000) Transcriptional silencing and promoter methylation triggered by double-stranded RNA. EMBO J 19:5194–5201
137. Mette MF, van der Winden J, Matzke MA, Matzke AJM (1999) Production of aberrant promoter transcripts contributes to methylation and silencing of unlinked homologous promoters in trans. EMBO J 18:241–248
138. Mourrain P, van Blokland R, Kooter JM, Vaucheret H (2007) A single transgene locus triggers both transcriptional and post-transcriptional silencing through double-stranded RNA production. Planta 225:365–379
139. Schubert D, Lechtenberg B, Forsbach A, Gils M, Bahadur S, Schmidt R (2004) Silencing in *Arabidopsis* T-DNA transformants: the predominant role of a gene-specific RNA sensing mechanism versus position effects. Plant Cell 16:2561–2572
140. Jorgensen RA, Snyder C, Jones JDG (1987) T-DNA is organized predominantly in inverted repeat structures in plants transformed with *Agrobacterium tumefaciens* C58 derivatives. Mol Gen Genet 207:471–477
141. De Block M, Debrouwer D (1991) Two T-DNAs co-transformed into *Brassica napus* by a double *Agrobacterium*

tumefaciens infection are mainly integrated at the same locus. Theor Appl Genet 82:257–263
142. Verma D, Daniell H (2007) Chloroplast vector systems for biotechnology applications. Plant Physiol 145:1129–1114
143. De Block M, Schell J, Van Montagu M (1985) Chloroplast transformation by *Agrobacterium tumefaciens*. EMBO J 4:1367–1372
144. Maliga P (2005) New vectors and marker excision systems mark progress in engineering the plastid genome of higher plants. Photochem Photobiol Sci 4:971–976
145. Boynton JE, Gillham NW, Harris EH, Hosler JP, Johnson AM, Jones AR, Randolph-Anderson BL, Robertson D, Klein TM, Shark KB, Sanford JC (1988) Chloroplast transformation in *Chlamydomonas* with high-velocity microprojectiles. Science 240:1534–1538
146. Svab Z, Hajdukiewcz P, Maliga P (1990) Stable transformation of plastids in higher plants. Proc Natl Acad Sci USA 87:8526–8530
147. Zoubenko OV, Allison LA, Svab Z, Maliga P (1994) Efficient targeting of foreign genes into the tobacco plastid genome. Nucleic Acids Res 22:3819–3824
148. Sinagawa-García SR, Tungsuchat-Huang T, Paredes-López O, Maliga P (2009) Next generation synthetic vectors for transformation of the plastid genome of higher plants. Plant Mol Biol 70:487–498
149. Hamilton CM (1997) A binary-BAC system for plant transformation with high molecular weight DNA. Gene 200:107–116
150. Liu YG, Shirano Y, Fukaki H, Yanai Y, Tasaka M, Tabata S, Shibata D (1999) Complementation of plant mutants with large genomic DNA fragments by a transformation-competent artificial chromosome vector accelerates positional cloning. Proc Natl Acad Sci USA 96:6535–6540
151. Hamilton CM, Frary A, Xu YM, Tanksley SD, Zhang HB (1999) Construction of tomato genomic DNA libraries in a binary-BAC (BIBAC) vector. Plant J 18:223–229
152. Shibata D, Lui Y-G (2000) *Agrobacterium*-mediated plant transformation with large DNA fragments. Trends Plant Sci 5:354–357
153. Vega JM, Yu W, Han F, Kato A, Peters EM, Zhang ZJ, Birchler JA (2008) *Agrobacterium*-mediated transformation of maize (*Zea mays*) with Cre-lox site specific recombination cassettes in BIBAC vectors. Plant Mol Biol 66:587–598
154. Schmidt MA, LaFayette PR, Artelt BA, Parrott WA (2008) A comparison of strategies for transformation with multiple genes via microprojectile-mediated bombardment. In Vitro Cell Dev Biol Plant 44:162–168
155. Mullen J, Adam G, Blowers A, Earle E (1998) Biolistic transfer of large DNA fragments to tobacco cells using YACs retrofitted for plant transformation. Mol Breed 4:449–457
156. Wada N, Kajiyama S, Akiyama Y, Kawakami S, No D, Uchiyama S, Otani M, Shimada T, Nose N, Suzuki G, Mukai Y, Fukui K (2009) Bioactive beads-mediated transformation of rice with large DNA fragments containing *Aegilops tauschii* genes. Plant Cell Rep 28:759–768
157. Carlson SR, Rudgers GW, Zieler H, Mach JM, Luo S, Grunden E, Krol C, Copenhaver GP, Preuss D (2007) Meiotic transmission of an *in-vitro*-assembled autonomous maize minichromosomes. PLoS Genet 3:1965–1974
158. Schaefer DG (2002) A new moss genetics: targeted mutagenesis in *Physcomitrella patens*. Annu Rev Plant Biol 53:477–501
159. Li J, Hsia AP, Schnable PS (2007) Recent advances in plant recombination. Curr Opin Plant Biol 10:131–135
160. Terada R, Urawa H, Inagaki V, Tsugane K, Lida S (2002) Efficient gene targeting by homologous recombination in rice. Nat Biotechnol 20:1030–1034
161. Cotsaftis O, Guiderdoni E (2005) Enhancing gene targeting efficiency in higher plants: rice is on the move. Transgenic Res 14:1–14
162. Kumar S, Allen GC, Thompson WF (2005) Gene targeting in plants: fingers on the move. Trends Plant Sci 11:159–161
163. Cai CQ, Doyon Y, Ainley WM, Miller JC, Dekelver RC, Moehle EA, Rock JM, Lee YL, Garrison R, Schulenberg L, Blue R, Worden A, Baker L, Faraji F, Zhang L, Holmes MC, Rebar EJ, Collingwood TN, Rubin-Wilson B, Gregory PD, Urnov FD, Petolino JF (2009) Targeted transgene integration in plant cells using designed zinc finger nucleases. Plant Mol Biol 69:699–709
164. Zeevi V, Tovkach A, Tzfira T (2008) Increasing cloning possibilities using artificial zinc finger nucleases. Proc Natl Acad Sci USA 105:12785–12790
165. Shukla VK, Doyon Y, Miller JC, DeKelver RC, Moehle EA, Worden SE, Mitchell JC, Arnold NL, Gopalan S, Meng X, Choi VM, Rock JM, Wu YY, Katibah GE, Zhifang G, McCaskill D, Simpson MA, Blakeslee B, Greenwalt SA, Butler HJ, Hinkley SJ, Zhang L, Rebar EJ, Gregory PD, Urnov FD (2009) Precise genome modification in the crop species *Zea mays* using zinc-finger nucleases. Nature 459:437–441
166. Townsend JA, Wright DA, Winfrey RJ, Fu F, Maeder ML, Joung JK, Voytas DF (2009) High-frequency modification of plant genes using engineered zinc-finger nucleases. Nature 459:442–445
167. Marjanac G, De Paepe A, Peck I, Jacobs A, De Buck S, Depicker A (2008) Evaluation of Cre-mediated excision approaches in *Arabidopsis thaliana*. Transgenic Res 17:239–250
168. Srivastava V, Ariza-Nieto M, Wilson AJ (2004) Cre-mediated site-specific gene integration for consistent transgene expression in rice. Plant Biotechnol J 2:169–179
169. Chawla R, Ariza-Nieto M, Wilson AJ, Moore SK, Srivastava V (2006) Transgene expression produced by biolistic-mediated, site-specific gene integration is consistently inherited by the subsequent generations. Plant Biotechnol J 4:209–218
170. Luo K, Duan H, Zhao D, Zheng X, Deng W, Chen Y, Stewart CN Jr, McAvoy R, Jiang X, Wu Y, He A, Pei Y, Li Y (2007) "GM-gene-deletor": fused *lox*P-FRT recognition sequences dramatically improve the efficiency of FLP or CRE recombinase on transgene excision from pollen and seed of tobacco plants. Plant Biotechnol J 5:263–274
171. Srivastava V, Anderson OD, Ow DW (1999) Single-copy transgenic wheat generated through the resolution of complex integration patterns. Proc Natl Acad Sci USA 96:11117–11121

Books and Reviews

Deblaere R, Reynaerts A, Hofte H, Hernalsteens JP, Leemans J, Van Montagu M (1987) Vectors for cloning in plant cells. Meth Enzymol 153:277–292

Kado CI (1998) *Agrobacterium*-mediated horizontal gene transfer. Genet Eng 20:1–24

Komari T, Ishida Y, Hiei Y (2004) Plant transformation technology: *Agrobacterium*-mediated transformation. In: Christou P, Klee H (eds) Handbook of plant biotechnology. Wiley, New York, pp 233–288

Slater A, Scott N, Fowler M (2003) Plant biotechnology. Oxford University Press, Oxford

Twyman RM (2006) Gene transfer to plants. In: Primrose SB, Twyman RM (eds) Principles of gene manipulation and genomics. Wiley-Blackwell, Oxford

Twyman RM, Stoger E, Kohli A, Christou P (2002) Foreign DNA: integration and expression in transgenic plants. In: Setlow JK (ed) Genetic engineering: principles and practice, vol 24. Kluwer Academic/Plenum Publishers, New York, pp 107–136

Valentine L (2003) *Agrobacterium tumefaciens* and the plant: the David and Goliath of modern genetics. Plant Physiol 133:948–955

Zupan J, Muth TR, Draper O, Zambryski P (2000) The transfer of DNA from *Agrobacterium tumefaciens* into plants: a feast of fundamental insights. Plant J 23:11–28

Crop Radiation Capture and Use Efficiency

Erik Murchie[1], Matthew Reynolds[2]

[1]Division of Plant and Crop Sciences, School of Biosciences, University of Nottingham, Sutton Bonington, UK

[2]International Maize and Wheat Improvement Centre (CIMMYT), Mexico DF, Mexico

Article Outline

Glossary
Definition of the Subject and Its Importance
Introduction and History
Determination of Radiation Use Efficiency
Radiation Capture by Crop Canopies
"Conversion" of Captured Radiation: Photosynthetic Mechanisms
Metabolic and Regulatory Constraints to RUE
Source–Sink Processes and Partitioning of Assimilates
Theoretical Considerations Related to the Improvement of RUE
Sources of Variation in Agricultural RUE
Future Directions
Bibliography

Glossary

C3 The C3 pathway of photosynthesis, found in most plant species, for example, rice, potato, and wheat.

C4 The C4 pathway of photosynthesis, found in some tropical species, for example, maize, sugarcane, sorghum.

PAR Photosynthetically active radiation. Solar radiation in the wavelength region 400–700 nm.

RUE Radiation use efficiency, the ratio of biomass produced per unit radiation intercepted.

Definition of the Subject and Its Importance

The rate of growth (the rate of the accumulation of dry matter) of all plants is entirely dependent on the interception of energy (electromagnetic radiation) from the sun in the wavelength range 400–700 nm. This energy is utilized by photosynthesis to synthesize carbohydrates and other biological molecules needed for essential plant processes.

The amount of energy intercepted or captured by the whole plant and community system (the canopy) is determined by the organization of leaves into an efficient spatial structure with a large total surface area. The amount of radiation captured will determine the rate of photosynthesis possible and the rate of growth. However, the final growth rate is then determined by *losses* in the system that originate from a number of sources, including the type of photosynthetic mechanism, metabolic and hydraulic constraints, the relationship between photosynthetic source and non-photosynthetic sink organ, variability in environmental conditions, and limitations imposed by management techniques.

The discovery that plant and crop growth is closely linked to the amount of intercepted radiation led to the establishment of methods for measuring radiation use efficiency (RUE). RUE is measured as the amount of dry matter produced per unit intercepted radiation over a given time period and it is often separated into key developmental stages within the life cycle of the crop. It was quickly established that values of RUE tend

to be stable for a given species, growth stage, and environment, but there are important differences across crop species and plant types. In the absence of other factors, RUE will set the theoretical limit to biomass production and ultimately crop yield. It is now accepted that RUE is a fundamental measurement which underpins potential crop productivity and yield and it has become embedded into modern methods of crop growth analysis.

In many cases, plants absorb more photosynthetically active radiation (PAR) radiation than they utilize for growth: given the current emphasis on global food security, there is currently much interest in raising the RUE of key crops in important agroecosystems.

Introduction and History

All green plants use sunlight as their sole energy source for assimilation of carbon dioxide into carbohydrates. At its most fundamental level, this process is the formation of energy-rich bonds in a form that is easily stored, transported, and utilized in most essential plant functions. This process is of course photosynthesis and it is the sole supplier of energy for almost all human nutrition and fuel requirements, via current and prehistoric photosynthesis.

The continuing expansion of the human population and the steady increase in consumption per capita is placing pressure on land availability. A variety of factors including urbanization and the erosion of existing land certainly necessitate production of more food and fuel per hectare with fewer inputs (water, fertilizer) and all of this within the uncertainty of changes in climate and increased pressure to use land which may be currently unsuitable for cultivation. For example, 700 million people depend on rice for calorific intake. Each hectare can currently feed around 27 people; by 2050 this will have to rise to 43 people per hectare [1]. This is compounded by the fact that Asian rice yield potential appears to be stagnating [2]. Wheat is grown on over 200 million hectares of land providing approximately one-fifth of the total calorific input of the world's population, and while there have been steady increases in productivity since the green revolution, global demand for wheat is predicted to increase at a faster rate than the annual genetic gains that are currently being realized [3]. Since the highest yields of major crops are usually only achieved within high input systems, it is not surprising that many suggest a reappraisal of the basis of crop productivity.

It seems clear that an increase in the rate of application of fertilizer or water is neither desirable nor even possible. Nitrogen fertilizer is heavily dependent on the continued availability (physically, financially, and politically) of fossil fuels. Water is increasingly scarce not just in equatorial regions but in temperate regions. One way to improve resource use efficiency is to increase the rate of overall biomass production and this is starting to be associated with yield progress of major crops such as rice and wheat [3, 4]. As shall be described, an increase in biomass production by crops, whilst helping to improve upon current rates of breeding progress in yield potential, would also (1) underpin future genetic improvements in adaptive processes, (2) improve the relative efficiency of resource use in terms of biomass production per unit water, light, and fertilizer, and therefore (3) increase the attractiveness of using waste products of arable crops for secondary uses such as fuel, and (4) if applied universally, reduce the competition for land between biofuel crops and food crops, and (5) increase the feasibility of using marginal land for fuel and food production.

A History of Radiation Use Efficiency

Given that it underlies so much of human activity and endeavor it is perhaps curious that the relationship between radiation and plant growth did not become explicitly defined and quantified until relatively recently. It has been suggested that a tendency to retain methods of classical crop growth analysis during the first half of the twentieth century delayed a mechanistic analysis of the processes of biomass accumulation [5]. In these early studies, growth (crop mass) was described as a function of time possibly because of the ease with which mass could be measured through the growing season. This approach was confounded by its inclusion in measurements of relative growth rate where crop biomass increase is closely related to existing biomass. The central role of light interception in growth was recognized by Watson [6] who suggested a measurement of net assimilation rate which worked in some situations but did not adequately account for the complex relationship

between leaf area and variation in assimilation rate (photosynthesis) of individual leaves.

Another advancement in understanding came with the consideration that efficiency of light use declined at high levels (light saturation) [7, 8] and that light levels were lower at the base of the canopy. In fact, as pointed out by Hirose [9], the first mathematical model of canopy photosynthesis was first produced by Monsi and Saeki in 1953 but this was not recognized for more than a decade. This resulted in the first real considerations of growth as a function of the amount of light intercepted by the plant canopy. At this time, it was observed that the amount of light intercepted by the canopy was closely related to dry matter accumulation [5]. Despite this there were many studies in the 1970s which used incident light rather than intercepted radiation to make key studies in agronomy and ecology.

The sole use of incident radiation measurements will lead to errors in the calculation of radiation use efficiency especially before canopy closure when not all radiation is absorbed and when crops possess differing rates of canopy development. Over the whole life cycle of the crop, the proportion of incident radiation that is intercepted and available for assimilation can be quite small. It was not until the mid 1970s that John Monteith established the relationship between accumulated intercepted radiation and accumulated biomass within canopies [10]. This was accompanied by experimental data demonstrating a level of conservation of radiation use efficiency of crop species when grown under optimal growth conditions with high resource availability and a consideration of the role of leaf photosynthetic capacity in crop canopies. This has since proved to be a robust approach and has remained a central feature of crop growth analysis ever since. Many studies attempted to provide values for RUE across a wide range of species and growth conditions across the world [11, 12]. It was quickly claimed (1) that it was possible to attain consistent values for a given species when growing conditions were good, (2) that suboptimal (e.g., nitrogen or water deficient) or stressful conditions caused RUE to decline, and (3) that there were clear differences between crop species: plants possessing the C4 photosynthetic mechanism had the highest RUE followed by most C3 plant species and finally legumes with the lowest RUE values. Early data suggested that RUE was a conservative or even constant value for a given species. However, data published since has demonstrated significant variation and it has been pointed out that close attention in each case must be paid to the methods of analysis, growth conditions, developmental phase, and genotype.

RUE is commonly used within the crop sciences although it is applicable to growth of any autotrophic organism and most ecosystems. Its calculation requires knowledge of the amount of radiation absorbed in a given time period and measurement of the resulting biomass and energy content. These are easier to measure in a uniform system like a monoculture. The historical development of RUE was no doubt dependent on the advancement in other areas of science such as photosynthetic regulation and the technical development of instruments to accurately measure key attributes, that is, radiation, photon flux density, and the rate of photosynthetic carbon assimilation.

The understanding that RUE is fundamental to crop productivity leads naturally to the question of whether it can be improved. The observation that C4 plants possess a higher RUE leads to the notion that such a change would give a higher biomass productivity which could be exploited to increase yield per hectare. The green revolution provided a step change in agricultural productivity that was able to prevent the tragedy of mass starvation in some regions and also to support population increase. As outlined here, a step change of similar magnitude now would probably require an improvement in RUE.

Determination of Radiation Use Efficiency

RUE is the ratio between accumulated plant biomass and the accumulated radiation intercepted by the crop. A note on terminology: some authors use the terms "radiation conversion factor" [13] and "radiation conversion efficiency." Some authors have pointed out that use of the word "conversion" is inappropriate because energy is not being directly converted to matter but rather converted from one form of energy to another (i.e., solar radiation to higher energy state of chlorophyll molecules) [5]. The term radiation use efficiency (RUE) shall be used.

To calculate RUE, it is necessary to know the amount of radiation arriving at the top of the canopy, the amount of radiation intercepted by the canopy, and

the biomass accumulated during a given period. In many studies, the energy content of the dry matter is also required. This section will summarize how RUE is measured in a practical sense and tackle some of the diversity in approaches that have been taken.

Radiation arrives at the edge of the earth's atmosphere at a mean rate of 1.4 kJ m^{-2} s^{-1}, the so-called solar constant. By the time photons reach the earth's surface a number of geometrical and atmospheric factors have reduced this value significantly. Cloud cover notwithstanding the greatest influx occurs in tropical regions at low latitudes. The greatest measured flux at the earth's surface itself occurs in low latitude regions where cloud cover is minimal (20–30°). High latitudes can have extremely low solar radiation levels.

Light is absorbed and scattered by molecules, aerosols, and particles in the atmosphere, reducing flux even further. Gas molecules such as CO_2, H_2O, and CH_4 absorb energy at specific infrared wavelengths whilst gas molecules O_2 and O_3 absorb at lower wavelengths. Photosynthesis is restricted to a range of wavelengths that approximate to those visible to the human eye: 400–700 nm. Higher wavelengths do not contain sufficient energy to drive photosynthesis. At ground level, this range of wavelengths makes up 49% of total solar energy. In other words, the photosynthetic process does not use over half of the energy available. However, longer wavelengths have an important heating effect which raises plant tissue temperature and accelerates metabolic and developmental processes such as leaf and canopy construction.

Variation from day to day means that it is necessary to integrate measurements of radiation over long time periods. This is often done by positioning devices above the canopy and below the canopy. Most commonly these have been fairly inexpensive tube solarimeters connected to a device that continually stores data produced. Reflection can be measured by inverting the device. Instantaneous measurements (spot measurements) of fractional interception (f) are also used but these can be misleading because they are most reliably taken at midday during the same, usually sunny, conditions and therefore do not account for cloud cover or low solar elevation and give lower values of f.

The proportion of PAR is higher in scattered light than direct beam radiation and so it is useful to distinguish between the two and a few commercially available devices are capable of doing so. This also means that the proportion of PAR changes according to solar elevation, although it is around 0.45 at elevations greater than 30° [5]. Growth in predominantly scattered radiation commonly causes an increase in RUE.

Wavelengths used for growth (400–700) are preferentially absorbed by chlorophyll within the canopy resulting in transmitted light that is depleted in red and blue and enriched in far-red. The formula for fractional interception is presented in its simplest form by Eq. 1.

$$f = 1 - \frac{(I + r)}{Io} \tag{1}$$

where f = fractional interception, Io = incident radiation, r = reflected radiation, I = intercepted radiation.

An alternative method for measuring f is spectral reflectance. This compares reflectance from the canopy in the red band and the near IR band to produce a normalized difference vegetation index (NDVI). It has been possible to show the relationship between NDVI and f in many crops [14] and is a technique that is possible to use remotely from satellites and aircraft. Although it is clearly convenient and rapid, one must be aware that it has the drawback of being a spot measurement. Measurements made from satellites suffer from problems of images that deviate from 90° to the earth's surface [15].

Photography is also used to estimate f using a camera fitted with a fish-eye lens positioned below or above the canopy. This has the advantage of encompassing a large area, producing permanent image and being taken rapidly in the field. This method has been shown in many cases to correlate with f measured using solarimeters; however, errors arise due to common bias in positioning the camera. All indirect measurements of f should consider the potential errors that may result.

RUE is usually calculated by measuring the difference in biomass between many consecutive harvests (i.e., accumulated intercepted growth) and plotting this against the measured accumulated intercepted radiation. This is usually a linear relationship and RUE is calculated as the slope of this relationship (Fig. 1). The points at which measurements are made are critical because RUE varies according to developmental state.

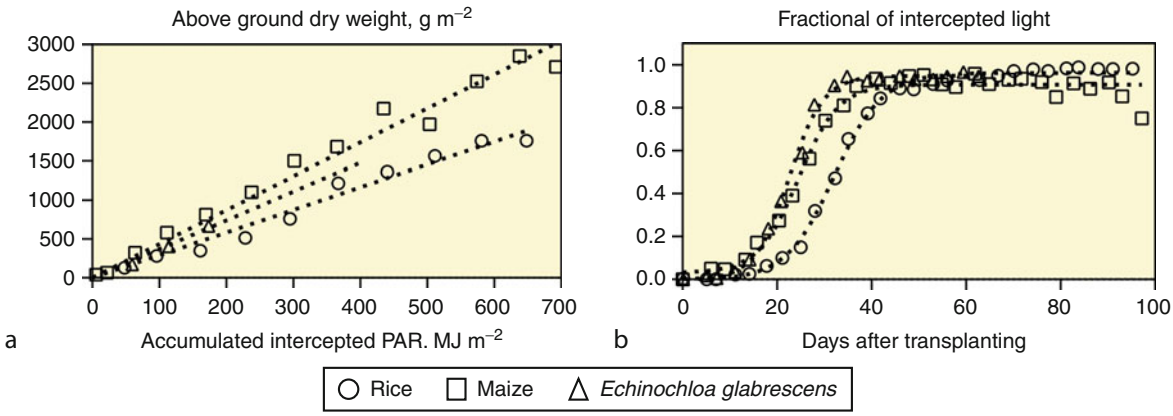

Crop Radiation Capture and Use Efficiency. Figure 1
An example of the relationship between accumulated intercepted radiation and accumulation of dry matter by three species : the C3 crop rice (*circle*), the C4 crop maize (*square*), and the C4 weed *Echinochloa glabrescens* (*triangle*). Note the higher slope for maize in (**a**), that maize reached full interception before rice in (**b**), and that the weed is the first to form a full canopy but does not achieve the same amount of biomass as the crop species (Redrawn from Sheehy et al. [1])

Care must be taken when comparing values from different sources [5, 13]. Some of the common sources of variation are as follows:

1. If root mass is not included then RUE values will be lower. However, it is extremely difficult to measure root mass directly and it is often ignored or assumed to be a fixed percentage of total plant mass. Nonuniform growth can therefore be a significant source of error. Energy required to grow and maintain roots is also a function of the biotic and abiotic environment of the soil.
2. Solar radiation flux density is measured using solarimeters, pyranometers, or radiometers which usually cover the wavelengths 300–3,000 nm. The photon flux density is commonly measured using sensors that detect within the photosynthetically active range of 400–700 nm. Therefore the conversion between energy and quanta-based measurements must take into account the energy of each waveband. Data based on different regions of the electromagnetic spectrum can cause inaccuracies, for example, the transmission of shortwave radiation through canopies differs from that of PAR [16]. However, the solar spectrum is fairly constant, and the reliable figure for this is 4.6 μmol quanta. Inaccuracies can arise from badly positioned, poorly leveled or uncalibrated instruments. It is common practice to keep devices free of anything that would attenuate radiation in a way that would bias the results, for example, dead leaves are removed and glass is cleaned.
3. It is important to distinguish *absorbed* from *intercepted radiation*. The latter does not take into account the reflection of PAR from the top surface of the canopy. This is generally assumed to be about 5% of total PAR but variation is likely. Not all of the plant tissues that absorbed energy are necessarily alive or of equal photosynthetic potential.
4. When comparing different species of plant with contrasting harvest organs it is important to consider the *energy content* of the organs involved. Lipid has a higher calorific content than protein, which in turn has a higher calorific content than carbohydrates [17]. The heats of combustion of carbohydrates, proteins, and lipids are 17.3, 22.7, and 37.7 kJ g^{-1}, respectively. Since RUE is comparing the input of energy to the output of dry matter it can vary according to the energy content per unit dry matter and it is essential to adjust RUE accordingly. For example, the RUE of crops that produce particularly oily seeds should decrease during the seed-filling period. However, the nutrient content of plant tissue does not greatly directly influence the measurement of RUE.

5. The stage of growth can have a large influence on the RUE measured (see section Source–Sink Processes and Partitioning of Assimilates). It can be common practice to calculate the RUE over the entire growing season but this does not necessarily represent the maximal RUE value. For example, in many crops RUE appears to be steady during the vegetative period but to decline following the onset of the reproductive phase.

Radiation Capture by Crop Canopies

Canopy structure and therefore the efficiency of light capture was a common feature in the domestication and the later improvement of many crop species. For example, the reduction of branching in maize and sunflower allowed dense planting [18] and there is evidence of further adaptation to higher planting density [19]. The reduction in height of cereals was a key factor in the green revolution, permitting an increase in harvest index and reduction in lodging. Crop canopies must intercept or capture as much radiation in the 400–700 nm bandwidth as possible. Most of the light interception occurs by leaves; however, stems, petioles, leaf sheaths, and reproductive structures can also absorb significant amounts of radiation. To achieve high interception, they must construct and present a canopy with large leaf area and in many crops the minimum leaf area index (L: the ratio of leaf area per unit ground area) is around three. The L can be expressed by the product of the number of plants per unit ground area, the number of leaves per plant, and the mean area of leaves per plant (plus green stem area). Light can penetrate the canopy and strike the ground below as direct beam radiation (so-called sunflecks), scattered radiation, or radiation that has passed through leaves and other plant organs, that is, transmitted. The amount of penetrated radiation is dependent on the three-dimensional arrangement of leaves in the canopy and for a given L will be a function of a large number of features such as leaf size, leaf density per cubic meter, the angle of individual leaves, heterogeneity of leaves in space (clumping), leaf thickness, and albedo. There is clear variation between species and even between crop varieties in these features. Additionally, it is possible to alter these features through management techniques such as planting density and the application of NPK fertilizer. Therefore there needs to be a way of describing radiation distribution within canopies mathematically and linking this to agronomic characteristics such as leaf area index and nitrogen content.

The relationship between L and fractional interception can be described by Monsi–Saeki equation (Eq. 2), a modification of Beer's law. This assumes that the canopy is a homogeneous medium whose leaves are randomly distributed in space, that is, there is no effect of row structure or clumping and under these conditions Beer's law will apply [9]. The Monsi–Saeki equation can be applied if the canopy is considered to be divided into horizontal layers with each layer possessing a particular L and the irradiance within each layer is measured. The irradiance at each layer will depend on the three-dimensional characteristics of the leaves both within that layer and the layers above. It has been found that this provides an accurate estimate in many crops in which this has been measured: $\ln(I/Io)$ against L provides a linear relationship, the slope of which gives the value k which provides a simple but useful mathematical description of the architecture of the crop canopy in question.

$$I = Io \exp(-kL) \tag{2}$$

I and Io as in Eq. 1, L = leaf area index, and k = extinction coefficient for a given waveband

Crops have been found to vary for the value of k and the major feature is the erectness of leaves. Canopies with erect and narrow leaves such as cereals have a lower value of K than those with flat, broad, and horizontal leaves. This also applies to differences within species, for example, rice varieties vary in erectness [20].

If the Monsi–Saeki equation holds and the k value for a given canopy type is known then it becomes possible to calculate f simply from a knowledge of L (Eq. 3).

$$f = 1 - \exp(-kL) \tag{3}$$

Equation 3, letters as Eqs. 1 and 2

This analysis is useful when canopies are considered to be a three-dimensional "box" of vegetation with radiation penetrating only from above. It can fail where plants are sparsely populated and do not achieve full ground cover or are simply planted in rows with space in between, which is the case for some crops that are tended by hand. The calculation of intercepted

radiation in these cases can become quite complex and impractical at high levels of heterogeneity although estimations are often made on the basis of incident radiation and leaf area per plant. Another source of error is angle of solar elevation which can significantly alter the proportion of reflected light and the proportion of scattered light within the canopy. It also does not account for the commonly seen variation in leaf angle that occurs between the top and the bottom of the canopy. Even at a point close to full canopy cover there can be a "bimodal" type of variation in crop canopies. For example, rice plants tend to form "inverted cone" shapes and this causes a complex three-dimensional variation in irradiance distribution especially during canopy development.

The optimal "design" of plant canopies must consider not just maximum interception but also the relationship with photosynthetic rate. In principle, a plant could achieve close to 100% interception with a single, planar chlorophyll-rich leaf and a L of 1.0. However, this does not result in optimum productivity largely due to the fact that photosynthesis saturates below full sunlight and this is especially marked in C3 plants. This is a central point: the response of leaf photosynthesis to irradiance is shown in Fig. 2. This is a useful measurement and easy to make with today's equipment. It provides not only a measurement of the maximum rate of photosynthesis (Amax) but also the potential quantum yield of photosynthesis.

A greater canopy carbon gain is achieved by reducing the proportion of leaves in the canopy that exist in the light-saturated state. The leaves lower in the canopy are retained at light limitation while those at the top will be prone to light saturation. If the irradiance increases (e.g., moving from cloud-cover to full sunlight) then those lower in the canopy will be able to respond accordingly. This has lead to the widely observed phenomenon that when irradiance is plotted against carbon-gain (photosynthesis) one commonly observes a linear response for canopies but a saturation in leaves (normally described by a non-rectangular hyperbola) (Fig. 3) [11]. This is important: if canopies demonstrated light saturation then this would severely limit their ability to improve RUE.

Canopy Properties and Photosynthesis

The optimum design for biomass production in terms of carbon gain is predicted to be one that permits

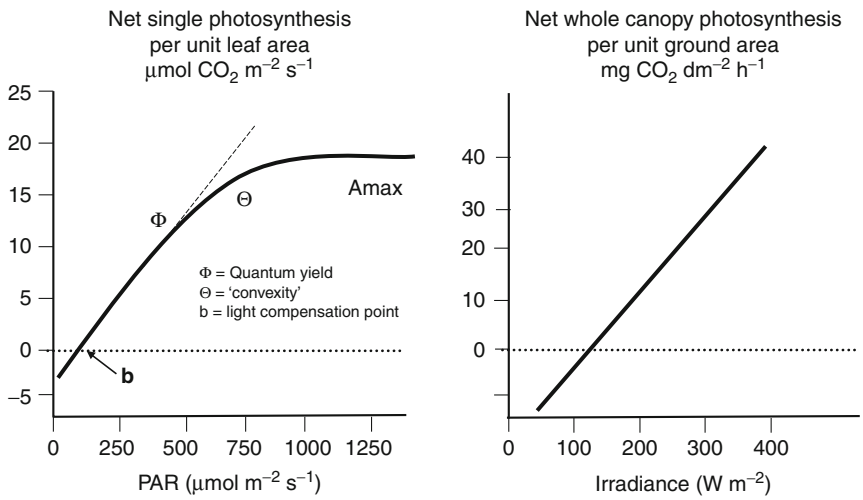

Crop Radiation Capture and Use Efficiency. Figure 2
The relationship between photosynthesis and *incident* radiation levels for (**a**) single leaves and (**b**) a full canopy: (**a**) typical features of the leaf response, the linear phase (maximum quantum efficiency), the light compensation point, convexity, and the light saturated rate (Amax, and (**b**) schematic figure: note the linear response of whole canopies in comparison to single leaves

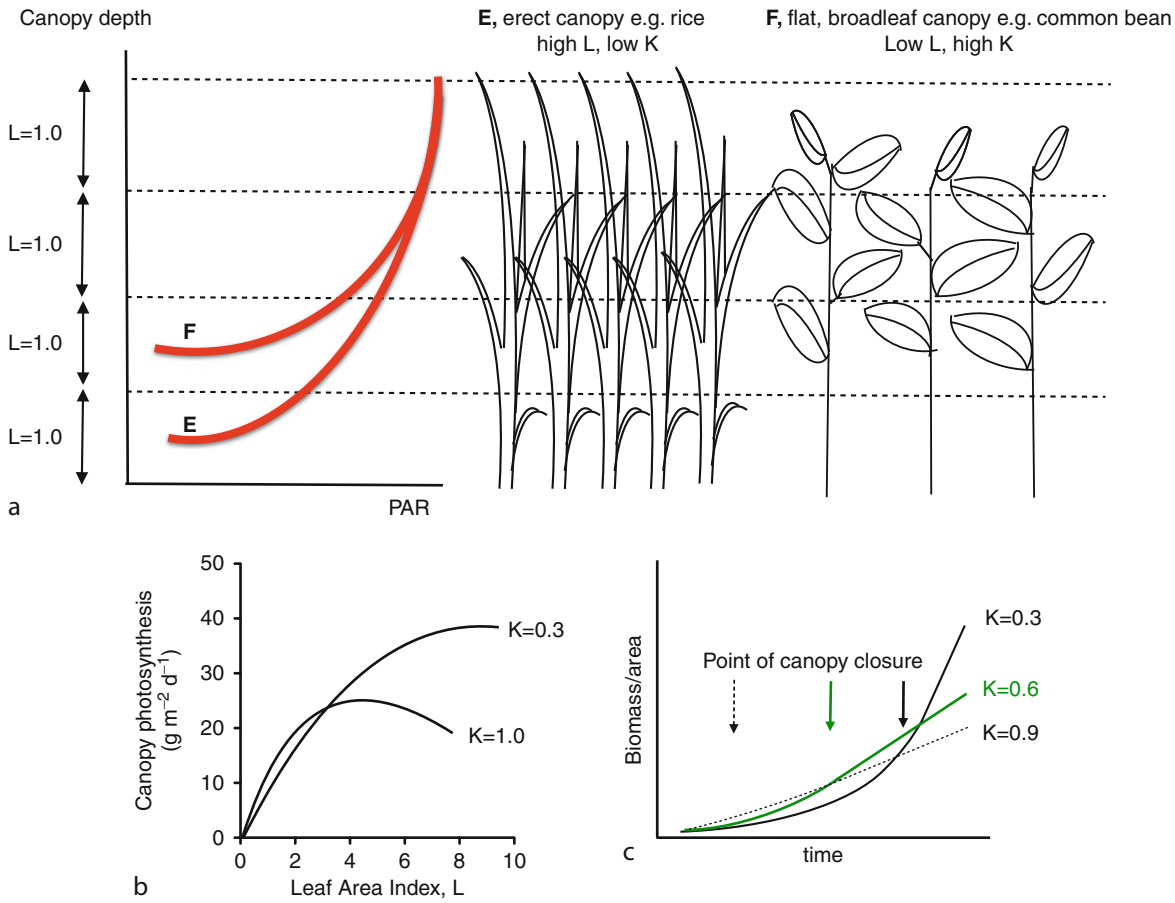

Crop Radiation Capture and Use Efficiency. Figure 3
Canopy structure and function according to leaf "architecture." (**a**) The schematic figure on the *left* shows canopy depth where the canopy has been divided into layers, each with a leaf area index (*L*) of 1.0. Attenuation of light in the canopy follows the Monsi–Saeki equation. For a broadleaf canopy, the radiation reaches extinction at a higher point and a lower *L* compared to an upright canopy. The canopy extinction coefficient value "*K*" is derived from Eq. 2 and provides a mathematical description of the link between *F* and *L*. (**b**) The calculated relationship between canopy photosynthesis and *L*, measured at irradiance saturating at the top of the canopy for species with two values of *k*. Note the higher maximum value of the species with higher *k* (Redrawn from [9]). (**c**) A highly schematic figure redrawn and adapted from Ong and Monteith [32] and shows the theoretical differences in canopy biomass accumulation over time in species with different values of *k*. Maximum values of carbon gain are achieved after canopy closure which occurs earlier in broadleaf species (high *k*). Species with a lower value of *k* have higher potential rates of total canopy photosynthesis

a higher proportion of radiation to penetrate to lower layers, whilst also reducing light saturation at the top (Fig. 3). Indeed, this seems to be the trend in species such as rice and wheat although the advantage here is thought to be greatest at lower latitudes where light is overhead for a greater proportion of the year and therefore penetration into the canopy is greater. This also has the advantage that it prevents the unwanted senescence of leaves when light levels drop below or close to the light compensation point [21].

This raises the question of whether there is room for improvement in canopy architecture to improve RUE. Early work found that canopies with a low *L* benefitted from horizontal posture while those with high *L* benefitted from upright posture [5, 22]. This work suggested that RUE would not be sensitive to extreme

upright posture of leaves. However, it is clear that upright leaves are associated with the highest yielding lines in wheat [23, 24] and it has been suggested that some cereal canopies may benefit from increasing erectness further [3, 23, 25]. There are relatively few genes controlling erectness and this should be straightforward to test, although work has shown that compensatory effects such as leaf size may be hard to account for.

Modern high-yielding rice lines also have highly erect leaves and it is assumed that this also results in higher potential productivity. In rice, this also permits denser planting which accelerates canopy closure and improves total radiation intercepted over a short tropical growing season.

A further feature is that leaves have different characteristics according to the light intensity to their canopy position. Most notably they have "sun leaf" and "shade leaf" characteristics, the former having higher light compensation points, higher photosynthetic capacity, and higher nitrogen and enzyme content. This is considered to be an efficient use of resources with nitrogen being located only where it is required for high photosynthetic activity. Additionally, there are a number of acclimation mechanisms to improve light harvesting in shade and diffuse light such as the synthesis of light harvesting complexes enriched in chlorophyll b [20, 26]. The efficiency of use of shade and diffuse light within the canopy is a relatively unexplored area in crops. This raises the question of whether leaf ageing or leaf acclimation gives rise to the nitrogen content of the leaf. There is evidence that both processes are at play: in fact the distribution of nitrogen in plant canopies should be closely related to photosynthesis and irradiance level [27, 28]. There is some indication that this has been achieved although the role of "storage" of assimilated nitrogen in leaves needs further analysis [20, 21].

Canopy development occurs by the successive emergence of leaves from primordia which are localized points of tissue formed around the apical dome of the vegetative shoot. The arrangements of these primordia will largely determine the positions of the leaves in the final canopy. Therefore there is great interest in the genetic manipulation of developmental processes in crops [29, 30]. The thermal time interval between the initiation of successive primordia is critical and determines the time taken for production of successive leaves. The genetic and molecular processes determining leaf development and expansion is an exciting area of research [31].

For annual crops with a limited growing season, it is critical that canopy development is synchronized with periods of high radiation. In temperate regions, low temperatures in Spring can increase the time taken for canopy closure. Since maximum rates of production are not attained until full canopy cover is achieved, this can be deleterious and is referred to as "lost time" [32]. Faster rates of canopy closure can be achieved by different strategies such as the application of nitrogen increasing planting density, irrigation, and the planting of crops in autumn so that the time taken for establishment is reduced. For example, in the UK, maximum radiation receipts occur in June, and for Spring-sown crops such as potato and sugar beet, productivity can depend on the establishment of a high L before this period. In rice, the remarkable erectness of leaves in some modern cultivars has allowed for extremely dense planting and a shift toward a reduction in tillering. This has the advantage that canopy closure can be achieved quickly and the so-called lost time is reduced.

There is no doubt that canopy structure is a central feature of crops with high RUE although the precise three-dimensional characteristics are difficult to quantify by direct measurement and this has meant that the techniques to describe crop canopies mathematically have remained relatively simple and continued to assume that they exist as randomly distributed photosynthetic elements in space. As shall be described in the next section, it will be essential to have a more sophisticated approach which links leaf arrangement and light distribution at higher resolutions and accounts for the dynamics of both light distribution and localized photosynthetic responses. For this various photographic and laser-based methods are available for "digitization" of plant and crop canopies although the high density of many crop canopies makes such measurements difficult in a practical sense. Mathematical modeling of plant canopy structure is progressing rapidly along with increased computing power and more sophisticated programming [33]. It would seem likely that methods that can use empirical measurements to model canopy architecture at high resolution and accurately predict photosynthetic light responses are not far away.

"Conversion" of Captured Radiation: Photosynthetic Mechanisms

The efficiency of radiation use by the whole canopy is the sum of photosynthesis occurring by each leaf and each leaf portion within the canopy. In turn, the photosynthetic rate of each leaf is determined by the sum of photosynthesis in the chlorophyll-containing organelles (chloroplasts). Each leaf and organelle will exist in a dynamic microenvironment and the photosynthetic productivity will depend on the resources available to it at a given moment in time (light, water, nutrients). Due to limitations placed on the photosynthetic process such as light saturation and CO_2 diffusion, the rate of photosynthesis at the leaf level is a strong determinant of canopy carbon gain. This section will describe the photosynthetic process, the different types of photosynthesis, and limitations to leaf level photosynthesis.

The vast majority of chloroplasts are located in leaves and they are numerous, with each mesophyll cell containing between 50 and 200 chloroplasts [34]. Chloroplasts are responsible for absorption of the 400–700 waveband in crop canopies and are the reason that plants appear green. They are sac-like subcellular organelles that contain membranous structures that possess the chlorophyll used for light harvesting. Most of the chlorophyll is contained within pigment protein complexes called "light harvesting complexes" and these are extremely efficient at absorbing visible light, and through a series of resonance transfer mechanisms, they pass the excitation energy to a reaction center where a special pair of chlorophyll molecules use this energy to generate a redox potential capable of oxidizing water via the oxygen evolving complex. The resulting electrons are passed through an electron transport chain and used to generate a proton gradient that synthesizes ATP. Ultimately, the electrons produce a reductant, NADPH. The NAPDPH and ATP are utilized within the Calvin–Benson or photosynthetic carbon reduction cycle to reduce CO_2 to triose phosphates that are used in hexose and starch synthesis or exported from the chloroplast for sucrose synthesis.

How Efficient Is Crop Photosynthesis?

It is useful to consider the amount of light energy arriving at a canopy top or leaf surface and calculate energy losses at each stage based on current knowledge of the photosynthetic process in order to estimate the potential system productivity [35, 36]. As mentioned, only 49% of solar energy is available for photosynthesis. Within the PAR range chlorophyll does not absorb strongly in the green band and the reasons for this adaptation have been well explored [37]. Green photons make up around 10% in the PAR range. Red and blue photons drive photosynthesis with equal efficiency despite the fact that blue light contains more energy per photon than red light. Chlorophyll is excited to higher energy states by blue photons but the extra absorbed energy is not used to drive photochemistry. This extra energy which is calculated to make up 6.6% of incident solar energy is effectively lost [36].

C3 photosynthesis is the dominant form among plant life which uses the enzyme ribulose bis phosphate carboxylase (Rubisco) to fix CO_2 where the initial product of photosynthesis contains three carbon atoms. Rubisco is part of the Calvin–Benson cycle. Examples of C3 crop species are rice, wheat, potato, soybean, cotton, and chickpea. In C3 photosynthesis, three ATP molecules and two NADPH molecules are used to assimilate one molecule of CO_2 and regenerate the acceptor, RuBP. Zhu et al. [36] provide a calculation of the energy required to fix one carbon atom and compare this to the energy contained within that one-sixth of a mole of glucose. A calculation of the quantum requirement of each ATP and NADPH molecule reveals that 8 mol of photons are needed for the fixation of CO_2 molecule and this represents 1,388 kJ of energy [36] whilst the energy content of this carbon atom within the glucose molecule is 477 kJ.

C3 plants operate the process of photorespiration. This is a consequence of the dual reaction of Rubisco: in addition to the fixation of CO_2 into carbohydrates, Rubisco also reacts with O_2 to produce glycolate. This molecule must be metabolized through the photorespiratory pathway, a process that consumes ATP, reducing power and releases CO_2. The product of this is phosphoglycerate which reenters the Calvin–Benson cycle. The losses caused by photorespiration are significant and are greatly dependent on temperature: the specificity of Rubisco for CO_2 and the solubility of CO_2 relative to O_2 in water declines with increasing temperature. In tropical C3 plants the rate of photorespiratory flux can be significant especially when stomata limit the internal leaf CO_2

concentration. In tropical rice in field temperatures of 35°C under otherwise optimal conditions, saturating leaves with CO_2 resulted in an increase in leaf photosynthesis of over 40% [38].

A subset of plants called C4 plants have evolved a fascinating mechanism which minimizes the oxygenase reaction of Rubisco to often insignificant levels. It does this by restricting Rubisco to a bundle sheath cell, which is oxygen free and non-leaky. Initial fixation of CO_2 takes place in mesophyll cells using an alternative enzyme, phosphoenol pyruvate carboxylase which generates C4 acids. These acids are pumped into the bundle sheath cell where they are de-carboxylated, and the CO_2 released is concentrated around Rubisco in the bundle sheath chloroplasts. This effectively reduces the extent of the oxygenase reaction and the photorespiratory pathway to insignificant levels. It is thought to have evolved in a climate where high temperatures, low CO_2 levels, and low humidity could all have been strong selective pressures. The C4 mechanism is largely found in warm regions. Measurements show that in many plants the advantage of the C4 mechanism over C3 starts to become particularly significant at growth temperatures above 25°C. C4 requires additional ATP synthesis which increases the quantum requirement of the photosynthetic process to 12 photons per CO_2 molecule, in comparison with 8 for C3 photosynthesis. However, this is more than overcome by the elimination of photorespiration and low activity of Rubisco resulting in a greatly enhanced capacity for carbon assimilation at most light intensities in C4 plants. Other advantages become apparent, for example, the higher efficiency of Rubisco means that lower amounts of this protein are needed. Since Rubisco can make up to 35% of total leaf protein in some C3 plants [20], this increases the photosynthetic nitrogen use efficiency of C4 plants. The CO_2 concentrating mechanism of C4 plants means that stomatal conductance does not need to be high and water loss can be reduced.

A substantial "loss" of biomass is mitochondrial respiration which has often been divided into growth respiration and maintenance respiration in accordance with the associated physiological process. Respiration is unsurprisingly difficult to measure and to define in practice [39]. The relative rates can vary substantially according to growth stage. For example, maintenance respiration increases substantially as a proportion of total carbon flux following ear emergence in barley [35]. During vegetative growth, growth respiration is substantially higher than maintenance respiration. Respiration as a whole can vary from 30% to 60% of total carbon exchange and therefore it has a significant impact on RUE. Studies have shown that it undergoes optimization according to the environment and developmental state: for example, it is well known that the relationship between L and respiration is not linear because this would result in a negative net carbon balance in the lower, shaded regions of the canopy. Attempts have been made to optimize respiratory rates to improve crop productivity but this is a difficult task because of the problems with measurement (especially with roots) on different scales from tissue to whole canopy, and of the separation between maintenance and growth respiration. It is often considered that there is greater scope for the improvement of maintenance respiration because this is more sensitive to prevailing conditions. Recent work suggests that the possibilities should be revisited [39, 40].

At any given moment in time photosynthesis can be limited by light level (e.g., under cloud cover or self-shading), stomatal conductance (this becomes severely limiting under conditions of low soil water), and Rubisco (under saturating irradiance and high stomatal conductance Rubisco limits photosynthetic rate in C3 plants). Interactions between growth condition and genotype will determine the final rate of photosynthesis. Growth under optimal conditions is considered: the imposition of resource limitation on RUE will be discussed in the final section.

Taking into account the minimum essential losses that occur, the percentage of "biomass energy" produced per unit solar radiation (total solar spectrum) for C3 and C4 plants is generally agreed to be 4.6% and 6%, respectively (calculated on a kJ/kJ basis) [36]. The highest recorded values are 2.4% and 3.7% [36] with common measured values being much lower than this, for example, [41]. The large difference between measured and attained photosynthetic efficiency of crop canopies is the cause of some debate and some mechanisms focusing on metabolic constraints are discussed here. It is possible that canopy architecture remains a limitation (discussed above). It is however noted that much of the observed reduction in RUE and

photosynthetic efficiency in agricultural systems is caused by growth under suboptimal conditions [36].

The above has considered photosynthetic efficiency in the context of a leaf canopy. However there is current interest in exploiting photosynthesis in non-leaf organs such as the green ear in wheat [42, 43] and the spikelets in rice. Despite the relatively small surface area (compared to LAI) it seems clear that the high exposure to radiation and close proximity to the grain sink may mean that their photosynthetic contribution has been underestimated [42]. In the case of oil seed rape, the photosynthesis in seed pods is the dominant supply due to a diminished leaf area [44]. This is a source of photosynthate that deserves closer investigation.

Metabolic and Regulatory Constraints to RUE

Although photosynthesis underpins growth and yield it has often been considered that it is a feature of primary metabolism which has undergone optimization through natural selection and empirical breeding. This view has partly arisen from the conservative nature of the basic mechanism and composition of the photosynthetic apparatus. However, firstly, it is clear that canopy photosynthesis has undergone improvement via total leaf area and nitrogen per unit leaf area (fertilizer) and, secondly, there is considerable genetic variation in leaf photosynthetic capacity and in the response of leaf photosynthesis to environmental factors and abiotic stress. Nevertheless, the role of any improvement in leaf photosynthesis in crop yield progress has been hard to quantify due to the difficulty of routinely measuring net leaf and canopy carbon gain and of eliminating compensating processes, although some success has been achieved [24, 45, 46]. and photosynthesis has been successfully linked to yield progress in some cases, for example, [24]. There is some recent evidence that leaf photosynthesis can exert an effect when biomass production is the dominant limiting factor [47–49]. Nevertheless leaf photosynthesis is considered to be the dominant factor determining RUE [5] and its improvement is increasingly viewed as an important target [49, 50].

Many of the suggested routes to the leaf CO_2 assimilation rate of crops have focused on Rubisco. Increasing the amount of Rubisco in the leaf is problematic: it is already at extremely high levels and to accumulate more would require an increase in nitrogen fertilizer application. There are indications that Rubisco may be accumulated to excess capacity in some leaves [51]. There may be opportunities to improve the properties of the Rubisco enzyme [52] and there is some natural variation among plants and algae in the properties of Rubisco. For example, forms of Rubisco present in the genus *Limonium* have a higher specificity factor than that in all crop species [53]. However, there is a well-cited inverse relationship between specificity for CO_2 and maximum catalytic activity [54]. It has been suggested that different forms of Rubisco could be assigned different roles within the plant according to environmental condition, tailored, for example, to high light or low light conditions. Other enzymes in the Calvin–Benson cycle have been shown to have promise for improvement such as sedoheptulose-1,7-bisphosphatase [55].

Elimination or reduction in photorespiration has been of interest for a long time even though the seemingly wasteful process has been assigned metabolic and photoprotective roles. The increased growth rates, biomass, and yield of plants grown under high CO_2 where photorespiratory flux is reduced indicates that the process is largely wasteful. Methods for blocking the pathway have proved ineffective [56] probably due to the accumulation of intermediates. A recent and novel approach has avoided this problem by using bacterial enzymes to "shortcut" the pathway [57]. In *Arabidopsis thaliana* plants, this has had the effect of improving biomass production and shows great promise although the precise mechanism of improved growth has not been described yet.

The greatest improvements in yield of crops native to warmer climates would come from the introduction of the C4 mechanism into C3 crop species. In the case of rice, for example, it has been calculated that this is the only way to bring about an increase in biomass production sufficient to meet a 50% improvement in yield by 2050 [1, 58]. Early attempts to introduce elements of the C4 pathway into rice by transformation with C4 genes from maize or other C4 species [59] are considered ambiguous or partially successful at best and introduction of the full "Kranz" anatomy seems to be the most likely way to achieve the required goal. Some natural C4 mechanisms exist in a single cell [60] but it is unclear whether this would provide sufficient rates of assimilation.

The evolution of the C4 syndrome independently on more than 60 occasions in angiosperms would suggest there is no intrinsic reason why the C4 pathway could not be introduced into a major crop such as rice or wheat. A combination of advanced molecular techniques, transformation of key genes and smart screening of germplasm may achieve this [61]. Indeed there is now a funded international consortium of scientists formed to address this task in rice (www.irri.org).

Recent modeling work suggests that photosynthesis may not be optimized in many plant species. For example, Zhu et al. [62] used an evolutionary algorithm to partition nitrogen between enzymes associated with different processes within a plant cell. The combination of enzyme amounts and activities that produced a higher photosynthetic rate was allowed to proceed to the next generation, and after 1,500 generations it was found that photosynthesis was substantially increased. It seems that an over investment in photorespiratory metabolism and an underinvestment in enzymes of the Calvin–Benson cycle may be critical. It is possible that this represents a lack of adaptation to contemporary higher CO_2 levels.

Photosynthesis is a dynamic process and constantly responds to changing environmental conditions. It is still debated as to whether the responses observed in situ are optimized. For example, when light is absorbed in excess of that required for photosynthesis, a series of regulatory mechanisms are activated which dissipate the excess excitation energy within the thylakoid membrane [63, 64]. This is considered a photoprotective process which reduces the likelihood of photooxidative stress. This process often has no impact on the light-saturated rate of CO_2 assimilation but it does reduce the quantum yield at low irradiance levels. Therefore, following a transfer to low light (caused, e.g., by cloud cover or leaf and solar movement), the slow relaxation of photoprotection causes a potential reduction in the rate of CO_2 assimilation. Given the large variation in irradiance in canopies in space and time, this has long been considered a factor in canopy photosynthesis. Indeed the manipulation of photoprotection has been shown to influence fitness in *A. thaliana* [65]. Recently, photoprotection was modeled in a tall three-dimensional canopy using ray tracing algorithms [66]. The reduction in canopy carbon gain was predicted to be as large as 30% under low temperature conditions. This would seem to indicate that there is room for improvement in terms of optimization of photoprotection.

Acclimation of photosynthetic capacity to environmental conditions such as irradiance can occur over longer timescales such as days and weeks. It has been hypothesized that acclimation conferred an advantage in terms of carbon gain [49]. Recent experiments using *A. thaliana* indicate that over long growth periods under naturally variable light levels this is indeed the case [67].

The question of whether plant and crop responses are appropriate for any switch in environmental conditions has been expanded to include those of growth and storage of carbon. For example, there is evidence that transfer of carbon to storage organs can occur at the expense of allocation to new organs [68]. Cross et al. [69] observed that accessions that allocated less carbon to storage at night had a higher growth rate. This concept has yet to be tested in crop species. Genes that are involved in the regulation are being identified, for example, DELLA proteins are negative growth regulators of central importance which are thought to integrate the effects of various growth-promoting hormones such as gibberellins and have been shown to have an effect on rates of tissue growth [70].

Source–Sink Processes and Partitioning of Assimilates

This section discusses the different assimilate sinks that have either direct or indirect effects on light interception (LI) and RUE in crops. As discussed, radiation capture is a highly dynamic process affected not only by sun angle and fluxes in radiation intensity, but also by gross morphological above ground structures that evolve over a plant's life cycle and include leaf area development, stem dynamics, and the emergence of floral structures. Within crop species, there is considerable interest in genetic effects on morpho-physiological traits that affect light interception and distribution. Genetic effects include early vigor; stem density (m^{-2}) and dynamics; leaf anatomy and geometry; the composition, distribution, and duration of light harvesting and photosynthetic proteins in the canopy; the architecture of floral structures; and the continual interaction of these with crop development. Crop management is an additional factor which will

affect radiation interception principally through row spacing, N fertilization, and irrigation, and by controlling biotic stresses that may reduce LI.

Direct Effects of Sinks on RI and RUE

It is axiomatic that all photosynthetic structures begin as carbon sinks while at some point becoming net exporters (i.e., assimilate sources). The exact investment strategy in these photosynthetic structures will determine the RUE of the "photosynthetic canopy" as a whole. In this context, leaf area index (L) is a useful parameter to consider. Typically L values above 3 are considered optimal for maximizing RUE in annual crops. However, theoretical considerations suggest that the relative distribution of leaf area and light harvesting and photosynthetic proteins among different layers of the canopy can also modulate RUE and are currently targets for genetic improvement [25].

In the context of canopy photosynthesis, two other important sinks with direct impact on RUE are the stems and the reproductive structures. Stems, as well as being covered with a green leaf sheath, provide the skeleton for leaf display and, therefore, to a large extent, determine the height and geometry of the leaf canopy. Stems are highly dynamic and may appear and disappear within the main part of the crop cycle. In small grain cereals, full light interception is typically accelerated through tiller development, a strategy which results in the subsequent shedding of nonproductive tillers after optimum L is achieved; the investment of assimilates in tillers apparently being offset by the increased L [71]. The strategy also has benefit under favorable years when a larger proportion of tillers achieve reproductive success. Reproduction requires a further investment of assimilates in floral structures, which, though often photosynthetic themselves, may also intercept incident light and, therefore, shade other photosynthetic tissue. Reducing panicle height for this reason has proved beneficial in rice [72]. Genetic modification of tiller dynamics and spike photosynthesis are both promising areas in crop breeding; neither has been systematically addressed yet as outlined above, and both traits interact with LI and potentially with RUE. There is considerable genetic diversity for tillering capacity in small grain cereals and a tiller inhibitor gene (*Tin*) has also been identified in wheat [73]. Considerable morphological diversity is also apparent in the reproductive structures of many crop species. However, those which are photosynthetic show a complex physiology, the measurement of LI and RUE is extremely challenging, and studies to establish genetic diversity are scant [43]. Nonetheless, shading studies in wheat have suggested genetic diversity for the contribution of spike photosynthesis to grain filling under drought, and given that reproductive structures intercept a significant proportion of light in many crops, it may be expedient to incorporate them into models of canopy photosynthesis.

Finally, non-photosynthetic sinks such as roots and structural components of the plant (stem wall, rachis, etc.) may impact on LI and RUE by competing with photosynthetic tissue for assimilates, however, these effects are not well documented [74].

Indirect Effects of Sinks on RI and RUE

There are other non-photosynthetic sinks which may also compete directly with photosynthetic tissue for assimilates but whose indirect effects may be much more significant in terms of overall RUE of the crop. These are (1) the accumulation and remobilization of carbohydrates (such as water-soluble carbohydrates in wheat and starch in rice) to and from stems and (2) the partitioning of assimilates to the reproductive spike.

While it seems clear that stem storage carbohydrates accumulate to provide a buffer against post-anthesis stress conditions when current photo-assimilates may be insufficient for grain filling [75–77], it is unclear what trade-offs may be involved in terms of assimilate partitioning. Given that genetic variation for storage carbohydrates is large and may constitute up to 50% of the stem dry weight shortly after anthesis, it could affect not only competition for assimilates from other sinks (e.g., roots, spike) but also RUE if, for example, the demand for stem storage carbohydrates is great enough to solicit feedback responses of the photosynthetic apparatus. While the latter has not been studied, feedback effects that influence RUE have been shown in response to partitioning of assimilates to the reproductive spikes.

A large body of evidence has shown that the number of reproductive sinks that are set in a crop is the main factor determining yield potential [78, 79].

Indeed the post anthesis sink size in wheat has been associated with RUE [80]. Sink strength associated with grain number is the most likely explanation for the relationships demonstrated between yield and photosynthetic rate, for example, in a historic series of wheat cultivars [24]. Furthermore, in other studies in spring wheat it was shown using both genetic and physiological treatments that RUE responded to increased spike fertility, resulting in increased yield and aboveground biomass [3]. It has been suggested that one way to enhance the sink capacity in wheat is to lengthen the stem elongation phase. The stem elongation phase encompasses the spike growth period and this would therefore result in a heavier spike during this period [3]. Another strategy would be to alter the sinks that compete with spike index, such as roots, stems, leaf sheaths, and infertile shoots. It must be ensured that any reduction in leaf lamina does not have an effect on LI and RUE. Reducing the allocation of biomass to roots may improve RUE by permitting increased partitioning to spikes (discussed in Reynolds et al. [3]). Some caution is urged since future yields may be dependent on increasing the ability to access soil water and nutrients. However, there is a possibility that the efficiency of uptake of water and nutrients could be improved with no change in root mass, for example, partitioning root length density at greater soil depths [81]. Structural stem carbohydrates (not the reserve carbohydrates discussed above) could be reduced by classical methods such as reducing plant height although wheat plant heights of below 70–90 cm are associated with lower biomass [3, 82]. Such approaches must be offset against increased lodging susceptibility. Other possible targets such as infertile tillers and awns are discussed in Reynolds et al. [3].

In particular, the maintenance of fertility under unpredictable environments is highlighted: in wheat, kernel set can be very sensitive to a number of environmental conditions such as moisture stress and irradiance. This is part of a set of evidence suggesting that plant signaling is involved in reducing grain number. The signaling (local or long distance within the plant) is a well-established phenomenon: the transport of molecules regulates growth, partitioning, and metabolism and is a fundamental feature of plant biology, likened in some cases to neural networks that sense, quantify, and memorize the environment around them [49, 68, 83]. The most well-known example is that drying soils induce the synthesis of abscisic acid in roots, and transport of this hormone to shoots induces a reduction in stomatal aperture to increase water use efficiency of remaining soil water [84]. It is possible that plant responses to environmental events are preemptive certainly but may also be simply too "conservative" predicting unfavorable conditions and setting seed size accordingly, while a higher yield can be attained by maintaining larger seed number under well-managed conditions. Floral abortion in maize in response to drought appears to be controlled by the up- or downregulation of a few enzymes [85]. In wheat, day length can alter sugar supply to fertile florets leading to cell death [86], and ethylene is a high-temperature signal leading to kernel abortion. Cytokinin appears to regulate the number of spikelets in rice [87]. Therefore, better targeted regulation of grain abortion before the onset of seed filling is a potential target for improvement of RUE and yield potential (Fig. 4).

Theoretical Considerations Related to the Improvement of RUE

The concept of RUE has received some criticism as being one that contains circular reasoning: one cannot have growth without biomass accumulation and vice versa. Additionally it is the product of almost every process in plant canopy growth and development, which makes a mechanistic description quite complex. However, it is established as a unifying concept in crop physiology, for example, [5, 10, 88]. Moreover the understanding of the component parts of the system and their integration is continually improving, and increasingly these parts are not viewed as a "black box," giving more options in the future with regard to RUE improvement.

For a given crop genotype, RUE is largely sensitive to leaf photosynthesis (and therefore nitrogen content) and the proportion of radiation that is diffuse or direct [89]. The latter is a much under-studied area in plant and crop physiology. The stability of RUE has been used to question whether it is possible to improve upon crops with existing C3 or C4 types.

Theoretical figures were outlined above for the maximum efficiency with which photosynthesis can

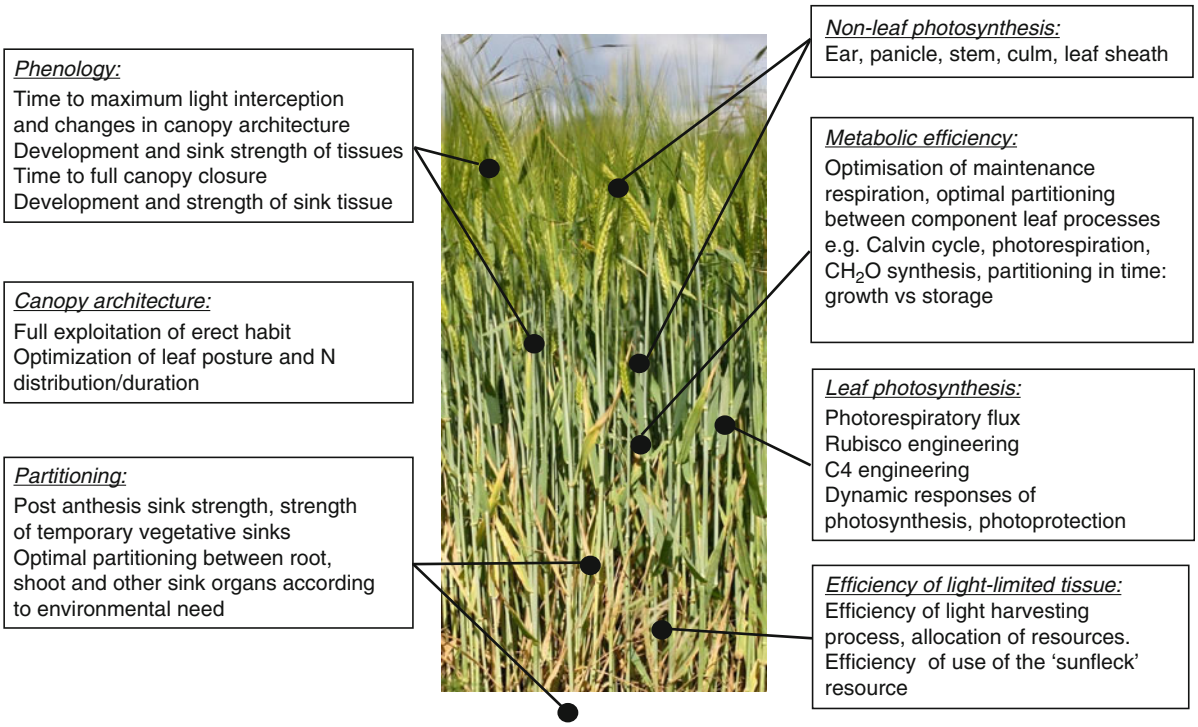

Crop Radiation Capture and Use Efficiency. Figure 4
Summary of the potential target areas which would result in an improvement of crop radiation use efficiency

operate and it was concluded that crops operate below this. However, what is the realistic "spare capacity" for RUE improvement in a major crop plant? Reynolds et al. [23] estimate potential productivity for the entire growth cycle of irrigated wheat in a specific and well-characterized location, NW Mexico. Radiation fluxes were measured throughout the season. Due to the time it takes for canopy establishment, large losses can occur before canopy closure, and this was taken into account using a model that used measured intercepted radiation and the time before canopy closure. A value of 1,748 MJ m^{-2} was obtained for radiation absorbed by photosynthetically active tissue. Estimates of field quantum requirement can vary between 10 and 30 mol quanta mol^{-1} CO_2, taking into account photorespiration and photochemical inefficiency. For a wheat crop, best estimates would seem to be in the range 15–24 mol quanta mol^{-1} CO_2 [90] which results in a range of RUE between 1.5 and 2.6 g carbohydrate MJ^{-1}. The calculated value of biomass ranges from 2,620 to 4,545 g m^{-2} whilst the measured value for wheat in this environment is up to 2,100 g m^{-2}. This suggests that improvements in field RUE are conceivable.

Sinclair and Horie [88] claimed that the observed stability of RUE arose from consistently high light-saturated leaf photosynthetic capacity (Amax). They plotted the leaf photosynthetic capacity against RUE for C3, C4, and leguminous crops types. The saturation of this response indicated that further modest increase in leaf photosynthetic capacity will only have a limited impact on the RUE, hence the stability of the RUE response [5]. However under conditions of restricted nitrogen, water, or under stress much lower values of photosynthetic capacity caused a larger reduction in RUE. This has been used as an argument that seeking modest improvements in leaf photosynthetic capacity may not be worthwhile. As pointed out here it is possible to trace improvements in biomass production that are linked to Amax. Biomass, yield, and Amax were associated in irrigated wheat cultivars in warm conditions [23] and in temperate conditions [24]. In the

latter case, higher Amax may reflect a feedback response caused by greater partitioning to reproductive structures – the differences in Amax were greatest during grain filling and not well associated with aboveground biomass.

There has been a lot of attention paid to the use of Amax in the selection of varieties with a higher photosynthetic potential, largely because it is convenient to measure and shows genetic variability. However, it should be clear from this entry that Amax will mostly be expressed at the top of the canopy (most leaves will not be at light saturation) and may not be a good proxy for canopy photosynthetic rate especially when integrated over long time periods. Care should be taken when extrapolating from spot measurements to whole canopy photosynthesis. It is not surprising then that attempts to improve yield by simply selecting for Amax have had largely unsuccessful results.

Perhaps more importantly, many of the improvements that show great promise are not solely associated with capacity at light saturation but rather to the dynamic responses of photosynthesis over time and therefore to total canopy carbon gain. These processes are much harder to measure experimentally although advances in techniques such as continual chlorophyll fluorescence monitoring may provide breakthroughs. As the knowledge of photosynthetic regulation improves, these should be installed into agricultural photosynthesis. It would seem necessary to tailor photosynthetic responses to improvements in canopy architecture.

Sources of Variation in Agricultural RUE

In any comparative analysis of RUE, it is necessary to ensure that the methods of analysis are directly comparable and provide an accurate estimate that do not contain any of the potential errors in measurement outlined above. Additionally, consideration must be taken when comparing different environments because varieties may not be well adapted to their locality and therefore able to "express" their maximum RUE. Other reviews, for example, Sinclair and Muchow [5] provide a comprehensive survey of the literature for many key crop species. A summary is provided here of the species and of the environmental factors affecting RUE in agriculture, and available information for a few key species has been provided.

It is in fact not common to find studies that specifically link RUE with yield progress; however, it has been shown, for example, that yield progress in wheat associates with both harvest index and total biomass production [74]. Some evidence also suggests that older wheat cultivars had a lower RUE and this was associated with a lower post-anthesis sink capacity [4, 80].

Species Variation in RUE

As pointed out by many workers, there is no "constant" for RUE and there is considerable variation between species. It is important to pay attention to the developmental stage of each crop in question and maximum attained RUE is referred to here. The highest recorded values for season-long RUE across C4 species are 3.4 g MJ^{-1} and those of C3 species 2.8 g MJ^{-1} [5, 35]. Mitchell et al. [13] reported that average values for RUE in rice, wheat, maize, and soybean in the vegetative stage were 2.2, 2.7, 3.3, and 1.9 g MJ^{-1}, respectively.

Therefore the tendency for a distinction between C3 and C4 crops seems to be consistent. However, care must be taken. For example, sorghum, a C4 species, possesses a relatively low RUE and this has been attributed to low leaf N content. Conversely, sugarcane, also a C4 species, seems to have an exceptionally high RUE. Potato, a C3 species, has shown values for RUE higher than all other C3 crops and even some C4 species (sorghum). It must once again be emphasized that the energy content of dry matter should be taken into account. It has been suggested that the high values for sugarcane and potato reported are due to the exceptionally low energy content of the products (sucrose and starch). It is often claimed that sugarcane has the highest radiation use efficiency among the plant kingdom, although there are relatively few studies.

A few studies have indicated the relatively low RUE of rice among C3 crops [13, 91], although there are surprisingly few studies available for this species and recent suggestions that RUE may not be currently closely linked to high yield potential [92].

Leguminous species such as soya bean have lower RUEs and a high percentage of PAR utilization. This is due to the higher lipid and protein content (see earlier section). However, even when the vegetative stage alone is considered, soybean has shown lower RUE values than wheat, rice, and maize [13, 93]. This has also

been observed in other grain legumes [5]. RUE of legumes may be an important future target. For detailed information on RUE values for each species, the reader is referred to detailed reviews such as [5].

In recent years, there has been much interest in "energy crops." These are crops that are grown for the sole purpose of fuel production or combustion for energy generation. This has been stimulated by concerns over emissions of greenhouse gasses and the growth of crops represents a CO_2-neutral strategy. Drawbacks include the clear competition with food supply and the possible threat to natural vegetation. Nevertheless it has been shown that certain species have the potential to be extremely productive in this regard, especially C4 grasses such as *Miscanthus* [94]. *Miscanthus* has the highest annual primary production of any crop species producing 50% more biomass than corn due to a high leaf area and longer duration, although the energy conversion rate is about the same [95]. Other examples of energy crops under study are willow, poplar, and oil crops such as *Jatropha*, although radiation use efficiency of this category of crop species is not well studied. These crops may find an application on land unsuitable for food crops and low input environments.

Developmental Stage

The stage of crop development has a clear effect on the RUE attained. Firstly the photosynthetic potential may be dependent on growth stage. Secondly the appearance and disappearance of vegetative and reproductive sinks can influence photosynthesis via the presence of feedback signaling mechanisms and carbohydrate accumulation; this has been discussed in detail above. In many species, a lower RUE was observed during earlier crop establishment stages in comparison with later stages and this was attributed to a lowered photosynthetic capacity [5]. The effect of senescence during the post flowering has the effect of reducing photosynthesis, and therefore RUE is usually observed to be higher during the vegetative stages than post flowering. Recent studies have indicated that post-anthesis RUE in wheat is strongly linked to sink size: Older cultivars with smaller sinks had significantly reduced RUE during this phase [4].

There is an indication in some studies that in rice this post-anthesis effect is not as pronounced [13]. In a recent study, Takai et al. [96] suggested that a maintenance of high growth rate and RUE in the late reproductive phase of rice is a key to higher grain yield potential in this species and may be linked to the short tropical life cycle and requirement for rapid photosynthesis during grain filling.

Environmental Factors

There are many practical difficulties involved with linking leaf-level photosynthesis with canopy-level RUE, even though it is technically straightforward to measure leaf photosynthesis. However, increasing the photosynthetic rate per unit leaf area of leaves has direct relationship with increasing RUE. It is frequently observed that the response between light-saturated photosynthetic *capacity* and RUE is curvilinear rather than linear. However, as discussed above it is critical to consider photosynthetic efficiency at all light levels. As a generalization it is fair to say that any factor, biotic or abiotic, that reduces the photosynthetic potential of a canopy is also likely to reduce the RUE. This applies to many of the common factors that reduce growing conditions below optimum such as water availability, nutrients, and extreme temperature.

It is not surprising that nitrogen has a significant impact upon RUE due to the close and well-established relationship with leaf photosynthesis. There is a strong nitrogen-dependent effect on leaf area and consequently light capture in plants, therefore, nitrogen content per unit leaf mass or per unit leaf area is considered. This has been the subject of a number of studies in several species: Usually a curvilinear response with leaf nitrogen is obtained, with RUE increasing up to a saturating value beyond which response is limited such as sunflower (average canopy leaf nitrogen [97]), soybean (specific leaf nitrogen [98]), and maize and sorghum (leaf nitrogen per unit leaf area [99]). However, this relationship is not always observed (see [5]). In examining species differences, the plant matter energy content and the nitrogen–photosynthesis relationship is important. For example, C4 plants have a higher potential photosynthetic nitrogen use efficiency [88]. Naturally site-variation in soil nitrogen is common and potentially a large source of variation in RUE.

Soil water and atmospheric humidity have the potential to reduce photosynthetic rate and therefore

RUE. In experiments that imposed soil water deficit, reductions in RUE have been observed in some cases [100] but not others [100]. It has been suggested that the variability in response is a result of variation in the extent of the soil water deficit: When this was measured in a quantitative manner, it could be established that RUE would decline when the level of extractable soil water declined below a certain limit (in this case 30%) [101].

An increase in vapor pressure deficit has been associated with lower RUE in some studies. It is noted that the impact in RUE was greater than that would have been predicted from leaf photosynthesis alone and it was suggested that environmental factors associated with vapor pressure deficit are involved. Other studies indicated only a small impact of vapor pressure deficit on RUE [5, 102].

Temperature has been associated with RUE when it has an influence on leaf CO_2 assimilation rate and this has also been shown to be related to the physiological effects of nighttime temperature [5].

Future Directions

Due to the effects of climate change caused by anthropogenic emissions, an altered environment for crop growth is likely to be required [103]. Some of these changes can be predicted with a high probability, for example, CO_2 is rising and is likely to continue at a similar rate to the current one with a slowing of rate according to internationally agreed emission cuts. Since 1750, atmospheric CO_2 has risen by around 100 ppm and continues to rise at the rate of around 2 ppm per year. By the end of the twenty-first century, temperature is predicted to rise by between 0.5°C and 4°C in response to levels of the greenhouse gasses CO_2, methane (CH_4), and nitrous oxide (N_2O). Agriculture itself is a major contributor to greenhouses gasses. Studies have already indicated that climate change is having an effect on productivity of crop systems [103–105].

These changes must be considered according to geographical region and in the context of deleterious effects such as a likely reduction in water availability, a rise in pollutants such as ozone, and the increasing frequency of extreme damaging events such as flooding, drought, and storms. They must also be weighed against possible beneficial effects such as higher photosynthetic rates induced by elevated CO_2 and a longer growing season at higher latitudes leading to higher biomass and higher yield. Accordingly, a reduction in yield in the tropics and a rise in temperate regions may be experienced. The effect of most of these factors on RUE has been discussed above and a detailed discussion of the wider impact of climate change on agriculture is beyond the scope of this article. Clearly suboptimal growing conditions will potentially reduce RUE and yield. However, it is important to ensure that the crops are adapted appropriately to future climates.

Experiments using completely enclosed or open topped chambers in the field in which CO_2 levels are elevated above ambient have shown significant increases in growth and yield. The reasons are clear and related to the suppression of photorespiration and consequently an increase in RUE. Additional beneficial effects related to a lowered stomatal conductance [25, 106]. These data have been used in models that predict an increase in future crop production in many northern regions. Experiments with more realistic field conditions (Free Air CO_2 Enrichment, FACE) have also demonstrated an increase crop yields but these were lower than those predicted by chamber experiments. This is lowered further when additional effects such as ozone and disease are accounted for and the net result may be negative [107, 108]. This suggests that the predicted beneficial effects of an increased atmospheric CO_2 on plant growth have been overestimated. However, as pointed out by Long et al. [107] there is still a paucity of data for CO_2 enrichment effects in many agroecosystems so a level of uncertainty remains.

There is also a need for further work into the adaptation of crops to high CO_2 levels: Theoretical work by Zhu et al. [62] using evolutionary algorithms to predict optimal levels of CO_2 for photosynthesis have shown that the relative levels of enzymes involved in primary metabolism are not optimized for carbon assimilation. It is possible that there has been insufficient adaptation during crop improvement since the start of the industrial revolution, raising the intriguing possibility that plants should be bred or engineered for adaptation to higher CO_2 levels of the future in order to maximize yield and RUE. Presumably this also applies to other environmental changes.

Therefore it is clear that there is a demand for greater crop yield per unit area of land with fewer resources available. This step change in yield will arise from an integrated set of targets, most of which have been outlined in this article. Assuming that management of the crop is optimal and improvement of partitioning and sink capacity reach their limits, it will be increasingly necessary to underpin any substantial yield improvements with increased biomass production and this means that RUE will need to increase.

RUE represents a complex system and as pointed out by Reynolds et al. [23], it is a less frequent outcome of the genetic recombination events required for breeding, in comparison to manipulation of sink size. It will be necessary to focus on methods for improving RUE of crops and to introduce this into breeding techniques. In addition, there have been significant advances in the plant molecular and genomic sciences in the past 2 decades and these should be exploited to raise RUE. The discovery of new genes and combinations of genes requires routine screening of large amounts of leaf material for photosynthetic potential. It is difficult to do this manually using traditional gas exchange techniques; however, there are a number of techniques developing rapidly that could be exploited to act as surrogates or proxies of CO_2 assimilation rate. For example, chlorophyll fluorescence is a rapid method that can be used to image leaf material for photosynthetic efficiency extremely rapidly. It is routine to image chlorophyll fluorescence; however, it is technically difficult to do this on a three-dimensional structure such as a canopy. Another method is canopy temperature depression which measures the difference between leaf and air temperature caused by evaporation. It therefore provides an indication of stomatal conductance and has been correlated with plant performance [109]. Considerable recent interest has been placed on the imaging plant growth leading to the emergence of the field of "plant phenomics." Advances in methods for rapid and high-resolution screening of plant material for photosynthetic performance can be anticipated. Additionally, the complexity of RUE means that a mathematical understanding of the integration and functioning of component processes will be critical. Given the difficulty of direct measurement, modeling of canopy photosynthesis is already used routinely and will be needed for the continued testing of new traits.

The Role in Wheat and Rice Research: Current Research at CIMMYT and IRRI

The challenge of improving photosynthesis and therefore RUE in crops during both optimal and suboptimal conditions has been recognized by the research organizations that were central to the last great agricultural revolution (the green revolution), the International Rice Research Institute (IRRI) in the Philippines and the International Maize and Wheat Improvement Centre (CIMMYT) in Mexico. IRRI has a number of research programs that are centered toward the sustainable improvement of rice yield in changing environments. Perhaps the most relevant here is the C4 rice consortium whose goal is a step change in rice photosynthesis through the introduction of the C4 pathway of photosynthesis (http://beta.irri.org/projects15/en/c4rice). The impact this would have on yield and resource use efficiency of the poorer rice growing regions of the world should not be underestimated.

Given the urgency of the current food crisis coupled with the likely negative impact of climate change on productivity, especially in less developed countries [110], both IRRI and CIMMYT have strategic initiatives to raise the yield potential of rice and wheat, respectively, by around 50%. The IRRI C4 rice initiative is already underway as mentioned. CIMMYT is currently facilitating a Wheat Yield Consortium (WYC) among a group of leading scientists with the view to raising the genetic yield threshold of wheat. A central issue is that the fundamental bottleneck to raising productivity, namely, photosynthetic capacity, has hardly changed since wheat breeding started. Nonetheless, basic research in photosynthesis suggests that substantial improvements in yield are theoretically possible. While increasing photosynthetic potential will require considerable research focused at cellular and subcellular processes (such as the genetic modification of Rubisco and its regulation), intervention at this level must go hand in hand with modification of structural and reproductive aspects of growth, since these will determine the net agronomic benefit of increased RUE .For example, even at current levels of yield potential, a significant portion of yield is lost to lodging damage each year so improved structural integrity will be prerequisite to realizing genetic gains in RUE and biomass. The other major factor determining yield

potential is adaptation of the reproductive processes which affect harvest index [3, 111] and whose physiological and genetic basis is relatively poorly understood [112]. The aim of the WYC is to develop or identify sources and genes for the combination of traits necessary to realize improved expression of wheat yield potential and combine them through strategic crossing using the most expedient combination of conventional, physiological, and molecular breeding approaches; the consortium approach is expected to realize impacts in farmers fields in a shorter time frame than if bottlenecks to yield potential are identified successively and investigated in relative isolation.

Bibliography

Primary Literature

1. Sheehy JE, Mitchell PL, Hardy B (2007) Charting pathways to C4 rice. International Rice Research Institute, Los Banos
2. Cassman K (1994) Breaking the yield barrier. In: Proceedings of a workshop on rice yield potential in favourable environments, International Rice Research Institute, Los Banos
3. Reynolds M, Foulkes MJ, Slafer GA, Berry P, Parry MAJ, Snape JW, Angus WJ (2009) Raising yield potential in wheat. J Exp Bot 60:1899–1918
4. Acreche MM, Briceno-Felix G, Sanchez JAM, Slafer GA (2009) Radiation interception and use efficiency as affected by breeding in Mediterranean wheat. Field Crops Res 110:91–97
5. Sinclair TR, Muchow RC (1999) Radiation use efficiency. Adv Agron 65:215–265
6. Watson DJ (1952) The physiological basis of variation in yield. In: Norman AG (ed) Advances in agronomy. Academic, New York
7. DeWit CT (1959) Potential photosynthesis of crop surfaces. Neth J Agric Sci 7:141–149
8. Loomis RS, Williams WA (1963) Maximum crop productivity: an estimate. Crop Sci 3:67–72
9. Hirose T (2005) Development of the Monsi-Saeki theory on canopy structure and function. Ann Bot 95:483–494
10. Monteith JL (1977) Climate and efficiency of crop production in Britain. Philos Trans R Soc Lond B Biol Sci 281:277–294
11. Gallagher JN, Biscoe PV (1978) Radiation absorption, growth and yield of cereals. J Agric Sci 91:47–60
12. Evans LT (1993) Crop evolution, adaptation and yield. Cambridge University Press, Cambridge
13. Mitchell PL, Sheehy JE, Woodward FI (1998) Potential yields and the efficiency of radiation use in rice. In: IRRI discussion paper series No. 32, International Rice Research Institute, Manila
14. Garcia R, Kanemasu ET, Blad BL, Bauer A, Hatfield JL, Major DJ, Reginato RJ, Hubbard KG (1988) Interception and use efficiency of light in winter-wheat under different nitrogen regimes. Agric For Meteorol 44:175–186
15. Hanan NP, Prince SD, Begue A (1995) Estimation of absorbed photosynthetically active radiation and vegetation net production efficiency using satellite data. Agric For Meteorol 76:259–276
16. Marshall B, Willey RW (1983) Radiation interception and growth in an intercrop of pearl-millet groundnut. Field Crops Res 7:141–160
17. Penningdevries FWT, Brunstin A, Vanlaar HH (1974) Products, requirements and efficiency of biosynthesis - a quantitative approach. J Theor Biol 45:339–377
18. Doebley JF, Gaut BS, Smith BD (2006) The molecular genetics of crop domestication. Cell 127:1309–1321
19. Duvick DN (2005) Genetic progress in yield of united states maize (*Zea mays* L.). Maydica 50:193–202
20. Murchie EH, Hubbart S, Chen YZ, Peng SB, Horton P (2002) Acclimation of rice photosynthesis to irradiance under field conditions. Plant Physiol 130:1999–2010
21. Sinclair TR, Sheehy JE (1999) Erect leaves and photosynthesis in rice. Science 283:1456–1457
22. Duncan WG (1971) Leaf angles, leaf area, and canopy photosynthesis. Crop Sci 11:482–485
23. Reynolds MP, van Ginkel M, Ribaut JM (2000) Avenues for genetic modification of radiation use efficiency in wheat. J Exp Bot 51:459–473
24. Fischer RA, Rees D, Sayre KD, Lu ZM, Condon AG, Saavedra AL (1998) Wheat yield progress associated with higher stomatal conductance and photosynthetic rate, and cooler canopies. Crop Sci 38:1467–1475
25. Long SP, Zhu XG, Naidu SL, Ort DR (2006) Can improvement in photosynthesis increase crop yields? Plant Cell Environ 29:315–330
26. Murchie EH, Horton P (1997) Acclimation of photosynthesis to irradiance and spectral quality in British plant species: Chlorophyll content, photosynthetic capacity and habitat preference. Plant Cell Environ 20:438–448
27. Murchie EH, Yang JC, Hubbart S, Horton P, Peng SB (2002) Are there associations between grain-filling rate and photosynthesis in the flag leaves of field-grown rice? J Exp Bot 53:2217–2224
28. Ackerly DD (1992) Light, leaf age, and leaf nitrogen concentration in a tropical vine. Oecologia 89:596–600
29. Morinaka Y, Sakamoto T, Inukai Y, Agetsuma M, Kitano H, Ashikari M, Matsuoka M (2006) Morphological alteration caused by brassinosteroid insensitivity increases the biomass and grain production of rice. Plant Physiol 141:924–931
30. Boccalandro HE, Ploschuk EL, Yanovsky MJ, Sanchez RA, Gatz C, Casal JJ (2003) Increased phytochrome B alleviates density effects on tuber yield of field potato crops. Plant Physiol 133:1539–1546
31. Fleming AJ (2005) The control of leaf development. New Phytol 166:9–20
32. Ong CK, Monteith JL (1992) Canopy establishment: light capture and loss by crop canopies. In: Baker NR, Thomas H (eds) Crop photosynthesis: spatial and temporal determinants. Elsevier, Amsterdam, pp 1–9
33. Watanabe T, Hanan JS, Room PM, Hasegawa T, Nakagawa H, Takahashi W (2005) Rice morphogenesis and plant

architecture: Measurement, specification and the reconstruction of structural development by 3D architectural modelling. Ann Bot 95:1131–1143
34. Pyke KA, Leech RM (1987) The control of chloroplast number in wheat mesophyll-cells. Planta 170:416–420
35. Hay R, Porter J (2006) The physiology of crop yield. Blackwell, Oxford
36. Zhu X-G, Long SP, Ort DR (2008) What is the maximum efficiency with which photosynthesis can convert solar energy into biomass? Curr Opin Biotechnol 19:153–159
37. Nishio JN (2000) Why are higher plants green? Evolution of the higher plant photosynthetic pigment complement. Plant Cell Environ 23:539–548
38. Murchie EH, Chen YZ, Hubbart S, Peng SB, Horton P (1999) Interactions between senescence and leaf orientation determine in situ patterns of photosynthesis and photoinhibition in field-grown rice. Plant Physiol 119:553–563
39. Amthor JS (2000) The McCree-de Wit-Penning de Vries-Thornley respiration paradigms: 30 years later. Ann Bot 86:1–20
40. Nunes-Nesi A, Carrari F, Lytovchenko A, Smith AMO, Ehlers Loureiro M, Ratcliffe RG, Sweetlove LJ, Fernie AR (2005) Enhanced photosynthetic performance and growth as a consequence of decreasing mitochondrial malate dehydrogenase activity in transgenic tomato plants. Plant Physiol 137:611–622
41. Beadle CL, Long SP (1985) Photosynthesis: is it limiting to biomass production. Biomass 8:119–168
42. Araus JL, Brown HR, Febrero A, Bort J, Serret MD (1993) Ear photosynthesis, carbon isotope discrimination and the contribution of respiratory CO_2 to differences in grain mass in durum-wheat. Plant Cell Environ 16:383–392
43. Tambussi EA, Bort J, Araus JL (2007) Water use efficiency in C-3 cereals under Mediterranean conditions: a review of physiological aspects. Ann Appl Biol 150:307–321
44. Diepenbrock W (2000) Yield analysis of winter oilseed rape (*Brassica napus* L.): a review. Field Crops Res 67:35–49
45. Watanabe N, Evans JR, Chow WS (1994) Changes in the photosynthetic properties of Australian wheat cultivars over the last century. Aust J Plant Physiol 21:169–183
46. Gutierrez-Rodriguez M, Reynolds MP, Larque-Saavedra A (2000) Photosynthesis of wheat in a warm, irrigated environment - II. Traits associated with genetic gains in yield. Field Crops Res 66:51–62
47. Peng S, Laza RC, Visperas RM, Sanico AL, Cassman KG, Khush GS (2000) Grain yield of rice cultivars and lines developed in the Philippines since 1966. Crop Sci 40:307–314
48. Hubbart S, Peng S, Horton P, Chen Y, Murchie EH (2007) Trends in leaf photosynthesis in historical rice varieties developed in the Philippines since 1966. J Exp Bot 58:3429–3438
49. Murchie EH, Pinto M, Horton P (2009) Agriculture and the new challenges for photosynthesis research. New Phytol 181:532–552
50. Horton P (2000) Prospects for crop improvement through the genetic manipulation of photosynthesis: morphological and biochemical aspects of light capture. J Exp Bot 51:475–485
51. Quick WP, Fichtner K, Schulze ED, Wendler R, Leegood RC, Mooney H, Rodermel SR, Bogorad L, Stitt M (1992) Decreased ribulose-1, 5-bisphosphate carboxylase-oxygenase in transgenic tobacco transformed with antisense rbcS. 4. Impact on photosynthesis in conditions of altered nitrogen supply. Planta 188:522–531
52. Parry MAJ, Andralojc PJ, Mitchell RAC, Madgwick PJ, Keys AJ (2003) Manipulation of Rubisco: the amount, activity, function and regulation. J Exp Bot 54:1321–1333
53. Galmes J, Flexas J, Keys AJ, Cifre J, Mitchell RAC, Madgwick PJ, Haslam RP, Medrano H, Parry MAJ (2005) Rubisco specificity factor tends to be larger in plant species from drier habitats and in species with persistent leaves. Plant Cell Environ 28:571–579
54. Zhu G, Spreitzer RJ (1996) Directed mutagenesis of chloroplast ribulose-1, 5-bisphosphate carboxylase/oxygenase. Loop 6 substitutions complement for structural stability but decrease catalytic efficiency. J Biol Chem 271:18494–18498
55. Raines CA (2006) Transgenic approaches to manipulate the environmental responses of the C-3 carbon fixation cycle. Plant Cell Environ 29:331–339
56. Medrano H, Keys AJ, Lawlor DW, Parry MAJ, Azconbieto J, Delgado E (1995) Improving plant-production by selection for survival at low CO_2 concentrations. J Exp Bot 46:1389–1396
57. Kebeish R, Niessen M, Thiruveedhi K, Bari R, Hirsch HJ, Rosenkranz R, Stabler N, Schonfeld B, Kreuzaler F, Peterhansel C (2007) Chloroplastic photorespiratory bypass increases photosynthesis and biomass production in *Arabidopsis thaliana*. Nat Biotechnol 25:593–599
58. Hibberd JM, Sheehy JE, Langdale JA (2008) Using C-4 photosynthesis to increase the yield of rice - rationale and feasibility. Curr Opin Plant Biol 11:228–231
59. Matsuoka M, Furbank RT, Fukayama H, Miyao M (2001) Molecular engineering of C4 photosynthesis. Annu Rev Plant Physiol Plant Mol Biol 52:297–314
60. Voznesenskaya EV, Franceschi VR, Kiirats O, Freitag H, Edwards GE (2001) Kranz anatomy is not essential for terrestrial C4 plant photosynthesis. Nature 414:543–546
61. Sage R, Sage T (2007) Learning from nature to develop strategies for the directed evolution of C4 rice. In: Sheehy JE, Mitchell PL, Hardy B (eds) Charting new pathways to C4 rice. International Rice Research Institute, Los Banos
62. Zhu X-G, de Sturler E, Long SP (2007) Optimizing the distribution of resources between enzymes of carbon metabolism can dramatically increase photosynthetic rate: a numerical simulation using an evolutionary algorithm. Plant Physiol 145:513–526
63. Horton P, Ruban AV, Walters RG (1996) Regulation of light harvesting in green plants. Annu Rev Plant Physiol Plant Mol Biol 47:655–684
64. Ruban AV, Berera R, Ilioaia C, van Stokkum IHM, Kennis JTM, Pascal AA, van Amerongen H, Robert B, Horton P, van Grondelle R (2007) Identification of a mechanism of photoprotective energy dissipation in higher plants. Nature 450:575–U522
65. Frenkel M, Bellafiore S, Rochaix JD, Jansson S (2007) Hierarchy amongst photosynthetic acclimation responses for plant fitness. Physiol Plant 129:455–459

66. Zhu XG, Ort DR, Whitmarsh J, Long SP (2004) The slow reversibility of photosystem II thermal energy dissipation on transfer from high to low light may cause large losses in carbon gain by crop canopies: a theoretical analysis. J Exp Bot 55:1167–1175
67. Athanasiou K, Dyson BC, Webster RE, Johnson GN (2010) Dynamic acclimation of photosynthesis increases plant fitness in changing environments. Plant Physiol 152:366–373
68. Smith AM, Stitt M (2007) Coordination of carbon supply and plant growth. Plant Cell Environ 30:1126–1149
69. Cross JM, von Korff M, Altmann T, Bartzetko L, Sulpice R, Gibon Y, Palacios N, Stitt M (2006) Variation of enzyme activities and metabolite levels in 24 arabidopsis accessions growing in carbon-limited conditions. Plant Physiol 142:1574–1588
70. Achard P, Renou JP, Berthome R, Harberd NP, Genschik P (2008) Plant DELLAs restrain growth and promote survival of adversity by reducing the levels of reactive oxygen species. Curr Biol 18:656–660
71. Berry PM, Spink JH, Foulkes MJ, Wade A (2003) Quantifying the contributions and losses of dry matter from non-surviving shoots in four cultivars of winter wheat. Field Crops Res 80:111–121
72. Setter TL, Conocono EA, Egdane JA, Kropff MJ (1995) Possibility of increasing yield potential of rice by reducing panicle height in the canopy. 1. Effects of panicles on light interception and canopy photosynthesis. Aust J Plant Physiol 22:441–451
73. Spielmeyer W, Richards RA (2004) Comparative mapping of wheat chromosome 1AS which contains the tiller inhibition gene (tin) with rice chromosome 5S. Theor Appl Genet 109:1303–1310
74. Shearman VJ, Sylvester-Bradley R, Scott RK, Foulkes MJ (2005) Physiological processes associated with wheat yield progress in the UK. Crop Sci 45:175–185
75. Blum A (1998) Improving wheat grain filling under stress by stem reserve mobilisation (Reprinted from Wheat: Prospects for global improvement, 1998). Euphytica 100:77–83
76. Foulkes MJ, Sylvester-Bradley R, Weightman R, Snape JW (2007) Identifying physiological traits associated with improved drought resistance in winter wheat. Field Crops Res 103:11–24
77. Yang J, Zhang J, Liu L, Wang Z, Zhu Q (2002) Carbon remobilization and grain filling in Japonica/Indica hybrid rice subjected to postanthesis water deficits. Agron J 94:102–109
78. Miralles DJ, Slafer GA (2007) Sink limitations to yield in wheat: how could it be reduced? J Agric Sci 145:139–149
79. Slafer GA, Calderini DF, Miralles DJ, Dreccer MF (1994) Preanthesis shading effects on the number of grains of 3 bread wheat cultivars of different potential number of grains. Field Crops Res 36:31–39
80. Acreche MM, Slafer GA (2009) Grain weight, radiation interception and use efficiency as affected by sink-strength in Mediterranean wheats released from 1940 to 2005. Field Crops Res 110:98–105
81. Reynolds M, Dreccer F, Trethowan R (2007) Drought-adaptive traits derived from wheat wild relatives and landraces. J Exp Bot 58:177–186
82. Miralles DJ, Slafer GA (1995) Yield, biomass and yield components in dwarf, semi-dwarf and tall isogenic lines of spring wheat under recommended and late sowing dates. Plant Breed 114:392–396
83. Brenner ED, Stahlberg R, Mancuso S, Vivanco J, Baluska F, Van Volkenburgh E (2006) Plant neurobiology: an integrated view of plant signaling. Trends Plant Sci 11:413–419
84. Davies WJ, Wilkinson S, Loveys B (2002) Stomatal control by chemical signalling and the exploitation of this mechanism to increase water use efficiency in agriculture. New Phytol 153:449–460
85. Boyer JS, McLaughlin JE (2007) Functional reversion to identify controlling genes in multigenic responses: analysis of floral abortion. J Exp Bot 58:267–277
86. Ghiglione HO, Gonzalez FG, Serrago R, Maldonado SB, Chilcott C, Cura JA, Miralles DJ, Zhu T, Casal JJ (2008) Autophagy regulated by day length determines the number of fertile florets in wheat. Plant J 55:1010–1024
87. Ashikari M, Sakakibara H, Lin SY, Yamamoto T, Takashi T, Nishimura A, Angeles ER, Qian Q, Kitano H, Matsuoka M (2005) Cytokinin oxidase regulates rice grain production. Science 309:741–745
88. Sinclair TR, Horie T (1989) Leaf nitrogen, photosynthesis, and crop radiation use efficiency - a review. Crop Sci 29:90–98
89. Hammer GL, Wright GC (1994) A theoretical-analysis of nitrogen and radiation effects on radiation use efficiency in peanut. Aust J Agric Res 45:575–589
90. Loomis RS, Amthor JS (1996) LImits to yield revisited. In: Reynolds M, Rajaram S, McNab A (eds) Increasing yield potential in wheat: breaking the barriers. CIMMYT, Mexico, pp 76–89
91. Inthapan P, Fukai S (1988) Growth and yield of rice cultivars under sprinkler irrigation in southeastern Queensland. 2. Comparison with maize and grain-sorghum under wet and dry conditions. Aust J Exp Agric 28:243–248
92. Zhang YB, Tang QY, Zou YB, Li DQ, Qin JQ, Yang SH, Chen LJ, Xia B, Peng SB (2009) Yield potential and radiation use efficiency of "super" hybrid rice grown under subtropical conditions. Field Crops Res 114:91–98
93. Rochette P, Desjardins RL, Pattey E, Lessard R (1995) Crop net carbon-dioxide exchange-rate and radiation use efficiency in soybean. Agron J 87:22–28
94. Heaton EA, Dohleman FG, Long SP (2008) Meeting US biofuel goals with less land: the potential of *Miscanthus*. Glob Change Biol 14:2000–2014
95. Dohleman FG, Heaton EA, Leakey ADB, Long SP (2009) Does greater leaf-level photosynthesis explain the larger solar energy conversion efficiency of *Miscanthus* relative to switchgrass? Plant Cell Environ 32:1525–1537
96. Takai T, Fukuta Y, Shiraiwa T, Horie T (2005) Time-related mapping of quantitative trait loci controlling grain-filling in rice (*Oryza sativa* L.). J Exp Bot 56:2107–2118
97. Hall AJ, Connor DJ, Sadras VO (1995) Radiation-use efficiency of sunflower crops - effects of specific leaf nitrogen and ontogeny. Field Crops Res 41:65–77

98. Sinclair TR, Shiraiwa T (1993) soybean radiation-use efficiency as influenced by nonuniform specific leaf nitrogen distribution and diffuse-radiation. Crop Sci 33:808–812
99. Muchow RC, Sinclair TR (1994) Nitrogen response of leaf photosynthesis and canopy radiation use efficiency in field-grown maize and sorghum. Crop Sci 34:721–727
100. Muchow RC (1989) Comparative productivity of maize, sorghum and pearl-millet in a semi-arid tropical environment. 2. Effect of water deficits. Field Crops Res 20:207–219
101. Singh P, Rama YV (1989) Influence of water deficit on transpiration and radiation use efficiency of chickpea (*Cicer-arietinum*-l). Agric For Meteorol 48:317–330
102. Sinclair TR, Muchow RC (1999) Occam's Razor, radiation-use efficiency, and vapor pressure deficit. Field Crops Res 62: 239–243
103. IPCC (2007) Summary for policymakers. In: Climate change 2007: the physical science basis. A report of working group I of the 4th assessment report of the Intergovernmental Panel on Climate Change, Cambridge University Press, Cambridge/New York
104. Parry M, Rosenzweig C, Livermore M (2005) Climate change, and risk global food supply of hunger. Philos Trans R Soc B Biol Sci 360:2125–2138
105. Peng SB, Huang JL, Sheehy JE, Laza RC, Visperas RM, Zhong XH, Centeno GS, Khush GS, Cassman KG (2004) Rice yields decline with higher night temperature from global warming. Proc Natl Acad Sci USA 101:9971–9975
106. Drake BG, GonzalezMeler MA, Long SP (1997) More efficient plants: A consequence of rising atmospheric CO2? Annu Rev Plant Physiol Plant Mol Biol 48:609–639
107. Long SP, Ainsworth EA, Leakey ADB, Morgan PB (2005) Global food insecurity. Treatment of major food crops with elevated carbon dioxide or ozone under large-scale fully open-air conditions suggests recent models may have overestimated future yields. Philos Trans R Soc B Biol Sci 360:2011–2020
108. Ainsworth EA, Long SP (2005) What have we learned from 15 years of free-air CO_2 enrichment (FACE)? A meta-analytic review of the responses of photosynthesis, canopy properties and plant production to rising CO_2. New Phytol 165:351–371
109. Amani I, Fischer RA, Reynolds MP (1996) Canopy temperature depression association with yield of irrigated spring wheat cultivars in a hot climate. J Agron Crop Sci 176:119–129
110. Lobell DB, Burke MB, Tebaldi C, Mastrandrea MD, Falcon WP, Naylor RL (2008) Prioritizing climate change adaptation needs for food security in 2030. Science 319:607–610
111. Reynolds MP, Delgado MI, Gutierrez-Rodriguez M, Larque-Saavedra A (2000) Photosynthesis of wheat in a warm, irrigated environment - I: Genetic diversity and crop productivity. Field Crops Res 66:37–50
112. Barnabas B, Jager K, Feher A (2008) The effect of drought and heat stress on reproductive processes in cereals. Plant Cell Environ 31:11–38

Books and Reviews

Bolhar-Nordenkampf HR, Leegood RC, Long SP (eds) (1993) Photosynthesis and productivity in a changing environment: a field and laboratory manual. Chapman & Hall, London

Laisk A, Nedbal L, Govindjee (eds) (2009) Photosynthesis in silico: understanding complexity from molecules to ecosystems. Springer, Dordrecht

Lawlor DW (2000) Photosynthesis. Taylor & Francis, Boca Raton

Reynolds MP, Rajaram S, McNab A (eds) (1996) Increasing yield potential in wheat: breaking the barriers. CIMMYT, Mexico

Russell G, Marshal B, Jarvis PG (eds) (1990) Plant canopies, their structure growth and function. Cambridge University Press, Cambridge

Sage RF, Monson RK (eds) (1999) C4 Plant biology. Academic, London

Crop Responses to Available Soil Water

Manuela M. Chaves[1,2], O. Zarrouk[1]
[1]Plant Molecular Ecophysiology Laboratory (LEM), Instituto de Tecnologia Química e Biológica, Universidade Nova de Lisboa, Oeiras, Portugal
[2]Instituto Superior de Agronomia, Universidade Técnica de Lisboa, Lisbon, Portugal

Article Outline

Glossary
Definition of the Subject
Introduction
Revisiting Plant Strategies to Cope with Water Scarcity: The Crop Perspective
Photoassimilates, Water Use, and Crop Yield
How Metabolic Processes Respond to Drought: Photosynthesis, Respiration, Photorespiration
Yield and Quality Under Water Scarcity
The Breeding Achievements
Future Directions
Bibliography

Glossary

Dehydration avoidance Dehydration avoidance is the strategy of the plants that are able to maintain tissue water potential as long (and as high) as possible under drought conditions.

Dehydration tolerance Dehydration tolerance is the strategy of the plants that are able to cope with severe tissue dehydration.

Harvest index Harvest index is the biomass of the harvested product expressed as a percentage of the total crop biomass.

Photoassimilates Photoassimilates is the energy-storing carbohydrates produced by photosynthesis in the green tissues of the plants.

Water-use efficiency (WUE) Water-use efficiency (WUE) is the carbon gain (or biomass formed) per unit of water transpired or the ratio between photosynthesis (A) and stomatal conductance (g_s), termed as intrinsic WUE.

Definition of the Subject

Sustainable intensification of global agriculture is a major purpose (and challenge) for twenty-first century scientific, social, and political communities, in order to guarantee food security, while preserving natural resources. Fast growing population and climate change could lead to a global crisis if efforts from different disciplines and countries are not congregated. Among limiting factors is water scarcity, which may dramatically decrease crop production worldwide.

Mitigation measures are therefore a major goal for sustaining crop production and they are based either on management practices that will enable water savings or on breeding efforts for more adequate crops. Improved physiological and molecular knowledge on plant's response to water deficits is essential to get improvements in crop yield under adverse environments. Because of the complexity of these responses, it is imperative to integrate disciplines as functional genomics, transcriptomics, proteomics, and metabolomics with plant physiology to improve breeding strategies.

According to the present knowledge, the key factors responsible for high yield under drought in annual plants include an appropriate phenology that will enable escaping drought and getting the timing of flowering right, as well as high water-use efficiency (WUE) and harvest index. On the other hand, the basic knowledge for fruit tree crop breeding under water scarcity is much more fragmented than for annuals because of the highest complexity of fruit trees. Therefore more efforts are needed in this area of research.

Introduction

Scarcity of water resources is an increasingly important issue since it will dictate global production of food and feed for the next generations, as dramatically described by The Economist (May 2010): "Water is the new oil: a resource long squandered; now growing expensive and soon to be overwhelmed by insatiable demand. Aquifers are falling, glaciers vanishing, reservoirs drying up and rivers no longer flowing to the sea. Climate change threatens to make the problems worse. Everyone must use less water if famine, pestilence and mass migration are not to sweep the globe."

The International Panel for Climate Change [1] predicts that water scarcity, together with incidence of high temperature, will increase in the near future in many regions of the globe with dramatic effects on agriculture. Of the world's water resources, c. 80% is currently consumed by irrigated agriculture. In this context, the investment in research for improving water use by the crops ("more crop per drop" as in the CGR program Challenge Program on Food and Water) [2], either through improved management technologies [3, 4] or more efficient genotypes [5, 6], is crucial. Increased water use by the crop can be obtained by agronomic practices that decrease water losses by soil evaporation, runoff, through-flow, deep drainage, and competing weeds, thereby making more water available for the crops, and in irrigated agriculture by using deficit irrigation practices.

Crop resistance to drought has been the subject of extensive research in the last decades, ranging from the physiological traits underlying resistance to water deficits [7–12] to breeding efforts [13, 14] including classical and genetic engineering approaches [15–17]. The world's most important crops for human and animal consumption in terms of total production – wheat, maize, rice, soybean, barley, and sorghum – have endured large yield increases during the twentieth century [18–22] and recently became the target of investigation aiming at improved performance under harsh environments, namely water scarcity [5, 6, 15, 23]. To articulate the knowledge obtained in different scientific disciplines (agronomy, breeding, physiology, and molecular biology) still remains a challenge, with the ultimate goal of providing farmers with better performing crops under water scarcity [7, 14].

Designing robust field trials is also essential in order to test improved crops under the multi-stress conditions they generally face under natural conditions. Indeed, there have been several reports of apparently promising biotechnological manipulations that have failed to deliver drought-tolerant crops in yield terms, when the novel material is transferred from the growth room to the field [4].

The key factors responsible for high yield under drought in annual plants are an appropriate phenology that will enable escaping drought and getting the timing of flowering right, high water-use efficiency (WUE) and a high harvest index [14, 24]. To get high WUE would involve the improvement in crop transpiration efficiency but the increased partitioning of biomass into the harvested product will also lead by itself to higher WUE. The relative importance of each of these processes will depend on how water is available during the crop cycle [13]. Indeed, it is noticeable that under most dryland situations where seasonal rainfall is unpredictable, maximizing soil moisture use is a crucial component of drought resistance (avoidance), which is generally expressed in lower WUE [25].

It is also important to recognize that many of the traits that explain plant adaptation to drought (e.g., phenology, the size and depth of the root system, xylem properties or the storage of reserves) are mostly constitutive [21, 26] and therefore can be found within the species population when it exhibits a large intraspecific variability. Moreover, there is the general recognition that the efficacy of high throughput screening of plant genetic material will speed-up crop improvement via breeding programs (see, e.g., [19]).

In fruit crop production, improvement under conditions of water scarcity has been achieved mostly by optimized management technologies such as deficit irrigation [3, 27], with breeding efforts being much more modest. Indeed the basic knowledge for tree crop breeding under water scarcity is much more fragmented than for annuals because of the highest complexity of fruit trees. In tree crops economic return is highly dependent on fruit quality, generally not related with total plant biomass produced and therefore water availability [3]. Moreover, yield-determining processes in fruit trees may not be sensitive to water deprivation at some developmental stages [28] and fruit quality may even beneficiate from a mild to moderate water deficits, as is well documented in grapevines [29]. High-density fruit orchards use composite plants – the scion cultivar grafted into a rootstock. The rootstock can alter the behavior of the scion, including its vegetative growth, flower numbers and flowering time, crop yield [30], and also drought tolerance [31]. The mechanisms underlying the regulation of scion growth and development by the rootstock are not fully understood [32].

Research in the so-called new climate proof crops such as *Chenopodium quinoa* Willd (quinoa) and *Amaranthus* spp is also developing. Quinoa is an Andean seed crop, very nutritious [33], showing high tolerance to drought, frost, salinity, and biotic factors [34–36]. Quinoa has been selected as one of the crops to secure food production in the twenty-first century [37]. The protein quantity and the quality of quinoa seed is superior to those of cereals, because of the high content of lysine, methionine, and threonine, in addition to a range of vitamins (B2) and minerals (iron, calcium). Although amaranth is less tolerant to a range of stresses as compared to quinoa, it tolerates higher temperatures because it is a C4 plant [38]. The protein content of amaranth grain ranges from 12% to 17%, with a high level of lysine, similar to quinoa [39].

In this review the focus is on the key factors responsible for sustained plant growth and production under water scarcity, referring to both annual and perennial (fruit) crops. During evolution, plants developed different strategies to successfully cope with water stress; they comprised either acclimation to a slowly developing water deficits or the response to a sudden drought. These issues will be discussed in the context of the agriculture needs and related to production (fruit) quality, a major target of modern agriculture nowadays.

Revisiting Plant Strategies to Cope with Water Scarcity: The Crop Perspective

Plants respond and adapt to stress at whole plant, root, reproductive structures, and leaves, by using mechanisms that are being unraveled at the cellular and molecular levels [7, 40].

Classically, plant resistance to drought has been divided into escape, avoidance, and tolerance strategies

[7, 41, 42]. However, in practice, most plants combine a range of these different strategies [43].

Plants that escape drought are able to adjust their phenology to the environment, being able to complete their life cycle before drought occurs. Escape strategies rely on successful flowering and therefore reproduction before the onset of severe stress. Plant ability to store reserves in stems and roots and to remobilize them for grain filling under water scarcity is extremely relevant for grain crops under water scarcity [44, 45], as it has been described in cereals such as wheat, maize, and rice [46–48], and legumes [49]. When stem reserve storage/utilization is insufficient to support fruit growth under stress, delayed-senescence genotypes may be desirable in crops where yield is source-limited [50]. High nitrogen availability can further increase the reuse of stored carbohydrates in cereals under moderate soil drying, leading to increased grain yield; under non-limiting water conditions, however, abundant nitrogen was shown to reduce grain yield in stay green genotypes [47].

Dehydration avoidance, which is common to both annuals and perennials, implies the maintenance of tissue water potential as long (and as high) as possible under drought conditions. This can be achieved either by (1) minimizing water loss or by (2) maximizing water uptake. Decreased water loss may derive from stomata closure and/or reduction of absorbed light, including leaf rolling [51], increased reflectance (with, e.g., trichomes), or steep leaf angles [52]. Shedding of older leaves is also relevant to reduce water loss, while allowing the reallocation of nutrients to younger leaves, when water deficit is relieved. Maximizing water uptake may be accomplished by increased investment in the roots at the expense of shoot growth (Fig. 1), which is generally inhibited very early on in response to decreasing water availability [8, 45]. Deep roots have been reported as important drought resistance traits for both annuals and perennials in semi-arid regions [26]. However, in arid environments, where rainfall is sporadic and of short duration, plants may take advantage of shallow roots that proliferate quickly near the soil surface allowing water uptake by the plant before it evaporates [53]. For example, *Zoysia japonica* was reported as having a relatively shallow root system, moderate WUE, while exhibiting a high capacity for osmotic adjustment [53]. High root plasticity is a key factor in this strategy because it will determine how fast roots grow in response to sporadic rain, following a period of drought stress.

Under slowly developing water deficits some plants show osmotic adjustment (OA), a cellular stress adaptive response that may improve tissue resistance to desiccation, by maintaining cell turgor, likely supporting crop yield under stress [25]. Because this mechanism allows plant water uptake at lower soil water potentials it is considered a dehydration avoidance strategy. The alterations observed under OA comprise increases in soluble sugars (like fructans and sucrose) [54], amino acids (e.g., proline, aspartic acid, and glutamic acid), methylated quartenary ammonium compounds (e.g., glycine betaine and alanine betaine), and some proteins, such as dehydrins [55] and cyclitols (e.g., D-pinitol, mannitol) ([56]; see also review [7]). In addition to the role played via the decrease in osmotic potential, these solutes may protect cell membrane and metabolic machinery under dehydration. According to Bohnert et al. [57] sequestration of H_2O molecules, reducing the solvent-protein interaction, may explain stabilization of protein complexes and membranes.

The positive role of osmotic adjustment on yield has been subject to much discussion since benefits were often not observed (see review by [58, 59]). A possible explanation is that turgor maintenance in cells is often associated with slow growth. It is also likely that osmoprotection mechanisms are not functional until severe dehydration occurs, with the implication that OA may be critical to survival rather than to promote plant growth and crop yield under drought [7].

Mechanisms of protection against oxidative stress are also fundamental to cope with drought and co-occurring stresses under arid semi-arid environments, as it will be discussed below.

Photoassimilates, Water Use, and Crop Yield

As proposed by Monteith [60], yield potential (Yp) of a crop at a given location can be defined as: $Yp = HI.Pn$ with $Pn = \Sigma(PAR^{*}ABSc^{*}\varepsilon c)$ and PAR being the incident solar radiation in the specific location, ABSc the fraction of the radiation intercepted by the crop, εc the efficiency of the conversion of intercepted radiation into biomass and Pn the primary productivity (total biomass produced over the growing season) and HI the

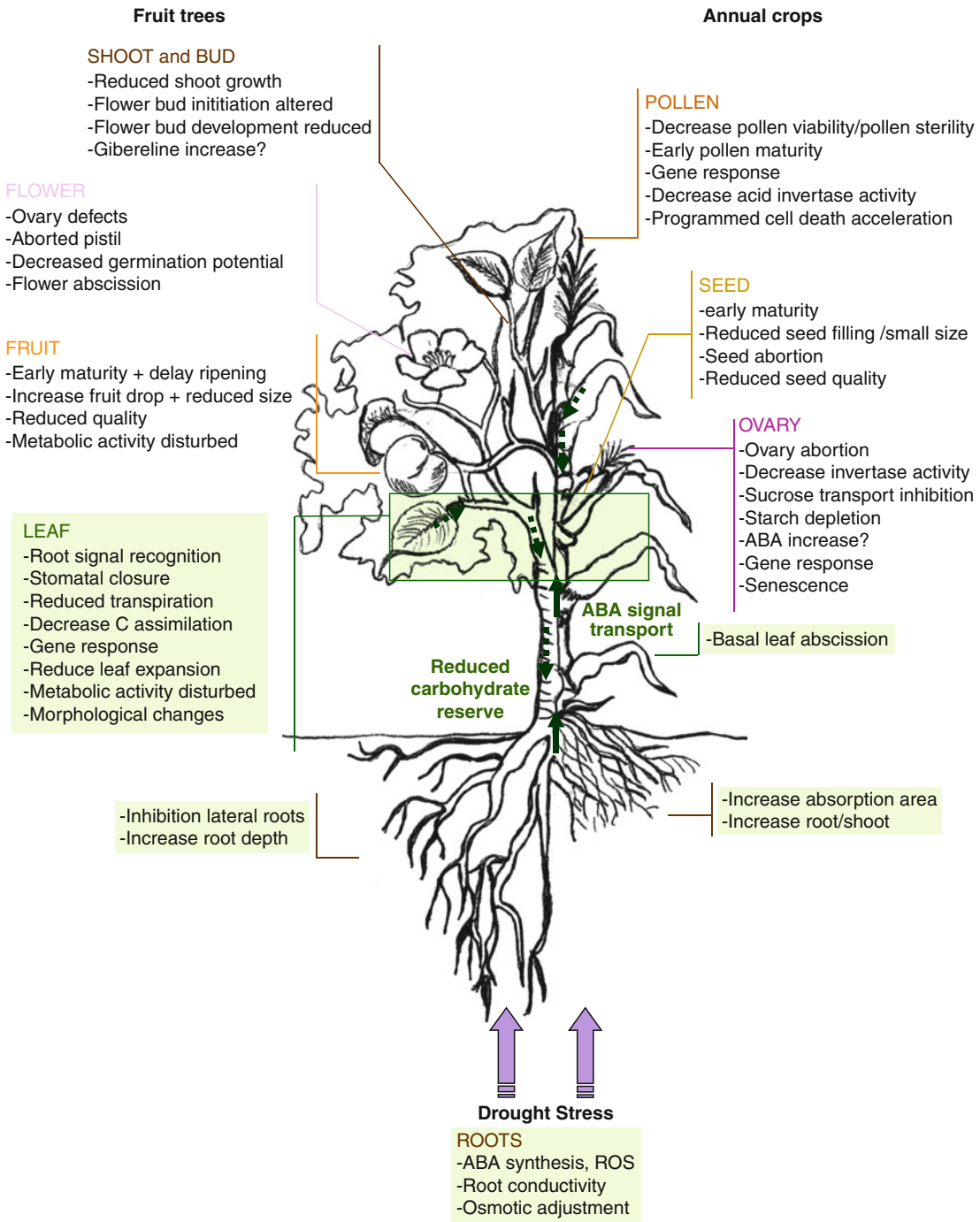

Crop Responses to Available Soil Water. Figure 1

Whole plant response to drought stress in fruit trees (*left*) and in annuals crops (*right*). Green boxes and letters correspond to shared responses between the species

harvest index (see also [61]). Under water scarcity a decrease in Yp may occur as a result of less intercepted radiation (due to lower total leaf area and smaller leaf angles) and a lower εc, as a result of a decrease in photosynthesis.

On the other hand, as judiciously proposed by Passioura ([62]; see also [14, 22, 63]), crop yield under water-limited conditions can be estimated by the product of transpiration efficiency (biomass/water transpired) × water transpired (WU) × harvest index (HI). Therefore, optimizing yield under such conditions has to be performed by increasing either water-use (amount and pattern), transpiration efficiency/WUE or partitioning of more biomass to grain. This can be achieved through better water management, the adjustment of crop phenology to the environment, or genetic improvement. The latter implies getting varieties that can give the so-called more crop per drop, either by improved carbon fixation under water deficits or having deeper roots to capture more water or converting more of the biomass into grain (increasing HI). Increasing WUE at the expenses o higher assimilated carbon rather than decreased WU is a desirable way to improve YP under water scarcity, but will generally require biotechnological interventions [17].

In the last decades, increases in Yp under non-limiting water conditions have been achieved with genotypes of cotton, wheat, and rice that exhibit high stomatal conductance and transpiration. This trait allows a decrease in leaf temperature and a greater CO_2 fixation per unit of leaf and land area [25, 64]. Under water-limited environments crop production has relied mostly in dehydration avoidance traits as described above, which maximize soil moisture use (when it becomes available for example, under sudden rainfall), but is generally associated with lower WUE. On the contrary, drought resistance traits that reduce WU, and are therefore associated with high WUE, will unavoidably reduce YP.

Few successful cases of breeding for water scarcity environments have been reported, one being the dryland wheat grain yield improvement, with selection for high WUE in Australia [65]. This success has been explained by the fact that wheat is grown there mainly on stored soil moisture. Furthermore, as suggested by Blum [2], a major opportunity for yield improvement under water scarcity is the control of WU during the earlier part of the growing season in order to avoid lack of soil moisture later on, during the reproduction phase. An attempt to achieve this was done by Richards and Passioura [66] by selecting for reduced root xylem diameter.

How Metabolic Processes Respond to Drought: Photosynthesis, Respiration, Photorespiration

Photosynthesis

Under water scarcity, restrictions in leaf carbon uptake take place as a result of increased resistance to CO_2 diffusion induced both by decreased stomatal aperture (Fig. 2) [7, 9] and decreased mesophyll conductance [67]. At the whole plant level, total carbon uptake is further reduced due to the concomitant or even earlier inhibition of shoot growth [8]. Metabolic inhibition of photosynthesis usually occurs under more severe stress conditions or when various stresses co-occur, such as high light and temperature [8, 10], although claims for earlier alterations in photosynthetic metabolism are reported by Lawlor and coworkers ([12]; see a review by [68]). Interestingly, alterations in gene expression are also observed very early on, although these alterations are generally not turned into differential expression of proteins or enzymes in the short term (see revision [9]).

Stomata are able to detect a decrease in water availability either in the soil or in the atmosphere by feedback and feed-forward mechanisms. Feedback mechanisms include the response to dehydration in the leaf itself that is transmitted to the guard cells, either by hydraulic or by chemical signals. Feed-forward responses are generally mediated by hormonal signals and may take place before any alteration in leaf tissue water status occurred. They comprise responses of guard cells to high vapor pressure deficit, whose mechanisms area still not fully resolved [69–71] and to dehydration taking place elsewhere in the plant, namely in the roots [72]. Hormones, with particular relevance to ABA, but also cytokinins and ethylene, have been implicated in the root–shoot signaling, either acting in isolation or concomitantly. This long distance signaling by hormones may be mediated by reactive oxygen species [73].

Primary events of photosynthesis including electron transport capacity are very resilient to moderate

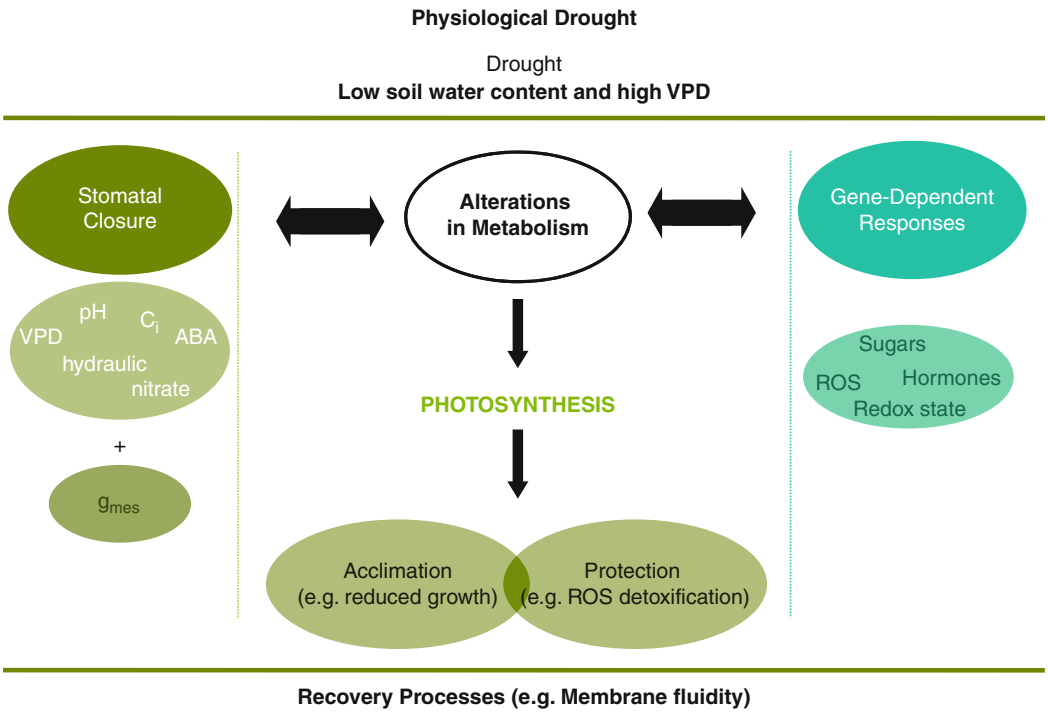

Crop Responses to Available Soil Water. Figure 2
Direct effects of drought on stomata and mesophyll (g_m) conductance as well as on gene expression, resulting in alterations of photosynthetic metabolism and ultimately on plant acclimation (Adapted from [9])

drought [74], with the decline in PSII photochemistry being explained by a decrease in substrate availability. In fact, PSII activity often declines concomitantly with carbon uptake under water deficits, suggesting that photosynthetic electron chain is finely tuned by available CO_2 [75]. However, under field conditions, when high light co-occur with water deficits, CO_2 deprivation at the chloroplast (driven by stomatal closure) may result in the production of excess reducing power and therefore in the decline of the quantum yield of PSII. These stresses also appear to inhibit the repair of PSII through suppression of the synthesis of PSII proteins, in particular, the production of D1 protein [76]. Protection mechanisms against reactive oxygen species (ROS) that are formed under such conditions are an essential component of plant survival [77]. Such protection may be achieved by the regulated thermal dissipation occurring in the light-harvesting complexes, involving the xanthophyll cycle [78, 79] and the lutein cycle [80]. Photoprotective mechanisms compete with photochemistry for the absorbed energy, thus leading to the downregulation of photosynthesis. If the limitation of the rate of CO_2 assimilation is accompanied by an increase in the activity of another sink for the absorbed energy, for example, photorespiration [81] or Mehler-peroxidase reaction [82], the decline in non-cyclic electron transport will be proportionally lower than the decrease observed in the rate of CO_2 assimilation. It was estimated that, in the absence of the repair mechanisms, photodamage would lower the yield of photosynthesis to less than 5% of the yield achieved now [83]. Although these responses have mainly been documented in plants native to semi-arid regions they may also occur in crop plants, even irrigated, when they are subjected to intense heat and irradiance, during the summer period. This is likely to increase its frequency in the near future.

As for Rubisco activity it was shown to be very resistant to water deficits [84, 85], being generally affected only after severe stress [86, 87]. The same authors also found evidence that low CO_2 concentration in the chloroplast (Cc) attained under severe water deficits could induce deactivation of Rubisco sites. It is further suggested that these effects are

species-dependent, with species adapted to low Cc being able to maintain active Rubisco longer in response to prolonged drought [87]. These findings are compatible with earlier data suggesting that decreased sink capacity (limited capacity to use photoassimilates), as induced, e.g., by shoot growth inhibition under drought, might feedback to decrease photosynthesis, namely by downregulating the enzymes of the photosynthetic carbon cycle [88].

When studying the effects of drought on photosynthesis it is also important to recognize that crop productivity is dependent on photoassimilates produced at the whole plant level, which partly explains why often there is no correlation between crop yield and leaf photosynthetic rate [61]. Therefore, the impact of drought on shoot and canopy growth may be as important to crop yield as the effects produced at the single leaf level. Indeed, water scarcity by inducing a significant decline in total plant leaf area via the inhibition of new leaf growth or the earlier senescence of older leaves will decrease total carbon uptake by the plant. Moreover, lower leaf angles induced by decreased leaf turgor will reduce total intercepted irradiance, with significant impact on crop yield (Pinheiro and Chaves, unpublished results). However, it must be emphasized that, at least in cereals (wheat, maize and soybean), yield is generally more limited by the sink than by the source [61, 89]. This explains why these crops have the potential to cope with moderate drought and still fill their grains. Of course, this is also possible due to the capacity of remobilizing photoassimilates, previously stored in the shoot, as was discussed above.

Respiration and Photorespiration

The effects of water deficits on *dark respiration* are still unclear, with reports of either decreases, maintenance, or increases in the rates of this process (see the review [90]). Inhibition of respiration under drought has been observed in mature leaves of crops and herbaceous species as well as in roots, and is presumably related with a decreased availability of substrate to mitochondria under conditions of low photosynthesis and growth (e.g., [86, 91, 92]). This may be explained by the need of herbaceous species to quickly respond to water scarcity, thereby lowering their respiration rates in order to optimize their carbon gain over shorter periods of time.

On the contrary, trees and shrubs seem to show slower responses to drought than short-lived species. As suggested by Flexas et al. [86] and Atkin and Macherel [93], a higher demand for respiratory ATP (higher respiration rates) may be required under severe water stress to compensate for the lowered ATP production in the chloroplasts. The increased maintenance respiration will support repair mechanisms needed under acclimation to drought that will ensure a better performance under extended periods of water scarcity.

In general, the changes observed in respiration in response to drought are smaller than those observed in photosynthesis, thereby implying that respiration increases proportionally in relation to photosynthesis, with likely impact on leaf intercellular CO_2 and on plant carbon balance [68].

The role of *photorespiration* during drought stress has been scarcely studied [81, 94], partly due to difficulties in quantifying the rate of photorespiration [95]. Since photorespiration and photosynthetic metabolism are strictly linked and photorespiration depends on the recycling of RuBP in the Benson–Calvin cycle, it may be hypothesized that severe drought stress should result in lower photorespiration. As suggested by Osmond et al. [96], photorespiration and the Mehler-peroxidase pathway could protect the photosynthetic apparatus against photoinhibition in drought-stressed leaves, by sustaining photon utilization in non-assimilatory electron flow, when electron consumption by CO_2 assimilation is reduced due to low internal CO_2 concentrations. However, other studies, such as the one by Brestic et al. [97] concluded that photorespiration was not important for photoprotection in drought-stressed French bean.

In a recent work with glycine decarboxylase-deficient plants, Igamberdiev et al. [98] showed that photorespiration contributes to stomatal regulation. The data obtained with these mutants revealed that the photorespiratory mutants were able to decrease the rate of photorespiration, but only at the expense of increased water loss. Indeed, the necessity to maintain a high CO_2 concentration near the site of carboxylation in the chloroplasts of plants deficient in photorespiratory enzymes required an increased opening of the stomata, with a corresponding increase in water loss and decrease in water-use efficiency.

Yield and Quality Under Water Scarcity

Agriculture depends to a large extent on the success of plant reproduction [99]. Drought affects crop productivity as much as all other environmental factors combined and its impact on crops differs according to the attained developmental stage. The effects of water scarcity are quite different in annuals and perennial species [100]. Reproductive development of cereals, from meiosis to seed set, is highly vulnerable to water deficit [101] and the meiosis stage appears to be the most stress sensitive period of reproduction in all studied species [102]. However, anthesis, pollen fertility, pollination, female fertility, and early zygote development were also reported to be susceptible and finally their failure altered the number and the final quality of grain [102]. Later in the development, water stress tends to reduce grain size [103]. In fruit trees, severe water stress during flowering was reflected in the final fruit number per tree, whereas water stress during the fruit-growth and maturity phases was reflected mainly in fruit size [104]. In addition, the timing and intensity of the drought period dictate the extent of alterations occurring in the final fruit quality [29].

Flower Initiation and Induction

Grain crops are very sensitive to drought during floral initiation and floral pre-meiotic differentiation [105]. Water deficit at this stage causes pollen sterility, but when stress is severe, it usually affects also female fertility. In cereals, water stress during flower induction and inflorescence development leads to a delay in flowering or even to its complete inhibition [105]. The increase of abscisic acid (ABA) in response to water stress has been suggested to play a role in this delay [106].

In woody plants, flower bud initiation is an important feature in fruit tree cultivation. However, the effect of drought on floral meristems is among the least understood aspects of crop reproductive development under water deficit [107]. In species where flowering takes place prior to leaf emergence as *Prunus* trees, flower development occurs in the absence of new photoassimilates and at the expense of pre-stored reserves (starch), either in the flower itself or other plant organs [108]. This explains why in *Prunus* water stress effects are only detected in the subsequent reproduction event and not in the same year. This is the case of peach, apricot, and sweet cherry trees, where drought stress during flower bud initiation markedly slowed the progression of floral differentiation by delaying the differentiation of pistil primordia [109, 110].

In opposition, water stress has been demonstrated experimentally to induce flowering by a direct stimuli on stem and bud in citrus [111], apple [112], and pear [113]. In these species, water stress showed to stimulate polyamine accumulation, which is linked to floral initiation, thus enhancing the production of floral primordia and re-flowering. However, severe water stress induces little flower production. Indeed, under severe stress during flower bud induction periods, gibberellins level increased, inducing a low level of flower production per shoot [114].

Flowering and Pollen Development

Loss of pollen fertility, spikelet death, and abortion of newly formed seed are associated with a decline in the water status of the reproductive structures and decline of carbohydrate availability [105]. By reducing photosynthesis, drought directly interferes with inflorescence and flower number, flowers life span, flowers opening, and maintenance of floral organs in crops [115] as well as maintenance of nectar production in floral organs [116]. In addition, water stress reduces flower size and sucrose content in nectar [117] leading to an extensive loss in yield [118].

Drought also affects seed yield of plants through an effect on availability and viability of pollen grains [119]. The effect of drought on pollen fertility/availability also depends on the species and it is considered a common symptom in angiosperms [120]. The hypothesis that ABA is a primary controlling agent in water stress induction of pollen viability still remains unanswered [102]. Recently in chickpea [119], water stress was shown to affect pollen growth in the pistil rather than affecting pollen viability. In fact, pistils from well watered plants pollinated with pollen of stressed ones showed fewer germinated pollen grains and fewer pollen tubes that reached the ovary, which suggested that drought has an effect on pollen tube growth, which is inhibited in the pistil [119]. Pollen viability is highly dependent on sugar unloading and

pre-anthesis stem reserve accumulation is considered a significant factor affecting flower development in water stressed plants (see Fig. 1) [121]. The decrease of acid invertase activity under low water potential impedes pollen to metabolize incoming sucrose in hexose in the developing pollen, which might lead to pollen sterility [122, 123]. This hypothesis is confirmed by the study of Koonjul et al. [124] who observed a downregulation of the soluble invertase gene *Ivr1* and *Irv5* in wheat microspores, which correlates with accumulation of reducing (fructose and glucose) and non reducing (sucrose) sugars in the ear [125]. Nevertheless, recent studies by Liu and Bennett [126] showed that stress induced sterility in rice is not only caused by disruption in sugar metabolism or by desiccation of reproductive tissue, but also by disturbance of anther pollen development and cell function. In wheat, microspores lost contact with the tapetum at first pollen grain mitosis and the filament degenerated in response to water stress, which resulted in total sterility [127]. The expression of various proteins related to anther wall degradation and cell wall modifications are modified in stressed rice anther [126]. Furthermore, pollen from stressed plants might have a shorter life span and reduced vigor, which explain that pollen tube growth fails to reach the ovule [128]. The depletion of the adenosine triphosphate pool, increased concentration of hydrogen peroxide, and downregulated transcripts in anthers of drought-stressed rice lead to a programmed cell death and may cause pollen sterility [129].

In woody species, as observed in apricot trees, post-harvest drought may induce an increase of aborted pistils in the subsequent year, decrease germination potential of pollen (see Fig. 1), and decrease the percentage of fruit set due to an increase of fruit drop [130]. In almond, the number of fruiting positions per tree is negatively associated with water stress [131]. However, drought stress during flower initiation does not influence the percentage of spurs that flowered or set fruit during subsequent years. Although water stress had no apparent effect on spur mortality in the first year, more than a half of spurs died within three subsequent years. In addition, water stress reduces flower bud development in grapevine [132] and peach [133] and increases flower abscission [134] and young fruit drop [135].

Ovary Development

Consequences of inhibited photosynthesis under drought and therefore insufficient assimilates are particularly striking around the time of pollination when reproductive events occur rapidly, namely ovary growth [136, 137]. In maize the pollen does not loose availability even at severe water stresses (water potential below −12.5 MPa) and low kernel number is explained by a poor receptivity of silks and/or by an ovary abortion. Maize ovaries are normally loaded with glucose and starch on the day of pollination [138, 139]. Under drought, sucrose, the main translocated product from the carbon fixed in photosynthesis, declines (see Fig. 1). The enzymes that convert incoming sucrose to glucose in ovary lose activity and starch starts to be hydrolyzed [137, 138]. Cell wall acid invertase hydrolyses sucrose in the apoplast of the upper pedicel tissues and its activity creates a steep gradient in glucose concentration between the upper pedicel and the nucellus of young ovary. Ovary abortion under drought was attributed to the decrease of glucose and invertase activity in upper pedicel, inhibiting sucrose transport [138]. Sucrose delivery decreased first in ovary and probably triggers an early downregulation of genes coding for sucrose processing enzymes (*INCW2* and *IVR2*). Glucose depletion occurs few days after and triggers an up-regulation of putative senescence genes as *ribosome inactivation protein 2* [139], which suggests the beginning of failed ribosome function and later induces an up-regulation of *phospholipase D1* gene leading to loss of plasma membrane integrity, indicating the onset of senescence [137, 140]. This probably causes the irreversible loss in viability found during abortion [139]. Feeding sucrose during water stress largely prevents these changes, which confirm that senescence genes are "monitoring" the sugar status of the ovary cells and when sugars content decreases these genes turn on in sequence and orchestrate cell death [137].

A transcriptional study of placenta and endosperm of maize under drought showed that both tissues responded differentially to water shortage [141]. While most of the responding genes in placenta involved up-regulation, in endosperm these were downregulated. Downregulated genes relate to cell division and to endosperm growth, which may explain

arrested growth and thus decreased demand of photosynthates [141].

These described events are common across crop species [137]. Although wheat requires water potentials to be much lower than maize to lose the same amount of photosynthetic activity [137], starch is also depleted in floral structures after drought (see Fig. 1) [142], inducing an impairment of ovule function [143]. Also in grapevine, drought induces lower availability of sugar due to decreased photosynthesis, which provokes ovary abnormalities and flower abscission [144].

Setter and coauthors [145] suggest an interaction between ABA and sugar that might induce a signal cascade that leads to the abortion process to initiate. The recent finding by Setter and Parra [146] supported the model of the interacting influence of carbohydrates and ABA at least at the pedicel-placenta tissues of basal kernels. Several studies in maize reported that water stress increases ABA in florets, suggesting it might trigger the abortion process [145, 147]. Young and Gallie [148] observed that regulation of programmed cell death during maize endosperm development involves the interaction of ABA and ethylene signaling pathways. However, Boyer and Westgate [99] explained that hormone effects are difficult to interpret because their expression on dry matter or water content basis can cause concentration to increase simply because the ovary dry mass or water content decreased, as it was shown in maize [149].

Yield

All described abnormalities of flowering, fertilization, and zygote development that may occur under drought stress induce yield losses, and the timing of the occurrence of drought stress determines the degree of disturbance. Water stress during ear formation and milk stages in maize was shown to induce early loss of lower leaves and a decrease in plant dry matter and in grain yield, as a result of reduced intercepted radiation [150]. Moreover, all the yield parameters were significantly affected. When water stress occurred at pre-anthesis a reduction in seed numbers was observed due to pollen sterility and ovary abortion. Post-anthesis water stress generally enhances whole-plant senescence and lead to a faster remobilization of carbon from vegetative tissues to seeds, thereby inducing earlier maturity and small seeds [119, 151–155]. This is a typical strategy of Mediterranean annuals, which exhibit a phenological drought-avoidance producing seed before water supplies are exhausted [45]. Remobilization of pre-stored carbon to the seed and acceleration of seed filling rate are associated to an alteration in the hormonal balance of grains, namely the decrease in gibberellins and the increase in ABA [48, 156]. The reduced duration of grain filling may partly result from reduced number and size of endosperm cells and therefore reduced capacity to accumulate starch following drought stress [157]. Additionally, seed cell expansion is driven by water uptake [158] and when cell expansion in the seed stops, the end of seed growth and seed maturation are predetermined. Indeed, Yang et al. [152] suggested the enhancing of sink strength with water stress is promoted by alterations in sucrose synthase and starch branching enzyme activities taking place in grain during stress. Severe drought stress during seed filling generally resulted in seeds that are shriveled and deformed and with a reduced weight [152, 159]. The shortening in the duration of seed fill limits seed size because grain fill process fails to finish in a short maturation period [155, 160], consequently reducing seed yield [161]. Seed size reduction was highest in late maturing wheat genotypes, suggesting that early maturing genotypes partially escaped late-season water stress [162]. However if water stress occurs after cell division is completed it does not affect yield since sink size per kernel is already predetermined [152]. In sesame, most drought-tolerant cultivars abort a higher proportion of their seeds, and in that case more efficiently shunt available nutrient resources to the healthy growth of remaining seeds [163].

In woody plants and especially in fruit trees, it is generally accepted that post-harvest water stress may negatively influence fruit set and crop load in the next season, as it is the case in peach [164–167], in almond [168] and in sweet cherry [169]. This reduction in fruit set is due to the limitation placed by reduction in the accumulation of carbohydrate reserves. In fact, in cultivated *Prunus* species, floral bud-break and fruit set significantly precede net carbon export from leaves [167]. In citrus, severe water stress taking place during flowering led to decreased fruit number per tree, whereas in water restrictions occurring during the

fruit-growth and maturity phases, the effects were reflected mainly in fruit size [104]. Olive tree has a reputation of being a drought resistant crop. However, drought incidence during winter, leading to a low level of soil moisture, may reduce vegetative growth [170] and have an important impact on flowering and fruit set, resulting in a drastic decrease on olive fruit number and size [171, 172]. In fact, severe water stress in phase I of fruit growth was shown to reduce mesocarp cell division and number [170, 173] suggesting a high sensitivity of olive mesocarp cell size to water stress. Grapevines are also well adapted to semi-arid climates, nonetheless severe water stress during the summer largely limit grapevine yield and cluster weight [27, 29]. This reduction is mainly observed in drought-avoiding genotypes, which optimize survival at expense of yield and reduced sugar allocation to reproductive tissues and thereby reducing fertility [174].

The effect of drought in crop plants is enhanced by high temperature and effects are usually difficult to separate [118]. Differences among genotypes are observed; for example barley is much less sensitive to short periods of very high temperature than wheat, and combined drought and high temperatures are more likely than high temperature alone to explain the reductions in grain weight observed in the field [175].

Fruit and Seed Quality

Drought influences end-use quality of major food crops in the world, as it is the case of wheat [176], barley, and maize [177]. Indeed, water stress in wheat changes the patterns of proteins [178]; in barley, grain β-glucan content and malt fine extract decreased with drought stress [179]; in soybean drought during seed development has a large effect on isoflavone concentration in the seeds [180]; in maize, water stress increases flavonoid content in seeds but reduces carotenoids and phenol content inducing a decrease in the antioxidant capacity of kernel oil [181]. In lupin seeds, raffinose quantity and accumulation pattern are reduced by water stress, suggesting an increase in nutritive values of seeds since raffinose is considered to be a major cause of flatulence in animals and humans [161].

Starch granule shape, volume and structure are important factors contributing to starch quality in wheat [182]. Post-anthesis water stress affects the proportions of different types of starch granules and increases the percentage of small granules per seed [183].

Protein content has an important implication in the processing qualities of cereals since it affects the functional properties of processed wheat products [184]. In wheat, grain protein content decreases linearly with the severity of drought stress during grain development [158]. Recently Zhao et al. [184] showed that the intensity of drought dictates the intensity of the effect on protein accumulation and reported a differential accumulation of proteins (especially gliadins and glutenins) in mature grains. The decrease in the accumulation of oil due to water stress was reported in wheat [184], soybean [185, 186], lupin [187] and chickpea [188].

In fruit trees, drought influences fruit development, metabolism, and final composition, and its timing and intensity dictate the extent of alterations occurring in final quality [29]. With regard to the effect of water stress on organoleptic properties, fruit quality is significantly affected by severe water stress during the fruit-growth and maturity periods [104]. Under water restriction, fruit maturity tends to be hastened, supporting the hypothesis that increasing water restriction might encourage early fruit maturity as observed in peach [189, 190]. Post-harvest water deficit was shown to increase fruit soluble solid concentration in the following season in peach [191, 192]. The opposite effect, reducing firmness and soluble solid concentration, was reported in sweet cherry [169].

Water stress was shown to decrease oil content and yield in young olive trees and induce lower level of phenolics in oil [172]. Olive fruits import assimilates from the canopy, but also produce them in situ by photosynthesis in the mesocarp; the fruit is capable of retaining chlorophyll even when its color change [193] and this makes a significant contribution to oil production [194]. This "autonomy" of olive fruits may explain the maintenance of oil quality in trees under water deficits [172]. In fact, although irrigation led to decreased contents of some undesirable sensory qualities as phenols, some favorable intense green notes were also reduced, which suggests complex effects of water stress on olive quality [195]. In grapevine, severe water stress influences final composition of the berries by delaying their ripening but also through an indirect

effect on berry size [196, 197] that affects sugar and flavonoids metabolism in the berry (review [29]). However, moderate water deficit was shown to have beneficial effects on grape berries, for example by enhancing photoprotection mechanisms [198] and likely having a positive effect on wine quality [29, 196]. Indeed, moderate water deficit promotes sugar accumulation by inhibition of shoot growth with a subsequent reallocation of carbohydrates to fruits [199] and by the activation of ABA-mediated uptake of hexoses [198]. Under such conditions, sugar accumulation in berries accelerates anthocyanin accumulation or/and biosynthesis [200, 201]. The enhancement of carotenoids content and the up-regulation of genes encoding enzymes involved in biosynthesis of berry aroma were also observed after mild stress imposition [198, 202]. Similar benefits of mild water deficit in fruit quality were also observed in apricot [203], citrus [104] and olive [204].

The Breeding Achievements

Conventional Breeding

To face drought, farm-management practices and plant breeding are used for the improvement of crop yield [18], being the second approach the most promising in the long term [64]. Drought is the most recalcitrant to breeders' efforts due to the complexity of plant drought-tolerance mechanisms [205] and breeders have no reliable method of distinguishing sensitive from tolerant germoplasm other than by measuring yield [19]. Therefore, the main objective of a drought-tolerance breeding program is to select the variety presenting the better yield under stress conditions [206]. However, yield is a trait which is characterized by low heritability, polygenic control, and a high genotype × environment interaction (G × E) [21, 207].

During the last 50 years, most of the progress has been derived from empirical (conventional) breeding [208, 209] by selecting desired traits recognized at the phenotypic level. Generally, there is a minimum of 4 years extensive yield testing to further selection at multiple locations before a new variety is released to farmers. Empirical selection for grain yield was effective during the last decades. However, when plants are crossed some undesirable traits may be transferred along with those of interest – including some with negative effects on yield potential. In addition, breeding can only be done between species inter-compatible, which limits the new traits that can be added to those that already exist in a particular species [206]. Furthermore, the variability of rainfall from year to year increases G × E and reduces heritability for yield, thereby limiting yield progress [19]. The indirect or analytical approach based on an understanding of the crop physiology, may help to target the key traits that are limiting yield [64]. Such an approach may therefore complement conventional breeding programs and hasten yield improvement [210–212].

A number of physiological studies have identified some traits which presence/expression are associated with plant adaptability to drought prone environment [205] and have been already successfully exploited in crop improvement [213]. Increasing water use by increasing early shoot vigor to escape dryer periods is a common strategy in Mediterranean region [214], but in very dry years this strategy may result in reduced yield. Early maturity by adjusting crop development with seasonal rainfall pattern in environments where they experiment terminal drought, or late flowering with short grain filling period in environments with early season drought, are examples of traits that are being used in breeding. Leaf cuticle waxes appear to play a key role in day and night transpiration and selecting for waxy leaves may reduce water loss and prevent leaf senescence during grain filling [215]. Enhancement of water extraction, by optimizing root architecture that resulted in greater water capture, has also the potential to significantly increase grain yield [63]. In addition, enhancement of root osmolytes accumulation was used in cereals, but a clear evidence of their beneficial role in crop yield was not observed [58].

Carbon isotope discrimination (Δ) is an attractive feature for C_3 plants breeders since it may provide an indirect sensing of transpiration efficiency (TE) [13]. In fact, genotypes showing higher TE (lower Δ) may be more productive under certain environmental conditions [216]. However, in the Mediterranean region the opposite was found and positive correlation between Δ and yield are reported [217], which is probably due to the fact that genotypes with lower TE have maintained a higher CO_2 conductance due to a better water status or by a faster plant development or better access to

water [216]. Aerial infrared (IR) methods on vegetative material offer the possibility to detect variation on TE and present the advantage to reduce the cost of measuring carbon isotope discrimination [19, 216].

Fruit tree species propagation is possible only by vegetative methods. However, with the spreading of different species in new areas, the use of rootstock has become the first alternative to adapt scion cultivars to soils or climatic conditions that are otherwise not fully suited to their cultivation. Climatic areas or soils subjected to transient drought conditions require rootstock capable of inducing efficient water use by the scion cultivar. Unfortunately, there is only limited understanding of how rootstock provides tolerance to drought [218] and the majority of rootstock breeding programs addresses fruit quality. Traditionally, rootstocks have been produced using conventional hybridization breeding techniques, which are time and space consuming. Initial selection of main rootstocks is made from open pollinated fruit tree germplasm, generating thereby intra- and interspecific hybrids. The extended use of interspecific hybrids is due to the lower susceptibility of this type of rootstocks to biotic and abiotic stresses and may also overcome soil problems as drought [219], which might derive from heterosis (hybrid vigor) or from the elevation of ploidy levels of these rootstocks [220]. However, the use of known drought-tolerant/resistant rootstocks may not fulfill grower's intents in terms of fruit commercial traits, mainly because they may provide excess vigor. In addition, the problem of graft compatibility of hybrid rootstocks with commercial scion complicated the use of a wide range of cultivars [221, 222].

New Breeding Approaches

Compared to conventional approaches, genomics offer unprecedented opportunities for dissecting quantitative traits into their single genetic determinants, the quantitative trait loci (QTLs), thus paving the way to marker-assisted selection (MAS) and, eventually, cloning of QTLs and their direct manipulation via genetic engineering. Several studies have reported QTLs for roots architecture and investigated their effect on yield under water stress in rice [223] and also in maize, where QTL reported for leaf ABA concentration showed an effect on root size and grain yield [224, 225]. In sorghum QTLs related to 'stay green' trait and yield were identified [226].

Some QTLs of one character were shown to overlap with QTLs of other characters. This is the case in maize, where QTLs of leaf growth sensitivity to water deficit overlapped with QTLs for leaf responses to evaporative demands, thus suggesting that hydraulic mechanisms are involved in that response [227]. Similarly, overlap between QTLs of leaf growth sensitivity with silk growth was observed [228]. QTLs were also reported for anthesis-silking interval in maize [15], for seed weight and yield under different water conditions in rice [229] and durum wheat [230]. It was also possible to identify WUE QTLs in brassica [231], rice [232], and wheat [233]. However, despite all the recent technological breakthroughs, the overall contribution of genomics-assisted breeding to the release of drought-tolerant cultivars has so far been marginal [234], in part due to the fact that a given QTL can have positive, null or negative additive effects depending on the drought scenario [235]. In addition, cloning QTLs for yield maintenance under drought conditions and drought physiological traits is limited because the unavailable information about the biochemistry of some of these traits [236].

In recent years, proteomic and transcriptomic studies have advanced the basic understanding of protein/gene regulatory networks that are active during the exposure of plants to water stress [237, 238] and there have been several reports of apparently promising biotechnological manipulations emerging from these tools [239]. Remarkable dehydration tolerance has been obtained under laboratory conditions using bacterial RNA chaperones overexpression [16], NFYB2 class transcriptionals regulators [240], as well as modulating the expression of dehydration response element binding (DBF/DREB1) transcription factor [241], using of detoxification of reactive oxygen species that accumulate under stress [242, 243] and of hormone intervening in drought signaling [244]. Introducing RNA silencing in some crops to downregulate poly ADP ribose polymerase and thus inducing tolerance to wide range of stresses [245] and overexpression of cyanobacterial flavodoxin [246] were also reported. However, these reports and others have failed to deliver

drought tolerance in yield terms when the novel material is transferred from the growth room to the field [4].

Fruit trees also have benefited from new technologies and it is now possible to reduce the breeding time by MAS. Very recently fruit breeders have begun to examine the possibilities of using such techniques in the production of new rootstocks. The aim is to improve an already good rootstock for yield by modifying its gene expression or introducing new genes to improve resistance to abiotic factors. Unfortunately, the mechanisms by which rootstocks bring about their beneficial effects on the vigor and cropping of scions are still very poorly understood. Until more research is conducted in this field and genes that control such processes are identified, progress in this area may be slow. Recent studies showed that ectopic expression of the transcription factor Osmyb4 gene in transgenic apple trees, improved water stress tolerance and might result in long term ameliorated productivity. Further experiments are required to assess the agronomic value of the plants produced and to verify to what extent the expression of *Osmyb4* may contribute to enhanced drought tolerance under field conditions [247].

Summarizing, to date increased drought resistance of the major crop plants (sustained yield under water scarcity) has been dependent upon the screening of a wide range of germoplasm in order to identify genetic variation in major traits involved in stress resistance [19, 248, 249]. In addition, the effective use by the crop of a limiting water supply has been achieved by adjusting crop phenology to its environment [2, 14] or by using agronomic practices aiming at an improved water use, such as deficit irrigation [4, 29]. A variety of approaches have been successful, particularly in the irrigation of top quality fruit and vineyards [3, 27, 29, 250, 251] but also in annual crops [252–255]. In addition to minimizing changes in shoot water status, deficit irrigation is able to control the balance between fruit and vegetative growth, with likely positive impact on fruit quality [8, 256].

Future Directions

Drought has a great impact on the vegetative and reproductive development of annual and fruit tree crops and thereby impacts on final yield and seed and fruit quality. The key factors responsible for high yield under drought in annual plants are an appropriate phenology that will enable escaping drought and getting the timing of flowering right, high water-use efficiency and a high harvest index. The impact of drought is highly complex and involves diverse processes as photosynthesis, respiration, reserve accumulation, fertilization, gamete and embryo development, and fruit and seed development. Due to the complexity of crop reproduction and the still incomplete knowledge of mechanisms underlying the response of reproductive events under water stress, it has been until now difficult to construct a model system to guarantee successful reproductive development and high yield under water scarcity. How resource availability (namely carbohydrate reserve) influence the development of reproductive organs under water stress is among the least understood aspects. On fruit trees, it is also urgent to understand (1) how rootstock confers resistance and/or tolerance to drought to the scion cultivar to better adjust breeding strategies; (2) the key events of fruit ripening. In addition, differences between species imply different strategies to improve/maintain yield and quality under such conditions. Spatial strategies also differ: a particular trait may be associated with higher yield in one environment and may have no/or negative effect in other environment [13].

Conventional breeding still appears to be the most effective for a significant drought-tolerance improvement of new cultivars. The application of modern molecular tools to understand responses of crops to water scarcity has only recently begun. In addition, to integrate them in breeding programs it is imperative to incorporate an accurate measurement of the phenotype under water stress. However, the speed of molecular technologies is not matched by the speed on phenotyping, being the latter one of major limitations to improve selection methods for water-limited environments [19]. Moreover, it is imperative to integrate disciplines, as functional genomics, transcriptomics, proteomics and metabolomics with plant physiology to improve breeding strategies. This would allow researchers to address drought tolerance/resistance through an integrated approach based on the knowledge of expression of genes and their products at a particular phenological and developmental stage of the crop.

Bibliography

1. IPCC (2007) Climate change 2007: the physical basis summary for policy makers. Cambridge University Press, Cambridge
2. Blum A (2009) Effective use of water (EUW) and not water-use efficiency (WUE) is the target of crop yield improvement under drought stress. Field Crops Res 112:119–123
3. Fereres E, Soriano MA (2007) Deficit irrigation for reducing agricultural water use. J Exp Bot 58:147–159
4. Chaves MM, Davies B (2010) Drought effects and water use efficiency: improving crop production in dry environments. Funct Plant Biol 37(2):iii–vi
5. Reynolds MP, Pierre CS, Saad ASI, Vargas M, Condon AG (2007) Evaluating potential grains in wheat associated with stress-adaptive trait expression in elite genetic resources under drought and heat stress. Crop Sci 47:172–189
6. Reynolds M, Foulkes MJ, Slafer G, Berry P, Parry MAJ, Snape JW, Angus WJ (2009) Raising yield potential in wheat. J Exp Bot 60:1899–1918
7. Chaves MM, Pereira JS, Maroco J (2003) Understanding plant response to drought – from genes to the whole plant. Funct Plant Biol 30:239–264
8. Chaves MM, Oliveira MM (2004) Mechanisms underlying plant resilience to water deficits – Prospects for water-saving agriculture. J Exp Bot 55:2365–2384
9. Chaves MM, Flexas J, Pinheiro C (2009) Photosynthesis under drought and salt stress: regulation mechanisms from whole plant to cell. Ann Bot 103:551–560
10. Flexas J, Bota J, Loreto F, Cornic G, Sharkey TD (2004) Diffusive and metabolic limitations to photosynthesis under drought and salinity in C3 plants. Plant Biol 6:269–279
11. Neumann PM (2008) Coping mechanisms for crop plants in drought-prone environments. Ann Bot 101(7):901–907
12. Lawlor DW (2009) Musings about the effects of environment on photosynthesis. Ann Bot 103:543–549
13. Condon AG, Richards RA, Rebetzke GJ, Farquhar GD (2004) Breeding for high water use efficiency. J Exp Bot 55(407):2447–2460
14. Passioura J (2007) The drought environment: physical, biological and agricultural perspectives. J Exp Bot 58:113–117
15. Ribaut JM, Ragot M (2007) Marker-assisted selection to improve drought adaptation in maize: the backcross approach, perspectives, limitations and alternatives. J Exp Bot 58(2):351–360
16. Castiglioni P, Warner D, Bensen RJ, Anstrom DC, Harrison J, Stoecker M, Abad M, Kumar G, Salvador S, D'Ordine R, Navarro S, Back S, Fernandes M, Targolli J, Dasgupta S, Bonin C, Luethy MH, Heard JE (2008) Bacterial RNA chaperones confer abiotic stress tolerance in plants and improved grain yield in maize under water-limited conditions. Plant Physiol 147:446–455
17. Parry MAJ, Madgwick PJ, Bayon C, Tearall K, Hernandez-Lopez A, Baudo M, Rakszegi M, Hamada W, Al-Yassin A, Ouabbou H, Labhilili M, Phillips AL (2009) Mutation discovery for crop improvement. J Exp Bot 60:2817–2825
18. Richards RA, Rebetzke GJ, Condon A, van Herwaarden AF (2002) Breeding opportunities for increasing the efficiency of water use and crop yield in temperate cereals. Crop Sci 42:111–121
19. Richards RA, Rebetzke GJ, Watt M, Condon AG, Spielmeye W, Dolferus R (2010) Breeding for improved water productivity in temperate cereals: phenotyping, quantitative trait loci, markers and the selection environment. Funct Plant Biol 37:85–97
20. Araus JL, Ferrio JP, Buxo R, Voltas J (2007) The historical perspective of dryland agriculture: lessons learned from 10 000 years of wheat cultivation. J Exp Bot 58(2):131–145
21. Passioura JB (2002) Environmental biology and crop improvement. Funct Plant Biol 29:537–546
22. Passioura J, Angus JF (2010) Improving productivity of crops in water-limited environments. Adv Agron 106:37–75
23. Lafitte HR, Yongsheng G, Yan Y, Li ZK (2007) Whole plant responses, key processes, and adaptation to drought stress: the case of rice. J Exp Bot 58(2):169–175
24. Richards RA (1991) Crop improvement for temperate Australia: future opportunities. Field Crops Res 26(2):141–169
25. Blum A (2005) Drought resistance, water-use efficiency, and yield potential- are they compatible, dissonant, or mutually exclusive? Aust J Agric Res 56:1159–1168
26. Blum A, Arkin GF (1984) Sorghum root growth and water-use as affected by water supply and growth duration. Field Crops Res 9:131–142
27. Chaves MM, Santos TP, Souza CR, Ortuno MF, Rodrigues ML, Lopes CM, Maroco JP, Pereira JS (2007) Deficit irrigation in grapevine improves water-use efficiency while controlling vigour and production quality. Ann Appl Biol 150:237–252
28. Johnson RS, Handley DF (2000) Using water stress to control vegetative growth and productivity of temperate fruit trees. HortScience 35:1048–1050
29. Chaves MM, Zarrouk O, Francisco R, Costa JM, Santos T, Regalado AP, Rodrigues ML, Lopes CM (2010) Grapevine under deficit irrigation: hints from physiological and molecular data. Ann Bot 105:661–676
30. Lockard RG, Schneider GW (1981) Stock and scion growth relationships and the dwarfing mechanism in apple. Hortic Rev 3:315–375
31. Landsberg JJ, Jones HG (1981) Apple orchards. In: Kozlowski TT (ed) Water deficits and plant growth, vol 6. Academic, London, pp 419–469
32. Atkinson CJ, Policarpo M, Webster AD, Kingswel G (2000) Drought tolerance of clonal Malus determined from measurements of stomatal conductance and leaf water potential. Tree Physiol 20:557–563
33. Repo-Carrasco R, Espinoza C, Jacobsen CE (2003) Nutritional value and use of the Andean crops quinoa (*Chenopodium quinoa*) and kañiwa (*Chenopodium pallidicaule*). Food Reviews Int 19:179–189
34. Jacobsen SE (2003) The worldwide potential for quinoa (*Chenopodium quinoa* Willd.). Food Reviews Int 19:167–177

35. Jacobsen SE, Monteros C, Corcuera LG, Bravo LA, Christiansen JL, Mujica A (2007) Frost resistance mechanisms in quinoa (*Chenopodium quinoa* Willd.). Eur J Agron 26:471–475
36. Bertero HD, de la Vega AJ, Correa G, Jacobsen SE, Mujica A (2004) Genotype and genotype-by-environment interaction effects for grain yield and grain size of quinoa (*Chenopodium quinoa* Willd.) as revealed by pattern analysis of multi-environment trials. Field Crops Res 89:299–318
37. FAO (2006) FAOSTAT data, FAO Statistical databases FAOSTAT. www.fao.org
38. Jacobsen SE, Mujica A (2003) The genetic resources of Andean grain amaranths (*Amaranthus caudatus* L., *A. cruentus* and *A. hipochondriacus* L.) in America. Plant Genet Resour Newsl 133:41–44
39. Bressani R, Gonzales JM, Zuniga J, Brauner M, Elias LG (1987) Yield, selected chemical composition and nutritive value of 14 selections of amaranth grain representing four species. J Sci Food Agric 38:347–356
40. Vinocur B, Altman A (2005) Recent advances in engineering plant tolerance to abiotic stress: achievements and limitations. Curr Opin Biotechnol 16(2):123–132
41. Levitt J (1972) Responses of plants to environmental stresses. Academic, New York
42. Turner NC (1986) Crop water deficits: a decade of progress. Adv Agron 39:1–51
43. Ludlow MM (1989) Strategies of response to water stress. In: Kreeb KH, Richter H, Hinckley TM (eds) Structural and functional responses to environmental stresses. SPB Academic, The Hague, pp 269–281
44. Blum A, Sinmena B, Mayer J, Golan G, Shpiler L (1994) Stem reserve mobilization supports wheat-grain filling under heat stress. Aust J Plant Physiol 21:771–781
45. Chaves MM, Pereira JS, Rodrigues ML, Ricardo CPP, Osório ML, Carvalho I, Faria T, Pinheiro C (2002) How plants cope with water stress in the field: photosynthesis and growth. Ann Bot 89:907–916
46. Bruce WB, Edmeades GO, Barker TC (2002) Molecular and physiological approaches to maize improvement for drought tolerance. J Exp Bot 53:13–25
47. Yang J, Zhang J, Huang Z, Zhu Q, Wang L (2000) Remobilization of carbon reserves is improved by controlled soil-drying during grain filling of wheat. Crop Sci 40: 1645–1655
48. Yang JC, Zhang JH, Wang ZQ, Zhu QS, Wang W (2001) Remobilization of carbon reserves in response to water deficit during grain filling of rice. Field Crops Res 71:47–55
49. Rodrigues ML, Pacheco CMA, Chaves MM (1995) Soil–plant relations, root distribution and biomass partitioning in *Lupinus albus* L. under drought conditions. J Exp Bot 46:947–956
50. Levy PE, Moncrieff JB, Massheder JM, Jarvis PG, Scott SL, Brouwer J (1997) CO_2 fluxes at leaf and canopy scale in millet, fallow and tiger bush vegetation at the HAPEX-Sahel southern super-site. J Hydrol 188–189:612–632
51. Ehleringer JR, Cooper TA (1992) On the role of orientation in reducing photoinhibitory damage in photosynthetic-twig desert shrubs. Plant Cell Environ 15:301–306
52. Larcher W (2000) Temperature stress and survival ability of Mediterranean sclerophyllous plants. Plant Biosyst 134: 279–295
53. Huang B (1997) Roots and drought resistance. Turfgrass performance during drought depends heavily on root characteristics. Golf Course Management June:55–58
54. Vijn I, Smeekens S (1999) Fructan: more than a reserve carbohydrate? Plant Physiol 120:351–359
55. Pinheiro C, Cruz de Carvalho MH, Bartels D, Ricardo CP, Chaves MM (2008) Dehydrins in *Lupinus albus*: pattern of protein accumulation and gene expression in response to drought. Funct Plant Biol 35:85–91
56. Anderson CM, Kohorn BD (2001) Inactivation of Arabidopsis SIP1 leads to reduced levels of sugars and drought tolerance. J Plant Physiol 158:1215–1219
57. Bohnert HJ, Nelson DE, Jensen RG (1995) Adaptations to environmental stresses. Plant Cell 7:1099–1111
58. Serraj R, Sinclair TR (2002) Osmolyte accumulation: can it really help increase crop yield under drought conditions? Plant Cell Environ 25:333–341
59. Turner NC, Abbo S, Berger JD, Chaturvedi SK, French RJ, Ludwig C, Mannur DM, Singh SJ, Yadava HS (2007) Osmotic adjustment in chickpea (Cicer arietinum L.) results in no yield benefit under terminal drought. J Exp Bot 58(2):187–194
60. Monteith JL (1977) Climate and the efficiency of crop production in Britain. Phil Trans R Soc Lond B 281:277–294
61. Long SP, Zhu X-G, Naidu SL, Ort DR (2006) Can improvement in photosynthesis increase crop yields? Plant Cell Environ 29: 315–330
62. Passioura JB (1977) Grain yield, harvest index, and water use of wheat. J Aust Inst Agric Sci 43:117–121
63. Passioura JB (2006) Increasing crop productivity when water is scarce – from breeding to field management. Agr Water Manage 80:176–196
64. Araus JL, Slafer GA, Reynolds MP, Royo C (2002) Plant breeding and water relations in C3 cereals: what should we breed for? Ann Bot 89:925–940
65. Condon AG, Richards RA, Rebetzke GJ, Farquhar GD (2002) Improving intrinsic water-use efficiency and crop yield. Crop Sci 42:122–131
66. Richards RA, Passioura JB (1989) A breeding program to reduce the diameter of the major xylem vessel in the seminal roots of wheat and its effect on grain yield in rain-fed environments. Aust J Agric Res 40:943–950
67. Flexas J, Ribas-Carbó M, Diaz-Espejo A, Galmés J, Medrano H (2008) Mesophyll conductance to CO2: current knowledge and future prospects. Plant Cell Environ 31:602–621
68. Lawlor DW, Tezara W (2009) Causes of decreased photosynthetic rate and metabolic capacity in water-deficient leaf cells: a critical evaluation of mechanisms and integration of processes. Ann Bot 103:561–579

69. Bunce JA (1997) Does transpiration control stomatal responses to water vapour pressure deficit? Plant Cell Environ 20:131–135
70. Franks PJ, Cowan IR, Farquhar GD (1997) The apparent feed forward response of stomata to air vapour pressure deficit: information revealed by different experimental procedures with two rainforest trees. Plant Cell Environ 20:142–145
71. Buckley TN, Mott KA, Farquhar GD (2003) A hydromechanical and biochemical model of stomatal conductance. Plant Cell Environ 26:1767–1785
72. Wilkinson S, Davies WJ (2002) ABA-based chemical signalling: the coordination of responses to stress in plants. Plant Cell Environ 25:195–210
73. Lake JA, Woodward FI, Quick WP (2002) Long-distance CO_2 signalling in plants. J Exp Bot 53:183–193
74. Cornic G, Gouvallec JL, Briantais JM, Hodges M (1989) Effect of dehydration and high light on photosynthesis of two C3 plants (*Phaseolus vulgaris* L. and *Elatastema repens* [Cour.] Hall f.). Planta 177:84–90
75. Loreto F, Tricoli D, Di Marco G (1995) On the relationship between electron transport rate and photosynthesis in leaves of the C4 plant Sorghum bicolor exposed to water stress, temperature changes and carbon metabolism inhibition. Aust J Plant Physiol 22:885–892
76. Takahashi S, Murata N (2008) How do environmental stresses accelerate photoinhibition? Trends Plant Sci 13:179–182
77. Foyer CH, Noctor G (2009) Redox regulation in photosynthetic organisms: signaling, acclimation, and practical Implications. Antioxid Redox Signal 11:861–905
78. Demmig-Adams B, Adams WW III (1996) The role of xanthophyll cycle carotenoids in the protection of photosynthesis. Trends Plant Sci 1:21–26
79. Ort DR (2001) When there is too much light. Plant Physiol 125:29–32
80. Matsubara S, Gilmore AM, Osmond CB (2001) Diurnal and acclimatory responses of violaxanthin and *lutein epoxide* in the Australianmistletoe *Amyema miquelii*. Aust J Plant Physiol 28:793–800
81. Wingler A, Lea PJ, Quick WP, Leegood RC (2000) Photorespiration, metabolic pathways and their role in stress protection. Phil Trans R Soc Lond B 355:1517–1529
82. Biehler K, Fock H (1996) Evidence for the contribution of the Mehler peroxidase reaction in dissipating excess electrons in drought-stressed wheat. Plant Physiol 112:265–272
83. Melis A (1999) Photosystem-II damage and repair cycle in chloroplasts: what modulates the rate of photodamage in vivo? Trends Plant Sci 4:130–135
84. Bota J, Medrano H, Flexas J (2004) Is photosynthesis limited by decreased Rubisco activity and RuBP content under progressive water stress? New Phytol 162:671–681
85. Grassi G, Magnani F (2005) Stomatal, mesophyll conductance and biochemical limitations to photosynthesis as affected by drought and leaf ontogeny in ash and oak trees. Plant Cell Environ 28:834–849
86. Flexas J, Ribas-Carbó M, Bota J, Galmés J, Henkle M, Martínez-Cañellas S, Medrano H (2006) Decreased Rubisco activity during water stress is induced by stomatal closure, not by decreased relative water content. New Phytol 172:73–82
87. Galmés J, Ribas-Carbó M, Medrano H, Flexas J (2010) Rubisco activity in Mediterranean species is regulated by the chloroplastic CO_2 concentration under water stress. J Exp Bot (in press)
88. Peet MM, Kramer PJ (1980) Effects of decreasing source-sink ratio in soybeans on photosynthesis, photorespiration, transpiration and yield. Plant Cell Environ 3:201–206
89. Borrás L, Slafer GA, Otegui ME (2004) Seed dry weight response to source-sink manipulations in wheat, maize and soybean: a quantitative reappraisal. Field Crops Res 86: 131–146
90. Gimeno TE, Sommerville KE, Valladares F, Atkin OK (2010) Homeostasis of respiration under drought and its important consequences for foliar carbon balance in a drier climate: insights from two contrasting Acacia species. Funct Plant Biol 37:323–333
91. Ribas-Carbo M, Taylor NL, Giles L, Busquets S, Finnegan PM, Day DA, Lambers H, Medrano H, Berry JA, Flexas J (2005) Effects of water stress on respiration in soybean (*Glycine max*. L.) leaves. Plant Physiol 139:466–473
92. Galmés J, Ribas-Carbo M, Medrano H, Flexas J (2007) Response of leaf respiration to water stress in Mediterranean species with different growth forms. J Arid Environ 68:206–222
93. Atkin OK, Macherel D (2009) Crucial role plant mitochondria orchestrating drought tolerance. Ann Bot 103:581–597
94. Wingler A, QuickWP BRA, Bailey KJ, Lea PJ, Leegood RC (1999) The role of photorespiration during drought stress, an analysis utilizing barley mutants with reduced activities of photorespiratory enzymes. Plant Cell Environ 22:361–373
95. Long SP, Bernacchi CJ (2003) Gas exchange measurements, what can they tell us about the underlying limitations to photosynthesis? Procedures and sources of error. J Exp Bot 54:2393–2401
96. Osmond CB, Badger MR, Maxwell K, Björkman O, Leegood RC (1997) Too many photons: photorespiration, photoinhibition and photooxidation. Trends Plant Sci 2:119–121
97. Brestic M, Cornic G, Fryer MJ, Baker NR (1995) Does photorespiration protect the photosynthetic apparatus in French bean leaves from photoinhibition during drought stress? Planta 196:450–457
98. Igamberdiev AU, Mikkelsen TN, Ambus P, Bauwe H, Lea PJ, Gardeström P (2004) Photorespiration contributes to stomatal regulation and carbon isotope fractionation: a study with barley, potato and Arabidopsis plants deficient in glycine decarboxylase. Photosynth Res 81:139–152
99. Boyer JS, Westgate ME (2004) Grain yields with limited water. J Exp Bot 55(407):2385–2394
100. Munns R, James RA, Sirault XR, Furbank RT, Jones HG (2010) New phenotyping methods for screening wheat and barley for beneficial responses to water deficit. J Exp Bot 61:3499–3507

101. Saini HS, Lalonde S (1998) Injuries to reproductive development under water stress, and their consequences for crop productivity. J Crop Prod 1:223–248
102. Saini HS, Westgate ME (2000) Reproductive development in grain crops during drought. In: Spartes DL (ed) Advances in agronomy, vol 68. Academic, SanDiego, pp 59–96
103. Boyer JS, McLaughlin JE (2007) Functional reversion to identify controlling genes in multigenic responses: analysis of floral abortion. J Exp Bot 58(2):267–277
104. García-Tejero I, Jiménez-Bocanegra JA, Martínez G, Romero R, Durán-Zuazo VH, Muriel-Fernández JL (2010) Positive impact of regulated deficit irrigation on yield and fruit quality in a commercial citrus orchard [*Citrus sinensis* (L.) Osbeck, cv. Salustiano]. Agr Water Manage 97(5):614–622
105. Winkel T, Renno JF, Payne WA (1997) Effect of the timing of water deficit on growth, phenology and yield of pearl millet (*Pennisetum glaucum* (L.) R. Br.) grown in Sahelian conditions. J Exp Bot 48:1001–1009
106. King RW, Evans LT (1977) Inhibition of flowering in *Lolium temulentum* L. by water stress: a role for abscisic acid. Aus J Plant Physiol 4:225–233
107. Saini HS, Aspinall D (1981) Effect of water deficit on sporogenesis in wheat (*Triticum aestivum* L.). Ann Bot 48:623–633
108. Rodrigo J, Hormaza IJ, Herrero M (2000) Ovary starch reserves and flower development in apricot (Prunus armeniaca). Physiol Plant 108(1):35–41
109. Engin H (2006) Scanning electron microscopy of floral initiation and developmental stages in 'Glohaven' peach under water deficit. Bangladesh J Bot 35(2):163–168
110. Alburquerque N, Burgos L, Egea J (2003) Apricot flower bud development and abscission related to chilling, irrigation and type of shoots. Sci Hortic 98(3):265–276
111. Southwick SM, Davenport TL (1986) Characterization of water stress and low temperature effects on floral induction in citrus. Plant Physiol 81:26–29
112. Jones HG (1987) Repeat flowering in apple caused by water stress or defoliation. Trees Struct Funct 1(3):135–138
113. Crisosto CH, Sugar D, Lombard P (1988) Effects of putrescine sprays at anthesis on 'Comice' pear yield component. Adv Hortic Sci 2:27–29
114. Koshita Y, Takahara T (2004) Effect of water stress on flower-bud formation and plant hormone content of satsuma mandarin (*Citrus unshiu* Marc.). Sci Hortic 99(3-4):301–307
115. Akhalalkatsi M, Losch R (2005) Water limitation effect on seed development and germination in *Trigonella coerulea* (Fabaceae). Flora 200:493–501
116. Mohan Ram HY, Rao IVR (1984) Physiology of flower bud growth and opening. Proc Indian Acad Sci Plant Sci 93: 253–274
117. Campbell DR (1996) Evolution of floral traits in a hermaphroditic plant: field measurements of heritabilities and genetic correlations. Evolution 50:1442–1453
118. Barnabas B, Jager K, Feher A (2008) The effect of drought and heat stress on reproductive processes in cereals. Plant Cell Environ 31:11–38
119. Fang X, Turner NC, Yan G, Li F, Siddique KHM (2010) Flower number, pod production, pollen viability, and pistil function are reduced and flower and pod abortion increased in chickpea (*Cicer arietinum* L.) under terminal drought. J Exp Bot 61(2):335–345
120. Porch TG, Jahn M (2001) Effect of high temperature stress on microsporogenesis in heat-sensitive and heat-tolerant genotypes of *Phaseolus vulgaris*. Plant Cell Environ 24:723–731
121. Blum A (1998) Improving wheat grain filling under stress by stem reserve mobilisation. Euphytica 100:77–83
122. Dorion S, Lalonde S, Saini HS (1996) Induction of male sterility in wheat by meiotic stage water deficit is preceded by a decline in invertase activity and changes in carbohydrate metabolism in anthers. Plant Physiol 111:137–145
123. Sheoran IS, Saini HS (1996) Drought-induced sterility in rice: changes in carbohydrate levels and enzyme activities associated with the inhibition of starch accumulation in pollen. Sex Plant Reprod 9:161–169
124. Koonjul PK, Minhas JS, Nunea C, Sheoran IS, Saini HS (2005) Selective transcriptional down-regulation of anther invertases precedes the failure of pollen development in water-stressed wheat. J Exp Bot 56:179–190
125. Xuemei JI, Shiran B, Wan J, Lewis DC, Jenkins CLD, Condon AG, Richards RA, Dolferus R (2010) Importance of pre-anthesis anther sink strength for maintenance of grain number during reproductive stage water stress in wheat. Plant Cell Environ 33:926–942
126. Liu JX, Bennett J (2010) Reversible and irreversible drought induced changes in the anther proteome of rice (*Oryza sativa* L.) genotypes IR64 and Moroberekan. Mol Plant. doi:10.1093/mp/ssq039
127. Saini HS, Sedgley M, Aspinall D (1984) Developmental anatomy in wheat of male sterility induced by heat stress, water deficit or abscisic acid. Aust J Plant Physiol 11:243–253
128. Turner LB (1993) The effect of water stress on florl characters, pollination and seed set in white clover (*Trifolium repens* L.). J Exp Bot 44:1155–1160
129. Nguyen GN, Hailstones DL, Wilkes M, Sutton BG (2009) Drought-induced oxidative conditions in rice anthers leading to a programmed cell death and pollen abortion. J Agron Crop Sci 195(3):157–164
130. Ruiz-Sanchez MC, Egea J, Galego R, Torrecillas A (1999) Floral biology of 'Bulida' apricot trees subjected to postharvest drought stress. Ann Appl Biol 135(2):523–528
131. Esparza G, DeJong TM, Weinbaum SA, Klein I (2001) Effects of irrigation deprivation during the harvest period on yield determinants in mature almond trees. Tree Physiol 21(14): 1073–1079
132. Matthews MA, Anderson MM (1989) Reproductive development in Vitis vinifera: responses to seasonal water deficits. Am J Enol Vitic 40:52–60
133. Johnson RS, Handley DF, DeJong TM (1992) Long-term response of early maturing peach trees to postharvest water deficits. J Am Soc Hortic Sci 117:881–886

134. Ussahatanonta S, Jackson DI, Rowe RN (1996) Effects of nutrient and water stress on vegetative and reproductive growth in *Vitis vinifera* L. Aust J Grape Wine Res 2:64–69
135. Torrecillas A, Domingo R, Galego R, Ruiz-Sánchez MC (2000) Apricot tree response to withholding irrigation at different phenological periods. Sci Hortic 85(3):201–215
136. Schussler JR, Westgate ME (1994) Increasing assimilate reserves does not prevent kernel abortion at low water potential in maize. Crop Sci 34:1569–1576
137. Boyer JS (2010) Drought decision-making. J Exp Bot 61(13):3493–3497
138. McLaughlin JE, Boyer JS (2004) Glucose localization in maize ovaries when kernel number decreases at low water potential and sucrose is fed to the stems. Ann Bot 94:75–86
139. McLaughlin JE, Boyer JS (2004) Sugar-responsive gene expression, invertase activity, and senescence in aborting maize ovaries at low water potentials. Ann Bot 94:675–689
140. Hiyane R, Hiyane S, Ching Tang A, Boyer JS (2010) Sucrose feeding reverses shade-induced kernel losses in maize. Ann Bot 106(3):395–403
141. Yu L, Setter TL (2003) Comparative transcriptional profiling of placenta and endosperm in developing maize kernels in response to water deficit. Plant Physiol 131:568–582
142. Ji X, Shiran B, Wan J, Lewis DC, Jenkins CLD, Condon AG, Richards RA, Dolferus R (2010) Importance of pre-anthesis anther sink strength for maintenance of grain number during reproductive stage water stress in wheat. Plant Cell Environ 33:926–942
143. Kokubun M, Shimada S, Takahashi M (2001) Flower abortion caused by pre-anthesis water deficit is not attributed to impairment of pollen in soybean. Crop Sci 4:1517–1521
144. Lebon G, Wojnarowiez G, Holzapfel B, Fontaine F, Vaillant-Gaveau N, Clément C (2008) Sugars and flowering g in the grapevine (*Vitis vinifera* L.). J Exp Bot 59((10):2565–2578
145. Setter TL, Flannigan BA, Melkonian J (2001) Loss of kernel set due to water deficit and shade in maize: carbohydrate supplies, abscisic acid, and cytokinins. Crop Sci 41:1530–1540
146. Setter TL, Parra R (2010) Relationship of carbohydrate and abscisic acid levels to kernel set in maize under post-pollination water deficit. Crop Sci 50:980–988
147. Zinselmeier C, Westgate ME, Schussler JR, Jones RJ (1995) Low water potential disrupts carbohydrate metabolism in maize (*Zea mays* L.) ovaries. Plant Physiol 107:385–391
148. Young TE, Gallie DR (2000) Regulation of programmed cell death in maize endosperm by abscisic acid. Plant Mol Biol 42:397–414
149. Mäkela P, McLaughlin JE, Boyer JS (2005) Imaging and quantifying carbohydrate transport to the developing ovaries of maize. Ann Bot 96:939–949
150. Çakir R (2004) Effect of water stress at different developmental stages on vegetative and reproductive growth of corn. Field Crop Res 89:1–16
151. Brevedan RE, Egli DB (2003) Crop physiology and metabolism: short period of water stress during seed filling, leaf senescence, and yield of soybean. Crop Sci 43:2083–2088
152. Yang J, Zhang J, Wang Z, Zhu Q, Liu L (2003) Activities of enzymes involved in sucrose-to-starch metabolism in rice grains subjected to water stress during grain filling. Field Crop Res 81:69–81
153. Yang JC, Zhang JH, Wang ZQ, Xu GW, Zhu QS (2004) Activities of key enzymes in sucrose-to-starch conversion in wheat grains subjected to water deficit during grain filling. Plant Physiol 135:1621–1629
154. Samarah NH (2005) Effects of drought stress on growth and yield of barley. Agron Sustain Dev 25(1):145–149
155. Mi G, Chen F, Zhang F (2009) Grain filling rate is limited by insufficient sugar supply in the large-grain wheat cultivar. J Plant Breed Crop Sci 1(3):60–64
156. Yang J, Zhang J (2005) Grain filling of cereals under soil drying. New Phytol 169:223–236
157. Nicolas ME, Gleadow RM, Dalling MJ (1985) Effect of post-anthesis drought on cell-division and starch accumulation in developing wheat grains. Ann Bot 55:433–444
158. Gooding MJ, Ellis RH, Shewry PR, Schofield JD (2003) Effects of restricted water availability and increased temperature on the grain filling, drying and quality of winter wheat. J Cereal Sci 37(3):295–309
159. Younesi O, Moradi A (2009) The effect of water limitation in the field on sorghum seed germination and vigor. Aust J Basic Appl Sci 3(2):1156–1159
160. Rotundo JL, Westgate ME (2009) Meta-analysis of environment effects on soybean seed composition. Field Crops Res 110:147–156
161. Pinheiro C, Rodrigues AP, Saraiva de Carvalho I, Chaves MM, Ricardo CP (2005) Sugar metabolism in developing lupin seeds affected by a short-term water deficit. J Exp Bot 56:2705–2712
162. Saint Pierre C, Peterson CJ, Ross AS, Ohm JB, Verhoeven MC, Larson M, Hoefer B (2008) White wheat grain quality changes with genotype, nitrogen fertilization and water stress. Agron J 100(2):414–420
163. Kim KS, Park SH, Jenks MA (2007) Changes in leaf cuticular waxes of sesame (*Sesamum indicum* L.) plants exposed to water deficit. J Plant Physiol 164(9):134–1143
164. Larson KD, DeJong TM, Johnson RS (1988) Physiological and growth responses of mature peach trees to postharvest water stress. J Am Soc Hortic Sci 113:296–300
165. Girona J, Mata M, Arbones A, Alegre S, Rufat J, Marsal J (2003) Peach tree response to single and combined regulated deficit irrigation regimes under shallow soils. J Am Soc Hortic Sci 128:432–440
166. Naor A, Stern R, Peres M, Greenblat Y, Gal Y, Flaishman MA (2005) Timing and severity of postharvest water stress affect following-year productivity and fruit quality of field-grown 'Snow Queen' nectarine. J Am Soc Hortic Sci 130:806–812
167. Lopez G, Girona J, Marsal J (2007) Response of winter root starch concentration to severe water stress and fruit load and its subsequent effects on early peach fruit development. Tree Physiol 27(11):1619–1626

168. Goldhamer DA, Viveros M (2000) Effects of preharvest irrigation cutoff durations and postharvest water deprivation on almond tree performance. Irrigation Sci 19:125–131
169. Marsal J, Lopez G, Arbones A, Mata M, Vallverdu X, Girona J (2009) Influence of postharvest deficit irrigation and pre-harvest fruit thinning on sweet cherry (cv. New Star) fruit firmness and quality. J Hortic Sci Biotechnol 84:273–278
170. Fernandes-silva AA, Ferreira TC, Correia CM, Malheiro AC, Villalobos FJ (2010) Influence of different irrigation regimes on crop yield and water use efficiency of olive. Plant Soil 333:35–47
171. Moriana A, Orgaz F, Pastor M, Fereres E (2003) Yield responses of a mature olive orchard to water deficits. J Am Soc Hortic Sci 128:425–431
172. Greven M, Neal S, Green S, Dichio B, Clothier B (2009) The effects of drought on the water use, fruit development and oil yield from young olive trees. Agric Water Manage 96:1525–1531
173. Gucci R, Lodolini EM, Rapoport HF (2009) Water deficit-induced changes in mesocarp cellular processes and the relationship between mesocarp and endocarp during olive fruit development. Tree Physiol 29(12):1575–1585
174. Medrano H, Escalona JM, Cifre J, Bota J, Flexas J (2003) A ten-year study on the physiology of two Spanish grapevine cultivars under field conditions: effects of water availability from leaf photosynthesis to grape yield and quality. Funct Plant Biol 30:607–619
175. Savin R, Nicolas ME (1996) Effects of short periods of drought and high temperature on grain growth and starch accumulation of two malting barley cultivars. Aust J Plant Physiol 23:201–21
176. Guttieri MJ, Bowen D, Gannon D, O'Brien K, Souza E (2001) Solvent retention capacities of irrigated soft white spring flours. Crop Sci 41:1054–1061
177. Tollenaar M, Lee ED (2002) Yield potential, yield stability and stress tolerance in maize. Field Crops Res 75:161–169
178. Gusta LV, Chen THH (1987) The physiology of water and temperature stress. In: Heyne EG (ed) Wheat and wheat improvement nº13, 2nd edn. ASA/CSSA/SSSA, Madison, pp 115–150
179. Coles GD, Jamieson PD, Haslemore RM (1991) Effects of moisture stress on malting quality in triumph barley. J Cereal Sci 14:161–177
180. Lozovaya VV, Lygin AV, Ulanov AV, Nelson RL, Daydé J, Widholm JM (2005) Effect of temperature and soil moisture status during seed development on soybean seed isoflavone concentration and composition. Crop Sci 45:1934–1940
181. Ali Q, Ashraf M, Anwar F (2010) Seed composition and seed oil antioxidant activity of maize under water stress. J Am Oil Chem Soc 87(10):1179–1187
182. Lindeboom N, Chang PR, Tyler RT (2004) Analytical, biochemical and physicochemical aspects of starch granule size, with emphasis on small granule starches: a review. Starch Starke 56:89–99
183. Dai Z (2009) Starch granule size distribution in grains at different positions on the spike of wheat (*Triticum aestivum* L.). Starch Stärke 61(10):582–589
184. Zhao CX, He MR, Wang ZL, Wang YF, Lin Q (2009) Effects of different water availability at post-anthesis stage on grain nutrition and quality in strong-gluten winter wheat. CR Biol 332(8):759–764
185. Kumar V, Rani A, Solanki S, Hussain SM (2006) Influence of growing environment on the biochemical composition and physical characteristics of soybean seed. J Food Compos Anal 19:188–195
186. Carrera C, Martinez MJ, Dardanelli J, Balzarini M (2009) Water deficit effect on the relationship between temperature during the seed fill period and soybean seed oil and protein concentrations. Crop Sci 49:990–998
187. Carvalho IS, Ricardo CPP, Chaves MM (2005) Seeds chemical composition of two lupines (*Lupinus albus* and *Lupinus mutabilis*) influenced by water stress. J Agron Crop Sci 191:95–98
188. Nayyar H, Singh S, Kaur S, Kumar S, Upadhyaya HD (2006) Differential sensitivity of macrocarpa and microcarpa types of chickpea (*Cicer arietinum* L.) to water stress: association of contrasting stress response with oxidative injury. J Integr Plant Biol 48:1318–1329
189. Genard M, Souty M, Holmes S, Reich M, Breuils L (1994) Correlations among quality parameters of peach fruit. J Sci Food Agric 66:241–245
190. Mercier V, Bussi C, Lescourret F, Genard M (2009) Effects of different irrigation regimes applied during the final stage of rapid growth on an early maturing peach cultivar. Irrigation Sci 27(4):297–306
191. Gelly M, Recasens I, Mata M, Arbones A, Rufat J, Girona J, Marsal J (2003) Effects of water deficit during stage II of peach fruit development and postharvest on fruit quality and ethylene production. J Hortic Sci Biotechnol 78:324–330
192. Gelly M, Recasens I, Girona J, Mata M, Arbones A, Rufat J, Marsal J (2004) Effects of stage II and postharvest deficit irrigation on peach quality during maturation and after cold storage. J Sci Food Agric 84:561–568
193. Connor DJ (2005) Adaptation of olive (*Olea europaea* L.) to water environments. Aust J Agric Res 56:1181–1189
194. Proietti P, Famiani F, Tombesi A (1999) Gas exchange in olive fruit. Photosynthetica 36(3):423–432
195. Stefanoudaki E, Williams M, Chartzoulakis K, Harwood J (2009) Effect of irrigation on quality attributes of olive oil. J Agric Food Chem 57(15):7048–7055
196. Bravdo B, Hepner Y, Loinger C, Tabacman H (1985) Effect of irrigation and crop level on growth, yield and wine quality of Cabernet Sauvignon. Am J Enol Vitic 36:132–139
197. Kennedy JA, Matthews MA, Waterhouse AL (2002) Effect of maturity and vine water status on grape skin and wine flavonoids. Am J Enol Vitic 53:268–274
198. Deluc LG, Quilici DR, Decendit A, Grimplet J, Wheatley MD, Schlauch KA, Mérillon JM, Cushman JC, Cramer GR (2009) Water deficit alters differentially metabolic pathways affecting

important flavour and quality traits in grape berries of Cabernet Sauvignon and Chardonnay. BMC Genomics 10:212
199. Coombe BG (1989) The grape berry as a sink. Acta Hortic 239:149–158
200. Gollop R, Farhi S, Perl A (2001) Regulation of the leucoanthocyanidin dioxygenase gene expression in Vitis vinifera. Plant Sci 161:579–588
201. Gollop R, Even S, Colova-Tsolova V, Perl A (2002) Expression of the grape dihydroflavonol reductase gene and analysis of its promoter region. J Exp Bot 53:1397–1409
202. Bindon KA, Dry PR, Loveys BR (2007) Influence of plant water status on the production of C13-norisoprenoid precursors in *Vitis vinifera* L. cv. Cabernet Sauvignon grape berries. J Agric Food Chem 55:4493–4500
203. Pérez-Pastor A, Ruiz-Sánchez MC, Martínez JA, Norte PA, Artés F, Domingo R (2007) Effect of deficit irrigation on apricot fruit quality at harvest and during storage. J Sci Food Agric 87(13):2409–2415
204. Gómez-Rico A, Salvador MD, Moriana A, Pérez D, Olmedilla N, Ribas F, Fregapane G (2007) Influence of different irrigation strategies in a traditional Cornicabra cv. olive orchard on virgin olive oil composition and quality. Food Chem 100(2):568–578
205. Cattivelli L, Rizza F, Badeck FW, Mazzucotelli E, Mastrangelo AM, Francia E, Mare C, Tondelli A, Stanca AM (2008) Drought tolerance improvement in crop plants: an integrated view from breeding to genomics. Field Crops Res 105(1–2):1–14
206. Atlin G (2003) Improving drought tolerance by selecting for yield. In: Fischer KS, Lafitte R, Fukai S, Atlin Q, Hardy B (eds) Breeding rice for drought-prone environments. IRRI, Los Bańos, Philippines, pp 14–22
207. Jackson P, Robertson M, Cooper M, Hammer G (1996) The role of physiological understanding in plant breeding; from a breeding perspective. Field Crops Res 49:11–39
208. Evans LT (1993) Crop evolution, adaptation and yield. Cambridge University Press, Cambridge
209. Loss SP, Siddique KHM (1994) Morphological and physiological traits associated with wheat yield increases in Mediterranean environments. Adv Agron 52:229–276
210. Araus JL (1996) Integrative physiological criteria associated with yield potential. In: Reynolds MP, Rajaram S, McNab A (eds) Increasing yield potential in wheat: breaking the barriers. CIMMYT, Mexico DF, pp 150–167
211. Richards RA (1996) Defining selection criteria to improve yield under drought. Plant Growth Regul 20:157–166
212. Slafer GA, Araus JL (1998) Improving wheat responses to abiotic stresses. In: Slinkard AE (ed) Proceedings of the 9th international wheat genetics symposium vol 1. University of Saskatchewan Extension Press, Saskatoon, pp 201–213
213. Edmeades GO, Bolaños J, Chapman SC, Lafitte HR, Banziger M (1999) Selection improves drought tolerance in tropical maize populations: I. Gains in biomass, grain yield, and harvest index. Crop Sci 39:1306–1315
214. López-Castañeda CR, Richards RA (1994) Variation in temperate cereals in rainfed environments. I. Grain yield, biomass and agronomic characteristics. Field Crops Res 37:51–62
215. Richards RA, Rawson HM, Jonhson DA (1986) Glaucousness in wheat: its development and effect on water-use efficiency, gas exchange and photosynthetic tissues temperatures. Aust J Plant Physiol 13:465–473
216. Araus JL, Bort J, Steduto P, Villegas D, Royo C (2003) Breeding cereals for Mediterranean conditions: ecophysiological clues for biotechnology application. Ann Appl Biol 142:129–141
217. Slafer GA, Araus JL (2007) Physiological traits for improving wheat yield under a wide range of conditions. In: Spiertz JHJ, Struik PC, van Laar HH (eds) Scale and complexity in plant systems research: gene-plant-crop relations. Springer, Dordrecht, pp 147–156
218. Webster T (2002) Dwarfing rootstocks: past, present and future. Compact Fruit Tree 35(3):67–72
219. Reighard GL, Loreti L (2009) Rootstock development. In: Layne DR, Bassi D (eds) The peach: botany production and uses. CABI, Cambridge, pp 193–220
220. Hammatt N (1992) Progress in the biotechnology of trees. World J Microbiol Biotechnol 8(4):369–377
221. Zarrouk O, Pinochet J, Gogorcena Y, Moreno MA (2006) Graft compatibility between peach cultivars and *Prunus* rootstocks. Hortic Sci 41:1389–1394
222. Zarrouk O, Testillano PS, Risueño MC, Moreno MA, Gogorcena Y (2010) Changes in cell/tissue organization and peroxidase activity as markers for early detection of graft incompatibility in peach/plum combinations. J Am Soc Hortic Sci 135:9–17
223. Steel KA, Virk DS, Kumar R, Prasad SC, Witcombe JR (2007) Field evaluation of upland rice lines selected for QTLs controlling root traits. Field Crops Res 101(2):180–186
224. Giuliani S, Sanguineti MC, Tuberosa R, Bellotti M, Salvi S, Landi P (2005) Root-ABA1, a major constitutive QTL, affects maize root architecture and leaf ABA concentration at different water regimes. J Exp Bot 56:3061–3070
225. Landi P, Sanguineti MC, Liu C, Li Y, Wang TY, Giuliani S, Belloti M, Salvi S, Tuberosa R (2007) Root-ABA1 QTL affects root lodging, grain yield, and other agronomic traits in maize grown under well-watered conditions. J Exp Bot 58:319–326
226. Harris K, Subudhi PK, Borrell A, Jordan D, Rosenow D, Nguyen H, Klein P, Klein R, Mullet J (2007) Sorghum stay-green QTL individually reduce post-flowering drought-induced leaf senescence. J Exp Bot 58:327–338
227. Sadok W, Naudin P, Boussuge B, Muller B, Welcker C, Tardieu F (2007) Leaf growth rate per unit thermal time follows QTL-dependent daily patterns in hundreds of maize lines under naturally fluctuating conditions. Plant Cell Environ 30(2):135–146
228. Welcker C, Boussuge B, Bencivenni C, Ribaut JM, Tardieu F (2007) Are source and sink strengths genetically linked in maize plants subjected to water deficit? A QTL study of the responses of leaf growth and of anthesis-silking interval to water deficit. J Exp Bot 58:339–349
229. Wang JW, Yang FP, Chen XQ, Liang RQ, Zhang LQ, Geng DM, Zhang XD, Song YZ, Zhang GS (2006) Induced expression of DREB transcriptional factor and study on its physiological

effects of drought tolerance in transgenic wheat. Acta Genetica Sinica 33:468–476
230. Maccaferri M, Sanguineti MC, Corneti S, Araus JL, Ben Salem M, Bort J, DeAmbrogio E, Garcia del Moral L, Demontis A, El-Ahmed A, Elouafi I, Maalouf F, Machlab H, Martos V, Nachit MN, Nserallah N, Ouabbou H, Royo C, Slama A, Villegas D, Tuberosa R (2008) Quantitative trait loci for grain yield and adaptation of durum wheat (*Triticum durum* Desf.) across a wide range of water availability. Genetics 178:489–511
231. Hall NM, Griffiths H, Corlett JA, Jones HG, Lynn J, King GJ (2005) Relationships between water-use traits and photosynthesis in Brassica oleracea resolved by quantitative genetic analysis. Plant Breed 124(6):557–564
232. Laza MR, Kondo M, Ideta O, Barlaan E, Imbe T (2006) Identification of quantitative trait loci for delta 13 C and productivity in irrigated lowland rice. Crop Sci 46:763–773
233. Spielmeyer W, Hyles J, Joaquim P, Azanza F, Bonnett D, Ellis ME, Moore C, Richards RA (2007) A QTL on chromosome 6A in bread wheat (*Triticum aestivum*) is associated with longer coleoptiles, greater seedling vigour and final plant height. Theor Appl Genet 115:59–66
234. Tuberosa R, Salvi S (2006) Genomics-based approaches to improve drought tolerance of crops. Trends Plant Sci 11:405–412
235. Vargas M, van Eeuwijk FA, Crossa J, Ribaut JM (2006) Mapping QTLs and QTL x environment interaction for CIMMYT maize drought stress program using factorial regression and partial least squares methods. Theor Appl Genet 112:1009–1023
236. Collins NC, Tardieu F, Tuberosa R (2008) Quantitative trait loci and crop performance under abiotic stress: where do we stand? Plant Physiol 147:469–486
237. Bogeat-Triboulot MB, Brosché M, Renaut J, Jouve L, Le Thiec D, Fayyaz P, Vinocur B, Witters E, Laukens K, Teichmann T, Altman A, Hausman JF, Polle A, Kangasjärvi J, Dreyer E (2007) Gradual soil water depletion results in reversible changes of gene expression, protein profiles, ecophysiology, and growth performance in *Populus euphratica*, a poplar growing in arid regions. Plant Physiol 143:876–892
238. Hummel I, Pantin F, Sulpice R, Piques M, Rolland G, Dauzat M, Christophe A, Pervent M, Bouteillé M, Stitt M, Gibon Y, Muller B (2010) Arabidopsis plants acclimate to water deficit at low cost through changes of carbon usage: an integrated perspective using growth, metabolite, enzyme, and gene expression analysis. Plant Physiol 154:357–372
239. Valliyodan B, Nguyen HT (2006) Understanding regulatory networks and engineering for enhanced drought tolerance in plants. Curr Opin Plant Biol 9(2):189–195
240. Nelson DE, Repetti PP, Adams TR, Creelman RA, Wu J, Warner DC, Anstrom DC, Bensen RJ, Castiglioni PP, Donnarummo MG, Hinchey BS, Kumimoto RW, Maszle DR, Canales RD (2007) Plant nuclear factor Y (NF-Y) B subunits confer drought tolerance and lead to improved corn yields on water-limited acres. Proc Natl Acad Sci 104: 16450–16455
241. Habash DZ, Kehel Z, Nachit M (2009) Genomic approaches for designing durum wheat ready for climate change with a focus on drought. J Exp Bot 60(10):2805–2815
242. Yang XH, Wen XG, Gong HM, Lu QT, Yang ZP, Tang YL, Liang Z, Lu CM (2007) Genetic engineering of the biosynthesis of glycinebetaine enhances thermotolerance of photosystem II in tobacco plants. Planta 225:719–733
243. Zhu JM, Alvarez S, Marsh EL, LeNoble ME, Cho IJ, Sivaguru M, Chen SX, Nguyen HT, Wu YJ, Schachtman DP et al (2007) Cell wall proteome in the maize primary root elongation zone. II. Region specific changes water soluble lightly ionically bound proteins water deficit. Plant Physiol 145:1533–1548
244. Rivero RM, Kojima M, Gepstein A, Sakakibara H, Mittler R, Gepstein S, Blumwald E (2007) Delayed leaf senescence induces extreme drought tolerance in a flowering plant. Proc Natl Acad Sci 104:19631–19636
245. Vanderauwera S, De Block M, Van de Steene N, van de Cotte B, Metzlaff M, Van Breusegem F (2007) Silencing of poly(ADP-ribose) polymerase in plants alters abiotic stress signal transduction. Proc Natl Acad Sci 104:15150–15155
246. Tognetti VB, Palatnik JF, Fillat MF, Melzer M, Hajirezaei M-R, Valle EM, Carrillo N (2006) Functional replacement of ferredoxin by a cyanobacterial flavodoxin in tobacco confers broad-range stress tolerance. Plant Cell 18:2035–2050
247. Pasquali G, Biricolti S, Locatelli F, Baldoni E, Mattana M (2008) Osmyb4 expression improves adaptive responses to drought and cold stress in transgenic apples. Plant Cell Rep 27: 1677–1686
248. Lopes MS, Reynolds MP (2010) Partitioning of assimilates to deeper roots is associated with cooler canopies and increased yield under drought in wheat. Funct Plant Biol 37:147–156
249. Saint Pierre C, Trethowan R, Reynolds M (2010) Stem solidness and its relationship to water-soluble carbohydrates: association with wheat yield under water deficit. Funct Plant Biol 37:166–174
250. Beis A, Patakas A (2010) Differences in stomatal responses and root: shoot signalling between two grapevine varieties subjected to drought. Funct Plant Biol 37:139–146
251. Collins MJ, Fuentes S, Barlow EWR (2010) Partial rootzone drying and deficit irrigation increase stomatal sensitivity to vapour pressure deficit in anisohydric grapevines. Funct Plant Biol 37:128–138
252. Kang S, Zhang J (2004) Controlled alternate partial root-zone irrigation: its physiological consequences and impact on water use efficiency. J Exp Bot 55:2437–2446
253. Dodd IC, Theobald JC, Bacon MA, Davies WJ (2006) Alternation of wet and dry sides during partial rootzone drying irrigation alters root-to-shoot signalling of abscisic acid. Funct Plant Biol 33:1081–1089
254. Kirda C, Topcu S, Cetin M, Dasgan HY, Kaman H, Topaloglu F, Derici MR, Ekici B (2007) Prospects of partial root zone irrigation for increasing irrigation water use efficiency of major crops in the Mediterranean region. Ann Appl Biol 150:281–291

255. Wang Y, Liu F, Andersen MN, Jensen CR (2010) Improved plant nitrogen nutrition contributes to higher water use efficiency in tomatoes under alternate partial root-zone irrigation. Funct Plant Biol 37:175–182
256. Davies WJ, Wilkinson S, Loveys B (2002) Stomatal control by chemical signalling and the exploitation of this mechanism to increase water use efficiency in agriculture. New Phytol 153:449–460

Crop Responses to Nitrogen

Gilles Lemaire
INRA, Lusignan, France

Article Outline

Glossary
Definition
Introduction
N in Plants
Crop N Demand
Regulation of Crop N Uptake
Diagnosis of Crop N Status: Nitrogen Nutrition Index
Crop Responses to N Deficiency
Nitrogen Use Efficiency in Crops
Conclusion
Future Directions
Bibliography

Glossary

Critical plant N concentration Critical plant N concentration is defined as the minimum plant nitrogen concentration of a crop corresponding to its maximum crop mass.

Critical crop N uptake Critical crop N uptake is defined as the minimum crop nitrogen uptake for achieving maximum crop mass.

Harvest index (HI) Harvest index (HI) is the ratio between harvested biomass Y (grains, tubers) and aboveground crop mass W at crop maturity.

Intercepted photosynthetic active radiation (IPAR) Intercepted Photosynthetic Active Radiation (IPAR) is the proportion of the incident PAR which is intercepted by the crop at a given time. This proportion is related to the size of the canopy, the Leaf Area Index, and depends also on canopy structure: leaf angle and geometry.

Leaf area index (LAI) Leaf area index (LAI) is the total canopy leaf area of a crop per unit of soil area. LAI allows the estimation of the proportion of the incident light which is intercepted by the canopy, and then which can be used for photosynthesis of the whole crop.

Nitrogen absorption efficiency (NAE) Nitrogen absorption efficiency (NAE) is the increase in crop nitrogen uptake per unit of supplemental N supply rate.

Nitrogen conversion efficiency (NCE) Nitrogen conversion efficiency (NCE) is the increase in crop dry mass (dW) or in crop yield (dY) per unit of supplemental crop N uptake corresponding to an increase in nitrogen supply rate.

Nitrogen use efficiency (NUE) Nitrogen use efficiency (NUE) is the increase in crop dry mass (dW) or in crop yield (dY) per unit of supplemental N supply rate. So NUE = NAE × NCE.

N dilution N dilution is the process corresponding to more rapid accumulation of nitrogen-free compounds than nitrogen compounds within plant as plant grows, leading to decline in plant nitrogen concentration with plant mass accumulation.

Nitrogen nutrition index (NNI) Nitrogen nutrition index (NNI) is an index which allows the estimation of the crop nitrogen status. This index is calculated at any moment as the ratio between the actual plant nitrogen concentration of the crop and the critical plant N concentration (see this definition) corresponding to the actual crop mass.

Photosynthetic active radiation (PAR) Photosynthetic active radiation (PAR) is the part of solar radiation spectrum corresponding to wavelengths that are active for photosynthesis.

Radiation use efficiency (RUE) Radiation use efficiency (RUE) is the ratio between the quantity of biomass accumulated within a crop and the quantity of photosynthetic active radiation (PAR) intercepted by this crop during the same period of time.

RuBPc-o Ribulose bisphophate carboxylase/oxygenase, the enzyme located within chloroplasts which allows the carboxylation of CO_2.

Definition

A prerequisite for the analysis of crop responses to nitrogen (N) is the determination of the plant nitrogen content and repartition. How much N is incorporated within plants and crops? Within which plant tissue? For which physiological function? Thus, according to the answers to these questions, it is possible to determine a *critical plant nitrogen status* as the minimum plant N concentration that allows the maximum plant (or crop) growth rate. It has been demonstrated that this critical plant N concentration decreases as plant grows as the result of an ontogenetic plant architecture development leading to a *dilution of N* compounds within increasing proportion of free-N compounds as plant gets bigger. This N dilution process can be formulated through a negative power relationship between plant N concentration and crop mass. This critical N dilution curve allows the discrimination of situations of N deficiency (below the curve) and situations of N luxury consumption (above the curve). So a Nitrogen Nutrition Index (NNI) can be calculated for quantifying the intensity of N deficiency or N luxury of any crop at any stage of its life cycle. This possibility for determination of crop N status and for quantification of N deficiency either in terms of intensity or timing allows the complete inversion of the approach: instead of response of crop to N supply, the problem is to study the response of crop to N deficiency. By this way, the check treatment is the non-limiting N conditions where crop growth potential is limited only by genetics and climate. Then the effect of intensity and timing of N deficiency period on the different plant growth processes and yield component elaboration can be studied with a more generic approach. This new method for analysis of the effect of plant N nutrition on crop yield allows the identification of physiological, agronomical, and genetical ways for improving nitrogen use efficiency of crops.

Introduction

Nitrogen is considered to be the most important limiting factor, after water deficit, for crop production worldwide. Over the last 50 years, the worldwide use of mineral fertilizers is one of the key elements for producing sufficient food to meet the demand of increasing human population [1, 2]. During this period, the use of mineral N fertilizers in agriculture systems increased sevenfold in parallel with the doubling of agricultural food production. This huge amount of mineral N is provided by industrial processes of chemical reduction of atmospheric nitrogen. So even if this resource can be considered as quantitatively non-limited, the energy cost of the Haber–Bosch process necessary to obtain mineral N fertilizers and the large greenhouse gas emission associated with oblige to reconsider the sustainability of the use of mineral N in agriculture. Moreover, the use of large amounts of N in intensive agriculture production systems has led to important environmental problems such as the eutrophication of freshwater [3] and marine ecosystems [4], pollution of ground water, and gaseous emissions of N oxides and ammonia in the atmosphere [5, 6]. In consequence, problems associated with sustainable development, global changes, environment protection, and global food security are now questioning the efficiency of use of N fertilizers in agricultural systems [7].

During the last decades, the relatively high products/fertilizer price ratio, incited farmers to adopt an insurance strategy in fertilizer management: applying excess of N to avoid any restriction in crop N supply and then any penalty in crop yield. These practices, when they were generalized on large agricultural areas led to a progressive increase in soil N surplus accumulation and an elevated risk of N leaching with dramatic consequences on ground water quality [8]. Adoption of a more restricted strategy for supplying and timing of N fertilizers is now a prerequisite for a more sustainable agriculture development. But such a strategy is difficult to be adopted in practice because of the non-predictable variations in weather which determines both soil N mineralization and crop growth potential. In consequence, a reduction in N application rates to avoid surplus of N in soils would increase the probability of temporary crop N nutrition deficiency, and then, as a consequence, an increased risk for a lower crop production and then a deterioration of the economic outputs the farmers are expecting. Therefore, optimizing crop production with the goal of reducing environment hazards requires an improvement in the understanding of the regulatory mechanisms by which crops absorb nitrogen from the soil and use it efficiently for yield component and quality elaboration.

But it requires also a better understanding of soil microbial processes and the interaction between C and N cycles in order to optimize crop N residue cycling, soil organic matter dynamics, and to improve the capacity to predict soil N supply.

Fertilization management has to be conceived as a mean to match as closely as possible crop N supply with crop N demand in order to limit accumulation of mineral N within soils, and then emissions to hydrosphere and atmosphere. By this way, matching timing of N supply with timing of crop N demand appears very necessary. It is fundamental to underline here the necessity for a high precision for adjustment of N supply to N demand: for an intensive wheat crop producing about 8 t ha^{-1} of grain, the total N demand is about 240 kgN ha^{-1} and the loss of only 20 kgN ha^{-1} through leaching (i.e., less than 10% of the total N demand) can lead to pass over the admissible limit of nitrate concentration (50 mg l^{-1}) in drainage water! Moreover, the loss of only 2–3 kgN ha^{-1} through emission of N_2O to atmosphere (that corresponds to 1% of the total N demand) is considered as highly detrimental for greenhouse gas effect. So the problem to face now is not to understand how the yield of the different crop species can be improved by addition of N fertilizers, but (i) to determine the dynamics of crop N demands all along the crop development cycle; (ii) to determine the timing of the soil N supply according to soil characteristics, climate, and soil agronomic management; (iii) to determine the crop responses to different intensity and timing of N nutrition deficiency; and then (iv) to manage timing of crop N fertilization using diagnostic and decision tools for optimizing trade-off between minimizing crop yield reduction and minimizing environmental impacts.

N in Plants

For most of the crop species, plant life cycle can be roughly divided into two main phases: (i) the vegetative growth phase, when young developing roots and leaves behave as sink organs that absorb and assimilate inorganic nitrogen for amino acid and protein synthesis, and (ii) the remobilization phase when senescing tissues start to behave as source organs translocating organic molecules to ensure formation of new developing and/or storage organs [9]. The first phase is dominated by the dynamic of leaf area expansion as a mean for light capture, and then the role of nitrogen in both leaf growth and leaf photosynthesis is capital. The second phase is dominated by the development of reproductive organs such as seeds, fruits, tubers, and bulbs, or by storage organs allowing survival for perennial species such as trunks for trees or roots and stubbles for herbaceous species like grasses. As a consequence, the same N absorbed by the plant can be used successively for different functions and then analysis of crop response to N nutrition cannot be simply reduced to an addition of different elementary functions, but as a complex and integrated adaptive system with strong interactions among different processes.

In plants, N is required primarily for the synthesis of proteins, both structural and enzymatic, as the more important components of cells. There is large variation in the composition of the different cell types within a plant according to the different types of tissues. Cells which store carbohydrates or are part of support and transport tissues have relatively lower protein and nucleic acid concentration than metabolically active cells within meristems and photosynthetic parenchyma [10]. The relative numbers of each type of cells determine the organ composition. So organs that have relatively slow metabolism but are specialized in support and transport, such as roots and stems, contain little protein and thus have small N concentration in dry matter. Organs which store starch or other carbohydrate, such as grains, fruits, and tubers, have also low N concentration. On the contrary, leaves having a high metabolic activity through photosynthesis have high N concentrations. So, plants are very heterogeneous systems in terms of N concentration at every level of organization: cells, tissues, and organs. Therefore plant N demand, i.e., the quantity of N required for the plant to achieve its potential growth and development, depends on the morphologic and histologic plant composition.

Leaves are essential organs by which plants capture light and assimilate carbon. Light capture, photosynthesis, and the associated respiratory processes require a large number of different enzymes, pigments, and proteins [11]. About 50% of the soluble protein of the leaf is in RuBPc-o enzyme alone, another 25% is in the light harvesting and electron transport components [11].

Thus the chloroplast, as the location of RuBPc-o and other photosynthetic enzymes, and according to its high protein membrane component, contains the major part of the total leaf N. Composition of leaves and their N concentration varies with age, development stage, and environment. Leaves of cereals have the greatest concentration of N just after their full expansion that corresponds to their maximum in photosynthetic activity. After a period the N concentration in the leaves decreases in parallel with metabolic activity as senescence progresses [12]. Remobilization of N-components occurs during the senescence process, and then amino acids from proteolysis are transported to younger developing leaves, or reproductive organs. A consequence of this ageing and senescing processes is that older leaves situated in the lower canopy where light intensity is limiting for photosynthesis, provide N for new leaf production at the top of the canopy. This recycling process thus tends to optimize photosynthesis in relation to N supply and light at the level of the canopy [13].

To achieve large rates of photosynthesis in well-illuminated conditions, leaves require a large concentration of RuBPc-o and other N-components and, hence, large N concentration [14]. As N supply rises, the amount of N per unit area in leaves increases, enhancing the rate of CO_2 assimilation [12, 15]. Thus, there is a good correlation between CO_2 assimilation rate and leaf N content. However, with very large N supply, leaf N content may increase without any increase of photosynthetic rate, unless larger CO_2 concentrations are used [16]. Plants with C_3 photosynthetic pathway contain more N per unit leaf area than those with C_4 metabolism. So C_4 crops use N more efficiently than C_3 ones [17]. Ample N increases the number of chloroplast compared with deficient N. Also the density of protein in the stroma is increased by large N supply. All these processes contribute to accumulate N within leaf tissues as plant N supply increases.

Although the primary role of RuBPc-o in plants is to assimilate CO_2, a storage function for N has been mooted for this enzyme [18, 19]. Thus, N of RuBPc-o have two successive functions within plants: CO_2 assimilation and source of N supply for reproductive and storage organs. Storage of N within the plants for further reuse can be considered as an adaptive mechanism for buffering plant N nutrition in highly variable soil N supply conditions. In this way, plants can store N reserves during periods of vegetative growth and large soil N availability, and then to reuse these N compounds at the end of their life cycle when mineral soil N is exhausted. Accumulation of RuBPc-o in excess within leaf tissues is not the only way for plant to store N. Accumulation of vegetative storage proteins (VSP) within different plant tissues or organs is a complementary way for storing N reserves, as demonstrated in alfalfa [20] and in perennial grasses [21]. For perennial plants, the storage of N reserves within perennial organs such as roots, rhizomes, tubers, or trunks is a prerequisite for regrowth after defoliation or after winter.

Due to the importance of light capture and photosynthesis for plant growth, much attention has been paid to allocation of N to leaves within canopies. However, allocation of N to other vegetative tissues is also quantitatively important. Green leaf N content represents only 53% of total shoot N in a lucerne crop [22], and only 30% of shoot N in a wheat crop at the beginning of the grain filling period [23]. Lemaire et al. [24] showed that for a large number of crop species there exists trade-off between accumulation of N in leaves for optimizing crop photosynthesis and accumulation of N within stem tissues for optimizing the plant architecture development and the elaboration of reproductive organs.

N compounds as amino acid and proteins are used within meristematic tissues for initiation and expansion of new organs: leaves, stem internodes, tillers, and branches and roots, and also inflorescences, fruits, and seeds. The use of N for leaf area expansion during vegetative growth period is of first importance because it determines the dynamics of LAI expansion of the crop and then the capacity of the crop to intercept light and to accumulate biomass. The rate at which N is supplied to meristems greatly determines cell production rate while the final cell size is only little affected [25–27]. As cells enlarge in size, their N concentration decreases through a dilution by accumulation of greater quantities of N-free compounds until final size is reached. So any limitation of N supply to meristem tissues leads to a reduction in the cell production rate and in the size of the final organ produced. For reproductive meristems, shortage of N reduces more the number of grains than the grain size [28–30].

When analyzed at the level of a plant population, it has been clearly demonstrated that N is allocated to individual plants according to their own contribution to interception of light [31]. N resources are allocated preferentially to dominant plants and then stressed plants cannot respond to N supply because of the lack of light. In consequence, competition for light among individual plants within a dense canopy determines greatly competition for N resources.

In conclusion, plants and canopies are very heterogeneous systems in terms of N content, concentration, and repartition. This heterogeneity can be analyzed at different levels of organization: organite, cell, tissue, organ, whole plant, and plant population. N compounds, mainly as proteins are involved in all metabolic processes and then they are used successively for different functions such as cell division, organ growth and development, light capture, photosynthesis and respiration, reserve formation and recycling. Once absorbed by the plant, N is used several times through internal recycling processes and reallocation to the different plant parts. So analysis of plant N nutrition is very complex because it involves several interdependent metabolic functions and due to constant feedback mechanisms, it can be studied only through a dynamic approach.

Crop N Demand

Crop N demand (N expressed in kg ha^{-1}) at any time of the crop cycle can be defined as the result of critical crop mass (Wc) that is the maximum crop mass attainable in a given environment without any limitation of nutrients and its critical plant N concentration % Nc [32]:

$$N = \%Nc\,Wc \tag{1}$$

The critical plant N concentration (%Nc) has been defined as the minimum plant N concentration corresponding to maximum crop mass [33]. This concept can be applied in dynamic terms, such that the daily crop N demand (or critical N uptake rate expressed in kg ha^{-1} day^{-1}) is the quantity of N the crop has to absorb each day to maintain its potential growth rate over a given period of time.

Many studies conducted on a large range of crop species (see [34] for a review) have shown that the critical plant N concentration (%Nc) is regularly decreasing as crop mass accumulates during the crop growth period. Moreover, it has been shown that this dynamic of decline in %Nc could be represented by a unique and constant relationship whatever the conditions and the genotypes for a same species [35]:

$$\%Nc = a(Wc)^{-b} \tag{2}$$

Coefficient a represents the critical plant N concentration for Wc = 1t ha^{-1}. Coefficient b is dimensionless, and it represents the dynamic of the dilution of N within the dry matter.

Mixing Eqs. 1 and 2 allows the expression of the dynamics of the critical crop N uptake, i.e., the crop N demand, in relation with the dynamics of potential crop biomass accumulation:

$$Nc = a'(Wc)^{1-b} \tag{3}$$

where coefficient a' is the crop N demand (or the critical N uptake) for a potential crop mass accumulation of 1 t ha^{-1}. Value of a' is equal to 10a, when a is expressed in % and a' is expressed in kg ha^{-1}.

Values of a (and a') and b have been established for the main cultivated species according to the method developed on wheat by Justes et al. [36]. This method as illustrated on Fig. 1 requires a family of response curves of plant N concentration (%N) vs crop mass (W) across increasing N supply rates. For each response curve, the critical plant N concentration (%Nc) is estimated as the intersection point between the oblique line representing the response of both %N and W to increased rate of N supply, and the vertical line representing the increase in %N with further N supply rates once the maximum crop mass (Wc) is reached that correspond to luxury N accumulation. As the determination of %Nc is done at different stages of growth for a large range of value of W, then it is possible to fit the series of %Nc–Wc data points for getting the critical N dilution curve and to calculate the value of coefficients a and b.

These values are presented in Table 1. For a given species, coefficients a (and a') and b remained constant whatever the climatic conditions (years and locations). Moreover, Lemaire et al. [37] showed that for wheat, maize, canola, sorghum, and sunflower the same value of coefficients holds either in temperate or in

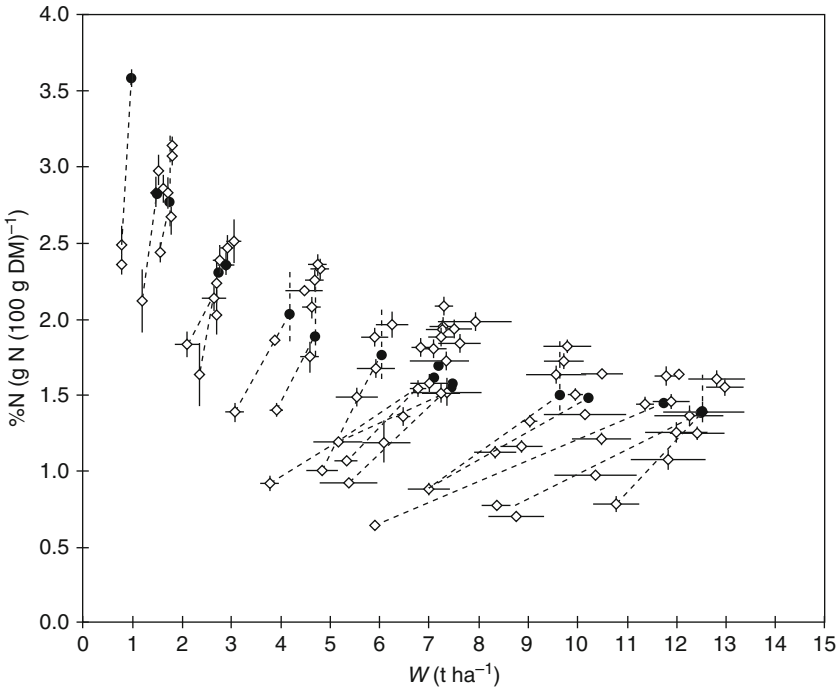

Crop Responses to Nitrogen. Figure 1
Determination of the critical plant nitrogen (N) concentration of maize crops as the intersection point between the *oblique line* corresponding to the response of both plant nitrogen concentration (%N) and crop mass (*W*) to increasing nitrogen supply rates, and the *vertical line* corresponding to the increases in plant N concentration without corresponding increase in crop mass that corresponds to luxury nitrogen accumulation [46]

subtropical conditions. Comparison among species allows a clear distinction between C_3 and C_4 groups for the value of coefficient a (and a') while coefficient b is unaffected by the type of the metabolic pathway. Within each of the metabolic groups, it is difficult to establish clear differences between species because of the high correlation between the coefficient a (or a') and b. Then the fitted curves corresponding to Eq. 2 for the different crop species are relatively close to each other [38].

The derivative of Eq. 3 allows the expression of the crop N demand in dynamic terms:

$$\frac{dN}{dt} = \frac{dN}{dW}\frac{dW}{dt} = a_c(1-b)W^{-b}\left(\frac{dW}{dt}\right) \quad (4)$$

Equation 4 shows that the daily crop N demand follows the daily crop growth rate, but for a similar daily crop growth rate, the daily crop N demand declines as the crop mass increases.

A theory has been developed for explaining the close relationship between crop N demand and crop biomass accumulation rate [33, 35]. The hypothesis is that plant mass W is composed of two compartments: Wm, the metabolic tissues involved directly in plant growth processes (photosynthesis and meristem activity) with a high N concentration %Nm; and Ws, the structural tissues involved in plant architecture and transport with a low N concentration %Ns. Then:

$$W = \mathrm{Wm} + \mathrm{Ws} \quad (5)$$

and:

$$\%\mathrm{N} = \frac{1}{\mathrm{W}}(\%\mathrm{Nm}\mathrm{Wm} + \%\mathrm{Ns}\mathrm{Ws}) \quad (6)$$

Supposing that Wm increases allometrically with W, then:

Crop Responses to Nitrogen. Table 1 Values of coefficient a' and b of Eq. 3, $N = a'(Wc)^{1-b}$, for different crop species

Crop species	a' (kgN ha^{-1})	b (dimensionless)	References
Temperate grasses (C_3)	48	0.32	[39, 40]
Alfalfa (C_3)	48	0.33	[41]
Pea (C_3)	51	0.32	[42]
Wheat (C_3)	53	0.44	[36]
Canola (C_3)	45	0.25	[43]
Rice (C_3)	52	0.52	[44]
Tomato (C_3)	45	0.33	[45]
Maize (C_4)	34	0.37	[46]
Sorghum (C_4)	39	0.39	[47]
Tropical grasses (C_4)	36	0.34	[48]

$$\mathrm{Wm} = kW^{\alpha} \tag{7}$$

and then:

$$\%\mathrm{N} = k(\%\mathrm{Nm} - \%\mathrm{Ns})W^{\alpha-1} + \%\mathrm{Ns} \tag{8}$$

This equation is very close to the empirical Eq. 2. The main difference is the asymptotic value of %Nc which is equal to %Ns and not to zero. But the difference is very little for the range of W from 1 to 15 t ha^{-1} [35].

Following Hardwick [49] assumptions, it can be postulated that because Wm is associated mainly with photosynthesis it scales for plant area, and then to crop Leaf Area Index (LAI):

$$\mathrm{Wm} = p(\mathrm{LAI}) \tag{9}$$

and then:

$$\mathrm{LAI} = \frac{k}{p}W^{\alpha} \tag{10}$$

So Eqs 3 and 10 indicate that both N uptake and LAI are allometrically related to crop mass. For a large range of crop species, cultivated either under temperate or sub-tropical climate, the hypothesis for a common value of coefficients b and α cannot be rejected, but then a direct relation of proportionality could be established between crop N uptake and crop LAI [37]:

$$\mathrm{N} = \frac{a'p}{k}\mathrm{LAI} \tag{11}$$

So, at crop level, the dynamic of expansion of LAI is driving the crop N demand.

Lemaire et al. [37] showed that the two coefficients b and α evolves in parallel during the time course of the crop growth. Just after seedling, and until a crop mass of approximately 1.5 t ha^{-1} is reached the value of b and α is high, close to 0.90–0.95 while it decreases rapidly to a value of 0.6–0.7 after this stage when competition for light between individual plants within the canopy is established.

Lemaire et al. [37] tried to determine among the two parameters, crop mass or LAI, who is the fundamental driver of crop N demand. They concluded that Eq. 3 was the more robust across genotypes and environments, but in fact the two Eqs. 3 and 11 each represent an incomplete expression of the feedback regulation by shoot growth of N absorption capacity of the roots and of N partitioning within the canopy as described within the above section. A more complex analysis of N allocation between leaf and stem and of remobilization of N from old leaves would be necessary to better capture genotypic differences in N uptake capacities. Nevertheless, the robustness of the relationship between critical crop N uptake (Nc) or critical crop N concentration (%Nc) with crop mass accumulation (W) across environments and genotypes allows the use of these empirical relationships as a base for the determination of crop N demand and for diagnosis of crop N status.

Regulation of Crop N Uptake

The theory developed above indicates that plant N uptake seems to be regulated by plant growth itself. In steady state N supply conditions, plant N uptake is feedback regulated by shoot signals, with a positive signal from photosynthetic C supply and a negative one from reduced N recirculation to roots [50–52]. So the relationship between N uptake and LAI as attested by Eq. 11 can be explained by the fact that LAI expansion allowing increased light interception provides larger C supply to roots, and also increases N storage capacities within expanding leaves as

RuBPc-o that avoids the depletion of N uptake by recirculating reduced N compounds in the phloem. This leads to the proportionality between crop N uptake and LAI for most of the species, but the slope of the relationships, i.e., the N uptake per unit LAI, is variable across species according to their morphology and, more particularly, their leaf/stem ratio. So leaf area expansion is not the only way for plant to store reduced N. Stem growth and leaf thickness increase are also a possibility for sequestrating N to avoid the repression of N uptake capacity of roots. In consequence, a more general and stable relationship between N uptake and crop mass can be obtained as attested by Eq. 3. Nevertheless, this relationship is not linear because N uptake per unit of crop mass decreases as the LAI per unit of crop mass, i.e., the leaf area ratio (LAR) of the crop, decreases, that determines the N dilution effect.

In the field, in a variable N supply condition, plant N uptake is co-regulated by both crop growth rate potential and the soil N availability. Two groups of transport systems, with low and high affinity for nitrate, operate in plants [53]. Devienne-Barret et al. [54] have proposed a model accounting for this co-regulation of plant N uptake by soil nitrate concentration and plant growth:

$$\frac{\mathrm{d}N}{\mathrm{d}t} = a_c(1-b)\,W^{-b}\left(\frac{\mathrm{d}W}{\mathrm{d}t}\right)_{\max} \left[V_{\mathrm{H}}\frac{C}{K_{\mathrm{H}}+C} + V_{\mathrm{L}}\frac{C}{K_{\mathrm{L}}+C}\right] \tag{12}$$

where V and K are coefficients of the Michaelis–Menten formula and subscripts describe the high (H) and the low (L) affinity transport systems for nitrate; C is the actual concentration of nitrate in soil solution, W is the crop mass in t ha^{-1} and b is the allometric coefficient of Eq. 3.

Figure 2 represents the crop N uptake vs crop mass trajectories for different steady-state N supply conditions, i.e., C = constant. Among these curves, it is then possible to identify the critical N uptake curve as defined above. It is also possible to imagine that the maximum N uptake curve corresponds to the higher quantity of N a crop is able to accumulate at a given crop mass. The difference between this curve and the critical curve correspond to the quantity of luxury N the crop is able to store.

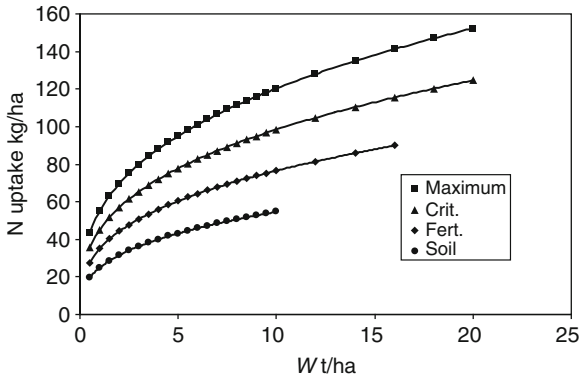

Crop Responses to Nitrogen. Figure 2
Nitrogen (N) Uptake – Crop Mass (W) trajectories for different steady states N supply: critical N uptake (Crit.), maximum N uptake (Maximum), non-fertilized (Soil), and suboptimal N application (Fert.). The two lines represent either (i) two growth stages of the same crop, (ii) two crops having different growth rate, or (iii) an environmental effect. The lines represent the response curves to increased N supply

So whatever the cause of the variation in crop mass provided that N supply remains at steady state, any increase in crop mass (ΔW) is accompanied by a corresponding increase in crop N uptake (ΔN). As soil N supply increases, plant N uptake increases as a consequence of both (i) the increase in soil N concentration (C) and (ii) the increase of plant growth rate itself. So, at any moment, crop growth rate is the consequence of crop N uptake and vice versa.

Diagnosis of Crop N Status: Nitrogen Nutrition Index

The main consequence of the theory developed above is that neither the plant N concentration nor the crop N uptake per se can indicate unequivocally the crop N nutrition status. Eqs. 2 and 3 indicate that these two variables have to be interpreted in relation with crop mass.

As shown in Fig. 2, the critical N uptake curve separate situations where N supply is limiting crop mass accumulation for situations where N is accumulated in excess without any supplemental increase in crop mass. For a given situation and at any time course of the growth period of the crop characterized by an actual crop N uptake (Na) corresponding to an actual

crop mass Wa, it is possible to determine a Nitrogen Nutrition Index (NNI) as the ratio between Na and the critical N uptake, Nc, corresponding to the same crop mass provided the critical N uptake of the crop species has been determined. NNI can also be determined directly from actual plant N concentration and dilution curves as illustrated in Fig. 3:

$$\mathrm{NNI} = \frac{\%\mathrm{Na}}{\%\mathrm{Nc}} \tag{13}$$

Values of NNI close to 1 indicate that at the date of the determination of Na or %Na the crop were in situation of non-limiting N supply. Values more than 1 indicate a luxury consumption of N. Values less than 1 indicate an N deficiency, the intensity of which can be estimated by the value of the NNI: a value of 0.6 indicating that crop N availability was only 60% of the critical level. Such an index of crop N status has been used as a diagnostic tool for analyzing a posteriori agronomical data from field experiments or farm observations in order to explain variations in yield by differences in crop N status [55].

Nevertheless, this approach does not take into account that the minimum plant N concentration is not 0 but is equal to %Ns (Eq. 8), which is the minimum plant N concentration for the plant to stay alive as postulated by Angus and Moncur [56]. So a more complex nitrogen nutrition index can be calculated:

$$\mathrm{NNI}' = \frac{\%\mathrm{Na} - \%\mathrm{Ns}}{\%\mathrm{Nc} - \%\mathrm{Ns}} \tag{14}$$

This new index, NNI′, is therefore physiologically more relevant than NNI, but it involves a greater degree of uncertainty related to the value of %Ns which has not been documented for many crop species. Lemaire and Gastal, [35] by using Eq. 8 derived a value of 0.77% and 0.82% for %Ns for wheat and maize, respectively. So variation in %Ns across crop species could be not very important. Therefore, the use of Eq. 2 for determining crop N status can be recommended owing to its simplicity.

NNI estimates the instantaneous crop N status at the period of time when actual plant N concentration %Na and actual crop mass Wa are estimated. But under changing N supply in the field, it is necessary to determine NNI several times during the growth cycle. An integrated value of NNI can be obtained by the weighted mean of NNI during the different growth periods, each time interval representing the duration in days or degree-days. Lemaire and Gastal [35] showed that it was possible to establish a linear relationship between the $\mathrm{NNI}_{\mathrm{int}}$ and the relative biomass accumulation as expressed as the ratio between actual (Wa) and potential (Wm) biomass:

$$\mathrm{Wa}/\mathrm{Wm} = K(\mathrm{NNI}_{\mathrm{int}} - \mathrm{NNI}_0) \tag{15}$$

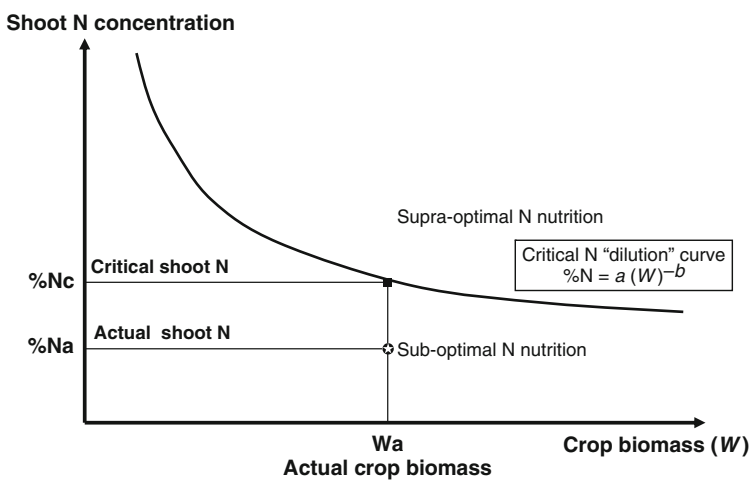

Crop Responses to Nitrogen. Figure 3
The use of the critical N dilution curve for the determination of the nitrogen nutrition index

where K is the response of the crop to increment in its average N nutrition status and NNI_0 is the minimum crop N status to allow plant growth. This minimum theoretically corresponds to %Ns.

Jeuffroy and Bouchard [57] characterizes the N deficiency period of a wheat crop by both its length (deficit N duration, (DD) and its intensity (ID) by means of the 1-NNI minimum observed value, and they calculated an integrated index of crop N status by the mean of the product ID × DD = IDD that represents about twice the area between the curve of NNIi dynamic and the horizontal line NNIi = 1 (Fig. 4). They showed that IDD explained 96% of the variation in grain number of wheat within a large experimental sites x years data set.

So it is clear that NNI is a good basic tool for analyzing actual plant status in crops, and then to interpret agronomical data in field conditions in order to detect if or not plant N deficiency periods occurred, with which intensity and timing and to analyze the consequences on crop growth and the crop yield components. But despite its high informative value as diagnostic tool for crop N status, NNI is difficult to use practically in field conditions and it remains more a research than an agronomical management tool. NNI determination is time consuming because of the necessity to determine crop mass. Then

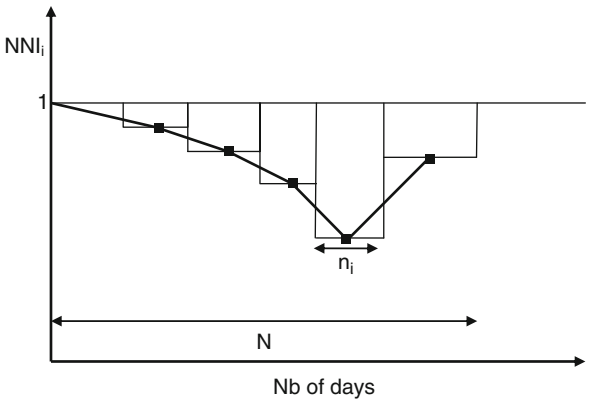

Crop Responses to Nitrogen. Figure 4
Estimation of NNIint from a sequential determination of NNI_i : $NNN_{int} = 1/N\ \Sigma NNI_i n_i$ The intensity of N deficiency (ID) is estimated by the lowest value of INN_i, and the duration of the deficiency (DD) is equal to the number of days with $NNI_i < 1$

it is necessary to use noninvasive and cost-effective methods for a rapid and operational determination of plant N status, and then to use NNI as a reference for calibration of these indirect methods.

The theory developed above showed that the N dilution effect and then the dependency of plant N concentration from the crop mass is the result of two processes: (i) the decline in plant leaf area ratio (LAR) as crop mass increases, and (ii) the preferential allocation of N to the well-illuminated upper layer of leaves as canopy develops. Therefore, Lemaire et al. [58] suggested that while plant N concentration declines with crop mass accumulation, the N content per unit of leaf area within the upper layer of leaves was more stable and would correlate well with the crop NNI. Then, it would be possible to use the N concentration of the well-illuminated leaf layer as an indicator of crop N status independently of the crop mass. Farrugia et al. (2004), using this correlation, were able to develop a method of diagnostics of grassland N status [59] and of maize crop N status [60]. The leaf N concentration can be measured directly from leaf samplings, but it can also be estimated indirectly by noninvasive methods. The leaf color chart (LCC) is an easy-to-use and inexpensive diagnostic tool for monitoring the relative greenness of a rice leaf as an indicator of the leaf and then of the plant N status [61]. The estimation of chlorophyll content of leaves by portable systems based on leaf transmittance or leaf reflectance in specific wave bands is also well correlated with leaf N content, and can be a method for crop N status diagnosis [62, 63]. But these predictions are in general dependant on cultivars and years [64]. Houlès et al. [65] demonstrated that through remote sensing it was possible to estimate both crop LAI and the quantity of chlorophyll per unit of soil area, and then the quantity of N within the canopy per unit of soil area. Therefore it would be possible to recalculate the NNI of the crop. Such an estimate can be intensively repeated in space and time that allows very precise information on the spatiotemporal dynamics of crop N status that is very useful for precision agriculture.

Crop Responses to N Deficiency

The use of the concept of critical crop N concentration and the possibility for diagnosis of the actual crop

N status totally reversed the approach of the response of crop to N fertilizers. The response of crop to N was studied by analyzing the response curve of yield to increasing fertilizer rates.

The difficulty for such an approach is that (i) the actual N supply for the crop is not known, because the quantity of N provided directly by the soil, and then the yield in absence of any fertilization is very variable, and (ii) the potential yield, i.e., the yield achievable in a given climatic condition when N supply can be considered as non-limiting is unknown. So, the crop N demand and the total crop N supply are unknown variables and it is possible to get only the regression between increment in yield and increments in N fertilization rates. This approach led to provide huge families of crop response curves to N fertilizers very variable to each other according to soils, climates, years, species, and cultivars, and the only way was to analyze this variability with statistic approaches with any possibility to identify and to quantify processes in order to develop prediction models.

The possibility for diagnosis crop N status allowed the identification of situations where crop growth and development were not limited by N deficiency, and then to develop crop potential growth models as resulting from climate conditions. Then using the critical N uptake concept, it was possible to derive from these models the dynamics of crop N demand all along the crop cycle. So instead of having the check treatment with no N fertilizer and to analyze response of crop to increments in N supply, the check treatment is now the crop with critical N status, and then the response of the crop to the occurrence of periods of N nutrition deficiency of different timing and intensity all along the crop growth cycle and the consequences on yield components and quality of the yield can be analyzed.

N Deficiency Effects on Crop Mass Accumulation

According to Monteith [66], crop mass accumulation is linearly related to the quantity of photosynthetic radiation (PAR) intercepted by a crop during its life cycle. The slope of this regression can be interpreted as the radiation use efficiency (RUE).

As illustrated in Fig. 5, and as shown by Bélanger et al. [67], N deficiency affects both the quantity of PAR intercepted by the crop and the efficiency with which

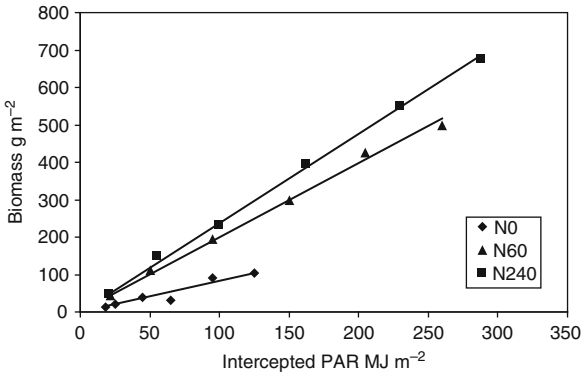

Crop Responses to Nitrogen. Figure 5
Relationships between the quantity of photosynthetic active radiation (*PAR*) intercepted by a tall fescue sward and the accumulation of aboveground biomass for three contrasted N supply rate: N0: no N application; N60: 60 kgN ha^{-1}; N240: 240 kgN ha^{-1}. The slope of the regression represents the radiation use efficiency [67]

the intercepted radiation is used for biomass elaboration (RUE). These authors, using NNI, have shown that in relative terms, RUE was more affected by moderate N deficiency (NNI = 0.6–0.8) than the quantity of PAR intercepted while for more severe deficiency, the response of the two variables converged. This type of response has been confirmed on sunflower [68] and on sorghum and maize [69]. LAI expansion seems a little bit more responsive to N deficiency than RUE: for an NNI of 0.6, RUE was reduced by 30% while LAI was reduced by 40% (Fig. 6).

RUE is an integrated variable accounting for photosynthesis and respiration, but also the allocation of assimilates to root [70]. These authors showed that, in fact, canopy gross photosynthesis was less affected by N deficiency than the accumulation of total biomass reflecting higher respiration losses in N-deficient crops, and the accumulation of shoot biomass was more affected than the accumulation of total biomass reflecting then an important increase of allocation of biomass to roots in N deficient situations. The lower shoot/root ratio in N deficient crops is widely documented [71, 72]. In fact this increased allocation of assimilate to roots is the consequence of the lower activity of shoot meristems (leaf and stem extension) that allows a greater quantity of carbon to be used for root growth. So the more sensible plant growth process

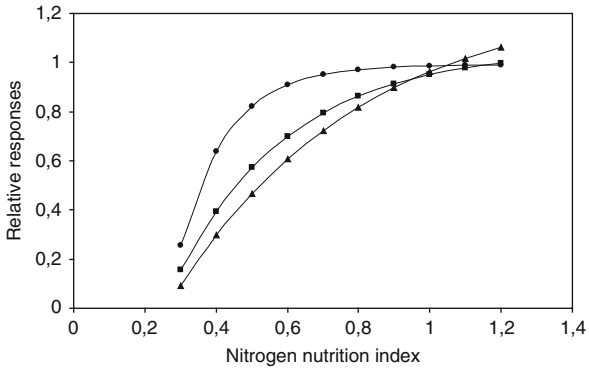

Crop Responses to Nitrogen. Figure 6
Effects of crop N status determined by the nitrogen nutrition index (*NNI*) of tall fescue swards receiving different N application rates and (i) the relative quantity of intercepted PAR, PAR_{act}/PAR_{max} (●), (ii) the relative Radiation Use Efficiency, RUE_{act}/RUE_{max} (■), and the relative LAI, LAI_{act}/LAI_{max} (▲). (Redrawn from [67])

to N deficiency appears to be the leaf area expansion rate, with two major consequences: (i) a reduction in the dynamic of light interception and then in the canopy photosynthesis and crop C supply and (ii) a preferential allocation of C for root growth that contributes to increase root foraging activity for a further increase in N uptake capacity.

The response of leaf area of plants and canopies to N deficiency is brought about by a decline in the expansion rate and size of individual leaves combined with reduction of branching or tillering. The accumulation of nonstructural carbohydrates in N-deficient leaves indicates that C supply is not the cause of the leaf area expansion under N deficiency [38].

N deficiency decrease the rates of cell division and cell expansion with little effect on final cell length [26], so the reduction of leaf size in N-deficient plants is mainly due to a reduction in cell number. Gastal et al. [73] proposed a quantitative relationship between the leaf elongation rate (LER) of tall fescue and the NNI of the sward:

$$\frac{\mathrm{LER}_{\mathrm{actual}}}{\mathrm{LER}_{\mathrm{critical}}} = 1.39 - 1.9e^{-1.49\mathrm{NNI}} \qquad (16)$$

Subscript "actual" corresponds to any suboptimal N condition, and subscript "critical" refers to a non-limiting N nutrition. For a severe limitation in N nutrition, NNI = 0.4, LER is then reduced to about 30% of its maximum value in non-limiting conditions. That demonstrates the high responsiveness of leaf expansion to N deficiency.

Lemaire et al. [24] used the relationship between LAI and crop mass (W) of Eq. 10 for studying the different types of response of crop species to N deficiency. This approach allows the separation of the reduction of LAI being directly associated with the reduction in crop mass (i.e., simply a crop size effect) from any specific reduction of LAI at similar crop mass (i.e., a modification of plant architecture through a reduction of leaf area ratio: LAR). They demonstrated that under a similar intensity of N deficiency as estimated through NNI, the reduction of LAI of maize is totally allometrically related to its reduction in crop mass (crop size effect), while for wheat N deficiency provokes in supplement a reduction of LAI at same crop mass, i.e., a reduction in LAR. These two types of responses represented two extremes and tall fescue behaves like maize while canola behaves like wheat; sorghum and sunflower having intermediate responses [24]. Hence classification of crops in either metabolic (C_3 vs C_4) or botanical (monocots vs dicots) groups does not correspond to any particular response type. In response to N deficiency, some species such as maize or tall fescue tend to maximize light interception by minimizing the reduction in LAI, at the expanse of N concentration per unit leaf area, and then leaf photosynthesis, while other species such as wheat and canola tend to develop an inverse response. Do these two opposite strategies mean that there exists a trade-off between photosynthesis per unit of LAI and leaf area expansion as already proposed by Sinclair and Horie [74]?

N Deficiency Effects on Leaf and Canopy Photosynthesis

The response of leaf photosynthesis to irradiance largely depends on the leaf N content. Leaf photosynthesis at saturating light intensity (A_{max}) increases asymptotically with leaf N content [75]. This relationship shows a positive intercept on the leaf N content axis, indicating that when leaf photosynthesis rate becomes zero, leaves would still contain significant amount of N, corresponding the structural leaf

N (N_s) of Eq. 8. The variation in the A_{max}/SLN (leaf N content per unit leaf area) relationship seems relatively limited among cultivated species of the same metabolic group [10, 76], despite Sinclair and Horie [74] showed a lower A_{max} at similar SLN for soybean. This variation among species could be due to (i) differences in nitrogen costs of PEP-carboxylase and RuBPc-o and the relative amounts of these two enzymes in leaves, and/or (ii) the possible accumulation of vegetative storage proteins within leaves of legume species such as soybean.

There is a large discussion whether A_{max} has to be related to either leaf N content per unit mass or per unit leaf area [75]. Lemaire and Gastal [32] indicated that none of these two relationships are completely right. The two components of photosynthesis, light harvesting by chlorophyll and CO_2 reduction by RuBPc-o, are affected by leaf N status, and these two processes have to be expressed on a leaf tissue volume basis, and not only on an area basis. Then leaf thickness is an important parameter to take into account. Specific leaf area (SLA) is the parameter allowing correspondence between leaf N content per unit area and per unit dry matter basis. But relationship between leaf thickness and SLA is weak because of the variations of nonstructural carbohydrate content within leaves.

The quantum efficiency that is the response of leaf photosynthesis to light at low irradiance is only little affected by N deficiency [77, 78]. Moreover, the dark respiration of leaves seems to increase with increasing leaf N [78]. Hence, as the leaves are progressively shaded within the canopy the effect of N deficiency on leaf net photosynthesis becomes lower and lower and then negligible.

Gastal and Bélanger [77] showed that canopy gross photosynthesis of a tall fescue sward at high irradiance (CGP_{max}) only responds smoothly to N deficiency: a reduction in NNI from 1 to 0.4 reduced the relative CGP_{max} from 1 to 0.6 only. This low responsiveness of canopy photosynthesis to N deficiency is due to the fact that as canopy develops, a greater number of leaves are shaded and then their photosynthesis does not respond to N shortage. When irradiance becomes more limited, the responsiveness of canopy photosynthesis to N deficiency becomes more limited. So when canopy photosynthesis is integrated over day and for a long period where crop LAI is high, the response of canopy photosynthesis to N deficiency appears relatively limited, which explains the limited influence of N deficiency on RUE.

N deficiency Effects on Harvest Index and Components of Grain Yield

For grain crops, yield is closely related to grain number per unit area of soil. The elaboration of grains depends on flows of C and N compounds to reproductive meristems during a narrow window period around flowering, anthesis, and very initial grain development, and also on environmental conditions (temperature, radiation, and water stress) during this period. This critical period coincides with the maximum rate of crop N uptake [79]. So any limitation of crop growth rate at this period by N deficiency decreases grain number and then grain yield on cereals such as maize [28], wheat [29, 80]. Jeuffroy and Bouchard [57] established for wheat a relationship between grain number and the severity and duration of the N deficiency before anthesis as calculated by NNI method. The effect of N deficiency on grain number is the consequence of two simultaneous effects: (i) a lower crop growth rate at anthesis restricting C supply to spikelets and then a spikelet abortion [81]; and (ii) a decrease in the N content in the spike stems [29] corresponding to a direct effect of N deficiency on floret fertility.

The other grain yield component, grain weight, is generally less affected by N deficiency at anthesis than the grain number [47]. However, it is necessary to take into account the negative correlation between grain weight and grain number: a reduced grain number resulting from pre-anthesis N deficiency can lead to a more favorable source:sink ration during grain filling period and then to an unaffected grain weight. Grain filling in both carbohydrates and proteins depends on (i) the recycling of C and N compounds previously accumulated within vegetative organs during pre-anthesis growth period, and (ii) post-anthesis photosynthesis and N absorption. The relative importance of these two components depends on plant species and their capacities to store C and N compounds in their vegetative organs. So some species such as wheat or rice are able to develop large LAI [7–9] and then to store large quantities of N, then they are able to feed 80–90%

of the N demand for grain development by recycling N stored within vegetative biomass, while other species such as maize, because they develop less LAI [4, 5] with lower N content because they have C_4 metabolism, are obliged to feed 40–60% of their grain N demand through post-anthesis N absorption. As a consequence, crop species like maize are more susceptible to terminal soil N shortage than crop species like wheat or rice.

Delaying leaf senescence for species like maize or sorghum should allow these species to continue to maintain high N absorption rate after anthesis. The supplement of carbohydrates allocated to roots permitted by this delayed leaf senescence allows the maintenance of root absorption capacity [82]. So using stay-green genotypes in low N supply conditions seems to be beneficial for both sorghum [83] and maize [84].

Nitrogen Use Efficiency in Crops

From an agronomic point of view, nitrogen use efficiency (NUE) of a crop represents its capacity to produce a supplement of yield (dY) for each added unit of N fertilizer (dNf) that corresponds to the derivative of the crop yield response curve to the rate of N supply: $Y = f(Nf)$. As this response curve is asymptotic, NUE generally declines with the higher rate of N supply, indicating that the first N unit applied is more efficiently converted into yield than later applications. According to the crop species types, Y can represent either the aboveground biomass, as for forage crops, or the grain part as for cereals, grain legumes, or oil seed crops.

Such a global approach does not allow a clear mechanistic analysis of the physiological traits controlling NUE between different species and cultivars because crops respond to total N supply (Nt) that include fertilizer supply (Nf) and soil N mineralization (Ns). So according to variations in Ns due both to soil and climatic conditions and to previous crop management, different value of Nt can be obtained with the same Nf, leading to large differences in NUE. For this reason, Moll et al. [85] propose to define NUE as the yield produced per unit of N available in the soil, considering two components:

1. The Nitrogen Absorption Efficiency (NAE) which measures the ability of a crop to uptake N from soil
2. The nitrogen conversion efficiency (NCE) which measures the ability of a crop to use absorbed N for dry matter and grain production

$$NUE = (NAE)(NCE) \tag{17}$$

Nitrogen Absorption Efficiency

Genotypic differences in N uptake at different levels of N supply have been shown in rice [86], wheat [87], and maize [88]. Modern cultivars have a higher N uptake capacity because they have a higher biomass production. This effect is accounted by Eq. (x) as it shows that the crop N uptake rate increases with crop growth rate. So any factor enhancing the potential crop growth rate, genotype or environment, increase de facto the N uptake capacity of the crop. More interesting from a plant breeding point of view would be to increase the N uptake capacity of crop at similar crop biomass production. Lemaire and Gastal [32] reported data comparing N uptake of tall fescue and cocksfoot swards at similar biomass. These data show that cocksfoot had a higher N uptake capacity than tall fescue under a sub-limiting N supply condition, while the two species had similar N uptake capacity under non-limiting N supply. Similarly, Lemaire et al. [89] showed that grain sorghum had a higher N uptake capacity than maize under limiting N supply, while the two species had similar N uptake under non-limiting N supply.

The fact that N uptake capacity and then nitrogen absorption efficiency (NAE) does not vary too much among crop species is due to the fact that the critical N uptake curve, as described by Eq. 2 is not very different among species of the same metabolic group (C_3 vs C_4). Then differences between crop species in NAE under non-limiting N supply conditions would reflect their differences in their potential biomass accumulation according to their respective metabolic group. Under limiting N supply conditions, clear differences emerge among species. As for cocksfoot vs tall fescue, sorghum appears to have a greater root length density than maize. This would confer these species a better capacity of interception of soil mineral N. Soil N recovery that determines NAE is the result of the nitrogen balance between crop N uptake rate, immobilization by soil microbial communities and losses through leaching, denitrification, and

volatilization [90]. Root architecture and biochemical composition, and perhaps root exudates could play an important role in this balance, and then on NAE. So because of a permanent turnover of N in soil, plants having a dense root system are able to compete more efficiently against microbes for capturing mineral N when the principal source of N is the mineralization of organic matter, i.e., in limiting N supply conditions. In non-limiting N supply conditions, there is ample mineral N in soil, the immobilization capacity of microbial community is saturated and then the differences among species tend to disappear. Only the difference in N uptake capacity linked to difference in crop growth capacity can then be observed.

Some coincidences between quantitative trait loci (QTL) for root architecture and NAE have been detected on wheat [91]. A large genotypic variability has been identified across maize lines for the density and length of lateral roots [92], suggesting that it would be possible to breed this species for improving its NAE under low N supply conditions. Similarly, genetic studies showed that NAE was the most important component of the Nitrogen use Efficiency in rice [93] and wheat [87].

Nitrogen Conversion Efficiency

The efficiency of conversion of absorbed N by crop into yield has to be analyzed at two levels:

- The efficiency for crop biomass production (W), i.e., the supplement of biomass (dW) associated to the supplement of N uptake (dN) when N supply increases
- The harvest index HI, i.e., the proportion of crop mass allocated to grain

Figure 7 allows a more detailed analysis of the NCE for crop mass production. This figure represents two N uptake vs crop mass (W) trajectories for crops at two level of N supply: a limiting N supply rate and a non-limiting one corresponding to critical N status. At each date the slope of the line joining data points corresponding to the two N supply rates is equal to $\Delta N_{upt}/\Delta W$ which is the reciprocal of NCE. The supplement of nitrogen taken up by the crop, ΔN_{upt}, due to the increase in N supply rate, can be defined as the sum of two components (i) $(\Delta N_{upt})_1$, the quantity of N the limiting N supply treatment should have been absorb in supplement for reaching the corresponding critical level, and (ii) $(\Delta N_{upt})_2$, the supplemental increase in N uptake associated to the accelerated growth rate

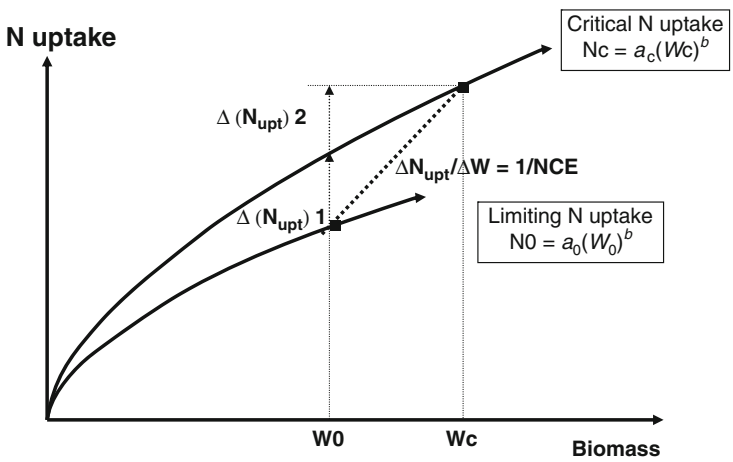

Crop Responses to Nitrogen. Figure 7
Schematic representation of the components of the nitrogen conversion efficiency. The first component $\Delta(N_{upt})1$ corresponds to the quantity of N necessary for crop to reach its critical N status, and its NCE is 0. The second component $\Delta(N_{upt})2$ corresponds to the quantity of N necessary for the synthesis the supplement of biomass ΔW and whose the NCE is $dW/dN = 1/ab(W)^{1-b}$ that increases with crop mass

resulting to the higher N supply level. The NCE of $(\Delta N_{upt})_1$ is 0 as the increment in N uptake is made at a constant crop mass. The NCE of $(\Delta N_{upt})_2$ is not constant and can be approached only for a given crop mass by the derivative of Eq. 3:

$$\frac{dN_{upt}}{dW} = ab(W)^{b-1} \quad (18)$$

This equation indicates that the efficiency of conversion of N absorbed into crop mass dW/dN_{upt} increases as crop mass increases. Such an analysis allows the identification of two different sources of variation for NCE: (i) when W is increased only by other factors than N supply, climate and/or genotype, then NCE increases with crop mass, and (ii) when W is increased by N supply, then NCE is lowered by the cost in N uptake for restoring the plant N status. This approach allows the study of NCE as a dynamic process where the time has to be explicitly taken into account through crop growth rate: the higher crop growth rate, the higher NCE of the crop. Then it allows the identification of the trivial effect of plant mass per se: a small crop, either because genetically small or because of unfavorable environmental conditions will have a lower NCE as compared to a bigger crop. This reason explains why a good correlation is observed between genotypes growing either in high or low N supply conditions [88]. In consequence, breeding for a high NCE must lead to the selection of genotypes to higher growth potential. There is no clear indication until now if NCE variation among genotypes would persist when comparisons are made at same crop mass. Since coefficients a and b of Eq. 2 differ little or not at all between species within C_3 or C_4 groups, the chances to find intraspecific differences in NCE when comparing plants having a similar growth potential remains very limited.

When considering yield (Y) and not only crop biomass (W), NCE can be highly variable among crop species as resulting to large genotypic variations in harvest index (HI). For grain crops as cereals, grain legumes, and oil seed species, HI is an important source of variation in grain yield per unit of N uptake. The repartition of N between the harvested and non-harvested plant parts that is the nitrogen harvested index (NHI) is then an important aspect of the grain nutritional quality [95]. Grain produced per unit of N uptake and grain N concentration are in general inversely related [96], and a variable proportion of the variation in yield per unit N uptake is accounted for by grain protein concentration or by NHI, according to crop type.

Grain protein N concentration is the result of two concomitant processes: (i) the rate of accumulation of proteins during grain filling and (ii) the rate of accumulation of free-N compounds (carbohydrates) within grains that lead to a dilution of N as grains develop. So a low grain N concentration can result in both a N deficiency during grain filling period and a large accumulation rate of starch. Thus, late application of N fertilizer to avoid any N shortage during grain filling can lead to an increase of the grain protein concentration. But as the capacity of roots for N absorption at this stage of the crop is largely impaired by the beginning of leaf senescence and the shortage of C allocated to roots, the recovery of this N application is low, and then, large mineral N residues in soil increase the risk for subsequent N leaching.

Conclusion

Since soil N availability, N uptake and distribution within plant and crop and finally crop growth are permanently interrelated during crop development and growth, the traditional view where crop N uptake was totally regulated by soil N supply must be reconsidered and replaced by a more dynamic approach where plant N uptake rate at any moment is co-regulated by both soil N supply and plant growth capacity itself. This co-regulation lead to the concept of critical plant N concentration and N dilution that link plant and crop N status to plant and crop mass. Such an approach allows the determination of the dynamics of plant N demand and plant N status all along their life-cycle. Critical N-curves are now available for most of the crop species growing either in temperate or tropical conditions. This allows the determination of the nitrogen nutrition index of any crop in any condition for diagnosis of its actual N status and estimating the necessity for applying N fertilizers. By this way, it would be possible now to adjust more precisely the quantity and the timing of N fertilizer supply for matching the crop N demand according to target yields. As a consequence, a reduction of the risk for

N losses to atmosphere and hydrosphere should be obtained while the crop productivity would be maintained.

One other perspective is to improve the efficiency of use of N within agro-systems. It appears that improving the ability of crops to absorb and accumulate N efficiently from soil (nitrogen absorption efficiency) is the first objective for high nitrogen use efficiency in cropping systems. This ability of plants and crops to take up mineral N from soil has to be investigated both at high or low N supply conditions. As demonstrated above, in both conditions, N uptake capacity of a crop is directly dependent upon its growth capacity as determined by (i) its own genetic potential, (ii) environmental conditions such as soil and climate, (iii) cropping management techniques, and (iv) interactions between these variables. So any improvement in crop growth capacity by both breeding cultivars and crop management (irrigation, P, K, S fertilization, planting density) will increase NAE of the crop and then will reduce the risk of accumulation of soil N mineral surplus with environmental hazards. But more important would be to improve NAE of crop species at similar crop growth potential. This would allow achieving a given target yield with less N fertilizer. Such an objective requires a more efficient root system to increase the competitive ability of the plant for using soil mineral N against microbial communities. This objective could be reached through a combination of plant breeding strategy and crop management techniques such as soil tillage and soil structure conservation.

Future Directions

The improvement of the ability of plants and crops to absorb and accumulate N efficiently from soil, that is measured by NAE, appears to be the first objective for a plant breeding strategy. As demonstrated above, the N uptake capacity of a crop primarily depends on its growth potential under given climatic conditions. So adaptation of genotypes for fast growth potential is the first way for improving its N uptake capacity. However, it should be also possible to increase the plant N uptake capacity at similar growth potential. By this way, it could be possible to increase the quantity of N a crop is able to uptake from soil in low N supply conditions and then to reduce the quantity of N fertilizers necessary to obtain a given target yield. Under low N supply conditions, root development and architecture as well as the interactions with rhizosphere through root exudates may be of major importance for the determination of the N uptake capacity of crops. Under high N supply conditions, it is the down regulation of root absorption capacities by shoot signals which determine the crop N uptake capacity. So for breeding genotypes with higher N uptake capacities both in low and in high N supply conditions, it is necessary to analyze more deeply all the regulation processes of N absorption at physiological and molecular levels. This kind of approach should be one of the major tasks in the next decade. The development of large-scale genomic, proteomic, and metabolomic studies is necessary for such an objective. However, the difficulty will be to integrate the huge amount of data generated by these studies. All elementary processes studied at cellular or molecular level have to be scaled up to the level of whole plant and crop where they are agronomically relevant. The nitrogen nutrition of crops and its efficiency for yield production is controlled by elementary physiological processes such as nitrate or ammonium transport through cell membranes in roots, nitrate reduction, ammonium assimilation, and protein synthesis. Each of these metabolic processes is regulated at molecular level, and then is susceptible to have more or less genetic variability. But when all processes are scaled up to whole plant or crop level, a large part of this elementary variability is buffered because of existing trade-off among elementary processes and feedback mechanisms. Quantitative genetics using both mutants and genetic engineering appears to be one of the most promising tools to allow the identification of key regulatory genes that are likely to control a variety of physiological and developmental processes involved in the determination of crop nitrogen absorption efficiency. But this approach must be always accompanied by a modeling approach in order to analyze all the feedback and trade-off at whole plant and crop level.

Breeding plants to increase nitrogen conversion efficiency for aboveground dry matter production appears to be more difficult because, apart from the difference between C_4 and C_3 groups, no clear interspecific differences are observed among cultivated crops. So it seems that intraspecific variability should

be very low. However, if the N efficiency for grain yield is considered, it should be possible to detect inter- and intraspecific differences. Detailed analysis of grain development and grain-filling processes should provide information about the genetic variability. The development of models describing both N partitioning and translocation within plant, and dynamics of grain development, taking into account the coupling between N and C fluxes between plant organs are necessary for detecting the key regulation processes for optimizing grain yield and quality. This approach will require a cooperative and integrated effort between plant molecular physiologists, geneticists, crop physiologists, and agronomists and the intensive use of bioinformatics.

Bibliography

Primary Literature

1. Angus JF (2001) Nitrogen demand and supply in Australian agriculture. Aust J Exp Agr 41:277–288
2. Eikhout B, Bouwman AF, Zeijts VH (2006) The role of nitrogen in world food production and food sustainability. Agric Ecosyst Environ 116:4–14
3. London JG (2005) Nitrogen study fertilizes fears of pollution. Nature 433:791
4. Beman JM, Arrigo K, Matson PM (2005) Agricultural runoff fuels large phytoplankton blooms in vulnerable areas of the ocean. Nature 434:211–214
5. Ramos C (1996) Effect of agricultural practices on the nitrogen losses in environment. In: Rodriguez-Barrueco C (ed) Fertilizer and environment. Kluwer, Dordrecht, pp 335–361
6. Stulen I, Perez-Soba M, De kok LJ, Van Der Eerden (1998) Impact of gaseous nitrogen deposition on plant functioning. New Phytol 139:61–70
7. Cassman KG (2007) Climate change, biofuels, and global food security. Environ Res Lett 2:11–12
8. Addiscott TM, Withmore AP, Powlson DS (1991) Farming, fertilizers and nitrate problem. CAB International, Wallingford, p 170
9. Hirel B, Lemaire G (2005) From agronomy and ecophysiology to molecular genetics for improving nitrogen use efficiency in crops. J Crop Imp 15:213–257
10. Evans JR (1983) Nitrogen and photosynthesis in the flag leaf of wheat (*Triticum aestivum* L.*)*. Plant Physiol 72:297–302
11. Lawlor DW (1995) Photosynthesis, productivity and environment. J Exp Bot 46:1449–1461
12. Lawlor DW, Konturri M, Young AT (1989) Photosynthesis by flag leaves of wheat in relation to protein, ribulose biphosphate carboxylase activity and nitrogen supply. J Exp Bot 40:43–52
13. Werger MJA (1991) Leaf nitrogen distribution and whole canopy photosynthetic carbon gain in herbaceous stands. Vegetatio 97:11–20
14. Nakano HM, Mae T (1997) The effects of elevated partial pressure of CO2 on the relationship between photosynthetic capacity and N content in rice leaves. Plant Physiol 115:191–198
15. Makino A, Mae T, Ohira K (1988) Differences between wheat and rice in the enzymic properties of ribulose-1, 5-biphosphate carboxylase/oxygenase and the relationship to photosynthetic gas exchange. Planta 174:30–38
16. Theobald JC, Mitchell RAC, Parry MAJ, Lawlor DW (1998) Estimating the excess investment in ribulose-1, 5-bisphophate carboxylase/oxygenase in leaves of spring wheat grown under elevated CO_2. Plant Physiol 118:945–955
17. Sage RF (1987) The nitrogen use efficiency of C3 and C4 plants. I- Leaf nitrogen, growth, and biomass partitioning in *Chenopodium album* (L.) and *Amaranthus retroflexus* (L.). Plant Physiol 84:954–958
18. Lawlor DW, Boyle FA, Keys AJ, Kendall AC, Young AT (1988) Nitrate nutrition and temperature effects on wheat: a synthesis of plant growth and nitrogen uptake in relation to metabolic and physiological processes. J Exp Bot 39:329–343
19. Millard P (1988) The accumulation and storage of nitrogen by herbaceous plants. Plant Cell Environ 11:1–8
20. Avice JC, Ourry A, Lemaire G, Volenec JJ, Boucaud J (1997) Root protein and vegetative storage protein are key organic nutrients for alfalfa shoot regrowth. Crop Sci 37:1187–1193
21. Ourry A, McDuff JH, Ougham H (1996) The relationship between mobilisation of N reserves and changes in translatable messages following defoliation in *Lolium temulentum* L. and *Lolium perenne* L. J Exp Bot 47:739–747
22. Lemaire G, Khaity M, Onillon B, Allirand JM, Chartier M, Gosse G (1992) Dynamics of accumulation and partitioning of N in leaves, stems and roots of lucerne in dense canopy. Ann Bot 70:429–435
23. Grindlay DJC, Sylvester-Bradley R, Scott RK (1995) The relationship between canopy green area and nitrogen in the shoot. In: Lemaire G, Burns IG (eds) Diagnostic procedures for crop N management. INRA Publication, Paris, pp 53–60, INRA-Editions, Collection "Les Colloques"
24. Lemaire G, van Oosterom E, Jeuffroz MH, Gastal F, Massignan A (2008) Crop species present different qualitative types of response to N deficiency during their vegetative growth. Field Crop Res 105:253–265
25. McAdam JW, Volenec JJ, Nelson CJ (1989) Effects of nitrogen on mesophyll cell division and epidermal cell elongation in tall fescue leaf blades. Plant Physiol 89:549–556
26. Gastal F, Nelson CJ (1994) Nitrogen use within growing leaf blade of tall fescue. Plant Physiol 105:191–197
27. Fricke W, McDonald AJS, Matson-Djos L (1997) Why do leaves and leaf cells of N-limited barley elongate at reduced rates? Planta 202:522–530
28. Uhart SA, Andrade FH (1995) Nitrogen deficiency on maize. I- Effects on crop growth, development, dry matter partitioning and kernel set. Crop Sci 35:1376–1383

29. Desmotes-Mainard S, Jeuffroy MH, Robin S (1999) Spike dry matter and nitrogen accumulation before anthesis in wheat as affected by nitrogen fertilizer: relationship to kernel per spike. Field Crop Res 64:249–259
30. Mae T (1997) Physiological nitrogen efficiency in rice: nitrogen utilization, photosynthesis, and yield potential. In: Ando T (ed) Plant nutrition for sustainable food production and environment. Kluwer, Dordrecht, pp 51–60
31. Lemaire G, Avice JC, Kim TH, Ourry A (2005) Development changes in shoot N dynamics of lucerne in relation to leaf growth dynamics as a function of plant density and hierarchical position within the canopy. J Exp Bot 56:935–943
32. Lemaire G, Gastal F (2009) Quantifying crop responses to nitrogen deficiency and avenues to improve nitrogen use efficiency. In: Sadras VO, Calderini DF (eds) Crop physiology: applications for genetic improvement and agronomy. Academic/Elsevier, Amsterdam, pp 171–199
33. Greenwood DJ, Lemaire G, Gosse G, Cruz P, Draycott A, Neeteson JJ (1990) Decline in percentage N of C3 and C4 crops with increasing plant mass. Ann Bot 66:425–436
34. Lemaire G, Jeuffroy MH, Gastal F (2008) Diagnostis tool for plant and crop N status in vegetative stage. Theory and practices for crop N management. Eur J Agron 28:614–624
35. Lemaire G, Gastal F (1997) N uptake and distribution in plant canopies. In: Lemaire G (ed) Diagnosis on the nitrogen status in crops. Springer, Heidelberg, pp 3–43
36. Justes E, Mary B, Meynard JM, Machet JM, Thellier-Huché L (1994) Determination of a critical nitrogen dilution curve for winter wheat crops. Ann Bot 74:397–407
37. Lemaire G, van Oosterom E, Sheehy J, Jeuffroy MH, Massignan A, Rossato L (2007) Is crop demand closely related to dry matter accumulation of leaf area expansion during vegetative growth? Field Crop Res 100:91–106
38. Gastal F, Lemaire G (2002) N uptake and distribution in crops: an agronomical and ecophysiological perspective. J Exp Bot 53:789–799
39. Lemaire G, Salette J (1984) Relation entre dynamique de croissance et dynamique de prélèvement d'azote par un peuplement de graminées fourragères. 1- Etude de l'effet du milieu. Agronomie 4:423–430
40. Lemaire G, Salette J (1984) Relation entre dynamique de croissance et dynamique de prélèvement d'azote par un peuplement de graminées fourragères. 2- Etude de la variabilité entre génotypes. Agronomie 4:431–436
41. Lemaire G, Cruz P, Gosse G, Chartier M (1985) Etude des relations entre la dynamique de prélèvement d'azote et la dynamique de croissance en matière sèche d'un peuplement de luzerne. Agronomie 5:685–692
42. Ney B, Doré T, Sagan M (1997) The nitrogen requirement of major agricultural crops: grain legumes. In: Lemaire G (ed) Diagnosis of the nitrogen status in crops. Springer, Heidelberg, pp 107–117
43. Colnenne C, Meynard JM, Reau R, Justes E, Merrien A (1998) Determination of a critical nitrogen dilution curve for winter oilseed rape. Ann Bot 81:311–317
44. Sheehy JE, Dionara MJA, Mitchell PL, Peng S, Cassman KG, Lemaire G, Williams RL (1998) Critical concentrations: implications for high-yielding rice (*Oryza sativa*, L.) cultivars in tropics. Field Crop Res 59:31–41
45. Tei F, Benincasa P, Guidici M (2002) Critical nitrogen concentration in processing tomato. Eur J Agron 18:45–56
46. Plénet D, Lemaire G (1999) Relationships between dynamics of nitrogen uptake and dry matter accumulation in maize crops. Determination of critical N concentration. Plant Soil 216:65–82
47. Plénet D, Cruz P (1997) The nitrogen requirement for major agricultural crops: maize and sorghum. In: Lemaire G (ed) Diagnosis of the nitrogen status in crops. Springer, Heidelberg, pp 93–106
48. Duru M, Lemaire G, Cruz P (1997) The nitrogen requirement for major agricultural crops: grasslands. In: Lemaire G (ed) Diagnosis of nitrogen status in crops. Springer, Heidelberg, pp 56–72
49. Hardwick RC (1987) The nitrogen content of plants and the self thinning rule in plant ecology: a test of the core-skin hypothesis. Ann Bot 60:439–446
50. Ismande J, Touraine B (1994) N demand and regulation of nitrate uptake. Plant Physiol 105:3–7
51. Lejay L, Tillard P, Petit M, Olive FD, Filleur S, Daniel-Vedele F, Gojon A (1999) Molecular and functional regulation of two NO3- uptake systems by N and C status of *Arabidopsis* plants. Plant J 18:509–519
52. Forde BG (2002) The role of long-distance signaling in plant response to nitrate and other nutrients. J Exp Bot 53:39–43
53. Glass ADM, Britto DT, Kaiser BN, Kinghorn JR, Kronzucker HJ, Kumar A, Okamoto M, Rwat S, Siddiqi MY, Unkless SE, Vidmar J (2002) The regulation of nitrate and ammonium transport systems in plants. J Exp Bot 53:855–864
54. Devienne-Barret F, Justes E, Machet JM, mary B (2000) Integrated control of nitrate uptake by crop growth rate and soil nitrate availability under field conditions. Ann Bot 86:995–1005
55. Lemaire G, Meynard JM (1997) Use of the nitrogen nutrition index for the analysis of agronomical data. In: Lemaire G (ed) Diagnosis of the nitrogen status in crops. Springer, Heidelberg, pp 45–56
56. Angus JF, Moncur MW (1985) Models of growth and development of wheat in relation to plant nitrogen. Aust J Agr Res 36:537–544
57. Jeuffroy MH, Bouchard C (1999) Intensity and duration of nitrogen deficiency on wheat grain number. Crop Sci 39:1385–1393
58. Lemaire G, Plénet D, Grindlay D (1997) Leaf N content as an indicator of crop N nutrition. In: Lemaire G (ed) Diagnosis on the nitrogen status in crops. Springer, Heidelberg, pp 189–199
59. Farrugia A, Gastal F, Scholefield D (2004) Assessement of nitrogen status of grasslands. Grass Forage Sci 59:113–120
60. Ziadi N, Bélanger G, Gastal F, Claesses A, lemaire G, Tremblay N (2009) Leaf nitrogen concentration as an indicator of corn nitrogen status. Agron J 101:947–957

61. Alam MM, Ladha JK, Rahman Khan S, Harun-Ur-Rashid Khan AH, Buresh RJ (2005) Leaf color chart for managing nitrogen fertilizer in lowland rice in Bangladesh. Agron J 97:949–959
62. Peng S, Garcia FV, Laza RC, Sanico AL, Visperas RM, Cassman KG (1996) Increased N-use efficiency using a chlorophyll meter on high-yielding irrigated rice. Field Crops Res 47:243–252
63. Feibo W, Lianghuan W, Fuha X (1998) Chlorophyll meter to predict nitrogen side dress requirements for short-season cotton. Field Crop Res 56:309–314
64. Le Bail M, Jeuffroy MH, Bouchard C, Barbotin A (2005) Is it possible to forecast the grain quality and yield of different varieties of winter wheat from minolta SPAD meter measurements? Eur J Agron 23:379–391
65. Houlès V, Guérif M, Mary B (2007) Elaboration of a nutrition indicator for winter wheat blades on leaf area index and chlorophyll meter content for making nitrogen recommendations. Eur J Agron 27:1–11
66. Monteith JL (1972) Solar radiation and productivity in tropical ecosystems. J Appl Ecol 9:747–766
67. Bélanger G, Gastal F, Lemaire G (1992) Growth analysis of a tall fescue sward fertilized with different rates of nitrogen. Crop Sci 6:1371–1376
68. Trapani N, Hall AJ (1996) Effects of leaf position and nitrogen supply on the expansion of leaves of field-grown sunflower. Plant Soil 184:331–340
69. Muchow RC, Davis R (1998) Effect of nitrogen supply on the comparative productivity of maize and sorghum in a semi-arid tropical environment. II- radiation interception and biomass accumulation. Field Crop Res 18:17–30
70. Bélanger G, Gastal F, Warembourg F (1994) Carbon balance on tall fescue: effects of nitrogen and growing season. Ann Bot 74:653–659
71. Robson MJ, Parsons AJ (1978) Nitrogen deficiency in small closed communities of S24 ryegrass. I-Photosynthesis, respiration, dry matter production and partition. Ann Bot 42:1185–1197
72. Jarvis SC, McDuff JH (1989) Nitrate nutrition of grasses from steady state supplies in flowing solution culture following nitrate deprivation and/or defoliation. J Exp Bot 40:695–975
73. Gastal F, Bélanger G, Lemaire G (1992) A model of the leaf extension rate of tall fescue in response to nitrogen and temperature. Ann Bot 70:437–442
74. Sinclair TR, Horie T (1989) Leaf nitrogen, photosynthesis, and crop radiation use efficiency: a review. Crop Sci 29:90–98
75. Grindlay DJC (1997) Towards an explanation of crop nitrogen demand based on leaf nitrogen per unit leaf area. J Sci Food Agric 63:116–123
76. Van Keulen H, Goudrian J, Seligman NG (1989) Modelling the effects of nitrogen on canopy development and crop growth. In: Rusell G, Marshall LB, Jarvis PG (eds) Plant canopies: their growth, form and function. Cambridge University Press, Cambridge, pp 83–104
77. Gastal F, Bélanger G (1993) The effects of nitrogen fertilization and the growing season on photosynthesis of fied-grown tall fescue canopies. Ann Bot 72:401–408
78. Connor DJ, Hall AJ, Sadras VO (1993) Effects of nitrogen content on the photosynthetic characteristics of sunflower crops during grain filling. Aust J Plant Physiol 20:251–263
79. Fischer RA (1993) Irrigated spring wheat and timing and amount of nitrogen fertilizer. II-Physiology of grain yield response. Field Crop Res 33:57–80
80. Martre P, Porter JR, Jamieson PD, Triboï E (2003) Modelling grain nitrogen accumulation and protein composition to understand the sink/source regulations of nitrogen utilization in wheat. Plant Physiol 133:1959–1967
81. Desmotes-Mainard S, Jeuffroy MH (2004) Effects of nitrogen and radiation on dry matter and nitrogen accumulation in spike of winter wheat. Field Crop Res 87:221–233
82. Dreccer MF (2005) Nitrogen use at the leaf and canopy level: a framework to improve N use efficiency. J Crop Imp 15: 97–125
83. Borell A, Hammer GL (2000) Nitrogen dynamics and the physiological basis for stay-green in sorghum. Crop Sci 40: 1295–1307
84. Mi C, Liu J, Chen F, Zhang F, Cui Z, Liu X (2003) Nitrogen uptake and remobilization in maize hybrids differing in leaf senescence. J Plant Nutr 26:447–459
85. Moll RH, Kamprath EJ, Jackson WA (1982) Analysis and interpretation of factors which contribute to efficiency of nitrogen utilization. Agron J 74:562–564
86. Borell A, Garside AL, Fukaï S, Reid DJ (1998) Season nitrogen rate and plant type affect nitrogen uptake and nitrogen use efficiency in rice. Aust J Agr Res 49:829–843
87. Le Gouis J, Béghin D, Heumez E, Pluchard P (2000) Genetic differences for nitrogen uptake and nitrogen utilization efficiencies in winter wheat. Eur J Agron 12:163–173
88. Bertin P, Gallais A (2001) Physiological and genetic basis of nitrogen use efficiency on maize. Maydica 46:53–68
89. Lemaire G, Charrier X, Hébert Y (1996) Nitrogen uptake capacities of maize and sorghum crops in different nitrogen and water supply conditions. Agronomie 16: 231–246
90. Lemaire G, Recous S, Mary B (2004) Managing residues and nitrogen in intensive cropping systems. New understandings for efficient recovery by crops. In: Proceedings of the 4th international crop science congress, Brisbane, Australia, 2004
91. Laperche A, Devienne-Barret F, Maury O, Le Gouis J, Ney B (2007) A simplified conceptual model of carbon and nitrogen functioning for QTL analysis of winter wheat adaptation to nitrogen deficiency. Theor Appl Genet 113: 1131–1146
92. Camus-Kulandaivelu L, Veyreiras JB, Madur D, Combes V, Fourman M, Barraud S, Dubreuil P, Gouesnard B, Manicacci D, Charcosset A (2006) Maize adaptation to temperate climate: relationship between population structure

and polymorphism in the Dwarf 8 gene. Genetics 172: 2449–2463
93. Singh U, Ladha JK, Castillo EG, Punzalan G, Tirol-Padre A, Duqueza M (1998) Genotypic variation in nitrogen use efficiency. I-medium and long-duration rice. Field Crop Res 58: 35–53
94. Sadras VO (2006) The N:P stoichiometry of cereal, grain legume and oilseed crops. Field Crop Res 95:13–29

Books and Reviews

Gastal F, Lemaire G (2002) N uptake and distribution in crops: an agronomical and ecophysiological perspective. J Exp Bot 53:789–799

Grindlay DJC (1997) Towards an explanation of crop nitrogen demand based on leaf nitrogen per unit leaf area. J Sci Food Agric 63:116–123

Hirel B, Lemaire G (2005) From agronomy and ecophysiology to molecular genetics for improving nitrogen use efficiency in crops. J Crop Imp 15:213–257

Justes E, Mary B, Meynard JM, Machet JM, Thellier-Huché L (1994) Determination of a critical nitrogen dilution curve for winter wheat crops. Ann Bot 74:397–407

Lemaire G, Gastal F (1997) N uptake and distribution in plant canopies. In: Lemaire G (ed) Diagnosis on the nitrogen status in crops. Springer, Heidelberg, pp 3–43

Lemaire G, Gastal F (2009) Quantifying crop responses to nitrogen deficiency and avenues to improve nitrogen use efficiency

Lemaire G, Jeuffroy MH, Gastal F (2008) Diagnostis tool for plant and crop N status in vegetative stage. Theory and practices for crop N management. Eur J Agron 28:614–624

Lemaire G, Recous S, Mary B (2004) Managing residues and nitrogen in intensive cropping systems. New understandings for efficient recovery by crops. In: Proceedings of the 4th international crop science congress, Brisbane, Australia, 2004

Lemaire G, van Oosterom E, Jeuffroz MH, Gastal F, Massignan A (2008) Crop species present different qualitative types of response to N deficiency during their vegetative growth. Field Crop Res 105:253–265

Lemaire G, van Oosterom E, Sheehy J, Jeuffroy MH, Massignan A, Rossato L (2007) Is crop demand closely related to dry matter accumulation of leaf area expansion during vegetative growth? Field Crop Res 100:91–106

Sinclair TR, Horie T (1989) Leaf nitrogen, photosynthesis, and crop radiation use efficiency: a review. Crop Sci 29:90–98

Sinclair TR (1998) Historical changes in harvest index crop N accumulation. Crop Sci 38:638–643

Van Keulen H, Goudrian J, Seligman NG (1989) Modelling the effects of nitrogen on canopy development and crop growth. In: Rusell G, Marshall LB, Jarvis PG (eds) Plant canopies: their growth, form and function. Cambridge University Press, Cambridge, pp 83–104

Crop Science and Technology, Introduction

Paul Christou[1,2], Roxana Savin[3]
[1]Department de Produccio Vegetal i Ciencia Forestal, Universitat de Lleida/ICREA, Lleida, Spain
[2]Institució Catalana de Recerca i Estudis Avançats, (ICREA), Barcelona, Spain
[3]Department of Crop and Forest Sciences, University of Lleida, Lleida, Spain

Article Outline

Transgenic Crops and Molecular Breeding
Crop Physiology and Agronomy

Population growth in the coming decades will put severe pressure on human food, animal feed, and fiber production. Bioenergy applications are already exerting increasing pressure on agricultural commodities and land use with severe economic consequences, particularly in the developing world. Any crop productivity increases must come necessarily from enhancing crop performance as further land expansion for agriculture is unlikely to take place. Environmental sustainability and social justice issues are becoming increasingly key elements in debates on how to assure adequate food for the ever-increasing global population. It is likely that the efficiency of increasing productivity would benefit by complementing the conventional empirical approaches with opportunities presented by the development of new knowledge and technologies in the field of Crop Science. Therefore, in this section a number of seminal articles by world experts in the field are featured. Through this collection of articles key advances in the field are highlighted and the reader is pointed to future directions in terms of opportunities and constraints for a more productive and sustainable agriculture. This is not meant to be an exhaustive list of topics; rather the aim is to highlight particular technologies and topics that have a real potential to make a substantial contribution to a more productive and environmentally friendlier agriculture in the short to medium term. This section comprises 45 articles that can be divided into two

parts: (a) molecular approaches and (b) crop physiology and agronomy.

Transgenic Crops and Molecular Breeding

World food and feed security are increasingly dependent on continuous crop improvement and in particular the development of crops with increased resistance to abiotic stresses (► Abiotic Stress Tolerant Crops: Genes, Pathways and Bottlenecks). Plants unlike animals are not mobile, consequently they need to develop strategies to combat natural enemies such as herbivores and environmental stresses. Drought, salinity, submergence, and temperature stresses amongst others are all important abiotic constraints which limit crop yields. Significant advances in our understanding of molecular mechanisms underpinning a plant's ability to combat abiotic stresses has resulted in the creation of transgenic plants with improved resistance to such stresses.

Sustainable, renewable resources are those derived from biological sources, primarily plant biomass which can be regenerated with minimal inputs using energy from the sun (► Biomass Crops for Biofuels and Bio-based Products). Biomass for biofuels includes many sources of material derived from agricultural harvests including grains, agricultural residues such as stalks and leaves, perennial crops such as hay and trees, animal manures, building waste wood, municipal solid waste such as paper, and various food industry wastes. Humans currently consume at least 25% more raw materials every year than are replaced through biological growth. In order to sustain quality of life and maintain adequate environmental resources, those resources must be balanced and renewable. Pressure on those resources has never been greater with the world population currently at seven billion people, and estimated to plateau at 10.5 billion by 2050.

Once a gene is introduced into a plant its expression may be controlled by a number of different factors (► Transgene Expression in Plants, Control of). Among these, promoters are most important as they regulate expression temporally and spatially. Transcriptional fusions of genes, with the Cauliflower Mosaic Virus 35S promoter when integrated into the plant genome (mostly dicotyledonous plants), result in transgenic plants with high and constitutive expression of the transgene. However, 35S-driven transgene expression is very variable with ca: 20% of the transformants exhibiting high expression levels, while the majority (ca: 80%) display an intermediate or low and unstable transgene expression. The possible causes of variation in transgene expression in a population of transgenic plants need to be identified and addressed in order to generate useful plants with stable and predictable levels of expression of introduced transgenes.

Plant transformation is a fundamental component of both basic and applied plant biology (► Crop Plants Transformation Methods). For basic research, transformation allows scientists to study how genes function and allows the study of both endogenous genes and transgenes. This has increased our understanding of how plants grow, develop, and defend themselves against pests, diseases, and harsh environments; how photosynthesis is controlled; and the basis of primary and secondary metabolism. For applied research, transformation can be used to improve the agronomic performance of crops, making them hardier, more nutritious, more productive, or converting them from conventional crops into green factories producing chemical precursors, novel oils, industrial enzymes, and pharmaceuticals. Plants have been cultivated for food and animal feed, fibers and structural materials, and small molecules that can be used as dyes, scents, and medicines since the dawn of history, and for the same length of time people have sought to improve plants by breeding them and selecting the better-performing and most useful varieties. The limitations of this approach, that is, the fact that breeders are restricted to the existing gene pool in each group of sexually compatible species, and that breeding takes a long time to achieve its goals, can be overcome by plant transformation, thus accelerating the development of plants with novel, beneficial traits. Plant transformation includes both the uptake of naked DNA (direct DNA transfer) and the transfer of DNA by the conjugation-like method adopted by *Agrobacterium tumefaciens* and *A. rhizogenes* (*Agrobacterium*-mediated transformation).

Genetics, molecular biology, genomics, and other disciplines have now provided us with an insight to the genes that encode important crop traits on which humans now depend. Knowledge of the molecular genetic basis of valuable crop traits will help provide solutions to our requirements for sustainable

existence, faced with a growing global population and diminishing natural resources (► Crop Traits: Gene Isolation). Isolated genes encoding useful traits and their use in plant transformation experiments allow the development of an in-depth understanding of the mechanisms that control such important crop traits. Thus, through such investigations that utilize isolated genes, one is able to understand and harness traits involved in plant domestication such as plant architecture, to those offering solutions for high crop production purposes such as growth under unfavorable environments or disease outbreaks. Cloning or identification of the genes involved in crop traits provide an insight into factors which determine gene–trait relationships. Understanding the molecular basis of crop traits provides a route to their controlled modulation ultimately leading to the development and implementation of novel genetic engineering solutions to create plants with superior and sustainable characteristics.

Conventional plant breeding practices alone will not be able to achieve sustainability in today's agriculture. Advances in plant genomics research are opening up a new era in plant breeding where the linkage of genes to specific traits will lead to more efficient and predictable breeding programs (► Crop Breeding for Sustainable Agriculture, Genomics Interventions in). Plant genomics is a rapidly developing field, which is radically improving our understanding of plant biology by making available novel tools for the improvement of plant properties relevant to sustainable agricultural production. Recent advances in high throughput genomics technologies including next generation sequencing and high-throughput genotyping have helped immensely in understanding the functions and regulation of genes in crop plants. The ever-increasing availability of genome sequences in crop plants has facilitated greatly the development of genomic resources that will allow us to address biological functions and a number of basic processes relevant to crop production leading to sustainable agriculture. It is therefore expected that genomics will be an integral part of the agricultural/plant breeding practices of the future for improving crop productivity to achieve food security and sustainable production.

Plants have been used as sources of small molecular weight compounds (secondary metabolites) with applications as medicines, flavors, and fragrances for millennia. However, many plants containing such high-value secondary metabolites are difficult to cultivate or are becoming endangered because of overharvesting. In addition, the chemical synthesis of plant-derived compounds is often uneconomical due to their highly complex structures. The biotechnological production of valuable secondary metabolites is an attractive alternative to the extraction of whole plant material (► Medicinal Plants, Engineering of Secondary Metabolites in Cell Cultures). Functional genomics may open entirely new avenues to screen unexplored medicinal plant species for their pharmacological value.

Molecular breeding (MB) allows the stacking of favorable alleles, or genomic regions, for target traits in a desired genetic background, thanks to the use of polymorphic molecular markers (MM) that monitor differences in genomic composition among cultivars, or genotypes, at specific genomic regions, or genes, involved in the expression of those target traits (► Molecular Breeding Platforms in World Agriculture). The use of MM generally increases the genetic gain per crop cycle compared to selection based on plant phenotyping only, and therefore reduces the number of needed selection cycles, hastening the delivery of improved crop varieties to the farmer. In contrast to the private sector, MB adoption is still limited in the public sector, and is hardly used at all in developing countries. The situation is critical in developing countries due to resource-limited breeding programs. As a result, the developing world has yet to benefit from the MB revolution, and most countries indeed lack the fundamental prerequisites for a move to informatics powered breeding. A sustainable web-based Molecular Breeding Platform (MBP) as a one-stop-shop for information, analytical tools and related services to help design and conduct marker-assisted breeding experiments in the most efficient way will alleviate many of these bottlenecks in the developing world. Such a platform will enable breeding programs in the public and private sectors in developing countries to accelerate variety development using marker technologies for different breeding objectives.

With the advent of molecular techniques, plants have the potential to serve as production vehicles for natural or engineered products that were previously limited to other hosts. Plant molecular pharming of industrial proteins refers to recombinant proteins used

in industrial processes and produced in plants (► Plant Molecular Pharming, Industrial Enzymes). Enormous quantities of a variety of enzymes go into making products such as paper, leather, detergents, pharmaceuticals, food, beverages, chemicals, and fabric, to name a few, and economical production of these industrially important enzymes is crucial to commerce. This production must be balanced with the need for sustainability and environmental stewardship. Sustainable production of industrial enzymes requires that resources are not overexploited and wastes are not polluting. The use of plants as "green" factories can meet both criteria. Combined with modern farming and containment methods, transgenic plants have the potential to produce large quantities of target material safely and sustainably.

The demand for recombinant medical proteins has increased in recent years and modern biotechnological methods have, until recently, ensured the production of safe and effective biopharmaceuticals to meet this demand. Various production platforms are currently used in the pharmaceutical industry, most based on the fermentation of engineered pro- and eukaryotic microorganisms, insect cells, or mammalian cells (► Plant Molecular Pharming, Pharmaceuticals for Human Health). The growth of the market for biopharmaceuticals is predicted to outpace production capacity using these platforms in the next decade, so alternatives are necessary. The production of pharmaceutical proteins in plants began with a monoclonal antibody expressed in transgenic tobacco plants more than 20 years ago. Since then many different plant species have been genetically engineered to produce valuable pharmaceutical proteins. Major progress has been achieved in transformation and expression technology, downstream processing of transgenic plant material, and the adaptation of regulatory procedures to encompass the new production platforms, allowing the first plant-made pharmaceuticals to begin clinical trials.

Since the successful expression of complete antibodies in transgenic plants and the first report of plant-based vaccine production in 1992 a large number of different vaccines, antibodies, as well as antibody fragments have been produced in plants for medical or veterinary purposes (► Plant Molecular Pharming, Veterinary Applications). Novel processing methods have been developed over the past several years to facilitate the development of recombinant proteins for veterinary applications.

Humankind has had an ever-increasing impact on the environment. With the increasing intensification of agriculture, particularly during the twentieth century, this impact has become even more pronounced, often with undesirable or unacceptable consequences, including water pollution, soil erosion, and loss of habitat, often accompanied by a loss of biodiversity (► Transgenic Crops, Environmental Impact). Pests, particularly weedy plants, demonstrate a remarkable ability to adapt to agricultural production systems. The practice of growing monocultures, typically used in intensive agriculture, increases the number of pests; these are currently predominantly controlled through use of pesticides. However, with increasing exposure to pesticides many pest populations are evolving resistance to these compounds. An additional problem encountered with many pesticides, and particularly insecticides, are their nontarget effects on beneficial insects. Transgenic crops expressing genes conferring resistance to insect pests and/or herbicides are becoming increasingly more widely grown and have the potential to eliminate many of the problems in conventional agriculture thus reducing agriculture's negative impact on the environment.

Annual losses worldwide due to plant diseases are estimated to be ~14% of total losses and about $220 billion. In addition, the need for measures to control diseases limits the acreage of land available for cultivation; restricts the crops that can be grown in fields already contaminated with certain pathogens; and necessitates the use of agrochemicals for treating seeds, fumigating soils, spraying plants, and applying postharvest treatments. Such control measures add to the cost of food production and toxic chemicals can be harmful to human health and the environment (► Transgenic Crops Resistant to Fungal, Bacterial and Viral Pathogens). Resistance to pathogens can be achieved by application of disease-suppressing cultural practices, use of plant defense-promoting substances, deployment of biological agents antagonistic to the pathogens that cause disease, agrochemicals, conventional breeding strategies, and genetic engineering. The need for controlling plant diseases effectively is not only a major challenge, but also a necessity to reduce food losses while improving food quality and safeguarding the environment.

Genetic Engineering can increase the nutritional quality of crops by increasing the availability of essential nutrients, which are often limited in human diets and lead to specific deficiency diseases (► Biotechnology and Nutritional Improvement of Crops). Food insecurity is one of the most important social issues faced today, with nearly one billion people enduring chronic hunger and an additional two billion people suffering from nutrient deficiencies, most in the developing world. Strategies to address food insecurity must ultimately address underlying problems such as poverty and poor governance/infrastructure, but the improvement of agricultural productivity in the developing world is an important goal, and biotechnology is one of a raft of measures being considered to achieve it.

The economic impact of transgenic crops has been immense (► Global Economic Impact of Transgenic/Biotech Crops (1996–2008)). This has been a major driver in their rates of adoption amongst farmers in the USA and other industrialized countries but perhaps more importantly by small holders in the developing world. Analysis on farm income effects through extensive analysis of existing farm level impact data for biotech crops confirms this to be a major reason for their broad adoption worldwide.

Biotechnology offers efficient and cost-effective means to produce a diverse array of novel, value-added products and tools. The first generation of commercialized biotechnology products were crops focusing largely on input agronomic traits whose value was often opaque to consumers. The coming generations of crop plants can be grouped into broad areas each presenting what, on the surface, may appear as unique challenges and opportunities (► Transgenic Crops, Next Generation). The present and future focus is on continuing improvement of agronomic traits such as yield and abiotic stress resistance in addition to the biotic stress tolerance of the present generation, crop plants as biomass feedstocks for biofuels and "bio-synthetics," value-added output traits such as improved nutrition and food functionality, and plants as production factories for therapeutics and industrial products. From a consumer perspective, the focus on value added traits, especially improved nutrition, is undoubtedly one of the areas of greatest interest.

The rapid development and deployment of modern biotechnology in the last decades has made biosafety a major issue. Although modern biotechnology can benefit agricultural productivity in developing countries transgenic crops remain an issue with regard to the conservation and sustainable use of biodiversity, as well as to human health. The perceived risks, which relate to the release of transgenic crops into the environment as well as the placement of genetically engineered crops onto the market, have as much to do with social values as scientific concerns. Regulatory frameworks for transgenic crops and the underpinning legislative frameworks have been or are being developed worldwide (► Commercialisation of GM Crops: Comparison of Regulatory Frameworks). These are viewed as essential components for the prudent deployment of transgenic crops worldwide.

The safety measures associated with transgenic crop deployment are embedded in process- or product-based regulatory approaches. The EU regulatory approach is process-based, precautionary, and includes mandatory labeling and traceability requirements for transgenic crops and their derived food and feed products (► Transgenic Crops, Risk Assessment and Regulatory Framework in the European Union). During its development, the EU regulatory system has become increasingly more stringent and unduly onerous. In the EU, the risk analysis consists of three components: risk assessment, risk management, and risk communication. When analyzing potential risks, it is important to bear in mind that the real choice is not between transgenic crops that are inherently risky and traditionally bred ones that are completely safe. The cultivation of existing crops and those with novel traits (including transgenic crops) will have both positive and negative consequences. To fully acknowledge the overall outcome of adopting specific crops, and to assess and manage more effectively the environmental footprint of agriculture as a whole, broader and more balanced legislative oversight is needed in the EU.

A framework for a better communication about science and regulation and production of GM crops is described in ► GM Crop Risk Debate, Science and Socioeconomics

While transgenic herbicide resistant crops have been a boon to agriculture, reducing both production costs and ecological impacts of farming, weeds have

rapidly evolved resistance to the major herbicide used in transgenic crops (glyphosate), rapidly rendering the technology less sustainable than had been thought (► Sustainable Herbicide-Resistant Crops). While no practice in agriculture has been sustainable forever, the period of sustainability can be extended. Methods to extend both the usefulness to crops where needed as well as the sustainability of transgenic herbicide technologies such as rotations of crops and herbicides, increasing the targets of herbicide action, suppressing herbicide targets in rotation, are needed.

Crop Physiology and Agronomy

Seed dormancy is a means of restricting germination to the season when environmental conditions are suitable for plant establishment. From an agricultural perspective, dormancy is a problem (► Seed Dormancy and Agriculture, Physiology). Many important challenges face agriculture in relation to dormancy and these apply to cultivated crops as well as noxious weeds. The physiological mechanisms responsible for the expression of the character are now better understood and molecular information underpinning the process is gradually being generated and incorporated into strategies to solve dormancy-related problems.

One of the first decisions a farmer needs to make is to choose the particular genotype to be grown in the fields based on anticipated or projected economic returns. This is a critical choice that determines the sustainability of the agricultural system (► Genotype by Environment Interaction and Adaptation). Identifying breeding implications on specific adaptive traits and the different statistical approaches for genotype by environment interaction characterization is important.

Attaining global food security by means of increased crop productivity will require an increase in gains from selection achieved through conventional breeding. The identification of molecular markers associated with loci controlling traits of agronomic interest coupled with the exploitation of marker-assisted breeding (MAB) approaches provides the opportunity to accelerate gain from selection (► Marker-Assisted Breeding in Crops). Genomic selection is already having a positive impact on the improvement of crop yield, mainly in the private sector where high-throughput infrastructures allow breeders to handle the large number of molecular data points that are needed for deploying genomic selection effectively. Ultimately, an effective exploitation of MAB to enhance crop performance will rely on a closer integration between molecular approaches and conventional breeding.

The next generation of highly productive crops in an increasingly variable and changing climate, will rely on genetic interventions based on process understanding, selection of target traits in managed environments, and high-throughput phenotyping and genotyping (► Plant Breeding Under a Changing Climate). Therefore, it is crucial to understand the recent advances in plant breeding for high yield potential environments and also those where abiotic stress is a major limitation to productivity.

Agronomic systems are defined as site-specific management of soils and crops on the basis of eco-regional and physiographic characteristics, and in the context of socioeconomic and policy environments. These systems are strong determinants of agricultural production, sustainable use of resources, and their environmental impact. Agricultural soils and ecosystems can also be used for sequestration of atmospheric CO_2 by enhancing photosynthesis, increasing net primary productivity (► Agronomic Interactions with CO_2 Sequestration).

Crop management comprises a set of agronomic practices such as tillage systems, methods of fertilization, and crop rotations (► Cropping Systems: Shaping Nature). Cropping system may vary among farms depending on availability of resources and particular constraints. The different cropping systems may determine water and nutrient availabilities, carbon cycle, erosion, and the pathogen inoculum in the soil.

Understanding plant development or the progression of plants through their life cycle is important because of the need to know and predict when harvestable products are at their optimum (► Crop Development Related to Temperature and Photoperiod). Current knowledge on how temperature (including vernalization) and photoperiod regulate crop development is of major interest and determines how crops adapt in a wide range of environments. Thus, it is critical to understand the physiology and genetic basis of crop development, and to predict as accurately as possible the timing of key developmental events.

Reduced crop productivity from the theoretical potential maximum commonly occurs because of high temperatures. In addition, air temperatures are predicted to increase during the twenty-first century. Crop physiological and developmental processes are sensitive to temperature so that high temperatures do frequently affect negatively crop productivity (► Sustainable Productivity, Heat Tolerance for). The effects of high temperature, elevated CO_2 and their interaction on crops, are therefore important to understand and subsequently to mitigate potential negative effects of genes that confer heat tolerance.

Since plants are immobile, their distribution greatly influences the ability of a crop to capture and use environmental resources (radiation, water, and nutrients), which are necessary for growth and yield. The spatial arrangement of plants and the temporal development of their structures (mainly leaves and roots) define the ► Spatial Crop Structure in agricultural systems. Density and spatial arrangement of crops may affect intraspecific competition and resource use efficiency, allowing full or partial use of available resources.

The rate of accumulation of dry plant matter is entirely dependent on the interception of energy from the sun in the wavelength range 400–700 nm. This energy is utilized by photosynthesis to synthesize carbohydrates and other biological molecules needed for essential plant processes (► Crop Radiation Capture and Use Efficiency). Given the current emphasis on global food security, there is currently much interest in raising the radiation use efficiency of key crops in important agro-ecosystems.

Scarcity of water resources is an increasingly important issue since it will dictate global production of food and feed for the next generations (► Crop Responses to Available Soil Water). Key factors responsible for sustained plant growth and production under water scarcity, for annual as well as perennial (fruit) crops are of paramount importance.

Irrigated agriculture is currently responsible for over 40% of total production on 17% of all cultivated land area. It is therefore imperative that irrigated agriculture not only sustains its current rates of productivity but also increases (► Irrigation Management for Efficient Crop Production). Irrigation expansion is currently under pressure from other sectors to reduce its share of the fresh water resources. Efficient crop production under irrigation in the future would be essential to produce more food with less water. This is an immense challenge, not easy to achieve without novel and innovative approaches in irrigation management and crop productivity.

Sustainability of fertilizer use is very important (► Fertilizer Science and Technology), as fertilizers are indispensable because nutrient supplies from the soil are normally inadequate for high-yielding crops and compensate for nutrient removals by previously cultivated crops. In addition, fertilizer may also improve the quality of human food and animal feed.

Nitrogen is the most important limiting factor, after water deficit, for crop production worldwide (► Crop Responses to Nitrogen). Therefore, understanding how the yield of different crops can be improved by addition of nitrogen (N) fertilizers is critical. There are several important issues regarding the dynamics of crop N demands during the crop development cycle, the timing of the soil N supply according to soil characteristics, climate and soil agronomic management, the crop responses to different intensity and timing of N nutrition deficiency, and the time management of crop N fertilization using diagnostic and decision-making tools to optimize trade-offs between minimizing crop yield reduction and minimizing environmental impacts.

A substantial increase in the effectiveness with which available water and nutrients are used is required to ensure food security and environmental protection. An essential component of crop improvement is breeding for deeper or denser root systems. These characteristics promote soil moisture and nutrient capture and high dry matter production in cultivars subjected to water and/or nutrient stresses (► Roots and Uptake of Water and Nutrients). The current understanding of the structure and functions of crop root systems and the avenues for the optimization of root anatomy and morphology traits that could be applied to the genetic and agronomic improvement of crop root systems for more effective below-ground resource capture are thus very important.

Lodging is the process by which the shoots of small grained cereals are permanently displaced from their vertical stance (► Lodging Resistance in Cereals). The reduced lodging risk of shorter varieties enabled them

to respond to greater amounts of fertilizers and this was a significant reason for the steady improvement in global cereal grain yields starting in the late 1960s. However, lodging is still a major problem in many countries and there is an urgent need to improve lodging resistance to further increase the yield of cereal species.

Plant growth and yield are severely affected by saline soils. High concentrations of salt in the soil make it difficult for plants to take up water, whilst the accumulated salts in cells, particularly sodium and chloride ions, are toxic to plant metabolism (► Increasing Salinity Tolerance of Crops). These two factors result in a reduction in plant growth, an increase in the rate of leaf senescence, and a loss in crop yield. Crop salinity tolerance can be improved, but a more in-depth understanding of osmotic and ionic stresses is needed.

Agroecology provides the basic ecological principles needed for studying, designing, and managing agroecosystems that are productive, sustainable, and economically viable (► Agroecological Basis for Managing Biotic Constraints). Rather than focusing on one particular component of the agroecosystem, agroecology emphasizes the interrelatedness of all of its components and the complex dynamics of ecological processes including all environmental and human elements. From a management perspective, the agroecological objective is to provide balanced environments, sustained yields, biologically mediated soil fertility, and natural pest regulation through the design of diversified agroecosystems and the use of low-input technologies.

Plant diseases cause substantial crop losses every year (► Crop Diseases, Management and Control of). Controlling plant diseases is therefore vital to maintaining crop productivity. Crop diseases can be controlled using a variety of methods; however, plant pathogens are genetically adaptable and can overcome plant resistance, and the toxic effects of pesticides. Ensuring that crops are adequately protected from diseases depends therefore on being a step ahead of the pathogens by improving existing control measures and developing new approaches.

Increase of crop yields may be achieved by maximizing the proportion of sunlight energy that is fixed by the crop or by reducing the amount of energy that is lost by insect pests, diseases, and weeds. More than 50% of the potential yield of agricultural crops is lost by the three constraints. ► Integrated Pest Management (IPM) aims to diminish losses caused by insect pests in agriculture, in an economically, ecologically, and sociologically acceptable manner. A major challenge for ecology is the development of a scientific approach to better understand processes in agroecosystems in order to implement more rapidly sustainable IPM systems.

Yield increases will continue to play a dominant role in world food security (► Crop Yields Around the World: Closing the Gap and Raising the Potential). Understanding the gaps between potential and actual yield is of paramount importance in order to increase actual yields. These include several aspects with respect to the natural resource base of the plot (climate, soil type, topography) and long-term management investments.

Grain quality of field crops is related to seed structure and composition. Grain composition is the major reason why only a limited number of plant species are used for food and fiber (► Grain Quality in Oil and Cereal Crops). It is impossible to put forward a unique grain quality definition for any species because this depends on the specific product end use. Therefore, understanding the physiological bases of seed composition and structure is essential to produce grains with a particular quality specification.

Agricultural production takes place under erratic and unpredictable conditions, particularly the availability and timing of radiation and rainfall patterns which are extremely difficult to predict. Their effects are compensated to some extend by the qualities of the land and the interventions of the farmer. Any methodology that would improve the predictability of the availability of resources and their impact on the performance of the production system could in principle improve performance and reduce the level of uncertainty (► Simulation Models as Tools for Crop Management). Crop growth simulation models are viewed as excellent tools for the reduction of this uncertainty. Advantages and limitations of such models need to be understood in the context of past experiences and the current state of the art in order to ascertain their best possible uses.

Crop Traits: Gene Isolation

Kurniawan Rudi Trijatmiko[1], Andy Pereira[2]
[1]International Rice Research Institute, Manila, Philippines
[2]University of Arkansas, Fayetteville, AR, USA

Article Outline

Glossary
Definition of the Subject and Its Importance
Introduction
Crop Traits: Gene Isolation
Future Directions
Bibliography

Glossary

Backcross To cross the progeny of a hybrid to one of its parents, which when repeated for many generations would yield advanced backcross progeny.

cDNA Complementary DNA (cDNA) refers to the DNA copy of RNA transcripts, which can be cloned into vectors to generate a library (collection) of different cDNAs.

Chromosomal recombination Breakage and rejoining of parental homologous chromosomes during meiosis, resulting in the exchange of chromosomal segments.

Cloning vector DNA molecule into which another DNA fragment can be integrated and replicated to produce large quantities of the cloned DNA. Examples are plasmids, lambda phage, cosmids, yeast artificial chromosomes (YACs), and bacterial artificial chromosomes (BACs).

Complementation A method of validating a gene cloning by using wild-type allele to rescue the function of mutant allele through genetic transformation.

Crop trait Any morphological, physiological, or other biological feature measurable at the plant level, present in different forms in different individuals that enable genetic analysis.

Domestication An artificial selection process conducted by humans to produce plants that have more desirable traits than wild plants.

EST Expressed sequence tag is a short subsequence from a transcribed cDNA sequence.

Forward genetics A strategy to identify or clone genes that are responsible for a phenotype of interest.

Gene A gene is an ordered sequence of nucleotides that encodes a specific functional product (i.e., a protein or RNA molecule).

Marker Molecular or genetic marker is a DNA sequence at a known location on a chromosome.

Mutation Changes in a genomic sequence, occurring naturally or artificially, that can either have no effect, alter the product of a gene, or prevent the gene from functioning properly or completely.

NIL Near-isogenic lines (NILs) refers to genotypes or lines that are genetically almost identical except for a small chromosome fragment or DNA sequence by which they differ.

ORF Open reading frame (ORF) refers to a DNA sequence that does not encode a stopcodon and predicted to encode a protein.

PCR Polymerase chain reaction, a method in which DNA is amplified or increased in number of copies, using oligonucleotide primers flanking the DNA sequence and an enzyme that carries out the reaction.

Polyploid Organism that has more than two paired sets of chromosomes that is present in a diploid.

Positional cloning A method of cloning genes based on their position in the genome, using molecular markers in a genetic map located close to the gene and then identifying cloned DNA fragments containing the gene of interest.

Quantitative trait locus A region on the genome associated with a particular phenotype showing continuous and measurable variation such as height or weight.

Reverse genetics A strategy to identify the function of genes revealed by DNA sequencing, by analyzing the phenotypic effects of the gene sequences by mutations or changes in expression.

RFLP Restriction fragment length polymorphism (RFLP) is a molecular marker revealed by differences in restriction fragments between homologous (similar) fragments of DNA.

STS marker A sequence-tagged site (STS) marker is a short DNA sequence at known location in the genome, with nucleotide differences/polymorphisms that make it a useful marker for mapping.

Transposon A piece of DNA that can move within the genome of an organism, and when inserted in genes can cause a mutation.

Definition of the Subject and Its Importance

Crop plants have been selected from their wild ancestors by humans for food, fiber, health, recreation, industry, and other special purposes. Crop breeding has then added on desired traits for convenience in crop production. Genetics, molecular biology, genomics, and other disciplines have now provided us an insight to the genes that encode these very important crop traits on which the human race now depends. Knowledge of the molecular genetic basis of valuable crop traits will help provide solutions to our requirements for sustainable existence, faced with the threats of growing population needs, climate change, and dwindling natural resources. This entry describes the historical and conceptual discoveries underlying the basis of important crop traits, leading from plant domestication such as in plant architecture to those offering solutions for high crop production purposes such as growth under unfavorable environments or disease outbreaks. Detailed descriptions are provided on the cloning or identification of the plant genes involved in crop traits that give an insight on the evidence required for establishing the relationship. In addition, the molecular basis of the crop trait provides an understanding of the biological processes involved, the interaction to other traits, and a framework that can be built on to engineer novel solutions to the future needs from crop plants.

Introduction

The domestication of the major crop plants from around 10,000 to 4,000 years ago resulted in the selection of crops on which humans are now dependent [1]. The crop traits involved in domestication, transformed the wild species to a crop species catered to the needs of this paradigm shift of human civilization to an agricultural lifestyle. These early crop traits that made agriculture possible were selections from wild species that allowed humans to collect grain from the sown crop involving non-shattering, larger grain and fruit, determinate growth with more synchronous harvest, easier accessibility to the grain from protective hard outer coat, and an overall increase in edibility along with a plethora of many specialized traits. The genetic analysis and molecular isolation of key domestication traits is now uncovering the gene, the regulatory processes, and the selective sweeps from the nearest wild ancestors that accompanied the domestication process [2].

Gene cloning and DNA sequencing from the simple bacterial organisms to that of the complex polyploids such as wheat, has enabled researchers to examine gene sequences one at a time and make conclusions on similarity between close and distantly related species, propose functions based on molecular and biological properties. In fact the generation of gene sequences of a multitude of organisms is the fastest growing dataset, which promises to reveal the identity and function of all living forms. Genome sequencing started with model and standard genomes. The model plant *Arabidopsis thaliana*, a common weed, was selected for genome sequencing and molecular genetics analysis [3], with the DNA sequence of a specific ecotype Columbia [4]. Now, the 1001 genomes project intends to finish off high-quality resequencing of Arabidopsis [5] that will provide sequences of genes from the ecotypes adapted to diverse environments, which might reveal the effect of natural selection and adaptation of this very effective weed species. This also opens up a new era of going beyond a "reference" genome sequence of an organism toward sequence-based maps of closely related genotypes, which can provide a more accurate landscape of differences between genes and genomes and the relationships to expressed traits. The power of this technology was demonstrated by revealing the low level of mutations that occur between plants following a few generations of self-fertilization [6].

Gene isolation and cloning in higher plants has now come a long way since the early days of struggling with genome size and complexity. Isolation of mRNA and characterization of translated proteins was one of the primary methods to demonstrate the function of specific nucleic acids as shown for soybean leghemoglobin mRNA [7], which was then proven to be transcribed from the soybean genome [8]. One of the first approaches in plants to characterize the different components of a plant cell in terms of the complexity of nuclear and polysomal RNA, was using tobacco an

early amenable model for biological studies [9], and then analysis of the proportion of the genome and the genes that were transcribed [10]. One of the first plant genes cloned from genomic DNA was a soybean ribosomal DNA (rDNA) gene from a lambda genomic DNA library [11]. Soybean continued to be a species of interest, resulting in the generation of a complementary DNA (cDNA) library for the analysis of auxin response [12]. In maize, differential expression of the gene for the chloroplast encoded large subunit of ribulose bisphosphate carboxylase was shown in bundle sheath cells and absent in mesophyll cells [13], describing the regulation of enzymes distinguishing C4 plant cell types. These early studies showed the potential to address different plant traits by the analysis of cloned or isolated characterized genes, and the novel insights they provided.

In the course of improvement in techniques for the isolation of plant genes, methods were developed to make a correlation or causative association between specific functions and gene sequences. These functions could be defined on the basis of specific proteins with a biological function or genes determining a phenotype as revealed by isolated mutants or naturally occurring variants.

One of the important technologies that helped bridge the gap between genes and functions was the development of transformation technologies that allowed the expression of isolated genes in plants and the monitoring of the resultant phenotype. Following early demonstrations of the transfer and expression of the *Agrobacterium tumefaciens* Ti-plasmid into plant cells [14], these Ti-plasmids were engineered to transfer DNA (T-DNA) and express genes in transformed plant cells, demonstrated by a number of research groups around the same time in 1983 [15–19]. In addition to *Agrobacterium*-mediated transformation systems, other methods were developed such as direct DNA transfer to plant protoplasts [20], electroporation [21], and particle bombardment [22].

Cloning of plant genes can presently be accomplished by a variety of high-throughput ways. The cloning of expressed genes in the form of cDNA libraries has been done in plasmids, lambda vectors, and other expression systems that allow the selection of specific genes based on hybridization, DNA sequencing, or functional expression assays. The plant genome can be fractionated into representative fragments and cloned in a variety of sizes in appropriate cloning vectors. Genome fragments, in progressively increasing sizes from a few kilobases (Kb) to megabases (Mb), can be cloned in vectors such as plasmids, lambda phage, cosmids, bacterial artificial chromosomes (BACs), yeast artificial chromosomes (YACs), and modifications to these. While the smaller clones are useful for characterizing single genes or fragments thereof, the larger clones are used in positional cloning methods to identify genes using molecular markers located close to the gene of interest.

To enable the isolation of plant genes that are associated with plant biological functions/processes or crop traits, a causal relationship has to be made between DNA sequence and observed phenotype. Genetic analysis of mutants or other genetic variants that are localized on the chromosome can be used to clone the corresponding genes by methods such as map-based cloning (Fig. 1) and transposon tagging (Fig. 2), which are the two most commonly used methods for cloning genes by a forward genetics strategy centered around the phenotype of interest. In positional or map-based cloning, with a general strategy described in Fig. 1, the mapped position of a gene on the chromosome/genome, which specifies a specific trait or phenotype is the starting point to identify molecular/genetic markers close to the gene and then using integrated physical and genetic maps "walk" or "land" closer to the gene. The proof of isolating the gene is by recombination analysis, complementation by transformation, analysis of genetic variants by sequencing, or mutational analysis of the candidate genes. In transposon tagging, described in a scheme in Fig. 2, an insertion sequence from a native or heterologous transposon is used to generate mutants of a specific phenotype or genetic locus, and analysis of the transposon/insertion-tagged mutant by co-segregation analysis to a transposon probe, transposon revertant analysis or complementation of the mutant by transformation, and among the many ways evidence can be obtained to prove the identity of the tagged gene. With the availability of genome sequences of many plant species, these quite anonymous sequences need to be assigned a function, generally through a reverse genetics strategy. In reverse genetics strategies many tools are available, in most models and important crops, to generate

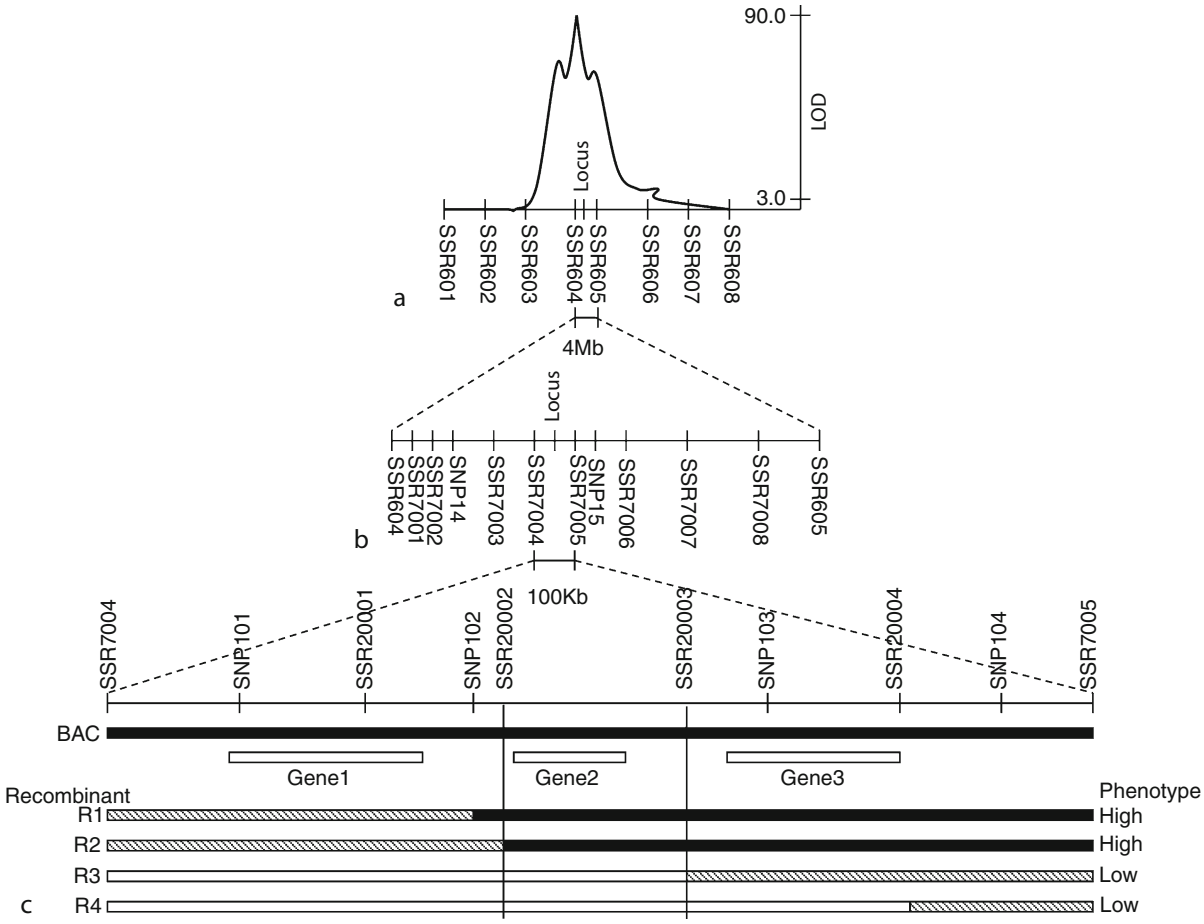

Crop Traits: Gene Isolation. Figure 1

Example of map-based cloning of a gene. (**a**) Locus mapped to a chromosome region between markers SSR604 and SSR605 via rough-scale mapping, with LOD (log of odds) score indicating linkage. (**b**) The gene further delimited to a 100-kb genomic region between markers SSR7004 and SSR7005 via fine mapping and physical mapping. (**c**) Precision mapping identified break points flanking a region containing a single gene. *Black bars* represent DNA from parent 1 (phenotype: high), *white bars* represent DNA from parent 2 (phenotype: low), and *patterned bars* represent DNA of heterozygote. The *vertical lines* show where recombination break points are positioned along the chromosome

or select mutations in specific genes and thus attribute functions by the analysis of the mutant phenotypes.

This entry describes the specific methods that have been used in the isolation and characterization of genes that determine important crop traits that agriculture is based on. The crop traits identified in many plants have homologues in the model plant Arabidopsis that can provide clues to the function. The examples described are described in some detail and others summarized in a table (Table 1) for the reader to refer to.

Crop Traits: Gene Isolation

Dwarfing Genes in Cereals

The biggest increase in agricultural production in the modern era, around the middle of the last century, is attributed to the "Green Revolution" where grain yields of the major world cereals, wheat and rice were improved along with complementary crop production practices [23, 24]. The spectacular increases in wheat and rice yields during the Green Revolution were

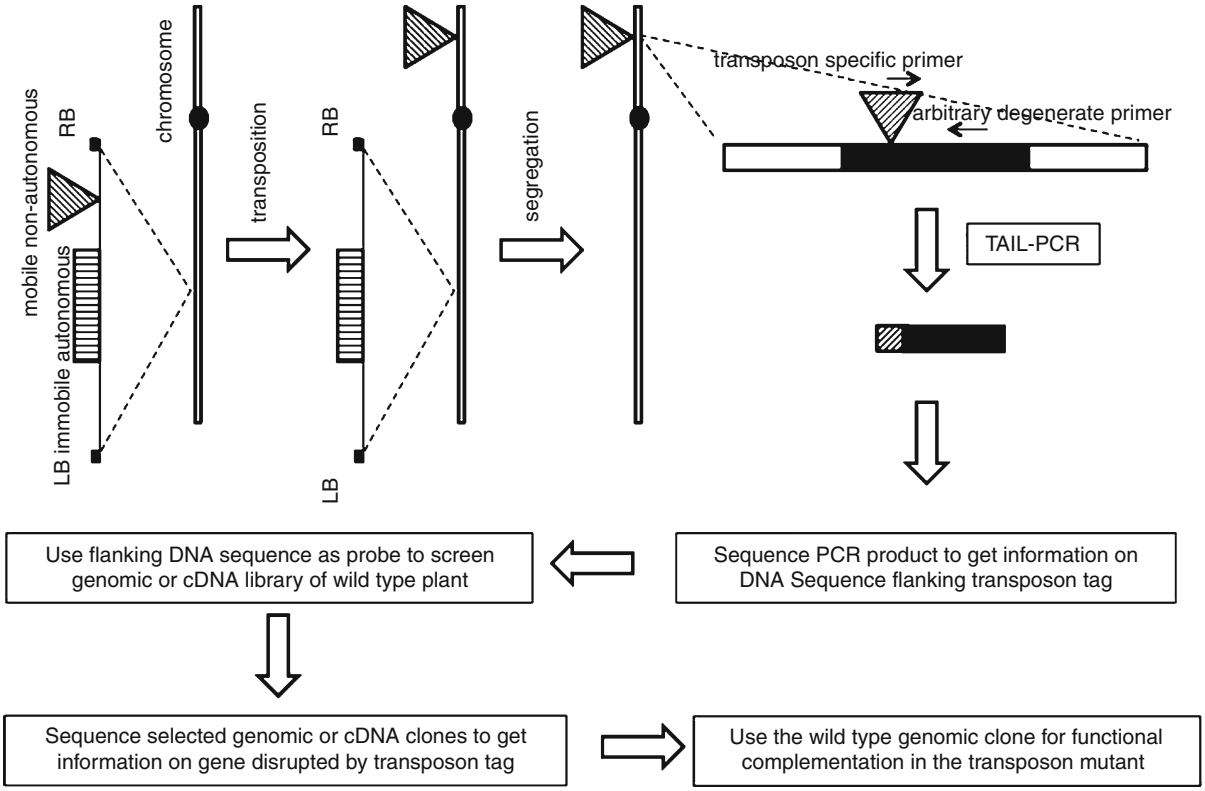

Crop Traits: Gene Isolation. Figure 2
Example of gene tagging using heterologous transposons. An "in cis two-component transposon construct" integrated into plant chromosome via *Agrobacterium*-mediated transformation. The construct contains a mobile nonautonomous transposon and an immobile transposase source. The transposase mediates transposition of the mobile nonautonomous transposon into new chromosomal positions. Segregation in the next generation creates stable mutants containing the transposon inserted in a gene with no transposase source. These stable mutants can be used in forward or reverse genetics. Identification of integration position is typically done by sequencing of DNA flanking the transposon isolated using techniques, for example, TAIL-PCR, Inverse PCR, or plasmid rescue. The flanking sequence is used as a probe to screen genomic and cDNA clones. Functional complementation is done by transforming wild-type genomic clone containing the tagged gene into the insertional mutant line

enabled by the introduction of dwarfing traits into the crop varieties. The founder of this Green Revolution, Norman Borlaug received the Nobel Peace prize in 1970 in recognition for his efforts in bringing food security to major parts of the developing world [25]. Identification of the genes responsible for these traits showed that they interfere with the action or production of the gibberellin (GA) plant hormones [26].

The dwarfing gene of wheat, *Reduced Height-1* (*Rht-1*), was isolated based on sequence similarity to the previously isolated Arabidopsis *GIBBERELLIN INSENSITIVE* (*GAI*) gene [27]. GAI is a member of the DELLA proteins and a repressor of GA responses [28]. The wheat *Rht-B1b* and *Rht-D1b* dwarfing mutants had similar characteristics to the Arabidopsis *gai* mutant, including reduced plant height, reduced responses to gibberellin, and increased *in planta* gibberellin levels. Compared to the wild-type *Rht-1* allele, the *Rht-B1b* and *Rht-D1b* dwarfing alleles each contained a nucleotide substitution that created a stop codon near the N-terminus of the protein [27]. It was proposed that translational reinitiation after these introduced stop codons might result in an N-terminally truncated product that confers the mutant phenotype.

Crop Traits: Gene Isolation. Table 1 Some isolated genes in crops

Gene (s)	Crop	Molecular and phenotypic function	Cloning method[a]	Validation method[b]	Causative change[c]	Reference (s)
1. Dwarfing gene						
Rht-1	Wheat	Transcriptional regulator (SH2); plant height	SS	Mut, HE	EStp	[27]
sd1	Rice	GA20 oxidase; plant height	SS, MBC	Var	Coding	[30–32]
d	Tomato	Cytochrome P450 enzyme; plant height	TT	FC		[141]
2. Flowering/heading date						
Hd6	Rice	Protein kinase; flowering time	MBC	FC	EStp	[33]
Hd1	Rice	Transcriptional regulator (zinc finger); flowering time	MBC	FC	Coding	[34]
Hd3a	Rice	Phosphatidylethanolamine-binding protein; flowering time	MBC	OE, Sil	-	[37]
Ehd1	Rice	B-type response regulator; flowering time	MBC	FC	AC	[142]
Vgt1	Maize	Transcriptional regulator (AP2); flowering time	MBC, AM	OE, Sil	Reg	[143]
E3	Soybean	Phytochrome A; flowering time	MBC	Mut	AC?	[144]
Vrn1	Wheat	Transcriptional regulator (MADS); vernalization	MBC	Var	Reg	[145]
Vrn2	Wheat	Transcriptional regulator (ZCCT); vernalization	MBC	Sil	AC	[146]
3. Fruit ripening, shape, and weight						
Rin	Tomato	Transcriptional regulator (MADS-box); fruit ripening	MBC	FC, Sil	Coding	[147]
Ovate	Tomato	Regulatory protein (OVATE); fruit shape	MBC	FC	EStp	[148]
fw2.2	Tomato	Cell signaling; fruit weight	MBC	FC	Reg	[40]
4. Grain yield						
Gn1	Rice	Cytokinin oxidase/dehydrogenase; grain number	MBC	Sil	Reg/EStp	[42]
GS3	Rice	VWFC module-containing protein; grain weight	MBC	Var	EStp	[44]
GW2	Rice	RING-type protein with E3 ubiquitin ligase activity; grain width	MBC	OE, Sil	EStp	[47]
5. Disease resistance						
Hm1	Maize	HC toxin reductase; resistance to the fungus *Cochliobolus carbonum*	TT	Co	Reg	[49]
Cf-9	Tomato	Leucine-rich repeat family of proteins; resistance to leaf mold fungus *Cladosporium fulvum*	TT	Co	Wild	[54]
RB/Rpi-blb1	Potato	CC–NBS–LRR-class R-gene analog; resistance to oomycete pathogen *Phytophthora infestans*	MBC	FC	Wild	[58, 59]
Rpi-blb2	Potato	NBS–LRR protein; resistance to oomycete pathogen *Phytophthora infestans*	MBC	FC	Wild	[60]

Crop Traits: Gene Isolation. Table 1 (Continued)

Gene (s)	Crop	Molecular and phenotypic function	Cloning method[a]	Validation method[b]	Causative change[c]	Reference (s)
mlo	Barley	Membrane-anchored protein; resistance against the fungal pathogen *Blumeria graminis* f. sp. *hordei* (Bgh)	MBC	Mut, RA	AC/EStp	[62]
Mi	Tomato	NBS–LRR protein; resistance to root-knot nematodes (*Meloidogyne* spp.)	MBC	FC	Wild	[72]
Tm-2^{2}	Tomato	CC–NBS–LRR class of R proteins; resistance to tomato mosaic virus (ToMV)	TT	FC	Wild	[76]
Pto	Tomato	Protein kinase; resistance to *Pseudomonas syringae* pv. *tomato*	MBC	FC	Wild	[149]
Xa21	Rice	Protein kinase; resistance to *Xanthomonas oryzae* pv. *oryzae*	MBC	FC	Wild	[150]
Cf-2	Tomato	LRR protein; resistance to leaf mold fungus *Cladosporium fulvum*	MBC	FC	Wild	[151]
N	Tobacco	LRR protein; resistance to tobacco mosaic virus (TMV)	TT	FC	Wild	[152]
Hs1^{pro-1}	Sugar beet	LRR protein; resistance to beet cyst nematode	MBC	FC	Wild	[153]
I2C	Tomato	NBS–LRR protein; resistance to *Fusarium oxysporum* f sp *1ycopersici*	MBC	Sil, OE	Wild	[154]
Ve	Tomato	Cell surface-like receptors; resistance to *Verticillium dahliae*	MBC	FC	-	[155]
R1	Potato	Leucine-zipper/NBS/LRR protein; resistance to *Phytophthora infestans*	MBC	FC	Wild	[156]
Rpg1	Barley	Receptor kinase; resistance to *Puccinia graminis* f. sp. *tritici*	MBC	Var	EStp, AC, FS	[157]
Hero	Tomato	NBS–LRR protein; resistance to potato cyst nematodes *Globodera rostochiensis*	MBC	FC	Wild	[158]
Lr10	Wheat	CC–NBS–LRR protein; resistance to *Puccinia triticina*	MBC, HS	OE	CD	[159]
Lr21	Wheat	NBS–LRR protein; resistance to *Puccinia triticina*	MBC	FC	Wild	[160]
Pm3b	Wheat	CC–NBS–LRR protein; resistance to *Blumeria graminis* f. sp. *tritici*	MBC	STA	-	[161]
Pi9	Rice	NBS–LRR protein; resistance to *Magnaporthe grisea*	MBC	FC	Wild	[162]
Rpg5	Barley	Protein kinase; resistance to *Puccinia graminis* f. sp. *secalis*	MBC	Sil	FS	[163]
Yr36 (WKS1)	Wheat	Kinase-START protein; resistance to *Puccinia striiformis* f. sp. *tritici*	MBC	FC	Wild	[164]
Rdg2a	Barley	CC–NB–LRR protein; resistance to *Pyrenophora graminea*	MBC	FC	Reg	[165]

Crop Traits: Gene Isolation. Table 1 (Continued)

Gene (s)	Crop	Molecular and phenotypic function	Cloning method[a]	Validation method[b]	Causative change[c]	Reference (s)
6. Plant and inflorescence architecture						
tb1	Maize	Transcriptional regulator (TCP); plant and inflorescence structure	TT	Co	Reg	[80]
tga1	Maize	Transcriptional regulator (SBP); seed casing	MBC	Mut	AC	[85]
Q	Wheat	Transcriptional regulator (AP2); inflorescence structure	MBC	Mut	Reg/AC	[92]
vrs1	Barley	Transcriptional regulator (HD-ZIP); spikelet morphology	MBC	Mut	AC/FS	[98]
nud	Barley	Transcriptional regulator (ERF); seed casing	MBC	Var, Mut	CD	[103]
MOC1	Rice	Transcriptional regulator (GRAS); tillering	MBC	FC	TE	[107]
PROG1	Rice	Transcriptional regulator (ZF); growth habit	MBC	FC	Reg/AC	[109]
7. Seed quality and color						
opaque-2	Maize	Transcriptional regulator (bZIP); endosperm characteristic	TT	Co	TE	[111]
Wx	Maize	Starch synthase; sticky grains	TT	Rev	TE	[113]
Wx	Rice	Starch synthase; sticky grains	SS	Var	Splice	[115, 116]
Sh2	Maize	Pyrophosphorylase; supersweet sweet corn	TT	Rev	TE	[118]
su1	Maize	Isoamylase; sweet corn gene	TT	Co	AC	[119]
Rc	Rice	Transcriptional regulator (bHLH); seed color	MBC	Mut	Coding	[121]
c1	Maize	Transcriptional regulator (MYB); kernel color	TT	Co	Reg	[166]
y1	Maize	Phytoene synthase; carotenoid content	TT	Rev	Reg	[167]
R	Pea	Starch branching enzyme; seed sugar content	IS	Co	TE	[168]
Brix9-2-5	Tomato	Invertase; fruit-soluble solid content	MBC	IR	Reg	[169]
8. Seed shattering						
sh4	Rice	Transcriptional regulator (Myb3); abscission layer formation, shattering	MBC	FC	Reg/AC	[128]
qSH1	Rice	Transcriptional regulator (homeodomain); abscission layer formation, shattering	MBC	FC	Reg	[129]
sh-h	Rice	CTD phosphatase; abscission layer differentiation, shattering	MBC	Mut, Sil	Splice	[131)
Jointless	Tomato	Transcriptional regulator (MADS); abscission zone development, shedding	MBC	FC, Sil	Coding	[170]
9. Tolerance to abiotic stresses						
SKC1	Rice	HKT-type transporters; salt tolerance	MBC	FC	AC	[134]
Sub1	Rice	Transcriptional regulator (ERF); submergence tolerance	MBC	FC	CD	[137]

Crop Traits: Gene Isolation. Table 1 (Continued)

Gene (s)	Crop	Molecular and phenotypic function	Cloning method[a]	Validation method[b]	Causative change[c]	Reference (s)
Alt1	Wheat	Aluminum-activated malate transporter; tolerance to aluminum toxicity	SH	Co, Var, HE	Reg/AC	[140]
Snorkel1, Snorkel2	Rice	Transcriptional regulator (ERF); deepwater tolerance	MBC	Var, OE	CD	[171]

[a]*MBC* map-based cloning, *TT* transposon tagging, *AM* association mapping, *HS* haplotype study, *SS* sequence similarity, *SH* subtractive hybridization, *IS* immunological screening

[b]*FC* functional complementation, *Rev* transposon revertant analysis, *Co* co-segregation analysis, *RA* recombination analysis, *Var* analysis of genetic variants by sequencing, *Mut* mutational analysis of the candidate genes, *OE* overexpression, *Sil* silencing, *IR* intragenic recombination, *HE* heterologous expression, *STA* single-cell transient assay

[c]*AC* amino acid change, *Coding* disrupted coding sequence, *FS* frame shift, *EStp* early stop codon, *Reg* regulatory change, *Splice* intron splicing defect, *CD* complete deletion, *Wild* introgression from wild relative,*TE* transposon insertion (Following Doebley et al. [1] with modification)

The rice *sd-1* dwarfing allele, with origin from cultivar Dee-Geo-Woo-Gen and used in the Green Revolution dwarf variety IR8, was mapped to the long arm of chromosome 1 [29]. Characterization and isolation of this gene was reported in 2002 by three different groups [30–32]. Biochemical analysis of the *sd-1* mutant showed that the activity of GA20 oxidase (GA20ox), a key enzyme in the biosynthesis of gibberellin, did not function effectively in the mutant. A wild-type *GA20ox* gene (*GA20ox-2*) was amplified by PCR using primers based on the conserved domain of *GA20ox* genes. Linkage mapping showed that this gene mapped to the long arm of chromosome 1, tightly linked to the *sd1* locus. Compared to the wild-type *Sd-1* allele, the *sd-1* dwarfing allele (in Dee-Geo-Woo-Gen and IR8) contained a 383-base-pair deletion which produces a frame shift that creates a stop codon [30]. Another study showed RFLP markers flanking the *sd-1* locus were positioned on a physical segment of chromosome 1 covered by contiguous BAC clones by using the physical map of the reference genome available in the database. A candidate gene search identified the *GA20ox-2* gene in this region. This gene was amplified in the wild type and mutant, and sequence comparison revealed a 280-bp deletion in the coding region of this gene in the mutant allele [31]. A third independent analysis of 3,477 segregants using several PCR-based markers localized the *sd-1* locus in a 6-kb candidate interval on chromosome 1, containing only one predictable ORF, that of *GA20ox-2*. The 3,477 segregants were derived from selfing of a backcross inbred line (BIL) having close chromosomal similarity to Sasanishiki (normal-type parent) over the whole genome length with the only heterozygous sequences located on *sd-1* locus. Sequence comparison showed that Habataki (semidwarf parent) has a 383-bp deletion from the middle of exon 1 to upstream of exon 2, including a 105-bp intron, resulting in a frame shift that produces a termination codon in exon 3 [32]. These evidence clearly defined the identity of the *Sd-1* dwarfing gene and the mutant *sd-1* alleles.

Flowering or Heading Date

Heading date or flowering time is an important trait for the adaptation of crops to different cultivation areas. In rice, heading date is determined mainly by two factors: duration of the basic vegetative growth and photoperiod sensitivity (PS) [33]. Genetic analysis of heading date in rice cultivars Kasalath and Nipponbare showed that a number of quantitative trait loci, termed Hd (heading date) determine the genetic variation for flowering time [34]. Day-length treatment sensitivity tests with an NIL of *Hd6* [NIL(*Hd6*)] revealed the *Hd6* PS phenotype, with the Kasalath allele increasing days-to-heading under natural and long-day conditions but not under short-day conditions. Linkage analysis of an advanced backcross progeny mapped *Hd6* on the long arm of chromosome 3 as a single Mendelian factor [35]. High-resolution mapping using 2,807 segregating plants derived from an advanced backcross progeny, in which the region around *Hd6* was heterozygous and

almost all other regions were homozygous for Nipponbare, delimited *Hd6* to a 26.4-kb genomic region. The sequence analysis of this region identified one gene with deduced amino acid sequence having high homology (>90%) to the α subunit of protein kinase CK2 (CK2α) in maize and Arabidopsis. Sequence comparison showed a single-nucleotide substitution within the coding region, which changed the lysine codon (AAG) in Kasalath to a premature stop codon (TAG) in Nipponbare. Functional complementation was performed by introducing the Kasalath genomic fragment carrying the CK2α gene into Nipponbare and the transgenic plants scored under natural day-length condition showed late heading, indicating that the Kasalath allele of CK2α increases days-to-heading [33].

Another heading date locus *Hd1* was characterized by high-resolution mapping using 1,505 early heading BC3F3 segregants derived from a cross between Nipponbare and Kasalath, which resolved the locus to a genomic region of 12 kb. Sequence analysis of the region identified one putative gene with considerable similarity to the *CONSTANS* (*CO*) gene, known to be involved in photoperiod response in Arabidopsis. Sequence comparison showed a 2-bp deletion in the second putative exon of the Kasalath allele resulting in a premature stop codon and a predicted shorter protein than the wild-type Nipponbare protein. Functional complementation was performed by transferring the candidate *Hd1* region from Nipponbare into a NIL of Nipponbare carrying an introgression of Kasalath nonfunctional *Hd1* allele. Transgenic plants showed earlier heading under short-day conditions than the NIL control and null-segregants. These results provide clear evidence that the *Hd1* sequence in the candidate genomic region retains the function of photoperiod response [34].

The *Hd3a* locus was roughly mapped on chromosome 6. NIL(*Hd3a*), an NIL homozygous for the Kasalath allele at the *Hd3a* locus in the genetic background of Nipponbare, headed earlier than Nipponbare under SD conditions and headed at almost the same date as Nipponbare under LD and natural field conditions [36]. High-resolution mapping using 2,207 segregants delimited *Hd3a* to a 20-kb genomic region, whose sequence revealed one putative gene with high similarity to the *FLOWERING LOCUS T* (*FT*) gene, which promotes flowering in Arabidopsis. In this study, the nucleotide polymorphism that caused the allelic difference between Kasalath and Nipponbare *Hd3a* could not be clarified [37].

Fruit Weight and Grain Yield

The domestication and improvement of crops has been accompanied by increase in size and yield of harvestable products. Cultivated tomatoes (*Solanum lycopersicum*) have hence undergone more than a 100-fold increase in mass over their wild relatives. A major quantitative trail locus (QTL) for fruit weight, *fw2.2*, was mapped to the same position on chromosome 2 in an introgression line F2 derived from *S. lycopersicum* x *Lycopersicon pennellii* and a backcross 1 (BC1) population derived from *S. lycopersicum* x. *Lycopersicon pimpinellifolium*. The *fw2.2* locus accounts for 30% and 47% of the total phenotypic variance in the *L. pimpinellifolium* and *L. pennellii* populations, respectively, indicating that this is a major QTL controlling fruit weight in both species. The small-fruit *L. pennellii* allele for *fw2.2* is semidominant to the large-fruit *S. lycopersicum* allele [38]. High-resolution mapping using 3,472 F2 plants derived from a cross between *S. lycopersicum* and a NIL containing a small introgression from *L. pennellii* narrowed down *fw2.2* to a less than 150-kb region [39]. A yeast artificial chromosome (YAC) containing *fw2.2* was used to screen a cDNA library constructed from the small-fruit *L. pennellii*. Four unique transcripts were identified and used to screen a *L. pennellii* cosmid library, identifying four positive, nonoverlapping cosmids (cos50, cos62, cos69, and cos84), one corresponding to each unique transcript. These four cosmid clones were transformed into two tomato cultivars carrying the partially recessive large-fruit allele of *fw2.2*. R1 progeny of primary transformants carrying cos50, but not other cosmids, showed a statistically significant reduction in fruit weight compared to null-segregants, indicated that *fw2.2* is contained within cos50. Sequence analysis of cos50 revealed two open reading frames (ORFs): one corresponding to cDNA44, which was used to isolate cos50, and another 663-nucleotide (nt) gene, *ORFX*, for which no corresponding transcript was detected in the initial cDNA library screen. Analysis on a single

recombination event used in the previous mapping showed that *ORFX* is the likely cause of the *fw2.2* QTL phenotype. Semiquantitative reverse transcriptase-polymerase chain reaction (RT-PCR) analysis showed that the relative level of the *ORFX* transcript in the carpels of the small-fruited NIL was significantly higher than in the large-fruited NIL. Analysis of the predicted amino acid sequence of *ORFX* indicated that it is a soluble protein with alpha/beta-type secondary structure, and has a structural similarity to the human oncogene c-H-ras p21. Sequence comparison of *L. pennellii* and *S. lycopersicum ORFX* regions indicated that the *fw2.2* phenotype is probably not caused by differences within the coding region of *ORFX*, but by one or more changes upstream in the promoter region of *ORFX* [40].

Grain yield is a complex crop trait determined mainly by the three component traits, number of panicles, number of grains per panicle, and grain weight; all of which are typical quantitative traits. In rice, the developments in genome mapping, sequencing, and functional genomic research have provided the necessary tools for dissecting the genetic and molecular bases of these quantitative traits [41].

The rice grain number gene *Gn1* was first roughly mapped on the short arm of chromosome 1 using 96 F2 individuals derived from heterozygote (*Gn1*/*gn1*) plants of NIL-*Gn1* carrying the *Gn1* region from cultivar Habataki in the Koshihikari background. Habataki plants have been known to produce more grains in their main panicle than Koshihikari plants. It was found that *Gn1* consisted of two loci, *QTL-Gn1a* and *QTL-Gn1b*. High-resolution mapping using 13,000 F2 plants derived from heterozygotes (*Gn1a*/*gn1a*) of NIL-*Gn1a* narrowed down the *Gn1a* region into a 6.3-kb interval containing one reading frame with high similarity to cytokinin oxidase/dehydrogenase (CKX), named *OsCKX2*. Sequence comparison between Habataki and Koshihikari revealed several nucleotide changes, including a 16-bp deletion in the 5′-untranslated region, a 6-bp deletion in the first exon, and three nucleotide changes resulting in amino acid variation in the first and fourth exons of the Habataki allele. However, protein expression study in *Saccharomyces cerevisiae* showed both Habataki and Koshihikari alleles of *OsCKX2* encode functional enzymes. Sequence analysis of 5150, a rice variety from China producing higher grain number, detected 11-bp deletion in the coding region of this gene creating a premature stop codon. The coincidence of the *OsCKX2* null allele and a higher grain number suggested that a reduction or loss of function of *OsCKX2* enhanced grain production. Confirmation was done by introducing antisense strands of *OsCKX2* into an easily transformable cultivar Taichung 65 (TC65), which possesses the Koshihikari allele of *OsCKX2*. Transgenic plants with reduced levels of expression developed higher grain numbers. Reverse Transcription (RT)-Southern blotting showed that the highest levels of *OsCKX2* expression in inflorescence meristems were found in Koshihikari, but were less abundant in Habataki and NIL-*Gn1a* and extremely low in 5150. These results suggested that the phenotypic differences observed might have been caused by differential transcription of *OsCKX2* [42].

The rice *GS3* grain weight gene was mapped to the pericentromeric region of chromosome 3 [43]. Near-isogenic lines (NILs) of *GS3* were developed by successive crossing and backcrossing Minghui 63 (large grain) with Chuan 7 (small grain), using Minghui 63 as the recurrent parent. High-resolution mapping using 1,384 BC3F2 individuals with the recessive phenotype (large grain) derived from one BC3F1 plant heterozygous for the *GS3* region and containing the least genetic background from Chuan 7 delimited the *GS3* region to 7.9 kb. A full-length cDNA was identified that matched well with the region, and sequence analysis of the predicted GS3 protein revealed the presence of a combination of multiple domains. Comparative sequencing analysis using six cultivars including three with long grains and three with short to medium grains indicated that all the large-grain varieties tested share the same nonsense mutation in the second exon of the *GS3* gene that causes a 178-aa truncation in the C-terminus of the predicted protein. These findings suggest that *GS3* may function as a negative regulator to prevent the growth and size of the grain [44].

Two QTLs for grain width were mapped to the short arm of chromosome 2 [45, 46). Subsequently, a major QTL for grain width GW2, was mapped to the same region using an F2 population derived from a cross between WY3 (1,000-grain weight, 41.9 ± 1.3 g) and Fengaizhan-1 (FAZ1) (1,000-grain weight, 17.9 ± 0.7 g). High-resolution mapping using 6,013 BC3F2

plants narrowed the GW2 locus to an 8.2-kb region. Only one predicted ORF was considered a viable candidate for GW2 in this region [47]. Homology search in databases showed that GW2 encodes a previously unknown RING-type protein with E3 ubiquitin ligase activity, which is known to function in the degradation by the ubiquitin–proteasome pathway. Comparison of the nucleotide sequences of the FAZ1 and WY3 alleles of GW2 uncovered a 1-bp deletion resulting in a premature stop codon in exon 4 of the WY3 allele. The premature stop codon led to truncation of 310 amino acid residues; the remaining portion of the protein consisted of a 115-residue polypeptide of ~13 kDa. Sequence analysis of GW2 from Oochikara, another rice variety that has a wider grain width, similar to WY3, showed a nucleotide sequence identical to the WY3 allele. These data indicate that reduction or loss of function of GW2 results in increased grain width. Rice transformation was used to produce transgenic plants expressing different levels of GW2. The transgenic plants with antisense strands of GW2 and with reduced levels of endogenous expression had a significantly wider grain width than plants containing the vector control. Transgenic plants overexpressing GW2 cDNA under the control of the 35S promoter, which produced high levels of expression, showed reduced grain width [47].

Disease Resistance

Disease resistance loci (R genes) conferring resistance to specific races of the pathogen, carrying corresponding avirulence (Avr) genes, have been studied in light of the gene-for-gene hypothesis proposed by Flor [48]. Plants that contain such race-specific R-genes with resistance to specific pathogen races, offer an interesting system to study plant pathogen interactions, although the genes are very rarely useful in the crop as they are quickly overcome by the pathogen gaining virulence.

In addition, there are non-race-specific disease resistance loci which provide plant resistance to a wider range or races of the pathogens. The first plant resistance gene cloned was *Hm1* from maize, which belonged to this class of resistance genes, was isolated by transposon tagging [49]. Two RFLP probes were mapped to 5 centimorgan (cM) proximal and distal to the *Hm1* locus, respectively, using progeny from the cross K61/Pr1 × K61 [50]. These two probes were used to classify segregating progeny of transposon insertion *hm1* mutants to determine which *HM1* alleles they had inherited. A transposable element probe was then used to identify a restriction fragment that cosegregated with *hm1* mutant allele. This fragment was isolated and sequenced, and the DNA flanking the transposon insertion was used as probe in northern blot analysis. A 1.3-kb RNA band was detected in polyadenylated [poly(A)$^+$] RNA from the resistant inbred strain Pr1 (*Hm1-Pr1*), while the susceptible strain, K61 (*hm1-2*), and the mutants either had no detectable hybridizing mRNA, or an mRNA of aberrant size. Difference at the transcriptional level between resistant and susceptible genotypes makes it unlikely that susceptible genotypes possess an alternative form of HM1 with specificity for a substrate other than HC toxin. A 1.6-kb cDNA clone was isolated by homology with the probe and sequenced. DNA sequence databases revealed homology between the *HM1* cDNA and the NADPH-dependent dihydroflavonol-4-reductase (DFR) genes of maize, petunia, and snapdragon. This homology supports the prediction that *HM1* encodes HC toxin reductase (HCTR) [49].

Among the race-specific R-genes, the tomato-leaf mold interaction has been well studied and yielded the first examples of cloned R-genes. The avirulence gene *Avr9* in the leaf mold fungus *Cladosporium fulvum* was shown to specify a 28-amino acid secreted peptide that elicits a necrotic response when injected into tomato plants carrying the *Cf-9* resistance gene [51]. The *Cf-9* gene was introgressed into cultivated tomato from wild species *L. pimpinellifolium* accession PI126915 [52]. The *Cf*-9 locus was mapped to the short arm of chromosome 1 [53], and a targeted transposon tagging strategy was employed to isolate the *Cf-9* gene [54]. A tomato line homozygous for *Cf*-9 was crossed to a transgenic tomato line carrying a *Ds* element located 3 cM from the *Cf*-9 locus, and additionally to a transgenic tomato plant containing a stabilized *Ac* (s*Ac*) element. The F1 plants were crossed and the progenies selected to produce tagging parents heterozygous for *Ds* and s*Ac* and homozygous for *Cf-9*. To tag *Cf*-9 the tagging lines were crossed as female parents to a tomato line homozygous for the *Avr9* transgene and lacking *Cf*-9. The progeny of this cross, which were heterozygous for *Cf*-9 and *Avr9*, became necrotic and died

shortly after seed germination, but the mutants for *Cf*-9 survived. Approximately 160,000 progeny were germinated and 118 survivors were recovered. A total of at least 37 independent *Ds* insertions into *Cf-9* were identified. Specific *Cf-9* primers were used in conjunction with *Ds* primers to map the *Ds* insertions on the basis of PCR product size. Twenty-eight *Ds* insertions were mapped to the same 3-kb region of the tomato genome. All stable mutants tested were susceptible to race 5 of *Cladosporium fulvum*, which indicates concordance between the loss of response to the *Avr9* transgene and loss of resistance to a race of the fungus carrying *Avr9*. Isolation via plasmid rescue and sequencing of the flanking genomic sequence showed that *Cf-9* encodes a putative membrane-anchored extracytoplasmic glycoprotein with homology to the leucine-rich repeat family of proteins [54].

Late blight caused by the oomycete pathogen *Phytophthora infestans*, and responsible for the Irish Potato Famine of the mid-nineteenth century that induced vast migration, is still one of the most devastating of plant diseases causing more than $3 billion loss annually [55]. The *P. infestans* pathogen easily overcomes the R-genes crossed in from various wild relatives of potato. Diploid *Solanum bulbocastanum* from Mexico, which was not easily crossable to potato (*Solanum tuberosum*) cultivars, had been characterized to have high resistance to *P. infestans* and was used to characterize the resistance gene loci. The *RB* (for "Resistance from *S.* b*ulbocastanum*") locus was mapped to chromosome 8 of *S. bulbocastanum* [56]. BAC walking by the reiterative screening of a BAC library using probes derived from the ends of previously identified BAC clones, was initiated using linked RFLP markers and the contig subsequently used to develop PCR-based markers to enhance map resolution in the *RB* region. High-resolution mapping using 542 BC2, 1,060 BC3, and 206 BC4 genotypes delimited the *RB* region to approximately 55 kb [57]. This region contained one truncated and four complete CC–NBS–LRR (coiled coil–nucleotide binding site–Leu-rich repeat)-class R-gene analogs (RGAs). Each of the four complete RGAs was amplified from *S. bulbocastanum* using Long Range-PCR and cloned into a binary vector for complementation studies. Katahdin, a late blight susceptible potato variety was transformed with the four complete R-gene analogs. Only the transgenic plants containing *RGA2*-PCR construct displayed resistance to all six isolates of *P. infestans*, including 126C18, a "super race" that overcomes all 11 major R genes identified in *Solanum demissum*, the complementation demonstrating that *RGA2* represents the functional *RB* gene [58].

In a simultaneous effort to the analysis of the RB locus, the *Rpi-blb1* resistance locus was characterized in intraspecific crosses between *S. bulbocastanum* accessions segregating for resistance, and mapped closely to marker CT88 on chromosome 8 [59]. A BAC contig was isolated across the *Rpi-blb1* locus, and sequence analysis revealed 4 RGAs of the CC–NBS–LRR class. One of the genes termed *Rpi-blb1* complemented potato and tomato cultivars to confer resistance to complex races of the *P. infestans* pathogen. In subsequent analysis of resistant complex interspecific hybrids designated ABPT derived from *S. bulbocastanum*, the *Rpi-blb2* locus was identified and mapped to a position on chromosome 6 at a similar position as the tomato *Mi* locus (see below) conferring resistance to nematode, aphids, and white flies. The *Rpi-blb2* locus harbored 15 Mi-1 gene homologues, one of which conferred *P. infestans* resistance in tomato and potato. The Rpi-blb2 protein shares 82% sequence identity to the tomato Mi-1 protein and exemplifies the evolution of a resistance gene cluster to confer diverse resistance specificity to a wide range of organisms such as nematodes, insects, and oomycetes [60].

The barley recessive *mlo* locus conferring resistance against the fungal pathogen *Blumeria graminis* f. sp. *hordei* (Bgh) has been mapped on chromosome 4 [61]. High-resolution mapping using 2,022 F2 segregants identified a DNA marker cosegregating with *mlo* and two flanking markers at a distance of 0.24 and 0.4 cM, respectively. Screening of a large insert yeast artificial chromosome (YAC) library identified three YAC clones containing the cosegregating marker and two flanking markers. Subcloning experiments of one YAC clone into bacterial artificial chromosome (BAC) vector and further mapping and sequencing delimited the *mlo* region to 30 kb. Sequence analysis identified one sequence contig of 5.8 kb, including the cosegregating marker, revealing an extensive region of high coding probability. Reverse transcriptase-PCR using a series of primers deduced from this region and sequencing revealed a single extensive open reading frame (ORF)

of 1,599 bp. The deduced 60 kDa protein was predicted to be membrane-anchored by at least six membrane-spanning helices. Genomic PCR-based sequencing of 11 mutagen-induced *mlo* resistance alleles and their corresponding wild-type DNAs identified nucleotide alterations (point mutations or deletions) in all tested mutant alleles that at the amino acid level result either in single amino acid substitutions or truncated versions of the predicted wild-type protein. A comparison among the wild-type gene sequences of seven tested barley cultivars indicated not a single amino acid difference. Inter-mutant crosses were performed using lines containing different mutant alleles. F2 seedlings were screened for rare disease–susceptible individuals after inoculation with an isolate of powdery mildew which is virulent on each of the parental *Mlo* wild-type cultivars. Homozygous susceptible F3 progeny were isolated and used for molecular analysis using RFLP markers tightly linked (<4 cM) on each side of the *Mlo* locus. Seven susceptible individuals exhibited flanking molecular marker exchange, indicating reciprocal crossover (CO) events. Genomic PCR-based sequencing demonstrated that all seven CO type recombinants restored wild-type sequences [62].

Root-knot nematodes (*Meloidogyne* spp.) are endoparasites of thousands of crop species and are important pests of tomato worldwide [63]. The root-knot nematode resistance gene (*Mi*) was introduced into cultivated tomato, *S. lycopersicum*, from its wild relative *Lycopersicon peruvianum* in the early 1940s [64], and today it provides the only form of genetic resistance against this pathogen. The *Mi* locus was localized to the short arm of chromosome 6 [65] and multiple markers linked to Mi were identified [66–69]. In these studies, it was found that the nematode-resistant tomato line Motelle, and related lines, retained only a small introgressed region (650 kb) from *L. peruvianum*. Efforts to localize the *Mi* gene were hampered for many years because of the severe repression of recombination near this gene in *Lycopersicon esculentum* lines carrying the introgressed *L. peruvianum* DNA [67, 68, 70]. This handicap was circumvented by screening large populations of tomato for recombinants and by identifying recombinants within *L. peruvianum* populations [71]. After data from *S. lycopersicum* and *L. peruvianum* recombinant analyses were combined, *Mi* could be localized to a genomic region of <65 kb. Subcloning experiments of one YAC clone containing the *Mi* locus identified four overlapping BACs hybridizing to the *Mi*-flanking DNA probes. Large-scale sequencing of two BACs identified six open reading frames; three of these are homologous to each other and to previously identified R genes of the nucleotide binding–LRR class. Two of them, *Mi-1.1* and *Mi-1.2*, appear to be intact genes; the third is a pseudogene predicted to not encode a functional product. Complementation studies were performed by transforming a nematode-susceptible tomato line using constructs containing the *Mi-1.1* and *Mi-1.2* genes. Eighty-seven percent of transformants carrying *Mi-1.2* were resistant to the root-knot nematode, whereas all transformants carrying *Mi-1.1* were completely susceptible, confirming *Mi-1.2* as the functional *Mi-1* gene [72].

In cultivated tomato, tomato mosaic virus (ToMV) infections are controlled by the introgressed *Tm-1*, *Tm-2*, and $Tm\text{-}2^2$ resistance (*R*) genes [73, 74]. Among these resistances the $Tm\text{-}2^2$ resistance was shown to be remarkably durable and, therefore, of ongoing practical importance. The $Tm\text{-}2^2$ locus has been localized to tomato chromosome 9, but map-based cloning of this gene has been shown to be difficult, especially due to the lack of recombination in the centromeric region [75]. The two-component Ac/Ds transposon system was utilized to isolate the tomato $Tm\text{-}2^2$ gene. A tomato line (homozygous $Tm\text{-}2^2$) was crossed with another line (homozygous for *sAc*). One F2 plant from this cross (homozygous for both *sAc* and $Tm\text{-}2^2$) was subsequently used in a cross with a tomato line having *Ds* transposon on chromosome 9 with distance 2 cM from the resistance gene. About 100 independent plants with the genotype *Ds*/–; *sAc*/–; $Tm\text{-}2^2/Tm\text{-}2^2$ were selected and used as males and females in a cross with a transgenic tomato line which is homozygous for the ToMV *MP* (Movement Protein) gene for a large-scale tagging experiment. Previous observation had shown a lethal combination of the $Tm\text{-}2^2$ gene and the *ToMV MP* transgene in the seedling stage of tomato plants. From about 30,000 seeds obtained from these crosses, five putative mutants were obtained. All contained the *Ds* element and the *MP* gene and only one mutant plant still contained *sAc*. To test whether these five putative mutants were really mutants in the $Tm\text{-}2^2$ gene, cuttings of these plants were inoculated with ToMV. All the five putative mutants were

susceptible to ToMV infection. Plasmid rescue was used to obtain transposon-flanking plant DNA from the mutant plants. Sequencing of 9.8 kb of rescued plant DNA identified an open reading frame (ORF) of 2,586 bp, which corresponds to a polypeptide of 861 amino acids. *In silico* analysis of the ORF did not predict the presence of introns. The polypeptide encoded by the 2,586-bp ORF shows the characteristics of the CC–NBS–LRR class of R proteins, and the 5′- and 3′-RACE experiments confirmed the prediction of the gene structure. Functional complementation was performed by introducing either *Tm-2*^{2} gene under the control of its own promoter and polyadenylation signal or *Tm-2*^{2} gene under the control of the CaMV 35S promoter and the NOS polyadenylation signal into a susceptible tomato line. The transgenic plants of the two constructs were resistant to ToMV [76].

Plant and Inflorescence Architecture

Maize Domestication Traits Most crop plants differ considerably from their wild ancestors in major morphological phenotypes that have probably resulted from visual selection of desired plant type. This is most dramatic in maize, where the major difference between maize and its probable wild ancestor teosinte is that teosinte typically has long branches with tassels at their tips whereas maize possesses short branches tipped by ears [77]. Most of the variation for the dramatic differences in inflorescence morphology between maize and teosinte is explained by five quantitative trait loci (QTLs) [78]. Complementation tests indicated that one of these QTLs, which is on chromosome arm 1L, is the locus for the maize mutant *teosinte branched l* (*tbl*) [79]. To isolate the *tb1* gene, homozygous *tb1-ref* (a spontaneous mutant in a maize population) plants were crossed to an active *Mu* transposon line, and 26,000 F1 plants were grown. Among these, three new *tb1* mutants (*tb1-mum1*, *tb1-mum2*, *tb1-mum3*) were observed. Each new mutant was crossed to maize inbred A532, and 14 progeny from each of these crosses were used for Southern blot analysis with marker loci that closely flank *tb1* to discriminate progeny that possessed the *tb1-ref* versus the new *Mu* alleles. The progeny were also screened by Southern blot analysis with *Mu* element probes, and a *Mu3* element that cosegregated with *tb1-mum*1 was identified. Overlapping genomic restriction fragments carrying the cosegregating *Mu3* element were cloned into λ vectors. Subclones of these were used for Southern blot analyses of the 20 progeny of each of the three mutant plants, showing that each of these mutants has an insertion into this region of the genome that did not exist in their sibs and the progenitor stocks. These observations provided the crucial evidence that the *tb1* has been newly tagged. Portions of the λ clones were sequenced and oligonucleotide primers were designed to be used in conjunction with a *Mu*-specific primer to amplify the insertion fragments for each of the three *Mu* alleles. DNA sequence analysis of these fragments identified the *Mu* insertion point of each allele. A 0.8-kb restriction fragment flanking the *Mu* element was used to screen a cDNA library derived from immature ear. A single clone with a 1,360-bp insert, excluding the poly(A)tail was obtained. The cDNA sequence is fully collinear with the genomic sequence of maize inbred A619, without any evidence for introns. BLAST analysis with the sequence showed that tb1 shares two short regions of homology with the snapdragon *cycloidea* gene. The pattern of *tb1* expression and the morphology of *tb1* mutant plants suggest that *tb1* acts both to repress the growth of axillary organs and to enable the formation of female inflorescence. The maize allele of *tb1* is expressed at twice the level of the teosinte allele, suggesting that gene regulatory changes underlie the evolutionary divergence of maize from teosinte [80]. Analysis of nucleotide polymorphism in *tb1* gene of maize and teosinte populations showed that during maize domestication the effects of selection were limited to the gene's regulatory region and could not be detected in the protein-coding region [81]. Fine mapping showed that the intergenic sequences approximately 58–69 kb 5′ to the *tb1* cDNA confer pleiotropic effects on *Zea mays* morphology. Moreover, an allele-specific expression assay showed that sequences >41 kb upstream of *tb1* act in *cis* to alter *tb1* transcription [82].

The most critical step in maize (*Zea mays* ssp. *mays*) domestication was the liberation of the kernel from the hardened, protective casing that envelops the kernel in the maize progenitor, teosinte [83]. This evolutionary step exposed the kernel on the surface of the ear, such that it could readily be used by humans as a food source. A large effect QTL for glume induration

(husk hardening) was mapped to chromosome 4 using two F2 populations derived from crosses between maize race Reventador (Nay 15) and Balsas teosinte, *Z. mays* ssp. *parviglumis* or between maize race Chapalote and *Z. mays* ssp. *mexicana* [84]. This large-effect QTL segregates as a single Mendelian locus in an isogenic background, and has been designated *tga1* [83]. Maize Mo17 bacterial artificial chromosome (BAC) libraries were screened using a marker on maize chromosome 4, which is tightly linked to *tga1* and a BAC contig near *tga1* was identified. The BAC end and other sequences from this contig were used to BLAST search the rice genome sequence, and a region on rice chromosome 8 that is collinear with the region near *tga1* on maize chromosome 4 was identified. Subsequent BLAST searches using the collinear rice sequence identified a second maize Mo17 contig near *tga1*. Marker analysis showed that these 2 contigs flank *tga1*. Maize B73 contigs that correspond to the two Mo17 contigs were subsequently identified. DNA sequence analysis revealed that the two B73 contigs overlap, and could be merged to a single supercontig of ~1.5 megabases. Fine mapping using 3,106 F2 plants delimited *tga1* to a 6-kb region. Further BLAST searches using the 6-kb region at *tga1* revealed that it has homology to SBP (squamosa-promoter binding protein) transcriptional regulators. DNA sequence analysis of the SPB gene for the *tga1-ems1* stock, another *tga1* allele generated by ethyl methanesulfonate mutagenesis of maize line W22 that matched the phenotype of the teosinte allele in homozygous state, revealed that it differs from its parental (W22) allele by a nonconservative amino acid substitution of a phenylalanine for a leucine at position 5. This mutation in the *tga1-ems1* allele confirmed the conclusion from positional cloning that *tga1* is the SBP gene, and demonstrated that a single amino acid substitution was sufficient to confer the difference between the maize and teosinte phenotypes. Northern blots, real-time PCR, and *in situ* hybridization did not show any quantitative or qualitative differences in *tga1* expression between the isogenic lines (W22 and W22: *tga1*) or between the maize inbred W22 and teosinte itself, suggesting that differences between the maize and teosinte proteins may be critical to phenotype. Further mapping using seven additional recombination events within the 6-kb region narrowed the location of the causative site for the functional difference between maize and teosinte phenotypes to a 1,042-bp segment. DNA sequence analysis of this 1,042-bp segment using 16 diverse maize and 12 teosinte individuals identified seven fixed differences between maize and teosinte. Six of these seven are single base-pair polymorphisms that lie just 5′ of the coding sequence and potentially affect *tga1* expression. The seventh difference encodes an amino acid substitution of lysine (K) in teosinte to asparagine (N) in maize at position 6. Western blot analysis showed that *tga1* protein encoded by the teosinte allele is more abundant than the one encoded by the maize allele over a range of developmental stages that might underlie the phenotypic differences. The K → N substitution might alter protein stability, or it might affect translation efficiency or protein function [85].

Wheat Inflorescence In wheat, the *Q* allele confers the square-headed phenotype and free-threshing character, and is possessed by most of the cultivated wheats, but most wild wheats have the *q* allele and, therefore, speltoid spikes that are not free threshing [86]. Early experiments involving the cytogenetic analysis of aneuploid (abnormal chromosome number) plants located the *Q* gene on the long arm of chromosome 5A [87, 88]. Using chromosome deletion lines, Endo and Gill (1996) physically mapped the *Q* gene to a submicroscopic deletion interval on the long arm of chromosome 5A [89]. Comparative mapping of anonymous RFLP clones, AFLP (amplified fragment length polymorphism) markers, and mRNA differential display analysis of lines which have deletion break points that flank the *Q* locus identified 18 markers within the *Q* gene deletion interval. These markers were used to construct a genetic linkage map of the region in F2 populations derived from chromosome 5A disomic (homologous chromosome pair) substitution lines. The genetic map corresponding to the deletion segment was 20-cM long, and markers as close as 0.7 cM to the *Q* gene were identified [90]. The closest marker to the *Q* gene was used to screen four high-density *Triticum monococcum* BAC filters resulting in the identification of one BAC clone. Chromosome walking involved the reiterative screening of the BAC library using probes derived from the ends of previously identified BAC clones. A BAC contig was then constructed that spans a physical distance of 300 kb

corresponding to a genetic distance of 0.9 cM. The physical map of *T. monococcum* had perfect colinearity with the genetic map of wheat chromosome arm 5AL. Analysis of fast neutron *q* mutants using markers derived from the BAC contig at the *Q* locus confirmed that the *T. monococcum* BAC contig spanned the *Q* locus and narrowed the region for prospective *Q* gene candidates to a 100-kb segment, which contains an APETALA2 (AP2)-like gene that cosegregates with *Q* [91]. Sequence analysis showed that this AP2 gene consists of ten exons and nine introns. The M2 generation of a population of *Triticum aestivum* cv.Chinese Spring (CS) EMS mutants was screened for the speltoid phenotype to identify putative knockouts. Three speltoid mutants harboring point mutations within the AP2 gene were identified. One mutant had a single base substitution in an AP2 DNA binding domain (exon 5) that resulted in the change of a cysteine to a tyrosine. Two other mutants had point mutations in the donor site of intron 2 and the acceptor site of intron 7, respectively, resulting in alternate splicing in these mutants. The sequence analysis of the mutants validated that the AP2 gene is the *Q* locus. Comparison of the genomic sequences of the AP2 gene revealed six conserved differences between *Q*- and *q*-containing genotypes. Four of these differences, including a variable microsatellite (DNA sequence repeat), were present in introns and one was in the 3′ UTR. One conserved nucleotide difference changed a predicted amino acid where, at position 329, all *Q*-containing genotypes possessed an isoleucine while all *q*-containing genotypes possessed a valine. Yeast two-hybrid analysis showed that the full-length Q protein has the ability to form a homodimer, whereas the point mutation of q greatly reduced homodimer formation of the full-length q protein. Rachis fragility, glume shape, and glume tenacity mimicked the q phenotype in transgenic plants exhibiting posttranscriptional silencing of the transgene and the endogenous *Q* gene. Variation in spike compactness and plant height were associated with the level of transgene transcription due to the dosage effects of *Q* [92].

Barley Inflorescence Barley spikes have a unique structure consisting of three one-flowered spikelets at each spike node. Cultivated barley, *Hordeum vulgare* subsp. *vulgare*, can be divided into two forms according to the morphology of the spikelets: two-rowed and six-rowed. The two-rowed condition is believed to be primitive, because wild barley, *Hordeum vulgare* subsp. *spontaneum*, is two-rowed. Row type is controlled by multiple alleles at the *vrs1* locus (formerly *v* for *vulgare*) on chromosome 2H [93, 94]. A recessive mutation from *Vrs1* to *vrs1* changes two-rowed barley to six-rowed barley. High-resolution mapping using 373 BC7F1 plants and 278 BC6F2 plants identified four RFLP-derived STS markers closely linked to the *vrs1* locus [95]. The orders of four marker loci and *vrs1* locus were the same in six different mapping populations developed from nine different barley cultivars (*H. vulgare* subsp. *vulgare*) or mutant and wild barley (*H. vulgare* subsp. *spontaneum*) [96]. Five AFLP markers within the 0.9-cM region associated with the *vrs1* locus were subsequently developed using well-characterized near-isogenic lines as plant materials [97]. Recombinants within the 0.9-cM region were analyzed further using STS markers generated from ESTs (expressed sequence tags) and BAC DNA sequences. PCR screening of BAC clones of cv. Morex using an STS marker located 0.01 cM proximal to the *vrs1* locus isolated one BAC clone. Chromosome walking identified six bacterial artificial chromosome (BAC) clones covering completely the candidate genomic region. The contig containing *vrs1* is composed of 518,343 bp. Annotation showed three predicted genes: *HvHox1* and *HvEP2* appeared to be intact genes, whereas *HvEP1* is highly degenerated and interrupted by several insertions of transposable elements. *HvHox1* is the only gene that lies between two markers that define the break points and is thus a likely candidate for *Vrs1*. The ORF of two-rowed barley encoded a polypeptide composed of 222 amino acid residues, including a homeodomain-leucine zipper (HD-ZIP) motif. Expression of *Vrs1* was strictly localized in the lateral-spikelet primordia of immature spikes, suggesting that the VRS1 protein suppresses development of the lateral rows. Loss of function of *Vrs1* resulted in complete conversion of the rudimentary lateral spikelets in two-rowed barley into fully developed fertile spikelets in the six-rowed phenotype [98].

The wild progenitor of barley, *H. vulgare* subsp. *spontaneum*, has covered (hulled) caryopses in which the hull (outer lemma and inner palea) is firmly adherent to the pericarp epidermis at maturity. In cultivated

barley, the hulled or naked caryopsis is one of the most important agronomic traits because of the direct link to its use. Most cultivars have the hulled caryopsis and are mainly used for animal feed and brewing malts. In contrast, naked barley has a caryopsis with easily separable husks upon threshing and is suitable for edible purposes. The naked caryopsis is considered a key domestication character in barley because extensive pearling to remove the hull is unnecessary [99]. The covered/naked caryopsis in barley is controlled by a single locus (*nud*, for nudum) located on chromosome arm 7HL [100]; the covered caryopsis allele (*Nud*) is dominant over the naked one (*nud*). Bulked segregant analysis on an F2 population derived from a cross between Kobinkatagi (naked type) and Triumph (hulled type) was performed using 1,894 primer combinations, and 12 AFLP markers were selected. Among them, five closely linked and two cosegregating AFLP markers were mapped around the *nud* locus using 151 F2 individuals [101]. High-resolution mapping using 2,380 segregants derived from five cross-combinations identified AFLP-derived markers flanking the *nud* locus at the 0.6-cM proximal and the 0.06-cM distal side, respectively [102]. Further mapping using 2,828 progeny segregating for the trait from two cross-combinations delimited the *nud* locus to a 0.64 cM interval. Integration of the flanking markers into a high-density barley expressed sequence tag (EST) map selected two barley ESTs flanking the *nud* locus. BLASTN analysis identified their respective homologous rice ESTs 370 kb apart on rice chromosome arm 6L. Two rice genes within the collinear region were used as vehicles to develop closer barley markers. A BAC library of the covered barley cultivar Haruna Nijo was screened using the closest marker to the *nud* locus. Seven rounds of chromosome walks selected 20 BAC clones and a 500 kb-contig spanning the *nud* locus was constructed. In the physical map, the *nud* locus was covered completely with four overlapping BAC clones. An ethylene response factor (ERF) family transcription factor was the only gene that lies in the region delimited by the genetic and physical mapping and, therefore, is considered as a *Nud* candidate gene [103]. Sequencing of the *nud* region obtained from two naked lines [Kobinkatagi (a Japanese landrace) and *nud*-Bowman (an isogenic line carrying the *nud* allele in the genetic background of the covered cultivar Bowman)] revealed a deletion of 16,680 bp relative to the corresponding region of the Haruna Nijo BAC contig sequence. The 16,680-bp deletion included the entire ERF gene. Thus, the gene structure analysis of naked cultivars supports the candidacy of the ERF gene. Sequence analysis of the candidate gene in two X-ray-induced naked mutants showed that each of the two mutants carried a different single base mutation in the putative functional motif of the ERF gene, but their wild-type varieties (Haisa's and Ackermann's Donaria, respectively) had a nucleotide sequence that is identical to that of Haruna Nijo. RNA in situ hybridization using the antisense probe revealed that, in Bowman, *Nud* was expressed strictly in the testa where adherence occurs, while no signal above background was detected in *nud*-Bowman. The *Nud* gene has homology to the Arabidopsis *WIN1*/*SHN1* transcription factor gene, whose deduced function is control of cuticular wax and cutin-related lipid biosynthesis pathways [104–106]. Staining with a lipophilic dye (Sudan black B) detected a lipid layer on the pericarp epidermis only in covered barley [103].

Rice Plant Architecture Tillering in rice (*Oryza sativa* L.) is an important agronomic trait for grain production. Screening of a collection derived from spontaneous mutations identified *monoculm 1* (*moc1*) mutant. The *moc1* plants nearly completely lose their tillering ability, producing only one main culm, in contrast to the multiple tillers in wild-type plants. Genetic analysis with reciprocal crosses between *moc1* and wild-type plants revealed that *moc1* is a single locus mutation. The *MOC1* locus was mapped to the long arm of chromosome 6 of *O. sativa* using 280 F2 mutant plants generated from the crosses between *moc1* and Minghui 63. Fine mapping using 2,010 F2 mutant plants and newly developed molecular markers delimited the *MOC1* locus to a 20-kb region. Annotation of the 20-kb sequence identified an ORF that encodes a protein highly homologous (44% identity) to the tomato *LATERAL SUPPRESSOR* (*LS*). The corresponding ORF from *moc1* and wild-type plants were amplified by PCR and sequenced. DNA sequence comparison revealed a 1.9-kb retrotransposon inserted in this ORF in the *moc1* mutant. Transformation of a binary plasmid carrying a 3.2-kb wild-type genomic

fragment containing the entire ORF plus a 1.5-kb upstream sequence and the 316-bp downstream sequence, but not the one carrying a 3′ truncated *MOC1* gene, was able to rescue the monoculm phenotype of the *moc1* mutant [107].

Typical common wild rice (*Oryza rufipogon*) tends to have a prostrate growth habit during the vegetative phase and develop erect panicle-bearing stalks during the reproductive phase. Cultivated rice has an erect-growth habit throughout the entire growth phase, which may increase plant density, enhance photosynthesis efficiency, and improve grain yield. A set of introgression lines was constructed using an accession of Yuanjiang common wild rice (YJCWR, *Oryza rufipogon*) with prostrate growth habit as a donor, and an elite indica cultivar Teqing (*O. sativa*) with erect-growth habit as a recipient [108]. One introgression line (YIL18) displaying prostrate growth was obtained, which harbored two YJCWR chromosomal segments on the long arm of chromosome 3 and the short arm of chromosome 7. The tiller angle of YIL18 was larger than that of Teqing. The grain number on the main panicle (GNP) in YIL18 was only 57.6% of that in the recipient Teqing, a result of the lesser number of primary branches and secondary branches on the main panicle. Genetic linkage analysis within 246 F2 individuals derived from the cross between YIL18 and Teqing showed that prostrate growth was completely associated with a marked decrease of GNP and controlled by a single semidominant gene, *PROG1* (*PROSTATE GROWTH 1*), located on short arm of chromosome 7. High-resolution mapping using 3,600 recessive homozygote plants with erect growth from the F2 population delimited *prog1* within an 8.8-kb region. Only one ORF was identified within this region that encodes a putative single Cys2-His2 zinc-finger protein. Transformation of a binary plasmid carrying the entire *O. rufipogon PROG1* with 596-bp or 2,914-bp 5′-flanking regions, but not the one carrying only the 2,914-bp 5′-flanking region, showed complementation of the prostrate growth phenotype. Comparison of the coding sequences of *PROG1* in YJCWR and *prog1* in Teqing showed 15 SNPs and 6 insertion/deletions (indels) that encoded 23 amino acid changes between *PROG1* and *prog1*. Sequencing of the *prog1* coding regions of 182 erect-growth varieties of cultivated rice, including 87 indica and 95 japonica cultivars from 17 countries showed that all the cultivars contained identical mutations as *prog1* in Teqing, including 15 SNPs and 6 indels [109].

Cereal Seed Quality and Color

Cereal grain is the staple food of most of the world, representing the major carbohydrate energy source in the diet. One of the most important crop traits is grain quality, which determines the price and variety of food that can be prepared from the cereal crop. Thus the major cereal crops such as rice, wheat, maize, barley, and oats have undergone selection from the onset of the crop domestication process. In comparison to other crop traits, seed quality and color are primarily biochemical traits and have been studied at the protein, gene, and metabolite or grain component level.

Maize Lysine Content The protein nutritional quality of maize is improved by increase in the essential amino acid lysine in the *opaque-2* (*o2*) mutant locus, which was localized on the short arm of chromosome 7 [110]. To isolate the gene by transposon tagging, normal maize strains (*O2*/*O2*) carrying a mutable allele of *C1* containing an autonomous *Spm* (*c1-m5*) or a mutable allele of *Wx* containing a nonautonomous, defective derivative of *Spm* (*dSpm*) (*wx-m8*) were used as pollen donors for opaque plants (*o2*/*o2*). Three opaque-mutable *o2*/*o2-m* kernels were selected from approximately 530,000 F1 seeds. These kernels were grown to maturity and self-pollinated. DNAs prepared from leaf samples of F2 individual plants were used for Southern blot analysis using a *Spm*-specific probe. The opaque-mutable plants contained a novel 8.4-kb band absent in both parents and missing from at least some of the individuals that had been classified as opaque. Those kernels that had been classified as opaque but possessed the fragment were evidently not mutable because of failure of the *Spm* to transpose, or else transposition occurred so late in endosperm development that revertant sectors were undetectable, giving the kernels an opaque rather than an obvious opaque-mutable phenotype. The fragment was cloned and restriction enzyme mapping of the clone revealed the presence of a full-length, autonomous 8.3 kb *Spm* and an adjacent sequence of about 150 bp. This non-*Spm* region was sequenced and used as a probe on Southern

blot using a BC1 population derived from a cross between opaque (*o2*/*o2*) and normal (*O2*/*O2*) plants. All the plants derived from opaque (*o2*/*o2*) seeds showed a single 6.5-kb fragment, whereas plants from seeds with a normal phenotype (*o2*/*O2*) had a 10-kb fragment in addition to the 6.5-kb fragment. This demonstrates that the 150-bp *Spm*-fanking sequence derived from the opaque-mutable plant represents a single-copy sequence that cosegregates with alleles of the *o2* locus. This fragment was subsequently used as a probe to clone a 17-kb *Hin*dIII fragment of the wild-type *O2* allele from the *c1-m5* parent [111]. A cDNA library prepared from wild-type endosperms was screened with probes derived from the *O2* genomic clone. Analysis of *O2* cDNA sequence showed that the deduced *02* protein sequence contains a "leucine-zipper" domain characteristic of some mammalian and fungal transcription activation factors. DNA binding assays demonstrated that the O2 protein or only a fragment specifying the leucine-zipper domain bound to two specific regions on the 5′ side of the coding sequence in a zein genomic clone [112].

Cereal Amylose Content The maize *Waxy* locus determines starch quality by the level of amylose and amylopectin. Isolation of the gene was carried out by a combination of identification of the protein and the gene associated with the kernel mutant phenotype. The mutant *wx-m6* and *wx-m9* alleles have *Ds* transposon inserts at the *Wx* locus, while the *wx-m8* allele is attributable to insertion of a defective transposon of the *Spm* transposon family. Starch granules from immature endosperm tissue of kernels carrying the *wx-m6*, *wx-m9*, and *wx-m8* alleles were isolated and the starch granule-bound proteins were analyzed on SDS-polyacrylamide gels [113]. When the kernels did not contain an autonomous controlling element (either *Ac* or *Spm*) and showed no somatic reversion of the *wx-m6*, *wx-m9*, or *wx-m8* mutations, the 58 kd protein was either not detectable or present at a very low level. When the *Spm* element was present with the *wx-m8* allele, sectors of endosperm tissue showed the *Wx* phenotype and a 58 kd protein was present in isolated starch granules. By contrast, when *Ac* was present together with the *wx-m6* allele, endosperm tissue showed sectors that were intermediate between the *Wx* and the *wx* phenotypes and a novel 60 kd protein was detectable on starch granules. Hence, reversion of the *wx-m6* mutation gives a protein that is structurally abnormal and appears to have an altered enzymatic activity. Only the 58 kd protein is present in starch granules from kernels that are heterozygous for the *wx-m6* and *wx-m8* alleles, but contain only the *Spm* element. Therefore, the structurally altered protein detected upon reversion of the *wx-m6* allele in the presence of *Ac* is not detected in the presence of *Spm*. Were the *Wx* locus a regulatory locus, both the 58 kd and the 60 kd proteins would be present in a kernel that is heterozygous for the *wx-m6* and *wx-m8* mutations and contains the *Spm* element. It was concluded that the *Wx* locus is the structural locus for the 58 kd protein [113].

Poly(A)$^+$ RNA purified from *Wx* and *wx* endosperms was translated in a rabbit reticulocyte in vitro translation system, and an antigenically related polypeptide was identified using antiserum raised against the *Wx* protein. No major 58 kd polypeptide was evident among the translation products, but a major 65 kd polypeptide was translated from *Wx*, and not from wx poly(A)$^+$ RNA. The 65 kd in vitro translation product may be a precursor that is synthesized, but not processed in the rabbit reticulocyte extract. Poly(A)$^+$ mRNA fractions substantially enriched for *Wx* mRNA were used to construct cDNA clones. Screening of cDNA clones was performed by selective hybridization to the mRNA sequence encoding the immunoprecipitable 65 kd *Wx* polypeptide. Further testing showed that the *Wx* cDNA hybridized to an abundant 2.3-kb poly(A) + RNA present in immature endosperm of plants homozygous for the *Wx* allele, but absent from immature endosperm tissue of a plant homozygous for a stable recessive *wx* allele. Finally, the *Wx* cDNA was shown to hybridize to a unique sequence in maize genomic DNA. That the unique sequence corresponds to the *Wx* locus was deduced from the results of hybridization analyses of DNA isolated from maize strains with and without a *Ds* insertion mutation at the *Wx* locus. The presence of the insertion at the *Wx* locus was correlated with the presence of a 2.4-kb insertion in the sequence homologous to the cloned *Wx* cDNA, unequivocally establishing the homology of the cDNA to the *Wx* locus [113]. Sequence analysis of genomic and cDNA clones of the wild-type *Wx* gene showed that the coding region comprises 3,718 bp and is composed

of 14 exons and 13 small introns. N-terminal sequencing of the mature Wx protein led to the identification of a maize amyloplast-specific transit peptide of 72 amino acid residues [114].

The *Wx* gene homologues were isolated from a number of species by isolating homologous clones or identification of DNA/protein sequences homologous to the maize *Wx* gene/protein. A rice genomic library was constructed in λEMBL-3 vector and screened using the maize *Waxy* gene DNA as probe. Two overlapping genomic clones containing the *Wx* gene sequence were identified. Sequencing and alignment with *Wx* gene of maize and barley revealed that the *Wx* gene in rice contains 13 introns and 14 exons. The full-length of rice *waxy* preprotein is 609 amino acid residues [115]. An analysis of Wx transcripts, Wx protein, and amylose content of 31 rice cultivars revealed that endosperm amylose and Wx protein contents are correlated with the ability of the cultivar to excise intron I from the leader sequence of the Wx transcript [116]. Sticky or glutinous rice quality is related to the low amount of amylose due to the mutant wx allele.

Sweet Corn The maize *sh2* mutant used in "supersweet" corn has negligible starch. The *Sh2* gene was predicted to be involved in carbohydrate metabolism, since the mutant *sh2* endosperm contains reduced starch. Candidate *Sh2* clones were identified from a cDNA library prepared from endosperm by differential screening with labeled cDNA of near-isogenic W64 *Sh2* and W64 *sh2* mRNA. The 1.3-kb cDNA clone pES6-66 hybridized to wild-type cDNA and not *sh2* cDNA. Clone pES6-66 was subsequently shown to hybridize to a restriction fragment length polymorphism (RFLP) associated with normal *Sh2* function in F2 segregants of *Sh2* × *sh2* crosses in three backgrounds [117]. To determine whether this clone was indeed *Sh2* or simply a closely linked gene, a series of maize stocks that differed only at the *Sh2* locus were used, including a wild-type *Sh2* allele (progenitor), *sh2-m1* (mutable) allele containing *Ds* at the *sh2* locus, and *Sh2* revertants [118]. Southern blot analysis using 500-bp fragment derived from pES6-66 as probe showed that *sh2-m1* yielded a fragment that is approximately 1,600 bp larger than that seen in the progenitor or revertant. The data are compatible with *sh2-m1* containing a 1,600-bp insertion. RNA gel blot analysis indicated that the size of the wild-type transcript is approximately 2.0–2.2 kb. A cDNA library constructed from poly A^+ RNA of *shrunken-1*, *bronze-mutable4* (*sh1 bz-m4*) was screened using probes derived from pES6-66. Eight of the 14 clones isolated had the 1.95-kb insert and were almost full length. The 900-bp and 1,050-bp *Eco*RI fragments from one of these clones were subcloned and sequenced. Examination of the 1.95-kb cDNA sequence identified only one open reading frame (ORF) coding for 542 amino acids and making up a polypeptide of 59,845 Da. Homology search identified the *Escherichia coli* glucose-l-phosphate adenyltransferase (ADP-glucose pyrophosphorylase or ADP-glucose synthetase, EC 2.7.7.27) was the only protein having significant similarity to the amino acid sequence of the *Sh2* cDNA [118].

The maize *sugary1* (*su1*) mutant accumulates twice as much sugar as sweet corn, having reduced starch. Mutations at the *su1* locus were generated by crossing active *Mutator* (*Mu*) plants with standard lines. Mutant alleles were identified following the self-pollinations of the F1 plants. Normal and sugary sibling kernels from a population segregating 1:1 for the nonmutant allele *Su1* and *su1-R4582*::*Mul* were germinated, and genomic DNA used for Southern blot analysis using the *Mu1* fragment as probe. A 4.0-kb *Eco*RI fragment containing sequences homologous to the transposon *Mu1* that cosegregated with *su1-R4582::Mu1* was identified. This 4.0-kb *Eco*RI fragment was subsequently cloned by screening a BAC library, based on hybridization to a probe internal to *Mu1*, and the genomic DNA insert was subcloned as part of plasmid pMJ60. The nucleotide sequence of both termini of the transposon were determined and found to match the known sequence of *Mul*. A 1.0-kb *Bam*HI-*Eco*RI genomic fragment flanking *Mu1* in the cloned DNA was purified and used as a hybridization probe (termed BE1000). This genomic probe detected a 4.0-kb *Eco*RI fragment that was present in all *su1-R4582::Mu1/su1-Ref* plants but was missing from all *Su1/su1-Ref* plants. Thus, the cloned *Mu* transposon is the same element that is within or tightly linked to the *su1* gene locus. Probe BE1000 identified a second *Eco*RI fragment of 2.6 kb that was present in all plants examined, and representative of the nonmutant progenitor allele. Presumably, insertion of the 1.4-kb transposon *Mul* within this

2.6-kb region resulted in the 4.0-kb *Eco*RI fragment that cosegregated with *su1-R4582::Mu1*. Mutations of the *su1* gene locus other than *su1-R4582::Mu1* were analyzed to determine whether they also cosegregated with physical alterations in the cloned region of the genome. Populations segregating for the nonmutant allele *Su1* and either *su1-R2412*, *su1-R7110*, or *su1-R3162* was digested with *Eco*RI and probed in DNA gel blot analysis with genomic fragment BE1000. In the *su1-R7110* and *su1-R3162* families, the 4.0-kb *Eco*RI fragment was present in all the seedlings grown from sugary kernels but was not observed in any seedlings grown from nonmutant sibling kernels. A different *Eco*RI fragment, 4.6 kb in length, was found to cosegregate with *su1-R2412*. The mutation *su1-R2412* is likely to have occurred via insertion of a 2.0-kb element into this same region. Approximately 200,000 lambda clones from a maize endosperm cDNA library were screened with genomic probe BE1000. DNA from eight different hybridizing clones was digested with EcoRI; the largest cDNA insert was 2.4 kb in length. Rapid amplification of cDNA ends (RACE) protocol was used to obtain the 5′ end of the *sul* cDNA. Sequencing of *su1* cDNA and BLAST search of the deducted amino acid sequence showed that *su1* cDNA specified a polypeptide of at least 742 amino acids, which is highly similar in amino acid sequence to bacterial enzymes that hydrolyze α-(1 → 6) glucosyl linkages of starch [119].

Rice Seed Color Red pericarp is ubiquitous among the wild ancestors of cultivated rice (*Oryza rufipogon*), in which it is closely associated with seed shattering and dormancy. On the other hand, most rice (*Oryza sativa*) that is grown and consumed throughout the world has white pericarp, showing that white pericarp is associated with domestication and remains under strong selection in most rice breeding programs today. A QTL associated with red pericarp, *rg7.1*, was mapped on chromosome 7 using two independent BC2 populations derived from crosses between an accession of *O. rufipogon* (IRGC-105,491) from Malaysia and, in one case, a US tropical japonica cultivar, Jefferson, and in the other case, a widely planted tropical indica cultivar, IR64. The log of the odds scores associated with the *rg7.1* QTL peaks in these two populations were 99 and 33, respectively [120, 121]. The peak of both QTLs corresponded to the previously mapped position of the mutant locus, brown pericarp, *Rc* [122]. Fine mapping using 1,410 BC2F3 plants and high-resolution mapping using 4,000 BC2F6 plants narrowed the rg7.1 QTL to an 18.5-kb region. Two genes encoding CACTA type, *En/Spm* subclass, transposon proteins, and one gene encoding bHLH protein were detected within the 18.5-kb target region. Sequence comparison of bHLH locus between cv Jefferson and H75, an *Rc* mutant stock belonging to the japonica subspecies, carrying a functional allele, but much more closely related to cv Jefferson than to *O. rufipogon*, showed that the coding sequence of the bHLH allele in H75 was identical to the cv Jefferson sequence except for a 14-bp indel in exon 6. This 14-bp sequence was present in the H75 stock as well as in *O. rufipogon*, but was deleted in cv Jefferson and cv Nipponbare. The deletion induces a frame shift in the sequence, resulting in two premature stop codons before the end of exon 6. The stop codons truncate the protein before the bHLH domain. Sequence analysis of bHLH of Surjamkuhi, an indica line that carries a third allele, *Rc-s*, conditioning light red seed pigmentation, showed that the sequence of this line differed from the *O. rufipogon* allele at only four sites (positions 96, 660, 1353, and 1833–1844). The first two changes proved to be synonymous substitutions. The change at position 1353 consisted of a C-to-A change in exon 6. This single-nucleotide polymorphism (SNP) was independent of any change seen in previous comparisons and represented a premature stop codon before the bHLH domain, truncating the protein and rendering the effect of the remaining indel immaterial. Conventional reverse transcriptase-PCR showed no expression of *Rc* in leaf tissue; however, expression was seen in panicles before fertilization, pericarp from grains in the milk or dough stage of filling, and pericarp from mature seeds. Similar expression levels of Rc were detected in cv Jefferson and *O. rufipogon* [121].

Seed Shattering

Wild plant species shatter their seed from the mature infloresence and thus disperse seed for the next generation to be seeded, while during domestication humans have selected for non-shattering plant types from which the seed can be harvested or gathered from the crop. Study of shattering has been very fruitful in

Arabidopsis, setting up the genetic models for shattering phenotypes [123] that have been also revealed in other crops like the cereals.

In rice, a major QTL for seed shattering, *sh4*, has been mapped on chromosome 4 using segregating populations derived from crosses between *O. sativa* ssp. indica and the wild perennial species *O. rufipogon* [124, 125], between *O. sativa* ssp. japonica and *O. rufipogon* and two other closely related wild species *O. glumaepetula* and *O. meridionalis* [126, 127], and between *O. sativa* ssp. indica and the wild annual species *Oryza nivara* [128]. High-resolution mapping using 12,000 F2 (*O. sativa* ssp. indica x *O. nivara*) delimited *sh4* to a 1.7-kb region of a gene with a previously unknown function. The comparison of the 1.7-kb sequences between the mapping parents revealed seven mutations located in the intron, exon, or 5′ upstream of the start codon. Sequencing of this 1.7-kb region from an additional 14 rice cultivars of *O. sativa*, 21 accessions of *O. nivara*, 6 accessions of *O. rufipogon*, and 1 accession of each of the four remaining wild A-genome species and their association with shattering phenotypes showed that a nucleotide substitution of G for T or an amino acid substitution of asparagine for lysine in the first exon was selected for the development of non-shattering cultivars during rice domestication. Annotation of the sh4 protein identified a Myb3 DNA binding domain and a nuclear localization signal, suggesting that *sh4* is a transcription factor. Transformation of a binary plasmid carrying *sh4-GFP* fusion under the control of *Ubi* promoter into rice cv. Taipei 309 determined the nuclear localization of GFP-tagged *sh4*. Transformation into rice cv. Taipei 309 of a binary plasmid carrying *O. nivara* sequence from the 3′ nontranslated region to the inclusion of the G-T mutation site and *O. sativa* sequence for the rest sequence until the 5′ regulatory region, but not the one carrying a shorter *O. nivara* sequence excluding the G-T mutation site, showed significantly reduced strength of grain attachment to pedicel [128].

A major QTL for seed shattering, *qSH1*, was first mapped on chromosome 1 using 182 F2 plants of a cross between Kasalath (a shattering-type *indica* cultivar) and Nipponbare (a non-shattering-type *japonica* cultivar). A near-isogenic line (NIL) was developed that contained a short chromosomal segment from Kasalath at the *qSH1* region in a Nipponbare genetic background. The NIL had a stronger seed-shattering phenotype than either Kasalath or Nipponbare. High-resolution mapping using 10,388 plants from the BC4F2 and BC3F2 populations segregating at the *qSH1* region succeeded in mapping the functional natural variation in 612 bp and only one single-nucleotide polymorphism (SNP) was found within this region. No distinct open reading frame (ORF) was identified in the SNP region based on gene prediction for the *qSH1* region in both Nipponbare and Kasalath genome sequences. However, one ORF for a rice ortholog of the Arabidopsis *REPLUMLESS* (*RPL*) gene was found 12 kb away from the SNP. The *RPL* gene encodes a BEL1-type homeobox and is involved in the formation of a dehiscence zone (or abscission layer) alongside the valve in the *Arabidopsis* fruit (silique). Transformation of 26-kb Kasalath genomic fragments scanning the predicted ORF and the SNP regions into the non-shattering Nipponbare cultivar showed complementation of the complete seed-shattering phenotype. The other fragments were not able to complement the phenotype, even if they contained the entire ORF region or the SNP region. These results indicated that both the ORF and the SNP regions were required for full shattering function. *In situ* hybridization analysis revealed that in the NIL the ORF was expressed at the inflorescence meristem in the stage of rachis meristem establishment [inflorescence stage 1 (In1)]. It was also expressed at both the anther region and the provisional abscission layer at the base of the spikelet in the stage of floral organ differentiation (In7) and in the stage of rapid elongation of the rachis and branches (In8). On the other hand, in Nipponbare, the ORF was expressed in the same way as in the NIL, except that it was not expressed at the provisional abscission layer in either In7 or In8. These results, together with the complementation results, indicated that this *RPL* ortholog was the *qSH1* gene and that the identified SNP affected only the spatial mRNA expression pattern of *qSH1* at the abscission layer [129].

A shattering mutant line of rice, Hsh, was derived from a non-shattering japonica variety, Hwacheong, by N-methyl-N-nitrosourea (MNU) treatment. Optical microscopy revealed that Hsh had a well-developed abscission layer similar to the wild rice *Oryza nivara*, while Hwacheong did not produce an abscission layer.

Genetic analysis showed that the easy shattering of Hsh was controlled by the single recessive gene *sh-h*. Using an F2 population consisting of 240 individuals derived from the Hsh/Blue&Gundil cross the *sh-h* was mapped on chromosome 7 [130]. Fine mapping using six newly developed SSR markers delimited the *sh-h* locus to a 150-kb region. Further mapping using three newly developed SNP markers on five F3 recombinant lines derived from F2 heterozygous plants narrowed the *sh-h* locus to a 34-kb region. Analysis of genomic sequences from Hwacheong, Hsh, and Blue&Gundil lines identified eight genes in this region. Among these, a gene which encodes a protein containing a conserved carboxy-terminal domain (CTD) phosphatase domain was considered to be a strong candidate for the *sh-h* locus because of the presence of a point mutation at the 3′ end splice site of its seventh intron. Sequencing of the RT-PCR products of Hwacheong and Hsh revealed that, compared with Hwacheong, a 15-bp deletion was induced by altered splicing in the mRNA isolated from Hsh. Because the consensus sequence for splicing at this "AG" site was changed to "TG," the next "AG" sequence, 15-bp downstream, was used as a new splice site. The 15-bp deletion in the Hsh mRNA resulted in the deletion of five amino acids in the C-terminal region of the CTD-like phosphatase domain (CPDc), which are situated within the phosphatase active site. Two transferred DNA (T-DNA) insertion mutants and one point mutant exhibited the enhanced shattering phenotype, confirming that this CTD phosphatase-like gene is indeed the *sh-h* gene. RNA interference (RNAi) transgenic lines with suppressed expression of this gene exhibited greater shattering [131].

Tolerance to Abiotic Stresses

Wild species are adapted to the environment where they are found; survive over long periods of time by creating diversity where environmental selection pressures allow the fit to reproduce and survive. The environmental stresses include abiotic stresses such as heat, cold, drought, salt, light, radiation, heavy metals, soil pH, and others. Plant response to these stresses has been studied and shows common and unique responses [132].

Salinity Stress Tolerance Salinity tolerance has been amenable to study for phenotypic variation and the genetic dissection into quantitative traits. In rice, a major QTL for shoot K + content under salt stress, *SKC1*, was mapped to chromosome 1 using 133 lines of an F2 and an equivalent F3 population derived from a cross between a salt-tolerant indica variety Nona Bokra, and a susceptible elite japonica variety Koshihikari [133]. Fine mapping was performed using 192 BC2F2 plants, and a high-resolution map was subsequently generated with 2,973 BC3F2 plants using markers newly developed on the basis of the PAC clone sequences. Progeny testing of fixed recombinant plants (BC3F4) delimited the *SKC1* locus to a 7.4-kb region, and only one predicted open reading frame (ORF) was identified in the region. The *SKC1* promoter region (2,554-bp upstream of the initial codon) and the coding region of the cDNA clone (1,665 bp) were ligated and subcloned into a plant binary vector. This construct was transferred into the japonica variety Zhonghua 11, which contained the same *SKC1* allele as Koshihikari and is salt susceptible. Shoot K + concentrations were substantially higher in all six T1 progeny containing the Nona Bokra *SKC1* transgene compared with plants containing the vector control under salt stress but not under normal condition. Database searches showed substantial similarity between SKC1 and the HKT-type transporters found in plants, bacteria, and fungi. Comparison of nucleotide sequences between Nona Bokra and Koshihikari alleles showed six nucleotide substitutions in the coding region that lead to four amino acid changes, which may be responsible for the functional difference between the two alleles. RT-PCR analysis in both Koshihikari and NIL (*SKC1*) showed that *SKC1* transcript levels were upregulated by salt stress in the root but not in the shoot. Under normal condition, K^+ and Na^+ contents in NIL (*SKC1*) shoots were not substantially different from those in Koshihikari. But under salt stress, NIL (*SKC1*) shoots had a higher K^+ content and lower Na^+ content than Koshihikari shoots. No substantial differences in K^+ and Na^+ contents were observed in the roots under either normal or stress condition. Consistent with the results of shoot analysis, K^+ and Na^+ contents in xylem sap were not different between NIL (*SKC1*) and Koshihikari; under salt stress, however, the xylem sap of NIL (*SKC1*) contained more K^+ and less Na^+ than that of Koshihikari. These results indicated that *SKC1* is involved in regulating K^+/Na^+ homeostasis in the shoots [134].

Submergence Tolerance A major QTL for submergence tolerance, *Sub1*, was mapped to chromosome 9 using 169 F2 plants and the resulting F3 families of a cross between a tolerant indica rice line, IR40931-26 (a descendant of FR13A), and a susceptible japonica line, PI543851 [135]. High-resolution mapping using 2,950 F2 individuals and the resulting F3 families of a cross between DX18-121 (a tolerant F3 plant from the first population) and M-202 (a submergence-susceptible japonica cultivar that is widely used in California) identified 2 AFLP markers localized within 0.2 cM of *Sub1* [136]. The *Sub1* locus was delimited to an interval of 0.06 centimorgan using 4,022 F2 individuals from the cross between DX18-121 and M-202. Physical mapping with five overlapping bacterial artificial chromosome (BAC) clones derived from submergence-intolerant indica rice varieties and a nearly complete contig of 13 binary clones from IR40931-26 showed that *Sub1* region physically spans over 182 kilobases (kb). This interval encodes three genes containing ethylene response factor (ERF) domains and designated *Sub1A*, *Sub1B*, and *Sub1C*, ten non-ERF genes including four transcribed and six hypothetical protein-coding genes, and >50% retrotransposon-related sequences. The corresponding region of the japonica genome represented by the sequenced variety Nipponbare spans 142 kb and is considerably rearranged. Notably, *Sub1A* is absent from the rice reference Nipponbare genome. Accumulation of *Sub1A* and *Sub1C* messenger RNAs was strongly but transiently promoted by submergence in seedling leaves of tolerant FR13A, while *Sub1B* transcripts increased only slightly during submergence. The ten non-ERF genes in the indica *Sub1* region showed no evidence of expression in seedling leaves before or during submergence in IR40931-26 or the intolerant variety M-202. A survey of the *Sub1* locus haplotypes in 17 indica and 4 japonica varieties identified 2 *Sub1A*, 9 *Sub1B*, and 7*Sub1C* alleles on the basis of variation in amino acid sequence. The *Sub1A-1* and *Sub1C-1* alleles are limited to all six submergence-tolerant accessions. There was no *Sub1B* allele identified as being specific to submergence tolerance. In the tolerant *Sub1A-1* allele, a single-nucleotide polymorphism at position 556 is responsible for a Pro 186 (intolerant) to Ser 186 (tolerant) substitution in a MAPK site. Conversely, the *Sub1C-1* allele of tolerant lines lacks a MAPK phosphorylation site present in the alleles of the intolerant accessions. A *Sub1A-1* full-length cDNA under the control of the maize Ubiquitin1 promoter was transformed into an intolerant japonica variety Liaogeng. A screen of seedlings after 11 days of submergence identified four T1 families, derived from independent T0 Ubi:Sub1A + lines, with submergence-tolerant transgenic individuals, and progeny from two families were examined in detail. T1 families one and three showed a correlation between high expression of the *Sub1A-1* transgene and submergence tolerance. As observed in the FR13A descendant IR40931-26, tolerant Sub1A-1+ plants showed a significant impairment of shoot elongation under submergence compared with the intolerant parent Liaogeng and non-transgenic siblings [137].

Aluminum Tolerance In wheat (*Triticum aestivum* L.) mechanisms that minimize the harmful effects of Al ions have been investigated using near-isogenic lines [ET8 (Al-tolerant) and ES8 (Al-sensitive)] that differ in Al tolerance at a single dominant locus designated as *Alt1*. The *Alt1* locus cosegregates with an Al-activated malate efflux from root apices [138, 139]. One cDNA clone more highly expressed in the root apices of ET8 compared to that of ES8 was isolated by subtractive hybridization. The full-length cDNA was obtained by rapid amplification of cDNA ends (RACE)-PCR. The predicted protein is hydrophobic having six to eight putative transmembrane regions. Heterologous expression of this gene in *Xenopus oocytes* indicated that this gene encodes an Al-activated transporter that facilitates the efflux of malate but not citrate. Based on this result, the gene was named *ALMT1* (aluminum-activated malate transporter). Sequencing the *ALMT1* cDNAs derived from ET8 and ES8 showed that the sequences differed at six nucleotides that resulted in the deduced proteins differing at two amino acid residues. Sequence of the *ALMT1* coding region in Atlas66 (Al-tolerant cultivar) was identical to that of the ET8 allele, while the sequence in Scout66 (Al-sensitive cultivar) was identical to that of ES8. As found for the ET8 and ES8 lines, the expression of *ALMT1* in the root apices was greater in Atlas66 compared to Scout66. Expression analysis of *ALMT1* in the 57 F2 individuals derived from a cross between ET7 and ES5, the near-isogenic progenitor lines of ET8 and ES8, showed that all the

Al-sensitive seedlings expressed the ES8 allele only, whereas Al-tolerant seedlings expressed either ET8 allele only or both ET8 and ES8 alleles. Thus, the ET8 allele was expressed only in the Al-tolerant seedlings, indicating that, in this population, the Al-tolerant phenotype was correlated with the higher expression of this allele. Evaluation of Al tolerance and genotype analyses using an RFLP marker and a PCR-based assay on 204 F3 families derived from a cross between ET8 and ES8 showed that the ET8 allele of *ALMT1* completely cosegregated with the Al-tolerant phenotypes and the Al-tolerance locus, *Alt1*. Heterologous expression of *ALMT1* in cultured tobacco cells increased the tolerance of tobacco cells to Al treatment [140].

Future Directions

The present era of plant sciences is distinguished by an integration of multiple disciplines toward a transdisciplinary/interdisciplinary approach of doing science, utilizing the technology and knowledge from computer science and bioinformatics, genomics, dedicated instrumentation for high-throughput automation of laboratory and field tasks, which can all together provide integrated models and technologies for the improvement of crop traits. The paradigm shift in genetics, due to the reduced cost in genome sequencing, is to be able to generate the genome sequence of any plant genotype of interest that will totally revolutionize the approach to use this information. With a few genetic crosses followed by whole genome sequencing of all genotypes, it would be possible to identify genes and useful alleles that can be incorporated into plant improvement programs. This would make the traditional ways of isolating or identifying gene sequences for crop traits obsolete. The lag will be in phenotyping individual genotypes, which will remain the challenge for the biologist. The association of genes to a trait will still require that traits be characterized, dissected into components and parameters that can be measured, and the candidate gene(s) validated by some reverse genetics strategies using methods such as mutant analysis, transformation, and complementation, at least till the function of every gene/allele is known and how these genes and their alleles interact together to determine the phenotype of a crop trait.

Bibliography

Primary Literature

1. Doebley JF, Gaut BS, Smith BD (2006) The molecular genetics of crop domestication. Cell 127:1309–1321
2. Vaughan DA, Balázs E, Heslop-Harrison JS (2007) From crop domestication to super-domestication. Ann Bot 100:893–901
3. Meinke DW, Cherry JM, Dean C, Rounsley SD, Koornneef M (1998) *Arabidopsis thaliana*: a model plant for genome analysis. Science 282:662–682
4. Arabidopsis Genome Initiative (2000) Analysis of the genome sequence of the flowering plant *Arabidopsis thaliana*. Nature 408:796–815
5. Ossowski S, Schneeberger K, Clark RM, Lanz C, Warthmann N, Weigel D (2008) Sequencing of natural strains of *Arabidopsis thaliana* with short reads. Genome Res 18:2024–2033
6. Ossowski S, Schneeberger K, Lucas-Lledó JI, Warthmann N, Clark RM, Shaw RG, Weigel D, Lynch M (2010) The rate and molecular spectrum of spontaneous mutations in *Arabidopsis thaliana*. Science 327:92–94
7. Verma DP, Nash DT, Schulman HM (1974) Isolation and in vitro translation of soybean leghaemoglobin mRNA. Nature 251:74–77
8. Baulcombe D, Verma DP (1978) Preparation of a complementary DNA for leghaemoglobin and direct demonstration that leghaemoglobin is encoded by the soybean genome. Nucleic Acids Res 5:4141–4155
9. Goldberg RB, Hoschek G, Kamalay JC, Timberlake WE (1978) Sequence complexity of nuclear and polysomal RNA in leaves of the tobacco plant. Cell 14:123–131
10. Kamalay JC, Goldberg RB (1980) Regulation of structural gene expression in tobacco. Cell 19:935–946
11. Varsanyi-Breiner A, Gusella JF, Keys C, Housman DE, Sullivan D, Brisson N, Verma DP (1979) The organization of a nuclear DNA sequence from a higher plant: molecular cloning and characterization of soybean ribosomal DNA. Gene 7:317–334
12. Baulcombe DC, Key JL (1980) Polyadenylated RNA sequences which are reduced in concentration following auxin treatment of soybean hypocotyls. J Biol Chem 255:88907–88913
13. Link G, Coen DM, Bogorad L (1978) Differential expression of the gene for the large subunit of ribulose bisphosphate carboxylase in maize leaf cell types. Cell 15:725–731
14. Schell J, Van Montagu M (1977) Transfer, maintenance, and expression of bacterial Ti-plasmid DNA in plant cells transformed with *A. tumefaciens*. Brookhaven Symp Biol 29:36–49
15. Joos H, Timmerman B, Montagu MV, Schell J (1983) Genetic analysis of transfer and stabilization of Agrobacterium DNA in plant cells. EMBO J 2:2151–2160
16. Herrera-Estrella L, Block MD, Messens E, Hernalsteens JP, Montagu MV, Schell J (1983) Chimeric genes as dominant selectable markers in plant cells. EMBO J 2:987–995
17. Caplan A, Herrera-Estrella L, Inzé D, Van Haute E, Van Montagu M, Schell J, Zambryski P (1983) Introduction of genetic material into plant cells. Science 222:815–821

18. Barton KA, Binns AN, Matzke AJ, Chilton MD (1983) Regeneration of intact tobacco plants containing full length copies of genetically engineered T-DNA, and transmission of T-DNA to R1 progeny. Cell 32:1033–1043
19. Fraley RT, Rogers SG, Horsch RB, Sanders PR, Flick JS, Adams SP, Bittner ML, Brand LA, Fink CL, Fry JS, Galluppi GR, Goldberg SB, Hoffmann NL, Woo SC (1983) Expression of bacterial genes in plant cells. Proc Natl Acad Sci USA 80:4803–4807
20. Paszkowski J, Shillito RD, Saul M, Mandák V, Hohn T, Hohn B, Potrykus I (1984) Direct gene transfer to plants. EMBO J 3:2717–2722
21. Fromm ME, Taylor LP, Walbot V (1986) Stable transformation of maize after gene transfer by electroporation. Nature 319:791–793
22. Klein TM, Kornstein L, Sanford JC, Fromm ME (1989) Genetic transformation of maize cells by particle bombardment. Plant Physiol 91:440–444
23. Jain HK (2010) The green revolution: history, impact and future, 1st edn. Studium Press, Houston, ISBN 1933699639
24. Khush GS (1999) Green revolution: preparing for the 21st century. Genome 42:646–655
25. Brown LR (1970) Nobel peace prize: developer of high-yield wheat receives award (Norman Ernest Borlaug). Science 170:518–519
26. Hedden P (2003) Constructing dwarf rice. Nat Biotechnol 21:873–874
27. Peng J, Richards DE, Hartley NM, Murphy GP, Devos KM, Flintham JE, Beales J, Fish LJ, Worland AJ, Pelica F, Sudhakar D, Christou P, Snape JW, Gale MD, Harberd NP (1999) "Green revolution" genes encode mutant gibberellin response modulators. Nature 400:256–261
28. Peng J, Carol P, Richards DE, King KE, Cowling RJ, Murphy GP, Harberd NP (1997) The Arabidopsis GAI gene defines a signaling pathway that negatively regulates gibberellin responses. Genes Dev 11:3194–3205
29. Maeda H, Ishii T, Mori H, Kuroda J, Horimoto M, Takamure I, Kinoshita T, Kamijima O (1997) High density molecular map of semidwarfing gene, sd-1, in rice (*Oryza sativa* L.). Breed Sci 47:317–320
30. Sasaki A, Ashikari M, Ueguchi-Tanaka M, Itoh H, Nishimura A, Swapan D, Ishiyama K, Saito T, Kobayashi M, Khush GS, Kitano H, Matsuoka M (2002) Green revolution: a mutant gibberellin-synthesis gene in rice. Nature 416:701–702
31. Spielmeyer W, Ellis MH, Chandler PM (2002) Semidwarf (sd-1), "green revolution" rice, contains a defective gibberellin 20-oxidase gene. Proc Natl Acad Sci USA 99:9043–9048
32. Monna L, Kitazawa N, Yoshino R, Suzuki J, Masuda H, Maehara Y, Tanji M, Sato M, Nasu S, Minobe Y (2002) Positional cloning of rice semidwarfing gene, sd-1: rice "green revolution gene" encodes a mutant enzyme involved in gibberellin synthesis. DNA Res 9:11–17
33. Takahashi Y, Shomura A, Sasaki T, Yano M (2001) Hd6, a rice quantitative trait locus involved in photoperiod sensitivity, encodes the alpha subunit of protein kinase CK2. Proc Natl Acad Sci USA 98:7922–7927
34. Yano M, Katayose Y, Ashikari M, Yamanouchi U, Monna L, Fuse T, Baba T, Yamamoto K, Umehara Y, Nagamura Y, Sasaki T (2000) Hd1, a major photoperiod sensitivity quantitative trait locus in rice, is closely related to the Arabidopsis flowering time gene CONSTANS. Plant Cell 12:2473–2484
35. Yamamoto T, Lin H, Sasaki T, Yano M (2000) Identification of heading date quantitative trait locus Hd6 and characterization of its epistatic interactions with Hd2 in rice using advanced backcross progeny. Genetics 154:885–891
36. Monna L, Lin HX, Kojima S, Sasaki T, Yano M (2002) Genetic dissection of a genomic region for quantitative trait locus, Hd3, into two loci, Hd3a and Hd3b, controlling heading date in rice. Theor Appl Genet 104:772–778
37. Kojima S, Takahashi Y, Kobayashi Y, Monna L, Sasaki T, Araki T, Yano M (2002) Hd3a, a rice ortholog of the Arabidopsis FT gene, promotes transition to flowering downstream of Hd1 under short-day conditions. Plant Cell Physiol 43:1096–1105
38. Alpert KB, Grandillo S, Tanksley SD (1995) fw2.2: a major QTL controlling fruit weight is common to both red and green-fruited tomato species. Theor Appl Genet 91:994–1000
39. Alpert KB, Tanksley SD (1996) High-resolution mapping and isolation of a yeast artificial chromosome contig containing fw2.2: a major fruit weight quantitative trait locus in tomato. Proc Natl Acad Sci USA 93:15503–15507
40. Frary A, Nesbitt TC, Grandillo S, Knaap E, Cong B, Liu J, Meller J, Elber R, Alpert KB, Tanksley SD (2000) fw2.2: a quantitative trait locus key to the evolution of tomato fruit size. Science 289:85–88
41. Xing Y, Zhang Q (2010) Genetic and molecular bases of rice yield. Annu Rev Plant Biol 61:421–442
42. Ashikari M, Sakakibara H, Lin S, Yamamoto T, Takashi T, Nishimura A, Angeles ER, Qian Q, Kitano H, Matsuoka M (2005) Cytokinin oxidase regulates rice grain production. Science 309:741–745
43. Li J, Thomson M, McCouch SR (2004) Fine mapping of a grain-weight quantitative trait locus in the pericentromeric region of rice chromosome 3. Genetics 168:2187–2195
44. Fan C, Xing Y, Mao H, Lu T, Han B, Xu C, Li X, Zhang Q (2006) GS3, a major QTL for grain length and weight and minor QTL for grain width and thickness in rice, encodes a putative transmembrane protein. Theor Appl Genet 112:1164–1171
45. Lin HX et al (1995) RFLP mapping of QTLs for grain shape traits in indica rice (*Oryza sativa* L. subsp. *indica*). Scientia Agricultura Sinica 28:1–7
46. Yoon DB, Kang KH, Kim HJ, Ju HG, Kwon SJ, Suh JP, Jeong OY, Ahn SN (2006) Mapping quantitative trait loci for yield components and morphological traits in an advanced backcross population between *Oryza grandiglumis* and the *O. sativa* japonica cultivar Hwaseongbyeo. Theor Appl Genet 112:1052–1062
47. Song XJ, Huang W, Shi M, Zhu MZ, Lin HX (2007) A QTL for rice grain width and weight encodes a previously unknown RING-type E3 ubiquitin ligase. Nat Genet 39:623–630
48. Flor HH (1955) Host-parasite interaction in flax rust – its genetics and other implications. Phytopathology 45:680–685

49. Johal GS, Briggs SP (1992) Reductase activity encoded by the HM1 disease resistance gene in maize. Science 258: 985–987
50. Johal GS, Briggs SP (1990) Placement of hm1 on the Pioneer RFLP map. Maize Genet Coop Newsl 64:37
51. Van den Ackerveken GF, Van Kan JA, De Wit PJ (1992) Molecular analysis of the avirulence gene avr9 of the fungal tomato pathogen Cladosporium fulvum fully supports the gene-for-gene hypothesis. Plant J 2:359–366
52. Stevens MA, Rick CM (1988) Genetics and breeding. In: Atherton JG, Rudich J (eds) The tomato crop. Chapman & Hall, London, pp 35–109
53. Jones DA, Dickinson MJ, Balint-Kurti PJ, Dixon MS, Jones JDG (1993) Two complex resistance loci revealed in tomato by classical and RFLP mapping of the Cf-2, Cf-4, Cf-5 and Cf-9 genes for resistance to *Cladosporium fulvum*. Mol Plant Microbe Interact 6:348–357
54. Jones DA, Thomas CM, Hammond-Kosack KE, Balint-Kurti PJ, Jones JD (1994) Isolation of the tomato Cf-9 gene for resistance to *Cladosporium fulvum* by transposon tagging. Science 266:789–793
55. Duncan JM (1999) Phytophthora – an abiding threat to our crops. Microbiol Today 26:114–116
56. Naess SK, Bradeen JM, Wielgus SM, Haberlach GT, McGrath JM, Helgeson JP (2000) Resistance to late blight in *Solanum bulbocastanum* is mapped to Chromosome 8. Theor Appl Genet 101:697–704
57. Bradeen JM, Naess SK, Song J, Haberlach GT, Wielgus SM, Buell CR, Jiang J, Helgeson JP (2003) Concomitant reiterative BAC walking and fine genetic mapping enable physical map development for the broad-spectrum late blight resistance region, RB. Mol Genet Genomics 269:603–611
58. Song J, Bradeen JM, Naess SK, Raasch JA, Wielgus SM, Haberlach GT, Liu J, Kuang H, Austin-Phillips S, Buell CR, Helgeson JP, Jiang J (2003) Gene RB cloned from *Solanum bulbocastanum* confers broad spectrum resistance to potato late blight. Proc Natl Acad Sci USA 100:9128–9133
59. van der Vossen E, Sikkema A, Hekkert BL, Gros J, Stevens P, Muskens M, Wouters D, Pereira A, Stiekema W, Allefs S (2003) An ancient R gene from the wild potato species *Solanum bulbocastanum* confers broad-spectrum resistance to *Phytophthora infestans* in cultivated potato and tomato. Plant J 36:867–882
60. van der Vossen EA, Gros J, Sikkema A, Muskens M, Wouters D, Wolters P, Pereira A, Allefs S (2005) The Rpi-blb2 gene from *Solanum bulbocastanum* is an Mi-1 gene homolog conferring broad-spectrum late blight resistance in potato. Plant J 44:208–222
61. Hinze K, Thompson RD, Ritter E, Salamini F, Schulze-Lefert P (1991) Restriction fragment length polymorphism-mediated targeting of the mlo resistance locus in barley (*Hordeum vulgare*). Proc Natl Acad Sci USA 88:3691–3695
62. Büschges R, Hollricher K, Panstruga R, Simons G, Wolter M, Frijters A, van Daelen R, van der Lee T, Diergaarde P, Groenendijk J, Töpsch S, Vos P, Salamini F, Schulze-Lefert P (1997) The barley Mlo gene: a novel control element of plant pathogen resistance. Cell 88:695–705
63. Williamson VM, Hussey RS (1996) Nematode pathogenesis and resistance in plants. Plant Cell 8:1735–1745
64. Smith PG (1944) Embryo culture of a tomato species hybrid. Proc Am Soc Hort Sci 44:413–416
65. Gilbert JC (1958) Some linkage studies with the Mi gene for resistance to root- knot nematodes. Rep Tomato Genet Coop 8:15–17
66. Klein-Lankhorst R, Rietveld P, Machiels B, Verkerk R, Weide R, Gebhardt C, Koornneef M, Zabel P (1991) RFLP markers linked to the root knot nematode resistance gene Mi in tomato. Theor Appl Genet 81:661–667
67. Messeguer R, Ganal M, Devicente MC, Young ND, Bolkan H, Tanksley SD (1991) High resolution RFLP map around the root knot nematode resistance gene (Mi) in tomato. Theor Appl Genet 82:529–536
68. Ho J-Y, Weide R, Ma HM, Wordragen MF, Lambert KN, Koornneef M, Zabel P, Williamson VM (1992) The root-knot nematode resistance gene (Mi) in tomato: construction of a molecular linkage map and identification of dominant cDNA markers in resistant genotypes. Plant J 2: 971–982
69. Williamson VM, Ho J-Y, Wu FF, Miller N, Kaloshian I (1994) A PCR-based marker tightly linked to the nematode resistance gene, Mi, in tomato. Theor Appl Genet 87:757–763
70. Liharska TB, Koornneef M, Van Wordragen M, Van Kammen A, Zabel P (1996) Tomato chromosome 6: effect of alien chromosomal segments on recombinant frequencies. Genome 39:485–491
71. Kaloshian I, Yaghoobi J, Liharska T, Hontelez J, Hanson D, Hogan P, Jesse T, Wijbrandi J, Simons G, Vos P, Zabel P, Williamson VM (1998) Genetic and physical localization of the root-knot nematode resistance locus Mi in tomato. Mol Gen Genet 257:376–385
72. Milligan SB, Bodeau J, Yaghoobi J, Kaloshian I, Zabel P, Williamson VM (1998) The root knot nematode resistance gene Mi from tomato is a member of the leucine zipper, nucleotide binding, leucine-rich repeat family of plant genes. Plant Cell 10:1307–1319
73. Pelham J (1966) Resistance in tomato to tobacco mosaic virus. Euphytica 15:258–267
74. Hall TJ (1980) Resistance at the Tm-2 locus in the tomato to tomato mosaic virus. Euphytica 29:189–197
75. Motoyoshi F, Ohmori T, Murata M (1996) Molecular characterization of heterochromatic regions around the Tm-2 locus in chromosome 9 of tomato. Symp Soc Exp Biol 50:65–70
76. Lanfermeijer FC, Dijkhuis J, Sturre MJ, de Haan P, Hille J (2003) Cloning and characterization of the durable tomato mosaic virus resistance gene Tm-2(2) from *Lycopersicon esculentum*. Plant Mol Biol 52:1037–1049
77. Iltis H (1983) From teosinte to maize: the catastrophic sexual transmutation. Science 222:886–894
78. Doebley J, Stec A (1991) Genetic analysis of the morphological differences between maize and teosinte. Genetics 129:285–295

79. Doebley J, Stec A, Gustus C (1995) Teosinte branched1 and the origin of maize: evidence for epistasis and the evolution of dominance. Genetics 141:333–346
80. Doebley J, Stec A, Hubbard L (1997) The evolution of apical dominance in maize. Nature 386:485–488
81. Wang R-L, Stec A, Hey J, Lukens L, Doebley J (1999) The limits of selection during maize domestication. Nature 398:236–239
82. Clark RM, Wagler TN, Quijada P, Doebley J (2006) A distant upstream enhancer at the maize domestication gene tb1 has pleiotropic effects on plant and inflorescent architecture. Nat Genet 38:594–597
83. Dorweiler J, Stec A, Kermicle J, Doebley J (1993) Teosinte glume architecture1: a genetic locus controlling a key step in maize evolution. Science 262:233–235
84. Doebley J, Stec A (1993) Inheritance of the morphological differences between maize and teosinte: comparison of results for two F2 populations. Genetics 134:559–570
85. Wang H, Nussbaum-Wagler T, Li B, Zhao Q, Vigouroux Y, Faller M, Bomblies K, Lukens L, Doebley JF (2005) The origin of the naked grains of maize. Nature 436:714–719
86. Muramatsu M (1986) The vulgare super gene, Q: its universality in durum wheat and its phenotypic effects in tetraploid and hexaploid wheats. Can J Genet Cytol 28:30–41
87. Unrau J, Smith WE, McGinnis RC (1950) Spike density, speltoidy and compactoidy in hexaploid wheat. Can J Res Sect C Bot Sci 28:273–276
88. MacKey J (1954) Neutron and X-ray experiments in wheat and a revision of the speltoid problem. Hereditas 40:65–180
89. Endo TR, Gill BS (1996) The deletion stocks of common wheat. J Hered 87:295–307
90. Faris JD, Gill BS (2002) Genomic targeting and high-resolution mapping of the domestication gene Q in wheat. Genome 45:706–718
91. Faris JD, Fellers JP, Brooks SA, Gill BS (2003) A bacterial artificial chromosome contig spanning the major domestication locus Q in wheat and identification of a candidate gene. Genetics 164:311–321
92. Simons KJ, Fellers JP, Trick HN, Zhang Z, Tai YS, Gill BS, Faris JD (2006) Molecular characterization of the major wheat domestication gene Q. Genetics 172:547–555
93. von Ubisch G (1916) Beitrag zu einer Faktorenanalyse von Gerste. Z Indukt Abstam Vererbungs 17:120–152
94. Robertson DW, Wiebe GA, Shands RG, Hagberg A (1965) A summary of linkage studies in cultivated barley, Hordeum species. (Suppl. III, 1954–1963). Crop Sci 5:33–43
95. Komatsuda T, Li W, Takaiwa F, Oka S (1999) High resolution map around the vrs1 locus controlling two- and six-rowed spike in barley, *Hordeum vulgare*. Genome 42:248–253
96. Komatsuda T, Tanno K (2004) Comparative high resolution map of the six-rowed spike locus 1 (vrs1) in several populations of barley, *Hordeum vulgare* L. Hereditas 141:68–73
97. He C, Sayed-Tabatabaei BE, Komatsuda T (2004) AFLP targeting of the 1-cM region conferring the vrs1 gene for six-rowed spike in barley, *Hordeum vulgare* L. Genome 47: 1122–1129
98. Komatsuda T, Pourkheirandish M, He C, Azhaguvel P, Kanamori H, Perovic D, Stein N, Graner A, Wicker T, Tagiri A, Lundqvist U, Fujimura T, Matsuoka M, Matsumoto T, Yano M (2007) Six-rowed barley originated from a mutation in a homeodomain-leucine zipper I-class homeobox gene. Proc Natl Acad Sci USA 104:1424–1429
99. Staudt G (1961) The origin of cultivated barleys: a discussion. Economic Bot 15:203–212
100. Franckowiack JD, Konishi T (1997) Naked caryopsis. Barley Genet Newsl 26:51–52
101. Kikuchi S, Taketa S, Ichii M, Kawasaki S (2003) Efficient fine mapping of the naked caryopsis gene (nud) by HEGS (high-efficiency genome scanning)/AFLP in barley. Theor Appl Genet 108:73–78
102. Taketa S, Awayama T, Amano S, Sakurai Y, Ichii M (2006) High-resolution mapping of the nud locus controlling the naked caryopsis in barley. Plant Breed 125:337–342
103. Taketa S, Amano S, Tsujino Y, Sato T, Saisho D, Kakeda K, Nomura M, Suzuki T, Matsumoto T, Sato K, Kanamori H, Kawasaki S, Takeda K (2008) Barley grain with adhering hulls is controlled by an ERF family transcription factor gene regulating a lipid biosynthesis pathway. Proc Natl Acad Sci USA 105:4062–4067
104. Aharoni A, Dixit S, Jetter R, Thoenes E, van Arkel G, Pereira A (2004) The SHINE clade of AP2 domain transcription factors activate wax biosynthesis, alter cuticle properties and confer drought tolerance when overexpressed in Arabidopsis. Plant Cell 16:2463–2480
105. Broun P, Poindexter P, Osborne E, Jiang CZ, Riechmann JL (2004) WIN1, a transcriptional activator of epidermal wax accumulation in Arabidopsis. Proc Natl Acad Sci USA 101:4706–4711
106. Kannangara R, Branigan C, Liu Y, Penfield T, Rao V, Mouille G, Höfte H, Pauly M, Riechmann JL, Broun P (2007) The transcription factor WIN1/SHN1 regulates Cutin biosynthesis in *Arabidopsis thaliana*. Plant Cell 19:1278–1294
107. Li X, Qian Q, Fu Z, Wang Y, Xiong G, Zeng D, Wang X, Liu X, Teng S, Hiroshi F, Yuan M, Luo D, Han B, Li J (2003) Control of tillering in rice. Nature 422:618–621
108. Tan L, Liu F, Xue W, Wang G, Ye S, Zhu Z, Fu Y, Wang X, Sun C (2007) Development of *Oryza rufipogon* and *Oryza sativa* introgression lines and assessment for yield-related quantitative trait loci. J Integr Plant Biol 49:871–884
109. Tan L, Li X, Liu F, Sun X, Li C, Zhu Z, Fu Y, Cai H, Wang X, Xie D, Sun C (2008) Control of a key transition from prostrate to erect growth in rice domestication. Nat Genet 40: 1360–1364
110. Coe EH Jr, Neuffer MG (1976) The genetics of corn. In: Corn and corn improvement, vol 18. American Society of Agronomy, Madison, pp 111–223
111. Schmidt RJ, Burr FA, Burr B (1987) Transposon tagging and molecular analysis of the maize regulatory locus opaque-2. Science 238:960–963

112. Schmidt RJ, Burr FA, Aukerman MJ, Burr B (1990) Maize regulatory gene opaque-2 encodes a protein with a "leucine-zipper" motif that binds to zein DNA. Proc Natl Acad Sci USA 87:46–50
113. Shure M, Wessler S, Fedoroff N (1983) Molecular identification and isolation of the Waxy locus in maize. Cell 35:225–233
114. Klosgen RB, Gierl A, Schwarz-Sommer Z, Saedler H (1986) Molecular analysis of the waxy locus of *Zea mays*. Mol Gen Genet 203:237–244
115. Wang ZY, Wu ZL, Xing YY, Zheng FG, Guo XL, Zhang WG, Hong MM (1990) Nucleotide sequence of rice waxy gene. Nucleic Acids Res 18:5898
116. Wang ZY, Zheng FQ, Shen GZ, Gao JP, Snustad DP, Li MG, Zhang JL, Hong MM (1995) The amylose content in rice endosperm is related to the post-transcriptional regulation of the waxy gene. Plant J 7:613–622
117. Barton C, Yang L, Galvin M, Sengupta-Gopalan C, Borelli T (1986) Isolation of the Shrunken-2 and Brittle-2 genes from maize. In: Shannon JC, Knievel DP, Boyer CD (eds) Regulation of Carbon and Nitrogen reduction and utilization in maize. American Society of Plant Physiologists, Rockville, pp 363–365
118. Bhave MR, Lawrence S, Barton C, Hannah LC (1990) Identification and molecular characterization of shrunken-2 cDNA clones of maize. Plant Cell 2:581–588
119. James MG, Robertson DS, Myers AM (1995) Characterization of the maize gene sugary1, a determinant of starch composition in kernels. Plant Cell 7:417–429
120. Septiningsih EM, Trijatmiko KR, Moeljopawiro S, McCouch SR (2003) Identification of quantitative trait loci for grain quality in an advanced backcross population derived from the *Oryza sativa* variety IR64 and the wild relative *O. rufipogon*. Theor Appl Genet 107:1433–1441
121. Sweeney MT, Thomson MJ, Pfeil BE, McCouch S (2006) Caught red-handed: Rc encodes a basic helix-loop-helix protein conditioning red pericarp in rice. Plant Cell 18:283–294
122. Kinoshita T (1998) Linkage mapping using mutant genes in rice. Rice Genet Newsl 15:13–74
123. Dinneny JR, Yanofsky MF (2005) Drawing lines and borders: how the dehiscent fruit of Arabidopsis is patterned. Bioessays 27:42–49
124. Xiong L, Liu K, Dai X, Xu C, Zhang Q (1999) Identification of genetic factors controlling domestication-related traits of rice using an F2 population of a cross between *Oryza sativa* and *O. rufipogon*. Theor Appl Genet 98:243–251
125. Cai HW, Morishima H (2000) Genomic regions affecting seed shattering and seed dormancy in rice. Theor Appl Genet 100:840–846
126. Sobrizal IK, Sanchez PL, Yoshimura A (1999) RFLP mapping of a seed shattering gene on chromosome 4 in rice. Rice Genet Newsl 16:74–75
127. Nagai YS, Sobrizal SPL, Kurakazu T, Doi K, Yoshimura A (2002) Sh3, a gene for seed shattering commonly found in wild rices. Rice Genet Newsl 19:74–75
128. Li C, Zhou A, Sang T (2006) Rice domestication by reducing shattering. Science 311:1936–1939
129. Konishi S, Izawa T, Lin SY, Ebana K, Fukuta Y, Sasaki T, Yano M (2006) An SNP caused loss of seed shattering during rice domestication. Science 312:1392–1396
130. Ji HS, Chu SH, Jiang W, Cho YI, Hahn JH, Eun MY, McCouch SR, Koh HJ (2006) Characterization and mapping of a shattering mutant in rice that corresponds to a block of domestication genes. Genetics 173:995–1005
131. Ji H, Kim SR, Kim YH, Kim H, Eun MY, Jin ID, Cha YS, Yun DW, Ahn BO, Lee MC, Lee GS, Yoon UH, Lee JS, Lee YH, Suh SC, Jiang W, Yang JI, Jin P, McCouch SR, An G, Koh HJ (2010) Inactivation of the CTD phosphatase-like gene OsCPL1 enhances the development of the abscission layer and seed shattering in rice. Plant J 61:96–106
132. Krishnan A, Ambavaram MMR, Harb A, Batlang U, Wittich PE, Pereira A (2009) Genetic networks underlying plant abiotic stress responses. In: Jenks MA, Wood AJ (eds) Genes for plant abiotic stress. Wiley, Ames
133. Lin HX, Zhu MZ, Yano M, Gao JP, Liang ZW, Su WA, Hu XH, Ren ZH, Chao DY (2004) QTLs for Na + and K + uptake of the shoots and roots controlling rice salt tolerance. Theor Appl Genet 108:253–260
134. Ren ZH, Gao JP, Li LG, Cai XL, Huang W, Chao DY, Zhu MZ, Wang ZY, Luan S, Lin HX (2005) A rice quantitative trait locus for salt tolerance encodes a sodium transporter. Nat Genet 37:1141–1146
135. Xu K, Mackill DJ (1996) A major locus for submergence tolerance mapped on rice chromosome 9. Mol Breed 2:219–224
136. Xu K, Xu X, Ronald PC, Mackill DJ (2000) A high-resolution linkage map of the vicinity of the rice submergence tolerance locus Sub1. Mol Gen Genet 263:681–689
137. Xu K, Xu X, Fukao T, Canlas P, Maghirang-Rodriguez R, Heuer S, Ismail AM, Bailey-Serres J, Ronald PC, Mackill DJ (2006) Sub1A is an ethylene-response-factor-like gene that confers submergence tolerance to rice. Nature 442: 705–708
138. Delhaize E, Craig S, Beaton CD, Bennet RJ, Jagadish VC, Randall PJ (1993) Aluminum tolerance in wheat (*Triticum aestivum* L.). Part I. Uptake and distribution of aluminum in root apices. Plant Physiol 103:685–693
139. Delhaize E, Ryan PR, Randall PJ (1993) Aluminum tolerance in wheat (*Triticum aestivum* L.). Part II. Aluminum-stimulated excretion of malic acid from root apices. Plant Physiol 103:695–702
140. Sasaki T, Yamamoto Y, Ezaki B, Katsuhara M, Ahn SJ, Ryan PR, Delhaize E, Matsumoto H (2004) A wheat gene encoding an aluminum-activated malate transporter. Plant J 37: 645–653
141. Bishop GJ, Harrison K, Jones JD (1996) The tomato Dwarf gene isolated by heterologous transposon tagging encodes the first member of a new cytochrome P450 family. Plant Cell 8:959–969

142. Doi K, Izawa T, Fuse T, Yamanouchi U, Kubo T, Shimatani Z, Yano M, Yoshimura A (2004) Ehd1, a B-type response regulator in rice, confers short-day promotion of flowering and controls FT-like gene expression independently of Hd1. Genes Dev 8:926–936
143. Salvi S, Sponza G, Morgante M, Tomes D, Niu X, Fengler KA, Meeley R, Ananiev EV, Svitashev S, Bruggemann E, Li B, Hainey CF, Radovic S, Zaina G, Rafalski JA, Tingey SV, Miao GH, Phillips RL, Tuberosa R (2007) Conserved noncoding genomic sequences associated with a flowering-time quantitative trait locus in maize. Proc Natl Acad Sci USA 104:11376–11381
144. Watanabe S, Hideshima R, Xia Z, Tsubokura Y, Sato S, Nakamoto Y, Yamanaka N, Takahashi R, Ishimoto M, Anai T, Tabata S, Harada K (2009) Map-based cloning of the gene associated with the soybean maturity locus E3. Genetics 182:1251–1262
145. Yan L, Loukoianov A, Tranquilli G, Helguera M, Fahima T, Dubcovsky J (2003) Positional cloning of the wheat vernalization gene VRN1. Proc Natl Acad Sci USA 100:6263–6268
146. Yan L, Loukoianov A, Blechl A, Tranquilli G, Ramakrishna W, SanMiguel P, Bennetzen JL, Echenique V, Dubcovsky J (2004) The wheat VRN2 gene is a flowering repressor down-regulated by vernalization. Science 303:1640–1643
147. Vrebalov J, Ruezinsky D, Padmanabhan V, White R, Medrano D, Drake R, Schuch W, Giovannoni J (2002) A MADS-box gene necessary for fruit ripening at the tomato ripening-inhibitor (rin) locus. Science 296:343–346
148. Liu J, Van Eck J, Cong B, Tanksley SD (2002) A new class of regulatory genes underlying the cause of pear-shaped tomato fruit. Proc Natl Acad Sci USA 99:13302–13306
149. Martin GB, Brommonschenkel SH, Chunwongse J, Frary A, Ganal MW, Spivey R, Wu T, Earle ED, Tanksley SD (1993) Map-based cloning of a protein kinase gene conferring disease resistance in tomato. Science 262:1432–1436
150. Song WY, Wang GL, Chen LL, Kim HS, Pi LY, Holsten T, Gardner J, Wang B, Zhai WX, Zhu LH, Fauquet C, Ronald P (1995) A receptor kinase-like protein encoded by the rice disease resistance gene, Xa21. Science 270:1804–1806
151. Dixon MS, Jones DA, Keddie JS, Thomas CM, Harrison K, Jones JD (1996) The tomato Cf-2 disease resistance locus comprises two functional genes encoding leucine-rich repeat proteins. Cell 84:451–459
152. Dinesh-Kumar SP, Whitham S, Choi D, Hehl R, Corr C, Baker B (1995) Transposon tagging of tobacco mosaic virus resistance gene N: its possible role in the TMV-N-mediated signal transduction pathway. Proc Natl Acad Sci USA 92:4175–4180
153. Cai D, Kleine M, Kifle S, Harloff HJ, Sandal NN, Marcker KA, Klein-Lankhorst RM, Salentijn EM, Lange W, Stiekema WJ, Wyss U, Grundler FM, Jung C (1997) Positional cloning of a gene for nematode resistance in sugar beet. Science 275:832–834
154. Ori N, Eshed Y, Paran I, Presting G, Aviv D, Tanksley S, Zamir D, Fluhr R (1997) The I2C family from the wilt disease resistance locus I2 belongs to the nucleotide binding, leucine-rich repeat superfamily of plant resistance genes. Plant Cell 9:521–532
155. Kawchuk LM, Hachey J, Lynch DR, Kulcsar F, van Rooijen G, Waterer DR, Robertson A, Kokko E, Byers R, Howard RJ, Fischer R, Prufer D (2001) Tomato Ve disease resistance genes encode cell surface-like receptors. Proc Natl Acad Sci USA 98:6511–6515
156. Ballvora A, Ercolano MR, Weiss J, Meksem K, Bormann CA, Oberhagemann P, Salamini F, Gebhardt C (2002) The R1 gene for potato resistance to late blight (*Phytophthora infestans*) belongs to the leucine zipper/NBS/LRR class of plant resistance genes. Plant J 30:361–371
157. Brueggeman R, Rostoks N, Kudrna D, Kilian A, Han F, Chen J, Druka A, Steffenson B, Kleinhofs A (2002) The barley stem rust-resistance gene Rpg1 is a novel disease-resistance gene with homology to receptor kinases. Proc Natl Acad Sci USA 99:9328–9333
158. Ernst K, Kumar A, Kriseleit D, Kloos DU, Phillips MS, Ganal MW (2002) The broad-spectrum potato cyst nematode resistance gene (Hero) from tomato is the only member of a large gene family of NBS-LRR genes with an unusual amino acid repeat in the LRR region. Plant J 31:127–136
159. Feuillet C, Travella S, Stein N, Albar L, Nublat A, Keller B (2003) Map-based isolation of the leaf rust disease resistance gene Lr10 from the hexaploid wheat (*Triticum aestivum* L.) genome. Proc Natl Acad Sci USA 100: 15253–15258
160. Huang L, Brooks SA, Li W, Fellers JP, Trick HN, Gill BS (2003) Map-based cloning of leaf rust resistance gene Lr21 from the large and polyploid genome of bread wheat. Genetics 164:655–664
161. Yahiaoui N, Srichumpa P, Dudler R, Keller B (2004) Genome analysis at different ploidy levels allows cloning of the powdery mildew resistance gene Pm3b from hexaploid wheat. Plant J 37:528–538
162. Qu S, Liu G, Zhou B, Bellizzi M, Zeng L, Dai L, Han B, Wang GL (2006) The broad-spectrum blast resistance gene Pi9 encodes a nucleotide-binding site-leucine-rich repeat protein and is a member of a multigene family in rice. Genetics 172: 1901–1914
163. Brueggeman R, Druka A, Nirmala J, Cavileer T, Drader T, Rostoks N, Mirlohi A, Bennypaul H, Gill U, Kudrna D, Whitelaw C, Kilian A, Han F, Sun Y, Gill K, Steffenson B, Kleinhofs A (2008) The stem rust resistance gene Rpg5 encodes a protein with nucleotide-binding-site, leucine-rich, and protein kinase domains. Proc Natl Acad Sci USA 105: 14970–14975
164. Fu D, Uauy C, Distelfeld A, Blechl A, Epstein L, Chen X, Sela H, Fahima T, Dubcovsky J (2009) A kinase-START gene confers temperature-dependent resistance to wheat stripe rust. Science 323:1357–1360
165. Bulgarelli D, Biselli C, Collins NC, Consonni G, Stanca AM, Schulze-Lefert P, Valè G (2010) The CC-NB-LRR-type Rdg2a resistance gene confers immunity

to the seed-borne barley leaf stripe pathogen in the absence of hypersensitive cell death. PLoS One 5(9):pii: e12599
166. Paz-Ares J, Wienand U, Peterson PA, Saedler H (1986) Molecular cloning of the c locus of *Zea mays*: a locus regulating the anthocyanin pathway. EMBO J 5:829–833
167. Buckner B, Kelson TL, Robertson DS (1990) Cloning of the y1 locus of maize, a gene involved in the biosynthesis of carotenoids. Plant Cell 2:867–876
168. Bhattacharyya M, Smith AM, Noel Ellis TH, Hedley C, Martin C (1990) The wrinkled-seed character of pea described by Mendel is caused by a transposon-like insertion in a gene encoding starch-branching enzyme. Cell 60:115–122
169. Fridman E, Pleban T, Zamir D (2000) A recombination hotspot delimits a wild-species quantitative trait locus for tomato sugar content to 484 bp within an invertase gene. Proc Natl Acad Sci USA 97:4718–4723
170. Mao L, Begum D, Chuang H, Budiman MA, Szymkowiak EJ, Irish EE, Wing RA (2000) JOINTLESS is a MADS-box gene controlling tomato flower abscission zone development. Nature 406:910–913
171. Hattori Y, Nagai K, Furukawa S, Song XJ, Kawano R, Sakakibara H, Wu J, Matsumoto T, Yoshimura A, Kitano H, Matsuoka M, Mori H, Ashikari M (2009) The ethylene response factors SNORKEL1 and SNORKEL2 allow rice to adapt to deep water. Nature 460:1026–1030

Books and Reviews

Charlesworth D, Willis JH (2009) The genetics of inbreeding depression. Nat Rev Genet 10:783–796
Doust A (2007) Architectural evolution and its implications for domestication in grasses. Ann Bot 100:941–950
Gibson S, Somerville C (1993) Isolating plant genes. Trends Biotechnol 11:306–313
Paterson AH (1995) Molecular dissection of quantitative traits: progress and prospects. Genome Res 5:321–333
Pereira A (2001) Transposon tagging methods in heterologous plants. In: Gilmartin P, Bowler C (eds), Molecular plant biology, vol I. Oxford University Press, Oxford, 294 p. ISBN: 0-19-963876-4
Salvi S, Tuberosa R (2005) To clone or not to clone plant QTLs: present and future challenges. Trends Plant Sci 10: 297–304
Sang T (2009) Genes and mutations underlying domestication transitions in grasses. Plant Physiol 149:63–70
Tanksley SD (1993) Mapping polygenes. Annu Rev Genet 27: 205–233
Tanksley SD, Ganal MW, Martin GB (1995) Chromosome landing: a paradigm for map-based gene cloning in plants with large genomes. Trends Genet 11:63–68
Wei H, Lin H-X (2010) Toward understanding genetic mechanisms of complex traits in rice. J Genet Genomics 37:653–664

Crop Yields Around the World: Closing the Gap and Raising the Potential

R. A. (Tony) Fischer
CSIRO Plant Industry, Canberra City, Australia

Article Outline

Glossary
Definition of Subject
Introduction
Estimates of Yield Gaps
Closing Yield Gaps
Lifting Potential Yield
Future Directions and Synthesis
Bibliography

Glossary

Allocative efficiency Efficiency with which given variable input(s) is used.

Attainable yield Yield reached by farmers with economically optimum management and reasonable risk aversion.

Ecotilling Seeking related alleles across germplasm collections based on DNA homology.

Farm yield Average grain yield across farms in a region.

Harvest index Ratio of grain dry weight to total above-ground dry weight at maturity.

Molecular markers Short sequences of DNA that are homologous with sequences close to or within important genes.

Potential yield Grain yield in the absence of manageable abiotic and biotic stresses.

Potential yield water limited Grain yield in the absence of manageable abiotic and biotic stresses apart from that imposed by water supply through inadequate rainfall.

Radiation use efficiency Above ground biomass produced per unit of total solar radiation intercepted by green crop tissue.

Technical efficiency Practices, timing, and technical skills adopted by farmer in using inputs.

Yield gap Difference between farm yield and potential yield.

Definition of Subject

The entry assumes that yield increase will continue to play a dominant role in world food security, as it has over the last 60 years. It is restricted to annual grain crops, since these dominate the world's arable landscape (>70%) and humankind's food supply (>70%), including grain used as livestock feed. Crop yield is the weight of grain, at some agreed standard moisture content, harvested per unit of land area per crop (note, there can be two or even three annual crops per year in some favored environments, meaning a cropping intensity of 200% or 300%, respectively). The starting point for yield is usually the field, district, regional, or national average yield in kg or t per hectare, as reported in surveys or local or national statistics. Here this is referred to as farm yield (FY, t/ha). This and many related cropping statistics are collated annually for all countries by FAO (http://faostat.fao.org/site/567/default.aspx#ancor). FY is usually expressed relative to harvested land area (note: this can fall well below planted area in some situations). Although FY is quoted and used widely, it may not be as accurate as it appears due to uncertain grain admixtures and/or poor collection of the statistics. With survey data sampling error can also arise.

At the highest end of the yield scale it is useful to define *potential yield* (PY), which is the yield to be expected with the best adapted cultivar, the best management of agronomic inputs, and in the absence of manageable abiotic and biotic stresses [1]. Many complications are hidden within this apparently simple definition. PY is usually determined in plots, with of course sampling error. In order to be relevant to the surrounding district, the natural resource base of the plot (climate, soil type, topography) needs to be comparable, including any long-term management investments to improve this aspect of the site (e.g., liming, tile drainage). Water supply must be adequate for PY determination as defined, and this can come from well-distributed rainfall close or equal to crop potential evapotranspiration (crop water use from sowing to harvest without water limitation) or from full or supplemental irrigation; in addition, pests, weeds, and diseases must be held at negligible levels through the use of biocides if necessary. Finally, crops experiencing relatively rare weather damage such as crop lodging or unseasonal frosting are excluded from PY measurement. Taken overall, it would seem PY might be impossibly difficult to measure, but it is reported often in the crop science literature, although not always with proper attention to the above caveats.

Since PY is usually measured in plots, edge effects arising from extra solar radiation or soil moisture or nutrients reaching outside plants must be avoided by discarding the plot edges. Two types of PY plots are commonest. Often they are well-managed yield trials to compare new varieties or advanced lines against older ones, or even historic ones, to give measures of breeding progress by plotting variety yield against year of release. The most useful such trials, for example those for wheat conducted by the UK Home Grown Cereals Authority (HGCA http://www.hgca.com/content.template/0/0/Home/Home/Home.mspx), measure yields with and without fungicide protection. Only the former yields are a measure of true PY, but fungicide protection is still not very common in such yield trials around the world, although visible disease levels are usually reported and can be negligible. The second source of PY data comes from experiments conducted by crop physiologists to calibrate and/or validate crop simulation models: the models, driven largely by various aspects of solar radiation and temperature, can then be used to predict PY in other environments (e.g., sowing dates, years, locations). For such purposes modeling accuracy has steadily improved, but models need to be updated with the latest varieties every few years, since breeders are steadily altering varieties (e.g., phasic development, improving PY). Sometimes, crop contest yields or crop record yields are considered to be synonymous with PY. But they need to be treated with caution, because they usually exceed PY measured as defined here, probably because they refer to very favorable circumstances (e.g., soils, weather, management), relative to the district average; nevertheless, we can learn from such yields if all site and management variables are quantified. For example, properly verified world record yields, invariably higher than PY values, not only extend our simulation models but also reveal that there is no anatomical limitation to very high yields, the main limitation evident with such yields being the stem strength needed to support them.

Since much of the world's grain crops are grown in rainfed situations where water supply from

precipitation plus starting soil storage falls well below the potential evapotranspiration, it is also useful to define a *water-limited potential yield* (PYw, t/ha): it is the yield obtained with no other manageable limitation to the crop apart from the water supply. Obviously, it will depend on the amount of water, so PYw is usually plotted relative to water supply (or use), the slope being the crop water use efficiency or water productivity, commonly reported in kilograms per hectare per millimeter. Complications can arise due to variation in rainfall distribution with respect to crop development stages, but PYw, defined as a linear function of the water supply, is a very useful simple benchmark, as argued in a recent in-depth review by Passioura and Angus [2], while simulation modeling has been especially useful in dealing with expected deviations due to variation in the distribution of water supply.

In any given region, between FY and PY (or PYw), there is another useful yield notion, namely *attainable yield* (AY, t/ha), which is defined here as the yield attained by a farmer with average natural resources adopting economically optimal practices and levels of inputs. Since risk of financial loss is almost always part of a farmer's decision to invest in increased inputs, the AY definition must temper "optimum level" with "prudent attention to risk"; as an example this could mean input investments must be expected to return at least 50% in net profit at the margin. Of course, AY will reflect the economic circumstances of the crop and region, in particular grain prices relative to input ones, all measured at the farm gate. Thus, it is not easy to know AY, but general experience suggests that it lies around 20–30% below PY in situations where world prices and reasonable transport costs operate. FY for wheat in the UK probably meets these conditions (Fig. 1). Where this does not occur, for example, in much of sub-Saharan Africa where infrastructure and institutions are weak, the AY as defined above may be much lower; alternatively where inputs and grain prices are heavily subsidized, AY could approach closer to PY. Because of these uncertainties, it is easier to talk of the *yield gap* in terms of the FY to PY gap, bearing in mind that even in the most advanced cropping situations in developed economies, operating at close to world prices, FY will remain significantly below PY. Since it is more appropriate to express this gap as a percentage of FY, it can be assumed from the literature that this minimal gap is reached when the PY–FY gap is about

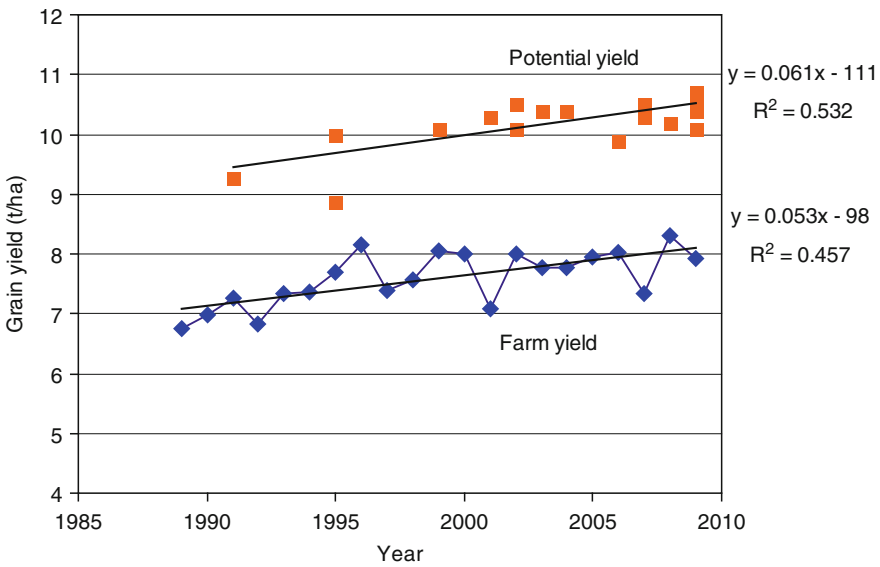

Crop Yields Around the World: Closing the Gap and Raising the Potential. Figure 1
Change in farm yield (FY) and potential yield (PY) with time for wheat in the UK. Source: FAOStat and HGCA. Note that in this and other figures (except Fig. 4), PY is plotted against year of variety release, for varieties are compared side by side in recent yield trials under modern management

30% (of FY). Any larger gap that this, which is usually the case, is often defined as an "economically exploitable yield gap," but bearing in mind that the expected exploitation can be as much a task for national and local government and agribusiness, as for the farmers.

Introduction

Crop yield has been the subject of attention since the days of Malthus and earlier. More recently, many have pointed out that the improved supply of food calories per capita globally, and reduced real costs of grain, over the last 60 years has been due almost entirely to global crop yields growing faster than the burgeoning world population (e.g., [4]), for there have been only small increases in cropped area (Fig. 2). The world population will grow to over nine billion by 2050, and grain demand is projected to increase around 60–70% (compared to 2000) [5], with others projecting even greater increases, and certainly more rapid increase coming early in this period. Seventy percent over 50 years amounts to an exponential increase of 1.1%; output growth must match this or real prices will increase (see also later). There is some potential new arable land of reasonable quality in South America and sub-Saharan Africa (and in northern latitudes of Russia), but increase in arable area demands heavy capital investment and brings negative environmental consequences; indeed, maintenance of arable area could be a challenge in densely populated fast-urbanizing regions like South and East Asia, and where there is continuing arable land degradation. Crop area can also increase through intensification of annual cropping but that usually depends on expansion in irrigation, which has in fact slowed markedly, especially in Asia where water availability for agriculture is now constrained. As a consequence, most argue that the projected increase in grain demand must continue to be met by yield increase.

Many grain crops have exceeded 1% exponential yield growth in the early decades of the modernization of agriculture last century, including the Green Revolution period for rice and wheat in Asia, but global yield growth trends for most crops over the last 20 years have slowed and have become linear, with current growth rates at or below 1%; maize at 1.6% and soybeans at 1.1% are the only major crops exceptions to this (Fig. 3; note growth rate is expressed here by

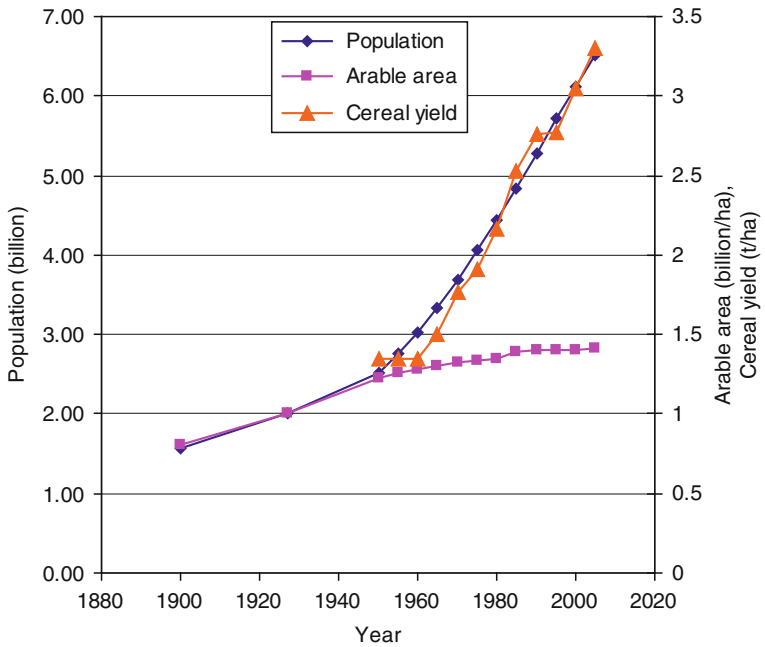

Crop Yields Around the World: Closing the Gap and Raising the Potential. Figure 2
Change in world population, global arable area, and cereal yield. Adapted with permission for Evans (1998)

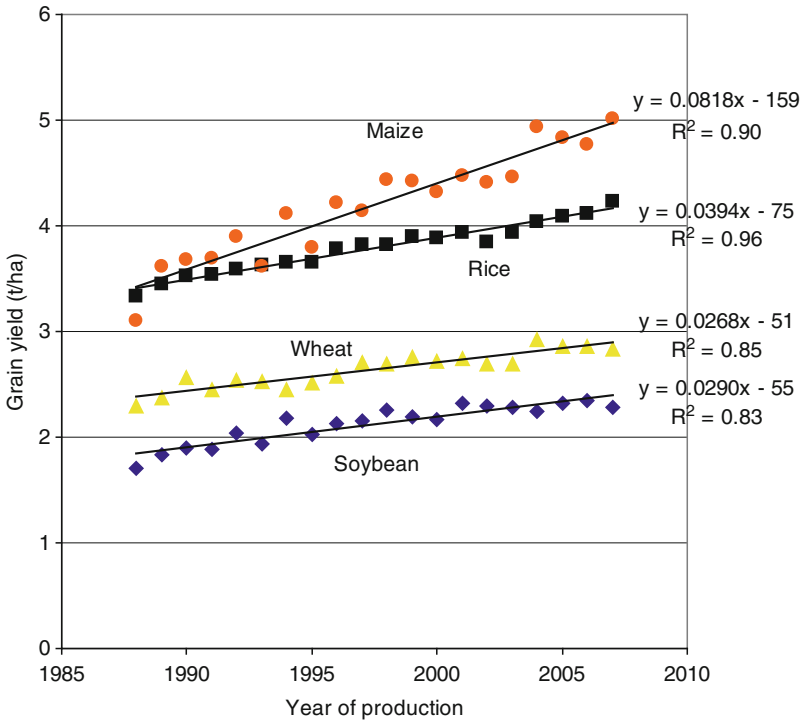

Crop Yields Around the World: Closing the Gap and Raising the Potential. Figure 3
World average yield versus time for wheat, rice, maize, and soybeans over last 20 years. Source: FAOStat

calculating the linear slope as a percentage of current predicted yield for each crop). Increasing the proportion of a crop which is irrigated can increase yield growth, as happened with wheat in Asia in the 1960s, but further increases in irrigation area are unlikely, due to cost and/or lack of water, except possibly in sub-Saharan Africa. This leaves the maintenance, or preferably boosting, of rates of yield increase in existing cropped situations as the major route for meeting growing demand for grain, and the major challenge facing agricultural science. And despite some media sentiment to the contrary, agricultural scientists are fully aware that this goal has to be met while sustaining, or better still, improving the natural resource base of cropping, and while confronting the uncertain and predominantly negative projected impacts of climate change.

From the definition of the subject, it can be seen that there are two sources of yield increase: raising PY and closing the PY to FY gap (see also Figs. 1, 4 and 5). In most situations, both processes contribute simultaneously to FY increase, with farmers adopting new

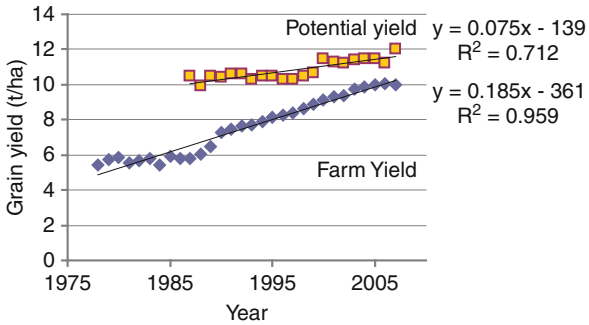

Crop Yields Around the World: Closing the Gap and Raising the Potential. Figure 4
Change in PY and in FY for rice in Egypt. Source: Badawi [3]; A. E. Draz, 2009, personal communication

technologies (varieties, management techniques, input levels) that have been developed years or decades earlier by researchers at which time the associated rise in PY occurred. Recently, two trends in this process are becoming evident. Firstly, management or agronomic innovations for increasing PY, including their positive

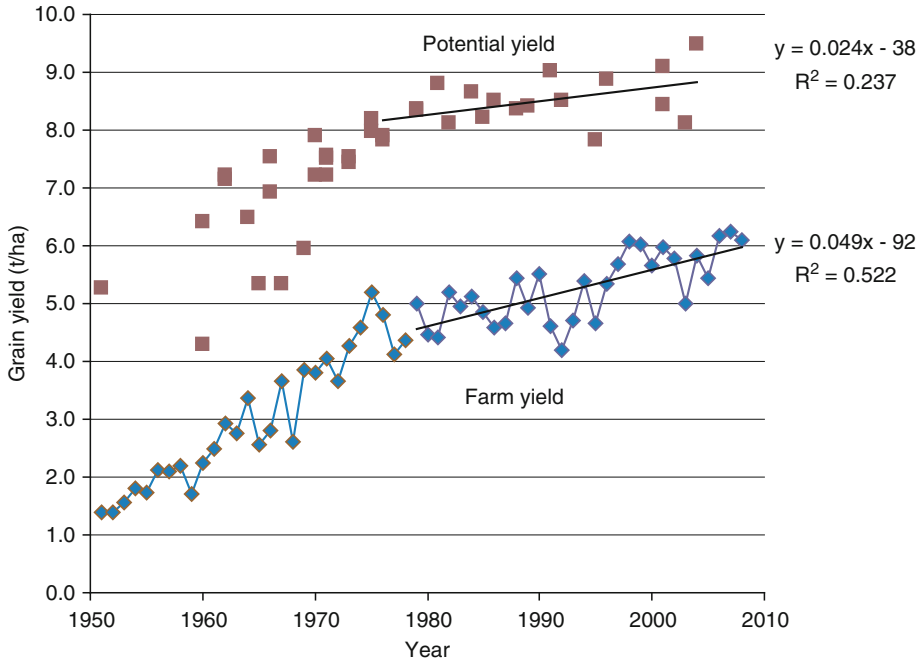

Crop Yields Around the World: Closing the Gap and Raising the Potential. Figure 5
Wheat PY and FY changes with time, Yaqui Valley, Mexico. Source: [5]

interactions with new varieties (e.g., the universal nitrogen by variety interaction in wheat and rice, or the plant density by hybrid variety interaction in maize), are becoming fewer, leaving a greater proportion of PY progress to breeding advances. This is a somewhat controversial observation but is clearly supported by analysis of the winter wheat yield changes in the UK [6]. Secondly, in some special situations, as mentioned earlier, the yield gap is approaching the minimal 30% or so dictated by current economics; examples include winter wheat in the UK (Fig. 1) and probably all of Western Europe), rice in Egypt (Fig. 4), and maize in the US corn belt (e.g., Iowa, see Fig. 6).

While it is not always easy to separate PY advance from gap closing, since this volume has given more attention to the former, in particular the possibilities arising with new molecular biological techniques becoming available to plant breeders, this entry will give more attention to closing the yield gap than to raising PY. Both issues have been more fully discussed in Fischer et al. [5]. Another reason for concentrating here on closing the yield gap is that, notwithstanding the evidence of small yield gaps in some situations, it is likely that yield gap closing offers better prospects globally for quickly lifting FY progress, as is needed, than does boosting PY progress. The entry continues by looking at the size of the yield gap in various key situations around the world. Passing then to gap closure, traditionally this is considered to arise from farmer adoption of yield-enhancing technologies, the area of agricultural extension or technology transfer. While there is a lively body of socioeconomic research on this process, which will be considered briefly, the way the yield gap is defined here, it is hard to see the new products of breeding and agronomic research reducing the yield gap. This is because their initial impact should be on PY as defined, actually increasing the gap, followed by their gradual adoption which, if complete, might be expected to reduce the gap to the same relative value as before, other things being equal. Needless to say the real situation is more complex and examples will be given of how such research, including progress in molecular biology, can help directly reduce the gap (e.g., more adoptable technologies, less costly ones, and better biotic stress resistance). The entry finishes by discussing briefly the current situation with progress in PY and PYw themselves. What will not be discussed further is the likelihood that

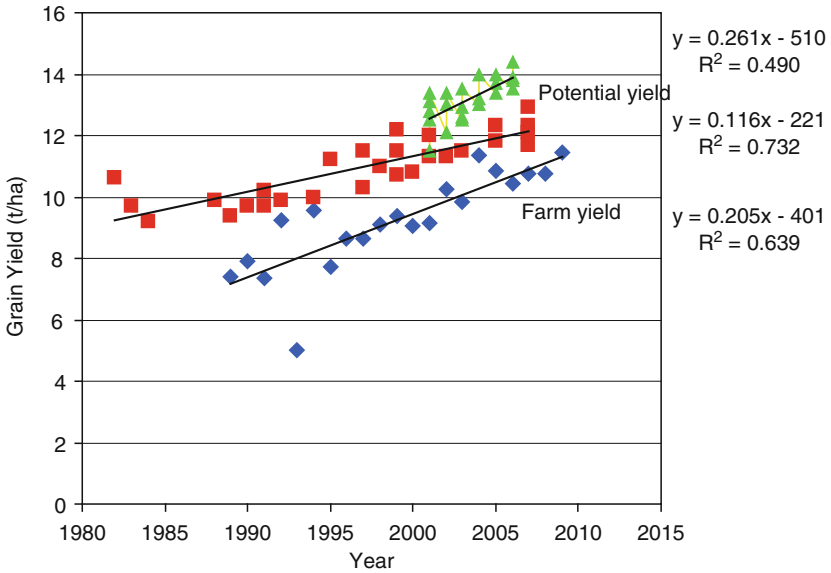

Crop Yields Around the World: Closing the Gap and Raising the Potential. Figure 6
Change in maize FY in Iowa compared to that in PY as estimated by Pioneer (Hammer et al. ([7], *red squares*) and de Kalb (Edgerton [8], *green triangles*) hybrid yields plotted against year of hybrid release

atmospheric CO_2 increase will continue to improve all grain yields, other things remaining equal, but the rate of increase is currently around only 0.2% in a C3 crop like wheat [9], and less for C4 crops.

Estimates of Yield Gaps

Fischer et al. [5] attempted to estimate yield gaps and their rate of change for a number of key representative cereal-producing regions in the world. The most reliable estimates are summarized in Table 1, supplemented with a few new crops and numbers.

The yield gap estimates for wheat are remarkably consistent at around 50% except for the UK, where as mentioned before the 25% gap probably implies that FY is approaching AY, an AY largely determined by ruling world prices in the UK. Figure 5 illustrates the Yaqui Valley data, where there was substantial yield gap closing as the modern semidwarf varieties took over in the 1960s; lately, however, the yield gap has remained fairly steady at 50%. Lobell et al. [12] recently presented 12 published estimations of the yield gap for wheat in developing countries, the gap ranged from 5% to 150% but the average was close to that in Table 1, namely 55%.

For rice, Table 1 shows gap values around 100% or more for most developing country situations except for Central Luzon in the wet season (65%), and a remarkably low 15% for Egypt (see also Fig. 4). The value of 55% for Japan reflects the heavy emphasis on producing high-quality grain, acting as brake on FY progress, because food-quality rice varieties and agronomy deliver lower yields. From the 41 rice estimates from developing countries in [12], the average gap was 65%, with modeling evidence that the gap was 120% in northwest India (cf. 110% in the Indian Punjab in Table 1).

Table 1 has only two cases for maize: Iowa at 25% contrasts with Kenya at 200+%; sub-Saharan Africa as a whole is similar to Kenya. Tittonell et al. [13] in a detailed survey of farm yields in three districts in the favored Kenyan Highlands confirms the figure shown in Table 1, recording a mean FY of 1.5 t/ha when PY was 6–7 t/ha. Lobell et al. [12] give nine examples of rainfed maize in tropical and subtropical developing countries (average gap 200%) and examples of irrigated and rainfed maize in Nebraska based on simulation of PY and PYw which suggest gaps of 35% and 55%, respectively, both larger than that for rainfed maize in the adjacent wetter state of Iowa (Table 1).

Crop Yields Around the World: Closing the Gap and Raising the Potential. Table 1 Estimates of current yield gaps for key crops and regions (compiled from [5] and elsewhere as noted)

Region	Environment	Crop area (M ha)	Yield (t/ha)[a] and gap(%), 2007 or 2008		
			FY	PY	Gap
Wheat					
Yaqui V, Mexico	Irrigated, low latitude	0.16	6	9	50
Punjab, India	Irrigated, low latitude	3.9	4.3	6.25	45
Western Australia	Subhumid, low latitude	4.5	1.8	2.6[b]	45
N. Dakota	Subhumid, high latitude	3.4	2.5	3.7[b]	50
UK	High rain, winter wheat	1.8	8.2	10.4	25
Eastern China	Irrigated, winter wheat	16	4.7	7	50
Kansas	Subhumid, winter wheat	3.6	2.6	3.9[b]	45
Rice					
Central Luzon	Wet season + irrigation	0.8	3.8	6	60
Punjab, India	Wet season + irrigation	2.4	3.8	8	110
Japan	Wet season + irrigation	3	6.5	10	55
South Asia	Wet season, rainfed	28.5	1.8	3.6	100
Central Luzon	Dry season, irrigated	0.4	4.5	9	100
Egypt	Dry season, irrigated	0.7	10.1	11.6	15
Maize					
Iowa	Temperate, high rainfall	5.3	10.8	15.5[c]	45
Kenya	All altitudes, moderate rain	1.75	1.8	6[b]	200+
Soybeans					
USA[d]	Temperate, high rainfall	30	2.8	3.6	30
India[e]	Subtropical, tropical, moderate rainfall	9	1	2.2[b]	120
Millet					
India[f]	Subtropical, rainfed	11	0.9	1.8[b]	100

[a]Predicted from linear trends
[b]Actually PYw
[c]Reestimated in Fischer and Edmeades [9]
[d]Estimate by R. A. Fischer, 2010 unpublished
[e]Bhatia et al. [10]
[f]Murty et al. [11]

While there is no doubt about the huge yield gap with maize in Africa, some uncertainty exists in these critical estimates from the USA, where maize is probably the most intensively researched and promoted crop in the world. No doubt the gap is quite small in Iowa and Nebraska, where it has been closing lately, and FY may be close to AY (Fig. 6), although more PY progress data is needed for a clearer conclusion.

The soybean examples in Table 1 also show a large difference in the yield gap between a developed and developing country, but do not show developing countries Argentina and Brazil, where FY across more than

35 M ha with favorable rainfall is as high as the USA, and PY is unlikely to be any higher. Finally, millet, grown in India under very harsh conditions, shows a gap no worse that of soybeans in adjacent more favorable areas of India.

Closing Yield Gaps

Yield gaps are reduced by farmers adopting new technologies or practices (new at least for them) or adopting higher rates of inputs (e.g., many farmers in western Kenya use added nutrients, either fertilizer or organic ones, but the rate of nutrients applied may be very low relative to the need/optimum (e.g., [13])). Some of this is usefully illustrated in Fig. 7 derived from Byerlee [14].

FY under traditional practices with low inputs is shown by point A on curve 1. Adopting new technologies such as an improved new variety and practices (e.g., line sowing and fertilizer) lifts technical efficiency and brings curve 2 into play. The farmer may move from point A to point B, as in the first years of the Green Revolution. Allocative efficiency could then rise further as fertilizer levels increase, following curve 2 to point C, approaching some economic optimum. An even newer variety and the best available practices (e.g., herbicides, conservation tillage) which together define current PY (point F) could lift the technical frontier further (the uppermost curve 3). Farmers might choose to further increase technical efficiency by moving to the uppermost curve, maximizing allocative efficiency at around point D, or sacrificing allocative efficiency, but not yield, by reducing inputs (point E). Of course, curve 3 is not static: for any given environment it may be moved further upward with new technologies, and it may also shift downward due to problems of resource degradation. This figure also serves to illustrate that the yield gap is not the same as an efficiency gap, gaps between curves are technical efficiency ones, gaps along curves are allocative ones, both combine to make up the FY to AY gap.

Adoption of New Technology

There is a rich agricultural economic literature on the adoption of new technologies by farmers. Examples for the adoption of two new technologies in the rainfed cropping in Australia are shown in Fig. 8a (a new crop, lupins, and a new practice, no till). The new crop was adopted faster than the new agronomic technique. Developing countries have proved equally fast in adopting new varieties (Fig. 8b) when the conditions are favorable. The well-recognized patterns of lag, rate of adoption, and ceiling adoption level clearly differ between technologies and farmers (regions); in addition, the infrastructural and institutional context is

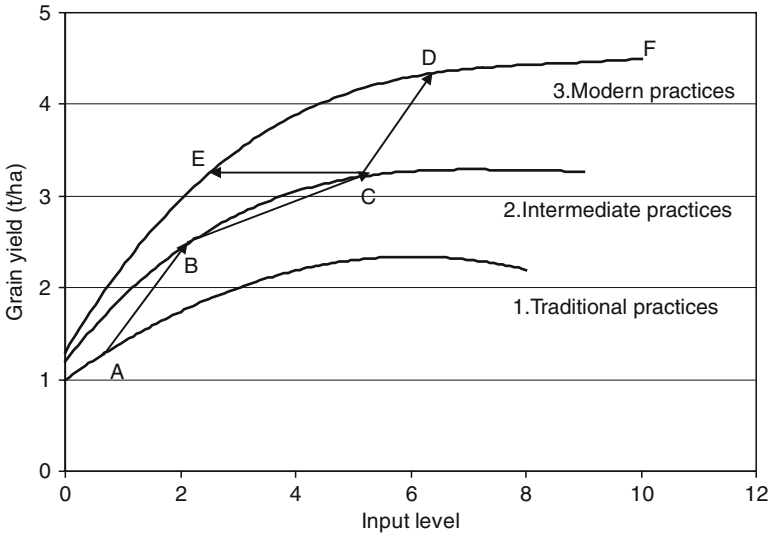

Crop Yields Around the World: Closing the Gap and Raising the Potential. Figure 7
Illustration of pathways from low FY to close the gap with PY; modified from Byerlee [14]

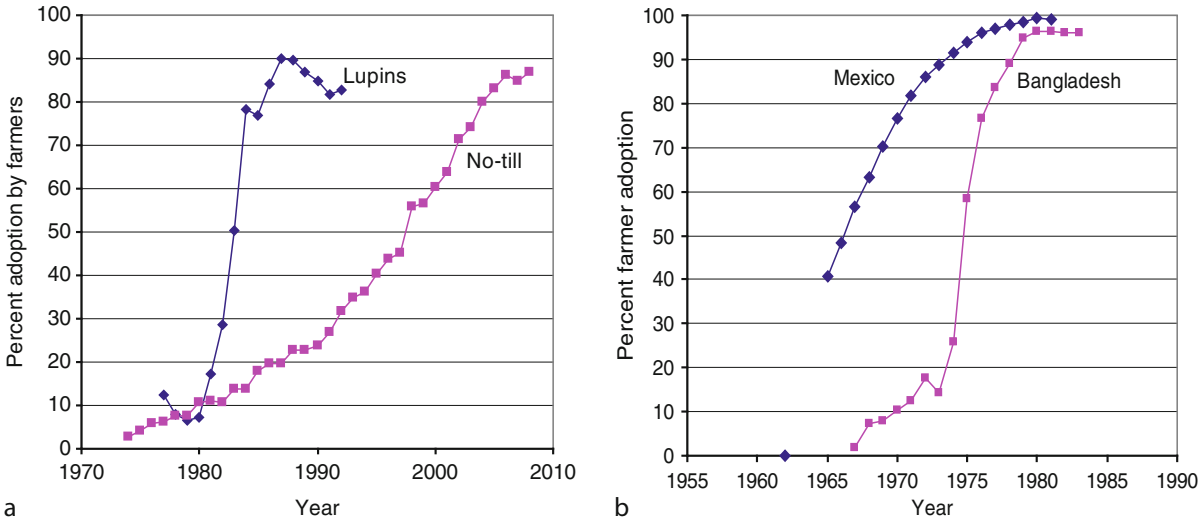

Crop Yields Around the World: Closing the Gap and Raising the Potential. Figure 8
Adoption of new technologies by (**a**) farmers in regions of Australia (lupins in Wongan Hills district [15] and no till in Loddon district [16]), and (**b**) semidwarf wheat varieties in Mexico and in Bangladesh [17]

important. For the technology itself, key elements are its perceived relative advantage (return over cost, risk of loss, convenience, etc.) over that which it replaces, and its trialability, meaning the ease with which a new technology can be tested on a small scale. Farmer characteristics influencing adoption are very diverse and can also interact with the nature of the innovation: education, age, health, exposure to extension and related media and demonstrations, group pressure, and support can be important. But there is little doubt that farmers around the world, large and especially the small, women and men, aspire to increase monetary return and given the means to do so, will adopt more profitable practices.

It is in the area of rural infrastructure and institutions that developed and developing country farmer circumstances differ most. One obvious example is the effect of poor roads on increasing input costs and reducing prices for surplus farm output. For example, the price ratio of N fertilizer to grain is on average double that in other regions of the world and higher still in inland landlocked regions of sub-Saharan Africa [18]. The high cost of credit, uncertainties surrounding contracts (including land tenure), the risk of poor-quality inputs, theft or unrest, and the prevalence of unfavorable and uncertain tax and pricing policies, all make adoption less attractive in many developing situations. Sometimes, price subsidy on inputs and outputs can compensate for these brakes on adoption, such as in the recent situation where a well-crafted fertilizer supply and subsidy policy permitted Malawi, a nation of small holders, to produce an unprecedented surplus of maize and to do so without a maize price collapse. But in general and especially in sub-Saharan Africa the lack of public investment in infrastructure, institutions and agricultural extension, and the lack of sound policy are the major contributors to the yield gap.

Looking at farm-level technical constraints that contribute to the yield gap, in any situation there are usually multiple constraints, and the challenge is to determine which constrains should take priority, while recognizing that interventions often interact positively and are thus more effective when adopted together [19, 20]. This can only be answered by on-farm survey and experimentation. Such work started many years ago with farming system research, farm management clubs, and rapid rural appraisal. It continues in many guises in the developed world, especially influenced by the privatization of agricultural extension, the use of remote sensing and ICT advances, and the entry of input suppliers, in particular seed companies, into agricultural extension.

In the developing world the more traditional approaches remain, although with growing emphasis

on farmer participation [21]. Lobell et al. [12] recount how IRRI conducted on-farm rice experiments in Asia in the 1970s to test high inputs, learning that farmer yields varied greatly between fields, as did responses to inputs especially fertilizer and insecticide, which were often uneconomic. This pointed to the importance of field-to-field variability, and the need to adjust inputs accordingly and as the season unfolds, whether by site-specific nutrient management, which reached maturity some 20 years later [22], or via field-level pest monitoring as part of IPM packages. Titonell et al. [13] recount a similar picture of substantial variability in soil fertility, resource use intensity, and yields among small farmer maize fields in western Kenya. Another lesson is surely that this is scientist-intensive expensive research, usually taken over by the farmer and his advisers in the industrial world, and explaining why large yield gaps often persist in the developing one, where circumstances demand innovative approaches in order to reach the billion small farmers (e.g., [21]).

Very recently IRRI again looked at rice yield gaps, this time using expert knowledge to assess constraints and possibilities for irrigated rice in South Asia [23]. For this crop, FY is currently 5.1 t/ha over 34.3 M ha; it was estimated that on average yield was constrained 1.9 t/ha (37%) by yield-limiting factors, which included individual constraints from nutrient insufficiency (10%), diseases (7%), weeds (7%), water shortage (5%), and rats (4%). The exercise was repeated for the 28.5 M ha of rainfed lowland and upland rice in South Asia with a current FY of 1.8 t/ha: yield-limiting factors amounted to 68% of FY, including nutrients (23%), disease (15%), and weeds (12%). The IRRI paper predicted that with a substantial research, development and extension effort, the adoption of existing technology and ongoing breeding over the next 15 years could reduce these losses by one third (irrigated rice) or one quarter (rainfed rice) adding about 1% to FY growth rate.

With wheat in the Yaqui Valley we have a recent concerted effort to understand the yield gap, PY–FY (currently 50%, Fig. 5, Table 1), this time using the latest high-resolution satellite imagery to estimate field-level yields for all fields in the Valley [24] and supplement a long history of farm surveys. Despite the moderate size and wealth of farms relative to India or Kenya, again field-to-field variability in yield was substantial. It was estimated from images over several years that wheat yields were constrained by late planting, delays in the first post-plant irrigation, and summer fallow weeds [25]. Improved institutions and farm management decisions could largely eliminate these constraints, which averaged over years totaled about 10–15% of FY, and would bridge about half of the gap to estimated *AY* in the Valley. These authors [26] used inter alia classification and regression trees to relate yield to constraints in their complex data sets. The same technique was used by Tittonell et al. [13] to explore management and soil constraints to 150 field-level maize yields in highland Kenya: the rate of added nutrients was the strongest explanatory variable, followed by date of planting and plant density, as yield ranged from 1.2 (low nutrients, late plant) to 4.2 t/ha (high nutrients, normal plant, high density).

Two recent studies illustrate for rainfed cropping the power of simulation modeling and water productivity boundary functions in understanding yield gaps in surveyed farmer fields and in particular removing that part of the apparent gap which is actually due to non-manageable weather (mostly rainfall distribution). Grassini et al. [27] found these distribution effects quite important for sunflower yield variation among fields in the western pampas of central Argentina. Hochman et al. [28] looking at farm wheat yields across Australia, found less influence of rainfall distribution, and more scope for farmers to lift water productivity via improved management (e.g., earlier planting, higher seeding density, higher N input). A weakness of both these studies is that they refer to better farmers rather than to a random sample of fields, for which the opportunities of gap-closing interventions are likely to be greater.

The persistence of large yield gaps in the developing world especially draws attention to situations where these gaps have been closed. Rice in Egyptian is an obvious example where strong R, D, and E engaged a small geographically focused industry of small holders under a sound price policy (Fig. 4). A second example of dramatic technology adoption, albeit with lesser immediate implications for FY than for sustainability of the whole cropping system, relates to the uptake of conservation tillage for wheat, maize, and soybeans in southern South America (Argentina, Brazil, and Paraguay), rising from nothing in 1970 to

24 M ha in 2000. This was very much driven by farmer groups and the farmers themselves faced with the threat of serious soil degradation and by the opportunity provided by knock-down herbicides and knowledge spillover from the North (e.g., [29]). This revolution has yet to reach other developing continents (but is beginning in northwest South Asia). A third success story among small poor farmers has recently appeared with the introduction and expansion of winter maize in northeastern India and Bangladesh.

Despite individual success stories like rice in Egypt, yield gaps in general appear to be quite persistent and close only slowly; this happens even when gaps are well above that to be expected from economics and risk aversion and even when PY progress has slowed such that catch-up through eliminating excessive lags in varietal adoption is not a big issue. The problem is that gap closing on the large scale needed requires massive investments in rural infrastructure and institutions as well as technology transfer, and these are not forthcoming, as maize in sub-Saharan Africa exemplifies. Elsewhere public sector agencies, in particular reaching the billion small farmers in Asia [21], aided by the private sector, in particular in Latin America, have made some inroads on the yield gap; they should continue to do so largely in proportion to the investments made, but there is also scope for innovation, for example, based on modern ICT technologies. The employment of agronomists by private seed companies is a pattern that is bound to be followed in the developing world as its seed industry grows in strength and competitiveness. With gap closing, there are no spill-ins as there are in the case of PY advance through R and D, innovations need to be adapted locally, but it can be argued that the Internet and mobile phones are relevant spill-in technologies for delivering information to farmers small and large, a role which could greatly expand.

Innovative Adoption-Friendly Crop Management and New Varieties

Research can facilitate the adoption of technologies to lessen those constraints which contribute to the FY to PY gaps. Table 2 lists common constraints, separating research targeting agronomic solutions from that involving breeding, while institutional and infrastructural solutions already mentioned are shown in the last column. Some agronomic technologies are still under development (e.g., improved seasonal weather forecasts), but much of the necessary agronomic research is adaptive, generally fitting technologies from more advanced farming systems. For example, the widespread adoption of direct seeding of wheat after rice in northwest India, which by saving on land preparation time has meant that sowing dates are less likely to be late and yield expectations are hence improved, required research and development on appropriate small-scale drills for this direct seeding operation. Sometimes, the agronomic technology comes from a "less-advanced" field cropping situations or from farmers themselves: for example, the use of plastic film mulches, quite common in northern China with wheat, maize, and oilseeds. Such mulches give substantial yield benefit through retaining soil moisture and aiding soil warming in the spring, and challenge agronomic researchers to adapt them in a sustainable fashion elsewhere, including developed countries.

It is with breeding that there are greater gap-closing opportunities. Considering that actual losses from diseases and insects globally exceed 20% of yield with wheat, rice, and maize [30], any improvement in genetic resistance has an immediate benefit for FY when the improved varieties are adopted. Conventional host plant resistance breeding continues to make progress on this front, while genetic engineering has brought exciting new opportunities. Although engineered resistance does not lift PY, it lifts FY wherever farmers cannot control pests and diseases with traditional means. The experience with Bt cotton in India shows how important this can be: small holder yields are at least 30% better simply because before the advent of Bt cotton they were unable to eliminate damage no matter how much insecticide was used [31]. It is likely that the advent of GM corn resistant to root worm is boosting farm yields in the USA because root worm damage went unnoticed beforehand (and is very difficult to treat with chemicals). Fungal diseases have yet to succumb to genetically engineered host plant resistance, but it is reasonable to expect varietal releases in this area in the next decade; engineered viral resistance has already been deployed in some crops [31]. Actual yield losses due to weeds are estimated globally at about 10% by

Crop Yields Around the World: Closing the Gap and Raising the Potential. Table 2 Constraining factors contributing to the farm yield–potential yield gap and their alleviation so that farm yield can approach the attainable yield corresponding to the current potential yield with realistic economics

Constraint	Resolution		
	Research		Institutional/infrastructural
	Agronomic	Breeding	
General farmer constraints			
Lack of farmer awareness or conviction or skill	On-farm demonstration	On-farm testing and selection	Education, media campaigns, extension
Risk aversion by farmer	Forecasts, tactical decision making (e.g., for N top dress)	Tolerance of extreme weather events, like drought, flooding, hail, frost, wind	Insurance schemes, favorable credit terms, price stability
Inadequate labor supply	Mechanization, reduced tillage, herbicides	Select for uniform maturity to favor mechanical harvesting	Facilitate labor migration; credit for mechanization
Technical constraints			
Lacking major long-term soil amelioration	Drainage, land leveling, liming, deep tillage, gypsum	Waterlogging, acidity, and salt tolerance	Long-term credit for major soil amelioration, secure tenure
Excess tillage and loss of moisture, soil compaction	Conservation tillage options and suitable machinery, controlled traffic	Suitable varieties: disease and herbicide tolerance	Credit for new machinery
Manageable topsoil soil toxicities	Ameliorate (e.g., lime for acidity)	Acidity, aluminum tolerance	Input suppliers, credit for lime
Suboptimal nutrient supply	Diagnostics, application of nutrients, slow release forms, tactics to match supply with need	Some scope for improved N, P, and Zn uptake and utilization efficiency	Infrastructure, input suppliers, credit, quality control
Soil variation within and between adjacent fields	Diagnostics to aid adjustment of application rates	Greater tolerance of soil stresses	
Growing old varieties, or use of poor seed	Better on-farm seed management and storage	F1 hybrids, licensed traits, royalties to encourage strong seed industry	Strong seed industry and proper regulation, credit
Incorrect time of sowing	Mechanize, reduced tillage to speed sowing; treatments to warm soil for spring sowing	Make available varieties with range of maturities; herbicide and cold tolerant varieties	Policy to favor mechanization, contract seeding
Poor plant population	Better drilling procedures and machines, quality seed storage	More robust varieties (e.g., long coleoptile in wheat, more tillering)	Seed testing and regulations
Diseases and pests, above and below ground	Biocides, sanitation, crop rotation, IPM	Host plant resistance	Input suppliers, pesticide quality control

Crop Yields Around the World: Closing the Gap and Raising the Potential. Table 2 (Continued)

Constraint	Resolution		
	Research		Institutional/infrastructural
	Agronomic	Breeding	
Weeds	Herbicides, cultivation, sanitation, crop rotation	Enhance crop plant competitiveness, herbicide tolerance	Herbicide quality control, release regulation
Poor water management in irrigated systems	Improve water application techniques and skills, land levelling	Greater tolerance water shortage and excess	Efficient supply systems to farm
Long-term soil degradation	Crop rotation, fertilizer, green manuring, farm yard manure, conservation tillage, amelioration	Varieties adapted to biotic and abiotic stresses of high plant residue levels, and with good residue production	Tenure regulations ensuring land ownership by farmer

Oerke [30], to which should be added the costs of current control measures. More competitive cultivars can help, but again genetic engineering has brought revolutionary advances in ease, cost, and effectiveness of weed control. Of course, with any chemical-based susceptibility of biotic stress agents, there will be the risk of resistance evolving in the target organism, but integrated management, albeit requiring greater farmer skills, can prevent that. Given proper R, D, and extension, the potential impact of herbicide-tolerant cultivars on FY in labor-limited African cropping is likely substantial. Of course, all breeding solutions to aid gap closing presuppose an effective seed production and distribution system. Systems are gradually improving in developing countries and most commercial farmers grow improved varieties although the rate of turnover of varieties is often too slow. There is little doubt that wherever plant breeding is privatized, competition drives quicker variety turnover; in advanced systems, it also drives significant agronomic extension by the breeding firms keen to maximize variety by management interactions and to retain clients.

Lifting Potential Yield

Although separated by a yield gap and a time lag, many situations show a close relationship between progress in PY and that in FY, as new technologies eventually find their way to farmers. Often the process is facilitated by new varieties linked to agronomic advances, for new varieties are fairly quickly adopted in most commercial farming. Sometimes, the PY advances owe more to innovative farmers than to researchers, as for example, when farmers moved to earlier planting permitted by direct seeding in southern Australia. In all cases, increase in PY is an important component driving increased FY, inevitably so where the yield gap is approaching the economic minimum (e.g., wheat in the UK), but less so where it is large (e.g., paddy or rainfed rice in India), and even less when the gap is huge (e.g., maize in sub-Saharan Africa).

Current rates of PY progress were summarized for the key cereals in [5]. These numbers come from breeders' and researchers' trials containing varieties of different vintage grown under modern agronomic management with little or no biotic stress; thus, the rates capture as well the positive interactions between new varieties and modern management. Linear regression is used to calculate the absolute rate of progress which is then expressed as a percentage of most recent predicted PY in the series, hopefully a recently released variety (>2006) but such data is not always available. For wheat, progress ranged from 0.3% to 1% p.a. with an average of 0.6% ($n = 6$) and with little difference between water-unlimited and water-limited PY progress (see also Figs. 1 and 5). For rice, the range was 0.2–0.7% (average of 0.4%, $n = 4$). Progress in PY at the International Rice Research Institute (IRRI) is disappointing, at close to zero; however, there is a one-off yield jump of 10–15% through the recent exploitation

of F1 hybrids feeding into the tropical rice regions, and following upon on a similar gain in China over the last 20 years as hybrids moved to >50% of their acreage. For maize, there is only one estimate in [5], coming from Iowa and showing 1%. Data of Luque et al. [32] in a somewhat similar environment in Argentina give a rather similar number for hybrids released up to 1997 (1.3%), but since then PY progress may have slowed (M. Otegui, 2009, personal communication). A subsequent report from Iowa with hybrids of a rival company showed progress at 1.7% but the breeding period sampled was only 2001–2006 [8]. In an irrigated favorable Mediterranean environment, data presented by Campos et al. [33] indicate PY progress in the Iowa Pioneer hybrids of 1% (but interestingly progress in PYw of 1.5% under artificial severe mid-season water stress). PY progress in cereals is discussed in more detail in [9]. Potential yield for soybeans in the USA appears to be progressing at 0.7% p.a. (R. A. Fischer, 2010, unpublished).

From the above, it is apparent that even in advanced situations with substantial breeding investment, potential yield progress from this source is currently at or well below 1%, with maize showing more progress than other major crops. Such PY progress is unlikely alone to drive FY progress at the rates needed. Prospects of lifting this rate of PY progress were now discussed briefly.

New Yield-Positive Agronomic Techniques

Improved agronomy has played a large if not dominant role in past yield increase (e.g., increased fertilizer use, better weed control, better seeding techniques for earlier seeding and more reliable crop stands, and water conserving reduced tillage), and most improvements have interacted positively with variety improvement (e.g., [20]). While many authors have consistently failed to anticipate agronomic advances in the past [34], currently it is hard to see any new ones raising PY or PYw (as distinct from advances specifically targeting improved input efficiency). One example might be improved seasonal forecasts which would permit the farmer to better tailor management and variety to expected weather, something currently limited by the low skill of forecasts. Another, which would clearly lift PYw, would be the reduction of soil evaporation with inexpensive plastic films (e.g., spray-applied nanofilms), copying a common practice seen in northwest China field crops, but designed so as not to contaminate the environment. Also it is possible advances can still come from better management of soil–root–microbe interactions, a complex and neglected area of research: poorly explained observations of "yield decline" and "break crop effects" point in this direction, as do reports of positive effects of increased soil organic matter (independent of nutrition), controlled traffic and reduced soil compaction.

Greater Investment in Current Conventional Breeding Efforts for Yield

Yield improvement through plant breeding is generally regarded as delivering benefits far in excess of the costs [35, 36]. Nevertheless, it has been suggested that returns from the investment in breeding personnel are diminishing, for example in maize, and that yield gains are getting harder to achieve [37]. This is occurring despite greater efficiency through computerization, advanced biometrics, mechanization, robotics, and techniques for rapid generation advance, all part of any conventional breeding today. What is quite unclear however is the marginal return on investment in conventional breeding; for example, what would happen if the number of breeders, and of crosses, selections, and yield trials, were increased say 50% in any currently substantial program? In crops where breeders are devoting many resources to maintaining disease resistance (e.g., wheat) or eating quality (e.g., wheat, rice), and thus unable to give full attention to yield, PY progress is likely to increase, although probably less proportionally that the proportional investment increase. A related question is whether any extra funds would be better spent on new breeding tools.

New Tools to Increase Progress in Conventional Breeding

Genetic variation is the basis of yield progress. It is unlikely that all or even the major part of the existing genetic variation has been utilized in any crop. Sampling germplasm collections is a formidable task, but new tools are becoming available for seeking out new and useful variation, such as the Focused Identification of Germplasm Strategy (FIGS, [39]) and Ecotilling [38]. Because of the low chance of success, this work

tends to be in the area of publically funded prebreeding, with only medium to long-term impacts on breeding, but it is worth noting that the steady reduction in genome sequencing costs is also opening up new ways of allele searching [40].

Both parental and especially early generation selection can benefit from the use of low cost performance-related markers. For the last 50 years or so, physiologists have attempted to identify such markers or traits, physiological or morphological, or even whole ideotypes, which would lead to greater yield. There have been some successes, for example, the first high-yielding semidwarf tropical rice variety, IR8, resulted from the pursuit of a specific ideotype [41], and breeding for resistance to some toxicities is usually based on early generation physiological screening (e.g., aluminum tolerance). However, indirect selection for both PYw and especially for PY has proved challenging, and much physiology has been restricted to the retrospective identification and understanding of traits which have changed as direct selection has increased yield. A good example are the many traits that have been found to change as maize yields increased in North America under direct selection for yield, lodging resistance, dry down, and disease resistance alone [37, 42]. As understanding of yield determination improves, including the recognition that seemingly useful traits can carry trade-offs, and as measurements of many traits become cheaper, especially through the use of remote sensing in the field, the possibilities for physiological traits have improved. At CIMMYT, maize breeding for drought (PYw) has definitely benefitted from the inclusion of physiological traits such as anthesis to silking interval in managed drought environments [43]. More recently, with wheat there has been testing of canopy temperature as an early generation selection criterion, a surrogate for stomatal conductance and possibly photosynthetic rate under irrigation, or possibly for rooting depth under drought; it shows promise under both conditions [44], as does multispectral canopy reflectance under irrigation [45]. In CSIRO, Australia, ideotrait selection for greater PYw has been under way for several decades, with focus on traits such as water use efficiency via carbon isotope discrimination, coleoptiles length, low tillering, and high stem carbohydrate content at flowering, with moderate success [46]. Very recent research points to genetic differences in wheat for grain set under drought and ways for screening this trait which is likely to be a significant bottleneck in PYw determination [47].

While physiology may be beginning to look more useful in early generation yield selection, it is now being challenged by the rapidly growing use of molecular markers for traits, initially qualitative ones but lately also quantitative traits, including yield itself. The huge decline in cost of detecting molecular markers, and their increasing density across crop genomes is driving this. Heffner et al. [48] review the possibilities of such marker-based genome selection in crops. Earthington et al. [49] describe in some detail the extent to which molecular markers are being incorporated into the Monsanto crop breeding programs: rates of progress in multiple trait indices (e.g., including yield, grain moisture, standability, and test weight for maize) can be doubled; indeed, for these authors marker-aided selection is the "new" conventional breeding. These approaches presume accurate phenotyping of genotypes for yield and its interactions with target environments, a challenge in all breeding. However, it is interesting that physiology hardly features in this new scenario, although other groups are busily mapping putatively useful physiological traits at the molecular level (e.g., [50, 51]). It remains to be seen whether physiological traits, either observed directly or identified by accurate markers, will have a place in marker-aided yield breeding, but it is possible some combination of markers and early generation trait phenotyping using smart remote sensing will prove an even more efficient strategy for PY advance. In addition physiology, just like plant pathology, will continue to identify individual traits whose incorporation into leading varieties may lift PY or PYw, a process which could benefit from the use of molecular trait markers, just as is becoming the case with new hard-to-screen host plant disease resistance genes.

Multilocation multiple-year yield testing remains the essential final step in all plant breeding for yield; testing under different management regimes (plant density, planting date, soil stored water) is also recognized as increasingly important. Crop simulation models are now good enough to help breeders understand the environmental and sometimes the genetic bases of the interactions encountered, and thus deploy the testing more efficiently, and more efficiently indentify the genotypes best suited to major

environment × management combinations. An excellent example is the analyses of multiple environment rainfed trials of sorghum in Queeensland [52].

Genetic Engineering for Yield

There are many claims of engineered traits that may increase crop yield, but very few of these have been backed up by yield measurements in the field. Crop physiologists have regularly pointed out how different is the performance of a genotype growing in a pot in the glass house from that of one at normal plant density in the field environment [53, 54]. For this reason, they remain skeptical of the value of these claims and await with much interest the results of field tests, for, to date, it appears that only a handful of papers describe performance in proper field tests. In an excellent example, wheat transformed with a more active ADP glucose pyrophosphorylase in the grain to increase grain sink strength and grain size, was thoroughly field tested, but there was no yield benefit [55]. More recently, Monsanto has reported increased PYw in field plots with maize transformed with two separate events [56, 57]; results in the latter case point to modest PYw increases and no change in PY, but the nature of the drought and of the crop physiological responses are not well described. More experimental data is needed before much confidence can be placed in this event, or in engineering for yield in general, for both genetic and physiological understanding of yield determination indicates that many processes are involved, and that the impact of any single transformation is likely to be small even if key regulatory genes or bottleneck processes are targeted. Indeed, it is now being recognized that if functional genomics is to have a significant impact on yield through engineering yield processes, it must pay more attention to the relevant plant and crop physiology connecting gene action to field performance [58]; even the current fashion for automated phenotyping in controlled facilities must be balanced by substantial investment in phenotyping in field plots in managed environments.

Some Tentative Conclusions on Future Potential Yield Progress

As PY increases, relative rates of PY progress are decreasing; this is probably more than the consequence of a linear rate of progress relative to a rising denominator, and may, in situations where the breeding investment is large (e.g., maize in North America, wheat in the UK and the rest of Western Europe), also reflect diminishing returns as biological limits are approached. Theoretical limits to harvest index are already being reached, but those to radiation use efficiency appear well above current measured values [59]. There have been a couple of attempts to project PY into the future. For example, Sylvester-Bradley et al. [60] propose that a longer period of light capture and a higher radiation use efficiency could lift PY of winter wheat in the UK to 17.4 t/ha by 2050, a linear rate of progress of 167 kg/ha/year, or two and half times the current rate of progress seen in Fig. 1. Taking a different tack, Monsanto has predicted a doubling of US maize yield between 2000 and 2030, based on equal contributions from conventional breeding, marker-aided selection, and genetic engineering, and amounting to a linear annual rate of progress which is 3.3% of today's yields. Physiological theory and commercial optimism both, however, have their limitations. Looking more cautiously at the ways of impacting PY progress outlined above, it is concluded that breeding progress will dominate in the future, that conventional breeding, including the exploitation of heterosis, will continue to deliver small but declining gains, while new approaches may boost gains enough to maintain current rates of linear PY progress at between 0.5% and 1%, other things such as climate remaining equal (note that given the way PY is defined here, this progress is independent of any direct effect of atmospheric CO_2 increase). Observers expect the investment in the relevant R and D to remain large, as the private sector involvement increases to balance a declining public sector, and many argue that it should grow further, although the marginal rate of return is not well known.

Future Directions and Synthesis

The key issue for future food security is the real grain price needed to balance burgeoning demand against increasing supply. World food production demand and supply to 2050 have recently been projected by Hubert et al. [61] with the IFPRI Impact model, and by Tweetin and Thompson [62]. Thus, the baseline case of the former paper projects a 56% increase in cereal

production over 2000, accompanied by substantial real price increases over the 2000 base, with negative effects on malnutrition. Demand growth is greater for maize and least for rice, such that the projected real price increases over 2000 are maize (97%), wheat (90%), and rice (60%). Clearly, a 56% increase in production is not enough. For Tweetin and Thompson [62], cereal supply rises somewhat more, by around 75% in 2050, but real prices still increase (on average 44%). The IFPRI projections allow for biofuel demand (peaking in the late 2020s at 16% of total maize consumption, after which second-generation biomass biofuel takes over), rising energy costs and likely restrictions on irrigation water supply. They also point to a much greater increase in grain demand in the first 25 years (1.4% pa) than in the second 25 years (0.4%), clearly placing more pressure on short- to medium-term yield progress. The IFPRI model contains crop area as a variable but, given the cost of developing new lands and its scarcity, this only increases significantly if prices more than double under a very low yield progress scenario.

In the IFPRI baseline projection, yield grows to meet demand at around 1% exponential projected over the whole period. In [62], it is expected to grow linearly at a rate equivalent to 1.4% of current yields. These rates compare to the current rates of world yield growth, which are wheat and rice (0.9%), maize (1.6%), and soybeans (1.1%), but it must be recalled that the actual rates all appear to be linear, not exponential, and that the projected rates in neither of the models are enough to hold real prices steady at 2000 levels. In addition, the elasticity of demand is such that a supply shortfall due to below baseline yield growth would be disastrous (as we saw 2 years ago although some other factors added to the sharp doubling of prices then): the projections in [61] suggest a 40% fall in yield growth below baseline (to 0.6% exponential) would lift 2050 real cereal prices to more than 200% above 2000 real prices!! Alternatively, 1.4% yield growth would mean continuing declines in real grain prices.

These numbers highlight the importance of yield growth that has been the subject of this entry and reveal that current FY growth rates are inadequate to hold real prices down. Since PY growth can contribute to FY growth everywhere, and is the only source of growth in advanced agricultural systems where FY is approaching PY, it assumes great underlying importance, even as current rates of growth, except possibly for maize, seem to be well below 1% and gradually falling as a percentage of yield. Unfortunately, the brief examination here suggests that the prospects of boosting PY growth, largely now relying on plant breeding, are small, or at least rather uncertain, especially in the short to medium term when yield increases are most critical. Much will depend on whether the molecular marker-aided yield selection can boost rates, for example, double them, as claimed by some; genetic engineering seems unlikely to lift PY in the short to medium term, although the prospects to lift PYw may be somewhat better if water stress-related yield bottlenecks can be relieved. And none of these projections have factored in the possible negative effects of climate change.

As a consequence of the above, yield gap closing assumes great importance for future world food security, especially as there still appear to be large exploitable gaps (>50%) in many situations, and as the way forward is clearer. There are few uncertainties regarding what needs to change at the farm level, but less optimism regarding how to achieve this quickly enough and from where the necessary resources will come. The biggest gaps are associated with small farmers in the developing world, and there is little doubt that strategies to help these farmers will have the greatest benefits for alleviating poverty and food insecurity. And note that the association between large yield gaps and small farmers is not an inevitable association, as can be seen among small holders in Egypt or parts of eastern China. This entry has emphasized that improvements in rural infrastructure and institutions are critical, but that breeding and agronomic research also has a role to play in gap closing, as is illustrated by the impact of simple direct seeding machinery and earlier sowing on wheat yields in the Indo-Gangetic Plains or of Bt cotton with Indian small holders. It is a great pity, however, that the types of on-farm adaptive research and development needed for gap closing in such situations are often thwarted by policy inertia toward agriculture in general, and poor rewards by science funders in particular, although the situation may be gradually improving. In developed countries, new paradigms seem to be emerging in which private sector companies, especially breeding and seed companies, invest not only in

developing better varieties but also in applied agronomic research linked to variety development and promotion, and this may account for some of the gap closing in the USA and Western Europe. In addition, and especially in Australia and the southern cone of South America, privately hired agronomists are assuming a critical role in yield gap closing and are rewarded accordingly. Taken overall such changes auger well for ongoing yield gap closing, even in the short to medium term, in the developed world, but their impact at the farm level in developing countries, and that of more traditional approaches, will remain limited by infrastructure and institutional constraints in the near to medium-term future. The cautious optimism expressed a decade ago by leading agricultural scientist Evans [4] regarding world food security may well be overly optimistic.

Bibliography

1. Evans LT, Fischer RA (1999) Yield potential: its definition, measurement and significance. Crop Sci 34:1544–1551
2. Passioura JB, Angus JF (2010) Improving productivity of crops in water limited environments. Adv Agron 106:37–75
3. Badawi AT (1998) Sustainability of rice production in Egypt, IRC 98/7-2. Cairo, Egypt
4. Evans LT (1998) Feeding the ten billion: plants and population growth. Cambridge University Press, Cambridge
5. Fischer RA, Byerlee D, Edmeades GO (2009) Can technology deliver on the yield change to 2050? Paper prepared for expert meeting on "How to Feed the World in 2050", FAO, Rome,24–26 June 2009. (www.fao.org/wsfs/forum2050/wsfs-background-documents/wsfs-expert-papers/en/)
6. Mackay I, Horwell S, Garner J, White J, McKee J, Philpott H (2010) Re-analysis of the historical series of UK variety trials to quantify the contributions of genetic and environmental factors to trends and variability in yield over time. Theor Appl Genet 121 (in press)
7. Hammer GL, Dong Z, McLean G, Doherty A, Messina C, Schussler J, Zinselmeier C, Paszkiewicz S, Cooper M (2009) Can changes in canopy and/or root system architecture explain historical maize yield trends in the U.S. Corn Belt? Crop Sci 49:299–312
8. Edgerton MD (2009) Increasing crop productivity to meet global needs for feed, food and fuel. Plant Physiol 149:7–13
9. Fischer RA, Edmeades GO (2010) Breeding and cereal yield progress. Crop Sci 50:S-85–S-98
10. Bhatia VS, Singh P, Wani SP, Chauhan GS, Rao AVRK, Misra AK, Sirinuas K (2008) Analysis of potential yields and yield gaps of rainfed soybean in India using CROPGRO-Soybean model. Agric Forest Meteorol 148:1252–1265
11. Murty MVR, Singh P, Wani SP, Khairwal IS, Srinivas K (2007) Yield gap analysis of sorghum and pearl millet in India using simulation modeling. J SAT Agric Res 5:1–85
12. Lobell DB, Cassman KG, Field CB (2009) Crop yield gaps: their importance, magnitudes, and causes. Annu Rev Environ Resour 34:4.1–4.26
13. Titonell P, Shepherd KD, Vanlauwe B, Giller KE (2008) Unravelling the effects of soil and crop management on maize productivity in smallholder agricultural systems of western Kenya – an application of classification and regression tree analysis. Agric Ecosyst Environ 123:137–150
14. Byerlee D (1992) Technical change, productivity, and sustainability in irrigated cropping systems of South Asia: Emerging issues in the post-green revolution Era. J Int Dev 4:477–496
15. Marsh SP, Pannell DJ, Lindner RK (2000) The impact of agricultural extension on adoption and diffusion of lupins as a new crop in western Australia. Aust J Exp Agric 40:571–583
16. Llewellyn RS, D'Emden FH (2009) Adoption of no-till cropping practices in Australian grain growing regions. Report to GRDC, Canberra
17. Byerlee D, Moya P (1993) Impacts of international wheat breeding research in the developing world, 1966–90. D.F. CIMMYT, Mexico
18. Morris M, Kelly VA, Kopicki RJ, Byerlee D (2007) Fertilizer use in African agriculture, Lessons learned and good practice guide. The World Bank, Washington
19. de Wit CT (1992) Resource use efficiency in agriculture. Agric Syst 40:125–131
20. Fischer RA (2009) Farming systems in Australia: exploiting the synergy between genetic improvement and agronomy. In: Sadras V, Calderini D (eds) Crop physiology: applications for genetic improvement and agronomy. Elsevier, Amsterdam, pp 23–54
21. Paroda RS (2004) Scaling up: how to reach a billion resource-poor farmers in developing countries. Plenary paper, 4th international crop science congress, Brisbane. (www.cropscience.org.au/icsc2004/plenary/4/223_paroda.htm)
22. Dobermann A, Witt C, Dawe D, Abdulrachman S, Gines HC, Nagarajan R, Satawathananont S, Son TT, Wang GH, Chien NV, Thoa VTK, Phung CV, Stalin P, Muthukrishnan P, Ravi V, Babu M, Chatuporn S, Sookthongsa J, Sun Q, Fu R, Simbahan GC, Adviento MAA (2002) Site-specific nutrient management for intensive rice cropping in Asia. Field Crops Res 74:37–66
23. Dobermann A, Mackill D (2008) Investment returns opportunities in rainfed/irrigated environments of South Asia. Unpublished discussion paper, IRRI, The Philippines, p 7
24. Lobell DB, Asner GP, Ortiz-Monasterio JI, Benning TL (2003) Remote sensing of regional crop production in the Yaqui Valley, Mexico: estimates and uncertainties. Agric Ecosyst Env 94:205–220
25. Ortiz-Monasterio JI, Lobell DB (2007) Remote sensing assessment of yield losses due to sub-optimal planting dates and fallow period weed management. Field Crops Res 101:80–87
26. Lobell DB, Ortiz-Monasterio JI, Asner GP, Naylor RL, Falcon WP (2005) Combining field surveys, remote sensing, and

regression trees to understand yield variations in an irrigated wheat landscape. Agron J 97:241–249
27. Grassini P, Hall AJ, Mercau J (2009) Benchmarking sunflower water productivity in semiarid environments. Field Crops Res 110:251–262
28. Hochman Z, Holzworth D, Hunt JR (2009) Potential to improve on-farm wheat yield and WUE in Australia. Crop Pasture Sci 60:708–716
29. Ekboir J (ed) (2002) CIMMYT 2000–2001 World wheat overview and outlook: developing no-till packages for small-scale farmers. D.F. CIMMYT, Mexico
30. Oerke EC (2006) Crop losses to pests. J Agric Sci 144:31–43
31. James C (2008) Global Status of Commercialized Biotech/GM Crops: 2008. ISAAA brief no. 39. ISAAA, Ithaca
32. Luque SF, Cirilo AG, Otegui ME (2006) Genetic gains in grain yield and related physiological attributes in Argentine maize hybrids. Field Crops Res 95:383–397
33. Campos H, Cooper M, Habben JE, Edmeades GO, Schussler JR (2004) Improving drought tolerance in maize: a view from industry. Field Crops Res 90:19–34
34. Evans LT (1993) Crop evolution, adaptation and yield. Cambridge University Press, Melbourne
35. Evenson RE, Gollin D (eds) (2003) Crop variety improvement and its effect on productivity: the impact of international agricultural research. CAB International, Wallingford
36. Byerlee D, Dubin HJ (2010) Crop improvement in the CGIAR as a global success story of open access and international collaboration. Int J Common 4:452–480
37. Duvick DN (2005) The contribution of breeding to yield advances in maize (*Zea mays* L.). Adv Agron 86:83–145
38. Comai L, Young K, Till BJ, Reynolds SH, Greene EA, Codomo CA, Enns LC, Johnson JE, Burtner C, Odden AR, Henikoff S (2004) Efficient discovery of DNA polymorphisms in natural populations by Ecotilling. Plant J 37:778–786
39. Bhullar NK, Street K, Mackay M, Yahiaoui N, Keller B (2009) Unlocking wheat genetic resources for the molecular identification of previously undescribed functional alleles at the Pm3 resistance locus. Proc Natl Acad Sci USA 106:9519–9524
40. Phillips R (2010) Mobilizing science to break yield barriers. Crop Sci 50:S-99–S-108
41. Jennings PR (1964) Plant type as a rice breeding objective. Crop Sci 4:13–15
42. Tollenaar M, Lee EA (2006) Dissection of physiological processes underlying grain yield in maize by examining genetic improvement and heterosis. Maydica 51:399–408
43. Edmeades GO, Bolaños J, Elings A, Ribaut J-M, Bänziger M, Westgate ME (2000) The role and regulation of the anthesis-silking interval in maize. In: Westgate ME, Boote KJ (eds) Physiology and modeling kernel set in Maize. Crop Science Society of America special publication no. 29. CSSA, Madison, pp 43–73
44. Brennan JP, Condon AG, Van Ginkel M, Reynolds MP (2007) An economic assessment of the use of physiological selection for stomatal aperture-related traits in the CIMMYT wheat breeding programme. J Agric Sci 145:187–194
45. Babar B, Reynolds MP, Van Ginkel M, Klatt AR, Raun WR, Stone ML (2006) Spectral reflectance to estimate genetic variation for in-season biomass, leaf chlorophyll, and canopy temperature in wheat. Crop Sci 46:1046–1057
46. Richards RA (2004) Physiological traits used in the breeding of new cultivars for water-scarce environments. In: Proceedings of the 4th international crop science congress, Brisbane. (www.cropscience.org.au/ICSC2004/symposia/1/3/1470_richardsr.htm)
47. Ji X, Shiran B, Wan J, Lewis DC, Jenkins CLD, Condon AG, Richards RA, Dolferus R (2010) Importance of pre-anthesis anther sink strength for maintenance of grain number during reproductive stage water stress in wheat. Plant Cell Environ 33(6):926–942
48. Heffner EL, Sorrells ME, Jannick J-L (2009) Genomic selection for crop improvement. Crop Sci 49:1–12
49. Eathington SR, Crosbie TM, Edwards MD, Reiter RS, Bull JK (2007) Molecular markers in a commercial breeding program. Crop Sci 47(S3):S154–S163
50. Rebetzke GJ, van Herwaarden AF, Jenkins C, Weiss M, Lewis D, Ruuska S, Tabe L, Fettell NA, Richards RA (2008) Quantitative trait loci for water-soluble carbohydrates and association with agronomic traits in wheat. Aust J Agric Res 59:891–905
51. Reynold M, Tuberosa R (2008) Translational research impacting on crop productivity in drought-prone environments. Curr Opin Plant Biol 11:171–179
52. Chapman SC, Cooper M, Hammer GL (2002) Using crop simulation to generate genotype by environment interaction effects for sorghum in water-limited environments. Aust J Agric Res 53:379–389
53. Sinclair TR, Purcell LC (2005) Is a physiological perspective relevant in a "genocentric" age? J Exp Bot 56:2777–2782
54. Fischer RA (2008) Improvements in wheat yield: Farrer, physiology and functional genomics. Agric Sci NS 1/08:6–18
55. Meyer FD, Talbert LE, Martin JM, Lanning SP, Greene TW, Giroux MJ (2007) Field evaluation of transgenic wheat expressing a modified ADP-glucose pyrophosphorylase large subunit. Crop Sci 47:336–347
56. Nelson DE, Repetti PP, Adams TR, Creelman RA, Wu J, Warner DC, Anstron DC, Benson RJ, Castiglioni PP, Donnarummo MG, Hinchley BS, Kumimoto RW, Maszle DR, Canales RD, Krolikowski KA, Dotson SB, Gutterson N, Ratcliffe OJ, Heard JE (2007) Plant nuclear factor Y(NF-Y) B subunits confer drought tolerance and lead to improved corn yields on water-limited acres. Proc Natl Acad Sci USA 104:16450–16455
57. Castiglioni P, Warner D, Bensen RJ, Anstrom DC, Harrison J, Stoecker M, Abad M, Kumar G, Salvador S, D'Ordine R, Navarro S, Back S, Fernandes M, Targolli J, Dasgupta S, Bonin C, Luethy M, Heard JE (2008) Bacterial RNA chaperones confer abiotic stress tolerance in plants and improved grain yield in maize under water-limited conditions. Plant Physiol 147:446–455
58. Spiertz JHJ, Struik PC, van Laar HH (eds) (2007) Scale and complexity in plant systems research: gene-plant-crop relations. Proc Frontis Workshop, Wageningen, The Netherlands, April 24–26, 2006. Springer-Verlag, New York

59. Zhu X-G, Long SP, Ort DR (2008) What is the maximum efficiency with which photosynthesis can convert solar energy into biomass? Curr Opin Biotech 19:153–159
60. Sylvester-Bradley R, Foulkes J, Reynolds M (2005) Future wheat yields: evidence, theory and conjecture. In Sylvester-Bradley R, Wiseman J (eds) Proc 61st Easter School in Agricultural Sciences. Yield of farmed species. Nottingham University Press, pp 233–260
61. Hubert B, Rosegrant MW, van Boekel MAJS, Ortiz R (2010) The future of food: scenarios for 2050. Crop Sci 50:S33–S50
62. Tweeten L, Thompson SR (2008) Long-term agricultural output supply-demand balance and real farm and food prices. Working paper AEDE-WP 0044-08, Ohio State University

Cropping Systems: Shaping Nature

Rafael J. López-Bellido, Luis López-Bellido
Departamento de Ciencias y Recursos Agrícolas y Forestales, University of Córdoba, Córdoba, Spain

Article Outline

Glossary
Definition of the Subject
Introduction
Components and Design
Anthropological View
Agricultural Practices' Footprint
Praise of Agricultural Science
Eradication of Fallow, Tillage, and Monoculture
Biological Synergism and Technical Synchronization
Dynamic Cropping Systems
Future Challenges
Bibliography

Glossary

Agriculture Agriculture and farming are often considered to be the same concept. However, both concepts can vary in their territorial scope of application. Agriculture is the production of food and goods through farming and forestry. Agriculture encompasses a wide variety of specialties and techniques. For this reason, its definition has developed to become: The science, art, and business of cultivating soil, producing crops, and raising livestock. The major agricultural products can be broadly grouped into foods, fibers, and raw materials. As of late, agriculture also uses plants to produce biofuels, biopharmaceuticals, and bioplastics.

Agricultural practices Agricultural practices are a set of techniques applied to on-farm production and postproduction processes, resulting in food and nonfood agricultural products.

Agronomic crops Agronomic crops typically involve a crop that is grown for grain, feed, or for processing into oil, starch, protein, or flour. Major agronomic crops include corn (grown for feed, ethanol, or processing), soybeans, wheat, hay (alfalfa and legume and grass mixtures), rice, peanuts, and cotton. Hay is also considered forage [1].

Agroecosystem An agricultural system or agricultural ecosystem is the basic unit of study for an agroecologist. This term is somewhat arbitrarily defined as a spatially and functionally coherent unit of agricultural activity, and includes the living and nonliving components involved in the unit as well as their interactions. An agroecosystem can be viewed as a subset of a conventional ecosystem. As the name implies, at the core of an agroecosystem lies the human activity of agriculture. However, an agroecosystem is not restricted to the immediate site of agricultural activity (e.g., the farm), but rather includes the region that is impacted by this activity, usually by changes to the complexity of species assemblages and energy flows, as well as to the net nutrient balance.

Agronomy The science which establishes the theory and practice of crop production and soil management [1].

Ecosystem A functioning community of nature that includes fauna and flora together with the chemical and physical environment with which they interact. Ecosystems vary greatly in size and characteristics, and can be a mud puddle, a field, or orchard, or a forest. An ecosystem provides a unit of biological study and can be a unit of management [2].

Environment The totality of the surrounding external conditions (biological, chemical, and physical) within which an organism, community, or object exists. The environment can be defined at any scale. The term is not exclusive in that organisms can be and usually are part of another organism's environment. Thus, one can speak of the environment as

that within which humankind lives (i.e., separate and external) or, of humankind as a component of the environment [2].

Definition of the Subject

Cropping system (CS) is a general term that describes how a producer or farmer might grow a crop [2]. Pragmatically, CSs effectively address the *what to grow*, *when to grow it*, and *how to grow it* considerations of crop production in the context of optimizing multiple goals [3]. A CS must bring together the biological, technical, economic, and sociological aspects of the land area farmed [4]. Therefore, a CS is a set of agronomic or agricultural practices used in a crop under specific conditions. The CS generates an agroecosystem, agri-environment, or agricultural system. Common synonyms of CS include crop management system, crop production system, farming system, crop production practices, etc. For example, a farming system is defined as a population of individual farm systems that have broadly similar resource bases, enterprise patterns, household livelihoods, and constraints, and for which similar development strategies and interventions would be appropriate [5].

The classification of CSs has been based on the following criteria: available natural resource base, including water, land, grazing areas, and forest; climate, of which altitude is one important determinant; landscape, including slope; farm size, tenure and organization; dominant pattern of farm activities and household livelihoods, including field crops, livestock, trees, aquaculture, hunting and gathering, processing and off-farm activities; and taking into account the main technologies used, which determine the intensity of production and integration of crops, livestock, and other activities [5]. Multiple cropping, in which several crops are grown sequentially in 1 year, and intercropping, when several crops are grown at the same time, are other kinds of annual CSs known as polycultures [6].

In general, each and every agronomic practice used in a CS affects different aspects of the system, i.e., the tillage system prepares the seedbed but affects the availability of water and nutrients, carbon cycle, erosion, diseases, etc. The use of the term CS is often applied to a rotation (wheat-fallow CS), tillage system (no-tillage CS), method of fertilization (organic CS), or agroecosystem (semiarid CSs) to simplify the designation of the CSs. However, it is important to note that a CS involves much more than a rotation, tillage system, fertilization method, or climatic conditions.

Introduction

Since the dawn of settled agriculture about 10 millennia ago, human beings have integrated different agronomic practices for application to selected plants (crops), and as a result generated CSs that transformed the natural ecosystem into agroecosystems. Agricultural practices such as genotype selection, crop rotation, natural fertilizers, irrigation, etc., were developed long ago, but have made great strides in the past century. The history of agriculture has played a major role in human history as agricultural progress has been a crucial factor in worldwide socioeconomic change. When human beings began to produce food beyond their needs, others activities began to take place. It is this agricultural surplus that made the development of civilization possible. A crucial time in the history of agricultural began with the discovery of America. A global exchange of previously local crops and livestock breeds occurred. Key crops involved in this exchange from the New World to the Old included the tomato, maize, potato, manioc, cocoa bean, and tobacco, with several varieties of wheat, spices, coffee, and sugar cane going from the Old World to the New. With the rapid rise of mechanization in the early twentieth century, particularly in the form of the tractor, farming tasks could be accomplished with a speed and on a scale previously impossible. Also during this period, the Haber–Bosch method for synthesizing ammonium nitrate represented a major breakthrough. Synthetic nitrogen, along with mined rock phosphate, pesticides, and mechanization, allowed crop yields to overcome previous constraints. Furthermore, global yield increases were experienced later in the twentieth century when high yield varieties of wheat, corn, and rice were introduced as a part of the Green Revolution. The Green Revolution exported technologies (including pesticides and synthetic nitrogen) from the developed world to the developing world. However, concerns have been raised over the sustainability of intensive agriculture. Intensive agriculture has become associated with

decreased soil quality, and there has been increased concern over the effects of fertilizers and pesticides on the environment, particularly as the population increases and food demand expands.

As a result, in the past few decades, a move toward sustainability in agriculture has also developed, integrating ideas of socioeconomic justice and conservation of resources and the environment within an agricultural system [7, 8]. Sustainable agriculture is defined as practices that meet current and future societal needs for food and fiber, for ecosystem services, and for healthy lives, and that do so by maximizing the net benefit to society when all costs and benefits of the practices are considered. If society is to maximize the net benefits of agriculture, there must be a fuller accounting of both the costs and the benefits of alternative agricultural practices, and such an accounting must become the basis of policy, ethics, and action. Additionally, the development of sustainable agriculture must accompany advances in the sustainability of energy use, manufacturing, transportation, and other economic sectors that also have significant environmental impacts [9]. Sustainable agriculture has renewed research in alternative technologies such as no-tillage, integrated pest management, etc. Recent mainstream technological developments include genetically modified (GM) crops. Also, agriculture has needed – and still needs – subsidies from many governments to ensure an adequate food supply and its competitivity in global markets. However, at times, these subsidies, especially when instituted by developed countries, have been noted as protectionist, inefficient, and environmentally damaging [10].

This chapter is not an overview of a subject as complex and broad as worldwide CSs, where oversights are inevitable. It must first be pointed out that about 85% of the Earth's cultivated land is planted with annual crops [11], and thus the principle CSs are used in herbaceous plants. Of these, wheat, rice, and maize provide more than 60% of human dietary calories, either as cereals for direct human consumption or embodied in livestock products produced from animals fed with feed grains and their by-products [9, 12]. Moreover, it is likely that these same cereal crops will continue to account for the bulk of future human food supply because they produce greater yields of human-edible food, are easily grown, stored, and transported, and require less fuel and labor for processing and cooking than other food crops [12]. Given their importance, this chapter focuses primarily on these crops, but also provides a general view that can be applied to any CS. The chapter starts off with a brief description of CS components and factors that must be taken into consideration during their design (*Components and Design*). To provide a new focus on defining CSs, and as a result agroecosystems, an anthropological view of a CS is then provided (*Anthropological View*). Following, the most important effects of these "human ecosystems" on the environment are reviewed (*Agricultural Practices' Footprint*). At this point, the chapter goes on to analyze the achievements of agricultural research and their importance to man (*Praise of Agricultural Science*). From here, agricultural practices that were unsuccessful in CSs and which must be urgently eliminated are studied (*Eradication of Fallow, Tillage, and Monoculture*). Afterward, the basic principles on which current and future CSs should be inspired are discussed. In fact, the application of these principles to a certain degree involves returning to techniques from the past, based on monitoring technologies of the future (*Biological Synergism and Technical Synchronization*). The application of these principles logically leads to what are called *Dynamic Cropping Systems*, which shift away from the application of a series of rigid agricultural practices to the agroecosystem at each growth stage. Finally, the chapter tackles the *Future Challenges* for CSs in the twenty-first century.

Components and Design

All agroecosystems generated by a CS break away from "natural" ecosystems, and the main effects are the loss of biodiversity and the export of resources. This causes environmental imbalance which means more or less of a struggle, depending on the intensity of the CS, to stabilize it. The more distant it is from a "natural" stable ecosystem, the more inputs are required by the CS as the result of a greater imbalance. In fact, one of the greatest concerns caused by agriculture, which has been a problem from the beginning due to the selection of few species, is the lack of biodiversity in many CSs. Advocates of diversification argue that it provides greater income stability [2].

Many CSs throughout the world are characterized by variable climate and soils, resulting in a high-risk condition for agricultural producers due to extreme variability in precipitation and seasonal temperatures [13]. In other words, crop production occurs in an environment that is always changing. With every growing season, producers must attend to numerous factors that influence their management decisions. Cropping systems vary among farms depending on the available resources and constraints; geography and climate of the farm; government policy; economic, social, and political pressures; and the philosophy and culture of the farmer [5, 6]. This is a daunting challenge, especially when one considers that producers' decisions are carried out in a financial environment of diminishing economic returns, where one wrong decision could mean financial hardship and potentially the end to a way of life [14].

A CS involves numerous interactive factors that may limit or facilitate crop production. The factors can be divided into the following groups [14]: (1) biophysical environment: weather/climate and soil; (2) socioeconomic externalities: market conditions and government programs; and (3) available technology. These three factors affect or guide the agricultural practices of the CS (crop election, rotation, tillage system, planting date, fertilization, crop protection, etc.), and are conceived on the basis of productive and economic objectives, as well as the social and environmental objectives that must be imposed by sociopolitical externalities.

Most developed countries' agriculture operates in a market-driven economy, although government policies can have an influence on what farmers produce and how they produce it. As with other businesses, agricultural producers respond to economic incentives and disincentives, and make decisions to maximize their welfare; usually measured as net income. Specifically, the farmer must consider the influence of technological advancements, income supports embodied in farm legislation, and changes in market structure and consumer demand. Many of the technological advancements have required large-scale production units to justify the investment. The influence of commodity support programs has been ambiguous. As farm legislation has evolved to decouple production decisions from program benefits, the incentives to specialize in program crops (crops that receive price and/or income benefits under governmental legislation) have diminished. However, wealth and risk effects, albeit small, may have promoted or inhibited the adoption of a more sustainable system. Changes in market structure, channels, and consumer demand in the past five decades have been dramatic with consolidation and specialization in both production and marketing sectors. However, the diversity of consumer demand has also created opportunities for more integrated farm operations. There is an increasing number of consumers who have become concerned about how and where their food has been produced (food security). While price and income supports may have been biased toward specialization (as these programs were targeted to specific commodities), the reduction in risk associated with the programs has enabled producers to expand the number and diversity of their production enterprises [15].

The rapid change in the agricultural industry driven by continuously arising challenges (climate change, market globalization, environmental concerns) requires the development of new methods of production in order to guarantee sustainable agriculture [16]. The design of a CS undergoes a study of the biophysical environment and socioeconomic externalities, and an inventory of available technologies. The first step in developing a CS is the definition of goals and constraints for the new CS. Constraints may result from soil and climate but also from environmental or economic concerns [17]. Afterward, a crop portfolio must be established, usually based on climate, and containing a diverse array of adaptable crop species, economic potential, crop production practices, and soil and water management considerations. The crop portfolio is used to screen adaptable crops for a region and includes the best management practices for the production of each adaptable crop [14]. In others words, it is the selection of crops compatible with the set of constraints. Next is the comparison and choice of the most satisfying crop and management options [16]. Designing new CSs is a long process and occurs in a rapidly changing environment. This is exemplified by climate but also by the economy (prices and policies) and the changing demands and functions that society assigns to agricultural systems. The design process must therefore integrate objectives of the resilience

and flexibility of CSs in an unpredictable environment [18]. Obviously, the use of models for the design of CSs can be an important tool for the farmer, although there are some drawbacks [16]. Geographic information systems, qualitative decision-matrix analyses, a simple rule-based model using multi-criteria evaluations, and a machine learning-based land-transformation model can be used harmoniously to study complex socio-ecological systems. Models evaluate how each technique performs in the study of complex socio-ecological systems using a multi-tier framework, detailing how each method analyzes the resource system, resource units, governance system, users and interactions, and outcomes in the system. Model use enhances our understanding of the land-use decision-making process [19].

Anthropological View

Beginning around 8,500 BC, the transition from the hunter–gatherer lifestyle to food production enabled people to settle down next to their permanent agricultural lands, instead of migrating to follow seasonal shifts in wild food supplies. Food production was accompanied by a human population explosion that has continued unabated to this day, resulting from two separate factors. First, the sedentary lifestyle permitted shorter birth intervals. Nomadic hunter–gatherers had previously spaced out birth intervals at 4 years or more because a mother shifting camp can carry only one infant or slow toddler. Second, plant and animal species that are edible to humans can be cultivated in much higher density in our agricultural land than in wild habitats [20].

Agriculture also led to an explosion of technology because sedentary living permitted the accumulation of heavy technology such as forges that nomadic hunter–gatherers could not carry and because the storable food surpluses resulting from agriculture could be used to feed full-time craftspeople and inventors. By also feeding full-time kings, bureaucrats, nobles, and soldiers, those food surpluses led to social stratification, political centralization, and standing armies. All of these overwhelming advantages are what enabled farmers to eventually displace hunter–gatherers [21].

Like all species, humans have exercised their impulse to perpetuate and propagate themselves. In doing so, humankind has "domesticated" ecosystems in ways that enhance its food supplies, reduce exposure to predators and natural dangers, and promote commerce. On average, the net benefits to humankind of "domesticated" nature have been positive. We have, of course, made mistakes, causing unforeseen changes in ecosystem attributes, while leaving few, if any, truly wild places on Earth [22]. Domestication of plants and animals may be the single most important feature of the human domination of our planet (Fig. 1). Domestication involves the selection of traits that fundamentally alter wild species to become more useful to us. Conservation has often been framed as the science aimed at protecting nature, and especially protecting nature from people. However, there really is no such thing as nature untainted by people [24]. Facing this reality should change the scientific focus of environmental science. Instead of recounting doom-and-gloom statistics, it would be more fruitful to consider the domestication of nature as the selection of certain desirable ecosystem attributes, such as increased food production, with consequent alteration to other ecosystem attributes that may not be desirable. Under this paradigm, our challenge is to understand and thoughtfully manage the trade-offs among ecosystem services that result from the inescapable domestication of nature [22].

It is clear that cities are the main consumers of most ecosystem services. This is important because the desire and value for these services determines the traits that humans select for preservation or elimination. For example, if humans want to maximize food production, landscapes will be domesticated to accommodate a few high productivity species, plus the human-associated species able to survive in these modified landscapes. If people want more wildlife for recreational hunting, populations of predators of game species will be reduced, and the edge habitat that a few game species prefer will be increased. The choices and actions of urban dwellers influence nature far removed from cities, yet urban dwellers are increasingly unaware of these impacts [22].

Agricultural Practices' Footprint

The huge magnitude of human impacts in the environment is recent, but the presence of impacts such as

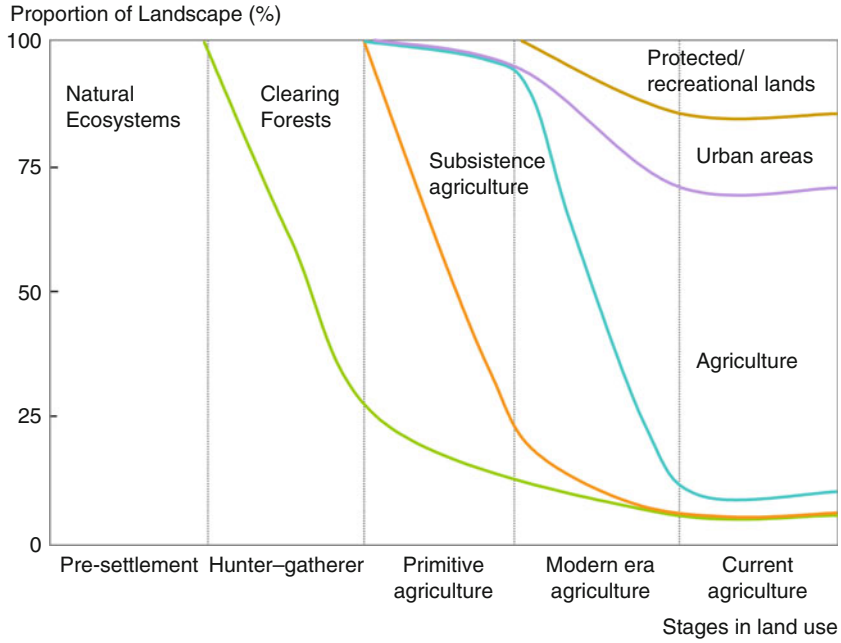

Cropping Systems: Shaping Nature. Figure 1
Stages in "domestication" of nature by human being in relation with the area occupied (Adapted from [23])

purposeful wildfires goes back thousands of years. The reality of the human footprint renders discussions about what areas of the world to set aside as wild and protected areas as somewhat irrelevant; more germane is a discussion of what trade-offs we are willing to accept as a result of the domestication of nature [22].

The main environmental impacts attributed to agriculture come from the conversion of "natural" ecosystems to agroecosystems by CSs [9]. Clearing land for agriculture, humans target wild species for harvest or elimination. Humans have so tamed nature that few locations in the world remain without human influence [22] (Fig. 1). The whole notion of a "virgin rainforest" may be erroneous, with extensive prehistoric human activity evident in what were once thought to be untouched forests in the Amazon and Congo [25]. Global maps of human impact indicate that, as of 1995, only 17% of the world's land area had escaped direct influence by humans [22]. Between 1700 and 1980, the total area of cultivated land worldwide increased 466%, and yields increased dramatically, particularly because of selectively bred, high-yielding varieties, fertilizers, pesticides, irrigation, and machinery. For example, irrigation increased corn yields in eastern Colorado by 400–500% from 1940 to 1997 [9]. Roughly 50% of the world's surface area has been converted to grazed land or cultivated crops [26]. Cropping systems (areas where at least 30% of the landscape is in croplands, confined livestock production, or freshwater aquaculture) now cover a quarter of the Earth's surface, partly by conversion of temperate grasslands, Mediterranean climate forests, and many tropical ecosystem types. More than half of the world's forests have been lost in this land conversion [26]. Forests have essentially disappeared from 25 countries, with 9.4 million hectares lost annually from the Earth's surface [27]. Species and populations of species are being lost at unprecedented rates, while at the same time, the global biota is becoming homogenized, owing to the introductions of alien species to new regions. These examples represent major losses of pieces of the biosphere machinery, which have a serious impact on the delivery of ecosystem-regulating services – impacts such as greater prevalence of infectious diseases in disrupted ecosystems, adverse effects on local climates by ecosystem modification, and the loss of flood protection [27].

Environmental damages have come from agricultural nutrients that pollute aquatic and terrestrial habitats and groundwater, and from pesticides, especially

bioaccumulating or persistent organic agricultural pollutants. Agricultural nutrients enter other ecosystems through leaching, volatilization, and the waste streams of livestock and humans. Pesticides can also harm human health, as can pathogens, including antibiotic-resistant pathogens associated with certain animal production practices [9]. Many CSs have degraded soil quality and necessitated the expense of increased fertilization, irrigation, and energy to maintain productivity [28]. Today, only 30–50% of applied nitrogen fertilizer [29] and ~45% of phosphorus fertilizer [30] is taken up by crops. A significant amount of the applied nitrogen and a smaller portion of the applied phosphorus are lost from agricultural fields. Nitrogen fertilization can increase the emission of gases that have critical roles in tropospheric and stratospheric chemistry and air pollution. Nitrogen oxides (NO_x) emitted from agricultural soils and through combustion increase tropospheric ozone, a component of smog that impacts human health, agricultural crops, and natural ecosystems. NO_x from agroecosystems can be transported atmospherically over long distances and deposited in terrestrial and aquatic ecosystems. Finally, nitrogen inputs to agricultural systems contribute to emissions of the greenhouse-gas nitrous oxide. Rice paddy agriculture and livestock production are the most important anthropogenic sources of the greenhouse-gas methane [31]. Much of agriculture in the developed world had for a time embraced potentially non-sustainable systems for economic reasons, over-utilizing monocropping, specialization and mechanization, which was damaging to soils and the environment [32]. Modern agroecosystems are also depleted in biodiversity and habitat heterogeneity, often with a reduction in resilience as a result of their biological monotony [22].

Cities are a good place to start when considering the broader implications of agroecosystems. The cumulative resource demands of cities are often expressed as the total land area required to supply those resources, called the "ecological footprint" [33]. Every city imports resources and exports waste into a region that is spatially much larger than the city's area. However, there is substantial variation in per capita ecological footprints between rich and poor regions, with the average resident of the United States using 6 times the area of the average sub-Saharan African [34].

Praise of Agricultural Science

To a conservationist interested mainly in biodiversity, we have degraded nature, but to an agronomist, we have shaped the nature to make it better serve humans [22]. It is paradoxical that current urban dwellers look down upon and lack an appreciation of agriculture when it is the key to our existence and to obtaining the energy needed for their daily activities. There is no question that humans have been successful in their efforts to produce food, thereby enhancing their well-being [22]. Contrary to Malthus's predictions, food production has kept up with, and even outpaced, human population growth [35]. Malthus did not take into account that "there is no gene for the human spirit" [36]. The massive increase in food supply has been achieved by focusing efforts on planting and consuming a small variety of plants [22]. As of 1999, barley, maize, rice, and wheat occupied almost 40% of global cropland [37].

Nowadays, few scientists think of agriculture as the chief, or model science. Many, indeed, do not consider it a science at all. Yet it was the first science – the mother of all sciences; it remains the science that makes human life possible; and it may well be that, before the century is over, the success or failure of Science as a whole will be judged by the success or failure of agriculture [38]. For too many years, the agricultural sciences have been disparaged in the science and education communities, perhaps because agronomy, soil science, plant pathology, and animal science use a problem-solving approach rather than simply seeking knowledge [39]. But as we move into a new era of shared accountability and responsibility, let's keep in mind that agricultural sciences affect us all, and when agricultural science is thriving, our communities likely are thriving too [39]. Agriculture is not seen as a source of solutions to many of the world's most pressing challenges. When science research funds are handed out, agriculture often gets left off the list. It is possible to suspect this because policy-makers and some scientists see "agriculture" as synonymous with "agribusiness" rather than as a purely scientific discipline, and they assume private funding will take care of agriculture-related research needs [39].

The benefits of agriculture have been immense. Before the dawn of agriculture, the hunter–gatherer

lifestyle supported about four million people globally [40]. Modern agriculture now feeds 6,000 million people. Global cereal production has doubled in the past 40 years, mainly from the increased yields resulting from greater inputs of fertilizer, water and pesticides, new crop strains, and other technologies of the "Green Revolution" [41] (Fig. 2). This has increased the global per capita food supply, reducing hunger, improving nutrition (and thus the ability of people to better reach their mental and physical potential), and sparing natural ecosystems from conversion to agriculture [43].

Agriculture is the science that has had and continues to have the greatest impact on humanity. The advancements are the result of countless researchers unknown to the general public and who deserve proper tribute and acknowledgement. We should be eternally grateful to people, many of whom are consigned to oblivion, such as Justus von Liebig, (1803–1873), who is known as the "father of the fertilizer industry," for his discovery of nitrogen as an essential plant nutrient and his formulation of the Law of the Minimum which described the effect of individual nutrients on crops; Sir John Bennet Lawes, (1814–1900) who experimented with crops and manures at his farm at Harpenden, nowadays known as Rothamsted, and established the first long-term field experiment in the world, the Broadbalk (1843); Daniel Albone, who invented, in 1902, the world's first successful light farm tractor; Fritz Haber and Carl Bosch, whose work led to the synthesis of the first N fertilizer in 1913, seeing that without the use of synthetic fertilizers, world food production could not have increased at the rate it did and more natural ecosystems would have been converted to agriculture [9]; Sir Ronald Aylmer Fisher, who, working in the long-term experiments at Rothamsted in 1925, established the basis of the modern statistics that so greatly benefited agricultural research and all other sciences; Erling Johnson, who in 1927 developed an industrial method for producing nitrophosphate; Paul Hermann Müller, who discovered that DDT was a very effective insecticide

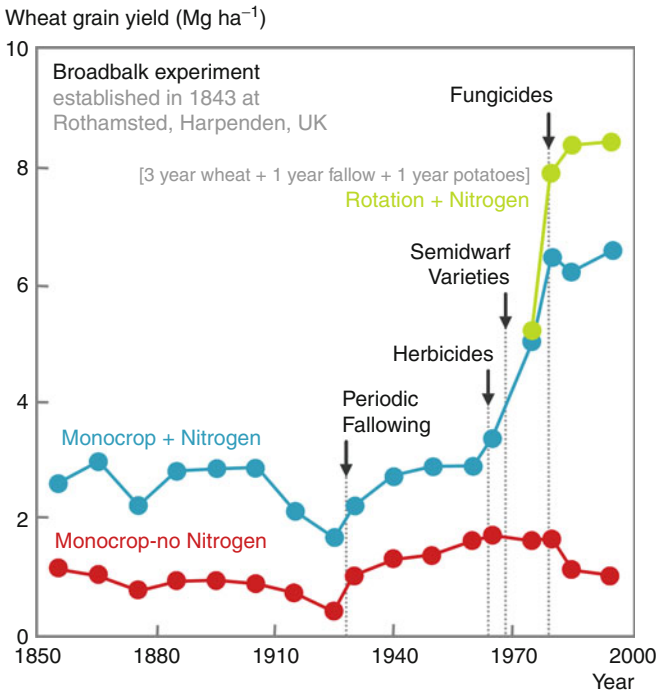

Cropping Systems: Shaping Nature. Figure 2
Changes with time in winter wheat yields from 1850 to 2000 with explanations for the trends due to new agricultural practice technologies introduced. Treatments show how important is nitrogen fertilization and crop rotation (Adapted from [42])

in 1939, in spite of the fact that it was later discovered to be hazardous for many living beings, the good it accomplished for humanity is immeasurable as it controlled mosquitoes spreading malaria and lice transmitting typhus; Judah Hirsch Quastel, who working at Rothamsted, developed the first herbicide (2,4-D) in 1946; Norman Ernest Borlaug, father of the "green revolution," led the introduction of high-yielding varieties, doubling wheat grain yield in many countries during the 1960s (Fig. 2); John E. Franz, who discovered Glyphosate in 1970, a broad-spectrum systemic herbicide; Marc Van Montagu and Jeff Schell discovered the gene transfer mechanism, developing the first transgenic plant in the 1980s; in addition to a long list of anonymous researchers who contributed their part to providing humanity with the food needed through techniques which have become increasingly more respectful of the environment and safer for consumption.

Eradication of Fallow, Tillage, and Monoculture

There are three agricultural practices that must tend to disappear from present and future CSs because it has been proven, in general, that they are more harmful than beneficial. Two of these, tillage and fallow, have been used since the beginning of agriculture, while the third, monoculture, emerged during the last century as a consequence of the incorporation of other techniques that made it apparently viable in the context of a great demand for food. These practices must be considered errors of the past that the present has allowed us to discover.

Soil is not naturally intended to be in a state of bare fallow. CSs must be inspired by or consider nature in their design. Soil is meant to be covered by vegetation as can be observed in most terrestrial ecosystems; therefore, when man included bare fallow in its group of agricultural practices, he committed a big mistake. Even in the conditions employed to allow low-fertility soils to rest, the most ideal option would be a change in crop, or if necessary, another option would be to not remove the crop. Although it was already known at the end of the last century that bare fallow was not useful, there have been policies, as is the case of the EU, which encouraged this practice as a result of market forces. Efforts to stabilize production of cereal crops led to the adoption of wheat–fallow CSs. This system, while popular with producers because it required limited equipment and managerial skills, has proven to be agronomically inefficient and environmentally unsustainable as shown through poor precipitation-use efficiency and decreased soil quality [44, 45]. In fact, at least 60% of the precipitation received during fallow is lost to evaporation [46]. Recognition of the drawbacks of wheat–fallow as well as advances in weed and residue management technology led to a reduction in the frequency of fallow [13]. Fallow time must be limited to those periods in which no water is available. Leaving a soil without residue shifts away from natural processes since in naturally dry ecosystems, the dry pasture leaves its residue protecting the soil against aggressive climatic events. All of the suggestions for intensifying cropping under dry-land conditions are contingent on maximum water capture and minimum losses to weeds, runoff, and evaporation. Ideally, crops should be synchronized so that there is always one crop in the field available to intercept possible rainfall [44]. Increased emphasis on crop diversity within annual CSs has allowed producers to take advantage of positive agronomic benefits derived from crop rotations [14]. Realizing these benefits requires knowledge of soil-water depletion and recharge characteristics for individual crops. Such knowledge is especially critical for areas where soil-water status can vary greatly between growing seasons [47].

Tillage, as is, is also not observed in nature. It was man, with the purpose of domesticating nature, who introduced it. No-tillage was used since ancient times by indigenous cultures. This was because tillage to any depth required more energy and power than was generally possible with hand labor. The ancient Egyptians and the Incas in the Andes of South America used a stick to make a hole in the ground and put seeds by hand into unprepared soil [48]. For thousands of years, agriculture and tillage were considered synonymous. It was simply not thought possible to grow crops without first tilling the soil before planting and for weed control [49]. Intensive tillage and use of heavy machinery have accelerated soil erosion, soil-C loss and nutrient depletion, soil compaction, acidification, pollution, and salinization [50]. The advent of modern herbicides permitted no-tillage to be developed and practiced on actual working family farms. No-tillage is generally defined as planting crops in unprepared soil with at

least 30% mulch cover [49]. Adoption of no-tillage after its successful demonstration in the 1950s was slow. Today, approximately 23% of the total cropland in the United States is planted using no-tillage [49]. No-tillage has revolutionized agricultural systems because it allows individual producers to manage greater amounts of land with reduced energy, labor, and machinery inputs. Maintenance of surface residue cover is essential to optimize CS performance as residue coverage minimizes erosion, enhances retention of limited precipitation, and improves soil quality [51]. Moreover, no-tillage substantially improves soil carbon, an area that is currently of great importance [45]. Crop residues, including the presence of crop stubble, can alter the soil environment in a number of ways by acting as a physical barrier, exudate of chemical suppressants (allelochemicals) from the residue, or enhancer of biological activity, and by providing a habitat for weed seed predators. These factors, as well as the buffering effect of crop residues on soil moisture and soil temperature and impacts on light availability, have a significant impact on weed-seed germination and emergence [52]. Lastly, the adoption of no-tillage has an economic benefit for farmers, reducing crop costs [53].

Monoculture, the lack of biodiversity, was a contributing factor to several agricultural disasters in history. Monoculture causes a loss of biodiversity in the "ecosystem" soil as a result of the monotony, leading to a yield loss with respect to a crop in rotation [54]. Practices that change species' composition or reduce biodiversity in agricultural systems may also diminish goods and services because the ability of ecosystems to provide some services depends both on the number and type of species in an ecosystem [9]. The supply of agricultural products and ecosystem services are both essential to human existence and quality of life. However, recent agricultural practices that have greatly increased global food supply have had inadvertent, detrimental impacts on the environment and on ecosystem services, highlighting the need for more sustainable agricultural methods [9]. Wheat, rice, and maize crops have become the three most abundant plants on Earth. A central conclusion of epidemiology is that both the number of diseases and disease incidence should increase proportionally to host abundance, and this disconcerting possibility illustrates the potential instability of a global strategy of food production in which just three crops account for so high a proportion of production [9]. The relative scarcity of outbreaks of diseases on these crops is a testament to plant breeding and cultivation practices. For all three cereals, breeders have been successful at improving resistances to abiotic stresses, pathogens, and diseases, and at deploying these defenses in space and time so as to maintain yield stability despite low crop diversity in continuous cereal systems [9]. However, it is unclear if such conventional breeding approaches can work indefinitely. Both integrated pest management and biotechnology that identifies durable resistance through multiple gene sources should play increasingly important roles [55]. Nonetheless, the evolutionary interactions among crops and their pathogens mean that any improvement in crop resistance to a pathogen is likely to be transitory [9]. Although the "Green Revolution" significantly increased rice yields in Asia, yield increases have not occurred in the past 15–20 years. The genetic "yield potential" has increased for wheat, but the yield potential for rice has not increased since 1966, and the yield potential for maize has "barely increased in 35 years." It takes a decade or two for herbicide-resistant weeds to emerge, and insects become resistant to insecticides within about a decade. Within about one or two decades of the introduction of each of seven major herbicides, herbicide-resistant weeds were observed. Crop rotation helps to prevent resistances [9].

Biological Synergism and Technical Synchronization

Agriculture should fulfill the economic, environmental, and social objectives of sustainable development. It is thus necessary to tailor current CSs to meet these needs as they are often too intensive and dependent on external inputs [56]. It is clear that the more we imitate nature or encourage natural processes, the greater the benefits for the CSs and fewer inputs that will be required. Two basic concepts should illustrate the design and management of CSs of the future: biological synergism and technical synchronization.

Biological Synergism

Biological synergic CSs should synchronize edaphoclimatic resources with the natural rhythms of

crops, this being a question of common sense that has not always been applied, and clearly speaks of the diversity which has been lost with intensive systems. Therefore, the increase in biodiversity in CSs is a clear consequence of the search for biological synergism in addition to the promotion of natural processes. Biodiversity is essential to ecosystem processes in ways that are not yet fully understood [57], and it is considered worth protecting in its own right. Crop diversification by itself, however, is of limited use without knowledge of how individual crops affect each other in a sequence. Consequently, a thorough understanding of crop sequencing effects – both positive and negative – on agronomic parameters is necessary to optimize CS performance [13, 46]. One problem associated with synergic CSs is how to choose and sequence crops to develop the inherent internal resources of the system while taking advantage of external resources such as weather, markets, government programs, and new technology [14]. Present CSs rely on extensive use of fertilizer and pesticides and the low cost of fossil fuel energy [46]. Future challenges for CSs will exploit synergism through crop sequencing to improve crop yields without additional inputs and to reduce deterioration of the environment [58].

Diversification of farming systems cannot be managed on a farm or field scale alone but also requires management on a regional scale. To improve biodiversity, the interaction with other stakeholders in the region is necessary as part of regional planning processes. This has consequences for agronomic research which thus far has had only limited attention for the regional scale. Spatial planning aimed at multifunctional agriculture can be seen as a negotiation process on environmental, social, and economic aspects of land use. Complexity arises due to the high number of stakeholders and due to limited knowledge, which is often organized along disciplinary divides [59].

Crop rotation is defined as the growing of different crops (spatial and temporal), in recurring succession, on the same land in contrast to monoculture cropping. Rotation usually is done to replenish soil fertility, create a diverse soil organism, and reduce pest populations in order to increase the potential for high levels of production in future years [2, 46]. Each crop or a closely related crop species should not be grown more than every 4 years because of increased pest problems [60, 61]. One of the most effective and inexpensive methods to control plant diseases in CSs is through crop rotation. Through the use of this practice, the need to breed for new disease resistance and to discover new pesticides can be reduced. Recently, an important and costly pathogen of rice was controlled in a large region of China by planting alternating rows of two rice varieties [62]. This tactic increased profitability and reduced the use of a potent pesticide. Specific crop-rotation effects on plant diseases, however, are poorly understood and contradictory results have been reported [13].

Changes in the weed flora of agroecosystems can occur as long-term changes or temporary fluctuations in species composition [52]. Agricultural weeds are a unique group of plant species because of their ability to infest and thrive in intensively disturbed habitats despite extensive efforts to eliminate them. Weed floras differ between fields, farms, regions, climatic zones, and CSs. Weeds are successful because they are generally plastic plants that adapt to and survive changes in the environment. In continuous CSs, changes in the environment may be as a result of differences in crop species, tillage, fertilizers, herbicides, and other weed-control tactics. Long-term population shifts are usually observed after repeated use of a control measure, which exerts a high selection pressure on a population, for example, the increased incidence of some annual grass weed species due to the intensification of cereal production and selective herbicides [52]. Studies have shown that the more diverse the CS, the more diverse the weed community, with less dominant and troublesome species as would occur in a simple rotation.

With diversified continuous cropping, there is greater opportunity to utilize crops that vary in N requirements [63]. Rotations with legumes are of great interest for strengthening the synergism of a CS. Legume crops are often planted to enhance nutrient cycling and availability to other crops in the rotation. Crops with high N demands are usually grown after legume crops. Grain legumes conserve soil N by fixing atmospheric N, thereby leaving residual N in place for the next crop. Wheat yields are often higher following legumes than following other cereals [54] and the N use efficiency of a wheat crop is greater following legumes than others crops [64]. The inclusion of a legume crop decreases its reliance on external fertilizer, supplying

a significant proportion of the N for the next crop and may moderate nitrate levels in the soil to avoid the potential for nitrate leaching [65] (Fig. 3).

Alternatives such as plurispecific CSs are of considerable interest for biological synergism because plant associations can provide environmental benefits in terms of better use of resources and provision of ecological services [67]. Yet they should also be able to maintain a level of productivity and production stability that fits with farmers' objectives. Intercrops (grass cover in the inter-rows) are now being introduced to an increasing extent due to the potential positive impacts on perennial crop and their environment: increased infiltration rate and decreased runoff due to modified soil surface characteristics [68], mitigation of soil erosion [69], limitation of herbicide use and weed control, better water-resource utilization by roots [70], and limitation of risks of diseases by reducing vegetative development [71]. However, intercropping also induces competition for soil resources, and vegetative development and yield can consequently be limited [56]. These different functions should be promoted through simultaneous adapted management of the two crops of the system.

Finally, an important link of biological synergism is the return provided by livestock to the CSs. There was always a crop–livestock pairing in ancient agriculture, but specialization caused this very important aspect of biodiversity and synergism to disappear. Research is needed to better understand interactions between crops and livestock with the intention of identifying management practices that maximize agroecosystem productivity and operational efficiency. This would save having to remove residues, part of which would be used directly by the livestock, partially allowing the recycling of nutrients. Inclusion of livestock in a CS complements both crops and livestock by adding value to grain, improving nutrient-use efficiency, and providing alternative uses for forages and crop residues [72]. It may create synergisms between the two enterprises, resulting in far greater productivity than either enterprise could attain alone [13, 73]. The inclusion of

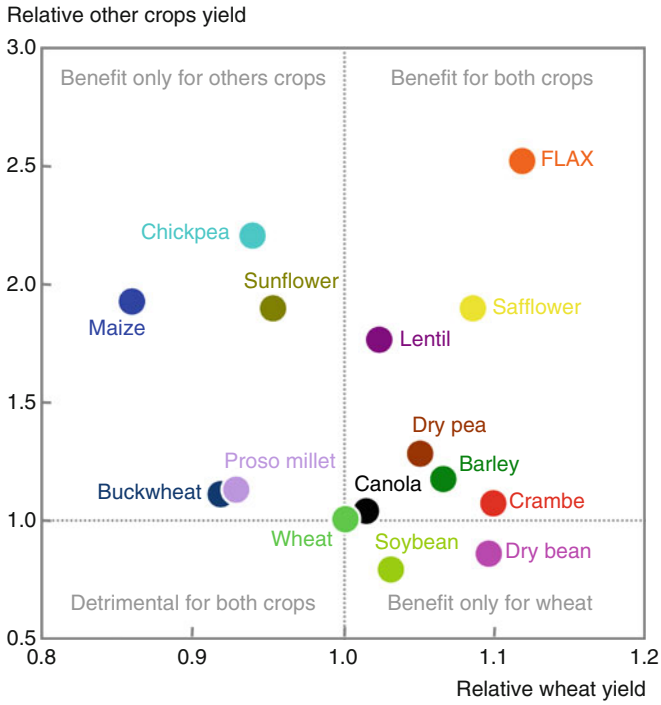

Cropping Systems: Shaping Nature. Figure 3
Effect of 14 previous crops on relative wheat yield and the effect of wheat, as a previous crop, on those crops in the Great Plains (Adapted from [46, 66])

livestock in CSs would also help alleviate the problems generated by livestock: high-density animal production operations can increase livestock disease incidence, the emergence of new, often antibiotic-resistant diseases, and air, groundwater, and surface water pollution associated with animal wastes. Current livestock operations are vulnerable to catastrophic loss of animals to disease. The handling and disposal of animal wastes are significant problems of high-density animal confinement facilities. Manure lagoons can release high levels of hydrogen sulfide and other toxic gases, volatilize ammonium that greatly increases regional nitrogen deposition, and contaminate surface and ground waters with nutrients, toxins, and pathogens. These animal wastes pose health and environmental risks similar to those of human wastes and should be treated accordingly. For example, animal wastes could be treated by composting to create a crop fertilizer that no longer harbors pathogens, and that is applied at appropriate rates and times and with methods that minimize nutrient leaching. This closing of the nutrient cycle decreases dependence on synthetic fertilizer production, and is more efficient when animal and crop production are combined locally [9].

Technical Synchronization

Technical synchronization must be defined as the concept on which precision agriculture is based, i.e., the temporal and spatial synchronization of agricultural techniques. All agricultural practices must be synchronized in time with the rhythms of the agroecosystem (time-specific management). This synchronization must take into account the growth stage of the crop, different soil characteristics (nutrients and water), weather forecasts, etc. On the other hand, there is the spatial synchronization that divides the land into homogeneous units for management (site-specific management) [63]. A basic principal of technical synchronization is the energetic efficiency when making decisions in relation to the agricultural practices to be carried out.

The key to the application of technical synchronization in a CS is the acquisition of data in order to make management decisions in time and space. There are an increasing number of data acquisition devices available to assist with decision making: global positioning (GPS), satellites or aerial images, information management tools (GIS), weather stations, soil sensors (water content, temperature, etc.), optical sensors (e.g., chlorophyll meters), and remote sensors (visible and near infrared spectral), etc. These tools allow the farmer to have a better understanding of the interaction of climate and management that causes tremendous year-to-year variation in on-farm yields and crop requirements.

Nonetheless, technical synchronization poses a problem when applied by the farmer. There is a large body of published research on technologies for increasing the technical synchronization of agricultural practices, but relatively few have been adopted by farmers because they are not cost-effective or practical. Adoption of improved technologies typically requires additional skills and labor or investments in new equipment. Information on expected costs and economic returns from such investments is required to convince farmers of the benefits from adoption [12]. A possible solution is cooperativism for the acquisition and sharing of these new technologies.

Dynamic Cropping Systems

It could be said that, until now, CSs have been static, i.e., year after year the same group of agricultural practices have been repeated, causing soil monotony in the agroecosystem. A dynamic CS must be flexible and go against repeated management practices, and the decisions must be made based on measured parameters and their determining factors. A dynamic CS is only the consequence of the application of the two previously stated principles: biological synergism and technical synchronization. Cropping systems need to be inherently flexible to take advantage of economic opportunities and/or adapt to environmental realities [13, 18]. The implementation of a management strategy requires knowing, understanding, planning, measuring, monitoring, and record keeping at each step of the production process. Dynamic CSs require the development and implementation of agricultural production systems that are highly productive, energy efficient, and environmentally non-degrading [12].

Dynamic CSs are a form of agricultural production that relies on an annual or pluri-annual strategy to optimize the outcome of (1) production, (2) economic,

and (3) resource-conservation goals using ecologically based management principles [74]. Implicit to this strategy is the need for producers to possess information necessary to respond to continual change. The key factors associated with dynamic CSs are diversity, adaptability, reduced input cost, multiple enterprise systems, and awareness of environment and information [14]. Greater crop diversity and sequencing flexibility within dynamic CSs may result in reduced weed, pest and disease infestations, greater nutrient- and precipitation-use efficiency, decreased requirements of exogenous inputs, and lower production risk [74]. To remain competitive in agricultural markets, increased diversity of systems will be required to minimize inputs and improve economic margins.

To increase responsiveness to externalities, opportunity/flex CS [75] or dynamic CS [14] concepts have been developed. These systems allow producers to adjust CS intensity and/or diversity based on externalities as well as management goals, such as soil-water status at planting, soil residual nitrogen, market demands, etc. This approach to crop sequencing possesses an inherent flexibility to adapt to high-risk conditions, and therefore may be more economically and environmentally sustainable than other approaches to crop sequencing [13]. However, the authors who established the principles of dynamic CSs have focused solely on rotation selection, which is erroneous, since a CS is more than its rotation selection, although the crop selection is without a doubt the most important decision made in a CS. Perhaps the concepts should be called dynamic or flexible crop election system. However, a dynamic CS makes more sense if each year all of the crop techniques used are reconsidered, i.e., crop selection, tillage, residue management, nitrogenous fertilization, etc. in such a way that there are dynamics in the selection of each and every one of the agricultural practices that depend on externalities.

Future Challenges

Agricultural science is ripe for a renaissance [39] as a consequence of the future challenges it must confront. The widespread adoption of CSs that are sustainable and environmentally benign is essential for the long-term survival of civilization [32]. Furthermore, through the use of strategic alliances, cooperation among producers on a regional basis may eventually lead to greater integration and diversification than could be achieved for the individual farm operation [15]. The primary challenges facing CSs in this century are: covering the demands of an increasing world population; water shortage; the inclusion and management of GM crops; harmonization of the production of biofuels and food production; and climate change, and the focus it brings to agricultural research. Obviously, there are many other challenges which have not been presented here, but which are intimately related to those mentioned such as: the biodiversity of CSs – as already previously mentioned – which should redound to a reduction of inputs and, therefore, a reduction of the negative effects on the environment, strategies to manage anthropogenic carbon emissions from terrestrial systems as well as fossil fuel and industrial sources, etc.

Nevertheless, together with these future challenges are a series of forces that may contribute or hinder their fulfillment: research policies, transference, and financing. In view of these challenges, governmental policies play an important role that may help or hurt the achieving of these objectives. For this reason, policymakers have a great responsibility, and their decisions should be guided by agricultural science professionals. Political intervention has an economic facet that arises as the result of the following question: How can society accomplish the dual objectives of improving food production and stability and of preserving the quality and quantity of ecosystem services provided by the Earth's land and water resources? Clearly, appropriate incentives are needed [9]. What incentives and policies could lead to the adoption of sustainable agricultural practices? Several policy initiatives have tried to level the playing field between agricultural production and the production of ecosystem services.

Another problem in the attempt to fulfill these objectives is the transference and application of new technologies in CSs. The earlier paradigm of science being developed at the international or perhaps national level and then disseminated to farmers should be replaced by an active exchange of information among scientists and farmers. Scientists in developing countries who understand the ecosystems, human culture, and demands on local agricultural systems must

be actively trained, promoted, and brought into the international scientific community [9].

The economic investment in agricultural research is the third problem. Organized public and private investment in agricultural R&D was a primary driver of the comparatively rapid growth in agricultural productivity experienced in the latter half of the twentieth century [76]. Substantially greater public and private investments in technology and human resources are needed internationally, especially in low-income nations, to make agricultural systems more sustainable. Global research expenditures are less than 2% of agricultural gross domestic product worldwide [77], being roughly 5.5% of agricultural GDP in developed countries, but less than 1% in developing countries (where most of the increased food demand will occur during the next 50 years). At present, there are few incentives for the private sector to increase investments in lower-income developing countries [78]. Moreover, funds have been redirected away from farm productivity toward other concerns, such as the environmental effects of agriculture; food safety and other aspects of food quality; and the medical, energy, and industrial uses of agricultural commodities. Without adequate investments, yield gains and environmental protection may be insufficient for a transition to sustainable agriculture [9].

Feeding the World: Priority Aim

In a recent update of earlier estimates, the Food and Agriculture Organization [79] of the United Nations reported that more than one billion people now suffer malnutrition [80]. By 2050, global population is projected to be 50% larger than at present and global grain demand is projected to double [28, 82], especially the economic growth of the fast-growing economies of Asia [81]. This doubling will result from a projected 2.4-fold increase in per capita real income and from dietary shifts toward a higher proportion of meat (much of it grain fed) associated with higher income. Further increases in agricultural output are essential for global political and social stability and equity. Doubling food production again and sustaining food production at this level are major challenges [82]. Doing so in ways that do not compromise environmental integrity and public health is a greater challenge still [9]. Agricultural productivity growth will be a pivotal determinant of long-term growth in the supply, availability, and price of food over the coming decades [81]. However, a slowdown in growth of agricultural productivity and grain yields has been documented. If this slowdown in productivity persists, it could have profound implications for food-price trends in the future [81].

A key trade-off in cultivated systems is between increasing the amount of cropland needed to meet growing food needs versus increasing the productivity of each hectare of cropland. The "land-sparing" impact of modern farming practices has mainly been achieved by yield increases from the use of crop monocultures with improved crop varieties, fertilizer inputs, and irrigation. For example, if yields of the six major crop groups that are cultivated on 80% of the total cultivated land area had remained at 1961 yield levels, it would require an additional 1.4 billion hectares of land in 2004 – more than double the amount currently used. This represents 34% of the total land area suitable for crop cultivation and would have required conversion of large areas of uncultivated land that support rain forests, grassland savannahs, and wetlands. In Asia alone, it would require an additional 600 million hectares, which represent 25% more land area than is suitable for cultivation on this continent. Asia would now be heavily dependent on food imports if crop yields had remained at 1961 yield levels. Although this increase in productivity has saved some land from conversion, it has resulted in greater impact on other services through water withdrawals, excessive nutrient loads and pesticide use. The key ecological question is, therefore, whether environmental services – other than food production at regional and global scales – would be enhanced by focusing food production on less land under intensive management with high yields, versus expanding cultivated area in lower-yielding systems using farming practices that preserve environmental services at the field and local levels. Few studies have addressed this issue using sound, ecological, analytical methods [27].

Water: Colorless Gold

Water is the principal factor limiting crop yield and is considered a luxury in many agroecosystems. In many

developing countries, water is a major factor constraining agricultural output, and income of the world's rural poor [83]. Forty percent of crop production comes from the 16% of agricultural land that is irrigated [84]. Irrigated lands account for a substantial portion of increased yields obtained during the Green Revolution [9]. Unless water-use efficiency is increased, greater agricultural production will require increased irrigation. However, the global rate of increase in irrigated area is declining, per capita irrigated area has declined by 5% since 1978, and new dam construction may allow only a 10% increase in water for irrigation over the next 30 years [84]. Irrigation return-flows typically carry more salt, nutrients, minerals, and pesticides into surface and ground waters than in source water, impacting downstream agricultural, natural systems, and drinking water. Technologies such as drip and pivot irrigation can improve water-use efficiency and decrease salinization while maintaining or increasing yields. They have been used in industrialized nations on high-value horticultural crops, but their expanded use currently is not economically viable for staple food crops. In developing countries, 15 million hectares have experienced reduced yields owing to salt accumulation and waterlogging [85]. The water-holding capacity of soil can be increased by adding manure or reducing tillage and by other approaches that maintain or increase soil organic matter. Cultivation of crops with high water-use efficiency and the development – through the use of biotechnology or conventional breeding – of crops with greater drought tolerance can also contribute to yield increases in water-limited production environments. Investment in such water-efficient technologies, however, is best facilitated when water is valued and priced appropriately [9].

However, most of the world's agricultural area corresponds to dry-land areas and therefore the challenge is to increase the efficiency of water use in these areas. Efficient use of limited water supplies in dry-land CSs is critical to system success. In the future, increases to semiarid dry-land system water-use efficiency and precipitation-use efficiency may come from continued improvement in managing residues (especially no-tillage), cropping sequences that minimize fallow periods, herbicides, and crop choice. However, continuous cropping under dry-land conditions remains risky due to the limited precipitation (erratic in distribution and frequency) and high-potential evaporation. In the future, the following are potentially fruitful areas of research that may improve system water-use efficiency [86]: (1) Increasing the amount and persistence of crop residues. (2) Implementation of flexible rotations (i.e., opportunity cropping). The occurrence of precipitation and, hence, the availability of adequate stored soil water for a crop is highly variable, especially in semiarid regions. Sometimes stored soil water at normal planting times for a crop in a given CS is limited; at other times, adequate water for a crop is available when the planting of a crop had not been planned. By practicing opportunity cropping, some crop generally could be planted when water becomes available. The goal should be to grow a crop whenever conditions are or become favorable and not according to some predetermined schedule [87]. (3) Matching of crop cultivar selection to prevailing weather conditions. Genetic yield potential is linked positively with maturity, so cultivar evaluation trials conducted under conditions of adequate soil water often favor longer-maturity cultivars and influence farmer choice. (4) Improvement of the timeliness of cultural operations, including early seeding of crops and optimum timing of weed control, and time operations to coincide with favorable conditions as predicted by short-term (48–72 h) weather forecasts.

Genetic Modified Crops: Essential

Genetically modified crops are a very important part of the "second Green Revolution," which may help to break the tendency toward the stabilization of work agricultural production. Genetically modified crops may offer the best hope for producing crops that can withstand drought, impoverished soils, and disease. Future GM products are likely to carry traits that will improve nutrition and health, help guard against drought, heat and cold, and allow plants to access and more efficiently utilize plant nutrients. All of these technologies have more benefits to offer society, and especially, poor farmers and consumers even more than rich ones [88].

Therefore, GM crops are an essential tool in feeding the growing world population and reducing the negative effects on the environment from the use of

pesticides. Nevertheless, this technology must be used properly by growers. Growers who adopt herbicide or pest tolerant crops in all cycles of the crop rotation will be at greater risk than those who choose to rotate crops and/or use other management strategies [89]. However, farmers must be proactive in protecting the longevity of the technology by reducing the likelihood of resistance occurring and providing alternative selection pressures on weeds and pests [52]. We must not forget that life always finds a way through barriers [90].

Biofuel Crops: A Controversial Birth

Recent analyses of the energy and greenhouse-gas performance of alternative biofuels have ignited a controversy that may be best resolved by applying two simple principles. In a world seeking solutions to its energy, environmental, and food challenges, society cannot afford to miss out on the global greenhouse-gas emission reductions and the local environmental and societal benefits when biofuels are done right. However, society also cannot accept the undesirable impacts of biofuels done wrong [91]. Biofuels done right can be produced in substantial quantities with little or no competition with food production.

The biofuel industry could have many positive social and environmental attributes, but it could also suffer from many of the sustainability issues if not implemented the right way. Putting biofuel crops on marginal lands, rather than on our most productive croplands, could mean preventing competition with food production and concomitant effects on commodity prices, as well as minimizing or even avoiding the carbon debt associated with land clearing. However, marginal lands can also be rich in biodiversity, may require sizable inputs of nutrients and water to make production economically viable, and may carry the opportunity cost of forgone future carbon sequestration [92].

Globally, the production of an important amount of energy with biofuels will require a large amount of land – perhaps as much as is in row crop agriculture today. This will change the landscape of Earth in a significant way. The identification of unintended consequences early in the development of alternative fuel strategies will help to avoid costly mistakes and regrets about the effects on the environment. Policies that support long-term sustainability of both our landscapes and our atmosphere are essential if we are to chart a low-carbon economy that is substantially better than business as usual. Sustainable biofuel production systems could play a highly positive role in mitigating climate change, enhancing environmental quality, and strengthening the global economy. But it will take sound, science-based policy and additional research effort to make this so [93].

Until now, the most convincing option for the production of biofuel has been the use of perennial plants as they require fewer inputs and can be grown on degraded lands abandoned from agricultural use [91]. Use of such lands minimizes competition with food crops. This also minimizes the potential for direct and indirect land-clearing associated with biofuel expansion, as well as the resultant creation of long-term carbon debt and biodiversity loss. Some initial analyses on the global potential of degraded lands suggest that they could meet meaningful amounts of current global demand for liquid transportation fuels [92, 94, 95]. The option of using crop residues from food crops, such as corn stover and straw from rice and wheat is a more controversial matter. Recent research suggests that it is to the benefit of farmers to leave substantial quantities of crop residues on the land [96], but that, nonetheless, even conservative removal rates can provide a sustainable biomass resource about as large as that from dedicated perennial crops grown on degraded lands.

Good public policy will ensure that biofuel production optimizes a bundle of benefits, including real energy gains, greenhouse-gas reductions, preservation of biodiversity, and maintenance of food security. Performance-based policies that provide incentives proportional to the benefits delivered are needed. This is a complex question that cannot be addressed with simplistic solutions and sound bites. It needs a new collaboration between environmentalists, economists, technologists, the agricultural community, engaged citizens, and governments around the world [91].

Climate Change: Technical Plasticity

The scenario produced, if indeed climate change becomes a greater reality, is unclear. There is

a "climate of suspicion" as published in the journal Nature at the beginning of January 2010. Climate researchers must emphasize that – although many holes remain to be filled – there is little uncertainty about the overall conclusions: greenhouse-gas emissions are rising sharply, they are very likely to be the cause of recent global warming and precipitation changes, and the world is on a trajectory that will shoot far past 2°C of warming unless emissions are cut substantially [97]. It is evident that CSs must have the ability to adapt to a more unpredictable amount of rainfall and high temperatures. According to the IPCC definition, the extent to which CSs are vulnerable to climate change depends on the actual exposure to climate change, their sensitivity, and adaptive capacity [98]. The adaptive capacity refers to the ability to cope with climate change, including climate variability and extremes, in order to (1) moderate potential damages, (2) take advantage of emerging opportunities, and/or (3) cope with its consequences [99].

Nonetheless, in spite of the uncertainty regarding climate change, primarily as a consequence of the increase in atmospheric CO_2 levels, there are some positive effects. When you step into a commercial greenhouse, the chances are you are stepping into the future. To plants, CO_2 is food, and greenhouse operators, knowing this, use it to fatten them up. While today's atmosphere contains about 380 parts per million of CO_2, commercial greenhouses often contain CO_2 concentrations of twice that or more – the sort of concentration that we might expect in the open air at the end of the century [100]. Many crop scientists believe that this carbon dioxide fertilization effect will go at least some way toward offsetting the losses in yield to be expected as a result of the higher temperatures, flooding, drought, and rising sea levels that the CO_2 greenhouse effect will bring. But some are not so sure. These researchers point to the known negative effects that increased CO_2 concentrations have on the protein content of crops. When Bruce Kimball started out in the 1970s, available technology for high-CO_2 research was limited. Based on current knowledge, he says, the net effect of increasing CO_2 is a good one: "As far as crops go, I think higher CO_2 is a definite benefit. Yes, a little less nutrition than before, but we get more food" [100]. But while Kimball thinks that, in general, the gains in yield are the most important thing, he is not blind to the drop in protein levels.

Agricultural Research: Return to the Field

In recent years, an important movement in agricultural research has emerged on an economic as well as human resource level, toward molecular aspects of plant growth and development. Progress in understanding plant molecular biology has been impressive, and useful applications are evident [101]. However, agronomy has been marginalized, with its field laboratories which require much more time to produce results. This migration could have something to do with the scientific productivity stimulated by the present scientific system since many agricultural research areas that do not conduct field work require less than a year from the start of experimental design until the results are published. On the contrary, field research requires at least 2 years before the results can be accepted by the scientific community. Most records used to assess ecosystem changes are based on short-term data or satellite imagery spanning only a few decades. In many instances, it is impossible to disentangle natural variability from other, potentially significant trends in these records partly because of their short time scale [102]. It is evident that the improvement of CSs requires research in CSs, and specially long-term experiments. Unless a return is made to the roots of research under field conditions, many of the challenges faced will not be overcome. The return to field research will contribute to the global public good by restoring and sustaining productivity growth over the long run, which in turn will mitigate hunger and poverty and, at the same time, reduce pressure on the natural resource base [81].

Nevertheless, in recent years, some agronomists have begun to once again stress the importance of this marginalized dimension of agricultural research, which is time, in relation to the consequences that CSs have on productivity and the environment. Within this framework, long-term experiments acquire a noteworthy relevance. The aim is to compare the biological and economic productivity of different CSs. The high annual fluctuations in rainfall, and resulting crop yields, may make several crop cycles necessary in order to detect significant differences. Likewise, the

differences between soils, water–soil relationship, and variability of pathogens and plagues could provide information that explains the differences in yield among CSs and suggest strategies in which crop sequences and management practices can be selected to increase efficiency in the use of water and nutrients, and control the populations of weed, plagues, and diseases. In this respect, long-term studies act as "laboratories" in which specific problems or mechanisms can be studied in continuous field conditions, where the crop and "input/output" history is well known, and also where tendencies of the quality of resources over time and crop yields can be examined [103]. The most convincing evidence regarding the sustainability of an agroecosystem comes from long-term experiments with positive results.

Bibliography

1. ASA (2010) Glossary of terms. American Society of Agronomy, https://www.agronomy.org
2. CRS (2005) Agriculture: a glossary of terms, programs, and laws. Congressional Research Service, Washington, DC
3. Sadras V, Roget D, Krause M (2003) Dynamic cropping strategies for risk management in dry-land farming systems. Agric Syst 76:920–948
4. Shrestha A (2003) Cropping systems: trends and advances. Food Products Press, Binghamton
5. FAO (2008) Analysis of farming systems. UN Food and Agriculture Organization, Rome
6. Acquaah G (2004) Agricultural production systems principles of crop production, theories, techniques and technology. Prentice Hall, Upper Saddle River, pp 283–317
7. Gold MV (1999) Sustainable agriculture: definitions and terms. USDA National Agriculture Library, Beltsville
8. Earles R, Williams P (2005) Sustainable agriculture: an introduction. ATTRA National Sustainable Agriculture Information Service, Fayetville
9. Tilman D, Cassman KG, Matson PA, Naylor R, Polasky S (2002) Agricultural sustainability and intensive production practices. Nature 418:671–677
10. Whitfield J (2006) How green was my subsidy? Nature 439:908–909
11. Marris E, Dodds P, Glover J, Hibberd J, Zhang JH, Sayre R (2008) Agronomy: five crop researchers who could change the world. Nature 456:563–568
12. Cassman KG, Dobermann A, Walters DT (2002) Agroecosystems, nitrogen-use efficiency and nitrogen management. Ambio 31:132–140
13. Liebig MA, Tanaka DL, Krupinsky JM, Merrill SD, Hanson JD (2007) Dynamic cropping systems: contributions to improve agroecosystem sustainability. Agron J 99:899–903
14. Tanaka DL, Krupinsky JM, Liebig MA, Merrill SD, Ries RE, Hendrickson JR, Johnson HA, Hanson JD (2002) Dynamic cropping systems: an adaptable approach to crop production in the Great Plains. Agron J 94:957–961
15. Halloran JM, Archer DW (2008) External economic drivers and US agricultural production systems. Renew Agr Food Syst 23:296–303
16. Bergez JE, Colbach N, Crespo O, Garcia F, Jeuffroy MH, Justes E, Loyce C, Munier-Jolain N, Sadok W (2010) Designing crop management systems by simulation. Euro J Agron 32:3–9
17. Loyce C, Wéry J (2006) Les outils des agronomes pour l'évaluation et la conception des systèmes de culture. In: Doré T, Le Bail M, Martin P, Ney B, Roger-Estrade J (eds) L'agronomie aujourd'hui. QUAE, Paris, pp 77–95
18. Wery J, Langeveld JWA (2010) Introduction to the EJA special issue on "Cropping systems design: new methods for new challenges". Euro J Agron 32:1–2
19. Washington-Ottombre C, Pijanowski B, Campbell D, Olson J, Maitima J, Musili A, Kibaki T, Kaburu H, Hayombe P, Owango E, Irigia B, Gichere S, Mwangi A (2010) Using a role-playing game to inform the development of land-use models for the study of a complex socio-ecological system. Agric Syst 103:117–126
20. Diamond J (2002) Evolution, consequences and future of plant and animal domestication. Nature 418:700–707
21. Diamond J (1997) Guns, germs, and steel: the fates of human societies. Norton, New York
22. Kareiva P, Watts S, McDonald R, Boucher T (2007) Domesticated nature: shaping landscapes and ecosystems for human welfare. Science 316:1866–1869
23. Foley JA, DeFries R, Asner GP, Barford C, Bonan G, Carpenter SR, Chapin FS, Coe MT, Daily GC, Gibbs HK, Helkowski JH, Holloway T, Howard EA, Kucharik CJ, Monfreda C, Patz JA, Prentice IC, Ramankutty N, Snyder PK (2005) Global consequences of land use. Science 309:570–574
24. Sanderson EW, Jaiteh M, Levy MA, Redford KH, Wannebo AV, Woolmer G (2002) The human footprint and the last of the wild. Bioscience 52:891–904
25. Willis K, Gillson L, Brncic T (2004) How "virgin" is virgin rainforest? Science 304:402–403
26. Millennium Ecosystem Assessment (2005) Ecosystems and human well-being: current state and trends. Island Press, Washington, DC
27. Mooney H, Cropper A, Reid W (2005) Confronting the human dilemma. Nature 434:561–562
28. Cassman KG (1999) Ecological intensification of cereal production systems: yield potential, soil quality, and precision agriculture. Proc Natl Acad Sci USA 96:5952–5959
29. Smil V (1999) Nitrogen in crop production: an account of global flows. Glob Biogeochem Cycl 13:647–662
30. Smil V (2000) Phosphorus in the environment: natural flows and human interferences. Annu Rev Energy Environ 25:53–88
31. Prather MD et al (2001) Atmospheric chemistry and greenhouse gases. In: Houghton JT et al (eds) Climate change 2001: the scientific basis. Cambridge University Press, Cambridge, pp 239–287

32. Boquet DJ, Breitenbeck GA (2004) Book reviews. Cropping systems: trends and advances. Crop Sci 44:2285
33. Wackernagel M, Onisto L, Bello P, Callejas Linares A, López Falfán IS, Méndez García J, Suárez Guerrero AI, Suárez Guerrero MG (1999) National natural capital accounting with the ecological footprint concept. Ecol Econ 29:375–390
34. van Vuuren DP, Bouwman LF (2005) Exploring past and future changes in the ecological footprint for world regions. Ecol Econ 52:43–62
35. Oki T, Kanae S (2006) Global hydrological cycles and world water resources. Science 313:1068–1072
36. Niccol A (1997) Gattaca trailer. Jersey Films, Columbia Pictures
37. Tilman D (1999) Global environmental impacts of agricultural expansion: the need for sustainable and efficient practices. Proc Natl Acad Sci USA 96:5995–6000
38. Mayer A, Mayer J (1974) Agriculture: island empire. Daedelus 103:83–95
39. Levine AS (2009) "Agriculture" is not a dirty word. Science 324:1140
40. Cohen JE (1995) How many people can the earth support? Norton, New York
41. Tilman D, Fargione J, Wolff B, D'Antonio C, Dobson A, Howarth R, Schindler D, Schlesinger WH, Simberloff D, Swackhamer D (2001) Forecasting agriculturally driven global environmental change. Science 292:281–284
42. Rasmussen PE, Goulding KWT, Brown JR, Grace PR, Janzen HH, Körschens M (1998) Long-term agroecosystem experiments: assessing agricultural sustainability and global change. Science 282:893–896
43. Waggoner PE (1995) How much land can ten billion people spare for nature? Does technology make a difference? Technol Soc 17:17–34
44. López-Bellido RJ, López-Bellido L, Benítez-Vega J, López-Bellido FJ (2007) Tillage system, preceding crop, and nitrogen fertilizer in wheat crop: II water utilization. Agron J 99:66–72
45. López-Bellido RJ, Fontán JM, López-Bellido FJ, López-Bellido L (2010) Carbon sequestration by tillage, rotation, and nitrogen fertilization in a Mediterranean Vertisol. Agron J 102:310–318
46. Tanaka DL, Anderson RL, Rao SC (2005) Crop sequencing to improve use of precipitation and synergize crop growth. Agron J 97:385–390
47. Merrill SD, Tanaka DL, Krupinsky JM, Ries RE (2004) Water use and depletion by diverse crop species on Haplustoll soil in the northern Great Plains. J Soil Water Conserv 59:176–183
48. Derpsch R (1998) Historical review of no-tillage cultivation of crops. JIRCAS Working Rep. 13:1–18. Japan International Research Centre for Agricultural Sciences, Ibaraki, Japan
49. Triplett GB Jr, Dick WA (2008) No-tillage crop production: a revolution in agriculture! Agron J 100:153–165
50. Lal R, Reicosky DC, Hanson JD (2007) Evolution of the plow over 10, 000 years and the rationale for no-till farming. Soil Tillage Res 93:1–12
51. Wienhold BJ, Pikul JL, Liebig MA, Mikha MM, Varvel GE, Doran JW, Andrews SS (2006) Cropping system effects on soil quality in the Great Plains: synthesis from a regional project. Renew Agr Food Syst 21:49–59
52. Murphy CE, Lemerle D (2006) Continuous cropping systems and weed selection. Euphytica 148:61–73
53. Nail EL, Young DL, Schillinger WF (2007) Diesel and glyphosate price changes benefit the economics of conservation tillage versus traditional tillage. Soil Tillage Res 94:321–327
54. López-Bellido L, López-Bellido RJ, Castillo JE, López-Bellido FJ (2000) Effects of tillage, crop rotation, and nitrogen fertilization on wheat under rainfed Mediterranean conditions. Agron J 92:1054–1063
55. DeVries J, Toenniessen G (2001) Securing the harvest: biotechnology, breeding, and seed systems for African crops. CAB International, Wallingford
56. Ripoche A, Celette F, Cinna JP, Gary C (2010) Design of intercrop management plans to fulfil production and environmental objectives in vineyards. Eur J Agron 32:30–39
57. Hooper CIIIFS, Ewel JJ, Hector A, Inchausti P, Lavorel S, Lawton JH, Lodge DM, Loreau M, Naeem S, Schmid B, Setälä H, Symstad AJ, Vandermeer J, Wardle DA (2005) Effects of biodiversity on ecosystem functioning: a consensus of current knowledge. Ecol Monogr 75:3–35
58. Kirschenmann F (2002) Why American agriculture is not sustainable. Renewable Resour J 20:6–11
59. Groot JCJ, Jellema A, Rossing WAH (2010) Designing a hedgerow network in a multifunctional agricultural landscape: balancing trade-offs among ecological quality, landscape character and implementation costs. Eur J Agron 32:112–119
60. Bailey KL, Gossen BD, Lafond GR, Watson PR, Derksen DA (2001) Effect of tillage and crop rotation on root and foliar diseases of wheat and pea in Saskatchewan from 1991 to 1998: univariate and multivariate analyses. Can J Plant Sci 81:789–803
61. Krupinsky JM, Bailey KL, McMullen MP, Gossen BD, Turkington TK (2002) Managing plant disease risk in diversified cropping systems. Agron J 94:198–209
62. Zhu Y, Chen H, Fan J, Wang Y, Li Y, Chen J, Fan J, Yang S, Hu L, Leung H, Mew TW, Teng PS, Wang Z, Mundt CC (2000) Genetic diversity and disease control in rice. Nature 406:718–722
63. Schlegel AJ, Grant CA, Havlin JL (2005) Challenging approaches to nitrogen fertilizer recommendations in continuous cropping systems in the Great Plains. Agron J 97:391–398
64. López-Bellido RJ, López-Bellido L (2001) Efficiency of nitrogen in wheat under Mediterranean conditions: effect of tillage, crop rotation and N fertilization. Field Crop Res 71:31–46
65. Grant CA, Peterson GA, Campbell CA (2002) Nutrient considerations for diversified cropping systems in the northern Great Plains. Agron J 94:186–198
66. Tanaka DL, Krupinsky JM, Merrill SD, Liebig MA, Hanson JD (2007) Dynamic cropping systems for sustainable crop production in the Northern Great Plains. Agron J 99:904–911
67. De Costa WAJM, Surentham P (2005) Tree-crop interactions in hedgerow intercropping with different tree species and tea in Sri Lanka: 1. Production and resource competition. Agroforest Syst 63:199–209

68. Léonard J, Andrieux P (1998) Infiltration characteristics of soils in Mediterranean vineyards in southern France. Catena 32:209–223
69. Battany MC, Grismer ME (2000) Rainfall runoff and erosion in Napa Valley vineyards: effects of slope, cover and surface roughness. Hydrol Process 14:1289–1304
70. Monteiro A, Lopes CM (2007) Influence of cover crop on water use and performance of vineyard in Mediterranean Portugal. Agric Ecosyst Environ 121:336–442
71. Valdés Gomez H, Fermaud M, Roudet J, Calonnec A, Gary C (2008) Grey mould incidence is reduced on grapevines with lower vegetative and reproductive growth. Crop Prot 27:1174–1186
72. Tanaka DL, Karn JF, Liebig MA, Kronberg SL, Hanson JD (2006) An integrated approach to crop/livestock systems: forage and grain production for swath grazing. Renew Agr Food Syst 20:223–231
73. Villano R, Fleming E, Fleming P (2010) Evidence of farm-level synergies in mixed-farming systems in the Australian wheat-sheep zone. Agric Syst 103:146–152
74. Hanson JD, Liebig MA, Merrill SD, Tanaka DL, Krupinsky JM, Stott DE (2007) Dynamic cropping systems: increasing adaptability amid an uncertain future. Agron J 99:939–943
75. Peterson GA, Westfall DG, Peairs FB, Sherrod L, Poss D, Gangloff W, Larson K, Thompson DL, Ahuja LR, Koch MD, Walker CB (2000) Sustainable dryland agroecosystem management. Agric Exp Stn Tech Bull TB00–3. Colorado State University, Fort Collins
76. Evenson RE (2002) Economic impacts of agricultural research and extension. In: Gardner BL, Rausser GC (eds) Handbook of agricultural economics, vol 1A, chapter 11. Elsevier, New York, pp 573–628
77. Pardey PG, Alston JM, Piggott RR (2006) Agricultural R&D in the developing world: too little, too late? International Food Policy Research Institute, Washington, DC
78. Falcon W, Fowler C (2002) Carving up the commons – emergence of a new international regime for germplasm development and transfer. Food Policy 27:197–222
79. FAO (2008) Hunger on the rise: soaring prices add 75 million people to global hunger rolls. Briefing paper, FAO, Rome
80. FAO (2009) More people than ever are victims of hunger. Press release, FAO, Rome
81. Alston JM, Beddow JM, Pardey PG (2009) Agricultural research, productivity, and food prices in the long run. Science 325:1209–1210
82. Alexandratos N (1999) World food and agriculture: outlook for the medium and longer term. Proc Natl Acad Sci USA 96:5908–5914
83. Namara RE, Hanjra MA, Castillo GE, Ravnborg HM, Smith L, Van Koppen B (2010) Agricultural water management and poverty linkages. Agric Water Manage 97:520–527
84. Postel SL, Daily GC, Ehrlich PR (1996) Human appropriation of renewable fresh water. Science 271:785–788
85. Naylor R (1996) Energy and resource constraints on intensive agricultural production. Annu Rev Energy Environ 21:99–123
86. Nielsen DC, Unger PW, Miller PR (2005) Efficient water use in dryland cropping systems in the Great Plains. Agron J 97:364–372
87. Miller PR, McConkey BG, Zentner RP, Campbell CA, Cochran VL (2003) Flexible cropping systems in the semiarid northern Great Plains. In: Hanson JD, Krupinsky JM (eds) Proceedings of dynamic cropping systems: principles, processes, and challenges, Bismark, ND, 4–7 Aug 2003. USDA-ARS, Mandan, pp 87–104
88. Borlaug NE (2007) Sixty-two years of fighting hunger: personal recollections. Euphytica 157:287–297
89. Diggle AJ, Neve PB, Smith FP (2003) Herbicides used in combination can reduce the probability of herbicide resistance in finite weed populations. Weed Res 43:371–382
90. Crichton M (1991) Jurassic park. Ballantine Books, The Random House Publishing Group, New York
91. Tilman D, Socolow R, Foley JA, Hill J, Larson E, Lynd L, Pacala S, Reilly J, Searchinger T, Somerville C, Williams R (2009) Beneficial biofuels – the food, energy, and environment trilemma. Science 325:270–271
92. Field CB, Campbell JE, Lobell DB (2008) Biomass energy: the scale of the potential resource. Trends Ecol Evol 23:65–72
93. Robertson GP, Dale VH, Doering OC, Hamburg SP, Melillo JM, Wander MM, Parton WJ, Adler PR, Barney JN, Cruse RM, Duke CS, Fearnside PM, Follett RF, Gibbs HK, Goldemberg J, Mladenoff DJ, Ojima D, Palmer MW, Sharpley A, Wallace L, Weathers KC, Wiens JA, Wilhelm WW (2008) Sustainable biofuels redux. Science 322:49–50
94. Tilman D, Hill J, Lehman C (2006) Carbon-negative biofuels from low-Input high-diversity grassland biomass. Science 314:1598–1600
95. Campbell JMF, Lobell DB, Genova RC, Field CB (2008) The global potential of bioenergy on abandoned agriculture lands. Environ Sci Technol 42:5791–5794
96. Wilhelm WW, Johnson JMF, Karlen DL, Lightle DT (2007) Corn stover to sustain soil organic carbon further constrains biomass supply. Agron J 99:1665–1667
97. Editorial (2010) Climate of suspicion. Nature 463:269
98. IPCC (2001) Climate change 2001. Impacts, adaptation and vulnerability. Cambridge University Press, Cambridge
99. Reidsma P, Ewert F, Oude Lansink A, Leemans R (2010) Adaptation to climate change and climate variability in European agriculture: the importance of farm level responses. Eur J Agron 32:91–102
100. Stafford N (2007) The other greenhouse effect. Nature 448:526–528
101. Borras L, Slafer GA (2008) Agronomy and plant breeding are key to combating food crisis. Nature 453:1177
102. Willis KJ, Birks HJB (2006) What is natural? The need for a long-term perspective in biodiversity conservation. Science 314:1261–1265
103. ICARDA (1995) Farm resource management program. Annual Report for 1994. International Center for Agricultural Research in the Dry Areas, Aleppo, Syria

Cryosphere, Modeling of

Cecilia M. Bitz[1], Shawn J. Marshall[2]
[1]Atmospheric Sciences Department, University of Washington, Seattle, WA, USA
[2]Department of Geography, Earth Sciences, University of Calgary, Calgary, AB, Canada

Article Outline

Glossary
Definition of Subject
Introduction
Thermodynamics of the Cryosphere
Land Ice Dynamics
Floating Ice Dynamics
Future Directions
Bibliography

Glossary

Ablation Snow and ice removed from an ice mass via meltwater runoff, sublimation, wind scour, or glacial calving (mechanical fracturing and separation).

Accretion Increase in ice mass by basal growth in the case of floating ice, the compression of snow into ice, or freezing of water that has pooled on the ice or percolated into snow from rain, meltwater, or flooding of sea/lake/river water.

Accumulation Snow and ice added to an ice mass via snowfall, frost deposition, rainfall that freezes on/in the ice mass, refrozen meltwater, wind-blown snow deposition, and avalanching.

Glacier A perennial terrestrial ice mass that shows evidence of motion/deformation under gravity.

Grounding line The transition zone between grounded and floating ice.

Ice sheet A large (i.e., continental-scale) dome of glacier ice that overwhelms the local bedrock topography, with the ice flow direction governed by the shape of the ice cap itself.

Ice shelf Glacier ice that has flowed into an ocean or lake and is floating, no longer supported by the bed.

Icefield A sheet of glacier ice in an alpine environment in which the ice is not thick enough to overwhelm the local bedrock topography, but is draped over and around it; glacier flow directions in an icefield are dictated by the bed topography.

Lake/river ice Floating ice on rivers or lakes, usually freshwater ice.

Mass balance The overall gain or loss of mass for a component of the cryosphere over a specified time interval, typically 1 year. This can be expressed as a rate of change of mass (kg year^{-1}), ice volume (m^3 year^{-1}), or water-equivalent volume (m^3 w.eq. year^{-1}). It is also common to express this as the area-averaged rate of change or the specific mass balance rate, with units of kg m^{-2} year^{-1} or m w.eq. year^{-1}.

Permafrost Perennially frozen ground, technically defined as ground that is at or below 0°C for at least 2 years.

Sea ice Floating ice from frozen seawater.

Snow Ice-crystal precipitation that accumulates on the surface.

Soil ice Ice in permafrost.

Definition of Subject

The global cryosphere encompasses snow and ice in all its forms in the natural environment, including glaciers and ice sheets, sea ice, lake and river ice, permafrost, seasonal snow, and ice crystals in the atmosphere. Cryospheric models are mathematical and numerical descriptions of these components of the Earth system, designed to simulate snow and ice processes and feedbacks in the context of the global climate system. This entry covers all forms of ice except ice crystals in the atmosphere, which are more appropriately combined with clouds and appear in entry ► Solar Radiation Management, Cloud Albedo Enhancement. We focus on models that are appropriate for global climate modeling. There are regional climate modeling applications that include some of the cryospheric components discussed here as well.

The cryosphere is critical to understanding global climate change owing to its control on Earth's surface reflectivity. In addition, storage of freshwater by the cryosphere and exchange of freshwater between the cryosphere and ocean are fundamental to ocean circulation and sea level rise. Sea ice and snow insulate the underlying surface and usually allow lower atmospheric temperatures than snow and ice environments.

Biogeochemical cycles in sea ice and permafrost influence carbon dioxide and methane concentrations in the atmosphere, and sea ice hosts organisms and nutrients important to marine ecosystems. Modeling cryosphere-climate interactions generally requires modeling the mass balance of ice on Earth and the key features of ice that interact with the climate system.

Perennial ice covers 10.8% of Earth's land, with most of this ice area in the great polar ice sheets in Greenland and Antarctica. Smaller glaciers and icefields are numerous – the global population is estimated at 160,000 – but these ice masses cover less than 1% of the landscape. An additional 15.4% of Earth's land surface is covered by permafrost: frozen ground that ranges from a few meters to 100 s of meters deep.

In contrast to this permanent land ice, seasonal snow and ice fluctuate dramatically. Snow cover is the largest-varying element of the cryosphere, with complete summer loss of this snow everywhere on Earth except over Antarctica, the interior of Greenland, and in the accumulation areas of other high-altitude and polar ice caps. In winter, the northern hemisphere snow cover reaches an average maximum extent of 45.2×10^6 km [1], based on data from 1966 to 2004). This amounts to 49% of the Northern Hemisphere land mass. Because the southern hemisphere continents are situated at lower latitudes (excepting Antarctica), southern snow cover is less extensive, with the seasonal snow cover estimated at 1.2×10^6 km. This combines with the permanent blanket of snow over Antarctica to give a peak southern hemisphere terrestrial snow cover of 15.0×10^6 km.

Relative to the snowpack, seasonal sea ice cycles are more hemispherically symmetric, although there are interesting north–south contrasts. Based on passive microwave remote sensing for the period 1979–2010, the average minimum Northern Hemisphere sea ice area is 4.4×10^6 km, typically reached in September [2]. Maximum ice cover is usually attained in March, with an average area of 13.1×10^6 km. The annual average Northern Hemisphere sea ice area is 9.4×10^6 km. The Southern Hemisphere sea ice has a larger seasonal cycle, with relatively little multiyear ice. Annual mean sea ice cover in the south is 8.7×10^6 km, varying from 1.9×10^6 km (February) to 14.5×10^6 km (September).

Introduction

The early energy balance modelers of the 1960s who investigated global climate recognized the importance of the high albedo of ice in the climate system [3, 4]. Their models parameterized snow and ice albedo by varying the land or ocean surface albedo with surface temperature, but no other physical characteristics of ice, such as its ability to insulate or store energy and freshwater, was simulated. When subject to climate forcing, such as a perturbation to the solar constants, the models nonetheless exhibited an amplification of temperature change in the high latitudes – a phenomenon widely known as polar amplification. The albedo difference between ice-covered and ice-free regions determined the strength of the polar amplification. Today we know ice-albedo feedback is only one of many important ways that ice and snow contribute to the climate system.

The next progression in ice modeling among global climate models was to include the major elements of the mass balance of snow on land [5] and sea ice [6], both implemented in the Geophysical Fluid Dynamics Laboratory (GFDL) in 1969. Yet the GFDL model and all other climate models for several more decades had no ice dynamics, continued to treat ice sheets as shallow snow fields with prescribed representative topography, and ignored soil ice altogether. The more advanced aspects of cryosphere modeling evolved in parallel with, but independent of global climate models.

In the 1950s, John Nye [7, 8] laid the theoretical foundations for glacier models, through the elucidation of the essential physics as well as several well-judged simplifications that permit analytical solutions. Theoretical and laboratory analyses by a contemporary materials scientist, John Glen, led to the understanding that glacier ice deforms as a nonlinear viscous fluid. Glen established a constitutive relation for the rheology of glacier ice that endures to this day [9, 10]. Combined with the conservation equations for mass, momentum, and energy, this provides the basis for modeling glaciers and ice sheets. By the late 1960s and 1970s, emerging computer power presented the opportunity to develop numerical models of glaciers [11–13]. Model development through the 1980s largely focused on regional

simulations [14] and ice flow in different regimes, such as ice shelves and ice streams [15, 16].

In the late 1980s, Philippe Huybrechts developed the first pragmatic, operational 3D thermomechanical ice sheet model [17, 18]. This model has been applied extensively to the Greenland and Antarctic Ice Sheets, helping to understand their past and present evolution, e.g., [19–22]. The Huybrechts model also underpins the projections of ice sheet response to climate change in the IPCC reports. Similar models have now been developed in several research groups, and intercomparison exercises have been carried out to evaluate model strengths and weaknesses [23, 24].

A few global climate models have incorporated a Huybrechts-type ice sheet model such that changes to the global climate can interact with the shape and extent of ice sheets in Greenland and Antarctica. The interaction occurs through changes in surface albedo as the ice sheet retreats or advances over bare soil, elevation-temperature feedbacks, and through changes in the atmospheric and oceanic circulation [21, 25–27].

The low-order glacier models implemented in global climate models to date are based on a simplified representation for ice sheet flow (see section "Land Ice Dynamics"), which is not well-suited to ice shelves, ice streams, and ice sheet margins. Because these features of ice sheets are known to be changing rapidly, current development efforts are focusing on higher-order solutions of ice dynamics [28–32]. Models of valley glacier dynamics have followed a similar evolution from simplified representations of ice dynamics, e.g., [33], to recent simulations that include a more complete representation of the glacier stress and strain regime [34–38]. Parallel to this recent effort are formal, community-scale programs to couple more sophisticated, high-resolution ice sheet models into global climate models [39], although fully coupled efforts with global climate models are still in their infancy.

The development of sea ice models took a rather different path than glacial models. Model development began later, but the methods, albeit often simplified, migrated more quickly into global climate models. Today the lag between developing new sea ice model physics and implementing them in global climate models is often only a few years.

The first sea ice rheology was proposed in the 1970s, roughly two decades after the glacier rheology proposed by Nye and Glen. Initially a plastic rheology was put forward as a way to produce deformation (ridging and rafting) for the Arctic Ice Dynamics Joint Experiment (AIDJEX) model spearheaded by Max Coon [40]. Models attempting to treat ice as a plastic were only appropriate for local-scale problems of a few weeks to a month duration and could not be used to investigate ice-climate interactions owing to their inherent numerical complexity [41]. In the late 1970s, William Hibler proposed a nonlinear viscous-plastic (VP) rheology – a simplification motivated on physical grounds [42]. In a 1979 landmark paper, Hibler applied his sea ice model to the whole Arctic Ocean basin and ran an 8-year simulation [43]. The AIDJEX and Hibler sea ice dynamics remains the foundation of modern sea ice models.

A subgridscale parameterization of the variety of sea ice thicknesses that are found in a typical model grid box, known as an ice thickness distribution (ITD), was developed by Alan Thorndike and colleagues [44] and implemented by Hibler at the basin-scale in 1980 [43]. Modeling the intricacies of sea ice thermodynamics to account for the thermal inertia of brine-pocket physics was developed slightly earlier by Norbert Untersteiner and Gary Maykut [45, 46], but it was only implemented in 1D until the present decade.

The first global climate models treated sea ice as a uniform slab without leads (openings among floes), melt ponds, or brine pockets, based on the simplifications proposed by Albert Semtner [47]. If the sea ice moved at all, it was advected with the surface currents – in what is known as "free drift." Once the sea ice thickness reached some threshold (4 m was common), it was then held motionless to prevent the sea ice from building to excess in regions of convergence [48–50].

It was not until Flato and Hibler [51] simplified the VP model by treating sea ice as a cavitating fluid (CF) that global climate modelers attempted to implement sea ice dynamics with a constitutive law. However, the lack of shear strength in the CF model degraded the accuracy of the simulation compared to the VP model. Soon after Hunke and Ducowicz [52] developed a technique of treating sea ice as an elastic-viscous-plastic (EVP) material – a numerical approximation to the VP model that asymptotes to the full VP solution and yet is efficient, highly parallelizable, and offers flexible grid choices. Zhang and Hibler [53] followed

suit by making the VP numerics more efficient and parallelizable. These new dynamical schemes ushered in a time of rapid improvement in the sea ice dynamics in climate models, and now EVP and VP dynamics are in wide use among climate models. Thermodynamic advances in global climate models have been slower. The use of an ITD and brine-pocket physics has only been recent in climate models [54, 55]. Melt pond parameterizations and radiative transfer that includes scattering have only been developed in one dimension and are in the early stages of production runs in the next generation of models.

Snow and permafrost models used for one- and two-dimensional applications also progressed significantly before their developments were brought into climate models, e.g., [56–58]. Permafrost models are typically based on one-dimensional thermal diffusion in the upper 2 km of the Earth surface, consisting of bedrock, sediments, and soils. Where temperatures are below freezing, ground ice occupies pore space and fractures in the rock. A freezing front propagates to a depth that is limited by the geothermal heat flux. Permafrost models simulate the aggradation or degradation of permafrost, based on mean annual surface (ground) temperatures and subject to geothermal heat flux from below. Detailed near-surface models can be added to simulate the seasonal melting/freezing of the surface active layer. In reality, more complex thermodynamic and hydrological processes are involved in permafrost dynamics. For instance, water flow can advect heat and there are 3D thermal effects associated with horizontal gradients in surface temperature, arising from variable surface vegetation, micro-topography, snow cover, and surface lakes. In addition, freezing of subsurface water is not always limited to the pore space; ice can accrue as "massive ice" deposits (e.g., ice lenses) through migration of water to the interstices of soils and sediments, driven by low capillary pressures. Simple permafrost models, as used in climate models, typically neglect these processes and focus on large-scale predictions of permafrost depth and 1D ground temperature structure.

For snow models, the chief physical processes that prove challenging to model are snow aging and grain size evolution influences on the albedo and density; liquid water infiltration and storage; snow blowing, redistribution, and collection by vegetation; and active layer depth dynamics. Many global climate models have developed terrestrial snow schemes to treat all but snow redistribution in the last few decades because these processes have a major impact on surface albedo, surface hydrology, and soil carbon storage [59–64]. Subgridscale snow distribution models exist [65] but have yet to be implemented in any global climate model that we are aware of. Models of snow on sea ice tend to be more primitive because transporting every variable that describes the snow is necessary and expensive.

In subsequent sections we describe the equations and methods used to model the cryosphere, followed by a brief outlook of future directions and priorities in cryospheric modeling. Components of the cryosphere are grouped into four types based on common characteristics and physics: Land ice refers to ice above the soil/bedrock (e.g., glaciers and ice sheets) and ice shelves; floating ice refers to river, lake, or sea ice; frozen soil includes permafrost and seasonally frozen soil; and finally snow, which may overly land ice, floating ice, or soil. The underlying equations for the dynamics of land and floating ice are rooted in a blend of continuum mechanics and fluid dynamics, but there are significant differences in their implementation, justifying separate descriptions. In contrast, thermodynamics cuts across all aspects of the cryosphere, and much about it can be described more generally.

Thermodynamics of the Cryosphere

Conservation of Energy

The governing equation for the thermodynamics of the cryosphere is conservation of energy:

$$\frac{Dq}{Dt} + \nabla \cdot (\mathbf{u}_v \phi q_v) = -\nabla \cdot (k \nabla T) + Q_{sw} + \Phi \tag{1}$$

which is written in terms of an enthalpy (q) for ice, snow, or mixed soil and ice, where q is expressed in units of Jm^{-3}, ϕ is the void (or pore) fraction within the solid where liquid water/vapor may exist, $\mathbf{u}_v$ is the velocity of liquid water/vapor moving in the voids, T is temperature in the solid and voids, q_v is the enthalpy of liquid water/vapor in the voids, k is the conductivity in solids and voids, Q_{sw} is the absorption of shortwave radiation over a finite thickness of the ice ($\mathrm{W\ m}^{-3}$), which is assumed to be significant only in ice, and Φ is

the strain heat production due to deformation work (significant for glaciers). The first term is a Lagrangian derivative of the heat required to raise the temperature and change the phase between solid and liquid. It is Lagrangian to account for the horizontal advection of heat in moving land and floating ice (see sections "Land Ice Dynamics" and "Floating Ice Dynamics"). The second term represents heat transport due to liquid water or vapor transport in the voids, and the third term is diffusion of heat in both solid and voids. In models of practical use today, vertical gradients in the enthalpy are far greater than those in the horizontal; therefore, the horizontal diffusion and horizontal liquid/vapor transport in the pore space are generally neglected.

The enthalpy can be written to a good approximation

$$q = c_i(T - T_o) + L_o(1 - \phi) \tag{2}$$

where c_i is the volumetric specific heat of ice or snow (or the ice and soil combination for permafrost), L_o is the volumetric latent heat of fusion for ice or snow, and ϕ is the fraction of the volume that is not composed of ice. This includes air- and liquid-filled pore space in the volume, and in frozen ground, it also includes the soil or rock matrix. Modern models of snow and frozen soil may allow liquid water to infiltrate and possibly supercool, and therefore, additional equations are needed to describe liquid infiltration and the conversion of liquid to ice and vice versa. Such equations may be devised such that the second term in Eq. 2 is not needed. The reader may refer to the Community Land Model, CLM version 4 for a description of one possible model of snow and frozen soil that is designed for a global climate model but is relatively complete [66].

The boundary conditions of Eq. 1 depend on the cryosphere component and possibly the climatic conditions. First consider the special case of floating ice where the basal temperature is always assumed to be at T_f. In these materials, the bottom boundary of Eq. 1 has a temperature boundary condition, and the net flux into the surface excluding the conductive flux in the ice is equal to the heat flux from the water below: $F|_{bottom} = F_W$ (fluxes are taken as positive toward the surface). In contrast, the base of land ice and the lowest point considered in a soil or snowpack model are generally not at the freezing point, in which case Eq. 1 has a flux boundary condition at the base equal to the geothermal heat flux: $F|_{bottom} = F_G$. At the top surface of ice or snow, one must test if the net flux into the top surface can balance the conductive flux (taking z as positive down):

$$F(T)|_{top} = k\left.\frac{\partial T}{\partial z}\right|_{top},$$

for a surface temperature below the freezing point ($T < T_f$). If so, then a flux boundary condition is used at that surface in Eq. 1. If the surface temperature is at or above the freezing point, then a temperature boundary condition is used at that surface in Eq. 1 with $T = T_f$.

Ablation, Accretion, and Accumulation

Models of land ice, floating ice, and snow usually employ a fixed number of layers and therefore layer thicknesses vary in time. This so-called moving boundary method requires a Stefan condition to describe ablation, accretion, and accumulation. The rate of change of the top surface position (z_o, positive down) for snow or ice from ablation is

$$q\left.\frac{dz_o}{dt}\right|_{\text{ablation}} = F(T)|_{top} - k\left.\frac{\partial T}{\partial z}\right|_{top} \quad \text{if } F(T)|_{top} > k\left.\frac{\partial T}{\partial z}\right|_{top}. \tag{3}$$

An additional equation is needed to account for snow processes that contribute to increasing the mass of ice and/or snow at the top surface:

$$\left.\frac{dz_o}{dt}\right|_{\text{accumulation}} = -S_{fall} + \delta, \tag{4}$$

where S_{fall} is the rate of falling snow, and δ is from snow densification, snow to ice conversion, snow redistribution, etc. The rate of change of the bottom surface position (z_b, positive down) for ice from accretion (if liquid water is available) or ablation is

$$q\frac{dz_b}{dt} = -F(T)\Big|_{bottom} - k\left.\frac{\partial T}{\partial z}\right|_{bottom}. \tag{5}$$

Floating ice may experience lateral accretion or ablation as well. Land and floating ice must also take into account the horizontal transport of ice, which is described in sections "Land Ice Dynamics" and "Floating Ice Dynamics".

Surface Energy Balance, Radiation, Surface Albedo, and Melt Ponds

The net flux entering the top surface of land and floating ice, soil, or snow is a sum of radiative and turbulent heat fluxes:

$$F(T)|_{top} = F_r(1-\alpha) - I_0 + F_L - \epsilon\sigma T^4 + F_s + F_e, \tag{6}$$

where $F_r(1-\alpha)$ is the net downward solar irradiance above the top surface, α is the surface albedo, I_o is the solar irradiance that penetrates the top surface, f_l is the downward longwave irradiance, $\epsilon\sigma T^4$ is the upward longwave irradiance (for T in Kelvin), ϵ is the emissivity, σ is the Stefan-Boltzmann constant, F_s and F_e are the downward sensible and latent heat fluxes, respectively.

In many ice and snow models, the surface albedo is a function of various quantities such as temperature, snow grain size, snow age, impurities, snow depth, ice thickness, and melt pond coverage. Often shortwave radiation is absorbed in the ice interior based on Beer's law, although Beer's law is inappropriate in materials with depth-dependent surface albedo parameterizations. Usually the temperature dependence of the surface albedo is a proxy for modeling melt pond, grain size, and/or surface scattering characteristics. These relatively crude methods are being revamped considerably in models at this time.

A better way is to design a highly interdependent set of physics for radiative transfer, ponding, and liquid infiltration. Ideally one would have radiative transfer account for multiple-scattering and be based on intrinsic optical properties that vary with impurity concentrations, snow grain size, ice bubbles, and brine pockets. Ponds would accumulate water above sea level when there is insufficient hydraulic connectivity to drain meltwater, and they would accumulate below sea level when there is hydraulic connectivity that is high enough to allow liquid water to rise up from below and flood the surface.

Influence of Salts and Other Impurities

Dissolved impurities such as salts in the pore water depress the freezing point. For ice to remain in local thermodynamic equilibrium, the pore water is always at the freezing point and freezing or melting must occur at the pore-ice interface to dilute or concentrate the solute. If we assume for simplicity that the voids are completely filled with liquid, then the void fraction is a function of temperature and the bulk solute concentration. The solute concentration in the voids, assuming freezing expels the solute completely into the voids, is a function of temperature according to the liquidus relation from the phase diagram of the binary material (ice plus solute). A few global climate models today have sea ice models that allow for such pore-ice interchange (also known as brine-pocket physics in sea ice) [54, 55]. However, these models assume the bulk solute concentration is fixed in time, and hence, they neglect the heat and solute transport in the voids. These simplifications made it possible for the first step, but they cannot capture the important structural evolution of young sea ice or rapidly changing permafrost. These processes should not be neglected in models that aim to model biogeochemistry in the polar regions.

Land Ice Dynamics

Glaciers are perennial ice masses that are large enough to experience gravitational deformation: the flow of ice under its own weight. Glaciers and ice sheets nucleate where snow accumulation exceeds snow and ice ablation over a period of many years or decades. With time, the accumulated snow is buried and compressed, metamorphosing into firn and then glacier ice. Ice behaves as a nonlinear, visco-plastic fluid; once the ice thickness is sufficient, internal gravitational stresses cause the ice to deform.

Snow accumulation is primarily meteoric (derived from atmospheric precipitation), but snow can also accumulate at a site through wind deposition or avalanching. Ablation refers to the loss of snow and ice through melting, sublimation, wind erosion, or calving, a process where slabs of ice at the glacier margin mechanically fracture and detach from the main ice mass. Iceberg calving is a very effective ablation mechanism for glacier and ice sheets that are in contact with the ocean. Melting occurs at the glacier surface – the ice-atmosphere interface – but there is also melting internally (englacially), at the glacier bed (subglacially), and on vertical ice cliffs that are common at the ice margin, particularly where glaciers reach

the sea and a large area of ice can be in contact with water. Melting only leads to ablation in the case where meltwater runs off and is removed from the system; some surface meltwater in the upper regions of glaciers and ice sheets percolates into the snowpack or ponds at the surface, where it can refreeze.

A glacier's mass balance is determined by the net accumulation minus ablation over a specific time period, typically 1 year. This can be expressed as a total balance (kg year^{-1} or m^3 year^{-1} water-equivalent for the entire glacier) or a specific balance, per unit area of the glacier (kgm^{-2} year^{-1} or m year^{-1} water-equivalent). There is no simple "threshold temperature" for a glacier to be viable; a mean annual temperature below 0°C is not a necessary or sufficient condition for glacier ice to exist. Tidewater glaciers are vivid examples of this. Because ice flow delivers large fluxes of ice to low elevations, glaciers can extend to sea level environments where mean annual temperatures are several degrees above 0°C. While most glaciers do not reach the ocean, this feature is intrinsic to all glaciers; glacier ice in the ablation area does not grow in situ, but is a consequence of ice transport from the accumulation area to the ablation area.

Glacier flow occurs through three different mechanisms: internal "creep" deformation, decoupled sliding at the ice-bed interface, and deformation of subglacial sediments (Fig. 1). The former is a function of ice rheology and the stress regime in the ice, while the latter two mechanisms are governed by conditions at the base of the glacier [67]. These processes are described in more detail below.

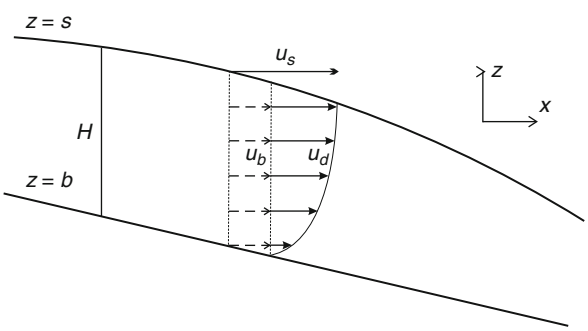

Cryosphere, Modeling of. Figure 1
Schematic of glacier flow mechanisms. The surface velocity $u_s = u_b + u_d(s)$. Basal velocity is the sum of deformation of underlying sediments and decoupled sliding at the ice-bed interface. Where ice is moving at the bed, these two processes can operate together, or only one of them may be active

Governing Equations for Glacier Dynamics

Similar to models of atmosphere or ocean dynamics, the flow of glaciers and ice sheets is mathematically described from the equations for the conservation of mass, momentum, and energy. For a point on the glacier with ice thickness H, the vertically integrated form of the conservation of mass is most commonly employed in glaciological models:

$$\frac{\partial H}{\partial t} = -\nabla \cdot (\overline{\mathbf{u}} H) + b. \tag{7}$$

Here $\overline{\mathbf{u}}$ is the average horizontal velocity in the vertically integrated ice column and b is the mass balance rate. The mass balance is computed generally from Eqs. 3–5 by

$$b = -\left.\frac{dz_o}{dt}\right|_{\text{ablation}} - \left.\frac{dz_o}{dt}\right|_{\text{accumulation}} + \frac{dz_b}{dt}. \tag{8}$$

The first term on the right-hand-side describes the horizontal divergence of ice flux, while the second term describes the net local source or sink of mass associated with accumulation and ablation. The vertically averaged velocity includes ice flow due to both internal deformation and basal flow: $\overline{\mathbf{u}} = \overline{\mathbf{u_d}} + \mathbf{u_b}$. Glacial ice moves slowly, so a year is typically adopted as the most convenient unit of time; hence, ice velocities are reported in m year^{-1} and b is expressed as m year^{-1} of ice-equivalent gain or loss of mass.

The main challenge in modeling glaciers and ice sheet is evaluation of the velocity field. Acceleration and inertial terms are negligible in glacier flow, so the Navier–Stokes equations that describe conservation of momentum reduce to a case of Stokes flow, where gravitational stress is balanced by internal deformation in the ice:

$$\nabla \cdot \sigma = -\rho \mathbf{g}, \tag{9}$$

where σ is the ice stress tensor, ρ is ice density, and $\mathbf{g}$ is the gravitational acceleration. Expanding this into the three directional components,

$$\frac{\partial \sigma_{xx}}{\partial x} + \frac{\partial \sigma_{xy}}{\partial y} + \frac{\partial \sigma_{xz}}{\partial z} = 0,$$
$$\frac{\partial \sigma_{yz}}{\partial x} + \frac{\partial \sigma_{yy}}{\partial y} + \frac{\partial \sigma_{yz}}{\partial z} = 0, \tag{10}$$
$$\frac{\partial \sigma_{xz}}{\partial x} + \frac{\partial \sigma_{yz}}{\partial y} + \frac{\partial \sigma_{zz}}{\partial z} = -\rho_i g.$$

Ice deformation is independent of confining (i.e., hydrostatic) pressure, so ice rheology is usually couched as a function of the deviatoric stress tensor, σ'. Under the assumption that ice is incompressible, the momentum equations can be analyzed to give the horizontal balances

$$2\frac{\partial \sigma'_{xx}}{\partial x} + \frac{\partial \sigma'_{yy}}{\partial x} + \frac{\partial \sigma'_{xy}}{\partial y} + \frac{\partial \sigma'_{xz}}{\partial z} = -\rho g \frac{\partial h}{\partial x},$$
$$\frac{\partial \sigma'_{yz}}{\partial x} + 2\frac{\partial \sigma'_{yy}}{\partial y} + \frac{\partial \sigma'_{xx}}{\partial y} + \frac{\partial \sigma'_{yz}}{\partial z} = -\rho g \frac{\partial h}{\partial y}. \tag{11}$$

The terms on the right-hand-side represent the surface slope, for the glacier surface $h(x, y)$. Greve and Blatter [129] present a detailed derivation of this full system of equations and their solution. A constitutive relation is needed to express internal stresses in terms of strain rates in the ice: $\dot{\epsilon}_{ij} = 0.5(\partial u_i/\partial x_j + \partial u_j/\partial x_i)$. Equation 11 can then be rewritten as a function of the 3D ice velocity field, providing a framework to solve for $\bar{u}$ and integrate Eq. 7 to model the evolution of glacier geometry in response to variations in ice dynamics or climate. The next section describes the constitutive relation that is most commonly used in glacier modeling.

Because ice rheology is strongly temperature-dependent, an additional equation is needed to solve for the 3D temperature distribution. As discussed in section "Thermodynamics of the Cryosphere," the local energy balance gives the governing equation for temperature evolution in the ice sheet in Eq. 1.

Given a 3D temperature distribution through the ice sheet, the effective rheology of the ice can be evaluated and the velocity field can be numerically determined. Knowledge of the temperature field is also essential to assessing whether the base of the ice sheet is at the pressure melting point or not; if so, liquid water can be present at the bed and the glacier or ice sheet is subject to basal flow.

Internal Deformation: Ice Rheology In order to solve the Stokes flow diagnostic equation, ice sheet stresses need to be expressed as velocity fields, via a constitutive relation for ice. The rheology of polycrystalline glacier ice is well-studied in laboratory and field environments [68]. Lab studies of tertiary ice deformation reveal that ice deforms as a nonlinear viscous fluid [9, 10, 69, 70]. The original form of the flow law proposed by Glen [9, 10] is broadly supported by field studies of tunnel and borehole deformation [7, 71], as well as observations and modeling of large-scale ice motion [72, 73].

This constitutive relation is known as Glen's flow law and is written as a function of the second invariant of the deviatoric stress tensor, $\sum_2' = \left(\sigma'_{ij}\,\sigma'_{ji}\right)/2$,

$$\dot{\epsilon}_{ij} = B(T) \sum_2'^{(n-1)/2} \sigma'_{ij}. \tag{12}$$

$B(T)$ is an "ice softness" term that follows an Arrhenius temperature dependence,

$$B(T) = B_0 \exp\left(\frac{-Q}{RT}\right). \tag{13}$$

B_0 is called the Glen flow law parameter, R is a constant, and Q is the creep activation energy. Lab and field studies of ice deformation suggest that B_0 can vary by a factor of about 10 [68]. Including the effects of strain-softening and temperature, the effective viscosity of ice varies by several orders of magnitude.

This formulation is an isotropic flow law that allows the first-order effects of ice temperature and deviatoric stress regime to be incorporated in estimates of ice deformation. Ice deformation is typically modeled as an $n = 3$ process. Where shear stress and shear deformation are dominant, as is often the case, this is well-approximated by

$$\dot{\epsilon}_{xz} = B(T)\,\sigma'^3_{xz}. \tag{14}$$

Glen's flow law is for pure, isotropic ice. There are numerous other complicating factors for ice deformation, such as anisotropic ice fabric [74–76], the potential impact of grain size [77, 78], and the presence of impurities and intergranular liquid water content [79]. These effects are not explicitly resolved in ice sheet models, but the flow rate parameter, b_0, is typically tuned to approximate the bulk effects of crystal fabric, grain size, and impurity content.

The strain rates in Eq. 12 or 14 can be expressed as velocity gradients, and then vertically integrated or

inverted and substituted into the momentum balance, Eq. 11, to give a set of equations for the horizontal ice velocity. Various numerical solutions to these equations have been adopted in glacier and ice sheet modeling, outlined in more detail in the next section.

Basal Flow In addition to internal deformation, glacier ice can flow at the base where the bed is at the pressure melting point, through some combination of subglacial sediment deformation and decoupled sliding over the bed. Large-scale basal flow generally requires pressurized subglacial meltwater, which can lubricate the bed, float the ice, or weaken subglacial sediments. Subglacial hydrology therefore plays a pivotal role in fast-flowing glaciers and ice streams [80, 81]. High subglacial water pressures can decouple the ice from the bed by reducing or eliminating basal friction. On local scales this may not entice a significant ice-dynamical response, as resistive stresses can be taken up at adjacent well-coupled regions of the bed, by side drag from valley walls or adjacent ice, or by longitudinal stress bridging (upstream and downstream resistance to flow). However, numerous observational studies report occasions where inputs of surface meltwater to the bed overwhelm these resistive stresses and produce localized speedups in valley glaciers, e.g., [82, 83] and in polar icefields [84–86].

For large-scale ice stream flow or surging of outlet glaciers, subglacial water must occupy a significant portion of the glacier bed, at pressures which are sufficient to drown geologic and topographic pinning points [83, 87]. In this situation, widespread ice-bed decoupling can permit high rates of basal flow (100–1,000 s of m year^{-1}) and a regime in which ice fluxes are dominated by basal flow.

In ice sheets that exhibit high rates of basal flow, there is ongoing uncertainty as to the relative importance of sliding flow along the ice-bed interface versus deformation of the underlying glacial sediment. High subglacial water pressures are conducive to both processes. Fast flow in West Antarctica's Siple Coast ice streams is associated with plastic failure of a thin layer of saturated marine sediment [88, 89], and similar processes are expected to be important wherever subglacial sediments and topographic features offer a relatively smooth, low-friction substrate [90].

Models make some allowance for basal flow, usually through a local sliding "law" relating basal flow, u_b, to gravitational shear stress at the bed, raised to some power m, $u_b \propto \tau_d^m$. In some applications, the effects of subglacial water pressure on basal flow are introduced, typically through the effective pressure p_e. This is the difference between glaciostatic (ice) pressure and subglacial water pressure: $p_e = pi - p_w$. An effective pressure of 0 indicates that ice is floating, so low or negative effective pressures promote ice-bed decoupling and enhanced basal flow. While it is safe to assume that $u_b \propto p_e^{-k}$, for some unknown power k, there is likely no generalized local relationship between u_b and p_e; actual basal flow is affected by regional-scale ice dynamics, not just local conditions. A prescription of the form $u_b = A\tau_d^m/p_e^k$ is unstable as this blows up as $p_e \to 0$. Local flotation is commonly observed in nature, so $p_e = 0$ is a physically acceptable possibility. The mathematical instability is simply a failure of the local form of the basal flow law. An alternative is to introduce a parameterization in terms of the flotation fraction p_w/p_i, with $u_b = 0$ when $p_w = 0$ and basal flow increasing with p_w/p_i. The local expression $u_b = A\tau_d^m f(p_w/p_i)$ can represent this, e.g., [91]. Basal flow observations are notoriously difficult to make so there is no clear recommendation as to the functional form of $f(p_w/p_i)$. Hydrological enabling of basal flow is expected to be a nonlinear, threshold process [92].

Modeling Glaciers and Ice Sheets

This section describes the physical approximations and numerical techniques in place for simulations of glacier and ice sheet dynamics, based on solution to Eqs. 7, 11, and 1.

One common reduction in ice sheet modeling, known as the shallow-ice approximation, involves a number of scaling assumptions that are valid when horizontal gradients in ice thickness and velocity are small and ice flows dominantly by vertical shear deformation. Under these conditions, Eq. 11 simplifies to

$$\frac{\partial \sigma'_{iz}}{\partial z} = -\rho g \frac{\partial h}{\partial x_i}. \tag{15}$$

where subscript i refers to the horizontal direction of interest (x, y). Equation 15 can be vertically integrated to give

$$\sigma'_{iz}(z) = -\rho g\,(h-z)\frac{\partial h}{\partial x_i}. \tag{16}$$

This vertical shear stress is commonly known as the gravitational driving stress, τ_d. It vanishes at the glacier surface ($z = h$) and $\tau_d = -\rho g\, H \nabla h$ at the glacier bed. Substituting for the strain rates based on Glen's flow law and representing strain rates in terms of velocity gradients gives

$$u_i(z) = u_{bi} - 2(\rho g)^n |\nabla h|^{n-1} \frac{\partial h}{\partial x_i} \int_b^z B(T)(h-z)^n dz, \tag{17}$$

for basal velocity $\mathbf{u_b}$.

For the shallow-ice approximation represented in Eq. 17, the vertically averaged ice velocity due to deformation is nonlinearly proportional to local surface slope and ice thickness,

$$\mathbf{u_d} \propto (\nabla h)^n H^{n+1}. \tag{18}$$

This treatment of ice dynamics has been adopted in most ice sheet modeling studies to date, e.g., [19, 20, 93]. The nonlinearity of Glen's flow law gives ice deformation rates that are exceptionally sensitive to the glacier thickness and surface slope. Under this approximation, ice velocity is solely a function of local ice geometry. This neglects "farfield" effects and other complicating influences on ice flow, such as longitudinal stretching/compression of the ice and horizontal shearing due to the friction of valley walls. The influence of longitudinal stress coupling on ice dynamics is significant in complex terrain such as valley glaciers and mesoscale icefields [34, 94]. It is also important in settings such as tidewater glaciers, ice shelves, ice streams, transition regions from inland to floating ice dynamics, and ice sheet divides [14, 28]. Many of the most interesting questions in ice sheet behavior involve these parts of the system, so more complete representations of ice dynamics are of great interest.

Doug MacAyeal [16, 130] introduced an approximation for ice shelf and ice stream flow that is essentially the complement of the shallow-ice approximation in Eq. 15. Because flow in ice streams is predominantly at the base, a plug-flow approximation, assuming no vertical shear, is reasonable. The gravitational driving stress is then taken up by longitudinal stress, horizontal shear stress, and basal friction. In ice shelves, the basal traction also vanishes. Under this approximation, Eq. 11 can be written

$$\begin{aligned} \frac{\partial}{\partial x}(2\sigma'_{xx} + \sigma'_{yy}) + \frac{\partial}{\partial y}(\sigma'_{xy}) &= -\rho g \frac{\partial h}{\partial x}, \\ \frac{\partial}{\partial x}(\sigma'_{xy}) + \frac{\partial}{\partial y}(\sigma'_{xx} + 2\sigma'_{yy}) &= -\rho g \frac{\partial h}{\partial y}. \end{aligned} \tag{19}$$

Substituting for strain rates and defining an effective viscosity μ_e from the inverted form of Glen's flow law [16],

$$\begin{aligned} \frac{\partial}{\partial x}\left[\mu_e\left(2\frac{\partial u}{\partial x} + \frac{\partial v}{\partial y}\right)\right] + \frac{\partial}{\partial y}\left[\frac{\mu_e}{2}\left(\frac{\partial u}{\partial y} + \frac{\partial v}{\partial x}\right)\right] &= -\rho g \frac{\partial h}{\partial x}, \\ \frac{\partial}{\partial x}\left[\frac{\mu_e}{2}\left(\frac{\partial u}{\partial y} + \frac{\partial v}{\partial x}\right)\right] + \frac{\partial}{\partial y}\left[\mu_e\left(\frac{\partial u}{\partial x} + 2\frac{\partial v}{\partial y}\right)\right] &= -\rho g \frac{\partial h}{\partial y}. \end{aligned} \tag{20}$$

A vertically integrated form of Eq. 20 is readily derived under the assumption that there is no vertical variation in strain rates. These equations can be numerically solved to give the horizontal velocity fields, subject to prescription of a basal shear stress as a boundary condition at the bed.

This set of equations provides a good representation of ice dynamics where vertical shear deformation is negligible. MacAyeal and colleagues have had good success in simulating Antarctic ice stream and ice shelf dynamics with this method. This approach to modeling ice dynamics has also been applied to former ice streams in the Laurentide Ice Sheet [95] and in studies of the inland propagation of ice-marginal thinning in the Amundsen Sea sector of West Antarctica [31]. Using control theory (inverse methods), these equations also provide an opportunity to construct the basal friction from known surface velocity fields [96, 97].

The assumptions that underlie both shallow-ice models and the "plug-flow" equations are limiting in mixed flow regimes where vertical and horizontal shear stresses and longitudinal stresses are all important. This is the case where ice flow goes through a transition from grounded to floating conditions (the grounding line), where there are large spatial gradients in basal flow, at ice divides, and in valley glaciers, where the shallow-ice approximation is not valid because the ice thickness is of similar magnitude to horizontal variations in ice thickness and velocity. To address this and

provide a modeling framework that is generic and self-consistent for all environments, recent efforts have explored solutions to the full Stokes system, Eq. 10, as well as intermediate stages of complexity between the shallow-ice approximation and the full Stokes solution. The development of theoretical and numerical solutions of full stress-field solutions is promising, and has become tractable on regional scales [28, 29, 32]. Full solutions are still computationally unwieldy on continental scales, and have yet to be applied to whole ice sheet simulations in Greenland or Antarctica.

Progress has been slower in numerical simulations of the subglacial geological and hydrological processes that give rise to basal flow. This remains absent or oversimplified in models, where basal sliding is often specified as a function of gravitational driving stress, subject to thermal regulation. Warm-based ice can slide, while ice frozen to the bed is subject to a no-slip boundary condition. Some recent efforts include explicit models of subglacial water flow and storage, permitting sliding-law formulations that model this control on basal flow [98–100], but the physical understanding and the numerical representation of these processes remain limited.

Computational Considerations

For whole ice sheet simulations, the horizontal grid spacing is typically 20–50 km, with some 30 layers in the vertical. Recent simulations have adopted grid sizes of 5–10 km. Such resolutions are tractable but the computational demand increases by an order of magnitude for each factor of two reduction in the resolution, due to a fourfold increase in grid cells and the necessary reduction in the solution time step.

Part of the computational challenge for full-stress solutions arises from the need for long spin-up simulations for the polar ice sheets. Both Greenland and Antarctica contain ice that is more than 200 k year old, and it is essential to model the temperature and thickness evolution of the ice sheets through the last one or two glacial cycles in order to provide a reasonable internal temperature field for present-day studies or future projections of the ice sheets. Present-day dynamical adjustments are ongoing from the long-term evolution of the ice sheets, and this provides a background signal that must be understood in order to evaluate the response of the ice sheets to recent climate change. Regions of the ice sheets are thickening and thinning as a result of the ice sheet and climate history, largely associated with the long timescales of thermal advection and diffusion. The ice sheets are also adjusting to the geometric changes that attended the last deglaciation, e.g., [101]. These "secular" effects are further compounded by the slow (10^3–10^4 year) timescale of isostatic adjustment to the last glacial maximum and the subsequent deglaciation, which also needs to be simulated for the ice sheet system.

Finite difference and finite element approaches have both been applied to glacier and ice sheet models. Finite elements are more versatile and applicable to the complex geometry of mountain glaciers and fixed, limited spatial domains such as ice shelves, and these have advantages for solution of the diagnostic equations for ice velocity. Time-adaptive, moving grids are needed to simulate the evolution of glacier geometry, however, and this combines with the simplicity of finite-difference methods to make these more popular for simulation of large-scale ice sheet dynamics.

Priorities and Challenges

Fundamental glaciological data are still sparse in large sectors of the polar ice sheets and mountain glaciers, including knowledge of ice thickness, thermal regime, and subglacial conditions. It is difficult to apply hydrological and basal flow models to much of Greenland and Antarctica, where groundwater drainage, sediment properties, and other details of the subglacial environment are poorly known. Better understanding of the essential subglacial processes physics is also needed [67], as well as methods to parameterize these subgrid-scale processes in large-scale models. Similar physical and numerical challenges are involved in simulation of iceberg calving; there is no established "calving law," as the underlying physics and environmental controls are not fully understood.

There is a recent emphasis on glacial systems modeling, including subglacial processes and hydrological evolution, e.g., [92], but these efforts are still in early stages. With these limitations in mind, there is potential for major progress on at least two fronts based on what is currently well-understood about glaciers and ice sheets: (1) through high-resolution, full Stokes

solutions, which are on the horizon, and (2) through improved coupling of ice sheet and climate models. Improved coupling with climate models is necessary and many research groups have initiated this effort in recent years, for both individual glaciers [102] and continental ice sheets [25, 103–105].

Improved representation of stress–strain regimes at ice sheet margins, within floating ice and grounding zones, and in drainage basins that feed fast-moving outlets will provide a better representation of interannual and decadal variability of the ice sheets. This will also improve model capability in simulating glacier and ice sheet sensitivity to climate change. Resolutions (and input bedrock and climate-forcing datasets) of order 1 km are needed for this advance in the polar ice sheets, at least in the areas of complex flow and steep gradients at the ice sheet margin. For valley glaciers, input fields and ice dynamics need to be simulated at resolutions of order 100 m, and closer to 10 m if one wishes to simulate interannual glacier terminus response to climate change. It is also important to recognize that even with full Stokes solutions, ice streams, surging behavior, summer speedups, ice shelf instabilities, and areas of fast flow within the ice sheets will not spontaneously arise in the correct places; these are associated with processes and forcings that are absent in most models. In particular, there is limited two-way interaction between oceans and ice sheets in modeling studies to date, despite recent evidence that ice sheets are highly responsive to ocean warming [106].

Floating Ice Dynamics

State-of-the-art climate models today treat the jumble of floating ice floes as a continuum. At present, in global models, the only floating ice with dynamics is sea ice, and lake and river ice models are generally thermodynamics only. There are specialized models of lakes and river ice with dynamics, and they are based on the same principles as in sea ice models, so we discuss their dynamics together here.

The physics of floating ice is strongly dependent on the thickness. Therefore, floating ice is generally described in terms of a distribution of ice thicknesses at the subgrid-scale. The ice motion is also considered for a continuum, rather than for individual floes. With this brief overview, a global-scale floating ice model can be developed from the description of thermodynamics given in section "Thermodynamics of the Cryosphere" and the additional governing equations for the dynamics and ice thickness distribution given in this section.

Ice-Thickness Distribution

The formulation of a floating ice model begins with the ice thickness distribution equation. The ITD is a probability density function (pdf), usually written $g(h)$, that describes the probability that the ice cover in a particular region has thickness h. A cruder alternative is to model the mean thickness of the pdf and the total ice concentration.

In a floating ice model, the ITD describes the pdf of a grid cell and thus it is sometimes called a subgrid-scale parameterization. A parameterization typically represents processes that are too small-scale or complex to be represented explicitly. For example, deformation is parameterized with a set of rules in a continuum model because there is no known differential equation that describes deformation in this type of model. The rules must select the portion of the ITD that will deform and then redistribute it within the ITD. In contrast, ice growth and melt alter the ITD in a way that is computed from first principles. Hence the ITD actually includes both parameterized and explicit physics.

The ITD equation is

$$\frac{Dg}{Dt} = -g\nabla \cdot \mathbf{u} + \Psi - \frac{\partial}{\partial h}(fg) + \mathcal{L} \tag{21}$$

where the left-hand-side is the Lagrangian derivative of g following an ice "parcel" and terms on the right-hand-side are the rate of change of g from parcel convergence, mechanical redistribution (Ψ, see Fig. 2), advection of g in ice thickness space from growth/melt (see Fig. 3), and the reduction rate of g from lateral melt ($\mathcal{L}$). Here, $\mathbf{u}$ is the horizontal ice velocity (vertical ice velocity is ignored) and f is the net growth rate. We use the variable f as is traditional in the ITD literature, though it is essentially equivalent to the mass balance b used to describe glaciers in Eqs. 7 and 8. The ITD equation was introduced by [44]. Models that specify the ITD, e.g., [107], or only permit a single ice thickness in the ice-covered fraction of a model grid cell,

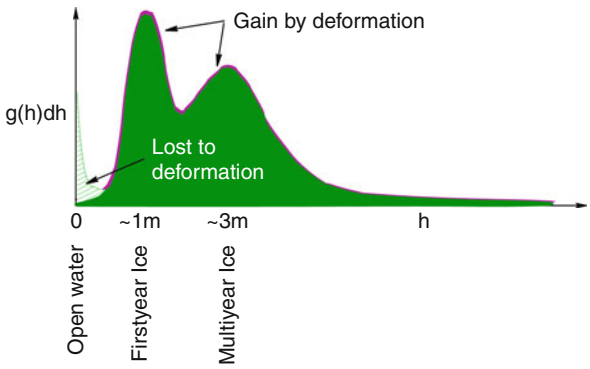

Cryosphere, Modeling of. Figure 2
Illustration of deformation. The portion of the distribution labeled "lost to deformation" is also known as the ice that participates in redistribution. It subsequently is redistributed to thicker parts of $g(h)$, where it is labeled "gain by deformation"

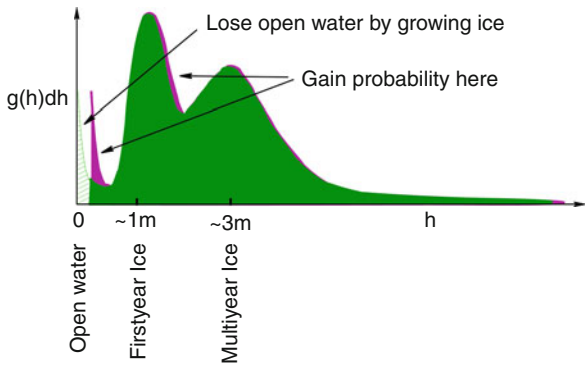

Cryosphere, Modeling of. Figure 3
Illustration of advection in thickness space

e.g., [108], would have an equation for the gridcell mean ice thickness instead.

There are two parts to deformation: a rate of opening (creating open water) and closing (closing open water and/or deforming and redistributing the ice), which depend on $\mathbf{u}$ and $g(h)$. The opening and closing rates depend on the convergence and/or shear in the ice motion field. It may not be obvious that shear would cause deformation. Imagine that the ice pack is composed of pieces with jagged edges. When shearing, the jagged edges can catch on one another and cause deformation, which converts kinetic energy into potential energy from piling up ice, or shearing can cause frictional loss of energy and no deformation. Thus the closing rates also depend on assumptions made about frictional losses, see e.g., [51, 54].

A mathematical representation of lead opening and mechanical redistribution is most conveniently written in terms of the divergence and shear of $\mathbf{u}$, $\dot{\epsilon}_I$ and $\dot{\epsilon}_{II}$, respectively. The parameterization follows from [44]:

$$\psi = |\dot{\epsilon}|[\alpha_0(\theta)\delta(h) + \alpha_r(\theta)w_r(h,g)], \tag{22}$$

where $|\dot{\epsilon}| = (\dot{\epsilon}_I^2 + \dot{\epsilon}_{II}^2)^{1/2}$, $\theta = \tan^{-1}(\dot{\epsilon}_{II}/\dot{\epsilon}_I)$, $\delta(h)$ (the delta function) is the opening mode and $w_r(h,g)$ is the ridging mode. The coefficients $|\dot{\epsilon}|\alpha_0(\theta)$ and $|\dot{\epsilon}|\alpha_r(\theta)$ are known as the lead opening and closing rates, respectively, and they are related such that their difference equals the divergence, $\dot{\epsilon}|\alpha_0(\theta) - |\dot{\epsilon}|\alpha_r(\theta) = \dot{\epsilon}_I$.

For the redistribution process, some portion of $g(h)$ is identified as potentially able to "participate" in redistribution (see Fig. 2). This is usually the thinnest 15% of $g(h)$. If the open water fraction exceeds 15%, then no redistribution takes place, and instead the open water closes under convergence and nothing happens under shear. The so-called participation function is weighted according to its thickness, so that the thinnest ice is most likely to deform. Then a rule is needed to redistribute the ice that ridges. Originally, Thorndike et al. [44] proposed that ridged ice would end-up five times thicker than its starting thickness. Other more complex redistribution schemes have been used since then [43, 109]. The interested reader can refer to these references, for examples, of parameterizations for $w_r(h,g)$.

The other primary mechanism that changes $g(h)$ is ice growth or melt, which cause $g(h)$ to shift in thickness space. This process is illustrated in Fig. 3. The growth/melt rate depends on thickness, so $g(h)$ becomes distorted in the process.

An explicit conservation equation for ice volume (or mass) is not given in this section because conservation of volume is contained in the equation for $g(h)$ (or at least it depends on the way $g(h)$ is discretized).

Momentum Equation

The second governing equation is conservation of momentum:

$$m\frac{D\mathbf{u}}{Dt} = -mf\mathbf{k} \times \mathbf{u} + \boldsymbol{\tau}_a + \boldsymbol{\tau}_w - mg_r\nabla Y + \nabla \cdot \sigma, \tag{23}$$

where the left-hand-side is the Lagrangian derivative of **u** following an ice parcel, the right-hand-side begins with a term representing Coriolis force, air and water stresses, the force due to ocean surface tilt, and the ice internal force. In this equation m is mass per unit area, f is the Coriolis parameter, g_r is gravity, Y is the sea surface height, and σ is the ice stress.

The force balance at two locations, one just north of Greenland and the other in the Weddell Gyre, is given in Fig. 4. The internal stress constitutes a very large internal force in the sea ice near Greenland, where the sea ice is converging against the coast. In contrast, at the Weddell location, the ice is nearly in free drift and the main force balance is between air and water drag. In both cases, the ice motion is perpendicular to the Coriolis Force, to the left in the upper panel and to the right in the lower.

Ice Rheology and the Constitutive Law

A constitutive law characterizes the relationship between the ice stress and strain rate and defines the nature of the ice dynamics. A simplistic picture of a converging ice pack with uniform thickness under an imposed compressive wind force is given in Fig. 5. Floating ice generally repels the compressive force somewhat even if it is deforming. The resulting internal force is associated with a nonzero stress state. In Fig. 5 the ice pack is converging such that its length L on one side decreases by δL in some time δt, so the ice experiences a strain $\dot{\epsilon} = \delta L/L$ and a strain rate $\dot{\epsilon} = \delta L/L\delta t$. A modeler chooses the constitutive law to relate σ and $\dot{\epsilon}$, which are actually two-dimensional tensors, not scalars as shown in Fig. 3 for illustrative purposes only. In two dimensions, the divergence and shear of the ice velocity can be conveniently used to describe the strain rate tensor as they are invariant across grid transformations.

The momentum equation depends on the ice internal force, which in turn depends on the ice stress tensor. The most common rheology used today is the viscous-plastic rheology from [108] (or a close derivative thereof) where the ice behavior is plastic at normal strain rates and viscous at very small strain rates.

The constitutive law for the viscous-plastic model of floating ice can be cast in terms of the invariants of stress (σ_I and σ_{II}) and strain rate ($\dot{\epsilon}_I$ and $\dot{\epsilon}_{II}$) with the pair of equations

$$\begin{aligned} \sigma_I &= \zeta\dot{\epsilon}_I - P/2 \\ \sigma_{II} &= \eta\dot{\epsilon}_{II}, \end{aligned} \tag{24}$$

where P is the ice strength and ζ and η are bulk and shear viscosities, respectively. The relationship between the viscosities and strain rate invariants is chosen so that the stress state lies on an elliptical yield curve,

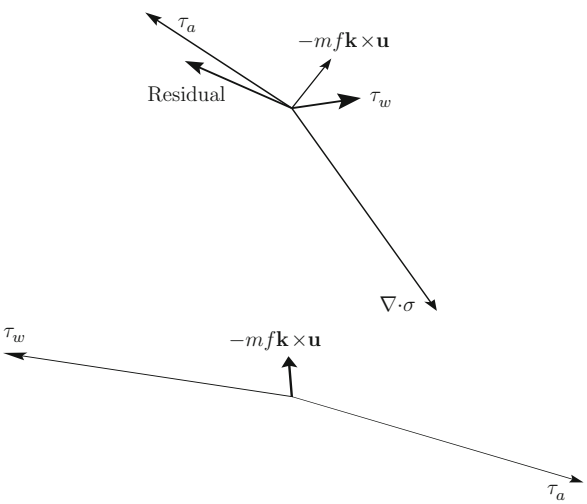

Cryosphere, Modeling of. Figure 4
Illustration of force balance from CCSM4 in October at 85N 65W (*upper*) and 64S 164W (*lower*). The residual force is the force needed to balance the other forces that are shown, and it is equal to the acceleration minus the force due to ocean tilt, the latter normally is very small. The forces from internal stress and the residual are negligible at the location of the *lower panel*

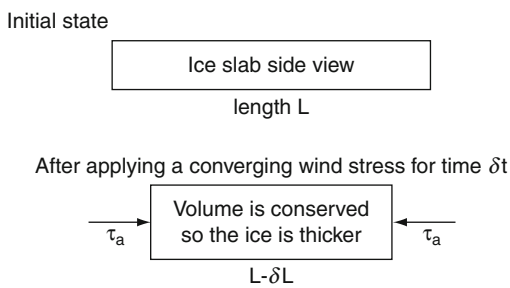

Cryosphere, Modeling of. Figure 5
Illustration of ice slab that deforms under compressive force

$$\frac{(\sigma_I + P/2)^2}{(P/2)^2} + \frac{\sigma_{II}^2}{(P/2e)^2} = 1, \tag{25}$$

where e is the ratio of the principal axes of the ellipse (the original Hibler model [108] used $e = 2$, which is still common today). Thus requiring

$$\begin{aligned} \zeta &= \frac{P}{2\Delta} \\ \eta &= \frac{\zeta}{e^2} \\ \Delta &= (\dot{\epsilon}_I^2 + \dot{\epsilon}_{II}^2 e^{-2})^{1/2} \end{aligned} \tag{26}$$

for plastic behavior. To avoid infinite viscosities as $\Delta \to 0$, ζ and η are assigned large constant values. In this case, the stress state lies inside the elliptical yield curve and the ice behaves like a viscous fluid, exhibiting creep.

The ice strength must be parameterized somehow. For a model with ridging, P can be based on the energetics argument proposed by Rothrock [110] for plastic deformation, where the compressive strength is equated to the potential energy increase per unit strain in pure convergence. Following [43], the potential energy is multiplied by a constant to account for the dissipation of kinetic energy by frictional energy loss during ridging,

$$P = ZC_p \int_0^\infty h^2 w_r(h)\,dh \tag{27}$$

where $C_p = 0.5(\rho_i/\rho_w)\hat{g}\,(\rho_w - \rho_i)$ and Z is the ratio of total energy dissipated to potential energy gain (ρ_i and ρ_w are the densities of ice and water and $\hat{g}$ is the acceleration due to gravity). [111] and [112] recommend $Z = 17$.

Computational Considerations

Computation time given to the sea ice component of a typical global climate models is roughly 10–20% for a ~100 km resolution ice grid, although it could easily be more or less depending on the relative resolution, sophistication, and optimization among components. Lake and river ice in global climate models take a trivial portion of the total computation time because their area is so small compared to the rest of the globe.

A key consideration for climate modelers is to design a model that can run the scenarios of interest in a time to meet publication deadlines. Choices must be made to balance model resolution, physics, parameterizations, and numerics. High-performance computers today have tens of thousands of cores and many have been constructed for the purpose of running climate models. Codes must parallelize well to take advantage of these machines, and sea ice codes generally do because there are relatively many processes that operate at the grid-scale (e.g., vertical heat equation) and subgrid-scale (e.g., deformation). The Los Alamos Sea Ice model CICE has already been successfully scaled beyond 10,000 cores on Cray XT equipment [113].

Future Directions

Most of the progress to date in modeling glaciers, ice sheets, permafrost, and snow science has stemmed from independent efforts by individual researchers. Advances have paralleled the much larger, coordinated research programs dedicated to the development of climate models, with little crossover or integration. This contrasts with modeling developments in sea ice studies, which are now fully integrated in most ocean–atmosphere general circulation models.

To date there have been few efforts to couple climate and ice sheet models. Most ice sheet simulations use "offline" forcing where climate model–derived fields are used to drive simulations of ice sheet evolution, through one-way forcing. The long timescale of ice sheet evolution means that this may be a reasonable approach, but evolution of ice sheet albedo and topography feeds back on atmospheric conditions on timescales of decades to millennia. Further, there are direct seasonal-timescale links between climate and the dynamics of glaciers and ice sheets, including the effects of surface meltwater and a possible link between coastal ocean temperature and sea ice conditions and outlet-glacier dynamics. These processes all require improved coupling between climate and ice sheet models. This is particularly true at the ice-ocean interface, where mass and energy exchanges are not physically modeled in current simulations.

In general, the mass balance fields (accumulation minus melt) simulated by climate models are not accurate enough for fully coupled ice sheet-climate modeling, nor can sophisticated atmospheric models be integrated over the millennial time scales of interest

for ice sheet evolution. However, the development of improved regional-scale meteorological and glacier mass balance models, e.g., [114–116], permit direct estimates of surface mass balance from meteorological models, and offer a good physically based method to simulate how these fields can be expected to change with ice sheet geometry.

The challenge is greater for the mass balance fields and surface climatological forcing of mountain glaciers and permafrost. Mountain glaciers reside in complex terrain where temperature and precipitation gradients are steep. The topography and relevant meteorological processes are not faithfully resolved in even regional climate models, so some form of climatic downscaling is needed to prescribe mass balance fields for glacier modeling [102]. These methods generally do not conserve energy or mass, and improved treatments are needed. There are different considerations for permafrost modeling, but they also relate to the resolution of the landscape and surface climate. The mean annual surface temperature that governs permafrost aggradation and degradation depends on local-scale vegetation, snowpack depth, hydrology, and soil properties, which commonly vary over a spatial scale of meters. Hence, global-scale permafrost and snow models should be interpreted "statistically" for a region (i.e., via a distribution of permafrost thickness and snow depth in a given climate model grid cell, based on the range of ground cover and snow conditions in the region).

In contrast to the terrestrial components of the cryosphere, the needs of global climate models often drive sea ice model developments. For example, models that use eddy-resolving ocean components are approaching the large floe-scale, where sea ice (assumed to be on the same grid) can no longer be considered a continuum. Rheologies that attempt to treat ice as a granular material hold promise as a means to extend the utility of continuum models to smaller length scales. Such rheologies often use Mohr-Coulomb or decohesive type yield curves, which depart from the standard elliptical yield curve particularly where the stress states on the ellipse resist breaking under tension. The floe models to date do well at modeling deformation but the process of joining floes at freeze-up has not been solved [111, 117].

Recent observations of sea ice reveal very long, narrow openings, or leads, in the ice that suggest oriented weaknesses occur. These regions have been dubbed linear kinematic features [118]. Such features occur in sea ice models with isotropic rheologies, such as the viscous-plastic type, with some level of realism at fine resolution [119]. However, models that account for such anisotropy explicitly by keeping track of lead orientation and computing resistance to opening depending on the orientation with respect to leads, e.g., [120, 121], may be able to match observations better [122].

The drive to model the carbon cycle and hence ecosystem dynamics in global climate models has spawned an effort to model sea ice algae and nutrient cycling. When seawater freezes, algae stick to the ice particles, and as the ice particles combine they trap brine, nutrients, and organisms in brine pockets. Biomass concentrations can be hundreds of times greater in sea ice than in seawater, and carbon and key nutrients in sea ice are a substantial fraction of the total in ice-covered regions. When sea ice melts it deposits these materials into the ocean precisely when solar input and meltwater runoff is highest, creating prime conditions for an ocean bloom. Models of these processes have been developed offline [123–127] and will soon be implemented in sea ice models of global climate models. Models of ecosystem dynamics in sea ice also require a treatment of seawater infiltration, brine drainage, and meltwater flushing, which necessarily involves modeling sea ice salinity [127].

Modeling the cryosphere today is concerned with far more than describing Earth's surface albedo. Global climate models need to be coupled to components of the cryosphere with adequate sophistication to investigate modern scientific problems involving sea level rise, Arctic sea ice retreat, permafrost thawing, and more. There is also evidence that models with better physics are among the models that agree best with observations [128].

Bibliography

1. Lemke P, Ren J, Alley RB, Allison I, Carrasco J, Flato G, Fujii Y, Kaser G, Mote P, Thomas RH, Zhang T (2007) Observations: changes in snow, ice and frozen ground. In: Solomon S, Qin D, Manning M, Chen Z, Marquis M, Avery K, Tignor M, Miller H (eds) Climate change 2007: the physical science basis. Contribution of working group I to the fourth assessment report of the intergovenmental panel on climate change. Cambridge University Press, Cambridge, UK, pp 337–384

2. Fetterer F, Knowles K, Meier W, Savoie M (2002) Sea ice index. National Snow and Ice Data Center, Boulder, CO, USA. Digital Media, updated 2009
3. Budyko MI (1969) The effect of solar radiation variations on the climate of the earth. Tellus 21:611–619
4. Sellers WD (1969) A global climate model based on the energy balance of the earth-atmosphere system. J Appl Meteorol 8:392–400
5. Manabe S (1969) Climate and the ocean circulation I. The atmospheric circulation and the hydrology of the Earth's surface. Mon Weather Rev 97:739–774
6. Bryan K (1969) Climate and the ocean circulation III. The ocean model. Mon Weather Rev 97:806–827
7. Nye JF (1953) The flow law of ice from measurements in glacier tunnels, laboratory experiments, and the Jungfraufirn borehole experiment. Proc R Soc Lond Ser A 219:477–489
8. Nye JF (1957) The distribution of stress and velocity in glaciers and ice sheets. Proc R Soc Lond Ser A 275:87–112
9. Glen JW (1955) The creep of polycrystalline ice. Proc R Soc Lond Ser A 228:519–538
10. Glen JW (1958) The flow law of ice. A discussion of the assumptions made in glacier theory, their experimental foundations and consequences. Int Assoc Hydrol Sci Publ 47:171–183
11. Budd WF (1970) The longitudinal stress and strain-rate gradients in ice masses. J Glaciol 9:29–48
12. Mahaffy MW (1976) A three-dimensional numerical model of ice sheets: tests on the Barnes Ice Cap, Northwest Territories. J Geophys Res 81:1059–1066
13. Jenssen D (1977) A three-dimensional polar ice sheet model. J Glaciol 18:373–389
14. Raymond CF (1983) Deformation in the vicinity of ice divides. J Glaciol 29:357–373
15. Thomas RA, MacAyeal DR (1982) Derived characteristics of the Ross ice shelf, Antarctica. J Glaciol 28(100):397–412
16. MacAyeal DR (1989) Large-scale flow over a viscous basal sediment: theory and application to Ice stream B, Antarctica. J Geophys Res 94(B4):4071–4088
17. Huybrechts P, Oerlemans J (1988) Evolution of the east Antarctic ice sheet: a numerical study of thermo-mechanical response patterns with changing climate. Ann Glaciol 11:52–59
18. Huybrechts P (1990) A 3-D model for the Antarctic ice sheet: a sensitivity study on the glacial-interglacial contrast. Clim Dyn 5:79–82
19. Huybrechts P, Letréguilly A, Reeh N (1991) The Greenland ice sheet and greenhouse warming. Palaeogeogr Palaeoclimatol Palaeoecol 89(4):399–412
20. Huybrechts P, de Wolde J (1999) The dynamic response of the Greenland and Antarctic ice sheets to multiple-century climatic warming. J Clim 12:2169–2188
21. Huybrechts P, Janssens I, Poncin C, Fichefet T (2002) The response of the Greenland ice sheet to climate changes in the 21st century by interactive coupling of an AOGCM with a thermomechanical ice-sheet model. Ann Glaciol 35:409–415
22. Huybrechts P, Gregory J, Janssens I, Wild M (2004) Modelling Antarctic and Greenland volume changes during the 20th and 21st centuries forced by GCM time slice integrations. Glob Planet Chang 42:83–105
23. MacAyeal DR, Rommelaere V, Huybrechts P, Hulbe CL, Determann J, Ritz C (1996) An ice-shelf model test based on the Ross ice shelf. Ann Glaciol 23:46–51
24. Payne AJ, Huybrechts P, Abe-Ouchi A, Calov R, Fastook JL, Greve R, Marshall SJ, Marsiat I, Ritz C, Tarasov L, Thomassen MPA (2000) Results from the EISMINT model intercomparison: the effects of thermomechanical coupling. J Glaciol 46(153):227–238
25. Ridley JK, Huybrechts P, Gregory J, Lowe J (2005) Elimination of the Greenland ice sheet in a high co_2 climate. J Clim 18:3409–3427
26. Driesschaert E, Fichefet T, Goosse H, Huybrechts P, Janssens I, Mouchet A, Munhoven G, Brovkin V, Weber SL (2007) Modeling the influence of Greenland ice sheet melting on the Atlantic meridional overturning circulation during the next millennia. Geophys Res Lett 34:L10707
27. Mikolajewicz U, Vizcaíno M, Jungclaus J, Schurgers G (2007) Effect of ice sheet interactions in anthropogenic climate change simulations. Geophys Res Lett 34(L18706). doi:10.1029/2007GL031173
28. Pattyn F (2003) A new three-dimensional higher-order thermomechanical ice sheet model: basic sensitivity, ice stream development and ice flow across subglacial lakes. J Geophys Res 108(B8):2382. doi:10.1029/2002JB002329
29. Pattyn F, Huyghe A, Brabander SD, Smedt BD (2006) The role of transition zones in marine ice sheet dynamics. J Geophys Res 111(F02004). doi:10.1029/2005JF000394
30. Pattyn F et al (2008) Benchmark experiments for higher-order and full stokes ice sheet models (ISMIP-HOM). The Cryosphere 2:95–108
31. Payne AJ, Vieli A, Shepherd A, Wingham DJ, Rignot E (2004) Recent dramatic thinning of largest west-Antarctic ice stream triggered by oceans. Geophys Res Lett 31:L23401
32. Price SF, Conway H, Waddington ED, Bindschadler RA (2008) Model investigations of inland migration of fast-flowing outlet glaciers and ice streams. J Glaciol 54:49–60
33. Oerlemans J, Anderson B, Hubbard A, Huybrechts P, Jóhannesson T, Knap WH, Schmeits M, Stroeven AP, van de Wal RSW, Wallinga J, Zuo Z (1998) Modelling the response of glaciers to climate warming. Clim Dyn 14:267–274
34. Blatter H (1995) Velocity and stress fields in grounded glaciers: a simple algorithm for including deviatoric stress gradients. J Glaciol 41:333–344
35. Albrecht O, Jansson P, Blatter H (2000) Modelling glacier response to measured mass balance forcing. Ann Glaciol 31:91–96
36. Schneeberger C, Albrecht O, Blatter H, Wild M, Hock R (2001) Modelling the response of glaciers to a doubling in atmospheric co2: a case study of storglaciaren, northern Sweden. Clim Dyn 17(11):825–834
37. Pattyn F (2002) Transient glacier response with a higher-order numerical ice-flow model. J Glaciol 48(162):467–477

38. Jarosch AH (2008) Icetools: a full stokes finite element model for glaciers. Comput Geosci 34(8):1005–1014
39. Rutt IC, Hagdorn M, Hulton NRJ, Payne AJ (2009) The glimmer community ice sheet model. J Geophys Res 114(F02004). doi:10.1029/2008JF001015
40. Coon MD, Maykut GA, Pritchard RS, Rothrock DA, Thorndike AS (1974) Modeling the pack ice as an elastic–plastic material. AIDJEX Bull 24:1–105
41. Coon MD (1980) A review of AIDJEX modeling. In: Pritchard RS (ed) Sea ice processes and models. University of Washington Press, Seattle, pp 12–27
42. Hibler WD (1980) Modeling pack ice as a viscous-plastic continuum: some preliminary results. In: Pritchard RS (ed) Sea ice processes and models. University of Washington Press, Seattle, pp 163–176
43. Hibler WD (1980) Modeling a variable thickness ice cover. Mon Weather Rev 108:1943–1973
44. Thorndike AS, Rothrock DS, Maykut GA, Colony R (1975) The thickness distribution of sea ice. J Geophys Res 80:4501–4513
45. Untersteiner N (1961) On the mass and heat budget of arctic sea ice. Arch Meteorol Geophys Bioklimatol Ser A 12:151–182
46. Maykut GA, Untersteiner N (1971) Some results from a time-dependent thermo-dynamic model of sea ice. J Geophys Res 76:1550–1575
47. Semtner AJ (1976) A model for the thermodynamic growth of sea ice in numerical investigaions of climate. J Phys Oceanogr 6:379–389
48. Washington WM, Meehl GA (1989) Climate sensitivity due to increased CO_2: experiments with a coupled atmosphere and ocean general circulation model. Clim Dyn 8:211–223
49. Manabe S, Stouffer RJ, Spellman MJ, Bryan K (1991) Transient responses of a coupled ocean–atmosphere model to gradual changes of atmospheric CO_2. Part I. Annual mean response. J Clim 4:785–818
50. McFarlane NA, Boer GJ, Blanchet J-P, Lazare M (1992) The Canadian climate centre second-generation general circulation model and its equilibrium climate. J Clim 5:1013–1044
51. Flato GM, Hibler WD III (1992) Modeling pack ice as a cavitating fluid. J Phys Oceanogr 22:626–651
52. Hunke EC, Dukowicz JK (1997) An elastic-viscous-plastic model for sea ice dynamics. J Phys Oceanogr 27:1849–1867
53. Zhang J, Hibler WD III (1997) On an efficient numerical method for modeling sea ice dynamics. J Geophys Res 102:8691–8702
54. Bitz CM, Holland MM, Weaver AJ, Eby M (2001) Simulating the ice-thickness distribution in a coupled climate model. J Geophys Res 106:2441–2464
55. Holland MM, Bitz CM, Hunke EC, Lipscomb WH, Schramm JL (2006) Influence of the sea ice thickness distribution on polar climate in CCSM3. J Clim 19:2398–2414
56. Goodrich LE (1978) Some results of a numerical study of ground thermal regimes, vol 1. National Research Council Canada, Ottawa, pp 29–34
57. Goodrich LE (1978) Efficient numerical technique for one-dimensional thermal problems with phase change. Int J Heat Mass Transf 21:615–621
58. Jordan R (1991) A one-dimensional temperature model for a snow cover. Special Report 91–16, Technical report. Cold Regions Research and Engineering Laboratory, Hanover, 49pp
59. Loth B, Graf H-F, Oberhuber JM (1993) Snow cover model for global climate simulations. J Geophys Res 98:10451–10464
60. Douville H, Royer JF, Mahfouf JF (1995) A new snow parameterization for the Météo-France climate model. 1. Validation in stand-alone experiments. Clim Dyn 12:21–35
61. Robock A, Vinnikov KY, Schlosser CA, Speranskaya NA, Xue Y (1995) Use of midlatitude soil moisture and meteorological observations to validate soil moisture simulations with biosphere and bucket models. J Clim 8:15–35
62. Yang ZL, Pitman AJ, McAvaney B, Sellers AH (1995) The impact of implementing the bare essentials of surface transfer land surface scheme into the BMRC GCM. Clim Dyn 11:279–297
63. Slater AG, Pitman AJ, Desborough CE (1998) The validation of a snow parameterization designed for use in general circulation models. Int J Clim 18:595–617
64. Slater AG, Pitman AJ, Desborough CE (1998) Simulation of freeze-thaw cycles in a general circulation model land surface scheme. J Clim 103:11,303–11,312
65. Dery S, Tremblay L-B (2004) Modelling the effects of wind redistribution on the snow mass budget of polar sea ice. J Phys Oceanogr 34:258–271
66. Oleson KW et al (2010) Technical description of version 4.0 of the community land model version (CLM). NCAR/TN-478+STR. National Center for Atmospheric Research, Boulder, CO, USA. http://www.cesm.ucar.edu/models/cesm1.0/clm/CLM4_Tech_Note.pdf
67. Clarke GKC (2005) Subglacial processes. Ann Rev Earth Planet Sci 33:247–276
68. Paterson WSB (1994) The physics of glaciers, vol 3. Elsevier, Amsterdam
69. Duval P (1981) Creep and fabrics of polycrystalline ice under shear and compression. J Glaciol 27:129–140
70. Mellor M, Cole DM (1982) Deformation and failure of ice under constant stress or constant strain-rate. Cold Reg Sci Technol 5:201–219
71. Hooke RL (1981) Flow law for polycrystalline ice in glaciers: comparison of theoretical predictions, laboratory data, and field measurements. Rev Geophys Space Phys 19:664–672
72. Adalgeirsdóttir G, Gudmundsson G, Bjornsson H (2000) The response of a glacier to a surface disturbance: a case study on Vatnajkull ice cap, Iceland. Ann Glaciol 31:104–110
73. Alley RB (1992) Flow-law hypotheses for ice-sheet modelling. J Glaciol 38:245–256
74. Shoji H, Langway CC (1988) Flow-law parameters of the dye 3, Greenland, deep ice core. Ann Glaciol 10:146–150
75. Thorsteinsson T, Waddington ED, Taylor KC, Alley RB, Blankenship DD (1999) Strain-rate enhancement at dye 3, Greenland. J Glaciol 45:338–345
76. Thorsteinsson T, Waddington ED, Fletcher RC (2003) Spatial and temporal scales of anisotropic effects in ice-sheet flow. Ann Glaciol 37:40–48

77. Cuffey KM, Thorsteinsson T, Waddington ED (2000) A renewed argument for crystal size control of ice sheet strain rates. J Geophys Res 105(B12):27,889–27,894
78. Durham W, Stern L, Kirby S (2001) Rheology of ice i at low stress and elevated confining pressure. J Geophys Res 106(B6):11,031–11,042
79. Paterson WSB (1991) Why ice-age ice is sometimes 'soft'. Cold Reg Sci Technol 20(1):75–98
80. Bindschadler RA (1983) The importance of pressurised subglacial water in separation and sliding at the glacier bed. J Glaciol 29:3–19
81. Clarke GKC (1987) Fast glacier flow: ice streams, surging, and tidewater glaciers. J Geophys Res 92:8835–8841
82. Iken A, Bindschadler RA (1986) Combined measurements of subglacial water pressure and surface velocity of Findelengletscher, Switzerland: conclusions about drainage system and sliding mechanism. J Glaciol 32(110):101–119
83. Kamb B (1987) Glacier surge mechanism based on linked cavity configuration of the basal water conduit system. J Geophys Res 92(B9):9083–9100
84. Copland L, Sharp MJ, Nienow P (2003) Links between short-term velocity variations and the subglacial hydrology of a predominantly cold polythermal glacier. J Glaciol 49:337–348
85. Zwally HJ, Herring T, Abdalati W, Larson K, Saba J, Steffen K (2002) Surface melt-induced acceleration of Greenland ice-sheet flow. Science 297:218–222
86. Joughin I, Das SB, King MA, Smith BE, Howat IM, Moon T (2008) Seasonal speedup along the western flank of the Greenland ice sheet. Science 320(5877):781–783
87. Alley RB (2000) Water pressure coupling of sliding and bed deformation. Space Sci Rev 92:295–310
88. Kamb B (1991) Rheological nonlinearity and flow instability in the deforming bed mechanism of ice stream flow. J Geophys Res 96(B10):16,585–16,595
89. Tulaczyk SM, Kamb B, Engelhardt H (2001) Basal mechanics of ice stream b, west Antarctica 1. Till mechanics. J Geophys Res 105(B1):463–481
90. Clark PU, Alley RB, Pollard D (1999) Northern hemisphere ice-sheet influences on global climate change. Science 286:1104–1111
91. Marshall SJ, Björnsson H, Flowers GE, Clarke GKC (2005) Modeling Vatnajökull ice cap dynamics. J Geophys Res 110(F03009). doi:10.1029/2004JF000262
92. Flowers GE, Marshall SJ, Björnsson H, Clarke GKC (2005) Sensitivity of Vatnajökull ice cap hydrology and dynamics to climate warming over the next two centuries. J Geophys Res 110(F02011). doi:10.1029/2004JF000200
93. Ritz C, Fabre A, Letréguilly A (1997) Sensitivity of a Greenland ice sheet model to ice flow and ablation parameters: consequences for the evolution through the last glacial cycle. Clim Dyn 13:11–24
94. Kamb B, Echelmeyer KA (1986) Stress-gradient coupling in glacier flow: I. Longitudinal averaging of the influence of ice thickness and surface slope. J Glaciol 32:267–279
95. Marshall SJ, Clarke GKC (1997) A continuum mixture model of ice stream thermomechanics in the Laurentide ice sheet, 2. Application to the Hudson strait ice stream. J Geophys Res 102(B9):20,615–20,638
96. MacAyeal DR, Bindschadler RA, Scambos TA (1995) Basal friction of Ice stream E, west Antarctica. J Glaciol 41:247–262
97. Vieli A, Payne AJ (2003) Application of control methods for modelling the flow of pine island glacier, west Antarctica. Ann Glaciol 36:197–203
98. Flowers GE, Clarke GKC (2002) A multicomponent coupled model of glacier hydrology. 1. Theory and synthetic example. J Geophys Res 107(B11). doi:10.1029/2001JB001122
99. Johnson J, Fastook JL (2002) Northern hemisphere glaciation and its sensitivity to basal melt water. Quat Int 95–96:65–74
100. Arnold NS, Sharp MJ (2002) Flow variability in the Scandinavian ice sheet: modelling the coupling between ice sheet flow and hydrology. Quat Sci Rev 21:485–502
101. Conway H, Hall BL, Denton GH, Gades AM, Waddington ED (1999) Past and future grounding-line retreat of the west Antarctic ice sheet. Science 286:280–283
102. Paul F, Kotlarski S (2010) Forcing a distributed glacier mass balance model with the regional climate model REMO. Part II: downscaling strategy and results for two Swiss glaciers. J Clim 23(6):1607–1620
103. Toniazzo T, Gregory JM, Huybrechts P (2004) Climate impact of a Greenland deglaciation and its possible irreversibility. J Clim 17:21–33
104. Ridley JK, Gregory J, Huybrechts P, Lowe J (2010) Thresholds for irreversible decline of the Greenland ice sheet. Clim Dyn 35(6):1049–1057
105. Vizcaíno M, Mikolajewicz U, Gröger M, Maier-Reimer E, Schurgers G, Winguth AME (2008) Long-term ice sheet-climate interactions under anthropogenic greenhouse forcing simulated with a complex earth system model. Clim Dyn 31:665–690
106. Holland DM, Thomas RH, Young BD, Ribergaard MH, Lyberth B (2008) Acceleration of Jakobshavn Isbræ triggered by warm subsurface ocean waters. Nat Geosci 1:659–664
107. Walsh JE, Hibler WD III, Ross B (1985) Numerical simultion of northern hemisphere sea ice variability 1951–1980. J Geophys Res 90:4847–4865
108. Hibler WD (1979) A dynamic thermodynamic sea ice model. J Phys Oceanogr 9:815–846
109. Lipscomb WH, Hunke EC, Maslowski W, Jakacki J (2007) Improving ridging schemes for high-resolution sea ice models. J Geophys Res 112:C03S91. doi:10.1029/2005JC003355
110. Rothrock DA (1975) The energetics of the plastic deformation of pack ice by ridging. J Geophys Res 80:4514–4519
111. Hopkins MA, Hibler WD III (1991) On the ridging of a thin sheet of lead ice. Ann Glaciol 15:81–86
112. Flato GM, Hibler WD III (1995) Ridging and strength in modelling the thickness distribution of Arctic sea ice. J Geophys Res C9:18,611–18,626

113. Dennis JM, Tufo HM (2008) Scaling climate simulation applications on the IBM blue gene/L system. IBM J Res Dev Appl Massively Parallel Syst 52(1/2):117–126
114. Box JE, Bromwich D, Veenhuis BA, Bai L-S, Stroeve JC, Rogers JC, Steffen K, Haran T, Wang S-H (2006) Greenland ice sheet surface mass balance variability (1988–2004) from calibrated polar MM5 output. J Clim 19(12):2783–2800
115. Fettweis X, Hanna E, Gallee H, Huybrechts P, Erpicum M (2008) Estimation of the Greenland ice sheet surface mass balance for the 20th and 21st centuries. The Cryosphere 2:117–129
116. Wake LM, Huybrechts P, Box JE, Hanna E, Janssens I, Milne GA (2009) Surface mass-balance changes of the Greenland ice sheet since 1866. Ann Glaciol 50:178–184
117. Hopkins MA (1996) On the mesoscale interaction of lead ice and floes. J Geophys Res 101:18315–18326
118. Kwok R (2001) Deformation of the Arctic ocean sea ice cover between November 1996 and April 1997: a qualitative survey. In: Dempsey J, Shen H, Shapiro L (eds) IUTAM scaling laws in Ice mechanics and ice dynamics. Kluwer Academic, Dordrecht, pp 315–322
119. Hutchings J, Heil P, Hibler W (2005) Modeling linear kinematic features in sea ice. Mon Weather Rev 133:3481–3497
120. Hibler WD, Schulson M (2000) On modeling the anisotropic failure and flow of flawed sea ice. J Geophys Res 105:17,105–17,120
121. Schreyer H, Sulsky D, Munday L, Coon M, Kwok R (2006) Elastic-decohesive constitutive model for sea ice. J Geophys Res 111:C11S26. doi:10.1029/2005JC003344
122. Coon M, Kwok R, Levy G, Prius M, Schreyer H, Sulsky D (2007) Arctic ice dynamics joint experiment (AIDJEX) assumptions revisited and found inadequate. J Geophys Res 112:C11S90. doi:10.1029/2005JC003393
123. Arrigo KR, Kremer JN, Sullivan CW (1993) A simulated Antarctic fast ice ecosystem. J Geophys Res 98:6929–6946
124. Arrigo KR, Worthen DL, Lizotte MP, Dixon P, Dieckmann G (1997) Primary production in Antarctic sea ice. Science 276:394–397
125. Lavoie D, Denman K, Michel C (2005) Modeling ice algal growth and decline in a seasonally ice-covered region of the arctic (resolute passage, Canadian archipelago). J Geophys Res 110:C11009. doi:10.1029/2005JC002922
126. Jin M, Deal CJ, Wang J, Tanaka N, Ikeda M (2007) Vertical mixing effect on the phytoplankton bloom in the southeastern Bering Sea midshelf. J Geophys Res 111:C03002. doi:10.1029/2005JC002994
127. Vancoppenolle M, Goosse H, de Montety A, Fichefet T, Tremblay B, Tison J-L (2010) Modelling brine and nutrient dynamics in Antarctic sea ice: the case of dissolved silica. J Geophys Res 115:C02005. doi:10.1029.2009JC005369
128. Bitz CM, Ridley JK, Holland MM, Cattle H (in press) Global climate models and 20th and 21st century arctic climate change. In: Lemke P (ed) Arctic climate change – the ACSYS decade and beyond. Springer
129. Greve, Blatter (2009) Dynamics of ice sheets and glaciers, Springer-Verlag, Berlin, pp 287
130. MacAyeal DR, Bindschadler RA, Scambos TA (1995) Basal friction of Ice Stream E, West Antarctica. J Glacio 41:247–262

D

Dairy Cattle Breeding

Filippo Miglior[1,2], Sarah Loker[3], Roger D. Shanks[4]
[1]Guelph Food Research Centre, Agriculture and Agri–Food Canada, ON, Canada
[2]Canadian Dairy Network, Guelph, ON, Canada
[3]Department of Animal and Poultry Science, University of Guelph, Guelph, ON, Canada
[4]Department of Animal Sciences, University of Illinois, Urbana, IL, USA

Article Outline

Glossary
Definition of the Subject
Introduction
Breeding Goals
Data Collection, Identification, and Pedigree Registration
Breeding Scheme
Purebred and Crossbred Cows
Genetic Evaluation
Future Directions
Bibliography

Glossary

Allele A variant form of a gene. Differences between alleles of a gene are a result of alternate DNA sequences.

Breeding value The sum of the independent allele effects on the trait of interest (i.e., the additive genetic worth).

Generation interval The average age of the parent when he/she is replaced by their offspring.

Genome-wide selection Selection of animals based on the value of their genomic profile. Animals are genotyped for several (thousands) of markers spanning the entire genome. These markers are so close together that they are thought to be linked with all genes in the genome.

Heritability A population measure depicting the strength of the relationship between performance and breeding value.

Indicator trait A trait genetically correlated with the trait of interest, but is easier, cheaper, or more convenient to measure and select in hopes of indirectly affecting the trait of interest in the population.

Mendelian sampling Describes the genetic variation of progeny of the same parents. More specifically, full-sibs are not expected to be genetically identical because of random segregation and recombination of genes from the sire and dam.

Reliability Regarding estimated breeding values, reliability, or accuracy of the estimated breeding value reflects the strength of the relationship between the estimated breeding value and the true breeding value.

Definition of the Subject

Dairy cattle breeding is the process of selecting and mating individuals in accordance with breeding goals, with the aim of changing genetic merit of future generations and bringing about an improvement in economic efficiency. For instance, a breeding goal may be designed to improve milk production, health, and fertility. Selection would then be for individuals who will produce offspring that genetically will earn greater profit through improved production at a lower cost (due to improved health and fertility).

Many factors have contributed to the vast improvement in dairy cattle production over the last century. One of the most important factors is the regular recording of phenotypic records. It is from these phenotypic records that the industry has estimated genetic worth. Improvement in methods for genetically evaluating dairy cattle is a large contributor to the

Robert A. Meyers (ed.), *Encyclopedia of Sustainability Science and Technology*, DOI 10.1007/978-1-4419-0851-3,
© Springer Science+Business Media, LLC 2012

substantial genetic improvement seen in this species. Such methods include the use of BLUP (Best Linear Unbiased Prediction), a method first proposed by C.R. Henderson in 1949 [1]. Another important milestone in the improvement of dairy cattle breeding was the development of techniques to freeze and store bovine semen in the early 1950s [2]. Because of this, semen can be stored for longer, shipped further, and therefore shared internationally. A large contributor to the success of dairy cattle breeding has been the implementation of progeny testing programs in the 1950s, which allowed for reliable genetic evaluations for bulls, especially for traits only expressed in daughters (such as milk production) [2]. To aid in the trade and use of dairy cattle genetics on an international basis, Schaeffer in 1994 developed MACE (multiple-trait across-country evaluation) [3]. This methodology allowed genetic evaluations to be converted to different countries' scales. In 2006, Shook [4] described the remarkable increase in yield traits from 1980 to 2000, revealing an increase of 3,500 kg of milk, 130 kg of fat, and 100 kg of protein per cow per lactation. While this increase is due to improvements of many factors, including genetics, nutrition, and management, Shook [4] determined that 55% of the gains in yield traits were due to genetics and that genetic change (versus altering environmental conditions) is permanent and cumulative.

Introduction

As seen in previous entries, genetic improvement in any livestock species requires: (a) identification of breeding goals; (b) accurate data collection, animal identification, and pedigree registration; (c) breeding scheme; and (d) genetic evaluation of measured traits. In dairy cattle breeding, artificial insemination is highly used and traits of interest are usually only expressed in females. Both points determine that males are very important in breeding scheme and genetic progress, but generation interval will be longer than in other species, given that males need to be proven based on progeny performance instead of their own. Another important aspect of dairy cattle breeding is an open international market for dairy genetics, where the male side is controlled through semen sales by a large number of AI organizations, some national and some multinational based. The female side, by contrast, is controlled by the dairy producers. Being an international market with high exchange of semen, and somewhat lower but still common exchange of embryos and live animals, a constant need is to obtain genetic values of foreign animals on local scales, a service provided via international genetic evaluations by the Interbull Centre in Sweden. Finally, in the last 2 years, the full sequence of the bovine genome has opened the way for genome-wide selection. The advent of genomic selection has provided new opportunities and challenges in the global dairy semen market. The market has already seen a partial shift from progeny tested sires to young genotyped bulls. After this transition time, provided one can confirm over the next few months that the genetic level and accuracy of evaluation of these young bulls are as high as expected, genomic selection will revolutionize dairy cattle breeding, and will decrease the importance of progeny testing for some bulls. This chapter will present all the characteristics of traditional dairy cattle breeding, the international aspects of this species breeding as well as the current application of genomic selection and its consequences.

Breeding Goals

Generally, the breeding goal of a dairy producer is to maximize the profitability of his/her dairy farm. The main return in a dairy farm derives from sales of milk production. Cost of milk varies across and within countries based on supply and demand and whether a quota system is present. Additionally, premiums are paid for high-quality milk, and higher percentages of fat and protein. Furthermore, penalization will apply for milk with somatic cell count (SCC) higher than a given threshold. The second return in a dairy farm originates from the sale of breeding stock, primarily young or pregnant heifers. This type of return is less common, being present only in dairy farms with high-genetic-value cows. The same type of farm will generate return from embryo sales by multiple flushings of their top cows. A more common but low return derives from the sale of male calves and cull cows. The most important variable cost in dairy farms is represented by feed costs, followed by veterinary and breeding costs.

For many years, most selection programs worldwide focused on increasing milk production. National selection indices were based on improving milk yield

and gradually shifted toward improving protein yield and, outside North America, toward increasing fat and especially protein content. This was true for most countries with the exception of the Scandinavian countries, whose selection indices also included health and reproduction; and North American countries, whose selection indices included conformation together with production. In the last 10 years, a growing interest has broadened selection indices to include functional traits such as reproduction and health. Main reasons for this shift were quota-based milk marketing systems, price constraints, or both, together with increasing producer and consumer concerns associated with the observed deterioration of the health and reproduction of dairy cows. Labor costs have increased relatively more than milk price in some countries. Several studies have shown that selection for production alone causes negative effects on udder health [5] and reproductive performance [6–8].

Figure 1 shows the relative emphasis on traits in national selection indices in October 2009. The main difference between selection indices in various countries was the relative emphasis on production. However, every country has now broadened their index by adding longevity, health, and reproduction to the usual production and conformation traits [9]. The search for the ideal balance between all of these important traits continues.

Data Collection, Identification, and Pedigree Registration

Proper identification, pedigree recording, and performance recording are crucial for genetic improvement of dairy cattle. Without them, accurate genetic evaluations would not be possible. In the past, animal identification was more important within the herd for management purposes [10]. However, it is now important to have proper animal identification for genetic evaluation purposes, which means that an animal's ID should be unique outside its herd. In some countries, a unique animal ID is mandatory. In the Canadian dairy cattle industry, a herd's lactation records only qualify for official publication if 80% of its first lactation animals are registered in a breed association herd book with a unique animal identification. Unique

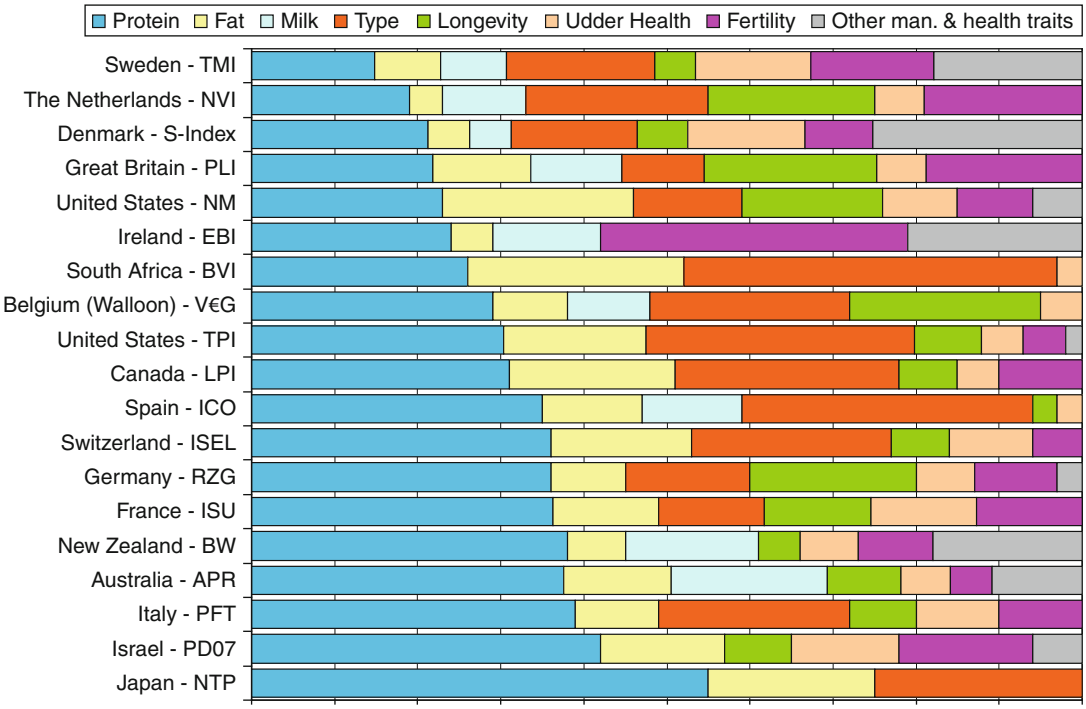

Dairy Cattle Breeding. Figure 1
Relative emphasis of traits for various national selection indexes around the world

animal identification is not without error, however. Larger ID numbers associated with unique national or international identifications are at risk of recording errors, and ID tags can become worn-out or lost. Identification errors can also lead to inaccurate pedigree recording, though pedigree errors can occur for various reasons. Banos et al. [11] and Israel and Weller [12] showed that pedigree errors resulted in biased estimated breeding values and reduced genetic gain. Also, faulty equipment and human error can lead to inaccurate data recording. Fortunately, several techniques correct or accommodate erroneous outliers in the data (e.g., robust procedures described by Jamrozik et al. [13]).

In summary, numerous errors can occur when recording performance and pedigree information. Therefore, to ensure better quality data, it is mandatory in most countries to follow the rules and standards established by the International Committee for Animal Recording before records can be used for genetic evaluation. Several traits are of economic importance in the dairy industry, but the relative importance of each depends on the country (Fig. 1).

Test-day models are used for the genetic evaluation of dairy cattle for milk production traits in many countries. These models necessitate the regular recording of milk production traits. A good recording scheme can therefore require records for 24-h milk, fat, protein, and somatic cell count (SCC) to be taken once monthly. These are called test-day records. Generally, production traits such as milk, fat, and protein yield are moderately heritable.

While milk production traits are important, many other traits are of economic importance in dairy cattle breeding, including conformation, longevity, reproduction, health, and workability traits. Conformation (or "type") traits describe the physical attributes of the cow that are generally associated with survival, health, and reproduction. Many traits (e.g., body condition score) require visual appraisal by the recorder, and are considered to be more subjective. In these cases, it is vital that assessors are highly trained to ensure repeatable and accurate recording. Many "type" traits are moderately heritable.

Because of the negative genetic correlations between milk production and fertility or health traits, long-term selection for improved milk production has led to reduced fertility and health in dairy cattle. As a result, routine genetic evaluations of reproductive and health traits are becoming more common, despite low heritabilities. A major challenge is that direct health data has not been recorded for very long and can be difficult to measure. In many cases, countries use indicator traits instead of measuring the health trait directly. An example of this is using somatic cell count as an indicator of mastitis.

Longevity (or survival) describes the length of a cow's survival in the herd, and has a low heritability as this trait can be greatly affected by herd management and other nongenetic factors. Workability includes traits such as milking speed and temperament during milking. Milking temperament has a low heritability, while milking speed has a moderate heritability.

Breeding Scheme

In general, a breeding scheme is the amalgamation of the processes involved in the selection and mating of livestock for the purpose of genetic improvement. Because of artificial insemination in the dairy cattle industry, semen from a single male can be used widely throughout the population. Therefore, genetic improvement is achieved largely through intense selection of males. However, most of the economically important traits in the industry (such as milk production traits) are expressed in the female. As a result, dairy cattle breeding relies on progeny testing schemes for genetic improvement. Data on various milk production and performance traits from daughters are collected and used to calculate estimated breeding values for bulls. The more daughters and daughter records are available for a bull, the greater the accuracy of the estimated breeding values. "Proven bulls" are bulls with very reliable estimated breeding values because they have many daughters with performance records. Estimated breeding values for bulls without progeny records are less reliable because they are calculated using the average of the estimated breeding values of the parents.

The major factors influencing rate of genetic progress for a given trait are the components of "the key equation" of animal breeding:

$$\frac{\Delta BV}{t} = \frac{r_{BV,\,\widehat{BV}}\, i\sigma_{BV}}{L} \tag{1}$$

where BV is true breeding value, t is time, $\widehat{BV}$= estimated breeding value, $r_{BV,\widehat{BV}}$ = accuracy of the estimated breeding value relative to the true breeding value (also the correlation between the estimated and true breeding values), i = selection intensity (a function of the proportion of the population chosen to be parents of the next generation), σ_{BV} is additive genetic standard deviation, and L is generation interval. The aim is to choose animals with superior genetics to be parents of the next generation to improve the genetics of the population. Increasing the reliability (accuracy) of prediction, selecting only the best animals as parents (increasing selection intensity), and decreasing the generation interval are important factors for increasing genetic improvement per unit time.

A major challenge in dairy cattle breeding is developing an optimum breeding program that maximizes genetic progress while minimizing cost. AI organizations are generally responsible for breeding schemes [14], and a typical AI organization can spend millions of dollars per year progeny testing bulls to find the best bull to market to the world [15]. However, dairy breeding is entering a new era in which genomic selection is possible. With genomic selection, bulls can be genotyped and selected at a young age. This improves the industry's traditional breeding scheme by reducing reliance on progeny testing (a lengthy and costly process), and will theoretically increase response to selection via a reduced generation interval [15]. Also, genomic values will increase the accuracy of genetic evaluations, especially for young sires for which traditional estimated breeding values are derived from parent averages [16].

Purebred and Crossbred Cows

The group of animals selected as parents of the next generation are expected to possess alleles that the industry considers favorable. Therefore, through selection, the frequency of favorable alleles in the population should increase with each generation while that of unfavorable alleles should decrease. The result is an increase in average breeding value, and improved performance of the dairy cattle population. The change in average breeding value over time defines the genetic trend.

As mentioned previously, artificial insemination has allowed for intense selection of sires for increased genetic improvement over time. This means that a few top bulls, with the best collection of favorable alleles, can be mated widely throughout the population. While this is a good way to progress more quickly toward fixing favorable alleles in the population, it reduces the effective population size of the breed which could raise inbreeding and reduce performance from the associated inbreeding depression. The dairy industry needs to find a compromise between selection of the best sires for use in artificial insemination, and minimization of inbreeding depression. This is, of course, less of a problem initially with crossbreeding, as sire and dam are unrelated. However, while several benefits exist with crossbreeding in general, heterosis obtained is too low to lead to more profitable animals than purebred Holsteins (the most widely used dairy breed) [17, 18]. Therefore, in the dairy industry, selection tends to occur within breeds.

Again, a large degree of dairy cattle genetic progress is achieved through the selection and use of semen of a few top bulls. However, it is important to understand that selection and consequent genetic progress within a breed is achieved via four selection pathways, all of which center around the progeny testing scheme.

Progeny testing is required so that the genetic merit of bulls can be calculated reliably via analysis of many performance records on many daughters. Every year, genetically superior bulls and cows are mated using artificial insemination to produce young bulls with high predicted genetic merit. On average, young bulls resulting from these matings will have high true genetic merit, but because of Mendelian sampling, it is not certain that these young bulls will be genetically superior. The young bulls therefore need to be proven via progeny testing. If a young bull is in fact of high genetic merit, he will yield daughters that perform well for traits of interest. The more daughters he produces with superior performance, the more certain it is that he is a genetically superior bull.

So far, two selection pathways have been discussed: selection of sires of young bulls, and of dams of young bulls. The sires of young bulls are proven and their semen can be used widely, so they can be selected very intensely, and their estimated breeding values are very reliable. Referring to Eq. 1, increased selection pressure and reliability will lead to increased genetic progress per unit time. Dams of young bulls can be selected

intensely because not many young bulls need to be produced for progeny testing (only about 400 a year in Canada and about 6,000 Holsteins worldwide). However, the reliability of estimated breeding values for dams of young bulls is not as high as that of the sires because the dams have fewer close relatives with records.

In a dairy herd, replacement heifers are required. Therefore, further potential for increasing genetic progress of the population is through two more selection pathways: selection of sires of cows and dams of cows. It takes several years for young bulls to be fully proven. However, when these bulls have a genomic evaluation or some daughter records (but not yet enough to achieve the reliability of a proven bull), they can be selected to produce replacement heifers with a reasonably high selection intensity. Dams of these future cows, however, cannot be selected so intensely for several reasons. Many replacement heifers are required, and because a female cannot breed as many times as a male, most cows will be selected for breeding. Also, female fertility in the dairy cattle population is typically low, so the industry cannot afford to be very selective with this pathway.

Genetic Evaluation

For progress in the dairy industry, it is important to accurately select genetically superior animals as parents of the next generation. Traditionally, genetic worth could only be estimated by evaluation of phenotypic records, which are a result of a combination of genetic and environmental factors (and sometimes an interaction of the two). Again, genomics is revolutionizing the way the industry evaluates dairy cattle, making it possible to genotype animals instead of waiting for phenotypic records. However, genomics is just one part of the process, and the collection of phenotypic records will still be important for some time.

The additive genetic value of an animal for a particular trait is the sum of the independent effects of that individual's alleles on that trait. On average, half of an animal's additive genetic worth is passed on to its offspring. The greater the animal's genetic worth, the more genetically superior its offspring are expected to be. The additive genetic value is therefore appropriately termed "breeding value." Breeding values of animals can be estimated from many different sources of information, including observations on the animal itself and observations from a variety of relatives. This reiterates the importance of quality phenotypic and pedigree data. True breeding value can never be known, only estimated from a very large (effectively infinite) number of genes with alleles each of which has a small effect on the trait of interest. Breeding values are estimated from limited phenotypic data using models that are not perfect. The accuracy of estimated breeding values (EBV) depends on a variety of factors, including the degree of relationship between the animals providing the phenotypic information and the animal being evaluated, the number of records available, and the heritability of the trait of interest. Of course, through genomics, perhaps one day the effect that each allele in the genome has on each trait could be quantified, bringing the industry closer to an animal's true breeding value for each trait.

Several traits of economic importance to the dairy industry were already discussed. So, a dairy bull or cow has several estimated breeding values, one for each trait. This makes selection complicated. For example, perhaps a potential sire has excellent estimated breeding values for milk production traits, but terrible values for health and fertility traits. Therefore, countries devise a national economic selection index, which incorporates estimated breeding values for traits of interest and their respective monetary worth into an equation that gives a single score for profitability ("aggregate breeding value") of each animal [19]. This makes selection much easier, as animals with the most favorable combination of estimated breeding values (e.g., high milk production and good health and fertility) are the most profitable.

Traditionally, selection index methods were used to combine weighting factors with adjusted phenotypic records from various sources (i.e., own records and records from various relatives) to derive estimated breeding values for traits. The phenotypic records were first adjusted for a variety of environmental influences including, for example, age of animal and effect of contemporary group. These methods of adjustment were not always effective for disentangling genetic effects from environmental influences. To improve the application of selection index methods, the dairy breeding industry began to use the statistical method

known as best linear unbiased prediction, or BLUP, in the 1970s. This method was first proposed by C.R. Henderson in 1949 [1]. Without going into too much detail, BLUP is able to simultaneously estimate environmental effects and predict breeding values while taking into account pedigree relationships.

Both the traits and the methodologies involved in national genetic evaluations vary substantially among countries [20]. Therefore, EBVs for one trait in one country may not be representative of EBVs for the same trait in another country. This makes comparing animals from different countries difficult. Dairy cattle genetics are shared internationally, especially sire genetics via artificial insemination. Therefore, the Interbull Centre was created to provide international evaluations. Specifically, the procedure carried out is called the multiple-trait across-country evaluation, or MACE [3]. This procedure allows Interbull to provide a separate list of International Genetic Evaluations to each participating country, expressed on that country's scale.

Future Directions

As previously mentioned, genome-wide selection is revolutionizing dairy cattle breeding. Young bulls benefit the most with a large increase in reliability of estimated breeding values at an earlier time in their lives, reducing the generation interval of these animals and hence increasing the speed of genetic improvement. It is fairly certain that future dairy cattle genetics research will focus on the improvement of genomic techniques.

Over the years, as quantitative geneticists improve upon techniques surrounding genome-wide selection for animal breeding, it is important to keep in mind the application of such techniques to human health. In 2008, Mardis [21] predicted that sequencing the entire human genome for $1,000 will be feasible in the near future. While animal breeders are currently using genomics to predict the genetic value of animals for complex traits, it may one day be possible to utilize genomics to predict human individuals' genetic risk for complex, multifactorial diseases, such as Crohn's disease [22]. Research in genomics in animal breeding will certainly pave the way for research and development of genomics applied to human health.

Bibliography

1. Henderson CR (1949) Estimation of changes in herd environment. J Dairy Sci 32:706 (Abstr)
2. Funk DA (2006) Major advances in globalization and consolidation of the artificial insemination industry. J Dairy Sci 89:1362–1368
3. Schaeffer LR (1994) Multiple-country comparison of dairy sires. J Dairy Sci 77:2671–2678
4. Shook GE (2006) Major advances in determining appropriate selection goals. J Dairy Sci 89:1349–1361
5. Heringstad B, Chang YM, Gianola D, Klemetsdal G (2003) Genetic analysis of longitudinal trajectory of clinical mastitis in first-lactation Norwegian cattle. J Dairy Sci 86: 2676–2683
6. Haile-Mariam M, Morton JM, Goddard ME (2003) Estimates of genetic parameters for fertility traits of Australian Holstein-Friesian cattle. Anim Sci 76:35–42
7. Kadarmideen HN, Thompson R, Coffey MP, Kossaibati MA (2003) Genetic parameters and evaluations from single- and multiple- trait analysis of dairy cow fertility and milk production. Livest Prod Sci 81:183–195
8. Veerkamp RF, Koenen EPC, De Jong G (2001) Genetic correlations among body condition score, yield, and fertility in first-parity cows estimated by random regression models. J Dairy Sci 84:2327–2335
9. Miglior F, Muir BL, Van Doormaal BJ (2005) Selection indices in Holstein cattle of various countries. J Dairy Sci 88:1255–1263
10. Jr Hooven NW (1978) Cow identification and recording systems. J Dairy Sci 61:1167–1180
11. Banos G, Wiggans GR, Powell RL (2001) Impact of paternity errors in cow identification on genetic evaluations and international comparisons. J Dairy Sci 84:2523–2529
12. Israel C, Weller JI (2000) Effect of misidentification on genetic gain and estimation of breeding value in dairy cattle populations. J Dairy Sci 83:181–187
13. Jamrozik J, Strandén I, Schaeffer LR (2004) Random regression test-day models with residuals following a Student's-*t* distribution. J Dairy Sci 87:699–705
14. Miglior F (2000) Impact of inbreeding – Managing a declining Holstein gene pool. In: Proceedings from 10th world Holstein Friesian federation conference – 30 Apr – 3 May 2000, Sydney, pp 108–113
15. Schaeffer LR (2006) Strategy for applying genome-wide selection in dairy cattle. J Anim Breed Genet 123:218–223
16. VanRaden PM, Van Tassell CP, Wiggans GR, Sonstegard TS, Schnabel RD, Taylor JF, Schenkel FS (2009) Invited review: reliability of genomic predictions for North American Holstein bulls. J Dairy Sci 92:16–24
17. Gunjal K, Menard L, Shanmugam R (1997) Economic analysis of crossbreeding dairy cattle. Agric Syst 54:327–339
18. VanRaden PM, Sanders AH (2003) Economic merit of crossbred and purebred US dairy cattle. J Dairy Sci 86:1036–1044
19. Hazel LN (1943) The genetic basis for constructing selection indexes. Genetics 28:476–490

20. Mark T (2004) Applied genetic evaluations for production and functional traits in dairy cattle. J Dairy Sci 87:2641–2652
21. Mardis ER (2008) Next-generation DNA sequencing methods. Annu Rev Genomics Hum Genet 9:387–402
22. Barrett JC, Hansoul S, Nicolae DL, Cho JH, Duerr RH et al (2008) Genome-wide association defines more than 30 distinct susceptibility loci for Crohn's disease. Nat Genet 40:955–962

Dam Engineering and its Environmental Aspects

Petar T. Milanović
Belgrade, Serbia

Article Outline

Glossary
Definition of the Subject
Introduction
Flood Regulation: Regional Impact on Population
Dam Failures
Reservoir Slope Instability
Tailings Dam Failures
Reservoir-Triggered Seismicity: Induced Seismicity
Dams and Heritage Protection
Dams and Ecosystems
Dams and Microclimate
Induced Subsidence (Collapse)
Spring Submergence Due to Dam Construction
Environmental Aspects of Dams in Karst
Further Directions
Bibliography

Glossary

Dam Civil structure planned, constructed, and operated to meet human needs in flood control, irrigation, supply of drinking water, electricity generation, recreation, and various other purposes.

Dam failure Collapse or movement of part of a dam or its foundation, so that the dam cannot retain water.

Guaranty ecological flow Required quantity and quality of flow to maintain the sustainability of the river ecosystem (ecological base flow).

Induced subsidence Collapse of the surface of the ground due to human activities, mostly reservoir operation and intensive pumping of groundwater.

Karst Terrain composed of highly soluble rocks (limestone, dolomite, gypsum, and salt), very risky environment for dams and reservoirs construction.

Large dams Dams having a height of 15 m from the foundation or, if the height is between 5 and 15 m, having a reservoir capacity of more than 3 million cubic meters.

Reservoir-triggered seismicity Seismic phenomena associated with impounding of reservoirs (Reservoir-Induced Seismicity).

Definition of the Subject

Construction of dams and reservoirs involves considerable natural and anthropogenic impacts. These impacts are for the most part positive, but can some negative influence on the environment. The main purposes of dam construction are focused on water regime improvement, and consequently to regional prosperity. Generally, the goal of dams and reservoirs is regional socioeconomic development by irrigation, flood control, power production, water supply, recreation purposes, reduction of deforestation, reduction of drought periods, for fishing farms, mining purposes, navigation, to enhance landscape including development of new infrastructure, and to provide new possibility for employment and many secondary benefits.

However, as a consequence of dam and reservoirs construction, a number of different and sometimes unpredictable negative environmental impacts and uncertainties cannot be avoided. Some common negative impacts are: the population migrates from inundated areas; the reservoirs cover arable land, settlements, and infrastructure; deep reservoirs provoke induced seismicity and induced collapses; water fluctuation provokes landslides along the reservoir banks; sedimentation of reservoirs; in some cases, important cultural and historical monuments are inundated; questionable impact on biodiversities, survival of wildlife, and endemic species is endangered; tailings may contain dangerous chemicals; and regime of surface and underground water is considerably changed. In a number of cases, socioeconomic constrains related to migration from submerged regions are very pronounced.

The worst most negative and disastrous impact is dam failures. The karst environment is a particularly sensitive influence on dams and reservoirs, and a variety of positive and negative consequences are numerous in such terrain.

Introduction

Since time immemorial, people have considered how to tame the surface waters to prevent floods and to use water for different purposes, irrigation, water supply, and much later, for electricity production. In many areas in the world, life was not determined by man, but by the rivers. The people have had to cope with two kinds of misfortune: flood and drought. In many cases, the consequences were disastrous. One single flood of the Yangtze River in China (1931) devastated 3.3 million hectares of arable land and caused the suffering of 28 million people and the loss of more than 145,000 lives [1].

From very ancient times, dams appeared as the only effective structures to tame river waters. Construction of dams started a few 1,000 years ago. Primary role of dams is to store or to divert waters. The oldest known are Jawa dams in Jordan (∼ 3000 BC). In Egypt, the Kosheish Dam was constructed during the period 3000–2900 BC and Saad El-Kafra Dam about 2610 BC. The Anfantang reservoir in China was built in sixth century BC, and a 30-m high gabion dam was constructed around 240 BC in Shanxi province. In Iran, dam constructions dates from before 2,000 years ago (Bahman Dam, Fig. 1); Shapour and Mizan dams were constructed during the reign of King Shapur I about 1,700 years ago; the Tilkan and Sheshtarz Dam, 1,000 years ago. The Amir Dam north of Shiraz, 1,000 years old, still is operational [2]. In Spain, the Proserpina Dam, 22 m high, was built in the second century and still is operational.

Later in the twentieth century, individual dams were constructed to control the large hydro-systems, which consist of a number of dams and reservoirs, to change water regime at large catchment areas: Tennessee Valley Authority (29 dams) USA; dams along the Yangtze River in China; Southeast Anatolia Project (21 dams); the Volga-Kama cascades, Russia (11 dams); dams at Karun River catchment in Iran (16 dams); or

Dam Engineering and its Environmental Aspects. Figure 1
Bahman Dam, Iran. Constructed approximately 2,200 years ago

dams in karst area the Hydro-system Trebišnjica, Bosnia and Herzegovina (BiH), and Croatia (6 dams).

In many cases, dam projects were initially controversial and potentially disastrous. Failures of dams and potential environmental impacts are the main reasons for controversy and fear. However, with increasing demand on water resources and electric power, at issue is how to keep the balance between the necessity for development and preservation of the environment. At many locations, dams are still structures of great importance.

According ICOLD World Register of Large Dams (1998), the main purpose of large dams is irrigation – 37%, multipurpose use – 22%, electricity generation – 16%, water supply – 12%, flood control – 6%, recreation – 3%, and other purposes – 4%. Tailing dams are excluded from this survey.

In the USA, considering all dams (not large dams only), the main purpose is recreation – 33.8%, flood control – 15.6%, fire control 13.7%, irrigation – 9.5%, water supply – 9.4%, electricity production – 2.9%, and rest for many different purposes.

Environmental problems are coupled with political (transboundary) problems if dams are constructed at rivers bordering countries: for example, the Iron Gate Dam at the Danube River between Serbia and Romania; the Aswan Reservoir at the Nile River between Egypt and Sudan; dams on the Euphrates and Tigris Rivers impacting Turkey, Syria, and Iraq; and the Itaipu Reservoir along the border between Brazil and Paraguay.

Flood Regulation: Regional Impact on Population

Historically, for thousands of years the primary role of dams was protection of settlements and arable land against flooding and for irrigation. Presently, flood control and irrigation are still of high importance, but usually dams and reservoirs are multifunctional, including power production, water supply, sediment control, landscape improvement, and recreation.

The Tennessee Valley Authority (Tennessee River, USA), founded in 1933, is one of the largest dam reservoir projects for flood control, navigation, power production, and irrigation [3]. Under natural conditions, the water regime was unfavorable for agriculture and life. Thirty percent of the population in the Tennessee Valley was affected by malaria. To construct 29 dams and reservoirs, more than 15,000 families were displaced. Electricity generation, flood control, and better organized water regimes have been of great benefit for the region. More than 1,000 km of navigation channels have been constructed as part of this project. One important positive environmental impact is control of surface waters with regard to malaria prevention.

Large floods were a regular occurrence along the Nile River under natural conditions. At the same time, floodwater deposited about 4 million tons of nutrient-rich sediments per year. To prevent floods, the first modern dam at Aswan was built in 1889. The first dam was not high or effective enough to control flooding, and a new Aswan High Dam was constructed during 1960–1970 a few kilometers upstream. Over 60,000 Nubians were relocated from the reservoir area. The reservoir contains a volume of 169 billion cubic meters. About 17% of the reservoir is in Sudan. After dam construction, the annual floods are under control and the navigation properties of the Nile River are considerably improved. However, artificial fertilizers have to be used instead of natural nutrients. Quality of the soil for farming has decreased. Negative impacts due to lack of rich sediments in the delta region is one negative environmental consequence.

Over the past two centuries, many people have died along the Yangtze River, China due to catastrophic floods. In 1840, about 156,000 persons lost their lives during flood periods; in 1931, 145,000; in 1954 about 33,000; and during more recent flooding in 1998, over 1,500 people died. Millions of hectares of arable land has been destroyed and is unusable. Numerous villages have completely disappeared. During the flood of 1954, 18 million were forced to evacuate from the area. For 3 months, Wuhan City with eight million people was covered with floodwater. After construction of the Three Gorges Dam (181 m high, 2,335 m long) the frequency of major floods has been reduced to a minimum and after project completion, large ships will be able to navigate from Shanghai 2,400 km upstream. Due to project requirements, about 1.24 million people had to be relocated.

As result of construction of the Chira-Piura irrigation system in Peru, including the 9-km long Poechos Dam, an area of 100,000 ha of uncultivated land has been turned into fertile farmland.

Construction of the Akosombo Dam in Ghana created one of the largest world reservoirs, Lake Volta; about 15,000 houses were inundated and 78,000 people were resettled.

The Gibe III Dam (240 m high at Omo River) in Ethiopia was controversial from its beginning. During the Omo River flood of 2006, at least 360 people and thousands of livestock were devastated. From an energy viewpoint, this project would provide great benefits for Ethiopia and Kenya. However, equally important is the projected negative impact on fisheries in adjoining Kenya's Lake Turkana, which threatens the livelihoods of about 0.5 million tribal people.

To construct the Ataturk Reservoir in Turkey, about 55,000 people were relocated, and from the Manantali Reservoir area (Mali) 15,000 people were displaced. It is estimated that the controversial Ilisu Dam Project (Turkey) would displace at least 55,000 people. For construction of the Everkiiskaya Dam (Central Siberia, Russia), about 7,000 local indigenous people would need to be relocated and a huge area flooded (9,000 km^2).

Dam Failures

One of the worst negative environmental impacts of dams is the risk of failure. The first known dam failure, as reported by Herodotus, was the collapse of the Saad Ei-Kafra Dam in Egypt during flooding ~2500 BC. In modern history, one of the oldest reported failures was the Blackbrook I Dam (Great Britain, 1799). Official worldwide database and case histories of dam incidents and failures are not still completed. According to the ICOLD Bulletin 99, Dam Failures, Statistical Analysis (without China), a total of 5,268 dams were built until 1950 (117 of them failed), 12,138 dams were built during the years 1951–1986, (59 of them failed).

Many incidents of dam failure occurred more than 50 years ago and involved older dams. In recent decades, the failure rate (particularly for dams more than 30 m high) has drastically decreased. At present, dams are constructed on the basis of thorough and detailed multidisciplinary investigations, including application of new technologies and detailed environmental studies and operational stability is regularly monitored.

The world's recorded dam disaster occurred 1975 in China (Banqiao Dam). Due to a strong hurricane and precipitation of 500 m over 3 days, the Banqiao Dam, together with Shimantan Dam and 62 small dams, was totally demolished. Water waves as high as 6–10 m and 12 km wide flooded more than a million hectares. More than 26,000 people were killed, and many more died afterward from resulting epidemics, for an estimated 150,000 total deaths. Eleven million people lost their homes.

Dam failures as a consequence of geology are sometimes catastrophic, causing loss of life or evacuation of thousands of people living downstream of the dams: for example, Malpasset (France), St. Francisco and St. Fernando (USA), Baldwin Hills (USA), and Teton (USA).

Total failure of the Malpasset concrete arch dam (66.5 m high) caused a huge flood on December 1959. Dam foundation consisted of gneissic rocks. Two sets of faults had crucial roles in the creation of a wedge failure. More than 325 persons lost their lives and a large area was devastated [4].

The worst American civil engineering failure of the twentieth century was the St. Francisco Dam (California, USA), killing 450 people along the St. Francisco Canyon and St. Clara Valley. Foundation rock of the concrete gravity dam (60 m high) is conglomerate. During March 12–13, 1928, the St. Francisco Dam collapsed due to a paleo-landslide at the left abutment and strong uplift. According to Cooper and Calow (1998), the failure was partially attributed to gypsum dissolution [5].

The Teton Dam (USA) failure happened on June 5, 1976, killing 14 people; that embankment dam was 93 m high above riverbed. Dam foundation consists of basalt and rhyolite rock. Piping was identified as the most probable cause of failure [4].

Catastrophic failure of San Juan earth dam (Spain) occurred during the first filling of reservoir (2001). Due to intensive dissolution of gypsum, part of dam collapsed, provoking a huge flood downstream [6]. The flood caused by failure of the Lower San Fernando Dam (California, USA, 1971) due to a strong earthquake (M = 6.6) caused temporary evacuation of 80,000 people from the downstream area [4]. The Baldwin Hills Reservoir (USA) failed in 1963 causing enormous damage downstream; however, thousands of inhabitants were evacuated in time [4].

Thousands of inhabitants downstream from dams all over the world are permanently under psychological

and mental pressure due to possible dam failure. Some of them seek relocation to safer places. If an area downstream from dam is populated, flood wave analysis in case of dam failure is very important. Analysis includes timing of water wave propagation, estimation of flood level, and installation of emergency alarm systems. Two important parameters are: time of flood wave between dam site and urban areas, and safe elevation for population evacuation – the elevation above which a disastrous wave is not effective.

In many cases, citizens living downstream from dams protest strongly against them, sometimes insisting on dam displacement. In the case of the Mulholland Dam (65-m high conrete gravity dam) because of disaster of St. Francisco, there was enormous protest from the citisens of Holliwood lining downstream from the dam. To solve this mostly psychological problem, the downstream dam face was covered in 1933 by a huge earthen mass, making it one of the most conservative dam structures in the world.

Reservoir Slope Instability

Reservoir slopes are exposed to different kinds of hazards. The most common is the potential for landslides to cause a wave which might overtop the dam crest, causing dam failure and disastrous flood wave downstream. According to Schuster (2006), at least 254 large dams worldwide have been subjected to landslide activity [7]. The most common types of hazard are instability of slopes and deterioration of reservoir water quality due to solution processes if the slope consists of evaporates. The most frequent remedial measures to prevent instable rock masses from sliding are retention walls, prestress anchors, galleries and other drainage structures, and grouting and cutting of sliding planes.

Due to hydrodynamic force caused by reservoir fluctuation, the slopes are exposed to sliding, creeping, and toppling. This process can have catastrophic consequences. The difficulty is how to predict potential for a landslide on the basis of geological data and geological history of reservoir rims. An attempt has been presented by Moon (1997) in New Zealand [8]. He has established a magnitude-frequency curve for landslides based on geomorphological evidence of sliding in a valley and the geomorphological history of a valley.

In the case of Vaiont Dam (261-m high dam in Italy), a huge landslide suddenly slid into the reservoir on October 9, 1963. The event lasted only 45 s, but a volume of about 300,000 million cubic meters plunged into the reservoir. The landslide length was 1.850 km and average thickness was 157 m. Maximal thickness of the slide rock mass was 330 m. A water wave was created which overtopped the 100-m high dam crest. The catastrophic water wave completely demolished the small town of Longarone, 2 km downstream, and six more settlements. About 1,700 inhabitants lost their lives and a number of industrial structures were completely destroyed [9]. The dam structure itself was not damaged at all.

In a number of cases, massive stabilization structures are constructed to eliminate hazards during reservoir operation. Induced slope stability is a problem along the 650 km of the Three Gorges Reservoir. The Lianziya potentially sliding rock mass, located about 25 km from the upper stream of the Sadoung dam site of the Three Gorges (China), has a volume of 2.26 million cubic meters. Deep prestress bolting, up to 3,000 kN, is used to improve slope stability [10].

Tailings Dam Failures

Tailings dams are more vulnerable than other dam types. In the case of failure, environmental impact is catastrophic and long lasting. Tailings usually contain high concentrations of different chemicals. They represent a potential threat of environmental contamination, in some cases by extremely dangerous chemicals such as heavy metals or cyanides. One of the latest incidents (Baia Mare, Romania) occurred in January 2000, and released about 100,000 m^3 cyanide contaminated water into the catchment area of Tisa River (tributary of Danube River), provoking great public concern in the huge and highly populated downstream area.

The last "Chronology of major tailings dam failure, 1960–2011" is prepared on the basis of Bulletin 121, published by United Nations Environmental Programme (UNDP), Division of Technology, Industry and Economics (DTIE), and International Commission on Large Dams (ICOLD), Paris 2001, 144 p., updated, March, 2011, (221 tailings dam incidents). Tailings dam failures occurred for many different

reasons, but mostly after heavy rainfall due to overtopping, seepage, foundation failure, or due to dam wall failure or liquefaction during earthquakes. Poor management and inadequate construction methods can also contribute to dam failure [11].

In many cases, failures are disastrous. Heavily polluted tailings flow can travel from a few 100 m up to more than 100 km. After failure of the tailing dam at Silverton, Colorado, USA (1975), tailings flow polluted 160 km of the Animas River; near Fort Mead, Florida, USA (1971), tailings flow traveled 120 km; in the Inez failure in Martin County, Kentucky, USA (2000), polluted flow traveled 120 km; in the case of Huancavelica, Peru (2010), the Escalera and Opamayo Rivers were contaminated 110 km downstream; and during dam failure of El Pocho, Bolivia (1996), 300 km of the Pilcomayo River were contaminated.

The worst impacts of tailings dam failure are the great number of people killed. From 1960 to 2010, 23 cases of tailings failures with fatalities were reported. Drastic examples are failure of the Sgorigrad, 1966 (Bulgaria), 488 people killed; the Stava, 1985 (Trento, Italy), 268 killed; Taoshi, 2008 (Shanxi province, China), 254 killed; El Cordobe, 1965 (Chile), 200 killed; Aberfan, 1966 (Wels, UK), 144 killed; Buffalo Creek, 1972 (W. Virginia, USA), 125 killed; and Mufulira 1970 (Zambia), 89 killed. Common impacts after tailing failures are demolition of homes, relocation of people, inundation of agricultural land, and catastrophic consequences for biodiversities in downstream areas, particularly for fish.

According Rico et al. [12], for a group of 147 cases of worldwide tailings failures, 39% happened in the USA, 12% in Chile, 10% in the UK, and 4.8% in the Philippines [12]. Twenty-six occurred in Europe. With regard to tailings dam height, a greater percentage of failures occur if the height is not higher than 30 m. Tailings failures are frequently related to heavy precipitation or due to seismic liquefaction. More than 85% of failures occurred during mine operation, and only 15% of incidents were related to inactive tailings dams.

Reservoir-Triggered Seismicity: Induced Seismicity

From the very beginning, reservoir-triggered seismicity has been controversial. The first documented case was the case of the Hoover Dam (Lake Mead, USA). Presently, more than 60 cases of reservoirs are frequently cited to have experienced reservoir-triggered seismicity (Perman et al. 1983 and Gupta 1992). Magnitudes are greater in the case of greater depths of reservoirs: Koyna (India), depth 100 m, M = 6.3; Kremasta (Greece), 120 m, M = 6.3; Kariba (Zambia), 122 m, M = 6.25; Hsingfengiang (China), 105 m, M = 6.0; Srinagarind (Thailand), 133 m, M = 5.9; Oroville (USA), 204 m, M = 5.8; Aswan (Egypt), 90 m, M = 5.2; Hoover (USA), 191 m, M = 5.0; Kurobe (Japan), 186 m, M = 4.9; and Mratinje (Montenegro), 220 m, M = 4.1. However, except for a few cases (Koyna and Hsingfengiang), human and material losses were negligible. The Hsingfengiang Dam was considerably damaged, but so far no dam has collapsed due to the effect of induced seismicity [13].

In general, triggered seismicity starts during the first impounding of the reservoir and increases with reservoir water levels; intensity of shaking sharply decreases with distance from the reservoir.

Certain earthquakes registered during reservoir impounding in karst indicate the role of karst in genesis of induced shocks. Those analyses indicate possible explosions of the compressed air during an abrupt reservoir impounding and simultaneous abrupt rising of the water table in the surrounding karst aquifer. Pressure of the air trapped in karst channels and siphons significantly increases. Trapped air pillows escape, creating strong explosions that are felt by inhabitants and recorded by seismographs at the surface. Environmental impact of this process is generally local, noisy, but not harmful. Small damage is possible in the case of older village structures.

Dams and Heritage Protection

During dam construction, in some cases, very important monuments and internationally recognized old civilization heritage sites are threatened by inundations. Some are world heritage sites protected by UNESCO. In many cases, reservoirs may flood national parks, caves of archeological importance, or old necropoli, monasteries, graveyards, and ancient bridges.

The most famous are the Abu Simbel temples in Egypt built in the middle of the Nubian Desert (present

reservoir) by Ramses II who ruled from 1290 to 1224 BC (19th dynasty). After construction of the Aswan Dam, both monuments of Ramses II and of his wife were sawn into 1,036 blocks, 30 t each, plus 1,110 blocks from surrounding rock. Monuments were reconstructed 90 m above the original level (Fig. 2).

Due to construction of dams along the Trebišnjica River (BiH), two ancient monasteries built in 1232 and during the first part of the fourteenth century, and one bridge constructed at the first part of the sixteenth century, nationally recognized cultural heritage sites have been relocated from the reservoir areas (Fig. 3).

Construction of the Lower Gordon dam in southwest Tasmania would have flooded a large karst area containing caves of great archeological importance. The project was abandoned for legal and environmental reasons in 1983 [14].

During construction of the Iron Gate Dam on the Danube River, a number of historical monuments, including ruins of the old bridge over the Danube River dating from 28 to 104 AD (time of Roman Emperors Tiberius, Claudius, and Traianus) have been flooded. To preserve the monument "Tabula Traiana," heavy limestone blocks of 250 t were sawn and lifted 20 m to be above the reservoir level. The old prehistoric settlement (Lepenski Vir) dated between five and six millennia BC, which represents one of the oldest cultures in this part of Europe, was relocated above the Danube Reservoir level.

Along the Three Gorges Reservoir (Yangtze River, China) about 1,300 archeological sites, including 30 Stone Age localities, have been carefully investigated. About 1,200 of them will be relocated to higher places. Some irreplaceable historical artifacts, however, have been permanently inundated.

The old Greek and Roman City of Zeugma, larger than Pompeii, founded in 300 BC, on the Euphrates River, was inundated after construction of the Birecik Dam, Southeast Anadolian Project, Turkey (1999). Zeugma mosaics have been declared one of the best preserved Roman Mosaic collections in the world. This ancient city is submerged, but its famous mosaics were placed in the museum of Gazi Antep.

The proposed Ilisu Dam (Southeast Anadolian Project, Turkey) upper Tigris River, 65 km from the Syrian border, threatens to inundate Hasankeyf, an

Dam Engineering and its Environmental Aspects. Figure 2
Abu Simbel monument replaced from Aswan Reservoir, Egypt

Dam Engineering and its Environmental Aspects. Figure 3
Old monasteries at bottom of Bileća Reservoir (BiH)

internationally recognized Roman, Byzantine, and Ottoman historical and cultural heritage site. Historical monuments include thousands of caves carved more than 2,000 years ago. About 50 villages and 15 small towns along the Tigris valley would be displaced [15].

A large part of Munzur National Park (Turkey) is to be flooded by construction of eight dams. Thousands of endemic species will become extinct after finalization of the project. Some of these dams are already constructed (Mercan and Uzuncayir dams).

A dam project in Coa Valley, Portugal was canceled because of the important Ice Age rock art. Many irreplaceable artifacts of an ancient Mesopotamian city (2000 BC) are endangered by construction of the Makhal Dam in Iraq. In the case of construction of Sardar Sarovar and Narmada Sagar dams at Narmada River (India) 250,000 people will be displaced and 3,000-year-old historical temples are potentially endangered.

Dams and Ecosystems

After dam construction, it is not simple to keep ecosystem parameters upstream and downstream at the same levels as preconstruction conditions. Most frequently, temperature and flow regime are disturbed, particularly if the purpose of the dam is power production, where a reservoir water body is not thermally and hydraulically homogenous. Magnitude and frequency of reservoir fluctuations are rapid and huge. Thermal stratification is quite pronounced. Intake structure position at the dam body is one of the important requirements to reduce the effect of complex processes in a reservoir. Water quality disturbances upstream from a dam are transferred to downstream flow. Enormous daily flow fluctuation and velocity due to hydroelectric power plant operation could have disastrous effects on flora, fauna, and physical properties of a riverbed. To minimize downstream negative environmental impacts, guaranty ecological flow is an essential requirement.

Guaranty ecological flow (or ecological base flow, or environmental flow requirements) is usually one of the controversial requirements in dam construction. Different methods are proposed to define base flow (for instance, the Tennant method). Compared with frequently used sustainable flow or biological minimum flow, the guaranty ecological flow is accepted as the quantity of water flow which guaranties natural ecosystem sustainability [16]. Flora and fauna are the

key parameters to establish balance between all ecological parameters, that is, to preserve ecosystem integrity. Adaptation processes may take place over many years before a new ecological balance is achieved. In the case of deep reservoirs for electricity production, with deep intake structures, the temperature of water downstream from a dam usually is much colder than under natural conditions. Daily, seasonal, and annual flows are quite different than under natural conditions. Consequently, the ecosystem is disturbed, and immediately below the dam structure, the water cannot be used for recreational purposes.

Dams reduce sediment load downstream. If a dam and a reservoir are constructed on a river close to a seacoast, the estuarial effect (saltwater intrusion) upstream is expected, that is, there can be a negative influence of brackish water on native biodiversity. Due to dam construction, the rate of deposition of sediments (fines, sand, and pebble) is reduced. If commercial excavation of sand and pebbles remains as before, the geometry of the riverbed drastically changes. If excavation of sand and pebbles occurred between the dam and the seacoast, the problem becomes more complicated. Excavated sediments cannot be naturally replaced; the river bottom becomes deeper and deeper. As a consequence, the saline water wedge penetrates upstream much faster. This effect can lead to declines in native aquatic vegetation, fish, and amphibian species. Over time, the natural balance is disturbed and brackish water species replace native species. In some cases, saltwater penetration endangers the quality of groundwater near riverbanks creating irrigation and water supply problem.

One of the most serious environmental consequences of dam construction is obstruction to fish migration. Dams are barriers for migratory fishes, such as salmon, trout, sturgeon, alewife, skate, eel, and many others. Construction of fish ways dates from about the seventeenth century in France. Presently, dams are widely equipped with several types of fish ways. These structures are not effective for all fishes or are only partially effective. In the case of downstream migration, mortality of fish passage through power plant turbines or over spillways is significant [17].

Particular problems appear in the case of reversible (pumping) power plants. When the power plant is in pumping regime, fishes can be sucked in by the turbines and transported through the pressure tube and headrace tunnel at the upper compensation reservoir.

Multiple dams along the river considerably worsen the situation for migratory fishes, but in the case of dams in the Glomma River system (Norway) efficient fish ways were constructed at eight dams along 122 km of river [18]. Four dams along the Peconies River (USA) have been equipped with fish ladders. Successful salmon migration has been studied in the case of Snake River dams, Lower Granite dams, and many other locations.

The Iron Gate Dam at the Danube River is not equipped with "fish ways." As a consequence, the caviar productive fish, sturgeon, and skate are unable to migrate from the Black Sea to the Danube River. The 11 dam cascades on the Volga and Kama rivers impede migration north from the Caspian Sea for several sturgeon migratory species including Beluga (Beluga caviar).

Construction of dams can negatively impact wetland ecosystems. Usually, wetlands are extremely rich in diversity of flora and fauna. Reduction of base flow which feeds wetland areas can lead to declines in aquatic vegetation, fish, and birds. Many wetlands are temporary recovery stations for migratory birds. Dam influence may cause reduction of some bird species; however, in some cases dam operation can be easily adapted to support, or even improve, wetland ecosystems.

Dams and Microclimate

As a consequence of damming, estimated total current reservoir surface is more than 400,000 km^2. Largest reservoirs are Lake Volta, Ghana – 8,502 km^2, Aswan Reservoir, Egypt/Sudan – 5,250 km^2, Itaipu Reservoir, Brazil/Paraguay – 1,350 km^2, Ataturk Reservoir, Turkey – 817 km^2, and Keban Reservoir, Turkey – 675 km^2. Due to hot weather or strong winds, evaporation from reservoir surfaces is estimated at about 2 m^3/m^2 per year.

Exact climatological measurements and analyses related to reservoir impact are rare. Measurements taken at the reservoirs at Pourinari and Mornos (Greece) and Bileća Reservoir (BiH) indicate negligible increase of temperature close to the reservoir areas. For more precise conclusions, long-term monitoring of different parameters is necessary.

According to subjective impressions of local people, there is some climatological influence. In karst areas, intensity of deforestation decreased, and fogs are registered much frequently after dam and reservoir construction. Impact of the Krasnojarsk Dam (Russia) on the Yenisei River reaches 200 km downstream and has an influence on local climate by increasing freezing fog.

Induced Subsidence (Collapse)

Origin of subsidence can be natural or induced. Induced subsidence is a consequence of human activities, but mainly due to groundwater extraction, mining, and dam construction [19–22].

Subsidence development is a common process as a consequence of dam construction and reservoir operation. Induced subsidence is a series of spatially independent random events created by reservoir operation. Events such as these are unpredictable and practically instantaneous. Some prominent examples are the following reservoirs: Wolf Creek (USA), Hutovo (BiH), Slano and Vrtac (Montenegro), Tarbela (Pakistan), Mavrovo (FYR Macedonia), Perdica (Greece), Hammam Grouz (Algeria), Kamskaya (Russia), Lar (Iran), Keban (Turkey), North Dike (Florida, USA), and Huoshipo Reservoir (China).

Subsidence is induced by extensive water level fluctuation in reservoirs and results in extensive water leakage. In some cases, subsidence occurred after many years of successful operation. In the case of Hammam Grouz (Fig. 4), subsidence occurred after 17 years, and in the case of Mavrovo, after 25 years.

In some cases, subsidence creates considerable environmental impact. For instance, the Mavrovo reservoir collapse resulted in heavy damage to local roads and surrounding houses.

In the case of Kamskaye Reservoir (Russia), after dam construction the dissolution process in gypsum has intensified in the vicinity of the reservoir [23]. During the period 1956–1961, 11 collapses occurred. Prior to dam construction, in the same area, only two collapses were registered during the previous 50 years.

Spring Submergence Due to Dam Construction

Submergence of large springs by artificial reservoirs and the consequences on environment and reservoir integrity are frequently discussed. After construction of the 185-m high Oymopinar Dam (Turkey), the large Dumanly spring Qmin = 35.6 m^3/s was flooded by 120 m of water head at maximum storage level; the Trebišnjica Spring (BiH), Qav = 80 m^3/s was flooded by 75 m of water column; the Neraidha Spring (Greece), Q = 10 m^3/s, was flooded by 40 m of Poliphiton Reservoir; the 220-m high Piva Dam (Montenegro) the large Pivsko Oko Spring, Qav = 25.5 m^3/s, was flooded by 70 m; the Rama spring zone (BiH) was submerged by 40–60 m of water column; and the Yarg Spring (Iran), Qav = 0.7 m^3/s was flooded after construction of the Salman Farsi Dam (136 m) by 27 m; Oko Spring (BiH) was flooded after construction of 35-m high Gorica Dam by 17 m of water column [24]. The Bel Spring (Iran) will be submerged by construction of the 230-m high Darian Dam.

The most important questions to be answered are as follows: Is the water used for water supply or water bottling, if so, how to keep quantity and quality at acceptable levels?; Are water losses from the reservoir possible?; What is the possible submergence effect on the hydrologic regime in upstream areas?; How could spring submergence affect induced seismicity in surrounding areas?. In many analyzed cases, spring submergence does not increase considerable environmental consequences.

One specific case is Bel Spring in Iran. Spring discharges vary between 150 l/s and 10 m^3/s. Two companies use water from the Bel Spring for bottling. By construction of the Darian Dam, the Bel Spring will be exposed to a water head of more than 150 m. The question is how to protect Bel Spring water for bottling (quantity and quality). A particular tapping structure is designed behind the spring to prevent reservoir water influence and preserve groundwater potential for bottling during reservoir operation.

The Oko Spring is the only water supply source for the town of Trebinje (BiH, 20,000 people). After construction of the Gorica Dam, the tapping structure is above the reservoir level. Three large diameter wells were drilled into the karst channel situated 25 m deeper than reservoir bottom. Impact of reservoir water to quality of potable water occurs only during extremely fast impounding of the reservoir.

Dam Engineering and its Environmental Aspects. Figure 4
Hammam Grouz Dam, Algeria. Subsidence occurred after 17 years of dam operation

Environmental Aspects of Dams in Karst

The complexity of karst presents a great variety of risk for dams and reservoirs in karst. The crucial role of dams and tunnels in karst is dewatering of temporarily flooded karst depressions, for water transfer from one catchment (or political entity) to another and for electricity production. By dam construction in karst regions, some temporarily flooded depressions are changed to permanent reservoirs or, in other cases, to farmland areas. By applying different geotechnical measures, the karstified and pervious riverbeds are transformed into permanent river flows.

Construction of dams and reservoirs in general has considerable influence on regime and quality of surface and underground water downstream. In the case of karst, impacts are sometimes registered at remote springs at distances of 10–30 km, leading to local and transboundary environmental and political problems.

In many cases, the purpose of dam structures is rerouting and transfer of water from one catchment to another. These solutions create conflicts between owners of the dams (reservoirs) and users of the springs. This situation is especially delicate if the reservoir and springs are in different political regions. For example, by construction of Grančarevo and Gorica dams at BiH, the average yearly discharge of Ombla Spring (Croatia) has been reduced from Qav = 33.8 m^3/s to Qav = 24.4 m^3/s. A large part of the water is transferred through the headrace tunnel toward the power plant of Dubrovnik located in Croatia. There was no change in the minimal discharge of Ombla Spring. By construction of dams, the karst aquifer was starved of about 4 billion cubic meters of water annually as a result of rerouting through the tunnels and paved channels for power production and drainage of many swallow holes [24].

Karst underground is very rich with various fauna. Often, as a result of dam construction in karst, a large volume of caverns in the aeration zone are flooded, or temporarily flooded karst channels become permanently dry. In both cases, cave habitat for a number of rare and endemic species is endangered, for example, Normandy Dam (Tennessee, USA), Melond Dam (California, USA), Scrivener Dam (Australia), Grančarevo and Gorica Dams (BiH), and Seymareh Dam (Iran).

A specific example is Popovo Polje in BiH (Fig. 5). Flooding under natural conditions before dam

Dam Engineering and its Environmental Aspects. Figure 5
Very pervious Trebišnjica riverbed covered by shotcrete. At hillside is visible line indicating flood level in natural conditions

construction reached a height of 40 m in the lowest section of the polje; the polje was under water an average of 253 days and was dry only 112 days. During maximum flood, 7,500 ha were under water. During dry periods the Trebišnjica River was dry also because of 65 m^3/s of seepage along the 65 km of riverbed [25]. The only variety of maize that grows here is called "hundred-day maize." In 100 days, it sprouts, grows, and bears fruit. After dam construction and the increase in impermeability of the riverbed, floods were almost eliminated and huge areas of arable land were created. New infrastructure (plantations, roads, irrigation canals, and settlements) changed complete environmental properties of the entire area.

Dewatering of the temporarily flooded Popovo Polje (BiH) has negative influence for aquatic organisms that inhabit temporary underground lakes during the dry period and ephemeral lakes during flood season. An example is the Gaovica fish (*Paraphoxinus ghetaldi*) which spends dry months in numerous siphon lakes and pools of the underground karst. During flood periods, the fish leaves the underground through karst channels and openings of estavelles. For the duration of inundation, the fish lives in the intermittent lakes at surface. For centuries, fishing at openings of estavelles was an important tradition and food source for inhabitants of Popovo Polje. By construction of two dams (Grančarevo and Gorica dams), the water regime has drastically changed; the Gaovica fish lost connections with the surface in most locations and is now threatened with extinction. As a consequence of the same project, the large concentrations of endemic worm *Mariphugia cavatica*, mollusk *Kongeria*, and cave-dwelling aquatic endemic species *Proteus anguinus*, known as "human fish" are seriously endangered [26]. Dam and reservoir construction decreased the activity time and discharge of a series of temporary and submarine springs along the seacoast. The operation of a commercial oyster and mollusk farm has been threatened because of reduced freshwater outflow through the submarine springs.

One of the richest caves with various fauna in the world is in the same area, Vjetrenica cave. Approximately 110 species have been identified in this cave. More than ten species are known only from this cave or the immediate vicinity [27].

From an environmental point of view, underground dams and reservoirs in karst have benefits. The main advantages of these unique structures are as follows: Arable land is not disturbed, water is not thermally stratified, water quality remains high and constant, catastrophic dam failure is not a possible outcome, and the landscape is not disturbed. In the karst regions of China, more than 20 underground reservoirs have been created with storage capacities between 1×10^5 and 1×10^7 m^3. Their purposes are water supply, irrigation, industry, and electricity production [28]. According to Yuan [29], in the Xiashi district (Guizhou Province) 16 underground dams have been constructed for irrigation of 3,624 acres of farmland [29].

To control concentrated infiltration through the large ponors (swallow holes) a specific type of dam is constructed in karst areas – cylindrical dams. The purpose of cylindrical dams is to prevent natural plugging of large ponors, that is, to ensure fast dewatering of floodwater from farmlands. Some cylindrical dams constructed at Peloponnesus (Greece) in fourteenth century are still operational (Fig. 6).

In the Dinaric karst area (BiH), cylindrical dams were used from ancient time until the middle of the twentieth century for mills. These dams were constructed above the large ponors at the riverbanks. Water sinking into the ponor propels wooden turbines and millstones. Mills were equipped with simple intake structures and gates to control quantity of water. Recently, cylindrical dams were used to prevent leakage from reservoirs in the case of large ponors or estavelles in Chinese karst and at some other locations.

During filling of Salanfe Reservoir (52-m high dam, Switzerland), new thermal springs appears in the Val d'Illes valley, at a distance of 8 km (1953). Springs are related to the leakage from Salanfe reservoir. The reservoir has never been filled completely since the first phase of impoundment [30].

Reservoirs in karst may fail to fill despite an extensive investigation program and sealing treatment. Dried reservoirs or reservoirs with unacceptable heavy leakage are common in many karst regions of the world: Hales Bar Dam (USA), Montejaque (Spain), Vrtac (Montenegro), Lar (Iran), May (Turkey), Perdikas (Greece), Wolf Creek (USA), Apa Reservoir (Turkey), and many others. A distinctive example is the

Dam Engineering and its Environmental Aspects. Figure 6
Ancient dam at Peloponnesus, Greece, to protect natural plugging of large ponor (swallow hole)

Dam Engineering and its Environmental Aspects. Figure 7
Montejaque Dam, abandoned due to huge leakage

Montejaque Dam in Spain. The dam was abandoned because of huge leakage from reservoir, and cavernous system downstream from the dam is presently used as a training area for speleologists (Fig. 7).

Further Directions

Optimal strategies for water resources development are a key requirement for socioeconomic development. With increasing demands on energy, particularly in many underdeveloped countries, dams and reservoirs are still necessary structures. The environment has been modified by dam construction with possible detrimental impacts. In most instances, impacts are positive: flood control, irrigation, water supply, power production, infrastructure improvement, reduction of deforestation, recreation, fishing, and many secondary benefits. Some negative impacts cannot be avoided: population replacement, inundation of arable land, historical and cultural monuments, influence on survival of endemic species and migratory fishes, deterioration of aquifers, the possibility of triggered seismicity, collapses, and similar events.

An important issue is how to keep the balance between the necessity for development and preservation of environment. Optimal environmental protection requires a multidisciplinary approach, including close cooperation of a wide spectrum of geologists, civil engineers, biologists, chemists, hydrologists, hydrogeologists, archeologists, sociologists, and many others. The ultimate aim is identification of crucial parameters that define causes and consequences between human activities (dam construction) and resulting impact on environment (cause-and-effect relations). Criteria for determining environmental protection, as well as regulatory procedures are important elements in the process.

Particularly, sensitive and complex is construction of large dams and reservoirs in highly developed karst because the majority of water flows through the underground karst conduits. Dam impacts on environment in karst may be unpredictable, occur rapidly, and may be unique. Similar situations are seldom, if ever, repeated. To expect the unexpected, should be permanently kept in the mind as the basic philosophy of dam construction in karst. The major aims of proper

planning of water resources systems in karst terrain are to minimize negative and to maximize positive environmental impacts by keeping water at surface level as much as possible.

Bibliography

Primary Literature

1. Liu J (1980) Changjiang (Yangtze River) China's largest river. Foreign Language Press, Beijing
2. Iranian National Committee on Large Dams (1993) A general view on Iranian dams, past-present-future. Ministry of Energy, Teheran
3. Tennessee Valley Authority (1949) Tennessee valley authority projects, geology, and foundation treatment. Technical report no 22, Knoxville, Tennessee
4. Flagg CHG (1979) Geological causes of dam incidents. Bull Int Assoc Eng Geol 20:196–201
5. Cooper AH, Calow RC (1998) Avoiding gypsum geohazards: guidance for planning and construction. British Geological Survey. Technical report WC/98/5
6. Gutierrez F, Desir G, Gutierrez M (2003) Causes of the catastrophic failure of an earth dam built on gypsiferous alluvium and dispersive clays, Altorricon, Huesca Province, NE Spain. Environ Geol 43:842–851
7. Schuster RL (2006) Interaction of dams and landslides. Case studies and mitigation. U.S. Geological survey professional paper 1723, p 107
8. Moon A (1997) Predicting low probability rapid landslides at Roxborough Gorge, New Zealand. In: Ctuden D, Fell R (eds) Landslides risk assessment. Balkema, Rotterdam, pp 272–284
9. Selli R, Trevisan L, Carloni GC, Mazzanti R, Ciabatti M (1946) La frana del Vaiont. Annali del museo geologico di Bolona, Bolongna
10. Lu Y (2001) Rational exploitation of resources and prevention of geohazards in karst regions. Acta geologica sinica (english edition). J Geol Soc China 75(3):239–248
11. Chronology of major tailings dam failure, 1960–2011 (prepared on the basis of) Bulletin 121, Published by United Nation Environmental Programme Division of Technology, Industry and Economics and International Commission on Large Dams, Paris 2001, p 144, updated March 2011, (221 tailings dam incidents)
12. Rico M, Benito G, Salgueiro AR, Diez-Herrero A, Pereira HG (2008) Reported tailings dam failures. A review of the European incidents in the worldwide context. J Hazard Mater 152:845–852, Elsevier
13. Bozovic A, Wieland M (2004) Reservoirs and seismicity, state of knowledge. ICOLD Committee on Seismic Aspects of Dam Design. Commission Internationale des Grands Barages, Haussmann, Paris
14. Kiernian K (1988) Human impacts and management responses in the karsts of Tasmania. In: Proceedings of the international Geographical Union, Study Group Man's Impact on Karst, Sydnay
15. Smith D (2000) Protest grow over plan for more Turkish dams. National Geographic News
16. Djordjević B, Dašić T (2007) Ecological guarantied discharge downstream from the hydropower plants. J Elektriprivreda 1. Belgrade, 5–13
17. Larinier M (2001) Environmental issues, dams and fish migration. In: Marmulla G (ed) Dams, fish and fisheries: opportunities, challenges and conflict resolution. FAO fisheries technical paper, 419. Food and Agriculture Organisation of the United Nations, Viale dell Terme di Caracalla, Rome
18. Linlokken A (1993) Efficiency of fishways and impact of dams on the migration of Grayling and Brown Trout in the Glomma river system, South-Eastern Norway. Regul River Res Manag 8:145–153, Wiley
19. Lamoreaux PE, Newton JG (1986) Catastrophic subsidences: an environmental hazard, Shelby County, Alabama. Environ Geol Water Sci 8(1/2):25
20. Hua SL (1987) Pumping subsidences of surface in some karst areas of China. In: Symposium on human influence on karst, Postojna
21. Tolmachev V, Ilyin A, Gantov B, Leonenko M, Khomenko V, Savarenski I (2003) The main results of engineering karstology research conducted in Dzerzinsk, Russia (1952–2002). In: Beck B (ed) Sinkholes and the engineering and environmental impacts of karst. Geotechnical special publication no 122. Alexander Bell Drive, Reston, Vurginia
22. Gutierrez F (2010) Hazards associated with karst. In: Alcantra-Ayala I, Goudie A (eds) Geomorphological hazards and disaster prevention. Cambridge University Press, Cambridge
23. Maximovich NG (2006) Safety of dams on soluble rock (The Kama hydroelectric power station as an example). On Russian. The Russian Federal Agency for Science and Innovations, Perm
24. Milanović P (2004) Water resources engineering in karst. CRC Press, Boca Raton
25. Milanović P (1981) Karst hydrogeology. Water Resources, Colorado
26. Milanović P (2002) The environmental impacts of human activities and engineering constructions in karst regions. Epizodes J Int Geosci 25(1):13–21
27. Sket B (2003) Vjetrenica Cave. In: Lučić I, Sket B (in Croatian), Zagreb-Ravno
28. Lu Y (1986) Some problems of subsurface reservoirs constructed in karst regions of China. Institute of Hydrogeology and Engineering Geology, Beijing
29. Yuan D (1990) The construction of underground dams on subterranean streams in South China karst. Institute of Karst Geology, Guilin, p 62
30. Roth P (1994) Reservoir induced earthquakes and thermal springs in valais. Proseis AG, Zurich

Books and Reviews

Abraham S (2008) Determining ecological baseflow needs for stream and springs in arid and semi-arid regions. Geological Society of America, Abstracts with programs 40(6): 87

Arthur HG (1977) Teton dam failure. In: The evaluation of dam safety: engineering foundation conference proceedings, ASCE, New York, pp 61–71

Avakyan AB, Romashkov EG, Chestnaya ET (1979) Fishways and dams (Trans: Gidrotechnickoe Stroitelstvo, 1970). Power Techn Eng 4(11)

Bergkamp G, McCartney M, Dugan P, Mcneely J, Acreman M (2000) Dams, ecosystem functions and envoronmental restoration: thematic review II. I World Commission on Dams, Cape Town

Bizer JR (2000) Avoiding, minimizing, mitigating and compensating the environmental impacts of large dams. IUCN, Gland

Bozovic A (1974) Review and appraisal of case histories related to seismic effects of reservoir impounding. Eng Geol 8(1–2):9–27

Chandler RJ, Tosatti G (1995) The Stava talings dam failure, Italy, July 1985. Proc Inst Civ Eng 113:67–79

Cogels FH, Coly A, Niang A (1977) Impact of dam construction on the hydrological regime and qualirty of a Sahelian Lake in the River Senegal Basin. Regul River Res Manag 13(1):27–41

Collier M, Webb RH, Schmidt JC (1996) Dams and rivers: a primer on the downstream effects of dams. US Geological survey circular 1126. US Geological Survey, Tuscon

Djordjevic B (1990) Cybernetics in water resources management. WRP, Colorado

Dobry R, Alvarez L (1967) Seismic failures of Chilean tailings dams. J Soil Mec Found Div 93:237–260

Fell R, Bowles DS, Anderson LR, Bell G (2010) The status of methods for estimation of the probability of failure of dams for use in quantitative risk assessment. In: International commission on large dams, 20th congress, Beijing

Ford D, Williams P (2007) Karst hydrogeology and geomorphology. John Wiley & Sons, Chichester

Fourie AB, Papageorfiou G, Blight GE (2000) Static liquefaction as an explanation for two catastrophic tailings dam failures in South Africa. In: Tailings and mine waste 2000, proceedings of the seventh international conference on tailings and mine waste 2000, Fort Collins, 23–26 Jan 2000, Balkema, Rotterdam, pp 149–158

Gupta HK (1992) Reservoir-induced earthquakes. Elsevier, Amsterdam

Helms SW (1981) Jawa, lost city of the black desert. Methuen and Co Ltd, USA

Holmgren R (2000) Experiences from the tailing dam failure at the boliden Atik and legal consequences, international report, County Administration of Norrbotten, Sweden

ICOLD Bulletin 99 (1995) Dam failure, statistical analysis. Commission Internatrionale des Grandes Barrages – 151, Paris

Jackson CD, Marmulla G (2001) The influence of dams on river fisheries. In: Marmulla G (ed) Dams, fish and fisheries: opportunities, challenges and conflict resolution. FAO, Fisheries technical paper, 419. Viale dell Terme di Carcalla, Roma

Jobin WR (1999) Dams and disease: ecological design and health impacts of large dams, canals, and irrigation systems. Taylor & Francis, London. ISBN 0419223606 (2)

Keffer ML, Bjornn TC, Peery CA, Tolotti KR, Ringe RR, Stuehrenberg L (2003) Adult spring and summer Chinook salmon passage through fishways and transition pools at Bonneville, McNary, Ice. A report for project MPE-P-95-1. U.S. Geological Survey, Idaho Cooperative Fish and Wildlife Research Unit, University of Idaho, Moscow, Idaho 83:844–1141

Lafitte R (2001) Ethics and dam engineers. Int J Hydropower Dams 4:58–59

Lamoreaux PE (1989) Water development for phosphate mining in a karst setting in Florida – a complex environmental problem. Environ Geol Water Sci 14(2):117–153

Liu JK, Yu ZT (1992) Water quality changes and efects on fish population in the Hanjiang River, China, following hydroelectric dam construction. Regul River Res Manag 7(4): 359–368

McCartney M (2009) Living with dams: managing the environmental impacts. Water Policy 11(Supp 1):121–139, IWA Publishing

McDonald MJ, Muldowny J (1982) TVA and the dispossessed: the resettlement of population in the Norris Dam. University of Tennessee Press, Knoxville

McKartney MP (2007) Decision support systems for large dam planning and operation in Africa. Working paper 119. International Water Management Institute, Colombo

Nations Environmental Programme (UNDP) Division of Technology, Industry and Economics (DTIE) and International Commission on Large Dams (ICOLD) (2001) Risk of dangerous occurrences, lessons learnt from practical experiences, Bulletin 121. Nations Environmental Programme (UNDP) Division of Technology, Industry and Economics (DTIE) and International Commission on Large Dams (ICOLD), Paris, p 144

Odum EP (1969) The strategy of ecosystem development. Science 164:262–270

Perman RC, Packer D, Coppersmith KJ, Kneupfer PL (1983) Collection of data bank on reservoir-induced seismicity. USGS contract no 14-08-0001-19132

Petrović P (2010) "The Kosheish Dam" has it really existed or not? Vodoprivreda no 246-248, Belgrade

Shen CK, Chen HC, Chang CH, Huang LS, Li TC, Yang CY, Wang TC, Lo HH (1973) Earthquakes induced by reservoir impounding and their effects on Hsingfeng dam. Sci Sin 17(2):232–272, Beijing, China

Simpson DW (1988) Two types of reservoir induced seismicity. Bull Seismol Soc Am 78:2025–2040

Tanaka E (2007) Protecting one of the best roman mosaic collections in the world: ownership and protection in the case of the roman mosaics from Zenguma Turkey. Stanford J Archeol 5:183–202

United Nations Environment Programe (1996) Environmental and safety incidents concerning tailings dams at mines: results of a survey for the years 1980–1996 by mining journal research services. United Nations Environment Programe, Industry and Environment, Paris, p 129

USCOLD (1997) Reservoir triggered seismicity. The sixtinth USCOLD Anual Meeting, LA. US Society of dams. Debver, CO

U.S. Army Corps of Engineers (1996) Harbour, and lower granite dams. Technical report 2003-5. U.S. Army Corps of Engineers, Portaland and Walla Walla District

U.S. Committee on Large Dams – USCOLD (1994) Tailings dam incidents. U.S. Committee on Large Dams – USCOLD, Denver, 82 p. 1-884575-03-X

Van Niekerk HJ, Viljoen MJ (2005) Causes and consequences of the Merreispruit and other tailings-dam failures. Land Degrad Dev 16:201–212

Vick SG (1990) Planning, design, and analysis of tailings dams. Bitech, Vancouver

Wieland M Dam safety aspects of reservoir-triggered seismicity. In: Wieland M, Ren Q, Tan SY, Taylor, Francis (eds) Book New Developments in Dam Engineering. pp 95–100

Daylight, Indoor Illumination, and Human Behavior

John Mardaljevic
Institute of Energy and Sustainable Development, De Montfort University, Leicester, UK

Article Outline

Glossary
Definition of the Subject
Introduction
Buildings and Daylight
Guidelines, Measures, and the Evaluation of Daylighting
Human Factors and Daylight
Recent Advances in Daylighting
Future Directions
Bibliography

Glossary

BTDF The bidirectional transmission distribution function. The BTDF characterizes the distribution in luminous output across the full hemisphere of transmitted rays and usually needs to be determined for every incident direction. It is needed to simulate the performance of complex glazing materials and systems.

Climate-based daylight modeling The prediction of various radiant or luminous quantities (e.g., irradiance, illuminance, radiance, and luminance) using sun and sky conditions that are derived from standardized annual meteorological datasets.

Daylight The totality of visible radiation originating from both the sun and the sky.

Daylight factor The ratio of internal illuminance to unobstructed external illuminance under the CIE standard overcast sky.

Daylight metric Some mathematical combination of (potentially disparate) measurements and/or dimensions and/or conditions of daylight represented on a continuous scale.

Illuminance The total luminous flux incident on a surface per unit area. It is a measure of the intensity of the incident light, wavelength-weighted by the eye's sensitivity to correlate with human brightness perception. SI unit: lux or lumens per square meter.

Luminance Photometric measure of the luminous intensity per unit area of light traveling in a given direction. It describes the amount of light that passes through or is emitted from a particular area, and falls within a given solid angle. The SI unit for luminance is candela per square meter.

Definition of the Subject

Daylight in buildings is the natural illumination experienced by the occupants of any man-made construction with openings to the outside, e.g., dwelling and workplace. The quantity and quality of daylight in buildings is continually varying due to the natural changes in sun and sky conditions from one moment to the next. These changes have components that are random (e.g., individual cloud formations), daily (i.e., progression from day to night), and seasonal (e.g., changing day length and prevailing weather patterns). For any given sky and sun condition the quantity and character of daylight in a space will depend on the size, orientation, and nature of the building apertures; the shape and aspect of the building and its surroundings; and the optical (i.e., reflective and transmissive) properties of all the surfaces comprising the building and its surroundings.

The purpose of the very earliest shelters – the forerunners of buildings – was to protect from the elements. The first buildings to include deliberate elements of daylighting design were often places of worship, many of which survive to this day. Only when glass became relatively commonplace in the

seventeenth century did the provision of daylight for everyday buildings become a consideration. Window design was invariably tailored to the prevailing climate, e.g., small with deep reveals for locales where the solar component of daylight needed to be controlled to prevent overheating. As the cities of the industrialized world became more populous, building densities increased and the provision of daylight for buildings became a planning issue. This eventually resulted in the formulation of the daylight factor which was intended to be a measure of the daylighting potential of a building, and which could be predicted at the design stage using a variety of methods. Devised in the first half of the twentieth century, the daylight factor still forms the basis of many guidelines and recommendations for building design, notwithstanding the fact that a daylight factor value is, by definition, completely insensitive to the building orientation and any consideration of climate.

Advances in glass making and window technology allowed architects to design buildings where the perimeter wall could be almost entirely glazed. Commercial buildings in particular became larger with deeper plan designs so that, despite the highly transparent facade, many occupants were situated far from the windows and so received little daylight. As conspicuous icons symbolizing modernity and prosperity, these designs became the exemplars for architects all over the world, and now many cities feature highly glazed buildings regardless of the local climatic conditions. Thus the daylighting characteristics of office buildings in particular tended to be dictated by considerations of architectural style rather than climate-adapted design. These trends were not hindered by the continued reliance on the daylight factor as an evaluative scheme since the measure is itself climate and orientation insensitive.

For the majority of buildings, it is incumbent on the occupants to moderate the internal daylight conditions using some form of blinds or shades. Occupants will deploy blinds/shades in an effort to moderate the internal environment according to their perceptions of both visual discomfort (e.g., daylight glare) and thermal discomfort (e.g., to avoid direct sun) which vary greatly from person to person. Also, once deployed, blinds/shades will tend to remain closed long after the external condition has passed. Thus it is common to see blinds closed for much of the occupied time. Consequently, the potential to exploit daylighting is often not realized because the blinds are left closed most of the time and the electric lights are left switched on.

Toward the end of 1990s, the daylighting of buildings began to achieve greater attention for a number of reasons. The two most important drivers were:

1. The widespread belief that the potential to save energy through effective daylighting was greatly underexploited.
2. The emergence of data suggesting that daylight exposure has many positive productivity, health, and well-being outcomes for building occupants.

The first of these concerns originated in the 1970s following the energy crisis and culminated with the widely accepted need to reduce carbon emissions from buildings in order to minimize the anticipated degree of anthropogenic climate change. This in turn led in the 1990s to the formulation of guides and recommendations to encourage the design and construction of low-energy buildings and also for the retrofit of existing buildings. All these guides contain recommendations on daylighting, invariably founded on the daylight factor or an equally simplistic schema such as glazing factors. The productivity, health, and well-being effects related to daylight exposure are not yet fully understood, and it is not yet known what the preferred exposure levels should be nor if existing guidelines would be effective for these quantities.

Almost concurrent with the emergence of the two key drivers noted above were a major advancement in the way daylight in buildings could be modeled and the development of numerous new glazing systems and materials to better exploit daylighting in buildings. These developments are expected to lead to significant changes in the way that daylight in buildings is both evaluated (through modeling) and exploited (by new glazing systems and materials).

Introduction

Daylight is generally taken to be the totality of visible radiation originating from the sky and, when visible, the sun during the hours of daytime. The source of all daylight is in fact the sun. Scattering of sunlight in the atmosphere by air, water droplets, and dust gives the sky the appearance of a self-luminous hemispherical

source of light. Sunlight is commonly referred to as direct light since it appears to originate from a small source and can be highly luminous casting sharp shadows. The sky, however, is an extended source of illumination that casts only soft shadows and so skylight is commonly referred to as diffuse light. In building science, diffuse light includes also light from the sky and/or the sun that has undergone one or more reflections from surfaces that are generally not mirrorlike in character.

Daylight may arrive at a point inside a building either directly or indirectly from the luminous source, i.e., from the sun or from the sky. Direct illumination generally results from having an unobstructed view of the source. Indirect illumination is when the light arrives at the point following one or more reflections. Thus, strictly speaking, there are direct and indirect components of illumination from both the sun and the sky (Fig. 1). Although the sun and the sky are both luminous sources, direct sunlight when present is given special consideration because of the small angular size of the sun and its potentially large contribution to illumination (and also its heating effect). Thus illumination from direct sunlight is commonly referred to as "direct light." In contrast, light from the sky – arriving either directly or indirectly – is commonly referred to as "diffuse light." Sunlight that has undergone one or more diffuse reflections is also commonly referred to as "diffuse light." Note that the mode of reflection of the direct sunlight is important: a specular (or "mirror") reflection of sunlight will produce a *redirected* beam of direct light rather than diffuse light. For reflections (and transmissions) that are part-specular and part-diffuse, the distinction between direct and diffuse light can become lost. Reflections can occur either internal or external to the building space under consideration.

Components of Daylight Illumination Indoors

The image shown in Fig. 2 is a simulation of the daylight distribution in a simple space under clear sky conditions. The viewpoint of the virtual camera is "looking" toward the south-facing window. The external conditions are those of a clear sky with sun, with the sun 30° west (i.e., to the right) of the view direction, and at an altitude of 45°. The direct sun illumination on the east wall and the floor is clearly visible. The space

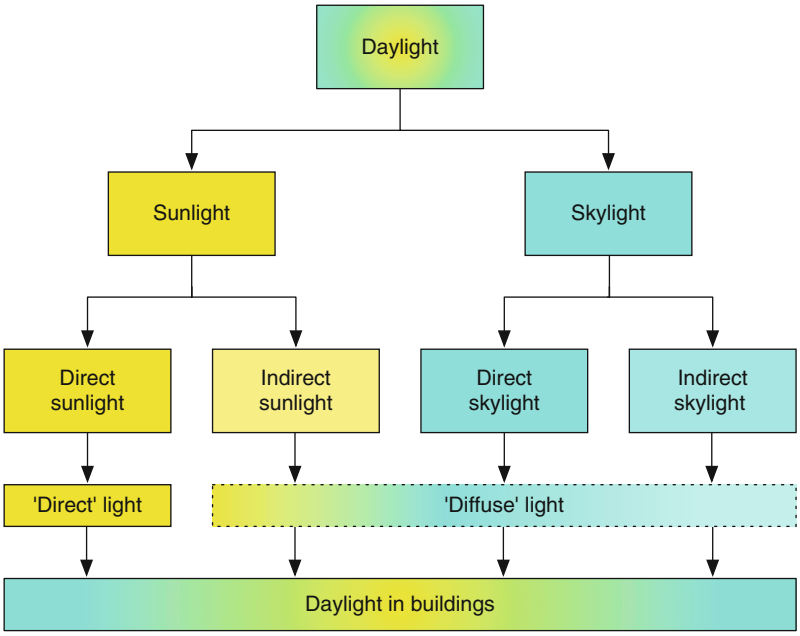

Daylight, Indoor Illumination, and Human Behavior. Figure 1
Components of daylight illumination in buildings

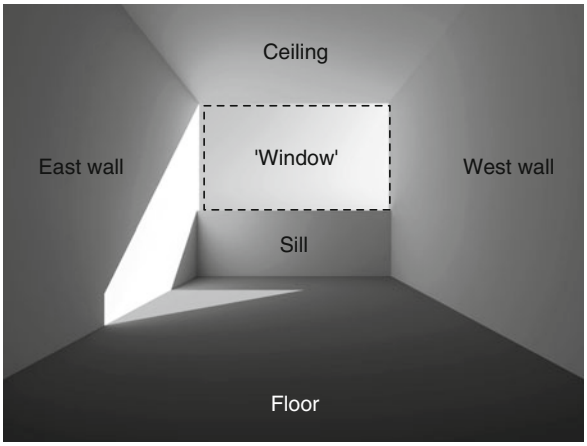

Daylight, Indoor Illumination, and Human Behavior. Figure 2
Simulated image of a simple space illuminated by sunny clear sky conditions

is 3.0 m wide, 9 m deep and 2.7 m high and it "sits" on a ground plane that is 100 m^2. The reflectance values assigned to the surfaces are typical of those commonly used for office buildings and the external ground plane. No glazing was used in the window aperture to eliminate potentially distracting reflection patterns for the example that follows. The simulation of the space was actually carried out in stages so that the individual components of illumination described above could be computed and shown individually. The image in Fig. 2 shows how the space might appear to the eye, in other words it is a representation of the predicted surface brightness (or luminance) of the scene. The light that is incident on a surface is termed the illuminance and is a measure of the illumination (i.e., the light arriving) at a particular point – this is what we would measure with a light or lux meter. The images in Fig. 3 show the distribution and relative proportions of the four components of daylight as illuminance values, together with a fifth image that shows the total illuminance (i.e., the sum of the four components). The magnitude of the illuminance is shown using color and the relation between the two can be read from the legend. Note that a logarithmic scale is used that covers the range from 100 to 10,000 lux. Areas where the illuminance value was zero are shaded gray and the window aperture has been shaded black.

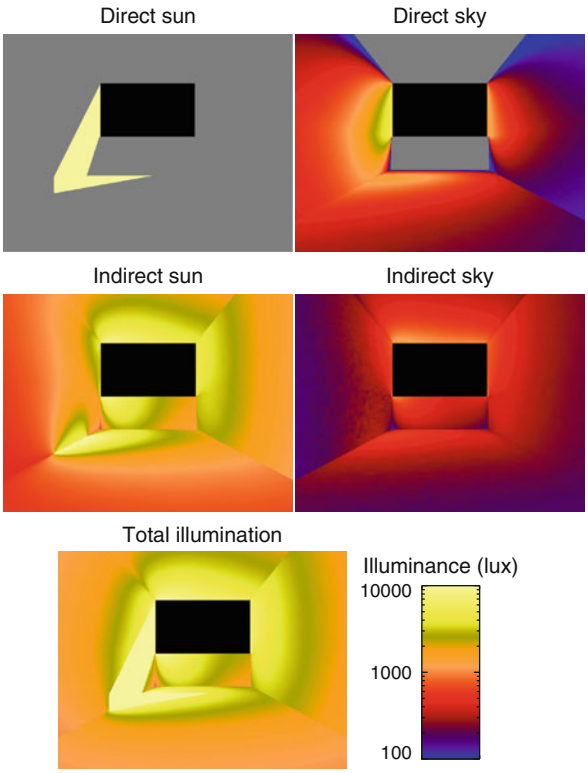

Daylight, Indoor Illumination, and Human Behavior. Figure 3
Components of illumination for the simple space shown in Fig. 2

Direct Components The direct sun image shows the pattern of sun illumination on the East wall and the floor. The illuminance value on the wall is around 40,000 lux (values higher than the legend maximum of 10,000 lux will all have the same shade). Because the scene contains no obstructions, all of the surfaces visible in the image except the ceiling and the sill (Fig. 2) have a direct "view" of the sky and so they receive some illumination directly from the sky. The amount of illumination received at a point depends on:

- The angular size of the patch of sky "seen" through the window (from that point)
- The brightness (i.e., luminance) of the patch of sky
- The transmission properties of the glazing (not used for this illustration)

The areas of wall nearest to the window have the best view of the sky, and they receive the largest

illumination. Note that the illuminance is greater on the East wall because this side "sees" the circumsolar region, i.e., the locus for the sun position and therefore the brightest part of the hemispherical clear sky pattern. The illuminance toward the back of the space (away from the window) reduces gradually as the apparent size of the window diminishes. The illuminance at the highest part of the walls drops off rapidly (i.e., blue shade) as the view of the sky reduces to zero.

Indirect Components The indirect components of illumination show the illuminance that results from multiple light reflections. These reflections usually introduce light from the external environment and also redistribute light within the space. The degree to which this occurs depends on the quantity of incident light (i.e., the direct components) and the reflective properties of the various surfaces. The images showing the indirect components do not include the direct component. The pattern of indirect sun illumination in Fig. 3 is quite complex, but it can be understood with reference to the direct sun pattern. The illuminance resulting from the first reflection of light will generally have the greatest contribution to the indirect component since the intensity of light diminishes with each subsequent reflection. Thus those areas of floor, wall, and ceiling that have the best "view" of the directly illuminated surfaces (inside and out) will have the highest indirect sun illuminance. The west wall "sees" the brightly illuminated sun patch on the east wall (together with the smaller sun patch on the floor) and so it receives a marked quantity of indirect (sun) illumination. For any given size of directly illuminated sun patch, the indirect illumination effect from one on the floor will be less than from one on the wall because the floor has a lower reflectivity. The ceiling will receive indirect sun light from both the sun patches inside the space and the sun-illuminated ground outside. Subsequent reflections will serve to redistribute this, but the bulk of the indirect sun illumination will be at the window end of the space, as is evident in Fig. 3. The indirect component of illuminance from the bulk of the indirect sun illumination will be at the window end of the space, as is evident in Fig. 3. The indirect component of illuminance from the sky shows a gradual diminution going away from the window and toward the back of the space. The slight asymmetry in illumination between the walls can be explained because, at the first reflection, the west wall "sees" the brighter east wall.

This illustration shows how complex the quantity, quality (i.e., direct, diffuse, etc.), and the patterns of natural illumination can be for even the simplest of indoor spaces under naturally occurring daylight conditions. For more realistic spaces, the patterns of illumination will be more complex and, of course, continually changing throughout the day/year.

Buildings and Daylight

The earliest windows were simply holes in the wall or roof of a building. They were providers of daylight and also ventilation, but could be covered with animal hide, cloth, or wood to protect the building occupants from the elements. Daylight would almost always be desirable inside the building, whereas ingress of cold air and rain would generally be avoided. The need for a light transmitting medium that would protect from the elements was first met by translucent materials such as flattened hides and thinly sliced sheets of marble. It was with the invention of glass that the story of daylighting design for buildings truly began.

The first recorded use of glass for windows was not until approximately 100 AD by the Romans. The largest panes that could be manufactured were fairly small. The use of vertical and horizontal dividers – called, respectively, mullions and transoms – increased the size of areas that could be glazed since small pieces of glass could be combined to create large windows. Substantial dividers could additionally form part of the load-bearing structure.

The Industrial Era: 1700s to the Present Day

Glass windows became common in homes in the most developed parts of Europe only in the early seventeenth century. With the advent of improved production techniques in the following century, the cost of glass became less of a limiting factor in its use, though its relative cost compared to other building components was still fairly high. Notwithstanding the high cost of glass, the real cost of artificial light (i.e., as a proportion of the overall household expenditure) was several thousand times what it is today on a per lumen of light basis [1].

The majority of building spaces were side-lit by vertical windows, though the size and arrangement of the windows depended on a number of factors, e.g., intended use, aspect and grandeur or otherwise of the property. Whatever the function or style of the building, window design was, with varying degrees, adapted to the local climatic conditions. Regardless of the size of the window, there would always be a trade-off between daylight provision, heat loss, and solar gain. Internal shutters, often in conjunction with curtains, tended to be used in colder climates where buildings were heated much of the year and heat loss through the windows was significant. In hotter climates where heating was rarely needed, overheating due to undue solar ingress was common in the summer months. Solar gain was moderated by having external shutters which could be closed to cover most or all of the window. Shutters usually had fixed or variable slats that were principally to allow ventilation but also some diffuse light, Fig. 4. Global warming has led to considerations that southern European architectural features such as external shutters may become commonplace in more northerly latitudes in the next 20–50 years.

Rooflights Rooflights began to appear in the mid 1700s when advances in the manufacturing process allowed the fabrication of large sheets of glass at a relatively low cost. Rooflights became a common feature in ordinary houses in the late nineteenth century when mass-produced rooflights with cast iron frames became available. By the late nineteenth century, glass had become relatively inexpensive and was available in good-quality large sheets. Factory buildings since the late 1800s were often designed to provide high levels of natural illumination evenly distributed across the workspace – a goal which is relatively easily achieved in single-story top-lit buildings. The potential for daylighting modern large-span buildings (e.g., storage facilities) was generally underexploited, but energy concerns have led to a rediscovery of this resource.

In domestic buildings, rooflights are now more common and more popular than ever before, particularly in attic conversions and in refurbished historic buildings. In newly designed dwellings, the rooflight is often seen as an integral feature of the daylighting design, and automated opening and blinds operation allows for high-level placement that would have been

Daylight, Indoor Illumination, and Human Behavior. Figure 4
Solar protection using moveable shutters (Dordorgne region, France)

Daylight, Indoor Illumination, and Human Behavior. Figure 5
Rooflights in a modern dwelling (Photo courtesy VELUX A/S)

impractical only 10 years ago, Fig. 5. Depending on the function and occupancy of the space, domestic rooflights can result in significant lighting energy savings [2].

Daylighting in Special-Purpose Buildings

Buildings such as art galleries and museums typically have special requirements for daylighting. Current display practice for highly light-sensitive objects is usually to exclude daylight and use subdued levels of electric lighting commensurate with recommendations for total annual exposure to illumination published by professional bodies and, in some countries, included in legislation. In the wider historical context, this is a relatively recent development since before the 1960s the use and control of light was largely an issue of household practice and museums were usually designed to maximize their use of available daylight through large areas of glazing. From the 1960s onward, daylight has been largely excluded from museum galleries with the exception of those used for art collections (particularly oil paintings) and historic interiors, where its exclusion was felt deleterious to the interpretation of the ensemble of interior and contents. While this move has been partially reversed, with designers expending a great deal of ingenuity trying to blend daylight with new designs of displays and galleries, the success of their work has been variable. In part this is related to our poor understanding of daylight's quantitative performance and the extremely limited techniques, most of them unchanged over half a century, by which daylight in interiors is predicted (see section "The Daylight Factor"). Daylighting design for museums remains one of the more challenging areas of architectural endeavor.

Daylighting Strategies

A daylighting strategy is any building feature that is intended to increase, enhance, or moderate the daylight entering a building. The term is not generally used to describe the typical vertical window with ordinary glazing, though readers may see it used in that way. The strategies can be loosely divided into those that:

1. Employ orthodox construction methods but the building apertures and windows use configurations other than the typical vertical perimeter arrangement
2. Make use of recent and emerging technologies to moderate and/or control the daylight

The first of these, what might be called basic daylighting strategies, are described in this section. The others are described in a later section "Advanced Glazing Systems and Materials". The basic daylighting strategies are essentially building configurations that depart from the norm of vertical glazing; however, they also include, e.g., simple exaggerations of standard building features such as the window reveal to improve the self-shading properties of the window. The various strategies do not occupy distinct categories and many designs feature elements of two or more. There are

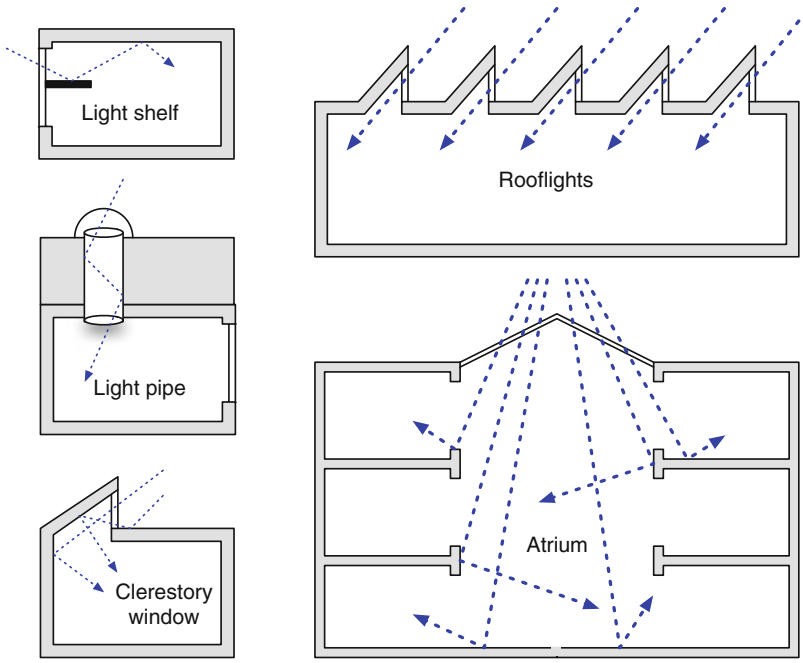

Daylight, Indoor Illumination, and Human Behavior. Figure 6
Daylighting strategies

a number of basic daylighting strategies that are commonly used in buildings. A few of the more common ones are illustrated in Fig. 6.

A light-shelf is any horizontal overhang which abuts and divides a vertical window. The upper and lower surfaces of the shelf are usually highly reflective, e.g., painted bright white, though the upper surface may have a mirror finish. The purpose of the light-shelf may be twofold: (a) to redirect daylight deeper into the space through multiple reflections and (b) to offer partial shading from direct sun for those occupants close to the light-shelf.

The clerestory is any window above eye-level height that allows light to penetrate deep into a space. Strictly speaking, the clerestory window in modern buildings is a distinct window aperture, so the upper part of a tall window separated by frame bars would not normally be described as a clerestory window. The effectiveness of a clerestory window for deep penetration of daylight generally improves with increased height of the window. Clerestory windows can feature on the perimeter facade, often above standard height glazing, or further back in the space to better illuminate those areas farthest from the main windows (Fig. 6).

A light-well is a shaft within a building that is open to the outside at the top to admit daylight. The sides of the light-well usually have a bright finish to encourage reflection of light deep into the well. Windows open onto the shaft to admit daylight to spaces that otherwise do not have any direct access to daylight. The level of daylight that a light-well provides to adjacent spaces tends to be fairly small and decreases rapidly away from the opening. The light-well may also serve as a means to encourage natural ventilation for those spaces deep in the core of the building. Where the primary function is ventilation, the structure is usually referred to as an air-shaft. Light-wells and air-shafts were a common feature in early-twentieth-century tenement buildings where the high density placed restrictions on the availability of natural light and air to core spaces.

The light-pipe, also known as light-tube or more generally as a tubular daylight guidance system (TDGS), is an evolution of the light-well design where a conduit transports light through multiple reflections (Fig. 6). A light-pipe is usually comprised of the collector at one end and the diffuser at the other, Fig. 7. The inside surface of the pipe usually has a metallic/mirror finish with a high reflectivity. Light-pipes can be

Daylight, Indoor Illumination, and Human Behavior. Figure 7
Typical light-pipe diffuser designed to appear like a luminaire. Note that the nearby luminaire is daylight sensing and switched off due to the daylight illumination provided by the light-pipe

made to almost any dimensions, though most are circular in cross section and less than 1 m in diameter, and they can be either straight or have minor bends. Light loss in bends will be higher than for the equivalent length of straight pipe, and so are avoided wherever possible. The efficiency of a light-pipe is the ratio of the lumens delivered into the room by the diffuser to the lumens received by the collector, expressed as a percentage [3]. The efficiency decreases with length of the tube, and so light-pipes are rarely longer than 5 m in length. In office buildings, the use of light-pipes is usually restricted to the topmost story, though they may occasionally be used to convey daylight to the next floor below also. For domestic dwellings, they are most commonly used to supply daylight to central areas such as upper-story stairwells that do not receive any light from perimeter windows. Thus the length of the pipe is governed by the distance traversed through the attic space between the ceiling diffuser and the collector on the roof.

Opened in 1993, the Queens Building at De Montfort University (Leicester, UK) is an award-winning low-energy design that incorporates a number of daylighting strategies. The core of the building is illuminated by several rooflights (which double as ventilation openings) and also "borrowed" light from well-daylit adjacent spaces, Fig. 8. The vertical facades on an enclosed courtyard area between two projecting wings have a high reflectivity finish to enhance the inter-reflected component of light that enters the windows, thus ameliorating to a degree the shading effect of the opposing obstructions, Fig. 9. Daylight penetration is encouraged by the use of high-level windows in combination with high ceilings, and a degree of solar protection is provided by having tall narrow windows set in deep reveals, Fig. 10.

The Decline of Climate-Adapted Building Design

Prior to the 1900s, buildings generally incorporated features that evolved from the need to temper the internal conditions in response to the prevailing climate for that locale. In hot climates with a high propensity for sunshine, buildings would be designed to include elements of solar control either by passive or active means. For example, on sun-exposed facades there would be small windows set in deep reveals to provide self-shading (passive control) or perhaps larger

Daylight, Indoor Illumination, and Human Behavior. Figure 8
Rooflights and glazing apertures to allow for light "spillage" from adjacent spaces

Daylight, Indoor Illumination, and Human Behavior. Figure 9
Highly reflective courtyard

windows with moveable shutters (active control). In less hot/sunny climates, window apertures would tend to be larger and solar control less of an issue – though there would be other concerns such as heat loss. Thus, all buildings contained to varying degrees features in their design that were climate-adapted, and which, over time, became an intrinsic part of that locale's vernacular architecture.

Daylight, Indoor Illumination, and Human Behavior. Figure 10
High-level glazing and deep window reveals

The latter half of the twentieth century witnessed a globalization in architectural form. The highly glazed office tower became the most conspicuous symbol of industrial progress, and hence an inspiration for architects and designers worldwide – regardless of their local climatic conditions. Designers typically rationalized the use of large glazing areas in terms of their daylight provision, but often it was more likely the pursuit of style. Aside perhaps from the possibility of a view to the outside, the daylighting benefit to the majority of occupants in a deep plan space was not great since very few would be close enough to the perimeter to gain any direct benefit in terms of daylight provision. Furthermore, the daylighting potential of highly glazed buildings was often not realized because the manually operated shades/blinds needed to control direct sun were typically left closed long after the external condition had changed. This is the case in fairly temperate climates such as the UK and Northern Europe, but the situation is worse still in sunnier locals. While internal shades do provide occupants with immediate protection from direct sun, they generally have only a limited overall heat rejection effect. Thus, solar radiation, once it has passed through glazing, will inject heat energy to the space which may need to be removed by active cooling (e.g., air-conditioning) if it causes overheating. The almost completely glazed building shown in Fig. 11 exemplifies the total abandonment of climate-adapted design in favor of architectural style. Solar gain will occur across the entire glazed area, and, since the internal shades are dark, virtually all of that solar gain will be instantly reprocessed into heat energy. Thus it is likely that the building will require air-conditioning throughout summer and also at spring/autumn times of the year whenever there is sun. The non-shaded glazed area (i.e., that which could provide daylight but not permanently covered by blinds) occupies approximately one fifth of the total glazed area. Compare that modern design, a tourist office in the Dordogne region, with the climate-adapted traditional design from the same locale shown in Fig. 4. A common practice with highly glazed buildings is to shield the exposed facades with a permanent structure known as a "brise-soleil" (from the French meaning "sun breaker"), Fig. 12. A brise-soleil can be almost any design providing that it offers some degree of solar protection. However, it is true that typical usage of brise-soleil is also more the product of architectural style than resulting from precise performance evaluation of their shading efficiency.

Daylight, Indoor Illumination, and Human Behavior. Figure 11
An almost completely glazed building (tourist office) in the Dordorgne region, France

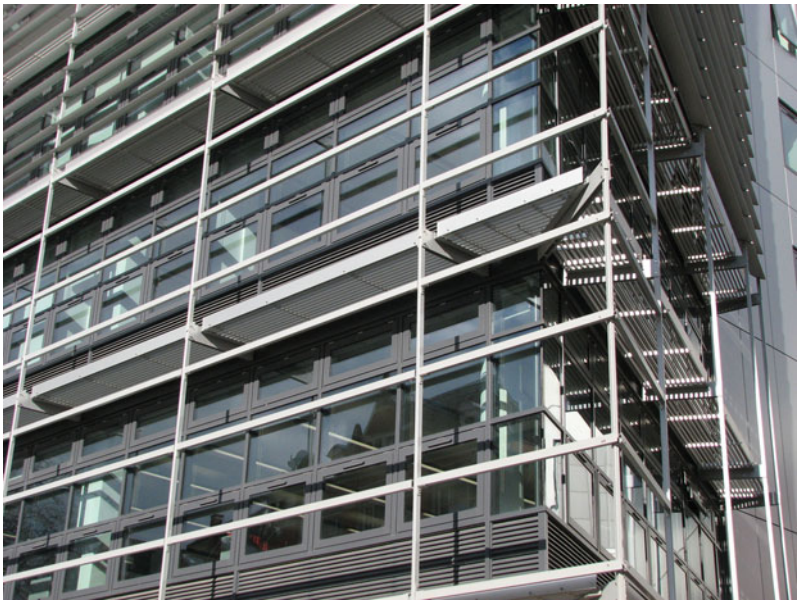

Daylight, Indoor Illumination, and Human Behavior. Figure 12
Solar protection provided by a brise-soleil, Hugh Aston Building, Leicester, UK

The "Well-Tempered" Daylit Environment

A "well-tempered" daylit environment is one where the fixed (i.e., static) architectural form provides both good daylighting and effective solar protection. Thus minimizing – though in practice rarely eliminating – the need for occupants to operate blinds/shades.

The potential for the fixed form to temper the daylighting of the space depends on the building type,

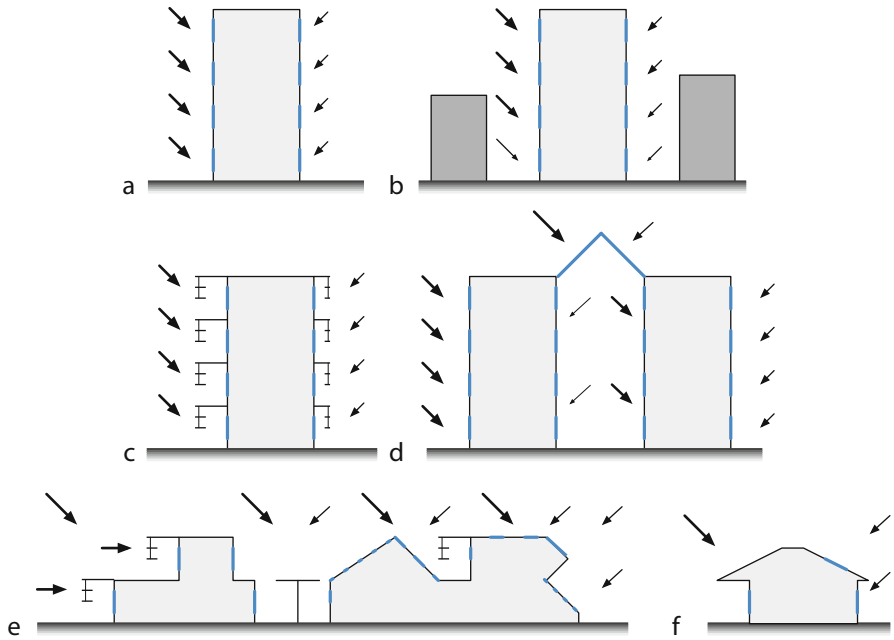

Daylight, Indoor Illumination, and Human Behavior. Figure 13
The "well-tempered" daylit environment

specifically on the richness/variety of the architectural form. This is illustrated by the schematic showing various building types given in Fig. 13. The weight of the arrows is used to indicate the degree of exposure to daylight, i.e., from both the sun and the sky. For the typical rectangular office building (in the northern hemisphere) the south-facing facade will be exposed to direct sun (Fig. 13a). For this type of building the scope to temper the daylit environment is limited to the manipulation of a few basic building parameters, e.g., glazing ratio, transmissivity, etc. Optimization of these will have some beneficial effect, but the occupants with a south-facing window will have to resort to frequent use of the blinds/shades to moderate the internal luminous environment. If shaded by a nearby building (Fig. 13b), the daylighting for the south-facing offices could actually be improved if the overshadowing was such that occurrence of direct sun was reduced but the diffuse daylight provision was still adequate. On the north-facing side of the building however, overshadowing could, in the main, lead to a reduced daylighting potential. Other features and design opportunities could serve to improve the daylighting of the space by tempering the direct sun while still admitting sufficient diffuse light. These include brise-soleil (Fig. 13c) and atria (Fig. 13d). The greater the potential for richness/variety in the architectural form, the greater the opportunity for producing a "well-tempered" daylit environment. Low-rise buildings such as schools (Fig. 13e) and also residential buildings (Fig. 13f) offer perhaps the greatest opportunity to realize a "well-tempered" daylit environment since the building mass and the apertures can be designed with the greatest flexibility to control the admittance of direct sun while providing adequate diffuse illumination.

At present, the realization of a "well-tempered" daylit building is more of an art than a science, relying more on the intuition and insight of the experienced daylight designer than what standard evaluative measures such as the daylight factor (see below) can inform.

Guidelines, Measures, and the Evaluation of Daylighting

Illuminance for Task

The absolute levels of illuminance that are needed for any particular task depend on the visual acuity required for the task and, to a lesser degree, the nature of the

environment in which the task is to be carried out. Most developed countries have produced design guides which give recommended illuminance levels depending on task and/or setting. The following is a selection of recommendations produced by the Chartered Institution of Building Services Engineers (CIBSE) [4]:

- 100 lux for interiors used rarely, with visual tasks confined to movement and casual seeing without perception of detail, e.g., corridors, changing rooms, bulk stores, auditoria
- 200 lux for interiors where the visual tasks do not require perception of detail, e.g., foyers and entrances
- 300 lux for interiors where visual tasks are moderately easy, e.g., libraries, sports and assembly halls, teaching spaces, and lecture theaters
- 500 lux for interiors where the visual tasks are moderately difficult and also where color judgment may be required, e.g., general offices, kitchens, laboratories and retail shops
- 1,000 lux for interiors where the visual tasks are very difficult, requiring small details to be perceived, e.g., general inspection, electronic assembly, retouching paintwork, cabinet making, and supermarkets

Recommended illumination levels were conceived primarily for the purpose of designing artificial lighting systems and not for the daylighting design of buildings because the variation in the provision of natural daylight is such that it is virtually impossible to deliver specific natural illumination levels without huge fluctuations occurring. For buildings therefore, design guidance was formulated in terms of building properties which are evaluated under a single, static "worst-case" daylight condition: an overcast sky. This is the basis of the daylight factor described in the following section. It is only with recent advances in daylight prediction techniques that absolute levels of daylight illumination under varying sky and sun conditions has become a consideration in the evaluation of the daylighting potential of a building (see section "Climate-Based Daylight Modeling").

The Daylight Factor

Design guidelines worldwide currently recommend daylight provision in terms of the long-established daylight factor (DF) [5]. The daylight factor at a point in an internal space is simply the ratio of internal illuminance E_{in} to unobstructed horizontal illuminance E_{out} under standard CIE overcast sky conditions, Fig. 14. It is usually expressed as a percentage, so there is no consideration of absolute illumination values:

$$DF = \frac{E_{in}}{E_{out}} 100\% \quad (1)$$

The luminance of the CIE standard overcast sky is rotationally symmetrical about the vertical axis, i.e., about the zenith. In other words, the illumination that the standard overcast sky delivers to an internal space will be the same regardless of the compass orientation of the building. And, since the sky is fully overcast, there is no sun. Thus for a given building design, the predicted DF is insensitive to either the building orientation (due to the symmetry of the sky) or the intended locale (since it is simply a ratio). Because the sun is not considered, any design strategies dependant on solar angle, solar intensity, redirection of sunlight, etc., can have no influence on the daylight factor value.

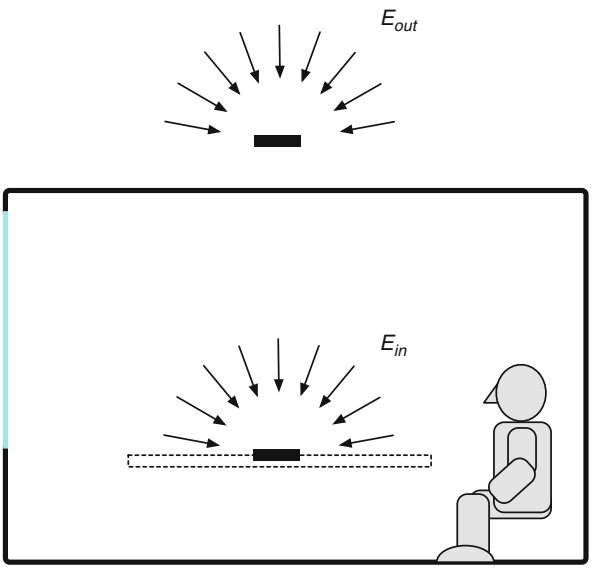

Daylight, Indoor Illumination, and Human Behavior. Figure 14
The daylight factor is the ratio of internal illuminance to unobstructed horizontal illuminance under standard CIE overcast sky conditions

The daylight factor was conceived as a means of rating daylighting performance independently of the actually occurring, instantaneous sky conditions. Hence it was defined as ratio. However, the external conditions still need to be defined since the luminance distribution of the sky will influence the value of the ratio. At the time that the daylight factor was first proposed, it was assumed that heavily overcast skies exhibited only moderate variation in brightness across the sky dome, and so they could be considered to be of constant (i.e., uniform) luminance. Measurements, however, revealed that a densely overcast sky exhibits a relative gradation from darker horizon to brighter zenith; this was recorded in 1901. With an improved, more sensitive measuring apparatus, it was shown that the zenith luminance is often three times greater than the horizon luminance [6]. A revised formulation for the luminance pattern of overcast skies was presented by Moon and Spencer in 1942, and it was adopted as a standard by the CIE in 1955. Normalized to the zenith luminance the luminance distribution of the CIE standard overcast it has the form:

$$L_\zeta = \frac{L_z(1 + 2\cos\zeta)}{3} \tag{2}$$

where L_ζ is the luminance at an angle ζ from the zenith and L_z is the zenith luminance. Comparisons with measured data have demonstrated the validity of the CIE standard overcast sky model as a representation of dull sky conditions [7]. Thus, since 1955, the daylight factor is strictly the ratio of internal to external illuminance determined under a sky luminance distribution that conforms to the CIE Standard overcast sky pattern (Eq. 2). Note that in papers and reports published prior to 1955, the "daylight factor" is likely to refer to a ratio determined for an actual or assumed uniform sky luminance pattern.

Influence of Building Properties on the Daylight Factor The daylight factor was intended to be a measure of the daylighting potential of a space. The key building properties that determine the magnitude and distribution of the daylight factor in a space are:

- The size, distribution, location, and transmission properties of the windows
- The size and configuration of the space
- The reflective properties of the internal and external surfaces
- The degree to which the external structures obscure the view of the sky

The importance of reflection in a space is illustrated in Fig. 15 which shows the distribution in daylight factor across a plane at desk height (0.8 m) in a rectangular space 3.0 m wide, 9 m deep, and 2.7 m high (i.e., the same space used for the earlier example).

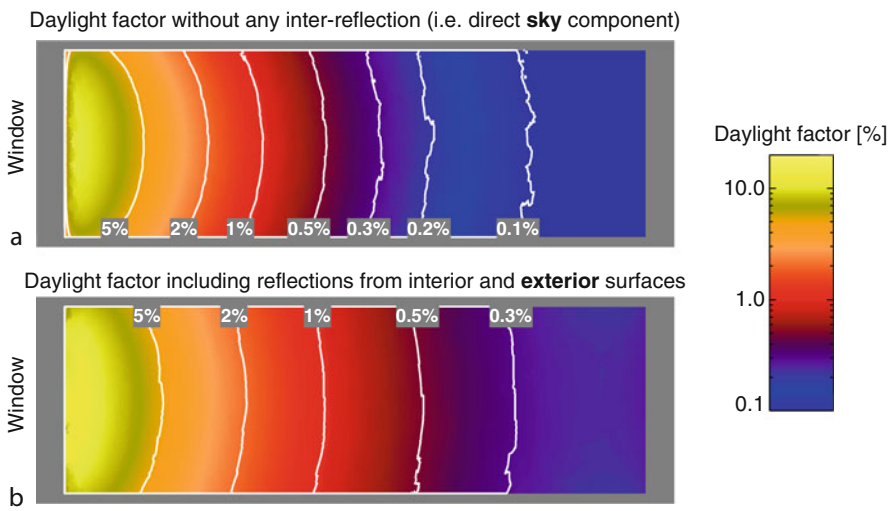

Daylight, Indoor Illumination, and Human Behavior. Figure 15
Example daylight factor

The upper plot shows the distribution in the daylight factor with no inter-reflection of light taking place. This would be the case if all the opaque surfaces had zero reflectance (i.e., perfectly black). This quantity is also known as the direct sky component of the daylight factor since it is entirely due to the sky which is directly "visible" from the point of calculation. The lower plot shows the same distribution but now including the effect of reflection from building surfaces having typical reflectivity values, i.e., 0.7 for the ceiling, 0.5 for the walls, and 0.2 for the floor and external ground. In both cases the daylight factor is greatest closest to the window; however, the proportion of the total that is due to reflected light increases with distance away from the window. At the back of the space, reflected light accounts for more than three quarters of the total daylight factor.

The mean daylight factor across the workplane including inter-reflection is 2.2%. The mean value however is greatly skewed by the high daylight factor values near to the window. The median daylight factor value is only 0.77%, i.e., half the floor area has a daylight factor less than this. One of the measures formulated to determine the evenness of the daylight distribution is called uniformity and it is defined as the minimum daylight factor divided by the mean value for daylight factor. Since the minimum DF value was 0.2%, the uniformity for this space was predicted to be 0.1.

Because the amount of sky visible at the workplane is a governing factor for general illumination, where obstructions are present it is common to estimate the "no-sky line," i.e., that point on the workplane where the sky just ceases to be visible, Fig. 16. If there is no obvious external horizon (i.e., no obstructions outside the window) then, as a rule of thumb, it is common to assume that natural light can penetrate into a space a distance twice that of the floor to ceiling height (for a window that extends from the workplane to the ceiling).

The Contribution of Sun to Daylight The potential for direct sun to enter and illuminate a space is a key consideration in architecture, albeit one that has been traditionally evaluated qualitatively. With scale models this is usually investigated independent of skylight illumination using a simple directional light source called a heliodon to represent the sun, and visually inspecting the resulting shadow patterns across and inside the model. At its most basic, a heliodon could be a small halogen lamp on a movable track. Rather than allowing for a full hemisphere of possible sun positions – and the space it would require – the light source in larger heliodons is usually kept fixed and the scale model is secured to a turntable that is free to rotate in all directions. Thus by positioning the turntable (and attached model) accordingly, it is possible to obtain the correct relative position between the sun (i.e., the light) and the model for a particular time of the day/year [8]. Heliodons have mostly been used by architects and students of architecture.

The shadow pattern approach is essentially qualitative. The brightness of the sun plays no part and light from the sky is not considered. The daylight factor approach (using a sunless sky) and the shadow-pattern approach (using a skyless sun) are essentially incompatible methodologies. Thus it is often difficult to

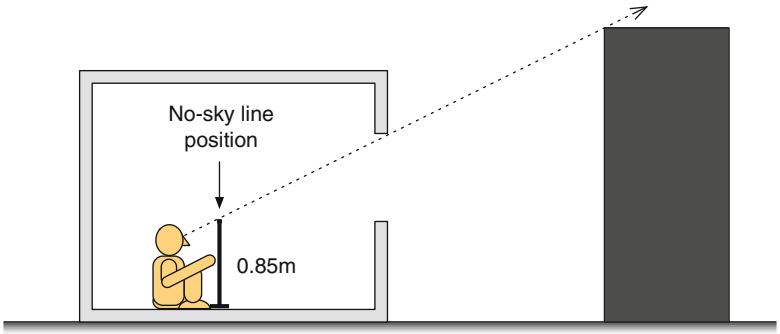

Daylight, Indoor Illumination, and Human Behavior. Figure 16
Estimating the no-sky line

reconcile the (qualitative) outcome of a shadow-pattern study with a quantitative measure of relative illumination under an overcast sky (i.e., a daylight factor). The inability to meaningfully evaluate daylight in its totality – light from the sun and the sky – in a single, unified schema is believed to be one of the major contributing factors leading to poor design decisions, e.g., overglazing of buildings and the ineffective application of brise-soleil. Computer modeling is used nowadays in preference to scale models to generate shadow patterns, and while this may be more convenient, especially for complicated geometries, the fundamental limitations of the approach are the same.

Determination of the Daylight Factor at the Design Stage

The various methods that can be used to predict daylight factors generally fall into one of the following categories:

- Physical, i.e., measurements in a scale model
- Graphical, tabular, and analytical methods
- Computer simulation, e.g., using a program such as *Radiance* [9]

Physical Modeling Architects have for centuries used physical scale models to study various aspects of building design including natural lighting, and the practice is still commonplace today. Daylight factors were first measured in scale models under actual overcast sky conditions. The measurements of internal and (unobstructed) external illuminance need to be taken simultaneously since the illuminance produced by an actual overcast sky can vary significantly over a period of a minute or even shorter. The daylight factor values obtained under actual conditions are to a fair degree approximations since many seemingly overcast skies have luminance patterns that diverge markedly from the CIE standard description [10]. An artificial sky provides a controlled means of illuminating a scale model for the purpose of taking measurements and also for qualitative appraisal [5]. The most common artificial sky is the "mirror box" design. This has a horizontal sheet of white diffusing material forming the top of the box. The sheet is evenly lit from behind (i.e., from above) by lamps. The four vertical sides of the box are mirrors. These create a sky vault that extends seemingly to infinity on all sides due to multiple reflections between the mirrors. Measurements have shown that the luminance pattern in mirror box skies can approximate that of the CIE overcast sky, and so these can provide a controlled luminous environment for the determination of daylight factors. Many of the larger schools of architecture had artificial skies at one time or another, but they tend to be less used since computer-based methods became more common.

Graphical, Tabular, and Analytical Methods The Waldram diagram is one of several graphical methods that were devised in the early 1900s to predict the direct sky component of illumination under simple sky conditions [5]. The principle of the Waldram diagram is that the half hemisphere of sky visible from a vertical window without obstruction is mapped onto a regular grid such that equal areas of the grid correspond to equal values of direct illumination from the sky. This involves applying a distortion to the representation of actual building features, e.g., the outline of a window, so that they can be shown on the diagram. The Waldram diagram is rarely used nowadays for daylighting evaluation, though some practitioners still resort to it for the arcane practice of determining a "right of light" [11].

Tabular methods such as the BRS tables were introduced in the 1950s and widely used at the time, though now they are only of historical interest. One of the many analytical methods commonly used is the equation to predict the average daylight factor. First proposed by Lynes in 1979 [12], the equation was revised by Crisp and Littlefair in 1984 following validation tests using scale models [13]. The revised equation is:

$$\overline{DF} = \frac{TW\theta M}{A(1 - R^2)} \tag{3}$$

Here T is the effective transmittance of the window(s); W is the net area of side window(s); θ is the angle in degrees subtended in vertical plane by sky visible from the center of a window; M is the maintenance factor; A is the total area of bounding surfaces of an interior, floor + ceiling + walls, including window(s); R is the area-weighted mean reflectance of interior

bounding surfaces. The equation is still used as a rule-of-thumb method at the design stage [14].

Daylight Prediction by Computer Simulation Computer programs that could predict internal daylight levels in buildings first became widely available in the late 1980s. One of the most commonly used is the freely available *Radiance* lighting simulation system [9]. Lighting simulation programs need to be distinguished from so-called photo-realistic rendering programs such as 3DS Max. The former, which includes *Radiance*, predict the transport of light in a virtual 3D scene using physically based models for the emission, transmission, reflection, and scattering of light. Thus the output can inform on how the actual building might perform, e.g., in terms of visual impression and predicted illuminance levels for a particular sky condition. Photo-realistic rendering in contrast uses various nonphysical means to quickly generate images that give an impression of what the real scene might look like in terms of its underlying 3D geometry, but the shading (i.e., lighting) applied to the surfaces is largely arbitrary. The image in Fig. 17 is a simulation of an atrium space under sunny sky conditions that was computed using *Radiance*. Below the visualization are two plots showing the distribution in predicted daylight factor (i.e., under CIE standard overcast sky) calculated at the workplane height across the floor plans for levels 1 and 3 (Fig. 17).

Accuracy of Daylight Factor Predictions Unlike scale models used to study thermal, acoustic, and structural properties, physical models for daylighting do not require any scaling factors. Thus the daylight conditions in a faithful scale model replica should be the same as for the full-sized building given identical external conditions. This fundamental property of illumination physics proved so compelling to practitioners, and indeed many researchers, that measurements of illuminance in scale models for daylight factor calculation assumed "benchmark" status even though the accuracy had not been rigorously proven.

One of the definitive studies on the accuracy of illumination studies using scale models was that carried out by Cannon-Brookes in 1997 [15]. The study found that the scale model measurements typically exceeded the illuminances in the actual space by 50–100% for overcast conditions and up to 250% for clear skies with sun. These findings, in addition to the inherent problems associated with sky simulator domes [16], have led most practitioners and researchers to choose computer simulation rather than physical models for the bulk of rigorous, quantitative work.

Computer simulation of lighting quantities including daylight has undergone numerous validation tests since the mid-1990s. The degree and exacting nature of these exceed those which physical modeling has been subjected to by a large margin. In particular, the *Radiance* system has undergone more validation studies than any other program, and many of the tests were under daylight conditions in actual spaces. In what is widely considered to be the definitive validation study of a simulation program under real sky daylight conditions, illuminance predictions from *Radiance* were compared with measurements taken in a full-size office space. Measured sky luminance patterns were "mapped" into the simulation program so that the absolute accuracy of the program could be evaluated without the uncertainties that are introduced when the sky luminance pattern has to be estimated using a sky model. The majority of *Radiance* illuminance predictions were shown to be within ±10% of the measured values [17–19]. This and other studies have led to the widespread adoption of *Radiance* by leading consulting engineers. For both researchers and practitioners worldwide, *Radiance* has become the de facto standard for a wide range of applications, not least the evaluation of daylight in buildings [20].

It needs to be borne in mind that validation studies reveal the *potential* accuracy of a daylight simulation program, and that the high accuracy shown in tests can only be approached in "live" projects if strict quality-control procedures are employed. Users of daylight simulation programs such as *Radiance* need to be fairly skilled and, ideally, have a good appreciation of the issues involved, e.g., how to construct a 3D model that is suitable for lighting simulation and how to set to key parameters for the simulation. Studies have revealed that users presented with the same design can produce widely differing predictions for, say, daylight factors, and that suitable training in the use of the simulation tool is vital [21].

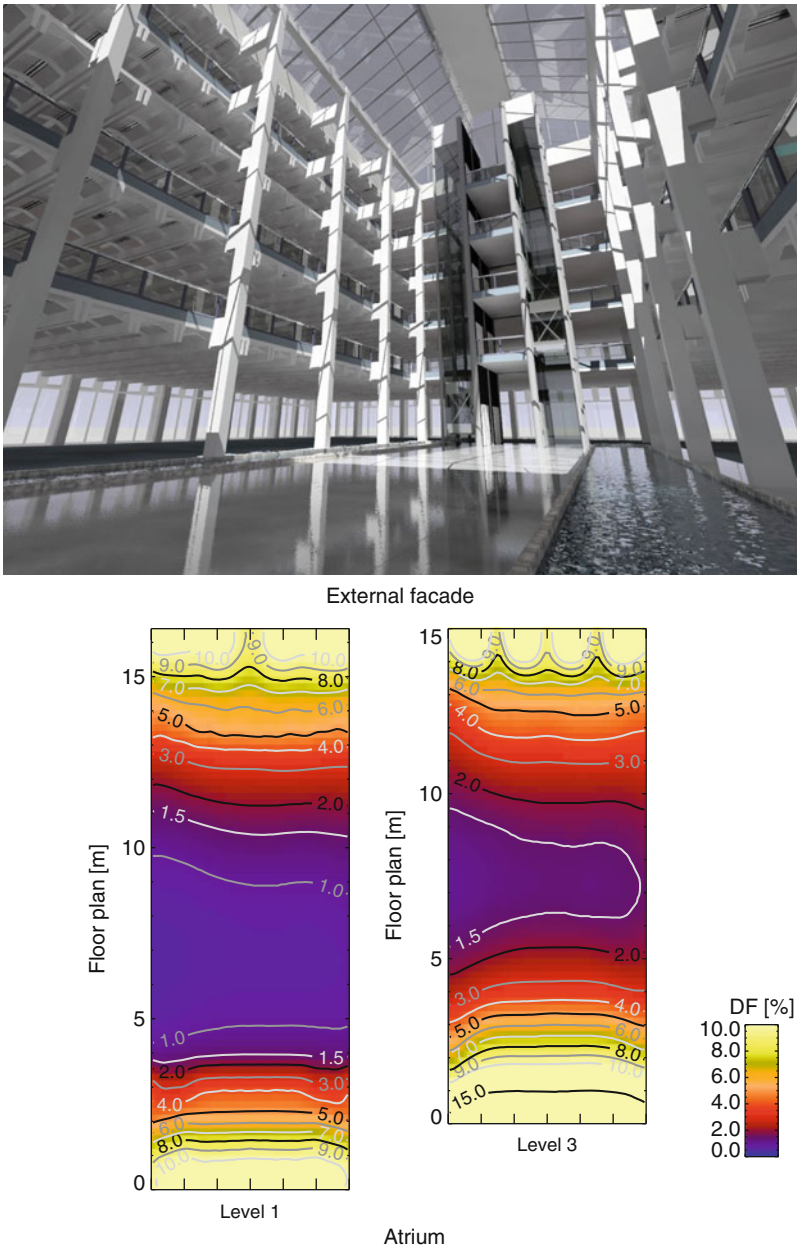

Daylight, Indoor Illumination, and Human Behavior. Figure 17
Visualization of atrium under sunny sky conditions and daylight factor plots under the CIE standard overcast sky

Despite the proliferation of computer-based tools for building evaluation and their proven accuracy, scale models still have a great appeal, especially to architects, because they offer an immediate and almost tactile feel for the relation between building geometry, surface properties, and the character of illumination. This is especially apparent when the spatiotemporal dynamic play of light in a model is observed using a heliodon to mimic the progression of sunlight through the day.

The Daylight Factor and Standards

Codes, standards, and guidelines for daylighting are invariably advisory rather than mandatory. As noted

earlier, codes, etc., worldwide are almost all founded on the daylight factor. One of the key standards documents for daylight in buildings is the British Standard 8206–2 *Lighting for buildings – Part 2: Code of practice for daylighting* [22]. That document gives the following recommendation:

- It is considered good practice to ensure that rooms in dwellings and in most other buildings have a predominantly daylit appearance. In order to achieve this, the average daylight factor should be at least 2%. If the average daylight factor in a space is at least 5% then electric lighting is not normally needed during the daytime, provided the uniformity is satisfactory. If the average daylight factor in a space is between 2% and 5%, supplementary electric lighting is usually required.

For uniformity, the same standard advises that

- . . . the minimum illuminance on a particular task area should not fall below 0.7 times the average illuminance on that task area.

This indicates that, for the 2% average criterion, the minimum daylight factor should be no less than 1.4%. It is instructive to compare this advice with the daylight factor distribution for a deep-plan office space shown in Fig. 15b. Although the mean daylight factor meets the requirement of 2%, the uniformity value for the space was only 0.1, much lower than the recommended minimum of 0.7. The median value of just below 0.8% better indicates just how much of the space falls below the minimum value of 1.4%. This simple example shows that there are quite fundamental limitations to the depth of daylight (strictly, *daylight factor*) penetration that can be achieved using only vertical glazing from one direction. Strategies to extend the penetration of daylight from perimeter windows include having large floor to ceiling heights with tall or clerestory windows (see section on "Daylighting Strategies"). If the window receives significant sun, then a light-shelf (Fig. 6) might serve the dual purpose of shading near to the window and redirecting sunlight deeper into the space. Note, however, that the effectiveness of a light-shelf design cannot be directly assessed using the daylight factor since neither sunlight nor sunny sky conditions figure in the evaluation.

Daylight, Indoor Illumination, and Human Behavior. Table 1 Typical daylight factor values recommended in guidelines during the latter half of the twentieth century

Nondomestic buildings	
Church	1% minimum
Factory	5% minimum
Office	2% minimum
Classroom	2% minimum
Hospital ward	1% minimum
Dwellings	
Bedroom	0.5% at 3/4 of room depth
Kitchen	2% at half of room depth
Living room	1% at half of room depth

Recommended Daylight Factor Values A set of daylight factor values as might be typically recommended in various guideline documents are presented in Table 1. Historically, the recommended values for factories have been high since these were often large-area, single-story buildings which could be very effectively daylit by rooflights (invariably configured to avoid the ingress of direct sun).

Deriving Absolute Values from Daylight Factors It is possible to convert a daylight factor value (i.e., a relative measure of illumination under a static sky condition) into an estimation of the annual provision of daylight using cumulative diffuse illuminance availability curves. An example curve based on measurements taken at Kew (near London, UK) is shown in Fig. 18. This curve gives the percentage of the year for which a diffuse horizontal illuminance is achieved during, say, normal working hours – in this case 09:00 to 17:30. Applying a simple technique, cumulative internal illuminance availability can be estimated from daylight factor values and the curves (or similar charts) of cumulative diffuse sky illuminance [23]. This gives a first-order approximation to annual daylighting provision from which supplementary lighting requirements can be estimated.

For example, suppose that the minimum required internal illuminance at a point in an office is 500 lux, and that a daylight factor evaluation using the CIE

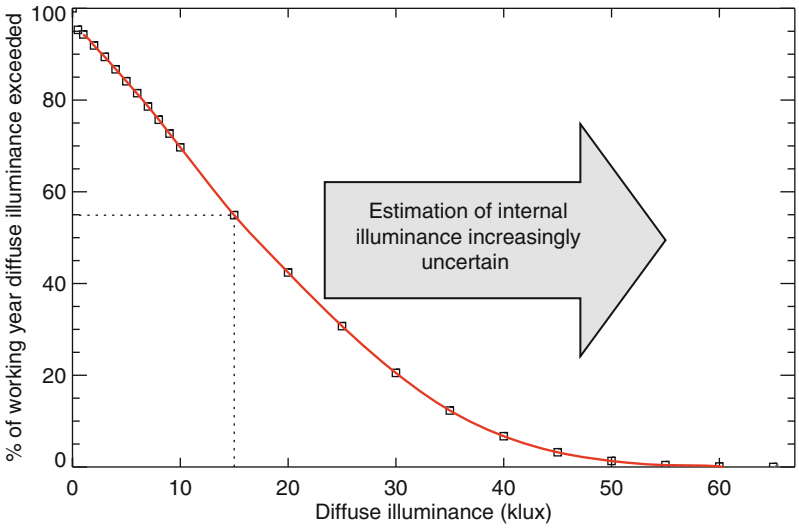

Daylight, Indoor Illumination, and Human Behavior. Figure 18
Cumulative diffuse illuminance availability, Kew, UK

standard overcast sky (equation, scale-model or simulation) predicts a daylight factor value of 3.3%. The minimum diffuse sky illuminance which provides an average internal illuminance of 500 lux is therefore:

$$\frac{500 \times 100}{3.3} \approx 15,000 \tag{4}$$

It can be determined from Fig. 18 that a diffuse sky illuminance of 15,000 lux is exceeded for about 55% of the normal working time. The CIE standard overcast sky is likely to be a reasonable approximation to some of the duller skies in the cumulative distribution. However, only about 40% of the skies in the Kew climate file for the UK can be classed as heavily overcast [18]. For locales sunnier than the UK, the percentage of overcast skies throughout the year will of course be lower. The fundamental weakness of this approach is that it tries to extend the daylight factor modeling paradigm (i.e., relative illumination under standard overcast sky conditions) to somehow account for the illumination effect of non-overcast skies. Since real non-overcast skies diverge enormously from overcast sky luminance patterns, the estimations of illuminance from the non-overcast skies in the distribution will be greatly in error. Additionally, the method cannot of course account for the illuminance contribution of the sun – either directly or from reflection. Thus the divergence between estimation and reality increases as higher illuminances in the cumulative distribution are considered (Fig. 18). Needless to say, this approach is highly inappropriate for building designs where the redistribution of direct beam radiation to provide diffuse illuminance is a significant feature of the daylighting system, as is the case with designs that make use of deep window reveals, light shelves, light wells, etc. Indeed, redirection of direct beam illumination will occur in all buildings to a greater or lesser degree even when it is not an explicit design feature. Despite the limitations, the cumulative illumination approach must be considered to be an advance on the daylight factor alone because the results, however flawed, do at least depend on absolute measures of the climate for the locale. In other words, the results for St. Petersburg will be different to those for Cairo. The effect of building orientation on internal illuminance, i.e., the difference between north- and south-facing glazing, can be roughly estimated by applying so-called orientation factors [24]. However it is believed that this is hardly ever used by practitioners.

Daylight Guidelines Post 2000 Since the year 2000, the role that daylight evaluation plays in the design process has acquired a new impetus as the need to demonstrate compliance with various "performance indicators" becomes ever more pressing. Two of the most used rating systems are BREEAM (The BRE

Environmental Assessment Method) and LEED (Leadership in Energy and Environmental Design) which originated in the UK and USA, respectively, though they are both used worldwide [25, 26]. Both the LEED and the BREEAM websites chart the growth in the building projects that have been certified using the respective schemes. These and similar rating systems are actively promoted by government departments and lobby groups. As a consequence, building designers are resorting more and more to prediction methods (invariably simulation) as a means of demonstrating compliance with the various schemes [20]. This, one might reasonably hope, would lead to noticeable improvements in the practice of design evaluation, which in turn should improve the likelihood of realizing a well-daylit building. However, basing design evaluation on the daylight factor has not been proven to result in better daylit buildings.

The Daylight Factor and Actual Daylighting Conditions

The daylight factor was formulated long before the computation of actual illumination levels became a practical possibility. Thus the simplifications inherent in the formulation were, back then, a necessary expediency. As noted, a major issue with the daylight factor is that actual daylight illumination conditions deviate markedly from that described by the overcast sky paradigm. This is so even for Northern Europe where there is a commonly held belief that skies are "mostly" overcast and so use of the daylight factor as a basis for evaluation is justified. A paper by Littlefair in 1998 gives annual cumulative internal illuminance measurements for a point in similar rooms with north- and south-facing glazing [27]. The rooms were unshaded and unoccupied. An illuminance of 200 lux was achieved for approximately 58% and 68% of the year for the north- and south-facing spaces respectively. However, an illuminance of 400 lux was achieved for only 12% of the year for the north-facing space with more than four times that occurrence (51%) for the south-facing space. Of course, for sunnier climates the effect of orientation on daylight illumination will be greater still.

An unfortunate consequence of the long-standing and often uncritical use of the daylight factor is that the terms "daylight" (as defined in the Introduction) and "skylight" are often used interchangeably. This leads to confusion where precise definitions are required. Some of this muddle has resulted from the conflation of "daylight" per se with what is predicted by the daylight factor. For example, expressions such as "the daylight factor was used to evaluate daylight levels" are common in both research and practice literature. The daylight factor is precisely what it was defined to be: a ratio of illuminances under a specific sky condition. The daylight factor therefore is, in reality, a proxy for actual daylight illumination. Thus, what the daylight factor communicates is in fact very different from the actual illumination levels that result from the full range of naturally occurring sun and sky conditions.

Extending the basis of the daylight factor approach by incremental means has proved problematic. It is a straightforward matter to use in a daylight simulation non-overcast sky conditions, e.g., the CIE clear sky luminance pattern with sun (see Fig. 17). To be useful for evaluation purposes however, the luminous output of the sun and sky must be known since absolute values and not ratios must be considered. Extending the daylight factor notion of ratios to non-overcast skies with sun results in essentially meaningless values and should be avoided. When absolute values for luminous quantities are predicted (e.g., lux at the workplane) then the values used to normalize the output from the sun and sky must be justified, e.g., diffuse horizontal illuminance for the sky and direct normal illuminance for the sun. Ideally, these should be based on typical values for, say, a clear, sunny day in summer. The predicted quantities however will be of very limited value for any estimation of prevailing daylight levels in the building since they are indicative only of conditions for particular sun and sky conditions occurring at a particular time of the day/year. In other words, such an evaluation would offer merely a single "snapshot" of the multitude of naturally occurring daylight conditions due to all the possible combinations of sun and sky conditions occurring at various times throughout the year. Estimating overall daylighting performance from snapshot evaluations could be highly misleading. The parameters governing the availability of daylight do not lend themselves to any form of averaging. While it can be informative to determine, say, a monthly average for a scalar quantity such as temperature, illumination is

strongly dependent on the directional character of the incident light. Associated with every non-overcast sky and sun condition are the solar altitude and azimuth which, of course, vary continuously throughout the day. In terms of providing a basis for predicting measures of illumination, the notion of "average" days is less than useful because an "average" sun position would give entirely misleading patterns of illumination. Some guidelines (e.g., LEED and ASHRAE) have allowed so-called clear sky options where a specified daylight illuminance must be achieved (usually at the workplane) for clear sky conditions at a particular time, e.g., at noon on the equinox. These approaches are problematic for a number of reasons. In particular, some of them provide no guidance on normalizing the sky output, a significant omission since absolute values are now the target. Furthermore, the method seems to recommend evaluation under clear sky conditions *without* a sun – a physically impossible illumination condition in nature.

The true nature of illumination from the sun and sky for any particular locale can only be appreciated by examining the luminous output from both the sun and the sky over a period of a full year. The principal sources of annual climate data are the standard weather files which were originally created for use by dynamic thermal modeling programs [28]. These datasets contain hourly averaged values for a full year, i.e., 8,760 values for each parameter. The key daylight parameters stored in the weather files are the diffuse horizontal illuminance and the direct normal illuminance. The diffuse horizontal illuminance is the visible light energy from the unobstructed sky that is incident on a horizontal surface. The direct normal illuminance is the visible light energy from the sun that is incident on a surface which is kept normal to the beam of radiation, i.e., the photocell always "points" directly to the sun. If the climate file contains only irradiance (i.e., total energy values), then it is converted to illuminance using a luminous efficacy model [29].

A visualization of the illuminance data from a standard weather file is given in Fig. 19. The time-series data of 8,760 values has been rearranged into an array of 365 days (x-axis) by 24 h (y-axis). The shading at each hour

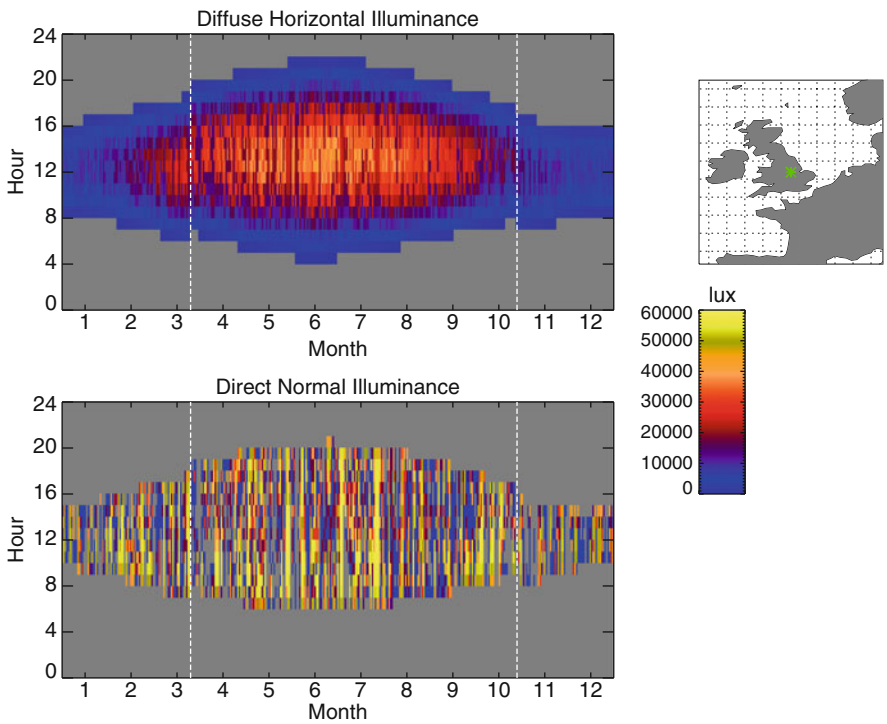

Daylight, Indoor Illumination, and Human Behavior. Figure 19
Illuminance data from the CIBSE standard climate file for Nottingham

indicates the magnitude of the illuminance – see legend – with zero values shaded gray. Presented in this way it is easy to appreciate both the prevailing patterns in either quantity and their short-term variability. Most obvious is the daily/seasonal pattern for both illuminances: short periods of daylight in the winter months, longer in summer. The hour-by-hour variation in the direct normal illuminance is clearly visible, though it is also present to a lesser degree in the diffuse horizontal illuminance (i.e., light from the sky). The data is for Nottingham, UK, the location of which is identified in the map above the legend. Local time is shown, i.e., summertime is local time plus one hour. The start and end period of summertime are indicated by vertical dashed lines in each of the figures. Recall the patterns of indoor illumination for the four components of daylight given in Fig. 3. Each of the 4,380 (i.e., the daylight hours) unique combinations of sky and sun conditions in the weather file (Fig. 19) will result in a unique pattern of internal daylight illumination.

Both diffuse and direct illuminances will, in reality, vary over periods much shorter than an hour. Interpolation of the dataset to a time-step shorter than one hour will provide a smoother traversal of the sun, which may be necessary when using the data for simulation of daylight. Interpolation alone, however, will not introduce short-term variability into the values for diffuse horizontal and direct normal illuminance. If required, this variability would have to be synthesized using stochastic models [30].

The illuminance data in the standardized weather files reveal the true nature of the patterns in daylight illumination from the sun and the sky. It is also evident from the visualization of the data (Fig. 19) that any "snapshot" evaluation using just part of the data would not be representative and could lead to highly flawed conclusions regarding the daylighting performance of the building. How these data might be used in their entirety to better predict actual building performance is described in the section on "Climate-Based Daylight Modeling."

Human Factors and Daylight

Daylight and Visual Comfort

A good provision of daylight is now considered to be highly desirable in terms of improving occupants' well-being and productivity [31, 32]. Daylight, however, can cause visual discomfort by inducing glare and veiling reflections. Efforts to control glare often result in the loss of predicted daylight benefit as occupants deploy blinds, etc., which may remain closed long after the glare condition has diminished.

In the CIBSE Lighting Guide LG7, glare is defined as a "Condition of vision in which there is discomfort or a reduction in the ability to see details or objects, caused by an unsuitable distribution or range of luminance, or to extreme contrasts" [33]. There are two types of glare: disability glare, where stray light reaching the eye results in a reduction of visibility and visual performance, and discomfort glare, which leads to users' discomfort, often with less immediately noticeable effects such as headaches or posture-related aches after work. Glare can be caused by direct sunlight through a window or by the luminance differences between bright areas such as windows with bright sky views and the darker task area. Furthermore, veiling reflections on reflective surfaces such as computer screens can affect visual comfort at workstations facing away from the window.

The majority of office workers now use (vertical) computer screens during all or part of their workday [34]. They are far more likely to be affected by glare from windows than their counterparts of 10 or 20 years ago who were largely occupied with paper-based tasks on horizontal surfaces [35]. It is considered an imperative, therefore, to attempt to minimize glare when designing for daylight provision in offices. Current international and European standards regarding visual comfort in the office environment aim to address this issue (EN ISO 9241–7:1998, EN 12464–1:2002, EN 29241–3:1993). A number of guidelines have been published which aid designers and architects in their efforts to reduce glare in order to achieve comfortable visual environments, such as the CIBSE Lighting Guides LG3 and LG7, the Code for Lighting [36], and CIBSE Guide A [4].

While there are accepted, albeit imperfect, models for the potential glare effect of (fixed output) luminaires, it is recognized that glare from daylight sources is poorly understood [37]. The first daylight glare formulations were extrapolations from studies of discomfort glare due to artificial lighting [38]. The light sources used in those studies subtended relatively

small solid angles from the viewpoint of the subject, and the luminance conditions (source and environment) were very different from typical daylit offices. In short, those extrapolations proved to be inadequate for the purpose of determining discomfort glare from daylight. There have been a number of attempts to improve glare formulations for use in daylight situations, such as Daylight Glare Index (DGI), Unified Glare Rating (UGR), and the New Daylight Glare Index (DGIN), but the problem persists. A review in 2005 by the chair of the International Commission on Illumination (CIE) Technical Committee on glare concluded that the "available assessment and prediction methods are of limited practical use in daylit situations" [37].

Numerous field studies have been carried out in order to investigate glare from daylight through windows. The earliest discomfort glare studies used large-area artificial light sources to mimic the effect of daylight through windows [5]. However, the sensation of discomfort that may arise from staring at a featureless (artificial) light source seems to be very different from that produced by viewing a comparably high-luminance natural scene [39, 40]. Moreover, as outlined in a recently published review of research regarding occupant satisfaction with the luminous environment, there are multiple additional factors that affect occupants' visual comfort, such as preferred light levels and access to lighting and shading controls [32]. Studies which have included occupant surveys in combination with controlled measurements of the luminance were often set in laboratory environments quite different from the usual workplace.

Considering that the natural variability in daylight contains seasonal, daily and short-term components and that discomfort glare is known to depend strongly on directional factors as well as the scalar magnitude and distribution of the luminous field, findings from existing studies have limited use when describing glare conditions experienced in real office spaces. Value judgments appear to be the only ground on which discomfort from glare may be assessed, but it is nevertheless essential that these subjective assessments are linked to objective and quantifiable data or phenomena [37]. New approaches to assessing glare that may overcome the current limitations in understanding are described in the section "New Approaches to Measuring the Daylit Environment."

Daylight and Health/Productivity

The primary concern in the daylighting of buildings has generally been to provide illumination for task, e.g., 500 lux on the horizontal workplane. However, in the last few decades there has been a gradual increase in awareness of the nonvisual effects of daylight/light received by the eye [41]. (We exclude from consideration here skin exposure effects such as tanning and the production of vitamin D.) It is well known that building occupants almost without exception will prefer a workstation with a view of the outdoor environment to a windowless office [42]. A view to the outside indicates of course the presence of daylight, although the relation between view and daylight provision is not straightforward, being dependent on many factors. Might there be productivity and well-being benefits in providing building occupants with well-daylit spaces? In addition to subjective preferences for daylit spaces, it is now firmly established that the light has measurable biochemical effects on the human body, in particular with respect to maintaining a healthy sleep-wake cycle. Could the quality and nature of the internal daylit environment have a significant effect on the health of the human body which can be proven through the measurement of, say, hormone levels? Evidence is suggestive of links between daylight exposure and both health and productivity; however, there is insufficient knowledge at present to conflate these two effects and so they are discussed separately in the following sections, beginning with health.

Health The daily cycle of day and night plays a major role in regulating and maintaining biochemical, physiological, and behavioral processes in human beings. This cycle is known as the circadian rhythm – the term "circadian" comes from the Latin circa, "around," and diem or dies, "day," meaning literally "approximately one day." Circadian rhythms occur in almost all organisms from bacteria to mammals. The circadian rhythm is endogenous meaning that it is produced from within the organism, i.e., what is commonly referred to as the "body clock." However, for many organisms the cycle

needs to be adjusted or entrained to the environment by external cues, the primary one of which is daylight.

The primary circadian "clock" in mammals is located in the suprachiasmatic nucleus (or nuclei) (SCN), a pair of distinct groups of cells located in the hypothalamus. The SCN receives information about illumination through the eyes. The retina of the eye contains not only the well-known photoreceptors which are used for vision (i.e., rods and cones) but ganglion cells which respond to light and are called photosensitive ganglion cells. The SCN in turn coveys signals to the pineal gland, which, in response, controls the secretion of the hormone melatonin. Secretion of melatonin peaks at night and ebbs during the day, i.e., its presence modulates the wake/sleep patterns.

The failure to maintain a circadian rhythm that is firmly entrained to the natural 24-h cycle of daylight results in many negative health outcomes for humans, though not all are fully understood. The degree and severity of the outcomes usually depends on the period over which the cycle is disturbed. A transitory disturbance to the circadian cycle familiar to many who have experienced a long-haul flight is jet lag. When traveling across a number of time zones, the body clock will be out of synchronization with the destination time, as it experiences daylight and darkness contrary to the rhythms to which it has grown accustomed. Depending on the individual, it can take a few days to reset the body clock to the local day-night cycle.

Less immediately obvious in its effects than jet lag is the chronic persistence of a poorly entrained circadian rhythm. This was first noticed in shift-workers; however, it is believed to be one of the factors in the increasing occurrence of sleep-disturbance and related conditions in the wider population of the developed world [43]. While the symptoms of sleep-disturbance can be at first mild, e.g., sleepiness, fatigue, and decreased mental acuity, the long-term persistence of the condition may result in significant impacts on both health and worker productivity.

The duration, intensity, and spectrum of the light received at the eye are the principal factors determining the degree of nonvisual effect, and thus a key factor in the entrainment of the circadian cycle. Another important factor is the time of day when the light is applied. Compared to the luminous efficiency function of the eye which has a peak value at 555 nm, the action spectrum for the suppression of melatonin is known to be shifted to the blue end of the spectrum and has a peak around 450–480 nm [44]. The relative suppression of melatonin as a function of light intensity and color temperature for artificial lighting was determined by Mclntyre et al. in 1989 [45]. The illuminances at the eye required for the effective suppression of melatonin are of the order of 1,000 lux depending on the spectrum. Note that the vertical illuminance at the eye is typically one fifth that delivered to the horizontal workplane by (overhead) artificial lights. Thus, a workplane illuminance of around 5,000 lux (much higher than the typical design levels of 300–500 lux) would be needed to provide 1,000 lux at the eye. Thus it is argued that interior lighting levels, as currently recommended and practiced, may be insufficient for circadian regulation [46]. Daylight often provides illuminances significantly higher than the design level, though this is only in close proximity to windows and perhaps also highly daylit spaces such as atria. If the typical illuminances in these zones are high – but not so great that blinds are needed – then those building users that regularly occupy the well-daylit spaces may perhaps experience stronger and more regular circadian entrainment stimuli than those users away from windows who are habitually exposed to lower illuminance at the eye level. These considerations have resulted in the notion that a building through its daylighting may possess a *circadian efficiency* [47]. However, such assertions are presently highly speculative and should be treated as such until the evidence becomes more compelling [48].

There is some evidence that daylight exposure can affect postoperative outcomes in patients and, consequently, that daylight should be a consideration in hospital design. One of the key studies in the literature is that by Walch et al. on patients recovering from elective cervical and lumbar spinal surgery. The patients were housed on either the "bright" or "dim" side of the same hospital unit. The study determined that sunlight exposure was associated with both improved subjective assessment of the patients and also reduced levels of analgesic medication routinely administered to control postoperative pain [49].

Productivity and Performance Bright lighting is generally believed to make people more alert, and

well-daylit spaces are generally perceived by occupants to be "better" than dim gloomy ones. The link between objective measures of productivity and the quality of the daylit environment is however elusive because worker productivity is influenced by numerous factors, and it is proving challenging to isolate the effect of just daylight. Furthermore, it is generally not a practical option to monitor the long-term daylight exposure for hundreds of subjects using light meters. Thus the daylighting potential is often estimated from space parameters that can be easily assessed by a site visit. This adds another measure of uncertainty to these studies since daylight exposure itself is a highly variable quantity. Some reports are mostly anecdotal, e.g., good daylighting has been identified as a factor in staff retention [50].

Perhaps the best known studies that have attempted to link productivity to daylight are those carried out by the Heschong-Mahone Group (HMG) in California, USA. The HMG schools' study claimed that

- ... students with the most daylighting in their classrooms progressed 20% faster on math tests and 26% on reading tests in one year than those with the least daylight. Similarly, students in classrooms with the largest window areas were found to progress 15% faster in math and 23% faster in reading than those with the least window areas. Students that had a well-designed skylight in their room, one that diffused the daylight throughout the room and allowed teachers to control the amount of daylight entering the room, also improved 19% to 20% faster than those students without a skylight [51].

Other studies by HMG have made similarly compelling claims in improved productivity for office workers and larger retail sales in well-daylit compared to poorly daylit spaces [52, 53]. However, until independent studies corroborate these reports, the findings must be considered suggestive of an effect rather than conclusive proof of a strong relationship between daylight and productivity/performance [54].

It should be noted that improved productivity has also been claimed for exposure to higher than usual levels of artificial lighting. In many regards, it is easier to isolate the effects of short periods of enhanced artificial lighting than it is for long periods of (highly variable) daylight. A Japanese study found that bright lighting in the office (2,500 lux compared to 750 lux, provided for 2 h in the morning and 1 h after lunch for several weeks) boosted alertness and mood, especially in the afternoon. It also seemed to promote melatonin secretion and fall in body temperature at night, changes that should improve the quality of sleep. Although this work was based on a small number of people and further work is needed, it shows promise for alterations in office lighting in terms of productivity and health of the workers [55]. These findings have led to developments in the use of artificial lighting where controlled exposure across the entire floor-plate of a building is a straightforward matter [56].

Daylight and the User Operation of Lights and Shades

Almost all the commonly used spaces in side-lit buildings will have some form of shading device, e.g., venetian blinds, that is either user-deployed or automatically controlled. Even if the fixed architectural form offers effective shading from direct sun much of the time, there are, nevertheless, likely to be occasions when blinds will need to be used to block either direct sun and/or the view of bright patches of sky. Blinds are usually formed either from individual sections called slats or are continuous. Slatted blinds can have either horizontal or vertical slats.

Users entering a space where there is little daylight will of course switch on the electric lights. The probability that users switch on electric lights was found to be correlated with the minimum daylight illuminance on the working plane [57]. The correlation presented by Hunt in 1980 was based on just a handful of samples and there was considerable scatter in the switch-on probability when the daylight illuminance was in the range 50–500 lux, which is typical of the range experienced in many buildings. A later study provided support for the Hunt model, but as with the original study there was large scatter in the measured daylight illuminances that triggered the switching on of lights [58]. In addition to the switch-on probability, there will also be switch-off probabilities. Relatively little field study data has been published regarding switch-off behavior, and determining a correlation with daylight is more confounding than for switch-on since other factors come into play. For example, switch-off probabilities

could be significantly determined by the overall appearance of the space and the particular design of the lights, since it is sometimes not obvious to the occupant that lights have been left on when daylight provision is high.

In an effort to account for the variability in occupants' light switching behavior, stochastic models were introduced in 1995 by Newsahm et al. [59]. This means that whenever a (simulated) user is confronted with a control decision, i.e., to switch on the lighting or not, a probabilistic (i.e., stochastic) process is initiated that determines the outcome of the decision. This approach was further refined by Reinhart in a model designated "Lightswitch-2002," which provides a unified modeling framework for both the switching on and off of electric lights and the operation of blinds/shades to control direct sun [60]. A key input parameter for the Lightswitch-2002 is the user type, of which there are four in the model. The type determines the degree to which the simulated user attempts to make the most of the daylight contribution by both optimizing the blinds and switching off unnecessary artificial lighting, and the results for, say, predicted energy use for lighting are highly sensitive to the assumed type.

Recent Advances in Daylighting

The consideration of daylight in buildings has recently undergone a radical reevaluation. For much of the latter half of the twentieth century, the "objective" evaluation of a building design relied almost exclusively on the daylight factor (section "The Daylight Factor"). Of arguably greater value than a daylight factor analysis was the advice of an experienced daylight designer. Although they commonly make use of the daylight factor, the real value of the designer's expertise however is in envisioning those many aspects of daylight provision that are *not* accounted for by the daylight factor. These aspects are many and varied. Key amongst them, however, are the contribution of the sun to the overall illumination of the building and the potential for glare resulting from direct sun and/or skylight. The first of these – the illumination contribution of the sun – can only be very approximately estimated. In truth, it is a qualitative judgment founded on experience and intuition rather than numerous computations of light transfer. The second depends in part on a consideration of geometrical relations between the progression of the sun and the configuration of the building, i.e., the windows of the building, their orientation, and any nearby obstructions. This involves envisioning the progression of the sun-illuminated surfaces inside the building, and estimating the potential for views of bright sky that might be a cause for glare. In other words, for either case there is an envisioning of sorts by the daylighting expert of the spatio-temporal dynamics of daylight illumination. These evaluations can be informed to a limited degree by shadow pattern studies of solar penetration. In addition, of course, an experienced designer will offer advice on a great many other, secondary aspects of daylighting design for the building. However valuable the advice offered by the daylight designer, it is not something that could be distilled into a codified scheme and, ultimately, some numerical measure of predicted performance. If daylighting experts were not part of the design team, then a routine daylight factor evaluation accompanied perhaps by a shadow-pattern study would be the sum total of the "daylighting evaluation." Thus a completed building with good daylighting was more likely to be a product of chance and good fortune than design. Inevitably, continued reliance on the half-century-old daylight factor led also to a sense of stagnation in sectors of the daylighting research community.

Two seemingly concurrent, but out-of-step and totally independent, developments have changed both the perceived importance and the nature of daylight evaluations. The first is the increasing demand to demonstrate compliance at the design stage with recommended measures of building performance, e.g., the LEED rating system. The need for this appears to be widely accepted throughout the developed world, and the rate of uptake by practitioners is ever increasing in response to pressure and encouragement from governments, regulatory bodies, etc. For those striving to effect good daylighting design, however, the race for compliance is by no means entirely good news because the recommendations are founded on schema such as the daylight factor that ignore fundamental parameters such as building orientation and prevailing climate. The second development is a major advancement in the way that daylight evaluations are carried out. This advancement, called climate-based daylight modeling, can address the very real concerns that practitioners and researchers are now voicing regarding the high

potential for "compliance chasing" resulting in poor design choices for buildings [61]. An important addition to these developments is the emergence of an array of new facade and glazing technologies for improving the daylighting of buildings, both new and existing. And in the last five years, camera-based measurement techniques that can characterize the luminous environment with an unprecedented level of coverage have become available to everyday practitioners. These developments, recently established and emerging, are described in the following sections.

Climate-Based Daylight Modeling

Climate-based daylight modeling is the prediction of various radiant or luminous quantities (e.g., irradiance, illuminance, radiance, and luminance) using sun and sky conditions that are derived from standardized annual meteorological datasets. Climate-based modeling delivers predictions of absolute quantities (e.g., illuminance) that are dependent both on the locale (i.e., geographically specific climate data is used) and the fenestration orientation (i.e., accounting for solar position and nonuniform sky conditions), in addition to the space's geometry and material properties. The operation of the space can also be modeled to varying degrees of precision depending on the type of device (e.g., luminaire and venetian blinds) and its assumed control strategy (e.g., automatic, by occupant, or some combination). The computational overhead and complexities introduced when attempting to model the operation of the space are discussed later.

The term "climate-based daylight modeling" does not yet have a formally accepted definition – it was first coined by Mardaljevic in the title of a paper given at the 2006 CIBSE National Conference [62]. However, it is generally taken to mean any evaluation that is founded on the totality (i.e., sun and sky components) of time-series daylight data appropriate to the locale over the course of a year. In practice, this means sun and sky parameters found in, or derived from, the standard meteorological data files which contain 8,760 hourly values for a full year. Given the self-evident nature of the seasonal pattern in sunlight availability, a function of both the sun position and the seasonal patterns of cloudiness, an evaluation period of 12 months is needed to capture all of the naturally occurring variation in conditions that is represented in the climate dataset. It is also possible to use real-time monitored weather for a given time period, if calibration to actual monitored conditions within a space is desired. Standardized climate datasets are derived from the prevailing conditions measured at the site over a period of years, and they are structured to represent both the averages and the range in variation that typically occurs. Standard climate data for a large number of locales across the world are freely available for download from several websites. One of the most comprehensive repositories is that compiled for use with the EnergyPlus thermal simulation program [63]. This contains freely available climate data for over 1,200 locations worldwide.

There are a number of possible ways to use climate-based daylight modeling [64–68]. The two principal analysis methods are cumulative and time-series. A cumulative analysis is the prediction of some aggregate measure of daylight (e.g., total annual illuminance) founded on the cumulative luminance effect of (hourly) sky and the sun conditions derived from the climate dataset. It is usually determined over a period of a full year, or on a seasonal or monthly basis, i.e., predicting a cumulative measure for each season or month in turn. Evaluating cumulative measures for periods shorter than one month is not recommended since the output will tend to be more revealing of the unique pattern in the climate dataset than of "typical" conditions for that period. The cumulative method can be used for predicting the microclimate and solar access in urban environments, the long-term exposure of art works to daylight, and quick assessments of seasonal daylight availability and/or the requirement for solar shading at the early design stage. Time-series analysis involves predicting instantaneous measures (e.g., illuminance) based on each of the hourly (or sub-hourly) values in the annual climate dataset. These predictions are used to evaluate, e.g., the overall daylighting potential of the building, the occurrence of excessive illuminances or luminances, as inputs to behavioral models for light switching and/or blinds usage, and the potential of daylight responsive lighting controls to reduce building energy usage. Thus a daylight performance metric would need to be based on a time-series of instantaneously occurring daylight illuminances since these cannot be reliably inferred from cumulative values. As noted, evaluations should

span an entire year. There is some debate as to whether the daily time period of analysis should be all daylit hours, which vary in length with the seasons, a standardized "working day" of 8, 10, or 12 h, or the actual occupancy pattern of the space. Different purposes are likely to favor different daily analysis periods.

How climate-based modeling compares to the standard method (daylight factors) and the more recent "clear sky options" is shown in Fig. 20. A daylight factor value can be converted into an estimate of the overall occurrence of daylight in a space by using a diffuse illuminance availability curve for that locale (as described in an earlier section). However, since the contribution of sunlight cannot be accounted for, the method must be considered a crude estimator. The various "clear sky" options generally do not require that the skies are normalized. Thus there is no link with prevailing climate. In contrast, climate-based daylight modeling uses the full year of irradiance or illuminance data found in the climate file, and derives the instantaneous sky and sun conditions from these.

Daylight Metrics

The purpose of a metric is to combine various factors that will successfully predict better or worse performance outcomes and so inform decision making.

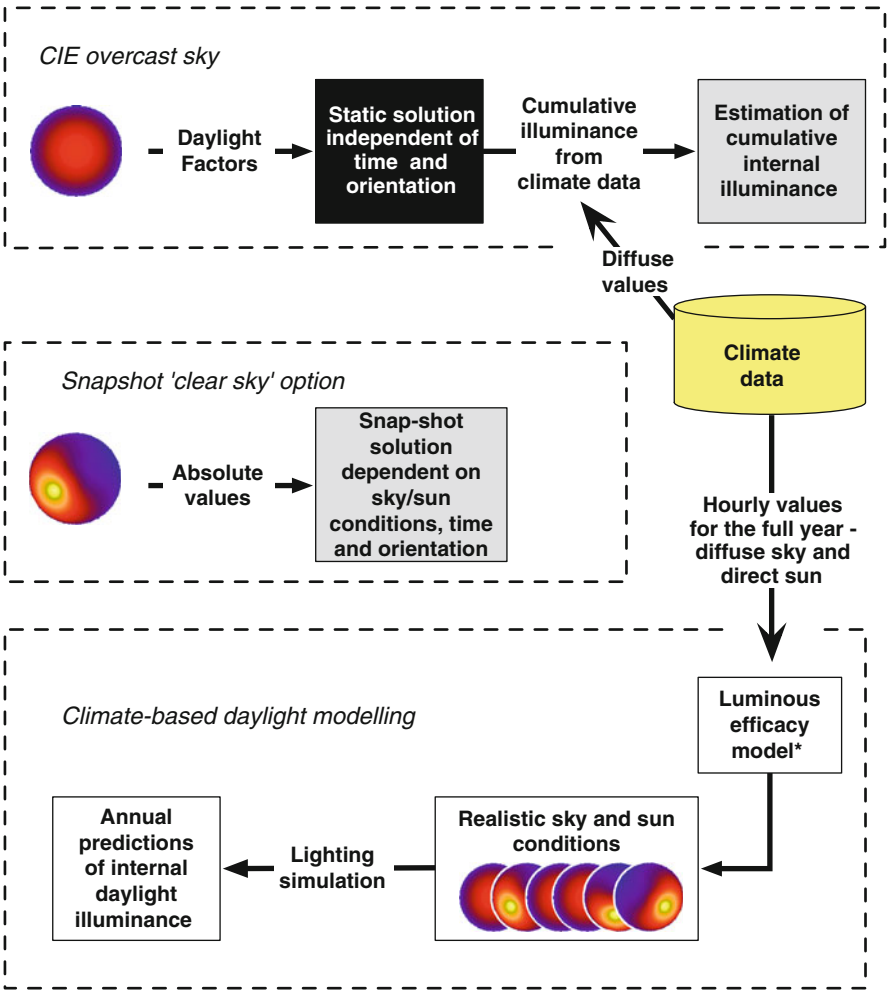

Daylight, Indoor Illumination, and Human Behavior. Figure 20
Climate-based daylight modeling compared to daylight factor and snap-shot "clear sky" options. Luminous efficacy model* is used if the data contains irradiance only

Performance may be described by more than one metric, i.e., it is not necessary to combine all significant factors into one metric. This implies a preference for simplicity so they can be intuitively understood, and a direct relation to measurable outcomes made. When metrics are sufficiently refined and understood and their predictive capabilities validated, then performance criteria can be set for various guidelines and recommendations.

As has been noted, metrics founded on the daylight factor are relatively straightforward since there is no time-varying component and so they simply report on the DF value at a point, some average DF value across a workplane, or perhaps some measure of uniformity of the DF across the workplane. Metrics founded on climate-based modeling are potentially far more complex since the simulations output illuminance data at each time-step for every point in the space. Thus, for all daylight hours in the year, a climate-based simulation would output approximately 4,380 values for every calculation point considered, and potentially several times this number if the simulations were run at a shorter time-step to, say, better resolve the progression of the solar patch across the internal space.

Various climate-based daylight metrics have been formulated since the emergence of climate-based modeling in the late 1990s. As of 2010, these metrics are being investigated by daylighting researchers in order to determine their potential to reliably characterize daylight in buildings for the purpose of discriminating between "good," "bad," and "mediocre" designs [61, 68]. One of the more straightforward climate-based metrics is daylight autonomy (DA) [69]. The DA metric determines the annual occurrence (within, say, working hours) of illuminances above a stated design level illuminance, e.g., 300 or 500 lux. It is well known, however, that occupants prefer daylight illumination not to exceed certain levels, although it is not clear what precisely those levels are since occupants vary greatly in their responses. The "useful daylight illuminance" (UDI) metric was formulated as a means to reduce the voluminous time-series data from a climate-based simulation to a form that is of comparative interpretative simplicity to the daylight factor method, but which nevertheless preserves a great deal of the significant information content of the illuminance time-series. The UDI metric informs on the occurrence of illuminances in the range that occupants either prefer or tolerate together with the propensity for excessive levels of daylight that are associated with occupant discomfort and unwanted solar gain [62]. Thus useful daylight illuminance is more firmly grounded on human factors than metrics which determine only sufficiency for task.

Achieved UDI is defined as the annual occurrence of illuminances across the workplane that are within a range considered "useful" by occupants. The range considered "useful" is based on a survey of reports of occupant preferences and behavior in daylit offices with user-operated shading devices. Daylight illuminances in the range 100–500 lux are considered effective either as the sole source of illumination or in conjunction with artificial lighting. Daylight illuminances in the range 500 to around 2,000 or maybe 3,000 lux are often perceived either as desirable or at least tolerable.

The range limits for UDI depend to a degree on the particular application, and, at the time of writing, there is no consensus on what precise values the upper and lower range limits should have. Nonetheless, the UDI scheme combines intuitive simplicity with rich information content. For the example shown below, UDI was defined as the annual occurrence of daylight illuminances that are between 100 and 3,000 lux. The UDI range is further subdivided into two ranges called UDI-supplementary and UDI-autonomous. UDI-supplementary gives the occurrence of daylight illuminances in the range 100–300 lux. For these levels of illuminance, additional artificial lighting *may* be needed to supplement the daylight for common tasks such as reading. UDI-autonomous gives the occurrence of daylight illuminances in the range 300–3,000 lux where additional artificial lighting will most likely not be needed. The UDI scheme is applied by determining at each calculation point the occurrence of daylight levels where:

- The illuminance is less than 100 lux, i.e., UDI "fell-short" (or UDI-f)
- The illuminance is greater than 100 lux and less than 300 lux, i.e., UDI supplementary (or UDI-s)
- The illuminance is greater than 300 lux and less than 3,000 lux, i.e., UDI autonomous (or UDI-a)
- The illuminance is greater than 3,000 lux, i.e., UDI exceeded (or UDI-e)

The same space that was used for the daylight factor example is employed again. Now, however, time-varying illuminances across the workplane during the hours of 09:00 to 18:00 were predicted for the entire year, i.e., a total of 3,285 h. Simulations were carried out for the space having, in turn, north- and south-facing glazing and the sun and sky conditions were derived from a standardized climate file for London, UK. For this illustration, there was no attempt to model user operation of blinds, etc.

The four UDI metrics determined from the illuminance data for both orientations of the space are shown in Fig. 21. The occurrence of the various UDI metrics is shown using color, and a zero value for the metric is shaded dark gray. The light gray perimeter indicates the space between the work and the walls of the space. In these plots we can readily see the contribution that sunlight has to overall illumination of the space by comparing the north and south orientations. In the absence of target values for the various UDI metrics, the approach is most useful to the designer when, e.g., various facade options need to be compared. Those that maximize the UDI-a metric without undue occurrence of UDI-e are likely to offer the best daylighting design – though it needs to be acknowledged that this supposition will need to be tested and proven.

Although there is no consensus yet on the type of climate-based daylight metric (e.g., UDI and DA) that should feature in future guidelines [68], there is

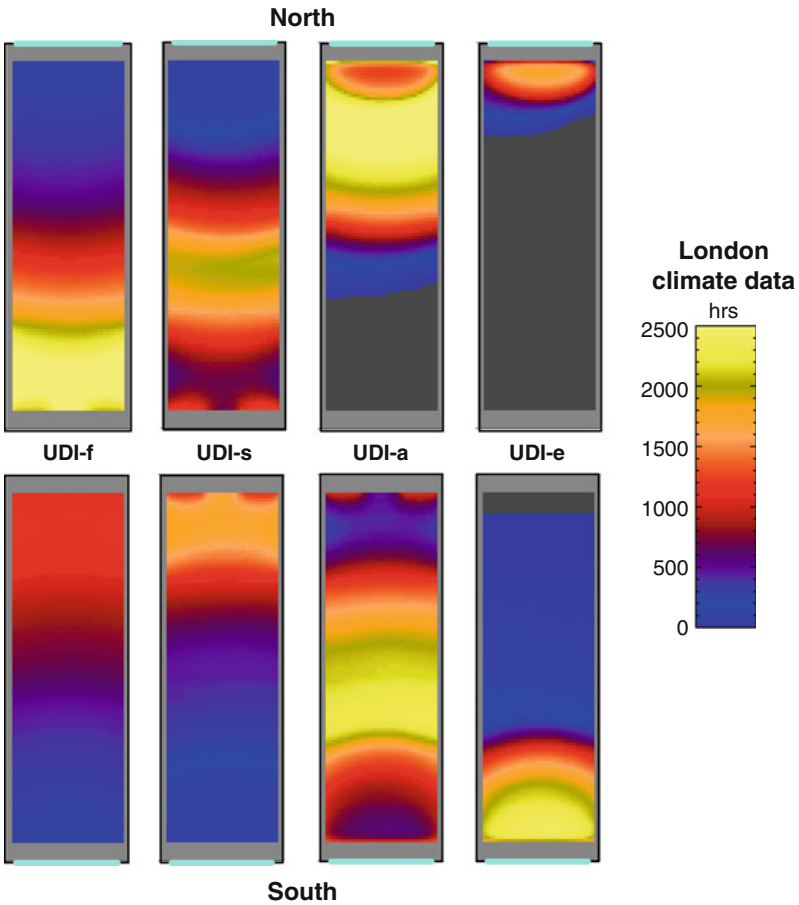

Daylight, Indoor Illumination, and Human Behavior. Figure 21
Annual occurrence of UDI metrics between the hours of 09:00 and 18:00 for north and south orientations (London, UK, climate data)

a groundswell of opinion that the half-century-old basis of daylight evaluation needs to be updated. In the meantime, climate-based modeling has made the transition from research to practice and is increasingly used by consulting engineers in their striving to achieve that elusive goal of the well-tempered daylit environment.

Metrics founded on climate-based daylight modeling will be the key to reliable evaluation of designs for well-daylit low-energy buildings. There remains, however, some work to ensure that future daylighting metrics will act in concert with other metrics, e.g., for thermal performance, and so not give conflicting guidance to the building designer.

Advanced Glazing Systems and Materials

The use of daylight in office buildings is generally considered to be a greatly underexploited resource. In large part this is because of both the highly variable nature of daylight illumination and its prevailing direction as it enters a space. Variability in daylight means that users will often need to use shades at least some of the time to moderate excessive ingress of daylight. Daylight illumination from perimeter glazing enters a space with a predominant downward direction. Those work areas close to the window may receive plentiful daylight; however, much of the natural light will arrive at the floor where it will be mostly absorbed due to the typically low reflectances of flooring materials. What little light there is reflected up from the floor may encounter significant obstructions (e.g., desk, chairs) before having the possibility of being reflected again – now downward off the ceiling – to contribute to illumination on the workplane. In short, reflection of light from the floor to help illuminate the space is a low efficiency process with limited effectiveness. Another key issue with traditional building facades that also serves to greatly impair the potential daylighting performance of a space is the design and user operation of the shading systems, e.g., venetian blinds, etc. Many shading systems act as a "shutter" that is either open or closed, with users rarely making the effort to optimize the shading for both daylight provision and solar/glare control. Furthermore, blinds are often left closed long after the external condition has changed. The exploitation of daylight in buildings, particularly those dominated by side-lighting from vertical windows, could be greatly improved by any of the following:

1. Redirecting the daylight that enters the space toward the ceiling and walls where subsequent reflections will help to better distribute the daylight deeper into a space
2. For a shading system, modulating the daylight gradually rather than an on/off shutter operation
3. Reducing, possibly even eliminating, the need for user interventions, e.g., the lowering of blinds

The purpose of the majority of so-called advanced glazing systems or materials (AGSM) is to improve overall daylighting in a space by achieving one or more of the above-mentioned goals.

AGSMs fall into to two broad categories: active and passive. Active systems vary some property (e.g., visible light transmittance) automatically according to some control parameter (e.g., illumination at the workplane), though they may often include an option for user override. A passive system is one that is invariably fixed requiring no external control either automatic or manual. However, some of the passive systems described below could have, say, automated movement though this would add considerably to the cost. Any of the systems discussed below will be subject to the same issues regarding visual quality (i.e., providing adequate views, avoiding glare, etc.) that are a consideration for conventional glazing.

Passive AGSMs The goal of most of the passive systems is to redirect daylight in some fashion, and any changes in the magnitude and distribution of the transmitted light is due to variation in the amount and direction of the incoming light. Passive AGSMs are usually in the form of a material applied to one of the glass surfaces of a window, or are themselves a glazing element, e.g., one part of a double glazing system where the other might be standard glass. The light redirection can be achieved by manipulating the specular and/or diffuse transmission properties of the material. Glazing systems in this category include light redirecting prismatic panels, laser-cut panels, diffusing materials, mirrored louvers, etc. Some of these materials have been available since the 1980s; however, the uptake has not been great. In part this is due to either limited

long-term performance data [70] and/or the inability to predict their daylighting performance at the design stage due to insufficient knowledge of the material's light transmission properties [71].

Anecdotal reports from some early installations of prismatic glazing suggests that the lack of a clear view to the outside together with secondary effects such as dispersion have not found favor with building occupants. More recent innovations have attempted to address these issues. The specular redirecting material marketed as Serraglaze provides a relatively clear view for an observer at normal incidence, but effectively blocks direct transmission of high-angle sun by redirecting it up toward the ceiling. Translucent materials such as Kalwall have very low thermal conductivity and can be used to replace sections of wall as well as glazing. However, these materials are essentially diffusing panels and so must be used in conjunction with clear glazing to provide views of the outside.

A common addition to windows to moderate both the solar gain and the daylight ingress is a film to reduce the overall transmissivity of the glazing. These films vary greatly in visible transmittance (from around 0.6 down to 0.1) and may have a pronounced color hue. Even films with the lowest transmittance usually need additional shading to moderate direct sun. The reduced transmittance of windows with films can, for the occupants, make views to the outside appear drab and gloomy, particularly on overcast days. A new approach to tempering daylight which, like films, can be applied as a retrofit is a novel treatment called Solaveil [72]. This material is fabricated using digital printing techniques which deposit microscale 3D structures on the substrate which act both as a "glare filter" and a redirecting "micro-light shelf." Before and after photographs for a retrofit installation of Solaveil are given in Fig. 22. The "before" image on the left shows how the building was typically used prior to the retrofit: the blinds are down to control glare and direct sun, and the electric lights are switched on. The "after" image on the right shows the treated area of the window which now acts as a diffusing light shelf redirecting light to the ceiling and protecting occupants from harsh, direct sun. Note that no additional shading has been installed and the lights – now photoelectrically controlled – are switched off. The lower untreated part of the window provides occupants with views to the outside. Initial findings indicate a significant potential for saving energy in both lighting and cooling from such interventions.

Active AGSMs The most established of the technologies in this category is the automated shading system where, say a motorized roller blind is deployed incrementally according to some sensor input, e.g., measured daylight level. This shading system features in the facade design throughout the majority of the 52 floors of the New York Times Building [73]. The design goals for the shading system were to

Daylight, Indoor Illumination, and Human Behavior. Figure 22
Photographs showing before and after cases where the standard glazing with blinds was replaced with a novel window treatment called Solaveil (Photos courtesy Solaveil)

- Maximize natural light
- Maximize occupant connectivity with the outdoors, i.e., external views
- Intercept sunlight penetration so as to avoid direct solar radiation on the occupants
- Maintain a glare-free environment
- Provide occupant manual override capability

The overall intent was to keep the shades up as much of the time as possible without causing thermal or visual discomfort. Thermal comfort is assured by solar tracking and the geometry of the external sun screens. Visual comfort is attained by managing the luminance on the window wall so that it does not exceed certain threshold values. A manual override system was specified because previous post occupancy evaluations of automated shade systems indicated that occupants were likely to complain if a manual override was not provided. A sequence of photographs showing incremental deployment of the shades is given in Fig. 23. Although a formal post-occupancy evaluation of the New York Times Building has yet to be carried out, anecdotal evidence from informal surveys indicates a high level of user satisfaction with the daylighting systems. Furthermore, effective daylighting has significantly reduced the energy consumed for artificial lighting. The NYT daylighting system provides a degree of modulation for the shading (they are deployed by increments) and has greatly reduced the need for user interventions.

In contrast to using standard shade materials deployed either manually or automatically, a glazing with a transmissivity that varies continuously between clear and dark extremes would offer a much greater degree of control over the luminous environment. Indeed, the dynamic control of daylight has been termed the "Holy Grail of the fenestration industry" [74]. In principle, the approach is simple: the transmission properties of the glazing are varied to achieve the best possible luminous environment. Formulations based on electrochromic (EC) principles, where the glazing transmission is modulated by a small applied voltage, are considered the most promising at present. In practice, the formulation and production of commercial-sized EC glazing has proved a formidable task. Recently, however, a number of technical hurdles have been overcome, preproduction samples of EC glazing have been deployed in test facilities for evaluation [75] and commercial installations have followed, Fig. 24. The optical properties of EC windows can be modulated using control variables such as incident or transmitted solar radiation, daylight illuminance, ambient air temperature, or space thermal load [76]. In the clear state the visible transmittance of EC glazing can be as high as 60%. However, to avoid the need for any additional shading (e.g., by venetian blinds), the visible transmittance in its tinted state has to be as low as 2%. This has now been achieved in production samples and, as prices fall, it is to be expected that EC glazings will become a more mainstream product.

In addition to the electrochromic method, there are also formulations for light modulating glazing where the visible transmittance varies autonomously in response to either the temperature of the material or the intensity of incident illumination, known as thermotropic and phototropic respectively. The phototropic glazings have a formulation which is similar to that commonly used in "reactive" sunglasses, whereas thermotropic glass consists of two panes of glass sandwiching a polymer gel that undergoes a transition from clear to cloudy at a threshold

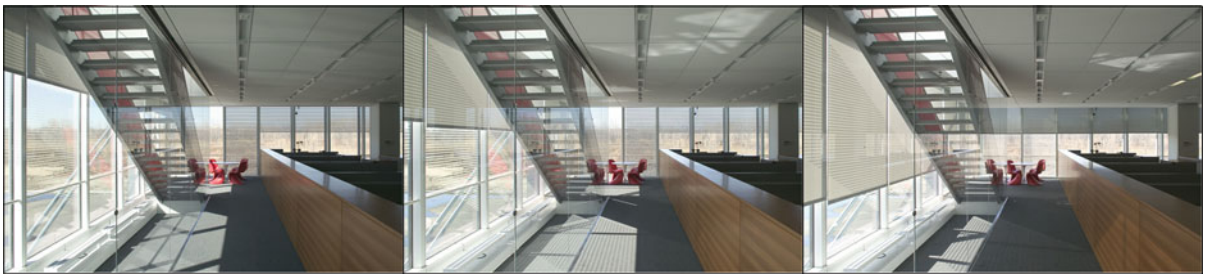

Daylight, Indoor Illumination, and Human Behavior. Figure 23
Sequence showing deployment of shades in a full-size mock-up of New York Times Building offices (Photos courtesy LBNL)

Daylight, Indoor Illumination, and Human Behavior. Figure 24
Images showing electrochromic glazing in clear and darkened state (Photos courtesy SAGE Electrochromics)

temperature [77]. These autonomous systems are largely confined to research studies at present, and the inability to control their transmission properties depending on some internally measured quantity, e.g., daylight levels, may ultimately prove to be a drawback rather than an advantage.

Evaluating AGSMs Advanced glazing systems/materials have the potential to enhance the daylighting performance of a space. Performance, cost, and user acceptance are key factors which determine the overall effectiveness of an installation. The first two of these factors can, in principle, be determined using simulation – the predicted performance could be judged against likely cost. It may even be possible to employ simulation to anticipate to some degree user acceptance of a novel glazing system/material, though the evaluation would have to be founded data from occupant-based studies to have credibility.

To simulate the performance of an advanced glazing system/material can be quite challenging due to their particular optical properties which often diverge greatly from standard glazing. The optical properties of ordinary clear glazing and reflective materials that have a matt finish are relatively easy to characterize for the purpose of lighting simulation. Less straightforward materials such as coated glazings and materials that produce part specular reflections are more challenging to both characterize and also to model accurately in a simulation. Tools such as Optics 5 and Window 6 can assist the creation of the necessary material description files for multilayer coated glazings [78]. The highlights resulting from even tiny specular reflections are an important part of the overall visual impression of a daylit space; however, the total light energy resulting from these reflections is usually very small and can be ignored when predicting illuminance quantities. Specular reflections are only important for overall light transfer in a space when significant amounts of the entrant direct and diffuse light are reflected, e.g., when a mirror light shelf is present. Large-scale reflecting/redirecting features such as light shelves or "skylight" wells can be modeled using standard *Radiance*.

A major issue with advanced glazing systems/materials however is that there is usually no straightforward relation between incident and transmitted light that can be determined a priori from simple, e.g., analytical, methods. Thus the optical properties of the AGSM need to be determined from either comprehensive measurements or, alternatively, simulation. For each light ray incident on an AGSM, there may be one or more strongly transmitted rays – which may be redirected in some fashion – together with, in most cases, a unique distribution of semi-diffuse or scattered light, Fig. 25. Thus, to fully characterize the material, the distribution in luminous output across the full hemisphere of transmitted rays needs to be determined for every incident direction [79]. This is the bidirectional transmission distribution function or BTDF [80]. The BTDF is challenging to characterize even for seemingly simple materials such as translucent

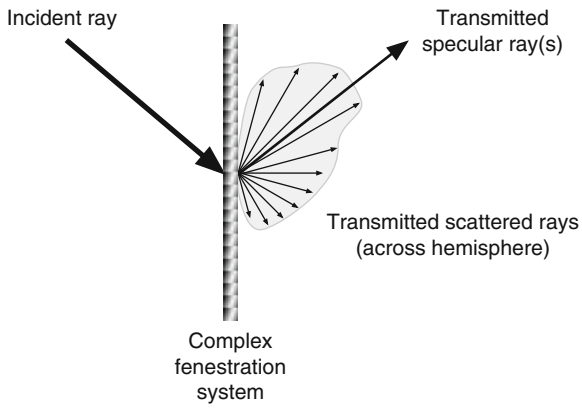

Daylight, Indoor Illumination, and Human Behavior. Figure 25
Schematic showing the distribution in transmitted light from a complex fenestration system

glazing [81]. Another approach to characterization of the BTDF is to predict it by simulation rather than by measuring it directly [82]. For this approach, the geometric microstructure of the material needs to be specified to a high degree of precision and the BTDF predicted using a forward ray-tracing program.

It is possible to model some AGSMs without going to the lengths of determining the full BTDF if the transmission properties of the materials can be adequately represented by an analytical function. This has been achieved for certain types of laser cut panels [83] and the redirecting material Serraglaze [84]. A limited set of angular-dependent transmission measurements will still need to be taken to calibrate the analytical model.

Note that although there are various approximations to model the light transmission through venetian blinds, even these commonplace devices have complex optical properties. Both the slat angle and the coverage of venetian blinds can be varied continuously and independently of each other. For any given sun position, either of these factors has a considerable effect on the overall light transmission, i.e., the BTDF [85]. Venetian blinds therefore can be more difficult to model accurately than many of the "advanced" systems/materials because their BTDF is dependent on the user operation.

Light-pipes (i.e., tubular daylighting devices) offer a potentially effective daylighting strategy for low-rise buildings. The performance of a light-pipe can be estimated using analytical methods or relatively simple software tools [86, 87]. The detailed simulation of light-pipe performance however remains quite challenging.

Characterization of BTDFs by either measurement or prediction is a highly specialized task, as is the use of these complex transmittance data in lighting simulations. There is considerable research to be carried out at all stages from characterization to implementation in a software tool before their use in lighting simulation becomes commonplace. The development of libraries of BTDF databases for various products, based on standardized test procedures, will be necessary to enable full utilization of these products in design optimization studies.

New Approaches to Measuring the Daylit Environment

Quantitative knowledge of the internal daylit environment has, until recently, been largely restricted to measurements of illuminance (typically at the workplane) and "spot" measurements of luminance taken by a narrow (e.g., 1°) field-of-view photometer. Illuminance at the workplane is rarely recorded over long periods in an occupied building due to the cost of the monitoring and the disruption caused by wires, etc. (though there are now largely autonomous wireless sensors available, albeit at a high cost). Humans have an almost 180° forward-facing field of view, so a measurement taken using a "spot" photometer with a 1° field-of-view records only a very small part of what is seen.

As noted in an earlier section, understanding of visual comfort in daylit environments is lacking in part because we have scant empirical data on the (constantly changing) visual field. A recent technology called high dynamic range (HDR) imaging has greatly expanded our capacity to measure and describe the visual field. An HDR image is one where every pixel contains a luminance reading for that point in the recorded scene, in other words: a measurement of luminance. There are a small number of specialist HDR cameras on the market; however, it is possible to create HDR images from multiple exposures taken by consumer digital cameras which can have up to

10 million or more pixels [88]. Furthermore, the consumer cameras can be fitted with a full fish-eye lens so the recorded image will be equivalent to or exceed the human field of view.

HDR image capture has been used in a number of daylight glare studies [89, 90] and also more generally to investigate lighting preferences in office spaces [91]. An example HDR image alongside a standard digital photograph is shown in Fig. 26. The view is of a workstation close to a window and with direct view of the sky. From the false-color HDR image it can be seen that the luminance of the sky is of the order of 7,000 cd m^{-2}. HDR imaging techniques were used to calibrate and commission the dynamic shading systems of the New York Times Building [73]. A key consideration in the design of the control system for the automated shades was to allow in as much daylight as possible without exceeding visual comfort criteria based on field-of-view (i.e., perceived) luminance. This was tested by measurement in the full-size mock-up of offices (Fig. 23) and evaluated more generally for the building using simulation (i.e., climate-based daylight modeling). The mock-up allowed only for limited scenarios, i.e., just two view directions with fixed external obstruction. The simulation, however, allowed multiple floors of the building to be evaluated in context (i.e., the surrounding buildings) and for all possible view directions. The images in Fig. 27 show long, medium, and close-up views of the highly detailed 3D model used for the simulation – model detail of the offices was generated on a per-floor basis for each of the floors evaluated.

High dynamic range imaging technology may become sufficiently compact and inexpensive to replace the traditional sensors that are currently used with daylight-responsive systems, e.g., photocell-controlled artificial lighting, automated shades/blinds and the transmission of electrochromic glazing [92].

Daylight and Saving Energy

It seems to be generally believed that "good" daylighting design will lead to reductions in electric lighting consumption, and also overall energy consumption. This belief results in part from common-sense notions and the pioneering work of Crisp and Hunt in the 1970s [93, 94]. The potential for energy savings was usually based on extrapolating internal illuminance from daylight factors and cumulative daylight distributions, and then applying some model of lighting control [95]. Lighting control models based on manual switching were derived from observed patterns of behavior [57, 96]. It was realized early on that occupant control alone was unlikely to lead to significant energy savings for the simple reason that lights were likely to remain switched on even when there was plentiful daylight. Some form of timed switching and/or automatic control was needed to ensure energy savings, and a number of largely theoretical formulations for occupancy-sensor and photoelectric control of lighting were devised [93]. The design and artificial lighting of nondomestic spaces has changed considerably over the last 30 years, and some of the findings noted in occupancy studies carried out three or more decades ago may not necessarily hold today.

Post-occupancy studies carried out in real buildings have shown that the actual energy performance is

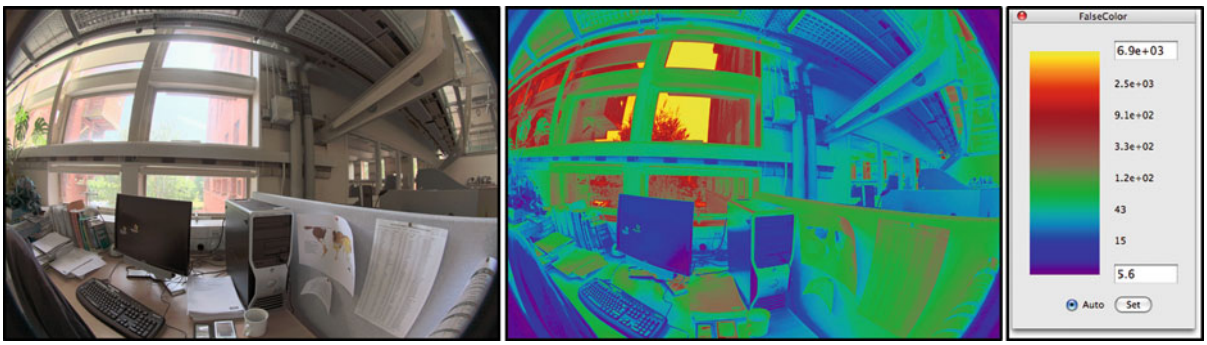

Daylight, Indoor Illumination, and Human Behavior. Figure 26
High dynamic range image used to measure the luminance of the occupants field of view

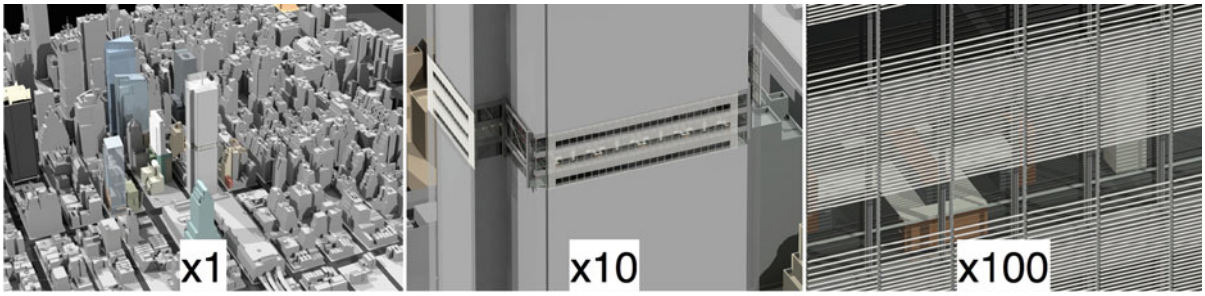

Daylight, Indoor Illumination, and Human Behavior. Figure 27
Highly detailed 3D model of the New York Times Building and surrounding Manhattan – full office detail modeled for floor 26

invariably markedly worse than that predicted at the design stage. The landmark PROBE study determined many of the reasons for this [97]. Some of the findings specific to lighting controls are noted below:

- Default states which are non-optimal, but cause the least trouble for occupants and management. The most common of these is blinds closed lights on, which has undermined many a daylight and lighting control strategy.

  Photocells used for perimeter dimming . . . were also confused by light redirected upwards onto them from the venetian blind slats, requiring control setpoints to be raised, so reducing the benefits of daylight-linked dimming.

The ratio of predicted to realized energy savings is defined as the "realized savings ratio" or RSR. Studies of automatic photocontrol performance in the USA have shown very high RSRs for simple top-lit spaces, and much lower RSRs for more complex side-lit spaces [98]. Predicting the performance of an automated lighting control system is a function of many factors, including not only space design and daylight availability, but also lighting system design, control settings, commissioning history, and occupant override behavior.

Daylight is merely the visible part of the radiant energy that enters through windows. Furthermore, the bulk of the daylight energy that enters a space is converted into thermal energy after just a few reflections. Many office buildings in moderate climates now have air-conditioning largely due to the high internal gains. In warmer climates cooling may be needed for large parts of the year. When cooling is needed in a space, both the use of electric lighting and the ingress of daylight will each add to the cooling load.

Attempts to provide good daylighting could therefore lead to a net *increase* in energy consumption if the additional cooling load due to daylight (i.e., including the solar component) exceeds the energy saved due to reduced electric lighting, or if the net heat gains and losses through the fenestration do not compensate for the lighting energy saved. In fact, an all too common scenario in over-glazed buildings is where the blinds are down to control glare and the lights are left on. This leads to the undesirable combination of high solar gains (blinds reject only a small part of the energy once it has passed through the glazing) and no "daylight benefit" in terms of displaced lighting energy or daylight provision. A full consideration of the potential for daylighting to save energy should, at some point, account also for the thermal effects of daylight. In which case, daylight metrics will need to be calibrated against criteria for whole building energy use and not just the potential to reduce the energy consumed for electric lighting. That was not a possibility with the standard daylight factor approach because the sun did not figure in the evaluation. However, with the emergence of climate-based daylight modeling, a truly holistic evaluative schema which can be applied at the design stage is now a likely prospect.

Good daylighting alone is unlikely to save energy unless it is part of an integrated design scheme. The typical lighting power densities (LPDs) in office spaces range from about 12–20 W/m^2, with those at the lower end considered "good practice." It is possible however

to achieve LPDs significantly lower than the good practice value – without recourse to emerging technologies such as light emitting diodes – using only good-quality low-energy fluorescent lights. This was successfully demonstrated in the New York Times Building which has an LPD of only 4.26 W/m^2.

A fully integrated low-energy daylighting design must necessarily be tailored to the local environment, in terms of both the climate and the surrounding built context. It is hoped that a new generation of daylight metrics founded on climate-based modeling will help designers to achieve that elusive balance between daylight provision and effective solar protection. And, importantly, offer design guidance that does not conflict with other criteria such as thermal performance of the building.

The potential for new technologies (e.g., electrochromic glazing) to save energy can only be reliably assessed using climate-based daylight modeling. Building facades may become electricity generators through the widespread adoption of various building-integrated photovoltaic (PV) technologies [99]. Semitransparent (PV) panels could serve as combined widows and electricity generators [100]. Thus daylight consideration could become closely linked with other performance aspects of the overall building.

Future Directions

Both the theoretical basis for and the practical application of daylighting in buildings are in the midst of a fundamental reappraisal. The emergence of findings that relate daylight exposure to positive outcomes in terms of productivity, health, and well-being have led to a renewed focus on daylighting in buildings. Throughout the developed world, governments and regulatory bodies are encouraging the adoption of design guides and recommendations in the hope that reduced energy consumption in buildings can be achieved, in part, through effective daylighting design. The theoretical basis for these guidelines, however, is a crude representation of actually occurring daylight conditions. A more realistic evaluative scheme has emerged with the development of climate-based daylight modeling, which it is widely believed will soon replace the daylight factor as the basis of a new generation of daylighting guidelines. A large number of advanced glazing systems and materials for enhancing the daylight in buildings have recently appeared on the market, and there are new formulations in the early stages of development. Market penetration of innovative daylighting systems has, until now, proven to be difficult because the standard "measure" of performance (i.e., the daylight factor) gives no indication of how much natural light and how often. Data on the magnitude and occurrence of absolute measures of natural illumination – precisely how much and how often – are vital to reliably assess both the performance-effectiveness and the cost-effectiveness of daylighting systems. Thus the hoped-for emergence of climate-based daylight metrics will greatly assist in the evaluation of these daylighting systems, and, for those shown to be effective, their marketing. Another consideration is the advances in measurement and control through techniques such as high dynamic range imaging. These theoretical and technological advances have the potential to radically improve our perception of what constitutes good daylighting in buildings, both in terms of basic design parameters and the use of novel glazing materials, thus paving the way for daylighting guidelines and codes that lead to the reliable and robust production of truly healthy, low-energy buildings.

Bibliography

1. Baker NV, Fanchiotti A, Steemers KA (1993) Daylighting in architecture: a European reference book. James & James, London. ISBN 1-873936-21-4
2. Mardaljevic J, Andersen M, Roy N, Christoffersen J (2011) Daylighting metrics for residential buildings. In: CIE 27th session, Sun City, South Africa
3. Al Marwaee M, Carter DJ (2006) A field study of tubular daylight guidance installations. Light Res Technol 38(3):241–258
4. CIBSE Guide A (2006) Environmental design. Chartered Institution of Building Services Engineers, London
5. Hopkinson RG (1963) Architectural physics – lighting. Her Majesty's Stationery Office, London
6. Moon P, Spencer DE (1942) Illuminations from a non-uniform sky. Illum Eng 37:707–726
7. Enarun D, Littlefair P (1995) Luminance models for overcast skies: assessment using measured data. Light Res Technol 27(1):53–58
8. Dufton AF, Beckett HE (1932) The heliodon: an instrument for demonstrating the apparent motion of the sun. J Sci Instrum 9(8):251
9. Ward Larson G, Shakespeare R (1998) Rendering with radiance: the art and science of lighting visualization. Morgan Kaufmann, San Francisco

10. Mardaljevic J (2004) Verification of program accuracy for illuminance modelling: assumptions, methodology and an examination of conflicting findings. Light Res Technol 36(3):217–239
11. Harris L (2007) Anstey's rights of light and how to deal with them, 4th edn. RICS Books, London
12. Lynes JA (1979) A sequence for daylighting design. Light Res Technol 11(2):102–106
13. Crisp VHC, Littlefair PJ (1984) Average daylight factor prediction. In: Proceedings of national lighting conference, Cambridge. CIBSE, London
14. Reinhart CF, LoVerso VRM (2010) A rules of thumb-based design sequence for diffuse daylight. Light Res Technol 42(1):7–31
15. Cannon-Brookes SWA (1997) Simple scale models for daylighting design: Analysis of sources of error in illuminance predictiont. Light Res Technol 29(3):135–142
16. Mardaljevic J (2002) Quantification of parallax errors in sky simulator domes for clear sky conditions. Light Res Technol 34(4):313–327
17. Mardaljevic J (1995) Validation of a lighting simulation program under real sky conditions. Light Res Technol 27(4): 181–188
18. Mardaljevic J (2000) Daylight simulation: validation, sky models and daylight coefficients. PhD thesis, De Montfort University, Leicester
19. Mardaljevic J (2001) The BRE-IDMP dataset: a new benchmark for the validation of illuminance prediction techniques. Light Res Technol 33(2):117–134
20. Reinhart CF, Fitz A (2006) Findings from a survey on the current use of daylight simulations in building design. Energ Buildings 38(7):824–835
21. Ibarra D, Reinhart CF (2009) Daylight factor simulations – how close do simulation beginners 'really' get? In: International Building Performance Simulation Association conference, Glasgow, Scotland, July 27–30, pp 196–203
22. BSI (2008) Lighting for buildings Code of practice for daylighting BS 8206–2. British Standards Institute, London
23. Hunt DRG (1979) Availability of daylight. BRE Report BR21, Building Research Establishment
24. Building Research Establishment (1985) Lighting controls and daylight use. BRE Digest 272
25. Building Research Establishment. BREEAM – the BRE environmental assessment method. http://www.breeam.org. Accessed 2011
26. The U.S. Green Building Council. LEED: leadership in energy and environmental design. http://www.usgbc.org/LEED. Accessed 2011
27. Littlefair PJ (1998) Predicting lighting energy use under daylight linked lighting controls. Build Res Inf 26(4):208–222
28. Clarke JA (2001) Energy simulation in building design, 2nd edn. Butterworth-Heinemann, Oxford
29. Littlefair PJ (1985) The luminous efficacy of daylight: a review. Light Res Technol 17(4):162–182
30. Skartveit A, Olseth JA (1992) The probability density and autocorrelation of short-term global and beam irradiance. Solar Energy 49(6):477–487
31. Begemann SHA, den Beld GJ, Tenner AD (1997) Daylight, artificial light, and people in an office environment: Overview of visual and biological responses. Int J Ind Ergon 20(3): 231–239
32. Galasiu AD, Veitch JA (2006) Occupant preferences and satisfaction with the luminous environment and control systems in daylit offices: a literature review. Energ Buildings 38(7): 728–742
33. LG7 CIBSE/SLL (2005) Lighting guide 7: office lighting. Chartered Institution of Building Services Engineers, London
34. EWCO (2005) Annual review of working conditions in the EU: 2004–2005. Technical report, European Foundation for the Improvement of Living and Working Conditions
35. CIBSE (1996) Lighting Guide 3: the visual environment for display screen use, addendum 2001. Chartered Institution of Building Services Engineers, London
36. CIBSE/SLL (2002) Code for lighting. Chartered Institution of Building Services Engineers/Society of Light and Lighting, London
37. Osterhaus WKE (2005) Discomfort glare assessment and prevention for daylight applications in office environments. Solar Energy 79(2):140–158
38. Chauvel P, Collins JB, Dogniaux R, Longmore J (1982) Glare from windows: current views of the problem. Light Res Technol 14(1):31–46
39. Velds M (2002) User acceptance studies to evaluate discomfort glare in daylit rooms. Solar Energy 73(2):95–103
40. Tuaycharoen N, Tregenza PR (2007) View and discomfort glare from windows. Light Res Technol 39(2):185–200
41. Webb AR (2006) Considerations for lighting in the built environment: Non-visual effects of light. Energ Buildings 38(7): 721–727
42. Collins BL (1976) Review of the psychological reaction to windows. Light Res Technol 8(2):80–88
43. Boyce PR, Beckstead JW, Eklund NH, Strobel RW, Rea MS (1997) Lighting the graveyard shift: The influence of a daylight-simulating skylight on the task performance and mood of night-shift workers. Light Res Technol 29(3):105–134
44. Brainard GC, Hanifin JP, Greeson JM, Byrne B, Glickman G, Gerner E, Rollag MD (2001) Action spectrum for melatonin regulation in humans: evidence for a novel circadian photoreceptor. J Neurosci 21(16):6405–6412
45. McIntyre IM, Norman TR, Burrows GD, Armstrong SM (1989) Human melatonin suppression by light is intensity dependent. J Pineal Res 6(2):149–156
46. Rea MS, Figueiro MG, Bullough JD (2002) Circadian photobiology: an emerging framework for lighting practice and research. Light Res Technol 34(3):177–187
47. Pechacek CS, Andersen M, Lockley SW (2008) Preliminary method for prospective analysis of the circadian efficacy of (day) light with applications to healthcare architecture. Leukos 5(1):1–26
48. Hubalek S, Brink M, Schierz C (2010) Office workers' daily exposure to light and its influence on sleep quality and mood. Light Res Technol 42(1):33–50

49. Walch JM, Rabin BS, Day R, Williams JN, Choi K, Kang JD (2005) The effect of sunlight on postoperative analgesic medication use: a prospective study of patients undergoing spinal surgery. Psychosom Med 67(1):156–163
50. Commission for Architecture and the Built Environment (2004) The role of hospital design in the recruitment, retention and performance of NHS nurses in England. CABE, pp 120–124
51. Heschong Mahone Group (1999) Daylighting in schools: an investigation into the relationship between daylight and human performance. Pacific Gas and Electric Company, San Francisco
52. Heschong Mahone Group (2003) Windows and offices: a study of office worker performance and the indoor environment. Heschong L (ed) CEC, California Energy Commission
53. Heschong Mahone Group (1999) Skylight and retails sales, an investigation into relationship between daylighting and human performance. Pacific Gas and Electric Company, San Francisco
54. National Research Council (2007) Green schools: attributes for health and learning. National Academies Press, Washington, DC, Committee to Review and Assess the Health and Productivity Benefits of Green Schools
55. Noguchi H, Itou T, Katayama S, Koyama E, Morita T, Sato M (2004) Effects of bright light exposure in the office (proceedings of the 7th international congress of physiological anthropology). J Physiol Anthropol Appl Hum Sci 23(6):368
56. Mills P, Tomkins S, Schlangen L (2007) The effect of high correlated colour temperature office lighting on employee wellbeing and work performance. J Circadian Rhythms 5(1):2
57. Hunt DRG (1980) Predicting artificial lighting use – a method based upon observed patterns of behaviour. Light Res Technol 12(1):7–14
58. Reinhart CF, Voss K (2003) Monitoring manual control of electric lighting and blinds. Light Res Technol 35(3):243–258
59. Newsham GR, Mahdavi A, Beausoleil-Morrison I (1995) Lightswitch: a stochastic model for predicting office lighting energy consumption. In: Proceedings of right light 3, Newcastle-upon-Tyne, UK
60. Reinhart CF (2004) Lightswitch-2002: a model for manual and automated control of electric lighting and blinds. Solar Energy 77(1):15–28
61. Mardaljevic J, Heschong L, Lee E (2009) Daylight metrics and energy savings. Light Res Technol 41(3):261–283
62. Mardaljevic J (2006) Examples of climate-based daylight modelling. In: CIBSE national conference 2006: engineering the future, Oval Cricket Ground, London, 21–22 Mar 2006
63. Crawley DB, Lawrie LK, Winkelmann FC, Buhl WF, Huang YJ, Pedersen CO, Strand RK, Liesen RJ, Fisher DE, Witte MJ, Glazer J (2001) EnergyPlus: creating a new-generation building energy simulation program. Energ Buildings 33(4):319–331
64. Mardaljevic J (2006) Time to see the light. Build Serv J September:59–62
65. Mardaljevic J (2000) Simulation of annual daylighting profiles for internal illuminance. Light Res Technol 32(3):111–118
66. Reinhart CF, Herkel S (2000) The simulation of annual daylight illuminance distributions – a state-of-the-art comparison of six RADIANCE-based methods. Energ Buildings 32(2):167–187
67. Nabil A, Mardaljevic J (2006) Useful daylight illuminances: a replacement for daylight factors. Energ Buildings 38(7):905–913
68. Reinhart CF, Mardaljevic J, Rogers Z (2006) Dynamic daylight performance metrics for sustainable building design. Leukos 3(1):7–31
69. Reinhart CF, Walkenhorst O (2001) Validation of dynamic radiance-based daylight simulations for a test office with external blinds. Energ Buildings 33(7):683–697
70. Littlefair PJ (1990) Review paper: Innovative daylighting: Review of systems and evaluation methods. Light Res Technol 22(1):1–17
71. Andersen M (2002) Light distribution through advanced fenestration systems. Build Res Inf 30(4):264–281
72. SolaVeil. http://www.solaveil.co.uk. Accessed 2011
73. Lee ES, Selkowitz SE, Hughes GD, Clear RD, Ward G, Mardaljevic J, Lai J, Inanici MN, Inkarojrit V (2005) Daylighting the New York Times headquarters building. Lawrence Berkeley National Laboratory. Final report LBNL-57602
74. Selkowitz S, Lee ES (1998) Advanced fenestration systems for improved daylight performance. In: Daylighting '98 conference proceedings, Ottawa, ON, Canada
75. Lee ES, DiBartolomeo DL (2002) Application issues for large-area electrochromic windows in commercial buildings. Sol Energ Mat Sol C 71(4):465–491
76. Sullivan R, Rubin M, Selkowitz S (1996) Energy performance analysis of prototype electrochromic windows, Report number: LBL-39905 BS-360. Technical report, Lawrence Berkeley Laboratory
77. Inoue T, Ichinose M, Ichikawa N (2008) Thermotropic glass with active dimming control for solar shading and daylighting. Energ Buildings 40(3):385–393
78. Optics5. Lawrence Berkeley National Laboratory. http://windows.lbl.gov/materials/optics5. Accessed 2011
79. Apian-Bennewitz P, von der Hardt J (1998) Enhancing and calibrating a goniophotometer. Sol Energ Mat Sol C 54(1–4): 309–322
80. Andersen M, Michel L, Roecker C, Scartezzini JL (2001) Experimental assessment of bi-directional transmission distribution functions using digital imaging techniques. Energ Buildings 33(5):417–431
81. Reinhart CF, Andersen M (2006) Development and validation of a Radiance model for a translucent panel. Energ Buildings 38(7):890–904
82. Andersen M, Rubin M, Powles R, Scartezzini JL (2005) Bi-directional transmission properties of venetian blinds: experimental assessment compared to ray-tracing calculations. Solar Energy 78(2):187–198
83. Greenup PJ, Edmonds IR, Compagnon R (2000) Radiance algorithm to simulate laser-cut panel light-redirecting elements. Light Res Technol 32(2):49–54
84. Mardaljevic J (2007) Climate-based daylight modelling for evaluation and education. In: VELUX daylight symposium, Bilbao, Spain, 6–7 May 2007
85. Breitenbach J, Lart S, Langle I, Rosenfeld JLJ (2001) Optical and thermal performance of glazing with integral venetian blinds. Energ Buildings 33(5):433–442

86. Carter DJ (2002) The measured and predicted performance of passive solar light pipe systems. Light Res Technol 34(1):39–51
87. Jenkins D, Muneer T, Kubie J (2005) A design tool for predicting the performances of light pipes. Energ Buildings 37(5):485–492
88. Reinhard E, Ward G, Pattanaik S, Debevec P (2005) High dynamic range imaging: acquisition, display, and image-based lighting (the Morgan Kaufmann series in computer graphics). Morgan Kaufmann Publishers Inc., San Francisco, CA, USA
89. Wienold J, Christoffersen J (2006) Evaluation methods and development of a new glare prediction model for daylight environments with the use of CCD cameras. Energ Buildings 38(7):743–757
90. Painter B, Fan D, Mardaljevic J (2009) Evidence-based daylight research: development of a new visual comfort monitoring method. Lux Europa, Istanbul, pp 953–960
91. Newsham GR, Aries MBC, Mancini S, Faye G (2008) Individual control of electric lighting in a daylit space. Light Res Technol 40(1):25–41
92. Newsham GR, Arsenault C (2009) A camera as a sensor for lighting and shading control. Light Res Technol 41(2):143–163
93. Crisp VHC (1977) Preliminary study of automatic daylight control of artificial lighting. Light Res Technol 9(1):31–41
94. Hunt DRG (1977) Simple expressions for predicting energy savings from photo-electric control of lighting. Light Res Technol 9(2):93–102
95. Hunt DRG (1979) Improved daylight data for predicting energy savings from photoelectric controls. Light Res Technol 11(1):9–23
96. Crisp VHC (1978) The light switch in buildings. Light Res Technol 10(2):69–82
97. Bordass B, Cohen R, Standeven M, Leaman A (2001) Assessing building performance in use 3: energy performance of the probe buildings. Build Res Inf 29(2):114–128
98. Heschong Mahone Group (2006) Sidelighting photocontrols field study. Final Report to Southern California Edison Co, Pacific Gas & Electric Company and Northwest Energy Efficiency Alliance
99. DTI (2000) Photovoltaics in buildings: BIPV projects programme – strategy document 1998–2002. Technical report, Dept. of Trade and Industry
100. Yoon S, Tak S, Kim J, Jun Y, Kang K, Park J (2011) Application of transparent dye-sensitized solar cells to building integrated photovoltaic systems. Build Environ 46(10):1899–1904

Daylighting Controls, Performance and Global Impacts

Helmut Köster
Köster Lichtplanung, Frankfurt am Main, Germany

Article Outline

Glossary
Definition of the Subject
Introduction: What Is Daylight?
The Benefits of Daylighting: Energy, Health, and Design Flexibility
The Challenges of Daylighting
Designing Effective Daylighting
Conclusion
Bibliography

Glossary

Brightness contrast/glare Risks of glare in daylighting

- Direct glare: sun is in user's immediate field of vision
- Background glare: brightness contrast between monitor and monitor background
- Reflected glare: mirroring effect on monitor surface

Daylight autonomy Daylight autonomy of a workplace is the percentage of normal working time without the requirement of electric lighting – i.e., the time in which the target illuminance can be maintained by daylight alone. This varies depending on the minimum illuminance required and is determined using daylight coefficient.

Direct/diffuse light Diffuse light illuminates a room or area contrast or shadow reduced. It is usually caused by extensive light sources like the overcast sky (5,000–20,000 cd/m^2). In contrast the clear sky has a luminance of up to 50,000 cd/m^2 which is caused by the high illuminance of the direct sun (100,000 lx).

Efficiency of daylight Depending on the type of building, 20–40% of its total energy requirement is used merely for electric lighting, primarily during the day. Using optimized daylight redirection systems, electric lighting demands can be reduced to less than 10% of total energy loads.

Heat gain from daylight versus electric light Outside, daylight produces up to 120 lm/W of energy. Inside – behind glass with controlled solar heat gain coefficients (SHGC) – daylight offers even greater 240 lm/W. Fluorescent luminaires, on the other hand, can only achieve approximately 70 lm/W, requiring much higher energy use per unit of lighting provided. As a result, the heat gain in buildings using daylight is less than 1/3 of the

heat generated by electric lighting, a gain taken into account in the energy balance of a building through the SHGC value.

Illuminance (lux/lumen/candela) Basic terms of lighting technology are:

- Illuminance E [lx]. The total luminous flux incident on a surface per illuminated surface area
- Luminous flux Φ [lm]. The radiated power emitted by a light source or the radiated power incidence on a surface
- Luminous intensity I [cd]. The directional luminous flux of a light source

Light distribution curves (LDC) Light distribution curves of daylight systems indicate the direction and the intensity of the light distribution. Given the sun's changing angles of incidence outside, factors to be considered in mapping the light distribution inside include light redirection elements and the potential for adjusted tilt angles to ensure freedom from glare.

Quality assurance for daylight control Quality assurance must ensure the simultaneity of three criteria:

- Reduction of solar irradiation in summer (F_c value) for passive cooling balanced by solar gain in winter
- Sufficient daylight supply on the task surfaces (daylight coefficient)/visual comfort
- Sufficient visual transmission for quality views

Conventional louvers are generally closed to protect against glare and overheating. This not only hinders the view outside, but also prevents sufficient daylight from coming in. Design for daylight, including light redirecting louvers, ensures simultaneity of all three qualities.

Reflectors – contoured prismatic, mirror and diffusing blinds Basic functions of mirror or prismatic light redirecting louvers include reflection of the light back to its source to protect against overheating (thermal comfort) and/or redirection of daylight into the space to improve the illumination in the room (visual comfort). Precise contours make it possible to calculate exactly the quantitative light distribution (both inside and outside) with reference to the louvers' tilt angle and the altitude of the sun. Mono-reflective light control refers to the redirection of light inside and its deflection back outside in a single reflection in order to minimize its absorption by the blinds and any resulting heat development. Mono-reflective light control is required to prevent undirected reflection of the rays back and forth between louvers to prevent unplanned light scattering or absorption.

Shading for passive cooling balanced by passive solar heating Shading is a critical protective function against overheating to avoid active cooling, achieved exclusively through reflection of solar irradiation. At the same time, "passive solar heating" relies on solar transparency to achieve high levels of solar gain to reduce mechanical heating requirements. To avoid the risk of overheating in summer, it is critical to provide seasonally or daily dynamic devices that balance light and heat gain.

Total solar energy transmission (g/SHGC) Total solar energy transmission through the glazed area (g-value, SHGC) defines the heat load resulting from solar irradiation, light transmission, and secondary heat radiation ($g = \tau_{verg} + q_i$). Design decisions include the total energy transmission for the window assembly and its interior and exterior layers that form an overall system including sun and light control. The F_c value for the system indicates the percentage by which the total energy transmission through the glazing is reduced through redirection of the light: $F_c = g_{tot}/g_{glazing}$.

Definition of the Subject

Worldwide, efforts are made to introduce energy saving regulations and laws requiring the use of regenerative energies. The focus so far has been on energy conversion systems to obtain power and heat. Yet, daylight is one of the most substantive renewable energies, and highly underutilized in buildings. It should be obvious that using the sun for natural illumination of indoor environments, without overheating, should be a primary goal for the building sector.

Improving the supply of natural daylight in workplaces rather than using electric lighting is a highly sustainable and economic resource that saves both energy and power. Over 30% of the total energy consumption of average buildings is used for electric lighting, and most of this during the daytime! Simply by redirecting daylight into the room, the use of electric

lighting can be reduced by at least 50%, and effective shading with daylight offers further cooling energy savings. Daylight management systems are thus the focal point of the latest strategies to save energy and reduce the carbon footprint of buildings.

This entry outlines the critical characteristics of daylighting design, incorporating reflection, redirection, and diffusion in the design of façades and their external and internal layers. The correct manipulation and exploitation of the sun and daylight is vital as an energy savings resource and must mature into a key element in the development of energy concepts. Daylight design must become central to a range of disciplines, including lighting technology, façade technology, energy technology and architecture, and ultimately calls for integrated design studies to provide training in planning and coordinating between the various disciplines.

Introduction: What Is Daylight?

Common parlance and building physics define "daylight" as follows: Daylight is perceived as brightness outdoors and includes all variants from twilight to the brightest time of day when the sun is highest, ranging from diffuse light in shaded areas or with cloudy skies to direct sunlight. The sun is the primary source of all variants of daylight (Photo 1).

Solar radiation is approximately 1 kW/m^2 on the earth's surface. The illuminance from direct sunlight is approximately 100,000 lx. A clear, blue sky has approximately 50,000 cd/m^2, a cloudy sky may have less or more – depending on the time of year – between 5,000 and 15,000–20,000 cd/m^2 [17].

Depending on the location, daylight is in the wavelength range from 350 to 750 nm – roughly 40–50% of light radiation in the sensitivity range of our vision (Figs. 2, 3b–d, 6).

Whereas the term "daylight" more likely conjures up an image of diffuse light without directional reference – i.e., uniform light distribution from all directions – the sun itself has clear directional reference, which indicates to us the exact time of day and year (Fig. 1).

The number of daylight hours varies depending on latitude and time of year, and the number of sunny hours varies depending on the climate zone. Germany gets between 1,200 and 1,500 h of sunlight per year [5].

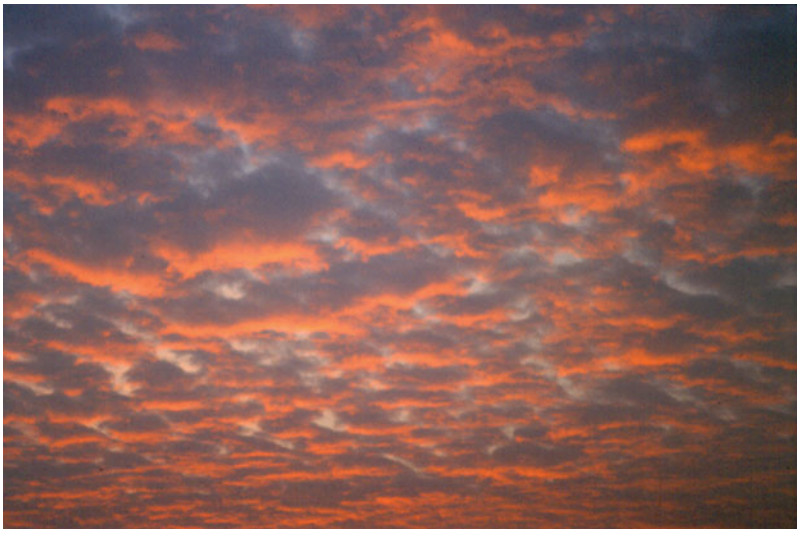

Daylighting Controls, Performance and Global Impacts. Photo 1
Daylight is an experience of color, season, and daytime and helps human beings to reintegrate themselves into the cycles of nature

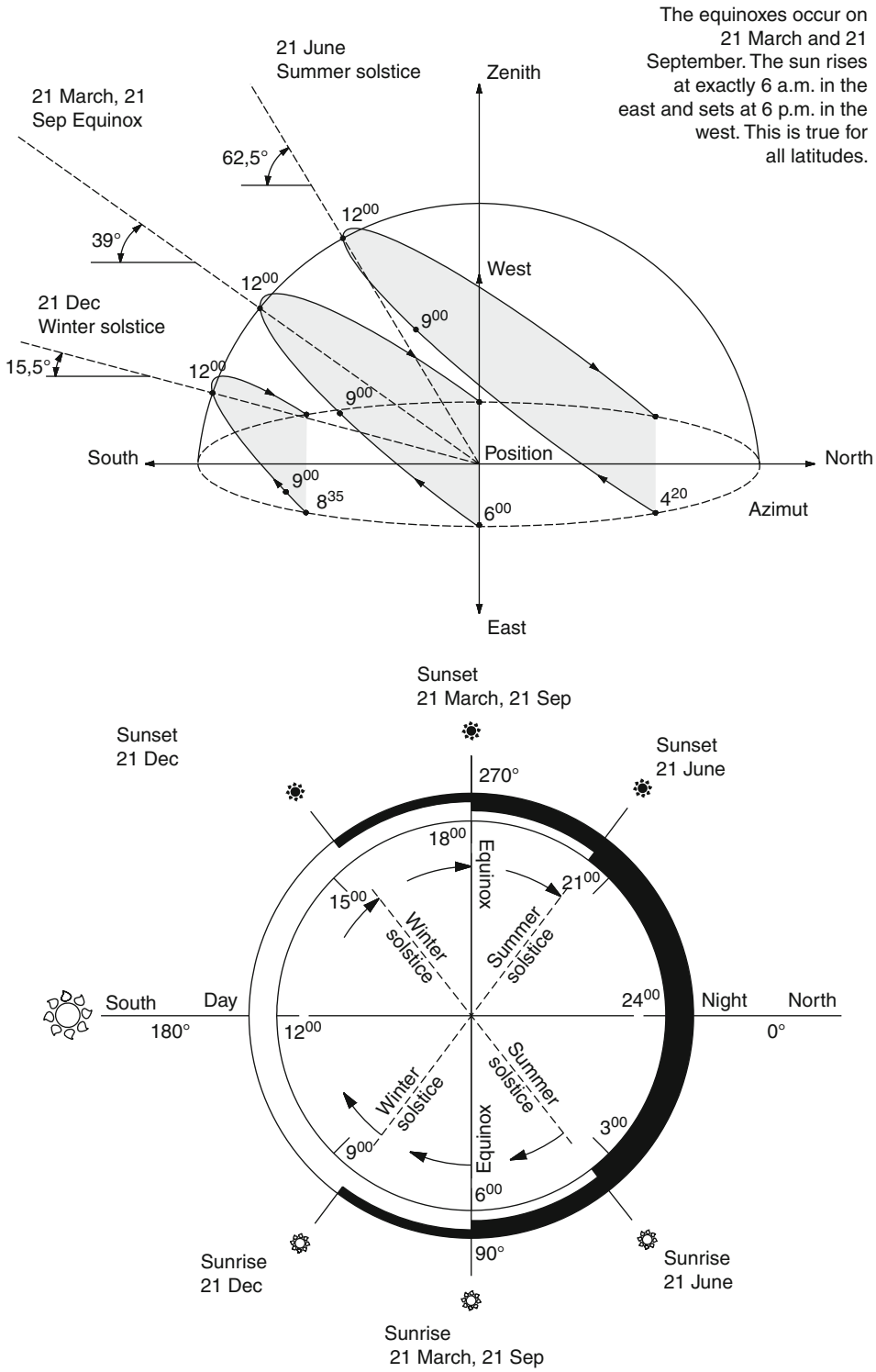

Daylighting Controls, Performance and Global Impacts. Figure 1
Illustration of the daily and annual paths of the sun at 51° latitude [14]

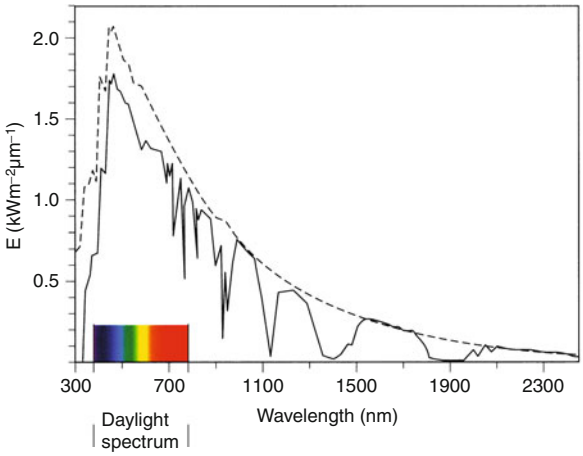

Daylighting Controls, Performance and Global Impacts. Figure 2
Spectral energy distribution of daylight [9]

In many parts of California, the sun shines over 3,000 h [23] of approximately 4,300 daytime hours a year.

Design for daylight must address diffuse sky and sunny conditions, as they vary by orientation, season, and climate. Daylight design must address illuminance, glare, brightness contrast, and view content for visual quality in addition to managing solar heat gain for thermal quality.

Given the dynamic nature of daylight, light-transmitting building elements (windows and skylights) must be supported by "daylight technologies" to manage light transmission and redirection, balancing the variations in the sun's angles of incidence (Fig. 14) against variations in desirable heat energy transmission. The aim of daylight technologies is to achieve specific lighting effects using defined reflection, transmission, and/or absorption characteristics. Its further purpose is to gain more heat in winter and ensure shading for passive comfort in summer.

Effective daylighting design is dependent on the size of the windows relative to the proportion of the room, the configuration of the windows and their adjacent surfaces (to manage brightness contrast), the arrangement of windows relative to each other and the surfaces to be lit in the room (bi-directional and indirect light), the type of glazing (e.g., transparency, translucency, diffusion) including color effects (e.g., church windows) and the layers placed inside or outside of the glass that may change the transmission or directionality of the light.

Balancing Light and Heat: The Optimization of Daylighting

Current research and development in daylight-optimized glazing technologies concentrates on optimizing the energy transmission proportional to light transmission. Standard glazing, therefore, is defined on the basis of three physical reference parameters:

- Light transmission $\tau_{L \text{ or } VT}$ (Fig. 3d)
- Total solar energy transmission or solar factor (g or SHGC) (Fig. 3a)
- Heat transmission coefficient U in W/m^2K (Fig. 3a)

Whereas τ_L and g are parameters related to the transmission of light and heat from the outside to the inside, the U-value is used to calculate the conductive heat losses from the inside to the outside. To maximize daylighting year round, while avoiding solar heat gain as cooling loads in summer, the τ_L and g-values (SHGC) will be critical (Fig. 3).

Thirty years ago, the visible light transmission (τ_L or $_{VT}$) of glass paralleled the heat transmission (SHGC or previously SC), with efforts to reduce heat transmission dominating specifications in an effort to minimize cooling loads. As a consequence, generations of dark or reflective glass buildings continue to be built, despite the fact that glazing innovations today allow for independent selection of visible transmission and shading values.

Typical glazing (6/16/6 and 4/12/4) of the latest developments has the following characteristics (Table 1).

The most recent developments in selective coatings applied to glass surfaces use sputtering methods to allow a ratio of τ_L/SHGC of approximately 2 for insulated (double-glazed) glass units. These advances ensure a high level of light transmission τ_L while keeping the total energy transmission g (SHGC) to a minimum. The competition among glazing producers can be reduced to the following formula:

"More light, less heat"

In spirit, this formula is a vast improvement over less heat ergo less light – the reflective glass era.

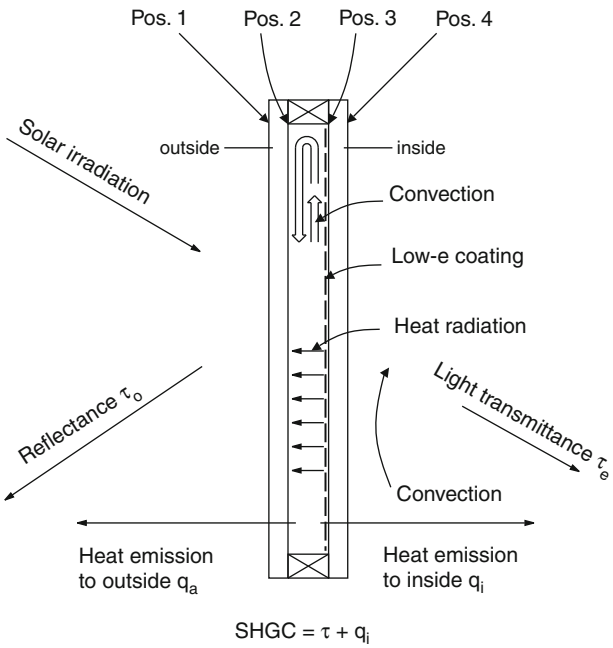

Typical design of insulation glazing in housing construction with low-e coating in pos. 3. (SHGC = 0.60)
The low-e coating of administrative buildings is found on pos. 2 (SHGC = 0.50)

U-value with double insulation glazing based on DIN 1.0 W/m^{2}K
a U-value with triple insulation glazing based on DIN 0.6 W/m^{2}K

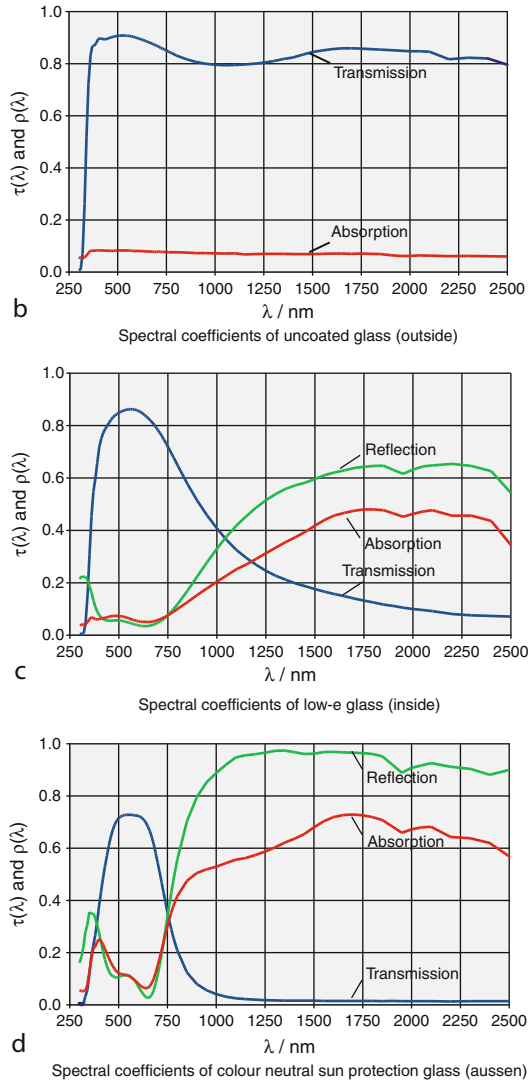

Daylighting Controls, Performance and Global Impacts. Figure 3
(**a**–**d**) Basics of building physics in daylight technology [12]

Daylighting Controls, Performance and Global Impacts. Table 1 Light to heat ratio [19]

	τ_L in %	SHGC in %
Sun protection glass	53	28
	61	44
	60	28
Low-e glass iplus 3LS	80	63
	78	61
	71	42

However, there are at least two other climate conditions that demand a more nuanced selection in glazing or glazing controls. First, climates that have high heating loads in both residential and commercial buildings will not benefit from low solar heat gain coefficient glazing materials. The potential for passive solar heat as a natural or renewable heating source is very significant (Table 1). In colder regions, it is best to use glazing with a high light and high total solar energy transmission to realize the additional solar gains in winter. Second, climates that are hot and sunny, with significant

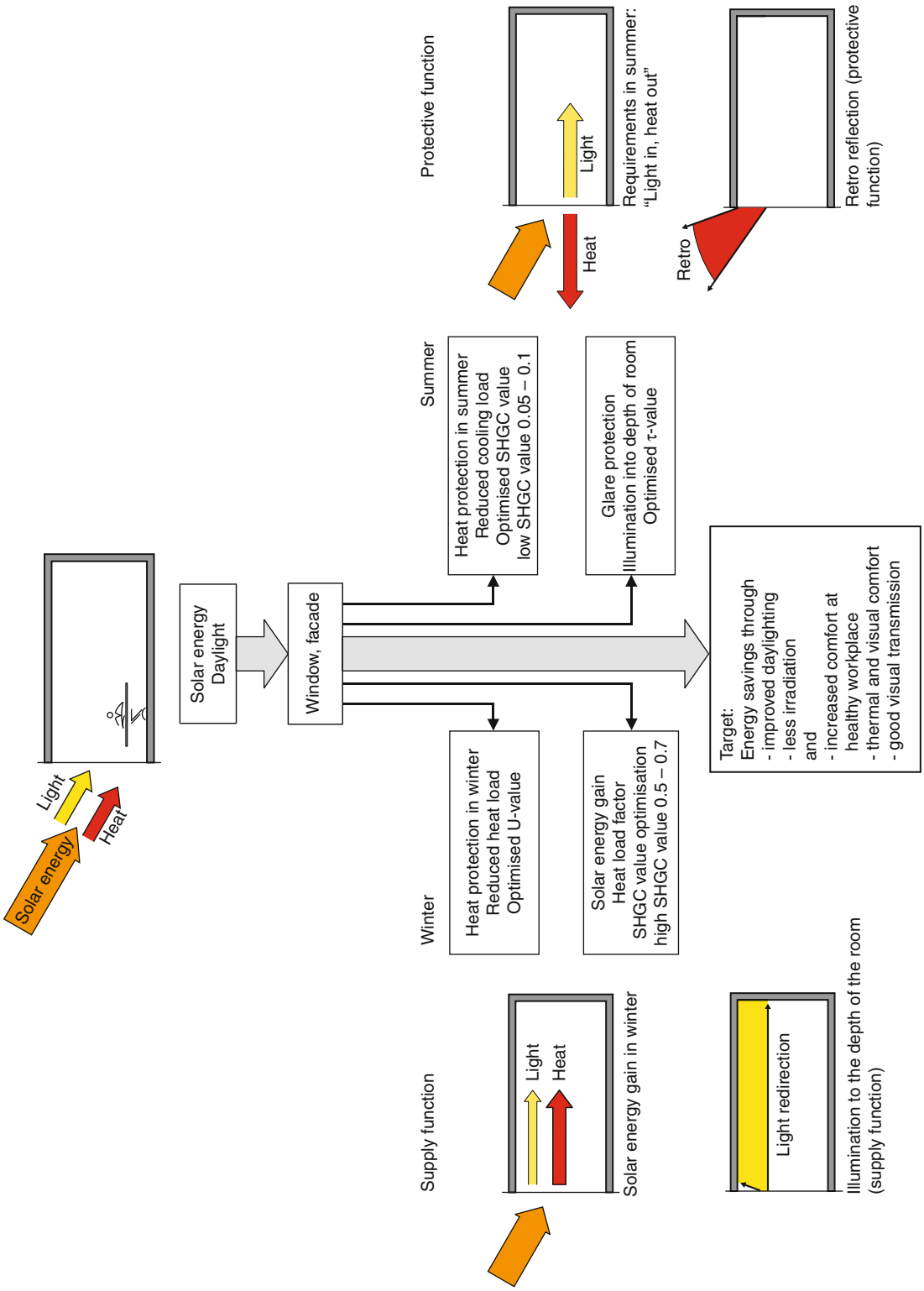

Daylighting Controls, Performance and Global Impacts. Figure 4
Tasks and functions of light-transmitting components in the conflict between required solar energy and passive cooling [14]

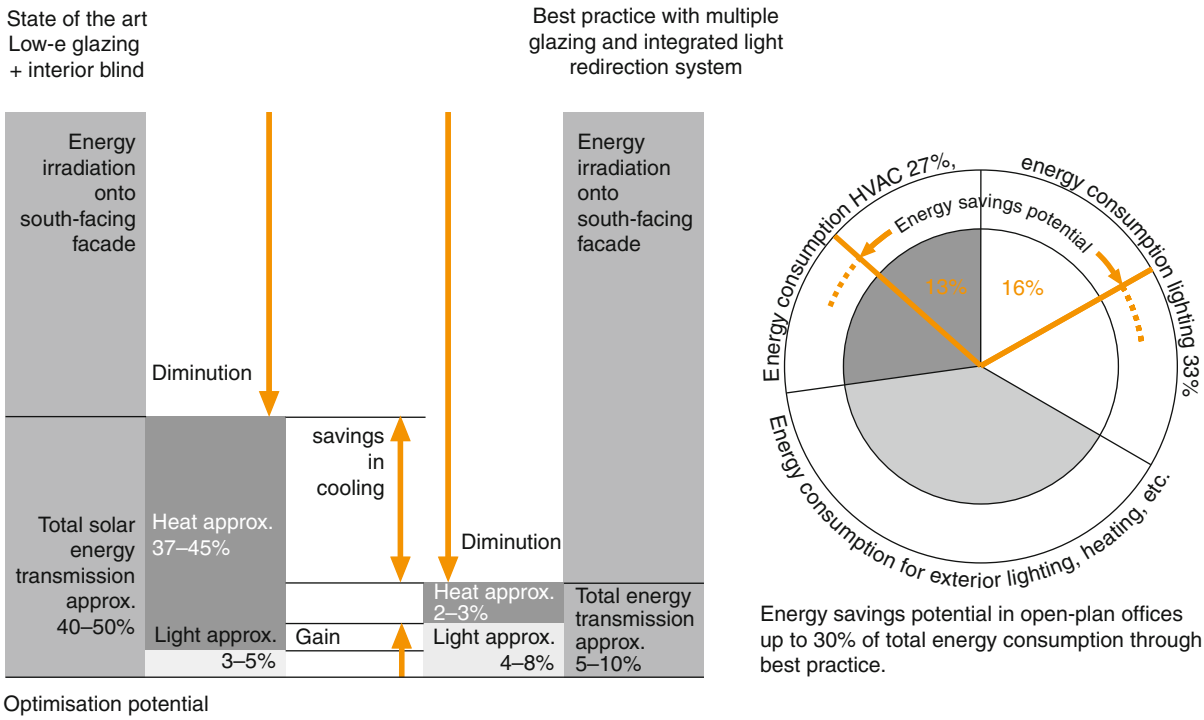

Daylighting Controls, Performance and Global Impacts. Figure 5
(**a**, **b**) Energy savings potential of a new, intelligent façade and daylight system in comparison to the state of the art

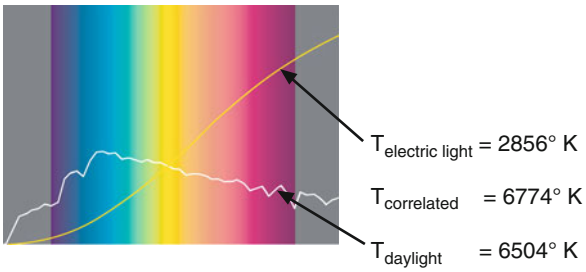

Daylighting Controls, Performance and Global Impacts. Figure 6
Spectral distribution of daylight [18]

ground reflectivity, such as desert regions, have an additional challenge of managing both heat gain and brightness contrast, suggesting lower light and heat transmission glazing choices (Fig. 3d). Both of these climates will benefit from the lowest heat transmission coefficient possible (U-value) to reduce heat loss and heat gain (Fig. 4).

The highest level of natural conditioning through daylighting, shading, and passive solar heating can only be achieved through the addition of dynamic layers, either inside or outside the glazing, to allow for the exact amount of light and heat that is needed given time of day, season, orientation, and space function, in each climate.

The addition of dynamic layers becomes even more important as the design community pursues all glass buildings with floor to ceiling transparencies, regardless of the climate in which they are built. One only needs to see the latest buildings in Dubai, Hamburg, or New York to realize that façade design will need to resolve the transmission of daylight, solar heat and heat loss with dynamic layers, to enable natural energies to offset the major conditioning demands these façades have generated.

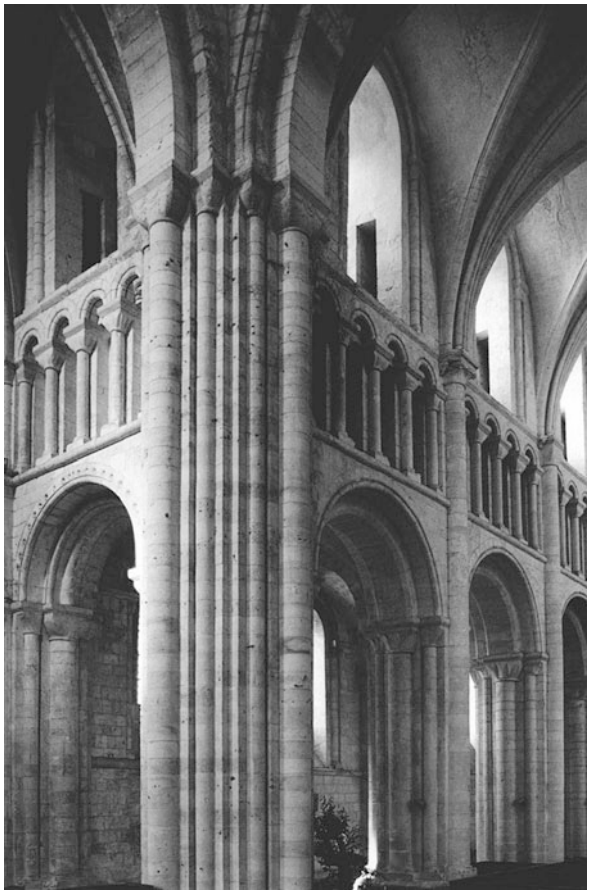

Daylighting Controls, Performance and Global Impacts. Photo 2
Examples from building history: Romanesque: interplay of wall relief and opening [14]

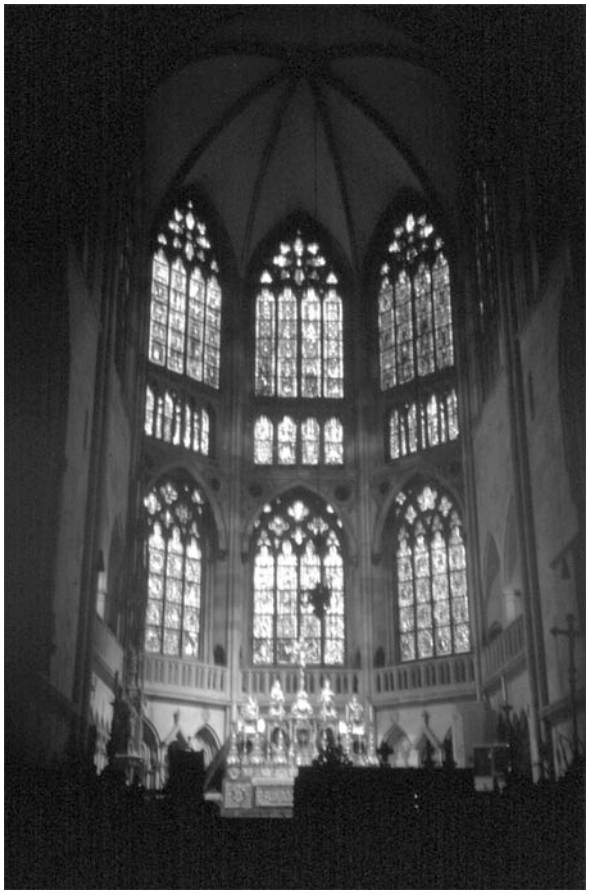

Daylighting Controls, Performance and Global Impacts. Photo 3
Examples from building history: Gothic: colored window [14]

The Benefits of Daylighting: Energy, Health, and Design Flexibility

Energy Saving Potential of Daylighting

Electric lighting energy consumption [kWh] in conventional office buildings today is as much as 35% of the total electric load – demands that are generated primarily during the day when daylight is abundant [8]! Since the energy drawn for electric lighting is ultimately converted into heat, there is additionally a load on the cooling system. Proportional to the total energy used, electric lighting can add as much as 16% to the cooling energy bill, such that the combined electricity costs for lighting and cooling are almost 50% of total electric demand (Fig. 5). While total energy consumption is made up of both electricity and fossil fuel energy uses, daylighting alone can reduce total energy use by as much as 25–30%, one of the most cost-effective investments for energy and carbon savings worldwide.

In the USA, where electric lighting is becoming pervasive during the daytime, the New Buildings Institute calculates that daylight harvesting systems can generate lighting energy savings of 35–60%. According to the US Department of Energy, daylight-response controls of skylights have demonstrated lighting energy savings in warehouses of 30–70%, without consideration of the additional cooling energy benefits.

Daylighting Controls, Performance and Global Impacts. Photo 4
Examples from building history: Baroque: indirect daylighting [14]

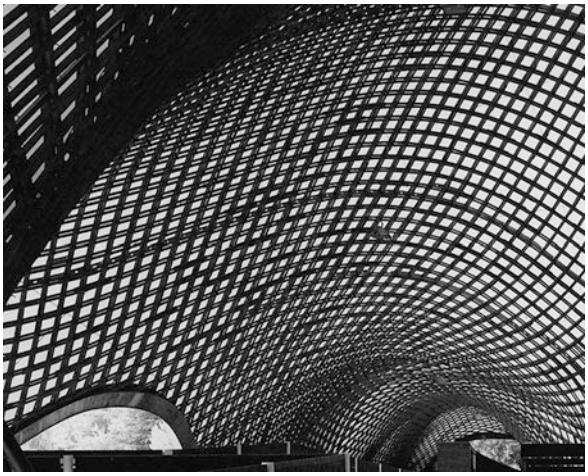

Daylighting Controls, Performance and Global Impacts. Photo 5
Examples of daylighting in modern architecture: Frei Otto: multipurpose hall and restaurant

Daylighting Controls, Performance and Global Impacts. Photo 6
Examples of daylighting in modern architecture: Jørn Utzon: church at Bagsvaerd

In a controlled experiment, the Energy Center of Wisconsin measured the additional cooling energy savings at 25% and fan energy savings at 3% (NBI, DOE, Wisconsin 2005).

The economic impact of ignoring daylight is even more problematic because it is an electric load in buildings – for which source or primary energy costs are significant. One kilowatt of power on site uses approximately 3–4 kW of primary energy, with the rest lost as heat up the chimney at the power plant. In conventional coal or oil fired power plants, only 35–40% of the primary energy is converted into power with a further 6% of the energy produced at the power plant lost in transmission [21]. In developed economies such as the USA, Japan, and Germany, power plants are to be blamed for approximately 50% of all CO_2 emissions! Over 40% of each nation's total energy consumption in developed economies is used for heating, cooling, air conditioning, lighting, and other power requirements in buildings [11].

Daylighting Controls, Performance and Global Impacts. Photo 7
Examples of daylighting in modern architecture: Paul Rudolph: Interdenominational Chapel

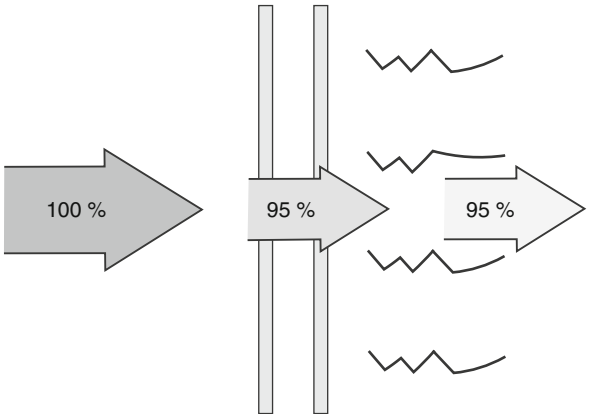

Daylighting Controls, Performance and Global Impacts. Figure 7
Color rendering of low-e glass 95–96%, color rendering of Retro louvers >99% eliminate?

Daylighting Controls, Performance and Global Impacts. Photo 8
Color shift through sun protection glass and electrochrome glazing

Daylight and Health

Humans, like plants, need to live and work in the full spectrum of light provided by [4] (Fig. 6). Daylight is critical for natural vitamin and hormone production, and is associated with numerous emotional values as well [9]. While the research on "daylight nutrient ingestion" through the human eye and the skin is still sparse, it is known that lethargy in winter and certain eating and hormonal disorders are due to a physiological lack of daylight [9]. These deficiency syndromes can be countered by using light treatments during which the patient stays, for hours, in "full-spectrum" settings for health.

One quality of full spectrum daylighting that is significant is its color rendering index. For this reason, it is important not to distort the natural color–rendering qualities of daylight by tinted glazing or colored blinds, screens, and fabrics that change the color composition of natural daylight (Photo 8, Fig. 7). As a result, quality assurance must also take into account the color-rendering index of the daylight transmitted through the window and blind assembly (Fig. 7).

These findings call for "healthy" building design guidelines that ensure full "value-added" daylight to the occupants of the building, changing the color composition of the daylight as little as possible. It is not enough to simply provide sufficient lighting for a visual

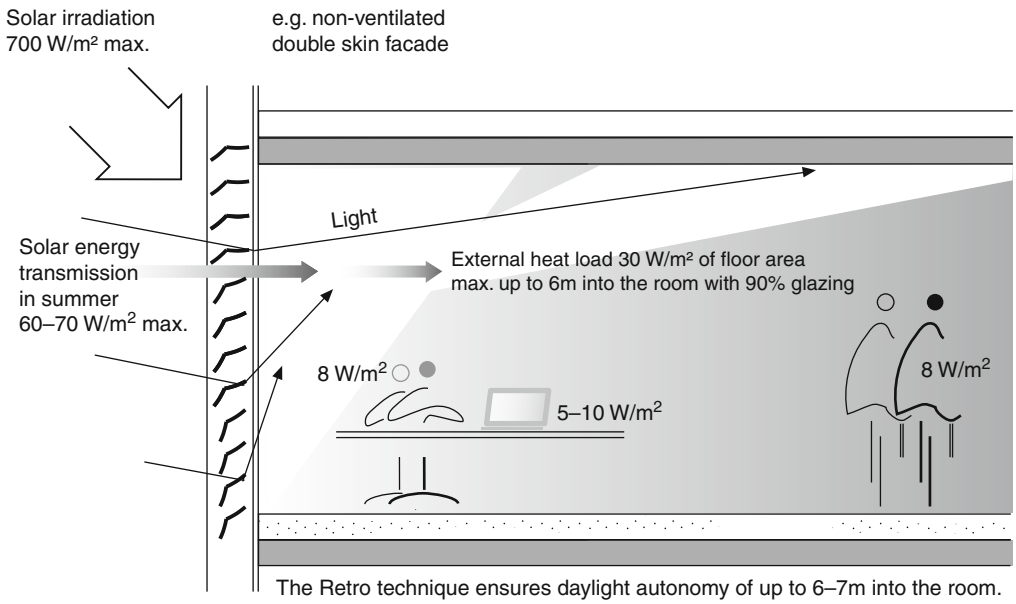

a External and internal heat loads in summer

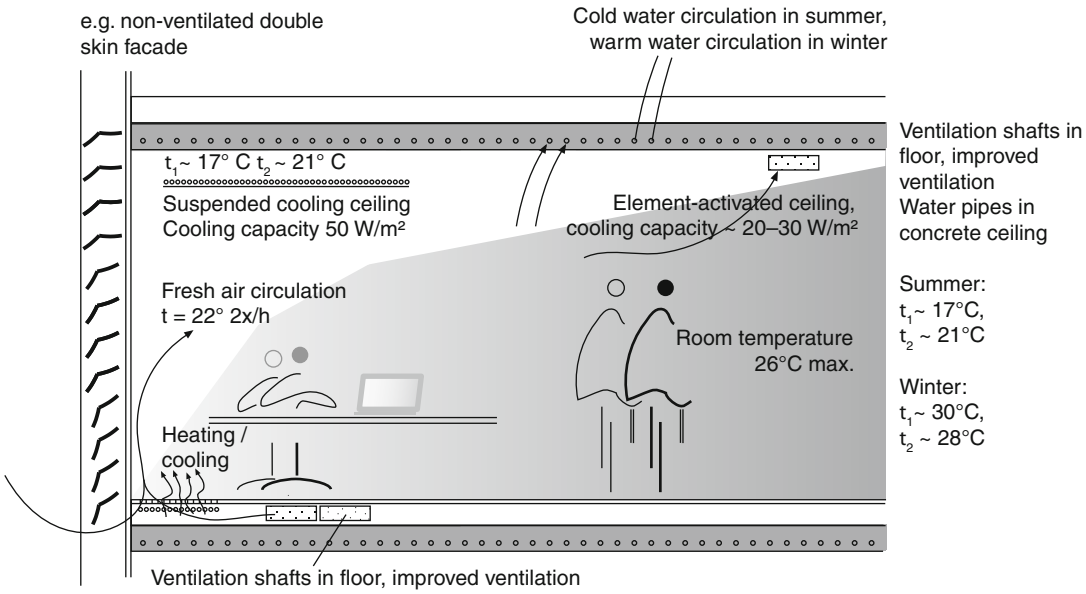

b Heating and AC system concept

Daylighting Controls, Performance and Global Impacts. Figure 8

The Retro technique dramatically reduces the high outer heat loads, making possible new concepts in AC systems. As a result, chilled ceilings are sufficient in most climates to cool a building. (**a**) External and internal heat loads in summer. (**b**) Heating and AC system concept

Daylighting Controls, Performance and Global Impacts. Photo 9
Mirror façades darken the interior, making it necessary to switch on the lights during the day (Photo: Helmut Köster) [21]

task; daylight designers must ensure that each individual receives the necessary light nutrition in their workplaces.

Daylighting and Design Flexibility

Effective daylighting design that manages cooling demands can also save building costs. The need for ceiling plenums are often driven by the demand for air conditioning, with air-based systems dominating the USA and now Asian building growth. The elimination of deep ceiling plenums for air-based cooling can save floor-to-floor heights, overall building height, and even associated elevator demands (Fig. 8).

Since managing solar heat and light can dramatically reduce cooling loads, the potential of radiant water-based cooling systems is unleashed. The use of water-based chilled ceilings, chilled beams, or radiant ceilings and walls for thermal cooling offers significant energy savings over air-based cooling [16]. In addition, the ducted systems can be dedicated to the delivery of fresh air, at 10% of the volume of air-based cooling systems. The ventilation-only systems can be focused on the quality and quantity of fresh air needed in each space, instead of ventilation that is dependent on the variability of cooling demands. Ventilation effectiveness is a measure of the delivery of outside air to the

	Consumption	Consumption
	Standard	Best practice
Interior lighting	25.2%	10.1%
Space cooling	12.5%	5.5%
Space heating	12.2%	8.5%
Ventilation (HVAC)	6.2%	4.7%
Water heating	6.0%	6.0%
Electronics	7.6%	7.6%
Computers	3.9%	3.9%
Refrigeration	4.2%	4.2%
Cooking	1.9%	1.9%
Other (4)	12.6%	12.6%
Adjust to SEDS	7.7%	7.7%

Savings in energy consumption: 27.3 %

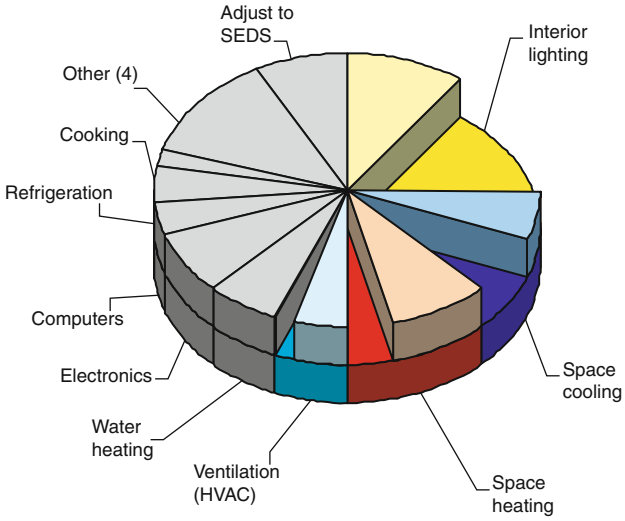

Daylighting Controls, Performance and Global Impacts. Figure 9
Energy consumption savings of approximately 27.3% in the climate of Sofia in office buildings by the use of intelligent daylight systems which help to reduce the cooling loads in summer and simultaneously improve the daylight transmission

Daylighting Controls, Performance and Global Impacts. Photo 10
Prisms are translucent but prevent visual transmission [14]

occupant, and many cooling-dominated ventilation systems have compromised ventilation effectiveness. The separation of thermal conditioning and ventilation offers both energy benefits and air quality benefits.

The savings in building and operating costs far exceed the investment costs for new daylight technology and the investments in façades with improved heat protection.

The Challenges of Daylighting

Despite generations of successfully daylit buildings, designing for effective daylighting poses a number of challenges. First, daylighting must be balanced against overheating due to solar gain, a time of day and seasonal design challenge. Second, daylighting is only successful if the brightness contrast of the window or other daylight source is fully managed, and direct glare must also be avoided. Heat loss and heat gain must be managed through the window and skylight areas, since they are typically less resistive to heat transfer than today's wall and roof constructions. Finally, view must be considered a critical component of effective daylight design.

Daylighting with Effective Shading

Over the past 40 years, the predominant strategy for shading to reduce solar energy transmission into the

Daylighting Controls, Performance and Global Impacts. Photo 11
Prisms are translucent but prevent visual transmission [14]

building is the selection of highly reflective or mirror glass. The low solar heat gain glass reduces the solar load by reflecting the solar gain at the outer skin with a measurable level of absorption in the glass as well. These low solar heat gain coefficients traditionally ensured low daylighting transmission as well, failing to provide the buildings with sufficient natural daylight. The resulting increase in energy use for electric lighting and associated cooling ensured that the glazed area in buildings had a negative energy balance (Fig. 29).

These sun protection strategies, which shade the inside but at the same time darken it to the point of requiring additional electric lighting even while the sun is shining, are, a priori, energetically highly counter-productive (Photo 9). While the use of reflective glass is the most problematic, many external and internal sun protection devices follow the same rule – darken the space to the point where electric light is necessary. This includes, in general, all interior roller shading systems, vertical louvers and colored blinds, and even many external sun shading devices. The loss of daylighting becomes even more profound when internal or external shading layers are used in combination with low transmission glazing.

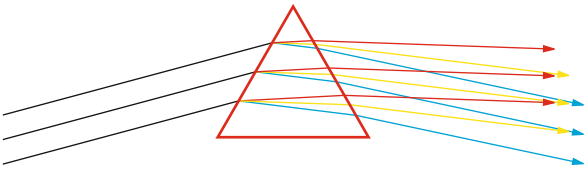

Daylighting Controls, Performance and Global Impacts. Figure 10
Breakup of light into its spectral colors through refraction in the prism

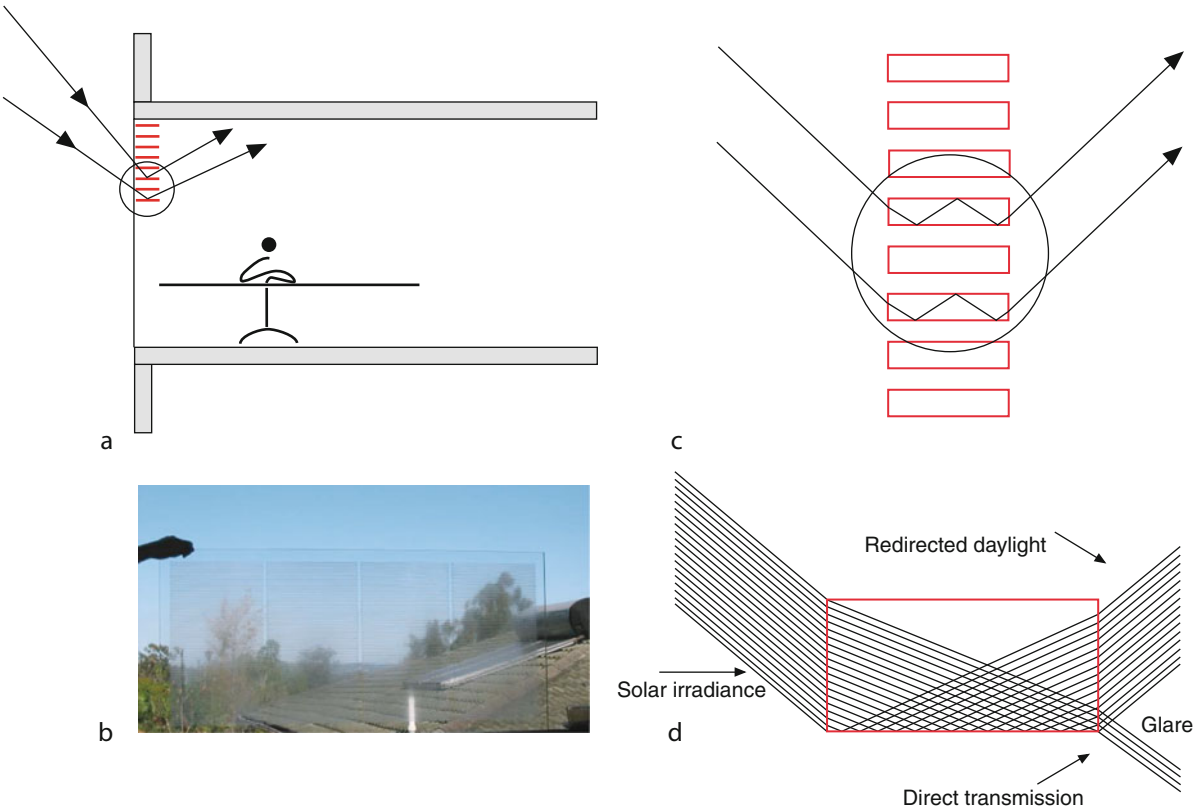

Daylighting Controls, Performance and Global Impacts. Figure 11
Light deflection using laser-cut panels, advantage: good visual transmission, disadvantage: risk of overheating

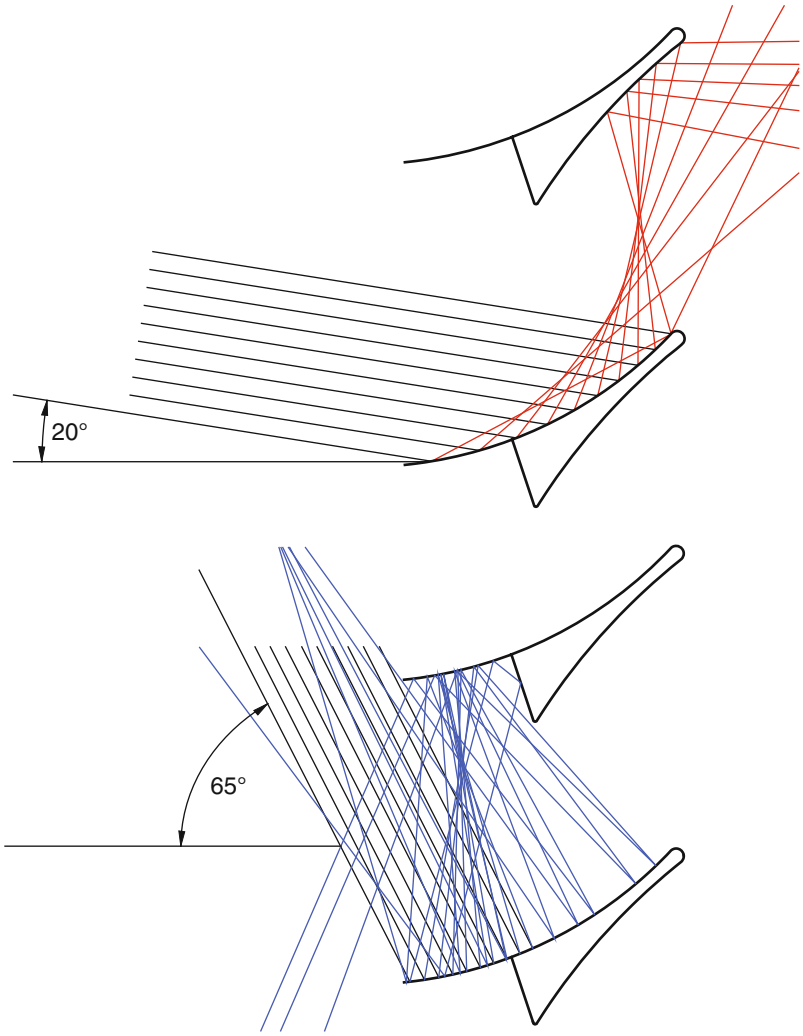

Daylighting Controls, Performance and Global Impacts. Figure 12
Okasolar light reflection louvers in a fixed position inside the glazing with resulting light redirection of the low winter sun and the high summer sun. A next step in the development of the systems involves mono-reflective light deflection which drastically improves the shading capacity of the technology (see also Fig. 16) [EP 0029442; US 4,715,358]

Shading strategies that do not include specific light redirection or light transmission solutions to improve the natural illumination in the room are a waste of the natural, free resource of daylight and of valuable electricity. Shading measures inside the glazing have further concerns relative to protecting the window zone from overheating, since they convert a percentage of the incident sun into heat through absorption. This is especially pronounced when the internal shades or blinds are dark, generating measurable cooling loads.

The pervasive loss of daylight as the dominant light source in modern buildings establishes the challenge to develop new strategies in ecological and sustainable building construction. A focus must be given to improving and optimizing the use of daylight without overheating the buildings through solar irradiation.

The first step is the introduction of high visible transmission glass combined with low solar transmission for any building that does not need passive solar heat. In cooling-dominated climates, this can be through high-visible, low-solar glazing materials.

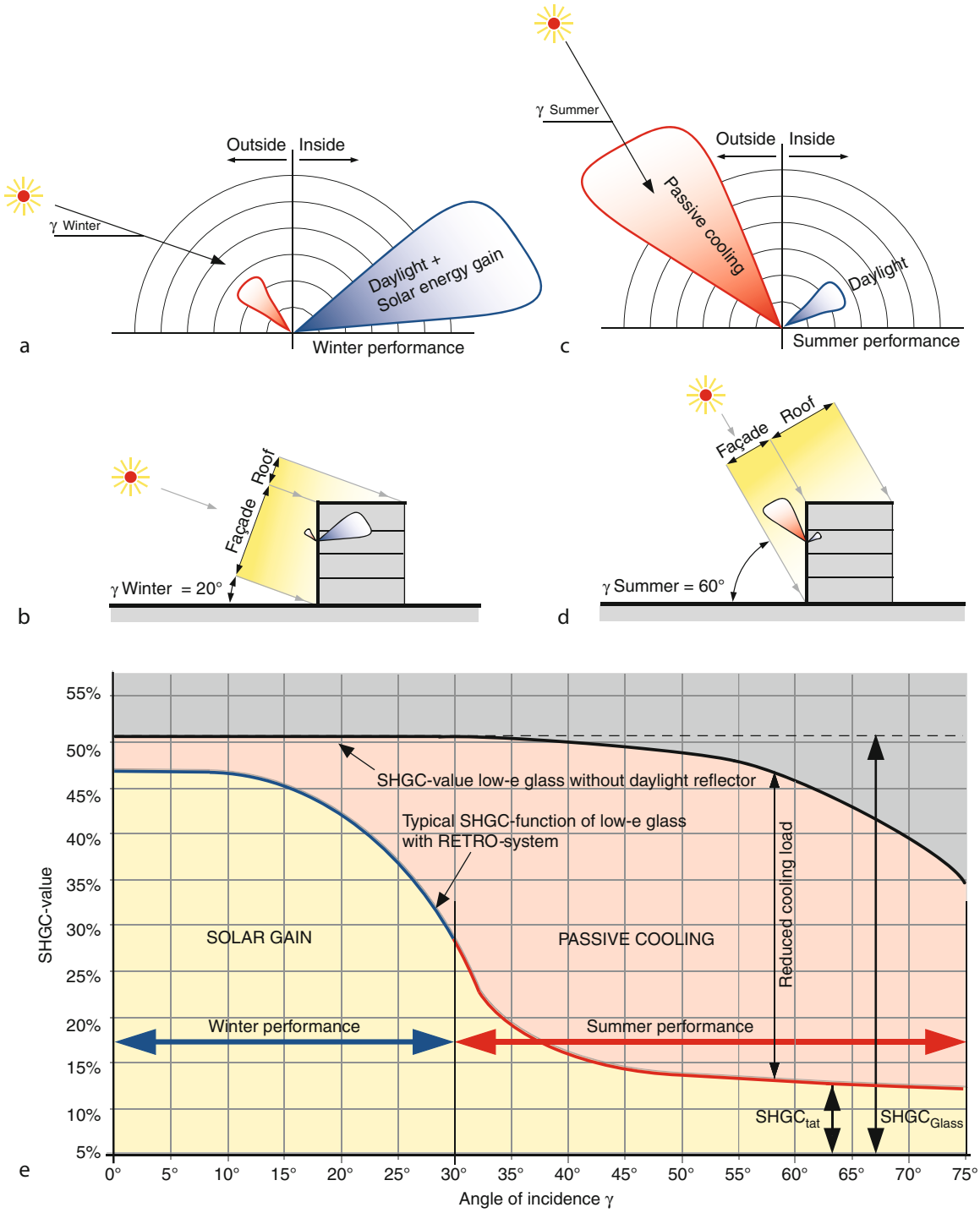

Daylighting Controls, Performance and Global Impacts. Figure 13
(**a**–**d**) Thermal loads for roofs and façades. (**e**) Given the distinctive heating and cooling periods in the European climate, intelligent daylight technologies can maximize solar energy gain in winter and achieve effective shading for natural cooling in summer. These two conflicting goals are achieved through utilization of the sun's changing angle of incidence even without tilting of the blinds

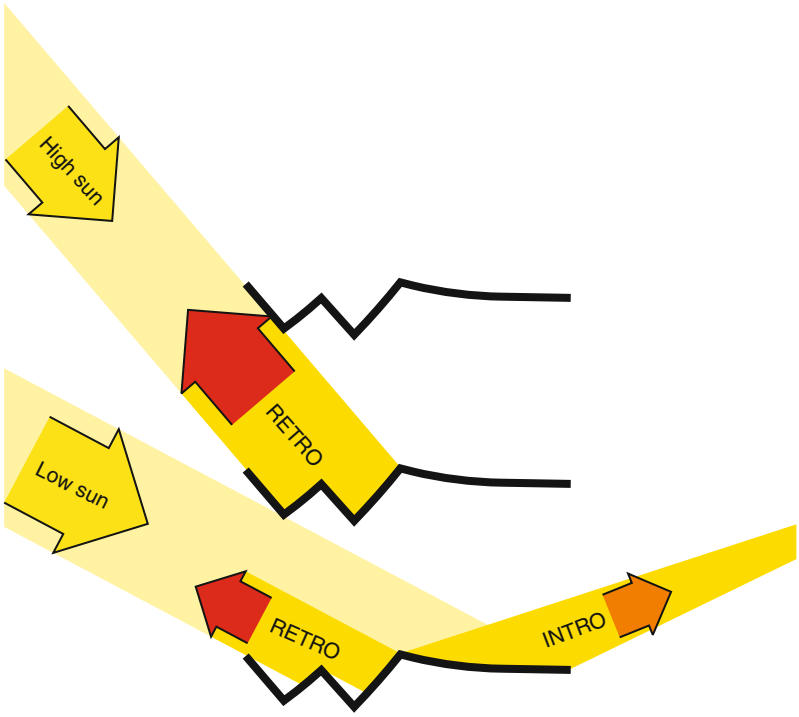

Daylighting Controls, Performance and Global Impacts. Figure 14
Light redirected on a RetroLux louver (see also Fig. 23). The overheating summer sun is retroreflected on the horizontal, open louvers. Daylight from diffuse sky and a low sun is supplied via the light shelf. [US 6,240,999; US 6,845,805; EP 0793761; EP 1212508]

However, in mixed or heating dominated climates, the provision of daylight must be accompanied by dynamic shading to ensure the ideal seasonal or even time-of-day energy management. The state of the art for buildings in Europe is low-e glass with a light transmission of 80% and a solar heat gain coefficient or g-value of 55% for year-round daylighting and winter solar heating. This is then combined with dynamic external and internal sun protection for summer SHGC-values as low as 8–15%. Technically, it is possible to lower the SHGC values for the high, overheating sun to less than 5% while still maintaining effective daylighting. These energetic advantages are primarily achieved through light redirection using reflective surfaces within a special, double skin façade (Figs. 5, 19, 31, 32).

It is critical to remember that a building will heat up less in summer as a result of improved daylighting when compared to the use of electric lighting combined with low transmission glazing or glazing assemblies. The sun produces a photometric radiation equivalent of approximately 100–120 lm/W. With low solar/high visible transmission glass assemblies, the lighting energy increases to 200–240 lm/W. On the other hand, the lighting efficacy of fluorescent luminaires is only 60–70 lm/W. Given comparable illuminance solutions (lux [lx = lm/m^2]), buildings are heated three times as much by fluorescent lights as by daylight [2].

Effective Daylight Distribution with Brightness Contrast Control

Admitting daylight through high-visible transmission glass is only the first challenge. The distribution of that light to task surfaces, as well as the balance of brightness of various surfaces to ensure managed brightness contrast, may be the greater challenge (Figs. 21, 23, 24, Photos 18, 28).

There are numerous textbooks on the design of window walls in relationship to room proportions

Daylighting Controls, Performance and Global Impacts. Photo 12
Holograms for light deflection produce excellent design effects using artificial lighting [14]

Daylighting Controls, Performance and Global Impacts. Photo 13
Holograms for light deflection produce excellent design effects using artificial lighting [14]

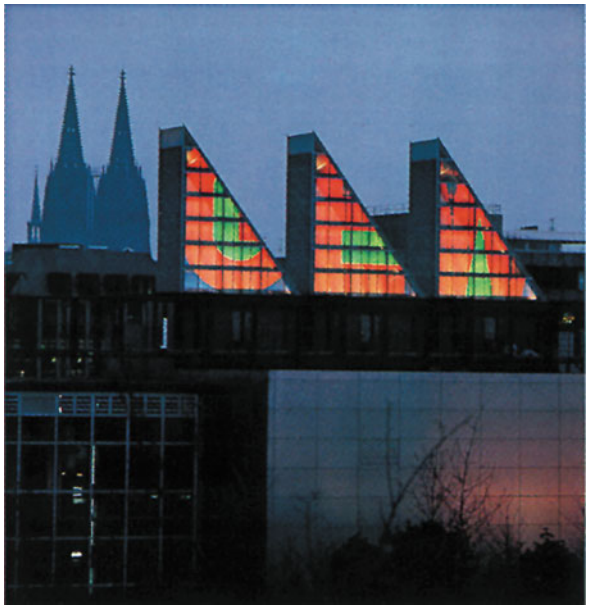

Daylighting Controls, Performance and Global Impacts. Photo 14
Holograms for light deflection produce excellent design effects using artificial lighting [14]

and surfaces for effective daylight distribution and brightness contrast control [20]. This entry does not intend to replicate these guidelines, or explain critical diagrams that illustrate the breadth and depth of these design imperatives. It is critical to state, however, that the design solution set will be significantly driven by climate and building function, and will have changing demands based on season and time of day.

Existing daylight design guidelines do not typically resolve the need for greater depth in daylight penetration for today's deeper buildings – to be achieved without glare or overheating. For this reason, it is critical to integrate dynamic controls of the daylight source – the windows and skylights – to ensure effective daylighting and control for solar heat gain. Dynamic

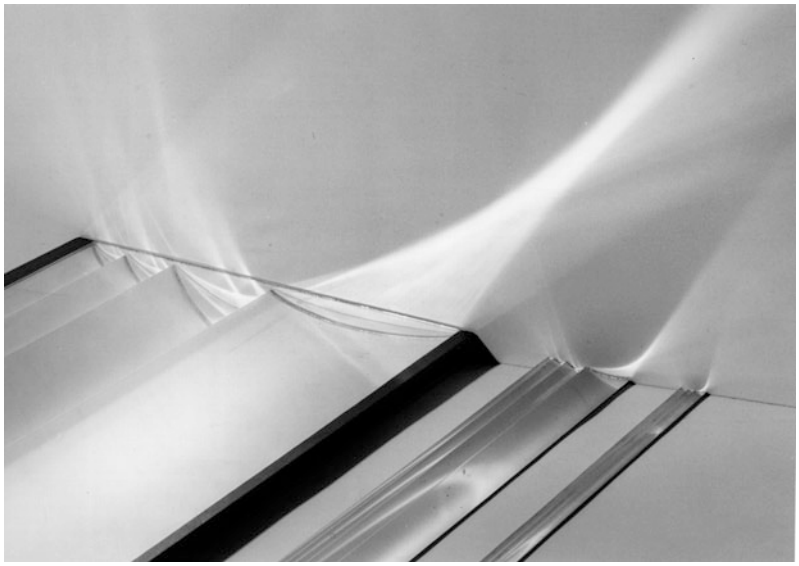

Daylighting Controls, Performance and Global Impacts. Photo 15
Light deflection using RetroLux™ louvers (see Fig. 7). Optical systems can be reduced or increased in size. The picture shows a 50-mm-wide louver, a 200-mm louver, and a large 2,500-mm louver. It illustrates how the high summer sun is reflected back outside while daylight is redirected to improve the illumination inside

Daylighting Controls, Performance and Global Impacts. Photo 16
Head office of Energie AG, Linz, Austria, Architects: Weber Hofer Partner, Zurich

controls for light distribution and shading are typically external or internal layers on the glazing, though they can be integral to the glass assembly. In designing the materials and surfaces of these layers, the following light redirection methods are important for consideration: prisms, holograms, mirrors, and hybrid systems.

Prisms redirect light through refraction in an optically denser medium, e.g., in acrylic or polycarbonate. Through total internal reflection, it is possible to prevent the light from passing through altogether due to retroreflective properties. The disadvantage of prisms is their lack of transparency. The systems are only transparent to light, offering translucency but not clear views (Photos 10, 11). When daylight passes through prisms and holographs, it is broken up into its spectral colors often creating colored patterns and striations on the walls and ceilings (Fig. 10). On the other hand, the use of laser-cut prismatic panels strategically placed on the inside or outside could ensure excellent views in combination with daylight redistribution (Fig. 11b). This installation, however, does not protect from overheating (Fig. 11c, d) [22].

Daylighting Controls, Performance and Global Impacts. Photo 17
Head office of Energie AG, Linz, Austria, Architects: Weber Hofer Partner, Zurich

Holograms are also useful for redirecting light into the depth of the room (Photos 12, 13, 14), but also eliminate transparency for views. They can be combined with electric lighting to offer some dramatic design effects in addition to effective daylight distribution. The foils onto which holograms are imprinted and which are embedded in glass, however, are still expensive, which makes it difficult to use them in larger quantities [13].

Mirror systems provide for a wide range of light redirection effects, depending on their mirror geometry, and they can be used on louvers or blinds inside the glass, within double skin façades (Figs. 31, 32, Photos 16, 17), outside the glass, or even installed in miniaturized form in the gap between the glass layers (Fig. 24, Photos 26, 29, 30).

Designing Effective Daylighting

The design of effective window and skylight systems for light and heat management as well as views requires consideration of a number of design variables: façade orientation and louver geometry, louver surface qualities and their relationship to ceiling diffusers, louver controls, and electric lighting interfaces.

Designing Daylighting: Orientation and Basic Louver Geometry

Internal, integral, or external louvers and blinds offer the most strategic solution to meeting the dynamic demands for balancing daylight distribution with effective shading. The surfaces of these louvers are critical to daylight distribution, but so is the louver geometry.

Effective daylighting requires varying design responses for different orientations. Japanese design standards for commercial buildings are focused on only providing occupied spaces with south and north orientations to ensure effective daylighting without the overheating or glare that is prevalent on the east and west (Fig. 1). Roofs are subject to much higher energy loads in the summer than east west façades, and significantly more than southern and northern façades. In short, design for effective daylighting without glare and overheating will require unique detailing for each orientation.

The first step to optimizing louver geometry is to recognize that blinds should be inverted from their conventional downward facing arc to an upward facing arc intended to move daylight further into the space, working in combination with the ceiling as a reflector (discussed in a later section).

The second step to optimizing louver geometry is to include the elevation angles of the sun in the design of even fixed systems, appropriately controlling thermal energy and light transmission by season. The sun in winter shines at a lower angle and in summer the angle is significantly higher. Consequently, it is necessary to design a louver geometry which redirects the low winter sun to a greater degree into the building, while reflecting the high summer sun to a greater degree back outside. This is in order to achieve a homeostatic

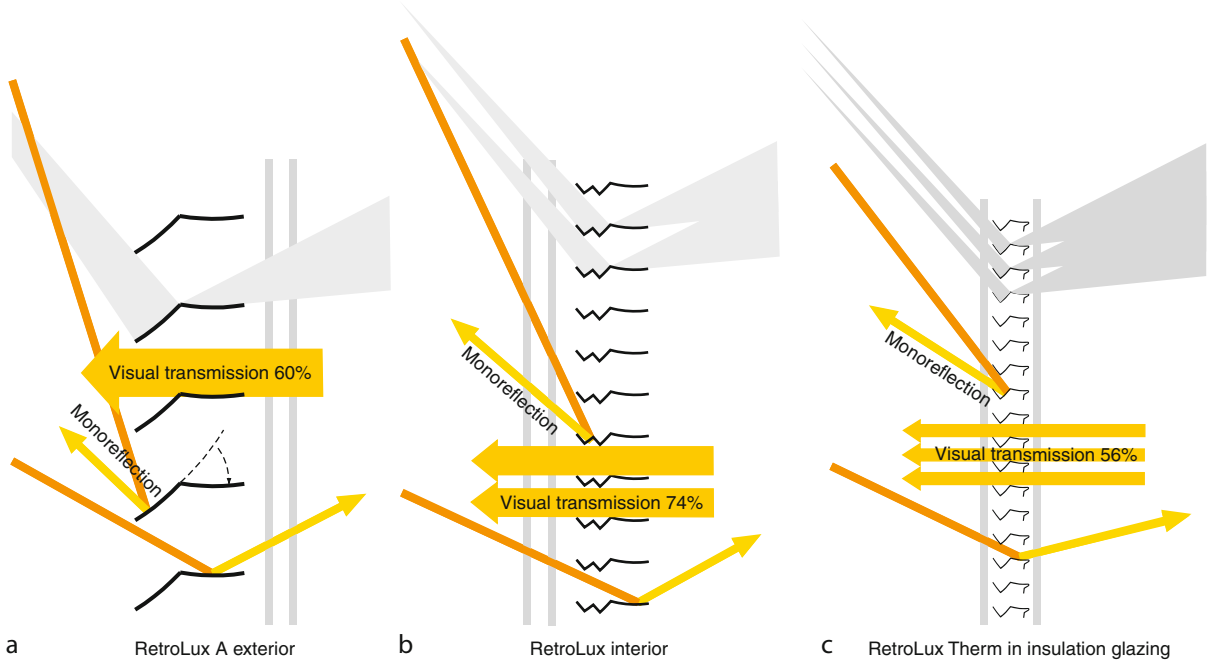

Daylighting Controls, Performance and Global Impacts. Figure 15
RetroLux systems ensure simultaneity of retroreflecting the overheating summer sun on the retroreflector, redirecting diffuse daylight on the light shelf and good visual transmission

balance of the building in accordance with the heating and cooling periods in different seasons (Fig. 15).

The development of light redirection systems is dependent on defining the friend/foe relationship with the sun in different climates and cultures: How much of the solar irradiation should be reflected back to the sky for passive cooling comfort? How much should be directed inside for daylighting of the interior? How much can the amount directed inside increase if passive solar heating is desired (Table 1, Fig. 13)

Such complex, contradictory demands for controlling energy transmission require precise mirror geometries. Horizontal louvers are most useful for refining energy transmission because they can respond to the solar altitude angle even without adjusting the louver position, and because they are best suited to ensure illumination into the depth of the room in combination with the unobstructed ceiling plane (Fig. 24). Vertical louvers or blinds, on the other hand, only respond to the azimuth of the sun without redirecting light toward the ceiling. They are merely suited to provide shade. The benefit of even fixed light redirection louvers with geometries optimized for summer shading is tremendous, as shown in Figs. 13 and 14.

Designing Daylighting: Louver Surface Qualities

Blinds should be designed both as shading devices and as light shelves. Maximizing the use of daylight with well-managed and comfortable illuminance levels, while minimizing solar overheating, can best be achieved through the louver contour and their optical characteristics. While mirrored surfaces are very effective for reflecting daylight deeper into the space, the surfaces of blinds can be significantly more refined to differentiate between high sun angle summer sun and low sun angle winter sun. Precise, mono-reflective surfaces can redirect daylight toward the ceiling and into the depth of the room.

Precise guidance of the daylight using optimized mirror geometries can also prevent the bottom sides of the louvers from exposure to sunlight, which would produce glare and turn the blind into an unwanted

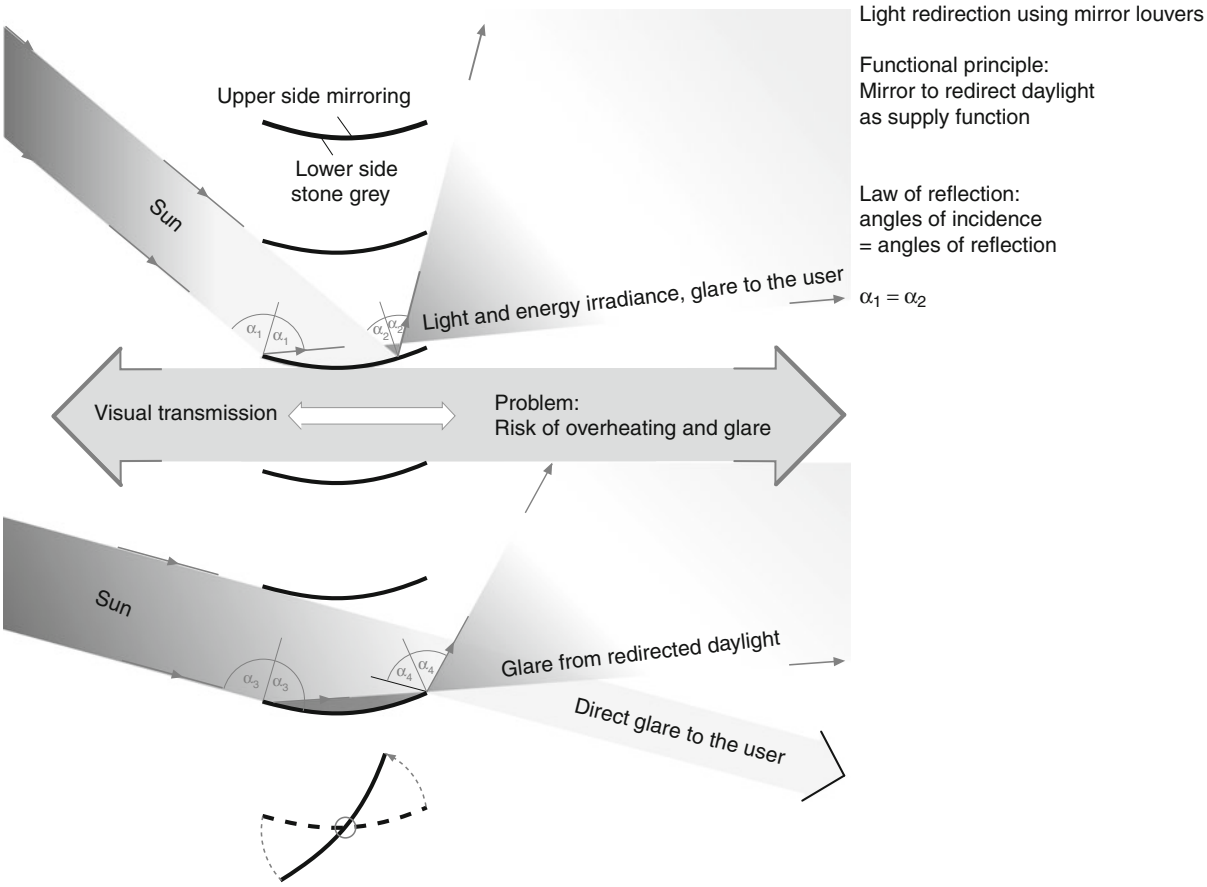

Daylighting Controls, Performance and Global Impacts. Figure 16
Mirror blinds open

surface emitter or even a heat radiator. Only mono-reflective structures ensure that incident sunlight is redirected either into the depth of the room and/or back outside, without a ping-pong effect between the louvers themselves (e.g., Fig. 12). Mono-reflective systems are easier to optimize in terms of their energetic and lighting capacity, and their thermal performance can be precisely calculated even in the building simulation phase (Figs. 18, 20, 23, 24). In addition, the underside of the blinds should not be mirrored, to avoid reflective glare.

Designing Daylighting: Innovative Louver Geometries and Surfaces

There are dozens of macro- and micro-design choices that can make a horizontal blind into an even more effective light fixture – with both glare and heat control. Surface reflectivity/absorptivity and finish, geometries of the outer and inner surfaces, W- and V-shaped blinds in addition to curved blinds with micro-features such as Fresnel surfaces, and innovative assemblies will be discussed further (Fig. 15).

If conventional blinds are inverted and mirrored on their concave upper side, they will indeed redistribute daylight to the ceiling and as a result to deeper portions of the room. However, the lower blinds will first direct light to the occupant, creating glare that makes it necessary to close at least the lower section of the blind (Fig. 16). As a result, visual contact with the outside is lost, and if the upper portion of the blind cannot be controlled independently, effective daylight will be lost. Even in the upper section of the window, open louvers can create glare in open plan offices whenever

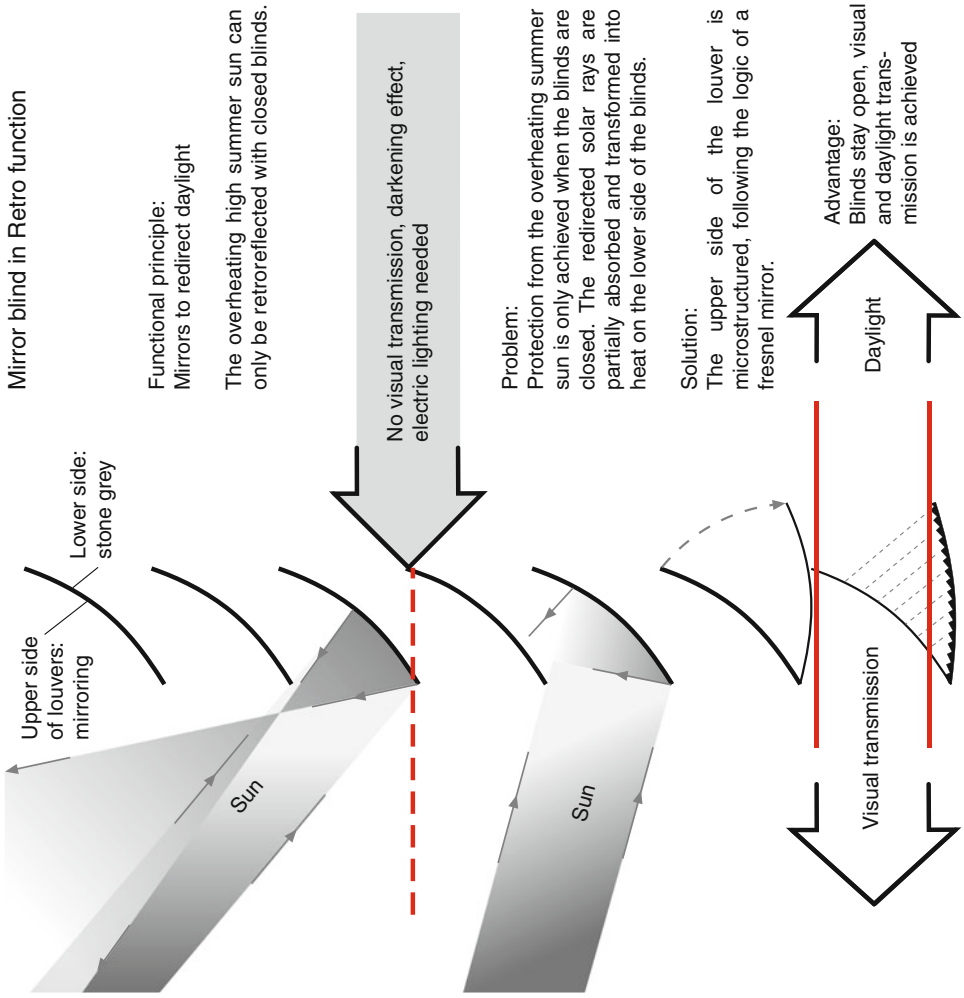

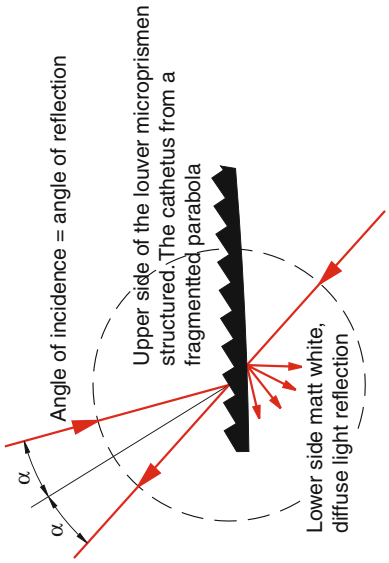

Daylighting Controls, Performance and Global Impacts. Figure 17
Genesis of a daylight reflecting louver [US 6,367,937; US 6,845,805; EP 1212508]

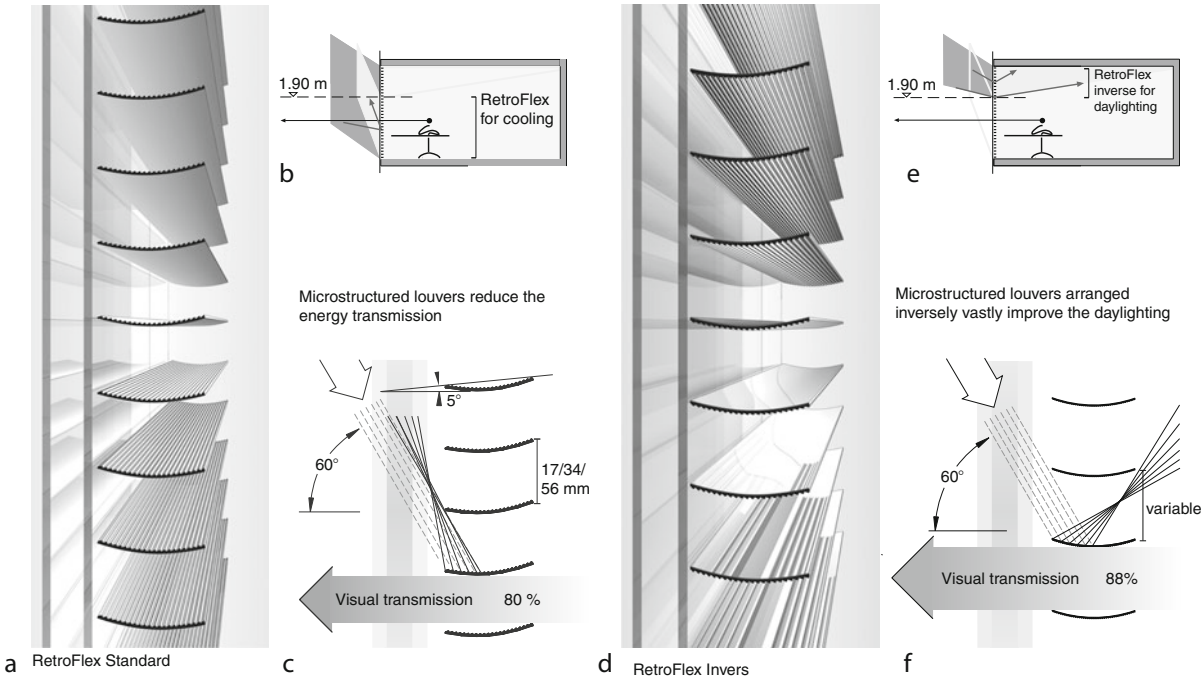

Daylighting Controls, Performance and Global Impacts. Figure 18
Louvers with microstructured upper surfaces to reflect solar heat gain back outside while supporting diffuse daylighting and views and micro-structured undersides to redirect daylighting into the depth of the room [US 6,367,937; US 6,845,805; EP 1212508]

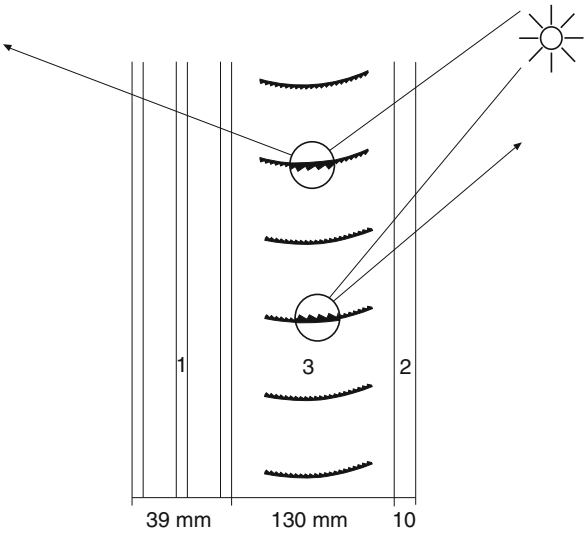

Daylighting Controls, Performance and Global Impacts. Figure 19
Non-ventilated double skin element façade with RetroFlex. U-value of façade 0.65 W/m^{2}K, SHGC value of glazing 0.05–0.1 with open louvers, depending on angle of incidence

the sun angle is low, streaming between the blinds into the space.

In addition, studies of daylight redirection blinds revealed a second area of concern. With higher sun angles in the summer, or a greater steepness for the blind, some of the daylight that is reflected off the blind will fall onto the bottom side of the louver above. The underside of the louvers will absorb a portion of this reflected light and heat up the window zone, even in summer (Fig. 17).

These studies led to the development of more optimized light redirecting louvers that combine surfaces and geometry to manage light in different seasons. One strategy would be to pursue micro-structural or prism innovations, embossing fresnel mirrors onto a concave louver (RetroFlex type louver systems) (Figs. 18a, c, 19, 31, 36). With a crafted fresnel surface, an open, horizontal louver will reflect the sun back to the outside to prevent overheating while allowing for 80% views and diffuse daylighting.

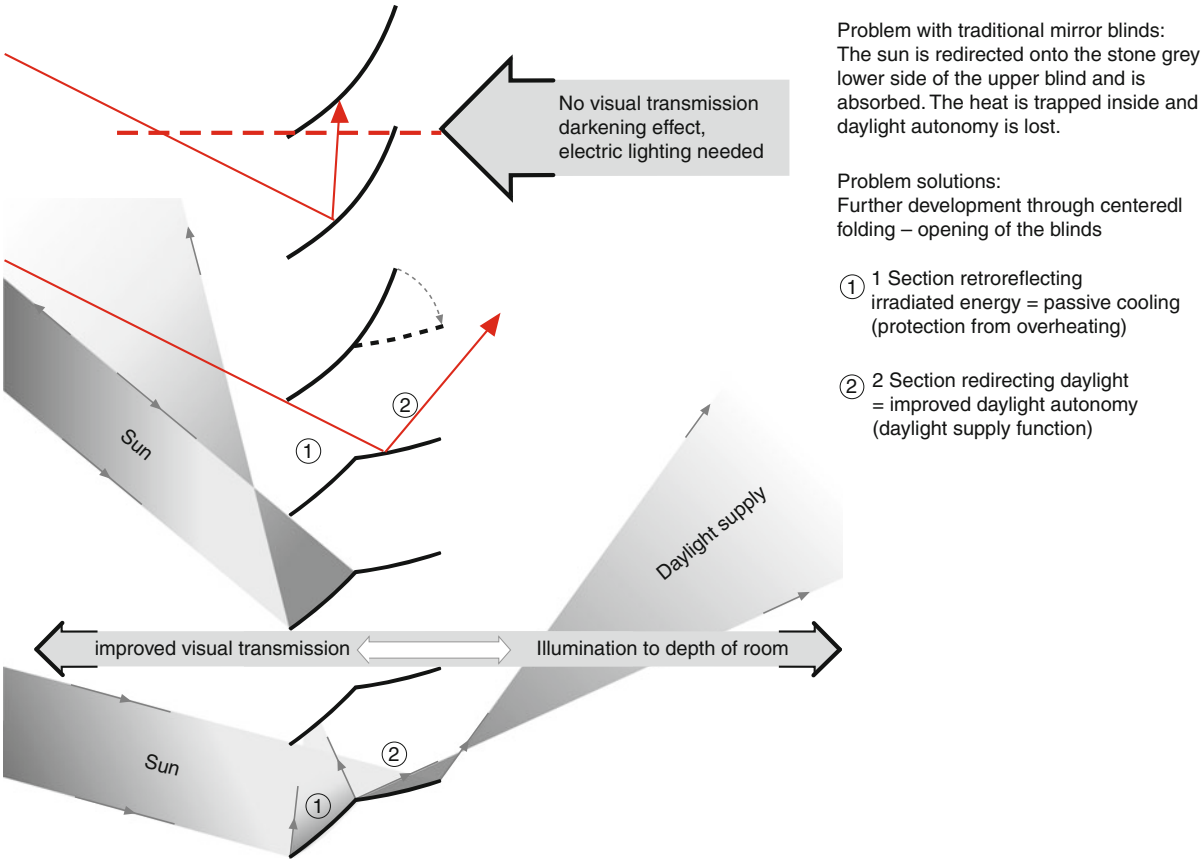

Daylighting Controls, Performance and Global Impacts. Figure 20
Folded mirror louvers as exterior blinds with integrated protection and supply functions through formation of two functional mirrors, a retroreflector toward the outside and a light shelf toward the inside [DE 10260711]

Above the seated window, the mirror prisms can be placed on the underside of the concave blind so that light falling onto their reflecting upper side is redirected to a greater degree into the depth of the room (Figs. 18d, f, 37).

The combination of sunlight-reflective louvers in the viewing area and underside micro-structured louvers above 1.8 m creates a blind assembly that protects the occupants near the window from overheating and glare, while ensuring more effective daylighting, entirely without the loss of views. Since all louvers are positioned identically depending on the sun's angle of incidence, they are easy to operate.

These micro-structured louvers are less than 0.4 mm thick, have a width between 25 and 80 mm depending on density desired, and be positioned inside or in-between a double skin façade (Photos 16, 17, Fig. 31).

While micro-structured louvers offer significant gains over conventional blinds, the best approaches to minimizing heat gain in summer while maximizing daylight requires more challenging geometric solutions. A critical first step is to divide each louver into two sections – redefining external and internal edges with different optical characteristics to respond to the different seasonal positions of the sun in the sky. Given the distance of the louvers from each other, the summer sun only falls onto the section of the louver oriented toward the outside. The outer half of the louver can then reflect the high, direct sun back out for natural

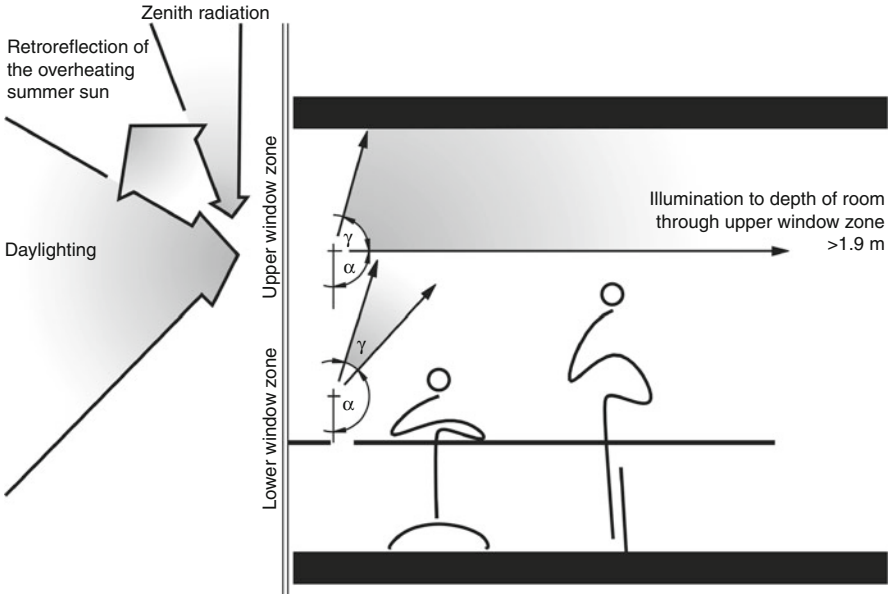

Daylighting Controls, Performance and Global Impacts. Figure 21
Angles of light redirection façade

cooling, while the inner half of the blind can direct the low-angled sun inside to improve illumination of the interior and support passive heating (Fig. 20).

Daylight-optimized louver geometries thus ensure solar heat control based on the sun's angle of incidence without the need for continuous readjustment of the louvers in line with the incident sunlight. On the outer section of the louver, the high summer sun is mono-reflectively redirected back into the sky (protective function) and on the inner section of the louver, low incident sun in winter is directed inside (supply function) (Figs. 15, 20, 22, 23). The blinds only need to be closed when the sun is very low and grazing light between the louvers causes glare. The geometries of these blinds and their degree of separation are established based on climate, latitude, and orientation, but there are some truisms for the designer. The further the building is from the equator, the lower the sun is and the longer the heating season is. The angle of incidence increases the closer you get to the equator, along with the temperatures.

The height of the work plane and the eye position of both seated and standing building occupants is an important consideration in daylight design for both glare control and quality views. While the use of reflected light off of the ceiling plane provides good uniformity over a greater depth of the space, any blinds below typical sill height of 1 m or less may create glare by reflecting light directly into the eyes of the occupants. To optimize the illumination into the depth of the room, it is necessary to split the façade into upper (clerestory), middle (viewing), and lower (below the sill) zones. In the upper, clerestory section of the window, daylight should be redirected at a shallow angle to maximize daylight distribution deep into the room. In the middle, viewing section of the window, a somewhat sharper angle is required to redirect the light toward the ceiling to eliminate direct glare, while still maintaining as clear a view as possible. In the lowest section of the window, below the normal sill line, the sharpest reflection angle is important (Figs. 21, 22, 15, 23) (Photo 18).

In addition to the V-shaped geometries described, a W geometry can also support effective daylighting and views with reduced glare and overheating. The W-shaped louver for interior use can offer a slimmer profile in manufacturing and support 76% visual transmission in an open position while the high summer sun is simultaneously reflected outside (Fig. 14).

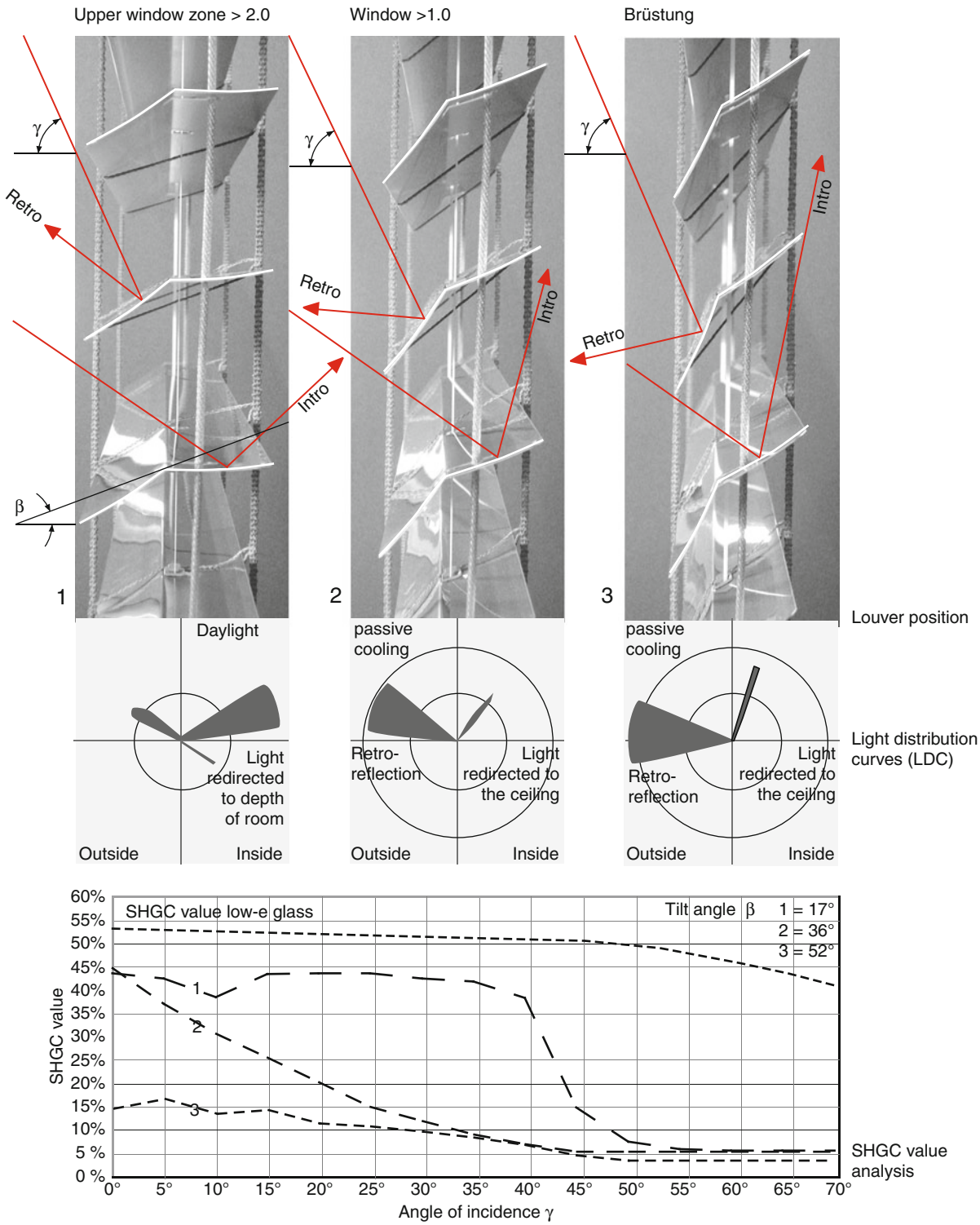

Daylighting Controls, Performance and Global Impacts. Figure 22

Three Louver positions in floor-to-ceiling blinds for optimum optical performance; analysis of the SHGC values of blind sections 1–3 are an average for all angles of incidence [DE 10260711]

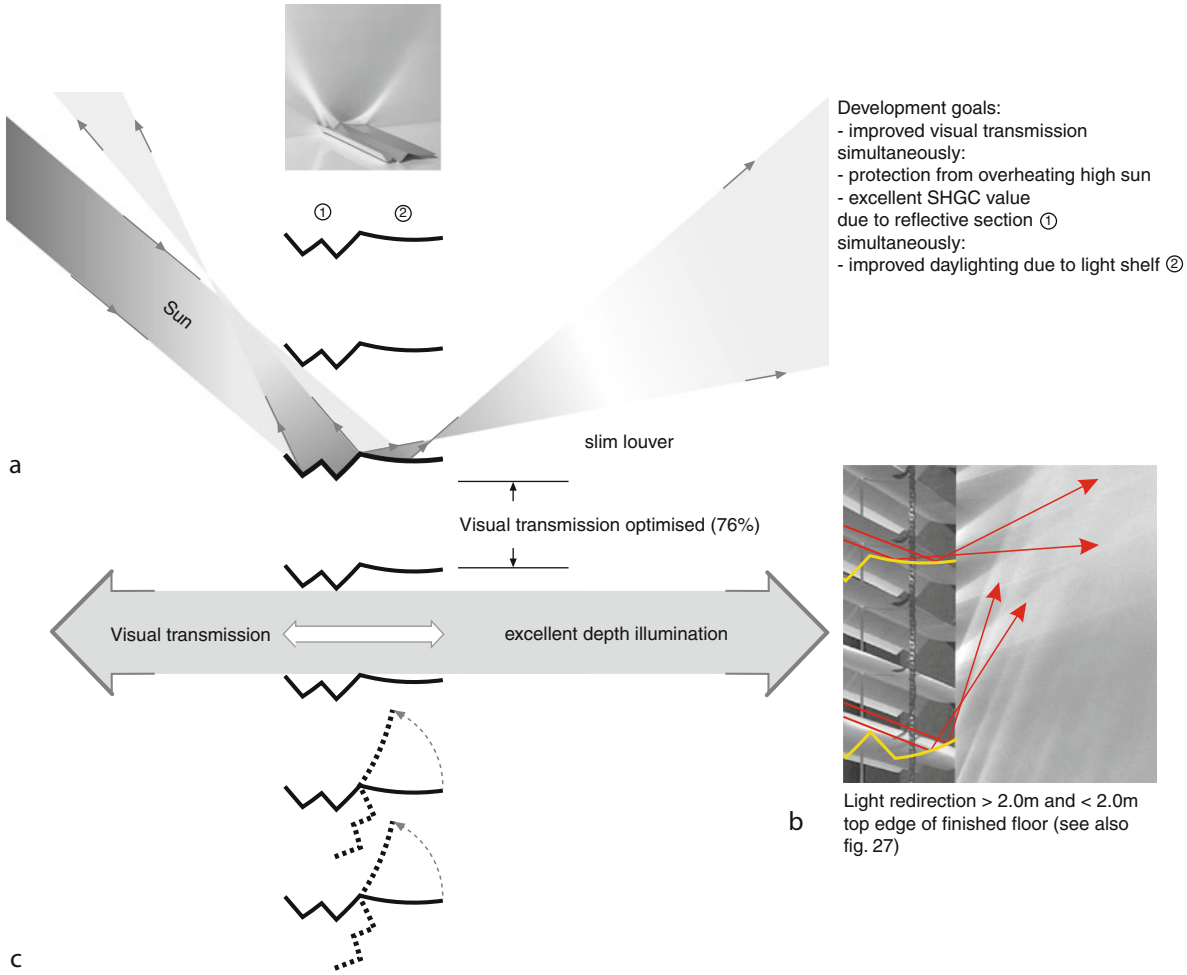

Daylighting Controls, Performance and Global Impacts. Figure 23
Functions of the macrostructured louver "RetroLux" in the upper and lower parts of the blind for glare-free redirection of daylight into the depth of the room and toward the ceiling [US 6,240,999; US 6,845,805; EP 0793761; EP 1212508]

The term "retro" refers to the deflection of light, i.e., the protective function of systems through which the sun is reflected back into the sky. The result, however, can be unwanted glare in the interior due to reflections from the glass. The skill in developing "retroreflective" systems is to guide the light in such a way that the sun rays do not glare in the glass (Photo 27a/b) and thus not visible from the seated position. The light redirection system must be designed such that the sun reflected in the glass hits the bottom side of an upper louver instead of reflecting inside. Louvers following this design rule ensure glare-free transparency of the glass. At a high solar elevation, the visual transmission of such blinds is between 70% and 80% [3].

Macrostructured louvers can also be designed as an integral component of insulated glazing. At 20 mm in width (Fig. 24; Photos 20, 21, 22), the louver section is designed in the shape of a V to stabilize the louver and keep it from bending (Photo 15).

Light-redirecting louvers can also be installed in glazed roofs and set at different angles. Here, the louvers should preferably be installed in a fixed, pre-calculated position in between the insulation glass.

Daylighting Controls, Performance and Global Impacts. Photo 18
Lighting requirements of a daylight façade for glare-free workplaces

Daylighting Controls, Performance and Global Impacts. Photo 19
Daylight façade with RetroLux (Fig. 15), municipal works, Bochum, Germany. Architects: Gattermann + Schossig, Cologne

Versions which can be tilted and tracked like blinds are, however, also possible (Photo 23).

Designing Daylighting: Controls – Balancing Light, Shade, and View

Managing glare, views, and shading as well as electric lighting and air-conditioning energy savings is strongly dependent on louver adjustability and control. On the one hand, controls should respond to weather changes, while on the other hand, changes should be kept to a minimum to avoid annoying users.

While energy optimization might recommend continuous blind adjustment, building occupants might prefer no adjustments, suggesting that louver controls be kept to a minimum of one to three positions throughout the day. East and west façades certainly will need the louvers to be adjusted when the sun rises and sets, and personal preferences will also suggest that some level of control be provided.

Cloudy skies specifically can cause significant glare due to sky brightness. Lights are often switched on during the daytime to avoid contrast glare between the bright sky and the unlit window frames or to compensate for lower illuminance further in the room. Sunny skies can result in direct glare whenever sun angles are low enough to enter directly, and blinds

Daylighting Controls, Performance and Global Impacts. Photo 20
RetroLux Therm in insulation glass (Fig. 24)

are often closed as a result. Some diffusing shades, designed to reduce direct glare and brightness contrast while allowing views, actually make the glare even worse, which also results in the turning on of electric lights. The key to effective daylighting is the ability to dim and redirect light and thermal energy from solar irradiation – independently.

Blinds can be controlled manually with simple guidelines, or controllers can be programmed to respond to calendar or light sensor information to adjust blinds for the optimum balance of view, daylight, and solar heat. Well-detailed blinds can ensure quality views, effective daylighting, at the same time as effective shading, with controls simply extending the long-term performance. Even with the blinds in a permanent down but open position, views can be excellent, while the carefully designed blind geometries and surfaces ensure seasonally differentiated daylight redistribution to the inside and solar heat reflection back to the outside (see Photos 24, 25).

Additional energy savings can then be provided through controls. During the summer, adjusting the light redirection louvers into a closed position when the sun is low on the east or west facing sides of the building can significantly reduce solar energy transmission. Closing the blinds at the end of each work day and opening them again in the morning before work begins can provide additional shade in the summer, or protection against heat loss in winter, during times when daylight and view are not needed (Fig. 25). It is, however, important to open the blinds during the day in order to gain sufficient daylight and views and save electric lighting energy.

In conclusion, the time of day and seasonal dimming and redirection of daylight can best be achieved by careful design of horizontal blinds – their geometries, surface qualities, and levels of adjustability (Photo 26, Fig. 17).

Designing Daylighting: Light Redirection Ceilings

The ceiling is an integral component in effective daylight distribution. Well-designed electric fixtures capitalize on the quality of the reflector as well as the effectiveness of the lamp and lens. Large windows without light redirection systems result in an uneven illumination of the room with excessively high illuminances in the window zone and considerable brightness contrasts (Photos 27a, b). Daylight redirection louvers shift the focal point of daylight design to the ceiling (Fig. 26).

Daylight reflected from the window to the ceiling allows light to be redirected onto the work surface with similar effects as those of conventional electric lighting, but without shadowing (Photos 29, 30).

Reflecting ceilings bear the risk of glare, particularly when viewed from deeper in the room. Consequently, light redirection ceilings and their reflective characteristics and geometry need to be carefully planned. At a very minimum, the ceilings must have the maximum possible light reflection properties, with a modest level of diffusion to reduce glare.

At an optimum, the design requirements for a light direction ceiling equal those of parabolic surfaces

Daylighting Controls, Performance and Global Impacts. Photo 21
The glazed facade is retro-reflecting the overheating sun but supplies the room with more daylight via the ceiling. The workplace is glare-free illuminated. In the openable window area the blinds are moved up to show the effect of the sun without redirecting louvers

Daylighting Controls, Performance and Global Impacts. Photo 22
Examples of illuminating a room using RetroLuxTherm in insulation glass as shown in Fig. 24 (Photo: Helmut Köster) [21]. The redirecting louvers are integrated as fixed systems within the insulation glass of the large glazing. Interior, behind the openable windows venetian blinds with redirecting RetroLux louvers are mounted

Daylighting Controls, Performance and Global Impacts. Photo 23
Light deflection in roof glazing either in insulation glazing or below the glass roof, e.g., with RetroFlex louvers

within luminaires. The light redirection and the cut-off angles of the ceiling must be precisely defined and are subject to the requirements of DIN EN 12 464. Superior redirection characteristics can be achieved by using micro-prism structures which redirect the light from the window downward in precise angles due to their angled prism edges. Prism-structured, convex-shaped louvers can be arranged parallel to the façade in order to ensure sufficient dispersion while reacting to different angles of incidence of the daylight.

Daylight reflective ceilings serve the purpose not only of redirecting daylight, but also of redirecting complementary electric lighting that may be installed at the façade, as described in the next section (Fig. 27).

Daylighting Controls, Performance and Global Impacts. Photo 24
RetroLux in solar protection position and closed position

Daylighting Controls, Performance and Global Impacts. Photo 25
RetroLux in solar protection position and closed position

Daylighting Controls, Performance and Global Impacts. Photo 26
View out of RetroFlex blinds in active sun protection position for β = 13

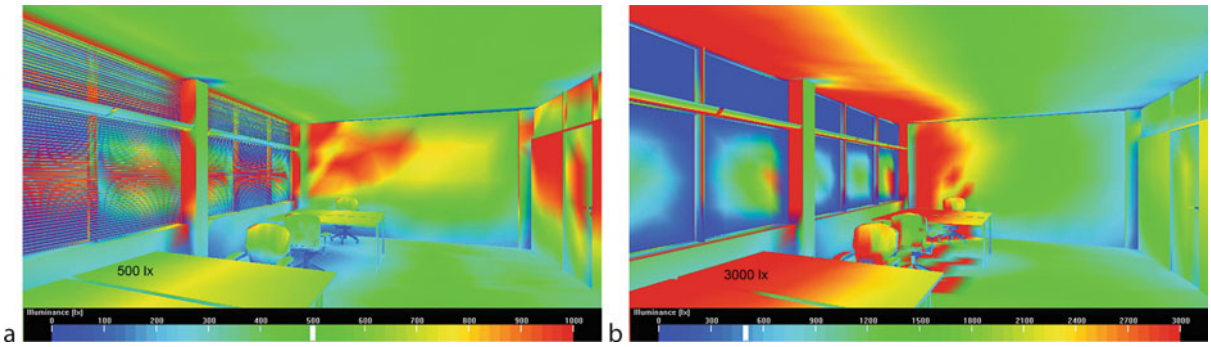

Daylighting Controls, Performance and Global Impacts. Photo 27
(**a**) Light irradiation as a false-color rendering – without redirected light: excessive overexposure (**b**) with redirected light: indirect daylighting (dimmed to comfortable level)

Integration of Daylight and Electric Lighting

European workplace regulations [1] often stipulate individual access to daylight and visual connection with the outside, such that permanent workplaces are frequently found within 6–7 m of windows. However, deep open-plan landscapes are common in many other countries, with boxed-in workplaces separated by seated or standing height partitions that eliminate effective daylight and visual access to the outdoors, and consequently necessitate daytime use of electric lighting.

In Europe, workplaces which do not provide a seated visual connection with the outside are considered inferior. In the USA, no laws exist to ensure seated views of daylight for workers, resulting in the extensive use of electric light during the daytime. In emerging hot countries as well, offices are being moved away from the window to reduce sunlight exposure. While on the surface, rooms without daylight exposure are easier to cool, the electricity used for lighting often exceeds that used for cooling. It is here, in particular, that daylight façades capable of managing solar factors and heat loads, climate by climate, will have the greatest benefits.

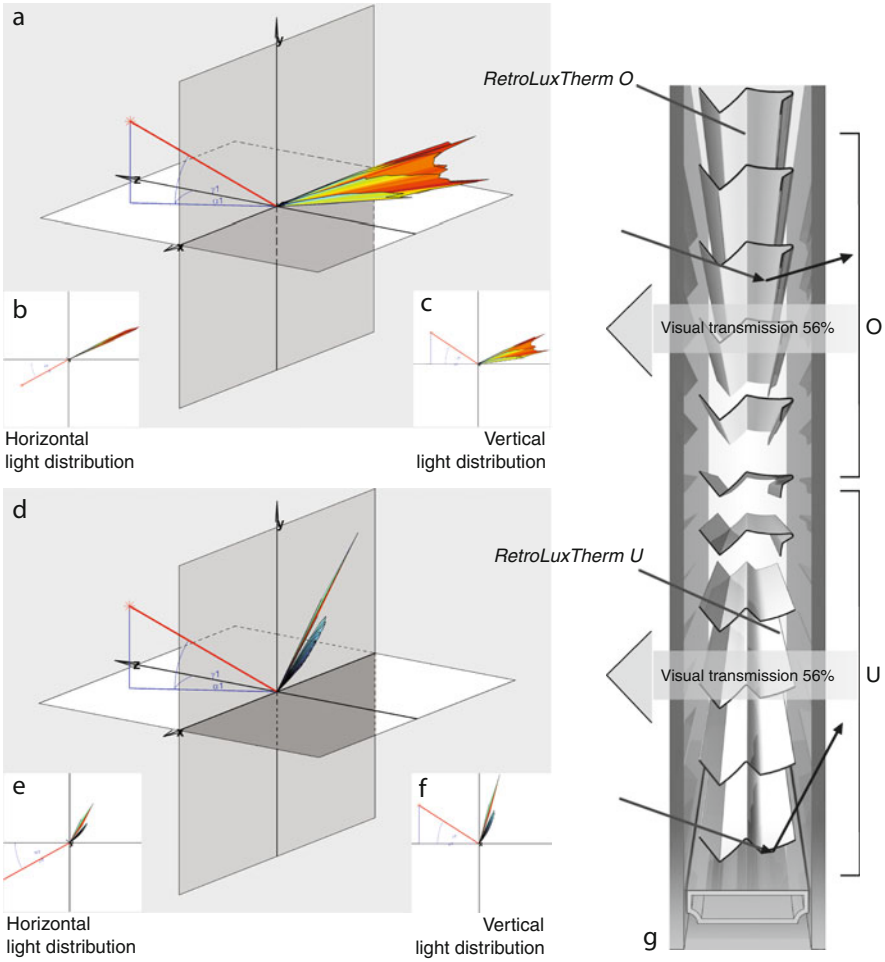

Spatial distribution of the luminance coefficient for $\alpha = 30°$ $\gamma = 30°$
Radiometrically measured values TU Berlin, Institute of Lighting Technology, Prof. Dr. Kaase / Dr. Aydinli

Daylighting Controls, Performance and Global Impacts. Figure 24
Macrostructured louver "RetroLux Therm" in insulation glazing. Analysis of light distribution to the inside for illumination into the depth of the room (type O) (Fig. 24a) and toward the ceiling in the lower window section (type U) (Fig. 24d)

First façades and interior layouts must be designed for effective daylighting, as previously discussed. Then, electric lighting must be designed to complement the daylight, filling in when and where daylight is inadequate.

Traditionally, lighting design considers buildings exclusively at night. To date, the dogma of uniform interior illumination has largely been the priority and a feature of good lighting design. The demands for uniformity may be one reason why daylighting has been so quickly abandoned, in addition to the unmanaged solar heat gain that often accompanies daylight. Workplaces in the window zone will always be brighter than those further inside. The uniformity of illumination can be improved by redirecting the light from the window via the white, reflective ceiling into the depth of the room. Diminishing daylight should then be complemented by increasing levels of electric light, shifting the lighting design goals from total uniformity to ensuring task lighting levels and managing brightness contrast throughout the workspace.

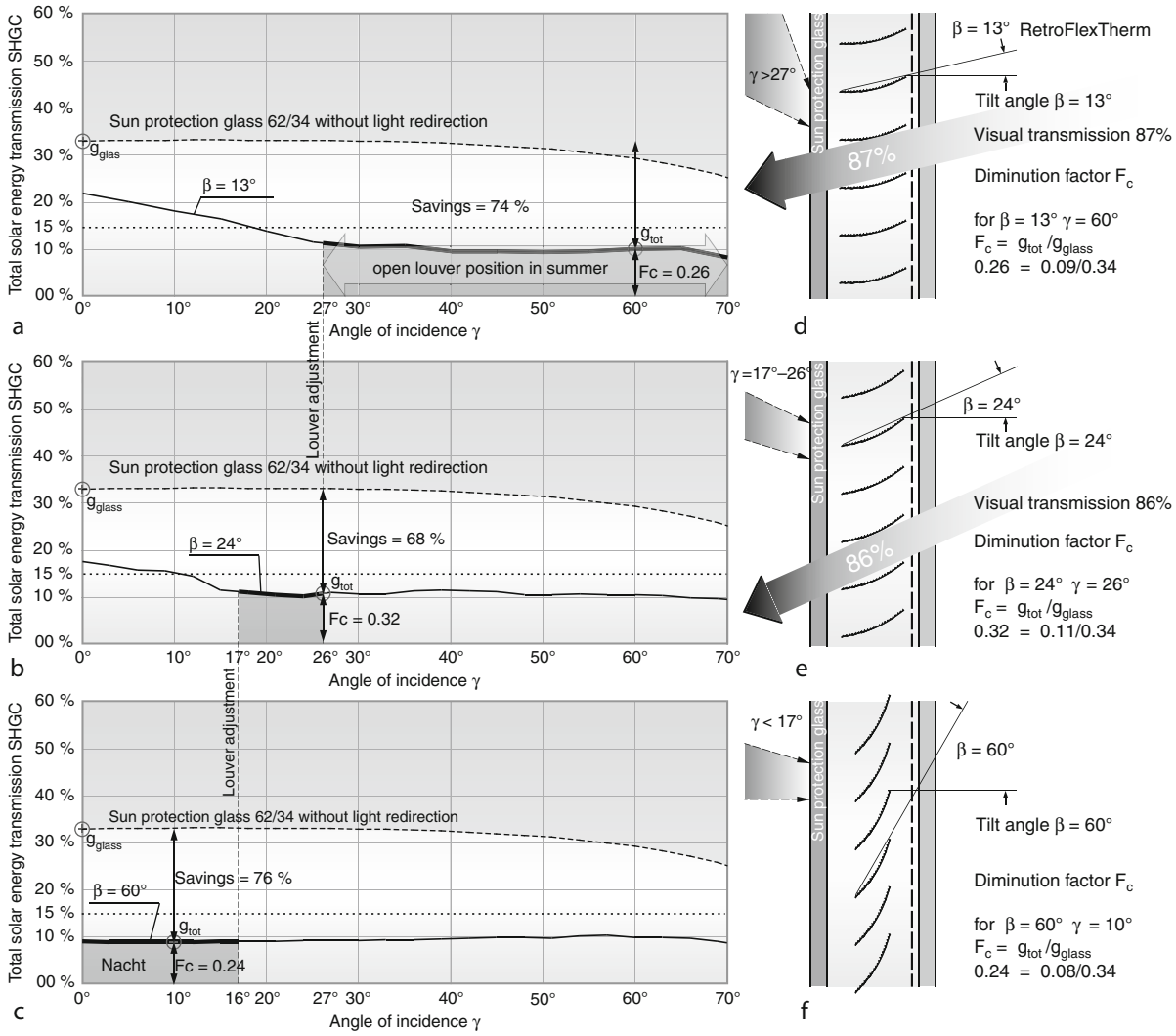

Daylighting Controls, Performance and Global Impacts. Figure 25
SHGC value analysis of a RetroFlex type blind (Fig. 25d–f) with microstructured louvers (fresnel optics) adjusted in two positions

Electric lighting can then be controlled based on the illumination levels needed at various workstations in the room. This is effected either through dimming of individual lamps as needed, or through cascade switching, where the lights furthest from the window are turned on first, cascading on row by row as daylight diminishes. Daylight-responsive controls for electric lighting are minimum requirements in energy-optimized building.

However, lights should remain switched off during the daytime, at least within the first 6 m of the window, to maximize use of the natural, free resource of daylight. Recently, a new generation of "integral" controls have become available which switch on the electric lighting whenever blinds are closed. These types of control are the result of observations that conventional interior or exterior blinds darken buildings even when the sun is shining outside! The promise of daylight technology cannot be fulfilled with such cross-purposes.

As a minimum requirement, daylight autonomy should be at least 80% for the first 6 m into the

Daylighting Controls, Performance and Global Impacts. Figure 26
RetroTop louvers have a microprism-structured surface. Used as a light ceiling parallel to the façade, they redirect both the electric light and daylight. The microstructuring of the RetroTop ceiling also provides for superior acoustic baffling boosted by louvers mounted in a freely oscillating system. By providing the louvers with water-filled tubes, the ceiling becomes a highly effective cooling system whose surface, enlarged through microstructuring, has a cooling effect as it absorbs heat

Daylighting Controls, Performance and Global Impacts. Photo 28
Light redirected through RetroFlex-blinds. To prevent overheating and overillumination only 2–3% of the solar irradiance is redirected onto the ceiling creating 500 lx in 7 m of room depth

room (Fig. 29). In hot climates, effective daylight should be provided without exceeding a maximum total solar energy transmission (heat load) of 10–12%. Indeed, good visual transmission (views) and optimized daylight conditions in the interior can be achieved at even 5% total solar heat energy transmission through the façade. In cold climates, heat gain with light gain will be paired goals, and geometrically optimized and controllable blind design can effectively manage climates that have both heating and cooling loads.

Daylighting Controls, Performance and Global Impacts. Photo 29
The light deflected from the façade to the ceiling is redirected in a conical shape onto the workplace through the concave design of the louvers. This ensures excellent illumination of the workplaces with glare-free top and side light

Daylighting Controls, Performance and Global Impacts. Photo 30
The light deflected from the façade to the ceiling is redirected in a conical shape onto the workplace through the concave design of the louvers. This ensures excellent illumination of the workplaces with glare-free top and side light

The aim of intelligent combined daylight–electric light controls must be:

- To modulate blinds to provide sufficient daylight for at least the first 6 m, while effectively shading and eliminating glare
- To modulate blinds to reduce the luminance of the window to a comfortable level to ensure both quality views and daylight transmission
- To modulate blinds to reflect out direct solar energy through mirroring in summer, while simultaneously redirecting a percent of the diffuse sky into the interior
- To modulate blinds to reflect in direct solar energy through mirroring in winter, ideally to thermally absorptive surfaces
- To infill electric light when and where daylight is inadequate for the task

To optimize the integration of daylight and electric lighting controls, at least one major source of electric lighting should shine from the window into the room. This is perfectly possible by integrating the luminous flux and arranging an asymmetrical luminaire with indirect lighting at the height of the window header (Photo 28). This ensures that the bottom sides of the

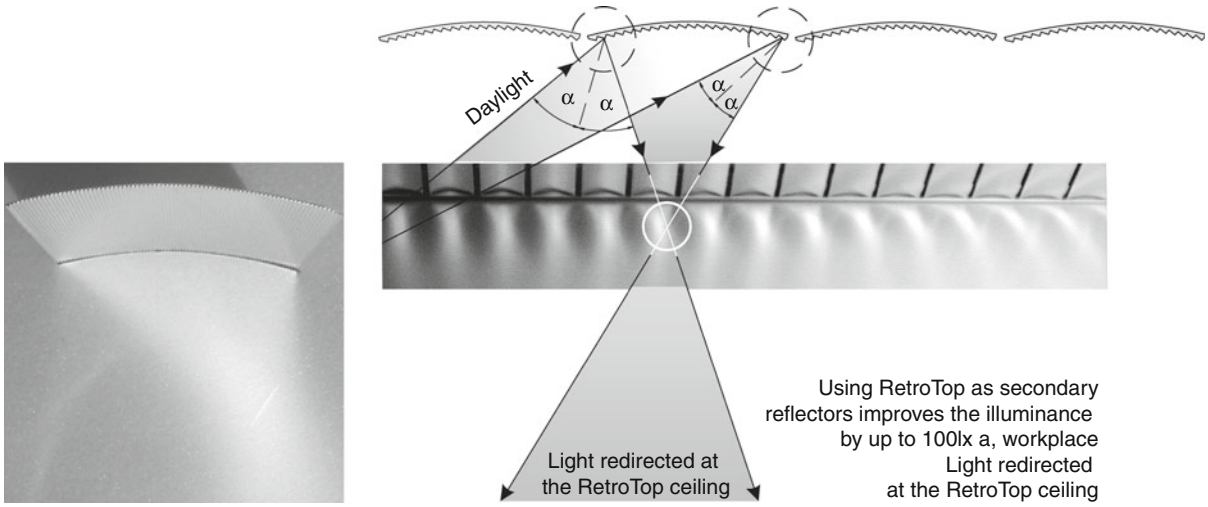

Daylighting Controls, Performance and Global Impacts. Figure 27
Light redirected by ceiling elements. Ceiling louvers with microprism-structured mirrors deflect the indirect daylight redirected toward the ceiling vertically onto the workplace

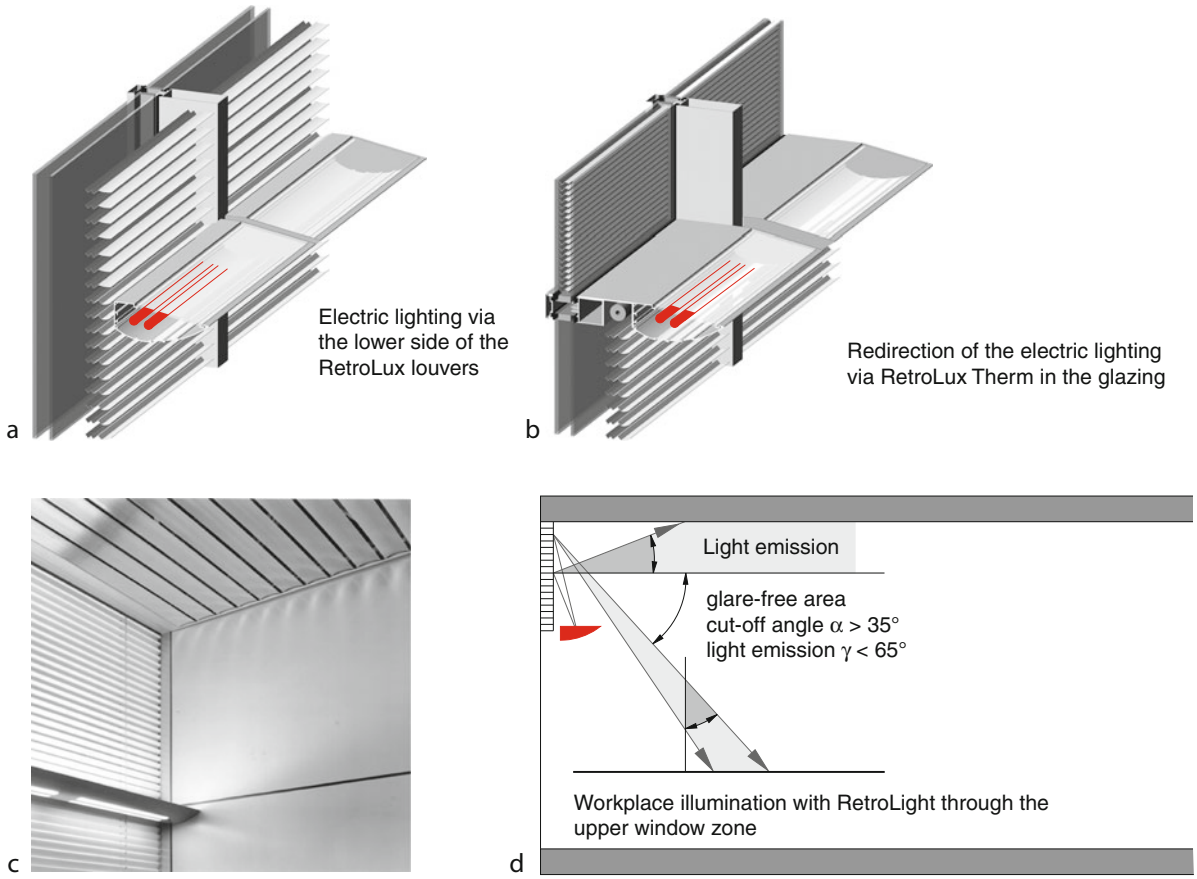

Daylighting Controls, Performance and Global Impacts. Figure 28
Electric lighting and daylight system optically integrated [EP 0461137; US P 5293305]

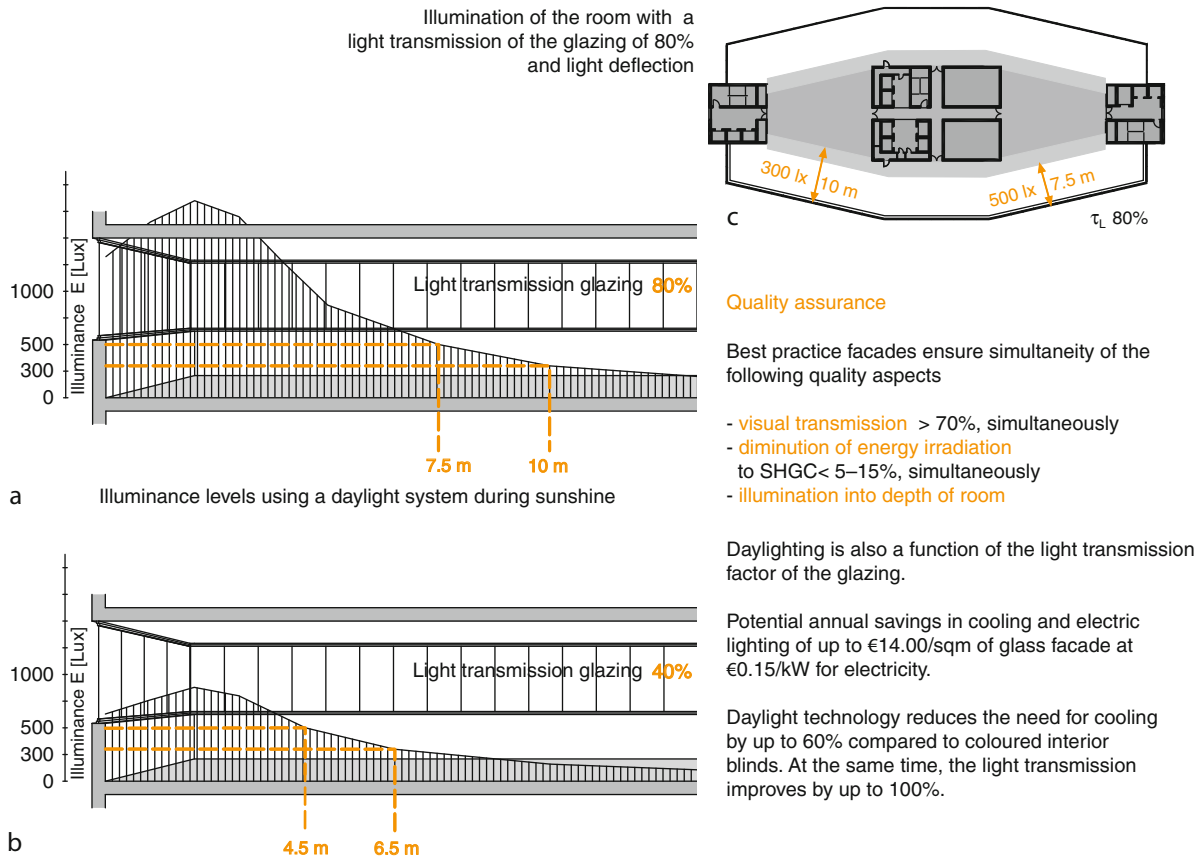

Daylighting Controls, Performance and Global Impacts. Figure 29
Comparison of illumination into the depth of room using a daylight redirection system for glazing with a light transmission of 40% and 80%, respectively

daylight redirection louvers are also used to redirect the electric lighting. The resulting integration of redirected daylight and electric lighting is symbiotic (Photo 31).

Quality Assurance in Daylighting Design

Both simulation and measurement techniques are critical for ensuring the highest level of daylight quality, solar heat management and views. Potential sources of error to be avoided include:

- Inappropriate louver geometry with required daylight reflected externally, without depth internally, or between the louvers themselves resulting in a rise in temperature due to absorption
- Inappropriate reflection characteristics of the surfaces with excessive absorption of heat and light
- Inappropriate louver control for time of day and seasonal variations
- Inappropriate electric lighting control to maximize the use of daylight
- Excessively dark glazing

Having looked at light redirection systems from a functional point of view, the question now arises as to their quantitative effectiveness as thermal and light management systems.

For a quantitative analysis of energy flows for heat and light it is important also to consider the totality of the glazing system including the light redirection system. Depending on the installation position of the light

Daylighting Controls, Performance and Global Impacts. Photo 31
Night Architecture using RetroLight, municipal works, Bochum, Germany, Architects: Gattermann + Schossig, Cologne

redirection system either before, behind, or in between the glass, there are complex, physical processes taking place between the light redirection system and the glazing, including echo reflections in the glass, absorption, heat build-up, etc. Daylighting calculation methods [6] often provide incorrect results, as they fail to consider the light redirection performance of the contoured louvers. For this reason, it is invaluable to physically measure the light and heat transmission of the overall glazing/light redirection system using calorimetric and radiometric measuring methods.

Calorimetric methods measure the electric energy required to keep a heat sink installed behind the window assembly at a constant temperature, and translate the results into the heat transfer of the system (SHGC or g-value). It combines measurement with calculation, given a set of tolerances, which is why measurements using the same window assembly may result in different SHGC values from different institutes.

Radiometric measurements are taken under an artificial sun. These measurements are highly accurate and easy to perform. Parameters measured include the wavelengths of the transmitted irradiation, from which the SHGC, or g-value is calculated (Fig. 30). Radiometric measurements can also determine the light distribution (LDC) of the glazing/light redirection system into the interior for different sun altitude and azimuth angles (Figs. 22, 24, 30).

According to DIN 4108–2, the effectiveness of a sun protection system is described using the diminution factor F_C. The total solar energy transmission of a glazed façade is thus calculated using the following equation:

$$g_{tot} = F_C \times g_{glass}$$

g_{tot} – Total solar energy transmission through glazing including sun protection

g_{glass} – g-value of the glazing

F_C – Diminution factor of the sun protection system

This calculation, however, is not sufficient for quality assurance of the façade design since it is focused on the thermal performance of the window relative to sunshine (Fig. 31). Best thermal performance of the façade will ensure low temperatures of the glazing (Fig. 32). However, windows are critical to effective daylighting, a factor that trumps cooling, so light transmission is equally important for consideration. The balance of solar heat and light is taken into account in the latest DIN EN 13363 standard – yet still without consideration of light-redirecting blinds, especially those that can distinguish high and low sun angle sunshine.

Windows have the additional goal of providing views, visual connections with the landscape and life on the ground plane. While very low solar heat gain factors are easy to achieve with highly reflective glass, or window assemblies that assume shades to be predominantly closed, these windows no longer ensure the views and daylight critical to building occupants (Photos 21, 22, 24, 26, 32). As a result, all

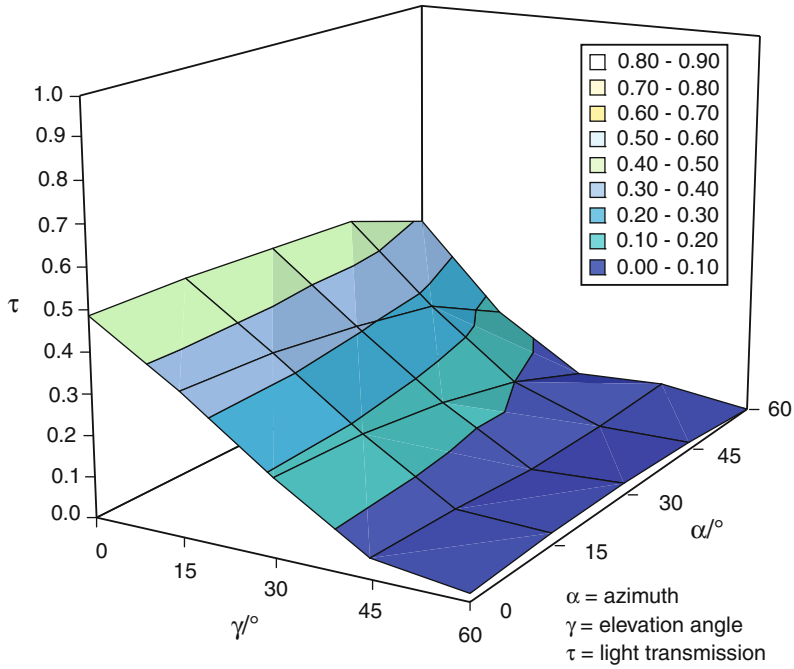

Daylighting Controls, Performance and Global Impacts. Figure 30
Example to illustrate the light transmittance τ for RetroLux Therm O with type 63/32 solar protection glazing (see also Fig. 24)

calculations should assume that blinds are in an adequately open position to ensure views and daylight effectiveness.

To evaluate the quality of the window assembly for thermal and visual performance, the g-value (SHGC) parameters must be complemented by light transmission and view clarity parameters. In other words, the g-value must be differentiated as a combined value of energy transmission for short-wave light radiation and long-wave heat radiation components. In the USA, a light to solar gain ratio (LSGR) has been introduced to give value to daylighting and views in relation to shading in the selection of glazing assemblies.

It is important to note that while glazing assemblies may be evaluated by combined values of daylight and view as well as shade, many internal and external layers – shade, louvers, overhangs – are not evaluated for their impact on daylighting. In addition, there are many climate periods when solar heat gain is desirable, such that dynamic properties for the entire window assembly are ideal.

Conclusion

Daylight and Solar Managing Façades as a Focal Point for Building Energy Futures

The largest primary energy load in buildings is for lighting, mostly during the daytime. The most rapidly increasing primary energy load in buildings is for cooling. This is where daylight technology offers the greatest opportunity for the design and engineering community. It not only reduces or manages the external solar load, but also eliminates the electric lighting load during the daytime along with the associated cooling loads.

Integrated design is critical to the detailing of façades for effective daylight and solar energy management. An interdisciplinary process can ensure that it meets a wide range of design goals. To date, it has been common practice in Europe to independently design sun shades and glare protection in different layers inside and outside the building. The design of fixtures

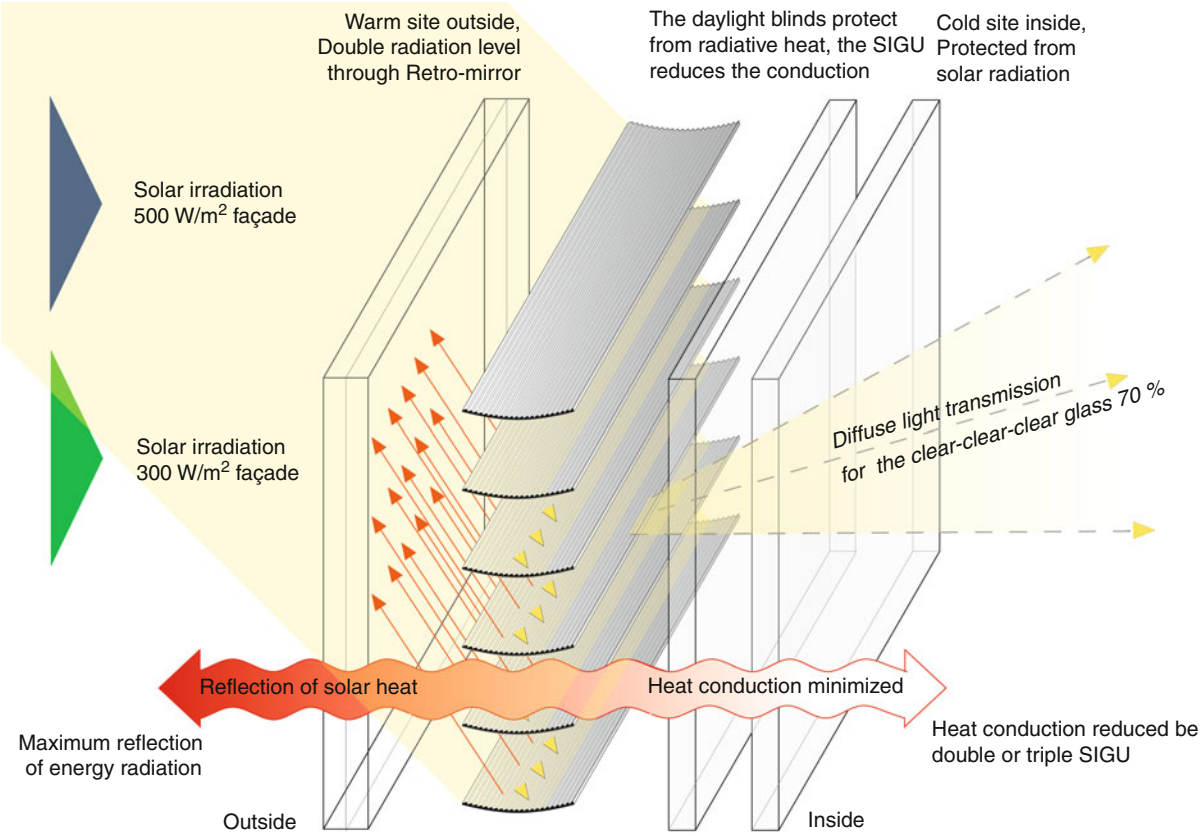

Daylighting Controls, Performance and Global Impacts. Figure 31
Example of optimized façade construction with a closed cavity: the outer pane is exposed to a double radiation load by incident and retroreflected sun. The outer pane should, therefore, be made from low-iron, color-neutral glass to prevent absorption and heat generation. The lower the temperature of the outer glazing is, the lower the heat radiation between the louvers will be on the inner glazing. The better the reflectivity of the light redirecting louvers is, the lower the heat-up of the air space will be

to diffuse light does not consider daylight. Structural design is typically independent of light or thermal design. Interior space layout and ceiling design is independent of daylight and often thermal conditioning. Breaking the building components into individual functional elements frequently led to excessive efforts and significant cost increases in the construction. Integrated design engages the architect, the lighting/daylighting designer, the mechanical engineer, and even the structural engineer in synergistic innovation (Figs. 33–37).

University curriculum must be revised to recognize the importance of integrated design. Every architect should be taught to be effective "system integrators," capable of orchestrating an interactive process that engages the expertise of the mix of disciplines early in the design process for maximizing synergistic innovation. An effective integrator must have a core competency in building physics, climate and energy management, and the full set of building technologies that impact heat, light, air, sound, and structural integrity – with the building façade and adjacent interiors as a primary focus for a sustainable future.

At the graduate level, universities must also take a far more proactive role in research related to daylighting technologies and system integration. The optical

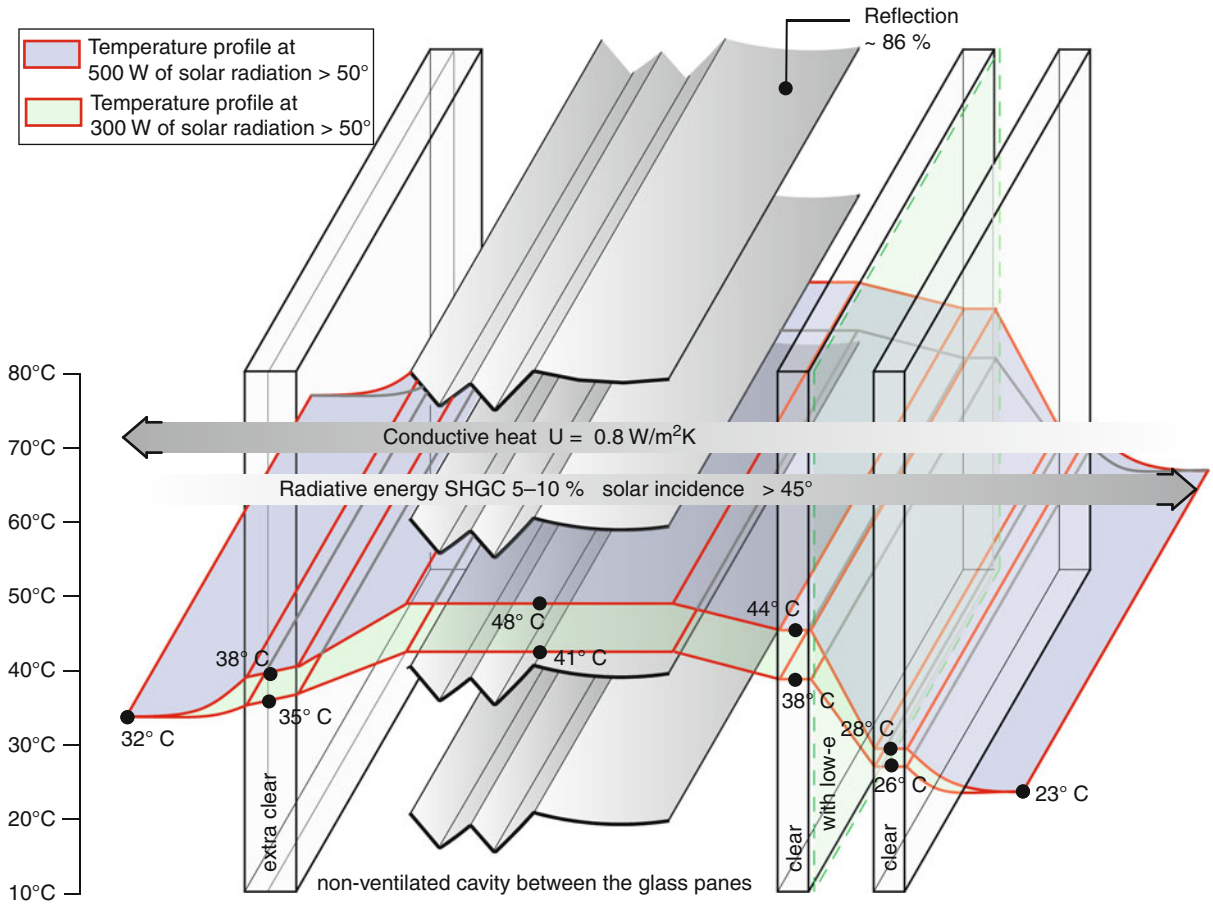

Daylighting Controls, Performance and Global Impacts. Figure 32
The above temperature profile in a closed cavity can be reached with RetroLux or RetroFlex blinds at angles of incidence >45°. The contour of the blinds is of crucial importance, because the low temperatures can be realized even in a horizontal louver position. Simultaneously a visual transmission of 70–80% between the louvers and the desired improved daylighting is achieved. The temperatures in the cavity should not exceed 60°C to ensure the longevity of the motors, plastic parts, and fibers

research inherent in fixtures that manage point light sources and linear light sources have not yet been applied to planar light sources such as a window. The geometry and positioning of light reflectors (internal, external, between glass installations) and critical dynamics given climate and time of day variations are critical areas of scientific and technical innovation. The interaction between glass coatings, such as reflective enhancing PVD coatings, and mirror systems, such as semi-specular, lacquered or anodized surfaces, offer enormous potential for the research and manufacturing community.

For the design community, algorithms and computational tools need to be developed to calculate the bi-directional energy- and light transmission values for dynamic tilt positions of the special mirror contours with reference to the positions of the sun. Existing simulation tools must be refined beyond qualitative transmission data, to describe the optical properties of reflected light to calculate the effectiveness of

Daylighting Controls, Performance and Global Impacts. Photo 32
Visual transmission of RetroLux

Daylighting Controls, Performance and Global Impacts. Photo 33
The Sopharma and Litex buildings in Sofia have a non-ventilated double-skin façade with a closed cavity (see Fig. 31) and RetroFlex blinds. The room temperature does not exceed 26°C even without chilling even at outside temperatures of 35°C and sunshine

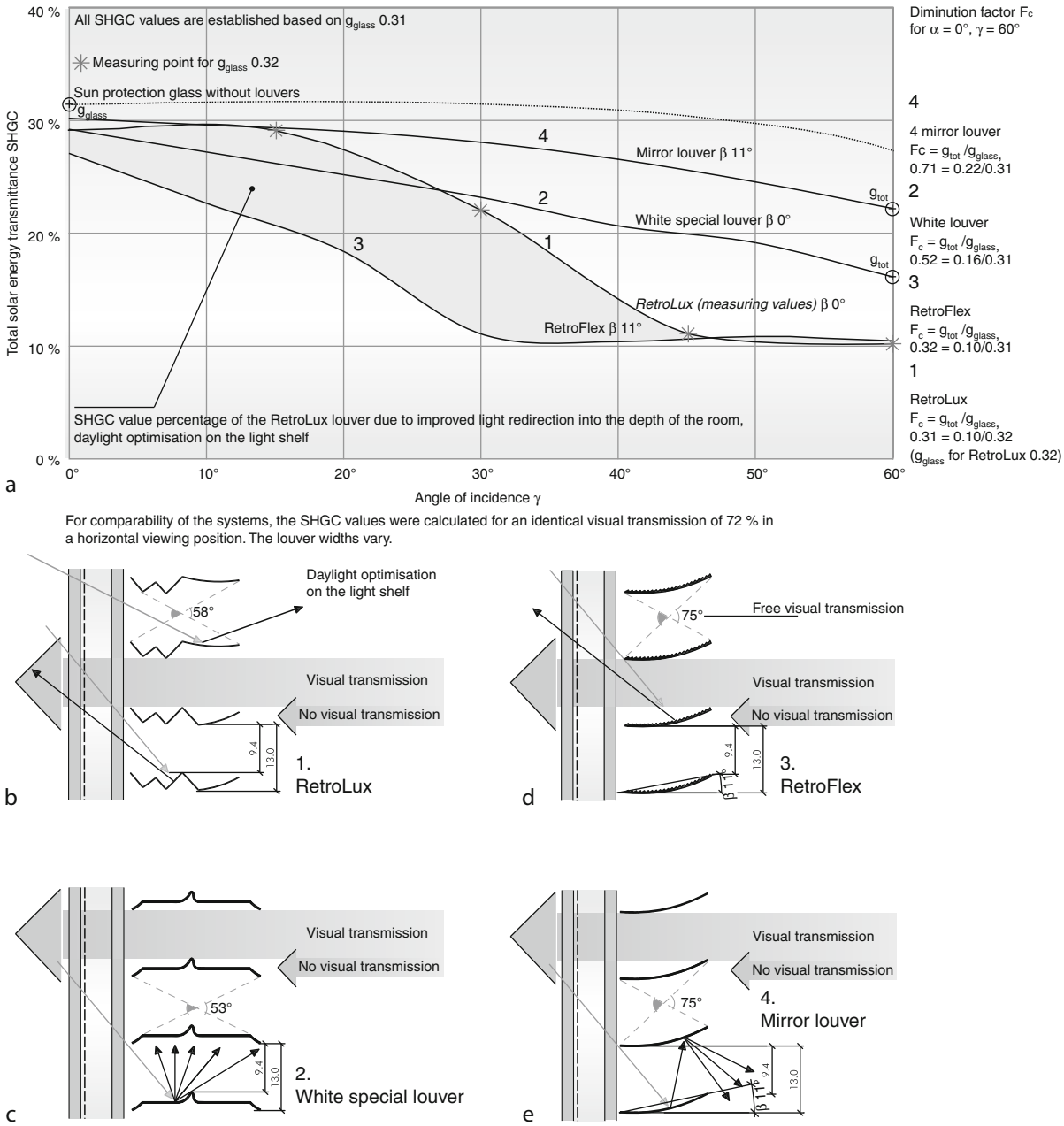

Daylighting Controls, Performance and Global Impacts. Figure 33

This illustration shows the dynamic SHGC values of different types of louvers based on condition of the same visual transmission for different angles of incidence. The mirror louver (Fig. 33e) performs very poorly, as the sun is reflected onto the gray lower side where it is absorbed and converted into heat. The white louver (Fig. 33c) shows better thermal properties. The RetroLux louvers (Fig. 33b) with light shelves in the second section produce a good light output with an excellent passive cooling capacity in the high summer sun. Despite open position, the RetroFlex louvers actively provide passive cooling even when the sun is low (Fig. 33d)

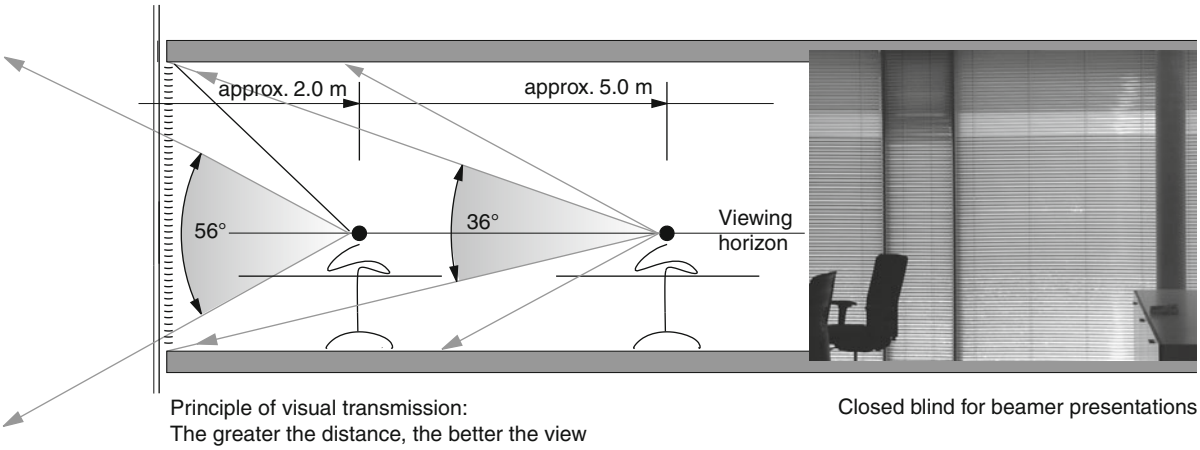

Daylighting Controls, Performance and Global Impacts. Figure 34
Analysis of visual transparency for RetroLux and RetroLux Therm during active protection from the high summer sun and closed blinds

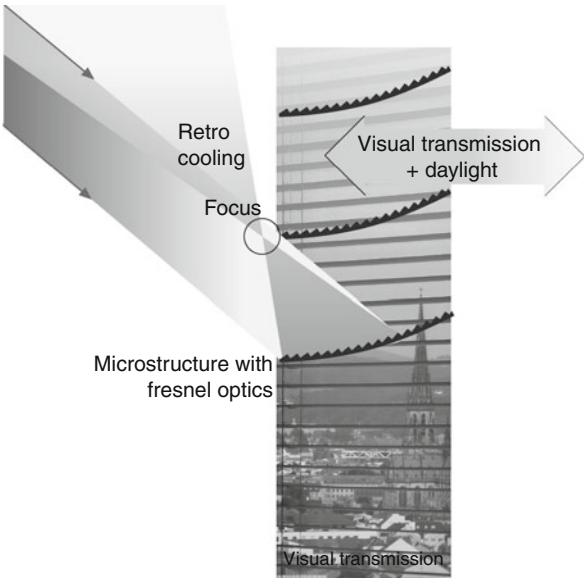

Daylighting Controls, Performance and Global Impacts. Figure 35
Visual transmission through RetroFlex louvers 74–80% (see also Figs. 17, 18)

daylighting for different sky and room conditions. Tools that accurately quantify annual and peak lighting, heating and cooling energy savings, and quantify the carbon benefits will be critical for designers as well as policy makers. Then standards such as DIN EN 13363–1 and 13363–2 [7] need to be refined to reflect the full energetic behavior of façades.

Appendix A. Daylight redirection-systems patents [excerpt]: Dr-Ing. Helmut Köster

EP 0793 761	Stepped Lamella for guiding Light Radiation
DE P 69514 005.1-08	Stepped Lamella for guiding Light Radiation
CH EP 0 793 761	Stepped Lamella for guiding Light Radiation
IT (EP) 0 793 761	Stepped Lamella for guiding Light Radiation
Fr (EP) 0 793 761	Stepped Lamella for guiding Light Radiation
GB EP 0 793 761	Stepped Lamella for guiding Light Radiation
NL (EP) 0 793 761	Lamelles en Gradins Destinees au Guidage de Rayonnement Lumineux
AT EP E 187 800	Stepped Lamella for guiding Light Radiation

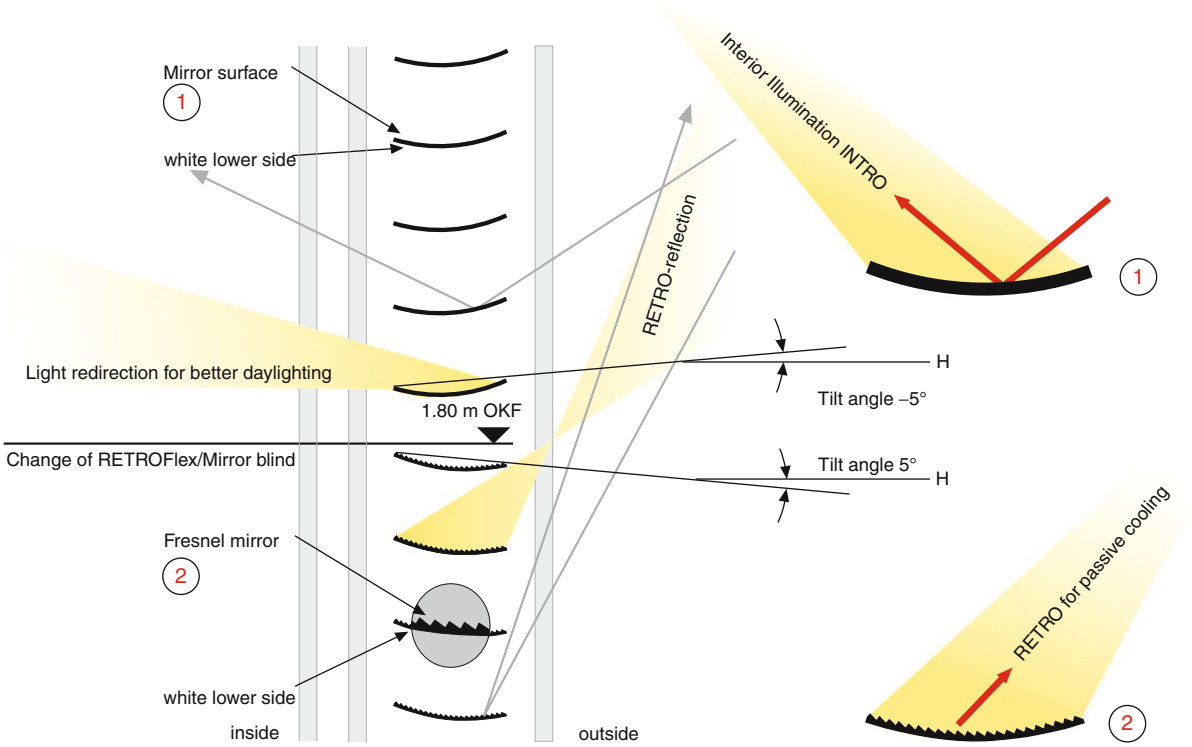

Daylighting Controls, Performance and Global Impacts. Figure 36
Strategy: within the retroreflective RetroFlex curtain a few mirror blinds with opposite qualities may be inserted in the upper window part to illuminate the working area in large depth (see also Fig. 37)

AU P 704 884	Stepped Lamella for guiding Light Radiation
CA P 2 205 560	Stepped Lamella for guiding Light Radiation
US 6,240,999	Stepped Lamella for guiding Light Radiation
EP 0461 137 B1	Lichtlenksystem für die Beleuchtung eines Innenraumes
DE P 590 09 101.8-08	Lichtlenksystem
US P 5 293 305	Light Guidance systems for the illumination of an interior area
USA 6,367,937	Sun Protection Installation.....
AT 411613	Sonnenschutzanlage mit Sonnenschutzlamellen.....

CH 694,947	Sonnenschutzanlage mit Sonnenschutzlamellen.....
NL 1010766	Zonwering met zonweringlamellen.....
GB 2332229	Sun Protection Installation.....
FR 9815482	Sun Protection Installation.....
IT - 1303650	Impianto di Protezione contra....
CA 2,255,302	Sun Protection Installation.....
AU 756628	Sun Protection Installation.....
AU 643429	Light deflecting system.....
DE 100 2006 006 855.6	Bewegliche Fixierung leiterartiger Bauelemente
DE 10 2005 028 6550	Medienfassade
DE 102 60 711	Blendfreie Jalousien

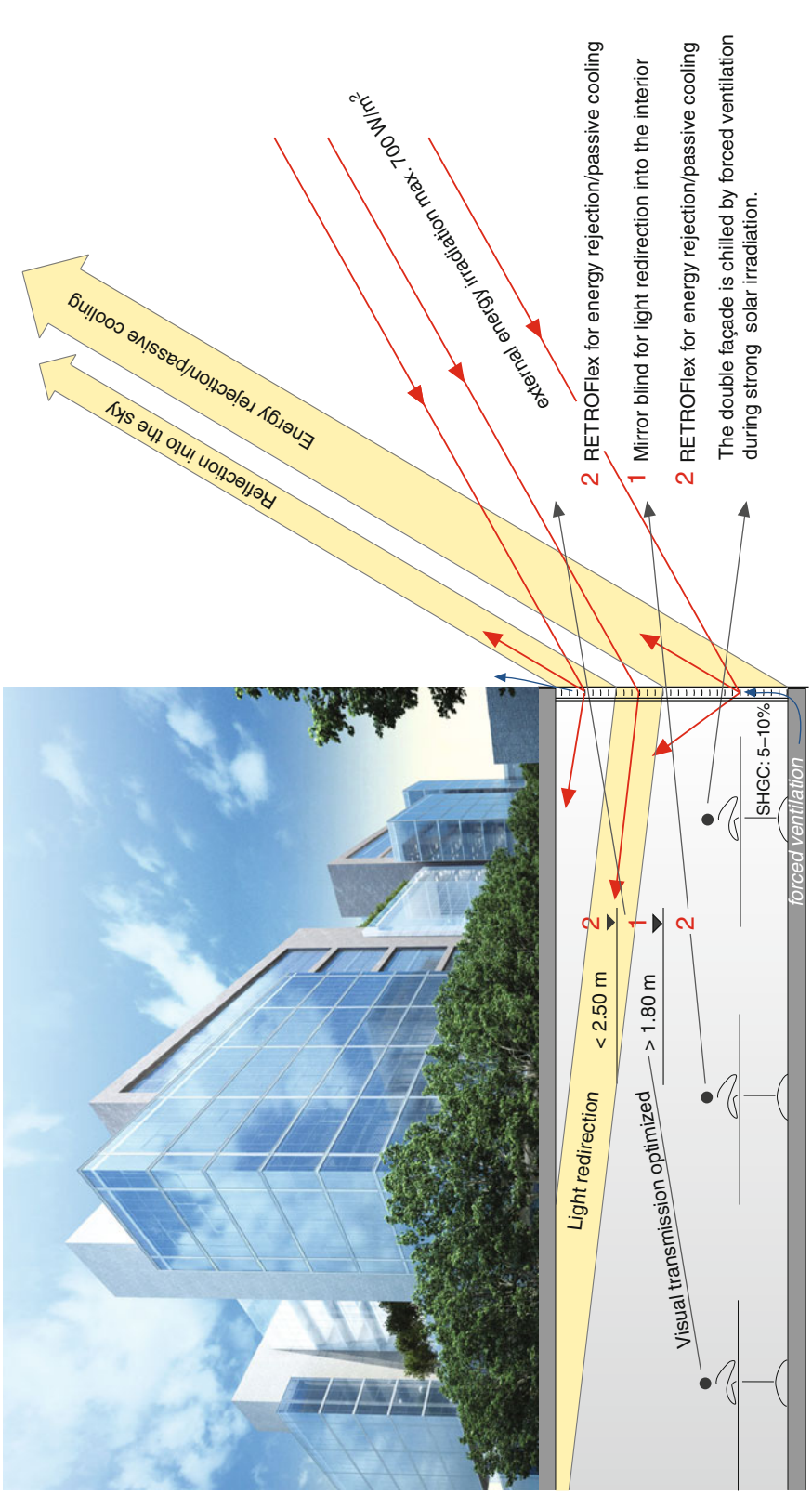

Daylighting Controls, Performance and Global Impacts. Figure 37
In the Standard Bank in Johannesburg, South Africa, the window is structured in three functional sections (see Fig. 36) with opposite values to ensure best daylighting in larger depths of the room without overheating

DE 100 18 451	Herstellung von linearen, prismatischen Strukturen auf einem lamellenartigen Festkörper
DE 198 28 543	Sonnenschutzanlage für Sonnenschutzlamellen, die eine gezahnte Oberseite aufweisen
DE 196 36 817	Sonnenschutzanlage mit Sonnen- schutzlamellen, die eine gezahnte Oberseite aufweisen
DE 44 42 870	Jalousielamelle zur präzisen Steuerung der direkten Sonneneinstrahlung
DE 000 331 483 -0001	Oberfläche für Jalousielamellem _ Oberfläche mirkostrukturiert, gezahnt
M9502488.3	Jalousie zur Tageslichtumlenkung
000 334 483 Alicante	selbst gefertigtes Lamellenprofil Retroflex
DE 401 04 706.7	Fassadenpfostenausbildung vorzugsweise für Glasfassaden mit und ohne Leuchte
DE 401 06 175.2	Lichtlenkdecken (1 Muster)
DE 401 09 455.3	Asymetrisch strahlendes Leuchtenmodul
DE 401 10 472.9	Oberlichtleuchte von Trennwänden
DE 402 02 313.7	Leuchten
DE 402 02 431.1	Trennwandleuchte II
DE 402 03 978	Lichtlenkjalousien bzw. Lichtlenkvorrichtung
DE 402 10 688	Jalousiebehang
DE 403 04 242	Lamellenvorhänge
DE 404 04 133.7	Lamellenvorhänge
M 9502488.3	Jalousie zur Tageslichtumlenkung
DM/052988 (15)	Blinds for reflecting sun and diffuse daylight as well as artificial light (2 x Retroluxtherm)
EP 00951306.0erteilt als EP 1212508	gezahnte Tageslichtlamelle
PCT/EP00/05929Intern. Application No.	gezahnte Tageslichtlamelle, toothed daylight blinds
CA 2,377,711	Toothed Daylight Blinds
USA 6,845,805	Toothed Daylight Blinds
AU 758 794	Toothed Daylight Blinds
EP 2006 005909	Medienfassade
PCT/EP2006/ 005909International Application No.	Medienfassade, s. auch, EP Anmeldenummer 06015154.5

Bibliography

Primary Literature

1. 2008: Verordnung über Arbeitsstätten (Arbeitsstätten-verordnung – ArbStättV), BGBl. I S. 2768
2. Arasteh D, Johnson R, Selkowitz S (1986) Definition and use of a daylight "Coolness" Index. In: International Daylighting Conference, Long Beach, 5–7 Nov 1986
3. ASR 7/1 Sichtverbindung nach außen; ASR 7/3 Künstliche Beleuchtung; ASR 7/4 Sicherheitsbeleuchtung
4. Cakir A, Cakir G (1994) Lixht und Gesundheit. Eine Untersuchung zum Stand der Beleuchtungstechnik in deutschen Büros. ERGONOMIC Institut für Arbeits- und Sozialforschung Forschungsgesellschaft mbH, Berlin
5. Deutscher Wetterdienst, Offenbach (2010) URL: http://www.dwd.de (Stand 09.04.2010). Accessed 9 Dec 2011
6. DIN 4108–2: Wärmeschutz und Energie-Einsparung in Gebäuden. Teil 2: Mindestanforderungen an den Wärmeschutz. Ausgabe: Juli 2003 DIN EN 13363: Sonnenschutzeinrichtungen in Kombination mit Verglasungen – Berechnung der Solarstrahlung und des Lichttransmissionsgrades. Ausgabe September 2007
7. DIN EN 13363–1: 2003 + A1:2007 (2003/2005/2007) Solar protection devices combined with glazing – Calculation of solar and light transmittance – Part 1: Simplified method. DIN EN 13363–2:2005 Solar protection devices combined with glazing – Calculation of total energy transmittance and light transmittance – Part 2: Detailed calculation method
8. Energy Policy Division of the Washington State Energy Office (Hg.): Washington State Energy Use Profile, Commercial Sector. URL: http://www.commerce.wa.gov/energy/archive/FILES/PRFL/docs/aboutweb.htm (Stand: 09.04.2010). Accessed 9 Dec 2011
9. Franke H (ed) (2007) Handbuch für Beleuchtung. Ecomed, Landsberg

10. Further daylight publications
11. Prof. Dr.-Ing. Dr. h.c. Hartkopf V (2009) Transnational endowment for sustainable built environments (TESBE). In: Green Building Conference, Carnegie Mellon University, Pittsburgh, 9 Nov 2009
12. Prof. Dr. Kaase, Heinrich: Ga-Nr.: HK-KÖ2-01 (2001) Gutachten über die Bestimmung der lichttechnischen und strahlungsphysikalischen Kennzahlen von zwei Retro-Lamellen als Innenjalousie. Institut für Elektronik und Lichttechnik der Technischen Universität Berlin
13. Klammt S, Müller H, Neyer A (2009) Advanced daylighting using micro-structured components. TU Dortmund. In: Proceedings of PLDC, Berlin, 27–31 Oct 2009
14. Köster H (2004) Tageslichtdynamische Architektur – Grundlagen, Systeme, Projekte, 1st edn. Birkhäuser, Basel (published in German, English, Chinese and Czech)
15. Patents: see Appendix
16. Dr. Pfafferrott J, Kalz D (2007) Thermoaktive Bauteilsysteme, FIZ Karlsruhe GmbH (Hg.). URL: http://www.bine.info/fileadmin/content/Publikationen/Themen-Infos/I_2007/themen0107internetx.pdf. Accessed 6 Dec 2011
17. Richtlinien VDI (2002) VDI 6011 Blatt 1: Optimierung von Tageslichtnutzung und künstlicher Beleuchtung – Grundlagen. Beuth, Berlin
18. Ruhstorfer W Computergrafik und Bildverarbeitung (1997) URL: http://www.uni-regensburg.de/EDV/Misc/CompGrafik/Script_5.html. Accessed 9 Dec 2011
19. Saint Gobain Glass, Memento (2005)
20. Twarowski M (1962) Sonne und Architektur. Georg D. W Callway, München
21. Umweltbundesamt. Daten zur Umwelt (2011) URL: http://www.umweltbundesamt-daten-zur-umwelt.de/umweltdaten/public/theme.do?nodeIdent=3437 [Stand: 09.04.2010]. Accessed 9 Dec 2011
22. SOLARTRAN Pty Ltd. URL: http://www.solartran.com.au/lasercutpanel.htm. Accessed 9 Dec 2011
23. World Data Center for Meteorology, Asheville. URL: http://www.ncdc.noaa.gov/oa/wdc/index.php?name=climateoftheworld. Accessed 9 Dec 2011

Books and Reviews

Goldmann M (2010) Gelenkte Lichtblicke, Deutsches Architektenblatt, Ausgabe Hessen/Rheinland-Pfalz/Saarland 06/10, S.38–S.40

Köster H (2010) Energiesparressource Tageslicht, Lichtlenkung. industrieBAU 56(2):S.36–S.41

Köster H (2010) Energiesparressource tageslichtlenkende Fassaden. In: Innovative Fassadentechnik, A 61029. Ernst & Sohn, Berlin, S.51–S.56

Köster H (2010) So sind Sie Ihrer Konkurrenz einen Schritt voraus, Diese Tipps von Köster Lichtplanung machen Sie zum Tageslichtexperten. Sicht + Sonnenschutz 9: S.16–S.19

www.koester-lighting-design.de

Desalination Technology for Sustainable Water Resource

Joon Ha Kim[1,2], Miriam Balaban[3]
[1]School of Environmental Science & Engineering, Gwangju Institute of Science & Technology (GIST), Gwangju, South Korea
[2]Sustainable Water Resource Technology Center (SWRTC), Gwangju, South Korea
[3]European Desalination Society (EDS), Tel Aviv, Israel

Article Outline

Glossary
Definition of the Subject and Its Importance
Introduction
Multistage Flash (MSF) Distillation
Multieffect Distillation (MED)
Reverse Osmosis (RO)
Forward Osmosis (FO)
Membrane Distillation (MD)
Future Directions
Bibliography

Glossary

Brine Water that contains a salt concentration greater than 50,000 ppm. Also, it is generally used in MSF processes to describe inlet seawater.

Concentration polarization Higher level of concentration profile of solute nearest to the upstream membrane surface compared with the more or less well-mixed bulk fluid far from the membrane surface.

Forward osmosis Process using osmotic pressure difference between brine and permeate as the driving force for water production.

Fouling The deposition of suspended or dissolved substances on the membrane surface, at the membrane pore, or within membrane pores.

Membrane distillation Thermal-driven membrane process, in which only water vapor can be transported through hydrophobic membranes.

Multieffect distillation Process uses multiple evaporators in a sequence at progressively low pressures. Generated vapor from each effect is used as a heat source in the next effect.

Multistage flash distillation Process using flash evaporation to convert a portion of the inlet seawater into steam in multiple stages and consequently condensate to product water.

Osmotic pressure Pressure causes the movement of solvent molecules through a semipermeable membrane into a region of higher solute concentration, aiming to equalize the solute concentrations on the two sides.

Permeate water Water product that leaves a membrane module and contains penetrants.

Pressure-retarded osmosis Process harvesting energy retrieved from the difference in the salt concentration between higher solute concentration and lower solute concentration solutions.

Reverse osmosis Process requiring application of transmembrane pressure on the liquid-phase pressure-driven separation process that causes the selective movement of solvent against its osmotic pressure difference.

Temperature polarization Temperatures at the membrane surfaces that differ from the bulk temperatures measured in the feed and permeate.

Definition of the Subject and Its Importance

As an alternative solution for eliminating water shortage, desalination processes have drawn an increasing amount of attention. Seawater desalination is a separation process to produce freshwater from saltwater, and can be categorized into two parts: thermal and membrane separation methods. Thermal separation methods are based on principles of the evaporation process and include multistage flash (MSF), multieffect distillation (MED), and mechanical vapor compression. On the other hand, the mechanisms of membrane separation methods are based on solution-diffusion or/and sieving processes. Among these processes, MSF and reverse osmosis (RO) currently cover more than 90% of the total market share. RO processes, in particular, have become competitive with other desalination processes due to their relatively low membrane cost and energy consumption.

Introduction

According to United Nations' reports, around 700 million people in various countries suffer from water shortage problems [1]. In addition, 1.8 billion people

are afflicted with severe water scarcity problems, and it is expected that up to two-thirds of the world population will encounter a number of difficulties from water stress. As such, it is predicted that conflicts may arise between regions where the suffering from water shortages become serious. Moreover, the absence of the freshwater may lead to similar sanitation problems as those that caused the deaths of 3.4 million people due to waterborne diseases in 2005 [2]. Important causes of water shortages include the acceleration of industrialization, increasing water demands, and severe climate changes as a result of global warming.

In order to overcome, or at least mitigate, these water scarcity problems, seawater can and should be considered as an alternative freshwater source. Seawater comprises the majority of the water present in the world, though it is not suitable for direct human consumption and/or industrial and agricultural use. To this end, desalination, which is the process of removing of salts and other minerals from feedwater, can offer a solution for achieving the required quality and quantity of freshwater. Desalination technologies can produce large amounts of water over a given time, and the construction period of desalination plants is relatively short compared to other technologies; therefore, a considerable amount of water can be produced relatively quickly. Moreover, some desalination technologies are independent of seasonal variations and weather conditions. Thus, the desalination industry has been rapidly developing over the past couple of decades, with the desalination market showing a corresponding growth (Fig. 1) [3].

Desalination can be divided into two primary technologies: thermal and membrane processes. Thermal methods are based on an engineering approach to replicating the earth's natural water cycle. The basic principle of the thermal method is to boil raw water and then condense it in order to get product water (distillate); MSF and MED are the two most dominant types of thermal desalination processes. Thermal methods can produce a high quality of product water and deal with the demands of large-scale production; however, these methods consume a large amount of energy. Typical membrane desalination processes using thermal methods are based on the characteristics of semipermeable membranes, with RO being the most popular. Since membrane desalination technologies do not utilize fossil fuels, like thermal processes do, they are referred to as energy-efficient desalination processes [4].

In order to meet their freshwater demands, a number of countries already rely on desalination technologies, especially in the Middle East and some parts of Europe. Figure 2 summarizes the capacity of seawater desalination plants in the world, based on typed over a period from 1981 to 2011 [5]. Until 2008, thermal methods dominated the market, mainly due to their use in fossil fuel–rich Middle Eastern countries. Other regions started to construct large-scale desalination plants about 10 years ago, and since that time, the method for desalination shifted from thermal to membrane-based processes. Indeed, the market share of membrane desalination processes has been increasing in the world, parallel with the water demand (Fig. 2) [3, 4].

This text includes chapters on thermal desalination (MSF and MED), membrane desalination (RO, FO, and MD), and future directions. In addition, each chapter consists mainly of sections on (1) process principles, (2) system investigation, (3) system model description, and (4) the advantages and limitations of each process.

Multistage Flash (MSF) Distillation

Principle

The basic principle of the multistage flash (MSF) distillation process is flash evaporation, which separates volatile components from a solution. When the operating pressure rapidly decreases below the saturated

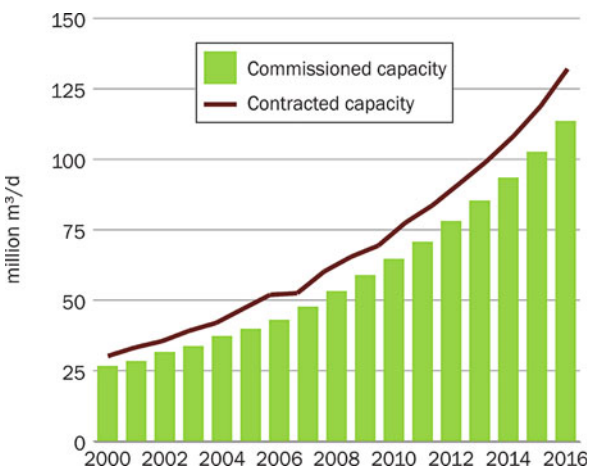

Desalination Technology for Sustainable Water Resource. Figure 1
Desalination market forecast; contracted and commissioned capacities [3]

vapor pressure at a given temperature, the latent heat of vaporization is removed from the contained heat of the liquid and flash evaporation occurs. In this process, the temperature of the inlet solution should be higher than the boiling point of the solution in the evaporation space; hence, a portion of the inlet solution can be vaporized based on the adiabatic equilibrium. Therefore, complete evaporation in the MSF process can be achieved by simultaneously increasing the temperature and decreasing the pressure.

System Investigation

MSF desalination plants consist of several flash chambers in series. The basic principles of the MSF desalination plant can be classified into three parts: heat input, heat recovery, and heat rejection (Fig. 3).

In brief, seawater is heated for the heat input, which is performed in a brine heater under low pressure conditions. The operating temperature of the boiled brine is generally kept between 90°C and 120°C in order to avoid scale formation. However, even though the system efficiency can be increased by using higher temperatures, this also increases the potential of scale formation. Scaling can accelerate the corrosion rate of devices, especially for parts that are in direct contact with the seawater. Note that a large-scale MSF desalination plant typically consists of 19–28 stages.

Seawater passes through the heat exchanger in the upper side of the flash chamber and flows into the brine heater. The boiled brine is then jetted through the orifice into the lower pressure chamber and vaporized. Any surplus energy can then be transferred to the partial latent heat; therefore, no additional external heat is required. The heating process continues until the seawater temperature reaches the boiling point of the flash chamber. In other words, flash distillation occurs based on the sequential reduction of pressure on the heated seawater. Further flash evaporation occurs when the liquid brine passes from one stage to the next lower pressure stage.

In order to minimize the loss of droplets from the brine, each evaporator stage is equipped with demisters. In this type of system, the evaporator is typically installed in conjunction with a decarbonator and deaerator in order to remove carbonate and eliminate dissolved gases. The decarbonator converts bicarbonate in the seawater to carbon dioxide by adding acid to the solution; bicarbonate is the main species in the seawater that leads to scaling. A steam jet ejector system then maintains the evaporation stage by extracting noncondensable gases from the system. The vaporized water is subsequently condensed using heat exchangers in order to produce distilled water. In these heat exchangers, latent heat from the flashed vapor is used to heat the inlet brine. The water quality produced from an MSF process normally contains around 2–10 ppm dissolved solids; as such, remineralization might be

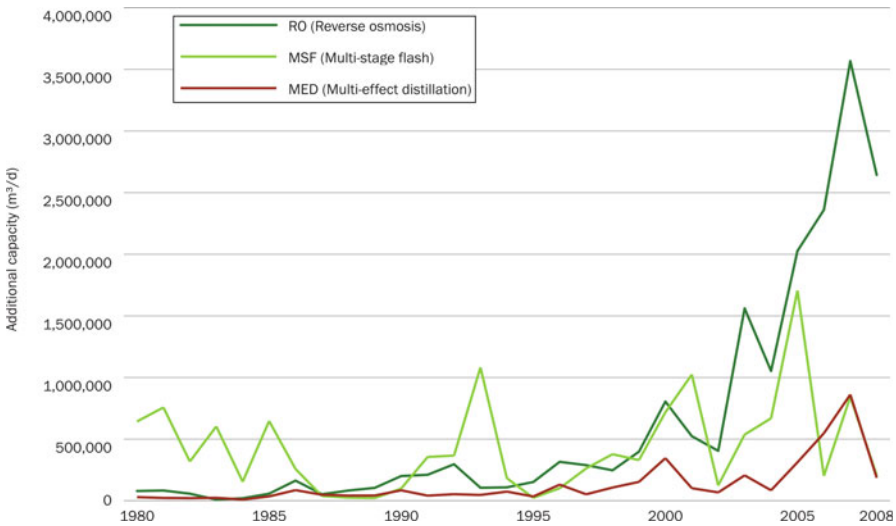

Desalination Technology for Sustainable Water Resource. Figure 2
Desalination process trend by contracted capacity [5]

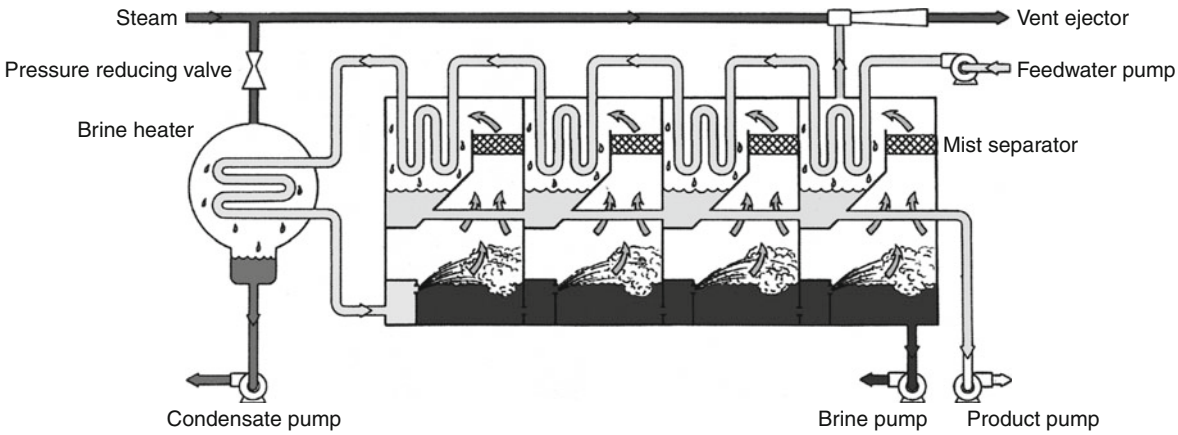

Desalination Technology for Sustainable Water Resource. Figure 3
Schematic of multistage flash (MSF) distillation [3]

required for potable water usage as the distilled water contains very low concentrations of salts [3, 4, 6].

System Model

Changes in the density of the cooling brine are negligible; therefore, the mass holdup of the cooling brine can be considered constant. In addition, as the heat transfer coefficient will be much larger for the condensation of vapor outside the tubes than inside the tubes, the tube temperature is assumed to be equal to the vapor temperature. Based on the above assumptions, the model equations are as follows [7]:

Mass and energy balance for the flash chamber

$$(M_b/1000)\frac{dC_{b,out}}{dt} = B_{in}(C_{b,in} - C_{b,out}) + VC_{b,o} \quad (1)$$

$$(M_b/1000)\frac{dh_{b,out}}{dt} = B_{in}(h_{b,in} - h_{b,out}) + V(H - h_{b,out}) \quad (2)$$

$$M_b = \rho_b A_b \cdot LE \quad (3)$$

where M, C, B, and V are the mass (kg), salt concentration, flashing brine flow rate (t/h), and vapor flow rate (t/h), respectively. In addition, h, H, and ρ are the liquid specific enthalpy (kcal/kg), vapor specific enthalpy (kcal/kg), and density (kg/m^3); A is the heat transfer area (m^2), and $LE$is the brine level (m). The subscripts in, out, and b indicate the input, output, and flashing brine.

Based on the assumption that the contents of the flash chamber are well mixed, Eqs. 1 and 2 can be rewritten. Therefore, the temperature, concentration, and specific enthalpy of the flash chamber will be equal to those of the outlet brine from the chamber.

Mass and energy balance for the brine heater

$$Q = 1000S(H_S - h_S) \quad (4)$$

$$M_{T,H}C_{P,ave}\frac{dT_F}{dt} = Q + 1000(F_{in}h_{F,in} - F_{out}h_{F,out}) \qquad F_i = F_o \quad (5)$$

$$M_{T,H} = \rho_F\left(\frac{\pi ID^2}{4}\right)_H L_H \cdot NT_H \quad (6)$$

where Q, S, and T are the heat transfer rate (kcal/h), steam flow rate (t/h), and temperature (°C), respectively. Also, C_p is the specific heat (kcal/kg°C) and F is the cooling brine flow rate (t/h); ID, L, and NT refer to the inner tube diameter (m), tube length (m), and number of tubes. The subscripts T, H, and F refer to the tubes, brine heater, and cooling brine.

Mass and energy balance for the condenser

$$D_{out} = D_{in} + V \quad (7)$$

$$T_D = T_b + T_L \quad (8)$$

where T_L is the total temperature loss caused the boiling point elevation, nonequilibrium, and pressure loss in the demister. Then,

$$D_{out}h_{D,out} = D_{in}h_{D,in} + Vh_D \quad (9)$$

where D is the distillate flow rate (t/h) and the subscript D is the distillate [7].

Advantages and Limitations

Since the core technologies of MSF desalination are well established, the application of MSF desalination is relatively easier than for other technologies. However, there is still a need for further development of materials and process design. In addition, by improving the process efficiency, the MSF life cycle can be extended by up to 30 years. Over the last several decades, MSF has been the dominant desalination technology; therefore, there is a corresponding strong background understanding of construction, maintenance, and operational expertise.

In spite of these advantages, however, MSF desalination has several limitations that need to be addressed. Recent increases in oil prices are an important limitation as they may lead to an inability to pay for MSF operations. In addition, the MSF desalination market is occupied by few major engineering companies, which limits the choice of alternative technologies to be introduced [3, 4] (Table 1).

Multieffect Distillation (MED)

Multieffect distillation (MED) is one of the oldest desalination processes, developed in the early nineteenth century. The MED process takes place in a series of evaporators, which are called effects. Similar to MSF, MED also uses the principle of the ambient pressure reduction; however, even though the MSF process replaced MED after its development, there has been a resurgence MED usage as new design approaches have been developed [3, 4, 8].

Desalination Technology for Sustainable Water Resource. Table 1 Advantages and limitations of MSF desalination process

Advantages	Limitations
Mature technology	Heat source cost
Longevity	Electrical consumption
Process simplicity for operating	Requirement to condensate
High product water quality	Higher energy costs
Easy to scale up (large scale)	Duopoly of the market
Requires minimum pretreatment	

Principle

The MED system consists of multiple evaporators in a sequence, which operates at progressively lower pressures. The vapor is generated from seawater within each effect, which is then transferred to the next effect as a heat source. While this vapor is being used as a heat source, product water condenses within the effect. A key benefit to this process is that once the vapor is generated at the first stage, there is no additional heat requirement for the rest of the process. The pressure and temperature sequentially decrease for each effect, from the first to the last stages [8].

System Investigation

After seawater enters the first effect, its temperature increases up to the boiling point. Cool seawater is then sprayed over a steam pipe to initiate the condensation process of the steam inside the pipe. At the same time, thin seawater layers boil outside the pipes as they absorb heat from the steam pipe. Freshly produced steam is then introduced into the pipes in the next effect, and this is repeated throughout the process. More recently, the introduction of vapor compression, which energizes low pressure steam, has been found to increase the overall efficiency of the MED process [3] (Fig. 4).

System Model

A "rigorous" model of MED columns includes the energy, material (overall), and component material balances. The balance equations for the distillation column are written as follows [9]:

Overall material balance

$$\frac{d\left(M_{\mathrm{L},i}+M_{\mathrm{V},i}\right)}{dt}=L_{i+1}+V_{i-1}-L_i-V_i \tag{10}$$

Component material balance

$$\frac{d\left(M_{\mathrm{L},i}x_{ij}+M_{\mathrm{V},i}y_{ij}\right)}{dt}=L_{i+1}x_{i+1,j}+V_{i-1}y_{i-1,j}-L_ix_{i,j}-V_iy_{i,j} \tag{11}$$

Energy balance

$$\frac{d\left(M_{\mathrm{L},i}u_{Li}+M_{\mathrm{V},i}u_{V,i}\right)}{dt}=L_{i+1}h_{\mathrm{L},i+1}+V_{i-1}h_{\mathrm{V},i-1}-L_ih_{\mathrm{L},i}-V_ih_{\mathrm{V},i} \tag{12}$$

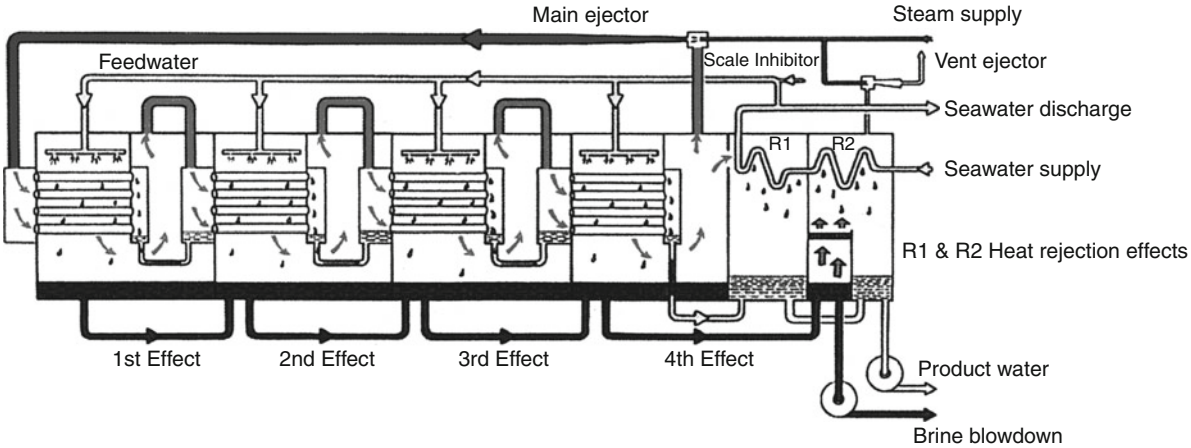

Desalination Technology for Sustainable Water Resource. Figure 4 Schematic of the MED process [3]

Here, $M_{L,i}$ and $M_{v,i}$ are the holdups in the liquid and vapor phases on stage i. In addition, index j denotes the component j, L and V are the liquid and vapor flows, x and y are component fractions in the liquid and vapor phases, and h_L and h_V are the liquid and vapor enthalpies.

Advantages and Limitations

Although MED is the oldest desalination technology, new developments for process efficiency, such as new design approaches, have rejuvenated the interest in MED applications. Even though MED technology is more complex than MSF – even with current developments – MED remains competitive with MSF. However, one of the major limitations for MED plant installation is the scarcity of titanium, which is used as a construction material [3, 4].

Desalination Technology for Sustainable Water Resource. Table 2 Advantages and limitations of MED desalination process

Advantages	Limitations
Rejuvenated technology	Complex technology
Competitive on a larger scale	Small unit size
High product water quality	Non-cost-competitive with RO process
Less cooling water required than MSF	Lack of track record
Lower capital cost than MSF	Lack of competition
Well established in certain markets	Titanium scarcity

Reverse Osmosis (RO)

Principle

Reverse osmosis (RO) is an unnatural process, which reverses water flow in an osmotic system. RO requires a larger transmembrane pressure than the typical transmembrane osmotic pressure used to push water from a high concentration zone to a low concentration zone through a semipermeable membrane [10]. The semipermeable membrane allows a solvent to pass to the permeate side, whereas solutes are rejected by the membrane. Note that RO processes can be categorized into two types according to their pressure strength: (1) high-pressure RO, which requires a pressure between 5.6 and 10.5 MPa, and can be used for seawater desalination; and (2) low-pressure RO, which requires a pressure between 1.4 and 4.2 MPa, and can be used for brackish water desalination. Both RO processes provide a high rejection efficiency (95–99%) of sodium chloride (NaCl) (Table 2).

Generally, RO membrane configurations can also be categorized into two types: flat (e.g., plate-and-frame and spiral-wound modules) and tubular (e.g., tubular, capillary, and hollow-fiber modules) [11]. However, the spiral-wound type has been more widely selected, due to its lower maintenance cost and simpler

design than is the case for other configurations [12]. The spiral-wound type consists of a central tube (used to collect the permeate water), membrane sheets (which are rolled onto the central tube), and a pressure vessel (which covers the system to ensure a stable pressurized environment) [13]. In practical applications, several spiral-wound elements are connected in series in one pressure vessel in order to increase the RO process efficiency.

To evaluate the process performance, recovery and rejection rates are broadly used as key parameters [14]. The performance of an RO membrane process is principally governed by site-specific variables (e.g., solute concentration, temperature, and pH), membrane variables (e.g., membrane type, module geometry, and module arrangement), and process variables (e.g., feed flow rate, operating pressure, and operating time) [15]. Moreover, the design, operation, and maintenance of an RO plant also influence the performance of the RO process. In order to maintain the feed flow rate, a high-pressure pump and a flow-regulating valve on the brine side can be used. The impact of each parameter on the membrane performance is shown in Fig. 5 [12]. Figure 6 then presents the schematic of a typical two-pass

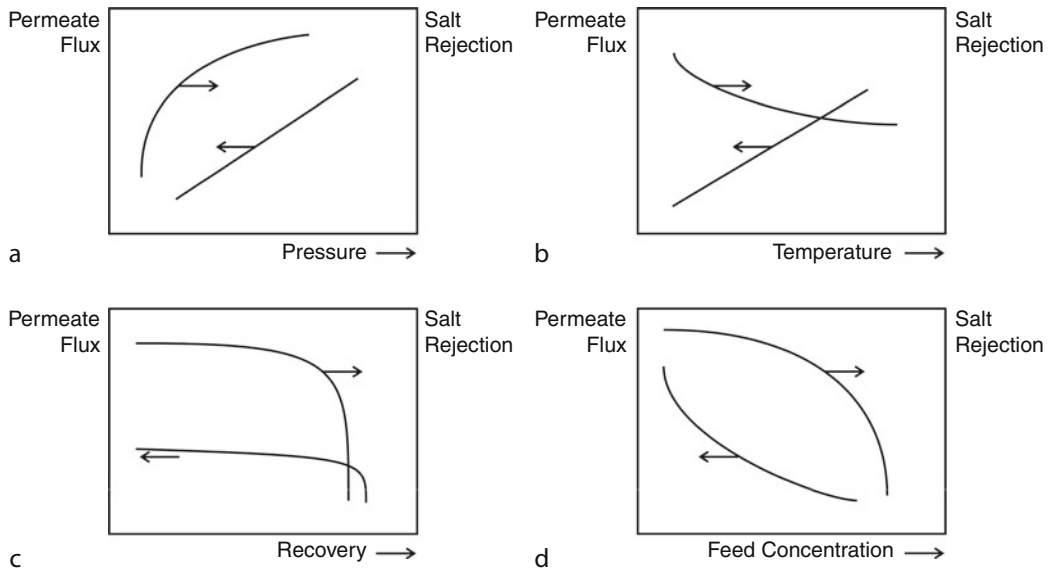

Desalination Technology for Sustainable Water Resource. Figure 5
Impact of several factors affecting membrane performance [12]

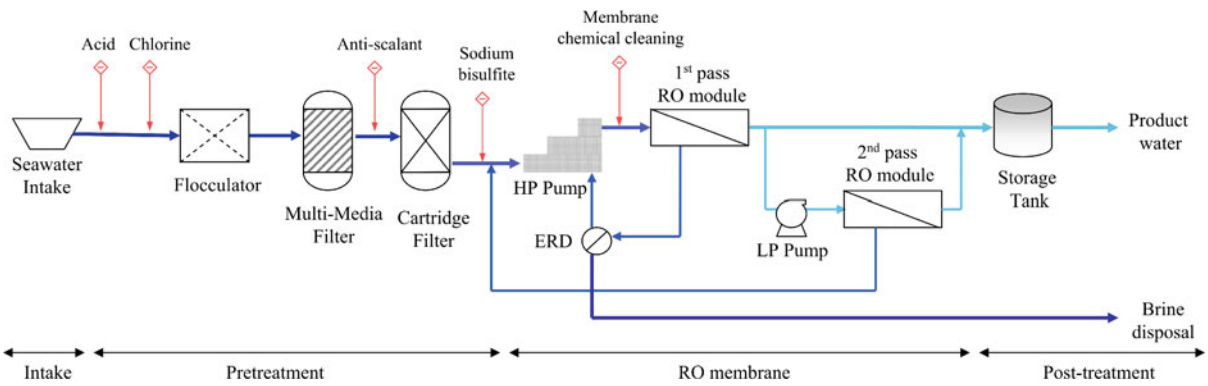

Desalination Technology for Sustainable Water Resource. Figure 6
Schematic of a typical SWRO desalination process [16]

seawater reverse osmosis (SWRO) desalination process, which includes a seawater intake, a pretreatment system, an RO system, and a posttreatment system.

Instead of using high-pressure RO systems for seawater desalination, nanofiltration (NF) can be considered as an alternative process as it has a lower pressure requirement. NF is also a pressure-driven membrane process and has a pore size between RO and ultrafiltration (UF) [17]. NF membranes have a molecular weight cutoff (MWCO) of about 200–1,000 Da, which make NF processes suitable for separating dissolved components with a molecular size of about 1 nm [18]. Separation mechanisms in the NF process are based on the sieving effect, solution-diffusion, Gibbs–Donnan effect, dielectric exclusion, and electromigration. Therefore, it is possible to separate both charged and uncharged organic solutes using NF [7]. NF also demonstrates a high rejection for divalent/multivalent ions, as well as for organic compounds that have molecular weights above 300 g/mol [17]. However, NF shows a low rejection efficiency for monovalent ions and nonionized organics, especially for those with a low molecular weight. Nonetheless, according to previous studies, NF membrane processes can be successfully applied to seawater desalination. For instance, results have shown that NF desalination could produce a water product that contains less than 1% salt content [19].

System Investigation

An SWRO distillation system generally consists of: an intake structure, a pretreatment process, an RO filtration process, a posttreatment process, and optionally an energy recovery process. System investigation for SWRO is important because it is helpful not only to increase the system efficiency but also to reduce the unit production costs. Moreover, the construction of large-scale RO plants can also reduce the cost per production unit. Thus, several large-scale plants have frequently been reported as effective and productive case studies. Table 3 presents a summary of the ten largest SWRO plants [20], where it should be noted that there are several issues that need to be evaluated prior to setting up a large-scale SWRO process.

Intake Structure and Site Area In order to ensure a high level of seawater quality, a subsurface seawater intake at 10–15 m below the sea surface is required [14]; therefore, the cost for logistics and construction will increase. Based on this requirement, desalination plants that are located close to the intake site might be considered to be more cost efficient.

Desalination Technology for Sustainable Water Resource. Table 3 Ten largest SWRO plants in the world [20]

Country	Location	Capacity (m^3/h)	Year of construction	Membrane manufacturer	Module
United Arab Emirates	Fujairah	7,083	2004	Hydranautics/Nitto	Spiral wound
Saudi Arabia	Median/Yanbu	5,333	1998	Toyobo	Hollowfilber
Spain	Carboneras	5,000	2003	Hydranautics/Nitto	Spiral wound
Trinidad and Tobago	Point Lisas	4,542	2002	Hydranautics/Nitto	Spiral wound
USA	Tampa Bay	3,917	2003	Hydranautics/Nitto	Spiral wound
Saudi Arabia	Al Jubail	3,750	2002	DuPont/Toray	Hollowfilber/spiral wound
Spain	Cartagena	2,708	2002	Hydranautics/Nitto	Wickelelement
Saudi Arabia	Jeddah I	2,367	1989	Toyobo	Hollowfilber
Saudi Arabia	Jeddah II	2,367	1994	Toyobo	Hollowfilber
Spain	Marbella	2,350	1998	DuPont	Hollowfilber

Raw Seawater Conditions Since raw seawater conditions depend on the specific location, it is important to investigate individual parameters when selecting the pretreatment process, RO system design, membrane material, and chemical cleaning methods [21]. Thus, it is necessary to continuously monitor the raw seawater conditions, in order to make prerequisite adjustments pertaining to the pretreatment process. A summary of raw seawater compositions from several sites in the world are given in Table 4 [22–31].

Pretreatment Processes

- *Conventional approach*
  As mentioned above, the seawater quality is a very important factor in RO process design and operation; since the plant operator cannot control the seawater quality, an effective pretreatment process is critical for improving overall SWRO system performance [27]. The basic components for the pretreatment process include screening, coagulation, flocculation, media filtration, and a cartridge filter. Table 5 summarizes several key issues that need to be considered during the pretreatment process [14, 25, 32, 33].
- *UF membrane approach*
  Ultrafiltration (UF) pretreatment processes are an alternative pretreatment method for the further improvement of feedwater quality. The major disadvantage of conventional pretreatments is the utilization of chemical agents, which tend to shorten the membrane lifetime [14, 26, 34, 35]. Therefore, UF can be a good candidate for SWRO processes. Table 6 presents a summary of advantages of UF over conventional pretreatments.

  Table 7 can also be used as a decision tree for the pretreatment selection for SWRO desalination systems.

RO Filtration Processes The major factors that can significantly affect the cost and performance of an RO membrane process are described as follows [36–48].

- *Permeate recovery and salt passage*
  Permeate recovery and salt passage rates are significant parameters that are commonly used to evaluate RO membrane performance. A high-efficiency RO membrane process should provide a high permeate recovery and low salt passage rates, which can be controlled by improving the membrane properties.
- *Concentration polarization*
  Concentration polarization affects solute adsorption and gel layer formation onto the active sides of the membranes. These phenomena increase the osmotic pressure and decrease the permeate flux. Polarization layers are formed by hydrophilic macromolecules, whereas gel layers are formed by hydrophobic macromolecules; both layers could lead to a severe flux decline.
- *Membrane fouling*
  Membrane fouling is an important factor that has an adverse effect on RO process performance. Membrane fouling occurs via the deposition of particles onto the membrane surface or into membrane pores. This phenomenon leads to an increase in the transmembrane pressure (TMP), followed by a decrease in the quantity and quality of the water product [49–51]. And although pretreatment processes are intended to remove majority of the foulants from raw seawater, pretreated water can still contain foulants such as dissolved organic compounds and tiny colloidal particles [52]. To date, numerous research groups have investigated the fouling mechanisms in attempts to predict fouling formation [53–56]; however, they could not provide a full explanation and/or solution for fouling occurrences. Therefore, membrane fouling remains as a significant factor limiting the further development of RO membrane processes. To this end, the major foulants are natural organic matter (NOM), colloidal particles, microorganisms, and inorganic particles. Scaling is the major inorganic fouling component, which forms by the precipitation of complex salts such as calcium carbonate ($CaCO_3$), calcium sulfate ($CaSO_4$), silica (SiO_2), and iron hydroxide ($Fe(OH)_3$), some of which occur during chemical pretreatment processes. Therefore, minimizing the chemicals used during pretreatment is required in order to reduce the fouling rate.
- *Chemical cleaning*
  Chemical cleaning is an inevitable process for RO in order to eliminate fouling and/or scaling on the membrane. Alkaline (NaOH), acid (citric acid or H_2PO_4), ethylenediaminetetraacetate (EDTA), chlorine (Cl_2), and surfactants/detergents are

Desalination Technology for Sustainable Water Resource. Table 4 Compositions of raw seawater at several sites in the world

	pH	TDS (mg/l)	Temp (°C)	Total alkalinity (mg/l)	Bicarbonate HCO_3^- (mg/l)	Sodium Na^+ (mg/l)	Potassium K^+ (mg/l)	Magnesium Mg^{2+} (mg/l)	Calcium Ca^{2+} (mg/l)	Fluoride F^+ (mg/l)	Chloride Cl^- (mg/l)	Sulfate SO_4^{2-}(mg/l)	Silica SiO_2^-(mg/l)	Barium Ba^{2+}(mg/l)	Phosphate PO_4^{3-}(mg/l)
Kifan site 1 [22]	7.21	11,435	28.6	133	133	2,462	39	303	693	2.15	4,013	3,016	2	0.18	<0.05
Kifan site 2 [23]	7.15	10,786.6	–	143.3	143.3	3,045	55.2	432.4	869.9	1.95	3,983.8	3,018.9	5.45	<0.05	<0.05
Canary Islands [30]	–	–	–	6,600	–	9,055.5	251.8	1,354.3	205.5	–	21,328.5	3,300	–	–	–
Crude seawater (Canary Islands) [25]	–	–	–	–	171.9	11,810	–	1,438.7	448.9	0.5	21,317.2	2,900	–	–	–
Atlantic Ocean [31]	8	40,077	17–20	162		12,255	441	1,477	464	1.5	22,019	3,075	1.4	0.4	–
Jeddah, Saudi Arabia (Red Sea) [28]	8	41,200	32	–	–	–	–	1,464	520	–	22,000	–	0.4	–	–
Yanbu City [26]	8.1–8.3	41,300–46,400	25	120–130	–	11,700–12,500	425–650	1,500–1,600	490–560	1.5	21,600–23,500	3,000–3,200	0.5	–	<0.1
Tajura, Libya [24]	8.3	38,000	–	–	163	11,600	419	1,427	455	–	20,987	2,915	–	2	–
Bocabarranco [29]	–	38,000	–	–	250	11,415	450	1,520	450	–	20,800	3,110	5	–	–
Surface seawater (open intake) [27]	8.07	–	19.3	–	161	10,945	410	1,471	441	1.55	20,900	2,965	0.2	10	0.02
Well seawater [27]	7.8	–	21.1	–	166	10,747	399	1,340	438	1.35	20,100	2,840	1.5	20	0.09
Combined water [27]	7.87–7.92	–	18.6–20.5	–	162	10,841	402	1,355	441	1.35	20,700	2,855	0.9	15	0.05

commonly used to eliminate NOM, inorganic scalants, scalants (e.g., $CaSO_4$), biofouling (biofilm), and colloids, respectively. In order to maximize the pretreatment efficiency, the type and concentration of the cleaning agent need to be considered. As an example, membranes can be cleaned via the cleaning-in-place (CIP) method, though this method requires information pertaining to interactions between the foulants/scalants and the membrane surface [39]. In CIP, the cleaning priority for essential foulants is as follows: silica colloids > adsorbed organic compounds > particulate matter (iron and aluminum colloids) > microorganisms > metallic oxides.

Energy Recovery Processes Since it is possible to transfer energy from the high-pressure brine stream to the feed stream [57], a suitable energy recovery process can be used. Current energy recovery technologies can allow us to reduce the total energy cost by up to 40% [20]. Typically, there are three types of energy recovery devices in SWRO systems [58–61]:

1. A Pelton wheel turbine (PWT) with an efficiency rate range of 40–60%
2. A pressure exchanger (PX) with a maximum efficiency rate as high as 95%
3. A hydraulic turbo charger (HTC) with an efficiency rate ranging from 50% to 65%

According to existing data, the PX shows the highest efficiency and most dynamic stability [59].

Posttreatment Processes In SWRO desalination processes, posttreatment is generally necessary in order to improve the quality of product water to meet potable water quality standards. Posttreatment processes include pH adjustment, minimal remineralization, disinfection, and boron removal [20, 62, 63]. The pH of desalinated water should also be adjusted to a range of 6.8–8.1, and disinfection techniques need to be applied to remove bacteria or other organisms from the product water. However, the concentration of disinfection by-products (DBPs) and bromate (BrO_3^-) in the final product should not exceed potable water quality standards; the concentration of boron should also meet these same standards. Previous studies reported that SWRO membrane systems could reject boron in a range from 92% to 94%; however, the boron rejection efficiency is strongly dependent on the pH level of the water. It was further reported that at a pH less than 9.5, approximately 50% of boron

Desalination Technology for Sustainable Water Resource. Table 5 Key issues to be considered in the pretreatment process

Foulant/parameter	Chemical
Microorganism	Sodium hypochlorite (NaOCl), Cl_2, $KMnO_4$, or O_3 can be used to control biofouling
	H_2SO_4 can be applied to assist the biocide action of NaOCl
Inorganic particles	Sodium hexametaphosphate $(NaPO_3)_6$ is usually added in doses to control scaling
	H_2SO_4 can be used to assist the action of scale inhibitors
pH adjustment	H_2SO_4 can be added to regulate the pH for polyamide-type RO membranes
Colloidal particles and dissolved organics	Ferric or alum salts are often used to coagulate and flocculate colloidal particles and dissolved organics
Suspended solids	Ferric or alum salts are often used to coagulate and flocculate colloidal particles and dissolved organics
	Anthracite (~1 mm) is often applied during the granular media filtration process to remove suspended solids
	A media backwashing process with air is followed by the granular media filtration process to remove particles captured in the filters
Particulate matter	Cartridge filters are usually tasked with preventing the sudden appearance of particulate matter
Neutralizing the residual active chlorine	Sodium metabisulfite ($NaHSO_3$) is primarily used to neutralize residual active chlorine, especially for polyamide-type RO membranes

Desalination Technology for Sustainable Water Resource. Table 6 Comparison of conventional and UF membrane pretreatments

	Conventional pretreatment	UF membrane pretreatment
Treated water quality	Unstable and fluctuating water quality depending on raw seawater (silt density index, SDI < 4.0)	Stable and constant water quality (SDI < 2.0)
Average RO flux	100%	20% higher
RO membrane fouling rate	High fouling potential	Lower fouling potential
RO membrane cleaning frequency	1–2 times per year	4–12 times per year
Typical lifetime	Filters: 20–30 years	UF/NF membranes: 5–10 years
	Cartridges: 2–8 weeks	Cartridges: not often needed
RO membrane replacement rate	100%	33% lower
Capital cost	100%	0–25% higher
Footprint	100%	30–60% smaller
Energy consumption	Lower than UF	Higher than conventional
Chemical dosing rate	High	Lower
Intake line	Long	Shorter
Operation/management cost	High	Lower
Miscellaneous	–	Better boron control

Desalination Technology for Sustainable Water Resource. Table 7 SWRO pretreatment process selection

Water quality process design (selection)	SDI < 4	SDI > 4				
	NTU < 0.5	0.5 ≤ NTU < 2	2 ≤ NTU < 20	20 ≤ NTU < 40	40 ≤ NTU < 100	100 ≤ NTU
Coagulation and flocculation		X	X	X	X	X
Sedimentation or DAF				X	X	
Enhanced sedimentation or DAF						X
Single-stage granular media filtration	X[a]	X[a]				
Two-stage granular media filtration			X[a]	X[a]	X[a]	X[a]
MF/UF membrane filtration	X[a]	X[a]	X[a]	X[a]	X[a]	X[a]

[a]Select either granular media or membrane filtration. For turbidity >20 NTU, consider using a combination of both

could be removed, and that at 10.5, the removal rates increased up to 100%. In addition, membrane material can also play an important role in the boron rejection rate. For example, polyamide-type membranes showed higher rejection rates for pH values of less than 9.5, though the most effective posttreatment for boron removal was found to be to use boron selective resins (BSR) because they are not affected by operating conditions such as temperature, pH, and/or salinity [64–66].

The Marin Municipal Water District (MMWD) SWRO pilot system in the city of Corte Madera in Sonoma County, California, developed the following general water quality objectives for after posttreatment stabilization (Table 8) [63].

Brine Disposal and Environmental Impact Brine from SWRO processes contains a high concentration of salts (TSD ~70,000 mg/L), in addition to remnants of chemical product/by-products, which are used in overall SWRO process. The effect of discharging this high concentration of salts and other chemicals into the environment should be seriously considered as these high concentrations could inhibit a natural mixing caused by density differences. Moreover, a leak of the brine pipeline into underlying aquifers could release heavy metals and cleaning agents into the environment, potentially leading to serious groundwater contamination. As such, environmentally friendly brine disposal methods should be selected, including methods with low carbon dioxide production and low energy consumption. Several options of brine disposal include: deep well injection into nonpotable aquifers, utilization of evaporation ponds (zero discharge), and connecting the brine pipeline to wastewater treatment plants and then treating it together with other discharged water [20, 30, 67–69].

System Model

Recently, desalination technology has shown remarkable improvements in many aspects: membrane material, equipment, and cost and energy reductions [70, 71]. However, in order to reduce the overall process cost, optimization of process operation and maintenance are required, as well as advanced control of the system. Therefore, a modeling approach is required for the system analysis of SWRO and also for the optimization of the technologies, in order to achieve an effective cost reduction.

A strong modeling approach can be used to predict performance and optimize process operations and process controls. Usually, advanced statistical models (e.g., artificial neural networks and genetic programming) are broadly applied because of their simplicity and user-friendly interfaces. And since these models are based on the input/output data, they do not require huge data sets. They have also been proven useful when a physical understanding is inadequate. For example, deterministic models, which are developed based on physical laws, can give a better physical insight of the system process. These models have also been used to provide a real time insight into process behavior monitoring, such as for state and measured variables.

Desalination Technology for Sustainable Water Resource. Table 8 Proposed general water quality objectives for after posttreatment stabilization for the MMWD SWRO pilot system in the city of Corte Madera in Sonoma County, California [63]

Parameter	Units	MMWD-treated reservoir			Sonoma County water			SWRO pilot objectives		
		Avg	Max	Min	Avg	Max	Min	Avg	Max	Min
TDS	mg/L	119	136	86	171	186	148	120	180	60
Hardness	mg/L	62	74	52	105	112	96	60	110	60
Alkalinity	mg/L	61	70	49	119	125	110	60	110	50
pH	Units	7.8	7.9	7.8	8.1	8.4	7.8	7.9	8.2	7.8
Color	CU	<3	<3	<3	<3	<3	<3	<3	<3	–
TOC	mg/L	1.6	2.4	1.1	0.9	1.2	0.7	<1	1	–
Sodium	mg/L	16	25	11	20	23	16	30	50	10
Chloride	mg/L	27	37	22	8	10	7	50	70	10
Boron	mg/L	<0.05	<0.05	<0.05	0.28	0.26	0.16	0.3	0.5	–
SAR	–	–	–	–	–	–	–	3	6	–

Pretreatment Process Models There have been several models developed for UF/MF pretreatment and posttreatment processes. These existing models are mostly described in a similar manner, based on mathematical approaches that can be applied to the specific desired process.

- *UF/MF*
  Microfiltration and ultrafiltration both resemble conventional coarse filtration; therefore, they are suitable for retaining suspensions and emissions. Darcy's law can be used to describe volume flow in UF/MF processes. Furthermore, for flux estimations, both the Hagen–Poiseuille and the Kozeny–Carman equations can be applied when laminar convective flow assumptions are valid [72].
- *Granular media filter*
  Models for granular media filters require a full understanding of particle transport and particle deposition phenomena in order to predict the fate of the colloidal particles. In this model, the main transport mechanisms of colloidal particles, from pore fluid to the surface of filter grains, are gravitational sedimentation and Brownian diffusion [73]. The first filtration model that was applied to a water treatment system was introduced by Yao et al. [74], though this model assumed that viscosity and van der Waals interactions have no effect on the system. Therefore, a prediction model for colloidal filtration must be developed based on a numerical approach that includes a convective-diffusion equation [75].

  However, a comprehensive solution of the convective-diffusion equation is not yet readily available. Thus, a semiempirical correlation model for the single-collector contact efficiency in granular filtration was introduced by Rajagopalan and Tien [76]. This model was developed by considering the effects of viscous and van der Waals interactions [73], which then was able to provide more realistic predictions than the original model. Recently, this model has been broadly applied to the prediction of single-collector contact efficiency in a granular filtration system [77].

SWRO Filtration Process Models There are three types of deterministic models for RO filtration processes: an irreversible thermodynamics-based model, a diffusion-based model, and a porous model [15]. These models have all been applied in attempts to evaluate the solvent and solute transport in RO filtration processes based on the membrane characteristics. RO transport models can also be classified into three categories: solution-diffusion (SD) models, irreversible thermodynamic (IT) phenomenological models, and pore-based models [15]. It should be noted, however, that numerous research groups have studied the solute transport mechanisms in RO processes more than the solvent transport because the solute flux is not proportional to the net driving pressure (NDP) [78]; several groups have also investigated membrane fouling via membrane resistance-in-series-based simulations [37, 55, 79, 80].

- *SWRO operational models*
  Operational models for SWRO processes can help to increase overall process efficiencies and production rates, and be used to determine the economic feasibility of the process. In additional, these models can also be used to improve the process management.

  The cost and total annual profit (TAP) estimations of an SWRO process are two of the most important criteria for establishing a feasible desalination process. Developed package models must be proven satisfactory in terms of permeate water flow rate and concentration, which can then be extended to estimate the operational cost of the system. Moreover, the results of cost estimation show that the models can successfully predict the TAP, according to operation time, feedwater TDS, and permeate water TDS [81].

  Most SWRO plants operate in isobaric conditions, which significantly reduce their ability to respond to an external disturbance. However, the permeate salinity significantly depends on the feed salinity and a change in the feed salinity can affect both process efficiency and operational costs. Therefore, a cost-effective SWRO process can be utilized by using a nonisobaric pressure control that considers possible fluctuations in the feed seawater concentrations [82]. Another study, which also investigated nonisobaric pressure control together with feed temperature control, showed that feed pressure required can be reduced by approximately 10 bars in an SWRO–MSF hybrid system [83].

An artificial neural network (ANN) model has been used to optimize the cost effectiveness of an SWRO–MSF hybrid system [84]. This study showed that feedwater temperature manipulation can directly improve the system performance, based on a linear increase with respect to the feed temperature over a 1-year period. Another SWRO–MSF hybrid system study also used feedwater temperature manipulation to increase the permeate flow rate [85]. It was seen that feedwater temperature manipulation can cause an increase in the permeate flow rate by up to 0.2% per day.

Lee et al. [86] proposed a membrane resistance model that utilizes temperature and pressure correction factors in order to evaluate membrane performances. The developed model requires a minimum parameter input to investigate the performance of the membranes under different conditions. This model can be used to suggest appropriate operating conditions for the desired water production.

- *SWRO network model*

Representations of RO network (RON) models developed by El-Halwagi [87] are now widely used to optimize the RO plants under various conditions [88–91]. In addition, RON models that can obtain realistic and economical solutions by optimizing total costs [41, 92] have also been developed.

A chronology of system engineering approaches for the modeling and optimization of the RO systems is given in Table 9.

The structure of an extended system analysis may start with the design of the seawater quality and the membrane modules. Then, a cost-effective RON configuration (RO modules, pumps, and energy recovery devices), the operating condition, and the optimal arrangement of membrane elements can be analyzed. The structure of this type of RO system analysis was first suggested and used by El-Halwagi [87] and Voros [90, 93]. Figure 7 shows a simplified RON representation that Lu et al. [94, 95] have recently developed by applying a stream split ratio, isobaric-mixing constraints, and a PX energy recovery device to the previous RON model.

Desalination Technology for Sustainable Water Resource. Table 9 Chronological systems engineering approaches for RO membranes

Year	Authors (et al.)	Systems engineering approaches for RO membranes
1965	Lonsdale	Homogeneous diffusion model for cellulose acetate (CA) membrane [96]
1969	Hatfield	Nonlinear program for maximal flux and optimal arrangement of RO systems in brackish water [97]
1980	Tweddle	Prediction of performance of membrane modules with system analysis [98]
1982	Sirkar	Analytical design to estimate the averaged permeate solute concentration in spiral-wound RO module [99]
1984	van Dijk	Optimal design of total unit water cost using raw water TDS, pressure, and recovery [100]
1985	Evangellsia	Graphical-analytical method to design straight-through and tapered reverse osmosis plants [101]
1992	El-Halwagi	Optimal arrangement, types, and sizes of RO units for reverse osmosis networks (RON) [87]
1993	Sekino	Analytical model of friction–concentration–polarization (FCP) in hollow fiber RO module [102]
1996	Malek	Minimal cost analysis per unit membrane area applying large-sized permeates [41]
	Robertson	Dynamic matrix simulations for control of RO desalination pilot plant [103]
	Voros	Mathematical models for the performance of various SWRO process units [90]
	Sekino	Analytical model of FCP with Kimura–Sourirajan algorithm applied to hollow fiber RO module [104]

Desalination Technology for Sustainable Water Resource. Table 9 (Continued)

Year	Authors (et al.)	Systems engineering approaches for RO membranes
1997	Zhu	Optimal design of flexible RON with mixed-integer nonlinear programming (MINLP) [91]
	Voros	Optimal design to minimize total cost of RON plant [93]
1998	van der Meer	Hydraulic model of the rejection of mono- and bivalent ions in spiral-wound RO modules [105]
1999	Al-Bastaki	Mass transport model to predict the performance of hollow fiber RO membranes [106]
	See	RON desalination plant cost analysis with MINLP based on optimal cleaning schedule [92]
2000	Maskan	Optimization of RON operating conditions with a constrained multivariable nonlinear algorithm [88]
	Al-Bastaki	Mathematical analysis of concentration polarization and pressure drop based on flux integration [107]
2001	Wilf	Economic feasibility analysis of SWRO systems based on recovery rate and feedwater salinity [108]
2003	Al-Enezi	Design calculations based on feed salinity and temperature in RO desalination process [36]
	Villafafila	Optimization of operating and design parameters using successive quadratic programming (SQP) [109]
	Helal	Optimization of minimum water cost in hybrid RO/MSF system [110]
2004	Chatterjee	Numerical analysis of hollow fiber RO module using three-parameter Spiegler–Kedem (S–K) model [111]
2005	Marcovecchio	Minimization of total cost of hollow fiber RO seawater desalination using Kimura–Sourirajan model [112]

Desalination Technology for Sustainable Water Resource. Table 9 (Continued)

Year	Authors (et al.)	Systems engineering approaches for RO membranes
	Abbas	Feedforward neural network (NN) model to predict performance of RO experimental setup [113]
	Vitor Geraldes	Longitudinal variation model for mass/momentum transport in the spiral-wound SWRO modules [114]
2006	Senthilmurugan	Mathematical model for the separation of two solutes from aqueous solutions in hollow fiber module [115]
	Lu	Optimum design of SWRO system considering membrane cleaning and replacing based on MINLP [94]
2007	Lu	Optimum design of SWRO system under different feed concentration and product specification [95]

Cost Analysis Models

- *Total Cost (CAPEX/OPEX)*
  The total cost of a desalination plant can be divided into two terms: capital costs and operation and maintenance (O&M) costs [41, 58]. The capital cost can be considered as the total expenditures of the plant construction, which is the largest portion of the capital cost (50–85%), other installation costs (equipment, piping, service utilities, etc.), engineering efforts, and administrative/financing activities. O&M costs consist of plant operation costs (energy, chemicals, replacement of consumables, and labor) and maintenance costs for plant equipment, buildings, and utilities. The O&M costs are generally reported as all operational expenditures per year (\$/year) or as operational costs for desalinated product water per volume (\$/m^3).
- *Factors Influencing Total Costs*
  Figure 8 summarizes the factors affecting the total costs; these factors should be considered in order to obtain an accurate optimization.

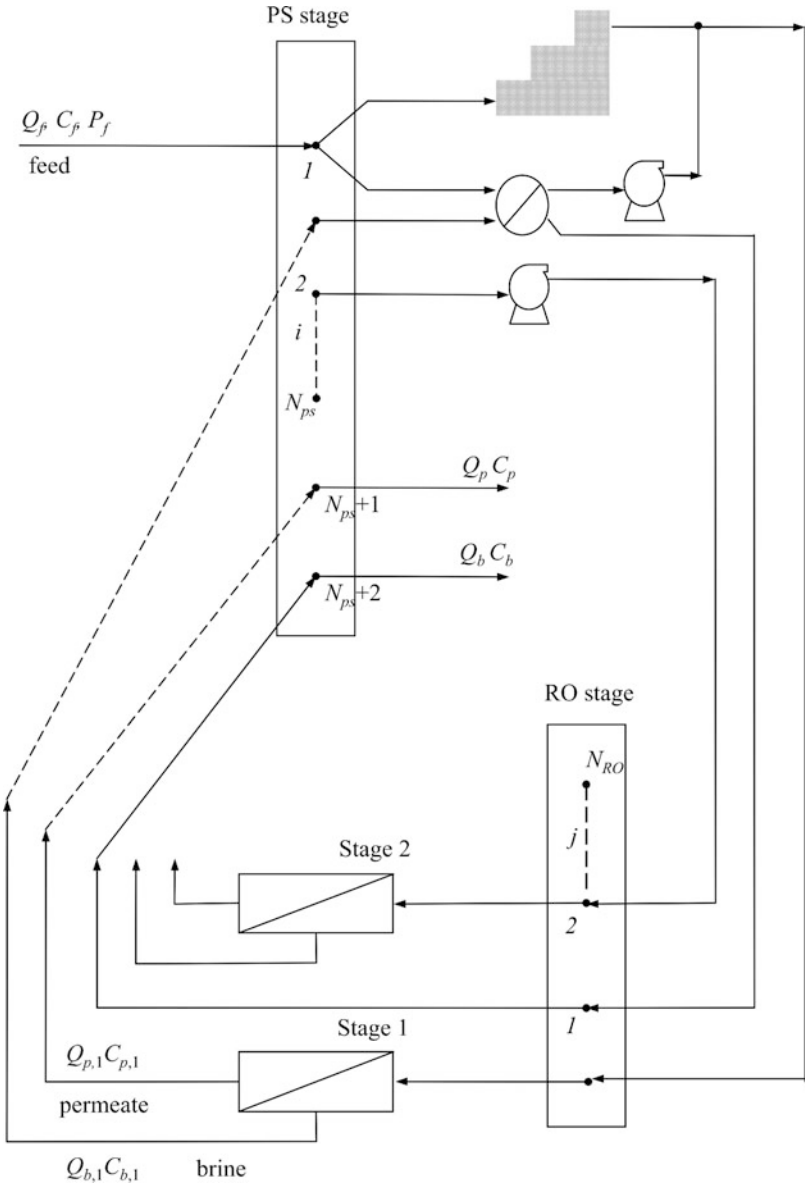

Desalination Technology for Sustainable Water Resource. Figure 7
Structural representation of an RO network (RON) [16]

- *Optimization of the Cost Model*
  There have been several models for estimating the membrane costs for seawater desalination plants released. For instance, the WTCost© Model was developed by the United States Bureau of Reclamation [116], and the Water Reuse Association in the US developed the WRA Model [117]. An example of the total cost optimization process that is commonly used in SWRO is given below [41, 91, 94, 95, 109, 112].

  A mixed-integer nonlinear programming (MINLP) model that minimizes the total cost can be solved by using an algebraic system. This model can be expressed as [94, 95]

$$J = \min_{\text{MINLP}} \; [C_T] \tag{13}$$

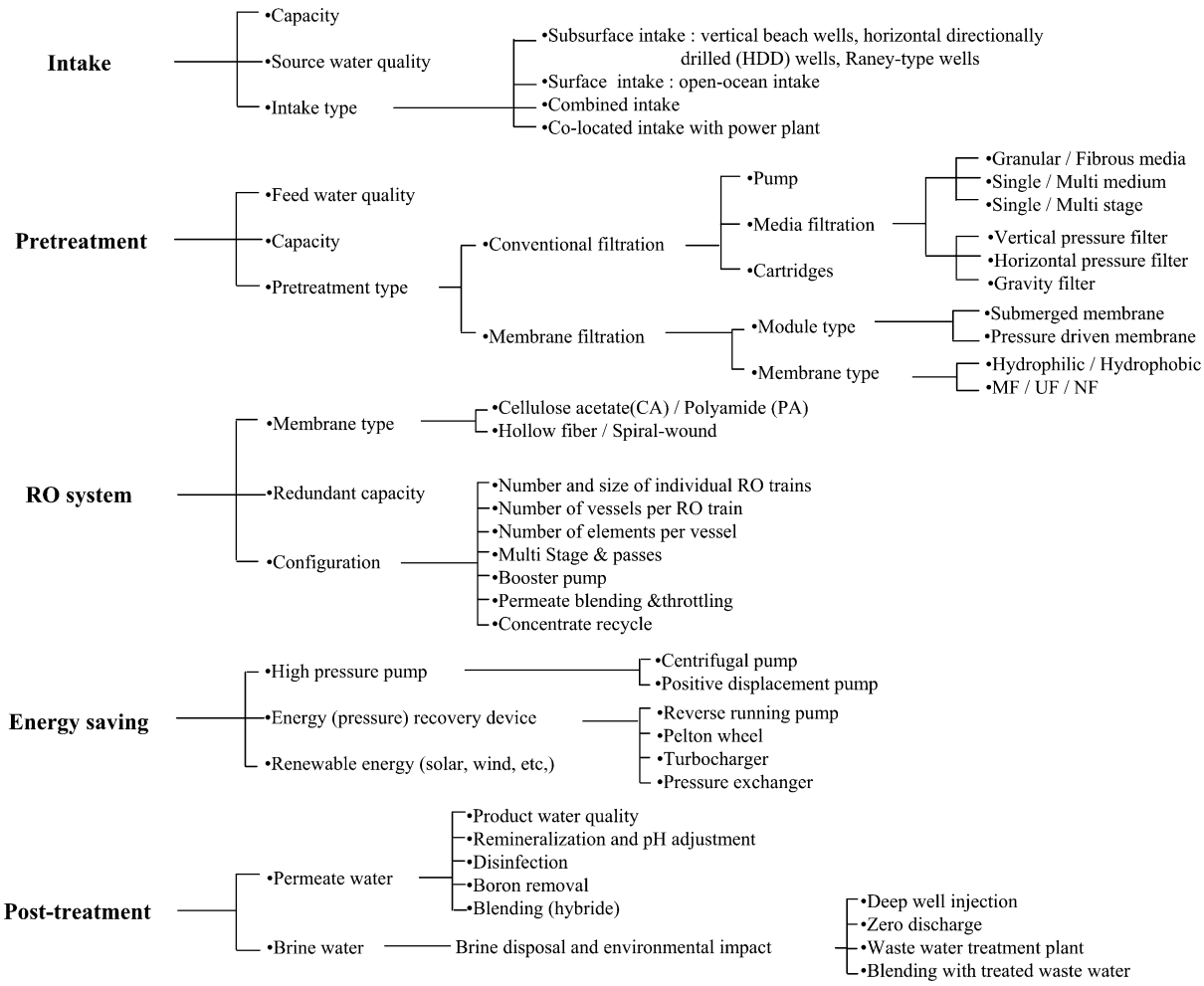

Desalination Technology for Sustainable Water Resource. Figure 8
System factors affecting the total cost in a large-scale SWRO plant [16]

where the objective function (J) is the total annualized cost (C_T).

$$C_T = (CC_{in} + CC_{hp} + CC_{px} + CC_{bp} + CC_m)1.411 \times 0.08 + OC_{in} + OC_{hp} + OC_{bp} + OC_m \quad (14)$$

In Eq. 14, CC and OC represent the annualized capital cost and annual operating cost, respectively; CC_{in}, CC_{hp}, CC_{px}, CC_{bp}, and CC_m represent the capital cost of the seawater intake pump, high-pressure pump, pressure exchanger, booster pump, and membrane purchase, and OC_{in}, OC_{hp}, and OC_{bp} indicate the energy costs for pump operations, and OC_m represents the maintenance cost for the membrane module, where 1.411 is the constant for the practice investment and 0.08 is the capital charge rate.

$$CC_{hp} = 52(\Delta P Q_{hp})^{0.96} \quad (15)$$

$$CC_{px} = 3134.7\ Q_{px}^{0.58} \quad (16)$$

$$Q_{ps,\,1} = Q_{hp} + Q_{px} \quad (17)$$

In Eqs. 15–17, P, Q_{hp}, and Q_{px} are the pressure and flow rates of the high-pressure pump and pressure exchanger, respectively; $Q_{ps,\,1}$ represents the flow rate of the first pressurization stage.

$$C_{\mathbf{m}} = \sum_{j=1}^{N_{RO}} \sum_{k=1}^{8} Z_{j,k}\, C_k\, m_{j,k} n_j + \sum_{j=1}^{N_{RO}} C_{\mathbf{pv}}\, n_j \quad (18)$$

In Eq. 18, C_m, C_k, and C_{pv} are the total cost of the membrane module, the price of the k_{th} membrane element, and the pressure vessel price, respectively. The indices j and k represent the j_{th} RO stage out of N_{RO} number of RO stages and the k_{th} membrane type out of a maximum of 8 elements. In addition, $Z_{j,\ k}$ is the binary variable, which is either 0 or 1; $m_{j,\ k}$ is the number of membrane elements in each pressure vessel; and n_j is the number of pressure vessels used in the j_{th} RO stage.

$$OC_{hp} = \frac{PQC_e f_c}{3.6\ \eta_{hp}\ \eta_{motor}} \tag{19}$$

$$\eta_{px} = \frac{\sum (PQ)_{\mathbf{out}}}{\sum (PQ)_{\mathbf{in}}} \times 100\% \tag{20}$$

In Eqs. 19 and 20, C_e is the electricity cost, and f_c is the load factor, where η_{hp}, η_{motor}, and η_{px} are the efficiencies of the high-pressure pumps, the electric motor, and PX, respectively.

Advantages and Limitations

RO membrane processes have a number of key advantages, such as a lower power requirement than other forms of desalination processes. They also require a smaller area for the RO membrane unit [50]; furthermore, RO processes can produce a high quality of water (i.e., TDS concentration between 100 and 500 ppm) [118], and can be operated automatically with minimal operator attention required [119].

However, fouling and scaling are crucial limitations of RO membrane processes [118]. Fouling and scaling of the RO membrane reduce the quantity and quality of the water product. These phenomena can also lead to an increase in the water production costs due to their requirement for chemical cleanings. Good pretreatment practices are also required in order to maintain stable performance [118], and RO membranes are sensitive to oxidizing compounds (e.g., chlorine oxides); thus, feedwater needs to be treated in order to prolong the lifetime of the membrane [118].

Forward Osmosis (FO)

Principle

Forward osmosis (FO) , often described as "engineered osmosis" or an "osmotically driven process," has been spotlighted as a promising water treatment and desalination process. FO is a membrane-based separation process that utilizes natural osmosis phenomena. In this process, water can be transported across a semipermeable membrane by osmosis [120].

Water permeates through a semipermeable membrane from a low-concentration region to high-concentration region in the FO process (Fig. 9) [121], an exact opposite to the RO process. This water movement can be explained based on the chemical potential difference across the membrane; the difference in the chemical potential on the two sides of the membrane leads the solvent (pure water) to move from a higher potential environment (generally a lower solute concentration) to a lower potential environment (higher solute concentration) until they reach an equilibrium [122]. As a practical term, instead of "chemical

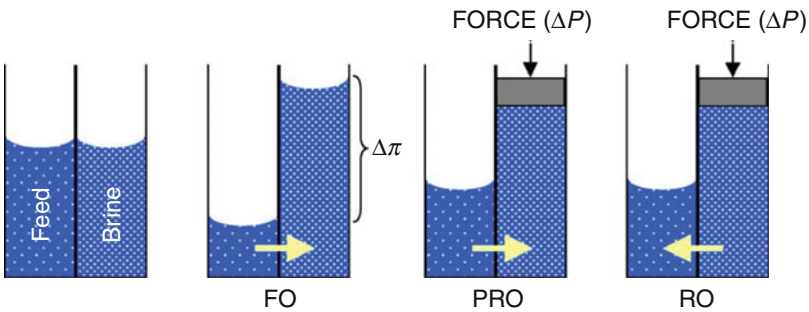

Desalination Technology for Sustainable Water Resource. Figure 9
Classification of membrane processes [121]. FO is naturally driven by osmotic pressure. If the applied pressure exceeds the osmotic pressure of the draw solution, the process is called RO. Pressure-retarded osmosis (PRO) refers to the case when the applied pressure is lower than the osmotic pressure

potential," osmotic pressure is used here to refer to the pressure that can induce the spontaneous net flow of water across a semipermeable membrane. Therefore, the driving force of this process is created by the transmembrane osmotic pressure difference. The higher concentration solution, exerting a higher osmotic pressure, is referred to as the draw solution.

System Investigation

Figure 10 presents the conceptual diagram of the FO process, which mainly consists of two major stages: (1) a membrane process and (2) the separation and recovery of the draw solution. During the membrane process, pure water spontaneously flows into the draw solution side due to the osmotic pressure difference. While the feedwater is concentrated and finally discarded as brine, the draw solution is simultaneously diluted with the permeating water. The diluted draw solution is then sent to the separation and recovery unit for the next step of the FO process. Next, the product water is separated from the diluted draw solution to yield potable water for several consumption purposes. Simultaneously, the draw solute is recovered and recycled back to the membrane process [124]. The currently suggested separation and recovery processes include evaporation/condensation, RO, distillation, membrane distillation (MD), and magnetic separation [125]. Note that the product water quality and draw solute recovery rate are the most important parameters for FO process as they reveal whether the process is feasible or not. During this closed-loop continuous process, loss of the draw solute should be minimized in order to lower its replenishment cost [126]. The draw solute can possibly be lost due to reverse diffusion during the membrane process and insufficient separation of the draw solute within the recovery unit [127].

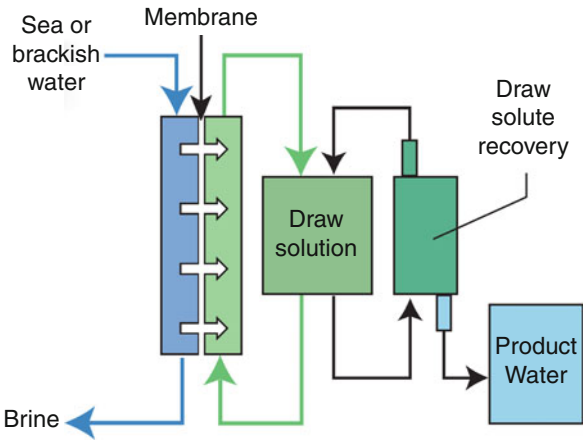

Desalination Technology for Sustainable Water Resource. Figure 10
Forward osmosis desalination process schematic adopted from McCutcheon et al. [123]

In addition to its water treatment/production applications, FO has been increasingly addressed for energy generation. FO can potentially be applied to generate energy by utilizing the concentration gradient between seawater and freshwater (Fig. 11) [126]. This process is referred to as pressure-retarded osmosis (PRO). In PRO, transmembrane water permeation pressurizes the draw solution side and power is harvested via depressurization through a hydro turbine. In 2009, Statkraft, located in Norway, opened the first prototype PRO installation; the plant configuration followed the original schematic proposed by Sidney Loeb.

System Model

In order to predict the flux performance in FO, a standard flux equation can be applied [123]:

$$J_w = A(\pi_{D,b} - \pi_{F,b}) \tag{21}$$

where A is the water permeability, and $\pi_{D,b}$ and $\pi_{F,b}$ are the bulk osmotic pressures at the feed and draw sides, respectively. This equation is representation of an FO process that is driven by the osmotic pressure difference. However, it has been found that actual membrane experiments have resulted in much less flux performance than was calculated from the bulk osmotic pressure difference [123]. These unexpected results were caused by a phenomenon referred to as the concentration polarization (CP). CP can be basically explained as the increased and/or decreased concentration on the membrane surface that thereby lowers the net osmotic pressure difference. Therefore, the osmotic pressure terms used in the standard flux equation should be modified by taking CP into account. Membrane orientation is an important factor for CP calculations; since the membranes normally adopted for FO are asymmetric, the position of the active layer also plays an important role.

The concentrations on both sides of the membrane affect the flux performance in FO, whereas RO only takes

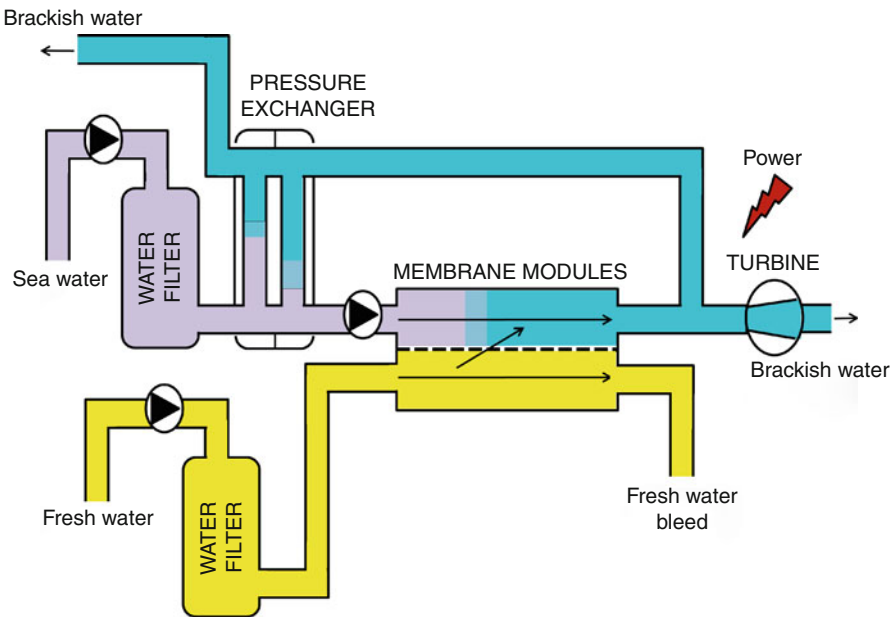

Desalination Technology for Sustainable Water Resource. Figure 11
Simplified process layout for a PRO power plant [121]

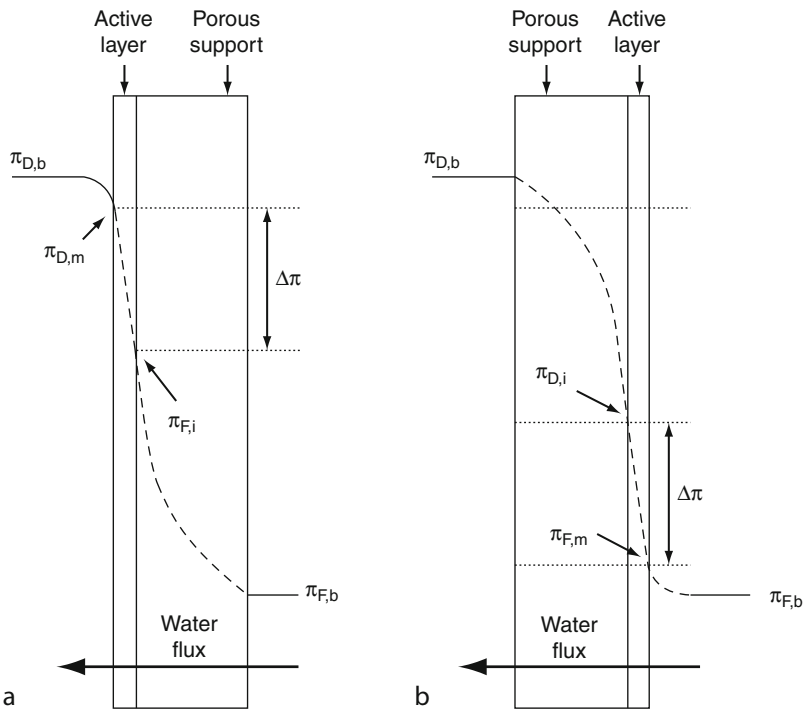

Desalination Technology for Sustainable Water Resource. Figure 12
Illustration of osmotic pressure profile in an asymmetric membrane [123]

the feed side concentration into account. As described in Fig. 12 [123], the actual driving force ($\Delta\pi$) is dramatically reduced by four types of CP. In PRO mode, dilutive external concentration polarization (ECP) at the left side of the membrane and concentrative internal concentration polarization (ICP) within the porous support layer can be observed. In FO mode, dilutive ICP inside the porous support layer and concentrative ECP on the active dense layer surface can be observed.

Based on the following equation, the ECP can be analyzed in a similar way as in RO [72]:

$$\frac{c_w - c_p}{c_0 - c_p} = \exp\left(\frac{\bar{v}}{k}\right) \tag{22}$$

where c_w, c_p, and c_0 are the solute concentrations on the membrane surface, in the permeate, and bulk solutions, respectively, $\bar{v}$ is the channel averaged permeate velocity, and k is the mass transfer coefficient. In order to model the ECP, the mass transfer coefficient (defined as $k = D/\delta$, where D is the diffusion coefficient of the solute and δ is the concentration boundary layer thickness) can be acquired based on the Sherwood relationship [72]:

$$\mathrm{Sh} = a\mathrm{Re}^b\mathrm{Sc}^c \tag{23}$$

If it is assumed that the membrane completely rejects the solutes and that the osmotic pressure and concentration are linearly proportional, the ECP modulus for both PRO and FO modes can then be given by the modification of Eq. 22 [123], such that

$$\frac{\pi_{D,m}}{\pi_{D,b}} = \exp\left(-\frac{J_w}{k}\right) \tag{24}$$

$$\frac{\pi_{F,m}}{\pi_{F,b}} = \exp\left(\frac{J_w}{k}\right) \tag{25}$$

where $\pi_{D,m}$ and $\pi_{D,b}$ refer to the osmotic pressures of the draw solution on the membrane surface and in the bulk solution, respectively, and $\pi_{F,m}$ and $\pi_{F,b}$ are the osmotic pressures of the feed solution on the membrane surface and in the bulk solution. Equation 24 defines the dilutive ECP and Eq. 25 is for the concentrative ECP.

The ICP phenomenon, particularly observed during mass transport, is the major factor that lowers the water flux in an FO process. The CP, which occurs inside a porous support layer, cannot be removed by physical methods such as increasing the cross flow velocity. Indeed, ICP originates from the characteristics of a symmetric membrane, which has a porous support layer that acts like an undisturbed concentration boundary layer.

Lee et al. [128] proposed a flux model for PRO based on a consideration of the ICP phenomenon. This model can be derived by applying the solute mass balance within the porous support layer to the boundary conditions:

$$B(C_{D,m} - C_{F,i}) = D\varepsilon\frac{dC(x)}{ds} - J_w C(x) \tag{26}$$

$$\begin{aligned} C(x) &= C_{F,i} \quad at\ x = 0 \\ C(x) &= C_{F,b} \quad at\ x = t\tau \end{aligned} \tag{27}$$

where B is solute permeability, ε is the porosity of the porous support layer, and t and τ are the thickness and tortuosity of the porous support layer, respectively ($t\tau$ corresponds to the distance of the effective boundary layer porous layer).

The following equation can then be obtained as a result of the integration of Eq. 26:

$$\frac{C_{F,i}}{C_{D,m}} = \frac{B[\exp(J_W K - 1) + J_W \frac{C_{F,b}}{C_{D,m}}\exp(J_w K)}{B[\exp(J_W K) - 1] + J_W} \tag{28}$$

where K is the solute resistivity (defined as $K = t\tau/D\varepsilon$), which describes how resistant the solute is to the porous layer. In order to simplify the equation, a linear relationship between the concentration and osmotic pressure is assumed. Therefore, the flux equation for PRO can be rewritten as

$$J_w = A\frac{1 - \frac{C_{F,b}}{C_{D,m}}\exp(J_w K)}{1 + \frac{B}{J_w}[\exp(J_W K) - 1]} \tag{29}$$

Loeb [128] further simplified Eq. 29 by applying the linear proportionality between the concentration and the osmotic pressure in order to obtain the solute resistivity:

$$K = \frac{1}{J_w}\left(\ln\frac{B + A\pi_{D,m} - J_w}{B + A\pi_{F,b}}\right) \text{ PRO mode} \tag{30}$$

$$K = \frac{1}{J_w}\left(\ln\frac{B + A\pi_{D,b}}{B + J_w + A\pi_{F,m}}\right) \text{ FO mode} \tag{31}$$

The ICP modulus can then be obtained from the above equations when perfect solute rejection ($B = 0$) is assumed:

$$\frac{\pi_{F,i}}{\pi_{F,b}} = \exp(J_w K) \tag{32}$$

$$\frac{\pi_{D,i}}{\pi_{D,b}} = \exp(-J_w K) \tag{33}$$

Equation 32 can define the concentrative ICP, whereas Eq. 33 is for the dilutive ICP. The modification of the osmotic pressure terms in Eq. 21 with ECP and ICP modulus gives the following final flux equations for the PRO and FO modes [123]:

$$J_w = A[\pi_{D,b}\exp(-\frac{J_w}{k}) - \pi_{F,b}\exp(-J_w K)]\ \text{PRO mode} \tag{34}$$

$$J_w = A[\pi_{D,b}\exp(-J_w K) - \pi_{F,b}\exp(\frac{J_w}{k})]\ \text{FO mode} \tag{35}$$

In another study, the effects of system parameters on FO membranes were simulated using a mathematical process model [129]. This model used CP for the plate and frame (PNF) module. Membrane orientation, flow direction, flow rate, and solute resistivity were selected as system parameters. It was found that the flow directions of the feed and draw solutions have no significant influence on the FO performance. In the case of membrane orientation, the all-inside case, in which the draw solution faces the active layer, displays a relatively higher performance than all-outside and all-up cases. Notably, the membrane performances were found to be affected by K, indicating the extent of the internal CP.

In order to investigate the importance of the membrane structure in FO process, the membrane structural parameter (S) was defined [130]; S was defined as being independent of the draw solution properties, assuming that osmotically active solutes do not physically affect the membrane layers. As such, S can be used to determine the degree of ICP in the porous support structure of an FO membrane [131].

$$S = KD = \frac{t_S \tau}{\varepsilon} \tag{36}$$

where K is the membrane support layer resistance to solute diffusion, D is the diffusion coefficient of the draw solute, t_s is the support layer thickness, τ the tortuosity, and ε the porosity. The intrinsic water permeability (A) and NaCl permeability coefficient (B), which are used to calculate the K value, were found to have an intricate interrelationship with S. Therefore A, B, and S were suggested to be tailored in order to improve the membrane performance.

The most influential factor causing inconsistent S values was found to be the assumption of identical concentration and osmotic pressure ratios, which are frequently used in FO modeling. Therefore, an FEM-based model was developed with the aim of obtaining a constant S parameter [131]. This developed model could successfully simulate the FO performance with a constant S value under different feed and draw concentrations.

Advantages and Limitations

Theoretically, FO processes have a low energy consumption rate because they do not require hydraulic pressure as the driving force. RO, on the other hand, requires a hydraulic pressure of at least more than twice the osmotic pressure of seawater (~25 bar) [132]. In addition, without hydraulic pressure, the fouling behavior of FO processes is significantly different than in RO. Fouling is relatively reversible in FO processes by physical cleaning because the fouling layer is less compact and sparser than that observed in RO [133]. The recovery rate in FO may also be higher than in other membrane processes and thus can result in less brine discharge to the environment [134]. Therefore, FO processes have significant potential advantages over pressure-driven membrane processes such as RO, NF, etc.

However, even though FO has a number of advantages over pressure-driven processes, the practical application of FO is still under investigation. Two major problems of FO processes that need to be resolved are the lack of suitable FO membranes and the development of separation and recovery technologies.

In order to enhance the flux performance in FO processes, appropriate membranes that can minimize ICP phenomenon should be developed since ICP is the major factor for flux decline. A suitable semipermeable membrane must have high water permeability

(a porous layer with less thickness and higher porosity) and a high solute rejection rate [135].

Challenges pertaining to the selection of a suitable draw solution also remain as priority; complete separation of the draw solute should be guaranteed for drinking water production [136]. In addition, the draw solute should be easily recovered by reconcentration or reconstitution in order for it to be recirculated in a closed-loop system without loss. Establishment of a stable technology for this separation and recovery process can enable continuous water production. For this task, draw solutions with high osmotic pressure, a relatively big molecular size, suitable separation properties (boiling point, vapor pressure, etc.), and high water solubility are recommended.

Membrane Distillation (MD)

Membrane distillation (MD) has been studied worldwide as an attractive membrane separation process. Since it was first introduced in 1960s, there have been key improvements and developments in the system, such as for membrane engineering [137–139]. Figure 13 presents the volume of related studies published in this field. The current level of interest in MD technology started from the late 1990s; however, further studies and developments are required for prior to actual industrial applications of the technology [140–142].

Principle

MD is a promising alternative technology to conventional separation processes such as RO and thermal distillation, with lower cost and energy requirements. MD can be defined as a thermal-driven membrane process, in which only molecular water in the form of steam can transport through microporous hydrophobic membranes [143]. In this process, the aqueous feed solution, which is in direct contact with the feed side of the membrane, cannot flow through the membrane pores because of its hydrophobic nature. Consequently, interfaces between the liquid and vapor phases are formed at the membrane pore entrance, such that the driving force of MD is the vapor pressure difference across the membrane.

System Investigation

In order to create and maintain the driving force through the membrane, there are four types of configurations for MD technology:

1. Direct contact membrane distillation (DCMD): the permeate side of the membrane is in direct contact with the liquid phase, which is colder than the feed solution.
2. Air gap membrane distillation (AGMD): an air gap is interposed between the membrane and the condensing surface.
3. Sweep gas membrane distillation (SGMD): cold inert gas is used for sweeping the permeate side of the membrane to carry the water vapor molecules.
4. Vacuum membrane distillation (VMD): a vacuum is used on the permeate side of the membrane in order to increase the driving force.

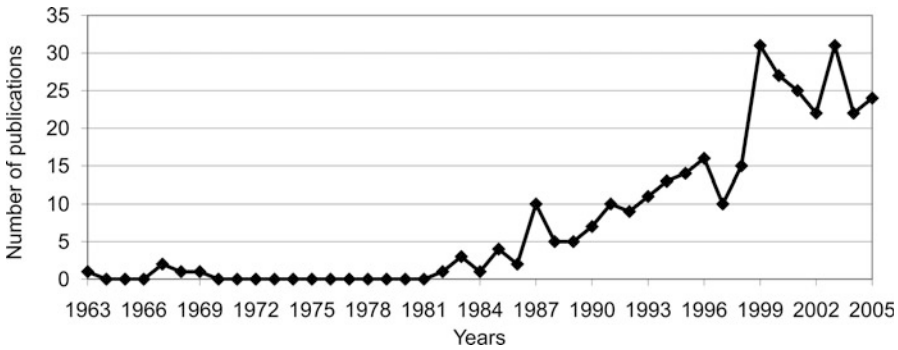

Desalination Technology for Sustainable Water Resource. Figure 13
Level of interest in MD processes [141]

Among these configurations, DCMD and AGMD are considered the most suitable for desalination technology [144–150].

System Model

Two of the main functions of an MD model are to predict the permeate flux and to estimate the temperature and concentration polarization coefficients, which are dependent on the membrane module design, operating variables, and membrane parameters. Furthermore, membrane selectivity can also be predicted for VMD configurations (Fig. 14).

As such, the effects of both temperature and concentration polarizations should be considered since heat and mass transfers occur simultaneously in MD processes (Figs. 15 and 16).

These phenomena are typically analyzed based on the assumption that vapor permeates through a microporous membrane. This flow of vapor consists of three contributions: the Knudsen flow, Poiseuille

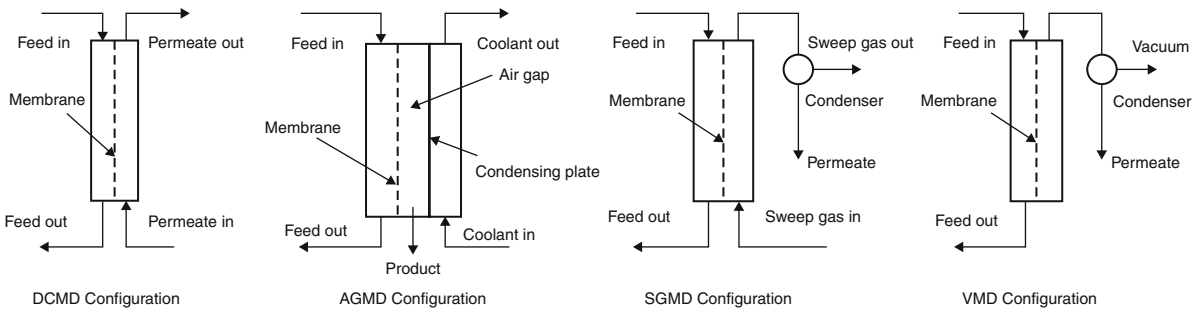

Desalination Technology for Sustainable Water Resource. Figure 14
MD configurations [141]

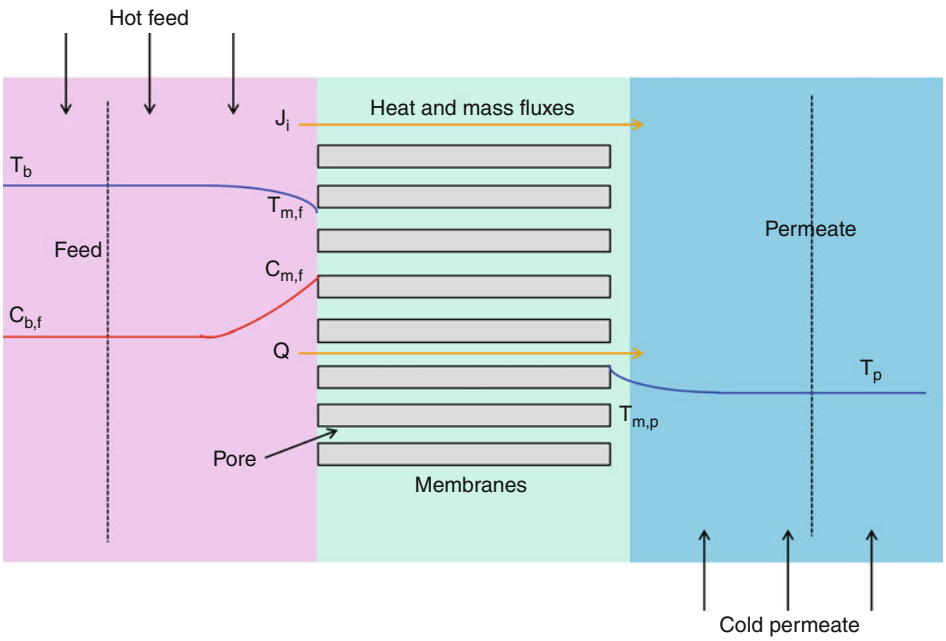

Desalination Technology for Sustainable Water Resource. Figure 15
Heat and mass transfer through the membrane in a DCMD configuration [151]

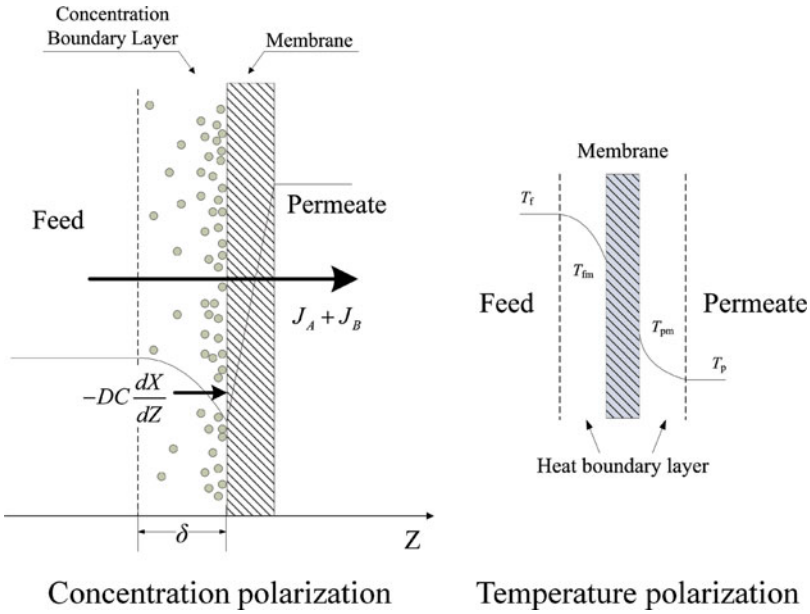

Desalination Technology for Sustainable Water Resource. Figure 16
Phenomena of temperature and concentration polarization

flow, molecular diffusion flow, and transitions between them. The dusty gas model is usually used to calculate the MD fluxes, and the molecular diffusion flow is not applied in VMD systems. Furthermore, numerical analyses have been developed by using momentum, energy, and diffusion equations.

Heat Transfer Heat transfer consists of four steps:

1. Heat transfer from the feed to the membrane surface across the thermal boundary layer on the feed side of the membrane, which can be associated with the temperature polarization effect
2. Heat transport by conduction, which is generated across the membrane matrix and heat loss occurs in the vapor filled pores
3. Mass transfer through the membrane pores as a result of the latent heat of vaporization
4. Heat transfer from the membrane surface to the permeate solution across the thermal boundary layer, which can be related to the temperature polarization effect on the feed side

In order to calculate the temperature polarization coefficient (TPC), which is defined as the fraction of difference between the transmembrane temperature and bulk temperature, the following equation is used:

$$TPC = \frac{T_{fm} - T_{pm}}{T_{fb} - T_{pb}} \tag{36}$$

where T_{fm}, T_{pm}, T_{fb}, T_{pb} are temperatures of the membrane surface and bulk on the feed and permeate sides. The latent heat for vaporization should be continuously transferred from the feed to the membrane surface because MD depends on the phase change. Thus, the equation of heat flux can be expressed as

$$\mathrm{Q_f} = \mathrm{h_f}(\mathrm{T_{fb}} - \mathrm{T_{fm}}) \tag{37}$$

where $\mathrm{Q_f}$ is the heat flux, which relies on the film heat transfer coefficient, and $\mathrm{h_f}$ is the temperature difference between the feed and membrane surface.

However, it should be noted that even though a higher feed temperature brings an exponential increase in the flux across the membrane, the effect of temperature polarization also increases with the feed temperature [148, 150].

Mass Transfer The phenomena of mass transport of volatile molecules can be explained as follows:

1. It takes place from the bulk feed to the membrane surface.
2. The vapor molecules are transported through the membrane pores.
3. It also takes place from the membrane surface to the bulk permeate phase on the permeate side.

The molar flux related to mass transport through the membrane pores can then be defined as

$$N = C\left[P_{\mathrm{fm}}(T_{\mathrm{fm}}) - P_{\mathrm{pm}}(T_{\mathrm{pm}})\right] \tag{38}$$

where C is the membrane distillation coefficient and $[P_{\mathrm{fm}}(T_{\mathrm{fm}}) - P_{\mathrm{pm}}(T_{\mathrm{pm}})]$ is the vapor pressure difference across the membrane [141].

Advantages and Limitations

Membrane distillation requires a low external energy for operation and has a relatively low capital cost for plant installation. In contrast to conventional distillation processes that require a large vapor space and high vapor velocities to provide vapor/liquid contact, MD uses a hydrophobic microporous membrane to create a vapor/liquid interface. Consequently, the MD module is much smaller than the conventional processes, which means it can minimize the capital cost and operate at much lower temperatures. In addition, the lower temperature with reduced equipment surface area can significantly decrease the heat loss [152, 153]. Therefore, alternative energy sources such as geothermal and solar energies can be applied in MD systems. Key advantages of the MD process are summarized below [143]:

- Hundred percent (theoretical) rejection of ions, macromolecules, colloids, and other nonvolatiles
- Reduced vapor spaces and lower operating temperatures compared to traditional distillation processes
- Lower operating pressures compared to conventional pressure-driven membrane separation processes
- Less chemical interaction between membrane and process solutions
- Reduction in required membrane mechanical properties

Although MD has notable advantages over other processes, a number of limitations for commercial applications in water desalination remain; these include [141]:

- A relatively low permeate flux in comparison with other separation process, such as RO
- Permeate flux decline because of concentration and temperature polarization effects, membrane fouling, and pore wetting
- A lack of membrane and module designs for MD
- High thermal energy consumption

Future Directions

Thermal Process Thermal desalination technologies, including MSF and MED, require an energy-intensive process; therefore, most research has focused on performance improvements and design simplifications.

- Development of alternative energy sources
- Mitigation and control of scaling and fouling
- Prevention and control of scaling and corrosion
- Alternative construction materials
- Optimization of process design
- Improvements in component design
- Control systems for optimizing consumables depletion

RO Process It is important to continue further development and investment efforts in SWRO desalination programs to resolve water scarcity problems in regions around the world, with the ultimate goal of reducing the cost of final water production. Subsequently, several researches to make the cost of product water more economical and enhance the process performance are suggested. These include:

- Optimization of pretreatment process design
- Development of membrane performance (durability, capacity, efficiency)
- Application of renewable energy resources
- Investigation of brine disposal (aimed for zero discharge)

There have been a number of new SWRO centers established, most by governments and big corporations, in order to promote and improve SWRO desalination. For example, the Seawater Engineering and Architecture of High Efficiency Reverse Osmosis (SeaHERO) center is one of the most important and

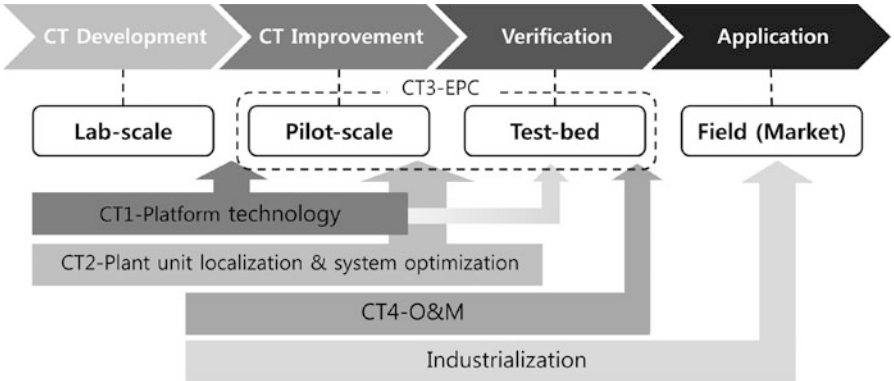

Desalination Technology for Sustainable Water Resource. Figure 17
SeaHERO's R&D strategy based on 4 CT projects and test-bed [154]

impressive centers, with a US $138.7 million budget, and involving 753 researchers from 50 different organizations. The R&D strategy of SeaHERO is based on test-bed-related core technology (CT) developments (Fig. 17).

In SeaHERO, there are four CT projects, including development of platform technologies for SWRO plant construction (CT 1: Platform technology), development of SWRO membranes and high-pressure pump component manufacturing and system optimization technologies (CT 2: Plant unit localization and system optimization), development of large-scale SWRO plant design and construction technology (CT 3: Engineering–procurement–construction (EPC)), and development of innovative operation and management (O&M) technology for large-scale SWRO plants (CT 4: O&M) [154, 155].

FO Process The ongoing studies related to FO are still at the lab-scale stage and have mainly focused on the membrane process. Therefore, FO is not currently available for water treatment applications as a stand-alone process, and will not be until these limitations can be resolved. This means that even though FO processes have been presumed to have great advantages, their practical application in real treatment plants is still far from reality, unless a reliable draw solution can be developed. Indeed, the forecast of low energy consumption, one of the biggest merits of FO, is theoretically based solely on the membrane process without considering the effective separation and recovery step. In order to be accepted as an economically feasible process, the development of membrane exclusively for FO should be progressed carefully, connected to advances in separation and recovery technologies. For the meantime, FO is expected to be hybridized with other processes, such as RO and MBR, since they have more feasible application possibilities for wastewater treatment or water reuse than for desalination.

MD Process There are several barriers that need to be overcome prior to the industrial implementation of MD processes, including [140, 141]:

- A lack of understanding pertaining to temperature and concentration polarizations, and surface membrane fouling.
- A lack of understanding of heat transfer in the MD process.

Therefore, these problems have to be investigated with respect to cost analysis, long-term operation, membrane modules, membrane fouling, and development of transfer models.

As a possible solution, in order to optimize energy requirements, hybrid systems such as RO/MD and NF/RO/MD can be offered [156]. However, although the energy consumption associated with coupling systems are higher than those of RO alone, the overall performance can be more efficient [157]. Thus, these integrated MD systems may yet be competitive alternatives to RO if thermal energy becomes readily available.

Bibliography

1. UNDP (2006) Human Development Report 2006
2. WHO (2005) The World Health Report 2005
3. Global Water Intelligence (2010) Global water market 2011, vol 1, pp 101–121, Media Analytics Ltd.
4. Khawaji A, Kutubkhanah I, Wie J (2008) Advances in seawater desalination technologies. Desalination 221:47–69
5. Global Water Intelligence (2011) DesalData.com
6. Abdul-Wahab SA, Reddy KV, Al-Weshahi MA, Al-Hatmi S, Tajeldin YM (2011) Development of a steady-state mathematical model for multistage flash (MSF) desalination plant. Int J Energy Res (doi:10.1002/er.1826)
7. Hussain AA, Nataraj SK, Abashar MEE, Al-Mutaz IS, Aminabhavi TM (2008) Prediction of physical properties of nanofiltration membranes using experiment and theoretical models. J Membr Sci 310:321–336
8. Zhao D, Xue J, Li S, Sun H, Zhang Q-D (2011) Theoretical analyses of thermal and economical aspects of multi-effect distillation desalination dealing with high-salinity wastewater. Desalination 273:292–298
9. Engelien HK, Larsson T, Skogestad S (2001) Simulation and optimization of heat integrated distillation columns. In: 42nd SIMS conference, Porsgrunn, Norway, pp 367–376
10. USEPA (2005) Membrane filtration guidance manual United States Environmental Protection Agency, EPA, 815-R-06-009
11. Van der Meer WGJ (2003) Mathematical modeling of NF and RO membrane filtration plants and modules. Ph.D. Thesis, Delft University of Technology, Netherlands
12. DOW filmtec (2005) Technical manual for FFILMTEC reverse osmosis membranes: liquid separation. Dow filmtec, Beulah, Michigan
13. Baker RW (2004) Membrane technology and applications, 2nd edn. Wiley, West Sussex
14. Wilf M (2007) The guidebook to membrane desalination technology: reverse osmosis, nanofiltration and hybrid systems, process, design, applications and economics. Balaban Desalination Publication, L'Aquila, Italy
15. Bhattacharyya D, Williams M (1992) Theory – reverse osmosis. Van Nostrand Reinhold, New York
16. Kim YM, Kim SJ, Kim YS, Lee S, Kim IS, Kim JH (2009) Overview of systems engineering approaches for a large-scale seawater desalination plant with a reverse osmosis network. Desalination 238:312–332
17. Eriksson P (1988) Nanofiltration extends the range of membrane filtration. Environ Prog 7:58–62
18. Van der Bruggen B, Vandecasteele C (2003) Removal of pollutants from surface water and groundwater by nanofiltration: overview of possible applications in the drinking water industry. Environ Pollut 122:435–445
19. Yu S, Gao C, Su H, Liu M (2001) Nanofiltration used for desalination and concentration in dye production. Desalination 140:97–100
20. Amy G (2007) Membrane-based water desalination – state of the art and future prospects. In: International seminar by center for seawater desalination plant, Seoul, Korea
21. El-Manharawy S, Hafez A (2001) Water type and guidelines for RO system design. Desalination 139:97–113
22. Al-Wazzan Y, Safar M, Ebrahim S, Burney N, Mesri A (2002) Desalting of subsurface water using spiral-wound reverse osmosis (RO) system: technical and economic assessment. Desalination 143:21–28
23. Ebrahim S, Al-Wazzan Y, Safar M, Burney N, Al-Mesri A (2000) Pilot study on renovation of subsurface water using a reverse osmosis desalting system. Desalination 131:315–324
24. El-Azizi IM, Omran AAM (2003) Design criteria of 10,000 m^3/d SWRO desalination plant of Tajura, Libya. Desalination 153:273–279
25. Elguera AM, Pérez Báez SO (2005) Development of the most adequate pre-treatment for high capacity seawater desalination plants with open intake. Desalination 184: 173–183
26. Khawaji AD, Kutubkhanah IK, Wie J-M (2007) A 13.3 MGD seawater RO desalination plant for Yanbu industrial city. Desalination 203:176–188
27. Leparc J, Rapenne S, Courties C, Lebaron P, Croué JP, Jacquemet V, Turner G (2007) Water quality and performance evaluation at seawater reverse osmosis plants through the use of advanced analytical tools. Desalination 203:243–255
28. Muirhead A, Beardsley S, Aboudiwan J (1982) Performance of the 12,000 m^3/d seawater reverse osmosis desalination plant at Jeddah, Saudi Arabia January 1979 through January 1981. Desalination 42:115–128
29. Sadhwani JJ, Veza JM, Santana C (2005) Case studies on environmental impact of seawater desalination. Desalination 185:1–8
30. Teuler A, Glucina K, Laîné JM (1999) Assessment of UF pretreatment prior RO membranes for seawater desalination. Desalination 125:89–96
31. Zidouri H (2000) Desalination in Morocco and presentation of design and operation of the Laayoune seawater reverse osmosis plant. Desalination 131:137–145
32. Kim SL, Paul CJ, Ting YP (2002) Study on feed pretreatment for membrane filtration of secondary effluent. Sep Purif Technol 29:171–179
33. Sheikholeslami R, Al-Mutaz IS, Koo T, Young A (2001) Pretreatment and the effect of cations and anions on prevention of silica fouling. Desalination 139:83–95
34. Pearce GK (2007) The case for UF/MF pretreatment to RO in seawater applications. Desalination 203:286–295
35. Wolf PH, Siverns S, Monti S (2005) UF membranes for RO desalination pretreatment. Desalination 182:293–300
36. Al-Enezi G, Fawzi N (2003) Design consideration of RO units: case studies. Desalination 153:281–286
37. Cho J, Amy G, Pellegrino J (2000) Membrane filtration of natural organic matter: factors and mechanisms affecting rejection and flux decline with charged ultrafiltration (UF) membrane. J Membr Sci 164:89–110
38. Kim S, Hoek EMV (2007) Interactions controlling biopolymer fouling of reverse osmosis membranes. Desalination 202: 333–342

39. Luo M, Wang Z (2001) Complex fouling and cleaning-in-place of a reverse osmosis desalination system. Desalination 141:15–22
40. Madaeni SS, Mohamamdi T, Moghadam MK (2001) Chemical cleaning of reverse osmosis membranes. Desalination 134:77–82
41. Malek A, Hawlader MNA, Ho JC (1996) Design and economics of RO seawater desalination. Desalination 105:245–261
42. Matsuura T (2001) Progress in membrane science and technology for seawater desalination - a review. Desalination 134:47–54
43. Pohland HW (1981) Seawater desalination and reverse osmosis plant design. In: Coating conference, proceedings of the technical association of the pulp and paper industry, Atlanta, pp 157–167
44. Sablani SS, Goosen MFA, Al-Belushi R, Wilf M (2001) Concentration polarization in ultrafiltration and reverse osmosis: a critical review. Desalination 141:269–289
45. Sheikholeslami R, Tan S (1999) Effects of water quality on silica fouling of desalination plants. Desalination 126:267–280
46. Tay KG, Song L (2005) A more effective method for fouling characterization in a full-scale reverse osmosis process. Desalination 177:95–107
47. Yiantsios SG, Sioutopoulos D, Karabelas AJ (2005) Colloidal fouling of RO membranes: an overview of key issues and efforts to develop improved prediction techniques. Desalination 183:257–272
48. Zhou W, Song L, Guan TK (2006) A numerical study on concentration polarization and system performance of spiral wound RO membrane modules. J Membr Sci 271:38–46
49. Barger M, Carnahan RP (1991) Fouling prediction in reverse osmosis processes. Desalination 83:3–33
50. Fritzmann C, Lowenberg J, Wintgens T, Melin T (2007) State-of-the-art of reverse osmosis desalination. Desalination 216:1–76
51. Hoek EMV, Allred J, Knoell T, Jeong B (2008) Modeling the effects of fouling on full-scale reverse osmosis process. J Membr Sci 314:33–49
52. Beier SP (2006) Pressure driven membrane processes, Ventus Publishing, Copenhagen, Denmark
53. Hoek EMV, Kim AS, Elimelech M (2002) Influence of crossflow membrane filter geometry and shear rate on colloidal fouling in reverse osmosis and nanofiltration separations. Environ Eng Sci 19:357–372
54. Kimura S, Nakao S (1975) Fouling of cellulose acetate tubular reverse osmosis modules treating the industrial water in Tokyo. Desalination 17:267–288
55. Ng HY, Elimelech M (2004) Influence of colloidal fouling on rejection of trace organic contaminants by reverse osmosis. J Membr Sci 244:215–226
56. Shaalan HF (2002) Development of fouling control strategies pertinent to nanofiltration membranes. Desalination 153: 125–131
57. Kurihara M, Yamamura H, Nakanishi T, Jinno S (2001) Operation and reliability of very high-recovery seawater desalination technologies by brine conversion two-stage RO desalination system. Desalination 138:191–199
58. Avlonitis SA (2002) Operational water cost and productivity improvements for small-size RO desalination plants. Desalination 142:295–304
59. Stover RL (2004) Development of a fourth generation energy recovery device. A 'CTO's notebook'. Desalination 165:313–321
60. Wilf M, Schierach MK (2001) Improved performance and cost reduction of RO seawater systems using UF pretreatment. Desalination 135:61–68
61. Wilf M, Bartels C (2005) Optimization of seawater RO systems design. Desalination 173:1–12
62. Bick A, Oron G (2005) Post-treatment design of seawater reverse osmosis plants: boron removal technology selection for potable water production and environmental control. Desalination 178:233–246
63. Reynolds T, Debroux J (2007) Seawater desalination pilot program: First and second pass RO permeate and finished water quality, Marin Municipal Water District, Corte Madera, CA
64. Jacob C (2007) Seawater desalination: boron removal by ion exchange technology. Desalination 205:47–52
65. Nadav N (1999) Boron removal from seawater reverse osmosis permeate utilizing selective ion exchange resin. Desalination 124:131–135
66. Taniguchi M, Kurihara M, Kimura S (2001) Boron reduction performance of reverse osmosis seawater desalination process. J Membr Sci 183:259–267
67. Ahmed M, Shayya WH, Hoey D, Al-Handaly J (2001) Brine disposal from reverse osmosis desalination plants in Oman and the United Arab Emirates. Desalination 133:135–147
68. Glueckstern P, Priel M (1997) Optimized brackish water desalination plants with minimum impact on the environment. Desalination 108:19–26
69. Morton AJ, Callister IK, Wade NM (1997) Environmental impacts of seawater distillation and reverse osmosis processes. Desalination 108:1–10
70. Global Water Intelligence (2008) IDA desalination yearbook 2007–2008. Media Analytics, Oxford, UK
71. Mickols WE, Busch M, Maeda Y, Tonner J (2005) A novel design approach for seawater plants. IDA World Congress, Singapore
72. Mulder M (1996) Basic principles of membrane technology, 2nd edn. Kluwer, Dordrecht/Boston
73. Tufenki N, Elimelech M (2004) Correlation equation for predicting single-collector efficiency in physicochemical filtration in saturated porous media. Environ Sci Technol 38:529–536
74. Yao KM, Habibian MT, O'Melia CR (1971) Water and waste water filtration: concepts and applications. Environ Sci Technol 5:1105–1112
75. Elimelech M, Gregory J, Jia X, Williams RA (1995) Particle deposition and aggregation: measurement, modelling, and simulation. Butterworth-Heinemann, Oxford
76. Rajagopalan R, Tien C (1976) Trajectory analysis of deep-bed filtration with sphere-in-cell porous-media model. AIChE Journal 22:523–533
77. Shin JY, O'Mella CR (2006) Pretreatment chemistry for dual media filtration: model simulations and experimental studies. Water Sci Technol 53:167–175

78. Soltanieh M, Gill WN (1981) Review of reverse osmosis membranes and transport models. Chem Eng Commun 12:279–363
79. Chen KL, Song L, Ong SL, Ng WJ (2004) The development of membrane fouling in full-scale RO processes. J Membr Sci 232:63–72
80. Visvanathan C, Ben Aim R (1989) Studies on colloidal membrane fouling mechanisms in crossflow microfiltration. J Membr Sci 45:3–15
81. Kim YM, Lee YS, Lee YG, Kim SJ, Yang DR, Kim IS, Kim JH (2009) Development of a package model for process simulation and cost estimation of seawater reverse osmosis desalination plant. Desalination 247:326–335
82. Kim SJ, Lee YG, Cho KH, Kim YM, Choi S, Kim IS, Yang DR, Kim JH (2009) Site-specific raw seawater quality impact study on SWRO process for optimizing operation of the pressurized step. Desalination 238:140–157
83. Kim SJ, Lee YG, Oh S, Lee YS, Kim YM, Jeon MG, Lee S, Kim IS, Kim JH (2009) Energy saving methodology for the SWRO desalination process: control of operating temperature and pressure. Desalination 247:260–270
84. Lee YG, Lee YS, Jeon JJ, Lee S, Yang DR, Kim IS, Kim JH (2009) Artificial neural network model for optimizing operation of a seawater reverse osmosis desalination plant. Desalination 247:180–189
85. Kim SJ, Oh S, Lee YG, Jeon MG, Kim IS, Kim JH (2009) A control methodology for the feed water temperature to optimize SWRO desalination process using genetic programming. Desalination 247:190–199
86. Lee YG, Kim DY, Kim YC, Lee YS, Jung DH, Park M, Park SJ, Lee S, Yang DR, Kim JH (2010) A rapid performance diagnosis of seawater reverse osmosis membranes: simulation approach. Desalin Water Treat 15:11–19
87. El-Halwagi MM (1992) Synthesis of reverse-osmosis networks for waste reduction. AIChE Journal 38:1185–1198
88. Maskan F, Wiley DE, Johnston LPM, Clements DJ (2000) Optimal design of reverse osmosis module networks. AIChE Journal 46:946–954
89. Nemeth JE (1998) Innovative system designs to optimize performance of ultra-low pressure reverse osmosis membranes. Desalination 118:63–71
90. Voros N, Maroulis ZB, Marinos-Kouris D (1996) Optimization of reverse osmosis networks for seawater desalination. Comput Chem Eng 20:S345–S350
91. Zhu M, El-Halwagi MM, Al-Ahmad M (1997) Optimal design and scheduling of flexible reverse osmosis networks. J Membr Sci 129:161–174
92. See HJ, Vassiliadis VS, Wilson DI (1999) Optimisation of membrane regeneration scheduling in reverse osmosis networks for seawater desalination. Desalination 125:37–54
93. Voros NG, Maroulis ZB, Marinos-Kouris D (1997) Short-cut structural design of reverse osmosis desalination plants. J Membr Sci 127:47–68
94. Lu Y-Y, Hu Y-D, Xu D-M, Wu L-Y (2006) Optimum design of reverse osmosis seawater desalination system considering membrane cleaning and replacing. J Membr Sci 282:7–13
95. Lu Y-Y, Hu Y-D, Zhang X-L, Wu L-Y, Liu Q-Z (2007) Optimum design of reverse osmosis system under different feed concentration and product specification. J Membr Sci 287: 219–229
96. Lonsdale HK, Merten U, Riley RL (1965) Transport properties of cellulose acetate osmotic membranes. J Appl Polym Sci 9:1341–1362
97. Hatfield GB, Graves GW (1970) Optimization of a reverse osmosis system using nonlinear programming. Desalination 7:147–177
98. Tweddle TA, Thayer WL, Matsuura T, Fu-Hung H, Sourirajan S (1980) Specification of commercial reverse osmosis modules and predictability of their performance for water treatment applications. Desalination 32:181–198
99. Sirkar KK, Dang PT, Rao GH (1982) Approximate design equations for reverse osmosis desalination by spiral-wound modules. Ind Eng Chem Process Des Dev 21:517–527
100. Van Dijk JC, De Moel PJ, Van Den Berkmortel HA (1984) Optimizing design and cost of seawater reverse osmosis systems. Desalination 52:57–73
101. Evangelista F (1985) A short cut method for the design of reverse osmosis desalination plants. Ind Eng Chem Proc Des Dev 24:211–223
102. Sekino M (1993) Precise analytical model of hollow fiber reverse osmosis modules. J Membr Sci 85:241–252
103. Robertson MW, Watters JC, Desphande PB, Assef JZ, Alatiqi IM (1996) Model based control for reverse osmosis desalination processes. Desalination 104:59–68
104. Sekino M (1995) Study of an analytical model for hollow fiber reverse osmosis module systems. Desalination 100:85–97
105. Van der Meer WGJ, Riemersma M, Van Dijk JC (1998) Only two membrane modules per pressure vessel? Hydraulic optimization of spiral-wound membrane filtration plants. Desalination 119:57–64
106. Al-Bastaki NM, Abbas A (1999) Modeling an industrial reverse osmosis unit. Desalination 126:33–39
107. Al-Bastaki NM, Abbas A (2000) Predicting the performance of RO membranes. Desalination 132:181–187
108. Wilf M, Klinko K (2001) Optimization of seawater RO systems design. Desalination 138:299–306
109. Villafafila A, Mujtaba IM (2003) Fresh water by reverse osmosis based desalination: simulation and optimisation. Desalination 155:1–13
110. Helal AM, El-Nashar AM, Al-Katheeri E, Al-Malek S (2003) Optimal design of hybrid RO/MSF desalination plants Part I: modeling and algorithms. Desalination 154:43–66
111. Chatterjee A, Ahluwalia A, Senthilmurugan S, Gupta SK (2004) Modeling of a radial flow hollow fiber module and estimation of model parameters using numerical techniques. J Membr Sci 236:1–16
112. Marcovecchio MG, Aguirre PA, Scenna NJ (2005) Global optimal design of reverse osmosis networks for seawater desalination: modeling and algorithm. Desalination 184:259–271
113. Abbas A, Al-Bastaki N (2005) Modeling of an RO water desalination unit using neural networks. Chem Eng J 114:139–143

114. Geraldes V, Pereira NE, Norberta de Pinho M (2005) Simulation and optimization of medium-sized seawater reverse osmosis processes with spiral-wound modules. Ind Eng Chem Res 44:1897–1905
115. Senthilmurugan S, Gupta SK (2006) Modeling of a radial flow hollow fiber module and estimation of model parameters for aqueous multi-component mixture using numerical techniques. J Membr Sci 279:466–478
116. Moch & Assiciates B.R.E. (2002) WTCcost, water treatment cost estimation program, US Bureau of Reclamation
117. Farrell MD, Cimino J (2003) Reverse osmosis desalination cost planning model. In: Proceedings of IDA World congress on desalination and water reuse, Bahamas
118. Van der Bruggen B, Vandecasteele C (2002) Distillation vs. membrane filtration: overview of process evolutions in seawater desalination. Desalination 143:207–218
119. Abdella DL (1994) Reverse osmosis desalination. Marine Technol 31:195–200
120. McGinnis RL, Elimelech M (2008) Global challenges in energy and water supply: the promise of engineered osmosis. Environ Sci Technol 42:8625–8629
121. Cath TY, Childress AE, Elimelech M (2006) Forward osmosis: principles, applications, and recent developments. J Membr Sci 281:70–87
122. Miller JE, Evans LR (2006) Forward osmosis: a new approach to water purification and desalination. Sandia National Laboratories, Albuquerque. Livermore
123. McCutcheon JR, Elimelech M (2006) Influence of concentrative and dilutive internal concentration polarization on flux behavior in forward osmosis. J Membr Sci 284: 237–247
124. McCutcheon JR, McGinnis RL, Elimelech M (2005) A novel ammonia-carbon dioxide forward (direct) osmosis desalination process. Desalination 174:1–11
125. Chung TS, Zhang S, Wang KY, Su J, Ling MM (2011) Forward osmosis processes: yesterday, today and tomorrow. Desalination (doi:10.1016/j.desal.2010.12.019)
126. Achilli A, Childress AE (2010) Pressure retarded osmosis: from the vision of Sidney Loeb to the first prototype installation – review. Desalination 261:205–211
127. Phillip WA, Yong JS, Elimelech M (2010) Reverse draw solute permeation in forward osmosis: modeling and experiments. Environ Sci Technol 44:5170–5176
128. Lee KL, Baker RW, Lonsdale HK (1981) Membranes for power generation by pressure-retarded osmosis. J Membr Sci 8: 141–171
129. Jung DH, Lee J, Kim DY, Lee YG, Park M, Lee S, Yang DR, Kim JH (2011) Simulation of forward osmosis membrane process: effect of membrane orientation and flow direction of feed and draw solutions. Desalination 277:83–91
130. Tiraferri A, Yip NY, Phillip WA, Schiffman JD, Elimelech M (2011) Relating performance of thin-film composite forward osmosis membranes to support layer formation and structure. J Membr Sci 367:340–352
131. Park M, Lee JJ, Lee S, Kim JH (2011) Determination of a constant membrane structure parameter in forward osmosis processes. J Membr Sci 375:241–248
132. Mallevialle JL, Odendaal PE, Wiesner MR (1996) Water treatment membrane processes. McGraw-Hill, New York/London
133. Mi B, Elimelech M (2010) Organic fouling of forward osmosis membranes: fouling reversibility and cleaning without chemical reagents. J Membr Sci 348:337–345
134. Elimelech M (2007) Yale constructs forward osmosis desalination pilot plant. Membrane Technol 2007:7–8
135. Tan CH, Ng HY (2008) Modified models to predict flux behavior in forward osmosis in consideration of external and internal concentration polarizations. J Membr Sci 324:209–219
136. Phuntsho S, Shon HK, Hong S, Lee S, Vigneswaran S (2011) A novel low energy fertilizer driven forward osmosis desalination for direct fertigation: evaluating the performance of fertilizer draw solutions. J Membr Sci 375:172–181
137. Bodell BR (1963) Silicone rubber vapor diffusion in saline water distillation. US Patent 285032
138. Findley ME (1967) Vaporization through porous membranes. IandEC Process Des Dev 6:226–230
139. Gore DW (1982) Gore-tex membrane distillation. In: Proceedings of the tenth annual convention of the water supply improvement association, Honolulu
140. Andersson SI, Kjellander N, Rodesjo B (1985) Design and field tests of a new membrane distillation desalination process. Desalination 56:345–354
141. El-Bourawi MS, Ding Z, Ma R, Khayet M (2006) A framework for better understanding membrane distillation separation process. J Membr Sci 285:4–29
142. Schneider K, Van Gassel TJ (1984) Membrane distillation. Membrane distillation 56:514–521
143. Lawson KW, Lloyd DR (1997) Membrane distillation. J Membr Sci 124:1–25
144. Banat FA, Simandl J (1994) Theoretical and experimental study in membrane distillation. Desalination 95:39–52
145. Bandini S, Gostoli C, Sarti GC (1992) Separation efficiency in vacuum membrane distillation. J Membr Sci 73:217–229
146. Khayet M, Godino P, Mengual JI (2000) Theory and experiments on sweeping gas membrane distillation. J Membr Sci 165:261–272
147. Kimura S, Nakao SI, Shimatani SI (1987) Transport phenomena in membrane distillation. J Membr Sci 33:285–298
148. Martínez-Díez L, Vázquez-González MI (1999) Temperature and concentration polarization in membrane distillation of aqueous salt solutions. J Membr Sci 156:265–273
149. Schofield RW, Fane AG, Fell CJD (1987) Heat and mass transfer in membrane distillation. J Membr Sci 33:299–313
150. Zhu C, Liu G (2000) Modeling of ultrasonic enhancement on membrane distillation. J Membr Sci 176:31–41
151. Khayet M (2011) Membranes and theoretical modeling of membrane distillation: a review. Adv Colloid Interface Sci 164:56–88
152. Hogan PA, Sudjito A, Fane AG, Morrison GL (1991) Desalination by solar heated membrane distillation. Desalination 81:81–90

153. Weyl PK (1967) Recovery of demineralized water from saline waters, United States Patent 3340186
154. Kim S, Cho D, Lee MS, Oh BS, Kim JH, Kim IS (2009) SEAHERO R&D program and key strategies for the scale-up of a seawater reverse osmosis (SWRO) system. Desalination 238:1–9
155. Park M, Lee YS, Lee YG, Kim JH (2010) SeaHERO core technology and its research scope for a seawater reverse osmosis desalination system. Desalin Water Treat 15:1–4
156. Criscuoli A, Drioli E (1999) Energetic and exergetic analysis of an integrated membrane desalination system. Desalination 124:243–249
157. Phattaranawik J, Jiraratananon R, Fane AG (2003) Heat transport and membrane distillation coefficients in direct contact membrane distillation. J Membr Sci 212:177–193

Desertification and Impact on Human Systems

David Mouat, Judith Lancaster
Division of Earth and Ecosystem Sciences,
Desert Research Institute, Reno, NV, USA

Article Outline

Glossary
Definition of the Subject
Introduction
Desertification and Human Systems
Discussion
Future Directions
Bibliography

Glossary

Adaptation changes made by organisms, including humans, to enable them to be more suitable for different conditions or situations.

Desertification the gradual change of habitable land which affects soils, flora, and fauna, and reduces productivity and an ecosystem's ability to adapt.

Drought a condition under which human demand for water exceeds its natural variability, usually considered to result from an extended period of reduced rainfall.

Drylands include arid, semi-arid, and dry sub-humid areas, and have a ratio of mean annual precipitation to mean annual potential evapotranspiration ranging between 0.05 and 0.65.

Ecosystem goods and services the benefits people obtain from ecosystems. These may be divided into provisioning (food and water), regulating (controlling floods and diseases), cultural (recreational, spiritual), and supporting services such as nutrient cycling.

Land degradation a temporary or permanent lowering of the biological and/or economic productive capacity of land, including changes to soil and vegetation.

Resilience the ability to recover quickly from change. Returning to the original state is often mentioned as part of a definition, but there are aspects of adaptation linked to resilience which implies that some change of state may be part of the process.

Vulnerability a condition of being at risk, and some difficulty in dealing with the situation.

Definition of the Subject

Desertification is not a new phenomenon, but it is seen to be increasing in severity and extent, with an estimated 10–20% of drylands degraded in 2005 [1]. The term "desertification" originates from the 1940s [2] although it was not widely recognized until the West African sub Sahelian droughts of the 1960s and 1970s. As Dietz and coauthors [3] discuss, the West African area has recovered from those droughts, not only because natural fluctuations in climate resulted in more rainfall but, and most importantly, because of human adaptation to the desertification "situation." In fact, desertification is not caused by a lack of rain – but by numerous interrelated contributing factors from both natural and social systems, which are acknowledged in this definition:

"Land degradation in arid, semi-arid and dry sub-humid areas resulting mainly from negative human impacts combined with difficult climatic and environmental conditions" [4].

Introduction

Faced with intensifying land degradation at the global scale, the United Nations Convention to Combat Desertification (UNCCD) was adopted in 1994, emphasizing sustainable development at the community level [5]. Regional and national assessments have been carried out [6] and research addresses many

issues. The UNCCD is committed to "bottom-up" action, recognition of traditional knowledge, and the importance of women, yet gaps among scientists, policy- and decision-makers, and communities still exist in many dryland areas hampering efforts to address this environmental, economic, and social problem.

Desertification affects arid, semi-arid, and dry subhumid regions, occurs on every continent, and affects more than two billion people who live in these areas. These are inherently fragile ecosystems often close to the tipping point between continued production of ecosystem goods and services [1] and a spiral of change leading to barren landscapes where people can no longer survive. Dryland regions tend to receive minimal attention from local or national agencies, and are typically poorly provided for in terms of education, health, and infrastructure services. Dryland peoples are thus marginalized [7], going unnoticed unless war, natural disasters, or famine draws attention to them. Poverty and desertification are strongly linked [1], and this situation is exacerbated by the political instability of many dryland regions.

Desertification and Human Systems

Changes in Production Systems

The extent, severity, and impacts of desertification vary in both space and time, driven by pressures people put on dryland ecosystems combined with the intensity of aridity [1]. Therefore, dryland productivity , the provision of goods and services – such as water, wood for fuel and building, and fodder for grazing – also varies. People have developed a range of coping mechanisms in response to the natural fluctuations of ecosystems, which include nomadism, shifting cultivation, and surplus accumulation. As pointed out by Reynolds and Stafford Smith [8] dryland peoples are not the "problem" in desertification, nor are they "victims," they are one part of an integrated system, and their responses to environmental change vary depending upon the severity, duration, and scale of the change. However, growth in both population and poverty may render previously effective coping mechanisms inadequate, and result in increased vulnerability to hunger, disease, and political pressures. With two billion people involved, these issues are serious and are likely to become more so as the implications of climate change are factored in.

Long-term trends to more intense and longer droughts and overall drying have been observed in the Sahel, Mediterranean, southern Africa, and areas in southern Asia [9] over the period 1900–2005. Climate change models for Africa indicate that temperatures are likely to increase 0.2–0.5°C per decade [10], which will contribute to increasing rainfall variability by more than one standard deviation from normal in many areas [11], and will, in turn, significantly decrease perennial surface runoff. In the Western Cape of South Africa, for example, up to half the present perennial water supply is likely to be lost – even based on a relatively optimistic climate model used by de Wit and Stankiewicz [10]. The Intergovernmental Panel on Climate Change (IPCC) [11] found that decreases in runoff totaled about 17% during the 1990s, which indicates that the trend has already started.

The IPCC Working Group 2 [in 9] reports that reduced rainfall when coupled with temperature increases, not only may lead to diminished surface water availability and less recharge, but also affects plants – to the point where current crop varieties may suffer reduced yields or not produce at all. IPCC Working Group 1 suggest that reduced rainfall in some areas juxtaposed with increased flooding in others, may make rain fed agriculture, which is practiced in many dryland areas, a precarious undertaking [9]. Rangeland, or natural pastures, upon which pastoralists depend for stock grazing are also likely to be affected with reductions in forage quantity and extent, and water points will become less reliable and productive.

These changes to natural resource viability will have, or are having, impacts beyond food shortages for dryland peoples. Competition for resources may weaken reciprocal arrangements which are inherent parts of coping mechanisms – increasing vulnerability, the possibility of conflict, migration, and the failure of social institutions such as tenure and inheritance systems, markets, and subsidies [8].

Response Strategies

Response strategies and social resilience to environmental change have been shown to be partially dependent upon the range of response options available – often at the individual household level [12]. In their analysis of building social resilience in arid ecosystems, Vogel and

Smith [12] suggest that households in the most marginal of environments tend to be poor in terms of options, lack resources for making changes, and therefore have not developed a diversified suite of production activities. Some level of household stratification exists in many parts of the southern African examples discussed by Vogel and Smith [12] and other authors in this entry.

In Namibia, unpredictable precipitation and concomitant productivity can result in cycles of abundance and paucity of natural resources and dryland agriculture crops. In the good years everyone "banks" for the future, whether it is literally in monetary terms as is the case for the wealthier individuals, or in terms of famine food stored for lean times by poorer families and communities. The stored food option is adequate until the natural cycles are changed by a prolonged drought (or climate change perhaps) when options run out, and vulnerability sets in.

Croppers and herders in Senegal have different levels of social resilience and decision-making options, yet coexist and have developed some intergroup adaptive strategies [13]. In describing their Social Resilience Model, Bradley and Grainger [13] discuss both social and environmental resilience, concluding that desertification in their study region was less severe than might be expected due to human behavior [cf.3]. By implication, adaptive strategies in the region are successful and maintain livelihoods despite climatic fluctuations, impacts of decisions by policy-makers, and the inherent variability of ecosystem resilience in time and space.

Also in Senegal, the National Action Plan initiated as part of the country's ratification of the UNCCD, established a national forum on the involvement of women. In Kenya, 30–50% of the participants in the formulation of the national action plan were women, and northeast Brazil is particularly active in promoting women's role in sustainable development [14]. Addressing gender inequalities in land tenure, inheritance, and decision making and recognizing the importance of women for dryland communities and ecosystems is a positive trend, which is gathering momentum in many countries.

Adaptation Systems and Improving Livelihoods

Most adaptation systems are of grass roots origin and local implementation, but this does not preclude their inclusion or performance within more formal organizational structures. National, Regional, and Subregional Action Programmes are key to implementing the United Nations Convention to Combat Desertification and although such programs might appear to be "imposed" or "top down," the UNCCD has recognized the importance of community level involvement, local knowledge, the role of women, and the value of synergistic activities between other UN programs [15]. The programs implemented by the UNCCD, and many in-country NGOs, operate at local level and aim to improve livelihoods within the context of desertification, rather than (or sometimes as well as) instigating remediation.

In several areas of northwestern China, desertification has been reduced over the past 5 years due to the application of new policies designed to change human activity and protect the environment. The "Grain for Green" and "Grazing Prohibition" policies are improving the environment, but other challenges remain – such as how to improve farmer's income and develop the economy. These questions were driving forces behind Zhou and Mouat's hypothetical study [16], which identified five uncertainties facing the Minqin region:

- Will there be sufficient water for agricultural and domestic use?
- What effect will climate change have?
- Is soil salinization likely to increase?
- What changes to the economy will occur, possibly as a result of government policy?
- Are land use patterns going to change?

Based upon the present land use status, one of the potential alternative futures for the region developed by Zhou and Mouat [16] focuses upon the development of high tech industry in the city of Wuwei. As a result of this, the city expands somewhat into the agricultural area, but the rural population remains on the land while taking advantage of new opportunities in the city. A policy to import high water use commodities initiated by the administration in Wuwei, combined with mandated water conservation, results in lowered water use for that area – and agriculture downstream, around Minqin, improves. Although based upon a hypothetical study, such diversification is an example of successful social resilience, which, in

conjunction with policy decisions, also enhances environmental resilience and minimizes increased desertification [cf. 13].

Management strategies – for land, water, and human resources – are critical for human existence in all ecosystems, but particularly those such as drylands which are fragile and where human–environmental interactions may have considerable implications. Traditional policies and organizations for water resource management are still effective for managing wells in southern Ethiopia [17]. However, Emiru [17] reports that newly constructed water points are often administered poorly due to newly instigated management committees. Not all "new" management strategies cause problems, as evidenced by the success of Conservancies (community-based conservation efforts, frequently targeting natural resources) [e.g., 18]. Many countries in Africa are adopting the Conservancy approach, which is usually focused on promoting conservation of natural resources and wildlife, plus sustainable utilization and sharing of resources. These organizations are a diversification from the single-family approach to management, and, recalling the arguments put forward by Bradley and Grainger [13], it is those who are able to maintain options and diversify who are most successful in living with desertification.

In western Senegal there are several strategies which are adopted by the pastoralist and agricultural groups in times of reduced productivity [13] – what is particularly interesting is how the groups vary in their perceptions and adaptations. The pastoralists move between their grazing, watering, and trade sites on a seasonal and long distance basis, both as an anticipatory and a response strategy. During these migrations, social networks and use rights are maintained on a regular basis. Both agriculturalists and pastoralists accumulate surpluses. Agriculturalists expand the area under cultivation, pastoralists build up herds with the idea that at least some of the animals would survive a future drought.

Both groups have some diversity in livelihoods including collection of forest products, trade, and spiritualist activities in addition to cropping and/or raising livestock. However, Bradley and Grainger [13] report that the pastoralists diversified more easily and had a confident approach to this adaptive strategy. In response to changing environmental conditions both groups maintained their customary production mode as long as possible, but, under pressure, pastoralists would increase their mobility, diversify stock type, or enter the gum-arabic trade. However, the response by agriculturalists is typically for some of the group to migrate to urban areas to look for work. It would appear that the pastoralists adapt readily and are innovative in their solutions, possibly as a result of the mobility and therefore flexibility inherent in their "normal" lifestyle.

Discussion

Human adaptations which improve both social and environmental resilience – such as diversification and development of reciprocal networks – are likely to be more successful, for human and ecosystems, than abandoning the land and migrating to cities. This latter strategy increases the potential for desertification, adds to the problem of urban poor, and presents a security risk for many regions.

Challenges from climate change, decreased productivity and biological diversity, poverty, and changing social institutions face the populations of the world's drylands, but Reynolds et al. [7] suggest a framework which can be used by managers and policy-makers to address the complexity of interlinked systems, and recognize what is important to change and where research can help. Based on the major characteristics of dryland ecosystems and social systems, Reynolds et al. [7] show how these relate to factors such as the maintenance of local environmental knowledge as key to functional coadaptation of both systems. This relationship is extrapolated to implications for research, management, and policy – for the local knowledge example above, this focuses on accelerating integration of science and local environmental knowledge at local and regional levels for management and policy.

Global climate change models operate at scales that do not permit a local level of analysis, and given the great spatial variability of dryland ecosystems there will be some areas which are less affected than others – even within the same ecosystem and climate regime [19]. This internal variability will impose additional social pressures upon dryland peoples, adding a further element of uncertainty to society, sustainability, and

human and environmental security. It is imperative that desertification is thought of as a process, a problem, a phenomenon that affects people not just in those places directly involved but globally as well.

Future Directions

In this entry, the process of desertification, especially as it integrates biophysical system and human use systems has been described. As Reynolds and Stafford Smith have stated, people are neither the problem nor the victims, they are a part of an integrated system. Causes and effects have been discussed as have International efforts to "combat," mitigate, and prevent desertification (UNCCD). Finally, response strategies and adaptation systems are discussed.

What will be the complexion of efforts to deal with desertification as the twenty-first century progresses? Increasing populations and concomitant competition for resources including water and arable land will require strategies to ameliorate a likely worsening situation. These include understanding how to use water and other resources more efficiently, developing salt and drought resistant crops, and developing local and green energy resources. As pointed out, at the local level, people faced with increasing land degradation and decreasing livelihoods adapt, revolt, migrate, or die. International, national, and NGOs are increasingly striving to communicate success stories across communities. These same organizations, at the very least, are drawing awareness to the problems that people living in drylands face. They are also raising awareness of the importance of developing bottom-up approaches, involving women and of using traditional knowledge in those same efforts. Developing infrastructure will assist. While early warning systems for forecasting drought have been around for decades, similar early warning systems for forecasting degradation are only in a nascent state.

Increasing our understanding of the causes and processes of desertification is important but so is the importance of figuring out how to use what is already known. It is important to ask questions about how drylands might change in the future including plausible alternatives. Assessing and analyzing the alternatives will allow one to pick pathways of development that will allow for positive futures. In our view, it is important to remain focused on the sustainability of desert ecosystems and for the people who live there, and it is essential to focus on the impacts of climate change on human use systems in the context of sustainability. While much attention is focused on ameliorating and mitigating the effects of desertification, it is important to prevent drylands from becoming desertified in the first place.

Bibliography

1. MEA (Millennium Ecosystem Assessment) (2005) Ecosystems and human well-being: desertification synthesis. World Resources Institute, Washington, p 25
2. Aubreville A (1949) Climats, forest, et desertification de l'Afrique Tropicale. Societe de Editions Geographiques, Maritime et Coloniales, Paris, p 255
3. Dietz AJ, Ruben R, Verhagen A (Eds) (2004) The impact of climate change on drylands: with a focus on West Africa. Environment and Policy Series, vol 39. Springer, New York, p 468
4. UNCED (United Nations Conference on Environment and Development) (1992) Earth summit agenda 21: programme of action for sustainable development. United Nations Department of Public Information, New York
5. The Convention. http://www.unccd.int/convention/menu.php. Accessed Nov 2010
6. Middleton N, Thomas D (eds) (1997) World atlas of desertification, 2nd edn. Arnold, London, p 182
7. Reynolds JF, Stafford Smith DM, Lambin EF, Turner BL II, Mortimore MN, Batterbury SPJ, Downing TE, Dowlatabadi H, Fernandez RJ, Herrick JE, Huber-Sannwald E, Jiang H, Leemans R, Lynam T, Maestre FT, Ayarza M, Walker B (2007) Global desertification: building a science for dryland development. Science 316:847–851, and www.sciencemag.org. May 11, 2007
8. Reynolds JF, Stafford Smith DM (2002) Do humans cause deserts?, pp 1–21. In: Reynolds JF, Stafford Smith DM (eds) Global desertification: do humans cause deserts?. Dahlem University Press, Berlin, p 437
9. CCDC (Commission on Climate Change and Development) (2008) Climate change and drylands. http://www.ccdcomission.org. Accessed Nov 2010
10. de Wit M, Stankiewicz J (2006) Changes in surface water supply across Africa with predicted climate change. Science 311:1917–1921
11. IPCC (Intergovernmental Panel on Climate Change) (2001) - Climate change: impacts, adaptation and vulnerability. World Meteorological Organization, Geneva
12. Vogel CH, Smith J (2002) Building social resilience in arid ecosystems, pp 149–165. In: Reynolds JF, Stafford Smith DM (eds) Global desertification: do humans cause deserts?. Dahlem University Press, Berlin, p 437

13. Bradley D, Grainger A (2004) Social resilience as a controlling influence on desertification in Senegal. Land Degrad Dev 15:451–470
14. (2004) Women and desertification: a dynamic relationship. Chapter 4, in UNEP, 2004, Women and the Environment, pp. 49–59. http://www.unep.org/pdf/women/chapterfour.pdf
15. UNCCD. http://www.unccd.int/main.php. Accessed Nov 2010
16. Zhou L, Mouat D (2007) Whose decisions impact land use change: the people or the government? Thoughts from Northwest China. Unpublished material
17. Emiru N (2010) Role of traditional institutions in water resource governance in the Borana lowlands, southern Ethiopia. Haramata 55:13–15
18. Who is CANAM. http://www.canam.iway.na/home.htm. Accessed Nov 2010
19. IUCC (Information Unit on Climate Change) (1993) Desertification and climate change. UNEP, Châtelaine

Direct Hydrocarbon Solid Oxide Fuel Cells

Michael van den Bossche[1], Steven McIntosh[1,2]
[1]Department of Chemical Engineering, University of Virginia, Charlottesville, VA, USA
[2]Department of Chemical Engineering, Lehigh University, Bethlehem, PA, USA

Article Outline

Glossary
Definition of the Subject
Introduction
Background
Copper-Ceria
Lanthanum Chromates
Double Perovskites
Strontium Titanates
Other Materials of Interest
Future Directions
Bibliography

Glossary

Electrical conductivity Also referred to as total conductivity. This total conductivity has three components: electronic n-type (electron charge carriers), electronic p-type (electron hole charge carriers), and ionic conductivity.

Electrocatalytic reaction Catalyzed reaction that involves charge transfer.

Humidified fuel In this text, humidified fuel refers to fuel that has been passed through room temperature water and hence contains 3 mol% H_2O.

OCP Open Circuit Potential. The potential difference measured between anode and cathode for an SOFC with an open electronic circuit. If the redox reactions occurring at the electrodes are known, the OCP can be predicted using the Nernst equation.

Overpotential The decrease in the maximum driving force (OCP), in a working SOFC. This is typically caused by charge transfer processes in the electrodes.

Oxygen stoichiometry The oxygen content of a solid oxide material. Most of the materials of interest in this study exhibit variable oxygen stoichiometry as a function of oxygen partial pressure and temperature while maintaining the cation structure.

Polarization resistance The electrical resistance of the electrode of an electrochemical device upon polarization.

SOFC Solid Oxide Fuel Cell. A fuel cell characterized as having a solid oxide electrolyte that separates the air electrode (cathode) from the fuel electrode (anode).

TEC Thermal Expansion Coefficient. Sometimes referred to as the coefficient of thermal expansion (CTE) and refers to the total expansion of the lattice cell as a function of temperature. For oxides with variable oxygen stoichiometry, the TEC consists of the thermal expansion and the chemical expansion. The latter is the expansion due to changes in oxygen stoichiometry. In this text it refers to the total expansion.

Definition of the Subject

Solid Oxide Fuel Cells (SOFCs) are one of the most promising technologies for future efficient conversion of the chemical energy stored in fuels to electrical energy. One of the primary advantages of SOFCs is the potential to operate with a wide variety of fuels. While H_2 is the fuel of choice for most fuel cells, operation with fossil-derived and bio-derived hydrocarbon fuels would bypass the costly requirement of a new H_2 infrastructure, and accelerate adoption of fuel

cell technology. This is feasible as SOFCs transport oxygen anions from the air electrode (cathode) to the fuel electrode (anode). The primary barrier to the realization of fuel flexible SOFCs is the anode material set. Traditional SOFC anodes are based on Ni composites. While these are very efficient for H_2 and CO fuels, Ni catalyzes graphite formation from dry hydrocarbons, leading to rapid degradation of cell performance and possible mechanical failure. This motivates the development of new anode materials and composites. The principle requirements of an anode are oxygen anion conductivity, electronic conductivity, and electrocatalytic activity toward the desired reaction. This entry reviews the primary issues in direct hydrocarbon anode development and discusses the new materials and composites that have been developed to meet this challenge.

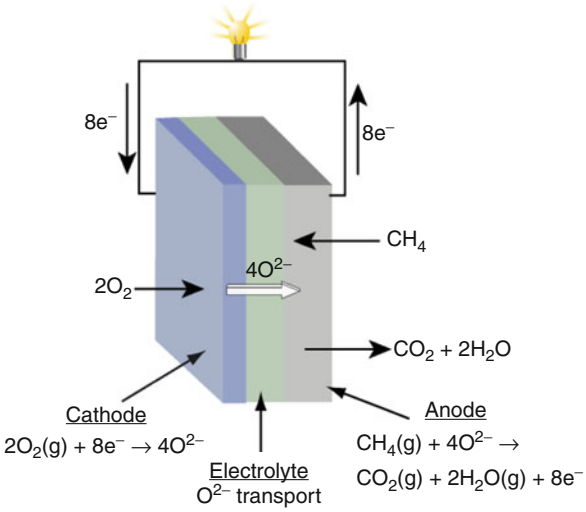

Direct Hydrocarbon Solid Oxide Fuel Cells. Figure 1 Solid Oxide Fuel Cell (SOFC) operating principle

Introduction

Traditional combustion-based methods of electrical power generation convert the chemical energy of a fuel to electrical energy via an intermediate thermal step. In contrast, electrochemical systems, such as batteries and fuel cells, promise increased efficiency through the direct conversion of chemical to electrical energy. This serves to reduce fuel demand and decrease associated greenhouse gas emissions per unit of electrical energy output. The defining difference between a fuel cell and a battery is that a battery is a closed system with a finite amount of "fuel," whereas a fuel cell is an open flow system with continuous feed of fuel and oxidant. Where a battery becomes depleted and must be recharged, a fuel cell continues to generate electrical power as long as both fuel and oxidant are supplied to the cell. Therefore, fuel cells are an efficient alternative for continuous power generation from a chemical fuel source.

There are many types of fuel cells with the primary differentiators between each type being the ion transported across the electrolyte and the operating temperature range. This entry focuses on solid oxide fuel cells (SOFCs) [1–5]. Like all fuel cells, SOFCs consist of three main components: a cathode (air electrode), an anode (fuel electrode), and an electrolyte (purely ion conducting membrane between the cathode and anode). Figure 1 is a schematic of the SOFC operating principle, showing operation with CH_4 fuel. The distinguishing feature of SOFCs is that the electrolyte is a dense, oxygen anion conducting but electronically insulating solid oxide. The SOFC operating mechanism is based upon the transport of oxygen anions from an oxygen-rich environment at the cathode (typically air) to an oxygen-lean fuel environment at the anode. The fuel and air chambers are physically and electronically separated by the dense electrolyte and the entire cell is sealed to prevent gas-phase mixing of fuel and air. The anode and cathode are ionically connected via the electrolyte, and electrically connected through an external circuit.

Under operation, electrons from the external circuit are utilized in the electrocatalytic reduction of molecular oxygen to oxygen anions at the cathode. These anions migrate through the electrolyte from the cathode to the anode. Fuel is electrocatalytically oxidized at the anode (consuming the oxygen anions) and the liberated electrons flow back to the cathode via external circuit, providing useful work. The electrochemical driving force for this process is the oxygen chemical potential difference between the cathode and anode compartments. The maximum theoretical thermodynamic driving force, the theoretical open circuit potential (OCP), can be calculated from the Nernst equation. This driving force is consumed as current is drawn

from the cell. The current generated for a given potential drop from OCP, or overpotential, is determined by the magnitude of the resistive processes within the cell electrodes and electrolyte. Assuming a constant cell temperature, electrolyte material, and electrolyte thickness, the cell current is maximized by minimizing losses associated with the reaction and transport in the electrodes. Since power is the product of potential and current, maximizing current at a high potential leads to maximum power output. The typical performance plot for an operating SOFC is a potential-current, or voltage-current (V-I) plot with accompanying power-current curve. An example is shown in Fig. 2 for an SOFC operating with H_2, CH_4, and n-C_4H_{10} fuels at 700°C.

The most commonly utilized SOFC electrolyte is 8 mol% yttria-stabilized zirconia (YSZ). YSZ is utilized as it is an almost pure oxygen ion conductor with acceptable conductivity, and is stable in both anode and cathode gas environments. The cathode [7] is a mixture of an electron or mixed oxygen ion and electron conducting oxide and the YSZ electrolyte. Typical cathode materials include $La_{0.2}Sr_{0.8}MnO_{3\pm\delta}$ (LSM) and the $La_{1-x}Sr_xCo_{1-y}Fe_yO_{3-\delta}$ (LSCF) family. The traditional anode is a combination of Ni metal and YSZ, where Ni provides electronic conductivity and electrocatalytic activity [3].

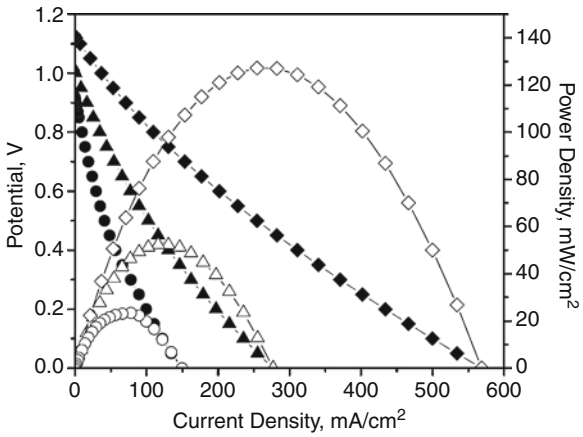

Direct Hydrocarbon Solid Oxide Fuel Cells. Figure 2 Cell potential (*closed symbols*) and power density (*open symbols*) as a function of current density in dry H_2 (*diamonds*), C_4H_{10} (*triangles*), and CH_4 (*circles*) fuels at 700°C. The cell had an LSM/YSZ cathode, 50 μm thick YSZ electrolyte, and 8/35/57 wt% $La_{0.75}Sr_{0.25}Cr_{0.5}Mn_{0.5}O_{3-\delta}$/Cu/YSZ anode. (Reproduced with permission from [6]. Copyright 2008, The Electrochemical Society)

Due to the high activation energy of ion transport in oxides, current SOFCs require operating temperatures greater than ~700°C. This high-temperature operation is advantageous in increasing efficiency, enabling the use of relatively inexpensive transition metal and metal oxide catalysts, and removing the issue of CO poisoning that plagues low temperature cells. In addition, the total system efficiency can be increased by utilizing the waste heat to generate more electrical power in a secondary turbine process. However, higher operating temperatures present challenges with regard to balance of plant material costs, startup and shutdown times, and system lifetime.

Full optimization of single cells and cell stacks requires optimization of all components, which is far beyond the scope of a single entry. There are a number of excellent reviews available in the literature that discuss SOFC development [2, 8–10]. The focus of our discussion is the direct utilization of hydrocarbon fuels in SOFC anodes. As such, the discussion here is limited to the anode material challenges and potential solution pathways specific to this goal.

The challenge for researchers is to design electrode materials and composites that provide sufficient ionic and electronic conductivity, and selectively catalyze hydrocarbon fuel oxidation. These materials must operate at high temperatures in highly reducing environments. This entry first provides background regarding the specific challenges and a brief introduction to the relevant materials chemistry. This is followed by more detailed discussions of possible solution pathways, grouped into broad material classes.

Background

Anodes for Hydrocarbon Fuels

Irrespective of the power generation route, any method that seeks to maximize electrical energy output via oxidation of a hydrocarbon fuel will emit the carbon content of the fuel as CO_2. This occurs irrespective of the number of intermediate chemical, electrochemical, or thermal steps. The goals for future power generation are thus to utilize both traditional fossil fuels and future

bio-derived hydrocarbons, minimize the amount of fuel used and CO_2 emitted per unit of electrical energy generated, and to generate the CO_2 in a high purity and more easily sequestered form.

Since SOFCs transport the oxidant (oxygen anions) to the fuel, Fig. 1, SOFCs can theoretically operate with any oxidizable fuel that can be supplied to the anode. The simplest and most commonly researched SOFC fuel is H_2 [2]. However, H_2 is not a primary energy source with ~96% of industrial hydrogen generated via energy intensive endothermic steam reforming of hydrocarbons, primarily CH_4. This is followed by high and low temperature water gas shift reactors to maximize H_2 production, and final product purification. The carbon content of the hydrocarbon is rejected as CO_2 at the point of H_2 generation. The remaining ~4% of industrial H_2 is generated by water electrolysis. The energy used to produce H_2, either by reforming or electrolysis, represents a parasitic load on the system that reduces efficiency and increases emissions. Furthermore, while hydrogen has a high mass-based energy density, the volumetric energy density is low and it is currently neither easily stored nor transported at the required scale. Direct utilization of hydrocarbon fuels would remove these barriers to fuel cell adoption and increase system efficiency.

Utilization of CO and H_2 mixtures can be considered a first step along the path to direct utilization of hydrocarbons. As with production of pure H_2, CO and H_2 mixtures are generated by hydrocarbon steam reforming. However, since the SOFC can utilize CO as a fuel, the water gas shift and H_2 purification steps are unnecessary. Hydrocarbon steam reforming can be performed either in an external reactor or internally on the SOFC anode itself. An external reactor operates as a typical hydrocarbon steam reforming system, while internal reforming requires addition of significant amounts of H_2O or O_2 to the fuel prior to feeding into the cell anode compartment. While both approaches remove the hydrogen production, storage, and transport demands, the system complexity increases and efficiency decreases compared to the promise of direct hydrocarbon utilization.

The goal for direct hydrocarbon anode design is to realize the complete electrochemical oxidation of the fuel to the total oxidation products H_2O and CO_2. This represents the full conversion of the chemical energy potential in the fuel to electrical energy in a single process unit. Where only one oxidation reaction is feasible for H_2, Eq. 1, hydrocarbons at high temperatures can undergo a large number of oxidation and polymerization reactions. The desired overall anode reaction is the total oxidation of fuel, shown in Eq. 2 for CH_4, as this represents complete utilization of the fuel and generates the maximum moles of electrons per mole of fuel consumed.

$$H_2 + O^{2-} \rightarrow H_2O + 2e^- \quad (1)$$

$$CH_4 + 4O^{2-} \rightarrow CO_2 + 2H_2O + 8e^- \quad (2)$$

By considering Eqs. 1 and 2, three clear requirements for SOFC anode materials can be derived. First, oxygen anion conductivity is required to transport the reactant oxygen anions to the reaction site. Second, the anode must selectively facilitate the desired electrocatalytic oxidation of the fuel. Third, facile electrical conductivity is required to transport the product electrons from the reaction site to the current collector wire. These material requirements are in addition to considerations of materials compatibility and stability during cell fabrication and operation, porosity in the electrode for fuel and product gas-phase diffusion, structural integrity, tolerance to impurities in the fuel and anode materials, and redox stability in case of accidental oxidation.

Current anodes for H_2 or humidified CO/H_2 fuelled SOFCs are Ni–YSZ composites. The electrolyte YSZ provides ionic conductivity, while metallic Ni is active for the oxidation of CO and H_2 and is a good electronic conductor. The operation of this anode is shown schematically in Fig. 3. Here operation with H_2 fuel is depicted, with the anode reaction given by Eq. 1. These electrodes are typically fabricated through slurry mixing and tape-casting of NiO and YSZ powders with or without pore former. The two materials are then co-fired at high temperature (>1,450°C) with the electrolyte. This is possible due to the high melting point of NiO (1,960°C) and lack of solid state reaction between NiO and YSZ. One limitation of utilizing two components is that the anode reaction can only take place at the interfaces between the Ni, YSZ, and gas phases as these are the only points at which all of the anode requirements are met – *the triple phase boundary (TPB)* highlighted red in Fig. 3. This disadvantage can

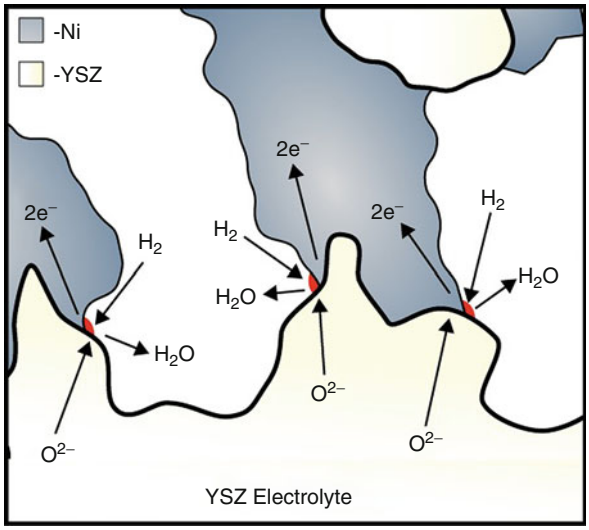

Direct Hydrocarbon Solid Oxide Fuel Cells. Figure 3 Schematic of Ni-YSZ based anode operating with H_2 fuel

be overcome by careful electrode design in terms of porosity and Ni/YSZ particle sizes and interconnectivity, and Ni-YSZ anodes do provide low overpotentials, and thus high cell power output, for H_2 and H_2/CO fuel mixtures.

The primary barrier to direct hydrocarbon utilization with these traditional anode materials is the activity of Ni toward the formation of graphitic carbon from dry hydrocarbons [11]. These carbon deposits rapidly build up in the anode structure and can generate sufficient stress to fracture the cell. While carbon formation can be suppressed by careful selection of cell operating parameters [12–16], this requires operating an inherently unstable system. For example, Barnett and coworkers demonstrated CH_4 utilization on a Ni-YSZ composite anode by using the oxygen anion flux through the electrolyte to suppress carbon formation [14]. This is impractical for application as the cell must be stable under all potential operating conditions. Thus a considerable effort has been expended to design materials and composites to replace Ni as the electronic and electrocatalytically active component.

Oxidation of Hydrocarbons in SOFC

Almost all studies regarding direct hydrocarbon SOFCs show comparatively poor performance (lower OCP and higher polarization resistance) with hydrocarbon fuels when compared to H_2 fuel, Fig. 2. Since most of these tests are performed by switching fuel on the same cell, the drop in performance must be linked to the anode. It is possible that the increased polarization resistance may be due to lower diffusivity of the hydrocarbon fuels, but the electrodes are typically highly porous and the current density per unit area is relatively low. In addition, the oxidation of 1 mole of hydrocarbon fuel yields a significantly greater number of electrons than 1 mole of H_2 fuel (H_2, CH_4, and C_4H_{10} total oxidation yield 2, 8, and 26 moles of electrons, respectively). Furthermore, the cell OCP is an equilibrium, zero current, measurement and is therefore not directly influenced by gas diffusivity. Therefore, it is unlikely that gas diffusivity limits the performance for pure fuels at low conversion. The conclusion must then be that the anode electrocatalytic activity toward hydrocarbon oxidation is the primary factor in reduced SOFC performance.

An ideal anode material would possess sufficient ionic conductivity, electronic conductivity, and electrocatalytic activity. With all of these properties present in a single mixed ionic-electronic conducting (MIEC) phase, the entire anode surface within the active region close to the electrolyte would be active toward fuel oxidation. This is depicted for CH_4 fuel in Fig. 4 with the active surface highlighted in red. The thickness of this active region would be dictated by the relative rates of oxygen ion transport and surface reaction rate [17]. If the surface reaction selectivity were 100% toward total oxidation of hydrocarbon fuel, it may be anticipated that all reactions would follow pathway 1 in Fig. 4. In this case, oxygen anions migrate from the electrolyte to the MIEC phase, and are utilized to oxidize CH_4 to CO_2 and H_2O in an electrocatalytic surface reaction. The product gases diffuse out of the anode pores with product electrons conducted through the MIEC phase to the surface current collector.

While a number of groups are pushing toward this goal, the idealized MIEC material shown in Fig. 4 has not yet been realized. All of the current materials are lacking in one or more of the critical material requirements. An alternative approach to seeking one multifunctional material is to utilize an increasing number of materials, each one meeting one or more requirements. As with the Ni-YSZ anode for H_2 and CO fuels, the combination of materials meets all of the anode

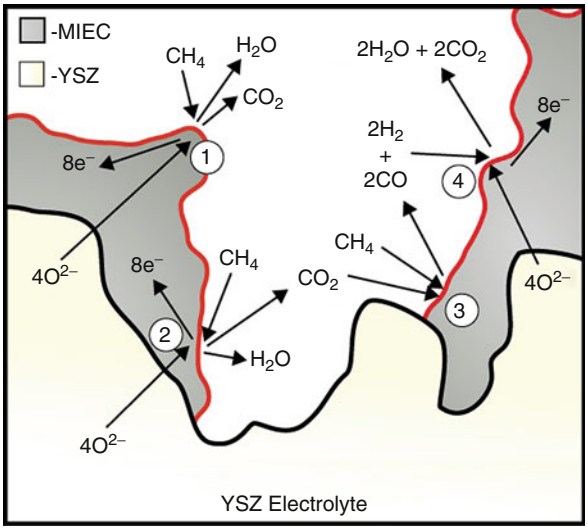

Direct Hydrocarbon Solid Oxide Fuel Cells. Figure 4 Simplified schematic of an idealized MIEC-YSZ based anode operating with CH_4

requirements and can provide high performance. However, more solid phases lead to increased complexity of the anode mechanism and increased complexity in device fabrication to ensure sufficient contact between phases.

In reality, it is unlikely that the catalyst will be 100% selective and it is also difficult to perceive that the required eight-electron charge transfer reaction will occur at a single point on the catalyst surface. Pathway 1 in Fig. 4 represents an idealized view of the target process. There are numerous alternative reaction pathways, one of which is highlighted by the steps 2–4 in Fig. 4. In this case, total oxidation of methane occurs as in step 1 above; however, the product CO_2 can react further in a dry reforming reaction with more CH_4 to form CO and H_2, step 3. These products then undergo further electrocatalytic oxidation to CO_2 and H_2O, step 4. This is, again, a representative oversimplification that serves only to demonstrate the complexity of the system. The number of possible reaction pathways for fuel oxidation is very large as products, intermediates, and reactants interact and compete for active heterogeneous reaction sites, and undergo homogenous gas-phase reactions at SOFC temperatures. This complexity only increases as the C-number of the hydrocarbon fuel is increased. Fully unraveling all of these possible reactions and their contributions toward determining fuel cell performance is very challenging.

Some insight into the dominant reaction in the anode can be provided by the cell OCP. The theoretical OCP for an electrochemical cell is given by the Nernst equation. For a cell conducting oxygen anions, this is given by:

$$E = -\frac{RT}{2F}\ln\frac{fO_2^{\frac{1}{2}(a)}}{fO_2^{\frac{1}{2}(c)}} \tag{3}$$

The fugacity of oxygen at the cathode is usually well determined as the cathode is typically exposed to air. For the anode side of the cell, the fugacity will be set by the reaction equilibria between the fuel and oxidation products. This is well defined for H_2 fuel as only one reaction can occur:

$$H_2 + \frac{1}{2}O_2 \leftrightarrow H_2O \tag{4}$$

Substituting this equilibrium expression for the anode fugacity and assuming an ideal gas yields:

$$E = E^0 - \frac{RT}{2F}\ln\frac{P_{H_2O}^{(a)}}{P_{H_2}^{(a)}P_{O_2}^{\frac{1}{2}(c)}} \tag{5}$$

where E^0 is the standard potential for the fuel oxidation reaction at the temperature of interest. The theoretical OCP for humidified H_2 at 700°C is 1.122 V and an H_2-fuelled cell should generate this well-defined OCP. Oxygen (or air) leaks through poor cell sealing or residual porosity in the electrolyte should be avoided as they will increase the oxygen fugacity at the anode and decrease the cell OCP. Electronic conductivity within the electrolyte will also reduce the OCP due to the presence of an electrical short circuit within the electrolyte. However, a well-constructed and sealed YSZ-based SOFC will generate the theoretical OCP for hydrogen fuel as YSZ is an almost pure ionic conductor.

The equivalent theoretical anode oxygen fugacity for hydrocarbon fuels is not set by a simple reaction equilibrium due to the complex reaction chemistry of these fuels. There are a large number of elementary steps, potential reaction pathways, and reaction intermediates. The most desirable reaction is the total oxidation of CH_4 to CO_2 and H_2O, Eq. 2. This provides both the highest OCP value and represents full utilization of the fuel. If the catalyst is 100% selective for this

reaction, the anode oxygen chemical potential will be set by this reaction equilibrium:

$$CH_4 + 2O_2 \leftrightarrow CO_2 + 2H_2O \tag{6}$$

In this case, the cell OCP would be fully defined by substituting this equilibrium expression into Eq. 3 to yield:

$$E = E^0 - \frac{RT}{8F} \ln \frac{P_{H_z}^{2(a)} P_{CO_2}^{(a)}}{P_{CH_4}^{(a)} P_{O_2}^{\frac{1}{2}(c)}} \tag{7}$$

However, as discussed with reference to Fig. 4, the complexity is large, even for CH_4. CH_4 can undergo total oxidation to CO_2 and H_2O, Eq. 2, or partial oxidation to CO, H_2, and/or H_2O, Eq. 8. CH_4 may also undergo surface catalyzed steam or dry reforming with product CO_2 or H_2O, Eqs. 9 and 10; react to form graphitic carbon and H_2, Eq. 11; or undergo gas phase cracking and free radical polymerization to deposit tar-like residue. All of these reaction equilibria and chemical species combine to set the anode oxygen fugacity and OCP. Furthermore, while it is desirable to selectively catalyze the electrochemical total oxidation of CH_4, this reaction involves the transfer of eight electrons. It is difficult (if not impossible) to ensure that each of these steps will occur electrocatalytically without desorption and further non-electrochemical reaction of partial oxidation products:

$$CH_4 + 3O^{2-} \rightarrow CO + 2H_2O + 6e^- \tag{8}$$

$$CH_4 + H_2O \rightarrow CO + 2H_2 \tag{9}$$

$$CH_4 + CO_2 \rightarrow 2CO + 2H_2 \tag{10}$$

$$CH_4 \rightarrow C + 2H_2 \tag{11}$$

The difficulty in defining fugacity, expected variation of anode catalyst reaction selectivity for heterogeneous reactions, and influence of anode gas residence time on the prevalence of homogeneous reactions leads to significant variation in reported cell OCP for hydrocarbon fuels. This also leads to some debate over the definition of "direct" oxidation or utilization. In this entry direct utilization refers to the direct feeding of a hydrocarbon fuel to the anode in the absence of significant diluent, H_2O, CO_2, or O_2, as adopted by McIntosh and Gorte [1].

One barrier to enhancing electrocatalytic activity is the current lack of knowledge regarding the electrocatalytic fuel oxidation mechanism in the anode. There are very few studies in the literature that seek to understand the mechanistic details of this process. In large part this is due to the complexity of the anode system and the relatively extreme anode operating environment. A classical surface science approach is not applicable to the study of SOFC systems. Many of the materials of interest have variable oxygen stoichiometry that controls the ion-electron conductivity and, most likely, catalytic properties of the material. Since oxygen stoichiometry is set by the gas-phase pO_2, temperature, and local electrochemical environment, measurements made under vacuum or at low temperature outside of a working electrochemical system are difficult, if not impossible, to relate to the performance and mechanisms of working SOFC. While one of the most intriguing and challenging aspects of SOFC systems is the unique environment in which the materials are placed, this environment presents considerable challenges to the researcher. For example, while rates of non-electrocatalytic reactions on a powder catalyst sample can be measured, it is not currently possible to accurately probe surface intermediate species under an applied potential. While some groups have attempted to relate externally measured activity to SOFC performance [6, 18–22] and have made steps toward measurements under realistic operating conditions [20], the current lack of in-situ spectroscopic tools is a significant barrier toward rational design of new SOFC electrocatalysts .

Structures and Defect Chemistry

The majority of new materials for SOFCs are perovskite structured oxides of general form $ABO_{3-\delta}$ [23]. The ideal perovskite structure is a cubic close-packed ABO_3 structure where the B-site cation sits within the octahedral interstices, Fig. 5. This structure is very flexible toward cation composition and tolerates large substitution fractions on either cation site. The Goldschmidt factor, a ratio of A, B, and O ionic radii, is often utilized to predict if a metal oxide will crystallize into the perovskite structure [24]. The A site of the commonly utilized perovskites is typically occupied by La, Ca, Sr, or Ba. The B site is typically a transition metal. Other structures investigated include double perovskites, apatites, and fluorites.

There are a number of excellent reviews and thorough treatments of the defect chemistry of oxides

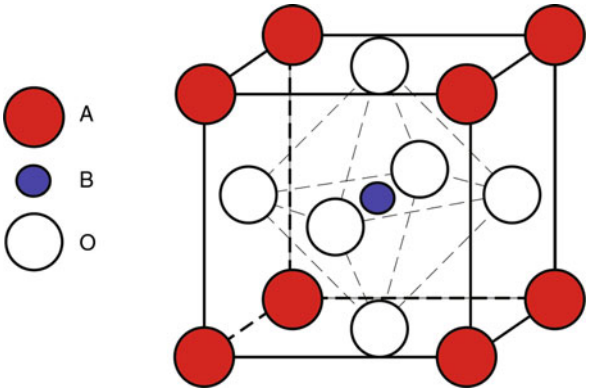

Direct Hydrocarbon Solid Oxide Fuel Cells. Figure 5 Schematic of the cubic perovskite structure

available in the literature, e.g., [25]. The brief overview below serves only to introduce the reader to primary concepts as a basis to the discussion in the rest of this entry. The following discussion is restricted to point defect models as these are predominant for most of the materials discussed.

Oxygen ion transport in these mixed oxides occurs primarily via oxygen anion hopping between oxygen vacancies. Cubic crystal structures are often considered desirable as all of the oxygen sites are geometrically equivalent. Structures with ordered oxygen vacancies may provide rapid transport through vacancy "channels" but perpendicular transport is frustrated by the ordered structure. In the absence of vacancy trapping or significant structural changes, ionic conductivity increases with increasing density of vacant oxygen sites and increasing mobility. Oxygen vacancies in these oxides are typically denoted as a deviation from the fully occupied lattice, the δ in 3-δ. Oxygen vacancies are formed either by reduction of a cation and/or by aliovalent doping.

Considering the very general system $A^{3+}B^{3+}O_{3-\delta}{}^{2-}$, a fully stoichiometric oxygen sublattice, $\delta = 0$, will exist while the combined charge on the A and B-sites is 6+, balancing the negative charge on the three O^{2-} anions. At elevated temperature and/or reduced gas-phase oxygen partial pressure, pO_2, the B-site transition metal cation may be reduced with the concomitant formation of oxygen vacancies. In Kröger–Vink notation:

$$2B_B^x + O_O^x \leftrightarrow 2B'_B + V'_O + \frac{1}{2}O_2 \qquad (12)$$

In addition to providing a mechanism for oxygen anion conduction, these oxygen vacancies can act as intrinsic electronic donors, with electronic conductivity occurring via a hopping mechanism between B and B′ sites.

An alternative approach to generate oxygen vacancies is aliovalent substitution of the element on the A or B site. For example, upon substituting X^{2+} for A^{3+}, the difference in charge can be compensated by two different mechanisms. The substitution can be compensated for through a change in the oxidation state of B to maintain a fully occupied oxygen sublattice:

$$XO + A_A^x + B_B^x + \frac{1}{4}O_2 \rightarrow X'_A + B^{\bullet}{}_B + \frac{1}{2}A_2O_3 \qquad (13)$$

In this case the number of electronic carriers is increased. Alternatively, the B site can maintain a constant charge and the A-site substitution is compensated through the formation of oxygen vacancies:

$$\begin{aligned} &2XO + 2A_A^x + 2B_B^x + O_O^x \\ &\rightarrow 2X'_A + 2B_B^x + V_O^{\bullet\bullet} + A_2O_3 \end{aligned} \qquad (14)$$

The dominant compensation mechanism, either cation reduction or vacancy formation, is a function of pO_2 and temperature. Thus by selecting materials with differing reducibility in the anode environment, electronic, ionic or mixed ionic, and electronic conductors can be created. An example of oxygen nonstoichiometry data for a candidate anode material is shown in Fig. 6. Note that the oxygen stoichiometry decreases with decreasing pO_2 and increasing temperature within the typical anode pO_2 and temperature range.

Electronic Conductivity for Direct Hydrocarbon Anodes

In order to minimize ohmic losses in the anode, the composite structure should have an electronic conductivity greater than 100 S/cm [4]. One option is to replace Ni with a metallic phase that is inert toward catalyzing carbon formation. This is the approach adopted by Gorte, Vohs and coworkers who developed direct hydrocarbon anodes utilizing Cu as the electronic conductor [1]. While this approach is very promising, the list of usable metals is very short as most transition metals either catalyze carbon formation or are prohibitively expensive.

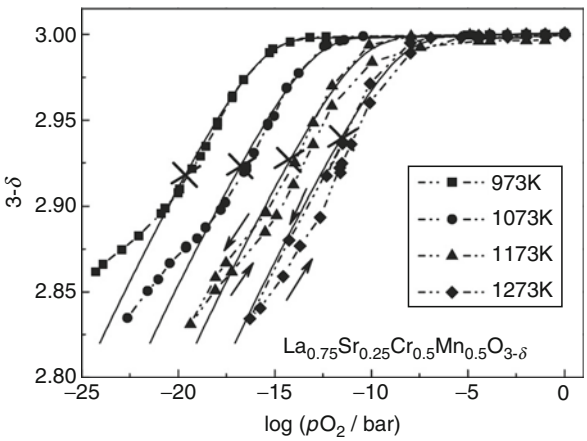

Direct Hydrocarbon Solid Oxide Fuel Cells. Figure 6 Oxygen non-stoichiometry of $La_{0.75}Sr_{0.25}Cr_{0.5}Mn_{0.5}O_{3-\delta}$ as a function of pO_2 and temperature (Reprinted from [26] with permission from Elsevier)

An alternative approach, and one with a wide possible material palette, is to develop stable and highly conductive oxides. The primary challenge is to meet the required target conductivity for both the pure material and a composite. When mixed with an electrolyte, the overall composite electronic conductivity will be considerably lower. Most attempts at this seek to boost the density of p-type carriers in the base lattice by substitution with lower valence cations. Charge compensation upon doping can be either electronic or ionic, and *n*- or *p*-type conductors can be pursued. Details specific to each material are discussed within the relevant sections in this entry.

Poisoning and Stability

Homogenous gas-phase cracking and subsequent free radical polymerization of hydrocarbon fuels at SOFC operating temperatures leads to the formation of tar-like carbon in the anode compartment [27]. This can lead to blocking of anode active sites but can also lead to improvements in anode electronic conductivity [27, 28]. This is an inherent property of hydrocarbon fuels and, as such, is a hurdle toward long-term operation for any hydrocarbon fuelled SOFC. Methods to control this carbon deposition include utilizing more stable hydrocarbons (typically CH_4), reducing cell operating temperature, co-feeding diluent or steam, or develop anodes that aid in removing these deposits by oxidation, steam reforming, and/or dry reforming with product H_2O and/or CO_2. It is essential to distinguish between this tar-like carbon formation and the catalytic formation of graphitic carbon that occurs on Ni-based anodes. This catalytic graphite formation is a property of Ni metal and must be avoided through the design of new anode materials and composites.

In addition to these undesirable side reactions, impurities in the feed must also be considered. Sulfur can be a significant poison, with its exact concentration and form dependent on the source of hydrocarbon fuel. While sulfur can be removed by preprocessing, at the time of writing (2010), the US Environmental Protection Agency requires a refinery average sulfur content of gasoline fuel of 30 ppm or lower, with a per gallon cap of 80 ppm. Pacific Gas and Electric Company in California allows a total sulfur content of 17 ppm. A number of additional impurities must be considered if coal is to be used as the carbon feedstock, including P, K, Ni, and Cl. While their influence on Ni-based anodes has been considered [29–31], this issue has not been addressed for other anode materials.

Copper-Ceria

Gorte, Vohs, and coworkers at the University of Pennsylvania pioneered the use of Cu-CeO_2-YSZ composite anodes for direct hydrocarbon utilization [1]. Their approach was to separate the anode material requirements between three materials: Cu to provide electronic conductivity without catalyzing graphitic carbon formation, CeO_2 to catalyze the oxidation of hydrocarbon fuel, and YSZ to provide ionic conductivity. These anodes cannot be manufactured utilizing the co-firing approach used for Ni/YSZ due to the relatively low melting point of CuO (1,336°C). Instead the anodes are fabricated by tape-casting a slurry of YSZ with pore formers [32]. This layer is then co-fired with the electrolyte to form a dense YSZ electrolyte supported on a thicker porous YSZ "skeleton." Following addition of the cathode, the CeO_2 and Cu phases are added via wet infiltration of metal nitrate salts followed by low temperature calcination (450°C). This infiltration approach to anode manufacture enables the incorporation of anode materials at lower temperatures. This expands the potential materials palette to materials that

would either melt, sinter heavily, decompose, or react with YSZ during high temperature sintering of the YSZ phase. This is a flexible technique that has been demonstrated for both anode and cathode manufacture [33–35]. The largest potential drawback is the time-consuming procedure of adding salt solutions, firing, and repeating until sufficient weight-loading is reached. The associated increases in cell performance must be weighed against increased manufacturing costs.

The ability to utilize hydrocarbon fuels is clearly an advantage to this approach. Cu-CeO_2-YSZ anodes have been demonstrated to operate with hydrogen fuel and via direct utilization with a range of hydrocarbon fuels from CH_4 to synthetic diesel fuel. Figure 7 shows operation of these cells with a variety of hydrocarbon fuels.

Conductivity

The YSZ in the Cu-CeO_2-YSZ composite anode is present as the primary ionic conductor. Since YSZ is a pure electrolyte, the electronic conductivity of the anode must be provided by a second phase. Although reduced CeO_2 has an electronic conductivity of greater than 1 S/cm at 1,000°C [37], the electronic conductivity in a 15 vol% CeO_2-YSZ composite was only 0.019 S/cm at 700°C in H_2 [38]. While this low electronic conductivity of CeO_2/YSZ composites is sufficient in a thin anode functional layer [39], a thicker anode structure requires higher electronic conductivity in order to minimize ohmic losses. As such, an additional phase is required. Unlike Ni, Cu does not catalyze the formation of graphitic carbon deposits in the anode, thus enabling the cell to operate with dry hydrocarbon fuel feed.

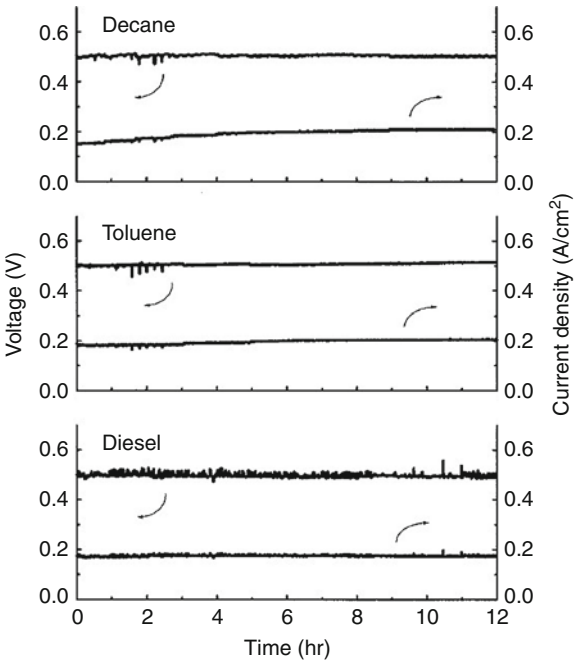

Direct Hydrocarbon Solid Oxide Fuel Cells. Figure 7 Cell voltage and current density versus time at 700°C for a cell with 10/20/70 wt% CeO_2/Cu/YSZ anode with various hydrocarbon fuels (Reproduced with permission from [36]. Copyright 2001, The Electrochemical Society)

It should also be noted that the electronic conductivity of a porous YSZ-based composite electrode will be significantly lower than that of the pure electronic conducting phases due to the porous and electron blocking YSZ. The loading of the electronic conductor required in the anode composite is dictated by percolation considerations. The electronic conductivity of a 15 vol% Cu-YSZ composite can be as high as 1,190 S/cm [38]. It should be noted that 15 vol% is much lower than the >40 vol% Ni typically utilized in Ni-YSZ anodes. This decrease in required metal loading is due to the difference in fabrication procedure. The Ni-YSZ powder processing leads to random mixing of the two phases and >40 vol% Ni is required to ensure percolation [3, 40]. In contrast, wet infiltration of Cu salt solution into a preformed porous YSZ structure leads to coating of the pore walls and formation of contiguous conducting pathways at lower volumetric loading. The electronic conductivity of the composite is thus a strong function of Cu loading, and the infiltration must be controlled to form the desired Cu structure [38].

Although Cu does not catalyze graphite formation, most hydrocarbon fuels undergo gas-phase free radical polymerization when fed undiluted into the anode compartment at SOFC operating temperatures. The long-chain and aromatic [22] products of this polymerization lead to tar-like deposits within the Cu-CeO_2-YSZ anode structure. While excessive deposition of these compounds may lead to blocking of the active sites within the anode, their electronic conductivity has a beneficial influence by reducing ohmic losses within the anode. McIntosh et al. [27] examined

the performance of SOFCs with varying Cu loading before and after exposure to dry n-C_4H_{10} at 700°C for 30 min. It was found that the initial ohmic resistance of cells with 10 wt% CeO_2 and either 5, 10 or 20 wt% Cu in H_2 fuel at 700°C was significantly higher than that calculated for the YSZ electrolyte (i.e., there was a significant ohmic resistance in the electrodes). For the cell with 20 wt% Cu, the ohmic resistance decreased dramatically upon exposure to n-C_4H_{10}, reaching the value predicted for the YSZ electrolyte. A cell with 10 wt% CeO_2 and 30 wt% Cu showed no change in ohmic resistance, matching that of the electrolyte before and after exposure to n-C_4H_{10}. This shift in ohmic resistance was ascribed to bridging gaps between isolated Cu particles with conducting tar-like carbon deposits. Indeed, further work [21] demonstrated operation of Cu-free cells utilizing only these deposits as the predominant electronic conductor.

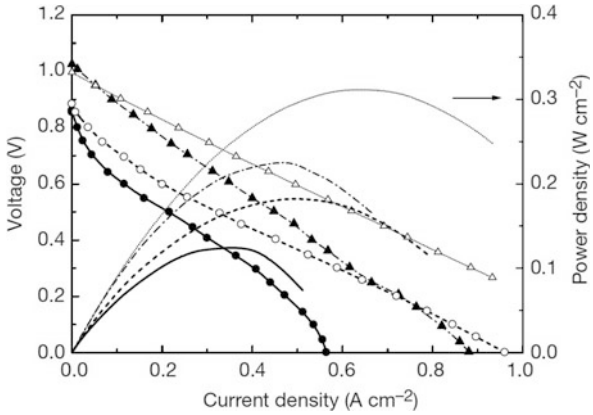

Direct Hydrocarbon Solid Oxide Fuel Cells. Figure 8 SOFC performance curves for cells with Cu-ceria composite anode. The cell had a 60-μm electrolyte, and data are shown for the following fuels: *filled circles*, *n*-butane at 700°C; *open circles*, *n*-butane at 800°C; *filled triangles*, H_2 at 700°C; and *open triangles*, H_2 at 800°C (Reprinted by permission from Macmillan Publishers, Ltd: Nature [43], copyright 2000)

Catalysis

While Cu can be utilized as a catalyst, it does not contribute significantly to the overall catalytic activity of the anode. This was verified by the low performance of Cu-only anodes, particularly in hydrocarbon fuels [22], and the identical performance achieved when Cu is replaced with catalytically inert bulk Au [41]. The role of CeO_2 as electrocatalyst for fuel oxidation was confirmed by replacing CeO_2 with other lanthanide oxides and comparing SOFC performance with the activity of the lanthanide toward fuel oxidation [22]. The cell performance tracked well with the n-C_4H_{10} light-off temperature of the lanthanide.

The performance of Cu-CeO_2-YSZ based cells (in terms of both cell OCP and maximum power density) is consistently lower for hydrocarbon fuels than for H_2. For example, Park et al. [42] reported cell OCP values of 1.05 and 0.9 V respectively for H_2 and CH_4 fuels at 700°C, with corresponding maximum power densities of 0.32 and 0.09 W/cm^2. A similar decrease is observed when comparing H_2 and n-butane fuel, Fig. 8. Kim et al. reported [36] a cell OCP of 1.1 V with current density at 0.5 V of 0.5 A/cm^2 at 700°C in H_2 fuel; these values decreased to 0.8 V and 0.2 A/cm^2 in 35 vol% toluene/N_2 fuel at the same temperature on the same SOFC.

Since the cathode and electrolyte are constant between tests, the electrocatalytic activity of the anode is the primary cause of this decrease. This limitation was partially overcome by utilizing precious metal dopants in the anode [21]. The addition of 1 wt% Pd added to a C-CeO_2-YSZ anode resulted in the same OCP, polarization resistance, and hence power density for CH_4 and H_2 fuels. The OCP in CH_4 increased from 1.0 V to 1.25 V and the maximum power density increased from 20 to 280 mW/cm^2 upon the addition of 1 wt% Pd to nominally identical anodes. This was attributed to the enhanced electrocatalytic activity of Pd-CeO_2 toward CH_4 oxidation compared to pure CeO_2. It should be noted that this cell utilized carbonaceous deposits as the electronic conducting component in the anode due to alloying between Pd and Cu. This result also suggests that care must be taken when utilizing precious metal current collectors to assess the performance of novel anodes. The current collector may inadvertently contribute significant catalytic activity to the anode.

While the influence of the electrocatalyst on cell power output is clear and trends in oxidation activity measured by traditional means track with cell

performance, very little is known about the fundamental reaction mechanism occurring in the anode. As discussed above, the thermal stability of hydrocarbons toward homogeneous cracking and free radical polymerization decreases with increasing carbon number. At SOFC operating temperatures, most hydrocarbons will readily undergo these gas-phase reactions in the hot areas of the fuel feed system and in the anode pores. Examining the OCPs reported for n-C_4H_{10} and longer-chain hydrocarbons on Cu-CeO_2 anodes finds that the OCPs are all very similar at around 0.8 V [28]. This suggests that the fuel species reaching the anode and the reactions occurring are similar for all these fuels, which makes sense when considering thermal cracking.

McIntosh et al. [21] studied the trend of OCP with CO_2 and H_2O content for H_2, CH_4, and n-C_4H_{10} fuels with CeO_2-C-YSZ anodes with and without the addition of Pd. For H_2, the trend of OCP with H_2O content for both anodes tracked the theoretical trend for total oxidation, as this is the only reaction equilibrium that can be established for H_2 fuel. For CH_4, Fig. 9, the trend for Pd-free anodes more closely follows the trend expected if CH_4 first undergoes reforming with the feed CO_2 and H_2O and it is the product H_2 that reacts at the anode. The trend line was calculated assuming the equilibrium amount of H_2 interacts with the anode. Upon addition of Pd, the measured OCP increased, with the trend line lying between the trend lines calculated for the reforming based mechanism of Pd-free electrodes and for direct CH_4 oxidation. This suggests that Pd-CeO_2 is active toward direct oxidation of CH_4. While an increase in OCP was measured upon addition of Pd for n-C_4H_{10} fuel, the increase was smaller. In addition, it was shown [27, 28] that the tar-like hydrocarbons formed by free radical polymerization are deposited in the anode structure of SOFCs with these longer-chain hydrocarbon fuels. It is likely that these deposits are the primary interaction species at OCP, even with precious metal catalyst dopants, but they may be removed from the active sites in the anode via oxidation with product H_2O under cell operation [28, 44].

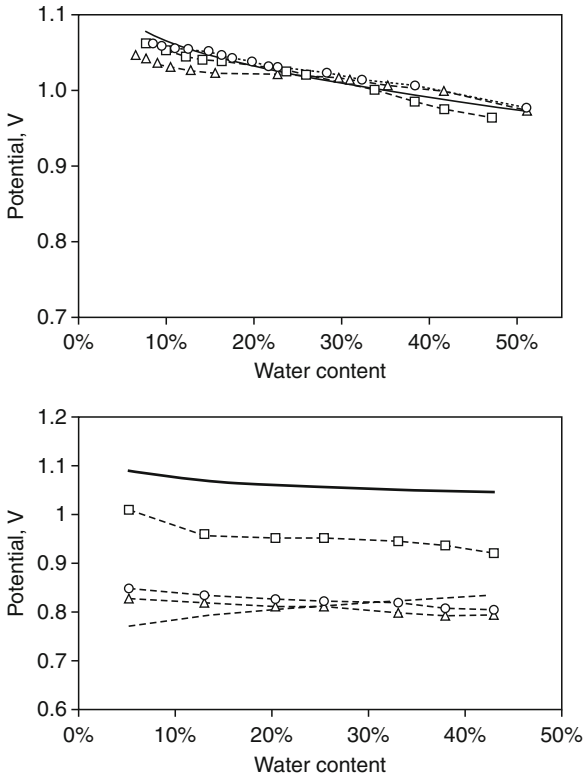

Direct Hydrocarbon Solid Oxide Fuel Cells. Figure 9 OCP as a function of H_2O content in H_2-H_2O (*top*) feed and CH_4-CO_2-H_2O (*bottom*) feed with CH_4:CO_2 ratio of 8. The calculated Nernst potentials for total oxidation of fuel are shown as bold lines (both figures) while the dashed line assumes reforming to form H_2 (*bottom*). Experimental results are shown for: C-ceria-YSZ (*triangles*); Cu-ceria-YSZ (*circles*); and C-Pd-ceria-YSZ (*squares*) anodes (Reproduced with permission from [21]. Copyright 2003, The Electrochemical Society)

Poisoning and Stability

The sulfur tolerance of these anodes is primarily dictated by the thermodynamics of ceria sulfide and oxysulfide formation, as the sulfur concentration required for Cu_2S formation is significantly higher [45]. Kim et al. demonstrated that stable operation could be achieved if the sulfur level in the fuel is reduced to 100 ppmv S as thiophene in 5 mol% n-$C_{10}H_{22}$ – this is below the concentration predicted from thermodynamics for Ce_2O_2S formation. This study was followed by work of He et al. who demonstrated stable operation up to 450 ppmv H_2S in H_2 [46], significantly higher than the tolerance levels reported for Ni-based anodes [47].

As these cells operate at temperatures relatively close to the melting point of Cu (1,085°C), concerns have been raised regarding the thermal stability of Cu. While Cu will sinter at SOFC operating temperatures, the thermal stability of the Cu phase is shown to be a strong function of the infiltration technique and precursor. These parameters influence the distribution of Cu throughout the anode structure [38]. Alloying may be utilized to increase the melting point, although alloy metals and alloy level must be chosen carefully in order to avoid nullifying the benefits of Cu with regard to graphitic carbon formation. Kim et al. [48] demonstrated the use of Cu-rich Ni alloys in preventing graphitic carbon formation and showed 500 h of operation in dry CH_4 with 80–20 mol% Cu-Ni replacing Cu in the anode. Lee et al. [49] expanded this to include Cu-Co based anodes and proposed that segregation and subsequent surface coverage of the Co by a Cu layer provided stable operation with dry hydrocarbon fuels. With regard to the CeO_2 phase, doping with Zr has been shown to significantly enhance thermal stability [50].

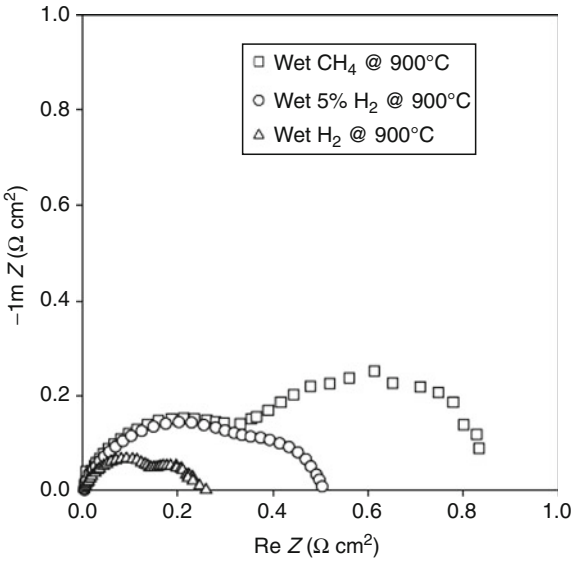

Direct Hydrocarbon Solid Oxide Fuel Cells. Figure 10 Electrode impedance of an optimized $La_{0.75}Sr_{0.25}Cr_{0.5}Mn_{0.5}O_3$ anode at 900°C, in different humidified fuel gas compositions. The electrolyte contribution has been subtracted from the overall impedance (Reprinted by permission from Macmillan Publishers, Ltd: Nature Materials [52], copyright 2003)

Lanthanum Chromates

Lanthanum chromate ($LaCrO_{3-\delta}$) is a reasonable electronic conductor and is stable up to high temperatures (> 1,000°C) in both oxidizing and reducing ($pO_2 < 10^{-21}$ atm) environments [51]. Perhaps the most promising material in the $LaCrO_{3-\delta}$ family so far is $La_{0.75}Sr_{0.25}Cr_{0.50}Mn_{0.50}O_{3-\delta}$ (LSCM). Single phase LSCM anodes showed low anode polarization resistances, 0.26 and 0.87 Ω·cm^2 in humidified H_2 and CH_4, respectively, at 900°C [52], Fig. 10. High power densities, 0.86 and 0.48 W/cm^2, were observed for SOFC with LSCM/Cu composite anodes in 850°C H_2 and CH_4, respectively [53]. Note that electrolyte thickness, electrode geometry, and cathode material can dictate power density as much as anode material, and that power densities should only be compared between nominally identical cells.

As $(La,Sr)CrO_3$ itself is not catalytically active toward hydrocarbon oxidation [54], Cr has been partially substituted with a variety of elements, limited mostly to first-row transition elements (Ti, V, Mn, Fe, Co, and Ni) and Ru, in an effort to enhance catalytic activity [55–58]. These substitutions significantly impact the stability of the perovskites. $(La,Sr)CrO_3$ with 5–25 mol% of Ru [59] on the B site or with large amounts (20–50 mol%) of Co [56], Fe [60] or Ni [56, 61] substituting for Cr are unstable, as the dopant cations exsolute from the perovskite lattice under reducing conditions. $LaCrO_3$ substituted with Ti is stable in reducing and oxidizing conditions, but has poor catalytic activity for fuel oxidation [56], showing large polarization resistances when used as anodes [62]. This is likely due to the low redox activity of Ti. Finally, the introduction of significant amounts (≥ 10 mol%) of V into the $(La,Sr)CrO_3$ lattice requires firing in highly reducing conditions [19]. It is likely that, as with LSV, V-substituted lanthanum chromates will not be stable in air [63].

The best substituent for Cr seems to be Mn, as LSCM shows stable performance in humidified CH_4 at 900°C [64], and has some catalytic activity for the total oxidation of hydrocarbons [65]. Although Zha et al. [66] reported that LSCM was stable in pure H_2 at 950°C ($pO_2 < 10^{-20}$ atm), Kawada found significant

quantities of the decomposition products $LaSrMnO_4$ and MnO in LSCM pellets after thermogravimetric measurements at lower temperatures and under less reducing conditions (900°C, $pO_2 = 10^{-20}$ atm) [26]. The same phases were encountered by other researchers after treating LSCM powder in humidified 20% H_2/N_2 at 800°C for 8 h [19]. These differences are expected to be due to variations in treatment times and synthesis procedures. The results indicate that LSCM may not be completely stable in pure fuel at very high temperatures. However, the actual pO_2 values in a working anode are expected to be higher than the pO_2 in the surrounding atmosphere due to the transport of oxygen through the SOFC, which could stabilize the anode material.

Conductivity

The total conductivity of $La_{0.75}Sr_{0.25}Cr_{0.50}Mn_{0.50}O_{3-\delta}$ was reported to be ~40 S/cm in air, and 1.5 S/cm in 5% H_2 at 900°C [64, 67] Fig. 11. While constant at high pO_2, total conductivity decreased sharply for $pO_2 < 10^{-10}$ atm [67], indicative of *p*-type conductivity [64, 68]. Positive values for the Seebeck coefficient under oxidizing conditions confirmed that conductivity in LSCM is *p*-type dominant [67, 69]. At low temperatures and in high pO_2 atm, the net negative charge created by the substitution of La^{3+} with Sr^{2+} is compensated by an increase in the average oxidation state of Mn, generating electron holes localized on Mn that are responsible for electronic conductivity [68], Eq. 15.

$$4SrO + 4La_{La}^{\times} + 4Mn_{Mn}^{\times} + O_2(g) \leftrightarrow 4Sr'_{La} + 2La_2O_3 + 4Mn_{Mn}^{\bullet} \quad (15)$$

The activation energy for the conductivity is on the order of 0.1 eV, indicative of conduction through a thermally activated polaron-hopping mechanism.

At elevated temperatures and in low pO_2 atm, Mn is reduced in average oxidation state and the net negative charge is now compensated by the formation of oxygen vacancies, Eq. 16, Fig. 6.

$$4Mn_{Mn}^{\bullet} + 2O_O^{x} \leftrightarrow 4Mn_{Mn}^{x} + 2V_O^{\bullet\bullet} + O_2(g) \quad (16)$$

The decrease in electron holes, evident from Eq. 16, results in a decrease in total conductivity in atmospheres with $pO_2 < 10^{-10}$ [67, 70]. Due to the generation of oxygen vacancies, this decrease is accompanied by an increase in oxygen ion conductivity, from $\sim 4\times10^{-5}$ S/cm at high pO_2 to $\sim 4 \times 10^{-4}$ at $pO_2 = 10^{-15}$, measured at 950°C. Although the ionic conductivity will be even higher in fuel atmospheres ($pO_2 \leq 10^{-21}$ atm), the conductivity under these conditions was found to remain dominated by electron holes [67].

The total conductivity of 1.5 S/cm in 5% H_2 is further reduced in the SOFC anode and by the use of composite porous GDC/LSCM or YSZ/LSCM anodes, to values of ~0.1 S/cm in humidified H_2 at 800°C for a YSZ/LSCM composite [71]. Although this value is much lower than the 100 S/cm suggested by Steele [4], thin YSZ/LSCM anodes with 1 wt% Ni show reasonable performance in H_2 nonetheless [34].

The substitution of La^{3+} with up to 50 mol% of Sr^{2+} has been attempted to enhance the electronic conductivity of LSCM [70]. However, the conductivity at low pO_2 is almost independent of the amount of Sr in the range of 0.20–0.30 mol% Sr [68], and the introduction of more than 0.25 mol% Sr did not significantly enhance electric conductivity. Furthermore, the presence of ≥ 30 mol% Sr resulted in higher solid state reactivity and decreased the compatibility with the YSZ electrolyte [70]. Increasing the amount of Mn on the B site was reported to enhance the conductivity both in air and reducing atmospheres, but decreased the stability at low pO_2 [66].

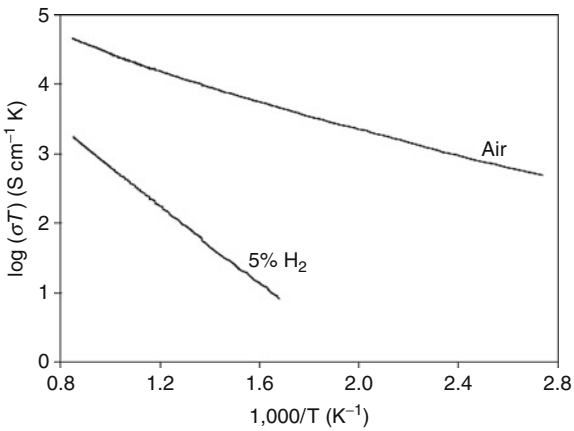

Direct Hydrocarbon Solid Oxide Fuel Cells. Figure 11 Temperature (T) dependence of total conductivity (σ) of $La_{0.75}Sr_{0.25}Cr_{0.5}Mn_{0.5}O_{3-\delta}$ in air and 5% H_2 (Reprinted by permission from Macmillan Publishers, Ltd: Nature Materials [52], copyright 2003)

Another method is the substitution of La^{3+} with alkaline earth elements other than Sr. Since the different alkaline earth elements are present in the 2+ oxidation state at the relevant conditions, the number of electron holes is not expected to change significantly for substitution with different alkaline earths. However, changes in lattice parameters and in the distance between the Mn centers, caused by differently sized A-site cations, could affect the electrical conductivity through changes in charge carrier mobility. The electrical conductivity was shown to change when substituting La with Mg and Ba, but this was mostly due to the formation of secondary phases [72]. Apart from Sr, only substitution with Ca resulted in a phase-pure perovskite, but without an increase in conductivity compared to LSCM [72]. Furthermore, the introduction of Ca is expected to result in the instability of LSCM under reducing conditions [73].

In practice, electronic conductivity has been increased by developing composite anodes of LSCM and an electronic conductor. Cu in particular has been used for the latter [6, 53], since it is an excellent electronic conductor and does not promote hydrocarbon cracking. Therefore, the large amounts of material required to achieve a percolation path can be added without carbon deposition during SOFC operation in hydrocarbon fuels. Although the electronic conductivity was not measured directly, Zhu measured a decrease in anode overpotential and a concomitant increase in SOFC power density with the addition of increasing amounts of Cu to LSCM [53], Fig. 12. The decrease in overpotential was mainly due to a decrease in the ohmic resistance of the SOFC. Since Cu replaced the catalyst LSCM, an optimum in Cu amount was expected. Indeed, this optimum was observed at 20 wt % Cu, at which point the current density was increased more than fourfold, compared to the pure LSCM anode. With the addition of more Cu, the low-frequency impedance part, ascribed to fuel-related oxidation processes, increased significantly. This may be due to blocking of the active area on the LSCM within the anode.

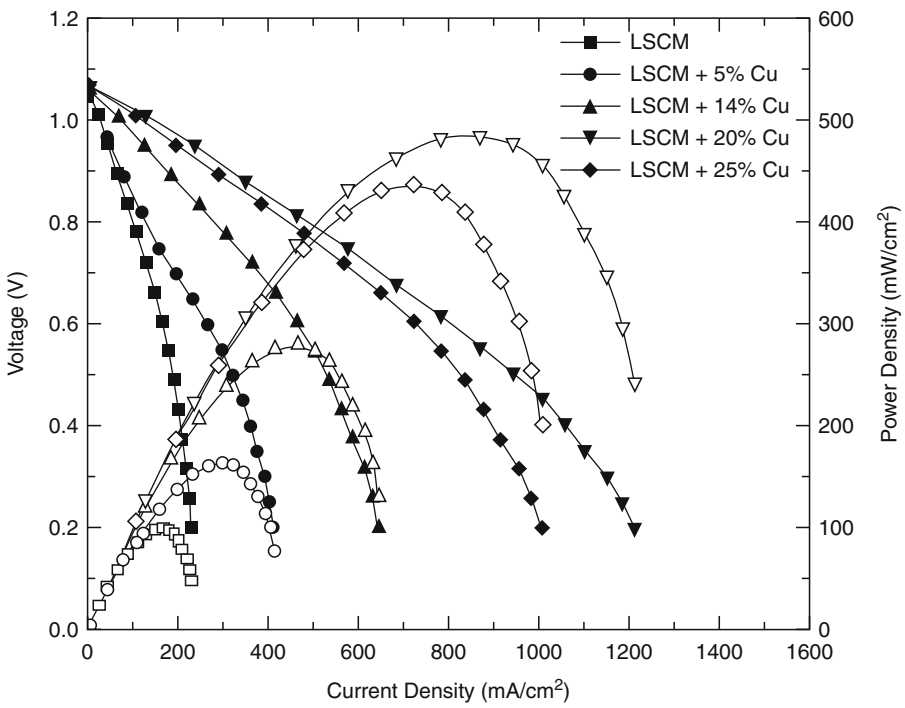

Direct Hydrocarbon Solid Oxide Fuel Cells. Figure 12
Voltage and power density for single cells with different LSCM + Cu composite anodes at 850°C in dry CH_4 (Reprinted from [53] with permission from Elsevier)

To our knowledge, a systematic enhancement of the ionic conductivity has not been attempted. Instead, SOFC anodes typically use a composite of LSCM with an electrolyte material, such as YSZ [71] or ceria [74]. Care has to be taken when attributing increases in cell performance to enhanced ionic conductivity, as ceria has some total oxidation activity and could function as a catalyst. Also, at least part of the increase in performance is likely to be structural, since the porous YSZ or GDC scaffold creates a large surface area for the oxidation reaction to take place.

Catalysis

Although the exact reaction mechanism is unclear, general concepts regarding the fuel oxidation reaction on LSCM have been described in the literature. Yamazoe and Teraoka pointed out that high-temperature oxidation reactions on perovskites typically occur through a reduction-oxidation cycle of the catalysts, otherwise known as a Mars-van Krevelen-type (MvK) mechanism [75], with the B-site elements serving as the redox centers. Studies suggest that this is the case for LSCM.

The active center of LSCM was identified by reducing air-annealed LSCM in fuel atmosphere, and comparing the energy levels of Cr and Mn before and after the reduction using X-ray Adsorption Near Edge Structure (XANES) analysis, Fig. 13. While the Cr K edge energies remained constant, the energy levels were different for Mn before and after reduction, attributed to a difference in oxygen coordination. This indicates that the average oxidation state of Mn decreases during reduction [68], identifying Mn as the active redox center. This is further supported by the poor catalytic activity of $LaCrO_{3-\delta}$ toward hydrocarbons, compared with the higher activity of $LaMnO_{3-\delta}$ [54].

Initial catalytic tests indicated that LSCM catalyzes the oxidation of hydrocarbon fuels, although it also has some activity toward dry reforming [65]. Compared to the conversion of CH_4 in a blank reactor, LSCM enhanced the reaction rate of CH_4, and increased the selectivity toward total oxidation. Even under relatively oxygen-lean conditions (CH_4:O_2 gas mixtures of 4:1), LSCM promoted the total oxidation of CH_4 to CO_2, up to 800°C. At 850°C, the CO_2/CO selectivity was still 98.6% in favor of CO_2. No significant steam reforming activity was measured.

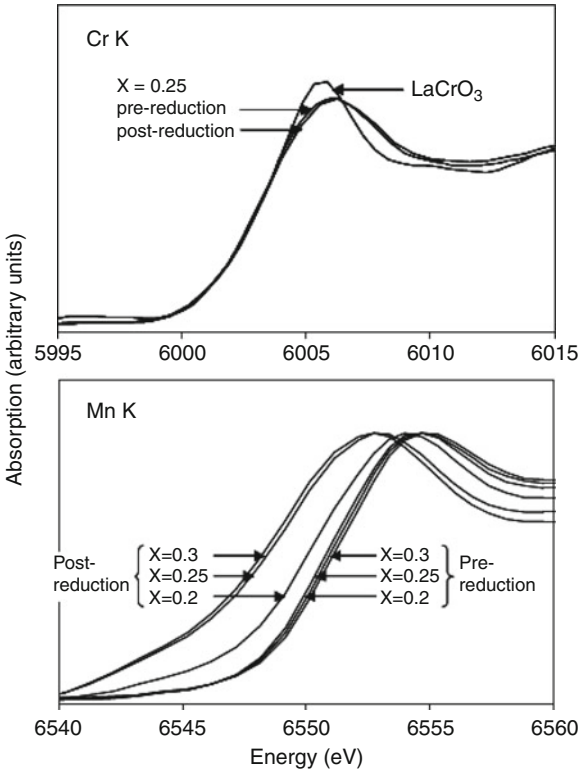

Direct Hydrocarbon Solid Oxide Fuel Cells. Figure 13 Cr and Mn K XANES spectra for $La_{1-x}Sr_xCr_{0.5}Mn_{0.5}O_{3-\delta}$ (Reprinted from [68] with permission from Elsevier)

The experiments described above were performed by co-feeding oxygen and CH_4, resulting in a $pO_2 \sim 10^{-1}$ atm, much higher than the pO_2 of $\sim 10^{-20}$ present at a working SOFC anode. Furthermore, the measured reaction rates are not differential rates as they were determined for 100% conversion. In order to determine the oxidation rate and the selectivity for total and partial oxidation of CH_4 under conditions similar to those of operating anodes, van den Bossche and McIntosh developed a pulse-type reactor [20]. In this set-up, pulses of CH_4 (or H_2) are fed to a reactor containing oxidized powder catalyst. No oxygen is co-fed with the fuel; instead, the fuel is oxidized utilizing oxygen from the oxide catalyst surface and bulk. Inert gas is fed between the short pulses of hydrocarbon fuel to allow re-equilibration of the surface oxidation states. This is necessary to prevent the measurement of a bulk oxygen diffusion limited rate. The pO_2 above the catalyst during a hydrocarbon pulse is that of pure fuel,

and the oxygen source is the same as in the anode. Thus the CO_x production rates and selectivity are those of the fuel cell. Furthermore, since each pulse titrates a small amount of oxygen from the lattice, multiple pulses and knowledge of the original stoichiometry enable measurement of rates and selectivity as a function of oxygen stoichiometry.

Pulse experiments on $La_{0.75}Sr_{0.25}Cr_{1-x}Mn_xO_{3-\delta}$ (x = 0.25 – 1) indicated that CH_4 oxidation rates increased with increasing Mn substitution and decreased with decreasing oxygen content. Both observations are in agreement with a modified MvK mechanism with Mn as the redox center. The oxygen stoichiometry (3-δ) of the perovskite influenced product selectivity. At high lattice oxygen content, $\delta \approx 0$, total oxidation was the preferred reaction for all Mn/Cr ratios, with 100% of CH_4 reacting to CO_2, Fig. 14. When less lattice oxygen was present, CO production dominated. The formation of CO was suggested to occur through the partial oxidation of CH_4, rather than secondary dry reforming.

Attempts have been made to link this shift in reaction rate and selectivity with oxygen stoichiometry to observed shifts in SOFC anode polarization resistance. At open circuit conditions at 700°C with CH_4 fuel, the LSCM oxygen stoichiometry is low as the material is at equilibrium with the fuel gas. This appears to promote cracking as the main reaction, with correspondingly high anode polarization resistance, ~12.3 $\Omega \cdot cm^2$ [6]. Upon application of current, it is suggested that the oxygen ion flux locally increases the oxygen stoichiometry of the perovskite. The pulse reactor studies suggest that this should shift the reaction mechanism toward total oxidation of the fuel and increase the activity. This is observed as a decrease in anode polarization (to 1 $\Omega \cdot cm^2$) and a shift toward CO_2 production with increasing SOFC current density.

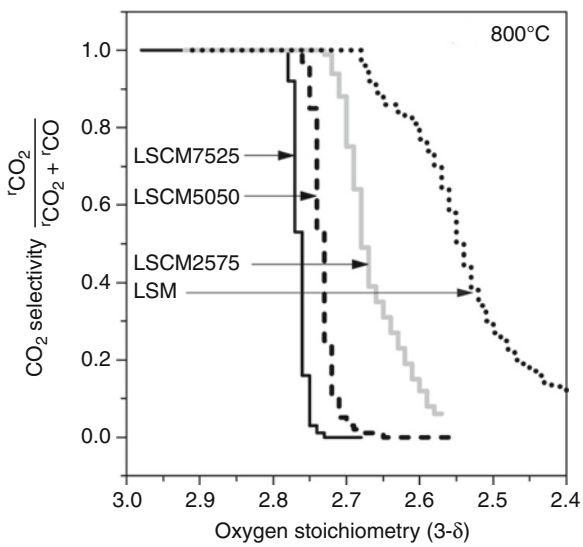

Direct Hydrocarbon Solid Oxide Fuel Cells. Figure 14 Selectivity toward total oxidation of methane at 800°C. The black solid line is LSCM with 75 mol% Cr and 25 mol% Mn (LSCM7525), dashed line is LSCM5050, gray solid line is LSCM2575 and dotted line is LSM (Reprinted from [20] with permission from Elsevier)

While these results are interesting, SOFC with LSCM anodes show significantly lower power outputs in C_4H_{10} and CH_4, when compared with H_2 fuel [6]. Since the change in fuel only influences anode conditions, the anode activity toward oxidation of hydrocarbons appears to be a performance-limiting process for these anodes. This was further illustrated by electrochemical measurements on SOFCs with dense LSCM films [18]. The OCP values measured for these SOFCs with CH_4 on the anode were comparable to the values measured in inert gas (He), ~0.06 V. It was suggested that the kinetics for CH_4 oxidation are slow, and that the contact time of the fuel on the relatively smooth surface was too short to set the CH_4 reaction equilibrium. The addition of small amounts of Pd as a catalyst to the anode resulted in reasonable OCP values, ~0.87 V, proving that the catalytic performance of LSCM toward CH_4 is low and must be improved.

To enhance catalytic activity, the B site of LSCM has been substituted with a third element that is suggested to be more active for hydrocarbon oxidation than Mn. Ni and Fe are attractive choices as their respective lanthanum perovskites show CH_4 conversion at lower temperatures than $LaMnO_3$ [54]. Also, Ni is used as the oxidation catalyst in traditional Ni/YSZ anodes. Although large amounts of Co, Fe, or Ni substitution are unstable [56, 61], small amounts of Ni (10 mol%) were suggested to be kinetically stable in the $LaCrO_3$ lattice [73]. Furthermore, the use of relatively small amounts of Co, Fe, or Ni, even if exsoluted, is not expected to lead to the mechanical failure that is caused by large amounts of especially Ni, as carbon formation and volume changes upon redox cycling will be limited.

Van den Bossche and McIntosh replaced 10 mol% of Mn with Co, Fe, or Ni and found that CH_4 oxidation rates were greatly enhanced on LSCMNi and LSCMCo, up to an order of magnitude compared to LSCM. This occurred only after the exsolution of the Co and Ni metals. The degree of carbon formation for LSCMNi and LSCMCo was similar to LSCM [19], suggesting that these compositions can be used as redox-stable, direct oxidation anodes.

Instead of introducing small amounts of catalytic elements into the perovskite, catalysts have also been successfully added to the anode as a separate phase. Again, Ni is the primary focus, as are precious metals such as Pd, Pt, and Rh. By adding a relatively small amount (4 wt%) of Ni to a GDC/LSCM (80% Cr) anode, Liu et al. [74] were able to increase the performance of SOFCs from ~50 to 80 mW/cm^2 in 750°C CH_4 (the relatively low power output resulted partly from a thick electrolyte). As the small amount of Ni was not expected to significantly increase the electronic conductivity, the increase in power output is mainly due to the enhancement in catalytic activity of the GDC/LSCM-Ni anode. Although the composite anodes with 4% Ni generated a small amount of carbon deposits in C_3H_8 fuel under open circuit conditions, no noticeable carbon formation occurred in working SOFCs. This was in contrast to composites with large amounts of Ni, which generated significant amounts of carbon, even under operating conditions. Although the SOFC power output of the GDC/LSCM anode with 4% Ni dropped slightly after a first redox-cycle, performance was stable during the next three cycles. Long-term electrochemical stability studies are required to determine the stability of this composite anode.

Using a similar method, Kin et al. obtained a power output of ~500 mW/cm^2 in humidified H_2 at 700°C utilizing YSZ/LSCM anodes with 0.5–1 wt% of either Pd, Rh or Ni added as a separate phase, Fig. 15. These values are to be compared to the power output of ~100 mW/cm^2 for YSZ/LSCM without metals added. The addition of 1 wt% Fe to YSZ/LSCM also increased power output to 400 mW/cm^2 [34]. An enhancement in SOFC performance with the addition of Pd was found by other researchers as well, but not to the extent of a fivefold increase [53]. The smaller impact may be due to other limiting processes, such as low ionic conductivity.

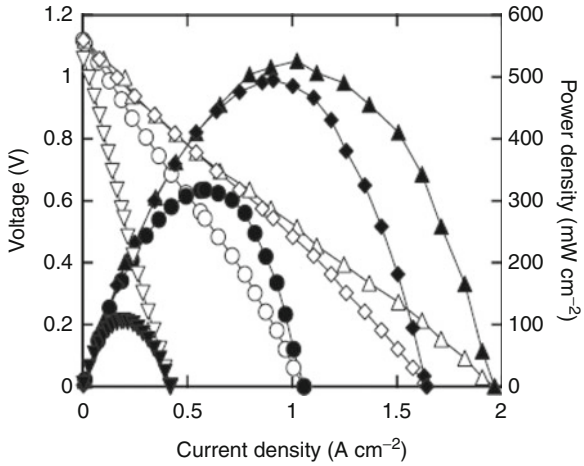

Direct Hydrocarbon Solid Oxide Fuel Cells. Figure 15 V-I polarization curves (open symbols) and power densities (filled symbols) in humidified H_2 at 700°C for cells having anodes with 45 wt% LSCM in YSZ, using various catalysts: (▼) no catalyst, (●) with 5 wt% ceria, (♦) with 0.5 wt% Pd, and (▲) with 5 wt% ceria and 0.5 wt% Pd (Reproduced with permission from [34]. Copyright 2009, The Electrochemical Society)

Pd and Rh may be prohibitively expensive for large-scale SOFC applications, but Ni or even Fe would be suitable. Long-term fuel cell tests using (sulfur-rich) CH_4 are required to assess the sulfur tolerance and sintering resistance of Ni in the YSZ/LSCM-Ni anode.

Stability

The LSCM anode is chemically compatible with the commonly used electrolytes, such as YSZ, up to 1,300°C [64] and LSGM, up to 1,100°C [76]. Values for the thermal expansion coefficient (TEC) of LSCM in air varied from 8.9 to 10.8 μK^{-1} at low temperatures (< ~500°C), and from 10.1 to 12.7 μK^{-1} at high temperatures, up to 950°C [64, 67]. These TEC values match well with those for YSZ (10.8 μK^{-1}), LSGM (11.1 μK^{-1}) and GDC (13.5 μK^{-1}) [8]. The change in TEC in LSCM with temperature is likely due to a change in space group from rhombohedral R-3 C to cubic Pm-3 m, occurring gradually over the range of 500–1,100°C in air [77]. As the associated change in volume is minimal, ~1% [64], this is not expected to cause instability during cell heating or

cooling. Furthermore, since the Pm-3 m phase is also observed for reduced LSCM, stresses due to redox cycling are expected to be small. Indeed, the difference in volume between the reduced and oxidized unit cells is only 1.7% at room temperature [77], while the difference in linear expansion between LSCM in air and in reducing atmospheres, $pO_2 = 2\times10^{-19}$, is limited to ~0.2% at 700°C [67].

The operation of SOFCs with LSCM anodes in sulfur-rich H_2 leads to a decrease in cell performance in a short amount of time. Liu reported a decrease in current density of 50% when exposing LSCM to 10% H_2S/H_2 at 950°C [66]. The decrease occurred over a period of 2 h, after which the performance stabilized. Ten percent H_2S is much higher than the typical ppm levels of sulfur present in natural gas and represents attempts to utilize H_2S as a fuel. However, even in H_2 with 50 ppmv H_2S, performance was observed to decrease significantly from 0.46 W/cm^2 to 0.09 W/cm^2, again in 2 h, at 850°C and constant current density of 625 mA/cm^2 [53]. The large deterioration of LSCM is due to La and Mn reacting with sulfur to form La_2O_2S, MnS, and α-MnOS [66]. Since Mn is the reactive site for fuel oxidation, the formation of these compositions is likely to have an adverse effect on anode performance.

There is no easy solution to decrease the susceptibility of LSCM to sulfur poisoning. Since LSV anodes have been shown to have excellent sulfur resistance [78], operating better in sulfur-rich fuel than in fuel without sulfur, it has been attempted to introduce 10 mol% V on the B site of LSCM. However, no phase-pure material could be obtained [19].

Interestingly, the use of sulfur-rich CH_4 instead of sulfur-containing H_2 led to an initial increase in performance on LSCM, compared to CH_4 without sulfur [56]. After 4–6 h though, the performance in 0.5% H_2S/CH_4 had stabilized to values similar to those in pure CH_4. This observation is consistent with the much smaller and slower decrease of power density of SOFC with LSCM anodes in 0.5% H_2S/CH_4, as compared to H_2S/H_2 mixtures [79].

Double Perovskites

Double perovskites are described by the general formula $A_2B'B''O_{6-\delta}$, and can be interpreted as a doubling of the regular perovskite $ABO_{3-\delta}$. The elements on the B′ site are different from those on the B″ site, and the two sites alternate to form a sublattice with a rock-salt structure. In a perfectly ordered lattice, every B′ ion would be coordinated by six perovskite unit cells with B″ ions and vice versa. This is illustrated in Fig. 16 for $Sr_2MgMoO_{6-\delta}$ (SMMO); the Mo ion (green) is surrounded by 6 Mg ions (red). The ordering is caused by large differences in the radii and charges between the B′ and B″ site ions. For example, in SMMO, the B′ site is occupied by the small Mg^{2+} ion, while the B″ site hosts the large and highly charged Mo^{6+} ion [80]. Although a regular perovskite can have two different elements on the B site as well, it is this particular B-site structure that classifies these materials as double perovskites.

The most investigated double perovskite anode material is SMMO. It has reasonable electrical conductivity, ~10 S/cm in pure H_2 at 800°C, good activity for direct CH_4 oxidation, and operates well in

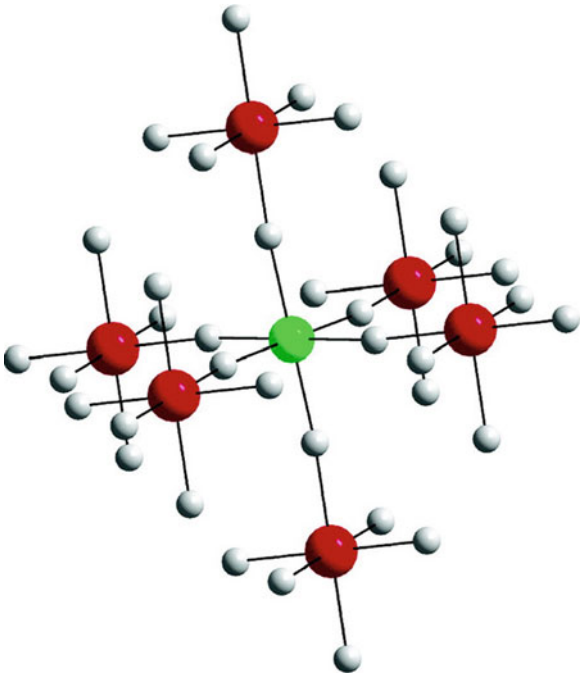

Direct Hydrocarbon Solid Oxide Fuel Cells. Figure 16 Mo (*green*) surrounded by six next-nearest-neighbor Mg (*red*) in a perfectly B-site ordered material; oxygen ions are white and strontium cations are omitted for clarity (Reprinted in part with permission from [80]. Copyright 2007 American Chemical Society)

sulfur-containing fuels [81]. The power output of an SOFC with a 300-μm-thick $La_{0.8}Sr_{0.2}Ga_{0.8}Mg_{0.2}O_{3-d}$ electrolyte, $SrCo_{0.8}Fe_{0.2}O_{3-d}$ cathode and SMMO anode reached 0.84 W/cm^2 in dry H_2 and 0.44 and 0.34 W/cm^2 in dry and wet CH_4, respectively, at 800°C [81], Fig. 17. Note that these values were obtained using Pt current collectors, which should be avoided as they contribute toward the catalytic activity of the anode [82], significantly increasing the performance for hydrocarbon fuels.

Conductivity

The electrical conductivity of SMMO was found to be ~1–4 S/cm in H_2/Ar and 10 S/cm in H_2, at 800°C [83, 84]. The slight differences in the values possibly result from differences in synthesis methods. The conductivity decreases with increasing pO_2, indicative of *n*-type conductivity. The charge carriers are electrons generated by the reduction of Mo(VI) to Mo(V) to compensate for the charge imbalance created by the formation of oxygen vacancies in the material [84]. No studies have yet been conducted to optimize the electrical conductivity.

Catalysis

The catalytic activity of SMMO is thought to result from the Mo ion. Whereas the Mg ion keeps a 2+ charge, Mo is reduced to some extent from predominantly Mo(VI) in air atmospheres, to a mixture of Mo (VI) and Mo(V) in reducing atmospheres [85]. The presence of a redox center would allow for the oxidation of fuel molecules according to a MvK mechanism, as suggested for the oxidation of CH_4 on LSCM [20]. Only a small amount of Mo(VI) is reduced to Mo(V), resulting in an oxygen non-stoichiometry of ~0.04–0.06 mol O/mol SMMO for samples reduced at 1,000–1,200°C in 5% H_2 [80, 84, 86]. The limited reduction of Mo(VI) could be due to the instability of Mg in a conformation with less than six surrounding oxygen ions. This is confirmed by the decreased B-site order after reduction, indicating that Mg ions relocate to maintain a sixfold oxygen coordination [80].

To increase the electrocatalytic activity of Mo-based double perovskites, Mg has been replaced by a number of transition metals. SOFC anodes have been prepared with Sr_2CoMoO_6, Sr_2FeMoO_6, Sr_2MnMoO_6 and Sr_2NiMoO_6, but none of those compounds were stable. SMMO with Co, Ni and Zn on the B′ site are easily synthesized in air, but are unstable in 5% H_2 at 800°C and above, due to exsolution of the metals [87, 88]. Higher initial power outputs were indeed observed for SOFCs made with Sr_2CoMoO_6 anodes, compared to similar SOFCs with SMMO anodes, but performance quickly deteriorated, likely due to the decomposition of

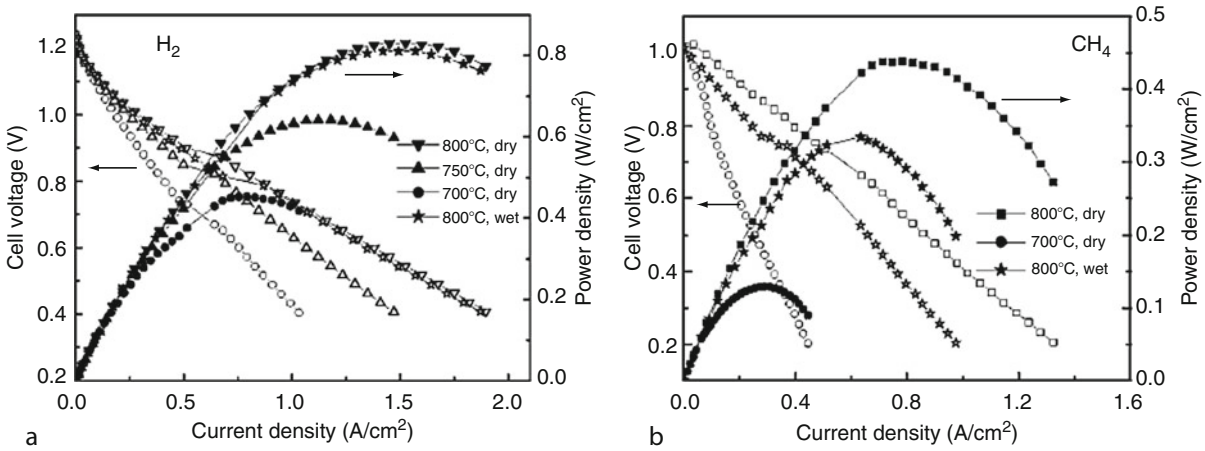

Direct Hydrocarbon Solid Oxide Fuel Cells. Figure 17
SMMO/LDC/LSGM/SCF cell voltage and power density as a function of current density in dry and wet: (**a**) H_2; and (**b**) CH_4. The open symbols represent the cell voltages while the closed symbols represent the power densities (Reproduced with permission from [83]. Copyright 2006, The Electrochemical Society)

SCMO. Sr_2FeMoO_6 and Sr_2MnMoO_6 are stable in reducing atmospheres, but unstable in >400°C air [88, 89].

More recently, the maximum oxygen non-stoichiometry in SMMO was successfully increased through partial substitution of Mo(VI) by Nb(V), without compromising the stability of the double perovskite [85]. The increase in oxygen non-stoichiometry suggests that more Mo^{6+}/Mo^{5+} redox centers are created, which are expected to increase both oxygen ion conductivity and fuel oxidation rates.

Stability

As suggested above, a significant challenge in the development of double perovskites is the synthesis of phase-pure, redox-stable compositions. The synthesis of SMMO, for example, is successful in air, but requires high temperatures, >1,200°C, to remove $SrMoO_4$ impurities [90]. The firing temperature can be brought down to 900°C if a 5% H_2 atm is used, but the use of such a reducing atmosphere could complicate large-scale SMMO production.

Because of the existence of $SrMoO_4$ impurities in air-fired SMMO, it is likely that the same impurities are formed upon treatment of H_2-synthesized SMMO in high temperature air. Depending on the thermal and chemical expansion properties of this phase, these impurities could result in a decrease in performance with redox cycling of SMMO. At room temperature in air, SMMO readily forms carbonates, such as $SrCO_3$, resulting in surface degradation and $SrMoO_4$ formation [84].

At elevated temperatures in reducing atmospheres, SMMO partly decomposes to MgO, SrO, and Mo. The temperature at which decomposition starts is subject to debate. In 5% H_2, decomposition temperatures have been reported as low as 900°C [80] up to 1,000°C [90] and even 1,200°C [83]. It has been suggested that the decomposition temperature is influenced by the preparation method, with the high temperatures utilized during air-firing or solid-state synthesis possibly leading to the evaporation of the volatile Mo, decreasing SMMO stability [90]. SMMO synthesized according to an EDTA-complexation route and fired at low temperatures in 5% H_2 is typically found to be stable up to 1,000°C in 5% H_2, at which point small amounts of the decomposition products appear. SOFC applications however run most efficiently on pure or humidified fuel, atmospheres that are more reducing than 5% H_2. The use of pure fuel could therefore lead to decomposition of the SMMO anode at temperatures lower than 900–1,000°C, which presents a problem for SOFC operating at 700–850°C.

Another potential issue is the chemical interaction of SMMO with the commonly used electrolytes YSZ and LSGM. When treated in 1,000°C air for 24 h, SMMO reacts with YSZ to form large amounts of $SrMoO_4$ and $SrZrO_3$, and it reacts with LSGM to form $(La,Sr)Ga_3O_7$ [84]. These reaction products have inferior properties compared to the reactants and are therefore to be avoided. In the case of LSGM, this has been done by using a thin ceria-based layer between anode and electrolyte [83]. The thermal expansion of SMMO, ~11.7–12.7 μK^{-1} [83] is compatible with values for YSZ (10.8), LSGM (11.1) and GDC (13.5).

SOFC with SMMO anodes have shown stable performance in dry H_2 fuel with 5 ppmv H_2S. The initial power output of fuel cells in 5 ppmv H_2S/H_2 fuel is similar to that in pure H_2 fuel, Fig. 18, and the cells show a similar decrease in power output, ~3% after 200 h of operation in both fuels at 800°C [83]. When, under otherwise similar conditions, the concentration of H_2S is raised to 50 ppmv, the initial power output of the cell was reduced to ~80–85% of its value in H_2 and P_{max} decreased ~5% in 200 h.

Strontium Titanates

Pure $SrTiO_3$ is a simple cubic perovskite that has a good thermal expansion match with YSZ and is stable under reducing conditions. However, undoped $SrTiO_3$ has insufficient electronic conductivity for an anode material [91]. In contrast, donor-doped (*n*-type) $SrTiO_3$ has attracted considerable interest due to its high electronic conductivity under reducing conditions, while maintaining a good thermal expansion match, and resistance to both coking and sulfur poisoning [92, 93]. Unfortunately, the performance of pure STO-based anodes is low, requiring additional catalytic materials to realize acceptable power densities [94]. As with the other oxides discussed in this entry, the conductivity and stability of this material is

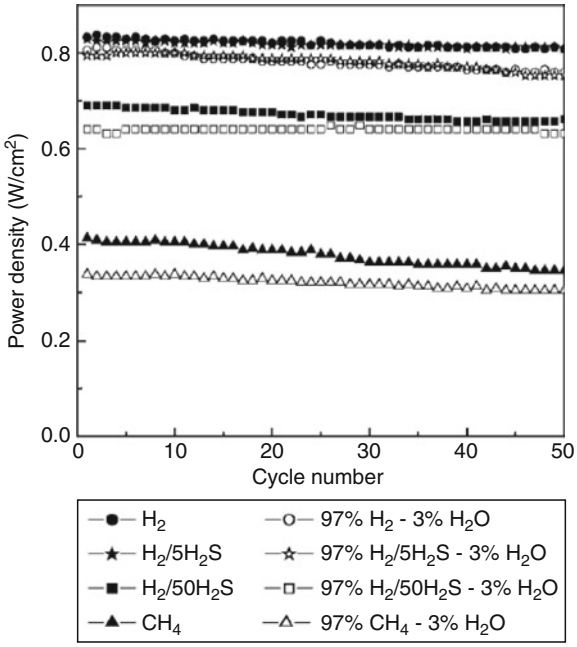

Direct Hydrocarbon Solid Oxide Fuel Cells. Figure 18 Maximum power density P_{max} at 800°C versus cycle number in dry and wet H_2, H_2/H_2S, and CH_4 (Reproduced with permission from [83]. Copyright 2006, The Electrochemical Society)

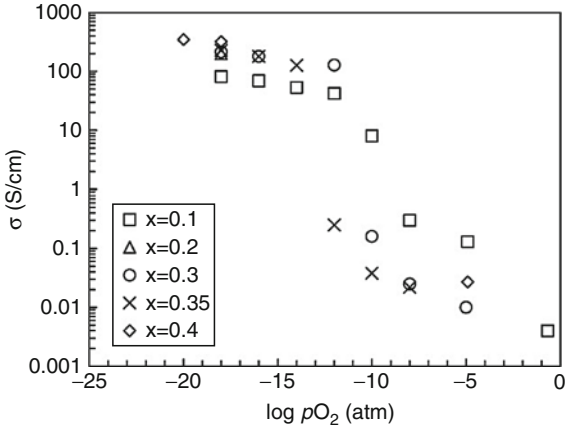

Direct Hydrocarbon Solid Oxide Fuel Cells. Figure 19 Electrical conductivity as a function of pO_2 for $La_xSr_{1-x}TiO_3$ sintered at 1650°C in H_2. Conductivity is measured at 1,000°C from low to high pO_2 (Reprinted from [96] with permission from Elsevier)

dominated by its defect chemistry. There are a number of articles that fully discuss the defect chemistry, for example [91]. This discussion is restricted to the essential points relevant to the use of STO as an SOFC anode.

Conductivity

There are two routes to doping of $SrTiO_3$: doping of trivalent cations onto the Sr site, and/or doping of pentavalent cations onto the Ti site. The most common trivalent dopants are La^{3+} and Y^{3+}. La^{3+} has high solubility, with only limited distortion of the lattice parameter at high dopant levels (>40%) [95]. Charge compensation upon doping can occur via electronic or ionic compensation, depending on the temperature and pO_2. At low pO_2, the compensation mechanism is electronic via reduction of Ti^{4+} to Ti^{3+} to form $Sr_{1-x}La_xTi'_xTi_{1-x}O_3$:

$$\frac{1}{2}La_2O_3 + Sr^x_{Sr} + Ti^x_{Ti} \rightarrow La^{\cdot}_{Sr} + Ti'_{TI} + SrO + \frac{1}{4}O_2 \quad (17)$$

A similar mechanism occurs for Y-doped STO under reducing conditions [97]. Assuming that dopant carriers dominate, the number of n-carriers is then directly correlated to the dopant level [98]; however, the correlation is not 100% as some electronic defects are associated with the donor atom. The creation of high concentrations of electronic defects leads to high conductivity. For example, Marina et al. reported conductivities for $La_{0.3}Sr_{0.7}TiO_3$ of over 100 S/cm at low pO_2, Fig. 19 [96].

At high pO_2, the compensation mechanism switches from electronic to cation vacancy compensation (or self compensation), where the donor charge is compensated by the formation of Sr vacancies [98, 99]. This is accompanied by the formation of a secondary Sr-rich phase. The nature of this phase is not fully determined and is suggested to be either an $Sr_{n+1}Ti_nO_{3n+1}$ phase within the matrix [100] or a separate SrO phase [101]. A separate phase is denoted below simply for clarity:

$$Sr^x_{Sr} + 2Ti'_{Ti} + \frac{1}{2}O_2 \leftrightarrow SrO + V''_{Sr} + 2Ti^x_{Ti} \quad (18)$$

This alternate charge compensation mechanism removes electronic carriers and thus greatly decreases the electronic conductivity of the material [98]. Indeed, the very high conductivities reported for La-doped

STO are only created upon sintering at high temperatures under very reducing conditions [92, 93, 96, 102].

Upon exposure to higher pO_2 at SOFC temperatures, the conductivity decreases slowly [96]. This is observed in Fig. 19 as the significant decrease in conductivity for all of the samples as the pO_2 is increased above $\sim 10^{-14}$ atm. The slow kinetics associated with this may be related to slow cation diffusion [101] and/or low oxygen mobility in these materials [103]. Slow reoxidation kinetics are beneficial to application in the SOFC anode where accidental and occasional exposure of the anode material to air may be expected. Of course, this assumes that a suitable and cost-effective cell synthesis procedure can be derived to initially form these highly conductive states. Furthermore, slow reoxidation may indicate slow surface oxygen exchange and low hydrocarbon oxidation activity.

Nb is the most common pentavalent dopant [104–108]. As with the trivalent A-site dopants, the additional charge is compensated by electronic carriers at low pO_2 leading to high electronic conductivity. These carriers are generated by reduction of Ti^{4+} to Ti^{3+}:

$$\frac{1}{2}Nb_2O_5 + 2Ti^{x}_{Ti} \rightarrow Nb^{\bullet}_{Ti} + Ti'_{Ti} + TiO_2 + \frac{1}{4}O_2 \tag{19}$$

Nb remains in the pentavalent oxidation state although there is evidence that Nb substitution improves the overlap between Ti atomic orbitals. As with the trivalent doped materials, conductivity decreases upon oxidation due to a shift toward ionic compensation via the formation of Sr vacancies. However, it has been reported that Nb-doped materials can provide adequate conductivity and are very slow to reoxidize [107].

Irvine et al. suggested deliberate introduction of Sr vacancies through the fabrication of A-site deficient materials with the A-site deficiency level set to compensate for the charge introduced through donor doping [103, 109]. While these materials show good electronic conductivity, recent work has suggested that A-site deficiency leads to precipitation of secondary Ti-rich phases [93, 110]. It should be noted that these secondary phases are not always observable by XRD but are observed upon SEM/EDX analysis.

Transition metal acceptor doping of A-site deficient $Sr_{0.85}Y_{0.1}Ti_{0.95}M_{0.05}O_{3-\delta}$ (M = V, Mn, Fe, Co, Ni, Cu, Zn, Mo, Mg, Zr, Al, Ga) leads to a decrease in total conductivity compared to the undoped composition. This is due to the acceptor dopant off-setting the influence of the donor dopant (Y^{3+} in this case). The ionic conductivity of these materials increases upon acceptor doping but it is still ~6 orders of magnitude lower than the electronic conductivity [111].

The ionic conductivity of doped STO is quite low although A-site deficient $(Y_{0.08}Sr_{0.92})_{1-x}TiO_{3-\delta}$ has been shown to have an ionic conductivity comparable to YSZ at 700°C; however, this occurs at the expense of lowering the electronic conductivity [112]. It may not be desirable to introduce significant oxygen ion conductivity as the low mobility of oxygen anions may play a significant role in preventing reoxidation of the material and concomitant loss of electronic carriers [96, 103]. The majority of SOFC anode studies utilize composites of doped STO and YSZ, where STO provide electronic conductivity and YSZ provides ionic conductivity [92].

Catalysis

Unfortunately, while able to provide sufficient electronic conductivity, the electrocatalytic activity of doped-$SrTiO_3$ is low [105]. As such, secondary catalysts are required to provide sufficient SOFC performance as cells without additional catalyst provide very low power density. For example, Lee et al. demonstrated a dramatic increasing in performance with H_2 fuel upon addition of 5 wt% CeO_2 and 0.5 wt% Pd. The power density increased from less than 20–780 mW/cm^2 at 800°C with no change in OCP [35]. Pd doping without CeO_2 has also been shown to enhance activity [94].

Avoiding precious metals, Fu et al. demonstrated a similar enhancement, realizing a two order of magnitude decrease in polarization resistance with an yttria-substituted $SrTiO_3$-YSZ composite upon infiltration of 5 vol% Ni [113]. Yang et al. also utilized Ni surface doping but did so in conjunction with Co doping of $Sr_{0.88}Y_{0.08}TiO_3$, finding an enhancement of activity attributed to the reducibility of Co within the lattice [114].

Only limited studies have discussed the activity of these materials toward hydrocarbon utilization. Vincent et al. showed that the performance of cells with $La_{0.4}Sr_{0.6-x}Ba_xTiO_3$ ($0 \leq x \leq 0.2$) based anodes

in CH_4 fuel was more than one order of magnitude lower than in H_2 fuel between 800 and 950°C [115]. The performance did increase slightly with an increase in Ba doping level but, perhaps most intriguingly, a more substantial improvement was observed upon the addition of H_2S to the feed gas. A role for Ba in enhancing oxygen surface exchange rates was confirmed, although with the caveat that it was measured under oxidizing conditions, when the surface is doped with Sr, Ba, or Ca [116]. Addition of CeO_2 to an $Sr_{0.88}Y_{0.08}O_3$-based anode significantly reduced the anode polarization resistance with both H_2 and CH_4 fuel [117, 118], likely due to enhanced catalytic activity of the composite.

Doping with a more reducible Mn cation to form $La_{0.4}Sr_{0.6}Ti_{0.4}Mn_{0.6}O_3$ leads to a decrease in electronic conductivity although it may slightly increase catalytic activity toward hydrocarbons. The resulting cell shows a low OCP in wet CH_4 of only 0.86 V at 856°C with a total cell R_P of ~1.4 $\Omega \cdot cm^2$ compared with an OCP of 1.05 V and total R_P of ~0.36 $\Omega \cdot cm^2$ in wet Ar/H_2 [119]. The difference in polarization resistance is not as dramatic as shown for Mn-free compositions.

Ruiz-Morales et al. took a unique approach by utilizing multiple dopants to control the oxygen stoichiometry and thus disrupt defect ordering to generate the single-phase perovskite anode material $La_4Sr_8Ti_{11}Mn_{0.5}Ga_{0.5}O_{37.5}$ [120]. The resulting cell generated 500 mW/cm^2 with H_2 fuel and 350 mW/cm^2 with CH_4 at 950°C, Fig. 19. The maximum power density and OCP in CH_4 fuel were both significantly higher than with 5% H_2 fuel, Fig. 20, suggesting that homogenous cracking of CH_4 to form H_2 was not the dominant reaction mechanism and that this material was active toward CH_4 oxidation.

$SrTiO_3$ based anodes have been shown to be quite tolerant to H_2S poisoning [121], operating with up to 1% H_2S [122] and up to 50 ppm H_2S when surface doped with Pd [94].

Other Materials of Interest

Pyrochlore structured oxides have received some attention for use in SOFC anodes, in particular the series $Gd_2Mo_xTi_{2-x}O_7$. SOFCs made with 250-micron thick YSZ electrolytes, LSCM cathodes, and $Gd_2Mo_{0.6}Ti_{1.4}O_7$ anodes have shown a stable power output of 340 mW/cm^2 in 950°C 10% H_2S/H_2, and an anode polarization resistance of ~0.23 $\Omega \cdot cm^2$ at OCP [123]. The substitution of Ti in the electrolyte $Gd_2Ti_2O_7$ with large amounts of Mo increases the total conductivity to ~70 and 25 S/cm in 1,000°C 5% H_2 for 70 and

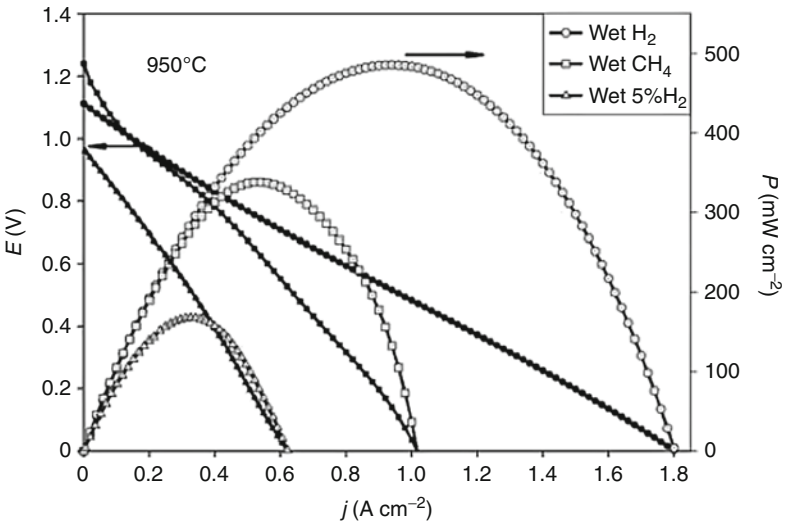

Direct Hydrocarbon Solid Oxide Fuel Cells. Figure 20
Fuel cell performance plots at 950°C of a cell with four-layer optimized $La_4Sr_8Ti_{11}Mn_{0.5}Ga_{0.5}O_{37.5}$ anode, 330 μm YSZ electrolyte, and $La_{0.8}Sr_{0.2}MnO_3$ cathode. Fuels humidified with 2.3% H_2O, cathode is in dry O_2 (Reprinted by permission from Macmillan Publishers, Ltd: Nature [120], copyright 2006)

50 mol% Mo respectively. The ionic conductivity under these conditions remains high, ~0.1 S/cm for 50 mol% Mo [124].

However, the introduction of large amounts of Mo is detrimental to the stability of $Gd_2Ti_2O_7$. Compositions with 70 mol% Mo are unstable and exist only in a very narrow pO_2 range, 10^{-13}–10^{-15} atm at 1,000°C. This range is extended for lower Mo contents, but even at 30 mol% Mo, compositions are not stable at 1,000°C in $pO_2 > 10^{-8}$ atm [124], Fig. 21. Sprague reported increased redox stability when co-substituting Ti with Mn instead of just Mo, but this has only been shown for small amounts of Ti substitution, $\leq$ 20 mol% [125].

More recently, the pyrochlore $Yb_{0.96}Ca_{1.04}TiNbO_7$ has been suggested as an anode material [126]. Based on $Yb_2Ti_2O_7$, the substitution of Yb with Ca increases the ionic conductivity [127], while the introduction of Nb greatly enhances the total conductivity, to 9 S/cm at 800°C in 5% H_2/N_2. The conductivity is n-type, and is therefore expected to increase further in more reducing atmospheres. In addition, $Yb_{0.96}Ca_{1.04}TiNbO_7$ is stable up to 1,450°C in air and 1,350°C in 5% H_2/N_2. The main drawback of the material appears to be slow oxygen ion exchange, which can be slightly enhanced with further substitution on the B site, for example, with Mn, Cr or Mg/Mo [126].

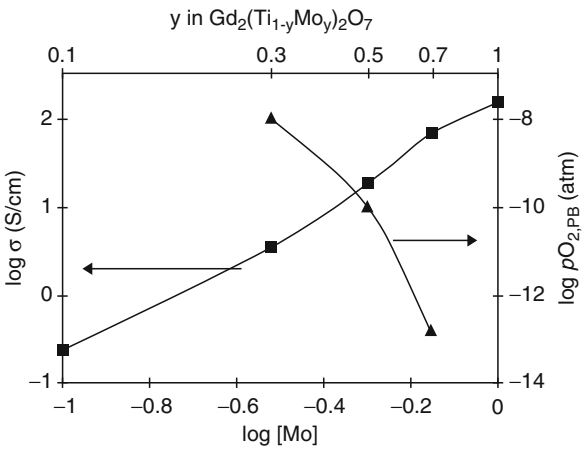

Direct Hydrocarbon Solid Oxide Fuel Cells. Figure 21 Electrical conductivity at $pO_2 = 10^{-18}$ bar and the pyrochlore phase boundary at high pO_2, $pO_{2,PB}$, vs. Mo concentration in $Gd_2Ti_2O_7$ at 1,000°C (Reprinted from [124] with permission from Elsevier)

Fluorite anodes, not including ceria, are typically based on YSZ and have been developed to ensure good thermo-mechanical and chemical compatibility with the widely used YSZ electrolyte. A purely ionic conductor, YSZ depends on the substitution of Zr with more reducible elements, such as Ti, to introduce electronic conductivity. The reduction of Ti^{4+} to Ti^{3+} in $Y_{0.18}Zr_{0.73}Ti_{0.09}O_{2-\sigma}$ (YZT) generates electronic charge carriers, but significant amounts of Ti^{3+} are only present at high temperatures and low pO_2. Even at 1,000°C and $pO_2 < 10^{-20}$ atm, the total conductivity is low, ~0.06 S/cm [128]. An additional drawback of substitution with Ti is the trapping of oxygen vacancies on Ti ions, reducing the ionic conductivity to ~0.04 S/cm.

By raising the amount of Ti to 18 at-%, the maximum amount that dissolves in the YSZ lattice, the electrical conductivity of $Y_{0.15}Zr_{0.67}Ti_{0.18}O_{2-\delta}$ is increased to 0.2 S/cm (at 930°C and $pO_2 = 10^{-20}$ atm), while the ionic conductivity is further reduced [129]. Introduction of Sc_2O_3 into YZT (ScYZT) slightly increased the electronic conductivity to 0.14 S/cm at 900°C [130]. SOFCs with ScYZT anodes were tested in 900°C 5% humidified H_2 (using Pt as electrode current collectors) and showed an estimated power output of 35 mW/cm^2 and an anode polarization resistance of ~5.5 Ω·cm^2 at OCP, using a 2 mm thick YSZ electrolyte and a Pt cathode [131].

Among the *Tungsten Bronzes*, formula $A_{0.6}BO_3$, the Nb-based $Sr_{0.2}Ba_{0.4}Ti_{0.2}Nb_{0.8}O_3$ is the best candidate for SOFC anodes. This composition is redox stable and has reasonable electrical conductivity, 3.4 S/cm at 930°C in 5% H_2/Ar [132]. Other compositions are unstable or have lower conductivity [132, 133]. $Sr_{0.2}Ba_{0.4}Ti_{0.2}Nb_{0.8}O_3$ has a much lower TEC than the electrolytes that are commonly used, ~6.7 μK^{-1}, and reacts with YSZ at 1,200°C. Also, the power output for symmetrical SOFCs made with this compound are low, with impedance data showing Warburg behavior, suggesting poor oxygen ion exchange and low oxygen ion conductivity [134].

Vanadates in the series $La_{1-x}Sr_xVO_3$ demonstrate sufficient electronic conductivity [63], and reasonable electrocatalytic activity at 1,000°C [135], coupled with stability toward sulfur poisoning [78]. Aguilar et al. demonstrated operation with 5% H_2S in both H_2 and N_2 [135]. In the latter case, the LSV-based anode utilized H_2S as the fuel source. Unfortunately, LSV is

only stable at low oxygen partial pressure, for example, $pO_2 < 10^{-17}$ atm at 800°C [63]. It transforms to the apatite phase $Sr_3V_2O_8$ [63] or $Sr_2V_2O_7$ [78] upon exposure to higher pO_2. This transformation is irreversible at SOFC operating temperatures [63].

Future Directions

As discussed in this entry, a number of novel materials and composites have been proposed as potential anodes for direct hydrocarbon solid oxide fuel cells. While many are promising, a commercially viable solution has not yet been found. The discussion in this entry is deliberately framed around the concepts of ionic and electronic conductivity, electrocatalysis, and stability. It is essential for future researchers to address all of these topics when discussing new materials. The schematic in Fig. 4 represents both the complexity of the problem and the simplicity that could potentially be achieved if a material meeting all of these requirements can be found.

One particular challenge for the field as a whole is the measurement of these properties under realistic conditions. Experimental tools to probe the surface or bulk of these materials in situ at the length scales relevant to the anode processes are not currently available. While significant consideration has been given to the bulk transport properties of potential materials, very little is known of the surface chemistry under realistic SOFC conditions. It is also necessary to develop techniques that can measure and quantify the electrocatalytic activity of these materials under operating conditions. While electrochemical impedance techniques can, in principle, provide a wealth of information, the fitting of such data can be ambiguous and it is not a replacement for a direct measurement of a fundamental property. This is a major hurdle that must be overcome if highly active and selective catalytic materials are to be developed for this application.

In combination with this increased knowledge of surface chemistry, a detailed knowledge of the material bulk is essential. It is clear from the discussion in this entry that the target materials set will be a multicomponent oxide with potentially complex cation and anion lattice structures. When material properties depend upon cation configuration, e.g., the double perovskites, or oxygen stoichiometry, these properties must be accurately determined in a working cell.

The barriers to direct hydrocarbon SOFCs will only be overcome through a combination of new material development and more detailed experimental systems that directly probe fundamental parameters on working SOFC electrodes.

Bibliography

Primary Literature

1. McIntosh S, Gorte RJ (2004) Direct hydrocarbon solid oxide fuel cells. Chem Rev 104:4845–4865
2. Minh NQ (2004) Solid oxide fuel cell technology–features and applications. Solid State Ionics 174:271
3. Minh NQ (1993) Ceramic fuel-cells. J Am Ceram Soc 76: 563–588
4. Steele BCH, Middleton PH, Rudkin RA (1990) Material science aspects of SOFC technology with special reference to anode development. Solid State Ionics 40–41:388
5. Tao SW, Irvine JTS (2004) Discovery and characterization of novel oxide anodes for solid oxide fuel cells. Chem Rec 4:83–95
6. Bruce MK, van den Bossche M, McIntosh S (2008) The influence of current density on the electrocatalytic activity of oxide-based direct hydrocarbon SOFC anodes. J Electrochem Soc 155:B1202–B1209
7. Adler SB (2004) Factors governing oxygen reduction in solid oxide fuel cell cathodes. Chem Rev 104:4791
8. Jacobson AJ (2009) Materials for solid oxide fuel cells. Chem Mater 22:660
9. Tsipis EV, Kharton VV (2008) Electrode materials and reaction mechanisms in solid oxide fuel cells: a brief review. J Solid State Electrochem 12:1367–1391
10. Brett DJL, Atkinson A, Brandon NP, Skinner SJ (2008) Intermediate temperature solid oxide fuel cells. Chem Soc Rev 37:1568–1578
11. He HP, Hill JM (2007) Carbon deposition on Ni/YSZ composites exposed to humidified methane. Appl Catal, A 317:284–292
12. Gupta GK, Hecht ES, Zhu H, Dean AM, Kee RJ (2006) Gas-phase reactions of methane and natural-gas with air and steam in non-catalytic regions of a solid-oxide fuel cell. J Power Sources 156:434–447
13. Walters KM, Dean AM, Zhu H, Kee RJ (2003) Homogeneous kinetics and equilibrium predictions of coking propensity in the anode channels of direct oxidation solid-oxide fuel cells using dry natural gas. J Power Sources 123:182–189
14. Lin YB, Zhan ZL, Liu J, Barnett SA (2005) Direct operation of solid oxide fuel cells with methane fuel. Solid State Ionics 176:1827–1835
15. Murray EP, Tsai T, Barnett SA (1999) A direct-methane fuel cell with a ceria-based anode. Nature 400:649
16. Zhan ZL, Barnett SA (2005) An octane-fueled solid oxide fuel cell. Science 308:844–847

17. Bouwmeester HJM, Kruidhof H, Burggraaf AJ (1994) Importance of the surface exchange kinetics as rate limiting step in oxygen permeation through mixed-conducting oxides. Solid State Ionics 72:185
18. van den Bossche M, Matthews R, Lichtenberger A, McIntosh S (2010) Insights into the fuel oxidation mechanism of $La_{0.75}Sr_{0.25}Cr_{0.5}Mn_{0.5}O_{3-d}$ SOFC anodes. J Electrochem Soc 157:B392–B399
19. van den Bossche M, McIntosh S (2010) Pulse reactor studies to assess the potential of $La_{0.75}Sr_{0.25}Cr_{0.5}Mn_{0.4}X_{0.1}O_{3-d}$ (X = co, fe, mn, ni, V) as direct hydrocarbon solid oxide fuel cell anodes. Chem Mater 22:5856–5865
20. van den Bossche M, McIntosh S (2008) Rate and selectivity of methane oxidation over $La_{0.75}Sr_{0.25}Cr_xMn_{1-x}O_{3-d}$ as a function of lattice oxygen stoichiometry under solid oxide fuel cell anode conditions. J Catal 255:313–323
21. McIntosh S, Vohs JM, Gorte RJ (2003) Effect of precious-metal dopants on SOFC anodes for direct utilization of hydrocarbons. Electrochem Solid State Lett 6:A240–A243
22. McIntosh S, Vohs JM, Gorte RJ (2002) An examination of lanthanide additives on the performance of cu-YSZ cermet anodes. Electrochim Acta 47:3815–3821
23. Bouwmeester HJM, Burggraaf AJ (1997) Dense ceramic membranes for oxygen separation. In: Gellings PJ, Bouwmeester HJM (eds) CRC handbook of solid state electrochemistry. CRC Press, Boca Raton
24. Goldschmidt VM (1926) Geochemische verteilungsgesetze der elemente. Akad Oslo I Mat Nat 2:7
25. Knauth P, Tuller HL (2002) Solid-state ionics: roots, status, and future prospects. J Am Ceram Soc 85:1654–1680
26. Oishi M, Yashiro K, Sato K, Mizusaki J, Kawada T (2008) Oxygen nonstoichiometry and defect structure analysis of B-site mixed perovskite-type oxide (la, sr)(cr, M)O_{3-d} (M = ti, mn and fe). J Solid State Chem 181:3177–3184
27. McIntosh S, He HP, Lee SI, Costa-Nunes O, Krishnan VV, Vohs JM, Gorte RJ (2004) An examination of carbonaceous deposits in direct-utilization SOFC anodes. J Electrochem Soc 151: A604–A608
28. McIntosh S, Vohs JM, Gorte RJ (2003) Role of hydrocarbon deposits in the enhanced performance of direct-oxidation SOFCs. J Electrochem Soc 150:A470–A476
29. Coyle CA, Marina OA, Thomsen EC, Edwards DJ, Cramer CD, Coffey GW, Pederson LR (2009) Interactions of nickel/zirconia solid oxide fuel cell anodes with coal gas containing arsenic. J Power Sources 193:730–738
30. Marina OA, Coyle CA, Thomsen EC, Edwards DJ, Coffey GW, Pederson LR (2010) Degradation mechanisms of SOFC anodes in coal gas containing phosphorus. Solid State Ionics 181:430–440
31. Marina OA, Pederson LR, Thomsen EC, Coyle CA, Yoon KJ (2010) Reversible poisoning of nickel/zirconia solid oxide fuel cell anodes by hydrogen chloride in coal gas. J Power Sources 195:7033–7037
32. Gorte RJ, Park S, Vohs JM, Wang C (2000) Anodes for direct oxidation of dry hydrocarbons in a solid-oxide fuel cell. Adv Mater 12:1465–1469
33. Vohs JM, Gorte RJ (2009) High-performance SOFC cathodes prepared by infiltration. Adv Mater 21(9):943–956
34. Kim G, Lee S, Shin JY, Corre G, Irvine JTS, Vohs JM, Gorte RJ (2009) Investigation of the structural and catalytic requirements for high-performance SOFC anodes formed by infiltration of LSCM. Electrochem Solid State Lett 12:B48–B52
35. Lee S, Kim G, Vohs JM, Gorte RJ (2008) SOFC anodes based on infiltration of $La_{0.3}Sr_{0.7}TiO_3$. J Electrochem Soc 155: B1179–B1183
36. Kim H, Park S, Vohs JM, Gorte RJ (2001) Direct oxidation of liquid fuels in a solid oxide fuel cell. J Electrochem Soc 148: A693–A695
37. Mogensen M, Sammes NM, Tompsett GA (2000) Physical, chemical and electrochemical properties of pure and doped ceria. Solid State Ionics 129:63–94
38. Jung S, Lu C, He H, Ahn K, Gorte RJ, Vohs JM (2006) Influence of composition and cu impregnation method on the performance of Cu/CeO_2/YSZ SOFC anodes. J Power Sources 154:42–50
39. Gross MD, Vohs JM, Gorte RJ (2007) An examination of SOFC anode functional layers based on ceria in YSZ. J Electrochem Soc 154:B694–B699
40. Jiang SP, Chan SH (2004) A review of anode materials development in solid oxide fuel cells. J Mater Sci 39:4405–4439
41. Lu C, Worrell WL, Vohs JM, Gorte RJ (2003) A comparison of cu-ceria-SDC and au-ceria-SDC composites for SOFC anodes. J Electrochem Soc 150:A1357–A1359
42. Park S, Gorte RJ, Vohs JM (2001) Tape cast solid-oxide fuel cells for the direct oxidation of hydrocarbons. J Electrochem Soc 148:A443–A447
43. Park S, Vohs JM, Gorte RJ (2000) Direct oxidation of hydrocarbons in a solid-oxide fuel cell. Nature 404:265
44. Kim T, Liu G, Boaro M, Lee S, Vohs JM, Gorte RJ, Al-Madhi OH, Dabbousi BO (2006) A study of carbon formation and prevention in hydrocarbon-fueled SOFC. J Power Sources 155:231–238
45. Kim H, Vohs JM, Gorte RJ (2001) Direct oxidation of sulfur-containing fuels in a solid oxide fuel cell. Chem Commun 22:2334–2335
46. He H, Gorte RJ, Vohs JM (2005) Highly sulfur tolerant cu-ceria anodes for SOFCs. Electrochem Solid State Lett 8:A279–A280
47. Rasmussen JFB, Hagen A (2009) The effect of H_2S on the performance of Ni–YSZ anodes in solid oxide fuel cells. J Power Sources 191:534–541
48. Kim H, Lu C, Worrell WL, Vohs JM, Gorte RJ (2002) Cu-ni cermet anodes for direct oxidation of methane in solid-oxide fuel cells. J Electrochem Soc 149:A247–A250
49. Lee S, Vohs JM, Gorte RJ (2004) A study of SOFC anodes based on cu-ni and cu-co bimetallics in CeO_2-YSZ. J Electrochem Soc 151:A1319–A1323
50. Ahn K, He H, Vohs JM, Gorte RJ (2005) Enhanced thermal stability of SOFC anodes made with CeO_2-ZrO_2 solutions. Electrochem Solid State Lett 8:A414–A417
51. Nakamura T, Petzow G, Gauckler LJ (1979) Stability of the perovskite phase $LaBO_3$ (B = V, cr, mn, fe, co, ni) in reducing atmosphere I. experimental results. Mater Res Bull 14:649

52. Tao SW, Irvine JTS (2003) A redox-stable efficient anode for solid-oxide fuel cells. Nat Mater 2:320–323
53. Lu XC, Zhu JH (2007) Cu(pd)-impregnated $La_{0.75}Sr_{0.25}Cr_{0.5}Mn_{0.5}O_{3-d}$ anodes for direct utilization of methane in SOFC. Solid State Ionics 178:1467–1475
54. Doshi R, Alcock CB, Gunasekaran N, Carberry JJ (1993) Carbon-monoxide and methane oxidation properties of oxide solid-solution catalysts. J Catal 140:557–563
55. Sfeir J, Buffat PA, Mockli P, Xanthopoulos N, Vasquez R, Mathieu HJ, Van herle J, Thampi KR (2001) Lanthanum chromite based catalysts for oxidation of methane directly on SOFC anodes. J Catal 202:229–244
56. Danilovic N, Vincent A, Luo J, Chuang KT, Hui R, Sanger AR (2009) Correlation of fuel cell anode electrocatalytic and ex situ catalytic activity of perovskites $La_{0.75}Sr_{0.25}Cr_{0.5}X_{0.5}O_{3-d}$ (X = ti, mn, fe, co). Chem Mater 22(3):957–965
57. Primdahl S, Hansen JR, Grahl-Madsen L, Larsen PH (2001) Sr-doped $LaCrO_3$ anode for solid oxide fuel cells. J Electrochem Soc 148:A74–A81
58. Vernoux P, Djurado E, Guillodo M (2001) Catalytic and electrochemical properties of doped lanthanum chromites as new anode materials for solid oxide fuel cells. J Am Ceram Soc 84:2289–2295
59. Kobsiriphat W, Madsen BD, Wang Y, Marks LD, Barnett SA (2009) $La_{0.8}Sr_{0.2}Cr_{1-x}Ru_xO_{3-d}$-$Gd_{0.1}Ce_{0.9}O_{1.95}$ solid oxide fuel cell anodes: Ru precipitation and electrochemical performance. Solid State Ionics 180:257
60. Tao SW, Irvine JTS (2004) Catalytic properties of the perovskite oxide $La_{0.75}Sr_{0.25}Cr_{0.5}Fe_{0.5}O_{3-d}$ in relation to its potential as a solid oxide fuel cell anode material. Chem Mater 16: 4116–4121
61. Jardiel T, Caldes MT, Moser F, Hamon J, Gauthier G, Joubert O (2010) New SOFC electrode materials: The ni-substituted LSCM-based compounds $(La_{0.75}Sr_{0.25})(Cr_{0.5}Mn_{0.5-x}Ni_x)O_{3-d}$ and $(La_{0.75}Sr_{0.25})(Cr_{0.5-x}Ni_xMn_{0.5})O_{3-d}$. Solid State Ionics 181:894
62. Pudmich G, Boukamp BA, Gonzalez-Cuenca M, Jungen W, Zipprich W, Tietz F (2000) Chromite/titanate based perovskites for application as anodes in solid oxide fuel cells. Solid State Ionics 135:433
63. Hui S, Petric A (2001) Conductivity and stability of $SrVO_3$ and mixed perovskites at low oxygen partial pressures. Solid State Ionics 143:275–283
64. Tao SW, Irvine JTS (2004) Synthesis and characterization of (La0.75Sr0.25)Cr0.5Mn0.5O3-d, a redox-stable, efficient perovskite anode for SOFCs. J Electrochem Soc 151:A252–A259
65. Tao SW, Irvine JTS, Plint SM (2006) Methane oxidation at redox stable fuel cell electrode $La_{0.75}Sr_{0.25}Cr_{0.5}Mn_{0.5}O_{3-d}$. J Phys Chem B 110:21771–21776
66. Zha SW, Tsang P, Cheng Z, Liu ML (2005) Electrical properties and sulfur tolerance of $La_{0.75}Sr_{0.25}Cr_{1-x}Mn_xO_3$ under anodic conditions. J Solid State Chem 178:1844–1850
67. Kharton VV, Tsipis EV, Marozau IP, Viskup AP, Frade JR, Irvine JTS (2007) Mixed conductivity and electrochemical behavior of (La0.75Sr0.25)(0.95)Cr0.5Mn0.5O3-delta. Solid State Ionics 178:101–113
68. Plint SM, Connor PA, Tao S, Irvine JTS (2006) Electronic transport in the novel SOFC anode material $La_{1-x}Sr_xCr_{0.5}Mn_{0.5}O_{3+/-d}$. Solid State Ionics 177:2005–2008
69. Wan J, Zhu JH, Goodenough JB (2006) $La_{0.75}Sr_{0.25}Cr_{0.5}Mn_{0.5}O_{3-d}$ + Cu composite anode running on H_2 and CH_4 fuels. Solid State Ionics 177:1211–1217
70. Fonseca FC, Muccillo ENS, Muccillo R, de Florio DZ (2008) Synthesis and electrical characterization of the ceramic anode $La_{1-x}Sr_xMn_{0.5}Cr_{0.5}O_3$. J Electrochem Soc 155:B483–B487
71. Kim G, Corre G, Irvine JTS, Vohs JM, Gorte RJ (2008) Engineering composite oxide SOFC anodes for efficient oxidation of methane. Electrochem Solid State Lett 11:B16–B19
72. Jiang SP, Liu L, Khuong POB, Ping WB, Li H, Pu H (2008) Electrical conductivity and performance of doped $LaCrO_3$ perovskite oxides for solid oxide fuel cells. J Power Sources 176:82–89
73. Sfeir J (2003) $LaCrO_3$-based anodes: stability considerations. J Power Sources 118:276–285
74. Liu J, Madsen BD, Ji ZQ, Barnett SA (2002) A fuel-flexible ceramic-based anode for solid oxide fuel cells. Electrochem Solid State Lett 5:A122–A124
75. Yamazoe N, Teraoka Y (1990) Oxidation catalysis of perovskites — relationships to bulk structure and composition (valency, defect, etc.). Catal Today 8:175
76. Pena-Martinez J, Marrero-Lopez D, Ruiz-Morales JC, Savaniu C, Nunez P, Irvine JTS (2006) Anodic performance and intermediate temperature fuel cell testing of $La_{0.75}Sr_{0.25}Cr_{0.5}Mn_{0.5}O_{3-d}$ at lanthanum gallate electrolytes. Chem Mater 18:1001–1006
77. Tao S, Irvine JTS (2006) Phase transition in perovskite oxide $La_{0.75}Sr_{0.25}Cr_{0.5}Mn_{0.5}O_{3-d}$ observed by in situ high-temperature neutron powder diffraction. Chem Mater 18:5453
78. Cheng Z, Zha S, Aguilar L, Liu M (2005) Chemical, electrical, and thermal properties of strontium doped lanthanum vanadate. Solid State Ionics 176:1921–1928
79. Chen XJ, Liu QL, Chan SH, Brandon NP, Khor KA (2007) Sulfur tolerance and hydrocarbon stability of $La_{0.75}Sr_{0.25}Cr_{0.5}Mn_{0.5}O_3$/$Gd_{0.2}Ce_{0.8}O_{1.9}$ composite anode under anodic polarization. J Electrochem Soc 154:B1206–B1210
80. Bernuy-Lopez C, Allix M, Bridges CA, Claridge JB, Rosseinsky MJ (2007) Sr_2MgMoO_{6-d}: structure, phase stability, and cation site order control of reduction. Chem Mater 19:1035–1043
81. Huang YH, Dass RI, Xing ZL, Goodenough JB (2006) Double perovskites as anode materials for solid-oxide fuel cells. Science 312:254–257
82. Otsuka K, Wang Y, Sunada E, Yamanaka I (1998) Direct partial oxidation of methane to synthesis gas by cerium oxide. J Catal 175:152–160
83. Huang YH, Dass RI, Denyszyn JC, Goodenough JB (2006) Synthesis and characterization of Sr_2MgMoO_{6-d} – an anode material for the solid oxide fuel cell. J Electrochem Soc 153: A1266–A1272
84. Marrero-López D, Peña-Martínez J, Ruiz-Morales JC, Gabás M, Núñez P, Aranda MAG, Ramos-Barrado JR (2009) Redox behaviour, chemical compatibility and electrochemical performance of Sr_2MgMoO_6 – [delta] as SOFC anode. Solid State Ionics 180:1672

85. Vasala S, Lehtimaki M, Haw SC, Chen JM, Liu RS, Yamauchi H, Karppinen M (2010) Isovalent and aliovalent substitution effects on redox chemistry of Sr_2MgMoO_{6-d} SOFC-anode material. Solid State Ionics 181:754–759
86. Matsuda Y, Karppinen M, Yamazaki Y, Yamauchi H (2009) Oxygen-vacancy concentration in A_2MgMoO_{6-d} double-perovskite oxides. J Solid State Chem 182:1713–1716
87. Huang Y, Liang G, Croft M, Lehtimaki M, Karppinen M, Goodenough JB (2009) Double-perovskite anode materials Sr_2MMoO_6 (M = co, ni) for solid oxide fuel cells. Chem Mater 21:2319–2326
88. Vasala S, Lehtimäki M, Huang YH, Yamauchi H, Goodenough JB, Karppinen M (2010) Degree of order and redox balance in B-site ordered double-perovskite oxides, Sr_2MMoO_{6-d} (M = Mg, mn, fe, co, ni, zn). J Solid State Chem 183:1007
89. Marrero-Lopez D, Pena-Martinez J, Ruiz-Morales JC, Martin-Sedeno MC, Nunez P (2009) High temperature phase transition in SOFC anodes based on Sr_2MgMoO_6-delta. J Solid State Chem 182:1027–1034
90. Marrero-Lopez D, Pena-Martinez J, Ruiz-Morales JC, Perez-Coll D, Aranda MAG, Nunez P (2008) Synthesis, phase stability and electrical conductivity of Sr_2MgMoO_{6-d} anode. Mater Res Bull 43:2441–2450
91. Moos R, Hardtl KH (1997) Defect chemistry of donor-doped and undoped strontium titanate ceramics between 1000° and 1400 °C. J Am Ceram Soc 80:2549–2562
92. Hui S, Petric A (2002) Evaluation of yttrium-doped $SrTiO_3$ as an anode for solid oxide fuel cells. J Eur Ceram Soc 22:1673–1681
93. Kolodiazhnyi T, Petric A (2005) The applicability of sr-deficient n-type SrTiO3 for SOFC anodes. J Electroceram 15:5–11
94. Lu XC, Zhu JH, Yang Z, Xia G, Stevenson JW (2009) Pd-impregnated SYT/LDC composite as sulfur-tolerant anode for solid oxide fuel cells. J Power Sources 192: 381–384
95. Moos R, Bischoff T, Menesklou W, Hardtl K (1997) Solubility of lanthanum in strontium titanate in oxygen-rich atmospheres. J Mater Sci 32:4247–4252
96. Marina OA, Canfield NL, Stevenson JW (2002) Thermal, electrical, and electrocatalytical properties of lanthanum-doped strontium titanate. Solid State Ionics 149:21–28
97. Huang X, Zhao H, Shen W, Qiu W, Wu W (2006) Effect of fabrication parameters on the electrical conductivity of YxSr1 − xTiO3 for anode materials. J Phys Chem Solids 67:2609–2613
98. Balachandran U, Eror NG (1982) Electrical conductivity in lanthanum-doped strontium titanate. J Electrochem Soc 129:1021–1026
99. Flandermeyer BF, Agarwal AK, Anderson HU, Nasrallah MM (1984) Oxidation-reduction behaviour of la-doped $SrTiO_3$. J Mater Sci 19:2593–2598
100. Battle PD, Bennett JE, Sloan J, Tilley RJD, Vente JF (2000) A-site cation-vacancy ordering in Sr1 − 3x/2LaxTiO$_3$: A study by HRTEM. J Solid State Chem 149:360–369
101. Meyer R, Waser R, Helmbold J, Borchardt G (2002) Cationic surface segregation in donor-doped $SrTiO_3$ under oxidizing conditions. J Electroceram 9:101–110
102. Fu QX, Mi SB, Wessel E, Tietz F (2008) Influence of sintering conditions on microstructure and electrical conductivity of yttrium-substituted SrTiO3. J Eur Ceram Soc 28:811–820
103. Slater PR, Fagg DP, Irvine JTS (1997) Synthesis and electrical characterisation of doped perovskite titanates as potentialanode materials for solid oxide fuel cells. J Mater Chem 7:2495–2498
104. Blennow P, Hagen A, Hansen KK, Wallenberg LR, Mogensen M (2008) Defect and electrical transport properties of nb-doped $SrTiO_3$. Solid State Ionics 179:2047–2058
105. Blennow P, Hansen KK, Wallenberg LR, Mogensen M (2009) Electrochemical characterization and redox behavior of nb-doped $SrTiO_3$. Solid State Ionics 180:63–70
106. Blennow P, Hansen KK, Wallenberg LR, Mogensen M (2007) Synthesis of nb-doped SrTiO3 by a modified glycine-nitrate process. J Eur Ceram Soc 27:3609–3612
107. Hashimoto S, Poulsen FW, Mogensen M (2007) Conductivity of SrTiO3 based oxides in the reducing atmosphere at high temperature. J Alloy Compd 439:232–236
108. Tufte ON, Chapman PW (1967) Electron mobility in semiconducting strontium titanate. Phys Rev 155:796
109. Irvine J, Slater P, Wright P (1996) Synthesis and electrical characterisation of the perovskite niobate-titanates, Sr1 − x/2Ti1 − xNbxO3 − δ. Ionics 2:213–216
110. Blennow P, Hansen KK, Reine Wallenberg L, Mogensen M (2006) Effects of Sr/Ti-ratio in SrTiO3-based SOFC anodes investigated by the use of cone-shaped electrodes. Electrochim Acta 52:1651–1661
111. Hui S, Petric A (2002) Electrical conductivity of yttrium-doped $SrTiO_3$: Influence of transition metal additives. Mater Res Bull 37:1215–1231
112. Zhao H, Gao F, Li X, Zhang C, Zhao Y (2009) Electrical properties of yttrium doped strontium titanate with A-site deficiency as potential anode materials for solid oxide fuel cells. Solid State Ionics 180:193
113. Fu Q, Tietz F, Sebold D, Tao S, Irvine JTS (2007) An efficient ceramic-based anode for solid oxide fuel cells. J Power Sources 171:663–669
114. Yang LM, De Jonghe LC, Jacobsen CP, Visco SJ (2007) B-site doping and catalytic activity of sr(Y)TiO_3. J Electrochem Soc 154:B949–B955
115. Vincent A, Luo J, Chuang KT, Sanger AR (2010) Effect of ba doping on performance of LST as anode in solid oxide fuel cells. J Power Sources 195:769
116. Wagner SF, Warnke C, Menesklou W, Argirusis C, Damjanovic T, Borchardt G, Ivers-Tiffée E (2006) Enhancement of oxygen surface kinetics of $SrTiO_3$ by alkaline earth metal oxides. Solid State Ionics 177:1607
117. Sun X, Wang S, Wang Z, Qian J, Wen T, Huang F (2009) Evaluation of $Sr_{0.88}Y_{0.08}TiO_3$–CeO_2 as composite anode for solid oxide fuel cells running on CH4 fuel. J Power Sources 187:85–89

118. Sun X, Wang S, Wang Z, Ye X, Wen T, Huang F (2008) Anode performance of LST–xCeO2 for solid oxide fuel cells. J Power Sources 183:114–117
119. Fu QX, Tietz F, Stover D (2006) $La_{0.4}Sr_{0.6}Ti_{1-x}Mn_xO_{3-d}$ perovskites as anode materials for solid oxide fuel cells. J Electrochem Soc 153:D74–D83
120. Ruiz-Morales J, Canales-Vázquez J, Savaniu C, Marrero-López D, Zhou W, Irvine JTS (2006) Disruption of extended defects in solid oxide fuel cell anodes for methane oxidation. Nature 439:568–571
121. Cheng Z, Zha S, Liu M (2006) Stability of materials as candidates for sulfur-resistant anodes of solid oxide fuel cells. J Electrochem Soc 153:A1302–A1309
122. Mukundan R, Brosha EL, Garzon FH (2004) Sulfur tolerant anodes for SOFCs. Electrochem Solid State Lett 7:A5–A7
123. Zha SW, Cheng Z, Liu ML (2005) A sulfur-tolerant anode material for SOFCs $Gd_2Ti_{1.4}Mo_{0.6}O_7$. Electrochem Solid State Lett 8:A406–A408
124. Porat O, Heremans C, Tuller HL (1997) Stability and mixed ionic electronic conduction in $Gd_2(Ti_{1-x}Mo_x)_2O_7$ under anodic conditions. Solid State Ionics 94:75
125. Sprague JJ, Tuller HL (1999) Mixed ionic and electronic conduction in Mn/Mo doped gadolinium titanate. J Eur Ceram Soc 19:803–806
126. Deng ZQ, Niu HJ, Kuang XJ, Allix M, Claridge JB, Rosseinsky MJ (2008) Highly conducting redox stable pyrochlore oxides. Chem Mater 20:6911–6916
127. Kramer S, Spears M, Tuller HL (1994) Conduction in titanate pyrochlores – role of dopants. Solid State Ionics 72:59–66
128. Naito H, Arashi H (1992) Electrical-properties of ZrO_2-TiO_2-Y_2O_3 system. Solid State Ionics 53:436–441
129. Kaiser A, Feighery A, Fagg D, Irvine J (1998) Electrical characterization of highly titania doped YSZ. Ionics 4:215
130. Tao S, Irvine JTS (2002) Optimization of mixed conducting properties of Y_2O_3-ZrO_2-TiO_2 and Sc_2O_3-Y_2O_3-ZrO_2-TiO_2 solid solutions as potential SOFC anode materials. J Solid State Chem 165:12–18
131. Tao SW, Irvine JTS (2004) Investigation of the mixed conducting oxide ScYZT as a potential SOFC anode material. J Electrochem Soc 151:A497–A503
132. Slater PR, Irvine JTS (1999) Niobium based tetragonal tungsten bronzes as potential anodes for solid oxide fuel cells: synthesis and electrical characterisation. Solid State Ionics 120:125–134
133. Slater PR, Irvine JTS (1999) Synthesis and electrical characterisation of the tetragonal tungsten bronze type phases, $(Ba/Sr/Ca/La)_{0-6}M_xNb_{1-x}O_{3-d}$ (M = mg, ni, mn, cr, fe, in, sn): evaluation as potential anode materials for solid oxide fuel cells. Solid State Ionics 124:61–72
134. Kaiser A, Bradley JL, Slater PR, Irvine JTS (2000) Tetragonal tungsten bronze type phases $(Sr_{1-x}Ba_x)_{0.6}Ti_{0.2}Nb_{0.8}O_{3-d}$: material characterisation and performance as SOFC anodes. Solid State Ionics 135:519–524
135. Aguilar L, Zha S, Cheng Z, Winnick J, Liu M (2004) A solid oxide fuel cell operating on hydrogen sulfide (H2S) and sulfur-containing fuels. J Power Sources 135:17–24

Books and Reviews

Atkinson A, Barnett S, Gorte RJ, Irvine JTS, McEvoy AJ, Mogensen M, Singhal SC, Vohs J (2004) Advanced anodes for high-temperature fuel cells. Nat Mater 3:17–27
Brandon NP, Skinner S, Steele BCH (2003) Recent advances in materials for fuel cells. Annu Rev Mater Res 33:183–213
Fergus JW (2006) Oxide anode materials for solid oxide fuel cells. Solid State Ionics 177:1529
Fleig J (2003) Solid oxide fuel cell cathodes: polarization mechanisms and modeling of the electrochemical performance. Annu Rev Mater Res 33:361–382
Gellings PJ, Bouwmeester HJM (2000) Solid state aspects of oxidation catalysis. Catal Today 58:1–53
Goodenough JB (2003) Oxide-ion electrolytes. Annu Rev Mater Res 33:91–128
Goodenough JB, Huang Y (2007) Alternative anode materials for solid oxide fuel cells. J Power Sources 173:1
Gong M, Liu X, Trembly J, Johnson C (2007) Sulfur-tolerant anode materials for solid oxide fuel cell application. J Power Sources 168:289
Gorte RJ, Vohs JM (2009) Nanostructured anodes for solid oxide fuel cells. Curr Opin Colloid Interface Sci 14:236–244

Disease-Resistant Transgenic Animals

Caroline Lassnig, Mathias Müller
Institute of Animal Breeding and Genetics & Biomodels Austria, University of Veterinary Medicine Vienna, Vienna, Austria

Article Outline

Glossary
Definition of the Subject and Its Importance
Introduction
Disease-Resistant Transgenic Animals
Future Directions
Bibliography

Glossary

Disease resistance/susceptibility The interplay of the genetically determined ability of an individual to prevent the reproduction of a pathogen or to reduce pathogen growth, host–pathogen interactions, and changing environmental conditions/factors decides on resistance/susceptibility.

Gene targeting Integration of exogenous DNA into the genome of an organism at specific sites as a result of homologous recombination. It can be used to disrupt or delete a gene, to remove or add sequences as well as to introduce point mutations at a given locus. Gene targeting can be permanent, i.e., ubiquitous with respect to tissue and developmental stage, or conditional, i.e., restricted to a specific time during development/life or limited to a specific tissue.

Genetic engineering Technological process resulting in a directed alteration of the genotype of a cell or organism. It combines recombinant nucleic acid technologies, in vitro culture technologies for gametes, embryos, tissues, or organisms, methods for the delivery of nucleic acids to the host genomes (gene transfer), and if needed, reproductive technologies to produce transgenic embryos and transfer them to foster organisms. With respect to inheritance ('transmission') to offspring, germline and somatic gene transfer methods are distinguished.

Knockdown Downregulation of expression of a specific gene by RNAi-based technologies.

Knockout/knockin Incorporation of a sequence into a specific site by homologous recombination (gene targeting) that results in disruption of gene function/altered gene function.

Quantitative trait loci (QTL) Genetic loci or chromosomal regions that contribute to variability in complex traits, as identified by statistical analysis. The genetic basis of these traits generally involves the effects of multiple genes and gene–environment interactions.

RNA interference (RNAi) The silencing of gene expression by the introduction of dsRNA that triggers the specific degradation of a homologous target mRNA, often accompanied by an attendant decrease in the production of the encoded protein.

Single nucleotide polymorphism (SNP) A variation in DNA sequence in which one nucleotide position is substituted for another by either nucleotide exchange, or deletion, or insertion. SNPs are the most frequent type of polymorphism in the genome.

Somatic cell nuclear transfer (SCNT) The nonsexual generation of nuclear genome-identical offspring ("cloned animals") by reconstitution of an enucleated oocyte with the diploid nucleus of a somatic cell to a zygote, which under appropriate culture conditions leads to reprogramming of the genome, enabling embryonic and fetal development.

Zoonotic infection The ability of a given pathogen to cross the host species barrier, from its current or long-term evolutionary host to animals and humans and thereby causing disease.

Definition of the Subject and Its Importance

Infectious diseases of livestock are a major risk to global animal health and welfare. In addition, human health is influenced due to the zoonotic potential of some of these infections.

Moreover, livestock diseases significantly impair food production and safety and cause enormous economic losses worldwide.

Transgenic technology was first developed as a research tool for studying gene function in mice in the early 1980s. The technique was extended and applied to other mammals in 1985. An interesting and challenging focus of agricultural transgenesis was the potential to increase disease resistance and/or reduce disease susceptibility by introducing new genes and/or deleting deleterious genes. The laborious improvements to original and recently developed transgene technologies lead to the generation of transgenic farm animals with improved resistance to infectious diseases, demonstrating the proof of principle that genetic engineering may potentially improve animal health and aid infectious disease control in livestock.

Introduction

Phenotype-driven traditional animal breeding and marker-assisted selection based on quantitative trait loci (QTLs) have been successfully used for the genetic improvement of many agricultural production traits such as body weight, carcass composition, or milk yield. However, these genetic selection strategies have not yet resulted in a significant increase in the resistance of farm animals to disease.

Currently, genomic sequences are available for several livestock species [1] and as a by-product of the sequencing, a huge number of single nucleotide

polymorphisms (SNPs) were discovered. The large panels of available SNPs were used in genome-wide association (GWA) studies for mapping and identifying genes [2]. GWA studies have already been successful in identifying causal genes and mutations for monogenic traits [3], but not for complex or quantitative traits such as resistance or susceptibility to disease.

Furthermore, traditional strategies in combating devastating infectious diseases of livestock, such as vaccination, antibiotic treatment, or even culling, have, to date, been unsuccessful (Fig. 1). Parasites evolved to resist chemical or vaccine control measures and bacteria developed resistance to many antibiotics. So far, a single infectious viral disease in livestock, rinderpest (cattle plague) could be eliminated through large-scale vaccination.

As an alternative to the traditional approaches, genetic engineering of livestock species may assist in the fight against infectious diseases.

The oldest and probably the most robust technique to produce transgenic farm animals is the injection of DNA sequences into the pronucleus of recently fertilized zygotes [4–6]. Pronuclear microinjection was successfully used to generate the most important livestock species, mainly for production of highly valuable human therapeutics. A more recent method for generating transgenic animals is the nuclear transfer technology, that is, 'cloning' [7, 8], which, together with a gene-targeting strategy allows the generation of specific gene-targeted animals [9, 10]. Recently, lentiviral vector-based strategies have been established which results in highly efficient production of transgenic livestock [11, 12]. This method in combination with the RNAi-technology may lead to the generation of disease-resistant transgenic livestock in the near future [13].

In the following section, the authors present an overview of the various transgenic methods used for the genetic enhancement of animal resistance to infectious diseases. Many studies were initially done using transgenic mouse models as this model often provides useful preliminary results prior to initiation of livestock studies.

Disease-Resistant Transgenic Animals

Reducing farm animal susceptibilty to infectious diseases via genetic engineering has been an ambitious goal since the first transgenic livestock was generated more than 20 years ago. Various transgenic strategies for improving animal health are described elsewhere [14–17].

In general, disease-resistant transgenic farm animals can be generated by two approaches: (1) introduction of resistance genes into the genome of the host (gain-of-function strategy) and (2) specific targeting of endogenous or exogenous susceptibility genes (loss or exchange-of-function strategy).

Improving Animal Health through Gain-of-Function Gene Transfer

In most cases, susceptibility to pathogens originates from the interplay of numerous genes, meaning susceptibility to pathogens is polygenic in nature. The murine *Mx* gene is one of the few examples of a single genetic (monogenic) locus encoding a disease-resistance trait. Mice and mouse fibroblast cell lines carrying the autosomal dominant *Mx1* allele are resistant to influenza virus infection [18, 19]. The transfer of the *Mx1* gene was able to restore virus resistance in mice lacking the *Mx1* allele [20] and inhibited influenza virus replication in avian cells [21]. However, the introduction of the murine *Mx1* gene into swine via pronuclear microinjection failed to produce influenza-resistant pigs [22]. The constitutive *Mx1* expression seemed to be detrimental to the pigs, whereas the expression from an inducible promoter was too low to produce detectable levels of *Mx1* protein. In the meantime, *Mx* genes of different farm animals have been identified, but their importance for disease susceptibility is not yet clear [23–25]. However, the ongoing detailed deciphering of the genomes of different farm animals, the improved techniques in generating transgenic animals [26–28], and the new tools for controlling transgene expression levels [29, 30] might allow the idea of generating influenza-resistant livestock by transferring a disease resistance gene to be addressed once more.

Antimicrobial peptides (AMPs) are an important component of the innate defense of most living organisms and there is a growing body of evidence to show that their role in defense against microbes is as important to the host as antibodies and innate and adaptive immune cells [31, 32]. AMPs are usually composed of

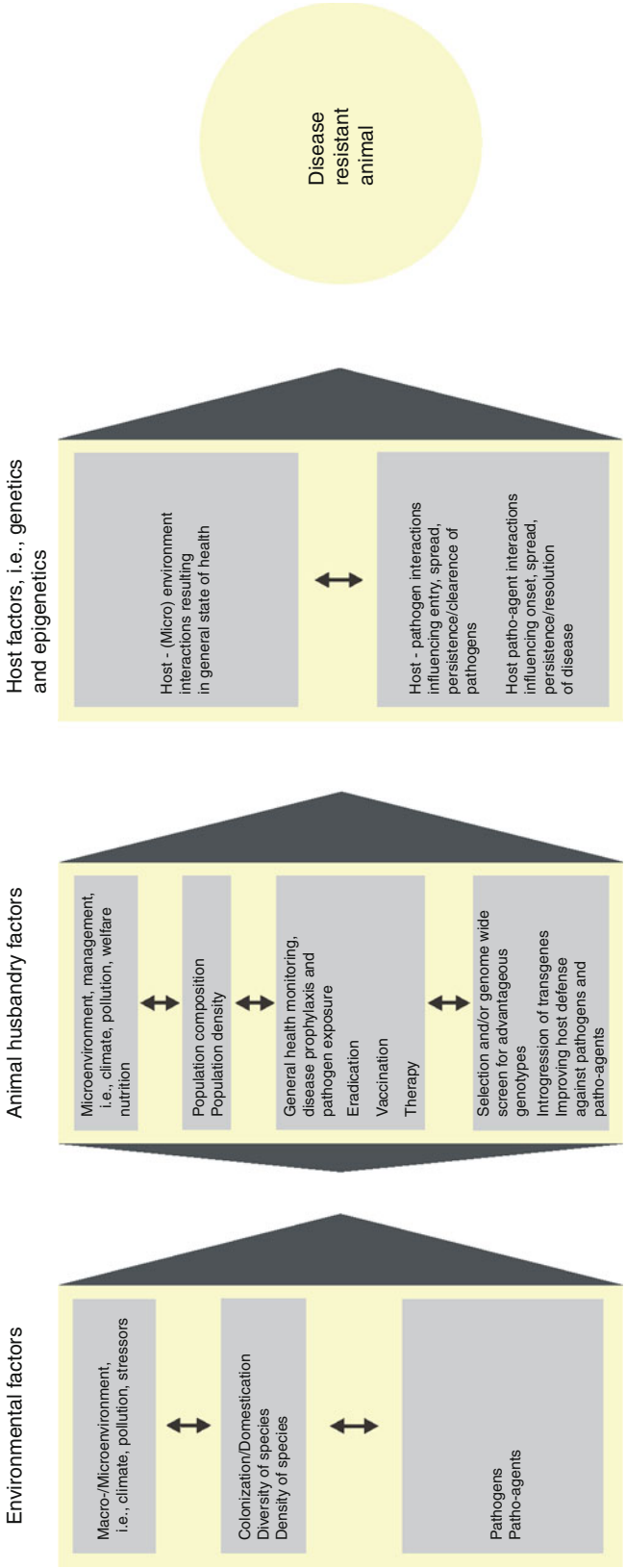

Disease-Resistant Transgenic Animals. Figure 1
Horizontal and vertical interrelations influencing the animal's health status, diseased versus nondiseased. The most specific measures to disrupt the pathogen/patho-agent flow toward the animal and/or improve the animal's disease defense mechanisms are highlighted

12–50 amino acids and synthesized by microorganisms as well as multicellular organisms, including plants and animals. They can have broad-spectrum antibacterial, antifungal, antiviral, antiprotozoan, and antisepsis properties. In addition to the wide range of these naturally occurring AMPs, many new ones have also been synthesized [33, 34]. Based on three-dimensional structural studies, the peptides are broadly classified into five major groups namely: (1) peptides that form alpha-helical structures; (2) peptides that form beta-sheets; (3) peptides rich in cysteine residues; (4) peptides rich in regular amino acids namely histatin, arginine, and proline; and (5) peptides composed of rare and modified amino acids [35, 36]. They can induce complete lysis of the organism by disrupting the membrane or by perturbing the membrane lipid bilayer, which allows for leakage of specific cellular components as well as dissipating the electrical potential of the membrane.

In initial engineering studies, the endogenous production of antimicrobial compounds in transgenic animals was shown to enhance disease resistance. Recombinant bovine tracheal antimicrobial peptide (bTAP) isolated from milk from transgenic mice, showed antimicrobial activity against *Escherichia coli*, without any deleterious side effects in suckling pups [37]. The antimicrobial activity of the synthetic alpha-helical peptide *Shiva 1a* was confirmed in transgenic mice, challenged with *Brucella abortus* [38]. The expression of the recombinant peptide significantly reduced both the bacterial colonization and the associated pathological changes in the genetically engineered mice.

Mastitis which is caused by bacterial infection of the mammary gland is reported to be the most costly disease in animal agriculture. It seriously affects animal well-being and is the most common reason for antibiotic use in diary cattle and the most frequent cause of antibiotic residues in milk [39]. The major contagious mastitis pathogen, *Staphylococcus aureus* is sensitive to lysostaphin, an antibacterial peptide naturally produced by a related bacterium, *Staphylococcus simulans* [40]. Kerr and colleagues showed that mammary gland expression of a bioactive variant of lysostaphin conferred protection against *S.aureus* infection in mice [41]. The staphylolytic activity in the milk of transgenic mice appeared to be 5–10 fold less active than bacterially derived lysostaphin, but was sufficient to confer substantial resistance to staphylococcal mastitis. Transgene production appeared to have no apparent effect on the physiology of the animal, the integrity of the mammary gland, or the milk it produces. Using nuclear transfer techniques, this approach was successfully extended to cattle, recently [42]. Transgenic dairy cows secreting lysostaphin constitutively in their milk were more resistant to *S. aureus* infections than nontransgenic animals. Lysostaphin concentrations in the milk of transgenic animals remained fairly constant during lactation. The recombinant lysostaphin was approximately 15% as active as bacterially derived protein. Challenge studies with *S. aureus* clearly demonstrated a direct correlation between the extent of protection against *S. aureus* infection with lysostaphin levels in the milk. Transgenic cows have been previously generated, primarily as bioreactors for large-scale production of pharmaceuticals and nutraceuticals. Thus, lysostaphin-transgenic cattle are the first example for enhancing disease resistance and animal welfare in livestock, and may allow substantial reductions in antibiotic use. This in turn will help to control the spread of antibiotic-resistant bacteria and to reduce bacterial and antibiotic contamination of milk and milk products.

The antibacterial effect of lysostaphin is restricted to *S. aureus* only and transgenic cows are not protected against other mastitis-causing pathogens. The additional expression of secondary antibacterial compounds in the milk might be necessary for further enhancing mastitis resistance.

Human lysozyme (hLZ), a bacteriostatic milk protein that is known to attack the peptidoglycan component of bacterial cell walls, was expressed in the mammary gland of transgenic mice [43] and transgenic dairy goats [44]. Milk from the transgenic animals showed significant bacteriostatic activity and slowed the growth of several bacteria responsible for causing mastitis and the cold-spoilage of milk. The somatic cell count (SCC) is applied as a measure for udder health and milk quality and a high SCC in milk is directly correlated with mastitis and an impairment of milk quality [45]. Analyzing the SCC in milk samples of transgenic diary goats revealed a significant lower SCC compared to milk samples from control animals suggesting an improved udder health in the transgenic animals [46]. Lysozyme plays a role in the defense

against gastrointestinal pathogens and reduces gastrointestinal illness in breastfed infants [47]. Feeding trials were conducted in pigs to evaluate putative health-promoting functions of hLZ-transgenic milk. Pigs are monogastric animals with a digestive system similar to humans and therefore are commonly used to study human health. Brundige and colleagues demonstrated that the consumption of pasteurized milk from hLZ-transgenic goats improved the gastrointestinal health of young piglets and was beneficial against a gastrointestinal infection with enteropathogenic *E. coli* [48].

A Chinese group enabled synthesis and secretion of bioactive bovine lactoferrin and bovine tracheal antibacterial peptides in goat mammary cells by use of plasmid-mediated gene transfer techniques [49], and the milk samples collected from these animals exhibited bacteriostatic effects against different mastitis-causing pathogens.

The authors summarize that genetic engineering for secretion of a broad range of AMPs in the mammary gland of dairy goats and cows reduces susceptibility to various microbial pathogens and is therefore a realistic approach to combat mastitis. Enhanced mastitis resistance will not only improve animal health and well-being, but also reduces bacterial contamination of milk and milk products in addition to reducing the costs incurred during disease prevention and cure.

Transgenic mice, expressing and processing a human enteric alpha-defensin peptide exclusively in specialized epithelia of the small intestinal crypt were generated, and were immune to an oral challenge with virulent *Salmonella typhimurium* [50].

Protegin-1 (PG-1) that is normally expressed in porcine myeloid cells and resides in secretory granules of neutrophils is another potent antimicrobial peptide targeting both gram-negative and gram-positive bacteria [51]. The ectopic expression of PG-1 in transgenic mice conferred enhanced respiratory resistance to an intranasal challenge with *Actinobacillus suis* [52], an opportunistic pathogen that may cause pneumonia, abortion, and fatal septicemia in pigs of all ages [53, 54]. Extending this concept to pigs and other somatic tissues beyond neutrophils will be another step toward the development of disease-resistant livestock.

The overexpression of dominant-negative mutants of viral proteins or pathogen receptors is another potent strategy to enhance animal disease resistance. The major focus has been to block viral attachment and penetration into a host cell by (1) producing viral proteins that block cellular receptors (antireceptor) or (2) altering known host molecular components, such as replacing host receptor genes with a modified version which is able to perform the receptor's physiological function but prevents attachment of the virus [55]. The first successful introduction of pathogen-mediated disease resistance in animals was reported 20 years ago. Transgenic chickens expressing the viral envelope of a recombinant avian leukosis retroviral genome were resistant to the corresponding subgroup of avian leukosis virus due to blockage of the virus receptors by the viral envelope proteins [56]. Using the same strategy, Clements et al. generated transgenic sheep expressing the maedi-visna virus envelope (E) gene, which is responsible for virus attachment to the host cells [57]. Maedi-visna virus is a prototype of ovine lentiviruses that cause encephalitis, pneumonia, and arthritis in sheep. Transgenic lambs expressing the viral E glycoprotein in monocytes/macrophages, the target cells for virus replication, were healthy and neither deleterious effects nor clinical abnormalities from the transgene was observed. However, up to date, challenge studies to determine the susceptibility of these animals to ovine lentiviruses have not been reported.

Transgenic mice expressing a soluble form of porcine nectin-1, the cellular receptor for α-herpesviruses were generated. These mice displayed high resistance to pseudorabies virus (PRV) infections [58]. In pigs, PRV causes lethal encephalitis, acute respiratory syndrome, abortion and infertility, and latent infections [59]. Analysis of transgenic mouse lines, ubiquitously expressing different soluble forms of the cellular receptor for the viral glycoprotein D revealed that the transgene encoding the soluble form of the entire ectodomain of porcine nectin-1 fused to the human IgG1 conferred highest resistance to intranasal and intraperitonal PRV infections without any side effects [60]. Surprisingly, the expression of a fusion protein consisting of the first Ig-like domain of nectin-1 and the Fc portion of porcine IgG1 not only resulted in reduced virus resistance but also caused microphthalmia and the lack of vitreous bodies [61, 62]. Before implementing this promising approach to the generation of α-herpesviruses-resistant swine, further investigations examining the

interactions of different soluble forms of nectin-1, endogenous nectins, and viral glycoprotein D and analysis of the influence of Fc domains of different species are required.

An alternative transgenic approach to protect livestock against infectious diseases is the expression of genes directing the synthesis of defined antibodies which target specific pathogens and thus induce immediate immunity without prior exposure to that pathogen.

Initial studies to express gene constructs encoding monoclonal antibodies in transgenic livestock were conducted nearly 20 years ago [63, 64]. However, the recombinant antibodies expressed in transgenic rabbits, sheep, and pigs showed aberrant sizes and only low antigen binding affinity. Nevertheless, following this idea, transgenic mice expressing coronavirus-neutralizing antibodies in the mammary gland were generated [65, 66]. High antibody expression titres throughout the lactation period provided complete protection against the enteric infection of newborns with transmissible gastroenteritis virus (TGEV), a pathogen which produces high mortality in suckling piglets, and also against a murine hepatitis virus (MHV)-induced encephalitis. Following this strategy, manipulating the lactogenic immunity in farm animals could improve the protection of suckling newborns through colostrium-delivered antibodies [67].

Enhancing Disease Resistance by Targeting Endogenous Susceptibility Genes

Transmissible spongiform encephalopathies (TSE) are fatal neurodegenerative disorders of the central nervous system which are termed scrapie in goat and sheep and bovine spongiform encephalopathy (BSE) in cattle. According to current knowledge, the causative agent of the brain pathology in diseased animals is the prion. Prion diseases are characterized by the accumulation of the abnormally folded and protease-resistant isoform (PrP^{Sc}) of the cellular prion protein (PrP^{C}) of the host [68, 69]. The generation of prion-free livestock resistant to TSE has been an ambitious goal since the BSE epidemic in cattle in the UK and the appearance of a new and highly lethal variant of Creutzfeldt-Jakob disease (vCJD) in humans. Early studies in mice revealed that reduction or loss of PrP^{C} expression did not affect normal development of the mice, but conferred protection against scrapie disease after inoculation with PrP^{Sc} prions [70–73]. With the development of nuclear transfer cloning techniques using genetically modified embryonic or somatic cell donors [7–10], the possible 'knock out' of the prion gene in transgenic sheep, goats, and cattle has opened new perspectives for the generation of disease-resistant livestock. A decade ago, Denning and colleagues generated the first PrP^{C}-targeted lambs. However, none of the cloned sheep survived more than 12 days [74]. Analyses of the targeted fetuses and lambs revealed defects that have been described in other nuclear transfer experiments with nontransfected cells and therefore, the authors expected that the early death of the lambs was not a consequence of the PrP^{C} disruption per se, but was probably due to the nuclear transfer procedures and/or the prolonged culture and drug selection of the primary fibroblasts used for nuclear transfer.

The functional disruption of the caprine PrP^{C} gene in cloned goats was first described by Yu et al. [75] and resulted in two goats lacking the prion protein [76]. The scientists confirmed the complete PrP^{C} ablation at mRNA and protein levels, and at 2 months age, the PrP^{C} null goats were healthy and showed no developmental or behavioral defects. The scientific community is awaiting the final proof of the concept – scrapie resistance of PrP^{C}-deficient goats after infection with PrP^{Sc} prions.

Richt and colleagues described the generation of the first PrP^{C}-deficient cattle [77]. They used a sequential gene targeting strategy which was demonstrated for the first time by the group of Kuroiwa et al. [78]. Male Holstein primary fibroblasts were transfected with two knockout vectors to sequentially disrupt the two alleles of the PrP^{C} gene. PrP^{C}-deficient fetal cell lines were established at 40–75 days of gestation and recloned for the generation of calves. The impact of PrP^{C} deficiency on calf development, on the immune system, on growth, and general health of the cattle for at least 20 months was analyzed in detail, and no negative influence of PrP^{C} ablation on animal health and well-being was detected. Importantly, brain homogenates from 10-month-old PrP^{C}-deficient cattle prevented PrP^{Sc} propagation in vitro, whereas in brain homogenates from wild-type cattle PrP^{Sc} proliferated. The researchers concluded that the presence of the

endogenous bovine PrP^C is essential for PrP^{Sc} propagation and that there are no other host-derived cellular factors that can support the in vitro PrP^{Sc} propagation in the absence of the endogenous bovine PrP^C. In vivo tests of resistance to prion propagation in PrP^C-deficient cattle are under way, but still will require some years to complete. Analyses of several PrP^C-targeted mouse lines indicated that the loss of the normal cellular function of PrP^C may adversely affect the animals. For example, PrP^C-deficient mice developed ataxia and cerebellar neurodegeneration [79, 80], slight alterations in sleep–wake circadian rhythm [81], and altered synaptic functions [82]. To date, none of the above-described alterations in PrP^C null mice could be observed in PrP^C-deficient cattle and goats, respectively, but further investigations on aged transgenic animals will be necessary to exclude these altered phenotypes.

Small interfering RNAs (siRNAs) can silence/shut down specific targeted genes by interfering with the RNA transcripts they produce [83, 84]. For a transient gene 'knock down,' synthetic siRNAs can be directly transfected into cells or early embryos. However, for stable gene expression and germline transmission, the siRNA sequences are incorporated into gene constructs which express short hairpin (sh)RNAs that are processed to siRNAs within the cell. Through stably integrated shRNA expression vectors, additional genetic information is introduced into an organism (gain-of-functions strategy), which then produces a 'knock down' phenotype that is functionally similar to a 'knock out' (loss of function). Thus, RNAi-transgenics is an interesting alternative to the homologous gene targeting strategies which are traditionally used for the generation of 'knock out' livestock.

One of the most interesting susceptibility genes in livestock is the PrP^C gene and in a preliminary in vitro experiment, it was demonstrated that siRNA suppression of the PrP^C gene abrogates the PrP^C synthesis and inhibits the formation of PrP^{SC} protein in chronically scrapie-infected murine neuroblastoma cells [85]. Shortly after, Golding and colleagues combined this RNAi-based technique with lentiviral transgenesis for targeting the PrP^C gene in an adult goat fibroblast cell line, which was then used for somatic cell nuclear transfer to produce a cloned goat fetus [13]. Protein analyses of brain tissues demonstrated that PrP^C expression was reduced >90% in the cloned transgenic fetus when compared with a control. In a further experiment, they injected the recombinant lentivirus directly into the perivitelline space of bovine ova. Development of more than 30% of injected ova to blastocysts and expression of the shRNA targeting the PrP^C gene in more than 70% provides strong evidence that this RNAi approach may be useful in creating genetically engineered farm animals with natural resistance to prion diseases.

In two further approaches, lentiviral-mediated delivery of shRNA expression vectors into the brain of scrapie-infected mice resulted in a clear reduction of the PrP^C protein level and a prolonged survival of infected mice [86, 87], inferring that RNAi-technology may also be used for therapeutic applications.

Enhancing Disease Resistance by Targeting Exogenous Susceptibility/Viral Genes

Another application of the RNAi-technology is the silencing of exogenous viral genes through the introduction of specific dsRNA molecules into cells, where they are targeted to essential genes or directly to the viral genome, thus inhibiting viral replication [88, 89]. Currently, the use of RNAi-based strategies for generation of viral disease-resistant livestock focuses on three pathogens: food and mouth disease virus (FMDV), bovine viral diarrhea virus (BVDV), and influenza A viruses.

FMDV is an extremely contagious pathogen that affects cattle, swine, and other livestock worldwide [90]. FMD is difficult to control by vaccination and impossible to eliminate by conservative natural breeding. Initial studies tested specific FMDV-siRNAs for their ability to inhibit virus replication in BHK-21 cells [91]. Transfection of BHK-21 cells with a mixture of siRNAs targeting highly conserved sequences of the 3B region and the 3D polymerase gene in all FMDV serotypes resulted in nearly 100% suppression of virus growth.

In another approach, siRNAs were designed to specifically target the viral VP1 gene, which plays a key role in virus attachment. This resulted in a nearly 90% reduction in FMDV VP1 expression and conferred resistance to FMDV challenge in cultured cells which are susceptible to this virus [92]. Encouragingly,

pretreatment with siRNAs before infection made suckling mice significantly less susceptible to FMDV, and expression of siRNAs directed against the viral nonstructural protein 2B clearly inhibited virus replication in infected porcine cells [93].

Another RNAi target of agricultural interest is the bovine viral diarrhea virus (BVDV), an ubiquitously occurring pathogen that affects cattle herds worldwide resulting in respiratory disorders and increased susceptibility to other pathogens [94]. Lambeth and his group demonstrated that BVDV replication in bovine cells can be efficiently suppressed by RNAi [95]. They transfected shRNA expression vectors and siRNAs targeting the 5′ nontranslated region (NTR) and the region encoding the C protein of the viral genome into MDBK cells. After challenging with BVDV, they detected reduced virus titres by both siRNA and shRNA-mediated RNAi.

Farm animals, in particular swine and poultry, serve as key links between the natural reservoir of influenza A viruses and epidemics and pandemics in human populations. Due to repeated reassortment or mixing of RNA segments between influenza viruses from different species, virulent strains emerge periodically and often lead to devastating human catastrophes [96]. However, the emergence of the RNAi technology has opened many new options for preventing influenza virus infections in animals.

In initial studies, a set of siRNAs specific for conserved regions of the influenza virus genome could potently inhibit virus production in MDCK cells and embryonated chicken eggs [97]. In subsequent approaches, this strategy was extended to an established animal model of influenza infections by two independent groups. Tompkins and colleagues used siRNAs for targeting highly conserved regions of the viral nucleoprotein (NP) and acidic polymerase (PA). After administration of influenza virus-specific siRNAs via hydrodynamic i.v. injection [98], BALB/c mice were infected intranasally with influenza A/H1N1. Virus titre in lung homogenates were significantly reduced in siRNAs-treated mice when compared to control mice 48 h p.i [99]. In addition, they demonstrated that influenza-specific siRNA treatment can protect mice from otherwise lethal virus challenges.

Ge and coworkers administered influenza virus-specific siRNAs intravenously along with lentiviral shRNA expression vectors into C57BL/6 mice. They demonstrated that siRNAs as well as shRNAs can reduce influenza virus production in the lung when given either before or after virus infection and that the simultaneous use of two or more siRNAs specific for different virus genes resulted in a more severe reduction of virus titres [100].

A promising approach for the generation of influenza-resistant livestock was published by Wise and colleagues [101]. They used shRNA expression vectors, targeting the viral NP and PA gene for lentiviral-mediated generation of transgenic mice. Expression of the siRNAs was confirmed by an RNAse protection assay, and thus far, stable transmission of the transgene was observed up to the third generation. Currently, transgenic mice are mated to generate homozygous lines for delivering the final proof for influenza virus resistance in vivo.

Recently the generation of transgenic chicken expressing a shRNA molecule able to inhibit influenza virus polymerase activity [115] was reported. Although the transgenic chicken did not exhibit a higher resistance to high challenge doses of H5N1, a highly pathogenic avian influenza virus, they showed strongly reduced transmission of the infection to transgenic and even non-transgenic birds housed in direct contact with them, demonstrating that this strategy may be used to prevent transmission and propagation of an infection at the flock level.

Future Directions

The past decade was dominated by large-scale and high throughput nucleic acid analyses allowing comparative genome sequencing and expression profiling projects. The comprehensive and ongoing analysis of the huge data sets led to the need for an updated definition of the term 'gene' and the introduction of the term 'epigenetics.' Taking into account that Mendel's and Morgan's elements of heredity include multifunctional protein coding, structural, regulatory, and RNAs of unknown functions and gene regulation is more complex than previously assumed, the 'gene' is suggested to be 'a union of genomic sequences encoding a coherent set of potentially overlapping functional products' [102] and 'epigenetics' is defined to describe 'stably inheritable phenotypes resulting from changes in

a chromosome without alterations of the DNA-sequence' [103]. The future challenge of the postgenomic era is subsumed as integrative, quantitative, and/or systems biology. 'Systems biology is the comprehensive and quantitative analysis of the interactions between all of the components of biological systems over time' [104]. 'Systems biology involves an iterative cycle, in which emerging biological problems drive the development of new technologies and computational tools' [104]. The further understanding of disease mechanisms also depends on these emerging disciplines.

The ongoing genome sequencing programs for various animal species and the increasing densities of SNP arrays will lead to the discovery of new QTLs underlying economically important traits such as disease resistance and susceptibility. In addition, complete genome sequences of many disease-causing pathogens are becoming available. Hence, genome data on host intrinsic factors and host–pathogen interactions causing disease can be used to increase the health of individuals or populations. Conventional breeding and genomic selection will increasingly benefit from the natural variations identified among the populations. This can be supplemented with gene transfer technologies allowing a more targeted approach toward desired animal breeding without the limitation of species barriers.

The future of transgene technologies is dependent on the simplification of the gene delivery systems along with targeted manipulation of animal genomes. The former aim is achieved by using lentiviral vectors which are highly efficient for domesticated animals including poultry [105, 106] and pets [107]. Gene targeting in species other than mice is limited as embryonic stem (ES) cells of farm or pet animals are unavailable and gene targeting via homologous recombination of embryonic and somatic cells and subsequent nuclear transfer is highly inefficient. However, the advent of the RNAi-technology offers new possibilities for specific gene targeting in animal species and will have a huge impact on transgenesis in the near future. Furthermore, the zinc finger nuclease (ZNF) technology has shown to be an attractive alternative to ES cell targeting and nuclear transfer technology [108] and was already applied successfully for targeted gene disruption in rats [109].

For further reading concerning the use of ZFN-technology in farm animals we refer to Kues and Niemann [116]. In addition, site-directed mutagenesis of genomes can be achieved by TALENs (transcription activator-like effector nucleases) which were originally identified in plant pathogens and recently were successfully used to generate knockout rats [117]. These site-specific nucleases may complement/enlarge the well established ZFN-technology for efficient gene targeting in livestock [118].

Last but not least, the cross-species generation of pluripotent/embryonic cell lines has gained new impetus through the induced pluripotent stem cell (iPS) technology, i.e., the reprogramming of somatic cells making them capable of embryogenesis (reviewed in [110]) and the recent isolation of authentic embryonic stem cells from rat blastocysts by novel culture conditions [111, 112]. In the future, animal transgenetics and animal disease resistance will be important in basic research and in the understanding of disease mechanisms. Bridging the gap between model and man by generating transgenic animals is fundamental to the development of novel therapeutics and disease prevention strategies.

Increased availability of genomic information of livestock species along with more sophisticated transgenic tools offers the potential to generate animal models to combat livestock diseases to a larger extent than ever before. However, animal geneticists/scientists must consider several important aspects. (1) The dissemination of the trait of interest such as disease resistance, introduced by a transgene will neither be simple nor fast, therefore cost–benefit calculations will probably decide on implementation of transgenic animals. For example, transgenic BSE-resistant cattle [77] will probably never gain importance in agriculture where culling is considered to meet demands with respect to cost efficiency and biosafety. However, BSE-resistant cattle may be engineered for the production of pharmaceuticals and therefore will have an enormous impact on providing safer drugs. (2) There is general public opposition to the use of transgenic livestock. However, if animals were resistant to zoonotic diseases, therefore resulting in reduced frequency of pandemics and epidemics such as those caused by influenza virus, attitudes of human societies might change [113]. In this context, recently, a trypansome lytic factor (TLF)

from baboons that protected mice both from animal and human-infective *Trypanosoma* subspecies was identified and suggested to be transferred to livestock [114]. Animal trypanosomiasis is one of the major parasitic diseases of livestock flocks and livestock are the major reservoir for human-pathogenic trypanosomes. (3) Scientists and society should clearly keep in mind that pathogens readily change their antigenic determinants and create novel subtypes to escape the 'resistant' host's immune system. Attempts to introduce resistance traits into animal populations either by conventional breeding or transgenesis should be subjected to thorough cost/detriment–benefit analyses.

Bibliography

1. de Koning DJ, Archibald A, Haley CS (2007) Livestock genomics: bridging the gap between mice and men. Trends Biotechnol 25:483–489
2. Goddard ME, Hayes BJ (2009) Mapping genes for complex traits in domestic animals and their use in breeding programmes. Nat Rev Genet 10:381–391
3. Charlier C, Coppieters W, Rollin F, Desmecht D, Agerholm JS, Cambisano N, Carta E, Dardano S, Dive M, Fasquelle C, Frennet JC, Hanset R, Hubin X, Jorgensen C, Karim L, Kent M, Harvey K, Pearce BR, Simon P, Tama N, Nie H, Vandeputte S, Lien S, Longeri M, Fredholm M, Harvey RJ, Georges M (2008) Highly effective SNP-based association mapping and management of recessive defects in livestock. Nat Genet 40:449–454
4. Hammer RE, Pursel VG, Rexroad CE Jr, Wall RJ, Bolt DJ, Ebert KM, Palmiter RD, Brinster RL (1985) Production of transgenic rabbits, sheep and pigs by microinjection. Nature 315:680–683
5. Brem G, Brenig B, Goodmann HM, Selden RC, Graf F, Kruff B, Springman K, Hondele J, Meyer J, Winnacker E-L, Kräußlich H (1985) Production of transgenic mice, rabbits and pigs by microinjection into pronuclei. Reprod Domest Anim 20:251–252
6. Pursel VG, Hammer RE, Bolt DJ, Palmiter RD, Brinster RL (1990) Integration, expression and germ-line transmission of growth-related genes in pigs. J Reprod Fertil Suppl 41:77–87
7. Cibelli JB, Stice SL, Golueke PJ, Kane JJ, Jerry J, Blackwell C, Ponce de Leon FA, Robl JM (1998) Cloned transgenic calves produced from nonquiescent fetal fibroblasts. Science 280:1256–1258
8. Wilmut I, Schnieke AE, McWhir J, Kind AJ, Campbell KH (1997) Viable offspring derived from fetal and adult mammalian cells. Nature 385:810–813
9. Campbell KH, McWhir J, Ritchie WA, Wilmut I (1996) Sheep cloned by nuclear transfer from a cultured cell line. Nature 380:64–66
10. Schnieke AE, Kind AJ, Ritchie WA, Mycock K, Scott AR, Ritchie M, Wilmut I, Colman A, Campbell KH (1997) Human factor IX transgenic sheep produced by transfer of nuclei from transfected fetal fibroblasts. Science 278:2130–2133
11. Hofmann A, Kessler B, Ewerling S, Weppert M, Vogg B, Ludwig H, Stojkovic M, Boelhauve M, Brem G, Wolf E, Pfeifer A (2003) Efficient transgenesis in farm animals by lentiviral vectors. EMBO Rep 4:1054–1060
12. Whitelaw CB, Radcliffe PA, Ritchie WA, Carlisle A, Ellard FM, Pena RN, Rowe J, Clark AJ, King TJ, Mitrophanous KA (2004) Efficient generation of transgenic pigs using equine infectious anaemia virus (EIAV) derived vector. FEBS Lett 571:233–236
13. Golding MC, Long CR, Carmell MA, Hannon GJ, Westhusin ME (2006) Suppression of prion protein in livestock by RNA interference. Proc Natl Acad Sci USA 103:5285–5290
14. Muller M, Brem G (1994) Transgenic strategies to increase disease resistance in livestock. Reprod Fertil Dev 6:605–613
15. Muller M, Brem G (1996) Intracellular, genetic or congenital immunisation–transgenic approaches to increase disease resistance of farm animals. J Biotechnol 44:233–242
16. Muller M, Brem G (1998) Transgenic approaches to the increase of disease resistance in farm animals. Rev Sci Tech 17:365–378
17. Whitelaw CB, Sang HM (2005) Disease-resistant genetically modified animals. Rev Sci Tech 24:275–283
18. Haller O, Arnheiter H, Gresser I, Lindenmann J (1981) Virus-specific interferon action. Protection of newborn Mx carriers against lethal infection with influenza virus. J Exp Med 154:199–203
19. Staeheli P, Haller O, Boll W, Lindenmann J, Weissmann C (1986) Mx protein: constitutive expression in 3T3 cells transformed with cloned Mx cDNA confers selective resistance to influenza virus. Cell 44:147–158
20. Arnheiter H, Skuntz S, Noteborn M, Chang S, Meier E (1990) Transgenic mice with intracellular immunity to influenza virus. Cell 62:51–61
21. Garber EA, Chute HT, Condra JH, Gotlib L, Colonno RJ, Smith RG (1991) Avian cells expressing the murine Mx1 protein are resistant to influenza virus infection. Virology 180:754–762
22. Muller M, Brenig B, Winnacker EL, Brem G (1992) Transgenic pigs carrying cDNA copies encoding the murine Mx1 protein which confers resistance to influenza virus infection. Gene 121:263–270
23. Ko JH, Jin HK, Asano A, Takada A, Ninomiya A, Kida H, Hokiyama H, Ohara M, Tsuzuki M, Nishibori M, Mizutani M, Watanabe T (2002) Polymorphisms and the differential antiviral activity of the chicken Mx gene. Genome Res 12:595–601
24. Thomas AV, Palm M, Broers AD, Zezafoun H, Desmecht DJ (2006) Genomic structure, promoter analysis, and expression of the porcine (Sus scrofa) Mx1 gene. Immunogenetics 58:383–389
25. Ellinwood NM, McCue JM, Gordy PW, Bowen RA (1998) Cloning and characterization of cDNAs for a bovine (Bos taurus) Mx protein. J Interferon Cytokine Res 18:745–755
26. Whitelaw CB, Lillico SG, King T (2008) Production of transgenic farm animals by viral vector-mediated gene transfer. Reprod Domest Anim 43(Suppl 2):355–358

27. Pfeifer A (2004) Lentiviral transgenesis. Transgenic Res 13:513–522
28. Park F (2007) Lentiviral vectors: are they the future of animal transgenesis? Physiol Genomics 31:159–173
29. Aigner B, Klymiuk N, Wolf E (2010) Transgenic pigs for xenotransplantation: selection of promoter sequences for reliable transgene expression. Curr Opin Organ Transplant 15(2):201–206
30. Kues WA, Schwinzer R, Wirth D, Verhoeyen E, Lemme E, Herrmann D, Barg-Kues B, Hauser H, Wonigeit K, Niemann H (2006) Epigenetic silencing and tissue independent expression of a novel tetracycline inducible system in double-transgenic pigs. FASEB J 20:1200–1202
31. Hancock RE, Diamond G (2000) The role of cationic antimicrobial peptides in innate host defences. Trends Microbiol 8:402–410
32. Selsted ME, Ouellette AJ (2005) Mammalian defensins in the antimicrobial immune response. Nat Immunol 6:551–557
33. Lee DG, Hahm KS, Shin SY (2004) Structure and fungicidal activity of a synthetic antimicrobial peptide, P18, and its truncated peptides. Biotechnol Lett 26:337–341
34. Powers JP, Hancock RE (2003) The relationship between peptide structure and antibacterial activity. Peptides 24:1681–1691
35. Epand RM, Vogel HJ (1999) Diversity of antimicrobial peptides and their mechanisms of action. Biochim Biophys Acta 1462:11–28
36. Reddy KV, Yedery RD, Aranha C (2004) Antimicrobial peptides: premises and promises. Int J Antimicrob Agents 24:536–547
37. Yarus S, Rosen JM, Cole AM, Diamond G (1996) Production of active bovine tracheal antimicrobial peptide in milk of transgenic mice. Proc Natl Acad Sci USA 93:14118–14121
38. Reed WA, Elzer PH, Enright FM, Jaynes JM, Morrey JD, White KL (1997) Interleukin 2 promoter/enhancer controlled expression of a synthetic cecropin-class lytic peptide in transgenic mice and subsequent resistance to Brucella abortus. Transgenic Res 6:337–347
39. Erskine RJ, Walker RD, Bolin CA, Bartlett PC, White DG (2002) Trends in antibacterial susceptibility of mastitis pathogens during a seven-year period. J Dairy Sci 85:1111–1118
40. Kumar JK (2008) Lysostaphin: an antistaphylococcal agent. Appl Microbiol Biotechnol 80:555–561
41. Kerr DE, Plaut K, Bramley AJ, Williamson CM, Lax AJ, Moore K, Wells KD, Wall RJ (2001) Lysostaphin expression in mammary glands confers protection against staphylococcal infection in transgenic mice. Nat Biotechnol 19:66–70
42. Wall RJ, Powell AM, Paape MJ, Kerr DE, Bannerman DD, Pursel VG, Wells KD, Talbot N, Hawk HW (2005) Genetically enhanced cows resist intramammary *Staphylococcus aureus* infection. Nat Biotechnol 23:445–451
43. Maga EA, Anderson GB, Huang MC, Murray JD (1994) Expression of human lysozyme mRNA in the mammary gland of transgenic mice. Transgenic Res 3:36–42
44. Maga EA, Shoemaker CF, Rowe JD, Bondurant RH, Anderson GB, Murray JD (2006) Production and processing of milk from transgenic goats expressing human lysozyme in the mammary gland. J Dairy Sci 89:518–524
45. Schukken YH, Wilson DJ, Welcome F, Garrison-Tikofsky L, Gonzalez RN (2003) Monitoring udder health and milk quality using somatic cell counts. Vet Res 34:579–596
46. Maga EA, Cullor JS, Smith W, Anderson GB, Murray JD (2006) Human lysozyme expressed in the mammary gland of transgenic dairy goats can inhibit the growth of bacteria that cause mastitis and the cold-spoilage of milk. Foodborne Pathog Dis 3:384–392
47. Lonnerdal B (2003) Nutritional and physiologic significance of human milk proteins. Am J Clin Nutr 77:1537S–1543S
48. Brundige DR, Maga EA, Klasing KC, Murray JD (2008) Lysozyme transgenic goats' milk influences gastrointestinal morphology in young pigs. J Nutr 138:921–926
49. Zhang J, Li L, Cai Y, Xu X, Chen J, Wu Y, Yu H, Yu G, Liu S, Zhang A, Cheng G (2008) Expression of active recombinant human lactoferrin in the milk of transgenic goats. Protein Expr Purif 57:127–135
50. Salzman NH, Ghosh D, Huttner KM, Paterson Y, Bevins CL (2003) Protection against enteric salmonellosis in transgenic mice expressing a human intestinal defensin. Nature 422:522–526
51. Panyutich A, Shi J, Boutz PL, Zhao C, Ganz T (1997) Porcine polymorphonuclear leukocytes generate extracellular microbicidal activity by elastase-mediated activation of secreted proprotegrins. Infect Immun 65:978–985
52. Cheung QC, Turner PV, Song C, Wu D, Cai HY, MacInnes JI, Li J (2008) Enhanced resistance to bacterial infection in protegrin-1 transgenic mice. Antimicrob Agents Chemother 52:1812–1819
53. Mauch C, Bilkei G (2004) Actinobacillus suis, a potential cause of abortion in gilts and low parity sows. Vet J 168:186–187
54. McManus MT, Sharp PA (2002) Gene silencing in mammals by small interfering RNAs. Nat Rev Genet 3:737–747
55. Gavora J (1996) Resistance to livestock to viruses: mechanisms and strategies for genetic engineering. Genet Sel Evol 28:385–414
56. Salter DW, Crittenden LB (1989) Artificial insertion of a dominant gene for resistance to avian leukosis virus into the germ line of the chicken. Theor Appl Genet 77:457–461
57. Clements JE, Wall RJ, Narayan O, Hauer D, Schoborg R, Sheffer D, Powell A, Carruth LM, Zink MC, Rexroad CE (1994) Development of transgenic sheep that express the visna virus envelope gene. Virology 200:370–380
58. Ono E, Amagai K, Taharaguchi S, Tomioka Y, Yoshino S, Watanabe Y, Cherel P, Houdebine LM, Adam M, Eloit M, Inobe M, Uede T (2004) Transgenic mice expressing a soluble form of porcine nectin-1/herpesvirus entry mediator C as a model for pseudorabies-resistant livestock. Proc Natl Acad Sci USA 101:16150–16155
59. Mulder WA, Pol JM, Gruys E, Jacobs L, De Jong MC, Peeters BP, Kimman TG (1997) Pseudorabies virus infections in pigs. Role of viral proteins in virulence, pathogenesis and transmission. Vet Res 28:1–17
60. Ono E, Tomioka Y, Watanabe Y, Amagai K, Taharaguchi S, Glenisson J, Cherel P (2006) The first immunoglobulin-like domain of porcine nectin-1 is sufficient to confer resistance

to pseudorabies virus infection in transgenic mice. Arch Virol 151:1827–1839
61. Tomioka Y, Morimatsu M, Amagai K, Kuramochi M, Watanabe Y, Kouda S, Wada T, Kuboki N, Ono E (2009) Fusion protein consisting of the first immunoglobulin-like domain of porcine nectin-1 and Fc portion of human IgG1 provides a marked resistance against pseudorabies virus infection to transgenic mice. Microbiol Immunol 53:8–15
62. Yoshida K, Tomioka Y, Kase S, Morimatsu M, Shinya K, Ohno S, Ono E (2008) Microphthalmia and lack of vitreous body in transgenic mice expressing the first immunoglobulin-like domain of nectin-1. Graefes Arch Clin Exp Ophthalmol 246:543–549
63. Lo D, Pursel V, Linton PJ, Sandgren E, Behringer R, Rexroad C, Palmiter RD, Brinster RL (1991) Expression of mouse IgA by transgenic mice, pigs and sheep. Eur J Immunol 21:1001–1006
64. Weidle UH, Lenz H, Brem G (1991) Genes encoding a mouse monoclonal antibody are expressed in transgenic mice, rabbits and pigs. Gene 98:185–191
65. Castilla J, Pintado B, Sola I, Sanchez-Morgado JM, Enjuanes L (1998) Engineering passive immunity in transgenic mice secreting virus-neutralizing antibodies in milk. Nat Biotechnol 16:349–354
66. Kolb AF, Pewe L, Webster J, Perlman S, Whitelaw CB, Siddell SG (2001) Virus-neutralizing monoclonal antibody expressed in milk of transgenic mice provides full protection against virus-induced encephalitis. J Virol 75:2803–2809
67. Saif LJ, Wheeler MB (1998) WAPping gastroenteritis with transgenic antibodies. Nat Biotechnol 16:334–335
68. Aguzzi A, Calella AM (2009) Prions: protein aggregation and infectious diseases. Physiol Rev 89:1105–1152
69. Aguzzi A, Sigurdson C, Heikenwaelder M (2008) Molecular mechanisms of prion pathogenesis. Annu Rev Pathol 3:11–40
70. Bueler H, Aguzzi A, Sailer A, Greiner RA, Autenried P, Aguet M, Weissmann C (1993) Mice devoid of PrP are resistant to scrapie. Cell 73:1339–1347
71. Bueler H, Fischer M, Lang Y, Bluethmann H, Lipp HP, DeArmond SJ, Prusiner SB, Aguet M, Weissmann C (1992) Normal development and behaviour of mice lacking the neuronal cell-surface PrP protein. Nature 356:577–582
72. Prusiner SB, Groth D, Serban A, Koehler R, Foster D, Torchia M, Burton D, Yang SL, DeArmond SJ (1993) Ablation of the prion protein (PrP) gene in mice prevents scrapie and facilitates production of anti-PrP antibodies. Proc Natl Acad Sci USA 90:10608–10612
73. Weissmann C, Bueler H, Fischer M, Sailer A, Aguzzi A, Aguet M (1994) PrP-deficient mice are resistant to scrapie. Ann NY Acad Sci 724:235–240
74. Denning C, Burl S, Ainslie A, Bracken J, Dinnyes A, Fletcher J, King T, Ritchie M, Ritchie WA, Rollo M, de Sousa P, Travers A, Wilmut I, Clark AJ (2001) Deletion of the alpha (1, 3) galactosyl transferase (GGTA1) gene and the prion protein (PrP) gene in sheep. Nat Biotechnol 19:559–562
75. Yu G, Chen J, Yu H, Liu S, Xu X, Sha H, Zhang X, Wu G, Xu S, Cheng G (2006) Functional disruption of the prion protein gene in cloned goats. J Gen Virol 87:1019–1027
76. Yu G, Chen J, Xu Y, Zhu C, Yu H, Liu S, Sha H, Xu X, Wu Y, Zhang A, Ma J, Cheng G (2009) Generation of goats lacking prion protein. Mol Reprod Dev 76:3
77. Richt JA, Kasinathan P, Hamir AN, Castilla J, Sathiyaseelan T, Vargas F, Sathiyaseelan J, Wu H, Matsushita H, Koster J, Kato S, Ishida I, Soto C, Robl JM, Kuroiwa Y (2007) Production of cattle lacking prion protein. Nat Biotechnol 25:132–138
78. Kuroiwa Y, Kasinathan P, Matsushita H, Sathiyaselan J, Sullivan EJ, Kakitani M, Tomizuka K, Ishida I, Robl JM (2004) Sequential targeting of the genes encoding immunoglobulin-mu and prion protein in cattle. Nat Genet 36:775–780
79. Moore RC, Lee IY, Silverman GL, Harrison PM, Strome R, Heinrich C, Karunaratne A, Pasternak SH, Chishti MA, Liang Y, Mastrangelo P, Wang K, Smit AF, Katamine S, Carlson GA, Cohen FE, Prusiner SB, Melton DW, Tremblay P, Hood LE, Westaway D (1999) Ataxia in prion protein (PrP)-deficient mice is associated with upregulation of the novel PrP-like protein doppel. J Mol Biol 292:797–817
80. Rossi D, Cozzio A, Flechsig E, Klein MA, Rulicke T, Aguzzi A, Weissmann C (2001) Onset of ataxia and Purkinje cell loss in PrP null mice inversely correlated with Dpl level in brain. EMBO J 20:694–702
81. Tobler I, Gaus SE, Deboer T, Achermann P, Fischer M, Rulicke T, Moser M, Oesch B, McBride PA, Manson JC (1996) Altered circadian activity rhythms and sleep in mice devoid of prion protein. Nature 380:639–642
82. Collinge J, Whittington MA, Sidle KC, Smith CJ, Palmer MS, Clarke AR, Jefferys JG (1994) Prion protein is necessary for normal synaptic function. Nature 370:295–297
83. Melo EO, Canavessi AM, Franco MM, Rumpf R (2007) Animal transgenesis: state of the art and applications. J Appl Genet 48:47–61
84. Hannon GJ (2002) RNA interference. Nature 418:244–251
85. Daude N, Marella M, Chabry J (2003) Specific inhibition of pathological prion protein accumulation by small interfering RNAs. J Cell Sci 116:2775–2779
86. Pfeifer A, Eigenbrod S, Al-Khadra S, Hofmann A, Mitteregger G, Moser M, Bertsch U, Kretzschmar H (2006) Lentivector-mediated RNAi efficiently suppresses prion protein and prolongs survival of scrapie-infected mice. J Clin Invest 116:3204–3210
87. White MD, Farmer M, Mirabile I, Brandner S, Collinge J, Mallucci GR (2008) Single treatment with RNAi against prion protein rescues early neuronal dysfunction and prolongs survival in mice with prion disease. Proc Natl Acad Sci USA 105:10238–10243
88. Berkhout B, Haasnoot J (2006) The interplay between virus infection and the cellular RNA interference machinery. FEBS Lett 580:2896–2902
89. Colbere-Garapin F, Blondel B, Saulnier A, Pelletier I, Labadie K (2005) Silencing viruses by RNA interference. Microbes Infect 7:767–775
90. Grubman MJ, Baxt B (2004) Foot-and-mouth disease. Clin Microbiol Rev 17:465–493

91. Kahana R, Kuznetzova L, Rogel A, Shemesh M, Hai D, Yadin H, Stram Y (2004) Inhibition of foot-and-mouth disease virus replication by small interfering RNA. J Gen Virol 85:3213–3217
92. Chen W, Yan W, Du Q, Fei L, Liu M, Ni Z, Sheng Z, Zheng Z (2004) RNA interference targeting VP1 inhibits foot-and-mouth disease virus replication in BHK-21 cells and suckling mice. J Virol 78:6900–6907
93. de Los Santos T, Wu Q, de Avila Botton S, Grubman MJ (2005) Short hairpin RNA targeted to the highly conserved 2B nonstructural protein coding region inhibits replication of multiple serotypes of foot-and-mouth disease virus. Virology 335:222–231
94. Lindberg AL (2003) Bovine viral diarrhoea virus infections and its control. A review. Vet Q 25:1–16
95. Lambeth LS, Moore RJ, Muralitharan MS, Doran TJ (2007) Suppression of bovine viral diarrhea virus replication by small interfering RNA and short hairpin RNA-mediated RNA interference. Vet Microbiol 119:132–143
96. Cox NJ, Subbarao K (2000) Global epidemiology of influenza: past and present. Annu Rev Med 51:407–421
97. Ge Q, McManus MT, Nguyen T, Shen CH, Sharp PA, Eisen HN, Chen J (2003) RNA interference of influenza virus production by directly targeting mRNA for degradation and indirectly inhibiting all viral RNA transcription. Proc Natl Acad Sci USA 100:2718–2723
98. Lewis DL, Hagstrom JE, Loomis AG, Wolff JA, Herweijer H (2002) Efficient delivery of siRNA for inhibition of gene expression in postnatal mice. Nat Genet 32:107–108
99. Tompkins SM, Lo CY, Tumpey TM, Epstein SL (2004) Protection against lethal influenza virus challenge by RNA interference in vivo. Proc Natl Acad Sci USA 101:8682–8686
100. Ge Q, Filip L, Bai A, Nguyen T, Eisen HN, Chen J (2004) Inhibition of influenza virus production in virus-infected mice by RNA interference. Proc Natl Acad Sci USA 101:8676–8681
101. Wise TG, Schafer DS, Lowenthal JW, Doran TJ (2008) The use of RNAi and transgenics to develop viral disease resistant livestock. Dev Biol (Basel) 132:377–382
102. Gerstein MB, Bruce C, Rozowsky JS, Zheng D, Du J, Korbel JO, Emanuelsson O, Zhang ZD, Weissman S, Snyder M (2007) What is a gene, post-ENCODE? History and updated definition. Genome Res 17:669–681
103. Berger SL, Kouzarides T, Shiekhattar R, Shilatifard A (2009) An operational definition of epigenetics. Genes Dev 23:781–783
104. Zak DE, Aderem A (2009) Systems biology of innate immunity. Immunol Rev 227:264–282
105. McGrew MJ, Sherman A, Ellard FM, Lillico SG, Gilhooley HJ, Kingsman AJ, Mitrophanous KA, Sang H (2004) Efficient production of germline transgenic chickens using lentiviral vectors. EMBO Rep 5:728–733
106. Scott BB, Lois C (2005) Generation of tissue-specific transgenic birds with lentiviral vectors. Proc Natl Acad Sci USA 102:16443–16447
107. Hong SG, Kim MK, Jang G, Oh HJ, Park JE, Kang JT, Koo OJ, Kim T, Kwon MS, Koo BC, Ra JC, Kim DY, Ko C, Lee BC (2009) Generation of red fluorescent protein transgenic dogs. Genesis 47:314–322
108. Le Provost F, Lillico S, Passet B, Young R, Whitelaw B, Vilotte JL (2010) Zinc finger nuclease technology heralds a new era in mammalian transgenesis. Trends Biotechnol 28(3):134–141
109. Geurts AM, Cost GJ, Freyvert Y, Zeitler B, Miller JC, Choi VM, Jenkins SS, Wood A, Cui X, Meng X, Vincent A, Lam S, Michalkiewicz M, Schilling R, Foeckler J, Kalloway S, Weiler H, Menoret S, Anegon I, Davis GD, Zhang L, Rebar EJ, Gregory PD, Urnov FD, Jacob HJ, Buelow R (2009) Knockout rats via embryo microinjection of zinc-finger nucleases. Science 325:433
110. Belmonte JC, Ellis J, Hochedlinger K, Yamanaka S (2009) Induced pluripotent stem cells and reprogramming: seeing the science through the hype. Nat Rev Genet 10:878–883
111. Buehr M, Meek S, Blair K, Yang J, Ure J, Silva J, McLay R, Hall J, Ying QL, Smith A (2008) Capture of authentic embryonic stem cells from rat blastocysts. Cell 135:1287–1298
112. Li P, Tong C, Mehrian-Shai R, Jia L, Wu N, Yan Y, Maxson RE, Schulze EN, Song H, Hsieh CL, Pera MF, Ying QL (2008) Germline competent embryonic stem cells derived from rat blastocysts. Cell 135:1299–1310
113. Chen J, Chen SC, Stern P, Scott BB, Lois C (2008) Genetic strategy to prevent influenza virus infections in animals. J Infect Dis 197(Suppl 1):S25–S28
114. Thomson R, Molina-Portela P, Mott H, Carrington M, Raper J (2009) Hydrodynamic gene delivery of baboon trypanosome lytic factor eliminates both animal and human-infective African trypanosomes. Proc Natl Acad Sci USA 106:19509–19514
115. Lyall J, Irvine RM, Sherman A, McKinley TJ, Núnez A, Purdie A, Outtrim L, Brown IH, Rolleston-Smith G, Sang H, Tiley L (2011) Suppression of avian influenza transmission in genetically modified chickens. Science 331:223–226
116. Kues WA, Niemann H (2011) Advances in farm transgenesis. PREVET, doi:10.1016
117. Tesson L, Usal C, Menoret S, Leung E, Niles BJ, Remy S, Santiago Y, Vincent AI, Meng X, Zhang L, Gregory PD, Anegon I, Cost GJ (2011) Knockout rats generated by embryo microinjection of TALENs. Nat Biotechnol 29:695–696
118. DeFrancesco L (2011) Move over ZFNs. Nat Biotechnol 29:681–684

Distribution Systems, Substations, and Integration of Distributed Generation

John D. McDonald[1], Bartosz Wojszczyk[2]
Byron Flynn[2], Ilia Voloh[2]
[1]GE Energy, Digital Energy, Atlanta, GA, USA
[2]GE Energy, Digital Energy, Norcross, GA, USA

Article Outline

Glossary
Definition of the Subject

Introduction
Distribution Systems
Substations
High Penetration of Distributed Generation and Its Impact on System Design and Operations
Future Directions
Bibliography

Glossary

Demand response Allows the management of customer consumption of electricity in response to supply conditions.

Distributed generation Electric energy that is distributed to the grid from many decentralized locations, such as from wind farms and solar panel installations.

Distribution grid The part of the grid dedicated to delivering electric energy directly to residential, commercial, and industrial electricity customers.

Distribution management system A smart grid automation technology that provides real time about the distribution network and allows utilities to remotely control devices in the grid.

Distribution substation Delivers electric energy to the distribution grid.

Distribution system The link from the distribution substation to the customer.

Renewable energy Energy from natural resources such as sunlight, wind, rain, tides, biofuels, and geothermal heat, which are naturally replenished.

Smart grid A modernization of the electricity delivery system so it monitors, protects, and automatically optimizes the operation of its interconnected elements.

Definition of the Subject

This entry describes the major components of the electricity distribution system – the distribution network, substations, and associated electrical equipment and controls – and how incorporating automated distribution management systems, devices, and controls into the system can create a "smart grid" capable of handling the integration of large amounts of distributed (decentralized) generation of sustainable, renewable energy sources.

Introduction

Distributed generation (DG) or decentralized generation is not a new industry concept. In 1882, Thomas Edison built his first commercial electric plant – "Pearl Street." The Pearl Street station provided 110 V direct current (DC) electric power to 59 customers in lower Manhattan. By 1887, there were 121 Edison power stations in the United States delivering DC electricity to customers. These early power plants ran on coal or water. Centralized power generation became possible when it was recognized that alternating current (AC) electricity could be transported at relatively low costs with reduced power losses across great distances by taking advantage of the ability to raise the voltage at the generation station and lower the voltage near customer loads. In addition, the concepts of improved system performance (system stability) and more effective generation asset utilization provided a platform for wide-area grid integration. Recently, there has been a rapidly growing interest in wide deployment of distributed generation, which is electricity distributed to the grid from a variety of decentralized locations. Commercially available technologies for distributed generation are based on wind turbines, combustion engines, micro- and mini-gas turbines, fuel cells, photovoltaic (solar) installations, low-head hydro units, and geothermal systems.

Deregulation of the electric utility industry, environmental concerns associated with traditional fossil fuel generation power plants, volatility of electric energy costs, federal and state regulatory support of "green" energy, and rapid technological developments all support the proliferation of distributed generation in electric utility systems. The growing rate of DG deployment also suggests that alternative energy-based solutions will play an increasingly important role in the smart grid and modern utility.

Large-scale implementation of distributed generation can lead to the evolution of the distribution network from a "passive" (local/limited automation, monitoring, and control) system to an "active" (global/integrated, self-monitoring, semiautomated) system that automatically responds to the various dynamics of the electric grid, resulting in higher efficiency, better load management, and fewer outages. However, distributed generation also poses a challenge for the design, operation, and management of the power grid because the network no longer

behaves as it once did. Consequently, the planning and operation of new systems must be approached differently, with a greater amount of attention paid to the challenges of an automated global system.

This entry describes the major components and interconnected workings of the electricity distribution system, and addresses the impact of large-scale deployment of distributed generation on grid design, reliability, performance, and operation. It also describes the distributed generation technology landscape, associated engineering and design challenges, and a vision of the modern utility.

Distribution Systems

Distribution systems serve as the link from the distribution substation to the customer. This system provides the safe and reliable transfer of electric energy to various customers throughout the service territory. Typical distribution systems begin as the medium-voltage three-phase circuit, typically about 30–60 kV, and terminate at a lower secondary three- or single-phase voltage typically below 1 kV at the customer's premise, usually at the meter.

Distribution feeder circuits usually consist of overhead and underground circuits in a mix of branching laterals from the station to the various customers. The circuit is designed around various requirements such as required peak load, voltage, distance to customers, and other local conditions such as terrain, visual regulations, or customer requirements. These various branching laterals can be operated in a radial configuration or as a looped configuration, where two or more parts of the feeder are connected together usually through a normally open distribution switch. High-density urban areas are often connected in a complex distribution underground network providing a highly redundant and reliable means connecting to customers. Most three-phase systems are for larger loads such as commercial or industrial customers. The three-phase systems are often drawn as one line as shown in the following distribution circuit drawing (Fig. 1) of three different types of circuits.

The secondary voltage in North America and parts of Latin America consists of a split single-phase service that provides the customer with 240 and 120 V, which the customer then connects to devices depending on their ratings. This is served from a three-phase distribution feeder normally connected in a Y configuration consisting of a neutral center conductor and a conductor for each phase, typically assigned a letter A, B, or C.

Single-phase customers are then connected by a small neighborhood distribution transformer connected from one of the phases to neutral, reducing the voltage from the primary feeder voltage to the secondary split service voltage. In North America, normally 10 or fewer customers are connected to a distribution transformer.

In most other parts of the world, the single-phase voltage of 220 or 230 V is provided directly from a larger neighborhood distribution transformer. This provides a secondary voltage circuit often serving hundreds of customers.

Figure 1 shows various substations and several feeders serving customers from those substations. In Fig. 1, the primary transformers are shown as blue boxes in the substation, various switches, breakers, or reclosers are shown as red (closed) or green (open) shapes, and fuses are shown as yellow boxes.

Distribution Devices

There are several distribution devices used to improve the safety, reliability, and power quality of the system. This section will review a few of those types of devices.

Switches: Distribution switches (Fig. 2) are used to disconnect various parts of the system from the feeder. These switches are manually, remotely, or automatically operated. Typically, switches are designed to break load current but not fault current and are used in underground circuits or tie switches.

Breakers: Like switches, distribution breakers are used to disconnect portions of the feeder. However, breakers have the ability to interrupt fault current. Typically, these are tied to a protective relay, which detects the fault conditions and issues the open command to the breaker.

Reclosers: These are a special type of breaker (Fig. 3), typically deployed only on overhead and are designed to reduce the outage times caused by momentary faults. These types of faults are caused by vegetation or temporary short circuits. During the reclose operation, the relay detects the fault, opens the switch, waits a few seconds, and issues a close. Many

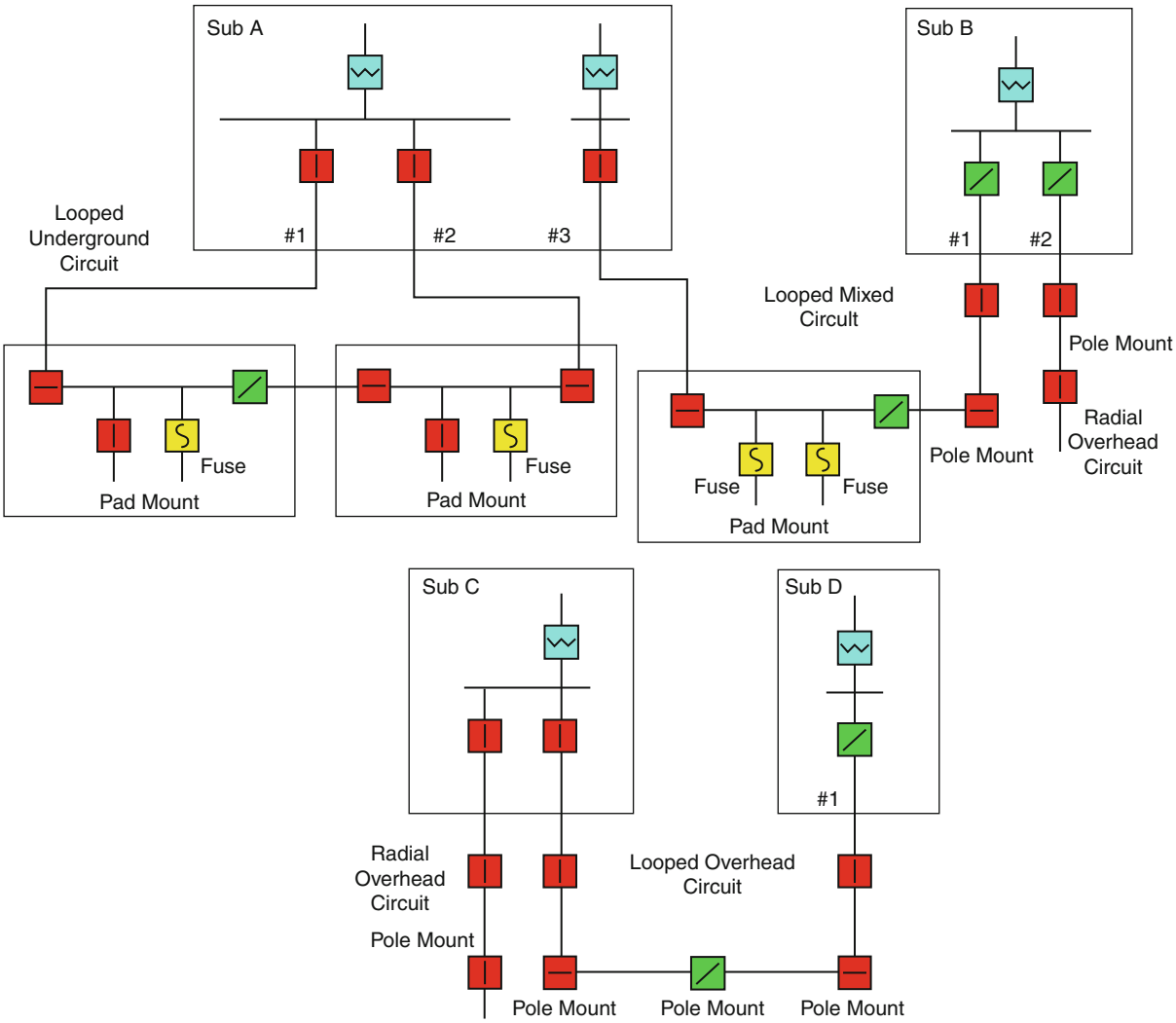

Distribution Systems, Substations, and Integration of Distributed Generation. Figure 1
Simple distribution system single line drawings

overhead distribution faults are successfully cleared and service is restored with this technique, significantly reducing outage times.

Capacitors: These are three-phase capacitors designed to inject volt amp reactives (VARs) into the distribution circuit, typically to help improve power factor or support system voltage (Fig. 4). They are operated in parallel with the feeder circuit and are controlled by a capacitor controller. These controllers are often connected to remote communications allowing for automatic or coordinated operation.

Fuses: These are standard devices used to protect portions of the circuit when a breaker is too expensive or too large. Fuses can be used to protect single-phase laterals off the feeder or to protect three-phase underground circuits.

Lightning arresters: These devices are designed to reduce the surge on the line when lightning strikes the circuit.

Automation Scheme: FDIR

The following description highlights an actual utility's FDIR automation scheme, their device decisions,

Distribution Systems, Substations, and Integration of Distributed Generation. Figure 2
Distribution pad-mount switch

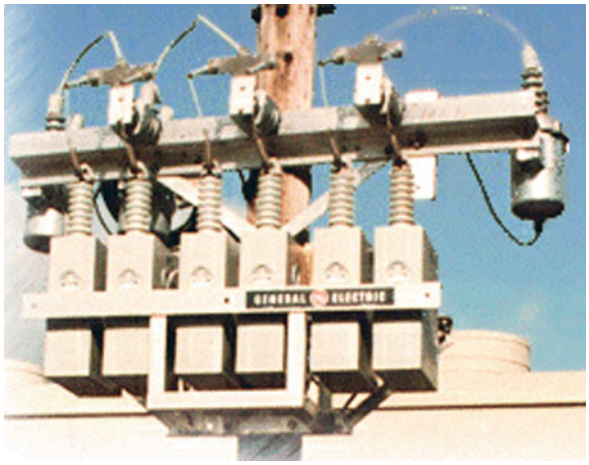

Distribution Systems, Substations, and Integration of Distributed Generation. Figure 4
Distribution overhead 600 kVA capacitor

Distribution Systems, Substations, and Integration of Distributed Generation. Figure 3
Distribution pole-mounted reclosing relay

functionality and system performance. Automation sequences include fault detection, localization, isolation, and load restoration (FDIR). These sequences will detect a fault, localize it to a segment of feeder, open the switches around the fault, and restore unfaulted sources via the substation and alternative sources as available. These algorithms work to safely minimize the fault duration and extent, significantly improving the SAIDI (system average interruption duration index) and SAIFI (system average interruption frequency Index) performance metric for the customers on those feeders. An additional important sequence is the automatic check of equipment loading and thermal limits to determine whether load transfers can safely take place.

Modern systems communicate using a secure broadband Ethernet radio system, which provides significant improvement over a serial system, including supporting peer-to-peer communications, multiple access to tie switches, and remote access by communications and automation maintenance personnel. The communication system utilizes an internet protocol (IP)–based communication system with included security routines designed to meet the latest NERC (North American Electric Reliability Corporation) or the distribution grid operator's requirements.

Feeder circuits to be automated are typically selected because they have relatively high SAIDI indices serving high-profile commercial sites. Scheme 1 utilized two pad-mount switches connected to one substation. Scheme 2 consisted of a mix of overhead and underground with vault switchgear and a pole-mounted recloser. Scheme 3 was installed on overhead circuits with three pole-mounted reclosers.

Automation Schemes 1, 2 and 3 (Fig. 5) were designed to sense distribution faults, isolate the appropriate faulted line sections, and restore unfaulted circuit sections as available alternate source capacity permitted.

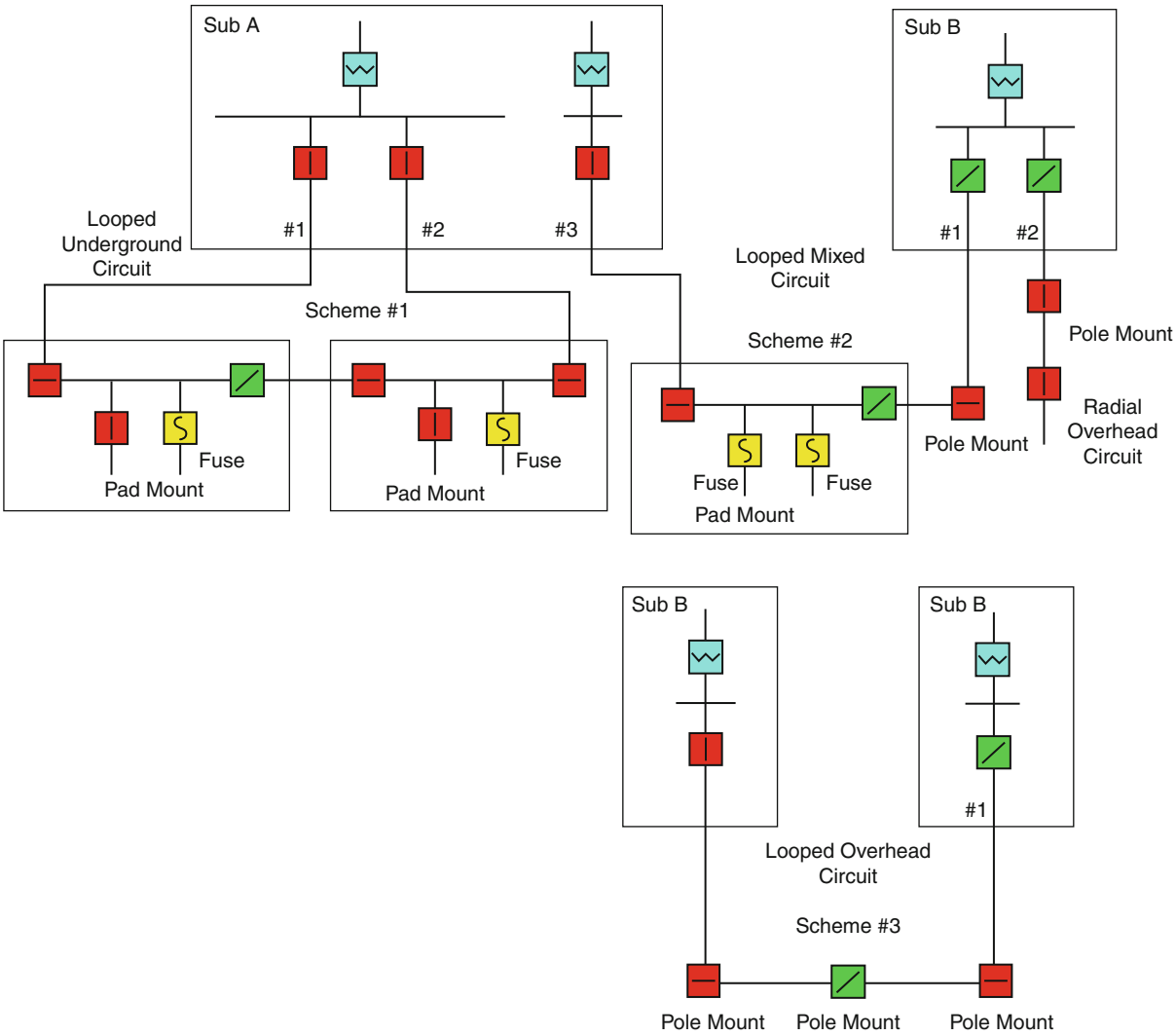

Distribution Systems, Substations, and Integration of Distributed Generation. Figure 5
Distribution automation (DA) system single lines

Safety Safety is a critical piece of system operation. Each algorithm has several safety checks before any operation occurs. Before the scheme logic is initialized, a series of checks occur, including:

- Auto Restoration is enabled on a specific scheme – dispatchers do this via the distribution management system or SCADA system.
- Auto Restoration has not been disabled by a crew in the field via enable/disable switches at each device location.
- Auto Restoration has been reset – each scheme must be reset by the dispatcher after DA has operated and system has been restored to normal configuration.
- Communications Status – verifies that all necessary devices are on-line and communicating.
- Switch Position – verifies that each appropriate line switch is in the appropriate position (see Fig. 1).
- Voltages – checks that the appropriate buses/feeders are energized.
- Feeder Breaker Position – verifies the faulted feeder breaker has locked open and was opened only by

Distribution Systems, Substations, and Integration of Distributed Generation. Figure 6
Pad-mount controller and pole-mount reclosing relay with enable/disable switches

a relay, not by SCADA or by the breaker control handle.

Prior to closing the tie switch and restoring customers in un-faulted sections, the following safety checks occur:

- Determine Pre-Fault Load – determine pre-fault load on un-faulted section of line.
- Compare Pre-Fault Load to Capacity – determine if alternate source can handle the un-faulted line section load.

After any DA algorithm executes:

- Notifies Dispatch of Status of DA System – success or failure of restoring load in un-faulted line sections.
- Reset is Necessary – algorithm is disabled until reset by dispatcher once the fault is repaired and the system is put back to normal configuration (see Fig. 1).

In summary, automation can occur *only* if these five conditions are true for every device on a scheme:

- Enable/Disable Switch is in enable position
- Local/Remote switch is in remote
- Breaker "hot-line" tag is off.
- Breaker opens from a relay trip and stays open for several seconds (that is, goes to lockout).
- Dispatch has reset the scheme(s) after the last automation activity.

Each pad-mounted or pole-mounted switch has a local enable/disable switch as shown in Fig. 6. Journeymen are to use these switches as the primary means of disabling a DA scheme before starting work on any of the six automated circuits or circuit breakers or any of the seven automated line switches.

FDIR System Components The automation system consists of controllers located in pad-mount switches, pole-mounted recloser controls (Fig. 7), and in substations (Fig. 8).

Pad-Mounted Controller The pad-mounted controller was selected according to the following criteria:

- Similar to existing substation controllers – simplifying configuration and overall compatibility
- Compatible with existing communications architecture
- Uses IEC 61131-3 programming
- Fault detection on multiple circuits
- Ethernet connection
- Supports multiple master stations
- Installed cost

The pad-mounted controller (Fig. 7) selected was an Ethernet-based controller that supported the necessary above requirements. The IEC 61131-3 programming languages include:

Distribution Systems, Substations, and Integration of Distributed Generation. Figure 7
Typical pad-mount and pole-mount switches

Distribution Systems, Substations, and Integration of Distributed Generation. Figure 8
Typical substation controller and vault switch

- Sequential Function Chart – describes operations of a sequential process using a simple graphical representation for the different steps of the process, and conditions that enable the change of active steps. It is considered to be the core of the controller configuration language, with other languages used to define the steps within the flowchart.
- Flowchart – a decision diagram composed of actions and tests programmed in structured text, instruction list, or ladder diagram languages. This is a proposed IEC 61131-3 language.
- Function Block Diagram – a graphic representation of many different types of equations. Rectangular boxes represent operators, with inputs on the left side of the box and outputs on the right. Custom function blocks may be created as well. Ladder diagram expressions may be a part of a function block program.
- Ladder Diagram – commonly referred to as "quick LD," the LD language provides a graphic representation of Boolean expressions. Function blocks can be inserted into LD programs.
- Structured Text – high-level structured language designed for expressing complex automation processes which cannot be easily expressed with graphic languages. Contains many expressions common to software programming languages (CASE, IF-THEN-ELSE, etc.). It is the default language for describing sequential function chart steps.
- Instruction List – a low-level instruction language analogous to assembly code.

Pole-Mounted Controller with Recloser The recloser controller was selected according to the following criteria:

- Similar requirements to pad-mounted controllers
- Control must provide needed analog and status outputs to DA remote terminal units (RTU)

Substation Controller The substation controller (Fig. 8) was selected per the following criteria:

- Similar to field controllers – simplifying configuration and overall compatibility
- Compatible with communications architecture
- Uses IEC 61131-3
- Ethernet and serial connections
- Supports multiple master stations including master station protocols
- Remote configuration is supported

Communications System

General The primary requirement of the communications system was to provide a secure channel between the various switches and the substation. The communication channel also needed to allow remote connection to the switchgear intelligent electronic devices (IEDs) for engineers and maintenance personnel. Additionally, the DA system also required the support for multiple substation devices to poll the controller at the tie switch. These requirements indicated the need for multi-channel or broadband radio.

Radio Communication Selection Criteria Primary considerations for selecting radio communications include:

- Security
- Supports remote configuration
- Broadband or multiple channels
- Compatible with multiple protocols
- From a major supplier
- Installed cost

The radio selected is a broadband radio operating over 900 MHz spread spectrum and 512 kbps of bandwidth. The wide-area network (WAN), Ethernet-based radio, supports the necessary protocols and provides multiple communications channels.

The communications network operates as a WAN providing the capability to communicate between any two points simply by plugging into the 10baseT communications port. A DA maintenance master was installed to communicate with the various controllers and to provide a detailed view of the DA system from the dispatch center. The DA system was also connected to the dispatch master station, which gives the dispatcher the ability to monitor and control the various DA algorithms and, in the future, typical SCADA control of the switches using distribution network protocol (DNP). (Since the dispatch master station currently does not support DNP over IP, a serial to Ethernet converter will be installed at the dispatch center to handle the conversion.) Figure 9 illustrates the communications architecture.

The radios communicate using point to multipoint with an access point radio operating as the base station radio and two types of remote radios, with serial or Ethernet. Some of the remote controllers only used DNP serial channels, requiring the radios to convert the serial connection to Ethernet. The remote Ethernet-based devices connect to the radios using a standard 10BaseT connection. Refer to Fig. 9.

For sites that require multiple DNP masters to connect to the serial controllers, the radios and the controllers have two serial connections. A new feature of the serial controllers is the support of point-to-point protocol (PPP). PPP provides a method for transmitting datagrams over serial point-to-point links. PPP contains three main components:

- A method for encapsulating datagrams over serial links. PPP uses the high-level data link control (HDLC) protocol as a basis for encapsulating datagrams over point-to-point links.
- An extensible Link Control Protocol (LCP) which is used to establish, configure, maintain, terminate, and test the data link connection.
- A family of network control protocols (NCP) for establishing and configuring different network layer protocols after LCP has established a connection. PPP is designed to allow the simultaneous use of multiple network layer protocols.

Establishing a PPP connection provides support for DNP multiple masters and a remote connection for maintenance over one serial communication line,

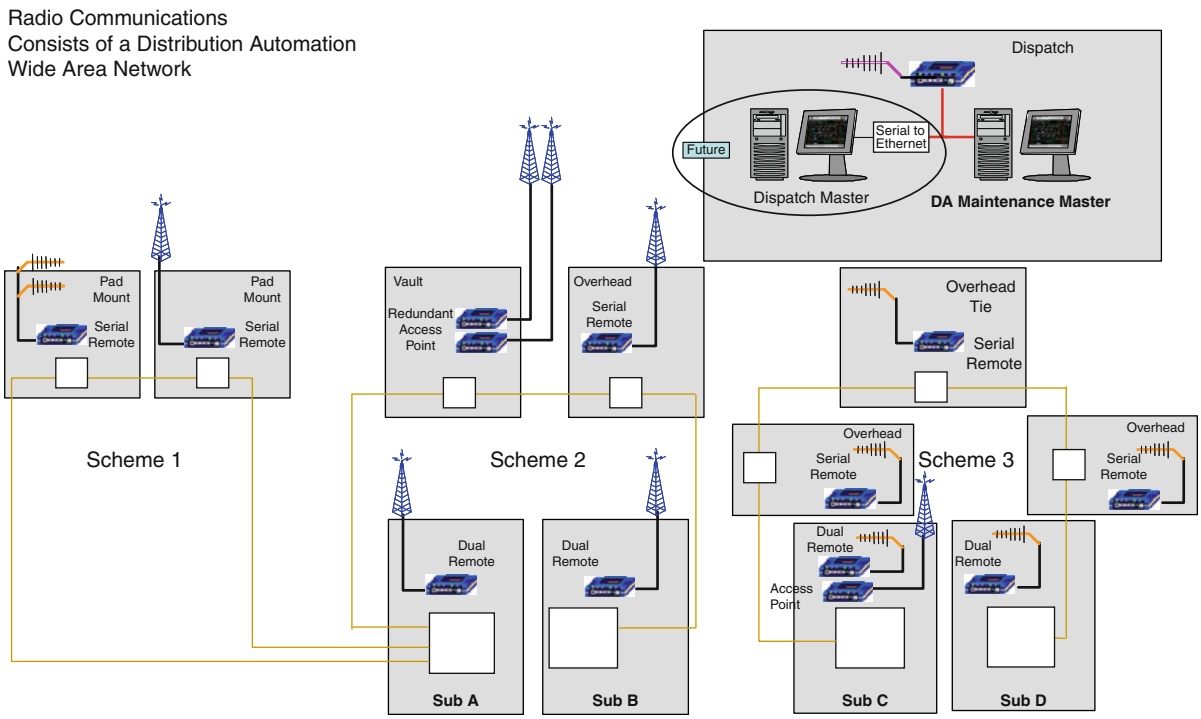

Distribution Systems, Substations, and Integration of Distributed Generation. Figure 9
DA communications infrastructure

effectively providing full Ethernet functionality over a single serial channel.

Security The wireless system contains several security features. Table 1 outlines the threat and the security measures implemented in the radio to meet these threats.

Automation Functionality

Distribution Automation Schemes Distribution automation (DA) scheme operation is discussed in this section. All three schemes are configured the same, differing only in the type of midpoint and tie point switches used and whether the two sources are in the same or different substations. All three are set up as two-zone circuit pairs, with one tie point and two midpoints. Only one scheme will be shown (Fig. 10), as the others are analogous. Scheme 1 operates on the system shown in Fig. 10. It consists of two pad-mount switches and one substation. The pad-mount controllers communicate with the controller in the substation and the substation controller communicates with the DA maintenance master station and, in the future, the dispatch master.

Zone 1 Permanent Fault Before the algorithm operates, the safety checks occur as previously described. Refer to Figs. 11 and 12. If a permanent Zone 1 fault occurs (between switch 1 and substation CB14) and the algorithm is enabled and the logic has been initialized, the following actions occur:

1. After relaying locks out the substation breaker, the algorithm communicates with the field devices and the station protection relays to localize the fault.
2. Algorithm determines fault is between the substation and SW1.
3. Algorithm opens the circuit at SW1 connected to the incoming line from the substation, isolating the fault.
4. Algorithm gathers pre-fault load of section downstream of SW1 from the field devices.
5. Algorithm determines if capacity exists on alternate source and alternate feeder.

Distribution Systems, Substations, and Integration of Distributed Generation. Table 1 Security risk management

Security threat	900 MHz radio security
Unauthorized access to the backbone network through a foreign remote radio	Approved remotes list. Only those remotes included in the AP list will connect
"Rogue" AP, where a foreign AP takes control of some or all remote radios and thus remote devices	Approved AP List. A remote will only associate to those AP included in its local
Dictionary attacks, where a hacker runs a program that sequentially tries to break a password	Failed-login lockdown. After three tries, the transceiver ignores login requests for 5 min. Critical event reports (traps) are generated as well
Denial of service, where Remote radios could be reconfigured with bad parameters bringing the network down	• Remote login
	• Local console login
	• Disabled HTTP and Telnet to allow only local management services
Airwave searching and other hackers in parking lots, etc.	• 900 MHz FHSS does not talk over the air with standard 802.11b cards.
	• The transceiver cannot be put in a promiscuous mode.
	• Proprietary data framing
Eavesdropping, intercepting messages	128-bit encryption
Key cracking	Automatic rotating key algorithm
Replaying messages	128-bit encryption with rotating keys
Unprotected access to configuration via SNMPv1	Implement SNMPv3 secure operation
Intrusion detection	Provides early warning via SNMP through critical event reports (unauthorized, logging attempts, etc.)

6. If so, algorithm closes the tie switch and backfeeds load, restoring customers on un-faulted line.
7. Reports successful operation to dispatch. The system is now as shown in Figs. 11 and 12, resulting in a reduction of SAIFI and SAIDI.

Zone 1 Permanent Fault: Load Too High to Safely Transfer In this case, a Zone 1 permanent fault occurs as shown in Fig. 13 and the previous example, except that this time loads are too high for the alternate source to accept load from the faulted feeder. Note the dispatch DA screens are descriptive and present information in plain language. Refer to Figs. 13 and 14.

Zone 2 Permanent Fault Depending on the type of the SW1 device (Fig. 15), the following actions occur:

If SW1 is a recloser (as in Schemes 2 and 3):

1. SW1 locks out in three shots. If SW1 is a pad-mount switch with no protection package (as in Scheme 1), the substation breaker goes to lockout. Fifty percent of CB11 customers remain in power.
2. This action occurs whether DA is enabled or disabled. That is, *existing circuit protection is unaffected by any DA scheme or logic.*
3. Safety checks are performed to ensure DA can safely proceed.
4. DA logic sees loss of voltage only beyond SW1 (recloser at lockout) and saw fault current through CB11 and SW1, so it recognizes that the line beyond SW1 is permanently faulted.
5. DA will not close into a faulted line, so the alternate source tie point (open point of SW2) remains open.
6. Customers between SW1 and SW2 lose power (about 50% of CB11 customers).

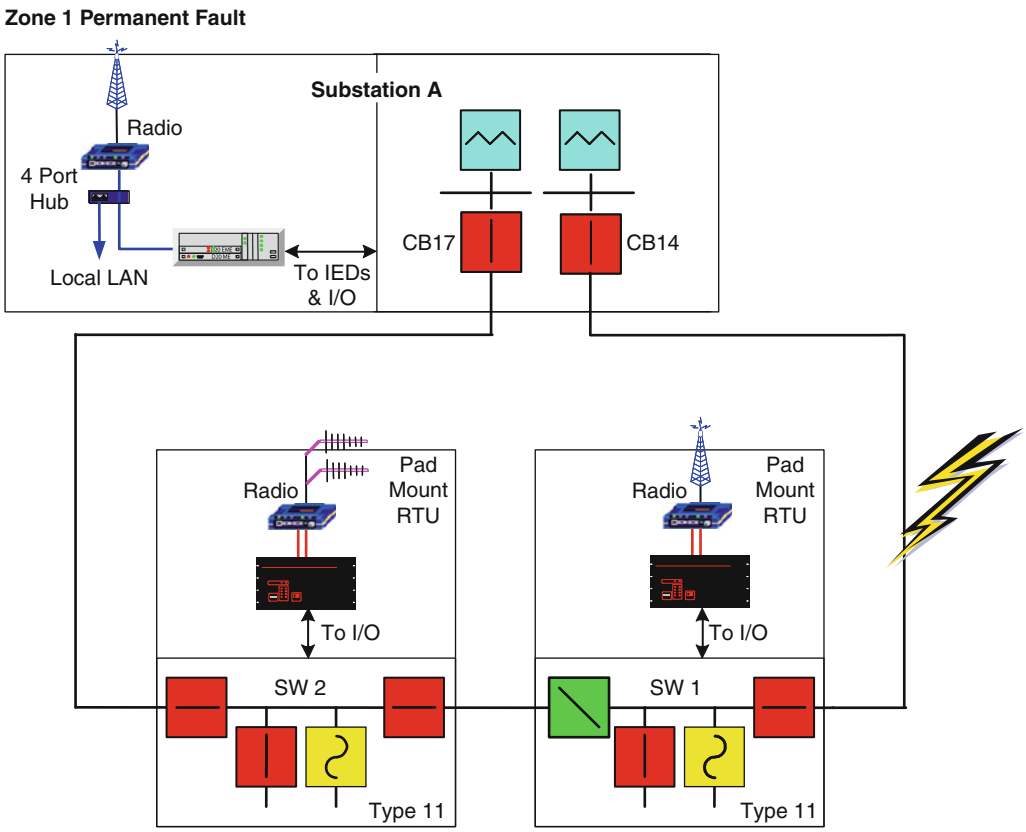

Distribution Systems, Substations, and Integration of Distributed Generation. Figure 10
Scheme 1 architecture

If SW1 is switchgear (as in Scheme 1):

1. Substation circuit breaker, CB11, locks out in three shots.
2. This action occurs whether DA is enabled or disabled. That is, *existing circuit protection is unaffected by any DA scheme or logic.*
3. Safety checks are performed to ensure DA can safely proceed.
4. DA logic sees loss of voltage beyond CB11 (CB at lockout) and saw fault current through CB11 and SW1, so it recognizes that the line beyond (not before) SW1 is permanently faulted.
5. Fault is isolated by DA logic, sending open command to SW1.
6. DA logic recognizes line upstream of SW1 is good (fault current sensed at two devices), and closes CB11, heating up line to source side of open SW1. Power is now restored to 50% of customers.
7. DA will not close into a faulted line, so the alternate source tie point (open point of SW2) remains open (Figs. 16 and 17).

System Operation In 5 months of operation thus far the DA system has operated for 21 faults; all were Zone 2 faults on Scheme 3 (all downstream of the midpoint SW1). Three of those faults were permanent and took the line recloser SW1 to lockout. As a result, in 5 months, the DA pilot has saved 550 customers 6 h of power outage time (i.e., saved 3,300 customer hours lost) and eliminated 18 momentaries for those same 550 customers.

There have been no Zone 1 faults on any scheme; therefore, no load transfers to alternate sources have taken place.

Automation Scheme: Volt/VAR Control (VVC)

General The various loads along distribution feeders result in resistive (I^2R) and reactive (I^2X) losses in the

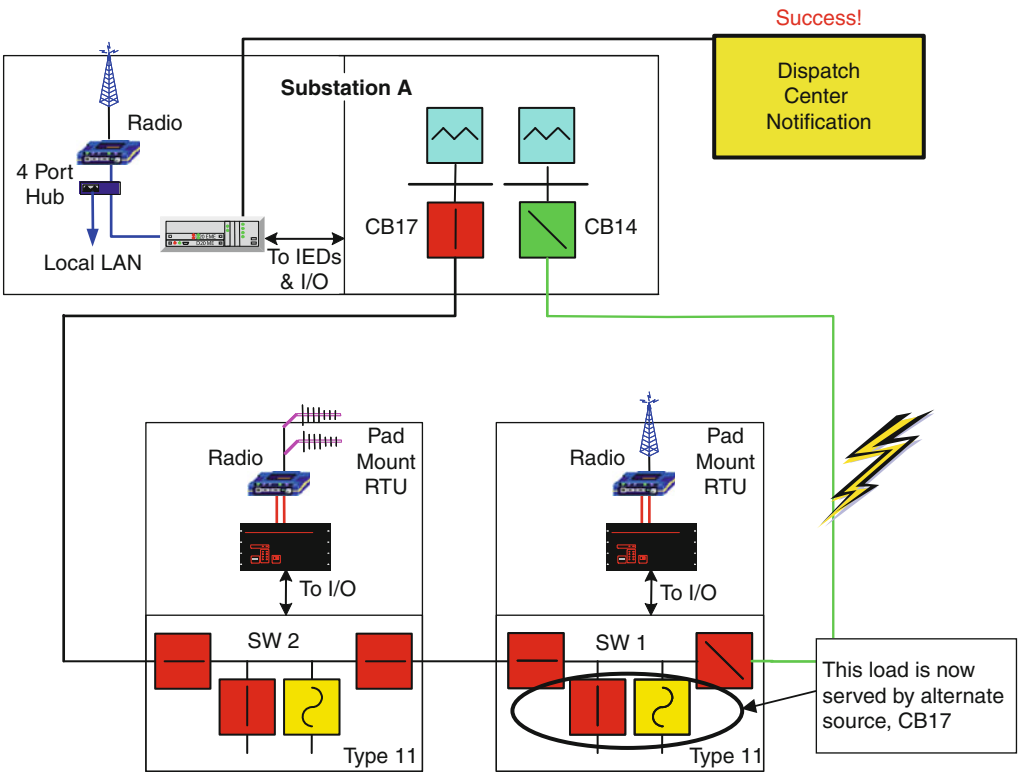

Distribution Systems, Substations, and Integration of Distributed Generation. Figure 11
Scheme 1 architecture after successful DA operation

distribution system. If these losses are left uncompensated, an additional problem of declining voltage profile along the feeder will result. The most common solution to these voltage problems is to deploy voltage regulators at the station or along the feeder and/or a transformer LTC (load tap changers) on the primary station transformer; additional capacitors at the station and at various points on the feeder also provide voltage support and compensate the reactive loads. Refer to Fig. 18.

Many utilities are looking for additional benefits through improved voltage management. Voltage management can provide significant benefits through improved load management and improved voltage profile management.

The station Volt/VAR equipment consists of a primary transformer with either an LTC (Fig. 18) or a station voltage regulator and possibly station capacitors. The distribution feeders include line capacitors and possibly line voltage regulators.

The LTC is controlled by an automatic tap changer controller (ATC). The substation capacitors are controlled by a station capacitor controller (SCC), the distribution capacitors are controlled by an automatic capacitor controller (ACC), and the regulators are controlled by an automatic regulator controller (ARC). These controllers are designed to operate when local monitoring indicates a need for an operation including voltage and current sensing. Distribution capacitors are typically controlled by local power factor, load current, voltage, VAR flow, temperature, or the time (hour and day of week).

Some utilities have realized additional system benefits by adding communications to the substation, and many modern controllers support standard station communications protocols such as DNP.

This system (shown in Figs. 19 and 20) includes the ability to remotely monitor and manually control the volt/VAR resources, as well as the ability to provide integrated volt/VAR control (IVVC).

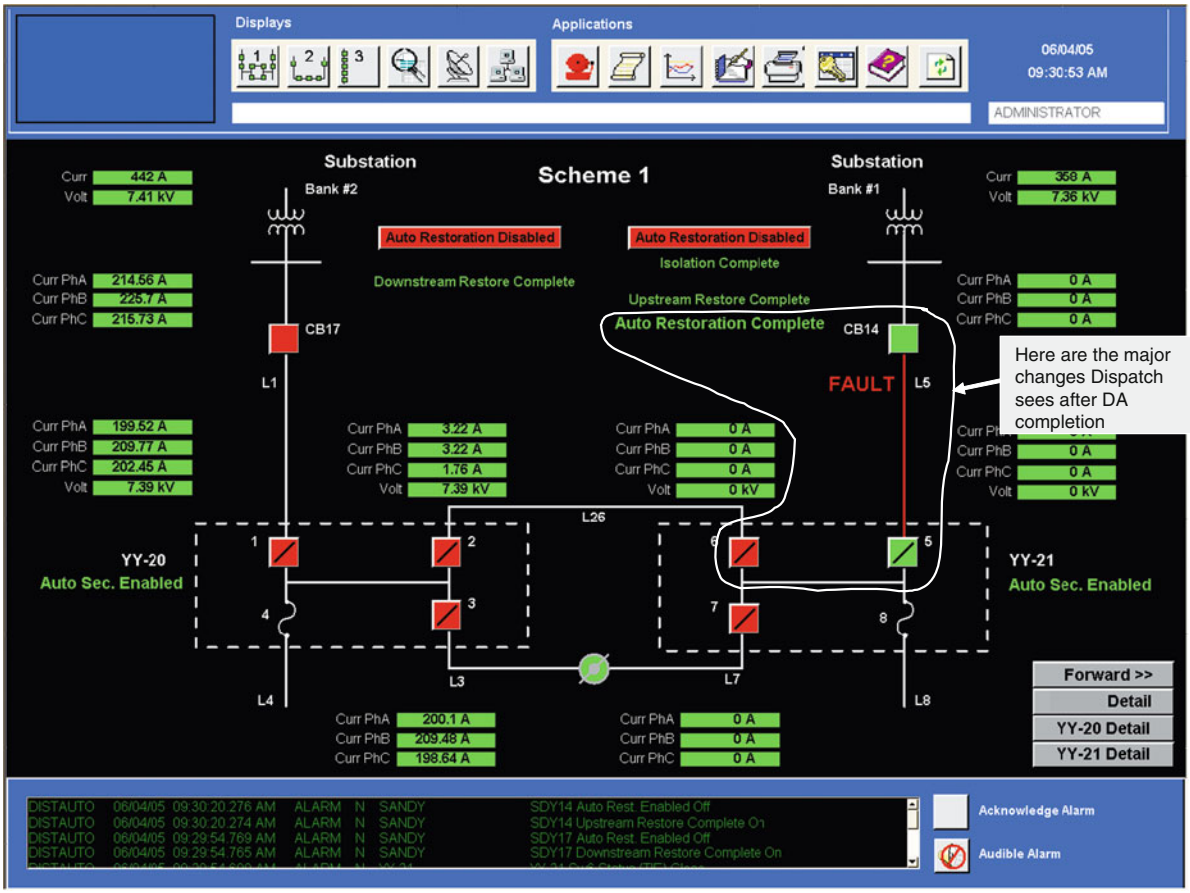

Distribution Systems, Substations, and Integration of Distributed Generation. Figure 12
Dispatch notification of scheme 1 isolation/restoration success

Benefits of Volt/VAR Control (VVC) The VAR control systems can benefit from improved power factor and the ability to detect a blown fuse on the distribution capacitor. Studies and actual field data have indicated that systems often add an average of about 1 MVAR to each feeder. This can result in about a 2% reduction in the losses on the feeder.

Based on the assumptions, the benefits for line loss optimization that some utilities have calculated represent a significant cost-benefit payback. However, one of the challenges utilities face is that the cost and benefits are often disconnected. The utility's distribution business usually bears the costs for an IVVC system. The loss reduction benefits often initially flow to the transmission business and eventually to the ratepayer, since losses are covered in rates. Successful implementation of a loss reduction system will depend on helping align the costs with the benefits. Many utilities have successfully reconnected these costs and benefits of a Volt/VAR system through the rate process.

The voltage control systems can provide benefit from reduced cost of generation during peak times and improved capacity availability. This allows rate recovery to replace the loss of revenue created from voltage reduction when it is applied at times other than for capacity or economic reasons. The benefits for these programs will be highly dependent on the rate design, but could result in significant benefits.

There is an additional benefit from voltage reduction to the end consumer during off-peak times. Some utilities are approaching voltage reduction as a method to reduce load similar to a demand response (DR) program. Rate programs supporting DR applications are usually designed to allow the utility to

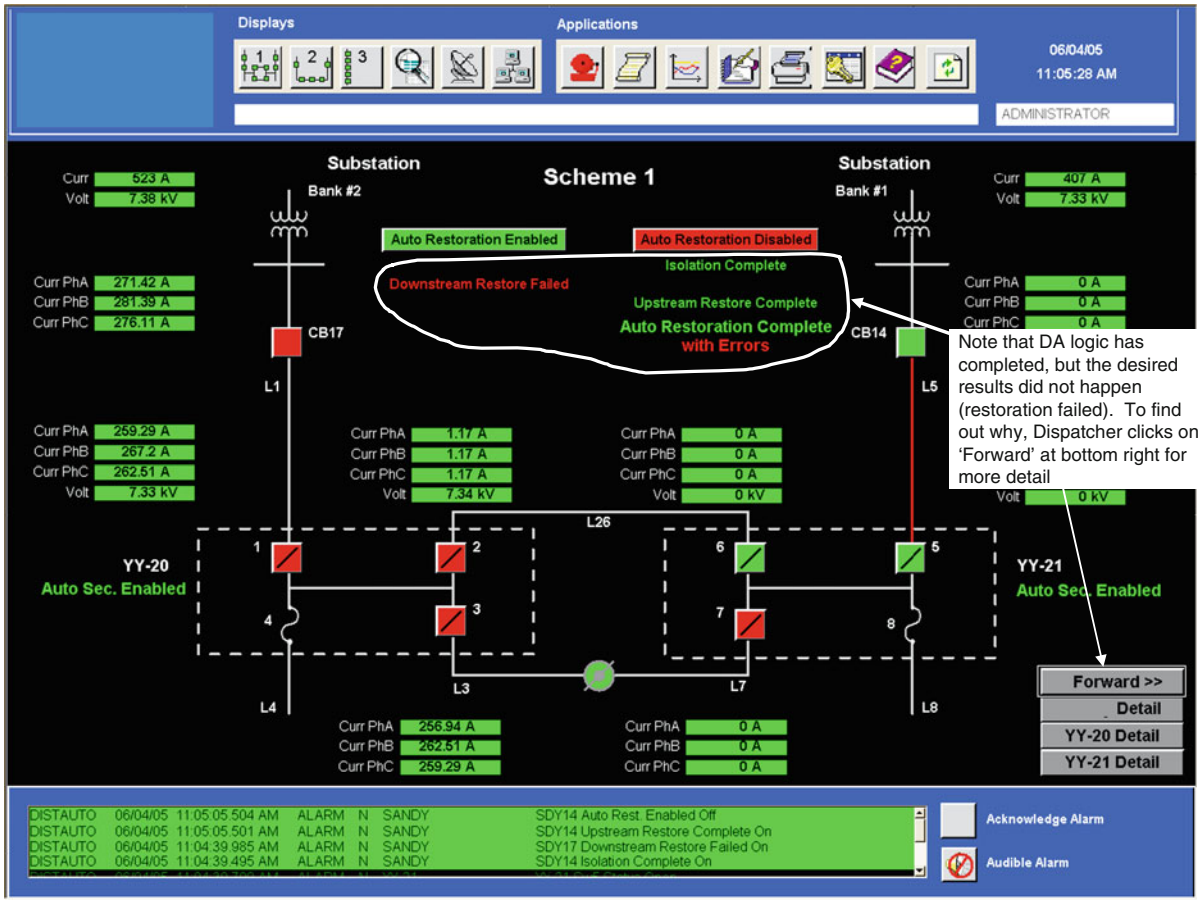

Distribution Systems, Substations, and Integration of Distributed Generation. Figure 13
Dispatch notification of scheme 1 restoration failure

recapture lost revenue resulting from a decreased load. In simplified terms, the consumer would pay the utility equal to the difference between their normal rate and the wholesale price of energy based on the amount of load reduction. Figure 21 highlights the impact of voltage as a load management tool.

This chart contains real data from a working feeder utilizing Volt/VAR control. As the chart indicates, with VVC, the feeder voltage profile is flatter and lower.

Considerations

Centralized, Decentralized, or Local Algorithm Given the increasing sophistication of various devices in the system, many utilities are facing a choice of location for the various algorithms (Fig. 22). Often it is driven by the unique characteristics of the devices installed or by the various alternatives provided by the automation equipment suppliers.

Table 2 compares the various schemes.

Safety and Work Processes The safety of workers, of the general public, and of equipment must not be compromised. This imposes the biggest challenge for deploying any automatic or remotely controlled systems. New automation systems often require new work processes. Utility work process and personnel must be well trained to safely operate and maintain the new automated distribution grid systems.

Operating practices and procedures must be reviewed and modified as necessary to address the presence of automatic switchgear.

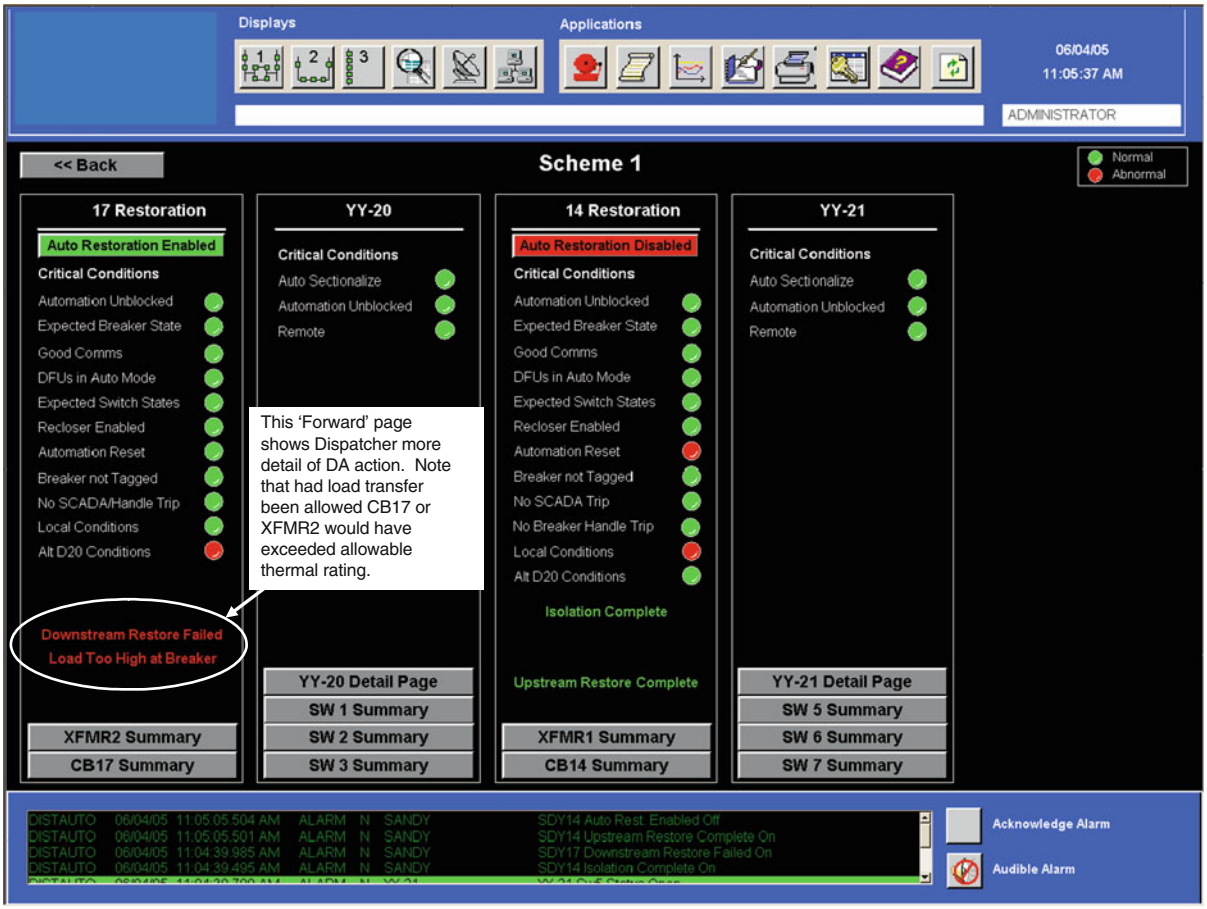

Distribution Systems, Substations, and Integration of Distributed Generation. Figure 14
Dispatch detail of scheme 1 restoration failure

Safety related recommendations include:

- Requirement for "visible gap" for disconnect switches
- No automatic closures after 2 min have elapsed following the initial fault to protect line crews
- System disabled during maintenance ("live line") work, typically locally and remotely

The Law of Diminishing Returns Larger utilities serve a range of customer types across a range of geographic densities. Consequently, the voltage profile and the exposure to outages are very different from circuit to circuit. Most utilities analyze distribution circuits and deploy automation on the most troublesome feeders first. Figure 23 depicts this difference.

Figure 23 highlights the decision by one utility to automate roughly 25% of feeders, which account for 70% of overall customer minutes interrupted.

The same analysis can be done on a circuit basis. The addition of each additional sensing and monitoring device to a feeder leads to a diminishing improvement to outage minutes as shown in Fig. 24.

Both of these elements are typically studied and modeled to determine the recommended amount of automation each utility is planning.

Substations

Role and Types of Substations

Substations are key parts of electrical generation, transmission, and distribution systems. Substations

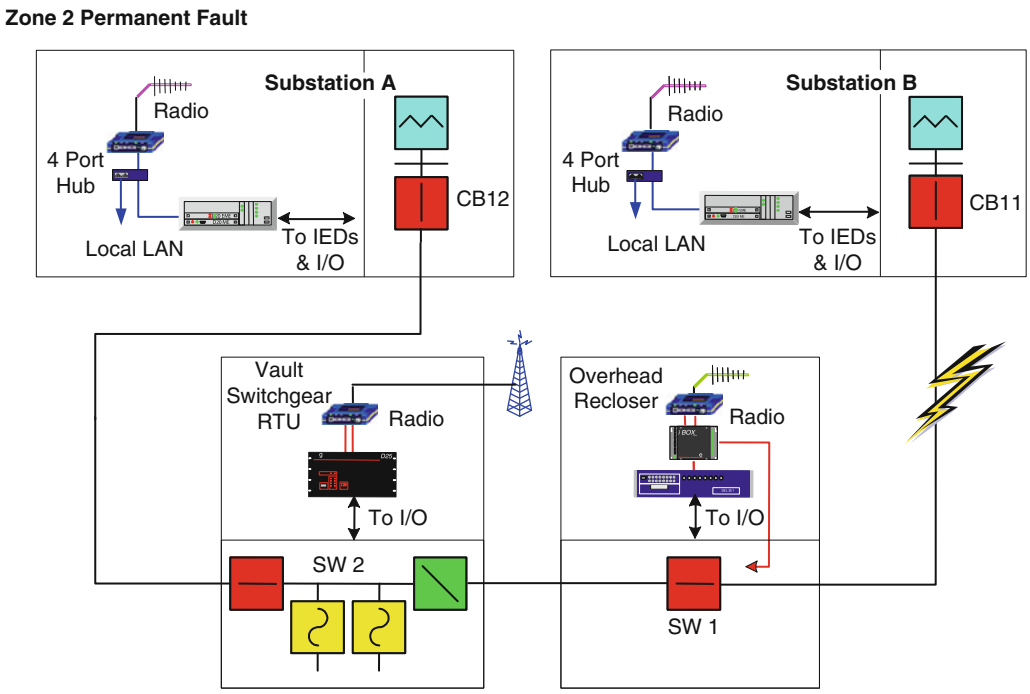

Distribution Systems, Substations, and Integration of Distributed Generation. Figure 15
Scheme 2 architecture

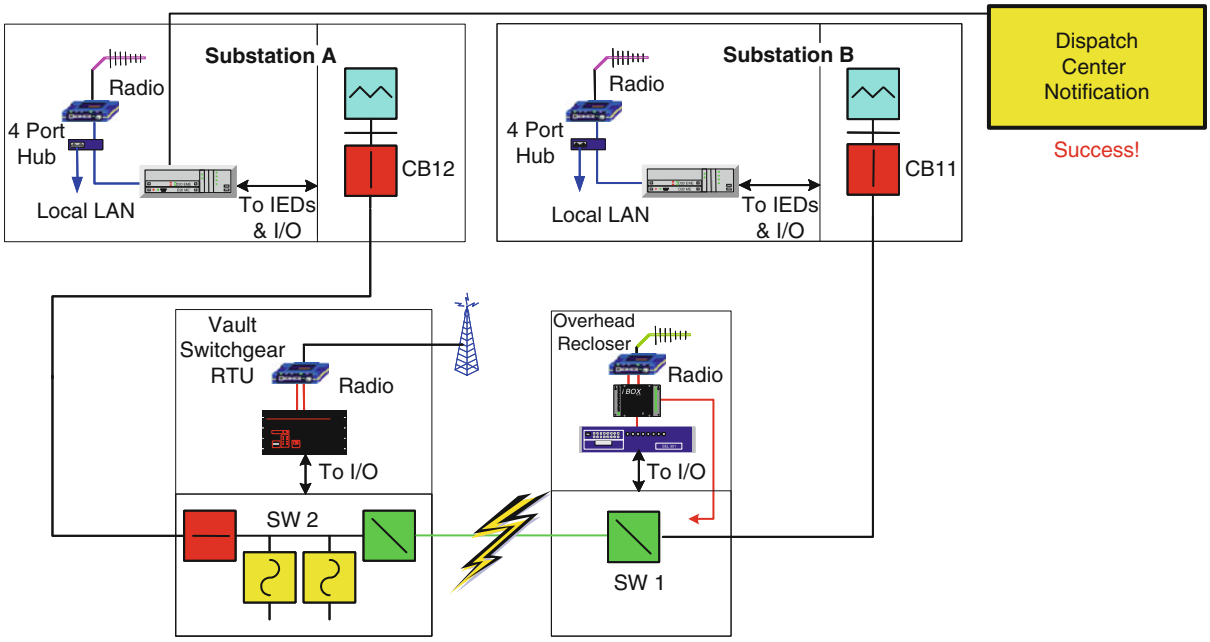

Distribution Systems, Substations, and Integration of Distributed Generation. Figure 16
Scheme 2 architecture after successful DA operation

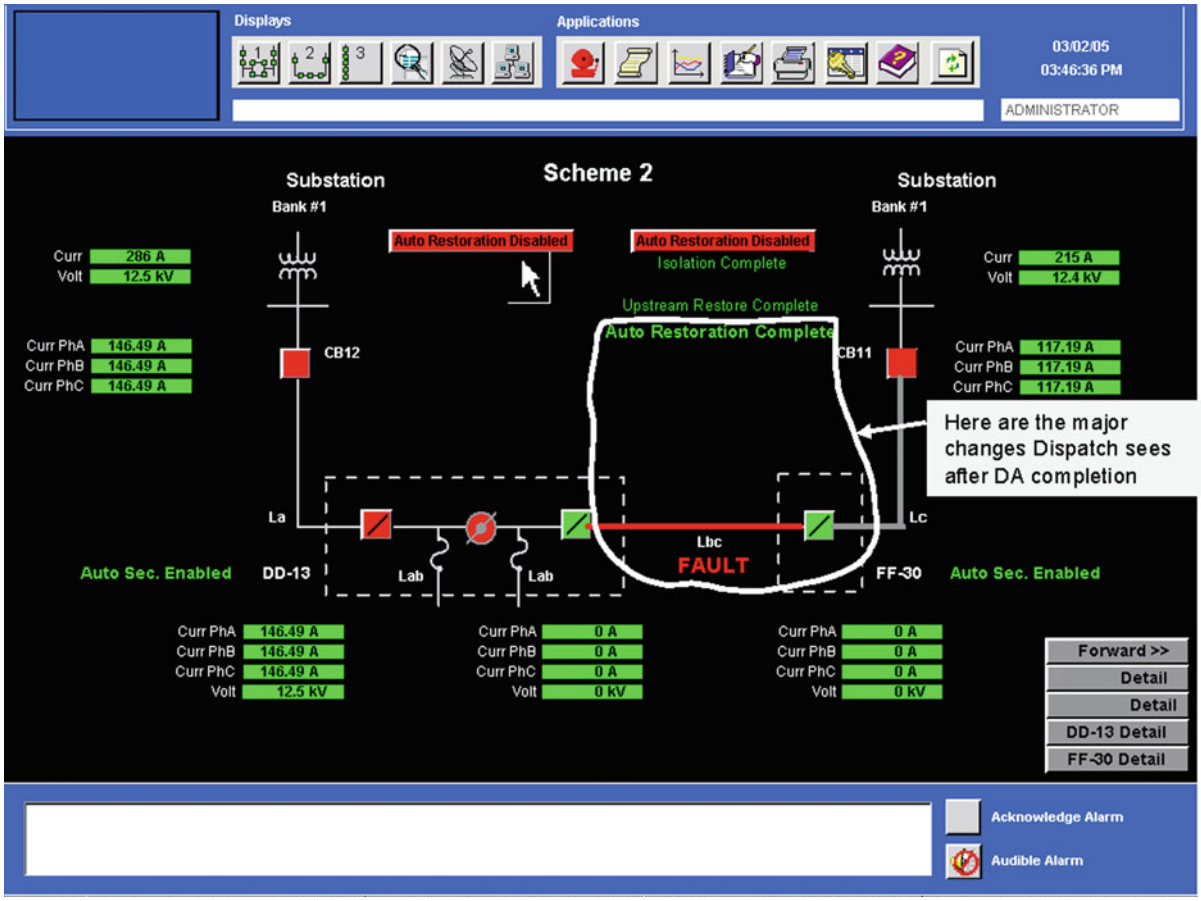

Distribution Systems, Substations, and Integration of Distributed Generation. Figure 17
Dispatch notification of scheme 2 isolation/restoration success

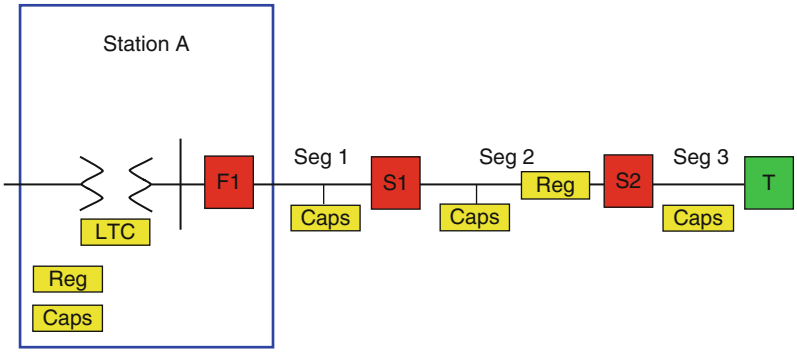

Distribution Systems, Substations, and Integration of Distributed Generation. Figure 18
Example station and feeder voltage/VAR control devices

Distribution Systems, Substations, and Integration of Distributed Generation. Figure 19
Example station and feeder voltage/VAR control devices

Distribution Systems, Substations, and Integration of Distributed Generation. Figure 20
Three-phase station voltage regulator

transform voltage from high to low or from low to high as necessary. Substations also dispatch electric power from generating stations to consumption centers. Electric power may flow through several substations between the generating plant and the consumer, and the voltage may be changed in several steps. Substations can be generally divided into three major types:

1. *Transmission substations* integrate the transmission lines into a network with multiple parallel interconnections so that power can flow freely over long distances from any generator to any consumer. This transmission grid is often called the bulk power system. Typically, transmission lines operate at voltages above 138 kV. Transmission substations often include transformation from one transmission voltage level to another.
2. *Sub-transmission substations* typically operate at 34.5 kV through 138 kV voltage levels, and transform the high voltages used for efficient

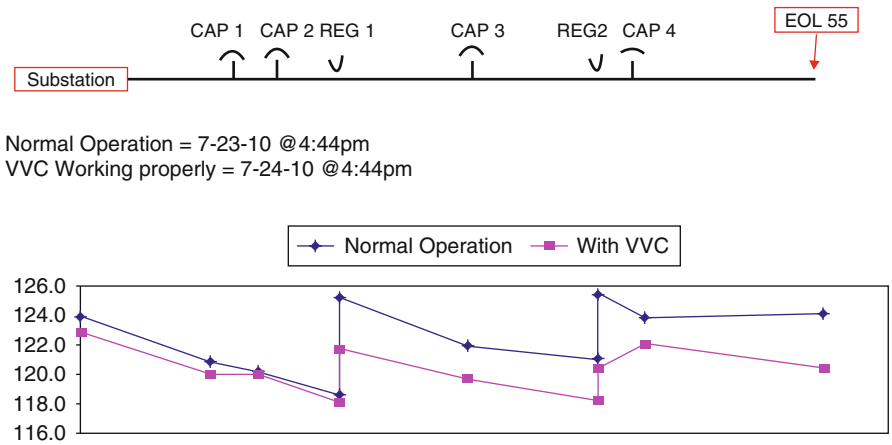

Distribution Systems, Substations, and Integration of Distributed Generation. Figure 21
Three-phase station voltage profile

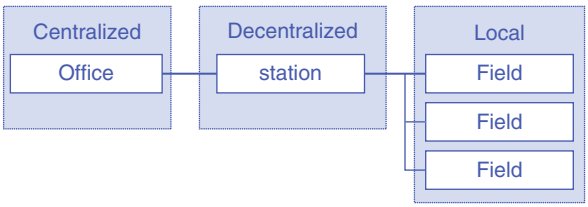

Distribution Systems, Substations, and Integration of Distributed Generation. Figure 22
Relationship automation at centralized, decentralized, and local areas

long distance transmission through the grid to the sub-transmission voltage levels for more cost-effective transmission of power through supply lines to the distribution substations in the surrounding regions. These supply lines are radial express feeders, each connecting the substation to a small number of distribution substations.

3. *Distribution substations* typically operate at 2.4–34.5 kV voltage levels, and deliver electric energy directly to industrial and residential consumers. Distribution feeders transport power from the distribution substations to the end consumers' premises. These feeders serve a large number of premises and usually contain many branches. At the consumers' premises, distribution transformers transform the distribution voltage to the service level voltage directly used in households and industrial plants, usually from 110 to 600 V.

Recently, distributed generation has started to play a larger role in the distribution system supply. These are small-scale power generation technologies (typically in the range of 3–10,000 kW) used to provide an alternative to or an enhancement of the traditional electric power system. Distributed generation includes combined heat and power (CHP), fuel cells, micro-combined heat and power (micro-CHP), micro-turbines, photovoltaic (PV) systems, reciprocating engines, small wind power systems, and Stirling engines, as well as renewable energy sources.

Renewable energy comes from natural resources such as sunlight, wind, rain, tides, and geothermal heat, which are naturally replenished. New renewables (small hydro, modern biomass, wind, solar, geothermal, and biofuels) are growing very rapidly.

A simplified one-line diagram showing all major electrical components from generation to a customer's service is shown in Fig. 25.

Distribution Substation Components

Distribution substations are comprised of the following major components.

Supply Line Distribution substations are connected to a sub-transmission system via at least one supply line, which is often called a primary feeder. However, it is typical for a distribution substation to be supplied by two or more supply lines to increase reliability of the

Distribution Systems, Substations, and Integration of Distributed Generation. Table 2 Three-phase station voltage profile

Centralized	Decentralized	Local
Supports more complex applications such as: Load Flow, DTS, Study	Most station IEDs support automation	Local IEDs often include local algorithms
Support for full network model	Faster response than centralized DA	Usually initiated after prolonged comms outage, e.g., local capacitor controller
Optimizes improvements	Smaller incremental deployment costs	Operates faster than other algorithms usually for protection, reclosing, and initial sectionalizing
Dynamic system configuration	Often used for initial deployment because of the reduced complexity and costs	Usually only operates based on local sensing or peer communications
Automation during abnormal conditions	Typical applications: include: initial response, measure pre-event	Less sophisticated and less expensive
Enables integration with other sources of data – EMS, OMS, AMI, GIS	Flexible, targeted, or custom solution	Easiest to begin deploying
Integration with other processes planning, design, dispatch	Usually cheaper and easier for initial deploy	Hardest to scale sophisticated solutions
Easier to scale, maintain, upgrade, and backup	Hard to scale sophisticated solutions	

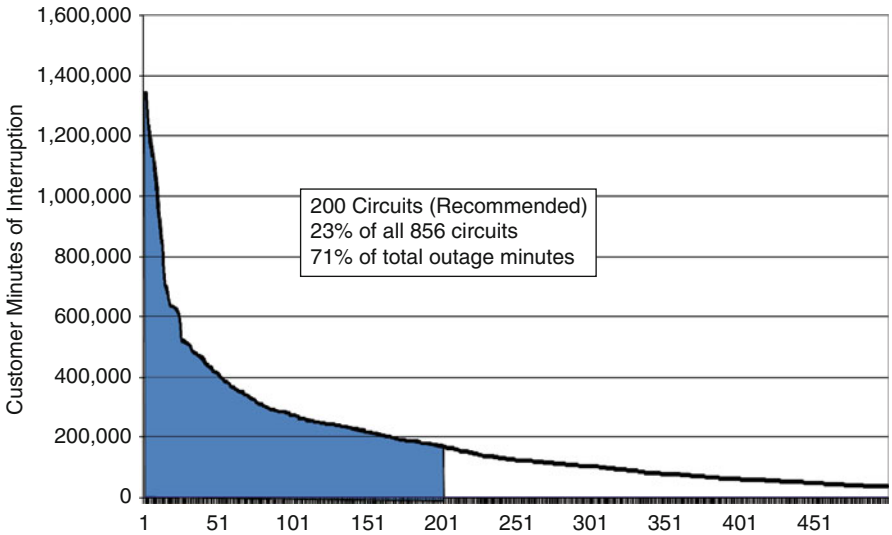

Distribution Systems, Substations, and Integration of Distributed Generation. Figure 23 Customer minutes interrupted by feeder

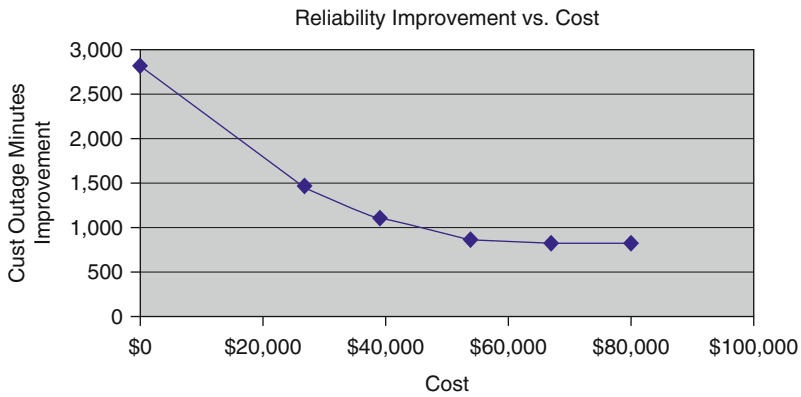

Distribution Systems, Substations, and Integration of Distributed Generation. Figure 24
Customer minutes interrupted by cost

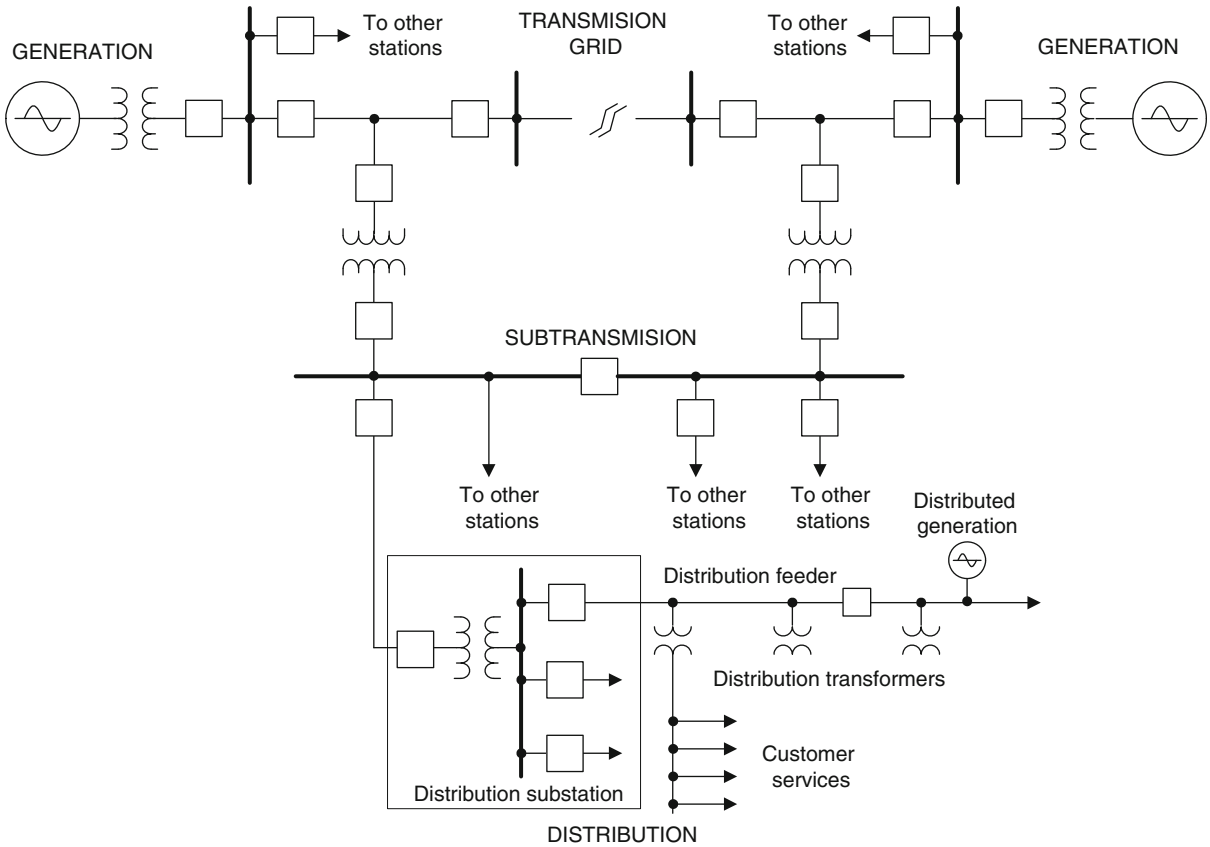

Distribution Systems, Substations, and Integration of Distributed Generation. Figure 25
One-line diagram of major components of power system from generation to consumption

power supply in case one supply line is disconnected. A supply line can be an overhead line or an underground feeder, depending on the location of the substation, with underground cable lines mostly in urban areas and overhead lines in rural areas and suburbs. Supply lines are connected to the substation via high-voltage disconnecting switches in order to isolate lines from substation to perform maintenance or repair work.

Distribution Systems, Substations, and Integration of Distributed Generation. Figure 26
Voltage transformers (Courtesy of General Electric)

Transformers Transformers "step down" supply line voltage to distribution level voltage. See Fig. 26. Distribution substations usually employ three-phase transformers; however, banks of single-phase transformers can also be used. For reliability and maintenance purposes, two transformers are typically employed at the substation, but the number can vary depending on the importance of the consumers fed from the substation and the distribution system design in general. Transformers can be classified by the following factors:

(a) *Power rating*, which is expressed in kilovolt-amperes (kVA) or megavolts-amperes (MVA), and indicates the amount of power that can be transferred through the transformer. Distribution substation transformers are typically in the range of 3 kVA to 25 MVA.
(b) *Insulation*, which includes liquid or dry types of transformer insulation. Liquid insulation can be mineral oil, nonflammable or low-flammable liquids. The dry type includes the ventilated, cast coil, enclosed non-ventilated, and sealed gas-filled types. Additionally, insulation can be a combination of the liquid-, vapor-, and gas-filled unit.
(c) *Voltage rating*, which is governed by the sub-transmission and distribution voltage levels substation to which the transformer is connected. Also, there are standard voltages nominal levels governed by applicable standards. Transformer voltage rating is indicated by the manufacturer. For example, 115/34.5 kV means the high-voltage winding of the transformer is rated at 115 kV, and the low-voltage winding is rated at 34.5 kV between different phases. Voltage rating dictates the construction and insulation requirements of the transformer to withstand rated voltage or higher voltages during system operation.
(d) *Cooling*, which is dictated by the transformer power rating and maximum allowable temperature rise at the expected peak demand. Transformer rating includes self-cooled rating at the specified temperature rise or forced-cooled rating of the transformer if so equipped. Typical transformer rated winding temperature rise is 55°C/65°C at ambient temperature of 30°C for liquid-filled transformers to permit 100% loading or higher if temporarily needed for system operation. Modern low-loss transformers allow even higher temperature rise; however, operating at higher temperatures may impact insulation and reduce transformer life.
(e) *Winding connections*, which indicates how the three phases of transformer windings are connected together at each side. There are two basic connections of transformer windings; delta (where the end of each phase winding is connected to the beginning of the next phase forming a triangle); and star (where the ends of each phase winding are connected together, forming a neutral point and the beginning of windings are connected outside). Typically, distribution transformer is connected delta at the high-voltage side and wye at the low-voltage side. Delta connection isolates the two systems with respect to some harmonics (especially third harmonic), which are not desirable in the system. A wye connection establishes a convenient neutral point for connection to the ground.
(f) *Voltage regulation*, which indicates that the transformer is capable of changing the low-voltage side voltage in order to maintain nominal voltage at customer service points. Voltage at customer

service points can fluctuate as a result of either primary system voltage fluctuation or excessive voltage drop due to the high load current. To achieve this, transformers are equipped with voltage tap regulators. Those can be either no-load type, requiring disconnecting the load to change the tap, or under-load type, allowing tap changing during transformer normal load conditions. Transformer taps effectively change the transformation ratio and allow voltage regulation of ±10–15% in steps of 1.75–2.5% per tap. Transformer tap changing can be manual or automatic; however, only under-load type tap changers can operate automatically.

Busbars Busbars (also called buses) can be found throughout the entire power system, from generation to industrial plants to electrical distribution boards. Busbars are used to carry large current and to distribute current to multiple circuits within switchgear or equipment (Fig. 27). Plug-in devices with circuit breakers or fusible switches may be installed and wired without de-energizing the busbars if so specified by the manufacturer.

Distribution Systems, Substations, and Integration of Distributed Generation. Figure 27
Outdoor switchgear busbar (upper conductors) with voltage transformers (Courtesy of General Electric)

Originally, busbars consisted of uncovered copper conductors supported on insulators, such as porcelain, mounted within a non-ventilated steel housing. This type of construction was adequate for current ratings of 225–600 A. As the use of busbars expanded and increased, loads demanded higher current ratings and housings were ventilated to provide better cooling at higher capacities. The busbars were also covered with insulation for safety and to permit closer spacing of bars of opposite polarity in order to achieve lower reactance and voltage drop.

By utilizing conduction, current densities are achieved for totally enclosed busbars that are comparable to those previously attained with ventilated busbars. Totally enclosed busbars have the same current rating regardless of mounting position. Bus configuration may be a stack of one busbar per phase (0–800 A), whereas higher ratings will use two (3,000 A) or three stacks (5,000 A). Each stack may contain all three phases, neutral, and grounding conductors to minimize circuit reactance.

Busbars' conductors and current-carrying parts can be either copper, aluminum, or copper alloy rated for the purpose. Compared to copper, electrical grade aluminum has lower conductivity and lower mechanical strength. Generally, for equal current-carrying ability, aluminum is lighter in weight and less costly. All contact locations on current-carrying parts are plated with tin or silver to prevent oxides or insulating film from building up on the surfaces.

In distribution substations, busbars are used at both high side and low side voltages to connect different circuits and to transfer power from the power supply to multiple outcoming feeders. Feeder busbars are available for indoor and outdoor construction. Outdoor busbars are designed to operate reliably despite exposure to the weather. Available current ratings range from 600 to 5,000 A continuous current. Available short-circuit current ratings are 42,000–200,000 A, symmetrical root mean square (RMS).

Switchgear Switchgear (Fig. 28) is a general term covering primary switching and interrupting devices together with its control and regulating equipment. Power switchgear includes breakers, disconnect switches, main bus conductors, interconnecting

Distribution Systems, Substations, and Integration of Distributed Generation. Figure 28
Indoor switchgear front view (Courtesy of General Electric)

wiring, support structures with insulators, enclosures, and secondary devices for monitoring and control. Power switchgear is used throughout the entire power system, from generation to industrial plants to connect incoming power supply and distribute power to consumers. Switchgear can be of outdoor or indoor types, or a combination of both. Outdoor switchgear is typically used for voltages above 26 kV, whereas indoor switchgear is commonly for voltages below 26 kV.

Indoor switchgear can be further classified into metal-enclosed switchgear and open switchgear, which is similar to outdoor switchgear but operates at lower voltages. Metal-enclosed switchgear can be further classified into metal-clad switchgear, low-voltage breaker switchgear, and interrupter switchgear. Metal-clad switchgear is commonly used throughout the industry for distributing supply voltage service above 1,000 V.

Metal-clad switchgear can be characterized as follows:

(a) The primary voltage breakers and switches are mounted on a removable mechanism to allow for movement and proper alignment.
(b) Grounded metal barriers enclose major parts of the primary circuit, such as breakers or switches, buses, potential transformers, and control power transformers.
(c) All live parts are enclosed within grounded metal compartments. Primary circuit elements are not exposed even when the removable element is in the test, disconnected, or in the fully withdrawn position.
(d) Primary bus conductors and connections are covered with insulating material throughout by means of insulated barriers between phases and between phase and ground.
(e) Mechanical and electrical interlocking ensures proper and safe operation.
(f) Grounded metal barriers isolate all primary circuit elements from meters, protective relays, secondary control devices, and wiring. Secondary control devices are mounted of the front panel, and are usually swing type as shown in Fig. 28.

Switchgear ratings indicate specific operating conditions, such as ambient temperature, altitude, frequency, short-circuit current withstand and duration, overvoltage withstand and duration, etc. The rated continuous current of a switchgear assembly is the maximum current in RMS (root mean square) amperes, at rated frequency, that can be carried continuously by the primary circuit components without causing temperatures in excess of the limits specified by applicable standards.

Outcoming Feeders A number of outcoming feeders are connected to the substation bus to carry power from the substation to points of service. Feeders can be run overhead along streets, or beneath streets, and carry power to distribution transformers at or near consumer premises. The feeders' breaker and isolator are part of the substation low-voltage switchgear and are typically the metal-clad type. When a fault occurs on the feeder, the protection will detect it and open the breaker. After detection, either automatically or manually, there may be one or more attempts to reenergize the feeder. If the fault is transient, the feeder will be reenergized and the breaker will remain closed. If the fault is permanent, the breaker will remain open and operating personnel will locate and isolate the faulted section of the feeder.

Switching Apparatus Switching apparatus is needed to connect or disconnect elements of the power system to or from other elements of the system. Switching apparatus includes switches, fuses, circuit breakers, and service protectors.

(a) *Switches* are used for isolation, load interruption, and transferring service between different sources of supply.

Isolating switches are used to provide visible disconnect to enable safe access to the isolated equipment. These switches usually have no interrupting current rating, meaning that the circuit must be opened by other means (such as breakers). Interlocking is generally provided to prevent operation when the switch is carrying current.

Load interrupting or a load-break switch combines the functions of a disconnecting switch and a load interrupter for interrupting at rated voltage and currents not exceeding the continuous-current rating of the switch. Load-break switches are of the air- or fluid-immersed type. The interrupter switch is usually manually operated and has a "quick-make, quick-break" mechanism which functions independently of the speed-of-handle operation. These types of switches are typically used on voltages above 600 V.

For services of 600 V and below, safety circuit breakers and switches are commonly used. Safety switches are enclosed and may be fused or un-fused. This type of switch is operated by a handle outside the enclosure and is interlocked so that the enclosure cannot be opened unless the switch is open or the interlock defeater is operated.

Transfer switches can be operated automatically or manually. Automatic transfer switches are of double-throw construction and are primarily used for emergency and standby power generation systems rated at 600 V and lower. These switches are used to provide protection against normal service failures.

(b) *Fuses* are used as an over-current-protective device with a circuit-opening fusible link that is heated and severed as over-current passes through it. Fuses are available in a wide range of voltage, current, and interrupting ratings, current-limiting types, and for indoor and outdoor applications. Fuses perform the same function as circuit breakers, and there is no general rule for using one versus the other. The decision to use a fuse or circuit breaker is usually based on the particular application, and factors such as the current interrupting requirement, coordination with adjacent protection devices, space requirements, capital and maintenance costs, automatic switching, etc.

(c) *Circuit breakers* (Fig. 29) are devices designed to open and close a circuit either automatically or manually. When applied within its rating, an automatic circuit breaker must be capable of opening a circuit automatically on a predetermined overload of current without damaging itself or adjacent elements. Circuit breakers are required to operate infrequently, although some classes of circuit breakers are suitable for more frequent operation. The interrupting and momentary ratings of a circuit breaker must be equal to or greater than the available system short-circuit currents.

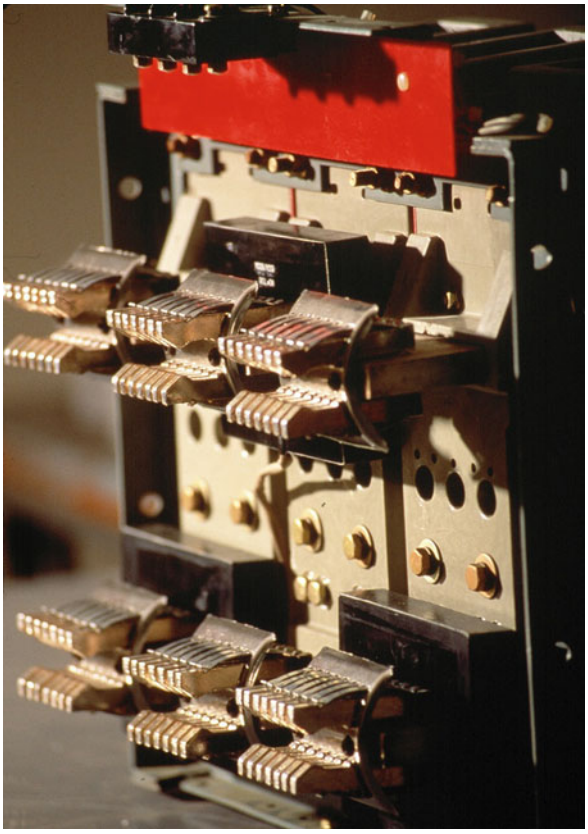

Distribution Systems, Substations, and Integration of Distributed Generation. Figure 29
Breaker of indoor switchgear, rear "bus" side (Courtesy of General Electric)

Circuit breakers are available for the entire system voltage range, and may be as furnished single-, double-, triple-, or four-pole, and arranged for indoor or outside use. Sulfur hexafluoride (SF_6) gas-insulated circuit breakers are available for medium and high voltages, such as gas-insulated substations.

When a current is interrupted, an arc is generated. This arc must be contained, cooled, and extinguished in a controlled way so that the gap between the contacts can again withstand the voltage in the circuit. Circuit breakers can use vacuum, air, insulating gas, or oil as the medium in which the arc forms. Different techniques are used to extinguish the arc, including:

- Lengthening the arc
- Intensive cooling (in jet chambers)
- Division into partial arcs
- Zero point quenching (contacts open at the zero current time crossing of the AC waveform, effectively breaking no-load current at the time of opening)
- Connecting capacitors in parallel with contacts in DC circuits

Traditionally, oil circuit breakers (Fig. 30) were used in the power industry, which use oil as a media to extinguish the arc and rely upon vaporization of some of the oil to blast a jet of oil through the arc.

Gas (usually sulfur hexafluoride) circuit breakers sometimes stretch the arc using a magnetic field, and then rely upon the dielectric strength of the sulfur hexafluoride to quench the stretched arc.

Vacuum circuit breakers have minimal arcing (as there is nothing to ionize other than the contact material), so the arc quenches when it is stretched by a very small amount (<2–3 mm). Vacuum circuit breakers are frequently used in modern medium-voltage switchgear up to 35 kV.

Air blast circuit breakers may use compressed air to blow out the arc, or alternatively, the contacts are rapidly swung into a small sealed chamber, where the escaping displaced air blows out the arc.

Circuit breakers are usually able to terminate all current very quickly: Typically the arc is extinguished between 30 and 150 ms after the mechanism has tripped, depending upon age and construction of the device.

Distribution Systems, Substations, and Integration of Distributed Generation. Figure 30
Outdoor medium-voltage oil-immersed circuit breaker (Courtesy of General Electric)

Indoor circuit breakers are rated to carry 1–3 kA current continuously, and interrupting 8–40 kA short-circuit current at rated voltage.

Surge Voltage Protection Transient overvoltages are due to natural and inherent characteristics of power systems. Overvoltages may be caused by lightning or by a sudden change of system conditions (such as switching operations, faults, load rejection, etc.), or both. Generally, the overvoltage types can be classified as lightning generated and as switching generated. The magnitude of overvoltages can be above maximum permissible levels, and therefore needs to be reduced and protected against to avoid damage to equipment and undesirable system performance.

The occurrence of abnormal applied overvoltage stresses, either short term or sustained steady state, contributes to premature insulation failure. Large amounts of current may be driven through the faulted

channel, producing large amounts of heat. Failure to suppress overvoltage quickly and effectively or interrupt high short-circuit current can cause massive damage of insulation in large parts of the power system, leading to lengthy repairs.

The appropriate application of surge-protective devices will lessen the magnitude and duration of voltage surges seen by the protected equipment. The problem is complicated by the fact that insulation failure results from impressed overvoltages, and because of the aggregate duration of repeated instances of overvoltages.

Surge arresters have been used in power systems to protect insulation from overvoltages. Historically, the evolution of surge arrester material technology has produced various arrester designs, starting with the valve-type arrester, which has been used almost exclusively on power system protection for decades. The active element (i.e., valve element) in these arresters is a nonlinear resistor that exhibits relatively high resistance (megaohms) at system operating voltages, and a much lower resistance (ohms) at fast rate-of-rise surge voltages.

In the mid-1970s, arresters with metal-oxide valve elements were introduced. Metal-oxide arresters have valve elements (also of sintered ceramic-like material) of a much greater nonlinearity than silicon carbide arresters, and series gaps are no longer required. The metal-oxide designs offer improved protective characteristics and improvement in various other characteristics compared to silicon carbide designs. As a result, metal-oxide arresters have replaced gapped silicon carbide arresters in new installations.

In the mid-1980s, polymer housings began to replace porcelain housings on metal-oxide surge arresters offered by some manufacturers. The polymer housings are made of either EPDM (ethylene propylene diene monomer [M-class] rubber) or silicone rubber. Distribution arrester housings were first made with polymer, and later expanded into the intermediate and some station class ratings. Polymer housing material reduces the risk of injuries and equipment damage due to surge arrester failures.

Arresters have a dual fundamental-frequency (RMS) voltage rating (i.e., duty-cycle voltage rating), and a corresponding maximum continuous operating voltage rating. Duty-cycle voltage is defined as the designated maximum permissible voltage between the terminals at which an arrester is designed to perform.

Grounding Grounding is divided into two categories: power system grounding and equipment grounding.

Power system grounding means that at some location in the system there are intentional electric connections between the electric system phase conductors and ground (earth). System grounding is needed to control overvoltages and to provide a path for ground-current flow in order to facilitate sensitive ground-fault protection based on detection of ground-current flow. System grounding can be as follows:

- Solidly grounded
- Ungrounded
- Resistance grounded

Each grounding arrangement has advantages and disadvantages, with choices driven by local and global standards and practices, and engineering judgment.

Solidly grounded systems are arranged such that circuit protective devices will detect a faulted circuit and isolate it from the system regardless of the type of fault. All transmission and most sub-transmission systems are solidly grounded for system stability purposes. Low-voltage service levels of 120–480 V four-wire systems must also be solidly grounded for safety of life. Solid grounding is achieved by connecting the neutral of the wye-connected winding of the power transformer to the ground.

Where service continuity is required, such as for a continuously operating process, the resistance grounded power system can be used. With this type of grounding, the intention is that any contact between one phase conductor and a ground will not cause the phase over-current protective device to operate. Resistance grounding is typically used from 480 V to 15 kV for three-wire systems. Resistance grounding is achieved by connecting the neutral of the wye-connected winding of the power transformer to the ground through the resistor, or by employing special grounding transformers.

The operating advantage of an ungrounded system is the ability to continue operations during a single phase-to-ground fault, which, if sustained, will not

result in an automatic trip of the circuit by protection. Ungrounded systems are usually employed at the distribution level and are originated from delta-connected power transformers.

Equipment grounding refers to the system of electric conductors (grounding conductor and ground buses) by which all non-current-carrying metallic structures within an industrial plant are interconnected and grounded. The main purposes of equipment grounding are:

- To maintain low potential difference between metallic structures or parts, minimizing the possibility of electric shocks to personnel in the area
- To contribute to adequate protective device performance of the electric system, and safety of personnel and equipment
- To avoid fires from volatile materials and the ignition of gases in combustible atmospheres by providing an effective electric conductor system for the flow of ground-fault currents and lightning and static discharges to eliminate arcing and other thermal distress in electrical equipment

Substation grounding systems are thoroughly engineered. In an electrical substation, a ground (earth) mat is a mesh of metal rods connected together with conductive material and installed beneath the earth surface. It is designed to prevent dangerous ground potential from rising at a place where personnel would be located when operating switches or other apparatus. It is bonded to the local supporting metal structure and to the switchgear so that the operator will not be exposed to a high differential voltage due to a fault in the substation.

Power Supply Quality The quality of electrical power may be described as a set of values or parameters, such as:

- Continuity of service
- Variation in voltage magnitude
- Transient voltages and currents
- Harmonic content in the supply voltages

Continuity of service is achieved by proper design, timely maintenance of equipment, reliability of all substation components, and proper operating procedures. Recently, remote monitoring and control have greatly improved the power supply continuity.

When the voltage at the terminals of utilization equipment deviates from the value on the nameplate of the equipment, the performance and the operating life of the equipment are affected. Some pieces of equipment are very sensitive to voltage variations (e.g., motors). Due to voltage drop down the supply line, voltage at the service point may be much lower compared with the voltage at substation. Abnormally low voltage occurs at the end of long circuits. Abnormally high voltage occurs at the beginning of circuits close to the source of supply, especially under lightly loaded conditions such as at night and during weekends. Voltage regulators are used at substations to improve the voltage level supplied from the distribution station. This is achieved by a tap changer mounted in the transformer and an automatic voltage regulator that senses voltage and voltage drop due to load current to increase or decrease voltage at the substation.

If the load power factor is low, capacitor banks (Fig. 31) may be installed at the substation to improve the power factor and reduce voltage drop. Capacitor banks are especially beneficial at substations near industrial customers where reactive power is needed for operation of motors.

Transients in voltages and currents may be caused by several factors, such as large motor stating, fault in the sub-transmission or distribution system, lightning, welding equipment and arc furnace operation, turning on or off large loads, etc. Lighting equipment output is sensitive to applied voltage, and people are sensitive to sudden illumination changes. A voltage change of 0.25–0.5% will cause a noticeable reduction in the light output of an incandescent lamp. Events causing such voltage effects are called flicker (fast change of the supply voltage), and voltage sags (depressed voltage for a noticeable time). Both flicker and sags have operational limits and are governed by industry and local standards.

Voltage and current on the ideal AC power system have pure single frequency sine wave shapes. Power systems have some distortion because an increasing number of loads require current that is not a pure sine wave. Single- and three-phase rectifiers, adjustable speed drives, arc furnaces, computers, and fluorescent lights are good examples. Capacitor failure, premature transformer failure, neutral overloads, excessive motor

Distribution Systems, Substations, and Integration of Distributed Generation. Figure 31
Capacitor Bank (Courtesy of General Electric)

heating, relay misoperation, and other problems are possible when harmonics are not properly controlled.

Harmonics content is governed by appropriate industry and local standards, which also provide recommendations for control of harmonics in power systems.

Substation Design Considerations

Distribution substation design is a combination of reliability and quality of the power supply, safety, economics, maintainability, simplicity of operation, and functionality.

Safety of life and preservation of property are the two most important factors in the design of the substation. Codes must be followed and recommended practices or standards should be followed in the selection and application of material and equipment. Following are the operating and design limits that should be considered in order to provide safe working conditions:

- Interrupting devices must be able to function safely and properly under the most severe duty to which they may be exposed.
- Accidental contact with energized conductors should be eliminated by means of enclosing the conductors, installing protective barriers, and interlocking.
- The substation should be designed so that maintenance work on circuits and equipment can be accomplished with these circuits and equipment de-energized and grounded.
- Warning signs should be installed on electric equipment accessible to both qualified and unqualified personnel, on fences surrounding electric equipment, on access doors to electrical rooms, and on conduits or cables above 600 V in areas that include other equipment.
- An adequate grounding system must be installed.
- Emergency lights should be provided where necessary to protect against sudden lighting failure.
- Operating and maintenance personnel should be provided with complete operating and maintenance instructions, including wiring diagrams, equipment ratings, and protective device settings.

A variety of basic circuit arrangements are available for distribution substations. Selection of the best system or combination of systems will depend upon the needs of the power supply process. In general, system costs increase with system reliability if component quality is equal. Maximum reliability per unit investment can be achieved by using properly applied and well-designed components.

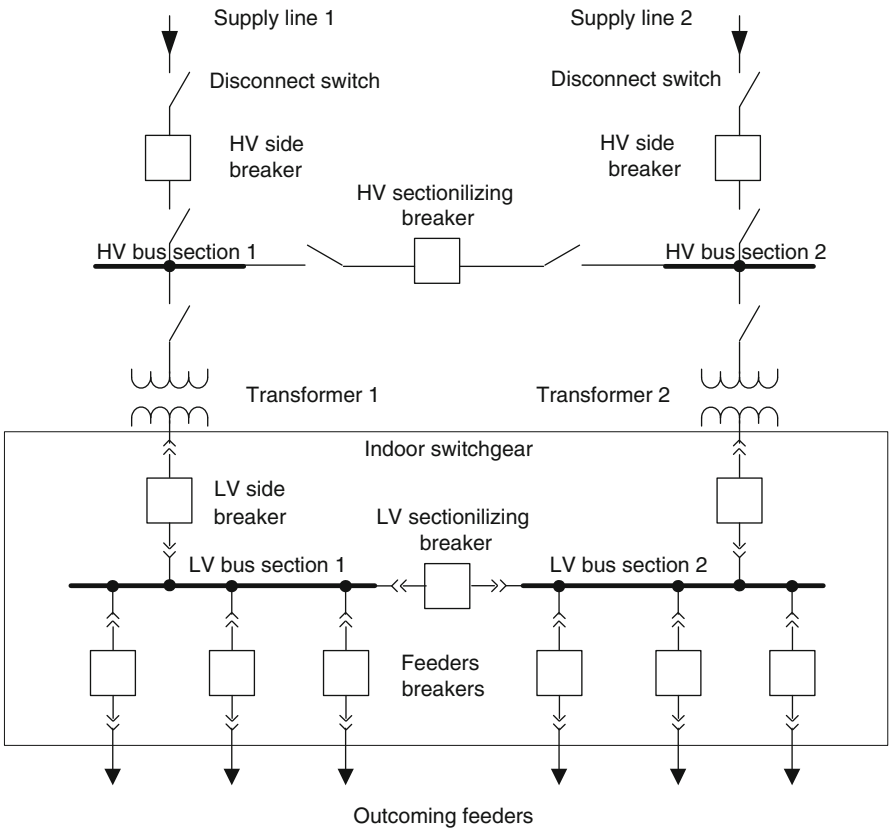

Distribution Systems, Substations, and Integration of Distributed Generation. Figure 32
Example one-line diagram of distribution substation with two transformers and two supply lines

Figure 32 provides an example of the distribution substation one-line diagram with two transformers, two supply lines, and two sections at both the high-voltage (HV) side and low-voltage (LV) sides, with sectionalizing breakers at both HV and LV voltages. Such an arrangement provides redundancy and reliability in case of any component failure by transferring the power supply from one section to another. Additionally, any component of the substation can be taken out of service for maintenance.

If the substation is designed to supply a manufacturing plant, continuity of service may be critical. Some plants can tolerate interruptions while others require the highest degree of service continuity. The system should always be designed to isolate faults with a minimum disturbance to the system, and should have features to provide the maximum dependability consistent with the plant requirements and justifiable cost. The majority of utilities today supply energy to medium and large industrial customers directly at 34.5, 69, 115, 138, 161, and 230 kV using dedicated substations. Small industrial complexes may receive power at voltages as low as 4 kV.

Poor voltage regulation is harmful to the life and operation of electrical equipment. Voltage at the utilization equipment must be maintained within equipment tolerance limits under all load conditions, or equipment must be selected to operate safely and efficiently within the voltage limits. Load-flow studies and motor-starting calculations are used to verify voltage regulation.

Substation Standardization

Standards, recommended practices, and guides are used extensively in communicating requirements for

design, installation, operation, and maintenance of substations. Standards establish specific definitions of electrical terms, methods of measurement and test procedures, and dimensions and ratings of equipment. Recommended practices suggest methods of accomplishing an objective for specific conditions. Guides specify the factors that should be considered in accomplishing a specific objective. All are grouped together as standards documents.

Standards are used to establish a small number agreed to by the substation community of alternative solutions from a range of possible solutions. This allows purchasers to select a specific standard solution knowing that multiple vendors will be prepared to supply that standard, and that different vendor's produces will be able to interoperate with each other. Conversely, this allows vendors to prepare a small number of solutions knowing that a large number of customers will be specifying those solutions. Expensive and trouble-prone custom "one-of-a-kind" design and manufacturing can be avoided. For example, out of the almost infinite range of voltage ratings for 3-wire 60 Hz distribution substation low side equipment, NEMA C84.1 standardizes only seven: 2,400, 4,160, 4,800, 6,900, 13,800, 23,000, and 34,500 V. Considerable experience and expertise goes into the creation and maintenance of standards, providing a high degree of confidence that solutions implemented according to a standard will perform as expected. Standards also allow purchasers to concisely and comprehensively state their requirements, and allow vendors to concisely and comprehensively state their products' performance.

There are several bodies publishing standards relevant to substations. Representative of these are the following:

The Institute of Electrical and Electronics Engineers (IEEE) is a nonprofit, transnational professional association having 38 societies, of which the Power and Energy Society (PES) is "involved in the planning, research, development, construction, installation, and operation of equipment and systems for the safe, reliable, and economic generation, transmission, distribution, measurement, and control of electric energy." PES includes several committees devoted to various aspects of substations that publish a large number of standards applicable to substations. For more information, visit www.ieee-pes.org.

The National Electrical Manufacturers Association (NEMA) is a trade association of the electrical manufacturing industry that manufactures products used in the generation, transmission and distribution, control, and end-use of electricity. NEMA provides a forum for the development of technical standards that are in the best interests of the industry and users; advocacy of industry policies on legislative and regulatory matters; and collection, analysis, and dissemination of industry data. For more information, visit www.nema.org.

American National Standards Institute (ANSI) oversees the creation, promulgation, and use of thousands of norms and guidelines that directly impact businesses in nearly every sector, including energy distribution. ANSI is also actively engaged in accrediting programs that assess conformance to standards – including globally recognized cross-sector programs such as the ISO 9000 (quality) and ISO 14000 (environmental) management systems. For more information, see www.ansi.org.

National Fire Protection Association (NFPA) is an international nonprofit organization established in 1896 to reduce the worldwide burden of fire and other hazards on the quality of life by providing and advocating consensus codes and standards, research, training, and education. NFPA develops, publishes, and disseminates more than 300 consensus codes and standards intended to minimize the possibility and effects of fire and other risks. Of particular interest to substations is the National Electrical Code (NEC). For more information, see www.nfpa.org.

International Electrotechnical Commission (IEC) technical committee is an organization for the preparation and publication of International Standards for all electrical, electronic, and related technologies. These are known collectively as "electrotechnology." IEC provides a platform to companies, industries, and governments for meeting, discussing, and developing the International Standards they require. All IEC International Standards are fully consensus based and represent the needs of key stakeholders of every nation

participating in IEC work. Every member country, no matter how large or small, has one vote and a say in what goes into an IEC International Standard. For more information, see www.iec.ch.

International Organization for Standardization (ISO) is a nongovernmental organization that forms a bridge between the public and private sectors. Many of its member institutes are part of the governmental structure of their countries, or are mandated by their government while other members have their roots uniquely in the private sector, having been set up by national partnerships of industry associations. ISO enables a consensus to be reached on solutions that meet both the requirements of business and the broader needs of society. For more information, see www.iso.org.

International Telecommunication Union (ITU) is the United Nations' agency for information and communication technology issues, and the global focal point for governments and the private sector in developing networks and services. For 145 years, ITU has coordinated the shared global use of the radio spectrum, promoted international cooperation in assigning satellite orbits, worked to improve telecommunication infrastructure in the developing world, established the worldwide standards that foster seamless interconnection of a vast range of communications systems, and addressed the global challenges of our times, such as mitigating climate change and strengthening cyber security. For more information, see www.iut.int.

Substation Physical Appearance

It is desirable to locate distribution substations as near as possible to the load center of its service area, though this requirement is often difficult to satisfy. Locations that are perfect from engineering and cost points of view are sometimes prohibited due to physical, electrical, neighboring, or aesthetic considerations. Given the required high- and low-voltage requirements and the required power capacity, a low-cost aboveground design will satisfy power supply needs. However, an aboveground design requires overhead sub-transmission line structures (Fig. 33), which are often undesirable structures for neighborhoods. Therefore, incoming lines are often

Distribution Systems, Substations, and Integration of Distributed Generation. Figure 33
Distribution substation view (Courtesy of General Electric)

underground cables, and the entire substation is designed to be as unobtrusive as possible.

Underground cables are more costly than overhead lines for the same voltage and capacity. Installation of underground cables in urban areas is also often inconvenient and potentially hazardous.

Local conditions or system-wide policy may require landscaping at a substation site or for housing the substation within a building. A fence with warning signs or other protective enclosures is typically provided to keep unauthorized persons from coming in close proximity of the high-voltage lines and substation equipment. Alarm systems and video surveillance are becoming normal practices for monitoring and preventing intrusion by unauthorized persons.

Protection and Automation

The purpose of protection in distribution substations is to isolate faulted power system elements, such as feeders and transformers, from sources of electrical supply in order to:

- Prevent damage to un-faulted equipment that might otherwise result from sustained fault-level currents and/or voltages

- Reduce the probability and degree of harm to the general public, utility personnel, and property
- Reduce the amount of damage the faulted element sustains, thus containing repair costs, service interruption duration, and impact on the environment
- Clear transient faults and restore service

To accomplish this, protection devices must be able to rapidly determine that a fault has occurred, determine which system element or which section of the system has faulted, and to open the circuit breakers and switches that will disconnect the faulted element. To do this reliably, means must be provided to clear faults even in the event of a single failure in the protection system.

Substation automation facilities complement protection at distribution substations. In the past, automation at distribution substations was limited to automatic tap changer control and capacitor auto-switching to regulate voltage. Automation and communication facilities in modern distribution substations provide visibility to the system operator of the state of the substation, allowing rapid identification of the source and cause of interruptions and other troubles, and providing the ability to dispatch repair personnel quickly to the correct location and with the necessary equipment and spares to effect a repair. In these modern distribution substations, automation facilities often provide operators with the ability to remotely open and close breakers and switches, allowing power rerouting to restore service.

The principle by which protection operates depends to a large degree on the element covered by the protection. Common element types are as follows.

Incoming Sub-transmission Supply Line Protection at Distribution Substations In the past, distribution substations supplied only loads; there was little if any distributed generation. With this arrangement, faults on the incoming sub-transmission supply line do not result in energy flowing out of the distribution substation and into the supply line (i.e., backfeed). In that event, opening of the distribution substation end of the supply line is not necessary to isolate supply line faults; opening of the source end by protection located there is all that is necessary.

Recently, distributed generation from windmills, bio-digesters, mini-hydraulics, and photovoltaic sources has been increasing dramatically, in some cases to the point where the contribution to the supply line faults and must be interrupted to extinguish the fault. Various protection technologies exist to detect such faults, including reverse flow, distance, and current differential.

Reverse flow protection detects the reversal from the normal direction of power and/or current flow. This type of protection is only suitable for cases where the amount of distributed generation in relation to the amount of load is small enough that under normal un-faulted conditions the flow from the supply line is always into the distribution substation. Reverse flow occurs when a supply line fault causes voltage depression to the point where load current essentially disappears, yet the distributed generators continue to source current.

Distance protection estimates the impedance of the supply line between the distribution substation and a fault on the supply line. Supply lines typically have a constant amount of impedance per unit distance (e.g., per kilometer), so the impedance seen at the distribution substation is larger for a fault beyond the end of the supply line than for a fault on the supply line. Distance protection thus can usually discriminate between these two faults, and avoid unnecessary tripping for faults beyond the supply line. To a first approximation, impedance is simply the voltage divided by the current.

Current differential protection is based on the fact that the algebraic sum of all supply line terminal currents is equal to the supply line fault current, if any. Current resulting from external faults and from load flowing into the supply line is canceled as it flows out. Charging current is typically negligible at sub-transmission voltage levels.

With each of these three methods, current transformers (CTs) are needed to measure supply line current, and except for current differential, voltage transformers (VTs) are needed to measure the voltage at the distribution substation. With current differential, a communications channel to the other end(s) of the supply line is needed. A relay (also known as an IED) is needed to detect the supply line fault and discriminate it from other conditions such as

faults on other elements. Also, a circuit breaker or circuit switcher is needed to interrupt the supply line connection on command from the relay.

Distribution Substation Transformer Protection In distribution substations with relatively small delta/wye transformers (typically less than 10 MVA), transformer protection often consists of simple fusing. A power fault in the transformer or on the low side bus typically produces a large current in the high side terminals that melts the fusible links, interrupting the fault. Internal turn-to-turn winding faults that produce only small terminal fault currents are allowed to burn until the fault evolves into a fault with current large enough to operate the fuses. This is acceptable because there is little or no difference in the commercial value of faulted transformers, and because small transformers on which fuses are used are less costly.

On larger (and more expensive) transformers, through-current restrained differential relays (Fig. 34) are most often employed. These protections require CTs measuring all current paths in and out of the transformer. Most often, the CTs are mounted on the high side terminals of the transformer and on the breaker(s) that directly connect to the low side terminals. Where there is no breaker between the transformer and the low side bus, the bus is also covered. The operating principle of transformer current differential protection is based on the incoming high side current under normal and under external fault conditions approximately equaling the sum of the outgoing low side currents after adjusting for the transformer's transformation ratio and internal connection (e.g., delta/wye). During internal fault conditions, there is a large inequality.

Distribution Systems, Substations, and Integration of Distributed Generation. Figure 34
Modern digital transformer protection relay (Courtesy of General Electric)

Invariably, there is actually some difference between these (even in a healthy transformer) that is a small but constant percentage of the current flowing through the transformer. An on-load tap changer is an example of what can cause such a difference. For large through-currents, such as occurring during external low side faults, the difference is substantial, so the relay employs through-current restraint. The differential operating threshold is made dynamic by including in the trip threshold a percentage of the measured through-current.

Another problem with transformer differential protection is that when the transformer itself is saturated, which usually occurs on energization, relatively large currents flow through the excitation impedance, which appear to the protection as differential current with no through-current. Energization current, however, contains a large harmonic component. Relays therefore monitor for the presence of such harmonics, most often the second harmonic, and when found block the differential element.

When a transformer fault is detected, the transformer is isolated by opening its high side connection. Where there are fuses, the fuses perform the interruption. Where there is a high side breaker or circuit switcher, they are tripped. Otherwise, a trip signal is sent to trip the remote end of the supply line. This signal may be via radio, optical fiber, or metallic pair, or may be the closing a switch that grounds one phase of the supply line causing the remote end to see and trip as for a supply line fault. Where there are distributed generators on the distribution system, the distributed generators or the distribution substation's low side breakers must be opened as well. Opening of low side breakers is often done even when there are no distributed generators.

Distribution Substation Bus Protection When fuses protect a distribution substation transformer and there is no transformer low side breaker and the differential

uses feeder breaker CTs, the transformer protection covers the low side bus as well as the transformer.

Where a separate bus protection is used, there are several alternatives for detecting bus faults, including low impedance current differential, high impedance differential, and zone-interlocked schemes.

Low impedance bus differential with through-current restraint operates on the same basic principle as transformer differential protection. Buses have no significant energization current, so harmonic blocking is not implemented. Also there is no need to adjust for transformer connection. However, there are typically many more feeders to measure than in transformer differential applications, so a relay designed for bus protection is required. Low impedance bus differential protections without through-current restraint have been deployed, but often have trouble with CT saturation, causing unnecessary tripping.

High impedance bus differential protections include a simple over-current relay with a large stabilizing resister connected in series. The relay current is from the parallel connection of the secondary windings of CTs measuring all bus connections. The CTs should be identical in type and ratio. With no fault, the current flowing into the bus is balanced by the current flowing out of the bus (a pattern that is matched in the CT secondary circuit), and thus little or no current flows through the over-current relay. The stabilizing resistor tends to prevent large external fault currents from saturating the CT of the faulted feeder and producing erroneous differential current.

Zone-interlocked schemes (also known as bus-blocking schemes) employ an over-current relay measuring infeed current from the main transformer. On detecting fault current, this over-current relay trips the bus unless one of the feeder protections sees a feeder fault and sends a blocking signal. Bus tripping is delayed by a short time to ensure that the feeder protections have sufficient time to detect and block for feeder faults.

No matter the detection method used, when a bus fault is detected, the fault current coming from the main transformer must be interrupted. Where there is a transformer low side breaker, it is opened. Otherwise, the transformer high side is opened using one or more of the methods described in the transformer protection section. Where there are distributed generators on the distribution system, the distributed generators or the distribution substation's low side breakers or circuit switchers must be opened as well. Opening of low side breakers is often done even when there are no distributed generators.

Distribution Feeder Protection Distribution feeder protection at distribution substations is most often instantaneous and timed over-current functionality. Very often, these functions are implemented within a recloser, which is essentially a circuit breaker packaged with a mechanism that repeatedly trips when current exceeds a set threshold, and then recloses or locks out after a series of set delays. Alternatively, an electronic relay with instantaneous and inverse time over-current features is used.

Distribution feeders (Fig. 35) typically have fuses along its length and/or on lateral sections intended to separate a faulted section, allowing the rest to be

Distribution Systems, Substations, and Integration of Distributed Generation. Figure 35
Modern digital feeder protection relay (Courtesy of General Electric)

supplied pending repair. Feeder protections usually implement either a fuse-saving or a trip-saving scheme.

Aerial feeders are prone to transient faults, faults that due to lightning or winding-induced swaying (the technical term is "galloping") disappear when the fault current is interrupted and the arc extinguished. A fuse-saving scheme is often used on these. Such a scheme has in normal conditions an instantaneous over-current element that trips the feeder breaker immediately upon detecting a fault. High speed tripping is used to prevent any fuses between the substation and the fault from melting. After the fault current has been interrupted, the instantaneous element is blocked, an inverse time element is enabled, and the feeder breaker reclosed. For transient faults, on reclosing, the fault will have disappeared and supply to all customers is restored. After a short delay of typically a few seconds, the scheme is reset and the instantaneous element placed back in service. For permanent faults, on reclosing, fault current will again flow, and the inverse time relay will start to operate. The inverse time relay is set to coordinate with the fuses such that if there is a fuse between the substation and the fault, the fuse will operate, interrupting customers on the section it supplies, but leaving all others energized. If the fault is located before any fuse, the inverse time relay will time out and trip the entire feeder.

Underground cable feeders rarely have transient faults; cable faults are almost always permanent. A trip-saving scheme is often used on these. Such a scheme has in normal conditions an inverse time element that trips the feeder only after sufficient time for any fuse between the substation and the fault to operate, interrupting customers on the section it supplies, but leaving all others energized. If the fault is located before any fuse, the inverse time relay will time out and trip the entire feeder. Following the feeder trip, an automatic reclose with instantaneous tripping may be attempted to restore service in cases of a fuse having melted but having been unable to interrupt fault current prior to the first trip.

Occasionally, distribution substation feeder protection includes distance supervision to prevent unnecessary tripping feeder tripping for faults on the low side of large distribution transformers near the substation. Such faults should instead be cleared at the distribution transformer location so that other customers on the feeder are not interrupted.

High Penetration of Distributed Generation and Its Impact on System Design and Operations

High penetration of distributed generation presents significant challenges to design and engineering practices as well as to the reliable operation of the electrical distribution system. The large-scale implementation of distributed energy resources (DER) on system design, performance, and reliable operation requires an integrated approach focused on interoperability, adaptability, and scalability.

Vision for Modern Utilities

Centralized Versus Distributed Generation The bulk of electric power used worldwide is produced at central power plants, most of which utilize large fossil fuel combustion, hydro or nuclear reactors. A majority of these central stations have an output between 30 MW (industrial plant) and 1,700 MW. This makes them relatively large in terms of both physical size and facility requirements as compared with DG alternatives. In contrast, DG is:

- Installed at various locations (closer to the load) throughout the power system
- Not centrally dispatched (although the development of "virtual" power plants, where many decentralized DG units operate as one single unit, may be an exception to this definition)
- Defined by power rating in a wide range from a few kW to tens of MW (in some countries MW limitation is defined by standards, e.g., US, IEEE 1547 defines DG up to 10 MW – either as a single unit or aggregate capacity)
- Connected to the distribution/medium-voltage network – which generally refers to the part of the network that has an operating voltage of 600 V up to 110 kV (depends on the utility/country)

The ownership of the DG is not a factor as to whether a power generator is classified as DG. DG can be owned or operated by electric customers, energy service companies, independent power producers (IPP), or utilities.

The main reasons why central, rather than distributed, generation still dominates current electricity production include economy of scale, fuel cost and availability, and lifetime. Increasing the size of a production unit decreases the cost per MW; however, the advantage of economy of scale is decreasing – technological advances in fuel conversion have improved the economy of small units. Fuel cost and availability is still another reason to keep building large power plants. Additionally, with a lifetime of 25–50 years, large power plants will continue to remain the prime source of electricity for many years to come [1].

The benefits of distributed generation include: higher efficiency; improved security of supply; improved demand-response capabilities; avoidance of overcapacity; better peak load management; reduction of grid losses; network infrastructure cost deferral (CAPEX deferral); power quality support; improved reliability; and environmental and aesthetic concerns (offers a wide range of alternatives to traditional power system design). DG offers extraordinary value because it provides a flexible range of combinations between cost and reliability. In addition, DG may eventually become a more desirable generation asset because it is "closer" to the customer and is more economical than central station generation and its associated transmission infrastructure [2]. The disadvantages of DG are ownership and operation, fuel delivery (machine-based DG, remote locations), cost of connection, dispatchability, and controllability (wind and solar).

Development of "Smart Grid"

In recent years, there has been rapidly growing interest in what is called "smart grid – digitized grid – grid of the future." The concept of smart grids has many definitions and interpretations dependent on the specific country, region, and industry stakeholder's drivers and desirable outcomes and benefits.

The Smart Grids European Technology Platform (which is comprised of European stakeholders, including the research community) defines "a Smart Grid [as] an electricity network that can intelligently integrate the actions of all users connected to it – generators, consumers and those that do both, in order to efficiently deliver sustainable, economic and secure electricity supply" [1].

In North America, the two dominant definitions of the smart grid come from the Department of Energy (DOE) and the Electric Power Research Institute (EPRI).

- *US DOE:* "Grid 2030 envisions a fully automated power delivery network that monitors and controls every customer and node, ensuring two-way flow of information and electricity between the power plant and the appliance, and all points in between" [2].
- *EPRI:* "The term 'Smart Grid' refers to a modernization of the electricity delivery system so it monitors, protects, and automatically optimizes the operation of its interconnected elements — from the central and distributed generator through the high-voltage network and distribution system, to industrial users and building automation systems, to energy storage installations and to end-use consumers and their thermostats, electric vehicles, appliances, and other household devices" [3].

Beyond a specific, stakeholder-driven definition, smart grids should refer to the entire power grid from generation through transmission and distribution infrastructure all the way to a wide array of electricity consumers (Fig. 36).

Effective deployment of smart grid technologies requires well-defined and quantified benefits. These benefits can be quantified in the areas of technical and business performance, environmental goals, security of electricity supply, and macro-economic growth and business sustainability development. One of the key components to effectively enable full-value realization is technology – the wide range of technical functionalities and capabilities deployed and integrated as one cohesive end-to-end solution supported by an approach focused on scalability, interoperability, and adaptability. Smart grid technologies can be broadly captured under the following areas:

- *Low Carbon:* For example, large-scale renewable generation, distributed energy resources (DER), electric vehicles (EV), and carbon capture and sequestration (CCS).
- *Grid Performance:* For example, advanced distribution and substation automation

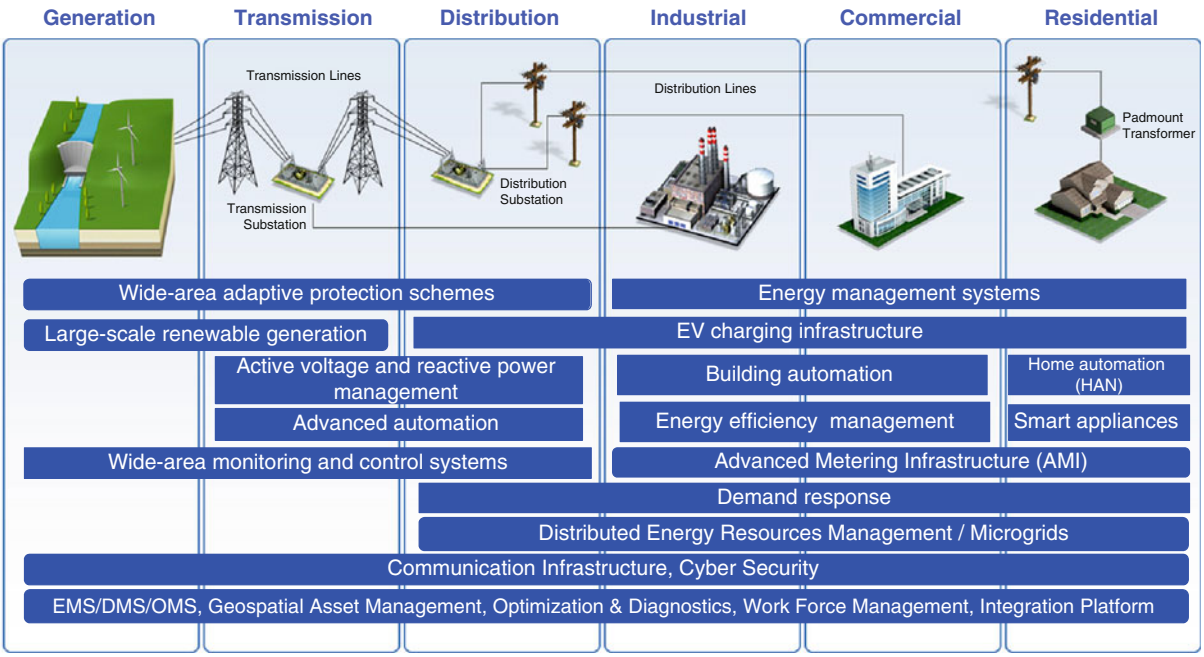

(Source: General Electric)

Distribution Systems, Substations, and Integration of Distributed Generation. Figure 36
Smart Grid Technologies span across the entire electric grid (Source: General Electric)

(self-healing); wide-area adaptive protection schemes (special protection schemes); wide-area monitoring and control systems (power management unit [PMU]-based situational awareness); asset performance optimization and conditioning (condition based monitoring); dynamic rating; advanced power electronics (e.g., flexible AC transmission system (FACTS), intelligent inverters, etc.), high temperature superconducting (HTS), and many others.

- *Grid-Enhanced Applications:* For example, distribution management systems (DMS); energy management systems (EMS); outage management systems (OMS); demand response (DR); advanced applications to enable active voltage and reactive power management (integrated voltage/VAR control (IVVC), coordinated voltage/VAR control (CVVC)); advanced analytics to support operational, non-operational and BI decision making; distributed energy resource management; microgrid and virtual power plant (VPP); work force management; geospatial asset management (geographic information system (GIS)); key performance indicator (KPI) dashboards and advanced visualization; and many others.
- *Customer:* For example, advanced metering infrastructure (AMI); home/building automation (home automation network (HAN)); energy management systems and display portals; electric vehicle (EV) charging stations; smart appliances, and many others.
- *Cyber Security and Data Privacy*
- *Communication and Integration Infrastructure*

Distributed Generation Technology Landscape

Common types of distributed generation include:

- Non-renewable generation:
  - Combustion turbine generators
  - Micro-turbines
  - Internal combustion
  - Small steam turbine units
- Renewable generation:
  - Low/high temperature fuel cells (e.g., alkaline fuel cell (AFC), molten carbonate fuel cell

(MCFC), phosphoric acid fuel cell (PAFC), polymer electrolyte membrane fuel cell (PEMFC), solid oxide fuel cell (SOFC), direct methanol fuel cell (DMFC))
- Photovoltaic (PV) (mono-, multicrystalline)
- Concentrated PV (CPV)
- Thin-film solar
- Solar thermal
- Hydro-electric (e.g., run-of-river)
- Wind/mini-wind turbines
- Tidal/wave
- Ocean thermal energy conversion (OTEC) (e.g., land-, shelf-, floating-based plants, open, close, and hybrid cycles)
- Energy storage (in the dispatch mode operations)

Each of these technologies is characterized by different electric efficiency, performance, installation footprint, and capital and operational costs.

Demand-Response Design and Operational Challenges

Demand-response (DR) interconnection engineering and engineering details depend on the specific installation size (kW vs. MW); however, the overall components of the installation should include the following:

- DG prime mover (or prime energy source) and its power converter
- Interface/step-up transformer
- Grounding (when needed – grounding type depends on utility-specific system requirements)
- Microprocessor protective relays for:
  - Three-, single-phase fault detection and DG overload (50, 51, 51V, 51N, 59N, 27N, 67)
  - Islanding and abnormal system conditions detection (81o/u, 81R, 27, 59)
  - Voltage and current unbalances detection (46, 47)
  - Undesirable reverse power detection (32)
  - Machine-based DG synchronization (25)
- Disconnect switches and/or switchgear(s)
- Metering, control, and data logging equipment
- Communication link(s) for transfer trip and dispatch control functions (when needed)

Table 3 summarizes the common DG interconnection requirements of utilities for various DG sizes (some details will vary based on utility-specific design and engineering practices).

Demand-Response Integration and "Penetration" Level

Integration of DG may have an impact on system performance. This impact can be assessed based on:

Distribution Systems, Substations, and Integration of Distributed Generation. Table 3 DG interconnection requirements of utilities

Requirements	DG less than 10 kW	DG 10–100 kW	DG 100–1,000 kW	DG > 1,000 kW or >20% feeder load
Disconnect switch	Yes	Yes	Yes	Yes
Protective relays: islanding prevention and synchronization	Yes	Yes	Yes	Yes
Other protective relays (e.g., unbalance)	Optional	Optional	Yes	Yes
Dedicated transformer	Optional	Optional	Yes	Yes
Grounding impedance (due to ground fault contribution current)	No	No	Optional	Often
Special monitoring and control requirements	No	Optional	Yes	Yes
Telecommunication and transfer trip	No	Optional	Optional	Yes

- Size and type of DG design: power converter type, unit rating, unit impedance, relay protection functions, interface transformer, grounding, etc.
- Type of DG prime mover: wind, PV, ICE (internal combustion engine), current transformer, etc.
- Interaction with other DG(s) or load(s)
- Location in the system and the characteristics of the grid, such as:
  - Network, auto-looped, radial, etc.
  - System impedance at connection point
  - Voltage control equipment types, locations, and settings
  - Grounding design
  - Protection equipment types, locations, and settings
  - Others

DR system impact is also dependent on the "penetration" level of the DG connected to the grid. There are a number of factors that should be considered when evaluating the penetration level of DG in the system. Examples of DG penetration level factors include:

- DG as a percent of feeder or local interconnection point peak load (varies with location on the feeder)
- DG as a percent of substation peak load or substation capacity
- DG source fault current contribution as a percent of the utility source fault current (at various locations)

Distributed Generation Impact on Voltage Regulation

Voltage regulation, and in particular voltage rise effect, is a key factor that limits the amount (penetration level) of DG that can be connected to the system. Figure 37 shows an example of the network with a relatively large (MW size) DG interconnected at close proximity to the utility substation.

Careful investigation of the voltage profile indicates that during heavy-load conditions, with connected DG, voltage levels may drop below acceptable or permissible by standards. The reason for this condition is that relatively large DG reduces the circuit current value seen by the load tap changer (LTC) in the substation (DG current contribution). Since the LTC sees "less" current (representing a light load) than the actual

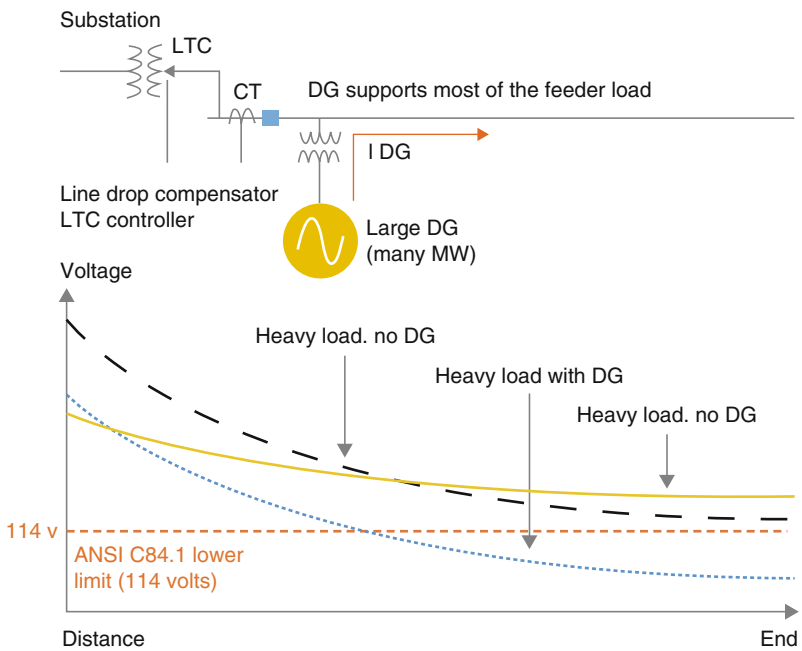

Distribution Systems, Substations, and Integration of Distributed Generation. Figure 37
DG connection close to the utility substation

value, it will lower the tap setting to avoid a "light-load, high-voltage" condition. This action makes the actual "heavy-load, low-voltage" condition worse. As a general rule, if the DG contributes less than 20% of the load current, then the DG current contribution effect will be minor and can probably be ignored in most cases.

Figures 38 and 39 show examples of the network with DG connected downstream from the bidirectional line voltage regulator (VR). During "normal" power flow conditions (Fig. 38), the VR detects the real power (P) flow condition from the source (substation) toward the end of the circuit. The VR will operate in "forward" mode (secondary control). This operation is as planned, even though the "load center" has shifted toward the voltage regulator.

However, if the real power (P) flow direction reverses toward the substation (Fig. 39), the VR will operate in the reverse mode (primary control). Since the voltage at the substation is a stronger source than the voltage at the DG (cannot be lowered by VR), the VR will increase the number of taps on the secondary side. Therefore, voltage on the secondary side increases dramatically.

Distributed Generation Impact on Power Quality

Two aspects of power quality are usually considered to be important during evaluation of DG impact on system performance: (1) voltage flicker conditions and (2) harmonic distortion of the voltage. Depending on the particular circumstance, a DG can either decrease or increase the quality of the voltage received by other users of the distribution/medium-voltage network. Power quality is an increasingly important issue and generation is generally subject to the same regulations as loads. The effect of increasing the grid fault current by adding generation often leads to improved power quality; however, it may also have a negative impact on other aspects of system performance (e.g., protection coordination). A notable exception is that a single large DG, or aggregate of small DG connected to a "weak" grid may lead to power quality problems during starting and stopping conditions or output

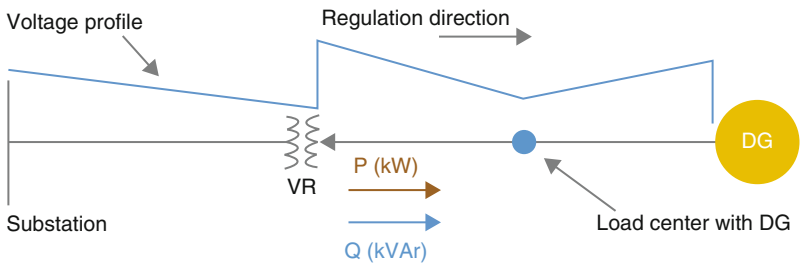

Distribution Systems, Substations, and Integration of Distributed Generation. Figure 38
VR bidirectional mode (normal flow)

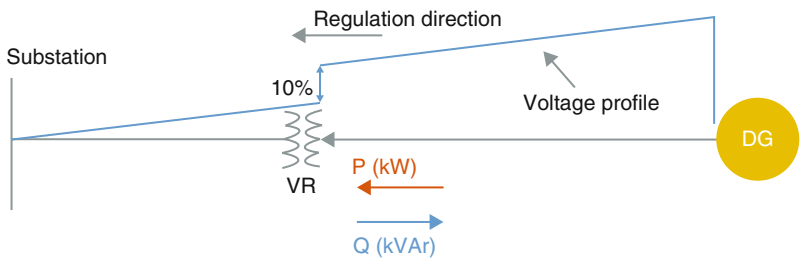

Distribution Systems, Substations, and Integration of Distributed Generation. Figure 39
VR bidirectional mode (reverse flow)

fluctuations (both normal and abnormal). For certain types of DG, such as wind turbines or PV, current fluctuations are a routine part of operation due to varying wind or sunlight conditions (Fig. 40).

Harmonics may cause interference with operation of some equipment, including overheating or de-rating of transformers, cables, and motors, leading to shorter life. In addition, they may interfere with some communication systems located in close proximity of the grid. In extreme cases they can cause resonant overvoltages, "blown" fuses, failed equipment, etc. DG technologies must comply with pre-specified by standards harmonic levels (Table 4).

In order to mitigate harmonic impact in the system, the following can be implemented:

- Use an interface transformer with a delta winding or ungrounded winding to minimize injection of triplen harmonics.
- Use a grounding reactor in neutral to minimize triplen harmonic injection.

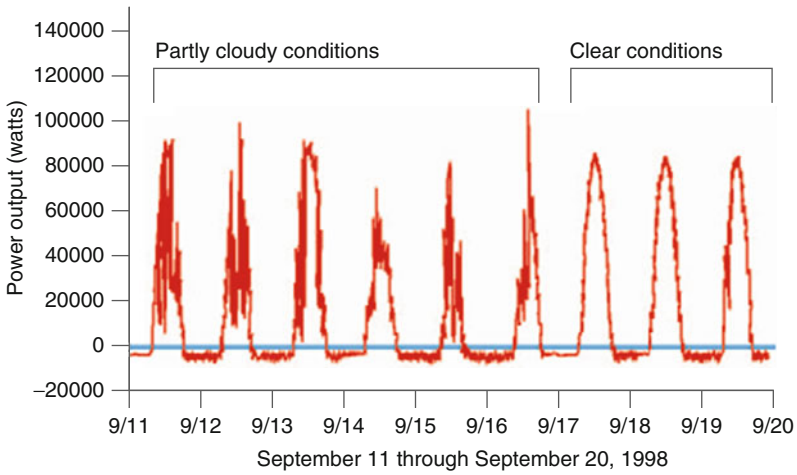

Distribution Systems, Substations, and Integration of Distributed Generation. Figure 40
Power output fluctuation for 100 kW PV plant

Distribution Systems, Substations, and Integration of Distributed Generation. Table 4 IEEE 519–1992, current distortion limits for general distribution systems

Maximum harmonic current distortion in % of I_L						
Individual harmonic order (odd harmonics)						
I_{SC}/I_L	<11	$11 \leq h < 17$	$17 \leq h < 23$	$23 \leq h < 35$	$35 \leq h$	TDD
<20[a]	4.0	2.0	1.5	0.6	0.3	5.0
$20 < 50$	7.0	3.5	2.5	1.0	0.5	8.0
$50 < 100$	10.0	4.5	4.0	1.5	0.7	12.0
$100 < 1{,}000$	12.0	5.5	5.0	2.0	1.0	15.0
$>1{,}000$	15.0	7.0	6.0	2.5	1.4	20.0

Even harmonics are limited to 25% of the odd harmonic limits. TDD refers to total demand distortion and is based on the average maximum demand current at the fundamental frequency, taken at the PCC

I_{SC} Maximum short circuit current at the PCC, I_L Maximum demand load current (fundamental) at the PCC, h Harmonic number

[a]All power generation equipment is limited to these values of current distortion regardless of $I_{SC}I_L$

- Specify rotating generator with 2/3 winding pitch design.
- Apply filters or use phase canceling transformers.
- For inverters: Specify pulse width modulation (PWM) inverters with high switching frequency. Avoid line-commutated inverters or low switching frequency PWM; otherwise, more filters may be needed.
- Place DG at locations with high ratios of utility short-circuit current to DG rating.

Distributed Generation Impact on Ferroresonance

Classic ferroresonance conditions can happen with or without interconnected DG (e.g., resonance between transformer magnetization reactance and underground cable capacitance on an open phase). However, by adding DG to the system, the case for overvoltage and resonance can increase for conditions such as: DG connected rated power is higher than the rated power of the connected load, presence of large capacitor banks (30–400% of unit rating), during DG formation on a non-grounded island.

DG Impact on System Protection

Some DG will contribute current to a circuit current on the feeder. The current contribution will raise fault levels and in some cases may change fault current flow direction. The impact of DG fault current contributions on system protection coordination must be considered. The amount of current contribution, its duration, and whether or not there are protection coordination issues depend on:

- Size and location of DG on the feeder
- Type of DG (inverter, synchronous machine, induction machine) and its impedance
- DG protection equipment settings (how fast it trips)
- Impedance, protection, and configuration of feeder
- Type of DG grounding and interface transformer

Machine-based DG (IEC, CT, some micro-turbines, and wind turbines) injects fault current levels of four to ten times their rated current with time contribution between 1/3 cycle and several cycles depending on the machine. Inverters contribute about one to two times their rated current to faults and can trip-off very quickly – many in less than one cycle under ideal conditions. Generally, if fault current levels are changed less than 5% by the DG, then it is unlikely that fault current contribution will have an impact on the existing system or equipment operation. Utilities must also consider interrupting capability of the equipment (e.g., circuit breakers, reclosers, and fuses must have sufficient capacity to interrupt the combined DG and utility source fault levels). Examples of DG fault contribution on system operation and possible protection mis-coordination are shown in Figs. 41 and 42.

Future Directions

Today's distribution systems are becoming more and more complicated. New methods of producing and storing electrical energy such as PV, fuel cells, and battery storage systems and new methods of consuming electric energy such as smart appliances and plug-in electric vehicles are being connected to the distribution grid. The rate of adoption of these devices will be driven faster as the economic and environmental benefits improve. In response, the automation systems used to monitor, control, and protect them will need to become more sophisticated.

Many utilities are facing these challenges today in increasingly larger areas of their distribution grid. Many developers are building new green communities that contain enough generation and storage to carry the community's load during an outage. Commonly referred to as microgrid operation, these areas of the distribution grid can be momentarily operated while isolated from the rest of main distribution grid. These microgrids can maintain service to un-faulted sections of the grid during some distribution outages. When these microgrids are connected to the distribution system, utilities are also investigating techniques to maximize the value of the distributed energy resources (DER) during times of economic peak or during capacity peaks. The electric energy in these devices can contribute watts, watt-hours, VARs, and voltage or frequency support during times of distribution system need.

The increasing complexity of the distribution grid will force a need to further integrate the various systems on that grid. The various systems described here will become increasingly integrated. These include the FDIR and Volt/VAR systems. As the FDIR system reconfigures

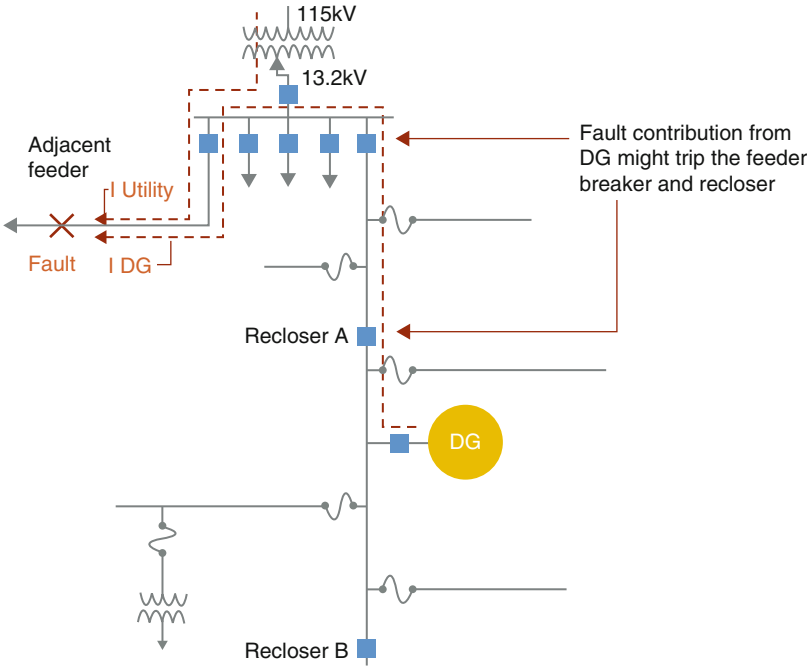

Distribution Systems, Substations, and Integration of Distributed Generation. Figure 41
Undesirable protection trip (back-feeding)

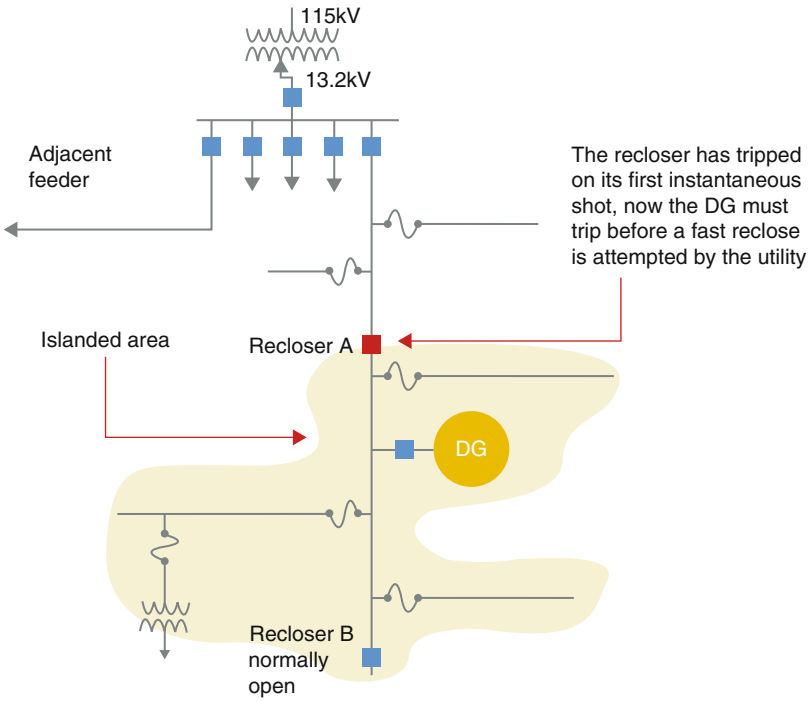

Distribution Systems, Substations, and Integration of Distributed Generation. Figure 42
Unintentional DG Islanding

the distribution system, the Volt/VAR system can then optimize the newly configured feeders. Information such as voltage and VARs from the consumers can be used to improve the amount of the Volt/VAR system can control the grid without violating limits at the consumer. Microgrid operation will further push the integration of all of the distribution systems to maintain a safe, reliable, and efficient distribution grid.

This will have the effect of reducing the costs and increasing the overall benefits of these technologies, while maintaining an improved quality and reliability of the electric energy provided to the customers on the distribution system. This stronger economic justification will drive the rate of advance of these new technologies causing a significant impact on the issues and elements of the design of the distribution system and associated automation systems.

There are vast developments happening in the power industry changing whole transmission and distribution world including substations. Smart grid technologies make their way into transmission and distribution world to improve power supply, make it more efficient and reliable, and decrease greenhouse emissions. This became possible due to rapid developments in power electronics and communications. Major areas of developments are as follows:

- Smart metering implies getting metering data from all possible measurement points including end of the feeder over communications in order to maintain proper distribution voltage level for all consumers. This includes deploying voltage regulators, capacitor banks, switches, and other devices in the distribution network.
- Advances in communications imply real-time, live communication between the consumer, the network, and the generation station, so the utility can balance load demand in both directions. Advanced communications are also needed for manual or automatic reconfiguration of the network in case some components of the network are experiencing failures or deficiencies.
- Advanced protective relays and other control devices with enhanced communications and algorithms capabilities to automatically detect, isolate, and reconfigure the grid to maintain uninterruptable power supply.
- Renewable energy sources will continue fast deployment in the distribution network. Wind power, solar power, hydro power units will increase their capacity and output; energy storage systems will be deployed to help system to meet peak demand and offload system generators. Microgrids will provide consumers with reliable and high-quality energy when connection with a transmission n system is lost or in case of isolated community.

A growing number of electric utilities worldwide are seeking ways to provide excellent energy services while becoming more customer focused, competitive, efficient, innovative, and environmentally responsible. Distributed generation is becoming an important element of the electric utility's smart grid portfolio in the twenty-first century. Present barriers to widespread implementation are being reduced as technologies mature and financial incentives (including government and investor supported funding) materialize. However, there are still technical challenges that need to be addressed and effectively overcome by utilities. Distributed generation should become part of a utility's day-to-day planning, design, and operational processes and practices, with special consideration given to:

- Transmission and distribution substation designs that are able to handle significant penetration of distributed generation
- Equipment rating margins for fault-level growth (due to added distributed generation)
- Protective relays and settings that can provide reliable and secure operation of the system with interconnected distributed generation (can handle multiple sources, reverse flow, variable fault levels, etc.)
- Feeder voltage regulation and voltage-drop design approaches that factor possible significant penetration of distributed generation
- Service restoration practices that reduce the chance of interference of distributed generation in the process and even take advantage of distributed generation to enhance reliability where possible
- Grounding practices and means to control distributed generation-induced ground-fault overvoltages.

Bibliography

Primary Literature

1. Smart Grids, European Union, http://www.smartgrids.eu/
2. United States Department of Energy, Office of Electric Transmission and Distribution (2003) Grid 2030: a national vision for electricity's second 100 years
3. EPRI (2009) Report to NIST on the smart grid's interoperability standards roadmap

Books and Reviews

Institute of Electrical and Electronics Engineers (1994) IEEE recommended practice for electric power distribution for industrial plants, IEEE Std 141-1993. Institute of Electrical and Electronics Engineers, New York. ISBN 978-1559373333

Killian C, OG&E, Flynn B (2009) Justifying distribution automation at OG&E. In: 2009 DistribuTECH conference, San Diego, 3–5 Feb 2009

Lathrop S, Flynn B, PacifiCorp (2006) Distribution automation pilot at PacifiCorp. In: Western Energy Institute, 2006 operations conference, Costa Mesa, 5–7 Apr 2006

Lemke JW, Duke Energy, Flynn B (2009) Distributed generation, storage and the smart grid. In: Autovation 2009, The utilimetrics smart metering conference and exposition, Denver Colorado, 13–16 Sep 2009

Stewart R, Flynn B, Pepco Holdings Incorporated (2007) Modeling DA improvements to reliability performance metrics. In: 2007 WPDAC, Spokane, Washington, DC, 3–5 Apr 2007

Weaver T, AEP, Flynn B (2011) Achieving energy efficiency through distribution system improvements: integrated volt/VAR control (IVVC). In: 2011 DistribuTECH conference, San Diego, 3–5 Feb 2011

Westinghouse Electric Corporation (1959) Electric utility engineering reference book, Distribution systems, vol 3. Westinghouse Electric Corporation, Pittsburgh

Dosimetry

John W. Poston, Sr.
Department of Nuclear Engineering, Texas A & M University, College Station, TX, USA

Article Outline

Glossary
Definition
Introduction
Thermoluminescence Dosimetry
Estimates of Absorbed Doses to Organs of the Body
Thermoluminescence Dosimetry for Neutron Radiations
Optically Stimulated Luminescence
Electronic Dosimeters
Summary
Future Directions
Bibliography

Glossary

Absorbed dose The amount of energy deposited by ionizing radiation per unit mass of the material. Usually expressed in the special radiologic unit rad or in the SI unit the gray (Gy). One Gy equals 1 J/kg or 100 rad.

Dosimeter Any device worn or carried by an individual to establish total exposure, absorbed dose, or equivalent (or the rates) in the area or to the individual worker while occupying the area.

Equivalent dose (Formally the dose equivalent) The product of the absorbed dose and the radiation-weighting factor (formerly the quality factor) for the type of radiation for which the absorbed dose is measured or calculated. The equivalent dose is used to express the effects of radiation-absorbed dose from many types of ionizing radiation on a common scale. The special radiologic unit is the rem or in the SI unit the sievert (Sv). One sievert is equal to 1 J/kg or 100 rem.

Exposure A quantity defined as the charge produced in air by photons interacting in a volume of air of known mass. An old quantity that is generally no longer used. Also, a general term used to indicate any situation in which an individual is being irradiated.

Ionization The process of removing one or more electrons from an atom or a molecule. The positively charged atom and the negatively charged electron are called an *ion pair*.

Isotope One of two or more atoms with the same number of protons but a different number of neutrons in their nuclei. A radioisotope is an isotope of a chemical element that is unstable and transforms by emission of nuclear particles and electromagnetic radiation to reach a more stable state. This term is often misused because unless the materials

are the same element this term should not be used (see radionuclide below).

Nuclide A general term to indicate an atomic nucleus characterized by its atomic number (number of protons), number of neutrons, atomic mass, and energy state.

Radiation Used in this section to mean ionizing radiation. That is, particles or electromagnetic radiation emitted from the nucleus with sufficient energy to cause ionization of atoms and molecules composing the material with which the radiation is interacting.

Radionuclide A nuclide that is radioactive and, upon decaying, emits ionizing radiation.

Definition

Dosimetry is best defined as "the theory and application of principles and techniques associated with the measurement of ionizing radiation" [1].

Introduction

The term "dosimetry" can be best explained by assuming it was derived from combining two words: "dose" and "measurement." The word dose is shorthand for several quantities associated with the profession of health physics (i.e., radiation protection and safety). The terms include the "absorbed dose," which is a measure of the energy deposited per unit mass of material, and the "equivalent dose," which includes consideration of the biological effects of different radiations, when the same absorbed dose is delivered to matter. The term "equivalent dose" is now used instead of the older term dose equivalent to signify changes in the ICRP recommended radiation and tissue weighting factors. There are many other "dose terms" used in health physics but these will not be included here because the fundamental quantity associated with dosimetry is the absorbed dose. Of course, the term measurement implies the use of some sort of detector that is sensitive to the ionizing radiation being measured. These "detectors" can take many forms from photographic film, first used more than 100 years ago, to sophisticated solid-state detectors being introduced today.

Scientists have been detecting radiation for more than a century using a wide variety of detectors. Initially, the detectors were either photographic film or simple ionization chambers filled with air. Crude scintillation systems led to the invention of detectors such as the Geiger–Mueller counter and more sophisticated proportional counters and detectors designed for specific applications and/or to detect a specific radiation. A discussion of these detectors would fill a textbook [2–5] and see also entry C. Radiation Detection Devices (in this encyclopedia). For this reason, this discussion of dosimetry will focus on two of the more modern dosimeters used to monitor the absorbed dose to occupationally exposed workers in nuclear facilities across the United States.

As indicated above, *Dosimetry* is best defined as "the theory and application of principles and techniques associated with measurement of ionizing radiation" [1]. In reality, two basic areas encompass the term "dosimetry." These are called external dosimetry and internal dosimetry. Again, these terms are shorthand descriptions of the more complex exposure conditions being considered. External dosimetry simply means the measurement of radiation that exists outside the human body. Basically, this type of dosimetry uses radiation detection devices and instrumentation to establish the characteristics of the radiation field. These measurements provide information in many forms, for example, the energy or energy spectrum of the radiation, the radiation intensity, the types of radiation present, and other useful information. In many cases, the radiation detectors used for these measurements are called "dosimeters"; an indication that the sole purpose is to measure the radiation-absorbed dose and which leads to an estimate of the equivalent dose. It is important to remember that, because the radiation source and the dosimeters are both outside the body, the measurement does not provide a direct measurement of the absorbed dose to the organs of the body. Methods used to provide estimates of the absorbed doses to organs and tissues of the body will be discussed later.

When a radionuclide or radionuclides are taken into the body, through inhalation, ingestion, injection, or assimilation through the intact skin, there is a completely different set of challenges facing the dosimetrist. Internal dosimetry is defined as "a process of measurement and calculation that results in an estimate of the absorbed dose to organs and tissues of the

body from an intake of radioactive material" [1]. Internal dosimetry is primarily confined to the use of mathematical models and calculational techniques based on an internationally agreed upon set of standard assumptions. The dose estimate relies on mathematical models that describe the uptake, distribution, and retention of the radioactive material in the body. However, the calculations may be based on a set of measurements, such as the concentration of airborne radioactivity in a work area, the activity of radioactive material deposited in the body or specific organs in the body, or measurement of the concentration of radioactivity in excreta, such as urine or feces. Even with these measurements as initial input, internal dosimetry must rely on models of a reference human and calculational techniques. These aspects will not be discussed here.

This section will focus on a discussion of external dosimetry methods, which are primarily used to monitor radiation exposures of occupationally exposed workers conducting licensed activities in the US. Radiation dosimeters that are no longer widely used, such as film badges and pocket ionization chambers will not be discussed.

Thermoluminescence Dosimetry

In 1950, Daniels suggested that the thermoluminescence (TL) phenomenon could be used as a radiation dosimeter [3]. This suggestion came late in the development of radiation dosimeters even though it was known that Henri Becquerel, as well as his father, had mentioned this phenomenon in his scientific papers. In addition, the relation between X-ray exposure and thermoluminescence was observed as early as 1904. Nevertheless, after many struggles and failures in the research of Cameron and his colleagues, thermoluminescence and thermoluminescence dosimetry (TLD) became a reality and flourished in the late 1960s and 1970s [3]. For a very long time, TLD has been the most popular method of personnel monitoring.

In these dosimeters, the absorbed dose is determined by observing the emitted light from an inorganic crystal after exposure to radiation. The light is released from the crystal as it is heated under controlled conditions. The heat energy originally was provided by electrical heating but subsequent developments in TLD led to the use of high-intensity light as an alternate method. Regardless of the method of heating, the amount of light emitted is directly proportional to the radiation energy deposited in the TL material. This light is normally measured with a photomultiplier tube sensitive to the wavelength of the emitted light. It must be remembered that the TLDs are not "absolute dosimeters" and, therefore, require proper calibration in the radiation fields to which the dosimeters will be exposed.

Detailed explanations of the TL phenomenon have been offered by a number of scientists but a simple bandgap model can be used to explain the basic mechanism. The usual procedure is to refer to the energy-level diagram in an insulating crystal. In a pure crystal, radiation impinging on the crystal would free electrons and these electrons would pass from the valence band to the conduction band. These electrons would not remain in the conduction band for a long period and would return to the valence band releasing the energy acquired in the form of light. In a pure crystal, this light would be absorbed and would not escape the crystal. In TLDs, dopants (impurities) are added to the crystal and these impurities reside in the forbidden or bandgap between the valence and conduction bands. When these crystals are exposed to radiation, the loss of electrons from the valence band creates positively charged atoms ("holes"). The electrons and holes may migrate through the crystal until they recombine or are "trapped" by the impurity atoms (dopants) residing in the bandgap. Thus, the energy absorbed by the crystal is stored until it is released, in the form of light, through heating the crystal (thus, thermoluminescence). This light, which is now characteristic of the impurity sites, can escape the crystal and can be measured with an external detector (i.e., a photomultiplier tube).

It is important to realize that these trapping sites may exist at many different levels in the bandgap and it is not correct to assume that all electrons (or holes) are trapped at exactly the same energy level. Thus, the light intensity may vary as a function of temperature and the plot of the light intensity as a function of temperature (called a "glow curve") may exhibit a number of peaks and valleys depending on the number of trapping levels in the crystal. Either the total light emitted or the height of a particular peak may be used to determine the absorbed dose (upon proper calibration). It is also important that the heating cycle be very reproducible to avoid causing fluctuations in the peak heights.

There are a large number of inorganic materials that have been studied for use as TLDs. Table 1 presents a summary of the characteristics of some of the most popular materials (but there are many other possible TLD materials). In dosimetry, it is common to use materials that are "tissue equivalent" in terms of the interactions of photons or other radiations with the dosimeters. Thus, the closer the effective atomic number of the material is to that of tissue (~7.6), the more tissue equivalent is the material. For historical reasons, LiF is the standard to which all other TLD materials are compared. The standard LiF is the natural form of lithium with the normal concentrations of the isotopes of Li-6 (7.4%) and Li-7 (92.6%). Also in this table are listed the temperatures of the "main peak." This designation is the peak in the TLD glow curve that is used to determine the absorbed dose. One big disadvantage of TLDs is that the dosimeter can only be read (evaluated) once. Heating the crystal essentially releases all the electrons or holes that are trapped and an opportunity to confirm the reading is not possible.

Table 2 compares other characteristics of the TLD materials. These include the "light output" of the material when exposed to ^{60}Co radiation compared to the light output for the standard, that is, LiF. The data for $Li_2B_4O_7$:Mn are somewhat misleading because the measurements quoted in this table were made with the standard photomultiplier tube used for all other TLD materials. However, because the wavelength of light from the $Li_2B_4O_7$:Mn is different, the output can be improved significantly by replacing the normal photomultiplier with one with a photocathode sensitive to the correct wavelength of light. The energy response is the ratio of the light output at energy of 30 keV to that from irradiation with ^{60}Co. Except for $Li_2B_4O_7$:Mn, most materials overrespond to low-energy photon radiation.

As can be seen in Table 2, the usual TLD materials are very sensitive to radiation with lower limits of detection in the range of tenths of microgray. Upper limits range from only 10 Gy to more than 10^4 Gy. The

Dosimetry. Table 1 Summary of characteristics of thermoluminescence dosimetry (TLD) materials

TLD material	Effective atomic number (Z_{eff})	Temperature of main peak
$CaSO_4$:Mn	15.3	110°C
$CaSO_4$:Dy	15.5	220°C
CaF_2:Mn	16.3	260°C
CaF_2:Dy	16.3	180°C
LiF:Mg,Ti[a]	8.2	195°C
$Li_2B_4O_7$:Mn	7.4	200°C
Al_2O_3:C	10.2	185°C

[a]LiF:Mg,Ti is the standard material to which all other TLD materials are compared

Dosimetry. Table 2 Summary of dosimetric characteristics of TLD materials

TLD material	Efficiency to Co-60	Energy response	Useful dose range	Fading
$CaSO_4$:Mn	70	~10	0.2 μGy–10^2 Gy	50% in 24 h
$CaSO_4$:Dy	20	~12.5	0.2 μGy–10^3 Gy	2% in 1 month 8% in 6 months
CaF_2:Mn	10	~13	10 μGy–3 × 10^3 Gy	10% in 16 h 15% in 2 weeks
CaF_2:Dy	30	~12.5	0.1 μGy–10^4 Gy	10% in 24 h 16% in 2 weeks
LiF:Mg,Ti	1.0	1.25	10 μGy–3 × 10^3 Gy	5% in 1 year
$Li_2B_4O_7$:Mn	0.15	0.9	0.5 μGy–10^4 + Gy	<5% in 3 months
Al_2O_3:C	70	2.9	0.5 μGy–10 Gy	<3% in 1 year

term "fading" is an indication of the ability of the TLD material to retain the stored energy and thus the stored information necessary to assign the absorbed dose from the wearing of the dosimeter. As is shown, LiF:Mg,Ti, $Li_2B_4O_7$:Mn, and Al_2O_3:C have good energy storage capability, which has led to a focus on these three materials.

Estimates of Absorbed Doses to Organs of the Body

In the United States, federal regulations require the reporting of three quantities for all occupationally exposed workers who are anticipated to receive doses in excess of 10% of the federal limits. These quantities are the "deep-dose equivalent," the "eye-dose equivalent," and the "shallow-dose equivalent." The deep-dose equivalent is defined as the dose at 1-cm depth in the body, which produces an overestimate of the absorbed doses because most organs and tissues of the body are located deeper than 1 cm (or 1,000 mg/cm^2). The eye-dose equivalent considers the dose to the lens of the eye, which is assumed to be at a depth of 300 mg/cm^2. Finally, the shallow-dose equivalent (or more properly the skin-dose equivalent) is assumed to be at a depth of 7 mg/cm^2.

Now the question arises, "How does one measure these absorbed doses, and the subsequent equivalent doses, with radiation dosimeters located outside the body of the worker?" The approach taken has been used for many years and is not new. It has been applied since the Manhattan Project era and is an accepted method to provide these dose estimates. The technique involves using multiple detector elements, that is, typically four TLDs, and covering these TLDs with different thicknesses of materials (called filters) to represent these depths. So, the TLD designated to measure the deep-dose equivalent is covered with a material having a density thickness of 1,000 mg/cm^2. The eye-dose equivalent is determined by covering the TLD with material with a density thickness of 300 mg/cm^2. Usually, there are two different materials of this density thickness in the dosimeter. Finally, there is a thin filter included to allow extrapolation to the depth of 7 mg/cm^2. It is very difficult to provide a direct measurement at such an extremely shallow depth.

Thermoluminescence Dosimetry for Neutron Radiations

TLDs have their primary application in dosimetry for X-ray and gamma-ray fields. In addition, the TLDs have limited sensitivity to beta radiation. Because certain materials in the TLDs interact with neutrons, TLDs can be used to measure both thermal and fast neutron dose – with proper calibrations. Table 3 lists the pertinent information regarding three types of LiF TLDs as these are applied to neutron dosimetry. As can be seen in this table, the natural LiF TLD has the normal concentrations on Li-6 and Li-7. This material is designated as TLD-100. The other two materials are designated TLD-600 and TLD-700. TLD-600 contains a high concentration of the isotope Li-6 with less that 5% Li-7. TLD-700 contains essentially all the isotope Li-7 with a very small amount of Li-6. Notice also the differences in the thermal neutron cross sections (probability to absorb neutrons) for these two isotopes. These differences play a role in the dosimetry of both thermal and fast neutrons.

Thermal neutron dosimetry is based on the "difference technique" used to separate the photon and thermal neutron dose from each other. This technique is similar in some ways to the standard method using bare and cadmium-covered gold foils to measure the thermal neutron fluence in a nuclear reactor core. Basically, the LiF TLD-600 is sensitive to photon radiation as well as to thermal neutron radiation. The LiF TLD-700 has the same photon sensitivity but essentially no sensitivity to thermal neutrons. Thus, when used in a mixed photon and thermal neutron field the TLD-600 will provide the absorbed dose for both the photons and the thermal neutrons. The TLD-700 will provide only the absorbed dose from the photon radiation and the

Dosimetry. Table 3 Characteristics of lithium fluoride TLDs for neutron dosimetry

TLD type	Li-6 percentage	Li-7 percentage	Thermal neutron cross section
Natural (TLD-100)	7.4%	92.6%	N/A
TLD-600	95.62%	4.38%	950 barns
TLD-700	0.007%	99.993%	0.033 barns

difference between the doses indicated by the two dosimeters is the thermal neutron dose.

Fast neutron dosimetry uses a similar technique but to obtain the fast neutron dose the "albedo technique" is used. The albedo technique relies upon the dosimeter being held closely to the body and the fast neutron dose is measured as the fast neutrons enter the body, are moderated there by tissue, are subsequently reflected from the body and hit the dosimeter. There are many designs of albedo fast neutron dosimeters but the concept is the same as that outlined above. The fast neutron dose is obtained by using the difference technique as before.

Note that using TLDs to measure either thermal neutron or fast neutron dose require very careful calibration of the dosimeters in radiation fields approximating those in which the exposures are anticipated. In addition, in very high photon radiation fields with a low percentage of thermal or fast neutrons, these dosimeters may provide data that is highly suspect. This is often the consequence of subtracting two very large numbers (large photon dose) to obtain an estimate of the very low thermal or fast neutron dose. Other methods of neutron dosimetry, for example, track-etch detectors, may be preferred in these situations.

Optically Stimulated Luminescence

Currently, the dosimetry method of choice for dosimetry appears to be optically stimulated luminescence (OSL). Even though film and TLD are still used to some extent, many facilities are switching over to this newer technology. OSL may be used, not only for personnel monitoring, but also for environmental monitoring and medical dosimetry. Basically, OSL is very similar to TLD in terms of the basic physics associated with the energy deposition, storage, and release. The major difference is that, instead of using heat, laser light is used to release ("detrap") the electrons. The laser is pulsed at a rate of 4,000 times per second and is directed to only a small area on the material. This provides an opportunity for multiple readings on the same dosimeter, if necessary, as the laser can be focused on another region of the crystal. In a similar fashion to the development of TLDs in the latter part of the twentieth century, many materials have been studied for possible use as OSL dosimeters. These materials include halides, sulfates, sulfides, and oxides [6].

However, the material of choice is an Al_2O_3:C crystalline detector. Single crystals of Al_2O_3:C are ground into a powder and mixed with a polyester base. This mixture is deposited on a polyester film about 0.03 cm thick, which can be fabricated in a thin strip for incorporation into a dosimeter. This material has a good response to photon radiation as well as a response to beta radiation. Copper (0.18 g/cm^2) and tin (0.39 g/cm^2) filters, as well as an open area, are used in the dosimeter (as described above) to provide the dosimetry quantities of interest. Commercially available dosimeters have a dose measurement range for photons of 1 mrem to 1,000 rem (10 μSv to 10 Sv) over an energy range from 5 keV to more than 40 MeV. For beta radiation, the dose measurement range is from 10 mrem to 1,000 rem (100 μSv to 10 Sv) over an energy range of 150 keV to 10 MeV (average energy). The commercially available OSL dosimeters may be used for up to 1 year. If the packaging is not compromised, the dosimeter is unaffected by heat, moisture, and pressure [7].

Electronic Dosimeters

Currently, in many situations, such as in a nuclear power plant, it is common to wear two types of dosimeters. One of these dosimeters is usually a TLD or an OSL-type. This dosimeter is usually designated as the "dosimeter of record." That is, these dosimeters are worn for long periods of time (i.e., 1 month, 3 months, or perhaps 1 year) and provide a measure of the total dose received by the exposed worker over the wearing period. It is these doses that are reported annually to the US Nuclear Regulatory Commission, as required by the federal regulations. The second dosimeter is a modern, electronic dosimeter that may contain as many as three small detector elements (usually solid-state detectors such as silicon diodes). Electronic dosimeters are used to monitor the work and may be worn for short periods of time. The primary function of these dosimeters is work and dose control. The dosimeters feature adjustable alarm points that may be set by a computer, before use, based on the anticipated total dose received or maximum dose rate encountered. Workers are trained to recognize the alarms and understand the proper response to these alarms.

There are many different electronic dosimeters but most have similar characteristics. A typical dosimeter would use small silicon diode detectors, which would be sensitive to both photons (50 keV to 6 MeV) and beta radiation (>60 keV up to more than 2 MeV). Doses from 0.1 mrem (1 μSv) to 10 Sv can be measured with dose rates ranging from 0.01 mrem/h (0.1 μSv/h) to 1,000 rem/h (10 Sv/h). Most dosimeters feature both audible and visible alarms. Typically, these dosimeters are lightweight, from 50 g up to perhaps 200 g. A unique feature of some of these dosimeters, and a good radiation protection practice, is the use of permanent stations throughout the plant that interrogate the dosimeters as the worker passes by the station and transmits this information to a central station. Other types of dosimeters contain small transmitters that transmit the accumulated dose (or dose rates) to central locations, which are monitored by the radiation safety staff. As technology moves forward, it is difficult to predict what the future holds in terms of the next generation of dosimeters.

Summary

The measurement of radiation energy deposited in material, that is, the measurement of the absorbed dose, is the primary goal of the practice of dosimetry. Over the last 100 years or more, dosimetry has taken many forms as science and technology have made significant progress. Many of the techniques have been relegated to the history books as other more advanced techniques have been introduced. This short discussion of dosimetry was intended to present the basic concepts and to provide two examples of modern dosimeters used to monitor personnel that are occupationally exposed to ionizing radiation, as well as to introduce the use of electronic dosimeters, which are used widely in nuclear utilities.

Future Directions

Approaches to dosimetry have changed rapidly with developments in electronics and computers. The last decade or so has seen the design and manufacture of dosimeters that are small but incorporate computer capabilities. These dosimeters allow the setting of dose and dose rate alarms, remote interrogation of the dosimeters to monitor worker exposure, and many other features. It appears these trends will continue as the demand for "smarter" dosimeters, with many more capabilities, for use in nuclear facilities as well as in emergency response continues to increase.

Bibliography

1. Poston JW Sr (1987) Dosimetry. In: Encyclopedia of physical science and technology, vol 6. Academic, New York
2. Knoll GF (2000) Radiation detection and measurements, 3rd edn. Wiley, New York
3. Eichholz GG, Poston JW (1979) Principles of nuclear radiation detection. Ann Arbor Science Publishers, Ann Arbor
4. Tsoulfanidis N (1995) Measurement & detection of radiation, 2nd edn. Taylor & Francis, Washington, DC
5. Kase KR, Bjarngard BE, Attix FH (eds) (1985) The dosimetry of ionizing radiation, vol I–III. Academic, New York
6. Boetter-Jensen L, McKeever SWS, Wintle AG (2000) Optically stimulated luminescence dosimetry. Elsevier, Maryland Heights
7. R. S. Landauer, Inc. (2010) http://www.osldosimetry.com/luxel/. Accessed 9 May 2010

Dredging Practices and Environmental Considerations

Craig Vogt[1], Gregory Hartman[2]
[1]Craig Vogt Inc, Hacks Neck, VA, USA
[2]Hartman Associates Inc, Waterway Engineering & Sediment Remediation, Port Orchard, WA, USA

Article Outline

Glossary
Definition of Subject
Introduction
Dredging and Dredged Material Management
Dredging
Transportation of Dredged Material
Dredged Material Disposal and Placement Alternatives
Control of Upstream Sources of Sediments and Contaminants
Future Directions: Sustainable Dredging and Dredged Material Management
Bibliography

Glossary

Beneficial use Placement or use of dredged material as resource materials in productive ways, which provide environmental, economic, or social benefits.

Confined disposal facility (CDF) An engineered structure for containment of dredged material consisting of dikes or other structures that enclose a disposal area above any adjacent water surface, isolating the dredged material from adjacent waters during placement. Other terms used for CDFs that appear in the literature include "confined disposal area," "confined disposal site," and "dredged material containment area."

Contaminant A chemical or biological substance in a form that can be incorporated into, onto, or be ingested by or harm aquatic organisms, consumers of aquatic organisms, or users of the aquatic environment.

Contaminated sediment or contaminated dredged material Contaminated sediments or contaminated dredged materials are defined as those that may cause an unacceptable adverse effect on human health or the environment.

Dredged material Material excavated from fresh, estuarine, or ocean waters. The term "dredged material" refers to material which has been dredged from a water body and disposed in a disposal site. The term "sediment" refers to material on the bed of a water body prior to the dredging process.

Dredging Underwater excavation is called dredging. "Dredging" is the term given to removal by digging, gathering, or pulling out materials from the bed to deepen waterways and to create harbors, channels, and berths. Dredging is also conducted for construction purposes, for mining, and for environmental cleanup and enhancement.

Habitat The specific area or environment in which a particular type of plant or animal lives. An organism's habitat provides all of the basic requirements for the maintenance of life. Typical coastal habitats include beaches, marshes, rocky shores, bottom sediments, mudflats, and the water itself.

Open-water disposal Placement of dredged material in rivers, lakes, estuaries, or oceans via pipeline or surface release from hopper dredges or barges, without confinement.

Sediment Material, such as sand, silt, or clay, suspended in or settled on the bottom of a water body. Sediment input to a body of water comes from natural sources, such as erosion of soils and weathering of rock, or as the result of anthropogenic activities, such as forest or agricultural practices, or construction activities. The term "dredged material" refers to material which has been dredged from a water body, while the term "sediment" refers to material in a water body prior to the dredging process.

Suspended solids Organic or inorganic particles that are suspended in water. The term includes sand, silt, and clay particles as well as other solids, such as biological material, suspended in the water column.

Toxicity Level of mortality or other end point demonstrated by a group of organisms that have been affected by the properties of a substance, such as contaminated water, sediment, or dredged material.

Toxic pollutant Pollutants, or combinations of pollutants, including disease-causing agents, that after discharge and upon exposure, ingestion, inhalation, or assimilation into any organism, either directly from the environment or indirectly by ingestion through food chains, will cause death, disease, behavioral abnormalities, cancer, genetic mutations, physiological malfunctions, or physical deformations in such organisms or their offspring.

Turbidity An optical measure of the amount of material suspended in the water. Increasing the turbidity of the water decreases the amount of light that penetrates the water column. Very high levels of turbidity can be harmful to aquatic life.

Definition of Subject

Underwater excavation is called dredging. Dredging is the term given to removal by digging, gathering, or pulling out materials from the bed to deepen waterways and to create harbors, channels, and berths. Dredging is also conducted for construction purposes, for mining, and for environmental cleanup and enhancement. The complete dredging activity includes sediment excavation and removal from the bed, and transport from the dredging site to a disposal area or placement site, which is located in either an open-water, nearshore, or upland location.

Operations that cause potential environmental impacts associated with the dredging process include (1) the sediment removal process from submerged excavation at the point of dredging and (2) the transport and placement for disposal of the dredged material. Environmental concerns relate to the location of the sediment removal by dredging and the disposal or placement site. General environmental considerations include:

- Turbidity in the water
- Acute and chronic toxicity due to chemicals in the dredged material
- Impacts to marine animals
- Loss of habitat
- Air pollutant emissions from the dredge
- Other general construction issues, such as underwater and surface equipment noise

Introduction

Dredges of various designs have been used for many years to create and maintain navigable waterways to move people, goods, and materials. It is theorized that thousands of years ago, blocks of stone that make up the pyramids in Egypt were barged from a distant quarry through a dredged canal. At that time, the canals were likely dredged using a barge with people using long-handled dipper shovels to raise solids out of a waterway and then place those solids on a haul barge deck for disposal elsewhere. Productivity gains likely came about when animal power was used to increase the digging power of early dredges. The late 1800s saw the development of electric and steam power units (Fig. 1), which enabled the construction of huge mechanical dredges with bucket ladders, backhoe dredges, and pipeline dredges with centrifugal pumps.

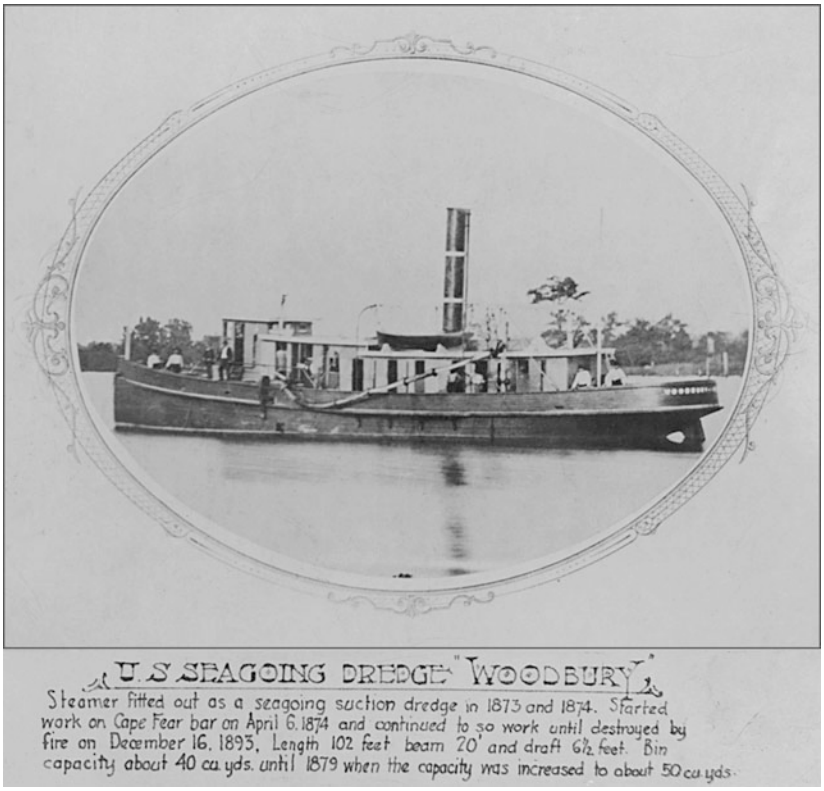

Dredging Practices and Environmental Considerations. Figure 1
US seagoing dredge "woodbury" – 1873 (Photo courtesy of Corps of Engineers)

Hydraulic technology made great advancements in the 1960s, with the result that hydraulic winches and hydraulic rotary cutter drives became a welcome replacement facilitating the removal of finer-grain sediment (compared to clunky and inefficient mechanical drives) [1].

Today, the dredge type can be hydraulic or mechanical and can be used for a multitude of purposes and projects. The primary purposes are navigation, environmental enhancement, and mining/construction [2].

Navigation Dredging

Most coastal and river ports, harbors, and navigation channels are not naturally deep enough or wide enough to support safe passage of vessels. Navigation channels need to be dredged to create waterway channels with adequate channel area, depth, and access to port and harbor facilities. Nearly all the major ports in the world have at some time required dredging to deepen and widen the access channels, to provide turning basins, and to achieve appropriate water depths to and from waterside facilities.

Virtually, all of the navigation channels created in rivers and harbors have and continue to require maintenance dredging, i.e., the removal of sediments which naturally accumulate on the bottom of the dredged channel. Navigation channel dredging can be categorized as two types. (1) New work dredging is the initial dredging conducted to excavate a channel with navigable depths greater than those that naturally exist. (2) Maintenance dredging is the dredging after new work, which removes accumulated sediments and ensures that the channel continues to provide adequate dimensions for vessels engaged in domestic and international commerce as well as for other types of vessels, such as recreational boating and commercial fishing.

Environmental Enhancement Dredging

In the last 3 decades, dredging has been successfully used to remove contaminated sediments from waterways, with the intention of improving water quality and restoring the health of aquatic ecosystems. Cleanup dredging for removal of contaminants is used in waterways, lakes, ports, and harbors, usually in highly industrialized or urbanized areas that are suffering from past toxic waste and wastewater disposal practices. After removal from the bed, the contaminated sediments are transported and disposed under strict environmental controls (e.g., lined upland confined disposal facilities). In some cases, the contaminated sediments may be treated, and some or all of the sediments used for beneficial objectives. Under proper conditions, a viable alternative to removal is in situ isolation, i.e., the placement of a cap (i.e., a cover of clean material) over the contaminated sediments in their original location.

Dredging is also used for environmental enhancement projects, such as beach nourishment (e.g., replacing lost sand to widen beaches) and providing sediments to enhance marshes and wetlands.

Reclamation, Mining, and Construction Dredging

Dredging is an integral tool in many types of water-related construction projects, such as emplacement of pipelines or immersed tunnels, underwater foundations, and maintaining storage capacity in water supply and recreational reservoirs. In addition, dredging is important in mining activities, with a primary use to provide sand and gravel for construction and reclamation projects. Dredged aggregates have a wide range of uses, including:

- Land reclamation: Pressures arising from population growth have created a need to raise the elevation of low-lying areas for port and infrastructure development and/or to construct new land areas. Such pressures are likely to continue, but loss of marine habitat is an opposing issue when creating new land.
- Construction materials: An increasing quantity of aggregate mined from marine and freshwater borrow sites is used in concrete and fill construction.

Dredging and Dredged Material Management

Dredging and dredged material management consists of the following three elements:

1. Excavation: The dislodgement and removal of sediments (clay, silt, sand, gravel, and rock) from the bed of the water body by a dredge, either mechanically, hydraulically, or by combination of the two dredging methods.
2. Transport: The transport of excavated material from the point of dredging to the final disposal

site. This can be accomplished by haul barges separate from the dredge equipment, or by a dredge equipped with hoppers, or by pipeline from the dredge to the disposal or placement site.

3. Disposal or placement: The final disposal or placement of dredged material. Whether dredged material is disposed or placed (and reused for another purpose, such as creation of a wetland) is determined by a range of factors, including the objectives of the dredging project. The disposal site factors to be considered include sediment type to be dredged (e.g., grain size), location of the dredging project versus the disposal site or beneficial use site, future disposal site utilization, physical and chemical characteristics of the sediment (e.g., is it contaminated?), and available funding.

Increasingly considered a resource, dredged material has a wide number of beneficial use applications that must be considered in dredged material disposal management. This includes consideration for beach nourishment, shoreline fill, and habitat creation or restoration. This concept as a resource is also an important environmental consideration for remedial and cleanup dredging. Dredged material from remedial dredging is usually placed into well-controlled upland confined facilities. Dredged material from clean sediment dredging is often used to cap, cover, and isolate contaminated sediment in the waterway.

Dredging

While specialized dredging equipment varies widely in many sizes and types, dredging is actually accomplished basically by only two dredge types. They are mechanical dredges and hydraulic dredges. The type of dredge is derived from the method of sediment capture and removal from the bed.

Selection of dredging equipment and the methods used to perform the dredging depends on the following factors [3]:

- Physical characteristics of material to be dredged
- Quantities of material to be dredged
- Depth of material to be dredged
- Method of disposal or placement
- Distance to disposal or placement site
- Physical environment of the dredging area(s)
- Physical environment of the disposal area(s)
- Level of contamination of the material to be dredged
- Dredge production capability
- Type of dredges available
- Time, environmental, and economic limits of the project

Mechanical Dredges

Mechanical dredges remove bottom sediment through the direct application of mechanical force to dislodge and excavate the material at almost in situ densities. The mechanical dredges (Fig. 2) are well suited to removing hard-packed material or debris and to working in confined areas, such as in environmental cleanup dredging. Cohesive sediments that are mechanically dredged usually remain intact, with large pieces retaining their in situ density and structure through the dredging and placement process. Sediments excavated with a mechanical dredge are generally placed into a haul barge or scow for transportation from the dredging site to the disposal or placement site.

Mechanical dredges use some form of bucket to excavate and lift the dredged material from the bottom, then load it on to a haul barge or scow. When the haul barge is loaded, a tug or other attendant vessel will take the barge to the disposal or placement site. Mechanical dredges are classified by how the bucket is connected to the dredge. The three standard classifications include:

- Wire rope connected – barge-mounted crane (clamshell or cable bucket)
- Structurally connected – articulated fixed-arm dredge (e.g., backhoe, excavator)
- Chain and structurally connected – bucket ladder

A mechanical dredge is often labeled a clamshell dredge. The clamshell is actually a type of cable-connected bucket used on a mechanical dredge and is the most common type of the mechanical dredges. Mechanical dredges that have the bucket with cable connection to the barge-mounted crane do use a number of different bucket designs for differing sediment characteristics, such as mud, gravel, rock, or boulders.

An articulated fixed-arm mechanical dredge can be a back-acting (backhoe) excavating machine, an advance cut (dipper, excavator) excavating machine, or a bucket (grab) excavating machine.

A bucket ladder dredge is the oldest and the most common type of mechanical dredge. It is primarily used for mining applications. A bucket ladder dredge consists of a large number of buckets linked together in an endless chain which is carried on a ladder that is raised and lowered by hoisting wires. The buckets dig into the face of the cut, and the sediment is carried up the ladder and dumped onto a conveyor belt.

Dredging for environmental cleanup requires much greater precision than navigation dredging and can be accomplished using articulated fixed-arm mechanical dredges, which are similar to conventional upland excavators placed on a barge. The rigid arm, as compared to the cable-connected bucket, provides greater positioning control in placing the bucket on the bottom. Bucket dredges that are designed for a level cut and equipped to be enclosed after the cut are also effective in environmental dredging. These buckets (Fig. 3) minimize the leakage of water and contaminants during the excavation and

Dredging Practices and Environmental Considerations. Figure 2
Mechanical backhoe dredge, New York (Courtesy Great Lakes Dredge & Dock Company)

Dredging Practices and Environmental Considerations. Figure 3
Mechanical dredges: environmental closed buckets (Courtesy Cable Arm Company)

placement of the contaminated material on the barge for transport.

The dragline bucket dredge is similar to the clamshell dredge. They are effective in excavation of gravels, sand, and compact silts. The dragline bucket is not an enclosed bucket and can cause significant turbidity in the water column. Dragline buckets can be operated as a dredge from shore or mounted on a barge. The bucket does not load vertically. Instead, it is lowered to the bottom and then loaded by dragging toward the crane. A dipper dredge is a floating face shovel that digs forward into the face of the excavation and is mounted on a spud barge.

Hydraulic Dredges

Hydraulic dredges are identified by two primary types. They are the pipeline cutterhead dredge and the trailing suction hopper dredge. The hydraulic dredge works by dislodging bed sediment and hydraulic removal of the sediment from the bed of the waterway by suction pipe.

The hydraulic pipeline dredge is generally comprised of the following equipment:

- Cutterhead. The pipeline dredge has an active cutterhead (Fig. 4) that rotates and dislodges the sediment from the bed. This allows the suction, created at the cutterhead by the suction pipe and pump, to be captured and pulled up the suction pipe.
- Suction pipe. The pipe that connects the cutterhead on the bed with the centrifugal pump in the dredge hull.
- Ladder. The ladder raises and lowers the suction pipe and the cutterhead.
- Barge hull. The pipeline dredge is a specialty barge that supports the machinery, pump cable winches, and other equipment in the hull with a lever room, anchor booms, and "walking" spuds on the hull.
- Discharge pipe. The discharge pipe transports the dredged material slurry from the pump to the disposal site.
- Dredge pump(s). The dredge pumps are large centrifugal pumps located on the dredge hull at the waterline and/or on the ladder near the suction mouth.
- Spuds/anchor wires. The spuds and anchor wires are used to anchor the dredge, swing the dredge across the cut, and move the dredge forward.

The pipeline dredge (Fig. 5) is not self-powered. It moves through the cut using the "walking" spud and then the working spud for dredging, thereby allowing

Dredging Practices and Environmental Considerations. Figure 4
Typical hydraulic cutterhead dredge (Courtesy Ellicott Dredges Company)

Dredging Practices and Environmental Considerations. Figure 5
Cutterhead pipeline dredge (CSD), Texas (Courtesy: Great Lakes Dredge & Dock)

the dredge to move forward as it swings the cutterhead from left to right and return.

The pipeline dredge size is classified by the size of the discharge pipe inner diameter. These dredges use hydraulic centrifugal pumps to provide the lifting force to capture and transport the dredged material in a liquid and solid slurry. Pipeline dredges usually work well in loose, "unconsolidated" silts, sands, gravels, and soft clays. In dense consolidated sediments, the hydraulic pipeline dredge depends on an active cutterhead and/or waterjets that can break up the consolidated material at the mouth of the suction pipe.

The centrifugal pump on the hydraulic dredge operates at or near the water surface elevation to pull water into the suction mouth at the cutterhead. The combination of the vacuum and atmospheric weight acts to move the bed material up through the suction pipe to the pump, and then the pump discharges the slurry into the discharge pipeline and directly to the disposal site. Because pipeline dredges pump directly to the disposal site, they operate continuously and can be very cost efficient. A booster pump is used for long distances to the disposal site (Fig. 6).

Cutterhead pipeline dredges work efficiently in large areas and in water depths up to 60–70 ft. The dredge production rate is the most efficient and creates minimum excess turbidity at the cutterhead when the loose sediment cut depth is equal or near the diameter of the dredge cutterhead. The dredged material slurry typically contains 90% water and 10% solids volume, and the water must be contained in the disposal site until the solids settle out. The dewatering is accomplished typically by discharging surface water in the disposal site back into the waterway. If it is contaminated sediment, discharge controls are required to minimize impacts to the receiving waters.

The discharge pipe can be a floating pipe on the surface or a submerged discharge pipe. Typically, the discharge line is a floating line, and they are not well suited for work in rough seas, where lines can be broken apart, or in high traffic areas, where the discharge pipeline can be an obstruction to navigation. The pipeline dredge is not an efficient dredge plant to work in an open estuary, entrance channel, or other open-water areas where significant wave conditions may occur. Rough waters with wave heights of significance will cause damage to the cutterhead, spuds, and the dredge hull, as well as the floating pipeline.

Hopper dredges are ships designed for dredging (Figs. 7 and 8). The trailing suction hopper dredge is

Dredging Practices and Environmental Considerations. Figure 6
Pipeline booster pump (Courtesy: Great Lakes Dredge & Dock)

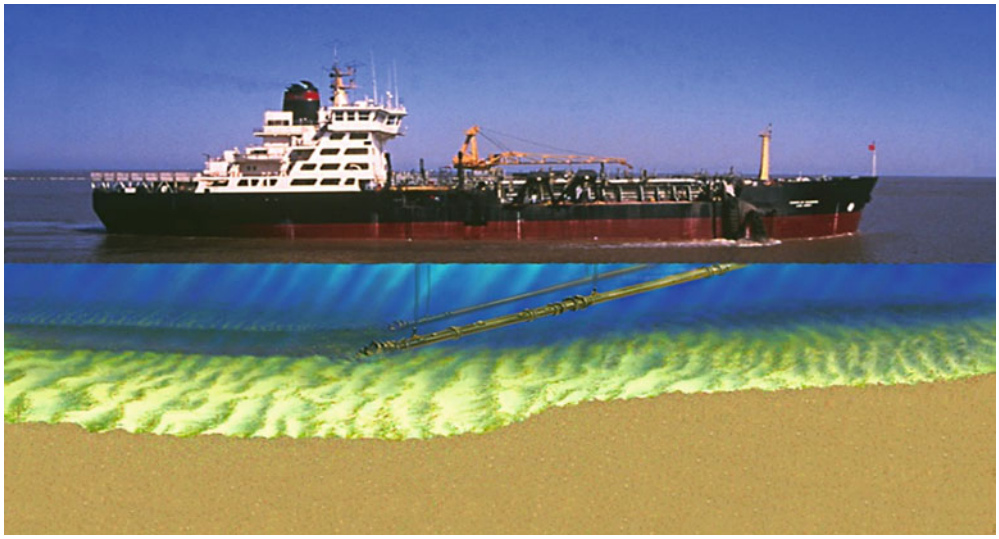

Dredging Practices and Environmental Considerations. Figure 7
Typical hopper dredge (Photo courtesy Corps of Engineers)

a self-propelled seagoing ship equipped with a suction pipe, which trails over the side of the vessel or through a well in the hull. The sediment and water slurry is transported through the pumps just as the pipeline dredge, but when the sediment and water slurry passes through the pump to the discharge pipeline, it is discharged immediately into the hoppers of the dredge. When the hoppers are full, the sediment

Dredging Practices and Environmental Considerations. Figure 8
Hopper dredge, Liberty Island (Photo courtesy of Great Lakes Dredge & Dock Company)

and water slurry is transported by the ship to the disposal site.

A hopper dredge can dispose of the dredged sediment in two manners. The split-hull hopper dredge design and the standard hopper dredge with bottom dump capability will discharge the dredged sediment to a submerged and acceptable disposal site. The alternative to bottom dumping is to pump out of the hoppers to an upland disposal site or to a shallow water area that the vessel draft prevents access.

The hydraulic hopper dredge is generally comprised of the following equipment:

- Drag arm. The drag arm on the hopper dredge serves the same purpose as the ladder on the pipeline dredge.
- Drag head. The drag head on the hopper dredge provides a similar purpose as the cutterhead on the pipeline dredge. Several designs of drag heads are used for different sediment types. The drag head design includes:
  - Erosional drag heads (unconsolidated fine sediment, sand, and gravel).
  - Mechanical drag head (silts, mud, light clay).
  - Combination drag head with waterjets (hard-packed sand to gravel).
- Gimbal joints. The gimbal joints allow the drag arm to articulate while the vessel moves, thereby keeping the drag head on the bed during mild to medium sea conditions.
- Swell compensator. The swell compensator acts much like a shock absorber and allows the hopper dredge to keep the drag heads on the bed and still work in relatively high-wave conditions (8–10 ft).

The slurry discharge is into the hoppers of the ship. Hopper dredge size, in terms of dredging, is defined by the capacity of the hoppers. The slurry of water and sediment is discharged into the top of the hopper. The sediments settle out in the hopper, while excess water is separated and discharged over the weir structure. It can be advantageous to overflow hopper dredges to increase the amount of sediment in the hopper; however, this is not always acceptable due to water quality concerns near the dredging site.

Hopper dredges are well suited to dredging heavy sands. They can maintain operations in relatively rough seas, and because they are mobile, they can be used in high-traffic areas. They are often used at ocean entrances where wave conditions prevent use of pipeline dredges and limit mechanical dredging capability. They cannot be used efficiently in confined or shallow

areas. Hopper dredges can move quickly to disposal sites under their own power. However, because the actual removal of sediment from the bed stops during the transit to and from the disposal area, the operation loses efficiency that can become critical when the haul distance to disposal is far.

There is a special hopper dredge class called side-casters and pipeline dredge called dustpan dredges. Both of these dredges are unique within their family of dredges. They are specialty dredges used for unusual waterway conditions. They work best when dredging loosely compacted, coarse-grained, clean sediment with disposal in areas close to the dredging activity. They are not widely used.

Environmental Cleanup Dredges

Dredging of contaminated sediments is potentially very harmful to the local environment during dredging and disposal. Contaminants can be remobilized and/or released into the water column where they can detrimentally affect aquatic life and pose a risk to human health. Technological advances have fostered modification of existing dredge equipment, and creation of new dredging equipment to address the environmental issues. Contaminated sediment dredging focuses on minimizing suspension and release of problem sediments in the water column while increasing the precision of dredging to reduce overdredging. Examples of contaminated sediment dredges include the following:

- Encapsulated bucket lines for bucket chain dredges.
- Closed buckets for backhoes.
- Closed clamshells for grab dredges.
- Auger dredges, disk cutter, scoop dredges, and sweep dredges (all modified cutter dredges) [4].

Transportation of Dredged Material

Transportation methods generally used to move clean and contaminated dredged materials are included in the three basic dredge types: pipelines, barges or scows, and hopper dredges.

- Pipeline transport is the method most commonly associated with cutterhead, dustpan, auger head, and other hydraulic dredges. Dredged material may be directly transported by hydraulic dredges through pipelines for distances of up to several miles, depending on a number of conditions. Longer pipeline pumping distances are feasible with the addition of booster pumps, but the cost of transport greatly increases proportionally with each booster pump added to the discharge line.
- Barges and scows, used in conjunction with mechanical dredges, have been one of the most widely applied methods of transporting large quantities of dredged material over long distances.
- Hopper dredges are capable of transporting the material for long distances in a self-contained hopper. Hopper dredges normally discharge the material from the bottom of the vessel hull by opening the hopper doors; however, most hopper dredges are equipped to pump out the material from the hopper and deliver the sediment much like a hydraulic pipeline dredge.

Dredged Material Disposal and Placement Alternatives

Evaluation and design of a proposed dredging project involves comprehensive assessment of alternatives for disposal or placement of the dredged material. Identification of the specific disposal site or beneficial use site involves a number of different considerations, including environmental, technical, and economic factors.

Three major disposal/placement alternatives are available:

- Open-water disposal in deep waters or along banks of a river outside the navigation channel
- Confined disposal in open water (confined aquatic disposal (CAD)) and on land (confined disposal facility (CDF))
- Placement for environmental and beneficial use

In the case of very contaminated sediments and cleanup/remedial dredging, treatment of the dredged material after temporary storage and before final disposal may be a necessary alternative.

Open-Water Disposal

Open-water disposal means that dredged material is placed at designated sites in oceans, estuaries, rivers, and lakes such that it is not isolated from the adjacent water. Clean dredged materials are the only acceptable dredged materials for disposal at open-water disposal

sites. The determination that dredged material is "clean" is based upon a series of chemical and biological tests, the results of which must meet national environmental regulations. The disposal of contaminated material can be considered for open-water disposal but only with appropriate control measures, such as capping the contaminated sediments by the use of clean capping materials.

The objective of capped in-water disposal is to isolate contaminated materials from the environment by covering the contaminated materials with clean materials, such as fine to coarse sand. The contaminated material is placed on a level bottom, in engineered deep constructed pits, or in bottom depressions. The cap of clean sediment that is placed on top must be designed to withstand erosion over time from bottom currents, waves, vessel movement, and prop wash, and burrowing bottom creatures (Fig. 9). Caps should be monitored over time to ensure their integrity [5].

Confined Disposal Facilities

Confined disposal is placement of dredged material within engineered diked nearshore or upland confined disposal facilities (CDFs) via pipeline or barge delivery of sediments. CDFs may be constructed as upland sites, nearshore sites with one or more sides in water (sometimes called intertidal sites), as island containment areas, or as subaqueous contained capped cells (Figs. 10–12).

The two objectives inherent in design and operation of CDFs are to provide for adequate storage capacity to meet dredged volume requirements and to maximize efficiency in retaining the solids. For facilities

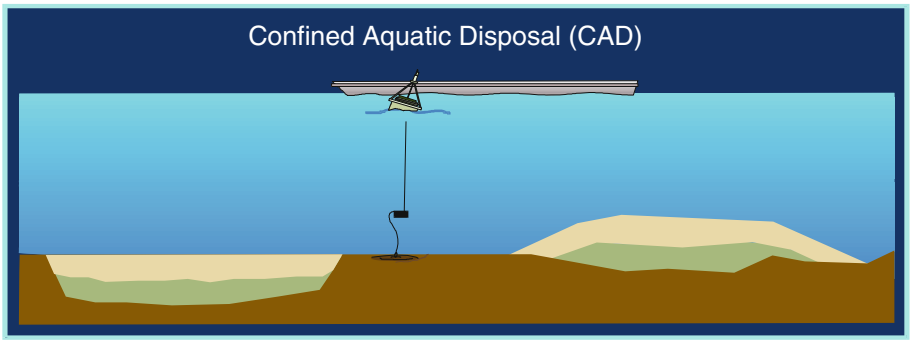

Dredging Practices and Environmental Considerations. Figure 9
Confined aquatic disposal (CAD) (Courtesy of Corps of Engineers)

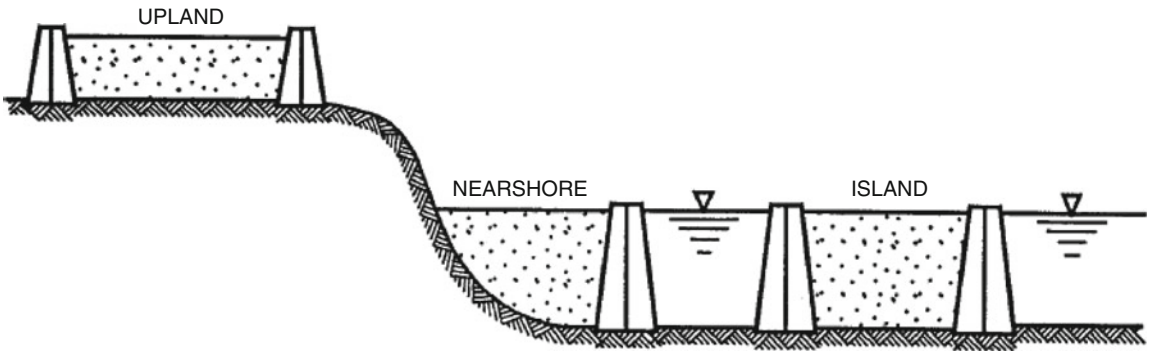

Dredging Practices and Environmental Considerations. Figure 10
Types of confined disposal facilities (Courtesy of Corps of Engineers)

Dredging Practices and Environmental Considerations. Figure 11
Nearshore CDF Huelva Estuary, Spain (Courtesy Spain government)

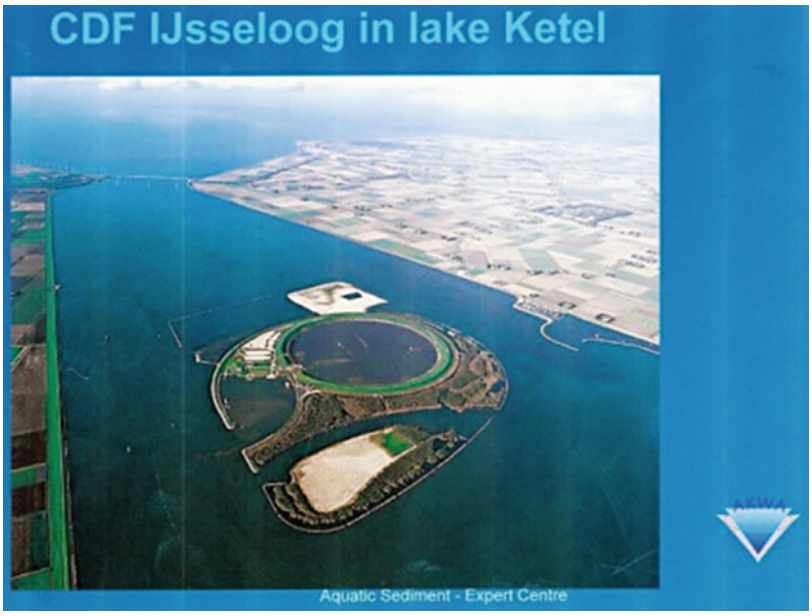

Dredging Practices and Environmental Considerations. Figure 12
Island CDF at IJsseloog, the Netherlands (Courtesy Dutch government)

receiving contaminated material, an additional objective is to provide the efficient isolation of contaminants from the surrounding area. To achieve these objectives, depending on the degree of intended isolation, CDFs may be equipped with a complex system of control measures, such as surface covers and bottom liners, treatment of effluent, surface runoff and leachate monitoring, and management controls.

Hydraulic dredging adds several volumes of water for each volume of sediment removed. This excess water is normally discharged as effluent from the CDF during the filling operation. The amount of water added depends on the design of the dredge, physical characteristics of the sediment, and operational factors, such as the pumping distance. When the dredged material is initially removed from the bed and deposited in the CDF, it can and will occupy several times its original volume. The settling process is a function of time, with sandy and gravelly sediment dewatering quickly and silts and clays dewatering very slowly. Silts and clays will eventually consolidate to the loose in situ volume or less if desiccation occurs. Adequate volume must be provided during the dredging operation to contain the total volume of sediment to be dredged, accounting for any volume changes during placement.

Beneficial Use of Dredged Material

Dredged material is increasingly regarded as a resource rather than as a waste. More than 90–95% of sediments from navigation dredging comprise sediments acceptable for open-water disposal; these are also considered acceptable for a wide range of environmentally and economically beneficial uses. The first step in examining dredged material management options is to consider possible beneficial uses of dredged material. Recent decades have seen the increasing use of dredged materials for habitat creation, habitat restoration, beach nourishment, and coastal protection (Fig. 13).

Beneficial use is defined as "*Utilizing dredged sediments as resource materials in productive ways, which provide environmental, economic, or social benefits*" [6]. Broad categories of beneficial uses of dredged material, based on the functional use of the dredged material or site, include:

- Habitat development and restoration
- Parks and recreation
- Coastal protection
  - Beach nourishment
  - Riverbank and lakeshore protection
- Nearshore placement/littoral zone sediment management
- Construction and agricultural
  - Construction and industrial/commercial development (roads, dikes, levees, parking lots)
  - Land reclamation/remediation (brownfield restoration, strip mine reclamation)
  - Agriculture, forestry, horticulture, and aquaculture

Dredging Practices and Environmental Considerations. Figure 13
Deer Island Marsh Creation: Mississippi, USA (Courtesy of Corps of Engineers)

Dredging Practices and Environmental Considerations. Figure 14
Beneficial use site: Evia Island Bird Nesting, Galveston Bay, Texas (Courtesy Port of Houston Authority)

Operational feasibility for these projects includes the availability of suitable material in the required amount at a particular time and within the project costs. These are crucial aspects of the most beneficial uses projects (Fig. 14).

Treatment of Dredged Material

In certain cases of environmental cleanup by dredging, treatment of the dredged material may be necessary prior to confined disposal or reuse. A variety of treatment technologies are available to reduce the quantity or to reduce the contamination of the dredged material.

Treatment methods range from separation techniques, in which contaminated sediments are separated from relatively clean sand, to incineration. Some techniques are well developed to date, but others are still in the early stages of development. The products of the treatment methods have a wide array of potential beneficial uses (e.g., construction grade cement, lightweight aggregate, bricks, and manufactured soil). The problem is that treatment is usually very expensive, thereby limiting project scale. As a result, the treatment of small volumes of contaminated material is more likely than that of large volumes.

Environmental Considerations

The potential environmental effects of navigation dredging and environmental cleanup dredging are the result of the actual dredging activity in the water and a result of the disposal of the dredged material (Fig. 15).

During dredging, effects may arise due to the excavation of sediments causing resuspension in the water column, loss of material during transfer to the barge, overflow from the dredge while loading and loss of material from the hopper dredge and/or pipelines during transport to disposal. Potential effects during disposal arise depend upon the physical and chemical characteristics of the dredged material and the selected disposal site (i.e., open-water, nearshore, or upland).

During all dredging operations, the removal of material from the seabed also removes the surface-based (benthic) animals living on and in the sediments (benthic animals). With the exception of deep-burrowing animals or mobile surface animals that may survive a dredging event through avoidance, dredging can initially result in the complete removal of surface-dwelling biota from the dredging site. Where the channel or berth has been subjected to regular maintenance dredging over many years, it is very unlikely that well-developed benthic communities will occur in or around

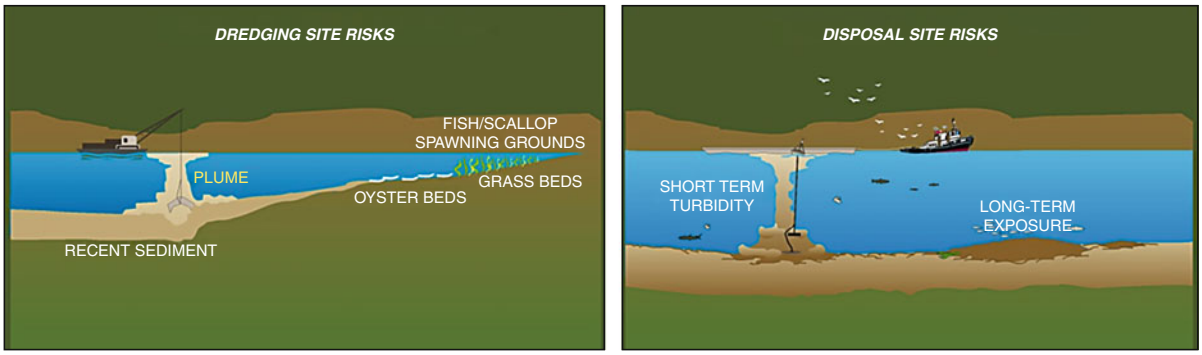

Dredging Practices and Environmental Considerations. Figure 15
Environmental risks: At the dredging and disposal sites (Courtesy Corps of Engineers)

the dredged area. The recovery of disturbed habitats following dredging ultimately depends upon the nature of the new sediment at the dredge site, sources and types of recolonizing benthos, river width and bank line, and the extent of the disturbance [7].

The environmental issues associated with dredging and dredged material management include:

- Physical and ecological impacts due to turbidity and sedimentation.
- Ecological and human health impacts: acute and chronic toxicity due to chemical contamination, e.g., PCBs, PAHs, dioxin, metals, such as lead, cadmium, and mercury.
- Loss of habitat – due to dredging or placement of dredged material.
- Impacts to endangered species (e.g., turtles) due to dredging.
- Impacts to fish migration and spawning due to turbidity and exposure to toxic chemicals from dredging and disposal.
- Impacts of noise from dredging operations upon aquatic living resources.
- Others: emissions of air pollutants, quality-of-life issues (e.g., noise, night lights).

When dredging and disposing of noncontaminated fine materials (e.g., silts, clays) in estuaries and coastal waters, the main environmental effects are associated with suspended sediments and increases in turbidity. All methods of dredging release suspended sediments into the water column during the excavation itself and during the overflow of dredging water from hoppers and barges. In many cases, the locally increased suspended sediments and turbidity associated with dredging and disposal are obvious from the turbidity "plumes," which may be seen trailing behind dredges and disposal sites [8].

- Increases in suspended sediments and turbidity levels from dredging and disposal operations may under certain conditions have adverse effects on marine animals and plants by reducing light penetration into the water column and by physical disturbance.
- Increases in suspended sediments can impact filter-feeding organisms, such as shellfish, through clogging and damaging feeding and breathing equipment. Similarly, young fish can be damaged if suspended sediments become trapped in their gills, and increased fatalities of young fish have been observed in heavily turbid waters. Adult fish are likely to move away from or avoid areas of short-term high suspended solids, such as dredging sites, unless food supplies are increased as a result of increases in organic material.
- In important spawning or nursery areas for fish and other marine animals, dredging can result in smothering eggs and larvae. Shellfish are particularly susceptible during the spring when spatfall occurs.
- Increases in turbidity result in a decrease in the depth that light is able to penetrate the water

column which may affect submerged seaweeds and plants, such as eelgrass *Zostera* species, by temporarily reducing productivity and growth rates.

The degree of resuspension of sediments and turbidity from dredging and disposal depends on four main variables:

- The sediments being dredged (size, density, and quality of the material).
- Method of dredging (and disposal).
- Hydrodynamic regime in the dredging and disposal area (current direction and speed, mixing rate, tidal state).
- The existing water quality and characteristics (background suspended sediment and turbidity levels).

The resuspension of sediments during dredging and disposal may also result in an increase in the levels of organic matter and nutrients available to marine organisms. In certain cases, nutrient enrichment can lead to the formation of algal blooms (eutrophication). These blooms can reduce the surrounding water quality by causing the removal of oxygen as the blooms break down, or occasionally, by the release of toxins, which may disturb marine wildlife.

Sediments dispersed during dredging and disposal may resettle over the seabed and the animals and plants that live on and within it. This blanketing can cause smothering of benthic animals and plants, may cause mortality, stress, and reduced rates of growth or reproduction, and, in the worst cases, the effects may be fatal. Generally, sediments settle within the vicinity of the dredged area, where they are likely to have little effect on the recently disturbed communities, particularly in areas where dredging is a well-established activity. However, in some cases, sediments are distributed more widely within the estuary or coastal area and may settle over adjacent subtidal or intertidal habitats possibly some distance from the dredged area.

When dredged materials are placed in open-water disposal sites, they will have a blanketing and smothering effect on benthic organisms in the immediate disposal site. The continual disposal of maintenance dredging at disposal sites may prevent the development of stable benthic communities and the partial or complete loss of benthic production and habitat. Recolonization is expected when disposal operations have been completed, depending on the characteristics of the dredged material and the changes to the hydrodynamic conditions at the disposal site.

A variety of harmful substances, including heavy metals, tributyl tin (TBT), polychlorinated biphenyls (PCBs), and pesticides, are in the sediments in certain ports, harbors, and waterways. These contaminants are often of historic origin and from local or upstream sources. The highest levels of contaminants generally occur in industrialized estuaries. Dredging and disposal can release these contaminants into the water column, making them available to be taken up by animals and plants, with the potential to cause adverse acute and chronic toxicity. The risk of this occurring depends upon the type and degree of sediment contamination. If contaminants are released into the water column or are in the sediments at the open-water disposal site, they may bioaccumulate in marine animals and plants and transfer up the food chain to fish and sea mammals, with associated risks to human health.

Dredging can cause direct threats to endangered species, such as sea turtles and their nearshore marine habitats. Hopper dredges have been directly responsible for the incidental capture and the death of hundreds, if not thousands, of sea turtles in the United States. Development of specially designed hopper dredge drag heads and institution of best management practices in areas of turtle populations has helped alleviate the majority of the takings of turtles during dredging operations [9].

Nearshore or upland CDFs are the most commonly used disposal technique for contaminated dredged material. Pathways for potential exposure to animals/plants and humans are similar for these two types of disposal sites. Comparison to open-water sites is not necessarily appropriate since open-water sites should be receiving clean dredged material, while nearshore and upland sites isolate contaminated dredged material from the surrounding environment. Potential pathways include the discharge into receiving waters (e.g., estuary or river) of the excess water from the dredged material, contamination of ground water, and exposure of birds and animals to the dredged material in the CDF. Depending upon the level of contamination, controls can be used to minimize

negative environmental impacts, such as using of impervious liners for disposal sites receiving dredged material from cleanup dredging.

Environmental Regulation of Dredging and Dredged Material Disposal/Placement

In addition to national and regional legislation and policies, the most widely applicable international regulatory instrument is the London Convention 1972 and London Protocol 1996 (LC/LP), which is part of the International Maritime Organization, an organization of the United Nations. The LC/LP regulates disposal of wastes into ocean waters, worldwide [10]. The LC/LP is an international treaty, which includes 90 country signatories. Member countries are required to implement the conditions of the treaty including the waste assessment procedures noted below.

The LC/LP Waste Assessment Guidelines for Dredged Material allow disposal of dredged material into ocean waters, provided that strict environmentally protective criteria are met. A step by step process to evaluate a dredging project, the alternatives for disposal or placement for beneficial use, and an action list for judging environmental acceptability of open-water disposal are specified in the Guidelines [11]. Components of the guidelines are shown in Fig. 16.

After an assessment of the need for dredging, major dredging or disposal projects should have studies carried out in order to ensure that any potential adverse effects are identified in advance and dealt with in an appropriate manner. Such investigations include characterization of the dredged material (physical, chemical, and toxicity), an examination of any sources of contamination and the potential to control those sources, an assessment of disposal or beneficial use placement alternatives, including identification and characteristics of the disposal site, and design of monitoring studies to determine whether any potential impacts are correctly predicted.

The environmental impact assessment should highlight both positive and negative, short- and long-term impacts. Appropriate testing may be required to determine the physical behavior of the material at the disposal site. Also, testing and assessments of potential contaminants of concern may be required, depending upon existing knowledge of the dredging site and any potential contaminant pathways. Where potentially adverse effects are anticipated, management techniques should be implemented to reduce risks to acceptable levels. Possible controls for open-water alternatives, include operational modifications, use of submerged discharges of dredged material, treatment, lateral containment, and capping or contained aquatic disposal. Possible controls for confined disposal facilities, include operational modifications, treatment, and various site controls (e.g., covers and liners).

An important component in development of the environmental impact assessment and in identifying potential impacts and implementing acceptable measures is the involvement of interested groups and organizations, consulting with them, and reaching a consensus in the early in the process of determining the alternatives. It is in the best interests of the project sponsors and stakeholders that the decision-making process is transparent, stakeholders are involved, and that the reasons for the selection of the preferred dredging and disposal or placement options are clearly understood.

Control of Upstream Sources of Sediments and Contaminants

Control of upstream sources of sediments and contaminants represents a significant part of the long-term solution to the continuing need for maintenance dredging of navigation channels and the continuing issues of contaminated dredged material. While control of upstream sources of sediments can contribute to lessening the need for dredging, sediments play a duel role in the watershed:

1. Sediments cause water quality problems and the need for more frequent dredging.
2. Sediments provide shoreline protection and maintaining habitats, such as marshes.

Sediments are increasingly recognized as scarce resources that can have costly impacts if not carefully managed, recycled, and conserved. Sediment overloading from land and stream erosion causes significant environmental and economic challenges, i.e., excessive needs for navigation dredging, and sediment in rivers, reservoirs, and estuaries may contribute to high turbidity, which can affect both habitat for aquatic life and human water uses, loss of flood storage

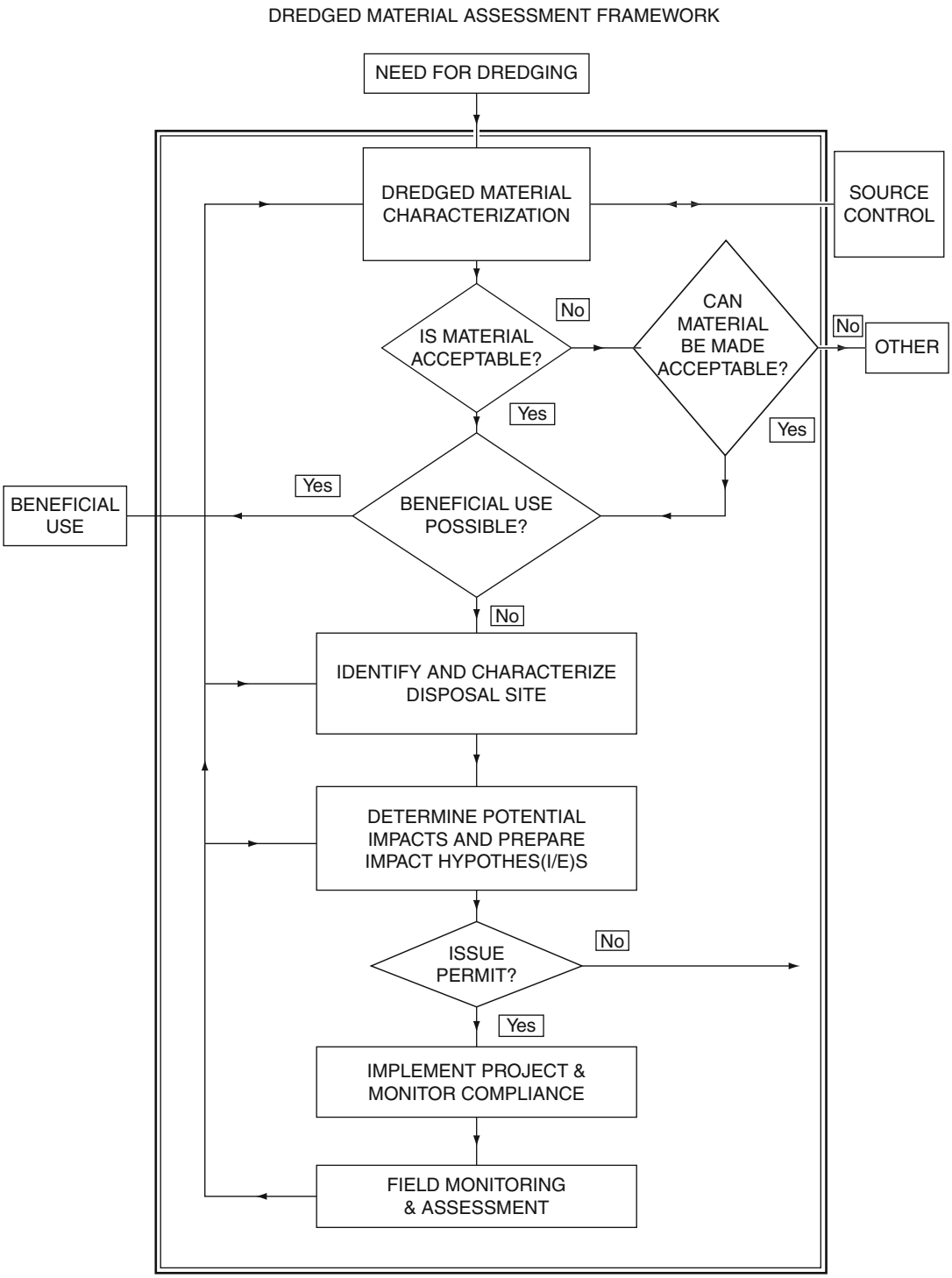

Dredging Practices and Environmental Considerations. Figure 16
International guidelines for assessment of dredged material (Courtesy London Convention)

capacity, and obstructions to waterway navigation and conveyance of floodwaters. Yet in other locations, a shortage of sediment can result in coastal and streambank erosion, and wetland loss. Many water resource projects are designed to remedy local sediment problems, but they must be well planned and thought out as they can create even larger problems upstream or downstream of the local problem.

Dredging and other projects affecting or involving sediment should be undertaken with awareness of the littoral or fluvial sediment system and the effects that proposed projects and actions may have on other stakeholders. Regulatory authorities and stakeholders are becoming increasingly aware of the necessity to manage sediments on a system-wide basis, dredging being one part of the overall river, lake, or coastal system [12].

Principles of Sustainable Sediment Management

- Recognize sediment as part of a system and as a valuable resource that is integral to economic and environmental vitality.
- Strive for balanced, economic, and environmentally sustainable solutions to sediment-related issues through integrated management of sediment from upland sources to estuaries and within coastal zones.
- Involve external and internal partners and stakeholders to integrate and balance objectives and to leverage resources in implementation.
- In project decision-making, consider the sediment implications beyond the local site, including intended and potential effects, and over long time scales (decades or more), and be effective stewards of sediment and related resources.

Dredging regulatory authorities and dredging sponsors need to embrace the concept of sediment management within the watershed. They should work with upstream pollution control authorities to address sediment management decisions such that the overall sediment system is evaluated in dredging projects. Similarly, upstream sources of contaminants from industrial and municipal sources as well as diffuse sources, such as storm runoff from farms or urban areas, need to be understood and comprehensive controls developed.

Achieving sediment management for source control usually involves substantial collaboration and cooperation between a number of organizations, agencies, and stakeholders. These groups must be willing to identify the source and take measures to reduce or prevent further contamination of waterways with sediments and chemicals. This is no easy task but it is the only viable way to guarantee a long-term successful outcome of our waterways development and environmental protection [13].

Future Directions: Sustainable Dredging and Dredged Material Management

The global economy and the dependence upon food and commodities via international trade require that vessels have sufficiently deep channels in ports, harbors, and waterways for safe passage. Other interests include national security as well as recreational opportunities.

While upstream sediment management controls will help, the natural erosion process in rivers and estuaries will continue. Thus, navigation dredging will continue to be needed over the very long term. Environmental cleanup dredging will be needed for decades to come, even as improved controls are placed upon waste and wastewater sources. Legacy contaminants already in the sediments will continue to pose aquatic and human health risks until they are removed or isolated from the surrounding aquatic environment. The environmental considerations relate to the quality and quantity of the sediment to be dredged, the potential environmental risks from the dredging itself, and what to do with the dredged material.

Over time, dredging and dredged material management practices will move towards sustainability concepts. The likely trends include:

Sediment Management

Dredging projects will be managed as part of the overall sediment system in the watershed, with dredged material being considered a resource. Opportunities for beneficial use of dredged material will increase as potential beneficial use projects (e.g., habitat restoration or creation, beach nourishment and coastal protection, restoration of brownfields, and construction

purposes) and their sponsors are identified early in the dredging project planning process.

Climate change can cause more erosion in some places and less in others, with associated changes in the quantities of sediment needed to be removed by dredging for navigation purposes. Continued focus upon control of local and upstream sources of sediment and contaminants will begin to pay dividends by reducing the frequency of navigation dredging. Improved chemical and toxicological quality of those sediments will occur as additional environmental controls are put in place to control municipal and industrial discharges and storm water runoff from urban and rural areas, including farmlands. Instituting environmental controls on the disposal of hazardous waste has helped control runoff from hazardous waste disposal sites and over decades will reduce the need for environmental cleanup dredging. Cleanup dredging, such as removal of PCB-contaminated sediments in the Hudson River, New York; Fox River, Wisconsin; and Passaic River, New Jersey, will contribute to improved sediment quality downstream.

Technological Innovations

Driven by concerns about the potential impacts to aquatic life and human health, technology will continue to evolve in dredging hardware, treatment of contaminated dredged material, and use of dredged material in beneficial use applications. Innovations in dredging technology are focused upon reduction in the disbursement of suspended solids and associated contaminants into the water column during dredging and disposal operations.

Further technological innovations in the types and efficiencies of treatment technologies will likely identify potential reuse opportunities for certain dredged materials, such as use as soil, fill, or aggregates. While the science and engineering of confined disposal facility design is well established, the likely trend is to increase use of confined aquatic disposal cells, ensuring the isolation of contaminated sediment from the aquatic environment.

Two other areas of dredging and disposal are likely to see significant changes:

1. Electric powered dredges will contribute fewer diesel emissions and NO_x in locations where compliance with air pollution standards is an issue or regulation.
2. Changes in navigation channel design to accommodate larger ships (deeper channels) will impact dredging projects, and improved channel design will be necessary due to limited project funding (e.g., narrower channels and institution of vessel operational controls, and fewer deep water ports with attendant increases in the use shallower draft vessels to move cargo between coastal ports).

Implementation of Regulations

International guidelines (i.e., London Convention/London Protocol) are in place for protection of the environment from dredged material disposal in ocean waters. National and local regulations are in place in many countries that implement the London Convention/London Protocol guidelines as well as for protection of internal country waters. These regulations are in various stages of implementation worldwide. Technical cooperation and assistance programs are ongoing to assist developing countries in their application.

One key aspect of the national and local regulations is the characterization of the dredged material prior to disposal. Updated procedures for testing dredged material will provide better techniques to assess its acceptability for open-water disposal or for specific beneficial uses; these include improved bioassays, interpretive guidance, and the application of risk assessment in cases where high uncertainties exist [14].

The final trend in the regulatory arena is the use of mitigation for unavoidable adverse impacts due to dredging and disposal. This will become more widespread as one of the tools for regulatory authorities.

Bibliography

Primary Literature

1. Willard (2009) *Willardsays*. . ..Dredge history done lite. http://www.willardsays.com/dredge_history.pdf. Accessed 25 May 2011
2. Cohen M (2005) Dredging: the environmental facts. Published by International Association of Dredging Companies; Typeset and printed by Opmeer Drukkerij bv, The Netherlands ISBN 90-75254-11-3. http://www.dredging.org/documents/ceda/downloads/publications-dredging_the_facts. Accessed 1 April 2011

3. U.S. Army Corps of Engineers, U.S. Environmental Protection Agency (2004) Evaluating environmental effects of dredged material management alternatives – A technical framework. EPA842-B-92-008
4. Bray RN, International Association of Dredging Contractors, Central Dredging Association (2008) Environmental aspects of dredging. Taylor and Francis/Balkema, Amsterdam
5. Otten MT, Hartman G (2002) Placing and capping fine-grained dredged material. In: ASCE conference proceedings of the third specialty conference on dredging and dredged material disposal, May 5–8, Orlando, Florida, 119
6. USEPA, Corps of Engineers (2007) Identifying, planning, and financing beneficial use projects using dredged material beneficial use planning manual. U.S. EPA, EPA842-B-07-001, Corps of Engineers, Washington, DC, USA
7. International Council for the Exploration of the Sea (ICES) (1992) Report of the ICES working group on the effects of extraction of marine sediments on fisheries. ICES cooperative research report # 182, Copenhagen (Denmark)
8. UK Marine Protected Areas Centre (2001) UK marine SACs project. Dredging and disposal. http://www.ukmarinesac.org.uk/activities/ports/ph5.htm. Accessed 2 April 2011
9. U.S. Corps of Engineers, Sea Turtle Data Warehouse. http://el.erdc.usace.army.mil/seaturtles/intro.cfm. Accessed 27 September 2011
10. IMO (2003) London convention 1972 and the 1996 protocol, 2nd edn. International Maritime Organization, London
11. IMO (2007) London convention 1972. Specific guidelines for assessment of dredged material
12. U.S. Army Corps of Engineers (2004) Regional sediment management – primer. U.S. Army Corps of Engineers, Washington, DC
13. Vogt C (2007) Dredged material management in a watershed context – seeking integrated solutions. In: Proceedings of 26th WEDA conference, San Diego
14. Moore DW, Bridges TS, Ruiz C, Cura J, Driscoll SK, Vorhees D, Peddicord D (1998) Environmental risk assessment and dredged material management: issues and application. In: Proceedings of workshop, San Diego

Books and Reviews

Adams JR, Herbich JB (1970) Gas removal systems. In: Proceeding world dredging conference, WODCON'70, Singapore

Addie GR, Whitlock L, Dresser J (2001) Dredge pump testing considerations. In: Proceedings of the Western Dredging Association 21st technical conference and 33rd Texas A & M Dredging seminar, Houston, TX, 24–27 Jun 2001

Albar A (2001) Modeling of a bucket wheel dredge system for offshore sand and tin mining. Ph.D. Dissertation, Ocean engineering program, Texas A & M University, Ocean engineering program, Civil Engineering Department, College Station, TX.

Ancheta C, Santiago R, Sherbin G (1998) An innovative approach to harbour remediation, Thunder Bay, Ontario, Canada. In: Proceedings of 15th world dredging congress, Las Vegas, NV

Board M (1997) Contaminated sediments in ports and waterways. National Research Council, National Academy Press, Washington, DC

Bray RN, Bates AD, Land JM (1997) Dredging: a handbook for engineers, 2nd edn. Arnold, London

Brandon DL, Price RA (2007). Summary of available guidance and best practices for determining suitability of dredged material for beneficial uses. ERDC/EL TR-07-27. U.S. Army Engineer Research and Development Center, Vicksburg

Bridges TS, Ells S, Hayes D, Mount D, Nadeau SC, Palermo MR, Patmont C, Schroeder P (2008) The four Rs of environmental dredging: resuspension, release, residual, and risk, ERDC/EL TR-08-4. U.S. Army Engineer Research and Development Center, Vicksburg

Briot JE, Doody JP, Romagnoli R, Miller MM (1999) Environmental dredging case studies: a look behind the numbers. In: Proceedings of the Western Dredging Association 19th technical conference and 31st Texas A & M Dredging seminar, Louisville, KY, 15–18 May 1999

Cura JJ, Heiger-Bernays W, Bridges TS, Moore DW (1999) Ecological and human health risk assessment guidance for aquatic environments. U.S. Army Corps of Engineers, Engineer Research and Development Center, Vicksburg

Demars KR (1995) Dredging, remediation, and containment of contaminated sediments. ASTM committee D-18 on soil and rock, environment, Canada

Dickerson DD, Nelson DA, Dickerson CE Jr, Reine KJ (1993) Dredging related sea turtle studies along the Southeastern U.S., Coastal Zone 93, New Orleans, LA

Eisma D (2005) Dredging in coastal waters. Taylor & Francis, London

Fredette TJ, Anderson G, Payne BS, Lunz JD (1986) Biological monitoring of open-water dredged material disposal sites. In: IEEE Oceans'86 conference proceedings, Washington, DC

Fredette TJ, Nelson DA, Clausner JE, Anders FJ (1990a) Guidelines for physical and biological monitoring of aquatic dredged material disposal sites, Technical report D-90-12. U.S. Army Engineer Waterways Experiment Station, Vicksburg

Fredette TJ, Nelson DA, Miller-Way T, Adair JA, Sotler VA, Clausner JE, Hands EB, Anders FJ (1990b) Selected tools and techniques for physical and biological monitoring of aquatic dredged material disposal sites, Technical report D-90-11. U.S. Army Engineer Waterways Experiment Station, Vicksburg

Graalum SJ, Randall RE, Edge BL (1999) Methodology for manufacturing topsoil using sediment dredged from the Texas Gulf intracoastal waterway. J Marine Environ Eng 1:1–38

Hayes DF (1986) Guide to selecting a dredge for minimizing resuspension of sediment, Environmental effects of dredging, Technical notes, EEDP-09-1. U.S. Army Engineer Waterways Experiment Station, Vicksburg

Hayes DF (1999) Turbidity Monitoring during boston harbor bucket dredge comparison study. Project report, Submitted to USAE Waterways Experiment Station, Vicksburg

Hayes DF, McLellan TN, Truitt CL (1988) Demonstration of innovative and conventional dredging equipment at Calumet

Harbor, Illinois, MP EL-88-01. U. S. Army Engineer Waterways Experiment Station, Vicksburg

Hayes DF, Raymond GL, McLellan TN (1984) Sediment resuspension from dredging activities. In: Dredging 1984. American Society of Civil Engineers, Clearwater

Herbich JB, Brahme SB (1991) A literature review and technical evaluation of sediment resuspension during dredging, Contract report HL-91-1. U.S. Army Engineer Waterways Experiment Station, Vicksburg

Herbich JB (2000) Dredge pumps. In: Herbich JB (ed) Handbook of dredging engineering. McGraw-Hill, New York, pp 3.36–3.58, Chapter 3

Herbich JB (2000) Removal of contaminated sediment by dredging. In: Dredging engineering short course notes, Center for Dredging Studies, Ocean Engineering Program, Civil Engineering Department, Texas A & M University, College Station

Herbich JB (2000) Handbook of dredging engineering, 2nd edn. McGraw-Hill, New York

Herbich JB (1995) Removal of contaminated sediments: equipment and recent field studies. In: Demars KR et al (eds) Dredging, remediation and containment of contaminated sediments. ASTM Publication Code Number (PCN) 04-012930-38, Philadelphia

History Channel (2005) Modern marvels: dredging

Huston J (1970) Hydraulic dredging. Cornell Maritime Press, Cambridge

Iwasaki M, Kuioka K, Izumi S, Miyata N (1992) High density dredging and pneumatic conveying system. In: Proceedings of XIIIth world dredging congress, WODCON XIII, Bombay, 7–10 Apr 1992, pp 773–792

Jaglal K, McLaughlin DB (1999) Evaluation of large scale environmental dredging as a remedial alternative. In: Proceedings of the Western Dredging Association 19th technical conference and 31st Texas A & M Dredging seminar, Louisville, KY, 15–18 May 1999

Kikeqawa K (1983) Sand overlying for bottom sediment improvement by sand spreader. In: Management of bottom sediments containing toxic substances: proceedings of the 7th US/Japan Experts meeting. Prepared for the U.S. Army Corps of Engineers Water Resources Support Center by the U.S. Army Engineer Waterways Experiment Station, Vicksburg, pp 79–103

Landin MC (2000) Beneficial uses of dredged material. In: Herbich JB (ed) Handbook of dredging engineering. McGraw-Hill, New York, Chapter 16

LaSalle MW, Clarke DG, Homziak J, Lunz JD, Fredette TJ (1991) A framework for assessing the need for seasonal restrictions on dredging and disposal operations, Technical report D-91-1. U.S. Army Engineer Waterways Experiment Station, Vicksburg

Lee CR (1997) Manufactured soil from toledo harbor dredged material and organic waste materials. In: International workshop on dredged material beneficial uses, Baltimore, MD, 28 July–1 Aug 1997

Marine Board (2001) A process for setting, managing and monitoring environmental windows for dredging projects. Transportation Research Board and Ocean Studies Board, National Research Council, National Academy Press, Washington, DC

Marine Board (1990) Managing troubled waters – The role of marine environmental monitoring. National Research Council, National Academy Press, Washington, DC

Marine Board, National Research Council (1997) Contaminated sediments in ports and waterways – cleanup strategies and technologies. National Academy Press, Washington, DC

Marine Board, National Research Council (1990) Managing coastal erosion. National Academy Press, Washington, DC

Marine Board, National Research Council (1987) Sedimentation control to reduce maintenance dredging of navigation facilities in Esturaries. National Academy Press, Washington, DC

Martin JL, McCutcheon SC (1992) Overview of processes affecting contaminant release from confined disposal facilities, Contract report D-92-1. U.S. Army Engineer Waterways Experiment Station, CE, Vicksburg, NTIS no AD A247 650

Matousek V (1997) Flow mechanism of sand-water mixtures in pipelines. Ph.D. Dissertation, Delft University of Technology, Delft, The Netherlands

McLellan TN, Havis RN, Hayes DF, Raymond GL (1989) Field studies of sediment resuspension characteristics of selected dredges, Technical report HL-89-9. U.S. Army Engineer Waterways Experiment Station, Vicksburg

Miertschin M, Randall RE (1998) A general cost estimation program for cutter suction dredges. In: Poceedings of 15th world dredging congress, Las Vegas, NV, pp 1099–1115

Myers TE, Brannon JM, Tardy BA (1996) Leachate testing and evaluation for estuarine sediments, Technical report D-96-1. U.S. Army Engineer Waterways Experiment Station, Vicksburg, NTIS no AD A306 421

National Dredging Team (2003) Dredged material management: action agenda for the next decade, Jacksonville, FL, 23–25 Jan 2003

Ocean Studies Board, National Research Council, Transportation Research Board (2001) A process for setting, managing and monitoring environmental windows for dredging projects; Special report 262

Otis MJ, Andon S, Bellmer R (1990) New bedford harbor superfund pilot study: evaluation of dredging and dredged material disposal. US Army Engineer Division, New England

Palermo MR, Clausner JE, Rollings MP, Williams GL, Myers TE, Fredette TJ, Randall RE (1998) Guidance for subaqueous dredged material capping, Technical report DOER-1. U.S. Army Corps of Engineers, Washington, DC

Palermo MR, Maynard S, Miller J, Reible DD (1996) Guidance for in-situ subaqueous capping of contaminated sediments. Environmental Protection Agency, EPA 905-B96-004, Great Lakes National Program Office, Chicago, IL

Palermo MR, Schroeder PR, Estes TJ, Francingues NR (2008) Technical guidelines for environmental dredging of contaminated sediments, ERDC/EL TR-08-29. U.S. Army Engineer Research and Development Center, Vicksburg

Parchure TM, Sturdivant CN (1997) Development of a portable innovative contaminated sediment dredge, Final report, CPAR-CHL-97-2, Construction productivity advancement research (CPAR) program. USAE Waterways Experiment Station, Vicksburg

Parchure TM (1996) Equipment for contaminated sediment dredging, Technical report HL-96-17. USAE Waterways Experiment Station, Vicksburg

Pearson TH (1987) Benthic ecology in an accumulation sludge-disposal site. In: Capuzzo JM, Kester DR (eds) Ocean processes and marine pollution, vol 1, Biological processes and wastes in the ocean. Krieger Publishing, Malabar, pp 195–200

Pelletier JP (1992) Collingwood harbour sediment removal demonstration. Preliminary report on the water quality monitoring program, environmental protection, Environment Canada, Toronto, ON, Canada

Pennekamp JGS, Quaak MP (1990) Impact on the environment of turbidity caused by dredging, Terra et Aqua, 42. International Association of Dredging Companies, The Hague

Pequegnat WE, Gallaway BJ, Wright TD (1990) Revised procedural guide for designation surveys of ocean dredged material disposal sites, Technical report D-90-8. U.S. Army Engineer Waterways Experiment station, Vicksburg

PIANC (1992) Beneficial uses of dredged material: a practical guide. PIANC, Brussels/Belgium

Pianc, EnviCom (2009) Dredging management practices for the environment, Pianc report 100

Pilarczyk KW (1996) Geotextile systems in coastal engineering, an overview. In: Proceedings of the twenty-fifth international conference on coastal engineering, vol 2, pp 2114–2127

Pilarczyk KW (1994) Novel systems in coastal engineering, geotextile systems and other methods, an overview. Rijkswaterstaat, Delft

Randall RE (1994) Dredging equipment alternatives for contaminated sediment removal. In: Conference on environmental dredging technology, East Brunswick, NJ, Sponsored by The Port Authority of New York/New Jersey, 21–22 Jun 1994

Randall RE (2000) Estimating dredging costs. In: Herbich JB (ed) Handbook of dredging engineering, 2nd edn. McGraw-Hill, New York, Appendix 9

Randall RE (2004) Dredging. In: Tsinker G (ed) Handbook of port engineering. McGraw-Hill, New York, Chapter 11

Randall RE (2000) Pipeline transport of dredged material. In: Herbich JB (ed) Handbook of dredging engineering, 2nd edn. McGraw-Hill, New York, Chapter 7, Section 2

Randall RE (1992) Equipment used for dredging contaminated sediments. In: 1992 international environmental dredging symposium proceedings, Erie County Environmental Education Institute, Buffalo, NY, 30 Sep–2 Oct 1992

Randall RE, Clausner JE, Johnson BH (1994) Modeling of Cap placement at the New York mud dump site. In: Dredging 94, Second international conference of dredging and dredged material placement, ASCE, Orlando, FL, 13–16 Nov 1994

Randall R, Edge B, Basilotto J, Cobb D, Graalum S, He Q, Miertschin M (2000) Texas gulf intracoastal waterway (GIWW): beneficial uses, estimating costs, disposal analysis alternatives, and separation techniques, Texas Transportation Institute, Project report no 1733-S, Texas A&M University System, College Station, Texas, Sep 2000

Reine KJ, Dickerson DD, Clarke DG (1998) Environmental windows associated with dredging operations, DOER technical notes collection (TNDOER-E2). U.S. Army Engineer Research and Development Center, Vicksburg

Richardson M (2001) The dynamics of dredging. Placer Management Corp, Irvine, California

Sanders L, Killgore J (1989) Seasonal restrictions on dredging operations in freshwater systems, environmental effects of dredging. Technical note EEDP-01-16. U.S. Army Engineer Waterways Experiment Station, Vicksburg

Sanderson WH, McKnight AL (1986) Survey of equipment and construction techniques for capping dredged material, Miscellaneous paper D-86-6. U.S. Army Engineer Waterways Experiment Station, Vicksburg

Santiago R (2000) Contaminated sediment removal general management options and support technologies, Dredging engineering short course notes, Center for Dredging Studies, Ocean Engineering Program, Civil Engineering Department, Texas A&M University, College Station, TX, Jan 2000

Schiller RE Jr (1992) Sediment transport in pipes. In: Herbich JB (ed) Handbook of dredging engineering. McGraw-Hill, New York, Chapter 6

Science Applications International Corporation (SAIC) (1995) Sediment capping of subaqueous dredged material disposal mounds: an overview of the New England experience, 1979–1993, DAMOS contribution #95, SAIC report no SAIC-90/7573&c84 prepared for the U.S. Army Engineer Division, New England, Waltham.

Shook CA, Rocco MC (1991) Slurry flow: principles and practice. Butterworth-Heinemann, Boston

Steevens J, Kennedy A, Farrar D, McNemar C, Reiss MR, Kropp RK, Doi J, Bridges T (2008) Dredged Material analysis tools; performance of acute and chronic sediment toxicity methods, ERDC/EL TR-08-16. U.S. Army Engineer Research and Development Center, Vicksburg

Sumeri A (1989) Confined aquatic disposal and capping of contaminated bottom sediments in puget sound. In: Proceedings of the WODCON XII, Dredging: technology, environmental, mining, world dredging congress, Orlando, FL, 2–5 May 1989

Togashi H (1983) Sand overlaying for sea bottom sediment improvement by conveyor barge. In: Management of bottom sediments containing toxic substances: proceedings of the 7th U.S./Japan experts meeting. Prepared for the U.S. Army Corps of Engineers Water Resources Support Center by the U.S. Army Engineer Waterways Experiment Station, Vicksburg, pp 59–78

Tsinker GP (2004) Port engineering: planning, construction, maintenance, and security. Wiley, Hoboken

Turner TM (1996) Fundamentals of hydraulic dredging, 2nd edn. ASCE Press, New York

USACE (1987a) Confined disposal of dredged material, Engineer manual, US Army Corps of Engineers, EM-1110-2-5027. US Government Printing Office, Washington, DC
USACE (1987b) Beneficial uses of dredged material, Engineer manual, US Army Corps of Engineers, EM-1110-2-5026. US Government Printing Office, Washington, DC
USACE (1983) Dredging and dredged material disposal, Engineer manual, US Army Corps of Engineers, EM-1110-2-5025. US Government Printing Office, Washington, DC
USEPA/USACE (1992) Evaluating environmental effects of dredged material management alternatives-A technical framework, EPA 842-B-92-008. US Government Printing Office, Washington, DC
USEPA/USACE (1996) Guidance document for development of site management plans for ocean dredged material disposal sites, USEPA, Office of Water, Washington, DC
USEPA/USACE (2007) The role of the federal standard in the beneficial use of dredged material from US Army Corps of Engineers new and maintenance navigation projects – Beneficial uses of dredged materials. USEPA/USACE, Washington, DC
USEPA/USACE (1996) Evaluation of dredged material proposed for discharge in inland and near-coastal waters – Testing manual. Office of Water, U.S. Environmental Protection Agency, Washington, DC
USEPA/USACE (1991) Evaluation of dredged material proposed for ocean disposal (Testing manual), EPA-503/8-91/001. Office of Water, U.S. Environmental Protection Agency, Washington, DC
Van Drimmelen C, Schut T (1992) New and adapted small dredges for remedial dredging operations. In: Proceedings of WODCON XIII, Bombay, India, pp 156–169
Vorhees DJ, Driscoll SBK, Stackelberg K, Bridges TS (1998) Improving dredged material management decisions with uncertainty analysis. U.S. Army Engineer Waterways Experiment Station, Vicksburg
Wilson KC, Addie GR, Sellgren A, Clift R (2006) Slurry transport using centrifugal pumps, 3rd edn. Blackie Academic, New York
Zappi PA, Hayes DF (1991) Innovative technologies for dredging contaminated sediments, Miscellaneous paper EL-91-20. U.S. Army Engineer Waterways Experiment Station, Vicksburg
Zeller RW, Wastler TA (1986) Tiered ocean disposal monitoring will minimize data requirements, Oceans '86, vol 3. Marine Technology Society, Washington, DC, pp 1004–1009

Driver Assistance System, Biologically Inspired

Moustapha Doumiati[1], Daniel Lechner[2]
[1]B2i Automotive Engineering Company, Massy, France
[2]Department of Accident Mechanism Analysis, IFSTTAR-MA Laboratory, Salon de Provence, France

Article Outline

Glossary
Definition of the Subject
Introduction
Estimation Process Description
Four-Wheel Vehicle Model
Tire–Road Interface
Observer's Design
Experimental Results
Conclusion and Future Perspectives
Acknowledgments
Bibliography

Glossary

Lateral tire forces They are responsible to hold on the vehicle during a turn.

Longitudinal tire forces They are responsible to accelerate/brake the vehicle.

Observer or estimator It models a real system in order to provide an estimate of its internal state, given measurements of the input and output of the real system.

Sideslip angle It is the angle between the velocity heading and the true heading of the vehicle.

Tire forces The developed forces (longitudinal and lateral) are function of tire properties (material, tread pattern, tread depth, profile, etc.), the normal load on the tire, and the velocities experienced by the tire.

Vehicle control systems They provide commands and instructions to control the movements of the vehicle in order to maintain stability and enhance passengers security and comfort.

Vehicle dynamics It includes analytical and experimental technology used to study and understand the dynamical responses of a vehicle in various in-motion situations.

Vertical (normal) tire forces They are responsible to support the weight of the vehicle.

Definition of the Subject

The principal concerns in driving safety with standard vehicles are understanding and preventing risky situations. A close examination of accident data reveals that losing the vehicle control is the main reason for most car accidents. To help the driver to prevent such accidents, vehicle control systems may be used. For their optimal operation, these control systems require certain input data concerning vehicle dynamic parameters

and vehicle–road interaction. Unfortunately, some fundamental parameters like the tire-road forces and the sideslip angle are difficult to measure in a car, for both technical and economic reasons. To face this problem, this entry presents a dynamic modeling and observation method to estimate these variables. The ability to accurately estimate lateral tire forces and sideslip angle is a critical determinant in the performances of many vehicle control systems. To address nonlinearities and unmodeled vehicle dynamics, an observer derived from unscented Kalman filtering technique is proposed. The estimation process method is based on the dynamic response of a vehicle instrumented with easily available and potentially integrable sensors. Performances are tested using an experimental car in real driving situations. Experimental results show the potential of the proposed estimation method.

Introduction

Vehicle dynamics and stability have been of considerable interest to automotive engineers, automobile manufacturers, government, public safety groups, and general public for a number of years. The obvious dilemma is that people naturally desire to drive faster and faster on the roads and highways, yet they expect their vehicles to be stable and safe during all normal and emergency maneuvers. For the most part, people pay little attention to the limited handling potential of their vehicles until some unusual behavior is observed that often results in fatality. According to statistics, worldwide, an estimated 1.2 million people are killed in road crashes each year and as many as 50 million are injured [1]. Preventing car accidents requires to know what determines vehicle dynamics during motion [2].

Today, automotive electronic technologies are developing for safe and comfortable traveling of drivers and passengers. Nowadays, there are a lot of vehicle control system such as the Anti-lock Braking System (ABS) that prevents wheel lock during braking [3], and the Electronic Stability Control (ESC) that enhances lateral vehicle stability [4, 5]. These control systems installation rate is increasing all around the world. Vehicle control algorithms have made great strides toward improving the handling and safety of vehicles. For example, experts estimate that ESC prevents 27% of loss-of-control accidents by intervening when emergency situations are detected [6]. While nowadays vehicle control algorithms are undoubtedly a life-saving technology, they are limited by the available vehicle state information.

Vehicle control systems currently available on production cars rely on available inexpensive measurements such as longitudinal velocity, accelerations, and the vehicle yaw rate. Sideslip rate can be evaluated using the yaw rate, lateral acceleration, and vehicle velocity [7]. Calculating the sideslip angle is possible from the sideslip rate integration. However, it is prone to uncertainty and errors from sensor bias. Besides, these control systems use unsophisticated, inaccurate tire models to evaluate lateral tire dynamics. In fact, measuring tire forces and sideslip angles is very difficult for technical and economic reasons. Therefore, these important data must be observed or estimated. If control systems were in possession of the complete set of lateral tire characteristics, namely, lateral forces, sideslip angle, and the tire–road friction coefficient, they could greatly enhance vehicle handling and increase passenger safety.

As the motion of a vehicle is governed by the forces generated between the tires and the road, knowledge of the tire forces is crucial when predicting vehicle motion. For example, a vehicle can turn because of the applied lateral tire forces. In fact, what happens is that when the front wheels of a vehicle are steered, a slip angle is created, which gives rise to a lateral force. This lateral force turns or yaws the vehicle. Under normal driving situations (low slip angle), a vehicle responds predictably to the driver's inputs. As the vehicle approaches the handling limits, for example, during an evasive emergency maneuver, or when a vehicle undergoes high accelerations, high slip angle occurs and the vehicle's dynamic becomes highly nonlinear and its response becomes less predictable and potentially very dangerous.

Accurate data about tire forces lead to a better evaluation of the vehicle possible trajectories, to a better vehicle control and rollover prevention. Moreover, it enables the development of a diagnostic tool for evaluating the potential risks of accidents related to poor adherence or dangerous maneuvers.

In the literature, many studies have looked at the vehicle dynamic states estimation. Several ones have

been conducted regarding the estimation of tire-road forces [8–20]. For example, in [8], a study of a 14-degrees-of-freedom (DOF) vehicle model is proposed where the dynamics of the roll center are used to calculate vertical tire forces. In [9], the authors propose an estimation method in order to estimate vertical and lateral forces per axle. The authors in [10–13] estimate the vehicle vertical forces and other dynamic states for a four-wheel vehicle model (FWVM) comprising four DOF. Consequently, lateral tire forces at each tire are calculated based on the estimated states and using a quasi-static tire model. In [14], Ray estimates the vehicle dynamic states and lateral tire forces per axle for a nine-DOF vehicle model. The author uses measurements of the applied torques as inputs to his model. We note that the torque is difficult to get in practice; it requires expensive sensors. More recently, authors in [15, 16] propose observers to estimate lateral forces per axle without using torque measures. In [17], the authors propose an estimation process based on a three-DOF vehicle model, as a lateral tire force estimator. In [15–17], lateral forces are modeled with a derivative equal to random noise. The authors in [17] remark that such modeling leads to a noticeable inaccuracy when estimating individual lateral tire forces, but not in axle lateral forces. This phenomenon is due to the non-representation of the lateral load transfer when modeling. Studies in [21–24] focus on the tire-road friction estimation.

The main goal of this entry is to present an estimation method that uses simple vehicle-road models and a certain number of valid measurements in order to estimate in real time and in accurate way the sideslip angle and the lateral force at each individual tire–road contact point. This entry presents two significant particularities:

1. First, the estimation process does not use the measurements of wheel torques which are very expensive.
2. Second, the estimation process uses accurate normal tire forces, in contrast to many existing approaches that assume constant vertical forces. This approach is more realistic since during cornering, accelerating, and braking, the load distribution varies significantly in a car, thus cornering stiffness and lateral forces evaluation are directly affected.

The developed estimation process is model based and built using Kalman filter technique. The Kalman filter is known as the most commonly used real-time estimator for linear and nonlinear systems. In order to show the effectiveness of the estimation method, some real-time validation tests were carried out on an instrumented vehicle in realistic driving situations.

Estimation Process Description

The estimation process is shown in its entirety by the block diagram in Fig. 1, where a_x and a_{ym} are respectively the longitudinal and lateral accelerations, $\dot{\psi}$ is the yaw rate, $\dot{\theta}$ is the roll rate, Δ_{ij} (i represents the front 1 or the rear 2 and j represents the left 1 or the right 2) is the suspension deflection, w_{ij} is the wheel velocity, F_{zij} and F_{yij} are respectively the normal and lateral tire-road forces, β is the sideslip angle at the center of gravity (cog). The whole estimation process consists of two blocks, and its role is to estimate sideslip angle at the cog, normal and lateral forces at each tire–road contact point, and consequently evaluate the used lateral friction coefficient. The following measurements are needed:

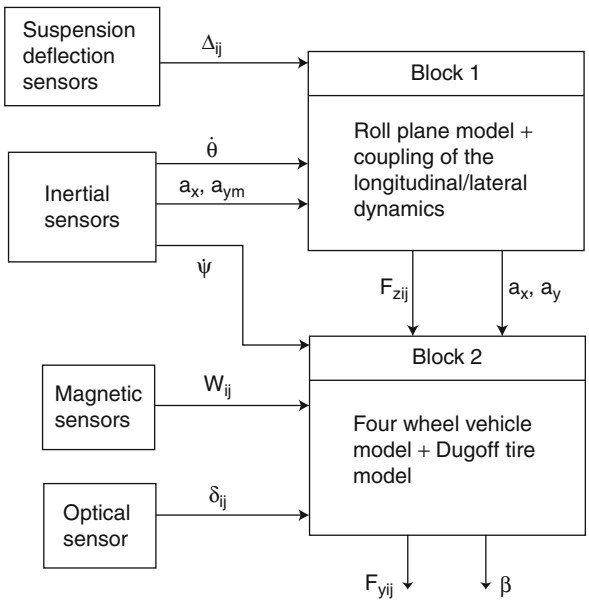

Driver Assistance System, Biologically Inspired. Figure 1 Process estimation diagram

- Yaw and roll rates measured by gyrometers
- Longitudinal and lateral accelerations measured by accelerometers
- Suspension deflections using suspension deflections sensors
- Steering angle measured by an optical sensor
- Rotational velocity for each wheel given by magnetic sensors

The first block aims to provide the vehicle's mass, lateral load transfer, normal tire forces, and the corrected lateral acceleration a_y (by canceling the gravitational acceleration component that distorts the accelerometer signal a_{ym}). It contains observers based on vehicle's roll dynamics and model that couples longitudinal and lateral accelerations. Authors have looked at the first block in some previous studies [10, 11]. This work focuses only on the second block, whose main role is to estimate individual lateral tire force and sideslip angle. The second block makes use of the estimations provided by the first block. In fact, as will be shown in the sections, the impact of including accurate normal forces in the calculation of lateral forces is fundamental.

One specificity of this estimation process is the use of blocks in series. By using cascaded observers, the observability problems entailed by an inappropriate use of the complete modeling equations are avoided, enabling the estimation process to be carried out in a simple and practical way. In the following, the model-based observer of the second block will be explained in details. Therefore, the vehicle-road model and the estimation method will be illustrated, respectively.

Four-Wheel Vehicle Model

The Four-Wheel Vehicle model (FWVM) is chosen for this entry because it is simple and corresponds sufficiently to our objectives. The FWVM is widely used to describe transversal vehicle dynamic behavior [12–14, 17, 18].

Figure 2 shows a simple diagram of the FWVM model in the longitudinal and lateral planes. In order to simplify the lateral and longitudinal dynamics, rolling resistance is neglected. Additionally, the front and rear track widths (E) are assumed to be equal. L_1 and L_2 represent the distance from the vehicle's center of gravity to the front and rear axles respectively. The

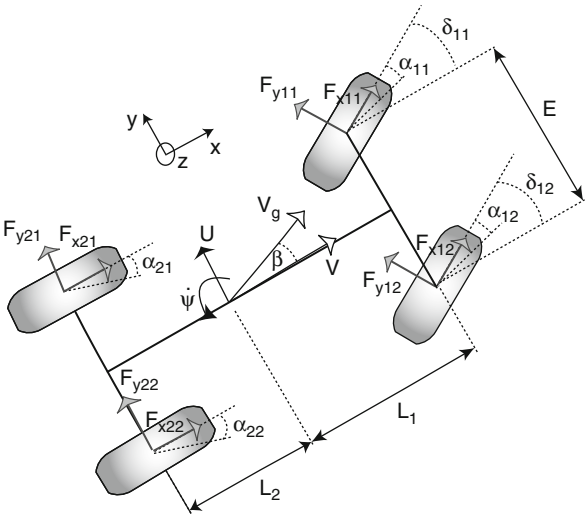

Driver Assistance System, Biologically Inspired. Figure 2 Four-wheel vehicle model

sideslip at the vehicle center of gravity (β) is the difference between the velocity heading (V_g) and the true heading of the vehicle (ψ). The yaw rate ($\dot{\psi}$) is the angular velocity of the vehicle about the center of gravity. The forward and lateral velocities are respectively $V$and U. The longitudinal and lateral forces ($F_{x,y,i,j}$) are shown for front and rear tires of the vehicle.

Longitudinal forces should be taken into account to enable accurate lateral forces estimation during vehicle braking or acceleration. While considering their effect is certainly important, its inclusion makes solving the lateral estimation problem considerably more complex. Thus, it may be desirable to solve the lateral estimation problem in the absence of longitudinal forces first and include them in later studies. This can be done by focusing on solving the estimation problem when the vehicle is driven at constant speeds [20].

This entry extended the hypothesis of moving in a constant speed and addresses the case of a front-wheel drive, where rear longitudinal forces are neglected relative to the front longitudinal forces. Longitudinal front axle forces are considered by assuming that:

$$F_{x1} = F_{x11} + F_{x12}. \tag{1}$$

The longitudinal force evolution is modeled with a random walk model, where its derivative is equal to random noise $\dot{F}_{x1} = 0$. This is due to the lack of

knowledge on the longitudinal slip and the effective radius of the tire [25].

The lateral dynamics of the vehicle can be obtained by summing the forces and moments about the vehicle's center of gravity. Consequently, the simplified FWVM is formulated as the following dynamic relationships [19]:

$$\begin{cases} \dot{V}_g = \frac{1}{m}\begin{bmatrix} F_{x1}\cos(\beta-\delta) + F_{y11}\sin(\beta-\delta) + \\ F_{y12}\sin(\beta-\delta) + (F_{y21}+F_{y22})\sin\beta \end{bmatrix}, \\ \ddot{\psi} = \frac{1}{I_z}\begin{bmatrix} L_1[F_{y11}\cos\delta + F_{y12}\cos\delta + F_{x1}\sin\delta] - \\ L_2[F_{y21}+F_{y22}] + \\ \frac{E}{2}[F_{y11}\sin\delta - F_{y12}\sin\delta] \end{bmatrix}, \\ \dot{\beta} = \frac{1}{mV_g}\begin{bmatrix} -F_{x1}\sin(\beta-\delta) + F_{y11}\cos(\beta-\delta) + \\ F_{y12}\cos(\beta-\delta) + (F_{y21}+F_{y22})\ \cos\ \beta \end{bmatrix} - \dot{\psi}, \\ a_y = \frac{1}{m}[F_{y11}\cos\ \delta + F_{y12}\cos\delta + (F_{y21}+F_{y22}) + F_{x1}\sin\delta], \\ a_x = \frac{1}{m}[-F_{y11}\sin\ \delta - F_{y12}\sin\delta + F_{x1}\cos\delta], \end{cases} \tag{2}$$

where m is the vehicle mass, and I_z is the yaw moment of inertia.

The tire slip angle (α_{ij}) as shown in Fig. 2, is the difference between the tire's longitudinal axis and the tire's velocity vector. The tire velocity vector can be obtained from the vehicle's velocity (at the cog) and the yaw rate. Assuming that rear steering angles are approximately null, the direction or heading of the rear tires is the same as that of the vehicle. The heading of the front tires includes the steering angle (δ). The front steering angles are assumed to be equal ($\delta_{11} = \delta_{12} = \delta$). The forward velocity V, steering angle δ, yaw rate $\dot{\psi}$, and the vehicle body slip angle β are then used to calculate the tire slip angles α_{ij}, where:

$$\begin{cases} \alpha_{11} = \delta - \arctan\left[\frac{V\beta + L_1\dot{\psi}}{V - E\dot{\psi}/2}\right], \\ \alpha_{12} = \delta - \arctan\left[\frac{V\beta + L_1\dot{\psi}}{V + E\dot{\psi}/2}\right], \\ \alpha_{21} = -\arctan\left[\frac{V\beta - L_2\dot{\psi}}{V - E\dot{\psi}/2}\right], \\ \alpha_{22} = -\arctan\left[\frac{V\beta - L_2\dot{\psi}}{V + E\dot{\psi}/2}\right]. \end{cases} \tag{3}$$

Tire–Road Interface

As the motion of a vehicle is governed by the forces generated between the tires and the road, knowledge of the tire forces is crucial in order to predict the vehicle's motion. This section presents the tire–road interaction phenomenon, especially the lateral tire forces. Since the quality of the observer largely depends on the accuracy of the tire model, the underlying model must be precise. Taking real-time calculation requirement, the tire model should also be simple.

Dugoff Tire Model

Many different tire models, based on the physical nature of the tire and/or on empirical formulations deriving from experimental data, can be found in the literature. These models include the Burckhardt, Dugoff, and Pacejka models [19, 26, 27]. One of the most commonly used model is the Pacejka's "Magic Formula." It is an effective method for predicting real tire behavior. However, it requires a large number of tire-specific parameters that are usually unknown. Another commonly used model is the Dugoff tire model. It synthesizes all the tire property parameters into two constants Cx and Cy, referred to as the longitudinal and cornering stiffness of the tire. Dugoff's model is the one used in this entry. Neglecting longitudinal forces, the simplified nonlinear lateral tire forces are given by:

$$\overline{F_{yij}} = -Cy_{ij}\, tan\alpha_{ij}\, f(\lambda), \tag{4}$$

where Cy_{ij} is the cornering stiffness, α_{ij} is the slip angle, and $f(\lambda)$ is given by:

$$f(\lambda) = \begin{cases} (2-\lambda)\lambda, & \text{if } \lambda < 1 \\ 1, & \text{if } \lambda < 1 \end{cases} \tag{5}$$

$$\lambda = \frac{\mu F_{zij}}{2C_{yij}|tan\alpha_{ij}|}. \tag{6}$$

In the above formulation, μ is the friction coefficient and F_{zij} is the vertical load on the tire. This simplified tire model assumes pure slip conditions with negligible longitudinal slip, a uniform pressure distribution, a rigid tire carcass, and a constant friction coefficient for sliding rubber. The original Dugoff tire model has

a constant stiffness in respect to weight transfer. It is worthy to note that, according to [28], load transfer affects the cornering stiffness Cy_{ij}. It can be represented by a second order polynomial with respect to the normal force as shown in equation (7):

$$Cy_{ij}(F_z) = \left(aFz_{ij} - bFz_{ij}^2\right), \tag{7}$$

where a and b are respectively the first and second order coefficient in the cornering stiffness polynomial. They are identified once using a set of experimental data treated offline, where the tires remain in their linear operation zone. Therefore, equation (7) is compared to the calculated cornering stiffness obtained from the ratio of the measured lateral force to the measured tire's slip angle. Hence, a and b are calculated, in such a way that the equation (7) fits the calculated cornering stiffness well.

This entry proposes a modified Dugoff tire model, where the cornering stiffness varies with respect to load.

As shown in equation (4), vertical forces and the tire slip angles can be used to find the lateral force on each tire. Figure 3, based on the modified Dugoff's tire model, is a graph of the lateral force versus tire slip angle. It will be noted that as the load increases, the peak lateral force occurs at somehow higher slip angle.

It is clear that for small slip angles the force profile can be defined by a linear region. When operating in this region, a vehicle responds predictably to the driver's inputs.

As the slip angle continues to grow, the tire begins to saturate and reaches a peak value; this area is commonly called the nonlinear region of the tire curve. It represents the tire limits and it is rarely reached under normal driving conditions. If the front tires saturate first, the vehicle is said to display understeer, and may plow out of a bend. If the rear tires saturate first, the vehicle limit oversteers and may spin out. Because most drivers are not accustomed to operate in the nonlinear handling regime, both of these responses are potentially very dangerous. Noting that oversteer situation is much more difficult to be controlled than the understeer [29].

Observer's Design

This section presents a description of the observer devoted to lateral tire forces and sideslip angle. The state-space formulation, the observability analysis, and the estimation method will be presented.

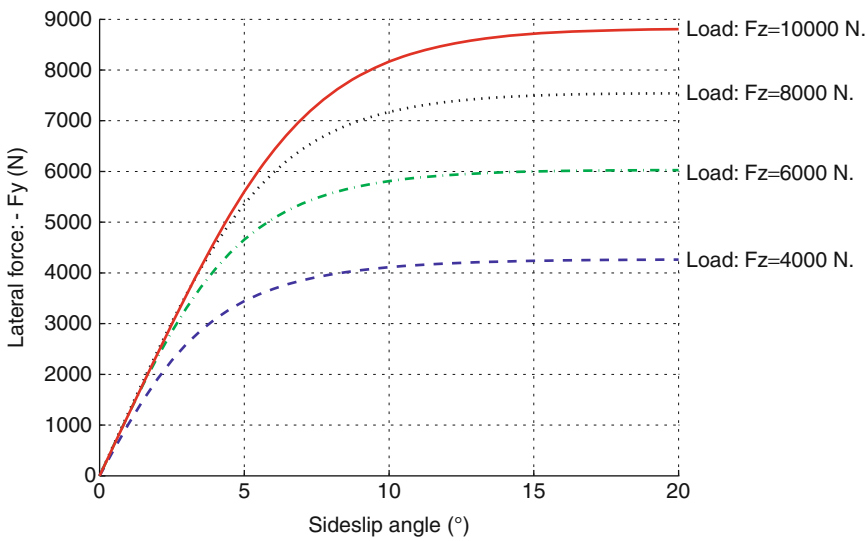

Driver Assistance System, Biologically Inspired. Figure 3
Generic tire curve: lateral force versus slip angle

Stochastic State-Space Representation

The nonlinear stochastic state-space representation of the system described in previous section is given as:

$$\begin{cases} \dot{X}(t) = f(X(t),\ U(t)) + w(t) \\ Y(t) = h(X(t),\ U(t)) + v(t) \end{cases} \tag{8}$$

The input vector, U, comprises the steering angle and the normal forces considered estimated by the first block (see Fig. 1):

$$\begin{aligned} U &= [\delta,\ \ F_{z11},\ \ F_{z12},\ \ F_{z21},\ \ F_{z22}]^T \\ &= [u_1,\ \ u_2,\ \ u_3,\ \ u_4,\ \ u_5]^T. \end{aligned} \tag{9}$$

The measure vector, Y, comprises yaw rate, vehicle velocity (approximated by the mean of the rear wheel velocities calculated from wheel-encoder data), and longitudinal and lateral accelerations:

$$Y = [\dot{\psi},\ \ V_g,\ \ a_x,\ \ a_y]^T = [y_1,\ \ y_2,\ \ y_3,\ \ y_4]^T. \tag{10}$$

The state vector, X, comprises yaw rate, vehicle velocity, sideslip angle at the cog, lateral forces, and the sum of the front longitudinal tire forces:

$$\begin{aligned} X &= [\dot{\psi},\ \ V_g,\ \ \beta,\ \ F_{y11},\ \ F_{y12},\ \ F_{y21},\ \ F_{y22},\ \ F_{x1}]^T \\ &= [x_1,\ \ x_2,\ \ x_3,\ \ x_4,\ \ x_5,\ \ x_6,\ \ x_7,\ \ x_8]^T. \end{aligned} \tag{11}$$

Authors would like to emphasize that the consideration of the lateral forces as states allows:

1. A better evaluation of the tire forces. In fact, whatever the complexity of the tire models, there are several reasons why such models do not match the actual tire forces perfectly [30]. From these reasons, we can cite especially the changes in the tire's pressure and temperature and the changes in the road characteristics. Therefore, authors believe that according to the closed loop observer theory, the integration of the tire forces in the state vector may lead to better results than just using an open loop tire model.
2. A better understanding of the tire behaviors using the relaxation-length formulation, especially in transient maneuvers [31].
3. The forces reconstruction to be done robustly with respect to some parameter variations. In fact, it is well known that the Kalman filters have proven to be robust to parameter changes.

Taking these observations in mind, one can infer the contribution of this entry with respect to other existing studies in the literature like [12, 13], which estimate dynamic variables of the vehicle, and then assess the tire forces using a properly adjusted tire model.

The process and measurements noise vectors, respectively w and v, are assumed to be white, zero mean and uncorrelated.

Consequently, the particular nonlinear function $f(.)$ of the state equations is given by:

$$\begin{cases} f_1 = \dfrac{1}{I_z}\begin{bmatrix} L_1[x_4\ \cos\ u_1 + x_5\ \cos\ u_1 + x_8\ \sin\ u_1] - \\ L_2[x_6 + x_7] + \\ \dfrac{E}{2}[x_4\ \sin\ u_1 - x_5\ \sin\ u_1] \end{bmatrix}, \\ f_2 = \dfrac{1}{m}\begin{bmatrix} x_8\cos(x_3 - u_1) + x_4\sin(x_3 - u_1) + \\ x_5\sin(x_3 - u_1) + (x_6 + x_7)\ \sin(x_3) \end{bmatrix}, \\ f_3 = \dfrac{1}{mx_2}\begin{bmatrix} -x_8\sin(x_3 - u_1) + x_4\cos(x_3 - u_1) \\ + x_5\cos(x_3 - u_1) + (x_6 + x_7)\cos x_3 \end{bmatrix} - x_1, \\ f_4 = \dfrac{x_2}{\sigma_2}\left(-x_4 + \overline{F_{y11}}\ (\alpha_{11},\ u_2)\right), \\ f_5 = \dfrac{x_2}{\sigma_2}\left(-x_5 + \overline{F_{y12}}\ (\alpha_{12},\ u_3)\right), \\ f_6 = \dfrac{x_2}{\sigma_2}\left(-x_6 + \overline{F_{y21}}\ (\alpha_{21},\ u_4)\right), \\ f_7 = \dfrac{x_2}{\sigma_2}\left(-x_7 + \overline{F_{y22}}\ (\alpha_{22},\ u_5)\right), \\ f_8 = 0. \end{cases} \tag{12}$$

The observation function $h(.)$ is:

$$\begin{cases} h_1 = x_1, \\ h_2 = x_2, \\ h_3 = \dfrac{1}{m}[-x_4\ \sin\ u_1 - x_5\sin\ u_1 + x_8\ \cos\ u_1], \\ h_4 = \dfrac{1}{m}\ [x_4\cos\ u_1 + x_5\cos\ u_1 + (x_6 + x_7) \\ \qquad + x_6\ \sin\ u_1]. \end{cases} \tag{13}$$

The state vector $X(t)$ will be estimated by applying the unscented Kalman filter technique.

Observability

Observability is a measure of how well the internal states of a system can be inferred from knowledge of its inputs and external outputs. This property is often presented as a rank condition on the observability matrix. Using the nonlinear state-space formulation of the system presented in section "Stochastic State-Space Representation," the observability definition is local and uses the Lie derivative [32]. An observability analysis of this system was undertaken in [33]. It was shown that the system is observable except when:

- Steering angles are null
- The vehicle is at rest ($V_g = 0$)

For these situations, we assume that lateral forces and sideslip angle are null, which approximately corresponds to the real cases.

Estimation Method: Kalman Filter Algorithms

The aim of an observer or a virtual sensor is to estimate a particular unmeasurable variable from available measurements and a system model in a closed loop observation scheme, as illustrated in Fig. 4. Because of the vehicle system-model mismatches (unmodeled dynamics, parameter variations, etc.) and the presence of unknown and unmeasurable disturbances, the calculation obtained from vehicle's model would deviate from the actual values over time. In order to reduce the estimation error, at least some of the measured outputs are compared to the same variables estimated by the observer. The difference is fed back into the observer after being multiplied by a gain matrix K, and so we have a closed loop observer (see Fig. 4). All developed observers are implemented in a first-order Euler approximation discrete form. At each iteration, the state vector is first calculated according to the evolution equation and then corrected online with the measurement errors (innovation) and filter gain K in a recursive prediction-correction mechanism. In this study, the gain is calculated using the Kalman filter method which is a set of mathematical equations and is widely represented in [34–36].

The EKF (Extended Kalman Filter) is probably the most commonly used estimator for nonlinear systems. However, in this study the UKF (Unscented Kalman Filter) [38–40] is chosen for the following fundamental reasons:

- The high nonlinearities of the vehicle-road model
- The calculation complexity of the Jacobian matrices which causes implementation difficulties

UKF Algorithm In this subsection, the principle of the UKF is summarized. Consider the general discrete nonlinear system:

$$\begin{cases} X_{k+1} = f(X_k,\ U_k) + w_k \\ Y_k = h(X_k) + v_k \end{cases} \tag{14}$$

where $X_k \in R^n$ is the state vector, $U_k \in R^r$ is the known input vector, $Y_k \in R^m$ is the output vector at time k. w_k and v_k are, respectively, the disturbance and sensor-noise vector, which are assumed to be Gaussian white noise with zero mean and uncorrelated.

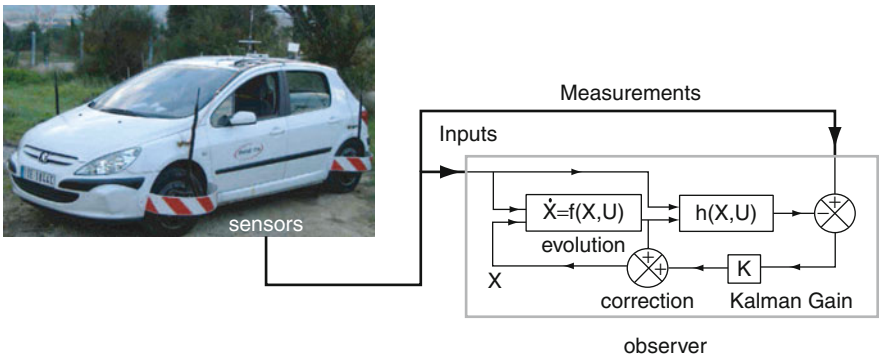

Driver Assistance System, Biologically Inspired. Figure 4
Process estimation diagram

The UKF can be formulated as follows [37–40]:
Initialization

$$\begin{cases} \bar{X}_0 = E[X_0] \\ P_0 = E[(X_0 - \bar{X}_0)(X_0 - \bar{X}_0)^T] \end{cases} \tag{15}$$

where $\bar{X}_0$ and P_0 are respectively the initial state and the initial covariance.

Sigma points calculation and time update

$$\begin{cases} \chi_{k-1} = \left[\bar{X}_{k-1},\ \bar{X}_{k-1} \pm \sqrt{(n+\lambda)P_{k-1}}\right] \\ \chi^*_{k|k-1} = f(\chi_{k-1},\ U_{k-1}) \\ \bar{x}_{k|k-1} = \sum_{i=0}^{2n} w_i^m\ \chi^*_{i,k|k-1} \\ P_{k|k-1} = \sum_{i=0}^{2n} w_i^c \left(\chi^*_{i,k|k-1} - \bar{X}_{k|k-1}\right) \\ \qquad \times \left(\gamma^*_{i,k|k-1} - \bar{X}_{k|k-1}\right)^T + Q \\ \chi_{k|k-1} = \left[\bar{X}_{k-1},\ \bar{X}_{k-1} \pm \sqrt{(n+\lambda)P_{k|k-1}}\right] \\ \gamma_{k|k-1} = h(\chi_{k|k-1}) \\ \bar{Y}_{k|k-1} = \sum_{i=0}^{2n} w_i^m \gamma_{i,k|k-1} \end{cases} \tag{16}$$

where

$$\begin{cases} w_0^m = \dfrac{\lambda}{n+\lambda} \\ w_0^c = \dfrac{\lambda}{n+\lambda} + (n - \alpha^2 + \beta) \\ w_i^m = w_i^c = \dfrac{1}{2(n+\lambda)} \quad i = 1, \ldots, 2n \\ \lambda = n(\alpha^2 - 1) \end{cases} \tag{17}$$

Measurement update

$$\begin{cases} P\bar{Y}_k\bar{Y}_k = \sum_{i=0}^{2n} w_i^c(\gamma_{i,k|k-1} - \bar{Y}_{k|k-1}) \\ \qquad \times (\gamma_{i,k|k-1} - \bar{Y}_{k|k-1})^T + R \\ P_{\bar{X}_k\bar{Y}_k} = \sum_{i=0}^{2n} w_i^c(\chi_{i,k|k-1} - \bar{X}_{k|k-1}) \\ \qquad \times (\gamma_{i,k|k-1} - \bar{Y}_{k|k-1})^T \\ K_k = P_{\bar{X}_k\bar{Y}_k} P^{-1}_{\bar{Y}_k\bar{Y}_k} \\ P_k = P_{k|k-1} - K_k P_{\bar{Y}_k\bar{Y}_k} K_k^T \\ \bar{X}_k = \bar{X}_{k|k-1} + K_k(Y_k - \bar{Y}_{k|k-1}) \end{cases} \tag{18}$$

where the variables are defined as follows: $\bar{X}_k$ and $\bar{Y}_{k|k-1}$ are the estimations respectively of the state and of the real measurement at each instant k. w_i is a set of scalar weights, and n is the state dimension; the parameter α determines the spread of the sigma points around $\bar{X}$ and is usually set to $1e-4 < \alpha < 1$. The constant β is used to incorporate part of the prior knowledge of the distribution of X, and for Gaussian distributions, $\beta = 2$ is optimal. Q and R are respectively the disturbance and sensor-noise covariance: R takes into account the uncertainty in the measured data and Q is tuned depending on the model quality. Remember that the computation of the Kalman gain is a subtle mix between process and observation noises. The less noise in the operation compared to the uncertainty in the model, the more the variables will be adapted to follow measurements. Since the lateral forces are modeled using a relaxation model based on reliable tire models, the uncertainty affected to them is not too high. However, the longitudinal force per front axle is not modeled at all; hence, it is represented by a high noise level. The other states (yaw rate, longitudinal and lateral vehicle velocity) are modeled using the vehicle's equations. Therefore, they are said to have an average noise. On the other hand, since the embedded sensors have good accuracy, the noises on the measurements are quite small. In order to reduce the complexity of the problem, both measurement covariance matrix, R, and the process covariance matrix, Q, are assumed to be constant and diagonal. The off-diagonal elements are set to 0. That means that both the measurement noises and the process noises are supposed uncorrelated.

Experimental Results

In this section, the experimental car used to evaluate the observer performances is presented. Moreover, the test conditions and the results of the previously developed observers are discussed and analyzed.

Experimental Car

The experimental vehicle shown in Fig. 4 is the INRETS-MA (Institut National de Recherche sur les Transports et leur Sécurité – Département Mécanismes d'Accidents) Laboratory's test vehicle [7]. It is a Peugeot 307 equipped with:

- Gyrometers and accelerometers that measure respectively the rotations (roll, pitch, and yaw

rates) and accelerations (longitudinal, lateral, and vertical) of the car body

- Suspension sensors that measure the distances between the wheels and the car body
- Three Correvit non-contact optical sensors:
  1. One is located in chassis rear overhanging position, and it measures longitudinal and lateral vehicle speeds.
  2. The other two are installed on the front right and rear right tires and they measure front and rear tires' longitudinal/lateral velocities and sideslip angles.
- Dynamometric wheels fitted on all four tires, which are able to measure tire forces and wheel torques in and around all three dimensions
- Steering-rack displacement sensor that is used to determine the steering angle
- Magnetic sensors that measure rotational velocity for each wheel

It is important to note that the Correvit and the wheel-force transducers (see Fig. 5) are very expensive sensors. They are used in this study as a reference for validating the estimation process. The sampling frequency of the different sensors is 100 Hz.

Test Conditions

Test data from nominal as well as adverse driving conditions were used to assess the performance of the observer presented in section "Observers Design," in realistic driving situations. We report a lane-change maneuver where the dynamic contributions play an important role. Figure 6 presents the Peugeot's trajectory (on a dry road), its speed, steering angle, and "g-g"

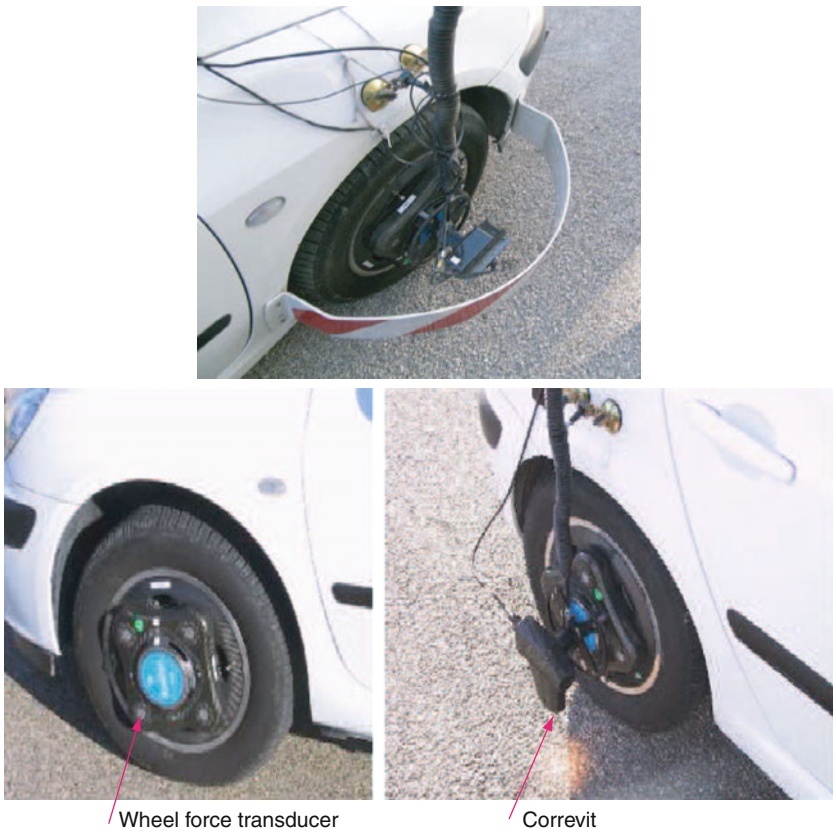

Driver Assistance System, Biologically Inspired. Figure 5
Wheel-force transducer and sideslip sensor installed at the tire level

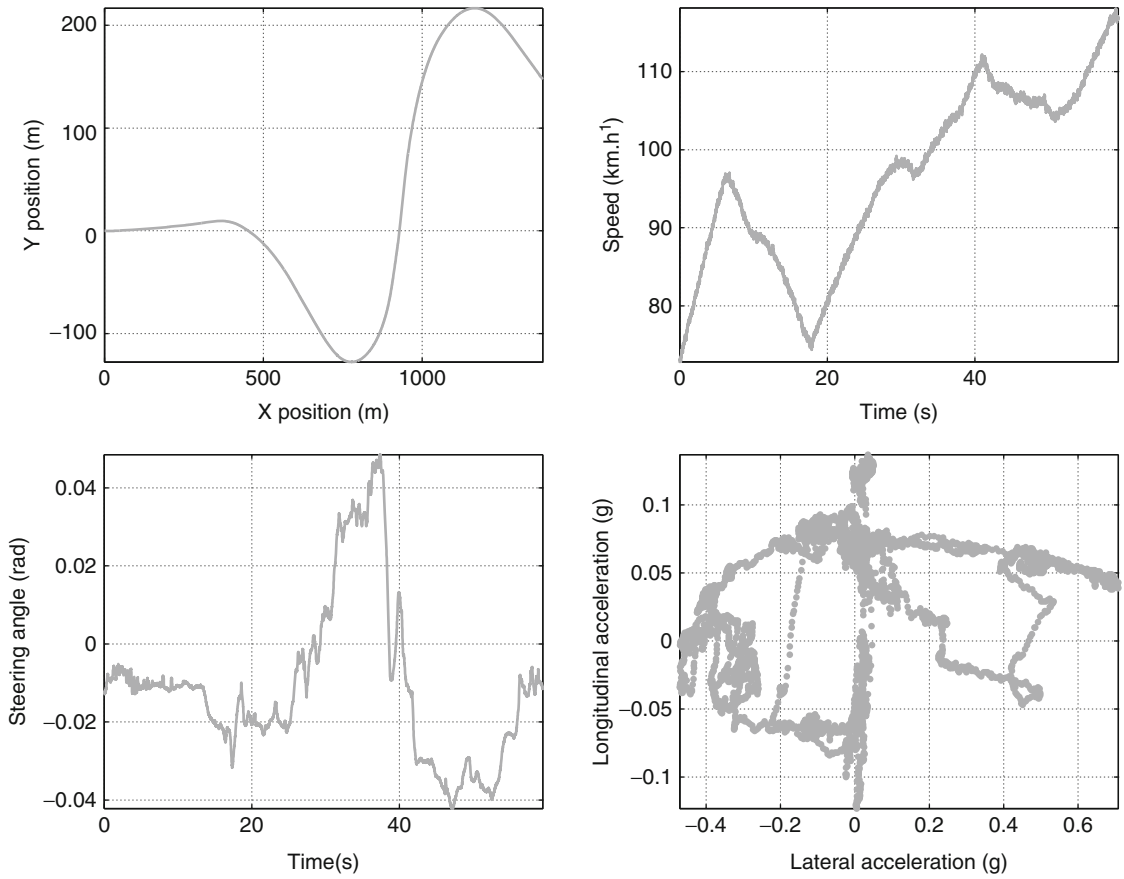

Driver Assistance System, Biologically Inspired. Figure 6
Experimental test: vehicle trajectory, speed, steering angle, and acceleration diagrams for the lane-change test

acceleration diagram during the course of the test. The acceleration diagram, which determines the maneuvering area utilized by the driver/vehicle, shows that large lateral accelerations were obtained (absolute value up to 0.6 g). This means that the experimental vehicle was put in a critical driving situation.

The estimation process algorithm was written in C++ and has been integrated into the laboratory car as a DLL (Dynamic Link Library) that functions according to the software acquisition system.

Validation of Observers

The observer results are presented in two forms: as tables of normalized errors and as figures comparing the measurements and the estimations. The normalized error for an estimation z is defined as:

$$\epsilon_z = 100 \times \frac{\| z_{obs} - z_{measured} \|}{max(\| z_{measured} \|)} \tag{19}$$

where z_{obs} is the variable calculated by the observer, $z_{measured}$ is the measured variable, and $max(||z_{measured}||)$ is the absolute maximum value of the measured variable during the test maneuver.

Figures 7 and 8 show lateral forces on the front and rear wheels. According to these plots, the observers are relatively good with respect to measurements. Some small differences during the trajectory are to be noted. These might be explained by neglected geometrical parameters, especially the camber angles, which also produce a lateral forces component [41]. It is also shown that the lateral forces on the right-hand tires exceed those on the left-hand tires. This result is clearly

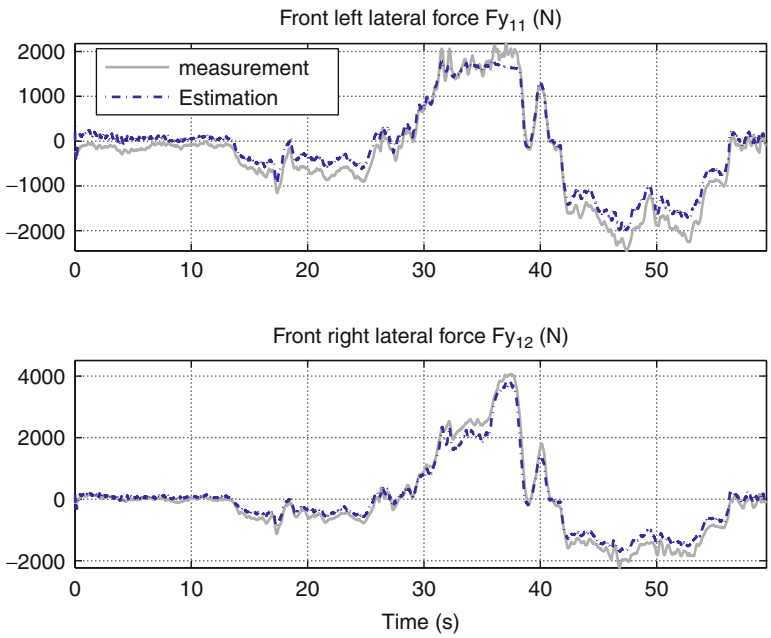

Driver Assistance System, Biologically Inspired. Figure 7
Estimation of front lateral tire forces

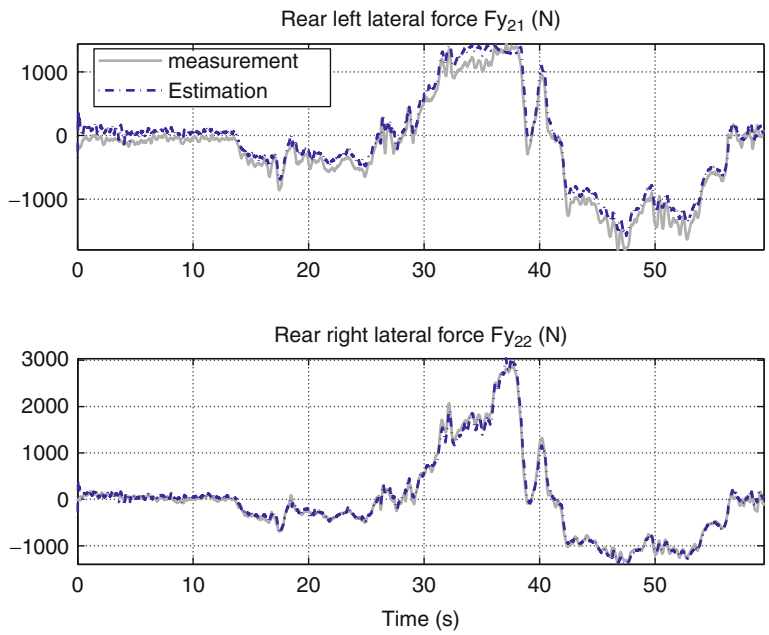

Driver Assistance System, Biologically Inspired. Figure 8
Estimation of rear lateral tire forces

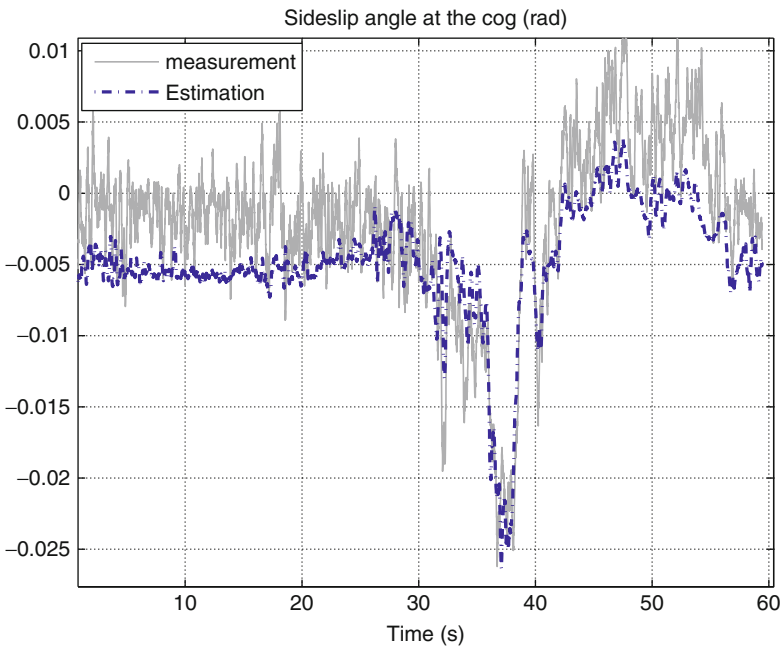

Driver Assistance System, Biologically Inspired. Figure 9
Estimation of the sideslip angle at the cog

a consequence of the load transfer produced during cornering from the left to the right-hand side of the vehicle. In fact, lateral force increases as normal force increases. Figure 9 shows how sideslip angle changes during the test. Reported results are relatively good.

Table 1 presents maximum absolute values, normalized mean errors, and normalized std (standard deviations) for lateral tire forces and sideslip angles. Despite the simplicity of the model, we can deduce that for this test, the performance of the observer is satisfactory, with normalized error globally less than 8%.

Given the vertical and lateral tire forces at each tire–road contact level, the estimation process is able to evaluate the used lateral friction coefficient μ. This is defined as the ratio of friction force to normal force, and is given by [29, 41]:

$$\mu_{ij} = \frac{Fy_{ij}}{Fz_{ij}} \tag{20}$$

The lateral friction coefficients in Fig. 10 show that the estimated μ_{ij} are close to the measured values.

Driver Assistance System, Biologically Inspired. Table 1
Maximum absolute values, normalized mean errors, and normalized std

	Max || ||	Mean %	Std %
F_{y11}	2180 (*N*)	8.23	4.80
F_{y12}	4070 (*N*)	3.70	3.74
F_{y21}	1441 (*N*)	7.51	3.52
F_{y22}	2889 (*N*)	1.91	1.77
β	0.027 (*rad*)	8.32	6.41

A closer investigation reveals that the used lateral friction coefficients μ_{12} and μ_{22} corresponding to the overloaded tires during cornering are lower than μ_{11} and μ_{21}. This phenomenon is due to the tire load sensitivity effect: the lateral friction coefficient is normally higher for the lighter loads, or conversely, falls off as the load increases [29, 41].

This test also demonstrates that μ_{11} and μ_{21} are high, especially for lateral accelerations up to 0.6,

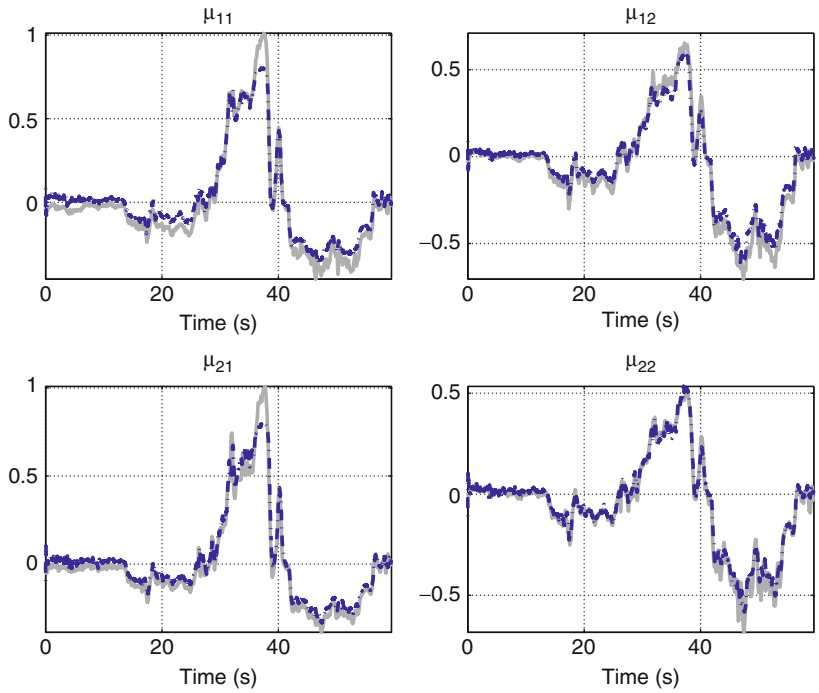

Driver Assistance System, Biologically Inspired. Figure 10
Used lateral friction coefficients developed by the tires

and that they attain the limit for the dry road friction coefficient. In fact, dry road surfaces show a high friction coefficient in the range 0.9–1.2 (implying that driving on these surfaces is safe), which means that for this test the limits of handling were reached.

Conclusion and Future Perspectives

This entry presents an interesting method for estimating lateral tire forces and sideslip angle, that is to say two of the most important parameters affecting vehicle stability and the risk of leaving the road. Consequently, the developed observer could feed control systems with fundamental vehicle-dynamics data in order to enhance vehicle safety.

The proposed observer is derived from a simplified four-wheel vehicle model and is based on unscented Kalman filtering technique. Tire–road interaction is represented by the Dugoff model. A comparison with real experimental data demonstrates the potential of the estimation process. It is shown that it may be possible to replace expensive correvit and dynamometric hub sensors by real-time software observers. This is one of the important results of this report. Another important result concerns the estimation of individual lateral forces acting on each tire. This can be seen as an advance with respect to the current vehicle-dynamics literature.

Future studies will improve the vehicle-road model in order to widen validity domains for the observer (take into account road irregularities and road bank angle), and make it adaptive with the road conditions (especially the road friction). Moreover, it will be of major importance to study the effect of coupling longitudinal/lateral dynamics on lateral tire behavior.

Acknowledgments

This work was done at Heudiasyc Laboratory UMR CNRS 6599, UTC University (Compiègne, France), in collaboration with Alessandro Victorino and Ali Charara.

Bibliography

Primary Literature

1. FARS (2007) Fatality analysis reporting system (FARS). Technical report, National Highway Traffic Safety Administration, National Center for Statistics and Analysis
2. Aparicio F, Paez P, Moreno F, Jimenez F, Lopez A (2005) Discussion of a new adaptive speed control system incorporating the geometric characteristics of the road International. J Veh Auton Syst 3(1):47–64
3. SAE Society of Automotive Engineers (2004) Bosch automotive handbook, 6th edn. SAE Society of Automotive Engineers, Warrendale
4. ESC (2003) Electronic stability control fact sheet. Technical report, ESC Coalition and DEKRA Automotive research
5. Van Zanten A (2002) Evolution of electronic control systems for improving the vehicle dynamic behavior. In: Proceedings of the 6th international symposium on advanced vehicle control (AVEC), Hiroshima, pp 7–15
6. Hsu Y, Gerdes JC (2005) Stabilization of a steerby-wire vehicle at the limits of handling using feedback linearization. In: Proceedings of IMECE 2005, AMSE international mechanical engineering congress and exposition, Florida
7. Lechner D (2008) Embedded laboratory for vehicle dynamic measurements. In: International symposium on advanced vehicle control, Kobe
8. Shim T, Ghike G (2007) Understanding the limitations of different vehicle models for roll dynamics studies. Veh Syst Dyn 45:191–216
9. Doumiati M, Baffet G, Lechner D, Victorino A, Charara A (2008) Embedded estimation of the tire/road forces and validation in a laboratory vehicle. International symposium on advanced vehicle control, Kobe
10. Doumiati M, Victorino A, Charara A, Lechner D, Baffet G (2008) An estimation process for vehicle wheelground contact normal forces. In: IFAC world congress, Seoul
11. Doumiati M, Victorino A, Charara A, Lechner D (2009) Lateral load transfer and normal forces estimation for vehicle safety experimental evaluation. Veh Syst Dyn 47(12):1511–1533
12. Wenzel TA, Burnham KJ, Blundell MV, Williams RA (2006) Estimation of the nonlinear suspension tyre cornering forces from experimental road test data. Veh Syst Dyn 44:153–171
13. Dakhlallah J, Glaser S, Mammar S, Sebsadji Y (2008) Tire-road forces estimation using extended Kalman filter and sideslip angle evaluation. American Control Conference, Seatle
14. Ray LR (1997) Nonlinear tire force estimation and road friction identification: simulation and experiments. Automatica 33(10):1819–1833
15. Baffet G, Charara A, Dherbomez G (2007) An observer of tire road forces and friction for active-security vehicle systems. Mechatronics, IEEE/ASME 12:651–661
16. Baffet G, Charara A, Lechner D, Thomas D (2008) Experimental evaluation of observers for tire-road forces, sideslip angle and wheel cornering stiffness. Veh Syst Dyn 45:191–216
17. Wilkin MA, Manning WJ, Crolla DA, Levesley MC (2006) Use of an extended Kalman filter as a robust tyre force estimator. Veh Syst Dyn 44:50–59
18. Venhovens PT, Naab K (1999) Vehicle dynamics estimation using Kalman filters. Veh Syst Dyn 32:171–184
19. Kiencke U, Daiss A (1997) Observation of lateral vehicle dynamics. Control Eng Pract 5(8):1145–1150
20. Hsu YHJ (2009) Estimation and control of lateral tire forces using steering torque. Ph.D., Department of mechanical engineering, Stanford University
21. Haffner L, Kozek M, Shi J, Jorgel HP (2008) Estimation of the maximum friction coefficient for a passenger vehicle using the instantaneous cornering stiffness. In: American control conference, Seatle
22. Gustafsson F (1997) Slip-based tire-road friction estimation. Automatica 33(6):1087–1099
23. Hahn JO, Rajamani R, Alexander L (2002) GPS-Based real time identification of tire-road friction coefficient. IEEE Trans Control Syst Technol 10(3):331–343
24. Uchanski MR (2001) Road friction estimation for automobiles using digital signal processing methods. Ph.D. thesis, University of California, Berkley
25. Koo SL, Tan HS (2007) Tire dynamic deflection and its impact on vehicle longitudinal dynamics and control. Mechatronics IEEE/ASME 12(6):623–631
26. Dugoff J, Fanches P, Segel L (1970) An analysis of tire properties and their influence on vehicle dynamic performance. Society of Automotive Engineers paper: 700377
27. Pacejka HB (2002) Tyre and vehicle dynamics. Elsevier, Amsterdam
28. Gillespie TD (1992) Fundamental of vehicle dynamics. SAE, Warrendale
29. Rajamani R (2005) Vehicle dynamics and control. Springer, New York
30. Lidner L (1993) Experience with the magic formula tyre model. In: Proceedings of the 1st international colloquium on tyre models for vehicle dynamic analysis, Amsterdam
31. Svendenius J (2007) Tire modeling and friction estimation. Ph.D. thesis, Lund University, Sweden
32. Nijmeijer H, Van der Schaft AJ (1991) Nonlinear dynamical control systems. Springer, New York
33. Doumiati M, Victorino A, Charara A, Lechner D (2009) Unscented Kalman filter for real-time vehicle lateral tire forces and sideslip angle estimation. In: IEEE intelligent vehicles symposium, Xi'an
34. Kalman RE (1960) A new approach to linear filtering and prediction problems. TransAS ME-J Basic Eng 82(D):35–45
35. Welch G, Bishop G (2001) An introduction to the Kalman filter. Course 8 University of North Carolina, Department of Computer Science
36. Durrant-Whyte H (2001) Multi sensor data fusion. Technical report, Australian center for field robotics, University of Sydney
37. Mohinder GS, Angus PA (1993) Kalman filtering theory and practice. Prentice Hall, Englewood Cliffs
38. Julier SJ, Uhlman JK (1997) A new extension of the Kalman filter to nonlinear systems. In: International symposium aerospace/defense sensing, simulation and controls, Orlando

39. Julier SJ, Uhlman JK, Durrant-Whyte HF (1995) A new extension approach for filtering nonlinear systems. In: American control conference, Seattle
40. Wan EA, Merwe RVD (2000) The unscented Kalman filter for nonlinear estimation. In: Proceedings of the adaptive systems for signal processing, communications, and control symposium, Atlanta, pp 153–158
41. Milliken W, Milliken DL (1995) Race car vehicle dynamics. SAE, Warrendale

Books and Reviews

Aga M, Okada A (2003) Analysis of vehicle stability control (VSC)'s effectiveness from accident data. In: Proceedings of the 18th international technical conference on the enhanced safety of vehicles, Nagoya

Aguirre LA, Letellier C (2005) Observability of multivariate differential embeddings. J Phys A Math Gen 38:6311–6326

Bakker E, PAcejka HB, Lidner L (1987) A new tire model with application in vehicle dynamic systems. SAE paper 890087

Besançon G (2007) Nonlinear observers and applications. Springer, Berlin

Bevly DM, Gerdes JC, Wilson C, Zheng G (2000) The use of GPS based velocity measurements for improved vehicle state estimation. In: Proceedings of the American control conference, Chicago

Brown T, Hac A, Martens J (2004) Detection of vehicle rollover. In: SAE world congress, Michigan

Doumiati M, Sename O, Martinez J, Poussot C, Dugard L (2010) Gain scheduled steering and braking control for improvement of vehicle handling and stability. In: IEEE conference on decision and control, Georgia

Doumiati M, Sename O, Martinez J, Dugard L, Gaspar P, Szabo Z, Bokor J (2011) Vehicle yaw control via coordinated use of steering/braking systems. In: IFAC world congress, Milano

Heydinger G, Howe J (2000) Analysis of vehicle response data measured during severe maneuvers. SAE paper 2000-01-1644

Jazar RN (2008) Vehicle dynamics, theory and application. Springer, New York

Smith ND (2004) Understanding parameters influencing tire modeling. Colorado State University, Formula SAE Platform

Driver Assistance Systems, Automatic Detection and Site Mapping

Andreas Wimmer, Klaus C. J. Dietmayer
Institute of Measurement, Control, and Microtechnology, University of Ulm, Ulm, Germany

Article Outline

Glossary
Definition of the Subject and Its Importance
Introduction
Sensors and Measurement Vehicle
Mapping of Safety Barriers
Detection of Beacons and Traffic Pylons
Detection and Mapping of Road Markings
Highly Accurate Road Work Map
Future Directions
Bibliography

Glossary

Advanced driver assistance system Driver assistance system with environmental perception which warns or informs the driver or even activates actuators for, for example, braking or steering.

Beacon, traffic pylon, guiding reflector post Infrastructure elements, which are often used at road construction sites for guiding motorists at areas where the traffic routing has changed or at potentially dangerous spots.

Environmental perception Concept of measuring and evaluating the environment, here: the surrounding of a vehicle.

Global Navigation Satellite System (GNSS) Satellite-based system for positioning in a global reference system, e.g., GPS, GLONASS.

Laser scanner Range sensor for environmental perception with a rotating laser beam and high angular resolution. The measurement principle is based on the time of flight of light.

Road construction site Area where a road is built or rehabilitated, also: road works, work zone.

Road marking Marking on the road to inform drivers, e.g., to delineate the traffic lanes.

Safety barrier Infrastructure element for physically separating traffic from an opposing lane or work zone, e.g., crash barrier/guard rail, Jersey barrier.

Definition of the Subject and Its Importance

Road construction sites are often the reason for traffic congestion and accidents on highways and freeways. This causes great economic and ecological costs to the society and environment through increasing travel time and additional fuel consumption. Driver assistance systems specifically designed for work zones will help to reduce the negative impact of construction sites for traffic flow. At road works, the lane width usually is

reduced, which makes lane keeping a challenging task, especially for heavy duty vehicles. It often happens that truck drivers slightly ride over the lane markings, thus preventing other vehicles to use the neighboring lane at dual carriageways. The aim is to provide lane keeping support for vehicles even in complex scenarios like road construction sites. An assistance system which laterally controls a heavy-duty vehicle highly depends on a robust and accurate estimation of the position of the vehicle within its lane. Depending on weather and lighting condition, this may not be achievable with a camera sensor only. Therefore, a system is proposed which additionally uses a laser scanner and a precise and detailed digital road work map, which might be regarded as an extension to standard navigation maps. This highly accurate map may be sent to vehicles via wireless communication technique as soon as they approach the road construction site. The following chapters describe how the layout and all typical elements of work zones on highways and freeways can be detected with modern sensors. Then, this data is used to automatically generate the above-mentioned highly accurate road work map.

Introduction

Mobility plays an important role in the society: people travel to work and goods are transported. The freight transport volume on roads constantly increases in many countries worldwide [1, 2]. On the one hand, the additional number of cars contributes to a higher possibility of congestion. On the other hand, heavy-duty vehicles cause high stress on the road surface, more than much lighter passenger cars. This makes it necessary to constantly maintain and repair the carriageways. On account of this, a road construction sites is set up.

Additionally, constructing new highways and freeways as well as the rehabilitation of existing ones is an accepted part of economic stimuli programs, as investments in the infrastructure are believed to have a high return on investment [3]. As a result, the number of road work zones is likely to increase in the future.

Road construction sites, on the contrary, account for additional stress and annoyance of car drivers due to the higher risk of traffic jams and delays caused by reduced speed limits. There is a survey, which reports an increased nervousness of drivers while traveling through a work zone [4]. Another survey on 1,700 car drivers [5] revealed that 41% regard a construction site as source of danger. Especially the reduced lane width is a reason why drivers feel uncomfortable.

If the number of lanes is reduced, the total throughput capacity may decrease as well, which is another reason for congestion. But not only discomfort of road users is an issue, there are several studies which identify a higher accident rate at a road work zones. Khattak et al. [6] extensively evaluated the effect of work zone presence on crashes in the USA. Approximately 24,000 injury crashes and 700 fatalities occur at US road construction sites every year. In this work, 36 observations have been examined, both on prework zone and during-work zone. They ascertained that the total work zone crash rate on highways is 21.5% higher than the prework zone crash rate. Similar analyses have been performed in other countries. The ARROWS project (Advanced Research on Road Work Zone Safety Standards in Europe [7]) states that "work zones generally have higher accident rates than the same road sections without a work zone". In detail, however, the data differs between countries [7, 8]. The main reasons for these accidents are driving errors and have been examined in [9]. Motorists have to recognize the work zone, assess geometry of their lane, and predict the behavior of other road users in dense traffic. An inadequate or late response may easily result in crashes [9].

The question arises, what can be done to make work zones less dangerous and stressful for drivers. Accidents statistics [10] show that rear-end collisions represent a high relative portion. This issue is addressed by driver assistance systems such as ACC (Adaptive Cruise Control) or AEB (Automatic Emergency Break) [11, 12], which are either already in series production or about to be released. But at work zones, sideswipe collisions occur more often than on regular roads. An assistance system which helps centering the vehicle within its lane will reduce the possibility for accidents of this type. There are several systems available, such as Lane Keeping Assist (LKA) which are designed for standard highways and freeways. The layout of a road construction site usually is much more complex and thus poses a great challenge for driver assistance systems. The following contribution deals with the special needs to

automatically interpret work zones for future driver assistance systems. This concept should serve several purposes: aligning the vehicle within its lane reduces the work load for the driver and thus enabling him to concentrate on the surrounding traffic, which reduces the risk of accidents. If a heavy duty vehicle is optimally laterally controlled, there will be enough space on the neighboring lane so that other vehicles can easily pass. This again reduces the stress on drivers and additionally helps to maintain the full throughput capacity as all lanes can be used.

The above-mentioned goals rely on a robust and accurate estimation of the position of the vehicle within the work zone and especially within its lane. The required robustness can be achieved by fusing information of different sensors. A single video camera designed for lane detection may not be able to detect and interpret the complex scenery of a road construction site if the lighting condition and weather is disadvantageous. Rain and thus a wet surface may produce reflections on the road, which might be misinterpreted as road marking. Adverse lighting, such as direct sunlight or fog, often decreases the contrast of the image. Longitudinal groove zones might erroneously be interpreted as lane markings and therefore lead to false detections. In dense traffic, some road markings may also be not detectable due to occlusions from other vehicles. If the road surface is covered by snow, a video-based detection of the road markings is not possible. For these reasons, a different approach has to be chosen. The idea is to use a detailed and highly accurate digital map (Road Work Map), which contains the positions of all important elements of a road construction site, for example, road markings, crash barriers, and pylons/beacons. This additional information is then used to fully reconstruct the environmental model of the vehicle, if parts of the surrounding cannot be measured with on-board sensors. For a robust detection, active sensors, such as lasers scanners or radar, are suitable as they are less susceptible to weather conditions. The laser scanner is not only able to detect other vehicles but also beacons, traffic pylons, and guard rails, which are commonly used at work zones. This data then is fused with the data of a video camera, a position estimate derived from GPS, and the detailed Road Work Map described above. Therefore, robust and reliable data can be supplied for assistance systems such as lane keeping.

Controlling a heavy-duty vehicle laterally is a demanding task [13–15]. Many systems require a look-ahead capability to enable a robust control. This can be easily provided, as the future road course can be extracted from the proposed Road Work Map.

The concept described above is divided into two parts (Fig. 1). First, the highly accurate map has to be created. For this, a measurement vehicle is equipped

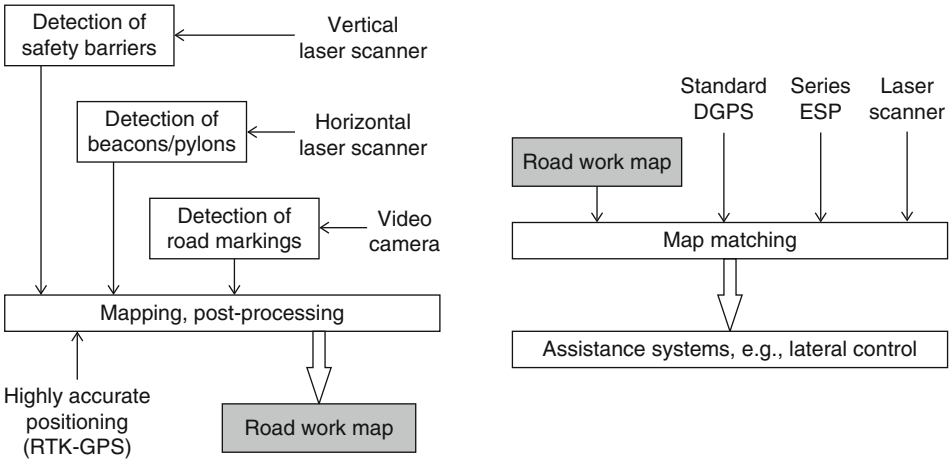

Driver Assistance Systems, Automatic Detection and Site Mapping. Figure 1
Overview over the modules for creating a highly accurate Road Work Map (*left*). Proposed system setup, which uses the Road Work Map to supply reliable data for advanced driver assistance systems (*right*)

with additional sensors. Each time when a new road construction site is set up, the vehicle will drive through the scenery and automatically detect and map all important elements. Here, post-processing and the use of additional and more accurate hardware are possible. This generated Road Work Map is transferred to facilities at the entrance of the road work zone.

The second part deals with the application for all vehicles driving through the construction site. It is assumed that cars and trucks receive a current map from the work zone via wireless communication. If the vehicles are equipped with a future sensor, for example, a laser scanner, they can match their current environmental model to the map and thus profit from additional information for assistance systems such as lane keeping assist.

The automatic generation of the Road Work Map will be presented in the following sections.

Sensors and Measurement Vehicle

The measurement vehicle is a standard car of series production, but additionally equipped with several sensors for environmental perception (Fig. 2). A front-facing gray-scale camera with a resolution of 640 × 480 pixels is used for the detection of road markings. A wide-angle lens allows the measurement of markings not only from the lanes of the host vehicle, but also from neighboring lanes.

Two Ibeo ALASCA XT laser scanners [16] are used for acquiring a horizontal and a vertical distance profile of the surrounding area. This type of sensor sends out a rotating laser beam and detects the echo reflected on obstacles. With the speed of light and the time of flight, the distance to an object can be derived. The laser scanner has an angular resolution between 0.125° and 0.5°, depending on the angle and scanning frequency. The total horizontal field of view is up to 240°; at this vehicle this is limited to 180° due to constraints of the housing and mounting position. The laser scanner provides four layers with a vertical angle shifted by 0.8°, resulting in a vertical opening angle of 3.2°. That feature enables the laser scanner to detect objects even in cases where the vehicle pitches, thus making tracking more robust. The detection range is up to 200 m, depending on the reflectivity. The good distance resolution of 4 cm enables a highly accurate detection and mapping. The front-facing laser scanner is used to detect beacons and traffic pylons as well as detecting the free space in front of the vehicle. At the rear of the vehicle, another laser scanner is mounted to acquire a vertical distance profile. This is used to detect and map safety barriers such as guard rails and Jersey barriers, which limit the road to the left and right.

Besides the novel environmental sensors, series sensors are used for estimating the position and movement of the host vehicle. Wheel encoders and a MEMS (micro-electro-mechanical systems) yaw rate sensor of a modern ESP (Electronic Stability Program) system are used for calculating the relative host vehicle movement between successive measurement frames. A standard DGPS (Differential Global Positioning System) provides global position information of about 3–10 m accuracy, depending on the measurement conditions of

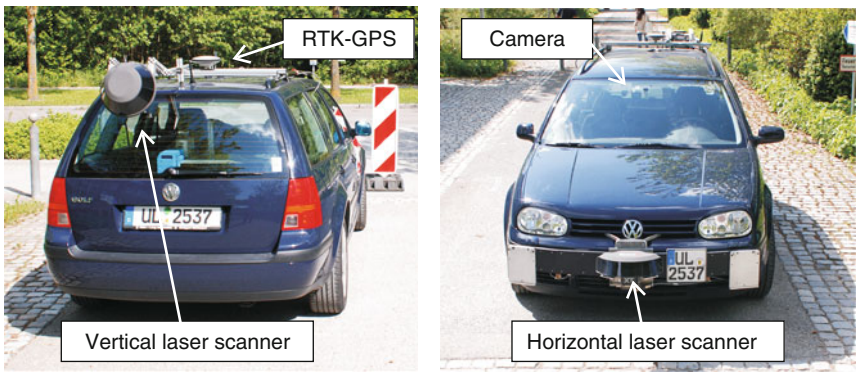

Driver Assistance Systems, Automatic Detection and Site Mapping. Figure 2
The measurement vehicle with two laser scanners, a video camera, and a highly accurate RTK-GPS

the satellites. This type of sensor is already part of series cars equipped with an on-board navigation system.

For generating the Road Work Map, a highly accurate position of the measurement vehicle must be known in a global coordinate system, for example, WGS84 [17] or UTM [18]. This position is acquired using a RTK-GPS (Real Time Kinematic GPS), which additionally uses online correction data of the land survey administration, thus enabling a horizontal position accuracy of 1 cm (RMS). This system not only uses GPS, but also GLONASS, the Russian Global Navigation Satellite System (GNSS). High accuracies can only be achieved under good measurement conditions. In cases where no or only a little number of satellites is visible (e.g., in tunnels or in street canyons), an IMU (inertial measurement unit), which contains highly accurate yaw velocity and acceleration sensors, is used. Both data is fused to obtain best position estimation (ADMA: Automotive Dynamic Motion Analyzer, [19]).

All data of position sensors and environmental sensors must be transformed to a global coordinate system. For that reason, the mounting position and alignment of each sensor relative to the vehicle must be known. Laser scanner and video camera have to be calibrated [20] and the position of the ADMA has to be known.

Besides this, timing of the sensors is similarly important on a moving platform like the measurement vehicle. Typical speeds at road work zones on highways are 80 km/h. This means, that a timing inconsistency of 5 ms already accounts for an error of over 11 cm. For that reason, laser scanner and video camera are hardware-triggered; the measurement frequency is set to 12.5 Hz. The highly accurate GPS system provides a trigger pulse every 20 ms (50 Hz). Both pulses are input to a trigger message controller which generates a time stamp message on the CAN bus (see Fig. 3). The data of the ESP is already present at the CAN bus. All of these messages are used to align sensor data from different sources to a common time reference.

Mapping of Safety Barriers

High speeds at highways and freeways even at road construction sites demand a mechanically robust protection system both for workers as well as motorists. Often, the traffic routing is changed significantly. A lane may be omitted, the width will be reduced and even one lane may be routed to the side of the opposing traffic. This poses a potential danger for all road users. For that reason, different safety barriers have been developed [21]. Crash barriers (guard rails) can be found on almost every dual carriageway. Especially for road construction sites, removable barriers are used. A commonly used type is the Jersey barrier, which is made of concrete and exists in different sizes. But steel barriers are also frequently used. Safety barriers in general serve different needs, which may contradict each other. On the one hand, these objects should have a preferably small profile to offer enough

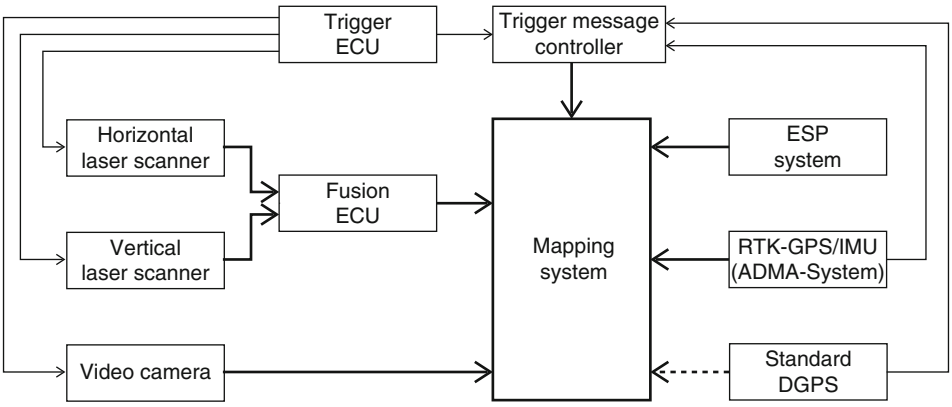

Driver Assistance Systems, Automatic Detection and Site Mapping. Figure 3
Schematic of sensors and modules of the measurement vehicle. All important sensors have trigger capability to provide accurate timing information

space for the actual traffic and the area of work. On the other hand, these barriers have to withstand impacts of heavy duty vehicles, so that these trucks can be kept within their lane in the event of a crash. Additionally, the barriers are designed to absorb some amount of crash energy, so that vehicles do not directly bounce off the wall. There are regulations which specify the physical characteristics in the event of a crash, subject to the total speed of the vehicle, its tonnage, and the angle under which it hits the barrier. Depending on the maximum speed limit and other operation purposes, different rules may apply [22]. The actual shape or material, however, is not regulated. For that reason, a detection system has to deal with numerous different outlines [21].

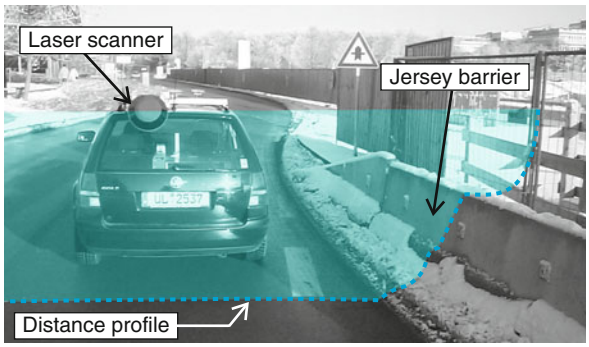

Driver Assistance Systems, Automatic Detection and Site Mapping. Figure 4
Measurement principle of a vertically mounted laser scanner. A vertical distance profile enables the detection of barriers, which are located *left* and *right* of the vehicle

A vertically scanning laser scanner mounted at the rear of the vehicle has been chosen as sensor setup for detecting and mapping safety barriers. The measurement principle is shown in Fig. 4. Because of the high angular resolution and the four layers, a detailed outline can be obtained. This data undergoes further analysis to distinguish between background (e.g., vegetation) and actual work zone infrastructure.

As a first step, the data is filtered to reduce measurement noise and to sharpen the contour [23]. A third-order Gaussian noise filter is applied on all raw laser scan points. On average roads, the mapping vehicle is subject to slight rolling, which distorts the measurement. Since the laser scanner acquires a distance profile of the road directly behind the rear of the vehicle, a regression line can be fit into the data. It can be assumed that the area which the vehicle is driving on is even. Therefore, a compensation of the roll angle is possible.

The structures of interest extend in vertical direction, as is illustrated in Fig. 5. That fact is exploited to extract suitable candidates for safety barriers. A histogram is applied on the data, where several vertical slots accumulate the number of scan points in this region. The distance between successive scan points

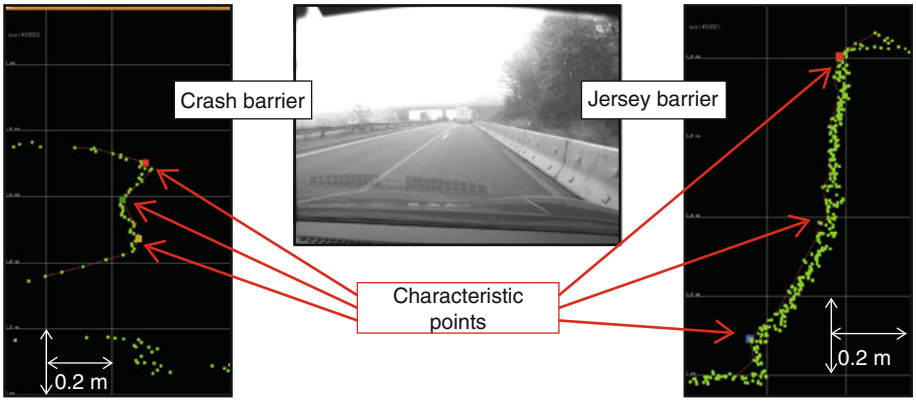

Driver Assistance Systems, Automatic Detection and Site Mapping. Figure 5
Real scan data example of a vertical scan. A guard rail is located on the *left* side, whereas a Jersey barrier is on the *right* side. As a result of the detection algorithm, three characteristic points can be extracted to incorporate them into the Road Work Map

increases in further distances from the vehicle due to the radial measurement principle of the scanner. This effect can be compensated before the accumulation is performed by applying different weights on the points based on the geometry [24]. The bins with a higher rating are regarded as valid candidates and are further examined.

Automatically detecting safety barriers requires distinguishing between background and actual infrastructure. Grass and bushes often grow underneath and around guard rails, which is also measured by the laser scanner. The Road Work Map, however, should not include background data, as this is not the border of the road. Preliminary tests have shown, that a rule-based separation of infrastructure and background only yields low detection rates. For that reason, a more sophisticated approach had to be chosen. As mentioned above, there is a variety of different safety barrier types. Extensive tests in Germany have shown that all different barriers can be grouped into a few different classes, which can be seen in Fig. 9. A similar analysis can be performed for other regions and barrier types. These types may not be totally the same structure, but they have a similar sensor reading, hence an analog outline. Separating between different classes leads to the use of a Bayesian classifier.

For making use of a Bayesian classifier, features have to be found, which best describe the different classes. The vertical distance profile of the laser scanner is processed to find a representation of the typical outline of safety barriers. As the scan points are subject to noise, a hull curve is fit into the measurement points. This hull curve is designed to represent the outer hull (closest to the vehicle), as a conservative approximation of the barrier with respect to the application. The hull curve is the basis for further feature extraction algorithms, which are based on the geometry of the structure. One obvious useful feature is the height of the barrier. Tall Jersey barriers reach approximately 1.2 m whereas guard rails have a typical height over ground of 0.8 m. Two other features are directly derived from the above-mentioned hull curve. One feature is the total length of the contour, the other one is the length of all vertical parts of the hull curve. Based on an angle interval criterion only those segments are accumulated, which are regarded as approximately vertical. Another two features are derived from the shape of guard rails. These structures show a typical grooving in the middle of the metal crash barrier. The height of this grooving is taken as one feature; the calculated width (horizontal distance of closest and furthest point to the vehicle) is taken as the other feature. For separating artificial structures like Jersey barriers from background vegetation a sixth feature is extracted: a regression line is fit into the vertical scan points. The variance of the horizontal distance of the points is regarded as a means for the smoothness of the structure. An illustration of all features can be seen in Fig. 6.

The features described above are evaluated for all different kinds of safety barriers. Several hundreds of data frames have been labeled manually to gain the typical distribution of the feature values. The result for one class and one feature value is exemplarily shown in Fig. 7. It can be seen that the class-conditional

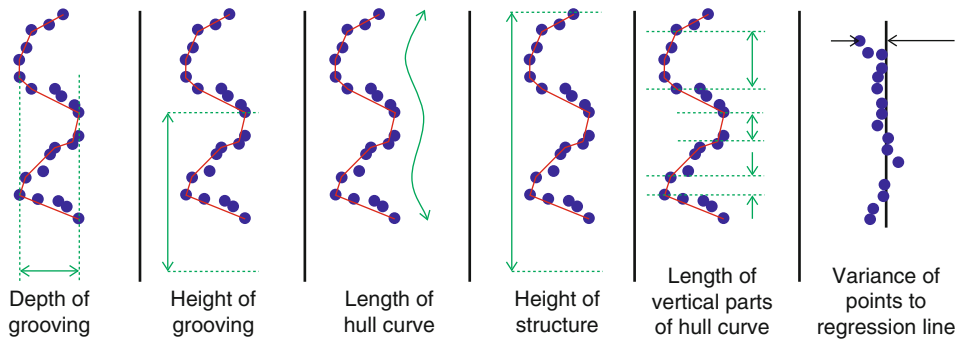

Driver Assistance Systems, Automatic Detection and Site Mapping. Figure 6
Several feature values can be calculated from the vertical scan based on the geometry of the structure. These features are used as an input for the Bayesian classifier

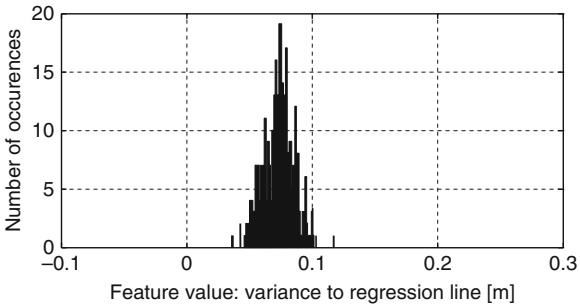

Driver Assistance Systems, Automatic Detection and Site Mapping. Figure 7
Number of occurrences of the feature values ("variance of points to regression line") for one barrier type (metal crash barrier)

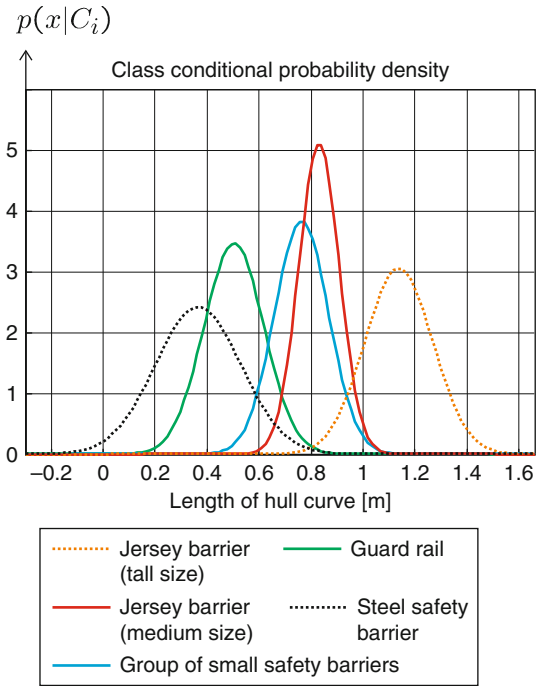

Driver Assistance Systems, Automatic Detection and Site Mapping. Figure 8
Class conditional probability density functions for five different types of barriers for the feature "length of hull curve"

probability density function $p(x|C_i)$ for a feature x and class C_i corresponds to a Gaussian distribution.

Hence, the density functions can be approximated by the mean μ and variance σ^2 of the features for every class. This fact motivates the use of a Bayesian classifier [25]. It is assumed, that all types of barriers (classes C_i) have equal prior probabilities $P(C_i)$. $P(C_i|x)$ is the probability that class i is true for the given feature value x (posterior probability) and should be calculated based on the measurement of all feature values and the predetermined class-conditional probability density functions.

This can be calculated for a one-dimensional feature and N classes:

$$P(C_i|x) = \frac{p(x|C_i)P(C_i)}{\sum_{j=1}^{N} p(x|C_j)P(C_j)}$$

The class-conditional probability density functions of all types of barriers for the feature "length of hull curve" can be seen in Fig. 8. For the six-dimensional ($d = 6$) feature vector $\underline{x}$ (mean vector $\underline{\mu}$ and covariance matrix $\underline{K}$), the class-conditional probability density is:

$$P(\underline{x}|C_i) = \frac{\exp\left(-0.5\left(\underline{x}-\underline{\mu}\right)^T \underline{K}^{-1}\left(\underline{x}-\underline{\mu}\right)\right)}{(2\pi)^{0.5d}\sqrt{|\underline{K}|}}$$

The extension to the multidimensional case results in a most probable class (type of barrier) for the given feature vector. This does not yet include the case, where the candidate structure is measured in the background. Therefore, only those measurements are regarded as valid, which lie in between the 2σ interval of its mean. This value has been found as best compromise between detection rate and the rate of non-detected safety barriers. Approximately 3,300 measurements have been labeled manually for evaluating the performance of the classifier. The overall detection rate is 97%, which indicates the differentiation between background and safety barriers. This number includes some misclassifications between different classes, that is, a Jersey barrier might have been mistaken as steel barrier (Fig. 9). Regarding correct class assignment, the correct classification rate is about 95%. Non-detected elements occur in 3% of the measurements, where the false positive rate (background erroneously detected as safety barrier) is only 2%.

After the classification of all candidates, a suitable representation of the structure is calculated. The top most and bottom point is extracted, as well as the position of the typical grooving for barriers which are

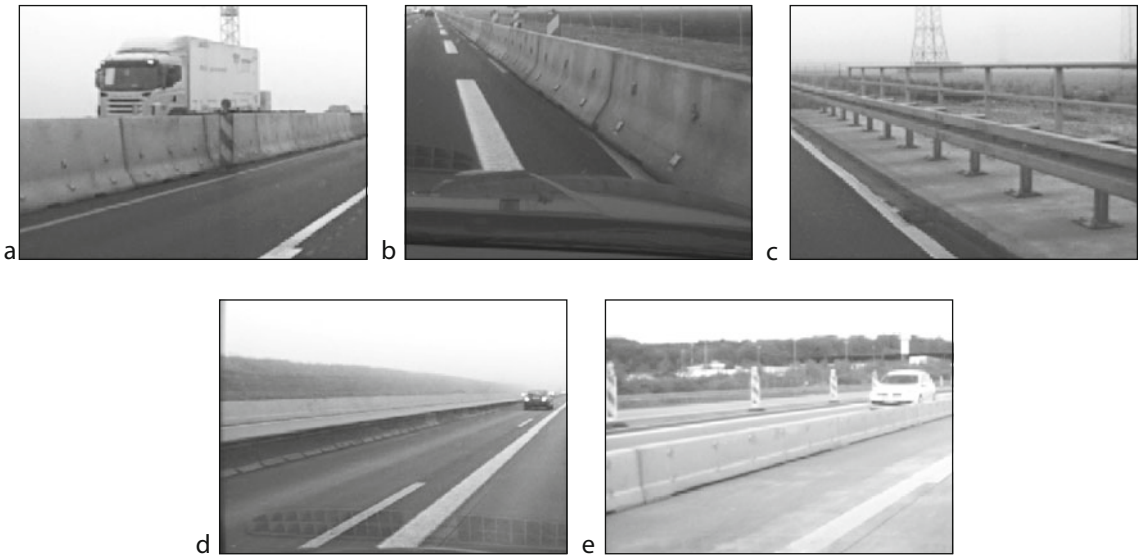

Driver Assistance Systems, Automatic Detection and Site Mapping. Figure 9
Examples of all five different types of barriers used for the classification algorithm: (**a**) tall Jersey barrier, (**b**) medium-size Jersey barrier, (**c**) standard guard rail, (**d**) steel safety barrier, (**e**) example of a group of different small safety barriers

classified as guard rails. For all other barriers, top and bottom points are derived as well, but additionally, the position of the bend of Jersey barriers is extracted. All safety barriers are now represented by three characteristic points (see Fig. 5). This enables a lower amount of data to be stored than using the whole hull curve. But on the other hand, the structure is still represented with high accuracy.

The above-mentioned process has been performed on a single frame basis. As the detection of safety barriers is meant for mapping, the connection of successive measurement points can be done with post-processing calculations. First of all, all measurement points are transformed from the local sensor coordinate system to a global frame using the position of the vehicle in global coordinates derived from the ADMA system. Then, all nodes which originate from the same class are grouped to segments. An outlier detection based on distance criteria removes false points of the classification process. All data of one segment is interpolated by a smoothing spline [26, 27]. On the one hand, this helps to bridge gaps between non measured areas (due to e.g., occlusion) and on the other hand, additional smoothing of noisy data is possible. A smoothing spline can be regarded as a combination of an interpolating spline, which connects all nodes by a piecewise continuous polynomial, and a regression line. A regression line minimizes the squared distance of all nodes to the function, where the spline, in contrast, minimizes the curvature of the function. The trade-off between those characteristics can be chosen by the smoothing factor λ. $S_i(x)$ is the polynomial in segment i and y_i the node with an assumed standard deviation of σ_i. Minimizing the function L gives the desired smoothing spline:

$$L = \lambda \sum_{i=0}^{n} \left(\frac{y_i - S_i(x)}{\sigma_i} \right)^2 + (1-\lambda) \int_{x_0}^{x_n} \{S_i''(x)\}^2 dx.$$

As the Road Work Map is designed to be transferred via wireless communication, the amount of data should be as low as possible. As the spline offers a very flexible representation of arbitrary curves, the user is able to omit nodes without losing too much accuracy. A maximum distance between the original node and the spline reconstruction of the barrier with less supporting points can be set to a value which is determined by the application. The exemplary relationship between the maximum loss of accuracy and the number of nodes of a sample barrier is shown in Fig. 10.

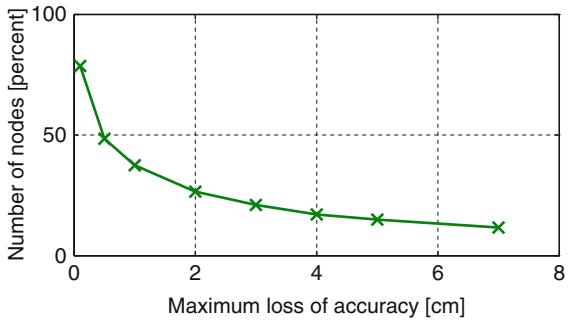

Driver Assistance Systems, Automatic Detection and Site Mapping. Figure 10
Exemplary relationship between the parameter "maximum loss of accuracy" and the number of nodes necessary for representing the barrier

Driver Assistance Systems, Automatic Detection and Site Mapping. Figure 11
Two infrastructure elements frequently used at road construction sites: beacon or guiding reflector post (*left*), traffic pylon or cone (*right*)

Besides the detection rate, the overall accuracy which can be achieved with that concept is of interest. For evaluating the preciseness of the algorithms mentioned above, the exact position of a guard rail has been manually derived by a static RTK-GPS measurement, which yields to a position accuracy of about 3 mm (1 σ interval) [28]. This is compared to the results of the automatic detection and mapping process. The evaluation shows a mean squared error of 7.1 cm and a standard deviation of 5.7 cm. This means that the proposed set-up produces results accurate enough for the generation of a detailed Road Work Map.

Detection of Beacons and Traffic Pylons

At the beginning and ending of road construction sites traffic pylons and guiding reflector posts (beacons) are often used (Fig. 11). They commonly mark the lead-in and exit tapers and guide drivers when traffic routing is changed. Pylons and Beacons are used especially for works of short duration [22], for example, when new road markings are applied on the road, as this is less time consuming than erecting safety barriers.

Both elements must have a reflecting surface. This fact is exploited when pylons and beacons should be detected with a laser scanner. The laser sensor not only measures the distance to objects but also the so called echo pulse width, which is proportional to the amount of energy returned from targets. The total amount of energy decreases with the distance of objects from the sensor. By comparing the data of reflecting and non-reflecting materials for different distances, a characteristic can be deduced, which is shown in Fig. 12. This characteristic enables the classification of each scan point to be reflector or non-reflector and is only slightly influenced by weather conditions.

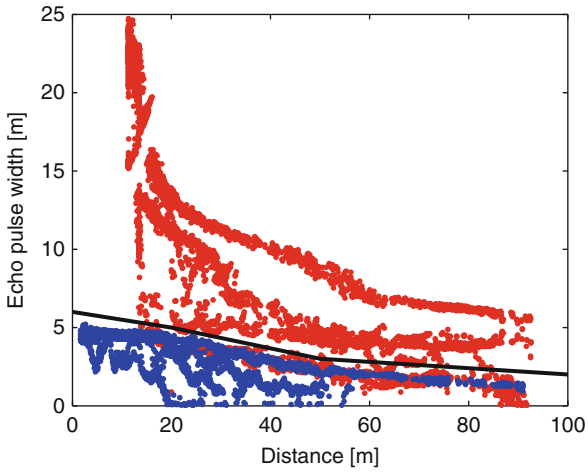

Driver Assistance Systems, Automatic Detection and Site Mapping. Figure 12
Distinguishing between reflecting and nonreflecting scan points based on the echo pulse width and the distance from the sensor. Scan points which originate from reflecting surfaces are drawn in *red*; points from nonreflecting surfaces are colored in *blue*. The *black* line shows the limiting curve which is used in the algorithm

Besides the reflector attribute, the size of the measured objects is taken into account as well. For extracting suitable beacon candidates, a measurement grid of the laser scan is used. This concept has been introduced in the field of robotics [29] and is now also used for automotive applications [30]. The area in front of the vehicle is segmented into a grid of squares with, for example, 20 cm edge length and initialized with probability value 0.5. For each scan point within one cell, the value is increased, depending on its distance and radial position to account for measurement noise. The area between the sensor and a measurement is assumed to be unoccupied, so the value of the cells on the way of the laser beam is decreased. Due to noise, this is also done distance dependent. The grid cell values can be visualized in grey scale color, where black means occupancy of 1 and white means 0 probability of occupancy (see also Fig. 13). As a result, the grid contains dark areas which are presumably occupied and hence denote the position of obstacles. Other grid cells have lighter color which means they are assumed to be on free space or the region is unknown, that is, the value remains 0.5. Based on this measurement grid, a contour extraction algorithm is applied to find the position of free standing objects with a certain size. If these objects additionally contain scan points marked as reflectors, they are regarded as candidates for pylons and beacons. After the object generation based on single frame, a tracking over time is applied. The position of all candidates of one measurement time is transformed into the next frame by compensating the host vehicle movement, as the pylons are assumed to be stationary. An association algorithm finds correspondences between last and current frame. In this way, random detections in the background can be filtered out, if no new measurements are found in this area. A track confirmation finally verifies pylon and beacon candidates. These positions can either be provided for online use while driving, or for incorporating the objects into the Road Work Map.

For assessing the preciseness of the detection and tracking algorithm, the position of some beacons and pylons has been determined manually with a static RTK-GPS measurement. The accuracy of this reference positions is approximately 3 mm (1 σ interval). This is compared to the automatic mapping process. The mean squared error evaluates to 7.3 – 7.7 cm for beacons and pylons respectively (see Fig. 14). With respect to the sensor resolution, this is a good value.

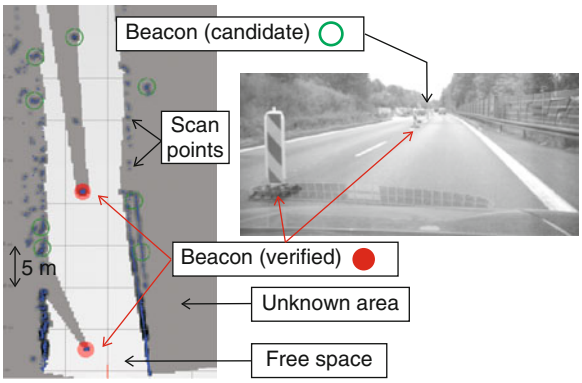

Driver Assistance Systems, Automatic Detection and Site Mapping. Figure 13
Detection of beacons using a front-facing laser scanner. Exploiting both size and reflectivity of objects enables the extraction of suitable candidates. A tracking algorithm verifies true beacons

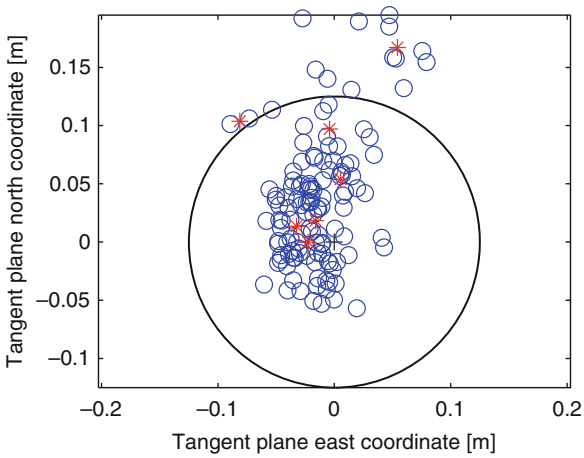

Driver Assistance Systems, Automatic Detection and Site Mapping. Figure 14
Accuracy of the mapping algorithm for traffic pylons. The true position (reference) is shown by a *black* circle with a diameter of 25 cm, which is the size of the bottom of the pylon. Each single measurement is drawn as a *blue* circle. The tracked position, which would be incorporated into the map, is shown as *red* star

Detection and Mapping of Road Markings

Road markings are used for guiding drivers on all major roads. They instruct motorists, if a lane change is possible or not. At lead-in and exit tapers, they are especially important for a safe and smooth guidance of all vehicles. At work zones the original marking (e.g., white color) may be invalidated by markings of another color (e.g., yellow), while the primary lines still remain on the road. That is the reason why lane recognition in road construction sites is such a demanding task. The Road Work Map described above should provide an interpreted description of the whole environment, including road markings.

Lane recognition with video cameras already has a long history in research. For well-structured scenarios such as highways and freeways, assistance systems for lane departure warning already exist on the market. The specific needs of such systems for road work zones, however, are not yet addressed. Current lane detection approaches offer a wide variety of concepts [31]. The first step usually is a feature extraction, followed by road modeling and finally a temporal tracking. These steps can be performed either based on monocular [32] or stereo [33] images. One of the most common concepts for feature extraction is to find edges in the image caused by a light-to-dark or dark-to-light transition of white or yellow markings on a darker road surface. Other approaches use color information or try to find areas of similar texture [34]. A template matching such as the Hough transform [32] can be applied to fit the data to a predefined model. Depending on the type of road which is mostly addressed by the application, an adapted mathematical curve is fit to the data. Commonly used are parabolic [31] or cubic curves, the assumption of constant curvature [32], or approximations for clothoids [35, 36]. The assumption of a flat world [31] may hold for many applications; otherwise, the road has to be modeled three dimensional [37]. A temporal filter such as a Kalman filter or particle filter can be applied to gain additional robustness against single frame detections [32, 34, 38].

The road markings in work zones have to be treated in a special case. The following paragraphs will describe all algorithms and adaptations for creating a highly accurate environmental model of road markings for the purpose of mapping. All lane markings should be detected at one single drive-through; therefore a video camera with wide-angle lens is used. This results in a detection range of about 20 – 35 m which is enough for mapping. Additionally, modeling a flat world in this range is a valid assumption on highways and freeways.

For edge detection, a Canny filter [39] has been chosen. This commonly used algorithm consists of multiple stages, among them are a Gaussian filter for noise reduction, an operator for determining magnitude and direction of the edge, and a non-maximum suppression. Road markings are assumed to have a left (dark to light transition) and right (light to dark transition) edge. This is exploited for finding appropriate pairs of edge points. The magnitude G and direction θ of the edge is calculated with the horizontal (x) and vertical (y) Sobel operator [39] on the image $\underline{I}$:

$$G_x = \begin{bmatrix} 1 & 0 & -1 \\ 2 & 0 & -2 \\ 1 & 0 & -1 \end{bmatrix} * \underline{I}$$

$$G_y = \begin{bmatrix} 1 & 2 & 1 \\ 0 & 0 & 0 \\ -1 & -2 & -1 \end{bmatrix} * \underline{I}$$

$$G = \sqrt{G_x^2 + G_y^2}$$

$$\theta = \arctan\left(\frac{G_y}{G_x}\right)$$

Due to image noise and blur there may be several edges in close distance. A local maximum gradient search finds the most probable position of the edge. These points are projected from image domain to vehicle coordinate system using a flat world assumption. The distance between left and right edge is the measured width of the road marking. Edge point pairs are only considered valid, if the distance matches the regulations for road marking widths [40] including some noise margin. Finally, only a little number of false detections remains.

After that, those point pairs which originate from the same road marking have to be associated. A linear extrapolation in the driving direction is calculated based on a least-square fit to associate adjacent measurement nodes. Point pairs are associated, if they have

a similar width and an appropriate distance to the preceding point pair. The measurement of lengths and widths is subject to noise. These errors can have several reasons and must be considered. The quantization through pixels results in different error values in the road plane, that is, they will be little in near distance from the vehicle and bigger in long distances. Additionally, pitching and rolling of the vehicle will result in errors because of the projection from image to flat road surface. These influences are taken into account before association. Point pairs, which cannot be associated are regarded as outliers and are neglected.

For separating one lane from the neighboring lane, dashed road markings are commonly used. The line length usually is 6 m, the gap between two line segments can be either 6 or 12 m [40, 41]. The detection algorithm only finds edges on the actual markings, so it is desirable to associate adjacent lines. Therefore, a higher order regression polynomial f_M is fit into the whole data of each line segment:

$$f_M(t, \underline{a}) = a_0 + a_1 t + \ldots + a_n t^n$$

where $a_0, \ldots, a_n$ are the polynomial coefficients and n the order of the polynomial, which can be adapted depending on the number of nodes. Finding the optimal parameters $\hat{\underline{a}}$ on a set of m data points y_i means minimizing the squared error sum S[42]:

$$\min_a S = \min_a \sum_{i=1}^{m} (y_i - f_M(t_i, \underline{a}))^2$$

This problem can be rewritten:

$$\begin{pmatrix} 1 & t_1 & t_1^2 & \cdots & t_1^n \\ 1 & t_2 & t_2^2 & \cdots & t_2^n \\ \vdots & \vdots & \vdots & \ddots & \vdots \\ 1 & t_m & t_m^2 & \cdots & t_m^n \end{pmatrix} \begin{pmatrix} a_0 \\ a_1 \\ \vdots \\ a_n \end{pmatrix} = \begin{pmatrix} y_1 \\ y_2 \\ \vdots \\ y_m \end{pmatrix}$$

$$\underline{B}\hat{\underline{a}} = \underline{y}$$

$$\hat{\underline{a}} = (\underline{B}^T \underline{B})^{-1} \underline{B}^T \underline{y}$$

The results are two polynomials which can be extrapolated and compared via distance criteria. If they overlap, these two lines are assumed to be part of the same lane marking. This method also helps to bridge gaps between non-detected segments (e.g., due to occlusion) of road markings. As road markings can have a curvature, especially when the traffic routing changes, this method assures a high flexibility for arbitrary curvatures within the field of view of the camera. Modeling curves for longer distances is done by splines in the post-processing step.

The detections based on single frames (illustrated in Fig. 15) are handed over to several post-processing stages. First, all data of the same road marking, which has been measured several times in different time steps has to be associated. This is based on distance criteria under consideration of the regulations for lane markings. As a result, there will be a lot of nodes of the same line, depending on the performance of the detection algorithm. For further processing, these nodes need to be clustered and, if necessary, the number of nodes can

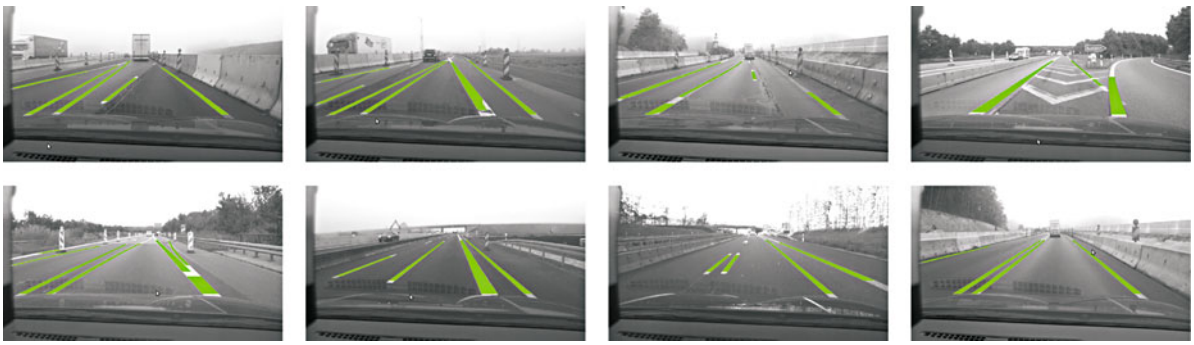

Driver Assistance Systems, Automatic Detection and Site Mapping. Figure 15
Examples of the road marking detection algorithm. The images show the performance for different lighting and surface conditions

be reduced. That is done by an algorithm inspired by the k-means clustering [43] with fixed cluster size, which preserves enough data points in areas with sparse number of points. After that, an outlier detection based on geometric parameters is applied. Background and beacons, which sometimes produce erroneous detections, can thus be removed, as they appear only in a limited number of frames and in inconsistent directions. Similar to the post-processing steps of the safety barrier mapping, a suppression of noise is achieved through the calculation of a smoothing spline and the number of nodes is reduced by an iterative process with predefined maximum error.

Highly Accurate Road Work Map

All three different elements of road construction sites can now be incorporated into the map. Beacons and traffic pylons have been measured by a front-facing laser scanner. Safety barriers are detected by a vertically scanning laser sensor and road markings are identified with a video camera. This data can now be interpreted with respect to valid and invalid lane markings. The idea is that vehicles which approach the work zones will receive a current and detailed Road Work Map. Usually, cars will not be equipped with highly accurate RTK-GPS sensors, but with standard DGPS already used for navigation applications. A matching algorithm aligns the map data with the current environmental perception, thus enabling a more accurate and extended model of the construction site. This is used as input for driver assistance systems such as lane keeping support.

Future Directions

Increasing traffic density makes driving more and more challenging. Assistance systems help to support motorists in their basic tasks. In the future, semiautomated vehicles are not completely unrealistic. Driving long distances on well-structured environments like freeways could partly be handed over from human to intelligent vehicles equipped with longitudinal and lateral control. More complex scenarios like urban traffic with pedestrians and cyclists sharing the same traffic area will still require human supervision, but there are already concepts for supporting the driver in more and more tasks.

The proposed concept of transferring maps to approaching cars and trucks requires infrastructure-to-vehicle communication. All major vehicle manufactures are involved in the research of applications for vehicle-to-vehicle or infrastructure-to-vehicle communication applications. The technical details are not yet fully specified, but the development shows a promising progress. This would enable the use of highly accurate infrastructure maps for many different future driver assistance systems [44]. These maps could also be extended by dynamic objects, such as pedestrians at intersections in urban areas.

Bibliography

1. Bureau of Transportation Statistics (2010) U.S. Department of Transportation, National Transportation Statistics, Washington
2. European Commission (ed) (2009) Panorama of transport, office for official publications of the European communities, Luxembourg
3. Helling A (1997) Transportation and economic development: a review. In: Little RG(ed) Public works management and policy, vol 2 (1). Sage, Thousand Oaks, CA, USA, pp 79–93
4. Benekohal R, Hashmi A, Orloski R (1993) Drivers' opinion on work zone traffic control. In: Transportation quarterly, 47 (1). ENO Foundation, Eno Transportation Foundation, Washington, DC, USA, pp 19–38
5. DEKRA (ed) (2009) Road works cause anxiety – Baustellen sorgen fuer Nervenflattern, DEKRA press and information, Stuttgart
6. Khattak Asad J, Khattak Aemal J, Council FM (2002) Effects of work zone presence on injury and non-injury crashes. In: Accident analysis and prevention, vol 34(1). England, Elsevier Science Ltd, Amsterdam, Netherlands, pp 19–29
7. ARROWS Consortium (1999) Advanced research on road work zone safety standards in Europe (arrows), road work zone safety, practical handbook, background report. National Technical University Athens
8. Board of Trustees for Traffic Safety (ed) (2007) Hazard area freeway road works? – Gefahrenstelle Autobahnbaustelle? Kuratorium für Verkehrssicherheit – Board of trustees for traffic safety, Austria
9. Twisk D, Mesken J (2007) PREVENT – Education to improve road safety around work zones. In: Larsson TJ Safety science monitor, vol 11(2). Perth, Australia
10. Wang J, Hughes WE, Council FM, Paniati JF (1996) Investigation of highway work zone crashes: what we know and what we don't know. In: Transportation research record 1529. TRB, National Research Council, Washington
11. Marsden G, McDonald M, Brackstone M (2000) Towards an understanding of adaptive cruise control. In: Transportation research part C. Elsevier Science, Pergamon

12. Bishop R (2000) A survey of intelligent vehicle applications worldwide. In: Proceedings of the IEEE intelligent vehicles symposium, Dearborn, 2000
13. Martini S, Murdocco V (2003) Lateral control of tractor-trailer vehicles. In: Proceedings of 2003 IEEE Conference on Control Applications, CCA
14. Wang J-Y (1999) Robust H∞ Lateral control of heavy-duty vehicles in automated highway system. In: Proceedings of the American control conference, San Diego
15. Fritz H (1999) Longitudinal and lateral control of heavy duty trucks for automated vehicle following in mixed traffic: experimental result from the CHAUFFEUR project. In: Proceedings of the 1999 IEEE international conference on control applications. Kohala Coast-Island of Hawai'i, Hawai'i
16. Ibeo Automobile Sensor GmbH (2006) ALASCA user manual, Hamburg
17. European Organisation for the Safety of Air Navigation (1998) WGS 84 implementation manual, European organisation for the safety of air navigation, Brussels, Belgium and Institute of Geodesy and Navigation University FAF Munich, Germany
18. Osborne P (2008) The mercator projections, edinburgh, http://mercator.myzen.co.uk/
19. GeneSys GmbH (2010) ADMA user manual, Offenburg
20. Kaempchen N (2007) Feature-level fusion of laser scanner and video data for advanced driver assistance systems. Ph.D. dissertation, University of Ulm, Ulm, Germany
21. Knoll E (ed) (2004) Der elsner – handbook for traffic and transportation. Otto Elsner Verlagsgesellschaft mbH & Co. KG, Dieburg, Germany
22. German Ministry of Transport (Bundesministerium für Verkehr, Bau- und Wohnungswesen, Abteilung Straßenbau (BMVBS)) (1995) Safety instructions for road construction sites – Richtlinien für die Sicherung von Arbeitsstellen an Straßen, Bonn, Germany
23. Wimmer A, Weiss T, Flögel F, Dietmayer K (2009) Automatic detection and classification of safety barriers in road construction sites using a laser scanner, In: IEEE proceedings of intelligent vehicles symposium, Xi'an, China
24. Weiss T, Dietmayer K (2007) Automatic detection of traffic infrastructure objects for the rapid generation of detailed digital maps using laser scanners. In: Proceedings of the 2007 IEEE intelligent vehicles symposium, Istanbul, Turkey
25. Duda RO, Hart PE, Stork DG (2000) Pattern classification. Wiley, New York
26. Reinsch CH (1967) Smoothing by spline functions. In: Reinsch CH (ed) Numerische mathematik, vol 10. Oxford University Press, New York, pp 177–183
27. Pollock D S G (1993) Smoothing with cubic splines, Department of Economics, Queen Mary College, University of London
28. NovAtel Inc (2007) Datasheet for receiver OEMV-3. NovAtel Inc, Canada
29. Thrun S, Fox D, Burgard W (2005) Probabilistic robotics. MIT Press, Cambridge
30. Weiss T, Schiele B, Dietmayer K (2007) Robust driving path detection in Urban and highway scenarios using a laser scanner and online occupancy grids. In: IEEE proceedings of intelligent vehicles symposium, Istanbul, Turkey
31. McCall JC, Trivedi M (2006) Video-based lane estimation and tracking for driver assistance: survey, system, and evaluation. In: IEEE transactions on intelligent transportation systems, Piscataway, NJ, USA
32. Taylor C, Koŝecká J, Blasi R, Malik J (1999) A comparative study of vision-based lateral control strategies for autonomous highway driving. I J Robotics Res, Sage Publications, Thousand Oaks, CA, USA
33. Bertozzi M, Broggi A (1998) GOLD: a parallel real-time stereo vision system for generic obstacle and lane detection. In: IEEE transactions on image processing, Piscataway, NJ, USA
34. Apostoloff N, Zelinsky A (2003) Robust vision based lane tracking using multiple cues and particle filtering. In: Proceedings of IEEE intelligent vehicles symposium, Piscataway, NJ, USA
35. Dickmanns ED, Mysliwetz BD (1992) Recursive 3-D road and relative ego-state recognition. In: IEEE transactions on pattern analysis and machine intelligence, vol 14(2), IEEE Computer Society, Washington, DC, USA, pp 199–213
36. Gumpp T, Nienhüser D, Liebig R, Zöllner JM (2009) Recognition and tracking of temporary lanes in motorway construction sites. In: IEEE proceedings of intelligent vehicles symposium, Xi'an, China, IEEE, Piscataway, NJ, USA
37. Nedevschi S, Schmidt R, Graf T, Danescu R (2004) 3D Lane detection system based on stereovision. In: IEEE intelligent transportation systems conference, Piscataway, NJ, USA
38. Loose H, Franke U, Stiller C (2009) Kalman particle filter for lane recognition on rural roads. In: IEEE proceedings of intelligent vehicles symposium, Xi'an, China, Piscataway, NJ, USA
39. Jähne B (2005) Digitale bildverarbeitung. Springer, Berlin
40. Bundesministerium für Verkehr (ed) (1993), Instructions for the construction of road markings – Richtlinien für die Markierung von Straßen, Bundesministerium für Verkehr – German Ministry of Transport, Köln
41. Research Association for Road and Transportation (ed) (1996) Instructions for the construction of roads – richtlinien für die anlage von Straßen, Forschungsgesellschaft für Straßen- und Verkehrswesen – Research association for road and transportation, Köln
42. Ljung L (1999) System identification: theory for the user. Prentice Hall, New Jersey
43. MacQueen J (1967) Some methods for classification and analysis of multivariate observations. In: Proceedings of fifth Berkeley symposium on mathematical statistics and probability, vol 1. University of California Press
44. Blervaque V, Mezger K, Beuk L, Loewenau J (2006) ADAS horizon – how digital maps can contribute to road safety. In: Proceedings of advanced microsystems for automotive applications Berlin

Driver Behavior at Intersections

Toshihisa Sato, Motoyuki Akamatsu
Human Technology Research Institute, National Institute of Advanced Industrial Science and Technology (AIST), Tsukuba-shi, Ibaraki, Japan

Article Outline

Glossary
Definition of the Subject and Its Importance
Introduction
Behavioral Data Collection in an Actual Road Environment
Analysis of Data Distribution Based on Traffic and Road Environments
Modeling of Driver's Preparatory Behavior Before Making Driver's Side Turn
Future Directions
Bibliography

Glossary

Driving simulator An indoor system providing a multisensory environment for a driver to perceive and control virtual vehicle movements. A standard simulator has a vehicle cockpit; a visual system, including screens and image generators; an audio system; and a motion system that gives the driver vehicle vibration and motion linked with the driver's operations.

HMI (human–machine interface/interaction) Interface or interaction between users and computer-based systems. The systems provide the users with visual, auditory, and/or haptic information. The users operate the systems using input devices, including a remote controller, a touch panel, and their voice.

Human-centered design Interface design of information contents or information devices that is adaptive to human cognitive and/or physical functions. In the automotive technology, research on the driver characteristics in perceptual, cognitive, and operational functions while driving is conducted for the purpose of applying the research findings to the interface design development of driver assistance systems, such as car navigation systems.

Instrumented vehicle A passenger vehicle equipped with various sensing technologies to detect and track internal and external conditions and a driving recorder system to save the measured data.

ITS (intelligent transport systems) Application of information, communication, and sensor technologies to multiple modes of transportation, including road, rail, air, and waterborne transports. Expected benefits by the introduction of ITS are reduction of traffic accidents, mitigation of traffic congestion, environmental improvement, positive economic impact, etc.

Naturalistic driving behavior Observation of driving behavior that takes place in its natural setting. The drivers are given no special instructions, no experimenter is present, and the data collection instrumentation is unobtrusive.

Preparatory behavior Driving behavior that occurs before making a turn at an intersection. This behavior includes activation of turn signal, release of the accelerator pedal, movement of driver's right foot to cover the brake pedal, and onset of pressure on the brake pedal.

Definition of the Subject and Its Importance

Vehicle navigation and communication systems play a role of an information center in road-traffic environments and a key component for realizing ITS (intelligent transport systems). The most popular function of the in-vehicle navigation systems is route guidance. The route guidance system presents drivers real-time, step-by-step driving instructions, such as preparation for turns, exits, or road changes. This function helps drivers choose and maintain efficient routes with less mental effort.

However, an inadequate interface design may lead to driver distraction or inattention to the primary driving tasks. This results in a reduction of driver acceptance of the route guidance as well as a reduction of driving safety. It is important to develop interface design of route guidance system in order for drivers to recognize the displayed contents correctly.

The in-vehicle navigation systems provide drivers with visual and auditory route guidance instruction as

well as a digital map with road information. The auditory message of the route guidance is usually presented three times while approaching the target intersection [1]. First, about 700 m before the target intersection, auditory information is provided for drivers to select the lane appropriate for the next turning direction. Second, guidance about 300 m before the intersection is presented when drivers can recognize a landmark. Third, just prior to reaching the intersection, a voice message (e.g., "turn to the right soon!") attracts attention to make the turn and can trigger a change in the driver's maneuvers from moving straightforward to preparing to make the turn. This essay focuses on the presentation timing of the last voice guidance. This last instruction is very important for the maneuver of tracing the provided route, especially where drivers have difficulty in recognizing the landmarks around the turning point due to complex road-traffic environments. Too early or too late presentation timing of the last message may lead to drivers' annoyance with the provided guidance and to drivers' navigational error, such as passing over the turning point. It is important to develop the presentation timing of the last voice guidance that enables drivers to begin preparing to make a turn at the same location as in their typical driving pattern. Understanding of the typical onset location of driver preparatory behavior for making a driver's side or curb side turn is necessary in the development of the optimal presentation timing.

When drivers missed correct turn, the navigation systems search the route again and update the guidance information. Rerouting requires a little time, and this delay may lead to a reduction in driver utilization of the route guidance. Prediction of the onset location of the driver's preparatory maneuvers prior to reaching the target intersection can contribute to enhancing navigation rerouting functions. For example, if a driver did not begin to prepare to make a turn after reaching the predicted onset point, the in-vehicle system can assess the driver's navigational error, determining whether he/she made an error by identifying an incorrect turning point or did not notice the information provided. The system can then reissue visual and/or auditory assistance information about the location of the target intersection or search the alternative route soon and present the updated route guidance. Modeling of the typical preparation behavior based on the driving behavior data is necessary to predict the onset location where the driver begins to prepare to make a turn under a specific road-traffic situation.

This essay describes a methodology of understanding drivers' typical preparatory behavior in a real road-traffic environment and of constructing preparatory behavior model using the behavioral data measured on the real road.

Introduction

Driving tasks have three levels of hierarchical structure: strategic, tactical, and operational [2]. The strategic level involves trip planning, determination of trip destination, and route choice, as well as general considerations about driving, including an evaluation of the costs, risks, satisfaction, and comfort. Tactical behaviors involve decision-making, such as the driving speeds, headway distances, and gaps in traffic. Operational behaviors involve the stable driving of the vehicle, including acceptable steering, and moderate acceleration and braking. The behavior at higher level has an effect on that at lower level, e.g., maneuvers at the tactical level (turning, overtaking, obstacle avoidance, and gap acceptance) must meet the criteria derived from the general goals set at the strategic level, and vice versa: e.g., a driver selects a route that includes many roads with less traffic volume when the driver likes a large margin to vehicles in the vicinity of his/her car.

Route guidance of in-vehicle navigation systems supports drivers' trip planning at the highest level of the driving tasks. In Japan, the route guidance systems presented a digital map, vehicle's current location on the map, and visual and auditory route guidance instructions to a destination as HMI in 1990s when the navigation systems began in widespread use. On the other hand, turn-by-turn displaying methods just indicating the next turning direction on the display were introduced in U.S. and Europe. Historically, the first type of the route guidance systems was developed by Honda in 1981. The contemporary navigation system indicating the vehicle's location on a map shown on a display device was mounted on the Crown of Toyota in 1987. Then, the first practical route guidance system which had real-time presentation of the vehicle location on a road map was the navigation system mounted

on the Nissan Cima, developed by Sumitomo Electric Industries, Ltd. in 1989. Please see literature [3] for development and commercialization process of navigation systems in Japan.

Route guidance systems using a digital map are now on the market all over the world. Recently, the navigation systems have more sophisticated functions, including real-time update of route guidance based on dynamic road-traffic information. These systems are integrated with several kinds of road sensors and road-traffic management center via multiple media. The systems provide the driver with the route guidance which takes into account current traffic jam conditions. In addition, the navigation systems present drivers with information on various facilities around the driving area, such as a car park.

The advanced functions of the in-vehicle navigation systems are expected to enhance road safety as well as to assist drivers in choosing and maintaining efficient routes with lower mental workload. However, the use of the new systems has strong concerns about driver confusion and distraction that can lead to an interference with the primary driving task and a reduction of driver acceptance of the provided information. Therefore, research on in-vehicle navigation systems with a human-centered design approach has been conducted and focused on the development of the interface design that is adapted to driver behavior in driving contexts [4].

The route guidance of in-vehicle navigation systems consists of visual and auditory information. The systems display a digital map with the route to a destination in real time while traveling. About 300 m before the target intersection, the systems present a magnified map of the vicinity of the intersection and the direction of the upcoming turn. The provision of the magnified map helps drivers identify the location of their next turn. Thus, visual information accompanying the magnified map is helpful in reducing drivers' misunderstanding of the target intersection. Human factor studies have investigated the information contents based on drivers' cognitive map and landmark designs that are suitable and acceptable to drivers [5–9].

In addition to the visual information, the navigation systems present auditory route guidance three times while approaching an intersection where to turn. The presentation timing is about 700 m before the intersection, about 300 m before it, and just prior to reaching it. The distance required for a lane change while approaching the target intersection, investigated by an empirical survey on urban roads [10], is "700 m." The distance where a landmark around the intersection (e.g., intersection sign, traffic signal, configuration of intersection) becomes recognizable and drivers identify the turning point is "300 m." The last guidance is important for drivers to leave the current road correctly because drivers frequently cannot recognize the landmarks around the turning point because of complex road-traffic environments, especially in urban areas. It is important to present the last guidance with appropriate timing that helps drivers begin preparing to make a turn at the same location as in their usual driving pattern. However, there may be some variations in the driving operations because the driving behavior is influenced by the road-traffic conditions [11]. Measurement and analysis of driver preparatory behavior prior to turning in an actual road environment are required and should clarify the influence of various road-traffic conditions – such as the presence of vehicles to the front and rear, the structure of the intersection, and the condition of the road surface – on the driver preparatory maneuvers. This essay focuses on the presentation timing of the last route guidance before making a driver's side turn at an intersection and deals with the existence of a lead and following vehicle and the intersection type (standard intersection, T-junction, and intersection after a curve). The behavior data described in this essay were collected on roads in Japan, where driving is on the left side of the road. Therefore, the right turn as driver's side in this essay corresponds to a left turn where driving is on the right side of the road, e.g., the United States.

Current navigation systems reroute when a driver failed to identify the turning point or failed to notice the provided guidance and he/she passed over the target intersection. Prediction of the onset location of the driver preparatory behavior can contribute to detecting the driver's navigational error before passing through the intersection at which to turn. The in-vehicle system can assess driver's failure of identifying the required turning point or his/her unawareness of the information provided if the driver does not begin to prepare for making a turn after reaching the predicted location.

Thus, the preparatory behavior prediction can lead to further advanced functions of the route guidance systems, such as restating the route guidance and quick rerouting and providing the updated route. The former function is expected to reduce the driver's error of passing over the target intersection, and the latter is expected to enhance usability of the route guidance systems. The influence of the road-traffic environments on the driver preparatory behavior should be evaluated quantitatively in order to predict the onset of the behavioral event. To accomplish this, a driving behavior model should be constructed based on naturalistic behavioral data measured repeatedly in a real environment.

Figure 1 presents a design concept of the presentation timing adapted to driver's typical preparatory behavior and the detection of driver navigational error based on prediction of the preparatory behavior onset. This essay describes a method of estimating typical onset location of driver behavior for preparing to make a driver's side turn and of predicting the onset location using statistical driver model.

Behavioral Data Collection in an Actual Road Environment

Overview of Data Collection Methods

Driving a vehicle in traffic is a task that is influenced by road-traffic environments. The preparatory behavior before making a turn is also influenced by traffic conditions while approaching an intersection where to turn and by road environments of the target intersection. It is essential to collect data on the external factors that affect the driver preparatory behavior in addition

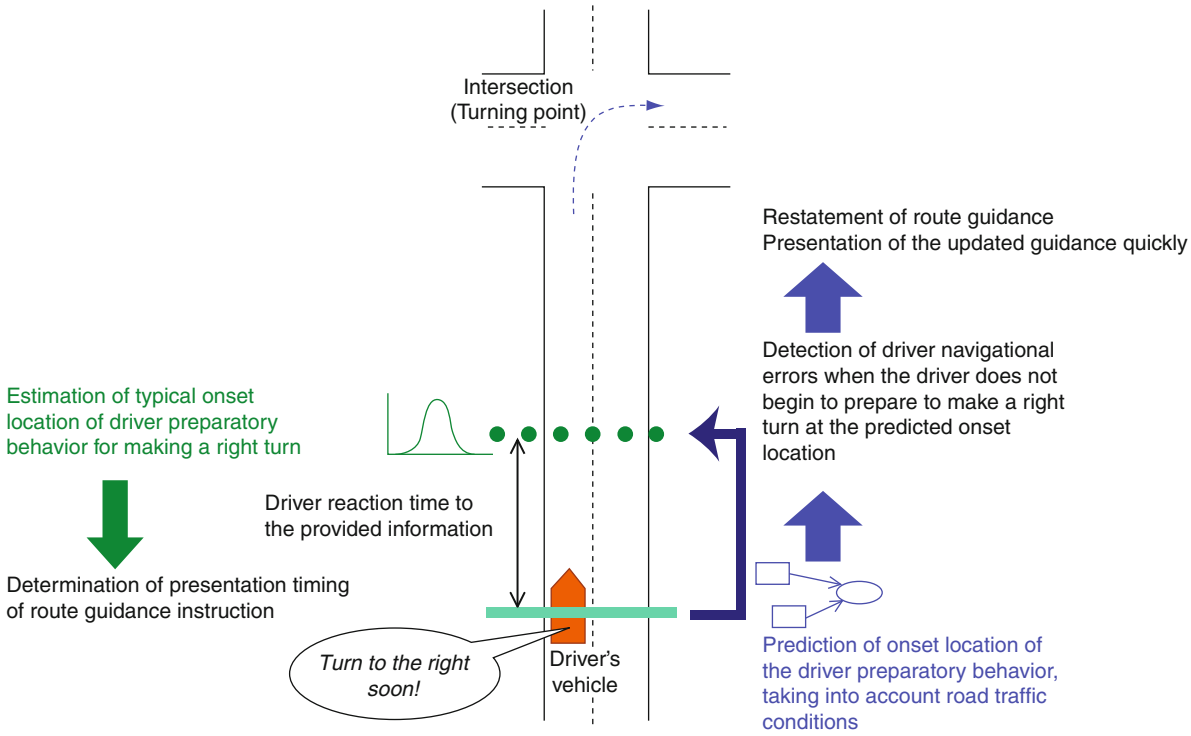

Driver Behavior at Intersections. Figure 1
Design concept of the presentation timing of last voice guidance compatible with driver behavior and the detection of driver navigational error. The typical onset location of driver preparation before making a driver's side turn is estimated based on measurement of naturalistic behavior data while approaching a target intersection. The driver navigational error is detected based on comparison between the actual behavior and prediction of the onset location using statistical driver model

to the data on the driver's operations for the preparations for making a turn.

A driver experiences only a few kinds of traffic conditions for a short term. For example, 1 day, there is a lead vehicle driving slowly in front of the driver's vehicle on one leg of a route; another day, there is a lead vehicle driving faster on the same leg; and the other days, he/she has no preceding vehicles on the same leg. Thus, a few days are too short to understand the driver's typical preparatory behavior under real traffic conditions. It is necessary to carry out repeated experiments on the same roads over a long term. The long term for the data collection is effective in recording the driver preparatory behavior on various kinds of road conditions, including dry, wet, and rainy roads. Analysis of the driving behavior that is measured on different intersections with various structures is necessary to investigate the influence of the road structures on the driver preparatory behavior. A driving route, which includes several kinds of intersection types – e.g., intersection on a straight road, intersection at the end of the road (T-junction), intersection after a curved road, and intersection after a slope – should be taken into account when designing and conducting an experiment.

Methodologies for the behavior data collection are point measurements, driving simulator experiments, and field experiments. Traffic-flow point measurements are conducted in which the number of vehicles, the time intervals between passing vehicles, and the traveling speeds are recorded via video cameras fitted at the site [12, 13]. However, the point measurements cannot clarify onset location and timing of driver decelerating operations.

Driving simulators have been used as experimental tools to measure driver operations and to examine the relationships between the external factors and the driving behavior [14–16]. Recently, image generation technologies, such as construction of geometric road structures based on CAD data and construction of scenery along the roads using texture mapping, have been applied to the development of realistic road environments [17]. However, the simulator cannot fully reproduce natural driving behavior in a real road-traffic environment due to mechanical restrictions, e.g., the lack of longitudinal movement during deceleration and the lack of speed and distance perception [18, 19]. These limitations negatively influence the driver operations before making a driver side turn. For example, a driver tends to apply the brake pedal several times before coming to a full stop at the target intersection in the driving simulator environment, whereas the stroke of the brake pedal is executed once and the driver presses down on the brake pedal gradually in the real road environment. Therefore, the onset location and timing of the preparatory behavior at a real intersection differ from those at the intersection of a driving simulator where the geometric structure and roadside landmarks are represented exactly similar to the real intersection.

Although repeated field experiments for a long period have a risk for traffic accidents, the real-world experiments are the most effective in collecting naturalistic data on the driver preparatory behavior. The recent development of memory devices to record large-scale data and sensing technologies to detect and track external conditions contributes to the realization of the field data collection. The following two approaches are used for the repeated experiments on an actual road: (1) installation of memory devices and sensors into drivers' owned passenger vehicles and (2) development of instrumented vehicles equipped with various sensors and a driving recorder system.

The representative project of the former method is the 100-Car Naturalistic Driving Study by Virginia Tech Transportation Institute [20]. In this project, several data collection devices, including speed sensor, GPS, accelerometers, front and rear radar sensors, and five channels of digital video, are installed into participants' owned vehicle. The large-scale behavior data have been recorded over 13 months with the primary purpose of collecting precrash and near-crash naturalistic driving data. The advantages of using privately owned vehicles are to eliminate the participants' unfamiliarity with an experimental vehicle and to eliminate their awareness of being monitored. This method has limitations from the viewpoint of driver preparatory behavior analysis in extracting a large amount of behavior data around the target intersections from the large-scale data.

Use of Instrumented Vehicles to Collect Behavioral Data

Instrumented vehicle is developed to collect driver behavior data as well as to measure the vehicle status and the

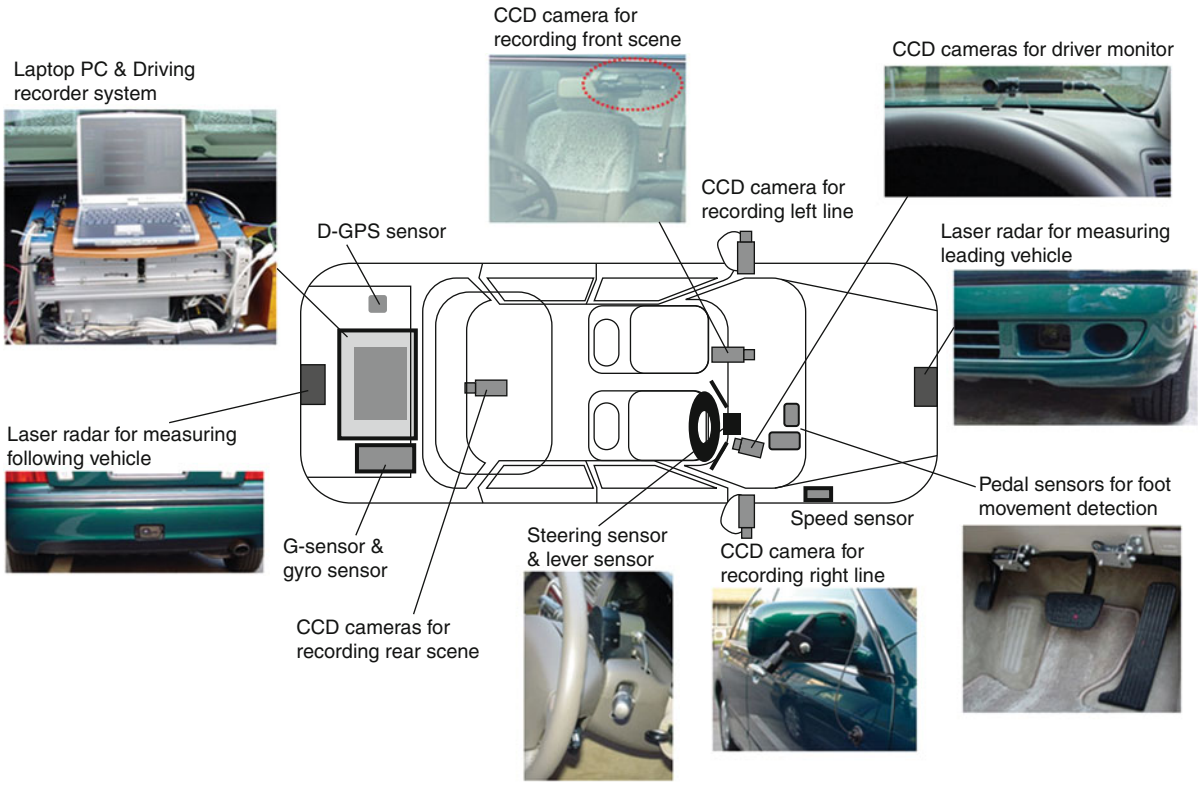

Driver Behavior at Intersections. Figure 2
Overview of the AIST instrumented vehicle. Several sensors and a driving recorder system are fixed inside the trunk where the drivers cannot see the instruments, thus encouraging naturalistic driving behavior. A participant drives alone this vehicle during measurement trials

traffic conditions around the vehicle. Figure 2 presents the AIST instrumented vehicle [21]. The following data sets are collected using the instrumented vehicle:

- Driving speed
- Vehicle acceleration (longitudinal, lateral, and vertical)
- Angular velocity (roll, pitch, and yaw)
- Geographical position of the vehicle
- Relative distance and speed to leading vehicle
- Relative distance and speed to following vehicle
- Application of accelerator and brake pedals
- Position of driver's right foot (covering the pedal without pressing)
- Steering wheel angle
- Turn signal activation
- Visual images (forward and backward traffic scenes, left and right lane positions, and the driver's face)

A speed sensor detects the driving speed using a speed pulse signal. A G-sensor detects the vehicle acceleration in longitudinal, lateral, and vertical directions, and a gyro sensor measures the angular velocity in roll, pitch, and yaw directions. A D-GPS sensor obtains the geographical position of the vehicle. Laser radar units fixed within the front and rear bumpers record the relative distance and relative speed to the leading and following vehicles. Potentiometers measure the applications of the accelerator and brake pedals. Laser sensors fitted above the pedal surfaces detect the position of the driver's right foot (covering the accelerator or brake pedal without pressing). Encoders added to the steering wheel and turn signal lever record the steering wheel angle and turn signal activation. A total of five CCD cameras are used to record visual images, including the forward and backward traffic scenes, left and right lane positions, and the

driver's face. These data are recorded on a laptop computer and mobile hard disks via a driving recorder system. The sampling frequency of all data except the visual images is 30 Hz; the visual images are sampled at eight frames/s. The abovementioned instruments are arranged so as to be as unobtrusive as possible (the recorder system is fixed inside the trunk of the vehicle) in order to encourage naturalistic driving behavior.

The disadvantage of using the instrumented vehicle is participants' unfamiliarity with the experiment vehicle. Practice drives before measurement trips are important in order for the participating drivers to be familiar with the instrumented vehicle and the experimental atmosphere as well as to drive from the start to the end without using any assistance, such as a map, a vehicle navigation system, and passengers. The driving route is predetermined, which included several left and right turns. The participant rides alone in the vehicle during the experiment trials, whereas the experimenter rides with the participants on the first day of the trials in order to confirm that the participants are following the correct route. Thus, the data from the first day are not used for subsequent data analyses and data modeling. The participating drivers are instructed only to drive in their typical manner.

Analysis of Data Distribution Based on Traffic and Road Environments

Driver preparatory behavior before making a turn is composed of turn signal activation and deceleration. The decelerating operations involve releasing the accelerator pedal, moving the right foot from the accelerator pedal to the brake pedal, and pressing the brake pedal. In this section, data analysis of the turn signal use and the foot movement to cover the brake pedal is introduced as representative maneuvers of the driver preparatory behavior. The accelerator pedal is released not only to decelerate for making turns but also to maintain an appropriate driving speed [22]. The brake pedal application is an operation after driver's decision-making on leaving the current road, and it is influenced by driver factors (such as driving skill) other than the decision to leave the current road [23]. Only the data acquired when there was a green light at the target intersection are analyzed in the following sections. The influence of traffic conditions on driver preparatory behavior differs between encountering green and red traffic lights. It is recommended to exclude the behavioral data recorded at the red traffic light when developing the presentation criteria of route guidance based on the measurement of the typical preparatory behavior [24].

Influence of Vehicle Velocity on Driver Preparatory Behavior

Vehicle velocity while approaching an intersection influences the driver decelerating operation before making a driver's side turn. In contrast, the onset location of the turn signal activation is almost stable regardless of the vehicle velocity. Figure 3 presents the onset locations of driver preparatory behavior in the five categorized vehicle velocities. Field experiments using the AIST instrumented vehicles were conducted, and the preparatory behavior data were collected before turning at an intersection with two traffic lanes and a designated lane for making a driver's side turn. The number of participants was four (three males and one female). The average age of the participants was 34.8 years, and the average driving experience was 16.3 years. The total trips for each participant were 40 over a period of about 2 months (weekdays). The four participants started driving on the identical route (total mileage, 15 km) at 10-min intervals. Please see literature [24] for detailed experiment methods and analyses. The vehicle velocity is measured when the driver moves the right foot from the accelerator pedal to the brake pedal because the velocity, when covering the brake pedal and when activating the turn signal, is almost the same.

The remaining distances to the center of the intersection when covering the brake pedal are directly proportional to the driving speeds, and the onset locations of the foot movement become closer to the intersection when approaching it more slowly. In contrast, the proportional relation between the speed and the turn signal use is not remarkable. The onset locations of the turn signal operation do not change in any categorized driving speeds.

Influence of Traffic Conditions on Driver Preparatory Behavior

Figure 4 presents the onset location of driver preparatory behavior in the four categories of the relative

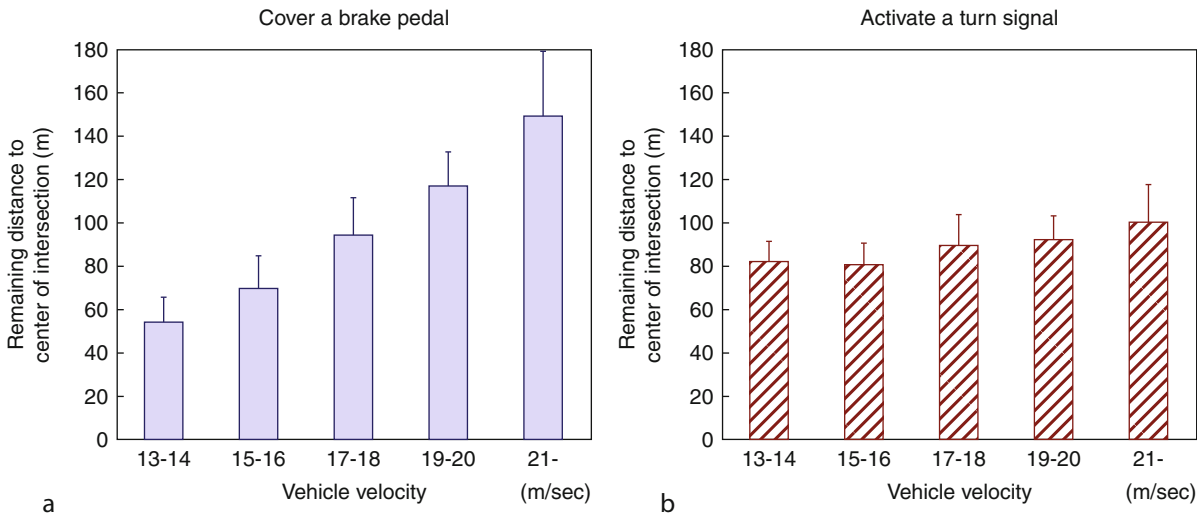

Driver Behavior at Intersections. Figure 3
Relationship between the onset location of driver preparatory behavior and vehicle velocity. The graphs present averages and standard deviations of the remaining distances to the center of the intersection when each behavioral event occurs in each category of the vehicle velocity. The data were collected at an intersection with two traffic lanes and a designated turn lane

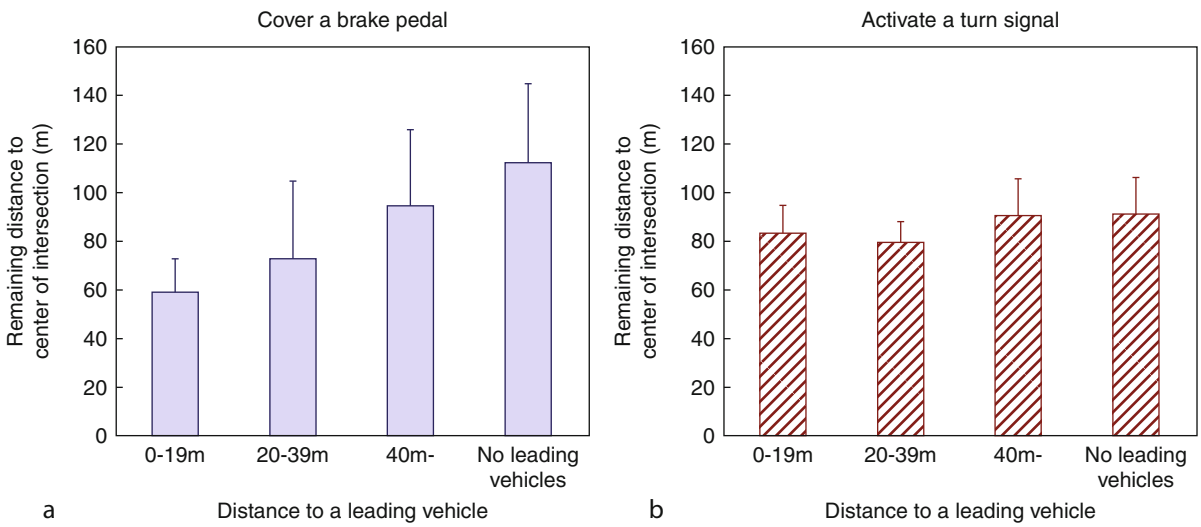

Driver Behavior at Intersections. Figure 4
Relationship between the onset location of driver preparatory behavior and relative distance to a leading vehicle. The graphs present averages and standard deviations of the remaining distances to the center of the intersection when each behavioral event occurs in each category of the relative position to the leading vehicle. The data were collected at the intersection with two traffic lanes and a designated turn lane

distance to the lead vehicle, including the absence of a leading vehicle. The data used are the same as those in Fig. 3. The relative distances from the leading vehicle are measured before the driver enters the designated turn lane. Here, the leading vehicle is a forward vehicle that travels straight toward the target intersection. The remaining distances to the center of the intersection when covering the brake pedal while driving with a leading vehicle are shorter than those during drives without a leading vehicle. In addition, shorter relative distances to the leading vehicle lead to shorter remaining distances at the onset of covering the brake pedal. On the other hand, the onset location of turn signal activation is at a remaining distance of between 80 and 90 m to the center of the target intersection. The turn signal use is independent of the existence of and relative distance to a leading vehicle.

Figure 5 presents the onset location of driver preparatory behavior in the four categories of the relative distance from a following vehicle, including the absence of a following vehicle. These data are also the same as those in Fig. 3. The relative distances from the following vehicle are measured before the driver enters the designated turn lane. Here, the following vehicle is a vehicle that follows the driver's vehicle in the same driving lane. The remaining distances when covering the brake pedal while driving with a following vehicle are shorter compared to driving without a following vehicle, particularly for a shorter relative distance between vehicles. On the other hand, the remaining distances when the turn signal is activated are almost stable in the four categories of the relative distance from the following vehicle, ranging from 80 to 90 m.

The vehicle velocity while approaching the intersection is correlated with the relative distance between the driver's vehicle and a leading or following vehicle. It is hypothesized that only the slower driving speed leads to a shorter remaining distance when covering the brake pedal. At a specific range of vehicle velocity (from 16.0 to 17.5 m/s), the onset locations when covering the brake pedal were compared among the four situations: driving with both leading and following vehicles, driving with only a leading vehicle, driving with only a following vehicle, and driving without either a leading or following vehicle. The remaining distance at the onset of covering the brake pedal was the shortest when driving with both leading and

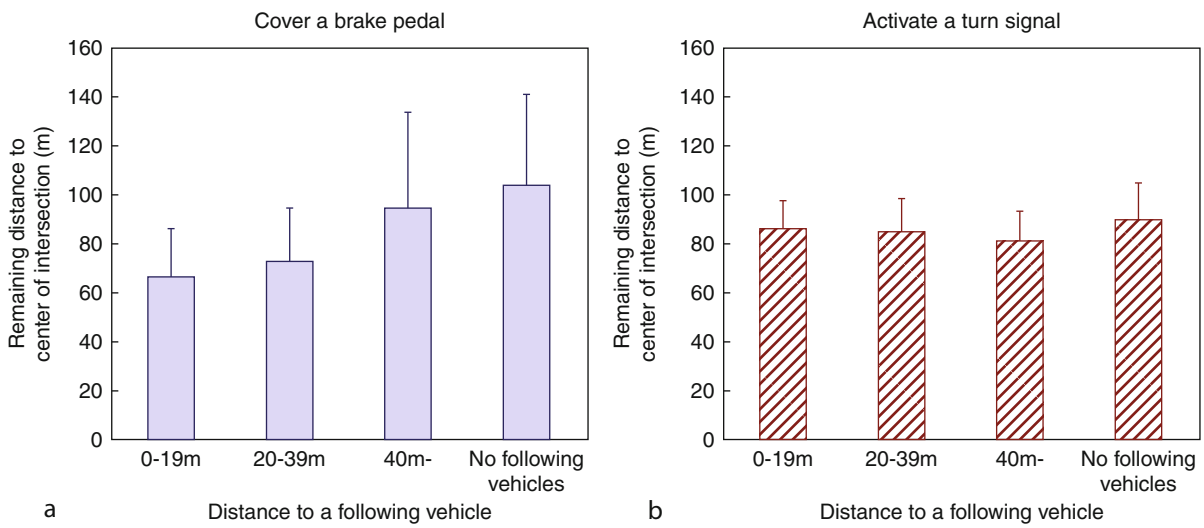

Driver Behavior at Intersections. Figure 5

Relationship between the onset location of driver preparatory behavior and relative distance to a following vehicle. The graphs present averages and standard deviations of the remaining distances to the center of the intersection when each behavioral event occurs in each category of the relative position from the following vehicle. The data were collected at the intersection with two traffic lanes and a designated turn lane

following vehicles. The onset location of covering the brake pedal was closer when driving with only a leading vehicle than that when driving with only a following vehicle.

Drivers begin to decelerate at a point closer to the center of the intersection under car-following conditions compared to free-running conditions at the same driving speed. The preparation point is the closest to the target intersection when drivers prepare to make a turn with a following vehicle in addition to a leading vehicle. Drivers following a forward vehicle pay attention to that vehicle in order to respond quickly to its actions [25, 26]. Additionally, they pay attention both forward and backward in so-called platoon conditions under which they travel a short distance to leading and following vehicles. Intense concentration on vehicles surrounding the driver's vehicle may lead to a delay in the onset of driver decelerating maneuvers before making a driver's side turn at an intersection.

The analyses of turn signal use within the specific range of the vehicle velocity reveal the fixed location of turn signal activation regardless of the traffic conditions surrounding the driver's vehicle. As mentioned from Figs. 3–5, the remaining distances to the center of the target intersection when activating the turn signal are almost constant in all ranges of the vehicle velocity and of the relative distance from the leading or following vehicle. The analyzed intersection has a designated turn lane (the distance between the entrance of the designated lane and the center of the intersection is 70 m). This road alignment feature may contribute to the constant location at which the drivers activate the turn signal.

Influence of Road Structure on Driver Preparatory Behavior

Traffic conditions (the existence of leading and/or following vehicles) influence the driver decelerating maneuver at a specific intersection with two traffic lanes and a designated turn lane. Moreover, the road structures of intersection where to turn influence the relations between the traffic conditions and the driver preparatory behavior for decelerating before a driver's side turn. Figure 6 presents the onset locations of covering the brake pedal in the four categorized traffic conditions at three kinds of intersections. The data collection methods were as follows: number of participants, eight (five males and three females); average age of the participants, 38.1 years; average driving experience, 18.1 years; total trips for each participant, 40 over a period of about 2 months (weekdays). Four participants started driving on the route, including the target intersections, at 10-min intervals. The other drivers made recorded trips at another period following the same procedures. Please see literature [27] for detailed experiment methods and analyses. Intersection A is a standard right-angle intersection on a straight road with one traffic lane. Intersection B is a T-junction at the end of the road. Intersection C is also a T-junction, and this intersection exists after drivers drive along a curved road (curve radius, 126.9 m).

At intersection A, the remaining distances while driving with leading and following vehicles and while driving with only a leading vehicle are shorter than those while driving without a leading or following vehicle. At intersection B, the onset locations of covering the brake pedal tend to be longer to the center of the intersection when there is a following vehicle compared to only a leading vehicle and without a leading or following vehicle. At intersection C, the remaining distances to the center of the intersection when covering the brake pedal are longer when there is a vehicle in front. The onset location is the longest among the four traffic conditions when driving with both leading and following vehicles.

The comparison between the standard intersection and the intersection with a designated turn lane indicates that the number of traffic lanes has less influence on the relationship between the traffic conditions and the driver decelerating behavior before making a driver's side turn. The behavioral analysis at the intersection after a curved road suggests that drivers begin to prepare for deceleration at an earlier point while approaching the intersection with leading and following vehicles and with only a leading vehicle compared to without such vehicles. Drivers cannot see the landmarks, including traffic lights, and cannot recognize the remaining distance to the turning point until just before the intersection after a curve. At the standard intersection, drivers can see and recognize the location of the intersection, and they may adapt their behavior to the leading vehicle until they are closer to the intersection. In contrast, drivers change their

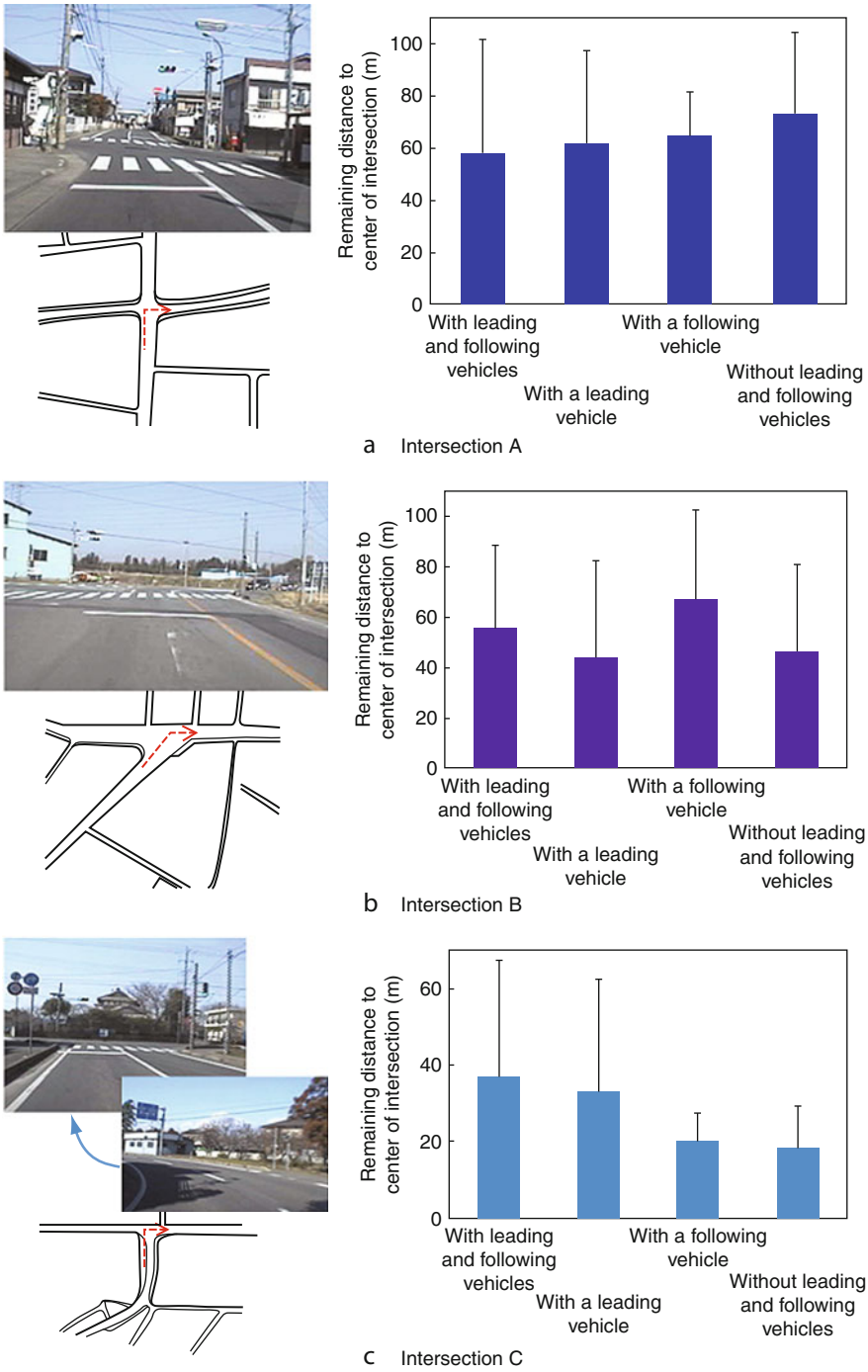

Driver Behavior at Intersections. Figure 6

Relationship between the onset locations of driver preparatory behavior and traffic conditions at three kinds of intersections. The graphs present averages and standard deviations of the remaining distances to the center of the intersection when the drivers move their right foot from the accelerator pedal to the brake pedal in each category of the traffic conditions

driving mode from following the leading vehicle to preparing to make a driver's side turn at an earlier point when the intersection cannot be recognized in advance.

Drivers begin to decelerate farther from the T-junction on a straight road when they have a vehicle following. In this case, drivers may intend to use their brake lights as a signal to the following driver to avoid a rear-end collision by the following vehicle. At T-junction, the leading vehicle always decelerates and turns right or left. Drivers can anticipate the deceleration of the lead vehicle, and they may pay more attention to the following vehicle compared to the movement of the lead vehicle while approaching the T-junction with leading and following vehicles. A driver's recognition of a following vehicle may lead to earlier preparation for deceleration. Intersection C is also a T-junction, but the onset location of covering the brake pedal when driving with only a following vehicle is similar to driving without leading or following vehicles. Drivers should pay attention to the inside of the curve during curve negotiation [28]. Thus, drivers might not recognize the presence of a following vehicle while approaching an intersection after a curve. When drivers notice the following vehicle before entering the curve, they may allocate more resources to the curve negotiation and may not pay attention to the rear vehicle.

Recommendations for Presentation Timing of Route Guidance

The presentation timing of route guidance instruction compatible with driver's typical preparatory behavior is recommended to enhance driver acceptance of the provided information. Data analyses described in section "Influence of Vehicle Velocity on Driver Preparatory Behavior, Influence of Traffic Conditions on Driver Preparatory Behavior, Influence of Road Structure on Driver Preparatory Behavior" suggest that it is effective to change the timing of the last route guidance presentation based on the vehicle velocity, the existence of and relative distance to leading and following vehicles, and the road structures of the turning point.

First of all, the presentation timing should be changed corresponding to the driving speeds while approaching a target intersection. Driving faster requires earlier presentation timing compared to driving slower. In addition to the vehicle velocity, the traffic conditions surrounding the driver's vehicle should be taken into account. Presenting the instruction closer to the intersection would be effective for guidance and compatible with driver preparatory behavior while approaching right-angle intersections on straight roads under close car-following conditions, whereas earlier presentation would be acceptable while driving with a leading and/or following vehicle at long range and while driving without leading or following vehicles. Moreover, the route guidance presentation with different timings at intersections with T-junctions and at intersections after curves is recommended. Earlier guidance would effectively enhance drivers' utilization of the instruction while approaching a T-junction on a straight road when driving with a following vehicle, independent of the existence of the lead vehicle. At intersections after curves, drivers cannot see or recognize the relation between their vehicle and the turning point until just before the target intersection. In these cases, the route guidance instructions should be provided earlier in car-following situations to improve the drivers' acceptance of the presented information.

Modeling of Driver's Preparatory Behavior Before Making Driver's Side Turn

Preparatory Behavior Model Using Structural Equation Modeling

Data analyses of driver preparatory behavior before making a driver's side turn at a specific intersection with a designated turn lane reveal linear relationships among the vehicle velocity, the traffic conditions in the vicinity of the driver's vehicle, and the preparatory behavior (sections "Influence of Vehicle Velocity on Driver Preparatory Behavior and Influence of Traffic Conditions on Driver Preparatory Behavior"). The onset locations of the foot movement to cover the brake pedal are positively correlated with the driving speeds or the remaining distances to leading and following vehicles. In contrast, the onset locations of the turn signal operation are almost constant, independent of the speeds and the traffic conditions. Structural equation modeling is an efficient modeling technique for quantifying the impact of independent variables on the dependent variables that suggests linear

relations [29]. Thus, the structural equation model can be applied to describe quantitatively the relationships among the vehicle velocity, the relative distances to the leading and following vehicles, and the onset locations of covering the brake pedal and activating the turn signal.

Structural equation modeling represents the interrelations among a set of variables comprising a model hypothesized by theory and empirical research. Observed and latent variables are used in the structural equation model: observed variables are directly collected and measured, and latent variables are inferred from the set of observed variables. The parameters specified in the structural equation model are estimated so as to minimize differences in the variance–covariance matrices between the hypothesized theoretical model and the measurement data. Various kinds of model fit indices evaluate whether or not the covariance matrix of the hypothesized model is as close as possible to that of the observed variables [30].

In the structural equation model of driver preparatory behavior, the following five observed variables are used: the driving speed, the relative distance to the leading vehicles, the relative distance to the following vehicles, the remaining distance to the center of the target intersection when covering the brake pedal, and the remaining distance to the center of the target intersection when activating the turn signal. Subsequently, the constructed model is applied to a prediction of the onset location of the driver preparatory maneuvers. Therefore, the independent variables, the driving speed and the headway and rear distances, at the onset of releasing the accelerator pedal are used in the model construction. Here, the release of the accelerator pedal is defined as the final release maneuver of the accelerator pedal, leading to right foot movement to cover the brake pedal. The cases where there are no leading and/or following vehicles when releasing the accelerator pedal have missing data for the relative distances to the leading and/or following vehicles. To overcome this limitation, having no leading and/or following vehicles around the driver's vehicle is defined as the condition in which leading and/or following vehicles are such a long way from the driver's vehicle that the laser radar cannot detect and measure them. The relative distances to the leading and following vehicles in the case of no leading and/or following vehicles are set to 100 m, a value which is beyond the detection limits of the laser radar unit.

The latent variables are important to obtain an acceptable model to data fit in the structural equation model specification of driver preparatory behavior. This is because the velocity and the headway and rear distances influence, not independently but interactively, the onset locations of driver preparations for making a driver's side turn. A latent variable, called the free-driving condition level, is input to the model specification as a latent factor describing the interaction between the leading or following vehicles and the driver's vehicle. This latent variable uses two indicator variables: the relative distance to the leading vehicle and the relative distance to the following vehicle. A higher free-driving condition level denotes that a driver drives without leading and following vehicles or remains a long distance from the front and rear vehicles. Conversely, a lower free-driving condition level denotes that a driver drives under close car-following conditions. In addition, a latent variable, called the location of transition to preparatory behavior, is introduced as a latent factor related to the onset location of the change in driving behavior from straight (going forward along the roadway) mode to the preparation mode. This latent variable comprises two indicator variables: the remaining distance to the center of the intersection when covering the brake pedal and the remaining distance to the center of the intersection when activating the turn signal. The location of transition to preparatory behavior denotes the degree to which a driver begins to prepare for making a driver's side turn at a long distance from the center of the intersection. A closer location of transition to preparatory behavior denotes that the onset location of the behavioral event is closer to the target intersection. Please see literature [31] for the details of the model construction.

Figure 7 presents a path diagram of the proposed structural equation model, the estimated path coefficients and factor loadings (standardized weights), and the results of model fit indices. The results of the model fit indices suggest that the estimated structural equation model fits the observed data well. The vehicle velocity and the free-driving condition level are positively related to the location of transition to preparatory behavior. The relation between the free-driving

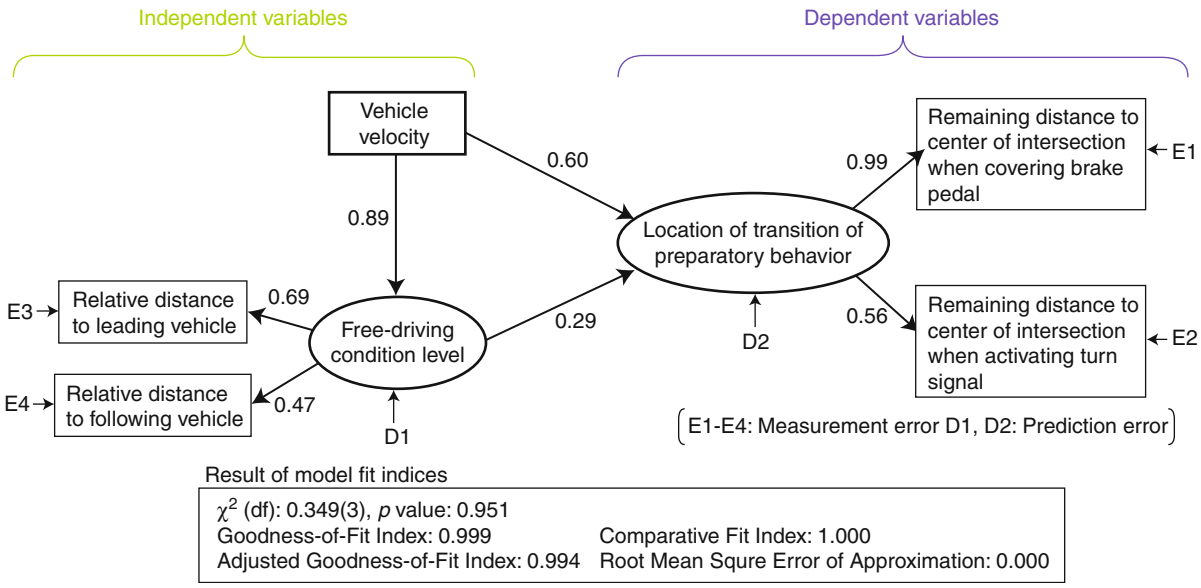

Driver Behavior at Intersections. Figure 7

Structural equation model of driver preparatory behavior. The values in the path diagram present the standardized path coefficient (among vehicle velocity, free-driving condition level, and location of transition to preparatory behavior) and factor loadings (between the latent variables and each indicator variable). The model was estimated using the maximum likelihood method. Total data sets are 119 for 4 drivers

condition level and each indicator variable (relative distances to leading and following vehicles) is also positive, suggesting that the location of transition to preparatory behavior is directly proportional to the headway and rear distances. The factor loading from the location of transition to preparatory behavior to the remaining distance at the onset of covering the brake pedal is higher than the factor loading for the remaining distance when activating turn signal. This means that higher driving speeds and free-driving conditions contribute to an earlier onset location when covering the brake pedal and that the independent variables have less effect on turn signal activation.

At T-junctions and intersections after curves, the relationships between the traffic conditions and the onset location of driver decelerating maneuver are different from those at the right-angle intersections on straight roads. In these cases, the structural equation model should be estimated at each intersection. The path diagram is the same among the intersections, and the path coefficients and/or the factor loadings will be changed according to the relationships observed at each intersection. At T-junctions, the factor loading between the free-driving condition level and the relative distance to the following vehicle will be negative. At intersections after curves, the path coefficients from the vehicle velocity and the free-driving condition level to the location of transition to preparatory behavior will be negative.

Prediction of Onset Location of Driver Preparatory Behavior

The path coefficients and factor loadings estimated in the structural equation model are used to predict the onset locations of driver preparatory operations. Figure 8 presents the method for predicting the onset locations of the driver preparatory behavior. The influences of the vehicle velocity on the location of transition to preparatory behavior are divided into direct influence and indirect influence via the free-driving condition level (Fig. 8a). The factor score for the free-driving condition level is calculated by using the factor loadings for the two indicator variables because the relationship between the free-driving condition level and the relative distances to the leading and

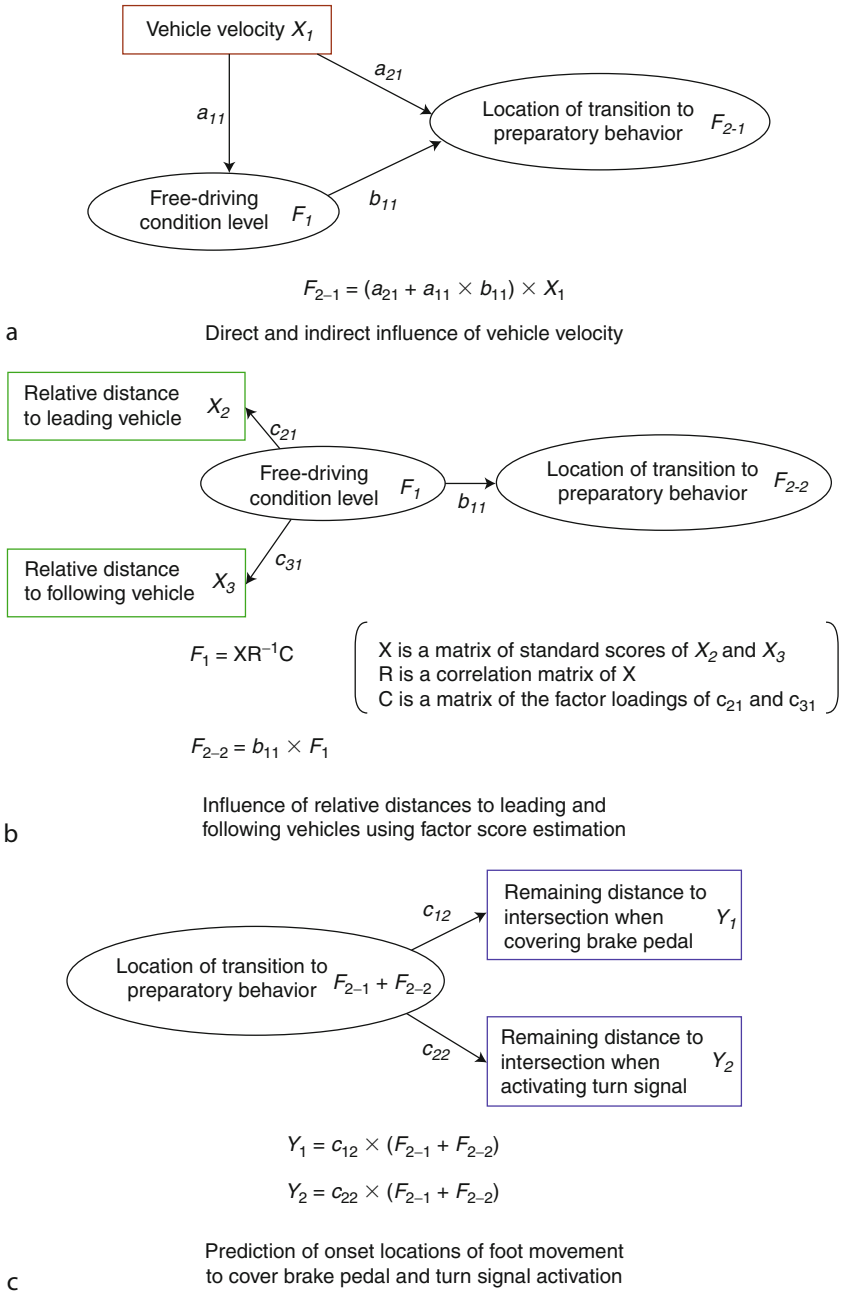

Driver Behavior at Intersections. Figure 8

Procedures for predicting the onset locations of driver preparatory maneuvers. The procedures are divided into three steps: the effect of vehicle velocity on location of transition to preparatory behavior, the effect of headway and rear distances on location of transition to preparatory behavior, and the calculation of remaining distances to intersection when covering brake pedal and activating turn signal from the latent variable. (**a**) Direct and indirect influence of vehicle velocity. (**b**) Influence of relative distances to leading and following vehicles using factor score estimation. (**c**) Prediction of onset locations of foot movement to cover brake pedal and turn signal activation

following vehicles corresponds to a confirmatory factor model [32]. Then, this score is used to calculate the direct effect of the free-driving condition level on the location of transition to preparatory behavior (Fig. 8b). Finally, the remaining distances to the center of the intersection when covering the brake pedal and when activating the turn signal are predicted by using the factor loadings between the location of transition to preparatory behavior and the onset location of each behavioral event (Fig. 8c).

The onset locations of covering the brake pedal and activating the turn signal can be predicted by applying estimated path coefficients and factor loadings to the recorded vehicle velocity and relative distances to leading and following vehicles. The estimated structural equation model uses the driving speed and the headway and rear distances when drivers release the accelerator pedal. The onset location of releasing the accelerator pedal may be almost the same as the last route guidance presentation that is determined based on drivers' typical preparatory behavior. The route guidance system linked with laser radar units and a speed pulse signal source can predict the driver decelerating maneuver and turn signal operation when the last voice message is presented. Sometimes a driver does not begin preparation after reaching the predicted onset location. In such cases, the system can infer a driver error that he/she did not accurately identify the turning point due to a misunderstanding of the provided information or did not notice the information provision. The systems could then restate the voice route guidance or quickly reroute and present the updated route.

Future Directions

Further data analyses reveal that the relationships among the onset location of driver preparatory behavior, the traffic conditions, and the road environments before making a curb side turn are similar to those before making a driver's side turn described in this essay [27]. Thus, the findings of understanding and modeling of typical preparatory maneuvers for a driver's side turn can be applied to the route guidance presentation timing and restatement before a curb side turn.

Understanding the driver usual preparatory behavior and developing the structural equation model need a large amount of measured data. Recording of the large-scale data by one vehicle requires a few weeks. After a driver bought an in-vehicle navigation system and used it in his/her daily lives for a few weeks, the route guidance system becomes sophisticated: the presentation timing becomes compatible with his/her typical preparatory behavior, and the advanced functions of the restatement of route guidance and the quick update of route become available when he/she misses the turning point.

Data analysis and modeling approach can be applied to driving tasks other than preparations for turning at intersections. The linear relations between the driving behavior and the traffic conditions are found in the driver's side turn behavior, and the structural equation modeling is adopted. If the measured data sets suggest nonlinear relationships, probabilistic models, including a Markov dynamic model and a Bayesian network model, will be used for modeling and predicting the driving behavior in a real environment (e.g., [33, 34]).

Bibliography

Primary Literature

1. Kimura K, Marunaka K, Sugiura S (1997) Human factors considerations for automotive navigation systems – legibility, comprehension, and voice guidance. In: Noy YI (ed) Ergonomics and safety of intelligent driver interfaces. Lawrence Erlbaum Associate, Mahwah, pp 153–167
2. Michon JA (1985) A critical view of driver behavior models: What do we know, what should we do? In: Evans L, Schwin RC (eds) Human behavior and traffic safety. Plenum, New York, pp 485–520
3. Ikeda H, Kobayashi Y, Hirano K (2011) How car navigation systems have been put into practical use – development management and commercialization process-. Synthesiology – English Edition 3:280–289
4. Pauzie A (2005) Methodologies for driver-centred evaluation of perceptive and cognitive requirements of in-vehicle display. In: Proceedings of 11th international conference on human-computer interaction, Las Vegas, CD-ROM
5. Pauzie A, Daimon T, Bruyas MP (1997) How to design landmarks for guidance systems? In: Proceedings of 4th world congress on intelligent transport systems, Berlin, CD-ROM
6. Daimon T, Nishimura M, Kawashima H (2000) Study of driver's behavioral characteristics for designing interfaces of in-vehicle navigation systems based on national and regional factors. JSAE Rev 21:379–384

7. Kawai M, Kawasumi M, Nakano T, Yamamoto S, (2003) Displaying method in on-board display – route guidance method based on sex differences. In: Proceedings of IEEE intelligent transportation systems council, Columbus, OH, pp 357–360
8. Ross T, May AJ, Grimsley PJ (2004) Using traffic light information as navigational cues: implications for navigation system design. Transp Res Part F 7:119–134
9. May AJ, Ross T (2006) Presence and quality of navigational landmarks: effect on driver performance and implications for design. Hum Factors 48:346–361
10. Kishi K, sugiura S (1993) Human factors considerations for voice route guidance. In: SAE SP-964 automotive display systems and IVHS. Society of Automotive Engineers, Warrendale, pp 99–109
11. Yoshioka M, Akamatsu M, Matsuoka K, Sato T (2003) Aim of "behavior-based human environment creation technology". In: Proceedings of the XVth triennial congress of the international ergonomics association, Seoul, CD-ROM
12. Vogel K (2002) What characterizes a "free vehicle" in an urban area? Transp Res Part F 5:15–29
13. Liu BS (2007) Association of intersection approach speed with driver characteristics, vehicle type and traffic conditions comparing urban and suburban areas. Accid Anal Prev 39:216–223
14. Akamatsu M, Okuwa M, Onuki M (2001) Development of hi-fidelity driving simulator for measuring driving behavior. J Robot Mechatron 13:409–418
15. Kappe B, Winsum W, Wolffelaar P (2002) A cost-effective driving simulator. In: Proceedings of DSC (driving simulation conference) 2002. INRETS-RENAULT, Paris, pp 123–134
16. The National Advanced Driving Simulator (2010) The University of Iowa. http://www.nads-sc.uiowa.edu/media/pdf/NADS_2010Overview.pdf. Accessed 19 May 2011
17. Akamatsu M, Onuki M (2008) Trends in technologies for representing the real world in driving simulator environment. Rev Automot Eng 29:611–618
18. Pinto M, Cavallo V, Ohlmann T, Espie S, Roge J (2004) The perception of longitudinal accelerations: what factors influence braking maneuvers in driving simulators?. In: Proceedings of DSC (driving simulation conference) 2004 Europe. INRETS-RENAULT, Paris, pp 139–151
19. Kemeny A, Panerai F (2003) Evaluating perception in driving simulation experiments. Trends Cogn Sci 7:31–37
20. Dingus TA, Klauer SG, Neale VL, Petersen A, Lee SE, Sudweeks J, Perez MA, Hankey J, Ramsey D, Gupta S, Bucher C, Doerzaph ZR, Jermeland J, Knipling RR (2006) The 100-car naturalistic driving study, phase 2 – results of the 100-car field experiment, Report no. DOT HS 810 593
21. Akamatsu M, Sakaguchi Y, Okuwa M, Kurahashi T, Takiguchi K (2003) Database of driving behavior measured with equipped vehicles in the real road environment. In: Proceedings of the XVth triennial congress of the international ergonomics association, Seoul, CD-ROM
22. Sato T, Akamatsu M (2006) Analysis of drivers' behaviour before making a right turn at an intersection based on driving behavior data on an actual road. RevAutomot Eng 27:287–294
23. Sato T, Akamatsu M, Daimon T (2006) Investigation on drivers' behaviour while approaching an intersection: comparison between real and simulated driving. In: Proceedings of driving simulation conference Asia/Pacific (DSC-AP 2006), Tsukuba, CD-ROM
24. Sato T, Akamatsu M (2007) Influence of traffic conditions on driver behaviour before making a right turn at an intersection: analysis of driver behaviour based on measured data on an actual road. Transp Res Part F 10:397–413
25. Brackstone M, McDonald M (2007) Driver headway: how close is too close on a motorway? Ergonomics 50:1183–1195
26. Ranney TA (1999) Psychological factors that influence car-following and car-following model development. Transp Res Part F 2:213–219
27. Sato T, Akamatsu M (2009) Analysis of drivers' preparatory behavior before turning at intersections. IET Intell Transp Syst 3:379–389
28. Land MF, Lee DN (1994) Where we look when we steer. Nature 369:742–744
29. Schumacker RE, Lomax RG (2004) SEM Basics. In: Riegert D (ed) A beginner's guide to structural equation modeling. Lawrence Erlbaum Associates, Mahwah, pp 61–78
30. Hu L, Bentler PM (1995) Evaluating model fit. In: Hoyle R (ed) Structural equation modeling: issues, concepts, and applications. Sage, Newbury, pp 76–99
31. Sato T, Akamatsu M (2008) Modeling and prediction of driver preparations for making a right turn based on vehicle velocity and traffic conditions while approaching an intersection. Transp Res Part F 11:242–258
32. Bollen KA (1989) Confirmatory factor analysis. In: Structural equations with latent variables. Wiley, New York, pp 226–318
33. Akamatsu M, Sakaguchi Y, Okuwa M (2003) Modeling of driving behavior when approaching an intersection based on measured behavioral data on an actual road. In: Proceedings of the human factors and ergonomics society 47th annual meeting, Denver, CL, pp 1895–1899
34. Pentland A, Liu A (1999) Modeling and prediction of human behavior. Neural Comput 11:229–242

Books and Reviews

Cacciabue C (2007) Modelling driver behavior in automotive environments: critical issues in driver interactions with intelligent transport systems. Springer, New York

Fuller R, Santos JA (2002) Human factors for highway engineers. Pergamon, Oxford, UK

Shinar D (2007) Traffic safety and human behavior. Emerald, Bingley

Takeda K, Hansen JHL, Erdogan H, Abut H (2009) In-vehicle corpus and signal processing for driver behavior. Springer, New York

Driver Characteristics Based on Driver Behavior

Jianqiang Wang[1], Lei Zhang[1], Xiaojia Lu[2], Keqiang Li[1]
[1]State Key Laboratory of Automotive Safety and Energy, Tsinghua University, Beijing, China
[2]China Agricultural University, Beijing, China

Article Outline

Glossary
Definition of the Subject
Introduction
Driver Behavior Questionnaire Design
Data Statistical Analysis and Quantification Analysis
Comparison and Discussion
Future Directions
Acknowledgments
Bibliography

Glossary

Driver Assistance System (DAS) Also called ADAS (Advanced Driver Assistance Systems), can prevent accidents caused by human errors or alleviate the damage by taking control of the vehicle just before an accident happens. It can contribute to improving traffic safety, environmental impact, energy efficiency, traffic homogeneity, and driver comfort and convenience. An adaptive Driver Assistance System ensures safe driving by assisting the driver in the following ways: reducing driver fatigue and maintaining driver performance by supporting a driver's "recognitions," "judgments," and "actions" displaying warning signs in the case that the actions are judged to be dangerous and taking control of the vehicle in the case that the driver is unable to avoid a collision.

Driver Characteristics The characteristics performed when driving, including the driver's operations to the vehicle (e.g., car-following and lane-changing), the physiological characteristics (e.g., response, cognition, and fatigue), and the psychological characteristics and so on. It has been studied mainly in two main aspects, i.e., driving skill and driving style.

Driver Behavior Questionnaire (DBQ) One of the most widely implemented measurement scales to examine self-reported driving behaviors, developed by Reason et al.

Factor Analysis Factor analysis was invented by psychologist Charles Spearman. It is a collection of methods used to examine how underlying constructs influence the responses on a number of measured variables. It is related to the principal component analysis but not identical; it estimates how much of the variability is due to common factors. It is performed by examining the pattern of correlations (or covariances) between the observed measures. Measures that are highly correlated (either positively or negatively) are likely influenced by the same factors, while those that are relatively uncorrelated are likely influenced by different factors.

Human Factors It is a theory that studies the physical and mental state of human beings when given different environments, products, and services.

Reliability It is the quality of being dependable or reliable. And it is defined as the proportion of the real variance in the total variance in the statistics. At present, the Cronbach's alpha reliability coefficient method is a commonly used measure. It is specially used for the reliability estimation of the accumulative Likert scale. It is defined as: the ratio of the sum variance of each item and the total variance of the whole scale.

***T*-Test** The *T*-test method is a common method for hypothesis testing. It is used to determine whether there are differences between the two samples (such as A and B) with an unknown but equal population variance. It can calculate the values simply, and is suitable for small sample testing.

Validity It is defined as the ratio of the variance of the scores that related to the measure purposes and the total variance. The content validity and discriminate validity are the two main indexes.

Definition of the Subject

According to the road traffic statistics and analysis information, most accidents can be directly attributed

to the driver mistake and violation behavior. In driving behavior research, the driving skill and style can be seen as the two main components of human factors [1]. The deficient driving skill and aggressive driving style may both lead to serious crash risk. Therefore, different kinds of Advanced Driver Assistance Systems based on intelligent technologies are developed by automotive manufacturers to increase driver skill and decrease driver workload, such as Forward Collision Warning System and Adaptive Cruise Control System [2]. The governments also conduct much work on the driver education and regulation to avoid aggressive behaviors. In order to optimize the effects of technical driving assistance and driver normalization, understanding and measuring of driver skill and style have become important research topics. However, because of the complication and variability of human drivers, it is challenging to convert the descriptive concepts of skill and style to quantitative mathematic variables.

Introduction

A self-reported survey is an effective method for studying the driver behavior, and it can be used to analyze the driver behavior, especially the relationship between abnormal behavior and driver characteristics. A number of driver measurement scales have been designed to investigate the driver characteristics and behavior, such as the Driver Anger Scale [3] and the Driving Skill Inventory [4]. In these methods, the Driver Behavior Questionnaire (DBQ) developed by Reason et al. [5] has recently become one of the most widely implemented measurement scales to examine self-reported driving behaviors. Based on this DBQ and its improved editions, many researches on driver behavior were carried out from different perspectives, e.g., the culture comparison [4], region diversity [6], and the gender and age influences [7]. Although the self-reported survey may affect the data of behavior scale by some subjective factors and objective factors (i.e., the uncertain factors from the outside), it cannot reflect the driver characteristics absolutely [8]. The existing research results show that this method has obvious advantages than previous methods, because a great quantity of behavior data about abnormal driving that cannot be obtained by experiments can be collected quickly and effectively. Meanwhile, the statistical methods that are involved in this paper (e.g., factor analysis, correlation analysis, and cluster analysis) provide an effective tool and basis for driver characteristics analysis. Thus, the indicated factors extracted from the behavior scale can accurately describe the abnormal driver characteristics of driver individual and population to a certain extent.

In this research, the DBQ is applied to explore a quantification method of driver characteristics. A self-reported survey based on DBQ is implemented with 33 Chinese driver participants. Factor analysis is used as the data processing method and a two-dimensional factor structure is established to describe the driver's characteristics of driving skill and driving style respectively. Some comparisons are also executed to validate the reasonability of this method.

Driver Behavior Questionnaire Design

Participants

The self-reported data in this survey are collected from 33 Chinese drivers with different occupations. There are 29 males (87.9%) and 4 females (12.1%). The average age of the participants is 45.54 years (S.D. = 9.86), and the age range is from 30 to 62 years. On average the participants hold their driving licenses for 13.21 years (S.D. = 8.29, range 3–38 years). The average driving mileage is 180.8000 km (S.D. = 18.33), and the driving range is from 20,000 to 600,000 km. Seventeen participants (51.5%) have traffic accidental history, and to them the average accident amount is 3.24 (S.D. = 2.77).

Driver Behavior Questionnaire Method

A self-reported survey is designed based on the Driver Behavior Questionnaire [9] and some modifications are made to adjust the items for Chinese traffic and driver conditions. The survey consists of three parts:

1. Individual information: including gender, age, driving experience (in terms of driving years), and traffic accidental history.
2. A self-evaluation on the driving skills and driving style, which uses an estimation method of Social Comparison [8]. The purpose of self-evaluation is to validate the quantification method. The participants were required to indicate on a six-point

scale (0 = never to 5 = nearly all the time) how often they commit each of the abnormal driving behavior. The skill is rated as five-point scales (0 = very strong and 4 = very weak), and so is the driving style (0 = very prudent and 4 = very aggressive).

3. The main body of the survey, including 20 items describing kinds of driver behaviors, which are extracted and transferred from the original questionnaire, as shown in Table 1. According to the definition and analysis of the original DBQ, the first to the tenth items are aggressive violation behaviors. The 11th to the 14th items are fatal errors which may cause serious accidents, and the 15th to the 20th items are just lapses, which are not very dangerous but may bring some troubles.

Driver Characteristics Based on Driver Behavior. Table 1 Driver behavior questionnaire and statistical analysis results

No	Item	Mean	S.D.	*r* with total score
1	Drive so close to the car in front that it would be difficult to stop in an emergency	0.8485	0.7953	0.471**
2	Cross-junction knowing traffic lights have already turned	0.5152	0.6185	0.289
3	Disregard the speed limit on a residential road	0.9697	0.8833	0.473**
4	Disregard the speed limit on a intercity highway	0.9394	0.8993	0.411*
5	Become angered by another driver and show anger to him	1.6364	1.0252	0.485**
6	Overtake a slow driver on the inside	1.5152	0.7953	0.576**
7	Race away from traffic lights to beat the car beside you	0.5152	0.6185	0.460**
8	Become angered by another driver and give chase	0.8485	0.7550	0.524**

Driver Characteristics Based on Driver Behavior. Table 1 (Continued)

No	Item	Mean	S.D.	*r* with total score
9	Sound your horn to indicate your annoyance to another road user	1.3636	0.7424	0.414*
10	Stay in a closing lane and force your way into another	0.5758	0.6629	0.439*
11	Fail to notice pedestrians are crossing in your path of traffic	0.5455	0.6170	0.367*
12	Fail to check your rearview mirror before pulling out, changing lanes, etc.	0.5758	0.7513	0.438*
13	Underestimate the speed of an oncoming vehicle when overtaking	1.0303	0.8095	0.321
14	Brake too quickly on a slippery road or steer the wrong way in a skid	0.5152	0.5658	0.473**
15	Get into the wrong lane approaching a roundabout or a junction	1.2121	0.7398	0.493**
16	Misread the signs and exit from a roundabout on the wrong road	1.2424	0.9024	0.692**
17	Forget where you left your car in a car park	1.2121	1.0828	0.587**
18	Hit something when reversing that you had not previously seen	1.0303	0.6840	0.460**
19	Intending to drive to destination A, find yourself on the road to destination B	0.5758	0.6629	0.567**
20	Have no clear recollection of the road along which you have just been traveling	1.0303	0.9180	0.444**
Total score		18.6970	7.3802	1.000

*$p < 0.05$
**$p < 0.01$

Questionnaire Validity and Reliability Analysis

In the statistical field, reliability, and validity are the two main indexes which can determine whether the results of such self-reported questionnaire are reliable and accurate. A questionnaire with high reliability and validity can be considered as the standard scale to test and quantify some characteristics of the participants [10]. In this section, reliability and validity have been analyzed and verified based on the simplified DBQ.

In statistics, reliability is defined as: the proportion of the real variance in the total variance [10]. When the scale has reliability larger than 0.6, it is persuasive. In general, the reliability of scale is estimated based on the sample values that measured, because the variance is hard to accurately calculate. At present, the Cronbach's alpha reliability coefficient method is the most commonly used method [11]. This method is specially used for the reliability estimation of the accumulative Likert scale. It is defined as: the ratio of the sum variance of each item and the total variance of the whole scale. According to the items shown in Table 1 and the total variance, the Cronbach's alpha reliability coefficient of the simplified questionnaire can be obtained as 0.8545, which indicates that the reliability of this scale is very high. Therefore, this scale is relatively persuasive.

Driver Characteristics Based on Driver Behavior. Table 2 DBQ score analysis of the driver groups

	N	Mean	S.D.	*T* value	*T* Sig.	Mean difference
Male	29	18.310	7.517	−0.806	0.426	−3.190
Female	4	21.500	6.455			
Age < 45 years	18	19.333	7.348	0.537	0.595	1.400
Age ≥ 45 years	15	17.933	7.601			
Driving years < 10 years	15	19.733	5.587	0.731	0.47	1.900
Driving years ≥ 10 years	18	17.833	8.665			
No accidental history	16	15.750	7.344	2.382	0.024*	−5.721
With accidental history	17	21.471	6.443			

*$p < 0.05$

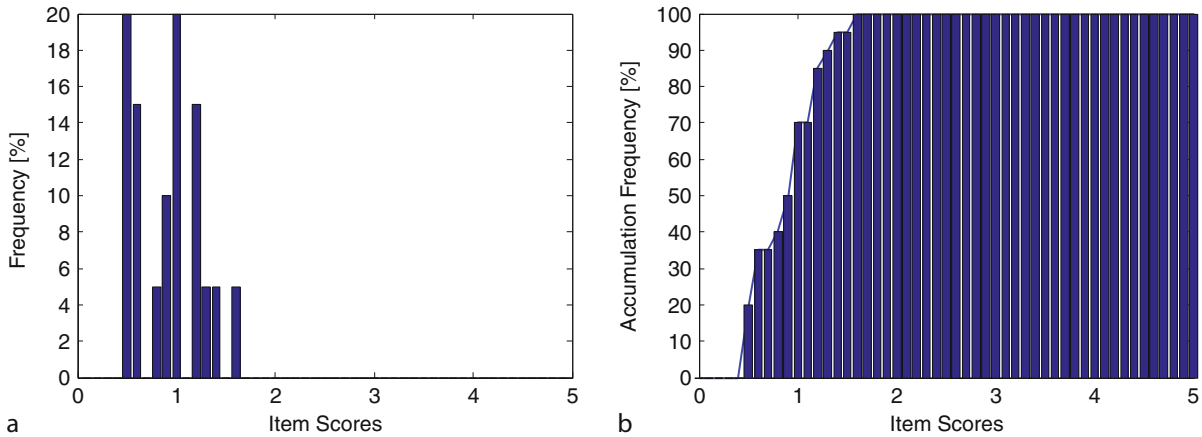

Driver Characteristics Based on Driver Behavior. Figure 1
Statistical results of item score frequency. (**a**) Frequency distribution and (**b**) accumulation frequency distribution

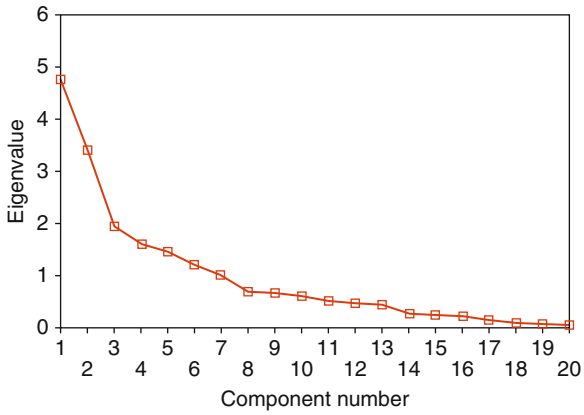

Driver Characteristics Based on Driver Behavior.
Figure 2
Scree plot of factor analysis

Driver Characteristics Based on Driver Behavior.
Table 3 Factor loading matrix

Item No.	Behavior	Factor 1	Factor 2
16	Lapse	0.795	
20	Lapse	0.749	
19	Lapse	0.746	
11	Error	0.641	
14	Error	0.638	
18	Lapse	0.574	
17	Lapse	0.554	
15	Lapse	0.507	
13	Error	0.469	
12	Error	0.466	
7	Violation		0.804
8	Violation		0.693
4	Violation		0.682
3	Violation		0.640
9	Violation		0.612
6	Violation		0.609
1	Violation		0.595
2	Violation		0.516
5	Violation		0.366
10	Violation		0.350

Validity is mainly used to express the ability that the scale is able to truly measure the desired information, i.e., the effective degree of the scale. It is defined as the ratio of the variance of the scores that related to the measure purposes and the total variance. In this section, the content validity and discriminate validity of the DBQ (the two items of the validity) are assessed by mainly utilizing the correlation analysis and average analysis method.

The content validity analysis can be used to demonstrate the validity of the scale by the correlation analysis of each item score and the total score. The more the correlation between each item score and the total score, the more the items involved in the scale reflect the same theme. The measure index of content validity is defined as the Pearson correlation coefficient (in terms of r_{xy}) between each item score and the total score, whose absolute value is less than 1. The judging rule is that: the closer $|r_{xy}|$ approaches to 1, the more significant the linear relation is. By analyzing the content validity of the DBQ in this paper, it can be seen that the correlation coefficients are all positive. In addition, 90% of the items have high positive interrelations with the total score under 0.05 and 0.01 significance levels. Therefore, this DBQ has a good content validity.

Discriminate validity is expressed as the ability of discriminating the characteristics of the measured sample from the scale. In this paper, it is desired that the scale can be used to analyze the driver characteristics, especially the driver behavior characteristics in traffic accidents. Therefore, the participants are divided into groups based on gender, age, driving years, mileage, and accidental history respectively, and in order to analyze the discriminate validity of the DBQ, *T*-test is carried out to investigate the difference between the groups. As Table 2 shown, the significant probability between groups divided by the accidental history is less than 0.05, which indicates that there is significant difference. Meanwhile, the total score of the group with accidental history is obviously higher than the group with no accidental history. It indicates that the participants having higher frequency behaviors are more likely to be involved in accidents. In addition, in groups divided by gender, age, and driving years, there are some differences between the average scores: the average score of the low age group is higher than that of the high age group, and average score of the low driving

Driver Characteristics Based on Driver Behavior.

Table 4 The factor score coefficient

Item No.	*a*	*b*
1	−0.001	0.154
2	−0.040	0.140
3	−0.014	0.168
4	−0.054	0.185
5	0.050	0.087
6	0.034	0.153
7	−0.061	0.218
8	0.002	0.180
9	−0.018	0.161
10	0.060	0.082
11	0.163	−0.063
12	0.112	0.001
13	0.119	−0.043
14	0.155	−0.010
15	0.117	0.033
16	0.188	0.022
17	0.125	0.059
18	0.139	−0.010
19	0.181	−0.013
20	0.189	−0.066

years is higher than that of the high driving years' group, but the difference is not significant. The average analysis indicates that the DBQ have a significant discriminate validity in the aspect of accidental history.

Data Statistical Analysis and Quantification Analysis

Data Statistical Analysis

The item scores of the questionnaire were analyzed, and the mean score, the standard deviation of the tested samples and that of the total scores are shown in Table 1. Figure 1 is the statistical results of item score frequency. It can be seen that the scores of the items are generally low, and almost all less than 2, more than 50% of these less than 1, which indicates that most of the abnormal driving behaviors in this DBQ are rare. The main reason for this phenomenon may be that most of the participants have high education background and good driving experience.

Quantification Analysis

Factor Analysis Factor analysis theory is applied to the data processing and extraction of this 20-item DBQ. Principle components analysis with oblique rotation is implemented as the factor analysis method to investigate the factor structure of the DBQ. A two-dimensional factor structure is established, too. This structure is also suggested in the scree plot shown in Fig. 2, and the curve becomes smooth from the third component. The two factors could account for 40.1% of the total variance. Table 3 shows the factor load matrix and the items with load less than 0.35 are omitted.

This factor analysis method distinguishes the different types of behaviors clearly. The first factor accounts for 20.8% of the total variance and contains ten items which are all lapse and error behaviors. The second factor contains the other ten items which describe violation behaviors. It could be assumed that both of the error and lapse are attributed to the driver's unintentional passive characteristics caused by the lack of driving skill. Taking the 12th item "Fail to check your rearview mirror before pulling out, changing lanes, etc.," as an example: the behavior occurs because the driver is short of training on this "mirror-checking" experience. As viewed from the behavior's property, this behavior is similar to the lapse behavior such as the 18th item "Hit something when reversing that you had not previously seen," and the diversities between these items are only the different driving skills presented by the behaviors. Therefore, the first factor could be defined as F_{skill} to describe the driver's characteristics on driving skills. The violation behaviors indicate the driver's intentional active characteristics attributed to driving style. The more aggressive style the driver is inclined to, the more violation behaviors may occur during his/her driving. Similarly, the second factor is defined as F_{style} to describe the driver's style characteristics. Based on the principle of factor analysis, these two factors are independent and represent the human driver's unintentional (not purposive) and intentional (purposive) behaviors respectively.

Driver Characteristics Quantification The factor analysis converts the 20 items to two factors F_{skill} and F_{style}, and provides a method to quantify individual driver's characteristics of driving skill and style based on the scale point data of self-reported questionnaire. The quantification of F_{skill} and F_{style} is calculated as the equation below. $X_1, X_2, \cdots, X_M$ are the standardized scale points of the DBQ items provided by the participants during self-reported survey, and a_1, $a_2 \cdots a_M$, b_1, $b_2 \cdots b_M$ are the factor score coefficients (M =20).

$$F_{skill} = a_1X_1 + a_2X_2 + \cdots + a_MX_M$$
$$F_{style} = b_1X_1 + b_2X_2 + \cdots + b_MX_M$$

Based on the original data of the 33 participants, the coefficients a_1, $a_2 \cdots a_M$, b_1, $b_2 \cdots b_M$ could be estimated with regression analysis and the results are shown in Table 4.

The quantified factors are normalized that the mean is 0 and the standard deviation is 1. The drivers with larger driving skill factor F_{skill} have higher frequency of error and lapse behaviors, and the larger value of driving style factor F_{style} means more violation behaviors. The data points of the 33 participants' characteristics factors distribute in all of the four quadrants, which are shown in Fig. 3. There are six participants (18.2%) in the first quadrant, 11 participants (33.3%) in the second quadrant, seven participants (21.2%) in the third quadrant, and nine participants (27.3%) in the fourth quadrant. This proportion of distribution indicates that the drivers are inclined to two main tendencies: one is aggressive style with better skill (quadrant II), and the other is prudent style with worse skill (quadrant IV). This result is coincident with the human psychological features.

Comparison and Discussion

The participants' self-evaluations on driving skill and style are collected during the survey, and the statistical results are shown in Table 5. According to the five-point scales, most participants are confident with

Driver Characteristics Based on Driver Behavior.
Table 5 Driver self-evaluation statistical results

	Skill	Style
Mean	1.212	1.879
S.D.	0.600	1.023

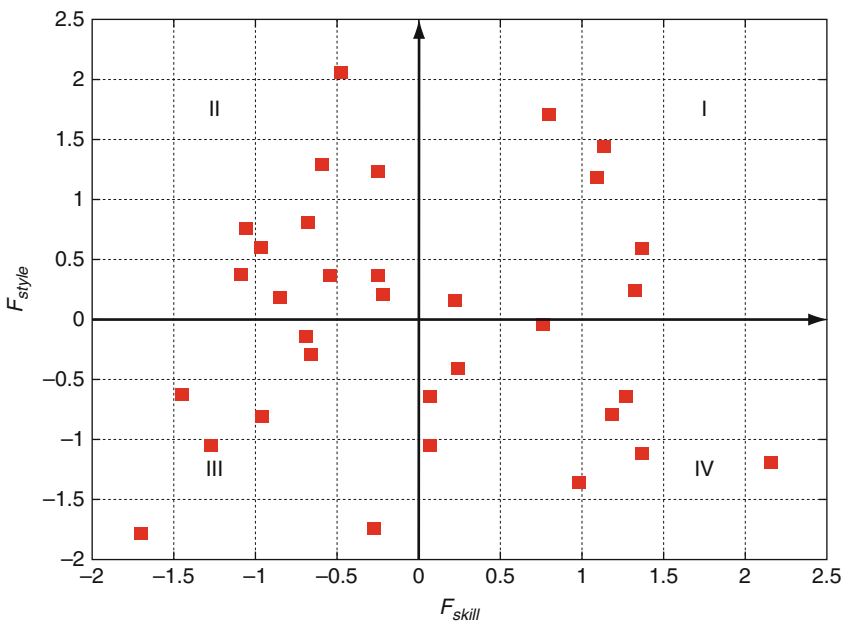

Driver Characteristics Based on Driver Behavior. Figure 3
Factor score distribution

Driver Characteristics Based on Driver Behavior. Table 6 Correlative coefficients analysis results of factor score and self-evaluation

	Self-evaluation of driving skill	Self-evaluation of driving style	Driving skill factor F_{skill}	Driving style factor F_{style}
Self-evaluation of driving skill	1	$r = -0.262$	$r = -0.542^{**}$	$r = -0.294$
		Sig = 0.140	Sig = 0.001	Sig = 0.096
Self-evaluation of driving style	–	1	r = 0.225	$r = 0.481^{**}$
			Sig = 0.208	Sig = 0.005
Driving skill factor F_{skill}	–	–	1	$r = 0.000$
				Sig = 1
Driving style factor F_{style}	–	–	–	1

$^{**}p < 0.01$

Driver Characteristics Based on Driver Behavior. Table 7 F_{skill} analysis of the driver groups

	N	Mean	S.D.	*T* value	*T* Sig.	Mean difference
Male	29	−0.129	0.987	−2.101	0.044^{**}	−1.065
Female	4	0.936	0.487			
Age < 45 years	18	0.047	0.924	0.290	0.774	0.103
Age ≥ 45 years	15	−0.056	1.115			
Driving years < years	15	0.231	0.894	1.222	0.231	0.424
Driving years ≥ 10 years	18	−0.192	1.067			
No accidental history	16	−0.301	0.971	−1.726	0.094^{*}	−0.584
With accidental history	17	0.283	0.970			

$^{*}p < 0.1$
$^{**}p < 0.05$

Driver Characteristics Based on Driver Behavior. Table 8 F_{style} analysis of the driver groups

	N	Mean	S.D.	*T* value	*T* Sig.	Mean difference
Male	29	0.049	0.975	0.754	0.456	0.405
Female	4	−0.356	1.263			
Age < 45 years	18	0.102	0.950	0.633	0.532	0.223
Age ≥ 45 years	15	−0.122	1.077			
Driving years < 10 years	15	−0.034	0.832	−0.177	0.860	−0.063
Driving years ≥ 10 years	18	0.029	1.144			
No accidental history	16	−0.229	0.893	−1.287	0.208	−0.444
With accidental history	17	0.215	1.073			

their driving skill and consider themselves as prudent drivers.

For the purpose of investigating the relationships between the driver background information, self-evaluation and the quantified factor scores, correlation analysis of these data is carried out. Table 6 shows the correlative coefficients analysis results of factor score and self-evaluation.

It can be seen that there are all positive correlations that with the significance level less than 0.01 between the driving skill factor F_{skill} and driving skill self-evaluation, the driving style factor F_{style} and driving style self-evaluation. These results show that the quantified factor scores are in accordance with the driver's self-evaluation.

The comparisons between the groups divided by gender, age, driving years, and accidental history are also conducted with T-test of F_{skill} and F_{style}, which are shown in Tables 7 and 8 respectively.

It can be seen that there are certain differences between the average values of common factors with the different groups. As for the group divided by gender, the average values of the driving skill factor F_{skill} of the female group are all higher than those of the male group. And the difference significant level is lower than 0.05, which indicates that there are certain differences for the driving ability of female participants compared with that of male participants. At the same time, the average values of driving style factor F_{style} with the female group are all lower than those of the male group, which indicates that the driving style of the female participant tends to be more conservative compared with the male participant. It accords with the gender characteristics to a certain extent.

As for the group divided by age and driving years, the average values of the driving skill factor F_{skill} of the low age group and the short driving years group is higher than those of the high age group and the long driving years' group. In addition, the average values of the driving style factor F_{style} with the low age group is higher than those of the high age group, and there is almost no difference between the short driving years group and the long driving years group. Then the difference also accords with the conventional understanding, but there is no significant difference among the most average values of the driving skill factor F_{skill}, and the same as the driving style factor F_{style}.

As for the group divided by accidental history, the average values of the driving skill factor F_{skill} with the no accidental history group are lower than those of the accidental history group and the significant level is lower than 0.1, which is an obvious difference. The above analysis indicates that the driver characteristics and the difference of the accident history can be reflected by the common factor. And the driver with the high driving skill factor F_{skill} or driving style factor F_{style} is much easier to have an accident.

Based on the comparisons between quantified factor scores and driver self-evaluation, the group analysis, the reasonability of the quantification method is validated that the quantified factors could embody the driver's characteristics tendencies on skill and style.

Future Directions

In this paper, a quantification method is explored to investigate the human driver behavior characteristics. Thirty-three Chinese drivers participate in a self-reported survey based on Driver Behavior Questionnaire (DBQ) and a two-dimensional factor structure is established from the original data with factor analysis theory.

The extracted F_{skill} and F_{style} factors can be calculated by the data of driver self-reported survey expediently, which describe the driver's unintentional driving skill and intentional driving style characteristics, respectively. Some comparisons and discussions are also carried out to validate this method. The quantification method of driving skill and driving style could be applied to the development of adaptive Driver Assistance Systems, e.g., providing more assistance to drivers with less driving skill and effective warning to the drivers with aggressive driving style. The quantified evaluation of drivers could also be utilized to train and educate drivers and help to improve the driving skill and correct the driving style. Meanwhile, the comparative analysis of the DBQ and real road experimental data can be carried out in the future work.

Acknowledgments

The project was supported by NSFC (No. 50705047). The authors especially thank Mr. Qing Xiao (China Agricultural University) and Mrs. Furui Yang (China Agricultural University) for their contribution to the preparation of the chapter.

Bibliography

1. Elander J, West R, French D (1993) Behavioral correlates of individual differences in road traffic crash risk: an examination of methods and findings. Psychol Bull 113:279–294
2. Aufrere R, Gowdy J, Mertz C, Thorpe C, Wang C, Yata T (2003) Perception for collision avoidance and autonomous driving. Mechatronics 13(10):1149–1161
3. Deffenbacher JL, Oetting ER, Lynch RS (1994) Development of a driving anger scale. Psychol Rep 74:83–91
4. Lajunen T, Parker D, Summala H (2003) The Manchester driver behaviour questionnaire: a cross-cultural study. Accid Anal Prev 942:1–8
5. Reason JT, Manstead ASR, Stradling SG, Baxter JS, Campbell K (1990) Errors and violations on the road: a real distinction? Ergonomics 33:1315–1332
6. Xie C, Parker D (2002) A social psychological approach to driving violations in two Chinese cities. Transport Res Part F: Traffic Psychol Behav 5(4):293–308
7. Ozkana T, Lajunen T, Summala H (2006) Driver behaviour questionnaire: a follow-up study. Accid Anal Prev 38:386–395
8. Lajunen T, Summala H (2003) Can we trust self-reports of driving? Effects of impression management on driver behavior questionnaire responses. Transp Res F 6:97–107
9. Davey J, Wishart D, Freeman J, Watson B (2007) An application of the driver behaviour questionnaire in an Australian organisational fleet setting. Transp Res F 10:11–21
10. Huixin K, Shen H (2005) The statistical analysis of the research, 2nd edn. The Press of China Media University, Beijing
11. Cronbach LJ (1951) Coefficient alpha and the internal structure of tests. Psychometrika 16(3):297–334

Driver Inattention Monitoring System for Intelligent Vehicles

Yanchao Dong[1], Zhencheng Hu[2]
[1]Graduate School of Science and Technology, Kumamoto University, Kumamoto, Japan
[2]Graduate School of Science and Technology, Computer Science Department, Kumamoto University, Kumamoto, Japan

Article Outline

Glossary
Definition of the Subject
Introduction
Distraction and Fatigue Effects on Driving Behavioral Performance
Commercial Products and Activities for Driver Inattention Detection
Current Methods to Detect Driver Inattention
Discussion: Future Directions
Conclusion
Bibliography

Glossary

DIMS Driver inattention monitoring system, to monitor the attention status of the driver.

Distraction Driver distraction is a diversion of attention away from activities critical for safe driving toward a competing activity.

Driver biological Utilize driver biological signals, e.g., electroencephalography (EEG), electrocardiogram (ECG), electro-oculography (EOG), surface electromyogram (sEMG), to estimate driver attention status.

Driver physical Utilize driver's physical signals, e.g., eye closure duration, blink frequency, nodding frequency, fixed gaze, and frontal face pose, to estimate driver attention status.

Driving performance Utilize driving performance, e.g., pressure distribution on the seat, car-following, steering wheel angle, accelerator pedal position, lane boundaries, and upcoming road curvature, to estimate driver attention status.

Fatigue Driver fatigue refers to a combination of symptoms such as impaired performance and a subjective feeling of drowsiness.

Hybrid Combining driver physical measures with driving performance measures to estimate driver attention status.

Inattention Driver inattention represents diminished attention to activities that are critical for safe driving in the absence of a competing activity.

Measures The way to estimate the driver's attention status.

Physical signal extraction The approaches for extracting driver physical signals.

Subjective report Subjective self-assessment of attention status.

Definition of the Subject

Driver inattention is a major factor in highway crashes. The National Highway Traffic Safety Administration (NHTSA) estimates that approximately 25% of police-reported crashes involve some forms of driver inattention – the driver is distracted, asleep or fatigued, or otherwise "lost in thought" [1]. This entry reviews

the state-of-the-art technologies for monitoring driver inattention, which can be classified into two main categories: distraction and fatigue. Driver inattention is a major factor in most traffic accidents. Research and development has been actively carried out for decades with the goal of precisely determining the drivers' state of mind. This entry summarizes these approaches by dividing them into five different types of measures:

1. Subjective report measures
2. Driver biological measures
3. Driver physical measures
4. Driving performance measures
5. Hybrid measures

Among these approaches, subjective report measures and driver biological measures are not suitable under real driving conditions, but could serve as some rough ground truth indicators. The hybrid measures are believed to give more reliable solutions compared with single driver physical measures or driving performance measures, because the hybrid measures minimize the number of false alarms and maintain a high recognition rate, which promote acceptance of the system. Also, a discussion on some nonlinear modeling techniques commonly used in the literature is made.

Introduction

Driver inattention is a major factor in highway crashes. The National Highway Traffic Safety Administration (NHTSA) estimates that approximately 25% of police-reported crashes involve some forms of driver inattention – the driver is distracted, asleep or fatigued, or otherwise "lost in thought" [1]. A common definition of driver inattention is given in [2]: "Driver inattention represents diminished attention to activities that are critical for safe driving in the absence of a competing activity."

A study by the AAA FTS (American Automobile Association Foundation for Traffic Safety) utilized five categories for the driver attention status: attentive, distracted, looked but did not see, sleepy, and unknown [3]. The category of looked but did not see can be considered to be a kind of cognitive distraction, and the word "sleepy" could be replaced by the more comprehensive word "fatigued." In this entry, two categories of inattention are proposed: *distraction* and *fatigue*.

The causes of driver distraction are diverse and pose large risk factors – over half of the crashes involving inattention were caused by driver distraction [1, 2]. After an intensive study on the various definitions of driver distraction appeared in the literature, a more general definition is proposed by Lee et al. [2]: "Driver distraction is a diversion of attention away from activities critical for safe driving toward a competing activity."

Thirteen types of potentially distracting activities are listed in [3]: eating or drinking, outside person, object or event, talking or listening on cellular phone, dialing cellular phone, using in-vehicle-technologies, etc. Because the distracting activities take many forms, the NHTSA classifies distractions into four categories from the viewpoint of the driver's functionality: visual distraction (e.g., looking away from the roadway), cognitive distraction (e.g., being lost in thought), auditory distraction (e.g., responding to a ringing cell phone), and biomechanical distraction (e.g., manually adjusting the radio volume) [1]. Two more categories are added by Lee et al. [2]: olfactory distraction and gustatory distraction. Many distracting activities can involve more than one of these components (e.g., talking to a phone while driving creates a biomechanical, auditory, and cognitive distraction).

The phenomenon of fatigue is different from that of distraction. The term "fatigue" refers to a combination of symptoms such as impaired performance and a subjective feeling of drowsiness [4]. Even with the intensive research that has been performed, the term "fatigue" still does not have a universally accepted definition [5]. Thus, it is difficult to determine the level of fatigue-related accidents. However, studies show that 25–30% of driving accidents are fatigue related [6]. In their definition, the European Transport Safety Council (ETSC) states that fatigue "concerns the inability or disinclination to continue an activity, generally because the activity has been going on for too long" [7]. From the viewpoint of individual organ functionality, there are different kinds of fatigue such as local physical fatigue (e.g., in a skeletal or ocular muscle), general physical fatigue (following heavy manual labor), central nervous fatigue (sleepiness), and mental fatigue (not having the energy to do anything). Central nervous fatigue and mental fatigue are the most dangerous types for driving, because these will

eventually lead to sleepiness, increasing the probability of an accident.

The ETSC defines four levels of sleepiness based on behavioral terms [7]: (a) completely awake, (b) moderate sleepiness, (c) severe sleepiness, and (d) sleep. In an attempt to avoid having an accident, most sleepy drivers will try to fight against sleep with different durations and sequences of the physiological events that precede the onset of sleep [8]. When a driver becomes fatigued and begins to fall asleep, the following symptoms can be observed: repeated yawning, confusion and thinking seems foggy, feeling depressed and irritable, slower reaction and responses, daydreaming, difficulty keeping eyes open and burning sensation in the eyes, lazy steering, difficulty maintaining concentration, swaying of head or body from nodding off, vehicle wanders from the road or into another lane, nodding off at the wheel, breathing becomes shallow, heart races, etc. Different individuals show different symptoms and the degrees vary. Thus, there is no concrete method to measure the level of fatigue. The ETSC's study [7] showed that the level of fatigue or sleepiness (sleepiness is the outside exhibition of fatigue) is a function of the amount of activity in relation to the brain's physiological waking capacity. Several factors can influence this physiological waking capacity, and hence lower the fatigue threshold [4, 5, 7, 9] such as disturbed sleep, the low point in the circadian rhythm, hard work prior to driving, etc. These factors are independent of the activity being undertaken, but result in the fatigue effect of that activity appearing more quickly. Thus, fatigue cannot be seen simply as a function of the duration of time engaged in driving.

Driving inattention includes two main categories and each of them includes a few subcategories, as shown in Fig. 1. The purpose of driving inattention monitoring system (**DIMS**) is to monitor the attention status of the driver and if driving inattention is detected some measures should be done to make the driving safe, depending on the inattention type and level.

Driving is a process involving situation awareness of the environment, decision making, and the performance of actions, as shown in Fig. 2 [10]. In this process, the most complicated stage is the situation awareness. In [10], a three-level situation awareness model is defined as "The perception of the elements in the environment within a volume of time and space, the comprehension of their meaning, and the projection of their status in the near future." The deployment of attention in the perception process acts to present certain constraints on a person's ability to accurately perceive multiple items in parallel, and is a major limitation on situation awareness. Direct attention is needed, not only for perceiving and processing the

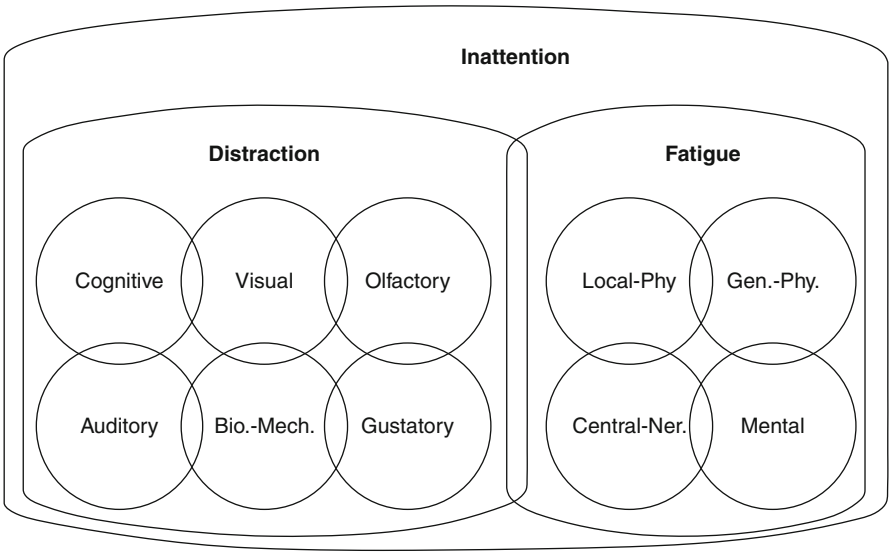

Driver Inattention Monitoring System for Intelligent Vehicles. Figure 1
Inattention categories

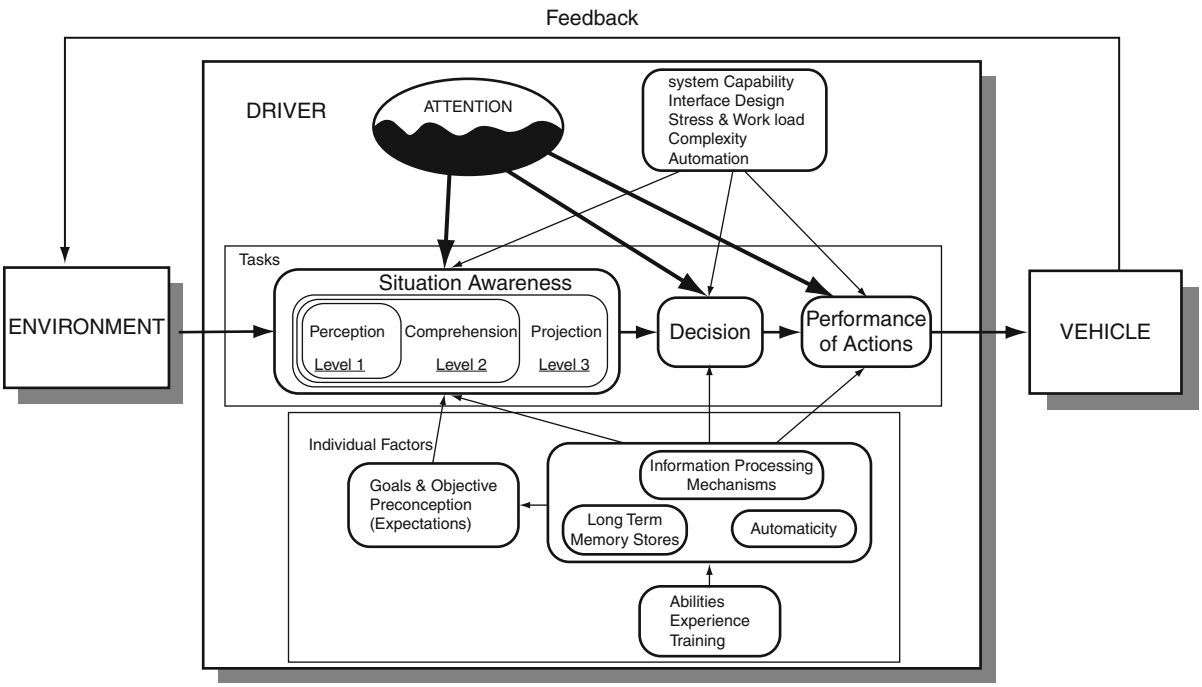

Driver Inattention Monitoring System for Intelligent Vehicles. Figure 2
Information processing and attention [10]

available cues, but also in the later stages of decision making and response execution. In a complex and dynamic driving environment, attention demands result from information overload, complex decision making, and the performance of multiple tasks. Thus, monitoring the attention status is vital for maintaining safe driving.

The purpose of the driver inattention monitoring system (**DIMS**) is to monitor the attention status of the driver. If driver inattention is detected, different countermeasures should be taken to maintain driving safety, depending on the types and levels of inattention. **DIMS** has been an active research field for decades. The first international conference on driver distraction and inattention was held in 2009 [11]. Some auto companies have already installed some simple function driver fatigue monitoring systems in their high-end vehicles. Yet, there is still a great need to develop a more reliable and fully functional **DIMS** using cost-efficient methods for a real driving context. It is believed that the development of signal processing and computer vision techniques will attract more attention to the study of this field in the coming years. With the intention of benefiting those interested in, or about to enter, this field, this entry gives a comprehensive review of the state of the knowledge on driver inattention. It thus provides a clear view of the previous achievements and the issues that still need to be considered.

The arrangement of this entry is as follows. We introduced the driver inattention concept in section "Introduction". Next, the effects of driver distraction and fatigue on driving performance are presented in section "Distraction and Fatigue Effects on Driving Behavioral Performance". Because some commercial products relative to inattention detection have emerged on the market in recent years, section "Commercial Products and Activities for Driver Inattention Detection" is devoted to reviewing these products. section "Current Methods to Detect Driver Inattention" presents a detailed review of the scientific researches on inattention detection. Five types of measures for inattention detection are presented in this section: (a) subjective report measures, (b) driver biological measures, (c) driver physical measures, (d) driving performance measures, and (e) hybrid measures. After a discussion of future directions in section

"Discussion: Future Directions", a conclusion is given in section "Conclusion".

Distraction and Fatigue Effects on Driving Behavioral Performance

This section concentrates on how distraction and fatigue affect a driver's behavior and driving performance. Exploring these effects could provide useful information for the development of real-time distraction and fatigue detection algorithms.

Effects of Distraction

Performing a cognitively demanding task while driving would influence both the driver's visual behavior and driving performance (as indicated by braking behavior).

Driver Behavior Patterns With an increase in the cognitive demand, many drivers changed their inspection patterns on the forward view. Angell et al. [12] indicated that the eye-glance pattern could be used to discriminate driving while performing a secondary task from driving alone, and could be used to discriminate high- from low-workload secondary tasks. More facts associated with cognitive distraction driving can be found in [13, 14]: Drivers narrowed their inspection of the outward view and spent more time looking directly ahead. They reduced their inspection of the instruments and mirrors, and reduced their glances at traffic signals and the area around an intersection. Rantanen and Goldberg [14] found that the visual field shrank by 7.8% during a moderate-workload counting task and by 13.6% during a cognitively demanding counting task. Drivers had fewer saccades per unit time, which was consistent with a reduction in glance frequency and less exploration of the driving environment, and in some cases drivers shed these tasks completely and did not inspect these areas at all [15]. Hayhoe [16] showed links between eye movement (fixation, saccade, and smooth pursuit), cognitive workload, and distraction. Fixations occur when an observer's eyes are nearly stationary. Saccades are very fast movements that occur when visual attention shifts from one location to another. Smooth pursuits occur when an observer tracks a moving object such as a passing vehicle. Saccade distance decreases as task complexity increases, which indicates that saccades may be a valuable index of mental workload [17]. In contrast, the amount of head movement increased when cognitive loads were imposed. It is believed that this is a compensatory action by which a driver attempts to obtain a wider field of view [18]. Miyaji et al. [18] proposed that the standard deviations of eye movement and head movement could be suitable for detecting the states of cognitive distraction in subjects. Both cognitive and visual distractions caused gaze concentration and slow saccades when drivers looked at the roadway, and cognitive distraction increased blink frequency [19]. Liang and Lee [19] found that visual distraction resulted in frequent, long off-road glances. A report from the Safety Vehicle Using Adaptive Interface Technology (SAVE-IT) program showed that eyes-off-road glance duration, head-off-road glance time, and standard deviation of lane position (SDLP) are good measures of visual distraction [20].

Other Physiological Responses When cognitive loads (conversation or arithmetic) were imposed on subjects, pupil dilation occurred by the acceleration of the sympathetic nerve [18]. The average heart rate also increased by approximately 8 beats per minute. However, the average value of the heart rate RRI decreased under the same situation [18]. Itoh [21] pointed out that performing a cognitively distracting secondary task (e.g., talking, thinking about something, etc.) during driving caused a decrease in the driver's temperature at the tip of the nose, and this effect was reproducible. It was reported in [22] that a considerable and consistent skin temperature increase in the supraorbital region could be observed during cognitive and visual distractions. Berka [23] found that the electroencephalography (EEG) signal also contained information about the task engagement level and mental workload.

Driving Performance Significant changes were observed in a driver's vehicle control as a consequence of performing the additional cognitive tasks while driving. Ranney [24] found that distraction may be associated with lapses in vehicle control, resulting in unintended speed changes or allowing the vehicle to drift outside the lane boundaries. Zhou et al. [25]

found the influences on the lane-changing behavior when a secondary task was being performed, which included a reduction in the frequency of the checking behavior (check a side mirror or speedometer), a delay in the checking behavior, and a longer time for the checking behavior. Carsten and Brookhuis [26] found that the effects of cognitive distraction on driving performance differed considerably from those of visual distraction. Visual distraction affects a driver's steering ability and lateral vehicle control, while cognitive distraction affects longitudinal vehicle control, particularly car-following. Liang and Lee [19] also found that cognitive distraction made steering less smooth, but improved lane maintenance. Liang and Lee [19] found that steering neglect and overcompensation are associated with visual distraction, while under-compensation is associated with cognitive distraction. Overall, visual distraction interferes with driving performance more than cognitive distraction. An apparently anomalous finding is that when secondary task cognitive demands increased, a driver's lateral control ability was found to improve [26]. Harbluk et al. [13, 15] found an increased incidence of hard braking associated with cognitive distraction driving.

Effects of Fatigue

When a driver is fatigued, certain physical and physiological phenomena can be observed. These include changes in brain waves or EEG, eye activity, facial expressions, head nodding, body sagging posture, heart rate, pulse, skin electric potential, gripping force on the steering wheel, and other changes in body activities.

Driver Behavior Patterns Eskandarian et al. [27] found that the follow actions were correlated with fatigue: Drivers exhibited a reflexive head nod after checking the side mirrors; the head motions were significantly less frequent; the number of times drivers touched or scratched their chin, face, head, ears, eyes, and legs significantly increased; drivers were inclined to turn their head to the left to relieve muscular tension in the neck; eye blinking activity radically increased; episodes of yawning were more frequent; and they tended to adopt more relaxed hand positions on the steering wheel. Particularly for eye blinking patterns, PERCLOS [28], the percentage of time the eye is more than 80% closed, is one of the most widely accepted measures in the scientific literature for drowsiness detection. It has been validated using both EEG data and subjective evaluation.

Other Physiological Responses The activity of a low frequency EEG ranging from 0 to 20 Hertz has a significant relationship with sleepiness. The spectral analysis of an EEG shows the transition from wakefulness to sleep can be described as a shift toward slower EEG frequencies. In the alert condition, the appearance of β activity is common in the EEG. α activity is also normally found in the occipital regions (O1 and O2) in the awake and relaxed condition. When a driver gets drowsy, a burst of α activity can often be seen in the central regions of the brain (C3 and C4). However, some people do not show any α activity. As the driver gets drowsier, the α activity is replaced by θ activity. When δ activity occurs in the EEG, the driver is no longer awake; this is an indicator of deep sleep [29].

Driving Performance It has been reported that sleep-deprived drivers have a lower frequency of steering reversals (every time the steering angle crosses zero degrees) [30], a deterioration of steering performance [31], a decrease in the steering wheel reversing rate [32], more frequent steering maneuvers during wakeful periods, no steering correction for a prolonged period of time followed by jerky motion during drowsy periods [33], low velocity steering [34], large amplitude steering wheel movements, and large standard deviations in the steering wheel angle [35]. Zhong et al. [36] found that when drivers had a fatigued status, the steering wheel angle and vehicle tracking became irregular, and the range of deviation greatly increased. Several researchers found that the lane-tracking ability decreased as the time on the task increased [31]. Variables such as the times of lane departures, SDLP, and maximum lane deviation were found to be highly correlated with eye closures [37]. The mean square of lane deviation, mean square of high pass lateral position, and SDLP showed good potential as drowsiness indicators [38].

Dingus et al. [34] found that the yaw deviation variance and the mean yaw deviation (calculated over a 3 min period) showed some promise as drowsiness indicators. However, no strong correlations between

drowsiness and braking or acceleration were found in [34, 39]. Generally, vehicle speed variability has not shown any strong correlation with drowsiness [39]. However, some reports found that the standard deviation of speed increased from the third driving hour with a time interval of 45 min [40].

Commercial Products and Activities for Driver Inattention Detection

Auto Companies

Many famous auto companies are currently conducting researches on driver inattention monitoring systems, including Toyota, Nissan, Volvo, Mercedes-Benz, and Saab.

Saab's Driver Attention Warning System [41, 42] is a project designed to counter two of the most common causes of road accidents: driver drowsiness and distraction. The system utilizes two miniature infrared cameras, one installed at the base of the driver's A-pillar and the other in the center of the main fascia, which are focused on the driver's eyes. It also utilizes SmartEye [43] software to get accurate eyelid, gaze, and head orientation information. In their algorithm, the driver's eye blinking frequency is measured. If a pattern of long duration eyelid closures is detected, it indicates the potential onset of drowsiness. A three-level warning interface was designed for drowsiness detection. This starts with a chime sound and text message, moves on to a spoken message, and finally a stronger warning tone audio message is persistently delivered until the driver presses the reset button. As soon as the driver's gaze moves away from what is defined as the "primary attention zone"-the central part of the windshield in front of the driver-a timer starts counting. If within 2 s of the timer being triggered the driver's eyes and head do not return to the "straight ahead" position, it is considered to be a distraction. In a case involving peripheral tasks such as looking in the rearview mirror, a side mirror, or turning a corner, the timer's elapse time becomes longer. Once the driver distraction has been detected, a seat vibration signal will be issued to warn the driver. However, there is no report about the robustness of this system during daytime and nighttime driving under different kinds of weather conditions, providing no driver status ground truth as a reference.

Toyota developed their Driver Monitoring System in 2006 for its latest Lexus models. This system features a camera, using near-infrared technology, mounted on top of the steering column cover. It monitors the exact position and angle of the driver's head while the vehicle is in motion. If the Advanced Pre-Crash Safety system detects an obstacle ahead, and at the same time the Driver Monitoring System establishes that the driver's head has been turned away from the road for too long, the system automatically activates pre-crash warnings. If the situation persists, the system can briefly apply the brakes to alert the driver [44]. In 2008, the Toyota Crown system went further. It can detect if the driver is becoming sleepy by monitoring their eyelids. Toyota's solution combines driver face orientation and environmental obstacle detection to determine accident potential, and utilizes eyelid activity to identify drowsiness.

In the spring of 2009, Mercedes-Benz introduced Attention Assist into its series production [45]. Attention Assist works by first observing a driver's behavior, and then using this information to create a unique driver profile. During operation, a series of tests continually monitor the driver input in relation to this profile, and in the event that a deviation is encountered, the system then determines whether or not the deviation is a result of fatigue. If it is, Attention Assist alerts the driver both visually and audibly that it is time to take a break. The factors taken into account to determine a driver's profile include the speed, longitudinal and lateral acceleration, angle of the steering wheel, way that the indicators and pedals are used, certain driver control actions, and even various external influences such as a side wind or an uneven road surface. The Attention Assist system only uses vehicle parameters to determine driver drowsiness, which requires no additional hardware setup. However, this system needs to establish individual profiles for different drivers, which would affect the acceptance of the system in real life.

In 2007, Volvo Cars introduced Driver Alert Control to alert tired and nonconcentrating drivers [46]. With the idea that the technology for monitoring a driver's eyes is not yet sufficiently mature and human behavior varies from one person to another, they developed their system based on the cars progress on the road. It is reported that Driver Alert Control

monitors the car's movements and assesses whether the vehicle is being driven in a controlled or uncontrolled way. It can also cover situations where the driver is focusing too much on his or her cell phone or children in the car, thereby not having full control of the vehicle.

Other Commercial Products and Activities

Technological approaches have continued to emerge in recent years, and hold promise for detecting and monitoring dangerous levels of driver inattention. While many of these projects are now in the development, validation testing, or early implementation stages, some companies can provide usable devices or prototype to give information about driver behavior. For the purpose of nonintrusive measurement, these devices mainly utilize video cameras and computer vision technologies.

Attention Technology, Inc. has designed and developed the DD850 Driver Fatigue Monitor (DFM), the only real-time, on-board drowsiness monitor that is currently being tested in an extensive field operational test. The DFM is a video-based drowsiness detection system that works by measuring slow eyelid closure. It is designed to mount on a vehicle's dashboard just to the right of the steering wheel, and provides a continuous real-time measurement of eye position and eyelid closure [47]. Specifically, the DFM estimates PERCLOS to determine drowsiness, which is the proportion of time the eyes are closed 80% or more over a specified time interval. The DFM uses a structured illumination approach to identify the driver's eyes. This approach obtains two consecutive images of the driver using a single camera. The first image is acquired using an infrared (IR) illumination source that produces a bright-pupil image. The second image uses an IR illumination source at a different wavelength to produce an image with dark pupils. These two images are essentially identical except for the brightness of the pupils in the images. A third image calculates the difference between these two images, enhancing the bright eyes and eliminating all image features except for the bright pupils. The driver's eyes are identified in this third image by applying a threshold to the pixel brightness. The bright pupil effect utilized by the DFM is a simple and effective eye-tracking approach for pupil detection based on a differential lighting scheme. However, the success of the bright pupil technique strongly depends on the brightness and size of the pupils, which are often functions of face orientation, external illumination interference, the distance of the subject from the camera, and race. For real-world in-vehicle applications, sunlight can interfere with IR illumination, reflections from eyeglasses can create confounding bright spots near the eyes, and sunglasses tend to disturb the IR light and make the bright-pupil phenomenon appear very weak.

Delphi believes that computer vision offers the most direct method for detecting the early onset of sleepiness and distraction, and it is also seen as an excellent platform to be shared with other vision-based driver assistance applications in the future. They integrated two products, the ForeWarn Drowsy Driver Alert and the ForeWarn Driver Distraction Alert, into a comprehensive Driver State Monitor (DSM) [47]. The DSM is a computer vision system that uses a single camera mounted on the dashboard directly in front of the driver and two IR illumination sources. Upon detecting and tracking the driver's facial features, the system analyzes eye closures and head pose over time to infer fatigue or distraction level. It provides an extended eye-closure warning for closures longer than 2.5 s, and also provides an extended distraction warning for nonforward gaze states in excess of 2.5 s. The fatigue detection algorithm predicts AVECLOS, the percentage of time the eyes are estimated to be fully closed over a 1-min interval. Because this is a less complex measure of drowsiness than PERCLOS, it permits the use of an automotive-grade data processor, in contrast to the high-grade PC processor required for PERCLOS.

Seeing Machines is engaged in the research, development, and production of advanced computer vision systems for research on human performance measurement, advanced driver assistance systems, transportation, etc. [48]. Their signature product, faceLAB, provides head and face tracking, as well as eye, eyelid, and gaze tracking for human subjects, using a noncontact, video-based sensor. faceLAB provides comprehensive blink analysis and PERCLOS assessment, including the delivery of raw data on the details of eyelid behavior. Instead of using traditional corneal reflection techniques, input is obtained using a stereo

camera pair. Seeing Machines's faceLAB has been employed extensively as a PC-based research tool. Although the device reportedly works very well in a simulator environment, the numerous challenges faced in a real driving environment prevent it from working robustly. Seeing Machines also provides another product, Driver State Sensor (DSS). It consists of one camera, two IR LED illuminators, and one special computing and communication unit. The goal of DSS is to detect driver fatigue by analyzing eyelid activity.

Smart Eye AB is another company that provides computer vision–based software for detecting human face/head movement, eye movement, and gaze direction [43]. Their product, Smart Eye Pro 3.0, is a machine vision system that estimates head pose using a simple and robust method based on tracking individual facial features and a three-dimensional (3D) head model. While the face is being tracked, the gaze direction and eyelid positions are determined by combining image edge information with 3D models of the eye and eyelids. A major advantage is that eye and head tracking can continue even if one camera is fully occluded or otherwise nonoperational. This also allows for large head motions (translation and rotation). Smart Eye has not developed an algorithm that monitors drowsiness.

SensoMotoric Instruments GmbH (SMI) [49] is a German company. Their product, InSight, can measure head position and orientation, gaze direction, eyelid opening, and pupil position and diameter. It uses a sampling rate of 120 Hz for head pose and gaze measurement, 120 Hz for eyelid closure and blink measurement, and 60 Hz for combined gaze, head pose, and eyelid measurement. It also provides PERCLOS information for drowsiness detection. It is a computer based system and needs user calibration.

Current Methods to Detect Driver Inattention

In the scientific literature, five main types of measures for inattention detection are commonly used: (a) subjective report measures, (b) driver biological measures, (c) driver physical measures, (d) driving performance measures, and (e) hybrid measures. With the exception of subjective report measures, these measures are based on nonlinear modeling techniques. This section briefly reviews the most common nonlinear modeling techniques. Then, the researches on the five main types of measures will be explored. Finally, the extraction of physical signals from a driver by image processing will be discussed at the end of this section, since driver physical measures offer distraction detection through eye gaze monitoring and fatigue detection through eye gaze, blink, head, and mouth tracking.

Nonlinear Modeling Techniques

Human cognition can hardly be represented by a linear model. Hence, nonlinear modeling techniques are greatly adopted in the driver inattention detection area. Nonlinear modeling with machine learning techniques can extract information from noisy data, and do not require prior knowledge before training. There are also some mechanisms in machine learning that can avoid over-fitting for nonlinear modeling, producing more robust and general models than traditional learning methods (e.g., logistic regression), which only minimize training error.

Artificial neural networks (ANNs) have been studied and utilized in numerous scientific and engineering fields. One of the main advantages of ANNs is that they infer solutions from data without any prior knowledge of the patterns in the data, that is to say, they extract the patterns empirically even if the equation between the inputs and outputs does not exist. This characteristic is very important because in most practical cases the exact input-output relationship is difficult to establish. ANNs also have the ability to generalize (i.e., they respond with a reasonable accuracy to patterns that are broadly similar to the original training patterns), which is very useful because real-world data is noisy, distorted, and often incomplete. ANNs are nonlinear, which allows them to solve some complex problems more accurately than linear techniques [27].

The fuzzy inference system (FIS) is famous for its well-known linguistic concept modeling ability. The fuzzy rule expression is close to an expert natural language. A fuzzy system then manages the uncertain knowledge and infers high-level behaviors from the observed data. On the other hand, as it is a universal approximator, the FIS can be used for knowledge induction processes [50].

Support vector machine (SVM) is based on the statistical learning technique and can be used for pattern classification and the inference of nonlinear relationships between variables. This method has been successfully applied to the detection, verification, and recognition of faces, objects, handwritten characters and digits, text, speech, and speakers, along with the retrieval of information and images [51]. The learning technique of the SVM method makes it suitable for measuring the cognitive states of humans. SVMs can generate both linear and nonlinear models and are able to compute the nonlinear models as efficiently as the linear ones. Given a set of input data, this method first transforms the input domain through a kernel, and then looks for a hyperplane in the transformed domain that separates the data with minimum error and maximum gain. Finally, the hyperplane is transformed back to the input domain to obtain the decision boundaries, which may potentially be nonlinear.

AdaBoost is a learning algorithm that uses the pattern recognition algorithm called Boosting [52]. Its advantages include a high classification performance, fast recognition process time, and the potential extension of recognition features. In AdaBoost, learning involves the creation of different classifiers while successively changing the weighting of the learning data. A weighted majority decision is then made for these multiple classifiers in order to obtain the final classifier function. Individual classifiers are referred to as "weak classifiers," while the combination of classifiers is a "strong classifier."

Bayesian networks (BNs) have several advantages that make them well suited for describing human behavior. First, the hierarchical structure of BNs can systematically present information from different sources and at different levels of abstraction, and can also capture probabilistic relationships. Second, a BN is not only a computational model but also a form of knowledge representation. Unlike other data mining approaches such as the SVM, BNs reveal the relationships that generate the model predictions. Third, BNs can handle situations with missing data. The certainty of the hypothesis will change according to the BN's reasoning, which incorporates new data using a probabilistic dependence network when new evidence is added. Because of these advantages, BNs are applicable to human-behavior modeling and have been used to detect inattention [53]. Despite these advantages, creating a correct and stable BN model requires extensive computational capability and a large amount of training data.

Another emerging trend has been to borrow techniques based on hidden Markov models (HMMs) from the speech processing and language technology field and apply these to driver behavior modeling for route recognition, driver identification, and distraction detection in a manner analogous to speech recognition, speaker identification, and stress detection in speech [54]. The foundation of HMM is a stochastic Markov process consisting of a number of states with corresponding transitions. At discrete time intervals, the Markov process moves from one state to another according to a set of transition probabilities. State changes in the Markov process are hidden from the user. Sathyanarayana et al. [54] constructed a hidden Markov model using vehicle speed, steering wheel angle, and braking force to predict route maneuvers (left turn, right turn, and lane change).

Subjective Report Measures

The Karolinska sleepiness scale (KSS) is the most commonly used tool for the subjective self-assessment of sleepiness; the values used in the KSS are shown in Table 1. Kaida et al. [55] investigated the validity and reliability of the KSS using EEG, behavioral, and other

Driver Inattention Monitoring System for Intelligent Vehicles. Table 1 Karolinska sleepiness scale (KSS)

KSS	Meaning
1	Extremely alert
2	Very alert
3	Alert
4	Rather alert
5	Neither alert nor sleepy
6	Some signs of sleepiness
7	Sleepy, no effort to stay awake
8	Sleepy, some effort to stay awake
9	Very sleepy, great effort to keep awake, fighting sleep

subjective indicators of sleepiness. Their study showed that the KSS was closely related to EEG and behavioral variables, which indicates that the KSS has a high validity for measuring sleepiness.

Ingre et al. [56] verified the close relationship between subjective sleepiness measured with the KSS and blink duration (BLINKD) and lane drifting, calculated as the standard deviation of the lateral position (SDLP) in a high-fidelity moving base driving simulator. Their experiments showed a significant effect of the KSS on both BLINKD and SDLP. A test for a quadratic trend suggested a curvilinear effect with a steeper increase at high KSS levels for both SDLP and BLINKD. Craig et al. [57] also found that psychological factors correlated consistently with self-reported fatigue. However, the KSS is recorded over relatively long time intervals, say every 15 min, as a trade-off between high temporal resolution and avoiding intrusive feedback. As a consequence, the KSS was not capable of recording sudden drowsiness variations caused by different situations.

Driver Biological Measures

Biological signals include EEG, electrocardiogram (ECG), electro-oculography (EOG), surface electromyogram (sEMG), etc. These signals are collected through electrodes in contact with the skin of the human body. Table 2 summarizes some typical methods used in this field. EEG has a spatial resolution of 20 mm and a temporal resolution of 0.001 s. It is widely used in the brain activity research field. Recent research has proposed various methods to extract features from a segment of raw EEG data for fatigue detection. In the time domain, the average value, standard deviation, and sum of the squares of EEG amplitude are the most commonly used features. In the frequency domain, the energy content of each band (β, α, θ, δ),

Driver Inattention Monitoring System for Intelligent Vehicles. Table 2 Summary of biological measures

References	Bio-signal type	Objective	Analysis methods	Result
[58]	EEG	Fatigue	Assess δ, θ, α, β	$(\theta + \alpha)/\beta \uparrow$
[59]			Sample entropy, phase synchronization	Sample entropy, phase synchronization ↑
[60]			SVM	Predict alert → drowsy
[61]			Probabilistic-SVM	Better than standard SVM
[62, 63]			ICA, FFT, correlation analysis, LRM	Est. drowsy level with 87% accuracy
[64]			KPCA algorithm	Complexity decreases as fatigue increases
[23]		Mental engagement	Inspection with second timescale	Different mental task can be detected
[65]			XCS	Different mental task can be detected
[66]	EEG, ECG	Fatigue	Dynamic Bayesian network	More features are favorable
[67]	ECG, PPG	PVT	Multi linear regression model	ECG, PPG is useful for est. PVT
[68]	EOG	Hypovigilance	Eight eye actives, fuzzy expert sys	Pre. sleep-related accidents with high acc
[69]	EOG	Drowsiness	Eleven eye actives, SVM	Accuracy is quite high for "very sleepy"
[70]	sEMG	Fatigue	Statistic analysis	Statistic trends were given
[71]			Frequency and statistic analysis	MDF, MNF, RMS show large change

mean frequency, and center of gravity of the EEG spectrum are commonly used. Other models such as the auto-regressive moving average (ARMA) and power spectrum estimation are also used by some researchers to extract EEG features. The most reliable patterns in terms of their consistency and occurrence for fatigue are the β, α, θ, and δ waves (see Fig. 3).

EEG is widely accepted as a good indicator of the transition between wakefulness and sleep, as well as between the different sleep stages. It is often referred to as the gold standard. Svensson [29] proposed objective sleepiness scoring (OSS), derived from EEG signals, as the ground truth for validating other drowsiness detection algorithms. The five-level OSS scores are described in [29], and are shown in Table 3.

The four EEG activities (β, α, θ, and δ) were assessed in [58] for 52 subjects during a monotonous driving session. The results showed an increasing trend for the ratio of slow wave to fast wave EEG activities over time. In [59], sample entropy and phase synchronization were adopted to detect fatigue from EEG signals, with the results showing that phase synchronization among the hemispheres gradually increased and sample entropy decreased, both pointing to a gradual increase in sleepiness, which is related to a decrease in EEG complexity. Yeo et al. [60] trained the SVM to classify EEG signals into four principal frequency bands, and then to predict the transition from alertness to drowsiness. Shen et al. [61] compared a probabilistic-based multi-class SVM and standard multi-class SVM as classifiers for distinguishing mental

Driver Inattention Monitoring System for Intelligent Vehicles. Table 3 Objective sleepiness scoring (OSS)

OSS score	EEG content
0	Background of continuous β waves, no α, no θ waves
1	Occurrence of α and/or θ waves, in at least two regions of the brain, for less than a cumulative length of 5 s
2	Occurrence of α and/or θ waves, in at least two regions of the brain, for less than a cumulative length of 5 s
	or
	Occurrence of α and/or θ waves, in at least two regions of the brain, for less than a cumulative length of 5 s
3	Occurrence of α and/or θ waves, in at least two regions of the brain, for less than a cumulative length of 5 s
4	Continuous α and/or θ waves

Source: Derived from EEG data [29]

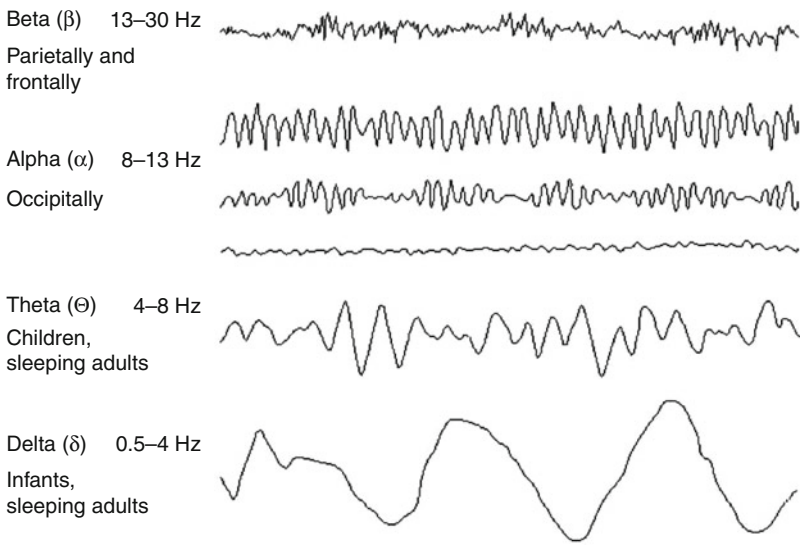

Driver Inattention Monitoring System for Intelligent Vehicles. Figure 3
Four types of EEG waves [29]

fatigue into five mental-fatigue levels, and showed that the accuracy of the probabilistic-based multi-class SVM was better. Lin et al. [62] established a linear regression model to estimate the drowsiness level from the ICA of 33-channel EEG signals, and could estimate the drowsiness level with 87% accuracy. They then implemented a real-time embedded EEG-based driver drowsiness estimate system in [63], which adopted only four channels of EEG data.

Although not apparently related, some researchers have shown that it is also possible to estimate the distraction level from EEG data. Berka et al. [23] tried to use EEG data to continuously and unobtrusively monitor the levels of task engagement and mental workload in an operational environment. An inspection on the EEG data using a second-by-second timescale revealed associations between the workload and engagement levels when aligned with specific task events, which provided preliminary evidence that second-by-second classifications reflect parameters of task performance. Skinner et al. [65] investigated the efficacy of the genetic-based learning classifier system XCS in classifying artifact-inclusive EEG signals into four mental tasks designed to elicit hemispheric responses. In Liu et al. [64], the KPCA algorithm was employed to extract nonlinear features from the complexity parameters of EEG (approximate entropy (ApEn) and Kolmogorov complexity (Kc)) and improve the generalization performance of an HMM. The result showed that both complexity parameters decreased significantly as the mental fatigue level increased, and the classification accuracy reached 84%.

In addition to EEG, other biological signals such as ECG, EOG, and sEMG have also been tested to estimate driver mental state. Yang et al. [66] employed a dynamic Bayesian network with EEG and ECG to estimate fatigue. A first-order hidden Markov model (HMM) was employed to compute the dynamics of a Bayesian network at two different time slices. The results showed that more features are favorable for inferring the driver fatigue more reliably and accurately. In Chua et al. [67], a multiple linear regression model was established to estimate PVT (psychomotor vigilance test) values from a combination of ECG and photoplethysmogram (PPG) data. Damousis and Tzovaras [68] selected eight eye activity features, extracted from EOG, to develop a fuzzy expert system (FES) for the detection of hypovigilance. Shuyan and Gangtie [69] employed an SVM to perform drowsiness prediction with 11 eyelid-related features extracted from EOG. These eyelid features included blink duration, blink duration 50–50, amplitude, lid closure speed, peak closing velocity, lid opening speed, peak opening velocity, delay of eyelid reopening, duration at 80%, closing time, and opening time. It was reported that the drowsiness detection accuracy was 86% for "sleepy." In Balasubramanian and Adalarasu [70], the surface sEMG of the shoulder and neck was analyzed while the participant was driving to determine the onset of fatigue and prove that the development of muscular fatigue is a consequence of driving. In Katsis et al. [71], frequency analysis and statistical analysis were performed on sEMG signals from the left bicep, right bicep, left forearm flexor, right forearm flexor, and frontal muscles. The results showed that the middle frequency decreased by about 9.5–18.9%, the mean frequency decreased by about 11.3–18.4%, and the root mean square amplitude increased by about 25.1–47.7% from their initial values for a predefined driving route.

Driver Physical Measures

Fatigue Detection In Bergasa et al. [50], PERCLOS, eye closure duration, blink frequency, nodding frequency, fixed gaze, and frontal face pose were normalized and used as inputs to the fuzzy inference system for fatigue detection. Different linguistic terms and their corresponding fuzzy sets were distributed in each of the inputs using induced knowledge based on the hierarchical fuzzy partitioning (HFP) method. They then chose the fast prototyping algorithm with the pruned method (FDT + P) to automatically generate fuzzy rules that were consistent, lacked redundancy, and were interpretable. Afterward, a simplification process was applied to achieve a more compact knowledge base to improve the interpretability and maintain the accuracy. Finally, three variables (fixed gaze, PERCLOS, and eye closure duration) were determined to be crucial cues for detecting a driver's fatigue. By fusing them with a fuzzy system, a final fatigue detection accuracy of 98% was achieved.

Fan et al. [72] utilized a Gabor-features representation of the face for fatigue detection. After the face was

located, Gabor wavelets were applied to the face area to obtain different scale and orientation features of the face. Then, features on the same scale were fused into a single one to reduce the dimension. Finally, the AdaBoost algorithm was used to extract the most critical features from the dynamic feature set and construct a strong classifier for fatigue detection. It was reported that this method worked well on a wide range of human subjects with different genders, poses, and illuminations.

Friedrichs and Yang [73] explore 18 features of eye movement for drowsiness detect. The features are listed in Table 4. Rather than using principal component analysis (PCA) or linear discriminate analysis (LDA) to reduce the dimension of the features, they chose the sequential floating forward selection (SFFS) [74] algorithm to select the most promising features to construct a classifier. The advantage of SFFS over feature transform techniques is its high transparency, because the selected features remain unchanged. An ANN classifier was trained to detect the drowsiness, and the results showed that as long as the blinking signals were correctly detected (high confidence), the drowsiness detection accuracy could reach 82.5%.

Driver Inattention Monitoring System for Intelligent Vehicles. Table 4 Eighteen features of eye movement [73]

Features
Average eye closure speed
Amplitude/velocity ratio (APVC)
APCV with regression
Blink amplitude
Blink duration
BLINKDUR baselined
Blinking frequency
Energy of blinking (EC)
EC baselined
Microsleep event 0.5 s rate
Microsleep event 1.0 s rate
Mean square eye closure
Mean eye closure
Percentage eyes >70% close (PERCLOS70)
Percentage eyes >80% closed (PERCLOS80)
PERCLOS70 baselined
PERCLOS80 EWMA baselined
Head nodding

Some other methods have also been used for fatigue detection. In Sun et al. [75], a Bayesian network was employed to infer fatigue from gaze information. Orazio et al. [76] used a mixture Gaussian model to model the "normal behavior" statistics from the eye closure duration (ECD) and frequency of eye closure (FEC) for each person, in order to identify anomalous behaviors. Suzuki et al. [77] derived three factors from the blinking waveform: the length of a blink, the closure rate, and the blink rate. These factors were then weighted using a multiple regression analysis for each individual to calculate the drowsiness level. In Senaratne et al. [78], four cues were fused using fuzzy logic to detect driver fatigue: PERCLOS, head nodding frequency, slouching frequency, and posture adjustment frequency. In addition to analyzing eye activities, some researches also analyzed mouth activities [79–81] to estimate the level of driver inattention. Fan et al. [80] used an LDA to classify the mouth into two states: normal and yawning. In Vural et al. [81], they used a BP ANN to estimate three mouth states from lip features: normal, yawning, and talking. Vural et al. [81] used a facial action coding system (FACS) to code facial expressions, and then employed machine learning to discover which facial configurations were suitable for fatigue detection, with 31 facial actions employed to predict drowsiness. This system claimed to be able to predict sleep-and-crash episodes with a 96% accuracy within subjects, and an accuracy above 90% across subjects.

Distraction Detection Kircher et al. [82] described and compared two different algorithms for gaze-based driver distraction detection, based on the eye-tracking data obtained in a field study. One algorithm relied on the metric "percent road center" (PRC) of gaze direction, where a PRC of more than 92% was considered to be indicative of a gaze concentration resulting from cognitive distraction, while a PRC below 58%, computed over 1 min, was a indicator of visual distraction. Fixations were used for the computation of PRC. The second algorithm was based on a 3D world model

with different interior zones such as the windshield, speedometer, mirrors, dashboard, etc., and on the time the driver spends glancing at those zones. A time-based "attention buffer" with a maximum value of 2 s was decreased over time when the driver looked away from the "field relevant for driving" (FRD), while it was increased when the driver's glance was inside the FRD, until the maximum value was reached. When the buffer reached zero the driver was considered to be distracted, and when further conditions were met (direction indicator not activated, speed above 50 km/h, no brake activation, and no extreme steering maneuvers), a warning was issued. The results showed that both algorithms have potential for detecting driver distraction, and that fully attentive drivers had a PRC of about 70–80%.

Pohl et al. [83] used head pose and eye gaze information to model the visual distraction level, which was time dependent on the visual focus, with the assumption that the visual distraction level was nonlinear: Visual distraction increased with time (the driver looked away from the road scene) but decreased nearly instantaneously (the driver refocused on the road scene). Based on the pose/eye signals, they established their algorithm for visual distraction detection. First, they used a distraction calculation to compute the instantaneous distraction level. Then, a distraction decision-maker determined whether the current distraction level represented a potentially distracted driver.

Bergasa et al. [84] tried to detect visual distraction with head pose and fatigue with yawning, eyebrow raising, and PERCLOS. Although they developed an algorithm for extracting the required cues, the algorithm for fusing them was unclear.

Driving Performance Measures

A change in the mental state can induce a change in driving performance. In Furugori et al. [85], the pressure distribution on the seat of male subjects was measured during simulated long-term driving, and the results showed there was a relationship between changes in the load center position (LCP) and driver reported subjective fatigue. Their algorithm to derive a fatigue index was calculated on a time interval of 10 min, which was a considerable delay.

Farid et al. [86] tried to distinguish between attentive and inattentive driving in car-following situations by analyzing the vehicle following distance and steering angle. They built up a real-time model using hidden Markov models with Gaussian mixtures to infer the intentions of the driver, and this model was able to detect a lane change half a second earlier than conventional approaches. Zhong et al. [36] performed a localized energy analysis of the steering wheel angle dynamics and vehicle tracking to detect driver fatigue, and found a trend of localized energy increase with driving time. In Takei and Furukawa [87], chaos theory was employed to explain the dynamics of steering wheel motion, and estimate driver fatigue. Using a proper time delay, they found the attractors, which involved the Chaos characteristics. They stated that they will study the Lyapunov exponent of this chaos to estimate the driver fatigue. In addition to an energy analysis, in [88], a Gaussian mixture model was adopted to identify the driver based on the driving behavior signals: forces on the pedals and vehicle velocity.

Kari Torkkola and Wood [89] adopted the steering wheel position, accelerator pedal position, lane boundaries, and upcoming road curvature to infer driver status. First, the original signals were preprocessed (averaging, entropy, etc.), which yielded a huge set of features. Then, random forest (RF) [90], a technique based on ensembles of learners, was employed to select the optimal parameters from the derived features. The classifier was also constructed using RF, and the final accuracy reached 80%.

In Ersal et al. [91], a radial-basis neural-network-based modeling framework was developed to characterize normal driving behavior. Then, in conjunction with an SVM, it was able to classify normal and distracted driving. Vehicle dynamics and driving performance data such as vehicle position, velocity, and acceleration, as well as throttle and brake pedal positions, were adopted to model normal driving. The average and standard deviations of the residuals (the differences between the actual and model-predicted driver actions) were chosen as the inputs for the SVM. The results showed that the accuracy varied between individuals.

Hybrid

Combining driver physical measures with driving performance measures could intuitively increase the inattention detection confidence. On the other hand,

road scene analysis and observations of the driver's face would make it possible to estimate what the driver knows, what the driver needs to know, and when the driver should know it. Combining driver gaze information with road scene information offers several potential benefits: context-relevant information selection, unnecessary information suppression, and anticipatory information selection. Table 5 shows a summary of some researches that utilized a hybrid method for detecting driver inattention.

Fatigue Detection Eskandarian et al. [27] utilized artificial neural networks (ANNs) to analyze vehicle parameter data and eye closure data to infer driver fatigue. The vehicle parameter data included speed, acceleration, vehicle lane position, steering angle, braking, and heading angle, which was recorded at a frequency of 20 Hz. The eye closure data was recorded at 60 Hz using PC-based equipment by Applied Science Laboratory (ASL), which recorded pupil diameter by capturing reflections from the pupils (bright pupil). Then they analyzed the data to identify the potential variables that were correlated with drowsiness. This analysis found four variables highly correlated with fatigue: PERCLOS, vehicle crash, vehicle lateral displacement, and steering wheel angle. Out of consideration for the simplicity and robustness of the data acquisition, Eskandarian et al. [27] implemented two ANN fatigue detectors: one utilized the steering wheel angle signal as an input and the other utilized both the steering wheel angle signal and the eyelid signal as inputs. The steering angle was preprocessed before being input in the ANN. The preprocessing scheme involved normalization for road curvature, discretization at different ranges, coding, and 15-s accumulation. For the eyelid signal, the preprocessing scheme was the same as that for the steering angle, except for eliminating the normalization stage. It was reported that after proper training and cross validation, the steering-eye ANN had an accuracy of 88%, with

Driver Inattention Monitoring System for Intelligent Vehicles. Table 5 Summary of hybrid measures

References	Raw signals	Fusion technique	Object
[27]	Vehicle parameter data and eye closure data	ANN	Fatigue detection
[18]	Eye gaze, head orientation, diameter of pupils, heart rate (RRI)	SVM and Adaboost	Cognitive distraction detection
[92]	Leg and head motions, CAN signals	K-nearest neighbors classifier	Distraction detection
[93]	Audio signal and CAN signals	GMM/UBM	Distraction detection
[94]	Head orientation and the surround salience map	Direct matching	Visual distraction detection
[95]	Gaze variables, driving data and road geometry	ANOVA and binary logistic regression.	Distraction detection
[51]	Eye movement and vehicle parameters	SVM	Cognitive distraction detection
[53]	Eye movement and vehicle parameters	Bayesian network	Cognitive distraction detection
[96]	Head/eye and vehicle parameters	SVM	Visual and cognitive distraction detection
[97]	Vehicle and environment parameters	ANFIS	Distraction estimation
[98]	Eye gaze, blink, head pose, and environment parameters	Region matching	Visual and cognitive distraction detection
[99]	Head dynamics, facial features, upper body posture information and vehicle dynamics	In developing	Driver assistance

a false alarm rate of 9%, while the steering-only ANN had an accuracy of 85%, with a false alarm rate of 14%.

Distraction Detection In Miyaji et al. [18], the standard deviations of eye gaze, head orientation, pupil diameter, and average heart rate (RRI) were combined to improve the accuracy of the driver cognitive distraction detection. The eye and head parameters were obtained using faceLAB, while the RRI data came from ECG. In Miyaji et al. [18], two machine learning techniques, SVM and Adaboost, were implemented under the same conditions. The results showed that the classification performance of Adaboost was slightly better than that of SVM, while the recognition time of AdaBoost was approximately 1/26 that of the SVM.

Sathyanarayana et al. [92] tried to detect distraction by combining motion signals from the leg and head with vehicle signals. The motion signals included the three-axis acceleration of the right leg and two-axis orientation of the head. The vehicle signals adopted included vehicle speed, braking, acceleration, and steering angle. Then, a group of features were derived from these signals based on the nature of the signals. The feature types are listed in Table 6. Next, these derived features were analyzed using LDA to reduce the dimension. Then, a K-nearest neighbors classifier was trained and verified.

Driver Inattention Monitoring System for Intelligent Vehicles. Table 6 Candidate signal features [92]

Signal features
Maximum value of the signal
Minimum value of the signal
Amplitude of the difference between the first value and the last value
Duration of the signal
Maximum difference between any two consecutive values
Median of the signal
Mean of the signal
Difference between the maximum and minimum value of the signal
Standard deviation of the signal
Root mean square value of the signal
Difference between the maximum and minimum value of the differential of signal

In order to cope with the variability between drivers and maneuvers (context), [93] utilized a GMM/universal background model (UBM) and likelihood maximization learning scheme to first identify the driver through an audio signal and then recognize the maneuvers (right/left turn and lane change) through CAN-bus signals. Finally, the CAN-bus signals were also used to detect distraction for a particular driver and particular maneuver. It was reported that this system could reach an accuracy of 70% for distraction detection.

Doshi and Trivedi [94] fused head orientation detection and a saliency map of the surroundings to determine whether there was a salient object in the driver's view, which gave an indication of whether a driver's head turn was motivated by the goal in his or her mind or some distracting object/event in the environment.

It is known that road geometry influences gaze behavior [100], and this aspect was taken into account by including road geometry as an additional factor when detecting driver distraction in [95]. They utilized an analysis of variance (ANOVA) and binary logistic regression to analyze and establish a model for distraction detection based on gaze variables and driving data: fixations (number and duration), scan path, standard deviation of gaze location, speed (minimum, maximum, average and percentage change in speed), lateral acceleration (maximum), and longitudinal deceleration (maximum). The results showed that the road geometry does influence the accuracy of distraction detection based on driving data, but gaze behavior is mainly influenced by distraction, with little or no influence by road geometry.

Liang et al. [51] tried to detect the driver cognitive distraction caused by interacting with In-Vehicle Information Systems (IVISs) in real time by fusing eye movement and driving performance using an SVM. The measured signals included fixation, saccade, smooth pursuit of eye (calculated from raw gaze vector obtained using faceLAB [48]), steering wheel angle, lane position, and steering error. These measures were summarized over various windows to create instances that became the SVM model inputs. After training, the SVM model could detect driver distraction with an average accuracy of 81.1% (sd = 9.05%). Lee et al. [53]

utilized the same conditions as [51] but adopted a Bayesian network to detect cognitive distraction, showing that compared to an SVM model, the dynamic Bayesian network produced better accuracy.

Markkula and Kutila [96] concentrated on processing head/eye and vehicle performance information to estimate both visual and cognitive distractions; their algorithm is shown in Fig. 4. The head/eye information derived from stereo cameras included head position, head orientation, gaze orientation, saccade, and blink identification, as well as confidence values. The vehicle performance information included lane position, vehicle speed, etc. Based on the head/eye information, they developed Gaze-World Mapping and Eyes-Off-Road Detection, which could detect momentary visual distraction. Another algorithm, visual time-sharing detection, was developed to measure longer term visual distractions. For cognitive distraction, they used three indicators to classify the cognitive tasks with an SVM: the standard deviation of gaze angle, standard deviation of head angle, and standard deviation of lane position. However, in the Gaze-World Mapping phase, which mapped gaze and head angles onto actual real-world targets of visual attention, the road-ahead target was static and determined off-line by inspecting the distribution of gaze angles for road-ahead data, and then manually enclosing the distribution in a rectangle.

Tango et al. [97] proposed a method to derive the distraction level from relevant vehicle and environment data using the adaptive neuro-fuzzy inference system (ANFIS). Rather than a binary "yes" or "no," they chose reaction time as the output to train, validate, and test their ANFIS model. The candidates to be selected as input for the ANFIS included the environment visibility, traffic density, and the standard deviations in speed, steering angle, lateral position, lateral acceleration, and deceleration jerk. After preprocessing, the level of difficulty of an IVIS and the standard deviation of steering angle were found to have the highest correlations with the reaction time. Thus, they were selected as the input. No accuracy information was provided in [97].

Fletcher and Zelinsky [98] utilized faceLAB to obtain information such as eye gaze direction, eye closure, and blink detection, as well as head position information. In this system, upper and lower bounds were placed on the percentage of time the driver spent observing the road ahead, called the percentage road center (PRC). A percentage that was too high (>90%) could indicate a fatigued state (e.g., vacant staring). A percentage that was too low (<20%) might indicate a distracted state (e.g., tuning radio). Similar to the PRC metric, they analyzed driver gaze to detect even shorter periods of driver distraction. They used gaze direction to reset a counter. When the driver looked forward at the road scene, the counter was reset. If the driver's gaze diverged, the counter began timing. When the gaze had been diverted for more than a specified time period, a warning was given. The time period for the permitted distraction was a function of the vehicle velocity. As the speed increased, the permitted time period would decrease, either as the inverse (reflecting time to impact) or the inverse squared (reflecting the

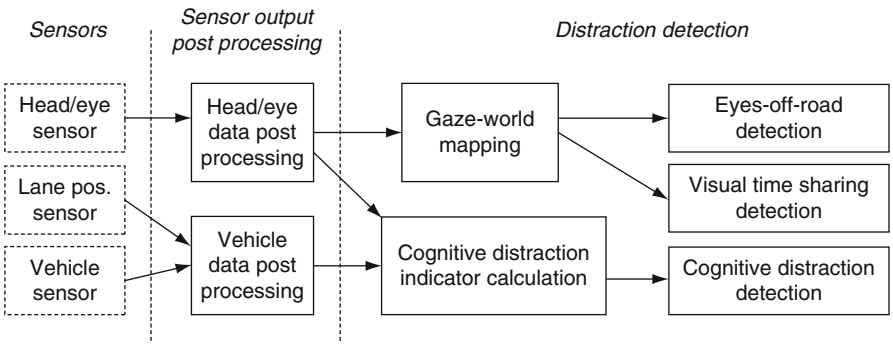

Driver Inattention Monitoring System for Intelligent Vehicles. Figure 4
Overview of the distraction detection algorithms [96]

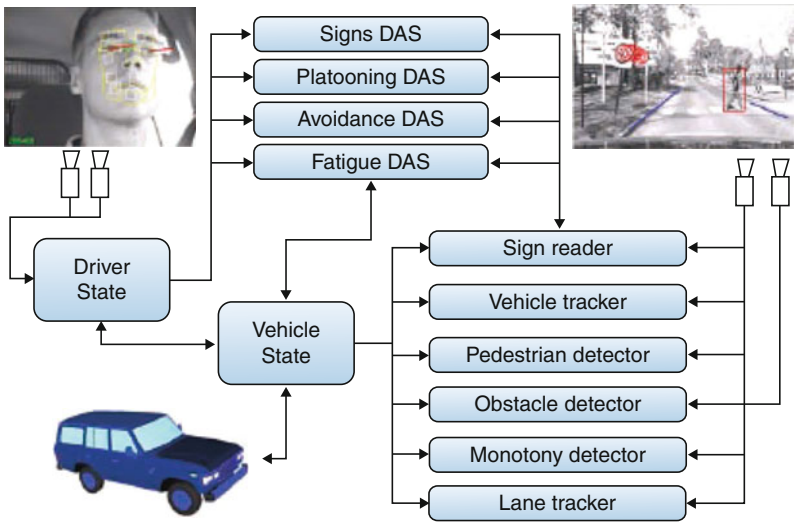

Driver Inattention Monitoring System for Intelligent Vehicles. Figure 5
The distributed modular software architecture [98]

stopping distance). They tried to integrate driver gaze information into other driver assist systems to make the system more acceptable and safer. The framework is shown in Fig. 5. They also spent a significant amount of effort on integrating driver gaze information into lane tracking and sign reading systems. The lane-tracking system was used to orient the driver gaze information. A strong correlation was found to exist between the eye gaze direction and the curvature of the road during normal driving [101], with a slight correlation being a potential indicator of inattention. Fletcher and Zelinsky [98] integrated driver visual information with sign detection to implement a Sign Driver Assist System. This system recognized critical signs in the environment. At the same time, the driver monitoring system verified whether the driver looked in the direction of the sign. If it appeared that the driver was aware of the sign, the information could be made available passively to the driver. In contrast, if it appeared that the driver was unaware of the information, it could be highlighted.

A driver's body posture information is potentially related to driver intent, driver affective state, and driver distraction. Tran and Trivedi [99] explored the role of 3D driver posture dynamics in relation to other contextual information (e.g., head dynamics, facial features, and vehicle dynamics) for driver assistance. It focused on head pose and upper body posture extraction, but no significant results on driver assistance were found.

Driver Physical Signal Extraction

Numerous researches have adopted commercial eye trackers to obtain the physical signals related to the face/eye, which have allowed them to concentrate on exploring the inattention detection algorithm rather than image processing. However, these commercial eye trackers can only work well under specific constrained environments. They do not normally work well for real road conditions. For example, [73] adopted the driver state sensor from the seeing machines [48] to obtain the eye signal. However, even after many improvements, there were still some issues: Reflections from glasses led to bad signal quality and varying light conditions during daytime driving posed problems for the eye signal tracking (see Fig. 6). Therefore, much research has been conducted to make the physical signals extracted using image processing more accurate and robust. The methods for physical signal extraction are summarized in Table 7.

For face segmentation in driver inattention detection, the commonly used methods in the literature include a boosted cascade of Haar-like features [102], adaptive boosting [75], landmark model matching [78], skin color [79], and gravity center template [80].

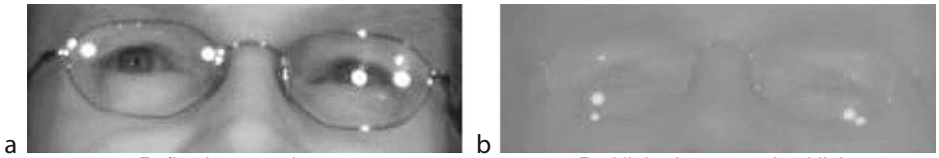

Driver Inattention Monitoring System for Intelligent Vehicles. Figure 6
Image processing problems [73]

Driver Inattention Monitoring System for Intelligent Vehicles. Table 7 Summary of physical signal extraction

Face segment	Eye segment	Blink feature	Gaze	Mouth segment	Mouth feature	Head pose
Boosted cascade of Haar-like features [102], adaptive boosting [75], landmark model matching [78], skin color [79], gravity center template [80], disparity map [103]	Darkest regions search [102], template matching method [75], neural network [77], edge map [78], p-tile and k-means algorithm [104], Hough transform + neural classifier [76], "bright pupil" [50] [105, 106], Sobel edges + SVM [107], templates matching [108]	Optical flow [102], derivative [77], SVM [78], finite state machine (FSM) [50], Kalman filtering [105]	Hough transform and gradient direction [75], Kalman filters and the FSM [50], relative position between pupil and glint [105], pupil features + eigenspace [105], headband + 3D eyeball model [106]	Fisher classifier [79], gravity center template [80]	Connected component analysis to determine lip [79], Gabor wavelet to get mouth corners [80]	Two eyes and the center of face [104], pupil and the nostril position [50], headband [106]

Eren et al. [103] adopted stereo cameras and extracted a face from a disparity map on the assumption that the driver's face had a smaller depth than the background. They then used an embedded HMM to recognize the forehead, eyes, nose, mouth, and chin.

After the face area has been segmented, it is necessary to extract the eye area and mouth area for further processing to obtain physical signals. In the literature, the following methods have been employed to extract the eye area. In Brandt et al. [102], the eyes were extracted by assuming that they were the darkest regions in the face; Sun et al. [75] located the eyes using a template matching method; Suzuki et al. [77] used a neural network to detect the eyes; Senaratne et al. [78] used an edge map to locate the irises of the eyes; and Su et al. [104] used a p-tile algorithm and k-means algorithm to locate the eyes. In [76], candidate eye regions were first extracted using a modified Hough transform, then symmetric regions in the candidates were chosen as further candidates, and finally a neural classifier was used to validate the presence of the eye in the image.

Another popularly adopted method for locating eyes involves the use of the "bright pupil" effect produced by near-infrared light. In [50, 105, 106], a camera equipped with a two-ring IR illuminator was adopted to acquire a driver image. The ring sizes were empirically calculated to obtain a dark pupil image when the outer ring was turned on, and a bright pupil image when the inner ring was turned on. A controller was designed to synchronize the IR illuminator with the image frame rate: to ensure that

the images with and without bright pupils were interlaced. Digitally subtracting the dark pupil image from the bright pupil image produced a difference image, where the pupils appear to be the brightest regions in the image, as can be seen in Fig. 7. The pupils were detected on the resulting image by searching the entire image to locate two bright blobs that satisfied certain constraints. After locating the eyes in the initial frames, Bergasa et al. [50] used two Kalman filters, one for each pupil, to continuously and robustly monitor a driver with eye closure or oblique face orientation. Huang et al. [107] eliminated the need for the synchronizer by acquiring the pupil location from a single image: First, pupil candidates were obtained through Sobel edges, and then they were identified using an SVM with a Gaussian kernel. In Zhu et al. [108], a round template two values matching algorithm was proposed for locating bright pupils, which had an accuracy of 96.4% but consumed 1,011 ms on a PIII 800 MHz computer.

After the location of the eye is extracted, the blinking and gaze parameters should be calculated. In Brandt et al. [102], blinks were measured by analyzing the optical flow of the eye region. Suzuki et al. [77] used a derivative method to detect the eyelids and produce a blinking waveform. Senaratne et al. [78] used an SVM to classify the state of the eye as open or closed to get the PERCLOS value. In the "bright pupil" condition, Bergasa et al. [50] implemented a finite state machine (FSM), with five states defined: tracking_ok, closing, closed, opening, and tracking_lost. The transitions between states were achieved from frame to frame as a function of the width/height ratio of the pupils. The ocular parameters such as eye closure duration, PERCLOS, eye closure/opening speed, and blink frequency were calculated as functions of the FSM. Ji and Yang [105] used Kalman filtering to track eyelid movements and compute the PERCLOS and average eye closure speed (AECS).

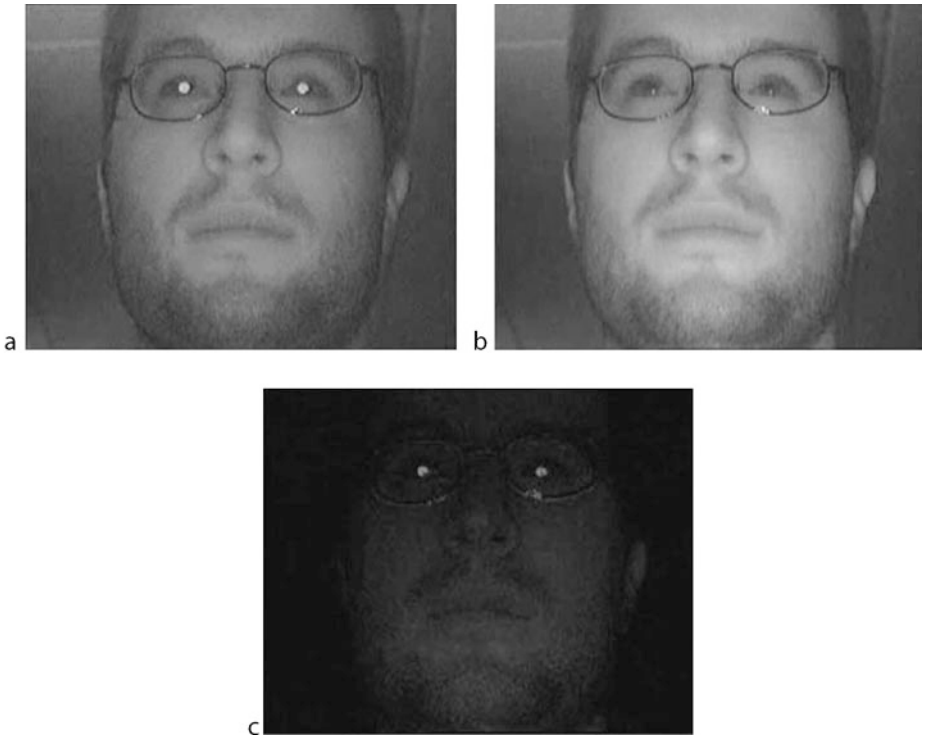

Driver Inattention Monitoring System for Intelligent Vehicles. Figure 7
Fields captured and subtraction. (**a**) Image obtained with inner IR ring. (**b**) Image obtained with outer IR ring. (**c**) Difference image [50]

The gaze was estimated by combining the Hough transform and gradient direction in [75], while Bergasa et al. [50] calculated the gaze based on the position and speed data using Kalman filters and the FSM. Ji and Yang [105] estimated gaze direction using information about the head movement and relative position between pupil and glint, with the gaze direction quantized into nine zones: left, front, right, up, down, upper left, upper right, lower left, and lower right. Cudalbu et al. [106] utilized a headband and a simplified 3D eyeball model to estimate the gaze orientation with an accuracy that varied from 1° to 3°.

Besides the eye, estimating the position of the mouth is also useful in fatigue detection. Rongben et al. [79] used a fisher classifier to extract the mouth area from the face region, while Fan et al. [80] used a gravity center template to extract the mouth area. Then, Rongben et al. [79] used connected component analysis to find the lips and [80] used a Gabor wavelet to get the corners of the mouth.

The head nodding frequency, slouching frequency, and posture adjustment frequency were derived from changes in the head position in [78]. Su et al. [104] clustered facial orientations into five clusters: frontal, left, right, up, and down, depending on the position of the eyes and the center of the face. Similarly, based on the pupil and nostril positions, Bergasa et al. [50] made a coarse 3-D face pose estimation. Ji and Yang [105] used an eigenspace algorithm to map seven pupil features (inter-pupil distance, sizes of left and right pupils, intensities of left and right pupils, and ellipse ratios of left and right pupils) to determine face orientation, which was quantized into seven angles: −45°, −30°, −15°, 0°, 15°, 30°, and 45°. Cudalbu et al. [106] employed a headband with IR reflective markers to estimate the 6 DOF head pose with an average error of 0.2°.

Discussion: Future Directions

Issues with Detection

The subjective report measures can produce some reasonable results in quantifying fatigue level. Because this kind of approach requires that the driver report his or her state frequently, both the fatigue level result and the driver himself or herself could cause interference. Large individual differences have been observed with the overall driving performance and blink duration independent of the KSS values [56]. In addition, [109] demonstrated that drivers have difficulty judging their fitness, especially after about 3 h of continuous monotonous daytime driving with increasing drowsiness. For these reasons, it is not sufficient to solely record the KSS. However, if only a rough fatigue level is needed and the lowest cost is required, this kind of approach may be the best choice. The driver biological measures directly measure biological signals from a driver's body, and have been found to be highly accurate when used to detect a driver's fatigue level. Svensson [29] even proposed an objective sleepiness scoring (OSS) method that relied on EEG. However, most of the driver biological measures are intrapersonal. The results of [71] showed that intrapersonal data had a good linear trend, while interpersonal data showed a different threshold. Bouchner [110] also showed that the EEG was very dynamic and very sensitive to outside factors. In addition, EEG patterns vary between individuals. Therefore, these two kinds of measures should be treated as rough ground truth indicators for other methods. Driver physical measures and driving performance measures are the most promising methods in the real driving context, because neither rely on intrusive measurements that might affect the driver.

For fatigue detection, the most popularly used parameter in driver physical measures is PERCLOS. However, one of the limitations of PERCLOS is that its prediction is good only when using large time intervals. Moreover, PERCLOS does not take into account the variability in human behavior, because blinking activity can significantly differ between individuals. Another challenge for driver physical measures is the robustness of the algorithm under all driving conditions (day and night, sunny and cloudy, etc.), because this type of method mainly relies on image processing. Many researchers have adopted infrared illumination techniques in image acquisition systems for three purposes. First, they minimize the impact of different ambient lighting conditions. Second, they allow the bright pupil effect to be produced, which makes eye detection easier. Third, because near-infrared is barely visible to the driver, it minimizes any interference with their driving. The "bright pupil" effect does benefit the eye extraction process, but it only works well under

some constrained lighting conditions. Moreover, in real driving scenarios, these constraints cannot be satisfied most of the time. In Bergasa et al. [50], three main illumination challenges were encountered: artificial light from elements outside the road (such as streetlights), vehicle lights, and sunlight, as shown in Fig. 8. The "bright pupil" effect will disappear under these conditions, which causes the eye detection to fail, and consequently influences the inattention detection. For example, sunlight and reflections from glasses could cause the performance to drop considerably, to 30% [50]. No matter how the hardware is adjusted, the "bright pupil" effect is not robust, especially in daytime [50] or when wearing glasses [27]. Even under constrained conditions, the reflection of the IR in the pupils varies by individual. Even with the same driver, the intensity depends on the gaze point, head position, and opening of the eye. Therefore, more reliable real-time eye detection algorithms are preferred over the "bright pupil" effect. As described in subsection "Driver Physical Signal Extraction", most studies have concentrated on image processing, and have estimated the driver physical parameters (e.g., gaze, face pose, mouth activity) quite roughly. Combining the image processing with some face mathematical models leads to more accurate estimation. Dong et al. [111] developed a real-time tracking kernel for stereo cameras to estimate face pose and face animation, including the movement of the eyelid, eyeball, eyebrow, and mouth, for driver inattention detection.

The advantage of driving performance measures is that the signals are meaningful and readily available. Moreover, the literature shows that they are useful for estimating driver fatigue, and show good promise in a real driving context. Although in subsection "Effects of Distraction", many researchers have found that driver distraction influences driving performance, few studies have utilized driving performance measures to detect distraction, with most concentrating instead on fatigue or abnormal detection.

One more issue that should be pointed out is that many of the researches claimed very high detection accuracies, which were true only for their particular hypothetical fatigue/distraction definitions. These hypothetical definitions usually covered a limited region of the whole fatigue/distraction definition. Without this condition, the accuracy rates had no meaning.

Because of the significant difficulties inherent in measuring driver attention, the magnitude, and particularly the safety implications, of driver distraction have been very difficult to determine. Indeed, unlike seat belt use, the driver's attention status cannot be categorized as "yes" or "no," but should be quantified in the same manner as blood alcohol level [24].

The factors that influence driver fatigue/drowsiness include greater daytime sleepiness, less sleep, a more difficult schedule, more hours of work, age, driving experience, cumulative sleep debt, the presence of a sleep disorder, and the time of day. This entry focused on real-time inattention detection technology, rather than on long-term sleep/wake regulation prediction technology. Biomathematical models that quantify the effects of the circadian and sleep/wake processes on the regulation of alertness and performance have been developed in an effort to predict the magnitude and timing of fatigue-related responses in transportation operations. These models of fatigue and

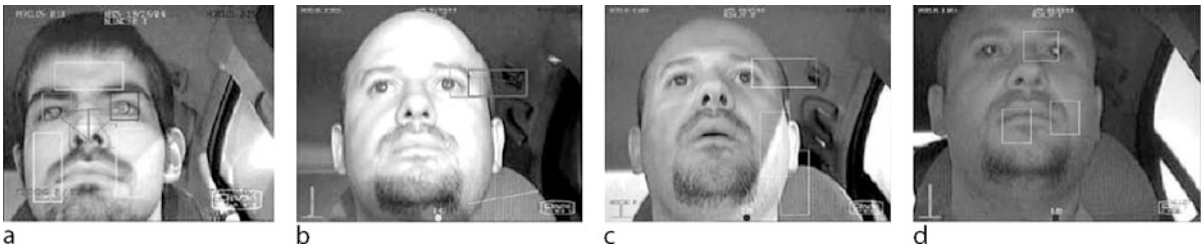

Driver Inattention Monitoring System for Intelligent Vehicles. Figure 8
Effects of external lights on the acquisition system. (**a**) Out-of-the-road lights effect. (**b**) Vehicle lights effect. (**c**) Sunlight effect. (**d**) Sunlight effect with filter [50]

performance typically use input information about sleep history, duration of wakefulness, work and rest patterns, and circadian phase to predict sleepiness, performance capability, and/or fatigue risk [47]. Researches on biomathematical models could enhance the confidence of the real-time estimation, because the former could be used to predict when the probability of sleepiness will become higher. For descriptions of these biomathematical models, see [47].

Systematical Design Consideration

This entry indicated that no single measure can be used to reliably detect inattentive driving. A combination of different measures is recommended, e.g., analyses of lateral control performance and eye blink patterns. According to the definition of driver distraction [2], when driver distraction occurs there should be some kind of distraction source that exists inside or outside of the vehicle. Therefore, fusing driver gaze information, vehiclears' ego state (steering, lane position, speed, and state of IVIS) with current road scenario (e.g., the type of road, weather conditions, and traffic density) will lead to a more comprehensive understanding and recognition of driver distraction.

The level of distraction associated with a given secondary task depends on the extent to which a driver is engaged in the task. Different secondary tasks have different requirements for concentration. Thereby, they have different levels of distraction. Based on the number of button presses and/or glances away from the forward road, Klauer et al. [112] defined three categories of secondary tasks: complex tasks, moderate tasks, and simple tasks. It was found that complex tasks carried three times the risk of involvement in a crash or near-crash as simple tasks or no secondary tasks. Specifically, for drivers performing complex secondary tasks, elevated likelihood ratios were found for the following conditions: dusk and unlighted darkness, rain, divided roads, and roads with grades (straight or curved). Therefore, identifying the environmental conditions is important to correctly assess the risk of the distraction.

Different environments contribute different risk levels for the same inattention state. Different environments could also induce the occurrences of different distractions. Specifically, Stutts et al. [3] reported that crashes associated with adjusting audio devices were more likely at night, those associated with moving objects inside the vehicle were more likely on nonlevel grades, and distractions involving communication with other occupants were more likely at intersections. Horne and Reyner [113] found various criteria associated with drowsiness-related accidents: the vehicle running off the road, no sign of braking, no mechanical defect, good weather, and the elimination of speeding. The NHTSA [27] reported some indirect cues: Accidents were more likely to be associated with the period from midnight to early morning, rural highways with a 55–65 mph speed limit, and fixed objects (trees, guardrail, highway sign, etc.). This, if these contextual cues could be taken into account when determining the risk level of an inattention occurrence and determining which countermeasure should be adopted, it would make the driver inattention monitoring system more reliable and acceptable.

Conclusion

This entry reviews the current state of the knowledge about driver inattention monitoring. Driver inattention increases driving risk, and has become a major factor in a considerable percentage of traffic accidents. Driver inattention has no universally accepted definition. However, based on a review of the literature, driver inattention is classified into two main categories, distraction and fatigue, each of which also contains a few subcategories. Summarily, distraction means the driver has the capability of paying attention, but their attention is shifted away from the primary driving task to some secondary task or attracted by some attractive object/event. Fatigue means the driver has exhausted his or her attention energy and cannot maintain sufficient attention for driving. The causes of distraction and fatigue are different, and they impose different influences on the driver and driving performance. Revealing these influences could help when selecting appropriate measures to develop a real-time inattention monitoring system. Recently, many commercial products relative to driver inattention monitoring have emerged. Auto companies such as Toyota, Nissan, Volvo, Mercedes-Benz, and Saab have installed driver inattention monitoring systems on their top-brand vehicles and/or are conducting researches on such

systems. A few third parties, like Seeing Machines and SmartEye, are providing camera-based nonintrusive tools for measuring driver physical signals such as gaze, head pose, and mouth activity. It should be pointed out that in most of the cases, neither the scientific and technological method behind, nor the exhaustive results of the performance can be provided for these commercial products.

Many articles have reported that these tools work well under constrained conditions, but are not robust under real driving conditions. Thus, there is still much progress to be made to improve the robustness and accuracy of the physical measuring tools. In the scientific literature, five different types of measures could be found for detecting driver inattention: (a) subjective report measures, (b) driver biological measures, (c) driver physical measures, (d) driving performance measures, and (e) hybrid measures. Although not suitable for a real life context, subjective report measures and driver biological measures could serve as some rough ground truth indicators. Because driver physical measures and driving performance measures have advantages and disadvantages, hybrid measures are believed to provide more reliable solutions, which will both accurately detect driver inattention and minimize the number of false alarms to promote acceptance of the system. After all, the goal of a driver inattention monitoring system is to reduce the driving risk. To obtain this goal, three distinct sources of data should be combined: driver physical variables, driving performance variables, and information from the IVIS. In addition to these variables, it is important to consider the characteristics of the driving environment (e.g., the type of road, weather conditions, and traffic density).

Bibliography

1. Ranney TA, Mazzae E, Garrott R, Goodman MJ (2000) Nhtsa driver distraction research: past, present, and future. Technical report, Transportation Research Center Inc
2. Lee JD, Young KL, Regon MA (2009) Driver distraction:. CRC Press/Taylor & Francis Group, London
3. Stutts JC, Reinfurt DW, Staplin L, Rodgman EA (2001) The role of driver distraction in traffic crashes. Technical report, American Automobile Association AAA Foundation for Traffic Safety
4. S.S.G. on Fatigue (2006) Canadian operational definition of driver fatigue. Technical report, STRID Sub-Group on Fatigue
5. Brill JC, Hancock PA, Gilson RD (2003) Driver fatigue: is something missing? In: Proceedings of the second international driving symposium on human factors in driver assessment, training and vehicle design, Park City, pp 138–142
6. T.R.S. for the Prevention of Accidents (2001) Driver fatigue and road accidents: a literature review and position paper. Technical report, The Royal Society for the Prevention of Accidents
7. Croo HD, Bandmann M, Mackay GM, Rumar K, Vollenhoven P (2001) The role of driver fatigue in commercial road transport crashes. Technical report, European Transport Safety Council
8. Horne J, Reyner L (1999) Vehicle accidents related to sleep: a review. Occup Environ Med 56(5):289–294
9. Nilson T, Nelson TM, Carlson D (1997) Accid Anal Prev 29(4):479
10. Endsley MR (1995) Hum Factors 37(1):32
11. http://www.chalmers.se/safer/driverdistraction-en/programme
12. Angell L, Auflick J, Austria A, Kochhar D, Tijerina L, Biever W, Diptiman T, Hogsett J, Kiger S (2006) Driver workload metrics project-task 2 final report. Technical report, U.S. Dept. of Transportation National Highway Traffic Safety Administration
13. Harbluk JL, Noy YI, Trbovich PL, Eizenman M (2007) Accid Anal Prev 39:372
14. Rantanen EM, Goldberg JH (1999) The effect of mental workload on the visual field size and shape. Ergonom 42(6): 816–834
15. Harbluk JL, Noy YI (2002) The impact of cognitive distraction on driver visual behaviour and vehicle control. Technical report, Ergonomics Division, Road Safety Directorate and Motor Vehicle Regulation Directorate
16. Hayhoe MM (2004) Infancy 6(2):267
17. May JG, Kennedy RS, Williams MC, Dunlap WP, Brannan JR (1990) Acta Psychol 75(1):75
18. Miyaji M, Kawanaka H, Oguri K (2009) Driver's cognitive distraction detection using physiological features by the adaboost. In: Proceedings of the 12th international IEEE conference on intelligent transportation systems, St. Louis, 2009
19. Liang Y, Lee JD (2010) Accid Anal Prev 42:881
20. Zhang H, Smith M, Dufour R (2008) A final report of safety vehicles using adaptive interface technology (phase ii: Task 7c): visual distraction. Technical report, Delphi Electronics and Safety
21. Itoh M (2009) Individual differences in effects of secondary cognitive activity during driving on temperature at the nose tip. In: Proceedings of the 2009 IEEE International conference on mechatronics and automation, Changchun, China, 2009
22. Wesley A, Shastri D, Pavlidis I (2010) A novel method to monitor driver's distractions. In: Proceedings of the 28th of the international conference extended abstracts on human factors in computing systems CHI EA 10 (2010), Atlanta, 2010
23. Berka C, Levendowski DJ, Lumicao MN, Yau A, Davis G, Zivkovic VT, Olmstead RE, Tremoulet PD, Craven PL (2007) Aviat Space Environ Med 78(5):B231
24. Ranney TA (2008) Driver distraction: a review of the current state-of-knowledge. Technical report, NHTSA
25. Zhou H, Itoh M, Inagaki T (2008) Influence of cognitively distracting activity on driver's eye movement during

preparation of changing lanes. In: SICE annual conference, Tokyo, 2008
26. Carsten OMJ, Brookhuis K (2005) Transp Res Part F: Traffic Psychol Behav 8:191
27. Eskandarian A, Sayed R, Delaigue P, Blum J, Mortazavi A (2007) Advanced driver fatigue research. Technical report, Report No. FMCSA-RRR-07-001. U.S. Department of Transportation Federal Motor Carrier Safety Administration
28. Dinges DF, Richard G (1998) Perclos: a valid psychophysiological measure of alertness as assessed by psychomotor vigilance. Technical report, Federal Highway Administration, Office of Motor Carriers
29. Svensson U, (2004) Electrooculogram analysis and development of a system for defining stages of drowsiness. Master's thesis, Department of Biomedical Engineering, Linkoping University, Sweden
30. Hulbert S (1972) Effects of driver fatigue. In: Forbes TW (ed) Human factors in highway traffic safety research. Wiley-Interscience, New York
31. Mast T, Jones H, Heimstra N (1989) Effects of fatigue on performance in a driving device. Highway research record. Technical report, Driver Fatigue Research: Development of Methodology, Haworth, Vulcan, Triggs, and Fildes (eds) Accident Research Center, Monash University Australia
32. Kahneman D (1973) Attention and effort. Technical report, Prentice Hall, Englewood Cliffs
33. Yabuta K, Iizuka H, Yanagishima T, Kataoka Y, Seno T (1985) The development of drowsiness warning devices. In: Proceedings of the 10th International technical Conference on Experimental Safety Vehicles, Washington, DC
34. Dingus TA, Hardee L, Wierwille WW (1985) Development of impaired driver detection measures. Technical report, Department of Industrial Engineering and Operations Research, Virginia Polytechnic Institute and State University, (Departmental Report 8504), Blacksburg
35. Elling M, Sherman P (1994) Evaluation of steering wheel measures for drowsy drivers. In 27th ISATA, Aachen, Germany
36. Zhong YJ, Du LP, Zhang K, Sun XH (2007) Wavelet Anal Pattern Recognit 4:1843
37. Skipper JH, Wierwille W, Hardee L (1984) An investigation of low level stimulus induced measures of driver drowsiness. Technical report, Virginia Polytechnic Institute and State University IEOR Department Report No.8402, Blacksburg
38. Stein AC (1995) Detecting fatigued drivers with vehicle simulators. Technical report, Drive r Impairment, Driver Fatigue and Driving Simulation, Hartley L (ed) Taylor & Francis, Bristol, pp 133–150
39. Safford R, Rockwell TH (1967) Highway Res Record 163:68
40. Riemersama JB, Sanders AF, Wildervack C, Gaillard AW (1977) Performance decrement during prolonged night driving. Technical report, Vigilance: Theory, Operational Performance and Physiological Correlates, Makie RR (ed) Plenum Press, New York
41. www.saabnet.com/tsn/press/071102.html
42. Nabo A (2009) Driver attention – dealing with drowsiness and distraction. Technical report, Saab Automobile AB
43. www.smarteye.se
44. www.testdriven.co.uk/lexus-ls-600h/
45. www.emercedesbenz.com
46. www.media.volvocars.com
47. Barr L, Popkin S, Howarth H (2009) An evaluation of emerging driver fatigue detection measures and technologies. Technical report, Volpe National Transportation Systems Center
48. www.seeingmachines.com
49. www.smivision.com
50. Bergasa L, Nuevo J, Sotelo M, Barea R, Lopez E (2006) IEEE Trans Intell Transp Syst 7(1):63
51. Liang Y, Reyes ML, Lee JD (2007) IEEE Trans Intell Transp Syst 8(2):340
52. Freund Y, Schapire RE (1997) J Comput Syst Sci 55:119
53. Lee J, Reyes M, Liang Y, Lee YC (2007) Safety vehicles using adaptive interface technology (task 5): algorithms to assess cognitive distraction. Technical report, The University of Iowa
54. Sathyanarayana A, Boyraz P, Hansen JHL (2008) Driver behavior analysis and route recognition by hidden markov models. In: Proceedings of the 2008 IEEE international conference on vehicular electronics and safety, Columbus, 2008
55. Kaida K, Takahashi M, Akerstedt T, Nakata A, Otsuka Y, Haratani T, Fukasawa K (2006) Clin Neurophysiol 117(7):1574
56. Ingre M, Akerstedt T, Peters B, Anund A, Kecklund G (2006) J Sleep Res 15(1):47
57. Craig A, Tran Y, Wijesuriya N, Boord P (2006) Biol Psychol 72:78
58. Jap BT, Lal S, Fischer P, Bekiaris E (2009) Expert SystAppl 36(2):2352
59. Chouvarda I, Papadelis C, Papadeli CK, Bamidis PD, Koufogiannis D, Bekiaris E, Maglaveras N (2007) Medinfo 12(2):1294
60. Yeo MVM, Li XP, Shen K, Smith EPW (2009) Safety Sci 47(1):115
61. Shen KQ, Li XP, Ong CJ, Shao SY, Smith EPW (2008) Clin Neurophysiol 119:1524
62. Lin CT, Wu RC, Liang SF, Chao WH, Chen YJ, Jung TP (2005) Circuits and systems I: regular papers, IEEE Trans 52(12):2726
63. Lin CT, Chen YC, Huang TY, Chiu TT, Ko LW, Liang SF, Hsieh HY, Hsu SH, Duann JR (2008) Biomed Eng IEEE Trans 55((5):1582
64. Liu J, Zhang C, Zheng C (2010) Biomed Signal Process Control 5:124
65. Skinner BT, Nguyen HT, Liu DK (2007) Classification of eeg signals using a genetic-based machine learning classifier. In: 29th annual international conference of the IEEE, Lyon. Engineering in Medicine and Biology Society, pp 3120–3123
66. Yang G, Lin Y, Bhattacharya P (2010) Inf Sci 180:1942
67. Chua CP, McDarby G, Heneghan C (2008) Physiol Meas 29(8):857

68. Damousis IG, Tzovaras D (2008) Intell Transp Syst IEEE Trans 9(3):491
69. Shuyan H, Gangtie Z (2009) Expert Syst Appl 36:7651
70. Balasubramanian V, Adalarasu K (2007) J Bodyw Mov Ther 11:151
71. Katsis CD, Ntouvas NE, Bafas CG, Fotiadis DI (2004) Assessment of muscle fatigue during driving using surface emg. In: Proceedings of the IASTED international conference on biomedical engineering, Article, Innsbruck, pp 259–262
72. Fan X, Sun Y, Yin B, Guo X (2010) Pattern Recognit Lett 31:234
73. Friedrichs F, Yang B (2010) Camera-based drowsiness reference for driver state classification under real driving conditions. In: 2010 IEEE intelligent vehicles symposium, San Diego, 2010
74. Pudil P, Ferrii FJ (1994) Floating search methods for feature selection with nonmonotonic criterion functions. In: Proceedings of the 12th international conference on pattern recognition, IAPR, Jerusalem, 1994
75. Sun XH, Xu L, Yang JY (2007) In: MIPPR 2007: automatic target recognition and image analysis; and multispectral image acquisition
76. Orazio TD, Leo M, Guaragnella C, Distante A (2007) Pattern Recognit 40(8):2341
77. Suzuki M, Yamamoto N, Yamamoto O, Nakano T, Yamamoto S (2006) Systems, Man Cybern 4:2891
78. Senaratne R, Hardy D, Vander B, Halgamuge S (2007) Lect Notes Comput Sci 4492:801
79. Rongben W, Lie G, Bingliang T, Lisheng J (2004) Monitoring mouth movement for driver fatigue or distraction with one camera. In: IEEE 7th conference on intelligent transportation systems, pp 314–319
80. Fan X, Yin BC, Sun YF (2007) Mach Learn Cybern 2:664
81. Vural E, Cetin M, Ercil A, Littlewort G, Bartlett M, Movellan J (2007) Drowsy driver detection through facial movement analysis. Springer, Berlin/Heidelberg
82. Kircher K, Ahlstrom C, Kircher A (2009) Comparison of two eye gaze based real-time driver distraction detection algorithms in a small-scale field operational test. In: Proceedings of the fifth international driving symposium on human factors in driver assessment, training and vehicle design, Big Sky, 2009
83. Pohl J, Birk W, Westervall L (2007) J Syst Control Eng 221(14)):541
84. Bergasa LM, Buenaposada JM, Nuevo J, Jimenez P, Baumela L (2008) Analysing driver's attention level using computer vision. In: 11th international IEEE conference on intelligent transportation systems, Beijing
85. Furugori S, Yoshizawa N, Iname C, Miura Y (2005) Rev Automot Eng 26(1):53
86. Farid M, Kopf M, Bubb H, Essaili A (2006) Safety Lit 1960:639
87. Takei Y, Furukawa Y (2005) IEEE international conference on systems, Man Cybern 2:1765
88. Wakita T, Ozawa K, Miyajima C, Igarashi K, Itou K, Takeda K, Itakura F (2006) IEICE Trans Inf Syst E89-D(3):1188
89. Torkkola K, Massey N, Wood C (2004) Driver inattention detection through intelligent analysis of readily available sensors. In: The 7th international IEEE conference on intelligent transportation systems, Washington, DC, 2004
90. Breiman L (2001) Random forests. Technical report, University of Califomia, Berkeley
91. Ersal T, Fuller HJA, Tsimhoni O, Stein JL, Fathy HK (2010) Model-based analysis and classification of driver distraction under secondary tasks. IEEE transactions on intelligent transportation systems 11(3):692–701
92. Sathyanarayana A, Nageswaren S, Ghasemzadeh H, Jafari R, Hansen JHL (2008) Body sensor networks for driver distraction identification. In: IEEE international conference on vehicular electronics and safety (ICVES), Columbus, 2008
93. Sathyanarayana A, Boyraz P, Hansen JHL (2011) Information fusion for robust 'context and driver aware' active vehicle safety systems. Inf Fusion 12(4):293–303
94. Doshi A, Trivedi M (2009) Investigating the relationships between gaze patterns, dynamic vehicle surround analysis, and driver intentions. In: Intelligent vehicles symposium. IEEE, Xi'an
95. Weller G, Schlag B (2009) In: European conference on human centred design for intelligent transport systems
96. Markkula G, Kutila M (2005) Online detection of driver distraction – preliminary results from the aide project. In: Proceedings of the 2005 international truck and bus safety and security symposium, Virginia, pp 86–96
97. Tango F, Calefato C, Minin L, Canovi L (2009) Moving attention from the road: a new methodology for the driver distraction evaluation using machine learning approaches. In: HSI 2009, Catania
98. Fletcher L, Zelinsky A (2007) Driver state monitoring to mitigate distraction. Technical report. In: Faulks IJ, Regan M, Stevenson M, Brown J, Porter A, Irwin JD (eds) Distracted driving. Sydney, NSW: Australasian College of Road Safety pp 487–523
99. Tran C, Trivedi MM (2010) Towards a vision-based system exploring 3d driver posture dynamics for driver assistance: issues and possibilities. In: 2010 IEEE intelligent vehicles symposium, San Diego, 2010
100. Land MF, Lee DN (1994) Nature 369:742
101. Apostoloff N, Zelinsky A (2003) Int J Robot Res 5:28
102. Brandt T, Stemmer R, Rakotonirainy A (2004) IEEE Int Conf Syst Man Cybern 17:6451
103. Eren H, Celik U, Poyraz M (2007) Stereo vision and statistical based behavior prediction of driver. In: Proceedings of IEEE intelligent vehicles symposium, Istanbul, 2007
104. Su MC, Hsiung CY, Huang DY (2006) Syst Man Cybern 1:429
105. Ji Q, Yang XJ (2002) Real-Time Imaging 8:357
106. Cudalbu C, Anastasiu B, Radu R, Cruceanu R, Schmidt E, Barth E (2005) Signals Circuits Syst 1:219
107. Huang H, Zhou YS, Zhang F, Liu FC (2007) Wavelet Anal Pattern Recognit 3:1144
108. Zhu ZW, Fujimura K, Ji Q (2007) Data Sci J 6:636
109. Schmidt EA, Schrauf M, Simona M, Fritzsche M, Buchnerb A, Kincsesa WE (2009) Accid Anal Prev 41:1087

110. Bouchner P (2006) WSEAS Trans Syst 5(1):84
111. Dong Y, Hu Z, Uchimura K, Murayama N (2010) A robust and efficient face tracking kernel for driver inattention monitoring system. In: Intelligent vehicles symposium (IV), 2010 IEE
112. Klauer SG, Dingus TA, Neale VL, Sudweeks JD, Ramsey DJ (2006) The impact of driver inattention on near-crash/crash risk: An analysis using the 100-car naturalistic driving study data. Technical report, National Highway Traffic Safety Administration, Washington, DC
113. Horne JA, Reyner LA (1995) Br Med J 310(6979):565

Driving Under Reduced Visibility Conditions for Older Adults

Rui Ni
Department of Psychology, Wichita State University, Wichita, KS, USA

Article Outline

Glossary
Definition of the Subject and Its Importance
Introduction
Car Following in Fog
Collision Detection in Fog
Steering Control Under Reduced Contrast Conditions
Spatial Integration in Processing Optical Flow Information
Future Directions
Bibliography

Glossary

Contrast sensitivity The ability to distinguish different levels of luminance for a given display.

Definition of the Subject and Its Importance

An important and consistent finding regarding driving safety is that accident risk increases for older driver populations [1–3]. Evans [2] systematically examined data from the FARS (Fatality Analysis Reporting System) and found steady increases in accident fatalities and rate of severe crashes for older drivers who were older than 60. This increased accident rate occurred for both men and women and was independent of miles driven.

For many people, driving gives us a sense of independence. This becomes even more important for older population to maintain the quality of life. Unfortunately, natural age-related functional deteriorations cause decreased driving performance and increased crash risks. There are an increasing number of older adults on the road today compared to 10 years ago [4], and the older driver population will continue to increase in the next few decades. Thus, it is important to understand older adults' driving behaviors and their limitations so that we can ultimately help them to sustain a healthy and active lifestyle.

Owsley [5] identified four main functional impairments that contribute to decreased driving performance: (1) visual, (2) visual-cognitive, (3) cognitive, and (4) physical. These impairments can come at any age but are more common among the older population. Research on visual impairments and driving has mainly focused on the decline of visual acuity for older drivers and visual acuity assessment has been a standard screening test for the driver's license test. However, it has been shown that visual acuity is not a good predictor for accident risk [6]. Instead, dynamic acuity, contrast sensitivity, and useful field of view [7] were proved to be much better candidates to predict accident risks. Wood and Owens [6] found that real-world recognition performance of all age groups was independent of visual acuity, which however was seriously degraded during night driving, and this impairment was greater for the older participants. McGwin, Chapman, and Owsley [8] found that contrast sensitivity was significantly associated with the frequency of making left-hand turns, driving on high-traffic roads, driving during rush hours, driving alone, and parallel parking. Glass [9] showed that contrast sensitivity accounted for more age-related variability and was highly correlated with high sensory-demand tasks as compared with low sensory-demand tasks. Thus, it is critical to systematically examine older drivers' driving behaviors under different contrast conditions.

Introduction

The increased crash risk for older drivers could result from a number of age-related factors. These factors range from sensory processing and perceptual processing to attention and cognitive ability.

Age-related declines in sensory processing have been found in accommodation [10], contrast sensitivity [11–13], dark adaptation [14, 15], visual acuity [16, 17], spatial vision [18], and dynamic visual acuity [19]. Age-related changes in perceptual processing have been found in motion perception [20–24], optical flow [22, 25, 26] and depth perception [27, 28].

These types of age-related changes have important implications for driving safety. For example, declines in motion and depth perception can result in performance decrements in detecting impending collisions during decelerations [25] and of approaching objects [26]. Age-related declines in attention include performance decrements for both focused [29, 30] and divided attention tasks [31]. One issue that has been extensively studied is the decline in the useful field of view [7, 32–35]. Finally, age-related declines in cognitive ability include a consistent result in generalized slowing of cognitive processing [36, 37].

Safely traveling in a vehicle relies on proper skills and capabilities performing complex tasks which can be categorized into three types of activities – strategic, tactical, and control [38]. Strategic tasks involve the planning of the trip and the overall goals for the driving. Before we even begin to drive, we must plan the route to our new destination. Choosing a route can be influenced by many factors. For example, we may choose a particular route because it is the shortest route in distance. Other times, we may decide on a route which is the shortest in travel time, the most familiar one, or the most fuel efficient one. Once a route is determined, the driver attempts to follow that route, experiencing a phenomenon called wayfinding. Wayfinding is the ability for a person to navigate through and around an environment. Subtasks of wayfinding that are equally important to safe driving include maintaining adequate heading, vehicle velocity [39], and developing a cognitive representation of the environment [40].

Tactical tasks of driving focus on the decisions made for the on-hand goals of arriving at a destination. These tasks include speed selection, decisions to pass other vehicles, and lane selection. For example, detection of an imminent collision is crucial in safe driving. Imagine a driver waiting to make a left turn at an intersection. If there are oncoming vehicles approaching the intersection, the driver needs to decide whether or not it is safe to make the turn. In other words, the driver has to judge whether there will be a collision before the turn is finished, by estimating the time-to-contact (TTC) from a stationary standpoint. It will be safe to make the left turn if the TTC is greater than the time that it would take for the driver to finish the turn. Now imagine you are sitting in the upcoming vehicle approaching this intersection. You need to estimate the TTC of the left-turning vehicle from a moving standpoint. If a collision is imminent, you should make a quick judgment and execute the proper reactions in attempt to avoid the collision, by either swerving, braking, or even speeding up.

Control tasks focus on the operation of the vehicle. These tasks include maintaining safe distances between cars, maintaining speeds, maintaining lane positions, and steering the vehicle. For example, proper car following entails maintaining a safe distance between a driver's vehicle and the lead vehicle in front. A safe following distance provides an ample amount of time for the driver to react appropriately to sudden hazards. It is very often that drivers have to gather information about the surroundings with just one glance. DeLucia [41] found that young drivers were able to derive motion information in car following scenes fairly well, even when visual information was partially absent. However, older drivers extrapolated this information much slower than their younger counterparts.

Lane keeping and lane changing are similar driving tasks. Lane keeping is the act of keeping the vehicle within the lane boundaries as the road and environment change, e.g., on a curved road. Lane changing is also necessary to avoid certain situations (e.g., avoid colliding into a car merging into the freeway) as well as maintaining safe, efficient wayfinding. Recent study by Macuga and colleagues [42] investigated whether people could perform a proper lane change with little or no visual information. When the needed heading direction was made implicit, participants were able to change lanes. Further, drivers were able to navigate properly even when all visual information was removed, by using inertial cues in a portable virtual reality vehicle. Again, research has demonstrated that drivers are able to perform certain driving tasks, such as lane changing, with little or no visual information within a certain amount of time.

Driving performance can also be assessed in terms of steering control error. Steering control is a basic task in driving that is to control the heading direction of the automobile. Steering control is also essential for many driving tasks that are previously discussed, e.g., car following, lane changing and keeping, and collision avoidance. Perceiving correct heading direction is necessary to maintain or adjust locomotion and may be the lowest-level steering control task. Therefore, it has been the primary driving performance measure for a large body of driving-related literature.

In the current article, a series of driving studies are reviewed that investigated age-related decrements in driving performance, especially in low visibility condition (i.e., in low contrast driving scenes). Several essential driving tasks are examined, including car following, collision detection, and steering control. In addition, the age-related spatial integration mechanism is proposed to account for age-related deficiency in driving in optical flow field. In the end, future research directions are considered briefly on both the advances of new technology and improving driving performance through training.

Car following in Fog

In this part age-related differences are examined in sensory and perceptual processing for a task important for driving safety – car following. Effective car following allows drivers to maintain safe distances that are necessary to take proper executions in case of emergency. Failure to correctly respond to lead vehicle (LV) speed changes can have serious consequences for the safety of the driver. For example, if a driver in a following vehicle fails to respond to a reduction in LV speed then the headway distance between the following and lead vehicle is reduced. This can result in a following distance that is too close (i.e., does not allow for sufficient response time should the LV suddenly decelerate), leading to an increased risk of a crash.

Previous research on car following [43, 44] has assumed that drivers have precise information regarding headway distance and speed of the lead and following vehicle. A limitation of this research is that drivers do not have access to this precise information. Instead, drivers can estimate distance and speed based on available sources of visual information. Recently, Andersen and Sauer [45] proposed a new model for car following, referred to as the DVA (driving by visual angle) model, based on the visual angle and speed information available to a driver. The DVA model consists of two components – one component provides information for distance perception (based on visual angle of the LV) and the second component provides information useful for speed perception (based on instantaneous changes in LV visual angle). The results of their study indicate that the DVA model, as compared to other car following models based on precise headway distance and LV speed, could better predict driver performance in both simulator and real-world driving conditions. In a related study, Andersen and Sauer [46] showed the use of the driving scene information in car following. The results indicated greater accuracy in driving performance when the surrounding scene was visible as compared to conditions when it was not visible. They argued that the surrounding scene is useful for specifying edge rate information, which is used to estimate the speed of the driver's vehicle.

Recent study by Ni, Kang, and Andersen [47] examined two hypotheses concerning age-related changes in car following performance. Previous studies have shown age-related differences in the use of scene information to judge distance and layout of a scene [48]. This finding suggests that older drivers, as compared to younger drivers, will have decrements in perceived distance to the LV. This hypothesis is referred to as the aging and distance perception hypothesis. Previous studies have also found age-related declines in judging speed of the driver's vehicle [25] and of the approaching objects [32, 49]. These findings suggest that older drivers, as compared to younger drivers, will have decrements in perceiving self-speed and relative speed change between the lead and following vehicle. This hypothesis is referred to as the aging and speed perception hypothesis.

In addition to examining age-related differences in car following performance, Ni's study [47] examined a set of environmental conditions, the presence of fog, that are likely to be problematic for older drivers. Fog reduces the overall contrast and visibility of the driving scene, with the magnitude of reduced visibility increasing as a function of distance. As a result, the ability to see detail of the driving scene is reduced as a function of

the distance between the driver and objects in the scene. Epidemiological studies of older driver crash rates have found increased crash risk for older drivers under reduced visibility conditions due to weather or dusk/nighttime conditions [1, 50–52]. A more recent study [53] found reduced car following performance for college-age drives under simulated fog conditions.

As discussed earlier, it is well documented in the literature that contrast sensitivity is reduced with increased age [11–13]. Indeed, studies have found that for photopic vision (daylight conditions) there is a 41% reduction of contrast sensitivity for 70 year old subjects as compared to 20 year old subjects in detecting mid- to high level spatial frequency targets [13]. These results suggest that older drivers are likely to have poorer car following performance than younger drivers because of reduced visibility of the LV under dense fog conditions.

Previous research [53, 54] has found decreased car following performance (failure to maintain following distance) under simulated fog conditions. Two factors may impact car following performance under foggy conditions. First, the reduced visibility of the scene may result in a compression of the overall perceived depth of the driving scene. This situation is likely to occur as the reduction in contrast of the surrounding scene will remove information important for perceiving scene depth such as texture gradients and linear perspective [55]. If the perceived depth is compressed then smaller headway distance at high fog density conditions is expected. Second, reduced visibility of the scene may result in increased difficulty in estimating speed. Previous research has found that edge rate information (the rate at which local edges cross a fixed reference point in the visual field) is important for determining the perceived speed of vehicle motion [56] and is used by drivers for tasks such as braking [57, 58]. If the reduced visibility of the scene from fog decreases the visibility of edge rate information in the driving scene then greater error in tracking changes in LV speed is expected.

The rest of this section then focuses on the study by Ni and colleagues [47]. In this study, Eight college students (age mean and standard deviation of 21.0 and 2.6, respectively) and eight older subjects (age mean and standard deviation of 72.6 and 4.6, respectively) participated in the study and all reported normal or corrected-to-normal vision and were currently licensed drivers. All drivers had experience driving in fog and reported driving at least 3 days per week.

The study was conducted in a fix-based driving simulator, in which the roadway in an urban setting consisted of three traffic lanes (representing a three lane one way road) with the driver and LV located in the center lane. Drivers were presented with a car following scenario in which the LV varied its speed according to a sum of three equal-energy sinusoids (i.e., the peak accelerations and decelerations of each sine wave in the signal were equivalent). At the beginning of each trial run, drivers were given 5 s of driving at a constant speed 18 m behind the constant speed LV. Drivers were instructed that the headway distance during this phase of the trial was the desired headway distance. Following 5 s a tone sounded to indicate to the driver that the LV speed would vary, which was based on the sum of three non-harmonic sine-wave frequencies. This signal does not repeat and thus prevents the driver from anticipating changes in LV speed.

To simulate realistic effects of fog, specific fog density values were selected to represent a range of conditions from high visibility (0.0 fog condition) to low visibility (0.16 fog condition). The low visibility condition was selected based on informal observations indicating that under this condition the visibility of the LV was considerably reduced at the desired following distance of 18 m. The LV was visible to all drivers under the simulated fog conditions at the predetermined driving distance.

Car following performance was assessed using a variety of measures that examine overall performance changes based on distance information and speed information. Specifically, mean and variance of distance headway are based on distance perception whereas RMS speed error is based on speed perception. If the age and distance perception hypothesis is correct, then age-related declines in measures based on distance perception are expected. If the age and speed perception hypothesis is correct, then age-related declines in measures based on speed perception are expected. In addition, if older drivers have greater difficulty in detecting and responding to speed changes then age-related declines should be greater as the overall speed of the LV is increased.

An important issue in car following is how to quantify a safe following distance. Time headway (THW) is a measure that is derived by the ratio of headway distance to the velocity of the driver vehicle. This measure indicates the time between two vehicles passing the same point traveling in the same direction and thus has been used as an indication of a safe margin between the driver and lead vehicle. In Ni's study they required drivers to maintain a fixed distance of 18 m across the three speed conditions. Thus, it is natural that THW would vary as a function of speed. The use of THW allows one to determine changes in safe driving performance as a function of fog density. For example, consider car following at a specific constant speed. If drivers have difficulty in maintaining a safe margin as a function of fog then increased fog density should result in a decrease in THW. If older drivers have greater difficulty than younger drivers under foggy conditions in determining distance and speed then they may follow at a closer distance resulting in a decrease in THW – an indication of increased crash risk.

The results showed that the mean distance headway (distance between driver and lead vehicle in meters) for the 0.0, 0.04, 0.08, 0.12, and 0.16 simulated fog density levels were 19.3, 20.1, 19.3, 18.2, and 17.9 m, respectively. Mean distance headway for the 40, 60, and 80 km/h speeds were 17.7, 19.2, and 20.0 m, respectively. The result also showed that older drivers maintained a slightly greater headway distance for the no fog (0.0 fog density) condition. However, at higher fog density levels and at increased speed older drivers maintained a closer headway distance than younger drivers. The largest age-related difference in distance headway occurred at the intermediate speed (60 km/h) and highest fog density condition. However, a notable exception was the highest fog density condition and highest speed. For this condition older drivers had a greater following distance than younger drivers. This result is likely due to a change in strategy employed by older drivers. Specifically, older drivers increased following distance at high speeds to minimize the likelihood of a collision because of difficulty in perceiving changes in the visual angle of the LV due to reduced contrast. In addition, the result indicated that older drivers had greater headway variance (mean variance of 25.6) compared to younger drivers (mean variance of 10.1). Analysis of RMS speed error showed greater RMS error for older drivers (mean RMS error of 6.17 km/h) as compared to younger drivers (mean RMS error of 4.83 km/h).

To examine the effects of fog on the safety margin for car following time headway (THW) data was derived. THW varied as a function of the average speed of the LV with THW decreasing at increased average speed of the LV. The result showed decreased THW as a function of fog density. These results showed that at the intermediate speed (60 km/h) THW decreased for both older and younger drivers with an increase in fog density. However, older drivers had the largest decrease in THW at the highest fog condition. This result indicates that older drivers, as compared to younger drivers, had a significant reduction in the safety margin at the highest fog density level. At the highest speed (80 km/h) both older and younger drivers had a decrease in THW with an increase in fog density with the exception of the highest fog density condition. For younger drivers THW continued to decrease at the highest fog density condition. However, for older drivers THW increased at the highest fog density condition. This result suggests that older drivers increased the following distance to increase the safety margin.

As discussed earlier, two hypotheses were examined in this study concerning age-related differences in car following performance under foggy conditions. According to the aging and distance perception hypothesis, older drivers, as compared to younger drivers, will have decrements in perceived distance to the LV. According to the aging and speed perception hypothesis, older drivers, as compared to younger drivers, will have decrements in perceived speed and relative speed change between the lead and following vehicle. The results of this study provided evidence in support of both of these hypotheses. With regard to distance information, they found that older drivers, as compared to younger drivers, followed at a closer headway distance with an increase in fog density. In addition, although mean headway distance varied for both younger and older drivers as a function of speed, older drivers showed a greater change as a result of speed. This effect was especially pronounced for the highest fog density conditions examined. They also found greater variance in distance headway for older drivers,

as compared to younger drivers. These results provide evidence in support of the age and distance perception hypothesis.

With regard to speed perception the results indicated that older drivers had greater RMS speed error than younger drivers. In addition, older drivers had lower squared coherence scores than younger drivers, indicating that older drivers had poorer performance in tracking local variations in speed at specific frequencies of LV speed. These results provide evidence in support of the age and speed perception hypothesis. The results, considered together, suggest that older drivers have decreased car following performance as a result of difficulty in judging both speed and distance.

An important finding in this study was the interaction of age, speed, and fog density for the distance headway measure. Of particular interest were the age-related performance differences for the 60 km/h speed condition under the highest fog density condition. Under this condition, older drivers followed at a very close distance and shorter THW. The authors believed that older drivers followed at a close distance because reduced visibility due to fog increased the difficulty to perceive LV speed changes. Collision risk can be assessed by deriving the THW. The shorter the THW, the less is the time available to the driver to avoid a collision. For the 60 km/h/0.16 fog density condition younger drivers had an average time gap of 1.1 s. However, older drivers had a time gap of 0.87 s, which represents a 21% reduction in available response time to avoid a collision. Given the well-documented finding of slower reaction time with age, this result suggests that older drivers may be at considerable risk of a collision under high fog density conditions at moderate speeds.

Collision Detection in Fog

In addition to car following, there is another important perceptual task for driving safety – collision detection. Failure to correctly detect an impending collision event can greatly increase accident risk for drivers. For example, if a driver in a vehicle fails to see an upcoming vehicle early enough or does not see it at all when making a left turn, then a crash might occur resulting in a severe injury or even death for the driver. Accurate detection of an impending collision is the basis of making appropriate responses, such as steering or braking to avoid a collision. DeLucia et al. [59] studied the age-related differences in detecting collision events when an object was moving toward the observer at a constant speed. They found an age-related decrement in sensitivity for older females but not older males. Andersen and Enriquez [26] found that older observers, as compared to younger observers, were less sensitive to collision events and required more time to process the visual information.

As reviewed earlier, previous studies of older driver have shown increased crash rates under reduced visibility conditions due to weather or dusk/nighttime conditions. Specifically, the presence of fog reduces the overall contrast and visibility of the driving scene, which results in reduced visible details as a function of increasing distance. Such reduced visibility of driving scene may lead to higher injury and death rates in accidents [60]. Driving simulation studies have found evidence of decreased driving performance under simulated fog conditions. Recent study [47] reviewed above on car following task has shown reduced performance under simulated fog conditions for older drivers compared with younger drivers. As discussed earlier, contrast sensitivity is reduced with increased age. These findings suggest that older observers may have more difficulty than younger observers in recovering visual information needed to correctly detect impending collision events under dense fog conditions.

In this section, I will review a most recent research [61] which investigated detecting collision events when an object was approaching the observer at a constant speed on a linear trajectory under foggy conditions. Two factors might affect collision detection performance in fog. First, the reduced visibility of the scene may result in a reduced visibility of bearing angle of the approaching object, which is crucial to judge the collision event on linear trajectory [62]. This situation is likely to occur as the reduction in contrast of the surrounding scene will remove information important for perceiving object distance such as the horizon, texture gradients, and linear perspective. If the information on object position in the visual field is compromised, then reduced collision detection performance at dense fog condition is expected. Second, reduced visibility of the scene may result in increased difficulty in estimating speed. Previous research has

found that edge rate information (the rate at which local edges cross a fixed reference point in the visual field) is important for determining the perceived speed of vehicle motion [56] and is used by drivers for tasks such as braking [25, 58]. When moving in the driving scene, drivers need to predict not only the motion path of the approaching object but also the vehicle position after a certain amount of time, which is dependent of estimated speed. Thus, it is expected that the decreased visibility of edges in the driving scene under dense fog condition will decrease collision detection performance.

In this study, they investigated the effects of fog on collision detection performance when optical variables (i.e., visual angle and change in visual angle of the object, and the relative speed between the object and the vehicle) were constant. Drivers were presented with a driving simulation scene of a straight roadway in a suburban setting. A spherical object traveled on a linear trajectory toward the vehicle for 9 s before it either collided with or passed the vehicle. The vehicle was either stationary in Experiment one or moved straight ahead at a constant speed in Experiment two while the relative speed between the object and the vehicle remained constant. Only a part of the travel path was presented and drivers were instructed to make a judgment whether the object would collide with the vehicle or not by pressing one of the two keys on the keyboard.

In the first experiment, three independent variables were examined: Age (younger and older drivers), simulated fog density (no fog, mild fog, medium fog, or dense fog, corresponding to 0, 0.08, 0.16, or 0.24 in density, respectively), and the time-to-contact (TTC) on the last frame of the display (2, 4, or 6 s).

In the second experiment, the stimuli were the same as in first experiment except that the vehicle moved at one of the three speeds (20, 50, and 80 km/h). Since the relative speed between object and observer was kept constant, which is 90 km/h, the object moved at a speed of 70, 40, or 10 km/h, respectively, depending on the vehicle moving speed. Four independent variables were examined: Age (younger and older drivers), simulated fog density (no fog or dense fog, corresponding to 0 or 0.24 in fog density, respectively), moving speed of the vehicle (20, 50, or 80 km/h), and TTC (2, 4, or 6 s).

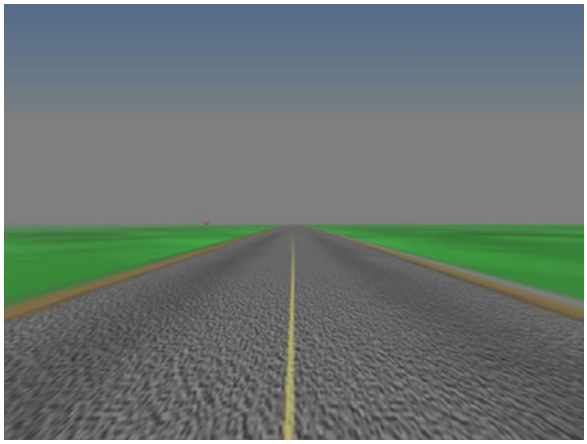

Driving Under Reduced Visibility Conditions for Older Adults. Figure 1
Example of the display in dense fog condition. A bright red spherical object moves along a linear trajectory toward the observer, which might or might not result in colliding with the observer

The displays simulated a 3D scene consisting of a roadway, roadway strip, textured ground, and an approaching bright red spherical object (See Fig. 1). The object motion trajectories were generated using the same method employed by Ni and Andersen [62]. The initial position of the object was chosen randomly from an arc (+/− 20° from the center of the display) at a fixed distance of 223 m from the viewpoint. The end position of the object was 50, 100, or 150 m from the view point for TTC of 2, 4, and 6 s, respectively. The 3D velocity for collision and non-collision events was constant. The simulated foggy effect was achieved using the same method described above. The low visibility condition was selected based on informal observations indicating that under this condition the visibility of the object was considerably reduced while still visible at the original position. All observers reported during debriefing that they were able to see the sphere in all conditions.

The two experiments were conducted in a darkened room. Observers viewed the monitor binocularly through a collimating lens with their head in a chin rest. They were informed that they would be shown a series of displays consisting of a 3D scene with a single object in a distance that was moving toward the

observer. Their task was to determine whether the moving object would hit the observer. Observers were next shown a series of demonstration displays of collision and non-collision stimuli in which the complete motion trajectory was displayed. After observers understood the task, they were presented with eight practice trials with complete 9-second events, half of which simulated a collision, and were asked to indicate whether or not the object was on a collision trajectory by pressing one of the two designated keys on a standard keyboard. Subjects pressed the number "6" key for non-collision responses and the number "4" key for collision responses. No feedback was given during the practice trials and experimental trials. Subjects were required to correctly identify seven out of the eight practice trials before proceeding to the experimental trials. Following the practice trials subjects were instructed that the experiment would include brief presentations of the collision and non-collision events. If they were uncertain of whether the display was a collision or non-collision event, they should make the best judgment possible.

The average proportion of hits (collision response for trials that simulated a collision) and false alarms (collision response for trials that did not simulate a collision) was calculated for each subject in each condition and used to derive sensitivity (d') and response bias (β) measures[63]. In conditions where observers performed perfectly (100% hit rate or 0% false alarm rate), d' and β were calculated based on the assumption that one error was made.

The analysis of d' values indicates that younger observers (mean $d' = 3.43$) had greater sensitivity than older observers (mean $d' = 2.78$). The increase of fog density resulted in decreased sensitivity for older observers but not for younger observers. When the TTC was 2 s, older observers performed as well as younger observers. As the TTC increased, the sensitivity for both age groups decreased. However, older observers' sensitivity decreased much faster than that of younger observers.

The analysis of β values suggests that both age groups were equally likely to make a collision judgment and the fog density did not bias the observers' likelihood to report a collision event. It was also found that observers were more likely to make a collision judgment with increased TTC.

The results of the second experiment are consistent with those in the first experiment, indicating that younger observers (mean d' = 2.65) had greater sensitivity than older observers (mean d' = 2.13). It was shown that with increased TTC the sensitivity for both age groups decreased. However, older observers' sensitivity decreased faster than that of younger observers. The analysis of β values suggests consistent results as in the first experiment that when fog was simulated or when the TTC increased, observers were more likely to respond that a collision would occur.

According to the contrast and bearing angle hypothesis, older drivers, as compared to younger drivers, will have more difficulty in perceiving constant bearing information under low contrast condition caused by fog. The results in Experiment 1 provide evidence supporting this hypothesis. It was found that older drivers, as compared to younger drivers, had significant decrements in sensitivity to detect an imminent collision event in dense foggy condition. In addition, although a decreased performance was found for both younger and older drivers with decreased display duration, older drivers showed greater decrements as a result of shorter display duration. This is a finding consistent with previous research (Andersen & Enriquez, 26). This result is probably due to the increased difficulty in discriminating bearing angle in driving scene with reduced contrast in distance.

Since reduced contrast in driving scene in dense fog condition caused decreased sensitivity of detecting collision events, one may ask whether this decrease can be predicted by contrast sensitivity. To address this concern, a linear regression between contrast sensitivity and the sensitivity of collision detection in fog was conducted for both age groups. The results indicated that contrast sensitivity was not a significant predictor for sensitivity of collision detection for either younger observers ($r^2 = 0.09$, $p = 0.37$) or older observers ($r^2 = 0.06$, $p = 0.46$). There are two explanations which might account for this result. First, the contrast sensitivity for each observer was measured using Pelli Robson test [64], which may not have sufficient precision to assess individual differences. For example, 10 out of 11 younger observers in this study had the same contrast sensitivity whereas their d' ranged from 2.38 to 3.24. An important issue for future research would be to precisely derive contrast sensitivity

thresholds. Second, the Pelli Robson test only measured contrast sensitivity in static scenes whereas our stimuli were in motion. Observers might have different contrast sensitivity when viewing motion stimuli as compared to when viewing static stimuli. A similar result has been found for studies examining sensitivity to binocular disparity [65]. Specifically this research has found that observers who were stereo-blind using static stimuli had sensitivity to disparity when the stimuli were moving. If similar conditions exist for low contrast stimuli, then the assessment of contrast sensitivity with static stimuli would not be predictive of sensitivity to low contrast moving stimuli.

With regard to edge rate information, it was found that both younger and older drivers had considerable decrease in their sensitivity to collision events when the vehicle is moving. The results in Experiment 2 were consistent with those in Experiment 1 in that decreased performance was found with decreased display duration (i.e., greater TTC). Considered together, these results suggest that under inclement weather conditions, such as fog, older drivers may be subject to an increased crash risk due to a decreased ability to detect impending collision events. One important finding in this study was the interaction of age and display duration, specifically the age-related difference for the 3 s condition. Under this condition, older drivers, as compared to younger drivers, had significant decrements in detecting the collision event which suggests a serious collision risk for older drivers. The longer it takes a driver to detect imminent collision events, the less time the driver has to take appropriate response, e.g., to decelerate or steer the vehicle. Given the well-documented finding of slower reaction time and reduced divided attention capacity with age this result suggests that older drivers may be at considerable risk of a collision under high fog density conditions.

Steering Control Under Reduced Contrast Conditions

Besides accelerating and decelerating the vehicle, the other control task that a driver performs during driving is steering control, which is to steer the vehicle to move in desired direction. To successfully steer the vehicle, one needs to first perceive the current status and moving direction from the visual information in the driving scene. Failure to accurately detect changes in the path of motion and make corrections to the vehicle's path of motion could have serious consequences for driver safety. One source of information that has been extensively studied for the perception and control of steering is optical flow – the perspective transformation of the optic array [66, 67]. Research on optical flow has demonstrated the usefulness of this information for the perception of heading [68, 69], the perception of self-motion [70], and the perception of egospeed [56]. A critical assumption of optical flow research is that the spatial and temporal characteristics of the stimuli result in a perception of apparent motion.

Previous research has demonstrated age-related decrements in the perception of motion and in the use of optical flow information for the perception of 3D shape [22]. In this part, I will introduce a most recent study on age-related differences in the use of optical flow for steering control under low contrast conditions. In the study by Nguyen et al. [71], drivers were presented with computer generated displays simulating forward vehicle motion through a 3D scene of random dots on a ground plane. The horizontal position of the vehicle was perturbed according to a sum of sinusoidal functions, and drivers were asked to steer the vehicle to maintain the initial straight path of motion.

Previous research has shown that the use of optical flow information for perceiving the path of observer motion requires the spatial integration of velocity information. Recently, it was found that older observers had a decreased ability to spatially integrate velocity information to perceive motion defined edge boundaries ([72], will be reviewed in details below). Nguyen et al. [71] proposed that older drivers, as compared to younger drivers, would show a decreased sensitivity to spatially integrate velocity information for steering control from optical flow, especially in low visibility conditions. This was referred to as the spatial integration hypothesis. To test this hypothesis they manipulated the dot density display (resulting in a greater spatial separation of the velocity information) and contrast of the dots display. If the spatial integration hypothesis is correct, then age-related differences in steering performance should be more pronounced at low as compared to high dot densities and at low-contrast conditions as compared to high-contrast conditions.

In their study, Nguyen et al. manipulated the number of dots in the optic flow field (25 or 325), and contrast level (low, medium, and high level, representing 0.15, 0.2, and 0.25 in Michelson contrast, respectively). The displays simulated driving through a 3D array of dots located on a ground plane, as illustrated in Fig. 2. The simulated speed was 72 km/h. The horizontal position of the dots pattern was perturbed according to a sum of three prime sine-wave functions. The frequencies, amplitudes, and phases of the sinusoidal functions were chosen in a similar way as in Ni et al [47] so that the output of the sum of three sine-wave functions was always zero at the beginning of each trial and unpredictable. The scene consisted either 25 or 325 randomly positioned white dots on a black background to form the ground plane. The background had an average luminance of 16 cd/m^2. The dots were randomly positioned at the beginning of each trial, and then moved to the observer. Any dot that moved out of view port would be randomly repositioned at the far end of the ground plane.

Drivers were instructed that their task was to maintain a fixed heading direction relative to the moving dots as if driving down a straight roadway with lateral wind gusts perturbing their positions on the roadway. Steering control performance was assessed by calculating RMS (root means square) steering error for each driver on each trial in each condition. The average results for RMS error in their study revealed that although both older and younger drivers had less steering error with a greater number of dots in the flow field, younger drivers had significantly less steering error (9.9) than older drivers (12.4). Under low dot density condition, in which less optical flow information was presented, both younger and older drivers showed decreased steering performance with decreased contrast of the scene. However, older drivers' performance deceased much faster with decreased contrast, as compared with younger drivers. This result suggests that older drivers are more prone to accident risk than younger drivers under low contrast condition, especially with less optical flow information.

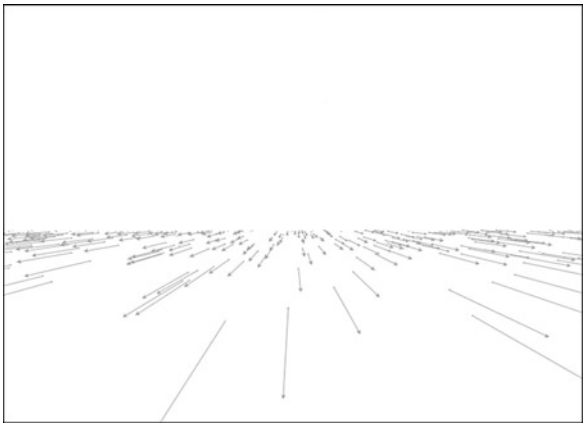

Driving Under Reduced Visibility Conditions for Older Adults. Figure 2
Low contrast optic flow showing straight ahead moving direction. In the actual experiment, the contrast was reversed so that *white dots* were displayed on a black background

Previous study by Ni and Andersen [73] found older drivers, as compared to younger drivers, relied more on optical flow than landmark information for their steering control task. One possible explanation for such result is that in their displays, only one color coded dot was present at a time which provided landmark information. In order to use landmarks for steering control, a driver must encode the spatial location of landmark positions and use this positional information as reference information to maintain the initial path of motion. Older drivers may have difficulty encoding and using landmark position information, which results in reduced accuracy in steering control, especially when small amount of landmark information is present. If this hypothesis is true, with increased landmark information there should be an increase in the steering performance for older drivers. However, older drivers might show less improved driving performance, which results from the extra landmark information added to optical flow field, as compared to younger drivers.

In a related study by Ni et al. [74], they used similar experimental setting as in the study by Nguyen et al. [71], except that different numbers of landmark dots were presented in the optic flow field (0, 1, 4, 7, and 10). Their result showed that younger drivers had significantly less steering error (5.8) than older drivers (9.9). Both older and younger drivers had less steering error with a greater number of landmark dots in the flow field. However, younger drivers, as compared to older drivers, were more efficient at using landmark information to improve steering control.

Overall, these findings indicate that older drivers may be more reliant on optical flow information for controlling a vehicle and may have a reduced ability to use alternative sources of information for steering control. The decreased reliance of landmark information for older drivers, when optical flow information is reduced, may result from age-related deficits in attention. Previous research [75] found that older subjects had greater difficulty than younger subjects in ignoring distracting items when scanning a display, presumably a result of difficulty in disengaging attention to irrelevant information. In Ni et al's study [74], older drivers may, under reduced optical flow conditions, focus their attention on the landmarks and have difficulty disengaging their attention from the landmarks to scan other parts of the scene. However, when more landmark information was presented on a dense optical flow ground plane, less steering control error occurred for older drivers since they can rely more on optical flow information in this condition.

Spatial Integration in Processing Optical Flow Information

Visual processing of optical flow information requires the integration of information over space and time. This section attempts to explain age-related difference in using optical flow information in terms of spatial integration. Now consider how the visual system perceives a 2D form from fragmented image information. In order to perceive the form, the visual system must combine local fragments (e.g., line segments) across space to recover the shape of the form. Information for perception can also be available from different time intervals. For example, consider the perception of a moving object partly obscured by nearer objects. In order to perceive the form, the visual system must integrate the different parts of the object visible at different time intervals. These examples highlight the role of spatial and temporal integration in vision.

Previous studies of neuronal activity in the visual system have shown evidence of spatial and temporal integration. For example, retina cells respond to information present over a limited region of the visual field [76]. The visual system combines or spatially integrates information from local receptive field regions via intracortical connections from other cells within a cortical region [77–79] and from cells in higher cortical regions [80–82]. Spatial integration has been demonstrated to be important for visual processing including motion perception [83] and form perception [84–86].

Neurophysiological studies have also examined the role of temporal integration by the visual system. For example, studies have examined the role of temporal integration for motion perception in primary visual cortex (V1) and extrastriate motion area (MT/V5) [87]. It has been argued that temporal integration at a neural level is due to the synchronous activity of groups of neurons rather than the firing rate of a single neuron [88]. Specifically, temporal integration has been shown to be important in visual processing in motion perception [89] and form perception [90–93].

Recently, Andersen and Ni [72] used a novel perceptual task to examine whether age-related declines in visual processing resulted from changes in spatial or temporal integration. To assess this issue, they used a visual task that requires both spatial and temporal integration – the recovery of 2D shape from kinetic occlusion. Kinetic occlusion can specify 2D shape by providing information regarding edge boundaries of an object based on the accretion and deletion of texture over time. Consider an opaque object positioned in front of a background (see Fig. 3). If the object and background have identical random texture (randomly positioned dots) then the object boundaries cannot be seen. However, when the object starts moving (or the background starts moving) the accretion and deletion of the background texture due to occlusion can be used

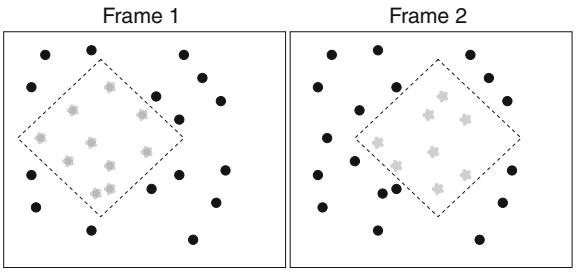

Driving Under Reduced Visibility Conditions for Older Adults. Figure 3
Illustration of 2D form perception results from occlusion when the form moves from frame 1 to frame 2. Note the *stars* in low contrast represent the *dots* that are occluded by 2D form above (a *diamond* in this illustration)

to reveal the boundaries of the object. In order to recover the object boundary, the visual system must integrate the accretion and deletion of texture over space (discrete samples of the edge boundary are specified by the local disappearance/reappearance of texture) and time (the accretion and deletion of texture occur in local intervals of time).

Previous research [90] examined the importance of kinetic occlusion for specifying the shape of 2D objects. College-age subjects were presented with displays of a moving opaque object with random dot texture against a random dot texture background. The velocity and texture of the display were varied and subjects were asked to identify which of four shapes were present. The results indicated that an increase in velocity and density resulted in greater accuracy in shape identification. The results also indicated that density was the primary factor in determining performance. An important issue examined in their study was whether performance was based on the rate of occlusion events (the number of occlusion events per unit time). To examine this issue, they compared performance across conditions in which velocity and density changed proportionally resulting in a constant rate of occlusion events. For example, an occlusion stimulus with a velocity of 0.8 deg/s and a density of 1.2 dots/deg^2 was compared to an occlusion stimulus with a velocity of 1.6 deg/s and a density of 0.6 dots/deg^2. These two conditions have identical rates of occlusion events (i.e., disappearance/reappearance of texture). The results indicated that performance varied across conditions with a constant rate of occlusion events, with performance increasing due to an increase in density. These findings led Andersen and Cortese to conclude that spatial integration from texture density was the primary factor in shape perception from kinetic occlusion.

In Andersen and Ni's study [72], they examined conditions similar to those examined by Andersen and Cortese [91]. Subjects were shown kinetic occlusion displays and were asked to identify the 2D shape of a moving form. Information for spatial and temporal integration was manipulated by changing velocity and texture density. Information for spatial and temporal integration was manipulated by changing the texture density of the display. Specifically, an increase in density will result in an increase in spatial and temporal information for the edge boundary. Information for temporal integration was manipulated by varying the speed of motion. Greater velocity of the object increases the rate of accretion and deletion, resulting in an increase in information for temporal integration. If age-related decrements in visual processing are due to changes in temporal integration, then it should be found that object identification performance will be significantly worse for older observers as compared to younger observers at slower speeds.

To isolate the role of spatial integration, they examined variations in performance when the rate of occlusion events remained constant. Specifically, if the velocity of the moving object is decreased and the texture density is increased proportionately, then the spatial separation of accretion and deletion of texture that defines the object boundary is decreased. If age-related decrements in visual processing are due to changes in spatial integration, then object identification performance will be significantly worse for older observers as compared to younger observers at lower texture densities under constant rates of occlusion.

Two experiments were conducted by Ander and Ni [72] to test their hypothesis. In the first experiment, they examined age-related decrements in the perception of 2D shape from kinetic occlusion. The displays consisted of random dots projected onto either a 2D shape (circle, square, diamond, or 5 point star) or the background. The primary variables of interest were dot density, velocity of object, and the absence/presence of background texture (i.e., providing kinetic occlusion information when background texture was present). If older observers have a decreased capacity for spatially integrating kinetic occlusion information, then poorer performance is expected for older observers with a decrease in dot density when background texture is present, particularly when the rate of occlusion is constant.

Older and younger observers showed similar levels of performance for the kinetic occlusion absent condition. When kinetic occlusion was added, both groups showed greater shape identification performance, but a greater increase in performance was found for the younger as compared to older observers. This result suggests that younger observers, as compared to older observers, had a greater capacity for integrating spatial and temporal information for identifying the boundaries of the object.

Based on these results, they conducted additional analyses of the data specifically for the condition when kinetic occlusion was present. No significant interactions were obtained between age and velocity, age and size, or any other higher order interactions with age. It was shown that age-related decrements in shape identification were approximately constant across variations in velocity. The lack of a significant interaction of age and velocity indicates that the age-related decrements are not due to a result of an age-related decline in temporal integration.

Andersen and Ni further examined the conditions in which two pairs of velocity/density combinations have identical spatial/temporal information. They found significant age effects between those conditions, such as between the combination of 1.2 deg/s velocity with 1.2 dots/deg^2 density and the combination of 0.6 deg/s velocity with 2.44 dots/deg^2 density. The interaction of age and performance for these two conditions was significant, indicating significant age effects when spatial/temporal information is constant. The greater age-related differences at lower density conditions indicate age-related decrements in spatial integration. Younger observers had a 32% increase in detection performance when kinetic occlusion information was present, as compared to an 11.5% increase for older observers.

To provide converging evidence in supporting spatial integration hypothesis, they conducted a second experiment. In this experiment, they managed to isolate the effects of spatial integration by manipulating limited lifetime of the stimuli, indicating the duration of individual dots was restricted. When limited lifetime displays are used, the object and background dots in the display would appear for a limited period of time before being randomly repositioned in the display. As a result, the salience of the edge boundary is considerably reduced because the disappearance/appearance of the dots can be either caused by occlusion or simply by the limited lifetime. In order to recover the boundary, the visual system must determine regions of local motion of limited duration and regions of no motion of limited duration. As a result, variations in the lifetime of the dots provide an opportunity to more directly assess the integration of information over time.

If the age-related decrements in using kinetic occlusion information were due to a loss in temporal integration, then decreasing the lifetime of local dot motion should greatly limit the temporal integration, resulting in a subsequent decrease in performance for older observers. Thus in their second experiment, the presentations of individual dots were shown for durations of 16, 33, 66, or 100 ms based on presentations of 2, 3, 4, or 6 frames. The proportion of dots repositioned from frame to frame varied as a function of lifetime. For example, for the two frame lifetime stimuli, 50% of the dots were repositioned on each frame; for the three frame lifetime stimuli, 33% were repositioned, etc.

The result showed a significant main effect of duration, indicating that an increase in lifetime result in increased detection performance. Surprisingly, planned comparisons of the effect of age at each duration condition showed no significant effects. These results suggest that age-related changes in visual processing are the result of changes in spatial integration.

An important question is that whether other aspects of visual processing, which are known to change with age (e.g., motion perception, pattern recognition, and face recognition), may be due to decreased spatial integration. Age-related changes have also been found in visual attention tasks that involve spatial information [94, 95]. Spatial integration may not only explain age-related effects in visual perception, but also be an important factor in age-related changes in performing driving-related visual tasks.

Future Directions

The results of the preset study suggest two practical applications in improving driving safety for older drivers. The first application concerns driving assisting system. Major automobile manufacturers have developed various intelligent safety systems, e.g., "Crash Mitigation Braking System" from Honda, Volvo's "City Safety," Toyota's "Pre-crash System," and Mercedes Benz's "Distronic Plus" system. However, there are two major concerns regarding the current assisting system prototypes. First, any system utilizing optical information, e.g., laser radar, is prone to weather change such as rain and fog. Second, most of these systems were tested on younger drivers which do not accommodate the specific characteristics of older driver population. A successful driving assisting system should take age-related differences in driving

performance into account, as well as the environmental changes in inclement weather conditions.

A second application concerns the potential improvement in driving performance through training for older drivers. Andersen et al. [96] found that following training with subthreshold stimuli, older observers were able to improve performance in a texture discrimination task, and that this improvement was retained for up to 3 months. Indeed, the training, which occurred over a 2 day period, made the older observers to perform equally well as compared to the pre-training performance of college age. In another study, Richards et al. [97] found that older observers could improve their performance in divided attention through repeated training with the UFOV (useful field of view) task. An interesting topic for future research would be to investigate whether older observers can improve driving performance under low visibility conditions using different training techniques.

Bibliography

1. Langford J, Koppel S (2006) Epidemiology of older driver crashes – identifying older driver risk factors and exposure patterns. Transp Res F Traffic Psychol Behav 9:309–321
2. Evans L (2004) Traffic safety. Science Serving Society, Bloomfield Hills, p 179
3. Owsley C, Ball K, Sloane ME, Roenker DL, Bruni JR (1991) Visual/cognitive correlates of vehicle accidents in older drivers. Psychol Aging 6:403–415
4. National Highway Traffic Safety Administration (2008) Traffic safety fact – 2007 data (NHTSA's national center for statistics and analysis. Publication No.DOT HS 810 992). Washington, DC
5. Owsley C, McGwin G Jr, Phillips JM, McNeal SF, Stalvey BT (2004) Impact of an educational program on the safety of high-risk, visually impaired, older drivers. Am J Prev Med 26:222–229
6. Wood JM, Owens DA (2005) Standard measures of visual acuity do not predict drivers' recognition performance under day or night conditions. Optom Vis Sci 82:698–705
7. Ball K, Owsley C, Beard B (1990) Clinical visual perimetry underestimates peripheral field problems in older adults. Clin Vis Sci 5:113–125
8. McGwin G, Chapman V, Owsley C (2000) Visual risk factors for driving difficulty among older driver. Accid Anal Prev 32(6):735–744
9. Glass JM (2007) Visual function and cognitive aging: differential role of contrast sensitivity in verbal versus spatial tasks. Psychol Aging 22:233–238
10. Schachar RA (2006) Effect of change in central lens thickness and lens shape on age-related decline in accommodation. J Cataract Refract Surg 32:1897–1898
11. Richards OW (1977) Effects of luminance and contrast on visual acuity, ages 16 to 90 years. Am J Optom Physiol Opt 54:178–184
12. Derefeldt G, Lennerstrand G, Lundh B (1979) Age variations in normal human contrast sensitivity. Acta Ophthalmol 57: 679–690
13. Owsley C, Sekuer R, Siemsen D (1983) Contrast sensitivity throughout adulthood. Vis Res 23:689–699
14. McFarland RA, Domey RG, Warren AB, Ward DC (1960) Dark adaptation as a function of age: I. A statistical analysis. J Gerontol 15:149–154
15. Domey RG, McFarland RA, Chadwick E (1960) Dark adaptation as a function of age and time. II. A derivation. J Gerontol 15:267–279
16. Chapanis A (1950) Relationships between age, visual acuity and color vision. Hum Biol 22:1–33
17. Kahn HA, Leibowitz HM, Ganley JP, Kini MM, Colton T, Nickerson RS et al (1977) The Framingham Eye Study I. Outline and major prevalence findings. Am J Epidemiol 106:17–32
18. Sekuler R, Hutman LP, Owsley CJ (1980) Human aging and spatial vision. Science 209:1255–1256
19. Long GM, Crambert RF (1990) The nature and basis of age-related changes in dynamic visual acuity. Psychol Aging 5:138–143
20. Trick GL, Silverman SE (1991) Visual sensitivity to motion: age-related changes and deficits in senile dementia of the Alzheimer type. Neurology 41:1437–1440
21. Gilmore GC, Wenk HE, Naylor LA, Stuve TA (1992) Motion perception and aging. Psychol Aging 7:654–660
22. Andersen GJ, Atchley P (1995) Age-related differences in the detection of three dimensional surfaces from optic flow. Psychol Aging 10:650–658
23. Betts LR, Taylor CP, Sekuler AB, Bennett PJ (2005) Aging reduces center-surround antagonism in visual motion processing. Neuron 45:361–366
24. Bennett PJ, Sekuler R, Sekuler AB (2007) The effects of aging on motion detection and direction identification. Vis Res 47:799–809
25. Andersen GJ, Cisneros J, Atchley P, Saidpour A (1999) Speed, size, and edge-rate information for the detection of collision events. J Exp Psychol Hum Percept Perform 25:256–269
26. Andersen GJ, Enriquez A (2006) Aging and the detection of observer and moving object collisions. Psychol Aging 21: 74–85
27. Norman FJ, Clayton AM, Shular CF, Thompson SR (2004) Aging and the perception of depth and shape from motion parallax. Psychol Aging 19:506–514
28. Norman FJ, Crabtree CE, Hermann D (2006) Aging and the perception of 3-D shape from kinetic patterns of binocular disparity. Percept Psychophys 68:94–101
29. Folk CL, Hoyer WJ (1992) Aging and shifts of visual spatial attention. Psychol Aging 7:453–465
30. Kramer AF, Hahn S, Irwin DE, Theeuwes J (1999) Attentional capture and aging: Implications for visual search performance and oculomotor control. Psychol Aging 14:135–154

31. Hartley AA, Little DM (1999) Age-related differences and similarities in dual-task interference. J Exp Psychol 128:416–449
32. Scialfa CT, Thomas DM, Joffe KM (1994) Age differences in the useful field of view: An eye movement analysis. Optom Vis Sci 71:736–742
33. Sekuler AB, Bennett PJ, Mamelak M (2000) Effects of aging on the useful field of view. Exp Aging Res 26:103–120
34. Owsley C, Sloane ME (1990) Vision and aging. In: Nebes RD, Corkin S (eds) Handbook of neuropsychology, vol 4. Elsevier Science, New York, pp 229–249
35. Hoffman L, McDowd JM, Atchely P, Dubinsky R (2005) The role of visual attention in predicting driving impairment in older adults. Psychol Aging 20:610–622
36. Salthouse TA, Somberg BL (1982) Time-accuracy relationships in young and old adults. J Gerontol 37:49–53
37. Salthouse TA, Somberg BL (1982) Isolating the age deficit in speeded performance. J Gerontol 37:59–63
38. Michon JA (1989) Explanatory pitfalls and rule-based driver models. Accid Anal Prev 21(4):341–353
39. Cutting JE (1996) Wayfinding from multiple sources of local information in retinal flow. J Exp Psychol Hum Percept Perform 22(5):1299–1313
40. Wilkniss SM, Jones MG, Korol DL, Gold PE, Manning CA (1997) Age-related differences in an ecologically based study of route learning. Psychol Aging 12(2):372–375
41. DeLucia PR, Mather RD (2006) Motion extrapolation of car-following scenes in younger and older drivers. J Hum Factors Ergon Soc 48(4):666–674
42. Macuga KL, Beall AC, Kelly JW, Smith RS, Loomis JM (2007) Changing lanes: inertial cues and explicit path information facilitate steering performance when visual feedback is removed. Exp Brain Res 178:141–150
43. Chandler RE, Herman R, Montroll EW (1958) Traffic dynamics: studies in car following. Oper Res 6:165–184
44. Brackstone M, McDonald M (1999) Car-following: a historical review. Transp Res Rec F 2:181–196
45. Andersen GJ, Sauer CW (2007) Optical information for car following: the driving by visual angle (DVA) model. Hum Factors 49:878–896
46. Andersen GJ, Sauer CW (2005) Visual information for car following by drivers: the role of scene information. Transp Res Rec F 1899:104–109
47. Ni R, Kang J, Andersen GJ (2010) Age-related declines in car following performance under simulated fog conditions. Accid Anal Prev 42(3):818–826
48. Bian Z, Andersen GJ (2008) Aging and the perceptual organization of 3-D scenes. Psychol Aging 23:342–352
49. Scialfa CT, Guzy LT, Leibowitz HW, Garvey PM et al (1991) Age differences in estimating vehicle velocity. Psychol Aging 6(1):60–66
50. Massie DL, Campbell KL, Williams AF (1995) Traffic accident involvement rates by driver age and gender. Accid Anal Prev 27:73–87
51. Stutts JC, Martell C (1992) Older driver population and crash involvement trends 1974–1988. Accid Anal Prev 24:317–327
52. McGwin G, Brown DB (1999) Characteristics of traffic crashes among young, middle-aged and older drivers. Accid Anal Prev 31:181–198
53. Kang JJ, Ni R, Andersen GJ (2008) The effects of reduced visibility from fog on car following performance. J Transp Res Board 2069:9–15
54. Broughton KLM, Switzer F, Scott D (2007) Car following decisions under three visibility conditions and two speeds tested with a driving simulator. Accid Anal Prev 39:106–116
55. Andersen GJ, Braunstein ML (1998) The perception of depth and slant from texture in 3D scenes. Perception 27:1087–1106
56. Larish JF, Flach JM (1990) Sources of information useful for perception of speed of rectilinear motion. J Exp Psychol Hum Percept Perform 16:295–302
57. Andersen GJ, Cisneros J, Saidpour A, Atchley P (2000) Age-related differences in collision detection during deceleration. Psychol Aging 15:241–252
58. Andersen GJ, Sauer CW (2004) Optical information for collision detection during deceleration. In: Hecht H, Kaiser M (eds) Theories of time to contact, advances in psychology series, North Holland. Elsevier, Amsterdam, pp 93–108
59. DeLucia PR, Bleckley MK, Meyer LE, Bush JM (2003) Judgments about collisions in younger and older drivers. Transp Res part F Traffic Psychol Behav 6:63–80
60. Al-Ghamdi AS (2007) Experimental evaluation of fog warning system. Accid Anal Prev 39:1065–1072
61. Bian Z, Ni R, Guindon A, Andersen GJ (2009) Aging and the detection of collision events in fog. In: Proceedings of the fifth international driving symposium on human factors in driver assessment, training and vehicle design, pp 69–75
62. Ni R, Andersen GJ (2008) Detection of collision events on curved trajectories. Percept Psychophys 70(7):1314–1324
63. Green DM, Swets JA (1966) Signal detection theory and psychophysics. Wiley, New York
64. Pelli DG, Robson JG, Wilkins AJ (1988) Designing a new letter chart for measuring contrast sensitivity. Clin Vis Neurosci 2:187–199
65. Braunstein ML, Andersen GJ, Rouse MW, Tittle JS (1986) Recovering viewer-centered depth from disparity, occlusion, and velocity gradients. Percept Psychophys 40:216–224
66. Gibson T (1979) The ecological approach to visual perception. Houghton Mifflin, Boston
67. Gibson T (1966) The senses considered as perceptual systems. Houghton Mifflin, Boston
68. Warren WH, Morris M, Kalish M (1988) Perception of translational heading from optical flow. J Exp Psychol Hum Percept Perform 14:646–660
69. Warren WH, Mestre DR, Blackwell AW, Morris MW (1991) Perception of circular heading from optical flow. J Exp Psychol Hum Percept Perform 17:28–43
70. Andersen GJ, Braunstein ML (1985) Induced self-motion in central vision. J Exp Psychol Hum Percept Perform 11:122–132
71. Nguyen B, Zhuo Y, Ni R (2011) Aging and the steering control under reduced visibility conditions. In: Proceedings of the

sixth international driving symposium on human factors in driver assessment, training and vehicle design (in press)
72. Andersen GJ, Ni R (2008) Aging and visual processing: declines in spatial not temporal integration. Vis Res 48:109–118
73. Ni R, Andersen GJ, Rizzo M (2005) Age related decrements in steering control: the effects of landmark and optical flow information. In: Proceedings of the third international driving symposium on human factors in driver assessment, training and vehicle design, pp 144–150
74. Ni R, Bian Z, Andersen GJ (2009) Age-related differences in using optical flow and landmark information for steering control. In: Proceedings of the IEEE intelligent vehicles symposium, 2009, pp 691–694
75. Ni R, Andersen GJ (2006) Age related performance in driving: steering and collision detection, vision in vehicles 11. Dublin, Ireland
76. Barlow HB (1953) Summation and inhibition in the frog's retina. J Physiol 119:69–88
77. Brown HA, Allison DD, Samonds JM, Bonds AB (2003) Nonlocal origin of response suppression from stimulation outside the classical receptive field in area 17 of the cat. Vis Neurosci 20:85–96
78. Das A, Gilbert CD (1999) Topography of contectural modulations mediated by short-range interactions in primary visual cortex. Nature 399:655–661
79. Stettler DD, Das A, Bennett J, Gilbert CD (2000) Lateral connectivity and contextual interactions in macaque primary visual cortex. Neuron 36:739–750
80. Bullier J, Hupe JM, James AC, Girard P (2001) The role of feedback connections in shaping the responses of visual cortical neurons. Prog Brain Res 134:193–204
81. Moore T, Armstrong KM (2003) Selective gating of visual signals by microstimulation of frontal cortex. Nature 421:370–373
82. Roberts MJ, Zinke W, Guio K, Robertson R, McDonald JS, Thiele A (2005) Acetylcholine kinetically controls spatial integration in Marmoset primary visual cortex. J Neurophysiol 93:2062–2072
83. Ledgeway T, Hess RF (2002) Rules for combining the outputs of local motion detectors to define simple contours. Vis Res 42:653–659
84. Field DJ, Hayes A, Hess RF (1993) Contour integration by the human visual system: evidence for a local 'association field'. Vis Res 33:173–193
85. Kovacs I (1996) Gestalten of today: early processing of visual contours and surfaces. Behav Brain Res 82:1–11
86. Aspell JE, Wattam-Bell J, Braddick O (2006) Interaction of spatial and temporal integration in global form processing. Vis Res 46:2834–2841
87. Bair W, Movshon JA (2004) Adaptive temporal integration in direction-selection neurons in Macaque visual cortex. J Neurosci 24:7305–7323
88. Shadlen MN, Movshon JA (1999) Synchrony unbound: a critical evaluation of the temporal binding hypothesis. Neuron 24:67–77
89. Baker CL, Braddick OJ (1985) Temporal properties of the short-range process in apparent motion. Perception 14:181–192
90. Andersen GJ, Cortese JM (1989) 2-D contour perception resulting from kinetic occlusion. Percept Psychophysic 46:49–55
91. Kellman PJ, Shipley TF (1992) Perceiving objects across gaps in space and time. Curr Dir Cogn Sci 1:193–199
92. Lee S-H, Blake R (1999) Visual form created solely from temporal structure. Science 284:1165–1168
93. Blake R, Lee S-H (2005) The role of temporal structure in human vision. Behav Cogn Neurosci Rev 4:21–42
94. Thorton WJL, Raz N (2006) Aging and the role of working memory resources in visuospatial attention. Aging Neuropsychol Cogn 13:36–61
95. Greenwood PM, Parasuraman R (2004) The scaling in visual search and its modification in healthy aging. Percept Psychophys 66:3–22
96. Andersen GJ, Ni R, Bower JD, Watanabe T (2010) Perceptual learning, aging, and improved visual performance in early stages of visual processing. J Vis 10(13):4, 1–13
97. Richards E, Bennett PJ, Sekuler AB (2006) Age related differences in learning with the useful field of view. Vis Res 46:4217–4231

Drug Discovery in Ocean

David J. Newman, Gordon M. Cragg, Paul G. Grothaus
Natural Products Branch Developmental Therapeutics Program, National Cancer Institute, NCI-Frederick, Frederick, MD, USA

Article Outline

Glossary
Definition of the Subject
Introduction
Antitumor Agents
Anti-infective Agents
Zinconotide, Cone Snail Toxin
Future Directions
Bibliography

Glossary

Biodiscovery The investigation of natural products (secondary metabolites) from organisms with the aim of determining if they have biological activities of utility in human diseases.

Derivatized A chemical structure that resembles a known published structure in general but has specific modifications made by nature or man.

Dredging collections Use of towed sledges or nets designed to skim the sea bed/ledges horizontally or at an angle, with organisms being separated at the surface.

Manned submersible A self-propelled small submarine equipped with collection devices that usually is used in the depth range of 50–1,000 m when used for biodiscovery.

Orthotopic tumor A tumor model where the human (or animal) tumor is implanted in its original site rather than in a subcutaneous or intraperitoneal site distinct from its site of nominal origin. An example would be the implanting of a brain-derived tumor into the cranial cavity of the animal instead of into the flank or peritoneum.

Proteasome inhibitor A chemical compound that blocks the protein degradation by cell organelle.

Remotely operated vehicle (ROV) A torpedo-shaped self-propelled underwater vehicle controlled via a tether from a mother ship, or autonomously via an internal guidance device. Collection baskets and video/tv recording devices are part of the general equipment.

Secondary metabolites Chemical compounds encoded by genes and produced by organisms that are not required for the basic life processes of the producer. These are usually considered to be produced when the organism needs to defend itself from attack, or wishes to attack another organism to gain an advantage.

Sessile organism A normally nonmotile marine organism that requires a "foothold" on a substrate in order to survive and grow. Almost all are filter feeders, moving large amounts of seawater through their bodies on a daily basis. Marine sponges (phylum Porifera) are prime examples of this type of organism.

Shallow water collections Usually considered to be from simple wading to the "regular" limit of SCUBA (self-contained underwater breathing apparatus) which is <50 m for well-trained and experienced divers.

Definition of the Subject

The oceans of the world cover roughly 71% of the planet and have a median depth of >3,000 m and a mean depth of 3,800 m. Of this vast expanse, less than 5% of the deep sea has been explored in any way and less than 0.01% of the deep sea floor has been sampled in detail [1]. What is often not realized is that, of the 36 animal phyla listed taxonomically, 34 are found in the marine environment [2] and of these, approximately half are only found in marine environments. Of the remainder, another approximate half are both marine and terrestrial (though predominately marine) and only one, the phylum Onychophora (the velvet worms) is exclusively terrestrial.

Although organisms had been recovered from depths in the 1800s and obviously had been seen for many centuries on coral reefs in shallow waters and beaches, it was not until the Challenger expedition in the 1872–6 time frame, and then the Galathea expedition in 1950–2 that collected live animals from the Philippines Trench at 10,190 M [3] that it was demonstrated that, with the possible exception of the anoxic zones in the Black Sea, living animals could be found at all depths. The reason for using "possible" as a modifier above is that the formaniferans tube worms found at "black smokers" are in anoxic environments and utilize microbes of the sulfur cycle to survive and grow.

Who first decided to investigate the marine environment as a source of medicaments is unknown, but the Japanese and Chinese herbals do contain various mixtures that were used as part of traditional medicines, and certainly, the toxic properties of marine-derived products were well-known centuries ago, with an example being the puffer fish (Fugu) in Japanese cuisine. From a historical perspective, "Tyrian Purple," a dyestuff from a Mediterranean mollusk used in Roman times, actually has significant activity in some cancers and was used as a part of traditional Chinese medicine (TCM) for the treatment of leukemia. It is only recently that it was realized that the active chemical compounds (marine sourced and plant sourced, respectively) were of the same basic chemical class.

Thus, this article will deal with the potential of the marine (aquatic) environment and its organisms as leads to agents of value to humans either directly or indirectly. What will become obvious as the stories unfold is that the original organism (usually a marine invertebrate) may or may not be the actual producer of the metabolite(s) of interest. Where the true producer is known, it will be identified, but in a significant

number of cases, the evidence is still circumstantial, though in other cases, the organism is directly identifiable.

Introduction

Though found in both marine and aquatic environments ranging from the Sea of Japan to Lake Victoria in Central Africa, one can argue that one of the first generally used "marine" invertebrate-sourced secondary metabolites was the toxin known as nereistoxin (Fig. 1) from the flatworm *Lumbrineris brevicirra* (also named *Lumbrineris heteropoda*). This worm had probably been used for centuries by fishermen to stun fish within the lake, thus permitting them to harvest their catches rather easily. One might almost call it a "chemical dynamite fishing system" by analogy to the explosive methods used by fishermen in countries such as the Philippines and other areas of SE Asia. In addition, Japanese fishermen had known for years that the flatworm had anti-insecticidal properties as it killed carnivorous insects when they landed on it.

In 1934, Nitta isolated the active principle in the flatworm with a structure being proposed by Okaichi and Hashimoto in 1962 and confirmed by total synthesis reported by Hagiwara et al. in 1965 [4]. This compound was shown to be an acetylcholine antagonist, and over the next few years, insecticides were developed from the base structure, with a close analog, Padan® (Fig. 1) being marketed by Takeda in 1967.

As mentioned earlier, there had been sporadic reports from at least two millennia ago of pharmacologically active agents being isolated and identified from marine organisms, but it was not until the twentieth century that any form of systematic investigation occurred. Thus in the early 1960s to early 1970s, academic groups in the USA and pharmaceutical company-linked organizations such as the Roche Institute for Marine Pharmacology in Australia reported their findings in a variety of formats. For information on these and earlier studies, one should consult the 1976 review by Ruggieri [5].

One may argue, and the authors and others have done so on a number of occasions [6, 7], that the seminal discoveries, and thus the impetus for the investigation of marine biodiversity and the subsequent vision of marine-derived drugs on the market, can be traced to identification by Bergmann in the early 1950s of the arabinose-containing bioactive nucleosides spongothymidine and spongouridine (Fig. 1) from

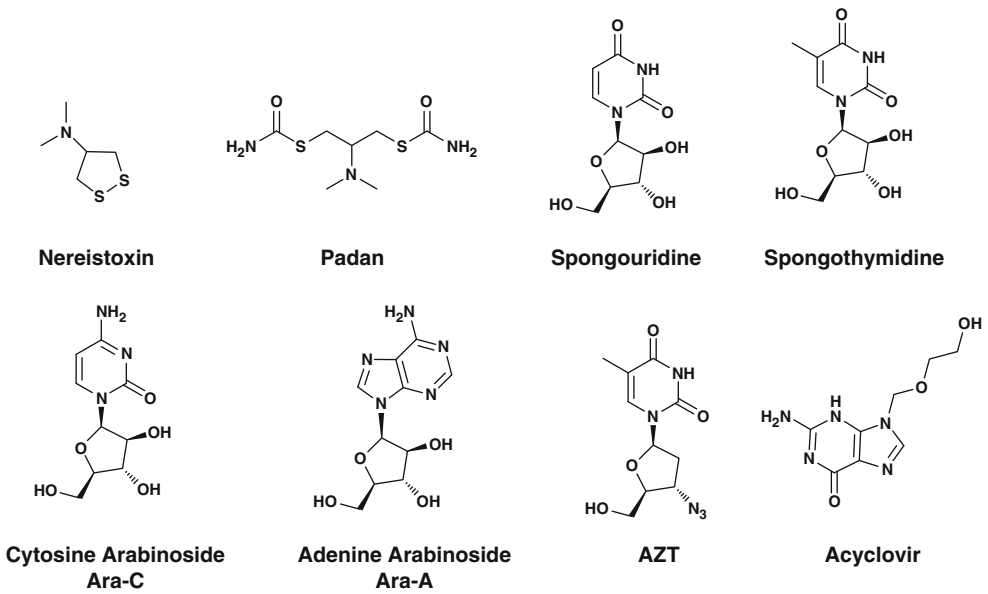

Drug Discovery in Ocean. Figure1
Early agents from marine sources and their subsequent derivatives

the Caribbean sponge *Tethya crypta* [8–10]. These discoveries overthrew the then current dogma that a nucleoside had to have either ribose or deoxyribose as the sugar moiety in order to demonstrate biological activity.

The subsequent explosion of compounds is described in the reviews by Suckling [6] and Newman et al. [7]. These discoveries led to the identification of a close analog, cytosine arabinoside (Fig. 1) as a potent antileukemic agent; this compound was subsequently commercialized by Upjohn (now Pfizer) as Ara-C. Other closely related compounds such as adenine arabinoside (Ara-A) (Fig. 1), an antiviral compound synthesized and commercialized by Burroughs Wellcome (now Glaxo SmithKline), and later found in the Mediterranean gorgonian *Eunicella cavolini*. Similar reasoning led to investigations on the minimum size of sugar rings and other substitutions on the sugar ring[s], thus azidothymidine (AZT) (Fig. 1) and even acyclovir (Fig. 1) can be traced back to this initial discovery.

In the subsequent sections, the discussion will be separated on the basis of pharmacologic activities rather than by nominal source since, as mentioned earlier, it is now being realized that what was thought to be the product of a marine invertebrate may well be produced by a microbe, a consortium of microbes, and/or interactions between microbe(s) and invertebrate host. Where data exist as to actual or probable source, the information will be cited.

Antitumor Agents

Introduction

By the early 1960s, the terrestrial plant world had been explored and reported by a number of groups from the 1940s onwards, with agents such as the Vinca alkaloids first being reported as potential antitumor agents in the late 1950s. Similarly, the terrestrial microbial world had been explored in a systematic fashion from roughly the late 1940s with success in both antibiotic and antitumor areas, and a number of agents still in current clinical use were first identified in the late 1950s to early 1960s in industry.

Similarly, although there had been a number of reports of biologically active agents from marine (and freshwater) environments (cf. discussion on arabinosides above), predominately by academic researchers who received funding from either NIH institutes or NSF for basic research, no systematic explorations had been performed on marine environments as sources of medicaments.

Starting in the early 1960s, the National Cancer Institute (NCI) the largest institute within the US government's National Institutes of Health (NIH), expanded its horizons beyond the testing of synthetic compounds as experimental antitumor agents and began large-scale studies of natural products. Plant materials were collected and recollected when required (and if feasible) in conjunction with the USDA. Microbial products were usually provided by pharmaceutical companies, and small numbers of marine invertebrates were also obtained by purchase from collectors.

These materials were then extracted by predominately academic groups; the extracts tested initially in whole animal models (mouse and rat tumors) and later in fast-growing animal leukemia cell lines by US government contract laboratories with "active materials" then being isolated and identified by academic collaborators. At the same time, academic investigators including those who were also acting as NCI collaborators were also expanding their investigator-initiated grant applications towards the marine environment with the aim of collecting and utilizing marine invertebrates as sources of drug leads (marine biodiscovery).

Early Marine-Sourced Antitumor Compounds

Introduction The two antitumor compounds that came from what might be considered as the earliest systematic investigations of the marine environment for such agents, as distinct from finding activities for isolated compounds (that might be considered as the marine equivalent of phytochemical investigations), were two agents reported by the Pettit group at Arizona State University working with the NCI. These were bryostatin 3 and dolastatin 10 (Fig. 2). The former was isolated from the well-known fouling organism *Bugula neritina* and the latter from the nudibranch *Dolabella auricularia*. Subsequently, each was found to be a representative of a family of somewhat similar compounds, examples of each going into extensive isolation/synthesis programs and then clinical trials in man over the next 20 plus years. The earlier history of both the dolastatins [11] and the bryostatins [12] was

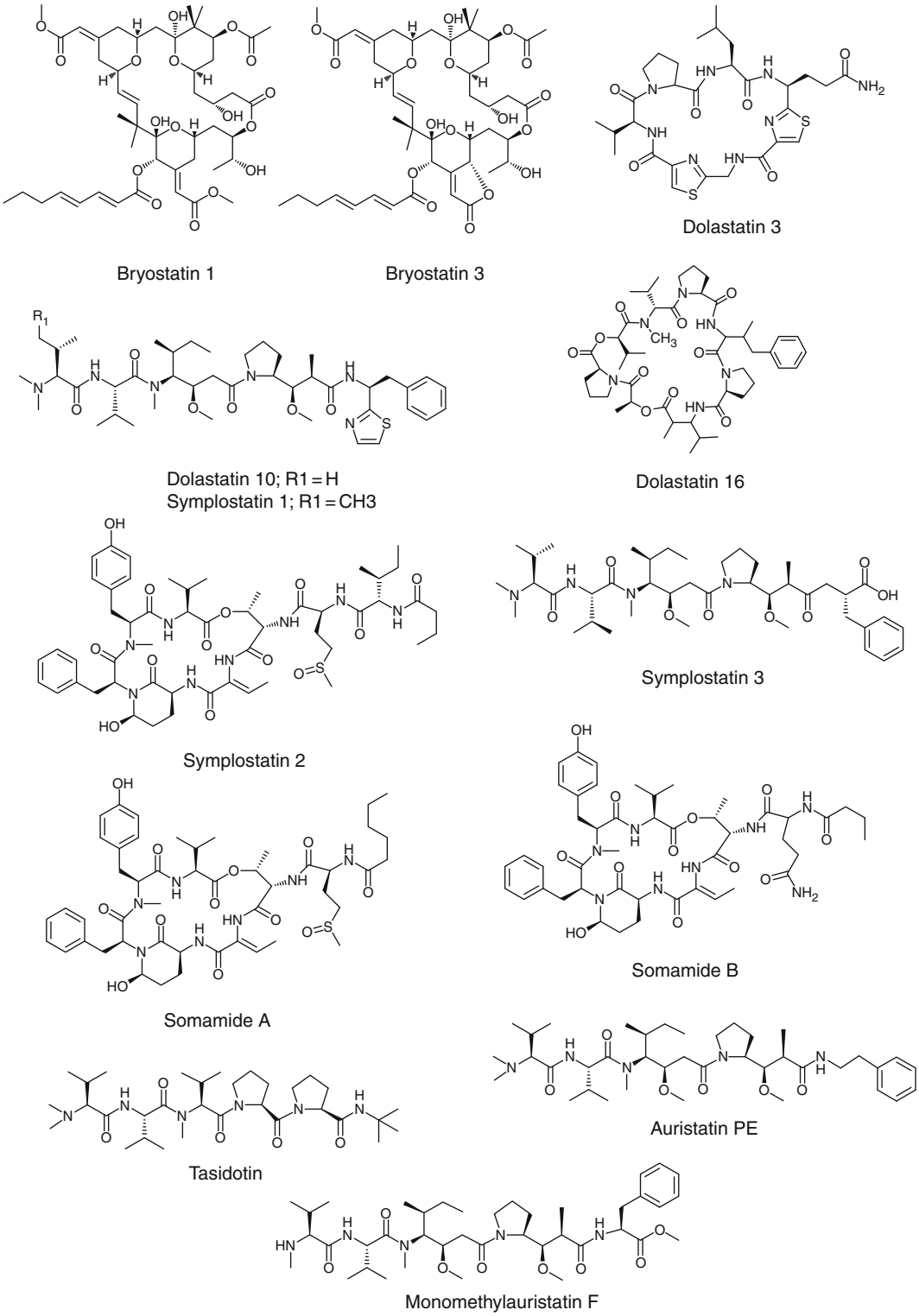

Drug Discovery in Ocean. Figure 2
Early antitumor agents from marine sources and chemical derivatives

reported in detail in the 2005 book *Anticancer Agents from Natural Products*. At that time, both classes of agents had been in multiple trials with only marginal success.

Bryostatins 1–20 and Bryologs In the case of the bryostatins, over the roughly 35 years since the initial report of bryostatin 3 in 1970 to the review in 2005, 19 variations on the bryostatin structure had been reported with syntheses of at least three in that time frame. From the early 1980s, bryostatin 1 (Fig. 2), which was the most abundant of the group and had been isolated and purified to cGMP quality mainly by workers at the NCI-Frederick in the late 1980s, and on a small scale by Pettit, went into a multiplicity of clinical trials (at phases I and II) as both a single agent and in conjunction with cytotoxins. However, to date, only a few patients showed responses to the agent in spite of being in over 80 clinical trials in this time frame. Currently, there are just two trials listed as of February 2011 that are still active. One phase II, studying paclitaxel and bryostatin 1 is active but not recruiting patients, and the other, a phase I trial with temsirolimus and bryostatin 1 that is listed as active and recruiting. What is of interest, however, is that the base molecule is now being investigated as a potential treatment for Alzheimer's disease, with a phase I trial approved in 2008 under the sponsorship of the Blanchette Rockefeller Neurosciences Institute in West Virginia, but the trial is not yet open for participants.

There have been some quite recent reviews and reports on the earlier syntheses of bryostatin and the simplified versions made by Wender that are known as the "bryologs," together with the research work that has led to the possibilities for the treatment of Alzheimer's disease referred to above. The interested reader should consult the excellent 2010 review article by Hale and Manaviazar [13] for a thorough discussion of all of the chemistry involved in the bryostatins, the papers by the West Virginia neurosciences groups [14–18] with a very interesting potential linkage to Alzheimer's treatment and bryologs recently published by Khan et al. [19].

Finally, the bryostatins may well be produced by an as yet non-cultured commensal microbe or microbes found in the pallial sinus of the larvae of the "nominal" producing organism *Bugula neritina*. As a result of extensive ecological and genomic analyses by Haygood and her collaborators, there is now very good evidence linking biosynthetic gene clusters from this commensal microbial organism (not yet identified; simply given the name "*Candidatus endobugula sertula*") to the formation of bryostatin. The discussion is beyond the scope of this article, but for readers who are interested, they should consult the following research papers that cover the discoveries [20–31]. One may ask whether the effort expended on the bryostain story was worth it? In the view of the authors, definitely! The chemistry, microbiology, studies of tumor systems, and their interactions would not have occurred without molecules such as these. The ultimate aim is to come up with chemical derivatives that will mimic the natural molecule but have better pharmacological properties.

Dolastatins and Derivatives (ILX651 and Auristatin PE) The dolastatins, unlike the bryostatins, had to be synthesized in order to obtain enough material for preclinical and clinical trials. The pre-2005 chemistry related to the synthesis of these compounds was discussed in detail by Flahive and Srirangam [11], though a little earlier, the proof that natural dolastatins and closely related peptides were definitively produced by cyanobacteria, was given in a series of publications. These reported the isolation of dolastatins 3, [32] 10, [33] 12–14 [34, 35], and 16 [36] directly from varieties of the blue-green algae *Lyngbya majuscula* and *Symploca hydnoides*, along with other novel closely related bioactive compounds such as the symplostatins 1–3 [37–39] and somamides A and B (Fig. 2) [35].

Dolastatin 10 was in a significant number of phase I and phase II clinical trials but was not successfully developed beyond that level. There are two "hold over" trials still listed as of Feb 2011 in the NCI's Clinical Trials web site, where it is reported as being studied as a single agent in a phase I study at M.D. Anderson as a treatment for various leukemias, and in a phase II study at the University of Chicago against liver-related carcinomas. No updates have been posted since 2008, nor have there been any publications directly related to the trials, but very recently, Siemann published a review on tumor-vascular disrupting agents that included dolastatin 10 and some close relatives within this mechanism of action category [40] including other agents that also bind to the colchicine-binding site of tubulin.

As a result of the experience with dolastatin syntheses, the Pettit group, and others, synthesized a variety of agents based upon dolastatin 10 and 15. Of these agents, ILX651 or tasidotin (Fig. 2), based upon dolastatin 15, entered clinical trials but currently, no active trials are shown, and the current owners of the compound, Genzyme (now owned by Sanofi-Aventis), reported in 2008 that they will continue investigating it at the preclinical level as an oral antitumor drug.

Another derivative, auristatin PE (Fig. 2) also entered clinical trials as both a tubulin interactive agent and also with potential as a vascular disrupting agent [40]. It too, did not demonstrate objective responses [41, 42]. This compound (some with subtle chemical modifications such as monomethyl auristatin E, also known as vedotin), and with or without a small chemical linker, was used as warheads by Seattle Genetics attached to selective monoclonal targeting antibodies. Variations differing in the antibody and the specific linker are currently in phase III (brentuximab vedotin, SGN-35), phase II (glembatumumab vedotin, CDX-011), phase I (PSMA-ADC, MEDI-547 and MN-immunoconjugate) with another (anti-CD19-vcMMAE), and in preclinical trials.

A variant of auristatin PE (known as auristatin F (Fig. 2) in which the C-terminal amino acid was changed to phenylalanine) provided another monoclonal antibody-warhead combination (1 F6-MMAF, SGN-75). This combination is currently in phase I clinical trials.

These clever modifications demonstrate how compounds based on marine natural products that exhibit interesting activities, but have pharmacologic properties that hinder clinical development, can be further optimized (rescued?) by clever chemistry and biology, with a new drug application (NDA) being filed by Seattle Genetics for SGN-35 late in 2010 for treatment of Hodgkin's lymphoma.

Antitumor Agents in Use

Trabectedin (Yondelis®, Et-743) The first, and currently only anticancer compound "directly from the sea," in the sense that the molecule approved is identical to the natural product for the treatment of cancer, is trabectedin (Yondelis®) (Fig. 3). This complex tetrahydroisoquinoline alkaloid was approved by the EMEA, the European equivalent of the FDA, in September 2007 for the treatment of sarcoma and was launched in Sweden, Germany and UK in late 2007 for that indication. Subsequently, it was approved for treatment, in conjunction with liposomal doxorubicin, of recurrent ovarian cancers that were sensitive to antitumor drugs containing platinum at the launching in 2009 in Sweden, UK and Spain. Currently, there are

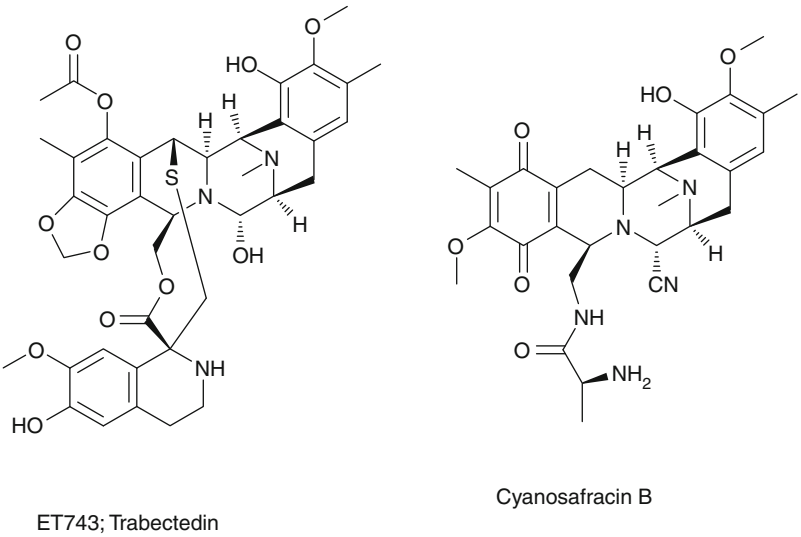

Drug Discovery in Ocean. Figure 3
The first "direct from the sea" antitumor agent and semisynthetic precursor

multiple clinical trials, all are ongoing and recruiting, listed in the NCI clinical trials database (http://clinicaltrials.gov), and details of the clinical trials that led to the ovarian cancer approval have recently been published [43, 44].

This compound belongs to a series of compounds originally reported by two different research groups in 1990 [45, 46]. The compound was recognized as a derivatized member of the well-known saframycin class of terrestrial antibiotics, and it was therefore possible that there might be a microbial component in the production of the compound by the invertebrate *Ecteinascidia turbinata*.

Trabectedin, then known by the abbreviation Et-743, was licensed by the discoverers to the Spanish pharmaceutical company, PharmaMar, and followed a very checkered development path including large-scale wild collections of the source tunicate *Ecteinascidia turbinata*, both in-sea and on-land aquaculture (all of which produced enough harvested materials for the initial and early clinical trials). The compound, though synthesized early in the study by Corey's group, was ultimately produced for later clinical trials by semisynthesis starting with cyanosafracin B (Fig. 3). This intermediate compound was produced by fermentation of a marine-derived *Pseudomonas fluorescens* and additional details of this agent can be found in the 2005 review by Henriquez et al. [47].

In addition to the review cited above, Velasco et al. reported the identification of the producing gene cluster for saframycin from the *P. fluorescens* culture used to produce the intermediate, thus presenting possibilities for combinatorial biosyntheses for trabectedin [48]. In addition to this report, approximately 2 years earlier, potential bacterial sources for trabectedin from Mediterranean Sea-sourced *Ecteinascidia turbinata* were identified by Moss et al. [49] which was followed in 2007 with an examination of the microbial assemblages associated with both Caribbean and Mediterranean isolates of *Ecteinascidia turbinata*.

In this report, five potentially persistent bacteria were identified, with one, *Candidatus Endoecteinascidia frumentensis*, occurring in *Ecteinascidia turbinata* in both geographical locations [50]. Although this is not absolute proof, such occurrences are indicative of microbial involvement in the production of trabectedin and require further investigation similar to the research conducted for the putative bryostatin producer (*vide infra*).

From a mechanistic aspect, a number of reports have been published in the literature over the last few years giving possibilities as to the mechanism of action (MOA) of trabectedin when tumor cells are treated in vitro. However, a significant problem with a number of these published reports is that the concentration(s) used in the experiments were frequently orders of magnitude greater than those that demonstrate activity in vitro. Since the "active" levels (in cellulo) are in the low nM to high pM range, care should be taken when evaluating published work on the MOA of this compound.

At physiologically relevant concentrations, the MOA(s) of trabectedin have been shown to include the following: effects on the transcription-coupled nucleotide excision repair process (TC-NER) and interaction between the Et-743 DNA adduct and DNA transcription factors, in particular, the NF-Y factor [51]. Recent pharmacogenomic analyses have identified a series of genes involved in the sensitivity of tumor cells to this agent, and the paper by Jimeno et al. [52] should be consulted in order to see the patterns identified.

In 2007, Soares et al. [53] demonstrated that adducts formed with ET-743 and DNA were stable and could convert into double-strand breaks (DSBs) a number of hours after initial formation. In addition, loss of the homologous recombination repair function, although having no effect on the initial number of DSBs, was associated with persistence of these lesions which could give rise to extensive chromosomal abnormalities, and thus, sensitivity to the drug. In addition to this report, two other papers that demonstrated other more subtle aspects of its cellular interactions have been published; the first in 2006, demonstrating that the demethylated analog ET-729 has a differential affinity for the CGA DNA triplet -binding site compared to ET-743 [54] and the second in 2007, demonstrating that sensitivity correlates with mutated p53 in low passage sarcoma cell lines [55].

Eribulin (Halaven®, E7389) This agent, which is a wholly synthetic molecule modeled on the ring structure of the naturally occurring antitubulin compound halichondrin B (Fig. 4), came from a tour-de-force

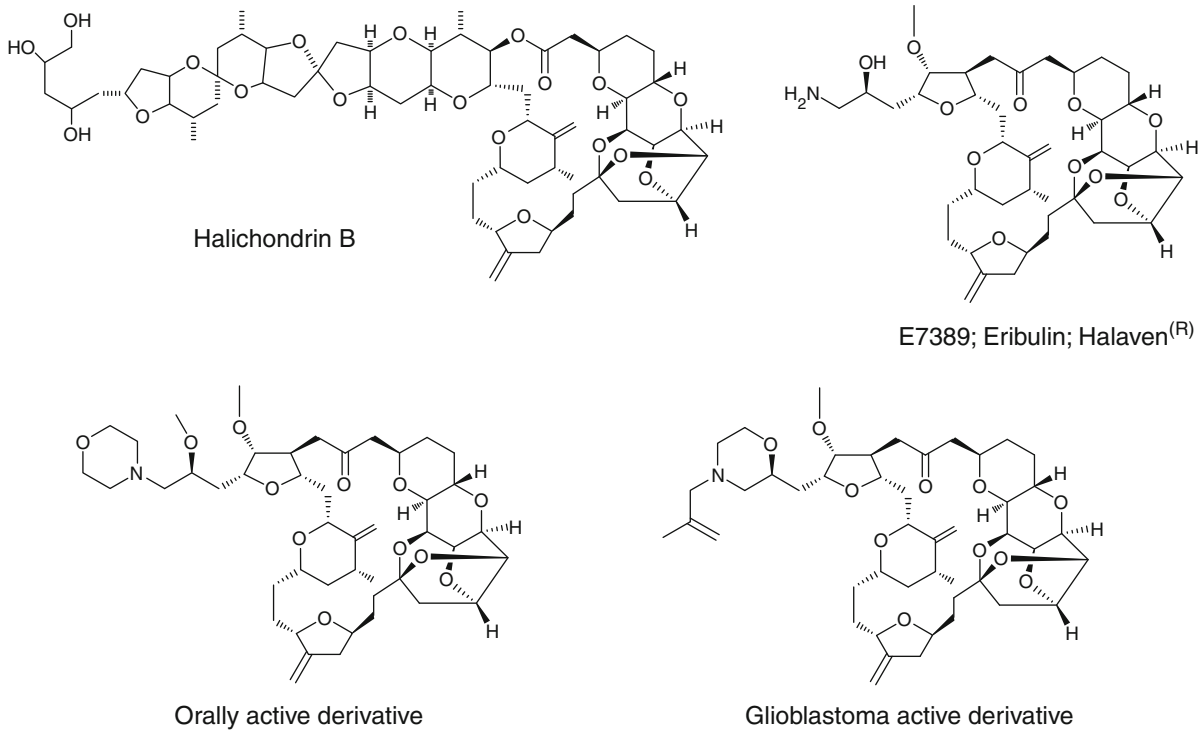

Drug Discovery in Ocean. Figure 4
Halichondrin B and the totally synthetic compounds derived from its structure

based upon the synthetic method for halichondrin B first reported by Kishi's group in 1992 [56]. During this synthesis and the investigation by scientists at the Eisai Research Institute (ERI) in Woburn, MA of the synthetic intermediates, Kishi and ERI scientists realized that the active part of the molecule resided in the macrolide ring (approx MW of 600) and not in the "tail" (the remaining 400 + of the overall 1,000 + MW). Chemists at the ERI, working very closely with the Kishi's group, synthesized over 200 molecules and, in conjunction with the Developmental Therapeutics Program (DTP) at NCI, they chose the modified truncated macrocyclic ketone (E7389) (Fig. 4) as the candidate compound when compared in in vitro and in vivo studies to pure halichondrin B (obtained by DTP in conjunction with New Zealand scientists). Much fuller details of the synthetic and base biological information were published by the leaders of the synthetic studies in 2005 [57]. This review article should be read by the interested reader for fuller details of the evolution of this compound through early 2005.

Eribulin, as with the "natural product parent," is a tubulin-interactive agent with very potent activity at the nanomolar level in in vitro studies. In 2005, Jordan et al. [58] reported that suppression of microtubule growth was the primary antimitotic mechanism of E7389 with differential effects due to concentration when studied in MCF7 cells. At low concentrations eribulin, potently inhibited microtubule dynamics resulting in prolonged arrest of mitosis and inducing apoptosis, whereas at tenfold the IC_{50} value (or higher concentrations), it induced depolymerization [58, 59] with extension of the experiments to demonstrate eribulin's interaction with centromere dynamics [60].

Within the same time frame, Jordan's group and others expanded studies to demonstrate that E7389/eribulin and halichondrin B could be modeled into a site close to the vinca site in tubulin [61] which was extended by use of analytical ultracentrifugation experiments by Alday and Correia [62]. Their data strongly suggested that eribulin is a strong inhibitor of the 1:2 stathmin-tubulin complex, and may also be a global inhibitor of tubulin polymer formation as a result of

disruption of tubulin–tubulin contacts at the interdimer interface. Also of interest in this work was the discovery that the penultimate precursor of eribulin (ER-076349), where the terminal amino group is an hydroxyl, is not as potent an inhibitor of the stathmin-tubulin complex formation as eribulin. Though it too, perturbs tubulin–tubulin contacts, it appears to have a more direct effect upon the tubulin polymer.

That the actual interaction of eribulin with tubulin may be even more complex than was originally thought is shown by the recent data reported by Jordan's group in a 2010 paper [63]. By using ^{3}H-eribulin, they reported a very high affinity site (K_d 400 ± 200 nM) on 25% of the tubulin mass (which might be the $\alpha\beta_{III}$ tubulin dimer) with a stoichiometry of 0.26 ± 0.12 moles of eribulin per tubulin dimer. Another high affinity site (K_d 3.5 ± 0.6 μM, stoichiometry of 14.7 ± 1.3 eribulin-tubulin dimer) was also identified together with a low affinity site ($K_d \sim 46 \pm 28$ μM, stoichiometry of 1.3 ± 0.4 saturable sites per tubulin dimer).

The binding isotherm from these results is highly complex which might well be due to competition for eribulin between soluble tubulin and microtubules, though there is photo and electron micrographic evidence in the paper, and in earlier ones from the same group, for binding to the plus end of microtubules and preferentially to β-tubulin. This is concordant with the ultracentrifugation data reported above [62]. As mentioned in the Smith et al. paper [63], further experimentation will be necessary in order to explain these complex results, including the inhibition of eribulin binding to microtubules in vitro by vinblastine when the eribulin concentration is <5 μM versus the reverse when >5 μM.

In the last 2 years or so, there have been three publications from the Kishi's group detailing improved methods for the synthesis of eribulin and, though written from an academic perspective, these papers consider the relative costs of production [64–66]. In addition, there was a 2007 review by Wang et al. [67] that gave extensive coverage of the patent routes to eribulin, with some duplication of the work presented in the 2005 review by Yu et al. [57]. This was followed in early 2009 by two excellent review articles from the Phillips group at the University of Colorado, covering the published syntheses by many groups of halichondrin B, norhalichondrin B, and E7389 [68, 69].

Very recently, three papers have been published by the Eisai group demonstrating that with only a relatively minor change to the "tail" of the molecule (Fig. 4), the base structure now had a much lower propensity for inducing P-glycoprotein susceptibility, when the diol that is the eribulin precursor was changed to either the dimethoxy substituent or the terminal amino group was changed to a methoxy group. Both compounds were potent in vivo and had a reduction of approximately 30-fold in terms of being substrates for P-glycoprotein compared to eribulin [70].

Continuing on with the eribulin studies, the Eisai group then demonstrated that by substituting a morpholine for the terminal amino group and changing the sidechain hydroxyl group to a methoxyl, the compound (Fig. 4) demonstrated oral activity in a subcutaneous LOX melanoma model and maintained a low susceptibility to P-glycoprotein induction [71].

Since there are very few treatments for brain tumors, the group then modified the base eribulin molecule by ring closure at the "tail" to give another morpholino derivative (Fig. 4). This molecule was subtly different from the orally active compound referred to above, and this molecule demonstrated intravenous in vivo activity in an orthotopic murine model of a human glioblastoma [72].

Although it effectively took from the original report on halichondrin B in 1985 until late 2010 to approve eribulin, the interplay of academic, industrial, and government laboratories in three continents led to the novel agent, perhaps the most complex drug molecule yet produced by total synthesis, but what is also of great import is that without the structure of the halichondrin B from a Japanese sponge and the subsequent purification of halichondrin B by NZ scientists and the NCI, eribulin would not have been approved, nor would, the very interesting and novel agents referred to in the preceding three paragraphs, have been synthesized.

Agents in Clinical Trials

Aplidine (Plitidepsin) Aplidin which is formally dehydrodidemnin B (Fig. 5), and thus, a very close chemical relative of the first direct-from-the-sea antitumor compound didemnin B (Fig. 5), was

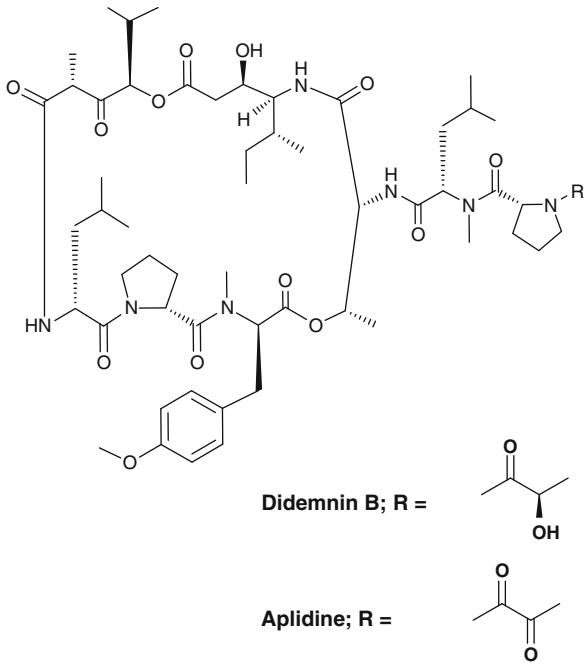

Drug Discovery in Ocean. Figure 5
Two compounds differing by two hydrogen atoms

originally isolated from *Aplidium albicans* and first reported in a patent application in 1989, with an UK patent issued in 1990. It was formally identified in the chemical literature in a paper from Rinehart's group in 1996 [73] on the structure-activity relationships among the didemnins. The earlier work on aplidin, its entry into phase I and II trials and the preferred method of synthesis, was described in detail through late 2004 by PharmaMar scientists [47]. At that time, the dose-limiting toxicity was muscle pain responsive to either dose limitation or addition of carnitine. Interestingly, in the presence of carnitine, the maximum tolerated dose could be increased by 40% to 7 mg/m^2. Since those earlier reports, significant numbers of phase I and II trials have been reported and or initiated in the USA and Europe. Currently, this agent is in three clinical trials listed in the NCI clinical trials database, including one phase III trial with or without dexamethasone against resistant multiple myeloma.

The precise MOA of this agent is not yet fully described, but it appears to block the vascular endothelial growth factor (VEGF) secretion and blocks the corresponding VEGF-Receptor-1 (also known as Flt1) autocrine loop in leukemic cells [74]. Using data from a series of ex vivo studies with leukemic blasts from pediatric and adult patients where cells underwent massive apoptosis at levels of 5 nM below the blood levels achievable in man [75], workers at PharmaMar developed a pharmacogenomic model that led to a molecular fingerprint for sensitivity to this agent using the "Oncochip" array. Full details are given in the 2006 paper [52]. Recently, a thorough analysis of the data available to PharmaMar scientists and their collaborators on the MOA of this agent was published, but even today, the exact mechanisms have not been identified, though effects upon the VEGF system are noted, together with the potential involvement of lipid rafts in cellular membranes [76].

What is interesting both chemically and pharmacologically is that the removal of two hydrogen atoms, i.e., conversion of a lactyl side chain in didemnin B to a pyruvyl side chain in aplidin, appears to significantly alter the toxicity profile as this is the only formal change between the two structures. However, the comments on dosage regimens for didemnin B from Vera and Joullie [77] should perhaps be taken into account in any future comparisons.

Kahalalide F This cyclic depsipeptide (Fig. 6) was first isolated as part of a number of similar molecules from the Sacoglossan mollusk, *Elysia rufescens*, after the mollusk grazed on the green macroalga *Bryopsis* sp. After isolation and identification from the invertebrate, it was discovered that the depsipeptide also occurred in the alga, but at a much lower weight basis when compared to the yield from the mollusk. Thus, the invertebrate significantly (20-fold or better) concentrated the depsipeptides [78]. The compound was licensed to PharmaMar by the University of Hawaii in the 1990s, and it entered preclinical testing. Using solid-phase peptide techniques, the compound was synthesized in a very efficient manner by a group in the chemistry department at the University of Barcelona [79], and kahalalide F entered phase I clinical trials in Europe in December 2000 for the treatment of androgen-independent prostate cancer.

A variety of mechanisms have been attributed to this compound. It was known to target lysosomes [80], which implied a selectivity for tumor cells such as prostate tumors that exhibited a high lysosomal

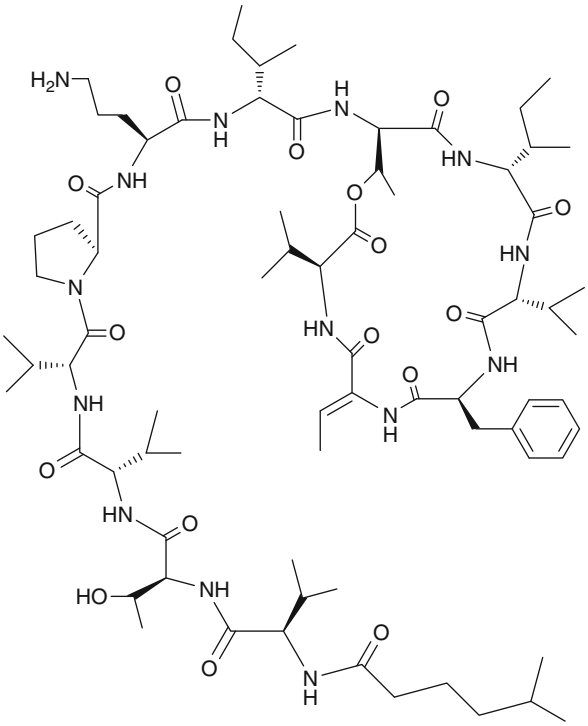

Drug Discovery in Ocean. Figure 6
Kahalalide F, A depsipeptide produced by an algal endophytic marine bacterium

activity. In addition, Suarez et al. [81] reported that kahalalide F induced cell death via "oncosis" (defined as the progression of cellular processes leading to necrotic cell death) possibly initiated by lysosomal membrane depolarization in both prostate and breast cancer cell lines. This was followed in 2005 by a report by Sewell et al. [82] that HepG2 cells treated with 300 nM kahalalide F demonstrated significant alterations in their membrane permeability, which was manifested as cell swelling and/or blebbing, thus implying specific interactions with membranes and/or proteins at this concentration. In 2005, it was reported that it induced a necrosis-like cell death that involved inhibition of Akt signaling and depletion of ErbB3 [83]. Extension of this work was reported in 2006, when it was suggested that ErbB3 may well be a marker for progress against suitable tumor types in patients and also implied that an ErbB3 kinase inhibitor may well increase efficacy [52].

In 2005, a PCT International Application was filed by Hill et al. [84], claiming production of kahalalide F and other derivatives from a Vibrio species isolated from *Bryopsis* and also *Elysia rufesens*. This report implied that the invertebrate obtained the producing microbe from the alga and then maintained the microbe(s) as symbionts [84]. Accordingly, there may well be a potential renewable source of these agents by use of microbial fermentation.

Although the compound went into phase II, clinical trials for cancer, it is currently in phase II clinical trials as a potential treatment for severe psoriasis, and over the last 2 years, two interesting papers have been published by PharmaMar scientists and/or their Spanish collaborators demonstrating that it is relatively easy to make over a 100 analogs with a variety of in vitro activities using solid state peptide synthesis techniques once the base structure was synthesized [85].

In addition to the antitumor and antipsoriasis activities reported above, it turns out that as well as having antifungal activity reported by one of the original discoverers of the class [86], in 2009, Cruz et al. reported that the molecule is also active against leishmanial infections [87].

Finally, Hawaii is not the only area with these peptides. Ashour et al. [88] reported new cyclic peptides of this class from the Indian Ocean mollusk, *Elysia grandifolia* and claimed a higher cytotoxicity in vitro than was reported for kahalalide F.

Zalypsis® (PM00104) This molecule (Fig. 7) is a "chemical cousin" of ET-743 (Yondelis®) though it is based upon the structures of two similar compound classes found in either mollusks (Jorumycin) (Fig. 7) or sponges (Renieramycin) (Fig. 7) [89–91]. PM00104 (Fig. 7) was derived from the base structure by subtle modifications and placed into preclinical and clinical trials by PharmaMar. It is currently in phase II trials against Ewing's sarcoma and endometrial and cervical cancers under PharmaMar auspices.

A fair number of papers dealing with the biochemical and pharmacological properties of PM00104 have recently been published [92, 93] together with an interesting report on the cross-resistance patterns demonstrated with paclitaxel and doxorubicin-resistant lines. It was shown that the expression of selected resistance markers does not correlate with the patterns shown

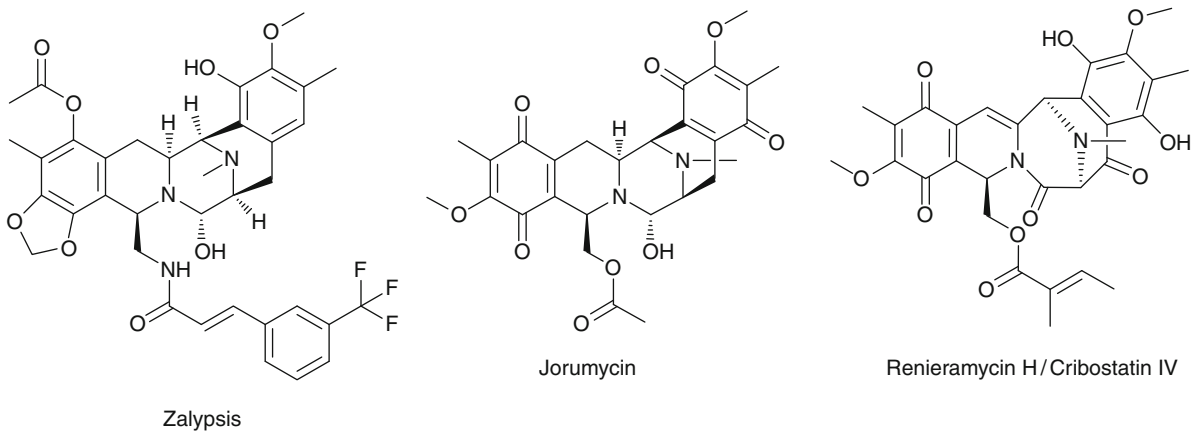

Drug Discovery in Ocean. Figure 7
Chemical cousins of trabectedin

with trabectedin and PM00104, and thus, subtly different genetic processes are involved with these two chemically similar compounds [94]. In addition, Pommier's group recently demonstrated that this compound and ET-743 differ in their interaction with DNA, with PM00104 demonstrating induction of a γ-H2AX response at nanomolar concentrations in Ewing's sarcoma cell lines; this observation suggests that PM00104 could serve as a pharmacodynamic marker for further clinical development of this agent in that particular cancer [95].

Salinosporamide A Salinosporamide A (Fig. 8) and the number of "chemical relatives" that have been reported since 2003 are vindication of an hypothesis that Fenical and Jensen had in the late 1980s to early 1990s that free-living microbes in the ocean or ocean sediments, in addition to those intimately involved with invertebrates, could produce compounds with pharmacologic potential. As in the case of the compounds descried earlier, due primarily to the source(s) of funding being either the NCI or related institutes at NIH, most of the investigations were directed towards antitumor agents from a practical aspect; however, the organisms were also studied from a microbial perspective by looking at the positions of isolated viable microbes in phylogenetic trees and, even more importantly, the basic genomic sequence(s) of metabolite-producing microbes from these pioneering studies as time progressed and techniques became available.

Salinosporamide A and its mechanism of action as a novel proteasome inhibitor was first reported by the Fenical and Jensen laboratories at the Scripps Institute of Oceanography in 2003 [96]; it was subsequently licensed to a small biotech company, Nereus Pharmaceuticals in San Diego, California for development. The compound had an unusual chlorine substitution pattern and within a year or so of the original publication, two academic groups had synthesized the base molecule and this was soon followed by a synthesis paper from Nereus scientists [97]. Subsequently, many groups reported improved syntheses with an excellent 2007 review covering almost all of the early studies [98].

In what was a highly significant breakthrough, the cooperation between Nereus scientists and the then fermentation group at IRL in New Zealand led to the production of the necessary current Good Manufacturing Practices (cGMP) product for clinical trials; this cGMP involves large-scale fermentation in a saline environment, the first time that this task had been successfully performed on any scale with a marine microbe. During these preparative studies, a significant number of other salinosporamide derivatives and other secondary metabolites were further explored [99–103]. Concomitantly, the mechanism of salinosporamide as a proteasome inhibitor was worked out using excellent X-ray crystallographic studies [104] together with studies on the stability of the β-lactone ring [105].

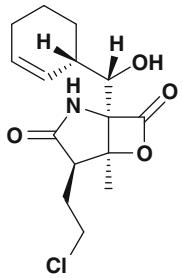

Salinosporamide A

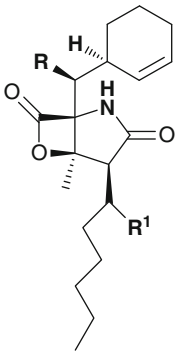

Cinnabaramide A; R = OH, R^1 = H
Cinnabaramide B; R = R^1 = OH
Cinnabaramide C; R = R^1 = H

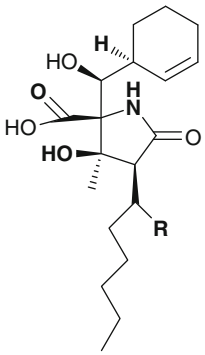

Cinnabaramide D; R = OH
Cinnabaramide E; R = H

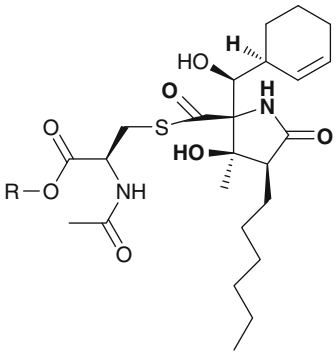

Cinnabaramide F; R = H
Cinnabaramide G; R = CH_3

Drug Discovery in Ocean. Figure 8
Marine and terrestrial proteasome inhibitors from microbes

In 2007, an interesting paper [106] was published on the isolation of similar molecules, the cinnabaramides A-G (Fig. 8), from a terrestrial microbial source, which was followed the same year by a number of papers on the genomic aspects of the salinosporamide A producing organism, *Salinispora tropica*. Inspection of the complete genomic sequence of *S. tropica* demonstrated that these marine streptomycetes, as with their terrestrial cousins, have many more "currently unexpressed" secondary metabolite clusters in their genomes, thus demonstrating that they are as biochemically diverse as the quintessential terrestrial microbe *S. coelicolor* [107, 108]. It was further reported that the *S. tropica* genome encodes for a very unusual chlorinase that can be substituted by other halogens [109].

Within the last 2 years, three excellent reviews have been published on salinosporamides. Two cover the initial discovery and drug potential from the industrial (Nereus Pharma) aspect [110, 111] and the other covers biosynthetic and genomic processes as well as syntheses [112]. Both of the 2010 reviews should be read by those interested in this subject as they complement each other.

In a recent publication in the journal *Blood*, Nereus scientists and collaborators at the Harvard Medical School reported that salinosporamide demonstrated both in vitro and in vivo synergistic activities with lenalidomide (the thalidomide analog currently in clinical use) in multiple myeloma models, thus, potentially expanding clinical models with salinosporamide in due course [113].

Salinosporamide A entered phase I clinical trials in May of 2006 initially against solid tumors and leukemias and in April of 2007, another phase I trial against multiple myeloma was initiated. Currently, there are four phase I trials still listed as recruiting in the clinical trials data base, with one involving the use of the

histone deacetylase (HDAC) inhibitor vorinostat in conjunction with salinosporamide A.

Anti-infective Agents

Introduction

To date, there have been no anti-infective agents from marine sources that have been approved by any governmental organization equivalent to the US FDA. However, over the last 10 plus years, as funding became available, scientists have extended their searches for biologically active metabolites from marine sources into the areas of antiviral and antibacterial agents with most of the initial systematic studies being offshoots of antitumor investigations. Later studies are now being funded in anti-infective areas as a result of some of these earlier results.

In this section, antiviral agents and antiparasitic agents are dealt with, and the section finishes with studies on antimicrobial agents against both bacteria and fungi. It again needs to be emphasized that these are not yet clinical studies. In some cases, particularly in the case of anti-HIV agents, some materials are close to a version of clinical trials.

Antiviral Agents

Griffithsin This agent, first reported in 2005, was isolated from the red alga *Griffithsia* sp., and it was shown to be a 121-residue peptide that was subsequently produced by transfer of the DNA sequence corresponding to the peptide and expressed in *E. coli* [114]. The material, either natural or recombinant, was ultimately shown to bind to specific mannose-rich regions of HIV viral proteins [115]. In 2009, it was reported that the compound could function as a topical microbicide with potential as an intravaginal agent to protect against HIV transmission [116]. Since that publication, O'Keefe et al. [117] have continued their work with griffithsin and demonstrated that it has significant activity against a variety of human viral diseases, including the SARS virus [117]. In addition, recently, Moulaei et al. [118] further elucidated its activity against HIV entry. Then, from meeting reports that are not formally cited, griffithsin was reported to have activity against Ebola in a murine in vivo model [119].

Antiparasitic Agents

Salinosporamide A In a paper published in 2008, Prudhomme et al., following testing of over 80 bacterial extracts and the pure marine-derived compound salinosporamide A (Fig. 8), demonstrated that this agent had significant activity against the erythrocytic stage of malaria, probably due to inhibition of the parasite's proteasome with an overall activity comparable to that of regular antimalarials such as chloroquin [120].

Other Agents In 2009, Fattoruso and Taglialatela-Scafati published an excellent review of the many marine-derived structures, including manzamine A (Fig. 9) derivatives that have demonstrated activity either in in vitro *or in vivo* models relevant to malaria [121]. Manzamine A (Fig. 9) and derivatives, though originally from a deepwater Indonesian sponge, are almost certainly produced by a commensal microbe and have shown activity in vivo against malarial models [122]. To date, however, no agents from marine sources have entered clinical trials.

Antibacterial or Fungal Agents

Since testing for antibacterial activities is a relatively simple and cheap operation, at least at the initial stage

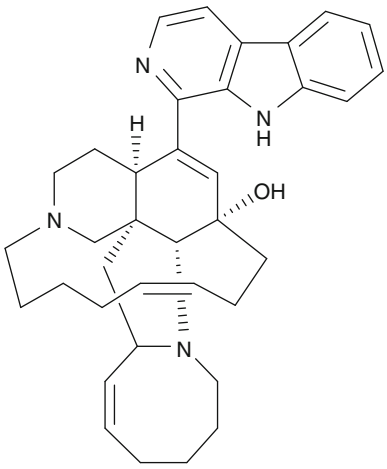

Drug Discovery in Ocean. Figure 9
Potential antiparasitic base structure from a deep water sponge

with crude extracts (simple disk diffusion assays against microbial lawns), a large number of groups have reported some antimicrobial activities for marine-derived structures. However, apart from some small companies and academic groups, no systematic investigations have yet been reported with marine-derived agents.

Fenical's group, among others, have realized the potential that is present in looking at invertebrate and marine microbial sourced extracts and compounds, and in a recent review article, they have demonstrated the potential for such a systematic investigation [123]. Obviously, they are not alone in this field. The 2007 review by Bull and Stach [124] and the very recent review on the biosynthetic potential of marine microbes from a genomic aspect must be read [125].

Ziconotide, Cone Snail Toxin

The fundamental work by Olivera et al. [126] on the peptide neurotoxins from fish-hunting cone snails led, over the next 20 years, to a massive amount of information as to the sources, utility in both the snail, and potential human use and to the first drug that was effectively directly from the sea as a human use pharmaceutical. This is the 25 residue highly cross-linked peptide known as ziconotide (Fig. 10), which was approved for severe chronic pain in 2005. Although ziconotide is made synthetically, it is chemically and biologically identical to the natural toxin.

The role of the *Conus* peptides in nature is as a method of paralyzing prey in order for the snail to be able to feed. From the information developed, mainly based on the pioneering work of Olivera's group, it is now only a matter of time before other cone snail-based drugs against a variety of disease of man will be coming out of clinical trials. That one can modify the base structure(s) and still maintain the desired activities, can be seen by the report from Craik's laboratories in Australia [127, 128], and when coupled to their predictive database of structures and potential pharmacology, the opportunities for the future development are significant [129].

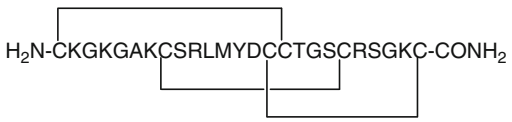

Ziconotide

Drug Discovery in Ocean. Figure 10
Cone snail toxin. Letters correspond to amino acids (www.biology.arizona.edu/biochemistry/problem_sets/aa/Dayhoff.html)

Future Directions

By its very nature, this article can only just "scratch the surface" of the potential for drug discovery from marine sources. As the understanding of the involvement of microbes of all domains expands, then it is highly probable that over the next decade or two, marine-sourced materials will be the building blocks, both literally and as leads to novel chemical structures, that will add to the armamentarium of drugs in areas that are in desperate need of novel agents.

If one looks at the multitude of reports on resistance to drugs by disease entities in anti-infective and antitumor areas to name but a few, then the absolute requirement for novel agents with new MOAs is quite apparent. That the marine area is a viable source for searching for such agents against a multitude of human diseases is now quite apparent as even though the costs and difficulties are very high, a significant number of the compounds that have been referred to in this chapter are completely different in their structures from anything yet found in terrestrial environments.

Bibliography

Primary Literature

1. Ramirez-Llodra E, Brandt A, Danovaro R, De Mol B, Escobar E, German CR, Levin LA, Martinez Arbizu P, Menot L, Buhl-Mortensen P, Narayanaswamy BE, Smith CR, Tittensor DP, Tyler PA, Vanreusel A, Vecchione M (2010) Deep, diverse and definitely different: unique attributes of the world's largest ecosystem. Biogeosciences 7:2851–2899
2. Arrieta JM, Arnaud-Haond S, Duarte CM (2010) What lies underneath: conserving the oceans' genetic resources. Proc Natl Acad Sci USA 107:18318–18324
3. Gage JD, Tyler PA (1991) Deep-sea biology: a natural history of organisms at the deep-sea floor. Cambridge University Press, Cambridge
4. Hagiwara H, Numata M, Konishi K, Oka Y (1965) Synthesis of nereistoxin and related compounds I. Chem Pharm Bull 13:253–260

5. Ruggieri GD (1976) Drugs from the sea. Science 194:491–497
6. Suckling CJ (1991) Chemical approaches to the discovery of new drugs. Sci Prog 75:323–359
7. Newman DJ, Cragg GM, Snader KM (2000) The influence of natural products upon drug discovery. Nat Prod Rep 17: 215–234
8. Bergmann W, Feeney RJ (1950) Isolation of a new thymine pentoside from sponges. J Am Chem Soc 72:2809–2810
9. Bergmann W, Feeney RJ (1951) Marine products XXXII. The nucleosides of sponges. I. J Org Chem 16:981–987
10. Bergmann W, Burke DC (1955) Marine products XXXIX. The nucleosides of sponges. III. Spongothymidine and spongouridine. J Org Chem 20:1501–1507
11. Flahive E, Srirangam J (2005) The dolastatins: novel antitumor agents from *Dolabella auricularia*. In: Cragg GM, Kingston DGI, Newman DJ (eds) Anticancer agents from natural products. Taylor and Francis, Boca Raton, pp 191–213
12. Newman DJ (2005) The bryostatins. In: Cragg GM, Kingston DGI, Newman DJ (eds) Anticancer agents from natural products. Taylor and Francis, Boca Raton, pp 137–150
13. Hale KJ, Manaviazar S (2010) New approaches to the total synthesis of the bryostatin antitumor macrolides. Chem Asian J 5:704–754
14. Alkon DA, Sun M-K, Nelson TJ (2006) PKC signaling deficits: a mechanistic hypothesis for the origins of Alzheimer's disease. Trends Pharmcal Sci 28:51–60
15. Etcheberrigaray R, Tan M, Dewachtert I, Kuipéri C, Van Der Auwera I, Wera S, Qiao L, Bank B, Nelson TJ, Kozikowski AP, Van Leuven F, Alkon DL (2004) Therapeutic effects of PKC activators in Alzheimer's disease transgenic mice. Proc Natl Acad Sci USA 101:11141–11146
16. Montaner J (2006) Latest advances and research in stroke: focus on diagnostic and therapeutic targets. Drug News Perspect 19:173–193
17. Sun M-K, Alkon DL (2006) Bryostatin-1: pharmacology and therapeutic potential as a CNS drug. CNS Drug Rev 12:1–8
18. Wang D, Darwish DS, Schreurs BG, Alkon DL (2008) Analysis of long-term cognitive-enhancing effects of bryostatin-1 on the rabbit (*Oryctolagus cuniculus*) nictitating membrane response. Behav Pharmacol 19:245–256
19. Khan TK, Nelson TJ, Verma VA, Wender PA, Alkon DA (2009) A cellular model of Alzheimer's disease therapeutic efficacy: PKC activation reverses A beta-induced biomarker abnormality on cultured fibroblasts. Neurobiol Dis 34:332–339
20. Davidson SK, Allen SW, Lim GE, Anderson CM, Haygood MG (2001) Evidence for the biosynthesis of bryostatins by the bacterial symbiont "*Candidatus* Endobugula sertula" of the bryozoan *Bugula neritina*. Appl Environ Microbiol 67: 4531–4537
21. Davidson SK, Haygood MG (1999) Identification of sibling species of the bryozoan *Bugula neritina* that produce different anticancer bryostatins and harbor distinct strains of the bacterial symbiont "*Candidatus* Endobugula sertula". Biol Bull 196:273–280
22. Haygood MG (2003) The role of a bacterial symbiont in the biosynthesis of bryostatins in the marine bryozoan *Bugula neritina*. Abstract paper 6th international marine biotechnology conference abstract S5-2A-K
23. Haygood MG, Davidson SK (1997) Small-subunit rRNA genes and in situ hybridization with oligonucleotides specific for the bacterial symbionts in the larvae of the bryozoan *Bugula neritina* and proposal of 'Candidatus Endobugula sertula'. Appl Environ Microbiol 63:4612–4616
24. Hildebran M, Waggoner LE, Lim GE, Sharp KH, Ridley CP, Haygood MG (2004) Approaches to identify, clone and express symbiont bioactive metabolite genes. Nat Prod Rep 21:122–142
25. Hildebrand M, Waggoner LE, Liu H, Sudek S, Allen S, Anderson C, Sherman DH, Haygood M (2004) *bryA*: an unusual modular polyketide synthase gene from the uncultivated bacterial symbiont of the marine bryozoan *Bugula neritina*. Chem Biol 11:1543–1552
26. Lim GE, Haygood MG (2004) *Candidatus* Endobugula glebosa, a specific bacterial symbiont of the marine bryozoan *Bugula simplex*. Appl Environ Microbiol 70(8):4921–4929
27. Lim-Fong GE, Regali LA, Haygood MG (2008) Evolutionary relationships of "*Candidatus Endobugula*" bacterial symbionts and their *Bugula* bryozoan hosts. Appl Environ Microbiol 74:3605–3609
28. Lopanik N, Targett NM, Lindquist N (2006) Isolation of two polyketide synthase gene fragments from the unclutured microbial symbiont of the marine bryozoan *Bugula neritina*. Appl Environ Microbiol 72:7941–7944
29. Lopanik NB, Shields JA, Buchholz TJ, Rath CM, Hothersall J, Haygood MG, Håkansson K, Thomas CM, Sherman DH (2008) In vivo and in vitro trans-acylation by *bryP*, the putative bryostatin pathway acyltransferase derived from an uncultured marine symbiont. Chem Biol 15:1175–1186
30. Sudek S, Lopanik NB, Waggoner LE, Hildebrand M, Anderson C, Liu H, Patel A, Sherman DH, Haygood MG (2007) Identification of the putative bryostatin polyketide synthase gene cluster from "*Candidatus Endobugula sertula*", the uncultivated microbial symbiont of the marine bryozoan *Bugula neritina*. J Nat Prod 70:67–74
31. Zimmermann K, Engeser M, Blunt JW, Munro MHG, Piel J (2009) Pederin-type pathways of uncultivated bacterial symbionts: analysis of O-methyltransferases and generation of a biosynthetic hybrid. J Am Chem Soc 131:2780–2781
32. Mitchell SS, Faulkner DJ, Rubins K, Bushman FD (2000) Dolastatin 3 and two novel cyclic peptides from a palauan collection of *Lyngbya majuscula*. J Nat Prod 63:279
33. Luesch H, Moore RE, Paul VJ, Mooberry SL, Corbett TH (2001) Isolation of dolastatin 10 from the marine cyanobacterium *Symploca* species VP642 and total stereochemistry and biological evaluation of its analogue symplostatin 1. J Nat Prod 64:907
34. Harrigan GG, Yoshida WY, Moore RE, Nagle DG, Park PU, Biggs J, Paul VJ, Mooberry SL, Corbett TH, Valeriote FA (1998) Isolation, structure determination, and biological activity of dolastatin 12

and lyngbyastatin I from *Lyngbya majuscula/Schizothrix calcicola* cyanobacterial assemblages. J Nat Prod 61:1221
35. Nogle LM, Williamson RT, Gerwick WH (2001) Somamides A and B, two new depsipeptide analogues of dolastatin 13 from a Fijian cyanobacterial assemblage of *Lyngbya majuscula* and *Schizothrix* species. J Nat Prod 64:716
36. Nogle LM, Gerwick WH (2002) Isolation of four new cyclic depsipeptides, antanapeptins A-D, and dolastatin 16 from a Madagascan collection of *Lyngbya majuscula*. J Nat Prod 65:21
37. Harrigan GG, Luesch H, Yoshida WY, Moore RE, Nagle DG, Paul VJ, Mooberry SL, Corbett TH, Valeriote FA (1998) Symplostatin 1: a dolastatin 10 analogue from the marine cyanobacterium *Symploca hydnoides*. J Nat Prod 61:1075
38. Harrigan GG, Luesch H, Yoshida WY, Moore RE, Nagle DG, Paul VJ (1999) Symplostatin 2: a dolastatin 13 analogue from the marine cyanobacterium *Symploca hydnoides*. J Nat Prod 62:655
39. Luesch H, Yoshida WY, Moore RE, Paul VJ, Mooberry SL, Corbett TH (2002) Symplostatin 3, a new dolastatin 10 analogue from the marine cyanobacterium *Symploca* sp VP452. J Nat Prod 65:16
40. Siemann DW (2011) The unique characteristics of tumor vasculature and preclinical evidence for its selective disruption by Tumor-Vascular Disrupting Agents. Cancer Treat Rev 31:63–74
41. Patel S, Keohan ML, Saif MW, Rushing D, Baez L, Feit K, DeJager R, Anderson S (2006) Phase II study of intravenous TZT-1027 in patients with advanced or metastatic soft-tissue sarcomas with prior exposure to anthracycline-based chemotherapy. Cancer 107:2881–2887
42. Riely GJ, Gadgeel S, Rothman I, Saidman B, Sabbath K, Feit K, Kris MG, Rizvi NA (2007) A phase 2 study of TZT-1027, administered weekly to patients with advanced non-small cell lung cancer following treatment with platinum-based chemotherapy. Lung Cancer 55(2):181–185
43. Carter NJ, Keam SJ (2010) Trabectedin: a review of its use in soft tissue sarcoma and ovarian cancer. Drugs 70(3):355–376
44. Poveda A, Vergote I, Tjulandin S, Kong B, Roy M, Chan S, Filipczyk-Cisarz E, Hagberg H, Kaye SB, Colombo N, Lebedinsky C, Parekh T, Gómez J, Park YC, Alfaro V, Monk BJ (2011) Trabectedin plus pegylated liposomal doxorubicin in relapsed ovarian cancer: outcomes in the partially platinum-sensitive (platinum-free interval 6–12 months) subpopulation of OVA-301 phase III randomized trial. Ann Oncol 22:39–48
45. Rinehart K, Holt TG, Fregeau NL, Stroh JG, Kiefer PA, Sun F, Li LH, Martin DG (1990) Ecteinascidins 729, 743, 745, 759A, 759B and 770: potent antitumor agents from the Caribbean tunicate *Ecteinascidia turbinata*. J Org Chem 55:4512–4515
46. Wright AE, Forleo DA, Gunawardana GP, Gunasekera SP, Koehn FE, McConnell OJ (1990) Antitumor tetrahydroisoquinoline alkaloids from the colonial ascidian *Ecteinascidia turbinata*. J Org Chem 55:4508–4512
47. Henriquez R, Faircloth G, Cuevas C (2005) Ecteinascidin 743 (ET-743; Yondelis™), aplidin, and kahalalide F. In: Cragg GM, Kingston DGI, Newman DJ (eds) Anticancer agents from natural products. Taylor and Francis, Boca Raton, pp 215–240
48. Velasco A, Acebo P, Gomez A, Schleissner C, Rodriguez P, Aparicio T, Conde S, Munoz R, de la Calle F, Garcia JL, Sanchez-Puelles JM (2005) Molecular characterization of the safracin biosynthetic pathway from *Pseudomonas fluorescens* A2-2: designing new cytoxic compounds. Mol Microbiol 56:144–154
49. Moss C, Green DH, Perez B, Velasco A, Henriquez R, McKenzie JD (2003) Intracellular bacteria associated with the ascidian *Ecteinascidia turbinata*: phylogenic and in situ hybridization analysis. Mar Biol 143:99–110
50. Perez-Matos AE, Rosado W, Govind NS (2007) Bacterial diversity associated with the Caribbean tunicate *Ecteinascidia turbinata*. Antonie van Leeuwenhoek 92:155–164
51. D'Incalci M, Galmarini CM (2010) A review of trabectedin (ET-743): a unique mechanism of action. Mol Cancer Ther 9:2157–2163
52. Jimeno J, Aracil M, Tercero JC (2006) Adding pharmacogenomics to the development of new marine-derived anticancer agents. J Transl Med 4:3
53. Soares DG, Escargueil AE, Poindessous V, Sarasin A, de Gramont A, Bonatto D, Henriques JAP, Larsen AK (2007) Replication and homologous recombination repair regulate DNA double-strand break formation by the antitumor alkylator ecteinascidin 743. Proc Natl Acad Sci USA 104:13062–13067
54. Marco E, David-Cordonnier M-H, Bailly C, Cuevas C, Gago F (2006) Further insight into the DNA recognition mechanism of trabectedin from the differential affinity of its demethylated analogue ecteinascidin ET729 for the triplet DNA binding site CGA. J Med Chem 49:6925–6929
55. Moneo V, Serelde BG, Fominaya J, Leal JFM, Blanco-Aparicio C, Romero L, Sanchez-Beato M, Cigudosa JC, Tercero JC, Piris MA, Jimeno J, Carnero A (2007) Extreme sensitivity to Yondelis(R) (Trabectedin, ET-743) in low passaged sarcoma cell lines correlates with mutated p53. J Cell Biochem 100:339–348
56. Aicher TD, Buszek KR, Fang FG, Forsyth CJ, Jung SH, Kishi Y, Matelich MC, Scola PM, Spero DM, Yoon SK (1992) Total synthesis of halichondrin B and norhalichondrin B. J Am Chem Soc 114:3162–3164
57. Yu MJ, Kishi Y, Littlefield BA (2005) Discovery of E7389, a fully synthetic macrocyclic ketone analog of halichondrin B. In: Cragg GM, Kingston DGI, Newman DJ (eds) Anticancer agents from natural products. Taylor and Francis, Boca Raton, pp 241–265
58. Jordan MA, Kamath K, Manna T, Okouneva T, Miller HP, Davis C, Littlefield BA, Wilson L (2005) The primary antimitotic mechanism of action of the synthetic halichondrin E7389 is suppression of microtubule growth. Mol Cancer Ther 4:1086–1095
59. Jordan MA, Kamath K (2007) How do microtubule-targeted drugs work? An overview. Curr Cancer Drug Targets 7:730–742
60. Okouneva T, Azarenko O, Wilson L, Littlefield BA, Jordan MA (2008) Inhibition of centromere dynamics by Eribulin (E7389) during mitotic metaphase. Mol Cancer Ther 7:2003–2011

61. Dabydeen DA, Burnett JC, Bai R, Verdier-Pinard P, Hickford SJH, Pettit GR, Blunt JW, Munro MHG, Gussio R, Hamel E (2006) Comparison of the activities of the truncated halichondrin B analog NSC 707389 (E7389) with those of the parent compound and a proposed binding site on tubulin. Mol Pharmacol 70:1866–1875
62. Allday PH, Correia JJ (2009) Macromolecular interaction of halichondrin B analogues eribulin (E7389) and ER-076349 with tubulin by analytical ultracentrifugation. Biochemistry 48:7927–7938
63. Smith JA, Wilson L, Azarenko O, Zhu X, Lewis BM, Littlefield BA, Jordan MA (2010) Eribulin binds at microtubule ends to a single site on tubulin to suppress dynamic instability. Biochemistry 49:1331–1337
64. Dong C-G, Henderson JA, Kaburagi Y, Sasaki T, Kim D-S, Kim JT, Urabe D, Guo H, Kishi Y (2009) New syntheses of E7389 C14-C35 and halichondrin C14-C38 building blocks: reductive cyclization and oxy-Michael cyclization approaches. J Am Chem Soc 131:15642–15646
65. Kim D-S, Dong C-G, Kim JT, Guo H, Huang J, Tiseni PS, Kishi Y (2009) New syntheses of E7389 C14-C35 and halichondrin C14-C38 building blocks: double-Inversion approach. J Am Chem Soc 131:15636–15641
66. Yang Y-R, Kim D-S, Kishi Y (2009) Second generation synthesis of C27-C35 building block of E7389, a synthetic halichondrin analogue. Org Lett 11:4516–4519
67. Wang Y, Serradell N, Bolos J, Rosa E (2007) Eribulin mesilate. Drugs Future 32:681–698
68. Jackson KL, Henderson JA, Phillips AJ (2009) The halichondrins and E7389. Chem Rev 109:3044–3079
69. Jackson KL, Henderson JA, Motoyoshi H, Phillips AJ (2009) A total synthesis of norhalichondrin B. Angew Chem Int Ed 48:2346–2350
70. Narayan S, Carlson EM, Cheng H, Du H, Hu Y, Jiang Y, Lewis BM, Seletsky BM, Tendyke K, Zhang H, Zheng W, Littlefield BA, Towle MJ, Yu MJ (2011) Novel second generation analogs of eribulin. Part I: compounds containing a lipophilic C32 sidechain overcome P-glycoprotein susceptibility. Bioorg Med Chem Lett 21:1630–1633
71. Narayan S, Carlson EM, Cheng H, Condon K, Du H, Eckley S, Hu Y, Jiang Y, Kumar V, Lewis BM, Saxton P, Schuck E, Seletsky BM, Tendyke K, Zhang H, Zheng W, Littlefield BA, Towle MJ, Yu MJ (2011) Novel second generation analogs of eribulin. Part II: orally available and active against resistant tumors in vivo. Bioorg Med Chem Lett 21:1634–1638
72. Narayan S, Carlson EM, Cheng H, Condon K, Du H, Eckley S, Hu Y, Jiang Y, Kumar V, Lewis BM, Saxton P, Schuck E, Seletsky BM, Tendyke K, Zhang H, Zheng W, Littlefield BA, Towle MJ, Yu MJ (2011) Novel second generation analogs of eribulin. Part III: blood-brain barrier permeability and in vivo activity in a brain tumor model. Bioorg Med Chem Lett 21:1639–1643
73. Sakai R, Rinehart KL, Kishore V, Kundu B, Faircloth G, Gloer JB, Carney JR, Manikoshi M, Sun F, Hughes RG Jr, Garcia-Gravalos D, Garcia de Quesada T, Wilson GR, Heid RM (1996) Structure-activity relationships of the didemnins. J Med Chem 39:2819–2834
74. Broggini M, Marchini SV, Galliera E, Borsotti P, Taraboletti G, Erba E, Sironi M, Jimeno J, Faircloth GT, Giavazzi R, D'Incalci M (2003) Aplidine, a new anticancer agent of marine origin, inhibits vascular endothelial growth factor (VEGF) secretion and blocks VEGF-VEGFR-1 (*flt-1*) autocrine loop in human leukemia cells MOLT-4. Leukemia 17:52–59
75. Erba E, Serafini M, Gaipa G, Tognon G, Marchini S, Celli N, Rotilio D, Broggini M, Jimeno J, Faircloth GT, Biondi A, D'Incalci M (2003) Effect of Aplidin in acute lymphoblastic leukaemia cells. Br J Cancer 89:763–773
76. Munoz-Alonzo MJ, Gonzalez-Santiago L, Martinez T, Losada A, Galmarini CM, Munoz A (2009) The mechanism of action of plitidepsin. Curr Opin Investig Drugs 10:536–542
77. Vera M, Joullie MM (2002) Natural products as probes of cell biology: 20 years of didemnin research. Med Res Rev 22:102–145
78. Hamann MT, Otto CS, Scheuer PJ, Dunbar DC (1996) Kahalalides: bioactive peptides from a marine mollusk *Elysia rufescens* and its algal diet *Bryopsis* sp. J Org Chem 61:6594–6600
79. Lopez-Macia A, Jimenez JC, Royo M, Giralt E, Alberico F (2001) Synthesis and structure determination of kahalalide F. J Am Chem Soc 123:11398–11401
80. Garcia-Rocha M, Bonay P, Avila J (1996) The antitumoral compound kahalalide F acts on cell lysosomes. Cancer Lett 99:43–50
81. Suarez Y, Gonzalez L, Cuadrado A, Berciano M, Lafarga M, Munoz A (2003) Kahalalide F, a new marine-derived compound, induces oncosis in human prostate and breast cancer cells. Mol Cancer Ther 2:863–872
82. Sewell JM, Mayer I, Langdon SP, Smyth JF, Jodrell DI, Guichard SM (2005) The mechanism of action of kahalalide F: variable cell permeability in human hepatoma cell lines. Eur J Cancer 41:1637–1644
83. Janmaat ML, Rodriguez JA, Jimeno J, Kruyt FAE, Giaccone G (2005) Kahalalide F induces necrosis-like cell death that involves depletion of ErbB3 and inhibition of Akt signaling. Mol Pharmacol 68:502–510
84. Hil RT, Hamann MT, Enticknap J, Karumanchi V (2005) Kahalalide-producing bacteria and methods of identifying kahalalide-producing bacteria and producing kahalalides. WO 2005042720
85. Jimenez JC, Lopez-Macia A, Gracia C, Varon S, Carrascal M, Caba JM, Royo M, Francesch AM, Cuevas C, Giralt E, Alberico F (2008) Structure-activity relationship of kahalalide F synthetic analogues. J Med Chem 51:4920–4931
86. Shilabin AG, Kasanah N, Wedge DE, Hamann MT (2007) Lysosome and HER3 (ErbB3) selective anticancer agent kahalalide F: semisynthetic modifications and antifungal lead exploration studies. J Med Chem 50:4340–4350
87. Cruz LJ, Luque-Ortega JR, Rivas L, Alberico F (2009) Kahalalide F, an antitumor depsipeptide in clinical trials, and its analogues as effective antileishmanial agents. Mol Pharm 6:813–824

88. Ashour M, Edrada RA, Ebel R, Wray V, Waetjen W, Padmakumar K, Mueller WEG, Lin WH, Proksch P (2006) Kahalalide derivatives from the Indian sacoglossan mollusk *Elysia grandifolia*. J Nat Prod 69:1547–1553
89. Fontana A, Cavaliere P, Wahidulla S, Naik CG, Cimino G (2000) A new antitumor isoquinoline alkaloid from the marine nudibranch *Jorunna funebris*. Tetrahedron 56:7305–7308
90. Saito N, Tanaka C, Koizumi Y-I, Suwanborirux K, Amnuoypol S, Pummangura S, Kubo A (2004) Chemistry of renieramycins. Part 6: transformation of renieramycin M into jorumycin and renieramycin J including oxidative degradation products, mimosamycin, renierone, and renierol acetate. Tetrahedron 60:3873–3881
91. Lane JW, Chen Y, William RM (2005) Asymmetric total syntheses of (−)-jorumycin, (−)-renieramycin G, 3-epi-jorumycin, and 3-epi-renieramycin G. J Am Chem Soc 127:12684–12690
92. Leal JFM, García-Hernández V, Moneo V, Domingo A, Bueren-Calabuig JA, Negri A, Gago F, Guillén-Navarro MJ, Avilés P, Cuevas C, García-Fernández LF, Galmarini CM (2009) Molecular pharmacology and antitumor activity of Zalypsis® in several human cancer cell lines. Biochem Pharmacol 78:162–170
93. Ocio EM, Maiso P, Chen X, Garayoa M, Álvarez-Fernández S, San-Segundo L, Vilanova D, López-Corral L, Montero JC, Hernández-Iglesias T, de Álava E, Galmarini C, Avilés P, Cuevas C, San-Miguel JF, Pandiella A (2009) Zalypsis: a novel marine-derived compound with potent antimyeloma activity that reveals high sensitivity of malignant plasma cells to DNA double-strand breaks. Blood 113:3781–3791
94. Duan Z, Choy E, Jimeno JM, Cuevas CD-M, Mankin HJ, Hornicek FJ (2009) Diverse cross-resistance phenotype to ET-743 and PM00104 in multi-drug resistant cell lines. Cancer Chemother Pharmacol 63:1121–1129
95. Guirouilh-Barbat J, Antony S, Pommier Y (2009) Zalypsis (PM00104) is a potent inducer of gamma-H2AX foci and reveals the importance of the C ring of trabectedin for transcription-coupled repair inhibition. Mol Cancer Ther 8:2007–2014
96. Feling RH, Buchanan GO, Mincer TJ, Kauffman CA, Jensen PR, Fenical W (2003) Salinosporamide A: a highly cytotoxic proteasome inhibitor from a novel microbial source, a marine bacterium of the new genus *Salinospora*. Angew Chem Int Ed 42:355–357
97. Macherla VR, Mitchell SS, Manam RR, Reed KA, Chao T-H, Nicholson B, Deyanat-Yazdi G, Mai B, Jensen PR, Fenical WF, Neuteboom STC, Lam KS, Palladino MA, Potts BCM (2005) Structure-activity relationship studies of salinosporamide A (NPI-0052), a novel marine derived proteasome inhibitor. J Med Chem 48:3684–3687
98. Shibasaki M, Kanai M, Fukuda N (2007) Total synthesis of lactacystin and salinosporamide A. Chem Asian J 2:20–38
99. Jensen PR, Williams PG, Oh D-C, Zeigler L, Fenical W (2007) Species-specific secondary metabolite production in marine actinomycetes of the genus *Salinispora*. Appl Environ Microbiol 73:1146–1152
100. Lam KS, Tsueng G, McArthur KA, Mitchell SS, Potts BCM, Xu J (2007) Effects of halogens on the production of salinosporamides by the obligate marine actinomycete *Salinispora tropica*. J Antibiot 60:13–19
101. Reed KA, Manam RR, Mitchell SS, Xu J, Teisan S, Chao T-H, Deyanat-Yazdi G, Neuteboom STC, Lam KS, Potts BCM (2007) Salinosporamides D-J from the marine actinomycete salinispora tropica, bromosalinosporamide, and thioester derivatives are potent inhibitors of the 20S proteasome. J Nat Prod 70:269–276
102. Tsueng G, Lam KS (2007) Stabilization effect of resin on the production of potent proteasome inhibitor NPI-0052 during submerged fermentation of *Salinispora tropica*. J Antibiot 60:469–472
103. Tsueng G, McArthur KA, Potts BCM, Lam KS (2007) Unique butyric acid incorporation patterns for salinosporamides A and B reveal distinct biosynthetic origins. Appl Microbiol Biotechnol 75:999–1005
104. Groll M, Huber R, Potts BCM (2006) Crystal structures of salinosporamide A (NPI-0052) and B (NPI-0047) in complex with the 20S proteasome reveal important consequences of beta-lactone ring opening and a mechanism for irreversible binding. J Am Chem Soc 128:5136–5141
105. Denora N, Potts BCM, Stella VJ (2007) A mechanistic and kinetic study of the β-lactone hydrolysis of salinosporamide A (NPI-0052), a novel proteasome inhibitor. J Pharm Sci 96:2037–2047
106. Stadler M, Bitzer J, Mayer-Bartschmid A, Mueller H, Benet-Buchholz J, Gantner F, Tichy H-V, Reinemer P, Bacon KB (2007) Cinnabaramides A-G: analogues of lactacystin and salinosporamide from a terrestrial streptomycete. J Nat Prod 70:246–252
107. Beer LL, Moore BS (2007) Biosynthetic convergence of salinosporamides A and B in the marine actinomycete *Salinispora tropica*. Org Lett 9:845–848
108. Udwary DW, Zeigler L, Asolkar RN, Singan V, Lapidus A, Fenical W, Jensen PR, Moore BS (2007) Genome sequencing reveals complex secondary metabolome in the marine actinomycete *Salinispora tropica*. Proc Natl Acad Sci USA 104:10376–10381
109. Eustaquio AS, Pojer F, Noel JP, Moore BS (2008) Discovery and characterization of a marine bacterial SAM-dependent chlorinase. Nat Chem Biol 4:69–74
110. Fenical W, Jensen PR, Palladino MA, Lam KS, Lloyd GK, Potts BC (2009) Discovery and development of the anticancer agent salinosporamide A (NPI-0052). Bioorg Med Chem 17(6):2175–2180
111. Potts BC, Lam KS (2010) Generating a generation of proteasome inhibitors: from microbial fermentation to total synthesis of salinosporamide A (Marizomib) and other salinosporamides. Mar Drugs 8:835–880
112. Gulder TAM, Moore BS (2010) Salinosporamide natural products: potent 20S proteasome inhibitors as promising cancer chemotherapeutics. Angew Chem Int Ed 49: 9346–9367

113. Chauhan D, Singh AV, Ciccarelli B, Richardson PG, Palladino MA, Anderson KC (2010) Combination of novel proteasome inhibitor NPI-0052 and lenalidomide trigger in vitro and in vivo synergistic cytotoxicity in multiple myeloma. Blood 115:834–845
114. Mori T, O'Keefe BR, Sowder RC II, Bringans S, Gardella R, Berg S, Cochran P, Turpin JA, Buckheit RW Jr, McMahon JB, Boyd MR (2005) Isolation and characterization of Griffithsin, a novel HIV-inactivating protein, from the red alga *Griffithsia* sp. J Biol Chem 280:9345–9353
115. Ziółkowska NE, Shenoy SR, O'Keefe BR, Wlodawer A (2007) Crystallographic studies of the complexes of antiviral protein griffithsin with glucose and N-acetylglucosamine. Protein Sci 16:1485–1489
116. O'Keefe BR, Vojdani F, Buffa V, Shattock RJ, Montefiori DC, Bakke J, Mirsalis J, d'Andrea A-L, Hume SD, Bratcher B, Saucedo CJ, McMahon JB, Pogue GP, Palmer KE (2009) Scaleable manufacture of HIV-1 entry inhibitor griffithsin and validation of its safety and efficacy as a topical microbicide component. Proc Natl Acad Sci USA 106:6099–6104
117. O'Keefe BR, Giomarelli B, Barnard DL, Shenoy SR, Chan PKS, McMahon JB, Palmer KE, Barnett BW, Meyerholz DK, Wohlford-Lenane CL, McCray PB Jr (2010) Broad-spectrum in vitro activity and in vivo efficacy of the antiviral protein griffithsin against emerging viruses of the family coronaviridae. J Virol 84:2511–2521
118. Moulaei T, Shenoy SR, Giomarelli B, Thomas C, McMahon JB, Dauter Z, O'Keefe BR, Wlodawer A (2010) Monomerization of viral entry inhibitor griffithsin elucidates the relationship between multivalent binding to carbohydrates and anti-HIV activity. Structure 18:1104–1115
119. Service RF (2009) Sugary achilles heel raises hope for broad-acting antiviral drugs. Science 325:1200
120. Prudhomme J, McDaniel E, Ponts N, Bertani S, Fenical W, Jensen PR, Le Roch K (2008) Marine actinomycetes: a new source of compounds against the human malaria parasite. PLoS One 3:e2335
121. Fattoruso E, Taglialatela-Scafati O (2009) Marina antimalarials. Mar Drugs 7:130–152
122. Ang KKH, Holmes MJ, Higa T, Hamann MT, Kara UAK (2000) In vivo antimalarial activity of the beta-carboline alkaloid, manzamine A. Antimicrob Agents Chemother 44: 1645–1649
123. Hughes CC, Fenical W (2010) Antibacterials from the sea. Chem Eur J 16:12512–12525
124. Bull AT, Stach JEM (2007) Marine actinobacteria: new opportunities for natural product search and discovery. Trends Microbiol 15:491–499
125. Lane AL, Moore BS (2011) A sea of biosynthesis: marine natural products meet the molecular age. Nat Prod Rep 28:411–428
126. Olivera BM, Gray WR, Zeikus R (1985) Peptide neurotoxins from fish-hunting cone snails. Science 230:1338–1343
127. Craik DJ, Adams DJ (2007) Chemical modification of conotoxins to improve stability and activity. ACS Chem Biol 2:457–468
128. Hala R, Craik DJ (2009) Conotoxins: natural product drug leads. Nat Prod Rep 26:526–536
129. Kaas Q, Westermann J-C, Craik DJ (2010) Conopeptide characterization and classifications: an analysis using ConoServer. Toxicon 55:1491–1509

Books and Reviews

Abraham DJ, Rotella DP (2010) Burger's medicinal chemistry, drug discovery and development, 7th edn. Wiley, Hoboken
Buss AD, Butler MS (2010) Natural product chemistry for drug discovery. RSC Publishing, Cambridge, UK
Chivian E, Bernstein A (2008) Sustaining life: how human health depends on biodiversity. Oxford University Press, Oxford
Rydzewski RM (2008) Real world drug discovery: a chemist's guide to biotech and pharmaceutical research. Elsevier, Amsterdam

Dynamic Environment Sensing Using an Intelligent Vehicle

Huijing Zhao, Long Xiong, Yiming Liu, Xiaolong Zhu, Yipu Zhao, Hongbin Zha
Key Lab of Machine Perception (MOE), Peking University, Beijing, China

Article Outline

Glossary
Definition of the Subject and Its Importance
Introduction
Sensor and System Architecture
Sensor Calibration and Data Alignment
Contextual Map Generation and Representation
Future Directions
Bibliography

Glossary

Classification Annotating a data segment or an object by a class label.

Contextual map A map containing high-level knowledge beyond geometry, such as object, class, and motion.

Data alignment Integrating the instantaneous measurements from sensors' coordinate system(s) to a global coordinate system.

Dynamic mapping A mapping technology that uses a dynamic procedure or generates a map of a dynamic environment.

Multi-laser sensing system A sensor system that makes collaborative use of a number of laser range scanners.

Range image A 2D image where the value of each pixel is a range distance, with the pixel index corresponding to range angle and scanning sequence, so that a 3D coordinate can be retrieved for each pixel of the range image.

Scene understanding Converting from low-level knowledge to high-level knowledge of an environment.

Segmentation Making partitions on a data set, where in each partition cell (i.e., segment), data has the property of certain homogeneity.

Sensor calibration Finding a set of parameters that describes internal or external sensor geometry.

Definition of the Subject and Its Importance

There have been numerous research efforts toward generating 2D/3D urban models using mobile robots. In addition, research has focused on robot-centric mapping and moving object detection/tracking for online perception and navigation. However, to date, there has been little work on generating a realistic 3D copy of a dynamic environment that describes the state of both static and dynamic objects at the moment. Toward the goal of developing omni-directional range sensing in a dynamic urban scene using an intelligent vehicle, research has mainly focused on the fundamental issues of multi-laser sensor system calibration and scene understanding in contextual map generation. Here, both system and algorithmic development are presented as well as experimental research demonstrating that a geometric and contextual representation of static objects such as buildings, trees, and roads, as well as the motion of dynamic entities such as people, bicycles, and cars, can be achieved using a vehicle robot.

Introduction

Traditionally, urban modeling has been thought of as generating maps of cities, in either 2D or 3D, for applications such as city planning, facility management, tourism, navigation, and cultural heritage. Numerous research efforts in photogrammetry and remote sensing [1] have been devoted to the study of aerial or satellite-based mapping technologies for the reconstruction of urban objects [2–4], yielding a vast amount of geographic databases. A summary of worldwide urban modeling projects can be found in [5]. Normally, aerial sensing can cover relatively wide area, but it fails to capture urban details due to the limitation of spatial resolution and a bird's eye viewpoint. Mobile mapping systems (MMS), which emerged at the end of the last decade [6–8], were initially considered as a complimentary mapping approach to aerial ones. This technological trend is described in [9, 10]. In such systems, ground vehicles are used as moving platforms carrying multi-modal sensors, so that city objects can be measured from nearby viewpoints on street. Early results [11–13] demonstrate thatrich data sets can be acquired, and highly realistic city models can be reconstructed using such a mapping technique. With the success of Google Earth [14] and Microsoft Virtual Earth [15], a broader community has found interest in visualizing cities in multi-levels of detail by combining data from both aerial and ground-based mapping techniques. Applications linking geographical maps with embedded 3D/2D visualization from street viewpoints are increasing. One of the most successful applications is Google StreetView [16], and a number of commercial systems using mobile mapping technologies [17–19] provide 3D/2D urban data. A review of the major approaches to large-scale modeling is given in [20]. However, these systems represent only the static entities of the environments, while the dynamic objects, such as cars and people, are either removed from the models or left on 2D images that do not reflect the current situation of the environment.

Mapping has been an active area of research in robotics and artificial intelligence for decades. Differing from photogrammetry and remote sensing, robotic mapping generates and maintains a spatial model of the robot's working environment, which is used to help

the robot's online perception and decision making. Maps vary in scale, dimension, content, and representation, according to the robot's function. A comprehensive survey of robotic mapping techniques, i.e. the key issues, major approaches and future challenges, is given in [21]. In recent years, interest in ground vehicle robots has grown rapidly. Especially with the DARPA Grand Challenges 2004, 2005 [22] and Urban Challenge 2007 [23], considerable enthusiasm and research interest have been inspired in the robotics and intelligent vehicle (IV) communities toward developing autonomous driving techniques and advanced driver assistance systems. The ground vehicle robot or intelligent vehicle must function in a complex outdoor environment [24, 25], where a map that eprovides knowledge of the highly dynamic environment is essential for the robot to achieve advanced online perception and decision. Generating maps of dynamic outdoor environments that contain the representations of both static and dynamic entities using mobile robots is still a fundamental issue.

There have been numerous research efforts to generate 2D/3D urban models using mobile robots [26–29]. There has also been work on robot-centric mapping and moving object detection/tracking for online perception and navigation [30–34]. However, to date, there has been little research on generating realistic 3D copies of a dynamic environment that describes the current situation of both static and dynamic objects at the moment. This research focuses on developing an intelligent vehicle system that conducts omni-directional range sensing to a dynamic urban scene, where a geometric and contextual representation of static objects such as buildings, trees, and roads,as well as the motion at the moment of dynamic entities such as people, bicycles, and cars, can be achieved after a run. In the following, sensor and system architecture is first addressed, followed by the description to the two major modules, sensor and data alignment, and map generation. Algorithms and experimental results are presented, and finally future directions are discussed.

Sensor and System Architecture

Sensor System

Over the past decade, laser range scanners, either 2D or 3D, have emerged as the dominant exteroceptive sensor for mobile robotics applications. Instead of using the 3D laser scanners, such as Velogyne HDL-64E [35], which has 64 laser heads and can achieve omni-directional 3D range sensing with a scan rate of 5–15 Hz, this research developed a multi-laser sensor system by integrating a number of single-row laser scanners (called LIDAR, for Light Detection and Ranging) in order to achieve low sensor cost and flexibility for a variety of applications. It is desirable that the software be adaptable to different numbers and layouts of laser scanners according to application requirements.

Figure 1 shows an example of sensor layout with five SICK LMS2**s [36] and a GPS (Global Positioning System)/IMU (Inertial Measurement Unit) based navigation unit. L1 is a horizontal scanning unit mounted in the center of the front bumper, which is used in combination with GPS/IMU so as to estimate vehicle position while generating a horizontal reference, i.e., a 2D grid map of the environment, and extracting motion trajectories of dynamic objects at a horizontal level (SLAMMODT [31]: Simultaneous Localization and Mapping [37, 38] with Moving Object Detection and Tracking [39, 40]). Other laser scanners are used to acquire 3D data about the environment along streets: L2 scans downwardly, measuring the lower part of objects on roadside, as well as road surface; L3 scans the upper part of objects on roadside, as well as those above the road surface, such as traffic signs and signal lights; L4 and L5 scan vertically to the left and right sides of the car. The data from each laser scanner can be represented in the form of 2D range images, as shown in Fig. 2, where the horizontal axis is time, and vertical strips correspond to laser scan lines, with each pixel valued by converting range distance into an intensity in [0, 255]. A piece of range segment, i.e., area "A" in Fig. 2, is enlarged in Fig. 3. It can be seen that a dynamic environment containing not only the stationary objects such as trees and poles, but also the moving objects such as pedestrians and cyclists, is vividly captured through such a range measurement.

Software Modules

Figure 4 describes software modules and major data flows (input and output). Module 1 is a sensor data logger, which records both GPS/IMU navigation inputs

Laser #	Scan mode	Major purpose
L1	Horizontal	SLAM with MODT
L2	Downward	Road geometry
L3	Upward	Objects above the road
L4	Vertical Right	Objects to the right of the car
L5	Vertical Left	Objects to the left of the car

Dynamic Environment Sensing Using an Intelligent Vehicle. Figure 1
A test-bed vehicle system designed for omni-directional range sensing [41]

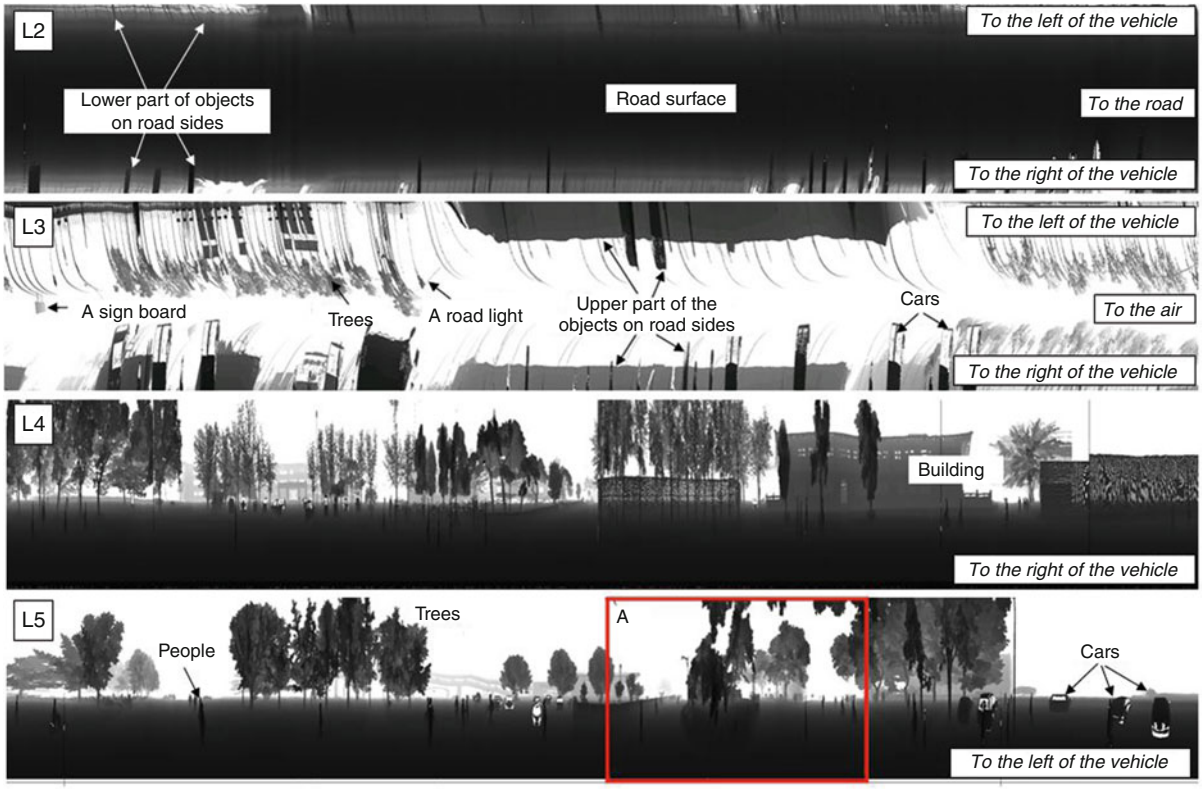

Dynamic Environment Sensing Using an Intelligent Vehicle. Figure 2
Range images of laser scan data L2–L5 [42]. Horizontal axis is scan line number (corresponding to time). Each vertical strip represents a line of range values of a certain laser scan

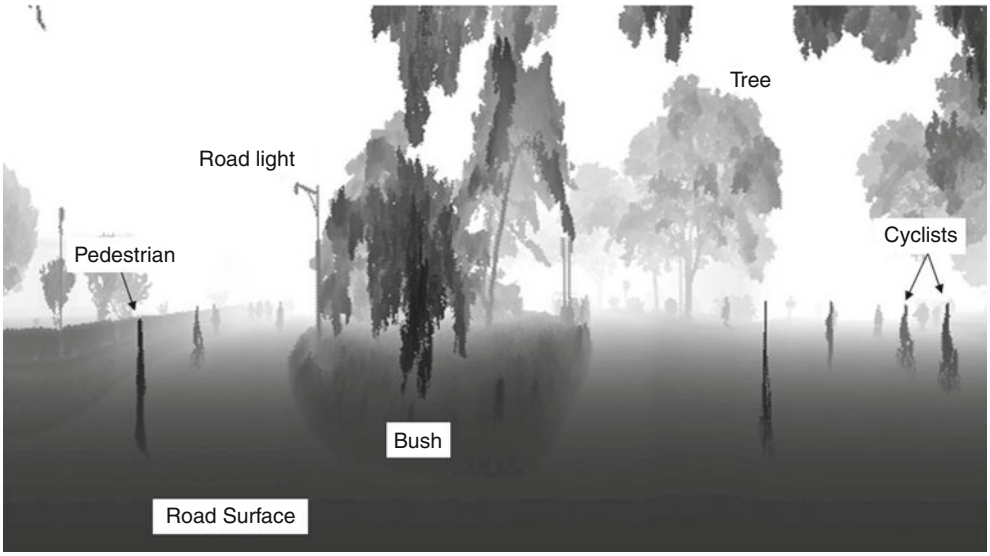

Dynamic Environment Sensing Using an Intelligent Vehicle. Figure 3
An enlarged range image by laser scanner L5 [42]

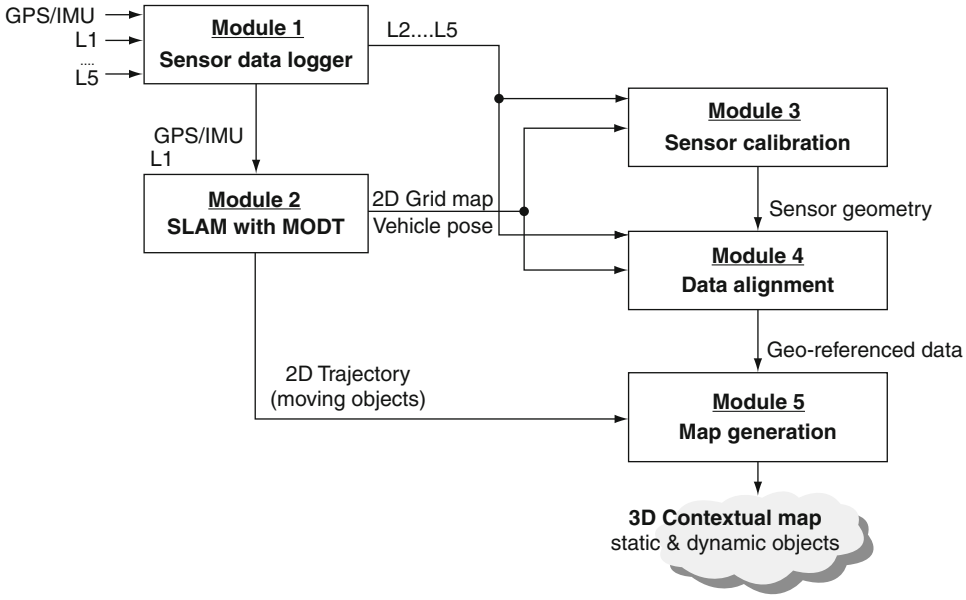

Dynamic Environment Sensing Using an Intelligent Vehicle. Figure 4
Software modules and major data flows

and all laser scan data, and then forwards the raw sensor logs to other modules through a wired local network, e.g., the data of L1 and GPS/IMU are forwarded to module 2, while those of L2–L5 are forwarded to processors 3 and 4.

In and urban environment, bridges, trees, tunnels, and buildings might obstruct GPS signals, and multi-path degrades the positioning accuracy of GPS/IMU based navigation units dramatically [43]. An algorithm of SLAMMODT was developed in the

authors' previous work [44], coupling a horizontal laser scanner with GPS/IMU, so that estimations of the robot's motion parameters can be refined by matching inter-frame sensing data to static objects (localization), meanwhile generating a consistent map in 2D grids, and detecting and tracking the data of dynamic entities at the horizontal level. The SLAMMODT is conducted in a horizontal level with an assumption that the ground surface is flat, and three kinds of outputs can be issued online-vehicle pose, a 2D grid map of static objects, and 2D trajectories of moving objects. A result after a cyclic run around a large building complex in a dynamic campus is shown in Fig. 5, where the course length is about 1 km.

In order to make collaborative usage of the data from different laser scanners, a calibration of sensor geometries is conducted in module 3 by referencing the sensor's coordinate system of L1. With the data of both sensor geometry and vehicle position, laser scans captured by different sensors at different vehicle positions can be integrated into a global coordinate system in module 4, so as to generate a map of the outside environment using the low-level primitive of 3D laser points. With such a representation, an operator can obtain visual knowledge of the environment, however, it is not informative for a robot, as such a map reflects only spatial existence through point sampling of object surface. In order for a robot to have semantic knowledge of the environment, such as objects, types, and their spatial relationships, a segmentation and classification of 3D laser points is conducted in module 5. A contextual map is finally reconstructed with each 3D object annotated, and the motion data of dynamic entities from processor 2 are integrated, which can be used to infer the relationships between different objects.

Currently, modules 1, 2, and 4 conduct online processing, module 3 is pre-processing directly after

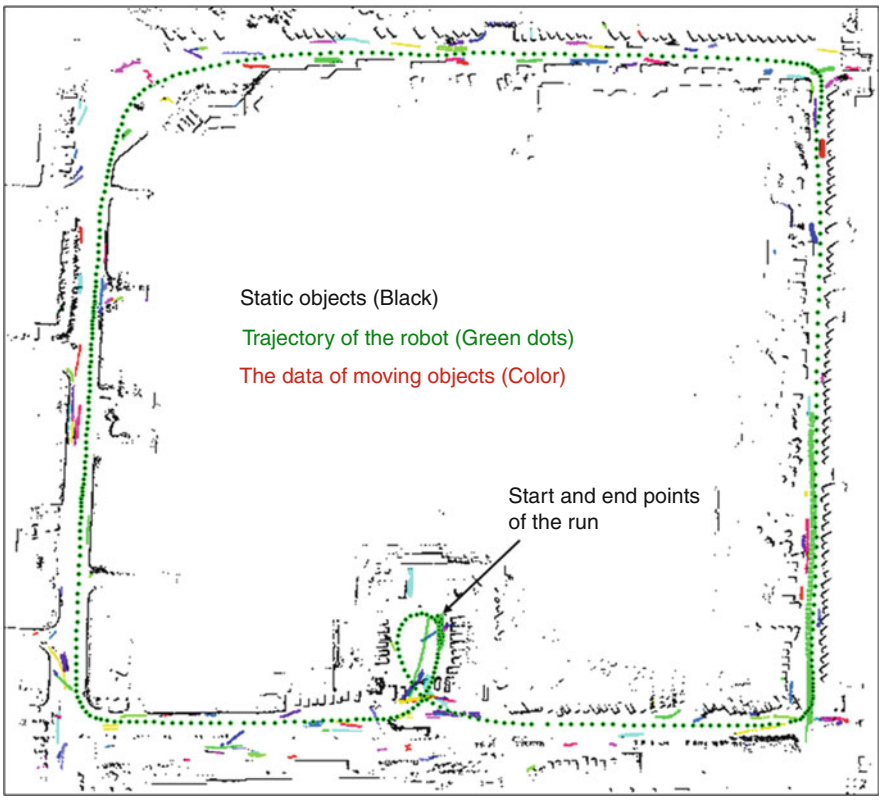

Dynamic Environment Sensing Using an Intelligent Vehicle. Figure 5
A result of SLAMMODT after a cyclic run in a dynamic campus

each sensor system setting, and module 5 is an off-line procedure after a vehicle run. The algorithm details as well as experiments with modules 3, 4 and 5 are described below; module 2 is described in [44].

Sensor Calibration and Data Alignment

Literature Review

There have been dozens of intelligent vehicle systems using laser scanners for perception. For example, all 11 finalists in the DARPA Urban Challenge relied upon laser scanners (LIDARs) as their primary exteroceptive sensing modality [24, 25]. Laser scanners can provide angle and range measurements, which are the samplings on object surface, and can be easily converted into 2D or 3D coordinates. However, a single laser scanner might have limited viewing angles and occluded sensing space, e.g., the widely accepted SICK LMS 2** conducts 2D scanning on a plane within 180°. Therefore, it is important for a robot to possess a number of laser scanners to achieve a better understanding of the whole 3D environment. In order to integrate the data from different sensors, calibration is required to find sensor geometries, i.e., transformation parameters between different sensor's coordinate systems.

Normally, calibration methods are decomposed into intrinsic and extrinsic calibrations. Intrinsic calibration finds the local geometry of each sensor, such as the camera's focal length, optical distortion, principal point, and so on. These parameters can be estimated independently with other sensors. They experience only slight changes in temperature and humidity. Extrinsic calibration finds the relative geometry, e.g. rotation and transformation parameters, between different sensors that compose a rigid body. These parameters change during sensors' removal and set-up, and need to be calibrated after the sensors are mounted on the vehicle. Calibration of the sensor system using laser scanner(s) is poorly documented, except for a few papers on intrinsic calibration of laser scanners [45, 46], extrinsic calibration of laser scanners with camera [47–49], and multi-laser systems [50].

The procedure for extrinsic calibration, especially for a large sensor system, is notoriously labor intensive.

Relative geometry between different sensors' coordinate systems can be estimated by registering their data sets, and a relationship between the data spaces can be established. Registration of range data has been studied for decades [51–53], where sensor geometry is supposed to be fixed during the measurement of each set of range data. However, registration of mobile laser scan data is different from that of a stationary platform.

This research focuses on extrinsic calibration of a multi-laser sensor system that uses a number of single-row laser scanners (LIDAR). A calibration method has been developed that is not restricted to the sensor system shown in Fig. 1, but is adaptable to different sensor numbers and layouts. Here, it is necessary to stress that (1) the laser beam of the laser scanners (e.g., SICK LMS2**) is invisible (near infrared band); (2) a traditional checkerboard is not useful here, as a single-row laser scan shoot only one line on it; and (3) locating a reflective target to catch a laser beam is labor intensive, especially with laser beams of upward scanning. A calibration method is desirable if it (1) does not require special facility and (2) uses the objects in the scene as landmarks.

Problem Statement

Without loss of generality, a laser scanner's coordinate system is defined as follows (see Fig. 6). The origin is at the principle point of the laser scanner. Laser beam

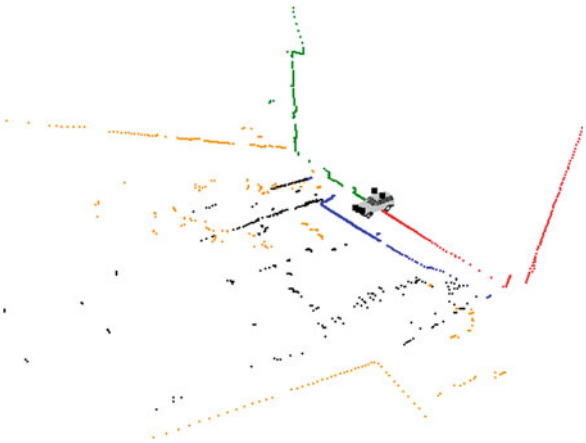

Dynamic Environment Sensing Using an Intelligent Vehicle. Figure 6
Instantaneous laser measurements at vehicle body frame

scans start from the x-axis, moving toward the y-axis. The z-axis is vertical to the laser beam's scanning plane, and xyz-axes compose a right-hand coordinate system. A range point $p_i^r = (k_i,\ r_i,\ s_i)$ is measured by the laser scanner p at scan line number k_i (corresponding to and denoted as "time" below), with range distance r_i, and data number s_i. $(k_i,\ s_i)$ locates the pixel index in range image (see Fig. 2), the value of which is assigned by $\frac{r_i \times 256}{r_{max}}$. Let α_{res} be the angular resolution for range sampling, e.g., $\alpha_{res} = 0.5$ in this research, s_i is converted to a scanning angle by $\alpha_i = s_i \times \alpha_{res}$, p_i^r is converted into a 2D coordinate at laser scanner p's coordinate system, and is represented in the following form.

$$p_i = (r_i \cos \alpha_i,\ r_i \sin \alpha_i,\ 0, 1)^t$$

Let T_{pv} be the geometric transformation from laser scanner p to the vehicle body frame, which is defined on that of L1, p_i can be converted to the vehicle body frame as follows.

$$p_v = (x_v,\ y_v,\ z_v,\ 1)^t = T_{pv} \cdot p_i$$

Given an initial set of sensor geometry (T_{pv}s), the laser points that are measured by L1–L5 at a certain moment can be integrated into the vehicle body frame as shown in Fig. 7, where colors denote for different sensor data: light blue for L1, dark blue for L2, orange for L3, green for L4, and red for L5. It can be found that, at any moment, an instantaneous measurement obtains data only on five 2D planes, which do not compose a 3D measurement of the whole environment. Also, even T_{pv}s are erroneous, it cannot be discriminated from the instantaneous laser scan lines, as there are no or few intersections between the data spaces of different sensors.

On the other hand, with module 2 – SLAMMODT, the vehicle robot is able to build a 2D grid map of the environment, meanwhile it determines its location and orientation within the map as shown in Fig. 5. The map can be a relative one, if referencing to the vehicle body frame at the starting point, or a global one if incorporating GPS/IMU inputs, where a fiducial vehicle body frame is defined on that of L1. Position estimation finds the location and orientation of the vehicle body frame

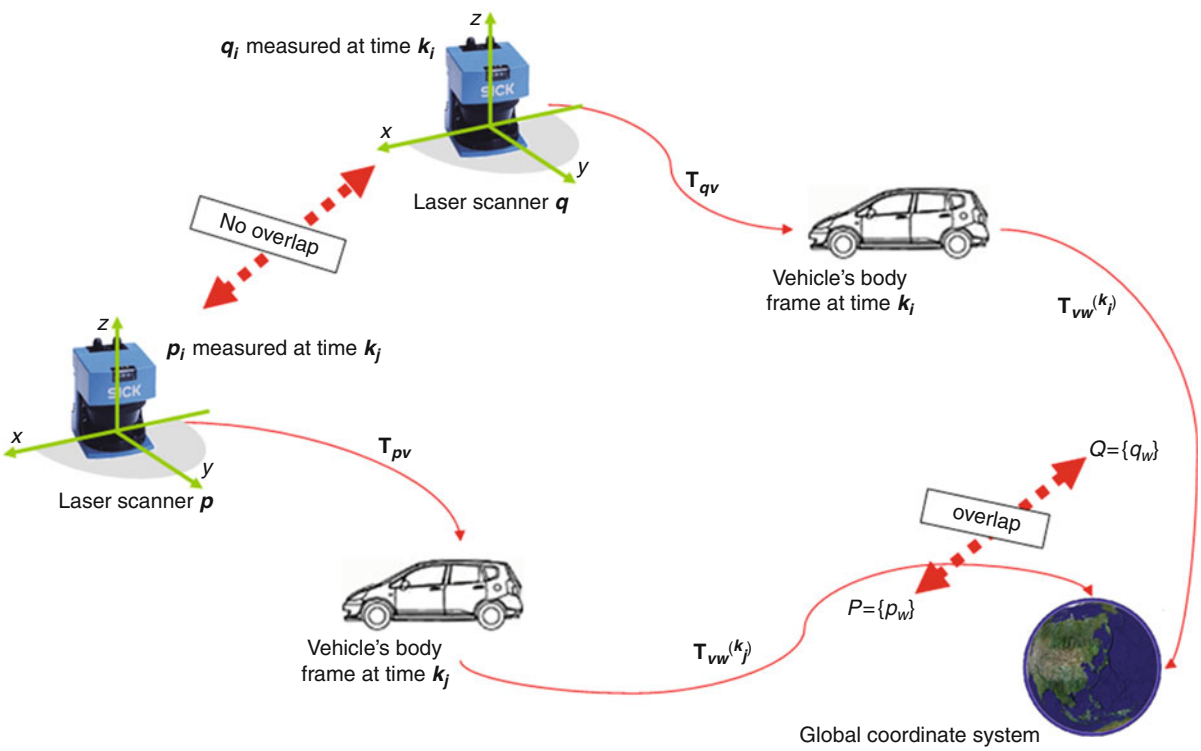

Dynamic Environment Sensing Using an Intelligent Vehicle. Figure 7
Sensor geometry and data geo-referencing [42]

with respect to the reference one (denoted as global coordinate system), as a result, a transformation matrix T_{vw}^{ki} is obtained at each time instance ki, associating the vehicle's body frame to the global one. With both sensor geometry T_{pv} and vehicle position T_{vw}^{ki} at time k_i, p_i can be converted to the global coordinate system as follows (see Fig. 7). $P_w = \{p_w\}$ denotes the geo-referenced data set of laser scanner p.

$$p_w = (x_w,\ y_w,\ z_w,\ 1)^t = T_{vw}^{ki} \cdot T_{pv} \cdot p_i$$

In the same way, let q be another laser scanner, q_i^r, q_i, q_w, and Q_w denote a range point, 2D coordinates at the sensor's coordinate system, a 3D point in the global coordinate system, and the geo-referenced data set of the laser scan measurements, respectively.

Figure 8 shows the geo-referenced 3D laser points, where the top-left, top-right, and bottom-left drawings are the data of each individual laser scanner, while the bottom-right is an integrated version. For the purposes of discrimination, colors in the drawings in the top row denote the local surface normal of the laser points, while colors in the drawings in the bottom row denote data from different sensors. It can be found that although the data generated by each individual sensor contains only partial knowledge of the whole environment, e.g., the data of L2 represents road surface only, the laser points have good consistency that describes object geometries in its vision field. However, when integrating the data from different sensors into a single one, displacement can be found in the duplicated measurements of common objects. It reflects that, although laser scanners have no intersection in their instantaneous measurement, a single object could be measured by different sensors at different time instances. When using the same vehicle position T_{vw}^{ki}s, the displacements come from the erroneous sensor geometries (T_{pv}s). This suggests that sensor geometries can be refined by minimizing the displacements between the overlapped measurements of different sensors after data geo-referencing, i.e., data registration. Let $T_{pq} = T_{pv}^{-1} \cdot T_{qv}$ denote the relative geometry between laser scanner p and q. Calibrating the sensor geometry between laser scanner p and q allows conversion into the following data registration problem:

$$T_{pq} = \arg\min_{T_{pq}}\ D(z(P_w), z(Q_w))$$

where $z(\cdot)$ is a function projecting P_w and Q_w to a matchable data space, and $D(\cdot\ ,\ \cdot)$ is a distance measure evaluating the displacement (i.e., distance) between two data sets. In solving the problem, a coarse-to-fine procedure is taken. Note that if q is L1, as the vehicle body frame is defined on L1, $T_{pq} = T_{pv}$.

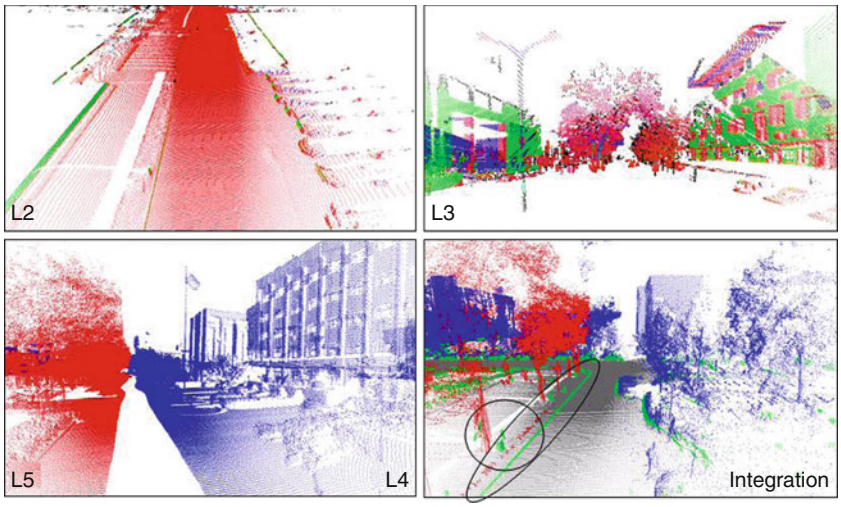

Dynamic Environment Sensing Using an Intelligent Vehicle. Figure 8
Geo-referenced 3D points of each individual laser scanner and their integration [42]

Coarse Registration

A geometric transformation T_{pq} is first initialized according to hardware design, then refined through matching their data sets, i.e., P_w and Q_w. If a direct correspondence between a number of landmark points in P_w and Q_w could be established, T_{pq} can be solved using a Least Squares Method. However, when laser scanners face different directions, partial observations and occlusions make direct correspondence an extremely difficult issue.

Recall the problem statement in previous section. A fiducial vehicle body coordinate system is defined on that of L1. Sensor calibration can be stated more specifically to achieve an alignment of all other laser scanners (L2–L5) with reference to L1. With the output of module 2 – SLAMMODT, a 2D grid map generates a horizontal reference of the environment, while T_{vw}^k locates a vehicle at any time k on the map as shown in Fig. 5. In a calibration procedure, vehicle positions T_{vw}^k s are considered adequately accurate, leaving T_{pq}s for refinement. In this research, a two-step procedure is designed in coarse registration: horizontal and vertical matching, both of which generate projections to a 2D grid map on a horizontal level.

Horizontal Matching Horizontal matching generates a projection $z_h(\cdot)$, so that the laser points of vertical features, such as buildings, poles, and tree branches, are projected to a horizontal grid map. The grid value $v(\cdot)_{ij}$ can be 1 or 0, representing that the number of laser points projected to the grid cell is greater than or less than a predefined threshold. The reason for thresholding is to filter out irregular laser points and enhance vertical features. Horizontal matching is conducted by taking a laser scanner p as reference, adjusting T_{pq} to minimize the distance between $z_h(P_w)$ and $z_h(Q_w)$. A distance measure is designed based on the following two criteria.

$$C_1 = \sum_i \sum_j v(\,\cdot\,)_{ij} \rightarrow \min$$

C_1 means that the sum of all grid values should be minimized. As each grid cell has a value of either 1 or 0, C_1 means also that the number of grid cells that has a value equal to 1 should be minimized. Ideally, a vertical wall is converted to a line by $z_h(\cdot)$, a pole becomes a point and so forth. Laser points belong to the vertical features, such as walls or poles, tend to be projected to the limited number of grid cells corresponding to the lines and points. A concentrated projection is highly evaluated comparing to a distributed projection.

$$C_2 = \sum_i \sum_j v(p)_{ij} \cdot v(q)_{ij} \rightarrow \min$$

C_2 means that the sum of a production between the grid values $v(p)_{ij}$ and $v(q)_{ij}$ should be maximized. As each grid cell has a value of either 1 or 0, it also means that the number of matched grid cells that have a value equal to 1 should be maximized. A distance measure is designed by summarizing the above criteria.

$$D_h(z_h(p),\ z(q)) = C_2(p,q) - C_1(q) \rightarrow \min$$

Vertical Matching Vertical matching generates a projection $z_v(\cdot)$, so that the laser points on ground surface are projected to a horizontal grid map. The grid value $u(\cdot)_{ij}$ represents the ground elevation at the grid cell, which is assigned by taking a mean of the z values of all laser points that are projected to the grid cell. A distance measure is designed as follows to evaluate the displacement between the elevation values:

$$D_v(z_v(p),\ z_v(q)) = \sum_i \sum_j |u(p)_{ij} - u(q)_{ij}| \rightarrow \min$$

Figure 9 shows an example of extracting the horizontal and vertical elements from the data of L4. A local surface normal is estimated for each laser point using its neighborhood data on scanning order. Either the horizontal and vertical elements are extracted by thresholding on their local surface normal. The vertical elements are used for horizontal matching, where an example of registering L4 on the 2D grid map of L1 is shown in Fig. 10. The horizontal elements, i.e., ground data, are used for vertical matching, where an example of registering L3 with L4 and L5 is shown in Fig. 11. In this research, both horizontal and vertical matching is conducted by adjusting the parameters of T_{pq}, so as to minimize D_h and D_v, respectively, in an exhaustive way.

Fine Registration

In coarse registration, data are represented in 2D grid maps at a horizontal plane, where resolution in

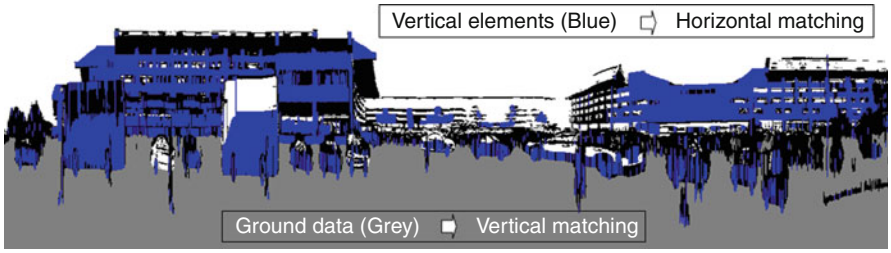

Dynamic Environment Sensing Using an Intelligent Vehicle. Figure 9
Example of extracting horizontal and vertical elements

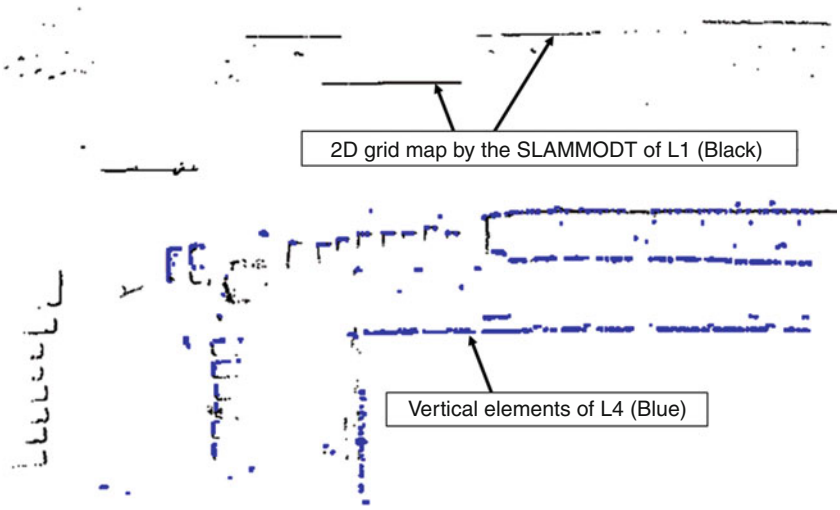

Dynamic Environment Sensing Using an Intelligent Vehicle. Figure 10
Example of horizontal matching of vertical elements from L4 and L1

describing object details as well as registration accuracy are limited by such a representation. Find registration approach is to refine the coarse registration results.

Given the sensor geometries of T_{pv} and T_{qv}, for any p_w measured by laser scanner p, a mirror range point ${}^{q}p_j^r = (k_j, r_j', s_j)$ is estimated at the range image frame of laser scanner q. Let $Q^r = \{q_j^r\}$ denote the range image measured by laser scanner q, while $Q_p^r = \{{}^{q}p_j^r\}$ for the mirror range image generated from the data measured by laser scanner p. The objective of fine registration is to find a T_{pv} that minimizes the difference between Q^r and Q_p^r. It is defined as follows:

$$T_{pv} = \arg\min_{T_{pv}} D(Q^r,\ Q_p^r)$$

Given p_w, a mirror range point ${}^{q}p_j^r = (k_j, r_j', s_j)$ is estimated, where k_j is the number of a scan line at laser scanner q's data space, s_j is the data number at k_j, r_j' is the range distance that p_w be measured on the scanning plane of k_j at range beam angle $\alpha_j = s_j * \alpha_{res}$. A mirror range point is estimated in an order of $k_j \rightarrow s_j \rightarrow r_j'$, where estimation of each parameter, as well as a definition to $D(\cdot\ ,\ \cdot)$ is described below.

Estimation of k_j For any laser scan k_j at the data space of laser scanner q, an orthogonal projection is done from p_w to the scanning plane as shown in Fig. 12, where r_x is the orthogonal distance, r_y is the Euclidean distance from sensor q's viewpoint at k_j to the

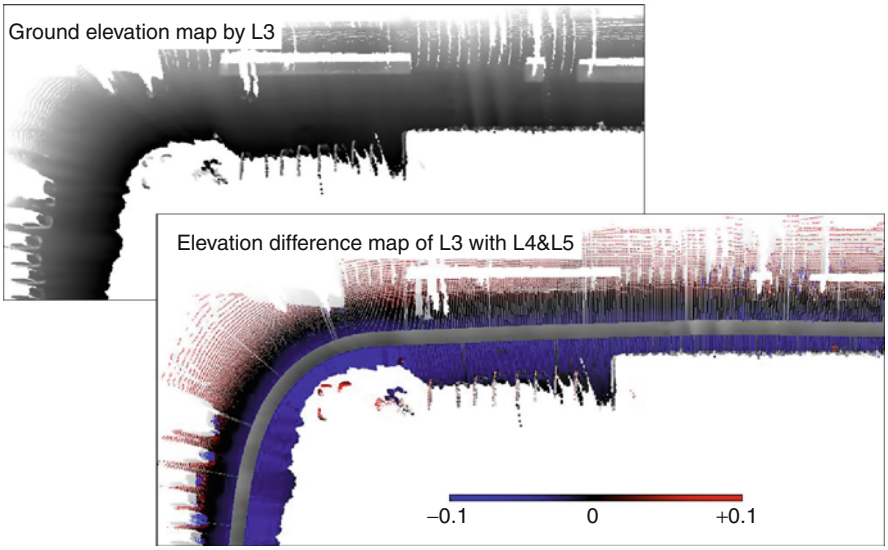

Dynamic Environment Sensing Using an Intelligent Vehicle. Figure 11
Example of vertical matching of ground data from L3 with L4 and L5

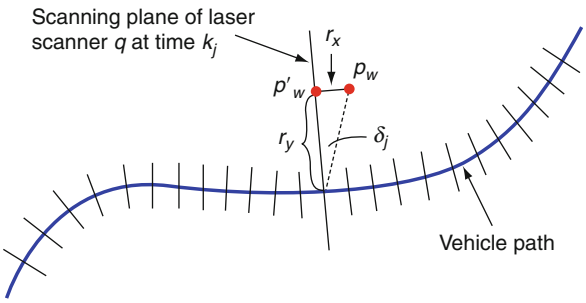

Dynamic Environment Sensing Using an Intelligent Vehicle. Figure 12
Locating a scan line k_j at the data space of q for a laser point p_w

orthogonal point $p_w{}'$, and $\delta_j = \arctan(\frac{r_y}{r_x})$. k_j is located as the laser scan of minimal δ_j and $\delta_j < \tau$, where τ is a threshold representing the diffusion of laser beam.

Estimation of s_j and $r_j{}'$ With the orthogonal point $p_w{}'$, a mirror point in sensor q's coordinate system is estimated as follows,

$$^{q}p_j = (^{q}x_i, {}^{q}y_i, {}^{q}z_i \approx 0, 1)^t = (T_{qv})^{-1} \cdot (T_{vw}^{kj})^{-1} \cdot p'_w$$

So that s_j and $r_j{}'$ are estimated as

$$s_j = \arctan(\frac{^{q}y_i}{^{q}x_i}) \Big/ \alpha_{res}$$

$$r_j{}' = \sqrt{(^{q}x_i)^2 + (^{q}y_i)^2}$$

Definition of $D(\cdot\,,\,\cdot)$ Let

$$sign_{ij} = \begin{cases} 1 & if\ \delta_{ij}^{q} \cdot {}^{q}\delta_{ij}^{p} \cdot (||r_{ij}^{q} - {}^{q}r_{ij}^{p}|| < \varsigma \\ 0 & otherwise \end{cases}$$

where δ_{ij}^{q} and $^{q}\delta_{ij}^{p}$ are binary values, denoting whether the range value r_{ij}^{q} at Q^r and $^{q}r_{ij}^{p}$ at Q_p^r, respectively, are valid (1 for valid). ς is a threshold, defining the bound for matched pair of range values. $sign_{ij} = 1$ denotes that the range points of Q^r and Q_p^r at pixel index (i,j) are matched ones. $D(\cdot\,,\,\cdot)$ is designed based on the following two criteria:

$$C_3 = \sum_{i=0}^{W}\sum_{j=0}^{H} sign_{ij} \rightarrow \max$$

$$C_4 = \sum_{i=0}^{W}\sum_{j=0}^{H} sign_{ij} * ||r_{ij}^{q} - {}^{q}r_{ij}^{p}|| \rightarrow \min$$

$$D(Q^r, Q_p^r) = C_4/C_3 - C_3$$

where C_3 counts for the number of matched range points, and C_4 is the sum of residuals between the matched range values. $D(\cdot\,,\,\cdot)$ is designed to maximize the number of matched range points, while minimizing the average of residuals between matched range values.

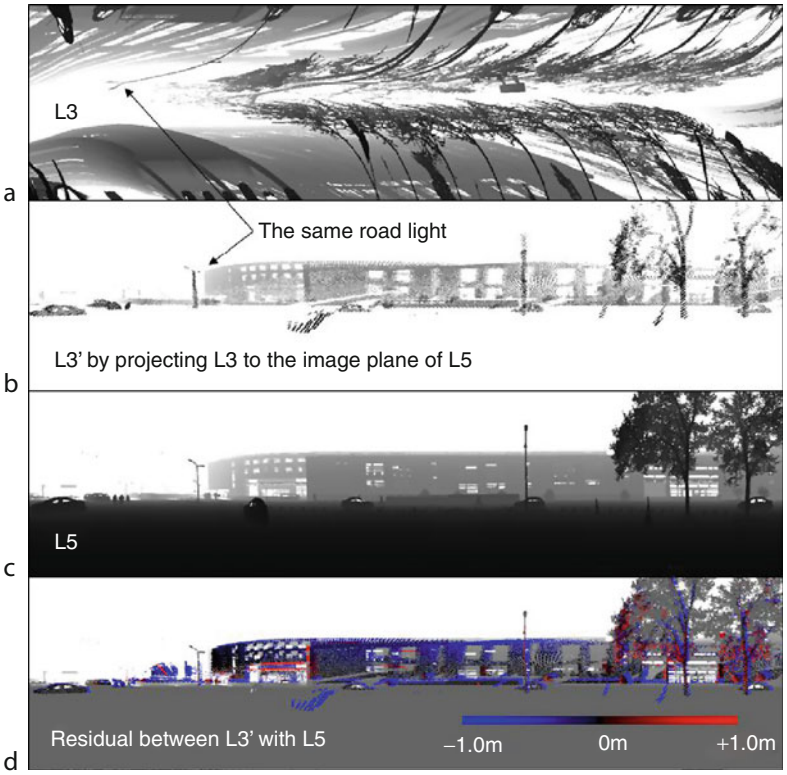

Dynamic Environment Sensing Using an Intelligent Vehicle. Figure 13
Explanation of the fine registration procedure using experimental results

Figure 13 explains the procedure of fine registration using experimental results, where the data of L3 (a) is projected to the range image frame of L5, and a new range image L3′ is generated as shown in (b). (c) shows the original range measurement by L5. A match is made between L3′ and L5, as shown in (d), where residuals between corresponding range points are represented in a color band of [blue-black-red], while the range points of L5 that do not have matched pair in L3′ are shown in grey. Some other results are also shown in Fig. 14, which are represented in both the residual maps between mirror and original range images, and their edge maps. In the edge map of L3′ and L5, it can be clearly found that a cyclist is captured by L5, however not in L3′. This might happen in the measurements to moving objects, where due to the difference in sensors' viewpoints, a single object (place) might be measured by sensors at a different time period. Although the cyclist is captured by L5, when L3 measured the place, it was not there, and L3 failed to capture the cyclist all the time due to its high dynamic motion. On the other hand, this phenomenon suggests that by matching the data from different sensors, the dynamic factors in the environment can be detected. Due to occlusion, viewpoint difference, and the dynamic entities of the environment, matching between the mirror and original range image is conducted manually in this research, where an automated method is to be developed through future research.

After sensor alignment, the laser points from different laser scanners can be integrated into a global coordinate system with more consistency, as shown in Fig. 15, where the ground data of L2 is shown in gray, non-ground data of L2 containing those of road edges are shown in green; L4 is in blue and L5 in red. It can be found that good consistency between the data of different sensors is achieved through a calibration procedure, and an omni-directional measure of the whole environment is achieved through the collaborative exploration of multiple single-row laser range scanners.

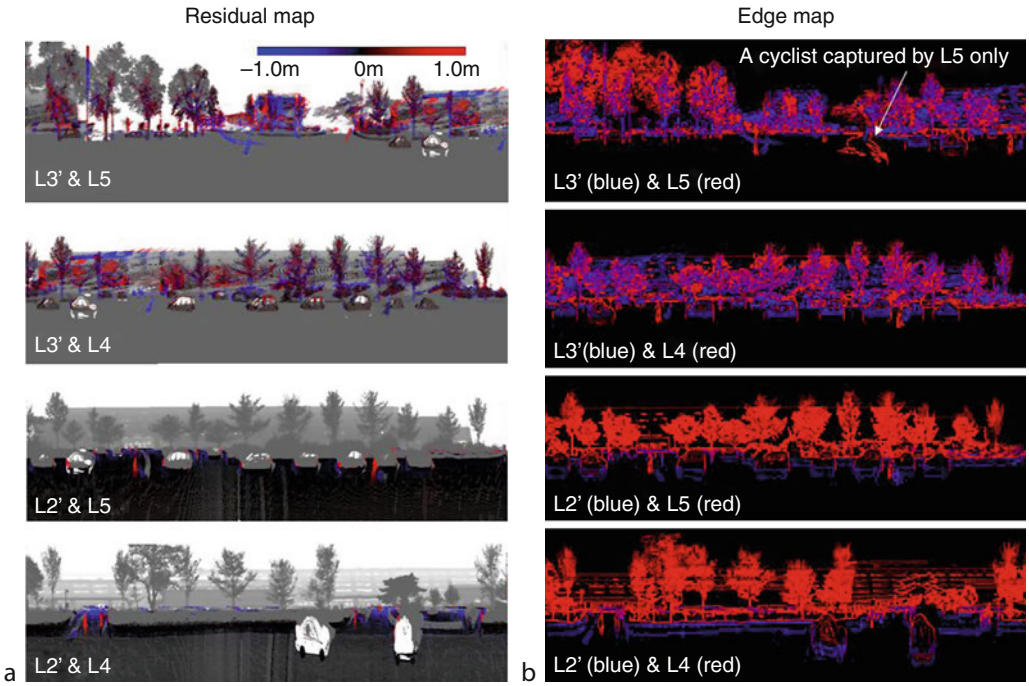

Dynamic Environment Sensing Using an Intelligent Vehicle. Figure 14
Some results of fine registration. *Left column*: residual map between mirror and original range images; *Right column*: edge points extracted from mirror (*blue*) and original (*red*) range images

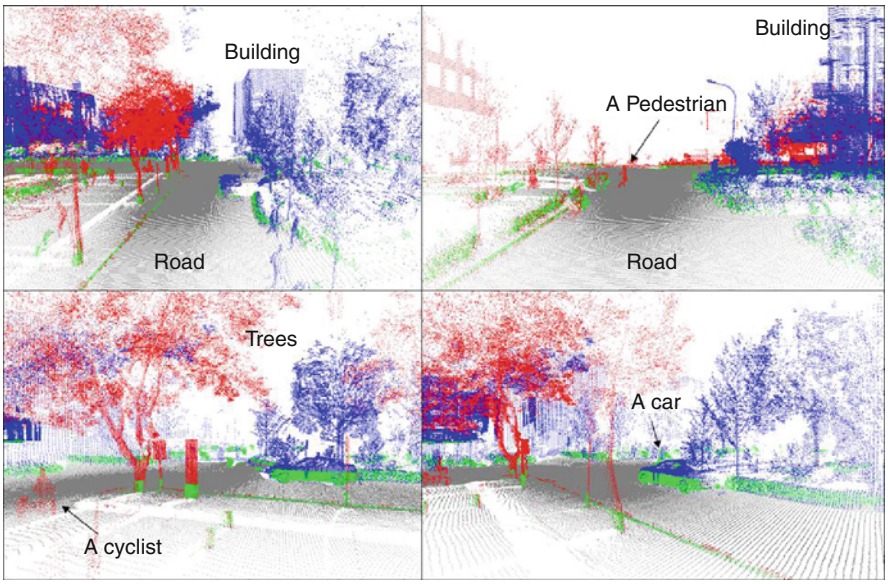

Dynamic Environment Sensing Using an Intelligent Vehicle. Figure 15
3D map of the environment created by integrating multi-laser sensing data [42]

Contextual Map Generation and Representation

An environmental map can be generated directly using the low-level geometric primitive of 3D laser points. However, such a map has limited capacity in representation, as it describes only spatial existence. An operator can easily understand from the data where objects are, and what kinds of objects they are, while a robot cannot. In order for a robot to have semantic knowledge of the environment, such as objects, types, and their spatial relationships, an automatic technique of converting a low-level map representation into a high-level one is important.

Literature Review

Through a bottom-up procedure, laser points can first be processed to find data clusters, i.e., laser points that are most likely to be the measurements of the same objects. They can then be recognized as certain kinds of objects, e.g., planar surfaces [54], line feature objects [55], cars [56], or natural objects [57]. In order to tackle the large number of laser points, [58, 59] tessellated the 3D space and projected laser points to voxels. The sequence of laser points can also be used as a whole to represent the geometric appearance of local surroundings, and a higher level knowledge of the robot's concurrent location, such as a doorway, corridor, or room, can then be inferred through machine learning techniques [60]. In addition, each individual laser measurement is considered to be dependent on its neighborhood in [61]. Their relationships are modeled using Markov networks, where labeling of each laser point is influenced by the labeling of others in its local vicinity. [62] also associated image cues with each laser point and varied the probabilistic framework using Conditional Random Field. Reference [63] further extended the method of [61], so that each node in the Markov network corresponds to a data patch, i.e., a superpixel (image patch) with corresponding laser points in successive scans, rather than a laser point. In addition, a recent report can be found in [63], where an aerial laser scan data is processed to label the small objects, such as posts, lights, and cars, in an urban environment. The problem is solved by localization, segmentation, representation, and classification procedures in a sequential way.

On the other hand, laser scan data can be represented in the form of a range image, where each pixel represents a depth value, and its index corresponds to the sequential order of measurements. Thus, beam origin and angle of each depth value can be retrieved, and depth value can then be easily extended to a 3D coordinate. There is a large body of work addressing range image segmentation. A famous report comparing the major segmentation methods can be found in [64]. Many of the methods are motivated by the needs for recognizing industry parts [65] or registering the data taken at different locations [66]. These works always assume simple or well-defined object geometry. There are still a few research works processing range images of real-world scenes. [67] considers a real-world indoor and outdoor scene by modeling the man-made objects using planes and conics, modeling free-form objects using splines, and modeling trees using 3D histogram; segmentation and model fitting for each segment is formulated in a data-driven Markov Chain Monte Carlo procedure.

Image segmentation and semantic interpretation have been studied extensively in the field of computer vision. As the data form of a range image is consistent with that of a visual image, many methods developed in the field of computer vision are of great reference for the processing of range image [68–71].

As shown in Figs. 2, 8, and 15, laser scan data can be represented in the forms of 2D range images or 3D laser points, where for a 2D range image, each pixel can be converted into a 3D point in a global coordinate system as addressed previously. In this research, range image is chosen as an interface for data representation. More specifically, this research concerns the segmentation and classification of range images in the real world, however estimations are conducted by retrieving the 3D coordinates of each range pixel. In dealing with the problem, a sequential flow as shown in Fig. 16a is generally used [72], where classification is conducted subsequently to segmentation. The framework is straightforward and easy to implement. However, when facing a complex environment with different kinds of objects, segmentation failures might happen due to the heterogeneous geometric properties between different kinds of objects. Unified frameworks are also proposed [68–71] that cope with the segmentation and classification problems simultaneously (see Fig. 16b).

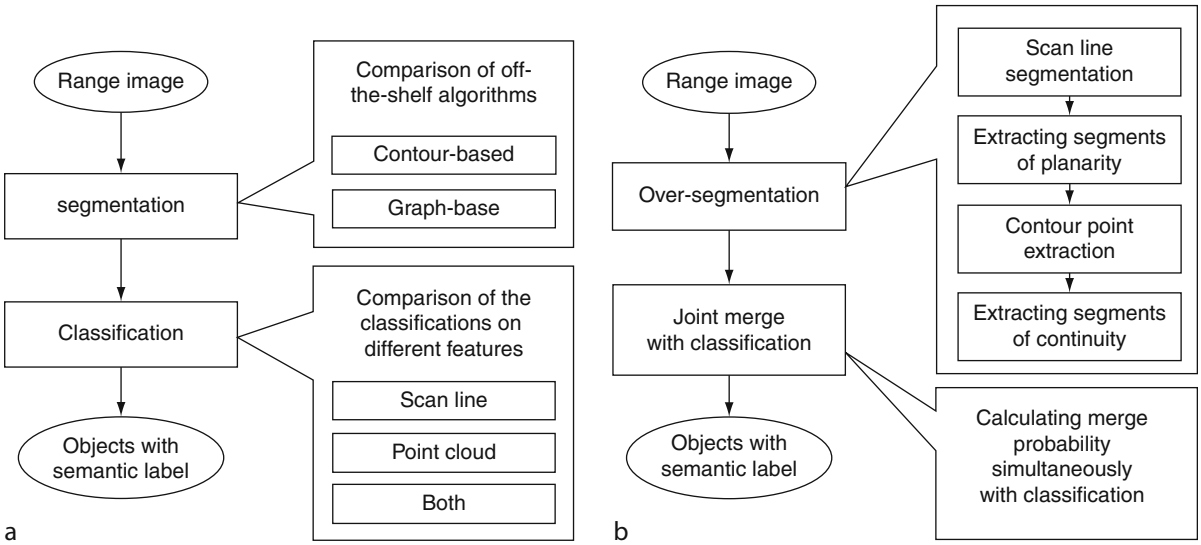

Dynamic Environment Sensing Using an Intelligent Vehicle. Figure 16
Sequential (**a**) and simultaneous (**b**) processing flows for range image segmentation and classification

This research examines the performances of both sequential and simultaneous processing flows in solving the problem of segmentation and classification of the range images in complex outdoor environments. The algorithmic and implementation details as well as experimental results are described below.

Segmentation

First, the data of the ground surface are discriminated and removed from the range image, so making the data of vertical objects spatially disconnected. Ground elevation at the point of host vehicle can be assumed, as the vehicle stands directly on the ground, and the sensor-vehicle is composed of a rigid body. For each laser scan line, segmentation is conducted, and the nearly horizontal line segment that has at least one end point within the bound of assumed ground elevation is extracted as the ground data, as the grey points in Fig. 17.

Contour-Based Segmentation In segmenting the rest of range image, contour points are first extracted, where the Euclidean distance between the 3D coordinates of each contour point with its four neighbors in range image is larger than a given threshold; a point-based region growing is then conducted to extract the data segments with spatial continuity (different color in Fig. 17 denotes a different segment). The method is efficient in extracting the data segments of most of the objects, and they are spatially disconnected. As shown in Fig. 17, although over-segmentation (i.e., a single object can be separated into a number of segments) occurs, especially for trees and pedestrians, most of the segments contain the data of a single object; with under-segmentation, different objects are merged into a single segment. Failure A merged the data of a piece of wall and a nearby car. Failure B merged the data of building surface and a clump of bush, where in some places, they are spatially close.

Graph-Based Segmentation Data acquired by laser scanner usually spatially connect with its neighbors in a range image. This property suggests a graph-based segmentation. The set of pixels can be represented as a weighted undirected graph $G = (V, E)$, where V is the set of nodes standing for pixels and E is the set of edges between pixels and their neighbors in 3D space. Thus, segmentation can be formulated as the problem of cutting an undirected graph G, where many mature algorithms exist [73, 74]. This research chose the FH algorithm [74] for its good performance in catching the

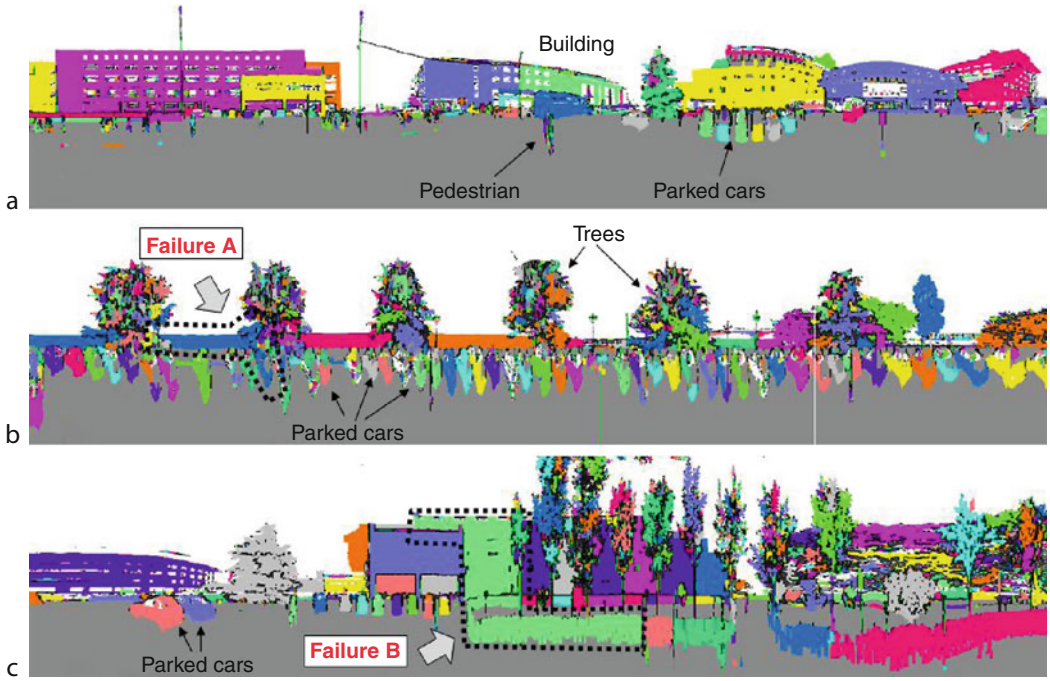

Dynamic Environment Sensing Using an Intelligent Vehicle. Figure 17
Results of contour-based segmentation

non-local properties and adaptability to online procedure. A range segment s is composed of a set of range points as well as weighed edges that represent the spatial relationships between neighbor range point pairs. The weight $w$of an edge $e$is assigned by the Euclidean distance between the 3D coordinates of two neighbor range points, which represents their spatial continuity. For any segment s that has ns range points, an internal difference ($Int(s) = \max_{e \in s} w(e)$) as well as a regulation term ($\tau(s) = \frac{k}{ns}$) is defined, where k is a predefined experimental factor. For any pair of segments (s_a and s_b), a minimum internal difference $MInt(s_a, s_b) = \min(Int(s_a) + \tau(s_a), Int(s_b) + \tau(s_b))$ is defined. The pair of segments s_a and s_b can be merged if and only if it has $MInt(s_a, s_b) < w(e_{a,b})$, where $e_{a,b}$ is an edge that has its two end points in s_a and s_b, respectively. Experimental results reflect that the parameter setting of k in the regulation term ($\tau(s) = \frac{k}{ns}$) is crucial to the segmentation result as described in Fig. 18. A small k causes objects to be over-segmented, while enlarging $k$might cause the data of different objects to merge. Figure 19 shows some of the results with $k = 1$. It can be found that the problem of over-segmentation is reduced compared with the results of a contour-based one, while under-segmentation is even heavier. Failure A merged the data of a number of trees and a clump of bush. Failure B merged the data of a banner and two neighboring trees.

Classification

A segment contains a set of 3D laser points, which describes the geometry of an object surface through the representation of point clouds. It is straightforward to extract data cues from the set of 3D laser points, and devise a classifier by evaluating their classification properties. On the other hand, a single-row laser scanner measures the environment in a mode of scan-line by scan-line. A scan-line measurement on a planar object, such as the surface of a building or road, can be modeled using a line segment. The measurement of a free-form object, such as a tree, yields many small line segments and isolated points. An isolated point can be considered as a specific type of line segment. A segment

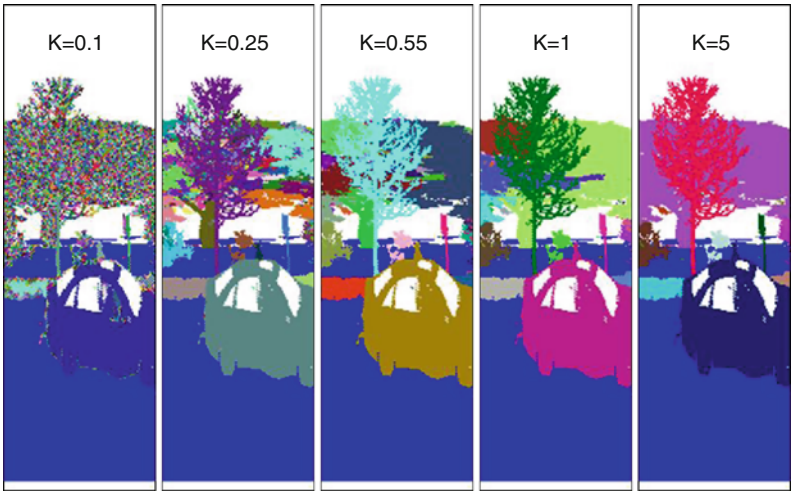

Dynamic Environment Sensing Using an Intelligent Vehicle. Figure 18
Parameter setting in graph-based segmentation

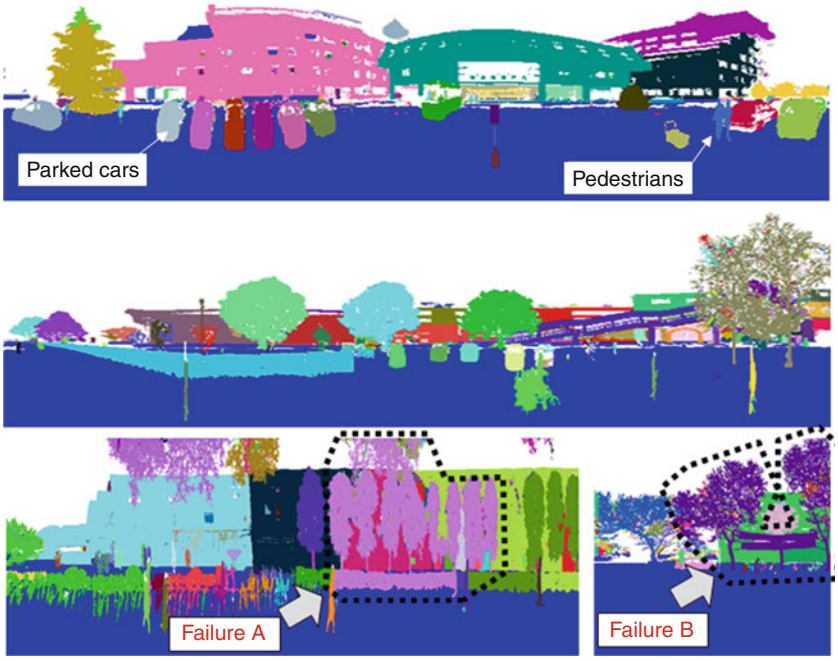

Dynamic Environment Sensing Using an Intelligent Vehicle. Figure 19
Results of contour-based segmentation

can also be considered as a set of scan line segments [75, 76], where data cues are extracted and evaluated to compose a classifier. Of course, a classifier can also be devised by a combinatory evaluation on the properties of 3D laser points and line segments. In this research, three classifiers are developed on line segments, 3D laser points, and their combinations, which are described below as well as an experimental comparison.

Classification on Scan Line Segments Let L denotes the set of object classes, i.e., $L = \{l|building, road, tree, person, car \cdots\}$, y be the label of a segment s,

and yk be the label of the kth line segment. Given data cue I, classification of segment s on scan line segments is formulated as follows.

$$y = \bar{l} = \arg\max_{l} \prod_{k} P(yk = l|I)$$

Let $I = \{d_1, d_2 ...\}$, the probability of a line segmentlabeled l, i.e., $P(yk = l|d_1, d_2, ...)$ can be further extended according to Bays' rule (i.e., a naïve Baysian classifier).

$$P(yk = l|d_1, d_2, ...) = P(yk = l) \prod_{i} P(d_i|yk = l)$$

where $P(yk = l)$ is a prior knowledge of a scan line segment labeled l. It is initialized as an equal distribution and updated after each iteration according to the percentages of data labeling.

$P(d_i|yk = l)$ is the likelihood measure (denoted by $\lambda_l^{yk}(d_i)$), when given a label $yk = l$, the probability d_i of the scan line segment can be observed. The data cues extracted from each scan line segment are listed in Table 1. For any pair of data cues d_i and object label $yk = l$, a likelihood measure $\lambda_l^{yk}(d_i)$ is trained using a set of manually labeled scan line segments. A histogram is first generated on data samples, then Gaussian fittings are conducted on each distinctive picks, followed by a normalization so that integration of the graph is 1. The likelihood measures trained in this research are shown in Fig. 20.

Classification on 3D Laser Points Let Y denote the label on the cloud of 3D laser points. Classification is formulated as follows:

Dynamic Environment Sensing Using an Intelligent Vehicle. Table 1 Data cues of a scan line segment

Feature	Definition
d_1	Length of the scan line segment
d_2	Maximal height value
d_3	Minimal height value
d_4	Z-coordinate of the directional vector
d_5	Mean of line regression
d_6	Variance of line regression

$$y = \bar{l} = \arg\max_{l} P(Y = l|I)$$

Data cues extracted from a cloud of 3D laser points are listed in Table 2. Differing from that of scan line segments, classification of 3D laser points does not evaluate the properties of each individual laser point but treats them as a whole. The likelihood measures $\lambda_l^{yk}(d_i)$ of a certain pair of data cues and object labels are generated as demonstrated in Fig. 21. However, due to the limited and unbalanced number of sample data (see Table 3), a naïve Baysian classifier did not yield satisfying results. In classification of 3D laser points, an off-the-shelf method, LIBSVM [77], is used.

Classification of Both 3D Laser Points and Scan Line Segments A classifier of both 3D laser points and scan line segments is designed through the multiplication of probabilistic estimations on each individual primitive, as follows:

$$y = \bar{l} = \arg\max_{l} P(Y = l|I) \cdot \prod_{k} P(yk = l|I)$$

Comparative Experimental Results In training the classifiers, an interactive tool is developed to generate training data samples. A range image is first processed to find local surface normal for each laser point, edge point that has discontinuous change in range value, scan line segments, super segments, etc. These results are compared by an operator to discriminate the boundaries of individual objects. For each object, the operator will manually draw a boundary and assign a label. The software will output the scan line segments that are inside the boundary, as well as the label, for training classifier $P(yk|I)$. The software will also output all laser points within the boundary, as well as the label, for training classifier $P(Y|I)$.

In experiments, two simultaneously measured range images from sensors L4 and L5 are manually labeled. The manually labeled data of L4 is used in training classifiers. The number of training samples with respect to each object class and classification method are listed in Table 3. Three classifiers are trained on the features of scan lines (classifier 1), 3D laser points (classifier 2), and their combination (classifier 3). On the other hand, the range image of L5 is first segmented then classified, and the result is compared with those of manually labeled

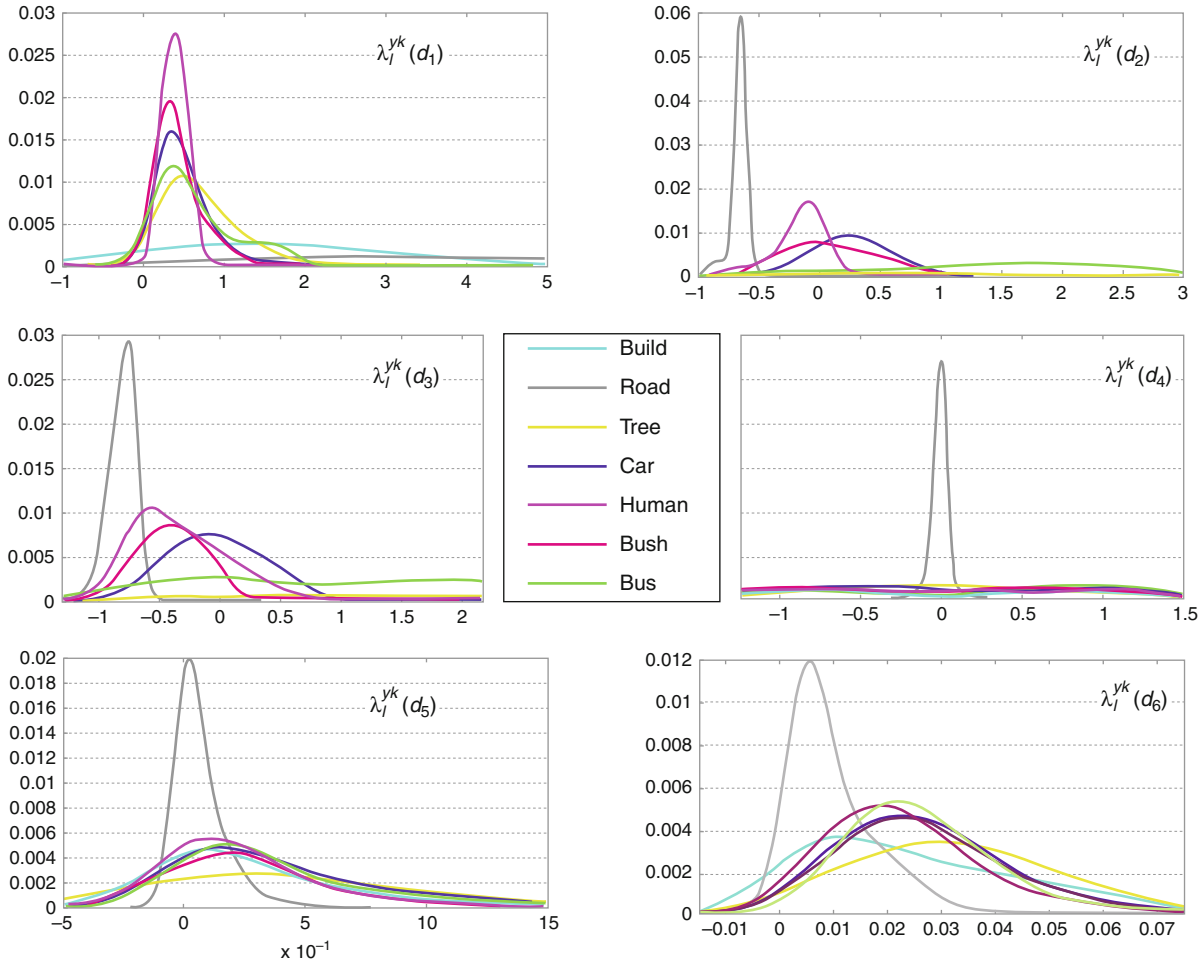

Dynamic Environment Sensing Using an Intelligent Vehicle. Figure 20
Likelihood measures for the classification of a scan line segment [41]

ones. Here, contour-based segmentation is exploited, and the segments are classified using each of the classifiers for comparison. A set of results is shown in Fig. 22, where a number of objects are highlighted. Object 1 includes cars that are correctly classified by all classifiers. Object 2 is a bus that is correctly classified by classifier 1 and 3, but failed in classifier 2. A reason might be the limited number of training samples. Objects 3 and 4 are pedestrians, which are failed in all three classifiers, pointing out that classification performance related to pedestrians needs to be improved through future work. Object 5 is a small house, the shape of which is similar to a bus. Classifier 1 misclassified it into a bus, while two others answered correctly.

Simultaneous Segmentation and Classification

As discussed previously, no matter whether it is a contour-based segmentation or a graph-based one, the same problem occurred. The balance between over-segmentation and under-segmentation can be guided through a parameter setting that is universal for all kinds of objects.

Segmentation is making a partition in data, where in each partition cell (i.e., segment), data has the property of certain homogeneity. However, in facing a complex environment that contains different kinds of objects, different kinds of objects might have different homogeneities. A segmentation method that applys

Dynamic Environment Sensing Using an Intelligent Vehicle. Table 2 Data cues extracted from a cloud of laser points

Feature	Definition
d_1	Minimal height value
d_2	Maximal height value
d_3	Ratio of boundary point number versus total point number
d_4	Mean of height values
d_5	Variance of a histogram distribution on normal vectors
d_6	Major picks of a histogram distribution on normal vectors
d_7	Ratio of width versus length

varied criteria for different object classes is required, where the segmentation and classification issues are considered in a unified form.

The processing flow is shown in Fig. 17b, where a super-segmentation is conducted using the bottom-up heuristics, such as scan-line segments and contour points at different scales, and then the super-segments are merged considering the factor of object class, which is modeled as a problem of joint merger with classification. In super-segmentation, scan line segments are first extracted [69, 70] and merged according to their planarity; a region growing is then conducted to merge the left points and isolated scan line segments according to their spatial connectivity, stopping when a contour point is met. Super-segmentation requires that each segment be a partial observation of an object; it should not be a mixture of different objects. Therefore, strict criteria are used in the above region growing procedures. In a merge procedure, a key problem is defining a model that evaluates the homogeneities for a variety of data segments. The probabilistic formulation is described below.

Probabilistic Model Let s_i and s_j be a pair of neighboring segments with the label of y_i and y_j, respectively. Let s_{i+j} denote the merged segment of s_i and s_j, and y_{i+j} for its label. The probability for s_i merged with s_j, i.e., $P(s_{i+j}|I)$, can be estimated as follows;

$$P(s_{i+j}|I) = \sum_{l \in L} P(y_i = l|I)P(y_j = l|I)P(s_{i+j}|y_{i+j} = l, I)$$

Where, given data cues I, $P(y_i = l|I)$ and $P(y_j = l|I)$ evaluate the probabilities of s_i and s_j labeled to l, respectively. Here, the classifier of both 3D laser points and scan line segments is exploited. $P(s_{i+j}|y_{i+j} = l, I)$ is a likelihood measure, where, given the knowledge of object class $y_{i+j} = l$ and data cues I, the probability of s_i and s_j are the measurements to a single object, i.e., s_i and s_j are merged to s_{i+j}. The likelihood measures with respect to different kinds of objects are defined below.

Definition to Likelihood Measures As the object class is given, an evaluation based on a prior knowledge of the object class is required. They are defined experimentally below.

1. y = building or road :

   Normally only a partial surface of building or road is measured, which could be modeled using a planar surface, with a certain volume (e.g., $\varepsilon = \pm 20$ cm) representing the errors in laser range measurements and modeling generalization. Let S denote the total number of laser points in the range segment, N the number of laser points within the volume, and α the angle between the surface normal and a vertical normal vector $(0, 0, 1)^t$. The likelihood measure is define

$$P(s|y = building,\ I) \propto \frac{N \times \sin\alpha}{S}$$

$$P(s|y = road,\ I) \propto \frac{N \times \cos\alpha}{S}$$

2. y = car:

   Normally data of a car can be restricted within a cube, so that τ_W, τ_L, and τ_H are defined according

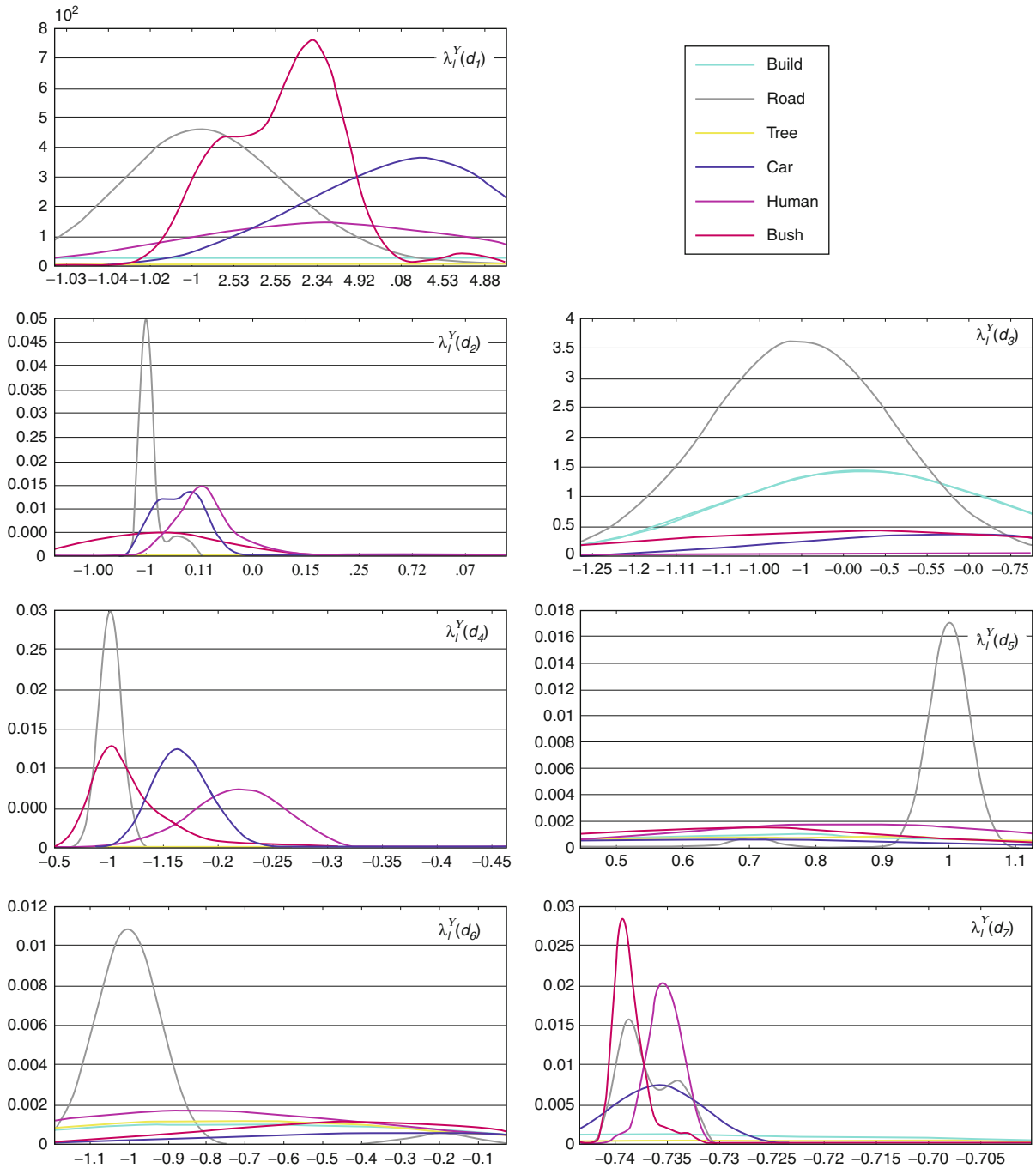

Dynamic Environment Sensing Using an Intelligent Vehicle. Figure 21
The likelihood measures for classifying a cloud of laser points [41]

to the largest width, length, and height of a normal car. A cubic model is used to fit on the laser points of the segment and obtain a width (W_f), a length (L_f), and a height (H_f). A step function is defined (see Fig. 23)

$$y = f(x,\ \alpha_1,\ \alpha_2)$$

and

$$\int_{\max(\alpha_1-\varepsilon,0)}^{\alpha_2+\varepsilon} y\ dx$$

The likelihood measure is defined

$$P(s|y = car,\ I) \propto f(W_f, 0, \tau_W) \times f(L_f, 0, \tau_L) \times f(H_f, 0, \tau_H)$$

3. y = bus:
   Similar with that of a car.
4. y = person:
   Normally data of a person can be restricted within a cylinder, so that a radius (τ_r) and a height threshold (τ_h) is defined according to the size of a normal person. A cylindrical model is used

Dynamic Environment Sensing Using an Intelligent Vehicle. Table 3 The number of sample data in training for classifiers

Class	Scan line segments	Segments of 3D Laser points
Building	9,394	96
Road	10,714	23
Tree	4,122	148
Car	6,080	41
People	394	120
Bush	1,176	39
Bus	253	1
Total	32,133	468

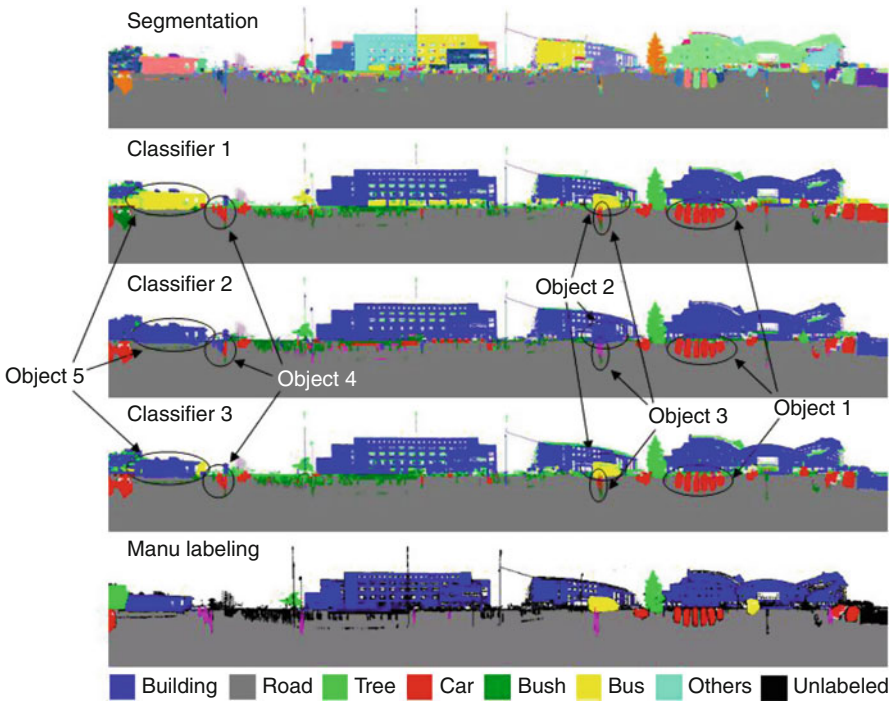

Dynamic Environment Sensing Using an Intelligent Vehicle. Figure 22 Comparative results of different classifiers

to fit on the laser points of the segment and obtain a radius (r_f) and a height (h_f). The likelihood measure is defined

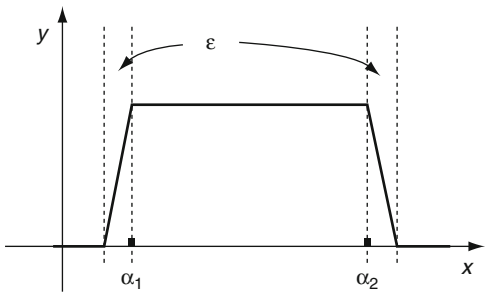

Dynamic Environment Sensing Using an Intelligent Vehicle. Figure 23
A step function for likelihood evaluation [41]

$$P(s|y = person,\ I) \propto \frac{\tau_r}{\max(\tau_r, r_f)} \times \frac{\tau_h}{\max(\tau_h, h_f)}$$

5. y = tree:
   Normally the range segment of a tree consists of many small line segments and edge points. Let S denote the total number of laser points of the range segment, and E the number of laser points on scan line segments. The likelihood measure is defined

$$P(s|y = tree,\ I) \propto \frac{E}{S}$$

6. y = bush:
   Similar with that of a car or bus.

Experimental Results Figures 24 and 25 show experimental results of simultaneous segmentation and classification, where in each figure, the first row is an

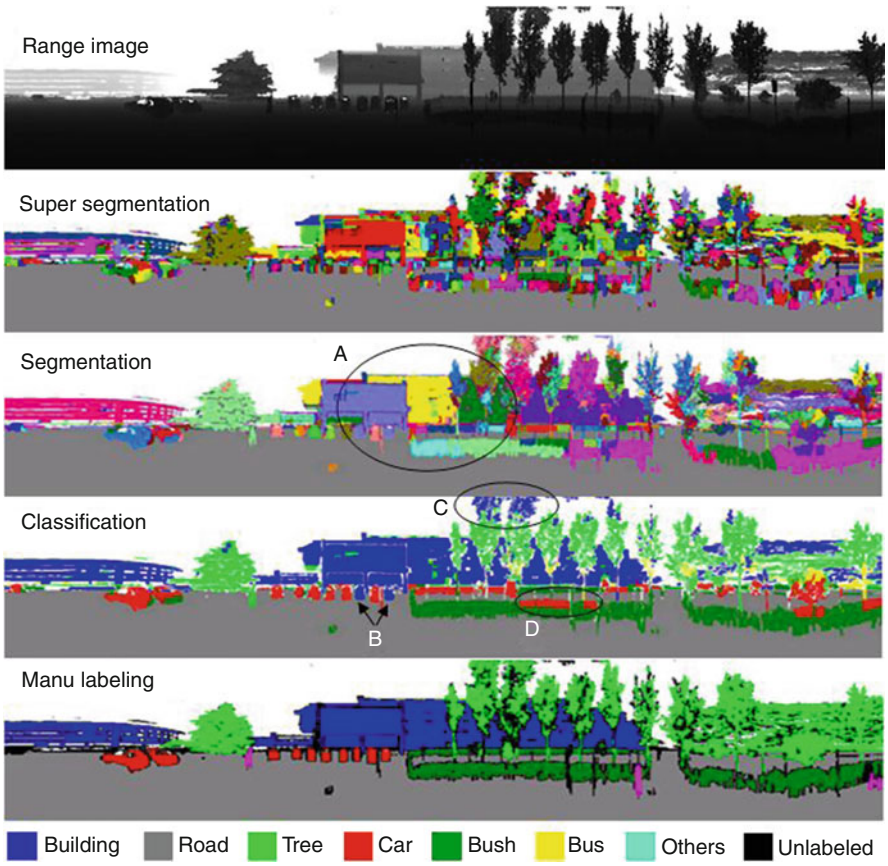

Dynamic Environment Sensing Using an Intelligent Vehicle. Figure 24
Results of simultaneous segmentation and classification

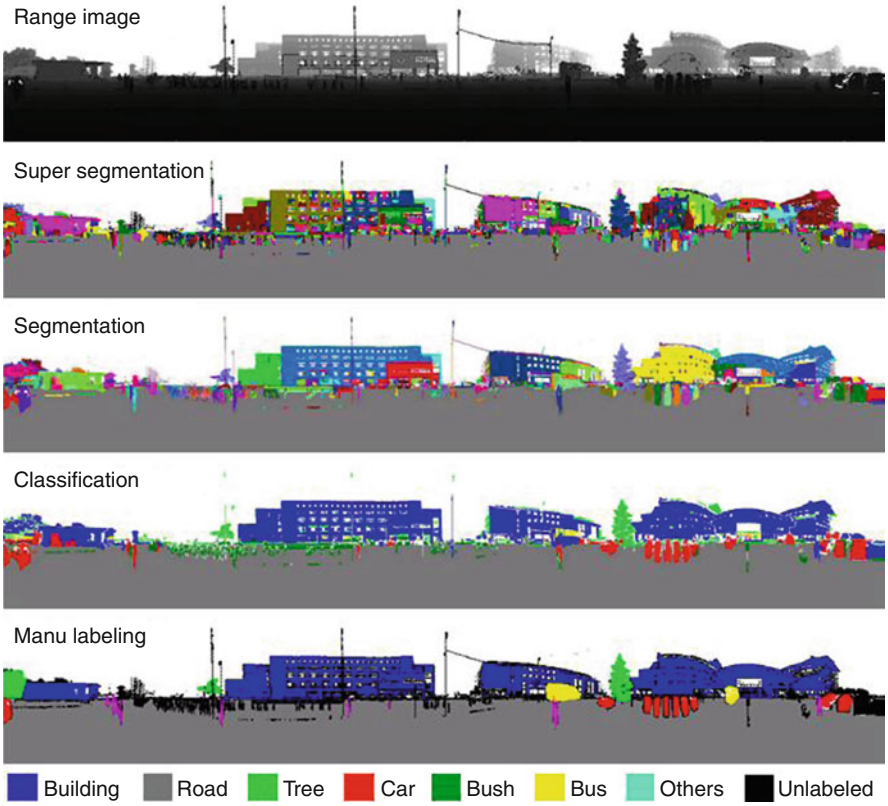

Dynamic Environment Sensing Using an Intelligent Vehicle. Figure 25
Results of simultaneous segmentation and classification [41]

original range image, and the second row shows the segments after super-segmentation. The third and fourth rows are simultaneously obtained results, which are the segments after merge and their class of the highest probability, respectively. For comparison, manually labeled results are also demonstrated at the last row. Generally speaking, the method has good performance with a majority of objects, especially large-scale ones, such as buildings and trees. Compared with the results of contour-based segmentation, over-segmentation in Fig. 24 is reduced greatly, and the problem of under-segmentation (as Failure B in Fig. 17) is solved in this result (highlighted by A in Fig. 24). However, classification errors still exist, where B indicates two cars that are misclassified as buildings, C is trees that are also misclassified as buildings, and D is clumps of bushes, however misclassified as cars. Classification accuracy will be improved through future work.

Contextual Map of Dynamic Environment

As discussed previously, a 3D coordinate can be retrieved for each range pixel, and a range image can be converted into a 3D representation using laser points. Figure 27 shows a map representation of an environment using the geo-reference 3D laser points of L4 and L5, where colors denote different sensor data. In such a map, laser points represent object geometry but do not suggest any contextual knowledge of the objects. Through segmentation and classification, range segments, i.e., laser point clouds, are extracted that represent the data of the same objects, and they are annotated by certain object classes. After segmentation and classification, the laser points of Fig. 26 are annotated and shown in Fig. 27. Here, the color legend is the same as that of Figs. 24 and 25. The result is compared with a manually labeled one, as shown in Fig. 28, where those laser points (i.e., range pixels) that are difficult in

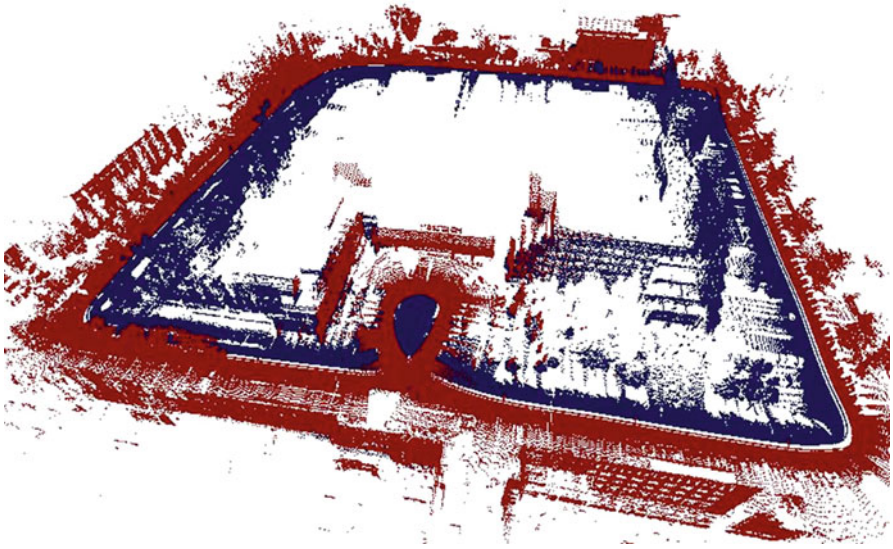

Dynamic Environment Sensing Using an Intelligent Vehicle. Figure 26
A map of the environment represented by unlabeled 3D laser points of L4 and L5 [41]

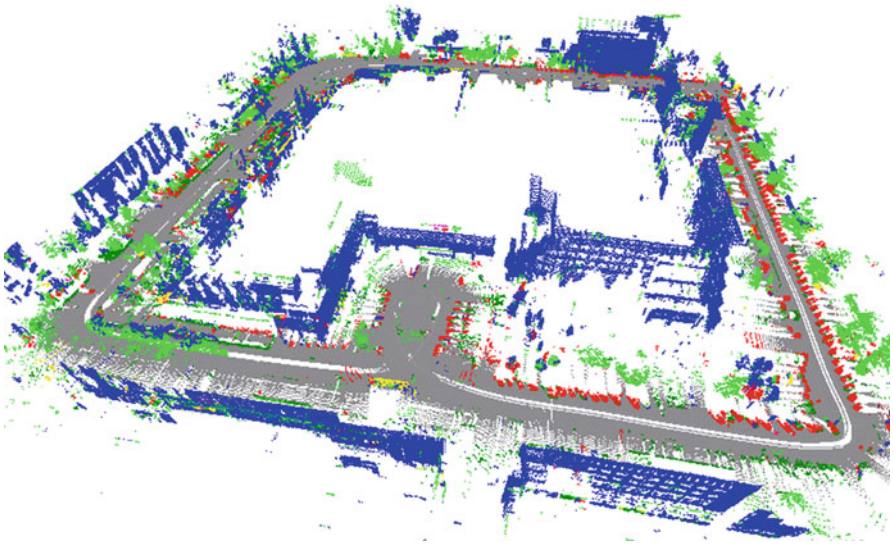

Dynamic Environment Sensing Using an Intelligent Vehicle. Figure 27
A map of the environment represented by annotated 3D laser points of L4 and L5 through simultaneous segmentation and classification [41]

manual discrimination (as the black points in Figs. 24 and 25) are not shown.

In geo-referencing laser measurements of Figs. 26 and 28, the vehicle position of Fig. 5 is used, which is an output of module 2 –SLAMMODT by combinatory exploration of GPS/IMU inputs and a horizontal laser scanner L1. Except for vehicle position, a set of motion trajectories is also obtained as the output of module 2,

which represents the motion of moving objects at a horizontal level that are captured by L1. With the result of Figs. 27 and 28, a 3D map representation of the potentially dynamic objects, such as cars and pedestrians, as well as those of static ones in the environment are generated. The motion trajectories from module 2 are the only direct measurements of the system to the dynamic entities at the environment, however, they are restricted within a horizontal plane. By fusing both of the data as shown in Fig. 29, where the motion trajectories are overlapped onto the 3D map as shown in light blue points, those true dynamic entities at the moment can be inferred. For example, there are almost no light blue points associated with the parked cars in

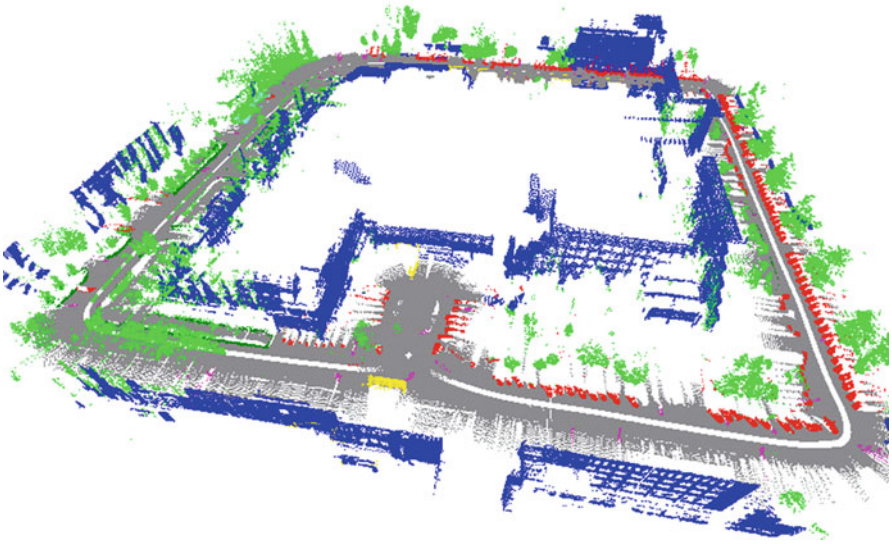

Dynamic Environment Sensing Using an Intelligent Vehicle. Figure 28
A map of the environment represented by annotated 3D laser points of L4 and L5 through manual labeling [41]

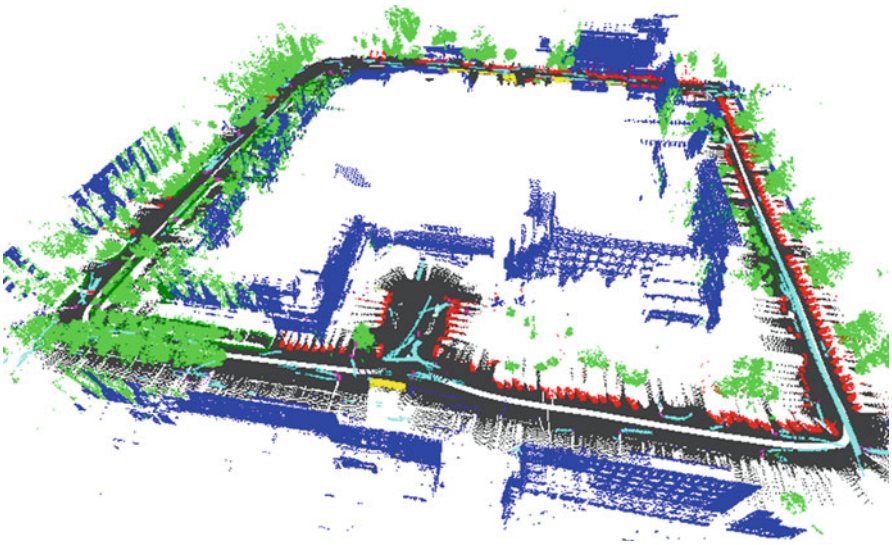

Dynamic Environment Sensing Using an Intelligent Vehicle. Figure 29
A map of the environment with the representation of both static and dynamic entities

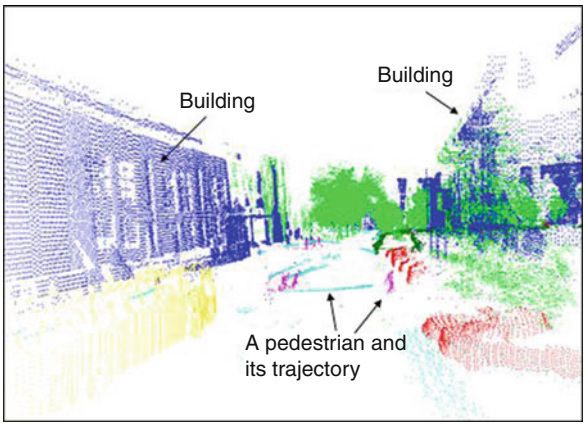

Dynamic Environment Sensing Using an Intelligent Vehicle. Figure 30
Rendered from a viewpoint on street

Fig. 29, which reflect that the potentially moving objects are static at the moment. A map is rendered in Fig. 30 from a street viewpoint, where a pedestrian as well as its motion is highlighted. The 3D shape of the pedestrian is vividly represented in the 3D map. A long, light blue tail can be associated with the pedestrian, which reflects its walking path. In addition, there is a building entrance nearby where the pedestrian is heading, suggesting a possible reason for such a motion.

Future Directions

In order to generate an omni-directional range sensing of a dynamic urban scene using an intelligent vehicle, a system and algorithmic developments for the fundamental issues of multi-laser sensor system calibration, and scene understanding in contextual map generation are presented, as well as experimental examinations. Although there are still open problems left in each of the key issues, this research intends to demonstrate that a geometric and contextual representation of static objects such as buildings, trees, and roads, as well as the motion at the moment of dynamic entities such as people, bicycles, and cars can be obtained using a vehicle robot system.

It is not only that such a representation is helpful in a robot's online perception and decision, but it is also useful in a broad range of potential applications. A city has not only static objects, such as buildings, trees, and roads, but also moving objects, such as people and cars. A study to analyze the interactions between static and dynamic objects is only available when a sensing technique is able to generate a copy of their simultaneous states. Knowledge of the statistical properties of the relationship between static and dynamic objects is important for an advanced online perception, such as surveillance, or offline systems, such as behavior analysis, architectural design, security planning, and so on. This research focused on a sensing system using an intelligent vehicle, where a 3D map representation of both the static and dynamic entities as well as motions in a dynamic environment can be generated. However, how to best make use of such a sensing technology for potential applications needs further research. The data sets that are generated in this research are in [78].

Bibliography

1. International Society of Photogrammetry and Remote Sensing. http://www.isprs.org/
2. Collins R, Hanson A, Riseman E (1994) Site model acquisition under the UMass RADIUS project. In: Proceedings of arpa image understanding workshop, Monterey, CA, pp 351–358
3. Gruen A (1998) TOBAGO – a semi-automated approach for the generation of 3-D building models. ISPRS J Photogramm Remote Sens 53(2):108–118
4. Forstner W (1999) 3D-city models: automatic and semiautomatic acquisition methods. In: Proceedings photogrammetric week, University of Stuttgart, Institute for photogrammetry, pp 291–303
5. Shiode N (2001) 3D urban model: recent developments in the digital modeling of urban environments in three-dimensions. GeoJournal 52(3):263–269
6. Ellum C, El-Sheimy N (2000) The development of a backpack mobile mapping system. Int Arch Photogramm Remote Sensing XXXII(B2):184–191, Amsterdam
7. He G, Orvets G (2000) Capturing road network data using mobile mapping technology. Int Arch Photogramm Remote Sensing XXXIII(B2):272–277, Amsterdam
8. Silva JFC, Camargo PO, Oliveira RA (2000) A street map built by a mobile mapping system. Int Arch Photogramm Remote Sensing XXXIII(B2):510–517, Amsterdam
9. El-Sheimy N (2000) Mobile multi-sensor systems: the new trend in mapping and GIS applications. IAG J Geodesy, vol. 121, Geodesy beyond 2000: the challenges of the first decade. Springer, Berlin/Heidelberg, pp 319–324
10. Li R (1997) Mobile mapping: an emerging technology for spatial data acquisition. Photogramm Eng Remote Sens 63(9):1085–1092

11. Früh C, Zakhor A (2004) An automated method for large-scale, ground-based city model acquisition. Int J Comput Vis 60(1):5–24
12. Ikeuchi K, Sakauchi M, Kawasaki H, Sato I (2004) Constructing virtual cities by using panoramic images. Int J Comput Vis 53(3):237–247
13. Zhao H, Shibasaki R (2003) Special issue on computer vision system: reconstructing textured CAD model of urban environment using vehicle-borne laser range scanners and line cameras. Mach Vis Appl 14(1):35–41
14. Google Earth (2004) http://earth.google.com
15. Microsoft Virtual Earth (2006) http://www.microsoft.com/virtualearth
16. Google StreetView (2007) http://maps.google.com/help/maps/streetview
17. StreetMapper (2007) http://www.streetmapper.net
18. City Grid (2006) http://www.cybercity.tv
19. Cyber City (2007) http://www.cybercity.tv
20. Hu J, You S, Neumann U (2003) Approaches to large-scale urban modeling. IEEE Comput Graph Appl 23(6):62–69
21. Thrun S (2002) Robotic mapping: a survey. CMU-CS-02-11
22. DARPA (2004) DARPA grand challenge rulebook. http://www.darpa.mil/grandchallenge05/Rules_8oct04.pdf
23. DARPA (2006) DARPA grand challenge rulebook. http://www.darpa.mil/grandchallenge/docs/Urban_Challenge_Rules_121106.pdf
24. Journal of Field Robotics: Special issue on the 2007 DARPA urban challenge, Part I 25(8)
25. Journal of Field Robotics: Special issue on the 2007 DARPA urban challenge, Part II 25(9)
26. Nuchter A, Lingemann K, Hertzberg J, Surmann H (2007) 6D SLAM – 3D mapping outdoor environments. J Field Robot 24(8/9):699–722
27. Zhao H, Shibasaki R (2003) A vehicle-borne urban 3D acquisition system using single-row laser range scanners. IEEE Trans SMC Part B: Cybern 33–4:658–666
28. Allen P, Atamos I, Gueorguiev A, Gold E, Blaer P (2001) AVENUE: automated site modeling in urban environments. In: Proceedings of the 3rd international conference on 3D digital imaging and modeling, Quebec City, pp 357–364
29. Georgiev A, Allen PK (2004) Localization methods for a mobile robot in urban environments. IEEE Trans Robot Automat (TRO) 20(5):851–864
30. Hahnel D, Burgard W, Fox D, Thrun S (2003) An efficient FastSLAM algorithm for generating maps of large-scale cyclic environments from raw laser range measurements. In: Proceedings of IEEE/RSJ international conference on intelligent robots and systems, Las Vegas, pp 206–211
31. Wang CC (2004) Simultaneous localization, mapping and moving object tracking. PhD dissertation, Carnegie Mellon University, CMU-RI-TR-04-23
32. Vu T, Aycard O, Appenrodt N (2007) Online localization and mapping with moving object tracking in dynamic outdoor environment. In: Proceedings IEEE intelligent vehicle symposium, Istanbul, pp 190–195
33. Weiss T, Schiele B, Dietmayer K (2007) Robust driving path detection in urban and highway scenarios using a laser scanner and online occupancy grids. In: Proceedings of the IEEE intelligent vehicle symposium, Istanbul, pp 184–189
34. Zhao H, Chiba M, Shibasaki R, Shao X, Cui J, Zha H (2008) SLAM in a dynamic large outdoor environment using a laser scanner. In: Proceedings of the IEEE international conference on robotics and automation (ICRA), Pasadena, CA, pp 1455–1462
35. Velodyne HDL-64E (2007) http://www.velodyne.com/lidar/products/overview.aspx
36. SICK LMS2** (2001) http://www.sick.com
37. Durrant-Whyte H, Bailey T (2006) Simultaneous localization and mapping: Part I. IEEE Rob Autom Mag 13(2):99–108
38. Bailey T, Durrant-Whyte H (2006) Simultaneous localization and mapping: Part II. IEEE Rob Autom Mag 13(3):108–117
39. Streller D, Dietmayer K (2004) Object tracking and classification using a multiple hypothesis approach. In: Proceedings of the IEEE intelligent vehicles symposium, Parma, pp 808–812
40. Fayad F, Cherfaoui V (2007) Tracking objects using a laser scanner in driving situation based on modeling target shape. In: Proceedings of the IEEE intelligent vehicle symposium, Istanbul, pp 44–49
41. Zhao H, Liu Y, Zhu X, Zhao Y, Zha H (2010) Scene understanding in a large dynamic environment through a laser-based sensing.In: IEEE international conference on robotics and automation, Anchorage, pp 127–133
42. Zhao H, Xiong L, Jiao Z, Cui J, Zha H (2009) Sensor alignment towards an omni-directional measurement using an intelligent vehicle. In: Proceedings of the IEEE intelligent vehicle symposium, Kobe, pp 292–298
43. Zhao H, Shibasaki R (2001) High accurate positioning and mapping in urban area using laser range scanner. In: Proceedings of IEEE intelligent vehicles symposium, Tokyo, pp 125–132
44. Zhao H, Chiba M, Shibasaki R, Shao X, Cui J, Zha H (2009) A laser scanner based approach towards driving safety and traffic data collection. IEEE Trans Intell Transport Syst 10(3):534–546
45. Cheok GS, Leigh S, Rukhin A (2002) Calibration experiments of a laser scanners. NISTIR 6922:121
46. Santala J, Joala V (2003) On the calibration of a ground-based laser scanner. TS12.4, FIG working week
47. Mahlisch M, Hering R, Ritter W, Dietmayer K (2006) Heterogeneous fusion of video, Lidar, ESP data for automotive ACC vehicle tracking. In: Proceedings of IEEE international conference on multisensor fusion and integration for intelligent systems, Heidelberg, pp 139–144
48. Rodriguez F, Sergio A, Fremont V, Bonnifait P (2008) Extrinsic calibration between a multi-layer LIDAR and a camera. In: Proceedings of IEEE international conference on multisensor fusion and integration for intelligent systems, Seoul, pp 214–219
49. Zhao H, Chen Y, Shibasaki R (2007) An efficient extrinsic calibration of a multiple laser scanners and cameras' sensor system on a mobile platform. In: IEEE intelligent vehicles symposium, Istanbul, pp 422–427

50. Gao C, Spletzer JR (2010) On-line calibration of multiple LIDARs on a mobile vehicle platform. In: Proceedings of IEEE international conference on robotics and automation, Anchorage, pp 279–284
51. Besl PJ, McKay ND (1992) A method for registration of 3-D shape. IEEE Trans Pattern Anal Mach Intell 14:239–256
52. Chen Y, Medion G (1992) Object modeling by registration of multiple range images. Image Vis Comput 10(3):145–155
53. Zhang Z (1994) Iterative point matching for registration of a free-from curves and surfaces. Int J Comput Vis 13:119–152
54. Hahnel D, Burgard W, Thrun S (2003) Learning compact 3d models of indoor and outdoor environments with a mobile robot. Rob Autom Syst 44:15–27
55. Althaus P, Christensen H (2003) Behavior coordination in structured environments. Adv Robot 17(7):657–674
56. Mendes A, Nunes U (2004) Situation-based multi-target detection and tracking with laserscanner in outdoor semi-structured environment. In: Proceedings IEEE/RSJ international conference on intelligent robots and systems, Sendai
57. Posner I, Cummins M, Newman P (2008) Online generation of scene descriptions in urban environments. Rob Autom Syst 56(11):901–914
58. Douillard B (2009) Vision and laser based classification in urban environments. PhD thesis, University of Sydney
59. Nuchter A, Lingemann K, Hertzberg J, Surmann H (2009) 6D SLAM – 3D mapping outdoor environments. J Field Robot 24(8–9):699–722
60. Martinez-Mozos O, Stachniss C, Burgard W (2005) Supervised learning of places from range data using AdaBoost. In: IEEE international conference on robotics and automation (ICRA), Barcelona, pp 1742–1747
61. Triebel R, Kersting K, Burgard W (2006) Robust 3D scan point classification using associative Markov networks. In: IEEE international conference on robotics and automation (ICRA), Orlando, FL
62. Douillard B, Fox D, Ramos FT (2008) Laser and vision based outdoor object mapping. In: Proceedings of robotics: science and systems, Zurich
63. Posner I, Cummins M, Newman P (2009) A generative framework for fast urban labeling using spatial and temporal context. Auton Robot 26(2–3):153–170
64. Hoover A, Jean-Baptiste G, Jiang X, Flynn PJ, Bunke H, Goldgof D, Bowyer K (1996) A comparison of range image segmentation algorithms. IEEE Trans Pattern Anal Mach Intell 18(7):673–689
65. Katsoulas D, Bastidas CC, Kosmopoulos D (2008) Superquadic segmentation in range image via fusion of region and boundary information. IEEE Trans Pattern Anal Mach Intell 20(5):781–795, 2008
66. Weingarten J, Siegwart R (2005) EKF-based 3D SLAM for structured environment. In: IEEE/RSJ international conference on intelligent robots and systems, Edmonton, Alberta, pp 2089–2094
67. Han F, Tu Z, Zhu SC (2004) Range image segmentation by an effective jump-diffusion method. IEEE Trans Pattern Anal Mach Intell 26(9):1138–1153
68. Borenstein E, Ullman S (2008) Combined top-down/bottom-up segmentation. IEEE Trans Pattern Anal Mach Intell 30(12):2109–2125
69. Malisiewicz T, Efros AA (2008) Recognition by association via learning per-exemplar distances. In: Proceedings of the IEEE conference on computer vision and pattern recognition (CVPR), Anchorage
70. Porway J, Wange K, Zhu SC (2008) A hierarchical and contextual model for aerial image understanding. In: Proceedings of the IEEE international conference on computer vision and pattern recognition (CVPR), Anchorage, pp 1–8
71. Tu Z, Chen X, Yuille A, Zhu SC (2005) Image parsing: unifying segmentation, detection and recognition. Int J Comput Vis 63(2):113–140
72. Golovinskiy A, Kim VG, Funkhouser T (2009) Shape-based recognition of 3D point clouds in urban environments. In: IEEE international conference on computer vision, Kyoto, pp 2154–2161
73. Shi J, Malik J (2000) Normalized cuts and image segmentation. IEEE Trans Pattern Anal Mach Intell 22:888–905
74. Felzenszwalb PF, Huttenlocher DP (2004) Efficient graph-based image segmentation. Int J Comput Vis 59:167–181
75. Jiang X, Bunke H (1994) Fast segmentation of range images into planar regions by scan line grouping. Mach Vis Appl 7:115–122
76. Rosin PL, West GAW (1995) Nonparametric segmentation of curves into various representations. IEEE Trans Pattern Anal Mach Intell 17:1140–1153. http://users.cs.cf.ac.uk/Paul.Rosin
77. Chang CC, Lin CJ (2001) LIBSVM: a library for support vector machines. http://www.csie.ntu.edu.tw/∼cjlin/libsvm
78. PKU Omni Smart Sensing – POSS (2010) http://www.poss.pku.edu.cn

E

Earth System Environmental Literacy

Sustainability Education: Challenges of Integrating Virtual Versus Real Nature in Science Education

Margaret Lowman
Nature Research Center, NC Museum of Natural Sciences and Professor, North Carolina State University, Raleigh, NC, USA
TREE Foundation, Sarasota, FL, USA

Article Outline

Glossary
Definition of Sustainability Education
Introduction
Short History of Sustainability Education and Related Education Initiatives
Sustainability Education in the Twenty-First Century
Future Directions
Bibliography

Glossary

Ecosystem services Benefits provided by natural systems that do not necessarily require significant financial maintenance, including water purification, clean air, pollination, soil decomposition, biodiversity, and many others. In accounting, balance sheets often overlook these free services provided by Mother Nature.

Finite resources In sustainability education, this involves those natural resources on planet Earth that require careful allocation into the future, such as fresh water, oil, and many others.

NEON Acronym for a long-term environmental monitoring program funded by Congress and mandated to include both research and education components, entitled "National Ecological Observatory Network."

Pedagogy The art, science, or profession of teaching and indirectly, the process of implementing assessments or outcomes as part of educational research in order to improve teaching.

STEM Acronym describing the major science subjects for education advancement, which include "science, technology, engineering, and mathematics."

Sustainability When a system functions indefinitely with regard to present and future needs, such as when human and natural systems operate indefinitely through careful resource allocation.

Virtual versus real In sustainability education, there is an underlying controversy between the importance of tools of teaching: newer techniques involve virtual tools (computers, handheld devices, simulated games, virtual field trips, and videos), whereas more conventional tools include real nature such as field trips, taxonomic collections, and hands-on natural science activities. Ideally, both virtual and real approaches contribute to effective learning.

Definition of Sustainability Education

▶ The best time to plant a tree is twenty years ago. The next best time is now. (African proverb)

If every citizen could read the above quote and understand its underlying ecological concepts, economic challenges, social services, and spiritual heritage, then it is likely that sustainability education would be achieved. The notion of a tree and its ecosystem services illustrate sustainability in the simplest yet most robust sense. To plant and grow a tree, economists struggle with volatile currencies; ecologists juggle development and conservation; religious leaders advocate stewardship; and social scientists examine equity in a world of declining resources. Sustainability education requires an integrated approach between ecology, risk analyses, economics, social sciences, biological sciences, political sciences, languages, biotechnology, physical sciences, health sciences, and religion.

Robert A. Meyers (ed.), *Encyclopedia of Sustainability Science and Technology*, DOI 10.1007/978-1-4419-0851-3,
© Springer Science+Business Media, LLC 2012

All these practitioners (and many others) contribute to sustainability education, an emerging discipline that requires an interdisciplinary synthesis of knowledge, translated into practice, to insure the future of life on Earth.

Introduction

Science education, also termed STEM (science, technology, engineering, and mathematics) is undergoing a revolution in America as well as overseas [1]. The clear links between our environment, human health, and economics have triggered a serious effort to improve science literacy into the twenty-first century. As global environmental setbacks including climate change, famine, and biodiversity extinction loom, Earth's living systems are fast approaching a tipping point beyond which life on earth may cease to exist as it is known now [2]. Yet never before have humans had such high levels of technology to achieve solutions to global challenges. How to integrate these new technologies with science education is one of the major priorities facing both local and national governments. Neighborhoods and communities face the challenges of air quality and fresh water; entire nations prepare to adapt to rising sea levels and volatile food prices due to droughts; and around the globe, nations struggle with increasing levels of carbon dioxide in our atmosphere and oceans [3]. All of these issues directly link to the quality of sustainability education, which translates into training the next generation to understand the links between a healthy environment, human health, a sound economy, and shared use of finite natural resources.

It is daunting to link the future health of planet Earth with the importance of learning about how our Earth operates. But science or sustainability education in this sense has become a direct metric for our future survival. In America, professional groups including National Academy of Sciences, National Science Foundation, American Association for Advancement of Science, National Association of Environmental Educators, Boy and Girl Scouts of America, American Association of Museums, almost all scientific societies, and even grassroots organization such as Children and Nature Network, local Sierra Club chapters, and religious networks have embraced the challenge of raising science literacy. Furthermore, science literacy is adopted here to umbrella many different aspects of STEM literacy. Diverse components of science literacy included under this umbrella range from marine literacy, environmental literacy, physics literacy, mathematics literacy, and to ecological literacy. Sustainability goes one step further from the collective science literacies in that it requires the integration of both social and physical/biological sciences. But one common denominator emerges for all of these efforts relating to science or sustainability literacy – the notion of sustainability education embraces our knowledge of how to continue to live on planet Earth without exhausting our resources.

Ultimately, sustainability education may be best achieved by a blend of hands-on (i.e., real) and virtual science education experiences. Building bridges between virtual and real environments, among scientists and citizens, and spanning ecology and economics were some of the central issues in recent summits and conferences of educators and other professionals in Washington, DC during 2009–2010. This chapter reviews some of the emerging informal science education priorities for integrating tools both virtual and real, ultimately to create effective sustainability education.

Short History of Sustainability Education and Related Education Initiatives

Over the past decade, myriad conferences, conversations, workshops, and white papers have been produced on the topic of science education, and on raising America's STEM literacy as part of its global economic competitiveness [4–13]. It is well recognized that the conventional methods of large lectures, textbooks, and short laboratory sessions are not able to cover the overwhelming body of scientific knowledge, and even worse, this format does not inspire today's students to pursue careers in science or even to achieve a minimal level of scientific literacy. Educators and scientists alike recognize that innovative, new pedagogies need implementation immediately, if America can regain her leadership in technology and innovation, especially in fields that relate to sustainability such as energy, conservation, biodiversity, ecosystem services, and environmental justice. This commitment

has gained center stage in editorials, publications, and conversations from the highest federal levels to the grassroots of small school PTAs; yet specific mechanisms for achieving a robust level of sustainability education have not yet been successfully documented. This remains a priority for both the current practitioners of STEM education, for educators, and for the stewards of natural resources, who recognize the need for interdisciplinary approaches in education to ensure sustainability for all.

Ecological Literacy

- There is one important difference between ecology and many other fascinating sciences and games: unsolved problems of chess, astronomy, or mathematics will not change if we ignore them. Our activity or lack of activity can alter the state of ecology. (Lawrence B. Slobodkin 2003)

Ecological or environmental literacy has been a cornerstone for both formal and informal science education [14]. In particular, the big challenge for ecology education is not a lack of information, but rather the need to provide the relevant context [15, 16] that will motivate the next generation of environmental scientists to collect, access, and interpret relevant information needed for ecological stewardship. A conceptual understanding of "healthy" ecosystems and related ecosystem services, ranging from food and energy to clean air and water, will be required – not only to serve as the foundation for sound economics, but also to sustain human health. Nature shapes, and is shaped, by communities where people live, and in this sense ecology education overlaps directly with sustainability education. When students bond with their natural surroundings, and then use virtual simulations to understand large-scale ecological processes and drivers, ecology education is achievable [17, 18].

During October 2010, a diverse group of organizations hosted a sustainability education summit, entitled Environmental Literacy for a Sustainable World (www.esa.org/eesummit). The mission of this summit was *not* to create a white paper to mail out to participants 6 months later, as is often the aftermath of conferences, but to create a decadal action plan embraced and activated by the participants to advance environmental literacy. One of the first notions of the summit was to agree that all the science literacies are closely related, and that the achievement of a sustainable world will only come about by raising the standards of ecological, environmental, and science literacy – or whatever the label. An open letter to government leaders about the importance of sustainability education was one of the first outcomes (for, e.g., 17 January 2011, www.heraldtribune.com). Additional action items include: (1) Produce a common set of 5–15 key concepts and principles that link human and natural systems for use by teachers and policy makers; (2) Engage communities to meet the challenges of an uncertain future; (3) Create a network of green-design built environments; create an "APP" (application for handheld mobile devices) that links personal behavior to the environment as an index of health; (4) Construct a "go-to" site for environmental materials, aka a technology infrastructure to inventory, synthesize and share best practices and programs; and others. These action items all have different timelines, with the ultimate goal of engaging diverse stakeholders in different elements of sustainability education by 2020.

Conservation Literacy

Like ecology, conservation biology represents another closely related discipline to sustainability, and hence the concepts and applications of an educational strategy will overlap. In the field of conservation biology, a lively debate about the creation of a conservation ethic started long ago with Aldo Leopold's seminal book, *The Sand County Almanac* [14]. Leopold articulated a value system with regard to land, "That land is a community is the basic concept of ecology, but that land is to be loved and respected is an extension of ethics. That land yields a cultural harvest is a fact long known, but latterly often forgotten."

The Society for Conservation Biology defined its goals and objectives as, "the education, at all levels, preparatory and continuing, of the public, of biologists, and of managers in the principles of conservation biology" [19]. Further, the Society's education committee articulated principles that seek to maintain Earth's biological diversity, ecological integrity, and ecological health. But the practitioners of conservation biology admit that their approach is very passive,

"Among conservation biologists the prevailing view of conservation education appears to rest on

a deep-seated belief that the basic function of conservation education should be to disseminate knowledge that scientists generate, essentially to transport information to the public and key groups in the expectation that it will eventually precipitate more appropriate conservation-related behaviors" [20]. This is not unusual, and most scientists have adopted a "speak and they will listen" approach to STEM education. But in a world of declining and finite resources, a tipping point is fast being approached in the education circles, whereby the methodologies need to drastically change in order to inspire a science-literate community as stewards of global health. Sustainability education – if launched with appropriate integration of virtual and real natural systems [21], facts and "oh-wow" responses, local and global perspectives, and interdisciplinary approaches [22, 23] – is critical to succeed.

Biological Literacy

As a biologist by training, I have tracked the notion of biological literacy as a component of science education throughout my career [1]. The world has witnessed an amazing explosion of knowledge in biology – ranging from genomics and nanotechnology to global climate change and how sea-level rise will impact Earth's resources.

The relevance of biology education may be the most focused of all the "science literacies" to date due to extensive support from NSF, AAAS, Association of American Medical Colleges (AAMC), and Howard Hughes Medical Institute (HHMI). In its most recent "conversation" that included over 500 biological sciences faculty, administrators, students, and other practitioners, AAAS published a white paper called "Vision and Change" (www.visionandchange.com) [1]. They summarized four academic concepts to implement change in biology education: (1) Integrate core concepts and competencies; (2) Focus on student-centered learning; (3) Promote a campus-wide commitment to change; and (4) Engage the biology community in the implementation of change. The outcome of the "conversation" was to encourage all biology educators to develop a coordinated and sustainable plan for implementation of principles that will improve the national standards of biology education.

Specific working groups to advance biology education (also termed "new biology") convened around different priorities needed for biology education: managing large, complex data sets; interdisciplinary approaches; making connections among different concepts and/or questions; and seek new inquiry-based learning activities rather than the conventional memorization and lecture-based approaches [1]. Advancing education in biological sciences directly impacts our nation's ability to respond to recent challenges, ranging from climate change to safe drinking water [10–12]. The core literacy concepts were delineated to include evolution, structure and function, information flow, and pathways and transformations of energy/matter, systems [1]. Core competencies were defined as the abilities to apply the process of science, use quantitative reasoning; use modeling/simulation; tap into the interdisciplinary nature of science; communicate/collaborate with other disciplines; and understand the relationship between science and society [1]. While these criteria were developed for biology education, many of the same elements would be relevant for sustainability education which concurrently embraces biology as well as other disciplines.

Sustainability Education in the Twenty-First Century

Achieving science literacy is vital in the twenty-first century. Sustainability education can be construed as that interdisciplinary platform whereby diverse members of global communities seek to understand the role of humans in their physical and social environments. As global environmental challenges loom at an unprecedented magnitude, "tipping points" that threaten to irreversibly damage Earth's living systems are fast approaching [16]. Yet, never before have humans had such a wealth of technology to achieve solutions at their disposal, allowing collaboration from virtually anywhere in the world, drawing ideas from multiple disciplines to process and analyze countless data points, and teaching the next generation to view our world in exciting, novel ways that inspire environmental stewardship.

In our teaching, environmental scientists must seek to balance cellular versus organismal biology, virtual models versus real-time data, and science blended with policy. Future stewards will need skills in assessing, predicting, managing, and communicating the dramatic ecological and societal risks and changes confronting us [1]. However, a major stumbling block in training the next generation of practitioners is the challenge of effectively integrating technology with in situ fieldwork. While most senior ecologists were inspired by their training in the field, younger scientists are more familiar with virtual ecosystems through gaming, social networking, and computer models, sometimes leading to so-called nature-deficit disorder. How can environmental practitioners blend "hands-on" fieldwork with "cutting-edge" technology? This conundrum is the subject of ongoing debate. Those born after 1980 spend more time indoors with electronic devices than going outdoors to experience nature first hand [17, 18].

On a positive note, new programs are emerging that successfully integrate virtual and real environments. The National Ecological Observatory Network (NEON) will conduct continental-scale environmental monitoring in situ, and their large databases will be accessible to students, citizen scientists, and policy makers ([20], see also www.neoninc.org). At the North Carolina Museum of Natural Sciences in North Carolina, the new Nature Research Center, with its mission "to engage the public in understanding the scientific research that affects their daily lives," will house state-of-the-art research laboratories, accessible to the public, a three-story Daily Planet immersion theater, broadcasting field science from remote sites via video-streaming, and dedicated virtual and real meet-the-scientist activities ([21], see also www.naturesearch.org) . These two examples illustrate the changing landscape for ecology education, and how technology can, and must, advance environmental literacy.

NEON

The National Ecological Observatory Network will take field measurements by scientists, citizens, and students collectively to a new level [24]. This continent-scale research platform will conduct long-term monitoring in America's major ecosystems, and create an important education outreach component as a parallel stream of the research program. Affectionately called the "ecologists' Hubble Telescope," this is the largest federally funded research project undertaken by the ecological community, and aspires to contribute data sets that will lead to best practices for solving environmental challenges in the future. Critical to NEON's success is the sustainability education and outreach component that have the potential to change how policy makers as well as citizens learn about sustainable solutions.

Citizen science has burgeoned in the past decade, in part due to Internet and handheld technological devices, but also because of a growing awareness that sustainability education is a community responsibility. Almost 20 years ago, the Jason Expedition (www.jason.org) pioneered distance learning for middle school youth, who not only visited marine and rain forest canopy environments, but also collected ecological data to share with other schools (e.g., [25]). Today, myriad programs including Project Budburst (www.budburst.org) and Project Nestwatch (www.nestwatch.org) rely on citizens' collecting data, which are collated at a central source for scientific use.

Planning for NEON took over a decade with hundreds of ecologists providing input. Projected to become fully operational by 2016, NEON's 20 field sites will be linked by high-capacity cyber infrastructure with the capacity to make forecasts about environmental changes. Important for sustainability education, these issues include six of the National Academies' grand challenges: biodiversity, climate change, ecohydrology, biogeochemistry, infectious disease, invasive species, and land use [26]. And even more critical to sustainability education is NEON's capacity to involve not just scientists – but also the public, students, teachers, and policy makers – to use the NEON interface for downloading data and learning by doing. NEON also pledges to prioritize science communication to diverse audiences [24] and foster the links between human health and healthy ecosystems. Will NEON's education vision be achieved, or will it become a pile of dusty papers on some university desks? Only time will tell, but NEON has the potential to advance sustainability education across an entire continent.

NRC

The Nature Research Center (NRC) at the North Carolina Museum of Natural Sciences is a new, 80,000-square foot wing of the existing 132-year-old Museum. While conventional museums focus on "what we know" about science, the new wing will engage the public in "how we know what we know" and in particular inspire the public to understand scientific research that affects their daily lives. The NRC goals are to conduct/communicate cutting-edge science, create exemplary role models to inspire diversity in the next generation of scientists, and integrate real and virtual science to engage youth about scientific discoveries. Four new labs will house scientists, educators, technology experts, students, and volunteers – all working together to understand how science works and communicate it to a diverse audience. In addition, the notion of scientists and educators and technology geeks all working together on the floor is unique to the Museum world, and seeks to assimilate "citizen science" into all components of research and education at the NRC. Many partners will insure a robust content for science communication – joint positions with the UNC system, partnerships with NOAA, NASA, National Geographic, and North Carolina government agencies, will all contribute to the creation of innovative science communication. The NRC has four unique learning platforms, facilitating the assessment of how different audiences learn best: (1) The Daily Planet, a high technology, immersion theater linked through the Ethernet highway to all classrooms in North Carolina and ultimately, around the world; (2) Citizen science labs, where participation in data collection by volunteers will contribute to answering important questions about our environment; scientific laboratories with glass walls allowing visitors to be involved in the research; (3) Investigate labs, where related research will be undertaken that involves school groups or other visitors; and (4) Hands-on exhibits where visitors are immersed in *how science works* (Fig. 1).

By "reinventing" the education pathways of conventional museums, the NRC hopes to inspire diverse students to become excited about science, and to inspire scientists to engage in successful education outreach, which links directly to creating a higher level of sustainability education.

Earth System Environmental Literacy. Figure 1
North Carolina's new Nature Research Center integrates cutting-edge research, education and technology for diverse audiences to foster environmental literacy

Future Directions

The future is ours by design, but there is a need to seek interdisciplinary solutions and then communicate them with one voice. When baby boomers think back to their childhood, they can probably recall a favorite tree house, scout camping trip, or neighborhood picnics. In today's world, children are not allowed unsupervised time outdoors, due in part to parents' distrust of issues ranging from strangers to global security. But knowledge of real nature is essential to raise levels of environmental literacy, and in turn achieve a higher degree of sustainability education. Harking back to the African proverb in the beginning of this entry, many children do not have a clear concept of what is required to sustain a tree. But knowledge of nature is their best weapon if young people are ultimately to make good decisions about personal health, climate change, and land-use management.

Despite the gloom and doom notions surrounding environmental literacy and our human aspiration to attain a sustainable lifestyle, there are exemplary actions providing amazing examples of best practices. What are some of the diverse projects exemplifying sustainable education? Here is a selection of sustainability education activities, perhaps useful to implement in your own community!

1. *Strategies for Ecology Education, Diversity and Sustainability (SEEDS). Diverse People for a Diverse Science.* SEEDS is an education program of the Ecological Society of America (Fig. 2). Its mission is to diversify and advance the ecology profession through opportunities that stimulate and nurture the interest of underrepresented students to not only participate in ecology, but to lead. Focused mainly at the undergraduate level, with extension services for communities, high schools, graduate students, and international collaborations, the SEEDS program promotes an ecology profession with wide representation to ensure environmental understanding and a sustainable future for all. (www.esa.org/seeds)
2. *Urban Farming.* In partnership with a neighboring community garden, Mill Creek Farm (MCF) transformed a vacant West Philadelphia lot into a thriving urban farm and intergenerational educational center (Fig. 3). Now starting on their sixth

Earth System Environmental Literacy. Figure 2
At the Ecological Society of America's annual meetings, SEEDS students are mentored to insure a diverse community of ecologists

Earth System Environmental Literacy. Figure 3
Mill Creek Farm, near Philadelphia Pennsylvania, examplifies the growing popularity of sustainable urban farming

field season, MCF engages and galvanizes the community by providing affordable and sustainable food to the surrounding neighborhoods, employing local high-school students, offering food justice education and much, much more. For more information (including a documentary and radio stories) visit: http://www.millcreekurbanfarm.org/

3. *Sustainability Education for Incarcerated Youth*. For 19 years, high school science teacher DC Randle taught biology and environmental sciences to middle and high school youth in the Minnesota correction system. Defined as emotionally, behaviorally disordered students, they thrived under a curriculum that allowed them to rediscover nature. Using the natural resources around their facility, their science teacher provided a strong backbone for sustainability education to these at-risk youth.
4. *Local-to-Global Connections*. As part of a fund raiser for a local canopy walkway, Meg Lowman started leading field trips to the Amazon for underserved youth in Florida. Called the Florida-Peru Connection, the local community funded scholarships for local Boys and Girls Club and Girls Inc. students. In return, young people have visited America from Amazonian villages along the Rio Napo in Peru. The link between local and global is an important concept for sustainability, and experiencing other ecosystems and culture first hand had a significant impact on the perspectives of both the Amazon and the American communities who were part of the exchange. As a result of shared global views, both Florida and the Amazon share a canopy walkway for education, where children (and others) conduct research on the biodiversity of forests (Fig. 4). More information is listed at www.treefoundation.og
5. *Student Outreach in Science (SOS)*. Environmental studies students at New College of Florida developed sustainability outreach activities appropriate for elementary and middle school classes. They developed a skillset in science communication, and then took their lessons to underserved schools in the districts, providing a student-teaching-student model that was well received by both the teachers and the students. Units ranged from climate change adaptation to growing local vegetables to invasive species to clean energy. Over 60 students at New College received the Sarasota County Conservation Education award based on their SOS program (www.canopymeg.com)

Earth System Environmental Literacy. Figure 4
At North America's first public canopy walkway in Florida, third graders conduct original research on forest canopies

6. *Master of Arts in Sustainable Communities, Northern Arizona University* (http://home.nau.edu/sus/). Students are admitted from all kinds of backgrounds – from political science and sociology to science and engineering to humanities and business. Students build their own programs of coursework from the university's very broad array of courses relevant to sustainability (of economies and of societies as well as of natural resources and environment). More important, they each develop independent, community-based research/thesis projects. Many come to this program as working professionals while some are more conventional students coming straight from a bachelor's degree. Graduates from this program are indeed transforming many communities around the intermountain west. Another unique program at NAU is the Professional Science Master's in Climate Science and Solutions. http://climatesciencesolutions.nau.edu/
7. *Measuring the Sustainability of Food to Table.* Professor David Cleveland at University of California, Santa Barbara engaged his environmental studies students in measuring the energy budget of regional agriculture, from farm to table. This agrifood systems analysis has the potential to change small-scale and local agriculture, and educate students in sustainable practices at the same time. It also earned David the award of Campus Sustainability Champion [27]. http://es.ucsb.edu/profile/cleveland
8. *Young Voices on Climate Change.* Author Lynn Cherry, finding resistance to teaching climate science, is producing inspiring, empowering short films to break down those barriers. The *Young Voices on Climate Change* documents inspiring success stories of kids shrinking their carbon footprint and fighting climate change. When climate change science is preceded with the showing of these films, youth and adults alike are more receptive to embracing the seriousness of environmental change rather than denying. Young people listen to others their own age and, in these films their peers model the skills, motivation, and confidence necessary to reduce CO_2 emissions.(www.YoungVoicesonClimateChange.com)
9. *Sustainability between Connecticut and Jamaica.* Eastern Connecticut State University recently had approved a new major in Sustainable Energy Studies – one interesting program associated with

students in this new major has been the service-learning project taking students to Jamaica to develop a small wind power system for the school in Lucea, Jamaica. The university has a long-standing relationship with Jamaican public schools because of our program to get their normal school teachers to complete their bachelor's degree in USA. This type of global experience in sustainability education is part of Eastern's two Strategic Plan Initiatives – Liberal Arts Work and Global Citizenship. Check out: http://www.diversityweb.org/DiversityDemocracy/vol14no2/loxsom.cfm?utm_source=pubs&utm_medium=blast&utm_campaign=divdemvol14no2

10. *The Perennials Collaborative*. The emerging generation of sustainability leaders brings new ideas for sustainability initiatives. Samir Doshi at University of Vermont and colleagues have undertaken a collective, action-oriented community project to inspire "Perennials," those visionary leaders who (like perennial plants) have roots in communities and become forces of vision and change. Doshi's team is making a documentary, web site, and hosting community workshops throughout the country, especially in at-risk areas such as Appalachia, to inspire more actions for sustainability. (www.perennialscollaborative.com).

America is at a crossroads for education in science, technology, engineering, and mathematics (STEM). Currently, a company can hire nine Mexicans or eight Indian engineers at the same cost as one American; 93% of middle school students learn physical sciences form a noncertified teacher; and Americans spend more on potato chips than the entire federal R&D budget for energy [6]. It is no wonder that America currently ranks 48th in terms of global STEM education. Recent reports by the National Academies of Science, Engineering and other focus groups have assessed America's current STEM education, and listed actions that federal policy makers could take to enhance STEM and allow America to increase her global competitiveness [5, 6]. Such actions include increasing America's economy by vastly improving K-12 STEM education; doubling federal investments in STEM research to fuel our economy, provide security, and foster sustainability; and encourage citizen science to raise STEM literacy. Will these actions be implemented, or will the Academies' report be overlooked? Only time will tell, but STEM and ultimately sustainability education collectively will invariably determine the quality of life for the next generation.

Bibliography

Primary Literature

1. Brewer CA, Smith D (2010) Vision and change in undergraduate education: a call to action. American Association for the Advancement of Sciences, Washington, DC, p 79
2. Pooley E (2010) The climate war. Harper Collins, New York
3. Braasch G (2007) Earth under fire. University of California Press, Berkeley, CA, USA, 286 pp
4. Council on Undergraduate Research (CUR) (2007) Developing and sustaining a research-supportive curriculum: a compendium of successful practices. CUR, Washington, DC
5. National Academy of Sciences (NAS) (2008) Rising above the gathering storm. National Academy of Sciences Press, Washington DC, USA
6. National Academy of Sciences (NAS) (2010) Rising above the gathering storm, revisited: rapidly approaching category 5. National Academies Press, Washington, DC
7. National Research Council (NRC) (1996) National science education standards. National Academies Press, Washington, DC
8. National Research Council (NRC) (1997) Science teaching reconsidered: a handbook. National Academies Press, Washington, DC
9. National Research Council (NRC) (1999) Transforming undergraduate education in science, mathematics, engineering, and technology. National Academies Press, Washington, DC
10. National Research Council (NRC) (2010a) Research at the intersection of the physical and life sciences. National Academies Press, Washington, DC
11. National Research Council (NRC) (2010b) Synthetic biology – building a nation's inspiration: interdisciplinary research team summaries. National Academies Press, Washington, DC
12. National Research Council (NRC) (2010c) Expanding underrepresented minority participation: America's science and technology talent at the crossroads. Committee on Underrepresented Groups and the Expansion of the Science and Engineering Workforce Pipeline. National Academies Press, Washington, DC
13. National Science Foundation (NSF) (1996) Shaping the future: new expectations for undergraduate education in science, mathematics, engineering, and technology. NSF, Washington, DC
14. Leopold A (1949) A sand county almanac. Oxford University Press, New York, NY, USA
15. National Research Council (2000) How people learn: brain, mind, experience, and school. National Academies Press, Washington, DC

16. National Science Foundation (2009) Advisory Committee for Environmental Education and Research. NSF, Washington, DC
17. Louv R (2006) Last child in the woods – saving our children from nature-deficit disorder. Algonquin Press, Chapel Hill
18. Lowman MD, Burgess E, Burgess J (2006) It's a jungle up there – more tales from the treetops. Yale University Press, New Haven
19. Trombulak SC, Omland KS, Robinson JA, Lusk JJ, Fleischner TL, Brown G, Domroese M (2004) Principles of conservation biology: recommended guidelines for conservation literacy from the education committee of the Society for Conservation Biology. Conserv Biol 18:1180–1190
20. Bride I (2006) The conundrum of conservation education and the conservation mission. Conserv Biol 20:1337–1339
21. Lowman M, Mourad T (2010) Bridging the divide between virtual and real nature. Front Ecol Environ 8(7):339
22. Balmford A, Cowling RM (2006) Fusion or failure? The future of conservation biology. Conserv Biol 20:692–695
23. Brewer C (2006) Translating data into meaning: education in conservation biology. Conserv Biol 20:689–691
24. Lowman M, D'Avanzo C, Brewer C (2009) A national ecological network for research and education. Science 323:1172–1173
25. Burgess E, Burgess J, Lowman MD (2003) Lowman and thousands of Jason X school students. 2003. Observations of a Coleopteran herbivore on a bromeliad in the Peruvian Amazon. J Bromel Soc 53:221–224
26. National Research Council (2001) Grand challenges in environmental sciences. National Academies Press, Washington, DC
27. Cleveland DA, Radko CN, Muller NM, Watson TD, Rekstein NJ, Van H, Wright M, Hollingshead SE (2011) Effect of localizing fruit and vegetable consumption on greenhouse gas emissions and nutrition, Santa Barbara County. Environ Sci Technol 45:4555–4562

Earth System Model, Modeling the Land Component of

Guo-Yue Niu[1], Xubin Zeng[2]
[1]Biosphere 2, University of Arizona, Oracle, AZ, USA
[2]The Department of Atmospheric Sciences, University of Arizona, Tucson, AZ, USA

Article Outline

Glossary
Definition of the Subject and Its Importance
Introduction
Major Processes Represented in an LSM
Future Directions
Acknowledgments
Bibliography

Glossary

Aerodynamic resistance Or drag or aerodynamic drag. The component of force exerted by the air on a liquid or solid object that is parallel and opposite to the direction of flow relative to the object.

Evapotranspiration A term used to describe the sum of evaporation and plants' transpiration from the Earth's land surface to the atmosphere.

LAI The ratio of total upper leaf surface area of vegetation divided by the surface area of the land on which the vegetation grows. LAI is a dimensionless value, typically ranging from 0 for bare ground to 6 for a dense forest.

Land surface processes The various biogeophysical and biogeochemical processes occurring within and over various land surface components and interacting with the atmospheric processes.

Parameterization A method or process to approximate the effect on the model resolved processes that would be generated by unresolved subgrid-scale processes using formulations containing empirical parameters.

Stomatal resistance The opposition to transport of quantities such as water vapor and carbon dioxide (CO_2) to or from the stomata of plant leaves.

Subgrid heterogeneity The spatial variation in land surface properties, for example, soil wetness, snow, vegetation, and terrain within an ESM grid cell, which is on the order of $\sim$100 km.

Tile method A method dealing with subgrid heterogeneity. It gathers similar homogeneous land patches at different geographic locations within an ESM grid-cell into a number of "tiles" or "mosaics"; computes surface fluxes over each "tile" using distinct parameters of each tile while sharing the same atmospheric forcing; and then averages the computed fluxes from the tiles, weighted by the fractional areas of each "tile."

Topographic index Or "wetness index," $= \ln(a/\tan\beta)$, where a is the specific catchment area, that is, the upstream area above a pixel that drains through the unit contour at the pixel, and $\tan\beta$ is the local surface topographic slope. A greater value corresponds to a pixel of lowland areas that are potentially wetter.

Definition of the Subject and Its Importance

Land covers about 29% of the Earth's surface and represents an important component of the Earth's climate system. The land surface encompasses soil, snow, vegetation, glaciers, urban, lakes and rivers, mountains, etc. Land surface processes refer to various biogeophysical and biogeochemical processes occurring within and over these components and interacting with the atmospheric processes. Land surface models (LSMs) are mathematical descriptions of the land surface processes, with particular attention to momentum, energy, and mass (water, carbon, dust, and other constituents) flux exchanges with its overlaying atmosphere; these fluxes are intimately related to their storages in these components. In the context of an earth system model (ESM), LSMs are designed to provide the atmospheric model with lower boundary conditions over global land areas, describing the interactions of the land surface with the atmosphere. In addition, LSMs provide ocean models with discharges of water, sediments, and solutes. In this chapter, the focus is on descriptions of processes related to momentum, energy, water, and carbon, while processes related to other mass constituents, like dust, sediment, solute transports will not be included. Readers can also further refer to reviews of land surface modeling such as Sellers et al. [1], Pitman [2], and Yang [3].

Most LSMs, if not all, for use in ESMs and operational weather forecasting models are vertically one-dimensional (1D) models solving soil temperature and moisture equations, while parameterizing the effects of lateral flows of surface and subsurface water driven by subgrid topography. Although three-dimensional (3D) hydrological models numerically describing lateral flows of surface and subsurface water and operating at a resolution of meters have existed for years, it is not practical to include them in a climate model due to their expensive computational cost. Vertically, an LSM extends down to a few meters of the soil (2–6 m in different models) and a few meters above the vegetation canopy or the urban canopy. Some LSMs extend their depth to tens of meters deep to consider the long-term effects of permafrost and unconfined aquifers [4].

LSMs describe processes at various spatial scales ranging from millimeter to continental scales. The energy flux exchanges between land surface and the atmosphere involve processes at various scales from scattering of photons by plants and latent and sensible heat transfer by surface layer small eddies to convective planetary boundary layer large eddies. The water flux exchange involves processes at scales from water infiltration and percolation through soil micropores, transpiration through plant stomata, hillslope overland flow to continental-scale hydrological processes. The subgrid, unresolvable small-scale processes are highly parameterized using empirical equations based on a basic understanding of the processes, but not attempting to represent the process by equations representing first principles. This is why LSMs are also referred to as land surface parameterization schemes.

The land surface processes can influence weather and climate at timescales ranging from seconds to millions of years. For instance, the convective atmospheric boundary layer is developed in response to land surface heating on timescales from seconds to hours. Atmospheric temperature and precipitation can be affected through changes in soil water and groundwater, seasonal variations in snow cover and frozen soil, and vegetation phenology on a scale ranging from days to seasons. Temperature and water availability can greatly influence vegetation structure and function from years to centuries [5]. The Earth's climate has been tightly coupled to atmospheric CO_2 levels through the carbonate silicate cycle and/or the organic carbon cycle on geological timescales spanning hundreds of millions of years [6].

Land surface processes are critical for understanding climate dynamics owing to its momentum, energy, and mass exchanges with the overlying atmosphere. Land surface can "memorize" climate dynamics by recording and filtering the signals of weather events through storages of energy, water, and carbon and feed back to the atmosphere through surface fluxes. Pitman [2] reviewed coupled model experiments including sensitivity studies of changing albedo (e.g., [7]), roughness length (e.g., [8]), LAI [9], water-holding capacity [10], and roots [11], etc., deforestation [12], desertification [13], land cover change (e.g., [14]), ecosystem feedback under doubling CO_2 [15], and vegetation-snow-albedo feedback [16]. These sensitivity experiments provided evidence that climate models are sensitive to the land surface processes [2].

In addition, land surface feedbacks may amplify and prolong sea surface temperature (SST) anomaly triggered droughts, playing a critical role in the persistence of droughts and mega-droughts [17, 18]. It is well known that global climate dynamics is greatly affected by ocean–atmosphere interactions. However, land surface processes are of great importance for seasonal, interannual, and decadal climate change over specific land areas. Koster et al. [19] revealed that land and ocean processes have essentially different geographic regions of influence on precipitation variance, that is, the ocean's influence is dominant mainly in the tropical land, while the land's influence is dominant over mid-latitude land areas. Koster et al. [20] identified the arid-to-wet transition regions over land as "hot spots" where changes in surface water fluxes associated with soil water storage have greater impacts on precipitation.

The land surface is more heterogeneous than other Earth surface components. Within one grid-cell of an ESM on the order of ∼100 km, different land surface types, for example, bare soil, snow, grass, crop, and forests, may coexist. An LSM has to parameterize the integral effects of these subgrid surfaces on surface energy, water, and carbon fluxes over the grid cell. A variety of methods are used, for example, effective parameters, "mosaic" (or tile) methods, probability density function (pdf) methods, or finer grids than the host climate model. LSMs are usually community efforts, because they are inherently interdisciplinary including atmospheric sciences, hydrology, ecology, soil and snow physics, etc., as well as social sciences related to land use and water use managements.

Introduction

LSMs have evolved for three generations [1, 2] since the advent of the first generation global climate models (GCMs). The first LSM was the "bucket model," which describes the land surface as a bucket with a fixed water holding capacity of 15 cm [21]. The bucket can be filled with precipitation and emptied by evaporation. Runoff is generated as the water that exceeds the bucket holding capacity, and evaporation is limited by the water content of the bucket. In the first generation models, the transfer of sensible and latent heat was based on simple aerodynamic bulk transfer formulations, using uniform and prescribed surface parameters, for example, water holding capacity, albedo, and roughness length. These models did not account for ecological processes (e.g., transpiration through plants' stomata) and more detailed hydrological processes (e.g., infiltration and capillary upward flow through soil micropores). Despite their simplifications, the first generation models represent a key step to describe land surface processes in ESMs, and their simulated soil moisture and evapotranspiration (ET) were comparable to more complex models at longer timescales.

From the 1980s to early 1990s, a second generation of models appeared. They explicitly represented vegetation effects and more complex soil hydrology in the calculation of surface energy and water balances [22–24]. Representative second-generation models are the Biosphere-Atmosphere Transfer Scheme (BATS) [23] and the Simple Biosphere Model (SiB) [24]. During this period, two dozen second-generation models were developed with emphasis on various specific processes (e.g., [25–28]). These models vary in detail, but they have many common features. They usually have a number of soil layers, a single canopy layer (or an additional understory canopy layer like in SiB), and a bulk snow layer. Micrometeorological, hydrological, and ecological processes are more explicitly represented in these models. Instead of the fixed surface albedo in the first-generation models, more explicit radiation transfer through the vegetation canopy differentiating visible and near-infrared and beam and diffusive lights was taken into account. Turbulent transfer of heat from multiple surface sources, for example, canopy leaves and the ground surface was considered, and the under-canopy and leaf boundary layer turbulences were parameterized based on atmospheric boundary layer similarity theories. Transpiration through plants' stomata were considered using the Jarvis-type stomatal conductance scheme [29], a simple empirical formulation as a function of light (photosynthetically active radiation; PAR), water (leaf water potential), and environmental conditions (temperature and humidity). Whether the soil moisture Richards equation is solved or not, vertical gravity and capillary flows of water were taken into account. Runoff was parameterized as various functions of soil water storage or excess above infiltration, neglecting topographic effects.

Accumulation and ablation of snow on the ground were represented with a bulk layer of snow, neglecting snowpack internal processes.

Since the early 1990s, third-generation models have been developed. The third-generation models were mainly characterized by the capability of simulating carbon uptake by plants and vegetation dynamics, or "greening" of the land surface [1, 2]. Other aspects of the model were substantially improved at the same time. Some models also began to incorporate treatments of nutrient dynamics and biogeography, so that vegetation systems can change location in response to climate shifts. Collatz et al. [30] and Sellers et al. [31] began to integrate stomatal conductance and photosynthesis into LSMs based on the work of Farquhar et al. [32]. A semiempirical model of leaf conductance was proposed [30] based on the understandings of the limitations on carbon assimilation by leaf and maximum use of water by plant [33].

During the same time period, LSMs were substantially improved in other aspects with regard to representations of hydrological processes in ESMs. LSMs started to account for subgrid variability in a more explicit way, for example, the "tile" approach to represent vegetation patchiness [34, 35] and the statistical approach to represent subgrid distribution of soil moisture and runoff generation [36], spatial variability of infiltration [37], topographic control on subgrid soil moisture distribution and runoff generation [38, 39], and subgrid snow distributions [40, 41]. LSMs started to include more physically based, multilayer snow submodels to accommodate more internal processes by parameterizing growth of grain size and liquid water retention and percolation within snowpack [42–44]. Ice content within soil (frozen soil) was explicitly resolved as a new prognostic variable, and its impacts on runoff and infiltration were investigated [45–47]. Most recently, groundwater processes were implemented in LSMs [48–52], and LSMs entered a new era involving multiple disciplinary sciences.

Major Processes Represented in an LSM

Subgrid Heterogeneity and Surface Data

Within an ESM grid on the order of ~100 km, land surface properties, for example, soil wetness, snow, vegetation, and terrain, vary at the scale of a few meters. Because of the strongly nonlinear dependence of surface fluxes on surface properties and states, for example, the dependence of ET on soil wetness, simple area-averaging approaches used to aggregate surface properties and states is problematic. The use of LSM grids whose resolution is higher than ESMs may partially improve the accuracy of grid cell averaged fluxes [53] but it is still very difficult to explicitly resolve the variability. Therefore, representing subgrid variability within ESMs will always remain a challenge no matter how fine the model resolution is [36, 54]. There are three major approaches to representing the subgrid heterogeneity, that is, effective parameters, "mosaic" or "tile" approach, and statistical approach.

Earlier LSMs used effective parameters to obtain the correct fluxes averaged over patches of a grid cell. Some effective parameters can be obtained by simply averaging the parameters for various patches, e.g., albedo, because of the linear relationship between radiative fluxes and surface albedo. But other effective parameters, which have a nonlinear relationship with surface fluxes, for example, the effective roughness length, cannot be obtained by simply averaging parameter values of individual patches and need to be derived in such a way that correct area-averaged fluxes [55–57] can be ensured.

The statistical approach uses pdf of input variables to derive grid cell averaged runoff and ET. Assuming point precipitation intensity and soil wetness are spatially distributed over a large ESM grid cell according to exponential and gamma distributions respectively, Entakhabi and Eagleson [36] derived grid cell mean surface runoff ratio (to grid cell mean precipitation), bare soil evaporation efficiency (ratio of actual to potential), and transpiration efficiency (ratio of actual to potential evaporation). Liang et al. [37] implemented spatially variability of infiltration capacity in the Variable Infiltration Capacity (VIC) model. Niu et al. [39] used an exponential distribution of topographic index (or wetness index) to parameterize fractional saturated area and saturation excess runoff.

The tile approach [34, 35] gathers similar homogeneous land patches at different geographic locations within an ESM grid cell into a number of "tiles" or "mosaics," computes surface fluxes over each "tile" using distinct parameters of each tile while sharing the same atmospheric forcing, and then averages the

computed fluxes from the tiles, weighted by the fractional areas of each "tile." The performance of the tile approach has been evaluated in numerous offline studies (e.g., [35]), boundary layer or mesoscale atmospheric models (e.g., [34]), and coupled ESMs [26, 58]. The tile can be also generated using different variables, for example, topographic index [38], soil wetness [54], or soil ice content [59]. The tile approach may overlap too much canopy shadows and thus induce errors in computing net solar radiation absorbed by the ground, especially over high latitude, boreal forest regions [60]. However, this approach is widely used in numerous second- and third-generation LSMs, because of its readiness to make full use of high-resolution satellite remotely sensed land surface data to generate the "tiles."

As an example, the National Center for Atmospheric Research (NCAR) Community Land Model version 4.0 (CLM4) [61] adopted the tile approach and parameterized some key processes using the statistical approach. CLM4 accounts for the subgrid heterogeneity as a nested subgrid hierarchy of landunits, soil/snow columns, and plant functional types (PFTs). Each grid cell can have a number of different landunits, for example, glacier, wetland, lake, urban, natural vegetation, and managed vegetation (crops). Each landunit can have a number of different columns (e.g., irrigated and rainfed soil), and each column can have multiple PFTs. CLM4 adopted the statistical method of Niu et al. [39] to parameterize surface saturated area and associated runoff. Surface datasets to feed CLM4 include percentages of glacier, lake, wetland, urban, and various PFTs to determine the fractional area of these surface tiles. PFTs are based on MODIS satellite data at 30 s (~1 km) resolution [62]. Prescribed PFT LAI was derived from the MODIS satellite data of Myneni et al. [63]. Prescribed PFT stem area index (SAI) is derived from PFT LAI phenology combined with the method of Zeng et al. [64]. Prescribed canopy top and bottom heights are from Bonan et al. [65]. Soil color dataset (affecting surface albedo) is based on Lawrence and Chase [62]. The IGBP soil dataset (Global Soil Data Task 2000) of 4,931 soil mapping units and their sand and clay content for each soil layer is used to create a mineral soil texture dataset [65] and an organic matter density dataset [66] that vary with depth.

Surface Energy Balance

Over an ESM grid cell, the net radiation (R_n) absorbed by the land surface is balanced by latent (LE), sensible (H), and ground heat fluxes (G):

$$R_n = LE + H + G \tag{1}$$

Note that the chemical energy stored during photosynthesis and released by respiration is not included in the above equation as it amounts to less than 1% of the absorbed insolation [2]. R_n includes net shortwave and net longwave radiation fluxes. LSMs that do not differentiate the vegetation canopy and the ground, for example, Noah [67] use the above equation and compute a single temperature for the land surface. More complex models that have a separate canopy layer from the ground, like versions of SiB and CLM, use two energy balance equations, one for the vegetation canopy and another for the ground surface, to solve their temperatures. The partitioning of available energy (R_n) into latent and sensible heat fluxes represented by Eq. 1 is greatly controlled by the land surface hydrological conditions. For an LSM using the tile subgrid approach, Eq. 1 is applied over each tile.

Net Shortwave Radiation LSMs compute net shortwave radiation over various land surfaces:

$$S_a = S(1 - \alpha_s) \tag{2}$$

where S is the incoming solar radiation from the host ESM, and α_s is the surface albedo, varying with solar zenith angle (SZA), vegetation types, snow cover, and soil moisture conditions. In earlier LSMs, α_s was prescribed for various land surface types. More complex second- and third-generation models used Beer's Law and two-stream approximation scheme [68, 69] to compute radiative transfer through the vegetation canopy, net radiation absorbed by the vegetation canopy and the ground, and the surface albedo.

Beer's law assumes that irradiance decreases exponentially with path length through an absorbing medium. Thus, the radiation reaching the ground, $S_g = Se^{(-\kappa LAI)}$, where κ is a constant attenuation coefficient, and LAI is the effective leaf area index of the canopy. However, Beer's law does not account for the scattering and multiple reflections by the canopy leaves [70].

The two-stream approximation [68, 69] accounts for beam and two main streams (vertical upward and downward) of diffusive radiation over two wavebands (visible and near-infrared). However, it assumes that the canopy leaves are evenly distributed within a grid cell. On the basis of complex radiation transfer models [71], Yang and Friedl [72] proposed a modified two-stream scheme to account for aggregation of the evenly distributed leaves represented by a two-stream scheme into canopy crowns with between-canopy and within-canopy gaps, which vary with radius and thickness of the canopy, tree density (the distance between trunks), and SZA. The scheme needs prescribed optical parameters, for example, reflectivity and absorptivity of the vegetation and ground, for various land surface types. The two-stream approximation also computes the fraction of sunlit and shaded leaves, which are crucial to photosynthesis processes.

Net Longwave Radiation The net longwave radiation (or infrared) is computed as the residual of the incoming ($L_\downarrow$) and emitted by the surface:

$$L_a = \varepsilon(L_\downarrow - \sigma T_s^4) \tag{3}$$

The upward longwave radiative flux emitted by the surface is based on the Stefan-Boltzmann Law. In the above equation σ is the Stefan-Boltzmann constant, ε is the emissivity of the land surface, and T_s is the surface skin temperature. For a model that has a canopy layer, computation of L_a becomes more complicated due to the interactions between the ground surface and its overlaying canopy [61].

Sensible and Latent Heat Fluxes The turbulent transfer of latent and sensible heat fluxes in most LSMs is based on Monin-Obukhov similarity theory [73, 74]. LSMs compute surface sensible and latent heat fluxes using the bulk transfer scheme:

$$H = \rho C_p C_H u(T_0 - T_a) \tag{4}$$

$$LE = \frac{\rho C_p}{\gamma} C_W u(e_0 - e_a) \tag{5}$$

where ρ is air density, C_p is the specific heat of dry air, γ is the psychrometric constant, C_H and C_W are the turbulent exchange coefficients for heat and water vapor, respectively, T_a and u are the air temperature and wind speed at the lowest layer of the host ESM, and T_0 and e_0 are the temperature and water vapor pressure at the height of the surface roughness length, z_0. The first-generation models prescribed C_H and C_W with different values for various land surfaces. The second- and third-generation models calculate C_H and C_W according to Monin-Obukhov similarity theory, accounting for surface stability conditions. For simplicity, $C_H = C_W$ and is assumed to be equivalent to that for momentum C_D in some LSMs. More elaborate schemes differentiate C_H (=C_W) from C_D using roughness lengths different for heat z_{0H} and momentum z_0; and usually $z_0 > z_{0H}$, because the transfer of momentum is more efficient (through pressure and diffusion) than those of heat and mass (through diffusion only). The value of $\ln(z_0/z_{0H})$ is about 2.0 over a range of vegetation surfaces, and in practical applications, $z_0/z_{0H} = 10$ [75]. In analogy with Ohm's law in electricity, the drag coefficient can be transformed to an aerodynamic resistance:

$$r_{a,\,H} = r_{a,W} = (C_H u)^{-1} \tag{6}$$

Shuttleworth [75] provided a review on formulations of the aerodynamic resistances for estimating surface ET and stability correction.

Complex models compute sensible and latent heat fluxes from multiple sources of the land surface such as soil, snow, plants' leaves, and stomata using equations similar to Eqs. 4 and 5. Over the soil surface, because of the strong temperature gradient between the soil skin (at 0 m) and z_0 as well as the difficulty in computing the temperature at z_0, LSMs use the skin temperature T_s to compute sensible and latent heat fluxes for convenience. The skin temperature over these surfaces can be computed iteratively using Eq. 1 till the surface energy is balanced. Because of the use of T_s rather than T_0 in Eqs. 4 and 5, an extra resistance, r_{soil}, is needed [76]:

$$H = \rho C_p \frac{(T_s - T_a)}{r_{a,H} + r_{soil}} \tag{7}$$

$$LE = \frac{\rho C_p}{\gamma} \frac{(e^*(T_s) - e_a)}{r_{a,W} + r_{soil}} \tag{8}$$

where $e^*(T_s)$ is the saturated vapor pressure at T_s, and r_{soil} accounts for the resistance to water vapor and heat transfer from the surface soil pore space to z_{0H} (roughness sub-layer) through molecular diffusion. Some

LSMs also added a relative humidity term before $e^*(T_s)$ to estimate the water vapor pressure within surface soil pore space. Sakaguchi and Zeng [77] reviewed numerous soil resistance schemes. This expression for soil surface evaporation is similar to that for transpiration through leaf stomata

$$LE = \frac{\rho C_p}{\gamma} \frac{(e^*(T_v) - e_a)}{r_{a,v} + r_c} \tag{9}$$

where T_v is the vegetation canopy temperature, $r_{a,v}$ is the leaf boundary layer resistance per unit LAI [73], and r_c is the canopy-scale stomatal resistance that is scaled up from the stomatal-scale stomatal resistance, r_{st}, using LAI: $r_c = r_{st}/LAI$. Most second-generation models implemented the Jarvis-type stomatal resistance [29], which relates r_{st} to multiplicative stress factors:

$$1/r_{st} = g_0 f_S(PAR) f_D(\Delta e) f_T(T_a) f_W(\psi_l) \tag{10}$$

where g_0 is a vegetation type-dependent maximum stomatal conductance and f_S, f_D, f_T, and f_W, all of which range from 0 to 1, are environmental stress factors associated with PAR, water vapor deficit of the surrounding air (Δe), air temperature (T_a), and leaf water potential that relates to root-zone soil moisture, respectively.

Ground Heat Flux The ground heat flux is controlled by the soil thermal diffusion (or conduction) process and can be expressed as

$$G = -\lambda \frac{T_1 - T_s}{\Delta z_1/2} \tag{11}$$

where λ is the soil thermal conductivity, T_1 is the temperature of the first soil layer, and Δz_1 is the layer thickness of the first soil layer. By definition ($G = -\lambda(\partial T/\partial z)_{z=0}$), the smaller Δz_1, the more accurate G is. In case of soil covered by snow, LSMs that have a bulk snow layer replace $\Delta z_1/2$ in the above equation with ($\Delta z_1/2 + h_{\text{snow}}$), where h_{snow} is the snow depth. Thus, when the snowpack becomes thicker, G becomes more inaccurate. This is one of the major reasons that complex models use a multilayer structure for the snowpack. G is then used as the upper boundary condition of soil temperature equation.

Heat Storage in the Soil and Snow The soil thermal conduction (or diffusion) equation is written as

$$C\frac{\partial T}{\partial t} = \frac{\partial}{\partial z}\left(\lambda \frac{\partial T}{\partial z}\right) \tag{12}$$

where C and λ are the volumetric heat capacity and thermal conductivity, respectively. LSMs solve the above equation using various methods, for example, the more efficient force-restore method [22, 78] as used in BATS and SiB and the finite difference method as used in the Noah and CLM4 models.

The force-restore method is based on an analytical solution of the above equation under two assumptions that the surface forcing is periodic and the soil thermal properties are uniform. It is named after the two terms controlling surface temperature, that is, the forcing term (G in Eq. 11) and a restoring term due to heat diffusion from surface to a deeper soil layer. Recognizing that the two assumptions are not always valid, Dickinson [78] took into consideration the nonuniform thermal properties induced by snow and soil moisture and generalized the force-restore method. However, the surface temperature solved through the force-restore method is not so responsive to variations in surface forcing with a frequency higher than diurnal (e.g., cloud effects on solar radiation) as the iterative method solving the surface energy balance equation (Eq. 1). Therefore, it may cause difficulties in resolving the available energy for snowmelt, which occurs at a sub-daily scale [60].

Current LSMs explicitly solve Eq. 12 using finite difference methods for layered soil and snow. The upper boundary condition is the surface forcing (G), and lower (bottom) boundary condition is either specified as a zero flux as used in CLM or as the long-term averaged surface air temperature at a deep soil layer (e.g., 8 m) as used in Noah [67]. The zero flux condition is more readily satisfied when the bottom layer is deeper. The accuracy of the solution increases as the number of layers increases. Due to the computational cost, the number of layers cannot be very large. CLM has ten soil layers, while many other LSMs have three to five layers. To account for the thermal inertia of deep ground, the number of soil layers of CLM4 is changed from 10 to 15 layers, extending the total depth of the soil column down to 42 m [4].

When covered by snow, the soil temperature is solved together with the temperature of snow of a varying number of layers [43, 60]. The layering of snowpack and the number of layers vary with the total snow depth and is more complex than layering soil (e.g., [43, 61]). For frozen soil, a source/sink term due to phase change, $\rho_{ice} L_f \partial\theta_{ice}/\partial t$, where ρ_{ice}, L_f, θ_{ice}, and t are density of ice, heat for fusion, volumetric ice content, and time, respectively, is added to the right-hand side of Eq. 12. This term accounts for the heat released by freezing liquid water or heat consumed to melt ice. It is usually combined with heat conductivity C and named as "apparent heat capacity," C_a,

$$C_a = C - \rho_{ice} L_f \frac{d\theta_{ice}}{dT} \tag{13}$$

Surface Water Balance

The temporal variation of the water storage (S) in a grid cell of an ESM is controlled by the water incident on land surface, that is, precipitation (P) and the water leaving the grid cell, that is, ET and runoff (R):

$$\frac{dS}{dt} = P - ET - R \tag{14}$$

The above equation neglects the lateral surface and subsurface flows that transport water to adjacent grid cells. The storage term in the above equation includes water (ice and liquid water) intercepted by the canopy, snow on the ground, water in the soil and aquifers. ET includes ground evaporation, canopy evaporation, and transpiration, which can be derived from their corresponding latent heat fluxes by dividing the heat of vaporization, L. For most LSMs, R includes surface runoff and subsurface runoff, which will be discussed later.

Canopy-Intercepted Water Although the amount of the canopy-intercepted water is relatively small compared to other water storages, it plays an important role in contributing to the total ET and altering the canopy reflectance by intercepting snowfall. Most LSMs takes into consideration liquid water interception by the vegetation canopy, while few LSMs explicitly consider additional processes of loading and unloading of snowfall [79, 80]. The temporal variation of the liquid water stored on the vegetation canopy, $W_{c,liq}$, is determined by the rates of interception (R_{intr}), evaporation/dew (E_c), and drip (R_{drip}):

$$\frac{dW_{c,liq}}{dt} = R_{\text{int}\ r} - E_c - R_{drip} \tag{15}$$

The interception rate is parameterized as a function of LAI and SAI. The interception capacity of the vegetation canopy is also related to the subgrid distribution of vegetation and precipitation. Considering only a fraction of the vegetation canopy within the large area of an ESM grid cell receives precipitation, CLM4 introduced a fractional area of precipitation as a limiting factor (0.25) to its interception rate [61]. However, this factor should vary with the distribution of precipitation that relates to the ratio of convective precipitation to total precipitation [39] and should be further investigated using high-resolution precipitation data.

The interception capacity for snow is estimated to be about 50 times greater than for rain [80]. Interception of snowfall by the vegetation canopy significantly reduces snow mass on the forest floor. About 30–40% of the annual snowfall over complete coniferous canopies sublimates from the canopy and thus never reaches the ground [80]. Depending on meteorological conditions, the intercepted snow may fall to the ground, sublimate, melt, or refreeze. Implementing a snowfall interception model and properly representing the sublimation of the canopy-intercepted snow can significantly improve the simulation of snow on the ground [81]. More importantly, properly representing interception of snow can significantly improve the simulation of surface albedo. However, most LSMs do not explicitly distinguish between solid and liquid phases of water on the canopy surface, and they use the same interception capacity for both snowfall and rainfall.

Based on the water stored on the vegetation canopy, a wet fraction of the canopy can be computed. Many LSMs (e.g., BATS and CLM) calculate the wet fraction as the 2/3 power of the ratio of canopy water to its maximum value, following Deardorff [22], while others (e.g., SiB) compute it as the ratio of the canopy water storage to its maximum value when the saturation vapor pressure at leaf temperature is less than the vapor pressure of the surrounding air. The maximum value of the canopy water is parameterized as a function of LAI.

Snow Water Snow cover is an important part of the climate system because of its high albedo, low thermal conductivity, and ability to absorb heat when melting. In addition, the snowmelt water is the primary source of stream flow and groundwater recharge in cold and alpine regions. The impacts of snow-cover processes on global and regional climate have been investigated by numerous researchers (e.g., [82–84]) using earlier GCMs. In addition, numerous sensitivity studies using GCMs found that the removal of all forests north of 45°N would lead to cooling and delay snowmelt because of the increased surface albedo (e.g., [12, 85]), indicating the important role of forest canopies in modifying the surface energy budget and climate over snow covered regions.

Snow covered area exhibits spatial and temporal fluctuations ranging from 7% to 40% seasonally in the Northern Hemisphere [86]. Snow cover extent in the Northern Hemisphere has been decreasing since the mid-1980s in response to a global warming trend [87, 88]. On the other hand, Arctic warming may be accelerated by decreases in snow cover due to the positive snow-albedo feedback. Chapin et al. [89] reported that Arctic summer warming is highly related to an increase in snow-free days and the transition from tundra (short to be easily buried by snow) to forest.

LSMs compute snow water equivalent (SWE), snow depth, and fractional area covered by snow. The representation of snow processes in the first- and second-generation LSMs was relatively simple using a bulk snow layer (e.g., [26, 90, 91]). Third-generation models tend to have multiple snow layers to resolve the internal processes of snowpack such as densification, liquid water flow, and multiphase changes of water [42–44, 92]. The multilayer structure also has a thin surface layer designed to produce a more accurate ground heat flux and snow skin temperature [60].

Bulk-layer models combine the snowpack with the top soil layer as a bulk layer. These models, for instance, BATS and SiB, use the force-restore approach to solve snow temperature. However, the force-restore approach cannot accurately resolve high-frequency variations in snow surface forcing and temperature, and thus induce errors in snowmelt. Most of the multilayer snow models were simplified from schemes with detailed internal processes such as grain-size growth and gravitational flows of liquid water within a snowpack (e.g., [93, 94]). In a multilayer model like CLM4, the snow mass balance includes ice and liquid water content, but neglects the vapor phase. Densification processes include destructive or equi-temperature metamorphism, compaction due to the weight of the overlying layers of snow mass, and melt metamorphism, following Anderson [93]. Excessive liquid water above the holding capacity (ratio of liquid water volume to the free space of a snow layer) flow down to next layer. The melting (or freezing) energy for a layer is assessed as the energy excess (or deficit) needed to change the temperature of the layer to the freezing point [60].

Researchers also recognized that snowpack modeling for hydrological applications and climate studies needs to account for the radiative effects of the vegetation canopy (e.g., [95]) and the impacts of the interception of snow by the vegetation canopy [80, 96]. In addition, the turbulent transfer of sensible heat flux below the vegetation canopy under a stable condition during melting season significantly affects melting snow on the ground [81]. However, these studies were not fully introduced into ESMs.

Snow depth varies greatly at subgrid-scales because of heterogeneities in land cover, terrain, snow deposition, snowmelt, and meteorological conditions [40]. In LSMs, subgrid snow distributions are represented as snow cover fraction (SCF), that is, the fraction of a grid cell covered by snow, through the relationship between SCF and snow depth. At an ESM grid cell scale, one of the largest uncertainties in modeling snow and its interactions with the atmosphere comes from SCF formulations and their associated parameters. Various SCF formulations as summarized in Liston [40] result in a wide spread of SCFs between models. ESMs vary significantly in simulating SCF, and most of them underestimate SCF [97] because of unrealistic SCF formulations. Most SCF formulations are parameterized as a function of grid cell mean snow depth and the ground roughness length [40, 41, 81, 90]. Some of them also considered the impact of subgrid topography variations on SCF [91]. Using gridded snow depth and SWE reanalysis and the advanced very high resolution radiometer (AVHRR) SCF [87], Niu and Yang [41] found the SCF–snow depth relationship varies with seasons and introduced snow density into an existing SCF formulation [90] to approximate the seasonal variation in the SCF–snow depth relationship.

Soil Water Although soil water accounts for a very small portion (~1%) of the terrestrial water storage, it plays an important role in the climate system through its controlling role on ET. Soil moisture anomalies (i.e., deviation from the mean) can persist from weeks to seasons [98, 99]. Numerous researchers have investigated its impact on climate predictability using GCMs (e.g., [100]). Koster et al. [19] revealed that the land's influence is dominant over midlatitude land areas. In analogy to the oceanic hot spot, for example, the eastern equatorial Pacific, playing a key role in the El Niño-La Niña cycle, Koster et al. [20] found the terrestrial "hot spots," that is, the arid-to-wet transition regions, where precipitation is affected by soil moisture anomalies during boreal summer. These hot spots were further confirmed by Zeng et al. [101] using an alternative index accounting for the land-precipitation coupling strength. For this reason, a proper initialization of soil moisture can enhance precipitation prediction skill over these hot spots [102–104]. Also, upgrades of LSMs with more elaborate representations of soil moisture can improve climate prediction skill especially during ENSO neutral years when the SST signal is relatively weak [104].

Temporal variation in the total soil moisture of a soil column within a certain depth (e.g., 3.4 m in CLM4) is controlled by infiltration, that is, the residual of precipitation minus runoff and evaporation at the soil surface, root uptake through transpiration, and the water flux at the bottom. The vertical distribution of soil water is controlled by vertical root distribution and soil property that determine gravitational and capillary water fluxes. Evolving from the first-generation "bucket" models, which neglects the capillary water flux, some second- and third-generation models directly solve the 1D, mass-based (θ) Richards equation to calculate the vertical distribution of soil moisture [61, 67]. Modern LSMs also tend to increase the number of soil layers to improve the accuracy of the solution. Various model intercomparison projects indicated that LSMs have a much better ability to simulate the soil moisture anomalies than to simulate the absolute value of soil moisture (e.g., [105, 106]).

The mass-based form (θ) of the Richards equation cannot resolve the soil water distribution at both unsaturated zone and saturated zone (groundwater) as continuously as a pressure-based (ψ) Richards equation. However, when solved through finite-difference numerical scheme, it conserves mass better than the pressure-based form. Zeng and Decker [107] demonstrated that a previous version of CLM cannot maintain the hydrostatic equilibrium of soil moisture distribution, and this problem cannot be resolved by increasing the vertical resolution of the soil column. In CLM4, they proposed a revised form of the Richard equation by explicitly subtracting the hydrostatic equilibrium pressure profile, $\psi_E(z)$, from the soil water pressure profile, $\psi(z)$.

Frozen Soil Frozen soil has a tremendous impact on soil thermal and hydrological properties, ecosystem diversity and productivity, and greenhouse gas release from the soil. Freezing of soil water delays the winter cooling of the land surface; thawing of the frozen soil delays the summer warming of the land surface. Frozen soil also affects the snowmelt runoff and soil hydrology by reducing the soil permeability. Runoff from the Arctic river systems is about 50% of the net flux of freshwater to the Arctic Ocean [108]. This is a large percentage when compared to the freshwater inputs to the tropical oceans, where freshwater input is dominated by precipitation. Runoff and the degree of freshening can affect ocean salinity, sea ice conditions, and thermohaline circulation.

Earlier LSMs did not explicitly solve soil ice content. These LSMs showed a much larger scatter in the simulated soil moisture and runoff in spring than in other seasons due to different representations of the effects of frozen soil on infiltration [109]. Some of them switched off infiltration for subfreezing temperatures, for example, in simplified SiB [25] and BATS [110]. This treatment failed to produce the spring peaks of soil moisture due to the underestimated infiltration [111, 112]. Xue et al. [112] improved SSiB's ability to simulate the spring peaks of soil moisture by gradually decreasing the hydraulic conductivity at a rate of 10% per degree for subfreezing temperatures following SiB2 [113]. Pitman et al. [45] implemented an explicit representation of the hydrological and thermal effects of soil ice in their LSM but found that the representation degraded runoff simulation in a large-scale river basin.

Field studies showed that the effect of frozen soil on infiltration depends on scale, surface conditions of

snow and vegetation, and soil structures. Shanley and Chalmers [114] showed that the effects of frozen soil on runoff are scale-dependent. There was no significant correlation between seasonal runoff ratios and ground frost depth for the 15 year of record from the Sleepers River watershed, USA, with an area of 111 km^2, while the increased runoff due to frozen ground was observed occasionally in its 0.59-km^2 agricultural subcatchment. Lindstrom et al. [115] also concluded that there were no clear effects of frozen soil on the timing and magnitude of runoff from an analysis of 16-year data in a 0.5-km^2 watershed in northern Sweden. Researchers have demonstrated that soil structure, air-filled porosity, ice content, and the number of freezing and thawing cycles are the governing factors affecting the infiltration capacity of frozen soil. Even at very local scales, recent laboratory and field studies using dye tracer techniques (e.g., [116]) revealed that water can infiltrate into deeper soil through preferential pathways where air-filled macropores exist at the time of freezing.

One-dimensional numerical models using the fully coupled heat and mass balance equations [46, 59, 117–119] used a variety of ways to parameterize the hydraulic properties of frozen soil. Some of the models [117, 119] assume that the freezing–thawing process is similar to the drying–wetting process with regard to the dependence of the soil matric potential on the liquid water content. This assumption leads to a very low infiltration rate or even upward water movements resulting in ice heave in surface layers. However, other modelers [46, 47, 59, 118] proposed various schemes to compute hydraulic properties as a means to produce greater infiltration rates. Stähli et al. [118] proposed two separate domains for the water infiltration into frozen soil: the low-flow domain where water flows through the liquid water film absorbed by the soil particles and the high-flow domain where water flows through the air-filled macropores. Koren et al. [46] assumed that frozen soil is permeable due to soil structural aggregates, cracks, dead root passages, and worm holes and reduced the effects of frozen soil on runoff production. Cherkauer and Lettenmaier [59] assumed that surface water tends to find areas of higher infiltration capacity as it flows across a frozen surface. They split their model domain into 10 bins with each having different ice content, which was derived from the observed spatial distribution of soil temperature, to increase the infiltration rate in VIC model. Niu and Yang [47] introduced fractional permeable area, which partitions an ESM grid cell into an impermeable fraction and a permeable fraction, and used the total soil moisture (liquid water and ice) to calculate soil matric potential and hydraulic conductivity over the permeable fraction.

When soil water freezes, the water closest to soil particles remains in liquid form due to the absorptive and capillary forces exerted by soil particles. For this reason, there is a certain amount of liquid water coexisting with ice over a wide range of temperatures below 0°C. This supercooled soil water at subfreezing temperatures can be computed with the freezing point depression equation [46, 47] or parameterized with observational data [120]. Most LSMs, for example, CLM4, consider ice and liquid water content but neglect the water vapor phase. The energy available for phase change between ice and liquid water is assessed in the same way as for snow except that only the excess above the supercooled liquid water can be frozen in the soil. Li et al. [121] provided a thorough summary of frozen soil models with different levels of complexity.

Groundwater Groundwater storage constitutes about 30% of the terrestrial water storage. Groundwater storage shows as large variations as that of soil water at monthly or longer timescales in Illinois [122]. The groundwater level also shows a strong diurnal cycle in aquifers where the water table depth is less than 2 m because of the water uptake by the roots of the aboveground plants [51]. The rise and fall of the water table directly interacts with soil moisture in the vegetation root zone and thus acts as a source term for ET. Groundwater dynamics also control runoff generation, which can further affect the computation of soil moisture and ET in a climate model. Observational data show that runoff is much more related to the water table depth than to precipitation at monthly timescale in Illinois [50].

Earlier LSMs did not explicitly account for groundwater storage and its interactions with soil moisture. When solving the soil moisture equation, these LSMs assumed zero flux or free drainage at the bottom of the soil column as the lower boundary condition. For instance, an earlier version of CLM (version 3.0) used gravitational free drainage as its lower boundary

condition at a depth of 3.4 m. Water drained from the soil bottom under gravity during wet seasons or wet years (parameterized as subsurface runoff) would never come back to the soil column in dry seasons or dry years. In reality, when the soil is drying, the soil can draw water through capillary suction from its underlying aquifer (or saturated layers), which has a longer memory of the past precipitation events than the soil. LSMs implicitly include such a process when the water table is shallow enough to be within the model soil layers. However, when the water table is below the model's soil bottom, LSMs neglect this upward water flow through capillary forces while taking into consideration gravitational free drainage at the model bottom, resulting in unrealistically dry deep soil.

During the past decade, the need for a groundwater component in LSMs has received increasing attention. As a result, a number of researchers have incorporated a groundwater component into LSMs [48–52, 123]. These models, for use in climate studies, can be divided in two categories: 3D models [51, 123] and 1D models [48–50, 52]. Because the horizontal transport of groundwater is more pronounced at a smaller scale, 3D models are more applicable to regional climate and water resource studies, while 1D models are often used in ESMs.

Researchers [48–50] have proposed more realistic solutions to solve the continuum of soil and relatively shallow aquifers at the expense of adding more integration elements, that is, 100 nodes, 50 layers, and 10 layers, respectively, in the above-referenced studies. Even with these additional layers, the models are only applicable for relatively shallow aquifers (<5 m) because of the prescribed depth of the model. Niu et al. [52] added a single integration element below the soil of CLM and parameterized groundwater recharge rate according to Darcy's law to account for the interactions between soil water and groundwater. Zeng and Decker [107] proposed another simple way to represent the groundwater recharge rate using the deviation of soil water pressure from its hydrostatic equilibrium at the soil bottom. All these developments represent a step forward from the current LSMs using gravitational free drainage or zero flux as their lower boundary condition. Further development and evaluation are needed to more realistically represent groundwater in ESMs.

Runoff Runoff is one of the major components of the global water cycle and accounts for about 40% of the precipitation that falls on land. It plays an important role in the global climate system by affecting ET and freshwater inputs to the oceans, which in turn affects the ocean thermohaline circulation. LSMs' runoff formulation directly affects the partitioning of precipitation into runoff and ET and soil moisture.

Runoff is conceptually difficult to represent in ESMs. The environmental factors that control runoff, precipitation, soil moisture, and topography, often vary considerably on local scales. The plethora of conceptualizations for runoff schemes reflects the uncertainties in understanding and representing fundamental runoff processes. Land model intercomparison projects (e.g., [106, 124]) summarized various implementations of runoff schemes ranging from simple bucket models to more sophisticated topography-based runoff models. The partitioning of precipitation into evapotranspiration, surface runoff and subsurface runoff (baseflow) varies widely among these LSMs. Climate models have been adjusted so that the global, multiyear average runoff production is about one third of the average precipitation. Runoff in BATS is divided approximately equally between surface and subsurface runoff to match the early observational estimates [110].

Most LSMs parameterize runoff processes as a sum of surface runoff (fast component) and subsurface runoff or base flow (slow component). The surface runoff is generated by two major mechanisms: Horton runoff (infiltration excess) and Dunne runoff (saturation excess). The former is assessed as the excess of precipitation intensity over soil infiltration capability, while the latter is estimated as the precipitation over saturated and impermeable surfaces. Horton runoff is more difficult to represent in ESMs because the precipitation intensity produced by ESMs is unrealistically small ("drizzle" problem) and thus precipitation needs to be distributed in both space and time to mimic storms. Hydrologists introduced the concept of fractional saturated area as the dominant control on surface runoff. Surface runoff is largely dominated by the fractional saturated area, that is, the saturated fraction of a grid cell of ESMs, where rainfall or snowmelt water immediately flows into local river systems [125–127].

The fractional saturated area is conceptually correlated with near-surface soil moisture as it is represented

in BATS [110]. More recent implementations [38, 39, 127–129] relate the fractional saturated area to the water table depth (or water deficit depth) and the subgrid characteristics of the topography following TOPMODEL [126, 130]. The latter is described by statistics of the "topographic index" (or "wetness index," $\lambda = \ln(a/\tan\beta)$, where a is the specific catchment area, i.e., the upstream area above a pixel that drains through the unit contour at the pixel, and $\tan\beta$ is the local surface topographic slope) computed from the high-resolution digital elevation model (DEM) [131]. Famiglietti and Wood [38] proposed a discretized framework in which the distribution of the topographic index was disaggregated into a number of bands, each representing a fraction of the watershed with similar water table depth and soil moisture, to parameterize the subgrid variability in soil moisture and runoff. However, its structural conflicts with climate models and its high computation costs impeded its application to ESMs. Most applications (e.g., [127–130]) used a three-parameter gamma distribution function to represent the pdf of the topographic index. By fitting the pdf of the topographic index with an exponential function, Niu et al. [39] simply expressed the saturated fraction as an exponential function of the water table depth.

The slow component was formulated as drainage under gravity in BATS [110] or a downslope lateral drainage in SiB [24]. TOPMODEL formulated its base flow as an exponential function of the soil water storage deficit [126] or the water table depth [130]. The TOPMODEL-based runoff schemes for ESMs also parameterized base flow as an exponential function of the catchment water storage deficit [128] or the water table depth [38, 39, 127, 129]. The exponential relationship between runoff (surface runoff and base flow) and the water table depth was demonstrated by observations [50].

Carbon Budgets and Vegetation Dynamics

The terrestrial ecosystem stores very large amounts of carbon, which is estimated at about 500 Pg of carbon (1 Pg C = 10^{15} g C) in plant biomass and 2,000 Pg of carbon in soil organic matter (top 1 m) [132]. The atmosphere, with a CO_2 concentration of 370 ppmv, contains about 785 Pg C as CO_2 [132]. Terrestrial ecosystem absorbs atmospheric CO_2 through photosynthesis at a rate of about 120 Pg C per year (gross primary productivity; GPP) and releases about half of that back to the atmosphere as CO_2 by respiration, resulting in net primary production (NPP) at about 60 Pg C per year. At the same time, heterotrophic respiration from soil and fire return about 60 Pg C per year back to atmospheric CO_2, closing the loop. The carbon fluxes between terrestrial ecosystem and the atmosphere have been quite stable for millennia. However, losses of C from land use change have been steadily increasing over the last one-and-half centuries, approaching rates of about 2 Pg C per year, mostly from tropical deforestation. Net cumulative CO_2 emissions from land use change may be close to 200 Pg C during the human history [132], about 25% of the atmospheric CO_2 at the level of 370 ppmv. Therefore, ESMs simulating the evolution of climate for centuries of the past and the future should represent these processes more realistically in their LSMs. ESMs also need to realistically simulate the relative role of land versus ocean in taking up the CO_2 released by anthropogenic sources.

Representing carbon budgets and vegetation dynamics is a major feature of the third-generation LSMs. The third-generation models try to fully represent plant physiology and phenology. Most of these LSMs use a semiempirical model of leaf conductance [1, 30, 33] to link the stomatal resistance with photosynthesis processes:

$$1/r_{st} = m\frac{A_n}{c_a}\frac{e_a}{e_{sat}}P + g_0 \tag{16}$$

where m is an empirical coefficient (~9 for most C_3 plants and ~4 for C_4 plants; a larger m means the leaf consumes more water to assimilate the same carbon), A_n is the net carbon assimilation rate, c_a and e_a are the CO_2 concentration and vapor pressure at the leaf surface, respectively, e_{sat} is the saturated vapor pressure at the leaf temperature, P is the atmospheric pressure, and g_0 is the minimum stomatal conductance.

The net carbon assimilation is calculated as the minimum of three limiting factors: the Rubisco-limited, light-limited, and export-limited rates of carboxylation rate for C_3 plants and PEP-carboxylase limitation for C_4 grasses based on Collatz et al. [30, 133]. Both Rubisco-limited and export-limited

rates of carboxylation are related to the maximum rate of carboxylation, which varies with temperature, foliage nitrogen, and soil water:

$$V_{\max} = V_{\max 25} a_{v\,\max}^{\frac{T_v - 25}{10}} f(N) f(T_v) \beta \tag{17}$$

where $V_{\max 25}$ is maximum carboxylation rate at 25°C depending on plant functional types (PFTs) and $\alpha_{v\,\max}$is the Q_{10} parameter (i.e., for an increase in temperature by 10°C, $V_{\max}$ would increase by $\alpha_{v\,\max}$), $f(T_v)$ is a function that mimics thermal breakdown of metabolic processes [30, 32], $f(N)$is a foliage nitrogen factor and, the β factor is the soil moisture stress factor.

Most third-generation models, for example, SiB2 [113], IBIS [5], MOSES [117], and CLM4 [61] represent plant physiology using the above formulations. To simulate the net carbon budgets from the terrestrial ecosystem, the models also included representations of autotrophic respiration and heterotrophic respiration. For instance, CLM4 represents autotrophic respiration as the sum of maintenance respiration and growth respiration. Maintenance respiration is a function of temperature and tissue nitrogen concentration for live biomass [134], while growth respiration is assumed to be about 0.3 of the total carbon in new growth on a given time step based on construction cost for a range of woody and nonwoody tissues. CLM4 also represents decomposition, mineralization, and immobilization processes of carbon and nitrogen stored in three litter pools, three soil organic matter pools, and a coarse woody debris pool, under the soil moisture and temperature controls [134].

These models also describe plant phenology. For instance, CLM4 predicts LAI, SAI, and vegetation heights, including three distinct phenological types: evergreen, seasonal-deciduous, and stress-deciduous. The seasonal-deciduous phenology algorithm is based on the parameterizations for leaf onset and offset for temperate deciduous broadleaf forest [135]. Initiation of leaf onset is triggered when a common degree-day summation exceeds a critical value, and leaf litterfall is initiated when daylength is shorter than a critical value. The stress-deciduous phenology algorithm is based in part on the grass phenology model proposed by White et al. [135]. The algorithm handles phenology for vegetation types such as grasses and tropical drought-deciduous trees that respond to both cold and drought stresses, and that can have multiple growing seasons per year. The overall reasonable performance of CLM4 has been documented in Lawrence et al. [4].

Future Directions

LSMs have been developed for more than 3 decades, focusing more on representations of biogeophysical processes, that is, the energy and water processes occurring in various terrestrial components, and are now at their third generation. They are becoming more complex and more realistically process based than earlier generations. The third-generation models already include terrestrial ecosystem dynamics and associated physiological effects on terrestrial carbon budgets. However, processes affecting greenhouse gas (GHG) emissions from various natural and anthropogenic sources over land are still not fully represented in these models. GHG emissions from various land surfaces are intimately coupled with various terrestrial biogeochemical processes. As suggested by Pitman [2], the need for an LSM to capture biogeochemical processes, which are tightly coupled to hydrological processes, is increasing and this provides focuses for future developments.

Numerous researchers have investigated the feedback of terrestrial ecosystem to climate change for the next century using the third-generation models (e.g., [15, 136]). Despite differences in details, these results demonstrate an important but uncertain role of the future ecosystems in the climate system. In these simulations, the terrestrial ecosystem functions as a sink through about 2050 and then turns into a source due to the collapse of the soil-carbon sink, resulting in an acceleration of global warming (1.5 K higher than without the carbon feedback). However, these results are questionable, because the terrestrial ecosystem and related biogeochemical processes are more complex than what are currently represented in these LSMs. For instance, these models do not fully represent key processes for stabilizing soil carbon, the hysteresis relationship between soil respiration and temperature, and the isoprene protective effects on photosynthesis under high temperature and light stress, etc. As an example, CLM4 includes the controlling role of soil temperature and water potential in the decomposition of leaf litter and soil organic carbon, but it lacks a representation of key processes such as biogeochemical weathering,

heteroaggregate formation, and microbial activities. To represent more sensitive links between climate, microbial physiology, and C transformations, the response of microbial enzymes and active fungi to bacteria ratios to climatic variation and plant cover should be included [137, 138]. CLM4 considered emissions of biogenic volatile organic carbon (BVOC) including isoprene and monoterpenes [139] based on the emission model of Guenther et al. [140]. However, CLM4 neglects the allocation of the assimilated carbon through photosynthesis to BVOC emissions versus respiratory CO_2 emissions and CO_2 inhibitive effects on isoprene emissions. As recently reviewed by Vickers et al. [141], a rich literature exists demonstrating the role of isoprene in protecting photosynthesis under high temperature and light stresses. Therefore, third-generation models have recently started to implement photosynthesis-based isoprene emission algorithms [142]. In addition, a growing body of evidence suggests a temperature-respiration relationship that exhibits a diurnal hysteresis pattern [143]. A representative model (based on a Q_{10} factor) that does not consider hysteresis would overestimate soil CO_2 efflux for the entire growing season [143]. It has also been found that the hysteresis is caused by the imbalance of production and diffusion of CO_2 within soil, and soil moisture controls the transition from the imbalanced hysteresis pattern under wet soil conditions to a balanced pattern without hysteresis under dry soil conditions. As such, Riveros-Iregui et al. [143] suggested that the role of soil moisture in controlling the hysteresis temperature–respiration relationship should be considered in models. In addition, autotrophic respiration from roots and more elaborate representation of vertical root distribution should also receive more attention.

A major indication of the anthropogenic effects on the climate system is the large-scale conversion of natural ecosystems to cropland throughout human history. Associated with this conversion are changes in GHG emissions and related water use. Global agriculture is a major contributor to increasing the GHGs, with ~18% of the total anthropogenic emissions, including 9% of the total CO_2 emissions due to land use (e.g., deforestation), 40% of the total CH_4 emissions due to rice cultivation, and 62% of the total N_2O emissions due to fertilizer application for year 2000 [144]. For irrigation, global cropland consumes about 2,500 km^3 of water each year, which represents almost 70% of the global fresh water withdrawal from surface reservoirs and aquifers [145]. LSMs have started to include crop models and irrigation schemes (e.g., CLM4). Fully representing agricultural practices, for example, sowing, dates, cultivars, irrigation, and fertilization and associated biogeochemical processes that affect GHG emissions and water use represents a direction in future LSM development. Crop models developed by the agriculture community and measurements from the Free-air Controlled Enhancement (FACE) [146] over various natural and agricultural ecosystems should be helpful for developing models and test models' response to enhanced temperature and CO_2 concentration.

Almost all LSMs for use in ESMs are 1D, solving the governing equations in the vertical direction. However, water flows also in lateral directions at surface and in subsurface driven by gravity; the lateral water flow controls the formation and persistence of wetlands and governs the dynamics of freshwater inputs to the oceans. There is an increasing need to implement 3D hydrologic model into LSMs for use in ESMs. Methane emission, which is the second largest contributor to the anthropogenic GHG, is highly related to wetland dynamics. Of all the natural and anthropogenic sources of methane, methane emission from wetlands is known to be the single largest [147]. However, most LSMs lack a representation of wetland dynamics, prescribing wetland area as a fixed value. To more realistically represent wetland area, Fan et al. [148] developed an efficient hydrologic framework to simulate wetlands for climate models, involving large-scale groundwater convergence that feeds wetland. The spatial resolution of ESMs is increasing (~10 km) with recent computational advances. Implementing a quasi 3D hydrological model, which describes lateral surface and saturated subsurface (groundwater) flows and operates at a high spatial resolution (1 km), to LSMs will become possible in the near future. The hydrology community recently proposed hyper-resolution (1 km) global land surface modeling for monitoring Earth's terrestrial water resources, studies of biogeochemical processes, and agricultural applications, etc. [149]. Lessons learned from developing such a hyper-resolution model will certainly be beneficial for developing advanced 3D LSMs for use in ESMs.

Acknowledgments

This review was partially supported by DOE (DE-SC0006773), NSF (AGS-0944101, and NASA (NNX09A021G).

Bibliography

Primary Literature

1. Sellers PJ, Dickinson RE, Randall DA, Betts AK, Hall FG, Berry JA, Collatz GJ, Denning AS, Mooney HA, Nobre CA, Sato N, Field CB, Henderson-Sellers A (1997) Modelling the exchanges of energy, water and carbon between continents and the atmosphere. Science 275:502–509
2. Pitman AJ (2003) The evolution of, and revolution in, land surface schemes designed for climate models. Int J Clim 23:479–510
3. Yang Z-L (2004) Modeling land surface processes in short-term weather and climate studies. In: Zhu X (ed) Observations, theory, and modeling of atmospheric variability, vol 3, World scientific series on meteorology of East Asia. World Scientific, Singapore, pp 288–313
4. Lawrence DM, Oleson KW, Flanner M, Thornton PE, Swenson SS, Lawrence PJ, Zeng X, Yang L, Levis S, Sakaguchi K, Bonan GB, Slater AG (2010) Parameterization improvements and functional and structural advances in version 4 of the community land model. J Adv Model Earth Syst 3:M03001, 27p. doi:10.1029/2011MS000045
5. Foley JA, Prentice IC, Ramankutty N, Levis S, Pollard D, Sitch S, Haxeltine A (1996) An integrated biosphere model of land surface processes, terrestrial carbon balance, and vegetation dynamics. Global Biogeochem Cycles 10:603–628
6. Pielke RA, Avissar R, Raupach M, Dolman AJ, Zeng X, Denning AS (1998) Interactions between the atmosphere and terrestrial ecosystems: influence on weather and climate. Glob Chang Biol 4:461–475
7. Charney J, Quirk WJ, Chow S-H, Kornfield J (1977) A comparative study of the effects of albedo change on drought in semi arid regions. J Atmos Sci 34:1366–1385
8. Sud YC, Shukla J, Mintz Y (1988) Influence of land surface roughness on atmospheric circulation and precipitation: a sensitivity study with a general circulation model. J Appl Meteorol 27:1036–1054
9. Chase TN, Pielke RA, Kittel TGF, Nemani R, Running SW (1996) Sensitivity of a general circulation model to global changes in leaf area index. J Geophys Res 101:7393–7408
10. Milly PCD (1997) Sensitivity of greenhouse summer dryness to changes in plant rooting characteristics. Geophys Res Lett 24:269–271
11. Zeng X, Dai J, Dickinson RE, Shaikh M (1998) The role of root distribution for climate simulation over land. Geophys Res Lett 25:4533–4536
12. Bonan GB, Pollard D, Thompson SL (1992) Effects of boreal forest vegetation on global climate. Nature 359:716–718
13. Xue Y (1997) Biosphere feedback on regional climate in tropical North Africa. Q J R Meteorol Soc 123:1483–1515
14. Betts RA (2000) Offset of the potential carbon sink from boreal forestation by decreases in surface albedo. Nature 408:187–190
15. Cox PM, Betts RA, Jones CD, Spall SA, Totterdell IJ (2000) Acceleration of global warming due to carbon-cycle feedbacks in a coupled climate model. Nature 408:184–187
16. Foley JA, Kutzback JE, Coe MT, Levis S (1994) Feedbacks between climate and boreal forests during the Holocene epoch. Nature 371:52–54
17. Hong SY, Kalnay E (2000) Role of sea surface temperature and soil-moisture feedback in the 1998 Oklahoma–Texas drought. Nature 408(6814):842–844
18. Schubert SD, Suarez MJ, Pegion PJ et al (2004) On the cause of the 1930s dust bowl. Science 303(5665):1855–1859
19. Koster RD, Suarez MJ, Heiser M (2000) Variance and predictability of precipitation at seasonal-to-interannual timescales. J Hydrometeorol 1(1):26–46
20. Koster RD et al (2004) Regions of strong coupling between soil moisture and precipitation. Science 305:1138–1140. doi:10.1126/science.1100217
21. Manabe S (1969) Climate and the ocean circulation: 1. The atmospheric circulation and the hydrology of the Earth's surface. Mon Weather Rev 97:739–805
22. Deardorff JW (1978) Efficient prediction of ground surface temperature and moisture with inclusion of a layer of vegetation. J Geophys Res 83:1889–1903
23. Dickinson RE (1984) Modelling evapotranspiration for three dimensional global climate models. In: Hansen JE, Takahasi T (eds) Climate processes and climate sensitivity, vol 29, Geophysical monograph. American Geophysical Union, Washington, DC, pp 58–72
24. Sellers PJ, Mintz Y, Sud YC, Dalcher A (1986) A simple biosphere model (SiB) for use within general circulation models. J Atmos Sci 43:505–531
25. Xue Y, Sellers PJ, Kinter JL, Shukla J (1991) A simplified biosphere model for climate studies. J Climate 4:345–364
26. Verseghy DL, McFarlane NA, Lazare M (1993) CLASS – a Canadian land surface scheme for GCMs. II: vegetation model and coupled runs. Int J Climatol 13:347–370
27. Thompson SL, Pollard D (1995) A global climate model (GENESIS) with a land-surface transfer scheme (LSX). Part 1: present climate simulation. J Climate 8:732–761
28. Desborough CE, Pitman AJ (1998) The BASE land surface model. Global Planet Change 19:3–18
29. Jarvis PG (1976) The interpretation of the variations in leaf water potential and stomatal conductance found in canopies in the field. Philos Trans R Soc Lond A Ser B 273:593–610
30. Collatz GJ, Ball JT, Grivet C, Berry JA (1991) Physiological and environmental regulation of stomatal conductance, photosynthesis and transpiration: a model that includes a laminar boundary layer. Agr Forest Meteorol 54:107–136
31. Sellers PJ, Berry JA, Collatz GJ, Field CB, Hall FG (1992) Canopy reflectance, photosynthesis and transpiration. III. A reanalysis

using improved leaf models and a new canopy integration scheme. Remote Sens Environ 42:187–216
32. Farquhar GD, von Caemmerer S, Berry JA (1980) A biochemical model of photosynthetic CO_2 assimilation in leaves of C3 species. Planta 149:78–90
33. Ball JT (1988) An analysis of stomatal conductance. PhD thesis, Stanford University, Stanford
34. Avissar R, Pielke RA (1989) A parameterization of heterogeneous land surfaces for atmospheric numerical models and its impact on regional meteorology. Mon Weather Rev 117:2113–2136
35. Koster RD, Suarez MJ (1992) Modelling the land surface boundary in climate models as a composite of independent vegetation stands. J Geophys Res 97:2697–2715
36. Entekhabi D, Eagleson PS (1989) Land surface hydrology parameterization for atmospheric general circulation models including subgrid scale spatial variability. J Climate 2:816–831
37. Liang X, Lettenmaier DP, Wood EF, Burges SJ (1994) A simple hydrologically based model of land surface water and energy fluxes for general circulation models. J Geophys Res 99:415–428
38. Famiglietti JS, Wood EF (1994) Multi-scale modeling of spatially variable water and energy balance processes. Water Resour Res 30(11):3061–3078
39. Niu G-Y, Yang Z-L, Dickinson RE, Gulden LE (2005) A simple TOPMODEL-based runoff parameterization (SIMTOP) for use in global climate models. J Geophys Res 110:D21106. doi:10.1029/2005JD006111
40. Liston GE (2004) Representing subgrid snow cover heterogeneities in regional and global models. J Climate 17:1381–1397
41. Niu G-Y, Yang Z-L (2007) An observation-based formulation of snow cover fraction and its evaluation over large North American river basins. J Geophys Res 112:D21101. doi:10.1029/2007JD008674
42. Jin JM, Gao X, Yang ZL, Bales RC, Sorooshian S, Dickinson RE (1999) Comparative analyses of physically based snowmelt models for climate simulations. J Climate 12:2643–2657
43. Dai Y et al (2003) The common land model (CLM). Bull Am Meteorol Soc 84(8):1013–1023
44. Yang Z-L, Niu G-Y (2003) The versatile integrator of surface and atmosphere processes (VISA) part 1: model description, global planet. Change 38:175–189
45. Pitman AJ, Slater AG, Desborough CE, Zhao M (1999) Uncertainty in the simulation of runoff due to the parameterization of frozen soil moisture using the GSWP methodology. J Geophys Res 104:16 879–16 888
46. Koren V, Schaake JC, Mitchell KE, Duan Q-Y, Chen F, Baker JM (1999) A parameterization of snowpack and frozen ground intended for NCEP weather and climate models. J Geophys Res 104:19,569–19,585. doi:10.1029/1999JD900232
47. Niu G-Y, Yang Z-L (2006) Effects of frozen soil on snowmelt runoff and soil water storage at a continental scale. J Hydrometeorol 7:937–952. doi:10.1175/JHM538.1
48. Liang X, Xie Z, Huang M (2003) A new parameterization for surface and groundwater interactions and its impact on water budgets with the variable infiltration capacity (VIC) land surface model. J Geophys Res 108(D16):8613. doi:10.1029/2002JD003090
49. Maxwell RM, Miller NL (2005) On the development of a coupled land surface and groundwater model. J Hydrometeorol 6:233–247
50. Yeh PJF, Eltahir EAB (2005) Representation of water table dynamics in a land surface scheme, part I: model development. J Climate 18(12):1861–1880
51. Fan Y, Miguez-Macho G, Weaver CP, Walko R, Robock A (2007) Incorporating water table dynamics in climate modeling: 1. Water table observation and equilibrium water table simulations. J Geophys Res 112:D10125. doi:10.1029/2006JD008111
52. Niu G-Y, Yang Z-L, Dickinson RE, Gulden LE, Su H (2007) Development of a simple groundwater model for use in climate models and evaluation with gravity recovery and climate experiment data. J Geophys Res 112:D07103. doi:10.1029/2006JD007522
53. Hahmann AN, Dickinson RE (2001) A fine-mesh land approach for general circulation models and its impact on regional climate. J Climate 14:1634–1646
54. Sellers PJ, Fennessy MJ, Dickinson RE (2007) A numerical approach to calculating soil wetness and evapotranspiration over large grid areas. J Geophys Res 112:D18106. doi:10.1029/2007JD008781
55. Mahrt L (1987) Grid-averaged surface fluxes. Mon Weather Rev 115:1550–1560
56. Mason PJ (1988) The formation of areally-averaged roughness lengths. Q J R Meteorol Soc 114:399–420
57. Garratt JR (1992) The atmospheric boundary layer. Cambridge University Press, Cambridge
58. Essery RLH, Besst MJ, Betts RA, Cox PM (2003) Explicit representation of subgrid heterogeneity in a GCM land surface scheme. J Hydrol 4:530–543
59. Cherkauer K, Lettenmaier DP (2003) Simulation of spatial varibility in snow and frozen soil. J Geophys Res 108:8858. doi:10.1029/2003JD003575
60. Niu G-Y et al (2011) The community Noah land surface model with multi-parameterization options (Noah-MP): 1. Model description and evaluation with local-scale measurements. J Geophys Res 116:D12109. doi:10.1029/2010JD015139
61. Oleson KW et al (2010) Technical description of version 4.0 of the community land model. NCAR Technical Note NCAR/TN-478+STR. National Center for Atmospheric Research, Boulder, 257 pp
62. Lawrence PJ, Chase TN (2007) Representing a MODIS consistent land surface in the community land model (CLM 3.0). J Geophys Res 112:G01023. doi:10.1029/2006JG000168
63. Myneni RB et al (2002) Global products of vegetation leaf area and fraction absorbed PAR from year one of MODIS data. Remote Sens Environ 83:214–231
64. Zeng X, Shaikh M, Dai Y, Dickinson RE, Myneni R (2002) Coupling of the common land model to the NCAR community climate model. J Climate 15:1832–1854

65. Bonan GB, Levis S, Kergoat L, Oleson KW (2002) Landscapes as patches of plant functional types: an integrating concept for climate and ecosystem models. Global Biogeochem Cycles 16:5.1–5.23
66. Lawrence DM, Slater AG (2008) Incorporating organic soil into a global climate model. Clim Dyn 30. doi:10.1007/s00382-007-0278-1
67. Ek MB, Mitchell KE, Lin Y, Rogers E, Grunmann P, Koren V, Gayno G, Tarpley JD (2003) Implementation of Noah land surface model advancements in the national centers for environmental prediction operational mesoscale Eta model. J Geophys Res 108(D22):8851. doi:10.1029/2002JD003296
68. Dickinson RE (1983) Land surface processes and climate-surface albedos and energy balance. In: Saltzman B (ed) Theory of climate, vol 25, Advances in geophysics. Academic, San Diego, pp 305–353
69. Sellers PJ (1985) Canopy reflectance, photosynthesis and transpiration. Int J Remote Sens 6:1335–1372. doi:10.1080/01431168508948283
70. Nijssen B, Lettenmaier D (1999) A simplified approach for predicting shortwave radiation transfer through boreal forest canopies. J Geophys Res 104(D22):27,859–27,868
71. Li X, Strahler AH, Woodcock CR (1995) A hybrid geometric optical and radiative transfer approach for modeling albedo and directional reflectance of discontinuous canopies. IEEE Trans Geosci Remote Sens 33(2):466–480
72. Yang R, Friedl M, Ni W (2001) Parameterization of shortwave radiation fluxes for nonuniform vegetation canopies in land surface models. J Geophys Res 106:14,275–14,286
73. Brutsaert WA (1982) Evaporation into the atmosphere. Reidel, Dordrecht, 299 pp
74. Garratt JR, Francey RJ (1978) Bulk characteristics of heat transfer on the instable baroclinic atmospheric boundary layer. Bound -Lay Meteorol 15:399–421
75. Shuttleworth WJ (2007) Putting the 'vap' into evaporation. Hydrol Earth Syst Sci 11(1):210–244
76. Zeng X, Dickinson RE (1998) Effect of surface sublayer on surface skin temperature and fluxes. J Climate 11:537–550
77. Sakaguchi K, Zeng X (2009) Effects of soil wetness, plant litter, and under-canopy atmospheric stability on ground evaporation in the community land model (CLM3.5). J Geophys Res 114:D01107. doi:10.1029/2008JD010834
78. Dickinson RE (1988) The force-restore model for surface temperatures and its generalizations. J Climate 1:1086–1097
79. Roesch A, Wild M, Gilgen H, Ohmura A (2001) A new snow cover fraction parameterization for ECHAM4 GCM. Clim Dyn 17:933–946
80. Hedstrom NR, Pomeroy JW (1998) Measurements and modeling of snow interception in the boreal forest. Hydrol Proc 12:1611–1625
81. Niu G-Y, Yang Z-L (2004) Effects of vegetation canopy processes on snow surface energy and mass balances. J Geophys Res 109:D23111. doi:10.1029/2004JD004884
82. Yeh T-C, Wetherald RT, Manabe S (1983) A model study of the short-term climate and hydrologic effects of sudden snow-cover removal. Mon Weather Rev 111:1013–1024
83. Walsh JE, Ross B (1988) Sensitivity of 30-day dynamical forecast to continental snow cover. J Climate 1:739–754
84. Cess RD et al (1991) Intercomparison of snow-feedback as produced by general circulation models. Science 253: 888–892
85. Douville H, Royer JF (1997) Influence of the temperate and boreal forests on the northern hemisphere climate in the meteo-France climate model. Clim Dyn 13:57–74
86. Hall DK (1988) Assessment of polar climate change using satellite technology. Rev Geophys 26:26–39
87. Robinson DA, Frei A (2000) Seasonal variability of northern hemisphere snow extent using visible satellite data. Prof Geogr 52(2):307–315
88. Brown RD (2000) North hemisphere snow cover variability and change, 1915–97. J Climate 13:2,339–2,355
89. Chapin FS, Sturm M, Serreze MC et al (2005) Role of land-surface changes in Arctic summer warming. Science 310:657–660
90. Yang Z-L, Dickinson RE, Robock A, Vinnikov KY (1997) Validation of the snow sub-model of the biosphere-atmosphere transfer scheme with Russian snow cover and meteorological observational data. J Climate 10:353–373
91. Douville H, Royer J-H, Mahfouf J-F (1995) A new snow parameterization for the meteo-France climate model, part I: validation in standalone experiment. Clim Dyn 12:21–35
92. Lynch-Stieglitz M (1994) The development and validation of a simple snow model for the GISS GCM. J Climate 7: 1842–1855
93. Anderson EA (1976) A point energy and mass balance model of a snow cover. NOAA Technical Report NWS 19. Office of Hydrology, National Weather Service, Silver Spring, 150 pp
94. Jordan R (1991) A one-dimensional temperature model for a snow cover. Special Report 91–16. Cold Regions Research and Engineering Laboratory, U.S. Army Corps of Engineers, Hanover
95. Davis RE, Hardy JP, Ni W, Woodcock C, McKenzie JC, Jordan R, Li X (1997) Variation of snow cover ablation in the boreal forest: a sensitivity study on the effects of conifer canopy. J Geophys Res 102:29,389–29,385
96. Essery R, Pomeroy J, Parviainen J, Storck P (2003) Sublimation of snow from coniferous forests in a climate model. J Climate 16(11):1855–1864
97. Frei A, Gong G (2005) Decadal to century scale trends in North America snow extent in coupled atmosphere–ocean general circulation models. Geophys Res Lett 32:L18502. doi:10.1029/2005GL023394
98. Pielke RA, Liston GE, Eastman JL, Lu L, Coughenour M (1999) Seasonal weather prediction as an initial value problem. J Geophys Res 104:19,463–19,479. doi:10.1029/1999JD900231

99. Schlosser CA, Milly PCD (2002) A model-based investigation of soil moisture predictability and associated climate predictability. J Hydrometeorol 3:483–501. doi:10.1175/1525-7541(2002) 003<0483: AMBIOS>2.0.CO;2
100. Shukla J, Mintz Y (1982) The influence of land-surface evapotranspiration on the Earth's climate. Science 215(4539):1498–1501
101. Zeng X, Barlage M, Castro C, Fling K (2010) Comparison of land-precipitation coupling strength using observations and models. J Hydrometeorol 11:980–995
102. Koster RD et al (2004) Realistic initialization of land surface states: impacts on subseasonal forecast skill. J Hydrometeorol 5:1049–1063. doi:10.1175/JHM-387.1
103. Koster RD et al (2010) Contribution of land surface initialization to subseasonal forecast skill: first results from a multi-model experiment. Geophys Res Lett 37:L02402. doi:10.1029/2009GL041677
104. Yang RQ, Mitchell K, Meng J, Ek M (2011) Summer-season forecast experiments with the NCEP climate forecast system using different land models and different initial land states. J Climate 24:2319–2334. doi:10.1175/2010JCLI3797.1
105. Entin JK, Robock A, Vinnikov KY, Zabelin V, Liu S, Namkhai A, Adyasuren T (1999) Evaluation of global soil wetness project soil moisture simulations. J Meteorol Soc Jpn 77:183–198
106. Boone A et al (2004) The Rhone-aggregation land surface scheme intercomparison project: an overview. J Climate 17:187–208
107. Zeng X, Decker M (2009) Improving the numerical solution of soil moisture-based Richards equation for land models with a deep or shallow water table. J Hydrometeorol 10:308–319. doi:10.1175/2008JHM1011.1
108. Barry RG, Serreze MC (2000) Atmospheric components of the Arctic Ocean freshwater balance and their interannual variability. In: Lewis EL et al (eds) The freshwater budget of the Arctic Ocean. Kluwer Academic Publishers, New York, pp 45–56
109. Luo LF et al (2003) Effects of frozen soil on soil temperature, spring infiltration, and runoff: results from the PILPS 2(d) experiment at Valdai, Russia. J Hydrometeorol 4:334–351
110. Dickinson RE, Henderson-Sellers A, Kennedy PJ (1993) Biosphere- atmosphere transfer scheme (BATS) version 1e as coupled to the NCAR community climate model. NCAR Technical Note, NCAR/TN- 387 + STR. National Center for Atmospheric Research, Boulder
111. Robock A, Vinnikov KY, Schlosser CA, Speranskaya NA, Xue Y (1995) Use of midlatitude soil moisture and meteorological observations to validate soil moisture simulations with biospere and bucket models. J Climate 8:15–35
112. Xue Y, Zeng FJ, Schlosser CA (1996) SSiB and its sensitivity to soil properties: a case study using HAPEX-mobilhy data. Global Planet Change 13:183–194
113. Sellers PJ, Randall DA, Collatz GJ, Berry JA, Field CB, Dazlich DA, Zhang C, Collelo GD, Bounoua L (1996) A revised land surface parameterization (SiB2) for atmospheric GCMs: part I. Modelformulation. J Climate 9:676–705. doi:10.1175/1520-0442(1996)009<0676:ARLSPF>2.0.CO;2
114. Shanley JB, Chalmers A (1999) The effect of frozen soil on snowmelt runoff at Sleepers River, Vermont. Hydrol Process 13:1843–1857
115. Lindstrom G, Bishop K, Lofvenius MO (2002) Soil frost and runoff at Svartberget, northern Sweden – measurements and model analysis. Hydrol Process 16:3379–3392
116. Stadler D, Stähli HM, Aeby P, Flühler H (2000) Dye tracing and image analysis for quantifying water infiltration into frozen soils. Soil Sci Soc Am J 64:505–516
117. Cox PM, Betts RA, Bunton CB, Essery RLH, Rowntree PR, Smith J (1999) The impact of new land surface physics on the GCM simulation of climate and climate sensitivity. Clim Dyn 15:183–203
118. Stähli M, Nyberg L, Mellander P-E, Jansson P-E, Bishop KH (2001) Soil frost effects on soil water and runoff dynamics along a boreal forest transact: 2. Simulations. Hydrol Process 15:927–941
119. Hansson K, Simunek J, Mizoguchi M, Lundin L-C, van Genuchten MT (2004) Water flow and heat transport in frozen soil: numerical solution and freeze-thaw applications. Vadose Zone J 3:693–704
120. Decker M, Zeng X (2006) An empirical formulation of soil ice fraction based on in situ observations. Geophys Res Lett 33: L05402. doi:10.1029/2005GL024914
121. Li Q, Sun S, Xue Y (2010) Analyses and development of a hierarchy of frozen soil models for cold region study. J Geophys Res 115:D03107. doi:10.1029/2009JD012530
122. Rodell M, Famiglietti JS (2001) An analysis of terrestrial water storage variations in Illinois with implications for the gravity recovery and climate experiment (GRACE). Water Resour Res 37(5):1327–1339
123. Kollet SJ, Maxwell RM (2008) Capturing the influence of groundwater dynamics on land surface processes using an integrated, distributed watershed model. Water Resour Res 44:W02402. doi:10.1029/2007WR006004
124. Bowling LC et al (2003) Simulation of high latitude hydrological processes in the torne-kalix basin: PILPS phase 2e. 1 – Experimental description and summary intercomparisons. Global Planet Change 38:1–30
125. Dunne T, Black RD (1970) Partial area contributions to storm runoff in a small New England watershed. Water Resour Res 6(5):1296–1311
126. Beven KJ, Kirkby MJ (1979) A physically based, variable contributing model of basin hydrology. Hydrol Sci Bull 24:43–69
127. Stieglitz M, Rind D, Famiglietti J, Rosenzweig C (1997) An efficient approach to modeling the topographic control of surface hydrology for regional and global modeling. J Climate 10:118–137
128. Ducharne A, Koster RD, Suarez MJ, Stieglitz M, Kumar P (2000) A catchment-based approach to modeling land surface

processes in a general circulation model: 2. Parameter estimation and model demonstration. J Geophys Res 105(D20):24,823–24,838
129. Chen J, Kumar P (2001) Topographic influence on the seasonal and inter-annual variation of water and energy balance of basins in North America. J Climate 14:1989–2014
130. Sivapalan M, Beven K, Wood EF (1987) On hydrologic similarity: 2. A scaled model of storm runoff production. Water Resour Res 23:2266–2278
131. Quinn PF, Beven J, Lamb R (1995) The ln(a/tan b) index: how to calculate it and how to use it within the TOPMODEL framework. Hydrol Process 9:161–182
132. Janzen HH (2004) Carbon cycling in earth systems – a soil science perspective. Agric Ecosyst Environ 104(3):399–417. doi:10.1016/j.agee.2004.01.040
133. Collatz GJ, Ribas-Carbo M, Berry JA (1992) A coupled photosynthesis–stomatal conductance model for leaves of C4 plants. Aust J Plant Physiol 19:519–538
134. Thornton PE, Rosenbloom NA (2005) Ecosystem model spin-up: estimating steady state conditions in a coupled terrestrial carbon and nitrogen cycle model. Ecol Model 189:25–48
135. White MA, Thornton PE, Running SW (1997) A continental phenology model for monitoring vegetation responses to interannual climatic variability. Global Biogeochem Cycle 11:217–234
136. Cramer W, Bondeau A, Woodward FI, Prentice IC, Betts RA, Brovkin V, Cox PM, Fisher V, Foley JA, Friend AD, Kucharik C, Lomas MR, Ramankutty N, Sitch S, Smith B, White A, Young-Molling C (2001) Global response of terrestrial ecosystem structure and function to CO_2 and climate change: results from six dynamic global vegetation models. Glob Chang Biol 7:357–373
137. Schimel JP, Weintraub MN (2003) The implications of exoenzyme activity on microbial carbon and nitrogen limitation in soil: a theoretical model. Soil Biol Biochem 35:549–563
138. Allison SD, Wallenstein MD, Bradford MA (2010) Soil-carbon response to warming dependent on microbial physiology. Nat Geosci. doi:10.1038/NGEO846 (Advance online publication)
139. Levis S, Wiedinmyer C, Bonan GB, Guenther A (2003) Simulating biogenic volatile organic compound emissions in the community climate system model. J Geophys Res 108(D21):4659. doi:10.1029/2002JD003203
140. Guenther A, Karl T, Harley P, Wiedinmyer C, Palmer PI, Geron C (2006) Estimates of global terrestrial isoprene emissions using MEGAN (model of emissions of gases and aerosols from nature). Atmos Chem Phys 6:3181–3210
141. Vickers CE, Gershenzon J, Lerdau MT, Loreto F (2009) A unified mechanism of action for volatile isoprenoids in plant abiotic stress. Nat Chem Biol 5:283–291
142. Pacifico F, Harrison SP, Jones CD, Arneth A, Sitch S, Weedon GP, Barkley MP, Palmer PI, Serca D, Potosnak M, Fu TM, Goldstein A, Bai J, Schurgers G (2011) Evaluation of a photosynthesis-based biogenic isoprene emission scheme in JULES and simulation of isoprene emissions under present-day climate conditions. Atmos Chem Phys 11:4371–4389
143. Riveros-Iregui DA, Emanuel RE, Muth DJ, McGlynn BL, Epstein HE, Welsch DL, Pacific VJ, Wraith JM (2007) Diurnal hysteresis between soil CO_2 and soil temperature is controlled by soil water content. Geophys Res Lett 34:L17404. doi:10.1029/2007GL030938
144. Olivier JGJ, Berdowski JJM (2001) Global emissions sources and sinks. In: Berdowski J, Guicherit R, Heij BJ (eds) The climate system. A.A. Balkema/Swets & Zeitlinger, Lisse, pp 33–78. ISBN 90 5809 255 0
145. Rost S, Gerten D, Bondeau A, Luncht W, Rohwer J, Schaphoff S (2008) Agricultural green and blue water consumption and its influence on the global water system. Water Resour Res 44:W09405. doi:10.1029/2007WR006331
146. Kimball BA (2011) Lessons from FACE: CO_2 effects and interactions with water, nitrogen, and temperature. In: Hillel D, Rosenzweig C (eds) Handbook of climate change and agroecosystems: impacts, adaptation, and mitigation. World Scientific, Singapore, pp 81–107
147. Houghton JT et al (eds) (2001) Projections of future climate change, climate change 2001: the scientific basis, contribution of working group I to the third assessment report of the intergovernmental panel on climate change. Cambridge University Press, New York, 881 pp
148. Fan Y, Miguez-Macho G (2011) A simple hydrologic framework for simulating wetlands in climate and earth system models. Clim Dyn 37:253–278. doi:10.1007/s00382-010-0829-8
149. Wood EF et al (2011) Hyperresolution global land surface modeling: meeting a grand challenge for monitoring Earth's terrestrial water. Water Resour Res 47:W05301. doi:10.1029/2010WR010090

Earth System Monitoring, Introduction

John Orcutt
Scripps Institution of Oceanography, University of California, San Diego, La Jolla, CA, USA

This section provides sensing and data collection methodologies, as well as an understanding of Earth's climate parameters and natural and man-made phenomena, to support a scientific assessment of the Earth system as a whole, and its response to natural and human-induced changes. The coverage ranges from climate change factors and extreme weather and fires to oil spill tracking and volcanic eruptions. This serves as a basis to enable improved prediction and response to

climate change, weather, and natural hazards as well as dissemination of the data and conclusions. The data collection systems include satellite remote sensing, aerial surveys, and land- and ocean-based monitoring stations. Our objective in this treatise is to provide a significant portion of the scientific and engineering basis of Earth system monitoring and to provide this in 17 detailed articles or chapters written at a level for use by university students through practicing professionals. The reader is also directed to the closely related sections on ► Ecological Systems, Introduction and also ► Climate Change Modeling Methodology, Introduction as well as ► Climate Change Remediation, Introduction to. For ease of use by students, each article begins with a glossary of terms, while at an average length of 25 print pages each, sufficient detail is presented for use by professionals in government, universities, and industries. The chapters are individually summarized below.

► Aircraft and Space Atmospheric Measurements Using Differential Absorption Lidar (DIAL) – A particular lidar technique called differential absorption lidar (DIAL) has proven to be an especially powerful method to measure atmospheric chemical species. It has been used both on the ground and in many aircraft to determine the concentration of gasses. DIAL systems can be deployed in fixed ground locations, in either piloted or unpiloted aircraft or in satellite platforms.

► Coral Reef Ecosystems – Over the millennia, coral reef ecosystems have served as the basis of human survival and sustenance in many coastal areas in the tropics and subtropics. They are significant geologic formations that provide crucial protection from destructive forces of the sea. They also harbor the greatest diversity of animal phyla of any other habitat on the planet. Threats due to climate change are detailed.

► Airborne and Space-borne Remote Sensing of Cryosphere – The cryosphere broadly constitutes all the components of the Earth system, which contain water in a frozen state. As such, glaciers, ice sheets, snow cover, lake and river ice, sea ice, and permafrost make up the terrestrial oceanic elements of the cryosphere. While ice particles in the upper atmosphere and icy precipitation near the surface are the representative members of the Cryosphere in atmospheric systems. Airborne and spaceborne remote sensing technologies are presented.

► Heat Content and Temperature of the Ocean – Following years of research and development in autonomous float technology, major international cooperation under the Argo Project led to the seeding of the global ocean with more than 3,000 floats each with the capability of profiling temperature and other properties between depths of 2,000 m and the surface approximately every 10 days. Measurements are relayed by satellite while the floats are at the surface in between each cycle of ascent and descent. Coverage is almost global. Measuring variability in sea level using satellite altimetry in situ temperature observations are complementary in efforts to infer changes in heat content.

► Hurricane and Monsoon Tracking with Driftsondes – During the international African Monsoon Multidisciplinary Analysis (AMMA) project, high flying balloons (called driftsondes) dropping meteorological sondes to take measurements over remote, but scientifically important locations, were deployed over West Africa and tropical Atlantic to study weak weather systems, called African easterly waves, that serve as seedlings for hurricanes.

► Large-Scale Ocean Circulation: Deep Circulation and Meridional Overturning – Observations from long-term moorings and deep floats have illustrated a dynamic deep ocean environment, with energetic variability observed at a wide range of space and time scales, including narrow jets, eddies, and recirculating gyres.

► Long-Term Ecological Research Network – The US Long Term Ecological Research (LTER) Network is the largest and longest-lived ecological network in the continental United States. Designed to provide long-term data from a broad range of key ecosystems, the LTER Network represents a unique national resource for addressing pressing environmental issues such as climate change, loss of biodiversity, and changes in patterns of land use.

► Ocean Acidification – The oceans have absorbed about one third of the anthropogenic carbon emissions, which in part ameliorates global warming induced by human activity. However, this capacity to absorb CO_2 is challenged by the accelerated increase in human activities including the increasing burning of fossil fuels, cement production, agriculture, and deforestation. The accelerated rate of increase in the concentration of atmospheric CO_2 and the parallel rise in dissolved CO_2 in seawater (and the associated chemical

changes) can affect marine life. For example, increases in CO_2 can potentially disrupt the acid base balance in tissues, fluids, and cells of marine organisms.

► Ocean Evaporation and Precipitation – Taken as a whole, the hydrological cycle is characterized by the evaporation of about half a million cubic kilometers of water per year, the bulk of which (86%) is from the ocean, with only 14% originating in the continents. The vast majority of the water that evaporates from the oceans (90%) is precipitated back into them, while the remaining 10% is transported to the continents, where it precipitates. About two thirds of this precipitation is recycled over the continents and only one third runs off directly into the oceans. This chapter covers the distribution of evaporation from the ocean and precipitation, oceanic heat reservoirs and evaporation, oceanic evaporation and monsoonal precipitation regimes, and the response of the relationship between evaporation and precipitation.

► Ocean Observatories and Information: Building a Global Ocean Observing Network – Ocean observatories are collections of networks of sensors that are deployed to sample the ocean physics, chemistry, and biology. The goal of these networks is to overcome chronic under-sampling of the oceans by providing sustained measurements in space and time. The data collected by these networks are used to address a range of basic and applied research questions, hindered by a lack of data. This chapter covers the need for a global ocean observing network, design considerations, platforms, and information systems.

► Oil Spill Remote Sensing – Remote sensing for oil spills is reviewed. The technical aspects of sensors are considered and the benefits and limitations of each sensor are assessed. Oil spill response often requires that remote sensing be used to detect, map and track the spill of interest. A wide variety of technologies are covered.

► The Gravity Recovery and Climate Experiment (GRACE) Detection of Ice Mass Loss, Terrestrial Mass Changes, and Ocean Mass Gains – The gravity field of Earth, caused by the distribution of masses inside and on the surface of Earth, changes in time due to the redistribution of mass. Such mass fluxes can be due both to natural processes (such as the seasonal water cycle, ocean dynamics, or atmospheric variations), as well as due to human actions, such as the systematic withdrawal of groundwater for human consumption. The GRACE satellite pair has provided the first global measurements at horizontal resolutions from 300 km to global, and time scales from 10 days to interannual. These measurements have been used to assess the mass variability in the oceans, terrestrial water storage, and loss of ice mass in glaciers and ice sheets. Long-term trends, episodic variations such as result from large earthquakes, and seasonal changes have all been measured with unprecedented accuracy and detail.

► Remote Sensing of Natural Disasters – Remote sensing involves the use of instruments to study phenomena from a distance. Natural disasters derive from hazards such as volcanoes, flooding, earthquake fires, and weather. Practically speaking, "remote sensing of natural disasters" principally refers to the use of airborne or spaceborne sensors to study natural disasters for detecting, modeling, predicting, analyzing, and mitigating effects on human populations and activities. Satellite instruments can provide imagery of large areas of Earth's surface and overflights can often easily provide data for hard to access locations (either due to terrain, weather, or causes of the disaster itself). Airborne instruments can also provide much of the same utility from remote sensing with the potential advantages of greater loiter or dwell time and rapid response.

► Remote Sensing of Ocean Color – The oceans cover over 70% of Earth's surface and the life inhabiting the oceans play an important role in shaping Earth's climate. Phytoplankton, the microscopic organisms in the surface ocean, are responsible for half of the photosynthesis on the planet. These organisms at the base of the food web take up light and carbon dioxide and fix carbon into biological structures releasing oxygen. Estimating the amount of microscopic phytoplankton and their associated primary productivity over the vast expanses of the ocean is extremely challenging from ships. However, as phytoplankton take up light for photosynthesis, they change the color of the surface ocean from blue to green. Such shifts in ocean color can be measured from sensors placed high above the sea on satellites or aircraft and are called "ocean color remote sensing." In open ocean waters, the ocean color is predominantly driven by the phytoplankton concentration and ocean color remote sensing has been used to estimate the amount of chlorophyll *a*, the primary light-absorbing pigment in all phytoplankton.

► Earth System Environmental Literacy – This chapter details the standards of ecological, environmental, and science literacy needed by the public to support decisions involved with assessing climate change data and predictions and taking the required actions.

► Contemporary Sea Level Variations, Observations and Causes – Sea-level change is a very sensitive index of climate change and variability. For example, as the ocean warms in response to global warming, seawaters expand, and thus sea level rises. When mountain glaciers melt in response to increasing air temperature, sea level rises because of freshwater mass input to the oceans. Similarly, ice mass loss from the ice sheets causes sea-level rise. Corresponding increases in freshwater transport into the oceans changes water salinity, hence seawater density as well as ocean circulation that in turn affects sea level and its spatial variability. Since the early 1990s, satellite altimetry has become the main tool for precisely and continuously measuring sea level with nearly global coverage and a few days revisit time. Compared to tide gauges which provide sea level relative to the ground, satellite altimetry measures "absolute" sea-level variations. The main factors causing current global mean sea-level rise are thermal expansion of seawaters, land ice loss, and freshwater mass exchange between oceans and land water reservoirs. These contributions vary in response to natural climate variability and to global climate change induced by anthropogenic greenhouse gas emissions.

► Volcanoes, Observations and Impact – Volcanoes are critical geologic hazards that challenge our ability to make long-term forecasts of their eruptive behaviors. They also have direct and indirect impacts on human lives and society. As is the case with many geologic phenomena, the time scales over which volcanoes evolve greatly exceed that of a human lifetime. On the other hand, the time scale over which a volcano can move from inactivity to eruption can be rather short: months, weeks, days, and even hours. Thus, the scientific study and monitoring of volcanoes is essential to mitigate risk as well as measure the influx of gasses and particulates into the atmosphere. There are thousands of volcanoes on Earth, and it is impractical to study and implement ground-based monitoring at them all. Fortunately, there are other effective means for volcano monitoring, including increasing capabilities for satellite-based technologies. The focus of this chapter is mainly on geophysical observations of volcanoes and calderas as they pertain to eruption forecasting and prediction.

Earthquake Faulting, Ground Motions and Deformations

Ömer Aydan
Geomechanics and Geoengineering, Tokai University, Ocean Research Institute, Shizuoka, Japan

Article Outline

Glossary
Definition of the Subject and Its Importance
Introduction
Ground Motions
Ground Deformations
Effects of Surface Ruptures on Structures
Future Directions
Bibliography

Glossary

Damage The damage is defined as the disruption of the integrity/failure of a structure or function of a system.

Earthquake fault It is the fault, along which relative ground displacement occur during an earthquake.

Engineering structures Structures (i.e., dam, tunnel, slope cut, pylon, bridge, viaduct, etc.) with a given function or purpose are those designed and built according to the principles of engineering.

Ground motions Ground motion is a change of a material point in space in a given time and is observed as displacement, velocity or acceleration and they are caused by the application of forces on a given material body (i.e., solid, fluid).

Definition of the Subject and Its Importance

Ground motion characteristics, deformation, and surface breaks of earthquakes depend upon the causative faults. Their effects on the seismic design of engineering structures are not considered in the present codes of

design, although there are attempts to include these factors in some countries (i.e., USA, Japan, Taiwan). This chapter describes ground motions and the effect of surface ruptures associated with earthquake faulting on response and stability of engineering structures.

Introduction

Earthquakes are known to be one of the natural disasters resulting in the huge losses of human lives and properties as experienced in the recent earthquakes. Since there is no way to prevent the occurrence of earthquakes in earthquake-prone countries such as Turkey, Japan, USA, and Taiwan, the design of structures and residential and industrial developments must be done according to possible faulting types of earthquakes (Fig. 1). It is well known that ground motion characteristics, deformation, and surface breaks of earthquakes depend upon the causative faults [1–13]. While many large earthquakes occur along the subduction zones, which are far from the land, and their effects appear as severe shaking, the large inland earthquakes may occur just beneath or nearby urban and industrial zones as observed in the recent great earthquakes.

The seismic design of engineering structures is generally formed by considering the possible shaking characteristics of the ground during earthquakes in a given region. It is a fact that the residual (permanent) relative displacement of the ground is not considered in any seismic code all over the world, except for very long linear structures such as pipelines. This problem is currently considered to be beyond the capability of seismic design concept for structures in the earthquake engineering, although it must be dealt with somewhat [1, 2].

In this chapter, the author first describes ground motions and deformations in view of laboratory experiments on rock samples and recordings in earthquakes having different faulting mechanisms. Then the effects of surface ruptures and deformations due to earthquake faulting on the response and stability of engineering structures through observations in recent great earthquakes are presented and discussed.

Ground Motions

It is observationally known that the ground motions induced by earthquakes could be much higher in the hanging-wall block or mobile side of the causative fault, as observed in the recent earthquakes such as the 1999 Kocaeli earthquake (strike-slip faulting), the 1999 Chi-chi earthquake (thrust faulting), the 2004 Chuetsu earthquake (blind thrust faulting), and the 2000 Shizuoka earthquake and L'Aquila earthquake (normal faulting) [7, 10, 12–15]. Figure 2 illustrates the effect of hanging-wall effect on the maximum ground accelerations observed in 1999 Chi-chi earthquake (Taiwan), 1999 Düzce earthquake (Turkey), and 2001 Geiyo earthquake (Japan) with different faulting mechanisms [9].

The recent advances in measurement, monitoring, and logging technologies enable measurement and monitoring of the dynamic responses of geomaterials during fracturing and slippage. Studies concerning the dynamic responses of geomaterials during fracturing and slippage can now be more easily undertaken than in the past. Such studies have been recently undertaken at several sites [1, 6–9, 16–19]. The experiments have been performed on geomaterials ranging from very soft materials to hard rocks such as siliceous sandstone by

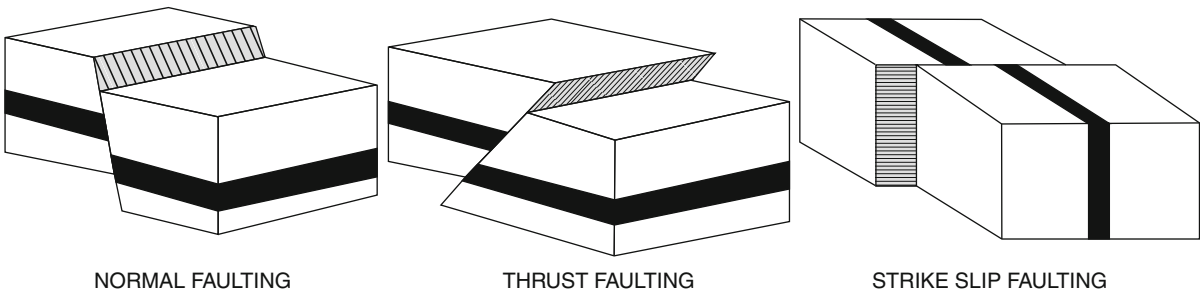

Earthquake Faulting, Ground Motions and Deformations. Figure 1
Fault types [1]

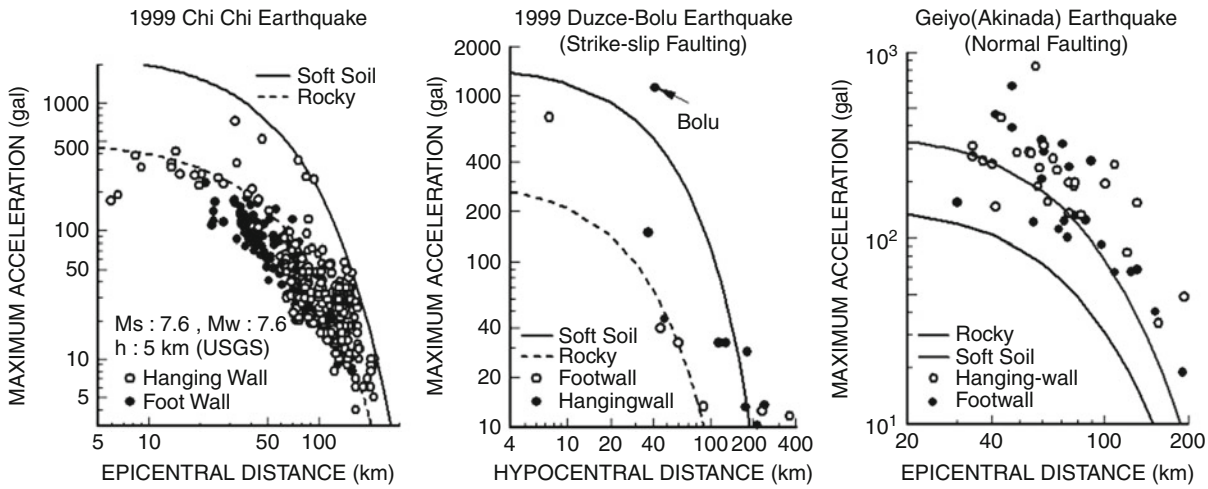

Earthquake Faulting, Ground Motions and Deformations. Figure 2
Attenuation of maximum ground accelerations for some earthquakes

using different loading schemes and loading frames and specially designed stick–slip experimental device.

Aydan and Ohta [3, 9] reported some tests on samples of various rocks such as Ryukyu limestone, tuff, granite, porphyrite, andesite, and sandstone. Two examples are Fuji-TV No.1 and Mitake Sandstone MS2. Fuji-TV No.1 granite is a prismatic sample (100 × 100 × 200 mm) (Fig. 3). The acceleration responses start to develop when the applied stress exceeds the peak strength, and it attains the largest value just before the residual state is achieved as seen in Fig. 3. Another important aspect is that the acceleration of the mobile platen is much larger than that of the stationary platen. This is a common feature in all experiments. In another words, the amplitude of accelerations of the mobile part of the loading system is higher than that of the stationary part.

It is well known that the ground motions are generally smaller than those at ground surface. Nasu [20] carried out first instrumental studies on tunnels during the aftershock activity following 1924 Izu earthquake with a 2.4-m offset. Kanai and Tanaka [21] measured ground acceleration in underground caverns and at the ground surface. These measurements indicated that the surface acceleration was generally twice or greater than twice of that at depth as expected theoretically.

Figure 4 shows the records of accelerations at the ground surface and at bedrock 260 m below at Ichinoseki strong-motion station (IWTH25) of KIK-NET [22] strong-motion network of Japan measured during the 2008 Iwate-Miyagi earthquake. The strong-motion station was located on the hanging-wall side of the fault, and it was very close to the surface rupture. As noted from the figure, the ground acceleration of the UD component was amplified by 5.67 times that at the bedrock. This record is also the highest strong motion recorded in the world so far.

Figure 5 shows the acceleration records measured on the ground surface (GSA) and underground gallery (GSG) during the 2009 Mw 6.3 L'Aquila earthquake [14, 23]. The GSA station is at Assergi, and the GSG station is located in an underground gallery of Gran Sasso Underground Physics Laboratory of Italy. Both stations are founded on Eocene limestone with a shear wave velocity of 1 km/s. Although the epicentral distances and ground conditions are almost the same, the acceleration at ground surface is amplified almost 6.4 times that in the underground gallery.

There are many empirical attenuation relations for estimating ground motions [24–28]. Including the possible next generation attenuation (NGA) relations, all these equations are essentially spherical or cylindrical attenuation relations and cannot take into account directivity effects. As it is shown in the beginning of this section, ground motions such as maximum ground acceleration (AMAX) and maximum ground

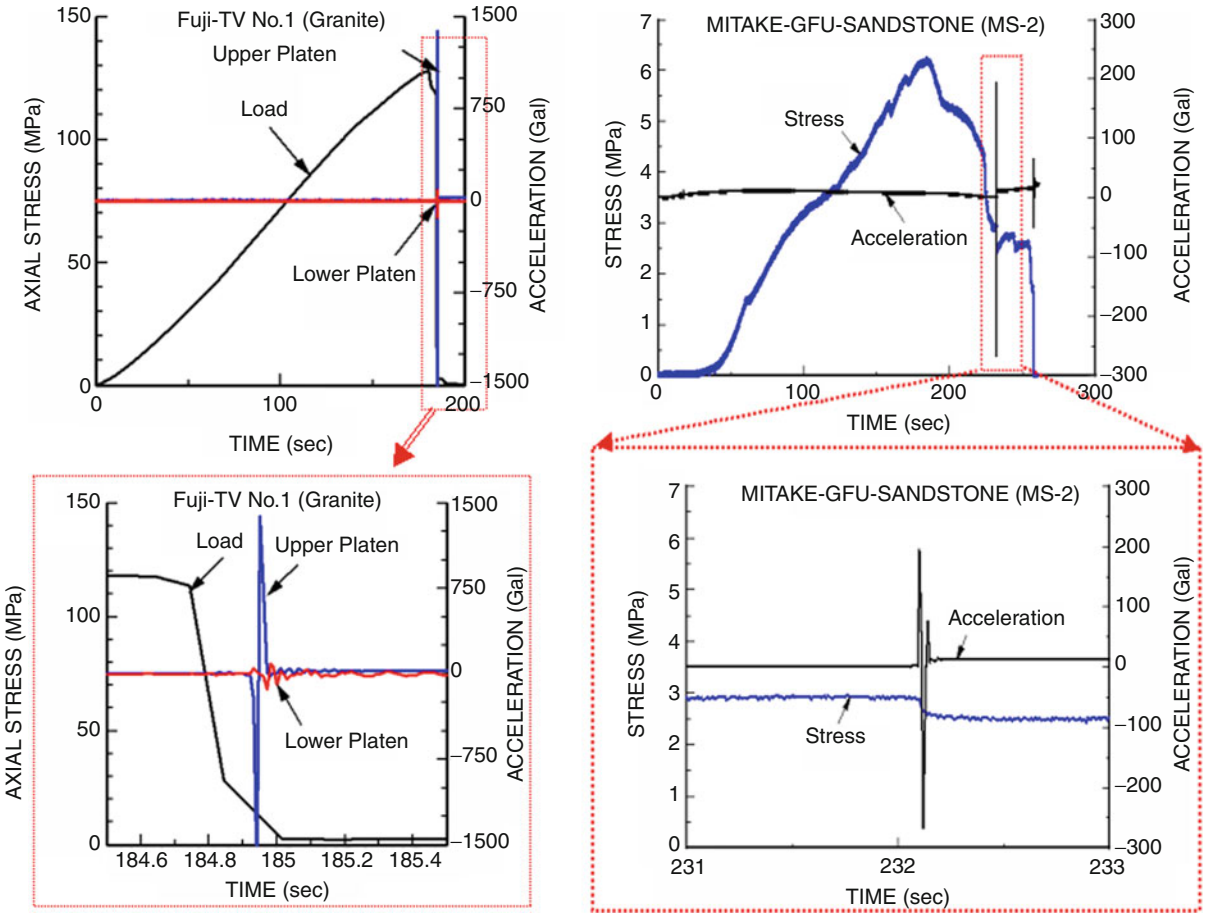

Earthquake Faulting, Ground Motions and Deformations. Figure 3
Acceleration and axial response of sandstone and granite samples

velocity (VMAX) have strong directivity effects in relation to fault orientation. Furthermore, these relations are generally far below the maximum ground acceleration, and they are incapable of obtaining the maximum ground acceleration (AMAX) or the preferred term "peak ground acceleration (PGA)."

Aydan and Ohta [4] proposed an attenuation relation by combining their previous proposals [5, 25, 26] together with the consideration of the inclination and length of earthquake fault using the following functional form (Fig. 6):

$$\alpha_{\max} = F_1(V_s) * F_2(R, \theta, \varphi, L^*) * F_3(M) \tag{1}$$

where V_s, θ, φ, L^*, and M are the shear velocity of ground, the angle of the location from the strike and dip of the fault (measured anticlockwise with the consideration of the mobile side of the fault), and earthquake magnitude. L^* (in km) is a parameter related to the half of the fault length.

The following specific forms of functions in Eq. 1 were put forward as:

$$F_1(V_s) = Ae^{-V_s/B} \tag{2a}$$

$$F_2(R, \theta, \varphi, L^*) = e^{-R(1-D\sin\theta+E\sin^2\theta)(1+F\cos\varphi)/L^*} \tag{2b}$$

$$F_3(M) = e^{M/G} - 1 \tag{2c}$$

The same form can be also used for estimating the maximum ground velocity ($V_{\max}$). The constants of the functions for maximum ground acceleration and velocity for intraplate earthquakes without consideration of faulting sense are given in Table 1.

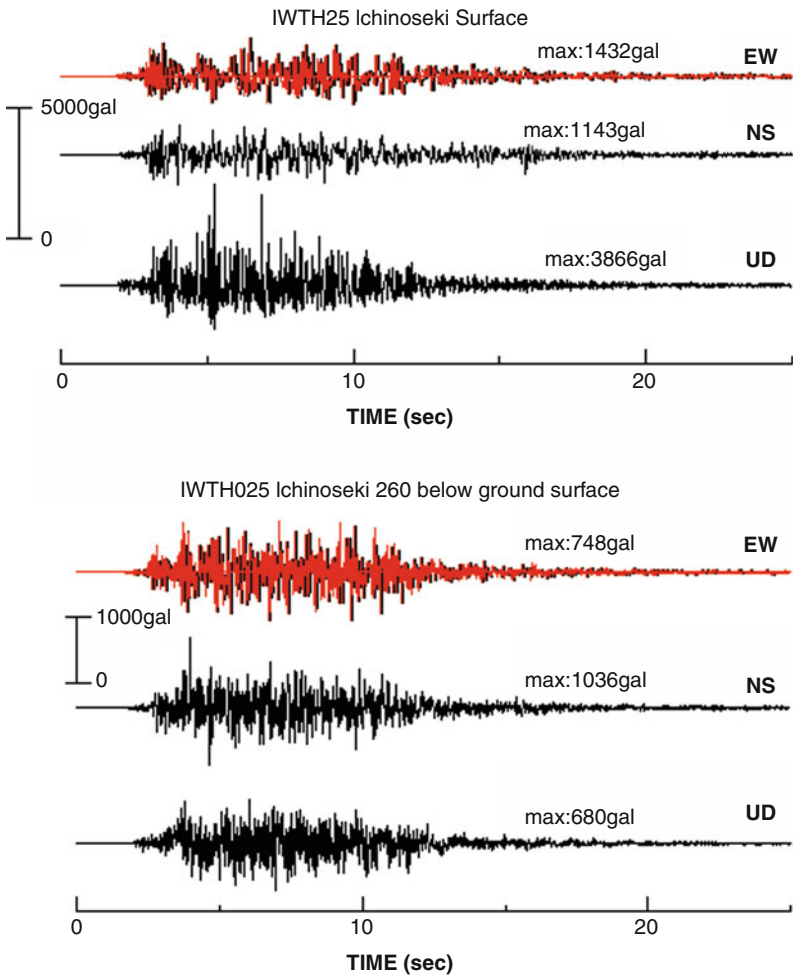

Earthquake Faulting, Ground Motions and Deformations. Figure 4
Acceleration records at ground surface and bedrock at Ichinoseki strong-motion station IWTH25 of KIK-NET in Iwate-Miyagi earthquake

For interplate and slab earthquakes, only the value of constant G is different, and it has the value of 1.05, while other parameters remain the same.

L^*, which is approximately associated with the half of the fault length, is related to the moment magnitude in the following form:

$$L^* = a + be^{cM_w}. \quad (3)$$

This parameter easily accounts for the effect of fault length. A similar form was initially proposed by Aydan et al. [18] for the effects of earthquake faults on underground structures. However, it should be noted that the attenuation characteristics of the earth's crust vary depending upon the location and the sense of faulting. The values of coefficients of Eq. 3 are given in Table 2.

Equation 1 takes into account the location of observation points with respect to earthquake fault and ground conditions, which are fundamentally the main causes of scattering of observational data seen in spherical models for attenuation of ground motions including NGA relations [24–28].

Ground Deformations

A fault is geologically defined as a discontinuity in geological medium along which a relative displacement

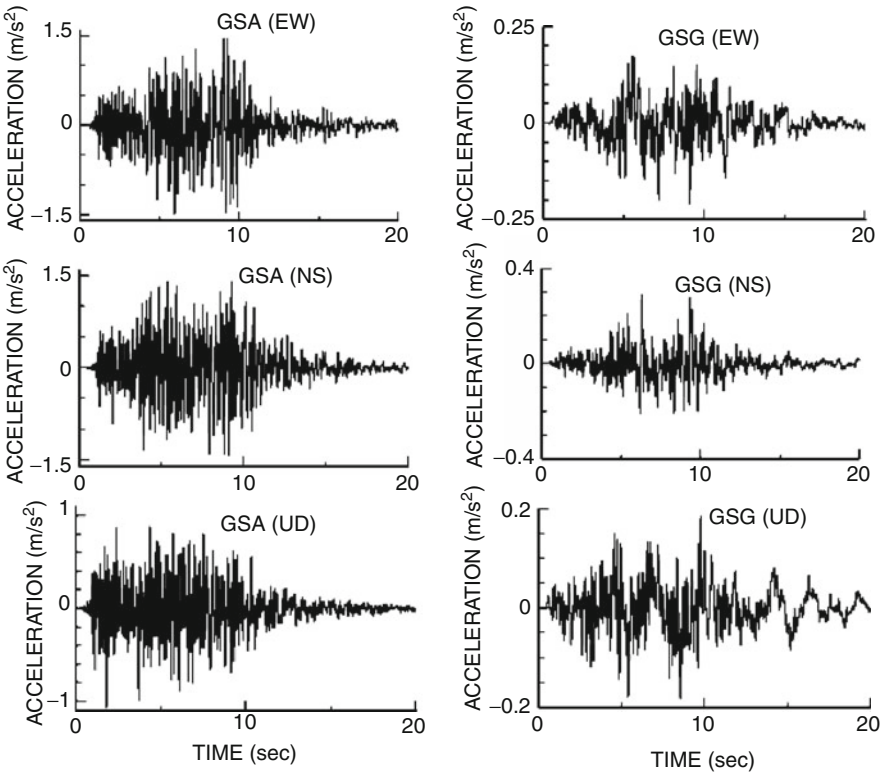

Earthquake Faulting, Ground Motions and Deformations. Figure 5
Acceleration records at GSA and GSG strong-motion stations [14]

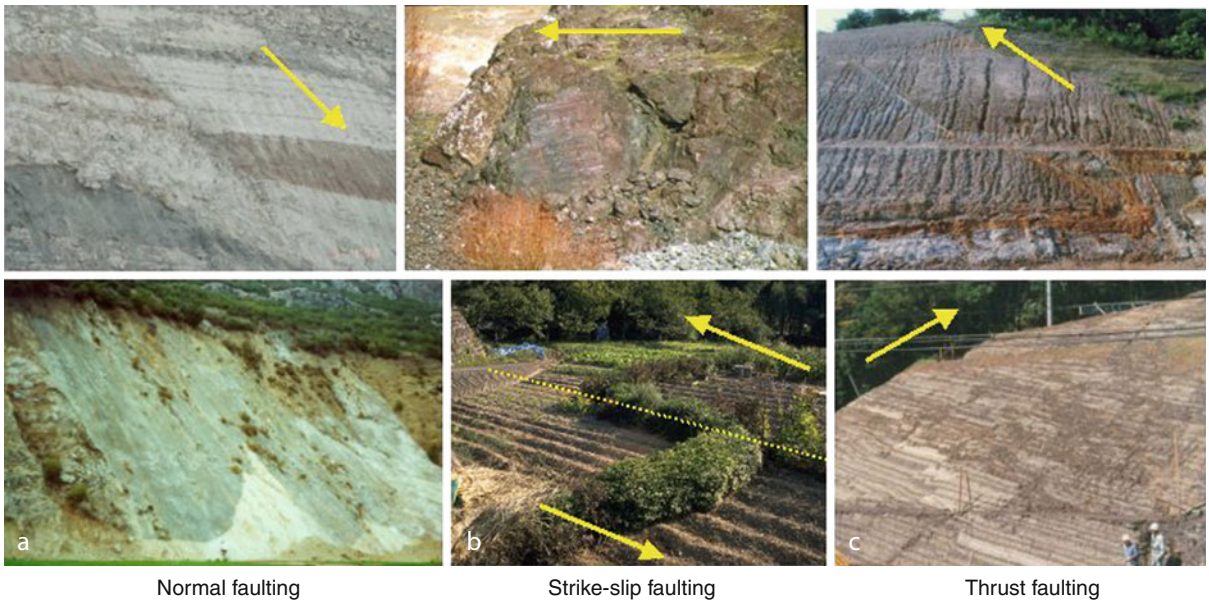

Earthquake Faulting, Ground Motions and Deformations. Figure 6
Some examples of faulting: (**a**) normal faulting; (**b**) strike-slip faulting; (**c**) thrust faulting

Earthquake Faulting, Ground Motions and Deformations. Table 1 Values of constants in Eq. 2 for intraplate earthquakes

	A	B(m/s)	D	E	F	G(M)	
						(Ms)	(Mw)
AMAX	2.8	1,000	0.5	1.5	0.5	1.11	1.16
VMAX	0.4	1,000	0.5	1.5	0.5	1.11	1.16

took place. Faults are broadly classified into three big groups, namely, normal faults, thrust faults, and strike-slip faults as seen in Figs. 1 and 6. A fault is geologically defined as active if a relative movement took place in a period of less than 2 million years previously. It is well known that a fault zone may involve various kinds of fractures, and it is a zone having a finite volume [29]. The appearance of ground breaks is closely related to geological structure, characteristics of sedimentary deposits, their geometry, the magnitude of earthquakes, and fault movements.

It is well known that the earth's crust is ruptured and contains numerous faults and various kinds of discontinuities, and it is almost impossible to find a piece of land without faults. During the construction of structures such as tunnels, dams, power plants, roadways, railways, power transmission lines, bridges, elevated expressways, etc., it is almost impossible not to cross a fault or faults. Therefore, one of the most important items is how to identify which fault segments observed on ground surface will move or rupture during an earthquake. A fault zone may involve various kinds of fractures as illustrated in Fig. 7, and it is a zone having a finite volume [29]. In other words, a fault is not a single plane. Furthermore, faults may have a negative or positive flower structure as a result of their transtensional or transpressional nature and the reduction of vertical stress near the earth's surface as shown in Fig. 8. For example, even a fault having a narrow thickness at depth may cause a quite broad rupture zone and numerous fractures on the ground surface during earthquakes. Furthermore, the movements of a fault zone may be diluted if a thick alluvial deposit is found on the top of the fault (i.e., 1992 Erzincan earthquake [30]).

The recent global positioning system (GPS) also showed that permanent deformations of the ground surface occur after each earthquake (Fig. 2). The permanent ground deformation may result from different causes such as faulting, slope failure, liquefaction, and plastic deformation induced by ground shaking [18]. These types of ground deformations will have limited effect on small structures as long as the surface breaks do not pass beneath those structures. However, such deformations may cause tremendous forces on long and/or large structures. The ground deformation may induce large tensile or compression forces, as well as bending stresses, in structures depending upon the character of permanent ground deformations. As an example, the ground deformations reported by Reilinger et al. [31] are shown in Fig. 9, which were caused by a strike-slip fault during the 1999 Kocaeli earthquake in Turkey. Blind faults and folding processes may also induce some peculiar ground deformations and associated folding of soft overlaying sedimentary layers. Such deformations caused tremendous damage on tunnels during the 2004 Chuetsu earthquake, although no distinct rupturing took place.

Earthquake Faulting, Ground Motions and Deformations. Table 2 Values of constants in Eq. 3

Faulting type	*a*	*b*	*c*
Normal faulting	30	0.002	1.35
Strike-slip faulting	20	0.002	1.40
Thrust faulting	30	0.003	1.45

Effects of Surface Ruptures on Structures

In this section, typical examples of damage to various structures induced by the fault breaks observed in recent large earthquakes since 1995 are presented [1, 2, 11, 32–50].

Roadways and Railways

The Trans-European Motorway (TEM) was damaged at three different locations by the earthquake fault caused by the 1999 Kocaeli earthquake. The motorway with east and west bounds having three lanes each was slightly elevated through embankments in the earthquake-affected region. The surfacing of the motorway was damaged by rupturing and buckling (Fig. 10). The railways were originally built on existing ground surface but were buckled near Tepetarla station where the earthquake fault crossed the railways at an angle of 50–55° with well-known "S" shape (Fig. 11).

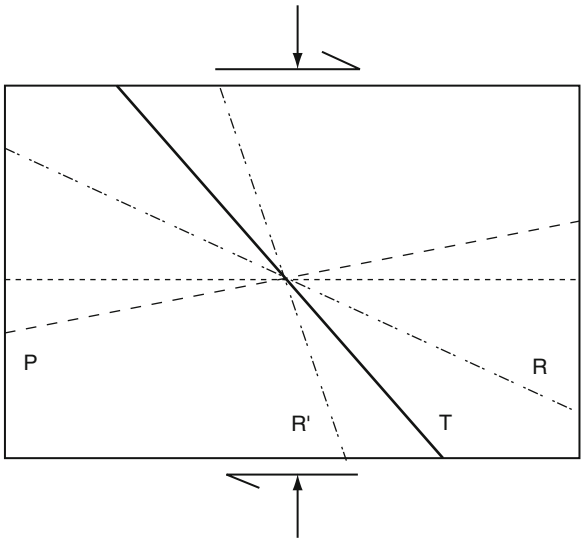

Earthquake Faulting, Ground Motions and Deformations. Figure 7
Fractures in a shear zone or fault [29]

Bridges and Viaducts

Along the damaged section of the TEM motorway mentioned above, there were several overpass bridges. Among them, a four-span overpass bridge at Arifiye junction collapsed as a result of faulting (Fig. 12). The fault rupture passed between the northern abutment and the adjacent pier. The overpass was designed as a simply supported structure according to the modified AASHTO standards, and girders had elastomeric bearings. However, the girders were connected to each other through prestressed cables. The angle between the motorway and the strike of the earthquake fault was approximately 15°, while the angle between the axis of the overpass bridge and the strike of the fault was 65°. The measurements of the relative displacement in the vicinity of the fault range between 330 and 450 cm. Therefore, an average value of 390 cm could be assumed for the relative displacement between the pier and the abutment of the bridge. The Pefong bridge collapsed due to thrust faulting in the 1999 Chi-chi earthquake, which passed between the piers near its southern abutment as seen in Fig. 13.

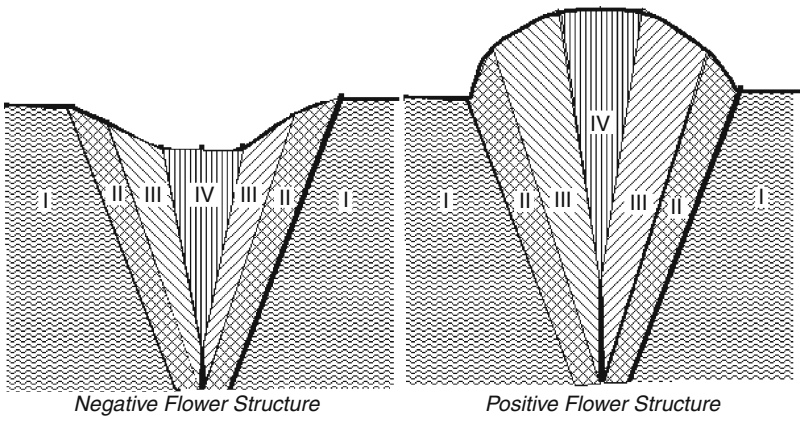

Earthquake Faulting, Ground Motions and Deformations. Figure 8
Negative and positive flower structures due to transtension or transpression faulting (Modified from [2, 11, 29])

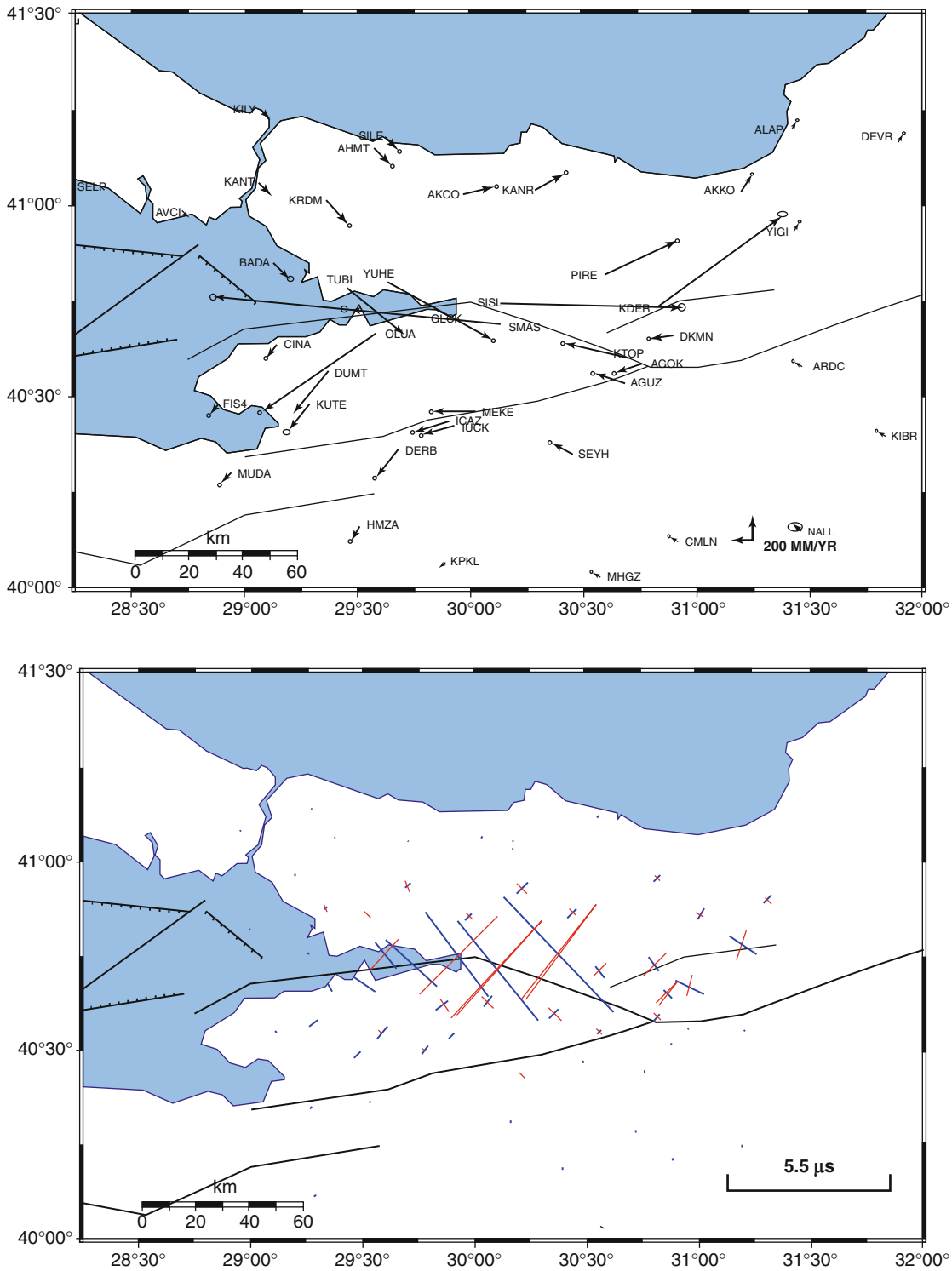

Earthquake Faulting, Ground Motions and Deformations. Figure 9
Permanent ground deformations and associated straining induced by the 1999 Kocaeli earthquake

Earthquake Faulting, Ground Motions and Deformations. Figure 10
Buckling of roadway surfacing

Earthquake Faulting, Ground Motions and Deformations. Figure 11
Buckled railways

Dams

The Shihkang dam, which is a concrete gravity dam with a height of 25 m, was ruptured by thrust-type faulting during the 1999 Chi-chi earthquake (Fig. 14). The relative displacement between the uplifted part of the dam was more than 980 cm. Liyutan rock-fill dam with a height of 90 m and a crest width of 210 m, which was on the overhanging block of Chelungpu fault, was not damaged even when the acceleration records at this dam showed that the acceleration was amplified 4.5 times of that at the base of the dam (105 Gal). The deformation zone of faulting during the 2008 Wenchuan earthquake caused some damage at Zipingpu dam with concrete facing.

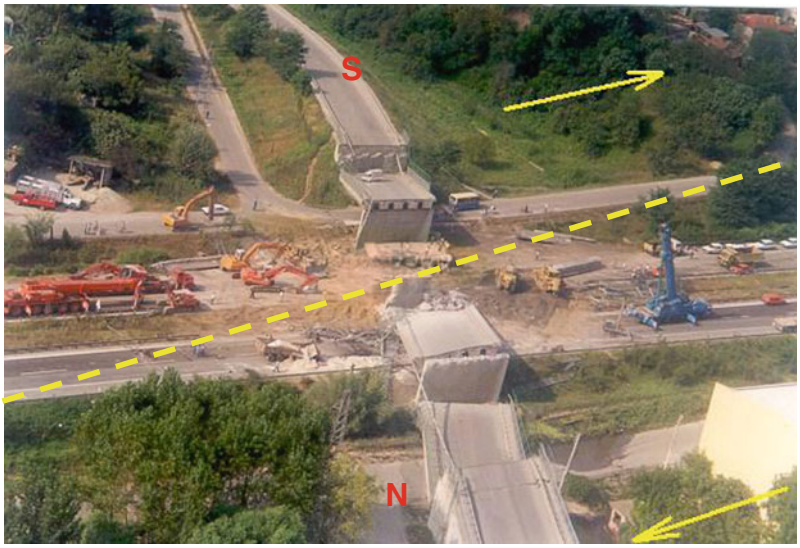

Earthquake Faulting, Ground Motions and Deformations. Figure 12
The collapse of the overpass bridge at Arifiye

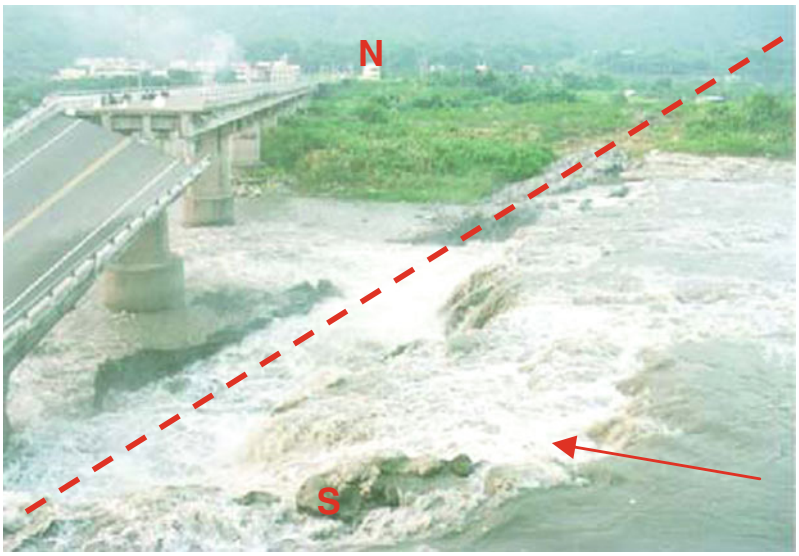

Earthquake Faulting, Ground Motions and Deformations. Figure 13
Collapse of Pefong bridge (note the uplifted ground on RHS)

Tunnels

The past experience on the performance of tunnels through active fault zone during earthquakes indicates that the damage is restricted into certain locations [18, 41–43]. Portals and the locations where the tunnel crosses the fault may be damaged as had occurred in the 2004 Chuetsu, 2005 Kashmir, and 2008 Wenchuan earthquakes (Fig. 15). A section nearby the Elmalık portal of Bolu tunnel collapsed (Fig. 16). This section of the tunnel was excavated under very heavy squeezing conditions [51]. Well-known examples of damage to

Earthquake Faulting, Ground Motions and Deformations. Figure 14
Failure of Shihkang dam due to thrust faulting

Earthquake Faulting, Ground Motions and Deformations. Figure 15
Examples of damaged portals of tunnels

Earthquake Faulting, Ground Motions and Deformations. Figure 16
Collapse of Bolu tunnel during the 1999 Düzce earthquake

tunnels at locations, where the fault rupture crossed the tunnel, are mainly observed in Japan. The Tanna fault ruptured during the 1930 Kita-Izu earthquake and caused damage to a railway tunnel, with a relative displacement of about 100 cm [52, 53]. The 1978 Izu-Oshima Kinkai earthquake induced damage to Inatori railway tunnel [54, 55]. A similar type of damage with a small amount of relative displacements due to motions of Rokko, Egeyama, and Koyo faults to the tunnels of Shinkansen and subway lines through Rokko mountains was also observed [33]. During the 1999 Chi-chi earthquake, the portal of the water intake tunnels was ruptured for a distance of 10 m as a result of thrust faulting. Except this section, the tunnel was undamaged for its entire length.

Jiujiaya tunnel is a 2,282-m-long double-lane tunnel 226.6 km away from the earthquake epicenter and about 3–5 km away from the earthquake fault of Wenchuan earthquake. The tunnel face was 983 m from the south portal at the time of the earthquake. The concrete lining follows the tunnel face at a distance of approximately 30 m. Thirty workers were working at the tunnel face, and one worker was killed by the flying pieces of rock bolts, shotcrete, and bearing plates caused by intense deformation of the tunnel face during the earthquake [17, 18]. The concrete lining was ruptured and fell down at several sections (Fig. 17). The effect of the unreinforced lining rupturing was quite large and intense in the vicinity of the tunnel face. The rupturing of the concrete lining generally occurred at the crown sections, although there was rupturing along the shoulders of the tunnel at several places. Furthermore, the invert was uplifted due to buckling at the middle sections.

Subways

The behavior of subways in active fault zones is basically quite similar to that of tunnels. The Daikai station of the subway line in Kobe was caused by the lateral strike-slip movement of Egeyama fault just beneath this station, although some have tried to associate the collapse of the station with the intensity of shaking (Fig. 18). The investigation of the collapse of this station showed that collapse was not due to shaking, as the

Earthquake Faulting, Ground Motions and Deformations. Figure 17
Earthquake damage at Jiujiaya tunnel due to permanent deformations [18]

Earthquake Faulting, Ground Motions and Deformations. Figure 18
The collapse of Daikai station

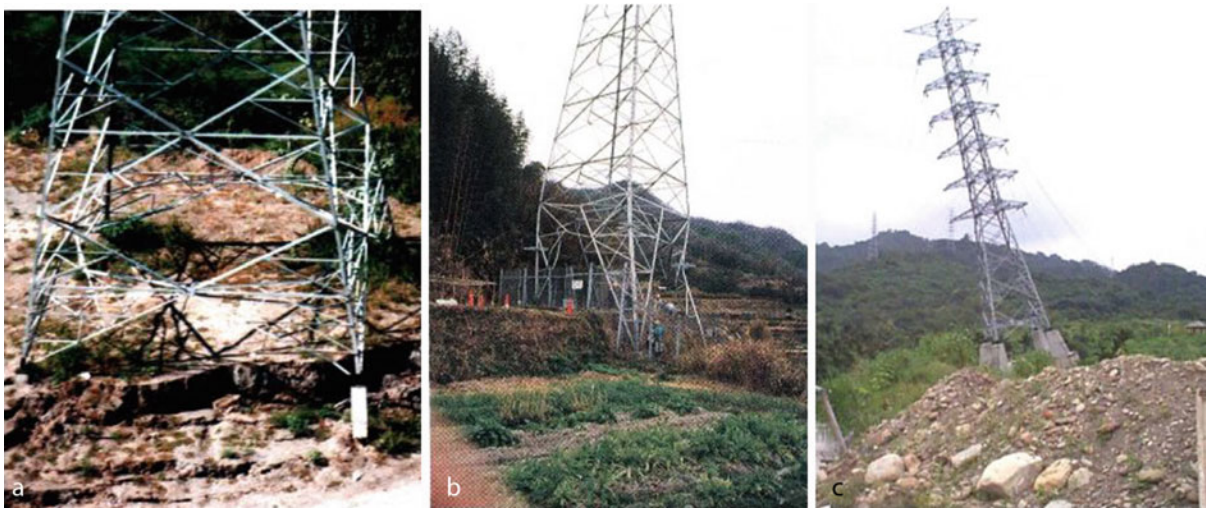

1999 Kocaeli earthquake | 1995 Kobe Earthquake | 1999 Chi-chi Earthquake

Earthquake Faulting, Ground Motions and Deformations. Figure 19
Damage to pylons due to faulting. (**a**) 1999 Kocaeli earthquake. (**b**) 1995 Kobe earthquake. (**c**) 1999 Chi-chi earthquake

central columns of the station were subjected to torsional failure due to the permanent ground displacement, consistent with the lateral strike-slip movement of Egeyama fault [33].

Power Transmission Lines

Power transmission lines generally consist of pylons and power transmission cables. The design of pylons and cables is generally based on the wind loads resulting from typhoons or hurricanes. The cables do not fail during earthquakes unless the pylons are toppled due to faulting, shaking, or slope failure. During the 1999 Kocaeli earthquake, only one pylon was damaged, at a site near Ford-Otosan automobile factory at Kavaklı district of Gölcük town. At this site, a normal fault, secondary to the main lateral strike-slip faulting event, crossed through the foundations of the pylon

and with a vertical lift of about 240 cm. One of the foundations of the pylon was pulled out of the ground and exposed (Fig. 19a). Some of its truss elements were slightly buckled. A similar type of damage to pylons straddling the Nojima fault break in the 1995 Kobe earthquake (Fig. 19b) and the Chelungpu fault during the 1999 Chi-chi earthquake has been observed as shown in Fig. 19c.

Line-Like and Tubular Structures

Tubular structures may be specifically designated as petrol and gas pipelines, water pipes, and sewage systems. They can be also classified as line-like structures. These structures may fail either by buckling or separation during a faulting event. Five such incidents were observed during the 1999 Kocaeli earthquake (Fig. 20). One of the incidents involved separation of a ductile iron pipe as a result of faulting near the collapsed overpass bridge. The second incident took place at the pumping facility of the Seka paper mill plant at Sapanca Lake. The third incident occurred near Tepetarla village where the railways buckled. The fourth and fifth incidents took place at Arifiye and nearby Başiskele. The fifth incident was quite important, since the fault caused a heavy damage to the main water pipe having a diameter of 2 m. Similar types of failures took place in the sewage pipe

Earthquake Faulting, Ground Motions and Deformations. Figure 20
Damage to pipes in the 1999 Kocaeli and 1999 Düzce earthquakes

networks whenever faulting breaks were observed. The natural gas pipelines crossing the İzmit gulf between Yalova and Pendik were undamaged. Some brittle asbestos water pipes were also damaged in Kaynaşlı and Fındıklı due the fault rupture of the 1999 Düzce earthquake.

Buildings

Many buildings along the earthquake faults of the 1999 Kocaeli, Düzce, Chi-chi, and Wenchuan earthquakes were affected in a similar manner. During the site investigation of the 1999 Kocaeli earthquake, one could see totally collapsed, severely damaged, or intact buildings on or adjacent to the traces of the fault breaks. Examples are many; it is difficult to note all of them. Two typical examples are briefly discussed. Nevertheless, this topic deserves more thorough investigation. The first example is a single-story reinforced concrete house with a raft foundation in Fındıklı village. The fault passed just underneath the building (Fig. 21a). The relative displacement of the fault break was about 200 cm with a 100-cm downthrow. The building was tilted, but no damage was observed. A very peculiar type of damage at an apartment complex consisting of 8 five-story apartment blocks was observed in Kullar village as shown in Fig. 21b. Seven apartment blocks failed in a pancake mode, while one apartment block remained standing. One of the failed apartment blocks just crossed the fault break which has a relative horizontal displacement of 240 cm and 20–25 cm vertical throw (north side down). The ground surface sloped to north. One of two apartment blocks on the southern side was damaged, while the other one collapsed toward the east in a pancake mode in accordance with the movement of its foundation. The five blocks on the northern side completely collapsed in a pancake mode toward west in accordance with the direction of shaking. Except for the apartment block over the fault break, the failure of the five apartment blocks on the northern side of the fault break may be considered to be purely due to shaking. The Bailu secondary school building of reinforced concrete survived the Wenchuan earthquake, even though the surface rupture of the thrust fault passed underneath the building (Fig. 21c). Although the intensity of shaking on the southern side of the fault break should be the same, the damaged self-standing apartment block deserves further consideration. Whatever the reason, it is of great interest that even the most vulnerable buildings may also survive within a distance of 5–6 m from the fault break during inland earthquakes.

Landslides and Rockfalls The recent large earthquakes caused megascale slope failures and rockfalls, particularly along the surface ruptures on the hanging-wall side of faults. The slope failure induced in Beichuan town during the 2008 Wenchuan earthquake [40, 50] is of great interest. In association with the sliding motion of the earthquake fault, NW- or SE-facing slopes failed during this earthquake. There were two large-scale slope failures (landslides) in Beichuan town, which destroyed numerous buildings

Düzce earthquake Kocaeli earthquake Wenchuan earthquake

Earthquake Faulting, Ground Motions and Deformations. Figure 21
The behavior of reinforced concrete buildings over surface ruptures. (**a**) Düzce earthquake. (**b**) Kocaeli earthquake. (**c**) Wenchuan earthquake

Earthquake Faulting, Ground Motions and Deformations. Figure 22
Views of landslides in Beichuan

and facilities. The NW-facing landslide (Jingjiashan) involved mainly limestone, while the SE-facing landslide (Wangjiaya) involved phyllite (mudstone, according to some) rock unit (Fig. 22). Limestone layers dip toward the valley side with an inclination of about 30°. There are several faults dipping parallel to the failure surface within the rock mass. The angles of the lower and upper parts of the failed slope are 60° and 30–35°, respectively. The existence of several faults dipping parallel to the slope with an inclination of about 60–65° creates a stepped failure surface.

The SE-facing slope (Wangjiaya landslide) may involve slippage along the steeply dipping bedding plane (fault plane?) and shearing through the layered rock mass. In other words, it may be classified as a combined sliding and shearing effect [56]. The angles of the lower and upper parts of the failed slope are 40–45° and 30–35°, respectively. The layers dip at an angle of 40° toward the valley, and the shearing plane is inclined at an angle of 20°.

Future Directions

The characteristics of ground motions and deformations associated with earthquake faulting are presented in this chapter. Furthermore, the response and damage to structures due to surface ruptures are illustrated through actual observations in recent great earthquakes.

The advanced strong-motion attenuation relations by Aydan and Ohta [4] seem to explain the wide range of observational data, which are considered to be scattering when spherical or cylindrical symmetric attenuation relations are used. A multisegmented or multisource model may be used for estimating strong motions [4] if surface ruptures due to earthquakes are relatively long.

The GPS measurements of ground deformations during earthquakes ($M > 6$) clearly indicated that permanent ground deformations do occur. The overall deformation response involves both coseismic and

time-dependent components. The permanent ground deformation may result from different causes such as faulting, slope failure, liquefaction, and plastic deformation induced by ground shaking. They may cause tremendous forces on long and/or large underground structures such as tunnels, powerhouses, and underground storage facilities of oil, gas, and nuclear wastes. Therefore, the current seismic design codes must be revised to include these effects.

As a conclusion, *it is almost impossible for mankind to prevent the damage to structures if a fault break happens to be just passing underneath the structures.* Nevertheless, the adverse effects of fault breaks on structures can be minimized to a negligible level in view of findings from the actual examples presented in this chapter. The following suggestions may be put forward for developing the seismic codes for structures in active fault zones:

1. Roadways and railways should not be elevated, and they should be constructed on the existing ground surface in active fault zones. In doing so, recovery of roadways and railways damaged by fault breaks in the event of the earthquakes would be very rapid. As a result, effective rescue and rehabilitation works would be possible.
2. Bridges and viaducts should be constructed as redundant structures, and simply supported structures should be avoided. Although prestressing can be used to increase the confinement of girders along the longitudinal axis of the bridge, the structures should not be wholly prestressed to prevent domino action in the event of failure. Furthermore, T-type piers must not be used as they constitute top-heavy situations which are undesirable in case of faulting as well as shaking caused by earthquakes.
3. Dams should never be built on active faults defined in engineering sense because of the risk of severe impacts to structures and residential areas downstream in the event of failure. If for some reason dams must be constructed in faulted zones, their height should be kept to a minimum and the type of dams should be rock-fill.
4. Observations and studies on various underground openings show that they are resistant to shaking. Nevertheless, the existence of discontinuities makes them vulnerable to collapse, particularly in case of shallow underground openings. This may have some important implications on areas where shallow abandoned mines, underground shelters, and old tunnels exist. As damage to tunnel linings due to fault breaks would be localized, there is no need for extra precautions at those locations. Underground openings crossing faults and fracture zones may be enlarged to accommodate relative slips along faults and fracture zones. The lining of the openings should be ductile to accommodate permanent ground deformations at such zones. Furthermore, the brittle linings of the existing underground structures should be lined with ductile thin plates or fiber-reinforced polymers together with rock bolts at fracture and fault zones, where permanent ground deformations may occur.
5. Tubular structures should be designed with the use of flexible joints to accommodate relative displacements with the consideration of likely relative displacement of the ground.
6. Buildings should be designed as rigid box-like structures with the use of shear walls. Walls with fragile hollow bricks having no structural strength must not be allowed during building construction. If the brick walls are to be used, the walls should be constructed before the construction of columns and beams in order to attain the necessary structural integrity, and they should be light, resistant, and ductile.
7. Vertical accelerations of inland earthquakes can be 0.65–0.75 times the maximum horizontal accelerations; sometimes they may even exceed maximum horizontal acceleration. The effect of vertical accelerations must be considered in structural design.
8. Structures of great importance should be sited on the rock foundations rather than on loose alluvial ground, since amplification of movement in loose ground may be several times that of rock foundation. The failure risk of structures during earthquakes could be drastically reduced by such a selection. Nuclear power plants and even arch dams built on rock foundation performed very well without any damage during the recent great earthquakes.
9. Global, regional, and local geological and geotechnical maps of cities and towns for residential and industrial developments in seismically active fault zones should be prepared. Furthermore, detailed

geological and geotechnical investigations should be required before any new development to reduce the seismic risks to structures during earthquakes in active fault zones.

Bibliography

Primary Literature

1. Aydan Ö (2003) Actual observations and numerical simulations of surface fault ruptures and their effects engineering structures. In: The 8th U.S.-Japan workshop on earthquake resistant design of lifeline facilities and countermeasures against liquefaction. Technical report, MCEER-03-0003, pp 227–237
2. Aydan Ö, Ulusay R, Hasgür Z, Hamada M (1999) The behaviour of structures built in active fault zones in view of actual examples from the 1999 Kocaeli and Chi-chi Earthquakes. In: ITU-IAHS international conference on the Kocaeli earthquake, 17 Aug 1999: a scientific assessment and recommendations for re-building, Istanbul, pp 131–142
3. Aydan Ö, Ohta Y (2006) The characteristics of ground motions in the neighbourhood of earthquake faults and their evaluation. In: Symposium on the records and issues of recent great earthquakes in Japan and overseas, EEC-JSCE, Tokyo, pp 114–120
4. Aydan Ö, Ohta Y (2011) A new proposal for strong ground motion estimations with the consideration of characteristics of earthquake fault. In: Seventh national conference on earthquake engineering, Istanbul, paper no 66
5. Aydan Ö (2007) Inference of seismic characteristics of possible earthquakes and liquefaction and landslide risks from active faults (in Turkish). In: The 6th national conference on earthquake engineering of Turkey, Istanbul, vol 1, pp 563–574
6. Ohta Y, Aydan Ö (2004) An experimental study on ground motions and permanent deformation nearby faults. J Sch Mar Sci Technol 2(3):1–12
7. Ohta Y (2011) A fundamental research on the effects of ground motions and permanent ground deformations neighborhood earthquake faults on civil engineering structures (in Japanese). Doctorate Thesis, Graduate School of Science and Technology, Tokai University, 272 p
8. Ohta Y, Aydan Ö (2009) An experimental and theoretical study on stick-slip phenomenon with some considerations from scientific and engineering viewpoints of earthquakes. J Sch Mar Sci Technol 8(3):53–67
9. Ohta Y, Aydan Ö (2010) The dynamic responses of geomaterials during fracturing and slippage. Rock Mech Rock Eng 43(6):727–740
10. Chang T-Y, Cotton F, Tsai Y-B, Angelier J (2004) Quantification of hanging-wall effects on ground motion: some insights from the 1999 Chi-Chi earthquake. Bull Seismol Soc Am 94(6):2186–2197
11. Ulusay R, Aydan Ö, Hamada M (2002) The behavior of structures built on active fault zones: examples from the recent earthquakes of Turkey. Struct Eng/Earthquake Eng JSCE 19(2):149–167
12. Somerville PG, Smith NF, Graves RW, Abrahamson NA (1997) Modification of empirical strong ground motion attenuation relations to include the amplitude and duration effects of rupture directivity. Seismol Res Lett 68: 199–222
13. Tsai YB, Huang MW (2000) Strong ground motion characteristics of the Chi-Chi Taiwan earthquake of 21 Sept 1999. In: 2000 NCHU-Waseda joint seminar on earthquake engineering, 17–18 Jul 2000, Taichung, pp 1–32
14. Aydan Ö, Kumsar H, Toprak S, Barla G (2009) Characteristics of 2009 l'Aquila earthquake with an emphasis on earthquake prediction and geotechnical damage. J Mar Sci Technol Tokai Univ 9(3):23–51
15. Abrahamson NA, Somerville PG (1996) Effects of the hanging wall and footwall on ground motions recorded during the Northridge earthquake. Bull Seismol Soc Am 86(1B): 593–599
16. Aydan Ö (2003) An experimental study on the dynamic responses of geomaterials during fracturing. J Sch Mar Sci Technol Tokai Univ 1(2):1–7
17. Aydan Ö, Ohta Y, Geniş M, Tokashiki N, Ohkubo K (2010) Response and earthquake induced damage of underground structures in rock mass. J Rock Mech Tunnell Technol 16(1):19–45
18. Aydan Ö, Ohta Y, Geniş M, Tokashiki N, Ohkubo K (2010) Response and stability of underground structures in rock mass during earthquakes. Rock Mech Rock Eng 43(6):857–875
19. Aydan Ö, Daido M, Tokashiki N, Bilgin A, Kawamoto T (2007) Acceleration response of rocks during fracturing and its implications in earthquake engineering. In: 11th ISRM Congress, Lisbon, vol 2, pp 1095–1100
20. Nasu N (1931) Comparative studies of earthquake motions above ground and in a tunnel. Bull Earthquake Res Inst Tokyo Univ 9:454–472
21. Kanai K, Tanaka T (1951) Observations of earthquake motion at different depths of the earth. Bull Earthquake Res Inst Tokyo Univer 28:107–113
22. K-NET, KiK-Net (2007, 2008) Digital acceleration records of earthquakes since 1998. http://www.k-net.bosai.go.jp/ and http://www.kik.bosai.go.jp/
23. Kawashima K, Aydan Ö, Aoki T, Kishimoto I, Konagai K, Matsui T, Sakuta J, Takahashi N, Teodori SP, Yashima A (2010) Reconnaissance investigation on the damage of the 2009 L'Aquila, Central Italy earthquake. J Earthquake Eng 14: 817–841
24. Joyner WB, Boore DM (1981) Peak horizontal acceleration and velocity from strong motion records from the 1979 Imperial Valley California earthquake. Bull Seismol Soc Am 71(6): 2011–2038
25. Aydan Ö, Sezaki M, Yarar R (1996) The seismic characteristics of Turkish earthquakes. In: The 11th World Conf. on Earthquake Eng., CD-2, Paper No:1270
26. Aydan Ö (2001) Comparison of suitability of submerged tunnel and shield tunnel for subsea passage of Bosphorus (in Turkish). Geol Eng J 25(1):1–17

27. Campbell KW (1981) Near source attenuation of peak horizontal acceleration. Bull Seismol Soc Am 71(6):2039–2070
28. Ambraseys NN (1988) Engineering seismology. Earthquake Eng Struct Dynam 17:1–105
29. Aydan Ö, Shimizu Y, Akagi T, Kawamoto T (1997) Development of fracture zones in rock masses. In: Int Symp. on deformation and progressive failure in geomechanics, IS-NAGOYA, Nagoya, pp 533–538
30. Hamada M, Aydan Ö (1992) A report on the site investigation of the March 13 earthquake of Erzincan, Turkey. ADEP, Association for Development of Earthquake Prediction, 86 p
31. Reilinger RE, Ergintav S, Burgmann R, McClusky S, Lenk O, Barka A, Gürkan O, Hearn L, Feigl KL, Çakmak R, Aktug B, Özener H, Toksöz MN (2000) Coseismic and postseismic fault slip for the 17 Aug 1999, M = 7.5, Izmit, Turkey earthquake. Science 289:1519–1524
32. Asakura T, Sato Y (1998) Mountain tunnels damage in the 1995 in Hyogo-ken Nanbu earthquake. Railway Tech Res Inst (RTRI) 39(1):9–16
33. Aydan Ö (1996) Faulting and characteristics of earthquake waves in Hyogo-ken Nanbu earthquake of 17 Jan 1995 (in Turkish). Jeoloji Mühendisliği 48:63–77
34. Aydan Ö, Kawamoto T (2004) The damage to abandoned lignite mines caused by the 2003 Miyagi-Hokubu earthquake and some considerations on its causes. In: 3rd Asian rock mechanics symposium, Kyoto, pp 525–530
35. Aydan Ö, Kumsar H (2010) An experimental and theoretical approach on the modeling of sliding response of rock wedges under dynamic loading. Rock Mech Rock Eng 43(6):821–830
36. Aydan Ö, Hamada M (2006) Damage to civil engineering structures by 8 Oct 2005 Kashmir earthquake and recommendations for recovery and reconstruction. J Disaster Res 1(3):1–9
37. Aydan Ö, Hamada M, Suzuki Y (2005) Some observations and considerations on the damage induced by the tsunami of the 2004 Sumatra earthquake on structures and coast. J Sch Mar Sci Technol 3(1):79–94
38. Aydan Ö, Miwa S, Kodama H, Suzuki T (2005) The characteristics of M8.7 Nias earthquake of 28 Mar 2005 and induced tsunami and structural damages. J Sch Mar Sci Technol Tokai Univ 3(2):66–83
39. Aydan Ö, Ohta Y, Hamada M (2009) Geotechnical evaluation of slope and ground failures during the 8 Oct 2005 Muzaffarabad earthquake in Pakistan. J Seismol 13(3):399–413
40. Aydan Ö, Hamada M, Itoh J, Ohkubo K (2009) Damage to civil engineering structures with an emphasis on rock slope failures and tunnel damage induced by the 2008 Wenchuan earthquake. J Disaster Res 4(2):153–164
41. Hashimoto S, Miwa K, Ohashi M, Fuse K (1999) Surface soil deformation and tunnel deformation caused by the 3 Sept 1998, Mid-North Iwate earthquake. In: 7th Tohoku regional convention, Japan Society of Engineering Geology
42. Yashiro K, Kojima Y, Shimizu M (2007) Historical earthquake damage to tunnels in Japan and case studies of railways tunnels in the 2004 Niigata-ken Chuetsu earthquake. Q RTRI 48(3):136–141
43. Asakura T, Shiba Y, Sato Y, Iwatate T (1996) Mountain tunnels performance in 1995 Hyogo-ken Nanbu earthquake. Special report of the 1995 Hyogo-ken Nanbu earthquake, Committee of Earthquake Engineering, JSCE
44. Aydan Ö, Kumsar H (1997) A site investigation of 1 Oct 1995 Dinar earthquake. Turkish Earthquake Foundation, TDV/DR 97–003, Istanbul, p 115
45. Aydan Ö, Ulusay R, Kumsar H, Sönmez H, Tuncay E (1998) A site investigation of Adana-Ceyhan earthquake of 27 June 1998. Turkish Earthquake Foundation, TDV/DR 006–30, 131 p
46. Aydan Ö, Ulusay R, Hasgür Z, Taşkın B (1999) A site investigation of Kocaeli earthquake of 17 Aug 1999. Turkish Earthquake Foundation, TDV/DR 08–49, 180 p
47. Aydan Ö, Ulusay R, Kumsar H, Tuncay E (2000a) Site investigation and engineering evaluation of the Düzce-Bolu earthquake of 12 Nov 1999. Turkish Earthquake Foundation, TDV/DR 095–51, 307 p
48. Ulusay R, Aydan Ö, Erken E, Kumsar H, Tuncay E, Kaya Z (2003) Site investigation and engineering evaluation of the Cay-Eber earthquake of 3 Feb 2002. Turkish Earthquake Foundation, TDV/DR 012–79, 213 p
49. Wang WL, Wang TT, Su JJ, Lin CH, Seng CR, Huang TH (2001) Assessment of damage in mountain tunnels due to the Taiwan Chi-Chi earthquake. Tunnel Undergr Space Technol 16:133–150
50. Aydan Ö, Ohta Y, Hamada M, Ito J, Ohkubo K (2009) The response and damage of structures along the fault rupture traces of the 2008 Wenchuan earthquake. In: International conference on earthquake engineering: the 1st anniversary of Wenchuan earthquake, Chengdu, pp 625–633
51. Aydan Ö, Dalgıç S, Kawamoto T (2000) Prediction of squeezing potential of rocks in tunnelling through a combination of an analytical method and rock mass classifications. Italian Geotech J 34(1):41–45
52. Kuno H (1935) The geologic section along the Tanna tunnel. Bull Earthquake Res Inst Univ Tokyo 14:92–103
53. Sakurai T (1999) A report on the earthquake fault appearing in the Tanna tunnel under construction by North-Izu earthquake 1930 (in Japanese). J Jpn Soc Eng Geol 39(6):540–544
54. Kawakami H (1984) Evaluation of deformation of tunnel structure due to Izu-Oshima Kinkai earthquake of 1978. Earthquake Eng Struct Dynam 12(3):369–383
55. Tsuneishi Y, Ito T, Kano K (1978) Surface faulting associated with the 1978 Izu-Oshima- Kinkai earthquake. Bull Earthquake Res Inst Univ Tokyo 53:649–674
56. Aydan, Shimizu Y, Kawamoto T (1992) The stability of rock slopes against combined shearing and sliding failures and their stabilisation. Int. Symp. on Rock Slopes, New Delhi, pp 203–210

Books and Reviews

Fowler CMR (1990) The solid earth – an introduction to global geophysics. Cambridge University Press, Cambridge

Okamoto S (1973) Introduction to earthquake engineering. Univ of Tokyo Press, Tokyo
Yeats RS, Sieh K, Allen CR (1997) The geology of earthquakes. Oxford University Press, Oxford/New York

Ecological and Health Risks at Low Doses

Kristine L. Willett[1], Christy M. Foran[2]
[1]Department of Pharmacology and Environmental Toxicology Research Program, University of Mississippi, School of Pharmacy, University, MS, USA
[2]Engineer Research and Development Center-Environmental Lab, Concord, MA, USA

Article Outline

Glossary
Definition of Subject
Introduction
Physiological Response to Low Doses
Specific Examples
Future Directions
Bibliography

Glossary

Acclimation A decline in response with previous exposure.

Adaptation Physiological changes that increase the fitness of a population in response to chronic exposure.

Epigenetic Mechanisms of altered gene expression that do not change primary DNA sequence.

Hormesis A beneficial effect from a low dose of a "poison" or contaminant.

NOAEL No-observed-adverse-effect level is the highest treatment level from which the response does not differ statistically from control groups.

Threshold dose Dose required to produce a measurable response.

Definition of Subject

The concept of "dose makes the poison" has been attributed to Paracelsus who lived in the 1500s. The goal of much of modern toxicology and pharmacology has since been to define the precise biological factors that dictate the relationship between dose and response following exposure to chemicals. One of the major challenges in risk assessment more recently appreciated is the difficulty in predicting with statistical certainty adverse effects at low doses when the probability of response in a population is low [1]. The nature of the risks at low doses may be qualitatively different from the nature of the risks at high doses. In other words, the risk at low doses is not just a smaller version of the risk at high doses, because the mechanism(s) responsible for the risk at low doses is often different.

Introduction

Paracelsus (1493–1541), or Theophrastus Phillippus Aureolus Bombastus von Hohenheim, is often credited as being the father of modern toxicology for development of the concept of a dose–response relationship. Paracelsus is quoted as saying "all things are poison and nothing is without poison; only the dose makes a thing not a poison" [2]. This principle tells us that even the most innocuous of substances, water for example, can be dangerous in excess. The public is generally aware that dehydration, or an excess of salt relative to water, can be life threatening. However, hyponatremia, an excess of water in the blood, is less widely accepted as a potentially fatal condition. As recently as 2007, a contestant in a radio contest died after consuming 6 l of water in 3 h [3]. The idea that the amount of the exposure or dose determines the frequency or magnitude of response is the fundamental basis for most toxicological research. In theory and practice, the principle that the dose determines the poison is the foundation for experimental toxicology even to this day.

Historically, the relationship between dose and response was considered to be in one direction (i.e., an increase in response with dose or a decrease in response with dose). This single direction, or monotonic, relationship is based on both an understanding of biological processes and mathematical descriptions of experimental outcomes [4]. The most common description of the relationship between dose and response is a sigmoidal curve (Fig. 1). This relationship describes the response expected from the log of the

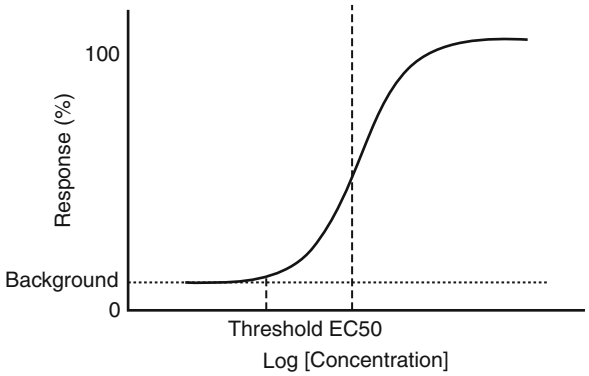

Ecological and Health Risks at Low Doses. Figure 1 The classical sigmoidal dose–response curve has doses or concentrations that elicit a 50% response (EC50). Theoretically, there is a threshold concentration or dose below which the response is the same as controls. This spontaneous response is the background rate in the absence of treatment

dose or concentration. Under this relationship, the lowest doses or exposures elicit no measureable response. In general, and in agreement with Paracelsus, organisms have some tolerance for exposure to poisons and toxicants. Some "threshold dose" is required to produce a measureable response. The response then increases exponentially until the midpoint of the curve, where it is half of the maximal response, a point referred to as the EC50 (effective concentration to produce 50% response). The rate of increase in the response decreases above the EC50 to zero where the response reaches its maximum. Increased doses or concentrations above the maximum (EC100) will not increase the response. The sigmoidal curve is the default assumption for the relationship between dose and response.

Despite this general convention, agreement on the shape of the dose–response curve at the low end has been controversial [4–6]. The classic sigmoidal dose–response relationship implies that there is a threshold for a biological response. Below that threshold value, exposure to a toxicant should have no measureable effect. Some responses to toxicants, such as the occurrence of tumors, occur spontaneously in control groups. In the absence of exposure, this rate of occurrence is considered the "background" level (Fig. 1). If an incremental dose increases this background rate of response, then the relationship between the incremental dose and response can be fitted linearly [4]. Furthermore, early studies of the biological basis of tumor formation led to the idea that a single molecule of a carcinogen could cause a mutation that led to tumor development. These "one hit" models have been disputed with both theoretical and physical lines of evidence [4]. For low-energy radiation, theoretical studies indicate that at least two hits of radiation are necessary for mutagenesis, potentially due to high DNA repair rates. Furthermore, cancer research indicates that tumor initiation requires a series of promotional changes even after mutations are incorporated into the genome.

For carcinogens, the precautionary assumption has been that every dose can elicit a response. In other words, there is not an observable no-effect threshold. The most common approach for estimating the low-dose effects of a carcinogen is to adequately describe the relationship between exposure and response over some range of treatments and then extrapolate to lower doses, generally using a linear function. If all poisons have a threshold dose, the linear extrapolation of low-dose response is a conservative assumption. There are reports of DNA adduct formation in proportion to dose even at extremely low concentrations. The US Environmental Protection Agency (EPA) has adopted a policy to utilize the formation of DNA and protein adducts as a means to extend the understanding of the shape of the dose–response relationship beyond the range that can be investigated with cancer bioassays [7]. The relationship between formation of DNA adducts and physiologically meaningful formation of tumors is not as clear. A review of the literature on biomarkers indicates that the dose–response relationship for biomarkers of exposure is not the same as the relationship for biomarkers of effect [7]. Recent descriptions of this debate include the historical progression of acceptance of linear extrapolation by the EPA [8].

In contrast to carcinogens, the assumption of a no-effect threshold has been used extensively for chemicals that are not considered carcinogenic. For these chemicals, the dose at which no adverse effects are detectable is a critical value incorporated into risk assessments. This dose is called the no-observed-adverse-effect level or NOAEL. The NOAEL is derived

from experimental data; it is the highest treatment level which does not differ statistically from the control groups. NOAEL is the basis for regulatory guidance such as acceptable intake levels. Data limitations and experimental design can limit the utility of the NOAEL. For example, note the chosen test concentrations represented by the gray vertical boxes in Fig. 2 for the NOAEL and the lowest observed adverse effects level (LOAEL). The doses in this hypothetical experiment might have been chosen to produce the maximum spread of responses or cover the relevant dose range for this compound. However, a higher concentration may have been chosen which would have still resulted in no significant response – and therefore a different value for the NOAEL. An alternative approach is to use a benchmark dose (BMD) [9]. The BMD is a derived value based on the effective range of the dose–response curve. Calculated BMD have the benefit of using a maximum likelihood approach to determine a confidence interval for the value. The variance in

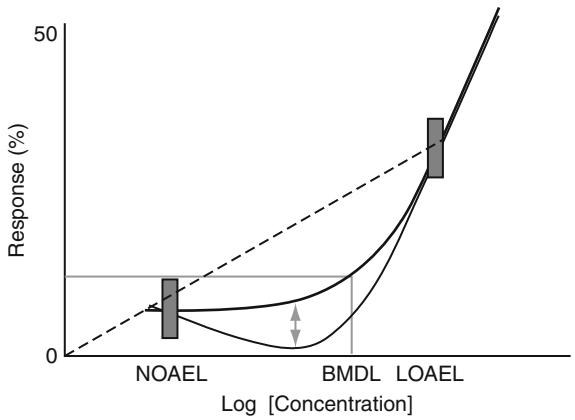

Ecological and Health Risks at Low Doses. Figure 2 The controversial low end of the dose–response curve is shown here. Experimental data determine the "lowest observed adverse effects level" (LOAEL) and the "no-observed-adverse-effects level" (NOAEL), indicated by the *vertical gray boxes*. Linear extrapolation from the LOAEL (*dashed line*) is a conservative estimation of the low-dose effects. Threshold dose can be estimated statistically using a lower bound benchmark dose (BMDL) through a proportion of the response (*gray bars*). In this hypothetical case, all extrapolations would overestimate toxicity if there were a hormetic response (*gray arrow*)

the response to the LOAEL or the EC50 can be used to estimate the concentration resulting in 5% response (or another level).

Extensive evidence now indicates that often the relationship between dose and response is biphasic. In other words, low-dose treatments may cause a decrease in response while higher doses cause an increase in response. An extensive review of the toxicological literature [10] found thousands of cases of these types of nonmonotonic dose–response relationships. In many of these cases, low-dose treatments with a toxicant induced a beneficial response – fewer tumors than unexposed controls, for example. A beneficial effect from a low dose of a "poison" or contaminant is referred to as hormesis. These beneficial effects have been reported over a range of responses from growth rate to carcinogenesis. Modeling studies indicate that hormetic response can be driven by a summation of the dose–response relationships for different steps in the biological response, specifically receptor binding, transcriptional activation, rate of DNA repair, and rate of cell division [5]. An example of how multiple physiological responses work together to result in a hormetic response is described below.

Alternatively, low-dose exposure may stimulate an increase in response while higher dose produces a lesser response. This "inverted U" shaped dose–response curve has also been observed in many cases. This relationship between dose and response is characterized by a heightened response to low doses and a depressed response to higher doses. A hypothetical example might be an increase in reproduction observed in response to a low concentration of estrogen and suppressed reproductive rates observed with higher treatments. The more complicated relationships between dose and response demonstrated in cases of hormesis and "inverted U" curves are likely to be observed in systems that require multiple steps to produce the response [5]. Systems biology and genomic/proteomic studies provide an opportunity to test summation hypotheses in a rigorous manner [1, 11]. Modeling and circuitry analysis provide an opportunity to test, or to generate new predictions about the responses of cells, individuals, and populations.

Further complicating the relationship between dose and response is the issue of exposure to mixtures [12]. Some cocontaminants will have the same mechanisms

of action and interact with the same receptors, while others will interact antagonistically through similar mechanisms of uptake, circulation, transformation, or elimination. EPA guidance recommends dose addition for chemicals which have similar mechanisms of action or exhibit response addition. However, predicting the toxicity of mixtures is difficult even when the mechanisms of action are understood.

The focus or target of a research study has a significant impact on predictions related to the dose–response relationship. Many cellular responses are either all or none switches (i.e., cell division). These cellular responses are described as being "quantal," and the sensitivity of the response in these cases will be described as a cumulative frequency of response at each dose. How the frequency of these incidences relates to specific biological response and adverse health outcomes is largely an unresolved issue [11]. By contrast, examination of a population of cells will produce a smooth dose–response curve as individual cells respond at different concentrations. An analogous dose–response relationship can be described in epidemiological studies [6]. Individuals participating in a study will either have a tumor or not; their response to their particular dose is quantal. However, different individuals will have different sensitivities based on their age, health, lifestyle, and previous exposure history [4]. Each individual is likely to have a different "threshold" for tumor incidence based on their situation. Summation of these different thresholds is expected to "smooth" the dose–response relationship in studies that include a diverse population. Indeed, most human epidemiological studies have a linear relationship between dose and response [6].

Physiological Response to Low Doses

As described above, the response of an organism to a toxicant may be nonmonotonic. One range of treatment may suppress a response while another may enhance the response [12]. Physiological mechanisms underlying these complicated hormetic responses are of much interest. The long history of these types of responses has been documented by Rozman and Doull [13]. Their review summarizes the notion that a beneficial response to a low dose of a poison is the result of homeostatic compensation in response to a stressor. Rozman and Doull make an analogy between low-dose treatment and physical exercise. Both are minor stressors and homeostatic response to those stimuli may ultimately enhance fitness. Adaptation to a low dose of a stressor, like recovery from physical exercise, may be the result of diverse physiological mechanisms. As a general phenomenon, adaptation or compensation induced by a low-dose treatment is believed to be the basis for hormesis [14].

In situations that result in a hormetic response, continuous exposure to a relatively constant dose should result in a continuous state of (over)compensation. This response has been described as steady-state hormesis induced by chronic exposure [15]. A critical cellular aspect involved in the maintenance of homeostasis is the suite of biotransformation and conjugation enzymes [16]. Three categories of enzymes, Phase I–III, are the basis for xenobiotic metabolism. Phase I enzymes include the cytochrome P450 family, which classically oxidize xenobiotics rendering them more water soluble. However, these Phase I enzymes also activate some procarcinogens and mutagens to reactive metabolites. Phase II enzymes conjugate solubilizing groups that further facilitate excretion. Phase III enzymes are membrane-bound transporters that export metabolized xenobiotics from the cell. A model of these xenobiotic metabolizing enzymes (XMEs) by Zhang and coworkers [17] has generated a mechanistic hypothesis for the hormetic response to many mutagens and carcinogens.

Zhang et al. [17] have described a multipart negative feedback and feedforward model of XMEs, including cross-induction of Phase I and II enzymes. Simulations of this model find a drop in the production of a reactive metabolite below baseline levels in response to 64 h of exposure to an exogenous procarcinogen. Activation of a homeostatic control mechanism, in this case transcriptional induction of XME in response to binding of a nuclear receptor (the aryl hydrocarbon receptor), will compensate for the poison and produce a new physiological state. Because of this hormetic compensation, the authors conclude that the response of biological systems will not be "linearly correlated with the dose of the stressing agent, especially in the low dose region" [17]. The regulation and induction of Phase I and II enzymes is a common cellular mechanism for coping with toxicants. In the cases where Phase I metabolism

activates a toxicant, the feedforward induction of these enzymes is a potential mechanism for hormetic responses at the cellular level. This model provides a hypothesis for the cellular basis of suppression of background levels of tumor induction in response to low-dose exposure to carcinogens to the extent that reactive metabolites are correlated with mutagenesis, apoptosis, and cell proliferation.

Low-level or subacute doses have the potential to produce long-term changes in the magnitude of the response elicited from a toxicant. A decline in response with exposure is called acclimation. The process of acclimation is best studied in relation to exposure of fish to heavy metals (reviewed by Hamilton and Mehrle [18]). Pretreatment of animals with metals, specifically cadmium, copper, mercury, and zinc, is protective for subsequent exposures. Exposure induces synthesis of thionein, a protein that normally occurs only in trace amounts in certain tissues (blood, gills, liver, kidney, and intestine). Binding of metals to this protein, then called metallothionein, reflects the relative concentrations of the metals present and their binding affinity. Chronic toxicity of metals that are sequestered by metallothionein has been described as "spillover"; once metallothionein's metal binding sites are saturated, the excess will cause tissue damage. This example of competition for a target will influence the shape of the dose–response curve at the low end. Metallothionein is induced by metal, and to a lesser extent, by glucocorticoids. Therefore, some protection or acclimation to metals may be produced by a number of different stressors that produce a glucocorticoid response. In this case, exposure to some classes of metals or heightened stress response will alter the threshold dose for tissue damage from toxicants such as mercury, cadmium, and silver.

Different populations will vary in their response to a toxicant, especially at the low range of the dose–response curve. If a mathematical description of the response indicates that 5% of the population should be impacted, a change in sensitivity of the population (not to mention sample size and health-related factors) will result in more variability in the reported response rate. Populations may differ in age, or individuals may have encountered a previous exposure as described above. Additionally, populations may have a history of chronic exposure that results in transgenerational changes in the dose–response curve. Genetic or epigenetic adaptation to a chronic stressor will impact the response of a population to exposure. Resistant phenotypes may have enhanced fitness under chronic exposure conditions. Those phenotypes would be expected to increase in frequency in subsequent generations. Experimental studies of killifish from a creosote-contaminated Elizabeth River (Virginia) location have documented resistance to the teratogenic effects of creosote exposure which is maintained through two generations of animals reared in clean conditions [19]. Transgenerational resistance to the polycyclic aromatic hydrocarbons (PAHs), which make up the majority of creosote, is not associated with a general increase in resilience. In fact, offspring of Elizabeth River–collected killifish exhibited higher mortality in response to hypoxic conditions. This study reveals that the magnitude of resistance to PAHs decreases with subsequent laboratory-raised generations (F2 vs. F1); therefore the mechanism of adaptation might not be conferred genetic resistance, but instead be a heritable change in gene regulation.

Epigenetic mechanisms are molecular phenomena, such as DNA methylation of CpG nucleotides, which regulate gene expression without changing the DNA sequence itself [20]. Methylation patterns are normally established two times during development in somatic cells during gastrulation and in the germ cells after sex determination [21]. Many common diseases (e.g., diabetes, osteoporosis, atherosclerosis etc.) have a sex-related incidence bias that may be a result of sex-specific (e.g., X-chromosome inactivation) epigenetic control [22]. As reviewed by Gabory and coworkers, environmental factors including xenobiotics, nutrition, or social factors can influence epigenetic marks throughout development [22]. Furthermore, when germ cells are adversely epigenically reprogrammed, sex-specific transgenerational effects have been reported. For example, when pregnant rats were exposed to the antiandrogen, vinclozolin, all subsequent generation (F1–F4) males had sperm cell defects and subfertility [21, 23]. Epigenetic changes are also becoming well-recognized mechanisms contributing to cancer and have been associated with all stages of tumor formation and progression [24]. Losses of DNA methylation in oncogenes, hypermethylation of tumor suppressor genes, and altered histone

modifications have all been noted during oncogenesis. The extent to which these epigenetic modifications of gene expression and/or their multigenerational consequences mediate xenobiotic low-dose effects are still largely unknown.

Specific Examples

While a list of xenobiotics that display different effects at high and low doses is likely to grow as "omic" tools and systems biology approaches are implemented in risk assessment, there are a number of examples already known. The bulk of the initial work on predicting low-dose effects was done with respect to carcinogen risk assessment [8]. Radiation and polycyclic aromatic hydrocarbons (PAHs) will be used to highlight issues in cancer low-dose predictions. Similar to cancer progression, neurotoxicological risk assessment has acknowledged that neurological effects are rarely unifactoral [25, 26]. Here, lead and organophosphate pesticides will be used as case studies. A focus of a National Toxicology Program Peer Review [27], certain endocrine disrupting chemicals including bisphenol A (BPA) also have been recognized for their potential to cause "biological change" at low doses. Accordingly, the specific examples described below will focus on carcinogens, neurotoxicants, and endocrine disruptors.

A recent review by Calabrese has provided the history of carcinogen risk assessment [8]. As he describes, the basis for the idea that carcinogen effects were linear at low doses was derived from the early work of Hermann Muller [28], wherein it was discovered that X-ray radiation induced mutations in *Drosophila*. The relationship between low-dose linearity and radiation-induced mutations in germ cells was further asserted in the 1956 Biological Effects of Atomic Radiation (BEAR) Report. The idea that mutations in somatic cells could lead to cancer also with a linear response at low doses was brought to public debate following publication of E.B Lewis' paper relating radiation risks and leukemia [29]. The criticisms of this manuscript are reviewed by Calabrese [8]; nonetheless, it was a key contribution to the adoption of a precautionary approach and low-dose linear risk assessment for both radiation and ultimately chemical carcinogens. The current risk assessment paradigm for radiation exposure includes a "single-cell origin, a radiation-induced mutation/aberration as the rate-limiting step, simple expectations of a linear non-threshold radiation response (LNT) at low doses and little or no other relevant contributions. . .to promotion or progression of the tumor" [30]. As pointed out by Goodhead, however, there are a number of radiobiological phenomena including bystander effects and genome instability that are not yet completely understood that may impact how risk of low doses should be assessed and ultimately how human radiation protection is performed. Bystander effects, effects in neighboring nonirradiated cells, are most apparent in the low-dose range where overt toxicity by direct radiation is not dominant [31]. The consequences of bystander effects would be supposed to be relevant to carcinogenicity in that they could be detrimental (toxic effects or mutations in adjacent cells) or beneficial (apoptosis of impacted cells, so no additional tumor progression possible); however, how to mechanistically account for their role in dose–response relationships and risk assessment is currently unknown [30]. Similarly, *de novo* genetic instability in cells generations after irradiation appears to display nonlinear dose responses, and the mechanisms are also unclear. Further research will certainly be necessary to establish the relevance of these more recently recognized potentially low-dose effects of radiation and whether a change in the radiation risk assessment paradigm is necessary [30].

With respect to chemical carcinogens, the Guidelines for Carcinogen Risk Assessment [32] establish a two-step process for dose–response assessment. First, animal or human effect data are used to model biological effects such as adduct, mutation, or tumor formation. The second step then is to extrapolate below the range of observation to the expected range of human exposure with considerations as appropriate or available to mode of action of the chemical, quality of data, and uncertainties therein. Because of the lack of human data, the high costs and low sensitivity of rodent cancer studies, and the goal to protect against one cancer per million, extrapolation of dose back five orders of magnitude is sometimes necessary [33]. Furthermore, it has recently become apparent that biomarkers of exposure (e.g., DNA adducts; linear response) do not have the same dose–response curve shape as biomarkers of effect (e.g., mutations;

threshold response) [7]. As reviewed by Swenberg et al., acrylamide, methymethanesulphonate, and ethylene oxide all represent examples wherein different exposure and effect curves have been reported [7]. Similarly, in a recent 40,800 animal study investigating ultralow-dose effects of the PAH dibenzo[a,l]pyrene in rainbow trout, the initial carcinogen-DNA adduct and the hepatic tumor response curves were "distinctly different" leading the authors to conclude that DNA adducts did not "provide an accurate biomarker for ultralow dose cancer risk evaluation" [33]. Additionally, the study design necessitated significantly less extrapolation below the modeled data set (200-fold vs. typical 100,000-fold) and found that the virtual safe dose for liver tumor formation was 500–1,500 times higher than the standard linear extrapolation from the lower confidence limit on the dose causing 10% incidence typically used in carcinogen risk assessment [33]. Mechanistically, the difference in these curves is relatively easy to appreciate. A specific PAH-DNA adduct will reflect exposure to that parent PAH exclusively. Furthermore, there exist very sensitive analytical methods of DNA adduct measurement. However, it is known that many adducts are not promutagenic. When mutagenic adducts formed, the excretion and repair rates of a particular adduct may be variable because of multiple gene interactions; yet, a relationship between adduct formation and initial exposure will exist. In contrast, mutations are caused by a number of initiating events. There always exists some background of mutations caused by endogenous chemicals or mistakes in DNA replication. Therefore, while physiologically more significant, mutation measurement in exposure experiments will ultimately approach a background frequency at low doses [7]. As these recent reports indicate, the way to measure and predict risks due to exposure to carcinogens is still relevant and continually being reevaluated even though this was one of the first areas in toxicology research to appreciate the need to estimate effects at low doses [8].

Effects of low doses are also important for acute acting compounds. Humans have used and been exposed to lead for thousands of years, and at high doses, a range of adverse effects can occur [34]. In humans, effects depend on developmental stage with the central nervous system as a target in children and peripheral neuropathies, nephrotoxicity, and cardiovascular effects common in adults [35]. Recent emphasis has been on how childhood low-dose, environmentally relevant lead exposure affects cognitive function. As more data were collected on lead's low-dose toxicity, the regulatory limit of concern for childhood lead intoxication reduced from its initial value of <60 μg/dl set in the 1960s, to 40 μg/dl in 1971, to 30 μg/dl in 1978, and 25 μg/dl in 1985 [36]. The current limit recommended by the Center for Disease Control and World Health Organization is <10 μg/dl. Studies from around the world have found blood lead concentrations far exceeding this level in particular study populations (reviewed in [34, 37]). For example, children from a lead-contaminated area of Ecuador had blood lead concentrations of 52.6 μg/dl (range 9.9–110.0 μg/dl) [38]. Findings from the National Health and Nutrition Examination Surveys (NHANES) in the United States show that average children's blood lead levels have been declining since the 1970s, and the prevalence of elevated levels in children was 0.7% in the 1999–2002 survey [39]. However, recent evidence suggests that blood lead concentrations below 10 μg/dl are not without adverse effect.

The 10 μg/dl standard was based, in part, on a study wherein children were grouped based on umbilical-cord blood concentrations (either <3 μg/dl, between 6 and 7 μg/dl, or >10 μg/dl). At 2 years of age, Mental Development Index scores were significantly lower in children from the >10 μg/dl group [40]. However, using the NHANES III cohort, Lanphear and coworkers found that, after results were corrected for confounding factors, there was an inverse relationship between blood lead concentration and cognitive functioning. Specifically, they reported "for every 1 μg/dl increase in blood lead concentration, there was a 0.7-point decrement in mean arithmetic scores, an approximately 1-point decrement in mean reading scores, a 0.1-point decrement in mean scores on a measure of nonverbal reasoning, and a 0.5-point decrement in mean scores on a measure of short-term memory" [41]. Importantly, these results included children who had blood lead concentrations less than 5 μg/dl. A more recent study by this laboratory followed 172 children measuring their blood lead concentrations at 6, 12, 18, 24, 36, 48, and 60 months of age and tested their performance on the Stanford-Binet

Intelligence Scale at 3 and 5 years of age [42]. They found that as lifetime average blood lead concentrations increased from 1 to 10 μg/dl, IQ declined by 7.4 points using a nonlinear model or 4.6 points with a linear model. Additionally, chelation therapy is largely ineffectual for children with blood lead concentrations between 20 and 44 μg/dl [43] and cognitive deficits due to lead exposure can last into adulthood [44]. These studies suggest that there is not a clear threshold for lead effects in children.

Unfortunately, the molecular targets and mechanistic reasons to explain low-dose effects of lead exposure are currently lacking. Clearly, critical neurodevelopmental processes occur in the early years of life that have profound effects on learning and memory. A current area of emphasis with respect to mechanisms of lead toxicity is focused on N-methyl-D-aspartate receptor (NMDAR)-mediated synaptic plasticity, specifically hippocampal long-term potentiation [37]. As reviewed by Toscano and Guilarte [37], in rodent models, environmentally relevant lead exposure alters NMDAR subunit expression and function including decreased calcium and nitric oxide signaling, both critical signaling pathways involved in learning and memory. Better understanding of the molecular targets of lead toxicity may in turn offer more effective therapeutic approaches to lead exposure in the future.

Organophosphate pesticides (OP), such as chlorpyrifos, have a well-recognized biomarker of exposure and effect in the irreversible inhibition of acetylcholinesterase (AChE). Significant inhibition of AChE causes a recognizable "cholinergic syndrome" causing accumulation of acetylcholine at cholinergic synapses and overstimulation of cholinergic receptors of the muscarinic and nicotinic type [45]. In addition to the acute cholinergic crisis, high-dose OP exposure can lead to OP-induced delayed polyneuropathy. Percent decreases in plasma pseudocholinesterase or red blood cell cholinesterase (e.g., 30% from baseline) are used in workplace surveillance even though the physiological significance of circulating cholinesterase activity is not known. Furthermore, signs of intoxication typically do not occur until cholinesterase inhibition is >70% [25]. Accordingly, organophosphate pesticides are another class of neurotoxicant that can exhibit strikingly different low- versus high-dose toxic effects.

Chlorpyrifos is one of the most widely applied OPs. In the United States, registrations for its use in residential settings were canceled in June 2000 [46]. Prior to this ban, chlorpyrifos was detected in 99.7% of personal air samples and 100% of indoor air in an urban pregnant woman cohort [47]. When pregnant rats are given chlorpyrifos at doses below those affecting acetylcholinesterase, their offspring have permanent deficits in learning and memory [25]. Work in the Slotkin laboratory has established persistent changes in serotonergic and dopaminergic systems in adult rats exposed either prenatally or neonatally to chlorpyrifos at doses that are devoid of systemic toxicity [48–50]. Furthermore, in rats exposed neonatally on gestational days 17–20 (during peak neurogenesis), there were sex-dependent behavioral impairments persistent to adulthood [51]. Intriguingly, in addition to the neurotoxicological effects of chlorpyrifos, adverse effects on adenyl cyclase cellular signaling cascades were noted in heart and liver of developmentally exposed rats [52]. As concluded by Slotkin, "The mechanisms for neurodevelopmental effects from toxins such as chlorpyrifos cannot be presumed to be based on known mechanisms for systemic toxicity in the adult" [25]. More recently, an epidemiologic study of inner-city children compared umbilical cord chlorpyrifos plasma concentrations and cognitive and motor development (at 12, 24, and 36 months of age) and behavior (at 36 months). A significantly higher proportion of children from the "highly exposed" group showed signs of mental and motor delays and were more likely to score in the clinical range for attention problems compared to the lower exposure group at 3 years of age [53]. Further insight into the mechanisms of chlorpyrifos and other organophosphates at low doses may further tighten regulatory control of this class of chemicals and/or offer therapeutic or psychological interventions to remediate low-dose and developmental exposures.

Endocrine disrupting chemicals (EDCs) can change endocrine function and cause adverse effects at the level of the organism, its progeny and/or (sub) populations of organisms. There have been a number of research conferences since the initial Wingspread Conference in 1991, spearheaded by Dr. Theo Colburn, to address the effects of EDCs. Germane to this chapter, in 2000, the

EPA and the National Institute of Environmental Health Sciences (NIEHS) held a peer review "aimed at evaluating the scientific evidence on reported low-dose effects and dose-response relationships for endocrine disrupting chemicals in mammalian species that pertain to assessments of effects on human health" [27]. Nine EDCs, not including dioxins or phthalates esters, were considered. More recently, as reviewed by Vandenberg and coworkers [54], bisphenol A (BPA) individually has been a focus of expert analysis and regulatory review.

Bisphenol A is a high-volume chemical used in polycarbonate plastic. Use of this chemical has recently received intense media scrutiny because of its occurrence in consumer products such as food container liners and baby bottles and ubiquitous occurrence in human samples [55]. Based on relatively low in vitro binding affinity to the estrogen receptor compared to estradiol, BPA was initially considered a weak environmental estrogen. However, more recently lower-dose effects are being noted at concentrations below those needed for nuclear estrogen receptor binding [56]. A number of in vitro studies measuring BPA-mediated effects in cell types as diverse as adipose explants, and pituitary, prostate cancer, and pancreatic cells have reported U-shaped nonmonotonic dose–response curves (reviewed in [54]). For example, cell proliferation was lower at both low and high doses of BPA compared to intermediate doses. In vivo, BPA-mediated effects on CD-1 mouse uterine endpoints also indicated nonmonotonic dose–response curves for some endpoints (e.g., vaginal opening and uterine wet weight) [57]. Fetal exposure to low doses of BPA causes changes in tissue organization and histoarchitecture of developing mammary gland in mice [58, 59]. In males, BPA causes adverse effects on the male reproductive system and sex-related behaviors [60, 61]. Important observations revealed from BPA studies, with particular relevance to low-dose effects, are that experimental design and study controls are critical. For example, compounds present in animal feeds can mask treatment effects, and different animal strains can have different sensitivities [62]. The exact mechanisms underlying BPA low-dose effects are still under investigation. It is important to remember that estrogen is a critical physiological mediator of many diverse tissue-dependent cellular processes. Furthermore, appropriate timing of sex steroid exposure is key in establishing the hypothalamus-pituitary-gonad feedback necessary for successful development and reproduction. Issues of timing of exposure would be expected to have profound impacts on effects of BPA.

Conclusions from the 2000 peer review included that relevant low-dose effects of BPA included increased prostate weight in male mice and advanced puberty in female mice after *in utero* exposure. Effects in rats (e.g., uterine growth and serum prolactin) were strain specific. They concluded "Data are insufficient to establish the shape of the dose-response curve for BPA in the low dose region, and the mechanism and biological relevance of reported low dose effects are unclear" [27]. In 2006, the NIEHS organized an additional meeting specifically addressing BPA. A product of this meeting was the Chapel Hill Consensus Statement [63], which concluded "...that human exposure to BPA is within the range that is predicted to be biologically active in over 95% of people sampled. The wide range of adverse effects of low doses of BPA in laboratory animals exposed both during development and in adulthood is a great cause for concern with regard to the potential for similar adverse effects in humans." Meanwhile, the National Toxicology Program's Center for the Evaluation of Risks to Human Reproduction (CERHR) evaluated the scientific data and concluded that some of the previously attributed effects of BPA (e.g., changes in prostate weight, reproductive tract malformations etc.) were not conclusive [64]. This report was highly criticized (see review [54]), and NTP released its own report finally concluding "there is *some concern* for effects on the brain, behavior, and prostate gland in fetuses, infants, and children at current human exposures" but "*minimal concern* for effects on the mammary gland and an earlier age for puberty for females" [65]. Importantly in August 2008, and in an interim update issued January 2010, the US Food and Drug Administration, which regulates food packaging etc., released a draft report finding that BPA remains safe in food contact materials [66]. Some of the questions plaguing the debates on BPA risk assessment include different routes of exposure and metabolism of BPA in animals and humans, lack of consistency in results between laboratory studies, and

the relevancy of the animal models to the human condition. Clearly, this is a timely ongoing debate that absolutely hinges on elucidating the consequences of low-dose environmentally relevant exposure to BPA.

Future Directions

The mechanisms of toxicity and the few selected xenobiotics used as examples here emphasize how timely and relevant the issue of effects at low doses is. Furthermore, answers to the issues raised are key for more informed and appropriate risk assessment. Toxicology studies historically have been limited to testing concentrations representing the high end of environmental relevance. The need to test higher doses was necessitated both by inability to measure/recognize subtle effects, and the need to achieve statistically significant results with the minimal number of test organisms and cost. Now with the realization that, in general, mechanisms of toxicity are not consistent from high to low doses, new robust experiments are needed to explain the more relevant low-dose effects. However, care must be taken so that the cost of regulatory measures that conservatively estimate the harm of low-dose effects is balanced with the cost of potential mechanisms that alter the response of current or future populations. Furthermore, when a biomarker of effect is recognized to not represent true risk of adverse effect (e.g., DNA adduct formation), then more appropriate endpoints (e.g., mutation) should be incorporated into risk assessment. As described above, many low-dose effects are critically linked to the developmental age at the time of exposure. Populations which differ in age or previous exposure are likely to have different responses to low-dose treatment of any contaminant. The World Health Organization has developed a multiple exposure/multiple effects children's health model incorporating the influence of social, economic, and demographic contexts on health outcomes and exposure in addition to the relationship between exposure and effect [67]. As the underlying system biology of test organisms becomes better understood, better evaluation of effects of xenobiotic exposure will be possible [1]. Finally, the field of risk assessment and society in general may ultimately have to deal with the ethical questions that arise associated with potential hormetic effects of chemicals that are toxic at high doses [31].

Bibliography

Primary Literature

1. Andersen ME, Thomas RS, Gaido KW, Conolly RB (2005) Dose-response modeling in reproductive toxicology in the systems biology era. Reprod Toxicol 19:327–337
2. Krieger WC (2001) Paracelsus dose response. In: Krieger WC (ed) Handbook of pesticide toxicology. Academic, New York
3. Ballantyne C (2007) Strange but true: drinking too much water can kill. Scientific American June 21, 2007. http://www.scientificamerican.com/article.cfm?id=strange-but-true-drinking-too-much-water-can-kill&print=true. Accessed 24 January 2010
4. Zeise L, Wilson R, Crouch EA (1987) Dose-response relationships for carcinogens: a review. Environ Health Perspect 73:259–306
5. Conolly RB, Lutz WK (2004) Nonmonotonic dose-response relationships: mechanistic basis, kinetic modeling, and implications for risk assessment. Toxicol Sci 77:151–157
6. Lutz WK (1990) Dose-response relationship and low dose extrapolation in chemical carcinogenesis. Carcinogenesis 11:1243–1247
7. Swenberg JA, Fryar-Tita E, Jeong YC, Boysen G, Starr T, Walker VE, Albertini RJ (2008) Biomarkers in toxicology and risk assessment: informing critical dose-response relationships. Chem Res Toxicol 21:253–265
8. Calabrese EJ (2009) The road to linearity: why linearity at low doses became the basis for carcinogen risk assessment. Arch Toxicol 83:203–225
9. Sand S, Victorin K, Filipsson AF (2008) The current state of knowledge on the use of the benchmark dose concept in risk assessment. J Appl Toxicol 28:405–421
10. Calabrese EJ, Baldwin LA (2001) Hormesis: a generalizable and unifying hypothesis. Crit Rev Toxicol 31:353–424
11. Andersen ME, Dennison JE, Thomas RS, Conolly RB (2005) New directions in incidence-dose modeling. Trends Biotechnol 23:122–127
12. Borgert CJ, Quill TF, McCarty LS, Mason AM (2004) Can mode of action predict mixture toxicity for risk assessment? Toxicol Appl Pharmacol 201:85–96
13. Rozman KK, Doull J (2003) Scientific foundations of hormesis. Part 2. Maturation, strengths, limitations, and possible applications in toxicology, pharmacology, and epidemiology. Crit Rev Toxicol 33:451–462
14. Stebbing AR (2003) Adaptive responses account for the beta-curve-hormesis is linked to acquired tolerance. Nonlinearity Biol Toxicol Med 1:493–511
15. Calabrese EJ, Bachmann KA, Bailer AJ, Bolger PM, Borak J, Cai L, Cedergreen N, Cherian MG, Chiueh CC, Clarkson TW, Cook RR, Diamond DM, Doolittle DJ, Dorato MA, Duke SO, Feinendegen L, Gardner DE, Hart RW, Hastings KL, Hayes AW, Hoffmann GR, Ives JA, Jaworowski Z, Johnson TE, Jonas WB, Kaminski NE, Keller JG, Klaunig JE, Knudsen TB, Kozumbo WJ, Lettieri T, Liu SZ, Maisseu A, Maynard KI, Masoro EJ, McClellan RO,

Mehendale HM, Mothersill C, Newlin DB, Nigg HN, Oehme FW, Phalen RF, Philbert MA, Rattan SI, Riviere JE, Rodricks J, Sapolsky RM, Scott BR, Seymour C, Sinclair DA, Smith-Sonneborn J, Snow ET, Spear L, Stevenson DE, Thomas Y, Tubiana M, Williams GM, Mattson MP (2007) Biological stress response terminology: integrating the concepts of adaptive response and preconditioning stress within a hormetic dose-response framework. Toxicol Appl Pharmacol 222:122–128

16. Parkinson A, Ogilvie BW (2008) Biotransformation of xenobiotics. In: Klaassen CD (ed) Casarett & Doull's toxicology: the basic science of poisons. McGraw Hill, New York, pp 161–304
17. Zhang Q, Pi J, Woods CG, Andersen ME (2009) Phase I to II cross-induction of xenobiotic metabolizing enzymes: a feedforward control mechanism for potential hormetic responses. Toxicol Appl Pharmacol 237:345–356
18. Hamilton SJ, Mehrle PM (1986) Metallothionein in fish: review of its importance in assessing stress from metal contaminants. Trans Am Fish Soc 115:596–609
19. Meyer JN, DiGiulio RT (2003) Heritable adaptation and fitness costs in killifish (*Fundulus heteroclitus*) inhabiting a polluted estuary. Ecol Adapt 13:490–503
20. Jones PA, Takai D (2001) The role of DNA methylation in mammalian epigenetics. Science 293:1068–1070
21. Anway MD, Skinner MK (2006) Epigenetic transgenerational actions of endocrine disruptors. Endocrinology 147:S43–S49
22. Gabory A, Attig L, Junien C (2009) Sexual dimorphism in environmental epigenetic programming. Mol Cell Endocrinol 304:8–18
23. Anway MD, Cupp AS, Uzumcu M, Skinner MK (2005) Epigenetic transgenerational actions of endocrine disruptors and male fertility. Science 308:1466–1469
24. Baylin SB, Ohm JE (2006) Epigenetic gene silencing in cancer – a mechanism for early oncogenic pathway addiction? Nat Rev Cancer 6:107–116
25. Connors SL, Levitt P, Matthews SG, Slotkin TA, Johnston MV, Kinney HC, Johnson WG, Dailey RM, Zimmerman AW (2008) Fetal mechanisms in neurodevelopmental disorders. Pediatr Neurol 38:163–176
26. Weiss B, Cory-Slechta D, Gilbert SG, Mergler D, Miller E, Miller C, Newland MC, Rice D, Schettler T (2008) The new tapestry of risk assessment. Neurotoxicology 29:883–890
27. National Toxicology Program (2001) National toxicology program's report of the endocrine disruptors low-dose peer review. NTP Office of Liaison and Scientific Review, Research Triangle Park
28. Muller HJ (1927) Artificial transmutation of the gene. Science 66:84–87
29. Lewis EB (1957) Leukemia and ionizing radiation. Science 125:965–972
30. Goodhead DT (2010) New radiobiological, radiation risk and radiation protection paradigms. Mutat Res 687(1–2):13–16
31. Hoffmann G, Stempsey W (2008) The hormesis concept and risk assessment: are there unique ethical and policy considerations? Hum Exp Toxicol 27:613–620
32. EPA US (2005) Guidelines for carcinogen risk assessment. US EPA, Washington DC
33. Bailey GS, Reddy AP, Pereira CB, Harttig U, Baird W, Spitsbergen JM, Hendricks JD, Orner GA, Williams DE, Swenberg JA (2009) Nonlinear cancer response at ultralow dose: a 40800-animal ED (001) tumor and biomarker study. Chem Res Toxicol 22:1264–1276
34. Tong S, von Schirnding YE, Prapamontol T (2000) Environmental lead exposure: a public health problem of global dimensions. Bull World Health Organ 78:1068–1077
35. Liu J, Goyer RA, Waalkes MP (2008) Toxic effects of metals. In: Klaassen CD (ed) Casarett and Doull's toxicology: the basic science of poisons. McGraw Hill, New York, pp 931–979
36. Landrigan PJ (2000) Pediatric lead poisoning: is there a threshold? Public Health Rep 115:530–531
37. Toscano CD, Guilarte TR (2005) Lead neurotoxicity: from exposure to molecular effects. Brain Res Brain Res Rev 49:529–554
38. Counter SA, Vahter M, Laurell G, Buchanan LH, Ortega F, Skerfving S (1997) High lead exposure and auditory sensory-neural function in Andean children. Environ Health Perspect 105:522–526
39. CDC (2005) Blood lead levels – United States, 1999–2002. MMWR 54:513–516
40. Bellinger D, Leviton A, Waternaux C, Needleman H, Rabinowitz M (1987) Longitudinal analyses of prenatal and postnatal lead exposure and early cognitive development. N Engl J Med 316:1037–1043
41. Lanphear BP, Dietrich K, Auinger P, Cox C (2000) Cognitive deficits associated with blood lead concentrations $<$10 microg/dL in US children and adolescents. Public Health Rep 115:521–529
42. Canfield RL, Henderson CR Jr, Cory-Slechta DA, Cox C, Jusko TA, Lanphear BP (2003) Intellectual impairment in children with blood lead concentrations below 10 microg per deciliter. N Engl J Med 348:1517–1526
43. Rogan WJ, Dietrich KN, Ware JH, Dockery DW, Salganik M, Radcliffe J, Jones RL, Ragan NB, Chisolm JJ Jr, Rhoads GG (2001) The effect of chelation therapy with succimer on neuropsychological development in children exposed to lead. N Engl J Med 344:1421–1426
44. White RF, Diamond R, Proctor S, Morey C, Hu H (1993) Residual cognitive deficits 50 years after lead poisoning during childhood. Br J Ind Med 50:613–622
45. Costa LG (2008) Toxic effects of pesticides. In: Klaassen CD (ed) Casarett & Doull's toxicology: the basic science of poisons. McGraw Hill, New York, pp 883–930
46. EPA US (2002) Interim reregistration eligibility decision for chlorpyrifos. US EPA, Washington DC, pp 1–235
47. Whyatt RM, Barr DB, Camann DE, Kinney PL, Barr JR, Andrews HF, Hoepner LA, Garfinkel R, Hazi Y, Reyes A, Ramirez J, Cosme Y, Perera FP (2003) Contemporary-use pesticides in personal air samples during pregnancy and blood samples at delivery among urban minority mothers and newborns. Environ Health Perspect 111:749–756

48. Aldridge JE, Meyer A, Seidler FJ, Slotkin TA (2005) Alterations in central nervous system serotonergic and dopaminergic synaptic activity in adulthood after prenatal or neonatal chlorpyrifos exposure. Environ Health Perspect 113:1027–1031
49. Roy TS, Sharma V, Seidler FJ, Slotkin TA (2005) Quantitative morphological assessment reveals neuronal and glial deficits in hippocampus after a brief subtoxic exposure to chlorpyrifos in neonatal rats. Brain Res Dev Brain Res 155:71–80
50. Slotkin TA, Seidler FJ (2005) The alterations in CNS serotonergic mechanisms caused by neonatal chlorpyrifos exposure are permanent. Brain Res Dev Brain Res 158:115–119
51. Levin ED, Addy N, Baruah A, Elias A, Christopher NC, Seidler FJ, Slotkin TA (2002) Prenatal chlorpyrifos exposure in rats causes persistent behavioral alterations. Neurotoxicol Teratol 24:733–741
52. Meyer A, Seidler FJ, Slotkin TA (2004) Developmental effects of chlorpyrifos extend beyond neurotoxicity: critical periods for immediate and delayed-onset effects on cardiac and hepatic cell signaling. Environ Health Perspect 112:170–178
53. Rauh VA, Garfinkel R, Perera FP, Andrews HF, Hoepner L, Barr DB, Whitehead R, Tang D, Whyatt RW (2006) Impact of prenatal chlorpyrifos exposure on neurodevelopment in the first 3 years of life among inner-city children. Pediatrics 118: e1845–e1859
54. Vandenberg LN, Maffini MV, Sonnenschein C, Rubin BS, Soto AM (2009) Bisphenol-A and the great divide: a review of controversies in the field of endocrine disruption. Endocr Rev 30:75–95
55. Calafat AM, Ye X, Wong LY, Reidy JA, Needham LL (2008) Exposure of the US population to bisphenol A and 4-tertiary-octylphenol: 2003–2004. Environ Health Perspect 116:39–44
56. Welshons WV, Nagel SC, vom Saal FS (2006) Large effects from small exposures III. Endocrine mechanisms mediating effects of bisphenol A at levels of human exposure. Endocrinology 147:S56–S69
57. Markey CM, Michaelson CL, Veson EC, Sonnenschein C, Soto AM (2001) The mouse uterotrophic assay: a reevaluation of its validity in assessing the estrogenicity of bisphenol A. Environ Health Perspect 109:55–60
58. Markey CM, Luque EH, De Munoz TM, Sonnenschein C, Soto AM (2001) In utero exposure to bisphenol A alters the development and tissue organization of the mouse mammary gland. Biol Reprod 65:1215–1223
59. Vandenberg LN, Maffini MV, Wadia PR, Sonnenschein C, Rubin BS, Soto AM (2007) Exposure to environmentally relevant doses of the xenoestrogen bisphenol-A alters development of the fetal mouse mammary gland. Endocrinology 148:116–127
60. Farabollini F, Porrini S, Della SD, Bianchi F, Dessi-Fulgheri F (2002) Effects of perinatal exposure to bisphenol A on sociosexual behavior of female and male rats. Environ Health Perspect 110(Suppl 3):409–414
61. Richter CA, Birnbaum LS, Farabollini F, Newbold RR, Rubin BS, Talsness CE, Vandenbergh JG, Walser-Kuntz DR, vom Saal FS (2007) In vivo effects of bisphenol A in laboratory rodent studies. Reprod Toxicol 24:199–224
62. Vom Saal FS, Richter CA, Ruhlen RR, Nagel SC, Timms BG, Welshons WV (2005) The importance of appropriate controls, animal feed, and animal models in interpreting results from low-dose studies of bisphenol A. Birth Defects Res A Clin Mol Teratol 73:140–145
63. vom Saal FS, Akingbemi BT, Belcher SM, Birnbaum LS, Crain DA, Eriksen M, Farabollini F, Guillette LJ Jr, Hauser R, Heindel JJ, Ho SM, Hunt PA, Iguchi T, Jobling S, Kanno J, Keri RA, Knudsen KE, Laufer H, LeBlanc GA, Marcus M, McLachlan JA, Myers JP, Nadal A, Newbold RR, Olea N, Prins GS, Richter CA, Rubin BS, Sonnenschein C, Soto AM, Talsness CE, Vandenbergh JG, Vandenberg LN, Walser-Kuntz DR, Watson CS, Welshons WV, Wetherill Y, Zoeller RT (2007) Chapel Hill bisphenol A expert panel consensus statement: integration of mechanisms, effects in animals and potential to impact human health at current levels of exposure. Reprod Toxicol 24:131–138
64. National Toxicology Program (2007) NTP-CERHR expert panel report on the reproductive and developmental toxicity of bisphenol A. In: Center for the Evaluation of Risks to Human Reproduction (ed) National toxicology program, pp 1–396
65. National Toxicology Program (2008) NTP-CERHR monograph on the potential human reproductive and developmental effects of bisphenol A. In: Center for the Evaluation of Risks to Human Reproduction (ed) National toxicology program, pp 1–321
66. US FDA (2010) Update on Bisphenol A for use in food contact applications. In: FDA (ed) US food and drug administration, pp 1–7
67. Briggs D (2003) Making a difference: indicators to improve children's environmental health. World Health Organization, Geneva, pp 1–17

Ecological Risk Assessment and Animal Models

Lisa J. Bain
Department of Biological Sciences, Clemson University, Clemson, SC, USA

Article Outline

Glossary
Definition of the Subject
Introduction
Animals Models in the Basic Framework of Risk Assessment
Considerations When Determining Which Organisms to Use for an Ecological Risk Assessment

Field Studies and Toxicity Testing
Other Assays Providing Support to Risk Assessments
Future Directions Using Animal Models in Risk Assessments
Bibliography

Glossary

Bioaccumulation factor (BAF) The concentration of contaminant in the organism divided by the concentration of the contaminant from all exposure sources, including water, air, soil, sediment, or food.

Bioconcentration factor (BCF) The concentration of contaminant in the organism divided by the concentration of the contaminant in the water.

Biomarkers A quantifiable change in a biochemical, physiological, or histological parameter that can be used as a measure of response to a toxicant.

Biological survey A systemic gathering of information on the presence, abundance, and condition of species at a given site to assess the health of those organisms.

EPT index The number of organisms in the orders *Ephemeroptera* (mayflies), *Plecoptera* (stonefiles), and *Trichoptera* (caddisflies). These orders are typically considered to be sensitive to contaminants.

LC_{50} The median lethal concentration, or the concentration of the medium that was lethal to 50% of the test organisms.

LOEC The lowest observed effect concentration, or the lowest concentration of test medium in which statistically significant toxic effects are seen.

NOEC No observed effect concentration, or the highest concentration of test medium in which no significant toxic effects are seen.

Toxicity test An assay in which organisms are exposed to soil, water, or air, and the effects of contaminants on processes such as survival, growth, and reproduction are determined.

Toxicogenomics Examining changes in gene expression, protein expression, and/or metabolite profiles in a response to an exposure by a toxicant.

Definition of the Subject

An ecological risk assessment attempts to determine the effects of contaminants or other environmental stressors on individuals, populations, and communities of species. Although ecological risk assessments can be used for regulating chemicals and managing watersheds, the most typical use is for the study and remediation of contaminated sites. The organismal effects that can be examined vary considerably, depending on the ultimate use of the assessment, but most often focus on the organisms' ability to survive, grow and develop appropriately, and reproduce. The choice of which organisms to use should be based on easily evaluated criteria, such as the ease of sampling a particular organism, ensuring that the organism can both respond to the toxicant or mixture of toxicants, and that the organismal response is graded with respect to increasing exposure concentrations and/or times. The specific endpoints measured in the risk assessment with respect to organisms can therefore include lethality, weight gain, population numbers, birth and death rates, alterations in community structure, among others. Some endpoints are easily quantified, such as lethality. Other endpoints may be much more difficult to measure, such as reproduction, development, productivity, and immune function. For these more subtle outcomes, one often uses biological markers to indirectly assess these endpoints, or surrogate species in the laboratory to find out more about the health of the population or community under study. Other methods to better refine the risk assessment include the use of models and the use of genomics. The underlying goal to conduct an effective assessment relies on the choice of the organism and the endpoint examined so that management decision is appropriate and protective of organismal health.

Introduction

The selection of which organisms to monitor or use is an important part of the risk assessment process. This entry first discusses the role of organismal selection and response in the basic framework of risk assessment. The criteria used when selecting an appropriate organism to use and the common organisms routinely used in assessments will be discussed. Laboratory toxicity tests, using either standard organisms as surrogate species or nontraditional organisms that are more representative of the site can be used. Field studies are also routinely conducted, which can monitor the presence and the abundance of a variety of species. Beyond typical field assessment, biotic indices are used as

measures of community structure, while biomarker data are used to assess sublethal impacts that often cannot be determined during standard laboratory toxicity testing. Finally, the entry will cover future directions in risk assessment, which may include the use of genomics, proteomics, other multi-end point analysis, and physiologically-based pharmacokinetic (PBPK) modeling.

Animal Models in the Basic Framework of Risk Assessment

Overview

The basic framework for risk assessment consists of four phases: problem formulation, analysis, risk characterization, and risk management [1, 2]. Much of this entry will focus on the first two phases, where the selection and analysis of organismal responses is most crucial. There is an additional step prior to the risk assessment itself, which is termed planning [3]. At the planning stage, the risk manager, risk assessors, and stakeholders should work together to identify the goals of the risk assessment. These goals should include developing clear objectives for what organisms the manager is most interested in protecting, determining what contaminants are most important to consider for the remediation effort, and indicating the acceptable levels of contaminants or the desired condition of the environment and organismal health after the remediation is completed [4].

During the problem formulation stage, a conceptual model should be developed to describe the relationships between the contaminants at the site and the organisms that may be affected by them. Although many species can be found at a site, the risk assessment is only concerned with those that could be adversely affected. Additionally, since there are always factors that mitigate or exacerbate the concentration of chemical that an organism encounters, these should be taken into account during model development. The risk assessor should identify the key ecological characteristics that allow or prohibit certain species to thrive. Potential confounding factors should be identified, such as physical manipulations, building and construction, other human disturbances, or competition by invasive species [4]. There is also the issue of indirect effects, in which the impact on a species affects another. Examples include a loss of a prey or predator species, or loss of vegetation that provides food and shelter. Once these factors are taken into account, then appropriate selection of the animal models to use in the risk assessment can occur.

During the analysis stage, there is both a characterization of the exposure and a characterization of the effects. Organisms may be sampled from the exposed site and changes due to the exposure determined. If suitable native species cannot be found or cannot be found in great enough numbers, outside organisms may be brought in and caged at the site to determine the amount of toxicant being taken into the organism and its resultant effects. More frequently, if a suitable field study cannot be performed on site, laboratory tests are conducted using surrogate species in standardized tests to determine the effects of contaminant exposure.

After data collection, one must determine whether there is a relationship between the contaminants and effects on organisms. One useful way to categorize the strength of the evidence is based upon the Bradford-Hill criteria [5], which provide a basic framework for assessing the strength of causal relationships. Although Hill originally published these criteria for human epidemiological work to determine the causes of diseases, they have been modified for ecotoxicology and risk assessments [6, 7]. The criteria or types of evidence a risk assessor is looking for to support a cause-effect relationship include:

1. *Spatial co-occurrence* – the effect should be observed only where the contaminant is present.
2. *Temporality* – there should be a cause-effect time relationship, in that the effect has to occur after the exposure to the contaminant.
3. *Biological Gradient* – this criterion describes the classical exposure-response relationship, in which higher exposure concentrations should lead to a greater incidence or more severe effects if the effect is due to the contaminant.
4. *Complete Exposure Pathway* – the contaminant has to be able to reach the organism in order to cause an effect. If the toxicant is in media that are

inaccessible to the organism of interest, than exposure will not occur.

5. *Consistency of Association* – if similar observations are documented by multiple investigators in multiple locations, this increases the likelihood that the effects seen are due to the contaminant.
6. *Experiment* – if the exposure is manipulated or modified, this should cause a decrease in effects. The manipulation can be conducted by using site media in the laboratory and altering the contaminant's concentration by dilution, or by conducting field experiments in which the exposure can be modified, contained, or eliminated.
7. *Plausibility* – this criterion asks whether the effects seen in the organisms can be explained because of a known or plausible biological mechanism. Additionally, the risk assessor should understand whether the effects would be expected at the concentration of contaminant seen at the site.
8. *Analogy* – this criterion examines uses case studies from contaminants that are similar in structure to the suspected contaminant, and asks whether the expected effects be the same.
9. *Specificity of Cause* – is the observed effect seen consistently associated with the contaminant or likely to only be caused by the contaminant. If so, the cause-effect relationship is quite strong.
10. *Predictive Performance* – this criterion asks whether side effects occurred as a result of the exposure, and if so, could they have been predicted based upon the contaminant's mode of action.

The first four provide the strongest evidence, since they are directly based upon the site being assessed. The next six are often considered less strong, since the data for these criteria typically come from laboratory studies or other field-based studies, which may or may not be completely applicable for the site in question. However, they provide corroborating evidence that, when coupled with the first four, can support the risk characterization process.

Monitoring Trends in the Environment

Knowing the baseline levels of contaminants and their impact on the health of populations and communities can support or act as a precursor to a risk assessment. Baseline levels are found by monitoring trends in the environment. Although these are not risk assessments, they can provide valuable information to the risk assessor. The US EPA's Environmental Monitoring and Assessment Program (EMAP) is one such large-scale endeavor that seeks to monitor sites in a particular region for many years, thus providing data on multiple spatial and temporal scales [8, 9]. EMAP data can include such information as contaminant levels, bacterial loads, and species distributions. Thus, the data can confirm trends in a particular area or provide baseline levels to serve as a reference site to aid risk assessors.

Biological surveys may also provide valuable information to support a risk assessment. Biological surveys most often are conducted in aquatic systems and often have data bases that span multiple sites and years. They are typically used to determine if an aquatic system is meeting its designated aquatic life uses, but have also been used to evaluate the effectiveness of controls and restoration activities, and characterize regional biotic attributes of reference sites. These surveys determine the presence or abundance of species at a given point in time. Information may also be collected on the numbers of sensitive or tolerant species, and may provide information on the overall community composition. These data is often converted and used in as a biotic index, which assigns numbers to analyzed sites to indicate the level of impact that external factors have on the community [10]. The survey can provide baseline data on the health of a particular system or region, which can be used as a reference during the risk assessment to determine whether the impacted site is similar or not.

Ecological epidemiology is another method to monitor trends in the environment. This is often used prior to a risk assessment, when the sources of contamination are either unknown or due to nonpoint sources [11]. Most often, this endeavor is initiated after reports of a noticeable environmental effect, such as the mortality of a large number of individuals, an increase in the number of deformities, or the decline of a species. The goal of the epidemiological study is to try to form a causal chain from source to exposure to effects. Once the cause is identified, those parties involved can then formulate the problem and continue on with the traditional risk assessment.

Considerations When Determining Which Organisms to Use for an Ecological Risk Assessment

The basic purpose of the risk assessment is either to estimate the exposure to the consumers or to the endpoint organisms, such as a carnivore higher up the food chain. Therefore, the relevance of the assessment heavily depends on choosing the appropriate organisms to monitor or study, or the appropriate species assemblages. There are certain criteria that are desirable when considering which organisms to use in the risk assessment [4]. First, the organism should be easily sampled. This suggests that the organism should be abundant in the area under study and amenable to capture and holding. Second, the organism should be sensitive to the contaminants in the system. If a particular species is known to be insensitive to PAHs, for example, than selecting it to determine effects of creosote contamination will not be protective of the environment. Third, the organism should respond to the toxicant under question in a predictable manner. Ideally, one wants a gradual change in response when the contaminant levels are increased. Ideally, a threshold should exist in which contaminant concentrations below these levels should be of little concern because they will not cause adverse effects [4, 12].

Levels of Biological Organization

There are different levels of biological organization that can be used in an ecological risk assessment: (1) monitoring or testing individual organisms; (2) testing or monitoring populations of a particular species; or (3) community level assessment (Table 1). The choice of level will ultimately depend upon a variety of factors, such as the types of organisms present, their abundance, and their types of interactions with one another. Using the assessment to investigate impacts on a rare species might necessitate only examining a few individual organisms. However, if during the problem formulation step, there is concern about indirect effects, in which the impact on one species affects another, than population or community levels may be most appropriate. For example, if the contaminant is thought to reduce levels of a prey species, then using a community level approach to determine predator–prey interactions might be in order.

Ecological Risk Assessment and Animal Models.
Table 1 Levels of biological organization and typical endpoints assessed during a risk assessment

Organism	Population	Community
Survival	Survival	Survival
Growth	Population density	Population density
Condition factor	Reproductive success	Community structure changes
Reproductive success	Productivity	Trophic imbalances
Tumors	Changes in genetic structure	Biomass
Behavioral alterations	Development of resistance	
Acetylcholinesterase inhibition	Biomass	
Stress proteins		
Changes in metabolism		
Immune system alterations		

The spatial characteristics of the site and the specific agent or agents being assessed will clearly influence the choice of biological organization, as will any temporal variations in the exposure. For example, if one is doing an assessment involving an effluent stream released once per month, this will necessitate a different strategy for testing and monitoring than an assessment for remediation of a contaminated site in which the organisms are continuously exposed. Along with temporal variations, the concentration of the agents may make a difference in the choice of scale as well. An exposure that is extremely high in concentration and pulsatile in nature would warrant different tests than a low level, chronic exposure [3].

The first level of organization is to monitor or test individual organisms. The endpoints garnered from these tests are typically survival, growth, and/or reproduction (Table 1). Depending on the organism used, these tests can take anywhere from hours to days. Population level tests typically are conducted via microcosms or mesocosms, using multiple organisms.

The endpoints assessed are usually survival and growth/production, which takes days to months to conduct. The effects on populations can also be determined in the field by either a designed test or, more often, by simply monitoring the environment. Examples of these types of investigations might include examining organisms in a lake or pond, or in gridded and staked terrestrial areas. Again, the endpoints often assessed are survival, growth, reproduction, and production, which may take days to years to conduct. Community assessments are conducted either using a mesocosm (a small community), field tests, or environmental monitoring. Beyond the typical endpoints of survival and growth, one can now examine changes in community structure and trophic balance.

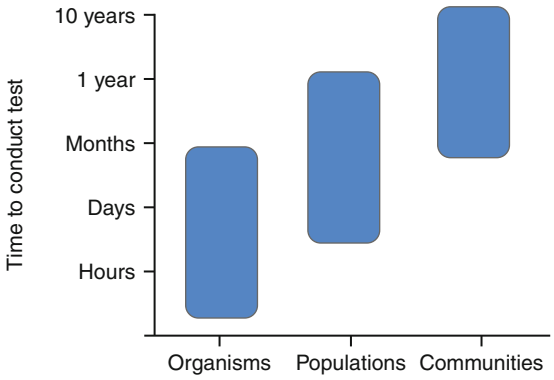

Ecological Risk Assessment and Animal Models. Figure 1 Time scale for collecting field or laboratory data to support the risk assessment

Exposure Time, Organismal Characteristics, and Exposure Routes

Once the level of biological organization is decided upon, the next step is to determine the types organism(s) to use and how long to expose or monitor them. Influencing factors for the exposure time and type of organism include the type of media that are contaminated (soil, sediment, water), the concentrations of the contaminants, and what types of organisms are present at the site, and how many of them are at the site.

The length of exposure time for each of these tests depends on the agent and how it is released or occurs in the area. If assessing the effects of a pesticide application, one may only need to conduct the test or monitor the environment for a few days. If assessing the effects of an oil spill, monitoring for months to years might be more appropriate (Fig. 1). The timing of when the test is conducted also needs to take into account issues like seasonal variability. Water and food may be limited at certain times during the year, and thus the organisms' exposure could be reduced. Additionally, breeding and migration times may pose issues for accurate monitoring and should be taken into account before beginning the study.

Most risk assessments focus on a limited number of organisms – typically no more than just a few species or a small community, if looking at invertebrates or algae. The choice of organisms to examine therefore becomes critical. Among the specific factors and organismal characteristics that should be taken into consideration is the mobility of the organism. Ideally, one would want to monitor an organism with limited mobility, such as earthworms or invertebrates, or to monitor those organisms with low mobility at some stage in their life cycle [12]. Another concern is the sensitivity of species toward the contaminant of interest. Ideally, one would want to use the most sensitive species, which would be protective of all other species. However, given that most sites have a suite of contaminants, finding the species most sensitive to the mixture may be difficult. A third consideration is the ecological function or role of the organism. Often, it is good to choose at least one primary producers to study because of their large contribution to the food chain. Other factors to take into account are choosing an organism that is easy to collect and choosing an organism of high relative abundance. Finally, one also needs to be concerned with a species that has a certain recognized value, either economic or symbolic, as the one that you want to protect. It may be necessary to monitor these types of species, even if they do not fit the other criteria for choice of an organism to use [12].

The last issue is to determine the most likely route of uptake, be it oral, dermal, or inhalation (for a recent review, see [13]). The oral route is the most likely exposure route (Table 2). However, organisms can also swim in water, absorb contaminants through dermal contact, and take up compounds via inhalation, so that depending upon the contaminants at the site, these minor routes of uptake may be more important. For terrestrial invertebrates, the most common type of

Ecological Risk Assessment and Animal Models.
Table 2 Routes of uptake in different organisms

Organism	Common uptake routes
Terrestrial invertebrates	Oral, dermal
Aquatic invertebrates	Oral, respiratory surfaces
Fish	Oral, gills, dermal
Mammals	Oral >> dermal, inhalation
Birds	Oral, inhalation
Amphibians	Dermal, oral
Reptiles	Oral

Routes listed are in the order of importance for each class of organism

organism to monitor is the earthworm. For these animals, exposure occurs either dermally or orally. Other arthropods can be examined, but these typically have an exoskeleton, so a food-borne exposure is more likely than dermal exposure. Aquatic invertebrates are most likely exposed through the oral route. Rather than conducting a test or monitoring these organisms, it is sometimes more desirable to use water or sediment bioaccumulation factors (BAFs) to estimate exposure. The uptake route of fish is typically oral but can also be via the gills or as a dermal exposure. As with aquatic invertebrates, one sometimes estimates the exposure to fish using BAFs or bioconcentration factors (BCFs). BAFs tend to be more consistent across different water chemistries and different organisms. They are also considered more realistic of an exposure since diet and food chain multipliers are included within the BAF. BCFs are determined in laboratory-based studies and are considered more precise. Therefore, a BCF is often what is used to estimate exposure, if available [3]. Exposure factors for many organisms can be found in the *Wildlife Exposure Factors Handbook* [14].

For most terrestrial organisms, the oral uptake route tends to be most important (for a recent review, see [13]). In mammals, the uptake of contaminants tends to be through the diet, while the dermal and inhalation routes tend to be negligible. Mammals have extremely varied feeding strategies, both in terms of prey preference and in feeding frequency. This can result in high exposures to some mammals while no exposure to others, so care must be taken in the risk assessment to choose a species that will come into contact with the contaminants of concern. Periods of fasting, hibernation, and migration can mobilize stored contaminants, resulting in toxicity without changing the body burden. Additionally, lacatational and placental transfer may occur from mothers to the developing offspring. In birds, the oral route is the most important uptake pathway, most commonly through the ingestion of contaminated prey items. During pesticide exposure, uptake via inhalation may contribute significantly to their body burdens. The transfer of contaminants from gravid females into their eggs may also represent a significant exposure source to embryos. In reptiles, the oral route is most important via ingestion of contaminated food items. The skin tends to inhibit some compounds from passing through dermally. As with avian species, contaminant transfer into eggs also represents an important exposure route. In contrast, the dermal route may be extremely important to amphibians due to their life cycle, which is spent in contact with both water and soil for parts of their life span.

When quantifying how much contaminant the organism had received during the exposure, one can determine its concentration in the whole body of the organism, its burden in an organ in which the toxicant is likely to exert a toxic effect, such as the liver, kidney, or brain, or in organs of accumulation, such as fat, hair, or feathers. As stated above, for aquatic organisms, BAFs or BCFs are often used to estimate exposure.

Field Studies and Toxicity Testing

Toxicity tests involve collecting contaminated soil, sediment, or water from the site, and then exposing organisms to that medium or those media in a laboratory setting. There are several different advantages of toxicity tests over field studies. First, a toxicity test can evaluate whether the contaminant was bioavailable to the organisms. Second, a toxicity test can enable a more informed assessment of the impact of mixtures of compounds than the use of data in the literature on single compounds. They can determine whether characteristics of the medium itself, such as hardness or pH, are influencing toxicity. Third, they can examine substances whose effects on wildlife are not well understood. Fourth, they are typically used for monitoring

to determine whether the risk mitigation strategy is working [2, 15].

Although a variety of endpoints can be measured from toxicity tests, the most common ones are survival, growth, and reproduction. Survival is most often assessed using a short term, acute toxicity test. An acute test typically lasts 24–96 h, during which the organisms are exposed to a medium from the site, plus a reference medium, and the number of deaths is recorded. Outcomes of this test include the medium lethal concentration or LC_{50}, which is the concentration of the medium that killed 50% of the test organisms. Other values that are typically obtained are the lowest observed effect concentration (LOEC), which is the lowest concentration of test medium in which statistically significant toxic effects are seen, and the no observed effect concentration (NOEC), which is the highest concentration of test medium in which no significant toxic effects are seen.

Sublethal endpoints, such as growth and reproduction, are best measured using a chronic toxicity test. These tests take a longer period of time to conduct, because they encompass either a critical developmental phase or the organism's entire life cycle, but give better resolution as to whether a toxic effect is occurring on site. Similar to an acute test, the values obtained are typically a median effective concentration (EC_{50}), or the concentration of medium that caused effects, such as reduced growth or reproduction, on 50% of the organisms. A LOEC and NOEC are typically calculated for chronic tests.

Generally, values such as the LC_{50}, NOEC, and LOEC for a single contaminant using standardized test organisms can be easily be obtained from the literature or using databases such as the EPA's ECOTOX database (http://cfpub.epa.gov/ecotox/) or the USGS's Contaminant Exposure and Effects-Terrestrial Vertebrates database (CEE-TV) (http://www.pwrc.usgs.gov/contaminants-online/pages/ceetv/ceetvintro.htm). This means that oftentimes, a *de novo* test may not be necessary. However, one should consider conducting a toxicity test if the data for the compound or interest is absent in the literature, if there is reason to suspect that conditions at the site, such as pH or organic matter, may be influencing bioavailability or toxicity to organisms, or if the interactions between mixtures of compounds are considered significant.

Standard Toxicity Tests

When the risk assessor decides that a *de novo* toxicity test is needed, there are several elements that need to be decided upon. First, the assessor should decide upon the level of effort needed to achieve the goals of the study. If he or she only wants to know whether the medium is toxic or not, using two test organisms and collecting medium from just a few sites may be sufficient to obtain the desired information. However, to fully characterize the site's toxicity, the study might use test organisms at different trophic levels, a number of sampling locations, and several dilutions of each test medium [15]. Second, a reference site should be included that is similar in characteristics to the site under study and is located as close to the study site as possible. Third, the test medium must be decided upon. Although it is most typical to use the water, sediment, or soil directly from the site, one can use soil or sediment elutriate to expose the test organisms. Finally, the test organisms themselves need to be selected. Whenever possible, a standardized organism should be used that is representative of the onsite organisms and is sensitive to the contaminant of concern [15, 16].

Several types of acute aquatic tests involving fish, macroinvertebrates, mysids, Daphnia, and algae have been developed (for a good overview, see [17]). Most of these are 48–96 h LC_{50} tests that measure survival as the endpoint (Table 3). Chronic tests generally involve either early life stage tests with juveniles, but there are some partial or full life cycle tests. Most of these measure endpoints such as survival, growth, and reproduction (Table 3).

Nonstandard Tests and Field Tests

If a laboratory test is needed to assess site medium, the risk assessor should try to choose a standardized test and a standardized organism (Table 3). This is not always possible, as the biota in a particular site may not be similar enough to a standardized organism, or the standardized organisms are not sensitive to the contaminant at the site. In these cases, using an alternative species is completely appropriate [2, 15]. Additionally, field studies are routinely conducted at the actual site. These studies are more concerned with effects on populations and communities, rather than

Ecological Risk Assessment and Animal Models. Table 3 Standard toxicity tests

Test	Organism	Test duration	Endpoints	Reference
Freshwater acute	*Daphnia magna* or *Daphnia pulex*	48–96 h	Survival	[18, 19]
	Fathead minnow	96 h	Survival	[18, 19]
	Rainbow trout	96 h	Survival	[18, 19]
	Brook trout	96 h	Survival	[18, 19]
Freshwater chronic	*Cerodaphnia dubia*	7 days	Survival, reproduction	[20]
	Daphnia magna	21 days	Survival, reproduction	[21]
	Fathead minnow larvae	7 days	Survival, growth	[22]
	Algae (*Selenastrum capricornutum*)	96 h	Cell density	[23]
Saltwater acute	Bivalve mollusk larvae	48 h	Abnormal shell development	[24]
	Silverside (*Menidia* sp)	48 h	Survival	[18, 19]
	Sheepshead minnow (*Cyprinodon variegates*)	48 h	Survival	[18, 19]
Saltwater chronic	Silverside larvae	7 days	Survival, growth	[18, 19]
	Sheepshead minnow	7 days	Survival, growth	[18, 19]
	Mysid shrimp	7 days	Survival, growth, reproduction	[25]
	Sea urchin (*Arbacia punctulata*)	20 min	Egg fertilization	[25]
	Algae (*Champia parvula*)	5–7 days	Fertilization	[26]
Freshwater sediment chronic	*Hyalella azteca*	10–30 days	Survival, growth, reproduction	[26]
	Midge (*Chironomid tetans* or *C. riparius*)	10–14 days	Survival, growth	[26]
Marine sediment chronic	Amphipod	10 days	Burrowing	[25]
Terrestrial	Earthworm (*Eisenia foetida*)	14 days	Survival	[27]
	Bobwhite quail	8 days	Survival, growth	[28]
	Mallard duck	8 days	Survival, growth	[28]

on individual organisms [12]. Reasons for doing a field study might include the fact that a current or future effect is likely, but there is not enough information to support a management decision, or it can provide additional evidence to link a site's contaminant and adverse effects. The key to conducting a good nonstandardized laboratory test or a field test is to find an appropriate reference site.

Studies of sites in which the contaminants of concern are found in the water should include the examination of the effects on periphyton, plankton, benthic macroinvertebrates, or fish [12]. Periphyton and plankton, such as algae, protozoa, and some crustaceans, are primary producers. Periphyton is typically collected by scraping or suction, or an artificial substrate may be deployed for a number of days to allow

attachment. Plankton is collected by pumping, netting, or trapping. Endpoints examined usually involve measures of community composition, such as species numbers, diversity, and richness.

Benthic macroinvertebrates are indicative of the effects of sediment contamination and are typically a good choice to examine if there are lipophilic contaminants at the site. They are collected by digging, netting, dredging, or grab sampling. Endpoints measured include the number and types of species, and other measures of species diversity. Macroinvertebrates can also easily be used in laboratory sediment toxicity tests, using either spiked artificial sediments or sediments taken from the site. Fish are good to examine because they can occupy different trophic levels, and they are relatively easy to collect by seining, passive netting, trawling, or electrofishing. Endpoints examined are often numbers and diversity, or sublethal effects such as behavior or tumor burden. Like benthic macroinvertebrates, fish are often used in laboratory toxicity tests.

Studies of sites in which the contaminants of concern are found in the soil often involve examination of effects on earthworms, nematodes, amphibians, mammals, or reptiles [29]. Earthworms and other soil nematodes are good for both metals and organics since they are in constant contact with the soil. Nematodes are collected by coring, sieving, or they can be driven from the soil by heat. Worms can be tested using spiked soil as the medium, or are examined directly on site, with typical endpoints being survival and reproduction [27]. Organisms such as amphibians, reptiles, and mammals are not used or collected as frequently. When they are, the risk assessor generally chooses a small species, since its home range is likely to be smaller and it tends to be more abundant than larger species. These types of organisms are generally collected by trapping, or their presence can simply be determined by examining surrogate measurements such as footprints, droppings, or carcasses [12]. Birds are not typically used or examined in a risk assessment because their home ranges can be quite large and their collection tends to be difficult and time intensive. When they are examined, they can be trapped to determine their numbers, or surrogate measures, such as auditory signals, used to determine their presence. Alternatively, the number of nests can be counted and the success of each nest can be documented.

Other Assays Providing Support to Risk Assessments

Beyond using standard toxicity tests to assess survival, growth, and reproduction, or looking for the presence of an organism during a field survey, there are several different ways to determine other types of adverse impacts, such as altered community composition, to estimate body burdens of toxicants, and to examine markers or exposure and/or effects.

Biological Surveys

Two such methods to examine altered community composition are biotic indices and rapid bioassessment protocols. These two types of surveys compare population and community compositions of macroinvertebrates, fish, or periphyton between a reference site and the site of interest. For both of these protocols, an initial survey is conducted to quantify the presence and abundance of different species at both sites. These quantities are then converted into numerical values that relate to the overall health of the community.

More than 50 different indices have been developed to assess community health [10]. Parameters examined include species richness, or the number of species in a community, density, dominance, diversity (the abundance of individuals in one taxon versus all other individuals), as well as the number of sensitive species, such as the number of species belonging to the Ephemeroptera (mayflies), Plecoptera (stonefiles), and Trichoptera (caddisflies) or the EPT index [30]. Other metrics include percent dominant taxon, percent tolerant taxa, and percent Chironomidae, all of which are predicted to increase in response to increased perturbation [10]. The Family Biotic Index is also a good measure of perturbation, as it uses tolerance values to weight abundance in an estimate of overall pollution [10]. Other indices such as the Simpson's Diversity Index and the Shannon-Wiener Diversity Index are also used to account for the richness and the evenness of the different species that make up the total community [31]. Finally, determining the percentage of

individuals in each of the five functional feeding groups can be used to determine whether the trophic structure is balanced [32].

Since many of this indices require a lot of time, expertise, and money, rapid bioassessment protocols (RBPs) have been developed since the 1980s to obtain these same measurements in a more cost effective and efficient way. These protocols were developed from previously existing bioassessment methods that were used by many state agencies. The RBPs examine other parameters besides numbers of organisms. In the case of streams, these include the available cover, embeddedness, velocity and depth of the river or stream, sediment deposition, channel flow status, channel alteration, frequency of riffles, bank stability, vegetative protection, and riparian vegetative zone width [10]. RBPs are appropriate for distinguishing the existence and severity of impairment of the water body, as well as identifying the causes of impairment. They are also used to determine if a stream is supporting a designated aquatic life use specified in state Water Quality Standards, evaluating the effectiveness of controls and various restoration activities, and characterizing regional reference conditions. Additional information on both types of bioassessments and their uses is provided in another entry.

Biomarkers and Toxicokinetic Models

A second method to estimate exposure of an organism to a contaminant is to use a biomarker. Biomarkers are defined as a quantifiable change in a biochemical, physiological, or histological parameter that can be used as a measure of response to a xenobiotic. The idea behind biomarkers is that they can detect more subtle adverse effects than lethality at lower chemical concentrations, which would better protect the population or community. Biomarkers can be indicators of either exposure or effects, although exposure biomarkers are much more common. Examples of biomarkers routinely used in environmental toxicology studies include the induction of cytochrome P4501A (CYP1A) to indicate PAH exposure, acetylcholinesterase activity to indicate organophosphate or carbamate pesticide exposure, metallothionein induction to indicate exposure to several metals, vitellogenin to indicate exposure to estrogenic compounds, and eggshell thinning to indicate organochlorine exposure. Additional information on biomarkers is provided in another entry.

A final strategy is to incorporate physiologically-based pharmacokinetic (PBPK) models into the risk assessment. These model the time course of disposition of toxicants in the whole organism, which gives an estimate of body burdens. In a PBPK model, the organism is represented by several different compartments in which toxicants might be expected to be absorbed in, distributed to, biotransformed in, and excreted from, such as the alimentary canal, blood, fat, liver, and kidney. Thus, one can use the model to predict concentrations of contaminants in an organism, rather than having to measure actual body burdens of contaminants, which can be time consuming and extremely expensive. Beyond cost, the models have other advantages, such as being able to provide a time course of distribution of toxicants to any organ or tissue, being able to estimate effects by changing physiological parameters such as food consumption, mobility, or reproductive status, and being able to use the same model to predict toxic action in different species. Although PBPK models can improve estimates in determining whether the contaminant will accumulate to high enough levels in the organism of interest to cause an adverse effect, there are a number of distinct disadvantages to their use compared to simply measuring body burdens. First and foremost, one needs information to build the model, such as blood volume, heart rate, breathing rate, and organ volumes. The fact that these parameters are often ill-defined for many species detracts from the power and utility of the model. Second, the mathematics, computational tools, and training needed to build and run the models may be out of reach for many risk assessors.

In spite of these obstacles, there are several PBPK models available for wildlife species, such as fish and polar bears, which can describe the body and tissue burdens of contaminants. For example, fish PBPK models have been built for rainbow trout and have been used to estimate tissue concentrations of paraoxon and cadmium [33–35]. Likewise, there is a PBPK model that estimates arsenic concentrations in the different organs of tilapia (*Oreochromis mossambicus*) [36]. Additionally, there are also models to assess ionizing radiation doses to a variety

of non-human species [37]. The models for polar bears are a bit more sophisticated than those built for fish, in that they can estimate tissue concentrations of organohalogenated compounds, such as dieldrin and PCBs, but can also be used to estimate risk of effects, such as adverse impacts on reproduction [38]. It is likely that they can be extended to other at-risk populations, such as orcas and the arctic fox [39].

There are a few models in reptiles and birds that were developed to be more applicable to veterinary uses, but could be used to estimate contaminant concentrations in wildlife. Examples include a model developed in red-eared sliders (*Trachemys scripta elegans*) to determine the pharmacokinetics and tissue distribution of buprenorphine, a potential analgesic drug for reptiles [40]; a model for midazolam developed in chickens, but able to accurately predict tissue residues in turkey, pheasant, and quail [41]; and a model used to determine tissue levels of lipophilic pesticides in chickens, ducks, geese, and turkeys [42]. Alternatively, there are many rodent models for environmental contaminants that could potentially be adapted for use in other species. One such recent example includes a PBPK model in rats for developmental exposure to polybrominated diphenyl ethers (PBDEs) [43].

Future Directions Using Animal Models in Risk Assessments

Some future directions for increasing the quality of risk assessment is to refine our understanding of sublethal effects rather than focusing on survival as an endpoint, and to better determine the mode of action of contaminants. One potential way to accomplish this goal is through the use of genomics – analyzing changes in gene, protein, and metabolite expression. Genomics has the advantage of examining thousands of genes or proteins simultaneously as opposed to traditional biomarkers, which often measure a single gene or protein at a time. Like biomarkers, genomic changes can be linked to both exposure and effect outcomes. For example, rather than looking for reproductive failure in a toxicity test, one could examine changes in genes involved in steroidogenesis. These genes should be differentially expressed at much lower toxicant concentrations, yet can still provide a predictive measure that adverse reproductive effects are likely to occur [44]. Thus, genomic techniques are more sensitive than traditional toxicity testing or biomonitoring and can be used to detect early indicators of environmental perturbation.

One of the issues encountered when using genomic data in a risk assessment is that baselines or control patterns of expression need to be established for a variety of species. This is true for those organisms routinely used in risk assessments, such as fathead minnows and Daphnia, but even more so for nontraditional species and those organisms collected in field studies, since the variation in natural populations can be quite significant [45]. Second, the data generated from a genomic study cannot be easily translated into terms familiar to many risk assessors, such as a NOEL or EC_{50} [46, 47]. Some recent studies have developed no observed transcriptional effect levels (NOTEL) for *Daphnia magna* exposed to copper, and these NOTELs were validated after exposing Daphnia to water samples collected upstream and downstream from two copper mines in California [48, 49]. However, there are almost no published studies using a NOTEL and relating that value to an adverse event. Third, there is often a lack of phenotype associated with the changes in mRNA levels, making it hard to interpret just what types of adverse effects would be occurring to organisms at the site [46, 47, 50]. Studies linking adverse effects, such as altered growth and reproduction, with transcriptomic changes have also been conducted (reviewed in [51], but there are too few of these published to support the current use of genomics in risk assessments. Finally, genomic studies are expensive and the computational needs are quite high.

The current policy at EPA is that toxicogenomics data may be used in a weight-of-evidence approach for ecological risk assessment, but must be provided in conjunction with other information. At this point, genomics data alone are insufficient for a risk assessment and any subsequent management decision [52, 53]. However, some potential uses for genomics in risk assessment for the foreseeable future are to guide the experimental design of monitoring programs so as to reduce the number of animals used, as an initial screening to rank or set priorities for further toxicity testing, and to help extrapolate the effects of contaminants across species [54].

Bibliography

Primary Literature

1. EPA (1992) Framework for ecological risk assessment. EPA/630/R-92/001, Risk Assessment Forum, Washington
2. EPA (1998) Guidelines for Ecological Risk Assessment. EPA/630/R-95/002F. Risk Assessment Forum, Washington
3. Suter GW II (2007) Ecological Risk Assessment, 2nd edn. CRC, Boca Raton, p 643
4. Dale VH, Mulholland PJ, Olsen LM, Feminella JW, Maloney KO, White DC, Peacock A, Foster T (2004) Selecting a suite of ecological indicators for resource management. In: Kapustka L et al (eds) Landscape ecology and wildlife habitat evaluation: critical information for ecological risk assessment, land-use mangement activities, and biodiversity enhancement practices. ASTM International, West Conshohocken
5. Hill AB (1965) The environment and disease: association or causation? Proc R Soc Med 58:295–300
6. Fox GA (1991) Practical causal inference for ecoepidemiologists. J Toxicol Environ Health 33:359–373
7. EPA (2000) Stressor identification guidance document. EPA/822/B-00/025. Office of Water, Washington
8. EPA (1997) Environmental monitoring and assessment program (EMAP): research strategy. EPA/620/R-98/001. Office of Research and Development, Washington
9. EPA (2002) Research strategy: environmental monitoring and assessment program. EPA 620/R-02/002. Office of Research and Development, Research Triangle Park
10. Barbour MT, Gerristen J, Snyder BD, and Stribling JB (1999) Rapid bioassessment protocols for use in streams and wadeable rivers: periphyton, benthic macroinvertebrates, and fish, 2nd edn. EPA 841-B-99-002, ed. U.S.E.P.A.O.o. Water, Washington
11. Suter GW II (2006) Ecological risk assessment and ecological epidemiology for contaminated sites. Hum Ecol Risk Assess 12:31–38
12. EPA (1994) ECO update: field studies for ecological risk assessment. Publication 9345.0-05I. Office of Emergency and Remedial Response, Washington
13. Smith PN, Cobb GP, Godard-Codding C, Hoff D, McMurry ST, Rainwater TR, Reynolds KD (2007) Contaminant exposure in terrestrial vertebrates. Environ Pollut 150:41–64
14. EPA (1993) Wildlife exposure factors handbook. EPA/600/R-93/187. Office of Research and Development, Washington
15. EPA (1994) ECO update: using toxicity tests in ecological risk assessments. Publication 9345.0-05I. Office of Solid Waste and Emergency Response, Washington
16. 04 AE (2004) Standard Guide for Selection of Resident Species as Test Organisms for Aquatic and Sediment Toxicity Tests. ASTM International, West Conshohocken, DOI: 10.1520/E1850-04
17. Landis WG, Yu M-H (2003) Introduction to environmental toxicology: impacts of chemicals upon ecological systems, 3rd edn. CRC, Boca Raton
18. 96 AE (2007) Standard guide for conducting acute toxicity tests on test materials with fishes, macroinvertebrates, and amphibians. ASTM International, West Conshohocken, DOI: 10.1520/E0729-96R07
19. 97 AE (2008) Standard guide for conducting acute toxicity tests on aqueous ambient samples and effluents with fishes, macroinvertebrates, and amphibians. ASTM International, West Conshohocken, DOI: 10.1520/E1192-97R08
20. 01 AE (2006) Standard guide for conducting three-brood, renewal toxicity tests with *Ceriodaphnia dubia*. ASTM International, West Conshohocken, DOI: 10.1520/E1295-01R06
21. E1193-97 AS (2004) Standard guide for conducting daphnia magna life-cycle toxicity tests. ASTM International, West Conshohocken, DOI: 10.1520/C0033-03
22. E1241-05 A (2005) Standard guide for conducting early life-stage toxicity tests with fishes. ASTM International, West Conshohocken, DOI: 10.1520/E1241-05
23. D3978-80 (1987) e1 (1997) Standard practice for algal growth potential testing with *Selenastrum capricornutum*. ASTM International, West Conshohocken
24. 98 AE (2004) Standard guide for conducting static acute toxicity tests starting with embryos of four species of saltwater bivalve molluscs. ASTM International, West Conshohocken, DOI: 10.1520/E0724-98R04
25. 03 AE (2008) Standard test method for measuring the toxicity of sediment-associated contaminants with estuarine and marine invertebrates. ASTM International, West Conshohocken, DOI: 10.1520/E1367-03R08
26. 05e1 AE (2005) Standard test method for measuring the toxicity of sediment-associated contaminants with freshwater invertebrates. ASTM International, West Conshohocken, DOI: 10.1520/E1706-05E01
27. 04 AE (2004) Standard guide for conducting laboratory soil toxicity or bioaccumulation tests with the lumbricid earthworm *Eisenia Fetida* and the Enchytraeid Potworm *Enchytraeus albidus*. ASTM International, West Conshohocken, DOI: 10.1520/E1676-04
28. 05e1 AE (2005) Standard practice for conducting subacute dietary toxicity tests with avian species. ASTM International, West Conshohocken, DOI: 10.1520/E0857-05E01
29. Golden NH, Rattner BA (2003) Ranking terrestrial vertebrate species for utility in biomonitoring and vulnerability to environmental contaminants. Rev Environ Contam Toxicol 176:67–136
30. Wallace JB, Grubaugh JW, Whiles MR (1996) Biotic indices and stream ecosystem processes: results from an experimental study. Ecol Appl 6:140–151
31. Lampert W, Sommer U (1997) Limnoecology: the ecology of lakes and streams, 2nd edn. Oxford University Press, New York
32. Merritt RW, Cummins KW (1995) An introduction to the aquatic insects of North America, 3rd edn. Kendall/Hunt, Iowa
33. Abbas R, Hayton WL (1997) A physiologically based pharmacokinetic and pharmacodynamic model for paraoxon in rainbow trout. Toxicol Appl Pharmacol 145:192–201

34. Thomann RV, Shkreli F, Harrison S (1997) A pharmacokinetic model of cadmium in rainbow trout. Environ Tox Chem 16:2268–2274
35. Franco-Uria A, Otero-Muras I, Balsa-Canto E, Alonso AA, Roca E (2010) Generic parameterization for a pharmacokinetic model to predict Cd concentrations in several tissues of different fish species. Chemosphere 79:377–386
36. Liao CM, Liang HM, Chen BC, Singh S, Tsai JW, Chou YH, Lin WT (2005) Dynamical coupling of PBPK/PD and AUC-based toxicity models for arsenic in tilapia *Oreochromis mossambicus* from blackfoot disease area in Taiwan. Environ Pollut 135: 221–233
37. Beresford NA, Barnett CL, Brown JE, Cheng JJ, Copplestone D, Filistovic V, Hosseini A, Howard BJ, Jones SR, Kamboj S, Kryshev A, Nedveckaite T, Olyslaegers G, Saxén R, Sazykina T, Vives I Batlle J, Vives-Lynch S, Yankovich T, Yu C (2008) Intercomparison of models to estimate radionuclide activity concentrations in non-human biota. Radiat Environ Biophys 47:491–514
38. Sonne C, Gustavson K, Rigét FF, Dietz R, Birkved M, Letcher RJ, Bossi R, Vorkamp K, Born EW, Petersen G (2009) Reproductive performance in East Greenland polar bears (*Ursus maritimus*) may be affected by organohalogen contaminants as shown by physiologically-based pharmacokinetic (PBPK) modelling. Chemosphere 77:1558–1568
39. Sonne C (2010) Health effects from long-range transported contaminants in Arctic top predators: An integrated review based on studies of polar bears and relevant model species. Environ Int 36:461–491
40. Kummrow MS, Tseng F, Hesse L, Court M (2008) Pharmacokinetics of buprenorphine after single-dose subcutaneous administration in red-eared sliders (*Trachemys scripta elegans*). J Zoo Wildl Med 39:590–595
41. Cortright KA, Wetzlich SE, Craigmill AL (2009) A PBPK model for midazolam in four avian species. J Vet Pharmacol Ther 32:552–565
42. MacLachlan DJ (2010) Physiologically based pharmacokinetic (PBPK) model for residues of lipophilic pesticides in poultry. Food Addit Contam A Chem Anal Control Expo Risk Assess 27:302–314
43. Emond C, Raymer JH, Studabaker WB, Garner CE, Birnbaum LS (2010) A physiologically based pharmacokinetic model for developmental exposure to BDE-47 in rats. Toxicol Appl Pharmacol 242:290–298
44. Kennedy SW, Euling S, Huggett DB, De Coen LW, Snape JR, Zacharewski TR, Kanno J (2008) Application of genomics to screening. In: Ankley GT et al (eds) Genomics in regulatory ecotoxicology. CRC, Pensacola
45. Oleksiak MF, Churchill GA, Crawford DL (2002) Variation in gene expression within and among natural populations. Nature Genet 31:261–266
46. Ankley GT, Daston GP, Degitz SJ, Denslow ND, Hoke RA, Kennedy SW, Miracle AL, Perkins EJ, Snape J, Tillitt DE, Tyler CR, Versteeg D (2006) Toxicogenomics in regulatory ecotoxicology. Environ Sci Technol 40:4055–4065
47. Boverhof DR, Zacharewski TR (2006) Toxicogenomics in risk assessment: applications and needs. Toxicol Sci 89: 352–360
48. Poynton HC, Loguinov AV, Varshavsky JR, Chan S, Perkins EJ, Vulpe CD (2008) Gene expression profiling in Daphnia magna part I: concentration-dependent profiles provide support for the No Observed Transcriptional Effect Level. Environ Sci Technol 42:6250–6256
49. Poynton HC, Zuzow R, Loguinov AV, Perkins EJ, Vulpe CD (2008) Gene expression profiling in Daphnia magna, Part II: validation of a copper specific gene expression signature with effluent from two copper mines in California. Environ Sci Technol 42:6257–6263
50. Degitz SJ, Hoke RA, Bradbury S, Brennan R, Ferguson L, Klaper R, Orban L, Spurgeon D, Tilton S (2008) Application of genomics to regulatory ecological risk assessments for pesticides. In: Ankley GT et al (eds) Genomics in regulatory ecotoxicology. CRC, Pensacola
51. Van Aggelen G, Ankley GT, Baldwin WS, Bearden DW, Benson WH, Chipman JK, Collette TW, Craft JA, Denslow ND, Embry MR, Falciani F, George SG, Helbing CC, Hoekstra PF, Iguchi T, Kagami Y, Katsiadaki I, Kille P, Liu L, Lord PG, McIntyre T, O'Neill A, Osachoff H, Perkins EJ, Santos EM, Skirrow RC, Snape JR, Tyler CR, Versteeg D, Viant MR, Volz DC, Williams TD, Yu L (2010) Integrating omic technologies into aquatic ecological risk assessment and environmental monitoring: hurdles, achievements, and future outlook. Environ Health Perspect 118:1–5
52. Dix DJ, Gallagher K, Benson WH, Groskinsky BL, McClintock JT, Dearfield KL, Farland WH (2006) A framework for the use of genomics data at the EPA. Nat Biotechnol 24:1108–1111
53. EPA (2007) Interim guidance for microarray-based assays: data submission, quality, analysis, management, and training considerations. Draft, Science Policy Council, Washington
54. Perkins EJ, Denslow N, Chipman JK, Guiney PD, Oris JT, Poynton H, Robidoux PY, Scroggins R, Van Der Kraak GJ (2008) Application of genomics to assessment of the ecological risk of complex mixtures. In: Ankley GT et al (eds) Genomics in regulatory ecotoxicology. CRC, Boca Raton

Books and Reviews

Barnthouse LW, Munns JWR, Sorensen MT (eds) (2008) Population-level ecological risk assessment. CRC, Boca Raton

Kapustka L, Biddinger G, Luxon M, Galbraith H (eds) (2004) Landscape ecology and wildlife habitat evaluation: critical information for ecological risk assessment, land-use management activities, and biodiversity enhancement practices. ASTM International, West Conshohocken

Solomon KR, Brock TCM, de Zwart D, Dyer SD, Posthuma L, Richards SM, Sanderson H, Sibley PK, van den Brink PJ (eds) (2008) Extrapolation practice for ecotoxicological effect characterization of chemicals. CRC, Boca Raton

Ware GW (2006) Reviews of environmental contamination and toxicology, vol 187. Springer, New York

Ecological Succession and Community Dynamics

Herman H. (Hank) Shugart
Department of Environmental Sciences,
The University of Virginia, Charlottesville, VA, USA

Article Outline

Glossary
Definition of the Subject and Its Importance
Introduction
Sustainability and Vegetation Dynamics
Future Directions
Bibliography

Glossary

Abstract community A group of organisms that recurs on the landscape with an implication of a level of integration among its parts that in extreme could be called organismal or quasi-organismal (see: Concrete Community).

Chronosequence A space-for-time substitution in which the successional vegetation is ordered in a regular fashion. An example would be the series of vegetation at the foot of a receding glacier or a series of sand dunes ordered in regularly aged series.

Clementsian succession An explanation of succession emphasizing the attributes of the community as if it functioned like a single living organism (see: Abstract Community).

Climax community An ecological community associated with a particular climate and in a state of dynamic equilibrium with the climate. The American ecologist, F.E. Clements, designated the climax community as the endpoint of ecological succession for a given climate condition and noted the common Greek root κλίμα (*clima*) or inclination, in both climax and climate as indicating their close relationship.

Concrete community The collection of organisms found at a specific place and time (see: Abstract Community).

Gleasonian succession theory An explanation of succession emphasizing the importance of the attributes of individual organisms as the fundamental basis.

Indicator species Plants or animals whose presence implies the past or present conditions at a given location.

Monoclimax The concept that one mature vegetation will eventually be produced by successional processes in a given region.

Polyclimax The concept that multiple mature, stable-vegetation types can develop from the successional processes operating in a given region.

SIGMATIST A school of vegetation science emphasizing the classification of vegetation.

Time-for-space substitution The collection of vegetation data from different locations at which succession has been initiated at different times in the past to piece together the pattern of succession.

Definition of the Subject and Its Importance

"Ecological Succession" is an ordered progression of structural and compositional changes in communities toward an eventual unchanging condition, the climax community [1–3]. The term "Community" is used in two ways [4]. The "Abstract Community" refers to an abstract group of organisms that recurs on the landscape, a definition, which usually carries with it an implication of a level of integration among its parts that in extreme could be called organismal or quasi-organismal; the "Concrete Community" concept refers to the collection of organisms found at a specific place and time. These terms and their meanings are topics of significant debate among ecologists, both historically and today [5, 6]. These differences in the meaning and cause of ecological succession strongly affect the formulation of policies for ecosystems management and restoration.

Succession is important in sustainability science for several reasons: Many of the laws and regulations regarding the maintenance and restoration of terrestrial ecosystems contain assumptions that are products of different theories as to how ecological succession proceeds in a given environment. Laws might require restoration to a natural condition, which is often the

vegetation that is considered the stable single vegetation type on a map that is itself based on the idea that vegetation undergoes succession a vegetation type appropriate to the climate (the climax vegetation). Further, the management of land systems often has as their basis concepts as to how succession works. For example, if one subscribes to a successional theory that abused land under an inappropriate management scheme will return to its natural state if the inappropriate management is relaxed, then one can utilize land until monitoring indicates the ecosystem is over stressed. If an alternate successional theory is applied, that abused land may not recover to its former when released from inappropriate management, then a much more cautious form of management is needed.

Introduction

Ecological succession and the dynamic change of communities is one of the pillars of modern ecology and it has considerable influence on sustainability science. The processes that drive succession and the regularly of patterns of succession have been the topic of considerable debate over the past century – due in no small part to the importance of the concept to basic and applied ecology. Succession is at its simplest level the pattern of change in ecological communities and these changes can be read on the landscape if one knows regional history or conversely can be used to interpret a landscape's history. In the former case, the historical pattern of land abandonment in the piedmont of the southeastern United States presents land elements abandoned and never reclaimed since the US Civil war in 1860, land left fallow in the First World War; farms left to ruin in the crushing economic Great Depression of the 1930s; more land left when the sons of farmers left for the Second World War; still other farm land taken out of production in agricultural programs reduce farm acreage in the 1950s. The landscape as one drives and automobile through Georgia or the Carolinas, is a kaleidoscopic montage with similar parcels of land cover types replicated on locations with similar history. In the latter case, a small patch of pine (*Pinus* sp.) trees on a slope bears witness to recovery from a past wildfire or a Beech (*Fagus*) forest of great stature indicates an area that has not burned, perhaps for centuries. The dependence of pine species on fire for regeneration or the sensitivity of the thin-barked beech to fire is written into the landscape response.

At the turn of the twentieth century, an American plant ecologist, F.E. Clements, framed many of the definitions and concepts in ecological succession and produced a theoretical system of concepts that explained the nature and function of ecological communities changing over time. Clements' definitions and approaches to understanding the dynamics of landscapes were used to develop regional systems of land management policies based on expectations, succession, and successional recovery. Clements also developed a niche-based concept of using what he called "indicator species" to evaluate the history and condition of land units [2]. For example, an overabundance of bitter or poisonous herbs might be indicators of overgrazing in a prairie systems; the occurrence of other species might indicate unusual soil chemistry and thus the presence of valuable minerals in the bedrock. The details of Clements' ideas were debated strongly by his contemporaries and other ecologists in the 1920s and 1930s found differences with parts of his successional concepts. For example, H.A. Gleason [7, 8] argued that the highly coordinated interactions in Clements concepts had at their basis the unique attributes of the individual plant species. These will be discussed below. Perhaps the most sharply pointed criticism was from the British ecologist, A.G. Tansley, who argued that the Clements' view of succession had so clouded the meaning of the term, community, that a new term, the ecosystem [5], was needed to replace and properly formalize these ideas. It is significant in understanding the emphases in ecosystem studies to note that A.G. Tansley was a coauthor to the 1899 edition of Spencer's *Principles of Biology*, the leading English biology text of the late nineteenth century. Tansley's definition of the ecosystem and his lack of acceptance of Clements' and Phillips' holistic view that the ecological community was a coherent, organism-like entity was not a rejection of a holistic view of ecology, it was a debate among holistic ecologists [9]. These and other continuing and sometimes rancorous [6, 10] debates will be discussed in more detail below.

The development of the attributes of ecological succession has from its beginning had two poles: one

Clementsian pole, which emphasizes holism, great interconnectedness of ecological systems and a successional progression toward an ultimate stable ecological system with an optimization of its attributes; a second Gleasonian pole, which sees the properties of ecological systems as deriving from the individual attributes of the organisms that comprise it and their interactions with their environment. The Gleasonian view is less dogmatic about the necessary outcomes of succession. Of course, sustainability science ultimately must take the measure of the dynamics of complex ecosystems, the natural and direction of their change under management. Debates among ecologists as to the nature of succession must be understood by scientists seeking to understand sustainability.

It is important to note that through the history of this strong Anglo-American debate on the nature of succession, there has been a continental European effort toward the goal of developing a taxonomic tradition in the issue of classifying vegetation into meaningful units, which is also an essential element of sustainable management. The so-called Zurich-Montpellier school (or as later called the SIGMATIST school) originated in the 1890s with work by C. Schröter and Charles Flahault. This effort was taken up and lead by J. Braun-Blanquet. This tradition emphasized a floristic description of vegetation and had the ultimate goal a classification of "associations" as the basic vegetation units of interest [11]. This interest in vegetation classification as a basis of mapping and prediction continues to the present. Significantly, vegetation classification is an ultimate element in organizing management plans and hence for sustainability as well.

Historical Development of the Concept of Ecological Succession

Different scientists in different locations have observed these patterns and drawn rather different conclusions about the root causes of succession and to the degree that it repeats itself over time and space. Figure 1 illustrates the relationships among several ecologists who have developed what might be best described as "iconic" views of succession. The two axes in the figure are the level of holism in the theories and the emphasis on the degree of importance of feedbacks between the biological community and the environment.

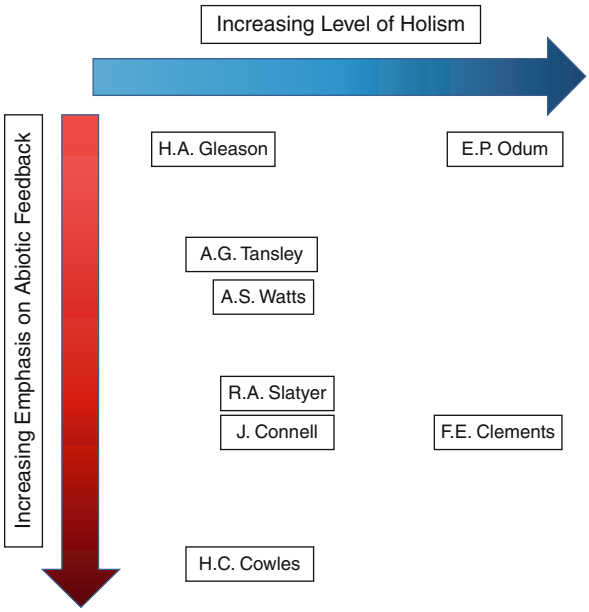

Ecological Succession and Community Dynamics. Figure 1
Iconic ecologists and their emphases on the attributes of successional systems

All of these scientists are holistic in that they focused on the larger system behavior of ecological systems. The most holistic of these scientists would see the community as a highly organized, perhaps highly coevolved systems described as an abstract community in the definition section of this paper (above). They also vary on the degree to which they emphasize feedbacks between the organisms and their environment.

F.E. Clements The iconic scientists in Fig. 1 represent different points of view in the formative debates on the nature of ecological succession in the formative period in the first third of the twentieth century. Clements was in some sense the dominant figure in these discussions. A.G. Tansley who represented strong opposition to many of Clements' fundamental concepts, wrote Clements obituary [12] for *The Journal of Ecology*,

- Though out of accord with many American ecologists, Clements had, throughout his career, a devoted following of younger men, and besides exercising a world-wide influence through his theory of vegetation, he

directly inspired a great deal of American ecological research. This was partly due to his powerful personality. He was decidedly puritan, even ascetic (he neither drank nor smoked, and it gave him real pain to see other people doing so), and his manner was apt to be tinged with a certain arrogance. These things naturally antagonized many people; but at the same time his capacity for hard work, his intense and complete devotion to his subject, his powerful intellect and unremitting search for fresh knowledge and satisfactory formulations, could not fail to inspire the highest respect.

Clements' concept [3] saw secondary succession as being initiated by an event that removed all of the vegetation. Nowadays, this would fall under the term "disturbance" [13]. Clements referred to this process as *nudation*. Seeds, spores, etc., would then disperse to the site in the process of *migration*. These would germinate and become established in a collective set of processes that he called "eccesis." The resultant plants would then interact with one another, notably through competition. Clements called these collection of interactions, "coaction." Successful plants would interact with the microenvironment at the site and, in a process called "reaction," would modify the local site conditions as to make it unsuitable for the plant species that were there and more suitable for other species, which would replace them. This interaction is often called "facilitation" in modern ecology texts. The plant communities generated by this process are called "seres." The feedback between each sere and the environment produces an ordered sequence of seres or seral stages of succession. This reaction-replacement process would continue until an assemblage of species, which were able to occupy the site after the plant-environment reaction process, became dominant ("stabilization"). This ultimate assemblage was the "climax community."

Clements' climax community concept is incorporated almost subliminally in a number of the ideas in plant ecology and landscape management, particularly in the Western United States. Maps of "potential vegetation" are often maps of climax vegetation in the style of Clements. This is reinforced by the two-dimensional nature of paper making it cumbersome to print maps with more than one potential vegetation in a given map location. Management of parks toward a "natural" condition often has a "climax community" concept as an underlying basis. Decisions to sustainably conserve land are straight-forward if there were a climax vegetation but should be difficult for successional seres, which might be expected to change over time. While Clements' concepts are ubiquitous in land management, several ecologist have noted difficulties with the concept. More frequent criticisms of Clements' concepts include:

1. The idea that the sere/environment feedbacks produce a necessary ordering of communities toward the climax community. Clements [11] noted, "The climax formation is the adult organism of which all the initial stages are but stages of development." Some of the more ardent Clementsian ecologists [14–16] likened the sequence of seres in succession as a direct analog to the embryological development of an organism. The rejection of this concept of the community as a superorganism concept by Tansley [5] motivated the invention of the neologism, "ecosystem," as a replacement for what he felt was a corrupted term, "community," in 1935.
2. The concept of facilitation. Facilitation has been attacked from evolutionary arguments to the effect that one would not expect a species to evolve to facilitate the success of a replacing competitive species. Field observations of species replacements support the existence of facilitation such as the presence of plants with nitrogen-fixing symbiotic organisms increase the nutrient status of a site and advantaging other species. There are also numerous counterexamples of species that hold sites tenaciously over generations before finally losing to competitors [6].
3. The progressive ecesis of different species relayed to the site for all the seral stages. In some successional sequences, all the species are present at the site from the first nudation event. In these cases, the progression of seral stages is a consequence of the differences in rate of maturation of herbaceous plants, shrubs, and trees [10].
4. The existence of a single stable climax community reached by a single sequence of seres. Several questions have arisen about the climax concept. Is there a single climax community or is there always change in the vegetation at a site? [17] Can there be multiple stable climaxes? [18–20] Can there be several

pathways to a particular community? [21] Can the pathways fork? Are the seres comparable at different locations?

These criticisms continue in no small part because of the importance of Clements and his students in the formulation of a grand theory of vegetation dynamics and their ability to translate their concepts into practical applications. Subsequent recognition that past conditions could leave stable relict communities (e.g., preclimaxes such as grassland patches in temperate deciduous forest). Human or natural disturbances (such as occasional wildfires) could leave in a region a persistent vegetation that could be expected to change to a climax vegetation if the disturbance were controlled ("disclimax"). Unusual soil conditions or variations in topography could produce persistent vegetation that was different from the regional stable vegetation ("preclimaxes and post climaxes"). These elaborations of the climax concept inspired a proliferation of conditional climax vegetations [3]. These extended definitions of the Clementsian succession concept that essentially preserved the ideas of a single succession to a climax community through an ordered series of seral communities, also allowed for special conditions (disturbance regime, human use of the land, historical antecedents and soils) to create deviations from this basic model [22].

The debate over these issues and its continuation over almost a century in some cases, speaks to the complexity of the issues and the importance of understanding succession in designing concepts to manage natural systems sustainably [11, 23]. The issues raised by the scientists in Fig. 1 are illustrated in Fig. 2 as deconstructions of the standard definition of ecological succession.

H.A. Gleason and the Individualistic Concept of Succession Henry Gleason represents a logical foil to Clements holistic idea of progression of succession toward a climax vegetation. In total, his publications were strongly focused on plant taxonomy [24] but the relatively smaller section of ecological papers that he produced had remarkable impact on his colleagues, an impact that continues to the present day. As early as 1910, Gleason [25] noted, "... it is impossible to state whether there is one definite climax vegetation in each province; it seems probable that there are several such association each characteristic of a limited proportion."

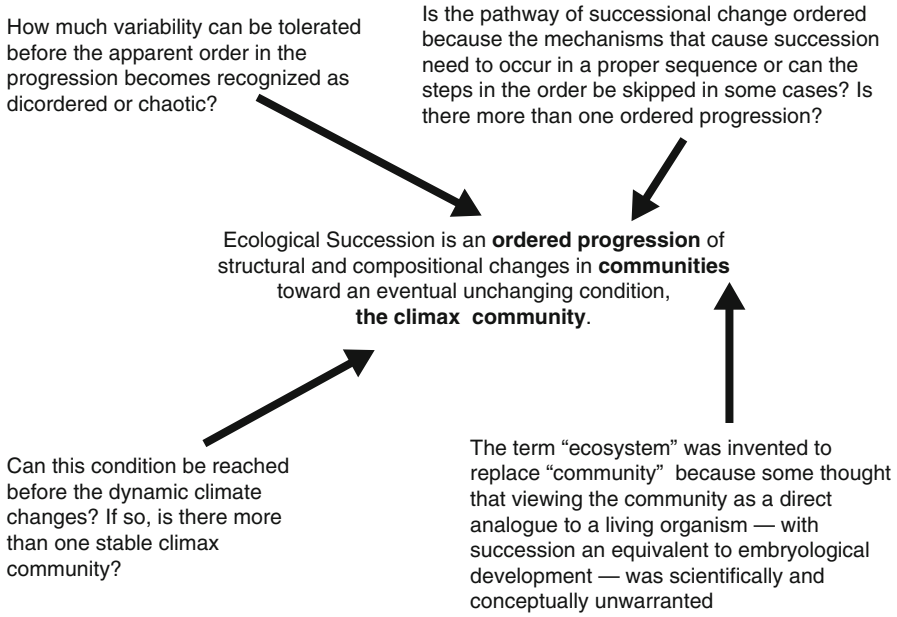

Ecological Succession and Community Dynamics. Figure 2
Some of the basic issues in the nature of ecological succession arising from a standard definition

Gleason's view of succession differed significantly from that of Clements. He recognized as early as 1908 [26] that succession to be retrograde as well as progressive as posited by Clements. Succession was not necessarily an irreversible trend toward the climax community. Gleason also recognized that the climate could change in contrast with Clements' theory of vegetation undergoing succession in an unchanging climate. Gleason developed what he called the "individualist concept" that succession is the result of environmental requirements of the individual species that comprise the vegetation. He also noted [27] that ". . . no two species make identical environmental demands."

Gleason's concept of succession was a much more fluid and much less stereotypical concept of succession than that of Clements. Succession reflected the interactions of individuals with the environment. It could change in its nature with different climatic and other environmental conditions. It could progress or regress to a more different, stable community depending on time and circumstance.

Henry Chandler Cowles One of the founders of ecological concepts of plant communities in the United States was the geologist turned ecologist, Henry C. Cowles, at the University of Chicago [11]. Cowles [28] studied the pattern of ecological succession in a set of sand dunes, the "Indiana Dunes," which are now protected by the State of Indiana's "Indiana Dunes State Park." These dunes were formed sequentially from sediment that was exposed with variation in Lake Michigan. The oldest of the dunes, which is the furthest away from the Lake Michigan beach, has a loamy brown forest soil and is covered by a Beech-Maple (*Fagus-Acer*) forest; the youngest dune at the beach front has windblown sand as a soil and is covered with a patchy beach-grassland. Cowles recognized this entire land pattern represented a chronosequence, with the spatial location of the dunes of different ages representing different stages of successional development. He later [29] produced the now famous phrase that "succession was a variable chasing a variable" – the changes in vegetation chase the changes in the climate. This insight was, and remains, a remarkable concept of vegetation function. What he meant by this was that the rate of change of vegetation succession, the variable, is sufficiently slow that one could expect the climate, the chased variable, to change by the time the succession process was completed.

Cowles was a remarkable and innovative scientist. He was honored in the 1935 issue of *Ecology*, the journal of the Ecological Society of America. The Henry Chandler Cowles issue (*Ecology*, Volume16, Number 3) is a collage of the central issues in plant ecology in its formative years: C.C. Adams, [30] an early researcher of ecological succession and the associated bird communities, along with F.E. Clements, [31] wrote on human ecology and ecology in the public service; Transeau [32] discussed the "Prairie Peninsula," a region of prairie vegetation jutting into a forests in the American Midwest, and emphasized that one must consider past climates as well as present climates to understand vegetation; Fuller [33] and Sears [34] made much the same point looking at paleoecological data; several students and colleagues of Cowles presented data on mature vegetation in different areas.

A.G. Tansley and the Ecosystem Concept The first of the papers in the Cowles issue and different in tone from the rest, was Tansley's now classic 1935 paper on "The use and abuse of vegetational concepts and terms." Tansley [5] discussed the ideas of the American, F.E. Clements, and the amplification of these ideas by the South African, John Phillips. Tansley declared his strong disagreement with three of Phillips' papers in the *Journal of Ecology* [14–16] characterizing ecological communities as "quasi-organisms" whose successional dynamics were analogous to embryological development, "The community is born, grows, matures, reproduces, and carries out various other biotic phenomena: it behaves in a manner similar to an individual, with obvious and natural differences inherent in its wholly divergent and far more complex structure, constitution and functions. It behaves in such a way as to justify the view that not only is it similar to an organism, but that it is a kind of organism . . ." This conceptualization is in keeping with the principle of holism from Aristotle's *Metaphysica* onward and often abbreviated as "the whole is greater than the sum of its parts." Phillips attributed many of his ideas to Jan Smuts' book, *Holism and Evolution* [35] and noted later in writing a eulogy for Clements, [36] that his colleague Smuts was profoundly influenced by the writings of Clements.

Tansley created the ecosystem concept as in contrast to Phillips' and Clements' views. It is significant that in his iconoclastic "ecosystem" definition, he emphasized ecosystems "were of the most various kinds and sizes." In doing so, Tansley basically defined an ecosystem as what systems scientists would nowadays call a *system of definition*: an arbitrary system defined by the specific considerations for a particular application [37]. Tansley's ecosystem definition conforms well to more mathematical, interactive-system concepts in other sciences. His definition includes the intrinsic consideration of scale found in other sciences, particularly physically based sciences.

Tanssley also endorsed the concept of the "polyclimax", the possibility of multiple stable ecosystems following from succession and a logical contrast to the Clements idea of the "monoclimax" as the eventual product of successional processes working in a region. An example of the polyclimax is shown in Fig. 3 for succession after fires in the boreal forests in the vicinity of Fairbanks, Alaska. In this case, the pattern of succession following a wildfire on

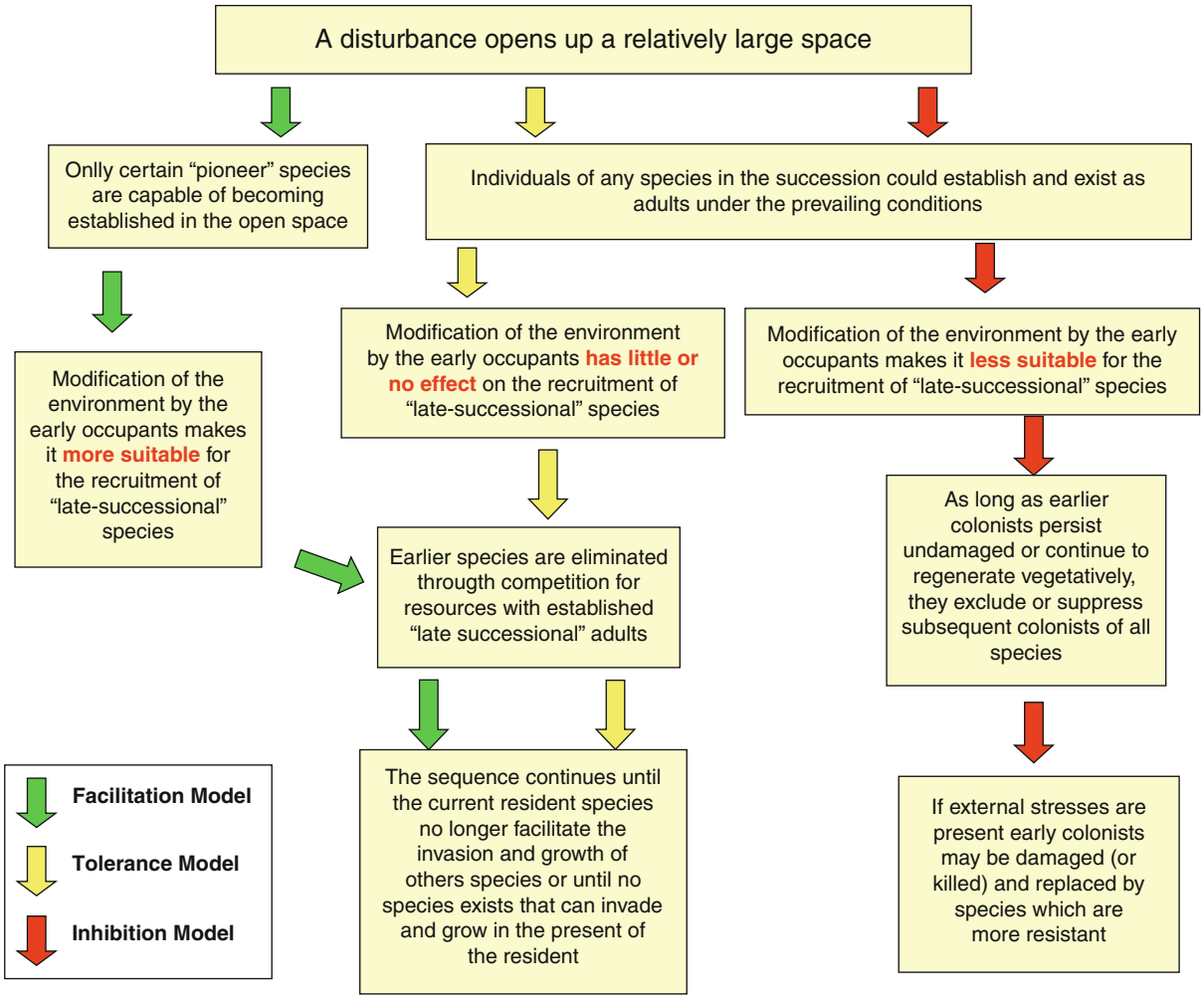

Ecological Succession and Community Dynamics. Figure 3
Three different models of ecological succession from J.H. Connell and R.O. Slatyer [19] depicting succession as arising from the resident species at a location encouraging the colonization of a subsequent set of species (Facilitation Model), by the resident species being relatively neutral to the other species (Tolerance Model), or by the resident species inhibiting the colonization by other species (Inhibition Model)

south-facing slopes eventually leads to a White Spruce (*Picea glauca*) forest that is quite different in its composition and character from the Black Spruce (*Picea marina*) forest seen on north-facing slopes. To some degree, Clements and his colleagues used terms such as disclimax, etc. (see above) to handle these sorts of cases in their monoclimax theory of succession.

A.S. Watt One of Tansley's outstanding students was Alexander Stuart Watt. He developed his doctorate in 1924 on the dynamics of Beech (*Fagus* sp.) forests [38]. He noted the structure of the beech forest was at the scale of the canopy controlled by a dominant large tree best characterized as a cyclical process of the regeneration in the patch of well-lighted area that followed the death of a canopy tree, the growth of these recruits and their competition with one, and the development of a dominate canopy tree in that location. The death of this large tree would then reinitiate the cycle. By 1947, Watt had become the president of the British Ecological Society and delivered one of the most important papers in ecology as his presidential address. This presidential address and the subsequent paper represented a synthesis of what nowadays might be called the "big picture" science view of his doctoral advisor, A.G. Tansley, with Watt's own insights based of his field experience and broad ecological interests. In his address, Watt represented the plant community as a "working mechanism" of interacting plant processes such as regeneration, growth, and death on individual plants producing the broader-scale pattern of plant communities. He stated, "The ultimate parts of the community are the individual plants, but a description of it in terms of the characters of these units and their spatial relations to each other is impractical at the individual level. It is, however feasible in terms of the aggregates of individuals and species which form different kinds of patches: these patches form a mosaic and together constitute the community. Recognition of the patch is fundamental to an understanding of the structure as analyzed here" [39]. To illustrate this communality in the underlying working dynamics of vegetation, he compared a diverse array of plant communities – heathlands, grasslands, bogs, montane vegetation and forests.

As was the case with Gleason, Watt noted that one must account for the results of individual plants interacting with one another, but he also felt such an accounting was "impractical at the individual level." Twenty years later, the explosive expansion of computational power that still continues to date has made such computations more and more feasible. With the development of increasingly powerful digital computers, starting in the 1960s and continuing to the present, several different scientific disciplines (physics, astronomy, ecology) independently began to apply computers to the tasks of "book-keeping" the changes and interactions of individual entities. Forest "gap" models (which will be discussed below) were one of this class of individual-based models or IBM's that brought Watt's insights on vegetation dynamics into a form that could be projected using computer simulation techniques.

Attempts at Synthesis: Connell and Slatyer The persistent dichotomy represented by Clementsian versus Gleasonian views of succession has consistently invited attempts to synthesis toward a unified concept. J.H. Connell and R.O. Slatyer [19] developed a synthesis that emphasized the individual attributes of plants and their feedback with their environment. Clementsian succession was a special case, which they called the "Facilitation Model" (Fig. 4). The replacement patterns in the Connell and Slatyer model were for sets of species, which also implies to some degree a replacement of one community with another, which also is more of a Clementsian concept. Succession was driven by transfers from one set of species as the facilitation model in which succession as arises from the resident species at a location encouraging the colonization of a subsequent set of species, as the tolerance model in which the resident set of species are relatively neutral in their interaction with other species, or as the inhibition model in which the resident species block the colonization by other species (Fig. 4).

Attempts at Synthesis: E.P. Odum Eugene Pleasants Odum was a significant figure in what Robert McIntosh called the rise of ecosystems science. In 1953, he wrote the first modern ecology textbook, [40] which was the standard text for an emerging formulation of ecology as a formal academic discipline. He and his brother H.T. Odum were instrumental in the use of energy transfers in ecosystems (ecological energetics) as

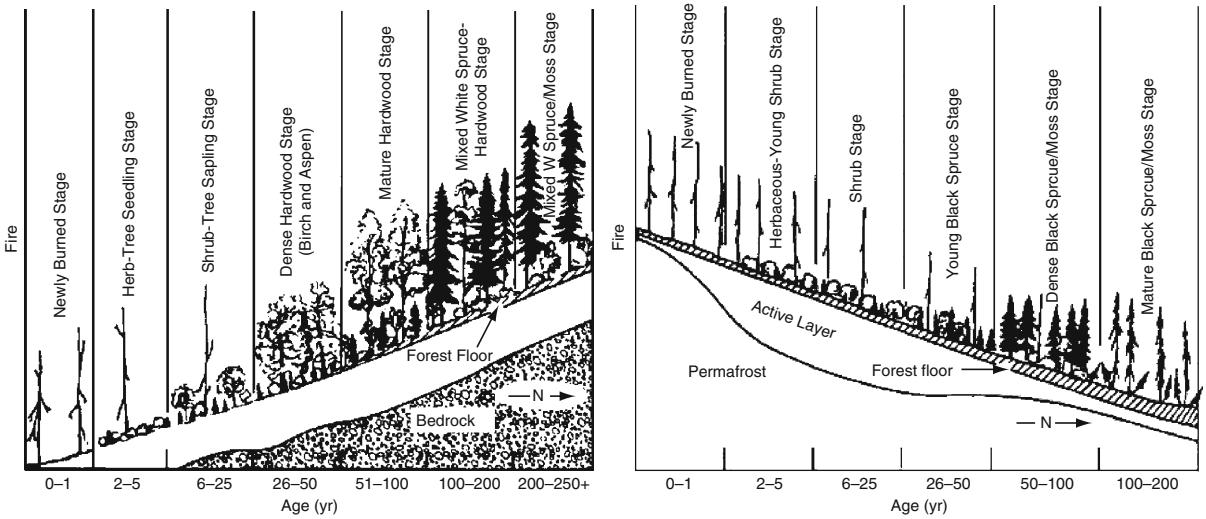

Ecological Succession and Community Dynamics. Figure 4
Ecological succession following wildfires in the vicinity of Fairbanks, Alaska (USA). *Left*. Ecological succession of a south facing slope. *Right*. Ecological succession on a north- facing slope [78]

a common currency for comparing ecosystems with one another. As the sons of a crusading sociologist, H.W. Odum, the two Odum brothers were drawn to include "human ecosystems" in their studies, particularly the energetics of human society and its interactions with the natural ecosystems. The impact of ecological energetics on ecology was profound in that it promoted large-system intercomparisons. The International Biological Programme, the first "big picture" synoptic study of ecosystems used ecological energetics as an organizing principle for projects that compared forests, grasslands, and other biomes, worldwide. These comparisons were often made using "compartment models," diagrams in which the transfers of energy in units of such as $Kcalm^2\ year^{-1}$ were indicated by arrows connecting boxes which expressed the integral of the arrows such as $Kcalm^2$. Compartment models were easily transformed into ordinary differential equations for model projections

Also in the 1950s and 1960s, the United States Atomic Energy Commission (USAEC) sponsored a large program studying the movement of radioactive isotopes in natural environments including whole ecosystem experiments and direct measurements of rates of transfer of isotopes through natural environments [41]. Large, linear compartment models developed in pharmacology [42], and used in ecological energetics were developed to predict the ecological transfer of these materials. There were several advantages to such linear models. They (even for complex linear models) can be solved at equilibrium by algebraic manipulations, an advantage given the modest computational power available in the 1950s and 1960s. When the transfer of material between compartments is a fixed percentage of the amount of material in a source compartment (called donor-controlled flow), linear models have the property that, with a constant input of material into the system, the equilibrium levels of materials are also the maximum amount. Importantly for models of radioisotope transport, radioactive decay of the isotope is a linear, donor-controlled process. Models of this formulation continue today in applications to determine the transfer of radioactive material to human populations from reactors or nuclear accidents such as the Chernobyl event.

In 1969, E.P. Odum wrote "The Strategy of Ecosystem Development," [43] a synthetic paper strongly based on ecological energetics and compartment models in ecosystems. The emphasis of the paper was strongly in the area that nowadays might be termed as sustainability science as is evidences by its first lines, "The principles of ecological succession bear importantly on the relationship between man and nature. The framework of successional theory

needs to be examined as a basis for resolving man's current environmental crisis." Odum's view of succession was summarized as a tabular model of ecological succession (Table 1). It was strongly Clementsian with some of the superorganism emphasis of Phillips added in. It also included a number of ideas that were popular in theoretical and population ecology at the time, such as the idea that biotic diversity in an ecosystem connotes ecosystem stability or the concept that succession was inherently driven to maximize some features (total biomass, biotic diversity, ratios of energy, or material transfers, etc.). These latter considerations can be seen as a logical continuation of Clements' concept that succession was progressive in its direction.

Ecological Succession and Community Dynamics.
Table 1 A "tabular model" of changes expected over ecological succession from E.P. Odum

Ecosystem attributes	Early succession	Late succession
GPP/respiration	> or <1	Approaches 1
GPP/biomass	High	Low
Biomass/energy	Low	High
Net community production (NPP)	High	Low
Food chains	Linear	Web-like
Total organic matter	Small	Large
Inorganic Nutrients	Extrabiotic	Intrabiotic
Species richness	Low	High
Species evenness	Low	High
Biochemical diversity	Low	High
Stratification and pattern	Poorly organized	Well organized
Niche specialization	Broad	Narrow
Size	Small	Large
Life cycles	Short, simple	Long, complex
Mineral cycles	Open	Closed
Nutrient exchange	Rapid	Slow
Role of detritus	Unimportant	Important
Selection on growth form	r-Selection	k-Selection
Selection on production	Quantity	Quality
Symbiosis	Undeveloped	Developed
Nutrient conservation	Poor	Good
Stability	Low	High
Entropy	High	Low
Information content	Low	High

GPP gross primary production (photosynthesis), *NPP* net primary production (GPP minus respiration)
Source: From Odum [40]

Odum's 1969 paper generated and still generates strong interest in the scientific community and continues to be influential these 40 years later. (At this writing in the end of year 2010, the Odum paper has been cited over 1,700 times with no diminution in citation rate.) As one might expect given its essential Clementsian theme updated with central topics in ecosystems ecology, the Odum's paper attracted several negative reviews from the ecologists of a Gleasonian persuasion, particularly given the ascendency of ideas association with Gleason's papers on succession [6]. Nevertheless, Odum's work has had a strong influence on the direction of sustainability science. Its rules on how change should progress toward appropriate natural goals provide guidelines to how ecological systems might be managed toward naturally appropriate goals. Its dogmatism makes it a target for criticism but also gives it an influential position in those wrestling with the difficult problem in a dynamical, strongly human-altered planet.

Sustainability and Vegetation Dynamics

In the historical review above, one finds succession to be a complex concept with different interpretations as to its causes and attributes over time. Ecologists such as F.E. Clements and E.P. Odum viewed succession as a process that drove change in vegetation everywhere. The generality of their application invited the inspection of local examples and the discovery of "exceptions to the rule" that could whittle away at the claimed generality. They also were drawn to applying these principles in understanding human changes on landscapes. Other ecologists such as H.A. Gleason and probably the majority of modern ecologists active in this area of research today developed a much more

diffuse notion of succession. How do these ideas contribute to sustainability sciences and how can they be applied?

Clementsian Succession and Sustainability Science

The importance of succession for sustainability science can be illustrated by two examples: The first is from the historical role of succession theory in land-use policy in the United States; the second involves the incorporation of succession theory into environmental policy. Both examples favor Clementsian successional approaches in application in sustainability science. A following section will discuss the application of more Gleasonian approaches to sustainability science.

Succession and the United States Land-use Policy The importance of succession theory in the land-use policy of the United States is can be illustrated in human connections associated with F.E. Clements. Clements' doctoral advisor at the University of Nebraska was Charles Edwin Bessey, a leading botanist of his era. Bessey came to the University of Nebraska in 1884. He was a leading college administrator; he wrote high school and college textbooks; he served as editor for the journal *Science*. He produced a remarkable set of students: the Pulitzer Prize winning novelist, Willa Cather; Frederic Clements and his wife, Edith; and Roscoe Pound, the leading jurist of his time. Pound and Clements wrote several papers together. Pound went on to the faculty at Harvard University, became Dean of the Harvard Law School, and eventually served as an advisor to President Franklin Roosevelt involved in the structuring of the "New Deal" reformulation of the structure of American government. Among the "New Deal" legislation came administrative structures and regulations for land-use policies, conservation and land protection, soil conservation, and other topics which nowadays would clearly fall in the rubric of sustainability. Pound eventually wrote an obituary/recollection for F.E. Clements [44].

The connections among these remarkable individuals from American heartlands are indicators of a deeper relationship between the ecology of Clements, his associates and students, and land-use policies in the United States. The Great Depression of the 1930s in America was acerbated by a collapse of agriculture in the "Dust Bowl" states through the middle of the nation. A complex combination of persistent land abuse, a climatic anomaly in the form of a drought, and bank collapse accompanying the collapse of family agriculture turned dryland farmers into unemployed refugees. The universities of the Midwest and the emergence of focused studies, such as the "Botanical Seminar" of Bessey at Nebraska (which had collected the Clements, Pound, and other students), had been in part a larger problem of understanding the difficulties in agriculture in the United States as farming moved westward from the forest of the East to the central grasslands [45]. Range management as an agricultural science grew from this tradition and particularly from the work of Clements and his colleagues [46, 47]. Thus, the emerging science of range management developing at the universities at the center of an ecological disaster involving the dynamics of grassland ecosystems produced information and applications on what could and should be done to restore stability. Political and policy advisors, such as Roscoe Pound, were in a position to translate this science and to put into laws concerning the sustainable use of grasslands, rangelands, and other ecosystems – in American and to a degree, worldwide.

Clarity of Clementsian Succession and the Formulation of Policy Environmental policy like most political processes eschews complexity. One of the features of modern is the need for "elevator speeches" – summaries of complex issues that can be delivered to a listening decision-maker in the length of time one might have riding an elevator to a meeting. These and the even shorter snippets of information present to the press convey the idea that good ideas necessarily can be expressed succinctly. Certainly the Principle of Parsimony or "Ockhams Razor" in the sciences, the idea that one should select the hypothesis that makes the fewest additional assumptions when hypotheses are otherwise equal and a founding concept in modern science, lends itself in some interpreters to this point of view. Readers of F.E. Clements works are almost always impressed by the formidable richness of details in his writings, which he produced to support relatively clear general statements as to how succession as a unified process works. E.P. Odum, in some sense an inheritor and elaborator of Clements concepts, wrote using rich analogies to convey simple principles that operate in complex systems.

Clements' and Odum's writings share the ability to convey complexity with simple principles has served to make succession a tangible concept for policy makers and to illustrate the application of these principles. These "ecological generalizations as principles" have been widely used to impress upon the general public an appreciation of a unified ecological view of succession. The seemingly less-focused, special-case orientation of Gleason and subsequent ecologists seems complicated by exceptions. Range management research, which today still has a Clementsian theme and which has been successful in producing widely applied and useful policies for sustainable land management, is a tangible example that this approach can work. It is being challenged with its application in developing nations and in areas with old soils and variable climates but it remains the central paradigm [48].

Even though most modern ecologist would see Gleasonian views of succession as most appropriate, the findings do not always lend themselves to the "elevator-speech" test. One might ask, "What does an application of Gleasonian succession theory in sustainability look like in its application?" The answer is in modern forest and the very root of the origin of the word sustainability. This is the topic of the following section.

Nachhaltigkeit, Sustainability and Modern Forestry

Throughout Europe in Medieval times there was a substantial clearing of forests and extensive regional deforestation [49]. As forests, conflicts over the use products of forests intensified. This eventually produced a class conflict and subsequently laws against poaching of animals, thieving of wood, and proscriptions against public use of forests, in general. In the mid-eighteenth century, a forest management concept called "Nachhaltigkeit" (translated into English as the neologism, "sustainability") was developed by the Germans. From about 1,800, this new forestry practice spread over Europe, particularly Northern Europe. Nachhaltigkeit involved detailed determination of how to best manage forests to produce wood and other goods in perpetuity. In German, the root Nachhaltigkeit alone means nothing more than having a lasting or sustained effect.

Nachhaltigkeit involved detailed determination of how to best manage forests to produce wood and other goods. Essential to this objective was manipulating density by spacing trees on a given site, either by planting trees or by thinning a naturally regenerated stand of trees following a timber harvest or a natural disturbance. Additionally, one needed to determine how long one should wait before harvesting a stand of trees and then planting a new stand. This spacing/length-of-rotation problem had long been solved for crop plants through experimentation and observation. To produce trees as long-lived crops, elaborate long-term data collection started on the height; size in diameter; amount of wood; size of crowns in forest stands of different densities at sites with different environmental conditions. Eventually, a forest modeling concept called the "yield table" approach developed and became the signature of modern forestry. Nowadays, some of the historical forest data-sets used in yield tables have grown to 200+ years of continual record [50].

On a given kind of site (same soils, same rainfall, etc.), trees growing in even-aged, single-species stands (such as forest plantations) tend to grow to the same height at a given age, regardless of density of trees [51, 52]. At low densities, trees have with large diameters and crowns and on an equivalent high-density location, the trees would have small diameters and crowns – but the heights of the trees would be the same in both cases. In a yield table, decades and sometimes centuries of forest stand data are arranged by the height of the trees at a given location reach at a given age, usually the typical age of tree harvest. The tree height at this standard age is called a "site index" and is used to signify the overall quality of a location for growing trees. A site index is the canopy height one would expect a forest to attain in a reference length of time. If, for example, the dominant trees in the canopy of a forest attain a height of 30 m in 50 years (the reference time) then the forest would have a site index of 30. Sites with larger site indices would reach the 30 m height earlier than 50 years; sites with lower site indices would reach 30 m later (if at all). Using yield tables, one can assess the volume of wood in managed stands of equivalent heights on different sites.

Site index is clearly defined in terms of the basic data that goes into a yield table and it can be directly determined by measuring the heights of trees on even-aged

stands at the reference age. Associating site index with actual plots of land is a learned skill and an art at the same time. A capable site surveyor can judge site index by reconnaissance of land in a particular region and can make a good wage practicing this trade. Along with such arcane practices as ax-throwing, log-rolling, and tree-felling, forestry schools have regular intercollegiate competitions of judging site indices among their students as part of "Forestry Field Day" celebrations. At the edge of most universities with a college of forestry, one finds plots of trees planted at different densities for field teaching on the calibration of yield tables. The yield table concept is the quantitative basis of modern forestry.

One significant observation found in yield tables is that the rate of mortality of trees in stands undergoing natural thinning is highest in stands with the highest site indices. Faster growing trees suppress their competitors at a higher rate than slower growing trees on low site-index locations. The trade-off between rapid tree growth versus high mortality on good sites is the basis of the development of thinning strategies for managed stands and for schemes to plant forest plantations at particular spacing of trees. Despite their elevated mortality, sites with high site indices are more productive than low site-index locations.

Nachhaltigkeit was fueled by social unrest. It resulted in laws and regulation based on scientific research and experimentation with inspiration stemming from a shared political necessity to better manage the forests of Europe. Nachhaltigkeit was also the origin of the initial use in English of the word, sustainability. Its development into modern forestry practice was an ongoing process that continues today. Modern forestry is significant in sustainability science as a first real-world application. Modern forestry and its Nachhaltigkeit origins also represent a model of Gleasonian approaches to forest dynamics into sustainability science. It focuses on individual organisms and their relationships with one another and with their environment. One of the significant implications is that quantitative ecology and in particular, ecological models, likely could have a significant role in sustainability science. Individual-based vegetation dynamics models have a logical intellectual inheritance from forestry studies and are an example of tools for the application of Gleasonian successional concepts. These are the topics of the next section.

Individual-Based Models: Computer Descendants of Gleasonian Succession

Currently, several factors are simultaneously arising that challenge the application of successional theory in sustainability science. Climate conditions are changing, perhaps with a greater rate of change than seen in the past [53]. The carbon dioxide composition of the atmosphere has been altered by human activities with potential effects on plant processes particularly photosynthesis and the efficiencies of plant water-use [54]. This issue was addressed several decades ago by foresters who realized that the elaborate calibrations used to develop long-term data on forest change were subject to less accurate predictions if selected genetic strains of trees were used, if forests were fertilized or if there were significant variations in climate.

Impressed by the power of computers and interested in developing a methodology to use highly detailed computer models to simulate the spatial relations among thinning of trees, tree growth, and spatial arrangement of trees, foresters developed individual-based dynamic models of forests (mostly for commercial forests) in the mid-1960s. Their computational innovation was being independently paralleled in other fields, notably astronomy, physics, and several engineering sciences [55, 56]. The early individual-tree-based forest models were quite complex. For example, the competition among individual trees was typically simulated by crown interactions involving the 3-dimensional geometry of each individual tree crown for all the trees in a stand; [57] the growth of the tree trunks of each tree were often simulated at multiple heights; [58, 59] a tree's mortality was related to 2- or 3-dimensional crown pruning among trees [60].

For vegetation dynamics, the earliest individual-based model of forests [57] was developed for Douglas-fir (*Pseudotsuga menziesii*) applications and there were soon several similar models developed as doctoral dissertations at several Schools of Forestry [37]. These early individual-based models of forests were inordinately complex, perhaps because they were applied to tree-spacing problems in even-aged and single-species forests or forest plantations. However, a most detailed early model [61] with multiple tree species, tree interactions based on interacting three-dimensional crown geometry, mapping exact locations of trees, calculating

the dispersion of seed-fall based on seed morphology, etc., exceeds the complexity of almost all of the individual-based models of today.

As noted above, Watt noted that to understand succession one must account for the results of individual plants interacting with one another, but that it is "impractical at the individual level." Twenty years later, the explosive expansion of computational power that still continues to date has made such computations more and more feasible. Early versions of these models in ecology were developed by population ecologists interested in including animal behavior in population models [62–64] and lead to a diverse array of applications for fish, insects, and birds [55]. An advantage of such models is that two implicit assumptions associated with traditional ecological modeling populations are not necessary, namely that:

1. The unique features of individuals (including their size and relative location) are sufficiently unimportant to the degree that individuals are assumed to be identical and
2. The population is "perfectly mixed" so that there are no local spatial interactions of any important magnitude [55].

As Watt noted, most ecologists are interested in variation between individuals (a basis for the theory of evolution and a frequently measured aspect of plants and animals) and appreciate spatial variation as being quite important. Assumption that this variation somehow is uniform seems particularly inappropriate for trees which are sessile and which vary greatly in size over their life span. This may be one of the reasons why tree-based forest models are among the earliest and most widely elaborated of this genre of models in ecology.

In 1972, Botkin and colleagues [65] produced an important simplification of the early forestry work (called the JABOWA model for the initials of its developers) and introduced this modeling approach to ecologists. They did not cite any of the antecedent forestry models and likely were not aware of them. The earlier forestry work remained sub rosa to most ecologists. The forestry models were mostly, but certainly not entirely, in sources not frequently read by forest ecologists. Additionally, some of the forestry models were seen as sufficiently useful that the models drifted into the realm of "industrial secrets" as their developers found employment in the timber industry.

In 1980, a paper reviewing some of this work [66] coined the term, "gap model," to describe this class of models. The gap-model designation was originally developed to emphasize that a principal simplifying assumption in these models (the assumption that the competition among individual trees on a small patch of land was homogeneous in the horizontal over a small area of land but spatially explicit in the vertical dimension) fitted well with the classic "gap dynamics" concept of A.S. Watt [39, 67]. At the time the term gap model was coined, Watt's concept had been significantly reintroduced to American ecologists by Frank Bormann and Gene Likens [68, 69]. A generation of forest ecologists have made numerous extensions of "gap models" and the term, nowadays, refers to a broad class of individual-based models of forests and other ecosystems of a natural character (mixed-age, mixed-species, natural disturbance regimes, etc.).

An Application of an Individual-Based Model on Sustainability of Russian Forests under Climate Change

Global climate model simulations indicate that the Northern Hemisphere's boreal forests and, in particular, the Siberian boreal forest zone, may not only respond to climate change but may affect the Earth's climate through feedbacks involving changes in the regional surface albedo, the degree to which the surface reflects incoming radiation. Bonan and his colleagues [70] altered surface albedo in order to simulate the clearing of the boreal forest in the National Center for Atmospheric Research (NCAR)'s Community Climate System Model version 1.0 (CCSM1). This substantially cooled the Earth not only in the boreal zone but across the Northern Hemisphere. Betts [71] used the Hadley Center Atmosphere Model (HadAM3) to simulate the climatic consequences of albedo changes from growing more trees, worldwide. He found that the surface albedo changes associated with the growth of coniferous evergreen trees in boreal regions led to significant increases in the average global temperature. These increases were large enough to overshadow the effect of the carbon storage that occurred as a result of growing evergreen forest in that region.

Field observations provide further evidence that changes in the boreal forest may impact the global climate. Larch forest, dominated by both *Larix sibirica* and *L. gmelinii*, covers extensive regions in Siberia. Shifts from larch to dark-conifer forests, dominated by trees such as spruce or fir that are tolerant of higher temperatures, have been documented [72, 73]. Because larch is a deciduous conifer, this shift in forest composition would lead to the similar albedo changes as the evergreen tree growth simulation presented by Betts. This reduction of albedo associated with a documented shift in forest type (larch to dark conifer) indicates that warming temperatures may lead to a positive feedback response: a warmer climate accelerates the natural succession from larch to dark-conifer forest; the resultant albedo change promotes additional warming.

Dynamic vegetation models, specifically forest gap models, are ideally suited to an exploration of the impacts that climate change may have on the structure and composition of boreal forests and the existence of a climate/land cover feedback in this region. The FAREAST [74] model was run at a total of 2,083 sites across the former USSR. FAREAST uses monthly climate parameters derived from historical station data to compute daily temperature and update soil water [75]. In particular, at each site, the model's climate inputs are drawn from a statistical distribution of monthly values for minimum and maximum mean temperature and precipitation which is derived from 60 years of data recorded at local weather stations [76]. The model also uses values for soil field capacity and soil carbon and nitrogen [77].

The birth, growth, and eventual death of individual trees are determined in response to local site parameters such as soil moisture and nutrient availability, which are updated annually with bio-environmental conditions, soil moisture, and available nutrients. Individual trees compete for light and nutrients with stochastic processes governing the birth and death of trees in a circular twelfth hectare plot, which approximates the size of a mature tree crown. Forty-four individual tree species are included in FAREAST simulations. These species represent the genera which dominate Northern Eurasian forests. Each species is characterized by 25 parameters which describe the species' fundamental silvics and determine which species has an advantage in terms of competition for light or nutrients, or tolerance to lack of water. At each of the 2,083 sites, 200 independent twelfth hectare plots were simulated and then the modeled biomass values were averaged for each species in each year of the model run.

The overall response of Russian boreal forests to climate change when the effects of changes in temperature and precipitation are separated show higher average precipitation leads to increased biomass (Fig. 5a), lower average precipitation results in decreased biomass (Fig. 5b), and warming causes decreases in biomass for certain regions, though in parts of Siberia, where average temperatures are extremely low, warming induces an increase in forest biomass (Fig. 5c). There are also genera specific patterns in the shifts in biomass that occur across Russia. Specifically, there are different patterns of change for *Larix* spp. and *Pinus* spp. in response to temperature warming. Both genera display a decrease in biomass in western and southwestern Russia and the Russian Far East. The number of sites that experience a biomass decrease for *Larix* spp. is larger than the number of sites that show a decline in *Pinus* spp. In particular, the sites that show a decline in *Larix* spp. extend further northward in both European Russia and the Russian Far East. A more detailed analysis is required to determine whether these patterns are the result of a replacement of *Larix* spp. with *Pinus* spp.

Future Directions

Ecological succession has a complex and controversy rich history. It is significant over this history that the importance of successional knowledge as a prerequisite to the wise management of landscapes has not been a point of issue. The debates in succession are not about its importance. Rather, the debates were and are over how succession works, how it should be understood, and how it can be wisely applied. This is all the more so in the case of sustainability science as a user of successional theory and succession concepts. To sustainably manage the planet, it is an absolute prerequisite to have a capability to predict the dynamic change of the world's vegetation. To the extent that the understanding of succession and vegetation dynamics is not complete, so too will be the state of the understanding of sustainable management.

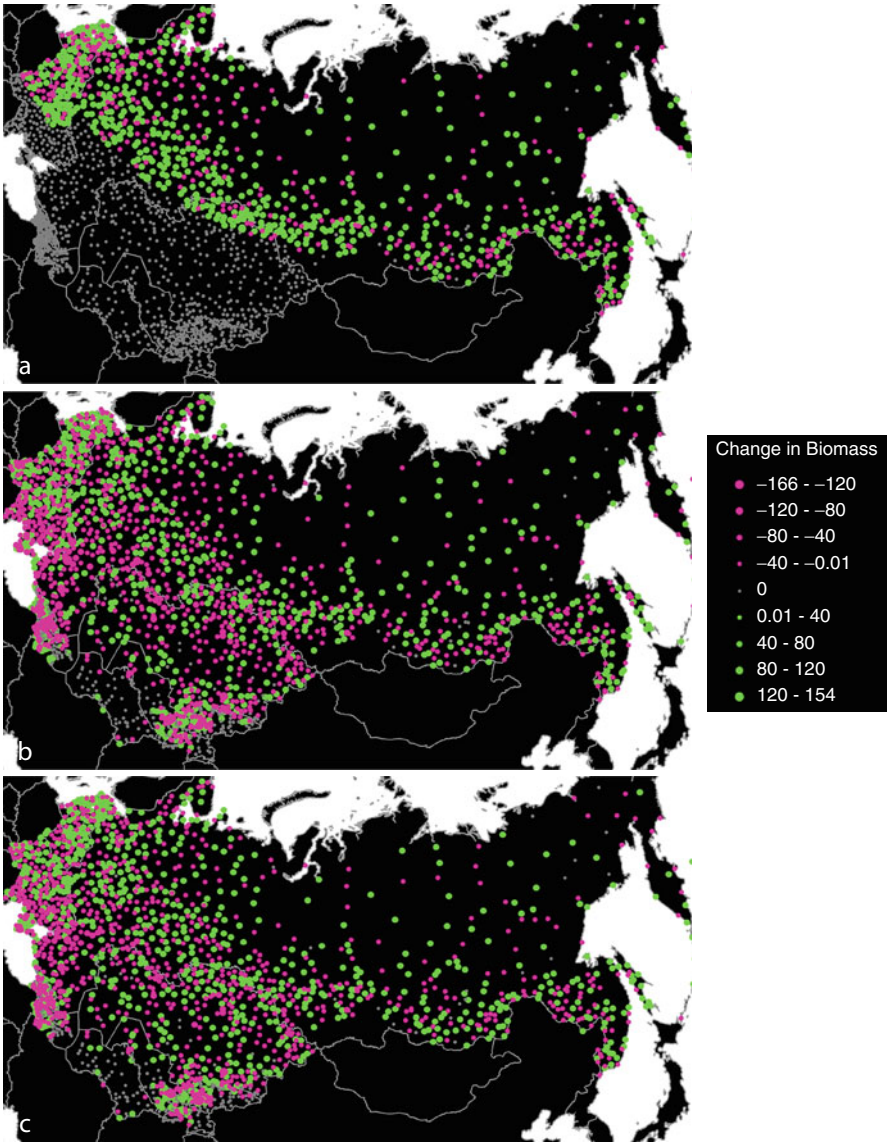

Ecological Succession and Community Dynamics. Figure 5
Decreasing biomass is shown in *pink* and increasing biomass is shown in *green*. Figure shows difference in magnitude of total forest biomass ($tCha^{-1}$) for year 200 between a baseline scenario with no change in climate, and: (**a**) climate scenario with a +10% precipitation showing an overall pattern toward increasing biomass; (**b**) climate scenario of −10% precipitation with pattern is toward decreasing biomass; (**c**) climate scenario with a 2°C increase with decreasing biomass in western and southwestern locations, but an inconsistent response across the region

Ecological models of vegetation dynamics have developed to a great degree over the past several decades. The capability to predict change in vegetation is much more today as it was 50 years ago. At the same time, the novel and large environmental changes that humankind is visiting upon the biosphere (changes in the gasses of the atmosphere, in the diversity of regions, in the local to global climate, etc.) conspire to challenge models to predict outside the range of conditions in which they were developed. Extrapolation is always a difficult endeavor for life scientists.

One would expect sustainability scientists to become more dependent on models when conditions are novel. This novelty conspires to make models potentially less reliable. Sustainability has a word origin in the word, Nachhaltigkeit. That legacy grew into modern forestry with a quantitative capability to predict the future changes of forests under active management. In some senses, however, forestry with its emphasis on single-species, even-aged forest stands has developed the simple case and provided an example of how much effort it takes to develop such the simple case. The task of understanding the complex cases of natural ecosystems in the face of novel conditions is both daunting and essential. The real challenges to sustainability science is the development of meaningful policies and protocols when the essentials, such as succession theory, are themselves changing with new discovery.

Bibliography

Primary Literature

1. Clements FE (1916) Plant succession: an analysis of the development of vegetation. Carnegie Institute, Washington, DC, Publication no 242
2. Clements FE (1928) Plant succession and indicators. Wilson, New York
3. Clements FE (1936) Nature and structure of the climax. J Ecol 24:252–284
4. McCune B, Grace JB, Urban DL (2002) Analysis of ecological communities. MjM Software Design, Gledenon, 304 pp
5. Tansley AG (1935) The use and abuse of vegetational concepts and terms. Ecology 16:284–307
6. Drury WH, Nisbet ICT (1973) Succession. J Arnold Arbor 54:331–368
7. Gleason HA (1926) The individualistic concept of the plant association. Bull Torrey Bot Club 53:1–20
8. Gleason HA (1939) The individualistic concept of the plant association. Am Midl Nat 21:92–110
9. Rich PH (1988) The origin of ecosystems by means of subjective selection. In: Pomeroy LR, Alberts JJ (eds) Concepts of ecosystem ecology. Springer, New York, pp 19–28
10. Egler FE (1954) Vegetation science concepts. I. Initial floristic composition – a factor in old-field vegetation development. Vegetatio 4:412–417
11. McIntosh RP (1985) The background of ecology: concept and theory. Cambridge University Press, Cambridge, 383 pp
12. Tansley AG (1947) Obituary notice. Frederic Edward Clements, 1874–1945. J Ecol 34:194–196
13. White PS (1979) Pattern, process and natural disturbance in vegetation. Bot Rev 45:229–299
14. Phillips J (1934) Succession, development, the climax and the complex organism: an analysis of concepts. I. J Ecol 22:554–571
15. Phillips J (1935) Succession, development, the climax and the complex organism: an analysis of concepts. II. J Ecol 23:210–246
16. Phillips J (1935) Succession, development, the climax and the complex organism: an analysis of concepts. III. J Ecol 23:488–508
17. Heinselman ML (1981) Fire and succession in the conifer forests of northern North America. In: West DC, Shugart HH, West DC (eds) Forest succession: concepts and application. Springer, New York, pp 374–405
18. Cattelino PJ, Noble IR, Slatyer RO, Kessell SR (1979) Predicting the multiple pathways of plant succession. Environ Manage 3:41–50
19. Connell JH, Slatyer RO (1977) Mechanisms of succession in natural communities and their role in community stability and organization. Am Nat 111:1119–1144
20. Glenn-Lewin DC, Peet RK, Veblin TT (eds) (1992) Plant succession: theory and prediction. Chapman and Hall, London
21. Kessell SR, Potter MW (1980) A quantitative succession model for nine Montana forest communities. Environ Manage 4:227–240
22. Weaver JE, Clements FE (1938) Plant ecology, 2nd edn. McGraw-Hill, New York, 520 pp
23. McIntosh RP (1981) Succession and ecological theory. In: West DC, Shugart HH, Botkin DB (eds) Forest succession: concepts and application. Springer, New York, pp 10–23
24. McIntosh RP (1975) H.A. Gleason – "Individualistic ecologist" 1882–1975; His contributions to theoretical ecology. Bull Torrey Bot Club 102:253–273
25. Gleason HA (1910) The vegetation of the inland sand deposits of Illinois. Bull Illinois State Lab Nat Hist 9:21–174
26. Gleason HA (1927) Further views on the succession concept. Ecology 8:299–326
27. Gleason HA (1917) The structure and development of the plant succession. Bull Torrey Bot Club 44:463–481
28. Cowles HC (1899) The ecological relations of the vegetation on the sand dunes of Lake Michigan. Bot Gaz 27:95–117, 176–202, 281–308, 361–369
29. Cowles HC (1901) The physiographic ecology of Chicago and vicinity. Bot Gaz 31:73–108
30. Adams CC (1935) The relation of general ecology to human ecology. Ecology 16:316–335
31. Clements FE (1935) Experimental ecology in the public service. Ecology 16:342–363
32. Transeau EN (1935) The prairie peninsula. Ecology 16:423–437
33. Fuller GD (1935) Postglacial vegetation of the Lake Michigan region. Ecology 16:473–487
34. Sears PB (1935) Types of North American pollen profiles. Ecology 16:488–499

35. Smuts JC (1926) Holism and evolution. Macmillan, London
36. Phillips J (1955) A tribute to Frederic E. Clements and his concepts in ecology. Ecology 35:114–115
37. Shugart HH (1998) Terrestrial ecosystems in changing environments. Cambridge University Press, Cambridge, 537 pp
38. Watt AS (1925) On the ecology of British beech woods with special reference to their regeneration. II. The development and structure of beech communities on the Sussex Downs. J Ecol 13:27–73
39. Watt AS (1947) Pattern and process in the plant community. J Ecol 35:1–22
40. Odum EP (1953) Fundamentals of ecology. W. B. Saunders, Philadelphia, 383 pp
41. Jordan CF (1986) Ecological effects of nuclear radiation. In: Orians GH (ed) Ecological knowledge and environmental problem solving: concepts and case studies. National Academy Press, Washington, DC, pp 331–344
42. Zilversmit DB, Entenmann C, Fishler MC (1943) On the calculation of turnover time and turnover rate from experiments involving the use of labeling agents. J Gen Physiol 26:325–331
43. Odum EP (1969) The strategy of ecosystem development. Science 164:262–270
44. Pound R (1954) Frederic E. Clements as I knew him. Ecology 35:112–113
45. Arthur JC (1895) Development of vegetable physiology. Science 44:164–184
46. Tobey R (1976) Theoretical science and technology in American ecology. Technol Cult 17:461–534
47. Tobey R (1981) Saving the prairies: the life cycle of the founding school of American plant ecology 1895–1955. University of California Press, Berkley
48. Washington-Allen RA, West NE, Douglas Ramsey R, Phillips DK, Shugart HH (2010) Retrospective assessment of soil stability on a landscape subject to commercial grazing. Environ Monit Assess 160:101–121
49. Williams E (2003) Deforesting the earth: from prehistory to global crisis. University of Chicago Press, Chicago, 689 pp
50. Pretzsch H (2009) Forest dynamics, yield and growth: from measurement to model. Springer, Berlin
51. Kimmins JP (1987) Forest ecology. Macmillan, Vancouver
52. Kira T (2001) Forest and environment: an approach to global environmental issues. Shin-Shisosha, Tokyo
53. Solomon S, Qin D, Manning M, Chen Z, Marquis M, Averyt KB, Tignor M, Miller HL (eds) (2007) Climate change 2007: the physical science basis. Contribution of working group I to the fourth assessment report of the intergovernmental panel on climate change. Cambridge University Press, Cambridge, UK/New York, 996 pp
54. Shugart HH, Woodward FI (2011) Global change and the terrestrial biosphere: achievements and challenges. Wiley-Blackwell, Oxford, 216 pp
55. Huston M, DeAngelis DL, Post WM (1988) New computer models unify ecological theory. Bioscience 38:682–691
56. DeAngelis DL, Gross LJ (eds) (1992) Individual-based models and approaches in ecology: populations, communities and ecosystems. Chapman and Hall, New York
57. Newnham RM (1964) The development of a stand model for Douglas-Fir. PhD thesis, University of British Columbia, Vancouver
58. Mitchell KJ (1969) Simulation of growth of even-aged stands of white spruce. Yale Univ Sch Forest Bull 75:1–48
59. Mitchell KJ (1975) Dynamics and simulated yield of Douglas-fir. Forest Sci Monogr 17:1–39
60. Hegyi F (1974) A simulation model for managing jack-pine stands. In: Fries J (ed) Growth models for tree and stand simulation. Royal College of Forestry, Stockholm, pp 74–90
61. Ek AR, Monserud RA (1974) FOREST: computer model for the growth and reproduction simulation for mixed species forest stands. Research report A2635, College of Agricultural and Life Sciences, University of Wisconsin, Madison
62. Holling CS (1961) Principles of insect predation. Annu Rev Entomol 6:163–182
63. Holling CS (1964) The analysis of complex population processes. Can Entomol 96:335–347
64. Rohlf FJ, Davenport D (1969) Simulation of simple models of animal behavior with a digital computer. J Theor Biol 23:400–424
65. Botkin DB, Janak JF, Wallis JR (1972) Some ecological consequences of a computer model of forest growth. J Ecol 60:849–872
66. Shugart HH, West DC (1980) Forest succession models. Bioscience 30:308–313
67. Watt AS (1925) On the ecology of British beech woods with special reference to their regeneration. II. The development and structure of beech communities on the Sussex Downs. J Ecol 13:27–73
68. Bormann FH, Likens GE (1979) Pattern and process in a forested ecosystem. Springer, New York
69. Bormann FH, Likens GE (1979) Catastrophic disturbance and the steady state in northern hardwood forests. Am Sci 67:660–669
70. Bonan GB, Pollard D, Thompson SL (1992) Effects of boreal forest vegetation on global climate. Nature 359:716–718
71. Betts RA (2000) Offset of the potential carbon sink from boreal forestation by decreases in surface albedo. Nature 408:187–190
72. Kharuk V, Ranson K, Dvinskaya M (2007) Evidence of evergreen conifer invasion into larch dominated forests during recent decades in Central Siberia. Eurasian J Forest Res 10: 163–171
73. Kharuk VI, Ranson KJ, Sergey TI, Dvinskaya ML (2009) Response of *Pinus sibirica* and *Larix sibirica* to climate change in southern Siberian alpine forest-tundra ecotone. Scand J Forest Res 24:130–139
74. Yan X, Shugart HH (2005) A forest gap model to simulate dynamics and patterns of Eastern Eurasian forests. J Biogeogr 32:1641–1658

75. Shuman JK, Shugart HH (2009) Evaluating sensitivity of Eurasian forest biomass to climate change using a dynamic vegetation model. Environ Res Lett 4:045024. doi:10.1088/1748-9326/4/4/045024
76. National Climate Data Center (NCDC) (2005) TD-9813 daily and sub-daily precipitation for the former USSR Version 1.0. NOAA National Climatic Data Center, Asheville
77. Stolbovoi V, McCallum I (eds) (2002) CD-ROM land resources of Russia. International Institute for Applied Systems Analysis and the Russian Academy of Science, Laxenburg
78. Van Cleve K, Viereck LA (1981) Forest succession in relation to nutrient cycling in the boreal forest of Alaska. In: West DC, Shugart HH, Botkin DB (eds) Forest succession: concepts and application. Springer, New York, pp 185–221

Ecological Systems, Introduction

Rik Leemans
Environmental Systems Analysis Group, Wageningen University, Wageningen, The Netherlands

It is estimated that there are roughly 8 million animal species, 600,000 fungi, 300,000 plants, and an unestimated number of microbial species on earth. It is further estimated that only about 25% of the animal, fungi, and plant species have been identified as yet. Further, the interactions among these species and their physical environment are known to an even lesser degree. Meanwhile, the earth's biota faces the prospect of climate change which may be either slow to manifest or extremely rapid, as we pass through a potential tipping point. In addition, human population is set to grow by two billion by 2045 from a present seven billion. This would certainly be rated as a population explosion, and these numbers together with expected (and hoped for) economic growth will stress the entire ecology of the earth. The question is how to cope with all of the above. That is actually the subject and goal of this entire *Encyclopedia* and our team of well over 700 scientists and engineers, and also the subject of this section from an ecological systems viewpoint. Our objective in this section is to provide a significant portion of the scientific and engineering basis of the systems ecology of the earth and to provide this in 14 detailed entries written at a level for use by university students through practicing professionals. Our approach is to recognize that we cannot wait for a complete data set for the biota before assessing and planning and acting to preserve the ecological balance of the earth. Therefore, methodology is presented aimed at identifying the key interactions and environmental effects and enabling a systems level understanding even at our present state of factual knowledge.

For, ease of use by students, each entry begins with a glossary of terms, while at an average length of 20 print pages each, sufficient detail is presented for utilization by professionals in government, universities, and industry. The reader is also directed to the closely related sections: ► Earth System Monitoring, Introduction and also ► Transport and Fate of Chemicals in the Environment, Introduction.

Each of the entries is summarized below.

► Ecosystems, Adaptive Management – Adaptive management is an approach to natural resource management that emphasizes learning through management based upon the philosophy that knowledge is incomplete and much of what is thought to be known is actually wrong, but despite uncertainty managers and policymakers must act. This entry includes: Structure Decision Making, Participatory Active Adaptive Management, Adaptive Governance, and Adaptive Management and Law.

► Marine Biogeochemistry – The biogeochemistry of the world oceans has been studied for many decades, and major advances in understanding have been linked with development of new techniques and tools that allow the accurate representation of various organic and inorganic pools within the water. It has been shown that some critical bioactive compounds (containing the elements: carbon, nitrogen, phosphorus, oxygen) occur with particular atomic ratios to one another that are relatively invariant over space and time pools. The following cycles are presented in detail: carbon ocean Acidification, nitrogen and phosphorous, iron (including iron ocean fertilization), sulfur, and oxygen.

► Atmospheric Biogeochemistry – Biogeochemistry represents the interaction of biology, chemistry, and geology in the Earth system. For many processes, an understanding of biological uptake and emission, chemical processing, and geological sequestration is necessary to resolve the sources and sinks of a particular constituent. For example to discover the

sources and sinks of atmospheric carbon dioxide, it is important to understand how biota take up carbon dioxide and chemically convert the carbon to organic carbon, and then how this organic carbon is used either to produce energy by biota or is deposited to the land or ocean surface and can become sequestered in geological formations. Often when biogeochemistry is referred to, one refers to the nutrient cycling of important nutrients. Atmospheric biogeochemistry, as defined in its narrowest sense, is the flux of nutrients and pollutants important for biogeochemistry through the atmosphere. In its broadest sense, atmospheric biogeochemistry is the interaction of the atmosphere and atmospheric processes with the biogeochemistry of the earth system. This broader definition is used here.

► Ecological Succession and Community Dynamics – Ecological succession and the dynamic change of communities is one of the pillars of modern ecology and it has considerable influence on sustainability science. The processes that drive succession and the regularly of patterns of succession have been the topic of considerable debate over the past century – due in no small part to the importance of the concept to basic and applied ecology. Succession is at its simplest level the pattern of change in ecological communities and these changes can be read on the landscape if one knows regional history or conversely can be used to interpret a landscape's history.

► Ecosystem Engineers, Keystone Species – This contribution focuses on two ecological phenomena. The first is "keystone species" which is defined as a species (mostly of high trophic status) whose activities exert a disproportionate influence on the patterns of species occurrence, distribution, and density in a community. The second is the concept of "ecosystem engineers" defined as organisms that directly or indirectly modulate the availability of resources (other than themselves) to other species by causing physical state changes in biotic or abiotic materials. Models have shown that the loss of species with a large number of trophic interactions can trigger high numbers of secondary extinctions with serious consequences for species persistence. The importance of keystone species can also be strongly linked with ecosystem engineering. For example, the large impact of sea otters in kelp forest ecosystems results from the coupling between engineering effects and a trophic cascade.

► Ecosystem Services – This entry provides an overview of issues concerning the identification, biophysical and economic characterization, and safeguarding of ecosystem services. The concept of ecosystem services has a long written history, reaching back at least as far as Plato. This review history focuses on recent advances such as the Millennium Ecosystem Assessment, and advances in spatial modeling, economic valuation, and policy implementation. Examples of novel finance and policy mechanisms, including water funds, marine spatial planning, land-use planning and human development, and global policy efforts are presented. The entry concludes with a discussion of the largest research and implementation challenges in this field, identifying the issues that will frame the future growth of the concept of ecosystem services.

► Ecosystems and Spatial patterns – Ecological processes such as forest disturbances act on ecosystems at multiple spatial and temporal scales to generate complex spatial patterns. These patterns in turn influence ecosystem dynamics and have important consequences for ecosystem sustainability. Analysis of ecosystem spatial structure is a first step toward understanding these dynamics and the uncertain interactions among processes. Quantitative characterization of spatial patterns and their rates of change in natural environments are essential to understanding ecological processes and to inform sustainable management techniques that aim to minimize degradation and alteration of ecosystem dynamics. This entry covers: sources of heterogeneity, spatial analysis, spatial analyses within the ecosystem and spatial analyses among ecosystems.

► Ecosystem Flow Analysis – It is necessary to understand the ecosystem as a thermodynamic system and how the energy flows enter, interconnect, and disperse from the environmental system. Ecological network methodologies exist to investigate and analyze these flows. In particular, partitioning the flow into boundary input, non-cycled internal flow, and cycled internal flow shows the extent to which reuse and recycling arise in ecosystems. The intricate, complex network structures are responsible for these processes all within the given thermodynamic constraints. Design of sustainable human systems could be informed by these organizational patterns, in order to use effectively the energy available. This entry

demonstrates the need for flow analysis, provides a brief example using a well-studied ecosystem, and discusses some of the ecosystem development tendencies which can be addressed using ecosystem flow analysis.

► Ecotones and Ecological Gradients – Ecotones are areas of steep transition between ecological communities, ecosystems, or ecological regions (such as Mediterranean and desert). Ecotones often occur along ecological gradients. Such gradients are created as a result of spatial shifts in elevation, climate, soil, and many other environmental factors. Ecotones commonly coincide with areas of sharp climatic transition along environmental gradients. They occur at multiple spatial scales, from continental-scale transitions between major biomes to small-scale ecotones where local vegetation communities and microhabitats coincide. They show a diversity of boundary types that range from natural boundaries (e.g., altitudinal, latitudinal transitions) to human-generated ecotones (e.g., forest clear-cut edges or urban ecotones). Ecotones have been studied in the past four decades in an ecological context and in recent years are receiving increasing attention in the context of biodiversity conservation. Various studies have shown that species richness and abundances tend to peak in ecotonal areas, though exceptions to these patterns occur. Ecotones are "natural laboratories" for studying a range of evolutionary processes, such as the process by which new species form, also termed speciation. Recent evidence suggests that ecotones may serve as speciation centers. Some researchers argue that ecotones deserve high conservation investment, potentially serving as speciation and biodiversity centers. Because ecotones are often small in size and relatively rich in biodiversity, conservation efforts in these areas may prove to be an efficient and cost-effective conservation strategy.

► Invasive Species – This entry describes the causes and consequences of biological invasions, by synthesizing concepts from population biology, community ecology, evolution, biogeography, and conservation biology. First, the patterns and process of invasion are explored; then, some of its potential ecological and socioeconomic impacts are examined. Some major hypotheses and theoretical concepts explaining patterns of colonization and impact are presented. Next, management approaches to assessing, preventing, and mitigating this problem are considered. The entry ends with a brief glimpse at some of the emerging issues that will likely be the foci of future research.

► Landscape Ecology – Landscapes are spatially heterogeneous areas characterized by diverse patches that differ in size, shape, contents, and history. When spatial heterogeneity is considered, scale matters and hierarchy emerges. Landscape ecology is the science and art of studying and improving the relationship between spatial pattern and ecological processes on a multitude of scales and organizational levels. In a broad sense, landscape ecology represents both a field of study and a scientific paradigm. As a highly interdisciplinary and transdisciplinary enterprise, landscape ecology integrates biophysical and analytical approaches with humanistic and holistic perspectives across natural and social sciences. Landscape ecology was initially developed in Europe. With theoretical developments in spatial ecology and technological advances in remote sensing and geospatial information processing, landscape ecology became an internationally recognized field of study in the 1980s. The most salient characteristics of landscape ecology are its emphasis on the pattern-process relationship and its focus on broad-scale ecological and environmental issues. Key research topics in landscape ecology include ecological flows in landscape mosaics, land use and land cover change, scaling, relating landscape pattern analysis with ecological processes, and landscape conservation and sustainability.

► Species Competition and Predation – Competition and predation are key interactions between species, and are major foci of thought and study in community ecology. They are believed to be major forces structuring natural communities, having critical roles in the determination of species diversity and species composition, and are regarded as important drivers of evolutionary processes. The relationships between the niches of different species determine how they interact through competition and predation, which then have key roles in assembly of local communities, and their reassembly following perturbations. Niches define patterns of linkages between species, their resources, and their natural enemies. These patterns include how linkages change over time, and between different spatial locations, and define

mechanisms by which similar species are able to coexist by their effects on competition and predation relationships. The human element in the environment has profound effects on these phenomena. Changing the environment shifts interactions between species, and profoundly modifies the structure of food webs. In the modern day, there is much community reassembly, potentially involving major shifts in competition and predation. Humans transport invasive species that act as predators, prey, and competitors with potentially major effects on the community reassembly process.

► Species Diversity Within and Among Ecosystems – Species diversity is a function of species richness, the number of species in a given locality and species evenness, the degree to which the relative abundances of species are similar. Commonly used quantification methods include constructing mathematical indices known as diversity indexes (the Shannon, Simpson, and Margalef indexes being the most widely used) or comparing observed patterns of species abundance to theoretical models. The scale of assessment may range from within a single site or habitat (known as α diversity) to the difference between two or more sites (β diversity); which can then be combined to give γ diversity – the diversity of the landscape. Early research tended to be concentrated on largely α diversity, but there has been a marked increase in studies investigating β and γ diversity during the last decade. The species richness aspect of diversity is often considered the iconic measure of biodiversity since it is well defined and aligns with our intuitive sense of the concept. As the species level is the level at which living organisms are most widely known, species have become the major taxonomic rank for describing biodiversity. Along with populations, it is also the level that most scientists, managers, and policy makers use when referring to biological diversity and it provides a useful means for both monitoring and priority setting. As the species level is one of three fundamental levels of biodiversity (the others are the genetic level and the ecosystem/community level), species diversity is thus an important component of conservation.

► Urban Ecology – Within the science of ecology, urban ecology is defined as the study of structure, dynamics, and processes in urban ecological systems. Urban ecology is the study of the relationships of human and nonhuman organisms in urban areas, the interactions of these organisms with the native and built physical environment, and the effects of these relationships on the fluxes of energy, materials, and information within individual urban systems and between urban and nonurban systems. Urban ecology applies the methods and concepts of the biological science of ecology to urban areas, but requires and integrates with the concerns, concepts, and approaches of social sciences to produce a hybrid discipline. Urban ecological systems include individual organisms, populations, communities, and landscapes, as well as buildings and infrastructure. Urban ecology further recognizes specific urban ecosystems as a part of the global biogeochemical, economic, and human demographic system.

Ecosystem Engineers, Keystone Species

Sanne de Visser[1], Elisa Thébault[2], Peter C. de Ruiter[3]
[1]Community and Conservation Ecology group, University of Groningen, Groningen, The Netherlands
[2]CNRS, UMR 7618 "Biogéochimie et écologie des milieux continentaux", Paris, France
[3]Biometris, Wageningen UR, Wageningen, The Netherlands

Article Outline

Glossary
Definition of the Subject
Introduction: Keystone Species and Ecosystem Engineers: Analysis of Concepts
Issue-1: How to Find Keystone Species and Ecosystem Engineers in Communities?
Issue-2: Usefulness for Management
Future Directions
Bibliography

Glossary

Connectance The proportion of possible ecological interaction links between species that are realized.

Ecosystem engineer An organism that creates or modifies its habitat [19].

Ecosystem functioning The way ecosystems work related to abiotic and biotic components, such as chemicals, water, soil, microbes, plants, and animals.

Keystone species A species that has a disproportionate effect on its environment relative to its biomass (Paine 1995).

Trophic level The position a species occupies in a food chain.

Definition of the Subject

This entry focuses on two ecological phenomena. The first is "keystone species" which is defined by Paine [1] as a species (mostly of high trophic status) whose activities exert a disproportionate influence on the patterns of species occurrence, distribution, and density in a community. The second is the concept of "ecosystem engineers" defined by Jones et al. [2] as organisms that directly or indirectly modulate the availability of resources (other than themselves) to other species by causing physical state changes in biotic or abiotic materials.

Introduction: Keystone Species and Ecosystem Engineers: Analysis of Concepts

Paine's definition of keystone species was inspired from the large effects of the removal of the carnivorous starfish (*Pisaster ochraceus*) from intertidal habitat, which reduced prey species diversity due to intense competition from mussel prey [3], and represents now a classic textbook in ecology. The original keystone species concept of Paine [1, 4] thus identified a very specific mechanism: the top-down regulation of community structure and diversity by a top predator (Fig. 1). The concept of keystone species has been later extended to a broader definition and now includes any species whose effect on ecosystems is disproportionately large relative to its low biomass in the community as a whole [5]. Keystone species are thus species which have large effects on communities and ecosystems through many different processes such as trophic interactions, pollination, or habitat modification [6, 7]. Examples include rabbits that can increase abundance and diversity of lizards [8] and sea otters whose hunting in the late nineteenth century caused a population explosion of their sea urchin prey and consequent overgrazing of kelp which led to numerous extinctions of local species [6].

The concept of ecosystem engineering was proposed two decades later than the "keystone species" concept by Jones and colleagues [2]. They defined ecosystem engineers as "organisms that directly or indirectly modulate the availability of resources

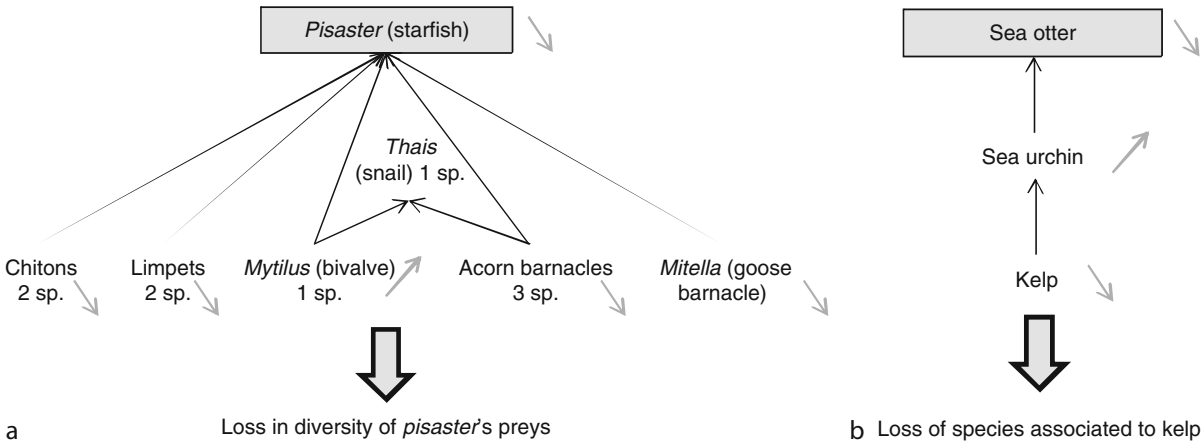

Ecosystem Engineers, Keystone Species. Figure 1
Two examples of keystone species impacts. (**a**) Effects of the removal of *Pisaster* on prey species diversity as a consequence of mussel population explosion. (**b**) Consequences of the removal of sea otters on species diversity due to overgrazing of kelp by sea urchins. Keystone species are represented in *grey boxes*. Small *grey arrows* indicate the direction of species abundance changes following the removal of the keystone species. The large *grey arrows* indicate the global consequences of keystone species loss on the ecosystem

(other than themselves) to other species by causing physical state changes in biotic or abiotic materials. In so doing they modify, maintain and/or create habitats" [2]. They further distinguish between two types of ecosystem engineers (Fig. 2): autogenic engineers that change the environment via their own physical structures, i.e., their living and dead tissues, and allogenic engineers that change the environment by transforming living or nonliving materials from one physical state to another via mechanical or other means. The idea that organisms can have important effects on abiotic processes occurring in the environment had been recognized before; indeed, Darwin devoted a whole book to the impact of earthworms on soil formation [9]. However, since the development of the concept of ecosystem engineer, engineering effects have been described for many organisms, from classic examples such as beavers, termites, or earthworms [10–12] to mollusks [13], fish [14], caterpillars [15], polychaete worms [16], grasses [17, 18], burrowing shrimp [19], ants [20], and many other species (see Table 1 of [21]).

Both the keystone species and the ecosystem engineer concepts point out to species which have important effects in ecological communities and ecosystems. Although these concepts partly overlap – an ecosystem engineer can be a keystone species – they however insist on different aspects: the keystone concept focuses on species which have disproportionate effects on community structure and ecosystem functioning ("outcome focused" sensu [22]) whereas the ecosystem engineering concept considers organisms which influence the abiotic environment with consequences on other species and related ecosystem processes ("process focused" sensu [22]). These differences between the two concepts are reflected in the literature: these concepts generally appear in distinct studies as less than 5% of the studies on these topics refer to both ecosystem engineers and keystone species (source: ISI Web of Science).

The keystone species concept has been strongly related to food web theory since its first definition [1, 23]. In particular, the identification of keystone species in food webs is an important issue. Theoretical studies have tried to pin down the characteristics of keystone species through food web models [24, 25] and several indices based on food web topology have been developed to identify keystones [26]. Models have

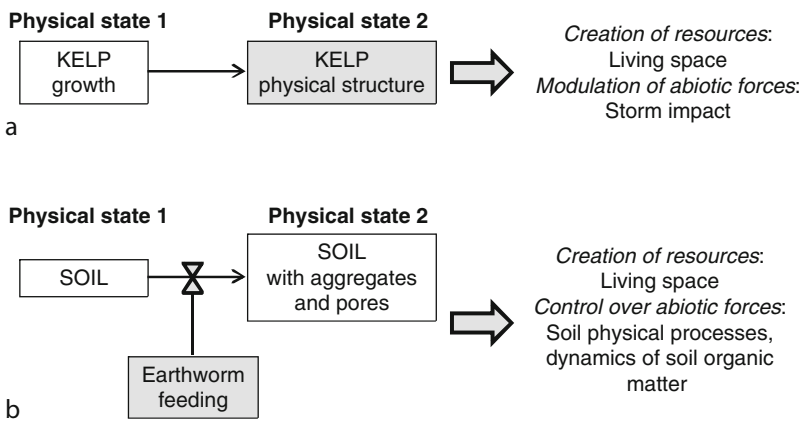

Ecosystem Engineers, Keystone Species. Figure 2
Two examples of ecosystem engineering with kelp (**a**) and earthworms (**b**) as ecosystem engineers. Ecosystem engineering corresponds to changes in physical state (state 1–2) of biotic (i.e., kelp for **a**) or abiotic (i.e., soil for **b**) materials. Ecosystem engineers are represented in *grey boxes*. (**a**) Case of autogenic engineering, the engineer is part of the new physical state (via growth here). (**b**) Case of allogenic engineering, the new physical state is caused by the engineer (⧖, caused via feeding here), but the engineer is not part of the new physical state

shown that the loss of species with a large number of trophic interactions can trigger high numbers of secondary extinctions with serious consequences for species persistence; a result which highlights the potential keystone role of highly connected species in food webs [24, 27, 28].

In contrast, the concept of ecosystem engineering has been rarely related to food web studies. Recent studies acknowledge that ecosystem engineers may also play an important role in the network of trophic interactions but separating the trophic effects from the engineering effects to determine their relative importance is difficult [20, 29–31].

The importance of keystone species can also be strongly linked with ecosystem engineering. For example, the large impact of sea otters in kelp forest ecosystems results from the coupling between engineering effects and a trophic cascade [32]. In these ecosystems, kelp provides habitat for many species and dampens wave action; the keystone effect of sea otters is thus mediated through their indirect trophic effect on kelp densities which is a main ecosystem engineer.

Issue-1: How to Find Keystone Species and Ecosystem Engineers in Communities?

Keystone species and ecosystem engineers may affect ecosystem processes, such as nutrient cycling, and thereby ecosystem functioning. In the face of rapid biodiversity loss, a considerable amount of studies were dedicated to investigate a possible link between species richness and ecosystem function [33] and the threat of diversity loss on the loss of ecosystem services to man. First indications show positive relationships between species richness and ecosystem productivity, stability, and sustainability, with more species being able to fully and complementarily run ecosystem functions due to niche differentiation and facilitative interactions (reviewed by [34]). However, there is now a growing consensus that functional diversity, rather than species numbers per se, strongly determines ecosystem functioning [35]. This means that the presence of a particular species with specific traits may play a larger role in determining ecosystem function than merely the number of species [36]. The apparent diversity-ecosystem function relationship can thus be partly caused by a greater chance of an influential species with particular traits being present in more diverse communities than in species-poor communities.

If it is possible to predict and identify a priori a set of species traits that determine keystone interactions in a system, this would greatly benefit management and conservation purposes. Species' traits determine how species contribute to ecosystem processes, so the presence and distribution of such traits can be utilized to indicate aspects of ecosystem functioning [37]. To identify keystone species various methods have been used ranging from experimental removal or addition manipulations to comparative studies and natural history observations [5]. Partly because of these methodological issues, identifying keystone species has so far proved elusive [5, 38] although some progress has been made and its concept now widely investigated in the context of complex ecological networks [25, 39–41]. Some examples of specific traits are for instance trophic level, body size, connectance, or traits concerning tolerance and resilience to disturbances. Organisms that influence their environment strongly and contribute disproportionately to the functioning of ecosystems often seem to occupy higher trophic levels in food webs [5]. Top predators have been described as highly interactive keystone species [42], have been shown to play an important role in stabilizing food webs [43], and play important roles in marine ecosystems [44] and terrestrial ecosystems [45].

Also, the loss of top predators has been linked to secondary extinctions [46, 47]. This has been attributed to their ecological role as suppressors of medium-sized predators (mesopredators) (e.g., [48, 49]) and generalist herbivores [50, 51]. In terrestrial ecosystems, organisms that influence their environment strongly also often seem to be large bodied (e.g., [52]). Larger bodied organisms require a high resource and energy use per individual [53, 54] and have greater mobility, home ranges, and longevity [55, 56] and, thereby, control more resources over greater and coarser spatial scales [52, 57]. It is also proposed that well-linked and interacting species as key interactors are more important for the community [28, 58–62]. This approach characterizes the interaction structure of species placed in an ecological network. Among plants, on the other hand, some studies have shown that species within the same functional types but with different requirements

and tolerances may provide insurance to the system in the form of long-term resilience against changes in environmental factors, such as global warming, grazing, drought or frost [35].

The latter example indicates that the keystone status of a species often appears to be context dependent, and may change with successional status, productivity, diversity, and other ecosystem traits [63]. It is therefore important to identify how the importance of traits that define keystone species change across a gradient of conditions, measuring environmental factors, community composition, trophic dynamics, and distribution of strong and weak links in the community (e.g., [24]). Without droughts, a specific plant species may not play an important role in maintaining community composition or ecosystem functioning. The Australian brushtail possum (*Trichosurus vulpecula*) may function as a keystone species in rata-kamahi forests by defoliating and killing canopy trees, but not in beech-dominated forests where floristic composition, but not forest structure, is typically affected [64–66]. A species in its native grounds may play no specific role in the system, whereas an invasive species may have devastating effects in the system it got introduced into, e.g., feral cats and rats on islands [67], Alewife (*Alosa pseudoharengus*) in nonnative freshwater lakes and ponds [68], and Cheatgrass (*Bromus tectorum*) in nonnative grasslands [69].

Identifying keystone species therefore is not without its problems. It is also important to notice that ecologically important species might not necessarily be the ones that are also considered important by traditional conservationists (i.e., rare species; [70]).

Issue-2: Usefulness for Management

Because of the limited resources available in comparison to conservation needs, it has been proposed to design protection of single species in the aim of indirectly protecting the regional biota. These "surrogate species" are roughly of three categories [71]: (1) flagships, charismatic species that attract public support; (2) umbrellas, species requiring such habitats that their protection might protect other species; and (3) biodiversity indicators, taxa whose presence may indicate high species richness. However the effectiveness of these policies has been questioned and [70] suggested that single-species management might be more effective when directed toward keystone species. Indeed, the importance of keystone species and ecosystem engineers in communities make these species particularly important conservation targets, since the loss of these species can affect entire communities and ecosystems [72]. However, the main difficulty for applying these concepts to conservation issues lays on both the identification of keystone species and ecosystem engineers in communities and on the context dependence of their impacts, as discussed in the previous section. Thus, although these concepts appear relevant for conservation policies, it is still a long way from providing general and practical recommendations for conservationists and managers [71].

The concepts of keystone species and of ecosystem engineers could also be useful for other management issues in natural and anthropized ecosystems, such as for ecosystem restoration or agriculture. For example, in agro-ecosystems, several well-known ecosystem engineers have been used to improve soil fertility and crop yield. In some countries, farmers make use of the soil fertilizing effect of termites by spreading termite mound soil in their field [73]. Similarly, earthworm inoculation has generally positive effects on crop yield [74].

Future Directions

The notions of ecosystem engineers and keystone species have been playing prominent roles in ecology for several decades, still many questions and uncertainties ask for further investigations. Three of them are briefly described here. The first is how keystone roles and engineering effects are related to body-size: Do larger organisms have larger effects than smaller organisms? The second regards the context dependence of keystone roles and engineering effects: As the composition and structure of ecological communities are dynamic both in terms of species composition and species abundances, what does that imply for the role species have in communities and ecosystem functioning? The third line of research might be the most relevant for our society: How can the concepts for nature conservation, biodiversity protection, and the enhancement of environmental quality be used?

Bibliography

Primary Literature

1. Paine RT (1969a) A note on trophic complexity and community stability. Am Nat 103:91–93
2. Jones CG, Lawton JH, Shachak M (1994) Organisms as ecosystem engineers. Oikos 69:373–386
3. Paine RT (1966) Food web complexity and species diversity. Am Nat 100:65–75
4. Paine RT (1969b) The *Pisaster-Tegula* interaction: prey patches, predator food preference, and intertidal community structure. Ecology 50:950–961
5. Power ME, Tilman D, Estes JA, Menge BA, Bond WJ, Mills LS, Daily G, Castilla JC, Lubchenco J, Paine RT (1996) Challenges in the quest for keystones. Bioscience 46:609–620
6. Estes JA, Palmisano JF (1974) Sea otters: their role in structuring nearshore communities. Science 185:1058–1060
7. Terborgh J (1986) Keystone plant resources in tropical forest. In: Soulé ME (ed) Conservation biology. Sinauer Associates, Sunderland, pp 330–344
8. Bravo LG, Belliure J, Rebollo S (2009) European rabbits as ecosystem engineers: warrens increase lizard density and diversity. Biodivers Conserv 18:869–885
9. Darwin CR (1881) The formation of vegetable mould through the action of worms, with observations of their habits. John Murray, London
10. Dangerfield JM, McCarthy TS, Ellery WN (1998) The mound-building termite *Macrotermes michaelseni* as an ecosystem engineer. J Trop Ecol 14:507–520
11. Eisenhauer N (2010) The action of an animal ecosystem engineer: identification of the main mechanisms of earthworm impacts on soil microarthropods. Pedobiologia 53: 343–352
12. Wright JP, Jones CG, Flecker AS (2002) An ecosystem engineer, the beaver, increases species richness at the landscape scale. Oecologia 132:96–101
13. Gutiérrez JL, Jones CG, Strayer DL, Iribarne OO (2003) Mollusks as ecosystem engineers: the role of shell production in aquatic habitats. Oikos 101:71–90
14. Flecker AS, Taylor BW (2004) Tropical fishes as biological bulldozers: density effects on resource heterogeneity and species diversity. Ecology 85:2267–2278
15. Lill JT, Marquis RI (2003) Ecosystem engineering by caterpillars increases insect herbivore diversity on white oak. Ecology 84:682–690
16. Schwindt E, De Francesco C, Iribarne OO (2004) Individual and reef growth of the non-native reef-building polychaete *Ficopomatus enigmaticus* in a south-western Atlantic coastal lagoon. J Mar Biol Assoc UK 84:987–93
17. Perelman SB, Burkart SE, León RJC (2003) The role of native tussock grass (*Paspalum quadrifarium* Lam.) in structuring plant communities in the Flooding Pampa grasslands, Argentina. Biodivers Conserv 12:225–238
18. Fogel BN, Crain CM, Bertness MD (2004) Community level engineering effects of *Triglochin maritima* (seaside arrowgrass) in a salt marsh in northern New England, USA. J Ecol 92:589–597
19. Berkenbusch K, Rowden AA (2003) Ecosystem engineering – moving away from 'just-so' stories. New Zeal J Ecol 27:67–73
20. Sanders D, van Veen FJF (2011) Ecosystem engineering and predation: the multi-trophic impact of two ant species. J Anim Ecol 80:569–765
21. Wright JP, Jones CG (2004) Predicting effects of ecosystem engineers on patch-scale species richness from primary productivity. Ecology 85:2071–2081
22. Wright JP, Jones CG (2006) The concept of organisms as ecosystem engineers ten years on: progress, limitations, and challenges. BioScience 56:203–209
23. De Ruiter PC, Wolters V, Moore JC, Winemiller KO (2005) Food web ecology, playing Jenga and beyond. Science 309:68–71
24. Christianou M, Ebenman B (2005) Keystone species and vulnerable species in ecological communities: strong or weak interactors? J Theor Biol 235:95–103
25. Libralato S, Christensen V, Pauly D (2006) A method for identifying keystone species in food web models. Ecol model 195:153–171
26. Jordán F, Liu W-C, Davis AJ (2006) Topological keystone species: measures of positional importance in food webs. Oikos 112:535–546
27. Solé RV, Montoya JM (2001) Complexity and fragility in ecological networks. P Roy Soc B-Biol Sci 268:2039–2045
28. Dunne JA, Williams RJ, Martinez ND (2002) Network structure and biodiversity loss in foodwebs: robustness increases with connectance. Ecol Lett 5:558–567
29. Wilby A, Shachak M, Boeken B (2001) Integration of ecosystem engineering and trophic effects of herbivores. Oikos 92: 436–444
30. Zhang YX, Richardson JS, Negishi JN (2004) Detritus processing, ecosystem engineering, and benthic diversity: a test of predator-omnivore interference. J Anim Ecol 73:756–766
31. De Visser SN, Freymann BP, Olff H (2011) The Serengeti food web: empirical quantification and analysis of topological changes under increasing human impact. J Anim Ecol 80:484–494
32. Jones CG, Lawton JH, Shachak M (1997) Positive and negative effects of organisms as physical ecosystem engineers. Ecology 78:1946–1957
33. Schwartz MW, Brigham CA, Hoeksema JD, Lyons KG, Mills MH, van Mantgem PJ (2000) Linking biodiversity to ecosystem function:implications for conservation ecology. Oecologia 122:297–305
34. Giller PS, O'Donovan G (2002) Biodiversity and ecosystem function: do species matter? Biol Environ 102B:129–139
35. Diaz S, Cabido M (2001) Vive la difference: plant functional diversity matters to ecosystem processes. Trends Ecol Evol 16:646–655

36. Sala OE, Lauenroth WK, McNaughton SJ, Rusch G, Zhang X (1996) Biodiversity and ecosystem functioning in grasslands. In: Mooney HA et al (eds) Functional role of biodiversity: a global perspective. Wiley, Chichester, pp 129–149
37. Bremner J (2008) Species' traits and ecological functioning in marine conservation and management. J Exp Marine Biol Ecol 366:37–47
38. Menge BA, Berlow EL, Balchette CA, Navarrete SA, Yamada SB (1994) The keystone species concept: variation in interaction strength in a rocky intertidal habitat. Ecol Monog 64: 249–286
39. Brose U, Berlow EL, Martinez LD (2005) Scaling up keystone effects from simple to complex ecological networks. Ecol Lett 8:1317–1325
40. Mills LS, Soulé ME, Doak DF (1993) The keystone-species concept in ecology and conservation. Bioscience 43:219–224
41. Okey TA, Banks S, Born AF, Bustamante RH, Calvopiña M, Edgar GJ, Espinoza E, Fariña JM, Garske LE, Reck GK, Salazar S, Shepherd S, Toral-Granda V, Wallem P (2004) A trophic model of a Galapagos subtidal rocky reef for evaluating fisheries and conservation strategies. Ecol Model 172:383–401
42. Soulé ME, Estes AJ, Miller B, Honnold DL (2005) Strongly interacting species: conservation policy, management and ethics. BioScience 55:168–176
43. Rooney N, McCann K, Gellner G, Moore JC (2006) Structural asymmetry and the stability of diverse food webs. Nature 442:265–269
44. Boyd I, Wanless S, Camphuysen CJ (eds) (2006) Top predators in marine ecosystems. Cambridge University Press, Cambridge, UK
45. Johnson CN (2010) Red in tooth and claw: how top predators shape terrestrial ecosystems. J Anim Ecol 79:723–725
46. Borrvall C, Ebenman B (2006) Early onset of secondary extinction in ecological communities following the loss of top predators. Ecol Lett 9:435–442
47. Henke SE, Bryant FC (1999) Effects of coyote removal on the faunal community in western Texas. J Wildlife Manage 63:1066–1081
48. Crooks JA, Soulé ME (1999) Lag times in population explosions of invasive species: causes and implications. In: Viken A (ed) Invasive species and biodiversity management. Kluwer, Dordrecht, pp 103–126
49. Letnic M, Koch F, Gordon C, Crowther MS, Dickman CR (2009) Keystone effects of an alien top-predator stem extinctions of native mammals. Proc Roy Soc Biol Sci 276:3249–3256
50. McLaren BE, Peterson RO (1994) Wolves, moose, and tree rings on isle royale. Science 266:1555–1558
51. Ripple WJ, Beschta RL (2003) Wolf reintroduction, predation risk, and cottonwood recovery in Yellowstone National Park. Forest Ecol Manag 184:299–313
52. Owen-Smith RN (1988) Megaherbivores: the influence of very large body size on ecology. Cambridge University Press, Cambridge, UK
53. Bush GL (1993) A reaffirmation of Santa Rosalia, or why are there so many kinds of small animals? In: Lees DR, Edwards D (eds) Evolutionary patterns and processes. Academic, London, pp 229–249
54. Olff H, Ritchie ME, Prins HHT (2002) Global environmental controls of diversity in large herbivores. Nature 415:901–904
55. Haskell JP, Ritchie ME, Olff H (2002) Fractal geometry predicts varying body size scaling relationships for mammal and bird home ranges. Nature 418:527–530
56. Peters RH (1983) The ecological implications of body size. Cambridge University Press, Cambridge, UK
57. Ritchie ME, Olff H (1999) Spatial scaling laws yield a synthetic theory of biodiversity. Nature 400:557–560
58. Allesina S, Bodini A, Bondavalli C (2006) Secondary extinctions in ecological networks: bottlenecks unveiled. Ecol Model 194:150–161
59. Dunne JA, Williams RJ, Martinez ND (2004) Network structure and robustness of marine food webs. Marine Ecol Prog Ser 273:291–302
60. Estrada E (2007) Characterisation of topological keystone species: local, global and "meso-scale" centralities in food webs. Ecol Complex 4:48–57
61. Jordán F, Benedek Z, Podani J (2007) Quantifying positional importance in food webs: a comparison of centrality indices. Ecol Model 205:270–275
62. Jordán F, Liu W-C, Mike A (2009) Trophic field overlap: a new approach to quantify keystone species. Ecol Model 220:2899–2907
63. De Ruiter PC, Neutel A, Moore JC (1995) Energetics, patterns of interaction strengths, and stability in real ecosystems. Science 269:1257–1260
64. Batcheler CL (1983) The possum and rata-kamahi dieback in New Zealand: a review. Pac Sci 37:415–426
65. Rose AB, Pekelharing CJ, Platt KH (1992) Magnitude of canopy dieback and implications for conservation of southern rata-kamahi (Metrosideros umbellate-Weinmannia racemosa) forests, central Westland, New Zealand. New Zeal J Ecol 16:23–32
66. Wardle JA (1984) The New Zealand beeches: ecology, utilization and management. New Zealand Forest Service, Christchurch, p 447
67. Holdaway RN (1999) A spatio-temporal model for the invasion of the New Zealand archipelago by the Pacific rat *Rattus exulans*. J Roy Soc New Zeal 29:91–105
68. Madenjian CP, Pothoven SA, Dettmers JM, Holuszko JD (2006) Changes in seasonal energy density of alewife (*Alosa pseudoharengus*) in Lake Michigan after invasion of dreissenid mussels. Can J Fish Aquat Sci 63:1–12
69. Knapp PA (1996) Cheatgrass (*Bromus tectorum* L.) dominance in the Great Basin desert. Global Environ Chang 6:37–52
70. Simberloff D (1998) Flagships, umbrellas, and keystones: is single-species management passé in the landscape era? Biol Conserv 83:247–257

71. Boogert NJ, Paterson DM, Laland KN (2006) The implications of niche construction and ecosystem engineering for conservation biology. BioScience 56:1–9
72. Crain CM, Bertness MD (2006) Ecosystem engineering across environmental gradients: implications for conservation and management. BioScience 56:211–218
73. Black HIJ, Okwakol MJN (1997) Agricultural intensification, soil biodiversity and agroecosystem function in the tropics: the role of termites. Appl Soil Ecol 6:37–54
74. Fragoso C, Brown GG, Patron JC, Blanchart E, Lavelle P, Pashanasi B, Senapati B, Kumar T (1997) Agricultural intensification, soil biodiversity and agroecosystem function in the tropics: the role of earthworms. Appl Soil Ecol 6:17–35
75. Paine RT (1995) A conversation on refining the concept of keystone species. Conserv Biol 9(4):962–964

Ecosystem Flow Analysis

Brian D. Fath
Biology Department, Towson University, Towson, MD, USA
Advanced Systems Analysis Program, International Institute for Applied Systems Analysis, Laxenburg, Austria

Article Outline

Glossary
Definition
Introduction
Investigation of Ecosystem Flows Using Network Analysis
Example: Cone Spring Ecosystem Model
Ecosystem Goal Functions
Conclusions and Future Directions
Bibliography

Glossary

Consumer Heterotrophic organism that consumes other organisms for their energy requirements.

Cycling The process by which energy or matter returns from its compartment of origin before exiting the system boundary.

Ecological goal function Tendency observed in the orientation or directional development of ecological systems.

Flow The transfer of energy or matter from one compartment in the system to another by active (feeding) or passive (death, egestion) means.

Network analysis A mathematical tool to study objects as part of a connected system and to identify and quantify the direct and indirect effects in that system.

Primary producer Photosynthesizing organism that captures external energy sources and brings it into the system as the basis for all subsequent thermodynamic activity.

Thermodynamic system A bounded system defined by the quantities of energy and matter flowing through it.

Definition

Ecosystem services provide the basis for all human activity. Maintaining their sustained function is of critical concern to the issues of sustainability addressed here in this encyclopedia. At root, the ecosystem is a thermodynamic system receiving, collecting, transforming, and dissipating solar energy. The energy pathways are varied and complex and lead to the diversity of form and services available on the earth. Therefore, it is necessary to understand the ecosystem as a thermodynamic system and how the energy flows enter, interconnect, and disperse from the environmental system. Ecological network methodologies exist to investigate and analyze these flows. In particular, partitioning the flow into boundary input, noncycled internal flow, and cycled internal flow shows the extent to which reuse and recycling arise in ecosystems. The intricate, complex network structures are responsible for these processes all within the given thermodynamic constraints. Design of sustainable human systems could be informed by these organizational patterns, in order to use effectively the energy available. This article demonstrates the need for flow analysis, provides a brief example using a well-studied ecosystem, and discusses some of the ecosystem development tendencies which can be addressed using ecosystem flow analysis.

Introduction

Ecosystems, like all environmental systems, are open, thermodynamic systems (Fig. 1). They take in energy

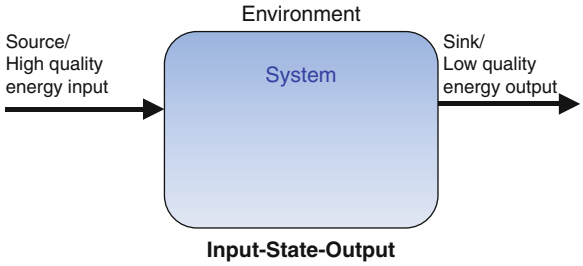

Ecosystem Flow Analysis. Figure 1
Environmental systems are open systems, connecting to the environment through inputs of high-quality energy and discarding low-quality outputs

from an external energy source – almost entirely from solar energy, although geothermal or geochemical energy drives some systems. Ecosystem structure is built with the energy, and then the degraded energy is passed back to the environment. For some time period the "stored solar energy" persists in the forms perceived on the earth's surface as biomass stores of living and nonliving organic material – such as all of us. In Frank Herbert's novel *Dune*, he envisioned that on an arid planet an important functional role of each individual was "carrying" water in oneself. In a world dominated by thermodynamic constraints, such as ours, everyone is an energy carrier. These stores are temporary and fluid. In this perspective, one could substitute the current object-mode paradigm with a flow-based, rheomode. In other words, *all stocks are flows*. The paper that one writes on now is only an ephemeral stage of the energy which started in the solar reactions, traveled to earth, was captured by a photosynthesizing organism, converted into storage in the xylem of that organism, and harvested and transformed into the useable product that one now holds. But that is not the end. Over time, the paper will slowly degrade or decompose, or perhaps the energy release will be sudden through combustion. In any case, the objects held are transitory states in a long-term dynamic from (energy) source to (energy) sink. Changing this view would help in appreciating better the difference between capital and income, because, for example, harvesting natural capital stock (i.e., a forest) into a flow (deforestation) is not equivalent yet treated as substitutable in the current accounts. The rheomode approach could help focus clearly on the difference and thus sustainability of stocks and flows.

Concerned about sustainability over a human time horizon, one must be aware of the constraints imposed by these sources and sinks. From the input side, clearly, it is necessary that one does not extract resources at a rate faster than they can regenerate. And concerning the output, the waste emissions should not exceed to the assimilative capacity of the local environment [1]. These are the most basic constraints imposed by open-system, thermodynamics. Humans have transformed the earth's surface to maximize the capture of photosynthetic energy – think of the millennia over which the Chinese, Romans, Babylonians, etc., have manipulated and manicured the landscape for agricultural production. Still, these societies rose and fell within the solar energy domain. These societies collapsed if they overconsumed the base resources or if they polluted their local environments [2]. In addition to these persistent input–output constraints, there is a third sustainability consideration currently observed in the anthropocene, in that it is not only the input–output relations, but also the structure which is created. Modern infrastructure demands the continual input of high-quality (low entropy) energy of a form not naturally delivered by ecosystem services. Furthermore, the created structure locks us into the necessity of immense energy flows for maintenance. Perhaps an apt analogy can be offered through the Greek myth of Erysichthon, who was King of Thessaly. He angered the gods by cutting down a sacred tree, and as punishment was insatiably hungry. Importantly, the more he ate, the hungrier he became. Our infrastructure, like Erysichthon, does not sit idle but continually demands upkeep such that the more structure, the more resources are needed to support this structure. It is not just about the present flows, but also the life cycle debt commitment as a result of the structure. Today that energy debt is paid almost entirely in the usage of fossil fuels – a nonrenewable resource. The scale of human activity seen today is because the application of fossil fuels to substitute solar fuels has released humans from one of the long-standing constraints on growth. And as a result, humans have exploded across the landscape. This growth was easy when there was sufficient energy to add to the system. In fact, the first growth form is *boundary growth*, taking energy into the system, and storing it as biomass. As long as there is more energy available, the system growth can occur unbound. The second stage

of growth, *network and information growth*, is squeezing more utility out of the available source by coupling processes and improving efficiencies [3]. This can occur in parallel with boundary growth, but becomes a necessity when boundary growth is limited. In human systems, those immediate constraints are looming at least given the current fuel-mix options.

Natural ecosystems, dependent on the solar energy flows developed extremely complex and beautiful structures within these thermodynamic constraints. And it is a useful guide to learn from these systems as a more eco-friendly design is incorporated. Below, some of the ecosystem flow analysis methodologies are explored and applied.

Investigation of Ecosystem Flows Using Network Analysis

"There are no trash cans in nature." This is a useful phrase reminding that waste from one entity is food/input for another. Energy, of course, has a higher dissipative factor in the reuse than material cycles such as nitrogen, phosphorus, and calcium, but still there is a complex network of pathways designed to utilize the energy available in natural ecosystems. In 1973, Hannon [4] introduced Leontief's input–output methodology into ecology, applying it to the energy flow structure of an ecosystem. The ecosystem is represented by n compartments, and the energy flowing into compartments, within compartments and exiting compartments.

A network flow model is essentially an ecological food web (energy–matter flow of who eats whom), which also includes energy input, and nonfeeding pathways such as dissipative export out of the system and pathways to detritus. The first step is to identify the system of interest and place a boundary (real or conceptual) around it. Energy–matter transfers within the system boundary comprise the network; transfers crossing the boundary are either input or output to the network, and all transactions starting and ending outside the boundary without crossing it are external to the system and are not considered. The energy inflows and intra-system flows can be considered the *production energy flow* and the flows with no consumers such as metabolic energy and exported biomass are the *respiration energy flow* [5].

The data required for ecological network analysis are as follows: for each compartment in the network, the biomass and physiological parameters, such as consumption (C), production (P), respiration (R), and egestion (E), must be quantified [6]. Furthermore, the diet of each compartment must be apportioned amongst the inputs from other compartments (consumption) in the network. This apportionment of "who eats whom and by how much" can be depicted in a dietary *flow matrix*, **F**, where energy flows from column elements j to row elements i. For all compartments, inputs should balance outputs (C = P + R + E) in accordance with the conservation of matter and the laws of thermodynamics.

The sum of the flow matrix elements, f_{ij}, gives the total inflow to compartmental i such that:

$$T_{i,in} = \sum_{j=1}^{n} f_{ij} + z_i$$

where z_i is the boundary flow into i. The outflow from i can be expressed as:

$$T_{i,\,out} = \sum_{j=1}^{n} f_{ji} + y_i$$

where y_i is the boundary outflow from i. At steady state, a necessary condition for the network flow analysis, $T_{i,in} = T_{i,out}$ and one compartmental throughflow vector can be written as $\mathbf{T} = (T_i)$. The total system throughflow (TST) is given by the sum of the compartmental throughflows:

$$TST = \sum_{j=1}^{n} T_i$$

The motivation for flow partitioning begins with nondimensional flow intensities (i.e., throughflow-specific flows) which result when flows are divided by throughflows of originating compartments: $g_{ij} = f_{ij}/T_j$. The elements of matrix $\mathbf{G} = (g_{ij})$ give the dimensionless transfer efficiencies corresponding to each direct flow, f_{ij}. Powers $\mathbf{G}^{\mathrm{m}}$ of this matrix give the indirect flow intensities associated with paths of lengths m = 2, 3, ... Due to dissipation, flow along these indirect paths approaches zero as m → ∞ so that the power series $\sum_{m=0}^{\infty} \mathbf{G}^{\mathrm{m}}$ representing the sum

of the initial, direct, and indirect flows converges to an integral flow intensity matrix, N:

$$\underbrace{\mathbf{N}}_{integral} = \underbrace{\mathbf{I}}_{initial} + \underbrace{\mathbf{G}}_{direct} + \underbrace{\mathbf{G}^2 + \mathbf{G}^3 + \ldots + \mathbf{G}^m + \ldots}_{indirect}$$
$$= (\mathbf{I} - \mathbf{G})^{-1}$$

N maps the steady-state input vector **z** into the steady-state system throughflow vector:

$$T = Nz = (\mathbf{I} + \mathbf{G} + \mathbf{G}^2 + \mathbf{G}^3 + \ldots + \mathbf{G}^m + \ldots)z$$

Term by term, flow intensities $\mathbf{G}^m$ of different orders m are propagated over paths of different lengths m. The first term, **I**, brings the input vector **z** across the system boundary as input z_j to each initiating compartment, j. The second term, **G**, produces the first-order direct transfers from each j to each i in the system. The remaining terms where m > 1 define m^{th} order indirect flows associated with length m paths. As stated before, these go to zero in the limit as m → ∞, which is necessary for series convergence. This demonstrates that each "direct" flow f_{ij} at steady state is actually composed of flow elements of all orders, m = 1, 2, ... In fact, a major result of this flow analysis is that indirect flows can dominate direct flows: $\sum_{m=2}^{\infty} \mathbf{G}^m > \mathbf{G}$. In the above developments **F**, **T**, **z**, and **y** represent matter or energy fluxes, and **G** and **N** are dimensionless intensive flows.

Finn [7] developed a cycling index using this basic approach and, Higashi et al. [8] described a three-mode partition of the flows, expanded by Fath et al. [9] into five modes (Table 1). Mode 0 is the boundary input into the system. Mode 1 accounts for all flow in which substance moves from node j to a terminal node i for the first time only without cycling. Mode 2 is flow cycled at terminal nodes i of each (i, j) pair. Mode 3 is component-wise dissipative flow in the sense that it exits from node i never to return again to i. Mode 4 is the boundary output from i constituting systemically dissipative flows exiting the system (Fig. 2). δ_{ij} is the Kronecker delta defined by $\delta_{ij} = 1$ for i = j and $\delta_{ij} = 0$ for i ≠ j.

Note, the symmetry in that quantitatively Mode 0 = Mode 4, and Mode 1 = Mode 3. This is due to the conservation of mass/energy and at steady state what comes in must go out. Mode 2 represents the cycled flow which has additional impact on the system by staying in the system longer, increasing the residence time, and returning to its source of emanation. Therefore, total system throughflow can be written as:

Ecosystem Flow Analysis. Table 1 Network representation of flow partitioning into five modes for any (i, j) pair in a system

	Pair-wise interaction	System-wide contribution
Mode 0 (boundary input)	$f_{j0}^{(0)} = z_j$	$f^{(0)} = \sum f_{j0}^{(0)}$
Mode 1 (first passage)	$f_{ij}^{(1)} = \left(\frac{n_{ij}}{n_{ii}} - \delta_{ij}\right) z_j$	$f^{(1)} = \sum\sum f_{ij}^{(1)}$
Mode 2 (cyclic)	$f_{ij}^{(2)} = \frac{n_{ij}}{n_{ii}}(n_{ii} - 1) z_j$	$f^{(2)} = \sum\sum f_{ij}^{(2)}$
Mode 3 (dissipation)	$f_{ij}^{(3)} = \left(\frac{n_{ij}}{n_{ii}} - \delta_{ij}\right) z_j$	$f^{(3)} = \sum\sum f_{ij}^{(3)}$
Mode 4 (boundary output)	$f_{0j}^{(4)} = y_j$	$f^{(4)} = \sum f_{0j}^{(4)}$

$$TST = f^{(0)} + f^{(1)} + f^{(2)} = f^{(2)} + f^{(3)} + f^{(4)}$$

And, on a nodal basis, throughflow is:

$$T_{ij} = f_{ij}^{(0)} + f_{ij}^{(1)} + f_{ij}^{(2)} = z_j\delta_{ij} + \left(\frac{n_{ij}}{n_{ii}} - \delta_{ij}\right) z_j + \frac{n_{ij}}{n_{ii}}(n_{ii} - 1) z_j$$
$$= \left(\delta_{ij} + \left(\frac{n_{ij}}{n_{ii}} - \delta_{ij}\right) + n_{ij} - \frac{n_{ij}}{n_{ii}}\right) z_j = n_{ij} z_j$$

The mode partition designation clearly shows the contribution of flow within the entire system of interactions.

Example: Cone Spring Ecosystem Model

A classic example is the Cone Spring ecosystem model developed by Tilly [10]. In this model, there are five compartments representing: (1) plants, (2) bacteria, (3) detritivores, (4) carnivores, and (5) detritus (Fig. 3). There are 2 external inputs (to plants and detritus), 8 internal flows, and each compartment has boundary outflow representing metabolic or egestion losses. The internal flows from columns j to rows i are given by:

$$\mathbf{F} = \begin{bmatrix} 0 & 0 & 0 & 0 & 0 \\ 8881 & 0 & 1600 & 200 & 167 \\ 0 & 5205 & 0 & 0 & 0 \\ 0 & 2309 & 75 & 0 & 0 \\ 0 & 0 & 0 & 370 & 0 \end{bmatrix}$$

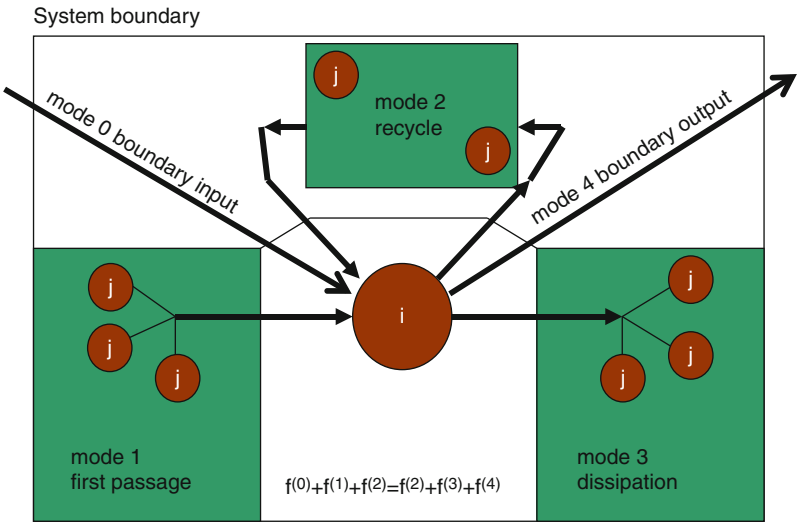

Ecosystem Flow Analysis. Figure 2

Schematic of flow partitioning for a central node i, in relation to other network compartments. Flow reaches the node directly across the boundary, $f^{(0)}$, by passing through other compartments before reaching i, $f^{(1)}$, and leaving i to cycle back again, $f^{(2)}$. Outflows symmetrically mirror these inputs

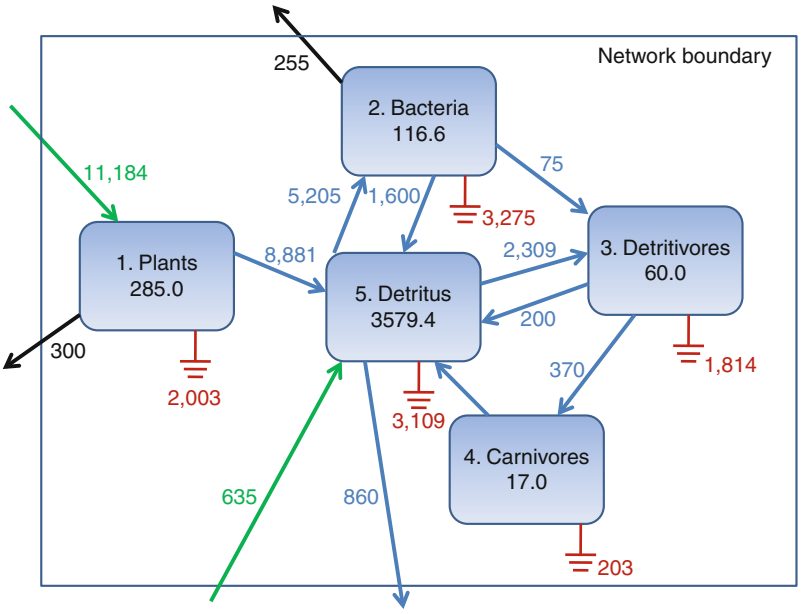

Ecosystem Flow Analysis. Figure 3

Network diagram of Cone Spring ecosystem energy flows [10]. All flows are in kcal/m^2/year. Biomasses are in kcal/m^2. *Green arrows* are exogenous boundary inflows. *Black arrows* are exports of useable energy. *Red ground* symbols represent metabolic energy loss

Compartmental throughflows are: T = [11 184, 11 484, 5 204, 2 384, 370] and TST = 30 627.

The nondimensional flow fractions are given by:

$$\mathbf{G} = \begin{bmatrix} 0 & 0 & 0 & 0 & 0 \\ 0.794 & 0 & 0.308 & 0.0840 & 0.451 \\ 0 & 0.453 & 0 & 0 & 0 \\ 0 & 0.201 & 0.014 & 0 & 0 \\ 0 & 0 & 0 & 0.155 & 0 \end{bmatrix}$$

And the integral flow matrix is:

$$\mathbf{N} = \begin{bmatrix} 1 & 0 & 0 & 0 & 0 \\ 0.958 & 1.207 & 0.374 & 0.186 & 0.545 \\ 0.434 & 0.547 & 1.169 & 0.084 & 0.247 \\ 0.199 & 0.251 & 0.092 & 1.039 & 0.113 \\ 0.031 & 0.039 & 0.014 & 0.161 & 1.018 \end{bmatrix}$$

Looking at Table 2, it is seen that over 38% of the flow comes directly to a node from the first instant across a system boundary and 52% of the flow originates from one compartment and enters another compartment for the first time without cycling. Slightly over 9% of the total energy flow is material that has cycled by exiting and reentering the same compartmental node. In other words, about 3,000 kcal/m^2/y of the total system throughflow is comprised of energy due to cyclic pathways which retain the energy in the system. This additional boost is important to the overall function of the Cone Spring ecosystem. A noticeable contribution of cycled flow is a common phenomenon in all ecosystems. Another way to demonstrate this importance of cycling, and the fundamental shift it has on how an ecosystem should be viewed, was given by Braner [11]. While investigating the same five-compartment Cone Spring model above, he showed that cyclic pathways identified by flow analysis reveal that the original boundary flow persists in the system much longer than obviously apparent. For contrast, in a five-compartment food chain model – a type often used, incorrectly, to represent an ecosystem – the longest path could only be four steps in length from X1 → *X*2 → X3 → X4 → X5. Real ecosystems have more complex structures with cycles. After those four steps, the original flow from compartment 1 would exit the system at compartment 5. According to Braner, more than 10% of the flow remains in the Cone Spring ecosystem after four steps. In fact, approximately 1% of the original flow remains after 9 steps and 0.001% is left after 15 steps (Fig. 4). A similar result is shown for two other ecosystems in the same figure. Therefore, the cycles, evident from flow analysis, play a very important role in the system having enough resource to function and provide ecosystem services.

Ecosystem Flow Analysis. Table 2 Results of the flow analysis partitioning for Cone Spring ecosystem. Values represent the fraction of total system throughflow for each mode

Mode 0	0.386
Mode 1	0.522
Mode 2	0.092
Mode 3	0.522
Mode 4	0.386

Ecosystem Goal Functions

Flow analysis has another useful feature related to understanding ecosystem dynamics. Odum [12] proposed 24 different attributes which describe the ecosystem development, for aspects such as community

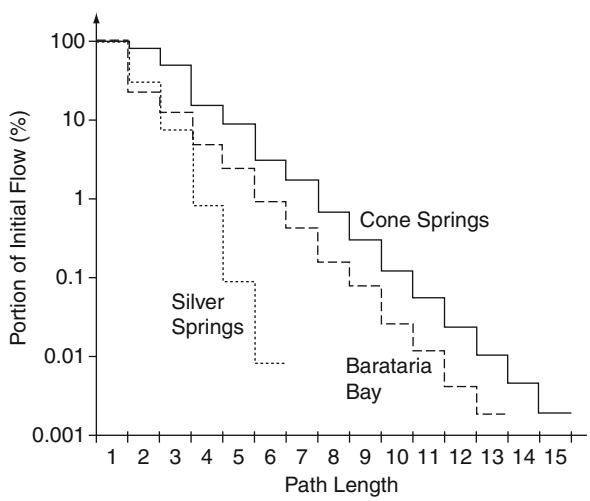

Ecosystem Flow Analysis. Figure 4 Portion of original energy that remains as path length increases (From Braner [11], reprinted with permission). There is still noticeable energy in the system after 10 steps

energetics, nutrient dynamics, and overall homeostasis. The attributes dealing with energetics, which change during the ecosystem development, have also been formulated as ecological goal functions – which describe observable macroscopic patterns over time. They are not strict goal functions in the sense of mathematical optimization models (neither is economic utility although it is used as such), but indicate the tendency for ecosystems to follow during development, for example, during succession from early r-selected species and r-selecting environments to late K-selected species and K-selecting environments. Some of the more common goal functions employed include: maximum power [13], maximum dissipation [14], maximum cycling [15], maximum residence time [16], minimum specific dissipation [17, 18], maximum energy [19], and maximum ascendency [20] (see [9], for a detailed description of these). The idea is that the ecological network self-organizes itself in a way that leads to directional change in the property of these values. For example, maximum power, interpreted to mean the maximum throughflow in the network is given by: $TST = f^{(0)} + f^{(1)} + f^{(2)}$. Therefore, TST increases when there is more boundary flow (mode 0), more first passage flow (mode 1), or more cycled flow (mode 2). The mechanisms for this to increase practically relate to the system's ability to capture more boundary flow by increasing the uptake. Both first passage flow and cycled flow also depend on the second stage of growth exemplified by the structure of the network and the efficiency of flows along each connection. Similar rationale can be made for the other goal functions listed above, and in fact it has been shown that the goal functions are complementary and mutually reinforcing in that the realization of one generally promotes the others. Together they provide a holistic view of ecosystem development through different thermodynamic perspectives. Again, the value of this ecosystem knowledge is obvious for application to design and to manage human systems sustainably. If ecosystem services are required, then the inherent dynamics of the systems used should be better understood. Human activities in line with these directions will be supported by natural processes, those that do not will experience additional resistance and therefore additional cost and difficulty. Humans are better off working with nature than against it if possible.

Conclusions and Future Directions

Ecosystem flow analysis clearly shows that the distribution of energy flow in a network is not simple. Some significant fraction of the energy remains in the system and cycles before exiting the system. This insight was evident in R. Lindeman's [21] seminal work on Cedar Bog Lake in which he referred to his eight-compartment ecosystem as a "food-cycle." Unfortunately, he did not have the quantitative tools at his disposal, like flow analysis, and to simplify the calculations, proceeded to analyze the system according to two distinct "food-chains," although in reality they are linked and contain cycles. Further work in this area also neglected the presence and significance of food cycles until research in the mid-1970s (such as [22–25], and others) when network analysis techniques developed sufficiently to provide a holistic investigation of the ecosystem function. As stated above, this changes the way one must look at ecosystems, as processors and stores of energy flow. The energy does not pass quickly through but can remain and impact the system indirectly. The good news is that this flow which remains in the system is able to positively drive ecosystem processes and contribute to the overall sustainability of the system.

However, the lesson to take is that in the design of human systems, industrial processes are built sequentially, which have raw material → processing → product → disposal. There is little room for cycling and reuse. Remember, there are no trash cans in nature. Everything has a use and reuse. Efforts are now seen in industrial ecology promoting closed loop engineering and cradle-to-cradle considerations, but there is a long way to go, as evidenced by the massive amounts of raw material input and solid waste generated on a daily basis by human activity. Also, the flow analysis must include all parts and processes of the holistic integrated socio-ecological system. Future work is needed to continue to understand energy cycles in natural systems and furthermore, how to implement lessons from these into the design of socio-ecological systems. Ecosystem flow analysis clearly shows the input–output orientation flow resources have at their disposal for maintaining functional activity and can aid in sustainability science.

Bibliography

Primary Literature

1. Daly HE, Townsend KN (1993) Valuing the earth: economics, ecology, ethics. MIT Press, Cambridge, MA, p 399
2. Diamond J (2005) Collapse: how societies choose to fail or succeed. Penguin Press, New York, p 575
3. Fath BD, Jørgensen SE, Patten BC, Straškraba M (2004) Ecosystem growth and development. Biosystems 77:213–228
4. Hannon B (1973) The structure of ecosystems. J Theor Biol 41:535–546
5. Levine SH (1977) Exploitation interactions and structure of ecosystems. J Theor Biol 69:345–355
6. Fath BD, Scharler U, Ulanowicz RE, Hannon B (2007) Ecological network analysis: network construction. Ecol Model 208:49–55
7. Finn JT (1976) Measures of ecosystem structure and function derived from analysis of flows. J Theor Biol 56:363–380
8. Higashi M, Patten BC, Burns TP (1993) Network trophic dynamics: the modes of energy utilization in ecosystems. Ecol Model 66:1–42
9. Fath BD, Patten BC, Choi JS (2001) Complementarity of ecological goal functions. J Theor Biol 208:493–506
10. Tilly LJ (1968) The structure and dynamics of Cone Spring. Ecol Monogr 38:169–197
11. Braner M (1985) A simple random path method for the analysis of flow networks. Ecol Model 28:165–180
12. Odum EP (1969) The strategy of ecosystem development. Science 164:262–270
13. Lotka AJ (1922) Contribution to the energetics of evolution. Proc Natl Acad Sci USA 8:147–151
14. Schneider ED, Kay JJ (1994) Life as a manifestation of the second law of thermodynamics. Math Comput Model 19:25–48
15. Morowitz HJ (1968) Energy flow in biology; biological organization as a problem in thermal physics. Academic, New York
16. Cheslak EF, Lamarra VA (1981) The residence time of energy as a measure of ecological organization. In: Mitsch WJ, Bossermann RW, Klopatek JM (eds) Energy and ecological modelling. Elsevier, Amsterdam, pp 591–600
17. Onsager L (1931) Reciprocal relations in irreversible processes. Phys Rev 37:405–426
18. Prigogine I, Wiame JM (1946) Biologie et Thermodynamique des Phenomenes Irreversible. Experientia II:451–453
19. Odum HT (1988) Self-organization, transformity, and information. Science 242:1132–1139
20. Ulanowicz RE (1997) Ecology, the ascendent perspective. Columbia University Press, New York
21. Lindeman RL (1942) The trophic dynamic aspect of ecology. Ecology 23:399–418
22. Pomeroy LR (1974) The ocean's food web, a changing paradigm. Bioscience 24:499–504
23. Finn JT (1976) Measures of ecosystem structure and function derived from analysis of flows. J Theor Biol 56:363–380
24. Patten BC (1978) Systems approach to the concept of environment. Ohio J Sci 78:206–222
25. Patten BC (1985) Energy cycling in the ecosystem. Ecol Model 28:1–71

Books and Reviews

Burns TP (1989) Lindeman's contradiction and the trophic structure of ecosystems. Ecology 70:1355–1362

Finn JT (1980) Flow analysis of models of the Hubbard Brook ecosystem. Ecology 61:562–571

Latham LG (2006) Network flow analysis algorithms. Ecol Model 192:586–600

Ulanowicz RE (1983) Identifying the structure of cycling in ecosystems. Math Biosci 65:219–237

Whipple SJ (1999) Analysis of ecosystem structure and function: extended path and flow analysis of a steady-state oyster reef model. Ecol Model 114:251–274

Ecosystem Services

Heather Tallis[1], Anne Guerry[1], Gretchen C. Daily[1,2]
[1]The Natural Capital Project, Department of Biology and Woods Institute, Stanford University, Stanford, CA, USA
[2]Department of Biological Sciences, Stanford University, Stanford, CA, USA

Article Outline

Glossary
Definition
Introduction
What are Ecosystem Services?
History of the Concept of Ecosystem Services
Incorporating Ecosystem Services into Decisions
Future Directions
Conclusions
Bibliography

Glossary

Ecosystem services The wide array of benefits that ecosystems, and their biodiversity, confer on humanity.

Marginal value The economic value of the next incremental unit of something. In this context, marginal values are those associated with managing the next

small unit of an ecosystem in a particular way (e.g., preserving, rather than clearing, the next unit of forest). They can also be the partial contribution of natural capital to a final good that is produced with other inputs. For example, the marginal value of irrigation water for crop production is the value of the incremental crop yield that can be attributed to irrigation, rather than to labor, fertilizer, and other inputs.

Natural capital Here we focus on living, renewable forms of natural capital, which constitute a stock – of an ecosystem and the biota that makes it up – that generates a flow of ecosystem services. For example, a forest constitutes a stock that generates a flow of timber, carbon sequestration, water quality, biodiversity, serenity, and other benefits, depending upon how it is managed. (Fossil fuels and other minerals constitute nonliving natural capital, which is generally nonrenewable on time scales of interest to society.)

Definition

Ecosystem services are essential to sustaining and fulfilling human life, and yet their supply is seriously threatened by the intensification of human impacts on the environment. Over the past decade, efforts to value and protect ecosystem services have been promoted by many as the last best hope for making conservation mainstream – attractive and commonplace worldwide. In theory, if institutions recognize the values of nature, then we can greatly enhance investments in conservation and foster human well-being at the same time. In practice, scientific and policy communities have not yet developed the scientific basis or the policy and finance mechanisms for integrating natural capital into resource and land-use decisions on a large scale.

Introduction

This entry provides an overview of issues concerning the identification, biophysical and economic characterization, and safeguarding of ecosystem services. The concept of ecosystem services has a long written history, reaching back at least as far as Plato. We review this history, including a focus on recent advances such as the Millennium Ecosystem Assessment, and advances in spatial modeling, economic valuation, and policy implementation. We provide examples of novel finance and policy mechanisms, including water funds, marine spatial planning, land-use planning and human development, and global policy efforts. We conclude with a discussion of the largest research and implementation challenges in this field, identifying the issues that will frame the future growth of the concept of ecosystem services.

What are Ecosystem Services?

Definition and Classification

Ecosystem services are defined simply as the benefits that people obtain from ecosystems [38]. They sustain and fulfill human life and flow from many conditions and processes of ecosystems, and the species making them up [14]. The processes and features generating ecosystem services (ES) are so tightly interconnected that any classification is inherently somewhat arbitrary. The most widely used classification was developed through the Millennium Ecosystem Assessment (MA) and identifies four classes of ES based on their types of benefits to society:

1. *Provisioning services* including the production of goods such as food, water, timber, and fiber
2. *Regulating services* that stabilize climate, moderate risk of flooding and disease, and protect or enhance water quality
3. *Cultural services* that provide recreational, aesthetic, educational, community, and spiritual opportunities
4. *Supporting services* that underlie provision of the other three classes of benefits, including soil formation, photosynthesis, nutrient cycling, and the preservation of options (Fig. 1; [38]).

The classification of ES is still a topic of debate and several other classification approaches have been suggested [7, 19, 22, 67].

System- and scale-neutral, the ecosystem services framework applies equally to terrestrial, freshwater, and marine ecosystems and their processes, anywhere on the spectrum from relatively pristine to heavily managed conditions. Indeed, all ecosystems provide, to differing degrees, a set of ES. Human conversion of ecosystems from one type to another is often motivated

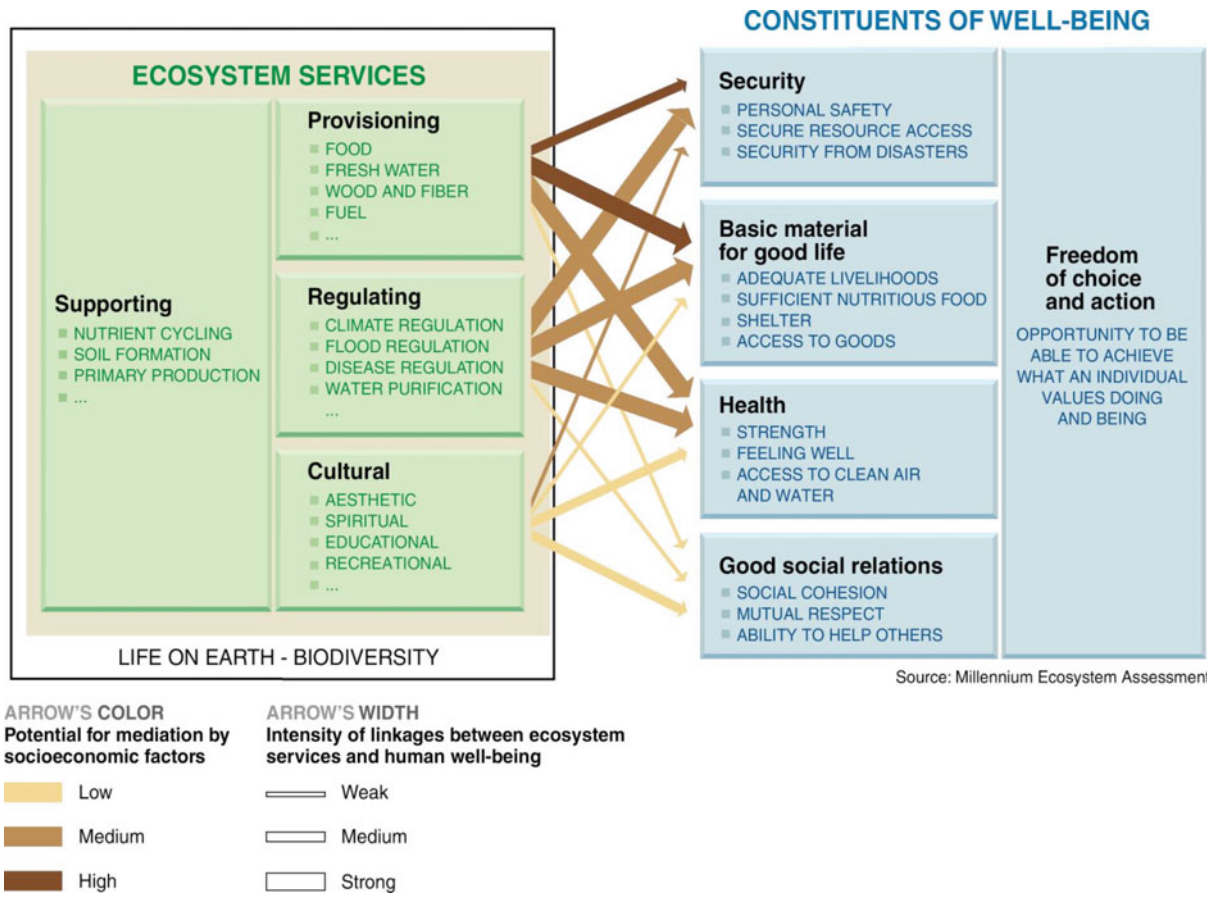

Ecosystem Services. Figure 1
Ecosystem service categories and their linkages to human well-being as described in the Millennium Ecosystem Assessment [38]

by a desire for a different set of ES, though consideration of the services of the two systems and their tradeoffs is often incomplete.

Ecosystem Services Across Systems

A wide range of ES is generated in the terrestrial realm, by croplands, natural and managed forests, grasslands, and wetlands. In each of these systems, for example, vegetation can protect and enhance soils, preventing their loss through erosion and improving fertility by retaining moisture and storing and recycling nutrients. Vegetation and soils together regulate the quantity, quality, and timing of water flows, thus moderating floods and droughts and providing cleaner, more reliable supplies [8].

Forests stand out as important in regulating water and carbon cycles [30]; in their strong influence on local, regional, and global climate [30, 49]; and because of the multiple, interacting threats to their future (e.g., [44, 66]). They also provide natural products for subsistence use or sale including timber, firewood, mushrooms, fruits and seeds, medicinal plants, rubber, cork, and bushmeat. Forest and woodland habitats harbor species that provide pollination and pest control to commercial or subsistence crops. Grassland and other dryland systems play these same critical roles in addition to supporting vast livestock populations [38]. Wetlands occupy a small fraction of Earth's surface, but dominate the landscape where they are concentrated and provide a wide array of water

quality, flood mitigation, coastal protection, and biogeochemical services [38]. Each of these systems, however natural or managed, can provide habitat for biodiversity and opportunities for recreational activities, spiritual experiences, and creative, cultural expression.

Freshwater ecosystems provide a suite of highly visible and widely appreciated ES [53]. The freshwater regulated by terrestrial systems and the atmosphere is used for drinking, hydropower production, irrigation, household activities (washing, etc.), industrial purposes (cooling, manufacturing, etc.), and cultural experiences. People also gain large revenues and nutrition from freshwater fisheries and aquaculture. Less appreciated is the value of sediment transport and deposition in rivers that supply river reaches and downstream beaches with important sand and gravel resources. Wetlands and other aquatic vegetation can regulate flood waters and cycle nutrients, improving water quality. Finally, freshwater systems serve as pathways for human transportation and recreational or cultural activities.

Marine ecosystems also provide all four classes of ecosystem services described in the MA. Marine fisheries and aquaculture provide nutrition, feed for animals, livelihoods, and important recreational and cultural opportunities. Harvests of other species for food additives, cosmetics, and pharmaceuticals also support health, nutrition, and livelihoods. Marine biogenic habitats (such as coral reefs, oyster reefs, and kelp forests) regulate natural hazards including storm surges, and may play a critical role in helping coastal communities adapt to sea level rise. Marine systems also transform, detoxify, and sequester wastes. In addition, oceans are the center of the global water cycle; they hold 96.5% of the Earth's water [24] and are a primary driver of the atmosphere's temperature, moisture content, and stability [12]. Oceans are also key players in the global cycles of carbon, nitrogen, oxygen, phosphorus, sulfur, and other major elements [51] and are responsible for approximately 40% of global net primary productivity [39, 61]. Finally, coastal communities reap many benefits from coastal tourism (one the one of world's most profitable industries [65]), and numerous coastal communities define their very identities in relation to the sea and all it brings.

The Ecosystem Service Supply Chain

Ecosystem services flow to people along a supply chain from biophysical systems to people [63]. All services are generated by some function or element of a natural or managed system (Fig. 2). The full suite of these elements or functions can best be considered in three discrete steps: supply, service, and benefit. For example, consider protection from coastal storm surges. Many different types of coastal elements (e.g., coral reefs, mangroves, oyster beds, barrier islands) confer protection from storm surges by attenuating waves. The full set of locations of these coastal elements represents the supply of protection from storms. People do not receive storm surge protection from all of these locations, however, because some are far from human infrastructure and settlement. Both the distribution of human infrastructure and settlement, together with the location and condition of supply, are required to give a clear picture of how much "service" is actually delivered at a given time. Finally, the service delivered to human communities is often valued differently, depending on the context. For example, coastal protection services provided by nearshore habitats to easily

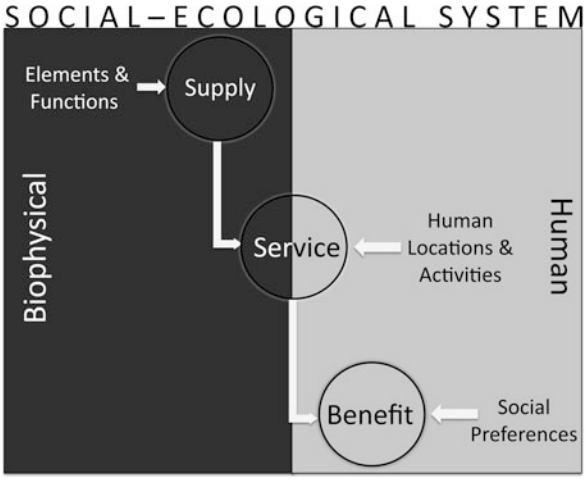

Ecosystem Services. Figure 2
Three measurement points for ecosystem services [63]. Supply metrics deal only with the biophysical system underpinning the service of interest. Service metrics include critical information linking supply to beneficiaries. Benefit metrics weigh the level of service based on people's preferences or social policy goals

accessible, popular, public beaches might be seen as more valuable, or providing greater benefit, than those to more remote sites.

History of the Concept of Ecosystem Services

It is primarily through disruption and loss that the nature and value of ecosystem services has been illuminated. For instance, deforestation has demonstrated the critical role of forests in the hydrological cycle – in particular, in mitigating floods, droughts, the erosive forces of wind and rain, and the silting of dams and irrigation canals. Release of toxic substances, whether accidental or deliberate, has revealed the nature and value of physical and chemical processes, governed in part by a diversity of microorganisms, that disperse and break down hazardous materials. Thinning of the stratospheric ozone layer sharpened awareness of the value of its service in screening out harmful ultraviolet radiation. And the loss of coastal wetlands has brought into relief their importance in regulating coastal hazards such as hurricanes and tsunamis.

Initial Development of the Ecosystem Services Concept

A cognizance of ecosystem services, expressed in terms of their loss, dates back at least to Plato and probably much earlier:

- What now remains of the formerly rich land is like the skeleton of a sick man with all the fat and soft earth having wasted away and only the bare framework remaining. Formerly, many of the mountains were arable. The plains that were full of rich soil are now marshes. Hills that were once covered with forests and produced abundant pasture now produce only food for bees. Once the land was enriched by yearly rains, which were not lost, as they are now, by flowing from the bare land into the sea. The soil was deep, it absorbed and kept the water…, and the water that soaked into the hills fed springs and running streams everywhere. Now the abandoned shrines at spots where formerly there were springs attest that our description of the land is true. (Plato)

Mooney and Ehrlich [40] trace modern concern for ecosystem services to George Perkins Marsh, a lawyer, politician, and scholar. Indeed, his 1864 book *Man and Nature* describes a wide array of services, again, often expressed in terms of their loss. Remarking on the terrain of the former Roman Empire, he notes that it "is either deserted by civilized man and surrendered to hopeless desolation, or at least greatly reduced in both productiveness and population" (p. 9). He continues, describing the reduction of hydrological services: "Vast forests have disappeared from mountain spurs and ridges, the vegetable earth … [is] washed away; meadows, once fertilized by irrigation, are waste and unproductive, because … the springs that fed them dried up; rivers famous in history and song have shrunk to humble brooklets" (p. 9). He also draws connections between deforestation and climate: "With the disappearance of the forest, all is changed. At one season, the Earth parts with its warmth by radiation to an open sky – receives, at another, an immoderate heat from the unobstructed rays of the sun. Hence the climate becomes excessive, and the soil is alternately parched by the fervors of summer, and seared by the rigors of winter. Bleak winds sweep unresisted over its surface, drift away the snow that sheltered it from the frost, and dry up its scanty moisture" (p. 186). Finally, he even wrote of decomposition services: "The carnivorous, and often the herbivorous insects render an important service to man by consuming dead and decaying animal and vegetable matter, the decomposition of which would otherwise fill the air with effluvia noxious to health" (p. 95).

Other eloquent writers on the environment emerged following World War II, including Fairfield Osborn (*Our Plundered Planet*, 1948), William Vogt (*Road to Survival*, 1948), and Aldo Leopold (*A Sand County Almanac and Sketches from Here and There*, 1949). Each discusses ecosystem services without using the term explicitly. In *The Population Bomb* (1968), Paul Ehrlich describes anthropogenic disruption of ecosystems and the societal consequences of doing so, addressing the need to maintain important aspects of ecosystem functioning. Along these lines, the *Study of Critical Environmental Problems* (1970) presents a list of key "environmental services" that would decline with a decline in "ecosystem function." This list was expanded upon by Holdren and Ehrlich [29]. Meanwhile, in the 1960s and 1970s, economists set out to measure "the value of services that natural areas provide" ([35], p. 12), with efforts focused on

agricultural production [3], renewable resources [11, 34], nonrenewable resources [18], and environmental amenities [23].

By the early 1980s, efforts were initiated to investigate two questions: the extent to which ecosystem function (and the delivery of services) depends on biodiversity, and the extent to which technological substitutes could replace ecosystem services. The first question is addressed in chapter ► Species Diversity Within and Among Ecosystems, this volume. The second question was tackled by Ehrlich and Mooney [21]. Work on these topics proliferated and, in 1997, a collective effort was made to synthesize the wealth of scientific information that had accumulated on the functioning of ecosystem services, with a preliminary exploration of their economic value, and of key issues meriting further work [14].

Recent Advances

Four major advances of the last decade have revitalized research on ecosystem services and brought them into the public eye. First, the MA represented a visionary and seminal step in global science – it was the first comprehensive global assessment of the status and trends of all of the world's major ecosystem services. It was requested by United Nations Secretary General Kofi Annan in 2000 and carried out between 2001 and 2005 with contributions from over 1,360 experts worldwide. The key finding of this assessment was that two thirds of the world's ecosystem services were declining [38]. This captured the attention of world leaders and emphasized the connections between human decisions and the natural environment that feed back to the human condition via changes in the flow of ecosystem services.

Work following the MA clarified this chain of connections (Fig. 3) [16]. Human decisions shape individuals' actions relating to the use of land, water, oceans, and other elements of natural capital. These actions often alter the state or functioning of ecosystems, which in turn provide altered flows of benefits (goods or services) to people. People express different values (monetary, cultural) associated with these altered streams of benefits and it is the expression of these values that leads to changes in institutions that guide decisions. The following three recent advances all concern the connections in this flow.

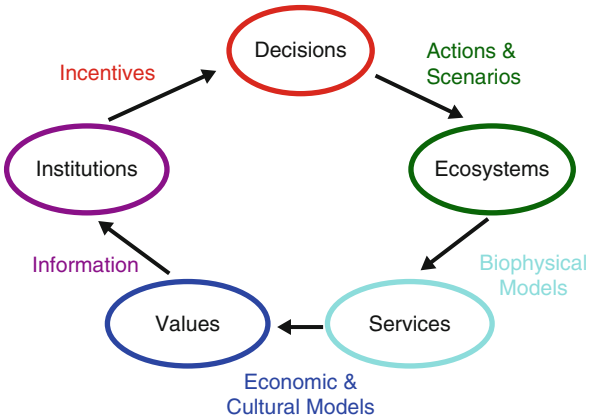

Ecosystem Services. Figure 3
A framework showing key elements for integrating ES into decision-making [16]. One could link any two ovals, in any direction, in different decision contexts

A suite of recent advances has greatly improved understanding of the links between ecosystem functions and processes and the provision of ecosystem services (Fig. 3). For some ecosystem services, we now better understand the key ecological system components that drive provision (e.g., [33]) and we can now measure (e.g., [56]) and model, with uncertainty, the impacts of land use and resource management decisions on a wider variety of ecosystem processes and associated services. Ecological science has also advanced spatially explicit modeling, which is essential for mapping ecosystem services and their flows to people (e.g., [10, 27, 43, 57]). Finally, we are starting to see patterns in how multiple ecosystem services and biodiversity change in relation to each other. Recent work has started characterizing bundles of ecosystem services, and exploring their synergies and trade-offs (e.g., [4, 6, 20, 42, 43]).

Further, economic valuation methods have been applied to the spatial provision of ecosystem services to estimate the monetary value of benefits and, in some cases, the distribution of those benefits to various segments of society [42, 45, 52, 64]. In addition, qualitative and quantitative methods from other social sciences have been applied to gain better understanding of the social and cultural importance of ecosystem services (e.g., [38]).

Lastly, experiments in payments for ecosystem services [47, 48, 69], in ecosystem-based management [2],

and in regional planning have begun, giving us opportunities to learn about how science can play a role in altering institutions, and how institutions alter decisions and the resulting flow of ecosystem services. The following section describes some of these efforts in more detail.

Incorporating Ecosystem Services into Decisions

Today, the urgent challenge is to move from theory to practical implementation of ES tools and approaches in resource decisions taken by individuals, communities, corporations, and governments. The framework in Fig. 3 connects the science of quantifying services with valuation and policy to devise payment schemes and management actions that take account of ecosystem services. This connection is expressed in the real world in a variety of ways across scales from local to global.

A great number and diversity of efforts to implement the ES framework have emerged worldwide over the past decade. Individually, most of these efforts are small and idiosyncratic. But collectively, they represent a powerful shift in the focus of conservation organizations and governments (primarily) toward a more inclusive, integrated, and effective set of strategies [15]. Taken together, these efforts span the globe and target a full suite of ecosystem services, including principally forest-generated services of carbon sequestration, water supply, flood control, biodiversity conservation, and enhancement of scenic beauty (and associated recreation/tourism values) [26, 62].

Many local or regional ES efforts focus on a single service that stands out as sufficiently important, from economic and political perspectives, to overcome the activation energy required to protect it. Under the institutional umbrella created for the focal service, it is possible that other services may be at least partially protected. Beginning in the late 1990s, larger-scale investment in natural capital for water flow regulation in China – and for a broad suite of ES in Costa Rica – set pioneering examples that are now being adapted elsewhere and scaled up.

Next, we briefly describe some contrasting models of success, at different scales and in different kinds of social-ecological systems. In each case, there is an acute or looming crisis, innovative leadership, and pursuit of dual goals: improving both human and ES condition.

Local Scale: Water Funds

New York City made one of the first and most famous investments in ecosystem service provision in recent history, in the mid-1990s. The city invested ca. USD1.5 billion in a variety of watershed protection activities to improve drinking water quality for 10 million users rather than spending the estimated USD6-8 billion needed (excluding annual operating and maintenance costs) for building a new filtration plant. This seminal example is widely cited as evidence of the business case for investing in natural capital instead of built capital [15]. Yet the effort remains very much an experiment in the science and policy of investing in natural capital, and one on which there is international focus.

Globally, watersheds are now emerging as the target of a range of creative policy and finance mechanisms that link beneficiaries to suppliers through a payment system. In these "water funds," water users voluntarily pay into a pool that is collectively managed by contributors and invested in watershed management improvements. The Nature Conservancy (TNC) has now established more than ten water funds in Latin America, has plans to create 22 more by 2015 [25], and is exploring the possibility of establishing some of the first funds in Africa.

Agua por la Vida y la Sostenibilidad, one of the recently established water funds, demonstrates the diversity of water users that are becoming engaged in these funds and the kinds of watershed management changes these funds motivate. Formally established in the Cauca Valley, Colombia in 2009, this water fund is supported by the region's sugarcane grower's association (PROCAÑA), the sugar producers' association (ASOCAÑA), 11 local watershed management groups, TNC and a Colombian peace and justice nongovernment organization (Vallenpaz). Each member of the water fund voluntarily pays a self-determined amount into the fund that is then jointly managed by the members to improve landscape management in 11 watersheds covering over 3,900 km^2.

Members in this fund have currently committed to contributing USD10 million over 5 years to be invested in five kinds of management changes: protection of native vegetation, restoration of denuded lands, enrichment of degraded forests, fencing of rangelands, and implementation of silvopastoral practices.

The fund is starting a monitoring program that will ensure that these investments lead to measurable improvements in water quality for approximately one million water users downstream and significant improvements in terrestrial and freshwater biodiversity.

Local Scale: Coastal and Marine Spatial Planning

People commonly think of oceans as relatively featureless expanses that defy the drawing of lines on maps. However, recent political and scientific advances have highlighted the need for a comprehensive approach to planning marine and coastal uses and the need for practical tools to make this more comprehensive approach a reality on the ground and in the water. In a marine spatial plan, a wide range of uses of the marine environment are put on one map. But an understanding of how such plans are likely to yield changes in the delivery of the broad range of services people receive from the system has, until recently, remained elusive.

Along the west coast of Vancouver Island Canada, multiple, often competing interests are struggling to define the future character of the place. Existing extractive, industrial, and commercial uses; traditional First Nations subsistence and ceremonial uses; recreation and tourism; and emerging ocean uses such as the extraction of wave energy are all in the mix. The West Coast Aquatic Management Board (WCA) is charged with creating a marine spatial plan for the region. WCA is a public-private partnership with participation from four levels of government (Federal, Provincial, local, and First Nations), and diverse stakeholders. Ultimately, WCA's vision is to manage resources for the benefit of current and future generations of people and nonhuman species and communities.

Some key pillars of the partnership's strategy are to: use a precautionary, ecosystem-based approach to protect, maintain, and restore marine and coastal resources; respect and protect First Nations' food, social and ceremonial requirements and treaty obligations; integrate expertise and knowledge from First Nations, local, scientific, and other sources; ensure broad participation in the planning process; and foster initiatives that maintain or enhance opportunities for coastal communities to benefit from local resources, while achieving sustainable social, cultural, and economic benefits for the region. WCA has partnered with the Natural Capital Project to explore how alternative spatial plans might affect a wide range of ES and to provide information about trade-offs among ES.

Key considerations for WCA and their stakeholders include balancing important industrial and commercial activities (such as shipping, mining, logging, aquaculture, and fisheries), increased development of tourism and recreation, renewable energy generation, and a strong cultural desire for sustaining the remote, wild feeling of the place. WCA is exploring the suitability of alternative regions for these different activities. For example, maps of coastal vulnerability to erosion and flooding from storm surge are helping to direct coastal development permits to low-risk areas. Similar maps of the value of captured wave energy are being overlaid with existing ocean uses (e.g., fishing and recreational activities) to highlight regions of high wave energy value, where wave energy generation facilities might be constructed while having minimal impacts on other activities. Examinations of trade-offs among aquaculture (finfish, shellfish), wild salmon fisheries, recreation (e.g., kayaking, whale watching, and diving), coastal development (on the coast, as well as floathomes), and habitat and water quality are underway.

The general framework of ES and ES modeling, in particular, is helping to articulate connections between human activities that are often considered in isolation, to align diverse stakeholders around common goals, and to make implicit decisions explicit. ES modeling results have informed early iterations of the marine spatial plan and will inform the creation of the final plan in 2012.

National Scale: Land-Use Planning and Human Development in China

The ecosystem service investments being made in China today are impressive in their goals, scale, duration, and innovation. Following massive droughts and flooding in 1997–1998, China implemented several national forestry and conservation initiatives, into which investments exceeded 700 billion yuan (ca. USD100 billion) over 2000–2010 [37, 70]. The larger and older of these initiatives are being rigorously evaluated to determine their biophysical and socioeconomic impacts, to improve their design and efficacy.

These initiatives have dual goals: to secure critical natural capital through targeted investments across landscapes and regions, and to alleviate poverty through targeted wealth transfers from coastal provinces to inland regions where many ES originate. The Chinese government aims to reduce the loss of soil, improve water retention, reduce desertification, and generally protect biodiversity and ecosystems in the west of the country for flood control, hydropower production efficiency, irrigation supply, more productive agriculture, and ecotourism. In addition, it wants to change the economic structure in rural areas to increase local household income while simultaneously making local households' patterns of land utilization and agricultural production more sustainable [36, 37].

The initiatives include two national PES programs, the Natural Forest Conservation Program (NFCP) and the Sloping Land Conversion Program (SLCP), established in 1998 and 1999 respectively. Implementation was tested in a few provinces, and then rapidly scaled to the whole country. Evaluation of the programs shows significant achievement of the biophysical goals, with remarkably rapid land conversion in the desired directions. For example, by the end of 2006, the SLCP had converted ca. 9 million hectares of cropland into forest/grassland and had afforested ca. 12 million hectares of barren land. Village-level field measurements have shown not only that the payments for ES have altered land use patterns, but in turn soil erosion has been decreased in some areas by as much as 68% [9].

Overall social impacts of the programs are mixed. In some places, payment levels and types are leading to improvements in economic measures of well-being, whereas in others payments were not sufficient to compensate for loss of income from shifting livelihoods [37]. In addition, in some places where participation in the SLCP has significant positive impacts upon household income, it has not yet transferred labor toward non-farming activities as the government wished [36]. Payments are now being adjusted to improve success in achieving goals of poverty alleviation and growth of new economic sectors in rural areas.

China is also now establishing a new network of Ecosystem Function Conservation Areas (EFCAs), specifically for ES provision. Their exact delineation is now being determined through quantitative ecosystem service mapping and valuation. They are expected to span ca. 25% of the country.

The current and potential future impacts of ES investments in China are enormous, certainly within the country – and also globally, in the form of enhanced carbon sequestration and reduced dust export, and perhaps most importantly in lessons on making the investments needed in natural capital and human well-being everywhere.

International Scale: Global Policy and Research Efforts

As described above, the MA was the first major effort to establish ES in the international policy arena. Activities stemming from that effort are now aimed at bringing countries together in making tangible commitments to safeguard ES (e.g., 2020 targets for the Convention on Biodiversity) and to assess national and international progress toward those commitments (e.g., through Group on Earth Observations Biodiversity Observation Network (GEO BON) and the Programme on Ecosystem Change and Society (PECS), which synthesize knowledge for the International Platform for Biodiversity and Ecosystem Services (IPBES), formally established in 2010). Several new international research efforts aim to feed into these international processes, including the Natural Capital Project, The Resilience Alliance, and the Stockholm Resilience Centre. Other entities are focused on establishing and tracking ES markets, as a mechanism for bringing larger attention to ES benefits to society (e.g., The Katoomba Group and The Ecosystem Marketplace, both initiated by Forest Trends). As an example of many burgeoning international efforts, we describe in greater detail the Natural Capital Project.

The Natural Capital Project (NatCap) (www.naturalcapitalproject.org) is an international partnership working to align economic forces with conservation, by developing tools that make incorporating natural capital into decisions easy and replicable; by demonstrating the power of these tools in important, contrasting places; and by engaging leaders globally. NatCap is developing InVEST, a family of tools for Integrated Valuation of Ecosystem Services and Tradeoffs.

InVEST helps decision makers visualize the impacts of potential policies by modeling and mapping the

delivery, distribution, and economic value of ES under alternative scenarios (for more information, see [30]). The outputs identify trade-offs and compatibilities between environmental, economic, and social benefits. InVEST is designed for use as part of an active decision-making process (Fig. 4) and can be applied at local, regional, or global scales. The first phase of the approach involves working with stakeholders to identify critical management decisions and to develop scenarios that project how the provision of services might change in response to those decisions as well as to changing climate, population, etc. Based on these scenarios, a modular set of models quantifies and maps ES. The outputs of these models provide decision makers with information about costs, benefits, trade-offs, and synergies of alternative investments in ES provision.

NatCap is using InVEST in major natural resource decisions in diverse contexts around the world, including in the three examples given above (water funds, coastal and marine spatial planning, and land-use planning and human development in China). The aim is to demonstrate the power of these approaches and to learn how to replicate and scale up models of success. The Project is engaged in a suite of international efforts, including GEO BON and IPBES, to offer a common, unifying platform for regional and national efforts that are spawned by these initiatives.

Future Directions

With the rapid rate of development of ES mapping, from the biophysical and economic modeling through to policy application in diverse socioeconomic contexts, it is likely that great advances will be made in coming years. What we report here is only a beginning. There are key arenas in which further learning is crucial to understand what drives variation in the provision of ES, how they percolate through various arms of society, and how social reaction leads to sustainable or unsustainable change in ES provision.

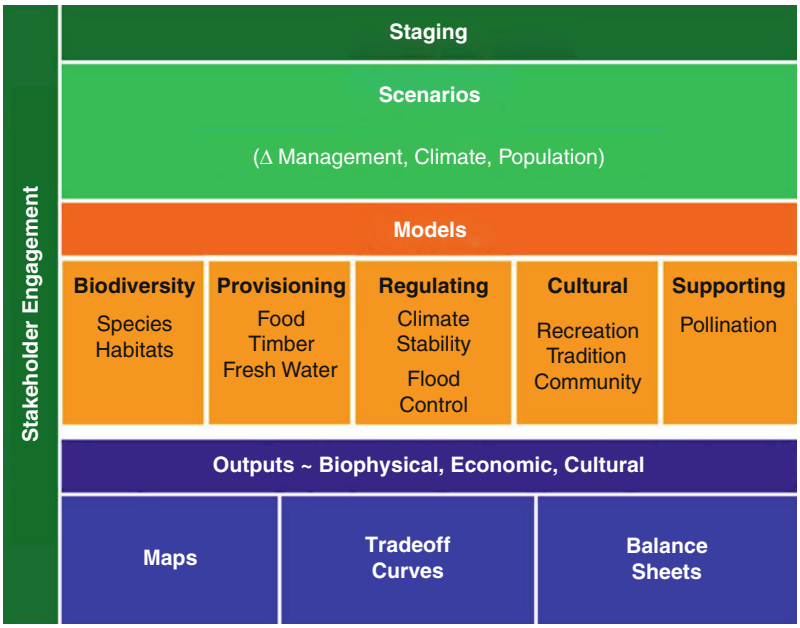

Ecosystem Services. Figure 4
An iterative process for integrating ecosystem services into decisions. The process begins with stakeholder engagement around impending decisions, with a focus on realistic, alternative scenarios for the future. The modeling is shaped by stakeholders, and typically focused on the services and scenarios deemed most important. Outputs are displayed in accordance with stakeholder preferences, in the form of maps, trade-off curves, and/or balance sheets. These can be expressed in biophysical (e.g., tons of carbon), economic (e.g., dollars), or cultural (e.g., visitor-days) terms

Relating Ecosystem Services and Human Health

The relationships between biophysical attributes of ecosystems and human health are complex [41]. Destruction of natural ecosystems can at times improve aspects of public health. Draining swamps, for example, can reduce habitat for the mosquito vector that transmits the parasite that causes malaria. On the other hand, destruction of other systems can have sharp negative consequences for human health. There is emerging evidence that loss of tropical forests, for example, leads to an increase in transmission of malaria [1, 50]. Similarly, fragmentation of, and biodiversity loss from, eastern North American forests is associated with an increase in lyme disease [32].

Natural and managed ecosystems provide many services that sustain human health, through provision of human nutrition (especially of protein and micronutrients); purification and regulation of drinking water; regulation of air quality; regulation of vector-borne disease; and psychological benefits. There is a great need for research illuminating the links between biodiversity, ecosystem conditions and processes, and human health.

Trade-offs and Synergies

The relationship between ES and biodiversity and among different ES varies with socio-ecological context. In some cases, clear trade-offs and synergies among services have been defined in specific contexts [54], but there is still much to be learned about what determines the nature of these relationships. Advancing this knowledge is essential because policies addressing management change can only be successful if management controls ES relationships. If policies are established to align multiple ecosystem services, but biophysical conditions in the system lead to innate trade-offs among services, management changes are bound to fail in delivering the desired improvements to social benefits.

Distributional Effects

Much of the science of mapping ES has focused on identifying where ES are generated and where they are delivered. However, less work has focused on identifying to whom ES actually flow. This connection is essential if policies addressing ES delivery are to be equitable and either improve the well-being of the poor or avoid unintended distributional consequences. Past work in this arena has focused on overlaying maps of ES provision with an array of poverty indicators (e.g., [68]). Missing from this spatial analysis is information on access to and ability to control the delivery of ES. In many cases (e.g., for services such as clean drinking water, hydropower production, agriculture, water for irrigation, wave power generation), the actual delivery of services to specific people is affected by the location of infrastructure or institutions regulating access to resources. New science is needed that allows the ready mapping of these connections and the prediction of how they will change under future conditions.

Dynamic Effects: Shocks and Uncertainty

Dynamic changes, such as in climate and in the nitrogen cycle – as well as changes arising through economic development and evolving human preferences over time – are very important. The possibility of feedbacks within ecosystems, and between ES and human behavior, is a key area for further development. Feedback effects can give rise to thresholds and rapid changes in systems that can fundamentally alter system outcomes [60]. The ability to incorporate shocks and the possibility of surprises is another area where further development is needed. Fires, droughts, and disease all can have major influences on ecosystems and affect the services produced. Changes in economic conditions or fads in human behavior can similarly cause major changes in systems (e.g., financial crises). The occurrence of each of these and other potential disturbances is difficult to predict but virtually certain to come about. Understanding their likely impacts on ecological and social systems will help us prepare for them.

Valuation in Monetary and Non-monetary Terms for Decision-Making

Monetary valuation of ES is not nearly as prevalent as sometimes assumed. More typically, real-world applications of the ES framework rely on biophysical values to inform policy design, such as measures of water quality or flood risk.

Value is not always easily characterized or fully captured in monetary terms, so it is important to characterize value in multiple dimensions, including

health, livelihood support, cultural significance, etc. (e.g., [17]). This will help ensure that valuation and broader decision-making approaches are inclusive of the range of benefits and people concerned [28]. Interdisciplinary efforts are presently underway to create a conceptual framework that is useful both in theory and in practice for a broad suite of cultural ES.

Institutional Design

However ES are measured, there is a need for political and social science research to design institutions and policy mechanisms that better capture externalities. Efforts such as national accounts are blossoming now, but it is unclear how they will evolve and how successful governments will be at incorporating natural capital into national measures of wealth. There is great work to be done in determining the merits and limitations of alternative policy and finance mechanisms, in different economic, governance, and other social contexts (e.g., [5, 46, 58, 59]). There is also great work to be done in developing institutions that achieve representation and participation by stakeholders as part of adaptive governance systems (e.g., [13, 55]).

Conclusions

Ecosystem services have had a relatively long history through indirect recognition of the importance of nature for the persistence of the human endeavor. There are scientific challenges for biogeochemists, hydrologists, ecologists, economists, anthropologists, and other social scientists to understand how human actions affect ecosystems, the provision of ES, and the value of those services. At least as demanding are the social and political questions associated with incorporating this understanding into decision-making. There is also a need to design effective and enduring institutions to manage, monitor, and provide incentives that reflect the social values of ecosystem services. Information is becoming more readily available for individuals, corporate managers, and government officials who make decisions affecting ecosystems and the services to consider a more complete set of costs and benefits associated with their choices. We are likely to see continuing growth in our scientific ability to measure and predict changes in ES, our ability to design policies and institutions that accurately represent these changes and in turn, the ability of the environment to continue providing the many benefits society needs to prosper.

Bibliography

Primary Literature

1. Afrane YA, Little TJ, Lawson BW, Githeko AK, Yan G (2008) Deforestation and vectorial capacity of *Anophiles gambiae* Giles mosquito in malaria transmission, Kenya. Emer Infect Dis 14:1533–1538
2. Barbier E, Koch E, Silliman B et al (2008) Coastal ecosystem-based management with non-linear ecological functions and values. Science 319:321–323
3. Beattie B, Taylor CR (1985) The economics of production. Wiley, New York
4. Bennett E, Peterson G, Gordon L (2009) Understanding relationships among multiple ecosystem services. Ecol Lett 12:1394–1404
5. Berkes F, Colding J, Folke C (2003) Navigating social-ecological systems. Cambridge University Press, Cambridge
6. Boody G, Vondracek B, Andow D et al (2005) Multifunctional agriculture in the United States. Bioscience 55:27–38
7. Boyd JW, Banzhaf HS (2005) Ecosystem services and government accountability: the need for a new way of judging Nature's value. Resources 158:16–19, Summer
8. Brauman KA, Daily GC, Duarte TK, Mooney HA (2007) The nature and value of ecosystem services: an overview highlighting hydrologic services. Annu Rev Environ Resour 32:67–98
9. Cao S, Zhong B, Yue H, Zeng H, Zeng J (2009) Development and testing of a sustainable environmental restoration policy on eradicating the poverty trap in China's Changting County. Proc Natl Acad Sci 106:10712–10716
10. Chan K, Shaw R, Cameron D et al (2006) Conservation planning for ecosystem services. Public Libr Sci Biol 4:2138–2152
11. Clark C (1990) Mathematical bioeconomics, 2nd edn. Wiley, New York
12. Colling A (2001) Ocean circulation. Butterworth Heineman/The Open University, Milton Keynes
13. Cowling R, Egoh B, Knight AT et al (2008) An operational model for mainstreaming ecosystem services for implementation. Proc Natl Acad Sci 105:9483–9488
14. Daily GC (ed) (1997) Nature's services. Island Press, Washington, DC
15. Daily GC, Ellison K (2002) The new economy of nature. Island Press, Washington, DC
16. Daily GC, Polasky S, Goldstein J et al (2009) Ecosystem services in decision-making: time to deliver. Front Ecol Environ 7:21–28
17. Dasgupta P (2001) Human well-being and the natural environment. Oxford University Press, Oxford
18. Dasgupta P, Heal G (1979) Economic theory and exhaustible resources. Cambridge University Press, Cambridge, UK
19. De Groot D, Wilson MA, Boumans RMJ (2002) A typology for the classification, description and valuation of ecosystem functions, goods and services. Ecol Econ 41:393–408

20. Egoh B, Reyers B, Rouget M et al (2008) Mapping ecosystem services for planning and management. Agric Ecosyst Environ 127:135–140
21. Ehrlich PR, Mooney HA (1983) Extinction, substitution, and ecosystem services. BioScience 33:248–254
22. Fisher B, Turner RK, Morling P (2008) Defining and classifying ecosystem services for decision making. Ecol Econ 68:643–653
23. Freeman AM III (1993) The measurement of environmental and resource values. Resources for the Future, Washington, DC
24. Gleick P (1996) Water resources. In: Schneider S (ed) Encyclopedia of climate and weather. Oxford University Press, New York, pp 817–823
25. Goldman R, Benítez S, Calvache A, Rámos A (2010) Water funds: protecting watersheds for nature and people. The Nature Conservancy, Arlington
26. Goldman RL, Tallis H, Kareiva P, Daily GC (2008) Field evidence that ecosystem service projects support biodiversity and diversify options. Proc Natl Acad Sci 105:9445–9448
27. Harrison J, Bouwman A, Mayorga E, Seitzinger S (2010) Magnitudes and sources of dissolved inorganic phosphorus inputs to surface fresh waters and the coastal zone: a new global model. Glob Biogeochem Cycles 24:271–279
28. Heal G (2000) Nature and the marketplace: capturing the value of ecosystem services. Island Press, Washington, DC
29. Holdren J, Ehrlich P (1974) Human population and the global environment. Am Sci 62:282–292
30. Jackson RB, Randerson JT, Canadell JG, Anderson RG, Avissar R, Baldocchi DD, Bonan GB, Caldeira K, Diffenbaugh NS, Field CB, Hungate BA, Jobbágy EG, Kueppers LM, Nosetto MD, Pataki DE (2008) Protecting climate with forests. Environ Res Lett 3:1–5
31. Kareiva PK, Tallis H, Ricketts TH, Daily GC, Polasky S (eds) (2011) Natural capital: theory & practice of mapping ecosystem services. Oxford University Press, Oxford
32. Keesing F et al (2010) Impacts of biodiversity on the emergence and transmission of infectious diseases. Nature 468:647–652
33. Kremen C (2005) Managing for ecosystem services: what do we need to know about their ecology? Ecol Lett 8:468–479
34. Krutilla JV (1967) Conservation reconsidered. Am Econ Rev 57:777–786
35. Krutilla JV, Fisher AC (1975) The economics of natural environments: studies in the valuation of commodity and amenity resources. Johns Hopkins University Press, Baltimore
36. Li J, Feldman M, Li S, Daily GC (2011) Rural household income and inequality under payment for ecosystem services: the Sloping Land Conversion Program in Western China. Proc Natl Acad Sci 108:7721–7725
37. Liu J, Li S, Ouyang Z et al (2008) Ecological and socioeconomic effects of China's policies for ecosystem services. Proc Natl Acad Sci 105:9489–9494
38. MA (Millennium Ecosystem Assessment) (2005) Ecosystems and human well-being: the assessment series (four volumes and summary). Island Press, Washington, DC
39. Melillo JM, Mcguire AD, Kicklighter DW, Moore B, Vorosmarty CJ, Schloss AL (1993) Global climate-change and terrestrial net primary production. Nature 363:234–240
40. Mooney HA, Ehrlich PR (1997) Ecosystem services: a fragmentary history. In: Daily GC (ed) Nature's services. Island Press, Washington, DC, pp 11–19
41. Myers S, Patz J (2009) Emerging threats to human health from global environmental change. Annu Rev Environ Resour 34:223–252
42. Naidoo R, Ricketts TH (2006) Mapping the economic costs and benefits of conservation. PLoS Biol 4:e360
43. Nelson E, Mendoza G, Regetz J et al (2009) Modeling multiple ecosystem services, biodiversity conservation, commodity production, and tradeoffs at landscape scales. Front Ecol Environ 7:4–11
44. Nepstad D, Carvalho G, Barros AC, Alencar A, Capobianco JP, Bishop J, Moutinho P, Lefebvre P, Silva UL, Prins E (2001) Road paving, fire regime feedbacks, and the future of Amazon forests. For Ecol Manag 154:395–407
45. NRC (National Research Council) (2005) Valuing ecosystem services: toward better environmental decision-making. National Academies, Washington, DC
46. Ostrom E (2005) Understanding institutional diversity. Princeton University Press, Princeton
47. Pagiola S, Arcenas A, Platais G (2005) Can payments for environmental services help reduce poverty? World Dev 33:237–253
48. Pagiola S, Bishop J, Landell-Mills N (2002) Selling forest environmental services. Earthscan, London
49. Parry ML, Canziani OF, Palutikof JP, van de Linden PJ, Hanson CE (eds) (2007) Contribution of working group II to the fourth assessment report of the intergovernmental panel on climate change. Cambridge University Press, Cambridge, UK
50. Patz JA, Olson SH (2006) Malaria risk and temperature: influences from global climate change and local land use practices. Proc Natl Acad Sci 103:5635–5636
51. Peterson C, Lubchenco J (1997) Marine ecosystem services. In: Daily G (ed) Nature's services. Island Press, Washington, DC
52. Polasky S, Nelson E, Pennington D, Johnson KA (2010) The impact of land-use change on ecosystem services, biodiversity and returns to landowners: a case study in the state of Minnesota. Environ Resour Econ 48:219–242
53. Postel S, Carpenter S (1997) Freshwater ecosystem services. In: Daily GC (ed) Nature's services. Island Press, Washington, DC, pp 195–214
54. Raudsepp-Hearne C, Peterson GC, Bennett EM (2010) Ecosystem service bundles for analyzing tradeoffs in diverse landscapes. Proc Natl Acad Sci 107:5242–5247
55. Rickenbach MG, Reed AS (2002) Cross-boundary cooperation in a watershed context: the sentiments of private forest landowners. Environ Manage 30:584–594
56. Ricketts T, Regetz J, Steffan-Dewenter I et al (2008) Landscape effects on crop pollination services: are there general patterns? Ecol Lett 11:499–515
57. Rokityanskiy D, Benítez P, Kraxner F et al (2007) Geographically explicit global modeling of land-use change, carbon sequestration, and biomass supply. Technol Forcasting Soc Chang 74:1057–1082

58. Ruhl JB, Kraft SE, Lant CL (2007) The law and policy of ecosystem services. Island Press, Washington, DC
59. Salzman J (2005) Creating markets for ecosystem services: notes from the field. NYU Law Rev 80:870–961
60. Scheffer M, Carpenter SR, Foley J et al (2001) Catastrophic shifts in ecosystems. Nature 413:591–596
61. Schlesinger W (1991) Biogeochemistry: an analysis of global change. Academic, San Diego
62. Tallis H, Goldman R, Uhl M, Brosi B (2009) Integrating conservation and development in the field: implementing ecosystem service projects. Front Ecol Environ 7:12–20
63. Tallis H, Lester SE, Ruckelshaus M, Plummer M, McLeod K, Guerry A, Andelman S, Caldwell MR, Conte M, Copps S, Fox D, Fujita R, Gaines SD, Gelfenbaum G, Gold B, Kareiva P, Kim C, Lee K, Papenfus M, Redman S, Silliman B, Wainger L, White C (2012) New metrics for managing and sustaining the ocean's bounty. Mar Policy 36:303–306
64. Troy A, Wilson M (2006) Mapping ecosystem services: practical challenges and opportunities in linking GIS and value transfer. Ecol Econ 60:435–449
65. United Nations Environment Programme (2006) Marine and coastal ecosystems and human well-being: a synthesis report based on the findings of the millennium ecosystem assessment. UN Environment Programme, Nairobi
66. van Mantgem PJ, Stephenson NL, Byrne JC, Daniels LD, Franklin JF, Fulé PZ, Harmon ME, Larson AJ, Smith JM, Taylor AH, Veblen TT (2009) Widespread increase of tree mortality rates in the Western United States. Science 323:521–524
67. Wallace K (2007) Classification of ecosystem services: problems and solutions. Biol Conserv 139:235–246
68. World Resources Institute (2007) Kenya poverty mapping
69. Wunder S, Engel S, Pagiola S (2008) Taking stock: a comparative analysis of payment for environmental services programs in developed and developing countries. Ecol Econ 65:834–852
70. Zhang P, Shao G, Zhao G et al (2000) China's Forest policy for the 21st century. Science 288:2135–2136

Ecosystems and Spatial Patterns

Patrick M. A. James[1], Marie-Josée Fortin[2]
[1]Department of Biological Sciences, University of Alberta, Edmonton, AB, Canada
[2]Department of Ecology and Evolutionary Biology, University of Toronto, Toronto, ON, Canada

Article Outline

Glossary
Definition of the Subject
Introduction
Sources of Heterogeneity
Spatial Analyses
Spatial Analyses within an Ecosystem
Spatial Analyses Among Ecosystem
Future Directions
Acknowledgments
Bibliography

Glossary

Disturbance A spatial process or event that reverts forest vegetation to early successional stages typically altering forest structure and composition.

Ecotone A region of interface between two communities, ecosystems, or biogeographic regions.

Legacy A persisting spatial feature or pattern that was generated by a historical disturbance. Legacies can constrain the spatial dynamics of contemporary disturbances.

Multi-scale analysis A method of spatial analysis that looks at the relative contributions of different scales of spatial pattern to a single observed spatial pattern.

Pattern A repeatable and identifiable feature in a spatial context.

Scale An attribute of a spatial process or data used to represent that process that describes its spatial dimensions. Scale includes elements of grain, extent, and thematic resolution.

Spatial autocorrelation The degree of correlation of a variable and itself as a function of the spatial distances among sample points.

Stationarity A feature of a spatial process in which the mean and variance of a process is consistent across the extent of a study area.

Variography A geostatistical modeling tool for describing spatial variance and semivariance as a function of spatial distance among pairs of points.

Definition of the Subject

Ecological processes such as forest disturbances act on ecosystems at multiple spatial and temporal scales to generate complex spatial patterns. These patterns in turn influence ecosystem dynamics and have important consequences for ecosystem sustainability. Analysis of ecosystem spatial structure is a first step toward understanding these dynamics and the uncertain interactions among processes. There are many spatial

statistics available to describe and test spatial pattern within ecosystems and to infer the character of the processes that generated them. Indeed, improving understanding of the processes that create spatial pattern is a central objective of spatial pattern analysis. In addition to standard tests of spatial autocorrelation and patch structure, methods for multi-scale decomposition of spatial data and identification of stationarity are necessary to determine the key spatial scales at which the processes operate and affect ecosystems and to identify meaningful spatial subunits within larger contexts. Finally, tools for identifying ecosystem boundaries are also important to monitor boundary movement and changes in local ecosystem characteristics through time.

Introduction

Spatial Patterns in Ecosystems

The spatial structure of ecological systems is important to examine and understand as spatial structure mediates the flows of individuals, materials, and information through space and time [1]. These flows bear on the probabilities of occurrence and persistence of floral and faunal populations which determine local and regional biological diversity as well as ecosystem functioning [2]. Interruptions and alterations of such flows within and among ecosystems in terms of rate, quantity, or both as a result of human interventions or natural dynamics such as disturbance can have important consequences for ecosystem sustainability and long-term population persistence. Quantitative characterization of spatial patterns and their rates of change in natural environments is essential to understanding ecological processes and to inform sustainable management techniques that aim to minimize degradation and alteration of ecosystem dynamics [3].

Spatial pattern, or simply spatial structure, refers to a quantifiable attribute of a spatial context. General definitions of the word pattern include a simple definition such as a distinctive or regular "form" or "order," or a feature that is repeated with some degree of "regularity" [4]. Recently, Wagner and Fortin [5] defined the more general term "spatial heterogeneity" as spatially structured variability in a property of interest. Both exogenous environmental (e.g., edaphic variability, elevation, climate) and endogenous ecological (e.g., species interactions, pollen, and seed dispersal) processes generate spatial structure. Each of these two types of spatial processes can produce spatial pattern in multiple forms and scales (Fig. 1). The simplest form of spatial pattern is a simple gradient (Fig. 1a). Spatial

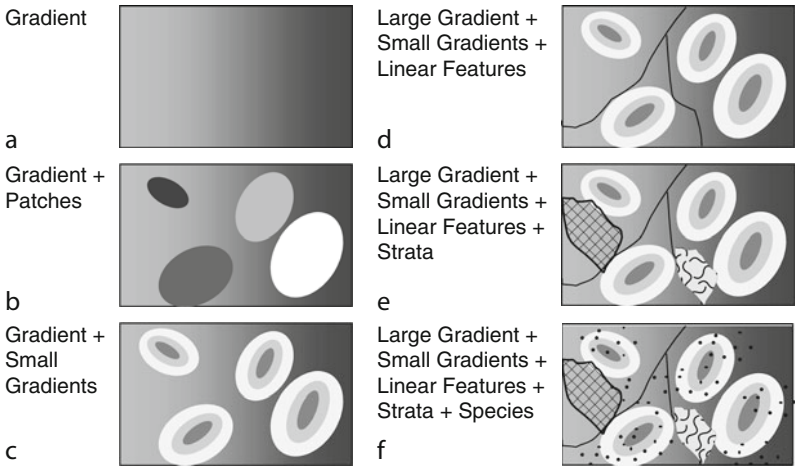

Ecosystems and Spatial Patterns. Figure 1
Spatial heterogeneity as a series of additive processes resulting in additive spatial patterns to which individual organisms (here represented points) may respond. Some or all of the different types of spatial heterogeneity may be present in any given landscape

structure can also be present in the form of patches, linear features, and points and can be superimposed on a gradient (Fig. 1b–f). When biological spatial structure is mostly responding to environmental conditions such as those depicted in Fig. 1, the resulting spatial structure is said to have spatial dependency to the environmental factors. However, when spatial structure emerges as a result of interactions among ecological processes, the pattern is said to be spatially autocorrelated [5].

Spatial patterns and heterogeneity can also be defined using spatial and topological characteristics. These characteristics can include, but are not limited to, a pattern's intensity, autocorrelation, degree of clustering, variability, and scale, which itself includes spatial grain and extent [6]. Importantly, a single pattern summarized using different characteristics can result in different interpretations of the processes behind that pattern [7, 8].

Because spatial pattern analysis is often interested in inferring the processes that created them, it is important to recognize that any single observed pattern represents but one realization of the stochastic process(es) that generated it [7, 9]. By acknowledging that an observed pattern is but a single "snapshot," its temporal dimension is recognized and that under different circumstances, the patterns seen may not be exactly the same. Hence, a main objective of studying spatial pattern is to try to tease apart stochastic processes and the patterns they create from their spatiotemporal conditionalities.

In addition to being driven by processes that are stochastic, patterns emerge as a result of multiple processes that operate at different spatial and temporal scales [10, 11]. These processes can be biotic or abiotic and are usually interconnected through dynamic, and occasionally nonlinear, feedback loops. For example, emergent spatial pattern following forest fires is conditional on the initial distribution of forest fuels as well as fire-weather conditions [12]. Similarly, patterns in forest vegetation composition are often related to patterns in abiotic factors such as moisture, drainage, and soil conditions. Patterns in the genetic composition in animal populations have also been shown to be influenced by the environmental variation (e.g., suitable vs. unsuitable habitat) between sampled populations [13]. These relationships are often nonlinear as the patterns that result from the interactions among pattern-generating processes tend to be different than any one process on its own [14, 15].

Novel spatial patterns created by contemporary anthropogenic processes have uncertain consequences for natural ecosystem dynamics. Anthropogenic processes including deforestation, development, land use change, and climate change do not replace natural processes, but have the capacity to interact with and alter them. As such, a significant question in modern ecology and ecosystem science is that of what are the effects of such novel patterns and processes on natural, or historical, system dynamics [16–18]. Not only do new sources of spatial variability influence natural dynamics through changing the patterns to which natural processes respond, but they also can alter the processes themselves. For example, with regard to forest fire dynamics, this is true where forest composition has been changed due to fire suppression and management (pattern change) and fire frequencies are increased due to increased ignitions near roads or changes in local weather patterns (process change). Similarly, with regard to animal population dynamics, movement and dispersal may be impeded through habitat loss and fragmentation (pattern change) and habitat loss can have an absolute effect on effective population size, rates of dispersal, and genetic variability (process change). Sophisticated spatial statistical analyses are required to begin to disentangle the contributions of different processes to observed spatial patterns to understand how best to manage natural systems to safeguard against further habitat-related losses to biodiversity [19].

Here the causes and consequences of spatial patterns in terrestrial forest ecosystems are reviewed with particular emphasis on patterns of forest vegetation generated through landscape level disturbance processes. Spatial patterns in forest vegetation are both ecologically and economically important in that they are directly relevant to wildlife habitat supply, timber supply, future disturbance dynamics, and represent future challenges to forest and land managers. Uncertainty regarding future disturbance dynamics, in particular fire and insects outbreaks, in the context of global climate change makes investigations into disturbance interactions and potential long-terms consequences for ecosystem spatial structure and functioning particularly relevant.

Forest Ecosystems

In North American forests, disturbance processes generally include landscape level fires, insect outbreaks, forest management (i.e., logging), and fine-scale local disturbances such as windthrow and fungal diseases. The patterns created through the interactions among disturbances can have important economic and ecological consequences. For example, Stadler et al. [20] demonstrated that hemlock wolly adelgid (*Adelges tsugae*) infestations in New England can affect both fast and slow ecosystem dynamics, nutrient cycling dynamics in the short term, and landscape-scale patterns of forest composition in the long term. Similarly, compounded disturbances (e.g., fire and logging) in the eastern boreal forest can result in alternate forest states [21], which can have consequences for biodiversity conservation. Economically, it has been clearly demonstrated that forests under risk of disturbance, either through fire or insect outbreaks, required longer rotation periods to accommodate for the losses [22].

Logging, fire, and insect outbreaks represent disturbance processes that revert forest stands to early seral stages. Succession describes processes of forest recovery, regeneration, and change that vary in response to different disturbances. Although multiple processes generate forest spatial heterogeneity, not all influence it in the same way. Spatial disturbance legacies vary in terms of shape, size, intensity, boundary characteristics, influence on forest succession, and effects on forest age structure [18, 23–25]. The interactions among processes, or more properly, interactions among current disturbance and existing spatial legacies, create and maintain heterogeneous forest landscapes. This cascade of effects and constraints creates mutual dynamic feedbacks among patterns (spatial legacies) and spatial processes (disturbances) [26, 27] with important consequences for ecosystem dynamics.

Different forest disturbances create different forms of spatial structure. Indeed, each disturbance imposes its own unique "spatial signature" on the landscape that also has different temporal characteristics contingent on a disturbance's interaction with succession (Fig. 2). Fires, for example, tend to produce relatively discrete patches that occur over a short time frame and vary in terms of the residual forest structure that is left behind [28]. Logging is somewhat similar to fires in that the patches created are discrete and occur over short time frames and forest managers have control over the scale and amount of residual structure. Insect disturbances, such as outbreaks of spruce budworm (*Choristoneura fumiferana*), forest tent caterpillar (*Malacasoma disstri*), and the mountain pine beetle (*Dendroctonus ponderosae*), are less discrete and tend to produce more complicated spatial structure and continue to affect forest structure at a given location for multiple consecutive years [29].

Each disturbance also has a unique relationship with forest regeneration processes [30] such that forest succession is tightly coupled to the type of disturbance that reinitiates stand development. These relationships determine future forest structure. Historically, fire and insects were the main disturbances in North American forest systems. Adaptations to disturbance such as serotiny in pine species (e.g., jack pine; *Pinus banksiana*) and advanced regeneration in the understory of spruce (e.g., *Picea spp.*) and balsam fir (*Abies balsamea*) stands that maintain spruce budworm host availability over time [31] are evidence of this dynamic feedback between disturbance and succession. The spatial patterns created through forest management and their influences on forest succession in turn influence future forest disturbances dynamics [32]. Spatial pattern analysis is important to better understand the effects of human activities on natural disturbance dynamics.

Sources of Heterogeneity

Understanding the nature and consequences of spatial heterogeneity in ecosystems requires an understanding of the processes that generate this heterogeneity. In this section, different types of spatial heterogeneity and how different types of processes may give rise to complex spatial patterns are described. The consequences and potential challenges involved in indentifying the relative contributions of these different and frequently interacting processes are discussed next [6].

Levels of Organization

Processes that generate spatial heterogeneity can be classified into a hierarchy of spatial processes that operate at different levels of ecological organization: (1) individual, (2) population, (3) community, and

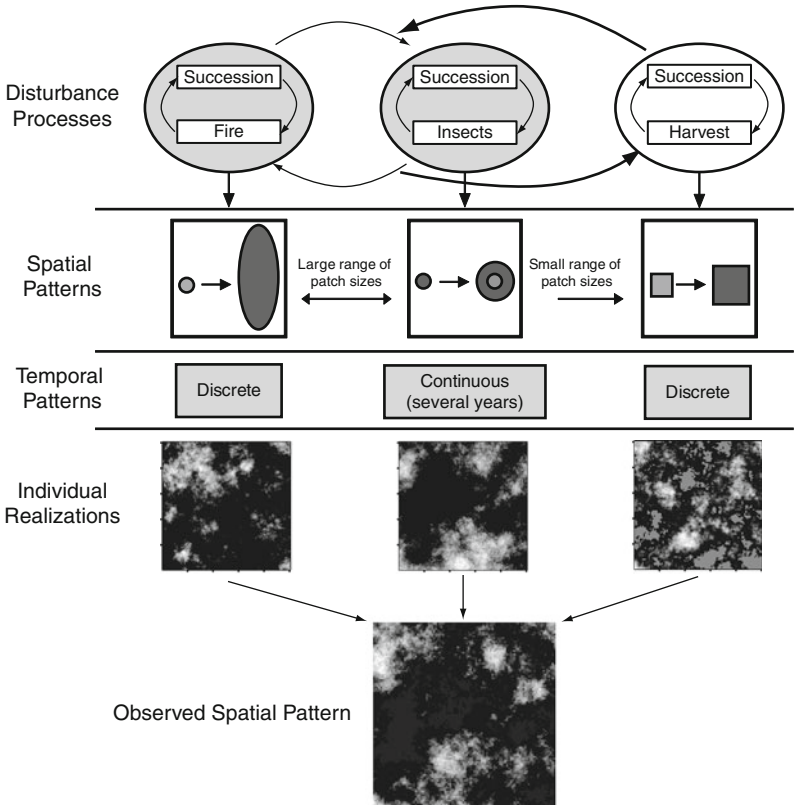

Ecosystems and Spatial Patterns. Figure 2
Spatial and temporal scales of forest disturbances. Interactions among disturbances are dependent on the unique successional responses to each disturbance (*row 1*). Historical forest systems were governed by interactions mainly between fire and insects (*arrows*) although presently, logging also interacts with these historical processes. Columns show the unique spatial and temporal attributes of each of the three main boreal forest disturbance agents: fire, insects (i.e., SBW), and harvesting (i.e., logging). These different spatial features result in different realization, or spatial signatures, of each disturbance (*row 4*). Interactions among these different processes produce a single observed spatial realization of spatial structure that contains elements of each of the different processes (*row 5*). Observed patterns contain elements of all three main processes; the objective of spatial analyses is to begin to tease apart the relative contributions of different processes to observed spatial pattern (*row 6*)

(4) landscape/ecosystem. Individual processes include organism dispersal and habitat selection; population processes can include demographic dynamics as well as immigration/emigration; community level processes are highly relevant to natural disturbance dynamics and can include successional changes and rates of species turnover. Examples of landscape/ecosystem level processes include disturbance, climate change, and migration.

Processes within this organizational hierarchy are not necessarily independent and can influence each other among levels. Such interactions can influence emergent patterns due to potential cross-scale interactions and amplifications [33] and can also further complicate efforts to identify clear cause-and-effect relationships. A recent example of such cross-scale amplification in a forest ecosystem can be found within the mountain pine beetle (*Dendroctonus ponderosae*) system of Western Canada, where the recent outbreaks of the lodgepole pine infesting beetle have affected an unprecedented millions of hectares [34]. Here, the local dynamics of population control by host tree defenses were overcome when population numbers increased dramatically due to persistent warmer temperatures in the early 2000s.

The interactions between these local- and landscape-level processes are thought to have led to a positive feedback that allowed the outbreak to expand as much as it did [34].

Interactions Among Spatial Processes

Spatial processes within ecosystems interact with each other directly as well as with the spatial legacies of previous, historical processes. In this way, spatial patterns and processes are connected through a dynamic and persistent feedback loop [32]. Spatial legacies can be thought of as a form of spatiotemporal connectivity among disjunct spatial processes or events that are mediated by forest succession and aging. The legacies of historical processes as represented by contemporary patterns can have long-lasting and significant impacts on biodiversity [16, 35] and efforts to sustainably manage forest ecosystems [23, 36].

Spatial legacies can be defined at different scales and describe persisting features within a stand, landscape, or ecosystem. The term "legacy" can refer to fine-scale structural complexity following windthrow [37], landscape level forest age structure [18, 38], disturbance-mediated seed availability [39], and residual forest structure following fire [39, 40]. Because patterns of historical land use can influence contemporary ecosystem composition, configuration, and ecosystem process dynamics long after the actual event [41], a better understanding of spatial legacies and their influence on ecosystem dynamics and landscape change over time is needed and requires novel spatial and temporal methods of investigation and analysis.

From the perspective of sustainability, spatial disturbance legacies, including those created through human activities, represent future ecosystem patterns and future challenges for sustainable management. Gustafson et al. [42] showed that new forest harvest goals are not easy to achieve due to existing conditions when examining shifting forest management rules. Wallin et al. [38] demonstrated that shifts from a dispersed to an aggregated harvest pattern did not immediately result in a change in forest attributes such as patch size and edge density. Instead, new harvest rules had to work around the legacies of previous patterns, and original patterns were enforced. Similarly, Gustafson and Rasmussen [43] found that when varying parameters in a harvest simulation model, the persistent legacies of previous harvest patterns resulted in timber harvest shortfalls. Using a simulation approach, James et al. [18] demonstrated that legacies in forest age structure created through forest management can persist for over 100 years. Ecologically, the consequences of these legacies interacting with new disturbances can result in greater system variability and gradual ecosystem degradation [43–45] or alternative stable states [21, 46].

Multiple Spatial Scales

Inferring the characteristics of spatial processes through analysis of spatial pattern is a central goal of most ecological studies as it is often very difficult to analyze the processes of interest directly. This can be particularly challenging when several types of pattern (Fig. 1) and underlying processes are present (Fig. 2). The challenge resides in the fact that the single observed pattern is an amalgamation of these multiple processes interacting with existing spatial structure and historical legacies; the functional relationships that connect these contributors to pattern are largely uncertain (Fig. 2). When analyzing the spatial structure of sampled data, it is not easy to disentangle the key spatial scales, and therefore processes, that act on the data. However, in the last decade, hierarchical decomposition methods (multi-scale ordination [47]; PCNM [48]; wavelets, [49] more detailed below) have been developed to identify the spatial scales at which data are most strongly structured and to decompose the data on the basis of scale-specific variances. Beyond simply describing patterns and the scales at which they are structured, it is also important to have a priori hypotheses about which scales and processes are the most relevant for the questions under study as these methods could reveal many patterns and spatial scales, many of which may not be of relevance [8]. Spatial pattern analysis will be more effective at describing underlying processes when used in an explicit and informed hypothesis testing framework.

Ecological Consequences of Spatial Heterogeneity

The consequences of changes in spatial pattern in forest landscapes are easily confounded by absolute losses in wildlife habitat [19]. That is, although both forest

composition and configuration are important, issues related to configuration are only relevant below a critical threshold of forest amount (usually 20–30% of area; [50]). Above the critical threshold, the landscape generally remains "connected" and organisms or disturbances can spread in the landscape [51]. Below such a critical threshold, species' response to the amount of habitat area is nonlinear as most species do not have enough habitat to meet their needs. Surrounding habitat quality (composition) and configuration become more important for local population persistence in this case. Moreover, fragmented landscapes with various landcover types can impede species abilities to move from habitat patches to another [52]. For example, nesting birds do not cross forest gaps larger than 25 m [53]. Impediments to movement across landscapes can influence population dynamics [54] as well as genetic heterogeneity [55], both of which affect the probability of population persistence.

Spatial Analyses

There are three main approaches to investigating the different aspects and consequences of spatial heterogeneity. Spatial statistics, landscape metrics, and statistical modeling, all approach the question of identifying spatial pattern in ecosystems in a slightly different way [5]. Owing to the varied history of approaches to studying spatial patterns including methods and concepts drawn from a diverse set of disciplines such as geography, geostatistics, and ecology, only the key concepts related to the most commonly used methods that quantify spatial structure within and among ecosystems are presented. Before describing the different types of analysis, some fundamental issues related to the spatial analysis of data are presented.

Assumption of Stationarity

To infer spatial pattern from samples spatial statistics require that the area under study is governed by the same underlying process (i.e., the assumption of stationarity; [7]). As it is often impossible to be sure that the underlying process is stationary, one needs either to assume it or to determine whether or not the observed data are stationary (i.e., their statistical properties such as mean, variance, isotropy do not vary with spatial distance). Nonstationary processes may arise when more than one process is present and that these multiple processes may be acting at different spatial or temporal scales. Yet, in most forest ecosystems, processes interact with one another, resulting in unique types and scales of spatial pattern which violate the assumption of stationarity. In such circumstances, it is required to first identify stationary subregions within such a larger spatial context. A few spatial analysis methods do not require the stationarity such as lacunarity analysis, local quadrat variance methods, and wavelets [7]. It is worth noting that these types of analyses although different and originating from different developmental histories are quite similar to one another mathematically [56].

Data Type

Spatial pattern within ecosystems can be represented using categorical or continuous data depending on the nature of the variable under investigation. Each type of data requires different methods of analysis (Fig. 3; [7]).

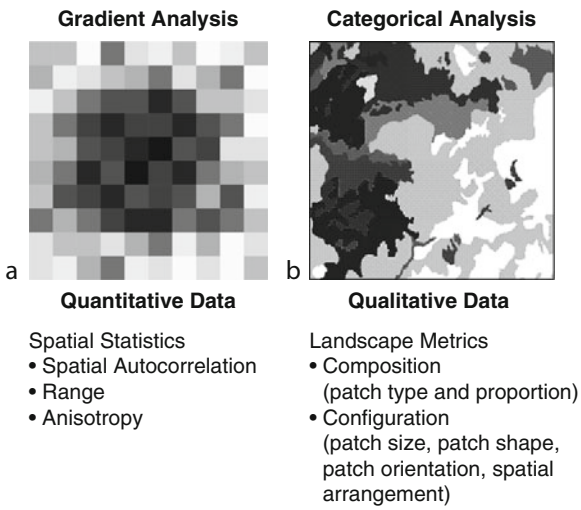

Ecosystems and Spatial Patterns. Figure 3
Spatial analysis can be undertaken on different types of spatial data. (**a**) Raster-based quantitative spatial data (e.g., forest height, basal area, NDVI) that can be analyzed using spatial statistics to determine the intensity, spatial range, and directionality (anisotropy) of the spatial pattern. (**b**) Categorical and qualitative forest data (e.g., species, stand age) require a different analytical approach that typically includes landscape pattern metrics

Categorical data can be described by the amount and configuration of the different discrete types on the landscape. Examples of categorical spatial data include forest type and age, or classified habitat patches. Both amount and configuration can be described in numerous ways using landscape pattern metrics [9, 57, 58]. Continuous data requires more subtlety in describing patterns and can include variables such as soil moisture, forest basal area, or remotely sensed reflectance indices (e.g., NDVI). Composition of continuous variables can be described using the density distribution of the variable and configuration is usually described by a spatial covariance function that captures the strength, directionality, and scale of autocorrelation of the variable [5, 7, 59].

In addition to the categorical/quantitative dichotomy of data types, patterns can be described using different geometric topologies of spatial features or units: the vector format (points, lines, polygons) and the raster (i.e., pixel) format [60]. Representation of spatial structure in one form of data does not preclude use of another form. For example, annual polygons of insect defoliation data can be converted into raster form and analyses can be undertaken using time series of raster values at a specific location [61]. Furthermore, binary rasters (presence/absence) can be converted to continuous rasters by increasing the cell size and counting the number of "presence" pixels surrounding a focal pixel using 4-neighbour, 8-neighbour, 16-neighbour rules and assigning this value to the to the new, larger pixel.

Raster data can be used to represent any continuous variable. In contrast to point data, in raster data types, the information fully covers the extent of the study area. There is also a unique grain (or cell size) to each raster "pixel" that determines the subarea of continuous space that is discretized by the raster cell. The selection of raster grain can have important consequences to the results of spatial analyses [6]. Raster data can be used to represent any number of spatial variables relevant to disturbance ecology including, but not limited to, tree species [62], stand age [18, 63], basal area [64], insect damage [61], and number of fire occurrences [65]. The continuous coverage of raster data makes it amenable to many different analytical techniques such local quadrat variance, lacunarity, and wavelets [56].

Spatial Analyses within an Ecosystem

Ecological variables that are geographically distributed in space and time tend to be more similar when compared close together [66]. Autocorrelation is a feature of most data and can be quantified by the degree of self-similarity or dissimilarity in a variable between pairs of locations at a given distance apart (i.e., spatial lag determined in terms of equidistant classes). Note that spatial statistics on their own cannot differentiate between spatial dependence to environmental factors and spatial autocorrelation due to ecological processes; only prior knowledge and multiple testing can differentiate between these two sources of spatial structure.

Spatial Description of the Pattern

The objective of many spatial statistics is often to characterize to what degree spatial data are autocorrelated, if they are oriented in a particular direction (anisotropy), and at what scale. As these spatial statistics have been thoroughly reviewed elsewhere [7, 58], we focus on three topics (1) methods of spatial pattern analysis devoted to identifying structure in point data, (2) methods of spatial analysis that are devoted to identifying structure and pattern in two-dimensional raster (pixel) or polygon data, and (3) methods of spatial analysis explicitly concerned with identifying the scale, or scales of structure that are present in either point or two-dimensional data. Both the data types discussed can be examined in uni-, bi-, and multivariate contexts and can include either categorically or continuously measured variables.

Point Pattern Analysis

Spatial point processes describe phenomena that produce events represented as points in space [67, 68]. The objective of point pattern analysis is to determine whether the distribution of events (points in space) is more or less spatially aggregated than is expected by chance and tests the null hypothesis of complete spatial randomness. The use of complete spatial randomness assumes that the underlying process is the same over the study area (i.e., stationarity). When it is not the case, the study area is said to "inhomogeneous" such that significance cannot be achieved using a single process such as complete spatial randomness. Modified

statistics and corrections have been developed to account for inhomogeneity within the study area [69, 70]. Point pattern analysis also assumes complete census of all point occurrences in the study area [7]. Fortin et al. [71] showed that the significance of spatial aggregation estimations is biased only when a subset of sample points is used rather than the entire set of points in the study area.

The most commonly used method of point pattern analysis is Ripley's *K* statistic [72]. New statistics have also been developed to compute local estimates [68]. Ripley's *K* statistic, and derived statistics, can be applied in one-, two-, or three-dimensional space to compare the degree of aggregation of points [68]. In cases where two (or more) point processes are operating, it may be of interest to assess whether one process influences the other and whether points of different types tend to cluster together. Examples of ecologically relevant spatial point processes include fire occurrence, plant occurrences [67], or the distribution of animal nesting or denning sites [72]. The bivariate, or cross-*K*, Ripley's *K* test assesses whether the co-occurrence of two types of points is clustered together more or less than is expected by chance [58]. Using this technique, Lynch and Moorcroft [73] examined co-occurrence of fire and insect outbreaks and found that contrary to expectation, insect-caused forest mortality does not increase the risk of forest fire.

Spatial Autocorrelation

Often, a researcher is interested in determining the scale and strength of spatial autocorrelation of a variable as well as whether there is a directional trend in the data (i.e., anisotropy). This can be achieved using spatial autocorrelation coefficients such as Moran's *I* which computes the product of the deviations of the values of the variable to its average according to various distance intervals (lags, classes) standardized by the variance at that spatial lag [7]. Moran's *I* behaves like a Pearson's correlation coefficient such that the null hypothesis is the absence of spatial autocorrelation, positive autocorrelation (mostly a short distance) indicates that values have comparable values, while negative values indicate that the values are very dissimilar. Moran's *I* assumes that the underlying process is the same over the entire study area (i.e., stationarity). Hence, the spatial autocorrelation coefficients computed at various distance classes are average values. Spatial autocorrelation in this sense can be referred to as a global spatial statistic that describes an attribute of the data over the entire study area [7]. Significance of each coefficient can be computed based on an asymptotic *t* or randomization procedure. In either case, stationarity is required. Moran's *I* is very sensitive to skewed data as the mean will be biased and in consequence all the deviations values based on it will also be biased. It is therefore recommended to check the distribution of the data before computing spatial autocorrelation and if needed transform the data to obtain a symmetric distribution.

Measures of spatial autocorrelation are also sensitive to sample size. When autocorrelation is estimated using too few locations, (e.g., <30 positions), spatial patterns may not be detected, even though present. Similarly, depending on the spacing among sampling locations, there will be different numbers of paired comparisons at each lag distance. Typically, there are few pairs at short distances due to the edge effects of the edge of the study area (no locations outside to compare too), most of the pairs at intermediate distances and very fewer at large distances (because of the overall size of the study area). To mitigate these unequal numbers of pair per distance lag, it is recommended to focus on lags distances equal to the length of the first half (up to two thirds) of the smallest edge of the study area as most spatial autocorrelation occurs at short distances and that the probability of detecting it is also highest in the first spatial lag [7].

A plot of spatial autocorrelation coefficients against distance lags is called a spatial correlogram. If the lags are based on distance only, the correlogram is said to be an omnidirectional correlogram. When the data contain directionality, the omnidirectional correlogram cannot reveal it and may, in fact, "mask" it. To detect the presence of anisotropic spatial pattern (i.e., not having the same sill and range according to direction), the samples need to be divided by distance class as well as direction angle range (usually 0°, 45°, 90°, 135°) to produce a set of directional correlograms.

In areas where several processes influence ecological data, Moran's *I* that assumes stationarity cannot be used. Instead, local indicator of spatial aggregation statistics, LISA (e.g., local Moran, local Getis), can be

used as they are computed at each sampling location and allow the identification of subareas that have similar high ("hot spots") or low ("cold spots") values [7].

Geostatistics

Spatial structure can be determined in terms of spatial autocorrelation as presented above or as spatial variance according to distance as computed using variograms which are part of the family of spatial statistical methods known as geostatistics [7, 58]. Variograms represent a global method of scale-specific analysis that has been used extensively in ecology to analyze spatial patterns [58]. Variograms model the relationship between lag distance and semivariance and can be calculated using continuous raster or point data. Semivariance is calculated as the sum of the squared differences between pairs of locations separated by a given lag distance divided by twice the number of pairs of locations at that particular lag distance [7]. From the observed, or empirical, variogram, three parameters can be estimated to fit a theoretical variogram: (1) range, or scale at which distance does not affect the estimate of variance, (2) sill, or the variance of the data, and (3) nugget effect, which represents the variability in the data that is not accounted for by spatial structure [58]. Theoretical variogram models can identify whether there is a directional trend in the data, that is, anisotropy as the spatial autocorrelation values. In addition to describing the attributes of spatial structure, geostatistical models can be used to "krige" (i.e., spatially interpolate) data [58] and to simulate spatial patterns using a chosen variogram model, process model, and parameter estimates [74].

Spatial Scale and Scaling

In addition to understanding the type (e.g., trend, patch) and strength (e.g., degree and distance) of a spatial pattern, it is useful to identify the spatial scale at which such patterns are present. Because patterns are the result of multiple processes that each have their own unique scales of spatial structure [75], disentangling the relative contributions of these processes and assigning relative importance to them and the scales at which they operate are of fundamental importance to ecology and improving the understanding of complex systems [11, 16]. Furthermore, the identification of the relative contributions of different processes and scales to observed patterns is necessary for understanding cross-scale interactions [33] which is necessary to make reliable predictions of system dynamics, ostensibly the objective of any spatial analysis [76].

As stated above, spatial pattern describes a "quantifiable attribute of a spatial context." Scale-specific analysis identifies the spatial scale at which that attribute is structured establishes its specific context. With regard to forest disturbance dynamics, for example, individual forest stands may seem unstable through the processes of destruction and renewal through disturbances such as fire, but the larger forest landscape (i.e., collection of stands) is in fact stable with respect to the proportion and relative configuration of the different stand types. This is what is meant when disturbance-mediated forest systems are described as a shifting mosaic [77]. Different conclusions would be drawn about forest stability and resilience (sensu [78]) depending on the spatial or temporal scale of investigation.

Scale generally describes the spatial extent, grain, and thematic resolution of a set of data [6]. However, scale can also be used to refer to a level within an organizational hierarchy to which such data pertain, such as a population, or community, or ecosystem [79]. It is important to note that scale in this latter sense is not directly equivalent to the former; scaling up, that is, increasing from local to a broader extent, or aggregating data from a fine to a coarse scale may move the analysis into another level or an organizational hierarchy, but not necessarily [80]. Although scale is best thought of as a feature of the phenomena of interest, it can also be a feature of sampling scheme imposed by a researcher, or the methods of analysis applied [6]. All of these features can influence a researcher's ability to identify scales of structure in spatial data and to make meaningful inferences regarding the underlying processes. It is therefore important to distinguish structure that is emergent from the data from those related to sampling or analytic scales (i.e., arbitrary scales; [10]), as such a priori scales may have little to do with the actual scale of structure in the ecological phenomena of interest [76].

The ability to identify meaningful scales of spatial structure depends on the methods used and the type of data being analyzed [77, 81]. Methods differ in their

ability to identify local vs. global scales of pattern. Global methods of scale-specific analysis summarize spatial pattern at a single scale and generally assume that the underlying processes are stationary. Examples of global methods of analysis include variography [58], spectral (i.e., Fourier) analysis [82], and global measures of spatial autocorrelation such as Moran's *I* and Geary's *c* [7]. Multi-scale methods of analysis identify both global and local scales of structure, can assign relative importance to difference scales, and do not assume stationarity. Instead, such methods can be used to identify boundaries and scale-specific stationary subregions within a larger spatial context [7, 74]. Multi-scale methods of analysis include lacunarity analysis [83], wavelets [74, 81, 84], distance-based Eigenvector methods (e.g., PCNM; [85]), and local spatial statistics [86].

Wavelet analysis is a particularly powerful method of local spatial analysis that can be used to decompose continuous data into its scale-specific components [87, 88]. A proportion of the total variance in the data set is associated with each level of the decomposition through use of the wavelet variance [84] and the relative contributions of different scales to overall structure can be assessed and visualized as a scalogram (Fig. 4b). Each of these scales of pattern can then be isolated using a multi-resolution decomposition (Fig. 5; [88]). Under conditions where observed spatial pattern is assumed to be the result of multiple interacting processes, such data decomposition provides an opportunity to assess the relationship among processes and individual scales of spatial structure present in the data. In combination with the scalogram (Fig. 4b), the relative importance of these different scales can also be determined and further analyses can be restricted to only those spatial layers that correspond to the scales of interest. Isolated scales of spatial pattern can then be examined independently or used as scale-specific predictors in further statistical analyses [89].

Whereas Fourier analysis assumes that observed patterns can be described as a sum of sine waves of different frequencies, wavelet analysis identifies global and local structure at different scales using a local wavelet template that can take on a wide variety of shapes and forms [90]. The majority of wavelet

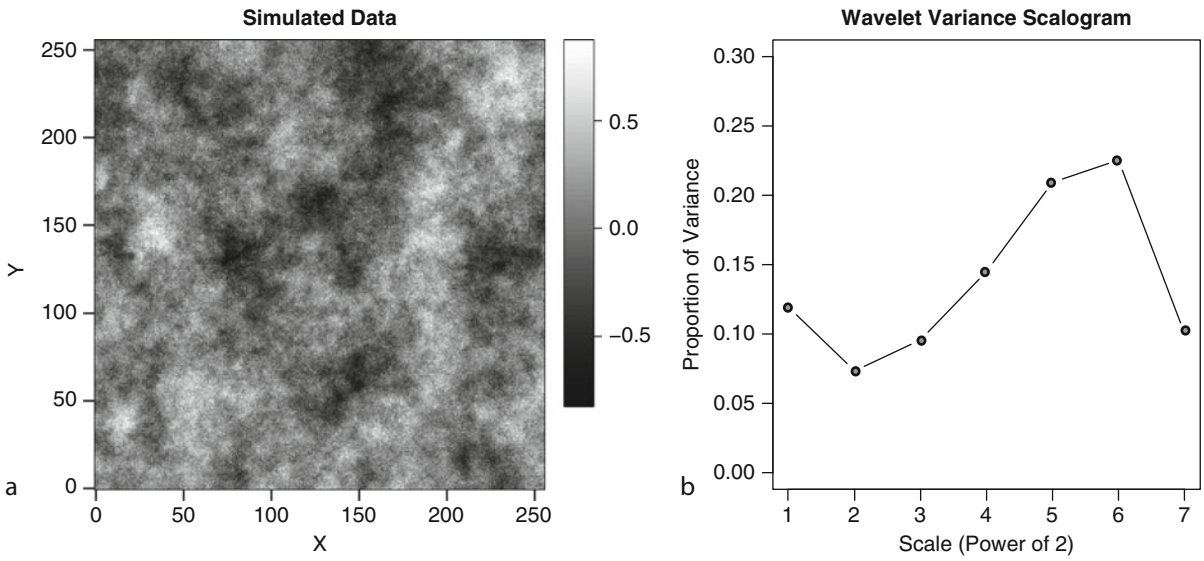

Ecosystems and Spatial Patterns. Figure 4

Example of a hierarchical multi-scale decomposition of two-dimensional, quantitative data using wavelets. (**a**) Simulated spatial data. (Data were simulated using an exponential variogram model with the following parameters: Sill = 1; Range = 40; Nugget = 0.1). (**b**) Scalogram that summarizes the proportion of total variance in the original data associated with each scale of the decomposition. Wavelet decomposition was accomplished using a maximal-overlap discrete wavelet transform (MODWT; Percival and Walden [109])

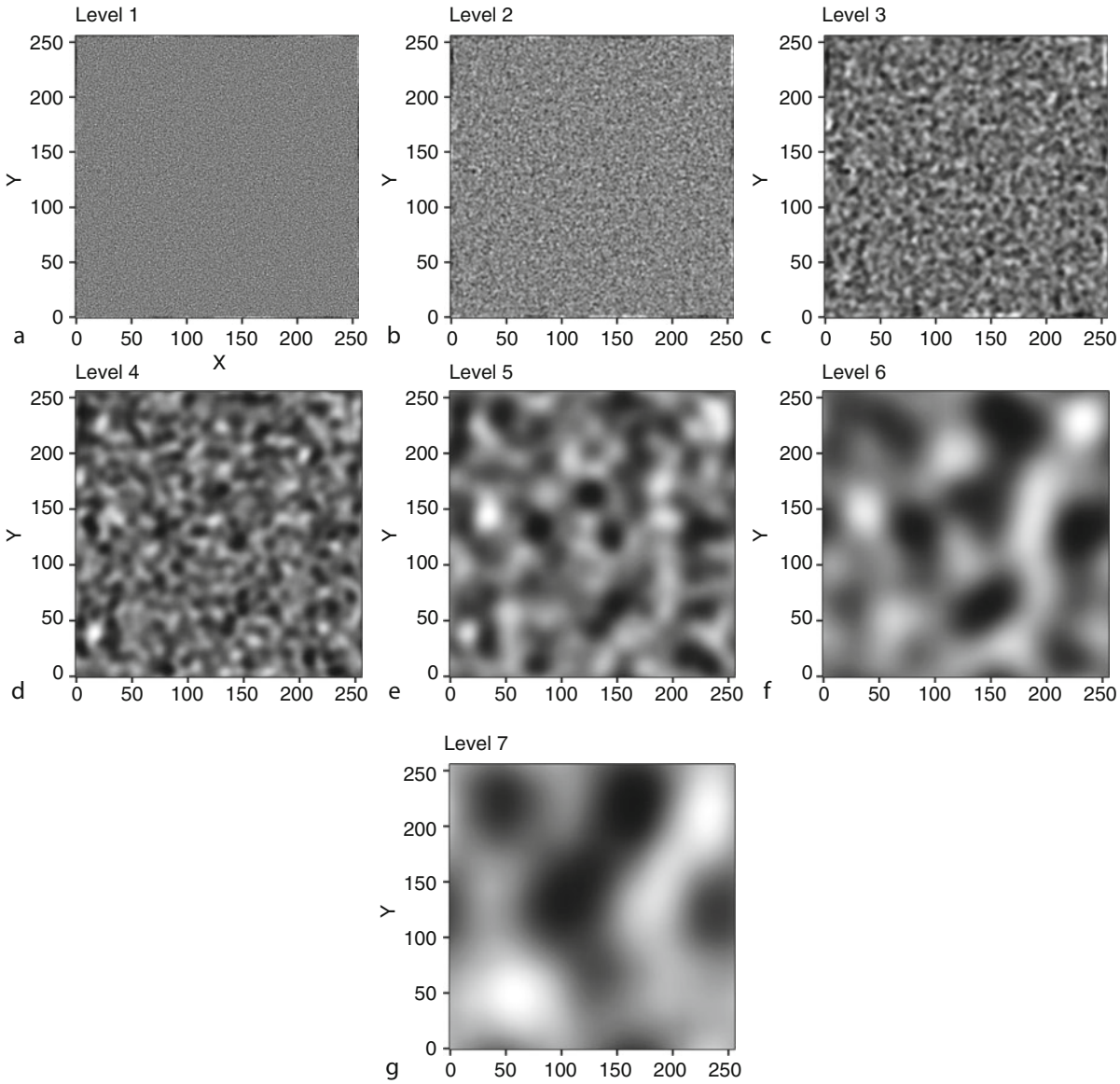

Ecosystems and Spatial Patterns. Figure 5
Back-transformed images from the decomposition of the data in Fig. 4a. Each panel shows the spatial structure at an individual isolated scale

applications have been in the analysis of temporal signals to identify periodicity in things such as climatic variability [91] and epidemiological time series [92, 93]. However, spatial applications of wavelet analysis in ecology continue to be developed and have been used to investigate one-dimensional forest canopy gap structure [87], vegetation reflectance [89], two-dimensional structure in grassland productivity [81], tree crown identification [94], and the significance of spatial structure in forest basal area [74].

When data are not sampled in a continuous way (i.e., they are irregularly spaced), multi-scale decompositions can be performed using spatial eigenfunction analyses such as principal coordinate analysis of neighbor matrices (PCNM) and Moran's eigenvector maps (MEM) [48, 95, 96]. These methods model spatial structure in

a multivariate framework using distance matrices where the spatial coordinates of the sampled sites are converted into a set of synthetic spatial variables that represent spatial structure at different spatial scales. These synthetic variables can then be used in combination with constrained ordination methods (e.g., canonical correspondence analysis and redundancy analysis; [95]) to identify the spatial scales at which data are dominantly structured. Jombert et al. [97] also proposed a multi-scale pattern analysis (MSPA) to determine which of these many scales are the most relevant to use as spatial predictors in subsequent analyses such as partial ordination or multiple regression [85].

Spatial Analyses Among Ecosystems

The ecotonal interfaces between ecosystems are important to delineate as they are the locations where the exchange of nutrients and species turnover occurs [7]. It is also important to determine not only the boundary location between ecosystems, that is, where one system begins and another ends, but also its width (i.e., sharp/line or gradual/zone) [98]. There are two different types of methods that can be used to determine the interface between ecosystems: by creating spatial clusters or by detecting boundaries [99]. In either case, the sampling design used to collect the data is crucial: The determination of a boundary (i.e., area of high rate of changes in the values of variables, hence a heterogeneous area) is relative to the two adjacent spatially homogeneous ecosystems. Therefore, the sampled data should cover enough of both ecosystems such that their interface can be detected.

Spatial Clustering

To delimit boundaries between ecosystems, spatially homogeneous clusters can be determined based on the degree of similarity of sample attributes and their spatial adjacencies [66, 99, 100]. The degree of similarity can be based on commonly used clustering algorithms (agglomerative, *k*-means, fuzzy logic, etc.) and adjacency can be based on network connectivity algorithms (e.g., nearest neighbors, minimum spanning tree, Gabriel network, Delaunay network; [7]). Spatial clustering provides the membership of each location to a spatial cluster and therefore, as a by-product, identifies boundaries among clusters. However, clustering procedures do not provide any information about the location and width of the identified boundaries between clusters. When information about location and width are needed, other methods should be used such as boundary detection methods ([99]; but see [101]).

Spatial Boundary Analyses

Ecological boundaries can be defined as areas of high rates of change or large absolute differences between adjacent locations [102]. Boundary detection methods [98] include edge detection algorithms (Laplacian, Canny, Sobel, Monomier, etc.), wavelet analysis [74, 81], and wombling (lattice, triangulation, categorical). The two former families of methods require the data to be in a contiguous fashion (grid) without any missing values while the latter one can either be used with contiguous or irregularly sampled data. All methods compute the magnitude of rate of change between adjacent locations over the entire extent of the study area. To determine which rates of changes are significantly higher than the others, different statistics and significance tests having been developed. Wombling typically uses arbitrary percentile thresholds of boundary elements to identify significant boundaries [7]. James et al. [74] proposed a series of restricted randomization procedures to test the significance of wavelet boundaries using variogram-based spatial null models. Oden et al. [103] developed boundary statistics to test the cohesiveness properties of the boundaries. Once cohesive boundaries have been detected and tested, subsequent hypothesis testing can be performed by comparing the spatial overlap and movement of boundaries using spatial overlap statistics [7, 104, 105] or polygon change analysis [106].

Future Directions

The detection and characterization of spatial structure is necessary for developing the understanding of ecosystem function and for ensuring sustainable management and use of landscape resources. Indeed, the current scale and pace of anthropogenic influence on the natural environment is without precedent and the ways in which novel human-created spatial patterns interact with and influence natural processes are uncertain. Even more uncertain are the relationships among different scales of spatial and temporal pattern and what such cross-scale

interactions may mean to ecosystem dynamics [107]. Future directions in the analysis of spatial pattern will require approaches and methods that can begin to tease apart the separate scales, both spatial and temporal, of processes that contribute to spatial patterns both within and among ecosystems. These methods should include multi-scale approaches such as the wavelet-based methods described above, tools to assess statistically significant changes over time, and methods that can identify local spatially significant subregions within larger spatial contexts [74]. Meaningful inference in these regards will only be possible if the spatial pattern analysis is applied within a hypothesis testing framework, where competing notions of how individual processes percolate through the landscape to produce pattern can be tested statistically [8]. Finally, increasing availability of remotely sensed data (e.g., NDVI, LiDAR, Quickbird, LANDSAT, MODIS) will allow people to detect spatial patterns at finer spatial and temporal scales over much larger spatial extents than has been previously possible. These huge amounts of data will also require focused, hypothesis-driven questions, the use of data-mining tools [108], and the further development of spatiotemporal statistics.

Acknowledgments

This work was funded by a Killam Postdoctoral fellowship at the University of Alberta to PMAJ and an NSERC Discovery grant to MJF.

Bibliography

Primary Literature

1. Lindenmayer DB, Fischer J (2006) Habitat fragmentation and landscape change. Island Press, Washington, DC
2. Loreau M, Naeem S, Inchausti P et al (2001) Biodiversity and ecosystem functioning: current knowledge and future challenges. Science 294:804–808
3. Lindenmayer DB, Franklin JF (2002) Conserving forest biodiversity. A comprehensive multiscaled approach. Island Press, London
4. Epperson BK (2003) Geographical genetics. Princeton University Press, Princeton
5. Wagner HH, Fortin M-J (2005) Spatial analysis of landscapes: concepts and statistics. Ecology 86:1975–1987
6. Dungan JL, Perry JN, Dale MRT et al (2002) A balanced view of scale in spatial statistical analysis. Ecography 25:626–640
7. Fortin M-J, Dale MRT (2005) Spatial analysis. Cambridge University Press, Cambridge
8. McIntire EJB, Fajardo A (2009) Beyond description: the active and effective way to infer processes from spatial patterns. Ecology 90:46–56
9. Fortin M-J, Boots B, Csillag F, Remmel TK (2003) On the role of spatial stochastic models in understanding landscape indices in ecology. Oikos 102:203–212
10. Wiens JA (1989) Spatial scaling in ecology. Funct Ecol 3:385–397
11. Levin SA (1992) The problem of pattern and scale in ecology. Ecology 73:1943–1967
12. Flannigan MD, Stocks BJ, Turetsky MR, Wotton BM (2008) Impact of climate change on fire activity and fire management in the circumboreal forest. Global Change Biol 14:1–12
13. McRae BH, Beier P (2007) Circuit theory predicts gene flow in plant and animal populations. Proc Natl Acad Sci USA 104:19885–19890
14. Veblen TT, Hadley KS, Nel EM et al (1994) Disturbance regime and disturbance interactions in a Rocky Mountain subalpine forest. J Ecol 82:125–135
15. Radeloff VC, Mladenoff DJ, Boyce MS (2000) Effects of interacting disturbances on landscape patterns: Budworm defoliation and salvage logging. Ecol Appl 10:233–247
16. Levin SA (2000) Multiple scales and the maintenance of biodiversity. Ecosystems 3:498–506
17. Cooke BJ, Nealis VG, Regniere J (2007) Insect defoliators as periodic disturbances in northern forest ecosystems. In: Johnson EA, Miyanishi K (eds) Plant disturbance ecology: the process and the response. Elsevier, Amsterdam, pp 1–10
18. James PMA, Fortin M-J, Fall A, Kneeshaw D, Messier C (2007) The effects of spatial legacies following shifting management practices and fire on boreal forest age structure. Ecosystems 10:1261–1277
19. Fahrig L (2003) Effects of habitat fragmentation on biodiversity. Ann Rev Ecol Evol Syst 34:487–515
20. Stadler B, Müller T, Orwig D, Cobb R (2005) Hemlock woolly adelgid in New England forests: canopy impacts transforming ecosystem processes and landscapes. Ecosystems 8:233–247
21. Jasinski JPP, Payette S (2005) The creation of alternative stable states in the southern boreal forest, Quebec, Canada. Ecol Monogr 75:561–583
22. MacLean DA, Erdle TA, MacKinnon WE et al (2001) The spruce budworm decision support system: forest protection planning to sustain long-term wood supply. Can J Forest Res 31: 1742–1757
23. Franklin JF, Forman RTT (1987) Creating landscape patterns by forest cutting: Ecological consequences and principles. Landscape Ecol 1:5–18
24. Fall A, Fortin M-J, Kneeshaw DD et al (2004) Consequences of various landscape-scale ecosystem management strategies and fire cycles on age-class structure and harvest in boreal forests. Can J Forest Res 34:310–322
25. Greene DF, Gauthier S, Noe J, Rousseau M, Bergeron Y (2006) A field experiment to determine the effect of post-fire salvage on seedbeds and tree regeneration. Front Ecol Environ 4:69–74
26. Watt AS (1947) Pattern and process in the plant community. J Ecol 25:1–22

27. Turner MG (1989) Landscape ecology: the effect of pattern on process. Ann Rev Ecol Evol Syst 20:171–197
28. Bergeron Y, Leduc A, Harvey BD, Gauthier S (2002) Natural fire regime: a guide for sustainable management of the Canadian boreal forest. Silva Fenn 36:81–95
29. Boulanger Y, Arseneault D (2004) Spruce budworm outbreaks in eastern Quebec over the last 450 years. Can J Forest Res 34:1035–1043
30. Schroeder D, Perera AH (2002) A comparison of large-scale spatial vegetation patterns following clearcuts and fires in Ontario's boreal forests. Forest Ecol Manage 159:217–230
31. Baskerville GL (1975) Spruce budworm: super silviculturist. Forestry Chron 51:138–140
32. Turner MG (1993) A revised concept of landscape equilibrium: disturbance and stability on scaled landscapes. Landscape Ecol 8:213–227
33. Peters DPC, Pielke RA, Bestelmeyer BT et al (2004) Cross-scale interactions, nonlinearities, and forecasting catastrophic events. Proc Natl Acad Sci 101:15130–15135
34. Raffa KF, Aukema BH, Bentz BJ et al (2008) Cross-scale drivers of natural disturbances prone to anthropogenic amplification: the dynamics of bark beetle eruptions. Bioscience 58:501–517
35. Peterson GD (2002) Contagious disturbance, ecological memory, and the emergence of landscape pattern. Ecosystems 5:329–338
36. Kohm KA, Franklin JF (1997) Creating a forestry for the 21st century. Island Press, Washinton, DC
37. Foster DR, Knight DH, Franklin JF (1998) Landscape patterns and legacies resulting from large, infrequent forest disturbances. Ecosystems 1:497–510
38. Wallin DO, Swanson FJ, Marks B (1994) Landscape pattern response to changes in pattern generation rules: land-use legacies in forestry. Ecol Appl 4:569–580
39. Tang SM, Franklin JF, Montgomery DR (1997) Forest harvest patterns and landscape disturbance processes. Landscape Ecol 12:349–363
40. McIntire EJB (2004) Understanding natural disturbance boundary formation using spatial data and path analysis. Ecology 85:1993–1943
41. Dupouey JL, Dambrine E, Lafitte JD, Moares C (2002) Irreversible impact of past land use on forest soils and biodiversity. Ecology 83:2978–2984
42. Gustafson EJ (1996) Expanding the scale of forest management: allocating timber harvests in time and space. Forest Ecol Manage 87:27–39
43. Gustafson EJ, Rasmussen LV (2002) Assessing the spatial implications of interactions among strategic forest management options using a Windows-based harvest simulator. Comput Electron Agric 33:179–196
44. Paine RT, Tegner MJ, Johnson EA (1998) Compounded perturbations yield ecological surprises. Ecosystems 1:535–545
45. Folke C, Carpenter S, Walker B et al (2004) Regime shifts, resilience, and biodiversity in ecosystem management. Ann Rev Ecol Evol Syst 35:557–581
46. Schröder A, Persson L, De Roos AM (2005) Direct experimental evidence for alternative stable states: a review. Oikos 110:3–19
47. Wagner H (2004) Direct multi-scale ordination with canonical correspondence analysis. Ecology 85:342–351
48. Borcard D, Legendre P, Avois-Jacquet C, Tuomisto H (2004) Dissecting the spatial structure of ecological data at multiple scales. Ecology 85:1826–1832
49. Keitt TH, Urban DL (2005) Scale-specific inference using wavelets. Ecology 86:2497–2504
50. Andrén H (1994) Effects of habitat fragmentation on birds and mammals in landscapes with different proportions of suitable habitat – a review. Oikos 71:355–366
51. Gardner RH, Milne BT, Turnei MG, O'Neill RV (1987) Neutral models for the analysis of broad-scale landscape pattern. Landscape Ecol 1:19–28
52. O'Brien D, Manseau M, Fall A, Fortin M-J (2006) Testing the importance of spatial configuration of winter habitat for woodland caribou: An application of graph theory. Biol Conserv 130:70–83
53. Bélisle M, Desrochers A, Fortin M-J (2001) Influence of forest cover on the movements of forest birds: a homing experiment. Ecology 82:1893–1904
54. Fahrig L, Merriam G (1985) Habitat patch connectivity and population survival. Ecology 66:1762–1768
55. Bohonak AJ (1999) Dispersal, gene flow, and population structure. Q Rev Biol 74:21–45
56. Dale MRT, Dixon P, Fortin M-J et al (2002) Conceptual and mathematical relationships among methods for spatial analysis. Ecography 25:558–577
57. Gustafason EJ (1998) Quantifying landscape spatial pattern: what is state of the art? Ecosystems 1:143–156
58. Cushman SA, McGarigal K (2008) Landscape metrics, scales of resolution. In: von Gadow K, Pukkala T (eds) Designing green landscapes. Springer, New York, pp 33–52
59. Cressie NA (1993) Statistics for spatial data. Wiley, New York
60. Burrough PA, McDonnell RA (1998) Principles of geographical information systems. Oxford University Press, Oxford
61. Candau J-N, Fleming R (2005) Landscape-scale spatial distribution of spruce budworm defoliation in relation to bioclimatic conditions. Can J Forest Res 35:2218–2232
62. Wolter PT, White MA (2002) Recent forest cover type transitions and landscape structural changes in northeast Minnesota, USA. Landscape Ecol 17:133–155
63. Didion M, Fortin M-J, Fall A (2007) Forest age structure as indicator of boreal forest sustainability under alternative management and fire regimes: a landscape level sensitivity analysis. Ecol Model 200:45–58
64. Townsend PA, Foster JR, Chastain RA, Currie WS (2003) Application of imaging spectroscopy to mapping canopy nitrogen in the forests of the central Appalachian mountains using Hyperion and AVIRIS. IEEE Trans Geosci Remote Sens 41:1347–1354
65. Wotton BM, Martell DL (2005) A lightning fire occurrence model for Ontario. Can J Forest Res 35:1389–1401

66. Legendre P, Fortin M-J (1989) Spatial pattern and ecological analysis. Vegetatio 80:107–138
67. Dale MRT (1999) Spatial pattern analysis in plant ecology. Cambridge University Press, Cambridge
68. Illian J, Penttinen A, Stoyan H, Stoyan D (2008) Statistical analysis and modelling of spatial point patterns. Wiley-Interscience, Chichester
69. Baddeley AJ, Moller J, Waagepetersen R (2000) Non-and semi-parametric estimation of interaction in inhomogeneous point patterns. Statistica Neerlandica 54:329–350
70. Wiegand T, Moloney KA (2004) Rings, circles and null-models for point pattern analysis in ecology. Oikos 104:209–229
71. Fortin M-J, Dale MRT, Bertazzon S (2010) Spatial analysis of wildlife distribution and disease spread. In: Huettmann F, Cushman SA (eds) Spatial complexity, informatics, and wildlife conservation. Springer, New York, pp 255–273
72. Ripley BD (1976) The second order analysis of stationary point processes. J Appl Probab 13:255–266
73. Lynch HJ, Moorcroft PR (2008) A spatiotemporal Ripley's K-function to analyze interactions between spruce budworm and fire in British Columbia, Canada. Can J Forest Res 38:3112–3119
74. James PMA, Fleming RA, Fortin M-J (2010) Identifying significant scale-specific spatial boundaries using wavelets and null models: spruce budworm defoliation in Ontario, Canada as a case study. Landscape Ecol 25:873–887
75. Holling CS (1992) Cross-scale morphology, geometry, and dynamics of ecosystems. Ecol Monogr 62:447–502
76. Gardner RH (1998) Pattern, Process, and the Analysis of Spatial Scales. In: Peterson DL, Parker VT (eds) Ecological scale. Columbia University Press, New York, pp 17–34
77. Saunders SC, Chen J, Drummer TD et al (2002) The patch mosaic and ecological decomposition across spatial scales in a managed landscape of northern Wisconsin, USA. Basic Appl Ecol 3:49–64
78. Holling CS (1973) Resilience and stability of ecological systems. Ann Rev Ecol Evol Syst 4:1–23
79. Allen TFH, Hoeskstra TW (1992) Toward a unified ecology. Columbia University Press, New York
80. O'Neill RV, Krummel JR, Gardner RH et al (1988) Indices of landscape pattern. Landscape Ecol 1:153–162
81. Csillag F, Kabos S (2002) Wavelets, boundaries, and the spatial analysis of landscape pattern. Ecoscience 9:177–190
82. Keitt TH (2000) Spectral representation of neutral landscapes. Landscape Ecol 15:479–494
83. Saunders SC, Brosofske KD, Chen J, Drummer TD, Gustafson EJ (2005) Identifying scales of pattern in ecological data: a comparison of lacunarity, spectral and wavelet analyses. Ecol Complex 2:87–105
84. Dale MRT, Mah M (1998) The use of wavelets for spatial pattern analysis in ecology. J Veg Sci 9:805–814
85. Borcard D, Legendre P (2002) All-scale spatial analysis of ecological data by means of principal coordinates of neighbour matrices. Ecol Model 153:51–68
86. Anselin L (1995) Local indicators of spatial association - LISA. Geogr Anal 27:93–115
87. Bradshaw RHW, Spies T (1992) Characterizing canopy gap structure in forests using wavelet analysis. J Ecol 80:205–215
88. Mallat S (1999) A wavelet tour of signal processing. Academic, New York
89. Keitt TH, Urban DL (2005) Scale-specific inference using wavelets. Ecology 86:2497–2504
90. Daubechies I (1992) Ten lectures on wavelets. SIAM, Philadelphia
91. Torrence C, Compo GP (1998) A practical guide to wavelet analysis. Bull Am Meteor Soc 79:61–78
92. Grenfell BT, Bjørnstad ON, Kappey J (2001) Travelling waves and spatial hierarchies in measles epidemics. Nature 414:716–723
93. Cazelles B, Chavez M, De Magny GC, Guegan JF, Hales S (2007) Time-dependent spectral analysis of epidemiological time-series with wavelets. J R Soc Interface 4(15):625–636
94. Falkowski MJ, Smith AMS, Hudak AT et al (2006) Automated estimation of individual conifer tree height and crown diameter via two-dimensional spatial wavelet analysis of lidar data. Can J Remote Sensing 32:153–161
95. Dray S, Legendre P, Peres-Neto PR (2006) Spatial modeling: a comprehensive framework for principal coordinate analysis of neighbor matrices (PCNM). Ecol Model 196:483–493
96. Griffith DA, Peres-Neto PR (2006) Spatial modelling in ecology: the flexibility of eigenfunction spatial analyses. Ecology 87:2603–2613
97. Jombart T, Dray S, Dufour AB (2009) Finding essential scales of spatial variation in ecological data: a multivariate approach. Ecography 32:161–168
98. Jacquez GM, Maruca S, Fortin M-J (2000) From fields to objects: a review of geographic boundary analysis. J Geograph Syst 2:221–241
99. Fortin M-J, Drapeau P (1995) Delineation of ecological boundaries: comparison of approaches and significance tests. Oikos 72:323–332
100. Fortin M-J, Keitt TH, Maurer B et al (2005) Species ranges and distributional limits: pattern analysis and statistical issues. Oikos 108:7–17
101. McIntire EJB, Fortin M-J (2006) Structure and function of wildfire and mountain pine bettle forest boundaries. Ecography 29:309–318
102. Fortin M-J (1994) Edge detection algorithms for two-dimensional ecological data. Ecology 75:956–965
103. Oden NL, Sokal RR, Fortin M-J, Goebl H (1993) Categorical wombling: detecting regions of significant change in spatially located categorical variables. Geogr Anal 25:315–336
104. Fortin MJ, Drapeau P, Jacquez GM (1996) Quantification of the spatial co-occurrences of ecological boundaries. Oikos 77:51–60
105. St-Louis V, Fortin M-J, Desrochers A (2004) Association between microhabitat and territory boundaries of two forest songbirds. Landscape Ecol 19:591–601

106. Sadahiro Y, Umemura M (2002) A computational approach for the analysis of changes in polygon distributions. J Geograph Syst 3:137–154
107. Peters DPC, Bestelmeyer BT, Turner MG (2007) Cross-scale interactions and changing pattern-process relationships: consequences for system dynamics. Ecosystems 10:790–796
108. Hastie T, Tibshirani R, Friedman J (2009) The elements of statistical learning: data mining, inference, and prediction, 2nd edn. Springer, New York
109. Percival and Walden (2000) Wavelet methods for time series analysis. Cambridge, Cambridge University Press

Ecosystems, Adaptive Management

Craig R. Allen[1], Joseph J. Fontaine[1], Ahjond S. Garmestani[2]
[1]U.S. Geological Survey, Nebraska Cooperative Fish and Wildlife Research Unit, School of Natural Resources, University of Nebraska, Lincoln, NE, USA
[2]U.S. Environmental Protection Agency, National Risk Management Research Laboratory, Cincinnati, OH, USA

Article Outline

Glossary
Definition of Adaptive Management
Introduction
Adaptive Management Today
Structured Decision Making
Participatory Active Adaptive Management
Adaptive Governance
Adaptive Management and Law
Conclusions
Future Directions
Acknowledgments
Bibliography

Glossary

Adaptive governance Institutional and political frameworks designed to adapt to changing relationships between society and ecosystems, institutional frameworks that enable adaptive management, and the facilitation of learning from adaptive management to policy.

Adaptive management A systematic process of natural resource management whereby management actions are treated as experiments to increase learning and improve subsequent management.

Natural resource management The management of natural resources including land, water, plants, and animals to meet societal goals, including conservation and exploitation.

Resilience The capacity of a system to absorb disturbance without altering states (undergoing a regime shift); a measure of the amount of disturbance a system can tolerate before collapsing.

Structured decision making A general term for a framework of analysis of problems to reach decisions based on evidence to meet stated goals.

Definition of Adaptive Management

Adaptive management is an approach to natural resource management that emphasizes learning through management based upon the philosophy that knowledge is incomplete and much of what is thought to be known is actually wrong, but despite uncertainty, managers and policymakers must act [1]. Although the concept of adaptive management has resonated with resource management scientists and practitioners following its formal introduction in 1978 [2], it has and continues to remain little practiced and much misunderstood. Misunderstanding is largely based upon the belief that adaptive management is what management has always been, a trial and error attempt to improve management outcomes. But unlike a trial and error approach, adaptive management has explicit structure, including a careful elucidation of goals, identification of alternative management objectives and hypotheses of causation, and procedures for the collection of data followed by evaluation and reiteration. Since its initial introduction and description, adaptive management has been hailed as a solution to endless trial and error approaches to complex natural resource management challenges and recently, it has become increasingly referenced under various forms (please refer to following sections) (Fig. 1). Regardless of the particular definition of adaptive management used, and there are many, adaptive management emphasizes learning and subsequent adaptation of management based upon that learning. The process is iterative, and

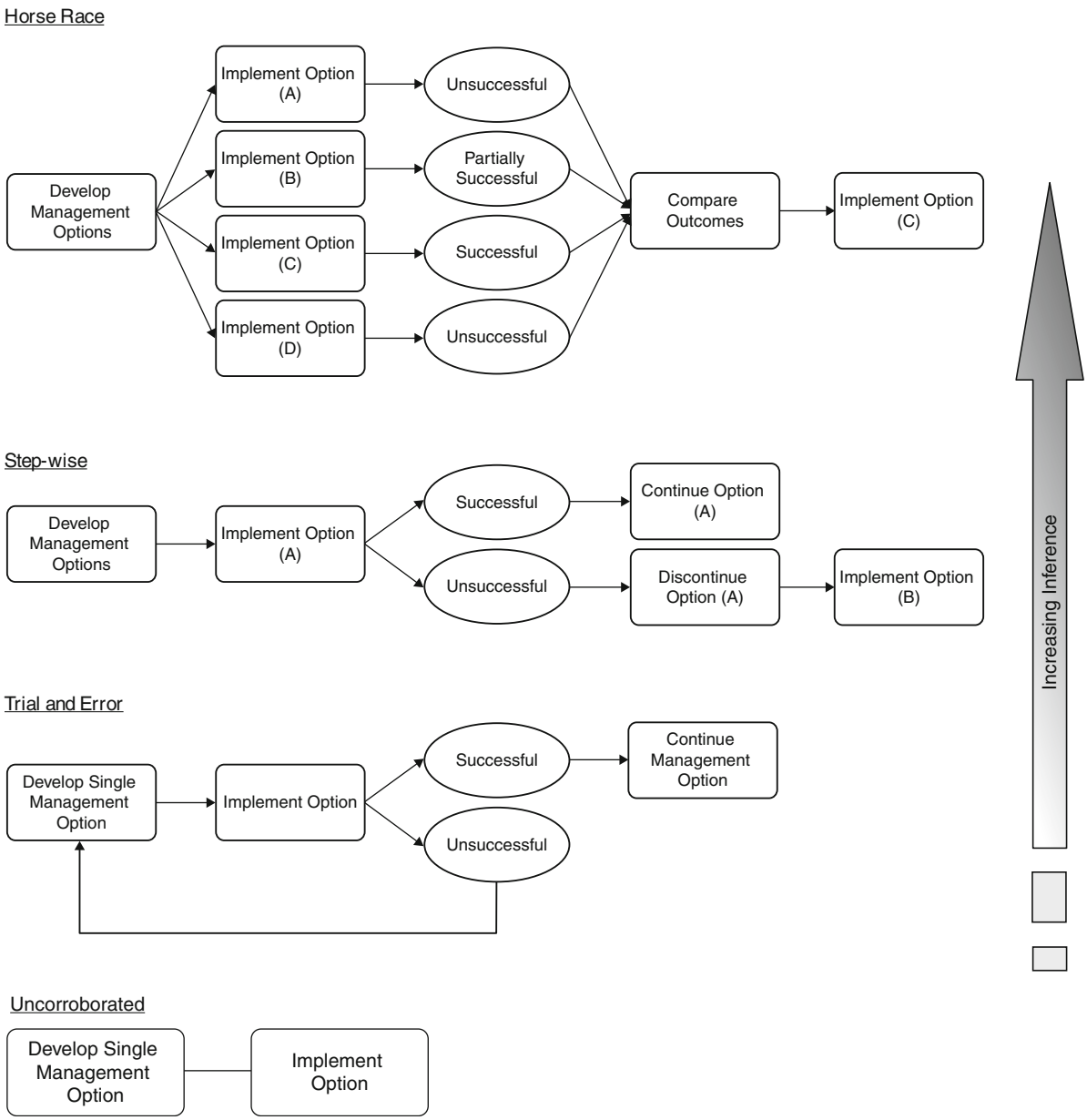

Ecosystems, Adaptive Management. Figure 1
Generalization of the different approaches to natural resource management

serves to reduce uncertainty, build knowledge, and improve management over time in a goal-oriented and structured process. However, adaptive management is not a panacea for the navigation of "wicked problems" [3, 4] as it does not produce easy answers, and is appropriate in only a subset of natural resource management problems where both uncertainty and controllability are high (Fig. 2) [5]. Where uncertainty is high but controllability is low, scenarios are a more appropriate approach. Adaptive management is a poor fit for solving problems of intricate complexity, high external influences, long time spans, high structural uncertainty, and with low confidence in assessments [5] (e.g., climate change). However, even in such

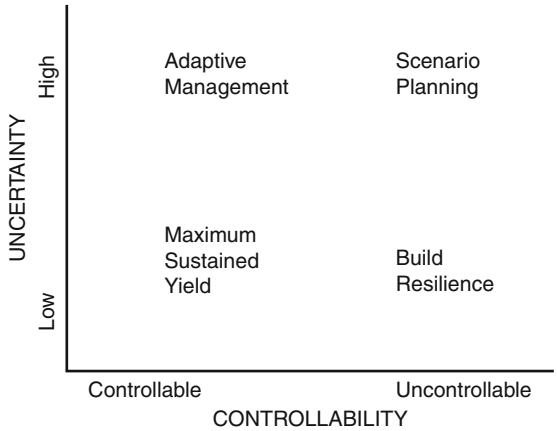

Ecosystems, Adaptive Management. Figure 2
Adaptive management and scenarios are complementary approaches to understanding complex systems. Adaptive management functions best when both uncertainty and controllability are high, which means the potential for learning is high, and the system can be manipulated (Adapted from [60])

situations, adaptive management may be the preferred alternative, and can be utilized to resolve or reduce structural uncertainty.

Clearly, adaptive management has matured, but it has also reached a crossroads. Its application is now common to a variety of complex resource management issues, and while practitioners and scientists have developed adaptive management and structured decision-making techniques, and mathematicians have developed approaches to reducing the uncertainties encountered in resource management, there continues to be misapplication of the method, and misunderstanding of its purpose.

Introduction

Adaptive management of natural resources did not spontaneously appear, but represents an evolving approach to natural resource management in particular, and structured decision making in general. Founded in the decision approaches of other fields [6] including business [7], experimental science [8], systems theory [9], and industrial ecology [10], the first reference to adaptive management philosophies in natural resource management may be traced back to Beverton and Holt [11] in fisheries management, though the term "adaptive management" was yet to be used (reviewed in [6]). The term "adaptive management" would not become a common vernacular until C.S. Holling, widely recognized as the "father" of adaptive management, produced his edited volume on the subject "Adaptive Environmental Assessment and Management" in 1978 [2]. The work was spawned by the experiences of Holling and colleagues at the University of British Columbia following from the development of resilience theory [12]. The concept of resilience, predicated upon the existence of more than one alternative stable state for ecosystems, had several ramifications. For one, it meant that managers should be very careful not to exceed a threshold that might change the state of the system being managed, and the location of those thresholds is unknown. Second, for ecological systems in a favorable state, management should focus on maintaining that state, and its resilience. Adaptive management, then, was a method to probe the dynamics and resilience of systems while continuing with "management," whereby management experiments were developed to enhance learning and reduce uncertainty, in a fail-safe manner. According to Holling (http://www.resalliance.org/2561.php):

- The resilience research led us to mobilize a series of studies of large scale ecosystems subject to management- terrestrial, fresh water and marine. All this was done with the key scientists and, in some cases, policy people who "owned" the systems and the data. So the process encouraged two major advances. One advance developed a sequence of workshop techniques so that we could work with experts to develop alternative explanatory models and suggestive policies. We learned an immense amount from the first experiment. That focused on the beautiful Gulf Islands, an archipelago off the coast of Vancouver. We chose to develop a recreational land simulation of recreational property. I knew little about speculation, but we made up a marvelous scheme that used the predation equations as the foundation- the land of various classes were the "prey," speculators were the "predators" and a highest bidder auction cleared the market each year. The equations were modifications of the general predation equations. The predictions were astonishingly effective and persisted so for at least a decade. As much as anything, it reinforced the earlier conclusion that

these equations were powerful and general. But the important conclusion concerned the workshop process and the people.

Eventually Carl Walters [1] built upon Holling's foundational contribution [12] and further developed the ideas, especially in the realm of mathematical modeling. Whereas Holling's original emphasis was in bridging the gap between science and practice, Walters emphasized treating management activities as designed experiments meant to reduce uncertainty. Both scientists sought an approach that allowed resource management and exploitation to continue while explicitly embracing uncertainties and seeking to reduce them through management. Walters [1] described the process of adaptive management as beginning "with the central tenet that management involves a continual learning process that cannot conveniently be separated into functions like research and ongoing regulatory activities, and probably never converges to a state of blissful equilibrium involving full knowledge and optimum productivity." He characterized adaptive management as the process of defining and bounding the management problem, identifying and representing what is known through models of dynamics that identify assumptions and predictions so experience can further learning, identifying possible sources of uncertainty and identifying alternate hypotheses, and finally the design of policies to allow continued resource management or production while enhancing learning.

A key focus of adaptive management is the identification and reduction, where possible, of uncertainty. Uncertainty is reduced through management experiments which enhance learning. Williams [6] describes four critical sources of uncertainty:

1. *Environmental variation* is often the most common source of uncertainty, and is largely uncontrollable. It may have a dominating influence on natural resource systems, through such factors as random variability in climate.
2. *Partial observability* refers to uncertainty about resource status. An example of this is the sampling variation that arises in resource monitoring.
3. *Partial controllability* arises when indirect means (e.g., regulations) are used to implement an action (e.g., setting a harvest rate), and it can lead to the misrepresentation of management interventions and thus to an inadequate accounting of their influence on resource behavior.
4. *Structural or process uncertainty* arises from a lack of understanding or agreement regarding the structure of biological and ecological relationships that drive resource dynamics.

Adaptive Management Today

Adaptive management has been referenced either implicitly [11] or explicitly [2, 13] for more than 50 years, but despite an illustrious theoretical history, there has remained imperfect realization of adaptive management in real world natural resource management decisions. The limited implementation of adaptive management stems from three fundamental problems: (1) a lack of clarity in definition and approach, (2) a paucity of success stories upon which to build [14–18], and (3) management, policy, and funding paradigms that favor reactive rather than proactive approaches to natural resource management [19, 20]. Each of these challenges has slowed the development of adaptive management as a paradigm for natural resource management and resulted in incomplete, inefficient, and even inappropriate implementation of adaptive management.

Although semantic arguments may seem the realm of ivory-towered professors, inconsistent and even contradictory approaches and definitions of adaptive management have resulted in confusion and limited the ability of management organizations to develop consistent and repeatable comprehensive adaptive management programs. Ironically, the confusion over the term "adaptive management" may stem from the flexibility inherent in the approach which has resulted in multiple interpretations of "adaptive management" that fall upon a continuum of complexity and *a priori* design, starting from the simple (e.g., "learning by doing") and progressing to the more explicit (e.g., "a rigorous process that should include sound planning and experimental design with a systematic evaluation process that links monitoring to management") [2, 21, 22]. Obviously, there is a clear distinction in intent, investment, and success between approaches that propose to learn from prior management decisions and those that outline a concise feedback mechanism dependent upon sound scientific principles on which

future management decisions will be made. The definition of "adaptive management" is further confused because one of the powerful attributes of adaptive management is the ability to simultaneously address multiple needs of managers, scientists, and stakeholders. The result has been published reports of adaptive management that emphasize definitions that focus on the needs of the authors and the ability of adaptive management to meet those needs (e.g., experimentation [14], uncertainty [23], changing management actions [24], monitoring [25], and stakeholder involvement [26]).

Despite the challenges in defining adaptive management, momentum and interest in the subject and its application continue to grow. The recent development by the United States Department of Interior of an adaptive management technical guide (http://www.doi.gov/initiatives/AdaptiveManagement/TechGuide.pdf) and the policies developed around this manual to:

- Incorporate adaptive management principles, as appropriate, into policies, plans, guidance, agreements, and other instruments for the management of resources under the Department's jurisdiction. – Department of Interior Manual (522 DM 1)

are an indication of the growing movement in natural resource management toward taking a more proactive role in management decisions. Unfortunately, this movement has little to build upon with one clear exception, the U.S. Fish and Wildlife Service (USFWS) Adaptive Harvest Management Plan (AHM) for mid-continent mallards. Worldwide, AHM is one of the few successful efforts to apply the principles of adaptive management and demonstrate how to successfully manage natural resources by improving the understanding of natural systems through management actions. The adaptive management processes of AHM have greatly improved the understanding of the harvest potential of waterfowl populations, the ability of managers to regulate harvest, and the importance of monitoring and assessment programs to support the decision-making process.

So why has AHM succeeded while so many other attempts to implement adaptive management have stalled? First, AHM developed a clear and concise objective: maximize long-term waterfowl harvest while ensuring long-term viability of waterfowl populations. The development and agreement by stakeholders to a concise set of fundamental objectives is paramount to ensuring the success of any adaptive management program. Failure to agree upon fundamental objectives and unwarranted attempts to alter objectives will ensure any attempt to manage, whether adaptive or not, will fail. The second key to the AHM success was due to simultaneous support for management, research, and monitoring. Waterfowl research and management in North America are nearly unequaled by almost any natural resource management program in terms of history, scope, and investment [27]. The enormity of historical and current data and the availability of resources for researchers and managers to utilize that data have facilitated the development of innumerable research and management activities all of which have fed back into the AHM process. In addition, the AHM program has arguably one of the most comprehensive monitoring programs for any ecological system currently under study. The combination of well-supported management, research, and monitoring programs has resulted in a clear reduction in the uncertainty of how waterfowl populations respond to management and enabled managers and policy makers to more effectively meet their stated objectives. Unfortunately, too often, attempts to implement adaptive management fail to address all of the requirements. In particular, resources for monitoring and research are often undervalued with the resultant outcome being a series of management actions with no understanding of their implications.

The final key to the success of AHM has been the ability to implement management and policy decisions based on the best information available. In many historical and current attempts to implement adaptive management, the regulatory body charged with implementation of management recommendations either is unable, or worse, is unwilling to implement actions proposed by the outcome of the adaptive management process. The body in charge of regulatory control is too often a stakeholder in the process of adaptive management with an agenda independent of regulating the resource alone. There may even be, and often are, several regulatory agencies controlling resources, each an independent stakeholder, each with an independent agenda. Such a situation can make implementation of a management

recommendation challenging, especially if it contradicts long-standing dogma. Consider for example, the management of Glen Canyon Dam and the waters of the Colorado River. Heralded by Congress as an adaptive management success story, the Colorado River Adaptive Management Program has fallen short of success because despite 13 years of work, the ecological status of the Colorado River and the conflict inherent to the development of an adaptive management program continue to worsen [28]. This is because the regulatory agency that controls the flow of water throughout the Colorado River Basin, the Bureau of Reclamation, is also one of the major stakeholders in the adaptive management process with an agenda (water storage) that conflicts with several other stakeholders and regulatory agencies that manage people and wildlife along the Colorado River (e.g., California Department of Water Resources, Mexican National Water Commission, USFWS). In contrast to the management of the Colorado River, there is a single centralized regulatory body governing waterfowl harvest in the United States (USFWS), and although there are many stakeholders that play a role in setting harvest management regulations, ultimately, decisions are made by the USFWS. Equally important, the interests of the USFWS parallel those of the other stakeholders. For the Colorado River, stakeholder interests are almost directly at odds. So from these examples is one to conclude that adaptive management is an unattainable mandate for the management of resources where various stakeholders and regulators are at odds? No, implementation of adaptive management is appropriate in both examples, possibly even more so for the management of the Colorado River. What the Colorado River example highlights is the importance of collaboration, the benefits of a single or superregulatory body, and the need to agree upon *a priori* objectives that guide long-term management decisions despite short-term political, societal, economic, or even environmental impacts.

Structured Decision Making

A key component of any management approach, whether it is adaptive or not, is deciding on the objectives, goals, and ultimately management options that may best achieve the desired goals (Fig. 3). Unfortunately, as with many decisions, deciding upon a proper set of objectives and the means to reach those objectives can prove challenging. Resource management decisions are further complicated because social-ecological systems are complex (e.g., multiple objectives and stakeholders, overlapping jurisdictions, short- and long-term effects) and are characterized by a high degree of uncertainty (e.g., appropriate management action or monitoring protocols, future economic or ecological conditions) and therefore present decision makers with challenging judgments (e.g., predicted consequences of proposed alternatives, value-based judgments about priorities, preferences, and risk tolerances) often under enormous pressure (economic, environmental, social, and political) and with limited resources to ensure success. The resulting outcome of such conditions too often leads to management paralysis, or continuation of the status quo, as managers and policy makers become overwhelmed by the process of the decision and lose track of the desired social-ecological conditions they are charged with achieving. Indeed, the process of resource management can be arduous and even controversial, particularly if there are a variety of stakeholders vying to push the agenda. Fortunately, there are methods to overcome these pitfalls and maximize the potential for success.

One method to overcome management paralysis and mediate multiple stakeholder interests is structured decision making. Borrowed from the sociological fields, structured decision making is an organized approach to identify and evaluate alternative resource management options by engaging stakeholders, experts, and decision makers in the decision process and addressing the complexity and uncertainty inherent in resource management in a proactive and transparent manner. Structured decision making uses a simple set of steps (Fig. 3) to evaluate a problem and integrate planning, analysis, and management into a transparent process that provides a roadmap focused on achieving the fundamental objectives of the program. It differs somewhat from "active" adaptive management in that it does not emphasize replicated management experiments (Fig. 4). Central to the success of the structured decision making process is the requirement to clearly articulate fundamental objectives, explicitly acknowledge uncertainty, and respond

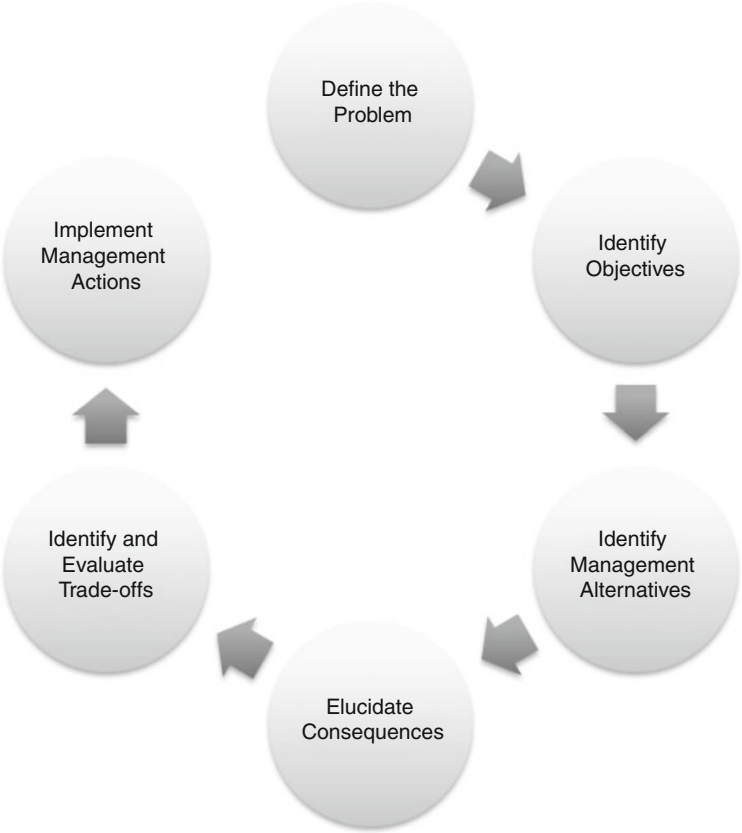

Ecosystems, Adaptive Management. Figure 3
The minimum steps necessary to implement a structured decision-making process: More complex integration of individual steps may be necessary if future steps clarify the process or if the decision is iterative over time

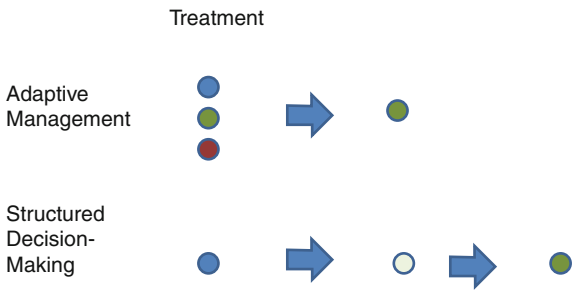

Ecosystems, Adaptive Management. Figure 4
Structured decision making and adaptive management differ somewhat, especially in that active adaptive management emphasizes the utilization of multiple replicated management experiments. As such, learning may be faster when such experiments are possible. However, adaptive management and structured decision making are terms often used interchangeably

transparently to all stakeholders' interests in the decision process. The conceptual simplicity inherent in structured decision making makes the process useful for all decisions from minor decisions to complex problems involving multiple stakeholders.

Structured Decision Making Steps

1. *Define the Problem* – The first step in a structured decision making process is a clear and concise evaluation and articulation of the problem being addressed and the motivation underlying the need to address the problem. Although identifying the problem may seem self-evident, failure to clearly articulate the problem to all stakeholders and subsequent agreement by stakeholders as to the nature of the problem is often cited as the primary reason management and policy actions fail, or worse, face

future litigation. To facilitate this process, decision makers need to ask:

(a) What specific decision(s) have to be made?
(b) What is scope of the decision (e.g., geographic, temporal)?
(c) Will the decision be iterated over time?
(d) What are the constraints within which the decision will be made (e.g., logistical, ecological, legal, temporal, financial)?
(e) What stakeholders should be involved in the decision process and what are their respective roles?

2. *Identify the Objectives* – The centerpiece of the structured decision making process is a set of clearly elucidated objectives. Together they define the "why do we care" about the decision and thereby facilitate the search for alternatives, and become the metric for comparing and evaluating management outcomes. When defining objectives, there are many considerations to ensure that decision makers can adequately evaluate alternatives. Ideally, objectives are stated in quantitative terms that relate to parameters that can be measured and thus evaluated. More importantly, objectives are meant to focus efforts on the importance of the decision in a consistent and transparent manner that exposes key trade-offs and uncertainties so decision makers can generate creative and proactive alternatives. Objectives should be complete, controllable, concise, measurable, and understandable [29]. To achieve this end requires "brainstorming" with stakeholders to identify what is important about the decision at hand. The outcome of such an effort may produce a wide variety and often extensive list of objectives that will need to be simplified to focus on things that matter and the direction they need to move (e.g., maximize deer harvest or minimize erosion). It is important to note, that unlike goals or targets, objectives do not have specific quantitative outcomes (e.g., 50% increase), but are meant to define the preferred ends and the direction of change to meet that ends.

   Once a list of objectives has been defined, it is important to separate the objectives into fundamental objectives (which reflect the ultimate goals) and means objectives (which are ways of achieving the ends) to ensure that management actions really effect the defined problem. For example, "maximize sandbars" may be an important objective for the management of a river like the Missouri or Platte, but if the river system is being managed for wildlife, sandbars are primarily important because they increase breeding habitat for threatened and endangered terns and plovers. "Maximize sandbars" is thus a means objective toward reaching the fundamental objective of "maximize tern and plover population size." Clearly, there are other means objectives that would also facilitate this fundamental objective (e.g., minimize nest predation, maximized food availability, etc.). The benefit of the process of distinguishing objectives is that the identification of means objectives can help lead to alternative management actions (e.g., build sandbars, release reservoir water), while the identification of fundamental objectives gives a basis for evaluating and comparing alternatives (annual tern and plover population size). Keep in mind, however, that the status of fundamental or means is not an innate quality of an objective, but rather is highly context dependent. Thus, what was a means objective for one decision, in the example "maximize sandbars," may be a fundamental objective for another if the decision problems shifts from say "wildlife management" to "aesthetics" or "flow."

   After developing a careful list of objectives, it can be useful to develop a hierarchy or means-ends diagram to group similar objectives and clarify the links and relationships between means and fundamental objectives. An objectives hierarchy can help clarify the context of each fundamental objective by identifying all the important elements that are affected by the decision process and demonstrate to stakeholders the importance of all objectives even those that are not "fundamental objectives."

3. *Identify Management Alternatives* – Management success is only as likely as the creativity and diversity of possible management alternatives. Unfortunately, management paralysis, "pet" management actions, and staying with the status quo too often limit managers and policy makers to few options and thereby impede management success. The process of identifying management alternatives, like the process of identifying objectives, starts with

brainstorming. Identifying alternative management actions is a process that should be addressed iteratively, as knowledge of best practices and the creativity to develop novel ideas should not be expected to develop instantaneously. The key is bringing the "right" people together. It is important to have a group with a set of interdisciplinary backgrounds that represent the larger decision to ensure that the needs of stakeholders are not overlooked. This is not to say that the stakeholders involved in identifying alternative management actions are the same as the larger stakeholder group, usually they are not. This is primarily due to the technical knowledge necessary to present plausible alternatives. Still there are opportunities where the benefit of being naive may present novel actions that might not otherwise be considered.

The brainstorming process should begin by identifying alternatives for individual objectives, but always be looking for opportunities when one action may fulfill the needs of multiple objectives. Identifying alternatives also means being mindful of those actions that must be done (e.g., standing policy), constraints (real or perceived) and potential trade-offs between objectives and various management actions. In developing alternatives, it is important that the "brainstorming" process focus on developing high-quality management actions that are: (1) explicitly designed to address the outlined objectives, (2) technically sound in that they build on the best known practices, (3) concise yet comprehensive enough to include the technical understanding for implementation, (4) designed to expose trade-offs between the decision process by having mutually exclusive strategies, and (5) developed to achieve the greatest good for the stakeholders involved.

Once an extensive list of alternatives has been identified, it can be useful to group them into strategies or portfolios based on general similarities in what they aim to achieve. Sometimes these portfolios can represent the needs of specific stakeholder groups or specific conditions that could be achieved. For example, management actions on a river system may be grouped together into portfolios that meet the needs of sport-fishery, endangered species, or irrigation; alternatively, they may be grouped based on their ability to return the river to 50%, 75%, or 95% of historical flows. Both methods have merit, the first in that it is generally clear to the stakeholders what objectives are being met and then where trade-offs must be considered, and the second in that the inherent interests of any particular group are not the driving factor and thus the process can be less contentious.

4. *Elucidate Consequences* – The list of alternative management actions is only effective if it creates an opportunity to evaluate and compare actions in light of the objectives before implementation. It is important to realize that the process of identifying management consequences is not a value judgment, but an analytical assessment of the most likely outcome of the action(s). Using the best scientific knowledge available, this process is a modeling exercise focused on predicting the likely outcomes of each alternative and thus the likelihood that each achieves the desired objective. Depending upon our knowledge of the system, this process can be highly quantitative where extensive data are modeled and probabilities assigned to each outcome or as is often the case, if little or nothing is known about the system, this process can depend heavily on expert opinion or comparisons to similar systems. In both cases, there is a degree of uncertainty associated with predicted outcomes as well as the parameters included in the modeling process. Indeed, because system function is rarely precisely understood, the effects of management actions are never certain and the future states are unknown, decisions are almost always made in the face of uncertainty. Uncertainty can make differentiating among alternatives difficult, but because uncertainty is an inherent part of the decision process, it must not be ignored. It is important that uncertainty be confronted throughout the decision process and that the uncertainties are identified and the possible impacts on the system and the ability to achieve stated objectives documented.

Once the modeling process has predicted the likely outcomes of each management action and the corresponding ability to address each objective, the next step is to develop a consequence table. The purpose of a consequence table is to produce

a visual summary of the consequences of each potential management action on each of the objectives in a table or matrix. A consequence table can take a variety of forms, from a simple rating system (e.g., consumer report 5-star rating) to a complex table with specific probabilities of outcomes and subsequent likelihoods of achieving each objective. Independent of the complexity of the underlying models that populate the matrix, the purpose of the consequence table is to ease and facilitate direct comparison of each management actions' ability to achieve each objective.

5. *Identify and Evaluate Tradeoffs* – Ideally the structured decision making process would lead to a clear management alternative that achieves the objectives of all interested parties; unfortunately, this is rarely the case. Generally, the process of developing a consequence table will clearly elucidate which options are the least likely to be effective, but if there are multiple stakeholders and thus multiple objectives, most decisions will require a trade-off between the ability of the remaining options to achieve each objective. The process of identifying where these trade-offs arise is analytical, but the decision process itself is highly value laden and thus dependent upon stakeholders. In most complex decisions, this will involve stakeholders choosing between less-than-perfect alternatives. There are a variety of methods to facilitate highly value-laden decisions by weighing options based on the values of the stakeholders and then comparing alternatives to find the "best" compromise solutions. However, trade-offs are real and it is unlikely that all parties will be totally satisfied with the eventual outcome. Indeed, although consensus is ideal, it is not necessary and is often unachievable; however, the benefit of the structured decision-making process is that even if there is disagreement, the process makes the disagreement transparent and enables stakeholders to re-evaluate using new knowledge and/or perspectives.
6. *Implement Management Action* – The final step in the structured decision-making process is implementation. Although this may always seem to be the desired outcome of a decision process, unfortunately, social and political pressures to reach "perfection" often impede implementation and leave decisions in a continuous state of inaction. To ensure success, managers, policy makers, and stakeholders must work together to move through the decision process in a timely manner to ensure action can be taken. Failure to take action is a decision, whether it is made passively or actively.

Participatory Active Adaptive Management

Panarchy is a useful model for characterizing ecological systems and the formal institutions that manage these systems [30]. One of the most critical aspects in the panarchy appears to be a bridging organization that can monitor the status of the social-ecological system, and manifest rapid change, if conditions are deteriorating [31]. Monitoring will allow for management to set new target levels, and modify policy to reach those target levels, as new information is generated on scale-specific system attributes [32]. In order for management entities operating at discrete scales to improve communication channels and create opportunities for collaboration, intermediate level entities may serve to facilitate these cross-scale linkages. Bridging organizations have the capacity to fulfill this role and organize cooperation between stakeholders across scales [33], but to do so successfully, one must formulate strategies, coordinate joint action, address uncertainty, and link diverse stakeholders in a world of increasing complexity. Brown [33] investigated bridging organizations from across the world, and from a variety of scopes (e.g., regional economic policy in the USA; small-scale irrigation projects in Indonesia; agricultural productivity in Zimbabwe) found that bridging organizations are independent of stakeholders in a social-ecological system, which allows them to negotiate with stakeholders and advocate multiple positions. This unique role in the management of social-ecological systems affords bridging organizations the capacity to catalyze the formation of policies that are flexible and reflective of the panarchy of ecosystems and institutions [33]. In addition, bridging organizations have the capacity to reduce transaction costs, and provide a mechanism to enforce adherence to desired policies, despite their lack of regulatory authority [34].

Examples of bridging organizations include: (1) assessment teams, which are made up of actors across sectors in a social-ecological system;

(2) nongovernmental organizations, which create an arena for trust-building, learning, conflict resolution, and adaptive co-management; and (3) the scientific community, which acts as a "watchdog," as well as a facilitator, for adaptive management. For purposes of environmental management, an example of a successful bridging organization is that of Ekomuseum Kristianstads Vattenrike (EKV), a small, municipal organization that facilitated progressive ecosystem management in southern Sweden [34]. EKV was tasked with managing water resources at a regional scale in Sweden, and was successful largely because it employed organizational flexibility that allowed for EKV to respond quickly to "surprise." This was achieved through leadership, a core interdisciplinary staff, and the facilitation of connections between individuals and organizations (i.e., the panarchy of institutions) in the social-ecological system. EKV was able to improve the social capacity to respond to "surprises" and create the trust necessary to push the social-ecological system toward improved adaptive management of resources.

The formal management institutions in place are likely to persist barring a large-scale perturbation to social-ecological systems. So, managers must operate within the limitations of these institutions, which complicates matters, but does not make the situation intractable. One possible option for improving environmental management, as highlighted in this section, appears to be in developing bridging organizations that catalyze cross-scale communication across the panarchy of institutions and ecosystems, and explicit recognition of the underlying cross-scale structure and nonlinear interactions of these linked systems, by both policy and policy makers. The lack of communication and cooperation between institutions at even small scales further illuminates that bridging organizations may help bring about effective management of natural resources at multiple scales [35]. Thus, bridging organizations should act as mini think tanks that facilitate communication between institutions, incubate new ideas for environmental management, and provide a forum for coming to agreements on contentious issues [36].

Bridging organizations play a critical role in facilitating adaptive comanagement and governance, and are essential to managing for resilience in social-ecological systems [37]. Perception of a particular policy can play a significant role in whether it is accepted by critical stakeholders in a social-ecological system [38]. Engaging stakeholders, implementing change at a suitable rate, and providing outreach to keep the public informed are all important for new environmental policy to be perceived of as positive and for a successful transition to a new policy regime [38]. This environmental management framework, which incorporates panarchy, adaptive management, and bridging organizations, could serve as one scenario in the suite of policy options for actualizing sustainability [30].

Adaptive Governance

Administrative agencies typically change incrementally [39], and as such, changes in policy are small because there is not enough information to make large overhauls of organization policy. Standard operating procedures are another mechanism that contributes to organizational inertia, as they slow the bureaucratic process [40]. Further, the lack of institutions matched to the appropriate scale is a significant barrier for sound environmental management [41]. Within this context, adaptive governance can help with this scale mismatch via collaboration of a diverse set of stakeholders at multiple scales [42]. Adaptive governance is a form of governance that incorporates formal institutions, informal groups/networks, and individuals at multiple scales for purposes of collaborative environmental management [43]. Bridging organizations, enabling legislation and government policies can also contribute to the success of an adaptive governance framework; governance creates a vision and management actualizes the vision [43].

Adaptive governance works via sharing of management power and responsibilities, and promotes a collaborative, participatory process, but is dependent upon adaptive comanagement, and adaptive comanagement is dependent upon social networks for success. Social networks have the capacity to allow for development of new ideas, to facilitate communication between entities, and to create the flexibility necessary for the interplay of the fluid (ecological systems) and the rigid (institutions) to be successful for environmental management [43]. Leadership has been well established as a critical factor in facilitating good environmental management. Leaders develop and facilitate a vision for

environmental management, incorporating local knowledge and information from social networks [43].

Olsson et al. [44] studied adaptive comanagement in Sweden and Canada and concluded that this form of management of ecological systems was most effective when there was: leadership with vision for the system of interest; legislation that created the environment for adaptive management; funds for adaptive management; monitoring of the ecological system; information flow (i.e., cross-scale linkages); combination of a variety of sources knowledge; and venue for collaboration. Olsson et al. [44] contend that these factors are critical to building resilience in social-ecological systems, as they help to protect the system from the failure of management decisions under uncertainty (i.e., imperfect information). Further, they assert that adaptive comanagement is necessary to facilitate adaptive governance. In turn, adaptive governance is facilitated by informal networks and leadership, which creates the capacity for development of novel ideas for environmental management [43]. These informal networks have the capacity to generate political, financial, and legal support for novel environmental management [43]. Further, adaptive governance is dependent upon polycentric institutions that are redundant (e.g., scale-specific) and are quasi-autonomous [45]. Olsson et al. [45] compared five case studies from around the world and concluded that in order for a social-ecological system to transition to adaptive governance, it must undergo a preparation and a transformation phase, linked by a window of opportunity.

In a well-cited example (Kristianstads Vattenrike) from Sweden, Olsson et al. [45] report the transition to adaptive governance was preceded by the development of a social network of parties interested in the management of the social-ecological system. The network consisted of members from local groups (environmental groups, farmers' associations), local government (municipality of Kristianstad, the County Administrative Board), and national scale (World Wildlife Fund, National Museum of Natural History, National Research Council). In case studies that have not resulted in a successful transition to adaptive governance, the social networks needed to help facilitate the transition were not well developed, and this hindered the changes needed for good environmental management [45].

The role of leadership has also been cited as critical to a transition to adaptive governance, and Olsson et al. [45] provide an example of leadership from Kristianstads Vattenrike. A key individual acted as a catalyst to social network formation, setting the research agenda, and mobilizing support at multiple scales for "new" environmental management. Critical to setting an agenda is defining how an issue becomes perceived as a "public problem because if most individuals accept a particular condition, negative feedback works to maintain public opinion in that particular regime" [46]. However, if the individuals in the regime develop a "critical mass" of distaste for a particular issue, public opinion can cross a threshold and reorganize into an alternative regime. Importantly, interest groups, the media, and other agents can have an effect on agenda setting and creating the "climate" necessary for a shift in public opinion [46]. There are critical roles to be played by individual actors in shifting policy from one regime to an alternate regime. For instance, social networkers that share information freely; individuals that have numerous, diverse connections; and individuals with powerful ability to persuade play key roles in policy change [47]. These individuals can interact to create the conditions necessary for regime shifts in public policy. In particular, the director of a municipal organization (Ekomuseum Kristianstads Vattenrike) filled this leadership role and served as a bridging organization that also was a significant factor in the transition to adaptive governance [45]. The leadership needed to foster a transition to adaptive governance is not necessarily the work of one individual, but rather is often encompassed by several individuals and entities [48].

There are two types of policy windows: a problem-driven window and a politically driven window [49]. A problem-driven window opens when a policymaker believes that a policy is necessary for a specific issue. A politically driven window is driven by a particular theme adopted by a policymaker, in which the policymaker looks for problems that fit within the theme. Significant changes in policy occur when conditions (e.g., problems, solutions, and politics) converge at the same time, which creates the window of opportunity for change [49]. In the Kristianstads Vattenrike example, social and ecological change at one scale triggered cross-scale effects which resulted in a window of opportunity for the transition to

adaptive governance [45]. In adaptive governance, decision making is not top-down but rather emerges from outreach and group meetings with stakeholders [50]. In order for adaptive governance to be effective, the policy requires strong leadership, communication, and incorporation of uncertainty, which allows for adaptation to changing circumstances [50].

Adaptive Management and Law

Legal certainty is an aspect of law that does not mesh well with environmental unpredictability. One of the most significant barriers for managing linked social-ecological systems is that often the aspects of a society that make it free (e.g., certainty of law) are not in concert with ecological realities (e.g., multi-regimes, nonlinear systems, and responses) [51]. The certainty of law and institutional rigidity often limit experimentation that is necessary for adaptive management [30]. This point is critical, as some scholars contend that environmental governance of the commons can only succeed if rules evolve with the system of interest [41].

Ecosystem management has been applied within the outdated framework of the Endangered Species Act (ESA), but ecosystem management is best implemented via adaptive management [52]. In its current form, the ESA does not have the necessary flexibility in its regulatory language to effectively implement adaptive responses to changing environmental conditions [52]. The legal constraints upon adaptive management in the American system of law do not stop there. The fundamental constraint to adaptive management is the current state of administrative law [53]. As the law now stands, the procedural rules require a vast amount of work before an agency promulgates a rule or issues a permit [54]. This "pre-decision" activity allows for public input and prepares agencies for judicial review. Ruhl [54] contends that "agencies will find that interest groups and courts relentlessly will erode adaptive agency behavior, using all the tools conventional administrative law puts at their disposal." Having to operate in an atmosphere where each policy is evaluated on the "front-end," in anticipation of public and legal scrutiny, has squelched agencies' appetite for adaptive management.

US administrative law is a two-step process, in which the first step allows for public comment on draft documents and alternative options [55]. The second step is final agency action, which creates "certainty" to the process and makes the decision subject to judicial review. This process is based on the assumption that agencies have the capacity to predict the consequences of a "final agency action" [55]. Thus, there is a fundamental conflict between linear legal processes (i.e., administrative law) based on "stationarity," versus environmental management frameworks (i.e., adaptive management) based on the realization of dynamic systems characterized by "surprise" [55]. Given this inherent conflict, adaptive management may not be possible under the current administrative law framework [54].

The adversarial character of administrative law, combined with the need for certainty (e.g., procedural rules) in the larger realm of American law, is likely incompatible with adaptive management [56]. Thus, environmental law is at odds with science, as the certainty required for socio-political stability makes it very difficult to apply a novel approach to ecosystem management (e.g., adaptive management) that requires institutional flexibility. Thus, if adaptive management is necessary for good environmental management, environmental law must be "adapted" to fit with adaptive management [54]. Karkkainen [56] argues that administrative law should proceed on two trajectories: (1) a fixed rule track that will apply unless an agency can justify otherwise; and (2) an adaptive management track, where a new set of administrative law standards specific to adaptive management would hold precedence, in order to actualize adaptive management as a tool for environmental policy.

Thus, some in the law community argue that adaptive management is not possible under the current administrative law framework [54]. The National Environmental Policy Act (NEPA) may act as a barrier to implementation of adaptive management (sensu Holling) [57]. NEPA could possibly be modified to an iterative process that could accommodate adaptive management [57]. Ruhl [54] contends that adaptive management is necessary for good environmental management, which in turn means that environmental law must be "adapted" to fit with adaptive management.

In effect, administrative agencies in the USA do not conduct adaptive management as it was originally conceived [55]. Rather, agencies conduct adaptive

management "lite," as the courts have provided some leeway to adaptive management projects, provided they have requirements that are legally enforceable [55]. The primary problem with adaptive management "lite" is that it does not measure up to the standards of adaptive management theory, nor does it hold up under the scrutiny of substantive and procedural law. Adaptive management (sensu Holling) is not likely until Congress provides more funding for adaptive management and clear standards for the adaptive management process [55].

Conclusions

The conceptual underpinnings for adaptive management are simple; there will always be inherent uncertainty and unpredictability in the dynamics and behavior of complex ecological systems as a result of nonlinear interactions among components and emergence, yet management decisions must still be made. The strength of adaptive management is in the recognition and confrontation of such uncertainty. Rather than ignore uncertainty, or use it to preclude management actions, adaptive management can foster resilience and flexibility to cope with an uncertain future, and develop safe-to-fail management approaches that acknowledge inevitable changes and surprises. Since its initial introduction, adaptive management has been hailed as a solution to endless trial and error approaches to complex natural resource management challenges. However, it does not produce easy answers, and it is appropriate in only a subset of natural resource management problems. Clearly adaptive management has great potential when applied appropriately.

Future Directions

Adaptive management is increasingly heralded as the future of natural resource management and has been adopted by many governmental and nongovernmental agencies. Institutions adopting adaptive management have utilized different definitions often focusing on a single strength of the process (i.e., experimentation, reducing uncertainty, involving stakeholders) and thus operationalize the practice uniquely. Some, like the U.S. Department of Interior, are highly focused on the decision process and the incorporation of structured decision making while others, such as the US Army Corps of Engineers, have embraced stakeholder involvement. Each approach has merit but adaptive management has failed to live up to its expectations [58]. The reasons for failure are many, and likely to be repeated, yet the great potential of adaptive management remains; unfortunately, it remains largely untapped. Translation of adaptive management approaches to "on-the-ground" natural resource managers is a critical step that has largely failed. Most natural resource managers are still unable to define adaptive management, let alone incorporate it into their normal management activities. The next decade will be critical: Will adaptive management remain in the domain of ivory towers, or will it become a tool for the trenches? Taking adaptive management to the practitioners will require the communication of adaptive management techniques in a clear, simple, and most importantly applicable manner. Currently, adaptive management fails because of an adherence to mathematical modeling above all else, its application to situations that are not conducive to replication or the measurement of success (e.g., large rivers such as the Missouri or the Colorado), and because adaptive management has not been adequately incorporated into natural resources management via appropriate legal mechanisms [59]. If the future of natural resource management is to be proactive and address the increasing uncertainties facing our world, adaptive approaches to resource management will require communication of the methodology and merits in a clear and simple manner.

Acknowledgments

The Nebraska Cooperative Fish and Wildlife Research Unit is jointly supported by a cooperative agreement between the United States Geological Survey, the Nebraska Game and Parks Commission, the University of Nebraska–Lincoln, the United States Fish and Wildlife Service and the Wildlife Management Institute. Any use of trade names is for descriptive purposes only and does not imply endorsement by the US Government.

Bibliography

1. Walters CJ (1986) Adaptive management of renewable resources. McMillan, New York
2. Holling CS (ed) (1978) Adaptive environmental assessment and management. Wiley, Chichester

3. Rittel HWJ, Webber MM (1973) Dilemmas in a general theory of planning. Policy Sci 4:155–173
4. Ludwig D (2001) The era of management is over. Ecosystems 4:758–764
5. Gregory R, Ohlson D, Arvai J (2006) Deconstructing adaptive management: criteria for applications to environmental management. Ecol Appl 16:2411–2425
6. Williams BK (2010) Adaptive management of natural resources – framework and issues. J Environ Manage 92(5):1346–1353
7. Senge PM (1990) The fifth discipline: the art and practice of the learning organization. Currency Doubleday, New York
8. Popper KR (1968) The logic of scientific discovery, 2nd edn. Harper and Row, New York
9. Ashworth MJ (1982) Feedback design of systems with significant uncertainty. Research Studies Press, Chichester
10. Allenby BR, Richards DJ (1994) The greening of industrial ecosystems. National Academy Press, Washington, DC
11. Beverton RJH, Holt SJ (1957) On the dynamics of exploited fish populations. Her Majesty's Stationery Office, London
12. Holling CS (1973) Resilience and stability of ecological systems. Annu Rev Ecol Syst 4:1–23
13. Walters CJ, Hilborn R (1978) Ecological optimization and adaptive management. Annu Rev Ecol Syst 9:157–188
14. Lee KN (1993) Compass and gyroscope: integrating science and politics for the environment. Island Press, Washington, DC
15. McLain RJ, Lee RG (1996) Adaptive management: promises and pitfalls. Environ Manage 20:437–448
16. Lee KN (1999) Appraising adaptive management. Conserv Ecol 3(2):3. http://www.consecol.org/vol3/iss2/art3/
17. Moir WH, Block WM (2001) Adaptive management on public lands in the United States: commitment or rhetoric? Environ Manage 28:141–148
18. Walters C (2007) Is adaptive management helping to solve fisheries problems? Ambio 36:304–307
19. Ascher W (2001) Coping with complexity and organizational interests in natural resource management. Ecosystems 4:742–757
20. Schreiber ESG, Bearlsin AR, Nicol J, Todd CR (2004) Adaptive management: a synthesis of current understanding and effective application. Ecol Manage Restor 5:177–182
21. Wilhere GF (2002) Adaptive management in habitat conservation plans. Conserv Biol 16:20–29
22. Aldridge CL, Boyce MS, Baydack RK (2004) Adaptive management of prairie grouse: how do we get there? Wildl Soc Bull 32:92–103
23. Williams BK, Johnson FA (1995) Adaptive management and the regulation of waterfowl harvests. Wildl Soc Bull 23:430–436
24. Rauscher HM (1999) Ecosystem management decision support for federal forests in the United States: a review. For Ecol Manage 114:173–197
25. Bormann BT, Haynes RW, Martin JR (2007) Adaptive management of forest ecosystems: did some rubber hit the road. Bioscience 57:186–191
26. Norton BG (1995) Ecological integrity and social values: at what scale? Ecosyst Health 1:228–241
27. Hawkins AS, Hanson RC, Nelson HK, Reeves HM (eds) (1984) Flyways: pioneering waterfowl management in North America. U.S. Government Printing Office, Washington, DC
28. Susskind L, Camacho AE, Schenk T (2010) Collaborative planning and adaptive management in Glen Canyon: a cautionary tale. Columbia J Environ Law 35:1–54
29. McDaniels T (2000) Creating and using objectives for ecological risk assessment and management. Environ Sci Policy 3:299–304
30. Garmestani AS, Allen CR, Cabezas H (2009) Panarchy, adaptive management and governance: policy options for building resilience. Neb Law Rev 87:1036–1054
31. Kinzig A, Starrett D, Arrow K, Aniyar S, Bolin B, Dasgupta P, Ehrlich P, Folke C, Hanemann M, Heal G, Hoel M, Jansson A, Jansson BO, Kautsky N, Levin S, Lubchenco J, Maler KG, Pacala SW, Schneider SH, Siniscalco D, Walker B (2003) Coping with uncertainty: a call for a new science-policy forum. Ambio 32:330–335
32. Karkkainen BC (2002) Collaborative ecosystem governance: scale, complexity and dynamism. Virginia Environ Law J 21:189–244
33. Brown LD (1993) Development bridging organizations and strategic management for social change. Adv Strat Manag 9:381–405
34. Hahn T, Olsson P, Folke C, Johansson K (2006) Trust-building, knowledge generation and organizational innovations: the role of a bridging organization for adaptive co-management of a wetland landscape around Kristianstad, Sweden. Hum Ecol 34:573–592
35. Roy AH, Wenger SJ, Fletcher TD, Walsh CJ, Ladson AR, Shuster WD, Thurston HW, Brown RR (2008) Impediments and solutions to sustainable, watershed- scale urban stormwater management: lessons from Australia and the United States. Environ Manage 42:344–359
36. Brown LD, Khagram S, Moore MH, Frumkin P (2000) Globalization, NGOs, and multi-sectoral relations. In: Nye JS, Donohue JD (eds) Governance in a globalizing world. Brooking Institution Press, Washington, DC, pp 271–296
37. Olsson P, Folke C, Galaz V, Hahn T, Schultz L (2007) Enhancing the fit through adaptive co-management: creating and maintaining bridging functions for matching scales in the Kristianstads Vattenrike Biosphere Reserve Sweden. Ecol Soc 12(1):28. http://www.ecologyandsociety.org/vol12/iss1/art28/
38. Marshall NA (2007) Can policy perception influence social resilience to policy change? Fish Res 86:216–227
39. Lindblom C (1959) The science of muddling through. Public Adm Rev 19:79–88
40. Allison G (1969) Conceptual models and the Cuban missile crisis. Am Political Sci Rev 63:689–718
41. Dietz T, Ostrom E, Stern PC (2003) The struggle to govern the commons. Science 302:1907–1912

42. Hughes TP, Bellwood DR, Folke C, Steneck RS, Wilson J (2005) New paradigms for supporting the resilience of marine ecosystems. Trends Ecol Evol 20:380–386
43. Folke C, Hahn T, Olsson P, Norberg J (2005) Adaptive governance of social- ecological systems. Annu Rev Environ Resour 30:441–473
44. Olsson P, Folke C, Berkes F (2004) Adaptive co-management for building resilience in social-ecological systems. Environ Manage 34:75–90
45. Olsson P, Gunderson LH, Carpenter SR, Ryan P, Lebel L, Folke C, Holling CS (2006) Shooting the rapids: navigating transitions to adaptive governance of social-ecological systems. Ecol Soc 11(1):18. http://www.ecologyandsociety.org/vol11/iss1/art18/
46. Wood BD, Doan A (2003) The politics of problem definition: applying and testing threshold models. Am J Political Sci 47:640–653
47. Gladwell M (2000) The tipping point – how little things can make a big difference. Little, Brown, Boston
48. Zellmer S, Gunderson L (2009) Why resilience may not always be a good thing: lessons in ecosystem restoration from Glen Canyon and the Everglades. Neb Law Rev 87:893–947
49. Kingdon JW (1995) Agendas, alternatives and public policies. Harper Collins College, New York
50. Steelman TA, Tucker DW (2005) The Camino Real: to care for the land and serve the people. In: Brunner RD et al (eds) Adaptive governance: integrating science, policy, and decision making. Columbia University Press, New York, pp 91–130
51. Folke C, Pritchard L, Berkes F, Colding J, Svedin U (2007) The problem of fit between ecosystems and institutions: ten years later. Ecol Soc 12(1):30. http://www.ecologyandsociety.org/vol12/iss1/art30/
52. Ruhl JB (2004) Taking adaptive management seriously: a case study of the Endangered Species Act. Univ Kans Law Rev 52:1249–1284
53. Ruhl JB (1998) The Endangered Species Act and private property: a matter of timing and location. Cornell J Law Public Policy 8:37–54
54. Ruhl JB (2008) Adaptive management for natural resources – inevitable, impossible, or both? Rocky Mountain Law Institute 54:11.01.-06
55. Ruhl JB, Fischman R (2010) Adaptive management in the courts. FSU College of Law, Public Law Research Paper No. 411; Indiana Legal Studies Research Paper No. 154. SSRN: http://ssrn.com/abstract=1542632
56. Karkkainen BC (2005) Panarchy and adaptive change: around the loop and back again. Minn J Law Sci Technol 7:59–77
57. Benson MH (2009) Integrating adaptive management and oil and gas development: existing obstacles and opportunities for reform. Environ Law Rep 39:10962–10978
58. Allen CR, Gunderson LH (2011) Pathology and failure in the design and implementation of adaptive management. J Environ Manag 92:1379–1384
59. Benson MH, Garmestani AS (2011) Embracing panarchy, building resilience and integrating adaptive management through a rebirth of the National Environmental Policy Act. J Environ Manag 92:1420–1427
60. Peterson GD, Cumming GS, Carpenter SR (2003) Scenario planning: a tool for conservation in an uncertain world. Conserv Biol 17:358–366

E

Ecotones and Ecological Gradients

Salit Kark
The Biodiversity Research Group, Department of Ecology, Evolution, and Behavior, The Hebrew University of Jerusalem, Jerusalem, Israel
ARC Centre for Environmental Decisions (CEED) School of Biological Sciences, The University of Queensland, St Lucia, QLD, Australia

Article Outline

Glossary
Definition of the Subject
Introduction
Conceptual Framework
History of Research on Ecotones and Biodiversity
Approaches for Measuring Ecotones
Patterns of Biodiversity in Ecotones
Processes Shaping Biodiversity and Sustainability in Ecotones
Implications for Biodiversity, Conservation Planning, and Sustainability
Future Directions
Bibliography

Glossary

Beta-diversity Also termed species turnover, beta-diversity refers to the change in species as one moves between habitats, communities, or ecosystems.

Divergence-with-gene-flow model of speciation A model explaining the process of species formation (speciation) in which new species diverge in the face of gene flow; the movement of genes within a group that results from mating with immigrant individuals.

Ecotone A transition zone between two or more different ecological communities or regions.

Ecotone effect The pattern of increased species richness (number of species) and abundance in ecotones and the occurrence of unique ecotonal species.

Edge effect The effect of the juxtaposition of contrasting environments on an ecosystem.

Geographic information systems (GIS) A computer-based system for creating and managing spatial data and associated attributes. It enables the capture, storage, retrieval, analysis, and display of spatial (location-based) data.

Remote sensing The science and art of obtaining information about an object, area, or phenomenon through the analysis of data acquired by a device that is not in contact with the object, area, or phenomenon under investigation (e.g., via a satellite image).

Definition of the Subject

Ecotones are areas of transition between ecological communities, ecosystems, or ecological regions (such as Mediterranean and desert). Ecotones often occur along ecological gradients. Such gradients are created as a result of spatial shifts in elevation, climate, soil, and many other environmental factors. Ecotones commonly coincide with areas of sharp climatic transition along environmental gradients. They occur at multiple spatial scales, from continental-scale transitions between major biomes to small-scale ecotones where local vegetation communities and microhabitats coincide. They show a diversity of boundary types that range from natural boundaries (e.g., altitudinal, latitudinal transitions) to human-generated ecotones (e.g., forest clear-cut edges or urban ecotones). Ecotones have been studied in the past four decades in an ecological context and in recent years are receiving increasing attention in the context of biodiversity conservation. Various studies have shown that species richness and abundances tend to peak in ecotonal areas, though exceptions to these patterns occur. Ecotones are "natural laboratories" for studying a range of evolutionary processes, such as the process by which new species form, also termed speciation. Some researchers argue that ecotones deserve high-conservation investment, potentially serving as speciation and biodiversity centers. Because ecotones are often small in size and relatively rich in biodiversity, conservation efforts in these areas may prove to be an efficient and cost-effective conservation strategy.

Introduction

While substantial research in the past decades has focused on distinct ecological regions, communities, and ecosystems, areas of transition between these regions have received much less attention. These areas, nevertheless, sustain rich and unique biodiversity and may have an important role in sustaining future biodiversity. However, studies have shown that species richness and abundances tend to peak in ecotonal areas, though exceptions to this pattern occur. This is likely because ecotonal areas hold species from two or more neighboring communities and possibly due to high spatial heterogeneity and high speciation rates in ecotonal areas. In addition, ecotones have been shown, in some cases, to hold ecotonal species and genotypes that are uniquely characteristic of the ecotone.

Several studies have found evidence that some species are diverging in ecotonal regions, suggesting that transitional areas may serve as speciation centers. Recent work has shown increased genetic and morphological diversity in ecotonal regions compared with neighboring areas. Ecotonal populations often coincide with peripheral populations along a species range. Some researchers suggest that because ecotones often hold marginal populations that depend on other parts of the range for the maintenance of genetic diversity, they do not deserve much conservation interest. Alternatively, in the face of global climate and environmental changes, it has also been argued that ecotones deserve special conservation investment, potentially being speciation and biodiversity hotspots that hold relatively resilient populations. This entry will provide a short overview of the history of ecotone research, recent novel findings in the area and the implications for future conservation, biodiversity, and sustainability research.

Conceptual Framework

Ecotones are areas where ecological communities, ecosystems, or biotic regions coincide. They often

occur in areas of steep environmental transition, along environmental gradients. In these transitional regions, the environment rapidly shifts from one type to another based on abiotic (e.g., climatic) and/or biotic (e.g., community structure) factors [13, 19]. The origin of the word "ecotone" is in the Greek roots "oikos" (home) and "tonus" (tension). Many different definitions and terms have been used in the literature to describe ecotones and areas of ecological transition. These include boundary regions, borders, meeting zones, transitional zones, tension zones, zones of intermingling, and zones of transgression [19]. The definition often contrasts ecotones with more homogenous areas found on both sides of the transition or to the landscape as a whole. Ecotones can occur in both terrestrial and aquatic systems, and cover several spatial scales, from large spatial-scale ecotones, where biomes meet [40] to local-scale transitions, such as mountain treelines ([11]; see Fig. 1). These areas are sometimes considered to be dynamic zones of interaction between communities, which are unstable over time [19]. As suggested by Odum [30], Ecotones do not simply represent a boundary or an edge; the concept of an ecotone assumes the existence of active interaction between two or more ecosystems with properties that do not exist in either of the adjacent ecosystems. Ecotonal regions show a diversity of transitions that range from natural transitions (e.g., altitudinal and latitudinal transitions) to human-generated ecotones, sometimes termed anthropogenic ecotones (e.g., forest clear-cut edges or urban ecotones) [24], as shown in Fig. 1.

History of Research on Ecotones and Biodiversity

For over 100 years, since the late nineteenth century, there has been scientific interest in boundary regions and edges of ecological systems. A conceptual ecological framework for the study of ecotones was given by Odum in 1953. Odum discussed the ecotone effect, which he characterized as increased richness and abundance in ecotones and the occurrence of unique ecotonal species. Until the 1970s, there was considerable interest in ecotones within the scientific community (reviewed by [32]). This interest subsided as focus on more homogenous and well-defined ecosystems and communities (e.g., tropical rain forests and tundra) became common. A revival of research in the field focusing on ecotones and their effects on biodiversity was seen in the late 1980s and 1990s, with the development of new research areas, especially those of landscape ecology and of conservation biology [11, 13]. Studies on ecotones in the 1980s often focused on material flow (e.g., water and nutrients) across communities and on ecosystem processes in these boundary regions [12]. Much of the work focused on wetlands and on riparian zones, where land–water interfaces occur (reviewed in [45]). Later work in the 1990s more directly examined the effect of ecotones on biological diversity, and especially on the relationship between ecotones and processes leading to morphological divergence, patterns of genetic and phenotypic diversity, species richness, rarity, and their conservation implications (reviewed in [17]).

Approaches for Measuring Ecotones

Due to the fact that ecotones can be rarely delimited by a fine line, their measurement and mapping is not simple. A wide range of research approaches and tools have been used to detect and quantify ecotones. These include, among others, simulation modeling, geographic information systems (GIS), remote sensing, and statistical tools that enable quantification and analysis of ecotones of different types and over several spatial scales. Diverse approaches for the quantification of the steepness of gradients exist [17]. Methods for measuring and characterizing ecotones depend on the data available (e.g., quantitative or qualitative, grid- or transect-based data), with one of the simplest approaches, proposed by Womble in 1951, being the quantification of the magnitude of the first and second derivatives (rates of change in a given variable or several variables along a spatial gradient) [44]. These approaches often examine the values of variables in an area (e.g., a 1 × 1 km grid square) relative to its neighboring regions. The basic idea is to detect areas of sharp environmental transition by finding the areas with the highest rate of change in the value of a given variable or several variables between adjacent squares (pixels). Specific software for the detection of boundary regions and analysis is now available (e.g., BoundarySeer: http://www.terraseer.com/products_boundaryseer.php), enabling more widespread use of advanced statistical tools for the study of areas of

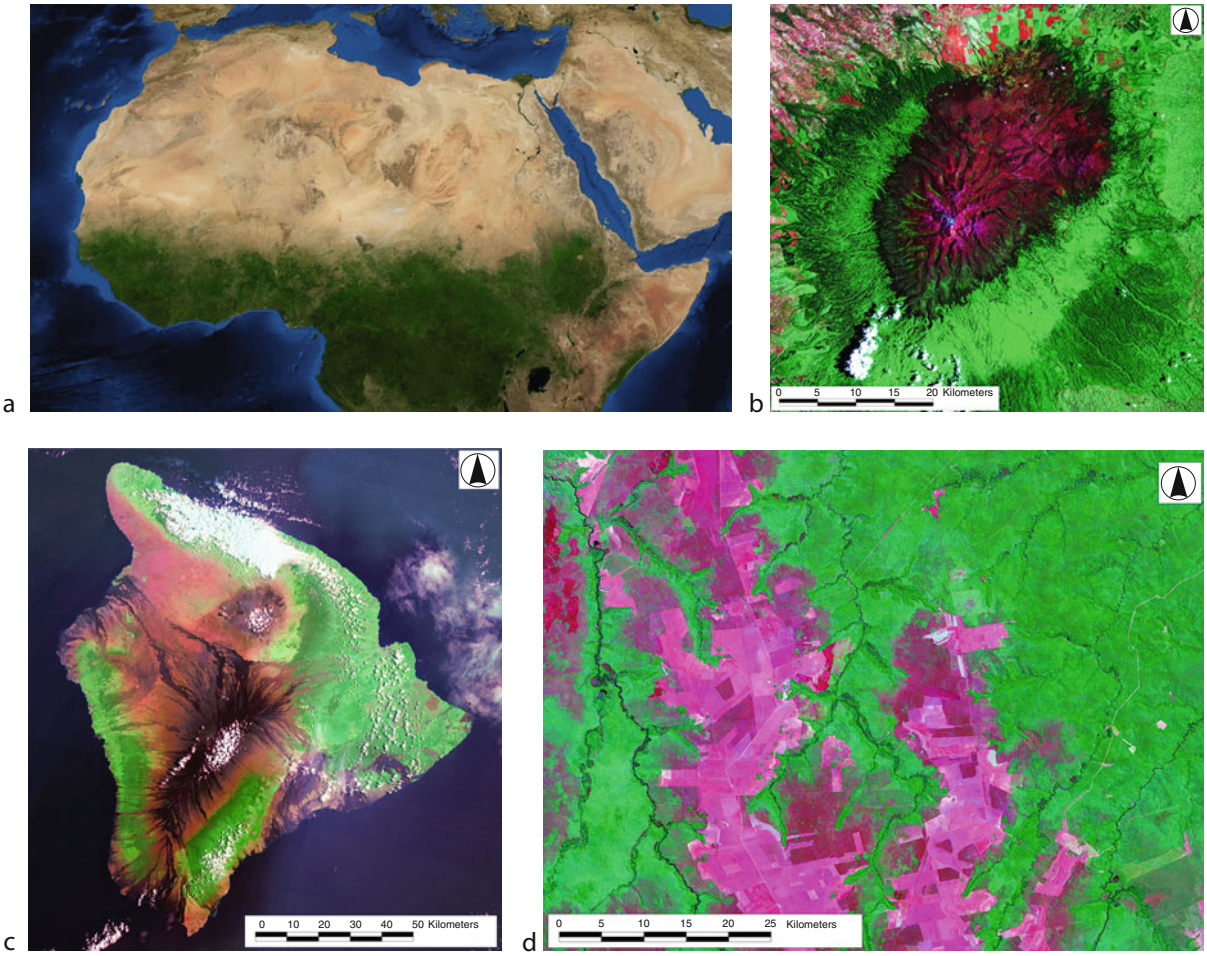

Ecotones and Ecological Gradients. Figure 1
Satellite images showing a variety of natural and human-generated ecotones at several spatial scales: (**a**) Ecotones in the Sahel region of Africa (see text). (**b**)Altitudinal ecotones between vegetation belts in Mt. Kenya. (**c**) Natural and human-made ecotones on Hawaii's big island. Ecotones vary over different slopes and elevations. Note also the sharper ecotones in areas where lava has flowed. (**d**) Human-related ecotones resulting from deforestation (in *pink*) in the Amazon Basin, Brazil. On the far *left* and far *right*, in dark green, natural riparian ecotones can be detected along the rivers. (Source of Fig. **a** Stöckli et al. [39] NASA Blue Marble Next Generation, August 2004. True color composite of MODIS satellite images. Downloaded from: http://visibleearth.nasa.gov/ [42].) (Source of Fig. **b**–**d** MDA Federal [25] NASA GeoCover circa 1990 Landsat images. False color composite of Landsat bands 7, 4 and 2. *Green shades* represent vegetation, *magenta* and *brown* represent bare soil, *black* represent water bodies, recent lava flows of shadows, *cyan shades* represent snow, and *white* represents clouds. Downloaded from: https://zulu.ssc.nasa.gov/mrsid/ [3].) (All images are public domain. The figures were produced by Noam Levin)

transition [5, 8]. These tools can also be applied to the study of ecotonal regions.

In recent years, new approaches to quantify changes in diversity across gradients and boundary regions have been developed and are being applied. Among these is a range of new beta-diversity estimates of species turnover in space [20, 26]. These have been developed in the past decades, since Wilson and Shmida's [43] review on beta-diversity estimates. Beta-diversity and species turnover are often used when studying gradients, and

although they do not focus necessarily on ecotonal areas, they can be applied to the study of ecotones.

One of the most promising directions in ecotone and boundary measurement is the use of tools developed in other areas of science. These include fields such as physics, remote sensing, and image analysis, where substantial advancements in boundary detection and gradient quantification methods have been made. Remote-sensing tools, for example, can use data occurring over several orders of magnitude, using satellite-derived data currently available at a resolution of 0.5 m to 100 km. Further application of these tools at multiple spatial resolutions will provide a better understanding of ecotones. Recent work has shown that remote sensing tools can be effectively used to detect ecotones and to predict species richness and rarity (e.g., range size rarity) in ecotones, especially in mountains where latitudinal gradients occur (e.g., [22, 23]).

Patterns of Biodiversity in Ecotones

There have been multiple studies on patterns of biodiversity in ecotonal areas, which have led to a range of results. Recent work is providing increasing evidence that boundary regions between ecological communities can be highly diverse at both the within-species and community levels. Ecotones have been shown to hold especially high biological diversity over several spatial scales, at both the community level (when examining species richness, i.e., the number of species in an area) and at the within-species level (morphological and genetic diversity) as reviewed by Kark and van Rensburg [17]. Other studies, however, have shown conflicting results, making it difficult to generalize without carefully examining each case, community, and region.

Early on, Odum [30] pointed at high species richness and abundance in ecotones and suggested that the ecotonal community commonly contains many species that are characteristic of, and sometimes restricted to, the ecotone. In a continental-scale study of New World birds, Kark et al. [16] examined the relationship between passerine richness and rarity of ~2,300 passeriform species in 4,889 one-degree New World grid cells and the distance of the cells to boundaries between adjacent plant-based ecoregions. They found that areas nearer to transitions between ecoregions had more bird species, and also scored more highly in terms of species rarity. The findings of their work suggest that transitional environments harbor many rare species, in addition to high richness. At the community level, there is also some evidence for high species richness in ecotonal areas in marine systems. For example, van Rensburg et al. [41] showed at the subcontinental scale in South Africa that species richness and range size rarity at a spatial resolution of quarter degree are generally negatively correlated with distance to areas of transition areas between vegetation communities for both birds and frogs. Areas with more range-restricted species were located significantly closer to areas of transition areas between vegetation communities than expected by chance [41]. Similarly, in the Gulf of Aden, Kemp and colleagues [18] found high-reef fish diversity in an ecotone harboring a unique mixing of the three distinct faunas of Oman, the Red Sea, and the Indian Ocean.

Processes Shaping Biodiversity and Sustainability in Ecotones

Ecotones and Evolutionary Processes

Ecotones are "natural laboratories" for studying a range of evolutionary processes, such as the process by which new species form, also termed speciation. This process is of major interest to evolutionary biologists who define three major types of speciation: allopatric, parapatric, and sympatric. These models are based on the degree of geographical subdivision between populations that lead to the formation of new species. Allopatric speciation happens in geographical isolation, and has been for many years considered the major form of speciation. Parapatric speciation occurs in adjacent populations with gene flow among them, often along clines. Sympatric speciation occurs when populations are geographically congruent, and are found in the same area. The study of ecotones has led to a better understanding of the potential importance of parapatric and sympatric speciation as mechanisms for speciation. Ecotones have been proposed by some authors to be centers of evolutionary novelty that maintain evolutionary process, and as regions where parapatric (or sympatric) speciation processes may take place [33]. As such, ecotones and areas of environmental transition have been suggested

as natural laboratories where evolutionary processes and barriers to gene flow can be examined [33].

A review by Moritz et al. [27] summarized the major models of evolutionary processes that promote diversification of rain forest faunas. They include the divergence-with-gene-flow model, which suggests that adaptive divergence caused by selection forces occurs across environmental gradients, leading to speciation even in the face of gene flow across ecotones. This means that speciation does not require isolation in cases where selection is strong enough to separate populations. This process is expected to occur especially where very different environments meet in the ecotone, for example, at the border between a dry and wet rain forest. This may mean that even when gene flow continues, strong selection pressures can lead to divergence.

Support for the divergence-with-gene-flow model comes from recent research examining divergence using molecular genetic, phenotypic, and experimental approaches [27, 33, 34, 37]. Smith et al. [37], studying the little greenbul (*Andropadus virens*), a passeriform bird in the rain forest–savannah ecotone region of Cameroon, found especially high morphological divergence in the ecotone. The authors proposed that when the ecotone is large enough, natural selection processes could be strong enough to generate morphological differences similar to those seen in reproductively isolated species even when high rates of gene flow occur. Their data support the divergence-with-gene-flow model of speciation [38], leading them to propose that ecotones may be integral to the production and maintenance of high biodiversity in tropical rain forests. Quantification of morphological and geographic distances in olive sunbird (*Nectarinia olivacea*) populations in West African forests and ecotones revealed similar divergence patterns [38].

Smith studied morphological divergence in another Central African species, the black-bellied seedcracker (*Pyrenestes ostrinus*). Seedcrackers show polymorphism in bill size. A megabilled morph was found in the ecotone that specializes on a very hard-seeded sedge found only in ecotonal areas [27]. This ecotonal megamorph was maintained in the population, despite high levels of gene flow with rain forest populations that had only smaller-billed morphs, owing to its selective advantage for feeding on the hard seeds. Morphological divergence between habitats across an ecotone was also found in leaf-litter skinks (*Carlia rubigularis*) in the wet tropical rain forest of Australia [34]. Adult skinks occurring across sharp ecotones from open (wet sclerophyll) forests to adjacent rain forests showed large morphological and life history differences over short distances despite moderate to high levels of mitochondrial gene flow [34]. Populations occurring across the ecotone had larger size differences than populations located dozens to hundreds of kilometers away that were geographically isolated millions of years ago, suggesting that in this case, and perhaps in others that await research, speciation with gene flow may have importance.

If ecotones regions harbor unique and endemic species and alleles, this may provide support for the notion that these regions may also have importance in speciation. If this is the case, ecotonal regions are expected to contain a preponderance of recently derived species that are yet to expand their ranges (neoendemics). Fjeldså and Rahbek [7] suggested that more recently evolved species are concentrated in transitional ecotones surrounding the main central African rain forest. This reasoning is consistent with the finding that terrestrial ecotones sustain high morphological divergence, providing evidence that current speciation processes may indeed be taking place in these regions [27, 33, 37].

Ecotones, Ecological Gradients, and Species Ranges

One of the important questions that arise is what are the processes that lead to higher species richness in ecotonal regions compared with adjacent areas? Evolutionary processes, as discussed above, may be one explanation. Ecological factors may also have importance in shaping this pattern. Several authors, such as Gosz [11] and Risser [32], have suggested that transitional areas not only share the two types of environments of the habitats that coincide in the ecotone, but also have a unique ecotonal environment. Indeed, Odum [30] proposed that transition zones often support a unique community with characteristics additional to those of the communities that adjoin the ecotone, although also commenting this is by no means a universal phenomenon. Studies testing these predictions show mixed results, some pointing toward

the occurrence of ecotonal species, while others not finding evidence for species unique and highly abundant in ecotones. The inconsistency among studies is complicated by the fact that different species, systems, scales, and regions were used in different studies or due to methodological factors, such as differences in sampling and analysis approaches.

In addition, ecotones tend to shift in space and time over several spatial scales [11, 19], as a response to climatic variation, other environmental changes [6, 19, 29], and human activity [10]. Ecotones show high spatial and temporal heterogeneity, which may serve as important factors contributing to their high genetic and species diversity [32]. For example, multiple ecotones can be defined within and around the African Sahel (Fig. 1a), depending on the scale of interest and on the definitions used [1]. The different transitions (e.g., that between the Sahel and the desert to the north) experience shifts in time and space, showing high spatiotemporal variability. Another, simpler, process shaping this pattern is that ecotones, comprising meeting areas between adjoining communities, include a combination of species from two or more community types [32]. Ecotonal areas often comprise the edge of the range for species on both sides and are where many peripheral populations occur [17, 35].

An important question is whether populations occurring in ecotonal areas are viable populations that exist over time within ecotones, or are rather present temporarily due to the constant flow of individuals from other parts of their range into the ecotone areas, are not self-sustainable over time, and will disappear if this flow is stopped. Shmida and Wilson [35] proposed that the high number of species in transitional areas could be due to a process they called the mass effect, which is the flow of individuals from favorable to unfavorable areas. For species that reach the margins of their range at the ecotone, this effect may result in some individuals of a given species establishing in ecotonal areas where they cannot maintain viable populations, existing in sinks adjacent to larger source populations [35]. This may lead to increased species richness in ecotonal areas, which is maintained by constant immigration of individuals from more favorable environments. Some evidence for the existence of mass effects can be found in the literature, yet these effects seem to be rather weak, and it is currently unclear whether they can indeed act as a major factor generating high diversity in ecotones [21].

The mass effect, however, does not predict the occurrence of unique or endemic ecotonal species or genotypes. If some species or genotypes are characteristic of an ecotone or occur at the ecotone in higher abundances than in the neighboring habitats, as proposed above, this could suggest that some ecotone populations are ecologically viable. Several recent studies have found peak genetic and morphological diversity within species in ecotone regions, with populations in these regions harboring unique and rare alleles not found elsewhere [17]. For example, a study examining allozyme (protein level) diversity within chukar partridge (*Alectoris chukar*) populations across a rainfall gradient from northern to southern Israel found that the highest levels of diversity occur in the sharp ecotone area between the Mediterranean region and the desert, in the northern Negev area. Populations in this area not only showed higher genetic diversity based on 32 loci (proteins) examined, but also had unique and rare alleles that did not occur elsewhere across the range [14]. The same species also had peak levels of morphological diversity in the ecotone region based on 35 traits and 23 ratios between traits [15]. More studies on genetic and species uniqueness in ecotonal areas are needed to enable generalizations.

Agricultural, Urban and Human-Related Ecotones

The early literature discussing ecotones largely dealt with natural ecotones that are generated by environmental factors such as soils, geology, and climate. More recent research is increasingly including human-related boundaries. Human activity is generating boundaries that did not exist before, changing their steepness and shifting ecotonal location. These boundaries include a diversity of ecotone types, such as forest clear-cut edges, margins between built-up and natural landscapes, and human-generated features, such as lakes and plantations. Research on these human-generated ecotones and their effects on biodiversity are related to a study area that is sometimes termed "countryside biogeography," examining biodiversity in human-dominated landscapes.

Another recently developing research area that is relevant is that of urban ecology. Sharp, human-caused transitions may result from human activities such as

urbanization, land-use changes, agriculture, grazing, or burning (see Fig. 1). These boundaries occur at multiple spatial scales, ranging from local ecotones between agricultural plots, urban areas, and roads, and their neighboring native habitat, to large-scale ecotones such as shifting desert borders owing to desertification processes and river divergence (Fig. 1). These ecotones may be either static and fixed in space or dynamic and shifting in location over space and time.

A substantial amount of work in both natural and human-related landscapes has focused on what has been called the "edge effect." This is the effect of the juxtaposition of contrasting environments on an ecosystem. It refers to how the local environment changes along some type of boundary, or edge and how biodiversity is affected by such edges. This idea is attributed by animal ecologists to Aldo Leopold and his 1933 book *Game Management*. It encompasses a wide range of both biotic and abiotic trends associated with boundaries between adjacent habitat types, natural or anthropogenic. Much of the reference to edge effects in the recent landscape ecology literature has been related to human-caused boundaries, and especially to boundaries between forest fragments and neighboring patches of habitat that have been cleared. Again, there are no clear-cut conclusions as to the effect of human-generated ecotones on biodiversity. The response largely depends on the type of edge and its history as well the species in focus.

Its conservation implications are therefore complex and deserve further scientific attention. A vast amount of research has been done on the effect of forest edges, especially the effect of human-made forest fragments and their edges on biodiversity. A review of edges [28] suggested there are many discrepancies in the literature, and a better understanding and search for general patterns requires a much more mechanistic approach to examine the processes underlying such patterns. In this context, there has been much effort to understand the effect of forest edges on predation, brood parasitism, and the breeding success of birds. Paton [31] found that in the majority of studies, nest success varied near edges with an increase in both depredation and brood parasitism rates. The most conclusive studies suggest that edge effects in birds usually occur within 50 m of an edge [31]. Since these reviews, multiple studies on dozens of species and regions have been conducted.

Implications for Biodiversity, Conservation Planning, and Sustainability

Whereas better understanding of the effects of ecotones on biodiversity is important for evolutionary and ecological pure science purposes, it also has many implications for conservation of biodiversity, sustainability, and practical decision-making. Some scientists have argued that because ecotones hold marginal populations at the edge of the range of many species, where abundances may be lower and populations more prone to local extinctions than other parts of the range, these ecotonal areas have low value for conservation as they will not persist over time, for example, if the surrounding environments become fragmented (e.g., [9]). There has been an interesting discussion in the literature in recent years regarding whether transitional areas are valuable for conservation (e.g., see Smith et al. [36] versus Brooks [4]). Substantial conservation attention has been given in recent years to the understanding and mapping of biodiversity patterns and the underlying processes, and toward predicting the effects of global change. Ecotone and boundary regions, where change, shifts, and variability occur naturally in both space and time, could serve as useful models for understanding, monitoring, and predicting the response of individuals, populations, and communities to changing environments [2, 6, 29]. In addition, while some scientists suggest that ecotone populations are more likely to be negatively affected by climate change [9], other researchers have argued that ecotonal areas sustain populations that are adapted to changing, fluctuating, and unstable environments and, as such, these populations may better be able to persist in the face of predicted change (see further discussion in [17]). This is especially relevant since climate shifts are expected, according to some studies, to be rapid and extreme in boundary regions between ecosystems [2]. By examining changes in ecotone locations over time, these areas may potentially serve as "early warning" indicators of global changes [6, 29]. However, the response depends on the spatial and temporal scales examined and may be a useful indicator mainly at global spatial scales and rather coarse timescales. Therefore, this area deserves further attention owing to the complexity of the factors shaping the location of ecotones in space and time.

Much research in the past decade has focused on prioritizing conservation efforts and determining what areas are most important and valuable for conservation. Two main approaches have been suggested: The first approach includes a search for biodiversity hotspots, or areas with especially high species richness, endemism, and rarity. A second approach has been to select areas that are complementary, and hold biodiversity not present in other areas. Ecotones may provide a unique opportunity to conserve both high species richness and high complementarity. Due to their relatively small size, it may prove a cost-effective strategy to further conserve ecotone regions and to explicitly include them in future systematic conservation planning, given they potentially provide a high return on investment having small area and high biodiversity. Undoubtedly, if these areas have the potential to maintain and to generate species richness as well as unique and novel species and forms, they deserve far greater research attention than they are currently receiving [36]. Nevertheless, conservation plans for ecotones should not be considered independent of their surrounding environments. Ecotonal regions are important for our understanding of evolutionary (such as speciation, divergence with gene flow, and adaptation) and ecological processes shaping biodiversity (e.g., response of populations to fluctuating environments). They may enable us to better predict the responses of populations to environmental change and to further identify previously neglected biodiversity hotspots valuable for biodiversity research and conservation.

Future Directions

Research on the effect of ecotones on biodiversity is an important future direction in the face of global change, including land-use and climate change. Because ecotones are areas where shifts in environmental conditions occur in space and time, they may serve as useful indicators of environmental change and of the response of ecosystems to shifts in climate. The degree of effectiveness of ecotones as early predictors of the impacts of change and the ways that ecological communities and systems respond to change may be an important future direction. Ecotones can sustain unique forms or species that are less abundant or do not occur elsewhere. In addition, studies suggest that ecotones are areas where some populations are diverging to new species in the face of gene flow (across the ecotone). It is important to examine the generality of these patterns and processes in different regions, spatial and temporal scales, and groups.

Another future direction is the application of multi-disciplinary approaches from other fields of science in studying and quantifying ecotones. For example, much work has been done in physics on transitions between states (liquid–solid etc.), which could be applied to work on environmental transitions ecotones. More work on the interactions between native and alien species and the role of ecotones in these interactions should be done to examine the hypothesis that ecotones are barriers to invasion between communities. The importance of ecotones to the generation and conservation of biodiversity, especially in the face of global climate and other environmental changes is an area of potential research and conservation investment that should further be explored and studied. The role of ecotones in promoting sustainability and its emerging science is an open area, which should be further explored in future work.

Bibliography

Primary Literature

1. Agnew CT, Chappell A (2000) Drought in the Sahel. Geo J 48:299–311
2. Allen CD, Breshears DD (1998) Drought-induced shift of a forest-woodland ecotone: rapid landscape response to climate variation. Proc Natl Acad Sci 95:14839–14842
3. Applied Sciences Directorate https://zulu.ssc.nasa.gov/mrsid/. Accessed Nov 2006
4. Brooks TM (2001) Prioritizing hotspots, representing transitions. Trends Ecol Evol 16:673
5. Colwell RK (2006) EstimateS: statistical estimation of species richness and shared species from samples. pp User's guide and application
6. Crumley CL (1993) Analyzing historic ecotonal shifts. Ecol Appl 3:377–384
7. Fjeldså J, Rahbek C (1998) Continent-wide conservation priorities and diversification processes. In: Mace G, Balmford A, Ginsberg J (eds) Conservation in a changing world. Cambridge University Press, Cambridge, pp 107–138
8. Fortin M-J, Olson RJ, Ferson S et al (2000) Issues related to the detection of boundaries. Landsc Ecol 15:453–466
9. Gaston KJ, Rodrigues ASL, van Rensburg BJ, Koleff P, Chown SL (2001) Complementary representation and zones of ecological transition. Ecol Lett 4:4–9

10. Gehrig Fasel J, Guisan A, Zimmermann N (2007) Tree line shifts in the Swiss Alps: climate change or land abandonment? J Veg Sci 18:571–582
11. Gosz JR (1993) Ecotone hierarchies. Ecol Appl 3:369–376
12. Hansen A, Di Castri F (1992) Landscape boundaries: consequences for biotic diversity and ecological flows. Springer, New York
13. Holland M, Risser P, Naiman R (1991) Ecotones. Chapman & Hall, New York
14. Kark S, Alkon PU, Safriel UN, Randi E (1999) Conservation priorities for chukar partridge in Israel based on genetic diversity across an ecological gradient. Conserv Biol 13:542–552
15. Kark S, Mukerji T, Safriel UN, Noy-Meir I, Nissani R, Darvasi A (2002) Peak phenotypic diversity in an ecotone unveiled in the chukar partridge by a novel estimator in a dependent sample (EDS). J Anim Ecol 71:1015–1029
16. Kark S, Allnutt TF, Levin N, Manne LL, Williams PH (2007) The role of transitional areas as avian biodiversity centres. Glob Ecol Biogeogr 16:187–196
17. Kark S, van Rensburg BJ (2006) Ecotones: marginal or central areas of transition? Israel J Ecol Evol 52:29–53
18. Kemp JM (2000) Zoogeography of the coral reef fishes of the north-eastern Gulf of Aden, with eight new records of reef fishes from Arabia. Fauna Arab 18:293–321
19. Kent M, Gill WJ, Weaver RE, Armitage RP (1997) Landscape and plant community boundaries in biogeography. Prog Phys Geogr 21:315–353
20. Koleff P, Gaston KJ, Lennon JJ (2003) Measuring beta diversity for presence–absence data. J Anim Ecol 72:367–382
21. Kunin WE (1998) Biodiversity at the edge: a test of the importance of spatial "mass effects" in the Rothamsted Park Grass experiments. Proc Natl Acad Sci 95:207–212
22. Levanoni O, Levin N, Turbé A, Pe'er G, Kark S (2011) Can we predict butterfly diversity along an elevation gradient from space? Ecography. doi:10.1111/j.1600-0587.2010.06460.x, In press
23. Levin N, Shmida A, Levanoni O, Tamari H, Kark S (2007) Predicting mountain plant richness and rarity from space using satellite derived vegetation indices. Divers Distrib 13:692–703
24. Lloyd KM, McQueen AAM, Lee BJ, Wilson RCB, Walker S, Wilson JB (2000) Evidence on ecotone concepts from switch, environmental and anthropogenic ecotones. J Veg Sci 11:903–910
25. MDA Federal (2004) Landsat Geocover (1990/TM) Edition Mosaics; Tiles N-37-00 and S-37-00 (Mt. Kenya), N-14-15_20 (Hawaii), and S-21-10 (Amazon). US Geological Survey, Sioux Falls, South Dakota
26. Mena J, Vázquez Domínguez E (2005) Species turnover on elevational gradients in small rodents. Glob Ecol Biogeogr 14:539–547
27. Moritz C, Patton JL, Schneider CJ, Smith TB (2000) Diversification of rainforest faunas: an integrated molecular approach. Annu Rev Ecol Syst 31:533–563
28. Murcia C (1995) Edge effects in fragmented forests: implications for conservation. Trends Ecol Evol 10:58–62
29. Neilson RP (1993) Transient ecotone response to climate change: some conceptual and modelling approaches. Ecol Appl 3:385–395
30. Odum EP (1953) Fundamentals of ecology. W. B. Saunders, Philadelphia
31. Paton PWC (1994) The effect of edge on avian nest success: how strong is the evidence? Conserv Biol 8:17–26
32. Risser PG (1995) The status of the science examining ecotones. Bioscience 45:318–325
33. Schilthuizen M (2000) Ecotone: speciation-prone. Trends Ecol Evol 15:130–131
34. Schneider CJ, Smith TB, Larison B, Moritz C et al (1999) A test of alternative models of diversification in tropical rainforests: ecological gradients vs. Rainforest refugia. Proc Natl Acad Sci 96:13869–13873
35. Shmida A, Wilson MV (1985) Biological determinants of species diversity. J Biogeogr 12:1–20
36. Smith TB, Kark S, Schneider CJ, Wayne RK, Moritz C (2001) Biodiversity hotspots and beyond: the need for conserving environmental transitions. Trends Ecol Evol 16:431
37. Smith TB, Wayne RK, Girman DJ, Bruford MW (1997) A role for ecotones in generating rainforest biodiversity. Science 276:1855–1857
38. Smith TB, Wayne RK, Girman DJ, Bruford MW (2000) Evaluating the divergence-with-gene-flow model in natural populations: the importance of ecotones in rainforest speciation. In: Bermingham E, Dick CW, Moritz C (eds) Rainforests past and future. University of Chicago Press, Chicago, pp 148–165
39. Stöckli R, Vermote E, Saleous N, Simmon R, Herring D (2005) The blue marble next generation – a true color earth dataset including seasonal dynamics from MODIS. NASA Earth Observatory, Goddard Space Flight Center, Greenbelt
40. van Rensburg BJ, Koleff P, Gaston KJ, Chown SL (2004) Spatial congruence of ecological transition at the regional scale in South Africa. J Biogeogr 31:843–854
41. van Rensburg BJ, Levin N, Kark S (2009) Spatial congruence between ecotones and range-restricted species: implications for conservation biogeography at the sub-continental scale. Divers Distrib 15:379–389
42. Visible Earth http://visibleearth.nasa.gov/
43. Wilson MV, Shmida A (1984) Measuring beta diversity with presence–absence data. J Ecol 72:1055–1064
44. Womble WH (1951) Differential systematics. Science 114:315–322
45. Zalewski M, Schiemer F, Thorpe J (2001) Fish and land-inland water ecotones: overview and synthesis. Ecohydrol Hydrobiol 1:261–266

Books and Reviews

Blake JG, Loiselle BA (2000) Diverstiy of birds along an elevational gradient in the Cordillera Central, Costa Rica. Auk 117:663–686

Kark S (2007, updated 2011) Effects of ecotones on biodiversity. In: Levin S (ed) Encyclopedia of biodiversity. Elsevier, Oxford, p 1–10

Kluge J, Kessler M, Dunn R (2006) What drives elevational patterns of diversity? A test of geometric constraints, climate and species pool effects for pteridophytes on an elevational gradient in Costa Rica. Glob Ecol Biogeogr 15:358–371

Mac Nally R, Molyneux G, Thomson J, Lake P, Read J (2008) Variation in widths of riparian-zone vegetation of higher-elevation streams and implications for conservation management. Plant Ecol 198:89–100

McCain C (2009) Global analysis of bird elevational diversity. Glob Ecol Biogeogr 18:346–360

Odum E, Barrett G (1971) Fundamentals of ecology, 5th edn. W.B. Saunders, Philadelphia

Oommen M, Shanker K (2005) Elevational species richness patterns emerge from multiple local mechanisms in Himalayan woody plants. Ecology 86:3039–3047

Sanchez-Rodriguez J, Baz A (1995) The effects of elevation on the butterfly communities of a Mediterranean mountain, Sierra de Javalambre, central Spain. J Lepid Soc 49:192–207

Senft A (2009) Species diversity patterns at ecotones MSc thesis, University of North Carolina, Chapel Hill

Terborgh J (1971) Distribution on environmetal gradients: theorand a preliminary interpretation of distributional patterns in the avifauna of the Cordillera Vicabamba, Peru. Ecology 52:23–40

Electric, Hybrid Electric and Fuel Cell Vehicles, Architectures of

Yimin Gao
Department of Electrical and Computer Engineering, Texas A&M University, College Station, TX, USA

Article Outline

Glossary
Definition of the Subject
Introduction
Architectures of Electric Vehicles
Architectures of Hybrid Vehicles
Architectures of Fuel Cell Vehicles
Future Directions
Bibliography

Glossary

Architecture The mechanical and/or electrical structure that defines the energy flow routes in a vehicle.

Electric coupling The method by which two electric powers are added together.

Electric vehicle An electric vehicle is referred to as a vehicle that uses electric energy as its energy source, generally chemical batteries and/or ultracapacitors and electric motor as its power source.

Fuel cell vehicle A fuel cell vehicle is referred to as a vehicle that uses fuel cells and electric motor as its power source.

Hybrid electric vehicle A hybrid electric vehicle is referred to as a vehicle in which two energy sources and correspondingly two power sources are installed, which are selectively used to power the vehicle. The primary energy source and power source may be chemical fuels and internal combustion engine. The secondary energy source and power source may be chemical batteries and electric motor.

Mechanical coupling The method by which two mechanical powers are added together.

Operation mode Drive train operation status in which power sources are selectively used as the active power mover to propel the vehicle.

Definition of the Subject

The architecture design of an electric vehicle is to design its energy flow route from the energy source to the energy destination. Usually, chemical batteries are used as its energy source and electric motors are used to produce mechanical power to propel the vehicle. For satisfying vehicle performance, the batteries, electric motor, and transmission should be properly designed.

A hybrid electric vehicle uses two power sources to power the vehicle. There are many methods to connect the two power sources together, each of which has its special operation characteristics. For different vehicles that have different mission requirements and operation environments, a special architecture should be used to fully use its advantages and avoid its shortcomings.

Fuel cell vehicle is the vehicle which is powered by a fuel cell system. Compared with internal combustion engine, fuel cell is more efficient and cleaner. Architectural design of a fuel cell vehicle consists in designing the drive train structure and components to meet the vehicle performance requirements.

Introduction

Electric vehicle (EV) is referred to as a vehicle that employs electric energy storage as its energy source and electric machines as its power source. Electric energy is a multisource energy type which can be obtained from many primary energy sources, such as traditional fossil energy sources (coal, petroleum, and natural gas), nuclear energy, hydraulic power, bioenergy, solar energy, wind energy, etc. With continuous depletion of petroleum resources and more and more concerns about environmental issues, it has been well recognized that electric vehicle is one the most viable substitutes to the current petroleum-fueled vehicle. Electric vehicle also possesses other advantages of absence emissions, high efficiency, quiet and smooth operation, etc. With continuous progress on the technologies of chemical batteries, electric propulsion systems, and electronic control, electric vehicles are much closer to meeting a user's requirements than ever before.

Compared with petroleum fuels, the energy density of chemical batteries is much lower, which results in shorter driving range per battery charge. Long time battery charging also causes incontinence to users. At present, the battery-powered electric vehicles cannot challenge the petroleum-powered vehicles in terms of performance and use convenience. Hybrid electric vehicles are the combination of conventional vehicles and battery-powered electric vehicles. They can adopt the advantages and avoid the shortcomings of both. It has been recognized that hybrid electric vehicles, especially plug-in hybrid vehicles, are the major substitutes of conventional vehicles before technologies of chemical batteries have substantive progress in energy density, safety, and cost.

Fuel cell vehicles have been considered to be the final solution as the future high-efficiency and clean vehicles. Compared with conventional vehicles, fuel cell vehicles are independent from the petroleum resource and potential has high efficiency and zero emission. Compared with battery-powered electric vehicles, they potentially have the advantages of long driving range and quick fuel replenishing. However, at present, the hydrogen sources and onboard storage are the major challenges.

Architectures of Electric Vehicles

In principle, electric vehicles share the common characteristics of internal combustion engine–powered vehicles. A chemical battery pack replaces the fuel tank as its energy storage. Electric machine replaces the internal combustion engine as the power source. Both share the similar performance requirements, such as, speed, acceleration, gradeability, and driving range. The design principles as discussed in the chapter of ► Vehicle Dynamics and Performance are still valid for electric vehicles. However, unique operating characteristics of the electric propulsion system have to be involved into the design process.

Previously, electric vehicles were designed to have a similar drive train structure to conventional internal combustion engine–powered vehicles as shown in Fig. 1. It simply replaces the engine with an electric motor and fuel tank with a chemical battery pack. With

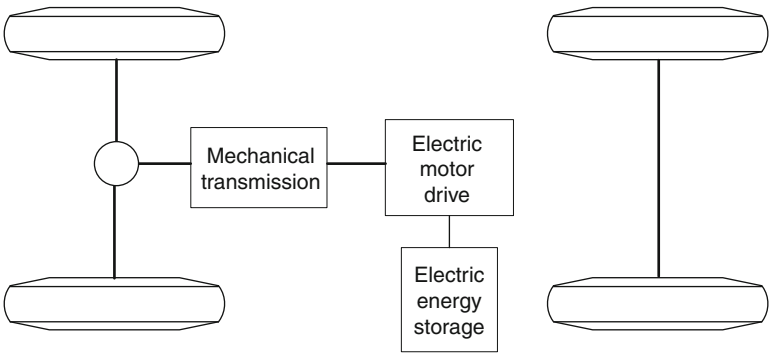

Electric, Hybrid Electric and Fuel Cell Vehicles, Architectures of. Figure 1
Primary electric vehicle drive train

development of the technologies of light weight, compact electric drive system, and advanced control, an electric vehicle drive train can be designed to various configurations as shown in Fig. 2 [1].

Figure 2a shows the first alternative configuration that is most alike a conventional one. An electric motor (EM) drive replaces the internal combustion engine. A clutch is used to connect the motor drive to or disconnect from the final drive and differential. A transmission gear box (GB) is used to modify the output speed–torque profile for meeting the performance requirement and supply a reverse gear. This drive train may be used for the motor drives which are only capable of operating in one or two quadrants, forward motoring and/or forward regeneration. Since a transmission gearbox is used, the torque-speed profile may not be required to close the ideal profile, which has constant torque in low speed range and constant power in high speed range. A motor drive with simple control may meet the requirement, such as series-excited DC motor.

Similar to the configuration shown in Fig. 2a, b shows the configuration in which clutch is not further needed. The motor starts producing its torque from zero speed. The transmission gear box may be either multi-gear or single gear, depending on the motor torque-speed profile. With a multi-gear transmission, the motor torque needs to be stopped during shifting. This can be carried out by cutting the current supply to the motor drive by the motor controller.

Figure 2c illustrates a configuration with a more compact design. A fixed gear ratio single gear transmission (FGB) is installed between the motor drive and the final drive (differential). This design requires the motor drive to be capable of producing a torque-speed profile which is closer to the ideal one. It also requires the motor be capable of operating in four quadrants, that is, forward and backward motoring and generating.

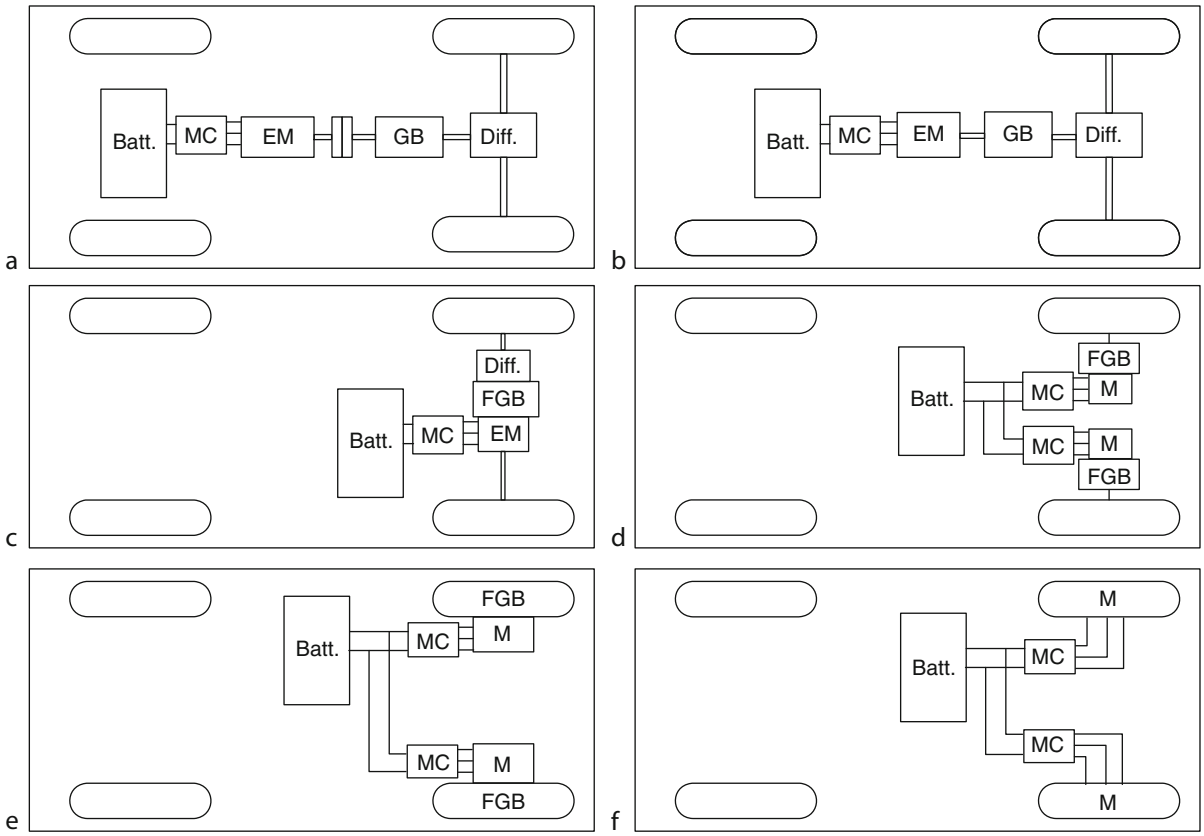

Electric, Hybrid Electric and Fuel Cell Vehicles, Architectures of. Figure 2
Possible electric vehicle configurations [1]

Figure 2d illustrates a configuration in which two motor drives are used. Each motor drives an individual wheel through a fixed gear ratio single gear box (FGB) which is used to match the motor speed to the wheel speed. A differential function is carried out by controlling the two motors. One advantage of this configuration is that it can fully utilize the road adhesive capability to improve the drivability of the vehicle. For example, when one wheel is on a slip road and loses its drive force, another wheel can produce a big driving force to help the vehicle get out of trouble.

The drive train shown in Fig. 2e is very similar to the one in Fig. 2d. The difference is that the two fixed gear ratio single gear boxes (FGB) are attached to wheels rather than to the vehicle frame. This design can save much space and may make packaging easier.

Figure 2f shows a simplest drive train structure, in which the wheel is designed as the rotor of the motor. This configuration is the most compact one and saves a lot space. This structure is generally termed as wheel motor. In the design of the drive trains shown in Fig. 2e, f, the impact of additional wheel weight to vehicle handing and vibration performance should be considered.

In all the architectures, the electric motors are powered by a battery pack and corresponding motor controller(s).

Except electric motor(s) and corresponding transmissions, a modern electric vehicle also needs other components for fulfilling its functions as shown in Fig. 3. The drive train consists of three major subsystems: electric propulsion subsystem, energy storage subsystem, and auxiliary subsystem. These three subsystems are interfaced through power routes and control signal routes. The electric energy from power grid is charged to the energy storage (batteries) through an energy charge system (battery charger). The energy storage delivers its energy to or absorbs energy from the electric motor through an electronic power converter which functions as a motor controller.

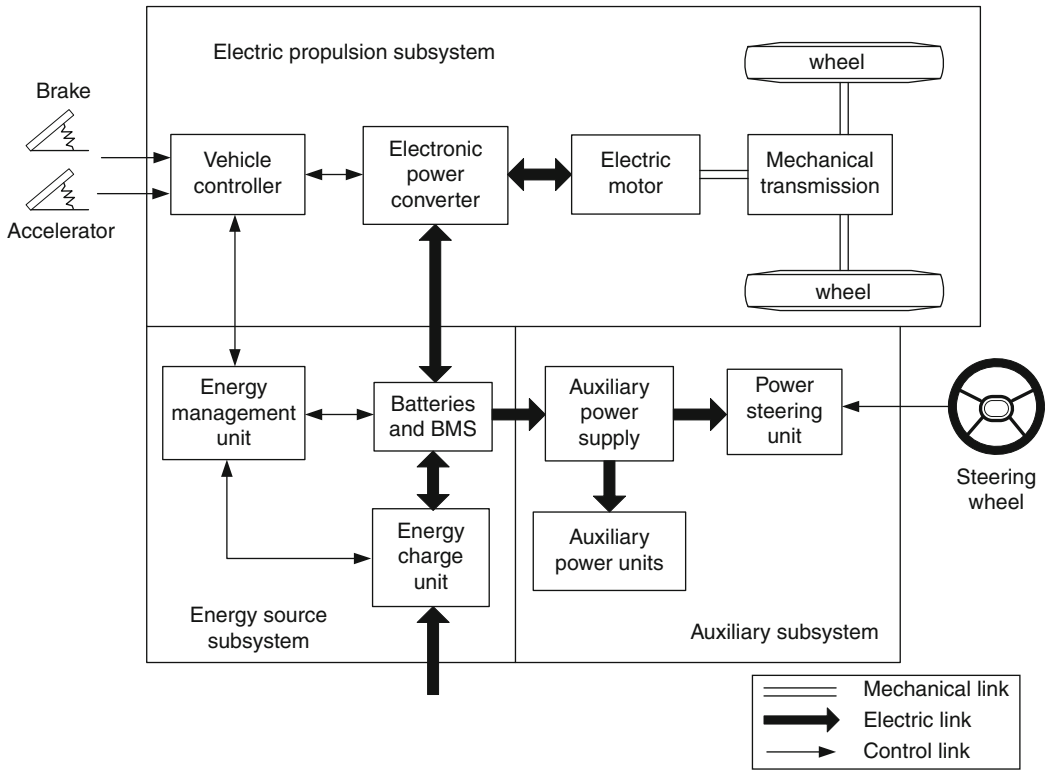

Electric, Hybrid Electric and Fuel Cell Vehicles, Architectures of. Figure 3
Conceptual illustration of an electric vehicle configuration [1]

The electric motor operation is controlled by a vehicle controller which commands the torque requirement to the motor controller based on the accelerator or brake pedal position and energy source operation parameters and energy management algorithm. The energy source also supplies energy to the vehicle auxiliaries. A battery management system (BMS) is used to monitor the operation of the battery pack, generate operation information, such as state-of-charge (SOC), and protect battery pack from abusing.

Architectures of Hybrid Vehicles

Hybrid vehicles (HV) are referred to as the vehicles that are powered by at least two energy sources and two power sources, in which at least one energy source and one power source have bidirectional energy flow capability, delivering energy to drive wheels and accepting energy from braking. When electric energy source and electric power source are used, they are referred to as hybrid electric vehicles (HEV). It is possible to replace the electric system with a hydraulic system. This kind of hybrid vehicle is referred to as hydraulic hybrid vehicles (HHV). Fuel cell vehicles (FCV) are usually referred to the vehicles in which fuel cells are used as the primacy power source. A fuel cell vehicle may use two energy sources, fuel cells and chemical batteries, which is referred to as fuel cell hybrid vehicles (FCHV).

Since there are two power sources and only one energy sink (wheels), there are many ways to combine the two powers together. The design of the energy flow routes are referred to as drive train architecture design. Control of the energy flows in hybrid drive train is referred to as vehicle control strategy.

Concept of Hybrid Vehicle

In a hybrid vehicle, two power sources supply powers to drive wheels. The total power should meet the vehicle performance requirements, in terms of maximum speed, gradeability, acceleration time requirement, and driving range. The vehicle performance requires the vehicle possessing sufficient power, and sufficient energy for continuous driving range. In operation, any one of the two power sources or both can be used for traction. Thus, there are many possible operation modes as shown in Fig. 4 [2].

The primary energy source and energy converter allows unidirectional energy flow, whereas, the secondary energy source and energy converter are required to have the capability of bidirectional energy flow. With today's technologies, the common primary energy sources are chemical fuels and primary energy converters are internal combustion engines (ICE) and fuel cells. The secondary energy sources are chemical batteries and/or ultracapacitors and the secondary energy converters are electric motors. The final destination of the energy flow (energy sink) is the vehicle wheels with the form of mechanical energy.

As shown in Fig. 4, the wheels can be powered by selecting power sources, which are referred to as operation modes, which include:

1. Primary power source alone propelling
2. Secondary power source alone propelling
3. Both power sources propelling (hybrid drive)
4. Regenerative braking (secondary power source absorbs energy form load)

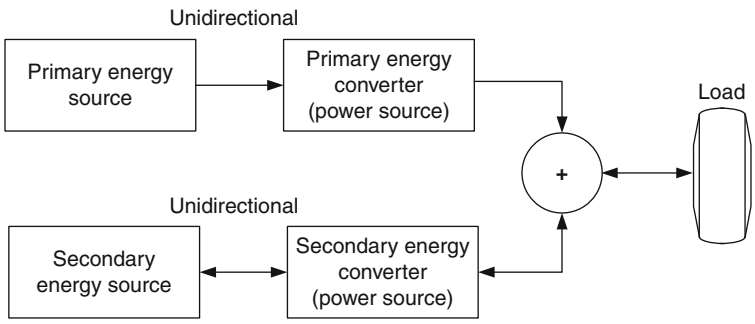

Electric, Hybrid Electric and Fuel Cell Vehicles, Architectures of. Figure 4
Concept of hybrid electric vehicles

5. Primary power source splitting for propelling and secondary power source charging

So many available operation modes create higher flexibility over single power source vehicles. It provides the drive train with opportunities for maximizing its operation efficiency and/or minimizing its emissions at any driving conditions by selectively using a best operation mode.

Vehicle load in normal driving varies randomly as shown in Fig. 5. Conceptually, the random load is composed of two components, one is the steady power (average) and the other is the dynamic power with zero average [2]. Ideally, hybrid vehicle can be designed and controlled in such a way that one power source supplies a constant power for the average load, which is referred to as energy source, since all the energy comes from it, and the other power source supplies dynamic power, which is named peaking power source, since it consumes zero energy in a whole driving cycle.

In normal driving, average power is relative small (few 10 kW). Thus, the primary power source can be designed with a small power capacity. When the internal combustion engine is used as a primary power source, it can be downsized and operated near its most efficient region. In addition, other types of engines may be used, such as Sterling engine, gas turbine engine, and others. The secondary power source may be batteries, ultracapacitors, flywheels and their combination, and electric motors.

Architectures of Hybrid Vehicles

Architecture of a hybrid vehicle is loosely defined as the ways by which the components of a hybrid drive train are connected and, therefore, the energy flow routes are schemed. Traditionally, hybrid vehicles are classified into series, parallel and series/parallel. However, the definitions of these configurations have not been clear. As discussed in a prior section, a hybrid vehicle has two power sources and one energy sink. Thus, there has to exist at least point at which two powers are merged together. At this point, the power forms have to be identical, mechanical or electrical. In this chapter, the terms of electric coupling and mechanical coupling are used rather than the traditional names. Figure 6 demonstrates the concepts of four configurations.

Figure 6a shows the configuration of an electric coupling, traditionally, a series configuration. Two powers are merged together at the power converter in the form of electrical. An internal combustion engine drives an electrical generator to supply electric power to the electronic converter, and at the same time, the battery pack also contributes its power to the power converter. The output power from the power converter flows to the electric motor to produce mechanical power and then drives vehicle wheels. The power shares are controlled by the power converter.

Figure 6b shows the configuration of mechanical coupling, traditionally, a parallel configuration. The internal combustion engine directly contributes its mechanical power to a mechanical coupler. At the same time, the battery pack supplies its power to the electric motor through a power converter which functions as the motor controller for controlling the motor torque. Two mechanical powers are merged together at the mechanical coupling and then delivered to drive wheels.

Figure 6c shows the configuration in which three power couplers are used, two mechanical and one electrical. There are plentiful available operation modes in the configuration that will be discussed in detail in following sections.

Figure 6d shows a configuration which is similar to Fig. 6c. The only difference is that the electric coupling function is moved from the power converter to the batteries and one more power converter is added between the motor/generator and the batteries [2].

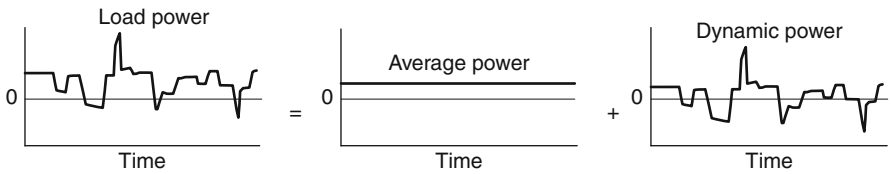

Electric, Hybrid Electric and Fuel Cell Vehicles, Architectures of. Figure 5
Steady power and dynamic power [2]

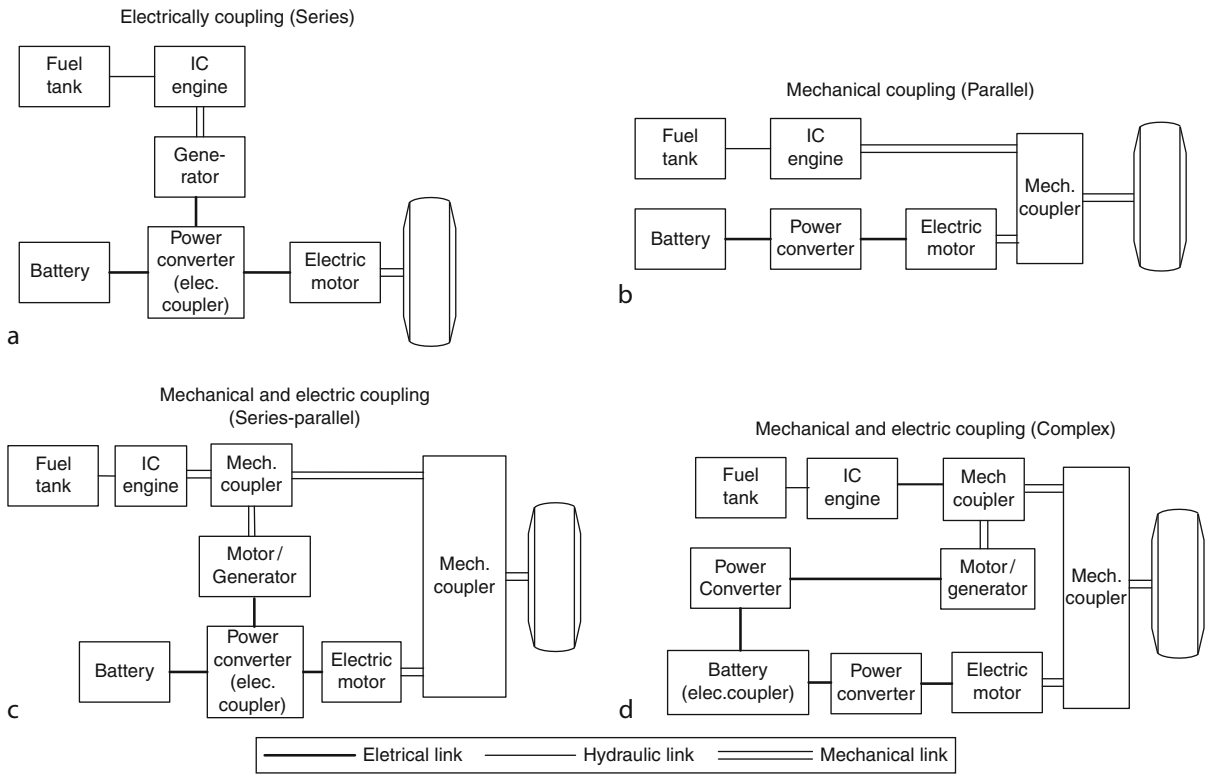

Electric, Hybrid Electric and Fuel Cell Vehicles, Architectures of. Figure 6
Various configurations of hybrid vehicles [1]

Electric Coupling HEV (Series)

The electric coupling configuration (series) is schematically shown in Fig. 7, on which, the possible power flow routes are also shown. This drive train may have been developed originally from pure electric vehicles by adding a "range extender" engine/generator set. The engine/generator unit is used to contribute part of the electric energy for compensation of battery energy shortage. An electric power converter is used for energy management purpose based on the states of charge (SOC) of the battery pack. As shown in Fig. 7, there are several operation modes available:

1. Pure electric propelling mode, in which the engine/generator is shut down and only batteries are used to propel the vehicle.
2. Pure engine/generator traction, in which batteries are isolated from the power supply route and engine/generator power follows the load power. This operation mode is also used by diesel-electric locomotives
3. Hybrid propelling mode, in which both batteries and engine/generator supply power to the traction motor. The power shares between batteries and the engine/generator are controlled by coordinate controls of the power electronic converter and engine/generator.
4. Engine/generator power split mode, in which the power of engine/generator is separated by the power converter, driving wheels and charging batteries.
5. Regenerative braking mode, in which the electric motor is operated to function as electric braking to slow down the vehicle and get the braking energy back to the batteries. The engine/generator may be shut down meanwhile.
6. Battery charging mode, in which the engine/generator is operated only for charging batteries while vehicle stop.
7. Hybrid battery charging mode, in which both the engine/generator and the regenerative braking charge the batteries.

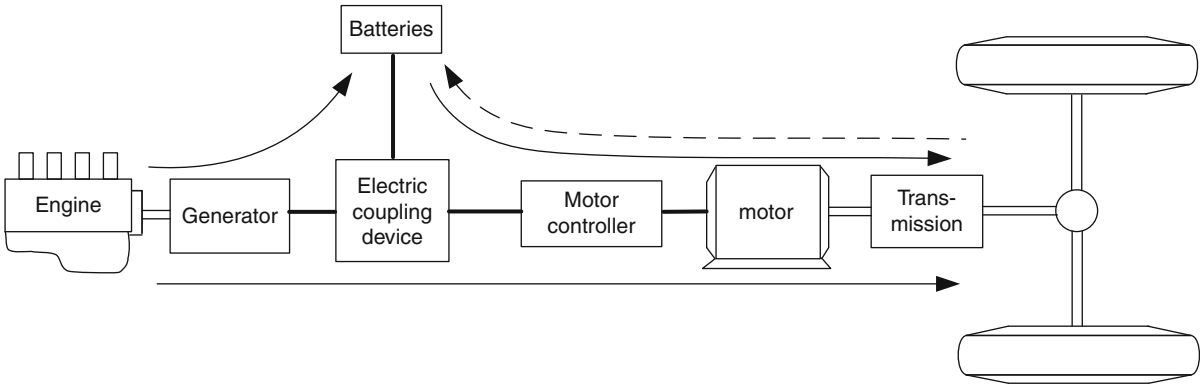

Electric, Hybrid Electric and Fuel Cell Vehicles, Architectures of. Figure 7
Electric coupling (series) hybrid drive train configuration and power flow scenario

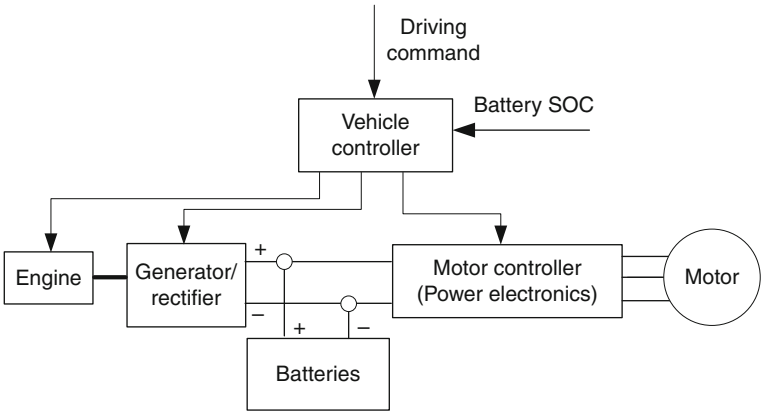

Electric, Hybrid Electric and Fuel Cell Vehicles, Architectures of. Figure 8
Directly connected power sources and motor drive

Electric Coupling Devices

The electric coupling device is the sole device at which two electrical powers are combined together. The operation modes discussed above can be carried out by coordinately controlling the electric coupling device and engine/generator. The simplest structure may be to directly connect the three terminals together as shown in Fig. 8.

The configuration in Fig. 8 has the features of identical voltage at the coupling point. The DC bus voltage is equal to the battery voltage. The power flows are only controlled by the voltage of the generator/rectifier, which depends on the operation speed of the generator and magnetic field. For battery charging, the engine/generator voltage has to be higher than the open circuit voltage of the batteries. In regenerative braking, the bus voltage has to be higher than the battery voltage. However, the voltage generated by the motor in generating mode is proportional to the motor speed. Thus, the regenerative braking capability at low speeds may be rather limited.

A DC/DC converter can be added between the batteries and the DC bus to release the voltage constraint as shown Fig. 9. This design may significantly improve the performance of the drive train. It has the following advantages: (1) variations in the battery voltage do not affect the bus voltage, thus the engine/generator can be operated at a constant speed; (2) the battery energy can be fully used, which is very important for a plug-in hybrid drive train; (3) low

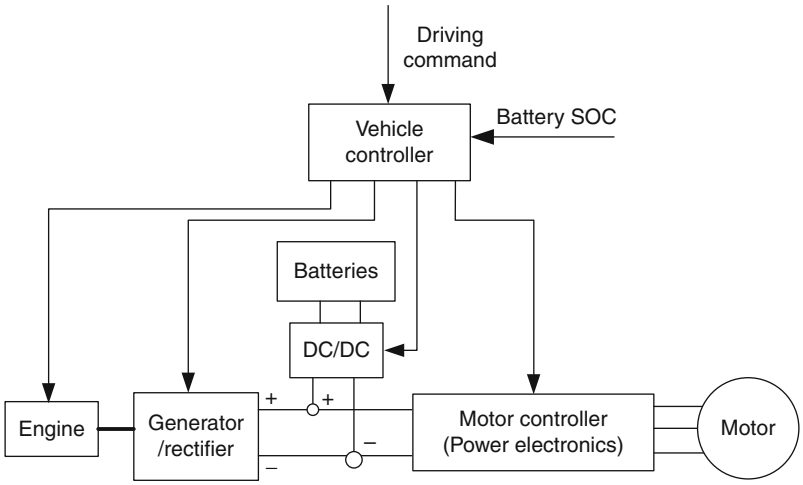

Electric, Hybrid Electric and Fuel Cell Vehicles, Architectures of. Figure 9 Configuration with a DC/DC converter

battery voltage and less battery cells can be used, which may lead to a small and light battery pack, low cost and high reliability; and (4) charging current of the batteries can be regulated during regenerative braking and charging from the engine/generator.

It is obvious that the DC/DC converter has to be bidirectional. It is considered to be the appropriate design with battery voltage lower than DC bus voltage. It boosts the battery voltage to match the DC bus voltage for propelling. On the other hand, it bucks the DC bus voltage to the level of the battery voltage for battery charging. In the situation of regenerative braking with the generated voltage by the motor higher than the battery voltage, the DC/DC operates in buck mode. However, at low speeds, the DC bus may be lower than the battery voltage. In this case, the DC/DC converter has to be operated in boost mode. The DC/DC operation mode is illustrated in Table 1 [2].

Figure 10 shows the topology of the four-quadrant DC/DC converter, operating in forward buck/boost and backward buck/boost by turning on or off the switches S_1, S_2, S_3, and S_4. The operation of the DC/DC converter is explained below.

Forward Bucking Forward operation is defined as the energy flow direction from batteries to DC bus. Forward bucking operation is that the DC/DC converter supplies current to the DC bus which has a voltage lower than battery voltage. In this operation,

Electric, Hybrid Electric and Fuel Cell Vehicles, Architectures of. Table 1 Basic function a DC/DC converter [2]

	Energy flow	
	Battery discharging	Battery charging
Battery alone traction mode	Boost	–
Battery charging from engine/generator	–	Buck
Regenerative braking	–	Buck/boost

switches S_2, S_3, and S_4 are turned off as shown in Fig. 11. Switch S_1 is operated on and off periodically. During the on period of S_1, the batteries supply current to the DC bus through S_1, L_d, and D_3 as shown in Fig. 11a, and during the off period, the batteries are isolated from the DC bus, and the current continuously flows through D_2, L_d, and D_3. The bus voltage depends on the duty cycle δ, of S_1, which is defined as the ratio of the on period, t_{on}, to whole period $T(T = t_{on} + t_{off})$. When $\delta = 0$, DC bus voltage is zero, and when $\delta = 1$, DC bus voltage equals to the battery voltage:

$$V_{bus} = \delta V_b. \quad (1)$$

The pulse width modulation (PWM) method is used to control the on and off operation of S_1 to obtain

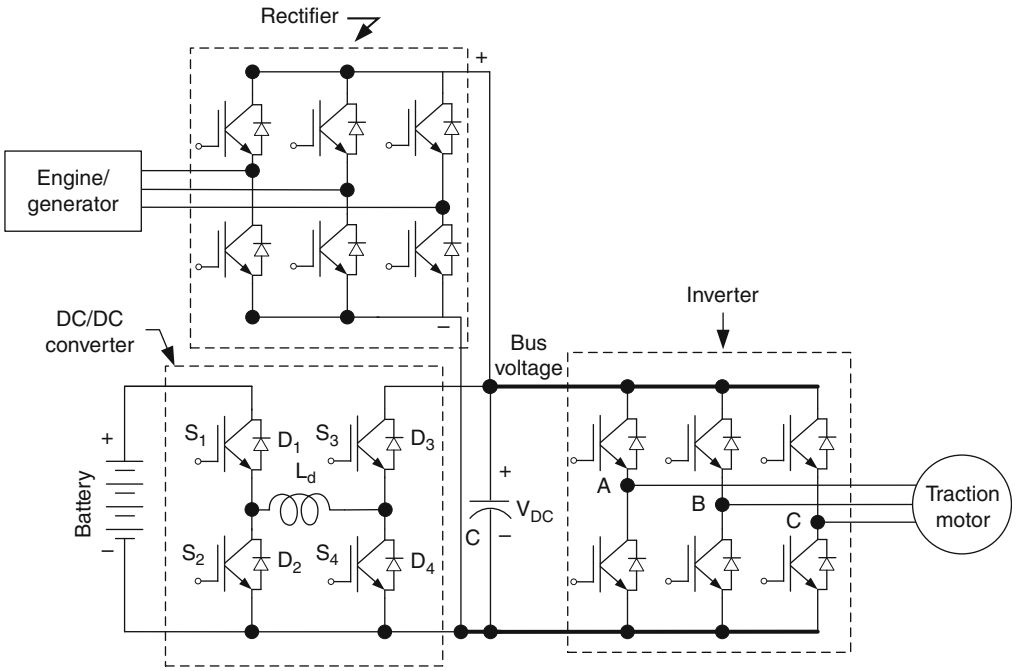

Electric, Hybrid Electric and Fuel Cell Vehicles, Architectures of. Figure 10
Bidirectional DC/DC converter [2]

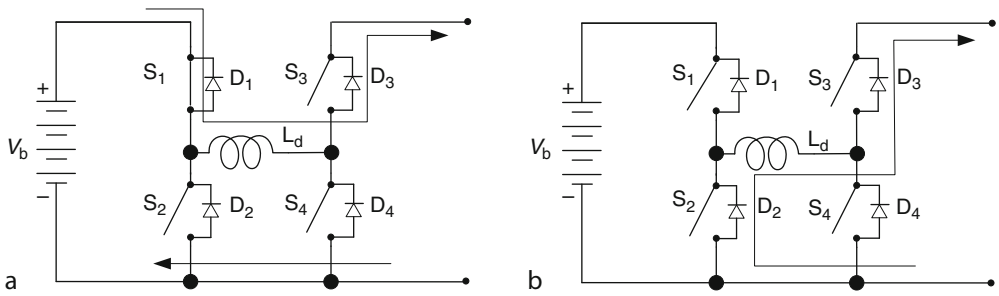

Electric, Hybrid Electric and Fuel Cell Vehicles, Architectures of. Figure 11
Forward bucking operation

the desired DC bus voltage. This case may not be used with a design that the battery voltage is lower than the DC bus voltage.

Forward Boosting When battery voltage is lower than the DC bus voltage, the DC/DC converter is operated for boosting the battery voltage for supplying current to the DC bus. In this case, switch S_1 is on, S_2 and S_3 are off, and S_4 is operated on and off periodically as shown in Fig. 12. During the on period of S_4, batteries charge the inductor L_d through S_1 and S_4 as shown in Fig. 12a. During the off period of S_4, both batteries and the inductor L_d supply current to the DC bus, which has a higher voltage than batteries. The DC bus voltage depends on the duty cycle of S_4:

$$V_{\text{bus}} = \frac{V_{\text{b}}}{1-\delta} \tag{2}$$

Backward Bucking Backward operation means the DC bus is supplying current to batteries from

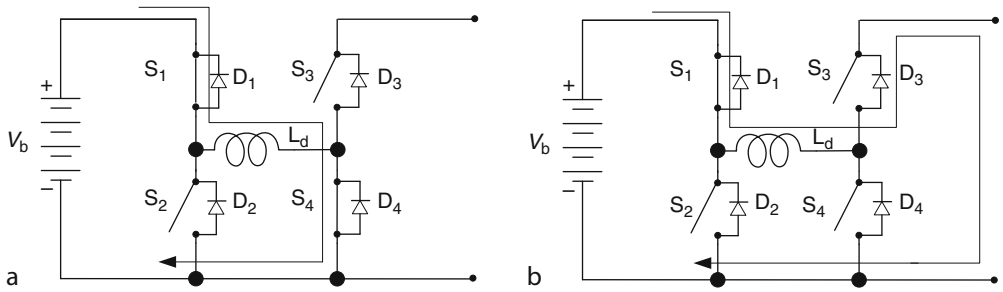

Electric, Hybrid Electric and Fuel Cell Vehicles, Architectures of. Figure 12
Forward boosting operation

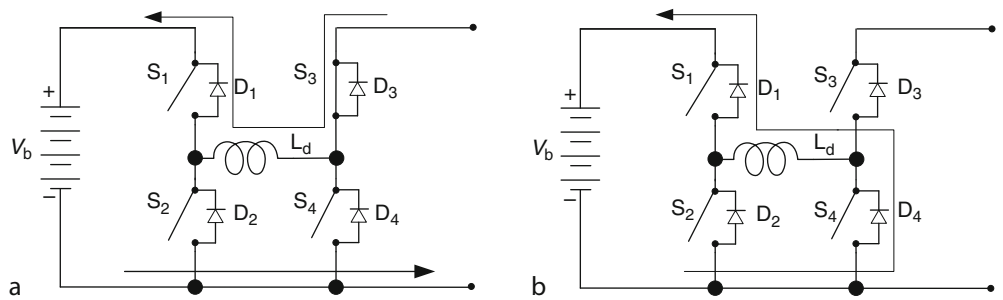

Electric, Hybrid Electric and Fuel Cell Vehicles, Architectures of. Figure 13
Backward bucking operation

regenerative braking or engine/generator. Bucking operation is to reduce the DC bus voltage to battery voltage level. In this operation, S_1, S_2, and S_4 are off and S_3 is operated on and off periodically. During the on period of S_3, the DC bus supplies current to batteries through S_3 and D_1 as shown in Fig. 13a. During the off period of S_3, the DC bus is isolated from the batteries. The batteries and DC bus have a voltage relation of

$$V_b = \delta\, V_{bus}. \tag{3}$$

This mode may be used in the situation of charging the batteries from engine/generator and regenerative braking at high vehicle speeds.

Backward Boosting This operation is to boost a low DC bus voltage to a high battery voltage. It may be used in regenerative braking at low vehicle speeds at which, the voltage generated by the motor is low. In this operation mode, S_1 and S_4 are off and S_3 is on and S_2 is operated on and off periodically. During the on period of S_2, the DC bus charges the inductor L_d through S_3 and S_2 as shown in Fig. 14a. During the off period of S_2, both the DC bus and inductor L_d supply energy to the batteries. The DC bus and batteries have the voltage relation:

$$V_b = \frac{V_{bus}}{1-\delta}. \tag{4}$$

Advantages and Disadvantages of Electric Coupling (Series) Drive Train

Electric coupling (series) hybrid vehicles have the advantages of:

1. Internal combustion engine is completely mechanically decoupled from wheels. Thus the engine operation can be operated in its most efficient speeds range. On the other hand, since batteries supply supplementary power, engine power is also decoupled from load power. Therefore, the engine can be operated in its most efficiency power range as shown in Fig. 15.
2. Since the engine can be potentially operated in a very narrow speed and power region, it becomes much easier for further improvement of fuel

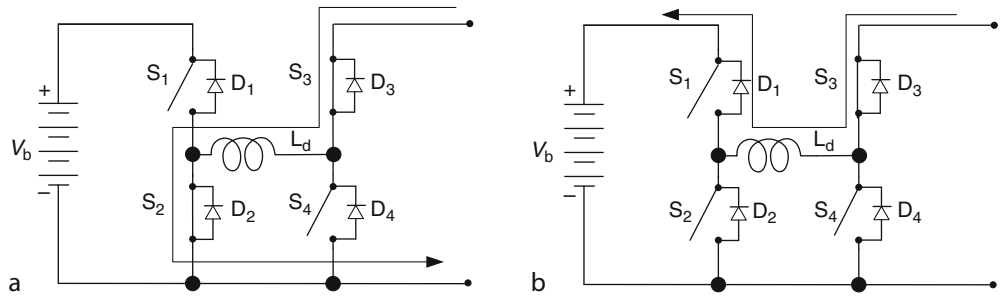

Electric, Hybrid Electric and Fuel Cell Vehicles, Architectures of. Figure 14
Backward boosting operation

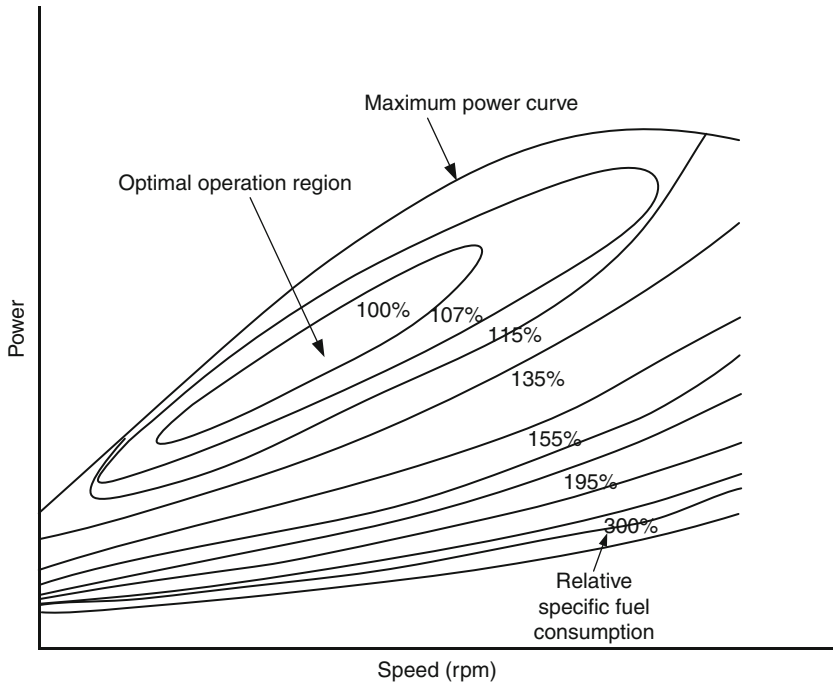

Electric, Hybrid Electric and Fuel Cell Vehicles, Architectures of. Figure 15
Illustration of a typical engine fuel consumption map

economy and emission characteristics by using some engine special design and control technologies in this narrow region than in the whole operation domain.

3. Completely mechanical decoupling of engine from driving wheels allows using engines that may not be suitable for direct vehicle propelling, such as gas turbine engine, sterling engine, etc.
4. A multi-gear transmission and torque converter may not be required, since the vehicle is solely driven by an electric motor, which has proper torque-speed profile for vehicle traction.
5. In-wheel motors may be used similar to a pure electric vehicle.
6. The control of the drive train may be simple, compared with other configurations.

However, electric coupling (series) drive train is also suffered from some disadvantages such as:

1. Two times energy form transformations from engine to wheels (mechanical to electrical and then to mechanical again) may cause significant energy losses.
2. Additional electric machine (generator) adds weight and cost.
3. Traction motor(s) have to be designed big enough to meet vehicle performance, such as maximum speed, acceleration, and gradeability.

Mechanical Coupling Hybrid Drive Trains

In mechanical coupling hybrid vehicles, mechanical coupling devices are used to couple two mechanical powers together. Mechanical power composes of force and speed in linear motion, and torque and angular speed in rotary motion. Accordingly, a mechanical coupling device may add to torques together or add two angular speeds together, depending on its mechanical structure.

Torque Couplers A torque coupler is a three-port mechanical device which adds two input torques together and delivers them to output port as conceptually illustrated in Fig. 16. Port 1 is a unidirectional input port (e.g., engine port), port 2 is bidirectional input port (e.g., electric motor port), and port 3 is a bidirectional output port (e.g., wheel port).

Ignoring losses and inertia effect, the total input power is always equal to the output power. Supposing port 1 and port 2 are inputs and port 3 is output, one obtains:

$$T_3\,\omega_3 = T_1\,\omega_1 + T_2\,\omega_2. \tag{5}$$

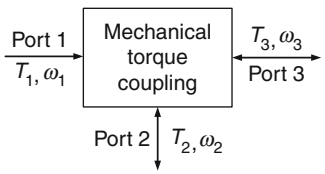

Electric, Hybrid Electric and Fuel Cell Vehicles, Architectures of. Figure 16
Concept of a mechanical coupling device

Inside the device, two torques, T_1 and T_2, are added together in the following way:

$$T_3 = k_1\,T_1 + k_2\,T_2\,, \tag{6}$$

where k_1 and k_2 are structural parameters which are constants or variables, depending on the structure design of the device. T_1 and T_2 are independent of each other and then can be independently controlled. Solving Eqs. 5 and 6 gives the relationship among the speeds:

$$\omega_3 = \frac{\omega_1}{k_1} = \frac{\omega_2}{k_2} \tag{7}$$

Obviously, three speeds are linked together by k_1 and k_2, and have a fixed relationship with each other. When a torque coupler is used in a hybrid vehicle, the engine torque can be decoupled from the wheel torque and motor torque is used for compensation. However, the engine speed varies with the vehicle speed. This feature provides the engine with an opportunity of always operating at its operation line at any vehicle load as shown in Fig. 17. Figure 18 shows the commonly used torque couplers.

Speed Couplers Similar to the torque coupler (also refer to Fig. 16), a mechanical speed coupler can be described as:

$$\omega_3 = k_1\,\omega_1 + k_2\,\omega_2 \tag{8}$$

where k_1 and k_2 are the constants or variables associated with the device structure design. Among these three speeds, two of them are independent and then can be controlled independently. Combining with Eq. 5, the torques are linked together by:

$$T_3 = \frac{T_1}{k_1} = \frac{T_2}{k_2} \tag{9}$$

A typical speed coupler is the planetary gear unit as shown in Fig. 19. It consists of a sun gear 1, a ring gear 2, and a yoke 3 which is hinged to the centers of several planetary gears (usually three or four gears for force balance). The relationship among ω_1, ω_2, and ω_3 is

$$\omega_3 = \frac{1}{1+g_r}\,\omega_1 + \frac{g_r}{1+g_r}\,\omega_2 \tag{10}$$

where g_r is the gear ratio of ring gear to sun gear ($R_2/R_1 = z_2/z_1$, where z_2 and z_1 are the tooth number

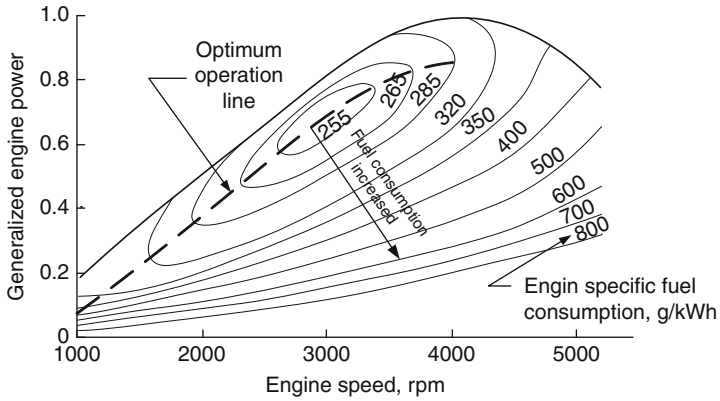

Electric, Hybrid Electric and Fuel Cell Vehicles, Architectures of. Figure 17
Engine fuel consumption map and its optimal operation line

of ring gear 2 and sun gear 1). Obviously, constants k_1 and k_2 in Eqs. 8 and 9 are $k_1 = 1/(1+g_r)$ and $k_2 = g_r/(1+g_r)$. The directions of the torques as shown in Fig. 19 (counterclockwise for sun and ring gears and clockwise for yoke) are defined as positive. The torque relationship can be expressed by Eq. 9. It can be seen from Fig. 19 that the torques on sun gear and ring gear always have the same direction and the torque on the yoke always has an opposite direction.

Another interesting speed coupling device is an electric motor with a floating stator [2], in which the stator, generally fixed to a stationary frame in conventional motor, is released and forms a double rotor motor as shown in Fig. 20. In this device, port 2 is an electric port, at which electric power is converted into mechanical power at the air gap between the inner and outer rotor to generate a relative speed ω_2. Obviously,

$$\omega_3 = \omega_1 + \omega_2, \tag{11}$$

and

$$T_3 = T_1 = T_2. \tag{12}$$

Here, $k_1 = 1$ and $k_2 = 1$ in Eqs. 8 and 9.

With a speed coupler, the engine speed is decoupled from the vehicle speed, thus the engine can always be operated within its optimal speed range.

Selective uses of electric coupling, mechanical torque, and speed couplings can create many hybrid vehicle configurations as discussed in following sections.

Hybrid Drive Train with One Torque Coupler

Hybrid drive train with one torque coupler is the simplest configuration which is traditionally referred to as parallel configuration. The torque coupler can be designed with different k_1 and k_2 values as indicated in Eqs. 6 and 7 and Fig. 16. A two-shaft configuration with gear box as its coupler and two transmissions is shown in Fig. 21.

In this configuration, the torque coupler can be designed with any parameter values of k_1 and k_2. In front of the torque coupler, two transmissions can be used, which may be multi-gear, single gear, or continuous varying transmission (CVT), depending on the engine and motor torque-speed characteristics and vehicle performance requirements. Actually, two transmissions and the torque coupler together can be taken as one assembly, which has the inputs of engine and motor and the output to final drive. The torque coupling assembly still has the same characteristic of the single torque coupler explained by Eqs. 6 and 7, except gear ratios of two transmissions being added, which can be expressed as:

$$T_o = k_1\, i_e\, T_e + k_2\, i_m\, T_m\,. \tag{13}$$

and

$$\omega_o = \frac{\omega_e}{k_1\, i_e} = \frac{\omega_m}{k_2\, i_m}, \tag{14}$$

where ω_e, T_e, ω_m, and T_m are the angular speeds and torques of the engine and motor, i_e and i_m are the

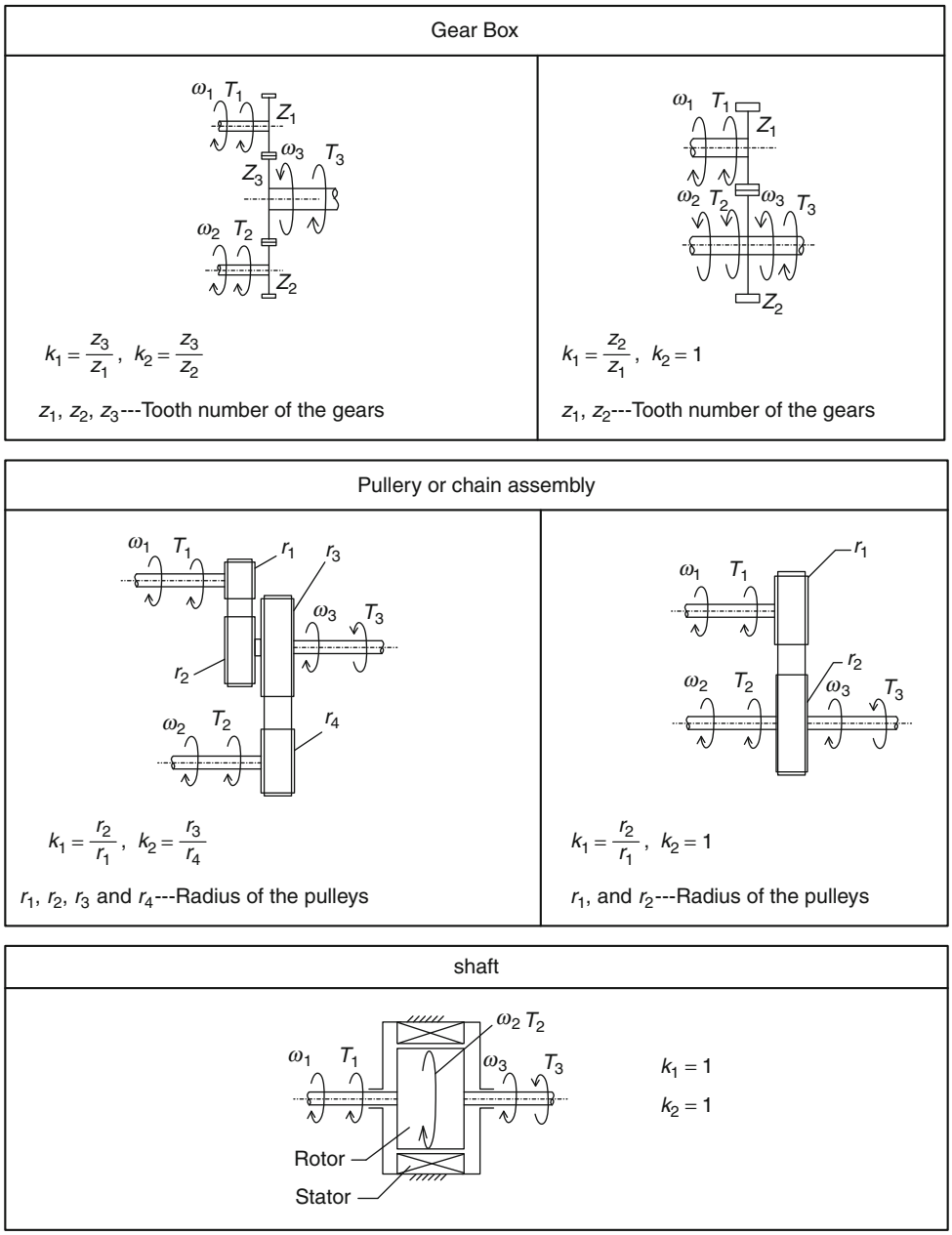

Electric, Hybrid Electric and Fuel Cell Vehicles, Architectures of. Figure 18
Commonly used torque coupling devices [2]

transmission gear ratios of the engine and motor transmissions, respectively.

Obviously, two multi-gear transmissions produce many tractive effort profiles [2]. For example, two three-gear transmissions produce nine tractive effort profiles (3 × 3). High vehicle acceleration and gradeability performance can be obtained. Further, high overall efficiency of the drive train can also be obtained by selecting proper gears for operating the engine and motor within their best region. This design also provides opportunity for using the engine and motor which may have less favorable characteristics.

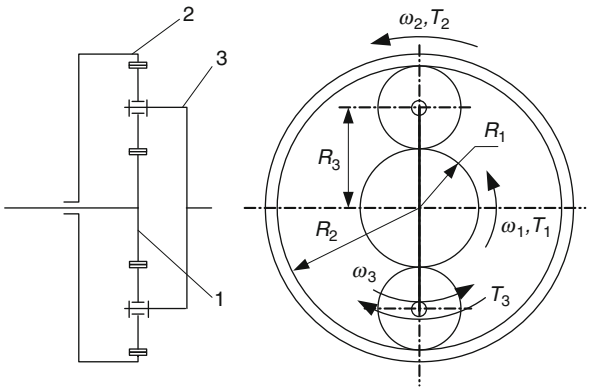

Electric, Hybrid Electric and Fuel Cell Vehicles, Architectures of. Figure 19
Planetary gear unit used as a speed coupler [2]

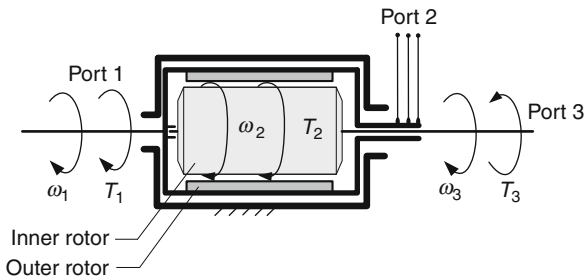

Electric, Hybrid Electric and Fuel Cell Vehicles, Architectures of. Figure 20
Electric motor with double rotors as a speed coupler [2]

However, this design makes it complicated for the control system for selecting proper gears.

Instead, a single gear transmission for the motor may be used, since electric motor generally has good torque-speed characteristics. The three-gear transmission for engine is used to modify the engine torque-speed profile and provides opportunity for engine operating closer to its high-efficiency region.

Another possible design is to use single gear transmission for engine and multi-gear transmission for engine. This design is considered to be an unfavorable design because it does not take advantage of the two power plants.

The simplest design is to use two single gear transmissions. When the engine and motor are designed to meet gradeability and acceleration performance, it is considered to be a good design.

Another two-shaft torque coupling hybrid configuration is to place a transmission behind the torque coupler as shown in Fig. 22 [1], in which, the engine and motor torque-speed profiles and the tractive effort are also illustrated. Obviously, the transmission modifies the engine and motor torques with the same scale. The gear ratio of the torque coupler (k_1 and k_2) is designed to matches the speeds of the engine and motor. This design may be a proper selection for the one with larger engine and small motor, such as mild hybrid drive train.

A simple shaft may be used as the torque coupler, which constitutes the configuration, traditionally called one-shaft parallel drive train. A transmission may be placed in front of the torque coupler as shown in Fig. 23. In this configuration, the rotor of the electric motor functions as the torque coupler, in which one end is connected to the engine and the other end to the transmission. Obviously, here, $k_1 = 1$ and $k_2 = 1$. This configuration has the similar operation characteristics. Since the motor directly drives the final drive, the motor speed is proportional to the vehicle speed, and the final drive gear ratio should be designed to match the motor speed and vehicle speed.

An alternative configuration is to place the transmission behind the motor as shown in Fig. 24. In this configuration, torques of both engine and motor are enhanced by the transmission. However, the engine and motor are directly coupled together; hence, they have to have the same operation speed range. The motor can serve as the engine start when a clutch is placed between the motor and transmission. When this configuration is used in a mild hybrid drive train, where motor alone operation mode is used, the clutch can be placed between the motor and transmission. The motor functions as an engine torque booster, engine start, generator, and regenerative braking.

Actually, the vehicle chassis and road can also used as a torque coupler. Figure 25 shows a hybrid drive train in which the engine and motor drive the front and rear wheels, respectively. The tractive efforts produced by the engine and motor are added together by the vehicle chassis and road. This configuration offers some advantages of keeping the original engine and transmission driveline and providing the vehicle with a four-wheel-drive capability.

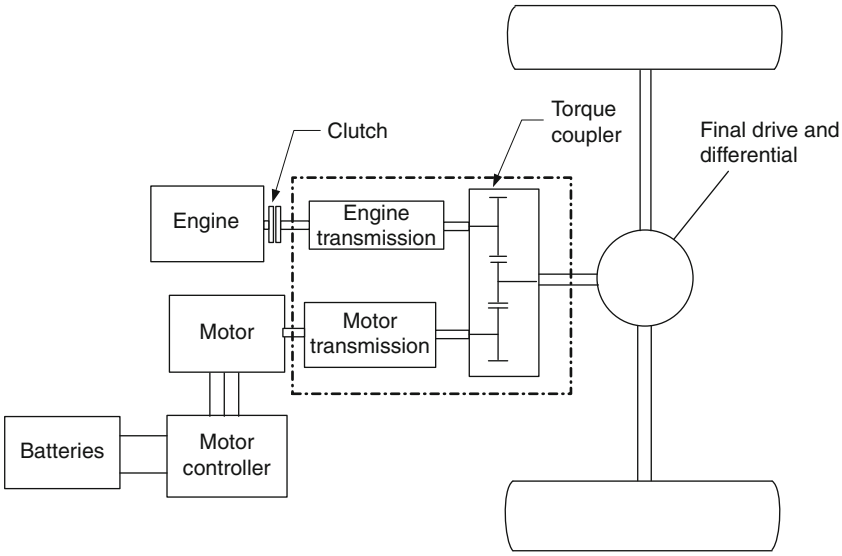

Electric, Hybrid Electric and Fuel Cell Vehicles, Architectures of. Figure 21
General torque coupling hybrid drive train [2]

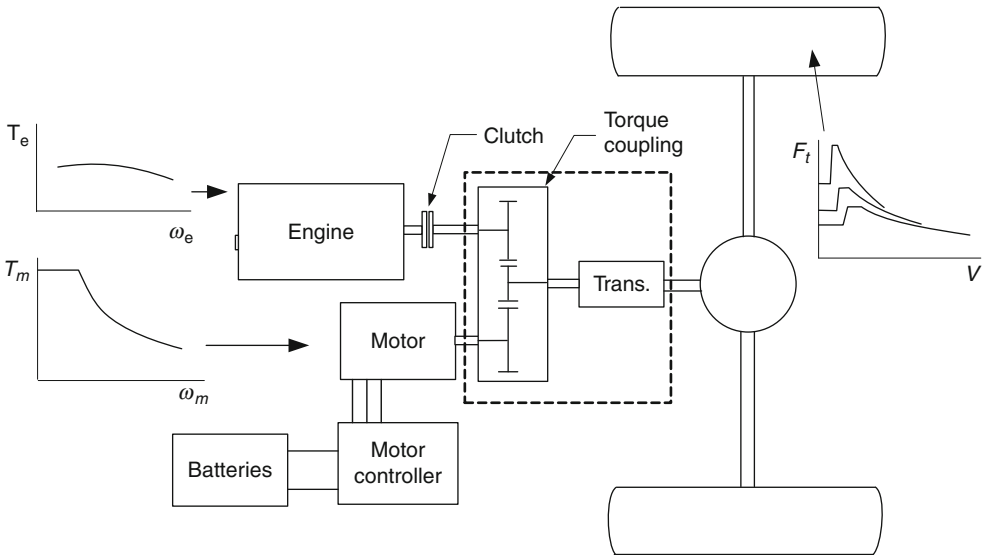

Electric, Hybrid Electric and Fuel Cell Vehicles, Architectures of. Figure 22
Two-shaft configuration with a transmission behind the torque coupler [2]

Hybrid Drive Trains with Torque and Speed Couplings

As discussed in prior sections, the torque coupler can decouple the engine torque from the wheel's torque demand, and speed coupler can decouple the engine speed from the wheel speed. Thus, it is possible to decouple the engine torque and speed from the wheels with two couplers. This concept is illustrated in Fig. 26.

A detailed drive train structure is shown in Fig. 27 [1]. The drive train uses a planetary gear unit as its speed coupler. Engine is connected to its yoke and

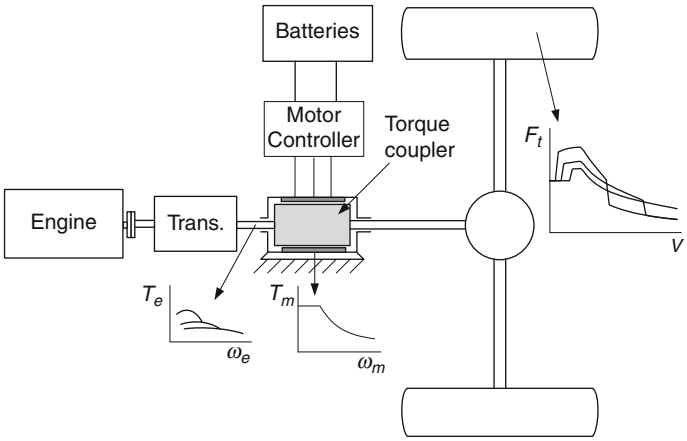

Electric, Hybrid Electric and Fuel Cell Vehicles, Architectures of. Figure 23
One-shaft configuration with a transmission in front of the torque coupler [1]

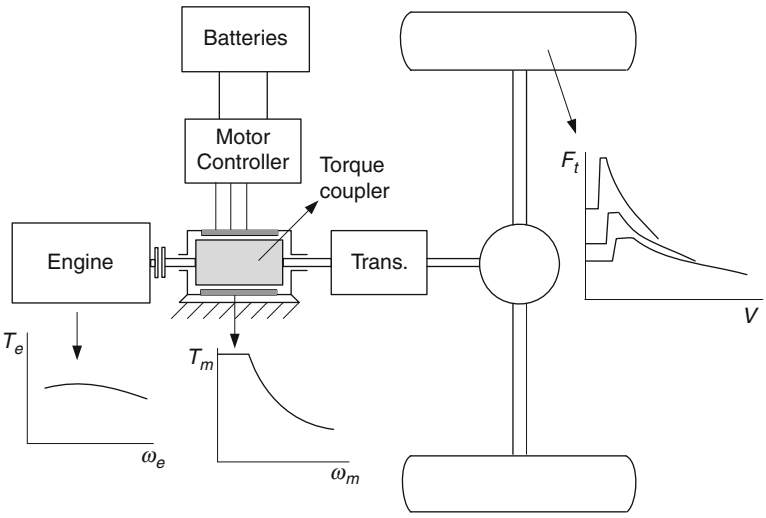

Electric, Hybrid Electric and Fuel Cell Vehicles, Architectures of. Figure 24
One-shaft configuration with a transmission behind the torque coupler [2]

a motor/generator to its sun gear. The ring gear as the output port is connected to a torque coupler which is a fixed shaft gear set. Another two ports of the torque coupler are connected to a traction motor and wheels.

As indicated in Eqs. 8 and 9, Fig. 19, the torque of the motor/generator always has an opposite direction as that of the engine and can rotate in two directions. When the rotating speed is in the same direction as its torque, it is a motor, otherwise, a generator. When it operates in the generating mode, it absorbs part of the engine power. Due to this reason, this hybrid drive train gets another name of engine power split hybrid drive train.

The torque of the motor/generator is always proportional to the engine torque. Thus, an ideal operation characteristic is a constant torque at the whole positive and negative speed domain. Also, the three controllable components (the engine, motor/generator, and traction motor) provide very plentiful operation modes, and hence, greater opportunity for high operating efficiency. However, very complex control is required [2].

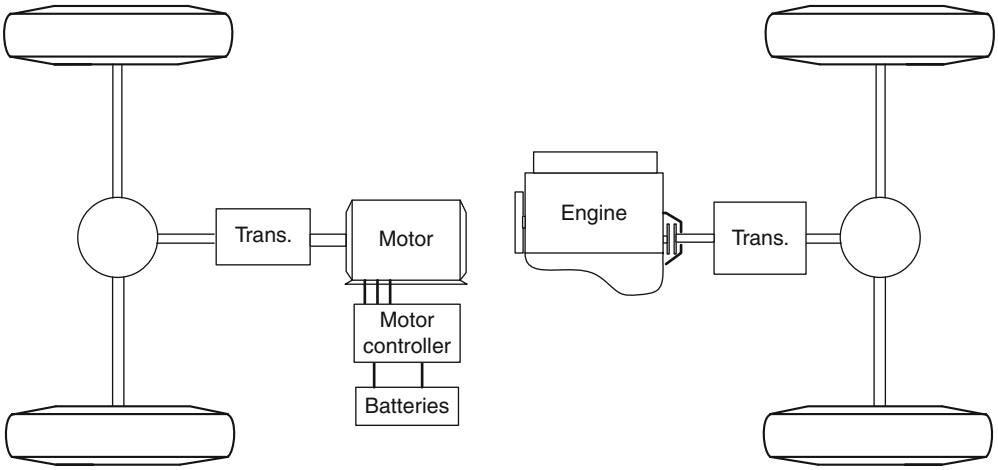

Electric, Hybrid Electric and Fuel Cell Vehicles, Architectures of. Figure 25
Front- and rear-wheel-driven hybrid vehicle

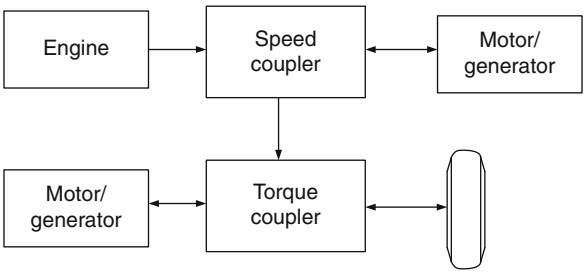

Electric, Hybrid Electric and Fuel Cell Vehicles, Architectures of. Figure 26
Concept of torque and speed coupling drive train

Architectures of Fuel Cell Vehicles

Fuel Cell System

A fuel cell is a chemical device that converts the chemical energy into electric energy by means of redox reaction with the operation principle exactly the same as in a chemical battery. In a battery cell, the reactive chemicals are pro-installed in the cell. When the active chemicals are used up, the cell is dead and has to be recovered by charging it from an outside electrical source. Instead, a fuel cell is fed with its reactive chemicals continuously from outside of the cell. It is more like an internal combustion engine which is fed with fuel and produces mechanical energy. However, the energy conversion efficiency in a fuel cell is higher than internal combustion engine due to its free from the Carnot cycle limitation. Compared to chemical batteries, it has the advantages of quick refueling and much more energy in an outside energy storage, similar to a fuel tank.

A fuel cell has a very similar structure of chemical battery cell, as shown in Fig. 28. Fuel and the oxidizing agency are continuously and separately fed into the anode and cathode electrodes, where they are ionized. Electrolyte is used to conduct positive ions from the anode to the cathode, and at the same time, electrons are conducted from the anode to the cathode through an electrical load.

A single fuel cell has very low voltage. In practice, a fuel cell stack may include hundreds of single cells serially connected together. A fuel stack needs auxiliaries to support its operation. The auxiliaries mainly include air circulating pump, coolant circulating pump, ventilation fan, fuel supply pump, and electric control devices. Part of the power developed from the fuel cell stack is used to support the operation of the auxiliaries as shown in Figs. 29 and 30.

Fuel Cell Technologies

There are several types of fuel cells, depending on their electrolytes. Table 2 lists the operation temperature and electrolytes.

Proton Exchange Membrane Fuel Cells (PEMFCs) PEMFCs work with hydrogen as fuel and oxygen as

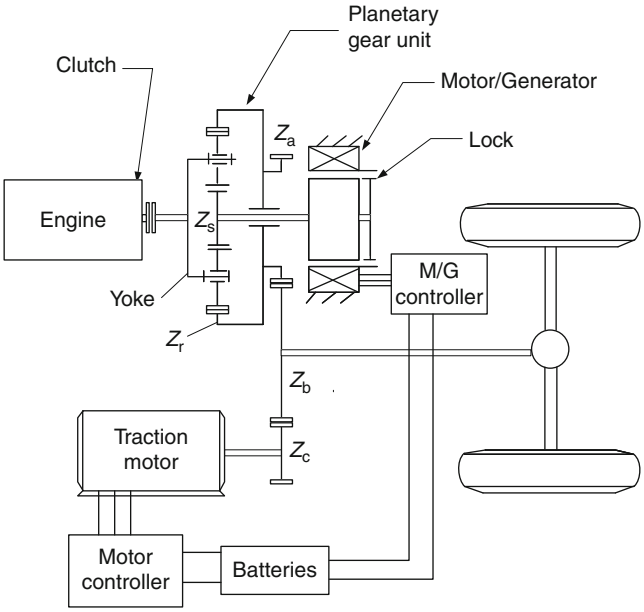

Electric, Hybrid Electric and Fuel Cell Vehicles, Architectures of. Figure 27
Hybrid drive train with speed and torque couplers

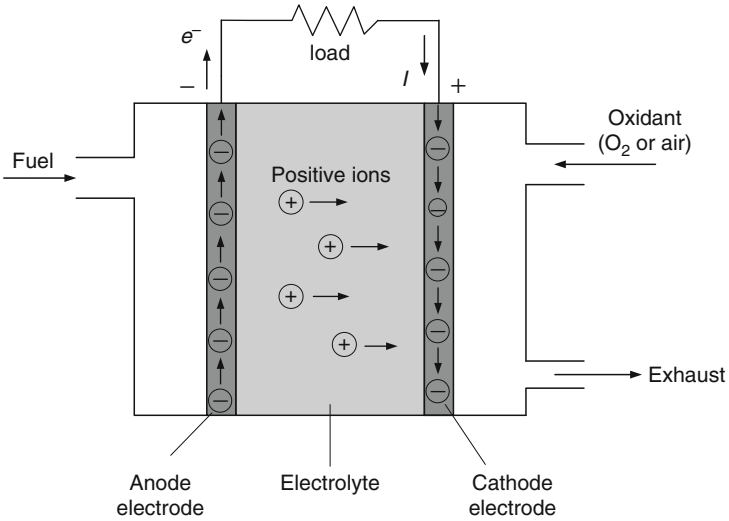

Electric, Hybrid Electric and Fuel Cell Vehicles, Architectures of. Figure 28
Illustration of fuel cell operation

oxidant. Hydrogen is supplied to the anode where it is oxidized, losing electrodes in the process. Positive hydrogen ions (protons) migrate across the electrolyte through the membrane to the cathode, at the same time, the electrons travel round the external circuit to the cathode. The oxygen is supplied to the cathode where it is reduced, picking up the electrons and the ions from the hydrogen to form water.

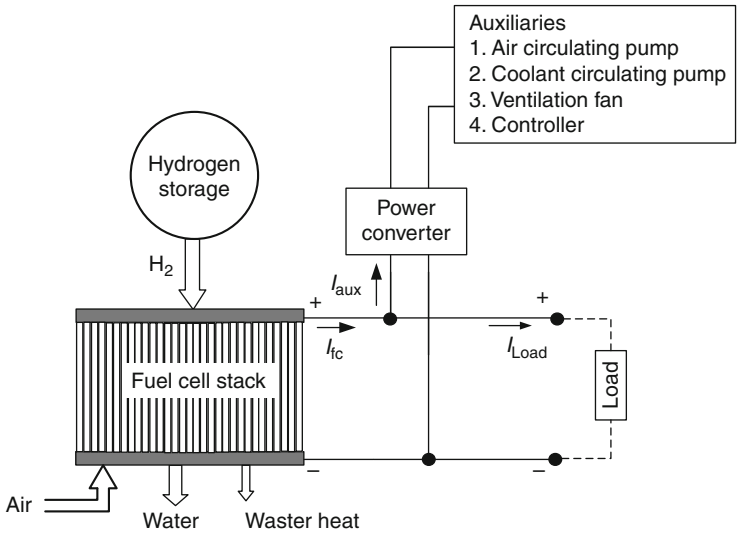

Electric, Hybrid Electric and Fuel Cell Vehicles, Architectures of. Figure 29
A hydrogen–air fuel cell system

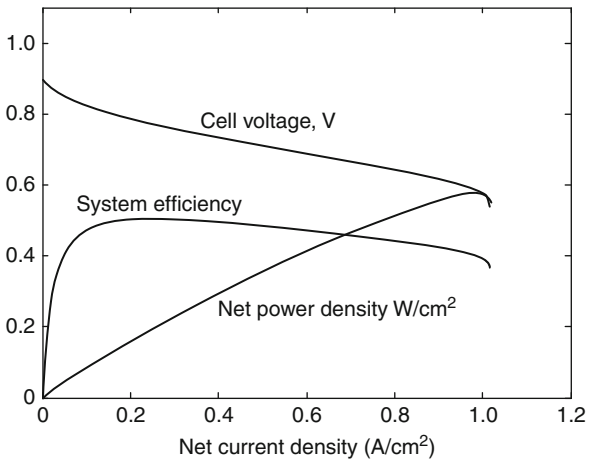

Electric, Hybrid Electric and Fuel Cell Vehicles, Architectures of. Figure 30
Cell voltage, system efficiency, and net power density varying along net current density of a hydrogen–oxygen fuel cell [2]

Electric, Hybrid Electric and Fuel Cell Vehicles, Architectures of. Table 2 Operating data of various fuel cell systems [3]

Cell system	Operating temperature, °C	Electrolyte
Proton exchange fuel cells (PEMFCs)	60–100	Solid
Alkaline fuel cells (AFCs)	80–230	Liquid
Phosphoric acid fuel cells (PAFCs)	60–200	Liquid
Molten carbonate fuel cells (MCFCs)	600–1000	Liquid
Solid oxide fuel cells (SOFCs)	1000–1200	Solid
Direct methanol fuel cells (DMFCs)	100	Solid

The electrodes of PEMFCs are made of porous carbon which allows the active gases to pass through. The electrode surfaces are coated with platinum as a catalyst which increases the rate of oxidation at the anode and the rate of reduction at the cathode. The platinum catalysts allow the chemical reaction to take place at a lower temperature. Alternatively to avoid the cost of expensive catalysts, some fuel cells are designed to work at elevated temperatures.

The platinum catalyst used in PEMFCs is very expensive and extremely sensitive to poisoning by even small amounts of carbon monoxide. Thus a high purity of hydrogen gas is necessary.

Electrolyte is a thin, fragile sheet of acidic, solid organic polymer about 50 μm thick which permits the

passage of hydrogen ions but is impermeable to electrons. Acidic compounds are fluids with free hydrogen ions and these are the fuel cell's charge carriers [4].

The first PEMFCs were developed in the 1960s for the need of a US-manned space program. It is nowadays the most investigated fuel cell technology for automotive applications. It operates at 60–100°C and can offer a power density of 0.35–0.6 W/cm^2. PEMFCs offer some definite advantages for electric and hybrid vehicle applications that include low temperature operation, high power density among all the available types of fuel cells, solid electrolyte that does not change, movement and vaporization from the cell, and most importantly, potentially high efficiency and being free of toxins and greenhouse gas emissions. The major problems are their requirements of expensive noble metal catalyst and membrane, and a need of high purity of hydrogen as its fuel.

Alkaline Fuel Cells (AFCs) Alkaline fuel cells use aqueous electrolytes of potassium hydroxide (KOH) to conduct ions between electrodes. Hydrogen and oxygen are used as the fuel and oxidant. The ion carried by the alkaline electrolyte is a hydroxide ion (OH^-). The half reactions are:

$$\text{Anode}: \ 2H_2 + 4OH^- \rightarrow 4H_2O + 4e^-$$

$$\text{Cathode}: \ O_2 + 2H_2O + 4e^- \rightarrow 4HO^-$$

AFCs are capable of operating over a wide range of temperature (80–230°C) and pressure (2.2–45 atm). AFCs are capable of achieving high operating efficiency because of the fast kinetics permitted by the hydroxide electrolyte. The fast kinetics in AFCs allows using silver or nickel as catalysts instead of expensive platinum.

The performance of AFCs can be further improved by circulating the electrolyte, which offers some advantages that include easy thermal management, more homogenous electrolyte concentration, easy replacement of electrolyte, and possible removal of the electrolyte when it is turned off. Of course, circulation of electrolyte needs additional equipments, such as circulation pump, heat exchanger, and evaporator. Further, it increases the risk of leakage (potassium hydroxide is highly corrosive and has a natural tendency to leak even through the tightest seals).

AFCs were some of the earliest practical cells and were used in the Apollo space program, generating drinking water as well as electric power. Although they are inexpensive compared with PEM cells, operating efficiencies of 60% are possible. Unfortunately they have a low power output and the catalyst is prone to poisoning from carbon dioxide in the atmosphere.

Phosphoric Acid Fuel Cells (PAFCs) PAFCs use acidic electrolyte to conduct hydrogen ions and the anode and cathode reactions are the same as in PEMFCs. PAFCs run at high temperature of around 200°C, delivering high power of a MegaWatt or more but with relatively low efficiency of around 35%. The poor conversion efficiency is the high heat generation in the fuel cell stack. Because of the high working temperature the efficiency losses can be mitigated by using the waste heat in combined heat and power (CHP) applications.

The advantage of PAFCs is the cheap electrolyte and disadvantages are the need of expensive catalyst (platinum), corrosion by acidic electrolyte, CO poising, and low efficiency.

Molten Carbonate Fuel Cells (MCFCs) MCFCs run at high temperatures of 650–1,000°C. They use molten carbonate salt to conduct ions, usually, lithium-potassium carbonate or lithium-sodium carbonate. Their unique chemistry needs carbon dioxide from the air as part of the process. Efficiencies achieved are 45% or more and power outputs of over 1 MW are typical in grid supply applications. Because of their high working temperature, they can operate directly with hydrocarbon gases which are reformed within the cell and do not need a separate hydrogen supply. The high temperature also means that less expensive catalysts are needed, but the molten electrolyte imposes special requirements on containment and anticorrosion measures.

Solid Oxide Fuel Cells (SOFCs) Solid oxide fuel cells also operate in the same or higher temperatures as the molten carbonate cells with the same fuel and catalyst advantages. The ceramic electrolyte which can run as hot as 800°C has the advantage that the electrolyte stays solid. They can deliver powers of several Megawatts but at a lower efficiency of around 35%.

Direct Methanol Fuel Cells (DMFCs) Direct methanol fuel cells are similar to PEM cells. Instead of pure hydrogen, they directly use liquid Methanol as fuel. It is sure that there are definite motivations for using DMFCs to vehicles. Methanol is a liquid fuel at room temperature that can be easily stored, distributed, and marketed through current infrastructures. Further, methanol is the simplest organic fuel that can be economically and efficiently produced on a large scale from fossil fuel, such as coal and natural gas. Further it can be also produced from biomass products.

Anode and cathode electrode of DMFC also need platinum or platinum alloys as catalyst. The electrolyte can be a trifluoromethane sulfonia acid or proton exchange membrane (PEM). The chemical reactions in a DMFC are:

$$\text{Anode}: \ CH_3OH + H_2O \rightarrow CO_2 + 6H^+ + 6e^-$$

$$\text{Cathode}: \ \frac{3}{2}O_2 + 6\,H^+ + 6e^- \rightarrow 3H_2O$$

$$\text{Overall}: \ CH_3OH + \frac{3}{2}O_2 \rightarrow CO_2 + 2H_2O$$

Like PEM fuel cells, DMFCs work at low temperatures in the range of about 50–120°C. They have a relatively low efficiency and power density. Output power using current technology is limited to about 1.5 kW which is enough to power most consumer goods but not sufficient for automotive applications. Nevertheless the ability to use liquid fuel coupled with the elimination of the reformer make these fuel cells very attractive.

Fuel Cell Vehicles

Fuel cell–powered vehicles potentially have the advantages of no toxic and greenhouse emissions and high operation efficiency. Compared to internal combustion engine, fuel cells have a prominent advantage of high operation efficiency at low power output which is coincident to a vehicle's normal driving situation. This means that fuel cells in a fuel cell–powered vehicle will naturally operate in their high-efficiency region in normal driving conditions.

Fuel cell–powered vehicles can be either fuel cell alone or hybridized with batteries and/or ultracapacitors. Fuel-cell-alone-powered vehicles have a very simple configuration, similar to pure electric vehicles by replacing the battery pack with a fuel cell system as shown in Fig. 31.

A fuel-cell-alone-powered vehicle is a single power source vehicle. The fuel cell power follows the load profile. The power rating of the fuel cell system is designed to meet the vehicle performance requirement. A fuel cell system management is required to manage the fuel cell operation, such as air supply, fuel supply, and cooling of the fuel cells for operating in their safe range.

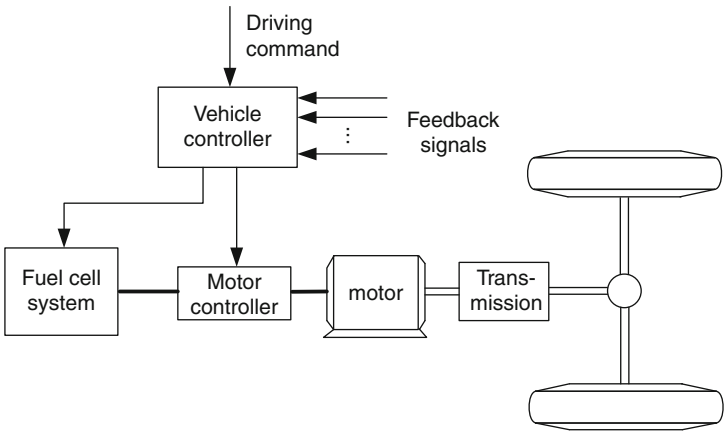

Electric, Hybrid Electric and Fuel Cell Vehicles, Architectures of. Figure 31
Configuration of fuel-cell-alone-powered vehicle drive train

Fuel cell is a unidirectional energy converter. It cannot operate in opposite directions to absorb energy from an electric energy source. Thus, a fuel-cell-alone-powered vehicle is not capable of recovering braking energy.

Fuel Cell–Powered Hybrid Vehicles

Fuel cell system, at today's technology, has low power density. For satisfying vehicle performance, a bulky and heavy fuel cell system is needed, which in turn, harms the vehicle performance and causes high energy losses. In addition, lack of regenerative braking capability is a major shortcoming of this drive train.

Hybridization of fuel cell system with a secondary power source, such as a battery pack and/or ultracapacitor pack is an effective technology to overcome these shortcomings. A fuel cell hybrid vehicle drive train is shown in Fig. 32.

Fuel cell hybrid vehicle drive train consists mainly of a fuel cell system as primary power source, a secondary power source that may be a battery pack and/or ultracapacitor pack. The powers of the fuel cells and secondary power source are coupled together at an electronic interface which is used to control the power flows. A vehicle controller is used to control the drive train based on the driver's command and system's feedback signals.

There are several operation modes that can be selectively used which are:

1. Fuel cell alone propelling: in which the electronic interface isolates the secondary power source from the power line and fuel cell pack alone supplies power to the electric motor.
2. Secondary power source alone propelling: in which the fuel cell pack is isolated from the power line and the secondary power source alone supplies power to the traction motor.
3. Hybrid propelling: in which both the fuel cell system and the secondary power source provide powers to traction motor simultaneously.
4. Fuel cell power split mode: in which fuel cell power is split into two parts by the electronic interface.

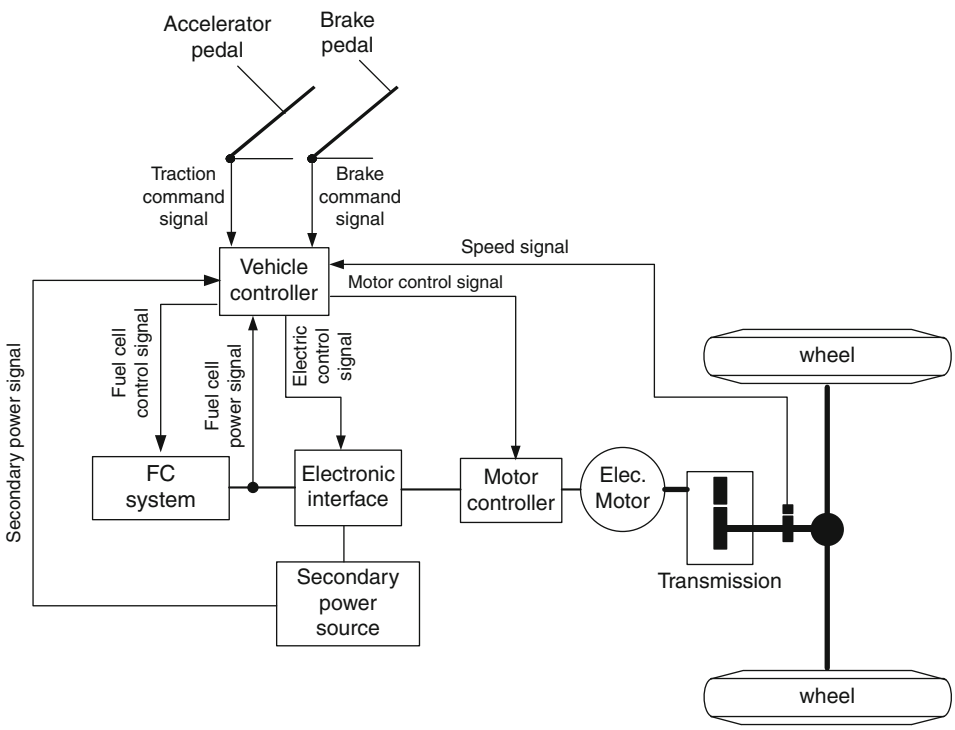

Electric, Hybrid Electric and Fuel Cell Vehicles, Architectures of. Figure 32
Configuration of a fuel cell–powered hybrid drive train

One part is used to power the traction motor and the other charges the secondary power source.

5. Regenerative braking: in which the traction motor functions as a generator to recover the braking energy and stores it in the secondary power source.

By electively using the operation modes, the fuel cells can be operated in their most efficient region as shown in Fig. 33.

The electronic interface plays a critical role in the drive train control. It should be designed with three ports and the ports to the secondary power source and electric motor are bidirectional. The configuration and operation principle are very similar as that used in engine/generator-based electric coupling (series) hybrid drive train.

Future Directions

The electric vehicle has a relatively simple power train structure. The most important components are the motor drive and the battery system. An advanced motor drive with high power density, high efficiency, and long extended speed range is the key technology. The success of an electric vehicle is almost determined by the performance of the battery system. The basic requirements for electric vehicle batteries are the high energy capacity for extended range, high power for vehicle performance, high safety, and low cost. At present, lithium-ion batteries are considered to be the most promising candidates. For hybrid vehicles, advanced primary power sources are very important that may include advantage engine technologies and alternative fuel engines. Advanced control strategies and real-time control algorithms are also very important. The key technologies for fuel cell vehicles include enhancement of fuel cell power density, reduction of cost, and, more importantly, hydrogen production and onboard storage.

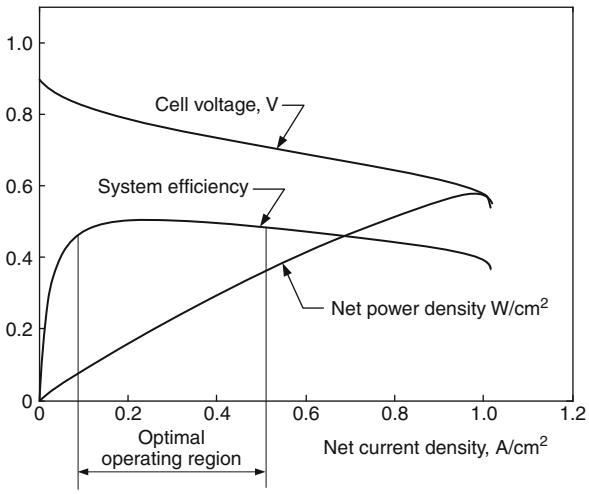

Electric, Hybrid Electric and Fuel Cell Vehicles, Architectures of. Figure 33
Optimal operation region of a fuel cell system

Bibliography

Primary Literature

1. Chan CC, Chau KT (2001) Modern electric and vehicle technology. Oxford University Press, New York
2. Ehsani M, Gao Y, Emadi A (2010) Modern electric, hybrid electric and fuel cell vehicles–Fundamentals, theory and design, CRC, FL, USA
3. Berlowwitz PJ, Darnell CP (2001) Fuel choice for fuel cell powered vehicles. Society of automotive engineers (SAE), Journal, Paper No. 2001-02-0003
4. http://www.mpoweruk.com/hydrogen_fuel.htm. Accessed Oct 2010

Books and Reviews

Miller JM (2004) Propulsion systems for hybrid vehicles. The Institution of Electrical Engineers, London

Messerle HK (1969) Energy conversion statics. Academic, New York

Larminie J, Dicks A (2000) Fuel cell system explained. Wiley, New York

Thomas CE, James BD, Lomax FD Jr, Kuhn IK Jr (2002) Societal impact of fuel options for fuel cell vehicles. SAE Journal, Paper No. 982496

Electric, Hybrid, and Fuel Cell Vehicles, Introduction

Mehrdad Ehsani
Department of Electrical & Computer Engineering, Texas A&M University, College Station, TX, USA

The success of internal combustion engine vehicles over the past century is one of the greatest technological achievements of mankind with a profound impact

on virtually every aspect of human life on the plant. However, the very widespread success of this technology has produced associated problems which can be the seeds of its own long-term demise. Solution of these problems will guarantee the long-term survival of personal and mass transit vehicles which are so essential to the economy and welfare of human beings. The proper combination of these solutions can bring about what is termed sustainable vehicles.

This section of the encyclopedia describes the important sustainable vehicle technical topics and the present state of the art on each topic. The following is a brief review of the entries in this section.

► Sustainable Transportation describes the technical and environmental problems that have to be addressed to achieve sustainable vehicles for the future. Issues of fuel, environment, and vehicle technologies are introduced.

► Electric, Hybrid Electric and Fuel cell Vehicles, Architectures of describes the basic configuration of the drivetrain of electric vehicles and hybrid electric vehicles. The various types of hybrid electric vehicles' drivetrains are presented. The basic operation of each of these systems and their components are described.

► Vehicle Dynamics and Performance describes vehicle drivability, fuel economy, braking performance, handling characteristics, noise, vibration, and harshness. Vehicle performance discussed in this entry is restricted to propelling and braking performance in terms of vehicle speed, acceleration, road grade climbing, braking deceleration, and braking force distribution on the front and rear wheels.

► Vehicle Energy Storage: Batteries gives an overview of batteries for vehicle applications and discusses the research and development roadmap of next-generation batteries for vehicle applications. It describes how the battery is used in EV and HEV and what the vehicle requirements on it are. It also presents the basic state of the art on the available batteries today.

► Battery Technologies describes the internal working of the electrochemical battery, the relationship between the internal resistance of the battery cell, maximum power output, energy efficiency in charging and discharging, and the issue of cell heating. A review of the characteristics of lead acid, nickel metal hydride, lithium-ion batteries, and super capacitors are then presented.

► Energy storage: Ultracapacitor describes the new technology of ultracapacitors for high-power energy storage and delivery. This is another approach to providing energy storage for hybrid vehicles. Ultracapacitors can be used either alone or in combination with batteries. In this approach, the batteries can be optimized for energy density and cycle life, and ultracapacitors can provide the power both for acceleration and regenerative braking.

► Hybrid Energy Storage Systems for Vehicle Applications describes the possibility of composing a high-energy, high-power hybrid energy storage system for vehicle applications, based on the analysis of inherent characteristics of different energy storage methods. The basic components in this system are chemical batteries, ultracapacitors, and flywheels (mechanical batteries). The objective is to fully utilize the advantages and suppress the disadvantages of each component to compose a compact energy storage system with high energy capacity and high power capability.

► Batteries, Battery Management, and Battery Charging Technology describes issues related battery charging and battery management. Battery management is one of the important engineering challenges of using batteries in vehicles. It starts with an overview of different types of rechargeable battery chemistries. Then, it discusses circuits for charging and managing vehicle batteries.

► Vehicle Traction Motors describes the role of the electric motor in EV and HEV drivetrains. The requirements that the vehicle put on the electric motor are explained. This is used as the basis to present the various traction motor drive technologies.

► AC Machines: Permanent Magnet Synchronous and Induction Machines describes the most common electric machines, motors, and generators that are used in EV and HEV drivetrains. It presents AC machines including induction machine (IM) and permanent magnet synchronous machine (PMSM). It is shown that both the IM and PMSM take advantage of the rotating magnetic field that is produced by their three-phase stator windings.

► Switched Reluctance Motor Drives for Propulsion and Regenerative Braking in EV and HEV describes a new basis for the selection of vehicle traction motor technology. The concept of extended speed

range at constant power and its benefit in vehicle traction application is introduced. On this basis, the modern switched reluctance motor drive technology is shown to be very attractive for future EV and HEV applications. In addition to having a wide speed range, these motors have a rugged and low-cost structure, reliable drive power converter topology, and high efficiency over a wide range of speed.

► Regenerative Braking describes the important technology of regenerative braking in EV and HEV drivetrains. Regenerative braking is responsible for most of the battery energy and fuel savings in these vehicles. This entry presents the principles of regenerative braking operation, design, and its hardware.

► Hybrid Electric and Hydraulic Technology Applications in Off-Road Vehicles describes a special call of HEV that are more suitable for off-road and heavy-duty applications. These include military vehicles, construction and mining vehicles, and similar industrial and special-purpose heavy uses. The special use of hydraulics in the drive train as part of the hybridization of the vehicle is of particular interest in this entry.

► Plug-in Hybrid Electric Vehicles describes a special class HEV that is called plug-in HEV (PHEV). It is shown that the PHEV has certain advantages over pure EV and HEV, such as (1) displacement of significant amount petroleum fuel by electric energy that comes from utility grid, (2) longer range than a pure EV, (3) no fuel consumption and emission during pure EV mode, and (4) lower overall fuel consumption and emission.

► PHEVs and BEVs in Coupled Power and Transportation Systems describes the role of utility electric power systems in the EV and HEV transportation system. The impact of plug-in HEV and battery-operated EV (PHEV/BEV) transportation systems on the utility power systems is discussed. The mutual benefits of charging the EV/HEV from the utility grid and some of their draw backs are addressed.

► Internal Combustion Engines, Alternative Fuels for describes the technical implications of alternative fuels on vehicle engines, their performance and emissions characteristics. The characteristics of the most dominant alternative fuels are defined and compared to conventional gasoline and diesel fuel. Of particular interests are the renewable alternative fuels.

► Vehicle Biofuels describes the nature and origins of liquid fuels for vehicle engines that are derived from biomass. Liquids biofuels are the most valuable because they are easily stored, have a high energy density, and are readily metered into engines. It is shown that biofuels are infinitely renewable provided appropriate agricultural practices are followed.

► Sustainable Vehicle Fuels, Well-to-Wheel Analysis describes the important stages, results, and key issues associated with the well-to-wheel stages of biofuels, hydrogen, and electricity as alternative transportation fuels. The importance of comparing alternative vehicle engine fuels with the conventional fossil fuels is presented from the fundamental point of view.

► Fuel Cell Powered HEV Design and Control describes different types of fuel cells and their electrolytes, sources of fuels for fuel cells, those applicable to the transportation sector, and the hybrid vehicle architecture. The ICE hybrid is also presented as a base model, since its operation is well understood by the general public.

Electrical Transmission Systems and Smart Grids, Introduction

Miroslav M. Begovic
School of Electrical and Computer Engineering, Georgia Institute of Technology, Atlanta, GA, USA

Transmission systems represent the backbone of the electric energy. They support transport of electric energy from large producers (power plants) to the load centers (residential areas, manufacturing facilities, business centers or a combination thereof). Those networks are probably among the largest human-made engineering systems – the transmission network in the United States covers over 300,000 km of lines and is served by 500 companies (electric utilities).

In contemporary power systems, the notion of net energy producers and net users is increasingly blurred as most economic generator capacities are of smaller size and can be (and often are) installed near users' locations – example of small photovoltaic generators or wind farms which can be installed on the roofs of

residential homes or in their vicinity illustrates that alternative, popular for many reasons (little or no maintenance needed, decreasing cost of electricity generated by such small generators, many of which are based on various renewable energy sources, reduction of congestion which is the result of carrying large amounts of power across vast distances, reduction of transmission losses, regulatory and policy-driven economic incentives for small owners of generators, reduction of carbon footprint, and enhancement of sustainability of such solutions, etc.) The need for electric energy systems is not only to run the equipment in manufacturing facilities or appliances in residential homes, but also to interact in various ways with other supporting infrastructures (water, gas, transportation, information, etc.) Those infrastructures are interdependent on one another and their efficient and reliable operation requires a thorough understanding of those interdependencies and adequate planning and operational support (see ► Energy and Water Interdependence, and Their Implications for Urban Areas).

As electric energy travels across waveguides (conductors), it incurs losses due to dissipation of current across the resistances of imperfect conductors. High-voltage overhead conductors do not need insulation. The conductor material is nearly always made of an aluminum alloy, which typically forms several strands and often is reinforced with steel strands for mechanical strength. Copper was more popular conductor choice in the past, but substantially lower weight and cost of aluminum and its only marginally inferior electrical performance have been the reasons for the current dominance of aluminum-based conductors in the transmission networks. As large amounts of power being transferred across the lines may incur considerable losses in transmission, typically such bulk transfers are performed at higher voltages, which require smaller currents (losses in the conductors are proportional to the square of the current, which means that operating the transmission line at double the voltage incurs only about 25% of the losses produced while operating at lower voltage). It is the need for changing the operating voltage levels as a function of the energy throughput that has forced design transition from the original DC transmission (introduced by Thomas Edison) into AC, originally deployed by Nikola Tesla and George Westinghouse in the 1880s to transfer power from the power plant at Niagara Falls, and nowadays used almost everywhere. Today, the highest operating AC transmission voltages can be up to 500 kV and even 800 kV. Ironically, when need for high power transfers calls for operation at voltages higher than 800 kV, it is done via DC transmission and with use of the large HVDC converter stations. The reason is inductances of the large overhead transmission lines, which at the highest voltages ultimately choke the efficient transmission of electric energy.

Transmission voltages are usually considered to be 110 kV and above. Lower voltages such as 66 kV and 33 kV are commonly called sub-transmission voltages. Voltages less than 33 kV are mostly used for distribution. Design of distribution networks is driven by their traditional role as infrastructure for disseminating bulk electric energy to a large number of customers. Such fragmentation of delivery requires distribution networks to operate somewhat analogous to capillaries in a cardiovascular system, at smaller capacities (and lower voltages) and covering large areas of sparsely populated customers (in rural areas) or densely populated smaller areas (in modern urban settings where increasingly large part of the world population now resides). Traditional design is evolving of radial distribution network, consisting of feeders supplied from the substations which interconnect them to the bulk power transmission networks. Such simple configurations were enabled by unidirectional flows of energy and simple distribution hardware which was supporting it. Transformation of distribution system into the site of both consumption and (distributed) generation of electric energy, as well as increasing need for enhanced interconnectivity at the distribution level, is imposing need for different designs. Part of the contemporary distribution networks are likely to experience a transition to microgrids (more meshed and better controlled distribution networks which can be used flexibly as reconfigurable autonomous, or grid-connected infrastructure for distribution of electric energy).

The structure and function of electric substations is also changing rapidly. Substations represent a vital part of the power grid infrastructure with many important functions (ability to reconfigure the system topology,

isolate equipment for maintenance and repair, monitor and communicate various system parameters and electrical variables to the control center or elsewhere, actuate control actions or protective relaying decisions, etc.) Substation automation represents one of the fastest evolving parts of the modern (smart) grids and will continue its evolution to keep up with the demands for more flexible and effective monitoring, control, and protection of power systems, both on the transmission and distribution side (see ► Distribution Systems, Substations, and Integration of Distributed Generation).

A growing part of the distribution networks, especially in developed countries, is being served by underground cables instead of overhead lines. There are many reasons in favor of such solutions (reliability, esthetics of the area where underground lines are installed, less vulnerability to the elements, etc.) and some against (considerably higher cost, faster pace of aging, especially due to moisture and impulse electrical stress, such as a consequence of lightning strikes in vicinity of the installations, and lack of effective diagnostic procedures to assess the operational status and effective remaining lifetime of the cables, more expensive repairs, etc.) Nevertheless, underground distribution (and in some places, underground transmission) represent a growing portion of the energy systems' assets, both in terms of importance and cost, and considerable care needs to be paid to their management and upkeep (see ► Underground Cable Systems).

Distributed generation (DG) can be defined as small-scale, dispersed, decentralized, and on-site electric energy systems. Currently, capacities of DGs vary typically in the range of several kW to hundreds of MW. As more DG penetrates the electric energy systems, more accurate and efficient system analysis algorithms are needed in order to analyze the impact of the DG system on various types of microgrids and distribution networks. Since DG can change the operation of the distribution system and interfere with its protection and control, electric power utilities are not motivated to interconnect customer-owned small generators to their distribution networks. Utilities tend to put nonutility generation under the extensive technical analysis. Conversely, the regulating authorities tend to act in favor of DG owners and support that the interconnection be as easy and transparent as possible. Nevertheless, the favorable economic features of small-scale distributed generators, especially those using the renewable energy resources as input, will make them increasingly popular and much more widespread than they are at the moment of creation of this text. Even now, many countries (Ireland, Spain, Denmark, etc.) possess considerable renewable resources as part of their generation portfolios. At the time when wind generation of electricity is the fastest growing new generation technology (in terms of new installed capacity) and when the energy produced by renewable resources (including hydro plants) is already larger than energy obtained from the nuclear power plants (United States in 2011), engineering challenges of planning, operating, controlling, and protecting the new power grids are substantial and require major transformative changes (see ► Renewable Generation, Integration of). This may become even more important as some countries elect to gradually abandon conventional nuclear generation and transition to other, more sustainable, generation resources.

One of the fundamental constraints in the transmission and distribution of electricity is that, for the most part, electrical energy cannot be stored, and therefore must be generated whenever needed. Few exceptions to that limitation have been found and exploited. The biggest problem is that currently available storage options cannot effectively be used at utility-scale capacities (pumped hydro plants are the best known among them). In the interim, a large number of smaller capacity storage technologies have been developed and advanced (superconductive magnetic storage, flywheel, battery storage, etc.), mostly to find applications as uninterruptible power supplies for critically important (but relatively small) loads and rarely exceed the capacities needed to achieve similar effects in the bulk power networks. When a storage technology is developed and commercialized to operate at such large capacity levels economically, it will trigger a major revolution in power grid planning and operation.

A very advanced infrastructure of monitoring, control, and protection (see ► Wide Area Monitoring, Protection and Control) is required to enable real-time balancing between electric generation and energy demand due to the lack of effective storage options.

If generation and consumption of electric energy are not in balance or if the complex infrastructure of voltage control across the system is challenged by the heavy loading conditions and/or the aftermath of an unforeseen major disruption in system operation (such as the outage of a major piece of equipment), generation plants and transmission lines can shut down which may lead to a major blackout. Sometimes such blackouts develop spontaneously in a cascading chain of equipment outages caused by spreading of the overloads through the equipment system-wide as a consequence of an initial disturbance, which may be relatively minor in its initial effects. These series of events may occur in unanticipated sequence, and can be hard to foresee even with large computers. An unexpected contingency may cause an amplifying effect of larger sequential outages and progressively stress the system to the point when the disturbance can no longer be contained. In the domain of large power grids, "flapping of the butterfly wings" in certain places can literally produce a "storm" in others (see ► Transmission Blackouts: Risk, Causes, and Mitigation).

To reduce the risk of such failures, electric transmission networks are highly meshed and interconnected into regional, national, or continental wide networks, providing multiple redundant alternate paths for energy to flow when needed. Considerable effort is expended by electric utility companies to ensure that sufficient spare capacity and redundant pathways for energy transfer are always available to mitigate the consequences of even large multiple disruptions of the network. In order to maintain sufficient security margins under the threat of multiple unpredictable contingencies, well-coordinated plans for preemptive (slower, based on extensive optimization algorithms applied to coordinate generation and control system wide) and preventive (much faster, emergency control and protection) actions need to be developed so that the system does not descend into a blackout and necessitate lengthy and costly restoration procedures (see ► Smart Grids, Distributed Control for). Particular focus should be on determining the ability of system to survive extreme contingencies, triggered by very unlikely chains of events, but capable of propagating into costly widespread outages with long-term consequences for both consumers and the power companies.

All of the above functional characteristics and solutions describe what is commonly referred to as smart grid. Gradual application of emerging technologies for advanced power grid management and control/protection represents an effective transition to smart grid, which from the perspective of different authors and researchers may assume different characteristics, but in general shares the following functional properties:

- Ability to resiliently recover to the extent possible from the effects of damaging or disruptive disturbances (self-healing)
- Providing opportunities for consumer participation in energy management and demand response (often via advanced metering options which may provide additional support and information, both for the utility and the customer, during normal operation)
- Ability to respond to, cope with, and resiliently enhance itself against physical and cyber attacks
- Providing power quality for modern equipment anticipated to be needed in the future
- Accommodating all generation and storage options
- Enabling new products, services, and markets
- Optimizing assets and operating efficiently

The transition to smart grid may in some cases be spontaneously driven by obvious benefits and cost-effectiveness, in others may be supported by regulatory and policy actions (see ► Sustainable Smart Grids, Emergence of a Policy Framework).

Electricity Generation with Small Wind Turbines

G. J. W. van Bussel
Aerospace Engineering Section Wind Energy,
Delft University of Technology, Delft, The Netherlands

Article Outline

Glossary
Definition of the Subject
Introduction
The Feasibility of Small Wind Turbines
Small Wind Turbine Technology

Performance of Drag-Driven Wind Turbines
Performance of Ducted Wind Turbines
Performance of Lift-Driven VAWTs
Control and Safety Systems
Costs of Small Wind Turbines
Bibliography

Glossary

COE Cost of Energy: A method to calculate the electricity costs taking into account investment and operation and maintenance costs.

Control and safety systems Systems to keep small wind turbines within their operational range and to bring them back into a normal operational mode.

Darrieus rotors A VAWT with curved rotor blades using a lift principle for its operation.

DAWT Diffuser-Augmented Wind Turbine or ducted wind turbine.

Drag Force in the direction of the incoming flow on a (streamlined) body.

HAWT Horizontal Axis Wind Turbine.

H-type VAWT A VAWT with rotor blades rotating along a cylindrical surface.

Lift Force perpendicular to the incoming flow on a (streamlined) body.

Savonius rotors "Crosswind" wind turbines with the main shaft perpendicular to the wind.

VAWT Vertical Axis Wind Turbine.

Definition of the Subject

Small wind systems can be seen in autonomous operation for pumping water, desalinization, and battery charging. A growing number of small wind turbines is connected to the grid, most of them behind the meter. This entry will focus on electricity-generating small wind turbines. Since the electricity production with wind turbines on buildings is a fairly new development with an interesting potential it will also be addressed. Safe and reliable operation of small wind turbines is technically challenging since they usually operate in more turbulent flows than large-scale wind turbines. A short description of the working principles of various types of small wind turbines is given; their safety and control systems are discussed as well as noise and vibrations. Furthermore, a treatment of the investment costs and the cost of energy is provided. Finally the implications for locating wind turbines on top of buildings are treated.

Nontechnical barriers such as legislatory and regulatory issues are not addressed, although they are very important for successful implementation of small wind turbines.

Introduction

There is a growing interest in the use of small wind turbines. The market is already significant and it is expected to grow at a similar rate as large-scale wind power. Small wind turbines are not only developed for remote applications in rural areas but also, to an increasing extent, for application in urban areas and on buildings. This entry will address small wind turbines for electricity generation. Other important applications, such as wind pumps for irrigation, drainage, and the provision for drinking water, are not addressed.

For further reading about wind pumping technology the reader is referred to Lysen [24] Kentfield [25] and de Jongh and Smulders [23].

In a strategy document issued by the American Wind Energy Association, a small wind turbine committee chaired by Bergey [2], a projected total of 75,000 MW wind power capacity by 2020 is provided by small- to medium-scale systems. With an average of 2 kW per turbine this would mean around 30–40 million units. Of this amount some 15,000 MW is foreseen at locations that are (also) suitable for rooftop mounting of wind turbines. A potential market of similar extent is present in the EU (Van Bussel 2005). Small wind turbines are also a very interesting option for small-scale energy supply at remote sites where no grid electricity is available and a grid extension would be too costly (e.g., for remote villages or homes). As such, they may have a great potential in developing countries. The most striking example is probably their dissemination among the nomads in Inner Mongolia (China), where over 100,000 small portable wind turbines (capacity about 100 W) are in use for "domestic" power supply. Such small off-the-grid wind turbines are often referred to as wind chargers [22].

Small wind turbines are not only developed for remote applications in rural areas but also, to an increasing extent, for application in urban areas and

on buildings. Yet the technology and the costs of small-scale wind deployment are not at the level of large-scale wind deployment. There is not a unique definition of what is regarded as a small wind turbine or a small wind system. The AWEA uses an upper limit of 100 kW and a maximum rotor diameter of 20 m [2] while the British Wind Energy Association [26] takes 15 kW and an annual production of 50,000 kWh as the upper limit without referring to any rotor size. Others [28] take a maximum swept area of 50 m^2 as the criterion. In this entry, the viewpoint is taken that a small wind turbine system is a system that is able to provide (part of the) electricity consumption for a local (private) customer.

Wind turbine deployment in the built environment is inherently more complicated than in rural, open spaces. In successfully exploiting wind energy in the built environment, three major issues can be identified: wind resource assessment and wind characterization around buildings, structural integration of wind turbines with buildings, and special urban wind turbine design requirements.

Safe and reliable deployment of wind turbines in the highly turbulent built environment is specialized and technically challenging. In almost all situations, the use of existing (small) wind turbines will be problematic due to the fact that they are not adapted to the complex wind environment and to additional building-related requirements. Some of these requirements are the severe noise restrictions and the ability to match the structural and esthetical integrity of buildings. This means that new ways need to be found in the design of new wind turbines that do fit the requirements for the built environment.

Nontechnical barriers such as economics, bureaucratic, and regulatory issues will not be addressed, although they are very important for successful implementation of wind turbines in the built environment.

The Feasibility of Small Wind Turbines

This section shows a comparison between large and small wind turbines. The comparison is performed in order to show if there is space for small wind turbines in the built environment from an economical point of view.

Consider a large wind turbine with a *rotor diameter* D of 70 m and a *swept rotor area* A_S of 3,848 m^2 (Fig. 1).

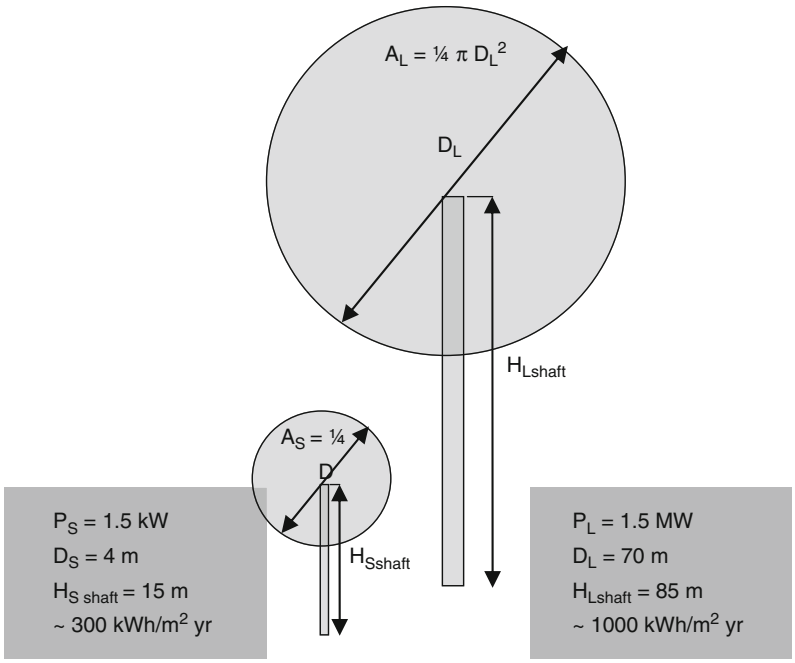

Electricity Generation with Small Wind Turbines. Figure 1
Comparison of large and small wind turbines

The *height from the ground to the nacelle and main shaft* H_{shaft} is 85 m. The wind turbine yield is assumed to be 800–1,100 kWh/m^2/year, evidently depended on its location. This means that around 3,000–4,500 MWh/year can be produced with a wind turbine of this size [8].

In the West European situation, this means that a few (3–10) m^2 of the swept surface suffices to meet the average electricity demand of one family.

Now take a small wind turbine with a diameter of 4 m at a 15-m tall mast. The swept area is then 12.57 m^2. With an average yield of 300 kWh/m^2/year (feasible in a very good wind climate: an average of at least 6 m/s at hub height) this is sufficient for one family (3,770 kWh/year). It thus takes 1,000 of these relatively small wind turbines to provide the same amount of electricity.

In normal utility grid operation it will be very difficult to be competitive in terms of the costs per kilowatt hour. eEither at remote locations where conventional electricity is very expensive and building large wind turbines is not possible or in situations where it is allowed to generate electricity behind the meter, since consumer price of electricity may easily be three times the production costs, small wind turbine may become a feasible solution.

The consumer's price of electricity was 0.22€/kWh in 2008 in the Netherlands. The Dutch consumer's price is roughly built up out of generation of electricity (30%), taxes (40% incl. carbon tax), and the distribution and administration costs (30%). This consumer's price may give an indication for the level of the cost of electricity which might make small wind turbines economically viable.

Small Wind Turbine Technology

Most of the modern small wind turbines typically have an upwind propeller type rotor, often directly coupled (without a gearbox) to an electrical generator (Fig. 2a). Such wind turbines are usually referred to as horizontal axis wind turbines (HAWTs). An increasing amount of small wind turbines pop up on the market with unconventional rotor topologies, such as Savonius rotors (Fig. 2b), Darrieus, and H-type vertical axis rotors (VAWTs) (Fig. 2c and d), as well as horizontal axis wind turbine rotors equipped with a duct (DAWTs) (Fig. 4a).

Vertical axis wind turbine can be further distinguished through their principle of operation. Some are driven by drag differences between the forward moving and the retracting blade; others use the lift principle, similar to that of "propeller"-type HAWTs.

Small wind turbines have mechanisms to limit the rotor speed and the forces on the rotor at high wind speeds. The rotor speed is usually allowed to vary with the wind speed. In the past, small wind turbines were often equipped with a direct current (DC) generator. Nowadays almost all machines are equipped with alternating current (AC) generators, most of them using Permanent Magnets (PM generators) which supply an electric output with variable voltage and variable frequency. An inverter is used to convert this variable speed AC into either fixed frequency AC to comply with the local grid convention, or to DC when the wind turbine operates in an off-the-grid mode using batteries for storage.

Since the principle of operation is an important issue with respect to the aerodynamic efficiency of the machine it is important to address the aerodynamic theory of these machines shortly.

Performance of Drag-Driven Wind Turbines

The conversion of wind energy into rotational energy of drag-driven wind turbines is based on the drag difference of rotating bluff bodies (as in Fig. 3).

An anemometer like drag-driven wind turbine is depicted. It consists of bluff bodies with different pressure drag induced by their shape. This difference in drag causes the turning moment.

The "tip speed ratio" λ is defined as $\lambda = \frac{\omega R}{U}$ where ω is the rotational speed, R the radius of the rotor, and U the incoming wind speed.

The aerodynamic efficiency defined as $C_P = \frac{P}{\frac{1}{2}\rho U^3 A}$ where A is the total area swept by the wind turbine rotor projected on a plane perpendicular to the wind direction and P is the (aerodynamic) power extracted from the wind. The nondimensional coefficient C_P is called the power coefficient and is a measure of the (aerodynamic) efficiency of the machine. Where the theoretical maximum power coefficient of lift-driven wind turbines is $C_P = \frac{16}{27}$, the maximum attainable C_P of a drag-driven wind turbine can be approximated by $C_P \approx \frac{4}{27} C_{Dr}$, where C_{Dr} is the drag

Electricity Generation with Small Wind Turbines. Figure 2
(**a**) Small HAWT (**b**) drag-driven VAWT (**c**) small lift-driven VAWT (**d**) H-type lift-driven VAWT

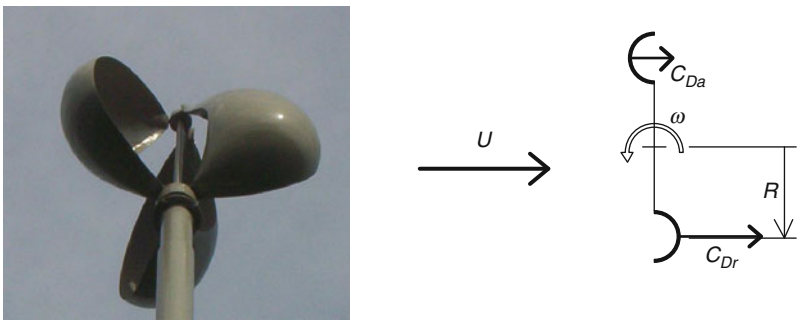

Electricity Generation with Small Wind Turbines. Figure 3
Left: AES drag-driven VAWT, *right*: aerodynamic working principle

coefficient of the retreating (moving with the wind) rotor blade. Here it is assumed that the drag coefficient of the advancing blade is zero: $C_{Da} = 0$, where this is only the case when the advancing blade is completely sheltered from the wind.

Drag coefficients of bluff bodies have maximum values up to 2; therefore the optimal aerodynamic efficiency of a drag-driven wind turbine will be up to $\frac{8}{27} \approx 0.3$. In practice, drag-driven wind turbines usually have power coefficients below 0.1. This is in contrast to lift-driven machines which are able to achieve significant larger power conversion efficiencies. Large-scale HAWTs do have C_P values ranging as high as 0.5 where small-scale wind turbines usually level off at values around $C_P = 0.35$.

Performance of Ducted Wind Turbines

The performance of wind turbines equipped with a duct may be larger than "bare" wind turbines. Figure 4 shows an example of a small DAWT.

As can be seen from the schematic on the right-hand side of Fig. 4, the duct is able to induce a larger mass flow through the rotor: the yellow and red colored areas indicate areas where increased velocities are found. This increased mass flow gives rise to larger performances of a propeller-type rotor located at that position. The performance of well-designed ducted wind turbines compares well with the performance of a "bare" HAWT when referencing to the exit diameter of the DAWT. In other words, if the exit diameter of a DAWT is the same as the rotor diameter of a HAWT, they are able to produce similar power at the same wind speed [6]. The duct of a DAWT acts as a tail vane and keeps the rotor oriented toward the wind. The possible largest advantages of a DAWT are the possibility to incorporate noise damping material into the duct and the fact that the outer area of the duct can be used for commercial and/or styling purposes. This, especially, holds for DAWTs operating on top of company buildings.

Performance of Lift-Driven VAWTs

The aerodynamic efficiency of a wind turbine depends upon other things on the way the wind energy is converted into mechanical power.

A high aerodynamic efficiency can be achieved when the working principle is based upon lift forces. Such wind turbines make use of airfoil-shaped blades in order to generate their driving force.

Lift-based VAWTs usually run fast and have slender blades (see Fig. 5), just like modern large-scale HAWTs. This is in contrast to drag-driven VAWTs, which achieve a significantly lower aerodynamic efficiency and use a large amount of rotor material. The Darrieus wind turbine (DWT) is the most widely known example of a lift-driven VAWT. Its working principle is depicted in Fig. 6. The energy extraction takes place during the cross-flow phases of the blades, that is, when the blades move perpendicular to the oncoming wind. With respect to a modern HAWT the Darrieus wind turbine has a somewhat lower efficiency (about 10%) in an ideal undisturbed low-turbulence wind environment. The main reason for this is that the rotor blades do not contribute to generating torque

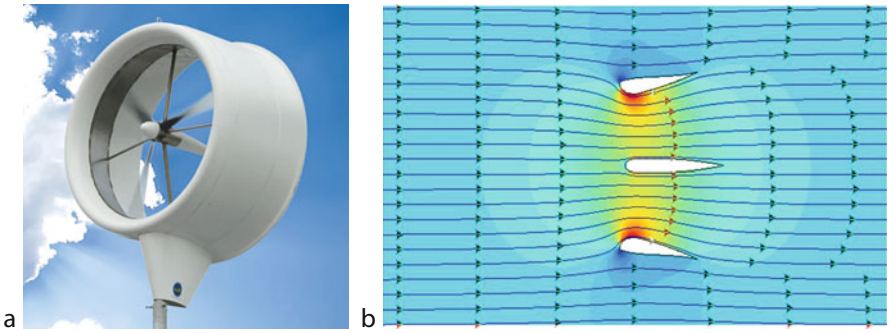

Electricity Generation with Small Wind Turbines. Figure 4
(**a**) small Donqi® DAWT wind turbine (**b**) aerodynamic operation principle of a duct around a DAWT

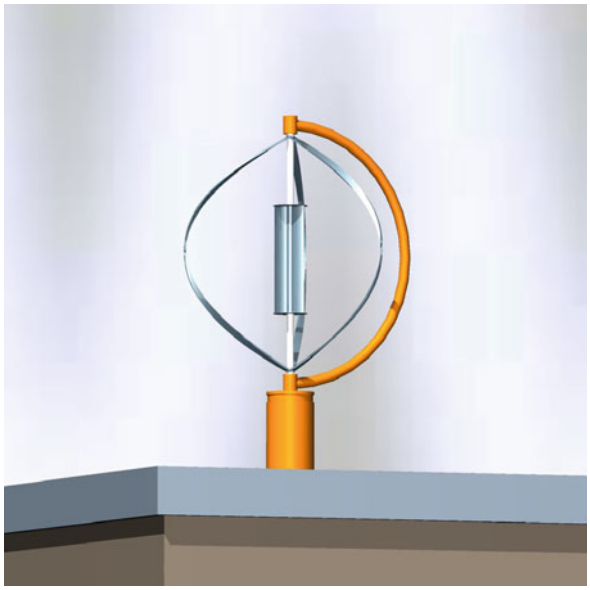

Electricity Generation with Small Wind Turbines.
Figure 5
Globuan, a modern Darrieus wind turbine located on a flat roof

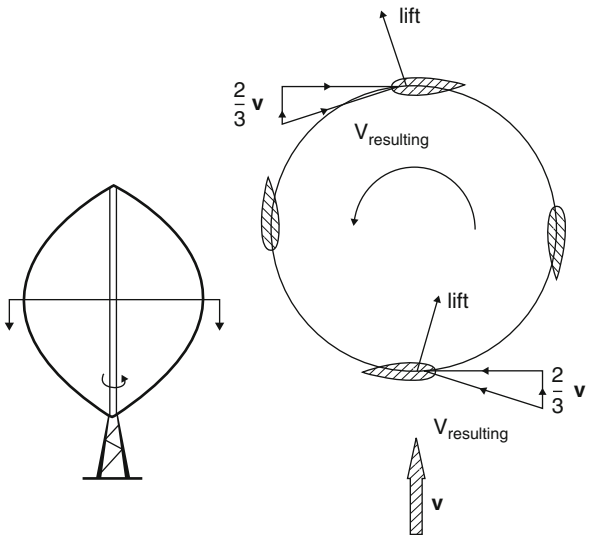

Electricity Generation with Small Wind Turbines.
Figure 6
Aerodynamic principle of operation of the Darrieus rotor

when they are at the retreating and at the advancing phases of the revolution. On the contrary, then they generate drag only which has a detrimental effect on the performance.

This also gives rise to a fluctuating torque. Novel small VAWTs have mitigated these torque fluctuations by introducing a blade sweep. In Fig. 17, examples are shown of VAWTs with blade sweep. A second, large advantage of blade sweep is the significant reduction of noise. Normally high tip speed ratio (slender blade) Darrieus-type VAWT machines are very noisy, where the noise generated resembles the noise of an ascending helicopter. Another disadvantage of a lift-driven VAWT is its incapability to deliver a starting torque. This means that auxiliary systems are needed to get the machine running. Sometimes a small Savonius rotor is used, as in Fig. 5, but that has the disadvantage that the aerodynamic performance of the total system is influenced negatively in the normal operation mode. For this reason a start-up procedure is often implemented in which the generator of the wind turbine is temporarily used as a motor, to acquire a sufficient rotational speed.

Control and Safety Systems

Each wind turbine needs a safety system to take action when the machine is getting out of its normal mode of operation. Also control systems are usually incorporated in the design. Control systems are used for maximizing energy production while keeping the forces on the system within limits. Control and safety systems can be implemented using the same wind turbine components, but in terms of hierarchy the safety system should always be able to overrule the control system.

Figure 7 shows a commonly used control and safety set up for a small HAWT. The machine is equipped with a tail vane. The first function of this tail vane is to keep the rotor oriented toward the wind. The tail vane of this system, however, is connected with a hinge to the body of the wind turbine. The tail vane hinge is tilted with respect to the direction of gravity (Fig. 7a). This causes the tail vane to prefer a “lowest” position due to the weight of the tail vane. For zero and low wind speeds the tail vane will be in this position keeping the rotor perpendicular to the wind and as such maximize the energy production for low wind speeds.

The rotor shaft, connected to the body of the turbine, has an offset with respect to the yaw bearing on top of the tower. Thrust on the rotor will initiate a yaw moment turning the rotor out of the wind. The

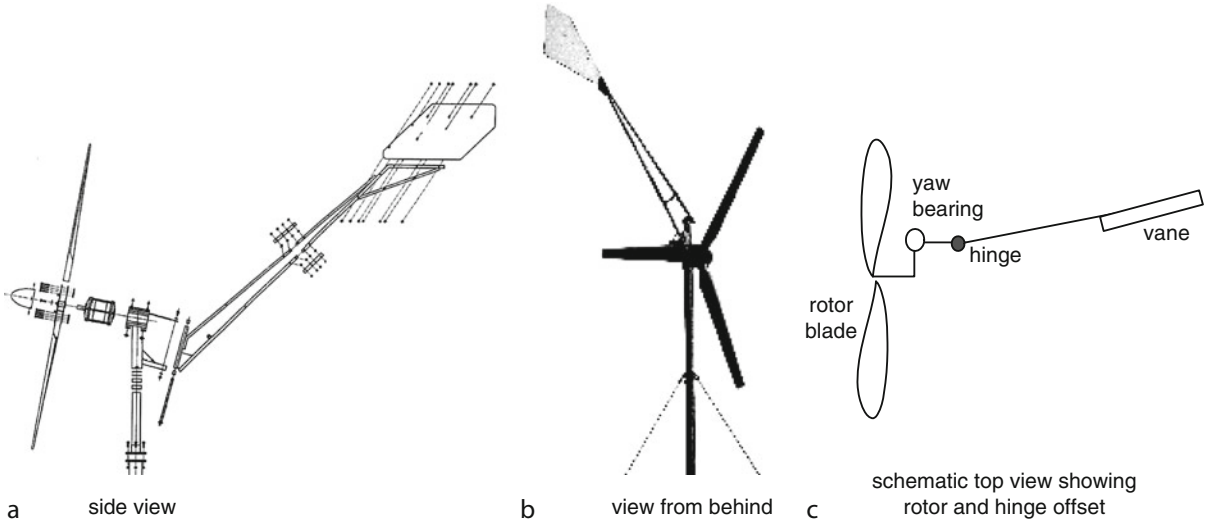

Electricity Generation with Small Wind Turbines. Figure 7
Fortis Montana® control and safety system

tail vane however prevents yawing. This is possible because the hinge of the tail vane has an offset and hence it can develop a yawing moment counteracting the yaw moment due to thrust on the rotor. But when the thrust on the rotor is getting too large, the aerodynamic force on the tail vane will cause the vane to rotate around its tilted hinge against gravity forces. This reduces the aerodynamic force on the tail vane and as a consequence, the thrust on the rotor will initiate a yawing movement leveling off the rotor thrust.

So in this hinged tail vane set up, the tilted hinged vane both has a control function as well as a safety function, since very large thrust forces are prevented by yawing the rotor out of the wind.

Apart from the tilted hinged vane other control and safety systems are found at small wind turbines.

Figure 8 shows two examples of safety systems activated by over speeding of the rotor. The ESI® wind turbine is equipped with tip brakes which are kept in place by springs in normal operation. Another commonly applied system uses centrifugal governors causing the blades to pitch toward feather when the rotational speed becomes too high.

Small wind turbines equipped with a permanent magnet direct-driven generator also may have a safety system through applying short circuit in the electric windings, causing the machine to stop.

This is a safety system that is also often applied in VAWTs since yawing the machine out of the wind and/or pitching the rotor blades are usually not an option in vertical axis designs.

Noise and Vibrations

For small wind turbines noise and vibration can be critical issues. Usually small wind turbines operate in the vicinity of people, which imply that noise levels should be within acceptable (legislation) levels.

Vibrations tend to reduce lifetime, but are a vital issue for roof top locations since they might give yield to induced noise inside the building.

Noise Background noise level in rural areas starts at 25 dB(A) [9] at a 10 min averaged wind speed of 4 m/s and increases with wind velocity (see Fig. 9).

The noise level in a built environment depends on local noise production, for instance, traffic. Due to an increased human activity noise in the built environment will be higher compared to rural areas.

When the wind turbine is modeled as a point source with hemispherical spreading, the noise shows a reduction of 6 dB(A) per doubling of distance to the source (Fig. 10). The distance from the source to the location of noise perception is important, and the sound produced by the wind turbine should ideally be at a level beneath or at least equal to the background level.

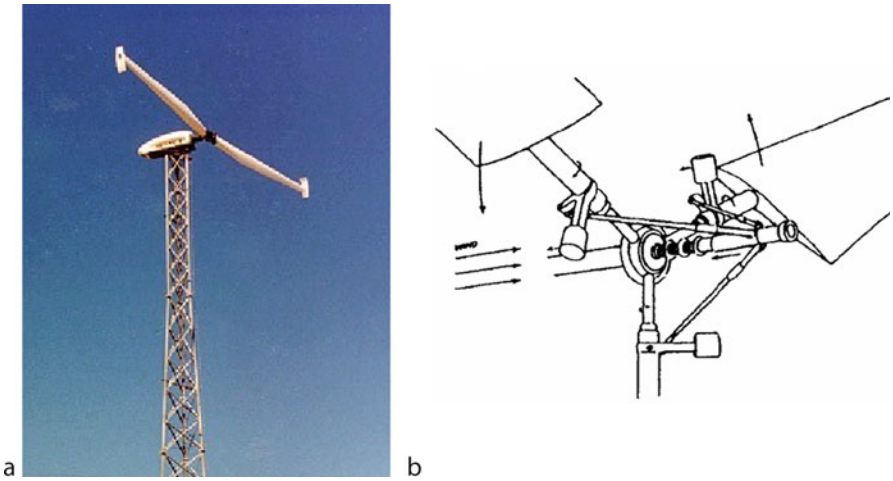

Electricity Generation with Small Wind Turbines. Figure 8
(**a**) ESI® wind turbine with tip brakes (**b**) passive pitch system using a centrifugal governor, reducing rotor thrust at high rotational speeds (e.g., [22])

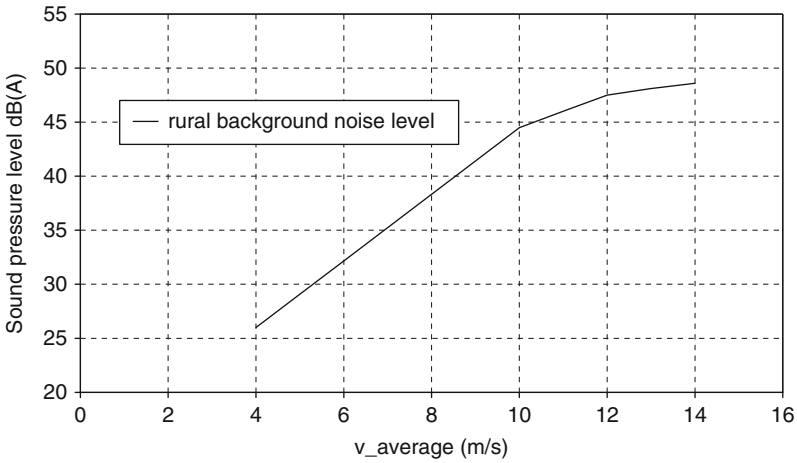

Electricity Generation with Small Wind Turbines. Figure 9
Prevailing background noise level in rural areas at an average 10 min [14]

An obvious approach to reduce aerodynamic noise emission is to lower the rotational speed of the wind turbine. Here a big advantage of drag-driven VAWTs comes in because of their inherently low rotational speed and hence noise production.

Lift-driven VAWTs have a big disadvantage with respect to noise production. Early (large-scale) Darrieus machines were notorious noise producers, where the cause of the noise production was the unsteady aerodynamic loading of the blades during a revolution. Mitigation of that noise source has taken place in modern small-scale VAWTs either by reducing the tip speed significantly (e.g., Fig. 2d) or by introducing a blade sweep (see Fig. 17c).

Vibrations Vibrations occurring in structures should be minimized since they cause fatigue damage. Proper design of the components of a small wind turbine and proper choice of tower and foundation should result into low vibrations. Crucial in this respect is the tuning

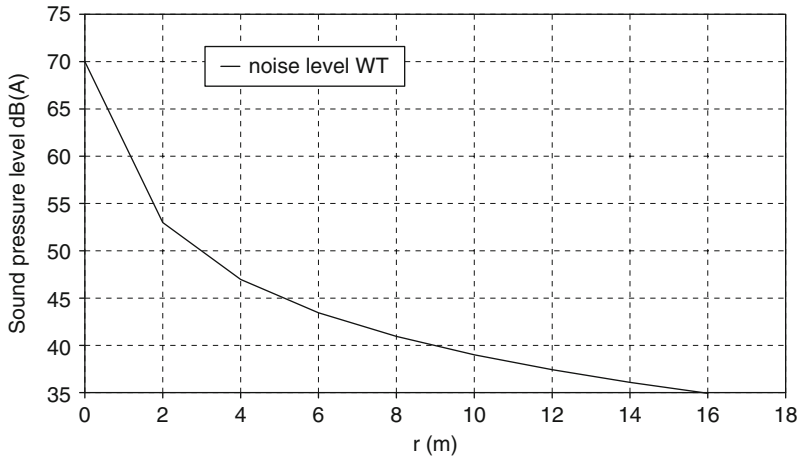

Electricity Generation with Small Wind Turbines. Figure 10
Wind turbine noise level at distance r for a point source noise emission of 70 dB(A) [14]

of the natural frequencies of the tower. They should be outside the rotational frequency/frequencies (and frequencies equal to n times the rotational frequency where n is the number of blades).

Compared to large machines, small wind turbines operate at a much larger rotational frequency ω. The reason is that the wind U does not scale with the size and since a rotor is designed to operate at a given tip speed ratio λ where $\lambda = \frac{\omega R}{U}$, the ω must be larger when the radius R goes down. This is a potential noise hazard since this might mean that vibration frequencies are getting in the audible range (>20 Hz) and as such may contribute to noise production.

Wind turbines may generate vibrations at frequencies starting at the rotational speed and the higher frequencies $in\omega$ where i is an integer, n is the number of blades, and ω is the rotational speed of the wind turbine. Vibration of the nacelle is often a consequence of mass and/or aerodynamic unbalance of the rotor and can thus be avoided by proper design and maintenance. But even well-balanced blades moving through turbulent structures in the incoming wind may cause vibration frequencies as well. Compared to large machines, small wind turbines operate at a much larger rotational frequency ω.

Lift-driven VAWTs will induce frequencies in the building at ω (mass unbalance) and $2in\omega$ (aerodynamic vibrations) since during one revolution a blade passes turbulent structures twice: first at the windward side of the VAWT and again at the leeward side of the VAWT.

Consequences for the operating wind turbines on buildings are evidently that operating at the natural frequencies of parts of the building, such as floors and walls should be avoided. The fundamental frequency of the building itself, which can be approximated by $f_e = \frac{46}{h_{geb}}$ according to Mertens [14], is usually well below the operating frequencies of the wind turbine.

Comparison of Different Types of Wind Turbines

The comparison of the wind turbines based upon their rotor topologies is provided in Table 1 below. The different systems are ranked according to their aerodynamic efficiencies. But this is evidently only one of the aspects that have to be taken into account. Auxiliary systems such as systems to yaw the machine in and out of the wind as well as control and safety systems need to be taken into account as well. Furthermore also the costs of the total system will play a role in considering what may be the best option.

Costs of Small Wind Turbines

The costs of small wind turbines are of evident importance. At first, the production of a given machine should always be considered in regard to the investment costs and the operational costs, and second, an assessment of the real total costs is important for making an economic trade-off between the choice of different (renewable) energy sources.

Electricity Generation with Small Wind Turbines. Table 1 Comparison of different small wind turbine systems based upon their rotor topology

	DAWTs (Diffuser-Augmented Wind Turbines)	HAWTs (Horizontal Axis Wind Turbines)	Lift-driven VAWTs (Vertical Axis Wind Turbines)	Drag-driven VAWTs (Vertical Axis Wind Turbines)
Advantages	Aerodynamically most efficient	Aerodynamically most efficient	Aerodynamically efficient	
			Wind direction insensitive	Wind direction insensitive
				Turbulence insensitive
				No noise
		Well proven	Easy access to generator	Easy access to generator
		Most widely used		Well proven
				Robust
Disadvantages	Large and expensive duct needed	Wind direction change sensitive	Needs start-up aid	Aerodynamically inefficient
		Tail vane/yaw system needed		Large amount of rotor material
		Does not perform well in highly fluctuating winds		

Cost of Energy

The *cost of energy* (COE) is calculated with a recommended procedure of the International Energy Agency (IAE) (e.g., [27]).

$$\mathrm{COE} = \frac{\mathrm{CRF} \cdot I}{\mathrm{APE}} + \frac{\mathrm{TOM}}{\mathrm{APE}}$$

where:

COE: *Cost of energy* [€/kWh]
I *Investment*: wind turbine costs [€]
CRF *Capital Recovery Factor*: yearly interest [%/year], depending on *interest rate* i and *economical lifetime* n:

$$\mathrm{CRF} = \frac{i \cdot (1+i)^n}{(1+i)^n - 1}$$

APE: *annually produced energy* [kWh]
TOM: *total yearly operation & maintenance costs* [€]

When an interest rate of 6% per year is assumed as well as an economical lifetime of 15 years [28], this results in a CRF of 0.103. The investment costs of main components of a small wind turbine will be discussed below.

Wind Turbine Costs

Information of wind turbine component costs has been gathered extensively by Van Beveren [4]. Wind turbine costs and component costs are determined based upon the values in the year 2006 and are valid for wind turbines with a nominal power up to 10 kW. Costs are given as costs per swept rotor area, since this is the best ratio for comparison. Wind turbine costs could also be divided by its nominal power P, but since this value is not unambiguous, often determined by wind turbine manufacturers themselves and seldom overestimated, it is not an objective measure. Note the vertical logarithmic scale. If wind turbine costs include costs for installation, this is indicated by the label.

The trend lines are shown in the Fig. 11.

Costs of HAWTs, the most common small wind turbine design as function of the swept rotor area,

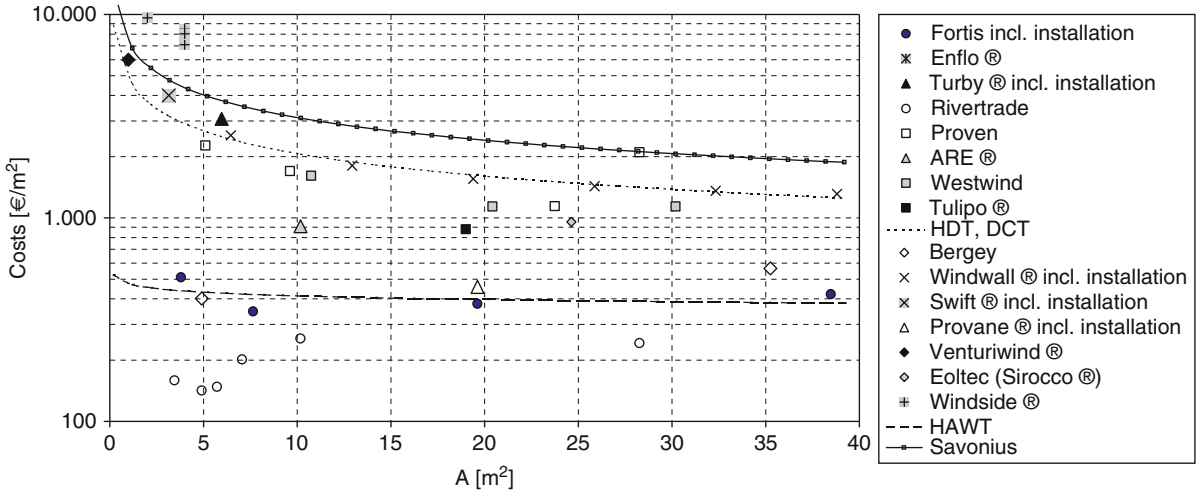

Electricity Generation with Small Wind Turbines. Figure 11
Year 2006 wind turbine costs and swept rotor area as specified by various manufacturers

comply roughly with $C_{\mathrm{HAWT}} = 500 \cdot A^{0.9}$, where the costs of DAWT and lift-driven DAWT can be described by $C_{\mathrm{DAWT}} = 4000 \cdot A^{0.6}$. The cost data of Windside® turbines, a typical drag-driven VAWT, show even higher costs and are described by $C_{\mathrm{Savonius}} = 6000 \cdot A^{0.6}$. These trend lines are also shown in Fig. 11.

As can be seen from this figure, the standard HAWT has by far the lowest cost to area ratio, though there is also a large spread in the values. The Proven machines turn out to be almost twice as expensive as the Bergey machines, while both are respected manufacturers with a relatively large production. What can be seen is that the small HAWT costs curve is only slightly dependent upon swept area (diameter in this case). The other types of wind turbines show a different trend. It should, however, be realized that the amount of data available for these machines is limited, as well as the number of produced machines.

Tower Costs

A distinction is made between lattice towers, steel guyed masts, supported tube towers, and free standing tube towers (see Fig. 12 taken from [4]). The costs of these towers as shown in the figure are for tower heights of 5–37 m.

The costs of the tubular towers of the lift-driven VAWT Turby® deviate substantially from the other designs. The most probable reason is that these are free-standing towers, where guyed towers are mostly used for Darrieus-type machines. Turby® though was designed for roof top application where guy wire connection may cause substantial additional installation costs, which are avoided in the current design.

Costs of Foundation and Installation

Costs of foundation and installation are based upon the WINEUR report [28] and further data of the manufacturers, a.o Fortis and Proven. Some towers need a foundation of concrete, others use a base plate with guyed wires attached to separate anchors. Evidently the installation and foundation costs depend very much on location, type of tower, and ground surface. Turby® has designed a special support structure for the installation upon a building. Of all cost elements of a small wind turbine these are costs which are most probably best suited for DIY activities, in order to bring the total investment down. A typical estimate for the professional costs of foundation and installation of small wind turbines is between 10% and 20% of the total investment.

Operation and Maintenance Costs

On top of the investment cost the Operation and maintenance (O&M) costs contribute to the total cost of energy. In the COE calculation, these are represented

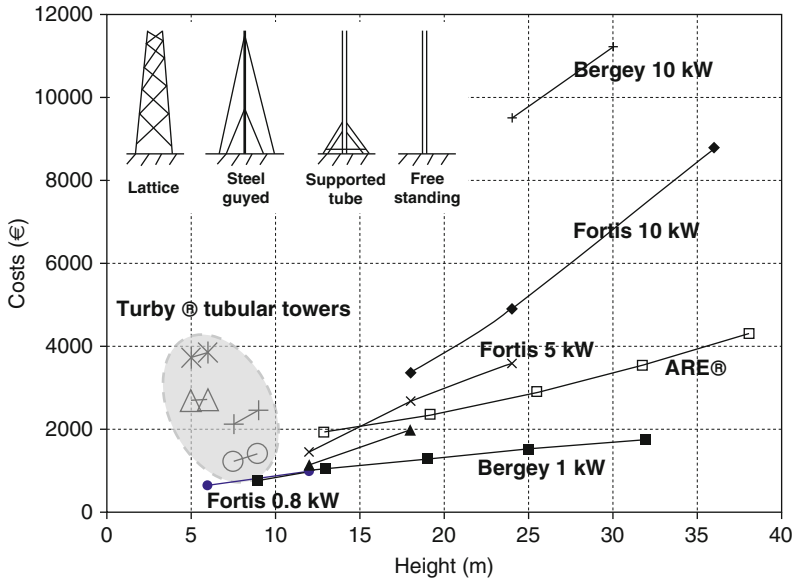

Electricity Generation with Small Wind Turbines. Figure 12
Tower costs as function of tower height

in the TOM component. Total O&M (TOM) costs are an addition of *inspection and maintenance costs* C_{IM} and the *cost of replaced parts* C_{RE} and thus: $\text{TOM} = C_{IM} + C_{RE}$.

Inspection and Maintenance Visit Costs Most wind turbine manufacturers advise to have the wind turbine checked at least twice a year. The costs associated are low if the wind turbine is inspected by the user. Normally inspection of the machine can be done within 1.5 h for an average-sized wind turbine with a swept rotor area of 10 m^2. Larger machines may take more time, mainly caused by the extra time and effort to access the nacelle at larger heights.

Replacement Costs The replacement costs are estimated with the *failure rate* of the wind turbine parts. These failure rates are based on an assessment of Van Beveren [4] covering a period of 10 operational years of small wind turbines and values for large-scale wind turbines of Van Bussel [3] (Table 2).

These values indicate that once every 1–3 years a part of a wind turbine fails and needs replacement. This is significantly better than for large-scale wind

Electricity Generation with Small Wind Turbines. Table 2 Estimate of failure rates of small wind turbine parts

No.	Wind turbine parts	Failures/year
1	Rotor blade	0.02–0.03
1S	Rotor blade Savonius	0.001–0.01
2	Shaft	0.001
3	Hub	0.001–0.05
4	Bearings	0.1–0.2
5	Generator	0.02–0.04
6	Power regulator	0.03–0.06
7	Inverter	0.1–0.2
8	Frame	0.002–0.004
9	Tail	0.03–0.06
10	Tower	0.01–0.02
11	Foundation	0.001
12	Cables	0.001
13	Anemometer and data logger	0.030
14	Lightning protector	0.001

turbines, maybe because smaller wind turbines allow for a larger safety margin in the design.

Impact of O&M Costs on Energy Production Downtime due to inspection, maintenance, and repair is not included in the TOM costs, but is found in the APE part of the COE calculation. Failure rates and inspection times, however, indicate that the availability (defined by the ability to produce if wind conditions are within the operational window) of small systems is larger than for large-scale systems. Since modern large-scale wind turbines show values beyond 98% downtime, production loss for small systems should not be an issue. But this is of course subject to the logistics of spare part handling.

Indications of APE cannot be given, since they strongly depend upon the local wind climate. In general terms, a kWh production of more than 1,000 kWh/m^2 per year swept rotor surface is feasible for large-scale wind turbines in good wind climates. Small-scale wind turbines are usually located at less favorable sites and operate at lower heights. Then a production level of 300 kWh/m^2 per year is considered to be feasible on a good location.

Application of Small Wind Turbines on Rooftops

A nice existing example of a wind turbine–building combination can be found at the Saxion Hogeschool in Deventer (NL). Figure 13 shows the building and the drag-driven VAWT on top of it.

The vertical axis wind turbine is used as an experimental setup for students. In the second instance, the similar wind turbine provides part of the electrical power for the illumination of the staircase. The wind turbines used on these buildings are modifications of existing products on the market.

Requirements for Wind Turbines on Rooftops The design of such urban wind turbines is driven by the following requirements:

- Good performance in complex winds
- Safe operation in the urban environment
- Low noise level
- Simple, rugged design
- Minimized maintenance
- Aesthetic appearance

With respect to the first point it already becomes clear that the design solution will look different for application on rooftops of buildings. HAWT-type wind turbines make use of a yawing system to track variations in wind direction. In urban areas, and definitively on top of buildings, wind direction variations can be considerable. HAWTs then have a clear disadvantage, since the yaw system is in general not able to follow these fast and extensive variations. This may

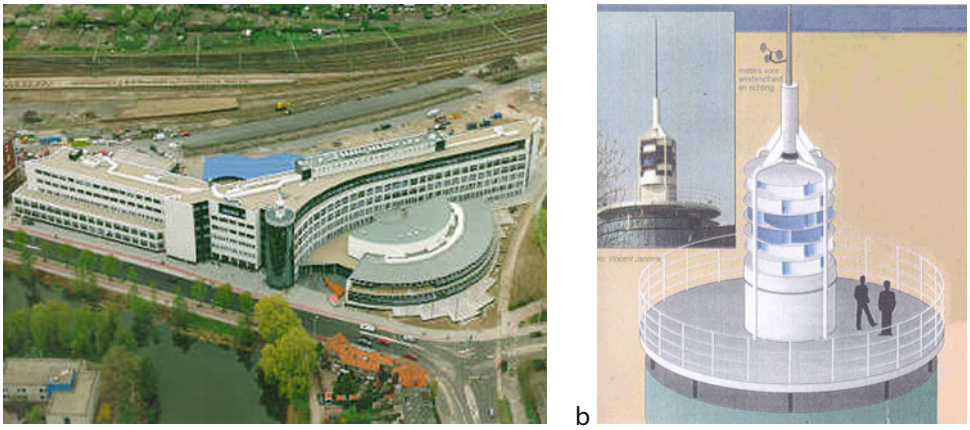

a b

Electricity Generation with Small Wind Turbines. Figure 13
(**a**) Saxion building, Deventer, the Netherlands; (**b**) Drag-driven VAWT wind turbine on top of the central stairway

result in a continuous misalignment of the wind turbine with the direction of the wind, and an inherent loss in efficiency. This is a major reason for introducing VAWTs for rooftop application.

Flows over Rooftops Flows around buildings are inherently complex. At first, the topology of the terrain in the oncoming direction of the wind determines the local wind structure in terms of average wind speed; vertical gradient and turbulence intensity. Second, the topology of the building itself and of adjacent buildings will determine the local structure.

An example of the complex flow conditions that occur around a square building is shown in Fig. 14. Here the flow around a square obstacle is visualized. A separation bubble on top of the obstacle, starting at the leading edge can be observed as well as a closed cell vortex on the windward side and a large separation area with recirculation at the leeward side. Unfortunately, the details of the flow, such as depicted in Fig. 14, are very difficult to predict, even with state-of-the-art advanced computational (CFD) methods. Yet Mertens [15] showed that it is possible to develop a fairly simple theoretical model to determine the performance of wind turbines located in such complex flows. His calculations show that a significant flow acceleration effect is present on top of the building just outside the separating streamline It is, however, restricted to a fairly small area. In this area, the wind will be about 20% higher than the undisturbed wind speed far in front of the building [14]. Figure 15 shows the result of the model for a high-rise building which is well exposed to the incoming wind.

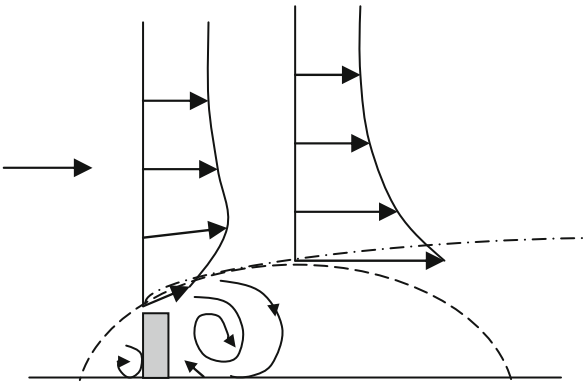

Electricity Generation with Small Wind Turbines. Figure 14
Flow over a high-rise building showing velocity increase and flow separation [14]

The results of the calculations of Mertens for a two-dimensional building (a building with infinite horizontal crosswind dimension) are shown in this figure for different values of the roughness height z_0 of the surface upwind of the building. The quantity b in this graph refers to the building depth, which is the horizontal size of the building in the direction of the incoming wind. Also shown is the result obtained by Wilson [21] for a square building. As can be seen there is a reasonable agreement between both results, for an upwind roughness height of 1 m, certainly for locations farther away from the windward edge of the building.

From further calculations of Mertens [15] it became clear that for a wind turbine located at the center of the roof a minimum height of 25% of the depth of a building is required for the lowest part of the rotor. For typical residential apartment buildings or office buildings this is in the order of 12–20 m. This means minimal tower height of 5 m underneath the rotor.

Suitable Wind Turbine Dimensions In the case the whole wind turbine is located in the higher wind speed region the energy increase is equal to the third power of 1.2. Thus, the aerodynamic power increase is 1.7 compared to a wind turbine in the same parallel flow without the building. When the wind turbine is located on the right spot on the roof this increase can be achieved for all wind directions. It, however, limits the dimensions of the wind turbine to something in the order of 20% of the characteristic height of a building. For uniform parallel oncoming flow over a mid- to high-rise its building height is equal to this characteristic height. Thus the limitation yields: $D \leq 0.2h$. For mid- to high-rise buildings with a characteristic dimension of say 50–100 m, the wind turbine diameter will, therefore, be from 10 up to about 20 m, in order to take full advantage of the speedup effect. Wind turbines of such sizes will generally not require significant modifications of the building structure, which is evidently an advantage when retrofitting buildings with renewable wind power.

Wind Turbines Developed for Operation on Buildings A number of companies have seen the potential for wind turbine application on top of existing buildings

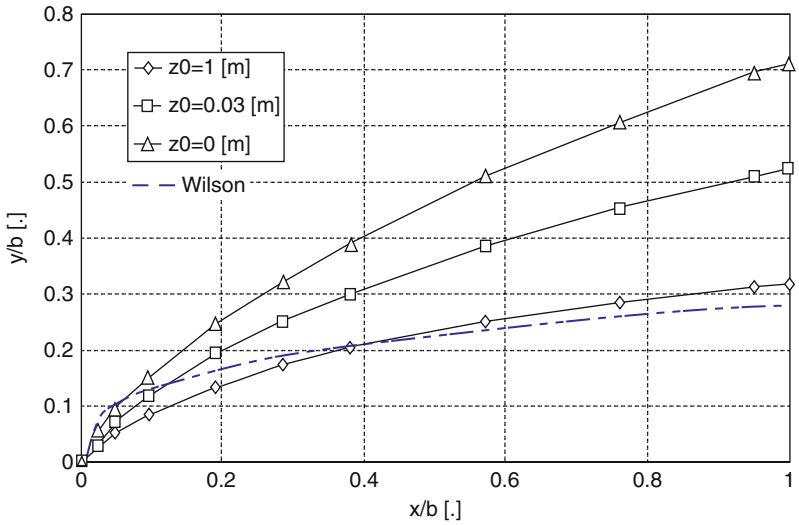

Electricity Generation with Small Wind Turbines. Figure 15
Location of the separating streamline for a two-dimensional building (20 m high, 10 m deep) [15]

Electricity Generation with Small Wind Turbines. Figure 16
High solidity and predominantly drag-driven VAWTs of various make

and have anticipated on the coming market with the development of dedicated machines. From the requirements for small wind turbines operating on buildings it is clear that vertical axis machines have a preference. Three examples of commercially available VAWTs for roof top application are shown in Fig. 16.

In similar fashion, examples of lift-driven VAWT designs are given in Fig. 17. It can be clearly seen that all three designs are derivatives of the Darrieus wind turbine depicted in Fig. 2c. In the DWT design use is made of curved blades, just as in the original design. The Neoga® adds skewness of the blades, whereas the Turby® combines a cylindrical swept area together with blade sweep.

Since Turby® is the most deviating design, when compared to the original Darrieus design, it is worthwhile examining this particular design somewhat further.

Electricity Generation with Small Wind Turbines. Figure 17
Lift-driven VAWTs of various make

H-type Lift-Driven VAWT with Skewed Blades The three blades of the Turby® rotate along a cylindrical surface. Compared to the classical Darrieus rotor this has the advantage that a larger swept area is obtained for the same blade length. A disadvantage is the addition of struts in the center necessary for structural reasons. They will contribute to the viscous drag of the machine and thus reduce its efficiency. Furthermore, the stress path in the blades due to centrifugal loads is no longer aligned with the blade itself. At this point it should, however, be noted that the design "tip" speed ratio of Turby®, the ratio between circumferential speed and wind speed, is significantly less than for a classical Darrieus rotor (speed ratio $\lambda = 3$ for Turby® where $\lambda = 5$–7 for classical Darrieus rotors).

The blades are furthermore swept. This complicates the load path through the rotor further, but is applied because it has a very favorable effect upon noise production. The combination of low λ together with blade sweep makes it possible to comply with the noise levels allowable in the built environment. More details regarding the development and the design of Turby® can be found in Van Bussel et al. [5]. The Quit Revolution lift-driven VAWT is another implementation of the above described design philosophy (see Fig. 18).

The fact that these machines are not self-starting is often seen as a major disadvantage. However, when located on top of building the grid infrastructure is present to use the generator of the wind turbine temporarily used as a motor for kick-starting the machine at sufficient wind speeds.

Electricity Generation with Small Wind Turbines. Figure 18
Turby® prototype at TU Delft open-air research site

Standards and Certification

Generic design requirements for small wind turbines are provided in the standard IEC 61400–2, ed.2, "Wind Turbines – Part 2: Design Requirements of Small Wind Turbines" provided by the International Electrotechnical Committee.

Local standards and testing procedures for small wind turbines are developed by consensus through independent third-party authorities, such as the Institute of Electrical and Electronic Engineers (IEEE) and Underwriters Laboratories (UL) in the USA. Often use is made of the above mentioned IEC 61400–2 standard and of (components of) standards for large wind turbines such as IEC 61400-12-1 ed.1, "Wind Turbines – Part 12–1: Power Performance Measurements of Electricity Producing Wind Turbines" and IEC 61400–11 ed.2, "Wind Turbine Generator Systems – Part 11: Acoustic Noise Measurement Techniques," and of other standards applied or modified for small wind turbines. According to AWEA [1], the standards UL 1741 and IEEE 929 have been successfully used to certify inverters for small wind turbines.

On top of that the IEEE is working on standard IEEE P1547 for intertied "distributed generation" technologies including small wind turbines [1].

Bibliography

1. AWEA (2009) AWEA small wind turbine performance and safety standard. AWEA 9.1 – 2009. American Wind Energy Association, Washington, DC
2. Bergey M Chair AWEA Small Wind turbine Committee (ed) (2002) Road map, a 20-year industry plan for small wind turbine technology. AWEA/Department of Energy, USA
3. van Bussel GJW (2003) Wind energy reliability data, a round-up from several data bases. In: Proceedings of the European wind energy conference & exhibition, Madrid, 16–19 June 2003
4. van Beveren SC (2008) Design of an urban wind turbine with diffuser. MSc thesis, TU Delft, Faculty of Aerospace Engineering, Delft University of Technology, Delft
5. van Bussel GJW, Mertens SM, Polinder H, Sidler HFA (2004) The development of turby, a small VAWT for the built environment. In: Proceedings of the global wind energy conference 2004, Chicago
6. van Bussel GJW (2007) The science of making more torque from wind: diffuser experiments and theory revisited. In: Proceedings of the science of making torque from wind. IOP, Lyngby
7. van Bussel GJW, Mertens SM (2005) Small wind turbines for the built environment. In: EACWE 4 conference proceedings, 11–15 July 2005, Prague, Paper No. 201
8. DWIA (2011) The guided tour. Danish Wind Industry Association, Denmark http://wiki.windpower.org/. Retrieved 20 Oct 2011
9. ETSU (1996) Working group on wind turbine noise, the assessment and rating of noise from wind farms. In: ETSU-R-97. ETSU, Harwell Didcot
10. IEC 61400–2, ed.2, Wind turbines – part 2: design requirements of small wind turbines. In: International electrotechnical committee, Geneva
11. Koehorst M (2001) De ontwikkeling van een windturbine voor toepassing in de gebouwde omgeving. M Sc thesis, TU Delft Faculty of Industrial Design, Delft
12. Lakeman LGJ (ed) (2002) Opwekking van windenergie in de gebouwde omgeving. Royal Haskoning, Nijmegen
13. Mertens SM (2001) Wind description for roof locating of wind turbines. Report 01173R, section Wind Energy. TU Delft, Delft
14. Mertens SM (2002) Notes on wind energy conversion in the built environment. Report 02187 R. TU Delft, Delft
15. Mertens SM (2005) Wind energy in the built environment. Phd thesis TU Delft, Faculty of Civil Engineering and Geosciences, Delft, The Netherlands
16. Put W (2000) Redesign of the Globuan Darrieus wind turbine. EJOK design for Industry, Rotterdam
17. Simiu E, Scanlan RH (1996) Wind effects on structures. Wiley, New York
18. Timmers G (ed) (2003) Eindverslag EET-Kiem project urban turbines. Ecofys, Utrecht
19. Toet S, Vermeer LJ (1996) Vermogensmetingen van een schaalmodel weerstandsturbine. Report IW96105R. Institute for Wind Energy, TU Delft, Delft
20. Van Dyke M (1968) An album of fluid motion. Parabolic, Stanford
21. Wilson DJ (1979) Flow patterns over flat-roofed buildings and application to exhaust stack design. ASHRAE Trans 28(2):284–294
22. Jacobs GJ (ed) (2003) Small wind turbine systems for battery charging. ARRAKIS, Veldhoven. www.arrakis.nl
23. de Jongh J, Smulders PT (2009) Introduction to wind pumps. ARRAKIS, Veldhoven. www.arrakis.nl
24. Lysen E (1983) Introduction to wind energy, CWD 82–1, 2nd edn. CWD, Amersfoort
25. Kentfield JAC (1996) The fundamentals of wind-driven water pumpers. Overseas Publishing Association, Amsterdam. ISBN 2-88449-239-9
26. Renewable UK (2010) Generate your own power, your guide to installing a small wind system. Renewable UK, London
27. Tande OJ (1994) Estimation of cost of energy from wind energy conversion systems, IEA recommended practices for wind turbine testing. International Energy Agency. http://www.ieawind.org/
28. WinEur (2006) Wind energy integration in the urban environment, Techno Economic Report, Jan 2006
29. Wood D (2011) Small wind turbines, analysis, design and application. Springer, London. ISBN 978-1-84996-175-2

Electrochemical Hydrogen Production

Marc T. M. Koper
Leiden Institute of Chemistry, Leiden University, Leiden, The Netherlands

Article Outline

Definition of the Subject
Introduction
General Theory
Hydrogen Evolution at Metal Electrodes
Hydrogen Evolution at (Electrodes Modified with) Molecular Catalysts in Aqueous and Nonaqueous Solvents
Concluding Remarks
Acknowledgments
Bibliography

Definition of the Subject

The electrochemical production of hydrogen by photoelectrolysis or electrolysis is one of the most promising ways for making high-purity hydrogen. Water electrolysis is as old as the field of electrochemistry itself, and this entry focuses on some of the fundamental principles that have been established through the years.

Introduction

Hydrogen (H_2) is considered by many as the fuel of the future. In view of the current interest and importance in securing the sustainability of our society's energy needs, many research efforts are invested in making hydrogen, storing hydrogen, and converting hydrogen back to work. One of the most promising ways to make *clean* "solar hydrogen" is by electrochemistry or electrolysis, either in combination with a photovoltaic cell or in an integrated photo-electrochemical device. A crucial component of such a device is the catalyst converting water (or protons) into hydrogen. Such a catalyst must be efficient, stable, robust, cheap (or "cost-effective") and be made from abundant sources.

This entry will consider some fundamental considerations associated with the catalysis of the electrochemical hydrogen production. The entry will focus on the energetic and thermodynamic requirements for such a catalyst [1–3] as opposed to the more usual approach (especially in the field of hydrogen evolution by molecular catalysts) in which emphasis is often on structural aspects of the catalyst. Of course, in an all-encompassing approach or theory, the two must be related, but in the author's view the approach emphasizing the energetic relationships provides a very useful general and basic framework for later, more detailed, approaches. The entry will also discuss these more detailed electrochemical models as well as the role of the solvent in the hydrogen evolution reaction (HER).

General Theory

Thermodynamic Theory

The hydrogen evolution reaction (HER), or the reverse hydrogen oxidation reaction (HOR), is a classic example of a two-electron transfer reaction

$$2H^+ + 2e^- \leftrightarrows H_2 \tag{1}$$

The reaction has a standard equilibrium potential $E^0_{H_2/H^+}$ of 0 V. The mechanism for the hydrogen oxidation/evolution reaction on metals will be considered first [4]. Later, this will be extended to a more general mechanism that encompasses the framework suggested for molecular catalysts. The classical electrochemical mechanism consists of three steps:

$$H^+ + * + e^- \leftrightarrows H_{ads} \tag{1a}$$

$$H_{ads} + H^+ + e^- \leftrightarrows H_2 + * \tag{1b}$$

$$2\,H_{ads} \leftrightarrows H_2 + 2^* \tag{1c}$$

known as the Volmer, Heyrovsky, and Tafel steps, respectively. The symbol $*$ stands for a free adsorption site on the metal electrode surface, but it may also be considered as a coordination site for hydrogen in a molecular catalyst. The H_{ads} intermediate is a hydrogen species chemisorbed to such a site on the surface or in the molecular catalyst. Note that in reactions 1a and 1b, the proton and electron transfer are assumed to take place simultaneously. The concerted character of the proton–electron transfer for the Volmer reaction on Pt(111) is supported by recent detailed ab initio density functional theory (DFT) calculations [5, 6].

The above multistep mechanism needs to satisfy thermodynamic constraints in the sense that the combined equilibrium constants need to conform to the Nernst equation of the overall reaction [7]. Let us assume that the reaction follows a Volmer–Heyrovsky mechanism, in which case:

$$\frac{E^0_{H^+/H_{ads}} + E^0_{H_{ads},H^+/H_2}}{2} = E^0_{H^+/H_2} = 0 \quad (2)$$

The equilibrium potential of a redox reaction involving an adsorbed or chemisorbed state can be calculated if one defines the concomitant standard state. Consider the Volmer reaction 1a, for which the equilibrium condition is

$$\Delta G(H_{ads}) = \Delta G(H^+ + e^-) \quad (3)$$

Following Nørskov et al. [8], the term on the right-hand side is 0 at $E = 0$ (vs NHE) by definition, and $-e_0E$ at any other potential E, assuming that when the potential is changed only the energy of the electrons changes, and nothing else. The latter assumption may be tested by DFT calculations, showing that the binding energy of H_{ads} does not depend strongly on potential, or on an applied electric field [9–12]. This implies that the static dipole moment of the H_{ads} bond to the surface is close to 0, and that the electrosorption valency corresponding to reaction 1a is close to 1 [12]. Therefore, the standard equilibrium potential for the Volmer reaction follows as:

$$E^0_{H^+/H_{ads}} = -\frac{\Delta G^0(H_{ads})}{e_0} \quad (4)$$

where $\Delta G^0(H_{ads})$ is the free adsorption energy of H_{ads} at some suitably defined standard state "0" (for instance, one-fourth coverage on a (111) surface), with respect to the energy of H_2, which is equal to 0 also by virtue of the above definition. If $\Delta G^0(H_{ads}) < 0$, i.e., H_{ads} formation onto the catalyst surface yields a thermodynamically more favorable situation than H_2 evolution, $E^0_{H^+/H_{ads}} > 0$. A well-known example of this is hydrogen underpotential deposition (UPD) on platinum and other transition-metal electrodes. Note, however, that in terms of the overall reaction, such a situation implies

$$E^0_{H^+/H_{ads}} = -E^0_{H_{ads},H^+/H_2} < 0 \quad (5)$$

so that the Heyrovsky reaction would have a standard equilibrium potential (defined for the same standard state) below 0 V. Neglecting kinetic factors, this analysis would suggest that if in the HER, H_{ads} formation would be a thermodynamically favorable reaction at $E = 0$, molecular hydrogen formation as in the Heyrovsky reaction must be thermodynamically unfavorable. Following Nørskov et al. [8], one could argue that in such a case, the minimal "thermodynamic overvoltage" for the overall reaction, η_T, would be equal to the standard equilibrium potential of the thermodynamically least favorable reaction, i.e., $\eta_T = E^0_{H^+,H_{ads}/H_2} - E^0_{H^+/H_2}$. This "thermodynamically least favorable reaction step" is termed the *potential-determining step* (not to be confused with the rate-determining step, though often they may correspond to the same reaction step). Since the lowest possible "thermodynamic overvoltage" is 0, it follows that, on the basis of these thermodynamic considerations, we are looking for a catalyst with:

$$\eta_T = E^0_{H^+/H_{ads}} = E^0_{H_{ads},H^+/H_2} = \frac{\Delta G^0(H_{ads})}{e_0} = 0 \quad (6)$$

Any catalyst with $\Delta G^0(H_{ads}) \neq 0$ will have a $\eta_T > 0$ as either the Volmer reaction has a standard equilibrium potential more negative than 0 ($\Delta G^0(H_{ads}) > 0$) or the Heyrovsky reaction has a standard equilibrium potential more negative than 0 ($\Delta G^0(H_{ads}) < 0$). Figure 1 plots η_T for the HER as a function of $\Delta G^0(H_{ads})$, and illustrates how the optimal catalyst is a compromise between strong and weak binding of H_{ads}, as expressed by the classical Sabatier principle [13]. Figure 1 is similar but not identical to a volcano relationship, in which the catalytic activity for a reaction is plotted as a function of some property of the catalyst, in this case the catalyst's ability to bind an intermediate. Typically such a plot leads to peak-shaped relationship of the catalytic activity versus the catalyst property, whence the name "volcano relationship." Such a catalyst property is also known as a "descriptor," as it gives a general but essential description of the catalyst properties. Although the "thermodynamic overpotential" of multistep electron transfer reactions is not a kinetic measure, the concept of the volcano relationship and associated Sabatier principle straightforwardly follow from thermodynamics combined with some very mild kinetic assumptions (one of the assumptions that one may make is that of a relation between activation energy

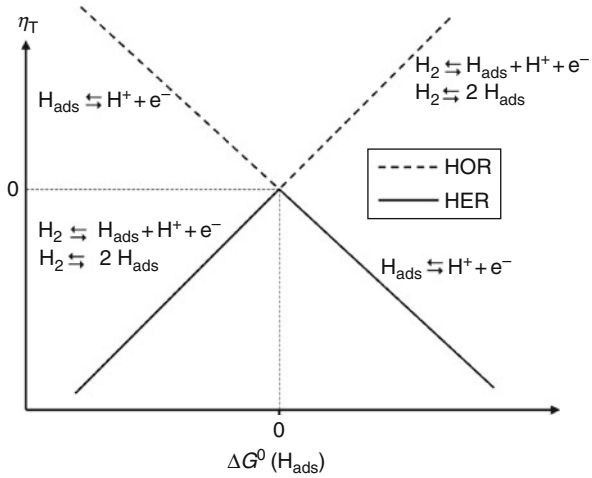

Electrochemical Hydrogen Production. Figure 1 "Thermodynamic" volcano plot for the hydrogen evolution reaction (*HER*) and the hydrogen oxidation reaction (*HOR*): thermodynamic overpotential (standard equilibrium potential of the potential-determining step) versus the free binding energy of hydrogen on the electrode surface [15, 17]. The *dashed line* gives the same plot for the HOR. The potential-determining steps corresponding to the various legs of the curves are indicated

and thermodynamic driving force, i.e., the Brønsted–Evans–Polanyi postulate [14]). Therefore, I consider Fig. 1 as a thermodynamic version of the kinetic volcano plot (i.e., log i_0 vs $\Delta G^0(\mathrm{H_{ads}})$, with i_0 the standard exchange current density), as originally suggested for the HER by Parsons [15] and Gerischer [16], and recently revived on the basis of DFT-calculated values for $\Delta G^0(\mathrm{H_{ads}})$ by Nørskov et al. [17]. Note that the same analysis can be applied to the HOR, leading to the dashed-line volcano plot in Fig. 1, illustrating that for a reduction reaction we obtain a "∧"-shaped plot, and for an oxidation reaction we obtain a "∨"-shaped plot.

The same analysis may be applied to a Volmer–Tafel mechanism for the HER/HOR. The only difference now is that reaction 1c does not have a standard equilibrium potential, because it is not an electrochemical reaction. However, combined with reaction 1a, it must still satisfy the overall thermodynamic constraints of reaction 1. Defining the standard equilibrium constant of reaction 1c as:

$$K_{\mathrm{H_{ads}/H_2}} = \exp\left[\frac{-\Delta G^0(\mathrm{H_{ads}})}{RT}\right], \tag{7}$$

the Tafel–Volmer mechanism has to obey the following relation:

$$E^0_{\mathrm{H^+/H_{ads}}} - \frac{\Delta G^0(\mathrm{H_{ads}})}{e_0} = 0 \tag{8}$$

In case $E^0_{\mathrm{H^+/H_{ads}}} < 0$, the thermodynamic overvoltage is $\eta_T = E^0_{\mathrm{H^+/H_{ads}}}$, as in the Heyrovsky–Volmer mechanism. In case $E^0_{\mathrm{H^+/H_{ads}}} > 0$, the Tafel reaction becomes endothermic (Eq. 8), and therefore thermodynamically unfavorable. The most straightforward definition of a "thermodynamic overvoltage" would then follow from Eq. 8, leading to $\eta_T = -E^0_{\mathrm{H^+/H_{ads}}}$. As a result, we see that the Heyrovsky–Volmer and the Tafel–Volmer mechanisms lead to "thermodynamic volcano curves" that are identical, and that more mechanistic assumptions are needed in order to distinguish between these two mechanisms. One important consequence of a volcano-type relationship such as that illustrated in Fig. 1 is that the potential-determining step is different on each side of the maximum. "Potential determining" means that this step determines the (over)potential at which a certain current density may be reached. For $\Delta G^0(H_{\mathrm{ads}}) > 0$, the Volmer reaction is potential determining; for $\Delta G^0(H_{\mathrm{ads}}) < 0$, either the Heyrovsky or Tafel reaction is potential determining. It is important to point out the difference between potential-determining and rate-determining step. Potential-determining steps are not always rate determining at the relevant potentials, as potential-determining steps suffer from an unfavorable thermodynamics, but not necessarily from an unfavorable kinetics at the potential at which the current finally starts flowing. Nevertheless, this simple analysis lucidly illustrates the thermodynamic constraints applicable to multistep multi-electron transfer reactions, and how catalysis may influence the "thermodynamic overvoltage" by optimizing the binding energy of the key intermediate, in this case $\mathrm{H_{ads}}$. The best catalyst, according to this analysis, is the one that binds hydrogen in such a way that there is no thermodynamic sink or barrier in going from reactant through intermediate to product. This is the essential point made already by Parsons more than 50 years ago [15]. Experimental volcano plots of the exchange current density of the HER have been suggested many years ago by Trasatti, [18] and such plots may be criticized for various (experimental)

reasons [19, 20]. In this section, we will summarize some of the main objections. The section Hydrogen Evolution at Metal Electrodes will review the experimental evidence for the existence of a volcano relationship for the HER. At this point, it is stressed again that the approach discussed here does not include explicitly any kinetic aspects of the reaction.

The idea recently suggested by Nørskov et al. [17] is that $\Delta G^0(H^*)$ may be calculated for many potential catalysts from first principles by using DFT in combination with some mild assumptions on entropic contributions. In a DFT calculation, one typically calculates the binding energy of the hydrogen atom (or radical):

$$\text{Catalyst} + H^\bullet \rightarrow \text{Catalyst} - H \quad E = E_{bind} \tag{9}$$

The free binding energy using H_2 as a reference can then be estimated from

$$\Delta G^0(H_{ads}) = E_{bind} - T^*\Delta S + \Delta ZPE + E(H^\bullet) \tag{10}$$

The term $T^*\Delta S$ takes into account the entropy contribution due to the vibration of hydrogen in its adsorbed state, and ΔZPE is the corresponding zero-point energy of the adsorbate. Their combined $(-T^*\Delta S + \Delta ZPE)$ value has been estimated for H adsorbed on metals as ca. 0.24 eV by Rossmeisl et al. [11]. $E(H^\bullet)$ is half the bond energy of the hydrogen molecule, which is 2.24 eV (including the molecule's ZPE).

Trends in $\Delta G^0(H_{ads})$ or E_{bind} among different metals often conform to the so-called d-band model proposed by Hammer and Nørskov [14, 21]. This model claims a close correspondence between the strength of a surface bond (of H, but also of other adsorbates such as O, OH, and CO) and the location of the center of the d band of the metal surface. The energy of the d band may be "engineered" by changing the properties of the metal surface, for instance by (surface) alloying and overlayer formation [22]. The d-band center also influences the activation energy for dissociative adsorption, primarily through the Brønsted–Evans–Polanyi relationship [14], which assumes a linear relation between reaction energy and activation energy. The role of the d band in bond breaking electron transfer reactions was recently modeled by Santos and Schmickler [23], and will be discussed briefly in the next section.

The above mechanism, based on reactions 1a–1c, is rather specific to the HER on metal electrodes. If such a mechanism takes place on a molecular catalyst, the catalyst typically has two nearby (metal) centers to coordinate the hydrogen and adsorbed hydrogen is often referred to as "hydride." The mechanism may be termed "homolytic" in this case, akin to the Volmer–Tafel mechanism. On many molecular catalysts or enzymes, however, the general mechanism tends to be different, and may be considered a variant of the Tafel–Heyrovsky mechanism, with the difference that the proton is not dissolved in the liquid phase, but also bound to a nearby "docking" site [1]. In such mechanisms, it is typically assumed that the release of the hydrogen molecule from the active site is an activated process (though the activation barrier may be small). Such a heterolytic mechanism may be written as follows:

$$H^+ + 2e^- + * \leftrightarrows H^-_{ch} \tag{11a}$$

$$H^+ + *' \leftrightarrows H^{+\prime}_{ch} \tag{11b}$$

$$H^-_{ch} + H^{+\prime}_{ch} \leftrightarrows H_{2,ch} \tag{11c}$$

$$H_{2,ch} \leftrightarrows H_2 + * + *' \tag{11d}$$

where the two different coordination sites have been labeled as * and $^{*\prime}$. The two-electron transfer character of reaction 11 should be considered as formal; the charge distinction between H^- and H^+ may be exaggerated. Note that we have now the binding energies of H^-_{ch} and H^+_{ch} as the main descriptors for the thermodynamics of hydrogen evolution, so strictly speaking we have two descriptors now. It is not difficult to understand from Eqs. 11 that the properties of this mechanism will depend on the basicity/acidity of the coordinating sites * and $^{*\prime}$. As a result, the overall activity for hydrogen evolution will normally be strongly pH dependent. By contrast, hydrogen evolution on metals, which only involves neutral hydrogen as intermediate (at least formally), is typically not strongly pH dependent [1, 4].

More Detailed Theories and Simulations

The phenomenological theory of the previous section has an old history in the electrochemistry literature, and can be given a much more detailed treatment than

given here, for which reference is made to the original literature [15–18, 20]. More detailed molecular-level simulations of the hydrogen evolution (and hydrogen oxidation) reaction have been carried out in recent years, and it is of interest to discuss the main results from those investigations.

Santos and Schmickler consider that modeling hydrogen oxidation or hydrogen evolution fully from first principles is currently still too ambitious a task, and more general insight can be obtained from taking a simpler approach [23–26]. They have formulated a simple Hamiltonian which includes two hydrogens and the metal, and the electronic interaction between them [27]. The interaction with the solvent is treated in a spirit similar to the Marcus model. The ground-state energy of the model Hamiltonian may be calculated (with some approximations) and the interaction parameters entering the expression for the ground-state energy (strength of electronic interaction between hydrogen atoms; strength of electronic interaction of the hydrogen with the metal states; metal surface electronic band structure; strength of interaction of the hydrogen with the solvent) may obtained from more detailed calculations, such as DFT. Although the effect of the simplifications of such an approach are somewhat difficult to estimate, the great advantage of this method is that it allows for a more detailed description of the HER/HOR without having to resort to extremely complicated calculations, which may have their own drawbacks. Moreover, the coupling between bond breaking and electron transfer can be followed in an instructive way. The activation energy in the theory of Santos and Schmickler is determined by the interaction of the bonding orbital of the hydrogen molecule with the d band of the metal catalyst as it passes the Fermi level of the metal. At this critical stage, the occupation probability of the bonding orbital is about one, so that one electron has already been transferred to the metal (in terms of the HOR). However, the activation energy for bond making or bond breaking does not only depend on the center of the d band as also predicted by the theory of Hammer and Nørskov. There is an additional important role of the electronic coupling between the hydrogen and the metal surface. The strength of the electronic coupling determines the broadening and splitting of the orbitals involved in the charge transfer reactions, and normally a stronger electronic coupling leads to a lowering of the activation energy. Electronic coupling strengths typically increase toward the lower left-hand corner of the relevant part of the periodic table containing the coinage and transition metals, because of the diffuseness of the metal orbitals involved in the interaction increases in that direction. Based on their detailed calculations, Santos and Schmickler have criticized the use of volcano relationships in understanding trends in the metal-dependent reactivity of the HER/HOR. First of all, for most of the metals for which calculations can be performed, the data points lie on the ascending branch of the volcano curve. Metals that bind hydrogen very strongly also tend to bind oxygen very strongly, and therefore points on the descending branch of the volcano (increasing hydrogen binding strength) pertain to metals covered by an oxide film under aqueous electrochemical conditions. Hence, the experimental evidence for a volcano relationship is weak, if any, according to Santos and Schmickler. While this argument may be correct for the "older" volcano curves encompassing a wide variety of metals, it may not apply to some recent volcano curves (to be discussed in the section Hydrogen Evolution at Metal Electrodes). Secondly, the activation energy for hydrogen evolution and hydrogen oxidation depends not only on the strength of the interaction between hydrogen and the metal surface, but also on effects not (directly) incorporated into the simple model discussed in the previous section, such as the strength of the electronic coupling. The weak electronic coupling between nickel and hydrogen may explain the rather low activity of nickel, whereas the strong electronic coupling between rhenium and hydrogen may explain the high HER activity of rhenium [28]. Santos and Schmickler have argued that these two metals indeed appear to deviate from the volcano plot, precisely for the reason mentioned. A final point raised by Santos and Schmickler that is not explicitly included in the analysis of the previous section is that the binding energy of hydrogen is coverage dependent and that different metals may show their optimum activity at different coverages. As a result, Santos and Schmickler refer to the volcano curve, as applied to the HER/HOR as a "venerable" but effectively "defunct" and "oversimplistic" concept.

One of the simplifications made in the Santos–Schmickler approach to the HER/HOR is the way in

which the role of the solvent is included. The atomic level modeling of the solvent in the initial stages of proton reduction, without resorting to fully ab initio methods, was considered by Wilhelm et al. [29, 30]. They took the so-called empirical valence bond model (EVBM) to describe proton exchange in water to include proton transfer to a Pt(111) electrode surface. The model was parameterized on the basis of density functional theory calculations. The advantage of this approach over fully ab initio simulations (see below) is that much longer simulation times can be probed and therefore a more meaningful statistics can be obtained. This setup allowed the authors to study the dynamics of proton transfer to Pt(111) as a function of the charge density on the electrode surface. Figure 2 shows the charge dependence of two rate constants obtained from their detailed simulations: the inverse time needed for the proton to reach the "final" adsorption state, still being a proton, and the inverse time needed for "adsorption-to-discharge." Figure 2 indicates that at strongly negative surface charge, the proton transfer reaction is dominated by the time the proton needs to approach the surface, and proton discharge is very fast. At less negative surface charge density, the rate for establishing an orientational fluctuation suitable for proton transfer to the surface is rate determining.

Otani et al. [5] have carried out a full ab initio molecular dynamics simulation of the proton transfer reaction on a Pt(111) surface. This was the first ab initio dynamical simulation of an electrode reaction, but it should also be emphasized that this was a single-trajectory simulation, without statistical sampling, and that proton transfer was obtained only if excessively high electric fields were applied. Nevertheless, expect more of this kind of work in the future, and combined with rare-event sampling techniques, this is a potentially very powerful method. More recently, Santana et al. have used a similar approach to study the HOR on Pt(110) [31].

An alternative approach to studying the dynamic aspects of proton reduction and/or hydrogen evolution is to compute the potential energy surface for such reactions from detailed DFT calculations. A potential energy surface is generated at zero temperature, and therefore it does not include any finite temperature effects. Such an ab initio treatment of the hydrogen evolution reaction has been carried out recently by Skulason et al. [6, 32]. They included the

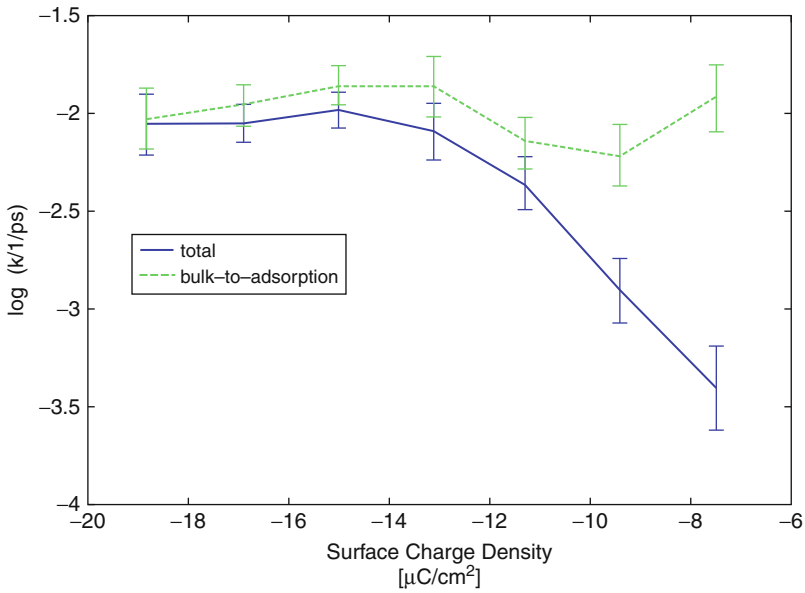

Electrochemical Hydrogen Production. Figure 2
Top: Logarithmic representation of the rate for proton discharge (*blue, full line*) and the proton bulk-to-adsorption rate (*green, dashed*) on Pt(111) (Reproduced with permission from Ref. [30])

effect of the electrode potential by considering various concentrations of protons (simulating different surface charge densities) within simulation cells of varying size, and extrapolating the obtained energies to infinite cell size to simulate a potentiostatic experiment. For the Volmer reaction on Pt(111), a barrier of ca. 0.5 eV was calculated. The Heyrovsky reaction was concluded to be the reaction with the highest barrier at 0 V, ca. 1.4 eV for the HER, whereas the Tafel reaction has a potential-independent barrier of ca. 0.8 eV at 0 V. As a result, the Tafel reaction is predicted to be the rate-determining step.

Hydrogen Evolution at Metal Electrodes

HER at Platinum Electrodes

As platinum is one of the best and most studied catalysts for the HER/HOR, as well as the one used in fuel cells and in many (acid) electrolyzers, it is useful to summarize here some of the pertinent experimental results. Platinum is generally agreed to be a very active catalyst for HER/HOR, and considered to be located near the apex of the volcano. Standard exchange current densities for the HOR are not easy to obtain because in general it is difficult to correct accurately for mass transport limitations and double-layer charging. Values from 10^{-3} to 1 A cm^{-2} have been reported for platinum [4, 33, 34] which would roughly correspond to a turnover rate of 0.1–100 s^{-1} per Pt active site, at the standard equilibrium potential. The Pt "active site" is not well known, and there has been quite some controversy as to whether the HER/HOR is structure sensitive on platinum or not. In contrast to early studies, [35] the groups of Markovic [33] and Conway [34] have found that the Pt(110) surface is the most active in catalyzing the HER/HOR, typically being an order of magnitude more active than the other low-index surfaces.

In electrochemical experiments, rate-determining steps are usually inferred from so-called Tafel slopes, which essentially express the overall potential dependence of the reaction rate (i.e., the current) in a certain potential range. If the Volmer reaction is rate determining and its rate obeys the Butler–Volmer model, then the potential dependence is equivalent to a Tafel slope of $\ln 10 \times RT/(\alpha FE) \approx 120$ mV/dec if $\alpha \approx 0.5$. If, on the other hand, the Heyrovsky reaction is rate determining, and the preceding Volmer reaction in "quasi-equilibrium," the potential dependence of the reaction is equivalent to a Tafel slope of $\ln 10 \times RT/[(1+\alpha)FE] \approx 40$ mV/dec if $\alpha \approx 0.5$. Finally, if the Tafel reaction is rate determining, the Tafel slope will be $\ln 10 \times RT/[2FE] \approx 30$ mV/dec. In these predictions of the Tafel slope, saturation effects on the surface are not included.

Markovic et al. [33] have measured Tafel slopes for both the HER and the HOR on Pt single-crystal electrodes in acidic media. Tafel slopes also appear to depend on the crystal plane; the most active Pt(110) surface exhibits the 30 mV/dec Tafel slope well known from polycrystalline Pt [34, 36]. This Tafel slope corresponds to a Tafel–Volmer mechanism, i.e., a combination of reactions 1a and 1c.

The HER/HOR reaction kinetics is first order in the proton concentration over a wide pH range (0–14), implying that overpotentials are similar on the RHE (reversible hydrogen electrode) scale, in full agreement with the idea that proton and electron transfer are coupled over the entire pH range. However, there is a nontrivial pH effect in the sense that in alkaline media, the rate of the reaction tends be about an order of magnitude lower than acidic media, at the same overpotential [37]. Conway et al. [37] have explained this effect by a more difficult abstraction of H from H_2O than from H_3O^+. Pt(110) is still the most active surface, also in alkaline media, but the Tafel slope seems to be different, closer to 60 mV/dec, although no clear straight line was obtained.

An important discussion in the surface electrochemistry literature concerns the nature of surface-adsorbed hydrogen that acts as a precursor for hydrogen evolution in the HER, or for proton formation in the HOR [4, 38]. It is well known that at potentials above the reversible hydrogen potential, from ca. 0.05 to 0.3 V versus RHE (i.e., where no hydrogen evolution takes place), adsorbed hydrogen is formed on platinum. This form of adsorbed hydrogen is referred to as "underpotential deposited" (upd) hydrogen [38]. The surface coverage of this H_{upd} follows a Frumkin isotherm on Pt(111) and Pt(100) [38–40] with weak repulsive interactions between the adsorbed hydrogens. The coverages of H_{upd} in acidic and alkaline media on Pt(111) are almost identical at the same overpotential,

but again the kinetics of its formation is much slower in alkaline media [41]. The adsorbed hydrogen that participates in the HER at potentials around 0 V, is usually termed "overpotential deposited" (opd) hydrogen. The exact relation between H_{upd} and H_{opd} has lead to ample discussion and speculation; for an illustrative account, see the paper by Conway and Jerkiewicz [42]. Most probably, H_{upd} and H_{opd} should primarily be distinguished on the basis of the different overall hydrogen coverages applicable to both states, with a typical H_{upd} coverage being lower than 0.5–1.0, and a typical H_{opd} coverage being close to or higher than 1 (i.e., including the H_{upd} coverage, implying more than 1 H per surface Pt atom), suggesting that H_{upd} and H_{opd} reside at different sites on the surface. The different coverages lead to different lateral interactions, different energetics, and site preferences, and therefore different activities toward H_2 evolution.

There have been a number of attempts to probe the adsorbed hydrogen on platinum using vibrational spectroscopy. A recent surface-enhanced infrared (IR) study on a platinum film electrode by Kunimatsu et al. [43] confirmed earlier results by absorption–reflection IR [44] that for potentials lower than ca. 0.1 V_{RHE}, atop-bonded Pt-H is formed. The signal of this band correlated with the hydrogen evolution current, and therefore this species was identified as the intermediate in the HER. Kunimatsu et al. suggest that H_{upd} adsorbs below 0.3 V_{RHE} in hollow sites, though this state has not been resolved spectroscopically, and that, in addition to H_{upd}, H_{opd} adsorbs below 0.1 V_{RHE} at atop sites, and serves as the reaction intermediate.

Experimental Evidence for Volcano Behavior on Strained Monolayer and Bimetallic Systems

The evidence for a volcano-type relationship has been collected by Trasatti [18], and more recently by Nørskov and Stimming and coworkers [17]. One problem with such a correlation is that it is partially based on including metals that under experimental conditions are most likely covered by an oxide [20]. Recent studies by Kibler et al. [45, 46] have employed the idea of using palladium monolayers on different substrates [from Pd on Re(0001) to Pd on Au(111)] to tune the reactivity toward hydrogen adsorption and hydrogen evolution. Since the potential of the H_{upd} peak observed in voltammetry is directly related to the adsorption energy of hydrogen (or more accurately, of H_{upd}), the authors could relate the peak potential to the theoretically predicted d-band shift with respect to Pd (111). The good correlation found suggested that this monolayer approach is a viable and controlled way to tune reactivity. In a subsequent study, the same systems were studied for their HER activity. Figure 3 shows the plot of the standard exchange current density versus the free energy of adsorption of hydrogen, clearly in agreement with the predictions of the Sabatier principle and the volcano plot. Note that from these results, an optimum standard exchange current density of ca. 0.01–0.1 A cm^{-2} is predicted.

Clearly, a catalyst consisting of Pd, Ru, and Pt is hardly an economical alternative for Pt, which is already quite a good catalyst for the HER/HOR. Therefore, Greeley et al. [47] have carried out an extensive computational study of bimetallic surfaces, screening for specific combinations with a $\Delta G^0(H^*)$ close to 0, with a negative formation energy to ensure stability of the material, and preferably consisting of cheaper elements. The counterintuitive combination of Pt and Bi emerged as one of the possibly attractive materials, with a $\Delta G^0(H^*)$ closer to zero than Pt. An appropriately prepared Pt-Bi surface alloy was subsequently found to indeed have a higher activity for the HER than Pt, showing the promise and usefulness of this computational screening strategy.

Hydrogen Evolution at (Electrodes Modified with) Molecular Catalysts in Aqueous and Nonaqueous Solvents

There have been ample efforts to develop molecular catalysts for hydrogen evolution, the majority of them inspired to mimic the activity of natural hydrogenases, resulting in an extensive literature on this subject that will not be summarized here. For some recent reviews, the reader may consult various recent sources [48–51]. These biomimetic complexes are usually organometallic compounds containing Fe, Ni, Co, and/or Ru. It is also known that certain nonmetal containing organic molecules (such as bipyridine) may enhance the HER on metal electrodes otherwise not particularly active for the HER, such as mercury or gold (see, e.g., Ref. [52] and references therein).

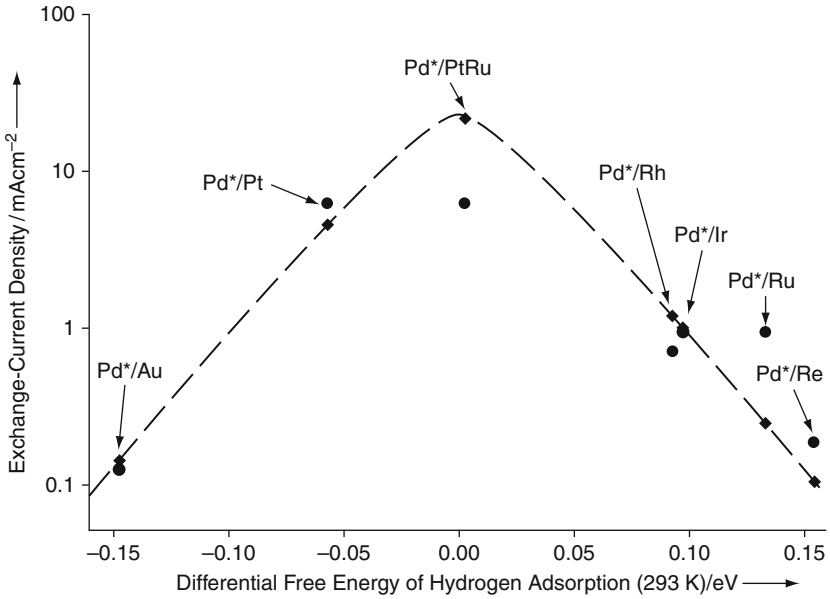

Electrochemical Hydrogen Production. Figure 3
Hydrogen evolution exchange current density as a function of the theoretical differential free energy of hydrogen adsorption, ΔG^0(H*). The *dashed line* shows the functional form of the theoretical exchange current density, and the *black diamonds* correspond to the predictions for specific overlayers. The *black circles* represent experimental measurements (the measured exchange current density determines the ordinate for these points, and the abscissa is specified by the theoretical ΔG^0(H*) value). Pd*/X denotes a pure overlayer of Pd on a substrate of metal X (Reproduced with permission from Ref. [46])

Hydrogenases themselves have also been investigated as hydrogen evolution catalysts, and when adsorbed on graphitic electrodes, have been shown to exhibit very good catalytic properties, comparable to platinum. This latter subject has been discussed and reviewed extensively by Armstrong and coworkers [53]. To elucidate the catalytic function of these enzymes, it is useful to discuss some existing DFT calculations on computational hydrogenase models within the framework of the theory discussed in the section General Theory.

All hydrogenases catalyze both HER and HOR. The [FeFe] hydrogenases are most active for hydrogen formation, while [NiFe] hydrogenases are poised for hydrogen oxidation. Mechanistic information has been obtained from enzyme kinetics, spectroscopy, X-ray structural data, and DFT calculations. A general feature is that hydrogen binding or dissociation, proton exchange, and electron transfer are separate steps. A second distinct difference with the metal surface-catalyzed reaction is the heterolytic splitting or formation of hydrogen (reactions 11). A proton is abstracted by a nearby base, and hydride is stabilized by the metal ions rather than H^*, although electron and spin densities are substantially delocalized. This is somewhat similar to the Heyrovsky reaction proposed for the mechanism on metals (reaction 1b). As mentioned, on a platinum electrode the homolytic bond splitting or making (Tafel reaction 1c) seems to be the preferred pathway.

The mechanism of the HER/HOR by [FeFe] hydrogenases, as suggested by DFT calculations and experimental data, can be summarized as follows: [54]

$$[Fe^{II}Fe^{I}]^{-1} + H^+ \rightarrow [Fe^{II}Fe^{I}H] \tag{12a}$$

$$[Fe^{II}Fe^{I}H] + e^- \rightarrow [Fe^{I}Fe^{I}H]^{-1} \tag{12b}$$

$$[Fe^{I}Fe^{I}H]^{-1} + H^+ \rightarrow [Fe^{I}Fe^{I}HH] \tag{12c}$$

$$\begin{aligned}[Fe^{I}Fe^{I}HH] + e^- &\rightarrow [Fe^{I}Fe^{0}HH]^{-1} \\ &\rightarrow [Fe^{II}Fe^{I}\eta - H_2]^{-1}\end{aligned} \tag{12d}$$

$$[Fe^{II}Fe^{I}\eta - H_2]^{-1} \rightarrow [Fe^{II}Fe^{I}]^{-1} + H_2 \tag{12e}$$

The electrons are rapidly transferred from the reductant (or the electrode) to the active site via the chain of [FeS] clusters. From an electrochemical perspective, these [FeS] clusters thus are intramolecular mediators. Although Fe–H–Fe bridging intermediates have been proposed, the most likely mechanism involves one-Fe bound H-species and side-on bound H_2. The secondary amine in the bridging ligand and Fe^I appear to be equally potent as catalytic base. The iron most distant from the nearby [FeS] cluster, called the Fe_d site that shuttles between the formal 1+ and neutral state in reactions 12a–e, appears as the actual binding site for H and H_2. By taking together the proton and electron transfer steps in reactions 12a–d, we can compare the DFT calculations performed by Sbraccia et al. [54] to the model presented in the section General Theory. For reactions 12a and 12b together

$$[Fe^{II}Fe^{I}]^{-1} + H^+ + e^- \rightarrow [Fe^{I}Fe^{I}H]^{-1} \qquad (12f)$$

the DFT-calculated reaction energy is −15.98 eV. Compared to the H_2 molecule, with a calculated total energy of 31.70 eV, the reaction energy is therefore −0.13 eV. For reactions 12c and 12d together:

$$[Fe^{I}Fe^{I}H]^{-1} + H^+ + e^- \rightarrow [Fe^{I}Fe^{0}HH]^{-1} \rightarrow [Fe^{II}Fe^{I}\eta - H_2]^{-1} \qquad (12g)$$

the DFT-calculated reaction energy is −15.43 eV, implying a reaction energy of +0.42 eV. For the final H_2 release, reaction 12e, the reaction energy is −0.29 eV (with a calculated activation energy of 0.07 eV). Note that the three calculated reaction energies now add up to 0, implying that we are considering the reaction at thermoneutral conditions. Although this is an analysis based on total energies, as calculated by DFT, and not on free energies, these numbers still suggest that: (1) for hydrogenases, the key to an efficient catalyst is also to have an active site that binds H just as strong as H_2 (see also Ref. [55]), and (2) that the addition of the second hydrogen, reaction 12g, is thermodymically uphill and hence the potential determining step, if we neglect zero-point energy contributions and entropy.

The organometallic nature of hydrogenase structural mimics makes them more soluble in nonaqueous solvents than in water. This has led to the development of activity tests in acetone, propylene carbonate, or acetonitrile for evaluation of model compounds. This is obviously not without consequences for the definition of pH and of the equilibrium potential of the redox couples. The equilibrium potential of the reference couple, $E^0_{H_2/H^+}$, is indeed strongly dependent on the nature of the protic species (solvated protons or weak acid). The overpotential for hydrogen evolution, which is the relevant experimental quantity when comparing different catalysts in different solutions, must therefore be referred to the reversible potential of the H^+/H_2 redox couple in the solvent under consideration. Working in a nonaqueous solvent has two important consequences for the determination of the reversible potential. First of all, the solvation energy of the proton is solvent dependent, and leads to a concomitant shift of the standard equilibrium potential. Second, many proton donors dissociate only incompletely in organic solvents, and therefore the dissociation constant should be taken into account in the definition of the standard equilibrium potential. Felton et al. [56] have described how to correct for both effects properly, and have given a useful comparison of various catalysts in a typical nonaqueous solvent, i.e., acetonitrile.

Considering the acid dissociation constant, $K^{sol}_{a,HA}$, in solvent "sol," of the reaction:

$$HA(sol) \leftrightarrows H^+ + A^- \qquad (13)$$

the standard equilibrium potential of the overall half reaction

$$2HA(sol) + 2e^- \leftrightarrows H_2(g) + 2A^- \qquad (14)$$

in the solvent "sol" is given by

$$E^{0,sol}_{H_2/HA} = E^{0,sol}_{H_2/H^+} - \left(\frac{2.303\,RT}{F}\right) pK^{sol}_{a,HA} \qquad (15)$$

In nonaqueous solvents, values for $E^{0,sol}_{H_2/H^+}$ or $E^{0,sol}_{H_2/HA}$ are often referred to the ferrocenium/ferrocene couple in the same solvent. The value of $E^{0,aq}_{H_2/H^+}$ would be a fundamentally more interesting reference, and if one is not interested in determining absolute electrode potentials, a simple way to look at the solvent dependence of $E^{0,sol}_{H_2/H^+}$, as referred to $E^{0,aq}_{H_2/H^+}$, is by considering the difference in the absolute solvation energies of the proton in "sol" and water:

$$E^{0,sol}_{H_2/H^+} = E^{0,aq}_{H_2/H^+} + \frac{[\mu^{sol}(H^+) - \mu^{aq}(H^+)]}{F} \qquad (16)$$

Values for the absolute solvation free energy (i.e., the Gibbs free energy of solvation not taking into account the surface potential of the solvent) of the proton in various solvents have been reconsidered recently by Fawcett [57] and the thus calculated values of $E^{0,sol}_{H_2/H^+}$ (vs $E^{0,aq}_{H_2/H^+}$) are given in Table 1. The experimental estimates of $E^{0,sol}_{H_2/H^+}$ have also been the subject of much work and debate. Fourmond et al. [58] have recently discussed their proper determination in a limited number of representative solvents, based on original data of Daniele et al. [59]. These values are, however, quoted versus an internal solvent standard, i.e., the ferrocenium/ferrocene $Fc^{+/0}$ couple. The equilibrium potential of this couple is usually considered solvent independent, although water appears to be an exception [60].

Using the tabulations provided in Ref. [60], the third and fourth columns in Table 1 have been generated, by first referring to decamethylferrocenium (DMFC)/decamethylferrocene couple (third column), which appears to be more solvent independent, and then rescaling such that in water the reference is at 0 V (fourth column). Although there is clearly a lack of data in this table to make any far-reaching conclusions, the differences between the theoretical and experimental values in acetonitrile and dimethylsulfoxide (DMSO) are typically within ±0.15 V. More data are obviously needed to further elucidate this correspondence.

To illustrate the influence of a nonaqueous solvent on the HER activity, a comparison of different catalysts in acetonitrile is given in Figs. 4 and 5 [56]. It is seen

Electrochemical Hydrogen Production. Table 1 dependence of the equilibrium potential of the hydrogen electrode

Sol	$E^{0,sol}_{H_2/H^+}$ versus SHE/V (From Eq. 16, Ref. [57])	$E^{0,sol}_{H_2/H^+}$ versus $E_{DMFc^{+/0}}$/V (From Refs. [58, 60])	$E^{0,sol}_{H_2/H^+}$ versus. SHE/V Combining [58, 60]
Water	0	−0.099	0
Acetonitrile	0.414	0.435	0.534
DMSO	−0.207	−0.202	−0.103
DMF	–	−0.162	−0.063
Methanol	0.083	–	–

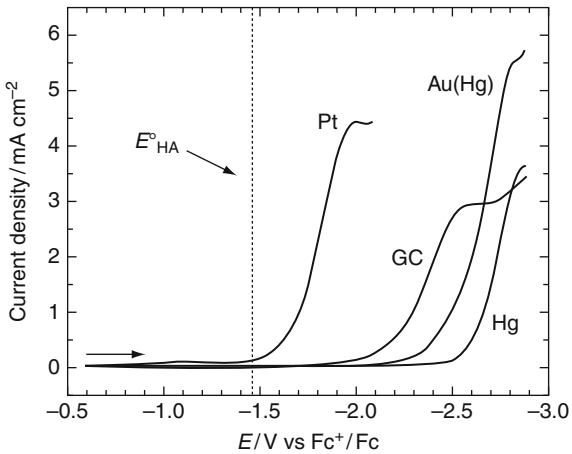

Electrochemical Hydrogen Production. Figure 4 Linear sweep voltammograms of hydrogen evolution for 10 mM acetic acid in acetonitrile with 0.10 M tetrabutylammonium hexafluorophosphate at 1.0 V/s. Electrodes as indicated (GC is glassy carbon). Reversible potential for reduction of acetic acid shown for comparison (Reproduced with permission from Ref. [56])

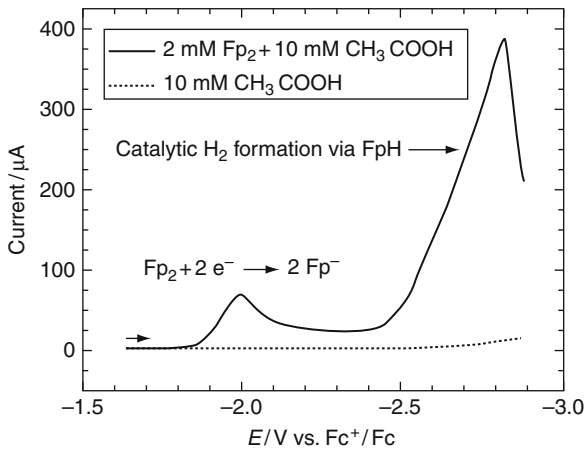

Electrochemical Hydrogen Production. Figure 5 Linear sweep voltammograms for 2 mM Fp2, an organometallic Fe compound, plus 10 mM acetic acid in acetonitrile with 0.10 M tetrabutylammonium hexafluorophosphate (*solid curve*) and 10 mM acetic acid alone (*dashed curve*). Hanging mercury drop electrode (area 0.0096 cm^2). Scan rate: 1.0 V/s (Reproduced with permission from Ref. [56])

that Pt is still the best catalyst of the four catalysts illustrated in Fig. 4, and also significantly better than the hydrogenase mimic in Fig. 5, but the overpotential is rather high compared to the situation in an aqueous solvent. As a practical compromise to comparing overpotentials, it has been suggested to compare half-wave potentials. A detailed discussion on the proper comparison of these half-wave potentials has been given recently by Fourmond et al. [58].

Concluding Remarks

This entry has attempted to address some fundamental issues with studying the electrochemical production of hydrogen under various conditions and with various catalysts. The aim was to provide a common theoretical framework first, and then to show how to build on this framework and to understand the similarities and differences between the different catalytic approaches that have been used to tackle this important problem. It is hoped that this approach may be useful in ultimately developing a cheap, robust, and active catalyst for the electrochemical production of hydrogen. A main future direction for the development of new catalysts for electrochemical hydrogen production could be the combination of heterogeneous and molecular catalysis.

Acknowledgments

I am grateful to the Catalysis Research Center of Hokkaido University, Sapporo, Japan, for the visiting professorship during which this entry was written, and to Prof. Masatoshi Osawa for his kind hospitality. I am grateful to Dr. Vincent Fourmond for a useful discussion on the correct generation of Table 1.

Bibliography

Primary Literature

1. Koper MTM, Heering HA (2010) In: Wieckowski A, Nørskov JK (eds) Fuel cell science: theory, fundamentals, and bio-catalysis. Wiley, New York, p 71
2. Koper MTM, Bouwman E (2010) Angew Chem Int Ed 49:3723
3. Koper MTM (2011) J Electroanal Chem (in press) doi: 10.1016/j.jelechem.2010.10.004
4. Markovic NM, Ross PN Jr (2002) Surf Sci Rep 45:117
5. Otani M, Hamada I, Sugino O, Morikawa Y, Okamoto Y, Ikeshoji T (2008) J Phys Soc Jpn 77:024802
6. Skúlason E, Karlberg GS, Rossmeisl J, Bligaard T, Greeley J, Jonsson H, Nørskov JK (2007) Phys Chem Chem Phys 9:3241
7. Bard AJ, Faulkner LR (2001) Electrochemical methods: fundamentals and applications. Wiley, New York
8. Nørskov JK, Rossmeisl J, Logadottir A, Lundqvist L, Kitchin JR, Bligaard T, Jónsson H (2004) J Phys Chem B 108:17886
9. Koper MTM, van Santen RA (1999) J Electroanal Chem 472:126
10. Hamada I, Morikawa Y (2008) J Phys Chem C 112:10889
11. Rossmeisl J, Nørskov JK, Taylor CD, Janik MJ, Neurock M (2006) J Phys Chem B 110:21833
12. Koper MTM (2008) Faraday Disc 140:11
13. Sabatier P (1911) Ber Deutsch Gem Ges 44:1984
14. Nørskov JK, Bligaard T, Hvolbaek B, Abild-Petersen F, Chorkendorff I, Christensen CH (2008) Chem Soc Rev 37:2163
15. Parsons R (1958) Trans Faraday Soc 34:1053
16. Gerischer H (1958) Bull Soc Chim Belg 67:506
17. Nørskov JK, Bligaard T, Logadottir A, Kitchin JR, Chen JG, Pandelov S, Stimming U (2005) J Electrochem Soc 152:J23
18. Trasatti S (1977) J Electroanal Chem 39:163
19. Petrii OA, Tsirlina GA (1994) Electrochim Acta 39:1739
20. Schmickler W, Trasatti S (2006) J Electrochem Soc 153:L31
21. Hammer B, Nørskov JK (1995) Nature 376:238
22. Hammer B, Nørskov JK (2000) Adv Catal 45:71
23. Santos E, Schmickler W (2007) Angew Chem Int Ed 46:8262
24. Santos E, Schmickler W (2007) Chem Phys 332:39
25. Santos E, Schmickler W (2008) Electrochim Acta 53:6149
26. Santos E, Lundin A, Pötting K, Quaino P, Schmickler W (2009) Phys Rev B 79:235436
27. Santos E, Koper MTM, Schmickler W (2008) Chem Phys 344:195
28. Schmickler W, Quaino P, Santos E (2010) In: Abstract for the 61st ISE meeting, Nice
29. Wilhelm F, Schmickler W, Nazmutdinov RR, Spohr E (2008) J Phys Chem C 112:10814
30. Wilhelm F, Schmickler W, Spohr E, Phys J (2010) Condens Matter 22:175001
31. Santana JA, Mateo JJ, Ishikawa Y (2010) J Phys Chem C 114:4995
32. Skulason E, Tripkovic V, Bjorketun M, Gudmundsdottir S, Karlberg G, Rossmeisl J, Bligaard T, Jonsson H, Norskov JK (2010) J Phys Chem C 114:18182
33. Markovic NM, Grgur BN, Ross PN (1997) J Phys Chem B 101:5405
34. Barber J, Morin S, Conway BE (1998) J Electroanal Chem 446:125
35. Gomez R, Fernandez-Vega A, Feliu JM, Aldaz A (1993) J Phys Chem 97:4769
36. Guerrini E, Trasatti S (2009) Electrocatalysis in water electrolysis. In: Barbaro P, Bianchini C (eds) Catalysis for sustainable energy production. Wiley, Weinheim, p 235
37. Barber JH, Conway BE (1999) J Electroanal Chem 461:80
38. Jerkiewicz G (1998) Prog Surf Sci 57:137
39. Koper MTM, Lukkien JJ (2000) J Electroanal Chem 485:161
40. Garcia-Araez N, Lukkien JJ, Koper MTM, Feliu JM (2006) J Electroanal Chem 588:1
41. Schouten KJP, van der Niet MJTC, Koper MTM (2010) Phys Chem Chem Phys 12:15217
42. Conway BE, Jerkiewicz G (2000) Electrochim Acta 45:4075

43. Kunimatsu K, Senzaki T, Samjeské G, Tsushima M, Osawa M (2007) Electrochim Acta 52:5715
44. Nichols RJ, Bewick A (1988) J Electroanal Chem 243:445
45. Kibler LA, El-Aziz AM, Hoyer R, Kolb DM (2005) Angew Chem Int Ed 44:2080
46. Greeley J, Nørskov JK, Kibler LA, El-Aziz AM, Kolb DM (2006) ChemPhysChem 7:1032
47. Greeley J, Jaramillo T, Bonde J, Chorkendorff I, Nørskov JK (2006) Nat Mater 5:909
48. Artero V, Fontecave M (2005) Coord Chem Rev 249:1518
49. Radkowski Dubois M, Dubois DL (2009) Acc Chem Res 42:1974
50. Dempsey JL, Brunschwig BS, Winkler JR, Gray HB (2009) Acc Chem Res 42:1995
51. Artero V, Fontecave M (2010) Energy Environ Sci 3:727
52. Uchida T, Mogami H, Yamakata A, Sasaki Y, Osawa M (2008) J Am Chem Soc 130:10863
53. Armstrong FA, Belsey NA, Cracknell JA, Goldet G, Parkin A, Reisner E, Vincent KA, Wait AF (2009) Chem Soc Rev 38:36
54. Sbraccia C, Zipoli F, Car R, Cohen MH, Dismukes GC, Selloni A (2008) J Phys Chem B 112:13381
55. Hinneman B, Moses PG, Bonde J, Jørgensen KP, Nielsen JH, Horch S, Chorkendorff I, Nørskov JK (2005) J Am Chem Soc 127:5308
56. Felton GAN, Glass RS, Lichtenberger DL, Evans DH (2006) Inorg Chem 45:9181
57. Fawcett WR (2008) Langmuir 24:9868
58. Fourmond V, Jacques P-A, Fontecave M, Artero V (2010) Inorg Chem 49:10338
59. Daniele S, Ugo P, Mazzochin G-A, Bontempelli G (1985) Anal Chim Acta 173:141
60. Noviandri I, Brown KN, Fleming DS, Gulyas PT, Lay PA, Masters AF, Phillips L (1999) J Phys Chem B 103:6713

Electrochemical Supercapacitors and Hybrid Systems

Katsuhiko Naoi
Institute of Symbiotic Science and Technology, Tokyo University of Agriculture & Technology, Koganei, Tokyo, Japan

Article Outline

Glossary
Definition of the Subject
Introduction
Electrochemical Capacitor and Battery
Operation Voltage of Electrochemical Capacitors
Attempts to Increase Energy Density of Capacitors
Hybrid or Asymmetric Capacitor Systems
Lithium-ion Capacitor (LIC)
Nanohybrid Capacitor (NHC)
Future Perspectives
Bibliography

Glossary

Activated carbon Also called activated charcoal or activated coal is a form of carbon that has been processed to make it extremely porous and thus to have a very large surface area available for EDLC, adsorption, or chemical reactions.

Carbon nanotube Carbon nanotubes (CNTs), not to be confused with carbon fiber, are allotropes of carbon with a cylindrical nanostructure. Nanotubes have been constructed with length-to-diameter ratio of up to 132,000,000:1, significantly larger than any other material. These cylindrical carbon molecules have novel properties, making EDLC performances excellent in power capability.

Electrochemical capacitor (EDLC) An electric double-layer capacitor, also known as supercapacitor, pseudocapacitor, electric double layer capacitor (EDLC), supercapacitor or ultracapacitor is an electrochemical capacitor with relatively high energy density. Compared to conventional capacitors the energy density is typically on the order of thousands of times greater than an electrolytic capacitor. In comparison with conventional batteries or fuel cells, EDLCs have lower energy density but a much higher power density.

Energy density or Specific energy is defined as the energy per unit mass or volume.

Hybrid (asymmetric) capacitor A hybrid capacitor consists of a battery-like (faradic) electrode and a capacitor-like (non-faradic) electrode, producing higher working voltage and capacitance. With these systems, one can certainly achieve twice or triple enhancements in energy density compared to the conventional EDLCs.

Lithium-ion capacitor A Lithium-Ion Capacitor (LIC) is a hybrid type of capacitor. Activated carbon is used as cathode. The anode of the LIC consists of carbon material which is pre-doped with lithium ion. This pre-doping process lowers the potential of the anode and allows a high output voltage and higher energy density.

Nanohybrid capacitor A new lithium-ion–based hybrid capacitor using the lithium titanate ($Li_4Ti_5O_{12}$) negative intercalation electrode that can operate at unusually high current densities. The high-rate $Li_4Ti_5O_{12}$ negative electrode has a unique nano-structure consisting of extremely small nano-crystalline $Li_4Ti_5O_{12}$ nucleated and grafted onto carbon nano-fiber anchors (nc-$Li_4Ti_5O_{12}$/CNF).

Power density Power density (or *volume power density* or *volume specific power*) is the amount of power (time rate of energy transfer) per unit volume.

Definition of the Subject

An electrochemical capacitor or electric double-layer capacitor (EDLC), also known as supercapacitor, pseudocapacitor, electrochemical double layer capacitor, or ultracapacitor is an energy storage device with high power and relatively high energy density. Compared to conventional electrolytic capacitors the energy density is typically 3 orders of magnitude greater. In comparison with conventional batteries or fuel cells, EDLCs show lower energy density but have a much higher power density. EDLCs have a variety of commercial applications, notably in energy-smoothing and momentary-load devices. They have applications as energy-storage devices used in vehicles, and applications like wind power solar energy systems where extremely fast charging required.

Historical Background

GE, General Electric engineers experimenting with devices using porous carbon electrodes first observed the EDLC effect in 1957. In 1966, SOHIO Standard Oil of Ohio developed the modern version of the devices, utilizing two layers of activated charcoal separated by a thin porous insulator. This basic cell design remains the basis of EDLCs. SOHIO failed to commercialize their device, licensing the technology to NEC, who finally marketed "supercapacitors" in 1978, as back-up of a computer memory. Around the mid-1990s various advances in materials science and refinement of the existing systems led to rapidly improving performance and an equally rapid reduction in cost. The first industrial applications were carried out for supporting the energy supply to robots.

In 2005, aerospace company, Diehl Luftfahrt Elektronik GmbH adopted EDLCs to power emergency actuation systems for doors and evacuation slides in airliners, including the new Airbus 380 jumbo jet. As of 2007 all solid state micrometer-scale electric double-layer capacitors based on advanced superionic conductors had been developed for low-voltage electronics.

Introduction

Environmental destruction are getting more and more serious in the global scale. It is urgent for human beings to cope with environmental and energy problems. The national development of each country greatly depends on economic activities oriented to environmental improvement business. Inevitably, in the future, it will be necessary to build an economic society taking into consideration the global ecology, that is, a society in which economic development is closely and directly related with eco-friendly activities such as carbon-reducing and energy-saving movements. Energy storage devices such as batteries and electrochemical capacitors hold an important key to solve the problems. The energy storage devices are some of the best fruits of our environmental technologies, and they have large potential for promoting our international contribution. Specifically, electrochemical capacitors are green devices having such excellent characteristics that they have long lifetimes and can be rapidly charged and discharged [7, 28, 31]. In particular, when combined with renewable energy plants (wind power, wave power and solar cell), they remarkably show their advantage and effectiveness [6]. In view of that, the electrochemical capacitors have been vigorously researched and developed in these days, and are expected to improve their energy densities. Thus, the technology is regarded as a promising art for storing electricity, and hence is expanding its possibilities.

Electrochemical Capacitor and Battery

Batteries store and deliver energy on the basis of chemical reactions, and hence their capacities depend on the redox reactions. In contrast, the energy storage or the charging–discharging mechanism by electrochemical capacitors are based on physical adsorption/desorption

behaviors of ions at the interface of electrode/electrolyte, namely, electric double-layer [3, 6, 7, 28, 31]. Accordingly, the electrochemical capacitors are often called "electric double-layer capacitor (EDLC)," and more recently they are called "Supercapacitor" or "Ultracapacitor" as they increase their performances like six characteristics described below:

1. High power densities capable of instantly charging and discharging.
2. Long lifetimes capable of more than 100,000 charge–discharge cycles. Free from maintenance capable of using for a long time until abandoned.
3. Excellent safety and reliability issues. Low heat generation during operation. Recoverable even after short-circuiting.
4. Wide operational temperature ranges. More than 10°C lower and 20°C higher temperature limits as compared with any battery systems.
5. No fear of material shortage. Activated carbon materials can be obtained from any organic substance.
6. Free of heavy metals and halogens and Low environmental load.

As described above, the electrochemical capacitors have various advantages such as high power, high charge–discharge cycleabilities, high safety, and favorable working temperature ranges. The above characteristics are remarkably contrastive with those of lithium ion batteries as shown in Fig. 1. The other cannot replace one of these devices. The contrasting two types of energy devices as represented by lithium ion batteries and electrochemical capacitors can be compared to two different energy-providing systems in a human body, i.e., aerobic reaction system and anaerobic reaction system. It is very interesting to see a human body from the viewpoint of its energy system. In a human body, ATP (adenosine triphosphate) efficiently takes charge of energy production and supply. The ATP is mainly produced by way of two routes (i.e., aerobic reactions and anaerobic reactions). The aerobic reactions, which proceed with oxygen obtained by breathing, slowly produce no less than 38 ATP molecules (from one glucose molecule), to provide large energy. On the other hand, the anaerobic reactions can rapidly produce two ATP molecules, to provide small but instant energy according to necessity. The combination of these systems realizes such smooth energy supply as can correspond to any movement of human body. In the same way, the combinations of lithium ion batteries and capacitors give very high synergy effects. Consequently, energy management can be conducted under any situation by use of the two contrasting energy devices in exquisite combination.

In many uses, lithium ion batteries and capacitors play complementary roles. Since the synergy effects obtained by their combinations are very high, practical

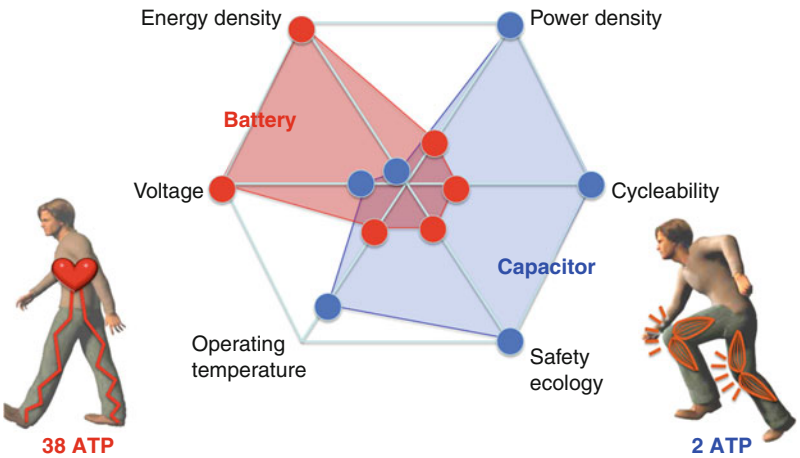

Electrochemical Supercapacitors and Hybrid Systems. Figure 1
Beautiful contrast of battery and capacitor

examples thereof are increasing in various fields. Further, the capacitors may be combined with devices other than the lithium ion batteries, for example, with fuel batteries or motor/inverters. At present, researchers pay their attention to smart systems employing the combinations of the capacitors and those devices. In consideration of necessity for effective and eco-friendly energy measures, it will be one of the large strategic aims to develop the composite energy storage systems.

Operation Voltage of Electrochemical Capacitors

However, since the EDLCs generally have low energy densities, their uses are limited and they cannot fully meet various performance demands required by the recent markets as shown in Fig. 2. Particularly in the field of automobiles, new energy devices are strongly desired to have hybrid characteristics between lithium ion batteries and EDLCs and thereby which can be suitably employed in idle reduction systems. Accordingly, it is expected for them to form a large market [28]. In order to satisfy the performance demands, it is often said to be necessary for the EDLCs to enhance their energy density to 20–30 Wh L^{-1}, which is approximately twice or more than present EDLCs, namely, 5–10 Wh L^{-1}. For realizing the above high energy density, hybrid capacitor systems comprising non-aqueous redox materials are being dynamically researched and developed in recent years [5, 6, 10, 16, 23, 31]. The present chapter deals with the recent contributions to get this high energy density by focusing on two major hybridized cell configurations in organic media.

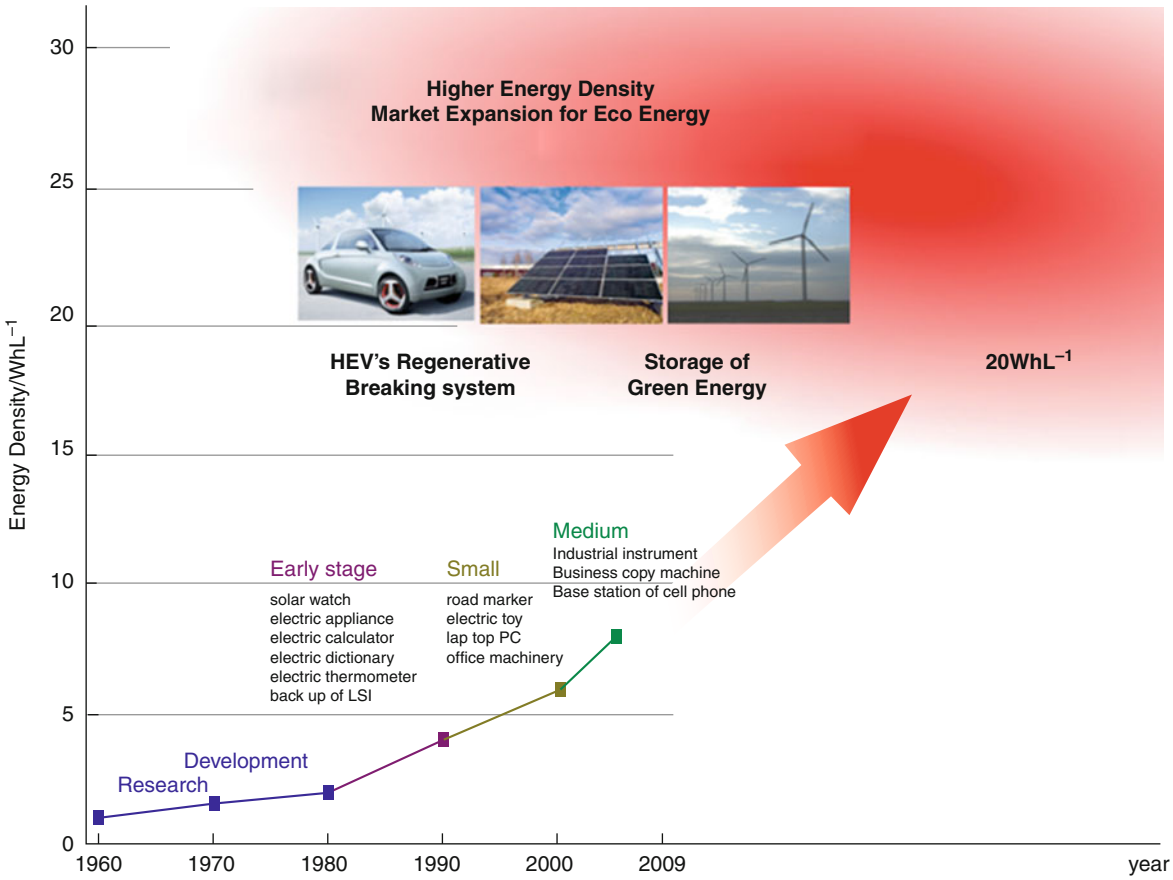

Electrochemical Supercapacitors and Hybrid Systems. Figure 2
Target value of the next-generation electrochemical capacitor

As is described above, increasing energy density is one of the most crucial matters. For conventional EDLC systems, designed with two symmetrical activated carbon electrodes, increasing voltage is more effective because the energy density increases in proportion to the squared voltage. Thus, it is essential to develop higher electrochemical durability at the electrode/electrolyte interface. Currently, the maximum voltage of an activated carbon-based EDLC (AC/AC) is limited to 2.5–2.7 V in Propylene carbonate (PC) and Acetonitrile (AN) electrolytes. At applied voltage over 2.7 V, there occurs a significant decrease in capacitance and an increase in internal resistance. In fact the float test revealed that the AC/AC capacitor lose its capacitance ($\Delta C < -13\%$ after 30 days) at 2.5 V, whereas at 2.9 V the capacitance loss became more significant ($\Delta C = -28\%$) for the same duration. The threshold cell voltages between 2.5 and 2.9 V certainly triggers a consecutive and fatal degradation. The undesired faradic process (failure modes) that leads to a capacitance fade is the most critical factor that determines the life of conventional EDLCs and needs to be further investigated as in the recent review article by Simon et al. [28]. Anyway this withstanding-voltage limitation (2.5–2.7 V) certainly exists because of a gas evolution at higher voltages and is a barrier for further enhancement of the energy density of the conventional activated-carbon–based EDLCs.

Attempts to Increase Energy Density of Capacitors

There is presently a major effort to increase the energy density of EDLCs up to a target value in the vicinity of 20–30 Wh kg^{-1} [7]. Many studies have been undertaken in order to enhance the energy density (E) of EDLC. There are mainly three approaches (Fig. 3): the first is to change the electrode (by higher-capacitance carbons or redox) and the second is to change electrolyte (by durable new electrolyte or ionic liquids).

① High working voltage(V)
② High double layer capacitance(C)

$$E = 1/2\,(CV^2)$$

(c : Capacitance (F), v : Working voltage(V))

Hybrid or Asymmetric Capacitor Systems

The third and the most important approach to meet the goal that is under serious investigation is to develop asymmetric (hybrid) capacitors. As shown in Fig. 3 various hybrid capacitor systems are possible by coupling redox-active materials (e.g., graphite [10, 31], metal oxides [5, 14], conducting polymers [17, 18]), and an activated carbon (AC). There are suggested two different systems, one is aqueous and the other is non-aqueous. Some of them are listed below in Fig. 4. These approaches can overcome the energy density limitation of the conventional EDLCs because it employs a hybrid system of a battery-like (faradic) electrode and a capacitor-like (non-faradic) electrode, producing higher working voltage and capacitance. With these systems, one can certainly achieve twice or triple enhancements in energy density compared to the conventional EDLCs.

FDK corporation proposes a "Dual Carbon Cell," which is a device behaving "like a capacitor" on the basis of faradic reactions on the electrodes. When the Dual Carbon Cell is charged, anions and cations (such as lithium ions) are intercalated into the positive graphite electrode and into the negative graphite electrode, respectively. As a result, an acceptor type graphite intercalation compound is formed on the positive electrode while a donor type one is formed on the negative electrode. Thus, the Dual Carbon Cell is charged or discharged like a capacitor is. It is reported that, if the positive electrode is made of graphite doped with boron, the Dual Carbon Cell can have improved load characteristics.

Meanwhile, many other hybrid capacitors are also proposed each of which utilizes a charge transfer reaction (faradic reaction) on either positive or negative electrode whereby one could have a good scenario attaining higher voltage and higher energy density. Figure 5 represents the voltage profiles of the conventional EDLC system (upper), Nanogate (middle), and LIC (lower). Examples of them include a "nanogate" capacitor or a "nanostorage" capacitor (Fig. 5, middle), in either of which the negative electrode is an activated carbon but the positive electrode is an amorphous carbon capable of undergoing an anion-intercalation

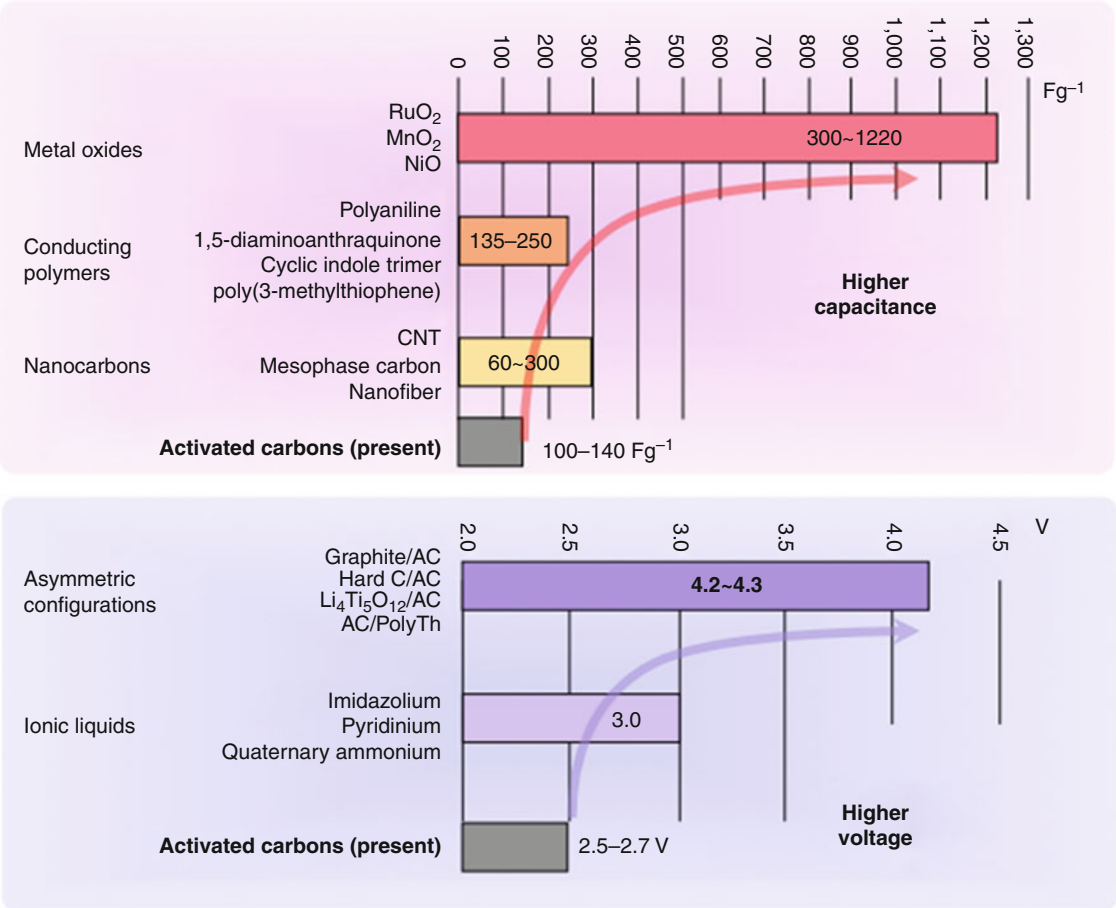

Electrochemical Supercapacitors and Hybrid Systems. Figure 3
Energy density enhancement of electrochemical capacitors

Aqueous hybrid capacitor	Non-aqueous hybrid capacitor	
Carbon/redox	**Carbon/Carbon**	**Carbon/redox**
$AC/LiMn_2O_4$ AC/PbO_2 AC/NiO	Graphite/Graphite Graphite/AC Graphite(Li^+)/AC AC/Graphite	$Li_4Ti_5O_{12}$/AC $Li_4Ti_5O_{12}$/AC+$LiCoO_2$ AC/pMeTh $Li_4Ti_5O_{12}$/pFPhTh

Electrochemical Supercapacitors and Hybrid Systems. Figure 4
Aqueous and non-aqueous hybrid capacitor systems

reaction at a high potential (not lower than 4.5 V vs. Li/Li^+), while a normal capacitor comprises both positive and negative electrodes made of activated carbon (Fig. 5, upper).

Lithium-Ion Capacitor (LIC)

Among high-energy hybrid capacitors comprising non-aqueous redox materials, a hybrid system called "lithium-ion capacitor (abbreviated as LIC)" has particularly attracted the attention in these days [10, 31]. The LIC is a hybrid capacitor in which the positive and negative electrodes are made of activated

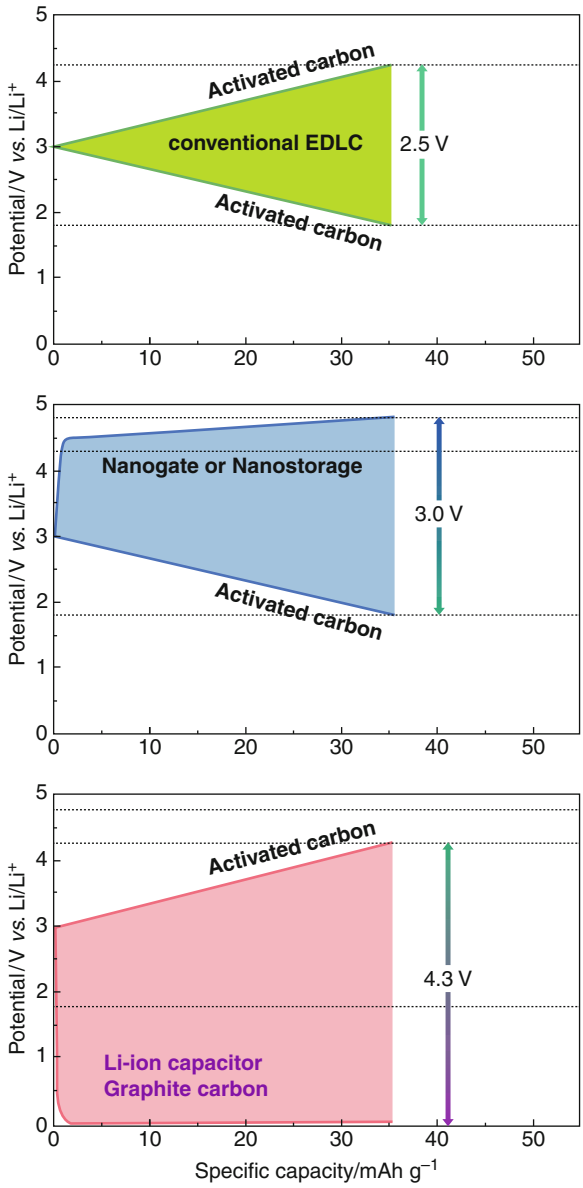

Electrochemical Supercapacitors and Hybrid Systems. Figure 5
Voltage profiles of a conventional EDLC, Nanogate, and LIC systems

carbon and of graphite pre-doped with lithium ions, respectively (Fig. 6).

Since the negative electrode of graphite undergoes the reaction at a potential a little over 0 V vs. Li/Li^+, the LIC has a high working voltage of 3.8 V to 4.0 V. This high working voltage enables the lithium-ion capacitor to realize both a high power density of approximately 5 kW kg^{-1} and an energy density of approximately 20–30 Wh kg^{-1}. The LIC thus exhibits favorable performance, and is regarded as a candidate of the next generation electrochemical capacitor. Hence, some Japanese companies including JM energy, FDK, ACT, etc. have already started commercializing LIC [10].

Generally speaking, instead of achieving energy density improvement, the high working voltage causes an electrolyte decomposition problem especially at negative graphite electrode [21] (Fig. 7). The limited charging rate and the low temperature performance are the possible drawbacks of the LIC because it has a lithium-intercalation negative electrode. The process of pre-lithiation of the graphite electrode may lead to poor cost-effectiveness or instability in the quality of the LIC device when they are mass-produced (see Fig. 8). This "pre-doing of Li^+" may bring about the same risks relevant to a long-term stability to keep low ESR. This is an issue that is specifically important for an electrochemical capacitor as a "power device" because it lead to create a high impedance electrode/electrolyte interface and thus eventually leads to a deteriorated power performance for longer cycles.

Nanohybrid Capacitor (NHC)

Very recently, Naoi's group and Nippon Chemi-con developed a hybrid capacitor system that certainly achieves a high energy density, high stability, and high safety. This is called "Nanohybrid Capacitor" (abbreviated as NHC) using a super-high-rate nano-structured lithium titanate ($Li_4Ti_5O_{12}$)/carbon composite negative electrode. They have kept their eyes on lithium titanate ($Li_4Ti_5O_{12}$) as a stable and safe redox material capable of increasing the energy densities of hybrid capacitors without sacrificing interfacial characteristics. The $Li_4Ti_5O_{12}$ operates at a potential (1.55 V *vs* Li/Li^+) out of the range where the electrolyte solution may be decomposed, and hence play key roles for providing capacitor systems as stable and safe as EDLCs (see Fig. 9). The $Li_4Ti_5O_{12}$ as a redox material for hybrid capacitors has the following essential advantages in energy density, in stability, and in safety:

1. It exhibits a high coulombic efficiency close to 100% during charge–discharge cycle

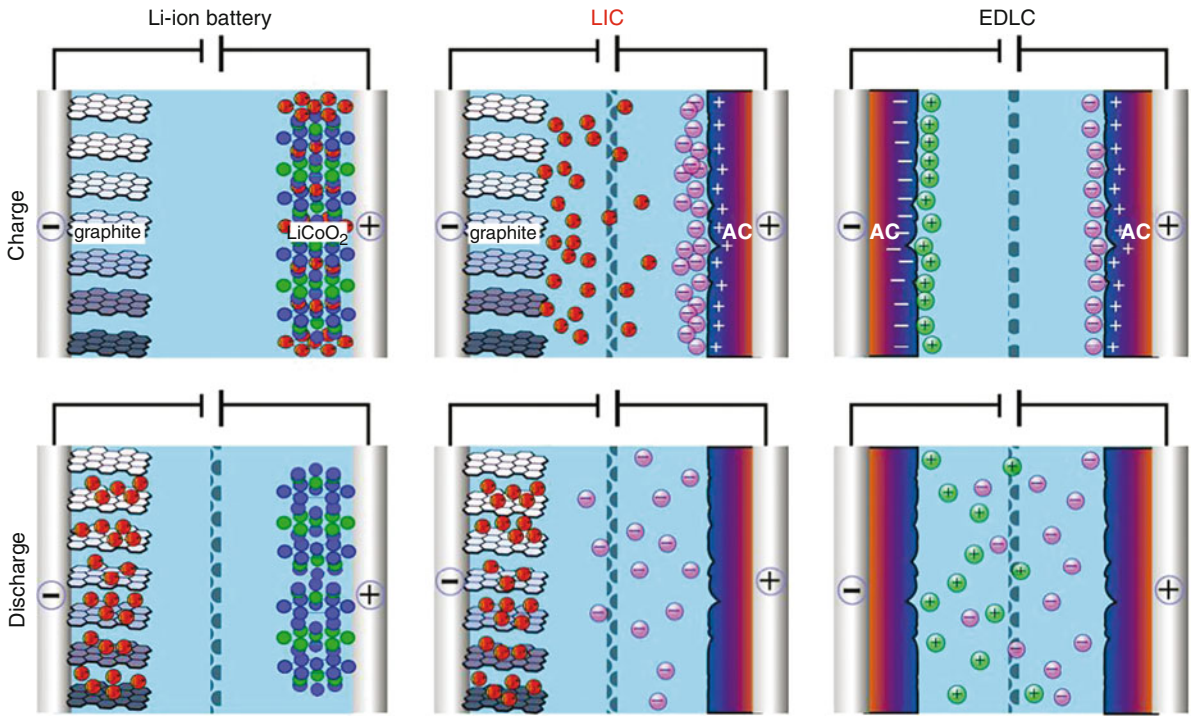

Electrochemical Supercapacitors and Hybrid Systems. Figure 6
Cell configurations of Li-ion Battery (LIB), EDLC, and LIC

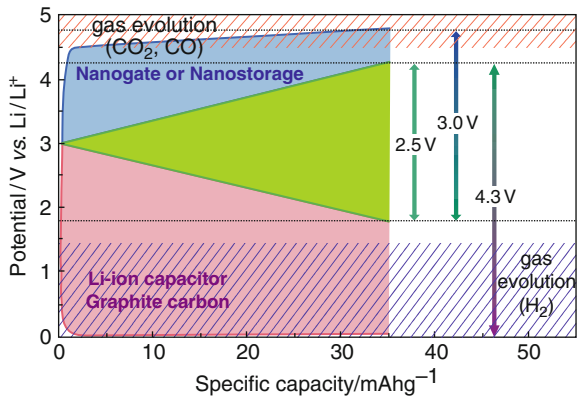

Electrochemical Supercapacitors and Hybrid Systems. Figure 7
Reliability and electrolyte decomposition at positive and negative electrodes of LIC systems

2. It has a theoretical capacity (175 mAh g^{-1}) four times higher than as activated carbon
3. It undergoes charging and discharging at a constant potential of 1.55 V vs. Li/Li^+, where the electrolyte solution is free from the fear of decomposition (no SEI formation and no gas evolution) [20, 27]
4. As shown in Fig. 10, it changes the volume to a very small degree (0.2%) in charging or discharging in intercalating or deintercalating Li^+ ions (zero-strain insertion)
5. Inexpensive raw material

As summarized in Table 1, a capacitor cell comprising $Li_4Ti_5O_{12}$ is, therefore, expected to be free from necessity for pre-doping of lithium ions (because of the above advantage (1)), to be capable of having a high energy density (because of the advantage (2)), and to be excellent in stability and in safety (because of the advantages (3) and (4)).

Amatucci et al. firstly introduced the $Li_4Ti_5O_{12}$/AC system as safer hybrid systems [1, 2]. However, the conventional $Li_4Ti_5O_{12}$ has the greatest problem of low power characteristics that stem from inherent poor Li^+ diffusion coefficient ($<10^{-6}$ cm^2 s^{-1}) [29] and poor electronic conductivity ($<10^{-13}$ Ω^{-1} cm^{-1}) [8].

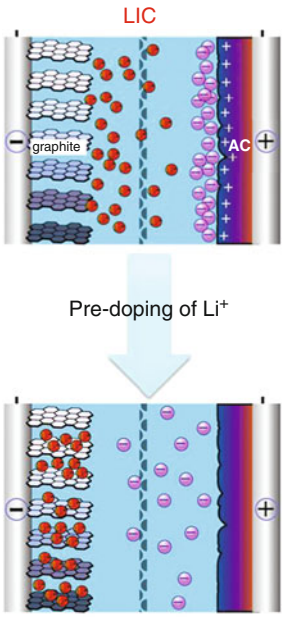

Electrochemical Supercapacitors and Hybrid Systems. Figure 8
Necessary pre-doing of Li^+ for LIC systems

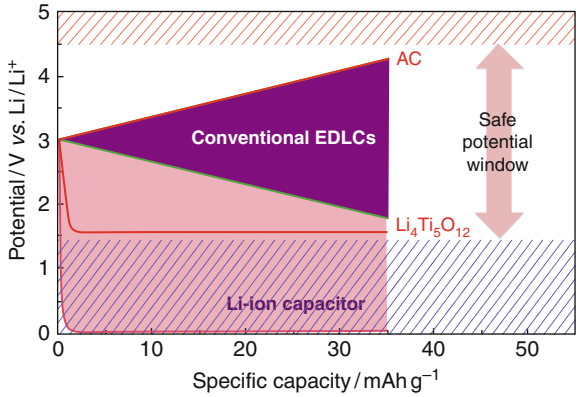

Electrochemical Supercapacitors and Hybrid Systems. Figure 9
Voltage profile of conventional EDLC, LIC, and NHC

Accordingly $Li_4Ti_5O_{12}$ had a big problem of slow output characteristics and was not fully developed for the application in electrochemical capacitors at that time. For the purpose of solving the problem of poor output performance, some measures can be thought of. For example, the $Li_4Ti_5O_{12}$ may be ground down to nano-sized particles and may be combined with an electro-conductive material to prepare a composite.

In the nano-sized $Li_4Ti_5O_{12}$ particles, it is expected that Li^+ ions diffuse and electrons migrate in distances reduced by 1/1,000 (see Figs. 11 and 12) or less as compared with the distances in normal micron-order $Li_4Ti_5O_{12}$ particles. Further, in the composite, electron paths are effectively formed in the electrode of nano-sized $Li_4Ti_5O_{12}$ particles (Fig. 13). On the basis of these expectations, a composite (nc-$Li_4Ti_5O_{12}$/CNF) has been synthesized by means of a new method referred to as "Ultracentrifugal force (UC) nanohybridization method" [19, 24]. Specifically, the composite (nc-$Li_4Ti_5O_{12}$/CNF) comprises nano-crystalline $Li_4Ti_5O_{12}$ particles hyper-dispersed on carbon nanofibers (CNFs) [13] having high electro-conductivity (25 $\Omega^{-1}\cdot cm^{-1}$). They utilized the composite as the negative electrode active material, and thereby succeeded in producing a novel hybrid capacitor (nanohybrid capacitor) realizing both high power and high energy density.

The nc-$Li_4Ti_5O_{12}$ negative electrode was developed to have a unique nano-structure that can operate at unusually high current densities. Nano-crystalline $Li_4Ti_5O_{12}$ attached onto carbon nano-fibers were prepared by a unique technique (UC method) of a mechano-chemical sol–gel reaction under ultracentrifugal force field [13, 19, 24], followed by an instantaneous heat treatment for very short duration (see Fig. 14a). The UC method is induced to form, anchor, and graft the nano-Li-Ti-O precursors on the CNF matrices. The subsequent instantaneous heat treatment is of prime importance to precisely achieve all of the following: high crystallization of $Li_4Ti_5O_{12}$, [13] inhibition of the CNF oxidation decomposition during the annealing at high temperature, [31] and suppression of the agglomeration of the $Li_4Ti_5O_{12}$ particles. These processes are quite simple and require only a few minutes. Actually, the power characteristic of the prepared composite (nc-$Li_4Ti_5O_{12}$/CNF) made a new bench mark (charge-discharge time = 12 s)

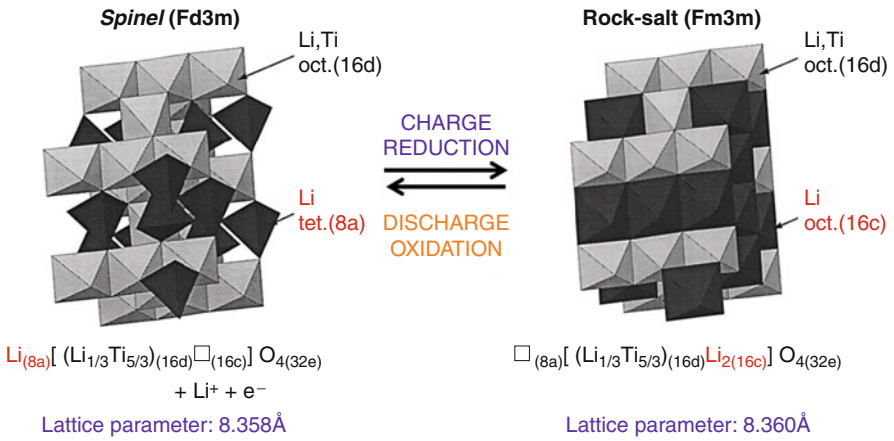

Electrochemical Supercapacitors and Hybrid Systems. Figure 10
Structural and volumetric changes at the charged and discharged states of $Li_4Ti_5O_{12}$

Electrochemical Supercapacitors and Hybrid Systems. Table 1 Comparison of LIC and NHC in their cell configurations

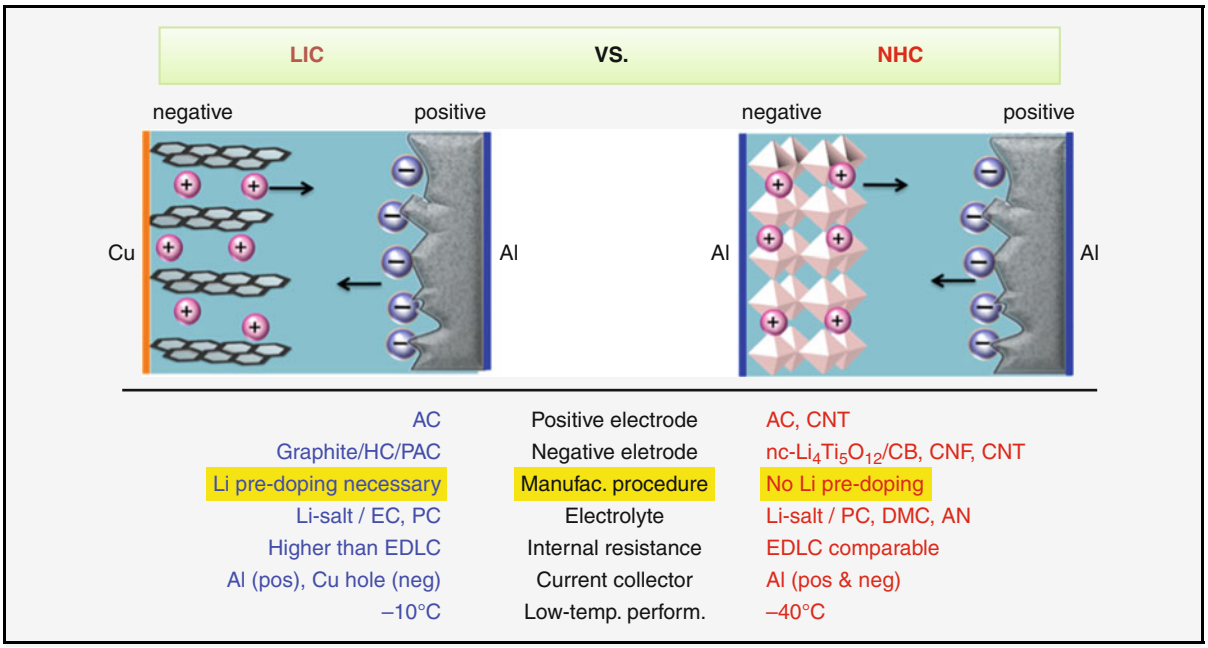

[4, 11, 12, 15, 24, 32] which exceeds greatly the shortest charge–discharge time that has ever been attained (see Fig. 14b).

XRD analysis was performed to confirm the formation of the nc-$Li_4Ti_5O_{12}$ and the presence of the CNF in the nc-$Li_4Ti_5O_{12}$/CNF composites. Figure 15a shows the XRD patterns of the prepared nc-$Li_4Ti_5O_{12}$/CNF composite and pristine CNF. The composite has several sharp diffraction peaks at $2\theta = 18$, 35, 42, 57, and 63°. These peaks correspond to (111), (311), (400), (511),

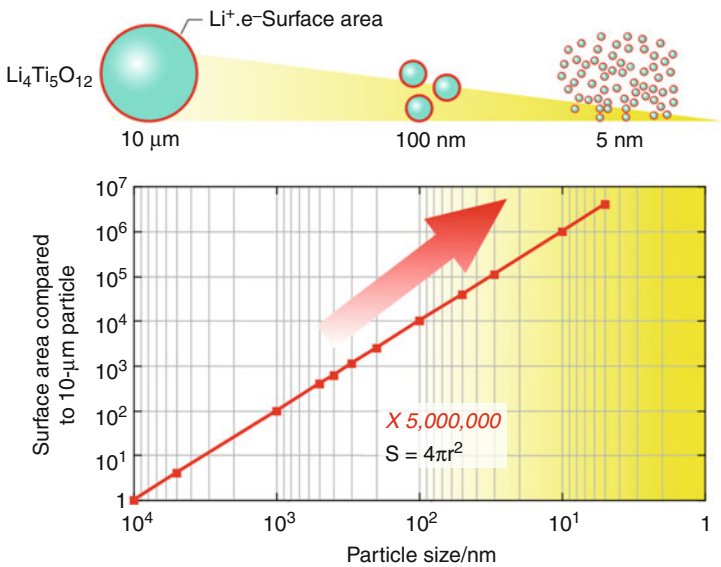

Electrochemical Supercapacitors and Hybrid Systems. Figure 11
Increased accessibility and surface area as a function of the particle size of $Li_4Ti_5O_{12}$

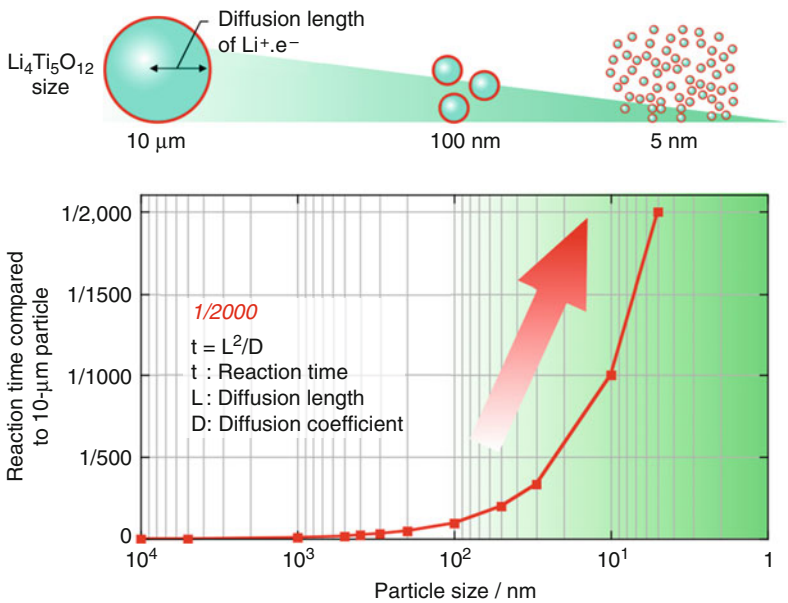

Electrochemical Supercapacitors and Hybrid Systems. Figure 12
Decreased diffusion length as a function of the particle size of $Li_4Ti_5O_{12}$

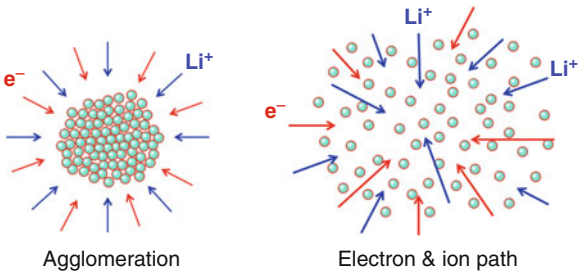

Electrochemical Supercapacitors and Hybrid Systems. Figure 13
Hyper-dispersion of the nano-size particles of $Li_4Ti_5O_{12}$

and (440) planes of a face-centered cubic spinel structure with $Fd\bar{3}m$ space group [22, 30], respectively, indicative of the formation of crystalline $Li_4Ti_5O_{12}$. Annealing at 900°C under vacuum well crystallizes the nano-particles of $Li_4Ti_5O_{12}$. A broad peak at around $2\theta = 24.5^{o}$ is observed which corresponds to the (002) plane of the pristine CNF [33]. This means that the CNF exists in the annealed composite and preserves its graphene layer structure. The fact that there are no other peaks observed corresponding to some possible impurities such as TiO_2, Li_2CO_3, and Li_2TiO_3 [9, 26] suggests that there are only two species, crystalline $Li_4Ti_5O_{12}$ and CNF.

Thermogravimetric (TG) measurement of the nc-$Li_4Ti_5O_{12}$/CNF composite was performed under air to estimate the residual weight ratio of the CNF. The obtained TG curve is shown in Fig. 15b. The weight loss at 400–600°C resulted by the oxidative decomposition of the CNF, and exactly 50 wt.% of the -nc-$Li_4Ti_5O_{12}$ remained. The 50 wt.% is well consistent with the weight ratio of the $Li_4Ti_5O_{12}$ to the CNF calculated on the basis of dosed Ti alkoxide weight before UC method. This fact implies that sol–gel reaction in the UC method stochiometrically proceeds, and the optimized (very short duration) annealing does not cause oxidative decomposition of the CNF. Such a stoichiometric preparation process (UC method and instantaneous annealing) is one of the important factors for cost-effectiveness of capacitor production.

The nano-structures and crystallinity of nc-$Li_4Ti_5O_{12}$ and CNF in the composite is observed by HR-TEM (see Fig. 16). The image indicates that the edge or defect sites of CNF graphenes accommodate and graft nc-$Li_4Ti_5O_{12}$ particles. The results support that the $Li_4Ti_5O_{12}$ particles are formed through a nucleation process onto the edge and defect CNF sites. The clear facet of $Li_4Ti_5O_{12}$ reflects the high crystallinity that is consistent with the sharp XRD spectrum (see Fig. 16a), despite such a nanosize. Such a high crystallinity resulted in a reversible, smooth Li^+ insertion performance, and ca. 100% of coulombic efficiency. Also, HR-TEM images of CNF show clear graphene layers indicative of crystalline structure. Thus, this composite is considered to be the junction material of two crystalline species, $Li_4Ti_5O_{12}$ and CNF. Of particular interest is that the lattice matching of the nc-$Li_4Ti_5O_{12}$ particles, and CNFs are perfect and they are firmly tied at the atomic level. This could bring about an establishment of good electronic paths between the two species (Fig. 16b).

Another closer view of an HR-TEM (see Figure 17) indicates the multiple attachments of the nc-$Li_4Ti_5O_{12}$ particles on the inside wall of the CNF graphene substrate as well as outside wall of the CNF matrices. This may indicate that the crystallization would be such efficient on CNF and more importantly one can enhance both the energy density and the specific gravity of the nc-$Li_4Ti_5O_{12}$.

Figure 18a shows the charge–discharge curve of the half-cell Li/(nc-$Li_4Ti_5O_{12}$/CNF) at 1 C. The horizontal axis represents specific capacity per unit weight of $Li_4Ti_5O_{12}$. The dominant plateau was observed at *ca.* 1.5 V versus Li/Li^+ that corresponds to the Li^+ intercalation–deintercalation process of the crystalline $Li_4Ti_5O_{12}$ [13, 24, 30], indicating that the capacity of the composite is determined by the redox capacity of nc-$Li_4Ti_5O_{12}$ in the composite. The obtained capacity was 167 mAh g^{-1} per $Li_4Ti_5O_{12}$, which is 95% of the theoretical capacity. It is noted here that the value of 167 mAh g^{-1} is obtained after subtracting the double-layer capacity of the CNF (8 mAh g^{-1}). This result indicates that almost all of the nc-$Li_4Ti_5O_{12}$

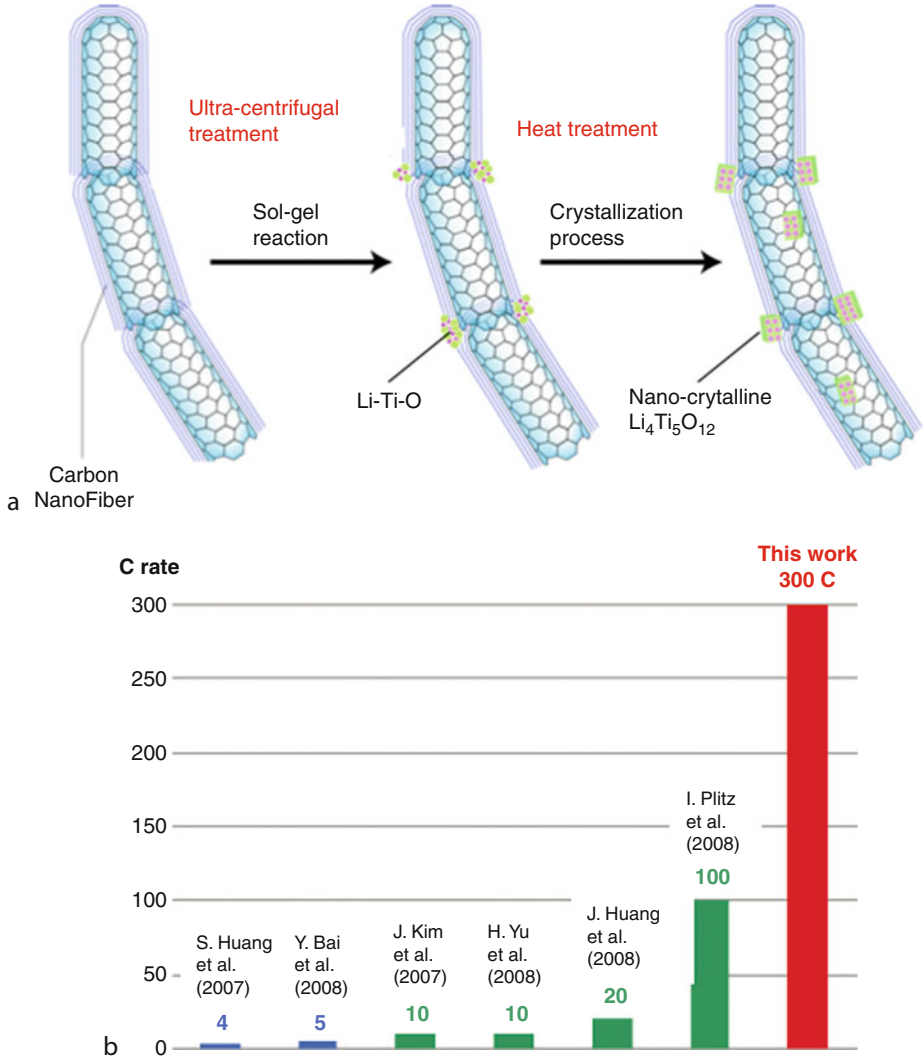

Electrochemical Supercapacitors and Hybrid Systems. Figure 14
Nano-structure model and high power performance of super-high-rate nano-crystalline $Li_4Ti_5O_{12}$ nested and grafted onto carbon nanofiber. (**a**) Schematic illustration for the two-step formation procedure of the nc-$Li_4Ti_5O_{12}$/CNF composite. (**b**) Maximum C rate values of the nc-$Li_4Ti_5O_{12}$/CNF composite and various $Li_4Ti_5O_{12}$ materials in literatures reported so far

particles in the composite are electrochemically active, meaning that ionic and electric paths are fully established in the composite. The rate capability of the obtained composite is shown in Fig. 18b.

Even at a high rate of 300 C, the composite shows reversible capacity of 158 mAh g^{-1} per $Li_4Ti_5O_{12}$ which correspond to 95% of the capacity obtained at 1 C. Such an excellent rate-capability indicates that the optimized nano-structure of the nc-$Li_4Ti_5O_{12}$/CNF composites as observed in HR-TEM image well overcome the inherent problems of $Li_4Ti_5O_{12}$ materials like poor Li^+ diffusivity and poor electronic conductivity. Probably,

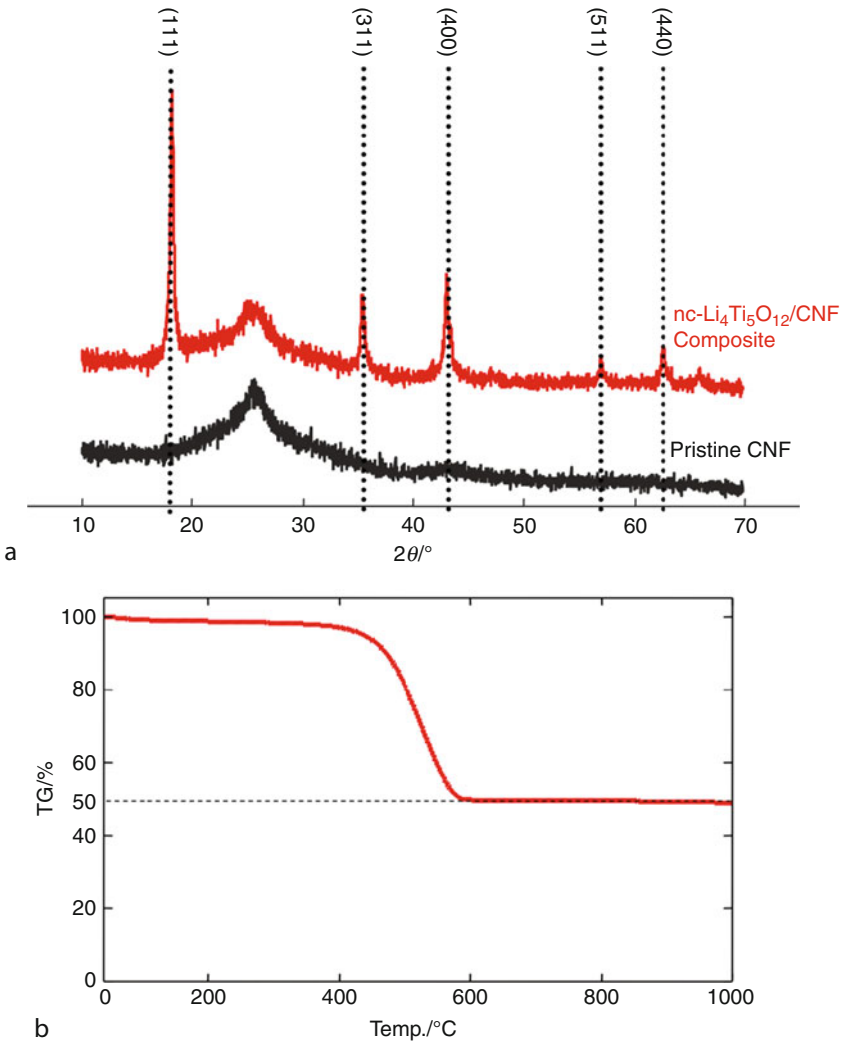

Electrochemical Supercapacitors and Hybrid Systems. Figure 15
Crystallinity and content of nc-$Li_4Ti_5O_{12}$ in the composite. (**a**) XRD patterns of the nc-$Li_4Ti_5O_{12}$/CNF composite and pristine CNF. (**b**) TG curve of the nc-$Li_4Ti_5O_{12}$/CNF composite at 1°C min^{-1} under air. The residual weight ratio corresponds to the content of nc-$Li_4Ti_5O_{12}$ in the composite

this is because the nano-crystallized $Li_4Ti_5O_{12}$ and $Li_4Ti_5O_{12}$/CNF junctions lead to facile ionic diffusion and electronic conduction, respectively. The cycleability of the composite is shown in Fig. 18c. Even after 9,000 cycles, 90% of the initial capacity is maintained, showing that the composite is electrochemically stable. The result strongly suggests that the aggregation and detachment of the nc-$Li_4Ti_5O_{12}$ particles hardly happen when they are operated at high-rate charge–discharge for a prolonged cycling.

Figure 19 shows Ragone plots obtained from charge–discharge measurements as laminate-type cell of the hybrid capacitor system ((nc-$Li_4Ti_5O_{12}$/CNF)/$LiBF_4$-PC/AC). The charge–discharge was performed

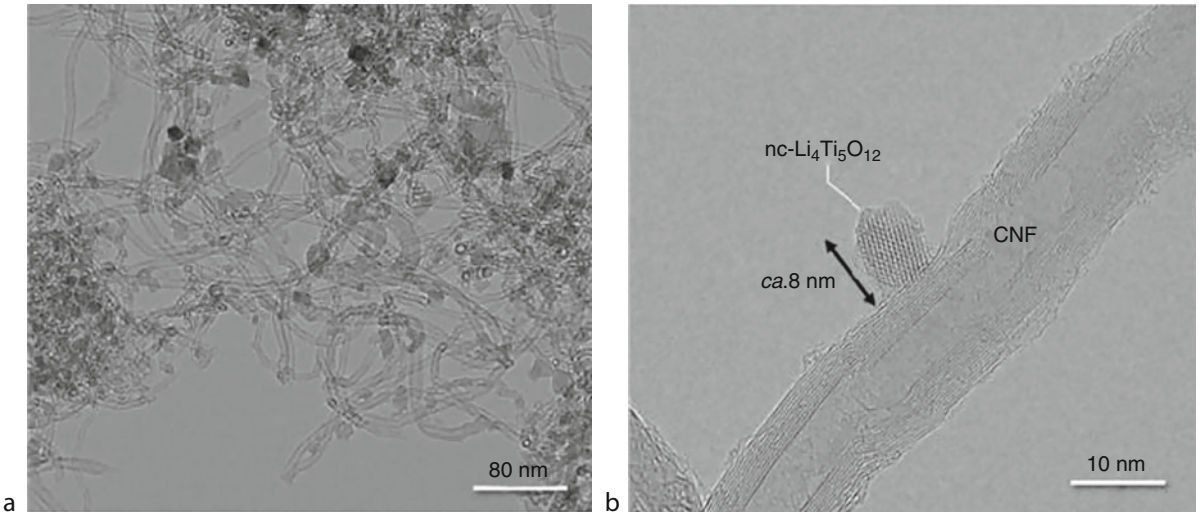

Electrochemical Supercapacitors and Hybrid Systems. Figure 16
Nano-structure of the nc-$Li_4Ti_5O_{12}$ and CNF. (**a**) A bird's eye view of a HR-TEM image of the nc-$Li_4Ti_5O_{12}$/CNF composite and (**b**) a worm's eye view focusing on the junction of the nc-$Li_4Ti_5O_{12}$ particle on CNF graphene surface

Electrochemical Supercapacitors and Hybrid Systems. Figure 17
Closer view of a HR-TEM image of multiple attachments of nc-$Li_4Ti_5O_{12}$ inside and outside wall of the CNF composite

between 1.5 and 3.0 V at various current densities ranging 0.2–30 mA cm^{-2} (0.18–26.8 A g^{-1}). For comparison, a conventional EDLC system (AC/$TEABF_4$-PC/AC) was also assembled and measured between 0 and 2.5 V. In a low power density range of 0.1–1 kW L^{-1}, the hybrid capacitor shows the energy density as high as 28–30 Wh L^{-1}, which is a value comparable to that of the Li-ion capacitors [31]. Even at a high power of 6 kW L^{-1}, the energy density of the hybrid capacitor remains at 15 Wh L^{-1} which is double that of the conventional EDLC system (AC/AC). The result reveals that the capacitor system can provide higher energy as compared with conventional EDLCs not only in the low power density region (0.1–1 kW L^{-1}) but also in the high power density region (1–6 kW L^{-1}). Accordingly, this configuration of capacitor system is anticipated as an energy device utilizable for both high energy and high power applications.

Future Perspectives

Hybrid capacitor systems are the promising approach to meet the goal to effectively increase the energy

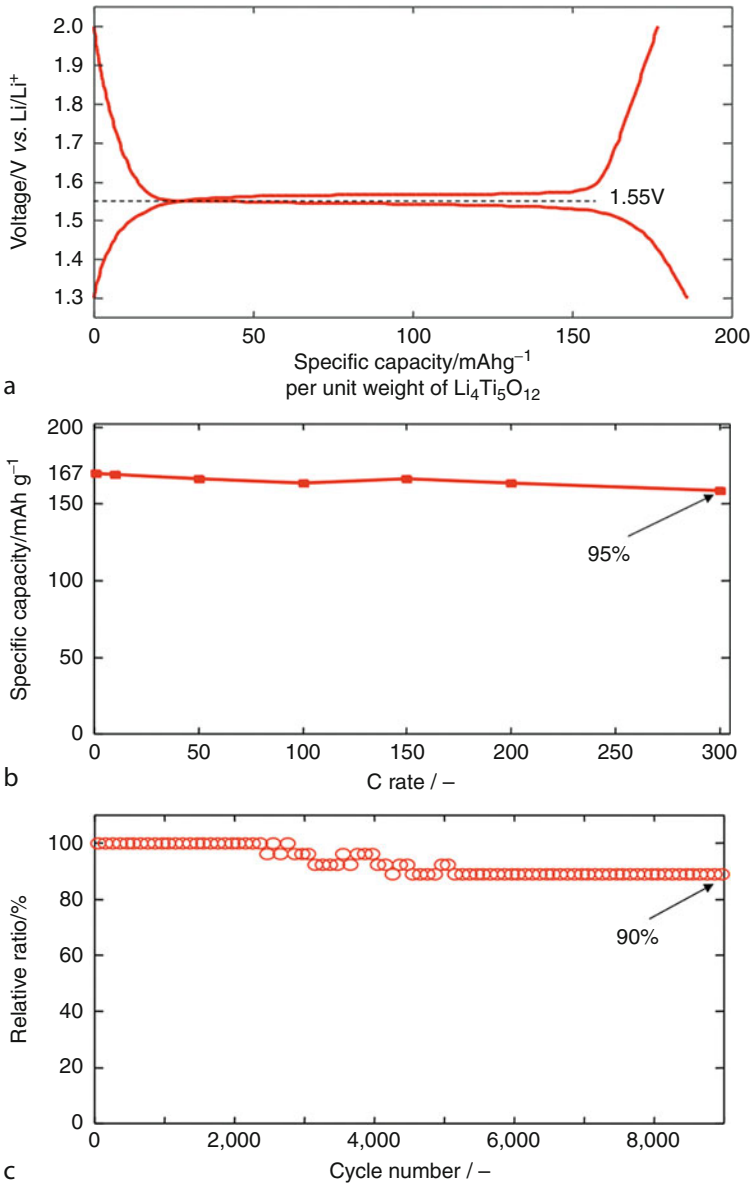

Electrochemical Supercapacitors and Hybrid Systems. Figure 18
Electrochemical properties of the nc-$Li_4Ti_5O_{12}$/CNF composite. (**a**) Charge–discharge curve of nc-$Li_4Ti_5O_{12}$/CNF composite between 1.0 and 3.0 V versus Li/Li^+ at 1 C. (**b**) Rate capability of the nc-$Li_4Ti_5O_{12}$/CNF composite in a C-rate ranges from 1 C to 300 C. (**c**) Cycleability of nc-$Li_4Ti_5O_{12}$/CNF composite between 1.0 and 3.0 V versus Li/Li^+ at 20 C. 1 M $LiBF_4$/EC + DEC(1:1) was used as the electrolyte

density. The investigation to develop hybrid capacitors has been initiated by "Li-ion capacitors (LIC)." And, now "Nanohybrid capacitor (NHC)" certainly achieves as high energy density as Li-ion capacitors with higher stability, higher safety, and higher productivity (see Fig. 20). Both LIC and NHC attain three-times higher energy density and are regarded as the next-generation supercapacitor systems.

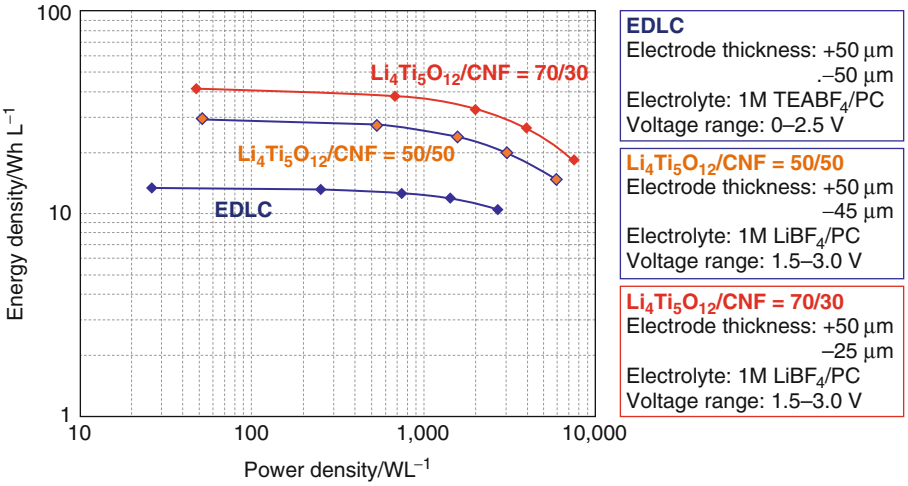

Electrochemical Supercapacitors and Hybrid Systems. Figure 19
Ragone plots of Nanohybrid capacitor systems ((nc-$Li_4Ti_5O_{12}$/CNF)/AC) with two different $Li_4Ti_5O_{12}$ loadings (50% and 70%) and conventional EDLC system (AC/AC) all in 1 M $LiBF_4$/PC

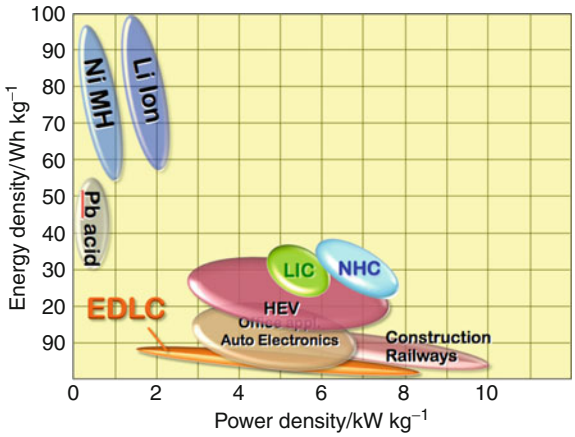

Electrochemical Supercapacitors and Hybrid Systems. Figure 20
Performances of lithium-ion capacitor (LIC) and nanohybrid capacitor (NHC) in Ragone plot

Bibliography

1. Amatucci GG, Badway F, Du. Pasquier A, Zheng T (1999) In: Abstract of 196th meeting of the Electrochemical Society, Honolulu, p 122
2. Amatucci GG, Badway F, Pasquier ADu, Zheng T (2001) An asymmetric hybrid nonaqueous energy storage cell. J Electrochem Soc 148:A930
3. Azaïs P, Tetrais F, Caumont O, Depond JD, Lejosne J (2009) Ageing study of advanced carbon/carbon ultracapacitor cells working in various organic electrolytes. In: Abstract of ISEE'Cap 09, p 19
4. Bai Y, Wang F, Wu F, Wu C, Bao L (2008) Influence of composite LiCl–KCl molten salt on microstructure and electrochemical performance of spinel $Li_4Ti_5O_{12}$. Electrochim Acta 54:322
5. Baldsing WG, Puffy NW, Newnham RH, Pandolfo AG (2007) High-energy asymmetric nickel-carbon supercapacitors. In: Proceedings advanced automotive battery and ultracapacitor conference, Long Beach
6. Burke A (2000) Ultracapacitors: why, how, and where is the technology. J Power Sources 91:37
7. Burke A (2007) R&D considerations for the performance and application of electrochemical capacitors. Electrochim Acta 53:1083
8. Chen CH, Vaughey JT, Jansen AN, Dees DW, Kahaian AJ, Goacher T, Thackeray MM (2001) Studies of Mg-substituted $Li_{4-x}Mg_xTi_5O_{12}$ spinel electrodes (0x1) for lithium batteries. J Electrochem Soc 148:A102
9. Hao Y, Lai Q, Xu Z, Liu X, Ji X (2005) Synthesis by TEA sol–gel method and electrochemical properties of $Li_4Ti_5O_{12}$ anode material for lithium-ion battery. Solid State Ionics 176:1201
10. Hatozaki O (2008) Lithium ion capacitor: electrode materials and cell performance. In: Proceedings advanced capacitor world summit 2008, San Diego (2008)
11. Huang J, Jiang Z (2008) The preparation and characterization of $Li_4Ti_5O_{12}$/carbon nano-tubes for lithium ion battery. Electrochim Acta 53:7756
12. Huang S, Wen Z, Zhu X, Gu Z (2004) Preparation and electrochemical performance of Ag doped $Li_4Ti_5O_{12}$. Electrochem Commun 6:1093
13. Jansen AN, Kahaian AJ, Kepler KD, Nelson PA, Amine K, Dees DW, Vissers DR (1999) High-rate nano-crystalline $Li_4Ti_5O_{12}$

attached on carbon nano-fibers for hybrid supercapacitors. J Power Sources 81–82:902
14. Kazaryan SA, Kharsov GG, Litvinrnko SV, Kogan VI (2007) Self-discharge related to iron ions and its effect on the parameters of HES $PbO_2|H_2SO_4|C$ Systems. J Electrochem Soc 154:A751
15. Kim J, Cho J (2007) Spinel $Li_4Ti_5O_{12}$ nanowires for high-rate Li-Ion intercalation electrode. Electrochem Solid State Lett 10:A81
16. Koetz R, Carlen M (2000) Principles and applications of electrochemical capacitors. Electrochim Acta 45:2483
17. Laforgue A, Simon P, Fauvarque JF, Mastrangostino M, Soavi F, Sarrau JF, Lailler P, Conte M, Rossi E, Saguatti S (2003) Activated carbon/conducting polymer hybrid supercapacitors. J Electrochem Soc 150:A645
18. Machida K, Suematsu S, Ishimoto S, Tamamitsu K (2008) High-voltage asymmetric electrochemical capacitor based on polyfluorene nanocomposite and activated carbon. J Electrochem Soc 155:A970
19. Naoi K, Ishimoto S, Ogihara N, Nakagawa Y, Hatta S (2009) Encapsulation of nanodot ruthenium oxide into KB for electrochemical capacitors. J Electrochem Soc 156:A52
20. Naoi K, Simon P (2008) New materials and new configurations for advanced electrochemical capacitors. Interface 17:34
21. Nikkei Electronics (2008) LIC prevails EDLCs?! 991:77
22. Ohzuku T, Ueda A, Yamamoto N (1995) Zero-strain insertion material of $Li[Li_{1/3}Ti_{5/3}]O_4$ for rechargeable lithium cells. J Electrochem Soc 142:1431
23. Pandolfo AG, Hollenkamp AF (2006) Carbon properties and their role in supercapacitors. J Power Sources 157:11
24. Plitz I, Dupasquier A, Badway F, Gural J, Pereira N, Gmitter A, Amatucci GG (2006) Nanohybrid capacitor: The next generation electrochemical capacitors. Appl Phys A 82:615
25. Scharner S, Weppner W, Schmind-Beurmann P (1999) Evidence of two-phase formation upon lithium insertion into the $Li_{1.33}Ti_{1.67}O_4$ spinel. J Electrochem Soc 146:857
26. Shen CM, Zhang XG, Zhou YK, Li HL (2002) Preparation and characterization of nanocrystalline $Li_4Ti_5O_{12}$ by sol–gel method. Mater Chem Phys 78:437
27. Shu J (2008) Study of the interface between $Li_4Ti_5O_{12}$ electrodes and standard electrolyte solutions in 0.0–5.0 V. Electrochem Solid State Lett 11:A238
28. Simon P, Gogotsi Y (2008) Materials for electrochemical capacitors. Nat Mater 7:845
29. Takai S, Kamata M, Fujiine S, Yoneda K, Kanda K, Esaka T (1999) Diffusion coefficient measurement of lithium ion in sintered $Li_{1.33}Ti_{1.67}O_4$ by means of neutron radiography. Solid State Ionics 123:165
30. Thackeray MM (1995) Structural considerations of layered and spinel lithiated oxides for lithium ion batteries. J Electrochem Soc 142:2558
31. Yoshino A, Tsubata T, Shimoyamada M, Satake H, Okano Y, Mori S, Yata S (2004) Development of a lithium-type advanced energy storage device. J Electrochem Soc 151:A2180
32. Yu H, Zhang X, Jalbout AF, Yan X, Pan X, Xie H, Wang R (2008) High-rate characteristics of novel anode $Li_4Ti_5O_{12}$/polyacene materials for Li-ion secondary batteries. Electrochim Acta 53:4200
33. Zhou JH, Sui ZJ, Li P, Chen D, Dai YC, Yuan WK (2006) Structural characterization of carbon nanofibers formed from different carbon-containing gases. Carbon 44:3255

Electronic Waste and Its Regulation

Shirley Thompson
Natural Resources Institute, University of Manitoba, Winnipeg, MB, Canada

Article Outline

Glossary
Definition of the Subject and Its Importance
Introduction
Regulation of Electronic Waste
Future Directions
Bibliography

Glossary

Design for environment (DfE) The various design approaches geared at reducing the overall environmental impact of a product, process, or service, considering environmental impacts across the product's life cycle.

Ecycling The process of recycling the components in used or discarded electronic equipment.

Electronic waste, e-waste and waste electrical and electronic equipment (WEEE) Old, end-of-life, or discarded appliances using electricity and includes computers, consumer electronics, fridges, etc. which have been disposed of by their original users.

Extended producer responsibility (EPR) Entails making manufacturers responsible for the entire life cycle of the products and packaging they produce based on the "polluter pays principle."

Persistent and bioaccumulative toxins (PBT) Compounds that are resistant to environmental degradation. Because of this, they have been observed to persist in the environment, bioaccumulate in human and animal tissue, and to have potential significant impacts on human health and the environment.

Toxicity characteristic leaching procedure (TCLP) A soil sample extraction method for chemical analysis employed as an analytical method to simulate leaching through a landfill.

Definition of the Subject and Its Importance

Electronic waste or "E-waste" is broadly defined as all surplus electronics. Electronic wastes are computers, television sets, mobile phones, etc., destined for reuse, resale, salvage, recycling, or disposal. Computers are a complex waste problem due to their volume, toxicity, and disposable, rather than recyclable, product design. Computers quickly become obsolete as technology rapidly changes. Everyday more than 160,000 obsolete computers and televisions are generated in the USA, weighing almost 3.2 thousand metric tons (3.5 thousand US tons). Electronic waste is about 4% of the total solid waste stream in North America but is growing two to three times faster than any other waste stream (i.e., paper, yard waste). For every new computer coming on the market there is an obsolete computer [1]. In 1998, of the 20 million computers taken out of service in the USA, only 2.3 million (slightly more than 10%) were recycled or Ecycled, mostly from large businesses and institutions. As well, 75% of "obsolete" computers are being stockpiled in people's homes [2].

Introduction

With rapid improvements in technology, most computers are disposed of within 2 years, rather than at the end of their functional life cycle of approximately 10 years [3]. Each new innovation in computer technology doubles its obsolescence rate, without increasing its repairability or recyclability. The consumer, targeted by advertising about the latest computers, finds buying a new computer cheaper and more convenient than upgrading their old one. Computers that cannot be upgraded become waste.

Electronic waste is a complex waste, made up of more than 30 compounds, many of which are hazardous substances. The presence of hazardous substances in computers makes landfilling or incinerating environmentally unsuitable for discarded computers. The use of toxic metals and other chemicals in computers results in environmental and health risks when computers are manufactured, incinerated, landfilled, burned, or melted down during recycling [4, 5]. E-waste emits billions of kilograms of toxic materials into the air, water, and soil, most of which are persistent and bioaccumulative toxins (PBTs). A cathode ray tube (CRT), the most common type of computer monitor until recently, typically contains four pounds of lead to protect users from the tubes' X-rays [2]. Lead is a teratogen and reproductive hazard. As well, lead causes damage to the central and peripheral nervous systems, blood system, and kidneys in humans. Circuit boards and batteries also contain lead, in addition to smaller amounts of mercury and hexavalent chromium, nickel, bromine, and zinc. In 2000, 90% of e-waste had no removal of components containing toxic mercury switches or nickel batteries before landfilling or incineration in Europe and North America. With these harmful chemicals, many consumer electronics fail the Toxicity Characteristic Leaching Procedure (TCLP) [6]. Leaching of heavy metals and brominated compounds occurs during landfilling, contaminating the soil and groundwater beneath a site and the surrounding area. For example, the European Commission estimates that consumer electronics constitute 40% of the lead found in landfills. Moreover, the workers in e-waste recycling operations face dangerous health and environmental risks. Hence the concerns about the trade, the technology in practice, and the existing poor disposal practices of e-waste in North America and many nations.

Increased regulation of electronic waste and concern over the environmental harm, which can result from toxic electronic waste has raised disposal costs. Regulation creates an economic disincentive to dispose of residue, unless strict restrictions enforce proper treatment. In extreme cases, brokers and others calling themselves recyclers export unscreened electronic waste to developing countries, avoiding the expense of removing items like bad cathode ray tubes (the processing of which is expensive and difficult).

Hazardous e-waste from developed countries (e.g., Western European countries, USA, Canada, and Japan) has a history of being recycled in developing countries and in Eastern Europe. These products are exported when the state has banned various metals in their landfills and incinerators, rather than pay the higher labor and environmental costs for recycling locally [7]. As much as 80% of all recycled e-waste in the USA were

shipped to Asia (e.g., China, Cambodia, India, Indonesia, Malaysia, Manila, and Pakistan) all of which have poor regulation and management of e-waste [8, 9, 10]. This shipping to places with low labor costs and environmental regulation occurs for the EU as well but the new WEEE-IT (Information Technology) regulation at least requires that their e-waste be recycled at facilities having as high or higher environmental and safety standards as in the EU.

A few demanufacturing operations exist in North America but are typically manned by unskilled or semiskilled labor such as prisoners, former welfare recipients, or mentally disabled individuals. These workers are exposed to hazardous conditions and often do not earn a living wage [11]. For example, 250 inmates, at the Atwater federal US penitentiary's recycling plant process 450 computers daily. The inmates receive only US $0.23–$1.15 per hour for this work and work without safety equipment, such as gloves, dust masks to reduce exposures to toxic lead, and barriers to prevent physical risks from cuts and lead exposure. Hammers are often used to break cathode ray tubes (CRT) rather than a sealed crushing machine, which is typical in commercial recycling, carrying out this work [12].

Regulation of Electronic Waste

Extended producer responsibility (EPR) regulations in Europe hold producers who are legally responsible in four ways for their products. They are responsible for having: (1) Economic responsibility to pay all or a portion of end-of-life management, (2) Physical responsibility to take possession of their products after the consumer discards it, (3) Information responsibility to provide mandatory product labeling such as component or material lists, and (4) Financial liability for environmental damage and clean-up costs from disposal of hazardous products [6, 13]. Generally, EPR policies have three characteristics: (1) a focus on end-of-life waste management to encourage redesign for environment, (2) a shift of physical and/or financial responsibilities from taxpayer or consumer to producer, and (3) an explicit target for waste reduction. Mandated programs "force producers to get involved in managing material streams" [14]. Consumers of WEEE products must have the opportunity to return waste items, without charge, to collection facilities with the producer responsible for product recovery.

Extended producer responsibility extends the "polluter pays principle" to consumer products, requiring "that the polluter should, in principle, bear the cost of pollution, with due regard to the public interest and without distorting international trade and investments" [15]. EPR policy places responsibility for a product's end-of-life environmental impacts on the original producer and seller of that product requiring producers: to take back their products and to meet recycling rate targets. This approach provides incentives for producers to optimize their internal logistics and recycling systems to minimize costs, create value, and integrate eco-design into business routines. Those changes should include improving product recyclability and reusability, reducing material usage and downsizing products, lower energy consumption and greenhouse gas production, reduce dependency on virgin materials, spur new business enterprises, generate new job opportunities, and provide financial and savings to companies improving their design, production, and distribution processes [16]. However, the ability to gain competitive advantage is restrained by the domination of collective compliance structures across the EU, over whose costs producers regard as difficult to manage or influence.

Despite new EU shipment rules banning the export of hazardous materials in waste electrical equipment to non-OECD countries from January 2002, a few exporters have transferred over two million old computer monitors and one million old TVs out of the EU for reuse. For example, of an estimated 121,000 metric tons (133,000 US tons) of computer and telecommunications equipment exported from the UK for re-use or recycling in 2003, 21,000 metric tons (23,000 US tons) was "grey market" equipment being exported without the full necessary documentation. This equipment is rarely tested or repaired before export to countries where dismantling takes place in unsafe conditions, or the equipment is simply dumped. Without criteria for the reuse of IT appliances (e.g., testing, minimal capacity, etc.) this environmental injustice can continue. Very little consumer-based electronic waste has true reuse value, and claims of export for reuse should be scrutinized carefully. Although Canada prohibits waste export to non-OECD nations, this occurs disguised as computer donations for reuse.

According to WEEE IT EU regulations, an average of 75% recovery by weight and of 65% component, material, and substance reuse and recycling must be achieved by December 31, 2006 [17]. These targets appear feasible, even low, based on pre-WEEE-IT programs surpassing these targets. Prior to WEEE, several member states within the EU (Belgium, the Netherlands, Sweden, Norway, and Switzerland) adopted national regulations and management schemes for e-wastes [6], with programs operating at a recycling rate (including energy recovery) of approximately 80–97% with 97% achieved by Switzerland [18]. Although high targets are being set and a good recycling/reuse rate is achieved, still a significant amount of waste (10–20%) is not recovered for recycling and reuse, presumably ending up in landfills or incinerators, releasing toxic chemicals. That some 91,000 metric tons (100,000 US tons) are incinerated or landfilled each year means computer waste has not been prevented and mass consumption of this disposal product continues to occur [19].

The USA and Canada have, rarely, if ever, mandated strict guidelines for product manufacturing, which includes both how the product is produced and what types of materials are used – perhaps as a result of the lack of political pressures to develop new waste management strategies amidst relatively plentiful landfill accommodations. Policy makers in North America are reluctant to require sustainable product management. A few companies, such as HP and Dell, do voluntarily take back their products, but at high costs that many consumers are unwilling to pay or have severe restrictions that limit acceptance to consumption of their new materials. The recycling rates of voluntary computer take-back programs in the USA and Canada conducted by a few companies, such as Dell, HP, Sony amount to only 14%, according to the most recent available figures, due to cost and acceptance of e-waste in landfills [2]. Many economically successful reuse and recycling programs are in effect [15, 20, 21, 22], even with producers' focus on productivity and the bottom-line. Hewlett-Packard (HP) was the first computer corporation to have a "tear it down" operation to accompany its successful "build it up" operation called Product Recycling Solutions (PRS), launching a take-back program in 1992 [15] in which HP committed to reuse or donate or environmentally sound recycle their products [7]. HP limits their financing to the pickup and transport of their printers and cartridges, requiring customers to pay $25–$50 Canadian for each e-waste component (CPU, monitor, scanner, server). HP witnessed numerous economic and market-share benefits from reducing resource and energy consumption of their products and production processes. An 87% landfill diversion rate reduced landfill costs, and reusing items accounted for $2.9 million Canadian in benefits for HP in addition to $2 million revenue for selling recycled materials in 2006 [23]. By applying reuse at HP, 15% of defects were reduced and productivity increased by 57% [22]. However, it should be noted that although the company avoided 16,000 metric tons (18,000 US tons) of carbon dioxide (CO_2) in 2006 through energy efficiency measures their emissions in 2006 were approximately 100x that at roughly 1,600,000 metric tons (1,800,000 US tons) of carbon dioxide [23]. The Electronic Product Stewardship Canada (2006) reports 91,000 metric tons (100,000 US tons) of electronics reach end of life in Canada annually and only 11% of this is currently recycled.

Future Directions

Policies can encourage redesign for reuse and upgrading for longevity, as well as recycling: Computers can be redesigned to have less material (de-materialization), facilitate upgrading through modularity, last longer, expend less energy and pollution in their production and use and that disassemble for reuse and recycling with ease after their useful life. Design for the Environment (DfE) promotes consideration of design issues related to environmental and human health over the life cycle of the product. Material selection, energy use, extended component life cycles, disassembly, reprocessing, remanufacturing must all be considered [24]. DfE has eight axioms: (1) manufacture without producing hazardous waste, (2) use clean technologies, (3) reduce product chemical emissions, (4) reduce product energy consumption, (5) use non-hazardous recyclable materials, (6) use recycled material and reused components, (7) design for ease of disassembly, and (8) product reuse or recycling at end of life [25]. Principles of ecodesign require products to be flexible, reliable, durable, adaptable, modular, dematerialized, and reusable. As applies to computers, improving environmental factors can

improve performance as well: work on optimization of environmental performance often spurs creativity and brings innovative design solutions into the product development process which allows improvement of its overall performance [26].

Policies can encourage reuse, as well as, recycling. Recycling is the series of activities by which discarded materials are collected, sorted, processed, and used in the production [27]. Although recycling reduces virgin material use, it still requires additional energy to be used to reform them into manufactured products [27]. Silicon Valley Toxics Coalition (2001) estimates that the cost of recycling computers ranges from $10 to $30 per unit. While this is less expensive than the estimated $25–50 per unit cost for disposal, the value of recycled materials in computers is $2.00–$3.00.

In contrast, remanufacturing, reconditioning, and repair should save money for the producer and reduce costs for the consumer. Over each computer's life cycle, reselling or upgrading computers saves 5–20 times more energy than recycling and would provide a public good if provided to organizations for educational purposes. For example, public schools have large needs for computers at 28.7 million computers in USA, which may be met by reusing or remanufactured computers, as recent state and local budget cuts otherwise severely limit the affordability of having computers in the classroom [28]. Reuse can include repair, recondition, or remanufacture. Also, it is environmentally preferable to reuse computers an extra 2 or 3 years than to recycle their components. Reducing the amount of computer waste relies heavily upon the reuse of systems that may be out of date, but fully functional [3]. Remanufacturing is considered the best strategy as the embodied energy of virgin production is maintained, preserving the intrinsic "added value" of the product for the manufacturer and enables the resultant products to be sold "as new" with updated features if necessary [27]. Components and materials from the end-of-life durable products can often be refurbished to substitute for virgin parts to be used as spares or in remanufacturing [29]. Upgrading individual components of a computer at the design stage, such as the hard drive, software, or processor, costs less than a new computer [3]. Lund, R. (1985) estimates that a remanufacturing product only requires 20–25% of the energy used in its initial formation and can be resold into lower-priced markets, typically costing 60% of the original production cost [27, 30]. However, the lack of a credible and stable demand for recycled or refurbished products is a barrier to remanufacturing [27, 31]. The noncommercial computer refurbishing field is a minuscule part of the overall computer recycling industry in the USA and Canada.

Designing for the environment (DfE) and implementing green production processes makes economic sense when life cycle environmental costs are required to be paid by the producer. DfE has producers considering "at the development phase of a products life cycle, the environmental impacts through enhancing the product design which includes resource consumption, both in material and energy terms and pollution prevention." Environmental considerations in product design include: waste minimization, reuse or recyclability, material conservation, pollution reduction, lower toxicity and "eco-design" [15, 32]. Six principles of Design for the Environment (DfE) are efficiency, appropriateness, sufficiency, equity, systems, and scale [33]. However, without extended producer responsibility internalizing environmental costs, manufacturers are typically unwilling to improve product and environmental quality if it costs more or compromises costs, quality, and scheduling constraints [24]. Firms are only willing to spend 0.1% more on a product to improve environmental quality [34]. Thus, usually design takes on the character of being a problem-solving activity for a component rather than product development from its conceptual stage [35, 36].

Bibliography

Primary Literature

1. Thompson S, Oh S (2006) Do sustainable computers result from design for environment and extended producer responsibility?: analyzing e-waste programs in Europe and Canada. ISWA/NVRD world congress 2006 conference proceedings. ISWA/NRVD, Copenhagen, Denmark, pp 145–161
2. Gattuso DJ (2005) Mandated recycling of computers: a lose-lose-lose proposition. Competitive Enterprise Institute (CEI)
3. Williams E, Sasaki Y (2003) Energy analysis of end-of-life options for computers: resell, upgrade, recycle. In: Proceedings of the 2003 IEEE international symposium on electronics and the environment, San Francisco, CA, pp187–192
4. Lincoln JD et al. (2005) Environmentally benign materials for electronics: A review current development and merging

technologies. In Proceedings. International symposium on advanced packaging materials: processes, properties and interfaces. IEEE, Piscataway, NJ
5. Schmidt CW (2002) E-Junk explosion. Environ Health Perspect 110(4):232–235
6. Sachs N (2006) Planning the funeral at the birth: extended producer responsibility in the European Union and the United States. Harv Environ Law Rev 30:51–98
7. McCarthy JE (2002) Recycling computer and electronic equipment: legislative and regulatory approaches for "E-Waste," Congressional Research Service, pp 1–21
8. Iles A (2004) Mapping environment justice in technology flows: computer waste impacts in Asia. Glob Environ Polit 4(4):76–105
9. Terazono A et al (2006) Current status and research on E-waste issues in Asia. J Mater Cycle Waste Manage 8:1–12
10. Yanez L et al (2002) Overview of human health and chemical mixtures: problems facing developing countries. Environ Health Perspect 10(110):901–909
11. Price JL (1999) Reclaiming end-of-life cathode ray tubes (CRTs), and electronics: a Florida update, hazardous material Management conference, Tucson, Arizona. 15 Nov 1999
12. Perry TS (2005) Recycling behind bars. IEEE Spectr 42(6):10–13
13. Toffel MW (2002) The regulatory and judicial roots of product stewardship in the United States. Haas School of Business/University of California, Berkeley
14. McKerlie K, Knight K, Thorpe B (2006) Advancing extended producer responsibility in Canada. J Cleaner Prod 14:616–628
15. Schwartz BJ, Gattuso DJ (2002) Extended producer responsibility: reexamining its role in environmental progress. Reason Public Policy Institute, Los Angeles, pp 1–65
16. Quinn L (2006) Extended producer responsibility: new direction for waste management. Eco-Journal (March/April)
17. Nakajima N, Vanderburg WH (2005) A failing grade for WEEE take–back programs for information technology equipment. Bull Sci Technol Soc 25(6):507–517
18. Vossennaar R, Santucci L, Ramungul N (2006) Environmental requirements and market access for development countries: the case of electrical and electronic equipment. Trade and environment review. United Nations, New York
19. Lin CK, Yan L, Davis AN (2002) Globalization, extended producer responsibility and the problem of discarded computers in China: an exploratory proposal for environmental protection. Georgetown Int Environ Law Rev 14:525
20. Bosch J (2002) Maturity and evolution in software product lines: approaches, artifacts and organization. In: Proceeding of the second software product line conference
21. Fiksel J (2001) Emergence of a sustainable business community. Pure Appl Chem 73:1265–1268
22. Tomer A, Kimchi E (2004) Evaluating software reuse alternatives: a model and its application to an industrial case study. IEEE Trans Software Eng 30(9):601–612
23. Hewett Packard (2007) HP global citizenship report: waste and recycling. http://www.hp.com/hpinfo/globalcitizenship/gcreport/operations/waste.html. Accessed 27 Mar 2007
24. Armstrong T (1997) Design for sustainability, sustainable consumption and production. IndEco Strategic Consulting, Ottawa
25. Hill B (1993) Industry's integration of environmental product design. In: 1993 IEEE international symposium on electronics and the environment. IEEE, Virginia
26. Thompson S, Sawyer J, Bonam R, Valdivia JE (2009) Building a better waste generation model: validating models with recovery rates at 35 Canadian landfills. Waste Manage 29:2085–2091
27. King AM, Burgess SC, Ijomah W, McMahon CA (2005) Reducing waste: repair, recondition, remanufacture or recycle?. Sust Dev
28. Lynch J (2004) Baseline study of noncommercial computer reuse in the United States. In: International symposium on electronics and the environment (IEEE). CompuMentor, San Francisco, pp 189–194
29. Toffel MW (2004) Strategic management of product recovery. Calif Manage Rev 46(2):120–141
30. Lund R (1985) Remanufacturing: the experience of the United States and implications for developing countries, UNDP project management report 2, World Bank Technical Paper No 31, pp 24–34. In: King AM, Burgess SC, Ijomah W2McMahon CA (2005) Reducing waste: repair, recondition, remanufacture or recycle? J Sustain Develop
31. Bras B, McIntosh MW (1999) Product, process and organizational design for remanufacture – an overview of research. Robot Comput-Integr Manuf 15:167–178
32. Calcott P, Walls M (2006) Can downstream waste disposal policies encourage upstream "design for environment"?. The American Economic Review: Papers and Proceeding of the One Hundred Twelfth Annual Meeting of the American Economic Association 90 (2), 233–237
33. Flecher K, Dewberry E (2002) Demi: a case study in design for sustainability. Int J Sustain High Educ 3(1):38–47
34. Matthews HS, McMichael FC, Hendrickson CT, Hart DJ (1997) Disposition and end-of-life options for personal computers. Green design initiative technical report #97–10
35. Fallman D (2003) Design-oriented human-computer interaction. Designing Des 5(1):225–232
36. Nichol S, Thompson S (2007) Policy options to reduce consumer waste to zero: comparing product stewardship and extended producer responsibility for refrigerator waste. Waste Manage Res 25(3):227–233

Books and Reviews

Boehm B (2003) Value-based software engineering. ACM SIGSOFT Softw EngNotes28(2):1–11

Bradner S, Mankin A (1995) The recommendation for the IP next generation protocol, Network Working Group

Bras B (1997) Incorporating environmental issues in product design and realization. Ind Environ 20(1–2):1–19

Business and Industry Advisory Committee (1998) Business and Industry Advisory Committee (BIAC) statement to the OECD EPR workshop 3 on extended and shared responsibility for products Washington, DC, 1–3 Dec 1998

Cull K, Malins J (2003) Designing a sustainable future: a new approach to influence design practice. http://www.ub.es/5ead/PDF/5%20/CullMalins.pdf
Farrell A (1996) Sustainability and the design of knowledge tools. Technol Soc Mag 15:17–21
Hauschild M, Wenzel H, Alting L (1999) Life cycle design: enroute to the sustainable industrial culture? Ann CIRP 48(1):393–396
Jacard M (2006) Mobilizing Producers toward Environmental Sustainability: The Prospects for Market-Oriented Regulations. In: Glen Toner (ed) Sustainable production: building Canadian capacity. UBC Press, Toronto
Lilly D, Lofthouse V Bhamra T (2005) Towards instinctive sustainable product use. In: Sustainable creating the culture, Aberdeen, 2–4th Nov
Macauley M, Palmer K, Shih J (2003) Dealing with electronic waste: modeling the costs and environmental benefits of computer monitor disposal. J Environ Manage 68:13–22
McDonough W, Braungart M (2002) Design for the triple top line: new tools for sustainable commerce. Corp Environ Strategy 9(3):251–258
Merola L (2006) The COTS software obsolescence threat. In: Fifth international conference on commercial-off-the-shelf (COTS)-based software systems, pp 127–133
Moffet J, Meyer S, Pezzack J (2006) Collaborative public policy for sustainable production: a broad agenda and a modest proposal. In: Toner G (ed) Sustainable production: building Canadian capacity. UBC Press, Toronto
National Safety Council (1999) Electronic product recovery and recycling baseline report: recycling of selected electronic products in the United States. National Safety Council, Washington, DC, p 29
Perdan S, Azapagic A, Clift R (2000) Teaching sustainable development to engineering students. Int J Sustain High Educ 1(3):267–279
Sheehan B, Spiegelman H (2005) Extended producer responsibility policies in the United States and Canada. In: Scheer D, Rubik F (eds) Governance of integrated product policy. Greenleaf Publishing, Sheffield, pp 202–223
Sheehan B, Spiegelman H (2005b) EPR in the US and Canada. Resour Recycling 2:18–21
Sheehan B, Spiegelman H (2006) Extended producer responsibility policies in the United States and Canada: history and status. Greenleaf Publishing, Sheffield. Silicon Valley Toxics Coalition, Poison PCs and Toxic TVs
Swanson M (2003) Canadian producer responsibility organizations. E4 Partners, pp 2–10. 15 Mar 2006
Walls M (2006) Extended producer responsibility and product design. Resource for the future
Wheeler D, Thomson K, Perkin M (2006) Sustainability, social capital and the Canadian ICT Secto. In: Glen Toner (ed) Sustainable production: building Canadian capacity. UBC Press, Toronto
Xu CY, Morrison PD (2005) Sustainable product development and business performance: a product life cycle approach. ANZMAC conference: entrepreneurship, innovation and new product development

Energy and Water Interdependence, and Their Implications for Urban Areas

Liz Minne[1], Arka Pandit[2], John C. Crittenden[3], Miroslav M. Begovic[4], Insu Kim[4], Hyunju Jeong[2], Jean-Ann James[2], Zhongming Lu[2], Ming Xu[5], Steve French[6], Muthukumar Subrahmanyam[6], Douglas Noonan[7], Marilyn A. Brown[7], Jess Chandler[7], Yongsheng Chen[8], Eric Williams[9], Reginald Desroches[8], Bert Bras[10], Ke Li[11], Michael Chang[2]
[1]Environmental Engineering, Brook Byers Institute for Sustainable Systems, Georgia Institute of Technology, Atlanta, GA, USA
[2]Brook Byers Institute for Sustainable Systems and the Department of Civil & Environmental Engineering, Georgia Institute of Technology, Atlanta, GA, USA
[3]Georgia Institute of Technology, Atlanta, GA, USA
[4]School of Electrical and Computer Engineering, Georgia Institute of Technology, Atlanta, GA, USA
[5]School of Natural Resources and Environment, University of Michigan, Ann Arbor, USA
[6]Center for Geographic Information Systems and the School of City and Regional Planning, Georgia Institute of Technology, Atlanta, GA, USA
[7]School of Public Policy, Georgia Institute of Technology, Atlanta, GA, USA
[8]Department of Civil & Environmental Engineering, Georgia Institute of Technology, Atlanta, GA, USA
[9]Golisano Institute of Sustainability, Rochester Institute of Technology, Rochester, NY, USA
[10]George W. Woodruff School of Mechanical Engineering, Georgia Institute of Technology, Atlanta, GA, USA
[11]Department of Biological and Agricultural Engineering, University of Georgia, Atlanta, GA, USA

Article Outline

Glossary
Definition of Subject
Introduction
Methodologies
Current Infrastructure
Water and Energy Nexus

Beyond the Water and Energy Nexus
Steps Toward a More Sustainable Future
Future Directions
Acknowledgments
Bibliography

Glossary

Anthroposphere That part of the environment that is developed or adapted by humans.

Life cycle assessment (LCA) Analysis of the impact of a product or service through all the stages of its life including raw resource acquisition, material processing, fabrication, assembly, transportation, operation, disposal, recycling, repurposing, or reusing.

Low-impact development (LID) A way of managing stormwater runoff through decentralized water systems, such as green roofs and rainwater harvesting.

Material flow analysis (MFA) Analysis of how resources move through the industrial, consumer, and ecological sectors.

Resilience The ability for a structure to maintain its fitness and function in response to indigenous and exogenous stressors; it is characterized by four measures:

Rapidity. A measure of the capacity to contain losses or prevent further degradation in a timely manner.

Redundancy. A measure of the inherent substitutability.

Resourcefulness. A measure of the capacity to mobilize resources to restore functionality in the event of disruption.

Robustness. An ability of the system to withstand a given level of stress and/or demand.

Sustainability The development of an anthrosphere that exists within the means of nature. Sustainability requires that humans use no more resources than nature can renewably provide and generate only wastes that nature can assimilate in a timely manner and without overwhelming natural cycles.

Urban heat-island effect The phenomenon where the temperature in a developed area with a high concentration of buildings, roads, and other physical infrastructure is significantly higher than in the surrounding undeveloped areas.

Urban sustainability An assessment of the long-term viability of a place considering the physical infrastructure (such as water, sewer, transportation, and buildings), socioeconomic issues (such as human well-being, health, wealth, safety, and security), and natural environment (such as resources, wildlife, and ecosystem health).

Definition of the Subject

There are many definitions for sustainability. Mathis Wackernagel, creator of the ecological footprint concept, defined sustainability as "securing people's quality of life within the means of nature" [1]. The United Nations' World Commission on Environment and Development (the Brundtland Commission) defined sustainable development as "development that meets the needs of the present without compromising the ability of future generations to meet their own needs" [2]. Throughout this report, sustainability will be defined as the development of the anthroposphere within the means of nature. Here, the anthroposphere is the built environment or the environment that humans created for security, wealth generation, and comfort. For it to exist within the means of nature implies that the anthroposphere must use resources that nature provides, and generate only the kind and amount of waste that can be assimilated into the environment without overwhelming natural cycles. At the global scale, there are several examples that suggest that current development patterns are unsustainable. Presently worldwide, there are approximately 7 billion people using 14 Gt of materials [3]. With only 5% of the global material use being renewable, the extraction of natural resources is beyond what nature can reasonably supply. At the other end, an enormous amount of synthetic and potentially toxic materials are being introduced into the global material cycle.

To fully understand sustainability, one needs to take a whole system approach. In the traditional reductive engineering paradigm, each of the individual infrastructure components such as water, energy, and transportation are optimized separately. However, since the function of all the component elements depend on each other, a more optimal solution can occur if all the urban pieces are considered together. These interdependencies form an ecosystem of infrastructure that,

if functioning properly, provides a lasting basis for human enterprise. An example of the interdependencies and the need for them to be considered together is the water energy nexus. In all but the most primitive cultures, it takes water to create useful energy and energy to create useful water. This nexus requires a comprehensive understanding not just of power generation or of water resource management, but of both and how they connect and interact at temporal and spatial scales that are both large and small. And on top of these engineering relationships, environmental, social, and economical concerns must also be integrated.

Why is sustainability, particularly urban sustainability, so important? The United Nations Environmental Program (UNEP) chief, Klaus Toepfer, stated in 2005 that "cities pull in huge amounts of resources including water, food, timber, metals and people. They export large amounts of wastes including household and industrial wastes, wastewater and the gases linked with global warming. Thus their impacts stretch beyond their physical borders, affecting countries, regions and the planet as a whole. So the battle for sustainable development, for delivering a more environmentally stable, just, and healthier world, is going to be largely won and lost in our cities" [4]. The UNEP expects 64% of the world's population to live in urban areas by 2040, a dramatic increase from 50.5% in 2010 [5]. For the developed countries like the United States, those in the European Union, and others, the share of urban population is projected to be 87% in the same time period [5]. With such an influx of people from rural areas to urban areas, cities must be prepared for this mass in-migration. With much of this movement expected in developing countries, those that adopt sustainability as a guiding framework for development could leapfrog other countries that are financially and systemically burdened with maintaining the status quo. For the developed world, a hybrid approach in which existing centralized systems are augmented by decentralized systems could help those cities remain competitive and viable. New or old, however, each city has different demographics, cultural values, fiscal and physical constraints, climate, and topology, and any solution to the demand for urban infrastructure – sustainable or not – will have to be uniquely tailored to consider these differences.

Introduction

Transmission grids are an integral piece of urban infrastructure. Understanding how electricity is used and finding ways to decrease the use of energy will be essential for developing more sustainable urban systems. Likely the greatest opportunities for improving efficiencies and increasing sustainability lies not in a single solution, but in how all the pieces – old technology and new – interconnect and work together. Transmission grids not only transmit energy to residencies and workplaces, but also to water treatment systems, to industries, to street lights, to trains, and to the gasoline stations where cars are fueled, just to name a few. These dependencies are not unidirectional, however. Energy production and demand are also significantly dependent on these systems. Pipelines move natural gas, oil, and water to refineries and power plants, while trains and ships transport coal for use in heating, manufacturing, and power production. Adding to this is the emergence of affordable and technologically feasible renewable or decentralized energy options such as photovoltaics, wind power, and microturbines. The most productive, healthy, and sustainable cities of the future will be the ones that learn to use all these resources to build and operate wholly integrated energy systems that meet the short- and long-term economic, social, and environmental needs and aspirations of their residents and region.

Urban areas are complex interconnected systems analogous to ecological food webs. For an urban area to function properly, water, energy, and transportation systems need to be effectively designed to support the area's desired land use. Similarly, the land-use pattern also should be governed according to the capacity of the area to host development. Beginning in the nineteenth century, these systems have increasingly been designed, built, and operated as isolated systems without considering how they interact. Water purveyors have been concerned about water distribution. Power companies examined energy production, distribution, and usage. Transportation planners examined ways to move people and goods safely and efficiently. Generally, they cared about optimizing their own processes to satisfy their own needs. However, in recent years, some cities have begun to realize that they could improve efficiency by considering how these different

systems interact and function together within the whole urban system, rather than as individual and independent parts. For example, energy generation requires water for steam production and cooling. The waste heat from energy production could be used to produce hot water, heat homes, or provide air-conditioning. In another example, a Pacific Northwest National Laboratory study in 2007 suggested that 73% of the United States' current light-duty vehicle fleet could be supported by the existing electric power infrastructure [6]. It is less clear, however, how the increased electricity demand required to electrify transportation would affect water demand. These are just two simple examples. Socioeconomics, policy, land use, and urban infrastructure form a complex system that makes up the city. When a holistic approach is adopted to analyze the urban infrastructure, many properties emerge that are not apparent when the components are analyzed individually. These emergent properties evolve from the economic and sociopolitical framework adopted by the stakeholders for the urban area. Hence, citizen capacity building, whereby informed citizens demand more sustainable infrastructure, is vital to driving the political agenda to improve the urban infrastructure.

A city is such a multifaceted and complex system that one cannot easily test the effect of certain decisions or actions. However, the impact of decisions can be estimated through modeling that simulates how agents change their behavior in reaction to different options. For example, a first-generation agent-based modeling analysis of urban infrastructure would include the following:

(a) A determination of the spatial and temporal demand for urban infrastructure due to development/redevelopment activities
(b) A listing of infrastructure alternatives that satisfy the needs of the development
(c) A calculation of the material and energy required for the different alternatives
(d) A determination of the vulnerability and resiliency of the urban infrastructure alternatives against exogenous or endogenous risks
(e) An assessment of the local, regional, and global impacts of the alternatives through life cycle analysis

A second-generation model would include feedback loops in which all previous decisions are reconsidered in light of outcomes revealed by the model. This is more realistic because of future decisions do depend on evolving properties. Once the model is verified, the dynamic policies and economic drivers (i.e., market forces) that will yield more sustainable and resilient urban infrastructure can be determined more accurately. More importantly, the model can be used to assess the sensitivity of outcomes to different inputs and resources can be focused on those components that will result in the greatest improvement.

Methodologies

There are many methods for evaluating sustainability. As with all methods, each has strengths and limitations. Some of the methods used to evaluate the sustainability of urban environments are discussed below.

Resiliency

Resiliency is the ability of a structure to maintain its functionality despite exogenous or endogenous stressors. Resilient systems are flexible and adaptable and typically provide a better return on material investments in the long term. There are four important attributes that compose resiliency: robustness, redundancy, resourcefulness, and rapidity. Robustness is the ability of the system to withstand a given level of stress or demand. Redundancy is a measure of the inherent substitutability, or the ease with which a component or a whole system, or the function that they provide, could be replaced in case of a failure. Resourcefulness is a measure of the capacity to mobilize resources in the event of disruption. Rapidity is a measure of the capacity to contain losses or prevent further degradation in a timely manner. These 4 "R's" can be used as metrics in determining the sustainability of a system or infrastructure [7]. Urban infrastructure that is designed to minimize material and energy investments may not in fact be sustainable in the long term if the reductions result in low resiliency and the functioning of the infrastructure is jeopardized. Resiliency serves as a check against short-sighted, but well intentioned, actions that do not contribute to longer-term sustainability.

Life Cycle Assessment

Life cycle assessment (LCA) is the analysis of the impact of one particular product across all phases of the product's "life." Life can be defined in multiple ways. The most common way an LCA is performed is from cradle-to-grave. This considers raw material extraction, manufacturing, use, and disposal. While a great deal of attention is often paid to a product's manufacturing phase, the use phase is often the most important phase based on a product's impact. For example, a car uses a great deal more energy and resources in the use phase than in the manufacturing phase.

If a product is recycled or reused instead of being disposed of, it is cradle-to-cradle, and the life of the product is extended. For example, plastic soda bottles made of polyethylene terephthalate (PET, recycling symbol number 1) can be recycled to make new plastic bottles or a variety of other products, like T-shirts and carpeting. Cradle-to-cradle aims to reduce waste and decrease the amount of virgin resources that are used in a product.

Other methods may shorten the view of an LCA, such as cradle-to-gate and gate-to-gate. Cradle-to-gate looks at the product from raw resources all the way through manufacture, but ends there. This might be useful particularly to a manufacturing plant or for products that have negligible effect in their use and disposal phase. Manufacturing also might look at a gate-to-gate LCA. This kind of LCA looks only at the production chain. This could be useful in comparing the efficiencies of different manufacturing methods and tools.

Two additional LCA methods that may be employed are the Economic Input-Output LCA (EIO-LCA) and the Ecologically based LCA (Eco-LCA). The EIO-LCA was developed at Carnegie Mellon, and is used to measure the economic effects of the materials and energy used to make a product [8]. Ohio State University developed the Eco-LCA [9]. This tool adds to the traditional cradle-to-grave LCA by emphasizing more analysis on the direct and indirect effects of a product on pollutant emissions and economic flows.

Life cycle assessment is a useful tool when looking at sustainability; however, it does have a number of limitations. Not all factors can be tracked or easily given a numerical value. For example, it is difficult to put a numerical value on the health effects of a product because toxicity and the transport and exposure routes may not be that easy to quantify.

One other limitation of LCA is the cutoff problem. For any product or process there are a large number of product stages or processes upstream and it is never possible to include all of them. Consider, for example, automobile manufacturing. An automobile needs parts for its manufacturing. The parts need a suite of metals. Mining equipment is required to obtain the required metals. But the metal needed for the mining equipment also required machines to obtain it. And so the chain continues. In LCA, the chain needs to be truncated somewhere resulting in errors of omission. Additionally, the different LCA methods and commercially available software, like SimaPro, that are widely used to conduct LCA may use different assumptions and data resulting in a variation of results that must be reconciled.

Material Flow Analysis

A material flow analysis (MFA) is a process used to assess the flow of mass and energy within a defined system. It can be conducted at national scales, at the scale of a product, or at any scale in between. Urban metabolism is a specific MFA tool looking at a defined urban area. This method tends to look at the city as a "black box." It considers the flows moving in or coming out of the city, but does not necessarily look at the mechanisms inside the city that cause these fluxes to occur. It does give a view of the amount of goods and energy needed to support a city, and how much waste the city produces. However, one constraint is the need for extensive input and output information for a huge number of materials. Some of these numbers are tracked at the national level, or are easy to track within one industry, but may be difficult to find or track for less controlled regions like states or cities. This approach works well for islands because all inputs are brought in by boats and recorded, and outputs also must go out on boat or stay on the island. With better data collection, this method will become increasingly useful. An improvement on urban metabolism would be to track the inflows of resources, the outflows of wastes, and the creation of infrastructure that creates wealth and comfort. The guiding principles would be to use fewer resources to create and operate the

infrastructure needed per capita. In practice, it can be difficult to compare one city to another because cities can be in different states of build-out of its infrastructure (e.g., a greenfield city as compared to a more mature city) and its climate, demographics, and topology can impose significant confounding effects.

Industrial Ecology

Industrial ecology can be defined as a multidisciplinary system-level study focusing on the interconnections between the industry, economics, and the natural environment. Industrial ecology utilizes a suite of different tools to analyze these interdependencies. Among these tools are life cycle assessment and material flow analysis, along with designing and manufacturing for the environment and ecological efficiency within the industry. The waste or by-products of one industry might be a resource for another industry, and if the two industries are located close enough for logistical viability, then the waste/by-product can be utilized by the other industry. For example, a cement manufacturer located near a power production facility may be able to use residual fly-ash from the power plant for its cement mix. And if a drywall production facility is also in the vicinity, it might be able to use the $CaSO_4$ from the cement plant as its raw material. Thus the net waste generation from these industries is reduced and their proximity saves significant fuel from the reduced need for transportation. This multitude of tools used in an industrial ecology assessment allows an industry or city to look at various designs and see how they affect inputs, outputs, and the overall effect on the economy.

Urban Sustainability

Urban sustainability is a systems-level holistic analysis of the sustainability of an urban system, particularly in regard to its infrastructure. Urban infrastructure is an intricate network of six major components: (1) private residences, (2) commercial establishments (including churches, schools, etc.), (3) water and wastewater, (4) energy, (5) transportation, and (6) land use. Urban sustainability also includes socioeconomic impacts and the policy drivers that cause the emergent properties of urban systems. With the demand for basic infrastructure growing with population, cities need to plan their infrastructures accordingly. Traditionally, urban areas were built with the "big-pipe concept," where the natural ecology was replaced with *hardscape* to provide for the urban infrastructure. *Nature* was restricted to curbside trees, and manicured parks and lawns filled with nonnative plants which require significantly more water and nutrients to thrive than the indigenous varieties. More recently, however, the importance of ecosystem services and preservation of natural ecology has been realized and natural alternatives, such as blue-belts for stormwater management, are increasingly being used in place of hardscapes. With this method, models are being developed to evaluate different options and to determine what social and economic decisions are needed to make them happen.

Current Infrastructure

Although current infrastructure may not be optimal, a large amount of capital has been invested in it and people still depend on it. One option for increasing sustainability is to develop a hybrid system of centralized and decentralized infrastructure, which increases redundancy without increasing the amount of requisite resources. Future planning also should guide how systems interact, and plan accordingly to save resources. Such interactions will now be described.

Water and Energy Nexus

Potable drinking water treatment provides clean drinking water, and wastewater treatment sanitizes sewage. Both use a great deal of energy in acquisition, treatment, and distribution. In 2000, the United States used more than 50 billion kWh of energy to attain, treat, and distribute drinking water and wastewater [10]. This is a huge demand for energy that is expected to continue to grow through 2050. The Electric Power Research Institute's (EPRI's) report on *Water and Sustainability* expects that by the year 2050, this number will reach over 75 billion kWh (Fig. 1). Already, water accounts for about 4% of the total energy sold in the United States. In California, it represents 18% of energy needs. And as water demand increases and good quality raw water becomes more difficult to find, these shares are likely to rise as advanced treatment technologies for reclaiming water or desalinating water are much more energy intensive. With this in mind, when a city is

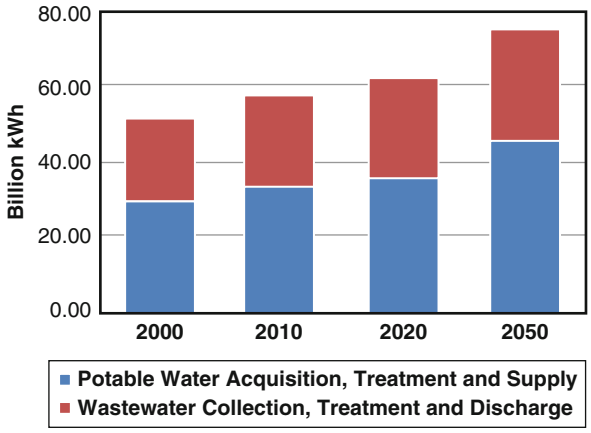

Energy and Water Interdependence, and Their Implications for Urban Areas. Figure 1
Energy needed for drinking water and wastewater processes in the United States with data from the year 2000 and predictions of use until 2050 [10]

considering their water infrastructure, it also may want to keep in mind the amount of energy needed for various treatments for water and wastewater.

French Nuclear Power

In 2003, France experienced what was then their hottest summer on record [15]. The higher temperatures increased the demand for air-conditioning and refrigeration, which translated into an increased demand for electricity. In turn, increased energy production created more waste heat, which required more water for cooling purposes. Though France had plenty of capacity to produce electricity – the nation obtains ~80% of its electricity from nuclear power – the heat wave and drought limited the amount of water available for operation of the nuclear power plants, and the country was forced to turn off or reduce production at 17 of its nuclear reactors. As a result, France could no longer export electricity, which had been sold at €95 per MW-h to other EU countries, but needed instead to import electricity at a cost of ~€1,000 per MW-h.

Water can be treated using different methods, and with methodology differences there also are differences in energy dependency. Surface water tends to be cleanest, and as such requires the least amount of energy to collect and treat (Table 1). Surface water is not available in all areas though. Groundwater requires slightly more energy to treat and seawater desalination can use up to 75 times the amount of energy as surface water.

Energy and Water Interdependence, and Their Implications for Urban Areas. Table 1 National average energy demand by various water treatment systems [10, 11]

Water treatment and collection	kWh/MGal
Surface water treatment [11]	1,422
Groundwater treatment [10]	1,824
Brackish groundwater desalination [11]	3,900–9,750
Seawater desalination [11]	9,780–16,500

Energy and Water Interdependence, and Their Implications for Urban Areas. Table 2 National average energy demand by various wastewater treatment systems [10]

Wastewater treatment and collection	kWh/MGal
Trickling filter	955
Activated sludge	1,322
Advanced treatment without nitrification	1,541
Advanced treatment with nitrification	1,911

For treating wastewater, methods include a trickling filter, activated sludge, advanced treatment without nitrification, and advanced treatment with nitrification. The energy demand, shown in Table 2, is lowest for the trickling filter and highest for advanced treatment with nitrification. The simplest treatments consume the least amount of energy, but they may not always be the most viable option given the quality of the water being treated and the requirements for the processed water. The gap in energy demand for the various approaches is much smaller in the case of wastewater than it is for water treatment.

Finally, power is also needed to distribute water. Logically, the farther that water needs to travel and the more difficult the water is to access, the more the energy that will be required to move it. Distributing water from lakes and rivers is the least energy intensive. It requires about 1,400 kWh/MGal to deliver [12].

Not all cities have lakes and rivers available to tap, however. For them, groundwater is more difficult to attain and requires slightly more energy. Lastly, discharging wastewater requires between 2,350 and 3,300 kWh/MGal on average.

The converse of energy being needed to provide, treat, and distribute water is that water is needed to produce, convert, and store energy. Water use in energy production varies depending on the source of energy. In the case of thermoelectric power generation, water is required for cooling purposes, while in case of hydroelectricity, water is used as the source of power. Water is also required for petroleum fuel processing, the primary energy source for transportation. Thus all forms of energy require water, which varies in the amount and purpose of its use depending on the energy source. Thermoelectric power accounts for 39% of freshwater withdrawals and 52% of our fresh surface water withdrawals [13].

The consumptive use of water for power generation is from evaporative losses. Every day thermoelectric power loses an average of 3.3 billion gallons of water to evaporation [13]. As one may suspect, certain kinds of power generation consume more water than others (Table 3). Accounting for the amount of energy produced and the water loss associated with each source, approximately 2 gal of water per kilowatt hour is lost to evaporation in the United States. Hydropower has an evaporative loss of 18.27 gal per kilowatt hour, which is more than 35 times the evaporative loss of water from coal-based thermal power. This implies that hydropower is feasible only in areas with an abundance of water. In contrast, photovoltaics and wind consume much less water.

Energy and Water Interdependence, and Their Implications for Urban Areas. Table 3 The evaporative loss of water by different energy sources in the United States [14]

Energy source	Gal/kWh (evaporative loss)
Hydro	18.27
Nuclear	0.62
Coal	0.49
Oil	0.43
PV solar	0.030
Wind	0.001

Example: Water and Energy Demand: A Tale of Two Cities

Atlanta and Phoenix are two cities with rapidly growing populations. As such, the demand on water and energy are rapidly growing. Being that they are in different regions, they have different demands for water. Table 4 describes how these cities are very different in terms of demand. For example, Atlanta uses more water indoors, but Phoenix uses a significant amount more outdoors. With long commutes and poor public transportation, Atlanta uses significantly more fuel per person per day than Phoenix. Some of the more important differences are due largely to Phoenix being a city in an arid region, very hot and dry, whereas Atlanta is more humid and wet generally. The water consumption for electricity production in Phoenix is more than four times that of Georgia. The electricity consumption for water supply and treatment also is around five times more in Phoenix than Georgia. With it being considerably more difficult to get water to Phoenix, these numbers are bound to become higher. The dependence of water on energy and energy on water in Phoenix are even greater than in Atlanta. Yet Atlanta has experienced a great deal of turmoil with its water resources, as described in the previous paragraph. So a strain on the Colorado River is subject to cause more damage, all things being the same. This table also shows that cities are not the same. No solution is right for all cities.

Beyond the Water and Energy Nexus

While water and energy are inherently connected, there are other connections that are equally important in the context of urban infrastructure (Fig. 2). Transportation needs energy to fuel vehicles, and the amount of energy available affects modes of transportation. Land use affects the amount of transportation activity in an area, and transportation is needed to made land accessible. The availability of water affects how land is used, and the way land is used affects the demand on water and the ways water can be treated. Likewise, the availability of energy affects land and water use, and the way the land is used affects the energy demands and the kind of energy that can be created. Additionally, water

Energy and Water Interdependence, and Their Implications for Urban Areas. Table 4 The relationship between water use and electricity use for the cities of Phoenix and Atlanta

		The City of Phoenix		The City of Atlanta	
Residential water demand	Indoor (gpcd)	48[a]	1999 data in Chap. 4 of The Water Environment of Cities [37]	71	2001 data in The World's Water 2008–2009: The Biennial Report on Freshwater Resources
	Outdoor (gpcd)	110[a]		20	
Power use	Residential electricity, kWh/person-day	36	2005 data [38]	41	2005 data Brown et al. (2008)
	Fuel, kWh/person-day	5.5		12.3	
Water consumption for electricity production	gal/kWh	7.85 (Arizona)	National Renewable Energy Laboratory (2003)	1.65 (Georgia)	Torcellini et al. (2003)
Electricity consumption for water supply and treatment	Water, kWh/MG	8,600	[39] Conveyance, 4600 Pumping, 2600 Water treatment, 100 Water distribution, 1300	1,700[b]	City of Atlanta Watershed Management, [13, 36]
	Wastewater, kWh/MG	10,700	[39] Wastewater collection and treatment, 1500 Reclaimed water, 9200	1,830[b]	

These data demonstrate the difference in use for the two different regions. Information of this sort must be considered when making energy and water plans for each city

[a]The numbers are modified assuming four people for one household

[b]The numbers are estimated based on the water and wastewater production of the City of Atlanta, the electricity use of the Atlanta Watershed Management Department (Thomas 2007), and the electricity demand for water supply and wastewater treatment of the South Atlantic Region (DOE [13])

is also used for extracting fuels and growing biofuels, which affects the transportation sector.

Energy for Transportation

Energy is needed to power a variety of transport vehicles including airplanes, trains, boats, trucks, and automobiles. The fuel used in these vehicles may be equally diverse and may include gasoline, diesel (both petro and bio based), ethanol, methanol, natural gas, electricity, hydrogen, solar, and even coal and wood (though these latter two are nearly negligible in the modern vehicle mix). The latest trend is to create hybrid vehicles that can utilize two or more fuel sources (e.g., gasoline and electricity). As of 2009, the transportation sector accounts for ~28% of the of total energy consumption in the United States and 72% of the nation's petroleum consumption [16]. Transportation also accounted for 3% of natural gas consumption and 12% of renewable energy use, mostly in the form of ethanol. Given these significant shares, the effect of transportation on energy needs to be considered when planning cities or city improvements.

Transportation, Land Use, and Energy

As the need for mobility increases, improving existing vehicle efficiency will lead to marginal reductions in the environmental impacts of transportation. Greater improvements, however, may be possible if switching to other modes of transportation is considered. In a 2007 study of plug-in hybrid electric vehicles, the

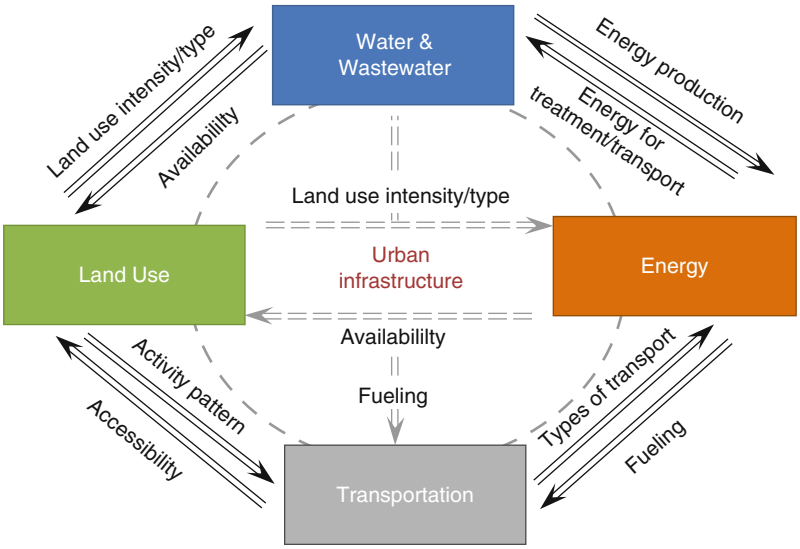

Energy and Water Interdependence, and Their Implications for Urban Areas. Figure 2
Water, energy, transportation, and land-use systems are interconnected in urban regions

Pacific Northwest National Lab [6] found that the current US electric power infrastructure could support the energy needs of 43–73% of the current light-duty vehicle fleet – the lower range resulting from the limiting of vehicle charging only to the 6 PM to 6 AM period. The study further estimated that if 73% of the US fleet was converted to electric vehicles, the United States would no longer need to import oil, and greenhouse emissions could be reduced by 27% (even if all electricity were generated by coal-fired power plants). While such broad-scale analyses are informative, it is important to note that complex local relationships underlie these bigger developments.

Bras recently completed an assessment of the energy and carbon dioxide emissions from different modes of transportation in Atlanta. Many kinds of vehicles and fuels were included in the study: conventional gasoline, diesel, compressed natural gas (CNG), ethanol 85 flexible-fuel vehicles (E85 FFV), spark-ignition (SI) gasoline hybrid electric vehicle (HEV), diesel HEV, SI plug-in hybrid electric vehicle (PHEV), diesel PHEV, electric vehicle, diesel vehicle, MARTA Clean Diesel bus, MARTA CNG bus, and MARTA rail. (MARTA is the Metropolitan Atlanta Rapid Transit Authority, which is the primary form of public transportation in Atlanta.) All of these transportation methods were evaluated on a Well-To-PUMP (WTP) and Pump-To-Wheels (PTW) basis for energy use and carbon dioxide emissions (see Figs. 3 and 4). Due to low ridership, MARTA's buses and rail are among the worst for both carbon dioxide emissions per passenger distance and for energy use per passenger distance. Increasing ridership would greatly improve these metrics. Other results suggest that electric vehicles do not fare much better than conventional gasoline and diesel. This is due, in part, to Georgia's dependence on older inefficient coal-fired power plants for energy. Overall, plug-in hybrid electric vehicles used the least energy and emitted the least carbon dioxide per passenger distance.

The implications of the effect of ridership on energy use and carbon dioxide emissions from various transportation modes in Atlanta suggest that other variables beyond just vehicles and fuel are also important. Planning and developing cities for growth with compact land use and transportation could significantly improve their sustainability and lower their dependence on energy. The way land is used affects the modes of transportation available and their efficiencies. For example, a compact city favors walking,

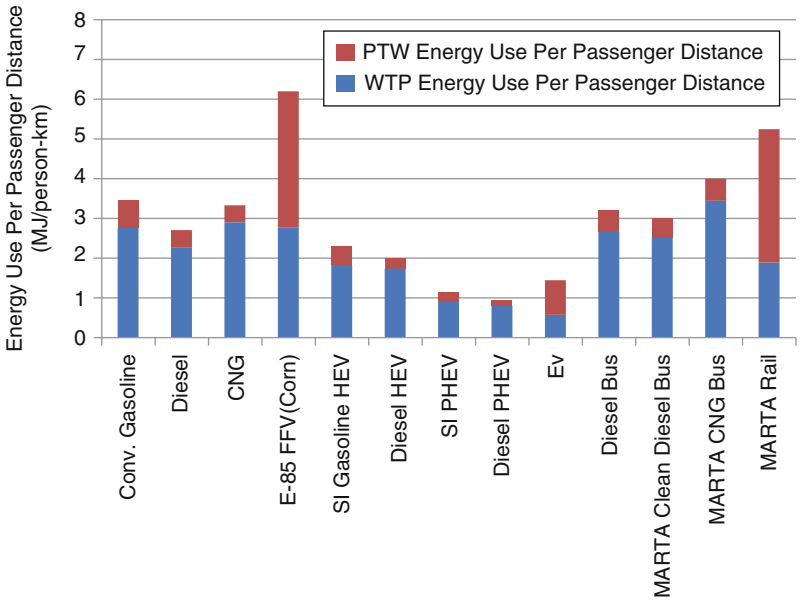

Energy and Water Interdependence, and Their Implications for Urban Areas. Figure 3
The energy use per passenger distance for various transportation modes in Atlanta, GA

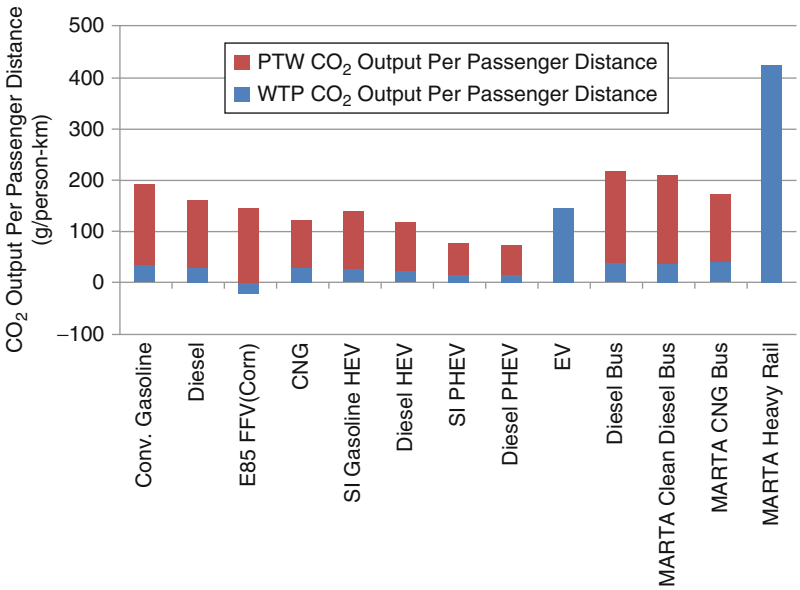

Energy and Water Interdependence, and Their Implications for Urban Areas. Figure 4
Carbon dioxide emissions per passenger distance for various transportation modes in Atlanta, GA

heavy rail, and other modes of efficient public transportation. New York City is a good example of this kind of city, where parking fees, gas expenses, and traffic lead the majority of the population to walk, take the subway, or ride the bus. An opposing example might be Atlanta, where the city is not compact enough to offer many people the option to walk or use public transportation.

Water for Transportation

Along with energy and land use, water is also intertwined with transportation. Department of Energy data [13], along with data from Harto's LCA of low carbon fuels [17], shows that oil consumes between 0.03 and 0.08 gal of water per kilowatt hour of energy [13] (see Table 5). Natural gas production uses a similar amount. Water needed to produce biodiesel from irrigated soy, though, is in the range of 0.39–9 gal of water per kilowatt hour. Corn-ethanol needs up to 19 gal of water per kilowatt hour, or ~500 times more than that for oil. From another perspective, Webber [12] found that a traditional gasoline car consumes around 7–14 gal of water per 100 miles traveled, PHEVs consume ~24 gal per 100 miles, and ethanol fueled vehicles require 130–6,200 gal per 100 miles.

The Compounding Power of Density

Urban density reaps a great many sustainable benefits. Public transportation is more accessible and commuting distances are generally shorter. Compact living also means that buildings can be closer to the infrastructures that provide them water and energy, which means less energy and materials are needed for distribution. It is also often the case that the more complex power and water networks that serve dense urban areas have built in redundancies that can compensate for component failures within the system. Finally, density affords other cross-pollinating opportunities such as combined heat and power, and low-impact development water infrastructure that also provides green space for recreation.

Energy and Water Interdependence, and Their Implications for Urban Areas. Table 5 The dependence of various transportation fuels on water

Unit: Gal/kWh	Low	High	
Coal [13]	0.007	0.027	Mining+washing
Petroleum/oil [13]	0.03	0.076	Extraction +refining
Natural gas [13]	0.01	0.01	Extraction +processing
Corn-ethanol [17]	1.26	19	Assuming 15% irrigation for USA
Cellulosic ethanol [17]	0.13	0.431	No irrigation
Cellulosic ethanol [17]	16	19	Irrigation
Soy-biodiesel [17]	0.392	8.98	Assuming 4% irrigation for USA
Algae biodiesel [17]	0.839	1.762	Enclosed
Algae biodiesel [17]	0.895	18.351	Open

Jobs, Quality of Life, and Tax Revenue

The nexus of infrastructure extends beyond the interconnection of the physical, functional, and environmental constituent pieces. It also has implications for a place's social and economic well-being. Consider again, for example, the benefits of compact urban design. Land consumed by large private residential lots cannot be used by the collective community. Small private lots, on the other hand, preserve the opportunity to leave larger tracts available for recreation, wildlife habitat, and other amenities that are not possible when the land is fragmented. These public conveniences and desired attributes improve the quality of life for everyone, create a more favorable, stable, and job-producing business climate, and raise property values. And when the resultant increase in tax revenues is reinvested in the infrastructure, an engine of prosperity is created (see Fig. 5).

Steps Toward a More Sustainable Future

Water

Rain water is a source of clean water that does not need much treatment. However, most cities currently do not handle this resource efficiently. In most cases, stormwater becomes contaminated when it falls onto urban or agricultural surfaces, or is shunted into the wastewater system. Collection and treatment of stormwater using low-impact development (LID) techniques offers a myriad of benefits. The first step is to separate the collection of stormwater from wastewater. One immediate benefit is that with less water to be treated, less energy is needed in the water treatment process. Reduced flow into the wastewater stream also reduces the risk of sewage overflow into surface waters.

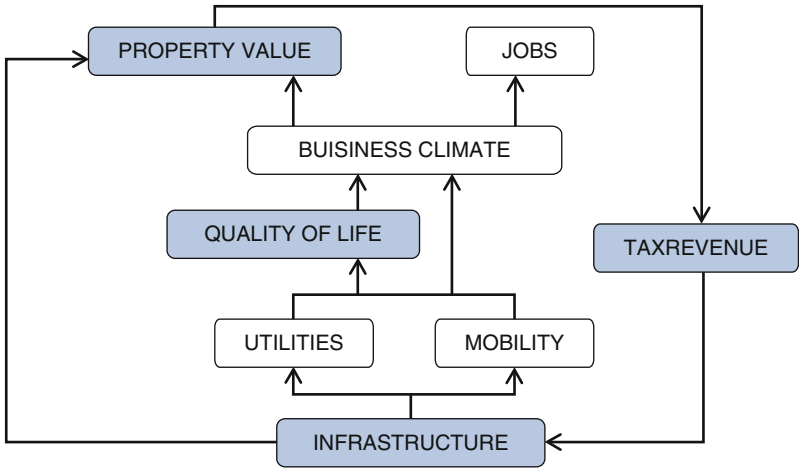

Energy and Water Interdependence, and Their Implications for Urban Areas. Figure 5
The relationship between improved infrastructure and an improved socioeconomic environment

The stormwater that is collected can be used to create green spaces, to flush toilets, for cooling, or for fire fighting. Below is a sample of LID techniques that can be used.

Vancouver

The City of Vancouver was concerned about the stormwater and sewage that was being discharged into its salmon-bearing rivers [18]. The city considered traditional separation and decentralized treatment, but after discovering that putting in a centralized stormwater treatment facility would cost the city an estimated $4 billion, it decided to look into different options. One approach that employed low-impact development and decentralized treatment satisfied the water treatment needs while also creating green space which increased property values and led to an estimated increase of $400 million in tax revenue. It also resolved the environmental problem for their salmon-bearing rivers, improved conditions for other wildlife, and reduced the urban heat-island effect.

Best Management Practices for Pollution Control

Best Management Practices (BMPs) are techniques used in controlling water pollution and the flow of water. They are put in place to control pesticides, herbicides, nutrients, other existing pollutants, and emerging contaminants like pharmaceuticals and personal care products from moving from the land to the water. Some of these techniques may simply reduce the amount of toxins used in a process or pesticides used for farming. Some structural techniques include detention basins, which are used to prevent flooding in storms, and pervious pavement, which allows water to flow through its pores while holding a number of pollutants in the soil. These techniques help manage the flow of stormwater so that wastewater systems are less likely to be overwhelmed. They often rely on natural techniques, such as bioremediation or wet land treatment, to clean the water and are often less expensive and less energy intensive alternatives.

New York

The Safe Drinking Water Act required New York City to build new water filtration plants at a cost of ~$8 billion. Balking at the cost, the city instead acquired undeveloped lands to buffer the watershed, initiated a host of Best Management Practices (BMPs), worked with the farming community to develop a Whole Farm Plan to reduce runoff pollution, used LID techniques to reduce stormwater flow, and made a few upgrades to existing sewer and septic systems in the region. In the end, these actions, in lieu of the $8 billion cost of new

filtration plants, enhanced the economic productivity of the land from recreation, farming, and the protection of the watershed from runoff [19].

Green Roofs Green roofs are roofs that are partially or wholly covered with vegetation. They increase urban green space, reduce stormwater runoff, sequester carbon dioxide directly, and reduce building energy consumption. They can be added to buildings in two ways, intensive or extensive. An intensive roof is normally between 8 and 12 in. thick and weighs 80–120 lb per square foot [20]. Extensive roofs are thinner and much lighter (10–50 lb per square foot). Intensive roofs are often built as gardens, but must be well supported due to the increased weight. Extensive roofs are not necessarily meant to be visited, but may be used for some of the same benefits, but at a lower cost.

Indigenous Plants Plants that are native to a region require less water, fertilizers, and pesticides than exotic plants. Indigenous plants have adapted to local conditions. Less effort is needed to maintain these plants, and they live longer than other plants would in their environment. Alternatively, plants with superior carbon sequestration qualities like yellow poplar and American sweet gums more effectively reduce the carbon footprint of a city relative to slower growing hardwood trees.

Pervious Pavement Pervious pavement allows water to pass through the pavement for groundwater recharge and thereby decreases the amount of rainfall that enters the wastewater system. Pervious pavement is ideal for large, low traffic uses like parking lots, driveways, bike paths, and sidewalks. Not only does pervious pavement reduce the load of stormwater on wastewater treatment systems, but it also reduces nutrient and metal loads from runoff (by 80% and 90%, respectively) [21].

LID techniques should be accessed city by city and based on a cost-to-benefit analysis, as not all techniques are proper for each city circumstance. But while most LID techniques are beneficial even within traditional centralized water systems, decentralized systems may offer additional benefits. With conveyance and distribution responsible for 80% of the energy demand in the water sector [10], decentralized systems can offer significant savings. In addition, due to the lower residence time of the water in the distribution system, the final water quality at the tap is less compromised. Decentralized systems also add resilience to the system due to higher redundancies than in centralized systems. That is, if a centralized system fails, all the customers that it serves are at risk of being disconnected from their water supply. When a decentralized system fails, another nearby station can supply the water needed until the damaged plant is fixed.

While newly developing areas may implement decentralized water systems, other cities with existing centralized water treatment systems should not look to totally disassemble their infrastructure. Instead they should consider developing a hybrid centralized/decentralized model. This might be as simple as adding a decentralized plant in a quickly growing area instead of expanding the centralized plant. And because LID techniques such as rainwater harvesting and low flow toilets reduce the output needed from a water treatment plant, LID techniques and decentralization simultaneously work to enable and enhance each other.

Energy

Fossil fuels are a limited resource. As such, their use needs to be judicious and efficient. Improving the efficiency of vehicles, lighting, appliances, electronics, heating, ventilation, and cooling is one strategy. Another strategy may be redesigning the energy system by distributing power and incorporating renewables, and truly integrating multiple resource planning. Below are described a sample of opportunities.

Combined Heat and Power A large amount of energy is lost in creating electric power; only about 30% of the energy input results in electricity delivered to the customer [23]. Seventy percent of the energy is lost in converting the primary fuel into electricity and distributing through the power grid. For that same amount of input energy, a combined heat and power

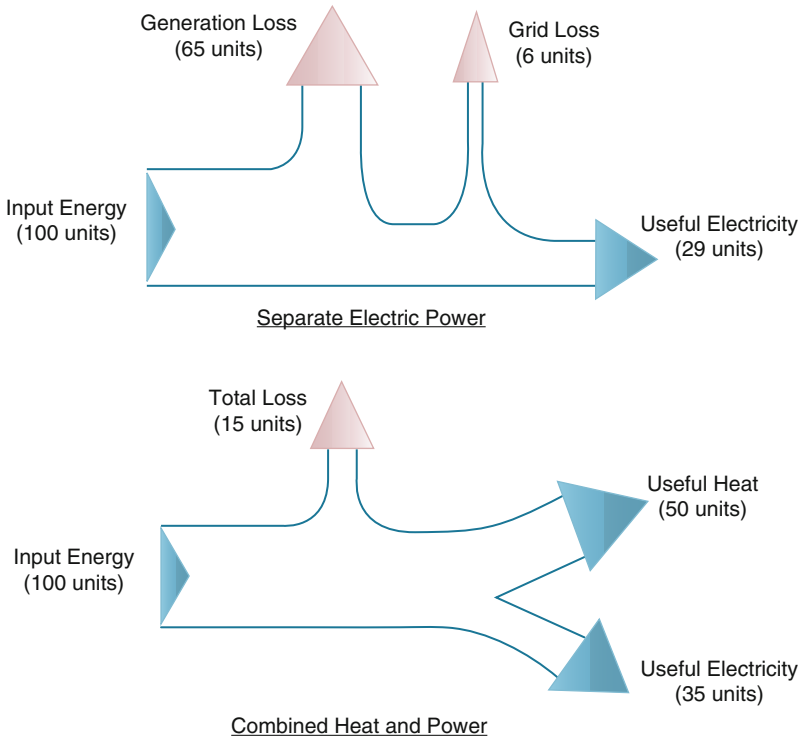

Energy and Water Interdependence, and Their Implications for Urban Areas. Figure 6
Utilization of energy for separate electric power and combined heat and power. The amount of energy lost is much higher in the separate system due to the recycling of heat to make more energy (Amended from [22])

system could utilize ~85% of the input energy (see Fig. 6). Combined heat and power has the potential to provide the United States 20% of the electricity by 2030, which could reduce an estimated 0.2 gigatons of carbon annually. This system also emits, on average, 1/10th of the nitrogen oxides (NO_x) per kWh as compared to the average grid electricity [24]. Helsinki Energy in Finland used combined heat and power, and has experienced great results [24]. Sulfur dioxide emissions from district heating were reduced around 90% from 1980 to 2004. This scheme also saved Finland six million tons of carbon emissions in 2004. Using less energy means fewer greenhouse gases are created, and with the climate changing so quickly, emission reduction is needed. Systems like these generate electricity and use the waste heat for a variety of processes like chemical manufacturing, heating buildings, or producing hot water, and thereby eliminate or reduce the energy and consequent environmental impacts needed for those demands [23, 24].

Energy Efficient Products In most existing applications, simply upgrading or modernizing energy demanding products will result in improved efficiencies and higher performance. Even low-end refrigerators produced today may be several times more efficient than refrigerators produced 20, 30, and 40 years ago, while also providing more features and functionality along with a relatively short payback period. When choosing new or replacement products, however, certified Energy Star products use 20–30% less energy than the federal standards require [25]. Eligible products include appliances, electronics, heating and cooling systems, lighting, fans, plumbing fixtures, and building products like insulation and roofing.

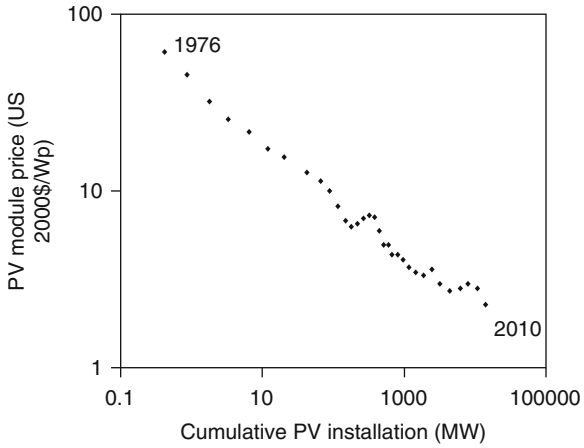

Energy and Water Interdependence, and Their Implications for Urban Areas. Figure 7
Price of a PV module per Watt peak (constant year 2000 US dollars) as a function of cumulative installation of PV in megawatts for the period 1976–2010 [27]

Energy and Water Interdependence, and Their Implications for Urban Areas. Table 6 A comparison of power generation from photovoltaic and coal energy sources

Energy Source	Photovoltaic	Coal
$\frac{\text{Energy output}}{\text{Energy invested}}$ [28]	9.0	5.0
Water use [29]	0.001 Gal/kWh	0.49 Gal/kWh
Land use	0.51 kWh/acre (RET Screen Simulation)	690 kWh/acre [30–33]
Overnight cost [34]	$4.75/kWh	$2.84/kWh
Total job-years/GW h (avg) [32]	0.87	0.11

Photovoltaics and Other Renewable Energy Sources Every day the sun provides more than enough energy to meet all the demands of humans and nature. But while nature has evolved to efficiently harvest this free energy, human made systems are only now becoming cost-effective (see Fig. 7). Comparing photovoltaic power generation to coal generation, Table 6 shows for each source the ratio of energy output to energy invested water use, land use, cost of power, and jobs. While the lower overnight cost of power still favors coal, the other attributes indicate that PV is already a competitive alternative. With costs continuing to drop, however, PV could soon become the preferred power source with coal becoming the less attractive alternative.

Wind, geothermal, biomass, and hydroelectricity are some of the other renewable energies that are growing in importance. For example, a recent working report suggested that there is an unrealized potential of 29,400 MW of hydroelectricity that could be developed in the United States [26]. One problem with renewable resources, though, is their inherent intermittency. In order for many renewables to become practical, large-scale inexpensive energy storage methods need to be developed. These methods may include various types or combinations of electrochemical batteries, flywheels, compressed air, superconductive magnetic storage, and the oldest, the least capacity-constrained and most popular when available, pumped hydro-storage.

Decentralizing Distribution Apart from the manner in which power is generated, system resiliency can be increased by changing how the power is distributed. The smaller scales inherent to renewable generators, such as PV, mean that these generators can more readily be located in various locations across the distribution feeder. Microgrids can be created by separating the distribution feeders into zones of balanced generation and load can by placing reclosers at the zone boundaries (reclosers are similar to circuit breakers, but do not have the capability to interrupt the fault current; see Fig. 8, e.g.). In the case of a feeder separated from one of its supply substations by a fault location, such a network may allow the feeder still to be energized and supplied by other generators while the faults are being mitigated. That would improve reliability as measured by indices such as SAIFI and SAIDI (system average interruption frequency and duration index), CAIFI and CAIDI (customer average interruption frequency and duration index), and ASUI and ASAI (average service (un)availability index). Improvements in such indices (or composite indices) usually mean better customer satisfaction and diminished losses associated with repetitive outages, that is, increased resiliency.

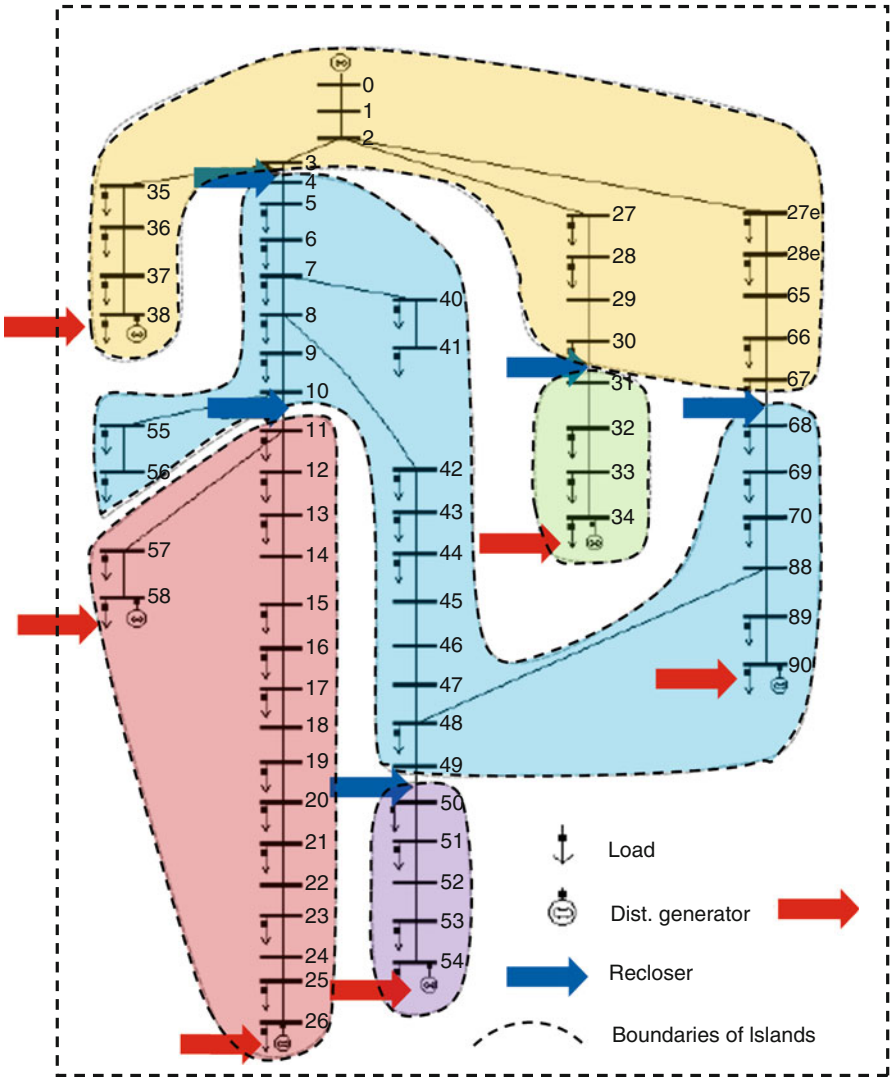

Energy and Water Interdependence, and Their Implications for Urban Areas. Figure 8
A depiction of an islanded distribution network. This system is split into multiple zones with balanced distributed generation and loads (as shown by the *dotted lines* and *multiple colors*). There are multiple distributed generators, and each island has a recloser at the boundaries with other zones. This allows the islands to cut off from each other in case of a disturbance, keeping the larger portion of the network supplied with energy. Once the problem is fixed, the islanded system can then automatically be reconnected to the grid (transmission network)

Example: Distributed Renewable PV Generation

Distributed generation consists of small-scale and decentralized electric energy systems. Capacities vary, typically in the range of several kW to hundreds of MW. Accurate and efficient system analysis algorithms are needed in order to analyze the impact of PV systems on various types of microgrids and distribution networks. The influence of uncertainties can be modeled via suitably optimized Monte Carlo techniques.

Commercial PV power industries started developing in the 1970s. In spite of a 70% reduction of the real price

of PV modules over 40 years, energy from PV remains too expensive to compete with conventional sources. Political changes in the United States in the early 1980s ended substantial funding for solar energy research and, since the nation represented nearly 80% of the global market for solar energy at that time, virtually halted solar energy development around the world. In 2004, renewable energy sources accounted for 9.6% of the electricity generated in the United States and 18.6% worldwide. China was the leading nation by renewable generation capacity in 2008 (598 TW h of renewable energy produced that year). A total of 3,584 TW h of renewable energy was produced in the world in 2008, of that only 12 TW h was from solar photovoltaic generators while, for example, 16% (3,288 TW h) of world electric energy was produced from hydroelectric plants. However, PV has become one of the most rapidly growing energy generation technologies. PV module shipments have grown at an average annual rate of 40% since 1996, up from 13% in the previous decade. The potential growth may transform PV into a $100 billion industry [35].

On the technical side of PV proliferation, electric power utilities are not motivated to allow interconnections of customer-owned generators (such as many PV installations would be) to their distribution networks (mostly for operational reasons). Utilities tend to put nonutility generation under the extensive technical analysis. Conversely, the regulating authorities tend to act in favor of DG owners and support that the interconnection be as easy and transparent as possible.

The main objective of PV installation is to boost the energy savings. Figure 9 shows annual estimated monthly PV generation output of an assumed PV system in the Atlanta area in the United States. Figure 10 presents how the total load demand is decreased due to the PV generation with capacity ranging 10–40% of the annual peak load at the same feeder. The figure represents the system performance on the 244th day of the year. If the distributed generator (DG) is owned by the customer, the actual benefit is cost saving in the electric bill. If the DG is owned by the utility, the benefit is avoided energy production from the less desirable or more expensive sources and reduction in transmission and distribution losses. This benefit means energy saving in both cases.

The second impact of solar electricity generation is the ecological impact. The PV output energy savings provide the opportunity to create the avoided carbon footprint by not using the more ecologically impactful technologies (coal, natural gas, etc.). In addition to reducing the effective feeder load in the distribution networks where it is installed (thus also reducing the transmission and distribution losses), PV generation can also bring about CO_2 reduction. It can also cause water footprint reduction through avoided thermoelectric and hydroelectric generation, and fuel reduction, such as coal, petroleum, and natural gas in the thermal power generation as in Table 6. The example assumes that the PV system is optimally oriented to maximize energy production. (If shaving of peak load levels is the main objective, it is possible to orient the PV system more westward, thereby boosting the PV output at the peak load times.)

Understanding Aggregate Demand A number of factors need to be considered in every city when making decisions to improve sustainability. Inputting all the data necessary to run a good model of a city is a massive undertaking, but the model could be a very useful tool.

For the modeling of Atlanta, Geographic Information System (GIS) tools were used to input infrastructure data. The What if?™ system was used to model Atlanta. This software was used to show the suitability of various infrastructures for an area. Figure 11 shows the suitability for eight different land-use types. As Atlanta continues to develop, this can be used as a tool to plan infrastructures for areas that are more suitable. Along with suitability factors, this program was used to predict the land use of Atlanta as it grows. Figure 12 shows Atlanta's use of land in 2010 and the prediction for land use in 2030, using the Business as Usual scenario. This scenario looks to grow the city in the traditional urban sprawl way, and the figure shows much of the land use going to residential use and employment centers expanding outward from the city center. Figure 13 offers a different comparison, this one of two different growth scenarios: Business as Usual and Compact Growth as predicted for 2030. This comparison shows the difference in how Atlanta

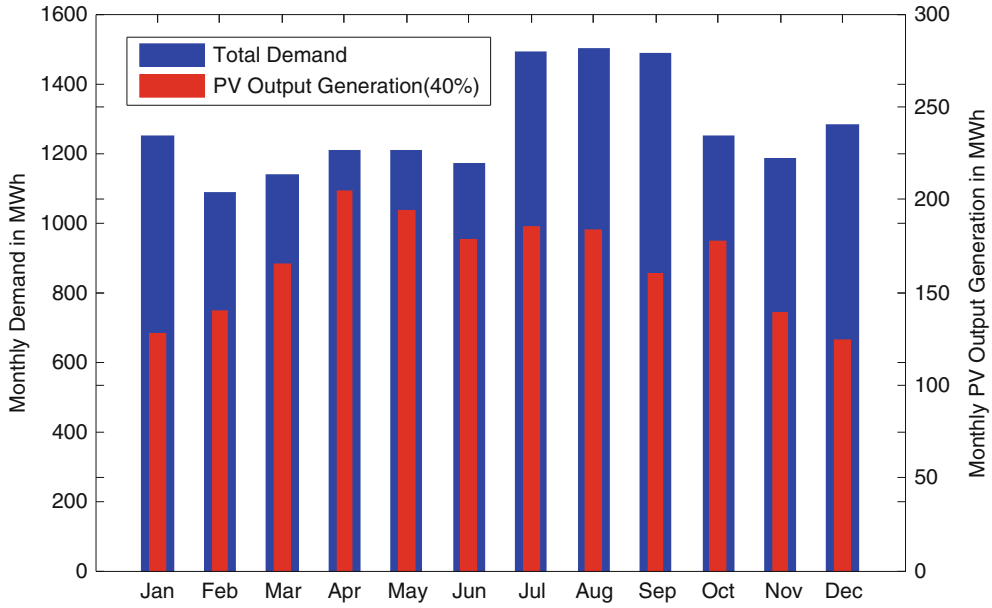

Energy and Water Interdependence, and Their Implications for Urban Areas. Figure 9
Annual PV generation and load demand on a typical distribution feeder. It is assumed that the total PV capacity is equal to 40% of the peak load demand

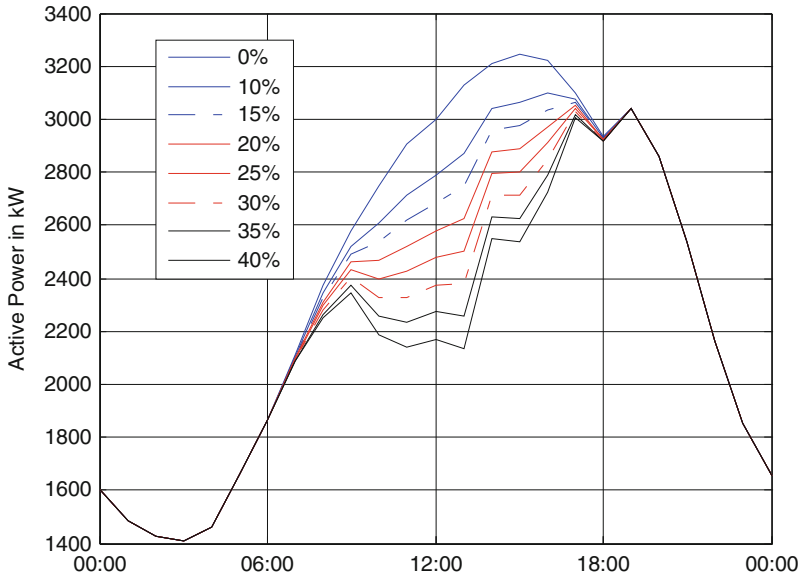

Energy and Water Interdependence, and Their Implications for Urban Areas. Figure 10
The effect of PV generation on a typical day of the year (horizontal axis represents time of the day). Assumed PV capacity is 40% of the annual peak load

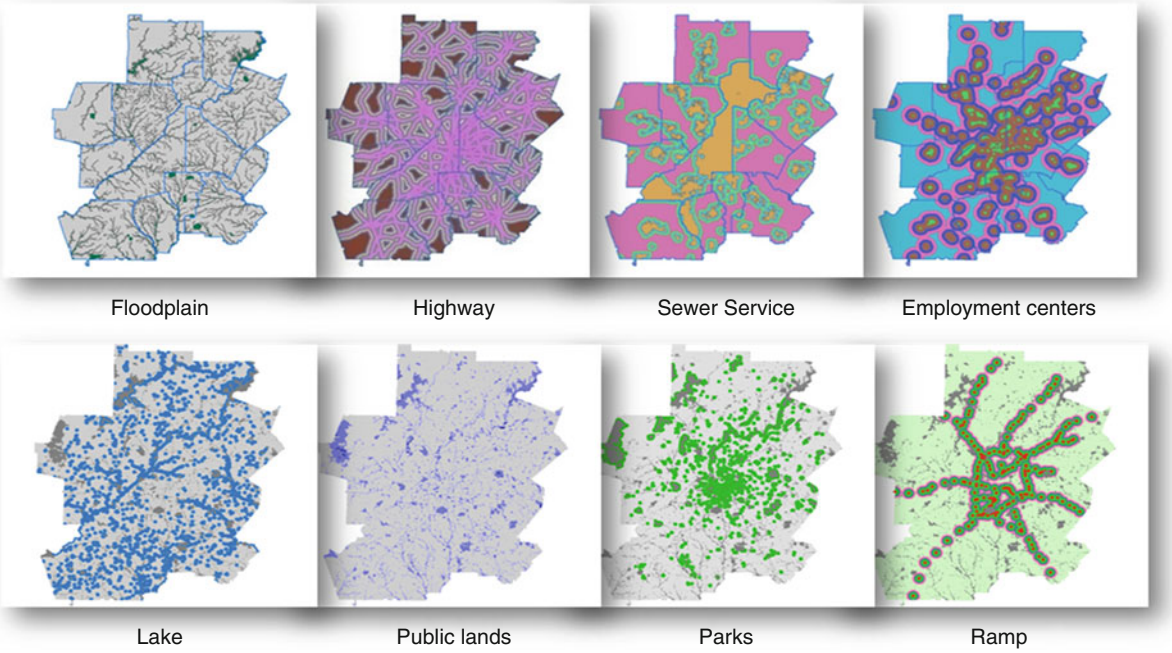

Energy and Water Interdependence, and Their Implications for Urban Areas. Figure 11
The maps show the 13 county metropolitan Atlanta area. Based on the land, the program What if?™ developed the suitability for different kinds of infrastructure and land use

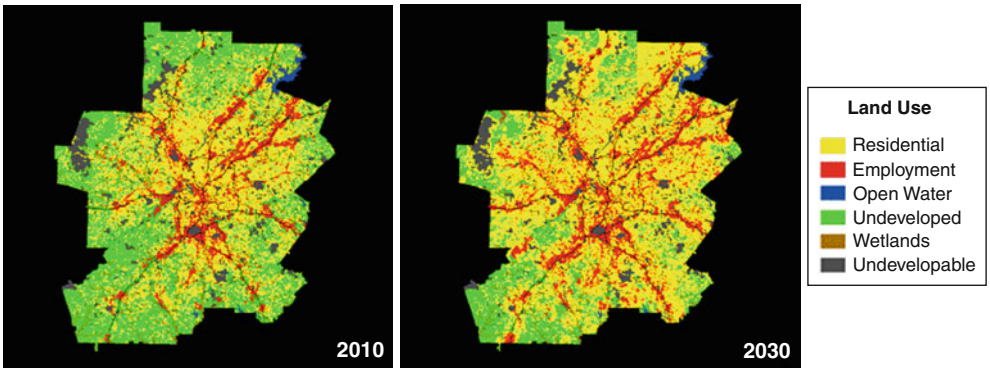

Energy and Water Interdependence, and Their Implications for Urban Areas. Figure 12
The 13 county metropolitan Atlanta area's land use. This shows the prospective land use using the Business as Usual scenario from the What if?™ software. Employment centers and residential areas expand outward over the 20 years, leaving very little area undeveloped

can grow, with more compact living and more undeveloped area, or with continued urban sprawl.

Programs such as What if?™ and UrbanSim give a rough prediction of the future, but the scenarios in these programs are not easily edited by the user. To date, infrastructure planning has been an exercise in developing a few different scenarios that fit the general tendencies of the agents and groups of agents that the infrastructure intends to serve. This approach, though, fails to account for a number of factors that affect the decision making of agents. Looking beyond a set of scenarios, agent-based modeling creates

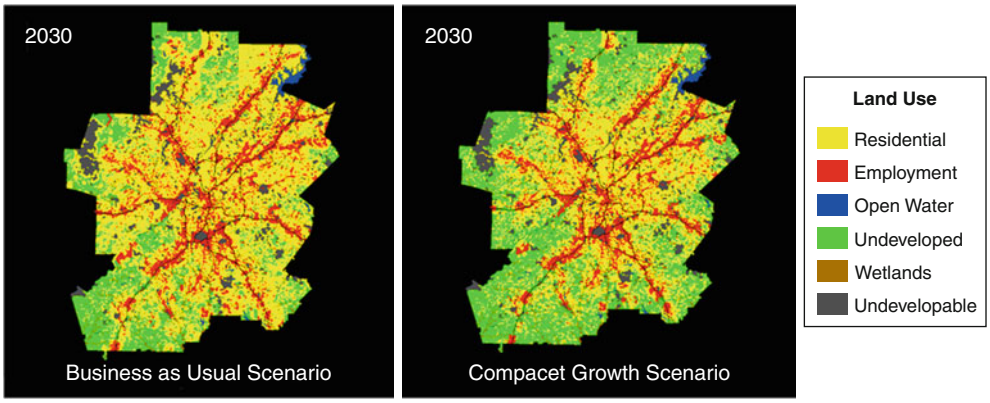

Energy and Water Interdependence, and Their Implications for Urban Areas. Figure 13
The 13 county metropolitan Atlanta area's prospective land use in 2030. This is according to the simulation run with the What if?™ software. These show the comparison of development based on two different scenarios, Business as Usual and Compact Growth. Compact Growth shows that much more land is left undeveloped and residences remain near the city, whereas Business as Usual shows an increase in urban sprawl

equations for how people react to different constraints and opportunities. For example, surveys and behavioral analyses can be used to develop algorithms that describe how people react to policy decisions or to gauge consumer awareness. These reactions though are tempered by the context of many other variables though such as economic feasibility, the state of current infrastructure, or the availability of technology. Modeling could provide a number of answers to questions concerning a city's sustainability. Some of the questions it could help address are as follows:

- What price are people willing to pay for renewable energies, and what kind of policies may be needed to encourage this choice?
- How can the transportation network be better planned in order to make public transportation efficient, and at what price will people pay to choose more sustainable forms of transportation?
- What incentives are needed for people to live in more compact spaces?
- How can consumption of nonrenewable resources be reduced?

Agent-based modeling, in combination with other modeling tools, is needed to predict the demand for urban infrastructure, how it should be built and designed, and what materials should be used.

Future Directions

For the future, there is a need to redesign our anthroposphere (the place where we live), so that it can exist within the means of nature: using only the renewable resources that nature can sustainably provide, while generating only wastes that nature can sustainably assimilate.

Future goals include:

- Monitor, model, visualize, and predict the emergent properties of urban infrastructure systems and their resilience to stressors.
- Understand the flow of resources and information as they move through the urban system with urban metabolism.
- Develop a pedagogy for the design of complex systems for sustainability within the context of urban systems.
- Integrate the human perspective into urban infrastructure so that socially sustainable policies and outcomes are produced.
- Research and develop sustainable alternative technologies for water treatment, and materials and energy production.

Acknowledgments

The authors would like to thank Brook Byers Institute for Sustainable Systems, High Tower Chair, and Georgia Research Alliance for their financial supports.

Funding for this research was provided by the US NSF grant 0836046: EFRI – RESIN Project: Sustainable Infrastructures for Energy and Water Supply (SINEWS). Any opinions, findings, conclusions, or recommendations expressed in this paper are those of the authors and do not necessarily reflect the view of the supporting organizations.

Bibliography

Primary Literature

1. GreenBiz (2000) Why tackle the sustainability challenge? GreenBiz.com
2. Committee on Education (1987) Our common future, from one earth to one world. In: UN Documents: gathering a body of global agreements, UNO
3. Xu M, Crittenden J, Chen Y, Thomas V, Noonan D, Desroches R, Brown M, French S (2010) Gigaton problems need gigaton solutions. Environ Sci Technol 44:4037–4041
4. Toepfer K (2005) One planet many people. In: UNEP press release, 2005/27
5. UNEP (2009) Population division of the department of economic and social affairs of the UN Secretariat (2009). World population prospects: the 2009 revision and world urbanization prospects. United Nations Population Division, New York
6. Kintner-Meyer M (2007) Impacts assessment of plug-in hybrid electric vehicles on electric utilities and regional US power grids part 1: technical analysis. Pacific Northwest National Laboratory, Richland
7. Bruneau M, Reinhorn A (2007) Exploring the concept of seismic resilience for acute care facilities. Earthq Spectra 23:42–62
8. Carnegie Mellon University Green Design Institute (2008) Economic input-output life cycle assessment. http://www.eiolca.net
9. Ohio State University Process Systems Engineering Group (2009) Ecologically-based life cycle assessment. http://resilience.eng.ohio-state.edu/eco-lca/index.htm
10. Goldstein R, Smith W (2002) Water and sustainability (vol 4): U.S. electricity consumption for water supply and treatment – the next half century. EPRI Technical Report 1006787, EPRI, Palo Alto
11. Klein G, Krebs M, Hall V, O'Brien T, Blevins BB (2005) California's water-energy relationship. In: Integrated energy policy report proceeding (04-IEPR-01E). California Energy Commission, Sacramento
12. Webber M (2008) Catch-22: water vs. energy. Sci Am 18:34–41
13. US Department of Energy (2006) Energy demands on water resources. Report to Congress on the interdependencies of energy and water. US DOE, Washington, DC
14. Gipe P (1995) Wind energy comes of age. Wiley, New York
15. Kanter J (2007) Climate change puts energy into hot water. New York Times, 20 May 2007
16. US Energy Information Administration (2010) Annual energy review 2009. US Department of Energy, Washington, DC
17. Harto C, Meyers R, Williams E (2010) Life cycle water use of low-carbon transport fuels. Energy Policy 38:4933–4944
18. Engineering Services, City of Vancouver (2005) Crown street, sustainable streetscapes and fish habitat enhancement project. Engineering Services, City of Vancouver, Vancouver
19. USAID Water Team (2003) USAID water team case study in integrated water resources management. USAID, Washington, DC. http://www.usaid.gov/our_work/environment/water/case_studies_success.html
20. Culligan P (2011) Solving urbanization challenges by design – the science of green roofs. Columbia University, The Earth Institute, New York
21. Minnesota Stormwater Steering Committee (2008) The Minnesota stormwater manual: version 2. Minnesota Pollution Control Agency, St. Paul, pp 352–353
22. EPA (2011) WaterSense®: program accomplishments. http://www.epa.gov/WaterSense/about_us/program_accomplishments.html
23. Elliott RN, Spurr M (1999) Combined heat and power: capturing wasted energy. ACEEE, Washington, DC
24. UNEP (2005) Combined heat and power: clean and efficient energy production. United Nations Environmental Programme, Governing Council, http://www.unep.org/GC/GCSS-IX/Documents/FINLAND-combinedheatpower.pdf
25. US Energy Information Administration Database
26. Weise E (2008) The shape of lights to come? Not everyone's buying it. USA Today, 28 Feb 2008
27. Brown M, Gumerman E, Baek Y, Morris C, Wang Y (2010) Renewable energy in the south: a policy brief. Working paper
28. Pandit A, Jeong H, Crittenden JC, Xu M, Ariaratnam S, Begovic M, Bras B, Brown M, DesRoches R, French S, Georgakakos A, Karady G, Li K, Noonan D, Perrings C, Williams E (2010) Sustainable and resilient urban infrastructure design: a holistic approach. In: The 6th international conference on sustainable water environment, session 4.7: Infrastructure, Newark, DE
29. Gagnon L (2002) Life-cycle assessment of electricity generation options: the status of research in 2001. Energy Policy 30(14):1267–1278
30. Georgia Power (n.d.) Plant Branch. Retrieved from Georgia Power. www.georgiapower.com/about/pdf/Plant%20branch%20Brochure.pdf
31. Georgia Power (n.d.) Plant Branch. Retrieved from Georgia Power. www.georgiapower.com/about/pdf/Plant%20branch%20Brochure.pdf
32. Georgia Power (n.d.) Plant Robert W. Scherer. Retrieved 2010, from Georgia Power. www.georgiapower.com/about/pdf/Plant%20sherer%20Brochure.pdf
33. Georgia Power (n.d.). Plant Wansley. Retrieved from Georgia Power. www.georgiapower.com/about/pdf/Plant%20Wansley%20Brochure.pdf
34. US Energy Information Administration (2010) Updated capital cost estimates for electricity generation plants
35. Miroslav M, Begovic IK (2011) Distributed renewable PV generation in urban distribution networks. In: PSCE 2011, IEEE power systems conference and exposition, Phoenix

36. Borin S, Wang J, Thomas V (2009) City of Atlanta greenhouse gas emissions inventory. Report to the City of Atlanta, Atlanta
37. Westerhoff P, Crittenden J (2009) Urban infrastructure and use of mass balance models for water and salt. In: LA Baker, ed. The Water Environment of Cities. Boston, MA: Springer US, pp 49–68
38. Brown MA, Southworth F, Sarzynski A (2008) Shrinking the carbon footprint of metropolitan America. The Brookings Institution, Washington, DC
39. Scott C, Pasqualetti M, Hoover J, Garfin G, Varady R, Guhathakurta S (2009) Water and energy sustainability with rapid energy growth and climate change in the Arizona-Sonora border region. Report to the Arizona water institute (closed)

Books and Reviews

Agence France-Presse (2006) Heat wave claims lives in Europe, and hottest days are still to come. New York Times-Europe, 19 July 2006

US EPA Region 2 (2006) Report on the City of New York's progress in implementing the watershed protection program, and complying with the filtration avoidance determination. US EPA Region 2. New York City watershed team and New York State Department of Health Bureau of water supply protection. US EPA, Washington, DC

Tugend A (2008) If your appliances are avocado, they probably aren't green. New York Times, 12 May 2008

Klein G (2009) The water-energy-carbon footprint connection

Wei M, Patadia S, Kammen D (2010) Putting renewables and energy efficiency to work: how many jobs can clean energy industry generate in the US? Energy Policy 38(2):919–931

Bruno L (1931) Magic plates, tap sun for power. Pop Sci 118:41

Torcellini P, Long N, Judkoff R (2003) Consumptive water use for U.S. power production. NREL, Golden, p 5, Dec 2003

Annual Energy Review (2009) U.S. Energy Information Administration. US DOE, Washington, DC, p 230, Aug 2010

Lazard Ltd (2009) Levelized cost of energy analysis, version 3.0. Lazard, New Orleans, p 2, Feb 2009

Energy Storage: Ultracapacitor

Andrew F. Burke
Institute of Transportation Studies, University of California-Davis, Davis, CA, USA

Article Outline

Glossary
Definition
Introduction
Energy Storage Characteristics of Ultracapacitors and Batteries
Systems Considerations and Advantages of Combining Ultracapacitors and Batteries
Laboratory and Vehicle Field Experiences Using Ultracapacitors
Hybrid Vehicle Simulations Using Ultracapacitors Alone
Plug-in Hybrid Vehicle Simulations Using Advanced Batteries And Ultracapacitors
Fuel Cell Vehicle Simulations Using Ultracapacitors
Economic Considerations
Future Directions of Ultracapacitor Development and Vehicle Applications
Summary
Bibliography

Glossary

Battery A cell in which electrical energy is stored and discharged via Faradaic electrochemical reactions occurring at a predetermined voltage dependent on the active materials in the two electrodes.

Control (power split) strategy The strategy used in a hybrid-electric vehicle to determine the fraction of the power demanded that is provided by the electric motor and engine, respectively.

Hybrid-electric vehicle (HEV) A vehicle having both an electric motor and internal combustion engine in which the battery is maintained near a fixed state-of-charge via electrical energy generated by the electric motor/generator driven by the engine.

Plug-in hybrid electric vehicle (PHEV) A vehicle having both an electric motor and internal combustion engine in which the battery is depleted by all-electric driving and recharged from the wall plug.

Pulse power efficiency The fraction of the discharge or charge energy from the battery or ultracapacitor during a short, high-power pulse that is available as electrical energy for use by the vehicle.

Ultracapacitor (electrochemical capacitor) A device in which electrical energy is stored and discharged via the electrostatic separation of charge in the micropores of activated carbon in two electrodes.

Vehicle simulations Computer calculations of the operation of a vehicle based on models of the various components in the driveline of the vehicle and a specified control strategy for its operation.

Definition

Most hybrid vehicles use batteries for energy storage. The batteries must provide both the energy and power required by the vehicle. In all cases, this requires compromises in designing the battery in that it cannot be optimized for either energy density or power capability. In addition, in most cases the battery unit is oversized (stores more energy than is used by the vehicle) in order to achieve long cycle life even for the shallow cycles experienced in charge-sustaining hybrid vehicles like the Toyota Prius. As discussed in this entry, another approach to providing energy storage for hybrid vehicles, both charge-sustaining and plug-in designs, is to utilize ultracapacitors either alone or in combination with batteries. In this approach, the batteries can be optimized for energy density and cycle life and ultracapacitors can provide the power both for acceleration and regenerative braking. The ultracapacitors, which are inherently high-power devices, would be deep discharged to one-half rated cell voltage and still provide cycle life of 500,000 to one million cycles.

The development of ultracapacitors suitable for use in vehicle powertrains started in about 1990 and steady progress in improving the performance of the devices has occurred since that time. This entry is concerned with the present status of commercially available cells and modules and projections of future developments based on the performance of prototype cells of both the carbon/carbon and hybrid carbon/pseudo-capacitive designs. The cost of ultracapacitors is currently the primary obstacle to the use of ultracapacitors in vehicle applications. In this entry, the future costs are projected and compared with high-power batteries based on the ultracapacitor material costs. Finally, applications of ultracapacitors in hybrid-electric vehicle powertrains are discussed. Key considerations are the relationships between the Wh stored in the ultracapacitor unit, system control strategy, and the fuel economy improvements attained for various driving cycles. These relationships are studied using detailed vehicle simulation results from Advisor.

Introduction

In the first section of the entry, the energy storage characteristics of lithium batteries and ultracapacitors are presented and compared. Of particular interest is the comparative power capability of lithium batteries and carbon/carbon ultracapacitors for charge/discharge conditions to be encountered in hybrid-electric vehicles. In the next section, system considerations and advantages of combining ultracapacitors and batteries for energy storage are discussed. Next laboratory and field experiences with ultracapacitors in hybrid-electric vehicles are reviewed for transit bus, light-duty, and fuel cell applications.

The final sections of the entry discuss in detail simulations of vehicles on various driving cycles using ultracapacitors alone and in combination with advanced batteries. The vehicle simulations treat charge-sustaining micro- and mild-hybrid designs, plug-in hybrids, and fuel cell–powered vehicles. The charge-sustaining hybrid vehicles using ultracapacitors alone in place of batteries are discussed in terms of the sizing of the ultracapacitor unit and control strategies that optimize the fuel economy improvements achievable. For the plug-in hybrids, the emphasis is on the use of ultracapacitors with advanced batteries having energy densities greater than 200 Wh/kg. It is likely that these batteries will not have proportionally high power density and will require the assist of ultracapacitors to achieve all-electric operation even on the FUDS driving cycle. The next section of the entry deals with fuel cell–powered vehicles and considers the use of ultracapacitors to load level the fuel cell to increase system efficiency and thus improve hydrogen consumption. In the final section of the entry, the cost of batteries and ultracapacitors are compared for charge-sustaining hybrid applications.

Energy Storage Characteristics of Ultracapacitors and Batteries

Lithium batteries and ultracapacitors have been tested in the laboratory at the University of California, Davis [1–3]. A summary of the test results for the batteries is given in Table 1 and for ultracapacitors in Table 2. For both energy storage technologies, the devices with the highest energy density typically have the lowest power capability. The pulse power capabilities shown in the tables were calculated using the following relationships:

Batteries: $P = EF(1-EF)\ V_{oc}^2/R$
Ultracapacitors: $P = 9/16(1-EF)\ V_{rated}^2/R$

Energy Storage: Ultracapacitor. Table 1 Summary of the performance characteristics of lithium-ion batteries of various chemistries

Battery developer/ cell type	Electrode chemistry	Voltage range	Ah	Resist. (mOhm)	Wh/kg	W/kg 90% effic.[a]	W/kg match. imped.	Wt. (kg)	Density (gm/cm^3)
Enerdel HEV	Graphite/ Ni MnO2	4.1–2.5	15	1.4	115	2,010	6,420	0.445	–
Enerdel EV/PHEV	Graphite/ Ni MnO2	4.1–2.5	15	2.7	127	1,076	3,494	0.424	–
Kokam prismatic	Graphite/ NiCoMnO2	4.1–3.2	30	1.5	140	1,220	3,388	0.787	2.4
Saft cylind.	Graphite/ NiCoAl	4.0–2.5	6.5	3.2	63	1,225	3,571	0.35	2.1
GAIA cylind.	Graphite/ NiCoMnO2	4.1–2.5	40	0.48	96	2,063	5,446	1.53	3.22
			7	3.6	78	1,310	3,472	0.32	–
A123 cylind.	Graphite/ iron phosph.	3.6–2.0	2.2	12	90	1,393	3,857	0.07	2.2
Altairnano prismatic	LiTiO/ NiMnO2	2.8–1.5	11	2.2	70	990	2,620	0.34	1.83
Altairnano prismatic	LiTiO/ NiMnO2	2.8–1.5	3.8	1.15	35	2,460	6,555	0.26	1.91
Quallion cylind.	Graphite/ NiCo	4.2–2.7	1.8	60	144	577	1,550	0.043	2.6
Quallion cylind.	Graphite/ NiCo	4.2–2.7	2.3	72	170	445	1,182	0.047	2.8
EIG prismatic	Graphite/ NiCoMnO2	4.2–3.0	20	3.1	165	1,278	3,147	0.41	–
EIG prismatic	Graphite/ iron phosph.	3.65–2.0	15	2.5	113	1,100	3,085	0.42	–
Panasonic EV prismatic	Ni metal hydride	7.2–5.4	6.5	11.4	46	395	1,093	1.04	1.8

[a]power density P=Eff.*(1−Eff.) Voc^2/R, $P_{match.\ imped.} = V^2/4R$

where EF is the efficiency of the pulse ($EF = V_{pulse}/V_{oc}$). The matched impedance power which is often cited for both battery and ultracapacitor devices is calculated as follows:

$$P_{matchimped.} = V^2/4R$$

These power relationships are derived in [4].

For charge-sustaining hybrids, it seems reasonable to cite the power capability of devices for pulse power efficiencies of 90–95%. For PHEVs and EVs operating in charge-depleting modes for the battery, it is reasonable to cite the power for efficiencies of 75–80%. In all instances, the power capability is proportional to V^2/R indicating that high power capability requires a low resistance R.

Comparisons of the Power Capabilities of Lithium Batteries and Ultracapacitors

There has been considerable discussion in the literature [4–6] comparing the power capability of lithium-ion

Energy Storage: Ultracapacitor. Table 2 Summary of ultracapacitor device characteristics

Device	V rated	C (F)	R (mOhm)	RC (s)	Wh/kg (1)	W/kg (95%) (2)	W/kg match. imped.	Wt. (kg)	Vol. (l)
Maxwell[a]	2.7	2,885	0.375	1.08	4.2	994	8,836	0.55	0.414
Maxwell	2.7	605	0.90	0.55	2.35	1,139	9,597	0.20	0.211
Skeleton technologies	2.8	1,600	1.3	2.1	5.8	800	7,140	0.22	0.13
Yunasko[b]	2.7	55	4	0.22	5.5	5,695	50,625	0.009	–
Yunasko[b]	2.7	450	1.3	0.58	5.89	2,766	24,595	0.057	0.045
Yunasko[b]	2.7	510	0.9	0.46	5.0	2,919	25,962	0.078	0.055
Ness	2.7	1,800	0.55	1.00	3.6	975	8,674	0.38	0.277
Ness	2.7	3,640	0.30	1.10	4.2	928	8,010	0.65	0.514
Ness (cyl.)	2.7	3,160	0.4	1.26	4.4	982	8,728	0.522	0.379
Asahi glass (propylene carbonate)	2.7	1,375	2.5	3.4	4.9	390	3,471	0.210 (estimated)	0.151
Panasonic (propylene carbonate)	2.5	1,200	1.0	1.2	2.3	514	4,596	0.34	0.245
EPCOS	2.7	3,400	0.45	1.5	4.3	760	6,750	0.60	0.48
LS Cable	2.8	3,200	0.25	0.80	3.7	1,400	12,400	0.63	0.47
BatScap	2.7	2,680	0.20	0.54	4.2	2,050	18,225	0.50	0.572
Power sys. (activated carbon, propylene carbonate)[b]	2.7	1,350	1.5	2.0	4.9	650	5,785	0.21	0.151
Power sys. (graphitic carbon, propylene carbonate)[b]	3.3	1,800	3.0	5.4	8.0	486	4,320	0.21	0.15
	3.3	1,500	1.7	2.5	6.0	776	6,903	0.23	0.15
JSR micro (AC/graphitic carbon)	3.8	1,000	4	4	11.2	900	7,987	0.113	0.073
		2,000	1.9	3.8	12.1	1,038	9,223	0.206	0.132

(1) Energy density at 400 W/kg constant power, Vrated – 1/2 Vrated
(2) Power based on P=9/16*(1−EF)*V2/R, EF=efficiency of discharge
[a]Except where noted, all the devices use acetonitrile as the electrolyte
[b]Except for these, all devices are packaged in metal containers

batteries and ultracapacitors. The conclusions vary from statements that lithium batteries have power capability equal to that of ultracapacitors to statements that ultracapacitors have an order of magnitude higher power capability than lithium batteries. Detailed comparisons of the power capability of ultracapacitors and batteries taken from [4] are shown in Table 3. As indicated in the table, neither of the extreme statements is valid in general and that comparisons should be made between specific devices for specific applications. Comparisons are often made based on the matched impedance power of the two types of devices. These comparisons indicate that most ultracapacitors have a power capability (W/kg) of three to six times that of lithium batteries. However, for vehicle applications the matched impedance power is not appropriate and should not be the basis of comparison.

For charge-sustaining HEV applications, a good basis of comparison is the W/kg at 95% efficiency at the SOC at which the devices will be used in the

Energy Storage: Ultracapacitor. Table 3 Comparisons of the power capabilities of various devices for HEVs and PHEVs using the different methods of calculation

Device Lithium batteries 60% SOC	Matched impedance	USABC Min/max	Efficient pulse EF =95%	Efficient pulse EF =80%
Kokam NCM 30 Ah	2,893	2,502	550	1,848
Enerdel HEV NCM 15 Ah	5,491	4,750	1,044	3,507
Enerdel EV NCM 15 Ah	2,988	2,584	568	1,908
EIG NCM 20 Ah	2,688	2,325	511	1,721
EIG FePhosph. 15 Ah	2,141	2,035	458	1,540
Altairnano LiTiO 11 Ah	1,841	1,750	350	1,180
Altairnano LiTiO 3.8 Ah	4,613	4,385	992	3,341
Ultracapacitors $V_0 = 3/4V_{Rated}$				
Maxwell 2,890 F	8,836	4,413	994	
Nesscap 3,100 F	8,730	4,360	982	
BatScap 2,700 F	18,224	9,102	2,050	
Yunasko 450 F	22,838	11,406	2,569	
LS Cable 3,200 F	12,446	4,609	1,038	
JSR 2,000 F	9,228	6,216	1,400	

vehicle. On this basis, there are lithium batteries with the same power capability as some carbon/carbon ultracapacitors, but there are some ultracapacitors with power capability twice that of the highest power lithium batteries presently available for vehicle applications. In other words, it is not possible to make general statements that are applicable to all devices of either type. The issue is further complicated when one notes that the density of the lithium batteries is about twice that of carbon/carbon ultracapacitors (2.2 g/cm^3 for the batteries and 1.2 g/cm^3 for the ultracapacitors). Hence on a volume basis W/l at 95% efficiency, the differences between the batteries and ultracapacitors are often quite small. Hence for HEVs, batteries alone and ultracapacitors alone can be an option with the decision being based on cycle life and cost in addition to relative power capability [7].

For plug-in hybrid and battery electric vehicle applications, the maximum usable power density from the lithium-ion battery can be higher than in an HEV because the peak power of the driveline is used less frequently and consequently charge/discharge efficiently is less important. For example, a pulse power efficiency of 80% is probably sufficient and most of the lithium batteries have a power capability of greater than 1,000 W/kg, 2,200 W/l for that efficiency.

In addition, the battery is larger (heavier) in these vehicles and as a result, the power density requirement is less demanding. For PHEVs and EVs, the best application of ultracapacitors is likely to be in combination with batteries designed for high energy density, long cycle life, and low cost. In those cases, as discussed in a later section of the entry, the ultracapacitors greatly reduce the peak currents and dynamic stress on the batteries and thus extend their cycle life.

Systems Considerations and Advantages of Combining Ultracapacitors and Batteries

Vehicle Design Considerations

The energy storage requirements vary a great deal depending on the type and size of the vehicle being designed and the characteristics of the electric powertrain to be used. Energy storage requirements for various vehicle designs and operating modes are shown in Table 4 for a midsize passenger car. Requirements are given for electric vehicles and both charge-sustaining and plug-in hybrids. These requirements can be utilized to size the energy storage unit in the vehicles when the characteristics of the energy storage cells are known. In some of the vehicle designs considered in Table 4, ultracapacitors are used to provide the peak power rather than batteries.

In the cases using only ultracapacitors, the key issue is the minimum energy (Wh) required to operate the vehicle in real-world driving because the energy density characteristics of ultracapacitors are such that the power and cycle life requirements will be met in most cases if the unit is large enough to met the energy storage requirement. As shown in Table 4, for passenger car applications, the energy storage in the ultracapacitor can be 150 Wh or less even if the ultracapacitor is used alone for the energy storage.

Reasons for Combining Ultracapacitors and Batteries

Most hybrid vehicles use batteries for energy storage. The batteries must provide both the energy and power required by the vehicle. In all cases, this requires compromises in designing the battery in that it cannot be optimized for either energy density or power capability. In addition, in most cases the battery is oversized (stores more energy than is used by the vehicle) in order to achieve long cycle life even for the shallow cycles experienced in charge-sustaining hybrid vehicles like the Toyota Prius. Combining ultracapacitors with batteries permits the design of the batteries to be optimized for energy density and cycle life and limits the magnitude and frequency of maximum power pulses experienced by the batteries during vehicle operation. The result will be a lighter, smaller, and lower cost battery which will have much longer cycle life (by as much as a factor of 2–3) and will operate over

Energy Storage: Ultracapacitor. Table 4 Energy storage unit requirements for various types of electric drive midsize passenger cars

Type of electric driveline	System voltage V	Usable energy storage	Maximum pulse power at 90–95% efficiency (kW)	Cycle life (number of cycles)	Usable depth-of-discharge
Electric	300–400	15–30 kWh	70–150	2,000–3,000	deep
					70–80%
Plug-in hybrid	300–400	6–12 kWh battery	50–70	2,500–3,500	deep
		100–150 Wh			60–80%
		ultracapacitors			
Charge-sustaining hybrid	150–200	100–150 Wh	25–35	300 K–500 K	Shallow
		ultracapacitors			5–10%
Micro-hybrid	45	30–50 Wh	5–10	300 K–500 K	Shallow
		ultracapacitors			5–10%

significantly narrower ranges of voltage and temperature than would be the case using only a battery. In addition, the cooling requirements and complexity of the battery management unit of the battery will be reduced and be less costly.

The ultracapacitors would provide the high-power pulses in discharge and accept all the charge pulses during regenerative braking of the vehicle. If needed, the ultracapacitors can be recharged at high rates during regenerative braking and/or using power from the engine or fuel cell. The ultracapacitors would be deep discharged (up to 75% of their rated energy) when that energy is needed to power the vehicle. Even for deep discharge operation, the ultracapacitors can be expected to have a cycle life of at least 500,000 cycles. As noted in Table 4, the energy stored (Wh) in the ultracapacitors can be quite limited being less than 150 Wh for midsize passenger cars. Larger ultracapacitor units would be needed for buses and trucks, but their advantages would be similar to those used in passenger cars. The weight and cost of the ultracapacitor unit would be proportional to the energy stored so it is advantageous to limit the energy stored to the minimum required for a particular application. As shown in Fig. 1, for most applications, it will be necessary to utilize interface electronics to control the power flow from the ultracapacitors because their voltage changes significantly during discharge. This permits a large fraction of the usable energy of the ultracapacitors to be utilized and minimizes their cost.

Sizing Components: Weight and Volume

Whether or not a vehicle designer will consider using ultracapacitors alone or in combination with batteries instead of a battery pack for energy storage will depend to a large extent on the relative weight, volume, and cost of the two systems.

Consider first the case of charge-sustaining hybrid vehicles (HEVs). In this case, the energy storage unit is sized by both usable power (kW) and energy storage (Wh) requirements. For batteries, the key issues are the power requirement and the minimum usable energy consistent with high cycle life for shallow cycles.

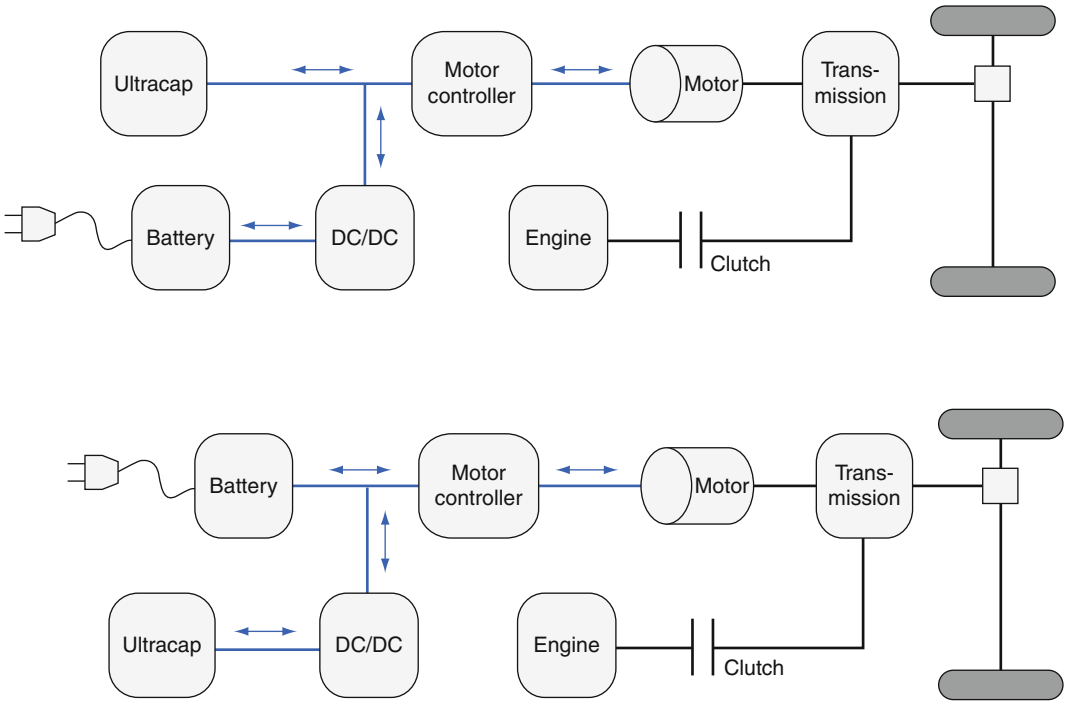

Energy Storage: Ultracapacitor. Figure 1
Schematics of powertrains using ultracapacitors and batteries

The total energy stored in the battery unit is of secondary importance as far as operation of the vehicle is concerned, but it has a strong effect on the weight, volume, and cost of the unit. For ultracapacitors, the key issue is the minimum energy (Wh) required to operate the vehicle in real-world driving because the energy density characteristics of ultracapacitors are such that the power and cycle life requirements will be met if the unit is large enough to meet the energy requirement.

Energy storage units for charge-sustaining hybrid powertrains for midsize passenger cars are shown in Table 5. For each application, the usable power and energy, total energy stored, and incremental state-of-charge for the unit and its weight and volume are shown in the table. The results shown in Table 5 indicate that for charge-sustaining hybrids, either batteries or ultracapacitors can be used alone. All the units listed should function satisfactorily for the applications indicated with the decision concerning their relative attractiveness based to a large extent on cost, which at the present time is uncertain for all the systems. The results in Table 5 also indicate that a combination of lead-acid batteries and ultracapacitors would result in a relatively low weight unit for a micro-hybrid having a maximum electric motor power of 5–10 kW. The economics of such a combination should be attractive because of the low cost of the lead-acid batteries.

Energy Storage: Ultracapacitor. Table 5 Characteristics of various technologies/types of batteries for use in charge-sustaining hybrid vehicle applications

Charge-sustaining hybrids (HEVs)								
Technology	C or Ah	System voltage	Δ SOC%	Total energy Wh[a]	Max. Power kW[b]	Pulse efficiency%	Weight of cells kg	Volume of cells l
Ultracapacitors								
Carbon/carbon	2,400	160	75	100	>40	90	22	15
microporous C/ graphitic C	2,400	160	75	150	27	90	18	13
Lithium-ion batteries								
Graphite/Ni Co Al	9	160	6.6	1,500	31	91	24	11
Iron phosphate 2.2 Ah cells	11	160	5.5	2,000	27	91	23	11
Lithium titanate 11 Ah	11	160	5.5	1,800	27	90	26	14
Lithium titanate 2.5 Ah	4	160	16.6	600	27	90	16	9
Nickel metal hydride (Prius)					14	90		
	10	160	6.25	1,600	25	80	35	19
Micro-hybrids								
Lead-acid	50	45	5	1,800	5	90	53	19
Lead-acid/ ultracapacitors	28		10	1,000			29	10
	4,000	45	75	50	15	95	10	8
							39 total	18 total
Nickel metal hydride (Prius)	24	45	10	1,100	10	90	24	13

[a]Total energy stored
[b]Power at the pulse efficiency indicated

Next consider energy storage units for plug-in hybrid vehicles (PHEVs). A key design parameter for PHEVs is the all-electric range. Energy storage units will be considered for all-electric ranges of 10, 15, 20, 30, and 40 miles. The acceleration performance of all the vehicles will be the same (0–60 mph in 8–9 s). For the batteries, the usable depth of discharge will be taken to be 70%. For the ultracapacitors, it is assumed that they can be cycled from rated to one-half rated voltage using 75% of the total stored energy. In the PHEVs, the battery will be sized by the energy needed to sustain a specified all-electric range. Hence the weight and volume of the battery pack follow directly from its energy density (Wh/kg, Wh/l). This means that battery technologies with high energy density will be strongly favored for PHEV applications. However, the batteries must also be able to meet the power requirements of the PHEV powertrain which can approach those of the battery-powered EV. Unfortunately, battery designs to attain the maximum energy density in most cases require a sacrifice in power capability as shown in Table 1. Calculated power density requirements for PHEVs of various ranges and maximum power [8] are given in Table 6 for batteries having energy densities of 70, 100, and 200 Wh/kg. The values shown are for a midsize passenger car having an energy usage of 250 Wh/mile in the all-electric mode and maximum electric motor power of 50 and 70 kW.

The required power densities for all-electric ranges of 20 miles and less are high especially for high energy density batteries. When the power density required exceeds that of the battery, it is of interest to consider using an ultracapacitor to augment the power of the battery. The usable pulse power from a battery depends on the efficiency that is acceptable for a particular application. The power densities for efficiencies of 95% and 80% for the various battery technologies are shown in Table 3. If it is assumed that 80% efficiency is satisfactory for use of the battery in the charge-depleting mode of the PHEV, it can be concluded from Tables 3 that ultracapacitors would be needed by the 200 Wh/kg lithium-ion and the 70 Wh/kg nickel metal hydride batteries. This result is shown in Table 7. The energy storage unit weights for the PHEVs of various all-electric ranges and battery energy density are given in Table 8. The combination of ultracapacitors and 200 Wh/kg lithium-ion batteries have the lowest weight for all the ranges. For higher energy density batteries (>250 Wh/kg), it seems even more likely that ultracapacitors will be needed to meet the power demands of PHEVs. The combination of ultracapacitors and batteries will also yield the highest efficiency during the charge-sustaining mode of vehicle operation after the energy of the batteries has been depleted.

As noted above, ultracapacitors can be used with 70 Wh/kg nickel metal hydride batteries for PHEV applications due to their limited power capability. Even using ultracapacitors, the all-electric range with nickel metal hydride batteries is limited to about 15 miles as otherwise the weight of the energy storage unit would exceed 100 kg.

Energy Storage: Ultracapacitor. Table 6 Battery sizing and power density for various ranges and motor power

Range miles	kWh [a]needed	kWh[b] stored	Battery 200 Wh/kg			Battery 100 Wh/kg			Battery 70 Wh/kg		
			[b] kg	50 kW kW/kg	70 kW kW/kg	kg	50 kW kW/kg	70 kW kW/kg	kg	50 kW kW/kg	70 kW kW/kg
10	2.52	3.6	18	2.78	3.89	36	1.39	1.94	51	0.98	1.37
15	3.78	5.4	27	1.85	2.59	54	0.92	1.30	77	0.65	0.91
20	5.04	7.2	36	1.39	1.94	72	0.69	0.97	103	0.49	0.68
30	7.56	10.8	54	0.93	1.30	108	0.46	0.65	154	0.32	0.46
40	10.1	14.4	72	0.69	0.97	144	0.35	0.49	206	0.24	0.34

[a]Vehicle energy usage from the battery: 250 Wh/mi

[b]Usable state-of-charge for batteries: 70%, weights shown are for cells only

Energy Storage: Ultracapacitor. Table 7 Battery/ultracapacitor combinations for various all-electric ranges

Wh/kg	100	200	100	90	70	70
Range miles	GAIA	Quallion 200	Quallion 100	A123	Altairnano	Panasonic Nickel mt.hyd.
10	N/N[a]	Y/Y	N/N	N/N	N/N	Y/Y
15	N/N	Y/Y	N/N	N/N	N/N	Y/Y
20	N/N	Y/Y	N/N	N/N	N/N	Y/Y
30	N/N	Y/Y	N/N	N/N	N/N	Y/Y
40	N/N	N/N	N/N	N/N	N/N	Y/Y

[a]X/X means need at 50 kW/need at 70 kW yes Y or no N

Energy Storage: Ultracapacitor. Table 8 Storage unit weights using a combination of batteries and ultracapacitors for various all-electric ranges

Wh/kg	5	200		100		70	
Range miles	Ultracap kg[a]	Battery Kg[b]	Combination kg	Battery kg	Combination kg	Battery kg	Combination kg
10	20	18	38	36	56	51	71
15	20	27	47	54	74	77	97
20	20	36	56	72	92	103	123
30	20	54	74	108	128	154	174
40	20	72	92	144	164	206	226

[a]The ultracapacitor unit stores 100 Wh usable energy
[b]Weights shown are for cells only, packaging into modules not Included

Power Split Strategies

As noted previously, interface electronics is needed (Fig. 1) in hybrid powertains using a combination of batteries and ultracapacitors to control the power split between the two energy storage units. Selection of a control strategy that will both limit the maximum power demanded of the batteries and improve the efficiency of the powertrain is critical to the design of attractive HEVs and PHEVs. One approach for the PHEV applications is to have the battery meet the average vehicle power requirement and the ultracapacitor meet the variable, pulse power requirement. The average vehicle power demand can be calculated over some specified time period (30–120 s) depending on the driving conditions. As discussed later, vehicle simulations indicate that this approach results in relatively slow variations in battery power and should lead to significantly increased battery cycle life and reduced need for high-power cells. Using this approach, the interface electronics could be directly attached to either the batteries or ultracapacitors (see Fig. 1).

As in the case of the HEVs, the key element of the system control strategy is how the ultracapacitors are recharged utilizing engine power via the motor/generator. The vehicle simulations have shown that the ultracaps should be recharged during periods in which the engine is needed to meet the vehicle power requirements. In this way, the engine operates nearly all the time at high efficiency and not at low output torque conditions resulting in large improvements (>35%) in fuel economy compared to the reference engine alone case.

Laboratory and Vehicle Field Experiences Using Ultracapacitors

Laboratory Testing of Ultracap/Battery Combinations

Most of the research [9–11] involving the testing of ultracap/battery combinations has been performed on bench-top arrangements. In most cases, these tests have included state-of-the-art interface electronics that controlled the currents from the ultracapacitors. The intent of these studies has been to show that the stress on the batteries due to repeated high current pulses was greatly reduced using ultracapacitors resulting in extended battery cycle life. The test data show clearly that the mean currents from the batteries are greatly reduced, but the effect on battery cycle life is not yet clear from the data. Much further testing of this type, especially using lithium batteries, is needed. The test results [12] from a simpler test utilizing small spiral wound lithium batteries (1.4 Ah) and 310 F ultracapacitors without interface electronics are shown in Fig. 2. The data show the effect of load leveling on the cycle life of the cells which were pulsed at the 5C rate. The magnitude of the effect (a factor of 7–8) is likely much greater than can be expected with larger batteries, but nevertheless, the data do indicate that load-leveling batteries can be expected to significantly improve cycle life.

Vehicle Field Experience Using Ultracapacitors

There has been continuing experience in demonstrating the use of ultracapacitors in hybrid-electric powertrains in heavy-duty [13–15] and light-duty [16–18] vehicles. In these applications, the capacitors provide the peak power for acceleration and recover energy during periods of braking. An engine generator or fuel cell is used to generate onboard electricity to

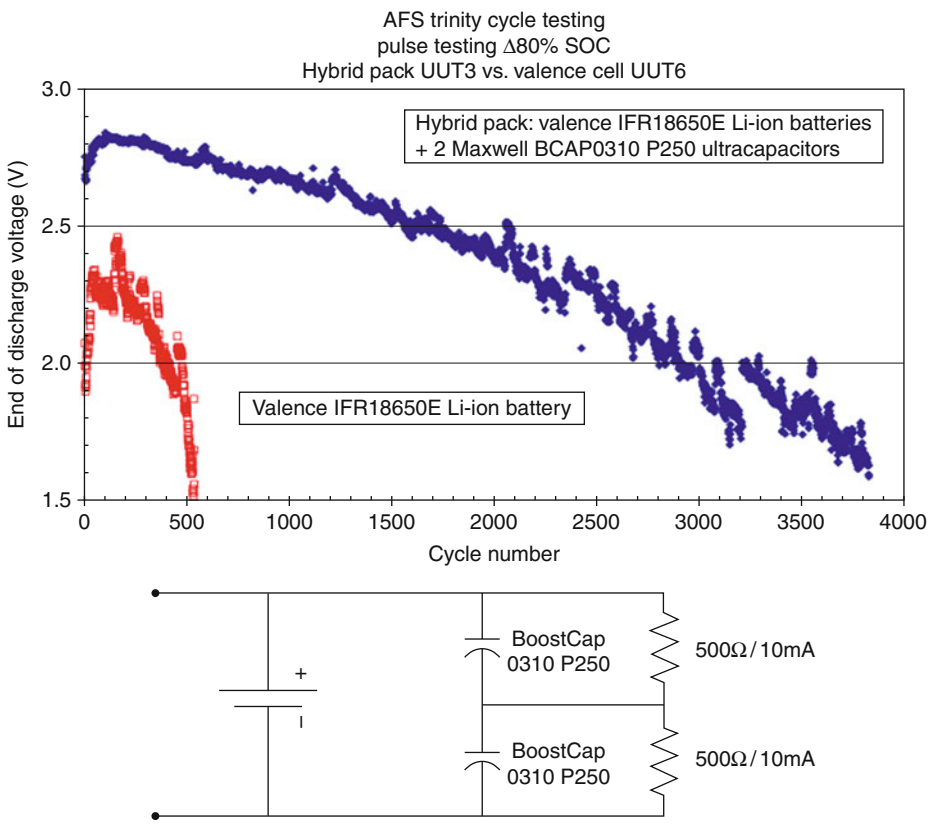

Energy Storage: Ultracapacitor. Figure 2
Pulsed discharge at average rate of 1 C comprising 5 C 5 s pulses at a 20% duty factor. Each cycle 80% (1.12 Ah)

recharge the capacitors as needed. The control strategy for the hybrid vehicle should be designed to operate the engine or fuel cell as close to the maximum efficiency condition as the driving cycle permits. Capacitor units for use in hybrid vehicles must be high voltage as the peak power for these applications is high (up to 200 kW). For passenger cars and SUVs, the voltage is likely to be about 300 V and for transit buses about 700 V. This would require 125 cells in series for the light-duty vehicles and 250 cells in series for the buses.

Transit Bus Applications In the USA, the company most active in utilizing ultracapacitors in hybrid-electric powertrains for buses and large trucks has been the ISE Corporation in San Diego, California [13]. ISE has developed a 360 V capacitor unit consisting of 144 2,600 F Maxwell cells connected in series (see Fig. 3). The weight and volume are 114 kg and 189 l, respectively. The unit stores 0.325 kWh of energy (0.245 kWh usable). In a transit bus, two of the units are used in series resulting in a voltage of 720 V and energy storage of 0.650 kWh. The peak power capability of the combined unit is over 300 kW. ISE utilizes this capacitor unit with a 225 kW electric motor in series hybrids using gasoline and diesel engines and hydrogen fuel cells. Since the capacitor unit stores only about 0.5 kWh, it can provide power only during vehicle acceleration and recovers energy during braking. The engine or fuel cell must provide all the power during cruise and hill climbing. ISE has built over 100 buses using the ultracapacitor energy storage units for transit companies in Southern California. The buses are in daily revenue service. Field experience has shown that the capacitor unit functions as planned with a high reliability. Field operation of the buses has shown a fuel economy improvement of 25% compared to the standard diesel engine buses [13].

Hybrid-Electric Passenger Car Applications Unlike the transit bus applications described in the previous section, there has not been a commercialized use of ultracapacitors in passenger cars as of 2010. In the last couple of years, there has been considerable discussion [19, 20] of marketing of micro-hybrids with stop-start

Nominal voltage	360V*
Peak voltage	403V**
Rated current	400A
Capacitance	18.05F
Total energy stored nominal / max.	0.325k Wh/0.407k Wh
Leakage current	5mA nominal
Operating temperature	–35 to 65°C
Weight	240lbs
Dimensions wxlxh	24″×40″×12″
Standard pack	144 capacitors
Fire suppression system	Heat activated halotron system

Energy Storage: Ultracapacitor. Figure 3
The ISE ultracapacitor unit (360 V, 0.325 kWh)

capability to improve fuel economy particularly in Europe. It is likely that when these cars are finally marketed some of them will use ultracapacitors. There have been several noteworthy demonstrations of ultracapacitors in hybrid-electric passenger cars. As discussed in the following paragraphs, these projects were very successful and showed that ultracapacitors can be used in place of batteries in mild hybrid vehicles with fuel economy improvements at least as high as with batteries.

The first project was termed "SUPERCAR" and was funded by the European Community (EC). It was a joint project between EPCOS [16], the ultracapacitor developer, and Siemens VDO [21], the vehicle integrator. The parallel hybrid passenger car (VW Golf) combined the ultracap module and lead-acid battery into a 42 V, 10 kW (peak) electric driveline with a 66 kW engine. The vehicle was tested on both the chassis dynamometer and the road. The tests showed a 16–18% improvement in fuel economy compared to the standard ICE car. The capacitor unit consisted of 24 3,600 F cells connected in series (see Table 2 for the cell characteristics). The rated voltage of the unit is 60 V and its capacitance and resistance are 150 F and 8 mOhm, respectively. The unit is shown in Fig. 4.

A second, more recent project (2009), is described in detail in [17]. This project was performed by the National Renewable Energy Laboratory (NREL) and General Motors (GM). It involved installing ultracapacitors in a 2007 Saturn Vue hybrid along with the nickel metal hydride battery. The vehicle could be operated on either of the energy storage units alone in order to make a direct comparison of its operation on the ultracapacitors and battery. The ultracapacitor energy storage unit consisted of one or two 48 V, 165 F modules from Maxwell. Each module, which consisted of 18 3,000 F cells connected in series (see Table 2 for the characteristics of the cells), stored about 35 Wh. A special UCAP state estimator was utilized to maintain the ultracapacitors in the required range of state-of-charge.

The 2007 Saturn Vue hybrid is a mild hybrid using a belt alternator/starter in parallel with a 127 kW, variable valve timing gasoline engine. The alternator/starter electric machine has a continuous rating of 3 kW and a peak power of 6–8 kW. The nickel metal hydride battery has a nominal rating of 36 V, but vehicle testing indicated it operates in the 38–42 V range most of the time at 75% state-of-charge. The characteristics of the energy storage units are compared in Table 9.

Extensive dynamometer testing of the vehicle was done operating on the ultracapacitors (both with one module and two modules) and the nickel metal hydride battery. The vehicle was tested on several driving cycles (FUDS, FHWY, and US06). The three energy storage options could be utilized interchangeably using the same vehicle operating strategy. The vehicle operated essentially the same on each of the energy storage options. The testing indicated that only 25–30 Wh was used from the ultracapacitor units even on the US06 driving cycle. When using only one ultracap module on the FUDS cycle, the state-of-charge (V/V_{rated}) of the ultracap unit varied from 75–90%. There was no difference in the measured fuel economy when the vehicle was operated on the ultracapacitors or the nickel metal hydride battery for any of the three

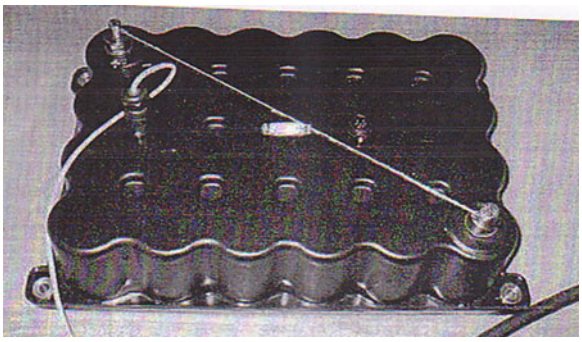

Energy Storage: Ultracapacitor. Figure 4 The EPCOS 60 V ECC module (150 F, 56 Wh)

Energy Storage: Ultracapacitor. Table 9 Characteristics of the energy storage units used in the Saturn Vue test vehicle

Storage unit	Weight (kg)	Volume (l)	Energy stored
Nickel metal hydride battery	24.7	15.4	1.1 kWh (estimated)
Ultracapacitors			
One 48 V module	14.8	11.2	35 Wh
Two 48 V modules	29.6	22.4	70 Wh

driving cycles. Test track acceleration tests of the vehicle indicated no differences in the acceleration times for 0–60 or 40–60 mph using the one module ultracapacitor and nickel metal hydride battery units.

Fuel Cell Vehicle Applications Ultracapacitors can also be used to meet the peak power transients in vehicles powered by fuel cells [22, 23]. The most publicized use of ultracapacitors in fuel cell vehicles has been that by Honda [22] in the "Honda FCV." In the Honda FCV, the capacitors were used to load level the fuel cell during accelerations and to recovery energy during regenerative braking. In the Honda fuel cell system, the ultracapacitors are used without interface electronics. The capacitors functioned very well and resulted in significant improvements in system energy efficiency.

A detailed study of the use of ultracapacitors in fuel cell–powered vehicles is given in [24]. The study showed that ultracapacitors are well suited to be used with fuel cells. This is especially true when the fuel cell and ultracapacitors are connected in parallel because the effective rest voltage of the capacitor is variable and their high-power capability permits them to meet the maximum power requirement of the system at all voltages between the rest voltage and the minimum voltage at which the fuel cell is to be operated. In this mode of operation, the system is self-controlling with the ultracapacitor and fuel cell sharing the power demand based on the system voltage of operation. Tests [24] were performed on a system (Fig. 5) consisting of the Ballard 1.2 kW Nexa fuel cell and an ultracapacitor bank made up of 17 Ness 2,500 F capacitors. The system was tested for 10 s pulses up to 5 kW. An analytical model of the fuel cell/capacitor system was derived and programmed using an EXCEL spreadsheet. Comparisons of the measured and modeled response of the system at various power levels (Fig. 6) indicated that the system operated as modeled and that the self-control of the fuel cell was as expected. SIMPLEV simulations [24] on the FUDS driving cycle were also performed for a midsize SUV powered by ultracapacitors connected in parallel with a fuel cell. It was found that the ultracapacitors significantly load leveled the fuel cell and the behavior of the system was much like that measured with the Ballard 1.2 kW Nexa fuel cell.

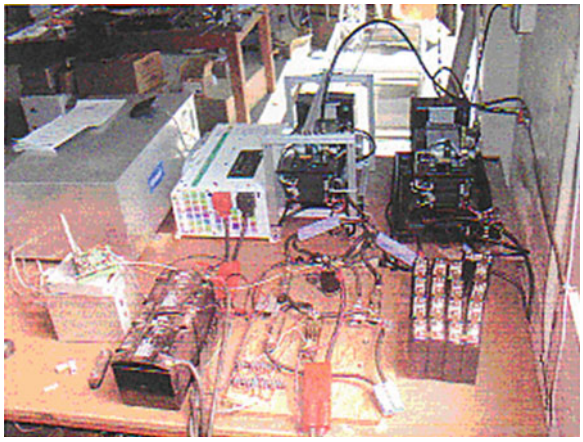

Energy Storage: Ultracapacitor. Figure 5
Photograph of the ultracapacitor/fuel cell test setup

Hybrid Vehicle Simulations Using Ultracapacitors Alone

Powertrain Control Strategies with Ultracapacitors Alone in Place of Batteries

Schematics of hybrid powertrains using ultracapacitors and batteries are shown in Fig. 1. If an ultracapacitor unit is used alone, there is no need for special electronics if the motor electronics can handle the increased voltage swing of the ultracapacitors. If that is not the case, then interface electronics is needed between the ultracapacitors and the motor electronics.

When ultracapacitors are used alone as the energy storage unit in a charge-sustaining hybrid (HEV), the objective of the control strategy is to permit the engine to operate near its maximum efficiency. As shown in [25–27], this can be done by operating the hybrid vehicle on the electric drive only when the power demand is less than the power capability of the electric motor; when the vehicle power demand exceeds that of the electric motor, the engine is operated to meet the vehicle power demand plus the power to recharge the ultracapacitor unit. In this mode, the electric machine is used as a generator and the engine operating point is selected along its maximum efficiency line (torque vs. RPM). The recharging power is limited by the power of the electric machine because ultracapacitors can have pulse power efficiency greater than 95% for W/kg values of over 2,000 W/kg (see Table 3). This control strategy is referred to as the "sawtooth" strategy

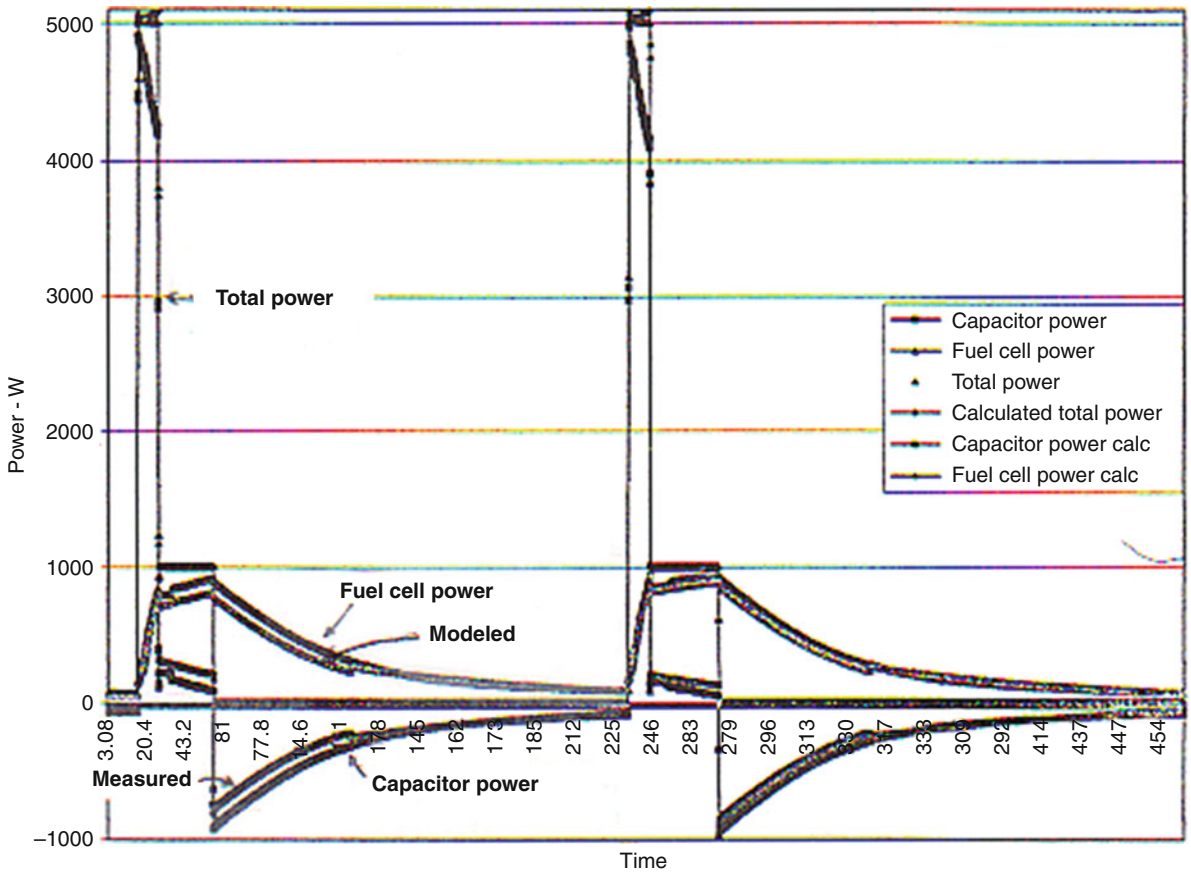

Energy Storage: Ultracapacitor. Figure 6
Comparison of the measured and modeled ultracapacitor and fuel cell powers for the 5 kW pulse power test

because a plot of the ultracapacitor state-of-charge (SOC) has the form of a saw blade. It can also be referred to as the "high engine efficiency" strategy.

Vehicle Simulation Results

Simulations of midsize passenger cars using the ultracapacitors in micro-hybrid and charge-sustaining hybrid powertrain designs have been performed using the **Advisor** vehicle simulation program modified with special routines at UC Davis [25–27]. All the powertrains were in the same vehicle having the following characteristics: test weight 1,660 kg, C_d =0.3, A_F = 2.25 m^2, RRCF = 0.009. The engine map used in the simulations was for a Ford Focus 2 l, 4-cylinder engine. The rated engine power was 120 kW for the conventional ICE vehicle and the micro-hybrid and 110 kW for the charge-sustaining hybrids. All the hybrids use the single-shaft arrangement similar to the Honda Civic hybrid. The same induction electric motor map was used for all the vehicle designs.

The simulation results are summarized in Table 10 for a conventional ICE vehicle and each of the hybrid designs. Results are given for fuel usage in terms of both l/100 km and mpg for various driving cycles. It is clear from Table 10 that large improvements in fuel usage are predicted for all the hybrid powertrains using ultracapacitors for energy storage. The simulation results will be discussed separately for each hybrid design.

Micro-hybrids The results for the micro-hybrids are particularly interesting and somewhat surprising, because of the large fuel economy improvements predicted. These improvements were about 40% on

Energy Storage: Ultracapacitor. Table 10 Summary of the vehicle fuel economy simulation results using ultracapacitors for various driving cycles

Driveline type	Energy storage type	Voltage and weight cells (kg)	EM Peak kW	L/100 km/mpg			
				FUDS	HWFET	US06	ECE-EUDC
ICE baseline				10/23.8	6.9/34.4	9.6/24.7	9.7/24.6
Micro-HEV	Lead-acid/ultracaps	48					
	Carbon/carbon	6 kg	6	5.7/41.7	5.3/44.7	7.8/30.6	5.9/40.2
	Hybrid carbon	3 kg	6	7.3/32.8	6.3/38.0	8.9/26.7	7.1/33.4
Charge-sustaining hybrid	Ultracaps	200					
	Carbon/carbon	30 kg	35	5.4/43.8	5.0/47.9	7.1/33.6	5.5/43.2
	Hybrid carbon	13 kg	35	5.8/40.9	5.2/45.8	8.0/29.9	5.8/41.3
Plug-in hybrid.	12 kWh Li battery (200 Wh/kg) and ultracaps	300	70 kW with 45 kW from caps				
	Carbon/carbon	40 kg	45	5.5/43.2	5.0/47.7	7.0/33.9	5.5/42.9
	Hybrid carbon	18 kg	45	5.8/41.2	5.2/46.2	7.9/30.2	5.8/41.2

the FUDS and ECE-EUD cycles and 20% on the Federal Highway and US06 cycles using the carbon/carbon ultracapacitors. The improvements are significantly less using the advanced hybrid carbon units because of their lower round-trip efficiencies. In the micro-hybrid designs, the rated engine power used was the same as that in the conventional ICE vehicle in order that the performance of the hybrid vehicle when the energy storage in the ultracapacitors is depleted would be the same as the conventional vehicle. The ultracapacitors were used to improve fuel economy with only a minimal change in vehicle acceleration performance. The control strategy used was the "saw-tooth" strategy discussed in the previous paragraph. As shown in Fig. 7, this resulted in a large improvement in average engine efficiency from 19% in the ICE vehicle to 30% in the micro-hybrid even though the electric motor had a peak power of only 6 kW.

Additional computer simulations were made for higher motor power (up to 12 kW) and larger ultracapacitor energy storage (up to 50 Wh). It was found that the improvements in fuel economy were only marginally greater. However, using a motor power of 3 kW reduced the fuel economy improvement on the FUDS by more than 50%. Note from Table 10 that the fuel economy improvements using the carbon/carbon ultracapacitors were for all the cycles greater than those using the advanced hybrid carbon devices. This was the case because the round-trip efficiencies for the carbon/carbon units were 95–98% and those of the hybrid carbon units were 75–90% for the various driving cycles. As shown in Table 2, the advanced hybrid carbon devices had higher energy density, but even though their power density for 95% efficiency was relatively high (1,050 W/kg), it was not proportionally higher – that is twice as high – as the carbon/carbon devices with lower energy density. These results show that it is essentially to develop high energy density ultracapacitors with proportionally higher power density; otherwise their use in vehicle applications will be compromised.

Charge-Sustaining Mild/Strong Hybrids The fuel economy simulation results for mild/strong charge-sustaining hybrids are also shown in Table 10 for a mid-size passenger car using both carbon/carbon and advanced hybrid carbon ultracapacitors. Using the carbon/carbon ultracapacitor unit, the fuel savings are about 45% for the FUDS and ECE-EUD cycles and about 27% for the Federal Highway and US06 cycles.

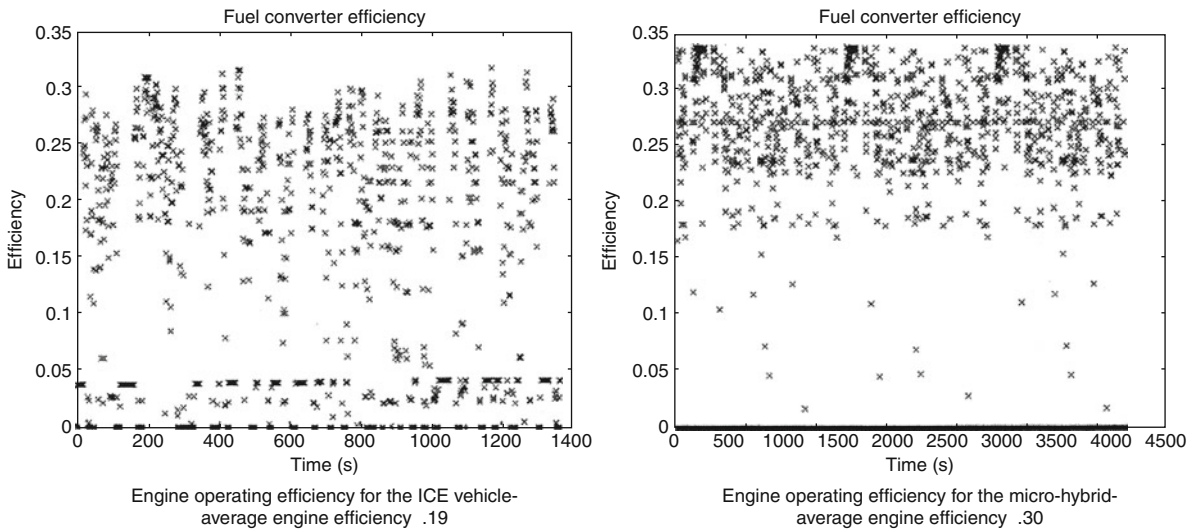

Energy Storage: Ultracapacitor. Figure 7
A comparison of engine efficiencies for a conventional ICE vehicle and a micro-hybrid on the FUDS cycle using carbon/carbon ultracapacitor

These improvement values are higher than for the micro-hybrid, but not by as large a factor as might be expected. The prime advantage of the high-power electric driveline in the mild/strong charge-sustaining hybrid is that it yields large fuel economy improvements even for high-power-requirement driving cycles like the US06. The fuel economy improvements using the advanced hybrid carbon ultracapacitor unit are not much less (5–10%) than those with the carbon/carbon unit even though the round-trip efficiency of the hybrid carbon unit is only 85–90% compared to 98% for the carbon/carbon unit. Since the weight/volume of the hybrid carbon unit is relatively small – 43% of that of the carbon/carbon unit, it appears that the mild/strong charge-sustaining hybrid application is a better one for the advanced hybrid carbon technology than the micro-hybrid application.

Plug-in Hybrid Vehicle Simulations Using Advanced Batteries and Ultracapacitors

Control Strategy for Plug-in Hybrid Vehicles (PHEVs)

For plug-in hybrid vehicles, batteries and ultracapacitors would be used in combination with the batteries providing the energy and the ultracapacitors the power. The powertrain schematics are shown in Fig. 1. The control strategy in the charge-depleting mode is to limit the power from the battery to the average power needed by the vehicle with the ultracapacitor providing the additional power during vehicle accelerations. The ultracapacitors also accept all the energy recovered during regenerative braking. If engine operation is needed, the "sawtooth" strategy is used with the ultracapacitors being recharged using engine power. In the charge-sustaining mode of operation of the PHEV, the electric drive is operated using only the ultracapacitors for energy storage like that previously described for mild/strong charge-sustaining hybrid vehicles. The PHEV operating strategies are summarized in Fig. 8.

Simulations of Plug-in Hybrid Vehicles Using Advanced Batteries and Ultracapacitors

A detailed study of plug-in hybrids using advanced batteries is presented in [8]. The characteristics of the advanced batteries used in the simulations are given in Table 11.

The battery and ultracapacitor units used in the simulations are given in Table 12. Simulations were

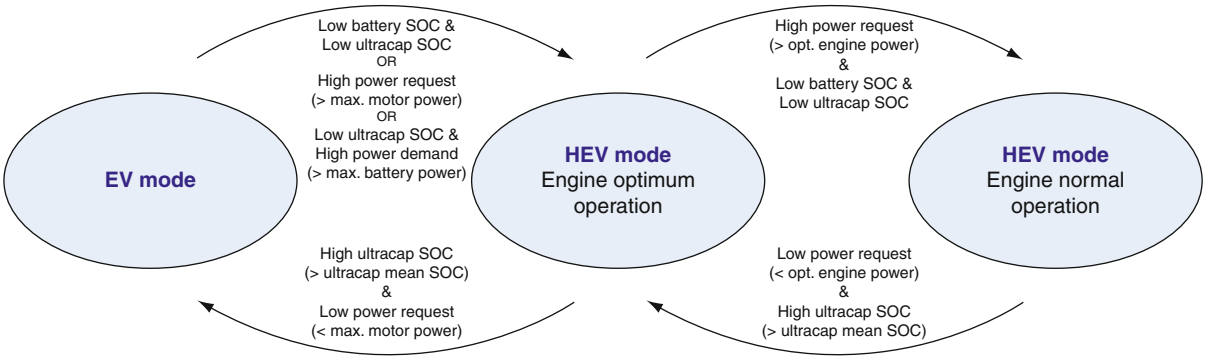

Energy Storage: Ultracapacitor. Figure 8
Summary of the operating strategy used in the simulation of plug-in hybrid vehicles

Energy Storage: Ultracapacitor. Table 11 Characteristics of present and future battery cell technologies for EVs and PHEVs

Chemistry Anode/ cathode	Cell voltage Max/nom.	Ah	Wgt. kg	R mOhm	EV Wh/ kg	HEV W/ kg 95%	EV W/ kg 75%	Cycle life (deep)	Thermal stability
Present technology batteries									
Graphite/$NiCoMnO_2$	4.2/3.6	30	0.787	1.5	140	521	2,060	2,000–3,000	fairly stable
Graphite/Mn spinel	4.0/3.6	15	0.424	2.7	127	540	2,120	1,500	fairly stable
Future technology batteries									
Graphite/composite MnO_2	4/3.6	5	0.09	20	200	250	1,350	–	fairly stable
Silicon carbon composites/ composite MnO_2	4/3.6	20	0.24	4.5	295	621	2,250	–	fairly stable
Rechargeable zinc–air	1.3/1.15	20	60	6.6	385	156	616	–	very stable
Present technology power devices									
supercapacitor activated carbon/ activated carbon	2.7/1.35	500 F	0.068	1.3	5.5	2,320	11,600	500 K	Very stable
Power battery lithium titanate oxide	2.8/2.5	4	0.23	1.15	40	1,310	5,170	20–50 K	Very stable

performed with the batteries alone and in combination with the ultracapacitors. The nominal energy storage unit voltage was 240 V in all cases with the maximum currents limited to about 300 A even in the cases of the batteries alone. In all cases, the batteries were depleted to 30% SOC from 100% SOC in the charge-depleting mode of vehicle operation.

Simulation Results for the PHEVs All the PHEV simulations were performed using the following vehicle inputs:

$C_D = 0.27$, $A_F = 2.2\ m^2$, $f_r = 0.008$, test weight = 1,650 kg (approx.)

Engine: Honda 1.3 l, iVTEC engine map, scaled to 90 kW

Energy Storage: Ultracapacitor. Table 12 The advanced battery and ultracapacitor units used in the simulations

Lithium-ion batteries				
EIG $NiCoMnO_2$	30 kg	20 Ah cells	60 in series	3.5 kWh usable
Composite MnO_2	32 kg	40 Ah cells	60 in series	4.6 kWh usable
Silicone composite	22 kg	30 Ah cells	60 in series	4.6 kWh usable
Zinc–air batteries				
Zn–air	32 kg	60 Ah cells	180 in series	9.5 kWh usable
Carbon/carbon ultracapacitors				
Symmetric C/C	20 kg	1,350 F cells	110 in series	100 Wh usable

Electric motor: Honda hybrid Civic AC PM 2006 efficiency map, scaled to 70 kW

DC/DC inverter: constant efficiency 0.96

Transmission: 5-speed manual (3.11, 2.11, 1.55, 1.0, 0.71, FD=3.95), automatically shifted in the model, but future models would incorporate the DCT (dual clutch transmission) as a convenient means to have smooth, fast shifting and to decouple the engine when it is not needed to provide power

Fuel and Electricity Use Characteristics The simulation results are summarized in Tables 13 and 14 showing results for vehicle operation in the charge-depleting and charge-sustaining modes of the PHEV.

With the batteries in combination with the ultracapacitors, the PHEVs were able to operate in the all-electric mode down to the battery SOC=30% on the FUDS and FDHW driving cycles. In all cases for the US06 driving cycle, the vehicle had blended operation (engine and electric drive both needed) in the charge-depleting mode. The use of the ultracapacitors with the batteries permitted all-electric operation over a wide range of driving conditions with higher Wh/mi for all the driving cycles. Hence in the charge-depleting mode, the fuel economy (mpg) is higher by 50–100% using the ultracapacitors for all the batteries. The fuel economy in the charge-sustaining mode is also higher for all the driving cycles using the ultracapacitors by 15–40%. The acceleration times of the vehicle were lower using the ultracapacitors than for the batteries alone. With the ultracapacitors, the acceleration times were 2.7 s for 0–30 mph and 6.9 s for 0–60 mph. For the batteries alone, the acceleration times varied somewhat with the battery used ranging from 2.9 to 3.2 s for 0–30 mph and from 8.6 to 9.8 s for 0–60 mph. Hence in all respects, vehicle performance was improved using the ultracapacitors for all the batteries studied.

Reductions in Battery Stress Using Ultracapacitors

The current and voltage responses of the batteries with and without the ultracapacitors are shown in Figs. 9–12 for the silicone carbon lithium-ion and the zinc–air batteries for the FUDS and US06 driving cycles. The effects of the load leveling of the power demand from the batteries using the ultracapacitors are evident in the figures. Both the average currents and the peak currents from the batteries are lower by a factor of 2–3 using the ultracapacitors. The minimum voltages of the batteries are significantly higher using the capacitors and the voltage dynamics (fluctuations) are dramatically reduced. Hence, the stress on the battery and resultant heating are much reduced. The simulation results in Figs. 9–12 also show that the ultracapacitors are utilized over a wide voltage range indicating that a large fraction of their usable energy storage (100 Wh) is being used to load level the batteries. This is only possible using a DC/DC converter between the battery and the DC bus.

The simulation results also indicate that using ultracapacitors, batteries with a wide range of power characteristics can be used in PHEVs and also EVs without sacrificing vehicle performance and subjecting the batteries to high stress and resultant shorter cycle life. This could be especially important in the future as high energy density batteries such as zinc–air and possibly lithium–air are developed. It is likely that those battery types will not have commensurate increases in usable power density and without ultracapacitors, the battery unit in PHEVs and EVs would be sized by the maximum power requirement (kW) rather than the range (mi)/energy requirement (kWh). This would significantly increase weight, volume, and the cost of the battery unit. It is also unlikely that the air electrode will have high charge acceptance

Energy Storage: Ultracapacitor. Table 13 Simulation results for the advanced batteries with ultracapacitors

Battery Type (1)	Cycle	Range mi.	kW max. control	kW max bat.	Eff. Bat.	kW max. Cap.	Eff. Cap.	Wh/ mi Bat.	Operat. mode	mpg 20mi	mpg 40mi	Ch. Sus. HEV mpg
Compos. MnO2	FUD	22	40	18	0.94	40	0.97	215	AE	none	97	52.8
32 kgbat	HW	20	45	18	0.91	45	0.96	227	AE	none	109	56.3
20 kgcap	US06	30	68	21	0.91	68	0.94	180	blended	71.9	56	38.3
Si Carb/ Compos. MnO2	FUD	20	40	18	0.94	40	0.97	220	AE	none	99	52.8
22 kgbat	HW	20	45	19	0.91	45	0.97	225	AE	none	110	56.8
20 kgcap	US06	30	68	21	0.91	68	0.94	190	blended	71.1	52	38.4
Rech. Zn–air	FUD	40	45	19	0.87	45	0.97	228	AE	none	none	54.5
32 kgbat	HW	38	45	19	0.81	45	0.97	242	AE	none	none	57.7
20 kgcap	US06	66	68	21	0.82	68	94	149	blended	62.4	60	38.8

(1) Weight of cells only

Energy Storage: Ultracapacitor. Table 14 Simulation results for the batteries alone

Battery Type (1)	Cycle	Range mi.	kW max. control	kW max bat.	Eff. Bat.	Wh/mi Bat.	Operat. mode	mpg 20mi.	mpg 40mi	Mpg Ch. sus. HEV
EIG NiCoMn	FUD	27	30	30	0.94	125	blended	134	85	47
30 kg	HW	24	20	20	0.93	137	blended	110	87	47
	US06	57	58	58	0.88		blended	48	45	37
Compos. MnO2	FUD	36	30	30	0.92	135	blended	134	104	46.9
32 kgbat	HW	31	20	20	0.91	147	blended	167	113	46.6
	US06	64	58	58	0.87	92	blended	48	48	34.1
Si Carb/Compos. MnO2	FUD	35	30	30	0.93	138	blended	138	106	46.9
22 kgbat	HW	32	20	20	0.92	148	blended	169	114	46.9
	US06	64	58	58	0.88	87	blended	48	48	35.7
Rech. Zn–air	FUD	66	30	30	0.84	139	blended	139	137	39.4
32 kgbat	HW	63	20	20	0.83	156	blended	169	169	41.1
	US06	93	36	36	0.72	101	blended	48.5	48.5	30.1

(1) Weight of cells only

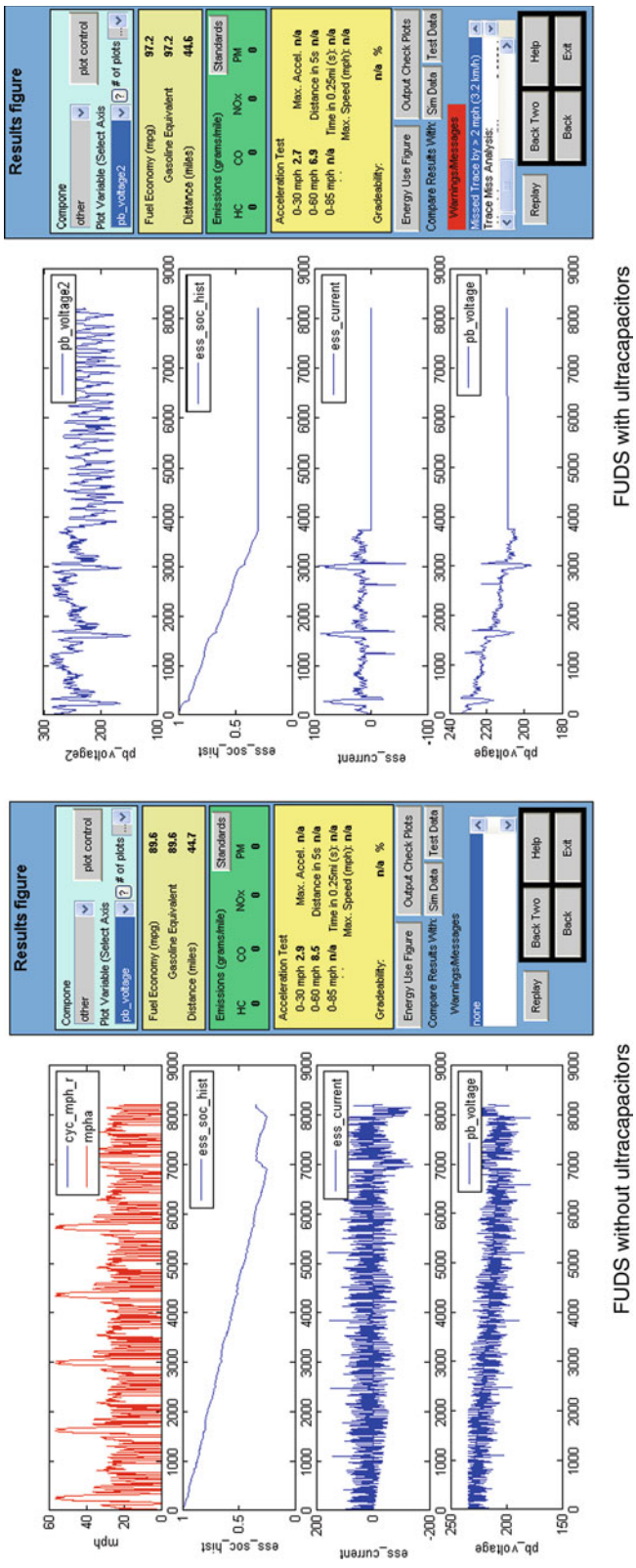

Energy Storage: Ultracapacitor. Figure 9
The Si carbon lithium battery on the FUDS with and without ultracapacitors

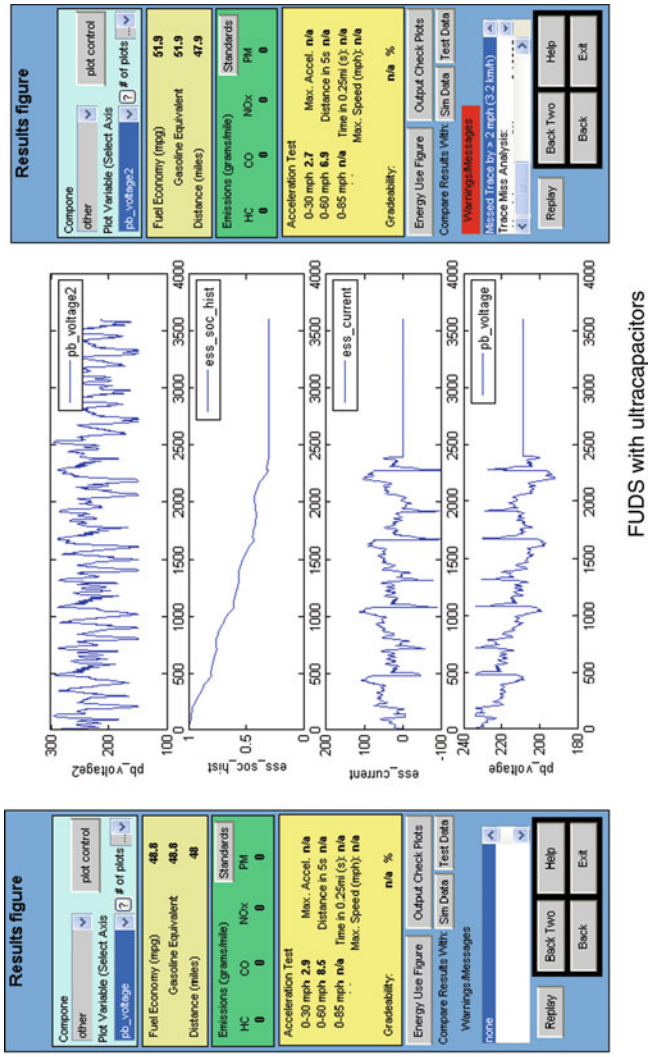

Energy Storage: Ultracapacitor. Figure 10
The Si carbon lithium battery on the US06 with and without ultracapacitors

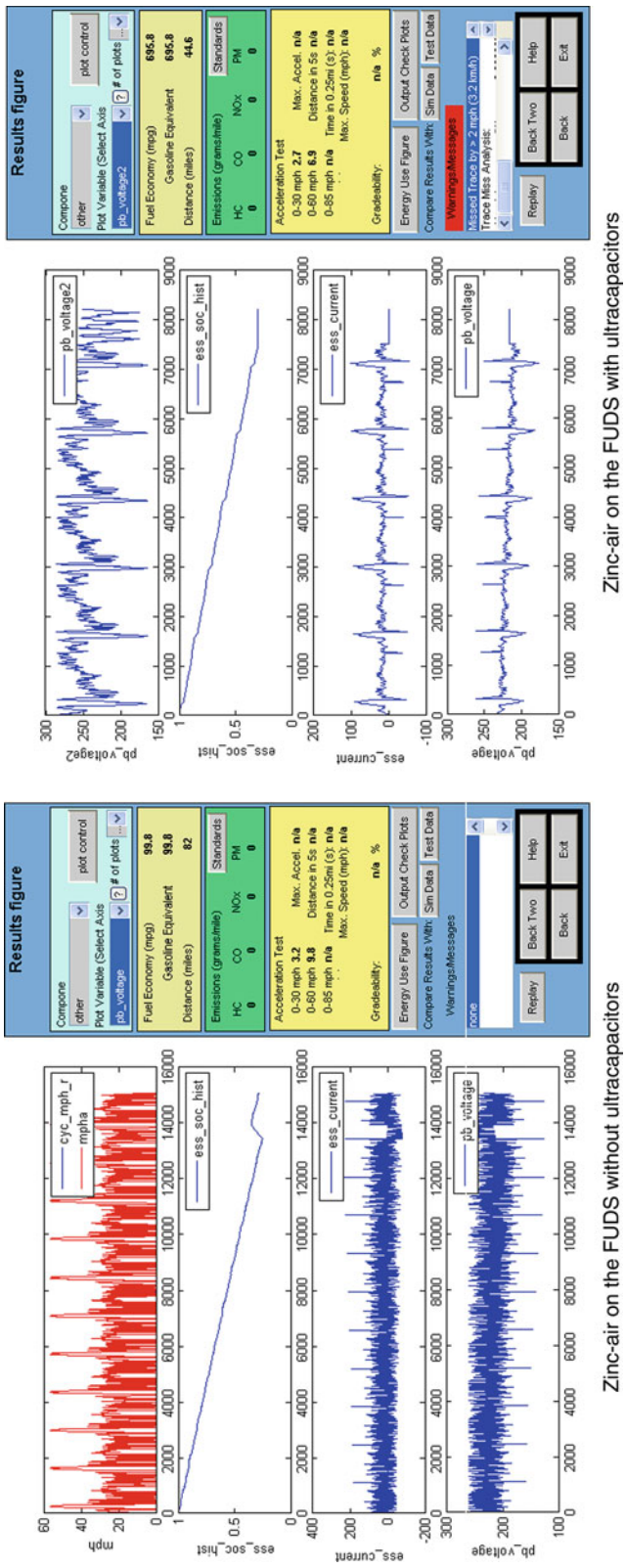

Energy Storage: Ultracapacitor. Figure 11
The zinc–air battery on the FUDS with and without ultracapacitors

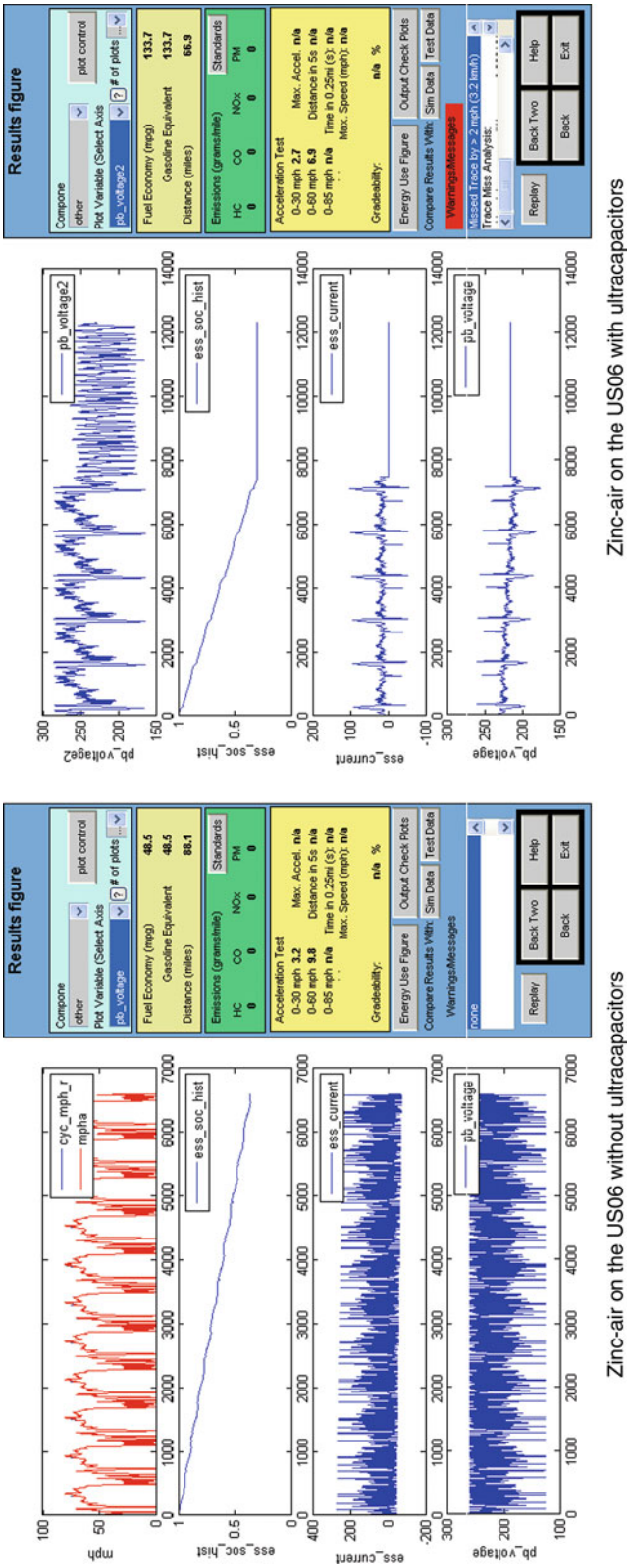

Energy Storage: Ultracapacitor. Figure 12
The zinc–air battery on the US06 with and without ultracapacitors

capability and thus regenerative braking performance approaching that of ultracapacitors or even lithium-ion batteries. This is another advantage of the use of ultracapacitors with the air-electrode batteries.

Fuel Cell Vehicle Simulations Using Ultracapacitors

Fuel Cell Powertrain Configurations and Power Split Strategies

A fuel cell vehicle powertrain consists of three elements: (1) a fuel cell unit that consists of a fuel cell stack, air and hydrogen supply, and water and thermal management systems; (2) an energy storage unit (ultracapacitors or batteries) that can store the electricity generated by the fuel cell as needed; (3) an interface electronics unit that controls the power split between the fuel cell and the energy storage unit. Fuel cells in combination with energy storage can create high power for vehicle traction with fast dynamic response, efficient capture of regenerative braking energy, and reduced stress on the fuel cell due to the elimination of high current pulses. Potentially the use of energy storage can also permit downsizing the fuel cell unit in some applications. As indicated in Fig. 13, there are several approaches to hybridizing the fuel cell system. These various powertrain configurations for fuel cell vehicles have been simulated [28–30] to determine the effect of the configuration used on vehicle hydrogen consumption and the dynamic stress on the fuel cell stack. Of particular interest in this entry are powertrains using ultracapacitors in place of batteries.

The key considerations in configuring the powertrain are whether interface electronics is used and where the electronics is positioned relative to the fuel cell and the energy storage unit. A powertrain without interface electronics is possible using ultracapacitors, but not with batteries. For fuel cell vehicles with ultracapacitors coupled directly in parallel with the fuel cell, a power diode is employed to prevent the flow of reverse current during braking periods.

In systems without interface electronics, the power sharing between the fuel cell and ultracapacitor is determined by the current–voltage characteristics of fuel cell and ultracapacitor because the voltages must be equal at all times.

$$V_{cap} = V_{fc} - V_{diode}$$

The voltage response of the fuel cell on various driving cycles is modeled in detail in [28–30].

Fuel cell vehicles with DC/DC interface electronics placed between the fuel cell and energy storage units have more flexibility for balancing the power flow between the fuel cell and the energy storage. The general control objective is to operate the fuel cell unit only

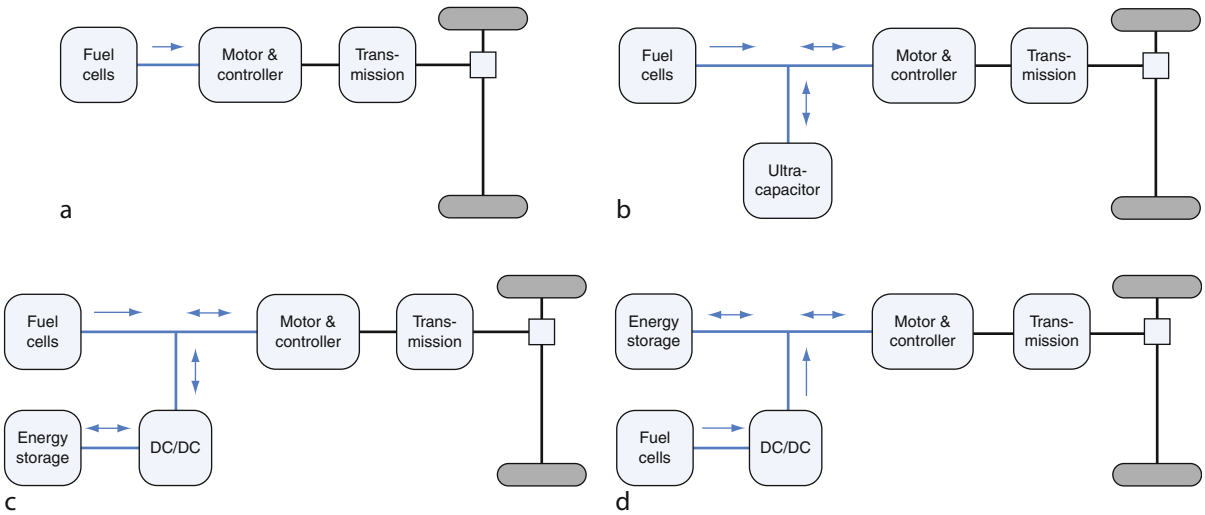

Energy Storage: Ultracapacitor. Figure 13
Powertrain configurations for hybridized fuel cells vehicles

in its high efficiency region and as close to constant or slowly varying power as possible. Two different control strategies, power assist and load leveling, can be employed [30]. Both control strategies maintain the SOC of the energy storage unit within a specified range. The *power assist control strategy* sets the current demand for the fuel cell based on the fuel cell voltage and the energy storage SOC. If the fuel cell voltage remains relatively high, it provides most of the current to the electric drive. When the fuel cell voltage becomes low and the energy storage SOC is high, the energy storage unit provides a large fraction of the current. In the *load-leveled control strategy*, the fuel cell provides relatively steady power and the energy storage unit provides transient power. The fuel cell power command is the vehicle demand averaged over a specified time period such as 60 s.

Simulation Results for Fuel Cell Vehicles

The performance and fuel consumption of midsize fuel cell vehicles were simulated for the different powertrain configurations and control strategies using the vehicle models developed at UC Davis [28–30]. Simulations were performed for the hybrid fuel cell vehicles with a dynamic fuel cell system operating in the optimal varying back pressure mode. The simulation parameters are listed in Table 15.

The simulations were performed over the FUDS and US06 driving cycles. The simulation results are discussed in detail in [30]. It was found that the use of energy storage significantly reduced the stress on the fuel cell stack by reducing the peak currents as well as the current fluctuations. There were no significant differences in the stack currents using batteries or ultracapacitors if interface electronics was positioned between the energy storage unit and the fuel cell bus; the results using ultracapacitors without interface electronics were nearly as advantageous as those with electronics.

The use of energy storage in the fuel cell vehicles resulted in improved fuel economy (reduced hydrogen consumption). As shown in Figs. 14 and 15, the improvements increase for larger energy storage units for both ultracapacitors and batteries. In general, the magnitudes of the improvements are much smaller than in hybrid-electric vehicles. This is due to the higher efficiency of the fuel cell and its smaller variation with power fraction than is the case for engines. Most of the improvement in fuel economy for fuel cell vehicles using energy storage is due to energy recovery during regenerative braking. Note from Figs. 14

Energy Storage: Ultracapacitor. Table 15 Vehicle simulation parameters

Vehicle and system parameters	
Drag coefficient	0.3
Frontal area (m^2)	2.2
Rolling resistance	0.01
Vehicle hotel load (kW)	0.3
Vehicle mass without energy storage (kg)[a]	1,500
Electric motor (kW)	75
Fuel cell stack and auxiliaries	
Max. net power (kW)	87.6
Gross power (kW)	106
Number of cells	440
Cell area (cm^2)	510
Compressor (kW)	17.2

[a]Weight includes all powertrain components except energy storage

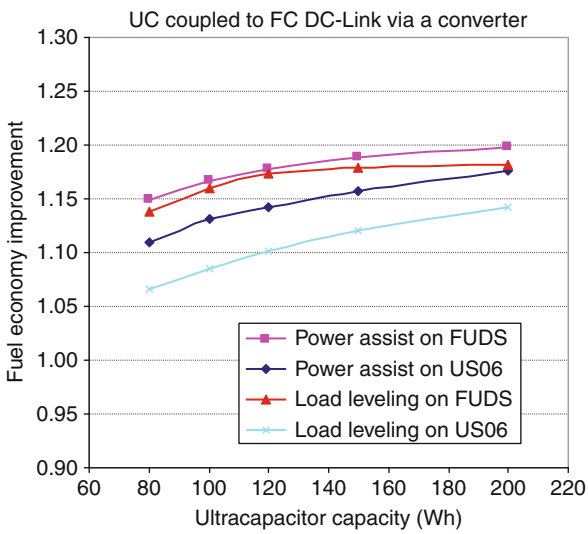

Energy Storage: Ultracapacitor. Figure 14 Fuel economy improvements using ultracapacitors

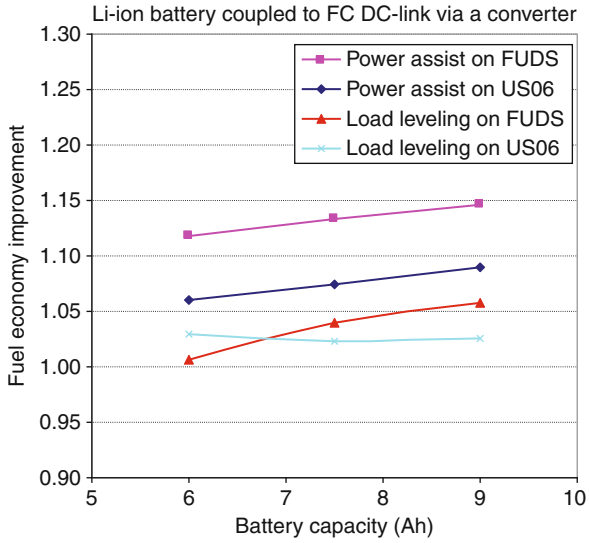

Energy Storage: Ultracapacitor. Figure 15
Fuel economy improvements using lithium batteries

and 15 that the fuel economy improvements with ultracapacitors are slightly larger than with batteries primarily due to the higher efficiency (lower losses) of the ultracapacitors.

Economic Considerations

Reducing the present high cost/price of ultracapacitors is a key issue in achieving high market penetration in the future especially of midsize and large devices. There are many applications for which ultracapacitors are presently precluded or even seriously considered because they remain too expensive even though their selling price has decreased significantly in recent years. The cost of manufacture of any product is closely tied to production volume with the cost decreasing rapidly with increased volume up to relatively high production rates. Sales of capacitors in the many millions of units per year are necessary to reduce the unit costs to levels at which large markets can develop. Semi-automated production facilities presently exist at a number of companies for ultracapacitors of all sizes. In fact, production capabilities exceed sales volumes for most devices and that is the reason the price of devices has decreased markedly in recent years. It is common to speak of the price of devices in terms of cents per Farad (cents/F) or $/Wh stored. It is easier to interpret the price information on the cents/F basis as it does not depend on the cell voltage or what fraction of energy stored can be used in a particular application. For example, for a 10 F device, if the price is quoted as 10 cent/F, the device cost would be $1. Similarly, a 2,500 F device would cost $25 at 1 cent/F.

The cost to manufacture a carbon/carbon device depends on the material and production costs. At the present time, material costs are high. The cost of carbon suitable for use in ultracapacitors can be as high as $100/kg with the average price being in the $30–50/kg range. The cost of the electrolyte solvent is also high in the range of $5–10/l for both propylene carbonate and acetonitrile. The ionic salts that dissociate in the solvent into the positive and negative ions that move into and out of the double layer in the microporous carbon to store the energy are also expensive being $50–100/kg. Since the analysis of ultracapacitors is straightforward, material costs can be calculated [31, 32] with good accuracy. The result of a typical costing exercise is shown in Table 16. Note the strong dependency of the cents/F and $/Wh unit costs for the device on the unit material costs. Presently the price of ultracapacitors is high because both the material and manufacturing costs are high. With more automated production and reduced material costs, it is anticipated that the price of ECCs in high volume can be in the range of 1–2 cents/F for small devices and 0.25–0.5 cents/F for large devices like those needed for vehicle applications.

Ultracapacitors cannot compete with batteries in terms of $/Wh, but they can compete in terms of $/kW and $/unit to satisfy a particular vehicle application. Both energy storage technologies must provide the same power and cycle life and sufficient energy (Wh) for the application. The weight of the battery is usually set by the system power requirement and cycle life and not the minimum energy storage requirement. Satisfying only the minimum energy storage requirement would result in a much smaller, lighter battery than is needed to meet the other requirements. On the other hand, the weight of the ultracapacitor is determined by the minimum energy storage requirement. The power and cycle life requirements are usually easily satisfied. Hence, the unit can be a more optimum solution for many applications and its weight can be less than that of the battery even though its energy density is less than one tenth that of the battery.

Energy Storage: Ultracapacitor. Table 16 Material costs for a 2.7 V, 3,500 F capacitor[a]

Carbon			Electrolyte ACN		Device	Unit	Costs		
F/gm	gmC/dev.	$/kg	$/l	$/kg salt	Total mat. $	$/kg	$/Wh	$/kW	Ct/F
75	187	50	10	125	17.0	29	6.4	29	0.48
120	117	100	10	125	15.5	26	6	26	0.44
75	187	5	2	50	3.6	6.0	1.3	6	0.10
120	117	10	2	50	2.5	4.2	0.93	4.2	0.070

[a]4.5 Wh/kg, 1,000 W/kg-95% eff.

Energy Storage: Ultracapacitor. Table 17 Relationships between capacitor and battery costs

Battery cost $/kWh	Battery cost[a] $/kW	Ultracap cost cents/F V_{cap} =2.6	Ultracap cost cents/F V_{cap} =3.0	Ultracap cost[b] $/kWh V_{cap} =3.0	Ultracap cost $/kW V_{cap} =3.0
300	30	0.25	0.34	3,626	7.3
400	40	0.34	0.45	4,800	9.6
500	50	0.42	0.56	5,973	11.9
700	70	0.59	0.78	8,320	16.6
900	90	0.76	1.0	10,667	21.3
1,000	100	0.84	1.12	11,947	23.9

[a]battery 100 Wh/kg, 1,000 W/kg
[b]capacitor 5 Wh/kg, 2,500 W/kg

Consider the example of a charge-sustaining hybrid like the Prius. If the energy stored in the capacitor unit is 125 Wh and that in the battery unit is 1,500 Wh, the unit costs of the capacitors and battery for equal unit cost are related by

$$(\$/\mathrm{Wh})_{\mathrm{cap}} = .012(\$/\mathrm{kWh})_{\mathrm{bat}}$$

The corresponding capacitor unit costs in terms of cents/Farad and $/kWh are given by

$$(\mathrm{cents/F})_{\mathrm{cap}} = .125 * 10^{-3} * (\$/\mathrm{kWh})_{\mathrm{bat}*} V_{\mathrm{cap}}{}^{2}$$

$$(\$/\mathrm{kWh})_{\mathrm{cap}} = 9.6 * 10^{4} (\mathrm{cents/F})_{\mathrm{cap}} / V_{\mathrm{r}}{}^{2}$$

and shown in Table 17 for a range of battery costs.

The results shown in Table 17 indicate that for the charge-sustaining hybrid application, ultracapacitor costs of 0.5–1.0 cents/F are competitive with lithium battery costs in the range of $500–700/kWh. Note also that the $/kW cost of the ultracapacitor are about one fourth those of the batteries.

Future Directions of Ultracapacitor Development and Vehicle Applications

Ultracapacitor Developments

Ultracapacitors for vehicle applications – that is devices having a capacitance greater than several hundred Farads – have been under development for over 20 years. This development is expected to continue with improvements in energy density as special carbons developed especially for the ultracapacitor application become available. Energy densities of about 10–15 Wh/kg can be expected using the advanced carbons and electrolytes permitting voltages of 3–3.5 V. The cost of ultracapacitors using activated carbon are presently 1–2 cents/F. It is expected that the cost will continue to decrease as the volume of production of ultracapacitors continues to increase. If the cost can be reduced to 0.25–0.50 cents/F, the market for ultracapacitors in vehicle applications will become large (millions of vehicles per year using the devices).

Development of ultracapacitors using pseudo-capacitance or Faradaic materials in at least one electrode will continue. These devices can use either activated carbon or an advanced carbon in one of the electrode. The energy density of these advanced devices could be greater than 20 Wh/kg. The key issues with the advanced devices are their power capability (W/kg for 95% pulse power efficiency) and cycle life. Research to date has indicated it is difficult to achieve large improvements in energy density without significant sacrifices in cycle life and power capability.

Vehicle Applications of Ultracapacitors

There have been numerous demonstrations of the use of ultracapacitors in vehicle applications, but except for a limited number of transit buses and heavy-duty trucks produced for sale, there has been no significant market for ultracapacitors for hybrid vehicles. This may be about to change (2011) as several auto companies are discussing the inclusion of ultracapacitors in micro-hybrids combined with lead-acid batteries. The success of this application is highly dependent on the cost of the ultracapacitors and will require a continuing decrease in their cost. If the energy density of the carbon/carbon devices can be increased to 8–10 Wh/kg with continuing cost reductions to 0.5–1.0 cents/F, it seems likely ultracapacitors will be used in charge-sustaining HEVs to further improve the fuel economy of those vehicles. This could be a very large market for ultracapacitors.

Applications of ultracapacitors in vehicles further in the future could involve their use in fuel cell–powered vehicles and electric and hybrid vehicles using advanced, high energy density (>250 Wh/kg) lithium batteries, which may not have corresponding higher power capability and need ultracapacitors to meet vehicle power requirements. These applications can be the focus of laboratory studies and field demonstrations in the next 5–10 years.

Summary

In this entry, various aspects of the use of ultracapacitors alone and in combination with batteries are discussed in relation to general system considerations and the performance of the energy storage systems in charge-sustaining and plug-in hybrid vehicles and fuel cell–powered vehicles. The performance of ultracapacitors and lithium batteries is reviewed based on test data taken at the University of California-Davis. It was found that ultracapacitors are commercially available with energy densities of 4.5–5 Wh/kg and power density of 1–2 kW/kg with a pulse efficiency of 95%. Lithium batteries of various chemistries were also tested. It was found that batteries consisting of graphite and manganese oxide/spinel had energy densities of 140–160 Wh/kg and power densities of 0.5–1.0 kW/kg with pulse efficiencies of 95%. High-power lithium batteries using lithium titanate oxide in the negative electrode were found to have an energy density of about 40 Wh/kg and a power density of 1.3 kW/kg with pulse efficiencies of 95%. Comparisons of the power densities of ultracapacitors and lithium batteries indicated that the best ultracapacitors had power densities a factor of 2–3 higher than the high-power batteries, but there are some batteries with higher power capability than the lower power capability capacitors. For use in hybrid vehicles, high power density is very important for ultracapacitors.

The application of ultracapacitors in hybrid-electric vehicles was considered in detail utilizing vehicle simulation results. The use of ultracapacitors alone is analyzed for micro- and mild/full charge-sustaining hybrids and in combination with high-energy density batteries for plug-in hybrids. It was found that ultracapacitors could be used in place of batteries in the charge-sustaining hybrids resulting in fuel economy improvements of 25–50% even for relatively small electric drive systems of 6–10 kW. The ultracapacitor units only stored 50–100 Wh of usable energy and their efficiency was high being 95–98%. In all cases, the ultracapacitors were used with interface electronics that permitted the use of a large fraction of their stored energy.

Vehicle simulations were also performed for plug-in hybrid vehicles that used ultracapacitors combined with advanced, high energy density batteries. The batteries had energy densities of 200–400 Wh/kg, but only moderate power capability of 300–1,000 W/kg for 90% efficient pulses. The simulation results indicated that the advanced batteries combined with ultracapacitors could provide all-electric operation on the FUDS and Federal Highway cycles in the charge-depleting mode and excellent fuel economy in the charge-sustaining mode. Vehicle operation with the advanced

batteries without the ultracapacitors required blended operation on all driving cycles. Comparisons of the current/voltage/power profiles of the batteries with and without the ultracapacitors indicated the peak currents and thus the stress on the batteries were reduced by about a factor of 3 using the ultracapacitors. This reduction is expected to lead to a large increase in battery cycle life.

Vehicle simulation results are also discussed for fuel cell vehicles using ultracapacitors or batteries for energy storage. It was found that the vehicle and fuel cell system functioned essentially the same with ultracapacitor or batteries. In the case of fuel cell vehicles, the ultracapacitor unit could be used without interface electronics with the resultant power split between the ultracapacitors and the fuel cell being self-controlled by the voltage–current characteristics of the respective devices. The fuel economy (hydrogen consumption) improvements using energy storage were 10–15% for the FUDS cycle and 5–10% for the US06 cycle with ultracapacitors and a few percent less using lithium batteries.

The long-term costs of both lithium batteries and ultracapacitors are uncertain. An analysis of ultracapacitor unit costs indicated that a battery cost of $500/kWh and ultracapacitor cost of 0.5 cents/F would result in a comparable energy storage unit cost for charge-sustaining hybrid vehicles.

Bibliography

1. Burke AF, Miller M (2009) Performance characteristics of lithium-ion batteries of various chemistries for plug-in hybrid vehicles, EVS-24, Stavanger (paper on the CD of the meeting)
2. Burke AF, Miller M (2009) Electrochemical capacitors as energy storage in hybrid-electric vehicles: present status and future prospects, EVS-24, Stavanger (paper on the CD of the meeting)
3. Burke AF, Miller M (2009) The UC Davis emerging lithium battery test project, Report UCD-ITS-RR-09-18
4. Burke AF, Miller M (2011) The power capability of ultracapacitors and lithium batteries for electric and hybrid vehicle applications. J Power Sources 196(1):514–522
5. US Department of Energy (2008) Battery test manual for plug-in hybrid electric vehicles, INL/EXT-07-12536
6. Yoshio M, Brodd RJ, Kozawa A (eds) (2009) Lithium-ion Batteries, chapter 12. In: HEV Applications. Springer, New York
7. Anderman M (2005) Could ultracapacitors become the preferred energy storage device for future vehicles? In: Proceedings of the 5th international advanced automotive battery conference, Honolulu, 15–17 June 2005
8. Burke A, Miller M (2010) Lithium batteries and ultracapacitors alone and in combination in hybrid vehicles: fuel economy and battery stress reduction advantages. Paper presented at the electric vehicle symposium 25, Shenzhen
9. Bohn T (2007) Plug-in hybrid vehicles: decoupling battery load transients with ultracapacitor storage. Paper presented at the advanced capacitor world summit 2007, San Diego
10. Miller JM, Bohn T, Deshpande U (2008) DC-DC converter buffered ultracapacitor in active parallel combination with lithium battery for plug-in hybrid electric vehicle energy storage. SAE paper 2008-01-1003, SAE World Congress, Detroit
11. Dixon J, Nakashima I, Ortuzar M (2010) Electric vehicle using a combination of ultracapacitors and ZEBRA battery. IEEE Trans Ind Electron 57(3):943–949
12. Bender J (2009) Life cycle testing of a ultracapacitor/lithium battery combination. Private communication from AFS Trinity
13. Bartley T (2005) Ultracapacitor energy storage in heavy-duty hybrid drive update. In: Proceedings of the advanced capacitor world summit 2005, San Diego
14. King RD et al (2003) Ultracapacitor enhanced zero emissions zinc air electric transit bus – performance test results. In: Proceedings of the 20th international electric vehicle symposium, Long Beach
15. Okamura M, Hayashi K, Ohta H (2006) Status report on ECaSS and Nanogate-capacitors. In: Proceedings of the 16th international seminar on double-layer capacitors & hybrid energy storage devices, Deerfield Beach
16. Schwake A (2006) EC-funded project "SUPERCAR": ultracapacitor modules for mild hybrid applications. In: Proceedings of the second international symposium on large ultracapacitor (EDLC) technology and application, Baltimore, 16–17 May 2006
17. Gonder J, Pesaran A, Lustbader J, Tataria H (2009) Fuel economy and performance of mild hybrids with ultracapacitor simulations and vehicle test results. Presentation at the 5th international symposium on large EC capacitor technology and applications, Long Beach
18. Armiroli P et al (2008) Valeo stars+system, ultracapacitors: the way for regen for micro-mild hybrids. In: Proceedings of the fourth international symposium on large ultracapacitor technology and application, Tampa
19. Peasaran A (2007) Factors and conditions for widespread use of ultracapacitors in automotive applications. In: Proceedings of the advanced capacitor world summit 2007, San Diego
20. Burke AF (2002) Cost-effective combinations of ultracapacitors and batteries for vehicle applications. In: Proceedings of the second international advanced battery conference, Las Vegas, 4–7 Feb 2002
21. Knorr R (2006) SUPERCAR – results of a European mild hybrid project. In: Proceedings of the 6th international advanced automotive battery and ultracapacitor conference, Baltimore, 17–19 May 2006

22. Knight B (2003) Information on the ultracapacitors used in the Honda fuel cell vehicle
23. Thounthong P, Rael S, Davat B (2009) Energy management of fuel cell/supercapacitor hybrid power source for vehicle applications. J Power Sources 193:376–385
24. Burke AF, Miller M (2003) Ultracapacitor and fuel cell applications. In: Proceedings of the 20th international electric vehicle symposium, Long Beach
25. Burke AF, Zhao H, Van Gelder E (2009) Simulated performance of alternative hybrid-electric powertrains in vehicles on various driving cycles, EVS-24, Stavanger, (paper on the CD of the meeting)
26. Burke AF, Van Gelder E (2008) Plug-in hybrid-electric vehicle powertrain design and control strategy options and simulation results with lithium-ion batteries. Paper presented at EET-2008 European Ele-drive conference, Geneva, 12 Mar 2008 (paper on CD of proceedings)
27. Burke AF (2007) Batteries and ultracapacitors for electric, hybrid, and fuel cell vehicles, IEEE Journal, Special issue on Electric Powertrains
28. Zhao H, Burke AF (2009) Optimum performance of direct hydrogen hybrid fuel cell vehicles, EVS-24, Stavanger (paper on the CD of the meeting)
29. Zhao H, Burke AF (2009) Optimization of fuel cell system operating conditions for fuel cell vehicles. J Power Sources 186(2):408–416
30. Zhao H, Burke AF (2010) Effects of powertrain configurations and control strategies on fuel economy of fuel cell vehicles. Paper presented at the electric vehicle symposium 25, Shenzhen
31. Burke AF (2010) Electrochemical capacitors. In: Handbook of batteries, 4th edn. McGraw-Hill, New York
32. Burke AF (2004) Key issues for the implementation and marketing of ultracapacitors in vehicle applications. In: Proceedings of the 14th international seminar on double-layer capacitors and similar energy storage devices, Deerfield Beach

Engineered Geothermal Systems, Development and Sustainability of

Roy Baria[1], L. Mortimer[2], G. Beardsmore[2]
[1]EGS Energy Ltd, Penance Cornwall, UK
[2]Hot Dry Rocks Pty Ltd, South Yarra, Victoria, Australia

Article Outline

Glossary
Definition of Engineered Geothermal Systems
Introduction
Future Directions
Acknowledgments
Bibliography

Glossary

Breakthrough time The time taken for a tracing element (chemicals) to travel through a specified media (a reservoir) indicating a degree of channeling or dispersion of injected fluid passing through the reservoir.

EGS Enhanced or Engineered Geothermal system; a geothermal system, a geothermal system engineered to mimic a natural system (hydrothermal) so that energy can be extracted from hot rocks at great depth.

Granite Granite is a common and widely occurring type of intrusive, felsic, igneous rock. Granites usually have a medium- to coarse-grained texture and can contain radiogenic material which produces heat in the rock.

Igneous rocks Igneous rock is formed through the cooling and solidification of magma or lava. Igneous rock may form with or without crystallization, either below the surface as intrusive (plutonic) rocks or on the surface as extrusive (volcanic) rocks.

In situ stress Forces that exits in the crustal plate and the three mutually orthogonal components are categorized as vertical, minimum horizontal, and maximum horizontal. It plays a very important part in the development of an EGS reservoir.

Joint network Term used to collectively describe fractures within a rock mass characterised by features such as fracture orientation, density, spacing, length and mechanical stiffness.

Permeability Permeability is defined by as a measure of flow through spacing between the two faces of a fracture open enough to allow fluid flow through it.

Reservoir A matrix of fractures are manipulated by injecting fluid under pressure for fractures to slide against each other, leaving a permanent increased aperture in the fracture so that fluid can pass through it to recover heat.

Shear failure A terminology used when two sides of a fracture slip over each other with minor permanent displacement.

Tensile failure A terminology used to create a new fracture by splitting the rock mass using fluid injection. The fracture remains open while the pressure is applied but closes once the pressure is taken off, leaving no residual gap between the two new faces of the fracture.

Thermal drawdown A process whereby the reservoir is progressively cooled over time by the passing through of cooler re-injected fluid.

Definition of Engineered Geothermal Systems

Engineered Geothermal System (EGS) is a relatively new technology with tremendous potential for providing heat and power, as well as helping to address the issue of reduction of CO_2 in the environment. The technology is complex, and it has taken some time for a series of research projects globally to understand the physical processes involved, to develop supporting technologies such as high temperature instrumentation, numerical models, and to validate the concept. In view of EGS being a new technology with very limited operating history, the issue of sustainability is difficult to address. It is important to assess the sustainability issue based on the current state of knowledge whilst also recognizing the fact that some existing data are inconclusive. Observations and conclusions reached at many of the EGS sites worldwide have been incorporated to give a broad-based qualitative assessment and to reduce the bias.

The most advanced and near commercial-scale EGS project is the European project at Soultz-sous-Forêts, north of Strasbourg in France. Knowledge gained from over 30 years of research carried out at other EGS projects formed the basis upon which the European project was built [1, 2]. To a large extent, the preceding national EGS projects were at a level of university research and subsequently remained starved of funds. This made it difficult to demonstrate the true potential of EGS. Establishing a European Project [3, 4] provided a big boost and allowed work to proceed on a realistic scale to address the technical and economic targets. The first successful circulation of an EGS system was achieved at Soultz in 1997, at a depth of around 3,600 m, and indicated that technically and economically the technology was promising [5]. Data from Soultz are drawn upon in this paper to support the case why this technology needs to move to a commercialization scenario, and how it can be scaled up to produce a large, sustainable power output to make it acceptable as a serious contender as an energy provider. It is important to re-emphasize that discussions and arguments for the sustainability of EGS presently remain theoretical as there are very few operating plants at present. However, our judgement and experience has been used to put forward sustainability scenarios based on the history of the development of this technology and observations to date.

Introduction

Global demand for energy is expected to continue to rise, but on the timescales of decades to centuries, the supply of traditional energy resources derived from hydrocarbon are unlikely to keep pace with the increasing demand. Additionally, there is increasing awareness of global warming, the political dimension to the generation of CO_2, and the importance of domestic energy security. Nations, industry, and the public are aware that low-emission energy resources will have to play an increasingly important role as people both choose and are forced to move away from hydrocarbon-based energy resources. The effect of digressions between the increasing demand and the limited supply of hydrocarbon-based energy will manifest itself as an increasing price of energy. The increasing prices should, in principle, make some renewables cost competitive.

The energy potentially available from Geothermal resources generally, and EGS in particular, is huge; almost beyond comprehension. Theoretical calculations indicate that cooling just 1 km^3 volume of rock from 200°C to 180°C (i.e., by 20°C) could provide enough thermal energy to power an electric generator of 10 MWe capacity for 20 years, the equivalent of 1.3 million tons of oil. For example, on a slightly larger scale (national scale), the estimate of the Technical Potential for EGS in Australia is around 6,800 GWe [6], which equates to 136 times the total current installed capacity in Australia from all energy sources.

Basic Concept of EGS

The concept of extracting heat energy from the deep, hot rock mass in the earth using EGS technology is relatively simple [7]. Drilling to an appropriate depth can provide access to any desired temperature, and

a reservoir (heat exchanger) can be created by pumping cold fluid at high pressure and flow rate from the surface to open up existing fractures, a process known as "reservoir stimulation". These fractures remain open permanently, giving the stimulated rock mass an enhanced permeability. A second, and sometimes a third, well is drilled into the heat exchanger some distance (typically around 600 m) from the first well. Cold water is pumped down the injection well, the water flows through the enhanced permeable zone (heat exchanger) where it heats up, and the hot water is returned to the surface via a production well in order to drive a turbine to produce electricity and/or space heating. The cooled fluid is then pumped down again and reheated, thus forming a continuous closed circuit loop (Fig. 1).

Although this was the initial concept of EGS, the term "EGS" now also encompasses the exploitation of fluid flow at depth in faults with favorable orientation within the prevailing stress field [8, 9]. Experience and knowledge to date indicate that some large faults that are approximately aligned in the maximum horizontal stress direction at depth are likely to be open and are able to deliver large flow rates of hot fluid for power generation [10]. A production well is drilled to orthogonally intersect at depth a large fault that is striking in the direction of maximum horizontal stress. Significant flow rates might be immediately achievable. If not, then stimulations may be necessary to enhance the flow rate by decreasing the flow impedance. A similar technique is used to drill a second well (injection well) some distance away and offset from the first fault. In planning such a strategy, it is important to recognize that stimulation of either or both wells may be necessary to decrease the natural impedance. An EGS project based on this model has already been commercialized in Landau, Germany (www.geox-gmbh.de/en). The EGS reservoir has been producing for around 3 years with no indication of reduction in the flow rate or thermal drawdown. The data from the project is not widely circulated due to the commercial nature of the project.

Numerical modeling of the stimulated deep reservoir at Soultz reveals that a reservoir of such dimensions should last for around 20+ years [11] before thermal drawdown reducing the rock temperature below commercial levels. But the results of the numerical models are yet to be confirmed through long-term circulation.

Any, even superficial, estimate of global EGS potential reveals a huge store of thermal energy at relatively shallow

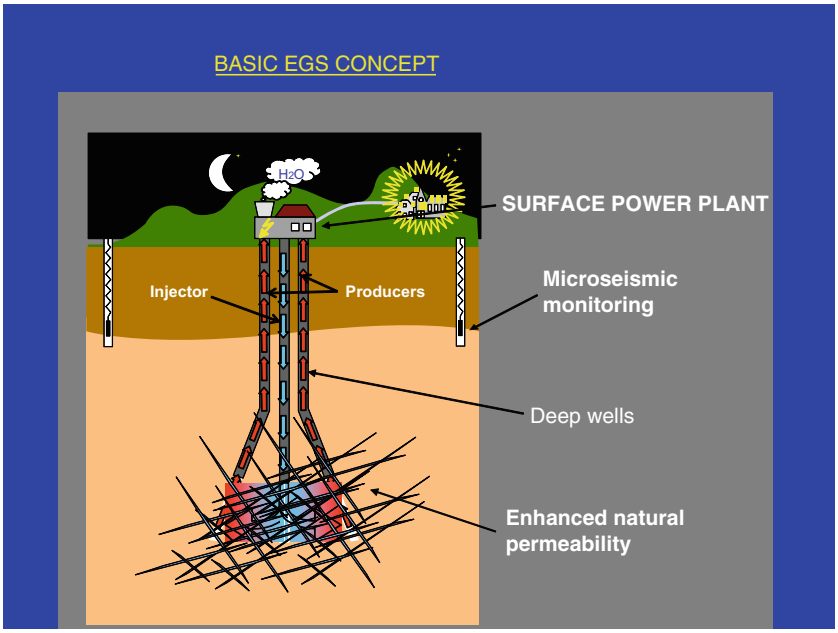

Engineered Geothermal Systems, Development and Sustainability of. Figure 1
Basic EGS concept

depths in the Earth's crust. Debate often surrounds issues such as whether the depth for estimating EGS potential should be limited to 5,000 or 10,000 m. A seminal report from the Massachusetts Institute of Technology in the USA [12] supported 10,000 m as the maximum depth of exploitation for EGS with a view that the technology to exploit energy at this depth is within the grasp of the hydrocarbon industry and therefore could be adapted to work for EGS in the future.

Global Potential of EGS

EGS technology has advanced significantly in the last 20 years. Some of the main questions now raised by potential investors are:

- What is the worldwide potential for EGS?
- Can present technology be scaled up to produce significant amounts of power?
- What are the risks associated with this technology?
- Are EGS reservoirs sustainable?

Taking notice of the concern of potential investors, one of the tasks under the auspices of "Geothermal Implementing Agreement" of the International Energy Agency (IEA/GIA) has been to assess the global potential for EGS. To this end, the Google organization has sponsored a mechanism to quantify the global potential by developing a Protocol, with the intention that it be adopted internationally [13]. Other questions are addressed later on in the paper.

Brief History of the Development of EGS

EGS projects have been activated in many countries, but only four are mentioned here to summarize the development of this technology.

The concept of extracting heat from hot, but low permeability, rocks at great depth and converting this to electricity came from Los Alamos, USA, in the early 1970s. The concept was called Hot Dry Rock (HDR), and a research project was established in a caldera near Los Alamos, New Mexico, USA [14, 15]. The concept relied on some basic assumptions at the time; primarily, that the system had to be in an igneous basement rock with low permeability so that it could be stimulated using high-pressure fluid injection to enhance permeability with minimal chance of losing water in the far field during circulation. The method of enhancing the permeability of the potential heat exchanger was borrowed from the hydrocarbon industry. It was felt that this technique could, in principle, be replicated worldwide to provide power and heat wherever necessary.

Although the concept appeared to be relatively simple, extensive supporting technologies had to be developed to overcome difficulties such as high temperatures encountered during drilling, casing and cementing, characterization of the development of the reservoir, and establishing the physics associated with it [2].

In the mid-1970s, a research project was established in the UK at the Rosemanowes site in Cornwall [16] to focus on and characterize the physics associated with the creation of an underground heat exchanger. The project targeted a much shallower depth and lower temperature than the Los Alamos site. This was done in recognition of the fact that the high temperature and complex stresses regime had created insurmountable difficulties for Los Alamos. The project at the Rosemanowes site was designed so that the physical processes involved in the development of an EGS reservoir could be easily observed and understood.

The Rosemanowes project addressed many of the uncertainties in the physical processes involved in the creation and characterization of an EGS reservoir, and in particular the influence of the prevailing tectonic stress regime on the fluid flow and water losses [17–19]. A 5-year-long circulation test was also carried out (the longest circulation so far in any EGS project), stimulations were carried out using various materials (explosives, gel with various viscosities, water, etc.). Attempts to define a number of economic targets for assessing the commercialization potential of the technology were also carried out [20].

By the early 1980s, as the definition and the concept of EGS grew broader, it was recognized that "*An EGS system is any system where reinjection is necessary to extract the heat at a commercial rate for a prolonged period*" [21]. If one accepts this definition, then a large proportion of hydrothermal systems may fall within the realms of EGS. Additionally, various names were given to the same concept (Hot Dry Rock) for political acceptance and because of variations in the in situ rock characteristics. Alternative names include "Enhanced Geothermal Systems," "Hot Fractured Rocks," and "Hot Wet Rocks," but, recently, all of these have been

grouped into a more coherent title, called *Engineered Geothermal Systems*. This recognizes the fact that there is not a single solution for creating a reservoir at depth due to the natural variation in rock properties, and that an engineered solution will need to be found to address local conditions based on past experience.

The Soultz project was established in late 1988 about 50 km north of Strasbourg in Alsace, France, near the German border [3, 22, 23]. The project was established as a European project, supported by the European Commission, incorporating Britain, France, and Germany (with Britain leaving the program around 1993). The program at Soultz had an international dimension and sufficient funds to take EGS technology to the next step in development, i.e., bring EGS closer to a commercial prospective by addressing/improving economic targets. The project successfully addressed some of the economic targets by initially creating an EGS reservoir at 3.5 km depth [24], and later at 5,000 m depth. Its international status (Fig. 2) helped to accumulate the knowledge gained in earlier projects and bring it into focus to address the further development required for commercial exploitation [24–28].

Economic Targets for Commercial Acceptance

A number of economics models have been generated in the past to assess the parameters necessary to make EGS commercially viable. One such economic model was prepared by Shock [29] for the UK DoE. That study identified a number of parameters (Fig. 3) that need to be demonstrated and quantified in real terms to gain confidence in a created EGS reservoir. These are:

Quantity of Power Output: 5–6 MWe This depends on the combination of output temperature, the delivered flow rate, and the density of the fluid. For example, at 200°C, one would require a flow rate of ~75 l/s using fresh water. The highest temperature accessed to date in an EGS project is 278°C at the Geodynamics site in Australia [30]. The highest flow rate produced to date is ~100 l/s at the Landau site, Germany.

Life of an EGS Reservoir at the Above Flow Rate In principle, a reservoir is designed to last around *20 years* with a temperature drawdown of *10%*. For example, if the initial temperature at the inlet of a power plant is 200°C, a temperature drawdown of 10% will bring this to 180°C. Once the system reaches around 180°C, the plant will be less efficient and is likely to be shut down, but this does not mean that there is no heat energy left in the rock mass.

For heat to be extracted efficiently, cold injected fluid has to come into contact with the hot rock so that heat can be transferred from the rock to the fluid. Numerical models suggest that about 1 million square

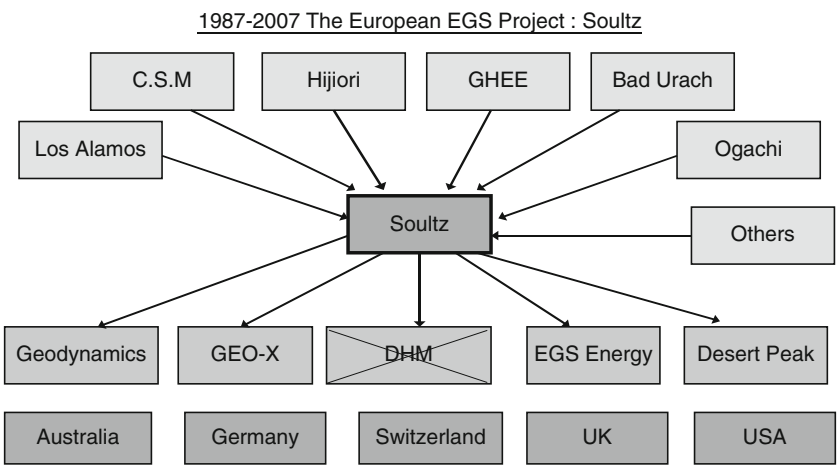

Engineered Geothermal Systems, Development and Sustainability of. Figure 2
Geothermal Systems, Engineered or Enhanced (EGS), Accumulation and dissemination of knowledge at the European EGS project at Soultz

ECONOMIC REQUIREMENTS	
DRIVEN BY ECONOMICS:	**Target 5–6 MWe/module**
• LIFE OF THE SYSTEM:	*~20 Years*
• TEMP/DEPTH OF THE WELLS:	~200 C
• SEPARATION BETWEEN WELLS:	~600 m
• PRODUCTION FLOW RATE:	*~75 Kg/s*
• FLOW IMPEDANCE:	*0.1 MPa/l/s*
• WATER LOSS:	~10% MAX
• THERMAL DRAWDOWN:	*~10%*
• CONTACT SURFACE AREA:	~10 million m^2
• RESERVOIR ROCK VOLUME:	~300 million m^3
• INTEREST RATE FOR THE CAPITAL:	~5%
• SUPPORT:	No CO_2 levy support etc
Economic study by Shock ~1986 for UK DoE	

Engineered Geothermal Systems, Development and Sustainability of. Figure 3
Main economic targets for EGS (From [29])

meters of contact surface area is required between the fluid and the rock mass [12]. For an EGS reservoir to last 20 years, a numerical model indicates that a total rock volume of around 200 million cubic meters is required [12]. Numerical modeling also indicates that this will necessitate a separation between the wells (injection and production) of around 600 m to achieve the above rock volume.

Parasitic Losses These are defined as a reduction in the net profit caused by the use of power required by various operations. Some of these are associated with the power required for pumping the fluid around the system and is quantified in MPa/L/s. Economic models suggest that 0.1 MPa/l/s is acceptable. Additionally, the system may lose some of the injected fluid in the far field due to the character of the site. In this case, additional water may be required to keep the system pressurized. This is normally quoted in a % of the exit flow. This additional water has to be paid for and comes out of the net profit. This is incorporated in the economic model, and around 10% is included as acceptable losses, but the lesser the amount of fluid losses, the better will be the return on the investment. Recent development of EGS reservoirs shows that typical water losses would be around 1–3%.

One of the key figures in the exploitation of the technology is the interest rate on the borrowed capital. This can play an important part in the net return on the investment as the construction of the overall plant may take anything from 3 to 4 years, depending on the depth, number of wells, etc.

More recently [31, 32], revisited economic modeling of a "Soultz-like" project. One of their key findings was that parasitic pumping power significantly impacts on the net power output from an EGS plant (see also section Parasitic Losses below). Higher flow rates require greater pumping power, and there will typically be an optimal pumping/flow rate to maximize the economic return of the system. The optimal pumping/flow rate might not necessarily be the maximum achievable flow rate.

Technical and Economic Achievements to Date

Reservoir Creation Mechanism The initial focus was on applying the hydrofrac technique used in the hydrocarbon industry for creating an EGS reservoir. This consisted of creating a penny-shaped single new fracture (tensile) by injecting fluid under high pressure [33–35]. Subsequently, it was recognized that this was not the way forward as a penny-shaped single fracture

does not create sufficient heat transfer area nor the fractured volume required for sustained heat extraction at high temperature for prolonged period.

Observations during the creation of EGS reservoirs showed that the reservoir in a natural-jointed rock mass grows by shear failure on existing fractures [17, 18]. Shear failure occurs when the pore pressure in the fracture increases and reaches the value of normal stress on the fracture, causing the fracture surfaces to part and for shear failure to take place. After shear failure, joints are propped open by asperities. Observations before and after stimulation at Soultz demonstrated an increase in "productivity index" of wells GPK2 and GPK4 by a factor of ~20 [36]. This, in turn, effectively reduces the pumping power required to circulate fluid through a system, as well as providing increased heat transfer area and fractured rock volume. Additionally, the shear mechanism produces microseismic noise, which is used to monitor the influence of stimulation in real time [18].

Size and Lifespan of the Reservoir The separation between the injection well and the production well, to a large extent, determines the size of the reservoir. Initially, this was in the range of 120–180 m because of a concern that hydrofracturing in granite would be difficult and that it might not be possible to link two wells hydraulically over many hundreds of meter. Following the change in the concept of reservoir creation mechanism (from predominant tensile to shear failure), a separation in excess of 600 m between the injection and production well is regarded as normal. The largest separation of wells at Soultz is 670 m [37–40], and over 1,000 m at the EGS project in Landau, Germany. Numerical modeling indicates that with a separation of this order, an EGS reservoir ought to last over 20 years [41] and that using three wells instead of two (i.e., one injector and two producers) may extend the life even longer. However, no EGS reservoir has yet been circulated this long for confirmation.

One of the methods used for assessing the size of an EGS reservoir is by using tracers [42]. Breakthrough time and model volume are good indicators.

At Soultz, it was felt that the required heat transfer and rock volume were achieved between GPK2 and GPK3, but not between GPK3 and GPK4. The poor connection between GPK3 and GPK4 was due to a poor stimulation strategy [38, 39], further explanation for this is given in section Parasitic Losses.

Parasitic Losses This was a big issue at the early stages of the development of EGS technology. One of the main energy losses is due to the power required to pump the fluid through the reservoir to collect the heat energy. This resistance to flow (impedance) is quantified as pressure required to flow per liter per second (MPa/l/s). In early days, until 1990, the best impedance achieved was around 0.4 MPa/l/s with a flow rate of 15 L/s with a separation between wells of around 200 m at the Rosemanowes site in the UK. At Soultz, this was reduced to ~0.23 MPa/l/s with a separation of 450 m between wells and a production flow of ~26 l/s. This EGS reservoir was at 3.6 km depth. It was felt that the impedance and flow rate could be improved further by having a three well system (one injector and two producers). Subsequently, three more wells (GPK2, GPK3 and GPK4) were drilled to 5,000 m depth to access ~200°C rocks, with a separation in excess of 600 m. Following stimulations of GPK2/GPK3, the flow impedance was found to be around 0.29 MPa/l/s, thus for three wells one would expect to half this to around 0.15 MPa/l/s [37, 38]. GPK4 was also stimulated, but a reduction in impedance was not achieved because GPK4 was poorly connected to GPK3, most likely, due to a change in the strategy for stimulation [38].

Stimulation between GPK2 and GPK3 was carried out using a newly developed stimulation technique [38] that involved injecting in both wells simultaneously ("focused stimulation"). GPK4 was stimulated by injection in one well only. Additionally, there was an indication that the previous stimulation in GPK3 may have created a stress barrier between GPK3 and GPK4. High pressures would have been required to break through this barrier, which might have been possible using focused stimulation [38] but was not possible by stimulating just one well.

Tracer tests indicated a breakthrough time between GPK3 and GPK2 in the order of 3.5 days, and between GPK3 and GPK4 of 28 days [42].

Power Output In view of the poor hydraulic connection between the wells GPK3 and GPK4 at Soultz, the flow rate achieved was lower than expected and

therefore the full potential of the system was not realized. Originally, it was planned to produce around 30–35 l/s from each production well, giving a total flow of around 60–70 l/s and power generation of 3–4 MWe. This proved impossible due to poor connection between GPK3 and GPK4. The plan at present is to produce around 2 MWe and gradually develop further to increase the flow rate and characterize the existing reservoir during the circulation period [36].

On the other hand, the EGS project at Landau increased the flow rate by stimulation from 50 to ~100 l/s, and power production of between 2.8 and 3.5 MWe has been achieved (personal communication).

Future Scenarios Which May Lead to a Mature EGS Technology

EGS has distinct advantages over other renewable energy sources in that it can deliver a base load or a peak load, it is a strategic (domestic) resource, has low visual impact, and has a very low carbon foot print (Fig. 4) in the range of 10 g CO_2/kWh.

Some of the disadvantages are finding the right environment for EGS development, the high cost of developing this technology, uncertainty about underground rock properties (although this is dramatically reduced after the drilling of the first well and obtaining the in situ properties), and community concern over generating seismic events (although experience suggests that this can be managed and mitigated). For example, the EGS project in Basel, Switzerland (DHM), generated a seismic event of the magnitude 3.4 while injecting to create a reservoir. The consequence was the shutdown of the project due to complaints of the local residents and consequence associated with it. This could have been avoided by taking the guide line provided by the protocol on induced seismicity [43] and a white paper published by IEA/GIA [44]. One of the recommendations in the protocol is to avoid establishing an EGS project in the area where there has been large earthquakes in the past or such continuous activities. In 1356, the city of Basel was almost entirely destroyed by a 6.5-magnitude earthquake. Basel is a known moderately active earthquake zone in Switzerland [45] and a possible way forward would have been to explain the situation to local residents, seek their agreement to go forward, and limit the stimulation to smaller volume.

Overall, the advantages of EGS appear to far outweigh the disadvantages, providing a power stimulus for continued development of the technology. Uptake will be progressive, starting with the technically and economically easiest styles of development and progressing to more challenging environments.

It is becoming apparent for the initial rapid take-up of this technology the easiest targets are large faults with high permeability, as at Landau, Germany. Observations at Soultz and other places have indicated that large faults often exist at great depth in granite basement, and those that are roughly aligned with the maximum horizontal stress orientation can potentially deliver increased geothermal fluid production by boosting the bulk permeability and fluid storage of a production zone. However, the hydromechanical properties of faults are inherently heterogeneous and anisotropic, making it challenging to distinguish between permeable and impermeable faults prior to drilling and testing. The probability of locating zones of enhanced fault permeability can be improved by preliminary fault stress state modeling. Such modeling can reduce the uncertainty and risk of exploring for fault-related geothermal targets, particularly in early stage exploration projects or in areas of unknown or complex geology [46].

One recent development has been the realization by the conventional geothermal industry that the heat

Mitigation potential of geothermal power plants in the world based on data of Table 6 and assumptions for emission of 120 g CO_2/kWh for today and 10 g CO_2/kWh for future technology (EGS).

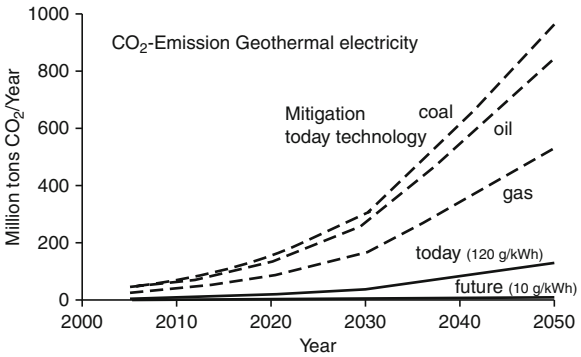

Engineered Geothermal Systems, Development and Sustainability of. Figure 4
CO_2 Emission from various energy resources

available in the vicinity of hydrothermal systems is significantly greater than what is produced from aquifers within those fields. The knowledge acquired from the development of EGS is being applied to extend existing hydrothermal fields to access much larger volumes of hot rock mass to contribute to the power production. Approaches include stimulations of existing dry wells and drilling new wells to connect to the hydrothermal reservoir, provided the wells are located in a favorable direction with respect to the local stress regime. ORMAT Technologies is carrying out pioneering work in this field at Desert Peak near Reno, USA. There is tremendous potential for the take-up of this technology once the concept is demonstrated.

The present economic conditions in many parts of the world mean that a combination of heat and power is likely to generate higher revenue for EGS plants rather than just power alone. This has been the policy pursued by some EGS companies, e.g., EGS Energy Ltd (www. egs-energy.com). The use and distribution of heat may not be applicable everywhere, but a serious consideration is essential to increase revenue and economic sustainability of projects.

Around 3–6 MWe EGS power plants are a starting point in the initial take-up of the technology, but much larger power generating capacity (25–50 MWe) must be demonstrated before the technology can be considered mature and acceptable as a big power player. In order to achieve such a goal, a concept put forward by EGS Energy Ltd, is to successfully replicate EGS reservoirs again and again. Taking the example of the achievement at Soultz and assuming that the connection between GPK3 and GPK4 could have had similar characteristics to that between GPK2 and GPK3, the module of one injector and two producers can be replicated again and again in parallel and serial configuration. Each module could produce around 5 MWe, so three stacked in series could give ~15 MWe (Fig. 5). Three 15 MWe systems stacked in parallel would produce ~45 MWe. This configuration could be extended/developed to generate a larger power the range of up to 100 MWe or more. An important criterion in developing such strategy is the uniformity of stress and thermal gradient so that once a prototype with appropriate characteristics has been developed and tested, it could be replicated with relative confidence. Minor occasional variations in characteristics can be rectified using an appropriate tool kit of responses as necessary.

Sustainability of EGS Systems

Sustainability can be briefly defined as "the capacity to endure, hold up or maintain." In the current atmosphere of community concern for the environment, the question of sustainability arises for any technology that is being developed for the future. For EGS, sustainability could relate to maintaining the temperature and pressure in the reservoir, the electricity output from the power plant, the economic return on investment, the lifespan of surface plant, or other measures. At present, the question of long-term sustainability for EGS is virtually impossible to quantify. Only one EGS commercial system is in existence, and this has been

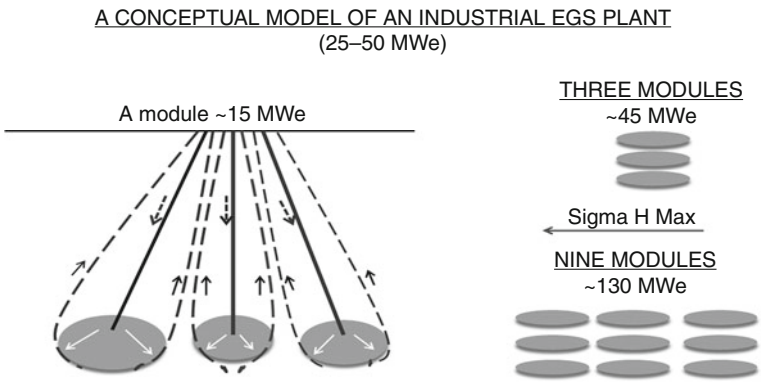

Engineered Geothermal Systems, Development and Sustainability of. Figure 5
Scaling up scenarios for producing 15–130 MWe (from EGS Energy Ltd)

operating only in the last few years. The question of sustainability still arises, however, and one can possibly address this at present through preliminary observations [47], numerical modeling, and value judgment from working in the development of such systems for over 30 years.

In an EGS power plant, one assumes the term "endurance" is aimed at the available thermal energy in the reservoir being able to recharge itself in a sufficient time to be used again in the future, and not associated with the mechanical items such as the casing of the well or the power plant. Sustainability questions will be raised when attempts are made to improve or extend the life of an existing EGS reservoir to conserve resource and/or improve profitability.

For example, calculations suggest that the recovery of the depleted heat in a fractured rock reservoir may take around 75 years to recover by the natural conduction process from the surrounding rocks [12]. This assumes that no convection process is involved, and all the heat transfer is by conduction. In order to extract heat from the upper crust using EGS methods, existing fractures must be opened up by a shearing mechanism to improve fluid flow. In this case, the fractured volume may internally act as convective cells [48]. A convection process is more efficient in transferring heat, and if this is the case, then it is possible that a depleted EGS reservoir might thermal recover in a shorter time than by conduction alone.

One of the observations during the 5-year circulation at the Rosemanowes site was that as the center part of the reservoir was cooling [49], causing a shrinking of the rock mass, the outer part of the reservoir was being opened up and played a greater part in the extraction of heat by the creation of new flow paths. This was concluded from tracer tests that suggested the generation of new flow paths. This suggests that if one manages the reservoir correctly, then there is a good possibility that additional channels could open up through time and thus improve sustainability.

Experience at Soultz demonstrates that a number of reservoirs can be created within the same granite body, above or beside each other (Fig. 6), depending on the stress regime. The upper reservoir (3,600 m) at Soultz was circulated initially for a while and was then sealed off. A new reservoir was created below the first at 5,000 m depth. This same concept could be used to create not just two but three EGS reservoirs, one stacked above the other. The bottom reservoir (system 3) would be exploited first. When it had been sufficiently depleted,

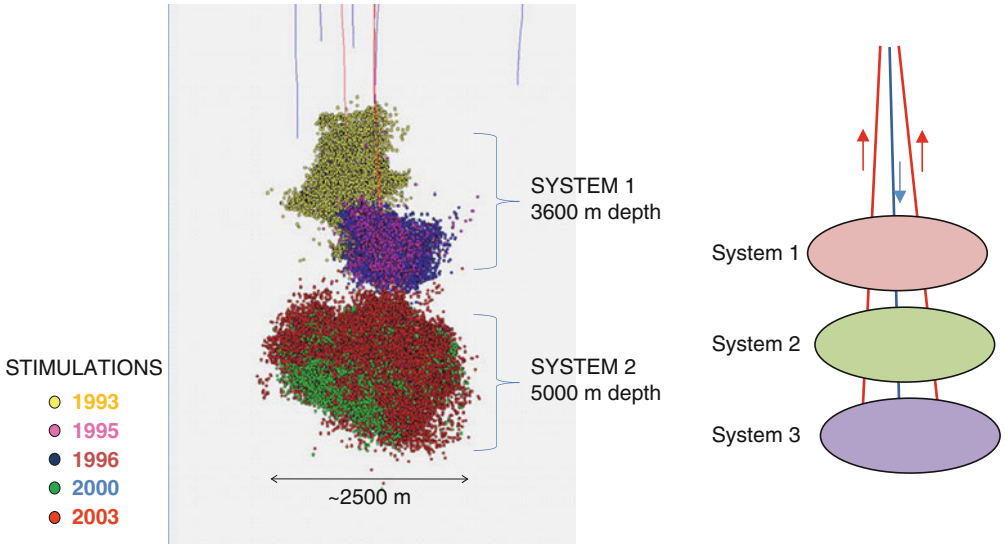

Engineered Geothermal Systems, Development and Sustainability of. Figure 6
Stacking up of EGS reservoirs (an example from Soultz and a conceptual model)

the reservoir would be isolated and the one above it opened and used for generating power. Once the second one is depleted, then that would also be isolated and the upper reservoir would be used. Assuming that each reservoir lasted for around 25 years, by the time the upper reservoir is depleted, the bottom reservoir would be recharged to almost the original temperature through conduction from the surrounding rocks. This suggests that the wells have to be completed in such a way that a number of EGS reservoirs can be created one above the other, such that any one can be isolated to operate independently of the others. A mechanism like this may make it possible for EGS reservoirs to be sustainable for a century or more.

Although EGS projects can offer a viable alternative renewable energy source, they should not be considered in isolation from other local constraints. For example, the creation and operation of an EGS project using a water-cooled power plant requires a local reliable source of water at reasonable cost. Furthermore, EGS field projects carried out throughout the world have experienced the impact of water losses through trial production testing. Controlling water losses is an important aspect of sustainability for a geothermal energy project particularly in areas of restricted water availability such as Geodynamic's Habanero project located in arid outback Australia. Water losses can have significantly negative economic and environmental impacts if not managed. Techniques proposed to control water losses include minimizing injection pressures to control reservoir growth during circulation, the use of injection proppants, and improving hydraulic connectivity between wells through the use of techniques such as "focused stimulation" [12, 50].

In hydrothermal systems, operators need to manage the system not just to prolong its life but also to make it economically attractive. This requires characterization of the reservoir using tracers to monitor the change in the reservoir properties and evaluation of the geochemistry to manage dissolution and precipitation effects. Geochemistry aspects associated with EGS reservoirs are still uncertain and not yet quantified [51, 52]. This is again a function of there being no long-term operating plants yet. Some of the experiments done at the Soultz site during various circulation tests suggest that dissolution, precipitation, and corrosion may be controlled by controlling the pH of the circulating fluid, maintaining back pressure on the production flow, introducing anti-corrosion agents in the system, and by pumping the production fluid back in to the formation without exposing the fluid to the open environment.

There has been some concern in the past that preferential flow paths may develop as the reservoir cools, and that this may cause the abandonment of a reservoir earlier than planned. This to some degree has been addressed by increasing the distances between injector and producer wells from ~200 m to over 600 m. The experience at Soultz suggests that these distances may be further increased to over 1,000 m if one uses a focused stimulation method. Focused stimulation allows the pressure to build up rapidly between the wells to shear existing joints at distances some hundreds of meters from any one well, and also takes significantly less time and volume of water. The result is a more consistent system of stimulated joints throughout the rock volume, and hence a lower probability of short circuits. Additionally, tracer tests carried out regularly in the reservoir would give an early indication of the development of preferential flow paths (short circuits), and then methods could be employed to seal them using various chemicals. Such sealing agents (calcite based) are currently being developed to seal a path temporarily or permanently. This, in principle, should help to extend the life and sustainability of a reservoir.

As mentioned earlier, sustainability is an issue that cannot completely be quantified until there are a number of operating EGS reservoirs for a long time, but the indications are that there is every probability that most issues affecting sustainability can be managed to provide an optimal return on investment.

Possible Road Map for EGS

There is a tremendous quantity of heat stored in the Earth (~10^{13} EJ, [47]), predominantly from the decay of natural radioisotopes. Some of this heat resource is being successfully exploited all over the world at the tectonic boundaries where the crust is thin. These resources have, to a great extent, large volumes of very hot fluid trapped underground and are accessed

by drilling in to them (Iceland, New Zealand, etc.). These resources are classified as a hydrothermal resource, but there are extensive areas of the world where the crust is not so thin, but extensive heat energy is available at greater depth.

EGS technology provides a mechanism to exploit this available heat resource at great depth by drilling in to it and creating an artificial reservoir by pumping fluid under pressure, opening up natural fractures to allow cold fluid to flow through it, and extract the heat to drive turbines at the surface. Only recently the technological and financial support was available to create such a system with relevant parameters to make it commercially viable. This was achieved under an international research environment which facilitated funds and scientists to address these problems and solve them.

International Energy Agency has recognized the potential of EGS worldwide and the cutting edge geothermal research required to make it successful. IEA has therefore set up a team to formulate a road map to assist the exploitation of this technology.

I suspect some of the aspects covered for the road map will be:

- What geophysical technique will help in selecting an ideal EGS site?
- How can one determine stress values and gradient in that specific area?
- How can one encourage joint international research to address some of the uncertainties, such as the behavior of an EGS reservoir in different stress regimes; how long will the reservoir last, etc.
- Can one support new drilling techniques to reduce the cost of drilling? Drilling can be over half of the cost of development of an EGS Project
- Facilitate a procedure of fast tracking for planning permission to reduce effective cost.
- Understand or develop mitigating methods to reduce large induced seismic events in EGS plants.
- Provide a mechanism such as insurance scheme to assist in any large drilling accidents.
- Long-term international research on the behavior of EGS reservoir and the control of likely geochemical, dissolution, and precipitation problems.
- Improve binary power plants to improve power conversion efficiency and reliability.

Future Directions

EGS is has gone through the fundamental research to scientific demonstration stage, and it is now ready for application in commercial environment, but, it does need supporting financial incentive to encourage potential investors.

These can be:

- A feed in tariff similar or better than that set by Germany will encourage potential investors to be prepared to take some risk.
- Additionally, the potential of being able to provide an abundant supply of hot water from an EGS plant has not been taken seriously, particularly as it can provide this 24 h a day and almost 95% of the time in a year.
- Environment friendly premium, as it has virtually no CO_2 emissions or any major pollutants.
- A separate feed in tariff for the supply of hot water.
- EGS has a potential for becoming a provider of large-scale power (200MWe +) and heat. This can become a strategic power base and additional financial support from government will help investors to expand in this direction.
- Insurance schemes to protect against unforeseen accidents during drilling.
- Establishment of fast tracking method in obtaining planning and fulfilling local regulations. This can take a long time and can become a major burden to investors at an early stage of development.

Acknowledgements

The authors would like to thank all the funding agencies that helped to establish and support the Soultz project, including the European Commission, Agence de l'Environnement et de la Maîtrise de l'Energie (France), the German Bundesministerium für Umwelt, Naturschutz und Reaktorsicherheit within the frame of the "Zukunftsinvestitionsprogramm," the Projektträger of the Forschungszentrum Jülich (Germany), the Department of Trade and Industry (DTI) (UK), and the Members of the EEIG "Exploitation Minière de la Chaleur."

The authors would also like to thank all the teams who contributed to the success of the projects at Rosemanowes and Soultz for over 30 years of research.

In particular, the authors would like to give special acknowledgement to Perry Moore (SII) who died on March 21, 2003, in Kazakhstan, and who played a significant part in the success of the Rosemanowes and Soultz projects.

Bibliography

1. Baria R, Baumgaertner J, Gérard A, Kappelmeyer O (1992) HDR project at Soultz-sous-Forêts. Geotherm Res Counc Trans 18:387–394
2. Abe H, Niitsuma H, Baria R (1999) Hot dry rock/Hot wet rock academic review: special issue. Geothermics 28(4/5). Pergamon Press, ISSN 0375-6505
3. Garnish JD (1985) Hot dry rock – a European perspective. In: Proceedings geothermal research council's international symposium on geothermal energy, international volume, Hawaii, pp 329–337
4. Baria R, Baumgaertner J, Gerard A, Jung R, Garnish J (1999) European HDR research program at Soultz-sous-Forets (France) 1987–1996. In: Abe H, Niitsuma H, Baria R (eds) Geothermics special issue, Hot dry rock/Hot wet rock, Academic review, 28(4/5). pp 665–669, ISSN 0375-6506
5. Baria R, Baumgaertner J, Gérard A, Jung R, Garnish J (1998) The European HDR research program at Soultz-Sous-Forets (France). In: Baria R, Baumgaertner J, Gerard A, Jung R (ed) International conference 4th HDR forum, Proceeding, 2002, Strasbourg, France, ISBN 3-510-95859-4
6. Hot Dry Rocks (2011) Summary of process and data sources used in the development of the EGS Potential maps and tables of Australia. Unpublished report (available from www.google.org/egs), 20 p
7. Smith MC (1975) The potential for the production of power from geothermal resources – Los Alamos scientific laboratory report, LA-UR-73-926
8. Barton CA, Zoback MD, Moos D (1995) Fluid flow along potentially active faults in crystalline rock. Geology 23:683–686
9. Finkbeiner T, Barton CA, Zoback MD (1997) Relationships among in-situ stress, fractures and faults, and fluid flow: Monterey formation, Santa Maria Basin. AAPG Bull 81(12):1975–1999
10. Barton CA, Hickman S, Morin R, Zoback MD, Finkbeiner T, Sass J, Benoit D (1997) Fracture permeability and its relationship to in-situ stress in the Dixie Valley, Nevada, geothermal reservoir. In: Proceedings 22nd workshop on geothermal reservoir engineering Stanford University, Stanford, 27–29 Jan 1997
11. Bruel D (1997) Heat exchange modelling using a discrete fracture network model with thermo-mechanical interactions – evaluation of the thermal performance of the reservoir developed at Soultz-sous-Forêts in 1996, ARMINES
12. M.I.T. Report (2006) The future of geothermal energy, impact of enhanced geothermal systems (EGS) in the United States in 21st century. Massachusetts institute of technology report. ISBN: 0-615-13438-6. (http://geothermal.inel.gov)
13. Beardsmore GR, Rybach L, Blackwell D, Baron C (2010) A protocol for estimating and mapping global EGS potential. GRC Trans 34:301–312
14. Potter RM, Robinson ES, Smith MC (1974) Methods of extracting heat from dry geothermal reservoirs, US Patent #3,786858
15. Brown DW, Duchane DV (1999) Scientific progress on the Fenton hill HDR project since 1983. In: Abe H, Niitsuma H, Baria R (eds) Geothermics special issue, Hot dry rock/Hot wet rock, Academic review, 28(4/5), pp 591–601, ISSN 0375-6506
16. Garnish JD (1976) Geothermal energy: the case for research in the United Kingdom. Energy paper no. 9, London, HMSO, 66 pp
17. Pine RJ, Batchelor AS (1984) Downward migration of shearing in jointed rock during hydraulic injections. Int J Rock Mech Min Sci 21(5):249–263
18. Baria R, Hearn KC, Batchelor AS (1985) Induced seismicity during the hydraulic stimulation of the potential hot dry rock geothermal reservoir – submitted to the fourth conference on acoustic emission/microseismic activity in geology structures and materials, Pennsylvania State University, 22–24 Oct 1985, 26 pp
19. Baria R, Green ASP (1989) Microseismics: a key to understanding reservoir growth. In: Roy Baria (ed) Hot dry rock geothermal energy. Proceedings Camborne school of mines international hot dry rock conference, Camborne School of Mines Redruth, UK, 27–30 June 1989. Robertson Scientific Publications, London, 1990, pp 363–377, ISBN 1-85365-217-2
20. Parker RH (1989) Hot dry rock geothermal energy. Phase 2B final report of the Camborne School of Mines project, vol 1 & 2. Pergamon, Oxford. ISBN 0-08-037929-X
21. Batchelor AS (1989) Hot dry rocks and its relationship to existing geothermal systems. In: Baria R (ed) Hot dry rock geothermal energy proceedings Camborne school of mines international hot dry rock conference, Camborne School of Mines Redruth, 27–30 June 1989. Robertson Scientific Publications, London, 1990, pp 13–29, ISBN 1-85365-217-2
22. Garnish JD (1986) Introduction: background to the workshop. In: Garnish J (ed) Proceedings of the first EEC/US workshop on geothermal hot dry rock technology, geothermics special issue, 16(4), 1987. Brussels, pp 323–330
23. Gérard A, Kappelmeyer O (1987) The Soultz-sous-Forêts Project. In: Garnish J (ed) Proceedings of the first EEC/US workshop on geothermal hot dry rock technology, geothermics special issue, 16(4), 1987, pp 393–399
24. Baumgärtner J, Gérard A, Baria R, Jung R, Tran-Viet T, Gandy T, Aquilina L, Garnish J (1998) Circulating the HDR reservoir at Soultz: maintaining production and injection flow in complete balance. In: Proceedings 23rd workshop of geothermal reservoir engineering, Stanford University, Stanford
25. Baria R, Baumgärtner J, Gérard A (1993) Heat mining in the Rhinegraben. Socomine internal project report
26. Baria R, Garnish J, Baumgärtner J, Gérard A, Jung R (1995) Recent development in the European HDR research programme at Soultz-sous-Forêts (France). Proceeding of the

world geothermal congress, Florence, International Geothermal Association, vol 4, pp 2631–2637, ISBN 0-473-03123-X
27. Baumgärtner J, Jung R, Gérard A, Baria R, Garnish J (1996) The European HDR project at Soultz-sous-Forêts: stimulation of the second deep well and first circulation experiments. In: Proceedings 21st workshop of geothermal reservoir engineering, Stanford University, Stanford, California, SGP-TR-151, pp 267–274
28. Gérard A, Baumgärtner J, Baria R (1997) An attempt towards a conceptual model derived from 1993–1996 hydraulic operations at Soultz. In: Proceedings of NEDO international geothermal symposium, Sendai, vol 2, pp 329–341
29. Shock RA (1986) An economic assessment of hot dry rocks as an energy source for the UK – Energy Technology Support Unit Report ETSU-R-34. Publ. HMSO (London), 215 p
30. Geodynamics (2010) Geodynamics company update. In: Proceedings Australian geothermal conference 2010, Adelaide, Australia, 16–19 Nov 2010
31. Heidinger P, Dornstädter J, Fabritius A (2006) HDR economic modelling: HDRec software. Geotherm 35:683–710
32. Heidinger P (2010) Integral modeling and financial impact of the geothermal situation and power plant at Soultz-sous-Forets. Comptes Rendus Geosci 342: 626–635. Elsevier Masson SAS
33. Abé H, Mura T, Keer LM (1976) Growth rate of a penny-shaped crack in hydraulic fracturing of rocks. J Geophys Res 81(29):5335–5340
34. Duffield RB, Nunz GJ, Smith MC, Wilson MG (1981) Hot dry rock – geothermal energy development program, annual report FY80, Los Alamos National Laboratory report, LA-8855-HDR, July 1981, 211 p
35. Hubbert MK, Willis DG (1957) Mechanics of hydraulic fracturing. Pet Trans AIME 210:153–168
36. Genter A, Fritsch D, Cuenot N, Baumgärtner J, Graff J-J (2009) Overview of the current activities of the European EGS Soultz project: from exploration to electricity generation. In: Proceedings thirty-fourth workshop on geothermal reservoir engineering, Stanford University, Stanford, 9–11 Feb 2009
37. Baria R, Michelet S, Baumgaertner J, Dyer B, Gerard A, Nicholls J, Hettkamp T, Teza D, Soma N, Asanuma H, Garnish J, Megel T (2004) Microseismic monitoring of the world's largest potential HDR reservoir. Twenty-ninth workshop on geothermal reservoir engineering, Stanford University, Stanford, California, 26-28 Jan 2004
38. Baria R, Michelet S, Baumgärtner J, Dyer B, Nicholls J, Hettkamp T, Teza D, Soma N, Asanuma H, Garnish J (2005) Creation and mapping of 5000m deep HDR/HFR reservoir to produce electricity. In: Proceedings WGC 2005 (CDROM), Antalya
39. Baria R, Jung R, Tischner T, Nicholls J, Michelet M, Sanjuan B, Soma N, Asanuma H, Dyer B, Garnish J (2006) Creation of an HDR reservoir at 5000m depth at the European HDR project. Thirty-first workshop on geothermal reservoir engineering. Stanford University, Stanford, 30 Jan–1 Feb 2006
40. Hettkamp T, Baumgaertner J, Baria R, Gerard A, Gandy T, Michelet S, Teza D (2004) Electricity production from hot rocks. In: Proceedings 29th workshop of geothermal reservoir engineering, Stanford University, Stanford, 26–28 Jan 2004, pp 184–193
41. Brown DW, DuTeaux R, Kruger P, Swenson D, Yamaguchi T (1999) Fluid circulation and heat extraction from engineered geothermal reservoirs. In: Abe H, Niitsuma H, Baria R (eds) Geothermics special issue, hot dry rock/hot wet rock, Academic review, 28(4/5), pp 553–572, ISSN 0375-6506
42. Sanjuan B, Pinault, Rose P, Gerard A, Brach M, Braibant G, Crouzet C, Foucher J-C, Gautier A, Touzelet S (2006) Tracer testing of the geothermal heat exchanger at Soultz-sous-Forets (France) between 2000 and 2005. Geotherm 35 (5–6):622–653
43. Majer E, Baria R, Stark M (2008) Protocol for induced seismicity associated with enhanced geothermal systems. Report produced in Task D Annex I (9 April 2008), International Energy Agency-Geothermal Implementing Agreement. http://www.iea-gia.org/publications.asp
44. Major E, Baria R, Stark M, Oates S, Bommer J, Smith B, Asanuma H (2007) Induced seismicity associated with Enhanced Geothermal Systems. Geotherm 36(2007):185–222
45. Helm JA, Hoang-Trong P (1993) Assessing the natural and induced seismic risk associated with a hot dry rock (HDR) geothermal energy project with specific reference to Soultz-sous- Forêts, N.E. France. American Geophysical Union, 1993 fall meeting, San Francisco
46. Mortimer L, Adnan, A, Simmons CT (2010) Targeting faults for geothermal fluid production: exploring for zones of enhanced permeability. In: Proceedings Australian geothermal conference 2010, Adelaide, 16-19 Nov 2010
47. Rybach L, Mongillo M (2006) Geothermal sustainability-a review with identified research needs. GRC Trans 30:1083–1090
48. Bächler D, Kohl T, Rybach L (2003) Impact of Graben-parallel faults on hydrothermal convection – Rhine Graben case study. Phys Chem Earth 28:431–441
49. Parker RH (1989) Geothermal energy at the Camborne school of mines. Geotherm Counc Bull 18(9):3–7
50. Cordon E, Driscoll JP (2008) Full life-cycle water requirements for deep geothermal energy developments in South Australia. Unpublished report to the Department of Primary Industries and Resources, South Australia. 50p. http://www.pir.sa.gov.au/__data/assets/pdf_file/0018/110556/TIG_4_PIRSA_Water_Project_26May09.pdf
51. André L, Rabemanana V, Vuataz F-D (2006) Influence of water-rock interactions on fracture permeability of the deep reservoir at Soultz-sous-Forêts, France. Geotherm 35(5–6):507–531
52. Vuataz F-D, Durst P (2001) Fluid-rock interactions and geochemical modelling of the formation brine in the fissured reservoir of the Soultz-sous-Forêts HDR test site. Final report, Federal office for education and science, project OFES N° 98.0008-3

Environmental Countermeasures and Restoration

Sergey V. Fesenko[1], Brenda J. Howard[2]
[1]Department of Nuclear Sciences and Applications, IAEA Environment Laboratories, International Atomic Energy Agency, Vienna, Austria
[2]Centre for Ecology and Hydrology, Lancaster Environment Centre, Bailrigg, Lancaster, UK

Article Outline

Glossary (According to the IAEA nuclear safety glossary [1])
Definition of the Subject and Its Importance
Introduction
Origin and Characteristics of Contaminants in the Environment
International Frameworks for Application of Countermeasures and Remediation of Contaminated Areas
Site Evaluation for Remediation Purposes
Management Options for the Application of Countermeasures and Remediation for Different Environments
Countermeasures and Remediation in Areas Affected by Radiation Accidents
Remediation of Sites Affected by Nuclear Testing
Remediation of Sites within Decommissioning of Facilities
Decision-Aiding Tools
Future Directions
Bibliography

Glossary (According to the IAEA nuclear safety glossary [1])

Acceptable limit A limit acceptable to the relevant regulatory body.

Accident Any unintended event, including operating errors, equipment failures or other mishaps, the consequences or potential consequences of which are not negligible from the point of view of protection or safety.

Action level The level of dose rate or activity concentration above which remedial actions or protective actions should be carried out in chronic exposure or emergency exposure situations.

Contamination Radioactive substances on surfaces, or within solids, liquids, or gases (including the human body), where their presence is unintended or undesirable, or the process giving rise to their presence in such places.

Cost–benefit analysis A systematic economic evaluation of the positive effects (benefits) and negative effects (disbenefits, including monetary costs) of undertaking an action.

Countermeasure An action aimed at alleviating the radiological consequences of an accident.

Decommissioning Administrative and technical actions taken to allow the removal of some or all of the *regulatory controls* from a *facility*.

Decontamination The complete or partial removal of contamination by a deliberate physical, chemical, or biological process.

Dose A measure of the energy deposited by radiation in a target.

Emergency A nonroutine situation or *event* that necessitates prompt action, primarily to mitigate a hazard or adverse consequences for human health and safety, quality of life, property, or the environment.

Evacuation The rapid, temporary removal of people from an area to avoid or reduce short-term radiation exposure in an emergency.

Exemption level A value established by a regulatory body and expressed in terms of activity concentration, total activity, dose rate, or radiation energy, at or below which a source of radiation may be granted exemption from regulatory control without further consideration.

Exposure pathway A route by which radiation or radionuclides can reach humans and cause exposure.

Exposure The act or condition of being subject to irradiation.

Intervention Any action intended to reduce or avert exposure or the likelihood of exposure to sources that are not part of a controlled practice or that are out of control as a consequence of an accident.

Justification (for intervention) The process of determining whether a proposed *intervention* is likely,

overall, to be beneficial, as required by ICRP's *System of Radiological Protection*, i.e., whether the benefits to individuals and to society (including the reduction in *radiation detriment*) from introducing or continuing the *intervention* outweigh the cost of the *intervention* and any harm or damage caused by the *intervention*.

Protective action An intervention intended to avoid or reduce doses to members of the public in emergencies or situations of chronic exposure.

Reference level An action level, intervention level, investigation level, or a recording level.

Relocation The nonurgent removal or extended exclusion of people from a contaminated area to avoid chronic exposure.

Remedial action Action taken when a specified action level is exceeded, to reduce radiation doses that might otherwise be received, in an intervention situation involving chronic exposure.

Remediation Any measures that is carried out to reduce the radiation exposure from existing contamination of land areas through actions applied to the contamination itself (the source) or to the exposure pathways to humans.

Risk A multi-attribute quantity expressing hazard, danger, or chance of harmful or injurious consequences associated with actual or *potential exposures*. It relates to quantities such as the probability that specific deleterious consequences may arise and the magnitude and character of such consequences.

Risk assessment Assessment of the radiological risks associated with normal operation and possible accidents involving a source or practice.

Site evaluation Analysis of those factors at a site that could affect the safety of a facility or activity on that site.

Waste management All administrative and operational activities involved in the handling, pretreatment, treatment, conditioning, transport, storage, and disposal of radioactive waste.

Definition of the Subject and Its Importance

There are a large number of sites around the world contaminated with radionuclides which, to varying extents, require attention. Some of these sites were contaminated by nuclear testing or radiation accidents while others became contaminated as a result of authorized discharges (e.g., hospitals) or inadequate waste management and/or waste disposal practices. In recent years, problems associated with radioactively contaminated sites have led to considerable concern amongst both the general public and decision makers. To a large extent, the concern has been stimulated by the occurrence of several radiation accidents, most notably the Chernobyl accident. These issues have also gained a particular importance because of an increased public concern about the safety of radioactive waste disposal and the associated justification of a sustainable development of nuclear power.

The first stage of any strategy responding to contamination is an evaluation of the need for action. Decisions to use any actions to protect the population or remediate the environment are normally based on a comprehensive site evaluation and justification of the intervention, if necessary. This analysis should then be able to identify appropriate management options.

Many factors govern the effectiveness and cost of countermeasures or remedial actions and need to be evaluated to identify a suitable strategy. The contributions of these factors are site specific, varying with the characteristics of the contamination and the receiving environment as well as on factors such as local and national priorities for remediation planning.

Environmental restoration is often considered as a system of actions having a final goal to return a site to the conditions that prevailed before the contamination. However, in practice, this is often not feasible, especially if vast areas are affected and require a response.

Planning of environmental countermeasures or remedial actions is a complicated, multidimensional task which needs to take account of radiological, ecological, and socioeconomic issues within a holistic approach. The challenge is to identify suitable, effective, individual actions or procedures (such as remediation technologies, communication strategies, or decision support technologies) within a holistic consideration of the entire range of available countermeasures and remediation actions.

Introduction

Contamination of the environment to an extent that requires countermeasures or remediation may occur

due to many different reasons. Obvious sources of radioactive contamination which may require the use of countermeasures include radiation accidents or incidents, but remediation may also be needed for radiation legacy sites [2–7]. Radioactive contamination can be caused inadvertently by human activities involving processes in which natural radionuclides can become concentrated in areas not normally controlled by regulatory bodies. Such activities can include conventional mining and processing of ores, production of phosphogypsum, etc. [8]. There are also many other sources of radioactive contamination such as the application of radionuclides in industry, research, and medicine. The responses to various accidents and existence of some highly contaminated legacy sites have required the development of a variety of countermeasure and remediation management options to protect human health or to remediate the environment.

According to the current international terminology, contamination refers to radioactive substances which occur on surfaces, or within solids, liquids, or gases (including the human body), where their presence is unintended or undesirable [1]. However, almost all human activities are accompanied by the release of contaminants into the environment and such releases are normally under strict regulatory frameworks.

The terms *countermeasure* and *remediation* are frequently used, but often applied differently by various authors. Such a situation can often lead to misinterpretations in descriptions of the activities applied to decrease radiation impact on the public and the environment in an emergency or in exposure situations when contamination is already present. To clarify the issue, the terms here are used consistently in the following way. Management options which have been applied in the case of emergency are countermeasures, and they can include both protective and remedial actions [1]. However, the same management options when applied in the situation of existing exposure are considered remedial actions. Existing exposure in this situation includes options applied when an emergency exposure situation has been declared to have ended or in areas contaminated by residual radioactive material from past practices, and are part of a *remediation process*. The more informal term *environmental countermeasure* is also used elsewhere for management options used as remedial actions.

There is no definitive set time period when an option will change from a countermeasure to a remediation in the case of emergencies. The transition from an emergency exposure situation to a subsequent existing exposure is characterized by a change in management, from countermeasure strategies mainly driven by urgency, with potentially high levels of exposures and predominantly central decisions to more decentralized remediation strategies aiming to improve living conditions and reduce exposures as low as reasonably achievable given the circumstances [9]. These strategies must take into account the long-term dimension of the situation with the possible direct involvement of the exposed individuals in their own protection [10].

There are some management option countermeasures such as evacuation or application of iodine tablets, which can be considered only as protection actions and never as remedial actions since they are only used in the acute or early phase of an emergency. Conversely, some management options can be used both as countermeasures and remedial actions, depending on the situation or interpretation of a purpose of the application, such as clean feeding of animals to decontaminate them.

A wide range of countermeasures and remedial actions have been developed, tested, and implemented in contaminated areas. As a result, a large amount of data on their effectiveness has been generated, together with information on ancillary factors such as the required resources and costs. These measures vary considerably in their effectiveness, cost, and practicability and this difference has led to a need to develop a variety of approaches and adequate decision-aiding technologies and Environmental Decision Support Systems (EDSSs) that can be effectively used for countermeasure or remediation planning and optimized application of such actions [11–13].

The main sources of the data on the effectiveness of management options has been the application of countermeasures in areas affected by major radiation accidents, remediation of nuclear testing sites, and areas affected by nuclear facilities or other human nuclear activities such as the use of radionuclides for medical, research, or industrial purposes. Analysis of the lessons learned from these case studies has been invaluable in demonstrating that the efficiency of protection of management options depends on many factors, including environmental conditions, properties of the radionuclides, management on the affected areas, and

response from the local population and stakeholders [11, 14–17]. This leads to a need to adopt a holistic approach, the application of which is to be facilitated by modern regulatory frameworks for countermeasures and remediation of contaminated areas [10], especially with a target of sustainable development of the environment.

Origin and Characteristics of Contaminants in the Environment

There are many different sources of radioactive substances in the environment. At present, the most important sources which have resulted (or which still result) in the need for the application of countermeasures or remediation can be divided into two main groups. The first group can be termed *radiation legacy*: this group includes military test explosions, radiation accidents, nuclear weapon accidents, early design nuclear fuel cycle facilities, and nuclear applications with inadequate operational and disposal practices [2, 4]. In some of these cases, the application of countermeasures was necessary to protect the population of the affected areas before remediation of these sites was considered.

The second group consists of *existing* human activities including uranium mining, processing of ore, fuel fabrication, energy generation, reprocessing of nuclear fuel, and various other applications of radionuclides in industry, research, and medicine. For all these activities countermeasures are not required because the corresponding discharges of radionuclides into the environment or the measured concentrations of radionuclides in the environment are below the acceptable limits. However, remediation is a planned and necessary part of the decommissioning of these facilities and the sites should be restored to the status which (under existing regulations) allows release of the site to unrestricted use (ideally) or for some specific purposes (restricted use) if the first option is not feasible.

Radiation Legacy Sites

Most sites requiring large-scale remediation are part of a "radiation legacy" [4]. Radionuclides of concern at such sites have a long physical half-life, high radiological toxicity, and high mobility in the environment or are elements (including analogs) which have an essential role in the biosphere [18].

During the period 1940–1970, many sites were heavily contaminated because of the prevailing radioactive waste disposal practices at facilities for nuclear weapons material production. In particular, large quantities of radioactive liquid wastes, sometimes mixed with other chemicals, were commonly disposed of directly into the ground, surface water bodies, or marine systems (for instance at the Mayak, Hanford, and Sellafield production facilities). These disposal practices led, in some instances, to serious environmental problems which required, or still require, remediation [2, 4, 17].

Another major legacy group arose from nuclear explosives, which have been detonated above ground, on the surface, and below ground at many test sites around the world. Nuclear weapons accidents have occurred around the world since the 1950s. Severe accidents include the losses of nuclear weapons from aircraft at Palomares (Spain) in 1966 and Thule in Greenland in 1968 [17, 19–21].

Additionally, about 100 civilian peaceful nuclear explosives have been performed in the former Soviet Union countries and in the USA for different purposes (constructions of dam, gas reservoirs, etc.). Although the contribution of these explosives to the global dose was very low [5], in some local areas contamination of the environment has required application of remedial actions [6, 22, 23].

Severe radiation accidents at the Mayak radiochemical plant (Kyshtym accident) in 1957 and the Chernobyl nuclear power plant in 1986 have led to significant contamination by long-lived radionuclides over many years, requiring long-term remediation [17, 24–26] after the acute phase.

In some cases, either through accidents or a lack of radiation safety culture, sites have been left contaminated with residues even from authorized operations. Such sites include factories where radium was used in luminescent paint and thorium was used in thorium-coated gas mantles [4].

Existing Nuclear Activities and Current Sources of Radioactive Contamination

Due to an improved radiation safety culture over the last several decades, the discharge of radionuclides into the environment has greatly declined in many countries [5]. Despite low discharges of radionuclides, nuclear

fuel cycle facilities still contribute to contamination of the environment (mainly within the facility) to a sufficient extent that remedial actions might be advisable even in the absence of radiation accidents. Naturally occurring radioactive materials (NORMs) such as ^{238}U, ^{232}Th, and their progeny are often the most significant environmental contaminants at such sites. NORMs can also occur in many ores containing metals such as copper, gold, coal, and monazite. Residues from the production of phosphoric acid and various phosphates may also cause contamination of the environment [27]. The combustion of coal for electricity generation, smelting processes, and heating leads to the release and dispersion of some natural radionuclides, mainly radium, in the environment.

Normally, remediation of all such sites is an obligatory part of the decommissioning process and is subject to special compliance monitoring [17, 28] which must prove that affected areas have been adequately remediated before it is permissible for them to be used for other purposes.

Currently, radionuclides are extensively used for a variety of scientific, medical, agricultural, and industrial purposes [2]. The major users of unsealed radioactive sources are hospitals where nuclear practices are used for diagnostic and therapeutic purposes, and to a lesser extent for treatments. Some of the radionuclides used for such activities (^{3}H, ^{14}C, ^{32}P, ^{35}S, and ^{131}I) occur in the liquid effluents which can be discharged into the environment [6]. These radionuclides are also in use in a range of research applications such as genetic studies, animal health or environmental studies, while ^{147}Pm is widely used in industry [4].

An additional long-term source of contamination of the environment is radioactive waste. Environmental contamination may occur during the collection, processing, storage, and disposal of wastes associated with the use of radioactive isotopes for industrial, research, and medical applications [4, 6].

International Frameworks for Application of Countermeasures and Remediation of Contaminated Areas

The major source of international recommendation on this subject is the International Commission on Radiological Protection (ICRP). The ICRP is the primary international body that recommends the fundamental principles and quantitative basis upon which appropriate radiation protection measures can be established. It leaves the responsibility of formulating the specific advice, codes of practice, or regulations tailored to the individual countries (http://www.icrp.org/about.asp).

Overall, the ICRP's recommendations serve as a major basis for all protective actions, including environmental countermeasures and any remedial actions. International standards and supporting technical documents, such as the International Basic Safety Standards for Protection Against Ionizing Radiation and for the Safety of Radiation Sources [29], are also based on ICRP recommendations.

The ICRP recently revised its approach to characterizing situations in which exposure to humans may occur. Instead of a process-based approach [30] distinguished by its use of two concepts, *practices* and *interventions*, the ICRP suggested a situation-based approach to characterize exposure situations [31]. This approach replaces reference to *practices* with *planned exposure situations* and replaces *interventions* with *emergency exposure situations* and *existing exposure situations* [9]. At present, the ICRP considers three major exposure situations [31]:

1. *Planned exposure situations* are situations involving the deliberate introduction and operation of radioactive sources.
2. *Emergency exposure situations* are situations that may occur during the operation of a planned situation, or from a malicious act, or from any other unexpected situation, and require urgent action to avoid or reduce undesirable consequences.
3. *Existing exposure situations* are situations that already exist when a decision on control has to be taken, including prolonged exposure situations following emergencies.

Overall, radiation protection is based on three fundamental principles, namely, *justification*, *optimization*, and *individual dose limitation*. Within the context of remediation, the fundamental principles can be formulated as justification of remediation, optimization of remedial actions, and restriction of residual individual doses [9]. Together, they provide a basic framework for the application of remediation in long-term exposure situations.

Any remediation should be justified and remedial measures shall do *more good than harm* and shall provide optimized arrangements to maximize the net benefit to society [1]. Thus, the total benefit of reduction of exposure through remediation must be greater than any detriment that the remediation may cause. Overall, remediation shall [1]:

(a) Reduce the doses to individuals or groups of individuals being exposed
(b) Avert doses to individuals or groups of individuals that are likely to arise in the future
(c) Prevent or reduce environmental impacts from the radionuclides present in the contaminated area

Justification of remediation shall go far beyond the scope of radiological protection and can include economic, political, environmental, social, and psychological facets. Justification of remediation should be based on cumulative benefits and impacts of individual remedial actions composing the remediation strategy. Some individually justified actions may be available, but may not provide a net benefit when considered as an overall strategy because, for example, collectively they bring too much social disruption for the considered exposed population as a whole, or they are too complex to manage. Conversely, a single protective action may not be justified alone, but may contribute to an overall net benefit when included as part of a protection strategy [9].

The responsibility for ensuring an overall benefit to society as well as to individuals when the population is allowed to continue living in contaminated territories is with governments or national authorities. At the same time, the current approach also emphasizes an important role to the individuals concerned. In existing exposure situations, justification should be considered for all remedial actions that may be included in a remediation strategy: those implemented centrally and locally by authorities, experts, and professionals and those directly implemented by the exposed individuals as self-help protective actions with the support of the authorities. The remediation strategy defined by the authorities should also take into account the ability of affected individuals to take self-help initiatives. However, as self-help protective actions are implemented – and thus largely decided – by the inhabitants themselves, they must be properly informed and even trained (to use the means and equipments provided by the authorities) to take decisions concerning their own protection with a net benefit.

The process of optimization of protection is intended for application to those situations for which the implementation of protection strategies has been justified. Thus, if justified, remediation of contaminated area should be optimized. The level of protection to be achieved by the remediation should be the best under the prevailing circumstances, maximizing the margin of benefit over harm.

Owing to its judgmental nature, there is a strong need for transparency of the optimization process. The decision-making process shall provide for the involvement of a wide range of interested parties in the definition, implementation, and verification of remediation programs and for regular public information exchange on the implementation of these programs [1]. All the data, parameters, assumptions, and the values that enter into the process should be presented and defined very clearly. This transparency assumes that all relevant information is provided to the involved parties, and that the traceability of the decision-making process is documented properly, aiming for an informed decision [31].

The optimization principle should be applied in the same manner in all exposure situations. Restrictions are applied with respect to the permitted dose to a nominal individual (or *representative person*). The representative person is an individual, who will almost always be a hypothetical construct, receives a dose that is representative of the more highly exposed individuals in the population [32]. The representative person is equivalent to, and replaces, the average member of the critical group recommended previously by the ICRP [33–35].

Options which result in the *representative* person receiving a greater dose than the restrictions permit should be rejected at the planning stage. Importantly, these dose restrictions are applied prospectively, as with optimization as a whole. If, following the implementation of an optimized protection strategy, it is subsequently shown that the permitted dose for the representative person has been exceeded, the reasons for this should be investigated but the exceeding alone should not necessarily encourage remedial action.

To avoid inadequate outputs of the optimization procedure, restrictions should be placed on the

potential doses or risks to individuals who remain in contaminated territory or implement remedial actions.

The main factors to be considered for setting the reference levels for existing exposure situations are the feasibility of controlling the situation, and the past experience with the management of similar situations. In most existing exposure situations, there is a desire from the exposed individual as well as from the authorities to reduce exposures to levels that are close or similar to situations considered as "normal." This applies particularly to situations of exposures from material resulting from human actions.

The experience gained in the aftermath of the Chernobyl accident has shown that nontechnical factors can affect remediation policies enormously [36]. The ICRP recommendations are based on objective assessments of the health risks associated with exposure levels and on radiological protection attributes of various exposure situations. However, members of the public (and sometimes their political representatives) may have personal views on radiation risks and feasibility of remedial actions intended for dose reductions. This can lead to different perceived needs for intervention and the extent of remediation, depending on the origin of the exposure. The public concerns are normally stronger when the environment is contaminated by artificial radionuclides than when these are of natural origin. An elevated exposure due to natural radiation sources are often ignored by the public, while relatively minor exposures to artificial long-lived radioactive residues are often a source of concern and sometimes lead to a request in remediation even it is not justifiable in terms of radiological protection standards.

As the long-term objective for existing exposure situations is *to reduce exposures to levels that are close or similar to situations considered as normal*, the ICRP recommends selecting the reference level for the optimization of protection of individuals living in contaminated territories in the lower part of the 1–20 mSv/year band [31].

The reference level represents the level of dose or risk above which it is judged to be inappropriate to plan to allow exposures to occur, and below which optimization of protection is implemented. Optimization is to be applied in emergency and existing exposure situations, even if the initial doses are below the defined reference levels.

Past experience has demonstrated that typical values used for constraining the optimization process in long-term postaccident situations fall in the range of the dose limit for planned exposure situations, namely, around 1 mSv/year [9]. National authority may take into account the prevailing circumstances and also usefully take account of the timing of the overall rehabilitation program to adopt intermediate reference levels to progressively improve the situation.

Although the above considerations were sometimes referred to the chronic exposures situation after the radiation accidents, the above framework is also entirely applicable for the sites of former practices and other similar exposure situations. Thus, if exposure level at the site of a former practice satisfies the reference level for all its future plausible uses, the site may be released for unrestricted use and the decommissioning phase of the practice can be terminated. If this is not feasible, the site may still be released for restricted use or released for unrestricted use after remediation. However, these restrictions and remedial actions (if any) can be considered a type of intervention since some form of institutional control will be still required [9].

Site Evaluation for Remediation Purposes

Remediation of any contaminated site starts with a site evaluation, which includes a comprehensive analysis of the factors that could affect the need of such actions and effectiveness of their application [37]. Overall, site evaluation should assist in making three major decisions. First, site evaluation should confirm that the site is contaminated to an extent requiring remediation. Second, it should be able to suggest appropriate management options if compliance with radiation safety criteria was not confirmed. And third, a site evaluation also includes a demonstration of remediation success and justification to release a site for future use [17, 28].

A site evaluation includes investigations covering [17]:

- Properties of both contaminants and the environment
- Detailed consideration of factors that could affect radiation safety at a site or of an activity that could result in a release of radioactive material and/or

could affect the dispersion of such material in the environment
- Population and access issues relevant to safety (e.g., feasibility of evacuation, location of people and resources)

To achieve these tasks, information on the site under evaluation should be made available and include data that is reliable and sufficient for making proper decisions.

If, after discovery of contamination, a radiological scan of a site shows high levels of radioactivity in some areas, then a grid survey using properly calibrated equipment is carried out. The property boundaries and pathways of the natural drainage system should be given special attention. This survey should also identify whether dose limits for members of the public or workers using a site might be exceeded under some circumstances within the boundaries of the site and to what extent [28].

If the need for application of countermeasures in the acute stage of the emergency or remediation was confirmed, a detailed site inspection needs to be undertaken. The aim of this survey is to determine the spatial extent of the problem, and to gather sufficient information to allow a full dose assessment for potential site occupiers and off-site populations. Any radiological threats to the environment from the existing situation, or from possible remediation actions, also have to be identified.

To achieve these objectives, an optimized sampling (measurement) program is required. The development of such program commences with the determination of baselines and comprises of a review of the history of all nuclear activities at the site. Alternatively, the presence of contamination has to be identified by measurements and expert judgment if no other information is available.

If a consideration of the results of this characterization leads to a decision to undertake protective actions, then detailed investigations are necessary to enable an optimized remediation strategy to be constructed. In addition, characterization of any waste stream may be necessary before the transport and disposal options for the waste are approved.

One final stage is required in the case of remediation, namely, a final survey (a compliance monitoring) to demonstrate that the objectives of remediation were successfully achieved. It also ensures that (1) radionuclide dispersion and migration will not have deleterious effects on the population and (2) the environment and the site can be reused following remediation. At that stage, compliance of residual concentrations of radionuclides in the environment with the acceptable levels must be verified and any areas with residual contamination must be identified and the nature, quantity, and distribution of the radioactivity determined. An example of the procedure, demonstrating interactions between a site remediation and evaluation within one generalized process is outlined in Fig. 1.

Management Options for the Application of Countermeasures and Remediation for Different Environments

The main objective of a management option as a countermeasure or as part of a remediation strategy is to reduce or prevent doses to humans. Although inhalation of resuspended material is a potential pathway, the doses in many situations arise largely from either the consumption of contaminated foodstuffs and water via ingestion or from exposure to contaminated surfaces in an inhabited area via external irradiation. A secondary objective is to provide reassurance to consumers and people living in contaminated areas and thereby maintain public confidence.

Countermeasures can be implemented at different phases of an emergency response extending from before the radioactive contamination is actually deposited and continuing for a varying amount of time depending on the characteristics of the accident or incident. The focus in the discussion here is on management options used after the acute phase of an accident and during remediation although countermeasures are mentioned to some extent.

The environmental behavior and mobility of radioactive contamination, and thus the potential severity of an emergency or existing exposure situation in terms of the predicted dose received by humans depends greatly on (1) the composition and physicochemical form of the radionuclides present and (2) the characteristics of the ecosystem affected by the contamination and how it is used by humans [38–43]. Thus, many different factors influence the selection of which management options are most appropriate to apply and when. When developing a remediation strategy for the long-term

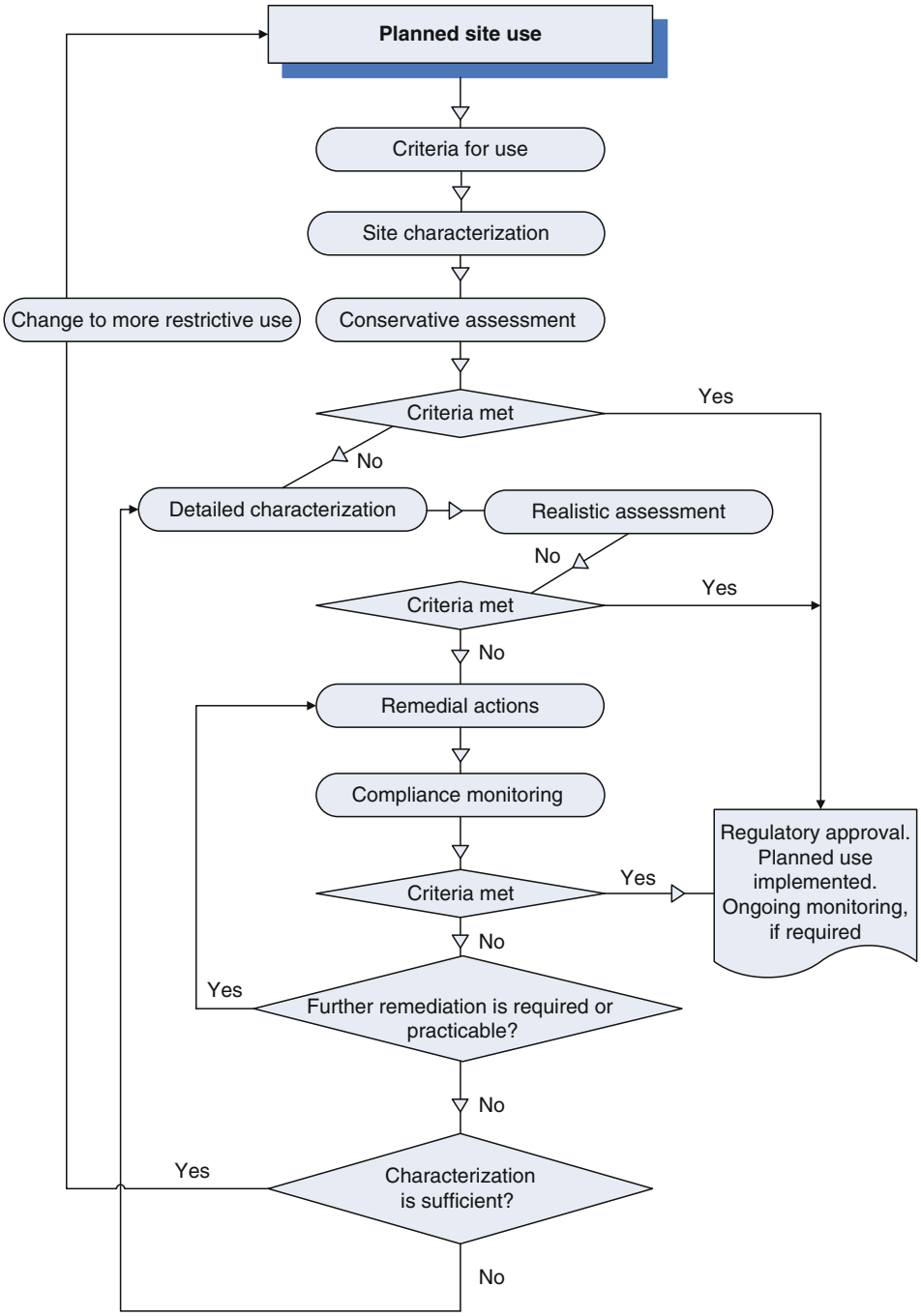

Environmental Countermeasures and Restoration. Figure 1
Key stages in remediation and release of contaminated sites (Adopted from [4])

recovery of contaminated areas, some of the most important factors to consider are described below.

Factors and Processes Influencing Management Options

Management options are largely designed to reduce (1) the ingestion dose from the consumption of contaminated foodstuffs and drinking water, (2) external dose rates from deposited radionuclides, and (3) inhalation dose from resuspended material. A wide range of factors can influence the administration, impact, and consequence of the use of various management options. Some of these factors are considered briefly below and others in more detail in subsequent sections.

Temporal Factors These include the time of year that the contamination happened, the variation in activity concentrations of the deposited radionuclides with time and their rate of movement in the environment. In the short term, prompt countermeasures may be necessary such as housing dairy cattle if they are grazing outdoors at the time of deposition. However, many management options take time to organize and implement. Where management options involve significant and/or irreversible actions, then stakeholder consultation is advisable if time permits, but this may often only be possible in the recovery phase of an accident when defining a remedial strategy.

Spatial Factors The size of the area affected, extent of contamination present, and land use will influence the choice of appropriate management options can be used. In heavily contaminated areas, priority has initially to be given to the direct protection of the population rather than options for agricultural production. In other less badly affected areas, restrictions on the entry of food into the food chain may be required or management options to reduce radioactive contamination in food products. Finally, adjacently, relatively unaffected areas will also need to be monitored in case of indirect effects and to maintain public confidence. The transfer of radionuclides may vary with factors such as soil type. In remediation situations, this may mean that less heavily contaminated areas outside the major zone of concern with sensitive soil types allowing higher radionuclide uptake into plants are actually producing more highly contaminated food products than those areas which received higher deposition [44–46].

Effectiveness of Management Options Information on effectiveness is generally presented as a percentage reduction in activity concentration in the target medium (i.e., soils, crops, building surfaces, roads) after implementation. There are some management options (such as live monitoring) which do not directly reduce doses but increase the effectiveness of other options and may also provide reassurance. Effectiveness is influenced by many factors including when it is applied relative to the time of deposition, application rates, duration of treatments, the radionuclide deposited and its form, biological half-live in animals, effective half-life in different ecosystems, timeliness of implementation, compliance, and acceptability.

Radiological Impact (Protection of Implementers) A radiological impact can occur due to incremental doses received by people who implement management options during procedures that are not part of normal practices. The magnitude of the doses received will depend on many variables such as the type of radionuclide released and what becomes contaminated, the exposure pathways (external, inhalation, ingestion, irradiation of the skin) resulting from carrying out the management options (including disposal of wastes) and length of exposure time. Doses to implementers are controllable so the ICRP principles of protection apply, namely, justification, optimization and, dose/risk limitation.

Economic Cost Many factors influence the monetary cost of implementing management options [47]. Direct costs which are more obvious are the cost of implementation, labor, consumables, equipment and transport, and the cost of handling wastes and carrying out environmental remediation. But there are other less often considered costs such as those incurred through loss of production, loss of retail sales, closure of businesses, and the provision of temporary premises. Indirect costs are often equally important, although they are inherently more difficult to quantify. Examples are loss of market share, regional impact on tourism, which could extend to area adjacent to those which are contaminated, and the impact on society when people cannot return to normal lifestyles.

Importantly, the option not to carry out any management options can also be a valid alternative. If authorities decide that countermeasures or remediation is not required, then it is important that this decision is accompanied by a monitoring strategy aimed at reassuring the local population. This option should be considered if measurements and assessments indicate that the doses to people living in the area would be low. No judgment is made here on what would constitute a low dose. Other factors could influence the decision not to implement any remediation, such as availability of limited resources or a very large area being affected.

A large number of management options have been developed and applied, especially since the Chernobyl accident. In the 1990s, initial efforts were made in the STRATEGY project to synthesize the information on available management options for the early to late phase after an accident, and to critically evaluate whether they were generally applicable and useful to areas other than those in which they had been applied [48]. The management options can be subdivided according to the different categories discussed below; some management options in one category are also applicable to others.

The most important generally applicable management option is the imposition of food bans to prevent contaminated food products from entering the food chain. This is a highly effective, but expensive option and would be an automatically imposed countermeasure due to regulatory procedures after accidents if contamination levels were predicted to exceed the relevant action levels. Alternatively, it may be considered appropriate in certain circumstances to raise action levels. For example, this was done in Scandinavia after the Chernobyl accident to protect the Saami way of life.

Countermeasure and Remedial Actions for Agricultural Food Chains

The agricultural food chain supplies the majority of food to humans. Therefore the application of management options to this exposure pathway is a critical part of any emergency response or remediation strategy. In food production systems, management options are targeted to various media and contamination pathways including soil, crops, livestock, and other animal products. They are not only aimed at addressing health concerns, but also a wide range of other issues such as the local economy, societal, and ethical concerns, and disposal of wastes.

In the pre-deposition phase, responses will obviously be dependent on the extent and quality of information available. Potential countermeasures include the prevention of contamination reaching food products such as switching off ventilation or irrigation systems in greenhouses, etc., or covering foodstuffs to prevent surface contamination. Livestock can also be sheltered from the contamination by being housed.

Agricultural food chain management options in the early to late phase can be divided into two types, namely, intervention along the soil-crop pathway and in animal production systems. The former focuses on reducing the contamination of crops including cereals, industrial crops, vegetables, and horticultural crops, food plants for domestic animals, and fruit. It is therefore largely aimed at reducing dose to humans. A management option which applies to both groups is the selection of alternative land uses whereby contaminated land may be used for nonfood production, such as flax, bioenergy, or biofuel crops, or for the production of leather and wool. Land may also be used for forestry, but this is unlikely to be the preferred option. The various available management options have one or more of the following aims:

- To remove contamination completely, usually through topsoil removal
- To reduce soil-to-plant transfer of radionuclides through a variety of techniques including deep, shallow, or skim and burial plowing, and soil treatment to reduce radionuclide transfer from soil to plants
- To reduce radionuclide contents at the food processing stage through chemical procedures or dilution.

If fodder plants are too highly contaminated for direct human consumption, they can still be fed to agricultural animals in the early stages of growth as long as there is sufficient time for decontamination thereafter, prior to slaughter.

Intervention in animal production systems is largely aimed at reducing the ingestion dose from meat, milk, and other dairy products, offal, eggs, and

other foodstuffs derived from agricultural animals [45, 49–52]. They generally involve:

- Decontamination of animals by feeding the animals uncontaminated feeds; the efficiency of "clean feeding" depends on the biological half-life of each radionuclide in the muscle or other products
- Reduce ingestion of contaminated feed by selective grazing regimes
- Reduce gut uptake of radionuclides by the addition of (1) specific radionuclide binders to the animal feed such as ammonium hexacyanoferrate for radiocaesium and (2) stable analogs such as Ca to suppress radiostrontium absorption
- Slaughtering of dairy livestock, which may be necessary if uncontaminated feed is not available (or other countermeasures are not possible); lactation might be suppressed in conjunction with this option
- Manipulating slaughter times to minimize the activity concentrations, by allowing physical decay of short-lived radionuclides and allowing longer finishing periods (sometimes with clean feed) to ensure that the meat is below action levels
- Reduce radionuclide contents at the food processing stage

Many of the above management options can be combined with live monitoring to determine whether activity concentration in animals are below the action limits and/or optimize application of the management options.

Countermeasures and Remedial Actions for Domestic and Free Foods from Extensive Ecosystems Including Forests

Extensive ecosystems include unimproved meadows (such as in mountainous areas or forest clearings) used for grazing livestock as well as forested areas. For grazing animals, some of the management options listed above may be applicable, although some animals in these areas are handled infrequently, so many of the most effective measures such as clean feeding are difficult to implement.

Forested areas are used by humans both for forestry, recreation, and as sources of wild foods. Dose pathways for forests may include external exposure from the forest floor, contamination in trees, handling of forestry material, and industrial production based on contaminated wood. Internal exposure arises from consumption of forest foods such as mushrooms, nuts, and berries. Finally inhalation of radionuclides can occur following forest fires or combustion of contaminated wood [53].

The reduction of some of the doses occurring in forests soon after deposition of radionuclides requires measures aimed at the atmospheric deposition process itself and are difficult to implement, so restricting access to the contaminated forest areas may be the most important short-term countermeasure. Over longer time periods, other available management options include selective harvesting to avoid the most contaminated wild foods, preventing forest fires, providing advice on use of wood ash and reducing soil-plant uptake.

Countermeasures and Remedial Actions for Aquatic Ecosystems

Aquatic ecosystems include lakes, rivers, groundwater, and marine waters, each of which has contrasting characteristics due to hydrological, hydrochemical, or morphological factors. The need for application of management options for aquatic ecosystems is, therefore, largely dependent on site-specific parameters which often severely constrain what can be done. Furthermore, management option application in contaminated waters may be expensive, including large engineering costs so cost–benefit analysis is particularly important.

In general, population doses from aquatic pathways are often less than from terrestrial pathways depending on food habits. The main dose pathways from aquatic sources are from their use as drinking water supplies and for irrigation, and as a source of aquatic foodstuffs. If lakes used in power production, which may alter lake volume, are contaminated then the occasional exposure of contaminated bottom sediments can lead to the risk of contaminated sediments becoming airborne. Due to the self-shielding of water, external doses from recreational use of contaminated lakes and rivers can often be relatively low.

Intervention in aquatic systems involves reducing:

- Contamination reaching the water body
- Uptake by fish
- Ingestion of contaminated feed

Management options for drinking water are targeted at public and private water supplies and can be divided into two main groups:

- Provide clean water through alternative supplies and changes to the source of the supply
- Treatment of water (blending and/or purification)

Many of the above groups of management options are more effective if combined with dietary advice, the provision of monitoring kits, food labeling, and compensation schemes.

Countermeasures and Remedial Actions for Inhabited Areas

The urban ecosystem is where most people live and constitutes a wide variety of different structures and natural surfaces such as grassed areas, paved areas, exterior walls, roof paving, trees, shrubs, and interior surfaces that can all become contaminated and contribute to dose. The relative magnitude of the dose contribution from these different structures and surfaces, and thus the specific needs for management options depends strongly on the release scenario. Clean-up may result in large volumes of contaminated material requiring disposal.

For contaminated surfaces there is a need to adequately identify and quantify the problem, including the type and spatial distribution of the radioactive contamination. This is because inadequate and incomplete application of management options which do not take account of the overall spatial and vertical distribution of radioactive contamination can be much less effective than expected when correctly applied [54].

Although most remediation techniques for inhabited areas are designed to reduce external dose [55, 56], non-acute inhalation doses received from resuspended contamination can be substantial. To reduce this pathway, techniques to fix contamination to the surface to suppress dust can be used in a later recovery phase [57].

Management options for inhabited areas comprise two main groups that (1) shield people from the contamination (shielding options) and (2) remove contamination (removal options also called decontamination or clean-up options). They may be further classified according to the type of target surface (i.e., buildings, road and paved areas, soils and grass, trees and shrubs).

Shielding options can be used to reduce both external exposure and the intake of contaminated material, and are effective in providing protection against both exposure pathways [58]. The effectiveness of a shielding option is defined as the reduction in the external dose rate from a surface (e.g., buildings, paved surfaces, grass, soil, and shrubs), generally expressed as a percentage, after the implementation of the option. If the primary aim is to reduce external exposure, shielding materials can be placed between the contamination and people (burial and covering of objects). The use of shielding materials is potentially a particularly effective option for short-lived radionuclides emitting alpha or beta radiation. Some more permanent shielding options, such as burial of contaminated material or the permanent relocation of people from a contaminated area are also effective for long-lived radionuclides and gamma-emitting radionuclides. There are three main types of shielding options:

- Burial and covering of objects including the use of clean topsoil or sand in gardens and other open areas and the turning of paving slabs, triple digging, and plowing in park areas
- Restricting people from gaining access to contaminated areas or objects, or relocating people from the area
- Fixing of contamination to the surface and restricting its mobility

Removal options involve the decontamination or clean-up of contaminated surfaces and objects. The effectiveness of a removal option is defined as the ratio of the activity initially present on a specific surface (e.g., buildings, paved surfaces, grass, soil, and shrubs) to that remaining after implementing the option. This ratio is usually called the decontamination factor (DF).

Surface treatments for buildings and infrastructure include road planning, vacuum sweeping of roads and walkways, high-pressure water hosing of walls and/or roofs, sandblasting of walls, ammonium treatment of walls, roof cleaning by cleaning device, intensive indoor surface cleaning, and firehosing of roads and walkways. One of the main disadvantages of these management options is that contaminated waste material is often produced in large quantities. Also,

decontamination techniques such as high-pressure hosing and sandblasting may damage old or poorly maintained brick or stone buildings.

Treatment of the gardens and parks can also be considered and available management options include snow removal, topsoil removal, lawn mowing and pruning, or removal of trees and shrubs.

Waste Disposal Options

Waste disposal options have been summarized most recently by Nisbet et al. [58, 59] in Recovery Handbooks and are summarized briefly here. For food production systems, considerable amounts of biodegradable waste can arise if food bans are implemented. Since the restrictions are based on statutory requirements they have to be carried out at short notice and appropriate routes of disposal need to be identified in advance of future accidents or incidents.

However, several management options also produce contaminated by-products and routes for their disposal must be considered. Contaminated produce that might require disposal include crops and by-products from processing of grass products (fresh grass, silage, hay), milk and by-products from processing, whole animal carcasses and meat, and soil.

Waste treatment options that can be carried out on-site include composting, land spreading of milk and/or slurry, and plowing in of a standing crop. Off-site options include biological treatment (digestion) of milk, burial of carcasses, disposal of contaminated milk to sea, incineration of crops, landfill, processing and storage of milk products for disposal, and rendering of animal carcasses (which converts waste animal tissue into stable, value-added materials).

The contamination of an inhabited area generates both solid and liquid waste regardless of whether any countermeasures are applied. In inhabited areas, contaminated items may need to be removed and facilities such as those for water treatment may become contaminated by waste water from management options such as firehosing buildings and by contaminated precipitation and runoff. The categories of radioactive waste are (1) contaminated waste (refuse) and goods, (2) solid and liquid waste from clean-up of the contaminated area and (3) waste water from precipitation and natural run-off. It is therefore important to consider the impact of the contaminated waste on the public, workers handling the waste, the environment, and normal waste disposal practices.

Waste disposal schemes for solid contaminated waste should preferably be planned for in advance, with potential disposal sites and resources identified if possible [54]. The selection of suitable disposal sites needs to take account of the proximity, cost, hydrogeological characteristics of the site, geological stability, and future land use.

Construction of a repository (Fig. 2) should consider a number of other factors:

- There should be adequate shielding so that the contamination in the repository does not contribute significantly to the external dose rate in the area.
- The ecological characteristics of the area should be assessed and intrusion by humans, animals, and plant roots needs to be prevented, usually by using suitable protective layers.
- Migration of radionuclides from the waste with rainwater must be prevented, usually by draining the rainwater off in a gravel layer on top of the waste layer.
- The repository should be protected against erosion.
- The acceptability of constructing repositories needs to be assessed.
- The repository may be equipped with a drainpipe at the bottom for inspection of the radionuclide contents in any water passing through the construction.
- The design should be simple, inexpensive, and possible to construct quickly.

Secondary (or Side) Effects of the Application of Management Options

Environmental impacts occurring due to the application of management options can be positive or negative, direct or indirect, and can lead to social disruption or damage to the environment [60]. Direct environmental impacts can include changes in biodiversity, soil fertility and structure, and enhanced soil erosion as well as pollution of air and aquatic ecosystems. Indirect effects may be less immediately obvious, but could include restrictions to an individual ability to follow their selected lifestyle.

The Chernobyl Forum, based on the related studies in areas affected by the Chernobyl accident, reported

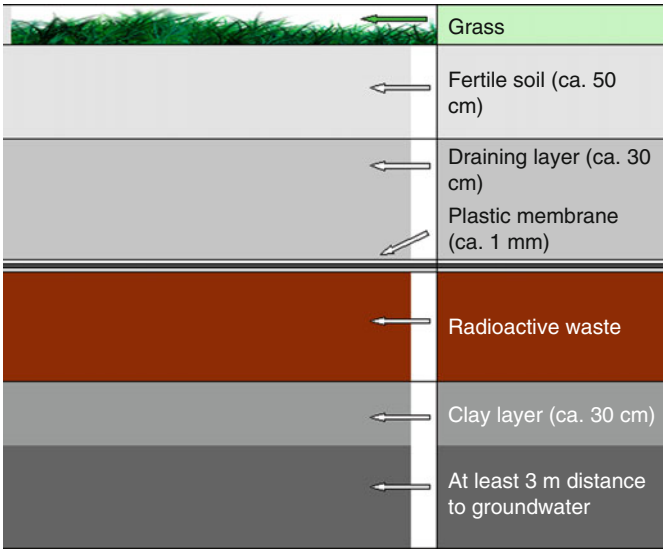

Environmental Countermeasures and Restoration. Figure 2
The principles of a simple ground repository for radioactively contaminated remediation waste (e.g., soil), as recommended by Junker et al. [53]

that some management options led to detrimental social and economic effects, particularly a breakdown in the social infrastructure [61] which could also be considered amongst the most serious consequences of the accident. Nevertheless, remediation can also include options to restore ecosystems, and secure livelihoods and the social structure of affected populations, or stabilize the economic situation [62].

Side or secondary effects of management options can be very diverse. If all access by the public is restricted and access for forestry is limited, major losses to the population would include a lack of locally collectible: wood for industrial purposes and for heating; berries and mushrooms; forest fodder for dairy cows and firewood for rural populations. The cost of forestry is also increased due to limitations on the time which forest workers can spend in contaminated forests which, in turn, can lead to deterioration in the maintenance of forests with negative ecological consequences. Application of restrictive management options such as limited access to forest in the areas affected by the Chernobyl accident had negative psychological and sociological consequences. The economic losses were also large [60, 62].

Implementation of soil-based agricultural actions can change soil properties or decrease air and water quality, while land use-based remedial options can change the landscape and its use, impacting the economic or recreation leisure value of an area [12, 48, 60].

Societal and Ethical Aspects

Overall, the primary factors and effects described above led to many ethical issues including assessment of the consequences of remedial actions implementation for future generations, sustainability, and comparing harm to the environment to benefits to humans. When both radiological factors and social aspects are taken into account, better acceptability of countermeasures by the public can be achieved [12, 61]. Thus, the impact on individual and communities needs to be considered. Local stakeholders need to be consulted in the identification of problems and their solution.

Some management options may have a negative impact on society by causing disruption (e.g., through restricting access or activities), anxiety, and stress (e.g., by causing panic, upheaval), and stigma (e.g., by affecting businesses or tourism). These need to be balanced against positive impacts through provision of reassurance and improvements to living conditions. There are also ethical issues to be addressed when selecting management

options, including: provision of self-help options that reinforce liberty and dignity, the distribution of doses over space and time and between different members of the community, animal welfare, environmental risk, and consequences for future generations [62].

The ethical acceptability of remediation is highly dependent on the ecological status of the area and the degree to which the actions diverge from usual practice. In most cases, environmental legislation must also be considered [63].

Studies on effectiveness of remediation implementation in many areas affected by the Chernobyl accident have identified a variety of factors that had a highly detrimental impact on the economic and social activities on contaminated areas. Practically all remedial options were too expensive to be competitive at the market, and required large subsidies from the state to support economic activity in the affected regions. In most cases, remedial actions imposed a stigma on the areas with contaminated environments [62]. Similar psychological effects have also been observed in some other European countries [64]. This constrained or prevented export of even high-quality products to nonaffected areas, constrained economic and social development of those regains, and promoted migration of some of the working-age population to areas with lower contamination levels. As a consequence, economies and social structures in affected communities deteriorated, alongside an apparent increase in poverty [62].

The provision of information, and how that information is communicated, will have a significant influence on how the authorities manage the situation, on society's response to the problem and on the overall success of the recovery strategy. Maintaining public confidence is paramount. Trust is easily lost and difficult to develop and/or regain so it is important to create a framework for information and communication strategies under noncrisis conditions with the involvement of stakeholders. The type of information disseminated should be targeted to meet a variety of needs. The form of communication should be adapted to different levels of understanding, circumstances and to address the relevant issues. This should be implemented at the same time as the development of restoration strategies.

Management option implementation is generally the responsibility of the authorities and carried out by designated personnel. Nevertheless, self-help implemented by the affected population can also be considered. Some of the simple management options that do not require any specific skills or experience to implement (such as lawn mowing, digging) are potentially suitable for implementation by affected inhabitants themselves [65]. This could, for instance, be beneficial in providing an extra labor force in situations where large areas need to be treated quickly. The involvement of affected persons in actions to improve their own situation can be psychologically beneficial and give a better feeling of control of the situation, which also prevents undue anxiety. Health and safety issues need to be carefully considered for people carrying out such "self-help" options, need careful communication and to be conducted with adequate supervision of individuals to ensure they are implemented correctly.

The Compendium of Management Options Datasheets

The concept of systematically describing all the key factors which need to be considered in the application of management options in a datasheet format was developed in the mid-1990s within the STRATEGY project [41, 48, 55, 66]. Standardized datasheets, mainly based on the Chernobyl experience, capturing key information required to carry out the management options and evaluate their feasibility, applicability, and practicality were developed to aid the decision-making process and to ensure that potentially important issues are not overlooked. They also described the resources needed. The information in the datasheets was intended to be generally applicable for use in different European countries. The rural and waste templates are being used by the joint FAO/IAEA division to be adapted to other climate types and to update the IAEA Handbook of parameter values for radionuclide transfer in the temperate environments 364 [67].

Stakeholder participation is an important mechanism to explore these additional benefits or disadvantages to the use of management options, and is an essential step in developing a decision framework which avoids problems previously experienced in emergency management [68]. Close liaison with the FARMING stakeholder network facilitated evaluation

of management options datasheets for rural ecosystems; while for other datasheets, stakeholders were consulted in small groups or individually. Stakeholder opinion suggested that some management options were as likely to be rejected on socio-ethical grounds as on technical and economic grounds. Rejection of specific management options can be expected to show site, context, and national differences.

The datasheets developed in STRATEGY have been gradually improved during the EURANOS project [69] with more detail provided and the scope widened to provide information representing more diverse conditions and for wider range of radiological hazards. Sources of contamination considered in the handbooks include nuclear accidents and radiological dispersion devices and the most relevant radionuclides are included. In addition, non-radiological considerations have been incorporated in the later generations of datasheets [48, 57], introducing viewpoints from experts on social, ethical, and economical sciences [68], and also considering documented reactions of the public and other participants during management option trials in the Former Soviet Union.

The most recent compendium of datasheets is integrated into decision-aiding handbooks for contaminated food production areas [58, 59] and inhabited areas [57]. These handbooks contain advice on the development of optimized strategies for remediation under specific conditions using a series of diagrams, tables, and decision-charts, which guide the user through a series of eliminations of unsuitable options. Site-specific factors need to be taken into account in this process, and it is recommended in the handbooks that they be customized and tailored for different users. The importance of adequately involving people in decisions that affect them is stressed.

The most recent revision of the datasheet template for food [58] and inhabited areas [55, 57] includes a wide range of criteria describing different aspects of each countermeasure including the objective and benefits, the target of the measure and the radionuclides targeted, constraints (e.g., legal and social), effectiveness, feasibility (equipment, skills, infrastructure needed), waste produced, doses to implements, costs, side effects of implementation, and stakeholder opinion of the measure.

The datasheets provide a comprehensive overview of management options [69] which are intended to be useful to "middle-level" decision makers who have to assess possible countermeasure options. They are not a comprehensive set of instructions, but provide a template to adapt to local conditions/languages. Their applicability will reduce across the world as climate, culture, production systems, and drinking water supply deviate from those currently encountered in Europe.

Countermeasures and Remediation in Areas Affected by Radiation Accidents

Various radiation accidents requiring an organized emergency response have resulted from a variety of different factors, including human error (Chernobyl accident), violations in procedures at a radioactive waste tank (Kyshtym accident), the crash of aircrafts and subsequent loss of nuclear weapons (e.g., Palamares, Spain and Thule, Greenland) and the loss or theft of sealed radioactive sources used for medical purposes (Goiânia, Brazil). Contamination scenarios and the radionuclides released differed in each case, thus requiring a variety of different countermeasures and remediation strategies.

Kyshtym Accident

An accident at a nuclear facility producing weapon grade plutonium in Chelyabinsk-40 (Soviet Union) led to one of the largest radioactive releases into the environment. Sr-90 was the most important dose forming radionuclide in the release and required extensive countermeasures and remediation. The resulting East Urals Radioactive Trace (EURT) was defined as the area where the ^{90}Sr contamination density at the time of the accident was above 3.7 kBq m^{-2}, a value which was twice that of global fallout of ^{90}Sr from nuclear tests. In the EURT area (23,000 km^2) there were 217 settlements with 270,000 inhabitants [70–74]. Within the EURT, a contamination density of 74 kBq m^{-2} for ^{90}Sr was used as the criterion to identify areas requiring management options [74]. Heavily contaminated areas were in a narrow band, 4.5–6 km wide and 105 km long covering an area of 1,000 km^2 (c. 5% of the EURT area). All economic activity within the contamination isolines of 74–150 kBq m^{-2} of ^{90}Sr was suspended

(resulting in a restriction zone of 700 km^2). In 1959, this area included 106,000 ha of which agricultural lands, forests, and lakes accounted for 54%, 36%, and 9%, respectively [70].

Agriculture The Kyshtym accident was the first case where vast areas received countermeasures soon after the accident and remediation activities in the long term. In the first phase, the major contributor to the dose was the internal exposure from ^{144}Ce uptake by humans with foodstuffs [73]. The maximum concentration of radionuclides in agricultural products on land closest to source areas (up to 20 km) reached 10–10,000 $kBqkg^{-1}$, ^{144}Ce and ^{95}Zr being the main contributors to these values except for milk where ^{90}Sr comprised a mean of 70% of the activity concentration present [25]. The radionuclide concentration in all environmental media, including farm products, declined with time reflecting the ecological half-life of the contaminated territory. After 5–8 years (after the ^{95}Zr, ^{106}Ru, and ^{144}Ce had largely decayed away), only ^{90}Sr, and to a very small extent ^{137}Cs, were relevant for determining radiation dose to humans [26]. In response, soil-based management options were a focus of the remediation strategy adopted (Table 1).

For some small areas with very high contamination levels, the decontamination of land by removal of the upper soil layer (5–10 cm depth) using bulldozers, graders, or scrapers with subsequent burial in special facilities was very effective (Table 2). This action was widely employed despite the high operational cost. Plowing rapidly after deposition greatly reduced external dose rate. Plowing of soil with the burial of the most contaminated upper layer (deep plowing) soon after the accident was one of the most effective methods that brought about a threefold reduction in external doses [74]. Plowing and burial were especially effective on chernozem soils with a thick humus horizon (up to 0.5 m); on low-fertility soils it was less effective. The decontamination effect from deep plowing was enhanced by adding mineral fertilizers at balanced rates (according to plant demand for mineral nutrients) and liming where appropriate. These widely used techniques provided up to a tenfold reduction in ^{90}Sr concentrations in plants compared with conventional plowing [26, 74]. Normal plowing (20–25 cm of soil)

Environmental Countermeasures and Restoration. Table 1 Effectiveness of soil-based options for different crop types [24–26]

Treatment	Soil type	Reduction factor of ^{90}Sr in root uptake
Liming:		
0.5 H_g[a]	Mineral	1.1–2.1
1 H_g		1.4–2.7
2 H_g		1.7–3.1
1 H_g	Organic	1.0–1.1
Mineral fertilizers:		
$N_{90}P_{180}K_{90}$	Mineral	1.1–1.4
$N_{60}P_{90}K_{120}$		1.3–1.9
Plowing:		
Plowing, depth of cultivation 20–25 cm	Mineral	1.0
Moldboard plowing, depth of cultivation 50 cm	Mineral	1.3–2.3
Plowing with turnover of upper layer	Mineral	1.6
Soil removal		5–15

[a]H_g Hydrolytic acidity

Environmental Countermeasures and Restoration. Table 2 Summary of reduction factors of soil based options used in the former Soviet Union countries after the Chernobyl accident [16, 49, 52]

Countermeasure	Reduction factor	
	^{137}Cs	^{90}Sr
Normal plowing (first year)	2.5–4.0	
Skim and burial plowing	8–16	
Liming	1.5–3.0	1.5–2.6
Mineral fertilizers	1.5–3.0	0.8–2.0
Organic fertilizers	1.5–2.0	1.2–1.5
Radical improvement (first application)	2.0–9.0 (2.0–3.0)[a]	1.5–3.5 (1.5–2.0)
Removal of soil (external dose)	1.5	Not relevant

[a]Multiple applications

for the first time after deposition achieved a 1.1–2.4-fold decrease in dose rate of γ-radiation. A further reduction in ^{90}Sr uptake in plants (including fodder for animals) was achieved through cultivation of plants with low ^{90}Sr accumulation giving a roughly tenfold reduction in the main farm crops although the reduction for some species was up to 60-fold [26, 74].

Management options to reduce ^{90}Sr accumulation in animal products mainly consisted of the provision of fodder with low amounts of ^{90}Sr to animals (clean feeding). The most effective feeds were based on potatoes, root vegetables, and grain which had much lower ^{90}Sr concentrations compared with feeds from unimproved lands typical of preaccident farming practice. In specialized agricultural farms this clean feeding resulted in a decrease of ^{90}Sr content in meat and milk by two- to sevenfold and three- to fourfold, respectively compared with normal farms [74, 75].

A reduction in ^{90}Sr transfer to animal products was also achieved through the administration of Ca additives or fodder rich in Ca (e.g., legume crops) resulting in a tenfold decline in ^{90}Sr concentrations in milk. Sr-90 reduction in meat was also achieved by preslaughter feeding with less contaminated fodder [26, 74].

Further reductions in the ^{90}Sr concentrations in food products and, hence, the internal doses to humans, was achieved by processing raw products. The processing of milk to fermented milk products and butter, which reduces ^{90}Sr concentration in butter 20-fold compared with raw milk was widely used. Conventional processing of grain reduces ^{90}Sr concentration in the final products by two to three times. Starch, alcohol, and vegetable oil were produced "clean" from the original contaminated agricultural products after the normally used processing [26, 74, 75].

Forest and Aquatic Ecosystems The key feature in the application of environmental management options in natural ecosystems affected by the accident was the identification and implementation of action limits for forest products including berries, mushrooms, game, and wood. The maximum permissible ^{90}Sr contamination density for forested areas used for pasture and haymaking was set at 92 kBq m^{-2} and for the production of industrial wood at 3.7 MBq m^{-2} [26, 74]. Successful implementation of these options was achieved by transferring the priority right to use these lands to specialized farms, and controlling public access to those areas.

Initial restrictions on the economic use of water bodies (fishing, use of aquatic vegetation as fodder for farm animals) were imposed on lakes in areas with ^{90}Sr density above 74 kBq m^{-2} [71]. By 1970, reutilization of lakes located in the affected area was possible for fish farming due to natural decontamination in lakes (the ^{90}Sr ecological half-life in water was 5–6 years) (Alexakhin et al. 2004 [25]). The remediation strategy was based on the presumption that lands should not be left vacant (with the caveat that occupational standards and dose limits to individuals must be observed) and their exploitation must partially compensate for damage from radioactive contamination. It was based on two main options: land use change and development of new economic activities, dependent on safe use of the environment. Land use differentiation into agriculture, forestry, and other branches of the rural economy using soil, plant, and water resources was based on the ability to produce products with permissible levels of ^{90}Sr contamination. Since farming was seriously restricted in the affected region (due to exceeding action levels), economic activities were focused on the production of industrial (nonfood) goods, development of forestry and local industry and the exploitation of peat, sand, gravel, and other mineral resources [26].

Effect of Remediation As a result of the remediation, a substantial decrease in the effective annual doses to the local population was achieved which ensured that these doses fell below those set out in the radiation safety standards present in the USSR at that time. The complex mixture of protective actions which was initially developed for areas affected by the Kyshtym accident was subsequently adopted for areas affected by the Chernobyl accident, with appropriate modifications to take account of the different circumstances [25, 70, 71].

Nuclear Weapon Accidents: Palomares Accident

Although a number of accidents involving nuclear weapons are currently known to have occurred (with different extent of reliability) (see http://www.atomicarchive.com/Almanac/Brokenarrows.shtml), a limited number, in particular accidents with losses of

nuclear weapons from aircraft, required remediation efforts.

In January 1966, near the south-eastern coast of Spain, two American air force aircrafts collided during air refueling. Of the four nuclear bombs that were onboard the aircraft, one was found in the Mediterranean Sea. The second bomb fell by parachute onto agricultural fields. The remaining two bombs were physically destroyed due to the explosion of their chemical detonators. Pyrophoric metallic plutonium caught fire and the resulting radioactive cloud, containing plutonium oxide, moved westward contaminating an area of 262 ha within a region of intensive farming, occupied by rural dwellings, agricultural fields, and forested areas [19].

The main remedial management options were applied to the soil. The soil was removed, placed into containers, and shipped to the US for disposal at the Savannah River plant at a Pu deposition density above 1.2 $MBq\,m^{-2}$. The total area of decontaminated soil was 2.2 ha, removed in 6,000 containers with a volume of 250 L each. Arable soil with Pu concentrations under 1.2 $MBq\,m^{-2}$ (17 ha) was re-plowed to a depth of 30 cm. In rocky areas where plowing was impossible and Pu levels exceeded 120 $kBq\,m^{2}$, soil was removed by hand and shipped to the USA [19].

Upon completion of mechanical decontamination, radiation monitoring of the air, soil, plants, farm animals, and the population was carried out. The major farm crops produced in the affected area were tomatoes, barley, alfalfa, maize, pepper, and fruit such as melon. Contamination levels in agricultural products were not sufficient to cause serious exposures to the public. Twenty-three years after the accident approximately 99% of the Pu still remains in the 0–5 cm surface soil layer [26].

The accident produced no serious health impacts, since doses were very low. The committed effective doses calculated for total Pu intake over 30 years amounted to 37 and 210 μSv for urban and agricultural workers (the most exposed population group), respectively [76].

Chernobyl Accident

The accident at the Chernobyl NPP was the most serious radiation accident in the history of nuclear energy generation. The accidental release comprised some highly environmentally mobile radionuclides including isotopes of radioiodine, radiostrontium, and radiocaesium, which had a serious impact on agriculture [12].

More than 15,000 settlements with a population of around six million people were living in areas with a ^{137}Cs deposition density above 37 $kBq\,m^{-2}$, and were therefore officially designated as contaminated. In the areas most severely affected, with ^{137}Cs contamination densities exceeding 555 kBq m^{-2}, there were 640 settlements, with 270,000 inhabitants [61, 77, 78].

Soon after the accident, a 30-km radius exclusion zone (the CEZ) was established around the reactor. Further population relocations took place in subsequent months and years in Belarus, the Russian Federation and Ukraine. Eventually, 116,000 persons were evacuated or relocated [61] with about 50,000 cattle, 13,000 pigs, 3,300 sheep, and 700 horses [12]. In the 30-km zone, more than 20,000 agricultural and domestic animals, including cats and dogs, were slaughtered and buried. In the first few years after the accident comprehensive surveys of contaminated lands and on-site inspection of foodstuffs were carried out. In 1989–1991, people from 470 settlements outside of the 30-km zone of the Chernobyl NPP were moved together with their agricultural animals to new locations [61].

Although decontamination of some settlements was carried out within the first few years after the accident, the main challenge for remediation after the accident was to retain the capability for agricultural production in contaminated areas. This task was of paramount importance to preserve the economy and the social and psychological stability of the population [12].

Agriculture The maximum radionuclide concentrations in agricultural products occurred in the farms surrounding the Chernobyl NPP in the first few days and weeks after the accident and considerably exceeded action levels [12]. During the first few weeks after the accident ^{131}I was the main contributor to internal dose leading to significant radiation doses through milk consumption [61]. In addition, plants and animals were also contaminated with a wide range of other radionuclides, in particular, radiocaesium isotopes which were the dominant contaminant in most environmental samples and food products from June 1986.

In the first weeks after the accident, the main goal of countermeasures was to prevent the consumption of contaminated milk and green vegetables by the population, and to decrease ^{131}I concentrations in milk [16]. This was largely achieved by (1) radiation monitoring of agricultural products and the rejection of foodstuffs in which ^{131}I activity concentrations were above action levels (3,700 Bql^{-1} at that time) and (2), processing rejected milk (mainly converting milk to storable products such as condensed or dried milk, cheese, or butter). Information on countermeasures was confined to managers and local authorities, and was not distributed in time to private farmers. As a result, application of the countermeasures was often delayed in rural settlements for privately produced milk, resulting in low countermeasure effectiveness in some areas.

The rural population around the ChNPP was the most heavily affected by both external and internal exposure pathways. The production of foodstuffs with radionuclide activity concentrations above action levels was considered by the population as evidence that the land and their lifestyle had been severely blighted. Therefore, the rapid deployment of optimized countermeasures was important not only to reduce the radiation doses but also for the social and psychological well being of the population of affected regions and helping to decrease their stress levels.

In the least contaminated zone (37–185 kBqm^{-2}) farming continued based on agricultural practices suitable for the soil and climate, except for areas with peaty soils, with high radiocaesium uptake by plants, where radical improvement was implemented. In the 185–555 kBqm^{-2} zone, plant production on arable soils continued without restrictions. Soils received increased doses of P and K or organic fertilizers. Natural meadows on sandy, sandy-loam, and peaty soils were subjected to radical improvement (which includes removing vegetation, plowing, liming, fertilization, and plants reseeding) with a 1.5-fold increase in the application rate of potassium and phosphorous fertilizers [12, 79] (Fig. 3). In the 555–1,480 kBqm^{-2} zone, there was a full-scale remediation. The areas receiving soil based management options in the 20 years following the Chernobyl accident are shown in Fig. 4 and the effectiveness of these actions is given in Table 2.

The provision of feed with low contamination levels to previously contaminated animals for an appropriate

Environmental Countermeasures and Restoration. Figure 3
Implementation of soil based remedial actions (radical improvement) in Rivno region of Ukraine (*upper photo*) and Tula region of Russian Federation (*photo in the mid*). Lower picture shows a meadow after radical improvement (Bryansk region, Russia). (Courtesy of Russian Institute of Agricultural Radiology and Agroecology Obninsk, Russia and Ukrainian Institute of Agricultural Radiology Kiev, Ukraine)

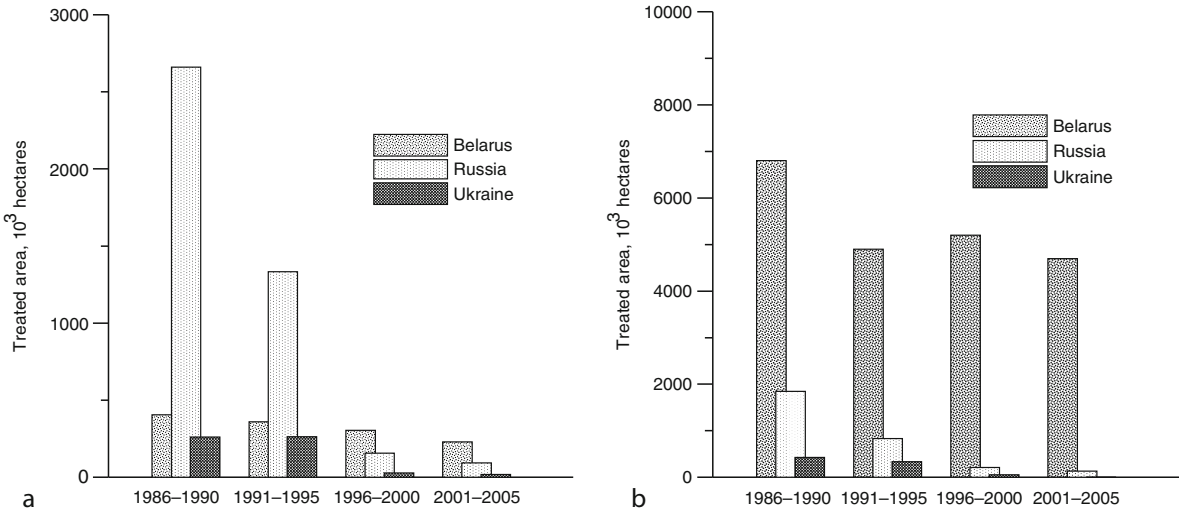

Environmental Countermeasures and Restoration. Figure 4
Changes with time in the extent of agricultural areas treated with liming (**a**) and mineral fertilizers (**b**) as a countermeasure in the USSR/fSU countries contaminated by the Chernobyl accident [12]

period before slaughter effectively reduced contamination in meat. Such "clean feeding" was normally combined with live monitoring of animals so that if radiocaesium transferred to meat was above action levels, the animals were returned to the farm for further clean feeding (Fig. 5).

Another important countermeasure used since the beginning of the 1990 s to reduce radiocaesium contamination in animal products was administration of cesium binders (Fig. 6). The Cs binder used was a hexacyanoferrate, widely referred to as Prussian blue [80] and was administered as a powder and as rumen dwelling boli.

This application has been especially useful and effective in settlements where the grazed meadows were not suitable for radical improvement. Various methods for milk processing to butter and sour-milk products were also developed and successfully implemented during food processing.

Forest and Aquatic Ecosystems More than 40,000 km^2 of forested areas had ^{137}Cs concentrations above 37 $kBq\,m^{-2}$ and in Russia alone about 50,000 forestry workers and members of their families lived in these affected areas [25].

In many of the most affected areas, the role of the forest as a source of food is essential to local communities [81]. Natural reductions in the ^{137}Cs concentrations in "forest products" was much slower compared with agricultural products; the effective half-lives for ^{137}Cs in mushrooms and berries were roughly 20 and 10 years, respectively [82, 83]. As a consequence, in the long term after the accident "forest products" (especially mushrooms) sometimes contributed more to the exposure of a population than did critical foodstuffs such as milk. This was particularly prevalent in settlements near forests [14, 39, 81].

Remedial actions in forests were mainly of a restrictive nature and the dose reduction achieved by various management options was small [84, 85]. Thus, in the affected forested areas, bans were imposed on the collection of mushrooms, berries, hunting game, and private cattle grazing on forest pastures and clearings; fire-control actions were also implemented. Management options in contaminated woods (such as the collection and removal of forest litter and leaves or reforestation) were either technologically ineffective, or economically expensive and ecologically unjustified.

The Chernobyl accident also affected many water bodies. Some 8 million people were exposed to additional radiation due to the consumption of drinking water and 32 million due to the consumption of fish and the use of water for irrigation purposes [61, 86].

Environmental Countermeasures and Restoration. Figure 5
Live monitoring measurements of animals in the settlements of the Bryansk region Russia affected by the ChNPP accident (Courtesy of Russian Institute of Agricultural Radiology and Agroecology, Obninsk, Russia)

Two major remediation strategies were implemented in water bodies affected by the Chernobyl accident: the implementation of remedial options to restrict radionuclide distribution with water movements; and restrictions on the consumption of aquatic foodstuffs and drinking water from the most contaminated water bodies. In the contaminated catchment area different hydro-technical constructions were implemented (dikes, dams, etc., as well as special channels). Also, to limit radionuclide migration and accumulation in fish, various sorbents were added to induce radionuclide sedimentation from water masses, and

Environmental Countermeasures and Restoration. Figure 6
Administration of the hexacyanoferrate boli to a sheep (Courtesy of Centre for Ecology & Hydrology, Lancaster Environment Centre, Lancaster, UK)

potassium fertilizers were added to reduce radionuclide accumulation in fish [87, 88] (see example in Fig. 7). These measures were rather costly and their effectiveness was generally low, especially compared with agricultural remedial options [26, 61].

Urban Ecosystems The decontamination of settlements following the Chernobyl accident was applied at a limited scale. For example, the Soviet army in 1989 decontaminated 93 rural settlements affected by the Chernobyl accident in the Bryansk region. The army units removed a layer of topsoil from areas around houses, from children gardens, and other public sites [54]. However, the dose reducing effect was only 1.1–1.5; which was much lower than expected [14]. Therefore, decontamination of inhabited areas ceased and relocation of the residents was continued in some cases. In later studies, carried out in 1997 it was shown that if soil removal is optimized in relation to the distribution of the contaminants in soil profile (e.g., using a mini-bulldozer, see Fig. 8), the external dose rate can be reduced by at least a factor of 6 [54, 89].

Effect of Remediation Countermeasures applied in the early phase of the Chernobyl accident had a considerable effect in averting doses to the affected population. However, they were only partially effective in reducing radioiodine intake via milk, because of the lack of timely information about the accident and

Environmental Countermeasures and Restoration. Figure 7
Application of potassium chloride fertilizer for reduction of ^{137}Cs concentration in the fish of the Svaytoe Lake (Belarus) (*left photo*) and the lake after the treatment (*right photo*). The fertilizers were colored red with a special neutral additive to track a potassium chloride application

Environmental Countermeasures and Restoration. Figure 8
Removal of contaminated topsoil with a "Bobcat" mini-bulldozer in the Bryansk region in 1997 [54]

advice on appropriate actions, particularly for private rural farmers [61].

Large-scale application of a range of management options achieved a sharp decrease in the amount of animal produce with radiocaesium activity concentrations above action levels in all three countries (Fig. 9).

The contribution of internal exposure to radiation doses of the general public caused by the Chernobyl radioactive release has been significant both in the short and long term. Agricultural management options were the most efficient in reducing dose, averting 30–40% of the collective internal dose to the affected population, excluding thyroid dose [12].

The current slow, natural decrease of ^{137}Cs availability in soil means that remediation actions after the Chernobyl accident will be important for around 70 years after the accident except for those areas (such as the 30-km zone around Chernobyl NPP) which have been withdrawn from economic use and for which this time period is longer.

Goiânia Accident

A serious radiation accident occurred in September 1987 in Goiânia in Brazil. One of the hospitals in Goiânia possessed a 50.9 TBq (1,375 Ci) ^{137}Cs ($^{137}CsCl$) sealed source for therapeutic applications [2, 3, 90]. Several unemployed young people penetrated the unguarded building and stole the device. They thought that the 50-kg metallic object was made from a valuable material so they separated the source from its biological shield and opened the source container. The source was sold at a junk yard; the junkyard

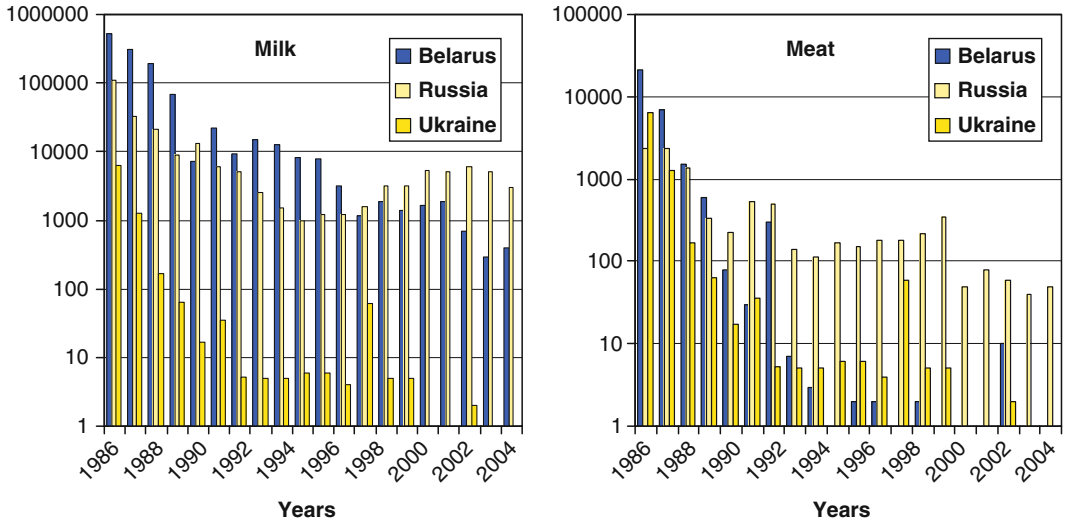

Environmental Countermeasures and Restoration. Figure 9
Variation with time in amounts of milk and meat exceeding action levels in Russia (all milk and meat – collective and private), Ukraine and Belarus (only milk and meat entering processing plants) after the Chernobyl accident, tones [12]

owner considered the material to be precious because of its blue luminescence. Dispersion of the radioactive substance then occurred as people came to look at the material, some of whom then took away pieces of it. Some people took parts of the source as souvenirs; others painted their faces with the blue powder for carnival.

As a result, the source was broken into small fragments and widely distributed. Radioactive substances were dispersed by high winds over a variety of vegetable gardens, houses, and roofs of buildings. Radioactive material even reached the main river in the region, the Meia-Ponte River with ^{137}Cs found in bottom sediments 12 km from the source site. In this incident some 250 persons were exposed to external and internal irradiation; 50 of which developed symptoms of whole-body and acute local irradiation; 14 of these had marrow failure. Doses of internal exposure in affected people ranged from 0.046 to 0.97 Gy [3].

Remediation actions for the Goiânia accident were carried out with international assistance. Some 755 professionals took part in remediation of the contaminated sites and were exposed to differing extents. Doses to around 70% of the participants were below 1 mSv and the maximum dose value reached was 16 mSv [91]. Very high contamination was found in 85 houses and residents from 41 houses were evacuated. The total area subject to radiation monitoring within the urban territory covered 67 km^2. In the city a γ-survey was performed by helicopter, followed by another γ-survey performed by vehicle.

The limits of contamination density chosen for the remediation actions in Goiânia (3.7 Bq cm^{-2} or 37 kBq m^{-2}) were the same as for the classification of the Chernobyl (1986)-affected area (areas with ^{137}Cs levels 37 kBq m^{-2} or 1 Ci km^{-2}). Once contaminated sites had been identified, more labor-intensive options were implemented. Various chemical solvents and abrasives were used for mechanical decontamination and radionuclide-containing materials were physically removed [92].

The identification of potential locations to store the collected radioactive materials was met with a highly negative public response. Ultimately, a site for temporary storage was chosen in the thinly populated town of Abadia de Goids (20 km outside the city of Goiânia). In the most affected areas houses were destroyed, soil was removed, and the decontaminated site was covered with concrete. In less-affected buildings, walls, floors, and roofs were decontaminated. Personal items that contained radioactive substances were designated as waste, since people refused to use them even after decontamination. In addition to houses, 45 public places including parts of streets, squares, parks, and

shops were decontaminated. By the end of December 1987, the main affected sites were decontaminated. Remediation after the Goiânia incident resulted in the bulk of the ^{137}Cs source (50.9 TBq) being localized in the 1.6-km^2 waste disposal area. The remediation in Goiânia thus largely comprised of the mechanical cleanup of contaminated territories, collection of various contaminated materials which were later assigned to radioactive waste, and their disposal at specially allocated storage sites [93].

Remediation of Sites Affected by Nuclear Testing

Radioactive contamination is often the result of human actions, the consequences of which were not fully understood at the time, as is the case for nuclear testing sites. Nuclear tests were conducted at a total of 16 sites, the most well known of which are the Nevada Test Site (the USA), Bikini and Enewetak (Marshall Islands), Emu, Maralinga, and Monte Bello Islands (Australia), Mururoa and Fangataufa (French Polynesia), Semipalatinsk (Kazakhstan), Novaya Zemlya (Russia), and Lop Nor (China) [6, 78, 94–97]. In total, about 29 mountains of fission yield were associated with radionuclides locally deposited at the test sites [98]. Another source of local contamination at the test sites were safety tests, in which nuclear weapons were destroyed using conventional explosives to simulate a possible accident.

Only two of these sites (Enewetak and Maralinga) have been remediated. Remediation at the other test sites was either not carried out or only partly performed, either because of low residual contamination (fractions of long-lived radionuclides in many types of nuclear explosions are very low), high financial costs, the remoteness of the site from populated areas or other political reasons. Even when a full remediation strategy was not applied at these sites, some remedial actions were usually conducted, especially where considerable plutonium residues resulting from safety tests were present [96].

Bikini Atoll Test Site

Nuclear tests were conducted at Bikini Atoll from 1946 to 1958. The regional fallout from the Bravo test caused widespread contamination of the Bikini Atoll and forced the evacuation of Marshallese people living on Rongelap and Utrik Atolls [96]. About 50% of the fission yield associated with near-surface nuclear detonations was deposited on a local or regional scale [99].

The 167 inhabitants of Bikini Island were evacuated prior to the first nuclear test in 1946. In August 1968, resettlement of the Bikinian people on the atoll was allowed and about 100 people returned to the atoll. Because of concerns expressed by Bikini residents about the safety of living on the atoll, in 1975–1978 a set of additional investigations were carried out gathering data for more precise dose estimates [100]. In 1978, a tenfold increase in the body content of ^{137}Cs compared to those measured in 1970 was identified, based on whole body measurements [101] which were associated with consumption of coconut fluid due to the limited availability of drinking water. In August and September 1978, in response to the uptake of cesium in the population, the Bikinians who had returned to Bikini Atoll were relocated once again [96].

The total annual dose to the potential residents of the atoll (above the natural background dose) was estimated in 1999 to be 4.0–15 mSv, depending on the ratio of local to imported foods in the diets of inhabitants. Cs-137 was identified as the main radionuclide contributing to the dose, while contributions of ^{90}Sr, $^{239+240}$Pu, and ^{241}Am were much lower. The intake of marine foods, stored rain water and groundwater, and inhalation of resuspended soil together accounted for less than 1% of the dose [102].

Although full-scale remedial actions at the site have not been applied, a few remedial options for Bikini were implemented and studied in detail. The interventions were based on projected dose to a hypothetical critical group. The assessed dose of 15 mSv [103] was higher than the action dose level for intervention of 10 mSv accepted at that time [29]. Therefore, the implementation of remediation was considered to be highly justified. The key remedial options used were (1) washing-out ^{137}Cs from the soil with large quantities of salt water, (2) application of ameliorants such as zeolites to soil to make ^{137}Cs less available for plant uptake, (3) planting vegetation with high biomass to remove ^{137}Cs from the soil and then burial of the contaminated biomass, (4) soil removal (40 cm top layer), and (5) treating soil with potassium fertilizers [96].

Soil removal and treatment with potassium fertilizers were identified as the most effective measures.

However, soil removal would necessitate moving about 30,000 mature coconuts, pandanus and papaya trees, and breadfruit and was therefore a complex and extremely expensive operation. In contrast, soil removal from dwelling areas would be more cost effective and the best option was to remove soil from around each house and replace it with a layer of crushed coral to minimize external exposure and possible ingestion of the remaining soil. Consideration was also given to the potential ecological effects of the proposed potassium fertilizer treatment; at the planned levels there was no significant alteration expected in the soil chemistry and the potential transfer of potassium to groundwater was very low [104]. Application of potassium fertilizer would be needed every 4 or 5 years to maintain the low ^{137}Cs activity concentrations in local foods. It has been estimated that after the potassium treatment of soil and the replacement of soil from around the living areas, the dose rate based on the assumption that residents were consuming only local food would be reduced by as much as a factor of 10 or slightly higher compared with the levels before remedial actions application [105].

Maralinga Test Site

Tests of the UK nuclear program at the Maralinga test site located on the Nullarbor Plain in South Australia began in 1955. The site was abandoned in 1967 following the advent of the Nuclear Non-proliferation Treaty and the banning of atmospheric nuclear tests because the site was not suitable for underground tests. Seven nuclear tests were performed at the site, with approximate yields ranging from 1–27 kt. The site was also used for hundreds of minor trials from 1955 to May 1963, many of which were safety tests intended to investigate the effects of fire or nonnuclear explosions on atomic weapons [106].

Since 1967, numerous surveys have been carried out to characterize the contamination within the site. Substantial contamination densities were found at many test sites, particularly at Taranaki site where the Vixen B nuclear test was performed. Several square kilometers of land were contaminated to levels exceeding 300 kBq m^2 of ^{239}Pu. Some limited areas at the site were 10- or 100-fold more contaminated. Initially, plutonium contamination consisted of the following isotopes: ^{238}Pu, ^{239}Pu, ^{240}Pu, and ^{241}Pu; radioactive decay resulted in ^{241}Pu being gradually replaced with ^{241}Am [96].

The first efforts to remediate the Maralinga site began in 1964. Initially, contaminated debris and most of the remaining infrastructure were buried in pits at a depth of 2–3 m. The Pu content of each of these pits was not well quantified, but was estimated to be in kilograms quantities [106]. In 1967, further steps were taken to reduce the plutonium surface concentrations by turning over and mixing the surface soil. Following the remediation the site was closed with a series of fences erected to enclose the burial pits containing significant quantities of plutonium at Taranaki and other sites [96].

Later assessments made for nomadic Aborigines living mainly an outdoor lifestyle identified the inhalation dose pathway as the contributor to the total doses to both adults and children [107]. As a result of this survey, a much more extensive remediation project was initiated at the site, within which three sets of criteria were established for making decisions on the remediation process, namely:

1. Contaminated soil was removed where the levels of dispersed ^{241}Am exceeded 40 kBq m^{-2} averaged over 1 ha, or where contaminated particles exceeding 100 kBq were found, or where the density of particles exceeding 20 kBq was greater than 1 in 10 m^2 (Soil-Removal Criteria).
2. Once soil was removed the residual levels of dispersed contamination in the cleared area was not to exceed 3 kBq m^{-2} for ^{241}Am, averaged over 1 ha, and particulate contamination was to meet the Soil-Removal Criteria (Clearance Criteria).
3. Permanent occupancy and unrestricted land-use was only to occur where levels of dispersed contamination were less than 3 kBq km^{-2} for ^{241}Am, averaged over 3 km^2, and the particulate contamination met the Soil-Removal Criteria (Unrestricted Use Criteria) [108–110].

To reduce the inhalation risk, the remediation criteria were guided by conservative principles and estimation of doses by realistic scenarios. These included the possibility of an Aboriginal group living for an entire year on the edge of the nonresidential area in regions of the highest activity permitted (approximately 3 kBq m^{-2} of ^{241}Am).

The first stage of the remediation project consisted of defining the boundaries at the sites contaminated with Pu (Taranaki, TMs, and Wewak), followed by bulk removal of contaminated soil from the three sites and burial in excavated burial trenches under at least 5 m of clean rock and soil. At the end of the remediation process, a compliance assessment was carried out to ensure that the whole Maralinga area had been made safe following the work undertaken during the 1994–2000 Maralinga project [96].

Following the remediation by removal and burial at depth of contaminated surface soil, all areas at Maralinga were shown to be within acceptable absorbed dose limits for all envisaged land uses. The restriction on permanent occupancy within the "restricted land-use" (nonresidential) boundary surrounding Taranaki was set as a precautionary measure as the inhalation doses for permanent occupancy of all but a few areas (essentially within the untreated plumes) were well below the 1 mSv a^{-1} limit for members of the public [96].

Remediation of Sites within Decommissioning of Facilities

The use of the term decommissioning implies that no further use of the facility (or part thereof) for its existing purpose is foreseen [111]. Decommissioning actions are taken at the end of the operating lifetime of a facility to remove it from service with due regard for the health and safety of workers and members of the public and the protection of the environment. Subject to national legal and regulatory requirements, a facility or its remaining parts may also be considered decommissioned if it is incorporated into a new or existing facility, or even if the site on which it is located is still under regulatory control or institutional control [112].

The actions taken during decommissioning will need to be such as to ensure the long protection of the public and the environment, and typically include reducing the levels of residual radionuclides in the materials and the site of the facility so that the materials can be safely recycled, reused, or disposed of as exempt waste or as radioactive waste, and the site can be released for unrestricted use or otherwise reused [111].

Remediation can be applied to both nuclear and nonnuclear contaminants that can affect human health and the environment. Remediation encompasses *inter alia* site characterization, identification of remedial action alternatives, implementation of a remedial action, and ongoing monitoring to assure the confinement or containment of residual contamination.

There are many facilities with different characteristics around the world contaminated with radionuclides and therefore, according to the legislation, require decommissioning. They can include nuclear power reactors, radiochemical processing facilities, uranium and thorium mines, research institutions and hospitals, and many other human activities [28]. Therefore, remediation activities can be also very different and vary from decontamination of selected pieces of equipment to large-scale soil removal near some uranium-mining facilities or demolition of large concrete structures and placing them into final or interim waste storage [111].

In contrast, nuclear laboratories or institutions with a good standard of radiation protection can be decommissioned after limited remediation efforts although in all cases, the decommissioning process must be well planned and sufficient resources must be available. Over time, without proper arrangements being made for decommissioning, shut down facilities deteriorate and ultimately constitute a radiological hazard in their vicinity from direct external exposure to radiation to the public and potential release of radioactive material to the environment [112]. Currently, a substantial discharge of radionuclides has only been observed within a few decommissioning projects, largely at uranium-mining and uranium-milling facilities [113].

Remediation goals are usually based on dose constraints and derived action levels expressed in concentrations of radionuclides in various media. Because of the high cost, remediation is more often aimed at achieving "restricted reuse" or "fit-for-purpose reuse" as opposed to "unrestricted reuse," though the latter would be the ideal goal. The remedial objectives for any restricted reuse are then based on meeting appropriate dose criteria associated with the intended land reuse. Where these doses are within the acceptable limit, regardless of the future uses of the site, then this enables a site to be released from any controls [61]. However, material originating from a released site needs to comply with the national requirements for

radiation protection for materials outside the scope of regulatory control [114].

The above aspects clearly show the importance of implementing a forward-looking planning process. While in the past, decommissioning and remediation activities have often been carried out as independent activities, optimization of effort, cost, impact, and risk can be achieved by carrying out decommissioning and remediation activities in an integrated manner as described in Falck et al. [112].

The high public concern regarding nuclear safety issues and the intention to build confidence to the remediation success has led to an acknowledgement of the need for stakeholder involvement. A system of the activities intended for providing transparency in remediation can be summarized as follows:

1. Development of an effective public-communication project policy (openness, transparency, truthfulness, effectiveness, timeliness etc.)
2. Development of the stakeholder involvement goals (no surprises, confidence generating)
3. Identification of relevant stakeholders to be involved into the decision conference
4. Selection of communication, consultation, and participation methods for training of project staff
5. Monitoring and review of success through local attitude survey; feedback from the stakeholders of different levels

As noted earlier, there are many differing facilities with distinct remediation goals, required remedial actions and further planned use of the contaminated site. Decommissioning of the Wismut uranium mine in Germany, based mainly on overview of remediation activities within decommissioning is an example of successful remedial activities typical for the decommissioning process.

Uranium mining in Saxony and Thuringia, known as Soviet-German Company (SDAG) Wismut, was in operation for more than 40 years. During that time, the Wismut company had mined around 231,000 t of uranium. Due to poor disposal practices in the first years of the operation, and routine natural radionuclides releases thereafter, vast areas mainly within the territory of the facility were contaminated. In total, the area of the Wismut Company covered 36.9 km^2, including 24.4 km^2 of mine dumps, 7.2 km^2 of tailings ponds, and 1.6 km^2 of open pit mine. The contamination of the site was represented by different radioactive materials, including: (1) scattered ore, (2) scattered tailings material (specific activity around 1–10 Bqg^{-1} for ^{226}Ra as the key nuclide, not in radioactive equilibrium), (3) lost uranium concentrate, (4) naturally leached uranium, for instance at sites from which waste dumps were removed [112].

In 1991, following integration of West and East Germany when the Federal Republic of Germany took responsibility for the SDAG Wismut Company, and the corresponding nuclear legacy, the Wismut Remediation Project was started. The project involves remedial activities at many sites, including four underground mines and two processing plants. In 1991, for a reuse of the sites, buildings, and materials contaminated by uranium mining activities, the German Commission on Radiological Protection recommended a reference level of effective dose of 1 mSv a^{-1}.

The extent of remedial measures which were undertaken at the site was justified based on site evaluation and remediation feasibility studies, rather than by applying uniform standards. Remediation of the Wismut legacy was viewed as an opportunity to return the affected land to productive use, thus enhancing the revitalization of the former mining areas in East Germany [112].

The Wismut site remediation took advantage of the open space available in unflooded mines and other sites to dispose of contaminated material in situ. The places used for disposal of contaminated material included:

- Underground storage sites ("dry" mine galleries above the groundwater level)
- Waste rock dumps (construction of cassettes, placement of the waste, coverage)
- Beach areas of tailings ponds (same technology as for dumps)
- Engineered hazardous waste disposal facility (constructed on top of a waste rock pile)

Special attention was given to the operational waste that resulted from the application of modern remediation technologies for the treatment of contaminated material. The contamination was concentrated in residues, reaching specific activities of up to 1,000 Bqg^{-1} ^{238}U and 20 Bqg^{-1} ^{226}Ra. Special techniques for the immobilization of these residues needed to be applied. Despite the lack of the space available for

disposal, separation of waste according to type and level of contamination and further recycling of low contaminated or uncontaminated materials were the key elements of the waste management practice at the Wismut site. In particular, salvaged uncontaminated metallic scraps and scraps with a total surface alpha activity lower than 0.5 $Bq cm^{-2}$ have been sold for smelting [112].

Former waste rock piles cannot always be completely remediated and they can be released for restricted reuse. In particular, such areas could be used for planting new forests, or in some cases even for fodder production or various industrial or trade applications. Forestry was an attractive cost-effective option which was considered sustainable in the long term.

Considerable efforts were made over the past years for the benefit and protection of the population inhibiting areas affected by mining activities at the Wismut site. The significant reduction of adverse environmental impacts and the reutilization of these areas for industrial use, housing construction, or as a nature reserve have revitalized these regions. The "New Horizons through Remediation" program became a key element of Remediation. Integrated state-of-the-art technologies from around the world were applied to conduct decommissioning and remediation of the radioactive legacies left by the uranium mining in an efficient and cost-effective way leading to sustainable solutions. Remediation has had a benefit for regional development at two former mining towns, leading to rebirth of the health spa of Schlema (Fig. 10) and the development of the Federal Garden and Landscape Exhibition in 2007 (BUGA, 2007) to be hosted by the towns of Ronneburg and Gera [112].

Overall, the Wismut Project provides evidence of the potential success of a value-added approach with no high additional (or not reimbursable) costs, if remediation is efficiently undertaken with a well-defined reutilization in mind. Such successful utilization goals can only be developed in cooperation with the envisaged future user (i.e., municipality or developer), the community and the regulatory authorities. If consensus is achieved with the stakeholders prior to remedial actions, then "remediation by objectives" becomes practicable, i.e., the objectives for the individual remedial steps can be determined, consistent with the ultimate utilization goal [112].

Environmental Countermeasures and Restoration. Figure 10
Former mining area near Schlema before (1991) and after (2009) remediation (http://www.wismut.de/)

Decision-Aiding Tools

The efficiency of countermeasures or remediation depends on many factors: the specific contamination scenario, the properties of the contaminants involved, characteristics of the affected environment, the perception of countermeasures or remedial actions by the local population amongst many others. The effectiveness of such actions, cost, and resources required for their implementation vary considerably with these various factors; this in turn affects the suitability of different countermeasures or remedial options for a given situation. Therefore, generalized recommendations which do not account for the diversity of local site-specific conditions can result in inadequate decision-making and may not be feasible to execute.

These multiple factors must be reconciled within a single optimization approach and there is a significant challenge in finding a balanced solution to the multidimensional problem each contamination scenario presents. This task can be facilitated with environmental decision support systems (EDSS), capable of providing advice on countermeasure/remediation strategies at different levels of the decision-making process, which take into account temporal and spatial variation in each factor. A conceptual framework and basic elements of such systems (*EDSS*) intended for support in remediation of contaminated areas is given in Fig. 11.

Following the Chernobyl accident, various EDSS, or models which underpin them, have been produced, such as FORCON [115], SAVE [40], RESTORE [116, 117], and CESAR [118] which have enhanced the ability to optimize remediation strategies in contaminated areas.

Decision-aiding techniques are useful tools to determine the level and kind of protection which will provide the best solution given the various factors and constraints involved, taking into account inherent uncertainties and value judgments. This can only be achieved on the basis of a clear identification of available alternative management options and the factors and constraints involved in the processes. Site-specific quantification is a difficult and time-consuming step in the decision-making process because all necessary data must be gathered or generated by models to then use in combination with decision-aiding techniques to optimize the decision-making process [119]. Decision-aiding techniques have been widely used to select preferable remedial options for contaminated areas, starting in the early 1980s when ICRP recommended the use of cost–benefit analyses [34, 35]. In these analyses, the cost of environmental deterioration as a result of radiological contamination which could be averted using protective measures was compared with the cost of the protective measures [34, 35, 120, 121]. For decisions of greater complexity, including considerations of large-scale remedial, decision-making can be improved by complementing the above methods with multi-criteria analysis [13].

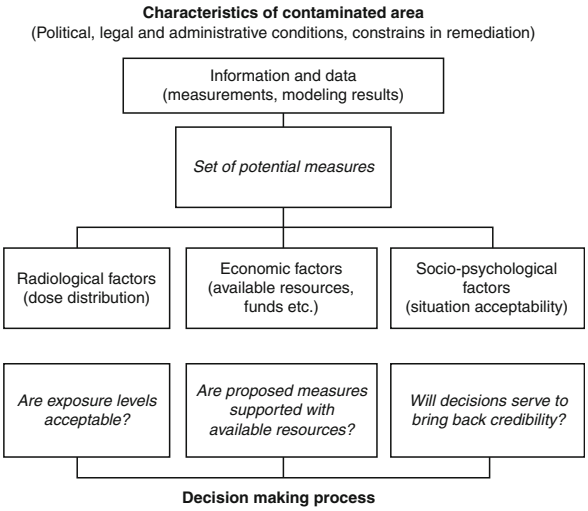

Environmental Countermeasures and Restoration. Figure 11
Key elements of the environmental decision support system (*EDSS*) for remedial measures on contaminated areas (Adopted from Shershakov et al. [13])

Cost-effectiveness and cost–benefit techniques are based on balancing the costs of management option implementation against the expected reduction of the collective dose, which is expressed in monetary value. The definition and use of the monetary value of collective doses, introduced by ICRP in Publication 22 [120], has been a key element of this approach; the implementation of this approach has been, and currently is, the subject of many debates on ethical grounds.

There are some clear differences between these two techniques. Cost-effectiveness analysis is intended mainly to eliminate low cost-effective management options and to rank the remaining options (see Fig. 12). The main elements of the approach are as follows:

1. Characterization of management options in terms of their cost and the corresponding residual collective doses following their implementation.
2. Selection of cost-effective options for which there are no alternative options either to reach the same residual collective dose at a lower protection cost or for the same protection cost to reach a lower residual collective dose.

This process is illustrated graphically in Fig. 12. Each management option is represented by a dot and all those dots situated along the cost-effectiveness curve

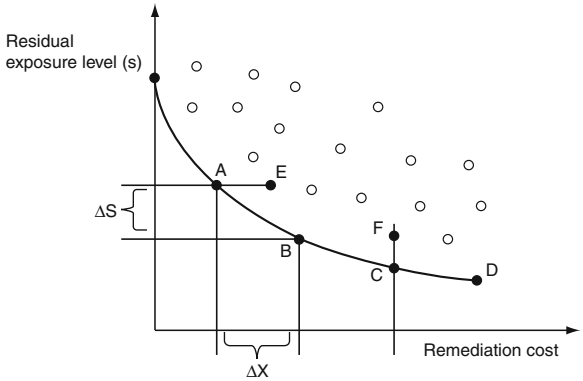

Environmental Countermeasures and Restoration. Figure 12
Cost-effectiveness analysis (Adopted from Lochard and Schneider [122])

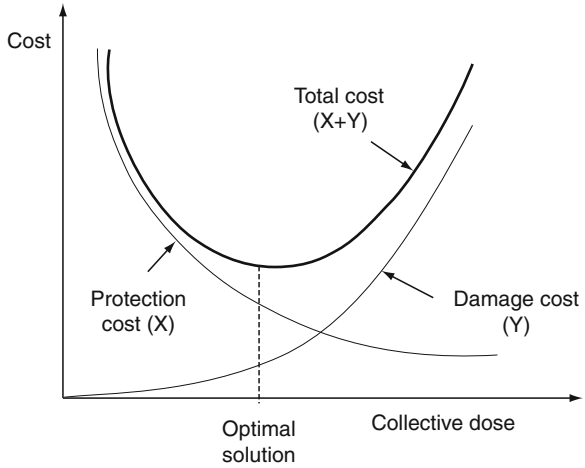

Environmental Countermeasures and Restoration. Figure 13
Cost-benefit analysis applied for the identification and justification of the optimal management option [34]

represent cost-effective options. For example option (A) allows for an equivalent residual collective at a lower cost than (E), and option (C) gives a lower residual collective dose for the same cost as (F). All the options which are above on the curve are called "totally dominated" (worse) options and must be discarded from further consideration (Lochard and Schneider 2001 [122]).

Cost-effectiveness is intended to assess the "marginal cost" of every management option, which has to be compared against the closest less or more expensive options. If a small additional cost would lead to a much higher effectiveness in terms of risk reduction, the option is not cost effective. Finally, each cost-effective option can be characterized by the increase in cost from one option to the next (DX) and the corresponding decrease in collective dose (DS). The quotient (DX/DS) is called the cost-effectiveness ratio and provides a basis for ranking the various options. However, determination of the cost-effectiveness curve and the corresponding cost-effectiveness ratios does not provide a basis for the selection of the optimum option. This is achieved by the introduction of a reference value for the cost-effectiveness ratio in the framework of the cost–benefit analysis [122].

The most widespread approach to performing the second technique, cost–benefit analyses is based on the determination, for each management option, of the sum of remediation costs and the cost of residual collective dose (expressed in monetary terms) resulting from that strategy, and then comparing them to identify which option has the lowest total cost. This option can be accepted as the optimum solution, as illustrated in Fig. 13 [34].

There are many factors to be taken into account as part of the process of remediation justification and some of them cannot be quantified either in monetary terms or in terms of any resources, although they may be quantifiable in other units or ranking parameters. In such a case the most straightforward way to justify an optimized remediation strategy is the application of multi-attribute-utility analysis (MAUA). This technique was first recommended by ICRP for the optimization of radiation protection efforts in ICRP Publication 55 [35]. The most recent ICRP Publications 103 and 104 emphasize the great impact of social and political factors on decisions regarding remediation which also encourage the use of MAUA as one of the basic approaches for remediation optimization [10, 31].

The basic principle of the multi-attribute-utility analysis technique is to construct a scoring scheme (or multi-attribute-utility function) for each option on the basis of all significant criteria which characterize

the situation (i.e., cost of remediation, collective or individual doses, perception of management options by the population, etc.). When the different remedial options are identified, the MAUA defines the relevant criteria for the decision process. The criteria are specified in compliance with specific strategies to ensure remediation success. These criteria normally include: economic attributes, human health impact and public safety attributes, socio-psychological attributes, environmental secondary effects and ethical considerations, criteria based on public opinions, and the interests of various population groups.

Every remediation alternative must be evaluated according to some or all of the above criteria, either quantitatively or qualitatively. Because of their diversity, possible options will be ranked differently for each criterion. In further steps, weighting-coefficients are assigned to each criterion to account for their relative importance. This is the most important and often difficult step in MAUA. Nevertheless, several techniques are available to derive this set of values, and whatever method is used, the choice of weighting coefficients should be justified. Formally, each option is qualified by its total utility (U) calculated as follows:

$$U_i = \sum k_j \cdot u_{ij},$$

Where i is the remediation alternative number; j is the criterion number; k_j is the weighting coefficient showing the relative importance of each option (normalized $\sum k_j = 1$); u_i is the utility of measure i.

The single utility associated with each criterion can be defined either as a linear function of the value expressing the criteria or as a nonlinear function to incorporate the preferences of the decision makers into the analysis. For example, it is possible to define utility functions which incorporate risk aversion according to the level of individual or collective exposures [35].

Finally, the management options which lead to the highest total utility should be selected. Since most of the weighting factors generally rely on decision makers' judgments, it is highly recommended that a sensitivity analysis be performed using different sets of weighting coefficients to test the "robustness" of the results.

Based on such an approach, a few specific decision-support systems for remediation of different environments: aquatic, forest, and rural were suggested and used for the long-term optimization of remediation strategies following the Chernobyl accident [85, 123–127].

Future Directions

Different nuclear applications have contributed to the rapid development of science and technology within the second half of the twentieth century. The use of numerous nuclear activities has, in many countries around the world, led to the contamination of significant parts of some ecosystems, which require remediation. Due to the variety of sources and the characteristics of the receiving environment, the scenario of contaminated sites varies greatly. Nuclear weapon testing and severe radiation accidents, in particular, have also greatly contributed to global concern about the need for reliable and comprehensive radiation risk assessment. In response, the development of countermeasures and remediation constitute two major radiation protection tools that can alleviate the radiological consequences of emergencies and reducing the radiation exposure from existing contamination, respectively.

Currently, the quality of assessments of the consequences of the contamination of the environment varies depending on the amount of available data on the environmental behavior of different radionuclides in the environment. While the data available on some key dose forming radionuclides, especially those released on the major accidents, are reasonably good, that of many other radionuclides is rather patchy. Therefore, there are some notable deficiencies in information on environmental behavior of many important radionuclides [128] and also in the associated radiation effects on many biological and ecological end points particularly in plants and animals. In some cases, contaminated sites already released for general use have had to be reclassified because of an insufficient understanding or quantification of the radiation risk at the time when they were released. The need for remediation of such sites was not fully appreciated as soon as it might have been if better information had been available on the environmental pathways of exposure.

Appropriate response to contamination of the environment with radionuclides requires a comprehensive multidisciplinary approach as outlined in this chapter. The paper is focused on actions to prevent exposure of humans but the challenge is greater than this in that the impact of countermeasures or remediation on wildlife is difficult to quantify on the basis of current knowledge. Therefore, there is a significant future challenge to consider the need for, and potential implementation of, a holistic framework for the response to environmental contamination considering both the protection of human beings and the environment itself.

Bibliography

Primary Literature

1. IAEA (2007) IAEA safety glossary: terminology used in nuclear, radiation, radioactive waste and transport safety. International Atomic Energy Agency, Vienna
2. Eisenbud M, Gessel T (1997) Environmental radioactivity from natural, industrial and military sources, 4th edn. Academic Press, San Diego, CA (ISBN 0-12-235154-1)
3. IAEA (1987) Dosimetric and medical aspects of the radiological accident in Goiania in, 1987. IAEA TECDOC-1009. International Atomic Energy Agency, Vienna
4. IAEA (1999) Technologies for the remediation of radioactively contaminated sites, International Atomic Energy Agency IAEA-TECDOC-1086. International Atomic Energy Agency, Vienna
5. UNSCEAR (2000) United Nations Scientific Committee on the effects of atomic radiation. Report to the general assembly. sources and effects of ionizing radiation. Scientific Annex C, UNSCEAR, New York, pp 157–252
6. Aarkrog A (2001) Manmade radioactivity. In: Van der Stricht E, Kirchman R (eds) Radioecology: radioactivity and ecosystems. Fortemps, Liege, pp 55–78
7. IAEA (2002) Radiation legacy of the 20th century: environmental restoration IAEA-TECDOC-1280. International Atomic Energy Agency, Vienna
8. IAEA (2003) Remediation of areas contaminated by past activities and accidents safety requirements IAEA safety standards series No.WS-R-3. International Atomic Energy Agency, Vienna
9. González AJ (2009) International approaches to remediation of territorial radioactive contamination. In: Voigt G, Fesenko S (eds) Remediation of contaminated environments. Elsevier, Amsterdam, pp 1–42
10. ICRP (2008) Scope of radiological protection control measures ICRP publication 104 Annals ICRP 37(5). Elsevier, Amsterdam
11. Voigt G, Eged K, Howard BJ, Kis Z, Nisbet AF, Oughton DH, Rafferty B, Salt CA, Smith JT, Vandenhove H (2000) A wider perspective on the selection of countermeasures. Rad Prot Dosim 92:45–48
12. Fesenko SV, Alexakhin RM, Balonov MI, Bogdevitch IM, Howard BJ, Kashparov VA, Sanzharova NI, Panov AV, Voigt G, Zhuchenka YM (2007) An extended critical review of twenty years of countermeasures used in agriculture after the Chernobyl accident. Sci Total Environ 383:1–24
13. Shershakov V, Fesenko S, Kryshev I, Semioshkina N (2009) Decision-aiding tools for remediation strategies. In: Voigt G, Fesenko S (eds) Remediation of contaminated environments. Amsterdam, Elsevier, pp 123–178
14. Jacob P, Fesenko SV, Firsakova SK, Likhtarev IA, Schotola C, Alexakhin RM, Zhuchenko YM, Kovgan L, Sanzharova NI, Ageyets V (2001) Remediation strategies for rural territories contaminated by the Chernobyl accident. J Environ Radioactiv 56:51–76
15. Lochard J (2004) Living in contaminated territories: a lesson in stakeholder involvement. In: Current trends in radiation protection (EDP Sciences)., pp 211–220
16. Fesenko SV, Alexakhin RM, Balonov MI, Bogdevich IM, Howard BJ, Kashparov VA, Sanzharova NI, Panov AV, Voigt G, Zhuchenko YuM (2006) Twenty years' application of agricultural countermeasures following the Chernobyl accident: lessons learned. J Radiol Prot 26(4):1–9
17. Fesenko S, Zeiller L, Voigt G (2009) Site characterisation and measurement strategies for remediation purposes. In: Voigt G, Fesenko S (eds) Remediation of contaminated environments. Elsevier, Amsterdam, pp 43–122
18. Shaw G (2007) Introduction. In: Shaw G (ed) Radioactivity in the terrestrial environment, Radioactivity in the environment. Elsevier, Amsterdam, pp 1–19
19. Iranzo E, Richmond CR (1987) Plutonium contamination twenty years after the nuclear accident in Spain. Oak Ridge National Laboratory, Tennessee
20. Wrenn MMN (1974) Environmental levels of plutonium and transplutonium elements WASH 1359 (Atomic Energy Commission). Washington, DC, USA, p 89
21. Eriksson M (2002) On weapons plutonium in the arctic environment (Thule, Greenland) Riso-R-1321(EN). Risø National Laboratory, Roskilde, Denmark
22. Strand P, Balonov M, Bewers M, Howard BJ, Tsaturov YS, Salo A, Aarkrog A (eds) (1997) Arctic pollution issues. radioactive contamination. A report from an international expert group to the arctic monitoring and assessment programme. Oslo, Norwegian Radiation Protection Authority, p 160
23. Ramzaev V, Mishin A, Golikov V, Argunova T, Ushnitsi V, Zhuravskaya A, Sobakin P, Brown J, Strand P (2008) Radioecological studies at the Kraton-3 underground nuclear explosion site in 1978–2007: a review In: Strand P, Brown J, Jølle T (eds) Proceedings of the international conference on radioecology and environmental radioactivity, NRPA, Norway, pp 448–451
24. Alexakhin RM, Fesenko SV, Sanzharova NI (1996) Serious radiation accidents and the radiological impact on agriculture. Radiat Prot Dosim 64:37–42
25. Alexakhin RM, Buldakov LA, Gubanov VA, YeG D, Ilyin LA, Kryshev II, Linge II, Romanov GN, Savkin MN, Saurov MM,

Tikhomirov FA, Kholina YuB (2004) Large radiation accidents: consequences and protective countermeasures. Moscow, IzdAT Publisher
26. Alexakhin RM (2009) Remediation of areas contaminated after radiation accidents. In: Voigt G, Fesenko S (eds) Remediation of contaminated environments. Elsevier, Amsterdam, pp 179–224
27. Cancio DJ, Gutierrez C, Rujz AS (1993) Radiological considerations related with the restoration of a phosphogypsum disposal site in Spain, European Commission Doc. XI-5027/94. In: Proceedings international symposium remediation and restoration of radioactive-contaminated sites in Europe, Antwerp. pp 645–652
28. IAEA (1999) Compliance monitoring for remediated sites, international atomic energy agency, IAEA-TECDOC-1118. International Atomic Energy Agency, Vienna
29. IAEA (1996) International basic safety standards for protection against ionizing radiation and for the safety of radiation sources. IAEA safety series No.115. International Atomic Energy Agency, Vienna
30. ICRP (1991) Recommendations of the international commission on radiological protection ICRP publication 60 Annals ICRP 21(1–3). Elsevier, Amsterdam
31. ICRP (2007) The 2007 recommendations of the international commission on radiological protection ICRP Publication 103 Annals ICRP 37(2–4). Elsevier, Amsterdam
32. ICRP (2006) Assessing dose of the representative person for the purpose of radiation protection of the public and the optimisation of radiological protection: broadening the process publication 101 Annals ICRP 36(3). Elsevier, Amsterdam
33. ICRP (1999) Protection of the public in situations of prolonged radiation exposure ICRP Publication 82 Annals ICRP 29(1/2). Elsevier, Amsterdam
34. ICRP (1983) Cost-benefit analysis in the optimisation of radiation protection ICRP publication 37. Annals ICRP 10(2/3). Pergamon Press, Oxford
35. ICRP (1989) Optimisation and decision-making in radiological protection. ICRP publication 55 Annals ICRP 20 (1). Pergamon Press, Oxford
36. IAEA (2002) Non-technical factors impacting on the decision making processes in environmental remediation IAEA-TECDOC-1279. International Atomic Energy Agency, Vienna
37. IAEA (2000) Site characterisation techniques used in environmental restoration activities, International Atomic Energy Agency IAEA-TECDOC-1148. International Atomic Energy Agency, Vienna
38. Fesenko SV, Colgan A, Sanzharova NI, Lissianski KB, Vazquez C, Guardans R (1997) The dynamics of the transfer of caesium-137 to animal fodder in areas of Russia affected by the Chernobyl accident and doses resulting from the consumption of milk and milk products. Radiat Prot Dosim 69:289–299
39. Fesenko SV, Jacob P, Alexakhin R, Sanzharova NI, Panov A, Fesenko G, Cecille L (2001) Important factors governing exposure of the population and countermeasure application in rural settlements of the Russian Federation in the long term after the Chernobyl accident. J Environ Radioactiv 56:77–98
40. Howard BJ, Wright SM (eds) (1999) Spatial analysis of vulnerable ecosystems in Europe: spatial and dynamic prediction of radiocaesium fluxes into European foods (SAVE). Final report. Commission of European Communities, Brussels
41. Howard BJ, Liland A, Beresford NA, Andersson KG, Cox G, Gil JM, Hunt J, Nisbet A, Oughton D, Voigt G (2004) A critical evaluation of the strategy project. Radiat Prot Dosim 109:63–67
42. Sanzharova NI, Fesenko SV, Alexakhin RM, Anisimov VS, Kuznetsov VK, Chernyayeva LG (1994) Changes in the forms of ^{137}Cs and its availability in plants as dependent on properties of fallout after the Chernobyl Nuclear Power Plant accident. Sci Total Environ 154:9–22
43. Dale P, Robertson I, Toner M (2008) Review: radioactive particles in dose assessments. J Environ Radioactiv 99:1589–1595
44. Alexakhin RA, Korneev NA (eds) (1991) Agricultural Radioecology. Ecology, Moscow (in Russian)
45. Prister BS, Perepelyatnikov GP, Perepelyatnikova LV (1993) Countermeasures used in the Ukraine to produce forage and animal food products with radionuclide levels below intervention limits after the Chernobyl accident. Sci Total Environ 137:183–198
46. Howard BJ (2000) The concept of radioecological sensitivity. Radiat Prot Dosim 92:29–34
47. Alvarez-Farizo B, Gil JM, Howard BJ (2009) Impacts from restoration strategies: assessment through valuation workshops. Ecol Econ 68:287–297
48. Howard BJ, Beresford NA, Nisbet A, Cox G, Oughton DH, Hunt J, Alvarez B, Andersson KG, Liland A, Voigt G (2005) The STRATEGY project: decision tools to aid sustainable restoration and long-term management of contaminated agricultural ecosystems. J Environ Radioactiv 83:275–295
49. Alexakhin RM (1993) Countermeasures in agricultural production as an effective means of mitigating the radiological consequences of the Chernobyl accident. Sci Total Environ 137:9–20
50. Prister B, Loshchilov N, Perepelyatnikova L, Perepelyatnikov G, Bondar P (1992) Efficiency of measures aimed at decreasing the contamination of agricultural products in areas contaminated by the Chernobyl NPP accident. Sci Total Environ 112:9–87
51. Howard BJ, Beresford NA, Voigt G (2001) Countermeasures for animal products: a review of effectiveness and potential usefulness after an accident. J Environ Radioactiv 56:115–137
52. Bogdevitch I, Sanzharova N, Prister B, Tarasiuk S (2002) Countermeasures on natural and agricultural areas after Chernobyl accident. In: Kolejka J (ed) Role of GIS in lifting the cloud off Chernobyl, Kluwer, Dordrecht, pp 147–158
53. Junker H, Jensen JM, Jørgensen HB, Roed J, Andersson KG, Kofman PD, Bøllehuus E, Baxter L, Grebenkov A (1998) Chernobyl bioenergy project, ELSAMPROJEKT report no. EP 8204-98-n600hju
54. Andersson K, Roos P (2009) Effectiveness of remedial techniques for environments contaminated by artificial radionuclides. In: Voigt G, Fesenko S (eds) Remediation of contaminated environments. Elsevier, Amsterdam, pp 375–426

55. Andersson KG, Roed J, Eged K, Kis Z, Voigt G, Meckbach R, Oughton DH, Hunt J, Lee R, Beresford NA, Sandalls FJ (2003) Physical countermeasures to sustain acceptable living and working conditions in radioactively contaminated residential areas, RISOE-R-1396(EN), ISBN 87-550-3190-0
56. Andersson KG, Brown J, Mortimer K, Jones JA, Charnock T, Thykier-Niellsen S, Kaiser JC, Proehl G, Nielsen SP (2008) New developments to support decision-making in contaminated inhabited areas following incidents involving a release of radioactivity to the environment. J Environ Radioactiv 99:439–454
57. Brown J, Mortimer K, Andersson K, Duranova T, Mrskova A, Hänninen R, Ikäheimonen T, Kirchner G, Bertsch V, Gallay F, Reales N (2008) Generic handbook for assisting in the management of contaminated inhabited areas in Europe following a radiological emergency, parts I-V, Final report of the EC-EURANOS project activities CAT1RTD02 and CAT1RTD04, EURANOS(CAT1)-RP(07). Health Protection Agency, UK
58. Nisbet A, Brown J, Jones A, Rochford H, Hammond D, Cabianca T (2009) HPA-RPD-064 – UK recovery handbooks for radiation incidents, HPA, Didcot
59. Nisbet AF, Brown J, Howard BJ, Beresford NA, Ollagnon H et al (2010) Decision aiding handbooks for managing contaminated food production systems, drinking water and inhabited areas in Europe. Radioprotection 45(5):S23–S37
60. Salt CA, Rafferty B (2001) Assessing potential secondary effects of countermeasures in agricultural systems: a review. J Environ Radioactiv 56:99–114
61. IAEA (2006) Environmental consequences of the Chernobyl accident and their remediation: twenty years of experience report of the Chernobyl forum expert group environment. International Atomic Energy Agency, Vienna
62. Oughton D, Bay-Larsen I, Voigt G (2009) Environmental, social, ethical and economic aspects of remediation. In: Voigt G, Fesenko S (eds) Remediation of contaminated environments. Elsevier, Amsterdam, pp 427–452
63. Oughton D, Forsberg E-M, Bay I, Kaiser M, Howard B (2004) An ethical dimension to sustainable restoration and long-term management of contaminated areas. J Environ Radioactiv 74:171–183
64. Gould P (1990) Fire in the rain: the democratic consequences of Chernobyl. Polity Press, Cambridge
65. Heriard Dubreuil G, Lochard J, Girard P, Guyonnet JF, Le Cardinal G, Lepicard S, Livolsi P, Monroy M, Ollagnon H, Pena-Vega A, Pupin V, Rigby J, Rolevitch I, Schneider T (1999) Chernobyl post-accident management: the ETHOS project. Health Phys 77:361–372
66. Eged K, Kis Z, Voigt G, Andersson KG, Roed J, Varga K (2003) Guidelines for planning interventions against external exposure in industrial area after a nuclear accident – Part I: a holistic approach of countermeasure application, GSF-Bericht 01/03, GSF – Forschungszentrum für Umwelt und Gesundheit GmbH, Neuherberg, ISSN 0721-1694, 67 p
67. IAEA (1994) Handbook of parameter values for radionuclide transfer in the temperate environments. Technical Report Series 364, International Atomic Energy Agency, Vienna
68. Nisbet A, Howard B, Beresford N, Voigt G (2005) Stakeholder involvement in post-accidental management. J Environ Radioactiv 83:259–435
69. Beresford NA, Howard BJ, Barnett CL, Rantavaara A, Rissanen K, Reales N, Gallay F, Papachristodoulou C, Ioannides K, Nisbet AF, Hesketh N, Oughton D, Bay I (2005) Compendium of countermeasures for the management of food production systems. Deliverable TN(05)-01 (including CD) for EURANOS project (Cat1). Available at http://www.euranos.fzk.de
70. Nikipelov BV, Romanov GN, Buldakov LA, Babaev NS, Kholina YuB, Mikerin EI (1987) The radiation accident in the South Urals in 1957. Atomnaya Energia 67:74–80 (in Russian)
71. Burnazyan AI (1990) Results of the studies and experience of mitigation of consequences of the accidental contamination of the territory by uranium fission products. Energoatomizdat, Moscow (in Russian)
72. Sokolov VE, Krivolutsky DA (eds) (1993) Environmental impacts of radioactive contamination in the South Urals. Nauka, Moscow, 336 p ISBN 5-02-005719-3 (in Russian)
73. Akleev AV, Kiselev MF (2001) Ecological and medical impacts of the 1957 accident at the PP "Mayak". RF Ministry of Health, Moscow
74. Romanov GN, Drozhko EG, Nikipelov BV, Teplyakov IG, Shilov VP (1993) Summing up: restoration of the economic activity. In: Sokolov VE, Krivolutsky DA (eds) Environmental impacts of radioactive contamination in the South Urals. Moscow, Nauka (in Russian)
75. Fetisov VI, Romanov GN, Drozhko EG (1993) Practice and problems of environment restoration at the location of the industrial association Mayak, 1994, European Commission Doc. XI-5027/94. In: Proceedings international symposium remediation and restoration of radioactive-contaminated sites in Europe, Antwerp, pp 507–521
76. Espinosa A, Aragon A, Stradling N, Hodgson A, Birchall A (1998) Assessment of doses to adult members of the public in Palamares from inhalation of plutonium and americium. Radiat Prot Dosim 79(1–4):161–164
77. Izrael YuA, Kvasnikova EV, Nazarov IM, Fridman ShD (1994) Global and regional contamination of the territory of the European part of the former USSR by ^{137}Cs. Meteorol Hydrol 5:5–9 (in Russian)
78. Izrael Yu (1999) Radioactive fallout after nuclear explosions and accidents. Environ Monit Assess 59(1):121–122
79. Sanzharova NI, Fesenko SV, Kotik VA, Spiridonov SI (1996) Behaviour of radionuclides in meadows and efficiency of countermeasures. Radiat Prot Dosim 64:43–48
80. Ratnikov AN, Vasiliev AV, Alexakhin RM, Krasnova EG, Pasternak AD, Howard BJ, Hove K, Strand P (1998) The use of hexacyanoferrates in different forms to reduce radiocesium contamination of animal products in Russia. Sci Total Environ 223:167–176
81. Strand P, Balonov M, Travnikova I, Hove K, Skuterud L, Prister B, Howard BJ (1999) Fluxes of radiocaesium in selected rural study sites in Russia and Ukraine. Sci Total Environ 231:159–171

82. Fesenko SV, Voigt G, Spiridonov SI, Sanzharova NI, Gontarenko IA, Belli M, Sansone U (2000) Analysis of the contribution of forest pathways to the radiation exposure of different population groups in Bryansk region of Russia. Radiat Environ Biophys 39:291–300
83. Shutov VN, Bruk GYa, Basalaeva LN, Vasiletskiy VN, Ivanova NP, Karlin IS (1996) The role of mushrooms and berries in the formation of internal exposure doses to the population of Russia after the Chernobyl accident. Radiat Prot Dosim 67:55–64
84. Tikhomirov FA, Shcheglov AI (1994) Main investigation results on the forest radioecology in the Kyshtym and Chernobyl accident zones. Sci Total Environ 157:45–57
85. Fesenko SV, Voigt G, Spiridonov SI, Gontarenko IA (2005) Decision making framework for application of forest countermeasures in the long term after the Chernobyl accident. J Environ Radioactiv 82:143–166
86. IAEA (2006) Radiological conditions in the Dnieper River Basin: assessment by an international expert team and recommendations for an action plan radioecological assessment report series. International Atomic Energy Agency, Vienna
87. Smith JT, Kudelsky AV, Ryabov IN, Hadderingh RH, Bulgakov AA (2003) Application of potassium chloride to a Chernobyl contaminated lake: modelling the dynamics of radiocaesium in an aquatic ecosystem and decontamination of fish. Sci Total Environ 305:217–227
88. Kudelsky AV, Smith JT, Petrovich AA (2002) An experiment to test the addition of potassium to a non-draining lake as a countermeasure to ^{137}Cs accumulation in fish. Radioprotection Colloques 37:621–626
89. Roed J, Andersson KG, Barkovsky AN, Fogh CL, Mishine AS, Ponamarjov AV, Ramzaev VP (2006) Reduction of external dose in a wet-contaminated housing area in the Bryansk Region. Russia J Environ Radioactiv 85:265–279
90. Rosenthal JJ, Cunha PO, Oliveira CA (1989) Aspects of the initial and recovery phases of the radiological accident in Goiania. In: Proceedings international symposium recovery operations in the event of a nuclear accident or radiological emergency, IAEA, Vienna, 593–597
91. Oliveira AR, Hunt JG, Valverde NJL, Brandao-Mello CE, Farina R (1991) Medical and related aspects of the Goiania accident: an overview. Health Phys 60(1):17–24
92. IAEA (1998) Dosimetric and medical aspects of the radiological accident in Goiania in, 1987. IAEA TECDOC-1009. International Atomic Energy Agency, Vienna
93. Rosenthal JJ, Almeida CE, Mendonca AH (1991) The radiological accident in Goiania, the remedial action. Health Phys 60:7–15
94. Anspaugh LR, Church BW (1986) Historical estimates of external γ exposure and collective external γ exposure from testing at the Nevada Test Site. I. Test series through Hardtack II, 1958. Health Phys 51:35–51
95. Donaldson LR, Seytnour AH, Nevissi'k AE (1997) University of Washington's radioecological studies in the Marshall islands, 1946-1977. Health Phys 73:214–222
96. Danesi PR (2009) Remediation of sites contaminated by nuclear weapon tests in the Marshall Islands and Australia. In: Voigt G, Fesenko S (eds) Remediation of contaminated environments. Elsevier, Amsterdam, pp 225–262
97. Carlsen TM, Peterson LE, Ulsh BA, Werner CA, Purvis KL, Sharber AC (2001) Radionuclide contamination at Kazakhstan's semipalatinsk test site: implications on human and ecological health. Lawrence Livermore National Laboratory, Livermore, CA. UCRL-JC-143920
98. Bennet BG (2000) Worldwide panorama of radioactive residues in the environment. In: Restoration of environments with radioactive residues, Proceedings International Symposium Arlington, Virginia, USA, 29 Nov.-3 Dec. 1999, IAEA, Vienna, pp 11–24
99. Hamilton TF (2004) Linking legacies of the cold war to arrival of anthropogenic radionuclides in the oceans through the 20th century. In: Livingston HD (ed) Radioactivity and the environment, vol 6. Elsevier Science, Amsterdam, pp 30–87
100. Robison WL, Phillis WA, Colsher CS (1977) Dose assessment at Bikini Atoll, Rep. UCRL-51879, Part 5, Lawrence Livermore National Laboratory, Livermore
101. Miltenberger RP, Greenhouse NA, Lessard ET (1980) Whole body counting results from 1974 to 1979 for Bikini Island residents. Health Phys 39:395–507
102. Robinson WL, Noshkin VE (1999) Radionuclide characterization and associated dose from long-live radionuclides in close-in fallout delivered to the marine environment at Bikini and Enewetak Atolls. Sci Total Environ 237–238:311–327
103. Simon SL, Graham JC (1997) Findings of the first comprehensive radiological monitoring program of the Republic of the Marshall Islands. Health Phys 73:66–85
104. IAEA (1998) Characterization of radioactively contaminated sites for remediation purposes, IAEA-TECDOC-1017. International Atomic Energy Agency, Vienna
105. Robison WL, Bogen KT, Conrado CL (1997) An updated assessment for resettlement options at Bikini Atoll U.S. nuclear test site. Health Phys 73:100–114
106. Symonds JL (1985) A history of British atomic tests in Australia. Australian Government Publishing Service, Canberra
107. Haywood SM, Smith JG (1992) Assessment of potential doses at the Maralinga and Emu test sites. Health Phys 63:624–630
108. Parkinson A (2000) Maralinga rehabilitation project. National Conference-MAPW Australia, http://www.mapw.org.au/conferences/mapw2000/papers/parkinson.html
109. Williams GA (ed) (1990) Inhalation hazard assessment at Maralinga and Emu, Technical Report ARL/TR087
110. Williams GA, Cooper MB, Martin LJ (1998) Plutonium contamination at Maralinga – dosimetry and clean-up criteria. In: Proceedings AIOH-98 17th annual conference of Australian institute of occupational hygienists (AIOH), December 1998, pp 117–126
111. IAEA (2005) Selection of decommissioning strategies: issues and factors. Report by an expert group IAEA-TECDOC-1478. International Atomic Energy Agency, Vienna

112. Falck WE, Seitz R, Pearl M, Audet M, Schmidt P, Fernandes HM (2009) Remediation as part of the decommissioning of nuclear facilities. In: Voigt G, Fesenko S (eds) Remediation of contaminated environments. Elsevier, Amsterdam, pp 263–374
113. NEA (2006) Releasing of the nuclear installations – a status report. NEA Publication No. 6187. OECD-Nuclear Energy Agency (OECD-NEA), Paris
114. IAEA (2004) Application of the concepts of exclusion, exemption and clearance, IAEA safety standard series No. RS-G-1.7. International Atomic Energy Agency, Vienna
115. Fesenko SV, Sanzharova NI, Wilkins BT, Nisbet AF (1996) FORCON: local decision support system for the provision of advice in agriculture – methodology and experience of practical implementation. Radiat Prot Dosim 64(1/2):157–164
116. Van der Perk M, Burrough PA, Voigt G (1998) GIS based modelling to identify regions of Ukraine, Belarus, and Russia affected by residues of the Chernobyl nuclear power plant accident. J Hazard Mater 61:85–90
117. Gillett AG, Crout NMJ, Absalom JP, Wright SM, Young SD, Howard BJ, Barnett CL, McGrath SP, Beresford NA, Voigt G (2001) Temporal and spatial prediction of radiocaesium transfer to food products. Radiat Environ Biophys 40:227–235
118. Jackson D, Wragg SK, Bousher A, Zeevaert T, Stiglund Y, Brendler V, Hedemann Jensen P, Nordlinder S (1999) Establishing a method for assessing and ranking restoration strategies for radioactively contaminated sites and their close surroundings. Nucl Energy 38:223–231
119. Shershakov VM, Trakhtengerts EA (1997) Decision-making in an emergency by using computer analysis with dynamically changeable rules. Radiat Prot Dosim 73:141–142
120. ICRP (1973) Implication of commission recommendations that doses be kept as low as readily achievable ICRP Publication 22. Pergamon Press, Oxford
121. ICRP (1977) Recommendations of the international commission on radiological protection ICRP publication 26, Annals ICRP 1(3). Pergamon Press, Oxford
122. Lochard J, Schneider T (2001) Application of decision aiding technologies for relocation strategies. In: Van der Stricht E, Kirchman R (eds) Radioecology: radioactivity and ecosystems. Fortemps, Liege, pp 504–536
123. IAEA (2000) Restoration of environments affected by residues from radiological accidents: approaches to decision making IAEA-TECDOC-1131. International Atomic Energy Agency, Vienna
124. Jacob P, Fesenko S, Bogdevitch I, Kashparov V, Sanzharova N, Grebenshikova N, Isamov N, Lazarev N, Panov A, Ulanovsky A, Zhuchenko Y, Zhurba M (2009) Rural areas affected by the Chernobyl accident: radiation exposure and remediation strategies. Sci Total Environ 408:14–25
125. Salt CA, Culligan Dunsmore M (2000) Development of a spatial decision support system for post-emergency management of radioactively contaminated land. J Environ Manage 58(3):169–178
126. Sazykina TG, Kryshev II (2006) Multi-criteria analysis for evaluating the radiological and ecological safety measures in radioactive waste management. Communications of Higher School. Nuclear Power Engineering (Izvestia vissikh uchebnikh zavedenij. Yadernaya energetica), Obninsk 1, pp 39–46 (in Russian)
127. Shaw G, Robinson C, Holm E, Frissel M, Crick M (2001) A cost-benefit analysis of long-term management options for forest following contamination with ^{137}Cs. J Environ Radioactiv 56:185–208
128. IAEA (2009) Quantification of radionuclide transfers in terrestrial and freshwater environments for radiological assessments IAEA-TECDOC-1616. International Atomic Energy Agency, Vienna

Books and Reviews

Brechignac F, Howard BJ (eds) (2001) Radioactive pollutants: impact on the environment and humans. EDP Science, Les Ulis

Brown J, Hammond DJ, Kwakman P (2009) Generic handbook for assisting in the management of contaminated drinking water in Europe following a radiological emergency. EURANOS (CAT1)-TN(09)-02

Ilyin LA, Gubanov VA (eds) (2004) Large radiation accidents: consequences and protective countermeasures. IzdAT Publisher, Moscow

International Atomic Energy Agency (2006) Environmental consequences of the Chernobyl accident and their remediation: twenty years of experience, Radiological assessment reports series. Report of the Chernobyl forum expert group "Environment." International Atomic Energy Agency, Vienna

Izrael YuA (2002) Radioactive fallout after nuclear explosions and accidents. Elsevier, Amsterdam

Nisbet AF, Jones A, Turcanu C, Camps J, Andersson KG, Hänninen R, Rantavaara A, Solatie D, Kostiainen E, Jullien T, Pupin V, Ollagnon H, Papachristodoulou C, Ioannides K, Oughton D (2009) Generic handbook for assisting in the management of contaminated food production systems in Europe following a radiological emergency v2. EURANOS (CAT1)-TN(09)-01. Available at http://www.euranos.fzk.de

Scott EM (ed) (2004) Modelling radioactivity in the environment. Elsevier, Amsterdam

Shaw G (ed) (2007) Radioactivity in the terrestrial environment. Elsevier, Amsterdam

Smith J, Beresford NA (2005) Chernobyl catastrophe and consequences. Praxis Publishing/Springer, Chichester

Van der Stricht E, Kirchman R (eds) (2001) Radioecology: radioactivity and ecosystems. IUR, Fortmeps, Liege

Voigt G (ed) (2001) Remediation strategies. Special Issue. J Environ Radioactiv 56

Voigt G, Fesenko S (eds) (2009) Remediation of contaminated environments. Elsevier, Amsterdam

Environmental Geology, Introduction

James W. LaMoreaux
P.E. LaMoreaux & Associates, Tuscaloosa, AL, USA

As world population increases, greater demand is placed on finite resources that earth can provide. Geographic areas once judged inadequate or inappropriate for construction, water and wastewater management, or transportation routes, among other activities, are being considered for and being used for development.

Environmental geology is the discipline which brings together these issues in a holistic approach to land use planning and utilization. This section of the encyclopedia examines some of the problems, techniques, and solutions for managing resources so that a balance can be maintained between development and the environment.

Natural disasters are reported frequently and have varying impacts depending upon the closeness of the disaster to population centers and the magnitude of the hazard. In all cases, the primary purpose of studying these phenomena is to minimize loss of human life and secondarily to minimize loss of infrastructure and impacts on present and future developments.

Each type of hazard impacts the environment in different ways, with some posing more danger to human life than others, and some posing more hazards to infrastructure and ongoing development. This section on environmental geology will address these various factors to provide a better understanding of how they occur, what can be done to minimize risk and how to plan better to address these concerns in the future.

Impacts of natural disasters including earthquakes and tsunamis and occurrence of sinkholes and landslides can have more devastating effects due to increases in world population. Two entries address earthquake issues: ► Earthquake Faulting, Ground Motions and Deformations and ► Construction Planning, Environmental Impact of Foundation Studies and Earthquake Issues. Earthquakes have occurred throughout history and left their traces as manifestations of geological processes on the geological record.

Many lessons have been learned from damages caused by earthquakes. Guidelines have been developed for design of earthquake resistant structures under different ground conditions. Education of the public has saved lives and continues to be a critical need as is research to develop mechanisms to forewarn the public.

Sinkholes and landslides are both naturally occurring and man induced. Both hazards can cause significant damages to various structures; however, they may not pose as significant a risk to human life as earthquakes. Protective measures can be performed to minimize the risks involved including preparing sinkhole maps which delineate the low, medium, and high risk areas subject to subsidence. If decisions are made to develop in sinkhole and landslide prone terrains, investigations of the geology and hydrogeology can determine where to seat structures into bedrock so as to minimize damages. In addition, engineering design can address the added stresses hazards pose and incorporate additional measures so that buildings and infrastructure can withstand them.

► Karst Terrane and Transportation Issues discusses various types of sinkholes, what their causes are and how to protect against their occurrence. This entry addresses ways to remediate damage and prevent future reoccurrence. ► Land Subsidence in Urban Environment reviews an emerging cause of subsidence in the burgeoning population centers of the world. Better management of water resources is required to prevent further subsidence from occurring in urban areas. Optimal utilization of water supplies must be implemented to correct existing situations and to minimize subsidence in the future.

Overuse of water supplies in concert with drought conditions and land degradation is creating desertification conditions rapidly in the world today. Desertification affects arid, semiarid, and dry subhumid regions; occurring on every continent, it impacts more than two billion people in these areas. Often these conditions occur across country borders and within areas of the world where tensions are already strained for political and religious reasons. ► Desertification and Impact on Human Systems discusses the activities of the United Nations Convention to Combat Desertification (UNCCD) and emphasizes the need for sustainable development at the local level. Stakeholders in these inherently fragile ecosystems must be brought

together to arrive at solutions that will allow continued production of ecosystem goods and services.

Not only do arid conditions require sustainable development, but urban areas do also. In The Interrelated Roles of Natural Resources and Sustainability in Urban Planning, cities are increasingly recognized as the most important global sustainability challenge of this century. Here too, stakeholders are critical in regard to resource access and distribution. Studies of urban metabolism are required to explore interactions among resource flows, urban transformation processes, waste streams, and quality of life. Results of these studies must be correlated to address the challenge of combining urban planning with sustainable resource management.

An integral part of continued growth and development of urban areas is detailed in ► Groundwater Salinity Due to Urban Growth. Understanding of groundwater is critical in regions where there is an increase in water demand and where shortages in water supply affect available and proposed infrastructure. Knowledge of water accessibility in terms of quantity and quality can help reduce the risk of saline intrusion in coastal areas from urban growth. Socioeconomic and environmental development programs require adequate political decision making and planning at local and regional levels. Proper space planning implies that proposed land use is in agreement with what land "attitude" and its environment can provide without putting in danger sustainability.

Geochemical modeling is applicable to investigations of water quality, as well as to many other fields. Modeling is a powerful and indispensable tool for research and investigations of environmental sustainability, science, and technology. It provides quantitative evaluation of complex processes and it can predict the extent and consequences of geochemical reactions in the order of tens of thousands of years. Basic concepts, information for accessing modeling codes and further readings are included in this chapter. More importantly, applications in the field are provided. An excellent example of the utility of geochemical modeling in environmental sustainability, science, and engineering is illustrated in geological carbon sequestration.

Much research is currently being performed on injection of carbon dioxide (CO_2) into deep geological formations as a climate mitigation tool. ► Geologic Carbon Sequestration: Sustainability and Environmental Risk provides an overview of the research and ideas about the future. National and local regulations will require risk assessments of wellbore integrity, well injectivity, and long-term performance in the order of thousands of years. The geology of each site differs and performance assessments are necessary at all stages of CO_2 storage operations: site assessment and selection, design, installation, operations and monitoring, and closure and post closure.

Drilling into deep geological formations is also taking place offshore in an activity known as Oceanic Hydrocarbon Investigation (OHI). OHI is currently increasing its production volume in an energy hungry society and the quest for finding and exploiting underground hydrocarbon resources is being continuously improved.

This is particularly true in relation to underwater mapping, inspection, and monitoring of the environment. ► Marine Life Associated with Offshore Drilling, Pipelines, and Platforms states that OHI has inflicted oil-spills on marine and coastal environments. At large, however, OHI appears to be environmentally friendly. This notion has been documented by extensive seafloor mapping and annual visual inspections of platforms, pipelines, and other infrastructure.

Environmental concerns in marine environments are also being addressed as they relate to dredging of navigable waterways. Dredges of various designs have been used for many years to create and maintain navigable waterways to move people, goods, and materials. ► Dredging Practices and Environmental Considerations discusses the history of dredging from the times of the pyramids when people used long-handled dipper shovels, to when productivity gains from using animals increased digging power. In the 1800s development of electric and steam power units enabled construction of mechanical, backhoe, and pipeline dredges. Hydraulic technology in the 1960s, utilizing hydraulic winches and hydraulic rotary cutter drives, facilitated removal of finer grade sediment. As technology improved, so too did concern for the environment, such that today there is much debate and research on the impacts of dredging. This concern has heightened with contaminated sediments in the picture and the question of whether to dredge or leave them in place.

Navigable waterways integrally relate to dam construction and movement of people, goods, and services. Construction of dams has a much greater impact on the environment. Since time immemorial, people have looked for ways to tame surface waters to prevent floods and use water for different purposes, including transportation, irrigation, water supply, and electricity production. ► Dam Engineering and its Environmental Aspects details the history of dams and their primary role to store or to divert waters. Many dam projects have been controversial and potentially disastrous. Failure of dams and their environmental impacts are the main reasons for controversy and fear. This is particularly true in karst environments which tend to be more sensitive to the influence of dams and reservoirs. With increasing demand on water resources and electric power, an important issue is how to maintain the balance between the necessity for development and preservation of the environment.

Energy continues to weave a thread through this section of the encyclopedia as the chapter on mining deals with mining of coal. Also addressed are impacts from mining of rare earth minerals, gold and copper among others. ► Mining and Its Environmental Impacts details the demands of the growing world population for increasing amounts of raw materials. To find acceptance and support in society, however, any future mining activity will demand state of the art environmental management and must incorporate sustainable development. A history of mining is provided, as well as an overview of the environmental effects of mining, differentiated by its relevant phases: exploration, exploitation and processing, decommissioning and rehabilitation.

Nuclear energy has its own inherent concerns which are increased in times of natural disasters. ► Groundwater Impacts of Radioactive Wastes and Associated Environmental Modeling Assessment discusses the long-term risks to human health and environment from radioactive waste contamination in soil and groundwater. Major sources of radioactive wastes and their impact on groundwater contamination are reviewed along with the major biogeochemical processes that control the transport and fate of radionuclide contaminants. The evolution of mathematical models designed to simulate and assess the transport and transformation of radionuclides are also described. Understanding the fate and transport of radionuclide contaminants can improve the ability to forecast contaminant destination and select cost effective remediation technologies.

Perhaps the greatest energy source known to man is from volcanoes. ► Volcanoes of Mexico includes an introduction to volcanoes: the reasons they form, where they are located, and the hazards presented by different types of eruption. Mexico is one of the world's most volcanic regions and a summary of Mexican volcanoes is presented. Volcanic eruptions can be divided into two broad categories: explosive or effusive. Various factors combine to determine how the magma emerges, the key ingredient of which is water. With the exception of ballistics, which do not reach very far from the volcano, volcanic hazards can present a major risk to populations living close by. Volcanologists need to investigate deposits of previous eruptions to understand what might happen in the future. Hazard maps can be created which indicate where eruptive products might accumulate.

Water, energy, minerals, and the environment all play a role in development and future growth of the world and its population. No single aspect can be addressed without including another. This section of the encyclopedia on environmental geology places these different factors into perspective so that scientists, politicians, economists, planners, and stakeholders can work together to develop solutions that provide an acceptable balance to development and the environment.

Environmental Impacts of an Open Ocean Mariculture Operation in Kona, Hawaii

Neil Anthony Sims
Kona Blue Water Farms, Inc, Kailua-Kona, HI, USA

Article Outline

Glossary
Definition of the Subject
Introduction
Overview of the Kona Blue Water Farms Operation

Farm Operations
Localized Environmental Concerns and Actual Impacts
Global Impacts: Fish Meal and Fish Oil Usage
Future Directions
Bibliography

Glossary

Sustainability The use of resources in such a manner as not to impinge upon the ability of future generations to enjoy similar use.

Open-ocean mariculture The culture of marine fish, invertebrates, or algae in exposed ocean locations.

Definition of the Subject

Open-ocean mariculture is the culture of marine fish, invertebrates, or algae in exposed ocean locations. The criteria for demarcation of open-ocean sites from inshore or nearshore aquaculture sites is often the subject of debate, with various schemes using some integration of distance from shore, depth of water, or exposure to open water and high sea conditions. A more meaningful definition is perhaps, simply, that an open-ocean mariculture site is a site where any of these conditions or criteria combine to disconnect the culture system from the surrounding substrates that might otherwise be subject to some significant environmental impact, or might become reservoirs for some ecological feedback with the culture system. Alternatively, rather than using a geographical or operational distinction, open-ocean mariculture might simply be described as culture of marine animals or plants at sites that are further offshore, or in deeper water. This definition reflects the evolving, aspirational, and incremental improvement in culture systems, rather than thinking of the open ocean as a final destination.

Whatever the definition, open-ocean mariculture offers the potential for a scalable production system for valuable, healthful seafood, with negligible environmental impacts.

Introduction

The Seafood Crisis

The oceans are in deep trouble. Even though the demand for seafood has increased, capture fisheries around the world are collapsing from overfishing, or are static. Wild stock fisheries cannot sustain any greater pressures, and clearly cannot scale to meet the growing needs of increasing population size, increasing affluence, and wider recognition of the health benefits of seafood.

The USA is both symptomatic of the seafood crisis and significantly contributive to the problem. In the USA, closures or buyback schemes to reduce effort have effectively shut down once-productive fisheries for Atlantic tunas and swordfish, the groundfish of Georges Bank and other Northeast fisheries, Pacific Coast sardines, albacore, and more recently, rockfish. Other environmental concerns for endangered species or marine mammals have seen closures or limitations placed on fisheries for shrimp in the Gulf of Mexico, purse seining for tuna in the Pacific, and long-lining for tuna and swordfish in Hawaii and the US Pacific. Currently, over 80% of the seafood consumed in the USA is imported, and more than half of those imports are from farmed sources.

Hawaii Fisheries Status The Hawaiian Islands represent a microcosm of the global fishing crisis. Increased fishing power – in terms of both the number of boats and available technologies – has seen the valuable deep bottom fish catches decline precipitously over the last few decades. GPS units allow deep bottom fishermen to return repeatedly and precisely to a "hot spot" until the fish are gone. Electric reels reduce the labor of hauling up from 60 fathoms to simply flicking a switch. Powerful echo sounders allow tuna fishermen to identify the location of individual fish tens of fathoms beneath their boat. At the same time, catches of sashimi-grade tuna have plummeted due to competing gear-types (seiners, long-liners, pole-and-line) and conflicting national interests throughout the range of these highly migratory species. Some 20 years ago, over 25 commercial fishing boats worked out of the local Honokohau Harbor in Kona, Hawaii, targeting deep-water snappers and big-eye tuna in the "ika-shibi" fishery. Today, there is only one commercial fishing vessel based there, and even that is only part-time.

The decreasing catch volume and decreasing average size of fish caught in the bottom fish fishery in Hawaii is causing increasing concern. By 1996, only 20% of the onaga (*Etelis coruscans*) catch in the main

Hawaiian Islands (MHI) had previously spawned; similar declines were evident among other species stocks. These species' biological characteristics make them vulnerable to recruitment overfishing; NOAA Fisheries staff estimate that an onaga attains maturity at about 4.1 years of age, at a size of 66 cm. With Federal and State data indicating significant overfishing of these stocks, increased regulation became imperative. In June 1998, new legislation went into effect, establishing limits on fishing gear, bag limits, registration of bottom fishing craft, and restricted fishing areas (up to 20% of the bottom fish ground was placed off limits) for the commercial and recreational fishery industry.

Further restrictions are still needed. Over the last two summers, the State declared all bottom fishing closed for the summer period from May 1st to September 30th, throughout the island range. State authorities have indicated that this seasonal closure may need to be repeated for coming years, as well, before there is any measurable improvement in stocks. The majority of high-value species consumed in Hawaii already are imported from other areas, such as the South Pacific and South East Asia.

Aquaculture as Part of the Solution Aquaculture offers the only viable solution to the growing demand for sustainable, healthy sources of seafood protein for human consumption. Fish farming reduces exploitative pressure on already depleted wild stocks, supports the growth of coastal and rural industries, and yields a product that is low in saturated fat and high in protein. The annual contribution of aquaculture to global aquatic production is now almost equal to that of wild catch (47% versus 53% [1]). In 1985, aquaculture represented only 5% of US fish consumption, yet today that figure stands at around 40%. Aquaculture growth is rapid, and is projected to increase in pace. The US Department of Commerce has set a goal of a fivefold increase in domestic aquaculture production value, to $5 billion, by 2025.

Domestic aquaculture production using existing methods or species cannot keep pace. Almost all US production is from freshwater species; the only marine species cultured in any quantity are salmon and striped bass, both of which are anadromous (freshwater spawning). It is almost impossible to obtain permits for nearshore farm sites; there is intense competition among different user groups for nearshore waters, and aquaculture has been besmirched in the conventional wisdom as environmentally destructive and unsustainable.

The Open-Ocean Potential Open-ocean mariculture technology has recently moved from the realm of science fiction [2, 3] to commercial reality. In the last few years, there have been dramatic advances in the legal and engineering fields, which have opened up the new fish farming frontier of offshore areas. New submersible net pen systems have been pioneered by OceanSpar, LLC, of Washington State ("Sea Station™" net pens), and Ocean Farm Technologies, Inc., of Maine ("Aquapod™" net pens). These new technologies have dramatically increased the workable extent of ocean farming, by providing seaworthy platforms for grow-out of fish in exposed offshore environments. These farms are therefore able to be located further offshore, in sites where currents, prevailing sea conditions or seasonal storm events may make surface pens inadvisable. These operations are also usually portrayed as having less environmental impact than nearshore fish farms. The rationale is that there is a cleaner and clearer disconnect between the farm and the underlying benthic substrate or the adjacent shoreline so that there is both minimal environmental impact and negligible potential for negative accumulative feedback from the environment to the culture system.

But how have these first open-ocean mariculture operations actually performed? Is there any basis in fact to these claims of environmentally sound mariculture in offshore locations? What are the opportunities for expansion of this industry, and what are the risks and precautions – both environmental, biological and economic – that should accompany such scaling?

This entry reviews some of the recent progress toward realizing this potential, as exemplified by one farm operation, in Kona, Hawaii. The environmental performance over the past 5 years of operation at Kona Blue Water Farms' site is instructive. It may demonstrate how open-ocean mariculture may represent a partial solution to the seafood crisis: a scalable, environmentally sound production system for high-value seafood. The environmental impacts of this one open-ocean mariculture site are reviewed here, in the context

of both local ecosystem effects and global marine resource use efficiency: the "footprint" on the oceans.

Overview of the Kona Blue Water Farms Operation

Prior to 1998, Hawaii's ocean-leasing legislation limited any potential project to a maximum of 4 acres, which had to be used for either educational or research purposes, and not for commercial gain. Through several years of work by industry aspirants, and strong leadership by the State Aquaculture Development Program, legislation was passed that allowed commercial offshore fish farms or energy projects.

The Kona Blue Water Farms principals had been involved through the legislative review, and with the passage of the bill, began research into developing hatchery culture techniques for high-value marine fish, simultaneously surveying the Kona Coastline for prospective offshore farm sites. After an extensive 3-year process of consultation and consensus-building with the community, Kona Blue was granted the requisite State and Federal permits for the original offshore farm site in March, 2004. The operation began deployment in February 2005 and first fish were harvested offshore in September, 2005. Since then, production has grown to the extent that Kona Blue has been harvesting up to 25,000 lb of sashimi-grade Kona Kampachi® per week, and up to 500 T per year. Kona Kampachi® (*Seriola rivoliana*) is also known as kahala, Long-fin Amberjack or Almaco Jack. It is related to the Japanese hamachi (*S. quinqueradiata*), but is native to Hawaii, and is distributed throughout the warm waters of the world.

The Offshore Farm Site and Farm Operations

The Lease Area Site selection is a critical component for any mariculture operation, but is particularly so for an innovative offshore farm that is pioneering both a new permitting process and a new net pen system. The original farm lease site was selected on the basis of the following criteria:

1. The selected site was in a deep-water area, over 200 ft deep, with brisk currents.
2. There was little or no public use of this area. The farm site lay between the limits of normal recreational scuba diving (around 120 ft) and the normal depths for offshore trolling for ono (wahoo, *Acanthocybium solandri*).
3. The site afforded some protection from both Kona storms and the strong trade winds (Figs. 1 and 2). The proximity to shore also allows for future telemetry links to shore for farm control and security.
4. There was ready access from Honokohau Harbor, 5 miles to the south, which provides support facilities such as slips, fueling, and land for staging of equipment and feed.
5. The site was directly offshore from the Kona International Airport and NELHA (Fig. 2), and, as such, its use was consistent with the adjacent land uses, and it represented no significant impact on the viewplane.

The farm site's topography and oceanography are distinguished by the depth of water, the bare sand substrate, the strong currents through the area, the exposure to high winter surf and strong trade winds, and the adjacent shoreline of a narrow coral bench reef with a steep basalt (lava) cliff. A few black sand beaches also lie along the coastline, to the north of the site, but these are little used, except by recreational fishermen. The preexisting uses of the farm lease area itself were negligible, because of its depth, the paucity of fish, and the barren benthos.

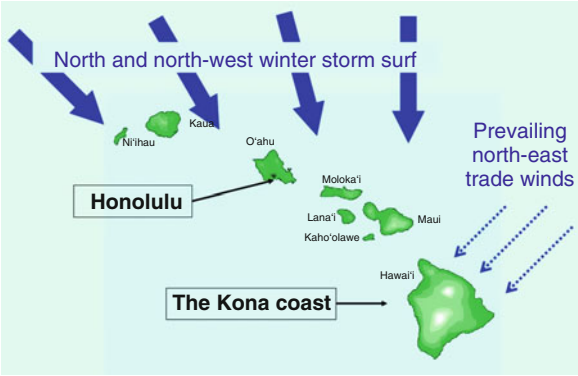

Environmental Impacts of an Open Ocean Mariculture Operation in Kona, Hawaii. Figure 1
Location of the Kona Coast on the western side of the Big Island of Hawaii affords moderate protection from trade winds and winter swells

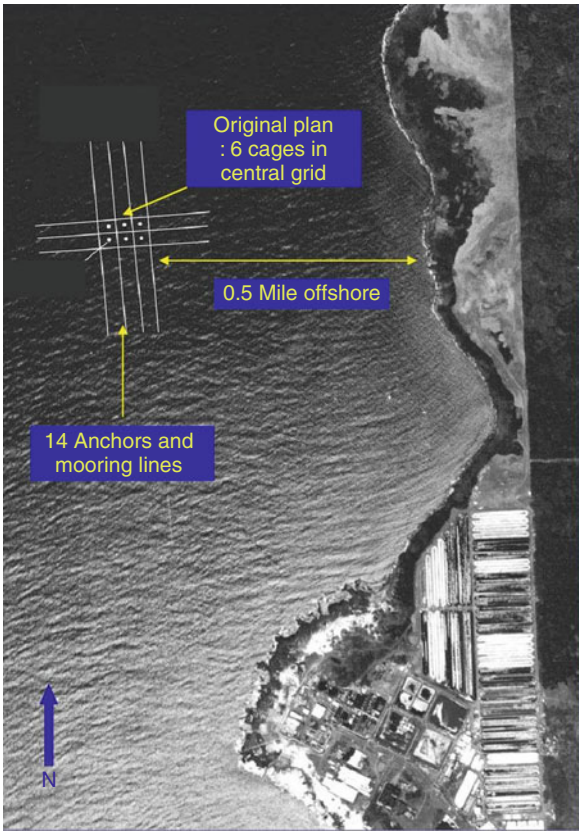

Environmental Impacts of an Open Ocean Mariculture Operation in Kona, Hawaii. Figure 2
Kona blue water farms' site located in waters over 200 ft deep over a sand bottom, a 1/2-mile offshore from a pristine coral fringing reef abutting lava cliffs. The site is a mile north of Keahole Point and west of the Kona International Airport

The net pens are all concentrated toward the center of the lease area (see Figs. 2 and 3), within two mooring arrays: one containing six net pens, and the other containing two net pens and the feed barge. The closest distance from the edge of the central grid array to shore is approximately 2,600 ft, or almost half a mile to the northeast, to Unualoha Point.

The farm site lease provides "negotiated exclusivity": Transit, trolling, hoop-net fishing and hook-and-line fishing are permitted throughout the lease area, but for liability, insurance, and safety reasons, there is no authorized anchoring, scuba diving, or swimming permitted.

The 90 acre lease area initially accommodated eight submersible Sea Station net pens, each of around 3,000 m^3 capacity (Fig. 4). The outermost area of the lease is used almost solely for mooring lines, which require a 5:1 scope. The net pens were originally tied into submerged grids that were anchored into the soft substrate using steel embedment anchors and chains. A series of buoys and weights ensure that the anchor lines are perpetually taut, to eliminate any risk of entanglement by marine mammals. Bridles from the mooring grid corners attach to the net pen rims, to hold the net pens in place in each grid square.

Farm Operations

The daily activities on the farm primarily consist of feeding the fish in the pens. Underwater video cameras inside the net pens are used to relay visual images to the operators on the feed barge. This enables the feed operators to regulate feed to ensure that no feed is wasted, and that excess feed does not fall below the net pen. Any fish carcasses are regularly removed by divers. Carcasses are disposed of as solid wastes in the county landfill.

Harvests usually occur twice each week. Fish are harvested into an ice-brine slurry, to quickly and humanely kill the animals with a minimum of damage. Fish are all transported whole, in ice-brine, to a single land-based processing facility, for packing and shipping. No fish processing occurs at sea during the harvests. Disposal of processing wastes is the responsibility of the wholesalers or other purchasers of the fish, but, at present, most trimmings from fillets go into the landfill.

Support activities for the existing operation are based out of Honokohau Harbor, where a half acre of land rented from the State accommodates containers for feed storage, gear storage areas, a closed workshop area, restroom, and office.

The farm is also serviced by a semipermanent feed barge/security platform vessel, which has been deployed on-site since October, 2007. A separate harvest boat – the 74 ft F.V. Kona Kampachi – transports the harvested product back from the farm site to the harbor. Several other smaller work boats are also used to support net pen and grid maintenance and cleaning, and other tasks.

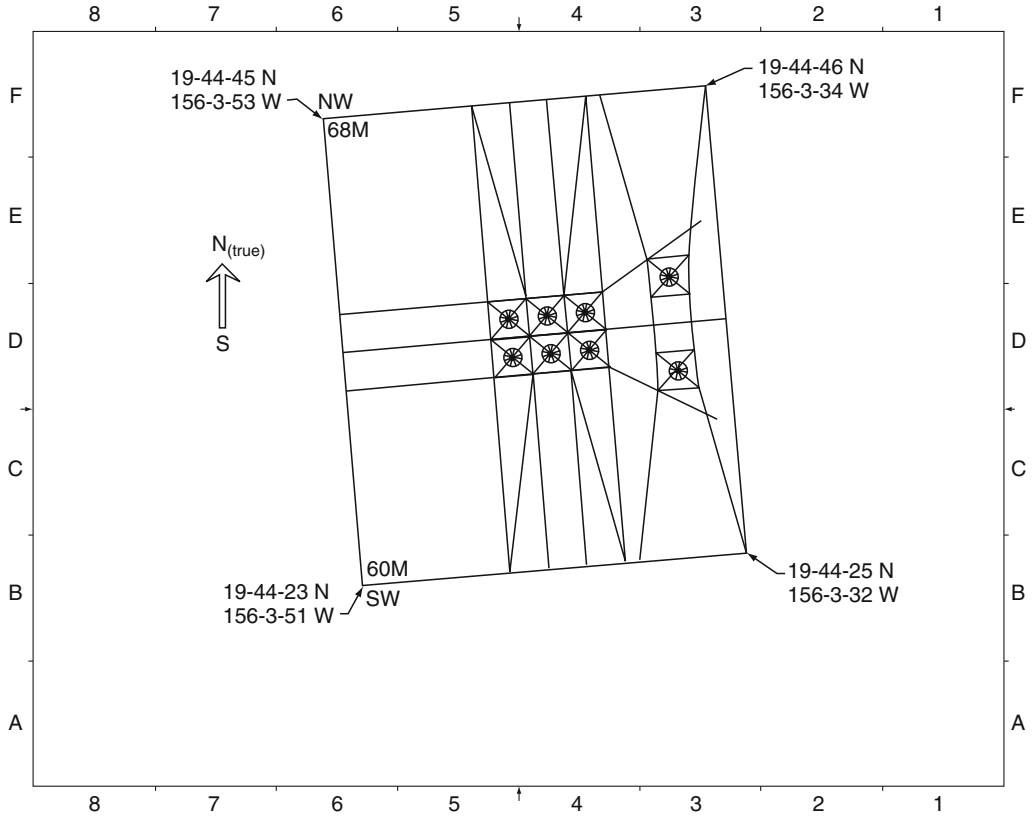

Environmental Impacts of an Open Ocean Mariculture Operation in Kona, Hawaii. Figure 3
Modified mooring array and grid dimensions – plan view. The number of net pens is presently being reduced from current eight smaller pens to five larger pens, with the same overall culture capacity (24,000 m^3). The submerged central grid remains at around 30 ft (9 m) beneath the surface

Localized Environmental Concerns and Actual Impacts

The Presumed Problems

Aquaculture – or indeed, development of any food production system – brings with it attendant environmental concerns. Fish farms are widely accused of environmental degradation. The concerns that are often voiced include the following local-affect possibilities:

- Detrimental impacts on water quality
- Nutrient enrichment of the substrate beneath the farm
- Antifoulant paints from net pens to contaminate the substrate
- Therapeutant or antibiotic misuse to harm the surrounding biota
- Escapes to outcompete wild fish for spawning grounds or feed
- Escapes to dilute the wild fish gene pool
- Proliferation of pests, parasites, and diseases inside the net pens, which can then be transferred to wild fish
- Entanglement of whales, dolphins, and other marine mammals
- Disruption of marine mammal or other species' migratory paths
- Harmful deterrents or fatal control measures against predators
- Excessive use of fish meal and fish oil, leading to overharvesting of the smaller pelagic species targeted by industrial reduction fisheries

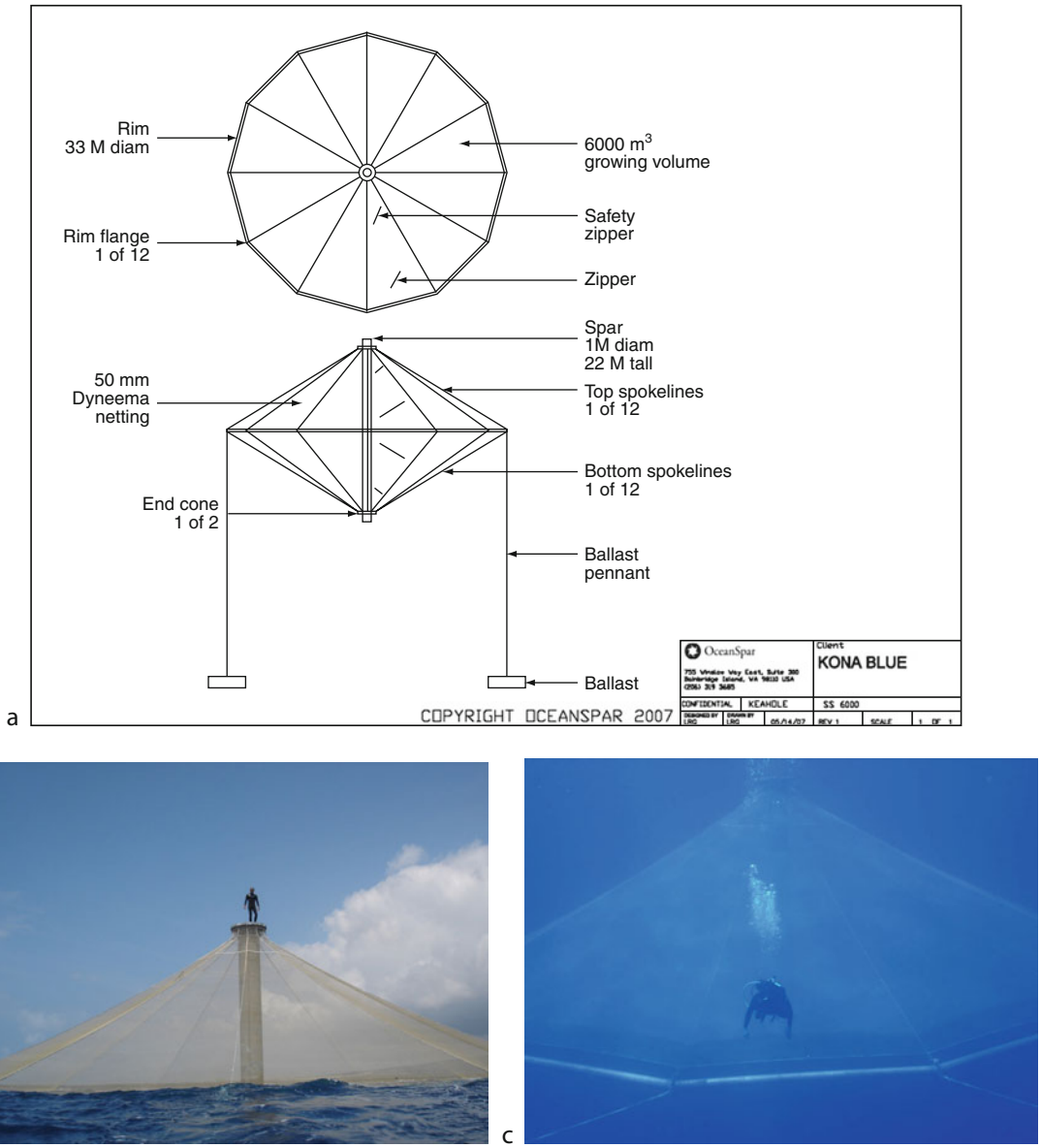

Environmental Impacts of an Open Ocean Mariculture Operation in Kona, Hawaii. Figure 4
Submersible Sea Station® Net Pens deployed on Kona Blue farm site. (**a**) Design of submersible SS6200 Sea Station net pens, with central steel spar and steel rim. (**b**) Sea Station SS3000 raised to rim-level on the Kona Blue farm site. (**c**) A submerged Sea Station SS3000 and diver on Kona Blue site

- Exclusion of other user groups from traditional, cultural, or recreational uses of the farm area
- Visual impact of the net pens on the viewplane

With almost 5 years' experience at the Kona Blue farm site, then, it is appropriate to evaluate the actual data and observations recorded at the Kona operation, and to compare this experience with the concerns that had been, and continue to be, voiced. Each of these issues is examined in detail, below, beginning with an evaluation of the de novo environmental status of the Kona Blue farm site, and then detailing the impacts that have occurred, their context, and their significance.

The Actual Observed Impacts: Locally

Water Quality and Effluent Impacts The water quality at the farm site is close to oceanic, with strong currents and low turbidity. Underwater visibility usually exceeds 100 ft or more.

General water movement patterns at the farm site are governed by the longshore currents past Keahole Point (the western-most point of the Big Island of Hawaii), 1 mile to the South. An S4 current meter deployed at the farm site over several periods since 2004 showed regular peak current speeds of over 50 cm/s (about 1 kt, at a depth of around 40 ft). Current headings were longshore: generally to the North (predominantly), but also to the South. The two points of first impact downstream from the farm site are therefore either Keahole Point, around 1 mile to the south of the site, or the Mahai'ula-Makalawena shelf area, around 3 miles to the north.

Because of the community concerns about potential impacts from the farm operation on water quality, the company had made commitments during the original permit process to a policy of ongoing transparency and objectivity in monitoring. These commitments included:

- Use of objective, third party experts to collect the water quality samples.
- Use of local water quality laboratories – such as NELHA Water Quality Lab, or local private laboratories – for conducting the sample analysis.
- Placement of copies of all monthly water quality monitoring reports at local repositories, such as the State Aquatic Resources office at Honokohau, or the NELHA library, so that local residents can review this data.
- Provision of reasonable access to Federal, State, and County officials for monitoring and oversight purposes.

Monthly measurements have been taken of ammonia and turbidity (the two most relevant water quality parameters for fish farming) at three depths (surface, mid-water – 50 ft deep, level with the submerged net pens, and at the bottom) and at a total of seven stations (two control stations upcurrent, one effluent station immediately downcurrent of the net pen with the greatest biomass, and four "zone of mixing" stations 4,000 ft downcurrent: Fig. 5). Quarterly measurements are also taken for a range of other parameters.

Detailed water quality data are available on the company's web site [4]. Figure 6 shows the mean for each sample site for turbidity for September, 2008, when the farm was at peak production of around 500 T annually. Turbidity is probably the best metric for fish feces and other particulates in the water, and so is most likely to reflect any impact from the farm's presence. These data are definitively clear – there is no discernible difference between water quality parameters at the upcurrent control sites, and the effluent site (1 m downcurrent of the net pen with the highest biomass) or the "zone of mixing" sites downcurrent. These results confirm that *there is no measureable impact* on water quality from the existing farm operations.

Benthic Impacts The substrate beneath the farm is over 200 ft deep, and almost exclusively comprises bare, coarse sand. Located along the shoreline, some 2,000 ft to the East (directly across the longshore currents) is a diverse coral reef community.

Impacts on Substrate Beneath and Around the Farm Site Prior to farm installation, a preliminary survey of the site was undertaken by repeated bounce dives, using scuba, to depths of 220 ft. Because the depth of the farm site is beyond the limits of normal safe diving, and the strength and unpredictability of the currents precluded ready use of grab samples or drop video cameras, the original permit provided that no benthic monitoring would be required. Over time, however, permit requirements were tightened to include grab sample monitoring of substrate chemistry and infaunal micromollusk community structure, and video monitoring using drop cameras. These samples have been conducted quarterly, and reports and video footage have been posted on Kona Blue's website [4].

These results generally indicate that there has been no measureable impact on the benthic community around the farm site. There have been episodic perturbances of substrate chemistry immediately underneath the cage footprint, with a few instances of anoxic conditions during 2007, during periods when a new feed distribution system was being tested. This resulted in some pulverization of pellets, and reduction of feed to a "slurry," rather than discrete pellets. Once

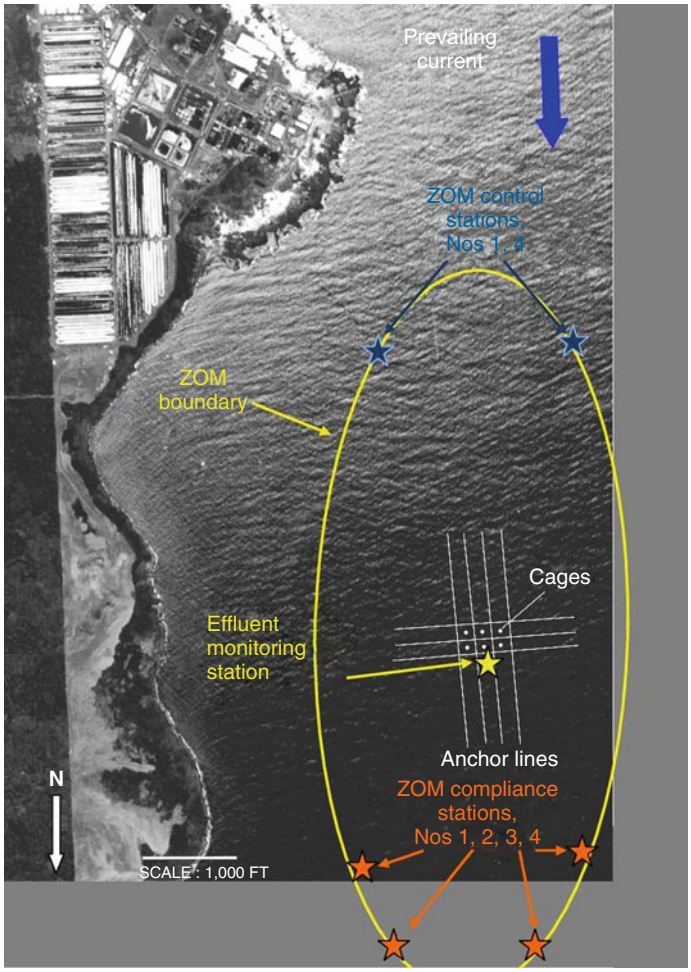

Environmental Impacts of an Open Ocean Mariculture Operation in Kona, Hawaii. Figure 5
Water quality sampling station map. Aerial photograph of the Kona Blue site showing water quality monitoring sampling station locations. Sampling stations under a prevailing N-setting current are shown. Under a S-setting current, control and compliance stations will be reversed. ZOM = Zone of Mixing

the feed system was refined, the substrate returned to its more normal condition, there was no further significant nutrient enrichment of the substrate.

Filamentous algae have also been visible in the drop-camera videos from around the farm site. These appear to have been detached from the cage mesh or the mooring lines, as the algae are not attached to the coarse sand substrate. Presumably, these algae are dispersed during periods of high current.

Monitoring of infaunal micromollusc assemblages in the substrate samples has also demonstrated that there has been no significant change in the community structure resulting from the farm presence (see reports on-line: [4]).

Impacts on the Adjacent Coral Reef Community A comprehensive survey of marine biota was conducted on the reef directly adjacent to the existing farm lease area, just south of Unualoha Point [5]. The survey of the benthic biota of the fringing reef crest used protocols identical to those employed by the State's Division of Aquatic Resources, in their West Hawaii Reef Management Task Force Survey. This provided an extensive set of "control" sites: the other benthic and

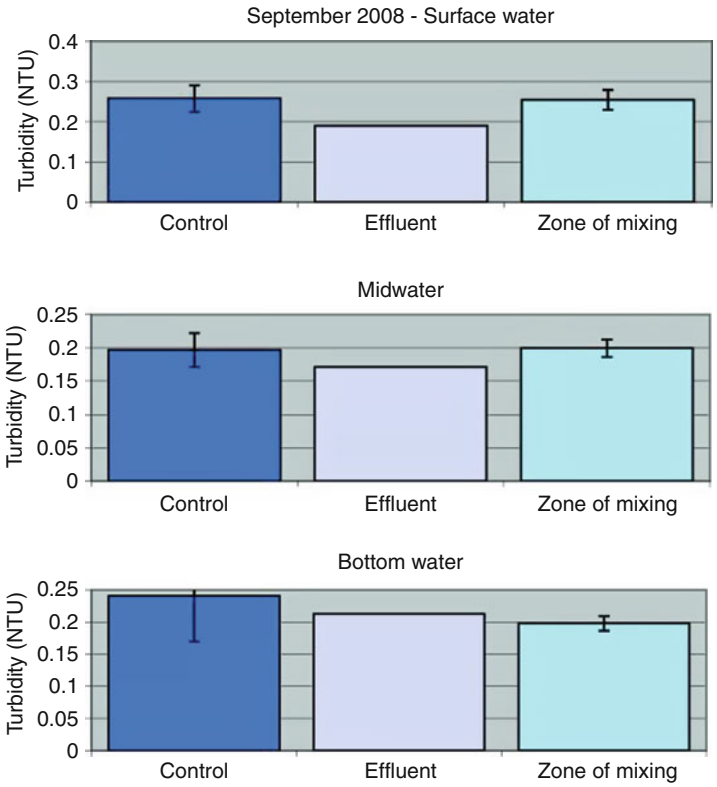

Environmental Impacts of an Open Ocean Mariculture Operation in Kona, Hawaii. Figure 6
Typical turbidity data from monthly sampling around the Kona Blue farm site. There is no discernible difference in water quality between the two Control sites (upcurrent), one Effluent site (immediately downcurrent) and four Zone of Mixing sites (4,000 ft downcurrent) of the farm site

fish data from the sites along the 90 miles of coastline on West Hawaii. A series of four transects of 25 m × 2 m extended parallelly to the reef crest, immediately shoreward of the seaward edge of the reef. Video footage was made of these transects, and digitized for selection of random points on the video frames.

The Makako Bay–Unualoha site has been repeatedly resurveyed since the original 2003 survey. Although no formal reports have been compiled, there have been no significant changes in benthic community composition or fish populations reported.

Biofouling on the Farm Structures There is also profuse growth of macro-invertebrate biofouling on the grid-lines and buoys of the mooring array, as well as on the bridle lines that attach the cages to the grid and the rims of the cages themselves (Fig. 7). This fouling includes diverse macroalgae, bivalves (several species of mussels and oysters: *Pteria* sp and *Pinctada* spp), corals (primarily *Pocillopora* and *Porites*), sea urchins (primarily *Echinothrix calamaris*) nudibranchs (*Stylocheilus longicauda*) and sponges. These all settle out of the plankton onto the farm structures, and their presence does not represent any significant or even measureable reduction in the available recruits to the nearby coral reef area. The growth of the corals, particularly, is compelling evidence that the presence of the fish farm operation is not deleterious to benthic organisms.

Apart from the one brief instance of anoxic conditions beneath the net pens, there have been no other adverse impacts on benthic communities in, underneath, or around the net pen area.

Pests, Parasites, and Pathogens Kona Blue employs an integrated pest management strategy to optimize fish health, reduce interactions or minimize impacts

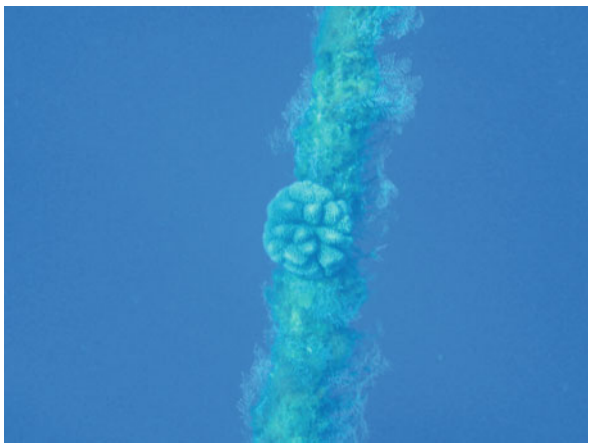

Environmental Impacts of an Open Ocean Mariculture Operation in Kona, Hawaii. Figure 7
A *Pocillopora damicornis* coral colony on a mooring grid line around the Kona Blue net pens (within about 15 m of net pen stocked with fish). The presence of coral colonies that are highly sensitive to nutrient enrichment on moorings and buoys confirms that the operation has no significant impact on marine biota in the area

on wild fish stocks, and reduce any potential environmental impacts from therapeutant use. As *Seriola rivoliana* is a new species, any therapeutant use must be conducted under an Investigational New Animal Drug (INAD) permit. INAD permits operate under the oversight of US Fish and Wildlife Service (USFWS), and the Food and Drug Administration (FDA), with State oversight through Office of Conservation and Coastal Lands (within Department of Land and Natural Resources) and Clean Water Branch (CWB, within the Department of Health). Federal Environmental Protection Agency (EPA) has oversight through the NPDES (National Pollutant Discharge Elimination System), which is administered by CWB.

As with almost all farmed animals, *S. rivoliana* is subjected to small external pests – in this case, the skin fluke, *Neobenedenia* sp, that attaches itself to the fish's skin. These flukes do not pose any risk to human health, and do not themselves detract from the quality of the harvested product, but may cause irritation to the fish. If left unchecked, the flukes can become a health problem for the animal, as the fish rub themselves on the netting to ease the irritation. Kona Blue uses occasional treatments of dilute hydrogen peroxide solution (at effective dosage rates of 200–300 ppm) to control levels of skin flukes among the fish in the net pens. Hydrogen peroxide (H_2O_2) breaks down rapidly in sunlight to form oxygen and water. Hydrogen peroxide is also considered an acceptable Organic aquaculture treatment under the draft USDA Organic aquaculture guidelines, and USDA Organic agriculture standards.

Under the permits in place at the existing site, such therapeutant use must demonstrate that there is no risk to the fish under treatment, or to the environment, or to human health. Monitoring of the effluent from any bath treatment at 100% concentration is mandated under the "Whole Effluent Toxicity" (WET Test) section of the NPDES permit. Results to date from the existing farm operation confirm that there are no significant environmental impacts from the use of the hydrogen peroxide. Ongoing effluent monitoring for WET test bioassays using larval fish (Pacific topsmelt, *Atherinops affinis*; conducted by Nautilus Laboratories in San Diego) demonstrate no significant difference in the rates of larval fish survival between control samples taken 4,000 ft upcurrent of the net pen, and samples taken of the whole effluent (100% concentration of the bath treatment water) at the conclusion of the bath treatments. There is therefore no mechanism for any measureable impact on the pelagic or benthic communities, or the surrounding water quality from the use of this therapeutant.

In addition, monitoring of wild kahala (*Seriola rivoliana*) stocks indicates that there is no significant proliferation of *Neobenedenia* sp. in the population around the farm area. Broodstock are collected periodically from around the farm area, to replenish the wild stocks in Kona Blue's hatchery. These fish are usually taken by commercial fishermen along the "drop off" of the marlin fishing grounds, about 1 mile to the South of the farm, and are sampled for ectoparasites upon capture, by immersion in a freshwater dip. Although these fish are usually infested with a number of other ectoparasites, the prevalence of *Neobenedenia* sp has never averaged much more than one individual per fish. By contrast, a parasitic copepod (sea lice, similar to *Caligus*) infests wild fish at average rates of around ten individuals per fish, and yet is not found at all on the farmed fish, and does not proliferate within the net pens.

A number of innovations, either in progress or planned, should also further reduce the proliferation of *Neobenedenia* on fish inside the net pens. The farm is being reconfigured to fewer, larger Sea Station net pens. With a planned reduction in the number of net pens, a reduction in the surface area-to-volume ratio of the remaining net pens (from double-cone net pens to a more cylindrical shape), the improved surface material characteristics and rigidity of the Kikkonet™ plastic monofilament net mesh (which make it easier to clean), and the improved access for offshore crew to regularly clean the nets from the surface (thereby breaking the skin fluke life cycle by dislodging the adhesive eggs on the mesh), the proliferative tendencies of the skin fluke should be further reduced.

Kona Blue does not use prophylactic antibiotics, but has, under the same regulatory oversights described above, and with veterinary guidance, used Florfenicol® to treat *Streptococcus iniae* infections that sometimes afflict juvenile fish after the stresses of transfer offshore. These treatments last for 10 days, and are also accompanied by WET test water quality monitoring. These WET tests have repeatedly demonstrated no impact on marine biota. A vaccine is available for *S. iniae*, which would avoid the need for these treatments, but regulatory requirements ironically prevent the use of the vaccine at this time. (The vaccine would qualify as an Organic treatment under draft USDA Organic aquaculture guidelines). *S. iniae* infections are not an issue with larger fish, once they have overcome the initial stress of transfer from the nursery to offshore.

Much of the concern over proliferative capacities for fish farm pests, parasites, or pathogens is derived from conflicts between salmon farming and wild salmon runs. Some research – though disputed – suggests that sea lice infestation rates can be exacerbated by the presence of salmon farms and can then be detrimental to survival rates of juvenile salmon as they migrate past the farms to the sea. Most marine fish, however, are broadcast spawners. Juvenile marine fish are therefore dispersed over vast areas of ocean and reef, and do not usually have vulnerable migratory patterns. Given such a distinct difference in life histories between salmonids and marine fish, there would seem to be limited applicability of the salmon and sea-lice research, or the concerns with impacts on vulnerable life stages, to open-ocean mariculture.

Interactions with Wild Fish Kona Blue cultures only Kona Kampachi® (*Seriola rivoliana*) on the offshore site, but the pertinent State permit also allows the company to possibly culture other amberjack (the other kahala species, *S. dumerili*), mahimahi (*Coryphaena hippurus*), and Pacific threadfin (*Polydactylus sexifilis*).

Aggregative Effects on Wild Fish Stocks The existing operation does have an aggregative impact on some species of fish in the area, but this is considered neither deleterious nor significant. Fish are attracted to the site for a number of possible reasons: the fouling on the net pen, the occasional release of small quantities of uneaten food from the net pen during periods of strong currents, and the aggregative nature of objects in open water (as for Fish Aggregation Devices). The makeup of the resident and transient fish communities around the net pens varies over time.

Pelagic or larger demersal fish frequently occurring around the Kona farm site include mackerel scad (opelu: *Decapterus macarellus*), ulua (giant trevally, *Caranx ignobilis*), wild kahala (*Seriola rivoliana* and *S. dumerili*), and barracuda (kaku, *Sphyraena barracuda*). Occasionally, schools of rainbow runners (kamanu, *Elegatis bipinnulatus*) and false albacore tuna (kawakawa: *Euthynnus alletteratus*) move through the net pen area. Larger pelagic fish, such as yellowfin tuna (ahi: *Thunnus alabacares*) and wahoo (ono: *Acanthocybium solandri*) are also occasionally attracted to the area by the baitfish, or by the net pens themselves.

A number of other, smaller fish that are more normally associated with coral reefs settle out of the plankton and assume residence either around the subsurface buoys or around the cages themselves. Such residents include schools of Sergeant majors (*Abudefduf abdominalis*), dascyllids (*Dascyllus albisella*), chromids (primarily *Chromis hanui* and *C. ovalis*) wrasses (primarily *Coris* spp and *Thalassoma* spp), and kyphosids (*Kyphosus* spp). As these fish are settled from the plankton, their presence is not considered a significant detraction from the biomass or diversity of the fish fauna on the adjacent reef.

Escaped Fish Interaction with Wild Stocks Concerns about potential negative impacts of escaped fish are often cited as one of the reasons for objections to fish

farming. However, this issue is most pressing only where non-native fish are cultured in areas where escapes might become established or compete with local species, such as Atlantic Salmon in the Pacific Coast of Canada. Kona Kampachi®, by contrast, is native to the waters of Kona. In addition, Kona Blue recognizes that the innovative net pen engineering employed means that there is some possibility of escape incidents over the initial proving period and development of refinements. In consideration of this, Kona Blue has deliberately not applied any selective breeding in the hatchery, and has not used any broodstock beyond F2 (i.e., all broodstock are either wild-caught, or first- or second-generation captive-reared). There is, therefore, no mechanism for development of any significant difference in the genetic makeup of the fish inside the net pen from the fish in the wild. This reduces any potential impact from escapes to merely direct ecological impacts.

Furthermore, the concerns with the effects of fish farm escapees on wild fish genetics are, again, largely a consequence of the conflicts between salmon-farming interests and wild salmon conservationists. Yet wild salmon stocks are unique, in that each river system or stream may have a genetically discrete stock from the adjacent watershed. Any blurring of this finer-scale differentiation, by interbreeding between escaped salmon and wild stocks, could represent a loss of genetic diversity. However, these concerns are not germane to farming of marine fish in the open ocean. As marine fish are broadcast spawners, there is only a coarse zoogeographic genetic granularity. Tagging research demonstrates that *Seriola* and other carangids migrate frequently between islands in the Main Hawaiian Archipelago. One *Seriola* migrated from French Frigate Shoals, in the Northwestern Hawaiian Islands, to the Big Island – a distance of 678 miles (over 1,000 km) over 3.6 years, at liberty [6]. The potential genetic impacts of Kona Kampachi® escapees on the wild stocks of *S. rivoliana* are therefore minimal.

Those Kona Kampachi® that have escaped from the Kona Blue net pens – either through "leakage" as divers enter or leave the pen through a submerged zipper, or from breaches in the netting – are invariably subjected to very heavy predation pressure. Individual escapees survive outside of the zipper for usually less than a minute before being eaten by either the ulua or the bottlenose dolphins that are frequently in the area. The long-term prospects for survival and reproductive success of any escapees are therefore highly dubious. In addition, any escapees that do survive in the wild are presumably entering a wide-open ecological niche, due to the severe depletion of other deep-water species – such as the deep-water snappers – by commercial fishing. There is little likelihood of escapees competing in any significant manner with the few remaining wild snapper stocks.

Other Wildlife Interactions

Sharks The single overarching feature of shark interaction with the offshore fish farm site has been – contrary to conventional wisdom and activist concerns prior to the farm deployment – the general absence of sharks around the net pens. For the first 8 months of operation, only one fleeting shark sighting occurred: a small tiger shark (mano: *Galeocerdo cuvier)*. Observations by farm workers suggest that there is a general pattern of brief influxes of tiger sharks to the area in the months of September and October of each year. Most of these animals appear individually, or in pairs, with a range of sizes from 8 to 15 ft in length, and they do not generally seem to take up residence on the farm site. Most tiger sharks only show interest in dead fish inside the net pens, and generally exhibit no interest in or aggression toward the farm workers.

In the first year of operation, however, a single tiger shark appeared to take up residence at the farm site. As the animal began to show aggression toward inanimate objects such as surface buoys, and then farm divers, it was humanely dispatched. Recognizing the long-term unacceptability of such predator control measures, Kona Blue sought alternative means of addressing this issue. A Shark Management Plan was then developed in consultation with State Aquatic Resources personnel in Kona and other experts, which included a range of measured responses, and nonterminal resolution if animals ever again become problematic at the site.

In subsequent years, tiger shark sightings usually increased in frequency at the farm site in the late-September early-October period. However, sharks were neither persistent, nor consistent. Farm operations had become more adept at removing dead fish, and the Shark Management Plan allowed divers to continue to work safely. One animal – or rarely two,

contemporaneously – may appear at the site, and remain for an hour or so, before moving away, presenting little inconvenience to farm operations, and no real risk to diver safety.

Kona Blue has also, in collaboration with DAR and HIMB researchers, established a receiver station on the farm site, as part of the larger research program for tracking tiger shark movements along the West Hawaii coastline. The first data series obtained suggested that the observations by the farm work crews were correct – that tiger sharks only very infrequently pass by the site, and rarely do they show any interest in the operation. From July 2006 to May 2007, there were a total of eight (8) records of tagged tiger sharks in the Kona Blue farm area. None of these sharks took up residence. One animal passed by the farm site three times in 2 months, another animal was recorded twice in 2 months, and three other animals had single records. (Fig. 8).

Over 2008 and 2009, however, further tiger shark tagging trials showed that two animals appeared to regularly return to the farm site over periods of up to 5 months. Two other sharks ranged over the entire Kona coast area, but for several weeks at a time were recorded exclusively from the farm site. All animals eventually moved on; one was later detected off Maui. While these results suggested that the farm site had become a "waypoint" for the animals over a few months, the "long-term entrainment (e.g., years) of tiger sharks is unlikely" [7].

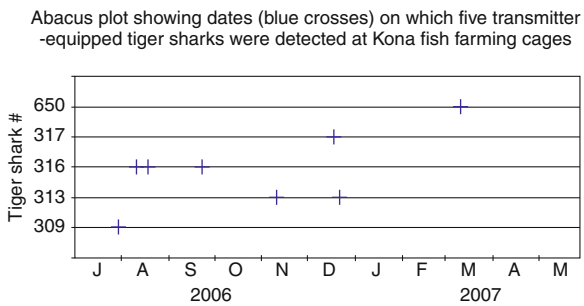

Environmental Impacts of an Open Ocean Mariculture Operation in Kona, Hawaii. Figure 8
Frequency of tagged tiger shark occurrence at Kona Blue farm site: 2006–2007. Five tagged sharks were recorded over an 11-month period, with the most frequently occurring shark being present three times over a 2-month period. No animals took up residence, or showed any strong site affinity

There have also been sightings of sandbar sharks (mano: *Carcharhinus plumbeus*) around the net pens. Initially, these were rare (none in the first year of operation), but since October, 2006, the frequency of sightings and number of sandbars has increased. These animals are usually seen in small groups (one to four sharks), below the net pens at depths of over 100 ft. They rarely rise up to the level of the net pens. Sandbar sharks are more secretive, and cannot readily be distinguished by any markings. No sandbar sharks were caught during the tagging trials in 2008–2009 [7]. It is therefore unclear if these are always the same individuals, or if they represent a larger population of animals that periodically move through the area.

In the period from June to August of 2008, there were a series of breaches of varying sizes in the Dyneema® webbing of one net pen that corresponded to shark bites. The same net pen was also breached in August 2009 by a small Galapagos shark that entered the net pen. The Galapagos was captured and released alive by company divers, unharmed except for a small dorsal fin notch for later identification. In each instance, breaches were sealed immediately on discovery. These incidents underscore the vulnerability of even sturdy Dyneema® nylon mesh, and have led to a plan for wholesale installation of Kikkonet® rigid plastic webbing across the farm. This material has been used in *Seriola* culture in Japan for over 25 years, and has been successfully used in crocodile and shark-infested waters by a sea-cage barramundi farmer in North Queensland, Australia. Kona Blue therefore anticipates that the use of Kikkonet webbing will reduce mesh breaches to negligible levels, and significantly reduce escapes and the attractant nature of the escapes to the bottlenose dolphins and sharks.

Overall, the evidence from the Kona Blue site confirms that there are no significant negative impacts from any aggregating effects of the net pens on sharks. The evolution of a nonterminal, humane plan for managing sharks on the farm site underscores the importance of commercial experience to improve open-ocean farming practices.

Turtles The threatened green sea turtle (*Chelonia mydas*) is common in the nearshore waters of the

main Hawaiian Islands. The endangered hawksbill turtle (*Eretmochelys imbricata*) is infrequently found in Hawaiian waters. The principal nesting site for the green turtle is in the Northwest Hawaiian Islands, on French Frigate Shoals [8]. No turtles have been observed in the area of the farm site, but it is possible that they occasionally transit through the site. If they were to do so, the taut-line mooring system and stiff-mesh net pens will prevent animals from becoming entangled.

Seabirds The submerged net pens used by Kona Blue do not significantly impact seabird populations. The farm area itself is infrequently used as a foraging area by seabirds. Most seabird activity in the area is confined to the fishing "grounds," which extend to the northwest of Keahole Point.

Monk Seals There are four conceivable ways for open-ocean fish farming to have a significant negative impact on rare, threatened, or endangered wildlife, such as monk seals, dolphins, or whales. The project may (1) present a significant obstruction to natural migratory patterns, either (2) attract, or (3) repel the animals and thereby disrupt their normal behavior, or (4) the animals may become entangled in the ropes or mesh of the net pens or moorings.

Monk Seals have been observed at the existing farm operation on two occasions, both in association with escape incidents from the nylon mesh nets on the surface nursery pens that were previously in use at that site. (These nylon mesh surface net pens were removed in 2006, as Kikkonet was, at that time, not yet available outside of Japan.) On each of these occasions, the Monk Seal was preying on the small, escaped Kona Kampachi®, but once the school was effectively eradicated by predators, the Monk Seals moved away. A radio tag allowed movement of one monk seal to be tracked from the Unualoha site to a beach on Maui the following day, clearly affirming that the animal did not take up residence, or become conditioned to the availability of escapees.

Dolphins Makako Bay, almost half a mile to the south of the farm site, is frequented by large schools of spinner dolphins (*Stenella longisrostris*), on nearly a daily basis. These animals usually follow a diurnal pattern of movement from the Makalawena shelf area to the north, along the reef edge to the shallow areas of Makako Bay, where they rest for some time during the middle of the day. Some concerns were expressed during preliminary hearings about the potential for the farm operation to interfere with the spinner dolphin patterns of movement or resting habits [5]. There is no evidence to suggest that this has been the case. There have only been some occasions over the 5 years of operation offshore when divers or workers on the farm site have witnessed spinner dolphins coming anywhere near the net pens. The net pens clearly do not impede the usual pattern of spinner dolphin movement toward Makako Bay; they do not attract or repel the animals, nor do they affect the resting pattern of the dolphins.

Over the last 3 years, the existing farm operation has demonstrated a propensity to attract bottlenose dolphins (*Tursiops truncatus*). No bottlenose dolphins were previously present on the farm site, but the animals have begun to appear regularly at the site since about October, 2006. Patterns of dolphin movement are best characterized as one or two animals, every day or so, with occasional instances of groups of up to seven or eight animals. There is no regularity to the animals' appearance on the farm site: they may be present all day, or only in the morning, or only in the afternoon.

Kona Blue staff monitor and report on dolphin activity to HIHWNMS and NOAA's PIRO PRD. The bottlenose dolphins are probably attracted to the farm site by a combination of (1) the presence of the mid-water structures acting as a Fish Aggregating Device and the associated fish community that is present around the net pens, (2) the occasional provisioning from "leakage" escapes when divers enter or exit a net pen, and from the rare larger escape incidents when predators have breached the Dyneema nylon webbing, and (3) interaction with divers outside of the net pen, as the divers move about the farm from boat to net pen and back.

One individual dolphin has taken up residence over 2009 and 2010. This animal was suffering from a large fishing hook and leader line that had become lodged in its jaw, and it was present on the farm site almost continuously during this period. For many months, the dolphin was lethargic and lost weight, but more recently (as of late 2009) has appeared to be more active and in better condition [9]. The aggregative effective of

the net pens for this one animal might therefore be interpreted as beneficial.

No other individual bottlenose dolphin has taken up permanent residence at the farm site. There are no other animals present on the farm site on around one-quarter to one-third of days. Even when other animals are present, they are often only there for part of the day, rather than the entire day. In October–November, 2008, for example, dolphins were present for some period of time on 22 days out of 34 days [10]. There were dolphins present at the farm site for some or all of the day on 65% of the days. On 35% of days, there were no dolphins reported as observed on the site. Only on 1 day were six dolphins present. Most other days, there were one or two animals present for some portion of the day.

Other dolphin species may be found in and around the proposed farm lease area, but they are usually most commonly seen on the "grounds" to the south of the site. Spotted dolphins (*Stenella attenuata*), rough-toothed dolphins (*Steno bredanensis*), and false killer whales (*Pseudorca crassidens*) have all been observed on the "grounds," or in other offshore waters of the Kona Coast, but have not been reported from the farm site.

In summation, although there has been behavior modification in one compromised individual, the presence of the farm operation has not had a significant negative impact on dolphin behavior. The overall long-term impact on dolphins from the farm operation will probably be further reduced. Modifications to net pens currently under way should help to alleviate the attractive nature of the farm to the dolphins, by reducing the potential for escapes through mesh breaches, and for leakage escapes, and by reducing the amount of time that divers need to operate outside of the net pens. Kona Blue will continue with the ongoing monitoring and reporting of marine mammal activity around the farm site, and continues to collaborate in this with HIHWNMS staff, PIRO PRD staff.

Humpback Whales Populations of the endangered humpback whale (*Megaptera novaeangliae*) winter in the Hawaiian Islands, and the project site lies around 1 mile inside the southernmost boundary of the Hawaiian Islands Humpback Whale National Marine Sanctuary (HIHWNMS). Humpbacks are known to frequent the entire Kona coast area in winter. The whales move throughout the general area, usually following a longshore track (north to south, or vice versa).

Concerns about the reduction in whale habitat by the existing project were previously expressed by HIHWNMS and DLNR/DAR officials. Some concerns were also earlier expressed with the potential for entanglement of whales in the mooring lines of the net pens. A comprehensive analysis of available records of whale entanglement (NMFS Stock Assessments), a review of interactions between marine mammals and Hawaii's fisheries [11], and details of marine mammal strandings compiled by NMFS Pacific Area Office (NMFS-PAO) shows that most whale entanglement events occur in slack net mesh (such as drift nets or fish weirs), slack vertical lines (such as crab pot or lobster pot floats), or surface lines (such as long-lining gear). Among all these observations, there is no record from any US aquaculture operation of entanglement of humpback whales, or other marine mammals, in the taut moorings or net panels of fish net pens. With heavy mooring gear, and taut lines and mesh, the potential for entanglement is considered negligible [12, 13].

Furthermore, it appears that the waters in the vicinity of Keahole Point are not as heavily frequented by the whales as are other waters of the Sanctuary, further to the north (Fig. 9). Observations from workers at the farm site suggest that the farm does not interfere with the movement of the humpback whales, beyond the immediate and obvious exclusion from the waters inside the net pens. The distance of around half-mile from the inshore side of the net pens to the shoreline offers ample room for the whales to move around the eastern end of the farm structures, without any chance for any funneling or bottleneck effects.

There is no definitive pattern of whales avoiding, or being attracted to the cages. Whales are occasionally seen within the lease area. On one instance, the farm workers witnessed a humpback on the surface inside the mooring grid array; the animal appeared to negotiate its path between the net pens and mooring lines with ease.

As part of the company's Marine Mammal Monitoring Plan (MMMP), farm workers provide data for assessing whale abundance and patterns of movement around the farm site. The MMMP describes Federal recommendations or instructions in the unlikely event of any entanglement, and also details ongoing

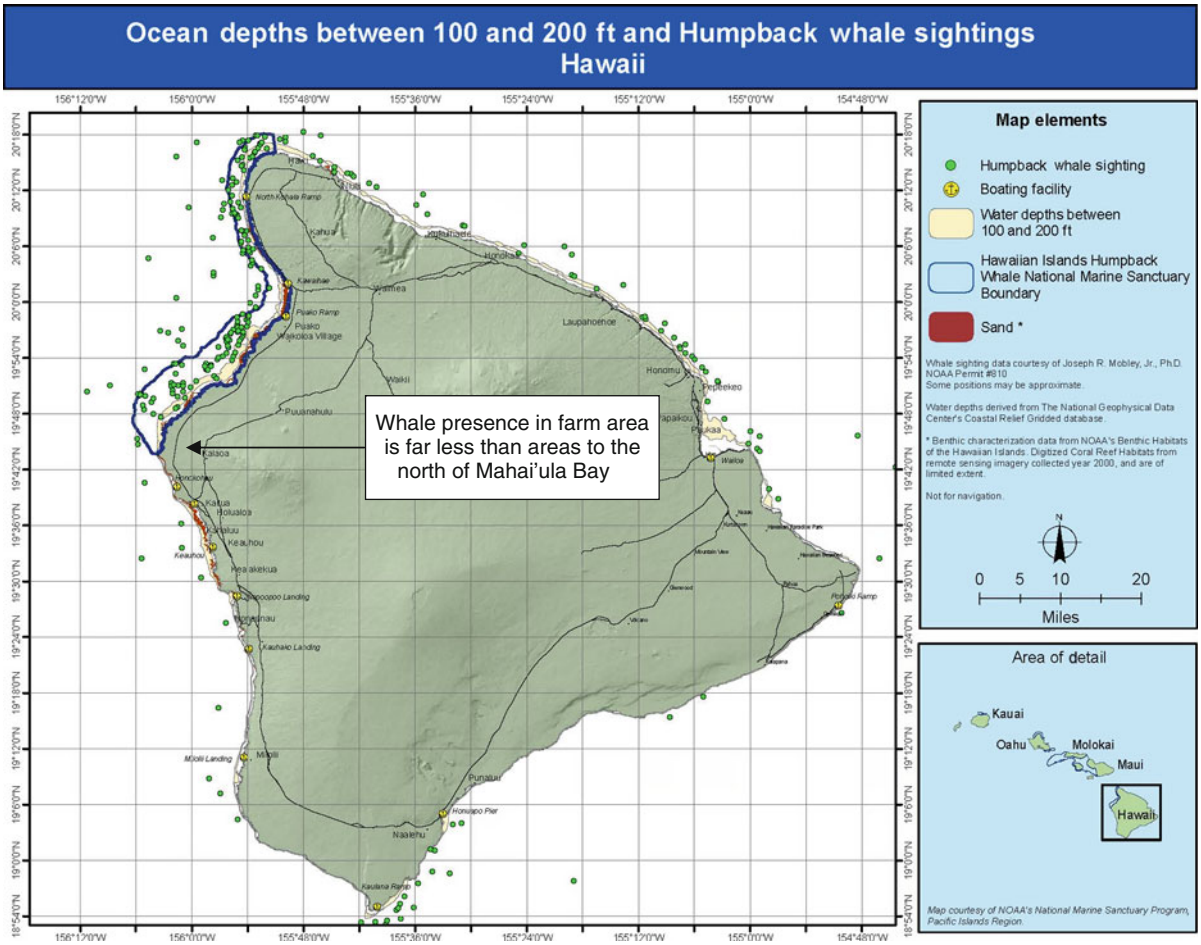

Environmental Impacts of an Open Ocean Mariculture Operation in Kona, Hawaii. Figure 9
Typical Humpback whale sighting patterns around the Big Island of Hawaii

reporting requirements for any close interaction with humpback whales, or any physical interaction between the farm array and other marine mammals.

Recreational Use Impacts The farm site lies offshore from the Natural Energy Laboratory of Hawaii Authority and the Kona International Airport, and as such, has little effect on shore-based recreation. The heavily used public recreation area of Kekaha Kai State Park (Mahai'ula) lies more than 3 miles further to the north.

A survey of recreational activity in the general area, north of Keahole Point was conducted prior to the farm installation, from August to September, 2001, in conjunction with the original farm site environmental assessment [14]. The survey covered 2 months of summer conditions, which was considered the best means of ensuring that the data represented the heaviest use of the area. The overarching finding of the survey was that the area is only used for transit: of the 150 observations made over the 61 consecutive days of the survey, only one boat was seen within the farm site – a boat transiting through the area. Most activity in the general Keahole-to-Unualoha area was recreational dive boats and commercial dive tour operations along the reef and shoreline south of Unualoha Point (directly inshore from the proposed farm site), and in Makako Bay itself.

Observations by the Kona Blue staff on the farm site suggest that this trend continues – the use of the farm lease area is merely for transit. Fishing boats now occasionally troll lines close to the central area, to try to take advantage of the aggregative effects of the net pens. There are no records of catch rates around the farm,

but anecdotal evidence indicates that catches are primarily ono (wahoo, *Acanthocybium solandri*), with infrequent catches of ahi (yellow-tuna, *Thunnus alalunga*).

Kona Blue's permit allows restricted public activities in the lease area, precluding anchoring, scuba diving, spearfishing, or swimming within the 90 acres. These limits are considered the minimum needed to protect the company's investment, to limit their liability (and retain insurance coverage), and to assure public safety. Fishing by the public from unanchored boats (trolling, or linefishing from drifting boats) is still permitted, but with the caveat that any fishing lines that become entangled in the net pen mooring lines must be left in place and cannot be retrieved by divers. The company also requests that fishermen not troll through the center of the farm site because of the potential for fishing lines to entangle divers, or for lures to hook into mooring lines or nets. Boats transiting the net pen area are also requested to observe a slow "no-wake" boat-speed to maximize safety for divers. Unguided recreational scuba diving or unauthorized commercial scuba dive tours are not permitted within the lease area because of liability, safety, and security concerns.

The loss of access to recreational activities within this relatively small area of ocean space is not considered significant. Kona Blue's ongoing observations affirm that there is virtually no fishing or other recreational use of the lease area, or the areas adjacent to the lease area, beyond trolling, which is probably enhanced by the farm's presence.

Viewplane Aesthetics Community value judgments and perceptions of how the oceans should be used largely govern the impact of the project on the community's aesthetic enjoyment of the area. In community meetings, Kona Blue generally enjoys strong support for the broad goals of the company. There is wide recognition of the severely depleted status of bottom fish species in Hawaii. The awareness of the global fisheries crisis has recently been amplified by several scientific studies, such as that of Worm et al. [15], which projected a collapse of world fish stocks by 2048, unless significant remedial changes are made to fisheries and marine ecosystem management.

The visual impact of the project is minor, compared with the adjoining properties of Kona International Airport and the aquaculture operations at the Natural Energy Laboratory of Hawaii Authority (NELHA). The major visual impact from the farm operation is from the experimental surface pens and the feed barge. There is also the additional presence of work and dive boats, and harvest boats, on some days. However, the impacts of these structures and activities are not significant, given the distance from the nearest residences, more than 3 miles away.

There is general community acceptance that the project fits in well with the overall ambience of innovative aquaculture at NELHA, and the need for Kona to develop alternative industries beyond tourism. Fisherfolk and other mariners recognize the validity of the criteria that Kona Blue has used to select this site (c.f. deeper or shallower sites), and have not expressed a strong preference for the project to be located elsewhere. Applicants for farm permits in other areas of the Kona Coast (around Kawaihae) have, on occasion, been told that their project would more appropriately be located "down near NELHA and Kona Blue."

Cultural Resources, Practices, and Mechanisms for Impact Prior to the 1801 lava flow that inundated the area, Keahole was the site of the largest fish pond in the Hawaiian islands. The Pai'ea pond (reputedly King Kamehameha's favorite pond) was approximately 3 miles long and 1/2 mile wide; canoes were used to traverse from one side to the other. The farm site is directly offshore from where Pai'ea once stood. Fish farming could therefore be considered historically and traditionally appropriate to the area.

The farm lease area is over a mile from the traditional marlin, tuna, and wahoo fishing grounds (Fig. 10). The site is too deep for free-diving or scuba diving activity but suitable for "blue-water" spearfishing. Usually, however, blue-water spearfishing is practiced close to a point or drop-off, rather than over bare sand substrate around 200 ft deep. There are no significant benthic plant or animal populations in the farm lease area, and there are virtually no benthic or pelagic fishing activities in this depth range. Kona crabs and nabeta (*Xyrichtys pavo*) are the only benthic resources that occur on sand bottom at this depth, but informants

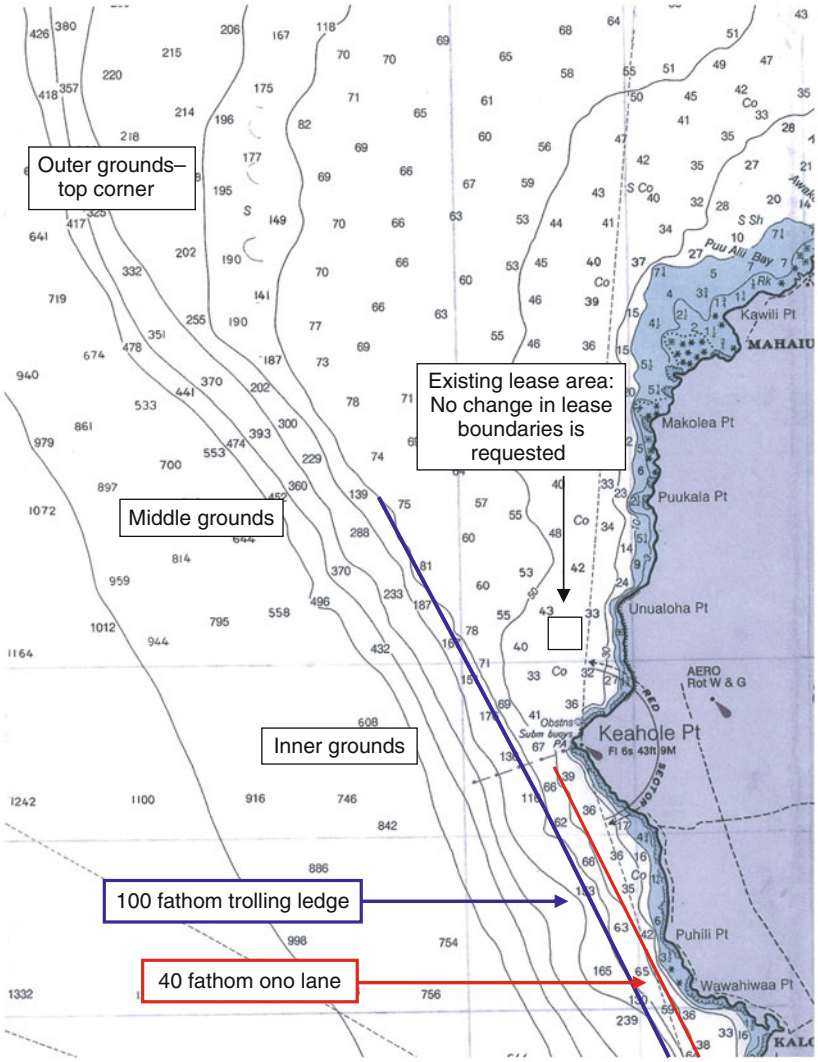

Environmental Impacts of an Open Ocean Mariculture Operation in Kona, Hawaii. Figure 10
Kona Blue's offshore fish farm site in relation to primary fishing areas. The farm site is well inside of both the 100 fathom (200 m) trolling ledge along the "grounds" offshore of Keahole Point and the 40 fathom (80 m) ono lane. Reef fishing and opelu ko'a are found well inshore of the proposed site, along the edge of the reef, in waters up to 120 ft deep (40 m). Fishing grounds for opelu at night are usually deeper than 40 fathoms (80 m)

suggest that the currents are too strong for any significant fishing effort this close to Keahole Point [16].

The only potentially impacted cultural resource that was cited during extensive discussions with community and kupuna (elder) groups for the original farm site was the several opelu ko'a ("holes" or schooling places for mackerel scad – *Decapterus macarellus*) that occur in the general region. The locations of these ko'a are considered to be part of traditional marine lore, and are considered inappropriate for publication, or for sharing outside of the families or community groups who have traditionally fished these ko'a. However, in private meetings with the most knowledgeable kupuna, the locations of the traditional opelu ko'a were determined to be outside of the proposed project location [17]. Opelu aggregations usually occur in water around 120 ft deep, close to reef drop-offs, and well shoreward of the farm area.

Access to, or practice of any other customary activities has not been significantly constrained by the farm array or operations. The exclusive control over the waters (and the fish) inside the net pens is consistent with traditional and cultural practices that identified fish traps or lobster traps – and the animals therein – as the private property of the trap owner. The same principles apply here.

Global Impacts: Fish Meal and Fish Oil Usage

Fish Meal and Fish Oil Usage

Fish such as *Seriola rivoliana* (Kona Kampachi®) usually feed toward the top of the trophic chain in the wild. They therefore possess digestive systems and nutritional requirements that are adapted for feeds with high protein and lipid levels, and low levels of carbohydrates.

Fish meal and fish oil usage in fish feeds can be considered a valid use of a natural, sustainable, renewable resource, so long as the fishery from where the fish meal and fish is sourced is responsibly managed. Although stocks such as the Peruvian anchovetta fishery are sustainable in the sense that they are very well managed, they are not scalable. If mariculture is going to fulfill its potential for increasing seafood consumption to meet growing demands, then some alternative sources of proteins and oils will be required.

Kona Blue has therefore been focused on reducing the inclusion rate of fish meal and fish oil, such as Peruvian anchovies, from targeted reduction fisheries and increasing the use of agricultural oils and proteins, such as soy, canola, wheat, corn and poultry meal, and oil.

Improving Feed Conversion Efficiencies: An Evolutionary Approach Though efficient use of fish meal and fish oil from targeted reduction fisheries is both rational and justifiable, this by no means suggests that these resources are unlimited, or that alternatives should not be searched for. If open-ocean mariculture is to develop into a food production system that can provide a significant proportion of the nutritional needs of a growing planet, then additional sources of sustainable proteins and oils for feedstuff must be found for this industry. The arc of Kona Blue's feed development strategies is perhaps instructive of directions that open-ocean mariculture, as a global industry, might follow to achieve such scalable sustainability.

Initially, Kona Blue Water Farms fed the Kona Kampachi® with a diet that was considered "organic" by European standards. At the time, USDA did not have (and still does not have) Organic standards for aquaculture feeds. In the EU, however, Organic fish food was considered to be that which was most similar to the animal's diet in the wild. This feed, therefore comprised largely comprised fish meal and fish oil derived from Peruvian anchovies.

With the recognition of the need for more scalable feedstuff alternatives, however, Kona Blue worked with the feed vendor to develop a new diet that lowered the inclusion rate of fish meal and fish oil from Peruvian anchovies to a combined total of 50%. This diet included soybean meal, wheat gluten, canola, and other grain proteins and oils. The biological efficiency for this diet, however, was still suboptimal, with a fish-in:fish-out ratio (FIFO) of over 2:1. (i.e., an input of more than 2 lb of anchovies for each pound of Kona Kampachi® produced).

The inclusion rate of agricultural proteins in diets for marine piscivorous fish is limited by the presence of a range of "anti-nutritional factors" in the grains and less-purified meals. (Aside: although often described as carnivorous, most marine fish such as groupers, snappers, jacks, and bream, are perhaps more accurately described as "carbohydrate intolerant." They require diets that are high in protein and lipid, and low in carbohydrate. There is no specific nutritional requirement that these fish eat meat). For this reason, soybean meal is restricted to about 20% of the diet for most marine fish. To reduce the fish meal and fish oil inclusion rate further, and to further lower the FIFO, would therefore require proteins and oils from other sources. By-products from both edible fishery processing and poultry processing were therefore included in the revised Kona Blue diet, allowing the Peruvian anchovy inclusion rate to be further reduced to 30% of the ration: 20% fish meal and 10% fish oil.

Inclusion of poultry processing by-products, however, meant that some customers, such as Whole Foods Markets (WFM), a high-end organic and natural foods retailer, would no longer carry Kona Kampachi®, even if the poultry used for the by-products was of Organic

origin. This position by WFM was out of consideration for those of their customers that were vegetarians, but still wanted to eat fish. WFM asserted that these customers would not want to eat that fish if fish had eaten a pellet that contained proteins or oils that were derived from mammals or birds. Kona Blue appealed to WFM to review their position, given the importance of reducing mankind's global footprint on the oceans, that is, the reliance of humans on natural marine resources – but as of 2010, there has been no change in this policy.

Kona Blue has recently tested two diets that completely eliminate from the Kona Kampachi® diet any fish meal and fish oil sourced from targeted reduction fisheries, and any land animal processing by-products. These innovative diets use processed by-products from sustainably managed fisheries intended for human consumption. As the trimmings from these sources would otherwise have been discarded, used as fertilizer, or burnt as fuel, the use of these fish meal and fish oil products in the Kona Kampachi® diet represents an ideal reuse of natural resources. These diets therefore would result in a zero FIFO ratio, that is, no targeted reduction fishery by-products included in the diet of the end product.

Alternative Feedstuffs for Open-Ocean Mariculture

Kona Blue is involved in testing a range of alternative feedstuffs for Kona Kampachi® diets, which also offer potential for other species of marine fish. Alternative soy products, other agricultural grain concentrates, yeast, and other single cell proteins, edible fishery by-products and – more recently, with the boom in microalgae culture for biodiesel production – defatted microalgae by-products, have all either been tested, or are under development for Kona Kampachi® feed trials.

Kona Blue has tested a range of soy-based diets, with soy protein concentrates and omega-3 oil rich strains of soybeans. These trials suggest that the inclusion rate of soy protein concentrates cannot, by itself, exceed the same 20% threshold that limits soybean meal. Above this level, growth rates and feed conversion ratios are depressed. With the inclusion of taurine in the formula, however, soy protein concentrates could replace fish meal as the source of protein up to 40% of the diet with no detriment to fish growth rates or feeding efficiencies.

There is a diverse array of edible fishery processing by-products that are available for use in aquaculture diets, and this direction offers tremendous potential for further development. The processing by-products from most wild salmon runs, for example, are woefully underutilized, and are often disposed of directly back into the rivers from which the fish are taken. Logistical and economic constraints limit the use of these trimmings, however, as the processing plants are usually small and isolated, the salmon runs are only of short duration, and storage and transport of fish meal or fish oil by-products from these villages to reduction facilities and feed mills is a challenge. Development of fish silage systems offers one potential, partial solution.

However, even the less-seasonal, larger-scale processing of farmed salmon in more centralized plants presents difficulties for the utilization of by-products. For biosecurity reasons, most fish feed plants will not run salmon-derived feed stuffs through their machinery because of the potential for contamination of feeds from viruses, bacteria, or other pathogenic vectors that may be found in the by-products. Screening for known pathogens is not an adequate solution: even though the chance could be considered very slim that some unknown pathogen may be unwittingly dispersed via extruded feed, the potential catastrophic consequences of such widespread and rapid disease dissemination are sufficient to ensure that no such chance be offered. This therefore excludes almost all large feed mills in salmon-farming regions from using salmon by-products.

Similar inefficiencies are found in the reuse of trimmings from the pollock fishery (*Theragra chalcogramma*) in the northern Pacific. This fishery primarily processes most of the catch at sea, into surimi. Trimmings from these fish constitute around 65% of the wet weight of the catch. For a fishery that has averaged around 1.3 million metric tonnes, this then represents around 850,000 tonnes of wet weight by-product annually that could be converted into fish meal and fish oil. For many years, much of this by-product was discarded back into the ocean, or the rendered fish oil was burnt in the diesel generators of the processing vessels. Some 8 million gallons of fish oil in Alaska is largely disposed of as biodiesel [18]. More recently, some proportion of these trimmings have been used to make a high-quality white fish meal that is largely exported to Asia, where it is valued in feeds for

farmed eels. However, the proportion of by-product that is reused or recycled is not reported. Again, economics and logistics conspire against development of a rational supplement to targeted reduction fisheries. The increasing prices of fish meal and fish oil, however, driven by the growing demand for animal feeds from developing economies (notably China and India) may be a greater incentive to resolve these constraints. Edible fishery by-products may yet play a significant role in aquacultue feedstuff sourcing.

There is ample evidence that some or all of these innovative feedstuffs could help to reduce the demand for fish meal and fish oil from clupeids in the medium- to long-term.

Is Aquaculture "Fishing down the Food Chain"?

Much interest has been recently focused on the problem of "fishing down the food chain," beginning with Pauly et al.[19], and Taylor et al.[20]. This is the trend over time for commercial fisheries – driven by serial stock depletion – to shift their target species to those lower on the trophic pyramid. Fishermen first start out exploiting the high-value, top-end predators, then move on to mid-level predators, and then down toward herbivores and detritivores – what was previously considered bycatch. Fisheries generally start out targeting the larger, sweeter-tasting species – tunas, snappers, groupers, and such. As these become increasingly scarce, fishermen apply greater fishing power, and fish longer and deeper, retaining or targeting what was previously considered "trash." The argument portends that at some stage, the food web is reduced to an ocean full of jellyfish. "Fishing down the food chain" is a condemnation of the inherent unsustainability of most commercial fisheries management – or rather, mismanagement.

Fish farming has somehow been implicated in this practice on the basis of farmed fish being fed pellets that are partly made up of fish meal and fish oil derived from anchovies, menhaden, sardines, or the like. These fish (collectively, the clupeiforms) usually form the first step in the ocean food chain beyond primary production. Some scientists and anti-aquaculture advocates misconstrue or deliberately misinterpret the complexities of ecological and economic cause-and-effect, and represent the use of clupeiforms as feed for farmed fish as wanton. This has been led by respected institutions such as the Monterey Bay Aquarium [21, 22], but has also spilled into mainstream media, such as the *NY Times* [23], *Conservation Magazine*'s article on "10 Solutions to Save the Ocean" [24], *The Ecologist* [25], and *The Economist* [26]. The notion that aquaculture is guilty of "fishing down the food chain" is now lodged within the public consciousness.

The bottom of the food chain, however, is where fishing should preferentially be done. It makes far more sense to use herbivores or planktivores from the base of the trophic pyramid as either human food or feed for farmed fish, than to be targeting top-end predators. This makes economic sense, but it also makes sense from other perspectives: it is better for the ocean's ecosystems, it is better from the viewpoint of bioenergetics transfer through the trophic pyramid, it is better for consumer health, and it makes for better fisheries management.

The economics are simple: Peruvian anchovies and menhaden are not highly valued in the market, so they are cheap. Maybe this will change in time, and prices for anchovies and sardines will increase, as more people develop a taste for oily baitfish, but it is more likely that most consumers will still prefer larger piscivorous marine fish as sashimi or fillets.

The ocean's ecosystem offers several reasons why the bottom of the trophic pyramid is a better place for humans to extract nutrition from the sea. It is, most simply, a matter of mass and mathematics. Herbivorous fish are more abundant, with greater biomass. Catching 1,000 t of Peruvian anchovies has little impact on the 6 million ton spawning biomass (around 0.025%). By contrast, 1,000 t of tuna represents around 10% of the Bluefin Tuna spawning stock in the Western Atlantic, the biomass of which is currently estimated at less than 10,000 t [27].

Moreover, Clupeiforms are classic "r-selected" species, with their smaller body size, faster maturing, and shorter life spans [28]. They are highly opportunistic: a decrease in population size in Peruvian anchovies often results in increased recruitment from the next spawning. From an ecological perspective, these species are precisely where fishing effort should be targeted, not the larger, more vulnerable, slower-growing "K-selected" species at the top of the food chain. In agricultural terms, most of the crops that humans raise

are strongly "r-selected" – wheat, corn, barley, rice, while targeting a "K-selected" species in agriculture might be the equivalent of chopping down oak trees to eat the acorns.

Herbivorous clupeiforms also grow and reproduce faster. Menhaden stock resilience to fishing pressure is "high" [29], with a population doubling time of only 15 months. Northern Bluefin Tuna, by contrast, have "low" stock resilience, and a minimum population doubling time of 4.5–14 years [30]. Therfore, if half the menhaden were harvested, it would take 15 months for the stock to recover. However, if half the tuna population was taken, it would take, at a minimum, between 4.5 and 14 years to recover. Southern bluefin tuna also do not begin to spawn until they are perhaps 11 years old, and may live to "at least 40 years of age" [30]. However, Peruvian anchovies are sexually mature within 1 year, and only live for around 3 years. The 3-year old anchovies then die and fall to the ocean floor.

The public health imperative should also provide impetus to source fish meal and fish oil from lower down the food chain. Menhaden and anchovies filter algae and zooplankton directly from the water. They are therefore high in heart-healthy omega-3 oils, yet low in the persistent organic pollutants, such as mercury and PCBs. These pollutants, however, are concentrated as they move further up the food chain. It is primarily top-level predators – sharks and tuna – that are on FDA advisories for pregnant and nursing mothers, and children. By contrast, an aquaculture species that can achieve a feed conversion efficiency of close to 1:1 (FIFO, or Fish In : Fish Out) contain essentially the same contaminant loading as the clupeiforms at the base of the food chain.

Clupeiform fisheries are also more readily managed, with relatively simple stock dynamics and ecosystem interactions. The major inputs to clupeiform stocks are the spawning biomass and primary productivity, which is usually driven by the strength of the nutrient-rich upwelling. Most of the fisheries occur within the EEZ of a single nation, where there are direct incentives for sound management and enforcement, and where access can be regulated. Tuna and swordfish, by contrast, are highly migratory species. Donut-holes of high-seas waters, beyond any country's 200-mile zone, provide opportunities for distant-water fishing nations to concentrate their boats and effort. Attempts at managing tuna stocks are typified by the International Commission for the Conservation of Atlantic Tunas (ICCAT), which has 46 members, and almost no enforcement capabilities. And while Hawaii's longline fishery targeting big-eye tuna may be very well managed, for example, heavily subsidized European or Asian purse-seiner fleets target the juveniles of the same stock in the South-Western Pacific.

Moreover, the carbon footprint of clupeiform fisheries is minimal. These fish are usually taken by purse-seiners, working close to the coast, encircling schools containing hundreds of tons at a time. The carbon footprint for species higher on the foodchain is much higher, with fish being caught by diesel-powered trawlers or trollers, or – for bluefin tuna and swordfish – by harpooning the fish, one at a time.

Most importantly, however, it is far better from a bioenergetic perspective to target fish closer to the bottom of the food chain. Applying the 10% trophic transfer rule means that the 1 lb of wild tuna sashimi on a consumer's plate needed to eat 10 lb of anchovies – or its equivalent in fish meal and fish oil. Or maybe, if there were two steps in the trophic pyramid, each pound of wild tuna required 100 lb of anchovies to first be converted into 10 lb of mackerel.

Aquaculture, by contrast, is always a single step – clupeiforms-to-crop. But aquaculture can also use alternative agricultural proteins and oils, such as corn and wheat gluten, soy proteins and oils, canola, and other animal processing by-products. These other proteins and oils reduce the fish meal and fish oil inputs to the extent that some of the purported "carnivores" can thrive on a diet that is around 20% fish meal and fish oil. On the "sustainability quotient" – the number of pounds of fish-in to produce 1 lb of fish-out (the FIFO) can then attain the perfectly efficient goal of parity, or 1:1 (i.e., every pound of Peruvian anchovies in the farmed fish diet produces 1 lb of product). The result is efficient conversion of a low-value anchovy into a high-value marine fish, without disrupting the fragile top of the trophic pyramid.

Larger, wild fish are more bioenergetically wanton. Wild fish lose energy through inefficient digestion, in hunting prey, trying to avoid predation, spawning, and succumbing to natural mortality. As wild fish grow larger, they also become increasingly inefficient – a greater proportion of energy is needed to maintain the animal's

metabolism. Any bycatch will compound these inefficiencies further. The global bycatch ratio is around 0.28 lb of discard for every pound of target species.

Earlier estimates [20] suggested that farmed fish might be more efficient than wild fish, based on a single trophic step, by a factor ranging from 2 to 5. Combining the life cycle inefficiencies, trophic inefficiencies, and bycatch inefficiencies of wild fish, however, means that farmed fish may be more efficient than wild fish by a factor of around 60 (Table 1, and [31]).

This reasoning does not advocate for greater fishing effort on anchovies. To the contrary – caution is called for. While most of these stocks are sustainably managed at current levels, they could not withstand any greater pressure. These clupeiform stocks should continue to be very closely monitored and highly regulated. Large marine protected areas should also be established to allow some clupeiform-based ecosystems to flourish in their natural state (rather than attempting ecosystem based management). But it is imperative that the

Environmental Impacts of an Open Ocean Mariculture Operation in Kona, Hawaii. Table 1 Relative ecological efficiencies of farmed and Wild-Caught fish. The table shows the compounded cost in terms of anchovy-equivalents for farmed and wild-caught fish. Low-end estimates and high-end estimates are provided for each type of fish and compared cross-ways to obtain a lowest relative rate and highest relative rate

	Farmed fish		Wild-Caught fish		Global mean
	Low-end estimate	High-end estimate	Low-end estimate	High-end estimate	Ratio of wild to farmed
Life cycle efficiency[a]	1	1	3	10	6
Trophic transfer efficiency[b]	1	8	10	100	7.3[c]
"Bycatch" efficiency	1	1	1[(4)]	11[e]	1.3[d]
Compounded "cost"	1	8	30	11,000	57

The lowest relative rate extrapolated from this table is that the least-sustainably farmed fish are around 4× more ecologically efficient than the most sustainably harvested wild fish (i.e., 30:8). The highest relative rate is that the most sustainably farmed fish could be 11,000× more ecologically efficient than the least-sustainably harvested wild fish (i.e., 11,000:1). The Global Mean of wild fish efficiency to farmed fish efficiency is around 57×

[a]There are no published estimates of the relative life cycle efficiencies of farmed versus wild fish. However, fish that reach reproductive age in captivity can see Feed Conversion Ratios increase by factors of 5 or 10 over juvenile and sub-adult fish. Natural mortality and the nutritional cost of maintenance of basal metabolic processes during periods of food depravation also increase the "Economic" Feed Conversion Ratio for wild fish populations

[b]In 1997, food conversion efficiencies (FCE) for farmed marine fish and farmed salmon were around 5:1 and 3:1, respectively (Naylor et al. 2000). By 2010, however, FCEs are projected to reach 1.5:1 for farmed marine fish, and as low as 1.2:1 for farmed salmon (Tacon 2005). Kona Blue has been able to culture Kona Kampachi® on a diet that equates to a 1:1 ratio of wet-fish-in to wet-fish-out. However, if a less-sustainably farmed fish is fed a pellet high in fish meal and fish oil (say, to meet the Scottish Soils Association's Organic standards, with around 80% fish meal and fish oil), this diet could equate to around 4 lb of wet anchovy-equivalents for every 1 lb of dry pellet (a wet-fish to fish-meal ratio of 5:1 is considered standard). On this diet, most commercially farmed species might have food conversion ratios of around 2:1 (dry pellet to wet fish), implying an FCE of 8 lb of wet-fish-in for every 1 lb of wet-fish-out

[c]Tacon's (ibid) estimate of FCEs for farmed salmon and farmed marine fish might be conservatively pooled at, say, 1.5:1, that is, 1.5 lb of anchovy-equivalents for every pound of farmed fish produced worldwide. There is a differential of around 1.1 trophic levels between global fishery landings (with a mean trophic level of around 3.3) and the Peruvian anchovetta fishery (with a trophic level of around 2.2: Pauly et al, [19]). At a presumed 10% biomass transfer efficiency up each trophic level, this implies 11 lb of anchovy-equivalents to produce a pound of harvested wild fish. The median ratio of wild to farmed trophic transfer efficiencies can therefore be estimated at 11:1.5, or 7.3:1 overall

[d]Harrington et al. (2005), report a "nationwide discard-to-landings ratio of 0.28" (i.e., for 3.7 million tons landed, some 1.06 million tons were discarded). However, for highly selective fishing methods, such as harpooning, bycatch is effectively zero, as for farmed fish

[e]For finfish, the ratio of bycatch to target fish (in the Northern Pacific) can be as high as 11:1 because the bycatch is either too young, out of season, or the vessel has no permit to keep it (Alverson 1998)

fisheries at the base of the food chain be better managed, and environmentally sound aquaculture endorsed so that pressure can be taken safely off the top of the food chain.

Fishing at the bottom of the food chain should therefore be encouraged preferentially over any other kind of fishing. This is not a function of recent overfishing: even 100 years ago, this principle would have still held true. People always *should have been* fishing at the bottom of the food chain. To continue to accuse aquaculture as being part of the problem of "fishing down the food chain" is therefore disingenuous. Aquaculture is an important part of the solution to the feeding of the growing humanity. To assert otherwise confuses the consumer and discourages the policy shifts needed toward more sustainable aquaculture, and healthier oceans.

Future Directions

The Challenge

Open-ocean mariculture must expand, but it must expand in an environmentally responsible manner. While opponents may cite the precautionary principle as reason to not move forward, or to do so only cautiously, with experimental site permits or restrictive legislation, there is an imperative for action. Extractive pressures cannot be increased on already depleted wild fishery resources, and the public health costs of limited seafood consumption cannot be accepted any more. These two trends must be turned around by finding alternative sources of healthful seafood. Open-ocean mariculture is the only practical means of achieving this. To urge inaction, then, is in effect advocating for either a greater fishing pressure on wild stocks, or the increasing human mortality and suffering from heart disease and stroke. If the consequences of inaction are so inevitable and so severe, and the potential consequences of action are only slight and temporary, then the precautionary principle insists that action must be taken. Therefore, the requisite regulatory framework for industry growth must expediently be set in place and the needed technologies and support industries developed to proceed forward.

The single greatest challenge will remain that of effecting a change in the mind-set of the environmental community to the extent that there is broad acceptance of the need for expansion of open-ocean mariculture as a conservation tool, that is, as an alternative to targeting larger wild fish. Until this is accomplished, then, this industry will continue to be smeared with irrational fears, community prejudice and consumer bias, and the promise it offers will be left woefully unfulfilled.

Further! Deeper!

The Kona Blue operations to date have produced annual harvests of around 500 T, and have demonstrated clearly that this can be achieved without any significant impact on ocean ecosystems or resources. The key now is to ensure that these impacts remain insignificant, as the industry scales. Expansion opportunities, in terms of broader acceptance and greater access, will be conditional on future farm sites being located further offshore and in increasingly deeper waters. The industry therefore needs to develop the technologies to support these trends and to ensure that carrying capacities and prudent biosecurity practices are adhered to as the industry grows.

There are economic and environmental drivers for larger-scale open-ocean mariculture operations in deeper water, further offshore. As the automation systems for net pen management become increasingly sophisticated [32], sea state becomes less of an impediment to more remote, more exposed sites. The major disincentive then becomes travel time to and from a site. Beyond about a 20 mile distance, it is increasingly difficult to maintain a farm site with day-workers, and some on-site residence becomes necessary. This, then, argues for further scaling: once a farm site is manned 24 h, with staff changes twice-weekly or weekly and periodic delivery of feed and other supplies, there are strong commercial reasons for the operation to grow in scale to support the inherent fixed costs.

Larger scale net pens present some challenges in the open ocean, particularly with fish handling, but there are dvantages as well. Larger pens are more cost-effective in terms of cost per unit of volume (i.e., cost per cubic meter) and in terms of managing the stock. A farmer manages a net pen, rather than a fish: a net pen of 3,000 m^3 and 50,000 fish requires roughly the same level of management as a net pen of 24,000 m^3 and 400,000 fish. Similarly, where there is a significant

cost to the netting material, or cost to maintaining the netting, then the lower surface area to volume ratios of larger net pens are increasingly attractive. Larger net pens also require larger hatcheries, to produce sufficient fish in one cohort to stock the pen, and this results in greater hatchery efficiencies.

New netting materials under development could revolutionize the net pen designs. Kikkonet™ appears to offer significant advantages over multi-strand nylon or cotton webbing, with greater rigidity and predator-breach resistance reducing the risk of escapes and easier cleaning capabilities with the single monofilament material. Similar advantages may be offered by new brass alloy materials under development, which almost completely eliminate biofouling and the attendant fish health concerns, as well as offering improved resistance to breaches from predators or mechanical tearing. Both Kikkonet™ and brass webbing, however, require rigid frames in open-ocean environments: constant wave and current movement can quickly destroy netting material if the net pen frame allows any excess movement. Each of these materials represents a significantly higher capital cost than nylon or cotton netting, but there are tremendous operational savings to be gained from reduced risk of failure and reduced labor for net changing, net washing, antifoulant dipping, and net loft work.

Although much discussion has focused on the advantages of surface and submerged net pens and the relative operational efficiencies of each, this may be the single most important deciding factor for pen design: rigid-framed nets such as the submersible Sea Station® and Aquapod® can support more robust, rigid netting materials. Flexible framed nets such as PolarCirkel®, or those that rely on gravity to maintain net shape, such as Wavemaster® can only support pliable nets of nylon and cotton in the higher wave and current conditions offshore. Where sea conditions or predator prevalence demand the more robust, rigid mesh forms of brass or Kikkonet, then submersible rigid-framed pens would appear to have operational advantages.

Letting Go

The potential for untethered "trans-ocean drifter net pen" fish farms has, up to now, been the stuff of science fiction [3]. However, the concept of untethered pens offers the potential for far larger scaling of operations, with almost negligible potential for any environmental impact; a net pen in very deep water is a nonpoint source for effluent impacts on water quality and substrate, and there is almost no potential for interaction with wild fish stocks (apart from aggregative effects). There are also advantages for fish health management on the farm – a drifter pen is essentially perpetually fallow. Drifter pens that ride regional ocean eddies or powered pens (either towed by a surface vessel, or where the fish containment is integrated into the vessel hull) are already moving from concept to prototype; within 5–10 years, some form of untethered net pen may become a commercial reality. Several examples are worth noting:

In June, 2008, a trial in Puerto Rico tested a submerged, self-propelled, 3,200 m^3. Aquapod as a demonstration of untethered aquaculture operations. The system was able to achieve 30 cm/s forward speed by using two electrically driven 2.5 m diameter propellers powered by a diesel generator set onboard a small towed vessel. The Aquapod was able to hold position in 25 cm/s currents and was easily maneuverable. The concept of remote-controlled or autonomous operation was judged feasible using cage-mounted sensors and buoy-mounted GPS and communications.

In October 2009, the State of Hawaii approved a tuna farm permit for a 247 acre site offshore of the Kohala Coast (north of the Kona Blue farm site) in water over 1,320 ft deep, for up to 12 untethered Oceanspheres. With no anchors, it is proposed that these fish farming platforms will be held in position by self-propulsive forces powered by a hybrid Solar Ocean Thermal Energy Generator. Hawaii Oceanic Technology, Inc. plans to deploy the first of these net pens in 2011.

A regional drifter pen concept under development by Kona Blue – christened the *Velella* system – is projected to remain within a prescribed geographical area without anchoring, by riding the eddies in the lee of oceanic islands such as Hawaii, or by riding the gyres found in semi-enclosed seas, such as the Sea of Cortez or the Gulf of Mexico. The advantages of this concept are that it then enables the operation to consistently

stock, feed, tend, and harvest the fish in the pen, as well as changing crew and other maintenance tasks. By being untethered, the *Velella* can be located in very deep water, beyond normal mooring depths, and any potential environmental impacts are reduced to de minimis levels.

As untethered net pens do not occupy a fixed geographical space, they do not require a lease but rather are more properly regulated as non-powered vessels. Where there is no point source effluent from a motile pen, the monitoring and regulatory requirements may also be those applied to vessels, rather than fixed farm locations. Projects such as *Velella* might also pass through or be deliberately sited in international waters, where no permits are presently required and where no regulatory framework is currently in place. This regulatory vacuum should be remedied, to both govern its growth but also encourage the development of this technology.

IMTA

Much interest is often focused on Integrated Multitrophic Aquaculture (IMTA) as a means of improving the sustainability of open-ocean fish farming, by mitigating effluent impacts and more fully utilizing the nutritional inputs. In nearshore systems, the siting of filter-feeding bivalves around fish farm net pens in IMTA systems has been shown to reduce particulates in the water column. Similarly, siting macroalgal culture systems downcurrent of the fish farm can also reduce dissolved organics. These polyculture systems also offer secondary products (such as edible seaweeds and mussels) that are themselves marketable.

In open-ocean mariculture systems, however, the applicability and utility of IMTA is somewhat dubious. The priority for siting open-ocean mariculture operations should be to strive for greater water clarity, depth, and current movement to optimize fish health and minimize any potential impacts on the effluent. These criteria are contrary to the desired characteristics of an IMTA operation, which presumes some entrainment of waters after it passes through the fish pen, with enrichment of the effluent providing benefits to the filter feeders and phototrophs. If open-ocean mariculture operations do indeed have no measureable impact on water quality, then presumably there is no benefit to be gained from co-siting the fish with filter feeders and plants.

Furthermore, the capital and maintenance costs for the secondary production systems would be prohibitive. Open-ocean mariculture, in the foreseeable future, will need to focus on high-value species such as tuna, yellowtails, snappers, and groupers to provide a reasonable return. Only with the development of far greater operational efficiencies, in later years, will lower-value finfish species become economically viable. The commercial returns from deploying and maintaining even lower-valued macroalgae and bivalve culture lines around an offshore site would be even further deferred.

In addition, the co-siting of mussels and seaweed, say, around an open-ocean site represents engineering and biological risks to the fish farm operation. The additional drag from the long-lines would add tremendous strain on the mooring system for the net pens. If moored separately, there would still be concerns that the secondary producer moorings could fail under load and entangle with the fish's net pen or moorings. The resting stages of pathogens or parasites might also be harbored in the cultured species or ecosystem that surrounds the long-lines, resulting in a proliferative feedback loop and elevated levels of these pests in the cultured fish.

The overarching goal of open-ocean mariculture is growing high-value species in near-pristine waters, with little potential for their interaction with surrounding biologically active substrates. The notion of burdening an offshore operation with lower-value production systems is antithetical to this goal. The fish carrying capacity should allow the natural assimilative capacities of the surrounding ecosystem to fully absorb the farm's ecological footprint. The nutritional by-products, that is, the nutrients in the effluent from open-ocean mariculture systems can still promote productivity on a broader scale, especially in oligotrophic tropical waters. However, a deeper ecological perspective would suggest that there is no need for man to capture this productivity for commercial gain. The oceans can use these inputs in other ways; they are not necessarily "lost."

Bibliography

Primary Literature

1. FAO (2009) The state of world fisheries and aquaculture. FAO, Rome. www.fao.org/docrep/011/i0250e/i0250e00.HTM
2. Clarke AC (1957) The deep range. Harcourt, New York, p 238
3. Mann CC (2004) The bluewater revolution. Wired Magazine, Issue 12.05 – May 2004
4. Environmental monitoring data for Kona Blue. www.kona-blue.com/emonitoring.php
5. See 2003 Final EA. www.kona-blue.com/permitapplication.php
6. Tagawa AW, Tam CKM (2006) Hawaii's Ulua and Papio tagging project 2000 to 2004. DAR Technical Report 06–01. DLNR, Honolulu, p 75
7. Meyer C (Personal communication, 2/17/2010)
8. Balazs GH (1980) Synopsis of biological data on the green turtle in the Hawaiian Islands. U.S. Dep. Commer., NOAA Tech. Memo. NOAA-TM-NMFS-SWFC-7, p 141
9. Viezbieke J (Personal communication)
10. 2009 Draft EA Appendix 2: Marine Mammal Report from Kona Blue to NOAA, dated 11/26/08, www.kona-blue.com/download/REVISED_DraftEnvironmentalAssessment2.pdf
11. Nitta ET, Henderson JR (1993) A review of interactions between Hawaii's fisheries and protected species. Mar Fish Rev 55(2):83–92
12. Celikkol B (1999) Biological assessment of the University of New Hampshire open ocean aquaculture demonstration project finfish component. Prepared for U.S. Army Corps of Engineers, New England Division, Concord, p 60, plus appendices
13. Wursig B, Gailey GA (2002) Marine mammals and aquaculture: conflicts and potential resolutions. In: Stickney RR, McVey JP (eds) Responsible marine aquaculture. CAB International, Wellington, pp 45–59
14. See Appendix III, Black Pearls, Inc., Final Environmental Assessment, 2003, http://www.kona-blue.com/permitapplication.php
15. Worm B, Barbier EB, Beaumont N, EmmetDuffy J, Folke C, Halpern BS, Jackson JBC, Lotze HK, Micheli F, Palumbi SR, Sala E, Sekoe KA, Stachowicz JJ, Watson R (2006) Impacts of biodiversity loss on ocean ecosystem services. Science 314(5800):787–790
16. Punihaole R (2003) Personal communication
17. Maly K, in litt, 8/26/02
18. Alaska Energy Authority, undated brochure
19. Pauly D, Christensen V, Dalsgaard J, Froese R, Torres F Jr (1998) Fishing down marine food webs. Science 279:860–863
20. Taylor R, Goldburg RJ, Primavera JH, Kautsky N, Beveridge MCM, Clay J, Folke C, Lubchenco J, Mooney H, Troell M (2000) Effect of aquaculture on world fish supplies. Nature 405:1017–1024
21. O'Neill B (2006) Seafood Watch®Seafood Report: U.S. Farmed Rainbow Trout, *Oncorhynchus mykiss*. Final Report. June 23, 2006. Monterey Bay Aquarium, p 26. www.montereybayaquarium.org/cr/cr_seafoodwatch/content/media/MBA_SeafoodWatch_FarmedTroutReport.pdf
22. Miranda IT, Peet C (2008) Seafood Watch®Seafood Report: Farmed Yellowtail, *Seriola* spp. Final Report. 22 Oct 2008, Monterey Bay Aquarium, p 73. www.montereybayaquarium.org/cr/cr_seafoodwatch/content/media/MBA_SeafoodWatch_FarmedYellowtailReport.pdf
23. Bittman M (2008) A seafood snob ponders the future of fish. The New York Times, 16 Nov 2008, p. WK1. http://www.nytimes.com/2008/11/16/weekinreview/16bittman.html
24. Simpson S (ed) (2007) 10 solutions to save the ocean. Conservation Magazine 8(3)
25. Wasley A, Wickens J (2008) Fishy business. The Ecologist, Dec 2008–Jan 2009, pp 24–29
26. The Economist (2009) Come, friends, and plough the sea – but make sure the farmed fish are veggies. The Economist: A Special Report on the Sea. 3 Jan 2009, p 11
27. ICCAT (2008) Report of the Standing Committee on Research and Statistics (SCRS); Madrid, Spain, September 29 to October 3, 2008. BFTW-Figure 2., p 89. International Commission for the Conservation of Atlantic Tuna, Madrid, Spain. http://www.iccat.int/Documents/Meetings/Docs/2008_SCRS_ENG.pdf
28. Pianka ER (1970) On r and K selection. Am Nat 104:592–597
29. Fishbase (2009a) *Brevoortia patronus,* Gulf menhaden. http://www.fishbase.org/Summary/SpeciesSummary.php?id=1589 (1/30/2009)
30. Fishbase (2009b) *Thunnus thynnus,* Northern bluefin tuna. http://www.fishbase.org/Summary/SpeciesSummary.php?id=147 (1/30/2009)
31. Pauly D, Christensen V (1995) Primary production required to sustain global fisheries. Nature 374:255–257
32. Langan R (2010) Technology needs for improved operational efficiency of open Ocean Cage Culture. J Marine Tech Soc 44(3):47–55

Books and Reviews

Bridger CJ, Costa-Pierce BP (2003) Open ocean aquaculture – from research to commercial reality. The World Aquaculture Society, Baton Rouge, p 351

ICES (2006) Report of the Working Group on Environmental Interactions of Mariculture (WGEIM). Narrangansett, Rhode Island, U.S.A. ICES CM 2006/MCC:03, p 195

IUCN (2004) Mediterranean marine aquaculture and environment; Identification of issues. IUCN Center for Mediterranean Cooperation, p 34

Halwart M, Soto D, Arthur JR (eds) (2007) Cage aquaculture. Regional reviews and global overview. FAO Fisheries Technical Paper No. 498. UN-FAO, Rome, p 254

Lee CS, O'Bryen PJ (eds) (2007) Open ocean aquaculture – moving forward. Oceanic Institute, Waimanalo, p 78

Marine Aquaculture Task Force (2007) Sustainable marine aquaculture: fulfilling the promise; managing the risks. Woods Hole Oceanographic Institute, Woods Hole, p 128

NOAA (2008) Offshore aquaculture in the United States: economic considerations, implications and opportunities. NOAA, Silver Spring, p 272. http://aquaculture.noaa.gov

Environmental Radioactivity and Ecotoxicology of Radioactive Substances, Introduction to

Glen A. Bird
EcoMetrix Incorporated, Mississauga, ON, Canada

Radioecology is a combination of radiobiology and ecology that involves the study of the behavior of radionuclides in the environment and their effects on organisms. Radioecology is multidisciplined involving studies of pathway analysis, speciation, bioaccumulation, food chain/food web transfer, radionuclide cycling, biological effects (radiobiology), modeling, prediction, environmental protection, risk assessment, and remediation, and may involve either ecosystem components or whole ecosystems. The goal of radioecology is to better understand, predict, and prevent environmental impacts due to radiation. This frequently involves the use of quantitative predictive models to assess the movement of radionuclides in the environment, and their transfer to biota where effects may be at the genetic, tissue/organ, individual, population, or community level.

The articles comprising this section describe the sources of radiation in the environment, the behavior of radionuclides in environmental media, their transfer to biota and potential radiation effects on biota. The basis and content of each of the 15 articles in this section are described below.

Radionuclides are ubiquitous in the environment and may be naturally occurring or the product of nuclear technology. Natural radiation consists of primordial radionuclides present since the formation of the earth and cosmogenic radionuclides. Primordial radionuclides include the ^{238}U, ^{232}Th, and ^{235}U decay chain radionuclides and ^{40}K which forms a small percentage of stable K (0.017%) present in all living organisms. Naturally occurring radioactive material is called NORM, whereas technologically enhanced naturally occurring radioactive material is called TENORM and includes mine/mill tailings, fertilizer, pulp and paper, and petroleum. Other sources of radiation are historic weapons testing, nuclear power plant operations, accidents (Chernobyl, Kyshtym), medical and industrial usage, and waste disposal (► Radiation in the Environment, Sources of).

In the nuclear fuel cycle, the mining and milling of uranium, reprocessing of spent fuel, and waste management represent the largest releases of radionuclides to the environment. Uranium is a common contaminant released from these activities. Uranium is more chemotoxic than radiotoxic and can be harmful at low concentrations especially to phytoplankton and zooplankton. Absorption of uranium in the digestive track of mammals is low and uranium does not biomagnify up the food chain. In vertebrates, damage is primarily to the kidney (► Uranium in the Environment: Behavior and Toxicity).

Tritium is a radioactive hydrogen atom that may be present as tritiated water (HTO), tritiated gas (HT), or organically bound tritium (OBT). Tritium exchanges readily with hydrogen atoms in media including water, so tritium moves rapidly through the environment by evaporation, transpiration, diffusion and isotope exchange, and enters biota and humans via inhalation and ingestion. Photosynthesis is the most important process converting tritium into OBT in complex molecules, increasing its retention in organisms. Dynamic models are available that account for isotopic discrimination and involve studies of atmospheric releases, model validation and uncertainty, and are process oriented (► Tritium in the Environment). Because tritium is a weak beta emitter, it is an internal hazard when inhaled, ingested, or absorbed into the body. Biological modeling of tritium in the body involves the use of dose models for inhalation and ingestion of tritiated water based on specific activity concepts to access potential effects such as teratogenic, reproductive, and carcinogenic effects (► Tritium, Health Effects and Dosimetry).

Within the terrestrial system the soil is the ultimate repository for radioactivity. Radionuclides are assimilated into soil organisms (microbes, invertebrates, and plant roots) or immobilized in abiotic components. Important properties of radionuclides are their biological half-life and ecological half-life. Chemical properties of radionuclides control their behavior and transport. Daughter products may have significantly different chemical properties from their parent. The soil hydrology is important in controlling the transport

and the buildup of radionuclides. Particle surface area to volume ratio, cation exchange capacity, metal oxide and hydroxides, organic matter, cation exchange, precipitation/dissolution, surface complexation, redox reactions, plant uptake, transfer factors, solute partitioning, dispersal coefficients, and retardation all interact to influence the behavior and effect of radionuclides in the soil environment (► Radionuclide Fate and Transport in Terrestrial Environments).

Soil erosion robs agricultural land of its productivity, deposits sediment in downstream areas and impacts water quality. Distinctive behavior of fallout radionuclides (^{137}Cs, ^{210}Pb, ^{7}Be) allow the quantification of sediment mobilization and deposition rates, tracing movement of fine sediment and associated contaminants through the landscape, discriminating the sources of sediment, and how this changes with change in land use/management practices (► Fallout Radionuclides and the Study of Erosion and Sedimentation).

In the arctic, lichens are the basis of the lichen/caribou/human (wolf) food chain and are important in the transfer of radionuclides to top predators. Lichens have a large surface area and no roots but scavenge nutrients/radionuclides from the air. Caribou and reindeer (*Rangifer tarandus*) are the only mammalian species that can subsist on a diet of lichen over the winter. Caribou populations are presently on the decline possibly because contaminants such as radiation may interact with other environmental stressors and weaken the overall ability of the animals to survive. Long-lived-artificial radionuclides (^{137}Cs and ^{90}Sr) and natural radionuclides (^{238}U and ^{232}Th decay chain radionuclides) accumulate in caribou. Following the Chernobyl accident high levels of radiation were found in Swedish reindeer, and chromosomal aberrations were observed in Norwegian reindeer calves (► Radiation Effects on Caribou and Reindeer).

To assess the contribution of foodstuffs to the internal doses received by humans and wildlife, models rely on transfer parameters which describe the empirical ratios of activity between two compartments. Transfer parameters such as soil to plant concentration ratios are lumped parameters that account for the various processes and interactions that result in radionuclide concentrations in these media: speciation, oxidation, reduction, transformations and interactions with soil components, clay and organic matter content, stable element concentration, pH, land management, and soil solutions. Transfer coefficients to farm animals consider metabolic rate, milk production rate, soil intake, stable element intake, transfer of radioiodine to milk, partition coefficients, and allometric relations (► Radiation Assessment, Use of Transfer Parameters).

Past practices and accidents have left radiation legacies. Remediation of these contaminated sites is receiving considerable attention. Many factors govern the effectiveness and cost of countermeasures, most of which are site specific. Environmental restoration is a complicated multidimensional task which needs to take into account radiological, ecological, and social-economic issues within a holistic approach. The ICRP principles of protection: justification, optimization, and dose risk limitation cost benefit analysis should be applied. Practitioners need to identify suitable, effective individual procedures, remediation technologies, communication strategies, and decision and management options. Spatial factors such as size of affected area, direct protection of the population, restriction of food, percent reduction in dose, and effectiveness must be considered (► Environmental Countermeasures and Restoration).

The behavior of radionuclides in freshwater ecosystems depends on the chemical characteristics of the radionuclide, the nature of the waterbody, and the physical state (particulate, dissolved, gaseous, colloidal) of the radionuclide. The chemical composition of the water (pH, dissolved organic content, alkalinity, hardness), partition coefficient, precipitation, uptake by phytoplankton, sedimentation, transfer to sediment, and sediment focusing interact to govern the behavior of radionuclides. Transfer to sediment depends on whether the radionuclide behaves as a conservative (nonreactive – remains dissolved in the water column,) or nonconservative (reactive – has a strong affinity for suspended particles and sediment) element, sediment type, organic and clay content, water temperature, hydrological flushing rate, lake/river morphology, redox conditions, decomposition, food web transfer, feeding behavior, and trophic level of organisms (See section on "Aquatic Ecosystems" in ► Uranium in the Environment: Behavior and Toxicity).

The release of radionuclides to the marine environment such as following the Fukushima accident in Japan

in April 2011 will result in interactions with individual organisms and food webs. The speciation of radionuclides in seawater differs from that in freshwater and affects the mobility of radionuclides; their interaction in the water column; interactions with sediments, suspended sediments, and colloids; and transfer to local communities of animals and plants and ultimately their toxicity. Radionuclides in seawater may behave as nonconservative substances (e.g., Pu and Am) or conservative substances (e.g., Cs, Sr, and Tc), which affects their loss to sediment and cycling in the food web (► Radioactivity in the Marine Environment).

Marine databases of radionuclide concentrations in seawater have been compiled by regional and global projects to assess the movement of ocean currents. Movement of conservative (^{3}H, ^{14}C, ^{90}Sr, ^{129}I, ^{137}Cs, etc.) and nonconservative radionuclides ($^{238, 239, 240}$Pu, ^{241}Am, etc.) have been used to study the circulation of ocean water in the Atlantic, Pacific, and Indian Oceans and interocean exchange of water. Models have been developed to describe currents such as the Great Ocean Conveyor Belt and Global Ocean Circulation Model. Radionuclide releases from Sellafield, UK and La Hague, France, have provided considerable information on the movement of water in the eastern North Atlantic and adjacent seas (► Radionuclides as Tracers of Ocean Currents).

Nuclear accidents such as the Chernobyl accident released large pulses of radionuclides (^{90}Sr and ^{137}Cs) that allow researchers to follow a pulse through the environment improving our understanding of the behavior of radionuclides and the predictability of models. The complex processes of radionuclide migration through a drainage basin are dependent on the characteristics of the specific radionuclide and the catchment. Movement of radionuclides is primarily governed by the hydrology and interactions with soil and, in aquatic systems, suspended and bottom sediment. The complex hydrological processes that control runoff such as water flow, sediment erosion, and physical and chemical processes of contaminant interactions with soil govern transport and can be described by radionuclide transfer functions per unit of deposition (► Radionuclide Migration from Catchments, Modeling). Models have been developed to predict inflow fluxes and outflow fluxes for rivers, lakes, and coastal regions. Dynamic models not only consider migration of contaminants in water bodies, removal to deeper waters, transfer to sediment, resuspension, and transfer through the food web, but incorporate biodilution and chemical dilution of radionuclides to fish and the biotic processes that control bioaccumulation and persistence in fish (► Nuclear Accidents, Chernobyl Fallout in Scandinavian Watersheds).

Chemical speciation affects the mobility, bioavailability, and toxicity of metals and radionuclides. This is discussed for the terrestrial (► Radionuclide Fate and Transport in Terrestrial Environments), and aquatic environment (► Speciation of Metals, Effects on Aquatic Biota) and uranium (► Uranium in the Environment: Behavior and Toxicity). The marine speciation of radionuclides differs from that in freshwater (► Radioactivity in the Marine Environment). An understanding of metal/radionuclide speciation allows the prediction of the interaction of dissolved metals/radionuclides with biological surfaces of organisms. The Biotic Ligand Model combines chemistry, physiology, and toxicology simultaneously to account for geochemical speciation and binding to specific sites to assess the bioaccumulation and toxicity of the chemical species. The Biotic Ligand Model is receiving considerable attention in the study of metal toxicity to aquatic organisms, but is equally relevant to the accumulation and toxicity of radionuclides by biota (► Speciation of Metals, Effects on Aquatic Biota).

The impact of radiation on organisms depends on the exposure rate, duration of exposure, time frame of biological repair and endpoint studied, which change with age. Exposures are either acute or chronic. Acute exposures in the environment are essentially restricted to the brief period following a major accident. The major consequence of chronic exposures at low dose rates as a result of routine releases is genetic effects. Chromosomal effects are also seen in organisms including humans living in areas of naturally elevated background levels of radiation. Radiation damage to DNA may include single- or double-strand breaks. Errors in DNA repair show up as chromosomal aberrations and may eventually result in genomic instability through the generation of dicentric or acentric chromosomal fragments and may be expressed at the population level several generations later. High exposure rates affect the rates of morbidity, reproduction,

and mortality depending upon such factors as tissue sensitivity, dose fractionation, relative biological effectiveness of the radiation type, and adaptive response. Since most exposures are to low dose rates, potential effects are small and difficult to quantify and are temporary in nature, the effect being reversible. The primitive germ cell is the most sensitive cell type. The biological effect is dependent on the number of cells struck by ionizing radiation, and energy type; alpha, beta, or gamma. The life history of the organism needs to be considered in the assessment of potential effects. Most vulnerable are long-lived, slow-reproducing species. Effects generally reported in exposed populations are life shortening, reproductive impairment, increased parasite loads, decreased survival of young, increased mutation rates, deformities, and genetic effects. However, it is difficult to differentiate the effect of radiation from that of other contaminants. Protection can be at the individual, population, or community level (► Ionizing Radiation on Nonhuman Biota, Effects of Low Levels of).

Environmental Toxicology, Introduction

Edward A. Laws
Louisiana State University, School of the Coast and Environment, Baton Rouge, LA, USA

Ecological Risk Assessment

Carroquino et al. (► Environmental Toxicology: Children at Risk) discuss the numerous factors that make children at greater risk from exposure to toxic substances than adults. They point out that children have higher exposures relative to body weight than adults because they drink more water (seven times more per kilogram), eat more food (three to four times as much per kilogram for children between the ages of 1 and 5), and breathe more air (up to twice as much per kilogram for a child less than 1 year old). Furthermore, during the time that their central nervous systems are developing, children are susceptible to permanent neurological damage from exposure to neurotoxins such as methyl mercury, lead, and ionizing radiation. And if endocrine disruptors send false signals to developing reproductive organs, there is a high probability that the resulting dysfunction will be permanent and irreversible. Babies in utero are especially sensitive to the use of addictive substances such as drugs and alcohol by their mothers, and studies have shown that maternal smoking during pregnancy increases the risk of pregnancy loss, stillbirth, and infant mortality.

Willett and Foran (► Ecological and Health Risks at Low Doses) discuss what is known and, more frequently, what is not known about the mechanisms associated with human health effects caused by exposure to low doses of xenobiotics. Traditional sigmoidal dose–response models lead to the conclusion that below a certain threshold dose, there are no adverse health effects. Application of such models has led to the use of so-called no observed adverse effect levels (NOAEL), which in turn have become the basis for setting acceptable daily intakes of substances known to cause adverse effects at higher doses.

In most cases, health effects at low doses are extrapolated from experimental results at much higher doses using a linear dose–response model. But in a number of cases, low-dose treatments with a toxicant have been shown to induce a beneficial response, a phenomenon called hormesis. And pretreatment of animals with metals, specifically cadmium, copper, mercury and zinc, is protective for subsequent exposures. The mechanism underlying the acclimation to metals is synthesis of thionein, a protein that normally only occurs in trace amounts in certain tissues (blood, gills, liver, kidney, and intestine) and can effectively sequester toxic metals if the dose is not too great. But in humans, at least, there is a growing consensus that any amount of lead in the body can be damaging, and especially so in children, in whom adverse effects of lead exposure are typically associated with brain damage. Exposure to neurotoxic organophosphorus pesticides such as chlorpyrifos and to endocrine disruptors such as Bisphenol A are additional examples of risks that are poorly quantified because of inadequate understanding of the mechanisms underlying effects at low doses.

Bain (► Ecological Risk Assessment and Animal Models) discusses the many issues associated with assessing the risk to plants and animals caused by damage/modification of the environment by human activities. As noted by Bain, this is a multistep process,

culminating ultimately in a phase characterized as risk management. The first few steps involve problem formulation and analysis, and these are the focus of the chapter. Much of the information upon which current environmental standards are based has come from either acute (short-term) or chronic (long-term) exposure of organisms to stress and observing the effects on survival, growth and development, and reproduction. Since the number of organisms potentially impacted by toxic substances and stresses is very large, care must be taken to carry out these bioassays with organisms that are in some sense representative of those found in the natural environment, including in particular some of the more sensitive species and life stages. Since such bioassays in most cases involve exposure to only one stress, an alternative, particularly when concern involves a combination of stresses and toxic substances, is to expose test organisms to, for example, contaminated soil or water and observe the impacts on survival, growth, and/or reproduction. In this way, the interaction of a combination of stresses is taken into account.

Alternatives to such bioassays include use of so-called bioaccumulation factors (BAFs) to estimate the effective degree of exposure based on the concentration(s) in the organism. In the last several decades, an approach to quantifying the overall health of a community of organisms has been the use of so-called biotic indices and rapid bioassessment protocols. Such surveys compare populations and community compositions of macroinvertebrates, fish, or periphyton (communities of organism and organic matter attached to surfaces) between a reference site and the site of interest. Finally, and most recently, molecular methods, so-called "omics" (genomics, proteomics, transcriptomics, and metabolomics), have begun to be used, with the expectation that their use will provide a more sensitive assay for stress than the proverbial canary in the coal mine. While this expectation is very likely true, the interpretation of results from omics studies with respect to issues such as risk management is an evolving art.

Medema (► Microbial Risk Assessment of Pathogens in Water) discusses the theoretical and practical issues associated with using quantitative microbial risk assessment (QMRA) to estimate the risk to public health from the presence of pathogens in drinking water derived from surface sources. This is an approach that has become popular in recent years because of the absence of relevant epidemiological data that might otherwise be used to estimate risks associated with drinking contaminated water. The use of QMRA has benefitted from the existence of a database that can be used to relate dose to the risk of infection by the protozoan pathogen *Cryptosporidium parvum*, a database, incidentally, derived from studies with human volunteers. An important point noted by Medema is that in many cases, the risk estimates are dominated by relatively infrequent so-called hazardous events, such as floods, when the water distribution system is compromised and/or the source water is seriously polluted. The water distribution system in New Orleans following Hurricane Katrina is a case in point.

The strategy in QMRA is to use mathematical and statistical models to follow drinking water from its source to a treatment system, through a distribution system, and finally to the consumer and to estimate the probability that a person drinking water from his/her tap would be infected by a particular pathogen. The process is an iterative one, and Medema notes that one of the important products of the modeling exercise is identification of knowledge gaps.

In addition to its role in estimating risks due to consumption of contaminated water, QMRA has been used to identify the risks associated with the use of reclaimed wastewater, for example, to irrigate golf courses and crops destined for human consumption, and for recreational water use. As in the case of drinking water, the strategy is to develop a probabilistic model of the public health risk associated with such practices. Persons and agencies responsible for risk management use the output of QMRA to make decisions about appropriate levels of drinking water treatment and to establish appropriate policies for water reuse and recycling.

Monitoring

Soelberg and Furlong (► Biosensors and Bioassays for Ecological Risk Monitoring and Assessment) describe a portable device for monitoring pollutants based on surface plasmon resonance (SPR) technology. This is a rather esoteric technology but simplistically takes advantage of the change in refractive index (RI) of

a solution adjacent to a gold surface when the solution contains a target compound. The gold surface is coated with so-called recognition elements that provide recognition element (e.g., antibody) attachment sites for the target compound. The technology is designed to detect targets dissolved or suspended in a liquid medium, but the chapter includes a discussion of methodologies for collecting/transferring substances/compounds from air or soil samples or from the surface of solid objects.

Details of the detection process depend on the size of the target, which may range from small molecules to single-celled organisms such as viruses and bacteria. Binding of small molecules to the sensor surface usually does not produce a change in RI large enough to be of practical use, but the detection of such small molecules can be achieved using a competition/inhibition assay involving another larger analyte. For larger molecules such as proteins, binding of the target may effect a change in RI sufficient for detection, but the signal can be amplified by addition of a second recognition element that binds to another site on the target molecule. Whole cells, which are generally too large to be directly detected by SPR technology, may, nevertheless, be detected indirectly as a result of their binding to an appropriate antibody, whose concentration is assayed by SPR in the presence and absence of the cells of interest. Because of the small size of the sensor chips, it is quite possible to design a flow-through system that can detect multiple analytes in sequential fashion. Future directions may involve the further miniaturization of the technology via illumination of an array of recognition element spots in a way that would allow detection of hundreds or perhaps thousands of analytes simultaneously.

Keum et al. (► Biomarkers and Metabolomics, Evidence of Stress) review the information and understanding of the effects of stress on organisms that has been derived from a study of metabolomics. This is an emerging area of omics research that lies downstream of genomics and proteomics. The rationale for identifying metabolic fingerprints associated with particular kinds of stress is to provide an early warning mechanism that could be used to trigger corrective action before serious damage has been done. To date, much of the metabolic work has involved single-celled microorganisms and plants and their responses to stresses such as nutrient deprivation, lack of water, pesticides, and/or salt stress. One of the more interesting metabolomic studies has been the investigation of the response of plants to attack by herbivorous insects and pathogens. Evolutionary arguments would lead one to expect that these responses provide some degree of defense for the plants, and elucidation of the relevant upstream portion(s) of the genome has enabled genetic engineers to produce crops resistant to attack by important plant pests. As noted by the authors, the metabolomes of mammals are more complex than those of plants and microorganisms, but ultimately, lessons learned from the study of relatively simple organisms will likely facilitate more informed investigations of the human metabolome, the etiology of various forms of cancer, and the metabolic pathways of preclinical drugs being obvious topics of interest.

Boehm and Soller (► Recreational Water Risk: Pathogens and Fecal Indicators) discuss the problems associated with determining the risk of infection associated with recreational water use. Although there is a long list of pathogens that could potentially infect swimmers, more than 95% of all non-food-borne illnesses in the United States are caused by only eight: the viruses norovirus, rotavirus, and adenovirus; the bacteria *Campylobacter*, *Salmonella*, and pathogenic *E. coli*; and the protozoans *Cryptosporidium* spp. and *Giardia lamblia*. Because the concentrations of such pathogens in recreational waters are typically low, monitoring of recreational waters has traditionally relied on the concentrations of so-called indicator organisms, which are found in relatively high concentrations in human feces but are not themselves pathogenic. Problems associated with the use of fecal indicator bacteria include the variable ratios of indicators to pathogens and the fact that epidemiological studies have shown that there is a human health risk associated with swimming in waters where there is no apparent source of human fecal contamination. In such cases, the risks of infection are presumably associated with animal excreta, including birds, pigs, and cattle.

A complement and possibly alternative to traditional recreational water quality monitoring techniques is quantitative microbial risk assessment (QMRA), a health risk modeling approach that translates microbial exposures into infection or illness risk

estimates. The input to such models includes information on the die-off rates of pathogens in the environment, assumptions about the amount of water swallowed by recreational swimmers, and the infectivity of the various pathogens. Comparisons of the output of QMRA models with the incidence of relevant infections have provided valuable insights concerning the likely contribution of land runoff and animal feces to the risks associated with recreational water use. Historically, the pathogen that has received the most attention in QMRA simulations is the rotavirus because of its high infectivity and the availability of dose–response information. More recent work has focused on the norovirus following publication of relevant dose–response information in 2008.

Mechanisms

Wilson (► Environmental Toxicology: Carcinogenesis) provides an excellent overview of the numerous and diverse mechanisms responsible for causing cancer. He points out that nine different conditions must be satisfied before a malignancy can develop and that to satisfy each of these conditions, one or more mutations are needed to alter the intracellular signaling pathways and/or response to the tissue microenvironment. The human body in fact has numerous defenses against cancer, including inter alia, DNA repair systems with phenomenally high fidelity, detoxifying enzymes for reactive species, glutathione to quench reactive electrophiles, and, in the case of mammalian and human cells, the ability to become terminally senescent or undergo self-suicide (apoptosis) upon self-recognition of excess DNA damage or perturbation of cell growth controls. However, these defenses are not infallible, and a variety of mutations generally classified as (1) single-base mutations, (2) chromosomal aberrations, (3) insertions and deletions (indels), and (4) epigenetic mutations can eventually lead to cancer, the probability being directly proportional to the dose and duration of carcinogen exposure.

With a few exceptions (e.g., mesothelioma and exposure to asbestos), most cancers have multiple etiological causes. Therefore, the development of a particular form of cancer does not, in most cases, implicate a mechanism. On the other hand, the mechanisms associated with some forms of stress are rather well established. Chronic alcohol consumption, for example, is associated with oral cavity, pharynx, larynx, esophageal, liver, and colorectal cancer, and breast cancer in women, and suspected to be involved in pancreatic and lung cancer. Alcohol (i.e., ethanol), however, is not itself genotoxic, but acetaldehyde, to which ethanol is converted in the liver, is mutagenic. Chronic alcohol use is associated with three carcinogenic pathways: DNA damage and mutation, inflammatory processes that promote proliferation, and vitamin deficiencies that perturb DNA epigenetic patterns. Exposure to ultraviolet radiation is associated with skin cancer, the most common cancer in the United States. Ultraviolet radiation in the wavelength range 290–320 nm causes DNA mutations leading to signature cyclobutane pyrimidine (6–4) pyrimidone photoproducts and pyrimidine dimers, which, if not repaired, result in signature C (cytosine) to T (thymine) and CC to TT mutations, respectively. Tobacco smoke, probably the most important anthropogenic carcinogen of the twentieth century, contains at least 300 known or suspected carcinogens and is believed to be an important etiological factor in many cases of oral cancers, esophageal, bladder, pancreatic, kidney, and possibly breast and cervical cancers. Many of the carcinogens in tobacco smoke alkylate or arylate DNA, with consequent production of promutagenic lesions, or produce DNA adducts that can lead to primarily G (guanine) to T (thymine) transversions, which are the most common single-base mutations in lung tumors. Despite the remarkable number of carcinogens in tobacco smoke, many years of smoking (~50 pack years in the case of lung cancer) are generally required before a tumor develops, a testimony, as noted by Wilson, "to the resilience of the human body to the bombardment of such a powerful combination of the carcinogens and toxic agents present in tobacco smoke."

Jones (► Environmental Toxicology: Oxidative Stress) points out that understanding of the mechanisms that underlie oxidative stress has changed significantly in recent years. Thirty years ago, oxidative stress was understood to reflect a predominance of prooxidants (agents that initiate radical reactions, oxidize biologic components, or interfere with normal reductive and antioxidant functions) over antioxidants, leading to macromolecular damage. If oxidative stress were as simple as that, supplementation with

antioxidants would be expected to provide protection but in fact has been found to be associated with little or no health benefits in humans. Furthermore, the discovery of NADPH oxidases that generate O_2^- and H_2O_2 as signaling molecules suggested that oxidative stress could involve disruption of redox signaling and control mechanisms. Living cells have a variety of mechanisms that almost completely prevent the sort of radical chain reactions associated with the more traditional concept of oxidative stress. Although such chain reactions may be relevant in cases of acute exposure, non-radical oxidants such as H_2O_2, lipid hydroperoxides, quinones, disulfides, and reactive nitrogen species are now believed to be far more important from the standpoint of chronic toxicity. The major mechanisms of non-radical oxidative stress involve primarily effects on thiols and selenols in proteins and secondarily mutagenic damage to DNA. Non-radical oxidants can interfere with reversible oxidation–reduction reactions of thiols or selenols (e.g., the thiol in cysteine, the thioether in methionine, and the selenol in selenocysteine) by causing abnormal oxidation or irreversible modification. These changes alter physiological function in receptor signaling, transcriptional regulation, cell proliferation, angiogenesis, and apoptosis. The hypothesized mechanisms presume that (1) all biological systems contain redox elements that function in cell signaling, (2) organization and coordination of the redox activity of these elements occurs through redox circuits dependent upon common control nodes, (3) the redox-sensitive elements are spatially and kinetically insulated, and (4) oxidative stress is a disruption of the function of these redox circuits caused by specific reaction with the redox-sensitive thiol/selenol elements, altered pathways of electron transfer, or interruption of the gating mechanisms controlling the flux through these pathways. Because biological systems are effectively engineered to conceal stress effects, subtoxic exposures can accumulate without overt signs of adverse effects. A redox proteomics/gene expression approach may therefore provide a means for systems analysis to detect evidence of oxidative stress before overt symptoms become apparent.

Laws (► Toxic Chemical Risks) note that most exposure to toxic chemicals is associated with lifestyle decisions and not, as might naively be expected, because a person lives downwind or downstream from a source of pollution. In the United States, by far, the biggest source of exposure is tobacco smoke, which, as noted by Wilson (vide supra), contains several hundred known or suspected human carcinogens. The list of toxic substances includes ammonia, arsenic, benzene, benzo[a]pyrene, cadmium, carbon monoxide, nicotine, and several compounds classified as tobacco-specific N-nitrosamines. The death toll from cigarette smoking accounts for about 20% of all deaths in the United States. Fortunately, the percentage of adults who smoke in the United States has been steadily declining from 42% in 1965 to 21% in 2008–2009.

After tobacco smoke, the most significant source of exposure to a toxic chemical in the United States is alcohol (ethanol) consumption. Health problems associated with chronic alcohol consumption include liver damage, a variety of reproductive system disorders, and damage to the digestive tract. Alcohol abuse accounts for about 100,000 deaths per year in the United States. The specific causes of death include drunken driving, cirrhosis of the liver, cancer, and stroke. In addition to these direct effects on human health, alcohol abuse is associated with half of all homicides and 40% of assaults. Alcohol consumption can be addictive, and about 8% of Americans abuse alcohol or are alcoholic.

Drug misuse/abuse follows alcohol in terms of the frequency with which people are exposed in the United States. The number of deaths associated with unintentional drug overdoses has been rising more or less exponentially during the last 30 years and is now approaching 30,000 per year. The biggest single source of exposure is abuse of prescription analgesics (painkillers). The painkillers in question are opioids, which puts them in the same drug category with drugs such as heroin and cocaine. They effectively block feelings of pain by binding to opioid receptors in the brain, spinal cord, and gastrointestinal tract, but they also produce feelings of euphoria, which accounts for their abuse and compulsive use. When used as prescribed, opioid analgesics seldom result in clinical addiction. Lethal effects are associated with the fact that unprescribed opioid use can lead to a suppression of breathing that may ultimately lead to respiratory failure.

Cocaine and heroin are both illegal opioid drugs. Cocaine has virtually no beneficial application, and there is no approved medication to treat cocaine

addiction. Heroin abuse is associated with a variety of health effects related to the tendency of addicts to inject the drug with a needle that in some cases is far from sterile. Thirty-six percent of AIDS cases and an estimated 70–80% of the new hepatitis C cases in the United States each year are attributable to injection drug use. Fortunately, there are a variety of effective treatments available for heroin addiction.

Obesity has become a major public health problem in the United States and reflects an old adage about toxic substances: the dose makes the poison. Food is essential for living organisms, but consumption of too much food can lead to serious health problems, including, in the case of humans, morbidity from hypertension, abnormal amounts of fat in the blood, type II diabetes, coronary heart disease, stroke, gallbladder disease, osteoarthritis, sleep apnea, respiratory problems, endometrial, and social stigmatization and discrimination. At the present time, roughly 100 million adults in the United States are overweight or obese. The solution is to consume fewer calories, but for many people, this is a difficult goal to achieve on a sustainable basis. Behavior therapy may be necessary to effect the necessary changes in lifestyle.

Of the problems with little or no lifestyle connection, lead intoxication appears to be the most pervasive. Several decades ago, the use of leaded gasoline was a significant source of exposure, but this practice was fortunately phased out in the United States in the 1970s. Today, the major lead-related issue is the fact that many residences were painted with lead-based paint prior to 1978, when the use of such paint was banned by the Environmental Protection Agency. Unfortunately, many people live in residences that were painted prior to 1978, and at the present time, it is estimated that 250,000 children in the U.S. have blood lead levels exceeding 100 μg/L, a concentration that the Centers for Disease Control feel should not be exceeded. Effects of lead intoxication are variable and depend on the degree of exposure. In children, the biggest concern is effects on the brain. The apparently obvious solution is to remove the lead-based paint in old homes, but doing so in a safe way requires special training and appropriate equipment.

Many of the other incidents of exposure to toxic chemicals involve accidents in the home. Among the most frequent involve ill-advised mixing of cleaning compounds, the most common examples being bleach mixed with either ammonia, vinegar, or toilet bowl cleaners. Chlorine gas, a highly toxic and corrosive gas, is often one of the products of such mixtures, and in some cases, the chemical reactions are very exothermic and can easily result in explosions.

Fate and Transport

Macauda and Hiscox (► Airborne Toxic Chemicals) use three case studies to illustrate issues related to the fate and transport of air toxics (atmospheric pollutants). Perchloroethylene (PERC) is the most common chemical associated with dry cleaning. It has been linked to liver and kidney tumors in rats and is considered to be a carcinogen by the EPA, which has ruled that the use of PERC in dry cleaning must be completely phased out by 2020. Persons living or working in close proximity to dry cleaning establishments are at greatest risk from exposure to PERC. In 2005, the EPA ruled that large dry cleaning establishments use state-of-the-art recovery systems to ensure that PERC is not emitted to the air, and that smaller dry cleaners use generally available control technologies to control emissions. Dry cleaners that operate in apartment buildings are particularly troublesome because residents are obviously living in close proximity to a source of PERC. For such establishments, the EPA has mandated the replacement of so-called transfer machines that require PERC-soaked clothes to be moved from washing to drying machines. These must be replaced by machines that both wash and dry.

Gasoline combustion creates air pollution problems on a broader scale geographically. The most troublesome issues relate to incomplete combustion of gasoline, which can result in the release of numerous pollutants. The pollutant of greatest concern from a public health standpoint is benzene, which has been linked to leukemia. Several approaches have been taken to mitigating the problems associated with incomplete gasoline combustion. First, many states now require gasoline pumps to be equipped with vapor recovery nozzles in order to trap gases that evaporate and would otherwise escape during refueling. Second, gasoline has been reformulated, primarily by addition of ethanol, to burn more completely. This reformulation has significantly reduced carbon monoxide emissions, a cause of

smog, but at the same time has led, in the case of California, to a 54% reduction in benzene emissions. A longer-term solution may be electric cars, which could be recharged at night when electric power demand is relatively low. However, such a transformative change would require an unprecedented degree of cooperation between the electric power and automobile industries.

Mercury emissions are an even longer-range problem, with emissions in Asia linked to mercury levels in North America. Although historically, industrial use of mercury has led to some very serious localized human health problems (e.g., Minamata Disease), on a global scale, coal combustion accounts for about 60% of atmospheric emissions. Inhalation of mercury vapor can lead to serious health effects because the mercury reaches the brain, where it can cause irreparable neurological damage. Ironically, the primary post-combustion technologies that reduce mercury emissions do not specifically target mercury but instead are designed to remove oxides of sulfur and nitrogen. In the USA, at least these stack gas–scrubbing technologies reduce mercury emissions by about 33%. In recent years, the USA has considered controlling the remaining mercury emissions from power plants using a cap-and-trade approach, but this idea was struck down by a Court of Appeals ruling. It now appears that mercury emissions from power plants will be regulated by the requirement for use of Maximum Achievable Control Technology.

Oliver and Heathwaite (Invisible Threats: Transfer of Pathogens and Nutrients Through and Across Agricultural Soils) discuss the tendency of agricultural soils to serve as conduits for pathogens and nutrients derived from agricultural activities. The nutrients of primary concern are nitrogen and phosphorus. The pathogens include a somewhat longer list or organisms (*E. coli* O157, *Salmonella* spp., *Campylobacter jejuni*, *Listeria monocytogenes*, *Cryptosporidium parvum*, and *Giardia intestinalis*) that are shed by livestock and are, coincidentally, pathogenic to humans. The ability of soils to sequester N is very much influenced by the fact that soil particles typically have a negative surface charge. Thus, the ammonium ion, NH_4^+, is effectively retained in soils, while nitrate, NO_3^-, is not. Phosphate, although negatively charged, is typically retained in soils because of its tendency to bind with ferric iron (Fe^{3+}), aluminum (Al^{3+}), or calcium (Ca^{2+}). The survival and movement of pathogens is very much influenced by the water content of the soil and the existence of conduits (e.g., macropores) for transport within the soil matrix. Under appropriate conditions, pathogens may survive within soils for literally months before being flushed out by seepage from storm events. Strategies such as no-till agriculture that are intended to minimize the use of pesticides and reduce nutrient runoff may actually exacerbate pathogen export by maintaining the continuity of macropores. In some cases, relatively simple strategies can be used to minimize pathogen problems, a case in point being the application of manure in a broadcast slurry to effect a more rapid destruction of associated bacteria through UV radiation and desiccation. Because of the potentially long time that pathogens and particularly nutrients may be sequestered in soils before being released, a considerable lag in time may exist between the implementation of management practices and discernible changes in the water quality of drainage systems. Awareness of this time lag is important to the informed assessment of management practices.

Bienfang et al. (► Bioaccumulation/Biomagnifications in Food Chains) discuss two somewhat different case studies that illustrate problems associated with the bioaccumulation and/or biomagnifications of toxic substances in food chains. Ciguatera fish poisoning (CFP) is the most common food-borne disease related to the consumption of marine finfish, with ~50,000 reported cases each year, but the actual number may be much larger. The toxin responsible for causing CFP comes in several dozen congeners. The various forms of ciguatoxin (CTX) are believed to be metabolites of gambiertoxins produced by various species of the dinoflagellate genus *Gambierdiscus*. Because CTX is toxic at very low concentrations, and in part because there are so many congeners, analytical detection of CTX has been problematic. In fact, virtually all reported cases of CFP are based on symptomology rather than detection of CTX. Short-term effects of CFP are a variety of gastrointestinal disturbances. The long-term and more troublesome effects are of a neurological nature.

As a high-molecular-weight lipid, CTX is a prime candidate for biomagnifications, but because of the aforementioned analytical detection issues, direct evidence of biomagnification of CTX is lacking.

The indirect evidence is the fact that the greatest number of reported cases of CFP and the most severe reported symptoms typically involve consumption of carnivorous as opposed to herbivorous fish.

Mercury is a well-known neurotoxin that is found in the environment in several different forms, by far the most troublesome of which is methyl mercury. In contrast to other forms of mercury that are rather efficiently eliminated from the human body, methyl mercury is, at least initially, retained with about 95% efficiency following consumption and is only slowly excreted at a rate of ~1% per day. The damaging effects of methyl mercury are associated with its ability to cross the blood-brain and placental barriers. As a result, exposure to methyl mercury can cause serious and permanent neurological damage. Fetuses appear to be particularly susceptible, as women evidencing no overt symptoms of mercury intoxication have been known to give birth to babies hopelessly brain damaged from the effects of methyl mercury.

Though methyl mercury has been reported at high concentrations in some fish populations, the documented cases of methyl mercury intoxication have all involved anthropogenic discharges. Natural concentrations of methyl mercury in fish are, with very few exceptions, invariably accompanied by even higher concentrations of selenium, the only exceptions being pilot whales and mako sharks. Evidence that has accumulated during the last 50 years has shown that mercury and selenium effectively sequester one another. The absence of any apparent mercury-related adverse health effects associated with the consumption of virtually any species of marine fish reflects the fact that any mercury in the fish is rendered inert by the selenium in the same fish.

Prevention

Kennedy and Tierney (► Xenobiotic Protection/Resistance Mechanisms in Organisms) point out that the toxic effects of xenobiotics can be mitigated either through acclimation or adaptation, the former involving intragenerational tolerance and the latter involving intergenerational resistance. Acclimation may involve nothing more complicated than avoidance, in some cases instinctive and in other cases the result of experiential learning. Adaptation involves selection for individuals in a population that for some reason are less sensitive/more resistant to a xenobiotic than other members of the population. Generally speaking, adaptation involves either (1) toxicokinetically derived mechanisms, which alter the way in which organisms absorb, biotransform, and excrete chemicals. and/or (2) toxicodynamically derived mechanisms, in which target sites are modified to reduce sensitivity. An important consideration in the case of toxicokinetic mechanisms is the fact that lipophilic chemicals such as PCBs and chlorinated hydrocarbons are not easily excreted because they partition back into cells and tissues from excretory media (e.g., urine, bile). Water-soluble chemicals are not reabsorbed because lipid membranes of cells lining excretory routes act as barriers to their reuptake. Thus, in the case of lipophilic toxins, toxicokinetic modes of adaptation involve transformation of the toxin into a more polar, water-soluble compound. This is generally accomplished through a series of reactions characterized as Phase I and Phase II. In Phase I reactions, a nucleophilic functional group is introduced or exposed in the parent molecule, and in Phase II, the Phase I metabolite or parent molecule already containing a functional group is conjugated to an endogenous molecule to form a water-soluble product. Cytochrome P-450 mixed-function oxidases, for example, are a superfamily of heme enzymes found in all living species that mediate Phase I transformations. Phase II involves conjugation reactions that produce substrates that are secreted with great efficiency. Glutathione conjugation mediated by glutathione S-transferases is a good example of a Phase II reaction.

Toxicodynamically derived resistance refers to alterations in xenobiotic-receptor interactions, which can be effected by alterations in target site, increased or decreased concentrations of target molecules, or circumvention of target function. Structural changes in the target site can significantly reduce binding of the xenobiotic but, as noted by the authors, can lead to biological effects from reduced functionality of the target in its normal physiological roles. So-called knockdown resistance, i.e., insensitivity of Na^+ channels to insecticide (e.g., DDT and pyrethroids) inhibition, may occur by one or another of several mechanisms, including a reduction in the number of Na^+ channels, changes in the fluidity of nerve membranes, or alterations in the binding characteristics

between Na^+ channels and insecticides. In the case of citrus-scale mites, an interesting adaptation to HCN, which interferes with cytochrome oxidase in the electron transport chain, is the use of an HCN-insensitive flavoprotein as an alternate electron carrier in the place of cytochrome oxidase. Application of molecular tools such as toxicogenomics, bioinformatics, and metabolomics has the potential to greatly enhance understanding of the mechanisms by which organisms, including humans, acclimate and adapt to xenobiotics.

Consumption of fish and shellfish is associated with a number of well-documented beneficial health effects, but Meujo and Hamann (► Science, Policy, and Risk Management: Case of Seafood Safety) point out that there are also health risks associated with fish and shellfish consumption. The risks reflect the fact that fish and shellfish may contain dangerous concentrations of pathogenic bacteria and viruses, parasites, toxic metals, pesticides, drugs, and a variety of toxins. In the United States, the Food and Drug Administration (FDA) is primarily responsible for ensuring that seafood is safe to eat, and the strategies taken by the FDA to fulfill this mission reflect the diverse sources of the contaminants of concern, practical issues associated with analytical detection and surveillance, and the extent to which postharvest processing can be used to reduce contaminant concentrations to an acceptable level.

Bacterial and viral pathogens can be very effectively eliminated by a process called high hydrostatic pressure (HHP) treatment. However, neither fish nor shellfish survive HHP, and that fact is a deal-killer for oysters destined for the raw oyster market. Two promising alternatives to HHP are X-ray treatment and supercritical CO_2 exposure. Both methods appear capable of killing the relevant pathogens (e.g., *Vibrio parahaemolyticus*) without killing the oysters.

Neurotoxins produced by a variety of microalgae can accumulate in fish and shellfish to levels that cause serious health effects on consumers. The most troublesome of these natural neurotoxins is ciguatoxin, but there is a long list of others, including brevitoxin, okadaic acid, and domoic acid. An additional neurotoxin, scombrotoxin, is not produced by microalgae but instead is a product of a catalytic reaction involving the conversion of histidine into histamine. One of the problematic issues with these neurotoxins is the fact that they are heat stabile, so cooking has little or no effect on the toxicity of seafood containing these compounds. From the standpoint of prevention, what is badly needed in the case of these neurotoxins is a simple and inexpensive test to determine whether seafood is safe to eat. In the case of brevitoxin, an antibody–antigen assay using ELISA (enzyme-linked immunosorbent assay) has recently been reported. The development of similar high-specificity probes for the other troublesome neurotoxins would clearly be desirable.

Correctives

Portier (► Bioremediation and Mitigation) describes several case studies in which heterotrophic microorganisms have been used to clean up organic waste in soil and water. The metabolic pathways involved in the biological degradation of various classes of organic compounds are reasonably well understood, and the ease/speed with which microbes can decompose different kinds of organic wastes have been the subject of numerous investigations. Normal alkanes, for example, are oxidized to primary alcohols, which are then further oxidized to carboxylic acids. The carboxylic acids are then converted via beta-oxidation enzymes to acetic acid and a simpler alcohol. Polycyclic aromatic hydrocarbons (PAHs) are generally considered to be the most toxic components of petroleum. Simple PAHs are initially converted via dioxygenase enzymes to catechols and substituted catechols. The strategy in bioremediation is to identify a community of microorganisms with metabolic pathways that enable them to effect such transformations and, insofar as possible, to create environmental conditions that encourage their catabolism of toxic substrates.

The examples cited by Portier illustrate some of the diverse strategies that may be employed to effect bioremediation. The first example concerns the application of adapted microbial consortia to remediate diesel-contaminated soils at an active rail yard. Total petroleum hydrocarbon concentrations in the soil were reduced by almost a factor of 20 over a 6-month timeframe. In the second example, an immobilized packed bed reactor filled with support media was used to provide a habitat for adapted microbes with enzyme systems capable of degrading wood preservative contaminants in groundwater. The contaminated

groundwater was pumped through the reactors and then used to irrigate surface vegetation and/or percolate back into the ground. The site in question is now zoned recreational, and groundwater is close to meeting federal maximum contaminant level water quality criteria. The third example involves in situ remediation of groundwater via use of soil seeding bioreactors called bioplugs or bioconduits. Through manipulation of subsurface hydrology, the contaminated groundwater is routed through the bioreactors. Surplus microbial biomass is allowed to escape into the surrounding soil, where the microbes infiltrate contaminated areas and further reduce the concentrations of toxic chemical constituents. Although bioremediation is not an option for all sorts of pollutant (e.g., heavy metals), the strategy has proven to be remarkably successful in cleaning up biodegradable wastes in terms of both cost and sustainability of treatment effects.

Jewett and Wascom (► CERCLA, Sustainability and Public and Environmental Health) discuss another kind of corrective strategy: legal action. The particular legal subject is the Comprehensive Environmental Response, Compensation, and Liability Act (CERCLA), one of the last pieces of legislation signed into effect during the administration of President Jimmy Carter. CERCLA was intended to provide a mechanism to clean up "facilities" contaminated by inappropriate disposal of hazardous substances, with the word facility very broadly defined. Hazardous substances are also broadly defined, with one notable exception: petroleum and petroleum products, natural gas, and synthetic gas used for fuel. This is the so-called Petroleum Exception.

Cleanup activities carried out under the "Superfund" component of CERCLA were originally financed by taxes imposed on the chemical and petroleum industries and an environmental tax on corporations. More recently, Superfund has been supported by allocations from the federal general fund and through additional legislation, such as the American Recovery and Reinvestment Act.

Thirty years after its passage, the report card on CERCLA is mixed. There have been some very noteworthy success stories. Of the more than 1,600 sites at one time or another on the National Priority List (NPL), 340 have been delisted, i.e., cleaned up. The case study discussed by Jewett and Wascom, the Agricultural Street Landfill in New Orleans, is a provocative example given the apparently sweeping powers the EPA has to investigate and correct problems at facilities contaminated by inappropriate disposal of hazardous substances. One certainly has to ask why a municipality would elect to locate residential housing and an elementary school on top of a landfill known, during its operative days, as Dante's Inferno. A hazard ranking score (HRS) of 28.5 is sufficient to place a facility on the NPL. The HRS for the Agricultural Street Landfill was 50.0. Why were the results of tests conducted at the site in the 1970s never made public? And why, when the presence of lead, mercury, and arsenic was detected in the soil, was a clay barrier not constructed (as recommended) to contain the contamination prior to the construction of an elementary school?

These are troublesome questions, but there is another side to the coin. The Small Business Liability Relief and Brownfields Revitalization Act has provided a defense for parties who have generated, transported, or arranged for transport of only small amounts of hazardous material and for so-called innocent landowners in the case of facilities acquired through inheritance or bequest. Such revisions have reshaped CERCLA to be more effective and fair, but, as noted by Jewett and Wascom, by no means supplant CERCLA. In summary, CERCLA is a piece of legislation with a very ambitious goal, and as time goes by may well be modified to make it more effective and fair. The need for such legislation is clearly apparent now and is unlikely to go away in the future.

Environmental Toxicology: Carcinogenesis

Vincent L. Wilson
Department of Environmental Sciences, Louisiana State University, Baton Rouge, LA, USA

Article Outline

Glossary
Definition of Subject
Introduction
Accumulation of Mutations
Properties of Cancer Cells

Oncogenic Mutations
Cytotoxicity and Cellular Turnover
Genomic Instability
Susceptible Individuals
Dose and Complex Dose
Environmental Carcinogens
Future Directions
Bibliography

Glossary

Complex dose The biologically effective (e.g., carcinogenic) dose of an agent that takes into account additive, subtractive, and synergistic interactions in a complex mixture

DNA adduct Any covalent addition or modification of a nucleotide or the phosphate backbone in DNA

Driver mutation Oncogenic mutations that are primary to the further advancement and development of a cancer

Genotoxic Causes DNA damage and/or mutations

Immortal stranding The retention of a specific strand of the DNA double helix by a stem cell regardless of how many times the cell divides

Initiation The formation of the first oncogenic mutation in a cell

Oncogenic process Any process that is involved in the development of a tumor

Proto-oncogene A normal gene that upon mutation produces an active oncogenic component in the development of cancer

Promotion The effect of encouraging the development of cancer by increasing cellular proliferation and turnover

Tumor suppressor gene A normal gene whose expression product appears to block the development of cancer

Definition of the Subject

Carcinogenesis is the induction of cancer by exposure to exogenous agents, chemical or physical carcinogens. Cancer is a large family of life-threatening environmental diseases. This definition is supported by the plethora of published evidence that cancer results from the accumulation of DNA mutations, which in turn depends upon progressive cell divisions. This process takes time. The accumulation of a sufficient allotment of oncogenic genetic errors for cancer to develop occurs over a large number of cell divisions (10s to 1,000s), which may take 10–50 years or more. Even without the intentional introduction of carcinogens into the human body by occupation or habits such as tobacco smoking, alcoholic use, and other life-style choices, our environment provides numerous opportunities and sources of DNA-damaging and potentially mutagenic lesions in our cells. Given enough time, the risk of cancer is inherent with life, while exposure(s) to carcinogenic agents not only shortens the time required to achieve tumor development, but also increases the probability of cancer occurrence.

In the present document, the term environmental carcinogenesis encompasses the induction of cancer by exposure to carcinogenic agents whether natural or man-made, present in our environment. The term environmental carcinogens will refer to all compounds foreign to the human or mammalian body, that is, xenobiotic and physical carcinogens. However, the development of cancer is a long and involved process that requires numerous cellular perturbations generally produced by both exogenous and endogenous reactive agents. As will be clarified in this chapter, for many cancers it is exceedingly difficult to separate out the contributions of the various etiological factors, including natural environmental carcinogens from man-made chemicals (see Table 1). For instance, a number of carcinogenic xenobiotics have been identified that are inherent in our food supply, for which the best-known examples are aflatoxins. Aflatoxins are present in fresh corn, peanuts (and peanut butter), and other grains, while other carcinogens such as PhIP (2-Amino-1-methyl-6-phenylimidazo[4,5-*b*]pyridine), are produced from cooking meat [1, 2]. The potent nephrotoxic aristolochic acid component of certain herbs sometimes used in herbal remedies produces urinary tract cancers [3–5]. To add to this disparaging viewpoint, the lack of proper nutrition, such as folate deficiency, also leads to genomic instabilities that are involved in carcinogenesis [6–8].

The contribution of a few environmental carcinogens is more clearly evident in selective cancer cases. Skin cancer induced by the ultraviolet (UV) radiation from sunlight is one of the more prominent environmental cancers in our world [9, 10]. Mesothelioma may result from inhalation of asbestos fibers [11].

Environmental Toxicology: Carcinogenesis. Table 1 The causes of cancer

Agent//Source	Examples	Associated cancer(s)
Chemical carcinogens[a]	Aflatoxins	Hepatocellular carcinoma
	Alcohol	Hepatic, breast, stomach, colorectal, oral, ovarian, pancreatic
	Aristolochic Acid	Urinary tract transitional cell carcinoma (renal, ureter, bladder)
	Asbestos	Mesothelioma and lung cancers
	Benzo(a)pyrene	Lung cancers (tobacco smoke associated)
	Benzene	AML and non-Hodgkin's lymphoma
	Formaldehyde	Nasopharyngeal
	Metals	
	Arsenic Beryllium Cadmium Chromium (VI) Nickel compounds	Skin, liver, lung, kidney, bladder Lung cancer Lung Lung, stomach Lung, nasopharyngeal
	Asbestos	Mesothelioma and lung cancers
	2-Naphthylamine	Bladder
	Tobacco Smoke	Lung cancers (also nasopharyngeal, esophageal, bladder, pancreatic, kidney)
	Tobacco Dip/Chew	Oral cancers
	Vinyl chloride	Hepatic angiosarcoma
Physical carcinogens[a]	Ionizing radiation (α, β, γ, X-rays, etc.)	multiple types of tumors
	Sunlight (Solar Radiation)	Skin (BCC, SCC, and melanoma)
Biological carcinogens Viruses	Hepatitis B, chronic infection	Hepatocellular carcinoma
	Hepatitis C, chronic infection	Hepatocellular carcinoma
	Epstein-barr virus	Burkits lymphoma, nasopharyngeal carcinoma
	HPV (high risk types)	Cervical cancer
Parasites (chronic inflammation)	Schistosoma hematobium	Bladder cancer
Chronic inflammation	Inflammatory bowel disease Crohn's disease Ulcerative colitis	Colon or intestinal cancers
	Chronic pancreatitis	Pancreatic cancer
	Barrett's esophagus	Esophageal carcinoma
	Helicobacter pylori, chronic gastritis	Stomach cancer
Fidelity limits of enzymatic processes	DNA Replication errors (1 to 3 errors per genome replication)[b]	Possibly all or most cancers
	Imperfect fidelity of DNA repair systems	Possibly all or most cancers

Environmental Toxicology: Carcinogenesis. Table 1 (Continued)

Agent//Source	Examples	Associated cancer(s)
Genetics (inherited predisposition)		
Cancer family syndromes	Breast cancer family (BRCA1 or BRCA2 gene mutation)	Breast cancer
	FAP (Familial adenomatous polyposis) (APC gene mutation)	Colorectal carcinoma
	Hereditary melanoma syndromes Dysplastic nevus syndrome Familial atypical mole-malignant melanoma syndrome Melanoma-astrocytoma syndrome	Melanoma
	HNPCC (Hereditary nonpolyposis colorectal carcinoma) (MSH2 or MLH1 gene mutation)	Colorectal carcinoma
	Li-Fraumeni cancer family syndrome (TP53 gene mutation in 70% cases)	Osteosarcoma, adrenocortical carcinoma, brain, breast, colon, leukemia, lung, pancreatic cancers, various sarcomas
	MEN2A and 2B (Multiple endocrine neoplasia, types 2A and 2B) (RET gene mutation)	Pheochromocytoma, thyroid carcinoma
	Neurofibromatosis types 1 and 2 (NF1 and NF2 gene mutations)	Neurofibromas, schwannomas, meningiomas, ependymomas, acoustic neuromas
	Retinoblastoma (RB gene mutation)	Retinoblastoma
	Von Hippel–Lindau Syndrome (VHL gene mutation)	Renal cell carcinoma, pheochromocytoma, hemangioblastomas
Other genetic diseases	Ataxia telangiectasia (AT)	Leukemias, lymphomas
	Bloom's syndrome	Leukemias, lymphomas, carcinomas
	Xeroderma pigmentosum (XP)	Skin (BCC, SCC, and melanoma)

[a]All chemical and physical carcinogens listed are classified as Group I: Carcinogenic to Humans, by the International Agency for Cancer Research (IARC), update January 16, 2009; http://monographs.iarc.fr/ENG/Classification/index.php
[b]DNA synthesis and the replication machinery has an astonishing fidelity of one error per 10^9 base pairs, which results in one to three errors every time the human genome is replicated [31, 32].

Exposures due to personal life-style choices and habits, such as tobacco smoking and alcohol use have been well studied and also provide clear examples of environmental carcinogenesis [12–16]. The carcinogenic impact of occupational exposures is another area that offers substantial clarification of mechanisms and risks involved in cancer development. Similarly, medical exposures, especially those involving chemotherapeutic agents and radiation therapy provide further risks of carcinogenic impacts, although these agents comprise risks of a spectrum of cancer types.

Since the same principles and mechanisms involved in the development of human cancer apply to various animal species, and the primary focus of environmental carcinogenic risk calculations is designed to protect humans, the human will be the primary focus of this chapter on environmental carcinogenesis.

Introduction

The biophysical aspects of this planet support and sustain life, while also being conducive to the

development of cancer in most multicellular species. Fortunately, the risk of cancer is low without the assistance of acute exposures to carcinogenic agents. However, the risk and incidence of cancer increases with age in the mammalian organism [17, 18]. The adage that "cancer is a disease of old age" has its foundings in empirical observation, while also demonstrating the requirement of extensive cell divisions (10s to 1,000s) for the development of tumors [19, 20]. The mixtures of gases that make up Earth's atmosphere sustain the carbon-based metazoan life forms on this planet due to the cellular oxidative metabolic processes. Low carbon dioxide (less than 0.04%) and high oxygen (20.9%) is crucial to the life-sustaining respiration of mammals. Unfortunately, the same life-sustaining oxidative metabolism functioning in the human cell also produces reactive oxygen species (ROS) that damage our cellular components including membranes, lipids, microfilaments, enzymes, and DNA. Additional ROS are produced by exposures to exogenous toxicants, including ionizing radiation, UV light, numerous toxic chemicals and heavy metals. The level of oxidative damage to mammalian DNA has been reported to be as high as 10,000 insults per cell per day [21, 22]. DNA replication (cell division) in the presence of oxidative damage leads to fixed mutations (permanent mutations). Endogenous DNA damage occurs in the form of modified nucleotides (e.g., 8-hydroxy-2′-deoxyguanosine, thymidine glycol, 5-hydroxymethyluracil, etc.), depurination, depyrimidination, deamination, and single and double strand breaks on a daily basis from oxidative processes [23–27]. Tallying up all these insults suggests that human DNA receives greater than 10,000 insults per cell per day. Other mammals receive similar insults at the level proportional to their basal metabolic rates, that is, mice and rats receive approximately tenfold more DNA damage per cell per day as humans. The DNA repair systems of the human cell have a phenomenally high fidelity, but even an error rate of only 0.0001% (the equivalent of one in a million) may lead to the accumulation of genetic errors on the order of 1 every 100 days for each and every cell [28, 29]. To add further insult to injury, the fidelities of DNA polymerases are also less than perfect, although remarkably precise in the human, such that errors are incorporated during DNA synthesis [30]. The reported occurrence of one to three mutations every time the human genome is duplicated further supports the limitations of cellular functions and endurances [31, 32]. Thus the processes involved in sustaining life also lead to DNA mutations. These endogenous life processes coupled with the environment that is so crucial in supporting and nurturing life leads to the accumulation of DNA mutations and, over many years, a significantly increased risk of cancer.

Nature maintains a balance between productive life and cancer risk. As with any genetic disease that terminates life before reaching a reproductive age or during the fertile years, the early occurrence of terminal cancer would be self-limiting. Barriers to cancer development are necessary for the survival and proliferation of the species. As advanced life forms evolved, so did a number of protective mechanisms that are quite effective in derailing tumor development. In addition to detoxifying enzymes for reactive species, glutathione to quench reactive electrophiles, and numerous DNA repair mechanisms, mammalian and human cells become terminally senescent or undergo self-suicide (apoptosis) upon self-recognition of excess DNA damage or perturbation of cell growth controls [33]. The processes involved in cellular aging, that is, loss of telomere length of chromosomes, shifts in gene expression, and responsiveness to external signals that finally lead to replicative senescence after a finite number of cell divisions, may actually be a means to block the development of cancer. Terminal differentiation programs, such as the short 4–5 day lifespan of the colonic mucosal cells, and the approximately 14 day lifespan of the squamous differentiating skin keratinocytes ensures that these cells will not be around if they pick up too many oncogenic DNA mutations during the rapid cell divisions that take place immediately prior to the final terminal differentiation processes [34]. Should these intracellular anticancer mechanisms fail, the local tissue microenvironment plays a role in containing or dampening the expansion of abnormal cells, and the body's immune system may take over and remove aberrant cells, thereby removing the threat of cancer [35–37]. Considering the low frequency of occurrence of cancer until old age, these endogenous protective anticancer mechanisms are advantageous for the human race, albeit not necessarily for the less fortunate individual statistical outlier.

Accumulation of Mutations

Avenues are available for the determined cell to find ways to circumvent these protective barriers against cancer development. With each protective mechanism, one or more DNA mutations enable cells to bypass this blockade and progress toward a neoplastic state. These "driver" mutations are the primary oncogenic errors involved in tumor development. Due to the number and variety of checks and balances opposing oncogenic development, a cell must accumulate a sufficient number of "driver" mutations to circumvent all the blockades for a tumor to develop, without meeting its demise by one of these protective mechanisms. This process is a statistical probability that weighs heavily on the healthy life side until old age, unless perturbed by carcinogenic exposures whereby the probability of tumor development increases (see Table 1). The rate of tumor development is increased sometimes many orders of magnitude above the spontaneous background rate by exposure to exogenous carcinogens. The timing of the onset of cancer is due to the dose and duration of carcinogen exposure and not to either chronological age or the age that exposure began [38, 39].

Properties of Cancer Cells

The product of carcinogenesis is a thriving cancer cell. The successful cancer cell has collected driver mutations that enable it to: (1) ignore antigrowth signals in the tissue microenvironment; (2) be at least partially independent of the requirements for exogenous mitogenic factors for cellular growth and proliferation; (3) block or inhibit differentiation programs; (4) evade apoptotic and senescence programs; (5) establish an extended replicative potential or immortality; (6) secrete factors that enhance and sustain angiogenesis; (7) acquire the ability to evade the immune system; and (8) acquire genomic instability [33, 35–37]. These are the minimal requirements for the development of a benign tumor. A malignancy has acquired one or more additional mutations that confer a ninth property, that of invasive and metastatic capabilities. For each of these nine properties of cancer, one or more mutations are needed to alter the intracellular signaling pathways and/or response to the tissue microenvironment. In some cases, only one driver mutation may be required to confer a specific property, but many of these nine properties are conferred only after multiple oncogenic mutations have been established in the developing cancer cell genome.

Oncogenic Mutations

The establishment of each driver mutation requires the successful negotiation of several protective molecular mechanisms. First of all, the formation of a DNA adduct, single or double strand break, or other form of DNA damage must occur due to exposure to a physical carcinogen (i.e., UV light or ionizing radiation), a chemical carcinogen, or the presence of an endogenous reactive species that has successfully negotiated the gamut of detoxifying enzymes and glutathione. This DNA damage must also have occurred in an oncogenically important base, gene, and/or sequence. Next this DNA damage must be converted into a permanent genetic alteration, a fixed mutation. The formation of a fixed mutation requires the combined failure of the cell's genome surveillance system to recognize and/or repair the DNA lesion, incorporation of an incorrect nucleotide (miss-pairing), and the survival of this mistake up to and through a second round of DNA synthesis, or through faulty repair [40–42] (Fig. 1). The frequency by which this occurs is exceedingly rare, as noted above by the high fidelity of the DNA repair system alone. The bombardment of cells in the human body by acute and chronic exposures to exogenous carcinogens increases the frequency of DNA damaging events and cellular turnover, both of which in turn increase the occurrence of fixed mutations and tips the balance of these processes toward an increased risk of cancer development (Fig. 1). The higher the dose received and the longer the exposure, the greater the risk of cancer.

There are several mechanisms by which carcinogens can influence the formation of DNA mutations, and the type of mutation(s) formed is dependent upon the mode of action of the carcinogen (see Table 2). Exogenous and endogenous agents can produce DNA mutations by directly damaging DNA, perturbing DNA replication machinery, polymerases, etc., inhibiting DNA repair systems, critically shortening telomere lengths, altering the cytoskeletal proteins, mitotic spindle fibers, enzymes involved in mitotic processes, and by stimulating cellular turnover and proliferation.

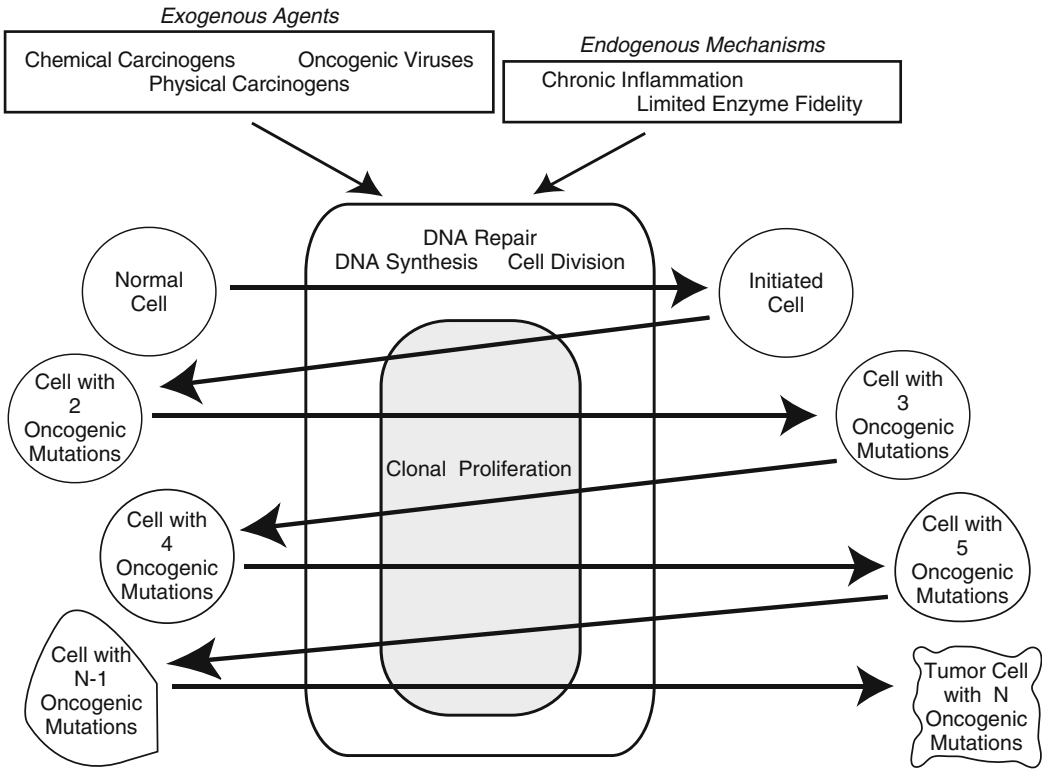

Environmental Toxicology: Carcinogenesis. Figure 1
A schematic representation of the accumulation of oncogenic mutations and the influences of exogenous agents and endogenous mechanisms on this process. Each time a cell completes the cell cycle and divides, there is a good chance that one or more mutations will occur. Fortunately, most of these DNA mutations are not oncogenic. However, the probability of an initiated cell or a cell with two or more oncogenic mutations, picking up another oncogenic mutation increases as clonal expansion occurs. A tumor develops once a sufficient number of oncogenic mutations have accumulated to bypass all of the protective barriers of the normal human cell

These different mechanistic impacts on cells encourage the formation of a variety of mutations, generally classified as single base mutations, chromosomal aberrations, insertions and deletions (indels), and epigenetic mutations.

Single Base Mutations

Single base mutations encompassing single base substitutions and single base indels represent a significant proportion of cancer-associated genetic errors. It is generally accepted that the more transformed a cell becomes, the more likely a single base substitution will occur in an activating site of a proto-oncogene or in deactivating site in a tumor suppressor gene. Most of the alkylating and arylating carcinogens listed in Table 1 are known to produce single base mutations, especially single base substitution mutations. Oxidation and the production of ROS and reactive nitrogen species (RNS), common with inflammatory processes, are also well known to produce single base mutations [25, 43]. The vast majority of errors produced by DNA polymerases and the DNA replication machinery are single base mutations [31, 32].

Single base substitution (SBS) mutations represent 85% or more of the activating and deactivating mutations in proto-oncogenes and tumor suppressor genes, respectively, in human tumors [44–48]. Although

Environmental Toxicology: Carcinogenesis. Table 2 Genotoxic and carcinogenic mechanisms

Mode of action	Effects	Mutations	Instability
1. Direct DNA damage (covalent alterations)	Base pair mismatch	Single base mutation (SBS and Indels)	NSI
	Depurination and depyrimidination	Indels (larger than one base) Epigenetic mutations	EIS
	Single strand break	Chromosomal aberrations (deletions, insertions, translocations)	CIN
	Double strand break		
2. Interference with DNA polymerases and replication machinery	Base pair mismatch	Single base mutation (SBS and Indels)	NSI
	Microsatellite slippage	Microsatellite length changes	MSI
	Perturbation of epigenetic patterns	Epigenetic mutations	EIS
3. Interference with cytoskeleton and mitotic spindle Mitotic proteins and enzymes	Nondisjunction	Aneuploidy	CIN
4. Interference with DNA repair systems	Faulty mismatch repair	Microsatellite length changes	MSI
	Improperly or unrepaired	Single base mutation Indels	NSI
	Single and double strand breaks	Chromosomal aberrations (translocation, inversions, deletions, etc.)	CIN
5. Interference with maintenance of telomeres	Critically shortened telomeres	Dicentric chromosomes aneuploidy	CIN
6. Cytotoxicity	Increased cell turnover	(Most types of mutations)	Any possible (NIS, MSI, CIN, EIS)
	Increased opportunity for accumulating mutations		
7. Stimulate cellular proliferation (promotion)	Clonal expansion	(Most types of mutations)	Any possible (NIS, MSI, CIN EIS)
	Increased probability for accumulating mutations		

CIN chromosomal instability, *EIS* epigenetic instability, *MSI* microsatellite instability, *NIS* nucleotide instability (also known as single base instability)

single base deletions and insertions are sometimes involved, SBSs represent the vast majority of these oncogenic errors [47, 49, 50]. This has been clearly demonstrated in human tissues for a number of proto-oncogenes and tumor suppressor genes, for example, Braf, H-, K-, and N-Ras, RB and TP53 [45–47, 49–51]. Missense SBS mutations alone comprise more than 75% of all identified disease-associated TP53 mutations [49].

Chromosomal Aberrations

Cancer-associated chromosomal errors have been known since the middle of the last century. Cytogenetic studies identified numerous leukemia-specific (and lymphoma-specific) chrosomal translocations [52]. The best-known example is the chronic myeloblastic leukemia (CML)-specific chromosomal translocation between chromosomes 9 and 22 [t(9;22)(q34:q11)], which forms the chimeric bcr-abl gene. Chromosomal

errors are prominent in many types of human tumors and most likely crucial to the development of at least some leukemias and lymphomas [52]. Aneuploidy is the most frequently identified mutation in human cancers, albeit cytogenetic analysis is routine medical care for cancers.

Disruption of cellular cytoskeleton, mitotic spindle apparatus, and/or enzymes involved in the processes of mitosis commonly lead to chromosomal errors. For example, asbestos fibers spear cells and bind proteins that are involved in mitosis, leading to non-disjunction and other chromosomal aberrations [53]. Polycyclic aromatic hydrocarbons (PAHs) also produce chromosomal errors by causing the rapid shortening of the telomere length [54]. Tobacco smoke constituents play a prominent role in the chromosomal aberrations [55–57].

Indel Mutations

Chemical and physical carcinogens are well known to cause single and double strand breaks in DNA. Some DNA adducts, such as the alkyl-N7-deoxyguanosine formed by alkylation (or aryl-N7-deoxyguanosine by arylation) may lead to a depurinic site, which weakens the strand and easily leads to a DNA strand break. The formation of the covalent adduction on the N7-position of purine residues in DNA destabilizes the guanidine-N9-1′-deoxyribose glycosidic linkage [58–60]. Single and double strand breaks also result from ionizing radiation. Two DNA strand breaks some distance apart can lead to deletions, the size of which is dependent upon the separation distance of the breaks. These carcinogen-initiated deletions may disrupt oncogenes such as RB or TP53, produce loss of heterozygosity (LOH), or result in chromosomal translocations [39, 45, 49]. Large deletions (and insertions) of one million bases or more are detectable by cytogenetics and will fall into the chromosomal aberration category.

The explanation for the formation of insertions is less clear, but may entail the same basic mechanisms as noted above for deletions, or by retrotransposition of viral or repeat sequences. The highly repeated Alu sequence, of approximately 300 nucleotides in length, is present in over a million copies in the human genome [61, 62]. Every so often, an Alu repeat sequence inserts itself in a new section of the DNA. This has been observed as a major oncogenic mutation in retinoblastoma and numerous genetic diseases [63]. However, these events are rare and retrotransposition is probably not a prominent mechanism in cancer development.

Epigenetic Mutations

Another form of DNA mutation that has been demonstrated in recent years to be crucially involved in cancer development is the alteration of patterns of DNA 5-methyldeoxycytidine (5mdC) and/or changes in DNA chromatin modification. This type of mutation is referred to as an "epigenetic mutation," since these changes do not alter the basic DNA coding sequence. To clarify firstly DNA 5mdC patterns, selective deoxycytidine residues in DNA are enzymatically modified by endogenous DNA methyltransferases (DNMTs) that catalyze the transfer of a methyl group from S-adenosylmethionine to the 5-position on the cytosine base, forming 5mdC [64]. In adult somatic cells, this normal DNA modification occurs almost exclusively at 5′-CpG-3′ sequences and duplex DNA is maintained in a symmetrically methylated state, so that the complementary 5′-CpG-3′ sequence is also methylated on the opposing strand [65, 66]. It should be noted that in stem cells, especially embryonic stem cells, a significant portion of the 5mdC also occurs in non-CpG sequences [65, 66]. The meaning of these non-CpG methylated sequences is presently unknown. Maintenance of symmetrically methylated duplex DNA ensures the mitotic heritability of these DNA 5mdC patterns in somatic cells by providing the 5mdC pattern template for each newly synthesized strand following semiconservative DNA synthesis. The level of 5mdC on a specific DNA locus or gene promoter region determines whether the sequences are expressed or not. Highly methylated promoter sequences 5′ to the coding sequence of a given gene indicate that the gene is not available for transcription [67]. Today this is commonly referred to as gene hypermethylation, which is identified frequently as an epigenetic mutation in one or more tumor suppressor genes in human cancers [67, 68]. Hypomethylation of these same promoter sequences opens the gene sequences up for transcription, but does not indicate that the gene is being transcribed since additional DNA binding proteins and transcription factors are required for expression of the gene.

Not surprisingly, DNA 5mdC patterns change during tumor development [69, 70], and chemical carcinogens are known to alter DNA 5mdC patterns [71–75].

Chromatin modifications are more complex than DNA 5mdC patterns and include a number of different molecular moieties. The basic repeating unit of chromatin is the nucleosome, which is composed of 147 base pairs of DNA wrapped around a core containing two copies each of four core histone proteins H2A, H2B, H3, and H4 [76, 77]. Various molecular modifications of the N-terminal tails of these core histones occur in mammalian cells. In 1964, Allfrey et al. [78] first reported histone N-terminal tail modification, acetylation, but it was many years later before the complexity and importance of this posttranslational modification became known. As it turns out, multiple histone modifications occur, consisting of methylation [79–81], acetylation [82], phosphorylation [83], ubiquitinylation [84], and sumoylation [85]. The patterns and combinations of these modifications are referred to as the histone code [86], which influences the chromatin structure and remodeling for either active expression or silencing of genes [87]. Euchromatin (active chromatin) along with active gene expression was associated with methylation of the lysine residue in the fourth position of the N-terminal tail of histone H3 (denoted as H3K4me), while H3K9me and K3K27me formation were linked to heterochromatin (silent chromatin) and repression of gene expression [79–81]. These patterns become even more complex as each of these histone lysine residues may be mono-, di-,or tri-methylated (i.e., H3K4me^1, H3K4me^2, and H3K4me^3) [88–91]. The importance of multiple methyl groups on lysine residues is presently only poorly understood. Histone methylation also takes place on other lysine residues on histone H3 K36 and K79, and histone H4 K20, and on arginine residues histone H3 R2, R17, and R26, and histone H4 R3.

Acetylation of the positively charged lysine residues decreases the effective ionic charge, reducing the affinity to the negatively charged phosphate backbone of DNA and creates a binding side for regulatory DNA proteins that activate transcription [92]. Essentially, histone acetylation alters the chromatin structure to a more transcriptionally supportive architecture. Acetylation of the amino group of lysine residues occurs on histone H2A K5 and K9, histone H2B K5, K11, K12, K15 and K20, histone H3 K9, K14, K18, K23 and K56, and histone H4 K5, K8, K12 and K16 [86]. Acetylation patterns are established by highly regulated histone acetyltransferases (HATs) and histone de-acetylases (HDACs) [93]. HAT enzymes are grouped into different family classes, GNAT family, MYST family, and CBP/p300 family [94]. Some transcription factors such as yeast protein Gcn5, a putative transcriptional adaptor, are HAT enzymes [95]. HDACs catalyze the removal of acetyl groups from histones by activation of a water molecule through a zinc ion in the active site [96, 97], and are involved in formation of heterochromatin and the silencing of genes. In human cells, 18 nonredundant HDACs have been identified [98], which have been divided into classes I, II, and III [99]. Class I HDACs are localized within the nucleus while Class II shuttle between the nucleus and cytoplasm [98]. Regulation of HDACs consists of protein–protein interactions, posttranslational modifications, cellular localization, and metabolic cofactors [100].

In 1967, Gutierrez and Hnilica [101] first reported histone phosphorylation of serine residues on H3S10 and H3S28. Histone phosphorylation appears to be involved in cell cycle chromatin condensation, active transcription, apoptosis, and DNA repair mechanisms [102, 103]. Histone H3T11 and H3S28 have been identified as mitosis-specific sites for phosphorylation [104, 105]. Histone phosphorylation is also involved with activation of early response genes such as c-fos, c-myc, and c-jun. This is a stimulant-dependent H3 phosphorylation, resulting in quick transcriptional activation of a subset of immediate-early genes [106]. Although, acetylation and phosphorylation are both linked to transcription activation, it is unknown whether the two modifications work independently, in parallel, or synergistically [107, 108]. Phosphorylation also occurs on serine and threonine residues on histone H2A S1, histone H2B S14, and histone H4 S1.

Histone ubiquitinylation and sumoylation are the least understood of the chromatin modifications [84, 85]. However, these modifications may be important in DNA damage response and repair, V(D)J recombination, meiotic and spermatogenesis remodeling, and chromosomal stability [109–114].

It is becoming clear that histones are major carriers of epigenetic information. Histone modifications provide mechanisms to generate and stabilize chromatin

structures. The study of chromatin modification patterns is a very young field, which will undoubtedly become very important to the delineation of carcinogenesis. In fact, evidence is already beginning to accumulate regarding alterations in chromatin histone modifications due to exogenous chemical carcinogen exposures [75, 115].

Cytotoxicity and Cellular Turnover

Most exogenous carcinogens are cytotoxic at recognized carcinogenic doses, and probably at much lower doses to impacted cells. This concept is easy to envision when considering agents that directly damage cellular macromolecules (i.e., ionizing radiation, alkylating and arylating carcinogens). Interference with cellular functions, enzymatic processes, cytoskeletal structure, mitochondrial electron transport and oxidative phosphorylation, etc. may lead to cell senescence or death. If the DNA is damaged to the extent that successful repair is doubtful, the cell undergoes apoptosis as mediated by TP53 [39, 116]. Both senescence and apoptotic pathways are protective means by which cells may avoid accumulating DNA mutations [33].

Concentrations of chemical carcinogens and doses of physical carcinogens that produce mutagenicity in experimental studies generally also produce a significant percentage of cell lethality [117]. Whether cell death is the result of cellular damage inflicted directly by the carcinogen or from triggering apoptosis, the loss of the cell leaves a gap to be filled by cellular turnover. In tissue, this leads to increased cell division to replace these lost cells. This damage-induced cell proliferation offers increased opportunities for the accumulation of mutations during DNA synthesis and mitotic division. Cells adjacent to the vacated space will have the chance to divide to replace the missing cell. One or more of these adjacent cells might harbor a mutation that confers a growth advantage enabling it to dominate over its neighbors and progress through cell division. Thus, the potential for clonal expansion and the continued accumulation of oncogenic mutations is encouraged by the impact of carcinogens on tissues.

The opportunity or encouragement of carcinogen exposed cells to undergo cell division provides yet another enhancement for mutation occurrence. Many of the cells that have the opportunity to divide have also received a carcinogen-induced damaging event, which if not repaired prior to DNA synthesis may lead to a fixed mutation [117]. For example, the presence of an alkyl-O^6dG adduct during DNA synthesis will result in the formation of a G to T mismatch approximately 50% of the time. Alkyl-O^6dG base pairs equally efficiently with either a thymidine or a cytidine residue [60, 118, 119]. Different DNA adducts and forms of damage will result in different mutational events following DNA synthesis. But the cytotoxic action of these carcinogens couples with the DNA damaging activity to induce mutations.

When carcinogen induced cell death involves a tissue stem cell, the dead cell is replaced by another stem cell. Most of cancer arises from tissue stem cells. The accumulation of mutations in a transit-amplifying progenitor cell will usually result in no consequence as the developing cancer cell will be terminally lost either by terminal differentiation and cell death or by being sloughed off the epithelial layer [34]. Stem cells have the capability of surviving long enough to accumulate the necessary mutations to become cancerous. Even in rapidly turning over tissues, stem cells appear to be long lived, with estimated lifetime division numbers totaling in the hundreds and higher [120]. But these stem cells also enjoy a slow or delayed cell cycle, dividing intermittently (only once every 7 or 8 days), and often sitting quiescent and in a nonproliferative or reserve stem cell state [121–123]. Stem cell division is generally considered to be asymmetric, giving rise to both a replacement stem cell and a progenitor cell that will undergo numerous symmetrical cell divisions and then terminally differentiate [120, 124–126]. This asymmetric cell division appears to also include the retention of the original DNA strand by the daughter stem cell replacement. Or stated differently, the original template DNA strand of the mother stem cell selectively segregates to the daughter stem cell replacement, while the newer DNA strand segregates to the transit-amplifying daughter cell. This is the Cairns' "immortal stranding" hypothesis [127], which appears to have experimental validity [124, 126]. DNA synthesis in human cells accumulates one to three mutations every time the genome is copied [31, 32]. "Immortal stranding" enables the stem cell to minimize the accumulation of DNA mutations, and thus limit the

number of mutations that are passed on to the transit-amplifying differentiating epithelial cells.

Adult stem cells are very sensitive to DNA damage, and rather than perform DNA repair, stem cells appear to undergo apoptosis in response to external exposure to DNA damaging agents [128]. Discarding the cell rather than risk faulty repair ensures that the accumulation of DNA mutations in stem cells does not occur. However, the loss of one or more stem cells due to external toxic exposure(s) (UV light, ionizing radiation, arylating or alkylating chemicals, or inflammation or infection produced ROS), requires the replacement of these stem cells. Stem cell replacement requires a symmetrical cell division to give rise to two daughter stem cells, which will produce one "aged" DNA template strand regardless of "immortal stranding." This process increases the number of mutations arising in the stem cells and increases the risk of disease. Alternatively, a transit-amplifying cell may undergo dedifferentiation, characteristic of mesenchymal-epithelial transition [129]. Unfortunately, this dedifferentiation process again produces a stem cell without the benefit of "immortal stranding" and increases the risk of mutations and disease developing in the tissue stem cell population.

Genomic Instability

Genomic instability is the loss of genomic stability and the increased probability for accruing DNA mutations. Restated, genomic instability is the inability of cells to maintain the integrity of their own genomic inheritance.

It is generally accepted that most cancers express one or more forms of genomic instability. However, among the scientific community there is still controversy as to whether the loss of genomic stability is required for the development of cancer. One argument states that genomic instability is not necessary for the accrual of a sufficient number of oncogenic mutations to reach a malignancy [130, 131]. The other argument states that human cells would not have the opportunity to accumulate a sufficient allotment of driver mutations to achieve a cancerous cell without an additional navigating mechanism(s) [132]. The statistical probability during a normal human life span has been proposed to be too low based on theoretical cell division numbers alone. However, many oncogenic mutations, such as in "caretaker" genes, result in the enhanced probability of initiated cells achieving more mutations and progressing along the road of tumor development [31, 40, 42, 133]. Caretakers are genes that code for cellular proteins and factors that protect the genome from mutation. Disruption of the finely balanced cellular network of monitoring and repair systems will lead to a loss of fidelity of these genome protection systems, increases in macromolecular damage, increased longevity of DNA damage, faulty repair, and an increased accumulation of DNA mutations. For example, a mutation that disrupts the normal function of a mismatch DNA repair gene leads to upward of a 100-fold increased rate of cellular DNA mutation [40].

Genomic instability is a hallmark of cancer and one of the trademarks of a number of inherited genetic diseases that predispose individuals to cancer [131] (see Table 1). By today's laboratory techniques, genomic instability manifests as chromatin instability (CIN), microsatellite instability (MSI) (sometimes referred to as MIN), nucleotide instability (NIS) (also called single base instability), and epigenetic instability (EIS) (see Table 2).

Chromosomal Instability (CIN)

The inability of the cell to properly repair single or double strand DNA breaks, perform appropriate recombination activities in somatic cells, or correctly perform the mitotic spindle functions during mitosis will lead to the development and accumulation of chromosomal aberrations, which is the manifestation of CIN [33, 134]. Cells expressing CIN miss-segregate chromosomes 10–100 times more frequently than chromosomally stable diploid cancer cells [135]. CIN may promote tumor evolution by enabling the clonal expansion of cells with proliferative advantages and/or metastatic potential [136–138].

Chemical and physical carcinogens can interfere with the cytoskeleton, mitotic spindle apparatus, or the various proteins and enzymes involved in mitosis. The impact of such carcinogenic damage is the increased probability of chromosomal mutations. As noted above, asbestos produces aneuploidy in skewered cells by interfering with the cytoskeleton and mitotic proteins [53]. Tobacco smoke PAHs, BPDE, and 4-aminobiphenyl enhance telomere shortening and produce CIN in vivo and in vitro studies [54–57].

Microsatellite Instability (MSI)

Microsatellites are relatively short sequences composed of tandemly repeated units of one to six bases in length [139]. The repeated unit of sequence may be only a mono-nucleotide repeat (e.g., AAAAAAA...), di-nucleotide repeat (e.g., CACACACACACACA...), tri-nucleotide repeat, etc., although microsatellites of imperfect and compound sequences also exist in the human genome (e.g., Bat25 and Bat26) [140]. The most common class of microsatellites in the human genome are composed of various tandemly repeated lengths of $(CA)_n$. Microsatellites are widely prevalent throughout the human genome, occurring more frequently in non-coding regions on all chromosomes, and act as gene promoters, as target sites for recombination, and as binding sites for DNA topoisomerases [139]. The length of a specific microsatellite is an inherited trait and therefore the same in all tissues. Insertion or deletion of one or more repeat units within a microsatellite occurs on rare occasion by slippage during DNA replication, resulting in a longer or shorter microsatellite sequence, respectively. These polymerase slippage errors are normally repaired by a post-replication mismatch repair system, and the presence of a microsatellite variant generally results from the lack of fidelity in the mismatch repair mechanism [141–143]. MSI is denoted by the presence of microsatellite variants of different lengths in tumors compared to normal tissue, and is a hallmark of mismatch repair deficient familial and sporadic cancers [144, 145].

In theory, a carcinogenic agent that interferes with DNA polymerases and/or the mismatch repair system would lead to MSI. For many types of cancer, MSI is the one genomic instability that is consistently acquired late in the tumorigenic process [139]. The major exception to this rule is the hereditary nonpolyposis colorectal cancer (HNPCC) syndrome, for which individuals inherit an error in the mismatch repair system and are at risk of developing colon cancer [146, 147]. However, airborne particulates ($PM_{2.5}$) have been associated with the development of MSI in human lung epithelial cells [148, 149]. Cancers induced by betel-quid chewing and chronic occupational exposure to chromium have been found to express MSI significantly more frequently than noncarcinogen-associated tumors [150, 151].

Nucleotide Instability (NIS)

Nucleotide instability may be one of the more easily induced instabilities by either exogenous or endogenous influences. Increases in the frequencies of various forms of DNA nucleotide damage and/or loss of cellular DNA damage surveillance and repair capacity, or the perturbation of the DNA polymerases or synthesis complex machinery result in increases in single base mutations [19, 46–48, 132]. With the possible exception of chromosomal translocations in leukemias and lymphomas, NIS is probably the most common genomic instability expressed in human cancer [47, 49, 50]. NIS may also be predominant in the earliest mechanisms of carcinogenesis as roughly 85% of the activating and deactivating mutations in proto-oncogenes and tumor suppressor genes, respectively, are single base substitution mutations [44–48]. Much of the NIS data in the literature has been accumulated from clonal expansion of mutations in tumor tissue, that is, TP53 mutation database and retinoblastoma gene mutations [49, 50]. The analysis of NIS has been hampered by the requirement of exceedingly sensitive techniques, and the limited viable ultrasensitive approaches are labor intensive [47]. However, with the present availability of the ultra-sensitive methods, the presence of NIS in non-tumor tissues and the induction of NIS by exogenous environmental carcinogens are beginning to unfold [48, 152].

Epigenetic Instability (EIS)

Although any alteration from normal of DNA 5mdC and/or chromatin modification patterns constitutes epigenetic instability, the majority of the scientific literature has focused on hypermethylation, that is, the transcriptional suppression of important anticancer genes by high levels of 5mdC present in the gene promoter sequences [67, 68]. In human cancer, a hypermethylation phenotype, referred to as CIMP (CpG island methylator phenotype), has been proposed [153]. The CIMP phenotype may have clinical significance, but the cause or mechanism underlying the CIMP tumor phenotype has yet to be identified [154–156]. Regardless of the gene specific hypermethylation ascertainment biased approach, cancer cells are globally hypomethylated and harbor 20–60% less genomic 5mdC than their normal counterpart. The hypomethylated sequences in cancer cells

may be mainly due to the loss of 5mdC levels in repetitive sequences, which are normally heavily methylated and comprise 20–30% of the human genome [157]. For at least some cancers, the level of global hypomethylation is associated with progression, becoming progressively more hypomethylated from normal to benign, to tumor and metastasis [158–160]. Indeed, transient global hypomethylation is inducible by either chemical carcinogens or hypoxia [71, 72, 161]. Interestingly, increased NO production that may occur in inflammatory disease, or in response to hypoxia, reduces S-adenosylmethionine levels by inactivating methionine adenosyltransferase, and produces hypomethylation [162]. Dietary deficiencies in either folic acid or methyl donor compounds, that is, methionine, also cause hypomethylation [6–8]. Hypomethylation of gene-specific sequences in cancer cells leads to ectopic gene expression, such as neuron-specific γ-synuclein expression in gastric cancers [163]. The degree of hypomethylation of the XIST gene correlates with prostate cancer aggressiveness [164].

There may be several mechanisms at work in the alterations of epigenetic signals during carcinogenesis as these patterns are intimately involved in all biological processes, that is, genomic imprinting, gametogenesis, embryogenesis, differentiation, aging, and carcinogenesis. As noted above, dietary deficits are known to alter DNA 5mdC levels and patterns [6–8]. Alkylation, arylation and other forms of DNA damage induced by carcinogens have been clearly shown to disrupt DNA 5mdC patterns [71, 72]. DNA epigenetic patterns may also be impacted by many other environmental factors, including tobacco use, drug use, physical exercise, and health status as DNA 5mdC patterns diverge with age in monozygotic twin pairs [165].

Chromatin modification patterns are well known to be involved in carcinogenesis and the development of cancer [166, 167]. However, this field is still developing, and the data regarding exogenous agent-induced changes in histone modifications are presently limited. Several in vitro tissue culture studies have been performed that suggest toxicants induced changes in selective histone residue methylation or acetylation (see review [75]), but the interpretation of these specific histone modification changes amid the complex arrays of epigenetic patterns and extrapolation to in vivo will require further analyses.

To summarize genomic instability, there are a large number of genes involved in the maintenance of the genome. Many of these genes, such as the DNA repair genes, have been referred to as caretaker genes for their role in genomic stability, while others such as the RB and TP53 genes have been denoted as gatekeeper genes due to their involvement in cell cycle control and the pathway to cancer development [168]. Each of these instabilities enhances the probability of accumulating oncogenic mutations and progression along the road of tumor development, the acquisition of invasive or metastatic capability, and/or resistance to chemotherapeutic regimens. This last effect has also been observed in non-chemotherapeutic carcinogens, whereby cells exhibiting selective genomic instabilities are resistant to the cytotoxic effects of some carcinogens. Cells expressing CIN were found to be resistant to the lethal effects of PhIP but not to the methylating carcinogen, *N*-methyl-*N*′-nitro-*N*-nitrosoquanidine (MNNG), while cells expressing MSI were resistant to MNNG but not to PhIP [169]. This provides yet another important mechanism by which chemical carcinogens may select for mutant cells and promote their clonal expansion by exerting cytotoxic effects on neighboring cells in the tissue.

Susceptible Individuals

Based on the above discussion of genomic instabilities, it is not surprising that some individuals in the human population have inherited genetic errors that render them more prone to developing cancer [47, 131] (see Table 1). For a portion of these susceptible individuals, the risk of cancer is quite high. For example, individuals who have inherited a mutation in one of the mismatch repair genes (i.e., MSH2, MLH1, MSH3, MSH6, PMS1, and PMS2) are carriers of hereditary nonpolyposis colorectal cancer (HNPCC) syndrome and are at high risk of colorectal carcinoma [139, 146, 147]. Inheritance of any one of several DNA repair gene mutations confers a genetic disease (i.e., xeroderma pigmentosum, ataxia telangiectasia, Fanconi anemia, Cockayne syndrome, and others), which is associated with adverse clinical symptoms including a substantially elevated risk of cancer. Individuals harboring a germ line mutation in the TP53 gene, referred to as the guardian of the genome gene, generally present as

a Li-Fraumeni Cancer Family Syndrome and are at a substantially elevated risk of multiple types of cancers during their lifetime [170]. More than 100 Mendelian diseases that confer predisposing cancer syndromes have been recorded in "McKusick's Online Mendelian Inheritance in Man" (OMIM), each with varying levels of cancer risk [171].

There are however heritable mutations that convey more subtle increases in cancer risk, especially when environmental exposures to exogenous carcinogens are involved [47, 172]. Polymorphisms in genes involved in the deactivation and elimination of toxic metabolites and carcinogens may confer to the individual a decreased ability to remove offending toxicants and/or reactive electrophiles before they can cause DNA damage, which provides a slightly increased probability of developing cancer. Examples of these susceptibility traits are found in polymorphisms among the phase I and phase II biotransformation enzymes, such as cytochrome P450 and glutathione-S-transferase genes [172–174]. These individuals are at an increased risk of cancer from exposures to polycyclic aromatic hydrocarbon (PAH) carcinogens commonly found in tobacco smoke and other combustion products [173, 175]. Depending upon the metabolic pathway used to activate, deactivate, and/or eliminate carcinogens, gene polymorphisms may render individuals more susceptible or less susceptible to cancer from exposure to selective carcinogenic agents.

Dose and Complex Dose

Humans are exposed to a plethora of toxic and carcinogenic materials in the environment. Exposure to complex toxic mixtures poses a higher risk of detrimental health effects than that represented by the toxicity of each separate individual constituent. When an individual or animal is exposed to a complex mixture of carcinogenic agents, the dose required to produce significant health problems and tumor development will be lower than that for each separate individual constituent. In toxicology, it is well recognized that exposures to significant levels of complex mixtures of toxic compounds results in increased detrimental health effects. This is also true for carcinogenic agents. The combined toxic effect of separate toxicants is generally predicted to be at a minimum additive, unless specific information exists to demonstrate a synergistic (above additive) or inhibitory (below additive) action. Many of these carcinogens target the same organs or tissues, and induce similar toxic effects in humans and animals. For example, alcohol use, foodborne aflatoxins and hepatitis B (or C) all adversely impact the liver and promote the development of hepatocellular carcinoma. Similarily, asbestos, arsenic, and tobacco smoke drive the development of lung cancer. For each of these examples, some differences in agent-specific direct DNA damage may exist, but similar mechanisms of cellular damage, enhanced cellular turnover, inflammatory responses, and ROS and RNS species involvement contribute to the development of cancer.

Although people are not generally exposed to an acute carcinogenic dose for each one of these environmental carcinogens, they may receive an accumulated dose sufficient to induce cancer due to long-term chronic low dose exposure. Damage to the skin from lifetime exposure to UV radiation from sunlight is one of the more obvious examples. However, the same may be true for a number of environmental chemical carcinogens, especially if one has been chronically exposed to tobacco smoke, whether as a smoker or nonsmoker. What is known regarding what constitutes a carcinogenic dose is based mostly on laboratory studies involving a single agent, not a complex mixture. It should note, however, that tobacco smoke is a complex mixture, and epidemiological studies have provided estimates of carcinogenic risk based on the number of cigarettes smoked per day and the number of pack years of smoking [176, 177]. Estimates of carcinogenic risk are generally derived from the carcinogenic dose of individual agents. The combined effects of exposures to multiple environmental carcinogens must certainly lower the carcinogenic dose threshold for individual carcinogens. Thus the chronic long-term low-dose exposure to a multitude of carcinogenic agents in our food, air, water, from sunlight, x-rays, and biological pathogens, enhances the risk of cancer as our bodies reach old age. Whether cancer is inherent with life or not, moderating one's exposure by avoiding habitual exposures, that is, tobacco smoke and alcohol abuse, and maintaining a healthy lifestyle significantly lowers one's lifetime risk of cancer.

Environmental Carcinogens

To reiterate, the rate of tumor development is increased sometimes many orders of magnitude above the spontaneous background rate by exposure to exogenous carcinogens. The timing of the onset of cancer is due to the dose and duration of carcinogen exposure and not to either the chronological age or the age that exposure began [38, 39]. Regardless of whether a cancer develops from carcinogen exposure(s) or endogenous processes, or the combination of exogenous and endogenous attacks (the most likely explanation), the accumulation of oncogenic driver mutations and a large number of cell divisions are required.

Separating the effects of exogenous versus endogenous genotoxic damage and cancer induction may not be an easy undertaking. More than likely, a tumor originating only from exogenous carcinogen exposure is rare if nonexistent. However, the impact of exogenous exposures to genotoxic agents is easily demonstrated by the significant increases in lung cancer of smokers [176], and by the patterns of oncogenic single base substitution mutations in the TP53 gene in lung cancers and breast carcinomas from smokers. Lung and breast tumors arising in smokers are twice and ten times, respectively, as likely to harbor a TP53 gene driver mutation of the G to T transversion type than similar tumors arising in nonsmokers [178, 179]. Benzo(a)pyrene and other PAHs are known to target deoxyguanosine in the most commonly mutated sites (codons 157, 248, and 273) observed in lung tumors, and to produce G to T transversion mutations in these same base sites [180–182]. Similar findings have reported for aflatoxin B1 adduction and G to T mutation of codon 249 of TP53 [183–185]. Sunlight (UV light) produces signature CC to TT mutations in TP53 and other DNA sequences that have been identified in sun exposed skin, which is well correlated with the occurrence of skin cancers [186–188]. Unfortunately, few carcinogens presently provide such clearly apparent tumor-associated agent-induced genotoxic damage. Signature diseases that aid in identifying the exogenous impact of toxicant exposure are also limited to only a few carcinogens, for which asbestos and mesothelioma are the best known examples. Many other cancers have multiple etiological causes, and delineation of specific carcinogen exposures in the causation is not easily identified (see Table 1).

The following are brief descriptions of the genotoxic processes and carcinogenic mechanisms for a few examples of common environmental carcinogens, which are provided here to clarify the discussions of the impact of these exposures on the development of human cancer. The discussions are not intended to be fully comprehensive. Extensive literature is available of each of these agents and numerous references are provided for the reader.

Alcohol

Chronic alcohol consumption is associated with oral cavity, pharynx, larynx, esophageal, liver, and colorectal cancer, and breast cancer in women [12, 13, 16]. Alcohol use is also suspected to be involved in the etiology of pancreatic and lung cancers. The development of alcohol-induced cirrhosis of the liver is a well-known etiology for hepatocellular carcinoma development [16], and the risk of hepatocellular carcinoma increases with the synergistic impact of tobacco smoke and alcohol, or of hepatitis (B or C) and alcohol [12]. However, pure ethanol itself is not genotoxic, but its primary metabolite acetaldehyde is mutagenic [189, 190].

The present theories regarding the carcinogenic mechanisms of alcohol are based on DNA damaging events, tissue inflammation and perturbation of nutrition and physiological functions [13, 14]. Acetaldehyde forms DNA adducts [189, 190], and damages hepatocytes and tissue architecture, which leads to increased cellular proliferation [191]. Alcohol induces CYP2E1, whose gene product (P450 2E1) adds to the metabolism of alcohol to acetaldehyde as well as activating tobacco carcinogens (i.e., nitrosamines) [12]. Alcohol also induces ROS & RNS [192], which leads to lipid peroxidation and further DNA damage from reactive electrophilic products of the lipid peroxidation reactions [193]. Alcohol intake interferes with folate metabolism [194] and folate deficiency increases the risk of colorectal carcinoma by two to five times [195]. Alcohol may also alter the absorption and metabolism of vitamins, such as vitamin B_{12}, B_6, and retinoic acid, and often results in malnourishment in the

alcoholic [13, 14, 194]. Thus chronic alcohol use utilizes at least three different avenues of carcinogenesis; DNA damage and mutation, inflammatory processes that promote proliferation, and vitamin deficiencies that are known to perturb DNA epigenetic patterns. It is not surprising that alcohol works synergistically with other carcinogens such as tobacco smoke to increase the occurrence of cancers [12].

Sunlight

UV light from the sun is probably the most important naturally occurring environmental carcinogen to which humans are exposed. Chronic exposure to sunlight and repeated sunburns are strongly correlated with nonmelanoma skin cancers (mainly squamous cell carcinoma and basal cell carcinoma), especially on the head, neck, forearms, and hands, which clothing generally leaves uncovered [196]. Skin cancer is one of the more frequent cancers in aging populations, and is the most common cancer in the USA [9, 10]. The lifetime risk of developing skin cancer in the USA is one in five. Fortunately, most skin cancers are amenable to early detection and a high cure rate. Melanoma is the exception, leading to a lethal disease course in greater than 10% of cases.

UV light is comprised of electromagnetic radiation wavelengths below 400 nm, and has been broken down to vacuum UV (100–200 nm), UVC (200–290 nm), UVB (290–320 nm), and UVA (320–400 nm). [Note that some authors refer to the wavelength ranges for UVB and UVA as 280–315 nm and 315–400 nm, respectively (e.g., Ridley et al. 2009 [197]).] The upper layers of the Earth's atmosphere filter out much of the harmful UV shorter wavelength, although this will become less effective and a potentially major health issue as the ozone layer thins over parts of the planet. The remaining UVA and UVB radiation reaches the ground. Both UVA and UVB damage cells and macromolecules in cells. UVB provides the major DNA mutational impact producing signature cyclobutane pyrimidine dimers and pyrimidine 6–4 pyrimidone photoproducts, which if not repaired, result in signature CC to TT and C to T mutations, respectively [186, 187, 198]. Cyclobutane pyrimidine dimers are responsible for approximately 80% of the UV light signature mutations, since the 6–4 photoproducts are repaired much more efficiently than the cyclobutane pyrimidine dimers [188, 197]. Cyclobutane pyrimidine dimers are only slowly repaired by a transcription-coupled repair system. These UV signature mutations are known to occur in at least one important tumor suppressor gene for human cancer, the TP53 gene [186]. UV-induced TP53 mutations probably represent an early step in the skin cancer carcinogenesis pathway for basal cell carcinoma and squamous cell carcinoma [186, 199].

UVA radiation also contributes to the carcinogenic impact of sunlight exposure. UVA radiation leads to DNA damage and mutations, albeit at more than a 1,000-fold lower extent than UVB. However, UVA penetrates more deeply into the skin than UVB and produces UV signature mutations in the basal layer, while the majority of UVB produces signature mutations in suprabasal keratinocytes [200]. UVA also initiates substantial cellular macromolecular damage, ROS, and lipid peroxidation [197].

UV light exposure may enhance the development of skin tumors both by inducing mutations and by interfering with the turnover of keratinocytes [201–203]. UV irradiation induces apoptosis in severely damaged keratinocytes. However, insulin-like growth factor-1 (IGF-1) produced by dermal fibroblasts opposes UV-induced apoptosis in keratinocytes and induces replicative senescence by NFκβ and TP53 signalling [201–204]. UV damaged keratinocytes that survive apoptosis still retain the capacity to divide unless held in check by IGF-1. Aging skin fibroblasts produce significantly less IGF-1, leading to the increased potential of damaged and mutant keratinocytes replicating. This may explain the increased incidence of nonmelanoma skin cancer in geriatric patients [205].

The combined effects of UVB and UVA to multiple cells in the epidermal layer result in localized tissue inflammation, which contributes to the melee of oxidative reactions and includes reactive nitrogen species [25, 27, 43]. The setting of cellular damage and inflammation results in a tissue microenvironment that encourages cellular turnover, promotes clonal expansion of mutated cells that leads to the accumulation of oncogenic mutations and ultimately to skin cancer development.

Tobacco Smoke

Tobacco smoke is the most frequent cause of lung cancer and probably the most important anthropogenic carcinogen of the last century. Whether by lifestyle choice of smoking or by exposure to side-stream smoke for the nonsmoker, tobacco smoke has been a primary etiological factor in lung cancer in the USA [176]. On average, lung cancer develops in cigarette smokers after 50 pack-years [177]. Tobacco smoke contains a large complex mixture of carcinogens, including many that may both initiate and promote the development of cancer. Cigarette smoke contains between 3,000 and 4,000 toxic compounds, more than 300 of which are known or suspected carcinogens, including the majority of the IARC Group I chemical carcinogens discussed in this chapter [206](see Table 1). Many of these toxic and carcinogenic components of tobacco smoke are readily absorbed systemically, and smoking is well associated with diseases such as cardiovascular disease and cancers in addition to lung [176, 177, 207]. Tobacco smoking is believed to be an important etiological factor in many cases of oral cancers, esophageal, bladder, pancreatic, kidney, and possibly breast and cervical cancers [208].

Many of the carcinogens in tobacco smoke alkylate or arylate DNA, producing promutagenic lesions. For example, benzo(a)pyrene is activated by the host cells' cytochrome P450 1A1 enzyme activity to the ultimate carcinogen, benzo(a)pyrene-7,8-dihydrodiol-9,10-epoxide (BPDE) form, which reacts with nucleophiles including the exocyclic amino group on deoxyguanine of DNA [209]. The BPDE-N^2dG adduct is a promutagenic lesion that leads most frequently to a G to T transversion mutation. Numerous other tobacco smoke carcinogenic PAHs, heterocyclic amines, and nitrosamines, produce DNA adducts that can lead to primarily G to T transversions. As noted above, G to T transversions are the most common single base mutations in lung tumors [178, 179]. A few of these carcinogenic nitrosamines are tobacco smoke specific, that is, 4-(methylnitrosamino)-1-(3-pridyl)-1-butanone (NNK) and N′-nitrosonornicotine (NNN) [207, 210]. The list of carcinogens in tobacco smoke is extensive and ensures multiple types of DNA damage and adverse impacts on other cellular macromolecules, enzymes, and structural components is complex [208]. It has been estimated that a developing preneoplastic clone of lung cells accumulates one DNA mutation for every 15 cigarettes smoked [211]. In addition to damaging DNA, most of these tobacco smoke toxicants also promote cellular turnover and inflammatory processes in lung tissue, providing another avenue of ROS and RNS species and altered microenvironments for clonal expansion of mutant cells [25, 43]. Particulates from tobacco smoke interfere with pulmonary function independent of the plethora of toxic chemicals, recovery and repair following exposure [148, 149]. In spite of all these genome destabilizing and tumor-promoting activities, many years of smoking history are generally required before a tumor develops, which is a testimony to the resilience of the human body to the bombardment of such a powerful combination of the carcinogens and toxic agents present in tobacco smoke.

Future Directions

It would be very difficult if not impossible for life on this planet to completely avoid exposure to environmental carcinogens. One can purposely avoid alcohol, tobacco smoke, and many occupational exposures, but the presence of carcinogenic substances in our food, air, water, and sunlight coupled with health, nutritional issues, and biological carcinogenic agents make avoiding all exposure to carcinogens very difficult. The extensive years of educating the public regarding the hazards of smoking, along with the banning of smoking in public buildings and other establishments has had a dramatic effect on the reduction in lung cancer and probably other cancers in recent years [176, 177]. Increased safety precautions and worker awareness to reduce occupational exposures remain a very important component in reducing cancer risk. Vaccinations against biological carcinogens, such as hepatitis B and C, may be important as well, and perhaps more important depending upon where one travels in the world. As people live longer and healthier lives, reductions in carcinogenic contaminants in our food, air, and water appears to be the only other viable avenue that society as a whole can take to diminish cancer risk. Individuals remain responsible for their

own nutritional health, exercise, and personal habits in avoiding carcinogenic exposures.

Fortunately, our food also contains anticarcinogens [212–214]. For example, the isothiocyanates in broccoli are suggested to aid in diminishing the carcinogenic impacts of a number of chemical carcinogens [215]. This is a relatively young, but growing field of research that has the potential to provide viable strategies for long-term reductions in cancer risks. Individuals may only have to monitor their dietary intake of selected vegetables and herbs to enjoy significantly reduced cancer risk. However, this may work for reducing some types of cancer and not others.

The relative contribution of endogenous versus exogenous causes of human cancer is still a matter of some debate. Since the carcinogenic impacts of endogenous and exogenous are completely intertwined, separating out individual contributions is very difficult. Only in selective cases where signature diseases and/or signature biomarkers such as specific DNA adducts and/or mutations are identifiable can the contributions be estimated in rough manner [116]. This is a problem that is likely to remain for many years to come. Learning and understanding many of the xenobiotics in our food and environment to which humans are presently exposed continues to be a prominent field of safety research. Add in the large influx of synthetic chemical compounds joining our environmental melee each year, many of which may contribute to the carcinogenic impacts, and identifying all carcinogens in our environment becomes a rather daunting undertaking. For example, the explosion in designed nanoparticles for industrial and medical purposes, introduces potentially genotoxic agents into the realm of human exposure. At least some synthetic nanomaterials have thus far been found to cause chromosomal aberrations, DNA breaks, point mutations, and oxidative DNA damage [216]. Control of occupational exposures and environmental releases of these new genotoxic synthetic compounds will be important in opposing additions to the causes of environmental carcinogenesis.

The lessons learned from the classical examples of environmental carcinogenesis (sunlight and skin cancer, tobacco smoke and lung cancer, and alflatoxin, hepatitis and liver cancer) have guided research studies and advances in understanding cancer development. Continued advances in understanding the tissue, cellular and molecular processes of carcinogenesis will enable the design of strategies to further diminish cancer incidence and reduce risks throughout life.

Bibliography

1. Ferguson LR, Philpott M (2008) Nutrition and mutagenesis. Annu Rev Nutr 28:313–329
2. Dybing E, O'Brien J, Renwick AG, Sanner T (2008) Risk assessment of dietary exposures to compounds that are genotoxic and carcinogenic–an overview. Toxicol Lett 180(2):110–117
3. Hashimoto K, Higuchi M, Makino B, Sakakibara I, Kubo M, Komatsu Y, Maruno M, Okada M (1999) Quantitative analysis of aristolochic acids, toxic compounds, contained in some medicinal plants. J Ethnopharmacol 64(2):185–189
4. Nortier JL, Martinez MC, Schmeiser HH, Arlt VM, Bieler CA, Petein M, Depierreux MF, De Pauw L, Abramowicz D, Vereerstraeten P, Vanherweghem JL (2000) Urothelial carcinoma associated with the use of a Chinese herb (Aristolochia fangchi). N Engl J Med 342(23):1686–1692
5. Lai MN, Wang SM, Chen PC, Chen YY, Wang JD (2010) Population-based case-control study of Chinese herbal products containing aristolochic acid and urinary tract cancer risk. J Natl Cancer Inst 102(3):179–186
6. Christman JK, Sheikhnejad G, Dizik M, Abileah S, Wainfan E (1993) Reversibility of changes in nucleic acid methylation and gene expression induced in rat liver by severe dietary methyl deficiency. Carcinogenesis 14(4):551–557
7. Pufulete M, Al-Ghnaniem R, Rennie JA, Appleby P, Harris N, Gout S, Emery PW, Sanders TA (2005) Influence of folate status on genomic DNA methylation in colonic mucosa of subjects without colorectal adenoma or cancer. Br J Cancer 92(5):838–842
8. Pogribny IP, Ross SA, Wise C, Pogribna M, Jones EA, Tryndyak VP, James SJ, Dragan YP, Poirier LA (2006) Irreversible global DNA hypomethylation as a key step in hepatocarcinogenesis induced by dietary methyl deficiency. Mutat Res 593(1–2):80–87
9. Robinson JK (2005) Sun exposure, sun protection, and vitamin D. JAMA 294(12):1541–1543
10. Rogers HW, Weinstock MA, Harris AR, Hinckley MR, Feldman SR, Fleischer AB, Coldiron BM (2010) Incidence estimate of nonmelanoma skin cancer in the United States, 2006. Arch Dermatol 146(3):283–287
11. Kao SC, Reid G, Lee K, Vardy J, Clarke S, van Zandwijk N (2010) Malignant mesothelioma. Intern Med J 40(11):742–750
12. Boffetta P, Hashibe M (2006) Alcohol and cancer. Lancet Oncol 7(2):149–156
13. Seitz HK, Stickel F (2007) Molecular mechanisms of alcohol-mediated carcinogenesis. Nat Rev Cancer 7(8):599–612
14. Pelucchi C, Gallus S, Garavello W, Bosetti C, La Vecchia C (2008) Alcohol and tobacco use, and cancer risk for upper aerodigestive tract and liver. Eur J Cancer Prev 17(4): 340–344

15. Hecht SS, Kassie F, Hatsukami DK (2009) Chemoprevention of lung carcinogenesis in addicted smokers and ex-smokers. Nat Rev Cancer 9(7):476–488
16. McKillop IH, Schrum LW (2009) Role of alcohol in liver carcinogenesis. Semin Liver Dis 29(2):222–232
17. He S, Nakada D, Morrison SJ (2009) Mechanisms of stem cell self-renewal. Annu Rev Cell Dev Biol 25:377–406
18. United States Cancer Statistics (USCS) (1999–2006) Cancer Incidence and Mortality Data, National Program of Cancer Registries (NPCR), Center for Disease Control and Prevention, Department of Health and Human Services, USA. http://apps.nccd.cdc.gov/uscs/index.aspx. Accessed March 2010
19. Bielas JH, Loeb LA (2005) Mutator phenotype in cancer: timing and perspectives. Environ Mol Mutagen 45(2–3):206–213
20. Stratton MR, Campbell PJ, Futreal PA (2009) The cancer genome. Nature 458(7239):719–724
21. Ames BN (1989) Endogenous oxidative DNA damage, aging, and cancer. Free Radic Res Commun 7(3–6):121–128
22. Loft S, Poulsen HE (1998) Estimation of oxidative DNA damage in man from urinary excretion of repair products. Acta Biochim Pol 45(1):133–144
23. Shigenaga MK, Gimeno CJ, Ames BN (1989) Urinary 8-hydroxy-2′-deoxyguanosine as a biological marker of in vivo oxidative DNA damage. Proc Natl Acad Sci USA 86(24):9697–9701
24. Cooke MS, Evans MD, Dizdaroglu M, Lunec J (2003) Oxidative DNA damage: mechanisms, mutation, and disease. FASEB J 17(10):1195–1214
25. Hussain SP, Harris CC (2007) Inflammation and cancer: an ancient link with novel potentials. Int J Cancer 121(11):2373–2380
26. Dahlmann HA, Vaidyanathan VG, Sturla SJ (2009) Investigating the biochemical impact of DNA damage with structure-based probes: abasic sites, photodimers, alkylation adducts, and oxidative lesions. Biochemistry 48(40):9347–9359
27. Sedelnikova OA, Redon CE, Dickey JS, Nakamura AJ, Georgakilas AG, Bonner WM (2010) Role of oxidatively induced DNA lesions in human pathogenesis. Mutat Res.
28. Yuan J, Narayanan L, Rockwell S, Glazer PM (2000) Diminished DNA repair and elevated mutagenesis in mammalian cells exposed to hypoxia and low pH. Cancer Res 60(16):4372–4376
29. Camenisch U, Naegeli H (2009) Role of DNA repair in the protection against genotoxic stress. EXS 99:111–150
30. Goldsby RE, Lawrence NA, Hays LE, Olmsted EA, Chen X, Singh M, Preston BD (2001) Defective DNA polymerase-delta proofreading causes cancer susceptibility in mice. Nat Med 7(6):638–639
31. Loeb LA, Bielas JH, Beckman RA (2008) Cancers exhibit a mutator phenotype: clinical implications. Cancer Res 68(10):3551–3557, discussion 3557
32. Zegerman P, Diffley JF (2009) DNA replication as a target of the DNA damage checkpoint. DNA Repair (Amst) 8(9):1077–1088
33. Hanahan D, Weinberg RA (2000) The hallmarks of cancer. Cell 100(1):57–70
34. van der Flier LG, Clevers H (2009) Stem cells, self-renewal, and differentiation in the intestinal epithelium. Annu Rev Physiol 71:241–260
35. Weinberg RA (2008) Mechanisms of malignant progression. Carcinogenesis 29(6):1092–1095
36. Weinberg RA (2008) Coevolution in the tumor microenvironment. Nat Genet 40(5):494–495
37. Chatten C, Bathe OF (2010) Immunoregulatory cells of the tumor microenvironment. Front Biosci 15:291–308
38. Peto J (2001) Cancer epidemiology in the last century and the next decade. Nature 411(6835):390–395
39. Loeb LA, Harris CC (2008) Advances in chemical carcinogenesis: a historical review and prospective. Cancer Res 68(17):6863–6872
40. Jiricny J (2006) The multifaceted mismatch-repair system. Nat Rev Mol Cell Biol 7(5):335–346
41. McCulloch SD, Kunkel TA (2008) The fidelity of DNA synthesis by eukaryotic replicative and translesion synthesis polymerases. Cell Res 18(1):148–161
42. Kunkel TA (2009) Evolving views of DNA replication (In)fidelity. Cold Spring Harbour Symp Quant Biol 74:91–101
43. Hussain SP, He P, Subleski J, Hofseth LJ, Trivers GE, Mechanic L, Hofseth AB, Bernard M, Schwank J, Nguyen G, Mathe E, Djurickovic D, Haines D, Weiss J, Back T, Gruys E, Laubach VE, Wiltrout RH, Harris CC (2008) Nitric oxide is a key component in inflammation-accelerated tumorigenesis. Cancer Res 68(17):7130–7136
44. Fearon ER, Vogelstein B (1990) A genetic model for colorectal tumorigenesis. Cell 61(5):759–767
45. Blanquet V, Turleau C, Gross-Morand MS, Senamaud-Beaufort C, Doz F, Besmond C (1995) Spectrum of germline mutations in the RB1 gene: a study of 232 patients with hereditary and non hereditary retinoblastoma. Hum Mol Genet 4(3):383–388
46. Hussain SP, Harris CC (1998) Molecular epidemiology of human cancer: contribution of mutation spectra studies of tumor suppressor genes. Cancer Res 58(18):4023–4037
47. Wilson VL (2001) Detecting rare mutations associated with cancer risk. Am J Pharmacogenomics 1(4):283–293
48. Tapp RA, Feng J, Jones JW, Carlson JA, Wilson VL (2007) Single base instability is promoted in vulvar lichen sclerosus. J Invest Dermatol 127(11):2563–2576
49. Petitjean A, Mathe E, Kato S, Ishioka C, Tavtigian SV, Hainaut P, Olivier M (2007) Impact of mutant p53 functional properties on TP53 mutation patterns and tumor phenotype: lessons from recent developments in the IARC TP53 database. Hum Mutat 28(6):622–629
50. Stenson PD, Mort M, Ball EV, Howells K, Phillips AD, Thomas NS, Cooper DN (2009) The Human Gene Mutation Database: 2008 update. Genome Med 1(1):13
51. Kumar R, Angelini S, Hemminki K (2003) Activating BRAF and N-Ras mutations in sporadic primary melanomas: an inverse association with allelic loss on chromosome 9. Oncogene 22(58):9217–9224
52. Aplan PD (2006) Causes of oncogenic chromosomal translocation. Trends Genet 22(1):46–55
53. MacCorkle RA, Slattery SD, Nash DR, Brinkley BR (2006) Intracellular protein binding to asbestos induces aneuploidy in human lung fibroblasts. Cell Motil Cytoskeleton 63(10):646–657

54. Pavanello S, Pesatori AC, Dioni L, Hoxha M, Bollati V, Siwinska E, Mielzynska D, Bolognesi C, Bertazzi PA, Baccarelli A (2010) Shorter telomere length in peripheral blood lymphocytes of workers exposed to polycyclic aromatic hydrocarbons. Carcinogenesis 31(2):216–221
55. Hirao T, Nelson HH, Ashok TD, Wain JC, Mark EJ, Christiani DC, Wiencke JK, Kelsey KT (2001) Tobacco smoke-induced DNA damage and an early age of smoking initiation induce chromosome loss at 3p21 in lung cancer. Cancer Res 61(2):612–615
56. Saletta F, Matullo G, Manuguerra M, Arena S, Bardelli A, Vineis P (2007) Exposure to the tobacco smoke constituent 4-aminobiphenyl induces chromosomal instability in human cancer cells. Cancer Res 67(15):7088–7094
57. Shinmura K, Iwaizumi M, Igarashi H, Nagura K, Yamada H, Suzuki M, Fukasawa K, Sugimura H (2008) Induction of centrosome amplification and chromosome instability in p53-deficient lung cancer cells exposed to benzo[a]pyrene diol epoxide (B[a]PDE). J Pathol 216(3):365–374
58. Groopman JD, Donahue PR, Zhu JQ, Chen JS, Wogan GN (1985) Aflatoxin metabolism in humans: detection of metabolites and nucleic acid adducts in urine by affinity chromatography. Proc Natl Acad Sci USA 82(19):6492–6496
59. Groopman JD, Wild CP, Hasler J, Junshi C, Wogan GN, Kensler TW (1993) Molecular epidemiology of aflatoxin exposures: validation of aflatoxin-N7-guanine levels in urine as a biomarker in experimental rat models and humans. Environ Health Perspect 99:107–113
60. Essigmann JM, Wood ML (1993) The relationship between the chemical structures and mutagenic specificities of the DNA lesions formed by chemical and physical mutagens. Toxicol Lett 67(1–3):29–39
61. Batzer MA, Deininger PL (2002) Alu repeats and human genomic diversity. Nat Rev Genet 3(5):370–379
62. Konkel MK, Batzer MA (2010) A mobile threat to genome stability: The impact of non-LTR retrotransposons upon the human genome. Semin Cancer Biol 20(4):211–221
63. Callinan PA, Batzer MA (2006) Retrotransposable elements and human disease. Genome Dyn 1:104–115
64. Jones PA, Liang G (2009) Rethinking how DNA methylation patterns are maintained. Nat Rev Genet 10(11):805–811
65. Lister R, Pelizzola M, Dowen RH, Hawkins RD, Hon G, Tonti-Filippini J, Nery JR, Lee L, Ye Z, Ngo QM, Edsall L, Antosiewicz-Bourget J, Stewart R, Ruotti V, Millar AH, Thomson JA, Ren B, Ecker JR (2009) Human DNA methylomes at base resolution show widespread epigenomic differences. Nature 462(7271):315–322
66. Schubeler D (2009) Epigenomics: Methylation matters. Nature 462(7271):296–297
67. Guil S, Esteller M (2009) DNA methylomes, histone codes and miRNAs: tying it all together. Int J Biochem Cell Biol 41(1):87–95
68. Lopez-Serra L, Esteller M (2008) Proteins that bind methylated DNA and human cancer: reading the wrong words. Br J Cancer 98(12):1881–1885
69. Esteller M (2008) Epigenetics in cancer. N Engl J Med 358(11):1148–1159
70. Sharma S, Kelly TK, Jones PA (2010) Epigenetics in cancer. Carcinogenesis 31(1):27–36
71. Wilson VL, Jones PA (1983) Inhibition of DNA methylation by chemical carcinogens in vitro. Cell 32(1):239–246
72. Wilson VL, Smith RA, Longoria J, Liotta MA, Harper CM, Harris CC (1987) Chemical carcinogen-induced decreases in genomic 5-methyldeoxycytidine content of normal human bronchial epithelial cells. Proc Natl Acad Sci USA 84(10):3298–3301
73. Chanda S, Dasgupta UB, Guhamazumder D, Gupta M, Chaudhuri U, Lahiri S, Das S, Ghosh N, Chatterjee D (2006) DNA hypermethylation of promoter of gene p53 and p16 in arsenic-exposed people with and without malignancy. Toxicol Sci 89(2):431–437
74. Bollati V, Baccarelli A, Hou L, Bonzini M, Fustinoni S, Cavallo D, Byun HM, Jiang J, Marinelli B, Pesatori AC, Bertazzi PA, Yang AS (2007) Changes in DNA methylation patterns in subjects exposed to low-dose benzene. Cancer Res 67(3):876–880
75. Baccarelli A, Bollati V (2009) Epigenetics and environmental chemicals. Curr Opin Pediatr 21(2):243–251
76. Luger K, Mader AW, Richmond RK, Sargent DF, Richmond TJ (1997) Crystal structure of the nucleosome core particle at 2.8 A resolution. Nature 389(6648):251–260
77. Malik HS, Henikoff S (2003) Phylogenomics of the nucleosome. Nat Struct Biol 10(11):882–891
78. Allfrey VG, Faulkner R, Mirsky AE (1964) Acetylation and Methylation of Histones and Their Possible Role in the Regulation of Rna Synthesis. Proc Natl Acad Sci USA 51:786–794
79. Kondo Y, Shen L, Yan PS, Huang TH, Issa JP (2004) Chromatin immunoprecipitation microarrays for identification of genes silenced by histone H3 lysine 9 methylation. Proc Natl Acad Sci USA 101(19):7398–7403
80. McKittrick E, Gafken PR, Ahmad K, Henikoff S (2004) Histone H3.3 is enriched in covalent modifications associated with active chromatin. Proc Natl Acad Sci USA 101(6):1525–1530
81. Kondo Y, Shen L, Ahmed S, Boumber Y, Sekido Y, Haddad BR, Issa JP (2008) Downregulation of histone H3 lysine 9 methyltransferase G9a induces centrosome disruption and chromosome instability in cancer cells. PLoS ONE 3(4):e2037
82. Yamada T, Mizuno K, Hirota K, Kon N, Wahls WP, Hartsuiker E, Murofushi H, Shibata T, Ohta K (2004) Roles of histone acetylation and chromatin remodeling factor in a meiotic recombination hotspot. EMBO J 23(8):1792–1803
83. Toh GW, O'Shaughnessy AM, Jimeno S, Dobbie IM, Grenon M, Maffini S, O'Rorke A, Lowndes NF (2006) Histone H2A phosphorylation and H3 methylation are required for a novel Rad9 DSB repair function following checkpoint activation. DNA Repair (Amst) 5(6):693–703
84. Shahbazian MD, Zhang K, Grunstein M (2005) Histone H2B ubiquitylation controls processive methylation but not monomethylation by Dot1 and Set1. Mol Cell 19(2):271–277
85. Iniguez-Lluhi JA (2006) For a healthy histone code, a little SUMO in the tail keeps the acetyl away. ACS Chem Biol 1(4):204–206
86. Biel M, Wascholowski V, Giannis A (2005) Epigenetics–an epicenter of gene regulation: histones and histone-modifying enzymes. Angew Chem Int Ed Engl 44(21):3186–3216

87. Henikoff S (2005) Histone modifications: combinatorial complexity or cumulative simplicity? Proc Natl Acad Sci USA 102(15):5308–5309
88. Talasz H, Lindner HH, Sarg B, Helliger W (2005) Histone H4-lysine 20 monomethylation is increased in promoter and coding regions of active genes and correlates with hyperacetylation. J Biol Chem 280(46):38814–38822
89. Schneider J, Wood A, Lee JS, Schuster R, Dueker J, Maguire C, Swanson SK, Florens L, Washburn MP, Shilatifard A (2005) Molecular regulation of histone H3 trimethylation by COMPASS and the regulation of gene expression. Mol Cell 19(6):849–856
90. Khalil AM, Driscoll DJ (2006) Histone H3 lysine 4 dimethylation is enriched on the inactive sex chromosomes in male meiosis but absent on the inactive X in female somatic cells. Cytogenet Genome Res 112(1–2):11–15
91. Kondo Y, Shen L, Cheng AS, Ahmed S, Boumber Y, Charo C, Yamochi T, Urano T, Furukawa K, Kwabi–Addo B, Gold DL, Sekido Y, Huang TH, Issa JP (2008) Gene silencing in cancer by histone H3 lysine 27 trimethylation independent of promoter DNA methylation. Nat Genet 40(6):741–750
92. Taverna SD, Li H, Ruthenburg AJ, Allis CD, Patel DJ (2007) How chromatin-binding modules interpret histone modifications: lessons from professional pocket pickers. Nat Struct Mol Biol 14(11):1025–1040
93. Kurdistani SK, Grunstein M (2003) Histone acetylation and deacetylation in yeast. Nat Rev Mol Cell Biol 4(4): 276–284
94. Roth SY, Denu JM, Allis CD (2001) Histone acetyltransferases. Annu Rev Biochem 70:81–120
95. Brownell JE, Zhou J, Ranalli T, Kobayashi R, Edmondson DG, Roth SY, Allis CD (1996) Tetrahymena histone acetyltransferase A: a homolog to yeast Gcn5p linking histone acetylation to gene activation. Cell 84(6):843–851
96. Finnin MS, Donigian JR, Cohen A, Richon VM, Rifkind RA, Marks PA, Breslow R, Pavletich NP (1999) Structures of a histone deacetylase homologue bound to the TSA and SAHA inhibitors. Nature 401(6749):188–193
97. Gray SG, Ekstrom TJ (2001) The human histone deacetylase family. Exp Cell Res 262(2):75–83
98. Dokmanovic M, Clarke C, Marks PA (2007) Histone deacetylase inhibitors: overview and perspectives. Mol Cancer Res 5(10):981–989
99. Verdin E, Dequiedt F, Kasler HG (2003) Class II histone deacetylases: versatile regulators. Trends Genet 19(5): 286–293
100. Sengupta N, Seto E (2004) Regulation of histone deacetylase activities. J Cell Biochem 93(1):57–67
101. Gutierrez RM, Hnilica LS (1967) Tissue specificity of histone phosphorylation. Science 157(794):1324–1325
102. Wei Y, Mizzen CA, Cook RG, Gorovsky MA, Allis CD (1998) Phosphorylation of histone H3 at serine 10 is correlated with chromosome condensation during mitosis and meiosis in Tetrahymena. Proc Natl Acad Sci USA 95(13):7480–7484
103. Hirota T, Lipp JJ, Toh BH, Peters JM (2005) Histone H3 serine 10 phosphorylation by Aurora B causes HP1 dissociation from heterochromatin. Nature 438(7071):1176–1180
104. Goto H, Tomono Y, Ajiro K, Kosako H, Fujita M, Sakurai M, Okawa K, Iwamatsu A, Okigaki T, Takahashi T, Inagaki M (1999) Identification of a novel phosphorylation site on histone H3 coupled with mitotic chromosome condensation. J Biol Chem 274(36):25543–25549
105. Preuss U, Landsberg G, Scheidtmann KH (2003) Novel mitosis-specific phosphorylation of histone H3 at Thr11 mediated by Dlk/ZIP kinase. Nucleic Acids Res 31(3):878–885
106. Barratt MJ, Hazzalin CA, Cano E, Mahadevan LC (1994) Mitogen-stimulated phosphorylation of histone H3 is targeted to a small hyperacetylation-sensitive fraction. Proc Natl Acad Sci USA 91(11):4781–4785
107. Cheung P, Tanner KG, Cheung WL, Sassone-Corsi P, Denu JM, Allis CD (2000) Synergistic coupling of histone H3 phosphorylation and acetylation in response to epidermal growth factor stimulation. Mol Cell 5(6):905–915
108. Clayton AL, Rose S, Barratt MJ, Mahadevan LC (2000) Phosphoacetylation of histone H3 on c-fos- and c-jun-associated nucleosomes upon gene activation. EMBO J 19(14):3714–3726
109. Panier S, Durocher D (2009) Regulatory ubiquitylation in response to DNA double-strand breaks. DNA Repair (Amst) 8(4):436–443
110. Galanty Y, Belotserkovskaya R, Coates J, Polo S, Miller KM, Jackson SP (2009) Mammalian SUMO E3-ligases PIAS1 and PIAS4 promote responses to DNA double-strand breaks. Nature 462(7275):935–939
111. Morris JR, Boutell C, Keppler M, Densham R, Weekes D, Alamshah A, Butler L, Galanty Y, Pangon L, Kiuchi T, Ng T, Solomon E (2009) The SUMO modification pathway is involved in the BRCA1 response to genotoxic stress. Nature 462(7275):886–890
112. An JY, Kim EA, Jiang Y, Zakrzewska A, Kim DE, Lee MJ, Mook-Jung I, Zhang Y, Kwon YT (2010) UBR2 mediates transcriptional silencing during spermatogenesis via histone ubiquitination. Proc Natl Acad Sci USA 107(5):1912–1917
113. Grazini U, Zanardi F, Citterio E, Casola S, Goding CR, McBlane F (2010) The RING domain of RAG1 ubiquitylates histone H3: a novel activity in chromatin-mediated regulation of V(D)J joining. Mol Cell 37(2):282–293
114. Lu LY, Wu J, Ye L, Gavrilina GB, Saunders TL, Yu X (2010) RNF8-dependent histone modifications regulate nucleosome removal during spermatogenesis. Dev Cell 18(3):371–384
115. Mabruk MJ, Toh LK, Murphy M, Leader M, Kay E, Murphy GM (2009) Investigation of the effect of UV irradiation on DNA damage: comparison between skin cancer patients and normal volunteers. J Cutan Pathol 36(7):760–765
116. Wogan GN, Hecht SS, Felton JS, Conney AH, Loeb LA (2004) Environmental and chemical carcinogenesis. Semin Cancer Biol 14(6):473–486
117. Lee WR, Perantie DC, Clark KB, Guillot DA, Wilson VL (2001) Effect of mutagen-induced cell lethality on the dose

response of germline mutations. Environ Mol Mutagen 37(4):340–344
118. Ellison KS, Dogliotti E, Connors TD, Basu AK, Essigmann JM (1989) Site-specific mutagenesis by O6-alkylguanines located in the chromosomes of mammalian cells: influence of the mammalian O6-alkylguanine-DNA alkyltransferase. Proc Natl Acad Sci USA 86(22):8620–8624
119. Dosanjh MK, Singer B, Essigmann JM (1991) Comparative mutagenesis of O6-methylguanine and O4-methylthymine in Escherichia coli. Biochemistry 30(28):7027–7033
120. Potten CS, Booth C (2002) Keratinocyte stem cells: a commentary. J Invest Dermatol 119(4):888–899
121. Bapat SA (2007) Evolution of cancer stem cells. Semin Cancer Biol 17(3):204–213
122. Orford KW, Scadden DT (2008) Deconstructing stem cell self-renewal: genetic insights into cell-cycle regulation. Nat Rev Genet 9(2):115–128
123. Yahata T, Muguruma Y, Yumino S, Sheng Y, Uno T, Matsuzawa H, Ito M, Kato S, Hotta T, Ando K (2008) Quiescent human hematopoietic stem cells in the bone marrow niches organize the hierarchical structure of hematopoiesis. Stem Cells 26(12):3228–3236
124. Karpowicz P, Morshead C, Kam A, Jervis E, Ramunas J, Cheng V, van der Kooy D (2005) Support for the immortal strand hypothesis: neural stem cells partition DNA asymmetrically in vitro. J Cell Biol 170(5):721–732
125. Lechler T, Fuchs E (2005) Asymmetric cell divisions promote stratification and differentiation of mammalian skin. Nature 437(7056):275–280
126. Smith GH (2005) Label-retaining epithelial cells in mouse mammary gland divide asymmetrically and retain their template DNA strands. Development 132(4):681–687
127. Cairns J (1975) Mutation selection and the natural history of cancer. Nature 255(5505):197–200
128. Potten CS, Grant HK (1998) The relationship between ionizing radiation-induced apoptosis and stem cells in the small and large intestine. Br J Cancer 78(8):993–1003
129. Lee JM, Dedhar S, Kalluri R, Thompson EW (2006) The epithelial-mesenchymal transition: new insights in signaling, development, and disease. J Cell Biol 172(7):973–981
130. Rubin H (2001) The role of selection in progressive neoplastic transformation. Adv Cancer Res 83:159–207
131. Negrini S, Gorgoulis VG, Halazonetis TD (2010) Genomic instability–an evolving hallmark of cancer. Nat Rev Mol Cell Biol 11(3):220–228
132. Beckman RA, Loeb LA (2006) Efficiency of carcinogenesis with and without a mutator mutation. Proc Natl Acad Sci USA 103(38):14140–14145
133. Chu WK, Hickson ID (2009) RecQ helicases: multifunctional genome caretakers. Nat Rev Cancer 9(9):644–654
134. Lengauer C, Kinzler KW, Vogelstein B (1998) Genetic instabilities in human cancers. Nature 396(6712):643–649
135. Ganem NJ, Godinho SA, Pellman D (2009) A mechanism linking extra centrosomes to chromosomal instability. Nature 460(7252):278–282
136. Weaver BA, Silk AD, Montagna C, Verdier-Pinard P, Cleveland DW (2007) Aneuploidy acts both oncogenically and as a tumor suppressor. Cancer Cell 11(1):25–36
137. Thompson SL, Compton DA (2008) Examining the link between chromosomal instability and aneuploidy in human cells. J Cell Biol 180(4):665–672
138. Torres EM, Williams BR, Amon A (2008) Aneuploidy: cells losing their balance. Genetics 179(2):737–746
139. Hussein MR, Wood GS (2002) Microsatellite instability and its relevance to cutaneous tumorigenesis. J Cutan Pathol 29(5):257–267
140. Dietmaier W, Wallinger S, Bocker T, Kullmann F, Fishel R, Ruschoff J (1997) Diagnostic microsatellite instability: definition and correlation with mismatch repair protein expression. Cancer Res 57(21):4749–4756
141. Boland CR, Thibodeau SN, Hamilton SR, Sidransky D, Eshleman JR, Burt RW, Meltzer SJ, Rodriguez-Bigas MA, Fodde R, Ranzani GN, Srivastava S (1998) A National Cancer Institute Workshop on Microsatellite Instability for cancer detection and familial predisposition: development of international criteria for the determination of microsatellite instability in colorectal cancer. Cancer Res 58(22): 5248–5257
142. Hoeijmakers JH (2001) Genome maintenance mechanisms for preventing cancer. Nature 411(6835):366–374
143. Jascur T, Boland CR (2006) Structure and function of the components of the human DNA mismatch repair system. Int J Cancer 119(9):2030–2035
144. Thibodeau SN, French AJ, Roche PC, Cunningham JM, Tester DJ, Lindor NM, Moslein G, Baker SM, Liskay RM, Burgart LJ, Honchel R, Halling KC (1996) Altered expression of hMSH2 and hMLH1 in tumors with microsatellite instability and genetic alterations in mismatch repair genes. Cancer Res 56(21):4836–4840
145. Hussein MR, Wood GS (2002) Microsatellite instability in human melanocytic skin tumors: an incidental finding or a pathogenetic mechanism? J Cutan Pathol 29(1):1–4
146. Fishel R, Lescoe MK, Rao MR, Copeland NG, Jenkins NA, Garber J, Kane M, Kolodner R (1993) The human mutator gene homolog MSH2 and its association with hereditary nonpolyposis colon cancer. Cell 75(5):1027–1038
147. Leach FS, Nicolaides NC, Papadopoulos N, Liu B, Jen J, Parsons R, Peltomaki P, Sistonen P, Aaltonen LA, Nystrom-Lahti M et al (1993) Mutations of a mutS homolog in hereditary nonpolyposis colorectal cancer. Cell 75(6):1215–1225
148. Garcon G, Dagher Z, Zerimech F, Ledoux F, Courcot D, Aboukais A, Puskaric E, Shirali P (2006) Dunkerque City air pollution particulate matter-induced cytotoxicity, oxidative stress and inflammation in human epithelial lung cells (L132) in culture. Toxicol In Vitro 20(4):519–528
149. Saint-Georges F, Garcon G, Escande F, Abbas I, Verdin A, Gosset P, Mulliez P, Shirali P (2009) Role of air pollution Particulate Matter (PM(2.5)) in the occurrence of loss of heterozygosity in multiple critical regions of 3p chromosome in human epithelial lung cells (L132). Toxicol Lett 187(3):172–179

150. Hirose T, Kondo K, Takahashi Y, Ishikura H, Fujino H, Tsuyuguchi M, Hashimoto M, Yokose T, Mukai K, Kodama T, Monden Y (2002) Frequent microsatellite instability in lung cancer from chromate-exposed workers. Mol Carcinog 33(3):172–180
151. Zienolddiny S, Aguelon AM, Mironov N, Mathew B, Thomas G, Sankaranarayanan R, Yamasaki H (2004) Genomic instability in oral squamous cell carcinoma: relationship to betel-quid chewing. Oral Oncol 40(3):298–303
152. Parsons BL, Marchant-Miros KE, Delongchamp RR, Verkler TL, Patterson TA, McKinzie PB, Kim LT (2010) ACB-PCR quantification of K-RAS codon 12 GAT and GTT mutant fraction in colon tumor and non-tumor tissue. Cancer Invest 28(4):364–375
153. Toyota M, Ahuja N, Ohe-Toyota M, Herman JG, Baylin SB, Issa JP (1999) CpG island methylator phenotype in colorectal cancer. Proc Natl Acad Sci USA 96(15):8681–8686
154. Teodoridis JM, Hardie C, Brown R (2008) CpG island methylator phenotype (CIMP) in cancer: causes and implications. Cancer Lett 268(2):177–186
155. Tanemura A, Terando AM, Sim MS, van Hoesel AQ, de Maat MF, Morton DL, Hoon DS (2009) CpG island methylator phenotype predicts progression of malignant melanoma. Clin Cancer Res 15(5):1801–1807
156. Yagi K, Akagi K, Hayashi H, Nagae G, Tsuji S, Isagawa T, Midorikawa Y, Nishimura Y, Sakamoto H, Seto Y, Aburatani H, Kaneda A (2010) Three DNA methylation epigenotypes in human colorectal cancer. Clin Cancer Res 16(1):21–33
157. Gaudet F, Hodgson JG, Eden A, Jackson-Grusby L, Dausman J, Gray JW, Leonhardt H, Jaenisch R (2003) Induction of tumors in mice by genomic hypomethylation. Science 300(5618):489–492
158. Gama-Sosa MA, Slagel VA, Trewyn RW, Oxenhandler R, Kuo KC, Gehrke CW, Ehrlich M (1983) The 5-methylcytosine content of DNA from human tumors. Nucleic Acids Res 11(19):6883–6894
159. Goelz SE, Vogelstein B, Hamilton SR, Feinberg AP (1985) Hypomethylation of DNA from benign and malignant human colon neoplasms. Science 228(4696):187–190
160. Kim YI, Giuliano A, Hatch KD, Schneider A, Nour MA, Dallal GE, Selhub J, Mason JB (1994) Global DNA hypomethylation increases progressively in cervical dysplasia and carcinoma. Cancer 74(3):893–899
161. Shahrzad S, Bertrand K, Minhas K, Coomber BL (2007) Induction of DNA hypomethylation by tumor hypoxia. Epigenetics 2(2):119–125
162. Avila MA, Carretero MV, Rodriguez EN, Mato JM (1998) Regulation by hypoxia of methionine adenosyltransferase activity and gene expression in rat hepatocytes. Gastroenterology 114(2):364–371
163. Yanagawa N, Tamura G, Honda T, Endoh M, Nishizuka S, Motoyama T (2004) Demethylation of the synuclein gamma gene CpG island in primary gastric cancers and gastric cancer cell lines. Clin Cancer Res 10(7):2447–2451
164. Laner T, Schulz WA, Engers R, Muller M, Florl AR (2005) Hypomethylation of the XIST gene promoter in prostate cancer. Oncol Res 15(5):257–264
165. Fraga MF, Ballestar E, Paz MF, Ropero S, Setien F, Ballestar ML, Heine-Suner D, Cigudosa JC, Urioste M, Benitez J, Boix-Chornet M, Sanchez-Aguilera A, Ling C, Carlsson E, Poulsen P, Vaag A, Stephan Z, Spector TD, Wu YZ, Plass C, Esteller M (2005) Epigenetic differences arise during the lifetime of monozygotic twins. Proc Natl Acad Sci USA 102(30): 10604–10609
166. Kampranis SC, Tsichlis PN (2009) Histone demethylases and cancer. Adv Cancer Res 102:103–169
167. Kristensen LS, Nielsen HM, Hansen LL (2009) Epigenetics and cancer treatment. Eur J Pharmacol 625(1–3):131–142
168. Kinzler KW, Vogelstein B (1997) Cancer-susceptibility genes. Gatekeepers and caretakers. Nature 386(6627):761–763
169. Bardelli A, Cahill DP, Lederer G, Speicher MR, Kinzler KW, Vogelstein B, Lengauer C (2001) Carcinogen-specific induction of genetic instability. Proc Natl Acad Sci USA 98(10):5770–5775
170. Palmero EI, Achatz MI, Ashton-Prolla P, Olivier M, Hainaut P (2010) Tumor protein 53 mutations and inherited cancer: beyond Li-Fraumeni syndrome. Curr Opin Oncol 22(1):64–69
171. Amberger J, Bocchini CA, Scott AF, Hamosh A (2009) McKusick's Online Mendelian Inheritance in Man (OMIM). Nucleic Acids Res. 37(Database issue): D793–D796
172. Cazier JB, Tomlinson I (2010) General lessons from large-scale studies to identify human cancer predisposition genes. J Pathol 220(2):255–262
173. Gresner P, Gromadzinska J, Wasowicz W (2007) Polymorphism of selected enzymes involved in detoxification and biotransformation in relation to lung cancer. Lung Cancer 57(1):1–25
174. Cote ML, Wenzlaff AS, Bock CH, Land SJ, Santer SK, Schwartz DR, Schwartz AG (2007) Combinations of cytochrome P-450 genotypes and risk of early-onset lung cancer in Caucasians and African Americans: a population-based study. Lung Cancer 55(3):255–262
175. Schwartz AG, Prysak GM, Bock CH, Cote ML (2007) The molecular epidemiology of lung cancer. Carcinogenesis 28(3):507–518
176. Cokkinides V, Bandi P, McMahon C, Jemal A, Glynn T, Ward E (2009) Tobacco control in the United States–recent progress and opportunities. CA Cancer J Clin 59(6):352–365
177. Lubin JH, Alavanja MC, Caporaso N, Brown LM, Brownson RC, Field RW, Garcia-Closas M, Hartge P, Hauptmann M, Hayes RB, Kleinerman R, Kogevinas M, Krewski D, Langholz B, Letourneau EG, Lynch CF, Malats N, Sandler DP, Schaffrath-Rosario A, Schoenberg JB, Silverman DT, Wang Z, Wichmann HE, Wilcox HB, Zielinski JM (2007) Cigarette smoking and cancer risk: modeling total exposure and intensity. Am J Epidemiol 166(4):479–489
178. Robles AI, Linke SP, Harris CC (2002) The p53 network in lung carcinogenesis. Oncogene 21(45):6898–6907
179. Olivier M, Hollstein M, Hainaut P (2010) TP53 Mutations in Human Cancers: Origins, Consequences, and Clinical Use. Cold Spring Harb Perspect Biol 2(1):a001008
180. Denissenko MF, Pao A, Tang M, Pfeifer GP (1996) Preferential formation of benzo[a]pyrene adducts at lung cancer mutational hotspots in P53. Science 274(5286):430–432

181. Greenblatt MS, Bennett WP, Hollstein M, Harris CC (1994) Mutations in the p53 tumor suppressor gene: clues to cancer etiology and molecular pathogenesis. Cancer Res 54(18):4855–4878
182. Bennett WP, Hussain SP, Vahakangas KH, Khan MA, Shields PG, Harris CC (1999) Molecular epidemiology of human cancer risk: gene-environment interactions and p53 mutation spectrum in human lung cancer. J Pathol 187(1):8–18
183. Hsu IC, Metcalf RA, Sun T, Welsh JA, Wang NJ, Harris CC (1991) Mutational hotspot in the p53 gene in human hepatocellular carcinomas. Nature 350(6317):427–428
184. Soini Y, Chia SC, Bennett WP, Groopman JD, Wang JS, DeBenedetti VM, Cawley H, Welsh JA, Hansen C, Bergasa NV, Jones EA, DiBisceglie AM, Trivers GE, Sandoval CA, Calderon IE, Munoz Espinosa LE, Harris CC (1996) An aflatoxin-associated mutational hotspot at codon 249 in the p53 tumor suppressor gene occurs in hepatocellular carcinomas from Mexico. Carcinogenesis 17(5):1007–1012
185. Gouas D, Shi H, Hainaut P (2009) The aflatoxin-induced TP53 mutation at codon 249 (R249S): biomarker of exposure, early detection and target for therapy. Cancer Lett 286(1): 29–37
186. Brash DE, Rudolph JA, Simon JA, Lin A, McKenna GJ, Baden HP, Halperin AJ, Ponten J (1991) A role for sunlight in skin cancer: UV-induced p53 mutations in squamous cell carcinoma. Proc Natl Acad Sci USA 88(22):10124–10128
187. Armstrong BK, Kricker A (2001) The epidemiology of UV induced skin cancer. J Photochem Photobiol B 63(1–3):8–18
188. Runger TM (2007) How different wavelengths of the ultraviolet spectrum contribute to skin carcinogenesis: the role of cellular damage responses. J Invest Dermatol 127(9):2103–2105
189. Fang JL, Vaca CE (1997) Detection of DNA adducts of acetaldehyde in peripheral white blood cells of alcohol abusers. Carcinogenesis 18(4):627–632
190. Vaca CE, Nilsson JA, Fang JL, Grafstrom RC (1998) Formation of DNA adducts in human buccal epithelial cells exposed to acetaldehyde and methylglyoxal in vitro. Chem Biol Interact 108(3):197–208
191. Clemens DL, Forman A, Jerrells TR, Sorrell MF, Tuma DJ (2002) Relationship between acetaldehyde levels and cell survival in ethanol-metabolizing hepatoma cells. Hepatology 35(5):1196–1204
192. Molina PE, Hoek JB, Nelson S, Guidot DM, Lang CH, Wands JR, Crawford JM (2003) Mechanisms of alcohol-induced tissue injury. Alcohol Clin Exp Res 27(3):563–575
193. el Ghissassi F, Barbin A, Nair J, Bartsch H (1995) Formation of 1,N6-ethenoadenine and 3,N4-ethenocytosine by lipid peroxidation products and nucleic acid bases. Chem Res Toxicol 8(2):278–283
194. Giovannucci E (2004) Alcohol, one-carbon metabolism, and colorectal cancer: recent insights from molecular studies. J Nutr 134(9):2475S–2481S
195. Giovannucci E (2002) Epidemiologic studies of folate and colorectal neoplasia: a review. J Nutr 132(8 Suppl): 2350S–2355S
196. Leiter U, Garbe C (2008) Epidemiology of melanoma and nonmelanoma skin cancer–the role of sunlight. Adv Exp Med Biol 624:89–103
197. Ridley AJ, Whiteside JR, McMillan TJ, Allinson SL (2009) Cellular and sub-cellular responses to UVA in relation to carcinogenesis. Int J Radiat Biol 85(3):177–195
198. Matsunaga T, Hieda K, Nikaido O (1991) Wavelength dependent formation of thymine dimers and (6–4) photoproducts in DNA by monochromatic ultraviolet light ranging from 150 to 365 nm. Photochem Photobiol 54(3):403–410
199. Lacour JP (2002) Carcinogenesis of basal cell carcinomas: genetics and molecular mechanisms. Br J Dermatol 146(Suppl 61):17–19
200. Agar NS, Halliday GM, Barnetson RS, Ananthaswamy HN, Wheeler M, Jones AM (2004) The basal layer in human squamous tumors harbors more UVA than UVB fingerprint mutations: a role for UVA in human skin carcinogenesis. Proc Natl Acad Sci USA 101(14):4954–4959
201. Kuhn C, Hurwitz SA, Kumar MG, Cotton J, Spandau DF (1999) Activation of the insulin-like growth factor-1 receptor promotes the survival of human keratinocytes following ultraviolet B irradiation. Int J Cancer 80(3):431–438
202. Lewis DA, Spandau DF (2007) UVB activation of NF-kappaB in normal human keratinocytes occurs via a unique mechanism. Arch Dermatol Res 299(2):93–101
203. Lewis DA, Yi Q, Travers JB, Spandau DF (2008) UVB-induced senescence in human keratinocytes requires a functional insulin-like growth factor-1 receptor and p53. Mol Biol Cell 19(4):1346–1353
204. Tavakkol A, Elder JT, Griffiths CE, Cooper KD, Talwar H, Fisher GJ, Keane KM, Foltin SK, Voorhees JJ (1992) Expression of growth hormone receptor, insulin-like growth factor 1 (IGF-1) and IGF-1 receptor mRNA and proteins in human skin. J Invest Dermatol 99(3):343–349
205. Ferber A, Chang C, Sell C, Ptasznik A, Cristofalo VJ, Hubbard K, Ozer HL, Adamo M, Roberts CT Jr, LeRoith D et al (1993) Failure of senescent human fibroblasts to express the insulin-like growth factor-1 gene. J Biol Chem 268: 17883–17888
206. Agents Classified by the IARC Monographs 1–100, Updated 30 August 2010; IARC Monographs on the Evaluation of Carcinogenic Risks to Humans. http://monographs.iarc.fr/ENG/Classification/index.php. Accessed November 2010
207. Hecht SS, Carmella SG, Murphy SE, Akerkar S, Brunnemann KD, Hoffmann D (1993) A tobacco-specific lung carcinogen in the urine of men exposed to cigarette smoke. N Engl J Med 329(21):1543–1546
208. Smoking and Tobacco Control Monograph 10, Health Effects of Exposure to Environmental Tobacco Smoke (August 1999), National Cancer Institute, National Institutes of Health, Bethesda, MD
209. Alexandrov K, Rojas M, Kadlubar FF, Lang NP, Bartsch H (1996) Evidence of anti-benzo[a]pyrene diolepoxide-DNA adduct formation in human colon mucosa. Carcinogenesis 17(9):2081–2083

210. Hecht SS, Hoffmann D (1988) Tobacco-specific nitrosamines, an important group of carcinogens in tobacco and tobacco smoke. Carcinogenesis 9(6):875–884
211. Pleasance ED, Stephens PJ, O'Meara S, McBride DJ, Meynert A, Jones D, Lin ML, Beare D, Lau KW, Greenman C, Varela I, Nik-Zainal S, Davies HR, Ordonez GR, Mudie LJ, Latimer C, Edkins S, Stebbings L, Chen L, Jia M, Leroy C, Marshall J, Menzies A, Butler A, Teague JW, Mangion J, Sun YA, McLaughlin SF, Peckham HE, Tsung EF, Costa GL, Lee CC, Minna JD, Gazdar A, Birney E, Rhodes MD, McKernan KJ, Stratton MR, Futreal PA, Campbell PJ (2010) A small-cell lung cancer genome with complex signatures of tobacco exposure. Nature 463(7278):184–190
212. McCullough ML, Giovannucci EL (2004) Diet and cancer prevention. Oncogene 23(38):6349–6364
213. Kensler TW, Groopman JD (2009) Is it time to advance the chemoprevention of environmental carcinogenesis with microdosing trials? Cancer Prev Res (Phila Pa) 2(12):1003–1007
214. Ju J, Picinich SC, Yang Z, Zhao Y, Suh N, Kong AN, Yang CS (2010) Cancer-preventive activities of tocopherols and tocotrienols. Carcinogenesis 31(4):533–542
215. Fowke JH (2007) Head and neck cancer: a case for inhibition by isothiocyanates and indoles from cruciferous vegetables. Eur J Cancer Prev 16(4):348–356
216. Singh N, Manshian B, Jenkins GJ, Griffiths SM, Williams PM, Maffeis TG, Wright CJ, Doak SH (2009) NanoGenotoxicology: the DNA damaging potential of engineered nanomaterials. Biomaterials 30(23–24):3891–3914

Environmental Toxicology: Children at Risk

Maria J. Carroquino[1], M. Posada[1], P. J. Landrigan[2]
[1]Instituto de Salud Carlos III, Madrid, Spain
[2]Department of Preventive Medicine, Mount Sinai School of Medicine, New York, NY, USA

Article Outline

Glossary
Definition of the Subject
Introduction: Brief History of the Issue of Children's Vulnerability to Environmental Hazards
Toxicological Basis of Children's Vulnerability to Environmental Hazards: Susceptibility and Exposure Factors Affecting Children's Vulnerability
Major Groups of Pollutants to Which Children are Exposed
Environmental Threats to Children on Specific Organ Systems
Future Directions
Bibliography

Glossary

Adult The time of life usually starting at 18 years (some systems such as skeleton and brain may continue to develop).

Adverse effect A treatment-related alteration from baseline that diminishes an organism's ability to survive, reproduce, or adapt to the environment.

Carcinogen Any substance that can cause cancer.

Critical period A specific phase during which a developing system is particularly susceptible.

Developmental disorders/effects Adverse effects such as altered growth, structural abnormality, functional deficiency, or death observed in a developing organism.

Dose (exposure)–response relationship Characterization of the relationship between administered dose or exposure and the biological change in organisms.

Embryonic period The period from fertilization to the end of major organogenesis.

Environmental exposures and environmental hazards For this entry, these terms refer to specific environmental chemicals and environmental pollutants.

Exposure Contact with a chemical by swallowing, by breathing, or by direct contact (such as through the skin or eyes). Exposure may be short term (acute) or long term (chronic).

Fetus The period from 8 weeks of pregnancy to birth.

Gestation Length of time between conception and birth.

Infant The period from 28 days of age to 1 year.

Lowest observed adverse effect level (LOAEL) The lowest concentration of a chemical in a study, or group of studies, that produces statistically or biologically significant increase in the frequency or severity of adverse effects between the exposed population and an appropriate control.

Mechanism of action The detailed molecular knowledge of the key events leading to an adverse effect in an organism.

Neonate The period from birth to 28 days of age.

Perinatal stage The period of 29 weeks of pregnancy to 7 days after birth.

Pregnancy The condition of having an implanted embryo or fetus in the body, after fusion of an ovum and spermatozoon.

Preterm birth A birth occurring at 24–37 weeks of pregnancy.

Risk assessment An empirically based paradigm that estimates the risk of adverse effect(s) from exposure of an individual or population to a chemical, physical, or biological agent. It includes the components of hazard identification, assessment of dose–response relationships, exposure assessment, and risk characterization.

Route of exposure Exposure route refers to the different ways a substance may enter the body. The route may be dermal, ingestion, or inhalation.

Sexual maturation Achievement of full development of the reproductive system and sexual function.

Susceptibility An individual's intrinsic or acquired traits that modify the risk of illness (e.g., high susceptibility to cancer).

Toxicokinetics The process of the uptake of potentially toxic substances by the body, the biotransformation they undergo, the distribution of the substances and their metabolites in the tissues, and the elimination of the substances and their metabolites from the body. Both the amounts and the concentrations of the substances and their metabolites are studied. (Pharmacokinetics is the term used to study pharmaceutical substances.)

Vulnerability A matrix of physical, chemical, biological, social, and cultural factors that result in certain communities and subpopulations being more susceptible to environmental factors because of greater exposure to such factors or a compromised ability to cope with and/or recover from such exposure.

Definition of the Subject

Children today live in a world that is vastly different from a few generations ago. While industrialization has maximized (for many) children's opportunities to survive, develop and enjoy high levels of health, education, recreation, and fulfillment, it has also added significant challenges to their development.

In the countries in the Organization for Economic Co-operation and Development (OECD), an infant born today has about 20 years longer life expectancy than one born at the beginning of the twentieth century [1]. Infant mortality has gone down by over 90%. Despite AIDS, SARS, West Nile virus, and the constant threat of other emerging infections, the ancient epidemics of smallpox, yellow fever, cholera, bubonic plague, polio, and measles are no longer the dominant causes of disease and death. However, an increase in the incidence (new cases) of many chronic diseases in children has been observed. These include asthma, cancer (which is the second leading cause of death in children after injuries), birth defects, developmental disabilities, and autism. For some of these conditions, an environmental origin has been established, and for others it is hypothesized.

Environmental threats to children's health range from asthma-inducing air pollution and lead-based paint in older homes, to treatment-resistant microbes in drinking water and persistent industrial chemicals that may cause cancer or result in reproductive or developmental changes.

Patterns of illness among children in the industrially developed nations have changed substantially. Infant mortality has declined. Life expectancy has increased. However, an increase in the incidence (new cases) of some diseases, such as asthma, birth defects, neurodevelopmental disorders and certain types of childhood and adolescence cancers, and obesity has been observed. Evidence is accumulating that toxic chemicals are responsible for at least some of these changing patterns of disease.

Children are uniquely susceptible to chemicals. This great vulnerability reflects the juxtaposition of two phenomena early in life: first, that infants and children have disproportionately greater exposures than adults to environmental chemicals, and second, that children are exquisitely sensitive to these exposures, because they are poorly equipped to metabolize many toxic compounds and because they are progressing through the complex, delicate, and easily disrupted stages of early development. The protection of children from environmental health hazards requires the consideration of their exposure patterns and susceptibility factors when conducting risk assessments, development of child protective legislation, and wider

application of the Precautionary Principle in the face of early warning of danger.

Introduction: Brief History of the Issue of Children's Vulnerability to Environmental Hazards

Children's risks from environmental health threats have received considerable political attention during the last two decades. In 1989, the United Nations Convention on the Rights of the Child laid down basic standards for the protection of children and proclaimed that they are entitled to special care and assistance. A year later, the World Summit for Children (WSC) adopted a Declaration on the Survival, Protection and Development for Children, in which the signatories agreed to join efforts on taking measures to protect the environment, so that all children can enjoy a safer and healthier future.

Agenda 21, adopted in 1992 at the United Nations Conference on Environment and Development ("the Earth Summit") gives attention to the protection of children from the effects of a deteriorating environment in several chapters. Chapter 6 of Agenda 21 "Protecting and Promoting Human Health" emphasizes the need to pay special attention to protecting vulnerable groups, particularly infants, young people, women, indigenous people, and the poor. Agenda 21 urges governments to develop programs to protect children from the effects of environmental and occupational toxic compounds.

In the USA, the National Research Council report [2] "Pesticides in the Diet of Infants and Children" was critical in raising awareness about the importance in risk assessment of children's environmental health. This report elevated concern on a broad national level about children's special vulnerabilities to environmental agents. It made clear that protection of the health of vulnerable populations would require a new approach to risk assessment. The NRC report recommended an approach to risk assessment that moved beyond consideration of average exposures based primarily on adult characteristics to one that accounted for the heterogeneity of exposures and for potential differential sensitivities of various life stages, particularly during prenatal development, infancy, and childhood.

Responding to recommendations in the NRC report [2], the US Government took decisive steps to attend to the growing concern on children susceptibility to environmental toxicants. In 1995, the EPA issued a National Policy to consistently and explicitly take into account health risks to children and infants from environmental hazards when conducting assessments of environmental risks. In 1997, the Clinton Administration issued an Executive Order, Executive Order 13045: Protection of Children from Environmental Health Risks and Safety Risks. The Executive Order requires all federal agencies to address health and safety risks to children, to coordinate research priorities on children's health, and to ensure that their standards take into account special risks to children. To implement the order, the US EPA established the Office of Children's Health Protection (OCHP) (renamed the Office of Children's Health Protection and Environmental Education – OCHPEE – in 2005), whose job is to work with Program and Regional Offices within the US EPA to promote a safe and healthy environment for children by ensuring that all regulations, standards, policies, and risk assessments take into account risks to children. Legislation, such as the Food Quality Protection Act and the Safe Drinking Water Act amendments, has made coverage of children's health issues more explicit, and research on children's health issues is continually expanding. As a result of the emphasis on children's risk, the US EPA Office of Research and Development (ORD) developed a strategy for research on environmental risks to children. The goal of this research agenda is to discover the environmental causes of disease in children and then to convert these research findings into blueprints for disease prevention and health promotion.

The 1997 Declaration of the Environmental Leaders of the Eight on Children's Environmental Health intensified their commitment to protecting children's health from environmental hazards. The Environment Ministers of the G8 countries acknowledged the special vulnerabilities of children and committed their countries to taking action on several specific environmental health issues such as lead, microbiologically safe drinking water, endocrine disrupting chemicals, environmental tobacco smoke (ETS), and air quality. They called on financial institutions, the World Health Organization (WHO), the United Nations Environment Program (UNEP), and other international bodies to continue ongoing

activities and to pay further attention to children's environmental health, in particular the economic and social dimensions of children's health. In addition, they committed their countries to fulfilling and to promoting the Organization for Economic Co-operation and Development (OECD) Declaration on Risk Reduction for Lead. The underlying rationale for each of these actions is that disease of environmental origin in children can be prevented by controlling harmful exposures in the environment.

International organizations such as the World Health Organization (WHO), the United Nations Environment Program (UNEP), and the European Union (EU) responded to this call and also developed initiatives on Children, Environment and Health. Children's Health and Environment has been the central focus of Europe wide Ministerial Conferences organized by WHO, and other EU initiatives, such as SCALE (Science, Children, Awareness, Legal Instrument, Evaluation). Thus, the protection of children from environmental hazards has been a subject of intense political and scientific attention and effort during the last two decades. Since the initial reports on this issue, research has intensified, and scientific literature abounds with new findings on children's differential vulnerability to environmental health threats that have provided the basis to maintaining the political attention on children's health.

Toxicological Basis of Children's Vulnerability to Environmental Hazards: Susceptibility and Exposure Factors Affecting Children's Vulnerability

Over the past 2 decades, a number of scientific reports have integrated the knowledge available on the susceptibility of children to environmental toxicants, have highlighted knowledge gaps, and have pointed to future directions of research to fill these gaps. This has expanded and deepened the knowledge of the differential susceptibility of children to environmental toxicants, and at the same time has allowed the firm establishment of certain fundamentals concerning children's susceptibility to environmental toxicants.

The International Life Science Institute (ILSI) and the EPA, recognizing the need for examining the scientific evidence on the broad question of the differential susceptibility of children to environmental hazards, organized in 1990 a conference titled: "Similarities and Differences Between Children and Adults: Implications for Risk Assessment." The results from this conference were summarized in the publication "Similarities and Differences Between Children and Adults" [3] and was incorporated into ongoing work of the National Research Committee on Pesticides in the Diets of Infants and Children. The National Academy of Science (NAS) published the NRC report "Pesticides in the Diets of Infants and Children" [2], which was critical in raising awareness of the importance of considering the vulnerable life stages of children when conducting risk assessment of exposures to children. In 2001, the International Life Sciences Institute convened a number of scientific experts to develop a conceptual framework for conducting health risk assessments of children exposures, which takes into consideration their unique characteristics and special vulnerabilities [4].

The ILSI report highlighted the fact that "children are not little adults," but a unique subpopulation that needs to be considered in risk assessment due to differential exposure patterns, immaturity in physiological development, or differential toxicant metabolism.

In 2006, the WHO published the Principles for Evaluating the Health Risks in Children Associated with Exposure to Chemicals in the Environmental Health Criteria 237 [5]. This publication constitutes the most recent monographic work of the subject of children susceptibility to environmental toxicants, and provides comprehensive information on children's developmental stages and the critical windows of susceptibility that appear through the course of their development.

In summary, it is clear from these three major scientific reports – NAS, ILSI, and WHO – that there is broad scientific consensus that risks to children from environmental health threats differ qualitatively or quantitatively from those of adults for a variety of reasons:

- Differential exposure patterns: Compared to adults, children have heavier exposures in relation to body weight because they drink more water, eat more food, and have higher breathing rates per unit of body weight than adults do. As a consequence, children have substantially heavier

exposures than adults to any toxicants that are present in water, food, or air.

- Children's ability to metabolize, detoxify, and excrete chemicals is different from that of adults. During the first months after birth, their metabolic pathways are immature. In some cases, children may actually have a higher metabolic capacity for some toxicants than adults. Commonly, however, they are less able to deal with toxic chemicals and thus are more vulnerable to them.
- Children undergo rapid growth and development, and their development phases are perfectly scheduled to achieve complete functional development. If a development phase is disturbed at a given time, its time to take place may be lost definitively. Thus, interferences with certain phases of development may have irreversible effects. If cells in a child's developing brain are destroyed by chemicals such as lead, mercury, or solvents, or if false signals are sent to the developing reproductive organs by endocrine disruptors, there is a high risk that the resulting dysfunction will be permanent and irreversible.
- Children's exposures are affected qualitatively and quantitatively by their behavior and the unique microenvironment in which they spend their time. Their hand-to-mouth behavior brings contaminated items or soil to their mouth, and living and playing closer to the ground also exposes them to pollutants in a different pattern than adults, both in quantitative and qualitative terms.
- Because children generally have more years of life ahead than adults, they have more time to develop chronic diseases triggered by early exposures. Many diseases, such as cancer and neurodegenerative diseases, are thought to arise through a series of stages that require years or even decades from initiation to actual manifestation of disease. Carcinogenic and toxic exposures, sustained early in life, including prenatal exposures, would then be more likely to lead to disease than similar exposures encountered later.

The purpose of this chapter has been to select, integrate, and summarize the most relevant and illustrative information that explains and highlights the potential susceptibility of children to environmental exposures. The goal of the chapter is to promote understanding of the issue of differential susceptibility and exposures of children to environmental threats among scientists from adjacent fields, and to encourage scientists to consider the issue of children's differential susceptibility and exposures in their research. Recognition of children's exquisite vulnerability to toxic exposures in the environment is critical to child-protective risk assessment and to disease prevention.

For a more in-depth study of any of the particular health issues or particular toxicants, extensive and rigorous reviews that are cited through this document can be consulted. The following sections will elaborate on the general toxicological aspects of children's susceptibility.

Exposure

There are several factors that influence the differential exposures of children to environmental toxicants. These are: (1) their higher ingestion, drinking, and breathing rates per unit of body weight, (2) their unique behaviors, (3) where they spend their time, and (4) their unique microenvironments.

Ingestion, Breathing, and Drinking Rates In toxicology, exposure is defined as the contact that occurs between a receptor (a living organism) and an environmental agent. The most commonly considered exposure pathways are inhalation, ingestion, and dermal absorption. For infants in the womb, transplacental transfer of toxic chemicals is another unique route of exposure, and for nursing infants, the proportion of the toxicant that enters the body through each of these pathways will depend on both external, environmental factors, and on biological factors that will determine the rate of uptake of the chemical by the organism. Exposure can also be referred to as the concentration that a target organ receives, once the chemical has been absorbed.

The environmental concentration and duration of exposure will determine the extent of exposure. In addition, other environmental factors such as for example, temperature, humidity, and pH, may alter pollutant concentrations. For example, the concentration of some volatile chemicals may vary under different temperature conditions. Sometimes, chemical reactions between pollutants in the environment may

change qualitatively the nature of exposure, such as in the case of ozone formation in the air from nitrogen oxides (NOx), carbon monoxide (CO), and volatile organic compounds (VOCs) in the presence of sunlight.

The patterns of exposure to ingested and inhaled toxicants are different between children and adults. Young children drink more water on a body weight basis than adults do (seven times as much water per kilogram of body weight). For the first 6 months, for example, children consume on average 88 mL/kg/day of tap water directly or indirectly (water added in the preparation of formula or fruit juice) compared to adults who drink 17 mL/kg/day [6]. As a result of this greater consumption of water, children may be disproportionately exposed to chemicals found in drinking water, including the water used to make infant formula [2].

Infants and young children have a higher resting metabolic rate and rate of oxygen consumption per unit body weight than adults. The oxygen consumption of a resting infant aged between 1 week and 1 year is 7 mL/kg body weight per minute, compared to that of an adult in the same condition, which is 3–5 L/kg/min [5]. Thus, on a body weight basis, the volume of air passing through the lungs of a resting infant is twice that of an adult, and therefore twice as much of any chemical in the atmosphere would pass through the lungs of an infant. An additional consideration is the smaller lung surface area per kilogram in the early stages of development. Thus, the higher amount of inspired air will affect a relatively smaller area of lung tissue. In addition, children have narrower airways than those of adults. Thus, irritation caused by air pollution that would produce only a slight response in an adult, can result in potentially significant obstruction in the airways of a young child [6]. Furthermore, the fact that children spend more time engaged in vigorous activities than adults exacerbates the differential effects. Children also ingest more food per unit of body weight than do adults. A 1–5 year old child eats three to four times more food per kilogram than the average adult, resulting in larger amounts of chemicals and infectious agents per unit of body mass [2, 7]. A child's diet is very different from an adult's. The diet of children contains more milk products and more fruits and vegetables per unit of body weight than adults. During the first year of life, human milk or cow milk–based products constitute most of their energy and nutrient source. The NRC report [2] reported that over the first year, cow milk products comprise 36% and 58% of the diets of nursing and non-nursing infants, respectively, compared to adults, where milk and milk products constitute only about 29% of their diet. Environmental pollutants, such as PCBs and dioxins, accumulate in fat and have been found in breast milk, although it is broadly accepted that the benefits of breast-feeding still outweigh the risks of exposure [5].

After the first few months of life, fruits and fruit juices constitute a large proportion of infants' diet. For example, the average consumption of apples for children between birth and 5 months of age is almost ten times that of an adult older than 20 years old [6]. Fruits can be contaminated with pesticides and other toxicants, causing children to be exposed to these chemicals.

Behavioral Patterns Influencing Exposure in Children Two characteristic behaviors of children have been considered and studied in relation to children's exposure to chemicals: mouthing behavior and pica behavior. Infants and toddlers pass through a developmental phase, characterized by intense oral exploratory behavior, when they indiscriminately bring their hands and objects to their mouths. Mouthing behavior can result in oral exposures to chemicals that may be part of the surfaces of objects, or adhered to them in dust particles.

Pica is a behavior of some children that has been defined as the craving or ingestion of nonfood items. The cravings found in patients with pica have been associated with a nutritional deficiency state, such as iron-deficient anemia; with pregnancy or with mental illness. Pica tends to disappear as children grow older, except for mentally retarded children [8]. Pica behavior can give rise to the ingestion of soil, paint, and other possibly contaminated substances. About 95% of children ingest 0.2 g of soil per day or less, but studies have shown that children with pica behavior ingest up to 60 g of soil per day [8]. Children living in neighborhoods built on soil contaminated with heavy metals (such as lead), aromatic hydrocarbons, and other compounds were found to be at increased risk for elevated blood levels [8].

Children may also have higher exposures because of their higher levels of physical activity, at least during certain stages of their development. When they are outdoors, they are more prone to run, jump, or play vigorously than adults do. Their breathing rates may reach exercise levels more frequently during a day than in adults. When near water, for example, children tend to spend more time in the water than adults. This can lead to higher exposures of air pollutants, such as ozone, or to toxicants in water due to the inhalation of volatilized chemicals, ingestion of pool water, and dermal exposures.

Other behaviors characteristic of children such as overexposure to sunlight for sun tanning among adolescents, or drug and alcohol ingestion, can also lead to disproportionately higher risks. However, in this chapter, the central focus is on those risks that are completely involuntary, and that would be difficult to change without altering the normal behavior of a child.

The Unique Microenvironment of Children The children's microenvironment is different from that of adults from the very beginning of conception. The womb, where the fetus is exposed to environmental chemicals and other agents from previous exposures of the mother is a unique environment to this developmental stage. In fact, humans are among the living mammals that have the longest gestational period, resulting in a long in-utero exposure. Many pollutants are known to cross the placenta and enter the fetal circulation, resulting in fetal exposure to toxicants present in the mother. Once the baby is born, breastfeeding can also result in exposures to chemicals accumulated in breast milk.

Children spend a large proportion of their time indoors, and because of their smaller stature and because they crawl and play on the floor, they are more highly exposed to ground-level contaminants. In indoor environments, for example, formaldehyde exposure from carpeting would be higher at ground level than about 4 or 6 ft above, the breathing zone of adults. House dust or particles to which pollutants adhere accumulate near the floor both in the indoor and outdoor air. Further, outdoors where there is traffic, their breathing zone is close to the height at which car exhaust systems expel their fumes.

Indoor air pollutants can originate indoors, such as formaldehyde from carpeting, fumes from home cooking, and solvents from freshly painted rooms, or can enter the inside of homes through windows or open airways. Sometimes, pollutants may be carried inside by persons entering the indoor environment. For example, children whose parents work on farms where pesticides are applied can be exposed to pesticides carried inside in the clothes and skin of adults who walk into the house. Studies have found higher levels of pesticides in farmworker households in agricultural areas compared with those in non-farmworker households in the same area [9]. In addition, some studies have demonstrated that degradation of pesticides is slower in the indoor environment, so pesticide exposure persists longer [9].

Toxicokinetics Once exposed, the amount of toxicant being absorbed, its metabolism, and excretion from children's bodies may be very different from that of adults. Rates of absorption through the oral, dermal, and respiratory pathways vary between children and adults. For example, children have a larger lung surface area per kilogram of body weight than adults and, under normal breathing, breathe 50% more air per kilogram of body weight than adults [6]. Therefore infants potentially receive a greater internal exposure to airborne compounds on a body weight basis.

Children's absorption of chemicals through the gastrointestinal route is also different from that of adults. For example, the absorption of lead from the intestine was found to be 40 times higher for children than for adults [3]. Gastric pH is higher in newborns than in adults, thus causing differences in ionization and absorption of certain chemicals. The alkaline gastric pH in newborns and infants may enhance the absorption of certain compounds.

The skin surface area of children relative to body weight is greater for children than for adults, resulting in a higher potential dose absorbed through the skin of about three times greater for infants than for adults [10]. In addition, hydration of the skin in neonates is greater than in older children, which potentially could result in them having a greater absorption of some hydrophilic chemicals. The permeability of the epidermal is incomplete in the preterm infant, resulting in greater percutaneous absorption of chemical agents [5].

Once absorbed, the different body composition of children will result in a different distribution and accumulation of chemicals compared to adults. For example, the relatively larger extracellular fluid volume of the infant means somewhat greater dilution of water-soluble chemicals. However, the lipid-soluble substances would be distributed in a smaller volume of fat in infants relative to adults. The body composition in terms of water, fat, and protein changes from birth to adulthood resulting in corresponding changes in the bioaccumulation, metabolism, and excretion of contaminants from the body throughout development. Water content, for example, decreases rapidly during the first 6 months of life and then remains fairly constant. Body fat, on the contrary, increases rapidly up to 6 months and then decreases, accounting for similar percentages of body weight at ages 4 and 12 months [5]. This can result in changes in the concentration of chemicals in different tissues and organs that can override the child's ability to metabolize and excrete the chemical.

Metabolism and elimination rates are generally lower in neonates than in adults. Many metabolic pathways are not fully developed in the infant. Renal clearance is lower in neonates than in older children and adults for all classes of chemicals. These factors will lead to differences in the bioaccumulation and persistence of environmental agents in children's and adult's bodies and the concentration of the agents in specific organs. The maturation of these metabolic and elimination rates can result in the mobilization of chemicals, and higher exposures of the target organs or systems to the products of metabolism. In terms of excretion, certain life stages such as pregnancy, lactation, and also menopause, will result in the mobilization of chemicals from fat or bone stores, and the exposure of other organs or the developing fetus and lactating child to the toxicants that were accumulated in the mother.

Developmental Aspects of Children's Susceptibility: Critical Periods of Development

Effects During Gestation From conception to birth, the human organism advances rapidly through a complex set of developmental processes that culminate in the newborn. These development processes include cell division, organ formation, and growth as well and functional development. During development, some biological processes occur only during certain stages of development and not in others, or they occur at a different rate in different developmental stages. For example, cell division in most organs takes place rapidly during early development and much more slowly at later stages. Other processes such as apoptosis, or programmed cell death, occur more widely during development and are less prominent during adulthood.

These biological processes need to be effectively coordinated and require the cellular and intercellular signaling systems to work correctly. Because of the complexity and speed at which these processes take place and the intricate relation between them, interference at the sequence of any of these processes can have damaging and irreversible effects. Exposure to environmental toxicants can have a completely different effect depending on whether it occurs at one developmental stage or another. In addition, damage due to environmental exposures may occur and manifest itself immediately, or may not appear until subsequent stages of development, after development is complete, including late adulthood.

Identifying and understanding these "critical" periods of unique susceptibility is essential to developing strategies to protect children from adverse health effects associated with environmental exposures. The following sections describe the current state of knowledge about the windows of susceptibility during childhood development.

Effects on Germ Cells Germ cells (sperm and egg cells) carry the genetic information from each parent that will provide the unique genetic blueprint for each child. In the male fetus, primordial germ cells develop in utero. From puberty to adulthood, these cells undergo cell division, mitosis, and meiosis, to produce mature sperm and continue to be produced from stem cells through adulthood. In females, primordial germ cells undergo mitosis and the first phase of meiosis during fetal life, and in women, mature oocytes are produced every month from follicular cells.

Environmental toxicants that harm germ cells can affect an adult's own fertility as well as the health of the offspring. In animal models, preconceptional carcinogenesis has been demonstrated for a variety of types of radiation and chemicals, with demonstrated sensitivity

for all stages from fetal gonocytes to postmeiotic germ cells [11]. Although this link in humans is not demonstrated, it is theoretically possible that environmental toxicants that harm germ cells can affect an adult's own fertility as well as the health of the offspring.

Results of environmental damage to germ cells may include reduced fertility later in life or offspring with congenital health problems [12, 13]. For example, men exposed to diethylstilbestrol (DES) in utero had lowered sperm count and increased frequency of abnormal sperm [14]. Women exposed to cigarette smoke during their mother's pregnancy had reduced fertility [13]. There is a substantial body of evidence demonstrating that exposures to environmental agents and medical radiation can injure germ cells in such a way as to cause increased incidence of cancer, particularly leukemia, among offspring of the exposed individuals. For example, paternal exposures to benzene have been linked to leukemia and lymphoma in children [15]. Animal studies support these findings [11].

Embryonic and Fetal Development During Pregnancy Several stages of embryonic and fetal development are susceptible to environmental harm. During development, gene expression is very active because a large number of genes are being "switched on" or "switched off" to control cellular activities. This high level of metabolic activity provides for a wide range of opportunities for environmental agents to interfere with cell development and growth.

Environmental toxicants may interact directly with DNA (e.g., alkylating agents) and disturb gene expression or may interact with the products of gene expression, such as enzymes and control molecules. A toxicant that interferes with gene expression may prevent the synthesis of enzymes necessary for toxicant metabolism, resulting in the accumulation of the toxicant in the body. DNA activation by a chemical may result in excessive synthesis of enzymes that catalyze the bioactivation of a toxicant (production of a toxicant metabolite more toxic than the compound originally present).

Chemicals can interfere with the activation or inactivation of genes that occur during early fetal life and that may be essential for the protection of the organism to external or internal harmful processes. For example, interference with genes involved in DNA repair, such as p53, a tumor suppressor gene important for DNA repair, may result in enhanced vulnerability to specific toxicants during development. Studies with transgenic mice that are missing this gene have shown an increased sensitivity of mice fetuses to benzo[a]pyrene exposure and an increased death rate when exposed to the chemical during gestation [16]. Damage to p53 in humans could likewise increase sensitivity to agents that damage genetic material.

If a toxicant interferes with cell differentiation, cells may not reach their specific form and function necessary for their final role in the body, and organ function may be compromised. Also, undifferentiated cells may be more vulnerable than differentiated cells to toxic effects. Some chemicals such as ethanol [17] and TCDD [18] have been demonstrated to affect specific types of undifferentiated cells.

Apoptosis or programmed cell death is a critical biological process for healthy development. Apoptosis involves the removal of certain cell types when they are no longer necessary. In some instances, one type of cell is succeeded by another during a specific developmental period. Apoptosis is involved, for example, in the elimination of cells in the immune system that, if they survived, could cause autoimmune disease [19]. Apoptosis is also critical in the development of the nervous system, where phases of cell proliferation alternate with phases of apoptosis on the basis of the progression of neuronal development [20] and remains active through the postnatal period because of ongoing nervous system development.

Normal patterns of apoptosis may be altered through altered gene expression or failure of signaling mechanisms resulting from environmental exposures. Certain autoimmune lympho-proliferative diseases and certain cancers have been related to the disruption of normal patterns of apoptosis. For example, Wilms' tumor, a relatively common childhood cancer, may arise from the transformation by postnatal exposures of renal stem cells that fail to disappear 4–6 weeks prior to birth [21].

Neuronal migration is an important process in nervous system development and its alteration may result in irreversible damage. For example, schizophrenia is thought to result, in part, from abnormal neuronal migration [22], but the role of prenatal exposures to environmental agents in causing

this disease is not clear. Exposures to ionizing radiation and methylmercury, for example, have been shown to affect the migration of neurons during development [20, 23].

During the period of organ development, which occurs (varying according to organ system) between the 3rd and 16th week, disruption of development can disrupt the large-scale structure of organs, often resulting in physical malformations (congenital anomalies). The best known example of such gestational damage is exposure to diethylstilbestrol (DES). DES caused genital anomalies among male children born of women who took the medication before the 11th week of gestation twice as often as among those who were exposed later in gestation [14].

Other effects such as low birth weight, pregnancy complications, or late fetal death have been shown to be a result of environmental exposures during later stages of prenatal development [24]. Disinfection by-products have been linked to the risk of spontaneous abortion for some time. There is now fairly consistent evidence for associations between early and late fetal deaths and indices of transplacental exposure to disinfection by-products [25–27]. Maternal smoking during pregnancy increases the risk of pregnancy loss, stillbirth, and infant mortality [28].

Development During Childhood Several organs and systems continue to grow and develop during childhood and in some cases almost until adulthood. For example, neuron migration, cell proliferation, and synapse formation are very active until 3 years of age, and myelination continues until adolescence [29] and possibly well into adulthood [20].

The immune response is also immature at birth and develops during infancy and childhood until about 1 year of age, while establishment of immunologic memory is not fully established until 18 years of age [30]. Exposure to environmental agents during early childhood may affect immune system development and may contribute to the development of certain diseases such as asthma and cancer later in life.

Physical growth and maturation of organ systems continues through adolescence. The process of sexual maturation is accompanied by complex interactions between the central nervous system and hormone-secreting organs, which can be affected by environmental exposures. For example, the risk of breast cancer has been found to be greater among women who were exposed to radiation before 20 years of age [31].

Cellular Metabolism and Biotransformation Many important metabolic and biotransformation processes are poorly developed in the fetus, and full metabolic activity is not fully developed until after childbirth. Metabolism can increase or decrease the toxicity of a chemical, depending on the metabolic products of the chemical and pathway involved. Metabolism may also make elimination from the body easier or harder, although the most common metabolic pathways usually render chemicals more hydrophilic and thus, more easily excreted. In some cases, the adult biotransformation of a certain chemical may consist of a bioactivation pathway that makes the compound more hazardous than the one originally present. The absence of a metabolic pathway may result in the bioaccumulation of the chemical in the body and a later bioavailability and disposition to exert its toxic effects. Immaturity could be an advantage if the activation pathway is not present in the fetus or child and there is an alternate pathway for the toxicant to be metabolized. However, according to [32], given the primary evolutionary function of detoxifying and eliminating potentially toxic chemicals, immature or underdeveloped metabolic pathways are likely to render infants and children more sensitive to common environmental contaminants.

Major Groups of Pollutants to Which Children are Exposed

Heavy Metals

Heavy metals are natural elements that have been extracted from the earth and used in human industry and products for centuries. As a consequence of human activity, concentrations of heavy metals in air, water, and surface soil today are hundreds of times higher than in the preindustrial era. Some metals are naturally found in the body and are essential to the functioning of critical enzyme systems. Iron, for example, prevents anemia, and zinc is a cofactor in over 100 enzyme reactions. Magnesium and copper are other familiar metals that, in minute amounts, are necessary for

proper metabolism to occur. The body has need for approximately 70 trace elements, but there are others, such as lead, mercury, aluminum, arsenic, cadmium, and nickel, that have no roles in human physiology and can be toxic at even trace levels of exposure. Nutritionally, heavy metals can compete with nutrient elements, such as the case of lead, which is stored in the bones in the place of calcium.

Metals are notable for their wide environmental dispersion, their tendency to accumulate in select tissues, and their overall potential to be toxic at even relatively minor levels of exposure. In general, heavy metals are systemic toxins with specific *neurotoxic*, *nephrotoxic*, *fetotoxic*, and *teratogenic* effects. Heavy metals can directly influence behavior by impairing mental and neurological function, influencing neurotransmitter production and utilization, and altering numerous metabolic body processes.

Exposure to heavy metals can occur through drinking water, air, or ingestion of heavy metal–contaminated soil. The amount that is actually absorbed from the digestive tract can vary widely, depending on the chemical form of the metal and the age and nutritional status of the individual. Once a metal is absorbed, it distributes in tissues and organs. Excretion of metals typically occurs through the kidneys and digestive tract, but they tend to persist in some storage sites, like the liver, bones, and kidneys, for years or decades.

Lead is one of the best known heavy metals in terms of its toxicity. Exposure to lead can occur in the prenatal stage through the placenta, and in infants through the mother's milk and the water used in milk formula [3]. During pregnancy, body stores of lead may be mobilized and transferred from the mother to the fetus [33]. Behavioral characteristics of children later on, such as the hand-to-mouth behavioral pattern of 1–3 year olds, can result in high exposure and internal levels of lead. Lead paint is a major source of environmental exposure for children who ingest flaking paint, paint chips, and weathered powdered paint (mostly from deteriorated housing units in urban areas). Lead can leach into drinking water from lead-based solder used in water pipes. Lead also leaches into foods or liquids stored in ceramic containers made with lead glazing, which is still used in some countries.

The absorption of lead from ingestion of lead-contaminated water is higher for children than for adults, so that for a given level of exposure, the resultant internal dose is higher in children than in adults [3]. Children are also more sensitive than adults to the toxicological effects of lead at a given internal exposure level. The lowest observed adverse effect levels (LOAELs) for several health endpoints occur at lower blood lead levels in children than in adults. The most sensitive targets for lead toxicity are the developing nervous system, the hematological and cardiovascular systems, and the kidney. There appear to be no safe exposure "thresholds" for lead or for other metals in early development.

Mercury is a ubiquitous heavy metal of both natural and anthropogenic sources. Mercury occurs in both inorganic and organic forms, and it is most hazardous in its organic form of methylmercury. The nervous system is very sensitive to all forms of mercury. Methylmercury and metallic mercury vapors are more harmful than other forms, because methylmercury can cross the blood brain barrier. Methylmercury in the marine and freshwater environment is absorbed by fish and shellfish and bioaccumulates in the food chain. Increased risk is of particular concern in children and in populations that have an increased dietary exposure to fish.

Arsenic occurs naturally in the environment and in some areas of the world is a natural contaminant of underground water that is used as drinking water. It is also an anthropogenic contaminant. Once absorbed into the body, arsenic undergoes some accumulation in soft tissue organs such as the liver, spleen, kidneys, and lungs, but the major long-term storage site for arsenic is keratin-rich tissues, such as skin, hair, and nails.

Cadmium is another chemical that is toxic to adults, although it has not been extensively studied in children. The US Department of Health and Human Services has determined that cadmium and cadmium compounds are known human carcinogens. Cadmium has been linked to diminished kidney function lung disease, chronic bronchitis, and lung, kidney, and prostate cancers. In the USA, smoking is the primary source of cadmium exposure, although high levels of cadmium can also be found in organ meats, shellfish, and vegetables.

Pesticides

Pesticides are substances that are used to prevent, repel, or destroy pests – organisms that compete for food supply, adversely affect comfort, or endanger human health (FIFRA 1996). More than 20,000 pesticide products with nearly 900 active ingredients are registered for use as insecticides, miticides, fumigants, wood preservatives, and plant growth regulators. It cannot be denied that pesticides have beneficial economic and also public health impacts. Pesticide usage helps improve human nutrition through greater availability, longer storage life, and lower costs of food. It also reduces human labor requirements and attendant risks of injury. Pesticides also assist in the control of food-borne and vector-borne diseases, such as malaria, which kill millions of persons in the world. Pesticides also pose human health concerns because they are toxic substances and widely spread in the environment. Although the toxic mechanisms on targeted pest species are well characterized, the potential for adverse health effects in humans is not fully known.

Pesticides are composed of several classes of chemicals with different mechanisms of action. Most insecticides work by interfering with nervous system function. Organophosphates, which account for approximately one-half of the insecticides used in the USA, and carbamates, which are widely used in homes and gardens, inhibit the activity of acetyl cholinesterase at nerve endings, resulting in an excess of acetylcholine in the synapsis and a depolarizing blockage of neural transmission. The effects of carbamates are readily reversible and of shorter duration. Organochlorines, such as dichlorodiphenyltrichloroethane (DDT) and lindane, interfere with nerve cell membrane cation transport, resulting in neural irritability and excitation of the central nervous system. Herbicides, including the chlorophenoxy compounds 2,4 D and 2,4,5 T are primarily irritative to the skin and respiratory tract during acute exposures and work by different mechanisms. Some substances, such as paraquat, are highly corrosive and can cause multisystem injury and progressive pulmonary failure [34].

Arsenical pesticides, such as copper chromium arsenate, have been used, until recently, as wood preservatives to prolong the useful life of exterior wooden structures. These compounds cause central nervous system depression at sufficient doses.

Pesticides are ubiquitous in the environment. They are found in food, water, homes, schools, workplaces, lawns, and gardens. They are present in soils that have been spread with pesticides or where pesticides from adjacent agricultural areas have drifted, and may reach water supplies from agricultural runoff. In the USA alone, more than 0.45 billion kilograms of pesticides are applied each year, in agriculture, in homes and gardens, and in schools and hospitals. In developing countries, many highly toxic and biologically persistent pesticides such as parathion, DDT, and paraquat, which are no longer permitted in many developed countries, are still in wide use and result in chronic exposures and acute, too often fatal poisonings of thousands of young children each year.

Most children in the world are exposed to some degree to pesticides. Children in rural and agricultural areas and especially children whose parents are farmworkers or pesticide applicators are at highest risk of having increased exposures to pesticides. Pesticides may reach their homes due to the drifting of pesticides that are applied to the ground through aerial spraying. Children may work or play near their parents in the fields where pesticides have been used. Parents who work with pesticides may bring pesticides to their homes, impregnated in their clothes and bodies. In countries where residential housing with gardens and lawn predominate, homes and garden pesticide use may result in significant levels of exposure [34].

Exposure of children to pesticides may occur through inhalation, ingestion, and dermal absorption. Ingestion of pesticides occurs either through accidental exposure due to pesticides stored in food containers (i.e., soft drink bottles), or through ingestion of pesticide-treated foods, particularly fruits and vegetables. Foods grown in pesticide-contaminated soils and fish from pesticide-contaminated water can also carry significant amounts of pesticides. Children may also ingest pesticides adhered to the surface of toys or other objects through their hand-to-mouth behavior. The potential of dermal exposure of children to pesticides is higher than that of adults because of their relatively large body surface area and extensive contact with lawns, gardens, and floors by crawling and playing on the ground.

Prenatal and early childhood exposures are of special concern because of the susceptibility of the

developing organ systems to pesticides (the central nervous system in particular) as well as behavioral, physiological, and dietary characteristics of children. Breast-feeding infants may ingest pesticides or pesticide metabolites present in the breast milk. The quantity of pesticide that is passed to the infant via breast milk is influenced by many variables such as maternal age and parity, maternal body burden of the chemical, and breast-feeding patterns. As infants are weaned and progress to solid foods, they consume, per unit of body weight, proportionally more fruit and more fruit juice than adults. The NAS in 1993 reported that children's dietary exposures to pesticides differed from adults both quantitatively and qualitatively and questioned the protection provided to infants and children from pesticide tolerances in effect at the time. The report estimated that 50% of lifetime pesticide exposure occurs during the first 5 years of life [2].

Environmental Tobacco Smoke

Environmental tobacco smoke (ETS), also known as second-hand smoke, is exhaled smoke and sidestream smoke emitted from the burning of the tip of the cigarette. The inhalation of ETS is known as "involuntary smoking" or "passive smoking." ETS contains more than 4,000 different chemical compounds, many of which are toxic. In 1992, the US Environmental Protection Agency (EPA) declared ETS as a Group A carcinogen.

The effects of passive smoking begin in utero, where constituents of tobacco smoke, such as PAHs, nicotine, and carbon monoxide, cross the placenta and are concentrated in the fetal circulation [35]. Children are also exposed during childhood if any of the parents smoke.

Persistent Organic Compounds: PCBs, Dioxins, and Related Organohalogens

Polychlorinated biphenyls are synthetic compounds with two linked phenyl rings and variable degrees of chlorination. They have been used for many years because of their thermal and chemical stability. They are nonvolatile, hydrophobic oils that are not easily biotransformed in the environment or metabolized by the human organism, so they are very persistent in the environment, and bioaccumulate in the food chain and in the fat compartment of the human body. Although they have been banned in the USA for more than 30 years, they are still widely present in the environment. They have been found in wildlife, human tissue, and human milk. Polychlorinated dibenzofurans (PCDFs) are partially oxidized PCBs that appear as contaminants of PCBs. Polychlorinated dibenzodioxins (PCDDs), commonly referred as dioxins, are formed during paper bleaching and waste incineration. One dioxin congener, 2,3,7,8-tetrachlorodibenzo-p-dioxin (TCDD), is considered to be the most toxic synthetic chemical known.

The most significant source of exposure is contaminated food, particularly fish at the top of their trophic chain. Of greatest concern are the populations that consume high amounts of fish. Because PCBs and PCDFs are not metabolized or excreted, they can accumulate in the fat tissue of the body, as well as in human milk, resulting in high exposures of the developing fetus and the newborn.

Disinfection By-products (DBPs)

Disinfection by-products (DBPs) form when disinfectants are added to drinking water and react with naturally occurring organic matter. Chlorine, the most widely used primary disinfectant, reacts with naturally occurring organic matter to form a range of unwanted by-products such as the trihalomethanes (THMs) which include chloroform, bromodichloromethane (BDCM), chlorodibromomethane (DBCM), and the haloacetic acids (HAAs), such as monochloroacetate, dichloroacetate, and trichloroacetate.

Exposure to DBPs occurs through ingestion of water or through inhalation and absorption during showering, bathing, and swimming. While there is some concern that these chemicals may pose a health risk, the potential risks arising from not treating drinking water are considerably greater, and the disinfection of water should never be compromised as a result.

Environmental Threats to Children on Specific Organ Systems

Nervous System

The developing nervous system is more susceptible than the adult brain to the disrupting effect of toxic

chemicals [5]. The lengthy period of brain development and the extensive number of processes needed to take place contribute to the susceptibility of the developing nervous system. In the 9 months of pregnancy, the human brain and spinal cord must develop from a thin strip of cells along the back of the embryo into a complex organ comprised of billions of precisely located, highly interconnected, and specialized cells. Brain development requires that neurons move along precise pathways from their points of origin to their assigned location, that they establish connections with other cells near and distant, and that they learn to intercommunicate. Each connection between and among neurons must be precisely established at a particular point in development, and redundant connections need to be pruned away through programmed cell death, apoptosis. All these processes must take place within a tightly controlled time frame, in which each developmental state must be reached on schedule and in the correct sequence.

Critical windows of vulnerability, which exist only in the 9 months of pregnancy and to a lesser extent in early childhood, are unique to early brain development. They have no counterpart in adult life. Exposure to toxic chemicals during these windows of vulnerability can cause devastating damage to the brain and nervous system.

Any toxic or other environmental exposure that interferes with the tightly orchestrated sequence of events involved in brain formation is likely to have profound effects on intellect, behavior, and other functions. If a developmental process in the brain is halted or inhibited, if cells fail to migrate the proper sequence to their assigned locations, if synapses fail to form, or if pathways are not established, there is only limited potential for late repair, and the consequences can be permanent [36].

Environmental toxicants can affect both the structural and functional development of the nervous system. Depending on the developmental stage at which exposure occurs, sensory development, intelligence, or behavior will be affected differentially. While early-developing neural systems have been considered the most vulnerable to chemical insult, scientists have called attention to the importance of chemical exposure that occurs late in childhood, as it has been recently suggested that behavioral and physiological foundations of cognition continue to develop during childhood and adolescence [5, 37].

Exposure to environmental toxicants such as lead, methylmercury, and certain pesticides and PCBs even at very low levels have been shown to produce neurobehavioral (functional) deficits, and increased susceptibility to neurodegenerative diseases much later in life [38]. Of critical concern is the possibility that developmental exposure to neurotoxicants may result in an acceleration of age-related decline in function that could lead to Parkinson Disease, Alzheimer Disease, and other forms of brain degeneration. This concern is compounded by the fact that developmental neurotoxicity that results in small effects on the individual at a particular stage can have a profound societal impact when considered in the whole population or across the life span of the individual [36]. For example, a five-point decline in average population intelligence (IQ score) can result in reduction by more than 50% in the number of children with superior IQ (>130) and concomitant doubling in the number of children with IQ scores in the retarded range (<70). Behavior is also disrupted, sometimes permanently, by such exposures.

The following sections will give a short overview of some neurotoxicological effects of the best known chemicals for their effect on the developing nervous system. Some toxicants such as ethanol have been excluded, as the focus of this chapter is on exposures to toxicants to which the majority of children are exposed.

Lead Lead is one of the best studied toxicants and one of the few pollutants for which susceptibility of children has been clearly established. The best known health effects on children are its neuropsychological effects although other effects have also been studied and are partially documented.

The neurotoxic effects of lead in children have been extensively studied. One distinctive characteristic of the research findings on lead neurotoxicity over the past 2–3 decades is that it has led to a progressive decline in the LOAELs (lowest observed adverse effect levels). The early finding in the 1970s by Landrigan et al. [39] and Needleman [40] that low-dose exposure to lead is associated with a significant decrease in intelligence quotient (IQ) has been confirmed in many

studies. The recommended action level of blood lead levels established by the Centers for Disease Control is 10 μg/dL of blood. However, epidemiological studies during the last decade have found strong evidence for cognitive deficits among school-aged children at blood lead levels below the current CDC action level [41, 42]. Further, in a pooled analysis of seven prospective longitudinal studies, the average IQ deficit associated with an increase in concurrent blood lead concentration from <1 to 10 μg/dL was about threefold that for an increase from 10 to 20 μg/dL [42]. Birth cohort studies have shown inverse dose-response relationships between transplacental lead exposure indices and central auditory processing indices among infants and children at maternal blood lead levels below 10 μg/dL [43].

Research has also demonstrated a link between developmental lead exposure and behavioral outcome. In a prospective study, the behavior of lead-exposed children at 8 years of age was significantly related to tooth dentine levels [44], suggesting that social and emotional difficulties correlate with lead exposure. In another prospective, longitudinal study, both prenatal and postnatal lead exposure was related to antisocial and delinquent behavior in adolescents [45]. It is generally accepted in the scientific and medical community that the adverse neurobehavioral consequences of lead are not reversible and remain in place across the life span [41]. Further, the possibility that a threshold level for the effects of lead does not exist has been suggested [42].

Mercury Methylmercury is a well-established neurotoxicant that can cause serious adverse effects on the development and functioning of the human central nervous system, especially when exposure occurs prenatally. The well-known episodes of community-wide poisoning in Japan and Iraq revealed the particular sensitivity of the fetus to the toxic effects from mercury exposure. In these communities, pregnant women exposed to methylmercury and who themselves had no or minimal symptoms, had babies with devastating neurological handicaps, including delayed attainment of developmental milestones, blindness, deafness, and cerebral palsy.

At levels of exposure lower than those encountered in the Minamata Bay, there is limited epidemiological evidence of neuropsychological effects. A birth cohort of 1,000 children was established at the Faroe Islands in 1986–1987, and the methylmercury exposure was determined from the mercury concentration in the cord blood [46]. More than 90% of these children were then examined at age 7 years. Neuropsychological effects in the areas of language, attention, and memory and to a lesser extent in visuospatial and motor functions were observed [46]. In Brazil, cross-sectional studies of Amazonian children aged 7–12 years show mercury-associated effects in agreement with the Faroe findings [47]. However, a large cohort study conducted in the Seychelles did not reveal consistent associations between perinatal methylmercury exposure indices and developmental milestones or neuropsychologic test scores up to age 5 years old [48].

Some studies have found an association between central auditory processing deficits and current childhood hair mercury levels as low as 5 μg/g [49]. These findings are supported by animal studies, showing that transplacental or postnatal methylmercury exposure affects auditory systems at the cortical level [50].

The important question is to which degree these findings relate to fish-consuming populations in general. Although this question cannot be answered with any confidence at this time, it looks like the recommended one to two fish meals per week during pregnancy would be very unlikely to cause any risk to the fetus, unless the seafood is severely contaminated. The National Academy of Sciences recommended that a limit of about 0.1 μg/kg of body weight per day should not be exceeded by pregnant women [51].

PCBs, Dioxins, and Related Organohalogens Polychlorinated biphenyls are known to interfere with thyroid hormones, some of which are critical for normal brain development, and this effect of PCBs on the thyroid function of the newborn has been postulated as the mechanism of action of neuropsychological effects [52].

The earliest evidence of PCB-related neurotoxicity comes from the poisoning episodes in Japan (Yusho) and Taiwan (Yucheng) where people became ill after ingesting rice oil that was highly contaminated with PCBs. Infants born to mothers who consumed PCB-contaminated rice oil during pregnancy were at increased risk for low birth weight, abnormal brown

pigmentation of the skin, and clinical abnormalities of the gingival, skin, nails, teeth, and lungs [53]. In addition, children of both cohorts had various neurobehavioral deficits such as delayed attainment of developmental milestones, lower scores on intelligence tests, and higher activity levels [54]. Children were followed and examined 6 years later and showed persistent behavioral abnormalities and ectodermal defects [55].

Many studies after the Taiwan event provide evidence of neuropsychological effects of PCBs [56]. The evidence indicates that PCBs cause neurobehavioral deficits in children who are exposed prenatally, while the evidence of effects of exposure to background levels commonly found in the general population is not conclusive. Studies support the association between low-level transplacental PCB exposure and childhood deficits in cognitive, psychomotor, memory, language, and attention functions [56, 57]. None of the studies up to date has been able to document an adverse effect of PCBs exposure from breast-feeding. It has been postulated that the larger fat compartment of the nursing infant than the fetus may make it possible to dilute somewhat the lipid-soluble contaminants absorbed through human milk. Thus, despite the occurrence of these contaminants in human milk, the advantages of breast-feeding for 4–6 months apparently override any limited neurotoxin damage due to the contaminants. Still, of particular concern would be the populations who frequently eat contaminated fish or who reside in contaminated areas and may still be exposed at levels that have been associated with adverse effect.

Pesticides Current knowledge about the neurotoxicological effects of pesticides is limited, despite the extensive knowledge available of the mechanisms of pesticide toxicity in animals. One observational study in children from a region in Mexico with intensive pesticide use found a variety of developmental delays compared with otherwise similar children living in a region where the population had not adopted a pesticide-based agriculture. The children were similar in growth and physical development, but significant delays were noted among the exposed children in physical stamina, gross and fine hand-eye coordination, short-term memory, and ability to draw a human figure [58]. However, these conclusions have been questioned, as pesticide levels were not reported for the individual children who received neuropsychological testing.

Fetal and neonatal animals are often more sensitive than adults to the neurotoxic effects of some organophosphates [2], and levels presumed to be nontoxic in adults may not be adequately protective of the developing organisms. For example, the young rat is deficient in the actions of two enzymes that detoxify chlorpyrifos, and young rats have increased sensitivity to chlorpyrifos toxicity [59]. In rats, chlorpyrifos appear to affect cholinergic function [60]. Infants may be particularly vulnerable to reductions in brain cholinesterase given that acetyl choline plays an important role in normal brain development and plasma and erythrocyte (and therefore probably brain) cholinesterase do not reach adult values until 6–12 months of age [61].

Animal studies suggest that exposure to pesticides such as DDT and its metabolites DDE and dichlorodiphenyldichloroethane at the levels found in the environment affect the developing brain. Ten-day old mice treated once with DDT showed behavioral changes compared with controls when tested at 4 months of age. These effects occur only after DDT dosing at 10 days of age and not after similar dosing at 3 or 19 days of age [62].

In spite of the absence of direct conclusive evidence of the neuropsychological effects of pesticides, the known subclinical effects observed in adults through neuropsychological testing, and what is known on the mechanism of action of pesticides and susceptibility of the developing brain, has led many investigators to infer that chronic low-dose exposure to certain pesticides might pose a potential hazard to the health and development of infants and children. Other investigations have concluded such inferences can be neither supported nor refuted at the present time.

Endocrine System

The endocrine system is one of the body's main communication networks and is responsible for controlling and coordinating numerous body functions. Hormones are first produced by the endocrine tissues,

such as the ovaries, testes, pituitary, thyroid, and pancreas, and then secreted into the blood to act as the body's chemical messengers. They direct communication and coordination among other tissues throughout the body, and they exert a powerful influence over growth and development of every organ system in the body.

The endocrine system regulates metabolic, nutritional, reproductive, and behavioral processes, as well as growth, responses to stress, and the function of the digestive, cardiovascular, renal, and immune system. Programming of endocrine set points is a unique aspect of endocrine system development that takes place during fetal/neonatal development, and exposure to toxicants during this critical period of programming can result in permanent abnormalities in endocrine function [5]. Disruption of endocrine function can have severe health consequences in adults, and exposures that interfere with the development of the endocrine system during early life stages can have even more far-ranging consequences [63].

Endocrine disruptors are natural compounds or man-made chemicals that may alter the production or activity of hormones of the endocrine system leading to adverse health effects. Although there is limited scientific information on the potential adverse human health effects, concern arises because endocrine disrupting chemicals, while present in the environment at very low levels, have been shown to have adverse effects in wildlife species, as well as in laboratory animals at these low levels. Many of these chemicals have been linked with developmental, reproductive, neural, immune, and other problems in wildlife and laboratory animals. The potential adverse effects of EDCs include neurodevelopmental and neurobehavioral abnormalities, reproductive disorders such as declined fertility, immune impairment, and certain hormone-related cancers [1].

An example of a phthalate is di(2-ethylhexyl) phthalate (DEHP). DEHP is a high-production-volume chemical used in the manufacture of a wide variety of consumer food packaging, some children's products, and some polyvinyl chloride medical devices. Recently, an independent panel of experts assembled by the National Toxicology Program (NTP) found that DEHP may pose a risk to human development, especially critically ill male infants.

In 2000, an independent panel of experts convened by the NIEHS and the National Toxicology Program (NTP) found that there was "credible evidence" that hormone-like chemicals can affect test animals' bodily functions at very low levels – well below the "no effect" levels determined by traditional testing. Although there is little evidence to prove that low-dose exposures are causing adverse human health effects, there is a large body of evidence in experimental animals and wildlife suggesting that endocrine disruptors may cause [1]:

- Reductions in male fertility and declines in the numbers of males born
- Abnormalities in male reproductive organs
- Female reproductive diseases including fertility problems, early puberty, and early reproductive senescence
- Increases in mammary, ovarian, and prostate cancers

Endocrine disruptors may interfere with the endocrine system through several mechanisms. Some mimic or partially mimic occurring hormones in the body like estrogens and androgens and thyroid hormones, potentially producing overstimulation. Another group of natural and synthetic substances interferes with the hormones at receptors. Substances that compete with a hormone at the receptor, and imitate its effect are called agonists, those that block the receptor are antagonists. Other chemicals interfere, or block the way natural hormones or their receptors are made or controlled, for example, by blocking their metabolism in the liver. Environmental chemicals with estrogenic activity are probably the most well studied; however chemicals with antiestrogen, androgen, antiandrogen, progesterone, or thyroid-like activity have also been identified.

A wide range of substances are thought to cause endocrine disruption. Chemicals that are known endocrine disruptors include diethylstilbestrol (DES), dioxin and dioxin-like compounds, PCBs, DDT, and some other pesticides. Some chemicals, particularly pesticides and plasticizers, such as Bisphenol A are suspected endocrine disruptors based on animal studies.

Phthalates, a class of chemicals that soften and increase the flexibility of polyvinyl chloride plastics, are considered to be endocrine disruptors on the basis of extensive animal research plus emerging studies in humans. An example of a phthalate is

di(2-ethylhexyl) phthalate (DEHP). DEHP is a high-production-volume chemical used in the manufacture of a wide variety of consumer food packaging, some children's products, and some polyvinyl chloride medical devices. Recently, an independent panel of experts assembled by the National Toxicology Program (NTP) found that DEHP may pose a risk to human development, especially critically ill male infants.

Research shows that endocrine disruptors may pose the greatest risk during prenatal and early postnatal development when organ and neural systems are developing. In animals, adverse consequences, such as subfertility, premature reproductive senescence, and cancer, are linked to early exposure, but they may not be apparent until much later in life.

There is some evidence that endocrine disruptors may not only impact the individual directly exposed but also future generations. It has been found that animals exposed to low doses of the natural human estrogen estradiol, or the environmental estrogen bisphenol A (BPA) (a chemical used in great quantities in the production of polycarbonates and epoxy resins), during fetal developmental and estradiol as adults were more likely to develop a precursor of prostate cancer than those who were not exposed [64]. This suggests that exposure to environmental and natural estrogens during fetal development could affect the way prostate genes behave, and may lead to higher rates of prostate disease during aging. It has also been shown that the adverse effects of diethylstilbestrol in mice can be passed to subsequent generations even though they were not directly exposed [64]. The increased susceptibility for tumors was seen in both granddaughters and grandsons of mice who were developmentally exposed to DES [65]. One study found that endocrine disruptors caused fertility defects in male rats that were passed down to nearly every male in subsequent generations [66]. These intergenerational effects may be the consequence of epigenetic changes caused by endocrine disruptors.

There is concern that alterations in thyroid hormone signaling by endocrine disruptors during fetal and neonatal development could disrupt central nervous system development. There have been several epidemiological studies of the neurobehavioral effects of in utero exposure to PCBs that have been mentioned in the section on nervous system effects. Thus far, few studies have directly linked neurobehavioral effects of exposure to polyhalogenated hydrocarbons to disruption of thyroid hormone signaling. One example is a study that showed that low-frequency hearing loss caused by developmental exposure in rats to PCBs could be partially reversed by replacement of T4 [67]. In animals, many polyhalogenated aromatic hydrocarbons such as dioxins and PCBs alter thyroxin levels via an increased metabolism and excretion of these hormones [52].

Perchlorates are another class of environmental chemicals that affect thyroid function via inhibition of iodine uptake by the thyroid gland, reducing T4 and T3 synthesis. There has been a concern that contamination of drinking water with perchlorates from industrial sites would suppress fetal thyroid hormone synthesis, disrupting central nervous system development. Increased rates of congenital hypothyroidism have been found in communities with detectable perchlorate levels in the drinking water [68], although others have not detected such elevated rates [69].

Evidence from epidemiological studies demonstrates that exposures during early life can result in greater susceptibility to diabetes and obesity later in life [70]. In the course of development of the pancreas and pancreatic function, for example, several windows of susceptibility have been identified [71]. Studies about the Dutch Famine Winter have shown that poor maternal nutrition, especially during the last trimester of pregnancy had an impact on glucose tolerance and insulin resistance, and that in terms of obesity, those individuals born to mothers who were exposed to the famine around the first half of pregnancy were more obese than those of mothers exposed during the last trimester [72]. A number of subsequent studies have documented the role of the intrauterine environment, and low birth weight in the development of diabetes [71, 73] and other metabolic disorders.

Reproductive System

The development of the reproductive system is a long process that takes place from the beginning of gestation, when organ development starts to take place, to maturation of the reproductive system during puberty. This long developmental period provides for several windows of susceptibility. Adverse effects of

reproductive toxicants can become manifest at birth (e.g., hypospadias and cryptorchidism in humans), in puberty (as delay or precocity), or in adulthood (e.g., infertility, alterations in accessory sex organs, disturbances in pregnancy maintenance, endometriosis, or premature reproductive senescence) [74].

The developmental susceptibility of the reproductive system was clearly demonstrated through the diethylstilbestrol (DES) exposure. In utero exposure of men to DES has been linked to increased incidence of meatal stenosis, epididymal cysts, testicular hypoplasia, cryptorchidism, microphallus, and sperm abnormalities. In females, DES exposure resulted in adenosis, clear cell adenocarcinoma, and structural defects of the cervix, vagina, uterus, and fallopian tubes [75].

Environmental tobacco smoke has been associated with decreased fecundity and earlier menopause in women smokers [76]. Women whose mothers smoked while pregnant also had reduced fecundity compared with women whose mothers did not smoke [13]. In men whose mothers smoked tobacco during pregnancy, reduced semen quality, smaller testis size, and reduced fecundability odds ratios have been observed [77].

Phthalates such as diethylhexyl phthalate (DEHP) are developmental toxicants in experimental animals. The organ system most sensitive to phthalates is the reproductive tract of immature males [78]. In utero exposure of male rats to some phthalate esters results in changes in the reproductive tract, such as decreased anogenital distance, hypospadias, cryptorchidism, disturbed development of prostate, epididymis, vas deferens, and seminal vesicles, retained nipples and decreased sperm production [79–82]. In humans, similar dysgenetic changes in the histology of the testis have been found in patients with testicular cancer, subfertility, or cryptorchidism [83, 84]. It has been hypothesized that all these human disorders (testicular germ cell cancer, cryptorchidism, hypospadias, and low sperm counts) have common origins in fetal life and that they all represent different symptoms testicular dysgenesis syndrome [87].

Neonatal Mortality, Growth Restriction, and Birth Defects

Birth defects are normally defined as structural problems in the newborn, attributable to faulty development or deformation, but defects in function, metabolism, or body chemistry that lead to physical or mental problems or to death may also be considered birth defects. The broader term "developmental disorders" is generally used when considering all effects observed on the conceptus from fertilization to sexual maturity. Developmental disorders include both structural birth defects and functional defects, such as blindness, deafness, or neurobehavioral disabilities.

The majority of birth defects are considered the result of multiple environmental and/or genetic causes acting together. Environmental toxicants studied for their relation with birth defects include maternal smoking and alcohol use, pesticides, disinfection by-products, plastics and plastic components, solvents, metals and numerous air pollutants [88]. Other environmental causes such as maternal diseases (e.g., rubella), and use of pharmaceuticals (e.g., valproic acid, an anticonvulsant, and mood stabilizers), have served to document the potential environmental role in developmental birth defects.

Many epidemiological studies have attempted to evaluate whether some chemical exposures are linked to increased rates of spontaneous abortions. For example, occupational exposure of the mother to organic solvents has been associated with spontaneous abortion in several studies [89, 90]. A review of six occupational studies found suggestive evidence for an association between toluene exposure and spontaneous abortion, although most workers were simultaneously exposed to multiple chemicals, which may have confounded the interpretation of results. According to this review, spontaneous abortion has generally not been observed as a major problem among highly exposed women who abuse toluene during pregnancy.

Many studies have investigated the effects of *disinfection by-products* (DBPs) on the developing fetus and children. Review of epidemiologic studies reveal that there is fairly consistent evidence for associations between early and late fetal deaths and indices of transplacental DBP exposure [25, 26, 89]. Associations between late fetal deaths and drinking water chloroform, bromodichloromethane, and total THM concentration at levels below the Canadian drinking water guideline of 100 μg/L have been found in Canada [90]. In England, increased risks of late fetal deaths among women living in regions with THM concentrations

above 30 μg/dL [91]. These findings are supported by animal studies, where high prenatal maternal exposure to chloroform, bromodichloromethane (BDCM), haloacetonitriles, or haloacetic acids produced fetal resorption and reduced fetal survival [26].

Evidence on the effects of maternal *DBP* exposure and SGA (small-for-gestational-age) effects is mixed. Recent reviews have found limited evidence for association with this effect [25, 26], but a cohort study in Massachusetts demonstrated associations between SGA and drinking water trihalomethanes and mutagenic activity levels during the third trimester in the town of maternal residence [92]. In experimental animals, high prenatal maternal exposure to chloroform, BDCM, haloacetonitriles, or haloacetic acids reduced fetal weight [26, 27].

The evidence of the effects of chlorination disinfection by-products in drinking water and birth defects is inconclusive. Some studies have shown an association between neural tube defects and prenatal maternal DBP [25, 26]. The evidence of effects of water disinfection from five previous studies with a cross-sectional study of all Taiwanese births in years 2001–2003 was reviewed [93] and evidence of an effect of exposure to chlorination by-products on the risk of neural tube defects, urinary system defects, and ventricular septal defects was concluded. However, a recent review of a small number of recent studies reported inconsistent results for an association between drinking water chlorination by-products and risk of al congenital anomalies combined and of specific groups of anomalies, and there was little evidence of an exposure–response relationship [94].

Maternal *smoking* during pregnancy increases the risk of pregnancy loss, stillbirth, and infant mortality [28]. There is some strong evidence that exposure to ETS increases the probability of preterm birth [95]. A large birth cohort study in California found borderline statistical association between maternal serum cotinine concentrations during early pregnancy and late fetal deaths (borderline statistical significance), preterm birth, and a significant association with reduced birth weight (significant) [24].

The association between sudden infant death syndrome (SIDS) and maternal smoking has been firmly established. As reported by Wigle et al. [98], a meta-analysis of 39 epidemiological studies and an expert panel review concluded that there is sufficient evidence of a causal association between sudden infant death syndrome and postnatal ETS exposure, independent of prenatal maternal active smoking [95]. Sudden infant death syndrome was also associated with paternal smoking, even when the mothers did not smoke.

Active *smoking* by mothers has been shown to significantly reduce the rate of fetal growth, and the effect was shown to be dose-dependent. DiFranza and Lew [97] using data from 23 studies, calculated an odds ratio of 1.82 for the association between maternal smoking and low birth weight (<2,500 g). The risk of intrauterine growth retardation caused by maternal smoking appears to increase with maternal age, from twofold for mothers aged 17 years to fivefold for mothers aged 35 years [98]. Although smoking throughout pregnancy is known to affect birth weight, there is some evidence that the final trimester may be particularly important [99]. In some studies, babies of smoking mothers have been reported to be shorter and to have smaller head circumferences at birth than babies of nonsmoking mothers [98].

Studies *on pesticide* exposures and birth defects have found evidence of associations between paternal pesticide exposure and cryptorchidism [99], although other studies have failed to find a similar association. Cryptorchidism was associated also with maternal serum DDT/DDE and hexachlorobenzene levels [100] and with adipose tissue or maternal serum DDE concentrations [101]. In animal studies, trans-placental exposure to the pesticides DDT/DDE vinclozolin, procymidone, or linuron, produce hypospadias, cryptorchidism, and other abnormalities [102]. The epidemiological evidence of the link between pesticide exposure and hypospadias is not conclusive enough to affirm a link between pesticide exposure and this type of birth defect.

Respiratory System

Lung development is a continuous process from embryonic life to adolescence. At birth, about 85% of the human alveoli are present. Alveolar number and lung surface area increase through childhood and begin to level off between 2 and 4 years of age, whereas lung expansion continues up to 8 years of age [5].

Immature (neonatal) differentiating cells of the respiratory tract are more sensitive to injury following exposure to respiratory toxicants than mature cells, and at dose levels that cause no effects in adult cells. Children are usually physically active, and have greater exposure to air pollutants. Because of their higher metabolic rates, they breathe more rapidly and inhale more pollutants per kilogram of body weight than adults. Their narrower airway passages compared to adults can be more easily obstructed in a greater proportion than in adults. Thus, because of the immaturity of the lungs during childhood and the greater exposures relative to body weight in children than in adults, it is inferred that children may be more susceptible to the effects of respiratory toxicants than adults, whose lung growth is complete.

Air pollution has been extensively studied in relation to respiratory health and in general it has been easier to demonstrate the effects of air pollution on exacerbation of certain conditions than on the causing of disease in previously normal individuals. Both outdoor and indoor air pollution have been identified as potential risk factors for both the initiation/induction and the exacerbation of respiratory diseases, especially asthma. Evidence of the effect of air contaminants such as ozone and ETS on lung function has been demonstrated in both animal and human studies. Air pollution is now linked to SIDS [103].

Indoor Air Pollution Indoor air pollution is the most important source of respiratory exposure to toxicants in children, given the fact that children spend up to 90% of their time indoors and the large range of pulmonary irritants that can be found in the home. Exposure to pollutants in the home environment in developed countries has increased with improved insulation and reduced ventilation and the use of chemical detergents and building or furnishing constituents that contain noxious pulmonary irritants [5]. Infants and young children in particular have little control over their exposure to pollutants in the home environment and are vulnerable to the activities of the adults (particularly ETS). Common indoor air pollutants include nitrogen dioxide, formaldehyde and other volatile organic compounds (VOCs), and ETS.

Environmental Tobacco Smoke Environmental tobacco smoke has been extensively studied in relation to children's respiratory health. The developing fetus can be involuntarily exposed to tobacco during pregnancy through a smoking mother or by the pregnant mother's exposure to environmental tobacco smoke. Exposure may continue throughout childhood if any of the parents smoke. The early exposures may have persistent adverse effects throughout life.

There is evidence of ETS effects on the increased risk of lower respiratory illness rates, especially in the first year of life, increased rates of chronic middle ear effusion in children, impairment of lung function and exacerbation of certain conditions such as asthma. Exposure to environmental tobacco smoke is a risk factor for sudden infant death syndrome. Children exposed to ETS are more likely to suffer from respiratory illness (bronchitis, pneumonia) and to be hospitalized because of the illness than unexposed children [103]. EPA estimates that between 150,000 and 300,000 of bronchitis and pneumonia cases annually in infants and young children up to 18 months of age are attributable to exposure to ETS. Of these, between 7,500 and 15,000 will result in hospitalization. Furthermore, there is evidence that exposure to ETS leads to increased infant mortality from respiratory illness as well as increased morbidity [104].

Exposure to pollutants during critical periods of lung development may have effects that would not be seen if exposure occurred during adulthood [105]. Maternal smoking during pregnancy was related to impaired lung function in newborn infants [106]. Permanent effects of parental smoking on lung function were found in adults of 30–59 years of age [107], indicating that the impairment of lung function persists through life.

The exacerbating effect of ETS on asthma has been known for some time, and many studies evidence this effect. ETS exposure increases the frequency of episodes and severity of symptoms and the rates of hospitalization in asthmatic children. In addition, ETS exposure is a risk factor for new cases of asthma in children who have not previously displayed symptoms (EPA http://www.epa.gov/smokefree/healtheffects.html) [69].

Another group of environmental agents that have been studied in relation to respiratory health are the bioaerosols. Bioaerosols include inhaled allergens (house dust mites and other insects, molds, pets, pollens) and bacterial (lipopolysaccharide) and

fungal (glucans) products. Sensitization to one or more common inhalant allergens is consistently associated with childhood asthma especially in developed countries [107]. An expert panel concluded that house-dust mite allergens produce incident (new onset) asthma and that cat, cockroach, and house-dust mite allergens induce episodes in sensitized asthmatics [96]. However, the relationship between exposure to inhaled allergens in early life and the development of asthma or wheeze in childhood is controversial [107]. Contrarily, it has been hypothesized that early exposure to some allergens may be protective of later development of asthma [109], although this hypothesis was discarded in later studies [110].

Outdoor Air Pollution Air pollution, from both vehicular and stationary sources, is associated with an increase in respiratory symptoms, a decrease in lung function, and the exacerbation of asthma symptoms among asthmatic children. Recent studies have evidenced the relationship between traffic air pollution and incident development of asthma. Most of these effects occur at levels within the ambient air quality standards of most countries that have the potential to affect a large population of children. Air pollution effects contribute significantly to children's respiratory morbidity and have a significant economic impact in terms of health expenses. Most studies attribute respiratory symptoms to particulate matter, although the close correlation of particulate matter levels with nitrogen dioxide and sulfur dioxide levels makes the contribution of individual pollutants difficult to determine [5].

There is a consistent body of evidence that outdoor air pollution is associated with increased respiratory symptoms, such as cough, bronchitis, respiratory infections, and upper respiratory tract illness in children [111]. Several studies have demonstrated an increase in respiratory symptoms such as cough and bronchitis associated with increases in PM10. A recent study in Eastern Germany evaluated the association between respiratory symptoms and air pollution levels before and after political reunification. A reduction in air pollution since reunification is associated with reductions in the rates of chronic cough and bronchitis symptoms in a new cohort of children, suggesting a potentially reversible effect of air pollution [112]. A similar dramatic effect was observed with children who moved out of an area to other areas of higher and lower PM10 concentrations. Those children who moved to areas of lower PM10 concentrations showed higher rates of growth in lung function, whereas the opposite effect was observed in children who moved to areas of higher PM10 concentrations than before [113].

The role of air pollution in the exacerbation of asthma is well established, and there is mounting evidence that air pollution, particularly from traffic, is implicated in the pathogenesis of asthma [114]. Because children with asthma have increased airway reactivity, the effects of air pollution on the respiratory system can be more serious for them. Children with asthma have been shown to experience more respiratory symptoms, use extra medication, produce chronic phlegm, and have more bronchitis following exposure to high levels of particulate pollution [115, 116]. Air pollution is also associated with increased school absenteeism due to respiratory illness [117], and increased admissions to hospital emergency department [118].

The role of the different components of air pollution in the development and exacerbation of asthma is difficult to elucidate. Oxidant gases such as nitrogen oxide and ozone have been associated with asthma prevalence [119]. Other studies suggest that traffic pollution, but probably not NO_2 from traffic, is associated with atopy and wheezing [120]. The authors suggested that diesel particles or some component of those particles, such as polycyclic aromatic hydrocarbons, may be the most important etiologic component. A recent review of the short-term effects of PM10 and NO_2 on respiratory health among children with asthma or *asthma*-like symptoms concluded there were clear effects of PM10 on the occurrence of asthma symptom episodes, and to a lesser extent on cough and PEF (pulmonary expiratory function). Results with respect to NO_2 were inconclusive [121].

Of great relevance have been recent studies that have related proximity to heavily trafficked roads with asthma and reduced lung functions as well as other respiratory symptoms such as wheeze and dry cough. Lin et al. [122] found significant odds ratios for living within 200 m of a street with the highest tertile of traffic density and asthma prevalence, and the children with

asthma were more likely to have truck traffic on their street. Although some studies showed no increased risk [123], the weight of evidence suggests that traffic pollution is associated with the risk of developing asthma [114].

Lung function is also affected by air pollution. Acute exposure to ozone, nitrogen dioxide, sulfur dioxide, and particulate matter is known to cause transient reversible decreases in lung function [124, 125]. Some recent studies indicate that long-term exposure to ozone and related co-pollutants (individually and synergistically) is associated with impairment of lung function capacity in children and adolescents [126], although other studies are not consistent. Further, it has been hypothesized that a fraction of the increases in the prevalence of chronic obstructive lung disease in adults who live in more polluted areas could be the result of exposures that occurred during childhood [127].

Cancer

Childhood cancers are relatively rare diseases during the first 2 decades of life, but are the leading cause of death of children in many countries. The most common types of childhood cancer are lymphoid neoplasms (leukemia, lymphoma) and cancers of the central nervous system. Other kinds of childhood tumors include embryonal tumors of the retina, sympathetic nervous system, kidney, and liver; tumors of bone and soft connective tissues; and certain gonadal neoplasms. Carcinomas in epithelial tissues, the most frequent type of cancer in adults, are rare in children. Neoplasms in adults resulting from known or iatrogenic exposure typically have latency periods of 20 years or more. Thus, cancers in children are qualitatively distinct from those in adults.

Although childhood cancer is a rare disease, the occurrence of new cancer cases among children has continued to rise during the last 2 decades. While medical advances have led to a sharp reduction in mortality from childhood cancer, it is still a group of diseases with potentially devastating outcomes, which can be at least partially prevented; so the study of the environmental causes of cancer is essential. A recent report from the European Automated Childhood Cancer Information System (EACCIS) provides evidence of a 1% increase per year in childhood cancers and 1.5% increase per year in adolescent cancer in Europe for the period 1970–1999. All of the common types of neoplasms showed significant increases, including leukemias, lymphomas, central nervous system tumors, neuroblastomas, soft tissue sarcomas, retinoblastoma, and germ cell, renal, hepatic, and bone tumors in children and carcinomas, lymphomas, soft-tissue sarcomas, and germ cell and CNS tumors in adolescents. There were in addition significant differences between Eastern and Western Europe with regard to leukemias, lymphomas, carcinomas, and central nervous system tumors in children, and carcinomas, lymphomas, leukemias, and soft-tissue tumors in adolescents. Earlier reports of European populations also noted increases in several of these types of childhood cancers. Similarly, in the USA, there was an overall increase of about 25% in childhood cancers between 1975 and 2000. While the reported increases in the 1980s may have reflected improvements in diagnosis and reporting, it is unlikely that the most recently reported trends reflect the same bias. Evidence from both epidemiological and mutagenicity/carcinogenicity studies suggest that environmental toxicants may be involved at least in the causation of some forms of cancers such as acute lymphoblastic leukemia (ALL), which is most common in industrialized countries.

Most cancers result from the interaction between genetic factors and the environment [128]. In this context, environment is defined broadly and includes diet, alcohol, drugs, tobacco, and all other nongenetic factors as well as classic environmental toxins. It has been estimated that about 80–90% of all cancers are attributable to environmental factors acting in conjunction with both genetic and acquired susceptibility. For cancer in adults, different opportunities for environmental exposure have commonly been considered a major (albeit not exclusive) reason for the geographical distribution of cancer. Geographical differences in incidence of most cancers (except lymphomas) are less marked for childhood than for adult cancer, thus suggesting that the fraction of childhood cancers due to environmental factors is probably lower than for adults [128].

The potentially higher susceptibility of the developing fetus and children to the effect of environmental carcinogens is based on several aspects. Chemical carcinogenesis is a multistep process involving genetic and epigenetic changes in susceptible cells that gain

a selective growth advantage and undergo clonal expansion as the result of activation of protooncogenes and/or inactivation of tumor-suppressor genes. The occurrence of these events is modulated by several factors that themselves change in the course of development. Thus, DNA damage may be repaired by the action of DNA repair enzymes, whose presence and activity may change with age. Similarly, changes in metabolism will determine whether carcinogenic metabolites are formed, thus allowing for the initiation of the cancer process.

DNA repair mechanisms play an important role in cancer protection. DNA repair enzymes have been found to be well expressed in embryos and fetuses. In fact, there are a number of DNA repair genes/activities that have higher expression in fetuses or embryos than in adults. Interference with the synthesis of DNA repair enzymes during development may result in increased susceptibility to cancer during childhood or later in life. An example of the important role of DNA repair mechanisms is the p53 gene, which encodes a protein that modulates DNA repair and cell division. Mutations of the p53 genes are involved in at least 50% of all cancers [129]. p53 mutations have been linked with tobacco smoking [130], and it is possible that p53 mutations occur in the offspring of smoking mothers.

The higher rates of cell proliferation during development can contribute to increased likelihood of carcinogenesis. For example, PAHs and aflatoxin B1 (AFB1) produce liver tumors when administered to newborn rodents but not when administered to older animals, presumably because the liver proliferates rapidly in the developing system but more slowly in older animals [131]. Women who were in their teens at the time of atomic bombings had the greatest risk of radiation-induced breast cancer [132]. Some organs, such as the brain, are fully developed in early childhood, whereas others such as the skeletal system do not achieve maturity until adolescence [131]. This may be the reason why osteosarcoma, the most common bone cancer, peaks in late adolescence, a period of rapid bone growth.

The immune system of the newborn is not fully developed until about 6 months of age. Chemicals that affect the immune system, such as halogenated aromatic hydrocarbons that bind to the Ah receptor [133], may modify the host defense mechanism against infection and cancer [134].

The susceptibility of children to cancer may be influenced by the presence/absence of metabolizing enzymes. The role of these enzymes is potentially complex, especially for those that carry out the phase I (usually detoxifying) reactions. Usually, chemical metabolism protects the adult and fetus from carcinogenicity, but the activity of enzymes can also result in bioactivation, such as in the case of bioactivation of benzo[a]pyrene to its carcinogenic form, which has been demonstrated by the observation of the formation of DNA adducts in mice and monkey fetuses, which probably originated in maternal liver [135].

The first step in metabolism is usually oxidation, carried out by cytochrome P450 enzymes. This group of enzymes are named as CYP enzymes and grouped in families according to their genotype and activity. Several groups of these enzymes are involved in the metabolism of exogenous carcinogens, such as the CYP families 1–3, which are thought to be the most relevant to effects of exogenous carcinogens. Other examples are the CYP4B1, which activates aromatic amines, and CYP2E1, which metabolizes nitrosamines and organic solvents that have been implicated in causation of childhood cancers.

Phase II detoxification enzymes have received less attention than CYPs in the perinatal context, though they are also likely to be important. For example, among the glutathione S-transferases (GSTs), the I (P) form is apparently expressed at the highest levels and in many tissues in human fetuses from early in gestation, and levels of total GST activity in all fetal tissues studied was comparable to that in the corresponding adult organ [135]. An increasing body of evidence implicates GST polymorphisms in risk of childhood leukemias. Glucuronidation, a type of Phase II reaction, catalyzed by uridine diphosphate-glucuronosyltransferase (UDG), is a key detoxification step for solubilization of high molecular weight carcinogens such as polycyclic aromatic hydrocarbons, heterocyclic amines, and tobacco-specific nitrosamines. Low expression of UDG in the fetus and neonate, and as a result of polymorphisms in children, could well increase sensitivity to carcinogenesis by some chemicals. Sulfotransferases (SULT) have been proposed to constitute a major enzymatic detoxification system in the fetus [136, 137]. However, these enzymes also catalyze activation of several types of

chemical carcinogens to DNA-damaging forms, including aromatic amines, polycyclic aromatic hydrocarbons, heterocyclic amines, 3-nitrobenzanthrone, and benzylic alcohols. This illustrates how alteration of enzymatic metabolism can greatly influence susceptibility to perinatal carcinogenesis.

While mutagenicity/carcinogenicity studies, as well as the study of enzymatic systems and DNA repair enzymes, provide mounting evidence that the interplay between chemical agents and these biological factors are significant in the development of cancer, epidemiological studies have only been of limited usefulness to confirm this hypothesis. The increasing trends over the last 20–30 years and the geographical distribution of childhood cancers, clearly point to environmental causes. However, few studies have been able to firmly establish the environmental origin of childhood cancers. Cumulative epidemiological evidence pertaining to childhood cancers, including international variation, time trends, and risk factor studies was reviewed and analyzed by Bunin [138]. This review concluded that ionizing radiation and a variety of genetic conditions are thought to explain 5–10% of childhood cancers. There are clear associations between Epstein-Barr virus infection and Burkitts lymphoma in Africa, and between human immunodeficiency virus and Kaposi's sarcoma [138].

Other risk factors have not been conclusively identified. Among the nongenetic causes, the pattern of international variation and associations with surrogates of infection suggested an infectious etiology for acute lymphoblastic leukemia, although no agent has been identified. For brain tumors, cured meats, polyomaviruses, and farm exposures were pointed out as potential causes. Changes in the incidence and characteristics of children with hepatoblastoma as well as risk factor studies suggest a role for an exposure of very low birth weight babies. High birth weight, tea or coffee consumption, and certain paternal occupations have shown some consistency in their association with Wilms' tumor. For most of the other cancers, very few epidemiologic studies have been conducted, so it is not surprising that nongenetic risk factors have not been detected. The most important difference between the cancers for which there are good etiologic clues and those for which there are not may be the number of relevant studies.

This section summarizes the evidence found in the recent literature of the associations between environmental factors and childhood cancer. Attention is given only for those agents for which there is at least limited evidence of an association between environmental agent and disease.

Ionizing Radiation

Evidence of the potential of ionizing radiation to induce childhood cancer comes from events such as Hiroshima and Nagasaki, populations affected by accidents at nuclear plants, as well as investigations on the longer effects of indoor radon and on the consequences of exposure to x-ray for diagnostic or therapeutic reasons.

Japanese children exposed to the atomic bombings of Hiroshima and Nagasaki had increased risks of adult cancers, including leukemia and solid tumors. The highest risk was that of children who were exposed in utero. Radiation-related leukemia started to occur 2–3 years after the bombing, reached its peak within 6–8 years, and has declined steadily since then. For people exposed as adults, the excess risk was lower than that of people exposed as children, but the excess risk appears to have persisted throughout the follow-up period [5].

Thyroid adult carcinomas were also increased in survivors who were children at the time of the bombings at Hiroshima and Nagasaki. The greatest risk for thyroid cancer occurred in individuals who received a radiation dose to the thyroid greater than 1 Sv before age of 10 years. Similarly, breast cancer risk among women survivors to the atomic bombings was highest for the women who were less than 10 years of age or between 10 and 20 years of age, lower for women who were between 20 and 40, and even lower for women exposed after 40 years of age [132].

Prenatal diagnostic X-irradiation has also been linked to increased risk of leukemia in offspring, as has therapeutic, high-dose, ionizing radiation in childhood for other cancers and for various non-neoplastic conditions [139].

The Chernobyl nuclear reactor accident in 1996 caused a significant increase in the incidence of thyroid cancer in children since 1990. Most of the tumors have been observed among individuals who were very young

at the time of the accident [31]. In Belarus, over half of the tumors occurred in people who were less than 6 years old at the time of the accident. In a series of 472 children with thyroid cancer diagnosed up to 1995 in Belarus, only 2% had been conceived after the accident, 9% had been exposed in utero, and 88% were under 15 years of age at the time of diagnosis [140]. The very early age at which the thyroid cancers have begun to be diagnosed is one of the most striking examples of the special sensitivity to a carcinogen other than an infectious agent occurring exclusively during preadult life.

UV Light

Sun exposure is known to be a risk factor for the development of skin cancer later in life. The occurrence of sunburn is an indicator of risk [141]. Numerous studies have assessed the carcinogenic effect of sunburn at different ages and concluded exposure to solar radiation before 10 years of age was a primary contributor to risk of melanoma. The IARC concluded that childhood is an especially vulnerable life stage [142] to the carcinogenic effect of UV radiation. While the use of sunscreen reduces the risk of sunburn, an expert working group convened by the International Agency for Research warned against the risk of relying solely on sunscreens for protection from ultraviolet radiation [143], as the use of sunscreens may lead to an extension of the duration of intentional sun exposure, which can increase the risk of melanoma.

Environmental Tobacco Smoke

Environmental tobacco smoke is an established human carcinogen by the International Agency for Research on Cancer [144]. Over 50 epidemiological studies have reported risk ratios of lung cancer for secondhand smoking in adults. A recent meta-analysis of epidemiological studies of lung cancer and adult exposure to environmental tobacco smoke resulted in risk ratios of 1.22 in women and 1.36 in men from workplace exposure. Other meta-analyses have produced similar results. The evidence of a causal relationship between ETS exposure and cancers in organs other than the lung is inconclusive.

Tobacco smoke contains many carcinogens, such as PAHs and 4-aminobiphenyl, that can cross the placenta and be transferred to the fetus. The genotoxicity of tobacco smoke to the fetal liver has been tested in an animal study. Sister chromatid exchange in the liver cells of fetal mice was analyzed at the 16th day of gestation after short-term exposure (twice, on the 15th and 16th days of gestation), long-term exposure (starting 4 weeks before mating and stopping on the 16th day of gestation), and prepregnancy exposure (4 weeks before mating). The number of sister chromatid exchanges was significantly increased in all exposure groups, and long-term exposure caused a significantly higher increase than did short-term exposure [145].

Most epidemiological studies on the link between exposure to ETS and childhood cancer have focused mainly on pregnant women. While most of studies of smoking by mothers reveal no effects on childhood cancer, many studies of smoking by fathers have shown a significant association with risk of cancer in their children, and when both mothers and fathers are included in the study, the effect appears to be greater for exposure of fathers than of mothers [135]. This effect has been attributed to germ-cell mutations during spermatogenesis caused by tobacco products [146]. Three reports from the Oxford Survey of Childhood Cancers have suggested that paternal but not maternal cigarette smoking is associated with increased risks for the generality of childhood cancers. Some, however, have produced conflicting findings. A large case control study conducted in the UK (the United Kingdom Childhood Cancer Study) concluded that there was no evidence that paternal smoking is a risk factor for childhood cancer in general [147]. A significant association was reported in this study, however, between hepatoblastoma risks and smoking by both parents relative to neither parent smoking. Sorahan and Lancashire speculated that the importance of both parents smoking in the etiology of hepatoblastoma might arise from the combination of oxidative damage to sperm DNA and damage to the fetal liver from carcinogenic metabolites in the blood of the pregnant mother [148]. Further, in a study where both preconception and postnatal smoking by the fathers was quantified, and few of the mothers smoked, the association with childhood cancer related significantly only to preconceptional paternal smoking levels [149]. Thus, second-hand exposure of the infants to smoke was less

likely. Transplacental effects of sidestream smoke were one possibility. In rats, sidestream smoke constituents received transplacentally caused oxidative DNA damage in fetal tissues [136]. In one epidemiological study, paternal smoking had a larger possible effect when mothers were nonsmokers [137], suggesting protective effects of detoxification enzymes induced in the placenta and in maternal tissues by maternal smoking.

Some studies have examined the relationship between exposure to environmental tobacco smoke during childhood and cancer risk. Sandler and colleagues [150] found that the overall cancer risk was greater for individuals with exposures to environmental tobacco smoke during both childhood and adulthood than for individuals with exposure during only one period. When specific cancer sites or types were considered, leukemia and lymphoma among adults were significantly related to exposure to maternal passive smoke before 10 years of age [150].

Pesticides and Cancer

Pesticides are biologically active molecules that are commonly used to destroy unwanted organisms in agricultural and residential environments. The widespread use of these chemicals has raised concerns over the potential of pesticides to cause childhood cancer.

Although the biochemical mechanisms relating pesticide exposures to childhood cancer have not been fully described, some evidence suggests that pesticides may promote the formation of chromosomal aberrations known to be associated with an increased cancer risk [149]. Studies in adult populations suggest that pesticide exposures may have a direct effect on chromosome structure, and therefore a causal relationship between pesticide exposures and childhood cancer is plausible [152].

Epidemiological studies have reported associations between childhood cancer and either parental or child exposures to pesticides. Research reviews have suggested an increase in the risk of brain cancer, leukemia, non-Hodgkins's lymphoma (NHO), Wilms' tumor, Ewing's sarcoma, and germ cell tumors associated with parental occupational and nonoccupational exposure to pesticides [153, 154]. The exposures observed occurred prior to and during pregnancy, as well as after the childbirth, thus involving different potential modes of action. Zahm and Ward [154] concluded that at least some childhood cancer could potentially be prevented by reducing or eliminating pesticide exposure, although methodological limitations common to many studies limit the possibility of making conclusions regarding the role of pesticides in the etiology of childhood cancers [153, 154].

Two extensive reviews were conducted after the Zahm and Ward review [154] that attempted to provide conclusions on the basis of cumulative evidence. In a review that evaluated 18 new studies conducted between 1998 and 2004, it was concluded that while collectively all studies seem to suggest an increase in the risk of different cancer types associated with exposure to pesticides, no conclusions could be drawn with respect to cancer types as well as to specific causative factors across studies [153]. Infante-Rivard and Weichenthal [152] reviewed studies conducted between 1999 and 2004 and critically evaluated the evidence on the associations between pesticide exposures and leukemia (12 studies), brain cancer (10 studies), neuroblastoma (4 studies), non-Hodgkin's lymphoma (3 studies), Wilm's tumor (2 studies), and Ewing's sarcoma (1 study), as in the Zahm and Ward review. The authors found recent studies to be consistent with the suggestion of Zahm and Ward of an association between pesticide exposure and childhood leukemia, brain tumors, neuroblastoma, and also non-Hodgkin's lymphoma and Wilm's tumor. Specifically childhood exposure to household insecticides and prenatal exposure to pesticides seemed to pose the greatest risks of leukemia and brain tumors. Exposure-response gradients were observed in some studies on pesticide exposure and risk of leukemia. For neuroblastoma, the authors found that all four recent studies reviewed showed an association between exposure of pesticides and risk of neuroblastoma that supported earlier findings by Zahm and Ward. A recent study also indicates that residential use of pesticides, and herbicides specifically, may increase the risk of neuroblastoma in children [153]. The risk of non-Hodgkin's lymphoma was found to be associated with residential exposure to pesticides, and two of the studies reviewed provided evidence of exposure response gradients in two of the three reviewed studies. With respect to Wilm's tumor, recent studies did not provide additional evidence of an association between insecticide exposures and parental

pesticide exposure before birth and Wilms' tumor that had been indicated in Zahm and ward's review. The evidence on Ewing's sarcoma was inconclusive.

A systematic review and meta-analysis of studies on childhood leukemia and parental occupational exposure to pesticides concluded that there was not sufficient evidence to affirm an overall association between childhood leukemia and any paternal occupational pesticide exposure among all studies combined or subgroups of studies [155]. An elevated childhood leukemia risk was found in relation to paternal occupational exposure to the broad pesticide classes of insecticides and herbicides, but the authors considered that the small number of studies showing this effect and the lack of exposure–risk relationships did not allow making firm conclusions. However, an association was found between childhood leukemia and prenatal maternal occupational pesticide exposures. The studies also showed associations between childhood leukemia and maternal occupational exposure to insecticides and herbicides. It was concluded that the overall evidence, though limited, warranted exposure prevention measures on the basis of the precautionary principle [152].

Many authors have pointed out the major shortcomings of epidemiological studies on pesticides exposures and childhood cancer [156]. One of the major shortcomings is exposure assessment, as many of the studies use very unspecific measures of exposure, such as "farming" as a measure of "exposures to pesticides." In most of the studies, the specific pesticide/s, timing and other concomitant exposures to which the population was exposed is not known. The authors recommended directing research efforts to the characterization of pesticide exposures in future research. Further they have remarked that "another 40 epidemiological studies similar to the majority of those conducted thus far will not provide clarity."

In spite of the limitations of epidemiological research on pesticide exposures and childhood cancers, many researchers find that there is sufficient evidence to be concerned about the potential role of pesticides in childhood cancers, and to recommend a precautionary approach. Infante-Rivard [152] contrasted the overall evidence against the Bradford Hill's causality criteria (strength, consistency, specificity, temporality, biological gradient, plausibility, coherence, experiment and analogy [157]). The strongest evidence in support of a causal relationship between pesticide exposure and childhood cancer was considered to be the repeated detection of statistically significant increased risks between childhood pesticide exposure and cancer. The authors concluded that there is sufficient evidence to conclude that there is at least some association between pesticide exposure and childhood cancer. In addition, the biological gradients observed in recent studies also suggest that there may be a causal relationship between childhood insecticide exposures and the development of ALL and NHL [158, 159]. Infante-Rivard [152] indicated that the development of childhood cancer probably depends on the presence of many factors, including genetic predisposition, and recommended the use of improved exposure assessments that include separate parental interview, specific pesticide exposure questions, and semiquantitative exposure measures that can be used to confirm exposure information obtained through questionnaires.

Disinfection By-products and Cancer

Disinfection by-products (DBPs), such as trihalomethanes (THMs), are regulated carcinogens in drinking water and have been detected in the blood and breath of swimmers and of nonswimmers at indoor pools. There are a few data on the effects of low doses on humans, particularly infants and children.

Villanueva et al. [160] conducted a pooled analysis of six epidemiological studies and calculated a summary relative risk of bladder cancer equal to 1.18 (95% CI 1.06, 1.32) for exposure above 1 μg/L of trihalomethanes. Boffetta [161] estimated the attributable fraction of bladder cancer on the basis of these figures to be about 10.3%.

Arsenic

Inorganic arsenic is a human carcinogen [162] which causes bladder, skin, and lung cancers in humans. At least in mice, inorganic arsenic is a much more potent carcinogen to the fetus than to adults. The modes of carcinogenic action of inorganic arsenic in rodents and in humans are not yet fully understood, but the possibility exists that inorganic arsenic in drinking water poses a special carcinogenic concern for pregnant women and their unborn infants.

Air Pollution and Childhood Cancer

There have been several studies during the last decade that have linked children's exposure to air pollutants to childhood cancer, leukemia in particular. Infante-Rivard [163] evaluated the results of epidemiological studies conducted between 1998 and 2008 on diverse chemical exposures and childhood leukemia. The review included nine case-control studies and four ecological studies. The latter showed an association between incidence rates of childhood leukemia and levels of air pollution in the area of residence of the population at the time of diagnosis. The lack of information about the place of residence of subjects prior to diagnosis (including during the preconception and gestation period) made it difficult to conclude an association between the exposure levels and risk of childhood leukemia. The review concluded that the weight of evidence from both case-control and ecological studies indicated no increased risk for childhood leukemia associated with exposure to traffic-related residential air pollution. The same conclusion was reached in another review conducted by Raaschou-Nielsen [164].

Endocrine Disruptors and Cancer

Increases in the incidence of cancer in certain parts of the world are often cited as evidence that widespread exposure to endocrine disruptors has adverse effects on human health. Of particular concern are the observed increased incidences of cancer at hormonally sensitive sites, such as breast, uterus, prostate, and testis in Europe and North America. These increases cannot be explained only on the basis of improved diagnostic techniques, and it has been argued that these trends coincide roughly with the increasing use and release of industrial chemicals into the environment. Concerns are also based on plausible mechanisms of action because both human and experimental animal studies show that these cancers are modulated hormonally.

Many epidemiological and experimental animal studies have attempted to evaluate the link between exposure to endocrine disruptors and increased risk of breast cancer. A direct association between these chemicals and increased risk of breast cancer has not been established. However, some researchers claim that the time of life when exposure takes place (e.g., prenatal, neonatal, childhood, adolescence) may have a major influence on the appearance of this and other health effects. The development of the mammary gland occurs in multiple stages. Fetal development of the mammary gland rudiment is governed by tissue interactions in both males and females. In females, the pubertal period drives ductal morphogenesis, and pregnancy results in massive differentiation of the mammary gland. Thus, the perinatal period and the period between age at menarche and age at first full-term pregnancy may be particularly important for breast tumor development and latency [165]. Young girls exposed to carcinogenic agents during puberty may be at high risk of future breast cancer due to susceptibility of rapidly growing breast tissue mediated by hormonal changes during this time. This claim is supported by data from atomic bomb survivors, where an increased risk of breast cancer was found in women exposed before 20 years of age [132]. Similarly, an elevated risk was found for women irradiated during childhood for medical reasons [166].

DES was extensively prescribed in developed countries from the late 1940s through the 1970s to women with high-risk pregnancies to prevent miscarriages and other complications of pregnancy. In the early 1970s, a rare form of female reproductive tract cancer, clear cell adenocarcinoma began to be detected among women whose mothers had taken DES during pregnancy [167]. Although clear cell adenocarcinoma occurs in only 0.1% of women who were exposed to DES in utero, this represents a 40-fold increased risk in comparison with the nonexposed population. In contrast, men who were exposed to DES in utero do not have a clear increased risk of any cancer, although a statistically nonsignificant threefold increased risk of testicular cancer has been reported [168]. While there is no epidemiological evidence for a link between exposure to estrogenic or anti-androgenic compounds and testicular cancer, some authors have hypothesized that the similar increases in the incidence of testicular cancer and in the incidence of cryptorchidism and hypospadias in similar geographical areas, suggest a common cause of similar environmental origin in both health effects [85].

Some studies have shown that women taking DES during pregnancy to prevent miscarriage have been shown to have a slightly increased risk of developing

breast cancer 30 years after taking the drug [169]. Data on the risks of breast cancer in daughters of DES-exposed women are not yet available.

Future Directions

During the last 2 decades, there has been an exponential increase of scientific literature about the susceptibility of children to the effects of environmental exposures. Evidence is accumulating that toxic chemicals are responsible for at least some of the changing patterns of disease. Well-studied examples include adenocarcinoma of the vagina in girls exposed prenatally to DES; asthma and pneumonia caused by smoke and particulate air pollutants; neurodevelopmental toxicity in infants exposed to lead, PCBs, methylmercury; and small head circumference at birth in infants exposed in utero to organophosphate pesticides.

Past discoveries of etiologic associations between toxic environmental exposures and diseases in children have led to successful programs of exposure control and disease prevention. Examples include reductions in the use of alcohol and tobacco during pregnancy, minimization during pregnancy of diagnostic x-rays, and removal of lead from gasoline. Sadly, though, the interval between initial recognition or suspicion of effects and their eventual control has been typically been far too long. Early warnings have frequently been ignored. The price of delayed action has been widespread increases in the incidence of certain diseases such as asthma and cancer.

When evaluating the health and social impact of environmental threats on children, it is necessary to take into account, not only their effects on childhood health, but also the long-term potential health effects throughout the lifelong span of the individual. It has been hypothesized that early exposure to environmental toxicants could affect the brain later in life. Consensus among scientists is based on experimental studies on associations between early life exposures to pesticides and Parkinson's disease, as well as on epidemiologic studies of the toxic and apparently irreversible effects on the developing brain of in utero exposure to lead, methylmercury, and polychlorinated biphenyls. A mechanistic hypothesis proposed that early exposure to neurotoxic chemicals reduce the number of neurons in critical areas of the brain such as the substantia nigra to levels below those needed to sustain function in the face of neuronal attrition associated with advancing age. In addition, as some researchers have pointed out, the effects at population level would add a substantial burden to society, in terms of health, economic, and human costs.

The difficulties in conducting environmental health research have been pointed out by many authors during the last 3 decades. Human populations are exposed to hundreds of chemicals through air, water, and food, under many different exposure situations. Environmental exposures are usually low, and often occur concomitantly with occupational exposures, smoking or naturally occurring agents. And when an association between with an exposure and a disease in found, such as for example, air pollution and asthma, a long path lies ahead to determine the specific causative agent of the disease, and the population and individual susceptibility factors that makes some individuals and not others become ill. The potential for interaction of different pollutant exposures makes the question with respect to the role of environmental exposures impact on health even more difficult to answer. The need for taking into account multiple and cumulative exposures has been clearly affirmed by the EPA and other government and research bodies.

Slowly, evidence is found to confirm or discard certain effects, but it seems that progress is too slow to catch up to the increases in incidence of certain diseases, such as asthma and cancer. It is possible that the statement of Olshan and Daniels [170] with respect to pesticide research, that "another 40 epidemiological studies similar to the majority of those conducted thus far will not provide clarity," should be applied to other groups of chemicals, such as disinfection byproducts, or endocrine disruptors, and that we need to think of a more effective way of examining evidence. Many authors have pointed out the need of better exposure assessment methods. In addition to continuing toxicological research, which is essential to elucidate the mechanisms of action, epidemiological research should probably incorporate exposure assessment methods that could enable detection of at least the specific exposures and exposure levels. Exposure assessment can be improved in many ways. In the extreme, if the body burden of a list of suspected carcinogens in the blood or adipose tissue of each

child diagnosed with cancer were determined, more specific associations between disease and toxic agent may be determined. The path to confirm and rule out some proposed environmental causes would probably be at least somewhat shorter. While this approach may be costly, it may be cost-efficient in the long run. There have been some efforts to integrate an environmental health perspective in the medical practice. These efforts should be further developed and supported.

Bibliography

Primary Literature

1. Tamburlini G, von Ehrenstein OS, Bertollini R (eds) (2002) Children's health and environment: A review of evidence. A joint report from the European Environment Agency and the WHO Regional Office for Europe. Environmental issue report No. 29. Office for Official Publications of the European Communities, Luxembourg
2. NRC (1993) Pesticides in the diets of infants and children. US National Research Council, National Academy Press, Washington, DC
3. ILSI (1992) Similarities and differences between children and adults: implications for risk assessment. International Life Sciences Institute Press, Washington, DC
4. ILSI (2003) Final report: workshop to develop a framework for assessing risks to children from exposure to environmental agents. International Life Sciences Institute Press, Washington, DC
5. WHO (2006) Principles for evaluating health risks in children. World Health Organization, Geneva
6. Moya J, Bearer CF, Etzel RA (2004) Children's behavior and physiology and how it affects exposure to environmental contaminants. Pediatrics 113(4 Suppl):996–1006
7. Landrigan PJ (2004) Children as a vulnerable population. Int J Occup Med Environ Health 17(1):175–177
8. Calabrese EJ, Stanek EJ, James RC, Roberts SM (1997) Soil ingestion: a concern for acute toxicity in children. Environ Health Perspect 105(12):1354–1358
9. Simcox NJ, Fenske RA, Wolz SA, Lee IC, Kalman DA (1995) Pesticides in household dust and soil: exposure pathways for children of agricultural families. Environ Health Perspect 103(12):1126–1134
10. Clewell HJ, Teeguarden J, McDonald T, Sarangapani R, Lawrence G, Covington T et al (2002) Review and evaluation of the potential impact of age- and gender-specific pharmacokinetic differences on tissue dosimetry. Crit Rev Toxicol 32(5):329–389
11. Anderson LM, Diwan BA, Fear NT, Roman E (2000) Critical windows of exposure for children's health: cancer in human epidemiological studies and neoplasms in experimental animal models. Environ Health Perspect 108(Suppl 3): 573–594
12. Loeffler IK, Peterson RE (1999) Interactive effects of TCDD and p, p′-DDE on male reproductive tract development in in utero and lactationally exposed rats. Toxicol Appl Pharmacol 154(1):28–39
13. Weinberg CR, Wilcox AJ, Baird DD (1989) Reduced fecundability in women with prenatal exposure to cigarette smoking. Am J Epidemiol 129(5):1072–1078
14. Wilcox AJ, Baird DD, Weinberg CR, Hornsby PP, Herbst AL (1995) Fertility in men exposed prenatally to diethylstilbestrol. N Engl J Med 332(21):1411–1416
15. Buckley JD, Robison LL, Swotinsky R, Garabrant DH, LeBeau M, Manchester P et al (1989) Occupational exposures of parents of children with acute nonlymphocytic leukemia: a report from the Children's Cancer Study Group. Cancer Res 49(14):4030–4037
16. Nicol CJ, Harrison ML, Laposa RR, Gimelshtein IL, Wells PG (1995) A teratologic suppressor role for p53 in benzo[a] pyrene-treated transgenic p53-deficient mice. Nat Genet 10(2):181–187
17. Mullikin-Kilpatrick D, Mehta ND, Hildebrandt JD, Treistman SN (1995) Gi is involved in ethanol inhibition of L-type calcium channels in undifferentiated but not differentiated PC-12 cells. Mol Pharmacol 47(5):997–1005
18. Murante FG, Gasiewicz TA (2000) Hemopoietic progenitor cells are sensitive targets of 2, 3, 7, 8-tetrachlorodibenzo-p-dioxin in C57BL/6J mice. Toxicol Sci 54(2):374–383
19. Amsen D, Kruisbeek AM (1998) Thymocyte selection: not by TCR alone. Immunol Rev 165:209–229
20. Rodier PM (2004) Environmental causes of central nervous system maldevelopment. Pediatrics 113(4 Suppl):1076–1083
21. Sharpe CR, Franco EL (1995) Etiology of Wilms' tumor. Epidemiol Rev 17(2):415–432
22. Bunney BG, Potkin SG, Bunney WE Jr (1995) New morphological and neuropathological findings in schizophrenia: a neurodevelopmental perspective. Clin Neurosci 3(2):81–88
23. Rodier PM (1995) Developing brain as a target of toxicity. Environ Health Perspect 103(Suppl 6):73–76
24. Kharrazi M, DeLorenze GN, Kaufman FL, Eskenazi B, Bernert JT Jr, Graham S et al (2004) Environmental tobacco smoke and pregnancy outcome. Epidemiology 15(6):660–670
25. Bove F, Shim Y, Zeitz P (2002) Drinking water contaminants and adverse pregnancy outcomes: a review. Environ Health Perspect 110(Suppl 1):61–74
26. Graves CG, Matanoski GM, Tardiff RG (2001) Weight of evidence for an association between adverse reproductive and developmental effects and exposure to disinfection by-products: a critical review. Regul Toxicol Pharmacol 34(2):103–124
27. Nieuwenhuijsen MJ, Toledano MB, Eaton NE, Fawell J, Elliott P (2000) Chlorination disinfection byproducts in water and their association with adverse reproductive outcomes: a review. Occup Environ Med 57(2):73–85
28. Platt RW, Joseph KS, Ananth CV, Grondines J, Abrahamowicz M, Kramer MS (2004) A proportional hazards model with time-dependent covariates and time-varying effects for analysis of fetal and infant death. Am J Epidemiol 160(3):199–206

29. Paus T, Zijdenbos A, Worsley K, Collins DL, Blumenthal J, Giedd JN et al (1999) Structural maturation of neural pathways in children and adolescents: in vivo study. Science 283(5409): 1908–1911
30. Dietert RR, Lee JE, Bunn TL (2002) Developmental immunotoxicology: emerging issues. Hum Exp Toxicol 21(9–10):479–485
31. International Agency for Research on Cancer (2001) IARC monographs on the evaluation of carcinogenic risks to humans: ionizing radiation, Part 2: some internally deposited radionuclides, vol 78. International Agency for Research on Cancer, Lyon, France
32. Altshuler K (2003) Critical periods in development. EPA . Paper Series on Children's Health and the Environment
33. Mahaffey KR (1991) Biokinetics of lead during pregnancy. Fundam Appl Toxicol 16(1):15–16
34. American Academy of Pediatrics Committee on Environmental Health (2003) Pediatric environmental health, 2nd edn. American Academy of Pediatrics, Elk Grove Village
35. Perera FP, Jedrychowski W, Rauh V, Whyatt RM (1999) Molecular epidemiologic research on the effects of environmental pollutants on the fetus. Environ Health Perspect 107(Suppl 3):451–460
36. Rice D, Barone S Jr (2000) Critical periods of vulnerability for the developing nervous system: evidence from humans and animal models. Environ Health Perspect 108(Suppl 3):511–533
37. Casey BJ, Tottenham N, Liston C, Durston S (2005) Imaging the developing brain: what have we learned about cognitive development? Trends Cogn Sci 9(3):104–110
38. Cory-Slechta DA, Thiruchelvam M, Barlow BK, Richfield EK (2005) Developmental pesticide models of the Parkinson disease phenotype. Environ Health Perspect 113(9):1263–1270
39. Landrigan PJ, Whitworth RH, Baloh RW, Staehling NW, Barthel WF, Rosenblum BF (1975) Neuropsychological dysfunction in children with chronic low-level lead absorption. Lancet 1(7909):708–712
40. Needleman HL (1979) Lead levels and children's psychologic performance. N Engl J Med 301(3):163
41. Bellinger DC (2004) Lead. Pediatrics 113(4 Suppl):1016–1022
42. Lanphear BP, Hornung R, Khoury J, Yolton K, Baghurst P, Bellinger DC et al (2005) Low-level environmental lead exposure and children's intellectual function: an international pooled analysis. Environ Health Perspect 113(7):894–899
43. Rothenberg SJ, Poblano A, Schnaas L (2000) Brainstem auditory evoked response at five years and prenatal and postnatal blood lead. Neurotoxicol Teratol 22(4):503–510
44. Bellinger D, Hu H, Titlebaum L, Needleman HL (1994) Attentional correlates of dentin and bone lead levels in adolescents. Arch Environ Health 49(2):98–105
45. Dietrich KN, Ris MD, Succop PA, Berger OG, Bornschein RL (2001) Early exposure to lead and juvenile delinquency. Neurotoxicol Teratol 23(6):511–518
46. Grandjean P, Weihe P, White RF, Debes F, Araki S, Yokoyama K et al (1997) Cognitive deficit in 7-year-old children with prenatal exposure to methylmercury. Neurotoxicol Teratol 19(6):417–428
47. Grandjean P, White RF, Nielsen A, Cleary D, Oliveira Santos EC (1999) Methylmercury neurotoxicity in Amazonian children downstream from gold mining. Environ Health Perspect 107(7):587–591
48. Davidson PW, Myers GJ, Weiss B (2004) Mercury exposure and child development outcomes. Pediatrics 113(4 Suppl): 1023–1029
49. Murata K, Weihe P, Budtz-Jorgensen E, Jorgensen PJ, Grandjean P (2004) Delayed brainstem auditory evoked potential latencies in 14-year-old children exposed to methylmercury. J Pediatr 144(2):177–183
50. Newland MC, Paletz EM (2000) Animal studies of methylmercury and PCBs: what do they tell us about expected effects in humans? Neurotoxicology 21(6):1003–1027
51. National Academy of Sciences CotTEM (2000) Toxicological effects of methylmercury. National Academy Press, Washington, DC
52. Brouwer A, Longnecker MP, Birnbaum LS, Cogliano J, Kostyniak P, Moore J et al (1999) Characterization of potential endocrine-related health effects at low-dose levels of exposure to PCBs. Environ Health Perspect 107(Suppl 4):639–649
53. Rogan WJ, Gladen BC, Hung KL, Koong SL, Shih LY, Taylor JS et al (1988) Congenital poisoning by polychlorinated biphenyls and their contaminants in Taiwan. Science 241(4863):334–336
54. Guo YL, Lambert GH, Hsu CC, Hsu MM (2004) Yucheng: health effects of prenatal exposure to polychlorinated biphenyls and dibenzofurans. Int Arch Occup Environ Health 77(3):153–158
55. Chen YC, Yu ML, Rogan WJ, Gladen BC, Hsu CC (1994) A 6-year follow-up of behavior and activity disorders in the Taiwan Yu-Cheng children. Am J Public Health 84(3):415–421
56. Ribas-Fito N, Sala M, Kogevinas M, Sunyer J (2001) Polychlorinated biphenyls (PCBs) and neurological development in children: a systematic review. J Epidemiol Community Health 55(8):537–546
57. Grandjean P, Weihe P, Burse VW, Needham LL, Storr-Hansen E, Heinzow B et al (2001) Neurobehavioral deficits associated with PCB in 7-year-old children prenatally exposed to seafood neurotoxicants. Neurotoxicol Teratol 23(4):305–317
58. Guillette EA, Meza MM, Aquilar MG, Soto AD, Garcia IE (1998) An anthropological approach to the evaluation of preschool children exposed to pesticides in Mexico. Environ Health Perspect 106(6):347–353
59. Moser VC, Chanda SM, Mortensen SR, Padilla S (1998) Age- and gender-related differences in sensitivity to chlorpyrifos in the rat reflect developmental profiles of esterase activities. Toxicol Sci 46(2):211–222
60. Slotkin TA, Tate CA, Cousins MM, Seidler FJ (2002) Functional alterations in CNS catecholamine systems in adolescence and adulthood after neonatal chlorpyrifos exposure. Brain Res Dev Brain Res 133(2):163–173
61. EPA (1997) Background document on cholinesterates. Attachment 4E presented to Environmental Protection Agency Scientific Advisory Panel Meeting of June 3–4, 1997. US EPA, Arlington

62. Weiss B, Amler S, Amler WR (2004) Pesticides. Pediatrics 113: 1030–1036
63. Damstra T (2002) Potential effects of certain persistent organic pollutants and endocrine disrupting chemicals on the health of children. J Toxicol Clin Toxicol 40(4):457–465
64. Ho SM, Tang WY, Belmonte DF, Prins GS (2006) Developmental exposure to estradiol and bisphenol A increases susceptibility to prostate carcinogenesis and epigenetically regulates phosphodiesterase type 4 variant 4. Cancer Res 66(11):5624–5632
65. Newbold RR, Hanson RB, Jefferson WN, Bullock BC, Haseman J, McLachlan JA (2000) Proliferative lesions and reproductive tract tumors in male descendants of mice exposed developmentally to diethylstilbestrol. Carcinogenesis 21(7):1355–1363
66. Anway MD, Cupp AS, Uzumcu M, Skinner MK (2005) Epigenetic transgenerational actions of endocrine disruptors and male fertility. Science 308(5727):1466–1469
67. Goldey ES, Crofton KM (1998) Thyroxine replacement attenuates hypothyroxinemia, hearing loss, and motor deficits following developmental exposure to Aroclor 1254 in rats. Toxicol Sci 45(1):94–105
68. Brechner RJ, Parkhurst GD, Humble WO, Brown MB, Herman WH (2000) Ammonium perchlorate contamination of Colorado River drinking water is associated with abnormal thyroid function in newborns in Arizona. J Occup Environ Med 42(8): 777–782
69. Kelsh MA, Buffler PA, Daaboul JJ, Rutherford GW, Lau EC, Barnard JC et al (2003) Primary congenital hypothyroidism, newborn thyroid function, and environmental perchlorate exposure among residents of a Southern California community. J Occup Environ Med 45(10):1116–1127
70. Lau C, Rogers JM (2004) Embryonic and fetal programming of physiological disorders in adulthood. Birth Defects Res C Embryo Today 72(4):300–312
71. Sadler TW (2000) Susceptible periods during embryogenesis of the heart and endocrine glands. Environ Health Perspect 108(Suppl 3):555–561
72. Ravelli AC, van der Meulen JH, Michels RP, Osmond C, Barker DJ, Hales CN et al (1998) Glucose tolerance in adults after prenatal exposure to famine. Lancet 351(9097): 173–177
73. Bo S, Cavallo-Perin P, Scaglione L, Ciccone G, Pagano G (2000) Low birthweight and metabolic abnormalities in twins with increased susceptibility to Type 2 diabetes mellitus. Diabet Med 17(5):365–370
74. Pryor JL, Hughes C, Foster W, Hales BF, Robaire B (2000) Critical windows of exposure for children's health: the reproductive system in animals and humans. Environ Health Perspect 108(Suppl 3):491–503
75. Stillman RJ (1982) In utero exposure to diethylstilbestrol: adverse effects on the reproductive tract and reproductive performance and male and female offspring. Am J Obstet Gynecol 142(7):905–921
76. Parente RC, Faerstein E, Celeste RK, Werneck GL (2008) The relationship between smoking and age at the menopause: a systematic review. Maturitas 61(4):287–298
77. Jensen TK, Joffe M, Scheike T, Skytthe A, Gaist D, Christensen K (2005) Time trends in waiting time to pregnancy among Danish twins. Hum Reprod 20(4):955–964
78. Shea KM (2003) Pediatric exposure and potential toxicity of phthalate plasticizers. Pediatrics 111(6 Pt 1):1467–1474
79. Weisbach V, Koch HM, Angerer J, Eckstein R (2006) Di(2-ethylhexyl)phthalate exposure of apheresis donors is procedure-related. Transfusion 46(8):1457–1458
80. Skakkebaek NE, Jorgensen N, Main KM, Rajpert-De Meyts E, Leffers H, Andersson AM et al (2006) Is human fecundity declining? Int J Androl 29(1):2–11
81. Lottrup G, Andersson AM, Leffers H, Mortensen GK, Toppari J, Skakkebaek NE et al (2006) Possible impact of phthalates on infant reproductive health. Int J Androl 29(1):172–180
82. Mylchreest E, Wallace DG, Cattley RC, Foster PM (2000) Dose-dependent alterations in androgen-regulated male reproductive development in rats exposed to Di(n-butyl) phthalate during late gestation. Toxicol Sci 55(1):143–151
83. Hoei-Hansen CE, Holm M, Rajpert-De Meyts E, Skakkebaek NE (2003) Histological evidence of testicular dysgenesis in contralateral biopsies from 218 patients with testicular germ cell cancer. J Pathol 200(3):370–374
84. Skakkebaek NE, Holm M, Hoei-Hansen C, Jorgensen N, Rajpert-De Meyts E (2003) Association between testicular dysgenesis syndrome (TDS) and testicular neoplasia: evidence from 20 adult patients with signs of maldevelopment of the testis. APMIS 111(1):1–9
85. Fisher JS, Macpherson S, Marchetti N, Sharpe RM (2003) Human 'testicular dysgenesis syndrome': a possible model using in-utero exposure of the rat to dibutyl phthalate. Hum Reprod 18(7):1383–1394
86. Weinhold B (2009) Environmental factors in birth defects: what we need to know. Environ Health Perspect 117: A440–A447
87. Lindbohm ML, Taskinen H, Sallmen M, Hemminki K (1990) Spontaneous abortions among women exposed to organic solvents. Am J Ind Med 17(4):449–463
88. Lipscomb JA, Fenster L, Wrensch M, Shusterman D, Swan S (1991) Pregnancy outcomes in women potentially exposed to occupational solvents and women working in the electronics industry. J Occup Med 33(5):597–604
89. Nieuwenhuijsen MJ, Toledano MB, Elliott P (2000) Uptake of chlorination disinfection by-products: a review and a discussion of its implications for exposure assessment in epidemiological studies. J Expo Anal Environ Epidemiol 10(6 Pt 1):586–599
90. Dodds L, King W, Allen AC, Armson BA, Fell DB, Nimrod C (2004) Trihalomethanes in public water supplies and risk of stillbirth. Epidemiology 15(2):179–186
91. Toledano MB, Nieuwenhuijsen MJ, Best N, Whitaker H, Hambly P, de Hoogh C et al (2005) Relation of trihalomethane concentrations in public water supplies to stillbirth and birth weight in three water regions in England. Environ Health Perspect 113(2):225–232

92. Wright JM, Schwartz J, Dockery DW (2004) The effect of disinfection by-products and mutagenic activity on birth weight and gestational duration. Environ Health Perspect 112(8):920–925
93. Hwang BF, Jaakkola JJ (2003) Water chlorination and birth defects: a systematic review and meta-analysis. Arch Environ Health 58(2):83–91
94. Nieuwenhuijsen MJ, Martinez D, Grellier J, Bennett J, Best N, Iszatt N et al (2009) Chlorination disinfection by-products in drinking water and congenital anomalies: review and meta-analyses. Environ Health Perspect 117(10): 1486–1493
95. California Environmental Protection Agency (2010) Proposed identification of environmental tobacco smoke as a toxic air contaminant. California Environmental Protection Agency, Sacramento
96. Wigle DT, Arbuckle TE, Walker M, Wade MG, Liu S, Krewski D (2007) Environmental hazards: evidence for effects on child health. J Toxicol Environ Health B Crit Rev 10(1–2):3–39
97. DiFranza JR, Lew RA (1995) Effect of maternal cigarette smoking on pregnancy complications and sudden infant death syndrome. J Fam Pract 40(4):385–394
98. Charlton A (1994) Children and passive smoking: a review. J Fam Pract 38(3):267–277
99. Wang J, Wang B (2002) Study on risk factors of cryptorchidism. Zhonghua Liu Xing Bing Xue Za Zhi 23(3): 190–193
100. Waliszewski SM, Infanzon RM, Arroyo SG, Pietrini RV, Carvajal O, Trujillo P et al (2005) Persistent organochlorine pesticides levels in blood serum lipids in women bearing babies with undescended testis. Bull Environ Contam Toxicol 75(5): 952–959
101. Longnecker MP, Klebanoff MA, Dunson DB, Guo X, Chen Z, Zhou H et al (2005) Maternal serum level of the DDT metabolite DDE in relation to fetal loss in previous pregnancies. Environ Res 97(2):127–133
102. Gray LE, Ostby J, Furr J, Wolf CJ, Lambright C, Parks L et al (2001) Effects of environmental antiandrogens on reproductive development in experimental animals. Hum Reprod Update 7(3):248–264
103. Woodruff TJ, Zeise L, Axelrad DA, Guyton KZ, Janssen S, Miller M et al (2008) Meeting report: moving upstream-evaluating adverse upstream end points for improved risk assessment and decision-making. Environ Health Perspect 116(11): 1568–1575
104. DiFranza JR, Aligne CA, Weitzman M (2004) Prenatal and postnatal environmental tobacco smoke exposure and children's health. Pediatrics 113(4 Suppl):1007–1015
105. Dietert RR, Etzel RA, Chen D, Halonen M, Holladay SD, Jarabek AM et al (2000) Workshop to identify critical windows of exposure for children's health: immune and respiratory systems work group summary. Environ Health Perspect 108(Suppl 3):483–490
106. Stick SM, Burton PR, Gurrin L, Sly PD, LeSouef PN (1996) Effects of maternal smoking during pregnancy and a family history of asthma on respiratory function in newborn infants. Lancet 348(9034):1060–1064
107. Upton MN, Watt GC, Davey SG, McConnachie A, Hart CL (1998) Permanent effects of maternal smoking on offsprings' lung function. Lancet 352(9126):453
108. Sporik R, Platts-Mills TA (2001) Allergen exposure and the development of asthma. Thorax 56(Suppl 2):ii58–ii63
109. Hesselmar B, Aberg N, Aberg B, Eriksson B, Bjorksten B (1999) Does early exposure to cat or dog protect against later allergy development? Clin Exp Allergy 29(5): 611–617
110. Merchant JA, Naleway AL, Svendsen ER, Kelly KM, Burmeister LF, Stromquist AM et al (2005) Asthma and farm exposures in a cohort of rural Iowa children. Environ Health Perspect 113(3):350–356
111. Schwela D (2000) Air pollution and health in urban areas. Rev Environ Health 15(1–2):13–42
112. Heinrich J (2003) Nonallergic respiratory morbidity improved along with a decline of traditional air pollution levels: a review. Eur Respir J Suppl 40:64s–69s
113. Avol EL, Gauderman WJ, Tan SM, London SJ, Peters JM (2001) Respiratory effects of relocating to areas of differing air pollution level. Am J Respir Crit Care Med 164(11): 2067–2072
114. Schwartz J (2004) Air pollution and children's health. Pediatrics 113(4 Suppl):1037–1043
115. Ostro B, Lipsett M, Mann J, Braxton-Owens H, White M (2001) Air pollution and exacerbation of asthma in African-American children in Los Angeles. Epidemiology 12(2):200–208
116. McConnell R, Berhane K, Gilliland F, Molitor J, Thomas D, Lurmann F et al (2003) Prospective study of air pollution and bronchitic symptoms in children with asthma. Am J Respir Crit Care Med 168(7):790–797
117. Gilliland FD, Berhane K, Rappaport EB, Thomas DC, Avol E, Gauderman WJ et al (2001) The effects of ambient air pollution on school absenteeism due to respiratory illnesses. Epidemiology 12(1):43–54
118. Tolbert PE, Mulholland JA, MacIntosh DL, Xu F, Daniels D, Devine OJ et al (2000) Air quality and pediatric emergency room visits for asthma in Atlanta, Georgia, USA. Am J Epidemiol 151(8):798–810
119. Studnicka M, Hackl E, Pischinger J, Fangmeyer C, Haschke N, Kuhr J et al (1997) Traffic-related NO_2 and the prevalence of asthma and respiratory symptoms in seven year olds. Eur Respir J 10(10):2275–2278
120. Kramer U, Koch T, Ranft U, Ring J, Behrendt H (2000) Traffic-related air pollution is associated with atopy in children living in urban areas. Epidemiology 11(1):64–70
121. Weinmayr G, Genuneit J, Nagel G, Bjorksten B, van Hage M, Priftanji A et al (2010) International variations in associations of allergic markers and diseases in children: ISAAC phase two. Allergy 65(6):766–775
122. Lin S, Munsie JP, Hwang SA, Fitzgerald E, Cayo MR (2002) Childhood asthma hospitalization and residential exposure to state route traffic. Environ Res 88(2):73–81

123. English P, Neutra R, Scalf R, Sullivan M, Waller L, Zhu L (1999) Examining associations between childhood asthma and traffic flow using a geographic information system. Environ Health Perspect 107(9):761–767
124. Vedal S, Petkau J, White R, Blair J (1998) Acute effects of ambient inhalable particles in asthmatic and non-asthmatic children. Am J Respir Crit Care Med 157(4 Pt 1): 1034–1043
125. Pekkanen J, Pearce N (1999) Defining asthma in epidemiological studies. Eur Respir J 14(4):951–957
126. Gauderman WJ, Gilliland GF, Vora H, Avol E, Stram D, McConnell R et al (2002) Association between air pollution and lung function growth in southern California children: results from a second cohort. Am J Respir Crit Care Med 166(1):76–84
127. American Academy of Pediatrics Committee on Environmental Health (2003) Air pollutants, outdoor. In: Etzel R (ed) Pediatric environmental health. American Academy of Pediatrics, Elk Grove Village, pp 69–86
128. Perera FP (1997) Environment and cancer: who are susceptible? Science 278(5340):1068–1073
129. Bartsch H, Hietanen E (1996) The role of individual susceptibility in cancer burden related to environmental exposure. Environ Health Perspect 104(Suppl 3):569–577
130. Husgafvel-Pursiainen K (2004) Genotoxicity of environmental tobacco smoke: a review. Mutat Res 567(2–3):427–445
131. National Research Council (1982) Diet, nutrition and cancer. National Academy Press, Washington, DC
132. Tokunaga M, Land CE, Tokuoka S, Nishimori I, Soda M, Akiba S (1994) Incidence of female breast cancer among atomic bomb survivors, 1950–1985. Radiat Res 138(2):209–223
133. Schiestl RH, Aubrecht J, Yap WY, Kandikonda S, Sidhom S (1997) Polychlorinated biphenyls and 2, 3, 7, 8-tetrachlorodibenzo-p-dioxin induce intrachromosomal recombination in vitro and in vivo. Cancer Res 57(19):4378–4383
134. Trizio D, Basketter DA, Botham PA, Graepel PH, Lambre C, Magda SJ et al (1988) Identification of immunotoxic effects of chemicals and assessment of their relevance to man. Food Chem Toxicol 26(6):527–539
135. Anderson LM (2006) Environmental genotoxicants/carcinogens and childhood cancer: bridgeable gaps in scientific knowledge. Mutat Res 608(2):136–156
136. Maciag A, Bialkowska A, Espiritu I, Powell D, Alvord WG, Kasprzak KS et al (2003) Gestation stage-specific oxidative deoxyribonucleic acid damage from sidestream smoke in pregnant rats and their fetuses. Arch Environ Health 58(4):238–244
137. Schuz J, Kaletsch U, Kaatsch P, Meinert R, Michaelis J (2001) Risk factors for pediatric tumors of the central nervous system: results from a German population-based case-control study. Med Pediatr Oncol 36(2):274–282
138. Bunin GR (2004) Nongenetic causes of childhood cancers: evidence from international variation, time trends, and risk factor studies. Toxicol Appl Pharmacol 199(2):91–103
139. Ron E, Modan B, Boice JD Jr, Alfandary E, Stovall M, Chetrit A et al (1988) Tumors of the brain and nervous system after radiotherapy in childhood. N Engl J Med 319(16): 1033–1039
140. Pacini F, Vorontsova T, Demidchik EP, Molinaro E, Agate L, Romei C et al (1997) Post-chernobyl thyroid carcinoma in Belarus children and adolescents: comparison with naturally occurring thyroid carcinoma in Italy and France. J Clin Endocrinol Metab 82(11):3563–3569
141. Whiteman DC, Whiteman CA, Green AC (2001) Childhood sun exposure as a risk factor for melanoma: a systematic review of epidemiologic studies. Cancer Causes Control 12(1):69–82
142. International Agency for Research on Cancer (1992) IARC monographs on the evaluation of carcinogenic risks to humans: solar and ultraviolet radiation, vol 55. International Agency for Research on Cancer, Lyon, France
143. Vainio H, Bianchini F (2000) Cancer-preventive effects of sunscreens are uncertain. Scand J Work Environ Health 26(6):529–531
144. International Agency for Research on Cancer (2004) IARC monographs on the evaluation of carcinogenic risks to humans: involuntary smoke, vol 83. International Agency for Research on Cancer, Lyon, France
145. Karube T, Odagiri Y, Takemoto K, Watanabe S (1989) Analyses of transplacentally induced sister chromatid exchanges and micronuclei in mouse fetal liver cells following maternal exposure to cigarette smoke. Cancer Res 49(13): 3550–3552
146. Wyrobek AJ, Adler ID (1996) Detection of aneuploidy in human and rodent sperm using FISH and applications of sperm assays of genetic damage in heritable risk evaluation. Mutat Res 352(1–2):173–179
147. Pang D, McNally R, Birch JM (2003) Parental smoking and childhood cancer: results from the United Kingdom Childhood Cancer Study. Br J Cancer 88(3):373–381
148. Sorahan T, Lancashire RJ (2004) Parental cigarette smoking and childhood risks of hepatoblastoma: OSCC data. Br J Cancer 90(5):1016–1018
149. Ji BT, Shu XO, Linet MS, Zheng W, Wacholder S, Gao YT et al (1997) Paternal cigarette smoking and the risk of childhood cancer among offspring of nonsmoking mothers. J Natl Cancer Inst 89(3):238–244
150. Sandler DP, Everson RB, Wilcox AJ, Browder JP (1985) Cancer risk in adulthood from early life exposure to parents' smoking. Am J Public Health 75(5):487–492
151. Abdollahi M, Ranjbar A, Shadnia S, Nikfar S, Rezaie A, Abdollahi M, Ranjbar A, Shadnia S, Nikfar S, Rezaie A (2004) Pesticides and oxidative stress: a review. Med Sci Monit 10(6): RA141–RA147
152. Infante-Rivard C, Weichenthal S (2007) Pesticides and childhood cancer: an update of Zahm and Ward's 1998 review. J Toxicol Environ Health B Crit Rev 10(1–2): 81–99

153. Daniels JL, Olshan AF, Teschke K, Hertz-Picciotto I, Savitz DA, Blatt J et al (2001) Residential pesticide exposure and neuroblastoma. Epidemiology 12(1):20–27
154. Zahm SH, Ward MH (1998) Pesticides and childhood cancer. Environ Health Perspect 106(Suppl 3):893–908
155. Wigle DT, Turner MC, Krewski D, Shannon M, Graef JW (2009) A systematic review and meta-analysis of childhood leukemia and parental occupational pesticide exposure. Lead intoxication from lead-contaminated water used to reconstitute infant formula. Environ Health Perspect 117(10):1505–1513
156. Nasterlack M (2006) Do pesticides cause childhood cancer? Int Arch Occup Environ Health 79(7):536–544
157. Hill AB (1965) The environment and disease: association or causation? Proceedings of the Royal Society of Medicine. 58:295–300
158. Buckley JD, Meadows AT, Kadin ME, Le Beau MM, Siegel S, Robison LL (2000) Pesticide exposures in children with non-Hodgkin lymphoma. Cancer 89(11):2315–2321
159. Infante-Rivard C, Sinnett D (1999) Preconceptional paternal exposure to pesticides and increased risk of childhood leukaemia. Lancet 354(9192):1819
160. Villanueva CM, Cantor KP, Cordier S, Jaakkola JJ, King WD, Lynch CF et al (2004) Disinfection byproducts and bladder cancer: a pooled analysis. Epidemiology 15(3):357–367
161. Boffetta P (2006) Human cancer from environmental pollutants: the epidemiological evidence. Mutat Res 608(2):157–162
162. International Agency for Research on Cancer (2004) Some drinking-water disinfectants and contaminants, including arsenic, vol 84. International Agency for Research on Cancer, Lyon, France
163. Infante-Rivard C (2008) Chemical risk factors and childhood leukaemia: a review of recent studies. Radiat Prot Dosim 132(2):220–227
164. Raaschou-Nielsen O, Reynolds P (2006) Air pollution and childhood cancer: a review of the epidemiological literature. Int J Cancer 118(12):2920–2929
165. Snedeker SM, Diaugustine RP (1996) Hormonal and environmental factors affecting cell proliferation and neoplasia in the mammary gland. Prog Clin Biol Res 394:211–253
166. Hildreth NG, Shore RE, Dvoretsky PM (1989) The risk of breast cancer after irradiation of the thymus in infancy. N Engl J Med 321(19):1281–1284
167. Herbst AL (1999) Diethylstilbestrol and adenocarcinoma of the vagina. Am J Obstet Gynecol 181(6):1576–1578
168. Strohsnitter WC, Noller KL, Hoover RN, Robboy SJ, Palmer JR, Titus-Ernstoff L et al (2001) Cancer risk in men exposed in utero to diethylstilbestrol. J Natl Cancer Inst 93(7):545–551
169. Colton T, Greenberg ER, Noller K, Resseguie L, Van Bennekom C, Heeren T et al (1993) Breast cancer in mothers prescribed diethylstilbestrol in pregnancy. Further follow-up. JAMA 269(16):2096–2100
170. Olshan AF, Daniels JL (2000) Invited Response: pesticides and childhood cancer. Am J Epidemiol 151:647–649

Environmental Toxicology: Oxidative Stress

Dean P. Jones
Division of Pulmonary, Allergy and Critical Care Medicine, Department of Medicine, Emory University School of Medicine, Atlanta, GA, USA

E

Article Outline

Glossary
Definition of the Subject
Introduction
Evolution of "Free Radical" and "Radical-free" Concepts of Oxidative Stress
Radical Mechanisms of Environmental Toxicity
Non-radical Mechanisms of Environmental Toxicity
Future Directions
Acknowledgment
Bibliography

Glossary

Antioxidant A term loosely defined as something that stops oxidation when present at a low amount. The term is used most specifically to mean a free radical-scavenging chemical that accepts or donates an electron to a radical to terminate radical chain reactions. The term is also used for agents that inactivate radical initiation and catalysis, such as metal ion chelators, agents that block radiation-induced oxidation, and agents that counter oxidation of a substance with reduction.

Disulfide An intermediate oxidation state of sulfur that is readily interconverted with the reduced (thiol) state and commonly found in biomolecules. Disulfides are important in protein structure, function, regulation, and translocation. Disulfide formation in proteins and low molecular mass sulfur-containing chemicals (glutathione, cysteine, Co-enzyme A) is a common and sensitive indicator of oxidative stress.

Electrophile (or electrophilic chemical) A chemical with a functional group that is deficient in electron density, such as a quinone or conjugated aldehyde,

and therefore reactive with a nucleophilic chemical containing electron-rich functional groups, such as a thiol. Electrophiles are important in toxicology because they react with nucleophilic centers in DNA, causing mutations and cancer, and with proteins, disrupting enzyme, receptor, transporter, gene expression, and other critical functions.

Lipid peroxidation A radical chain reaction involving polyunsaturated fatty acids (PUFA) and O_2. The process is initiated by agents that abstract a hydrogen atom from the carbon skeleton to form a carbon-centered radical, propagated by addition of O_2 and abstraction of a hydrogen atom from another carbon skeleton with creation of a lipid hydroperoxide and another radical, and ultimately terminated by reaction of radicals with each other to create non-radical species. The process causes fats and oils to become rancid and is common in decaying organic matter.

Oxidative stress A process or outcome in which an imbalance in prooxidant and antioxidant reactions causes macromolecular damage and/or disruption of biologic redox signaling and control. All classes of macromolecules and any biologic function can be affected. Effects on DNA are important in mutagenesis and cancer, effects on proteins contribute to many acute and chronic toxicities, effects on lipids contribute to dysfunctional energy metabolism and immunity, and effects on carbohydrates affect biological lubricants in joints and cellular identity.

Prooxidant An agent that stimulates aberrant electron transfer in biologic systems and causes oxidative stress. This includes agents that initiate radical reactions, oxidize biologic components, or interfere with normal reductive and antioxidant functions.

Radical (or free radical) An organic molecule with an unpaired electron. Radicals are important in biologic systems because they are reactive and can disrupt biologic functions. Radicals participate in a unique type of chemical reaction sequence termed a chain reaction. A radical chain reaction, such as that illustrated by lipid peroxidation, is initiated by an agent that removes (or adds) an electron from a non-radical chemical to form a radical. The chemical structure is modified, and the radical product becomes a non-radical by accepting or donating an electron to another non-radical species, thereby propagating the reaction sequence. The process is ultimately terminated by reaction of radicals with each other to create non-radical species.

Reactive oxygen species (ROS), sometimes reactive oxygen intermediates (ROI) One or more oxygen-containing chemicals that are reactive with organic molecules. This term is often used to refer to superoxide anion radical, hydrogen peroxide, lipid hydroperoxide, and related oxygen-centered radicals, but may also include reactive nitrogen species (RNS), such as nitric oxide, peroxynitrite, and other oxides of nitrogen (NOx), which also contain oxygen. The term is most often used because the chemistry is too complex and/or the analytic methods are insufficient to identify specific reactive species.

Redox cycling A process in which a chemical accepts an electron from a biological reductant and transfers that electron to O_2 or other acceptor to create aberrant radical generation. Many quinones and other aromatic chemicals do this by interacting with flavoproteins. The process is considered "cycling" because the chemical functions only as a catalyst. After donating the electron to an acceptor, the original form is regenerated so that it can accept another electron. If electrons are transferred between redox-signaling pathways, this creates a "short circuit," disrupting cell regulation.

Redox signaling A mechanism for cellular communication involving an oxidation–reduction reaction. This process commonly involves generation of a small diffusible redox-active chemical that transfers a signal to a biologic receptor. Redox signaling is highly integrated with kinase signaling and other central cell communication mechanisms, and difficult to discriminate from a more general process of redox sensing, which coordinates cellular functions via widely distributed redox-sensitive cysteine residues in proteins.

Thiol An organic form of sulfur containing a sulfur-hydrogen covalent bond. This is the reduced form of sulfur in the amino acid cysteine, in the antioxidant glutathione, and in most cysteine residues in cellular proteins. In proteins, thiols are also termed "sulfhydryl groups." The thiol functional group supports diverse reactivity and catalytic functions of proteins. Interconversion with disulfides and

other forms allows thiols to serve as structural transducers as well as chemical signal transducers.

Xenobiotic A chemical that is foreign to an organism. Although often used to refer to man-made chemicals, the term is also used to discriminate chemicals derived exogenously from the environment from those that are generated endogenously as a consequence of intermediary metabolism.

Definition of the Subject

Oxidative stress is a process or outcome in which an imbalance in prooxidant and antioxidant reactions causes macromolecular damage and/or disruption of biologic redox signaling and control (Fig. 1) [1]. Oxidation–reduction reactions, or "redox" reactions, are reactions involving electron transfer. These reactions are central to energy metabolism and maintenance of metabolic and physical organization of living organisms. Environmental agents that interfere with redox reactions or promote abnormal redox reactions are highly destructive to biologic macromolecules and metabolic organization. Electron transfer reactions in the atmosphere, water, and soil are common and important subjects of environmental sciences. In many

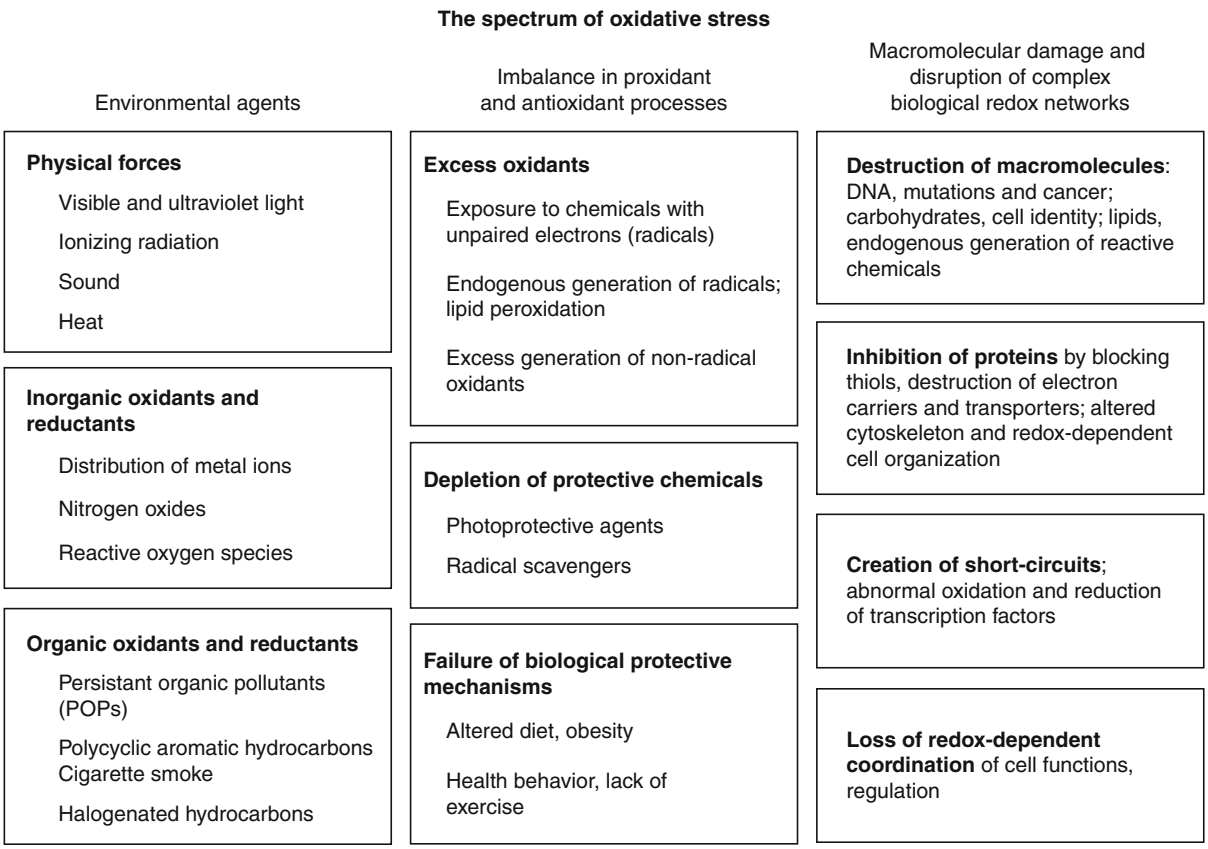

Environmental Toxicology: Oxidative Stress. Figure 1
The spectrum of oxidative stress in environmental toxicology. Oxidative stress refers to adverse effects (*right*) as well as the processes (*center*) that cause adverse effects in biologic systems. Environmental factors that contribute to oxidative stress (*left*) include physical, inorganic, and organic agents. These agents create imbalances in specific prooxidant and antioxidant reactions or reaction pathways (*center*) due to excess oxidants, depletion of protective chemicals, or failure of endogenous protective mechanisms. The imbalances result in the generation of reactive radicals and non-radical oxidants that cause macromolecular damage, inhibit thiol-dependent proteins, short-circuit redox pathways, and disrupt regulatory mechanisms (*right*)

cases, physical processes and inorganic chemicals are relevant causes of oxidative stress to living organisms. Oxidative stress can also occur endogenously within an organism due to organic chemicals derived from the environment. This entry focuses on oxidative stress within living organisms, recognizing that the environmental exposures causing oxidative stress in an organism are highly variable (Fig. 1, left). Many of these are addressed in detail in other sections of this Encyclopedia.

Living organisms depend upon the capability to maintain chemical and physical homeostasis despite variations in environmental exposures. Exposures that cause oxidative stress include chemical oxidants such as ozone and nitrogen oxides of the atmosphere [2, 3], transition metals such as iron [4] and cadmium [5–7], visible and ultraviolet radiation from the sun [8, 9], ionizing radiation from radioactive decay [10, 11], and a large number of pharmaceuticals [12] and chemicals from commercial products and industrial wastes [13, 14]. In some cases there is no real change in the amount of environmental toxicant, only a change in distribution that affects exposure of living organisms [15]. In other cases, there is an accumulation of environmental toxicant due to human activity. Some of these are recognized as persistent organic pollutants (POPs) [16–18] and other times they are persistent products of organic pollutants (P-POPs), some of which are not currently known to accumulate or represent a hazard. For instance, the recent investigation of PFOA, a product of fluorocarbons that is of unknown origin [19, 20], suggests that other unidentified chemicals derived from human activity may exist. Biologic defense mechanisms are diverse and include physical barriers, chemical detoxification mechanisms, repair mechanisms, and avoidance behaviors. Considerable scientific data are available in each of these areas, and efforts are currently being initiated to assemble this knowledge in a systematic description of the "exposome," i.e., the summation of all environmental exposures from conception throughout the life of an individual [21, 22].

The concepts of oxidative stress are currently undergoing revision from the earlier definition as an imbalance of prooxidants and antioxidants that cause macromolecular damage [23] to one that also includes oxidative stress as a disruption of vital signaling and control processes within a biologic system [1, 24]. In human health, the accumulating data suggest that the latter is more relevant. However, in environmental toxicology, both macromolecular damage and disruption of redox signaling and control mechanisms are relevant. Importantly, new developments in systems biology [25, 26], including powerful new molecular approaches and analytic tools to study genomics [27] and epigenomics [28], gene expression (transcriptomics) [29], protein modifications (proteomics) [30, 31] and chemical profiles (metabolomics) [32, 33] provide capabilities to improve surveillance, mechanistic understanding, and risk reduction.

Introduction

Two-electron and one-electron transfers in biologic systems. Living organisms obtain the energy necessary to sustain organization, delineation from their external environment, and reproduction, through electron transfer reactions. Loss of electrons is termed "oxidation," while gain of electrons is termed "reduction" (Fig. 2a–c). Because of the conservation of matter in chemical reactions, the processes are always coupled, so the terms "oxidation–reduction" reactions and "redox" (short for "reduction–oxidation") reactions are usually more correct. However, the common process of oxidation of chemicals in the presence of atmospheric O_2 (with water as the reduction product) explains the bias in terminology. Excessive reduction can also occur, termed "reductive stress" [34, 35], and is especially relevant to hypoxic and anoxic environmental conditions.

The major elements of life, carbon, hydrogen, oxygen, nitrogen, phosphorus, and sulfur form multiple stable biochemical structures in which pairs of electrons are shared. The major macromolecules (protein, nucleic acids, lipids, carbohydrates) are formed from smaller biochemicals (building blocks: e.g., amino acids, nucleotides, fatty acids, sugars) that include these elements. The biochemical structures are interconverted through chemical reactions that involve conservation of these pairs of electrons. The interconversions are often slow without a catalyst. Biologically, this involves two-electron transfers by NADH or

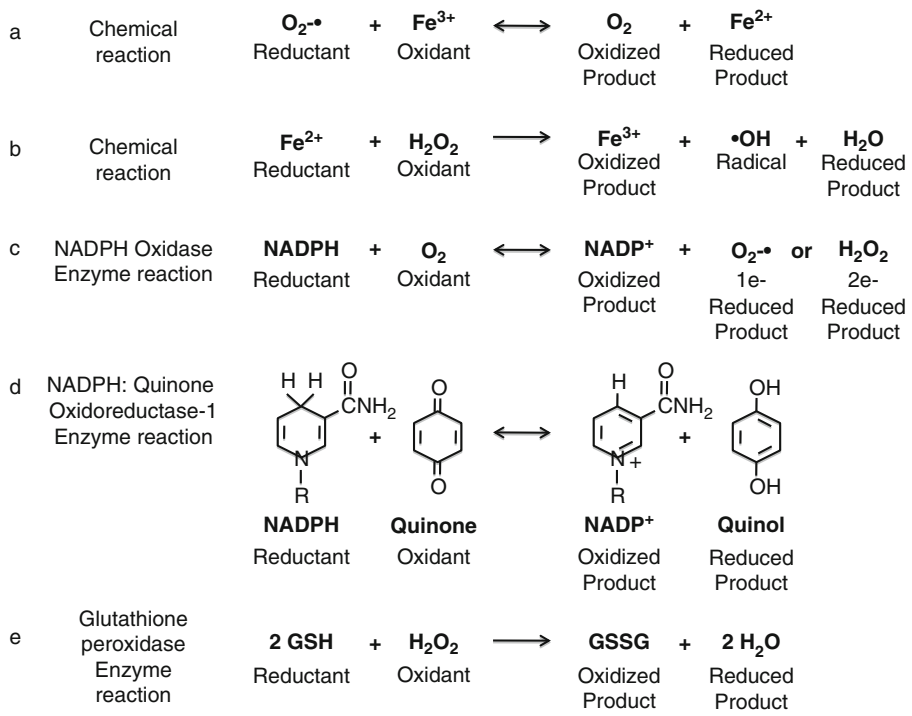

Environmental Toxicology: Oxidative Stress. Figure 2

Oxidation–reduction reactions. (**a**) One-electron transfer reaction from superoxide anion radical ($O_2^{-\bullet}$) to Fe^{3+}, as occurs in transfer from superoxide to oxidized cytochrome *c*. In this reaction, superoxide anion radical is oxidized to molecular oxygen (O_2), while the iron is reduced from Fe^{3+} to Fe^{2+}. Although the reaction can occur in the opposite direction, such as the generation of superoxide by electron transfer in oxy-hemoglobin, energetics in biologic systems usually favor the forward direction as written. (**b**) One-electron transfer from Fe^{2+} to hydrogen peroxide (H_2O_2). This energetically favorable reaction generates three products, Fe^{3+}, hydroxyl radical ($^{\bullet}OH$), and water. The hydroxyl radical is extremely reactive and destructive to biochemicals. Combination of reaction A and B constitutes the iron-catalyzed Haber–Weiss reaction, also known as the Fenton reaction, which has a central role in radical-mediated macromolecular damage. This process is very destructive when appropriate concentrations of superoxide, H_2O_2, and iron are present. (**c**) Flavin-containing enzymes, such as NADPH oxidases, catalyze both 1-e^- and 2-e^- transfers to O_2, thereby forming both superoxide and H_2O_2. Aerobic cells contain NADPH, O_2, and flavoproteins so that conditions are poised to support Fenton chemistry (A + B) when these enzymes are active. The most potent NADPH oxidase, Nox2, is present in phagocytic cells and activated to kill the invading microorganisms. (**d**) Two-electron transfer, shown for the detoxification enzyme NADPH:quinone reductase-1 (NQO1), is used to support chemical interconversions in intermediary metabolism. The niacinamide group shown for NADPH is identical to that in NADH, and serves to transfer a pair of electrons as a hydride ion (H^-) without radical formation. The reaction shown is an important detoxification reaction by which common environmental quinones are reduced to quinols for phase 2 conjugation and excretion. Quinones can function either as oxidants or electrophiles, and can also generate radicals through redox cycling (see Fig. 3). These adverse reactions are prevented by the NQO1 reaction. (**e**) Thiols are used as reductants to eliminate H_2O_2. In the glutathione (GSH) peroxidase reaction shown, two molecules of GSH are used to reduce H_2O_2 to water without forming radicals as intermediates. Reduction of the oxidized product, GSSG, by an NADPH-dependent reductase (not shown) completes a detoxification cycle for peroxides. This reaction cycle is complemented by a thioredoxin/peroxiredoxin system to maintain peroxide concentrations very low in cells despite continuous generation. In some cases thiol radicals are formed, but these rapidly react to form disulfides, thereby minimizing toxic effects

NADPH, with the electrons being transferred as a hydride (H^-) ion (Fig. 2c–e). Enzymes serve as catalysts to enhance rates of reactions so that the presence of enzymes largely determines the biochemical pathways for interconversion of the carbon-containing biochemicals. Many of these interconversions involve reaction of "electrophiles," chemicals with orbitals deficient in electrons, and "nucleophiles," chemicals with orbitals with excess electron density.

The two-electron (2-e^-) transfer reactions are contrasted by one-electron (1-e^-) transfers, which are predominant reactions of many biologically important metals, such as iron and copper, environmentally important metals, such as cadmium, chromium, and tin, and atmospheric reactions driven by ionizing and non-ionizing radiation. Living organisms are dependent upon 1-e^- chemistry because the central energy capture and transfer reactions of photosynthesis and mitochondrial respiration involve 1-e^- transfers. However, these 1-e^- transfers are physically contained within subcellular structures (chloroplasts and mitochondria), so that both 1-e^- and 2-e^- chemistries can occur simultaneously and be used to provide critical reaction pathways in biological systems. The incompatibility is illustrated by the combination of reactions A and B in Fig. 2, where superoxide donates an electron to Fe^{3+} to form Fe^{2+}, and Fe^{2+} reacts with hydrogen peroxide to form the highly reactive and destructive hydroxyl radical. The 1-e^- systems of mitochondria and chloroplasts are important in environmental toxicology because they represent a loaded gun; these systems have very high electron transfer rates, are sensitive to visible and ultraviolet light, trace metals, oxidants and electrophiles, and cause extensive destruction to other biologic components when triggered by environmental toxicants.

The 2-e^- and 1-e^- pathways are connected through flavoproteins and hydroquinone/quinone structures that exist in interconvertible fully oxidized, 1-e^--reduced and 2-e^--reduced forms. Flavoproteins are widely used in biology to support 2-e^- transfer reactions involving NADH and NADPH. In addition, they are critical to connect 2-e^- pathways to 1-e^- pathways, accepting 2 e^- from NADH or NADPH and transferring 1 e^- to electron acceptors. An illustration is given in Fig. 2c, where different NADPH oxidases support both 1- and 2-e^- reduction of O_2. Flavoproteins catalyze 1-e^- transfer to the mitochondrial respiratory chain, the major enzyme systems for oxidation of xenobiotics, and to O_2 to form ROS for signaling and defense against invading microorganisms. They also are a major source of toxic oxidant generation by initiating lipid peroxidation (Fig. 3). The planar aromatic structure interacts with polycyclic aromatic structures, facilitating the generation of reactive chemicals with an unpaired electron, termed "radicals," in a process known as redox cycling [36]. Flavins and flavoproteins are also photoreactive because they absorb visible light, and this activates electrons for transfer to other chemicals.

Antioxidants include chemicals that are relatively stable as radicals and donate or accept an electron to reactive radicals to decrease their destructive chemistry. This is highly beneficial by preventing radical-mediated destruction of macromolecules. Vitamin C (ascorbic acid) and vitamin E (α-tocopherol) are radical-scavenging antioxidants and function to terminate free radical chain reactions (See Fig. 3). Vitamin C is water soluble and synthesized by most animals but not by humans. Vitamin E is fat soluble and one of several lipophilic chemicals that blocks radical reactions in biologic systems. Plants are rich in radical-scavenging antioxidants, and also in carotenoids, light-absorbing chemicals that protect against light-induced oxidative damage.

Evolution of "Free Radical" and "Radical-Free" Concepts of Oxidative Stress

Joseph Priestley, an eighteenth century theologian and chemist credited with the first publication demonstrating production of O_2 [37], intimated that "dephlogisticated air" was toxic even before Lavoisier demonstrated that "dephlogisticated air" was oxygen [38]. Priestley said of breathing dephlogisticated air "...I fancied that my breast felt peculiarly light and easy for some time..." and "a candle burns out much faster in dephlogisticated air than in common air, so we might, as may be said, live out too fast, and the animal powers be too soon exhausted in the pure kind of air. A moralist, at least, may say, that the air which nature has provided for us is as good as we deserve" [39].

This conclusion of the late eighteenth century presaged a cliché of late twentieth century science, that

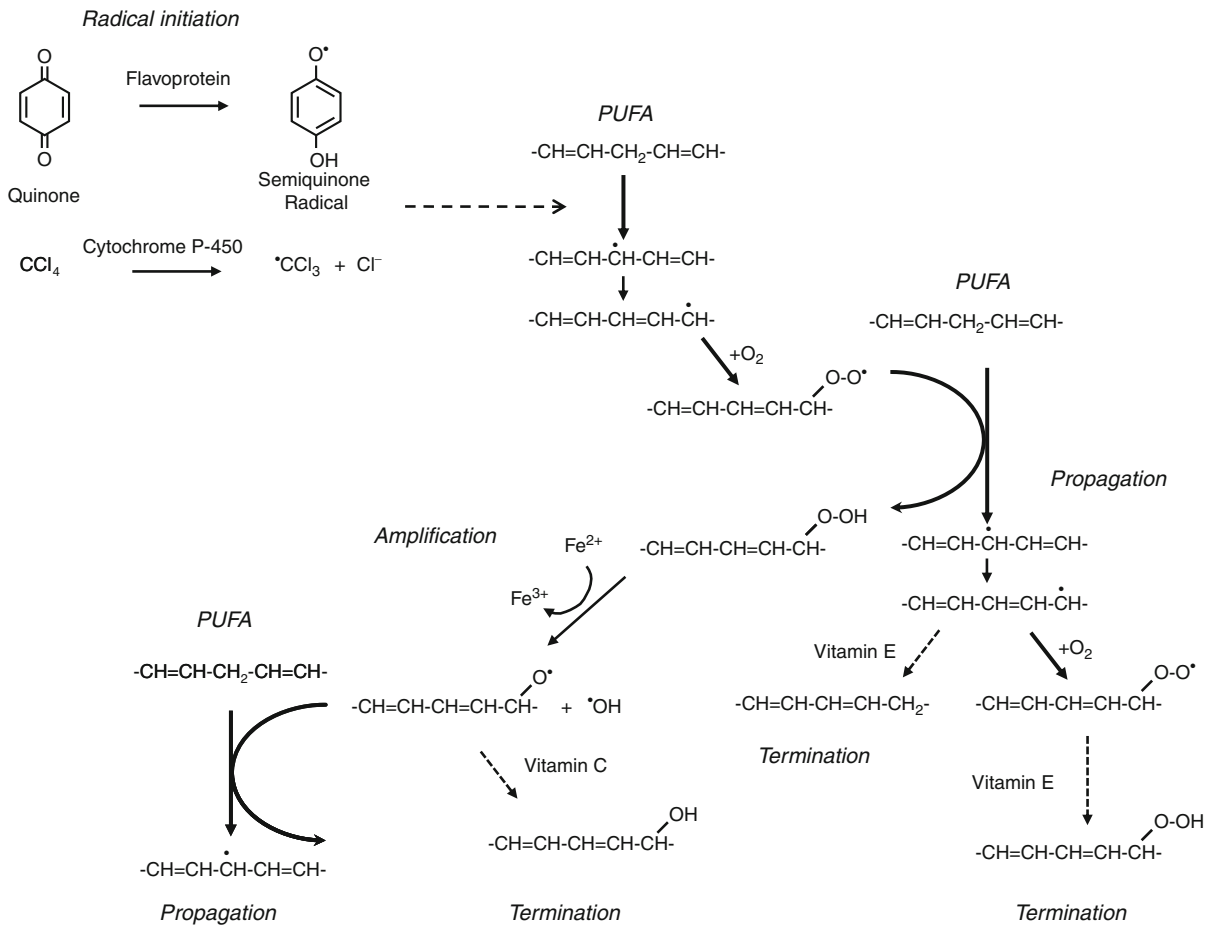

Environmental Toxicology: Oxidative Stress. Figure 3

Lipid peroxidation is a common radical chain reaction that occurs in biologic systems. Radical chain reactions include initiation, propagation, and termination events. In biologic systems, initiation (*top left*) often occurs by redox cycling of quinone compounds and reductive activation of halogenated hydrocarbons (e.g., CCl_4). In redox cycling, quinones accept an electron from a reduced flavoprotein, forming a radical. The radical can donate or accept an electron through a hydrogen abstraction from a polyunsaturated fatty acid (PUFA) (*top middle*). Normally this is most energetically favorable at a carbon adjacent to carbons with double bonds. The resulting radical rearranges to form a conjugated double bond system with an adjacent carbon-centered radical. Under aerobic conditions, O_2 rapidly adds to form a peroxyl radical (*center*). The peroxyl radical reacts with another PUFA (*right middle*) to propagate the free radical chain reaction. In this reaction, the peroxyl radical is reduced to a lipid hydroperoxide, which is normally reduced by GSH peroxidases or peroxiredoxin-6 (not shown). When activities of the latter systems are impaired and free iron is present, the process can amplify lipid peroxidation by Fe^{2+}-dependent initiation of another radical chain reaction (*bottom left*). In the presence of efficient radical scavengers, such as vitamin C and vitamin E, the chain reactions are terminated. Note that vitamins C and E are most active with different types of radicals and thus complement each other in function. Free radical chain reactions are limited in normal living tissues due to the presence of antioxidants and very high protein concentration. Lipid peroxidation in oils, fats, and decaying matter is very active when antioxidants are depleted

"oxygen is a double-edged sword." While science is usually better than cliché, the cliché was highly effective in promoting science, and in this case, an almost religious fervor to introduce "antioxidants" in dietary, cosmetic, and other commercial product development. Failure of large-scale, double-blind interventional trials with antioxidants in humans [40–47] has led to a backlash [48]. Some scientists now have a dismissive attitude concerning the importance of oxidative stress. However, the scientific knowledge of the mechanisms of oxidative stress is very strong and clearly establishes oxidative stress as relevant to environmental toxicology. A brief look at the evolution of concepts facilitates resolution of apparent conflicts between the extensive biomedical literature on oxidative stress and implications for environmental health.

Catalase was one of the first enzymes to be studied [49], and its association with aerobic life was recognized by early biochemists [50]. Hydrogen peroxide (H_2O_2) was recognized as a toxic reactive oxygen species (ROS) associated with O_2 exposure [51]. Early studies also included 1-e^--transfer reactions of the mitochondrial electron transfer pathway, begun by Keilin in the 1920s [52]. During this time, the environmental agent paraquat (methyl viologen) was introduced as an "electron mediator" to transfer electrons into the mitochondrial pathway [53]. The concepts of oxidative stress, though, are perhaps better traced to the concept of "free radicals," organic molecules with an unpaired electron, and their damaging effects on biological systems. The chemical terminology for a free radical has been changed to "radical," but the former is still more commonly used.

The study of radicals in biologic systems was popularized by the discovery of lipid peroxidation (Fig. 3) and antioxidant actions of vitamin E [54] and selenium-dependent glutathione peroxidase [55, 56]. Additional toxicologic studies of carbon tetrachloride (Fig. 3) showed that radical reactions of lipid peroxidation were responsible for hepatotoxicity [57, 58]. Finally, Denham Harmon attracted attention through his hypothesis that free radicals contributed to aging [59].

Lipid peroxidation is a free radical chain reaction contributing to rancidity of oils and fats and invariably present in dead and decaying matter [60]. Radical chain reactions involve an initiation event in which a radical is formed, subsequent propagation events, and finally termination reactions that eliminate the radicals (Fig. 3). Chemicals, such as quinones, that interact with flavoproteins and redox cycle [36] are a common source of initiation (Fig. 3, top left). Another process involves activation of halogenated hydrocarbons and other environmental chemicals to free radicals by the hemoproteins of the cytochrome P450 (CYP) family (Fig. 3, top left). These radicals abstract a hydrogen atom from polyunsaturated fatty acids (PUFA; Fig. 3, top center), which result in the rearrangement of the newly formed fatty acid radical to a more stable form with conjugated double bonds (Fig. 3, center). O_2 readily adds to this intermediate to form a peroxyl radical, which then propagates the chain reaction by the abstraction of a hydrogen atom from another PUFA (Fig. 3, right center). In the presence of trace Fe^{2+}, the process can be amplified by the creation of a new radical from the lipid hydroperoxide (Fig. 3, lower left). Vitamins C and E terminate the process by reducing the reactive intermediates and breaking the chain reaction.

While this constellation of findings and conceptual developments advanced the biochemical study of free radicals, the unanticipated finding of an enzyme that detoxifies superoxide attracted the attention of the broad spectrum of respiratory biologists and invigorated a new field of free radical biology and medicine. Study of the O_2-dependent reduction of cytochrome *c* by xanthine oxidase led to the discovery that the abundant blood protein erythrocuprein was an enzyme that converted the 1-e^- reduction product of O_2, i.e., the superoxide anion radical ($O_2^{-\cdot}$) to O_2 plus H_2O_2 [61]. The discovery of this enzyme, superoxide dismutase [62], was seminal because it provided evidence that biological systems had evolved an enzyme to eliminate radicals. This provided clear evidence that radicals must be commonly produced and be a threat to biological systems.

Chance et al. [63] provided an authoritative review on hydroperoxides that served as a platform for the integration of concepts of biologic damage by 1-e^- and 2-e^- oxidative processes by Sies [23] in the first monograph entitled "Oxidative Stress." In this volume, Sies [23] defined oxidative stress as "an imbalance of prooxidants and antioxidants in which the former predominates and causes macromolecular damage." This clear and simple definition proved useful to stimulate

research on oxidative stress as a mechanism of disease and aging, and antioxidants as means to protect against these deleterious processes.

The contemporary definition of oxidative stress has been refined based upon research findings of the turn of the century [1, 24, 64, 65]. Discovery of a family of enzymes, NADPH oxidases, that generates $O_2^{-\cdot}$ and H_2O_2 as signaling molecules [66, 67] showed that one cannot simply equate ROS with harmful chemistry, i.e., oxidative stress.

At the same time, results of large-scale, double-blind interventional studies with radical-scavenging antioxidants began to appear in the literature [40–47]. These studies showed that supplementation with antioxidants, i.e., shifting the "balance" toward protection, had little or no health benefit in humans. Consequently, the original definition of oxidative stress needs to be qualified in the sense that an "imbalance" is only considered in terms of specific reactions or pathways and not in terms of a global imbalance. In other words, an imbalance in a specific reaction or pathway can cause damage without an overall imbalance in the system, and a change in overall balance of prooxidants and antioxidants can occur without causing damage.

The contemporary view of oxidative stress has also been impacted by the development of new –omic technologies and systems biology. Instead of being limited to overall measures such as cell death [68], lipid peroxidation [69], or protein carbonylation [70], one can now measure effects on expression of specific genes [29], modification of specific lipids [71], and oxidation of specific proteins [72]. This research now shows that oxidative stress as it applies to environmental toxicology involves two processes: one related to earlier concepts of radical-mediated macromolecular damage and the other related to disruption of redox signaling and control mechanisms, which are largely non-radical in nature.

Radical Mechanisms of Environmental Toxicity

The lipid peroxidation mechanisms described above (Fig. 3) are more complex in living organisms because of the high concentrations of protein, the abundance of free radical scavenging antioxidants, and the processes of biologic turnover, which eliminate and replace damaged macromolecules and cells. In addition to redox cycling agents and halogenated hydrocarbons, a number of other initiators occur, including transition metals, ionizing and non-ionizing radiation, and sound. Because of the high concentration of protein in cells, the number of propagation reactions tends to be small, emphasizing the importance of initiation events in toxicity.

In pure lipid systems, free radical chain reactions can occur in which an initiation event causes modification of 200–400 molecules of fatty acid prior to being terminated by radicals reacting with each other. However, in biologic systems, such a chain reaction does not occur for several reasons. One is that initiation events are prevented by keeping free metal ion concentrations very low, and blocking other common initiation events. Another is that the concentration of protein is so high that H· is often abstracted from proteins rather than other polyunsaturated lipids, thereby decreasing propagation. Biologic systems also contain high concentrations of radical scavengers, such as vitamin C and vitamin E, which function as chain-terminating antioxidants. Amplification is also effectively prevented by the removal of lipid hydroperoxides by the peroxidases.

The propagation reactions are also not simple because multiple rearrangement products can occur. In addition to the rearrangement shown in Fig. 3, PUFA radicals can rearrange to eliminate a conjugated aldehyde, such as 4-hydroxynonenal (HNE). HNE is a reactive conjugated aldehyde that can react with proteins or DNA. The reactions generating HNE also generate carbon-centered radicals that propagate chain reactions. A number of other products can be formed, including epoxides (Fig. 4), which can be important as more stable forms with greater specificity in reaction with macromolecules, and isoprostanes [73], rearrangement products that are useful as biomarkers of this chemical reaction sequence. Conjugated aldehydes react with thiols and amines of proteins, creating modified proteins and degradation products that are universally detectable in biologic systems. Thus, lipid peroxidation appears to be an ongoing process. These are measured as protein carbonyls, another useful way to monitor oxidative stress in biologic systems [70].

Lipid peroxides are also formed enzymatically and are metabolized by several peroxidase systems. The most extensively studied enzymes are the glutathione

Ozone	O_3
Singlet oxygen	$^1O_2$
Hydrogen peroxide	H_2O_2
Hypochlorous acid	HOCl
Hydroperoxide	ROOH
Nitrous acid	HNO_2
Dinitrogen tetraoxide	N_2O_4
Peroxynitrite	$ONOO^-$
Alkylperoxynitrite	ROONO
Disulfide	RSSR′
Sulfenate	RSO^-
Sulfinate	RSO_2^-

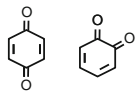

Quinones

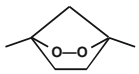

Endoperoxide

Epoxide

Environmental Toxicology: Oxidative Stress. Figure 4 Non-radical oxidants in biologic systems. Difficulties in quantifying oxidants and their rates of generation, as well as complexities in adaptive and toxic responses to long-term oxidant exposure and a generally conservative approach to terminology, have resulted in widespread use of the term "reactive oxygen species" (ROS). Although convenient, this term does not discriminate between radical and non-radical species and carries a bias that relevant biologic oxidants are closely related to O_2. A large number of non-radical oxidants, some of which are listed in this figure, exist in the environment and in biologic systems. Ozone and singlet oxygen (triplet O_2 is ground state) are common in the atmosphere, while H_2O_2, hypochlorous acid and lipid hydroperoxides are generated enzymatically and non-enzymatically in biologic systems. A number of other reactive carbon oxidation species occur, such as endoperoxides, epoxides and quinones (*right*). Reactive nitrogen oxidation products are also relevant biological oxidants. Nitrous acid and dinitrogen tetroxide are common in the atmosphere and also in biologic systems. Peroxynitrite is a reactive oxidant produced by reaction of two radicals, nitric oxide and superoxide. Nitric oxide (NO·) is a protective signaling molecule in the vascular system and is converted to peroxynitrite in the presence of superoxide. Alkylperoxynitrites can similarly form from nitric oxide and lipid peroxyl radicals. Other oxidants can also occur, such as disulfides of cysteine and other low molecular weight thiols. Other sulfur oxidation products, such as sulfenates and sulfinates, can also function as oxidants

(GSH) peroxidases [74], but more recent data indicate that a thioredoxin-dependent peroxidase, peroxiredoxin-6, is more active in the elimination of lipid hydroperoxides [75, 76]. The lipid peroxides can be very important in lipid peroxidation by providing a mechanism for amplification of lipid peroxidation [60]. Trace metal ions, such as Fe^{2+} or Cu^{1+}, can donate an electron to the peroxide to form another radical initiation event.

Because of these processes, radical chain reactions are almost completely prevented in living cells. In contrast, oxidative processes are a component of cellular destruction mechanisms used to kill microorganisms, to establish physical barriers to prevent infection, and to degrade and remove dead and dying cells. Phagocytes have a respiratory burst in which NADPH oxidase-2 generates ROS to kill microorganisms [67]. During apoptosis, a mitochondrial respiratory burst is created by the release of mitochondrial cytochrome *c* and switching the electron transfer chain to one that generates O_2^- [77]. Thus, unlike the interpretation that continuous generation of biomarkers of oxidative stress indicates that O_2 is a double-edged sword, the evidence shows that oxidative activities are part of normal biologic processes and that there is reserve capacity to protect against catastrophic collapse. Chain reactions of lipid peroxidation do not provide a major, central toxicologic process, but rather, when lipid peroxidation occurs, it mostly occurs by radical initiation events directly from environmental cause rather than as a consequence of chain reactions.

In summary, radical mechanisms are important for environmental toxicology because environmental agents can directly cause initiation of radical reactions that damage all types of macromolecules. Methods are available to evaluate radical-dependent mechanisms of oxidative stress in biological materials, especially through measurement of isoprostanes, protein carbonyls, and other well-documented oxidation products. Low levels of these products are found in normal cells, and healthy organisms are well protected against these reactions. Based upon extensive double-blind interventional studies with free radical scavengers in humans, these reactions do not contribute significantly to long-term health even though many studies show

short-term reductions in biomarkers of oxidative stress. Thus, in the absence of high concentrations of acute environmental exposure, the radical mechanisms appear to be secondary to non-radical oxidative mechanisms of toxicity [78].

Non-radical Mechanisms of Environmental Toxicity

The principles of non-radical mechanisms of oxidative stress are outlined in detail in "Radical-free biology of oxidative stress" [78]. Research has provided extensive knowledge of radical chemistry and antioxidants studied in purified systems and subcellular fractions of biologic systems, often with little regard to biologic relevance [79]. Most critically, biologic systems generate more non-radical oxidants (Fig. 4) than radicals, and the effective radical scavenging processes largely convert radicals to non-radicals or otherwise limit their destructive potential [78]. Important non-radical oxidants (Fig. 4) include H_2O_2, lipid hydroperoxides, quinones, disulfides, and reactive nitrogen species (RNS), especially peroxynitrite [80]. Peroxynitrite is a major oxidant formed by reaction of superoxide with nitric oxide, a protective signaling molecule controlling microcirculation and immune function [80, 81].

In the xanthine oxidase system, which provided the discovery of superoxide dismutase, the predominant product is H_2O_2, not the radical superoxide anion [82]. Under optimal conditions for univalent flux to form superoxide, this represents only 30% of the total flux, i.e., under all conditions divalent flux to form H_2O_2 predominated [82]. The univalent flux was considerably less under most conditions, consistent with partitioning of radical and non-radical oxidant production as depicted in Fig. 5. Many redox proteins that generate superoxide show rapid, sequential univalent transfer so that H_2O_2 is a common product of these reactions. Furthermore, dismutation of superoxide anion to H_2O_2 and O_2 occurs at a rapid rate (46) and, as indicated above, reaction of radicals with radical scavengers results in efficient conversion to non-radical oxidants. Consequently, the 2-e^-, non-radical oxidant, H_2O_2, is produced at a higher rate and appears to represent the major oxidant burden. This rate has

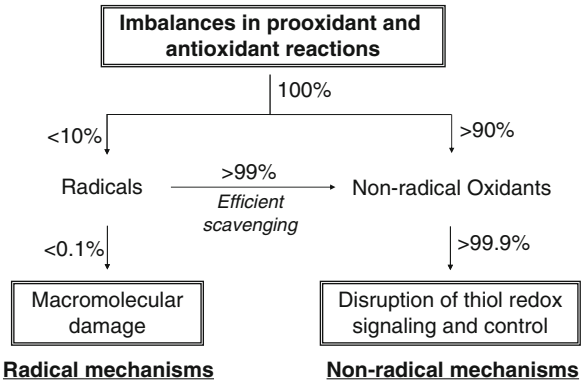

Environmental Toxicology: Oxidative Stress. Figure 5 Non-radical mechanisms of oxidative stress are quantitatively important in chronic and delayed toxicities. Although toxicity due to radical-induced macromolecular damage occurs under some conditions of acute toxicity, accumulating evidence indicates that non-radical mechanisms are important under other conditions. In this figure, the total rate of O_2 reduction to generate reactive oxygen species is expressed as 100%. Two-electron transfers predominate at biologic active sites that reduce O_2 to superoxide and H_2O_2, so that radicals are always produced at lower rates (e.g., <10% of total) than 2-electron products, such as H_2O_2 (>90% of total). Radical scavengers, including superoxide dismutase, are highly efficient (e.g., >99%) so that the radicals are largely converted to non-radical oxidants. This results in a low level of radical-mediated macromolecular damage and oxidative stress predominantly caused by non-radical oxidants. Non-radical oxidants preferentially target reactive thiols of redox signaling and control pathways, resulting in a disruption of signaling and control. Disruption of signaling and control mechanisms result in long-term dysfunction and reproductive and developmental toxicities. These can be insidious and pose a risk for environmental sustainability

been estimated to be 1–4% of the rate of O_2 consumption in mammalian systems [63], but rates can be higher in some compartments like the peroxisomes [83], or lower, such as in the cytoplasm or nuclei [84].

With non-radical oxidants being quantitatively most important and radical scavenging antioxidants converting some of the radicals to non-radical

oxidants, it is not surprising that radical-scavenging antioxidants do not provide protection against disease [40–47]. Perhaps a better way to view this in terms of environmental toxicity is that radical mechanisms are likely to contribute to acute toxicities but not as likely to contribute to chronic toxicities. In these reactions, macromolecular damage is of major concern, and all classes of macromolecules are potentially vulnerable. On the other hand, non-radical mechanisms can contribute to both; as described below, these are most relevant to chronic toxicity and can have effects through disruption of redox signaling and control, whether or not macromolecular damage occurs.

The major mechanisms of non-radical oxidative stress involve effects on thiols in proteins [78], although mutagenic damage to DNA also occurs [11, 85, 86]. Non-radical oxidants can interfere with reversible oxidation–reduction reactions of thiols by causing abnormal oxidation or irreversible modification. These changes alter physiological function in receptor signaling, transcriptional regulation, cell proliferation, angiogenesis, and apoptosis. Whether or not macromolecular damage occurs, the disruption of these functions alters cell fate and impacts physiologic health. Such changes can be adaptive and protective, in the process known as hormesis [87], but also can cause maladaptation and disease. These processes can occur due to a number of specific environmental agents, can occur in combination, and can be insidious in their long-term effects.

These concepts have been formalized in the redox hypothesis of oxidative stress [78], which provides four postulates to guide investigation into detailed mechanisms, ways to detect oxidative stress, and strategies to intervene to avoid or minimize oxidative stress. These postulates point to a need to incorporate systems biology, modern –omic technologies and bioinformatics into environmental health research, specifically to address environmental toxicities. These four postulates are:

1. All biologic systems contain redox elements (e.g., redox-sensitive cysteine, Cys, residues) that function in cell signaling, macromolecular trafficking, and physiologic regulation.
2. Organization and coordination of the redox activity of these elements occurs through redox circuits dependent upon common control nodes (e.g., thioredoxin, GSH).
3. The redox-sensitive elements are spatially and kinetically insulated so that "gated" redox circuits can be activated by translocation/aggregation and/or catalytic mechanisms.
4. Oxidative stress is a disruption of the function of these redox circuits caused by specific reaction with the redox-sensitive thiol elements, altered pathways of electron transfer, or interruption of the gating mechanisms controlling the flux through these pathways.

Proteins contain three functional groups that undergo reversible oxidation, the thiol in cysteine (Cys), the thioether in methionine (Met), and the selenol in selenocysteine (Sec). Cys has been studied most extensively, with relevant oxidation states including the thiol (-SH), disulfide (-SS-), sulfenate ($-SO^-$), sulfinate ($-SO_2^-$), and sulfonate ($-SO_3^-$). Thiyl radicals (-RS·) generated from thiols in the presence of oxygen-centered radicals [88], as well as other reactive sulfur species [89], can also be considered as toxic species in oxidative stress. Thiyl radicals rapidly react to form disulfides [90], and this may serve as a convergence point between 1-e^- and 2-e^- events. Relatively unstable sulfenates are converted to disulfides in the presence of thiols, and in some protein structures are stabilized as sulfenamides [91, 92]. Higher oxidation states, sulfinates and sulfonates, are typically not reversible in mammalian systems. A yeast enzyme (sulfiredoxin) reduces sulfinate in peroxiredoxin [93] and could be important in redox signaling mechanisms [94, 95].

Reversible oxidations of Met residues [96, 97] and the less common amino acid, selenocysteine (Sec) [98, 99], can also be important in toxicologic mechanisms. Met oxidation to methionine sulfoxide occurs in oxidative stress and aging [97, 100]. A good example, studied extensively in association with cigarette smoking, is the increased lung rigidity associated with loss of α1-antitrypsin inhibitor activity upon Met oxidation [101]. The loss of inhibition of elastase results in damage to lung structures and contributes to obstructive lung disease. Additional research shows that two types of methionine sulfoxide reductases (MSR) are important in protecting against distinct S- and

R-sulfoxides in methionine residues [96, 102, 103]. These MSR activities are dependent upon thioredoxins [103] and are associated with longevity [104–107]. This less frequently studied type of oxidation involves both Met and Sec, and probably deserves much greater attention in environmental oxidative stress due to the variable environmental availability of Met and Sec. The selenol of Sec undergoes reversible oxidation–reduction during catalytic functions of thioredoxin reductases and Se-dependent glutathione peroxidases [98, 99], enzymes present at key positions in both thioredoxin and GSH pathways and critically important to protect against non-radical oxidative stress.

Key points of oxidative stress according to the redox hypothesis include recognition of mechanisms of oxidative stress other than an imbalance of prooxidants and antioxidants. One of these involves altered function of redox circuits caused by specific reaction with redox-sensitive thiol elements (Fig. 6). This differs from the earlier concepts of macromolecular damage in that it could affect adaptability or tolerance of an organism without overt toxicity. For instance, redox-sensing thiols could govern tolerance to cold or prolonged starvation. Modification of these thiols would have no effect without the environmental challenge but would have catastrophic outcome with cold exposure or starvation. Environmental exposures could also create new pathways for electron transfer, effectively creating short circuits. Such short circuits may be accommodated by the stability of a network structure but create an overall vulnerability to other exposures.

Finally, a redox system design using low-flux systems to control high-flux systems is economical in terms of energy utilization [64]. Such a structure can be highly sensitive to low level exposures because it allows toxic agents to interrupt the gating mechanisms that control flux through these pathways. Because of this, accumulation of low levels of certain agents may induce a loss of function.

Future Directions

Oxidative stress and environmental sustainability. The view of oxidative stress as a disruption of redox signaling and control, as opposed to an imbalance of prooxidants and antioxidants, has different implications for sustainability in the environment. If oxidative stress were simply an imbalance, then oxidative stress caused by environmental agents could be eliminated by removing the source or directly compensated by increased antioxidants. Cleanup efforts generally approach the problem as though eliminating the source were sufficient. However, this simplistic approach, like the antioxidant supplementation trials, does not effectively address the problem with regard to environmental sustainability.

A critical issue is that complex systems respond to challenges with adaptation to maintain function. Because of this, subtoxic exposures can accumulate without overt signs of adverse effects. In the long term, this is not sustainable. Consequently, studies to evaluate impact can provide reassuring evidence that specific environmental challenges are not a problem, when the data may really mean that the biologic systems are effectively engineered to conceal hazards. While this may seem overly paranoid, millions of new chemicals have been synthesized in research efforts, and tens of thousands are in commercial use. Consequently, to consider sustainability in terms of oxidative stress, one must evaluate sustainability in terms of the impacts of cumulative exposures and acknowledge the reality that one cannot correct oxidative stress simply by shifting the balance with antioxidants.

Unfortunately, the scientific method is not well designed to deal with complex systems. The range of responses to multiple exposures within complex systems over long periods of exposure cannot be evaluated or predicted accurately with contemporary methods. Sustainability in the environment necessitates new ways to evaluate exposures and biologic responses.

From the standpoint of oxidative stress, a redox proteomics approach provides means for systems analysis. With a currently available liquid chromatography-mass spectrometry approach, one can measure the percent oxidation of specific cysteine residues in hundreds of proteins [108]. These Cys residues represent only a fraction of the total Cys encoded by the genome, which is about 200,000 in the 18,000 proteins in humans, but none-the-less provide an indication of the steady-state oxidation of the individual. The Cys residues change in oxidation state in response to exposures so that one could, in principle, establish sentinel species to examine environmental oxidative stress.

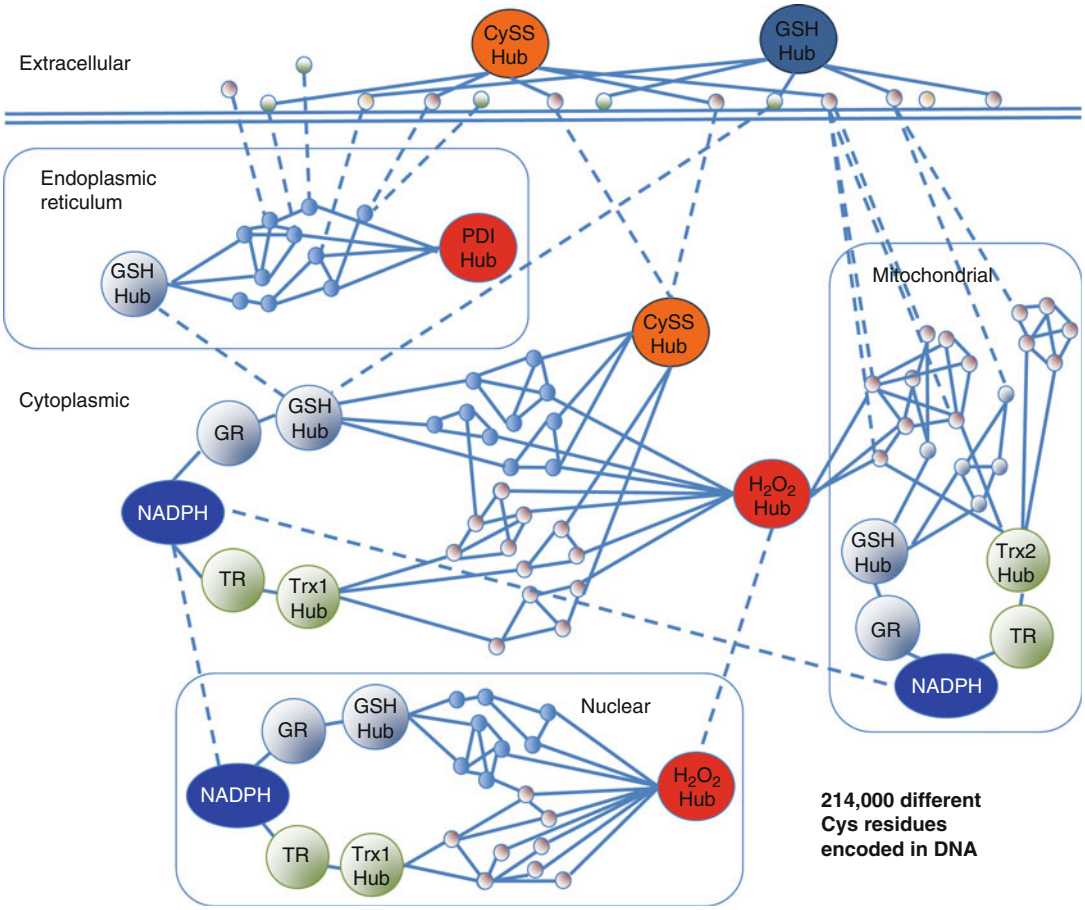

Environmental Toxicology: Oxidative Stress. Figure 6

Targets of oxidative stress include redox-sensitive thiols functioning in subcellular compartments. The human genome encodes 214,000 different cysteine residues. The resulting cysteine proteome is distributed among cellular compartments, with extracellular protein thiols (indicated as nodes) interacting with free cysteine and cystine, designated as a CySS redox-control hub, in the plasma and interstitial space. Solid connectors (edges) indicate direct interactions in a network structure. On the alveolar surface of the lung and lining of the gastrointestinal tract, GSH and GSSG appear to serve as the predominant redox-control hub. The extracellular thiol/disulfide systems are connected to intracellular systems (designated by broken lines) principally through transport systems or other indirect mechanisms. Within the cytoplasm, a CySS hub and a H_2O_2 hub function in the oxidation of cytoplasmic proteins. These oxidative reactions are ongoing and are countered by two major NADPH-dependent thiol reduction systems, represented by thioredoxin-1 (Trx1) and GSH/GSSG hubs. The relative rates for different proteins vary, with the majority of Cys residues being largely reduced under steady-state conditions. Trx1 is translocated into nuclei during oxidative stress; in the nuclei, Trx1 is maintained at a more reduced state than in the cytoplasm. Both nuclear Trx1 and nuclear GSSG hubs function are at least partially independent of respective cytoplasmic hubs. These hubs are important for redox control of transcription and are, therefore, critical nuclear targets of oxidative stress. Mitochondria contain Trx2 and GSH/GSSG hubs that control redox states of mitochondrial proteins. Lipophilic cationic oxidants can be especially toxic because they accumulate in mitochondria and disrupt bioenergetic control. In the secretory pathway, protein disulfide isomerase (PDI) is oxidized by an endoplasmic reticulum oxidase system (EROS) and functions as a redox hub controlling Cys oxidation in proteins destined for the plasma membrane or extracellular compartments. The range of organelle function in specialized tissues results in organ system–specific oxidative stress.

Two types of data can be obtained, one giving maps of electron transfer circuits and the other giving functional pathway maps linked by Cys oxidation [108]. Such a biomonitoring approach could be used to establish cumulative databases, providing a strategy to quantify deterioration of environmental conditions in terms of disruption of protein redox systems in the sentinel species. Of course, humans could be one of the sentinel species, and evaluation of protein oxidation in human samples could be useful to document oxidative stress. Similar information could be obtained from gene expression profiling; complete genomic information is available now for several species, so that multiple options are available to test the feasibility of such approaches.

Unfortunately, changes in redox proteomics or gene expression only reveal whether deterioration has occurred, and do not provide insight into the underlying causes. Exposure information will be needed to link environmental deterioration to specific causes. Current environmental surveillance methods are poorly equipped to address this problem because analyses are highly targeted to a relatively small number of hazardous agents. Newer methods are available to profile chemicals in biologic extracts, which show that thousands of chemicals can be detected in a single analysis [33]. Less than half of the chemicals detected in human plasma have been identified, meaning that humans are exposed to a large number of unidentified chemicals. Some of these may be environmental degradation products of known hazardous and nonhazardous chemicals. Whether these chemicals are helpful or harmful is not known, but multivariate analysis and modern bioinformatic methods can support studies linking alteration in metabolic characteristics with abundance of specific chemicals in biologic samples. Clearly, investment in new methods as well as cumulative environmental health data registries will be needed to address critical questions of environmental sustainability with regard to oxidative stress.

During the past decade, methods have been developed to allow study of oxidative stress within specific subcellular compartments [84, 109]. Mammalian cells contain about 214,000 Cys residues encoded in the genome, and redox biochemical approaches are beginning to provide an understanding of the organization of the redox network structure [108, 110, 111]. This research has revealed that oxidative stress is not uniform within cells but rather selectively affects specific pathways in compartments. The extracellular compartments of plasma and interstitial space are generally more oxidized than cellular compartments (Fig. 6) [84], have fewer antioxidant systems, and are vulnerable to oxidants. The lung alveoli, oral mucosa, and intestinal lumen are supplied with the thiol antioxidant GSH, and have protective enzymes associated with the mucous-lining layer. Thus, the maintenance of these surface barriers is critical for the protection of an organism because the lung lining is first exposed to airborne toxicants, while the intestine is first exposed to ingested toxicants.

Within cells, different redox systems function in the organelles. The endoplasmic reticulum (ER) and secretory pathway use protein disulfide isomerase (PDI) and an oxidase system (EROS) to oxidize proteins during processing for secretion ([112]; Fig. 6). Disruption of this oxidative pathway activates cell death through an ER stress mechanism [112, 113]. Nuclei and mitochondria are more reduced [84], and each has specific redox-sensitive proteins. Mitochondria have a unique thioredoxin-2, Trx2, and glutaredoxin-2, Grx2, while thioredoxin-1 and glutaredoxin-1 are found in the cytoplasm. Trx1 is translocated into nuclei during oxidative stress [114], and nuclei also contain Grx2, at least when over-expressed in cells [110]. Accumulating evidence indicates that most agents that cause oxidative stress do so by disrupting specific redox control pathways associated with specific organelles (Fig. 6).

Finally, there is a possibility that artificial intelligence may provide a more cost-effective means to monitor environmental sustainability. Irregularity of biologic data often reflects adaptability and health of the system. In essence, the accommodation of oxidative challenges can be expected to decrease the flexibility of the system. Thus, if appropriate methods were developed, it may be possible to evaluate health (or sustainability of a system) in terms of irregularity of metabolic or protein data [115]. Such an approach could potentially be accomplished using monofractality or multifractality, such as expressed by Hurst or Holder exponents [116]. While these are not traditional approaches used by experimental or environmental biologists, they could be very useful to approach the rather difficult problem of environmental

sustainability in the face of such a large number of newly introduced and accumulating abundance of environmental agents.

In summary, oxidative stress is an important concern in environmental toxicology, both as a cause of acute toxicity and as a contributor to chronic toxicity. In terms of sustainability, agents causing acute toxicity due to oxidative stress are more readily identified and managed by containment and cleanup, in some cases complemented by use of metal chelators and free radical scavenging antioxidants. Agents that cause chronic toxicity or delayed reproductive or developmental toxicity are of greater concern because of the difficulty of identification and association with the toxicity. At present, there is no way to evaluate whether this is a minor or major problem, but halogenated hydrocarbons are commonly used. Some of these could accumulate in the biosphere, and most of these are likely to contribute to oxidative stress. Safety testing mostly is performed only on commercial materials and not on products formed by the modification of these materials after release into the environment. Mass spectrometry analyses of human plasma reveal thousands of unidentified ions with unknown biologic effects. Currently there is no environmental exposure census to reveal whether or not such chemicals are accumulating due to human activity. Thus, there is considerable opportunity and need to enhance understanding of the environmental load of chemicals that could accumulate and cause adverse effects due to oxidative stress [117–122].

Acknowledgment

Research support provided by grants from the National Institutes of Environmental Health Sciences ES009047 and ES011195.

Bibliography

1. Sies H, Jones DP (2007) Oxidative stress. In: Fink G (ed) Encyclopedia of stress. Elsevier, San Diego, pp 45–48
2. Ruidavets JB, Cournot M, Cassadou S, Giroux M, Meybeck M, Ferrieres J (2005) Ozone air pollution is associated with acute myocardial infarction. Circulation 111:563–569
3. Seinfeld JH, Pandis SN (2006) Atmospheric chemistry and physics – from air pollution to climate change, 2nd edn. Wiley, New York, 1225 pp
4. Becana M, Moran JF, Iturbe-Ormaetxe I (1998) Iron-dependent oxygen free radical generation in plants subjected to environmental stress: toxicity and antioxidant protection. Plant Soil 201:137–147
5. Das P, Samantaray S, Rout GR (1997) Studies on cadmium toxicity in plants: a review. Environ Pollut 98:29–36
6. Klaassen CD, Liu J, Choudhuri S (1999) Metallothionein: an intracellular protein to protect against cadmium toxicity. Annu Rev Pharmacol Toxicol 39:267–294
7. Ragunathan N, Dairou J, Sanfins E, Busi F, Noll C, Janel N, Dupret JM, Rodrigues-Lima F (2010) Cadmium alters the biotransformation of carcinogenic aromatic amines by arylamine n-acetyltransferase xenobiotic-metabolizing enzymes: molecular, cellular, and in vivo studies. Environ Health Perspect 118:1685–1691
8. Hideg E, Vass I (1996) Uv-b induced free radical production in plant leaves and isolated thylakoid membranes. Plant Sci 115:251–260
9. Jurkiewicz BA, Buettner GR (1996) Epr detection of free radicals in uv-irradiated skin: mouse versus human. Photochem Photobiol 64:918–922
10. Bernhard WA (2009) Radical reaction pathways initiated by direct energy deposition in DNA by ionizing radiation. In: Greenberg MM (ed) Radical and radical ion reactivity in nucleic acid chemistry. Wiley, Hoboken, pp 41–68
11. Jackson SP, Bartek J (2009) The DNA-damage response in human biology and disease. Nature 461:1071–1078
12. Tafazoli S, Spehar DD, O'Brien PJ (2005) Oxidative stress mediated idiosyncratic drug toxicity. Drug Metab Rev 37:311–325
13. Araujo JA, Barajas B, Kleinman M, Wang X, Bennett BJ, Gong KW, Navab M, Harkema J, Sioutas C, Lusis AJ, Nel AE (2008) Ambient particulate pollutants in the ultrafine range promote early atherosclerosis and systemic oxidative stress. Circ Res 102:589–596
14. Siddique HR, Gupta SC, Mitra K, Bajpai VK, Mathur N, Murthy RC, Saxena DK, Chowdhuri DK (2008) Adverse effect of tannery waste leachates in transgenic drosophila melanogaster: role of Ros in modulation of Hsp70, oxidative stress and apoptosis. J Appl Toxicol 28:734–748
15. Matschullat J, Birmann K, Borba RP, Ciminelli V, Deschamps EM, Figueiredo BR, Gabrio T, Haßler S, Hilscher A, Junghänel I, de Oliveira N, Raßbach K, Schmidt H, Schwenk M, de Oliveira Vilhena MJ, Weidner U, Abmjbrz BP, Richard HL (2007) Long-term environmental impact of arsenic-dispersion in Minas Gerais, Brazil. In: Bundschuh J, Zevenhoven R, Loeppert RH (eds) Trace metals and other contaminants in the environment. Elsevier, Great Lakes, pp 365–382
16. Jones KC, de Voogt P (1999) Persistent organic pollutants (pops): state of the science. Environ Pollut 100:209–221
17. Ruzzin J, Petersen R, Meugnier E, Madsen L, Lock EJ, Lillefosse H, Ma T, Pesenti S, Sonne SB, Marstrand TT, Malde MK, Du ZY, Chavey C, Fajas L, Lundebye AK, Brand CL, Vidal H, Kristiansen K, Froyland L (2010) Persistent organic pollutant exposure leads to insulin resistance syndrome. Environ Health Perspect 118:465–471
18. Wania F, Mackay D (1996) Tracking the distribution of persistent organic pollutants. Environ Sci Technol 30:A390–A396

19. Apelberg BJ, Witter FR, Herbstman JB, Calafat AM, Halden RU, Needham LL, Goldman LR (2007) Cord serum concentrations of perfluorooctane sulfonate (PFOS) and perfluorooctanoate (PFOA) in relation to weight and size at birth. Environ Health Perspect 115:1670–1676
20. Wallington TJ, Hurley MD, Xia J, Wuebbles DJ, Sillman S, Ito A, Penner JE, Ellis DA, Martin J, Mabury SA, Nielsen OJ, Sulbaek Andersen MP (2006) Formation of C7F15COOH (PFOA) and other perfluorocarboxylic acids during the atmospheric oxidation of 8:2 fluorotelomer alcohol. Environ Sci Technol 40:924–930
21. Rappaport SM (2010) Implications of the exposome for exposure science. J Expo Sci Environ Epidemiol 21:5–9
22. Wild CP (2005) Complementing the genome with an "Exposome": the outstanding challenge of environmental exposure measurement in molecular epidemiology. Cancer Epidemiol Biomark Prev 14:1847–1850
23. Sies H (1985) Oxidative stress: introductory remarks. In: Sies H (ed) Oxidative stress. Academic, London, pp 1–8
24. Jones DP (2006) Redefining oxidative stress. Antioxid Redox Signal 8:1865–1879
25. Voit E, Neves AR, Santos H (2006) The intricate side of systems biology. Proc Natl Acad Sci USA 103:9452–9457
26. Voit EO, Qi Z, Miller GW (2008) Steps of modeling complex biological systems. Pharmacopsychiatry 41(Suppl 1):S78–S84
27. Schuster SC (2008) Next-generation sequencing transforms today's biology. Nat Meth 5:16–18
28. Callinan PA, Feinberg AP (2006) The emerging science of epigenomics. Hum Mol Genet 15(Spec No 1):R95–R101
29. Bammler T, Beyer RP, Bhattacharya S, Boorman GA, Boyles A, Bradford BU, Bumgarner RE, Bushel PR, Chaturvedi K, Choi D, Cunningham ML, Deng S, Dressman HK, Fannin RD, Farin FM, Freedman JH, Fry RC, Harper A, Humble MC, Hurban P, Kavanagh TJ, Kaufmann WK, Kerr KF, Jing L, Lapidus JA, Lasarev MR, Li J, Li YJ, Lobenhofer EK, Lu X, Malek RL, Milton S, Nagalla SR, O'Malley JP, Palmer VS, Pattee P, Paules RS, Perou CM, Phillips K, Qin LX, Qiu Y, Quigley SD, Rodland M, Rusyn I, Samson LD, Schwartz DA, Shi Y, Shin JL, Sieber SO, Slifer S, Speer MC, Spencer PS, Sproles DI, Swenberg JA, Suk WA, Sullivan RC, Tian R, Tennant RW, Todd SA, Tucker CJ, Van Houten B, Weis BK, Xuan S, Zarbl H (2005) Standardizing global gene expression analysis between laboratories and across platforms. Nat Meth 2:351–356
30. Li H, Grigoryan H, Funk WE, Lu SS, Rose S, Williams ER, Rappaport SM (2010) Profiling Cys34 adducts of human serum albumin by fixed-step selected reaction monitoring. Mol Cell Proteomics (Ahead of print)
31. Funk WE, Li H, Iavarone AT, Williams ER, Riby J, Rappaport SM (2010) Enrichment of cysteinyl adducts of human serum albumin. Anal Biochem 400:61–68
32. Evans AM, DeHaven CD, Barrett T, Mitchell M, Milgram E (2009) Integrated, nontargeted ultrahigh performance liquid chromatography/electrospray ionization tandem mass spectrometry platform for the identification and relative quantification of the small-molecule complement of biological systems. Anal Chem 81:6656–6667
33. Johnson JM, Yu T, Strobel FH, Jones DP (2010) A practical approach to detect unique metabolic patterns for personalized medicine. Analyst 135:2864–2870
34. Namakkal Soorappan R, Varadharaj S, Khanderao GD, Davidson CJ, Kannan S, Firpo MA, Zweier J, Benjamin I (2010) Sustained activation of nrf2/are signaling promotes reductive stress in the human mutant protein aggregation cardiomyopathy in mice. Antioxid Redox Signal (Ahead of print)
35. Zhang X, Min X, Li C, Benjamin IJ, Qian B, Ding Z, Gao X, Yao Y, Ma Y, Cheng Y, Liu L (2010) Involvement of reductive stress in the cardiomyopathy in transgenic mice with cardiac-specific overexpression of heat shock protein 27. Hypertension 55:1412–1417
36. Kappus H, Sies H (1981) Toxic drug effects associated with oxygen metabolism: redox cycling and lipid peroxidation. Experientia 37:1233–1241
37. Priestley J (1775) Letter to sir john pringle. Philos Trans 65:384–390
38. Bitterman N, Bitterman H (2006) Oxygen toxicity. In: Mathiew D (ed) Handbook on hyperbaric medicine. Dordrecht, Springer
39. Silverman WA (2004) A cautionary tale about supplemental oxygen: the albatross of neonatal medicine. Pediatrics 113:394–396
40. The Alpha-Tocopherol, Beta Carotene Cancer Prevention Study Group (1994) The effect of vitamin E and beta carotene on the incidence of lung cancer and other cancers in male smokers. N Engl J Med 330:1029–1035
41. Gruppo Italiano Per Lo Studio Della Sopravvivenza Nell'infarto Miocardico (1999) Dietary supplementation with n-3 polyunsaturated fatty acids and vitamin e after myocardial infarction: results of the gissi-prevenzione trial. Lancet 354:447–455
42. Age-Related Eye Disease Study Research Group (2001) A randomized, placebo-controlled, clinical trial of high-dose supplementation with vitamins C and E, beta carotene, and zinc for age-related macular degeneration and vision loss: AREDS Report no. 8. Arch Ophthalmol 119:1417–1436
43. de Gaetano G (2001) Low-dose aspirin and vitamin e in people at cardiovascular risk: a randomised trial in general practice. Collaborative group of the primary prevention project. Lancet 357:89–95
44. Hennekens CH, Buring JE, Manson JE, Stampfer M, Rosner B, Cook NR, Belanger C, LaMotte F, Gaziano JM, Ridker PM, Willett W, Peto R (1996) Lack of effect of long-term supplementation with beta carotene on the incidence of malignant neoplasms and cardiovascular disease. N Engl J Med 334:1145–1149
45. Lonn E, Bosch J, Yusuf S, Sheridan P, Pogue J, Arnold JM, Ross C, Arnold A, Sleight P, Probstfield J, Dagenais GR (2005) Effects of long-term vitamin E supplementation on cardiovascular events and cancer: a randomized controlled trial. J Am Med Assoc 293:1338–1347
46. Yusuf S, Dagenais G, Pogue J, Bosch J, Sleight P (2000) Vitamin e supplementation and cardiovascular events in high-risk patients. The heart outcomes prevention evaluation study investigators. N Engl J Med 342:154–160

47. Zureik M, Galan P, Bertrais S, Mennen L, Czernichow S, Blacher J, Ducimetiere P, Hercberg S (2004) Effects of long-term daily low-dose supplementation with antioxidant vitamins and minerals on structure and function of large arteries. Arterioscler Thromb Vasc Biol 24:1485–1491
48. Williams KJ, Fisher EA (2005) Oxidation, lipoproteins, and atherosclerosis: which is wrong, the antioxidants or the theory? Curr Opin Clin Nutr Metab Care 8:139–146
49. Loew O (1901) Catalase, a new enzyme of general occurrence. U.S. Department of Agriculture Report no. 68, pp 47–55
50. Chelikani P, Fita I, Loewen PC (2004) Diversity of structures and properties among catalases. Cell Mol Life Sci 61:192–208
51. Maehly AC, Chance B (1954) The assay of catalases and peroxidases. Meth Biochem Anal 1:357–424
52. Keilin D (1925) On cytochrome, a respiratory pigment, common to animals, yeast, and higher plants. Proc R Soc Lond B – Containing Pap Biol Character 98:312–339
53. Dutton PL, Wilson DF (1974) Redox potentiometry in mitochondrial and photosynthetic bioenergetics. Biochim Biophys Acta 346:165–212
54. Wolf G (2005) The discovery of the antioxidant function of vitamin E: the contribution of Henry A. Mattill J Nutr 135:363–366
55. Mills GC (1957) Hemoglobin catabolism. I. Glutathione peroxidase, an erythrocyte enzyme which protects hemoglobin from oxidative breakdown. J Biol Chem 229:189–197
56. Rotruck JT, Pope AL, Ganther HE, Swanson AB, Hafeman DG, Hoekstra WG (1973) Selenium: biochemical role as a component of glutathione peroxidase. Science 179:588–590
57. Recknagel RO, Ghoshal AK (1966) Lipoperoxidation of rat liver microsomal lipids induced by carbon tetrachloride. Nature 210:1162–1163
58. Recknagel RO, Ghoshal AK (1966) Lipoperoxidation as a vector in carbon tetrachloride hepatotoxicity. Lab Invest 15:132–148
59. Harman D (1956) Aging: a theory based on free radical and radiation chemistry. J Gerontol 11:298–300
60. Tribble DL, Aw TY, Jones DP (1987) The pathophysiological significance of lipid peroxidation in oxidative cell injury. Hepatology 7:377–386
61. Fridovich I (1997) Superoxide anion radical ($O_2^{-\bullet}$), superoxide dismutases, and related matters. J Biol Chem 272:18515–18517
62. McCord JM, Fridovich I (1969) Superoxide dismutase. An enzymic function for erythrocuprein (hemocuprein). J Biol Chem 244:6049–6055
63. Chance B, Sies H, Boveris A (1979) Hydroperoxide metabolism in mammalian organs. Physiol Rev 59:527–605
64. Jones DP (2006) Disruption of mitochondrial redox circuitry in oxidative stress. Chem Biol Interact 163:38–53
65. Jones DP (2006) Extracellular redox state: refining the definition of oxidative stress in aging. Rejuvenation Res 9:169–181
66. Griendling KK (2006) Nadph oxidases: new regulators of old functions. Antioxid Redox Signal 8:1443–1445
67. Lambeth JD (2004) Nox enzymes and the biology of reactive oxygen. Nat Rev Immunol 4:181–189
68. Orrenius S (2004) Mitochondrial regulation of apoptotic cell death. Toxicol Lett 149:19–23
69. Morrow JD, Roberts LJ 2nd (1999) Mass spectrometric quantification of F2-isoprostanes in biological fluids and tissues as measure of oxidant stress. Meth Enzymol 300:3–12
70. Levine RL, Garland D, Oliver CN, Amici A, Climent I, Lenz AG, Ahn BW, Shaltiel S, Stadtman ER (1990) Determination of carbonyl content in oxidatively modified proteins. Meth Enzymol 186:464–478
71. Kagan VE, Borisenko GG, Tyurina YY, Tyurin VA, Jiang J, Potapovich AI, Kini V, Amoscato AA, Fujii Y (2004) Oxidative lipidomics of apoptosis: redox catalytic interactions of cytochrome c with cardiolipin and phosphatidylserine. Free Radic Biol Med 37:1963–1985
72. Go YM, Park H, Koval M, Orr M, Reed M, Liang Y, Smith D, Pohl J, Jones DP (2010) A key role for mitochondria in endothelial signaling by plasma cysteine/cystine redox potential. Free Radic Biol Med 48:275–283
73. Morrow JD, Roberts LJ 2nd (2002) Mass spectrometric quantification of F2-isoprostanes as indicators of oxidant stress. Meth Mol Biol 186:57–66
74. Brigelius-Flohe R (1999) Tissue-specific functions of individual glutathione peroxidases. Free Radic Biol Med 27:951–965
75. Fisher AB, Dodia C, Manevich Y, Chen JW, Feinstein SI (1999) Phospholipid hydroperoxides are substrates for non-selenium glutathione peroxidase. J Biol Chem 274:21326–21334
76. Wang Y, Phelan SA, Manevich Y, Feinstein SI, Fisher AB (2006) Transgenic mice overexpressing peroxiredoxin 6 show increased resistance to lung injury in hyperoxia. Am J Respir Cell Mol Biol 34:481–486
77. Cai J, Jones DP (1998) Superoxide in apoptosis. Mitochondrial generation triggered by cytochrome C loss. J Biol Chem 273:11401–11404
78. Jones DP (2008) Radical-free biology of oxidative stress. Am J Physiol Cell Physiol 295:C849–C868
79. Halliwell B (2007) Oxidative stress and cancer: have we moved forward? Biochem J 401:1–11
80. Thomas DD, Liu X, Kantrow SP, Lancaster JR Jr (2001) The biological lifetime of nitric oxide: implications for the perivascular dynamics of NO and O_2. Proc Natl Acad Sci USA 98:355–360
81. Thomas DD, Ridnour LA, Espey MG, Donzelli S, Ambs S, Hussain SP, Harris CC, DeGraff W, Roberts DD, Mitchell JB, Wink DA (2006) Superoxide fluxes limit nitric oxide-induced signaling. J Biol Chem 281:25984–25993
82. Fridovich I (1970) Quantitative aspects of the production of superoxide anion radical by milk xanthine oxidase. J Biol Chem 245:4053–4057
83. Jones DP, Eklow L, Thor H, Orrenius S (1981) Metabolism of hydrogen peroxide in isolated hepatocytes: relative contributions of catalase and glutathione peroxidase in decomposition of endogenously generated H_2O_2. Arch Biochem Biophys 210:505–516
84. Go YM, Jones DP (2008) Redox compartmentalization in eukaryotic cells. Biochim Biophys Acta 1780(11):1273–1290

85. Barja G (2002) Endogenous oxidative stress: relationship to aging, longevity and caloric restriction. Ageing Res Rev 1:397–411
86. Doudican NA, Song B, Shadel GS, Doetsch PW (2005) Oxidative DNA damage causes mitochondrial genomic instability in saccharomyces cerevisiae. Mol Cell Biol 25:5196–5204
87. Calabrese EJ, Baldwin LA (2003) The hormetic dose-response model is more common than the threshold model in toxicology. Toxicol Sci 71:246–250
88. Winterbourn CC, Metodiewa D (1994) The reaction of superoxide with reduced glutathione. Arch Biochem Biophys 314:284–290
89. Giles GI, Tasker KM, Jacob C (2001) Hypothesis: the role of reactive sulfur species in oxidative stress. Free Radic Biol Med 31:1279–1283
90. Starke DW, Chock PB, Mieyal JJ (2003) Glutathione-thiyl radical scavenging and transferase properties of human glutaredoxin (thioltransferase). Potential role in redox signal transduction. J Biol Chem 278:14607–14613
91. Salmeen A, Andersen JN, Myers MP, Meng TC, Hinks JA, Tonks NK, Barford D (2003) Redox regulation of protein tyrosine phosphatase 1B involves a sulphenyl-amide intermediate. Nature 423:769–773
92. van Montfort RL, Congreve M, Tisi D, Carr R, Jhoti H (2003) Oxidation state of the active-site cysteine in protein tyrosine phosphatase 1B. Nature 423:773–777
93. Biteau B, Labarre J, Toledano MB (2003) Atp-dependent reduction of cysteine-sulphinic acid by S. cerevisiae sulphiredoxin. Nature 425:980–984
94. Woo HA, Chae HZ, Hwang SC, Yang KS, Kang SW, Kim K, Rhee SG (2003) Reversing the inactivation of peroxiredoxins caused by cysteine sulfinic acid formation. Science 300:653–656
95. Woo HA, Kang SW, Kim HK, Yang KS, Chae HZ, Rhee SG (2003) Reversible oxidation of the active site cysteine of peroxiredoxins to cysteine sulfinic acid. Immunoblot detection with antibodies specific for the hyperoxidized cysteine-containing sequence. J Biol Chem 278:47361–47364
96. Kim HY, Gladyshev VN (2004) Methionine sulfoxide reduction in mammals: characterization of methionine-r-sulfoxide reductases. Mol Biol Cell 15:1055–1064
97. Stadtman ER, Van Remmen H, Richardson A, Wehr NB, Levine RL (2005) Methionine oxidation and aging. Biochim Biophys Acta 1703:135–140
98. Gladyshev VN, Hatfield DL (1999) Selenocysteine-containing proteins in mammals. J Biomed Sci 6:151–160
99. Kryukov GV, Castellano S, Novoselov SV, Lobanov AV, Zehtab O, Guigo R, Gladyshev VN (2003) Characterization of mammalian selenoproteomes. Science 300:1439–1443
100. Stadtman ER, Levine RL (2003) Free radical-mediated oxidation of free amino acids and amino acid residues in proteins. Amino Acids 25:207–218
101. Carp H, Miller F, Hoidal JR, Janoff A (1982) Potential mechanism of emphysema: alpha 1-proteinase inhibitor recovered from lungs of cigarette smokers contains oxidized methionine and has decreased elastase inhibitory capacity. Proc Natl Acad Sci USA 79:2041–2045
102. Hansel A, Kuschel L, Hehl S, Lemke C, Agricola HJ, Hoshi T, Heinemann SH (2002) Mitochondrial targeting of the human peptide methionine sulfoxide reductase (MSRA), an enzyme involved in the repair of oxidized proteins. FASEB J 16:911–913
103. Weissbach H, Etienne F, Hoshi T, Heinemann SH, Lowther WT, Matthews B, St John G, Nathan C, Brot N (2002) Peptide methionine sulfoxide reductase: structure, mechanism of action, and biological function. Arch Biochem Biophys 397:172–178
104. Miller RA, Buehner G, Chang Y, Harper JM, Sigler R, Smith-Wheelock M (2005) Methionine-deficient diet extends mouse lifespan, slows immune and lens aging, alters glucose, T4, IGF-I and insulin levels, and increases hepatocyte MIF levels and stress resistance. Aging Cell 4:119–125
105. Moskovitz J, Bar-Noy S, Williams WM, Requena J, Berlett BS, Stadtman ER (2001) Methionine sulfoxide reductase (MSRA) is a regulator of antioxidant defense and lifespan in mammals. Proc Natl Acad Sci USA 98:12920–12925
106. Richie JP Jr, Leutzinger Y, Parthasarathy S, Malloy V, Orentreich N, Zimmerman JA (1994) Methionine restriction increases blood glutathione and longevity in F344 rats. FASEB J 8:1302–1307
107. Sanz A, Caro P, Ayala V, Portero-Otin M, Pamplona R, Barja G (2006) Methionine restriction decreases mitochondrial oxygen radical generation and leak as well as oxidative damage to mitochondrial DNA and proteins. FASEB J 20: 1064–1073
108. Jones DP, Go YM (2010) Mapping the cysteine proteome: analysis of redox-sensing thiols. Curr Opin Chem Biol 15: 1–10
109. Hansen JM, Go YM, Jones DP (2006) Nuclear and mitochondrial compartmentation of oxidative stress and redox signaling. Annu Rev Pharmacol Toxicol 46:215–234
110. Gallogly MM, Starke DW, Mieyal JJ (2009) Mechanistic and kinetic details of catalysis of thiol-disulfide exchange by glutaredoxins and potential mechanisms of regulation. Antioxid Redox Signal 11:1059–1081
111. Kemp M, Go YM, Jones DP (2008) Nonequilibrium thermodynamics of thiol/disulfide redox systems: a perspective on redox systems biology. Free Radic Biol Med 44:921–937
112. Cenci S, Sitia R (2007) Managing and exploiting stress in the antibody factory. FEBS Lett 581:3652–3657
113. Todd DJ, Lee AH, Glimcher LH (2008) The endoplasmic reticulum stress response in immunity and autoimmunity. Nat Rev Immunol 8:663–674
114. Go YM, Jones DP (2010) Redox control systems in the nucleus: mechanisms and functions. Antioxid Redox Signal 13:489–509
115. Goldberger AL, Amaral LA, Hausdorff JM, Ivanov P, Peng CK, Stanley HE (2002) Fractal dynamics in physiology: alterations with disease and aging. Proc Natl Acad Sci USA 99(Suppl 1):2466–2472

116. Ivanov PC, Amaral LA, Goldberger AL, Havlin S, Rosenblum MG, Struzik ZR, Stanley HE (1999) Multifractality in human heartbeat dynamics. Nature 399:461–465
117. Greenberg M (2009) Radical and radical ion reactivity in nucleic acid chemistry. Wiley, New York, 466 pp
118. Sarkar D, Datta R, Hannigan R (2007) Concepts and applications in environmental geochemistry. Elsevier, Amsterdam, 761 pp
119. Keilin D (1966) The history of cell respiration and cytochrome. In: Keilin D (ed) The history of cell respiration and cytochrome. Cambridge University Press, Cambridge
120. Finkel T (2003) Oxidant signals and oxidative stress. Curr Opin Cell Biol 15:247–254
121. Wu JJ, Quijano C, Chen E, Liu H, Cao L, Fergusson MM, Rovira II, Gutkind S, Daniels MP, Komatsu M, Finkel T (2009) Mitochondrial dysfunction and oxidative stress mediate the physiological impairment induced by the disruption of autophagy. Aging 1:425–437
122. Swanson RA, Siesjo B (2002) Oxidative stress in cerebrovascular disease. In: Swanson RA, Siesjo B (eds) Oxidative stress in cerebrovascular disease. Cambridge University Press, Cambridge

F

Facades and Enclosures, Building for Sustainability

Volker Hartkopf[1], Azizan Aziz[1], Vivian Loftness[2]
[1]Center for Building Performance and Diagnostics, Carnegie Mellon University, Pittsburgh, USA
[2]Center for Building Performance and Diagnostics, Carnegie Mellon University, Pittsburgh, PA, USA

Article Outline

Glossary
Definition of the Subject
Introduction
Facades that Maximize Individual Access to the Natural Environment
Facades that Ensure Daylighting as the Dominant Source for Both Task and Ambient Lighting
Facades that Ensure Natural Ventilation as the Dominant Fresh Air and Cooling Source Combined with Mixed-Mode HVAC Conditioning
Facades that Minimize Enclosure Heat Loss/Heat Gain
Facades that Integrate Climate-Responsive Shading and Glare Control
Facades that Engineer Load Balancing and Mean Radiant Temperature Control
Facades that Integrate Passive and Active Solar Heating, Cooling, and Power
Facades Designed to Manage Water
Facades that Maximize Enclosure Life
Future Directions: Facade Innovation Through Systems Integration
Bibliography

Glossary

Facade enclosure envelope Throughout this entry, Facade is a subset of Enclosure and Enclosure is considered the same as Envelope.

Carbon neutral net-zero and the 2030 challenge Carbon-neutral buildings and net-zero buildings are typically defined as buildings designed to achieve net-zero in green house gas emissions during their lifetime. This has been set as a requirement for all new buildings by 2030 in the 2030 Challenge™ (url).

Passive survivability Environmental Building News uses the term passive survivability to describe a building's ability to maintain critical life-support conditions in the event of extended loss of power, heating fuel, or water, or in the event of extraordinary heat spells.

Biophilia Introduced by E.O. Wilson, the biophilia hypothesis suggests that there is an instinctive bond between human beings and other living systems that must be met by buildings that ensure critical connections.

Ambient and task lighting Ambient lighting is the light needed for safe movement and non-visual tasks, while task lighting is linked to visual acuity at task and must be glare-free. Daylight can be used for both, but requires significantly greater design resolution for task lighting.

Mixed-mode or Hybrid HVAC An approach to space conditioning that combines natural ventilation from operable windows or vents with mechanical heating, cooling, and ventilation systems (HVAC).

Night ventilation An approach to space conditioning that utilizes cool night air to precool the buildings' thermal mass in order to reduce daytime cooling demands.

Thermal bridge A conductive or non-insulated element in the facade assembly that allows heat to be unnecessarily lost or gained, and allows condensation to occur, to be addressed by well-designed thermal breaks.

PassivHaus™ A standard that codifies energy conservation and passive conditioning requirements for residential and small commercial buildings.

Robert A. Meyers (ed.), *Encyclopedia of Sustainability Science and Technology*, DOI 10.1007/978-1-4419-0851-3,
© Springer Science+Business Media, LLC 2012

Double envelope The introduction of two facades with a captured air space and static or dynamic components that support orientation- and season-specific modulation of climate conditions.

Rainscreen An independent layer on the facade to manage weather challenges, separated by vent spaces from the structural, thermal, and vapor management of the primary facade.

Definition of the Subject

Sustainable buildings have enclosures that ensure the highest level of thermal, visual, acoustic, and air quality, as well as design for change, through system flexibility, and for long-term building integrity (Fig. 1). Sustainable enclosure design clearly demonstrates advances in enclosure components and assembly design, as well as their effective integration with interior systems, structural systems, mechanical conditioning systems, lighting systems, telecommunications and power systems. Sustainable enclosures effectively address ten major responsibilities, indeed areas of major innovative opportunity, in the pursuit of aesthetics, comfort, and resource conservation:

1. Access to the natural environment
2. Daylighting
3. Natural ventilation
4. Heat loss/heat gain control
5. Solar control
6. Load balancing
7. Passive and active solar
8. Water
9. Enclosure life
10. Systems integration

In addition to performance goals for building roofs and exposed floors, the design of high-performance building enclosures must fully resolve at least 12 facade layers: the transom, viewing field, kick plate, and spandrel (top to bottom) and the interior, integral and exterior layers (inside to out) to resolve each of the 10 performance goals (The relative importance of facade components and layers to each performance outcome will be highlighted in graphics with deepest shading for the most important design decisions.)

Introduction

Architecture Unplugged: Superefficient Buildings that Environmentally Surf

Carbon-neutral buildings, net-zero buildings, and the 2030 challenge. To meet these goals, the next generation

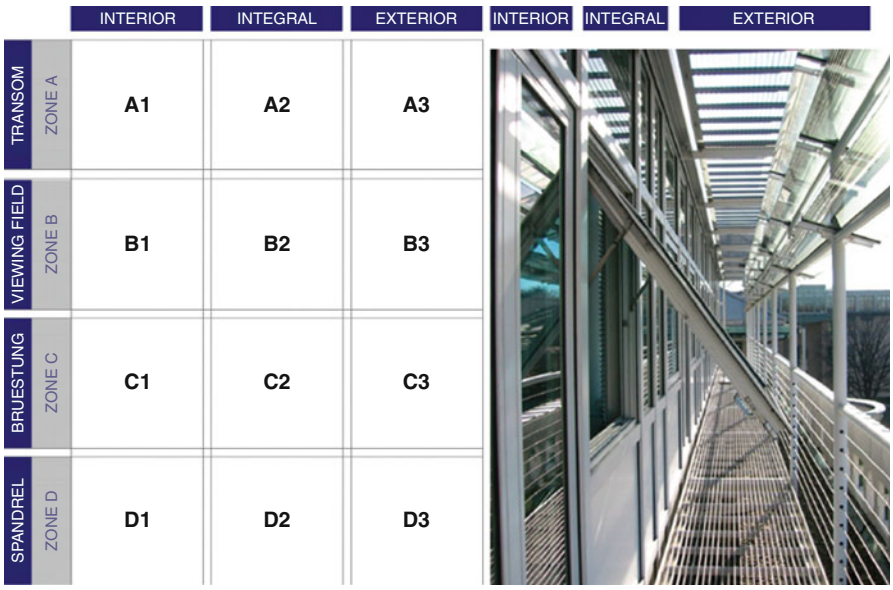

Facades and Enclosures, Building for Sustainability. Figure 1
Diagram illustrating 12 areas in the facade critical to various performance outcomes

of buildings must be designed to use so little energy that on-site renewable energy can fully meet the heating, cooling, and lighting loads – loads that represent over 35% of all US energy.

For the first generation of projects, these challenges are being met by tight buildings, with superefficient equipment, fed in part by solar installations. While this will help ensure a 30% reduction, it will never achieve carbon neutrality .

Carbon neutrality is critically dependent on the maximum use of nature's renewable energies – daylight, natural ventilation, natural cooling, and passive solar heating. Building systems will need to be turned off as long as possible – ensuring buildings that "free-roll" or better yet "environmentally surf" through hours, days, months, and seasons with natural conditioning. The beauty of free-rolling buildings goes beyond energy and carbon, however, to support health, productivity, and a higher quality of life.

The most critical early design decisions relate to building massing – the height, depth, and orientation of buildings – which has a major impact on indoor environmental quality and energy loads. Neither "the tallest building in the world" nor "the largest building under one roof" will offer sustainable work environments in a power failure. Indeed, these buildings create significantly higher-energy loads in almost every climate since they eliminate the use of daylight, natural ventilation, or the natural dissipation of internal heat gains through the building skin [1], and must be abandoned in a power outage. If air quality, comfort, and energy are drivers for building form, then the next generation of buildings will strive toward controlling the building depth, height, and orientation to achieve environmental comfort for a maximum percentage of the year – unplugged.

"Architecture Unplugged" would require enclosures that demonstrate serious attention to the management of solar gain, heat transfer, moisture migration, and day-night load balancing – a form of environmental surfing that depends on dynamic facades that recognize time of day, season, and variability of climate. These mass, color, venting, and thermal insulation characteristics are key to energy conservation in buildings, and require entirely regional solutions. Heavy capacitance masonry facades will be seen in desert climates with large diurnal swings; heavily shaded and highly operable facades will be seen in warm, humid climates; and solar exposed yet well-insulated facades will be seen in cold climates. In each climate, the massing, orientation, and selection of facade materials will be regional in character, providing the maximum natural comfort before mechanical systems need to be introduced (Figs. 2 and 3).

Facades that Maximize Individual Access to the Natural Environment

The most significant step that designers, engineers, and building managers can take to move toward healthier and more sustainable buildings is the commitment to increasing individual contact with the outside environment. The emerging field of "biophilia" has identified the importance of access to nature to human well-being [2–5], exploring a range of qualities of the natural environment: views, daylight, sunlight, fresh air, breezes, access to outdoor spaces and activities, circadian rhythms, seasonal and daily climate variations, and nature's sounds, smells and habitat. Windows and doors connect building occupants with a richness that may be critical to individual health. At the same time, windows and doors provide those outside the building with a level of transparency, oversight, and contact that may be critical to community.

Europe and Scandinavia have guaranteed every worker seated access to a window with views, setting a maximum distance of 7 m, or 20 ft from the window wall. In Switzerland and Scandinavia, they have further guaranteed access to *operable* windows in each workplace [6]. With these standards, buildings typically do not exceed 60 ft from window wall to window wall, and always maintain operable, dynamic facades instead of sealed, seasonally unchanging building enclosures.

Driven by the advent of air conditioning and inexpensive electricity, the "obese" buildings of today (maximum volume – minimum surface area buildings) have actually resulted in a dramatic increase in the length of the cooling "season" for buildings in all climates. They have also resulted in a significant increase in lighting loads during daylight hours, in combination often contributing more than 50% of the total energy demand in buildings. The study of the Building

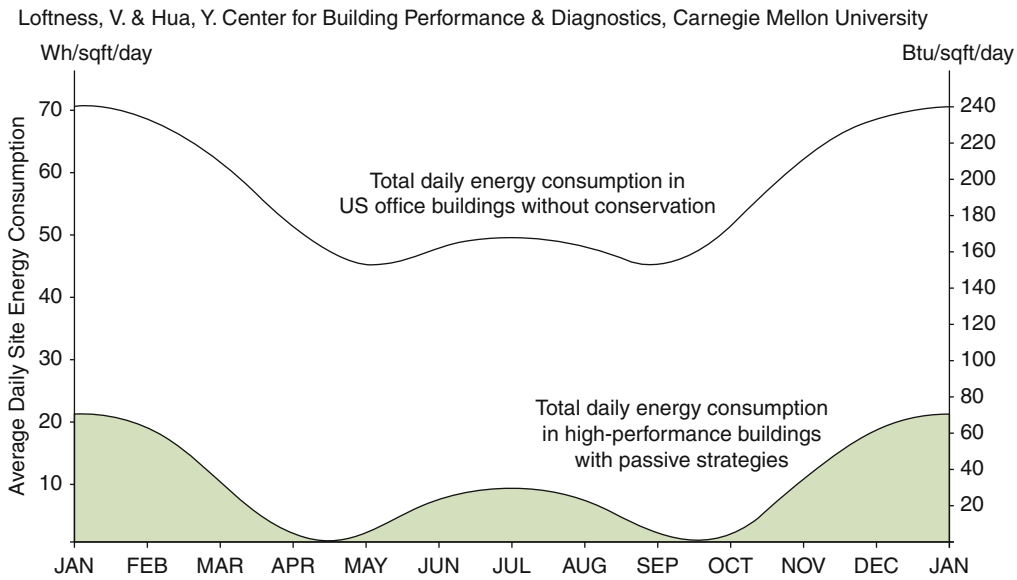

Facades and Enclosures, Building for Sustainability. Figure 2
Deep energy conservation combined with passive conditioning including daylighting, natural ventilation, and passive solar can dramatically reduce energy consumption

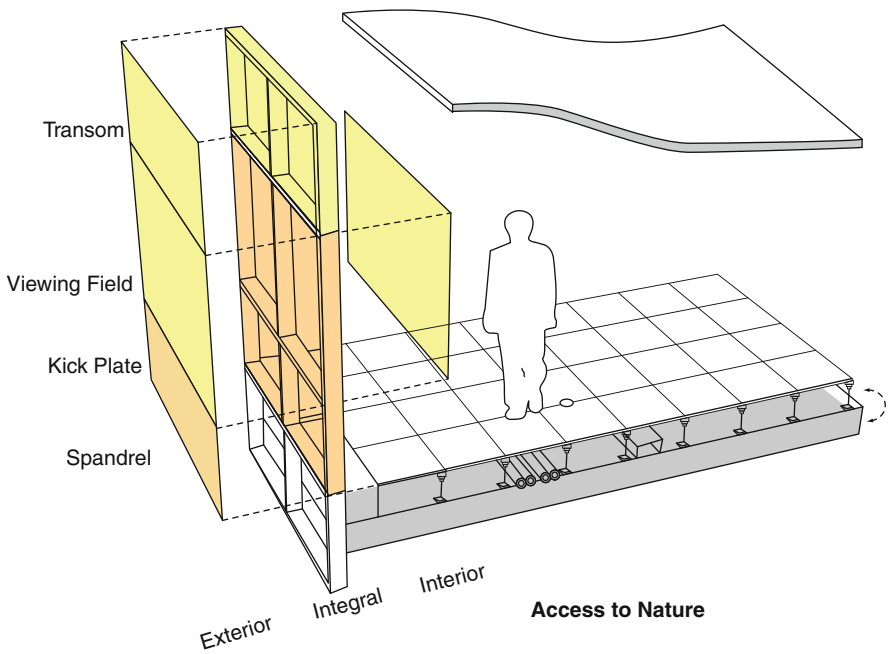

Facades and Enclosures, Building for Sustainability. Figure 3
Critical facade elements to maximize access to the natural environment

Research Establishment of a portfolio of UK office buildings clearly illustrates the energy penalty of sealed, deep floor plan "prestige" buildings [7].

While there is significant debate about the importance of indoor daylight or sunshine for human health or performance, there seems to be a growing consensus that access to views is significant. Beginning with the seminal work of Ulrich [8], then Mendell [9], Heschong Mahone Group [10], and now Kellert [4], seated views of nature and proximity to windows are being linked to reduced length of stay after surgery, reduced sick building syndrome, increased performance at task, and overall improved emotional health.

In a 1990 survey of over 2,000 employees in two buildings at the US Department of Energy, Carnegie Mellon University's Center for Building Performance identified 10–20% lower sick building symptoms among employees with seated views of windows, controlling for rank [11]. Whether user perception of personal health is improved due to the light, the view, the perimeter conditioning systems, or an increased level of environmental control (blinds, HVAC controls) at the window is unclear. Regardless, there is a measurable benefit to ensuring that a workforce has fewer health symptoms across the board (Fig. 4).

Two case studies that frame the conclusion that views are a significant factor in health and productivity are captured below from the Carnegie Mellon Building Investment Decision Support Tool (BIDS™) [7, 8, 10]:

Window View of Nature = Health

In a 1984 observational field study at a Pennsylvania hospital, Ulrich identifies an 8.5% reduction in postoperative hospital stay (8.7 days vs. 7.96 days) for gall bladder surgery patients who had a view of a natural scene from their hospital room, as compared to those with a view of a brick wall. Patients with a view of a natural scene also received fewer negative evaluations from nurses and took fewer strong analgesics (Pennsylvania Hospital/Ulrich [8]).

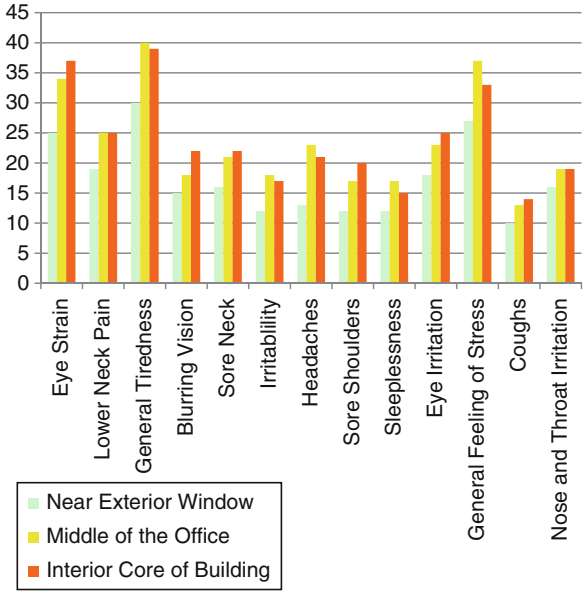

Facades and Enclosures, Building for Sustainability. Figure 4
Window proximity correlates to a 5–25% reduction in health complaints among 2,000 workers in two US office buildings, controlled for rank [11]

Window View of Nature = Productivity

In a 2003 building case study of the Sacramento Municipal Utility District (SMUD) Call Center, Heschong et al. identify a 6–7% faster Average Handling Time (AHT) for employees with seated access to views through larger windows with vegetation content from their cubicles, as compared to employees with no view of the outdoors (SMUD/Heschong Mahone Group [10]).

These studies illustrate the value of windows with views for all occupied spaces, alongside effective design of window size and orientation, sight lines, and view content. The studies suggest that views of the outdoors should be with "biophilic" content – views of pedestrians and trees and community life – to critically maintain our sense of time and season. At the same time, it will be imperative for designers to ensure that requirements for glare control, heat gain and noise

control, privacy and security are equally met—the definition of quality design (Fig. 5).

In pursuing design for sustainability, the challenge to designers is not only to connect indoor spaces with the outdoors visually, but to physically connect building occupants with nature – each site's unique climate and seasons, the textures, sounds, smells, and diversity of landscape and species. This not only suggests a shift away from mega-plexes and high-rise buildings toward open-air campus and village planning, but a commitment to operable windows, and distributed doors, terraces, and landscapes.

The physiological and psychological benefits of an ongoing connection to the locally unique and seasonally dynamic natural environment still need quantification. For example, studies in early childhood development reveal the academic and emotional benefits of natural playgrounds as opposed to hard-top play yards [12]. Sustainable buildings must incorporate physical access to outdoor spaces for a host of reasons, including physical exercise, exposure to sunshine and circadian rhythms, variations in thermal stimuli, and access to community (Fig. 6).

Facades that Ensure Daylighting as the Dominant Source for Both Task and Ambient Lighting

- *"A building with lights on during the daytime is not a sustainable building."*

Electric lighting is almost 25% of our primary energy use and over 35% of all electric energy use in the USA [13] – and much of that is during the daytime! Energy-efficient lamps, ballasts, and fixtures are obvious first steps for ensuring 30% lighting energy savings, and daylight responsive and occupancy responsive controls for these fixtures can reduce the next 20% (reference: see [14]). The giant leap, however, is achieved by buildings designed for daylighting as the *dominant* light source—environmentally "surfing" for 90% of the day without electric demand for lighting. This is more than rediscovering the design expertise of the nineteenth century. Good daylighting design demands effective integration of new glazing technologies, introducing light redirection and shading layers that enrich and regionalize architecture. Critically, buildings must be articulated, in finger or courtyard shapes, to ensure universal access to daylight.

Facades and Enclosures, Building for Sustainability. Figure 5
Designing window dimensions, orientations, and sight lines as well as adjacent landscaped spaces (with substantial storm water management benefits) are critical to ensuring access to views with "biophilic" content

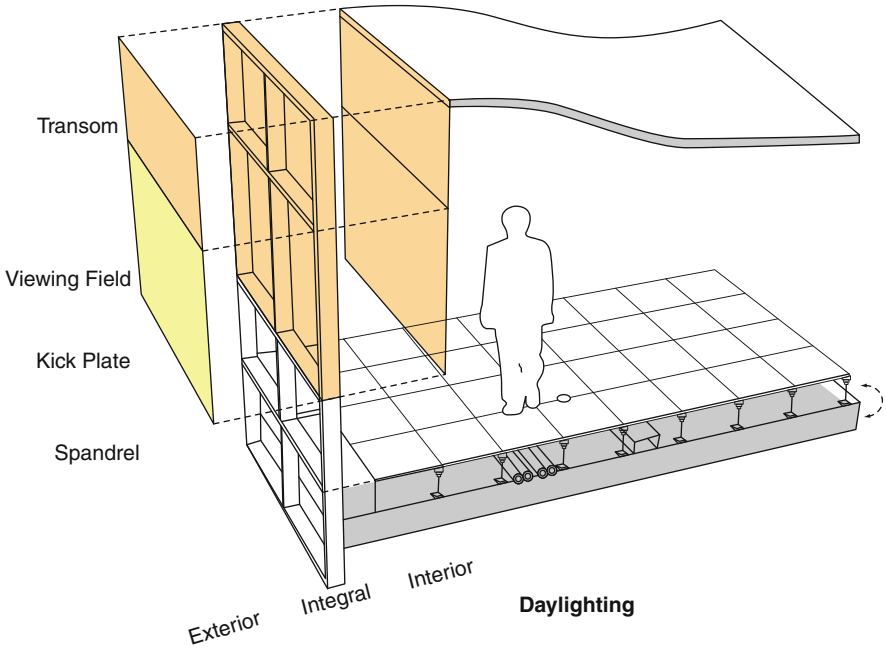

Facades and Enclosures, Building for Sustainability. Figure 6
Critical facade elements to ensure daylighting as the dominant light source

There are two main alternatives in the use of daylight in work environments. The first is the use of daylight for ambient lighting requirements of 200–300 lx and for spatial highlights. The second is the use of daylight as the dominant task lighting source at the work surface. This second alternative offers the greatest energy savings but also the greatest design challenge, since both the daylight "fixture" and the electric lighting interface need to be effectively designed. The daylight fixture – window, transom, or skylight – will need appropriate orientation, size, reflector-frame design and lens-blind design as well as the corresponding design of the room to ensure effective light distribution without glare.

There are a broad range of traditional and innovative technologies to be considered for effective daylighting of buildings to achieve both ambient and task lighting needs. New developments in glazing enable architects to specify high visual transmittance (short wave energy) while controlling solar transmittance and heat loss (long wave energy). Given innovations in glazing technology, it is possible to achieve high light transmittance over 50% while maintaining shading coefficients below 40% in cooling load–dominant climates, or above 60% in heating load–dominant climates.

However, sustainable design recognizes that not all shading should be solved with the glass selection, since this can rob spaces of daylight and solar heat where needed.

Each window must be designed as a lighting "fixture" in relation to space configuration and layout. If lighting engineers can design effective reflectors and diffusers for point and linear sources, they can design for planar sources as well. Transom glazing will be critical to effective distribution, combined with exterior, integral, or interior light redirection devices to ensure a more even distribution of daylight and to reduce glare from the window. If there is a shortage of window access, it should never be given to circulation aisles in a sustainable design (Fig. 7).

The rules for effective daylighting in offices, schools, and hospitals have long been established, relating to percent of aperture, ceiling height, room depth and color, as well as glare control and light redirection devices at the window. Today, high-performance

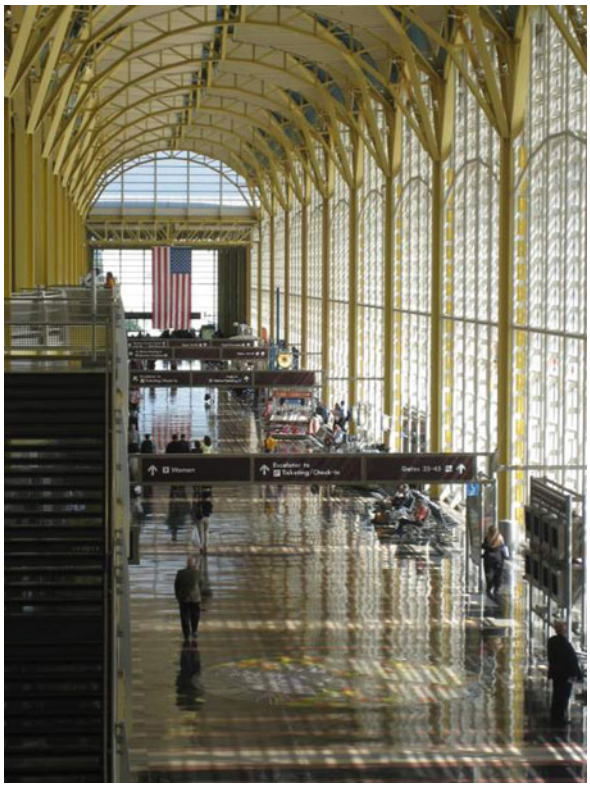

Facades and Enclosures, Building for Sustainability. Figure 7
Daylight is celebrated at Reagan National Airport, Washington DC

enclosures go even further, fully exploring the benefits of a layered facade. The design of layered facades enables seasonally and daily dynamic control of the light, heat, and ventilation energies available in the natural environment. All three layers should be designed together – external shading and light shelves to distribute daylight and reduce high sun angle glare; integral high visible transmittance glazing with climate responsive or dynamic shading coefficients; and internal light redirection blinds that sustain views while diminishing low sun angle glare. It is critical that the design of these layered facades be entirely regional in character, and suited to the function of the building, as they control light, glare, solar heat, heat loss/gain, even thermal mass. By displacing mechanical and electrical loads, these facades provide long-term energy savings. In retrofitting deep buildings for daylighting, the sustainable design community is exploring atria, light wells, light ducts, and light pipes. Bank of America in San Francisco cut an atrium into an overly deep building to bring daylight to all spaces. Innovations in light pipes, reflective ducts, and tracking/beaming heliostats all have potential for increasing daylight effectiveness and delight (Fig. 8).

At the same time, the daylighting "system" must give the appropriate information to the electric lighting interface so that it can offer the appropriate "infill" through continuous dimming control. Studies indicate that the selection, placement, and installation of the photo-sensor is critical, concluding that a ceiling-mounted photosensor shielded from direct window light will ensure the best correlation with daylight work-plane illuminance [15]. The net impact of daylighting and electric lighting integration is significant energy savings [16] and improved workplace satisfaction.

Emerging research is revealing that day-lit offices, classrooms, and hospitals may measurably contribute to greater health and performance at task. Light levels can be higher without energy penalty; full spectrum light offers rich color rendition and 3-dimensional modeling; circadian rhythms set by daylight variations throughout the day trigger melatonin production and sleep patterns; and views meet fundamental human needs.

Sustainable buildings are designed for daylight to meet all ambient and task requirements during the day. The investment in a layered facade for daylight effectiveness will simultaneously support natural ventilation, night ventilation, thermal load balancing, and passive solar heating – the full complement of regional opportunities for natural conditioning.

Daylight Lighting Control = Energy Savings

In a 1997 before and after building case study of the New York City federal building, the Electric Power Research Institute (EPRI) identifies 64% lighting energy savings and net HVAC energy savings of 0.07 kWh per square foot annually following the installation of an energy-efficient lighting system with daylight dimming and lumen maintenance controls (NYC Federal Building/ EPRI [16]).

Facades and Enclosures, Building for Sustainability. Figure 8
The central atrium and "sky gardens" at Commerzbank in Frankfurt bring daylight to all spaces and provide occupants with access to nature in a dense urban environment

Daylight Spectrum and Timing = Individual Productivity

In a 1997 controlled experiment, Boyce et al. identify a 1.6–12.8% improvement in night-shift workers' performance on short-term memory and logical reasoning tasks under large skylight-simulating fixtures with hidden fluorescent lamps, capable of providing fixed or variable illuminance from 200 lx to 2800 lx. Performance was enhanced by fixed high illuminance of 2800 lx and by steadily decreasing illuminance that simulated daylight from midday to dusk, as compared to fixed low illuminance of 250 lx or steadily increasing illuminance that simulated daylight from dawn to midday (Boyce et al. [17]).

Natural Ventilation = Health

In a 1991 multiple building study of 880 workers in eleven office buildings in the San Francisco bay area, Mendell identified 20–81% reductions in reported SBS symptoms for occupants of naturally ventilated buildings as compared to occupants of office buildings with air conditioning or mechanical ventilation (CA Healthy Building Study/ Mendell [9]).

Natural Ventilation = Health + Individual Productivity

In a 2004 multiple building study of professional middle-aged women in France, Preziosi et al. identify a 57.1% reduction in absenteeism, a 16.7% reduction in medical services use (doctor visits), and a 34.8% reduction in hospital stays among subjects with natural ventilation in their workplace, as compared to those with air conditioning (Preziosi et al. [18]).

Facades that Ensure Natural Ventilation as the Dominant Fresh Air and Cooling Source Combined with Mixed-Mode HVAC Conditioning

► *"A sealed building is not a sustainable building."*

The use of *natural ventilation and natural cooling* with direct outside air for swing and winter seasons ensure affordable high levels of fresh air with the greatest energy efficiency (Fig. 9). International studies consistently link increases in outdoor air supply to both productivity and health gains in the workplace [9].

In addition, the substantial opportunity for "free cooling" through the use of outside air is significantly underestimated by calculations focused on only "comfort zone" natural ventilation. Natural cooling is possible whenever outside conditions are within or below the comfort zone both in the day and at night, as long

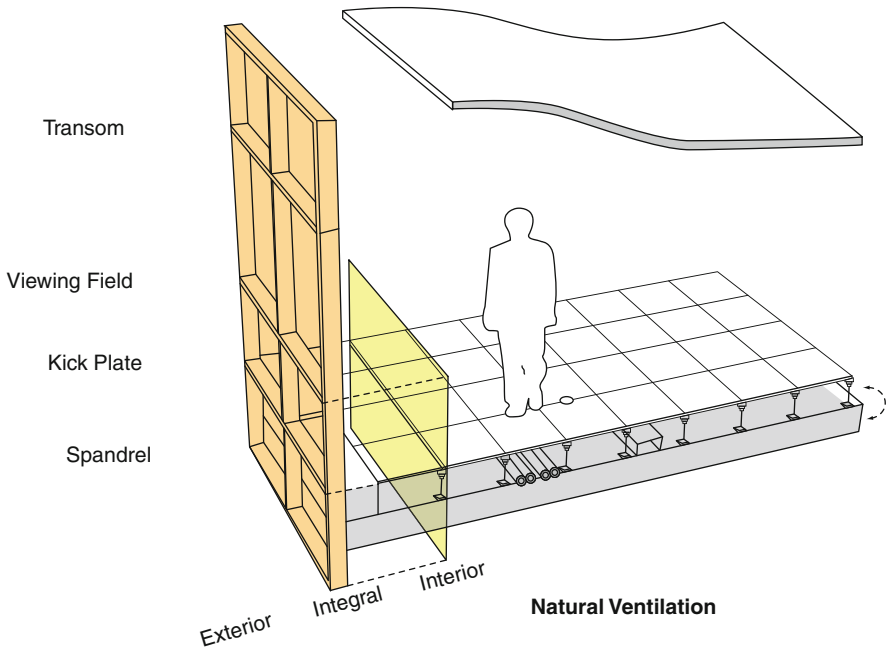

Facades and Enclosures, Building for Sustainability. Figure 9
Critical facade elements to ensure natural ventilation as the dominant fresh air and cooling source

as drafts can be effectively managed through mixing or heat recovery. The use of both passive (open windows) and active economizer cycles can save from 50% to 100% of the cooling demand in various regions of the USA, when including the benefits of nighttime cooling of the building's thermal mass [19].

Natural Ventilation = Individual Productivity + Energy Savings

In a 2002 multiple building study of 39 Australian office settings, Rowe identifies a 13.8% perceived productivity improvement, a 15% improvement in overall comfort, and 79% annual HVAC energy savings due to replacing a mechanical air-conditioning system with mixed-mode HVAC that supports both natural ventilation and air conditioning (Australian Offices/ Rowe [20]).

Design for effective natural ventilation and natural cooling of the building mass and its occupants requires multi-disciplinary expertise to ensure that building shape, orientation, atria/courtyards, chimneys, window types (awning, casement, double hung), sizes, and locations ensure effective cross and stack ventilation. Cross and stack ventilation demands that building form and space layout reflect prevailing wind directions and the potential for thermal and solar assist, often studied through wind model testing or computational fluid dynamic simulations. In climates with day-night temperature swings, night ventilation should be explored and building materials or storage selected to store cooler temperature, creating a thermal "flywheel" for the following day.

In many climates, *"mixed-mode" HVAC systems* are designed to support natural ventilation and to provide air conditioning and ventilation – when and where natural ventilation is inadequate. There are three types of mixed-mode HVAC systems [7]:

- Concurrent systems, which use natural ventilation and mechanical HVAC simultaneously. Occupants are free to open windows and the HVAC system provides supplemental ventilation, dehumidification, and cooling, while an advanced control system coordinates zone air supply rates with window positions.

- Changeover systems, where the building alternates between natural and mechanical mode on a seasonal or daily basis.
- Zoned systems, in which different conditioning strategies are used simultaneously in different zones of a building.

Concerns related to outdoor air pollution, pollen, and humidity can be effectively addressed with well-designed mixed-mode conditioning systems (Fig. 10). Natural ventilation in high-rise buildings demands both architectural and engineering innovations to manage both pressurization issues and stack effect. This has been accomplished through the design of stacked 6–8-story buildings such as the Commerzbank in Frankfurt, and through double envelope designs, where wind and pressure are moderated through intermediate facade spaces.

For both natural ventilation and mechanically assisted ventilation, it is critical to engineer *ventilation effectiveness*, ensuring adequate fresh air volumes through large apertures or economizers; accessible, large volume fresh air paths from air-intake locations to occupants, such as in displacement ventilation systems; multiple fresh air sources with operable windows, distributed air handlers or facade integrated HVAC; and adequate exhaust without recirculation or contamination of the air flow paths. Air intakes especially should be strategically located, not near loading docks with idling engines or on roof decks with standing water, but in non-polluted areas, without standing water or solar overheating. Indeed, air sources should be freshest where prevailing breezes travel through shaded, landscaped areas with some level of natural air purification and cooling.

To achieve effective natural ventilation with mixed-mode mechanical conditioning, the design team must work together to engineer and integrate the natural ventilation/natural cooling controls and the HVAC controls to maximize air quality, user control, passive conditioning, and energy efficiency. Given a growing body of research illustrated below, natural ventilation with mixed-mode conditioning should be the norm in

Facades and Enclosures, Building for Sustainability. Figure 10
Operable windows at Commerzbank, a high-rise structure, provide natural conditioning for the occupants, linked with mechanical cooling in a hybrid system. The atrium at Institute for Forestry and Nature Research in Wageningen provides a protected space for natural ventilation in the offices while giving occupants a natural setting for meetings and relaxation

all commercial buildings for human health and productivity, energy efficiency, and the viability of occupied spaces in the face of electricity shortages.

Facades that Minimize Enclosure Heat Loss/Heat Gain

One of the earliest decisions affecting the sustainability of buildings is the overall massing of the building and the *orientation of major facade and roof surfaces* (Fig. 11). While very harsh climates might benefit from minimum surface area to usable space enclosed, there are climate-specific arguments for increasing building enclosure for daylighting, natural ventilation, passive solar heating, and even the dissipation of excessive internal heat gains (see Load Balancing). These increased exposures must be strategic, however, avoiding solar overheating, cold air infiltration, and increased heat loss or heat gain. Serious re-evaluation of vast roof exposures and cantilevered floors is needed, minimizing excessive heat losses or heat gains unless they have corresponding benefits from natural conditioning. Even the location of the HVAC system will be significant, with rooftop and west facing cooling equipment measurably less efficient due to solar heat gains. Design goals should be set for building shape and orientation to ensure the best integration of passive conditioning while reducing environmental loads.

Architects make major decisions about the thermal performance of buildings through the specification of *window to wall ratios*. Sustainable designers weigh heat loss and heat gain against daylighting, natural ventilation, passive solar heating, and load balancing through the facade, alongside the spatial flexibility needed by dynamic organizations. Innovative building enclosures are designed to act like the human skin, dynamically supporting heat, air, and moisture dissipation for the health of the occupants in changing climates. The sustainable design community has rediscovered the opportunities for dynamic thermal performance of building enclosures, with high-resistance louvers, curtains, and dynamic layered facades changing heat transfer characteristics hour by hour, day to night, or season by season.

Needless to say, *the highest level of thermal resistance* to heat loss and heat gain is pursued for both the wall and window assemblies in sustainable buildings. Innovations in wall insulation have supported shifts from

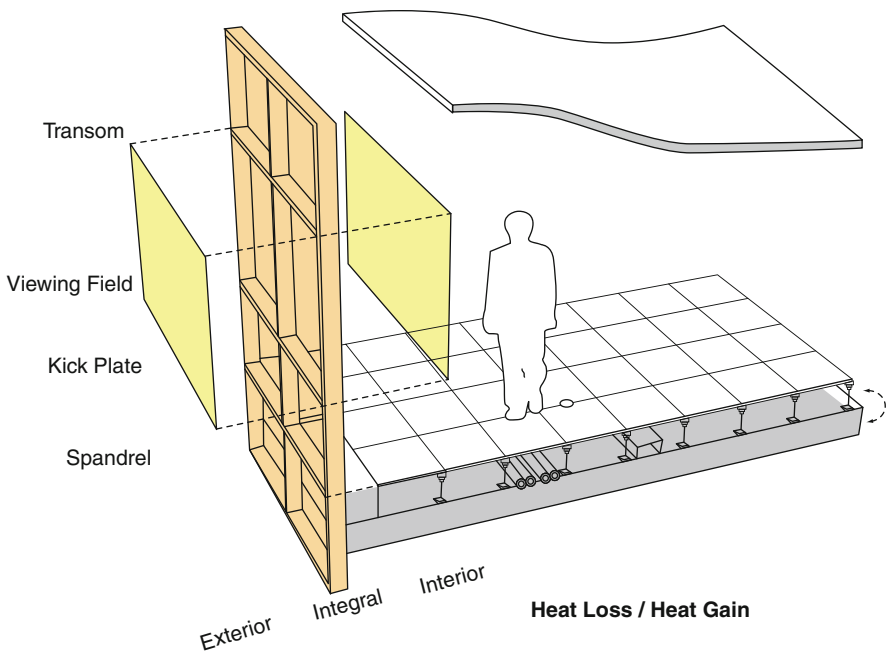

Facades and Enclosures, Building for Sustainability. Figure 11
Critical facade elements to minimize enclosure heat loss/heat gain

R5 per inch to R10 per inch – a doubling of performance specifications. Window innovations also abound, with R2 double glazed assemblies replaced by R4, R8, and even R12 assemblies as a result of low-e, gas filled assemblies with innovative spacer and frame technologies, even while visible transmission is critically kept above 50%. At the same time, low solar heat gain coefficients (SHGC) of 0.35–0.50 can be achieved where needed to reduce overheating at the facade without loss of visual connection to the outside. At a very minimum, these three window variables – resistance to heat transfer (R), visible transmission (t_v), and solar heat gain coefficients (SHGC, solar transmission) – must be balanced in response to each climate and building type.

Facade Temperature Control = Individual Productivity

In a 2000 field case study of telecommunication office workers in Finland, Hannula et al. identify a 2.8% increase in measured productivity in north-facing offices with an average temperature of 23.6°C (range 21.9–27.8°C) as compared to south-facing offices with an average temperature of 25.2°C (range 22.8–28°C), supporting the need for improved heat gain control by orientation (Telecommunication Office/ Hannula et al. [21]).

Finally, sustainable enclosure design detailing ensures the *lowest level of thermal bridging* through walls, roofs, floors, and foundations. Structural and enclosure designers must work together to ensure the elimination or minimization of structural elements that connect indoor heated or cooled areas with the outdoors, including the facade, roof, floor, and foundation. Ideally the thermal "wrapper" is continuous and fully outside the structural frame, except at foundation connections that might indeed support ground source conditioning (see Thermal Load Balancing). Cantilevered balconies, overhangs, floors, and roof elements can contribute to significant heat loss, moisture and vapor migration, and condensation that lead to building degradation (see Enclosure Life). Not only the structural integration, but also product specification, enclosure detailing, and design for constructability are critical to the thermal performance of facades. There are numerous conditions where well-insulated facades, roofs, and foundations are compromised by penetrations that were not anticipated in the drawings (vents, tie rods, utility meters, etc.), or not adequately sequenced in construction to ensure the continuity of the thermal envelope.

One of the most exciting new developments in enclosure design is *green roofs and green walls*. Green roofs and their layers of waterproofing, insulation, soils, and vegetation have the potential to improve roof resistance to heat gain by 50% (NRC reference – see [22]), improve roof longevity by a factor of 2 [23], reduce storm water runoff by 50% [24], reduce air plane noise transmission, as well as reduce urban heat islands and air pollution [25, 26]. Green walls are also offering measurable gains by reducing solar heat gain, providing evaporative cooling, and creating seasonal qualities for our buildings (Fig. 12).

Green Walls + Double Skin Façade = Energy Savings

In a 2005 controlled lab experiment in the Netherlands, Stec et al. identify an 18% reduction in cooling system capacity requirements and a 19% reduction in cooling energy consumption for a double skin façade with plants in the cavity rather than blinds, due to a 20% reduction in temperature on the interior wall of the façade (Stec et al. [27]).

Facades that Integrate Climate-Responsive Shading and Glare Control

As with heat loss and heat gain, managing solar overheating and glare begins with the careful *sizing and location of windows* to ensure shade and light without glare (Fig. 13). East and West orientations are the most problematic, since sun angles are too low to effectively block with overhangs or open blinds. Skylights in horizontal roofs can also be problematic since they receive excessive solar heat in summer and significantly less winter energy (when solar energy is most beneficial). Window sizes and locations should be uniquely considered for each building face, as well as the detailing of internal and external controls.

Facades and Enclosures, Building for Sustainability. Figure 12
Green walls at Musee Branly reduce heat gain in summer

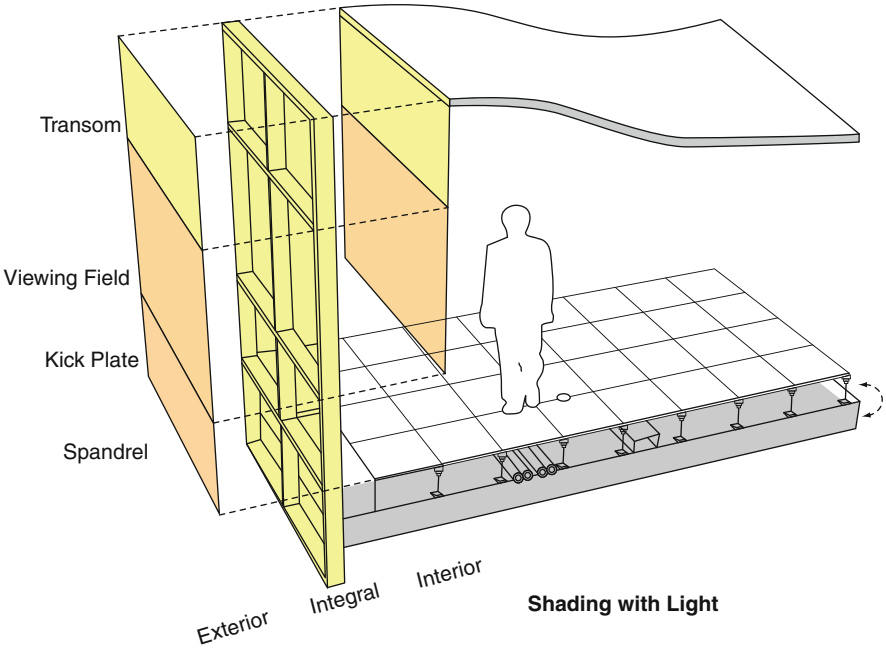

Facades and Enclosures, Building for Sustainability. Figure 13
Critical facade elements for climate-responsive shading and glare control

Integral shading devices, the selection of reflective or low transmission glazing, or the introduction of "frit" patterns to reduce solar transmission, are the most common strategies for shading and glare control. Unfortunately, low solar transmission glass will block useful gain in winter as well, and can also result in low daylight transmission. Many high reflectivity glass specifications inhibit daylighting, passive solar heating,

and clear views of the landscape. However, new developments in glazing support high visible transmittance (daylight and view) with low solar transmittance (solar heat) for buildings in hot climates. Just as low-e glazing is becoming the norm for improved thermal resistance in glazing assemblies, this high-visible, low-solar glazing must become the norm for all buildings where cooling loads dominate on the perimeter.

A number of new glazing materials are emerging that support seasonally dynamic management of solar heat and light. Electrochromic, prismatic, and holographic glazing assemblies are in development that would enable the seasonal or hourly separation of light and heat spectrums, and the depth and color of the beamed light, so that building spaces can be naturally conditioned with the least amount of solar overheating or glare. The combination of these heat and light redirection devices with exterior and interior shading devices enable the appropriate percentages of the solar light and heat to be independently tapped.

Exterior shading devices, overhangs, light shelves, blinds, fins, and shades are the most effective means of reducing solar load while maintaining visual connection with the landscape. Clearly, the shading devices must be designed for each orientation, and for each site's climate and latitude. At least six types of exterior devices can be explored: an overhang/light shelf, recessed windows that act as an "egg-crate" shading device, dynamic shades or awnings, exterior blinds, exterior green walls, and a second dynamic facade (Fig. 14).

Just as a baseball cap allows a clear view of the action without glare in the eye, overhangs or light shelves can allow for views without glare and solar overheating. While an overhang provides shade from high sun angles, it could act as a light shelf and reflect sunlight deeper into the space when positioned below the upper (transom) portion of the window wall. Fully retractable exterior blinds can support both seasonal shading and daylighting goals, and enable views to be fully enjoyed during those hours when the sun is away from the facade. Awnings offer seasonally and daily adjustable shading on all orientations, full views when the summer sun has passed, and a colorful gaiety to the building. Landscape materials are re-emerging as effective shading for roofs, walls, windows, and terraces, self-regulating their density of shade to match the seasons, and offering potential to manage storm water as well.

Green Walls = Energy Savings

In a 2000 controlled experiment at Tanz Greenhouse at the University of Toronto and a follow-up computer simulation study, Bass and Baskaran identify a 23% reduction in cooling load and a 20% reduction in the fan energy use, for an 8% reduction in total annual energy consumption, when a green wall was used to shade an exterior surface of the building, as compared to an unshaded surface (Tanz Greenhouse/Bass and Baskaran [28]).

Facades and Enclosures, Building for Sustainability. Figure 14
Exterior shading devices at the Chesapeake Bay Foundation Headquarters are designed to account for different building orientations

The line of last defense, *interior shading devices* are somewhat less effective than exterior shading at minimizing solar load (heat gain from the sun), since the energy is able to enter the building before it can be reflected. While roll-down mesh shades provide a level of solar heat and glare control, inverted horizontal venetian blinds provide heat and glare control as well as daylight contribution for sustainable buildings. Research at the Lawrence Berkeley National Laboratories demonstrates that exterior operable shading devices, and even interior shading devices, are more cost effective and energy/resource effective than highly tinted (low visible transmission) glass *in all regions of the USA*, from Los Angeles to Chicago to Miami [29]. The selection of interior blinds should maximize light reflection, typically with a white or metallic color; maximize light distribution in the room, typically through inverted blinds and carefully shaped blinds that act as effective light shelves; and provide adjustable slat angles to maximize view potential while also maximizing work-plane illuminance [30] (Fig. 15).

If they are combined with exterior shades in a multi-layered facade, interior shades and blinds can be dedicated to light diffusion and glare management, with fabric/color selection designed to minimize brightness contrast between the window and its surroundings. Coupled with operable exterior shading devices, interior blinds could also be selected to *absorb* solar heat for perimeter heat gain in winter months. As innovations in phase change materials emerge, it is possible to imagine internal shutters or shades that absorb solar heat during the day, and then are reversed at night to radiate solar heat to the occupied space.

The most far reaching facade development in the past 10 years has been the development of *the double envelope*. When a second facade is introduced 1–3 m from the window wall, the intermediate space can be used to moderate the environment – heat, light, wind, noise, pollution, and other environmental stressors. These second facades house layers of shading, light redirection, air redirection, thermal load balancing, mechanical conditioning, and even dynamic levels of resistance to heat loss and gain. The research on the life cycle benefits of these innovations reveals significant variations in both costs and performance [31]. If double envelopes provide the greatest number of hours, days, and months without mechanical conditioning, they will be invaluable to carbon-neutral designers. The following section explores a number of enclosure solutions that use dimensioned "circulatory systems," such as double envelope designs, to reduce environmental loads in buildings (Fig. 16).

Facades that Engineer Load Balancing and Mean Radiant Temperature Control

To work toward healthier buildings with higher levels of local/individual comfort, it is imperative that the thermal imbalances, *mean radiant imbalances*, and conductive losses in buildings be addressed (Fig. 17).

Facades and Enclosures, Building for Sustainability. Figure 15
The dynamic light redirection louvers in the Robert L. Preger Intelligent Workplace can be configured to increase daylight levels in the interior spaces while reducing glare at the perimeter. Interior venetian blinds have engineered w-sections that manage low and high angle sun differently, reducing direct glare while maximizing view and daylighting

Facades and Enclosures, Building for Sustainability. Figure 16
Light shelves in the double envelope combined with external overhangs provide wonderful daylight and views for the new Cambridge public library

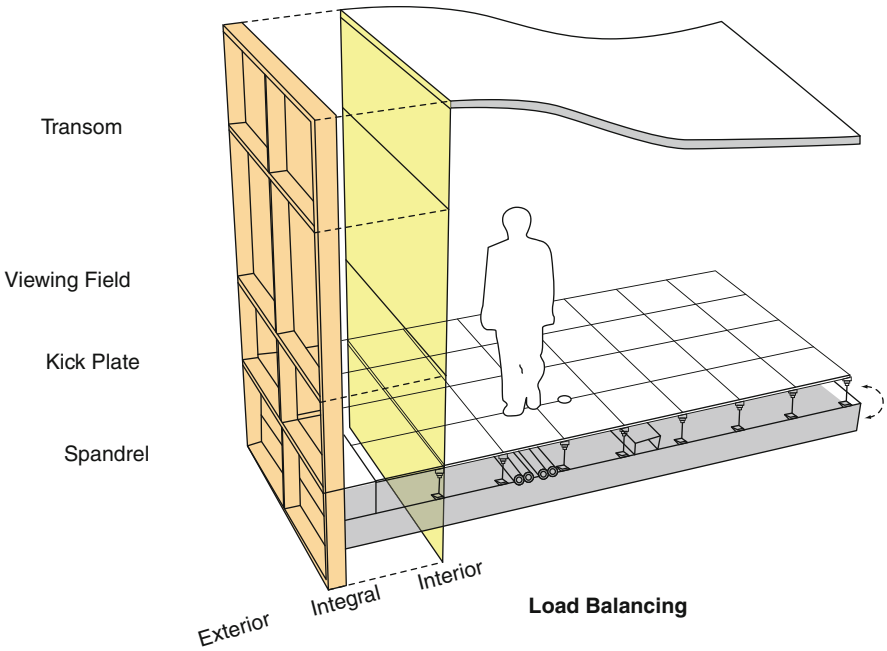

Facades and Enclosures, Building for Sustainability. Figure 17
Critical facade elements for load balancing and mean radiant temperature control

The engineering team is equally responsible with the architect for ensuring that the building enclosure detailing fully resolves thermal bridges and radiant imbalances.

As the internal heat gains in buildings have increased with office automation, the disparity in temperature conditions between facades and interior spaces has grown. Surprisingly, some designers have removed or reduced perimeter conditioning on the assumption that the interior loads will compensate for perimeter losses. This convective exchange will not be effective, however, without specifying super-insulated facade assemblies and/or deliberate load balancing by mechanically moving "core" heated air or water through the window wall.

Both air flow windows and water flow mullion systems enable excess heat from the building core – heat from occupancy, lights, and equipment – to be effectively dissipated through the facade. By taking return air through the "glass duct" of a triple glazed air-flow window, core cooling loads are dramatically reduced and perimeter heating is almost eliminated through *core-to-perimeter load balancing*. Water mullions (thermally broken from the outdoors) can also use "waste" heat from the core to minimize loads. In this system, waste heat from building cooling or power generating systems can be circulated through the facade to eliminate perimeter heating requirements and radiant imbalance, while allowing an increase in building periphery for views and light at every workstation. Indeed, the building facade could be seen as the natural dissipater of energy, a "circulatory system" resembling that of a healthy human – with appropriate surface to volume ratios. Given the constant increases in internal loads today, there is a real justification for increasing the periphery of buildings with the facade designed as an integral part of the mechanical system.

In addition to core and perimeter load differences, there are also significant load imbalances at different facade orientations, typically driven by solar load differentials (Fig. 18). One facade mechanical system of note is the use of double envelopes to provide *north-south-east-west load balancing* in climates where solar loads are significant and beneficial. The Occidental building in Niagara Falls is one of the earliest examples of a double envelope construction. When solar energy is received on the east, a natural convective loop of solar-heated air wraps the entire building. This continues throughout the day to eliminate simultaneous heating and cooling, to maximize passive solar

Facades and Enclosures, Building for Sustainability. Figure 18
In addition to radiant ceiling panels, radiant water mullions are integrated into the facade to balance temperatures year round in the Intelligent Workplace using water for energy-efficient load balancing

contributions to the heating load, and to ensure excellent mean radiant conditions. In summer, the double envelope is vented to the outside, and precautions are taken for fire protection. The Occidental building uses 70% less heating and cooling energy than a conventional office building in upstate New York [32].

A third strategy for reducing or eliminating the need for mechanical cooling is the use of *day-night load balancing* strategies. Night ventilation of a building's structural mass can successfully reduce or eliminate cooling loads in cooler climates, or climates with day-night temperature swings. Combined with the careful monitoring of dew point temperatures to avoid overcooling and condensation, nighttime cooling of a building's mass can provide adequate capacitance to absorb an entire day of internal gains. Thermal mass can be achieved through "heavy" or high-capacitance building walls and floors, or through the strategic introduction of phase change materials (PCM) to absorb and radiate heat as designed. A corollary to nighttime ventilation is the use of off-peak nighttime electricity to generate chilled water and ice or to chill PCMs for daytime cooling. This "ice storage" cooling strategy can be effectively bundled with nighttime ventilation of a building's thermal mass to absorb daytime overheating loads without peak electricity demands. Phase change materials also offer the potential for storing daytime solar heat for nighttime use, a strategy integrated into a number of PassivHaus projects [33].

For opaque enclosure surfaces, the value of high reflectivity surfaces in all overheated climates has led to a new era of "cool roof" design [34]. The combination of high reflectivity and night venting of enclosure mass in climates with day-night temperature swings has the greatest potential for natural comfort and low energy cooling [35].

Cool Roof = Energy Savings + Peak Demand Reduction + Extended Roof Life

In a 2002 multiple building controlled experiment in Florida, Parker et al. of the Florida Solar Energy Center identify 17.8–24.9% annual cooling energy savings and a 28.5–35.5% peak cooling load reduction from highly reflective white metal, white barrel tile, and white flat tile roofing; 9.5% annual cooling energy savings and a 12.9% peak cooling load reduction from terra cotta tile roofing; and 3.2% annual cooling energy savings and a 17.2% peak cooling load reduction from white asphalt shingles, as compared to dark asphalt shingles, on a single-family house (Florida Sustainable Energy Center/Parker et al. [35]).

The final load-balancing strategy for reducing heating and cooling loads in buildings is to take advantage of ground and aquifer temperatures through *ground-coupling*. Ten feet below ground, and in underground aquifers, the temperatures are surprisingly stable at year-round (inter-seasonal) averages of approximately 12–18°C (55–65°F). Given excellent temperatures for radiant, water and air-based cooling, high-performance building designers have tapped into this natural cooling potential through earth sheltered construction, large diameter "cool tubes," and aquifer or ground sourced chilled water loops that serve radiant, fan coil, or heat pump systems. Ground coupling significantly impacts foundation and flooring design, and might impact the facade "circulatory" systems as well (Fig. 19).

The benefits of active (mechanically integrated) load balancing to resolve mean radiant imbalances – from core to perimeter, from N/S to E/W, from day to night, and inter-seasonally through ground coupling – are many and are as follows: improved individual comfort, productivity, and health [36, 37]; reduced building material degradation from thermal differentials and condensation; significant energy conservation; and the potential to replace mechanical heating or cooling first costs and operating costs with high-performance building enclosures [38] (Fig. 20).

Radiant Cooling = Individual Productivity + Energy Savings

In a 1999 controlled field experiment and simulation study, Takehito et al. identify a measured 22% increase in speed and a 1.5% improvement in accuracy on simple tasks among women subjects and a simulated 10% HVAC energy savings in the Tokyo climate from a radiant ceiling cooling system as compared to conventional ceiling-based air conditioning (Imanari et al. [36]).

Facades and Enclosures, Building for Sustainability. Figure 19
"Cool tubes" beneath the greenhouses at Phipps Conservatory provide free cooling

Night Ventilation Cooling = Individual Productivity

In a 2003 meta-analysis study, Seppänen et al. identify a productivity increase equivalent to 0.39 h of work per day (4.9% for an 8-h workday) due to nighttime ventilation cooling of thermal mass, a very energy-efficient method of reducing daytime indoor temperatures by using nighttime air to cool a building's structure and furnishings (Seppanen et al. [37]).

Geothermal Heat Pump = Energy Savings + First Cost Savings

In a 1998 field study of Maxey Elementary School in Lincoln, Nebraska, Shonder et al. identify an average 47% reduction in annual HVAC energy use with a geothermal heat pump system as compared to the alternatives of VAV systems with air- or water-cooled chillers, as well as a first cost savings of $1.80/sf. Geothermal heat pump systems were found to have the lowest first cost, operational cost, and life cycle emissions of the three systems (Maxey Elementary School/Schonder et al. [38]).

Facades that Integrate Passive and Active Solar Heating, Cooling, and Power

The most direct use of solar energy in buildings is for *passive solar heating* (Fig. 21). The design of building enclosures to support direct gain through high solar transmission glass can effectively offset over 50% of the heat loss of buildings in many climates. Indeed, it is critical that glazing be carefully selected to ensure high solar transmission in cold climates to enable passive solar heating. In locations where direct gain would cause excessive daytime overheating or glare, the design of indirect gain passive solar facades – glazed mass walls or Trombe walls [39], water walls, or phase change walls – can strategically collect solar heat for nighttime heating. Recent developments in phase change materials that can be embedded in common construction or finish materials will help ensure that adequate solar heat storage exists to shift daytime solar gain to nighttime loads. Each of these solar heating strategies can be fully passive, utilizing no mechanical energy to collect, store, or distribute solar heat while providing potential health benefits to building occupants [40] (Fig. 22).

Sunlight = Health

In a 2005 building case study of Inha University Hospital in Korea, Choi identified a 41% reduction (3.2 days) in average length of stay among gynecology patients in brightly daylit rooms (317 lx average), as compared to those in dull rooms, in the spring, and an average 26% reduction (1.9 days) in average length of stay among surgery ward patients in bright rooms, as compared to those in dull rooms, in the fall. Across all seasons, the average daylight illuminance in bright rooms was 317 lx, compared to 190 lx in dull rooms (Inha University Hospital/ Choi [40]).

The solar heat gained in building atria or double envelope facades can also be actively transferred to a range of storage media, from rock storage to phase change storage to underfloor air systems with thermal mass. *Active solar hot water* collectors integrated into building roofs or facades can also transfer solar heat to architectural or mechanical heat exchangers. The effective integration of solar heat gain with the ventilation air systems in buildings can significantly reduce heating loads while supporting greater ventilation rates for human health.

While solar thermal collectors can provide excellent hot water temperatures for heating, *concentrating solar thermal* collectors can generate the extreme high temperatures needed for cooling and power generation. Bundled with the latest in absorption chillers and steam power generators, a new generation of solar-evacuated tube and concentrating collectors are beginning to transform building enclosures to help meet the growing electrical demands in buildings for air conditioning (Fig. 23).

Finally, integrating *photovoltaic solar* (PV) elements into the building curtain wall or roof can generate on-site power for feeding into the grid or for immediate use in the building. For maximum efficiency, PV energy could be used directly as DC electricity (without transformer loses to AC) to meet the power demands of fans and air conditioners, plug loads, and dynamic facade elements – from operable windows to light shelves and shading devices. Recent thin film developments have significantly improved the performance of building integrated photovoltaics (BIPV), supporting a range of design choices regarding shape, orientation, transparency, and color. For windows, new PV glazing assemblies can provide effective shading, daylight distribution, and a competitive power source. The next generation of building windows may absorb solar energy in almost transparent coatings and carry the electricity to window mullions for transport to the grid. For roofs and walls, the early PV assemblies that were rigidly sandwiched behind glass have been replaced by newer flexible PV materials that can replace common building materials, with 3–10-year life-cycle justifications. The vast areas of roof and facade that absorb or reflect long hours of sunshine can be turned into an asset even in hot climates, with building integrated photovoltaics playing a major role in generating distributed power, eliminating the source and

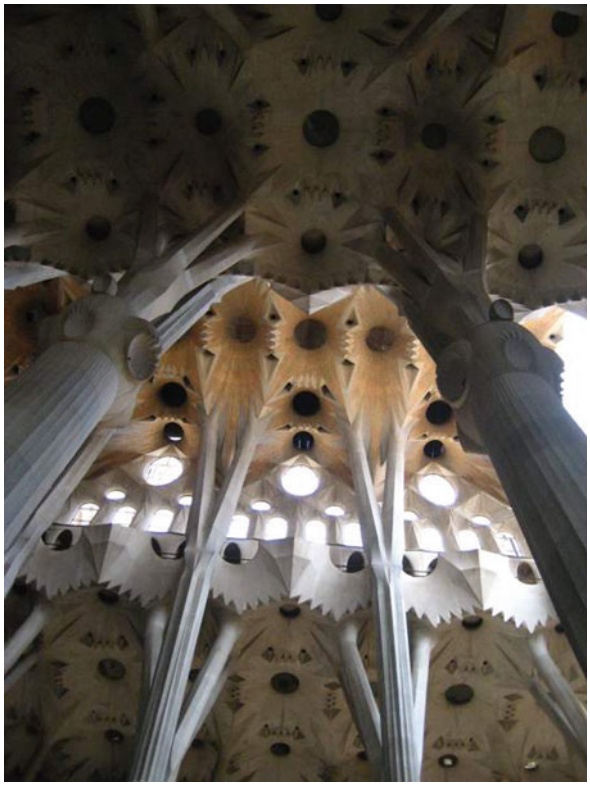

Facades and Enclosures, Building for Sustainability. Figure 20
Architecturally articulated thermal mass at Gaudi's Sagrada Familia minimizes daily temperature swings by night ventilation through architecturally expressive openings

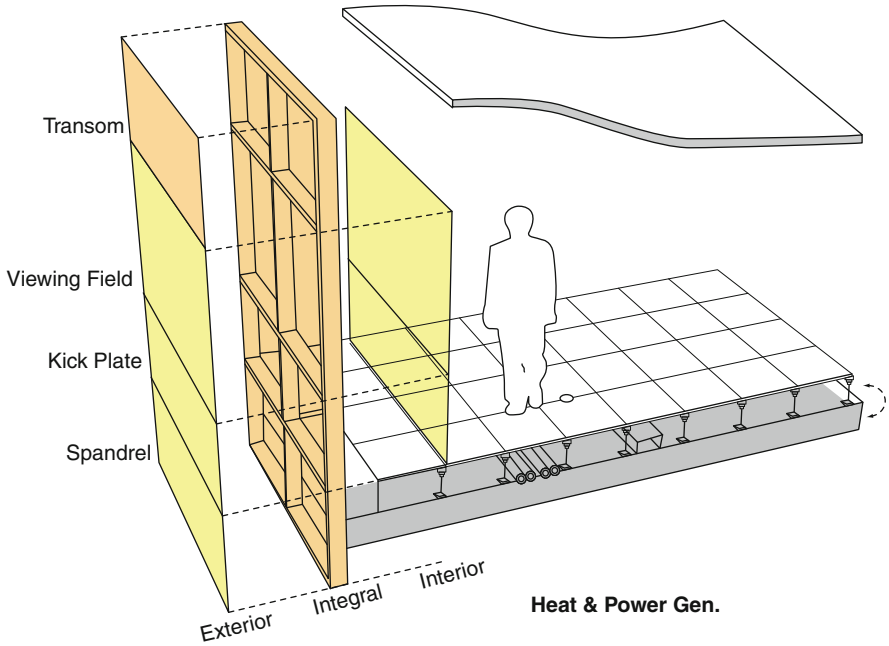

Facades and Enclosures, Building for Sustainability. Figure 21
Critical facade elements for passive and active solar heating, cooling, and power

Facades and Enclosures, Building for Sustainability. Figure 22
Interior and exterior views of the south facade at Fraunhofer Institute in Freiburg illustrate the integration of active and passive solar strategies

distribution inefficiencies of conventional power production for greatly reduced carbon impacts.

Wind power generation can also be integrated with building facades and roofs. A new generation of micro-turbines may create the parapets of future buildings, and large wind farms may occupy the upper floors of skyscrapers, as proposed in early solutions for the World Trade Center by Battle Engineering [41].

Facades and Enclosures, Building for Sustainability. Figure 23
Concentrating solar thermal collectors on the roof of the Intelligent Workplace produce steam in the summer to power absorption chillers to cool the space

Photovoltaic System = Energy Savings

In a building case study of Bren Hall, a LEED Platinum-rated building at the University of California, Santa Barbara (UCSB), Aigner identified that the building's 47 kW rooftop photovoltaic system reduces purchased electricity consumption by 7–10% annually, at a first cost of $240,000, for an ROI of 5% (Bren Hall/ Aigner [42]).

Facades Designed to Manage Water

A fundamental role for high-performance building enclosures is the management of water. It is imperative that roofs and facades effectively *manage rainfall* through material selection and articulated detailing from top to bottom (Fig. 24). While gargoyles and expressive cornices that were once the solution to ensure heavy rains were shed away from the building, modern facades rely far too heavily on the caulked joint – often with poor results as the facades age (Fig. 25).

A lesser understood role for building facades is to *manage the vapor migration* that might lead to condensation on embedded surfaces that are below dew point temperature. This is typically achieved through the design of continuous vapor barriers on the "warm side of the facade" to stop the humidity from migrating into the wall. Detailing in design and construction supervision is critical, especially in complex climates where humidity and cold temperatures may both be from the inside or outside. In addition, moisture that is trapped in construction materials must be released naturally as well, typically through a vapor porous skin or vented air spaces [43]. *Rain screens* are an innovative solution to managing both rain and vapor migration. Rain screens introduce an uncaulked and vented second skin for the facade – typically of ceramic tile or metal or wood panels – that sheds the rain and utilizes the vented air space to eliminate moisture buildup.

As we embrace a greater set of sustainability challenges, building enclosures also need to collect rainwater today. As we face declining sources of fresh water, and increasing storm runoff challenges, the importance of designing building enclosures to *catch and store water* is of growing importance (Fig. 26).

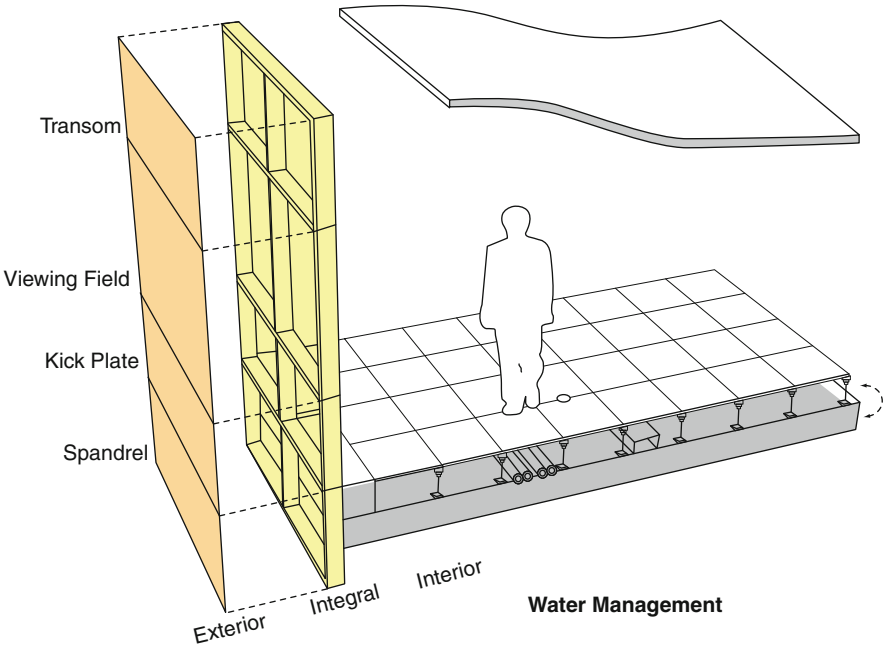

Facades and Enclosures, Building for Sustainability. Figure 24
Critical facade elements to manage rainwater and moisture migration

Facades and Enclosures, Building for Sustainability. Figure 25
On the *left*, water sculpture by Herbert Dreisetl playfully manages storm water, enticing visitors to return in the rain to watch. On the *right*, rainwater capture provides acoustic and visual richness in the Dockside Green development by Joe Van Bellingham

Green Roof = Energy Savings + Peak Load Reduction + Storm Water Retention

In a 2002 building case study of the Chicago City Hall, the city of Chicago identified annual cooling energy savings of 0.02 kWh/square foot and annual heating energy savings of 0.02 therms/square foot, as well as a 70% reduction in storm water runoff, from installation of a 20,000 sf green roof (Chicago City Hall/ City of Chicago [44]).

Green Roof = Energy Savings + Storm Water Retention

In a 2003 building case study of the 901 Cherry Offices of Gap, Inc. in San Bruno, CA, Green Roofs for Healthy Cities identify a 100% reduction in storm water runoff (7.54 gal/sf of roof area) and a simple payback of 11 years from energy cost savings alone (equivalent to 7% annual energy savings in a baseline building) due to installation of an extensive green roof (901 Cherry (GAP)/ Green Roofs for Healthy Cities [45]).

Facades that Maximize Enclosure Life

High-performance building enclosures will need to *use materials sustainably* (Fig. 27). Wherever possible, existing enclosures should be preserved to protect their "embodied" energy, or built of 100% recycled content materials. If virgin materials are used, their "chain of custody" should be known in relation to energy, carbon, rare materials, and toxicity. Toxic materials should be avoided in all assemblies, or designed for retrieval during disassembly.

Enclosure assemblies should be designed for their longevity, for natural *weathering and effective maintainability*. Most critically, enclosures should be designed and built for *cherish-ability*, the desire on the part of owners and the community to want to preserve the building rather than tear it down. This is typically ensured by the use of quality materials, assembled for longevity, and a high level of craftsmanship (Fig. 28).

Enclosure design must also address the needs for *human safety* in the face of manmade and natural disasters. This includes structural integrity in the face of earthquakes, hurricanes, and cyclones as well material integrity in the face of fires, floods, and blasts.

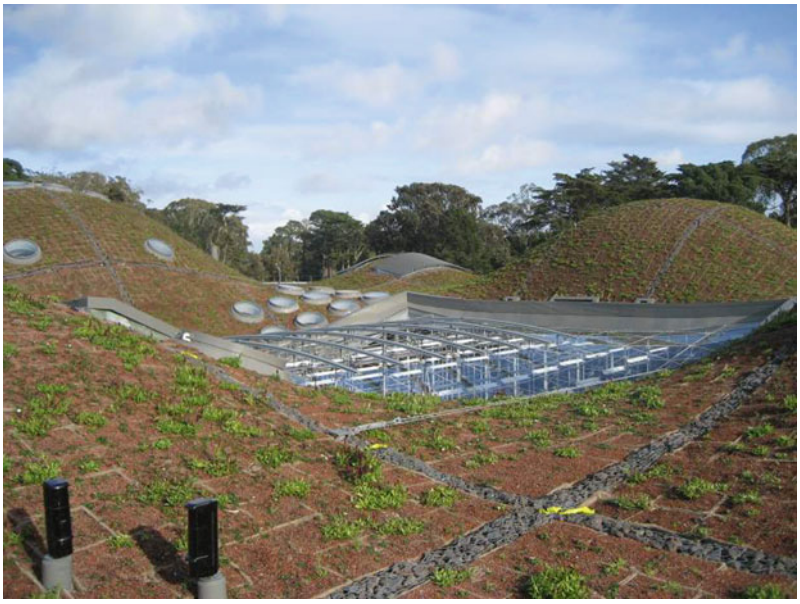

Facades and Enclosures, Building for Sustainability. Figure 26
Green roofs at the California Academy of Sciences capture storm water while providing a learning environment for landscape and habitats

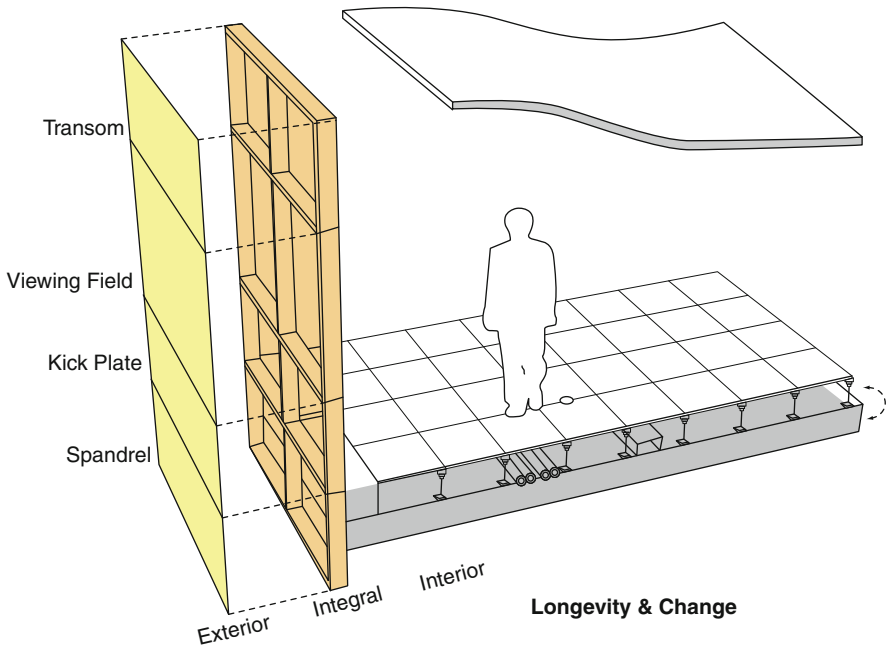

Facades and Enclosures, Building for Sustainability. Figure 27
Critical facade elements to maximize enclosure life

Design for disaster protection should be about human safety not building protection, ensuring adequate egress and adequate safe harbors. Design for human safety must also ensure adequate access to water, breathing air, and light, even in the face of power outages – a redundancy that can be best achieved by sustainable facade design that fully incorporates natural conditioning.

At the same time, building enclosures need to be *designed for change* – for expansion or contraction, for changes in use or function. Change can be supported through building generosity, floor-to-floor heights, size of openings, and level of building articulation. Change can be supported by modularity, with a kit of parts that anticipates the evolution of scale and function over the life of the building. Change can also be accommodated by *design for disassembly*, by which the building and/or its enclosure can be relocated to a second or third life. All high-performance enclosure components, such as window and door assemblies, water management systems, and ornamental parapets, should be designed to be recovered as the "value-added" assemblies that they are well beyond the value of the raw materials (Fig. 29).

Construction Waste Management = Salvage/Waste Savings

In a 2004 building case study of the renovation of the Boston Scientific Company, Inc. office building, the Institutional Recycling Network identified a 32% reduction in disposal costs due to a comprehensive waste management process, compared to the cost of renovation with conventional landfill disposal of material waste. A site separation process allowed materials to be disposed of at lower costs than co-mingled materials and resulted in a 92% recycling rate by weight (Boston Scientific Company/ Institution Recycling Network [46]).

Construction Waste Management = Salvage/Waste Savings

In a 2000–2001 building case study of the demolition of the 133,000 square foot Hume Residence Hall on the campus of the University of Florida, Guy and Strong identify new revenues, reduced disposal costs, and cost avoidance from substitutions of reclaimed

Facades and Enclosures, Building for Sustainability. Figure 28
Historical structures were designed and built to last a lifetime

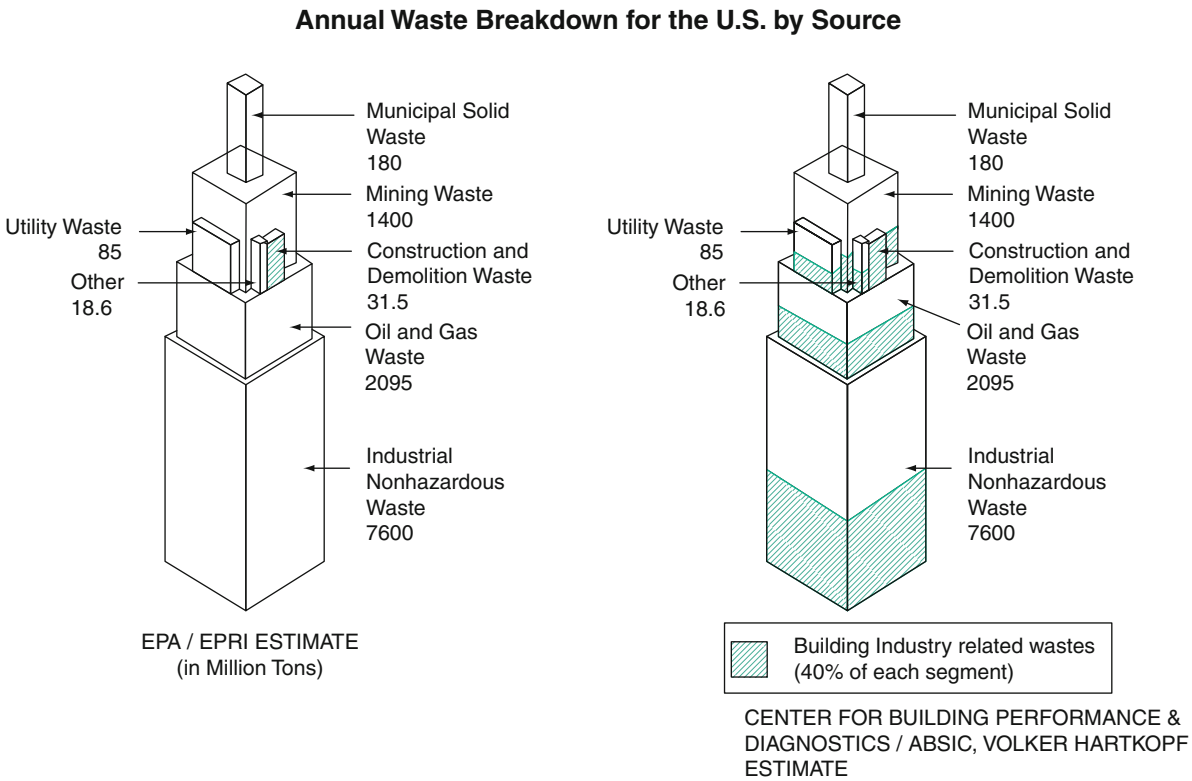

Facades and Enclosures, Building for Sustainability. Figure 29
Forty percent of the total waste stream can be attributed to the construction industry

materials, achieved through a process of salvage and source separation of "debris" building materials. A comprehensive C&D debris management process resulted in a *net savings* of 4% compared to the cost of conventional demolition with extensive landfill disposal (University of Florida Hume Residence Hall/Guy and Strong [47]).

Future Directions: Facade Innovation Through Systems Integration

In times of limited resources and limited building budgets, some of the most innovative high-performance facades are achieved through systems integration (Fig. 30). At a very minimum, high-performance sustainable building facades will have to be collaboratively designed to:

- Integrate structure and enclosure to ensure heat loss/heat gain control, provide shading and glare control, and support daylighting.
- Integrate fire and enclosure to support load balancing innovations.
- Integrate HVAC and enclosure to support natural ventilation, load balancing, and passive and active solar energy utilization.
- Integrate interior systems and enclosure systems for access to nature, daylighting, natural ventilation, shade and glare control, and passive solar heating.
- Ensure design for enclosure life and design for change without waste.

When expert disciplines work collaboratively early in the design process, a range of innovations are generated – structural systems that offer shading and light redirection; enclosures that are integral with the mechanical duct or piping; fire egress that provides shade and access for maintenance; ornament that manages water; and expressions of function, culture, or ambition that serve a critical purpose for ensuring the highest level of indoor environmental quality and environmental sustainability. Sustainable building enclosures are the deliverables of integrated design teams and integrated building delivery processes that in turn are pivotal to achieving the highest level of health, productivity, energy, and environmental benefits (Fig. 31).

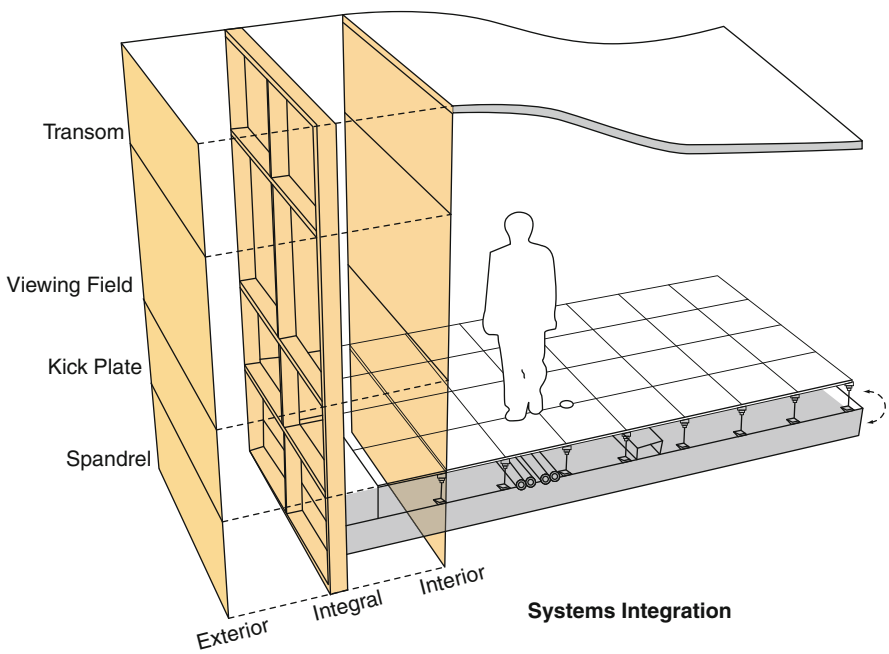

Facades and Enclosures, Building for Sustainability. Figure 30
Critical facade elements for innovation through systems integration

Whole Building = Energy Savings

In a 2000 building case study of BRE's Environmental office building in Garston, UK, Fisher et al. identify a 66% annual energy savings compared to a typical type III UK office building due to the use of thermal mass, natural ventilation, passive and low energy cooling, daylighting, high-performance electric lighting, and on-site power generation (BRE Environmental Building/Fisher et al. [48]).

Floor-Based Ventilation + Increased Outside Air = Health

In a 2000 multiple building study of 39 schools in Sweden, Smedje and Norback identify a 69% reduction in the 2-year incidence of asthma among students in schools that received a new displacement ventilation system with increased fresh air supply rates and dedicated exhaust, as compared to students in schools that did not receive a new ventilation system (Elementary School/Smedje and Norback [49]).

High-Performance Building = Energy Savings + Rent Premium

In a 2004 building case study of the Phillips Eco-Enterprise Center in Minneapolis, Brinkema identifies $0.31/sf energy savings and a 5–10% lease premium for the building owner (a financial gain of $0.62/sf) due to high-performance building design that incorporates passive solar and geothermal heating and cooling, daylighting and high efficiency electric lighting, salvaged building materials, nontoxic paints and finishes and landscaping with native plants (Philips Eco-Enterprise Center/ Brinkema [50]).

High-Performance Building = Energy Savings + Individual Productivity

In a 1992 building case study of ING Bank in Amsterdam, Bill Browning of Rocky Mountain Institute identifies a 92% reduction in primary energy consumption and a 15% reduction in employee absenteeism compared

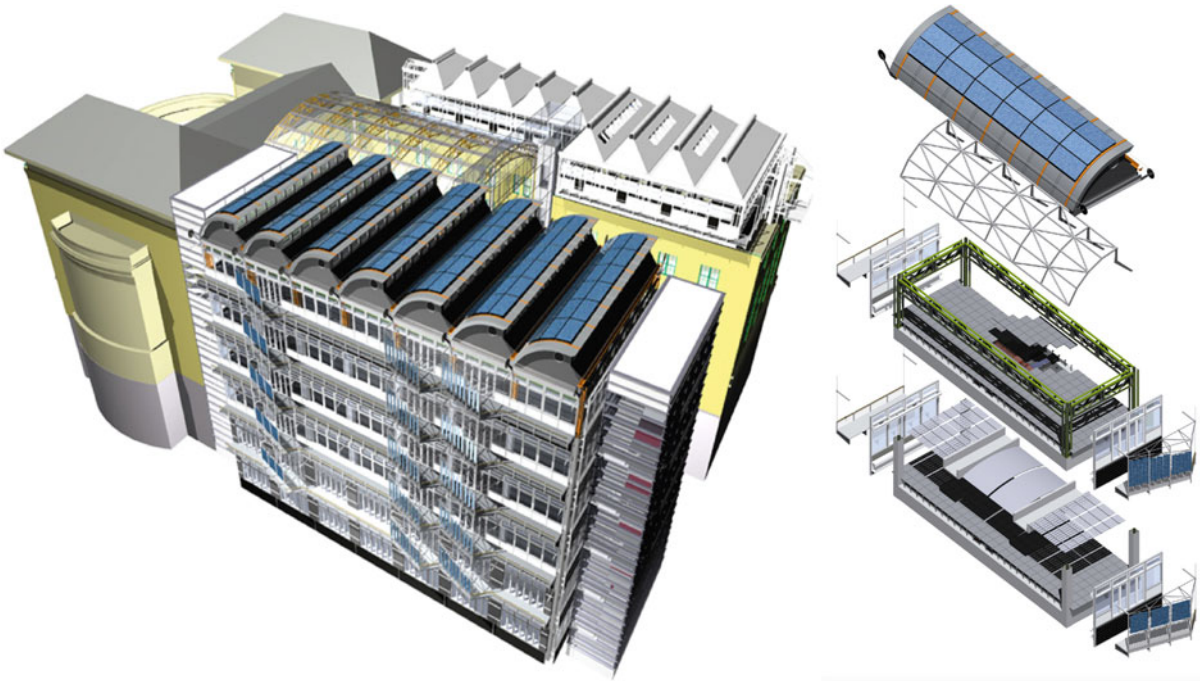

Facades and Enclosures, Building for Sustainability. Figure 31
The proposed "Building As Power Plant" at Carnegie Mellon University attempts to integrate all building systems, assemblies, and components to export unneeded renewable energy while providing optimum comfort for the occupants

to the bank's former headquarters, due to high-performance design strategies including daylight, a narrow floor plan that allows landscaped views for every occupant, passive solar conditioning, co-generation, and the use of heat exchangers (ING Bank/ Browning [51]).

Bibliography

1. Mahdavi A, Brahme R, Mathew P (1996) The "LEK"-concept and its applicability for the energy analysis of commercial buildings. Build Environ 31(5):409–415
2. Wilson E (1984) Biophilia. Harvard University Press, Cambridge
3. Kellert S, Wilson E (1993) The biophilia hypothesis. Island Press, Washington, DC
4. Kellert SR (2005) Building for life: designing and understanding the human-nature connection. Island Press, Washington, DC
5. Kellert S, Heerwagen J, Mador M (2008) Biophilic design: the theory, science and practice of bringing buildings to life. Wiley, Hoboken
6. NKB (1991) Indoor climate – air quality, Nordic Committee on Building Regulations. NKB Publication No 61E, June 1991
7. CBPD (n. d.) *eBIDS* – Energy building investment building support. http://cbpd.arc.cmu.edu/ebids/pages/home.aspx. Accessed 7 Feb 2011
8. Ulrich RS (1984) View through a window may influence recovery from surgery. Science 224(4647):420–421
9. Mendell MJ (1991) Risk factors for work-related symptoms in northern California Office workers. Indoor Environment Program Lawrence Berkeley Lab, CA, Unpublished doctoral dissertation, University of California, CA Department of Health Services, and NIOSH, Sponsoring Org. USDOE, Washington, DC, 1991
10. Heschong Mahone Group (2003) Windows and offices: a study of office worker performance and the indoor environment. CEC PIER Report, Oct 2003
11. Loftness V (1994) Major recommendations for action: forrestal and germantown building evaluation team. Field Study. Center for building performance and diagnostics, Carnegie Mellon University, Pittsburgh, 17–18 Oct 1994
12. Moore RC, Marcus CC (2008) Healthy planet, healthy children: designing nature into the daily spaces of childhood. In: Kellert S, Heerwagen J, Mador M (eds) Biophilic design: theory, science and practice of bringing buildings to life. Wiley, Hoboken, pp 153–203
13. US DOE (2009) *2008 Building energy data book*. Prepared for the Building Technologies Program Energy Efficiency and Renewable Energy, U.S. Department of Energy. By D&R International. Under contract to National Energy Technology Laboratory, 2006 Energy Consumption
14. Loftness V, Aziz A, Choi J (2008) Energy savings and performance gains in GSA buildings: seven cost-effective strategies. GSA Public Buildings Service, Washington, DC
15. Rubenstein F, Jennings J, Avery D, Blanc S (1998) Preliminary results from an advanced lighting controls testbed. In: 1998 illuminating engineering society of north america annual conference, San Antonio, TX, USA, 10–12 Aug 1998
16. EPRI (1997) Performance evaluation of energy efficient lighting and office technologies in New York City – Final Report. Electric Power Research Institute, EPRI, Palo Alto, June 1997
17. Boyce PR, Beckstead JW, Eklund NH, Strobel RW, Rea MS (1997) Lighting the graveyard shift: the influence of a daylight-simulating skylight on the task performance and mood of night-shift workers. Light Res Technol 29(3):105–134
18. Preziosi P, Czernichow S, Gehanno P, Hercberg S (2004) Workplace air-conditioning and health services attendance among French middle-aged women: a prospective cohort study. Int J Epidemiol 33(5):1120–1123
19. Emmerich SJ, Persily AK, Stuart Dols W, Axley JW (2003) Impact of natural ventilation strategies and design issues for California applications, including input to ASHRAE Standard 62 and California Title 24. NISTIR 7062, 2003
20. Rowe D (2002) Pilot study report: Wilkinson building. The University of Sydney, Sydney
21. Hannula M, Niemela R, Rautio S, Reijula K (2000) The effects of indoor climate on productivity. In: Proceedings of healthy buildings. Helsinki, pp 659–664
22. Loftness V, Baird N, Snyder M (2011) The triple bottom line of green roofs: assessing the life cycle economic, environmental and human benefits of green roof. Carnegie Mellon University, Pittsburgh
23. Kosareo L, Ries R (2007) Comparative environmental life cycle assessment of green roofs. Build Environ 42(7):2606–2613
24. Gangnes D (2007) Seattle green roof evaluation project final report. Magnusson Klemencic, Seattle: Seattle.gov
25. Currie BA (2005) Air pollution mitigation with green roofs using the UFORE model. Ryerson University,Toronto
26. Onmura S, Matsumoto M, Hokoi S (2001) Study on evaporative cooling effect of roof lawn gardens. Energy Build 33(7):653–666
27. Stec WJ, van Paassen AHC, Maziarz A (2005) Modelling the double skin façade with plants. Energy Build 37(5):419–427
28. Bass B, Baskaran B (2003) Evaluating rooftop and vertical gardens as an adaptation strategy for urban areas. National Research Council Canada, Report No. NRCC-46737, Toronto, Canada, pp 74–86
29. Winkelmann FC, Lokmanhekim M (1981) Life-cycle cost and energy-use analysis of sun-control and daylighting options in a high-rise office building. Report No. LBL-12298, University of California, Lawrence Berkley Laboratory, Berkeley
30. Koster E (1998) Natuur onder architectuur = architecture for nature: IBN-DLO Wageningen, architect stefan Behnisch. Schuyt, Haarlem
31. Oesterle E, Lieb RD, Lutz M, Heusler W (2001) Double skin facades: integrated planning: building physics, construction, aerophysics, air-conditioning, economic viability. Munich, Prestel, London\New York
32. Bazjanac V (1980) Architectural energy analysis. Prog Architect 61(4):98–101

33. Feist W (1999) Das Passivhaus. CF Mueller, Heidelberg
34. Akbari H, Levinson R (2008) Evolution of cool-roof standards in the US. In: Santamouris M (ed) Advances in building energy research (ABER), vol 2. Earthscan, London, pp 1–32
35. Parker D, Sonne J, Sherwin J (2002) Comparative evaluation of the impact of roofing systems on residential cooling energy demand in Florida. In: Proceedings of ACEEE 2002 summer study, American Council for an energy efficient economy, Washington DC, August 2002
36. Imanari T, Omori T, Bogaki K (1999) Thermal comfort and energy consumption of the radiant ceiling panel system. Comparison with the conventional all-air system. Energy Build 30(2):167–175
37. Seppanen O, Fisk WJ, Faulkner D (2003) Cost benefit analysis of the night-time ventilative cooling in office building. Lawrence Berkeley National Laboratory, Berkeley. LBNL Paper LBNL-53191, 1 June 2003
38. Shonder JA, Martin MA, Hughes PJ, Thornton J (2000) Geothermal heat pumps in K-12 schools: a case study of the Lincoln Nebraska, schools. ORNL/TM-2000/80, Oak Ridge National Laboratory, Oak Ridge
39. Hastings R, Wall M (2007) Sustainable solar housing: exemplary buildings and technologies. International Energy Agency. Solar Heating and Cooling Programme, IEA energy conservation in buildings and community systems Programme, vol 2. Earthscan, London\Sterling
40. Choi J (2005) Study of the relationship between indoor daylight environments and patient average length of stay (ALOS) in healthcare facilities. Unpublished Master's Thesis, Department of Architecture, Texas A&M University. College Station, TX, USA
41. Ragheb M (2008) Wind turbines in the urban environment. Wind power systems: Harvesting the wind. University of Illinois at Urbana-Champaign, 30 Dec 2008. https://netfiles.uiuc.edu/mragheb/www/NPRE%20475%20Wind%20Power%20Systems/Wind%20Turbines%20in%20the%20Urban%20Environment.pdf. Accessed 7 Feb 2011
42. Aigner DJ (2002) Bren Hall – a living laboratory. Solar Today, 28–31 July/Aug 2002
43. Lstiburek J, Carmody J (1996) Moisture control handbook: principles and practices for residential and small commercial buildings. Wiley, New York
44. City of Chicago (2000) Department of environment, extensive green roofs fact sheet
45. Green Roofs for Healthy Cities (2003) Green roof awards of excellence – profile of award winners. In: The First annual green roof infrastructure conference. Illinois, Chicago, 29–30 May 2003
46. Institution Recycling Network (2004) Boston Scientific Company, Inc. (BSCI) Office Park Renovation, Marlborough, MA, 2004. http://www.wastemiser.com/CS-BSCI-10-06.pdf. Accessed 18 Nov 2007
47. Guy GB, Strong KS (2001) Deconstructing Hume residence hall. Report of the Powell Center for Construction and Environment, University of Florida, Gainesville
48. Fisher J, NíRiain C, MacKenzie F, Littler J (2000) BRE's environmental building: energy performance in use. In: CIBSE Conference Paper, Dublin
49. Smedje G, Norbäck D (2000) New ventilation systems at select schools in Sweden – effects on asthma and exposure. Arch Environ Health 55(1):18–25
50. Brinkema C (2004) EIN and real estate development. EIDC Roundtable. Fall, Vancouver
51. Browning W (1992) NMB bank headquarters: the impressive performance of a green building. Urban Land, June 1992, pp 23–25

F

Fallout Radionuclides and the Study of Erosion and Sedimentation

Desmond E. Walling
Department of Geography, College of Life and Environmental Sciences, University of Exeter, Exeter, UK

Article Outline

Glossary
Definition of the Subject
Introduction
A Brief History of the Use of Fallout Radionuclides in Erosion and Sedimentation Studies
Fallout Sources and Inputs
Fallout Radionuclides in the Soil and Soil Inventories
Using Fallout Radionuclides as Tracers to Investigate Soil and Sediment Redistribution within the Landscape
Field and Laboratory Techniques
Some Examples of the Application of Fallout Radionuclides in Erosion and Sedimentation Investigations
Future Directions
Bibliography

Glossary

Activity The concentration of a given radionuclide in a soil or sediment per unit mass, also referred to as the mass activity density.

Erosion The mobilization of soil and sediment from its original location or a temporary store within the landscape by a range of agents, including water and wind.

Fallout radionuclides Radionuclides that enter the terrestrial and aquatic environments as fallout.

Fluvial system Landscape systems associated with streams and rivers and driven by rainfall and runoff.

Gamma spectrometry Measurement of the gamma-emitted radioactivity in soils and sediment, using a gamma spectrometer.

Gross erosion The total amount of soil mobilized by erosion within a given area.

Half-life The time taken for a radionuclide to decay to the point where its activity is half the original activity.

Inventory An alternative term for the areal activity density, which represents the total radionuclide content of a soil or sediment deposit per unit surface area.

Net erosion The total amount of eroded sediment transported out of a given area. This represents the gross erosion within that area minus the deposition occurring within that area.

Off-site impacts The impacts of soil erosion associated with the transport of eroded soil away from the original point of erosion, for example, by streams and rivers.

On-site impacts The impacts of soil erosion associated with the point where erosion occurs and including reduction in soil depth, loss of productivity, and destruction of agricultural land.

Sediment budget A conceptual model of the sources, transfers, sinks, and outputs of sediment for a catchment or river basin. The model may quantify mobilization, transfer, storage, and output.

Sediment delivery ratio This represents the ratio of the amount of sediment leaving a field or catchment to the total amount of sediment mobilized by erosion within that area. It provides a measure of the efficiency of sediment transfer out of the system considered. The sediment delivery ratio will decrease as deposition increases.

Sediment Material transported or deposited within fluvial, aeolian, and other erosional systems.

Sediment source fingerprinting Use of a range of biogeochemical properties to characterize or fingerprint different potential sediment sources. The properties of transported or deposited sediment are compared with those fingerprints, in order to determine its source.

Sediment source The point, place, or area from which sediment was mobilized.

Sedimentation A term frequently used to refer to the study of sediment transport in fluvial systems, including sediment mobilization, transport, and deposition, but also used in a more narrow sense to refer to deposition of sediment in sinks including river channels and floodplains, lakes and reservoirs, and estuaries and coastal environments.

Definition of the Subject

Soil erosion is an important problem in many areas of the world, where it reduces soil productivity, destroys agricultural land, and can threaten food security and the sustainable management of soil resources. The on-site effects of soil erosion are coupled with off-site effects, which relate to the downstream or downwind impact of the eroded soil. The resulting transport of increased amounts of fine sediment, particularly in streams and rivers, and the deposition of this sediment in downstream sinks gives rise to a range of important environmental problems. These include the degradation of water quality and aquatic habitats. Concern for the sustainable management of both soil resources and catchments and river basins has directed attention to the need to develop effective erosion and sediment control strategies. Designing and implementing such strategies requires an improved understanding and quantification of the mobilization, transfer, and deposition of sediment within the landscape, so that mitigation measures can be targeted to optimize their effectiveness. Existing measurement techniques for assembling data on erosion and sedimentation within the landscape face many limitations, and the potential for using fallout radionuclides to assemble the information required has attracted increasing attention over the past 30 years. Fallout radionuclides offer unique opportunities to document sediment mobilization and deposition rates and to trace the movement of fine sediment through the landscape. This entry reviews the important needs for information on erosion and sedimentation and the history of the application of fallout radionuclides in this field, describes and explains the basis for using fallout radionuclides in erosion and sedimentation investigations, and provides several different examples of their successful use.

Introduction

Soil erosion represents the removal of soil from the location where it developed by erosion processes. These processes are driven by several agents, the most important of which are water and wind. Water erosion is the most widespread cause of soil loss and occurs in a wide range of environments. Wind erosion can be equally destructive, but its occurrence is more limited. Soil erosion can be viewed as a natural process, but rates of soil loss are commonly very low in natural undisturbed landscapes, where the soil will generally be well protected by vegetation from the destructive effects of rainsplash, surface runoff, and deflation. Under these conditions, the rate of soil loss is likely to be balanced by the rate of soil formation and the soil will be in a quasi-equilibrium. When, however, the vegetation cover is removed or reduced by human activities, such as land clearance and cultivation, excessive grazing or forestry activity, rates of soil loss can increase by several orders of magnitude. Such accelerated soil erosion can represent a serious threat to the sustainability of the soil resource and to food security, through both reduced crop productivity and the loss of agricultural land as a result of soil removal, gully development, and other destructive effects of erosion. Recent estimates indicate that ca. 1,000 Mha of the earth's surface is currently adversely affected by water erosion and ca. 500 Mha by wind erosion, with about 80% of these totals being associated with the developing world [1]. Much of this erosion occurs on agricultural land. It has been estimated that about 80% of the world's agricultural land suffers from moderate-to-severe erosion and that about 10% suffers from slight-to-moderate erosion [2]. Even in developed countries, such as the USA, where soil conservation measures are widely applied, soil erosion represents a major problem, and it has been reported that in the USA, about 23 million hectares of cropland experience excessive soil erosion and that erosion rates exceed the tolerable soil loss on about a further 20 million hectares [3].

The annual global loss of agricultural land due to accelerated erosion has been estimated to be ca. 3 million hectares [4] and the progressive destruction of the global soil resource by erosion is emphasized by the calculation that the world's croplands are losing about 23 billion tons of soil in excess of new soil formation each year [5]. The rate of soil formation will be influenced by a wide range of factors, but a value of 1 t ha^{-1} $year^{-1}$ is frequently cited as a typical value. This value is often referred to as the soil loss tolerance, since, if erosion rates exceed this value, the soil depth will progressively reduce and crop productivity is likely to decline. Global models have been used to assess the extent to which this value of 1 t ha^{-1} $year^{-1}$ is exceeded and, based on the global pattern of land use in the 1980s, the global mean soil erosion has been estimated to be 10.2 t ha^{-1} $year^{-1}$, a value which is an order of magnitude greater [6]. Average erosion rates were shown to be highest in Asia (12.2 t ha^{-1} $year^{-1}$) and lowest in Australia (3.0 t ha^{-1} $year^{-1}$).

Current concern for the impact of climate change and global warming has directed attention to likely changes in soil erosion rates. In most areas of the world, predictions suggest that soil erosion rates will increase and, in the global modeling exercise referred to above [6], climate change predictions associated with a doubling of CO_2 concentrations were coupled with erosion models to estimate that at the global scale, soil loss would increase by 9% by the 2090s as a result of climate change. When this prediction was coupled with likely changes in land use by the 2090s, soil erosion increased by 14%. Soils play a key role in the global carbon cycle by storing carbon. Accelerated erosion perturbs this cycle by mobilizing soil carbon that may be subsequently oxidized causing increased CO_2 emissions, and by redistributing soil carbon and sequestering it in longer-term depositional sinks [7, 8]. Both past and likely future increases in soil erosion therefore have important implications for the global carbon cycle.

Although concern for soil erosion has traditionally focused on the on-site effects linked to loss of agricultural land and reduced productivity, it is important to recognize that much of the sediment mobilized by accelerated water erosion will find its way into streams and river systems leading to increased sediment loads. Increased sediment loads can give rise to a range of environmental problems linked to degradation of water quality and aquatic habitats, damage caused to infrastructure during floods, and increased deposition of sediment in river channels, lakes, and reservoirs [9]. These impacts are frequently referred to as off-site impacts, to distinguish them from the on-site effects

highlighted above. In many situations, the off-site impacts of soil erosion will be more serious than the on-site effects. Taken together, they represent a very large economic cost and it has been estimated that worldwide, the annual cost of both the on-site and off-site impacts of soil erosion on agricultural land amounts to about $400 billion [10]. However, it is difficult to quantify the economic cost of loss of biodiversity, changes in the carbon cycle, and impacts on ecosystem services, and the real cost may therefore be substantially greater.

The deposition of sediment within the landscape and in water bodies, such as rivers, lakes, reservoirs, and marshes, must be seen as an inevitable complement to the mobilization of sediment by erosion and such processes are frequently referred to as sedimentation. Most attention is generally directed to sedimentation associated with water erosion, since sediment mobilized by such erosion can be deposited before reaching the stream network and, once entering the river system, there will be many further opportunities for sedimentation downstream. A substantial proportion of the sediment moving through the river system will reach the outlet of the river basin and may then be deposited in estuaries, in coastal areas and in the deeper ocean. In contrast, soil mobilized by wind erosion is usually deposited locally, although the finer fractions can be transported over substantial distances and it may be less easy to link erosion and sedimentation. Equally, such sediment is likely to be deposited over large areas and its impact is likely to be much less. Again, sedimentation must be seen as a natural process, but accelerated erosion will frequently be coupled with increased sedimentation, which can lead to environmental problems. These problems relate not only to the physical presence of deposited sediment, which can, for example, greatly reduce the water holding or storage capacity of a water body, but also to the nutrients and contaminants, such as pesticides, associated with the sediment. Release of nutrients and contaminants from sediment deposited in water bodies can cause eutrophication and pollution of those water bodies. Similarly, deposition of contaminated sediment or sediment with a high-nutrient content on river floodplains can cause contamination of soil and crops and changes in the species composition of native vegetation communities, in response to the changing nutrient status of the soil. Estimates suggest that the world's large reservoirs are currently losing about 1% of their total storage each year [11]. Such losses can have important implications for water supply and the annual cost of replacing this lost storage has been estimated to be ca. $6 billion. When this cost is combined with the problems of finding new dam sites, when existing reservoirs are filled with sediment and can no longer operate effectively, the serious consequences of reservoir sedimentation are clear.

Against this background, there is an increasing need to assemble information on soil erosion and sedimentation rates to inform and support the sustainable management of soils, catchments, and associated water bodies. Such demands have increased with the development and use of numerical models as management tools, since such models commonly require data for calibration and validation. Although a range of techniques have been developed for documenting soil erosion and sedimentation rates [12, 13], these techniques have important limitations. For example, in the case of soil erosion, erosion plots are widely used to obtain information on rates of soil loss under particular conditions. (e.g., different soil types, slope gradients, crop types, cultivation practices, etc.). However, such plots are costly to install, they need to be operated for an extended period to obtain reliable information on mean annual rates of soil loss due to the inherent temporal variability of erosional events, and the results obtained from a small bounded plot may be unrepresentative of the natural landscape with its more complex topographic form. In the latter context, plot measurements relate to the export of material across the lower boundary of the plot and thus only provide spatially averaged estimates of net soil loss. They cannot provide information on deposition of mobilized soil within the plot and thus soil redistribution rates more generally (i.e., gross erosion, deposition, and net erosion). Furthermore, soil redistribution rates may vary markedly according to location within a field in relation to the local topography (e.g., ridges and hollows and concave and convex slope profiles). To meet the requirements of the current generation of distributed numerical models, spatially distributed information on erosion and deposition rates will frequently be required. Similar problems are faced by attempts to document deposition rates on river

floodplains and in water bodies, such as lakes, reservoirs, and wetlands. Short-term variation of sediment deposition rates and spatial variability of deposition rates may introduce the need to quantify such variability.

The limitations of traditional measurement techniques referred to above have directed attention to the potential for using environmental radionuclides to provide information on soil erosion and sedimentation rates. The fallout radionuclides cesium-137 (^{137}Cs), unsupported or excess lead-210 ($^{210}Pb_{ex}$), and beryllium-7 (^{7}Be) have proved particularly useful in this context, because they are rapidly and strongly fixed on reaching the soil or sediment surface as fallout and their post-fallout redistribution provides a means of documenting soil and sediment redistribution within the landscape. In essence, measurements of the radionuclide areal activity density or inventory (Bq m^{-2}) are made at a number of points across a field by collecting soil cores. By comparing the results of these measurements with a measurement of the reference inventory, which represents the inventory found in an adjacent undisturbed area, areas or points experiencing erosion and deposition can be identified. In the former case, the inventory at the sampling point will be less than the reference inventory, and in the latter case, the inventory will exceed the reference inventory. The degree to which the inventory departs from the reference inventory is a direct reflection of the magnitude of the erosion or deposition rate, and a range of conversion models have been developed to estimate erosion and deposition rates from the measurements obtained. In a similar way, fallout inputs to water bodies, which are subsequently incorporated into sediment deposits can provide a means of establishing the chronology of sediment deposits. In the case of ^{137}Cs, the occurrence of peak fallout in 1963 provides a time marker for that year and the rate of decrease of $^{210}Pb_{ex}$ activity with depth affords a means of estimating the time elapsed since the deposition of sediment from a specific depth and thus the sedimentation rate.

Early work on the use of fallout radionuclides to document erosion and sedimentation processes focused on ^{137}Cs and dates from the aftermath of the bomb testing of the 1950s and early 1960s. Cesium-137 can provide information relating to the redistribution of fallout received in the late 1950s and the 1960s, which currently provides a timeframe of ca. 50 years. The use of ^{137}Cs has been complemented more recently by the use of $^{210}Pb_{ex}$ and ^{7}Be, which provide information relating to longer (i.e., ca. 100 years) and much shorter (i.e., the past few weeks) timeframes, respectively [14]. Fallout radionuclides are being increasingly used in soil erosion and sedimentation investigations in many different areas of the world, and they are able to provide essentially unique information on rates and spatial patterns of erosion and sedimentation that cannot be obtained using traditional approaches. Particular advantages in terms of documenting erosion and sedimentation and particularly soil erosion include the ability to:

- Provide retrospective information on average rates of soil redistribution or sediment deposition (e.g., for the past 50 or 100 years) on the basis of contemporary sampling often involving only a single site visit.
- Provide both time-integrated data relating to the past 50 or 100 years (^{137}Cs and $^{210}Pb_{ex}$) and data relating to individual events or short periods of heavy rainfall occurring at present (^{7}Be).
- Integrate the various processes contributing to the redistribution of soil and sediment particles in the landscape.
- Obtain information from the "natural" landscape without the need for special installations or significant disturbance of the study area.
- Avoid the need for costly long-term monitoring.
- Assemble spatially distributed information that is directly compatible with recent advances in the development of physically based distributed models and the application of GIS and geostatistics to modeling erosion and sedimentation.
- Provide an approach that is applicable to several different components of the system, including erosion, sediment delivery, and sediment storage and deposition, as well as to tracing sediment sources. In the case of water erosion, it is also able to integrate processes associated with sheet erosion, rill erosion, and tillage erosion.
- Provide an approach that is applicable throughout the world, since fallout radionuclide fluxes and inventories are of sufficient magnitude to permit their use in most areas of the globe.

This entry provides an overview of the basis for using fallout radionuclides in the study of erosion and sedimentation and of the information that can be obtained. It provides a brief history of the approach; a description of the key characteristics of the individual fallout radionuclides, including their source, fallout input, and post-fallout behavior; a discussion of their use to document soil erosion and soil redistribution, as well as sediment deposition; a brief review of field and laboratory techniques and key issues that need to be addressed; and some examples of applications, based on the work of the author over the past 30 years.

A Brief History of the Use of Fallout Radionuclides in Erosion and Sedimentation Studies

As indicated above, work on the use of fallout radionuclides in soil erosion and sedimentation investigations largely dates from the aftermath of the nuclear weapons testing that occurred in the 1950s and early 1960s, although early work on the use of $^{210}Pb_{ex}$ to establish the chronology of sediment cores [15] developed essentially independently of this. The nuclear weapons testing that occurred in the 1950s and 1960s caused the fallout of a range of radionuclides, including strontium-90 (^{90}Sr) and ^{137}Cs. Menzel was arguably the first to recognize the link between radionuclide loss and soil loss from plots [16], although his work focused on ^{90}Sr. Subsequent studies [17–19] highlighted the link between ^{137}Cs loss and soil loss, and McHenry and Ritchie demonstrated that the spatial pattern of ^{137}Cs inventories within a field could be used to identify areas of erosion and deposition [20]. Based on this early work, the potential for using ^{137}Cs to document soil erosion and sediment redistribution rates has been successfully exploited in many different areas of the world. In addition to the very important lead provided by Ritchie working in the USA, particular reference can be made to pioneering work undertaken in Canada [21, 22], Australia [23–25], and the UK [26, 27]. The Chernobyl accident in 1986 also provided a significant input to the expansion of work on the application of ^{137}Cs measurements, by directing renewed attention to the behavior and fate of radiocesium in the environment and providing new opportunities to exploit the approach [28]. A further important stimulus to work in the field was provided by the International Atomic Energy Agency (IAEA). This body sponsored two Coordinated Research Projects between 1995 and 2001 aimed at promoting and standardizing procedures for using ^{137}Cs measurements in soil erosion and sedimentation investigations. These two Coordinated Research Projects culminated in the publication of a handbook for the assessment of soil erosion and sedimentation using environmental radionuclides that focused on the use of ^{137}Cs [29].

A clear and useful demonstration of the near exponential growth of studies involving the application of ^{137}Cs in soil erosion and sedimentation investigations between the late 1960s and the mid 1990s is provided by the number of entries for specific years included in the bibliography of publications of ^{137}Cs studies related to erosion and sediment deposition, compiled by Ritchie and Ritchie [30]. Although some of the publications included in this bibliography relate to broader aspects of the behavior of ^{137}Cs in the environment and to related radionuclides, the trend demonstrated in Fig. 1 provides a graphic indication of the rapid expansion of work in this field.

Although they focused attention on ^{137}Cs, the two IAEA Coordinated Research Projects referred to above also aimed to promote the use of other fallout radionuclides, and more particularly ^{7}Be and $^{210}Pb_{ex}$, in soil erosion investigations. The development of studies using these two fallout radionuclides commenced in the early and mid-1990s and important early work includes that of Wallbrink and Murray [31], Blake et al. [32], Walling et al. [33], Matisoff et al. [34], and Wilson et al. [35] with ^{7}Be, and Wallbrink and Murray [36], Walling and coworkers [37–39] and Matisoff et al. [34] with $^{210}Pb_{ex}$. Important drivers in promoting this work with additional fallout radionuclides included the possibility of addressing different timescales, with $^{210}Pb_{ex}$ covering up to ca. 100 years and ^{7}Be providing information on individual events and short periods of heavy rainfall. Another driver was the opportunity to increase the potential for using fallout radionuclides in areas of the world where ^{137}Cs inventories are very low and where these inventories will decline further in the near future, due to radioactive decay and the lack of contemporary fallout inputs.

Application of ^{137}Cs measurements to the study of sedimentation rates in depositional environments and to establishing the recent chronology for sediment

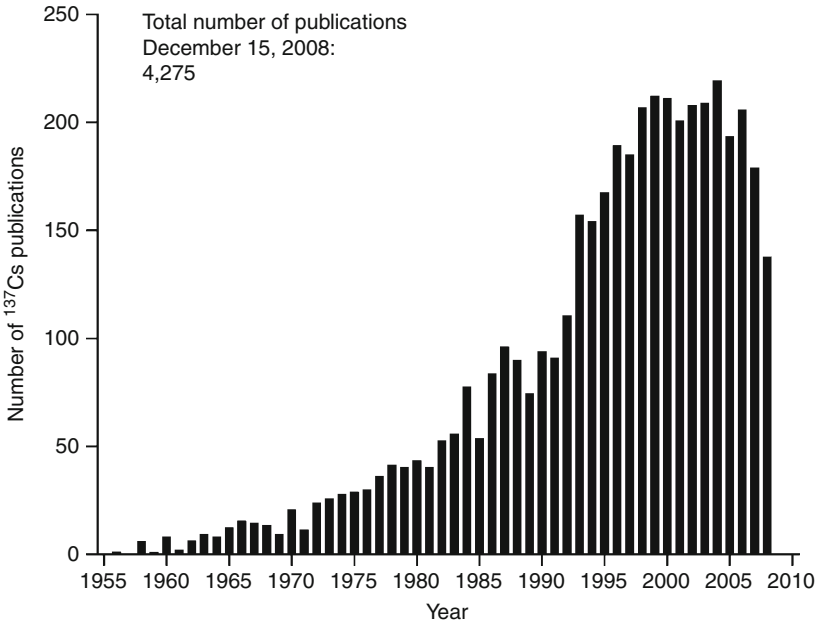

Fallout Radionuclides and the Study of Erosion and Sedimentation. Figure 1
The growth in the annual number of publications reporting work involving ^{137}Cs listed in the bibliography produced by Ritchie and Ritchie [30]

cores from lakes and reservoirs can again be traced back to the immediate aftermath of the bomb tests of the late 1950s and early 1960s [40]. The potential for using the peak fallout input in 1963 (or 1964 in the southern hemisphere) as a time marker was rapidly exploited by many investigators, and the approach was applied to a range of depositional sinks, in addition to lakes and reservoirs, including wetlands [41, 42], estuaries and coastal saltmarshes [43, 44], and river floodplains [45, 46]. The further fallout input provided by the Chernobyl accident introduced a second time marker in many areas of Europe and adjacent areas, which has improved the temporal resolution that can be achieved. Work by limnologists and sedimentologists on the application of $^{210}Pb_{ex}$ in establishing the chronology of sediment cores over the past ca. 100 years again developed in the early 1970s [47, 48] but proceeded essentially independently of work with ^{137}Cs. This in part reflects the different principle involved, namely, the reduction in activity with depth in response to decay, which was not dependent on the timing of weapons testing. The first application of the approach was to the accumulation of ice sheets and was described by Goldberg in the early 1960s [15]. Since the 1970s, key developments have included the use of direct measurements of $^{210}Pb_{ex}$ using gamma spectrometry as an alternative to its measurement using alpha spectrometry, which is considerably more demanding in terms of the chemical extraction required, and the development of improved models for interpreting the $^{210}Pb_{ex}$ depth distribution and establishing the chronology [49–51]. Because of its short half-life (53 days), ^{7}Be is commonly limited to the thin upper layer of sediment cores and is of little value for dating or establishing sedimentation rates. However, this radionuclide has been used since the 1980s to distinguish very recent sediment from older sediment and to quantify sediment mixing [52] and to estimate depths of overbank sedimentation on river floodplains associated with individual flood events [53].

Fallout Sources and Inputs

As indicated above, this contribution focuses on the application of three fallout radionuclides, namely, ^{137}Cs, $^{210}Pb_{ex}$, and ^{7}Be, in soil erosion and sedimentation investigations. These three radionuclides differ in terms of their half-lives, their sources, their fallout inputs, and the temporal variation of the resulting soil

inventories, and it is these differences that mean that they are able to be used to provide different, but complementary, information. It is important that their sources and the key features of their fallout input should be understood, since they have important implications for the interpretation of the measurements used to derive estimates of erosion and sedimentation rates. A brief overview of the source and fallout input of the three radionuclides is therefore provided below.

Cesium-137

Cesium-137 ($t_{½}$ 30.1 years) differs from the other two radionuclides in that whereas they are of natural origin, this radionuclide is manmade. It is found in the global environment primarily as a result of the testing of thermonuclear weapons (bomb tests) that took place during the period extending from the early 1950s to the early 1960s. In addition, a further fallout input occurred in parts of Europe and adjacent regions as a result of the Chernobyl accident in 1986. The bomb tests injected ^{137}Cs into the stratosphere, where it mixed and circulated globally before being redeposited as fallout. The first high-yield bomb test took place in 1952, but ^{137}Cs fallout was below detection in most areas of the world prior to 1954. The subsequent temporal pattern of fallout reflected the magnitude and number of bomb tests and the residence time of the ^{137}Cs in the stratosphere (ca. 1–10 years). Figure 2 summarizes available data on the temporal distribution of the annual fallout resulting from the bomb tests in the 1950s and 1960s, by combining data for New York, USA, and Milford Haven, UK to provide a typical record for the northern hemisphere, and from Adelaide and Brisbane to provide a typical record for the southern hemisphere. ^{137}Cs was not routinely monitored during the main period of bomb fallout, but reliable estimates can be derived from the measurements of ^{90}Sr fallout made at this time, since the two radionuclides are found in a fixed ratio. Most bomb tests were located in the northern hemisphere and Fig. 2 shows a gradual increase in ^{137}Cs fallout in the northern hemisphere up to 1959, when the temporary moratorium on bomb tests imposed in 1958 caused a reduction in fallout, followed by a further increase in fallout up to 1963 when the Nuclear Test Ban Treaty resulted in a cessation of bomb tests and fallout began to decline. Fallout levels fell below detection by the early 1980s. The further fallout input that occurred in 1986, as a result of the Chernobyl accident, was localized and more short-lived, because the radiocesium plume released from the accident was only dispersed into the troposphere. The data presented in Fig. 2 are estimates of annual fallout input. During a given year, the pattern of fallout is likely to have reflected that of precipitation, because most of the fallout occurred as wet fallout.

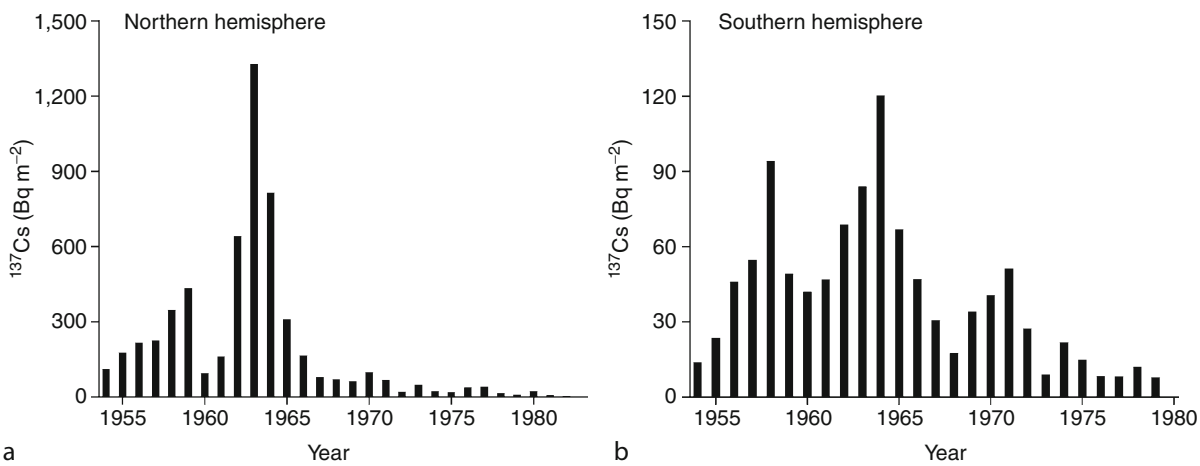

Fallout Radionuclides and the Study of Erosion and Sedimentation. Figure 2
Typical ^{137}Cs fallout records for the northern (New York, USA/Milford Haven, UK) and southern (Adelaide/Brisbane, Australia) hemispheres

The bomb tests injected ^{137}Cs into the stratosphere, and it was globally distributed. The global pattern of fallout reflects the global pattern of precipitation, since most fallout occurs as wet fallout in association with precipitation, the location of the bomb tests, and the pattern of stratospheric mixing. Because most tests occurred in the northern hemisphere, the global pattern of fallout evidences a clear latitudinal zonation. Figure 3 presents a generalized map of the global pattern of ^{137}Cs fallout associated with the bomb tests, as represented by the inventories found in 2000. Maximum fallout occurred in the mid-latitudes of the northern hemisphere and minimum fallout occurred around the equator. Overall, the amount of fallout received in the southern hemisphere was only about 30% of that received in the northern hemisphere. This feature of the global fallout pattern introduces some limitations on use of ^{137}Cs in the southern hemisphere, since the considerably lower inventories can introduce some measurement constraints.

It has been estimated that the amount of ^{137}Cs released by the Chernobyl disaster was of the order of 15% of that produced by the bomb tests. Because of its more limited tropospheric transport and dispersal, significant Chernobyl fallout is found over a more limited area of the globe located around the Chernobyl source (see Fig. 4). Here the pattern reflects the trajectory of the plume of contaminant released from Chernobyl and the distribution of precipitation during the immediate post-accident period. Considerable local variability has been reported in the case of Chernobyl fallout and this partly reflects the fact that the fallout was associated with a small number of rainfall events occurring within a short period. This contrasts with the situation for bomb fallout, which was distributed over a ca. 20-year period during which local variability is likely to have been smoothed. Reports of the magnitude of the depositional fluxes that occurred in the immediate vicinity of Chernobyl suggest that these were as high as 1,480 kBq m^{-2} and therefore more than two orders of magnitude greater than the total fallout received in areas of high bomb fallout. In many areas affected by Chernobyl fallout, that fallout input will now dominate the total inventory and this must be taken into account when using ^{137}Cs measurements to document soil erosion and sedimentation rates. However, there are also many areas in Europe where the two fallout inputs are of a similar magnitude and this may

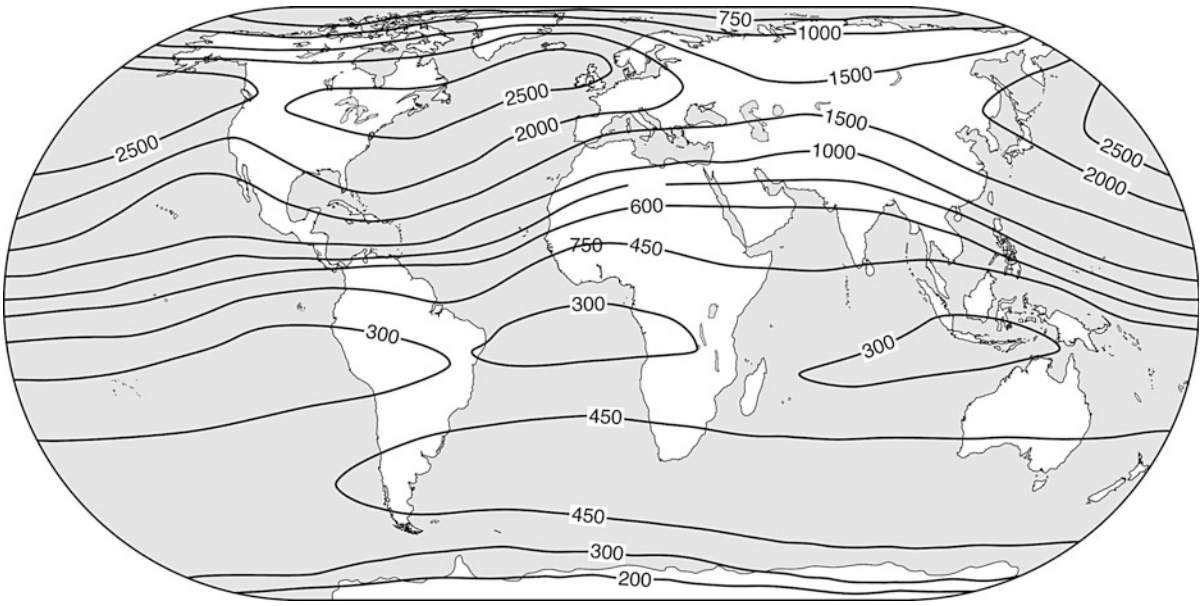

Fallout Radionuclides and the Study of Erosion and Sedimentation. Figure 3
The global pattern of ^{137}Cs inventories (Bq m^{-2}) in 2000 (based on Walling and He [54])

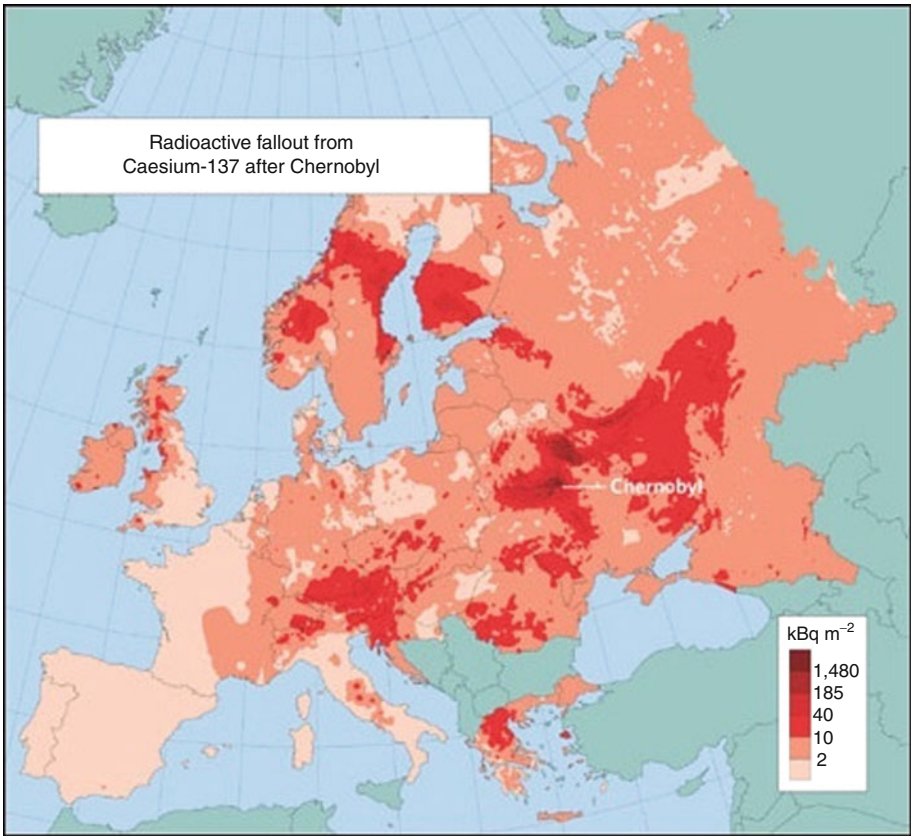

Fallout Radionuclides and the Study of Erosion and Sedimentation. Figure 4
The pattern of ^{137}Cs fallout over Europe resulting from the Chernobyl disaster (Based on Smith and Beresford [55])

introduce problems when interpreting contemporary measurements of ^{137}Cs inventories. In the period immediately after the Chernobyl accident, it was possible to distinguish the two components of the total ^{137}Cs inventory by also measuring the cesium-134 (^{134}Cs) activity. ^{134}Cs ($t_{½}$ 2.06 years) occurred in a fixed ratio to ^{137}Cs in Chernobyl fallout and this provided a means of quantifying the proportion of the total ^{137}Cs inventory attributable to Chernobyl fallout. Because of its short half-life, this approach could only be used for a few years immediately after the Chernobyl accident. However, scope exists to use the plutonium (^{239,240}Pu) content of the current inventory to establish the relative contribution of Chernobyl and bomb fallout, since ^{239,240}Pu was absent from Chernobyl fallout.

As emphasized by Fig. 2, a key feature of ^{137}Cs fallout is that in most areas of the globe, virtually all of this fallout input occurred during the period 1955–1970, with a peak in 1963. The basis for using this radionuclide to obtain estimates of erosion and sedimentation rates reflects this pattern of input. By studying the subsequent redistribution of the ^{137}Cs fallout in the landscape, it is possible to obtain information on soil and sediment redistribution over the past ca. 45 years. In addition, the occurrence of peak fallout in 1963 provides a valuable time marker in many depositional environments. Additional fallout inputs associated with the Chernobyl accident may mean that the main fallout input occurred in 1986 or if the inputs were of a similar magnitude that there were two periods of fallout input, one extending from 1955 to 1970 and the other occurring in 1986. The occurrence of the second fallout input can introduce a second time marker in sediment deposits which can prove very useful in establishing the chronology of a core.

Excess Lead-210

Lead-210 (^{210}Pb, $t_{½}$ 22.3 years) is a natural geogenic radionuclide that is produced in the Uranium-238 (^{238}U) decay chain. Radium-226 (^{226}Ra, $t_{½}$ 1,600 years) is a product of that chain and is found in most soils and rocks. This decays to gaseous Radon-222 (^{222}Ra, $t_{½}$ 3.8 days) which in turn undergoes a series of short-lived decays to ^{210}Pb. During its short half-life, some of the ^{222}Rn escapes from the soil into the overlying atmosphere, where it decays to ^{210}Pb, which returns to the earth's surface as fallout. The residence time of ^{210}Pb in the atmosphere is estimated to be only a few days. The ^{222}Rn that remains in the soil also decays to ^{210}Pb and, since this is an in situ product of the ^{226}Ra, it is commonly referred to as supported ^{210}Pb. It is possible to calculate the amount of supported ^{210}Pb that should theoretically exist in the soil, given the level of ^{226}Ra, by assuming equilibrium between the two radionuclides. However, the actual amount is likely to be less, since, under most conditions, some of the ^{222}Rn would have escaped to the overlying atmosphere. Without such escape or exhalation, supply of ^{222}Rn to the atmosphere and subsequent ^{210}Pb fallout would not occur. To distinguish the ^{210}Pb reaching the soil surface as fallout from that produced in situ within the soil, the former is commonly referred to as unsupported or excess ^{210}Pb ($^{210}Pb_{ex}$). The total inventory (Bq m^{-2}) of ^{210}Pb contained in a given depth of soil can therefore be partitioned into a supported and an unsupported or excess component. The former can be estimated from the amount of ^{210}Pb that would be expected if it was in equilibrium with the ^{226}Ra, reduced by a factor reflecting the proportion of the ^{222}Rn that escaped to the overlying atmosphere. It is not easy to establish this factor empirically, but it can be estimated by considering the difference between the theoretical estimate of supported ^{210}Pb activity (assuming equilibrium between ^{226}Ra and ^{210}Pb) in soil or sediment below the depth influenced by surface inputs of $^{210}Pb_{ex}$ and the measured activity at that depth. Since the fallout radionuclide (i.e., $^{210}Pb_{ex}$) is the component of interest for use in documenting erosion and sedimentation rates, it is important to direct attention to this, rather than the total ^{210}Pb activity. Other sources of ^{210}Pb fallout include exhalation of ^{222}Rn from the surface of the oceans, release of ^{226}Ra, ^{222}Rn, and ^{210}Pb from volcanic eruptions, and industrial emissions. Because the amount of ^{210}Pb produced over the oceans as a result of release and decay of ^{222}Rn is about two orders of magnitude less than that over land, this source is of limited importance for terrestrial fallout. The contribution of volcanic eruptions and industrial emissions to global fallout of ^{210}Pb is again minimal, but these sources can be locally significant.

In contrast to ^{137}Cs, the annual fallout of $^{210}Pb_{ex}$ at a given location can be viewed as being essentially constant in the medium term. If it is assumed that the total fallout of $^{210}Pb_{ex}$ is retained in the upper horizons of the soil of a stable reference site, that experiences neither erosion nor deposition, the mean annual fallout input can be estimated by assuming a steady-state equilibrium between fallout input and loss through radioactive decay. There are few longer-term records of annual $^{210}Pb_{ex}$ fallout involving direct measurements that can be used to assess the degree of inter-annual variability, but a record from Munich-Neuherberg in southern Germany for the period 1981–1999 [56] demonstrated a twofold variation in annual fallout, with values ranging from 120 to 250 Bq m^{-2} year^{-1}, with a mean of 180 Bq m^{-2} year^{-1}. A similar factor of two for the inter-annual variability of ^{210}Pb fallout has been reported by other studies. This inter-annual variability can be partly accounted for by variations in annual precipitation, but the relationship between the annual ^{210}Pb fallout flux and annual rainfall is not always well defined. The distribution of fallout within the year will reflect both the precipitation regime and seasonal variation of the concentration of $^{210}Pb_{ex}$ in the atmosphere, as well as the degree of mixing of the atmosphere and the volume of air scavenged by the rainfall. High concentrations are often found in the atmosphere during late spring and summer when drier soils and the absence of snow cover increase the exhalation of ^{222}Rn to the atmosphere from the soil [57]. Valles et al. [58] report a twofold variation in monthly ^{210}Pb concentrations in air sampled at Barcelona, Spain and at this location, concentrations were substantially higher in summer and autumn. However, equivalent information on air concentrations reported for Munich-Neuherberg [56] showed a contrasting pattern, with maximum values between September and February. At this site, maximum

monthly fallout fluxes occurred in the summer months between June and August, in response to the higher precipitation during these months.

Less is currently known about the global variation of $^{210}Pb_{ex}$ fallout than for ^{137}Cs. Values of annual fallout reported in the literature range over more than an order of magnitude from <50 Bq m^{-2} year^{-1} to in excess of 500 Bq m^{-2} year^{-1} (see Table 1). In terms of the global pattern, available information suggests that, although annual fallout fluxes will reflect annual rainfall, they are generally lower in the western areas of the continents, where the dominant air mass movements are off the oceans where very little ^{222}Rn will be produced. In contrast, higher annual fluxes are commonly found in the eastern areas of continents where the air mass tracks pass over large areas of land where ^{222}Rn is produced and concentrations of dust increase. A clear latitudinal zonation in annual fallout of ^{210}Pb has also been reported [59], with much lower values being documented in the southern hemisphere, due to the greater expanse of ocean. The values listed in Table 1 are consistent with these general controls. However, it is important to note that there may be appreciable local variability in annual fallout deposition. Values of annual ^{210}Pb deposition of 59 and 85 Bq m^{-2} year^{-1} in 1990 have been reported for two sites in the southern Netherlands that are only 5 km apart [60].

Fallout Radionuclides and the Study of Erosion and Sedimentation. Table 1 Mean annual deposition of $^{210}Pb_{ex}$ at different locations

Location	Mean ^{210}Pb fallout (Bq m^{-2} year^{-1})
Tatsunokuchi, Japan[a]	840
Hokkaido, Japan	367
Bombay, India	250
Munich, Germany[b]	180
Galveston, USA[c]	172
New Haven, USA	153
Geneva, Switzerland[d]	150
Delhi, India	133
Moscow, Russia	115
Bermuda[e]	115
Calcutta, India	102
Darwin, Australia	95
Milford Haven, UK	85
Suva, Fiji	80
Groningen, the Netherlands[f]	71
Alice Springs, Australia	57
Sydney, Australia	53
Auckland, New Zealand	50
East Antarctica[g]	31

Adapted from Beks et al. [60], with additions.
[a]From Turekian et al. [61]
[b]From Winkler and Rosner [56]
[c]From Yamamoto et al. [62]
[d]From Baskaran et al. [63]
[e]From Beks et al. [60]
[f]From Preiss et al. [59]
[g]From Caillet et al. [64]

Beryllium-7

Beryllium-7 (^{7}Be $t_{½}$ 53.3 days) is, like ^{210}Pb, a naturally occurring fallout radionuclide. In this case, its origin is cosmogenic and it is produced in the troposphere and stratosphere by the cosmic ray spallation of nitrogen and oxygen. The production of ^{7}Be is controlled by the cosmic ray flux which varies with altitude, latitude, and solar activity [66]. Production is reported to be greatest at altitudes between 12 and 20 km, depending on latitude, and decreases almost exponentially toward the earth's surface, where it is about three orders of magnitude lower [67]. Globally, production increases from the equator toward the poles and this increase is characterized by a factor of approximately 1–3 for the troposphere and 4–5 for the stratosphere [67]. Because ^{7}Be production is influenced by solar activity, it has been linked to sunspot numbers and the 11-year solar cycle. The increased incidence of sunspots reduces the cosmic ray flux to the earth and thus ^{7}Be production. Because of the longer residence times of aerosols in the stratosphere, ^{7}Be activity remains relatively constant in the stratosphere. However, with lower production rates and shorter aerosol residence times due to rapid washout, ^{7}Be concentrations in the troposphere are one or two orders of magnitude less than that in the stratosphere. Available evidence suggests that >90% of ^{7}Be deposition occurs as wet deposition [68].

There are relatively few records of ^{7}Be fallout to provide a detailed basis for defining its characteristics, but available evidence indicates that in addition to inter-annual variability connected to sunspot activity, ^{7}Be concentrations in precipitation and fallout fluxes vary seasonally. These variations will reflect the incidence of mixing between the stratosphere and troposphere, the altitude of precipitation generation, and precipitation amounts. Maximum concentrations and fluxes are often recorded in spring and early summer in mid-latitudes, in response to increased stratosphere-troposphere exchange and increased convection due to warming of the land surface. Considerable variability in ^{7}Be concentrations may be associated with individual rainfall events, with some researchers reporting that activities can vary by a factor of greater than 20 between events. However, fairly well-defined relationships between ^{7}Be depositional flux and event rainfall are commonly found [64]. Because of its short half-life, it is more important to understand the magnitude and timing of fallout inputs, since these will have a much greater effect on the soil inventory than in the case of ^{137}Cs and $^{210}Pb_{ex}$, where the inventory of these radionuclides will remain essentially constant in the short term and reflect the long-term pattern of fallout.

As with ^{210}Pb, there are currently insufficient measurements to obtain a clear picture of the global pattern of annual ^{7}Be deposition. However, available measurements indicate that annual fluxes range between ca. 500 and 6,500 Bq m^{-2} year^{-1} (see Table 2). The influence of annual rainfall amount is readily demonstrated by the high annual deposition of 6,350 Bq m^{-2} year^{-1} reported for Hokitika in South Island, New Zealand [68], where the annual rainfall was ca. 2,800 mm. Since most available measurements are from the mid-latitudes, it is difficult to identify the latitudinal

Fallout Radionuclides and the Study of Erosion and Sedimentation. Table 2 Annual deposition of ^{7}Be recorded at different locations

Place	Mean annual precipitation (mm)	Annual ^{7}Be fallout (Bq m^{-2} year^{-1})	Source
Hokitika, New Zealand	2,800	6,350	Harvey and Matthews [69]
Tatsunokuchi, Japan	–	5,300	Yamamoto et al. [62]
New Haven, CT, USA	1,390	3,780	Turekian et al. [70]
Bermuda	1,700	2,850	Turekian et al. [70]
Galveston, USA	1,167	2,450	Baskaran et al. [63]
Geneva, Switzerland	966	2,087	Caillet et al. [64]
Norfolk, VA, USA	1,313	2,075	Todd et al. [71]
Milford Haven, UK	1,328	1,618	Peirson [72]
Bombay, India	2,277	1,267	Lal et al. [73]
Heidelberg, Germany	810	1,249	Schumann and Stoeppler [74]
Canberra, South Eastern Australia	660	1,030	Wallbrink and Murray [68]
Chilton, UK	822	898	Peirson [72]
Arkansas, USA	1,070	867	Lee et al. [75]
Westwood, NJ, USA	787	717	Walton and Fried [76]
Damascus, Syria	153	528	Othman et al. [77]
East Antarctica	–	700	Nijampurkar and Rao [65]
Malaga, Spain	308	412	Duenas et al. [78]

influence that could be expected to result from the latitudinal variation in ^{7}Be production noted above. Because of its cosmogenic origin and the importance of production in the stratosphere, ^{7}Be deposition fluxes can be expected to be similar in both the northern and southern hemispheres. This contrasts with ^{137}Cs and ^{210}Pb, where the location of the bomb tests and the much larger extent of the oceans in the southern hemisphere, respectively, exert an important influence in reducing fallout inputs in the southern hemisphere.

Fallout Radionuclides in the Soil and Soil Inventories

^{137}Cs, ^{210}Pb$_{ex}$, and ^{7}Be fallout reaches the soil surface as positively charged cations, and in most environments, the fallout will be rapidly and strongly adsorbed by mineral particles and organic material and become essentially non-exchangeable [79–83]. Preferential adsorption by clay minerals and fine particles has been reported in many studies [84]. The strong affinity of these radionuclides for the soil is reflected by their high partition coefficients (K_d) which are commonly of the order of 10^4–10^5 L kg^{-1}. Existing evidence suggests that whereas ^{137}Cs is primarily associated with the mineral fraction of soils, the organic fraction is also important in the uptake of ^{7}Be and ^{210}Pb$_{ex}$. The speed of uptake and the kinetics of the adsorption are less well defined, but time spans for uptake or adsorption ranging from a few minutes to less than an hour are often cited. It is, however, important to recognize that in some environments, the fallout radionuclides reaching the soil surface may be less strongly fixed. This, for example, appears to be case for ^{137}Cs and peat soils, because there are a number of reports of Chernobyl fallout being poorly fixed by peat soils and remaining mobile within the soil and runoff.

Where the soil supports a vegetation canopy, this will complicate the transfer of the radionuclides to the surface soil. In the case of ^{137}Cs and ^{210}Pb$_{ex}$ where emphasis is usually placed on the longer-term accumulation and fate of the fallout input in the landscape, such interception is of limited importance, since the radionuclides can be subsequently transferred to the soil by leaching and wash-off and by decay when the vegetation dies back or sheds its leaves. For, ^{7}Be, however, this interception can be more important, since the short half-life of the radionuclide can mean that a significant proportion of the fallout input may be intercepted and subsequently lost from the vegetation canopy through radioactive decay and therefore never reach the soil surface. Work in forested areas in Maine, USA, has indicated that as much as 50% of the fallout input could be held in the forest canopy [85] and a study of ^{7}Be interception by grass undertaken at Bologna, Italy similarly indicated that more than 50% of the total inventory was held in the grass layer above the soil [86]. Kaste et al. [66] also suggest that soils with a grass cover are frequently characterized by a higher total areal activity density than bare soils, pointing to the role of the grass in trapping atmospheric aerosols. This interception has important implications for the use of ^{7}Be as a tracer of soil redistribution, since in areas with a vegetation canopy, it is likely to result in considerable local-scale variability in the soil inventory and it may prove impossible to establish a reference inventory for the soil itself which can be used to identify areas of erosion (i.e., reduced ^{7}Be inventories) and deposition (i.e., areas with increased ^{7}Be inventories).

Because of the rapid and strong adsorption of the fallout input by the surface horizons of the soil, the total inventory or areal activity density (Bq m^{-2}) measured at a reference site, defined as a stable undisturbed site which has experienced neither erosion nor deposition, will directly reflect the prior fallout input to the site, assuming that the transfer to the soil has not been influenced by a vegetation canopy as discussed above. Figure 5 provides a schematic representation of the variation of that inventory over the timescale relevant to the use of a particular fallout radionuclide as a tracer. For ^{137}Cs and ^{210}Pb, with half-lives extending to decades, this timescale covers ca. 50–100 years, whereas for ^{7}Be, with a much shorter half-life, it extends over ca. 6 months. For ^{137}Cs (Fig. 5a), the key feature of the variation of the inventory over the period of interest is the absence of ^{137}Cs in the soil prior to the early 1950s, the subsequent rapid increase in the inventory until the mid-1960s, due to the bomb tests during the period extending from the mid-1950s until 1963, and the subsequent decline in the inventory since the mid-1960s, when loss from the inventory due to radioactive decay exceeded the residual fallout input from the bomb tests. In the absence of new ^{137}Cs fallout, the inventory will continue to progressively decline to

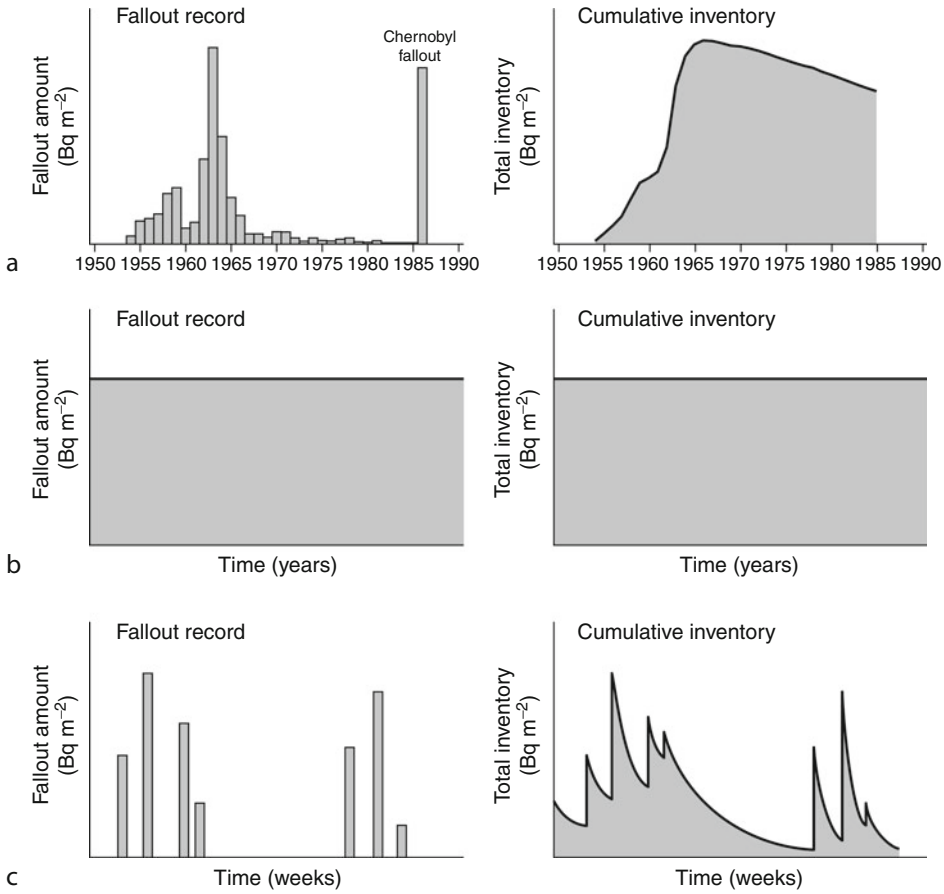

Fallout Radionuclides and the Study of Erosion and Sedimentation. Figure 5
A schematic representation of the interaction between the fallout input and the (**a**) ^{137}Cs, (**b**) $^{210}Pb_{ex}$, and (**c**) ^{7}Be inventory in the soil of a reference site over the timescale relevant to the use of the individual fallout radionuclides as tracers of soil and sediment redistribution

the point where it will fall below the level of detection and the radionuclide can no longer be used as a tracer. This point is likely to be reached earlier in equatorial regions and in the southern hemisphere, where inventories are lower. In locations where an additional input of ^{137}Cs occurred in 1986, as a result of the Chernobyl accident, this input would have caused an increase in the inventory and a temporary halt to the decline. However, since Chernobyl fallout was short-lived, the declining trend was soon restored.

For $^{210}Pb_{ex}$, the pattern of variation of the inventory is very different from that of ^{137}Cs and the inventory can be seen as essentially constant through time (Fig. 5b), with new fallout inputs balanced by losses caused by radioactive decay. For a reference site with a mean annual fallout input of 250 Bq m^{-2} $year^{-1}$, the steady-state inventory will be ~8,169 Bq m^{-2}. In reality, there will be small variations in the total inventory due to inter-annual variations in the fallout input, but since the annual fallout input represents only a relatively small proportion of the total inventory (i.e., ca. 3%), the effect of these fluctuations will be small. In the case of ^{7}Be, however, the magnitude and timing of the fallout inputs will exert a key influence on the variation of the inventory through time, due to the short half-life of this radionuclide. In the absence of further fallout, the inventory would decline to near-zero within about 6 months and the temporal pattern of fallout inputs will dominate the variation of the inventory through time. A timescale of ca. 6 months

has therefore been used in Fig. 5c to represent the key features of the variation of the ^{7}Be inventory through time.

When considering in more detail the storage or the longer-term fate of fallout radionuclides within the soil, there is a need to distinguish undisturbed and cultivated soils. In the former, redistribution of the fallout input within the soil profile will be governed primarily by physicochemical diffusion and migration processes, including biological activity, whereas in the latter case, tillage will commonly mix the upper horizons of the soil and cause the radionuclide activity to be relatively uniformly distributed through the plow layer. Figure 6 presents typical ^{137}Cs, ^{210}Pb$_{ex}$, and ^{7}Be depth distributions for undisturbed (i.e., permanent pasture) and adjacent cultivated area documented by the author

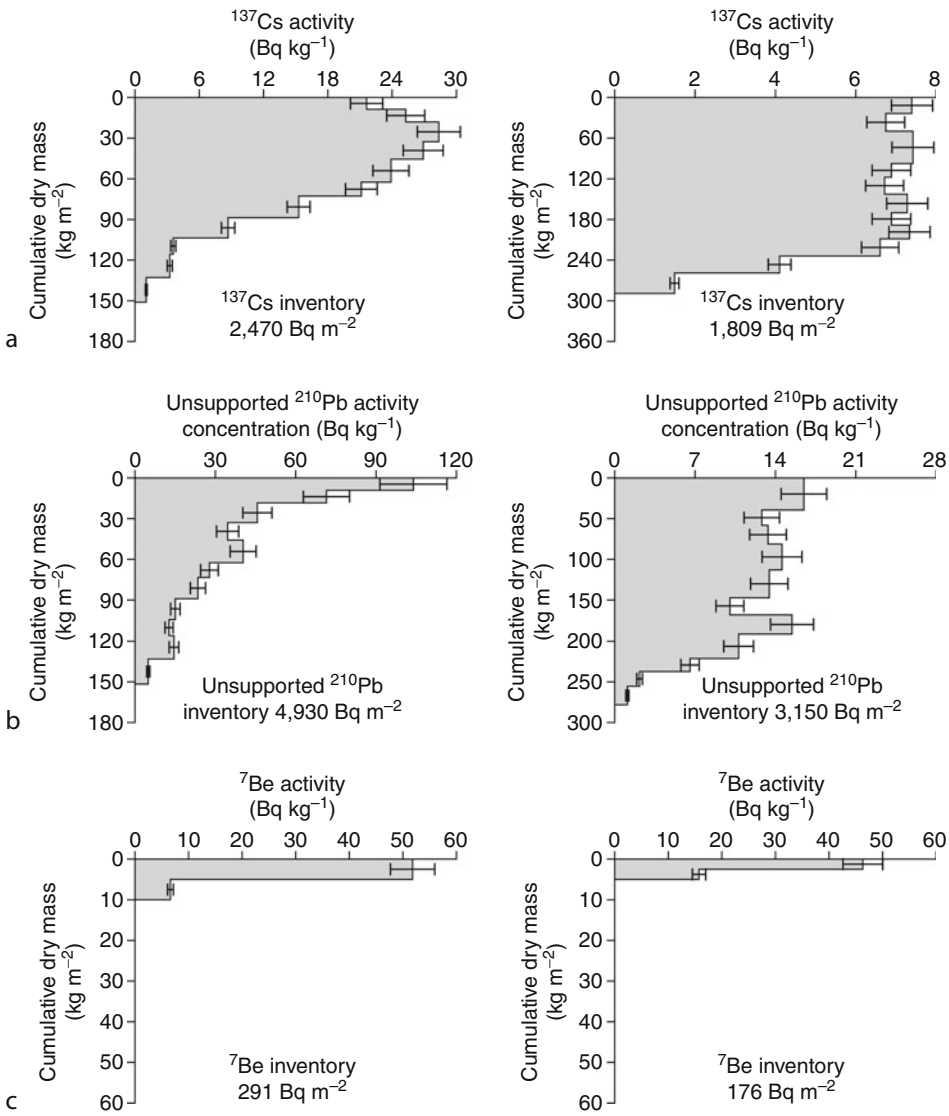

Fallout Radionuclides and the Study of Erosion and Sedimentation. Figure 6
Characteristic depth distributions of ^{137}Cs, ^{210}Pb$_{ex}$, and ^{7}Be in undisturbed pasture soils (*left*) and cultivated soils (*right*) in Devon, UK. The precision of the radionuclide measurements at the 95% level of confidence is indicated by the error bars

and his coworkers for a site near Crediton in Devon, UK. Depth distributions of similar shape are likely to be found in different areas of the world, although the total inventory will vary. In Fig. 6, the depth scale has been expressed as a mass depth (kg m^{-2}), since this removes the need to take account of variations in bulk density within the upper levels of the soil in influencing the precise form of the depth distribution. For ^{137}Cs, the depth distribution for an undisturbed soil shown in Fig. 6a is characterized by the typical exponential decline in activity with depth that has been widely reported for undisturbed soils. In this case, ca. 80% of the total inventory is found within the upper 10 cm of the soil profile. This depth distribution can be readily accounted for by the surface input of ^{137}Cs as fallout and its subsequent downward movement by diffusion-like processes. These processes include biological activity (e.g., earthworms), which cause mixing. In many undisturbed soil profiles, such as that illustrated here, the peak activity is found just below the surface, rather than at the surface, and this can be seen as reflecting the absence of significant fallout since the 1980s (in the absence of Chernobyl fallout), biological activity moving soil from depth to the surface, and the accumulation of dead organic material at the surface. The depth distribution of $^{210}Pb_{ex}$ for an undisturbed soil, illustrated in Fig. 6b, is, as might be expected, very similar to that of ^{137}Cs. However, in this case, the fallout input is continuous and the maximum activity is commonly found at the surface, where it is maintained by the fresh fallout. The depth distribution of ^{7}Be associated with an undisturbed soil shown in Fig. 6c differs substantially from that of the other two fallout radionuclides, in that all the inventory is contained within the upper ca. 10 mm of the soil and most is within the upper 5 mm. This situation reflects the continuing input of ^{7}Be fallout to the surface and the short half-life of the radionuclide, which means that any ^{7}Be slowly moving deeper into the soil disappears quite rapidly due to decay.

In the case of ^{137}Cs and $^{210}Pb_{ex}$, the depth distributions illustrated for an undisturbed soil in Fig. 6 can be viewed as essentially constant over a timescale of several years. The $^{210}Pb_{ex}$ profile is likely to remain constant over a longer timescale, as the fallout input and downward movement are balanced by decay. In the longer term, the ^{137}Cs depth distribution would have changed, through time, reflecting the beginning of the fallout input in the 1950s, when most of the radiocesium would have been found near the surface, the subsequent progressive downward movement of the radionuclide, the cessation of significant fallout in the 1980s, and the gradual reduction in the total inventory after the mid-1960s, when loss by decay started to exceed the input of new fallout. Existing experimental evidence, based on the artificial application of radiocesium to bare soil surfaces, indicates that fresh fallout is initially distributed within the top few millimeters of the soil. This situation is essentially replicated by the ^{7}Be depth distribution, since decay removes the evidence of medium-term downward movement. Because of its short half-life, the ^{7}Be depth distribution will be more dynamic, reflecting short-term changes in the total inventory in response to fresh fallout and its subsequent redistribution within the shallow upper soil layer, as well as ongoing decay. Figure 7 illustrates the evolution of the depth distribution of ^{7}Be within a bare undisturbed soil in an area of cleared forest near Valdivia in southern Chile, from summer through the wet season (autumn and winter) to the following spring [87]. Over the period of measurement, the total inventory varies over nearly an order of magnitude from 181 to 1,401 Bq m^{-2}. In Fig. 7, the depth distributions are represented by the total inventory recorded above a given depth and the individual distributions show a clear exponential form. The h_0 values listed represent the relaxation depths of the exponential distributions and increased values reflect greater penetration. During the initial period, which represents the end of the dry season, the inventory declines, but it subsequently increases at the onset of the wet season. At this stage, the new input of fallout to the surface causes an increase in the inventory held close to the surface and the h_0 values decline. As the wet season continues, however, the depth distribution deepens and the h_0 values increase to reflect the greater proportion of ^{7}Be held at depth.

As shown in Fig. 6, the depth distributions of ^{137}Cs and $^{210}Pb_{ex}$ in cultivated soils are dominated by the influence of soil mixing caused by tillage. The profiles are characterized by a fairly uniform radionuclide activity in the plow layer, which is well mixed by tillage, but the activity rapidly declines below the plow depth.

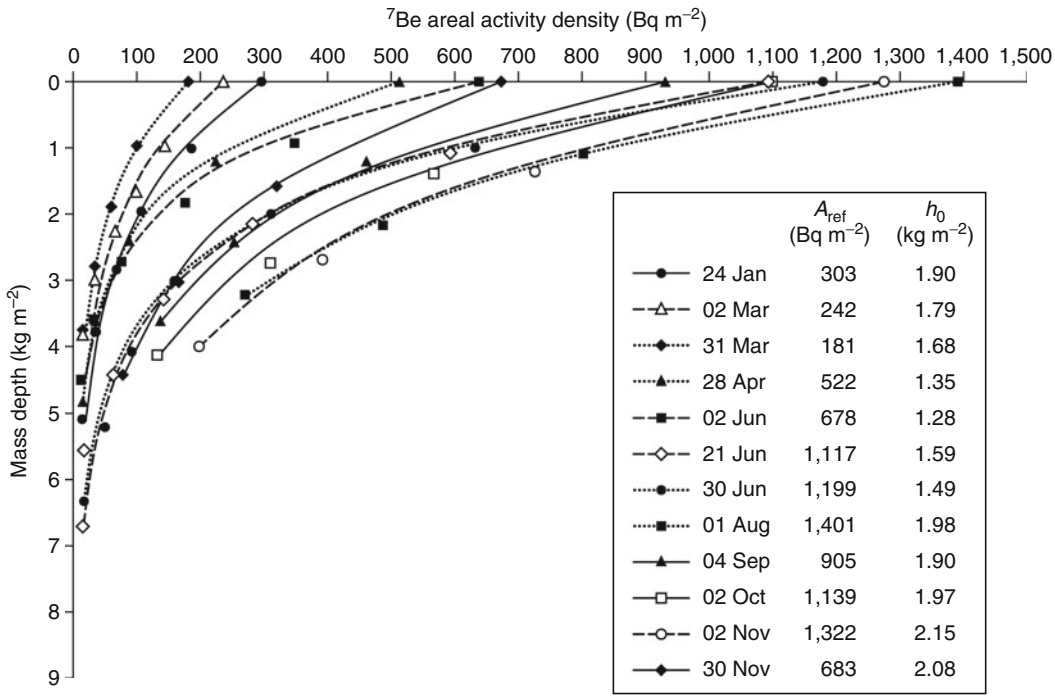

Fallout Radionuclides and the Study of Erosion and Sedimentation. Figure 7
Depth distributions of ^{7}Be recorded in a bare forest soil at a reference site near Valdivia in southern Chile over the seasonal cycle. The inventories (A_{ref}) and relaxation depths (h_0) associated with the individual depth distributions are listed in the key (Based on [87])

Most profiles evidence a small "tail" extending below the plow depth, reflecting some limited downward movement of the radionuclide to greater depth. The ^{137}Cs and ^{210}Pb$_{ex}$ profiles for cultivated soils portrayed in Fig. 6 were taken from eroding areas within a cultivated field, and the total inventories are less than those associated with the equivalent cores from an adjacent area of undisturbed grassland. The reduced inventories reflect the progressive loss of soil containing ^{137}Cs or ^{210}Pb$_{ex}$ from the surface of the profile by erosion. As erosion proceeds, both the inventory and the ^{137}Cs activity in the plow layer will decline, as plowing incorporates subsoil containing little ^{137}Cs or ^{210}Pb$_{ex}$ into the plow layer. In the absence of erosion, the depth distribution would be characterized by a total inventory similar to that associated with the undisturbed stable site. The shape of the profile would also be similar to those presented in Fig. 6 for cultivated soils, but the activity within the plow layer would be greater.

In contrast to the ^{137}Cs and ^{210}Pb$_{ex}$ profiles depicted in Fig. 6, the depth distribution of ^{7}Be for the cultivated field is almost identical to that recorded for the undisturbed area. The reason is that the ^{7}Be fallout accumulates in the upper few millimeters of the soil and when the field is plowed, the action of mixing the accumulated ^{7}Be into the plow layer reduces the activity to below the level of detection. After plowing and cultivation, new fallout will again accumulate near the surface and as time progresses and the inventory grows, the depth distribution will closely resemble the depth distribution associated with the undisturbed area. The reduced ^{7}Be inventory associated with the depth distribution for the cultivated field relative to the adjacent undisturbed field could reflect the timing of the prior plowing and the limited time available for the inventory to be restored. However, in this instance, the plowing occurred many months previously and the reduced inventory reflects the loss of surface soil by erosion. This situation is confirmed by the reduced depth to which ^{7}Be is found.

Where soil redistribution within the landscape caused by erosion produces areas of deposition, the

depth distributions of the fallout radionuclides associated with such depositional areas will differ from those for stable and eroding areas presented in Fig. 6. Assuming that the mobilized sediment which is subsequently deposited contains ^{137}Cs, $^{210}Pb_{ex}$, or ^{7}Be, by virtue of its source within the landscape, the deposition of sediment, for example at the foot of a slope or on a river floodplain, will cause the inventory to increase and the depth distribution to change due to upward extension and thus an increase in the depth of soil or sediment containing the radionuclide. Figure 8 provides some examples of such changes associated with a river floodplain site in Devon, UK. In this case, the depth distributions were documented for both a point on the river floodplain and an adjacent area of undisturbed pasture above the level of inundation, with no evidence of either erosion or deposition. In both cases, the soils were uncultivated and the profiles are therefore undisturbed by tillage mixing. In the case of the ^{137}Cs depth distributions, the profile from the floodplain has an inventory that is considerably greater than the profile from the area above the level of inundation, as a result of deposition of sediment containing ^{137}Cs. The profile shape also provides clear evidence of deposition. The shape of the ^{137}Cs depth distribution shown for the floodplain reflects the progressive reduction of the ^{137}Cs content of the sediment sources within the catchment, and thus also of the deposited sediment, as a result of the ongoing loss of ^{137}Cs through erosion.

As with ^{137}Cs, the total inventory associated with the $^{210}Pb_{ex}$ depth distribution from the depositional site on the floodplain shown on Fig. 8 is substantially greater than that of the $^{210}Pb_{ex}$ profile for the undisturbed site above the level of inundation. This again reflects the input of $^{210}Pb_{ex}$ to the floodplain profile from both fallout to the floodplain surface and the deposition of sediment containing $^{210}Pb_{ex}$. The depositional environment is again further confirmed by the substantially greater depth to which $^{210}Pb_{ex}$ is found in the floodplain profile. Since the fallout input of $^{210}Pb_{ex}$ to both the upstream catchment and the floodplain surface is essentially continuous, there is no reduction in activity toward the surface of the floodplain profile. The rate of decrease of the $^{210}Pb_{ex}$ activity with depth will reflect the rate of sediment accretion and the rate of decay of the $^{210}Pb_{ex}$ contained in the buried sediment. Since the latter is known, it is possible to estimate the rate of sediment accretion from the rate of decrease of activity with depth in the profile (see section "Estimating Sedimentation Rates and Establishing Chronologies in Depositional Sinks"). Comparison of the two ^{7}Be depth distributions presented in Fig. 8 again provide clear evidence of deposition, as reflected by the increased inventory and depth of the ^{7}Be profile from the accreting floodplain, when compared with the profile from the site above the level of inundation. Both these features of the floodplain profile indicate that the deposition occurred only a short time prior to the time that the ^{7}Be depth distributions were documented, since in the absence of new sediment deposition, any difference between the two ^{7}Be profiles would soon disappear. The higher ^{7}Be surface activity associated with the floodplain profile reflects the two sources of ^{7}Be input to the surface, namely, direct fallout and deposition of sediment containing ^{7}Be mobilized from the upstream catchment.

The fallout radionuclide profiles from a depositional site illustrated in Fig. 8 relate to an area of undisturbed permanent pasture on a river floodplain. Similar profiles will be found in other depositional sinks, such as areas of deposition at the foot of a slope, where the soil surface will receive both direct fallout and an input of radionuclide-bearing sediment eroded from upslope. In many instances, depositional sites will also be cultivated. In cultivated areas, the depth distribution of ^{137}Cs and $^{210}Pb_{ex}$ associated with depositional areas will again be characterized by increased inventories and the occurrence of the two radionuclides to greater depths. However, the action of tillage will commonly introduce greater homogeneity into the depth profile and in many cases, the magnitude of the increase in inventory rather than the shape of the depth distribution will provide the key evidence as to the rate of deposition.

Using Fallout Radionuclides as Tracers to Investigate Soil and Sediment Redistribution within the Landscape

A sound understanding of the input and redistribution of ^{137}Cs, $^{210}Pb_{ex}$, and ^{7}Be within the landscape provides the key to using these three radionuclides to estimate rates of soil and sediment redistribution.

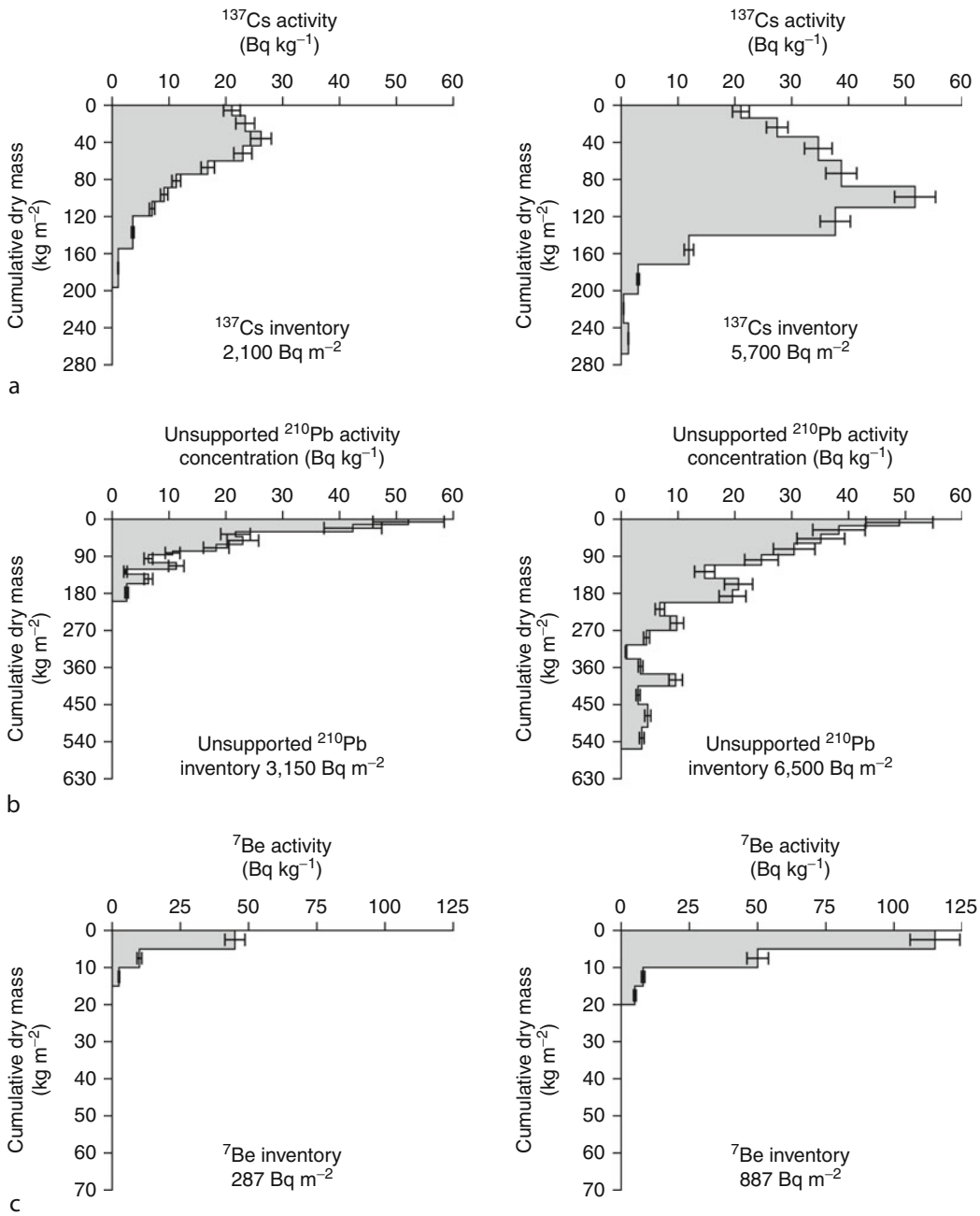

Fallout Radionuclides and the Study of Erosion and Sedimentation. Figure 8
Characteristic depth distributions of ^{137}Cs, $^{210}Pb_{ex}$, and ^{7}Be from an undisturbed pasture site (*left*) and from a neighboring regularly inundated river floodplain (*right*) in Devon, UK. The precision of the radionuclide measurements at the 95% level of confidence is indicated by the error bars

Their distinctive behavior at erosional and depositional sites, in particular, provides a basis for quantifying erosion and deposition rates and discriminating fine sediment sources. Further discussion of the principles involved will consider: firstly, quantification of soil redistribution within the landscape by soil erosion, secondly, the estimation of sedimentation rates in depositional sinks such as lakes, reservoirs, and river

floodplains and establishing chronologies for the associated sediment deposits, and thirdly, discriminating the potential sources of fine sediment in catchments and river basins. In each case, there is a need to take account of differences between the three fallout radionuclides in terms of the temporal pattern of fallout and the timescale of interest and the consequent need for different approaches.

Quantification of Soil Redistribution Within the Landscape by Soil Erosion

As demonstrated by Figs. 6 and 8, both the total inventory and the depth distribution of ^{137}Cs, $^{210}Pb_{ex}$, and ^{7}Be in soil or sediment can provide information on past soil redistribution at that point. Because the inventory can generally be obtained with a single measurement, whereas a substantial number of measurements will be needed to establish the depth distribution, and the number of samples that can be measured is frequently limited by detector availability and the count times involved (see section "Laboratory Procedures and Techniques"), attention usually focuses on inventory measurements. In most studies, the approach taken involves establishing a reference inventory, which represents the inventory associated with an undisturbed location experiencing neither erosion nor deposition, and comparing the inventories obtained for other sampling points with this value. Where they are less than the reference inventory, it is assumed that erosion has occurred and, where they exceed the reference inventory, this is assumed to reflect deposition. In the case of ^{137}Cs, the soil redistribution resulting in the reduced or increased inventory is assumed to have occurred over the period since the main period of ^{137}Cs fallout in the late 1950s and early 1960s, whereas for $^{210}Pb_{ex}$ and ^{7}Be, the period is defined by considering the half-life of the radionuclide and the extent to which the current inventory will reflect past fallout and redistribution of that fallout. It is important that this comparison should take account of the uncertainty associated with both the precision of the laboratory measurements of the radionuclide activity used to establish the inventories of the sampling points and any uncertainty associated with the value used for the reference inventory. The latter will reflect both the measurement precision and the uncertainty introduced by small-scale spatial variability of the soil inventory and the sampling procedure (see section "Field Techniques for Sample Collection").

In a few studies involving ^{137}Cs, a different repeat sampling approach has been employed and soil redistribution rates are estimated by comparing the inventories measured on two occasions at the individual sampling points [88]. The principle involved is very similar to the use of a reference inventory, in that a reduction in inventory over time is assumed to reflect erosion, whereas an increase is taken to indicate deposition. Although this alternative approach has the advantage that the period during which soil redistribution processes have been operating to cause the changing inventory is precisely defined and the need to establish the local reference inventory is removed, it also has several important limitations which are likely to restrict its application. The first is the need for repeat measurements and thus the inability to obtain results quickly and without preplanning. Studies where the approach has been used have generally been able to make use of data fortuitously provided from earlier sampling programs, but these will rarely be available. Secondly, there is a need to ensure that the period elapsed between the two surveys is of sufficient duration to produce a significant reduction or increase in the inventory, bearing in mind the uncertainty associated with the measured inventories, which will reflect both analytical precision and variability introduced by sampling. Finally, relocating sampling points may prove difficult. Even in areas where erosion and deposition rates are relatively high, it has been estimated that a period of 10 years between sampling campaigns may be required to ensure that there is a significant difference between the two sets of measurements. Where soil redistribution rates are relatively low, the length of the period will increase. This contribution will focus on the standard approach using a reference inventory.

Use of ^{137}Cs Measurements Figure 9 provides a schematic representation of the principles involved in using ^{137}Cs measurements to estimate soil redistribution rates. Here, an orchard is used as a reference site and the cores used to define the reference inventory and the characteristic depth distribution are collected between the trees where the presence of the trees will have had

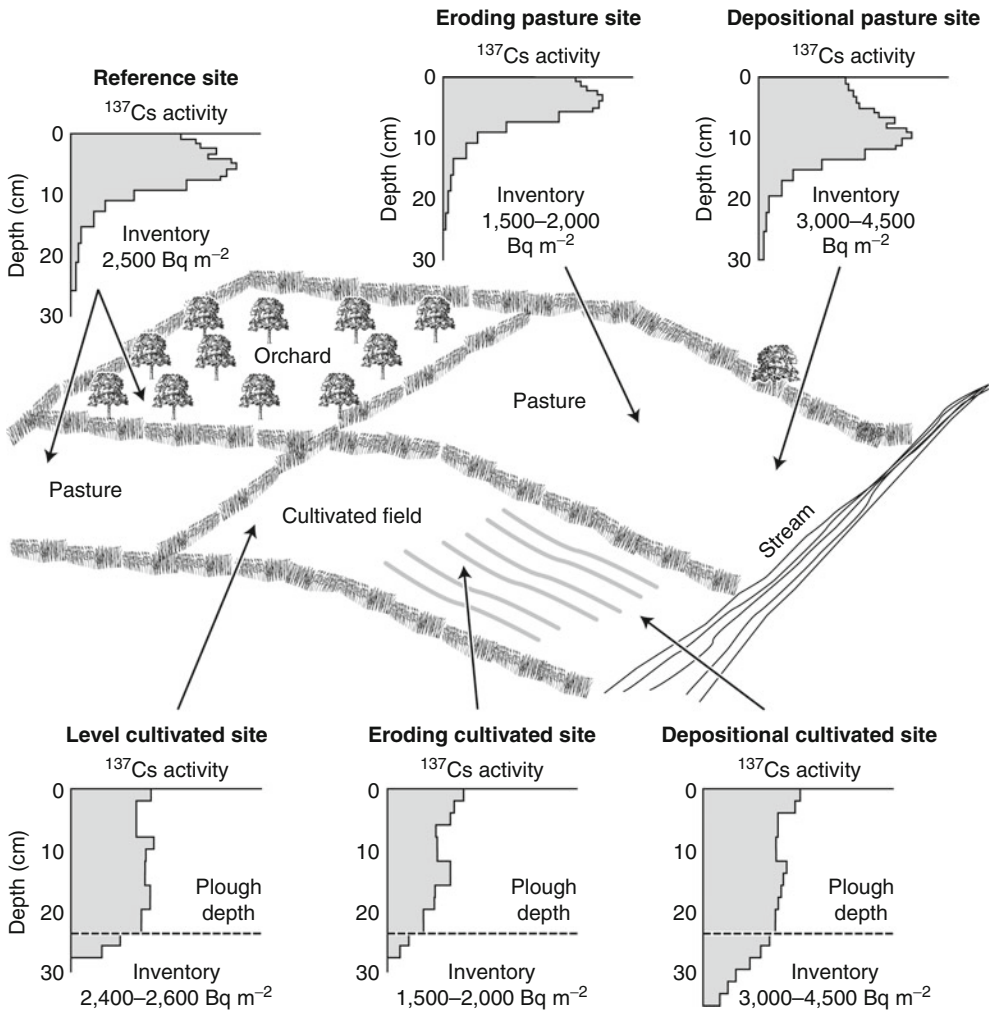

Fallout Radionuclides and the Study of Erosion and Sedimentation. Figure 9
A schematic representation of the principles involved in the use of ^{137}Cs measurements to estimate soil redistribution rates

little or no influence on fallout receipt. Eroding areas within both pasture and cultivated areas will be characterized by reduced inventories. Similarly, areas of deposition are reflected by increased inventories. The depth distributions provide further evidence of the incidence and magnitude of erosion and deposition. As indicated above, the soil redistribution reflected by the departure of the measured inventory values from the reference value is assumed to have occurred over the period between the main period of ^{137}Cs fallout in the late 1950s and 1960s and the present. Although information on ^{137}Cs inventories and depth distributions, such as that shown in Fig. 9, provides *qualitative* information on the magnitude and spatial distribution of soil redistribution rates within the landscape, for most purposes, there will be a need for quantitative estimates of soil redistribution rates. To obtain such estimates, it is necessary to apply what have become known as "conversion models" to the measured inventory values.

Reviews of the various conversion models used with ^{137}Cs measurements (e.g., [89–91]) commonly distinguish between *empirical* models and *theoretical* models. Empirical models, as might be expected, are based on

the use of empirical measurements to establish the relationship between the magnitude of the loss or gain of ^{137}Cs inventory relative to the reference inventory and the soil redistribution rate. Such data are difficult to obtain, but there have been some attempts to use data from a range of erosion plots for this purpose, as in Australia, where relationships between rate of soil erosion and the reduction in ^{137}Cs inventory have been established for both cultivated and uncultivated soils [92]. In this case, the measured soil loss from the plots Y (t ha^{-1} year^{-1}) was related to the reduction in ^{137}Cs inventory within the plot, X (%), using a function of the form

$$Y = aX^b \tag{1}$$

However, the development and use of such empirical models involves several important problems. Perhaps most importantly, any relationship developed will be time specific. This constraint is particularly important. For example, loss of 20% of the inventory by 1980 would reflect a much higher erosion rate than loss of 20% of the inventory by 2000 and a relationship established using data for 1980 would overestimate erosion rates if applied to recent measurements of the reduction in inventory. Equally, it is difficult to use this approach to estimate deposition rates, although, in some investigations, it has been assumed that the equation can simply be rearranged using the same constant and coefficient to estimate deposition.

Because of the lack of data that can be used to establish empirical models and the inherent limitations noted above, most of the conversion models that have been successfully used for estimating soil redistribution rates from ^{137}Cs measurements fall into the second group, namely, theoretical models. By definition, such models use existing understanding of the behavior and fate of fallout inputs in response to soil redistribution processes to derive a theoretical relationship between soil redistribution rate and the loss or gain of inventory relative to the reference inventory. The proportional model [21, 93] provides a very simple example of such a model that has been quite widely used for cultivated soils. In this case, the plow depth H (m) is determined and the depth of soil lost, as a proportion of H, is estimated by simply assuming that this proportion will be the same as X (%), the proportion of the inventory that has been lost. If the bulk density of the soil B (kg m^{-3}) and the period over which erosion T (years) has occurred are known, the depth of soil lost can be used to estimate the erosion rate Y, that is,

$$Y = 10\frac{BdX}{100T} \tag{2}$$

Although attractive in its simplicity, the basic assumptions underlying the proportional model are flawed, since it takes no account of the fact that as soil is eroded from the surface of the plow layer in a cultivated field, the depth of the plow layer will be maintained by incorporation of subsoil from below the original plow layer. Therefore, if a depth equivalent to the depth of the plow layer was removed by erosion, the soil would still contain a significant proportion of the original inventory and not an inventory of zero. Use of the proportional model will therefore *underestimate* erosion rates, and it has been shown [91] that with high rates of soil loss (e.g., loss of ca. 60% of the original inventory), the estimated erosion rate is likely to underestimate the erosion rate by ca. 40%. The simple assumptions underlying the proportional model relate to an eroding soil and the model does not explicitly provide a means of estimating deposition rates, where the measured inventory exceeds the reference inventory. However, in several studies, the equation has been extended to estimate the deposition rate, by again assuming that the depth of deposition represents a proportion of H, equivalent to the percentage increase in inventory, relative to the reference inventory. Use of this procedure is, however, likely to underestimate the deposition rate, since the deposited soil eroded from upslope and deposited at a sampling point is likely to be characterized by a lower ^{137}Cs activity than that assumed by the model.

Other attempts to develop conversion models have aimed to provide a more realistic representation of the behavior of ^{137}Cs in the soil at locations characterized by erosion and deposition [90, 91]. In providing a brief overview of some of these models, it is useful to distinguish between those developed for cultivated soils and those developed for uncultivated soils, for example, soils found on pasture or rangeland. In most circumstances, reduction of the soil inventory by a given percentage will reflect a much higher erosion rate for a cultivated soil, than for an uncultivated soil, since

the incorporation of the ^{137}Cs inventory into the plow layer means that a much greater depth of soil will need to be eroded to reduce the soil inventory by a given amount. For an uncultivated soil, most of the ^{137}Cs inventory is likely to be found close to the surface and reduction of the inventory by a given proportion is likely to reflect a much lower erosion rate than for a cultivated soil.

Since they have attracted most attention in terms of conversion model development, attention will be directed first to the use of theoretical conversion models developed for use with cultivated soils. Most of these models, which aim to overcome the fundamental inadequacy of the proportional model, use a mass balance approach and attempt to model the changes in the ^{137}Cs content of the plow layer in response to fallout inputs, radioactive decay, loss of ^{137}Cs from the surface by erosion, and incorporation of soil containing no ^{137}Cs from beneath the plow depth by ongoing plowing, over the period since the commencement of ^{137}Cs fallout. By running the model with a range of erosion rates, it is possible to establish a relationship between erosion rate and the degree of reduction of the ^{137}Cs inventory relative to the reference inventory. The basic form of the mass balance model for an eroding site can be represented as follows:

$$\frac{\mathrm{d}A(t)}{\mathrm{d}t} = I(t) - \left(\lambda + \frac{R}{d_m}\right)A(t) \tag{3}$$

where $A(t)$ = cumulative inventory (Bq m^{-2}), t = time since onset of ^{137}Cs fallout (years), R = erosion rate (kg m^{-2} year^{-1}), d_m = average plow depth expressed as a mass depth (kg m^{-2}), λ = decay constant for ^{137}Cs (year^{-1}), and $I(t)$ = annual deposition flux at time t (Bq m^{-2} year^{-1}).

For many locations, detailed information on the annual ^{137}Cs deposition is unlikely to be available and in this situation, the fallout record from a representative station in the same hemisphere (see Fig. 2) can be scaled to match the measured reference inventory for the study site. In order to estimate deposition rates R' (kg m^{-2} year^{-1}) using the same mass balance approach, there is a need to take account of the magnitude of the increase in the ^{137}Cs inventory. In this case, the deposition rate will reflect the ^{137}Cs activity in the deposited sediment, $C_d(t')$ (Bq kg^{-1}) according to:

$$R' = \frac{A(t) - A_{\mathrm{ref}}}{\int_{t_0}^{t} C_d(t')\mathrm{e}^{-\lambda(t-t')}\mathrm{d}t'} \tag{4}$$

where $C_d(t')$ = the ^{137}Cs activity of deposited sediment in year t' (Bq kg^{-1}).

The ^{137}Cs activity of deposited sediment can be estimated as the weighted mean ^{137}Cs activity of sediment mobilized from the upslope contributing area (i.e., from the data provided by eroding points upslope).

The general framework provided by Eqs. 3 and 4 has been extended by various workers to take account of other processes and factors that can be expected to influence the relationship between the erosion rate and the percentage reduction in the inventory relative to the reference inventory (e.g., [90, 94, 95]). These include the fate of fresh fallout which can be removed by erosion prior to incorporation into the plow layer by tillage, the particle size selectivity of erosion and deposition processes and the preferential association of ^{137}Cs with the finer fractions of the soil and with organic matter, and the role of tillage erosion in influencing ^{137}Cs redistribution. In the latter case, it has proved possible to develop conversion models that permit separation of water erosion and tillage erosion and provide separate estimates of each. In a overview of the conversion models available for cultivated soils, Walling and He [90, 91] provide further details of a simple mass balance model which assumes that all fallout was received in 1963, a more comprehensive mass balance model incorporating the fate of fresh fallout and the size selective nature of erosion and deposition and the further extension of that model to incorporate the effects of ^{137}Cs redistribution by tillage.

In the case of uncultivated soils, the conversion model needs to take account of the shape of the depth distribution, since this will influence the relationship between erosion rate and the depletion of the total ^{137}Cs inventory. Two main approaches have been used in developing models for uncultivated soils [91]. The first, which is often termed the profile distribution model, is based on the assumption that the ^{137}Cs depth distribution in most uncultivated soils is

exponential in form and can be characterized by a relaxation depth h_0 (kg m^{-2}). The greater the value of h_0 the greater the depth to which the ^{137}Cs extends into the soil. If the value of h_0 is determined for the reference site and it is assumed that at eroding sites, loss of surface soil will cause the exponential depth distribution to be truncated, comparison of the inventory at the sampling point with the reference inventory provides a means of estimating the depth of soil which must have been removed to reduce the inventory by the documented amount. The erosion rate can be estimated by dividing the total depth of soil removed by the number of years elapsed since 1963, the year of peak fallout, namely,

$$Y - \frac{10}{t - 1963} \ln\left[\left(1 - \frac{X}{100}\right)\right] h_0 \qquad (5)$$

where t = the year of sample collection.

Where the measured inventory at a sampling point exceeds the reference inventory, indicating that deposition has occurred, the deposition rates can be estimated from the magnitude of the increase in inventory and the ^{137}Cs concentration of deposited sediment, using the same approach as used for cultivated soils in Eq. 4.

Use of the profile distribution model assumes that the exponential depth distribution found at the reference site would have developed at the eroding point by 1963 and was subsequently truncated by erosion. This is clearly an oversimplification, since the depth distribution will evolve through time as a result of the time-variant fallout input, the progressive downward movement of the ^{137}Cs fallout received at the soil surface, and the removal of some fresh fallout from the soil surface by erosion shortly after its deposition. As a result, estimates of rates of soil loss provided by the profile distribution model are likely to overestimate erosion and deposition rates. However, a study aimed at testing the model within a small catchment in southern Italy [96], by comparing the measured sediment yield from the catchment with the estimate of mean annual net soil loss provided by the application of the profile distribution model to ^{137}Cs measurements obtained from the catchment, demonstrated good agreement between the two independent results.

Uncertainties regarding the assumptions implicit in the profile distribution model have encouraged the development of an alternative approach, commonly referred to as the diffusion and migration model [91]. This model involves a mass balance approach taking account of the time-variant fallout input and the slow downward movement of the ^{137}Cs fallout received at the surface. As such, it takes account of the evolution of the ^{137}Cs depth distribution through time, rather than assuming a constant form. This downward movement is governed by two lumped parameters loosely referred to as the diffusion and migration coefficients, which can be estimated from the form of the depth distribution found at the reference site. With this model, it is again possible to estimate the deposition rate associated with a sampling point where the inventory exceeds the local reference inventory. The approach taken is similar to that represented in Eq. 4. Since this model more closely replicates existing understanding of the post-fallout redistribution of ^{137}Cs in undisturbed soils and its interaction with erosion, it is likely to provide more reliable estimates of soil redistribution rates in areas with uncultivated soils.

Although most studies employing ^{137}Cs to investigate erosion and soil redistribution rates have focused on water erosion, there have been some studies that have attempted to extend its application to wind erosion. These studies have employed broadly the same approach of comparing the reference inventory at an undisturbed site unaffected by erosion or deposition with the inventories measured at a range of sampling points. Points with reduced inventories are assumed to represent eroding points, and points with increased inventories are assumed to represent points where deposition has occurred. In most instances, conversion models based on those developed for water erosion have been used, since the mechanisms involved are similar, that is, removal of soil from the surface and addition of sediment to the original surface by deposition. As with water erosion, a range of different approaches have been used in the models. These include the proportional model [97, 98], mass balance models [99, 100], and a profile distribution model [100, 101]. However, the available evidence suggests that wind erosion introduces greater complexity into the post-fallout redistribution of ^{137}Cs and the use of

^{137}Cs measurements to estimate soil and sediment redistribution rates. Important issues include the potential importance of selective winnowing of fines by deflation processes and the possibility that reference sites could be influenced by dust accumulation, which could increase the measured inventory [102].

As indicated above, estimates of soil redistribution rates obtained using ^{137}Cs measurements generally relate to the period extending from either the onset or the peak period of fallout in the 1950s or 1960s to the time of sampling. In many respects, the lengthy period covered by the measurements represents an advantage of the ^{137}Cs approach, because it integrates the natural temporal variability of soil erosion rates. However, it can also represent a limitation of the approach, in that it generates an average erosion rate for the period and it is not possible to document changes in erosion rates resulting from land use change. However, where land clearance for agriculture and the onset of significant erosion postdates the main period of ^{137}Cs fallout, the conversion models can be modified to provide an estimate of soil redistribution relating only to the post-clearance period. In another specialist application, it proved possible to produce estimates of erosion rates associated with two contrasting land management practices that characterized the period of interest [103, 104]. In this case, it was possible to reconstruct the erosion rates occurring during a period of conventional cultivation extending from 1954 to 1986 and a subsequent period under no-till management extending from 1986 to 2003. By measuring the current ^{137}Cs activity of the former plow layer associated with the period of conventional tillage, it was possible to reconstruct the inventory of a sampling point at the end of this period and thus estimate the erosion rate under conventional tillage using a mass balance conversion model. Similarly, the current depth of the original plow layer was estimated from measurements of the current total ^{137}Cs inventory and the current ^{137}Cs activity of the plow layer at individual sampling points and this value was compared with the plow depth during the period of conventional cultivation to provide an estimate of the depth of soil eroded during the period under no-till management. To use this approach, it is important that the overall period covered by the ^{137}Cs measurements (i.e., ca. 50 years) should include substantial periods under both management practices and thus that the change in management should coincide approximately with the middle of the period covered by the ^{137}Cs measurements.

Use of $^{210}Pb_{ex}$ Measurements The use of $^{210}Pb_{ex}$ measurements to investigate rates and patterns of soil redistribution within the landscape involves similar principles to those involved in the use of ^{137}Cs and shown schematically in Fig. 9. As with ^{137}Cs, the inventories and depth distributions documented at individual measuring points can be compared with equivalent information obtained from an undisturbed reference site and a conversion model is used to estimate soil redistribution rates. The key differences between the use of ^{137}Cs and $^{210}Pb_{ex}$ measurements relate to the contrasting nature of the fallout input and the shorter half-life of $^{210}Pb_{ex}$ (22.3 years vs 30.17 years). The essentially continuous nature of $^{210}Pb_{ex}$ fallout means that, unlike the situation with ^{137}Cs, there is no well-defined period (e.g., from the commencement of fallout to the time of sampling) for which soil redistribution rates are documented. The $^{210}Pb_{ex}$ inventory measured at a sampling point will reflect the interaction between the fallout input and soil redistribution processes over an extended period. This period will reflect the half-life of the radionuclide, such that the impact of past soil redistribution on the present day inventory will become progressively less as the period extends back into the past. It is frequently indicated that $^{210}Pb_{ex}$ measurements can be used to estimate the erosion occurring over a period representing about five half-lives and thus over the past ca. 100 years. In principle, this is correct, but it must be recognized that erosion occurring 100 or even 50 years ago will have much less influence on the current inventory than erosion occurring in the past 10 or 20 years. Thus, although $^{210}Pb_{ex}$ measurements will reflect erosion and soil redistribution taking place over a longer period than ^{137}Cs, the measurements are likely to be more sensitive to recent erosional activity than ^{137}Cs measurements.

Walling and his coworkers [38, 105] describe several conversion models which have been developed for deriving estimates of soil redistribution rates, based on the degree of reduction or increase in the $^{210}Pb_{ex}$ inventory relative to the reference value. These models

are very similar to several of those developed for ^{137}Cs and described above, the key difference being the need to incorporate a continuous and essentially constant annual fallout input, rather than fallout input over a limited period. The mass balance model for cultivated soils incorporates many of the refinements associated with the comprehensive mass balance model for ^{137}Cs described by the same authors. These include size selective sediment mobilization and deposition and the fate of fresh fallout prior to its incorporation into the plow layer by tillage. The mass balance model has also been extended to incorporate the effects of soil displacement by tillage. Because $^{210}Pb_{ex}$ fallout is continuous and essentially constant through time, it is particularly important that the fate of fresh fallout, prior to incorporation into the soil by tillage, should be represented in a physically realistic manner, since this will exert a key control on the $^{210}Pb_{ex}$ inventory. If erosion occurs whilst the recent fallout remains at the surface, a relatively small amount of erosion could remove a significant proportion of the fresh input, whereas once the fresh fallout is mixed into the plow layer, the same amount of erosion will remove a much smaller amount of $^{210}Pb_{ex}$.

Because the $^{210}Pb_{ex}$ fallout is continuous, it is not possible to use a conversion model equivalent to the profile distribution model developed for ^{137}Cs, when investigating soil redistribution on uncultivated soils. That model assumes that the depth distribution is established during the main period of ^{137}Cs fallout and is subsequently truncated by surface erosion. With $^{210}Pb_{ex}$, the continuous fallout will replenish the $^{210}Pb_{ex}$ removed from the upper part of the soil by erosion and the depth distribution is likely to achieve a quasi steady state. Under these circumstances, a model very similar to the diffusion and migration model developed for ^{137}Cs has been developed.

A different approach to estimating soil erosion rates using $^{210}Pb_{ex}$ measurements is described by Wallbrink and Murray [36]. This approach, which was applicable to uncultivated soils combined measurements of both ^{137}Cs and $^{210}Pb_{ex}$ and was recommended for use in areas, such as forests, where local variability of ^{137}Cs fallout made it difficult to establish a ^{137}Cs reference inventory. In this case, attention was directed to the contrasting depth distributions of the two fallout radionuclides, with ^{137}Cs evidencing deeper penetration than $^{210}Pb_{ex}$ in the study area in Tasmania, Australia. The different penetration depths resulted in a change in the ratio between the $^{210}Pb_{ex}$ inventory (below a specific depth in the profile) and the inventory of ^{137}Cs below the same depth. The ratio decreased monotonically with depth, down to ca. 8 cm, with values of >2.0 near the surface and <1.0 at depths of ca. 4 cm. The ratio provides a unique measure of the depth within the profile and can be used to estimate the depth of erosion that has occurred at a particular point, either over the period since the occurrence of bomb fallout or since erosion commenced as a result of land clearance or disturbance, if this occurred later. Once the depth distribution of the $^{210}Pb_{ex}/^{137}Cs$ ratio is established for the study site using an undisturbed reference site, bulk cores are collected from individual sampling points and measurement of the ^{137}Cs and $^{210}Pb_{ex}$ inventories permits the ratio to be calculated and the depth of soil eroded to be estimated. The approach is in many respects similar to the use of the profile distribution model to estimate the depth of erosion on an uncultivated soil from measurements of the ^{137}Cs inventory undertaken on bulk cores. In that case, the exponential depth distribution of ^{137}Cs provides a means of estimating the depth of soil removed by erosion, whereas with this approach, the depth distribution of the ratio provides the means of estimating the depth of soil removed from the inventory ratios calculated for individual bulk cores.

Use of ^{7}Be Measurements In contrast to ^{137}Cs and $^{210}Pb_{ex}$, the value of ^{7}Be for documenting soil redistribution rates reflects its short half-life (53 days) and its potential for obtaining information relating to individual events or short periods of heavy rainfall (e.g., 1–2 weeks). However, although there is increasing interest in this potential, relatively little work has been undertaken to date using this fallout radionuclide. One early attempt to use ^{7}Be to estimate soil redistribution rates employed a mass balance approach, analogous to the repeat monitoring approach developed for use with ^{137}Cs [35]. In this approach, the ^{7}Be inventory was documented for a number of sampling points immediately prior to the event or short study period. At the end of the event or period of interest, the ^{7}Be inventory was measured again at adjacent points. The ^{7}Be fallout input during the intervening period was

estimated using a rainfall collector. If the period studied is sufficiently short to permit the effects of radioactive decay to be ignored, the amount of erosion E (kg m^{-2}) at the sampling point associated with the period between the collection of the two sets of samples can be estimated as:

$$E = \frac{(A_0 + D - A_1)}{C} \tag{6}$$

where A_0 and A_1 are the ^{7}Be inventories (Bq m^{-2}) at the beginning and end of the study period, respectively; D (Bq m^{-2}) is the fallout input during the study period; and C is the ^{7}Be content of the eroded soil (Bq kg^{-1}).

The study undertaken by Wilson et al. [35] was undertaken on an erosion plot, and in this case, C could be established by collecting the eroded sediment and measuring its ^{7}Be content. In that study, C could also have been estimated by using the measurements of soil loss available from the erosion plot to estimate the depth of erosion during the event or study period and to then determine C from the depth distribution of ^{7}Be established using sectioned cores. In other applications, it is likely to prove more difficult to determine C, which is clearly a critical component of Eq. 6. Use of this mass balance approach must be seen as rather complex, since it involves a set of "before" and "after" measurements, as well as measurements of fallout input during the period of interest and information on the ^{7}Be content of eroded sediment. As such, it could be seen as providing experimental validation of the potential for using ^{7}Be to document short-term soil redistribution rates, rather than a more generally applicable procedure.

Most other attempts to use ^{7}Be for documenting soil redistribution rates (e.g., [32, 33, 106, 107]) have adopted a simpler approach more similar to that employed with ^{137}Cs and ^{210}Pb$_{ex.}$ This involves comparison of the inventories documented at a number of sampling points at the end of the period of interest using bulk cores, with a reference inventory, also measured at the end of the period of interest, in order to establish the magnitude of the increase or decrease in inventory in response to soil redistribution. However, the basis of the approach differs in several respects from that associated with ^{137}Cs and ^{210}Pb$_{ex}$. Firstly, as indicated above, attention focuses on short periods, usually a single storm event or a short period of heavy rainfall (e.g., 1–2 weeks). Secondly, study areas are usually unvegetated. Where a vegetation cover exists, a significant proportion of the ^{7}Be fallout input to a site is likely to be intercepted and will be retained by the vegetation cover until it is lost by decay. This situation differs from that for ^{137}Cs and ^{210}Pb$_{ex}$, where, by virtue of their much longer half-lives, the fallout will still eventually reach the soil surface after leaf fall or decay of the vegetation cover. This interception of the incident ^{7}Be fallout by the vegetation cover is likely to cause the fallout input to the soil surface itself to be spatially variable and it is not possible to assume a spatially uniform reference inventory. Equally, if the total inventory contained in both the vegetation canopy and the soil is considered, variable partitioning of the inventory between the two components makes it difficult to link changes in the inventory to soil redistribution. For this reason, the use of ^{7}Be to study soil erosion and soil redistribution rates is generally restricted to bare cultivated soils.

As emphasized by Figs. 6 and 7, a key feature of the depth distribution of ^{7}Be in the soil is its restriction to a very shallow layer of the surface soil, generally only ca. 1–2 cm deep. Within this layer, the depth distribution is commonly characterized by a rapid exponential decrease with depth. Little difference is found between the depth distributions associated with cultivated and undisturbed soils, since both are dominated by the fallout input to the surface. Where cultivation occurs, mixing of the ^{7}Be into the plow layer will cause the activity to fall below the level of detection. The conversion models generally used with ^{7}Be measurements (e.g., [33, 107]) are very similar to the profile distribution model employed with ^{137}Cs measurements. The ^{7}Be exponential depth distribution at the reference site can be characterized by the relaxation depth h_0 kg m^{-2} and the mass depth of soil eroded from a sampling point R kg m^{-2} can be estimated by comparing the ^{7}Be inventory at the sampling point A Bq m^{-2} with that for the reference site A_{ref} Bq m^{-2}, and relating the difference to h_0, namely,

$$R = h_0 \ln\left(\frac{A_{ref}}{A}\right) \tag{7}$$

Where the measured ^{7}Be inventory exceeds the reference inventory, deposition is assumed to have occurred and the mass depth of deposition can be estimated, as with ^{137}Cs (Eq. 4), by dividing the excess ^{7}Be inventory

by the mean ^{7}Be content of sediment mobilized by erosion from the upslope contributing area.

The procedure commonly used with ^{7}Be measurements is to visit the study site after a storm event or short period of heavy rainfall (e.g., 1 week) and to collect cores from a reference site and from the study site. The cores collected from the reference site should include a sectioned core that is used to determine h_0. By applying Eq. 7, it is possible to estimate the soil redistribution that occurred during the period considered. The short half-life of ^{7}Be and the emphasis on documenting individual events do, however, impose a number of constraints on the use of ^{7}Be for estimating soil redistribution which do not apply to the use of ^{137}Cs and $^{210}Pb_{ex}$ to estimate longer-term erosion rates covering periods of several decades [14]. Most important is the assumption that the spatial pattern of inventories documented by the cores collected after an event or period of heavy rainfall reflects soil redistribution occurring during that period and that the preexisting ^{7}Be inventory can be considered to have been spatially uniform across the study area. This means that this approach can only be applied to events or periods of heavy rainfall separated by relatively long periods with little rainfall or at least rainfall or insufficient intensity to cause erosion and soil redistribution. A period of ca. 5 months (i.e., three half-lives) is ideally required to ensure that the spatial variability of the ^{7}Be inventory inherited from previous events has effectively disappeared as a result of decay. Cultivation of a field provides an alternative means of removing or resetting the signal from past events, since the existing inventory will be mixed into the plow layer and is likely to be below the level of detection. This constraint can seriously limit the potential for using ^{7}Be measurements to document short-term erosion rates, since effectively only the first period of heavy rainfall following an extended dry period or the cultivation of the study site can be studied. In many environments, the events of most interest may occur later in the wet season or it might be important to consider the whole wet season. As the length of the period of rainfall studied increases, the estimate of erosion or soil redistribution obtained will underestimate the true value to a progressively greater degree. Walling et al. [87] used a hypothetical example to demonstrate that if the period extends to 6–7 weeks and this includes a number of rainfall events of similar magnitude distributed through that period, the amount of soil eroded could be underestimated by as much as 50%.

Increasing recognition of the potential value of ^{7}Be in providing a means of documenting short-term erosion rates, to complement the estimates of longer-term erosion rates provided by ^{137}Cs and $^{210}Pb_{ex}$, has directed attention to the possibility of extending the timescale over which ^{7}Be measurements can be applied and removing the constraint of only being able to document the first events occurring after a dry period. Such developments will necessarily increase the complexity of the approach and the need for additional information on, for example, fallout inputs, changing values of h_0, and the distribution of erosion within the period considered. Walling et al. [87] recently reported the development of a novel procedure for applying ^{7}Be measurements, involving such additional information, which permitted erosion and soil redistribution to be quantified over a period of ca. 3 months. The procedure was developed for application in Chile where soil erosion during the period following forest harvesting was being studied and there was a need to document erosion occurring during the entire wet season.

Estimating Sedimentation Rates and Establishing Chronologies in Depositional Sinks

The fallout radionuclides ^{137}Cs and $^{210}Pb_{ex}$ have been widely used to provide estimates of sedimentation rates in depositional sinks, including water bodies such as lakes and reservoirs, wetlands and river floodplains and for establishing the chronology of sediment cores collected from such sinks. In some studies, the emphasis may be on documenting sedimentation rates (g cm^{-2} year^{-1} or mm year^{-1}) and thus quantifying sediment accretion or sediment storage, whereas in others, attention may focus on the chronology. In the latter context, there may, for example, be a need to establish the chronology of changes in the contaminant content of sediment from different depths in a core, in order to reconstruct the pollution history of a study site and the upstream catchment area. Some attempts have been made to use ^{7}Be for these purposes, but this radionuclide has been less widely applied in sedimentation studies, partly because of its short half-life. With ^{137}Cs, the radionuclide provides information relating

to the period extending from the main period of bomb fallout to the present (i.e., ca. 50 years). In areas where significant Chernobyl fallout occurred, it may be possible to separate the periods before and after 1986. With $^{210}Pb_{ex}$, the timescale extends back ca. 100 years. In contrast, where ^{7}Be is used, it can provide information on very recent sedimentation rates or confirm the presence of recently deposited sediment. Much of the early work using ^{137}Cs and $^{210}Pb_{ex}$ for dating sediment cores and estimating sedimentation rates focused on lakes, and there is now a large body of literature on this topic (e.g., [47–51, 108–110]). Less work has been undertaken on other sediment sinks, such as river floodplains, and these will therefore be emphasized in this contribution, in order to demonstrate the potential for using fallout radionuclides to study the movement of sediment through the landscape.

Use of ^{137}Cs Measurements Figure 10 provides an example of the depth distributions of ^{137}Cs and $^{210}Pb_{ex}$ in cores collected from the overbank deposits on the floodplain of two UK rivers, the River Arun and the River Tone, and these provide a useful background for outlining the various approaches that can be used to estimate sedimentation rates and to establish age/depth relationships for sediment cores collected from sediment sinks. The contrasting features of ^{137}Cs and $^{210}Pb_{ex}$ fallout, and more particularly the event-related (i.e., bomb testing) nature of the former and the continuous nature of the latter, are reflected by the different principles involved in the use of the two radionuclides. With ^{137}Cs, attention focuses on the known fallout record (see Fig. 2), reflecting the first appearance of significant fallout in the early to mid-1950s and the occurrence of peak fallout in 1963 and in some locations a further short-lived input in 1986, as a result of the Chernobyl disaster. The ^{137}Cs activity of the sediment deposited in a lake, floodplain, or other sediment sink can be expected to reflect this fallout record through two mechanisms. The first mechanism represents direct fallout to surface of the sediment sink that will be incorporated into the depositing sediment. In the case of a lake or reservoir, the ^{137}Cs fallout to the surface of the water body will be dispersed within the water and adsorbed by sediment in the water column, which is subsequently deposited. With a floodplain or marsh, the fallout will be delivered directly to the surface of the accreting sediment, where it will "label" the surficial sediment. The second mechanism represents a catchment-derived contribution, reflecting ^{137}Cs associated with deposited sediment that was mobilized from the catchment surface, which would itself have received ^{137}Cs fallout. As demonstrated in Fig. 5, the cumulative inventory of the catchment surface, and thus the ^{137}Cs content of eroded sediment, will also vary through time and follow a similar pattern to the direct fallout, peaking around 1963. The precise shape of the ^{137}Cs depth distribution found in a lake or on a river floodplain will reflect the relative contribution of direct fallout and catchment-derived ^{137}Cs to the accumulating sediment [111, 112], but in most situations, the sediment deposited in or around 1963 will possess the highest ^{137}Cs activity. This provides a well-defined time marker. Thus, the clear ^{137}Cs peaks evident at mass depths of ~18 and 15 g cm^{-2} for the cores from the Rivers Tone and Arun, respectively, in Fig. 10 can be dated to 1963 and a mean sedimentation rate can be calculated by dividing the total mass or depth of sediment by the period elapsed between 1963 and the date of core collection. Some workers have used the depth of the first appearance of ^{137}Cs as an alternative time marker, which can be dated to ca. 1954. However, this approach is not to be recommended, since there is clear evidence that in most depositional sinks, the "tail" of the ^{137}Cs depth distribution will be influenced by post-depositional downward migration that will cause overestimation of the sedimentation rate. As indicated above, in some locations influenced by Chernobyl fallout, the existence of ^{137}Cs peaks in a sediment core that can be linked to 1963 and 1986 can provide a basis for estimating sedimentation rates for two periods (i.e., 1963–1986 and 1986 to present) [113, 114], and evaluating recent changes in sedimentation rates associated with changes in land use or land management.

The depth at which the ^{137}Cs peak is found is generally considered to be unaffected by downward migration in lake sediment deposits, where mixing is commonly assumed to be of limited importance. However, the possibility of some downward migration must be considered when studying floodplain deposits, since the peak ^{137}Cs activity is commonly found just below the surface in natural soils. The ^{137}Cs depth distribution from a representative undisturbed soil adjacent to

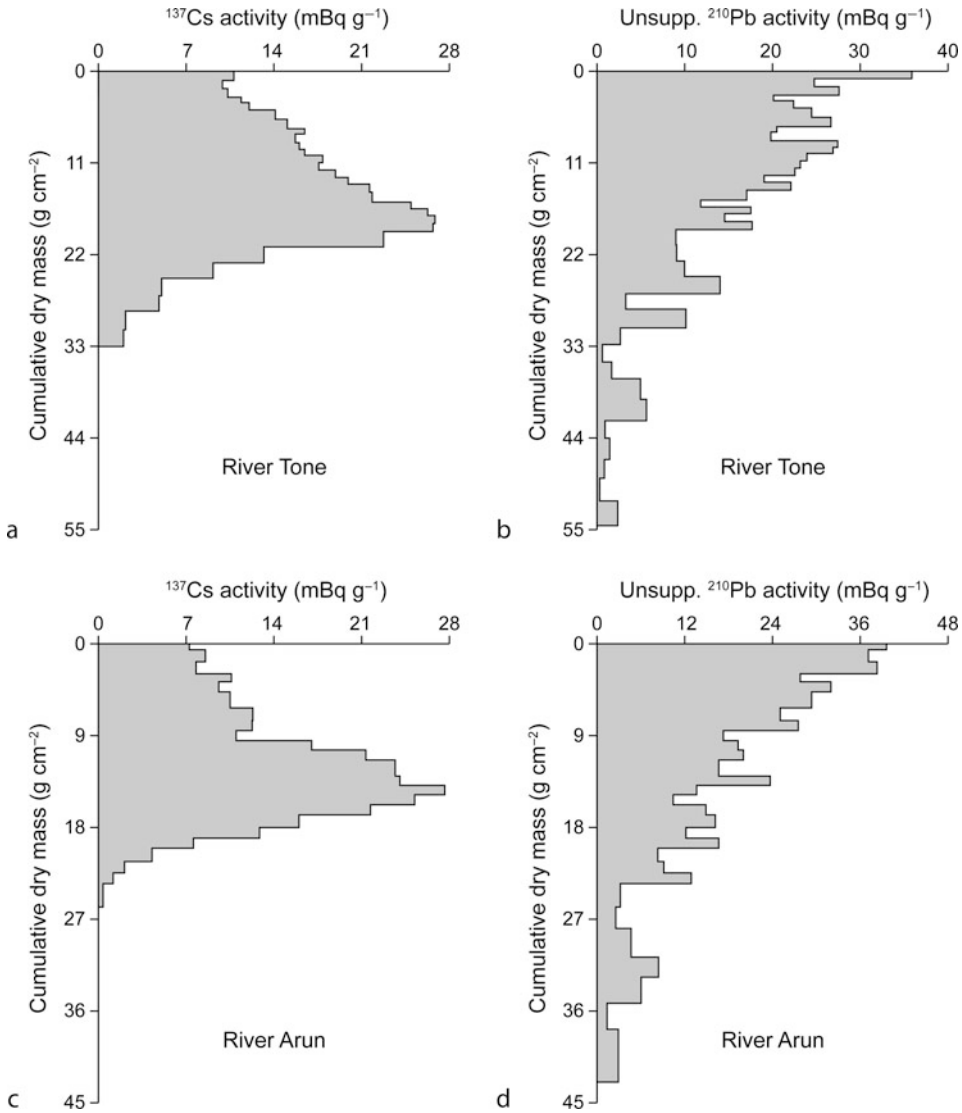

Fallout Radionuclides and the Study of Erosion and Sedimentation. Figure 10
Depth distributions of ^{137}Cs and ^{210}Pb$_{ex}$ measured in sediment cores collected from the floodplains of the River Arun and River Tone, UK

the floodplain study site can be used to estimate the likely downward migration rate of the ^{137}Cs peak R_m (kg m^{-2} year^{-1}) by dividing the present depth of that peak (expressed as a mass depth) by the time elapsed between the year of peak fallout and the present T_p (years). Thus, if the mass depth at which the peak ^{137}Cs activity occurs in the floodplain core D_{pk} (kg m^{-2}) is known, and R_m has been estimated, the mean sedimentation rate on the floodplain R' (kg m^{-2} year^{-1}) can be estimated as:

$$R' = \left(\frac{D_{pk}}{T_p}\right) - R_m \tag{8}$$

It is important to recognize that R', as estimated using Eq. 8 or simply from the depth of the ^{137}Cs peak in a sediment deposit, represents an *average* sedimentation rate and that for some sediment sinks, there may be marked inter-annual variability in the amount of deposition. On some floodplains, for example, most deposition may be associated with

infrequent high magnitude floods with recurrence intervals of >10 years.

The above approach to estimating sedimentation rates assumes that the sediment core is from an undisturbed location and therefore that the ^{137}Cs depth distribution reflects the interaction of the fallout input with the progressive sediment accumulation and any associated catchment contribution of ^{137}Cs. In some locations, the floodplain surface may be cultivated and this will cause mixing of the sediment within the plow layer. In this situation, it will no longer be possible to use the ^{137}Cs depth distribution to estimate the sedimentation rate. However, several studies [115–117] have shown that it is still possible to estimate the sedimentation rate, if the floodplain has been regularly cultivated since the beginning of ^{137}Cs fallout. If no sedimentation has occurred, ^{137}Cs will only be found to a depth equivalent to the plow depth. If, however, sedimentation has occurred, its depth can be estimated from the depth to which ^{137}Cs is found below the plow depth, due to the progressive accretion of the surface. Comparison of the total depth of the ^{137}Cs profile which has been homogenized by plowing D_t (kg m^{-2}) with the plow depth D_{pl} (kg m^{-2}) provides a means of estimating the sedimentation rate, namely,

$$R' = \frac{D_t - D_{pl}}{T_p} \tag{9}$$

The need to obtain detailed information on the depth distribution of ^{137}Cs within a sediment core can represent an important constraint in the application of the approach embodied in Eq. 8, which requires information on the depth of the ^{137}Cs peak. Due to likely limitations on the number of core slices that can be assayed, due to cost or time constraints, it may not be possible to document the small-scale spatial variability of sedimentation rates. This may be less of a problem in lakes, where sedimentation is likely to be relative uniform within a small area, but it can be a significant problem for river floodplain investigations, where sedimentation rates can be characterized by marked spatial variability, in response to the floodplain microtopography, distance from the main channel, and the vegetation cover (e.g., [45]). Walling and He [118] provide a means of addressing this problem by describing a procedure for estimating the sedimentation rate from measurements of the total inventory (Bq m^{-2}) of bulk cores collected from individual points on the floodplain. The bulk cores are assumed to contain the total depth of ^{137}Cs for the sampling points and the key feature of the approach is the estimation of the excess inventory, which is defined as the total inventory less the direct fallout contribution. The latter can be established using cores collected from adjacent reference site located above the level of flood inundation. The excess inventory I_{ex} (Bq m^{-2}) represents the ^{137}Cs input associated with deposited sediment, and its magnitude will reflect the rate of deposition and the ^{137}Cs concentration in the deposited sediment. The latter will clearly vary through time in response to the accumulation of ^{137}Cs in the catchment soils and its subsequent mobilization by erosion. Walling and He [118] describe a model that can be used to estimate the time-weighted mean concentration of the deposited sediment and thus the deposition rate. However, they also propose a simpler and more direct approach for estimating the deposition rate for individual sampling points, based on measurements of the inventories of bulk cores. This makes the assumption that the temporal variation of the ^{137}Cs content of the deposited sediment would have been similar across the floodplain surface and that the main factor accounting for spatial variation in the ^{137}Cs content of deposited sediment will be its grain-size composition. If the sedimentation rate R'_0 (kg m^{-2} year^{-1}) and excess ^{137}Cs inventory $I_{ex,0}$ are known for a specific representative point on the floodplain for which a well-defined ^{137}Cs profile obtained from a sectioned core is available, the sedimentation rate R' at other points on the floodplain can be estimated from a comparison of the values of excess inventory I_{ex} and the grain-size composition of the sediment at those points with the equivalent information for the reference point, that is,

$$R' = R'_0 \frac{I_{ex}}{I_{ex,0}} \left[\frac{S_{d,0}}{S_d}\right]^{\nu} \tag{10}$$

where $S_{d,0}$ and S_d represent the specific surface area of surface sediment (m^2 g^{-1}) from the reference point and the sampling point, respectively, and ν = a constant reflecting the form of the relationship between ^{137}Cs concentration and specific surface area, which has been shown to have a value of ca. 0.65–0.7 [84].

It is important that the second term in Eq. 10 should be included, in order to take account of the

influence of grain-size composition on ^{137}Cs activity and the preferential association of ^{137}Cs with finer sediment. In Eq. 10, the assumption is made that the grain-size composition of surface sediment is representative of that for the entire depth profile. The approach involving the use of measurements of the inventory of bulk cores represented by Eq. 10 can also be used for cultivated floodplains, although in this case, R'_0 will be estimated using Eq. 9 rather than Eq. 8. The use of bulk core measurements in the estimation of floodplain accretion rates depends heavily on the assumption that the deposited sediment is characterized by a significant ^{137}Cs activity, which in turn results in readily measurable excess inventories. In some environments, the deposited sediment may contain low levels of ^{137}Cs or no ^{137}Cs, because of the nature of the sediment sources in the upstream catchment or the low inventories existing in the catchment. In this situation, it may be difficult to quantify the limited excess inventory due to the low precision of the gamma spectrometer measurements and the ^{137}Cs depth distribution may represent the only viable approach to quantify the deposition rate. A situation of this nature has been described for the floodplain of a river in central Queensland Australia [119].

Use of $^{210}Pb_{ex}$ Measurements Because of the essentially continuous nature of $^{210}Pb_{ex}$ fallout, the $^{210}Pb_{ex}$ depth distributions associated with sediment sinks do not provide a distinct time marker, as provided by ^{137}Cs. As with ^{137}Cs, the $^{210}Pb_{ex}$ content of the accreting sediment will reflect both direct fallout to the lake or floodplain surface and $^{210}Pb_{ex}$ associated with sediment mobilized from the upstream catchment. If it is assumed that the sediment surface is progressively buried by deposition, the $^{210}Pb_{ex}$ activity of the sediment in a core will decline with depth due to radioactive decay. The rate of decline in the $^{210}Pb_{ex}$ activity with depth provides a means of estimating the age of the sediment at different depths and thus the sedimentation rate. The $^{210}Pb_{ex}$ depth distributions for the floodplain of the Rivers Tone and Arun shown in Fig. 10, for example, demonstrate that the $^{210}Pb_{ex}$ activity declines to zero at a mass depth of about 45–55 kg m^{-2}. Since it is normally assumed that $^{210}Pb_{ex}$ activity will decline to near-zero after ca. five half-lives, the sediment at this depth can be estimated to be about 110 years old. A preliminary estimate of the sediment age at different depths can be obtained by assuming that the $^{210}Pb_{ex}$ activity in the deposited sediment declines exponentially with time in accordance with the radioactive decay law, namely,

$$C_d = C_0\, e^{-\lambda t} \tag{11}$$

where C_d is the activity at a given time, C_0 is the initial activity of the deposited sediment, λ is the decay constant for ^{210}Pb (0.03114 year^{-1}), and t is the number of years since burial.

Use of Eq. 11 to estimate sediment age assumes that the activity of the sediment at the time of its initial deposition is constant through time and thus that the activity is not influenced by the sedimentation rate. In the real world, these assumptions may not apply and a range of different models of varying complexity have been developed for interpreting the $^{210}Pb_{ex}$ depth distributions in sediment cores, in order to obtain reliable estimates of sediment age or sedimentation rates. In these models, depths are commonly expressed as mass depths (g cm^{-2}) to avoid complications due to sediment compaction and downcore variations in bulk density. The models involve a number of different assumptions. In the simplest model, often referred to as the Constant Flux, Constant Sedimentation rate (CFCS) model, a constant initial concentration for the deposited sediment C_0 Bq kg^{-1} and a constant dry mass sedimentation rate r g cm^{-2} year^{-1}, and therefore a constant depositional flux are assumed, resulting in the following relationship:

$$C_m = C_0 e^{-\lambda m/r} \tag{12}$$

where C_0 and C_m are the $^{210}Pb_{ex}$ concentrations at the surface of the core and at mass depth m, respectively.

When log C_m is plotted against m, the resulting plot will be linear and the mean sedimentation rate r can be estimated from the slope of the best-fit line.

In many situations, however, it is unrealistic to assume a constant sedimentation rate, particularly in environments where extreme events play an important role in the operation of erosion and sedimentation processes. Equally, and perhaps more importantly, human impact on erosion rates as a result of land clearance and land use change will mean that sedimentation rates cannot be treated as stationary, but must be seen as being likely to have changed significantly over

the past 100–150 years covered by the $^{210}Pb_{ex}$ measurements. Two models, generally referred to as the Constant Rate of Supply (CRS) and Constant Initial Concentration (CIC) models, have been developed to take account of variable sedimentation rates [49, 120, 121]. In the first model, the annual supply of $^{210}Pb_{ex}$ to the accreting sediment is assumed to be constant, meaning that the activity of the sediment deposited in a given year will vary according to the amount of sediment deposited. If this is high, the activity will be reduced. With the CIC model, the initial activity of the deposited sediment is assumed to remain constant through time. Neither assumption is necessarily a close fit to reality. In this context, it is important to recognize the two sources of supply of $^{210}Pb_{ex}$ to the accreting sediment, namely, direct fallout to the lake or floodplain surface and supply of $^{210}Pb_{ex}$ in association with the eroded sediment. Temporal variation of the magnitude of the latter in response to changes in erosion rates and sediment flux will breach the assumption of the CRS model. Equally, variation of the mass of sediment deposited will mean that the initial $^{210}Pb_{ex}$ concentration associated with that sediment will vary through time, since the direct fallout input will be mixed with a variable mass of sediment. Furthermore, the initial $^{210}Pb_{ex}$ activity of the sediment mobilized from the upstream catchment can be expected to vary as sediment sources change as a result of land clearance and land use change within the catchment. If, for example, gully erosion assumes increasing importance, the $^{210}Pb_{ex}$ activity of the sediment mobilized from the upstream catchment might be expected to decline.

Appleby [109] provides an explanation of the procedures involved in applying the CRS model which permits the age t of the sediment at a given depth m to be calculated as:

$$t = \frac{1}{\lambda}\ln\left(\frac{A_0}{A_m}\right) \tag{13}$$

where A_0 and A_m are the total inventories below the surface and below the given depth m, respectively.

The sedimentation rate r g cm^{-2} year^{-1} at time t can also be calculated as:

$$r = \frac{\lambda A_m}{C_m} \tag{14}$$

where C_m is the $^{210}Pb_{ex}$ concentration at depth m and time t and A_m is the total inventory below this depth.

With the CIC model, the initial $^{210}Pb_{ex}$ concentration of the sediment at depth m and of age t is assumed to have been the same as the current concentration of sediment at the sediment–water interface or floodplain surface C_0. If the present concentration C of the sediment at this depth is known, its age t can be calculated using the relationship defined in Eq. 11, that is,

$$C = C_0 e^{-\lambda t}$$

The CIC model implicitly assumes that the supply rate of $^{210}Pb_{ex}$ is proportional to the sedimentation rate and this situation will not generally apply. For this reason, the CRS model is often assumed to provide more meaningful estimates of the sedimentation rate and, in the case of lakes, this has been confirmed by the similarity of CRS model–derived chronologies to the ^{137}Cs chronology and independent measures of sediment age based on counting of annual laminae. To date, little attention has been given to validating the models when applied to sediment cores from river floodplains.

As with the interpretation of ^{137}Cs depth distributions or profiles, use of the above models to estimate sedimentation rates or sediment age requires detailed information on the $^{210}Pb_{ex}$ depth distribution and this may introduce constraints on the number of cores that can be studied. Such limitations may be of limited importance in lakes, where sedimentation rates are unlikely to vary markedly over short distances, but for river floodplains and other terrestrial sediment sinks, such as wetlands, much greater spatial variability may occur and there may be a need to document this. Faced with the need to document the detailed patterns of sediment deposition on river floodplains, He and Walling [122] described a model which could be applied to bulk cores for which a measurement of the total $^{210}Pb_{ex}$ inventory was available. In this case, the complexity introduced by the dual source of $^{210}Pb_{ex}$, namely, direct fallout to the floodplain surface and $^{210}Pb_{ex}$ associated with the sediment mobilized from the upstream catchment, was reduced by focusing only on the latter component. This was calculated by subtracting the local reference inventory A_{ref} from the total inventory A_{total}, since the former represents solely the fallout input. The model assumed a constant initial concentration for the deposited sediment C_r and

a constant sedimentation rate r (averaged over a period of ca. 100 years) and was termed the CICCS model. The mean sedimentation rate for the past ca. 100 years (i.e., ca. five half-lives) can be estimated as:

$$r = \lambda \frac{A_{\text{total}} - A_{\text{ref}}}{C_r} \tag{15}$$

C_r is a key parameter in Eq. 15 and its estimation may prove difficult. It can be determined empirically by using sedimentation traps (e.g., [123]) to collect samples of the sediment deposited during overbank flood events and measuring its $^{210}Pb_{ex}$ content. Equally, it can be estimated from measurements of the $^{210}Pb_{ex}$ activity of suspended sediment transported during flood events, although potential contrasts between the $^{210}Pb_{ex}$ activity of suspended sediment and deposited sediment associated with contrasts in grain-size composition should be taken into account. In the absence of such direct measurements, C_r can also be estimated from measurements of the $^{210}Pb_{ex}$ activity of surface sediment from the floodplain and subtracting the direct fallout contribution to that concentration. Figure 11 presents the age–depth relationships derived from the ^{137}Cs and $^{210}Pb_{ex}$ depth distributions presented in Fig. 10 using Eq. 8 for ^{137}Cs and the CICC model for $^{210}Pb_{ex}$. There is good agreement between the estimates provided by the two radionuclides, although the results suggest that deposition rates in more recent years have increased for the River Tone and decreased for the River Arun. Such changes could reflect a range of factors, including changing sediment loads and changes in the frequency and depth of overbank flooding related to either changes in flood generation in the catchment or the effects of progressive floodplain accretion in increasing the bankfull stage. The latter would give rise to a reduction in the frequency and depth of overbank inundation.

In addition to the relatively simple conceptual models for deriving estimates of sedimentation rates within sediment sinks from $^{210}Pb_{ex}$ depth distributions, described above, more complex inductive models that permit the interpretation of $^{210}Pb_{ex}$ profiles in situations where both sedimentation rates and $^{210}Pb_{ex}$ fluxes vary with time have been developed [51, 124]. In this case, signal theory is used to compare the actual $^{210}Pb_{ex}$ profile with model profiles produced using realistic values of the various parameters and, by minimizing an objective function, it is possible to deduce the model form and the sedimentation rate. The Sediment Isotope Tomography (SITS) model described by Carroll and Lerche [51] is probably the

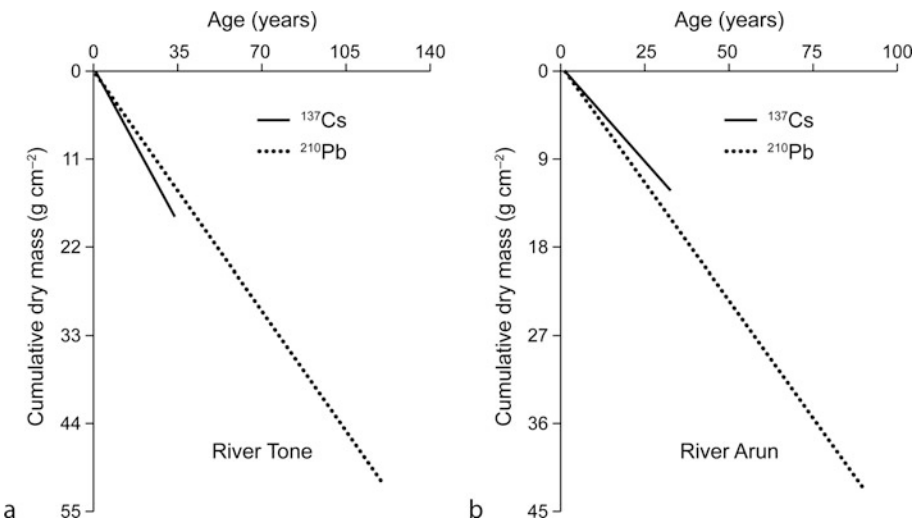

Fallout Radionuclides and the Study of Erosion and Sedimentation. Figure 11
A comparison of the age–depth relationships established for the floodplain cores illustrated in Fig. 10, using the ^{137}Cs depth distribution and the $^{210}Pb_{ex}$ depth distribution coupled with the CICC model

most widely applied model of this type, and some success has been achieved in incorporating bioturbation and mixing into the model structure.

For most sediment sinks, it is reasonable to assume quasi-continuous sedimentation, even though sedimentation rates may vary from year to year and over longer periods. This is the situation on many river floodplains where the river inundates the floodplain several times a year and accretion is ongoing. In some situations, however, sedimentation may be episodic and this introduces complications for interpreting the sediment profile, as this may reflect episodic accumulation of sediment, separated by periods of several years, or even a decade, with no sedimentation. A situation of this nature has been described for the floodplains of the Beni and Mamore Rivers in the Andean-Amazonian Foreland [125], but it still proved possible to use $^{210}Pb_{ex}$ measurements to reconstruct the sedimentation history of the floodplain over the past 100 years and to demonstrate the importance of extreme ENSO (El Niño/La Niña) events within this history. Eleven major events in the past 90 years were identified. In this case, a model referred to as the CIRCAUS (constant initial reach clay activity, unknown sedimentation) model was used. When applying this model, the $^{210}Pb_{ex}$ activity is normalized to reflect the clay (<4 μm) content of the sample, since most of that activity was shown to be associated with the clay fraction. The same CIRCAUS model was successfully used to study the chronology of floodplain sedimentation for the Strickland River in Papua, New Guinea [126].

Using ^{7}Be Measurements In comparison with ^{137}Cs and $^{210}Pb_{ex}$, relatively little use has been made of ^{7}Be to date for investigating sedimentation rates within sediment sinks in fluvial systems. Its use for this purpose has, however, been more fully exploited in coastal environments. Because of the short half-life of ^{7}Be (53 days), it can provide an effective means of identifying recently deposited sediment. Older sediment can be assumed to contain no ^{7}Be. This approach has been successfully used in shallow marine environments [127, 128] and a similar approach was employed in a study of the deposition and resuspension of PCB-rich sediments in the Fox River, Wisconsin, USA [129]. That study emphasized that appreciable short-term deposition and remobilization occurred, with short-term accumulation rates greatly exceeding the longer-term rates documented using ^{137}Cs measurements.

Although it is normally assumed that fallout radionuclides such as ^{7}Be will be preferentially associated with fine sediment, and particularly the clay fraction, recent work has demonstrated how coarser sand-sized (63 μm–2 mm) fluvial sediment can also retain ^{7}Be and that the radionuclide can be used to provide information on the residence time of such sediment in channel bars in rivers and on the sedimentation rates associated with such bars [130]. In a study of the Ducktrap River in Maine, USA, the evolution of channel bars associated with obstructions caused by large woody debris and the associated bar accumulation rates were investigated using ^{7}Be measurements and the application of a variant of the CIC model to interpret the depth distribution of ^{7}Be in the channel bars.

^{7}Be measurements can also be used in a similar manner to ^{137}Cs and $^{210}Pb_{ex}$ to estimate floodplain sedimentation rates. However, because of its short half-life, attention focuses on the sedimentation associated with individual events, rather than longer-term average rates of accretion. If shallow cores are collected from a floodplain after a flood event, the ^{7}Be inventories of those cores will reflect both the recent fallout to the floodplain surface and ^{7}Be associated with the sediment mobilized from the upstream catchment and deposited on the floodplain. If the local reference inventory for the time of sampling A_{ref} Bq m^{-2} is established, by collecting shallow cores from an adjacent reference site above the level of the inundating floodwaters, subtraction of this value from the inventories measured for the individual sampling points enables the excess inventory A_{ex} Bq m^{-2} associated with the deposited sediment to be calculated. The magnitude of this value will directly reflect the amount of sediment deposited and if the ^{7}Be concentration of the newly deposited sediment C_d Bq kg^{-1} is known, the amount of sediment deposited D_f kg m^{-2} can be estimated, namely,

$$D_f = \frac{A_{ex}}{C_d} \tag{16}$$

C_d is an important parameter in Eq. 16 and can prove difficult to establish. It could be measured directly by collecting samples of the deposited sediment using a sedimentation trap, or the ^{7}Be activity of the

suspended sediment transported by the river sampled during the flood event could be used as a surrogate. In both cases, however, the effects of the particle size composition of the sediment in influencing its ^{7}Be concentration must be considered. If the first approach is used, it is unlikely to prove feasible to install sediment traps adjacent to each sampling point and only a single sample or a composite sample comprising sediment collected from several traps may be available. In this situation, the ^{7}Be activity of the sample of deposited sediment C_t must be adjusted to provide an estimate of C_d for each sampling point by taking account of any difference in particle size between the sediment deposited at the sampling point and the sediment collected using the sediment trap. As with Eq. 10, which applied a similar approach for correcting ^{137}Cs activity to reflect the variation of the grain-size composition of sediment between individual sampling points, the measure of specific surface area ($m^2\ g^{-1}$) provides a convenient means of comparing the particle size composition of samples. If surface samples are collected adjacent to each sampling point and the specific surface area of those samples S_d and the sample collected by the sediment trap S_t is measured, C_d for individual sampling points can be estimated as:

$$C_d = C_t \left[\frac{S_d}{S_t}\right]^{v} \tag{17}$$

where v = a constant reflecting the form of the relationship between ^{7}Be concentration and specific surface area with a value of ca. 0.64 [53]. If the estimate of C_d is based on measurement of the ^{7}Be activity of suspended sediment, the values of C_t and S_t in Eq. 17 must be replaced by the values for the suspended sediment.

The procedure outlined above has been successfully used to document the spatial variability of sediment deposition during a single overbank flood event within a reach of the River Culm floodplain in Devon, UK [53]. When applying this approach, it important to ensure that the excess inventory inherited from previous events is minimal and this means that the overbank flood studied should be preceded by a period of ca. 5 months with no inundation of the floodplain. To overcome this constraint, it might be possible to collect cores from the floodplain both before and after the event, but this may introduce problems in terms of forecasting the occurrence of the flood that is to be studied and collecting samples from closely adjacent points, so that the pre- and post-flood ^{7}Be inventories can be directly compared. Since most floodplain surfaces are vegetated, the presence of grass and other vegetation can also introduce problems, but this is less significant than for studies of soil redistribution within fields. The shallow cores should include the vegetation mat, and because the amount of sedimentation is calculated from the excess inventory, no assumption is made as to whether the deposited sediment is held within the vegetation mat or if it is on the floodplain surface.

As indicated above, most work on using fallout radionuclides to estimate sedimentation rates and sediment chronologies for sediment sinks has focused on lakes and reservoirs, which commonly represent simpler systems than other sinks, such as river floodplains and wetlands. For example, it is generally assumed that the fallout input to a lake surface will be mixed within the body of the lake and will be attached to depositing sediment particles, which may already contain the same radionuclide by virtue of having been mobilized from the upstream catchment. As such, the two components of the total activity of the deposited sediment associated with a given year will be closely integrated and contained within the sediment deposit for that year. In the case of a river floodplain, however, the fallout to the floodplain surface will be deposited on the sediment surface over the course of the year and will be distributed within the shallow surface layer according to its initial distribution. If overbank sedimentation occurs during a flood, this will be deposited on top of the fallout input and the two may not be integrated. Furthermore, depending on the relative magnitude of the deposition rate and the relaxation depth of the initial distribution, the fallout input may be distributed through the sediment deposited over several years, or alternatively, it may only penetrate the upper part of the sediment deposited in a given year. Equally, there is likely to be greater temporal variability in the gain size composition of sediment deposited on a river floodplain, according to the magnitude of the flood events and this may influence the depth distribution of the fallout radionuclide, with coarser horizons being marked by lower activity. As noted above, Aalto and his coworkers have overcome this problem in their

studies of the floodplains of large rivers, such as the Amazon and the Strickland River in Papua New Guinea [125, 126], by normalizing the $^{210}Pb_{ex}$ measurements for the clay (<4 μm) content of the individual sediment sections recovered from the cores.

Tracing Suspended Sediment Sources and Sediment Transfer

In addition to their use for estimating soil redistribution rates and rates of sedimentation in sediment sinks, such as lakes and river floodplains, fallout radionuclides also provide important opportunities for tracing suspended sediment sources and for developing an improved understanding of sediment transfers in catchments and river basins. Concern for the off-site impacts of soil erosion in providing increased inputs of fine sediment to watercourses and for the many adverse impacts of increased fine sediment loads in river systems has focused attention on the need for sediment management or control strategies aimed at reducing sediment mobilization and transport. A range of control measures have been developed and successfully employed to reduce fine sediment fluxes, but the design of effective control strategies requires that control measures should target the key sediment sources and transfer pathways, in order to optimize the return on expenditure. Expenditure on reducing soil loss from cultivated areas could, for example, bring limited return if much of the sediment transported by a stream is mobilized by channel erosion. For this reason, an assessment of the primary suspended sediment sources in a catchment is often seen as an essential precursor to designing and implementing a sediment control strategy [131].

Sediment source fingerprinting techniques are increasingly used to provide information on sediment sources [132]. In essence, these techniques involve collecting samples of the fine sediment transported by a stream or river or deposited on its bed and comparing the chemical and physical properties of this sediment with those of potential sources. Such comparisons can be used to identify the primary source of the sediment and if a numerical mixing model is used (e.g., [131–135]), it is possible to quantify the relative contribution of a range of potential sources. In this context, *source* can represent *spatial sources* (e.g., different subcatchments or zones within a catchment), but more often emphasis will be placed on what can be referred to as *source types*, which reflect the nature of the erosion process or sediment source, for example, rill and interrill erosion on cultivated fields, and on land occupied by pasture or rangeland, gully erosion, erosion of tracks and unmetalled roads, and bank and channel erosion.

The success of sediment source fingerprinting studies depends heavily on the availability of tracer or fingerprint properties that are able to discriminate between potential sources. If the aim is to assess the relative importance of a number of different sources, several fingerprint properties will commonly be used. A wide range of sediment properties have been successfully used as source fingerprints, and these include inorganic and organic geochemistry, mineral magnetism, sediment color, stable isotopes and radionuclides. Fallout radionuclides, and particularly ^{137}Cs, ^{7}Be, and $^{210}Pb_{ex}$, have proved particularly useful as source fingerprints, since their fallout origin makes them essentially independent of the underlying geology or soil type and underpins their successful use for discriminating between different potential sediment source types [135]. In this context, the surface of a catchment will be exposed to direct fallout and the activity found in surface soils will be substantially greater than that associated with sediment exposed in channel banks and ditches or in gullies. Equally, where the soil is cultivated, the activity of ^{137}Cs and $^{210}Pb_{ex}$ in the surface soil can be expected to be significantly lower than in an undisturbed soil, such as might be found in an area of pasture or rangeland. Furthermore, the different nature and behavior of ^{7}Be fallout can provide potential for further discrimination, since this will only label the upper 1 or 2 cm of a cultivated soil, whereas ^{137}Cs and $^{210}Pb_{ex}$ will be mixed throughout the plow layer. This can provide a means of distinguishing sediment mobilized by sheet or interrill erosion and rill erosion, since the surface layer mobilized by sheet or interrill erosion will be characterized by high ^{7}Be activity, whereas the ^{7}Be activity of sediment mobilized by rill erosion will be lower, as it includes sediment mobilized from a greater depth within the plow layer.

Figure 12 provides a further demonstration of the ability of fallout radionuclides, in this case ^{137}Cs and ^{7}Be, to discriminate between potential sediment

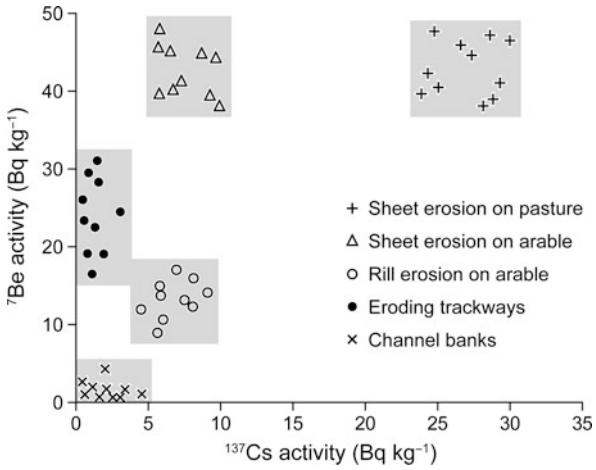

Fallout Radionuclides and the Study of Erosion and Sedimentation. Figure 12
The use of ^{7}Be and ^{137}Cs activity to discriminate between five potential suspended sediment sources in a small 1 km^2 catchment in Devon, UK

sources in a small (ca. 1 km^2) catchment in Devon, UK. By considering both the ^{137}Cs and ^{7}Be activities, it is possible to distinguish sediment mobilized from five potential sources. Sediment mobilized by sheet erosion from cultivated and pasture fields is characterized by a high ^{7}Be activity, by virtue of its surface origin, but the cultivated and pasture sources are clearly distinguished by their ^{137}Cs activity, which is much lower in the cultivated soil, due to the homogenization of the plow layer by tillage. Where rill erosion is the dominant erosion process on cultivated land, the ^{137}Cs activity of the mobilized sediment is close to that associated with sediment mobilized from cultivated land by interrill erosion, but the ^{7}Be activity is much lower, due to the inclusion of soil from below the surface containing little or no ^{7}Be. In contrast, channel banks are characterized by both low ^{137}Cs and ^{7}Be activities, because of the limited exposure of the face to fallout and the presence of both radionuclides in only the upper part of the bank profile. Eroding trackways are also distinguished by their radionuclide fingerprint. As erosion proceeds, the existing ^{137}Cs inventory is removed and the eroded surface material is characterized by a low ^{137}Cs activity. However, the ^{7}Be activity of sediment from this source is seen to be intermediate between that associated with channel banks and sediment mobilized from the surface of cultivated and pasture fields by sheet erosion. Because the ^{7}Be content of surface material is continually replenished by fresh fallout, the surface of eroding trackways can be characterized by an appreciable ^{7}Be activity. The sediment mobilized from the surface of eroding trackways is, however, likely to have a higher activity than that mobilized by rill erosion from cultivated fields, since the rills will penetrate deeper and mobilize some sediment with a low ^{7}Be activity. The addition of $^{210}Pb_{ex}$ to the results presented in Fig. 12 is likely to demonstrate further contrasts between the potential sources, since the ongoing nature of $^{210}Pb_{ex}$ fallout will provide some replenishment of the stock of this radionuclide in the surface horizons of eroding areas, whereas the effective cessation of ^{137}Cs fallout in the late 1970s means that no replenishment has occurred since that time.

The discrimination between various potential sediment sources provided by ^{7}Be and ^{137}Cs activity that is demonstrated in Fig. 12 means that these two fallout radionuclides are valuable fingerprint properties and the potential to distinguish sources could be increased further by looking also at $^{210}Pb_{ex}$ activity. However, additional fingerprint properties are likely to be required if a mixing model is used to provide definitive estimates of the relative contribution of the potential sources to the sediment sampled at the outlet of a catchment, in order to avoid problems of equifinality. Statistical procedures, such as multiple discriminant function analysis [131, 136], can be used to identify the optimum set of fingerprint properties or composite fingerprint, as it is often termed, for discriminating between all of the potential sources. There is also a need to recognize that contrasts in particle size composition and organic content between the sediment sampled at the catchment outlet or in the river, and the source material can mean that it is not possible to compare sediment and source material properties directly, and that some correction of the property values for particle size and organic matter content may be required [136]. Recent work has recognized the many uncertainties associated with characterizing the fingerprints of potential sources, and Monte Carlo techniques and Bayesian statistics have been used to explicitly recognize this uncertainty within the mixing models used to establish the relative contribution of different sources [137, 138].

The use of fallout radionuclides as sediment source fingerprints, both alone and with other sediment properties, has been successfully demonstrated at a range of scales. At the plot scale, for example, the contrasting depth distributions of ^{7}Be, ^{137}Cs, and ^{210}Pb$_{ex}$ have been shown to provide a means of establishing the relative contribution of sheet and rill erosion to the sediment output from small erosion plots under rainfall simulators and documenting the temporal variation of the sediment contributions from the two sources [139, 140]. At the larger field scale, Whiting and coworkers [141] investigated the erosion processes operating on a 6.03 ha cultivated field near Treynor, Iowa, USA, and used information on the different depth distributions associated with ^{7}Be, ^{137}Cs, and ^{210}Pb$_{ex}$ and measurements of the radionuclide content of the sediment output from the field during a storm event in mass balance calculations to estimate the areal extent of rill and sheet erosion and the characteristic depths of erosion associated with each process. Rill erosion was found to produce 29 times more sediment than sheet erosion, with rills eroding 0.38% of the field to a depth of 35 mm and sheet wash eroding 37% of the field to a depth of 0.012 mm. Within larger catchments, He and Owens [142] describe the use of ^{137}Cs, ^{210}Pb$_{ex}$, and ^{226}Ra activities to establish radionuclide fingerprints for cultivated land, uncultivated land, and channel banks within the 273 km^2 catchment of the River Culm in Devon UK and the application of these fingerprints to estimate the relative contribution of the three sources to the sediment output from the catchment. Similarly, Whiting et al. [143] working within the Yellowstone River catchment in Montana, USA, used measurements of ^{7}Be and ^{210}Pb$_{ex}$ to discriminate two primary sediment sources, namely, the catchment surface and eroding channel banks, and to estimate the changing relative importance of these sources along a 423 km^2 reach of the river.

In addition to their use as source fingerprints, fallout radionuclides have also been used as tracers to provide an improved understanding of the movement or transfer of sediment through river systems. In the study undertaken in the Yellowstone River in Montana [143] referred to above, radionuclide activities in the suspended sediment sampled at different locations along the river were used to investigate the sediment transport dynamics. Fine sediment transport distances were estimated from the exponential decrease in ^{137}Cs, ^{210}Pb$_{ex}$, and ^{7}Be concentrations downstream, and the transport distance was found to increase from a few km in the headwaters to hundreds of km downstream. Measurements of the ^{137}Cs and ^{7}Be activities of suspended sediment and fine bed sediment collected within the catchment of the River Clyst in Devon, UK were also used by Blake and coworkers [53] to explore the importance of short-term storage and remobilization of sediment within the channel system to downstream sediment delivery. The ratio of ^{7}Be to ^{210}Pb$_{ex}$ has also been successfully employed to assess the importance of recently resuspended bottom sediment to the suspended sediment moving within the Savannah Estuary, USA [144]. In this estuary, ^{7}Be activities were very low in the bottom sediment, when compared to those associated with recent suspended sediment inputs, while there was little difference in ^{210}Pb$_{ex}$ activity between the two sediment types.

As noted above, ^{7}Be has been found to provide a useful chronometer for coarser sand-sized fluvial sediment (transitional bedload) deposited in channel bars [130] and the labeling of this coarser sediment with ^{7}Be has also been exploited to document bedload transport velocities and the residence time of bed deposits [145]. In that study undertaken in Vermont, USA, the ratio of ^{7}Be to total ^{210}Pb was used in preference to ^{7}Be alone, since use of the ratio takes account of variations in grain size between samples. When sediment is deposited and stored on the riverbed, its ^{7}Be activity declines through time through decay, whereas the ^{210}Pb activity remains essentially constant. The magnitude of the ratio can therefore provide information on the short-term history of sediment deposition, remobilization, and replenishment at a site. The existence of a flood control dam on a river also provided the opportunity to investigate bedload transport velocities. Closure of the dam gate in early December caused the trapping of bedload and when the dam gate was opened in late March, the bedload which had been stored for several months and therefore had a near-zero ^{7}Be activity was released. By studying the downstream migration of this "dead" sediment, it was possible to document bedload transport velocities and to establish the length of the reach over which the influence of the dam in controlling bedload transport was evident.

Field and Laboratory Techniques

A detailed description and discussion of the field and laboratory techniques and procedures associated with the use of fallout radionuclides in the study of erosion and sedimentation falls outside the scope of this contribution. The reader is referred to the *Handbook for the Assessment of Soil Erosion and Sedimentation Using Environmental Radionuclides* edited by F. Zapata and published by Kluwer Academic Publishers in 2002 [29] for a detailed discussion of most of the field techniques and laboratory procedures employed when using ^{137}Cs measurements. Many of these are common to ^{7}Be and $^{210}Pb_{ex}$. Some further description and discussion of techniques will also be included in the case studies or examples presented at the end of this contribution. However, a brief overview of some key features of the field and laboratory techniques employed and important issues that frequently need to be addressed is provided below. This deals firstly with field techniques for sample collection, and secondly with laboratory analysis of the samples collected.

Field Techniques for Sample Collection

In most cases, the application of fallout radionuclides in soil erosion and sedimentation investigations involves the collection of samples from the field, for example, soil cores for use in studies of soil redistribution, cores from lakes or river floodplains for documenting sedimentation rates or establishing the chronology of sediment deposits, or samples from potential sources and samples of suspended sediment for use in sediment source fingerprinting investigations. As with most environmental sampling, there is an important need to ensure that the samples are representative and that they will provide results that can be readily interpreted. A carefully designed sampling program is therefore an essential precursor to the program of laboratory analysis. The need for representative samples involves both a temporal and a spatial dimension and both dimensions are important. When collecting samples of suspended sediment for establishing suspended sediment sources, for example, the temporal dimension can be very important and it is necessary to recognize that the properties of the sediment passing a sampling point may vary considerably through time, in response to different stages of the hydrograph and the routing of sediment from different parts of the catchment which may contribute at different times. It will therefore often be necessary to collect time-integrated samples, in order to provide representative information on the source of the sediment. Time integrating suspended sediment samplers or traps [146] provide one means of collecting such samples. These traps also have the advantage that they collect relatively large samples. Sizeable amounts of sediment may be required for subsequent laboratory analysis and if instantaneous samples are collected, a continuous flow centrifuge may be required to recover the sediment from large water samples [147].

When sampling fields to investigate patterns and rates of soil redistribution or collecting cores from lakes or river floodplains to document sedimentation rates, the temporal dimension will generally be of very limited importance for studies employing ^{137}Cs and $^{210}Pb_{ex}$, since these radionuclides provide information on medium- or longer-term process rates (i.e., 50–100 years) and their inventories are unlikely to be influenced by the conditions immediately preceding the time of sampling. However, when ^{7}Be is being used, the timing of sampling can be a key consideration in terms of providing definitive results, since there is need to avoid the possibility of past events influencing the measurements obtained.

Important issues related to the spatial dimension extend across the sampling associated with most applications of fallout radionuclides in the study of erosion and sedimentation. A key consideration here is that the cores, which frequently represent the main means of sample collection in studies of soil redistribution or sedimentation, are generally of relatively small diameter and are therefore characterized by a small or, perhaps more correctly, a very small, surface area. Sampling points must be carefully selected and the sampling scheme must be carefully designed to obtain representative data. When studying soil redistribution within fields, a density of 20 cores ha^{-1} is likely to be considered fairly dense, but such cores are typically ca. 8 cm in diameter and the cores will therefore typically only cover $<0.001\%$ of the surface area under investigation. Transects and sampling grids are frequently employed in studies of soil redistribution or sedimentation patterns and rates to provide representative data, but it is important to also recognize the uncertainty

that is likely to be introduced by microscale sampling variability, such that if the core was taken a few centimeters away from the initial sampling point, a different inventory value might be obtained [148]. Problems of sampling variability assume particular importance when samples are collected to define the local reference inventory [149, 150]. In addition to carefully selecting a stable undisturbed site that should provide a reliable estimate of the reference inventory, there is a need to collect an appreciable number of cores from the site, the results for which can be averaged, in order to obtain a reliable estimate of that inventory. The inventories measured for individual cores collected from a reference site can frequently be characterized by a coefficient of variation of ca. 20%, or perhaps more, and this means that about 16 cores would need to be collected to provide a mean value that was within 10% of the true mean at the 95% level of confidence. The use of a scraper plate [151], which collects the sample from a larger area, as an alternative to cores, can help provide more representative samples. Similar considerations apply when collecting samples to be used to represent the fingerprint properties of potential sources in source fingerprinting investigations. It is important to ensure that the samples collected are representative of the sediment that might be mobilized from a given source and the uncertainty introduced by representing the final fingerprint by mean property values must be recognized. Problems of spatial variability are generally less important when selecting the locations for collection of cores to be used for determination of the chronology of sediment deposits, but again it is important to collect the core from a representative position and it is generally considerably more difficult to appreciate potential subsurface variability or heterogeneity than variability related to readily visible surface conditions.

Corers will be a key requirement in many investigations employing fallout radionuclides to document soil and sediment redistribution and sedimentation. A range of different corers have been developed for use in different materials and environments, including lakes and reservoirs, wetlands, and soils and these are described in the literature. Sample size may be an important constraint, particularly with sectioned cores, and large diameter corers may be required to provide sufficient mass for the analysis of radionuclide activity, if the core is sectioned into small depth increments (e.g., 1 cm). For soils, cylindrical core tubes are commonly used, but if soils are compacted and dry, it may prove difficult to propel the core tube into the soil to the required depth (e.g., 60 cm). In this situation, a motorized percussion driver is often used to insert the core tube and a winch device may be required to extract the core tube. A scraper plate [151] can provide an alternative to a core, particularly if detailed depth incremental sampling is required, but use of these devices can prove very time consuming relative to the use of sectioned cores. One particular problem commonly faced when using ^{7}Be measurements is the need to section a shallow core into very fine depth increments (e.g., 2 mm), in order to define the precise shape of the depth distribution, which may only extend down to ca. 15 mm. In order to obtain samples of sufficient mass for the individual depth increments, a corer with a sizeable diameter will be required and devices involving a piston moved by a screw thread have been developed to permit the extrusion of the core to be carefully controlled.

Laboratory Procedures and Techniques

A key feature of the use of fallout radionuclides is that for most applications, the activities of the radionuclides of interest can be readily measured by gamma spectrometry and, provided suitable detectors are available, the radionuclides can be measured contemporaneously during the same counting operation. This removes the need for separate analyses. Gamma spectrometry is therefore the main analytical technique employed in fallout radionuclide investigations, although, in some studies focusing on ^{210}Pb, alternative analytical procedures using radiochemical separations and alpha counting are used [152]. However, this approach involves chemical extractions which require a substantial time input; furthermore, it can only provide measurements of total ^{210}Pb. Additional gamma spectrometry measurements would still be needed to quantify the ^{226}Ra and supported ^{210}Pb activity and thus calculate the $^{210}Pb_{ex}$ activity. In the case of sediment cores, collection of samples from depths below the likely influence of $^{210}Pb_{ex}$ fallout, where the measured ^{210}Pb activity can be assumed to represent supported ^{210}Pb, can provide a means of establishing the likely supported ^{210}Pb activity of the sediment,

although this value could change upcore. Another important advantage of gamma spectrometry is that only minimal sample preparation is required. Samples need only to be dried and disaggregated and possibly sieved prior to placing in containers to be counted. However, one key limitation of the assay of environmental samples by gamma spectrometry is the long count times involved. These are commonly of the order of 6–12 h per sample, and where activities are lower, count times of 24 h or more may be necessary. The long count times will frequently impose important limitations on the number of samples that can be analyzed within an investigation, since gamma detectors are relatively expensive and it is likely to be possible to operate only a limited number of detectors in a laboratory. With ^{137}Cs and ^{210}Pb$_{ex}$, dealing with large backlogs of samples may not represent too great a problem, apart from the time required to complete a study. However, with ^{7}Be, the short half-life means that samples must be analyzed relatively quickly after collection and this will commonly impose a limit on the number of samples that can be collected and analyzed within a particular study. It is important that such studies should be carefully planned to take account of these constraints to ensure that the final data set is complete.

Further details of the instrumentation required for analysis of samples by gamma spectrometry and of the procedures employed when analyzing soil and sediment samples are available in specialist handbooks [153]. Measurement of ^{137}Cs, ^{7}Be, and ^{210}Pb$_{ex}$ activities is undertaken using Germanium detectors, which have a high resolution and are therefore able to distinguish the signals produced by different radionuclides at similar energy levels. Figure 13 provides a useful summary of the main features of the various Germanium gamma detectors that are available, and attention should be directed to both the geometry and the energy ranges of these detectors. Although ^{137}Cs and ^{7}Be can be measured on standard gamma detectors, the measurement of ^{210}Pb requires a low-energy detector that is capable of undertaking measurements at the low-energy level (46 keV) associated with this radionuclide. Fortunately, the low-energy detectors needed for ^{210}Pb can, if required, also be used to measure ^{137}Cs and ^{7}Be, as well as to make the necessary measurements to determine the ^{226}Ra content of the sample required to calculate the supported ^{210}Pb activity. Where large samples (e.g., 1 kg) are involved, Marinelli beakers are commonly used as the sample container, as these fit over the detector head and are designed to optimize the positioning of the sample relative to the detector for

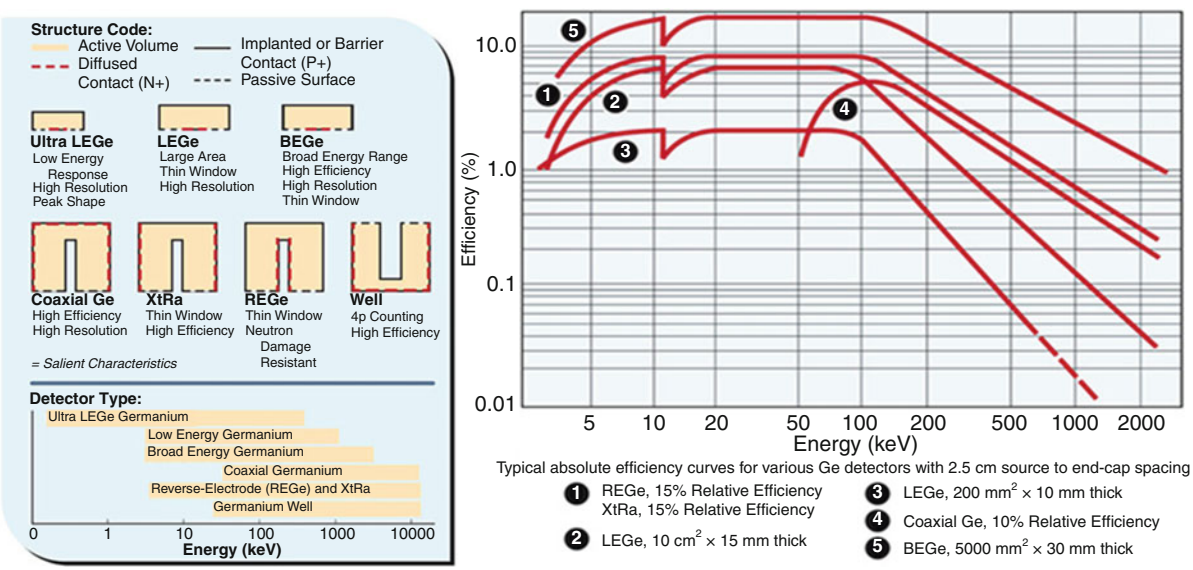

Fallout Radionuclides and the Study of Erosion and Sedimentation. Figure 13
The configuration, geometry, and response characteristics of Germanium detectors used for gamma spectrometry [154]

counting. Where small samples (e.g., 50–100 g) are counted, these can be put into small plastic pots that are placed on the detector head. For smaller samples (e.g., ca. 10 g), such as may be obtained from the sectioning of small diameter sectioned cores or from small samples of suspended sediment collected from a river, a well detector is commonly used. In this case, the sample is placed in a tube which is inserted into a hole in the top of the detector in order to optimize the counting geometry.

Although gamma spectrometry is relatively undemanding in terms of sample preparation, the detectors must be carefully calibrated to provide accurate measurements [153]. In the case of ^{210}Pb measurements, self-absorption effects can introduce problems and must be considered. The principle of measurement, which depends on the interaction of gamma rays (photons) produced by the disintegration of the radionuclide, an essentially random process, with the germanium crystal, means that the precision of the results obtained is heavily dependent on the number of disintegrations counted. This in turn depends on the activity of the sample, the efficiency of the detector, and the counting time. All results should therefore be accompanied by an indication of their likely precision, and this uncertainty must be recognized when using the results. The precision is typically of the order of ±5–10% at the 95% level of confidence. In the case of ^{137}Cs and ^{7}Be, the radionuclides can be measured directly by gamma spectrometry, but determination of $^{210}Pb_{ex}$ requires two measurements. The first quantifies the total ^{210}Pb content of the sample and the second establishes the ^{226}Ra content, which is used to calculate the supported ^{210}Pb activity by assuming equilibrium between ^{226}Ra and ^{210}Pb. The $^{210}Pb_{ex}$ activity is then calculated by subtracting the supported ^{210}Pb activity from the total ^{210}Pb activity. The Radium-226 content of a sample is usually determined by measuring the activity of its daughters ^{214}Bi and ^{214}Pb, because its direct measurement is complicated by interference from other radionuclides. The need for two measurements and the subsequent subtraction means that the precision of the final estimates of $^{210}Pb_{ex}$ activity is usually lower than that associated with ^{137}Cs and ^{7}Be measurements.

Although gamma spectrometry measurements are generally undertaken in the laboratory, to which samples collected in the field are transported, attention has been directed to the potential for using in situ detectors [155, 156]. In this case, the detector is deployed in the field in a portable configuration. The detector head is positioned ca. 1.5 m above the soil surface, and the gamma rays received from the soil are counted. Because gamma rays will be received from a relatively large area, the approach overcomes some of the sampling variability problems associated with the collection of small core samples and this, as well as the possibility of obtaining immediate results, are seen as important potential advantages. However, problems can arise in calibrating the measurements, since the precise area of soil from which gamma rays are received can prove difficult to define, due to attenuation effects. Equally a given radionuclide inventory can produce different signals according to the depth distribution of the radionuclide in the soil, and there is a need to make certain assumptions regarding the likely form of the depth distribution. Self-absorption effects also mean that the approach is unlikely to be applicable to ^{210}Pb measurements. Furthermore, in most environments, substantial count times (e.g., ca. 1 h) will be required and this may limit the number of points for which measurements can be collected. As a result, the use of field portable detectors has not been widely adopted and further research is required to assess more fully the potential and limitations of the approach. However, the approach has proved more successful for ^{137}Cs measurements in areas that received substantial amounts of Chernobyl fallout, since the high activities in such areas greatly reduced the count times required [157]. Furthermore, with such high activities, the ^{137}Cs signal is more readily distinguished from those of other radionuclides with similar energy levels and low cost scintillation detectors can be used in place of more costly Germanium detectors.

Uncertainty Considerations in the Use of Fallout Radionuclide Measurements

The brief overview of field and laboratory techniques provided above has emphasized the potential uncertainty introduced into the application of fallout radionuclide measurements by sampling variability and measurement precision. Any measurement of the

fallout radionuclide activity or inventory is likely to involve a significant degree of uncertainty by virtue of both the heterogeneity of natural soils and sediments and the associated sampling variability and the limited precision of gamma spectrometry measurements. It is important that this uncertainty should be recognized, at least implicitly, if not explicitly, and if possible propagated through subsequent use of the data, for example to derive estimates of soil redistribution rates by comparing measurements of the fallout radionuclide inventory made at individual sampling points with the local reference inventory.

Some Examples of the Application of Fallout Radionuclides in Erosion and Sedimentation Investigations

Further consideration of the application of fallout radionuclides in the study of erosion and sedimentation within the environment can usefully involve a brief overview of several case studies, based on investigations undertaken by the author and his coworkers, which demonstrate the potential of the approach across a range of applications. These include soil erosion, floodplain sedimentation, and sediment source tracing.

Soil Erosion: A Field Scale Investigation

Although most work involving the use of fallout radionuclides in soil erosion investigations has been based on measurements of ^{137}Cs, both $^{210}Pb_{ex}$ and ^{7}Be have also been used in similar applications. By collecting cores from a study site, measuring the ^{137}Cs, $^{210}Pb_{ex}$, or ^{7}Be inventories, and applying a conversion model, it is possible to derive point estimates of the erosion and deposition rates associated with the cores. The time base of the erosion rate estimates will depend on the radionuclide used. These values can then be used to establish the spatial pattern of soil redistribution, and by integrating the values across the study site, it is possible to calculate the gross and net erosion and the sediment delivery ratio. The latter represents the proportion of the eroded soil that is transported out of the study site and provides important information on the likelihood of eroded soil reaching watercourses. By making measurements of more than one radionuclide, it is often possible to obtain additional information, by virtue of the different half-lives or fallout histories of the radionuclides. Figure 14 presents the results of an investigation of rates and patterns of soil redistribution within a 6.7-ha field at Higher Walton Farm near Crediton in Devon, UK [33]. The area covered by the field represents a valley head depression with slopes of up to 15° converging toward its outlet. In this case, measurements of both ^{137}Cs and ^{7}Be activities were undertaken, with the former providing estimates of average rates of soil redistribution over the past ~45 years, and the latter estimates of the erosion rates associated with a particular period of heavy rainfall (69 mm in 7 days) that occurred in early January 1998.

In this study, the soil cores used for the ^{137}Cs and ^{7}Be measurements were collected during two separate campaigns, although they could have been collected together. In both cases, the cores were collected at the intersections of a 20 m × 20 m grid, resulting in a suite of ~140 cores from each sampling campaign. Cores were also collected from adjacent areas of undisturbed land, which were not expected to have experienced either erosion or deposition, in order to establish the reference inventory. For the ^{137}Cs measurements, the cores were collected in August 1996, using a motorized percussion corer equipped with a 6.9-cm internal diameter steel core tube, which was inserted into the soil to a depth of ~60 cm. The cores used for the ^{7}Be measurements were, in contrast, much shallower and were collected manually to depths of 3–5 cm using a 15-cm diameter plastic core tube, in January 1998. During the preceding spring/summer of 1997, the field had been cultivated and sown to maize and the crop was harvested in early November 1997, when the soil was compacted by the harvesting equipment. After harvesting, the field was left bare and uncultivated over the winter and the period of heavy rainfall in early January 1998 resulted in substantial surface runoff and soil erosion. The pattern of ^{137}Cs inventories documented for the study field is presented in Fig. 14a. The cores collected from the adjacent undisturbed sites provided an estimate of the local ^{137}Cs reference inventory at the time of sampling of ~2,500 Bq m^{-2} and the pattern of ^{137}Cs inventories shows clear evidence of both erosion (reduced inventories) and deposition (increased inventories). Use of a mass balance conversion model incorporating the effects of soil redistribution by tillage enabled estimates of mean annual soil

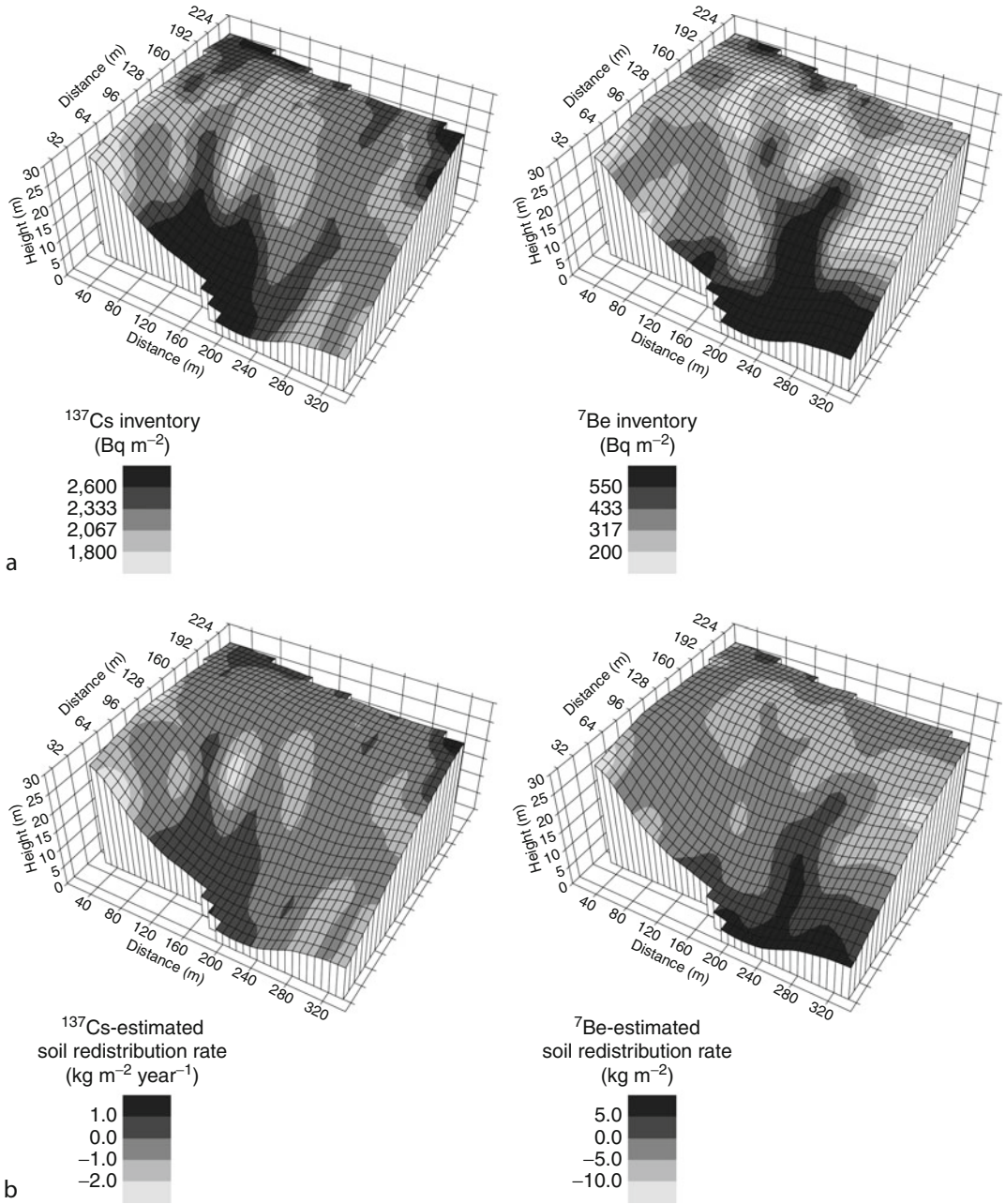

Fallout Radionuclides and the Study of Erosion and Sedimentation. Figure 14
The spatial distribution of ^{137}Cs and ^{7}Be inventories within a field at Higher Walton Farm, near Crediton, UK (**a**) and of the estimates of soil redistribution rates derived from these inventories (**b**)

redistribution rates to be derived from the measured inventories. These soil redistribution rates relate to the period of ca. ~45 years prior to the sampling campaign in 1996. The pattern shown has been mapped in Fig. 14b and the data have been summarized in Table 3, which presents values for the range of the documented soil redistribution rates, the mean erosion rate for the eroding areas, the mean deposition rate for the

depositional areas, the net soil loss from the field, and the sediment delivery ratio.

The spatial distribution of ^{7}Be inventories within the study field measured at the end of the period of heavy rainfall in early January 1998 is also presented in Fig. 14a. The equivalent value for the local reference inventory was estimated to be 533 Bq m^{-2} and the pattern depicted provides clear evidence of areas with both reduced and increased inventories, which in turn reflect both erosion and deposition within the field. In order to interpret this pattern in terms of soil redistribution rates associated with the period of heavy rainfall in early January, it was important to consider the extent to which it might reflect spatial variability inherited from previous erosion events. However, the preceding autumn and early winter had been relatively dry and there was no evidence of surface erosion having occurred during the previous 6 months. In this situation, the ^{7}Be inventory within the field immediately prior to the period of heavy rainfall in early January 1998 could be expected to be spatially uniform, since it would reflect the wet fallout associated with rainfall over the preceding months. Any spatial variability produced by soil redistribution associated with erosion events much earlier in 1997 would have been rendered insignificant by radioactive decay, due to the short half-life of ^{7}Be. It was therefore possible to assume that the spatial variability in ^{7}Be inventories within the study field evident in Fig. 14a reflects soil redistribution associated with the period of heavy rainfall in early January 1998. By using the conversion model for ^{7}Be measurements described previously in this chapter (i.e., Eq. 7), which takes account of the increase or decrease in inventory relative to the reference inventory and the depth distribution of ^{7}Be in uneroded soil within the field, it was possible to estimate the soil redistribution rates associated with the period of heavy rainfall preceding the sampling campaign. The pattern of soil redistribution rates demonstrated by these results is presented in Fig. 14b and summary data, equivalent to that provided for the ^{137}Cs measurements, are listed in Table 3. The soil redistribution rates (kg m^{-2}) associated with the period of heavy rainfall in early January 1998 estimated from the ^{7}Be measurements are substantially higher than the equivalent longer-term mean annual soil redistribution rates estimated using the ^{137}Cs measurements. However, the sediment delivery ratios are closely similar, indicating that ~80% of the eroded sediment was transported out of the field. The high sediment redistribution rates associated with the period of heavy rainfall in early January 1998 reflect both the extreme nature of this period of rainfall and, perhaps more importantly, the condition of the field, which having been compacted by the maize harvesting machinery and left bare after the harvest was particularly susceptible to surface runoff and erosion. Such results underscore the potential significance of a small number of extreme events and the incidence of particular land use conditions in controlling erosion from the study field.

Fallout Radionuclides and the Study of Erosion and Sedimentation. Table 3 A comparison of rates of soil redistribution within a field at Higher Walton Farm, near Crediton, UK, estimated using the ^{137}Cs and ^{7}Be measurements made on soil cores collected from the field

Measure	^{137}Cs (kg m^{-2} year^{-1})	^{7}Be (kg m^{-2})
Range	−4.5 to 2.0	−11.9 to 9.8
Mean erosion rate for eroding area	−1.1	−5.3
Mean deposition rate for depositional area	0.69	4.0
Net soil loss	−0.48	−2.5
Sediment delivery ratio	0.83	0.80

Based on Walling et al. [33]

Soil Erosion: A Countrywide Survey

A key feature of most existing studies involving the use of measurements of ^{137}Cs and other fallout radionuclides in soil erosion investigations has been the emphasis on small areas, frequently individual fields. It has been argued that if fallout radionuclides are to be more widely used as an operational tool to support policy, as distinct from a research tool, there is a need to upscale their application. Analytical constraints, including the relative long count times and the substantial cost of gamma spectrometers, which inevitably

limit the number of detectors available in most laboratories, means that it is not feasible to upscale by simply collecting and analyzing a greatly increased number of samples. There is a need to devise novel sampling strategies that permit the use of ^{137}Cs measurements at the reconnaissance scale. Work by Loughran and coworkers [92] in Australia attempted to develop a national soil erosion survey based on ^{137}Cs measurements, and, in this case, 206 sites located in many different parts of the country were sampled using single downslope transects comprising about 20 sampling points. Recent work in the UK [158] has attempted to develop this approach further by reducing the number of samples collected from a site, while still obtaining a representative estimate of the gross and net erosion rate and thereby increasing the number of sites for which data can be assembled. By selecting fields of similar size and simple topography, but representative of a wide range of conditions known to influence soil erosion rates, including soil texture, slope steepness, effective rainfall and land use, it was possible to commence the assembly of a national scale database on soil erosion rates on agricultural land.

In the initial stages of this study, detailed investigations were undertaken in a number of fields to confirm the potential for using a small number of samples (e.g., [10–15]) collected along a carefully positioned downslope transect to provide a meaningful assessment of the gross and net erosion rates in a given field. The information on ^{137}Cs inventories provided by the transects was used to estimate soil redistribution rates, using a conventional mass balance model and the diffusion and migration model for cultivated and non-cultivated fields, respectively. Estimates of the gross and net erosion rates for individual fields were derived by integrating the resulting estimates of soil redistribution rate along the length of the transect. Comparison of the results provided by the single transect with those provided by much denser grid or transect sampling networks, using the same conversion models, confirmed the validity of the approach and indicated that a transect comprising ca. 10–15 sampling points was capable of providing a reliable estimate of the gross and net erosion rates within individual fields.

A national sampling campaign was subsequently undertaken to obtain estimates of gross and net erosion rates for 248 fields located in different areas of England and Wales. The data collected are summarized in Fig. 15, which distinguishes the erosion rate estimates obtained for arable and pasture fields. These data have provided a basis for assessing the range of erosion rates occurring on agricultural land in England and Wales. The gross and net erosion rates documented for arable fields ranged between 1.2 and 29.3 t ha^{-1} year^{-1} and 0.0 and 27.3 t ha^{-1} year^{-1}, with median rates of 6.6 and 5.2 t ha^{-1} year^{-1}, respectively. The equivalent ranges for pasture were 0.7–13.0 and 0.0–11.7 t ha^{-1} year^{-1}, with median values of gross and net erosion of 2.6 and

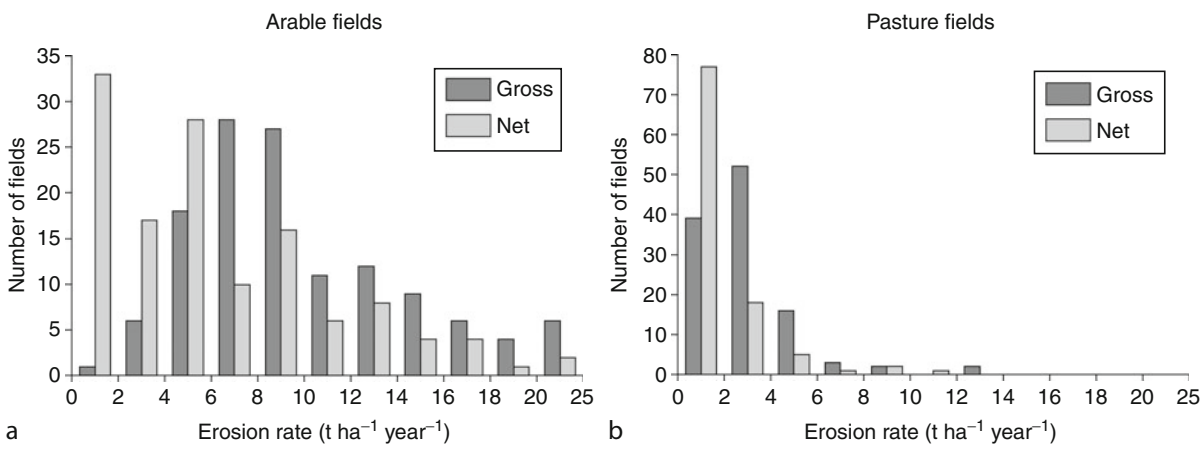

Fallout Radionuclides and the Study of Erosion and Sedimentation. Figure 15
Frequency distributions of mean annual gross and net erosion rates for the arable and pasture fields in England and Wales sampled in the national survey undertaken by Walling and Zhang (2010) [158]

1.8 t ha^{-1} $year^{-1}$, respectively. The ratio of net to gross erosion, which provides a useful measure of potential sediment delivery to watercourses, was typically >0.6 for arable fields and <0.6 for pasture fields, emphasizing the lower efficiency of sediment delivery from pasture areas. Comparison of the erosion rates obtained from the study with existing erosion hazard assessments, based on soil texture, confirmed the broad consistency of the results. The assembled dataset also provided a basis for exploring the influence of a range of potential controlling variables on soil erosion rates, using statistical tests. No very strong relationships existed, but several statistically significant relationships between the erosion rate variables and slope gradient and soil texture were found. The data have also been used to develop a typology for extrapolating the assembled information on gross and net erosion rates, based on land use, soil texture, and slope steepness and this has been employed within a GIS to produce national scale maps of gross and net rates of soil loss from agricultural land in England and Wales and a preliminary national scale inventory of soil loss for England and Wales.

Documenting Floodplain Sedimentation Rates

Overbank deposition on river floodplains during flood events represents an important potential sink for suspended sediment transported through a river system, and recent studies have demonstrated that such conveyance losses can be as high as ~40% of the suspended sediment load delivered to the main channel system [159]. Where attempts are made to reduce downstream sediment loads through improved land management and other sediment control measures, it can be important to document rates of overbank sedimentation on river floodplains, in order to quantify the potential magnitude of this sediment sink. In addition to representing a conveyance loss, the sediment deposited on the floodplain can also give rise to environmental problems, if it contains high levels of contaminants, such as heavy metals, or nutrients, particularly phosphorus. Again, information on rates of overbank sedimentation can represent an important requirement to assess such hazards. Since overbank inundation is commonly infrequent and difficult to forecast, direct measurements of associated sedimentation rates, using sediment traps and related techniques, can prove difficult to implement. Furthermore, there will often be a need to establish longer-term rates of sedimentation to take account of the frequency of floods of different magnitude. In this context, the use of ^{137}Cs and $^{210}Pb_{ex}$ measurements to document longer-term mean annual sedimentation rates offers considerable potential. As an example, Fig. 16 shows how ^{137}Cs and $^{210}Pb_{ex}$ measurements were used to document overbank sedimentation rates along a short reach of the floodplain of the River Severn near Buildwas in Shropshire, UK. In this study, 124 sediment cores were collected at the intersections of a 25 m × 25 m grid using a motorized percussion corer equipped with a 6.9-cm internal diameter core tube. Cores were collected to a depth of ~70 cm to ensure that they included the complete ^{137}Cs and unsupported ^{210}Pb profiles. Measurements of the ^{137}Cs and $^{210}Pb_{ex}$ inventories of the cores were used to estimate the mean annual sedimentation rates at the coring points using the procedures documented by [118, 122] and described previously. In the case of ^{137}Cs, the estimate of the sedimentation rate derived from a sectioned core and the depth of the ^{137}Cs peak (see Eq. 8) was extrapolated to the other sampling points where bulk cores were collected, using the procedure represented in Eq. 10. In the case of the $^{210}Pbex$ measurements, the values of total inventory obtained for the individual bulk cores collected from the sampling points were used with the CICCS model (Eq. 15) to estimate the sedimentation rates at those points. These estimates of sedimentation rate were used to map the patterns of sedimentation within the reach presented in Fig. 16. These patterns reflect the interaction of a number of controls on the sedimentation rate, including depth of inundation, distance from the channel, and the local microtopography. It is also possible to compare the sedimentation rate estimates derived from the ^{137}Cs measurements, which relate to the past ~40 years, with those based on the unsupported ^{210}Pb measurements, which relate to the past ~100 years, in order to assess longer-term changes in sedimentation at this location. The mean annual sedimentation rate at this site over the past 40 years is 0.28 g cm^{-2} $year^{-1}$, whereas the equivalent rate for the past 100 years is 0.33 g cm^{-2} $year^{-1}$. This suggests that rates of overbank sedimentation have decreased slightly toward the present. This decrease could reflect changes in the

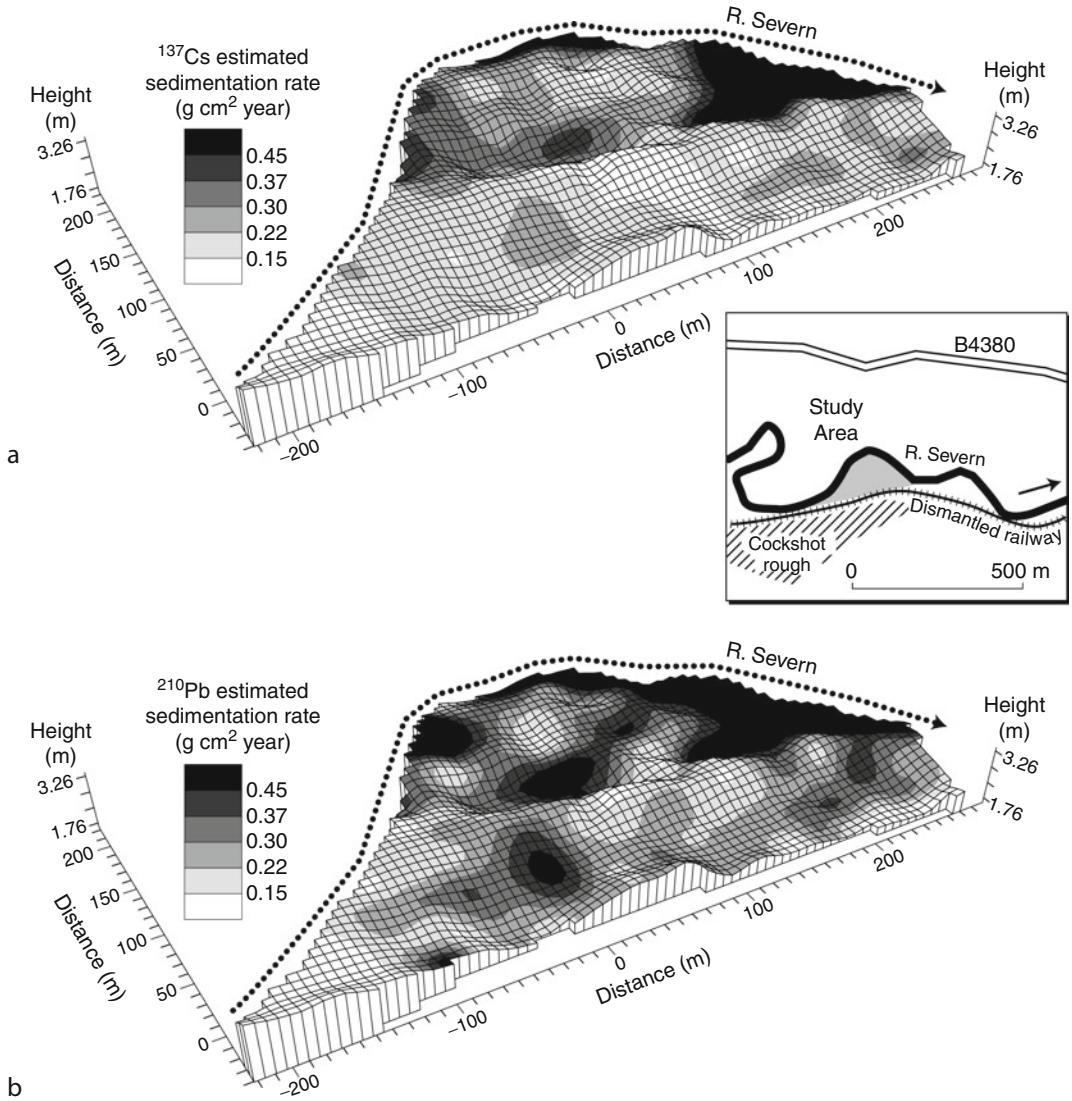

Fallout Radionuclides and the Study of Erosion and Sedimentation. Figure 16
The spatial distribution of overbank sedimentation rates within a small reach of the floodplain of the River Severn near Buildwas, Shropshire, UK derived from ^{137}Cs and $^{210}Pb_{ex}$ measurements undertaken on floodplain cores

magnitude and frequency of flood inundation, but it might also reflect a progressive reduction in inundation depths as the level of the floodplain surface gradually increased in height as a result of overbank deposition.

Using Floodplain Deposits to Reconstruct Changes in the Properties of Sediment Transported by a River

Where post-depositional changes in sediment geochemistry can be assumed to be of limited importance, it is possible to use downcore changes in the geochemistry of overbank deposits to reconstruct changes in the properties of the suspended sediment transported by a river. The overbank deposits effectively preserve a record of the suspended sediment transported by the river in the recent past [160] and fallout radionuclides can be used to provide information on the chronology of such deposits. A useful example of this approach is provided by a study undertaken by the author and his coworkers on the floodplain bordering

the main channel of the River Axe, which drains a 303 km^2 catchment in Devon, UK, aimed at reconstructing changes in the phosphorus content of the deposited sediment. Floodplain cores were collected from three representative sites in the upper, middle, and lower reaches of the river basin (see Fig. 17a) and measurements of both the ^{137}Cs activity and the total-P content of the sectioned cores were undertaken, in order to establish the associated depth profiles. The total-P profiles shown in Fig. 17 indicate that the total-P content of sediment deposited on the river floodplains at the three sites has more than doubled in recent decades, in response to increased fertilizer application and livestock densities in the upstream catchments and increased effluent discharges from sewage works and related point sources. The ^{137}Cs measurements were used to establish an approximate chronology for these changes by defining the level of the floodplain surface in 1963, the year of peak ^{137}Cs fallout (Fig. 17b), and assuming a constant annual sedimentation rate. This chronology was used to derive the plots of the changing total-P content of deposited sediment since 1950 presented in Fig. 17c. At all three sites, the total-P content of deposited sediment has increased by more than 100% over the past 50 years, but higher concentrations are found in the middle and lower reaches of the catchment where agriculture is more intensive and effluent discharges are greater. Although not clearly defined, there is some evidence of a reduced total-P content in deposited sediment in the last 10 years and this could reflect a response to improved land management and treatment of waste water discharges. Information of this nature can afford a valuable basis for defining baseline levels for fluvial sediment properties and assessing the impact of changing land management and wastewater treatment in reducing the inputs of P and other sediment-associated nutrients and contaminants to river systems.

Use of Fallout Radionuclides for Sediment Source Fingerprinting: An Example from the UK

The siltation of spawning gravels has been increasingly identified as a key factor contributing to the declining success of salmon fisheries in British rivers. Concern for this problem has focused attention on the need to reduce gravel siltation and thus to reduce fine sediment mobilization and transport in impacted catchments, through the establishment of sediment control programs. The development of effective sediment control programs requires information on the likely sources of the fine sediment accumulating in spawning gravels, since these sources must be targeted if the control program is to prove effective. In an attempt to provide such information, a reconnaissance source fingerprinting survey of several representative rivers, located in different parts of Britain, was undertaken by the author and his coworkers in collaboration with the Environment Agency [161].

Samples of interstitial fine sediment were recovered from salmonid spawning gravels within a representative selection of rivers in England and Wales (Fig. 18), during a national fieldwork program conducted by the Environment Agency over the period 1999–2000. Sample collection was based on the use of retrievable basket samplers, which were installed in artificial redds constructed in spawning gravels at representative locations. Between one and five basket samplers were installed in each of the rivers identified on Fig. 18. The basket samplers were filled with clean framework gravel (>6.4 mm) prior to their installation, and they were retrieved ca. 3 months later. The gravel contained within the basket was subsequently wet sieved to recover the fine (<0.125 mm) interstitial sediment that had accumulated within the gravel during the period of deployment and this fraction was used for sediment source fingerprinting. By virtue of the reconnaissance nature of the study, which included 18 catchments, sampling of potential source materials focused on the broad distinction between surface and channel bank/subsurface sources, and a total of 672 source material samples were collected from the different study areas. These samples were sieved to <0.125 mm to facilitate direct comparison with the samples of fine interstitial sediment. The limited resources available to the study also precluded the use of an extensive range of fingerprint properties to discriminate the two potential sources and emphasis was placed on the use of radiometric (^{137}Cs, $^{210}Pb_{ex}$, ^{226}Ra) measurements, coupled with information on the organic properties (C and N content) of the potential sources. Mean values of these properties were used to characterize the two potential sources in each of the river basins investigated.

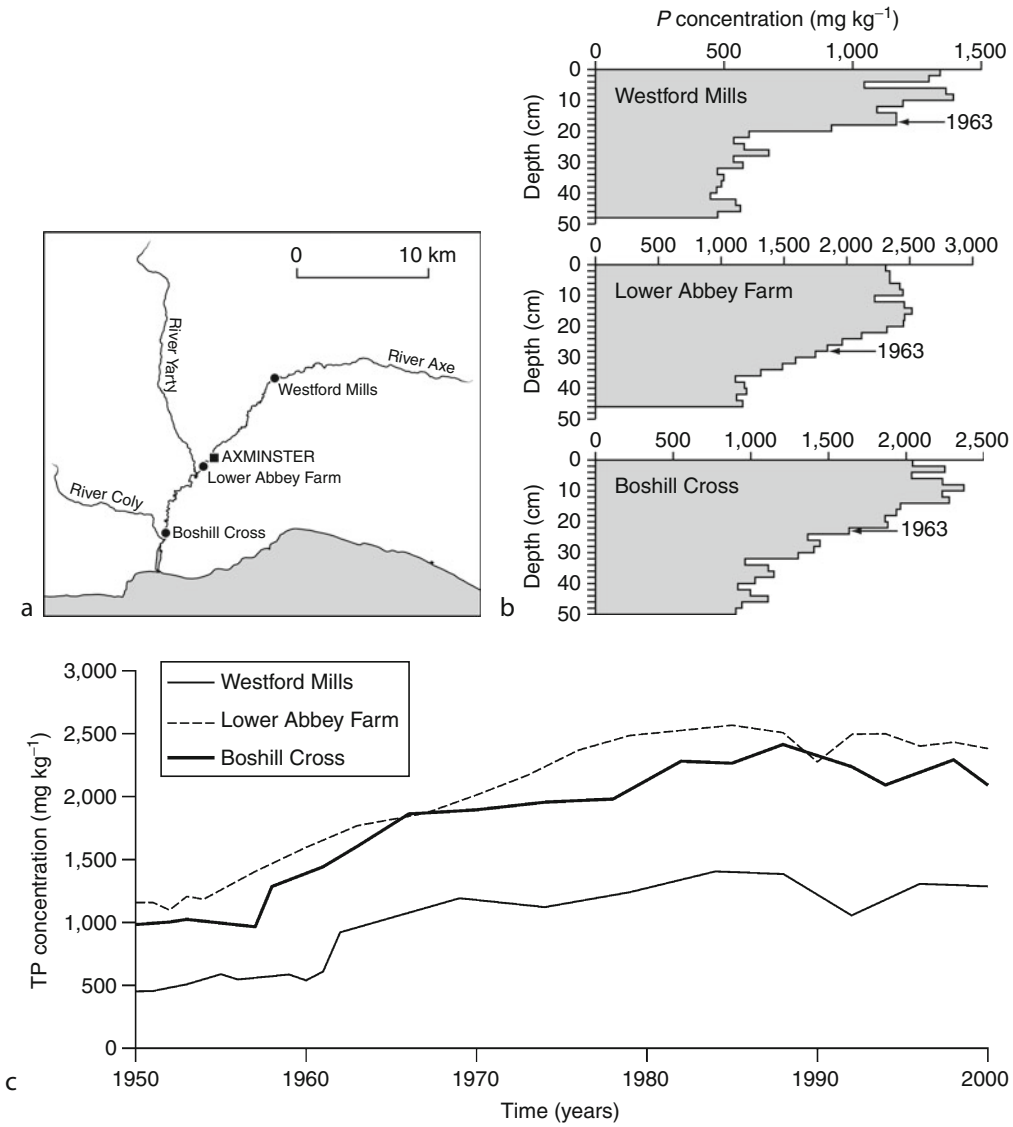

Fallout Radionuclides and the Study of Erosion and Sedimentation. Figure 17
The changing total-P content of fine sediment deposited on the floodplain of the River Axe over the past 50 years, showing (**a**) the location of the coring points, (**b**) the total-P depth distributions, and (**c**) the reconstructed trends in the total-P content of fine sediment deposited on the floodplain over the past 50 years

A multicomponent mixing model, incorporating correction for the effects of contrasts in particle size and organic matter content between the samples of interstitial sediment and the source material, was used to estimate the relative contributions of surface and channel bank/subsurface sources to the fine sediment recovered from the spawning gravels. The results of these computations for different regions of England and Wales are presented in Fig. 18. Significant contrasts in the relative contributions of the two sources are apparent between the regions, with, for example, surface sources accounting for >90% of the fine interstitial sediment in north Wales and southern England, but only 16% and 39% in south-west England and south and mid Wales, respectively. These regional contrasts reflect the interaction of land use and both erosion

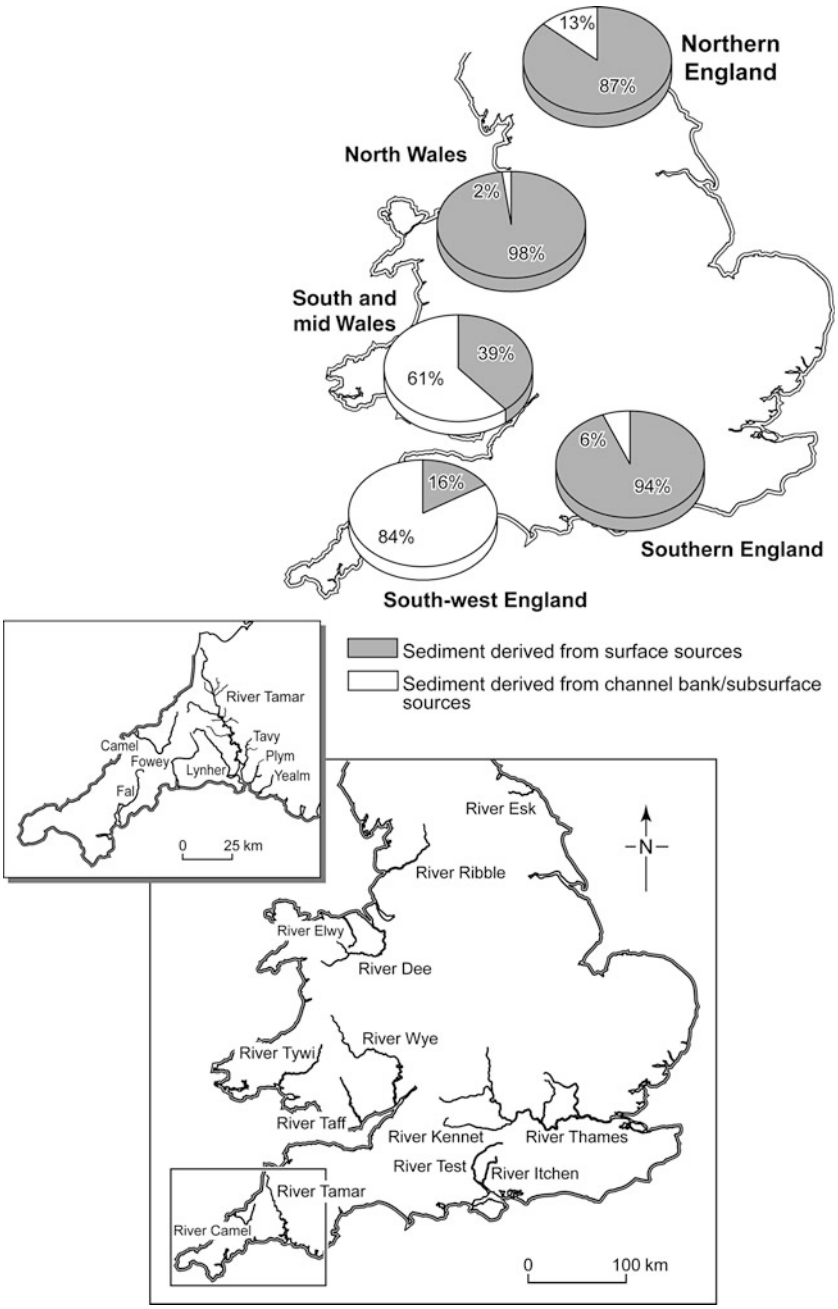

Fallout Radionuclides and the Study of Erosion and Sedimentation. Figure 18
Fingerprinting the source of fine sediment accumulating in salmon spawning gravels, showing the location of the sampled rivers and regional contrasts in the source of the fine sediment (Based on [161])

processes and the efficiency of sediment transfer to the channel network. In south-west England, where stocking densities are frequently high, drainage densities are relatively high and river channels are generally incised, a combination of livestock trampling of channel banks and erosion of unstable well-developed vertical channel banks mean that channel and subsurface sources are the dominant source of fine interstitial sediment.

In contrast, the greater importance of arable farming and more specifically soil erosion on large cultivated fields with few boundaries to interrupt slope-channel connectivity, combined with the relative stability of the well-vegetated channel banks, result in surface soils providing the dominant source (94%) of the samples of fine interstitial sediment recovered from spawning gravels in southern England. Surface sources are also important in the upland areas of northern England and north Wales, where high rainfall and grazing pressure promote the erosion of surface soils under upland pasture or moorland and the steep topography combined with an absence of field boundaries results in the efficient routing of sediment to the river channels.

The contrasts in the relative importance of surface and channel bank/subsurface sources in different regions of England and Wales outlined above have important implications for the design and implementation of effective sediment control strategies. Where bank erosion is the dominant source, attention should clearly focus on reduction of livestock trampling of channel margins and improvement of bank stability (e.g., by fencing and revegetation of channel margins). However, such measures are likely to be of little value in areas where surface sources are dominant and where emphasis should be placed on controlling sediment mobilization and transfer within the catchment more generally.

Use of Fallout Radionuclides for Sediment Source Fingerprinting: An Example from China

Another example of the potential for using environmental radionuclides, and more particularly ^{137}Cs, for fingerprinting sediment sources is drawn from work in the rolling loess plateau region of Shaanxi Province, China [162]. The landscape in the study area comprises two contrasting geomorphological units, representing the rolling plateau surface and the gully systems which dissect the plateau surface The very high sediment yields in this environment ($\sim$10,000 t km^{-2} year^{-1}) cause major downstream problems in terms of reservoir and channel siltation, and this has focused attention on the need to reduce sediment yields through soil and water conservation and sediment control measures. In planning such measures, there is a need to establish the relative importance of soil erosion from the cultivated areas of the rolling plateau and erosion occurring within the gully systems, in contributing to downstream sediment yields, since these two potential sediment sources require very different approaches to reduction in sediment mobilization and transfer.

A study aimed at establishing the relative importance of the two main sediment sources was undertaken in the 3.86 km^2 Zhaojia gully catchment, where the plateau surface and gully systems were of similar spatial extent and accounted for 53% and 47% of the catchment area respectively (Fig. 19). A check dam had been constructed across the channel in the middle portion of the catchment in early 1991 (Fig. 19), and when the catchment was visited in October 1993, the deposits associated with two floods occurring during the period July–August 1993 were clearly distinguishable in sediment cores collected from the area of sediment deposition above the check dam. The total depth of sediment deposition associated with the two events was $\sim$33 cm. Based on an analysis of three cores, the mean ^{137}Cs content of sediment deposited by the first flood was 0.74 Bq kg^{-1}, whereas that for the second flood was 1.06 Bq kg^{-1}. In attempting to decipher the main sources of the deposited sediment and thus the sediment yield from the catchment, attention was directed to variations in the ^{137}Cs concentration of potential sources within the two main sediment sources areas. Mean ^{137}Cs concentrations associated with these sources exhibited significant variations and offered an effective means of discriminating the sources. A summary of the ^{137}Cs content of potential source materials in the Zhaojia Gully catchment is provided in Table 4.

When the average ^{137}Cs content of the sediment deposits associated with the two floods occurring in 1993 was compared with that of potential source material collected shortly after the flood (cf. Table 4), it was found to be similar to that of cultivated soil from the steep gully slopes, lower than that of soil from the cultivated land on the plateau crests and steeper lower slopes of the rolling plateau, and considerably lower than that of topsoil from the grass covered areas. It was also very substantially higher than that of surface material from steep bare slopes and from recent mass movement deposits within the gully area. In view of either

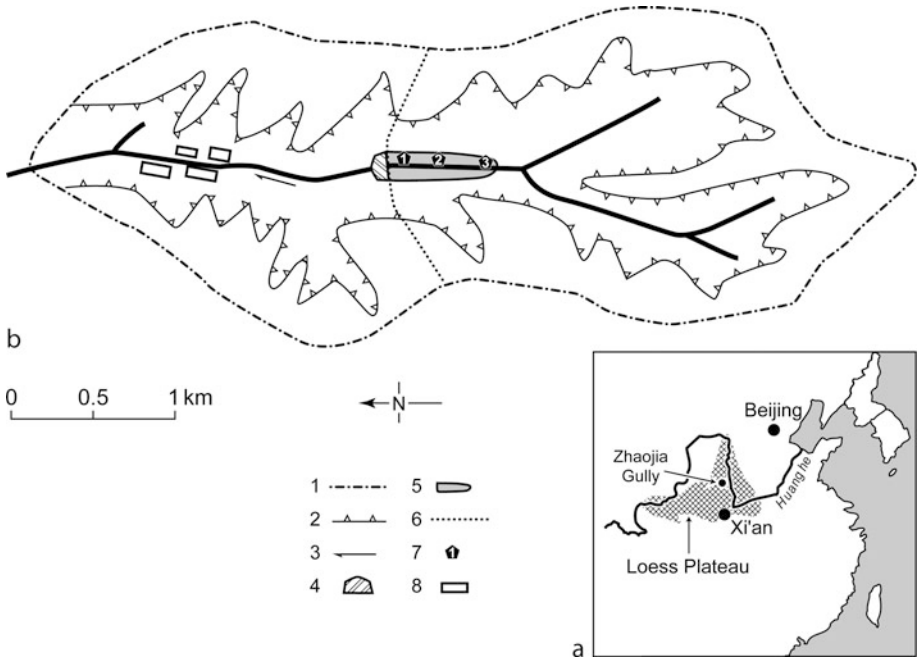

Fallout Radionuclides and the Study of Erosion and Sedimentation. Figure 19
The Zhaojia Gully catchment showing its location (**a**) and its main features (**b**). 1, catchment divide; 2, the boundary between the rolling plateau and the gully areas; 3, the main channel; 4, the check dam; 5, area of sediment deposition associated with the check dam; 6, divide of the catchment contributing to the sediment trap reservoir; 7, sampling sites for sediment deposits; 8, village (Based on [162])

Fallout Radionuclides and the Study of Erosion and Sedimentation. Table 4 The ^{137}Cs content of potential source materials in the Zhaojia Gully catchment from different topographic locations and under different land use conditions

Zone	Source material and land type	Catchment area (in %)	No. of samples	Mean ^{137}Cs content (Bq kg^{-1})	Erosional behavior
Gully (47%)	Surface soil on grassland of gully slopes	21	8	7.0	Slight sheet and rill erosion
	Plowed soil on steep gully slopes	2	7	1.2	Very severe sheet and rill erosion
	Surface soil on bare slopes and mass movement deposits	19	7	0.02	Very severe sheet and rill erosion on bare slopes and active mass movements
	Village area, cultivated land on terrace and gully floor and tracks	5	–	–	
Rolling plateau (53%)	Cultivated soil of crest slopes	14	36	6.4	Moderately severe sheet and rill erosion
	Cultivated soil of lower slopes	36	32	3.4	Severe sheet and rill erosion
	Surface soil on grassland	3	–	–	

Based on Walling et al. [162]

their limited extent or their low erosion rates, the cultivated land on the steep gully slopes and the grassland within the gully area were deemed unlikely to represent important sediment sources and the cultivated areas of the rolling plateau and the steep bare slopes and recent mass movement deposits within the gully area were identified as representing the primary sediment sources. Taking account of the relative extents of the cultivated areas on the crests and the steeper upper slopes of the rolling plateau and estimates of erosion rates obtained from these areas using ^{137}Cs measurements, a weighted average ^{137}Cs content for sediment mobilized from these cultivated areas of the rolling plateau of 3.9 Bq kg^{-1} was estimated.

Assuming that the average ^{137}Cs content of surface material from the steep bare gully slopes and recent mass movement deposits (0.02 Bq kg^{-1}) was representative of sediment from the gully area and that the minor contributions from the cultivated areas and areas of grass cover within the gully could be ignored, a simple mixing model was used to estimate the relative contribution of sediment derived from the gully area and the cultivated areas of the rolling plateau to the flood deposits. The results provided by the mixing model are presented in Table 5. These indicate that during the first flood, 18.6% of the sediment was derived from the rolling plateau and 81.4% from the gully area. During the second event, the equivalent values were 26.8% and 73.2%. Taking the two events together, the values were 23% from the rolling plateau and 77% from the gully area. These results emphasized the importance of the gully area and the associated gully erosion and mass movement processes as the main sediment source within the Zhaojia Gully catchment and clearly demonstrated that any strategy aimed at reducing sediment yields from this catchment and from similar landscapes in the local area should focus on reducing sediment production within the gully area. Such measures could include check dams and other gully stabilization measures.

Future Directions

As demonstrated by the above overview, the use of fallout radionuclides in soil erosion and sedimentation investigations now has a history that stretches back over more than 30 years. Over this period, there have been advances in measurement technology and whereas early work primarily focused on the use of ^{137}Cs, $^{210}Pb_{ex}$ and ^{7}Be are now also quite widely used both as an alternative and a complement to ^{137}Cs. Equally, whereas most early work focused on documenting patterns and rates of soil erosion and establishing chronologies for lake cores, subsequent work has expanded the various applications to include other sediment sinks, particularly river floodplains and wetlands, and sediment source fingerprinting. These expanding applications have been promoted by two key drivers. The first is the growing recognition of both the many environmental problems associated with the mobilization and transfer of fine sediment within the landscape and the need to document and develop an improved understanding of the source, mobilization, and transfer of fine sediment, in order to develop effective management and control strategies. The second is the essentially unique information that can be provided by the use of fallout radionuclides as tracers and the need to develop the use of tracers to complement more traditional monitoring techniques [163]. Future developments are likely to expand further this field of work and four areas in particular can be identified as potential areas for expansion or advances.

Fallout Radionuclides and the Study of Erosion and Sedimentation. Table 5 The relative contribution of sediment from the rolling plateau and gully areas of the Zhaojia Gully catchment during the floods of 1993

Flood	Date of flood deposit	Deposit thickness (cm)	^{137}Cs content of sediment deposits (Bq kg^{-1})	Relative contribution (%)	
				Rolling plateau	Gully
2	August 21, 1993	18.3	1.06	26.8	73.2
1	July 21–August 1, 1993	14.7	0.74	18.6	81.4

Based on Walling et al. [162]

These include: firstly, the use of other radionuclides; secondly, the further development and improvement of measurement techniques; thirdly, greater integration of the various applications and approaches; and finally, the progressive incorporation of fallout radionuclide tracers into sediment-based catchment investigations, as an operational rather than as a research tool. Each of these future directions will be briefly considered.

Use of Other Radionuclides

^{137}Cs, ^{210}Pb$_{ex}$, and ^{7}Be are now firmly established as the key fallout radionuclides for use in sediment tracing investigations. Their different half-lives and contrasting fallout patterns usefully complement each other. However, in recent years, some attention has been given to the potential for using Plutonium-239 and 240 (^{239,240}Pu) as an alternative to ^{137}Cs [164–167]. These radionuclides are also a product of bomb testing and have been shown to demonstrate very similar behavior to ^{137}Cs in terms of their distribution within the soil profile [168], their post-fallout redistribution within the landscape and thus their potential for studying soil redistribution, [169, 170], dating sediment cores [167, 171, 172], and fingerprinting sediment sources [166]. However, some contrasts with ^{137}Cs in terms of their post-fallout redistribution have been reported [173] and it has been suggested that ^{239,240}Pu is likely to be less mobile than ^{137}Cs in sediment cores [167].

The likely advantages of ^{239,240}Pu over ^{137}Cs lie primarily in their longer half-lives (24,110 and 6,561 years, respectively) and secondarily in analytical requirements. In the first context, the relatively short half-life of ^{137}Cs (30.1 years) means that activities of this radionuclide are beginning to decline significantly in the environment, since it is now almost 50 years since the period of peak fallout around 1963. Where fallout fluxes were relatively low, as, for example, in the southern hemisphere, this can represent a problem for gamma spectrometry analysis. Reduced activities mean longer count times and are likely to be coupled with reduced measurement precision and increased minimum levels of detection. With their long half-lives, ^{239,240}Pu do not face this problem. In addition, ^{239,240}Pu can provide additional chronomarkers associated with changes in the Pu isotopic composition of fallout during the 1950s and 1960s. In particular, the ^{238}Pu/$^{239+240}$Pu activity ratio shows distinct shifts in the early 1950s and the mid-to-late 1960s, providing important known-age horizons in southern hemisphere sediments. In the second context, recent advances in analytical techniques have provided the possibility of analyzing ^{239,240}Pu by mass spectrometry (ICPMS and AMS), thereby providing a means of greatly increasing sample throughput, relative to ^{137}Cs, where individual samples collected in areas with low fallout inventories can require a count time of ~24 h or more. A further feature of ^{239,240}Pu fallout is that, unlike ^{137}Cs, it was not associated with both bomb and Chernobyl fallout. It was only associated with the former. In some areas of the world affected by Chernobyl fallout, ^{239,240}Pu may therefore offer opportunities to distinguish fallout inputs from both sources [174] and to exploit their differences in timing to obtain additional information on the erosional history of a study area.

Another radionuclide which has attracted attention for its use as an alternative to ^{137}Cs in dating lake cores, due to the likelihood of reduced mobility, is ^{241}Am. ^{241}Am is a product of the decay of ^{241}Pu from bomb fallout and therefore has the advantage that activities are currently increasing rather than decreasing.

Development and Improvement of Measurement Technology

It is possible that advances in technology might also lead to alternatives to gamma spectrometry for the analysis of ^{137}Cs, ^{7}Be, and ^{210}Pb. The potential to increase sample throughput would offer considerable scope for increasing the size of the area that can be investigated and/or the spatial resolution of the results. Other areas of measurement technology, where advances have begun to occur, include the remote sensing of spatial patterns of radionuclide inventories using airborne sensors. The successful use of this approach for ^{137}Cs has been reported in Northern England and Northern Ireland [175, 176]. As yet, the spatial resolution is limited and the approach is more suited to documenting spatial variability of the original fallout input rather than post-fallout redistribution. Furthermore, its use may be restricted to areas receiving additional Chernobyl fallout where ^{137}Cs inventories

are higher. However, the possibility of collecting detailed information on the spatial distribution of inventories across an area would clearly introduce important new opportunities for expanding the scale of sediment redistribution investigations.

Increased Integration of Radionuclides and Approaches

Two important features of the use of fallout radionuclides as tracers in erosion and sedimentation investigations are: firstly, that conjunctive use of different radionuclides can provide increased information on the functioning of the system under investigation, and secondly, that it is possible to use the same tracers to document various components of a catchment sediment budget, for example, soil redistribution rates on the slopes; the deposition and storage of fine sediment on downstream floodplains; the dynamics of sediment mobilization, deposition, and remobilization within the channel system; and the relative contribution of key sediment sources to the sediment output from the catchment. Furthermore, where a long-term sink, such as a lake or well-developed floodplain or wetland, exists at the outlet of the catchment, it is possible to use the same radionuclides to establish a chronology for sediment cores to assist in interpreting the erosional history of the catchment. The potential for conjunctive use of several radionuclides is being increasingly recognized, and Blake and coworkers [177] provide an interesting example of this potential in their study of sediment redistribution by erosion after a wildfire at a site in Australia. Equally, the potential for integrating work on several different components of the sediment budget is provided by Zhang and Walling [178] who showed how it is possible to use the information provided by ^{137}Cs depth distributions in lake and reservoir sediments to provide information on both erosion rates in the contributing catchments and the dominant sediment sources.

To date, however, studies involving different components of the sediment budget have often been compartmentalized and considerable scope exists to integrate them more closely to provide a comprehensive assessment of the catchment sediment budget. In this context, there will be a need to make use of other measurements and approaches to complete the picture, but fallout radionuclide measurements can provide the key to establishing the sediment budget of a catchment [163, 179–181]. As indicated previously, the catchment sediment budget represents a key source of information for designing and implementing effective sediment management strategies for catchments and river basins [182]. Further work is required to integrate the various applications of fallout radionuclides in sediment budget investigations and to develop the comprehensive toolbox that will be required to exploit their full potential.

Moving from a Research Tool to an Operational and Management Tool

To date, most of the studies aimed at exploring and developing the potential for using fallout radionuclides in studies of erosion and sedimentation have been curiosity-driven research investigations. In some instances, the starting point has been the potential application, which has then been demonstrated. In others, the starting point has been the need to solve a problem or to obtain an improved understanding of a particular part of the system, and fallout radionuclides have been successfully used as the tool to achieve that objective. However, as the comprehensive toolbox referred to above is progressively developed, it is to be hoped that the wide-ranging potential of the approach will gain increasing recognition and that the use of fallout radionuclides will become more routine and thus a more widely used tool to support the sustainable management of the environment.

Bibliography

Primary Literature

1. Oldeman LR (1994) The global extent of land degradation. In: Greenland DJ, Szabolcs I (eds) Land resilience and sustainable land use. CABI, Wallingford, pp 99–118
2. Speth JG (1994) Desertification convention essential for food security. Environ Conserv 21:4–5
3. Toy TJ, Foster GR, Renard KG (2002) Soil erosion: processes, prediction, measurement and control. Wiley, New York, 352 p
4. Buringh P (1981) An assessment of the losses and degradation of productive agricultural land in the world. FAO Working Group on Soils Policy, Rome
5. Brown LR (1984) Conserving soils. In: Brown LR (ed) State of the world 1984. Norton, New York, pp 53–75

6. Yang D, Kanae S, Oki T, Koike T, Muslake K (2003) Global potential soil erosion with reference to land use and climate changes. Hydrol Process 17:2913–2928
7. Lal R (2003) Soil erosion and the global carbon budget. Environ Int 29:437–450
8. Van Oost K, Quine TA, Govers G, De Gryze S, Six J, Harden JW, Ritchie JC, McCarty GW, Heckrath G, Kosmas C, Giraldez JV, Marques da Silva JR, Merckx R (2007) The impact of agricultural soil erosion on the global carbon budget. Science 318:626–629
9. Clark EH, Haverkamp JA, Chapman W (1985) Eroding soils: the off-farm impacts. The Conservation Foundation, Washington, DC
10. Pimentel D, Harvey C, Resosuarmo P, Sinclair K, Kurz D, McNair M, Crist S, Shpritz L, Fitton L, Saffourni R, Blair R (1995) Environmental and economic costs of soil erosion and conservation benefits. Science 267:1117–1123
11. Mahmood K (1987) Reservoir sedimentation: Impact, extent and mitigation. World Bank Technical Paper no. 71. The World Bank, Washington, DC
12. Lal R (1994) Soil erosion research methods. St. Lucie Press, Boca Raton, 340 p
13. Morris GL, Fan J (1998) Reservoir sedimentation handbook: design, and management of dams, reservoirs and watersheds for sustainable use. McGraw Hill, New York, 750 p
14. Mabit L, Benmansour M, Walling DE (2008) Comparative advantages and limitations of the fallout radionuclides ^{137}Cs, $^{210}Pb_{ex}$ and ^{7}Be for assessing soil erosion and sedimentation. J Environ Radioactiv 99:1799–1807
15. Goldberg ED (1963) Geochronology with Pb-210 in radioactive dating. In: Proceedings of a symposium on radioactive dating, International Atomic Energy Agency, Vienna. Contribution 1510, pp 121–131
16. Menzel RG (1960) Transport of strontium-90 in runoff. Science 131:499–500
17. Yamagata N, Matsuda S, Kodaira K (1963) Run-off of caesium-137 and strontium-90 from rivers. Nature 200:668–669
18. Rogowski AS, Tamura T (1965) Movement of ^{137}Cs by runoff, erosion and infiltration on the alluvial Captina silt loam. Health Phys 11:1333–1340
19. Ritchie JC, Spraberry JA, McHenry JR (1974) Estimating soil erosion from the redistribution of fallout ^{137}Cs. Soil Sci Soc Am J 38:137–139
20. McHenry JR, Ritchie JC (1977) Estimating field erosion losses from fallout Cs-137 measurements. International Association of Hydrological Sciences Publication no. 122. IAHS, Wallingford, pp 26–33
21. de Jong E, Begg CBM, Kachanoski RG (1983) Estimates of soil erosion and deposition from some Saskatchewan soils. Can J Soil Sci 63:607–617
22. Kachanoski RG, de Jong E (1984) Predicting the temporal relationship between cesium-137 and erosion rate. J Environ Qual 13:301–304
23. McCallan ME, O'Leary BM, Rose CW (1980) Redistribution of caesium-137 by erosion and deposition on an Australian soil. Aust J Soil Sci 18:119–128
24. Campbell BL, Loughran RJ, Elliott GL (1982) Caesium-137 as an indicator of geomorphic processes in a drainage system. Aust Geogr Stud 20:49–64
25. Loughran RJ, Elliott GL, Campbell BL, Shelly DJ (1988) Estimation of soil erosion from caesium-137 measurements in a small cultivated catchment in Australia. Appl Radiat Isot 39:1153–1157
26. Walling DE, Bradley SB (1988) The use of caesium-137 measurements to investigate sediment delivery from cultivated areas in Devon, UK. International Association of Hydrological Sciences Publication no. 174. IAHS, Wallingford, pp 325–335
27. Walling DE, Quine TA (1991) The use of ^{137}Cs measurements to investigate soil erosion on arable fields in the U.K.: potential applications and limitations. J Soil Sci 42:147–165
28. Golosov VN, Panin AV, Markelov MV (1999) Chernobyl Cs-137 redistribution in the small basin of the Lokna river, Central Russia. Phys Chem Earth A 24:881–885
29. Zapata F (ed) (2002) Handbook for the assessment of soil erosion and sedimentation using environmental radionuclides. Kluwer, Dordrecht, 219 p
30. Ritchie JC, Ritchie CA (2008) Bibliography of publications of ^{137}Cesium studies related to erosion and sediment deposition. USDA-ARS Hydrology and Remote Sensing Laboratory Occasional Paper HRSL-2008-02
31. Wallbrink PJ, Murray AS (1996) Distribution of ^{7}Be in soils under different surface cover conditions and its potential for describing soil redistribution processes. Water Resour Res 32:467–476
32. Blake WH, Walling DE, He Q (1999) Fallout beryllium-7 as a tracer in soil erosion investigations. Appl Radiat Isot 51:599–605
33. Walling DE, He Q, Blake W (1999) Use of Be-7 and Cs-137 measurements to document short- and medium-term rates of water-induced soil erosion on agricultural land. Water Resour Res 35:3865–3874
34. Matisoff G, Bonniwell EC, Whiting PJ (2002) Soil erosion and sediment sources in an Ohio watershed using Beryllium-7, Cesium-137, and Lead-210. J Environ Qual 31:54–61
35. Wilson CG, Matisoff G, Whiting PJ (2003) Short-term erosion rates from a Be-7 inventory balance. Earth Surf Process Land 28:967–977
36. Wallbrink PJ, Murray AS (1996) Measuring soil loss using the inventory ratio of excess lead-210 to cesium-137. Soil Sci Soc Am J 60:1201–1208
37. Walling DE, He Q, Quine TA (1995) Use of caesium-137 and lead-210 as tracers in soil erosion investigations. International Association of Hydrological Sciences Publication no. 229. IAHS, Wallingford, pp 163–172
38. Walling DE, He Q (1999) Using fallout lead-210 measurements to estimate soil erosion on cultivated land. Soil Sci Soc Am J 63:1404–1412
39. Walling DE, Collins AL, Sichingabula HM (2003) Using unsupported lead-210 measurements to investigate soil erosion and sediment delivery in a small Zambian catchment. Geomorphology 52:193–213

40. Ritchie JC, McHenry JR, Gill AC, Hawks PH (1972) Fallout Cs-137 in reservoir sediments. Health Phys 22:97–98
41. McIntyre SC, Naney JW (1991) Sediment deposition in a forested inland wetland with a steep-farmed watershed. J Soil Water Conserv 46:64–66
42. Craft CB, Casey WP (2000) Sediment and nutrient accumulation in floodplain and depressional freshwater wetlands of Georgia, USA. Wetlands 20:323–332
43. DeLaune RD, Patrick WH Jr, Buresh RJ (1978) Sedimentation rates determined by ^{137}Cs dating in a rapidly accreting salt marsh. Nature 275:532–533
44. Oenema O, DeLaune RD (1988) Accretion rates in salt marshes in Eastern Scheldt, South-west Netherlands. Estuaries Coast Shelf Sci 26:379–394
45. Walling DE, He Q (1998) The spatial variability of overbank sedimentation on river floodplains. Geomorphology 24:209–223
46. Terry JP, Garimella S, Kostaschuk RA (2002) Rates of floodplain accretion in a tropical island river system impacted by cyclones and large floods. Geomorphology 42:171–182
47. Krishnaswamy S, Lal D, Martin JM, Meybeck M (1971) Geochronology of lake sediments. Earth Planet Sci Lett 11:407–414
48. Robbins JA, Edgington DN (1975) Determination of recent sedimentation rates in Lake Michigan with Pb-210 and Cs-137. Geochim Cosmochim Acta 39:285–304
49. Appleby PG, Oldfield F (1978) The calculation of lead-210 dates assuming a constant rate of supply of unsupported lead-210 to the sediment. Catena 5:1–8
50. Robbins JA, Edgington DN, Kemp LW (1978) Comparative ^{210}Pb, ^{137}Cs, and pollen geochronologies of sediments from Lake Ontario and Erie. Quatern Res 10:256–278
51. Carroll J, Lerche I (2003) Sedimentary processes: quantification using radionuclides. Elsevier, Oxford
52. Krishnaswami S, Benninger LK, Aller RC, Von Damm KL (1980) Atmospherically-derived radionuclides as tracers of sediment mixing and accumulation in near-shore marine and lake sediments: evidence from ^{7}Be, ^{210}Pb and ^{239,240}Pu. Earth Planet Sci Lett 47:307–318
53. Blake WH, Walling DE, He Q (2002) Using cosmogenic beryllium-7 as a tracer in sediment budget investigations. Geogr Ann A Phys Geogr 84A:89–102
54. Walling DE, He Q (2000) The global distribution of bomb-derived ^{137}Cs reference inventories. Unpublished report to the International Atomic Energy Agency
55. Smith JT, Beresford NA (2005) Chernobyl: catastrophe and consequences. Praxis, Chichester, 305 p
56. Winkler R, Rosner G (2000) Seasonal and long-term variation of ^{210}Pb concentration in air, atmospheric deposition rate and total deposition velocity in South Germany. Sci Total Environ 263:57–68
57. Olsen CR, Larsen IL, Lowry PD, Cutshall NH, Todd JF, Wong GTF, Casey WH (1985) Atmospheric fluxes and marsh-soil inventories of ^{7}Be and ^{210}Pb. J Geophys Res 90:10487–10495
58. Valles I, Camacho A, Ortega X (2009) Natural and anthropogenic radionuclides in airborne particulate samples collected in Barcelona (Spain). J Environ Radioactiv 100:102–107
59. Preiss N, Mélières MA, Pourchet M (1996) A compilation of data on lead-210 concentration in surface air and fluxes at the air-surface and water-sediment interfaces. J Geophys Res 101:28847–28862
60. Beks JP, Eisma D, van der Plicht J (1998) A record of atmospheric ^{210}Pb deposition in the Netherlands. Sci Total Environ 222:35–44
61. Turekian KK, Nozaki Y, Benninger LK (1977) Geochemistry of atmospheric radon and radon producers. Annu Rev Earth Planet Sci 5:227–255
62. Yamamoto M, Sakaguchi A, Sasaki K, Hirose K, Igarashi Y, Kim CK (2006) ^{210} Pb and ^{7}Be deposition: features of the Japan Sea side of Japan. J Environ Radioactiv 55:121–123
63. Baskaran M, Coleman CH, Santschi PH (1993) Atmospheric depositional fluxes of Be-7 and Pb-210 at Galveston and College Station, Texas. J Geophys Res 98:20555–20571
64. Caillet S, Arpagaus P, Monna F, Dominik J (2001) Factors controlling Be-7 and Pb-210 atmospheric deposition as revealed by sampling individual rain events in the region of Geneva, Switzerland. J Environ Radioactiv 53:241–256
65. Nijampurkur VN, Rao DK (1993) Polar fallout of radionuclides ^{32}Si, ^{7}Be and ^{210}Pb and past accumulation rate of ice at Indian station, Dakshin Gangotri, East Antarctica. J Environ Radioactiv 21:107–117
66. Kaste JM, Norton SA, Hess CT (2002) Environmental chemistry of beryllium-7. Rev Mineral Geochem 50:271–289
67. Lal D, Malhotra PK, Peters B (1958) On the production of radioisotopes in the atmosphere by cosmic radiation and their application to meteorology. J Atmos Terr Phys 12:306–328
68. Wallbrink PJ, Murray AS (1994) Fallout of ^{7}Be over south eastern Australia. J Environ Radioactiv 25:213–228
69. Harvey MJ, Matthews KM (1989) ^{7}Be deposition in a high rainfall area of New Zealand. J Atmos Chem 8:299–306
70. Turekian KK, Benninger LK, Dion EP (1983) ^{7}Be and ^{210}Pb total deposition fluxes at New Haven, Connecticut, and at Bermuda. J Geophys Res 88:5411–5415
71. Todd JF, Wong GRF, Olsen CR, Larsen IL (1989) Atmospheric depositional characteristics of Beryllium-7 and Lead 210 along the southeastern Virginia Coast. J Geophys Res 94:11106–11116
72. Peirson DH (1963) Beryllium-7 in air and rain. J Geophys Res 68:3831–3832
73. Lal D, Nijampurkar VN, Rajagopalan G, Somayajulu BLK (1979) Annual fallout of ^{32}Si, ^{210}Pb, ^{22}Na, ^{35}S and ^{7}Be in rains in India. Proc Indian Acad Sci 88A:29–40
74. Schumann G, Stoeppler M (1963) Beryllium 7 in the atmosphere. J Geophys Res 68:3827–3830
75. Lee SC, Saleh AI, Babavali AD, Jonoby L, Kuroda PK (1985) - Beryllium-7 deposition at Fayetteville, Arkansas and excess polonium-210 from the 1980 eruption of Mount St Helens. Geochem J 19:317–322
76. Walton A, Fried RE (1962) The deposition of beryllium-7 and phosphorus-32 in precipitation at north temperate latitudes. J Geophys Res 67:5335–5340

77. Othman I, Al-Masri MS, Hassan M (1998) Fallout of ^{7}Be in Damascus city. J Radioanal Nucl Chem 238:187–191
78. Duenas C, Fernandez MC, Carretero J, Liger E, Canete S (2002) Atmospheric deposition of ^{7}Be at a coastal Mediterranean station. J Geophys Res 106:34059–34065
79. Lomenick TF, Tamura T (1965) Naturally occurring fixation of cesium-137 on sediments of lacustrine origin. Soil Sci Soc Am Proc 29:383–386
80. Squire HM, Middleton LJ (1966) Behavior of ^{137}Cs in soils and pastures – a long term experiment. Radiat Bot 6:413–423
81. Frissel MJ, Pennders R (1983) Models for the accumulation and migration of ^{90}Sr, ^{137}Cs, $^{239+240}$Pu and ^{241}Am in the upper layer of soils. In: Coughtrey PJ, Bell JNB, Roberts TM (eds) Ecological aspects of radionuclide release. Blackwell, Oxford, pp 63–72
82. Jamsangton J, Parkpian P, Delaune RD, Jugsujinda A (2004) Retention of ^{137}cesium in acid sulphate soils of South Central Thailand. Chem Ecol 20:241–256
83. Romney EM, Childress JD (1965) Effects of beryllium in plants and soil. Soil Sci 100:210–217
84. He Q, Walling DE (1996) Interpreting particle size effects in the absorption of ^{137}Cs and unsupported ^{210}Pb by mineral soils and sediments. J Environ Radioactiv 30:117–137
85. Kaste JM, Norton SA, Fernandez IJ, Hess CT (1999) Delivery of cosmogenic beryllium-7 to forested ecosystems in Maine. Geol Soc Am Abstr 31:A305
86. Bettoli MG, Cantelli L, Degetto S, Tositti L, Tubertini O, Valcher S (1995) Preliminary investigations on ^{7}Be as a tracer in the study of environmental processes. J Radioanal Nucl Chem 190:137–147
87. Walling DE, Schuller P, Zhang Y, Iroumé A (2009) Extending the timescale for using beryllium-7 measurements to document soil redistribution by erosion. Water Resour Res 45:W02418. doi:10.1029/2008WR007143
88. Tiessen KHD, Li S, Lobb DA, Mehuys GR, Rees HW, Chow TL (2009) Using repeated measurements of ^{137}Cs and modelling to identify spatial patterns of tillage and water erosion within potato production in Atlantic Canada. Geoderma 153:104–118
89. Walling DE, Quine TA (1991) Calibration of caesium-137 measurements to provide quantitative erosion rate data. Land Degrad Rehabil 2:161–175
90. Walling DE, He Q (1999) Improved models for estimating soil erosion rates from cesium-137 measurements. J Environ Qual 28:611–622
91. Walling DE, He Q, Appleby PC (2002) Conversion models for use in soil-erosion, soil-redistribution, and sedimentation investigations. In: Zapata F (ed) Handbook for the assessment of soil erosion and sedimentation using environmental radionuclides. Kluwer, Dordrecht, pp 111–164
92. Loughran RJ, Elliott GL (1996) Rates of soil erosion in Australia determined by the caesium-137 technique: a national reconnaissance survey. International Association of Hydrological Sciences Publication No. 236. IAHS, Wallingford, pp 275–282
93. Mitchell JK, Bubenzer GD, McHenry JR, Ritchie JC (1980) Soil loss estimation from fallout cesium-137 measurements. In: DeBoodt M, Gabriels D (eds) Assessment of erosion. Wiley, Chichester, pp 393–401
94. Van Oost K, Govers G, Van Muysen W (2003) A process-based conversion model for caesium-137 derived erosion rates on agricultural land: an integrated spatial approach. Earth Surf Process Land 28:187–207
95. Quine TA, Walling DE, Govers G (1996) Simulation of radiocaesium redistribution on cultivated hillslopes using a mass-balance model: an aid to process interpretation and erosion rate estimation. In: Anderson MG, Brookes S (eds) Advances in hillslope processes. Wiley, Chichester, pp 561–588
96. Porto P, Walling DE, Ferro V (2001) Validating the use of caesium-137 measurements to estimate soil erosion rates in a small drainage basin in Calabria, southern Italy. J Hydrol 248:93–108
97. Sutherland RA (1992) Caesium-137 estimates of erosion in agricultural areas. Hydrol Process 6:215–225
98. Yan P, Dong Z, Dong G, Zhang X, Zhang Y (2001) Preliminary results of using ^{137}Cs to study wind erosion in the Qinghai-Tibet Plateau. J Arid Environ 47:443–452
99. Chappell A, Warren M (2003) Spatial scales of Cs-137-derived soil flux by wind in a 25 km^{2} arable area of eastern England. Catena 52:209–234
100. Chappell A, Warren A, Oliver M, Charlton M (1998) The utility of ^{137}Cs for measuring soil redistribution rates in southwest Niger. Geoderma 81:313–337
101. Basher LR, Webb TH (1997) Wind erosion rates on terraces in the Mackenzie Basin. J R Soc NZ 27:499–512
102. Chappell A (1999) The limitations of using Cs-137 for estimating soil redistribution in semi-arid environments. Geomorphology 29:135–152
103. Schuller P, Walling DE, Sepulveda A, Trumper RE, Rouanet JL, Pino I, Castillo A (2004) Use of Cs-137 measurements to estimate changes in soil erosion rates associated with changes in soil management practices on cultivated land. Appl Radiat Isot 60:759–766
104. Schuller P, Walling DE, Sepulveda A, Castillo A, Pino I (2007) Changes in soil erosion associated with the shift from conventional tillage to a no-tillage system, documented using Cs-137 measurements. Soil Tillage Res 94:183–192
105. Walling DE, Zhang Y, He Q Models for deriving estimates of erosion and deposition rates from fallout radionuclide (caesium-137, excess lead-210 and beryllium-7) measurements and the development of user-friendly software for model implementation. In: IAEA TECDOC D1.50.08. IAEA, Vienna, (in press)
106. Schuller P, Iroumé A, Walling DE, Mancilla HB, Castillo A, Trumper RE (2006) Use of beryllium-7 to document soil redistribution following forest harvesting operations. J Environ Qual 35:1756–1763
107. Sepúlveda A, Schuller P, Walling DE (2008) Use of ^{7}Be to document erosion associated with a short period of extreme rainfall. J Environ Radioactiv 99:35–49

108. Olsson IU (1986) Radiometric dating. In: Berglund BE (ed) Handbook of holocene palaeoecology and palaeohydrology. Wiley, Chichester, pp 273–312
109. Appleby PG (2002) Chronostratigraphic techniques in recent sediments. In: Last WM, Smol JP (eds) Tracing environmental change using lake sediments, vol 1. Kluwer, Dordrecht, pp 171–203
110. Erten HN (1997) Radiochronology of lake sediments. Pure Appl Chem 69:71–76
111. Walling DE, He Q (1992) Interpretation of cesium-137 profile in lacustrine and other sediments - The role of catchment derived inputs. Hydrobiologia 235(236):219–230
112. Walling DE, He Q (1993) Toward improved interpretation of caesium-137 profile in lake sediments. In: McManus J, Duck R (eds) Geomorphology and sedimentology of lakes and reservoirs. Wiley, Chichester, pp 31–53
113. Walling DE (2010) Using fallout radionuclides to investigate erosion and sediment delivery: some recent advances. In: Sediment dynamics for a changing future, Proceedings of the Warsaw symposium, IAHS Publication no. 337. IAHS, Wallingford, pp 3–16
114. Golosov VN, Belyaev VR, Markelov MV, Kislenko KS (2010) Overbank sedimentation rates on the flood plains of small rivers in Central European Russia. In: Sediment dynamics for a changing future, Proceedings of the Warsaw symposium, IAHS Publication no. 337. IAHS, Wallingford, pp 129–136
115. Allison MA, Kuehl SA, Martin TC, Hassan A (1998) Importance of flood-plain sedimentation for river sediment budgets and terrigenous input to the oceans: insights from the Brahmaputra–Jamuna river. Geology 26:175–178
116. Walling DE, Owens PN, Leeks GJL (1998) The role of channel and floodplain storage in the suspended sediment budget of the River Ouse, Yorkshire, UK. Geomorphology 22:225–242
117. Walling DE, Owens PN, Leeks GJL (1999) Rates of contemporary overbank sedimentation and sediment storage on the floodplains of the main channel systems of the Yorkshire Ouse and the River Tweed, UK. Hydrol Process 13:993–1009
118. Walling DE, He Q (1997) Use of fallout ^{137}Cs in investigations of overbank sediment deposition on river floodplains. Catena 29:263–282
119. Hughes AO, Olley J, Croke JC, Webster IT (2009) Determining floodplain sedimentation rates using ^{137}Cs in a low fallout environment dominated by channel- and cultivation-derived sediment inputs, central Queensland, Australia. J Environ Radioactiv 100:858–865
120. Appleby PG, Oldfield F (1983) The assessment of ^{210}Pb data from sites with varying sediment accumulation rates. Hydrobiologia 103:29–35
121. Robbins JA (1978) Geochemistry and geophysical application of radioactive lead. In: Nriagu JO (ed) The Biochemistry of lead in the environment. Elsevier, Amsterdam, pp 285–393
122. He Q, Walling DE (1996) Use of fallout Pb-210 measurements to investigate longer-term rates and patterns of overbank sediment deposition on the floodplains of lowland rivers. Earth Surf Process Land 21:141–154
123. Lambert CP, Walling DE (1987) Floodplain sedimentation: a preliminary investigation of contemporary deposition within the lower reaches of the River Culm, Devon, UK. Geogr Ann 69A:393–404
124. Liu J, Carroll J, Lerche I (1991) A technique for disentangling temporal source and sediment variations from radioisotope measurements with depth. Nucl Geophys 5:31–45
125. Aalto R, Maurice-Bourgoin L, Dunne T, Montgomery DR, Nittrouer CA, Guyot J-L (2003) Episodic sediment accumulation on Amazonian flood plains influenced by El Niño/southern oscillation. Nature 425:493–497
126. Aalto R, Dietrich W (2005) Sediment accumulation determined with ^{210}Pb geochronology for Strickland River flood plains. In: Sediment budgets I, Proceedings of the Foz do Iguaçu Symposium, Brazil, April 2005. International Association of Hydrological Sciences Publication No. 291. IAHS, Wallingford, pp 303–309
127. Canuel EA, Martens CS, Benninger LK (1980) Seasonal variations in the ^{7}Be activity in the sediments of Cape Lookout Bight. Geochim Cosmochem Acta 54:237–245
128. Dibb JE, Rice DL (1989) Temporal and spatial distribution of beryllium-7 in the sediments of Chesapeake Bay. Estuar Coast Shelf Sci 28:395–406
129. Fitzgerald SA, Klump JV, Swarzenski PW, Mackenzie RA, Richards KD (2001) Beryllium-7 as a tracer of short-term sediment deposition and resuspension in the Fox River, Wisconsin. Environ Sci Technol 35:300–305
130. Fisher GB, Magilligan FJ, Kaste JM, Nislow KH (2010) Constraining the timescales of sediment sequestration with large woody debris using cosmogenic ^{7}Be. J Geophys Res 115:F01013. doi:10.1029/2009JF001352
131. Walling DE (2005) Tracing suspended sediment sources in catchments and river systems. Sci Total Environ 344: 159–184
132. Collins AL, Walling DE, Leeks GJL (1998) The use of composite fingerprints to determine the provenance of the contemporary suspended sediment load transported by rivers. Earth Surf Process Land 23:31–52
133. Walling DE, Woodward JC (1995) Tracing sources of suspended sediment in river basins. Mar Freshwater Res 46:327–336
134. Walling DE, Owens PN, Leeks GJL (1999) Fingerprinting suspended sediment sources in the catchment of the River Ouse, Yorkshire, UK. Hydrol Process 13:955–975
135. Walling DE, Woodward JC (1992) Use of radiometric fingerprints to derive information on suspended sediment sources. International Association of Hydrological Sciences Publication No. 210. IAHS, Wallingford, pp 153–164
136. Collins AL, Walling DE, Leeks GJL (1997) Source type ascription for fluvial suspended sediment based on a quantitative composite fingerprinting technique. Catena 29:1–27
137. Collins AL, Walling DE, Webb L, King P (2010) Apportioning catchment scale sediment sources using a modified composite fingerprinting technique incorporating property weightings and prior information. Geoderma 155:249–261

138. Palmer MJ, Douglas GB (2008) A Bayesian statistical model for end member analysis of sediment geochemistry, incorporating spatial dependences. Appl Stat 57:313–327
139. Wallbrink PJ, Murray AS (1993) The use of fallout radionuclide as indicators of erosion processes. Hydrol Process 7:297–304
140. Yang M-Y, Walling DE, Tian J-L, Liu P-L (2006) Partitioning the contributions of sheet and rill erosion using Beryllium-7 and Cesium-137. Soil Sci Soc Am J 70:1579–1590
141. Whiting PJ, Bonniwell EC, Matisoff G (2001) Depth and areal extent of sheet and rill erosion based on radionuclides in soils and suspended sediment. Geology 29:1131–1134
142. He Q, Owens P (1995) Determination of suspended sediment provenance using caesium-137, unsupported lead-210 and radium-226: a numerical mixing model approach. In: Foster IDL, Gurnell AM, Webb BW (eds) Sediment and water quality in river catchments. Wiley, Chichester, pp 207–227
143. Whiting PJ, Matisoff G, Fornes W, Soster F (2005) Suspended sediment sources and transport distances in the Yellowstone basin. Geol Soc Am Bull 117:515–529
144. Olsen CR, Thein M, Larsen IL, Mulholland PJ, Cutshall NH, Byrd JT, Windom HL (1989) Plutonium, lead-210, and carbon isotopes in the Savannah estuary; Riverborne versus marine sources. Environ Sci Technol 23:1475–1481
145. Salant NL, Renshaw CE, Magilligan FJ, Kaste JM, Nislow KH, Heimsath AM (2006) The use of short-lived radionuclides to quantify transitional bed material transport in a regulated river. Earth Surf Process Land 32:509–524
146. Phillips JM, Russell MA, Walling DE (2000) Time-integrated sampling of fluvial suspended sediment: a simple methodology for small catchments. Hydrol Process 14:2589–2602
147. Ongley ED, Thomas RL (1989) Dewatering suspended solids by continuous-flow centrifugation: practical considerations. Hydrol Process 3:255–260
148. Owens PN, Walling DE (1996) Spatial variability of caesium-137 inventories at reference sites: an example from two contrasting sites in England and Zimbabwe. Appl Radiat Isot 47:699–707
149. Sutherland RA (1994) Spatial variability of ^{137}Cs and the influence of sampling on estimates of sediment redistribution. Catena 21:57–71
150. Sutherland RA (1996) Caesium-137 soil sampling and inventory variability in reference samples; literature survey. Hydrol Process 10:34–54
151. Campbell BL, Loughran RJ, Elliott GL (1988) A method for determining sediment budgets using caesium-137. International Association of Hydrological Sciences Publication No. 174. IAHS, Wallingford, pp 171–179
152. Zaborska A, Caroll J, Papucci C, Pempkowiak J (2007) Intercomparison of alpha and gamma spectrometry techniques used in ^{210}Pb geochronology. J Environ Radioactiv 93:38–50
153. Wallbrink PJ, Walling DE, He Q (2002) Radionuclide measurement using HPGe gamma spectrometry. In: Zapata P (ed) Handbook for the assessment of soil erosion and sedimentation using environmental radionuclides. Kluwer, Dordrecht, pp 67–96
154. Canberra (2010) Catalogue. http://www.Canberra.com
155. He Q, Walling DE (2000) Calibration of a field-portable gamma detector to obtain in situ measurements of the ^{137}Cs inventories in cultivated and floodplain sediments. Appl Radiat Isot 52:865–872
156. Benke RR, Kearfott KJ (2001) An improved in situ method for determining depth distributions of gamma-ray emitting radionuclides. Nucl Instrum Meth Phys Res A 463:393–412
157. Golosov VN, Walling DE, Kvasnikova EV, Stukin ED, Nikolaev AN, Panin AV (2000) Application of a field-portable scintillation detector for studying the distribution of ^{137}Cs inventories in a small basin in central Russia. J Environ Radioactiv 48:79–94
158. Walling DE, Zhang Y (2010) A national assessment of soil erosion based on caesium-137 measurements. Adv Geoecol 41:89–97
159. Walling DE, Owens PN (2002) The role of floodplain sedimentation in catchment sediment and contaminant budgets. In: The structure and management implications of fluvial sedimentary systems, Proceedings of the international symposium held at Alice Springs, September 2002, IAHS Publication 276. IAHS, Wallingford, pp 407–416
160. Walling DE (2000) Linking land use, erosion and sediment yields in river basins. Hydrobiologia 410:223–240
161. Walling DE, Collins AL, McMellin GK (2003) A reconnaissance survey of the source of interstitial fine sediment recovered from salmonid spawning gravels in England and Wales. Hydrobiologia 497:91–108
162. Zhang X, Walling DE, Quine TA, Wen A (1997) Use of reservoir deposits and Cs-137 measurements to investigate the erosional response of a small drainage basin in the rolling loess plateau region of China. Land Degrad Dev 8:1–16
163. Walling DE (2006) Tracing versus monitoring: new challenges and opportunities in erosion and sediment delivery research. In: Owens PN, Collins AJ (eds) Soil erosion and sediment redistribution in river catchments. CABI, Wallingford, pp 13–27
164. Ketterer ME, Watson BR, Matisoff G, Wilson CG (2002) Rapid dating of recent aquatic sediments using Pu activities and ^{240}Pu/^{239}Pu as determined by quadrupole inductively coupled plasma mass spectrometry. Environ Sci Technol 36:1307–1311
165. Everett SE, Tims SG, Hancock GJ, Bartley R, Fifield LK (2008) Comparison of Pu and ^{137}Cs as tracers of soil and sediment transport in a terrestrial environment. J Environ Radioactiv 99:383–393
166. Tims SG, Everett SE, Fifield LK, Hancock GJ, Bartley R (2010) Plutonium as a tracer of soil and sediment movement in the Herbert River, Australia. Nucl Instrum Meth Phys Res B 268:1150–1154
167. Wu FC, Zheng J, Liao H, Yamada M (2010) Vertical distributions of plutonium and ^{137}Cs in lacustrine sediments in northwestern China: quantifying sediment accumulation rates and source identifications. Environ Sci Technol 44:2911–2917

168. Kim CS, Lee MH, Kim CK, Kim KH (2008) ^{90}Sr, ^{137}Cs, ^{239,240}Pu and ^{238}Pu concentrations in surface soils of Korea. J Environ Radioactiv 40:75–88
169. Van Pelt RS, Ketterer M, Zobeck TM, Ritchie JC (2009) Anthropogenic radioisotopes to estimate rates of soil redistribution by wind [abstract]. American Society of Agronomy, Crop Science Society of America, Soil Science Society of America. 1–5 Nov 2009. Pittsburgh. Abstract No. 2009.55438
170. Schimmack W, Auerswald K, Bunzl K (2002) Estimation of soil erosion and deposition rates at an agricultural site in Bavaria, Germany, as derived from fallout radiocesium and plutonium as tracers. Naturwissenschaften 89:43–46
171. Hancock GJ, Leslie C, Everett SE, Tims SG, Brunskill GJ, Haese R Plutonium as a chronomarker in Australian and New Zealand sediments: a comparison with ^{137}Cs. J Environmental Radioactivity (in press)
172. Amos KJ, Croke JC, Timmers H, Owens PN, Thompson C (2009) The application of caesium-137 measurements to investigate floodplain deposition in a large semi-arid catchment in Queensland, Australia: a low-fallout environment. Earth Surf Process Land 34:515–529
173. Schimmack W, Auerswald K, Bunzl K (2001) Can $^{239+240}$Pu replace ^{137}Cs as an erosion tracer in agricultural landscapes contaminated with Chernobyl fallout? J Environ Radioactiv 53:41–57
174. Ketterer ME, Hafer KM, Mietelski JW (2004) Resolving Chernobyl vs global fallout contributions in soils from Poland using Plutonium atom ratios measured by inductively coupled plasma mass spectrometry. J Environ Radioactiv 73:183–201
175. Rawlins BG, Scheib C, Beamish D, Webster R, Tyler AN, Young ME (2010) Landscape-scale controls on the spatial distribution of caesium-137: a case study across Northern Ireland. Earth Surf Process Landforms. doi:10.1002/esp. 2026
176. Scheib C, Beamish D (2010) High spatial resolution observations of ^{137}Cs in northern Britain and Ireland from airborne geophysical survey. J Environ Radioactiv 101:670–680
177. Blake WH, Wallbrink PJ, Wilkinson S, Humphreys GS, Doerr SH, Shakesby RA, Tomkins K (2009) Deriving hillslope sediment budgets in wildfire-affected forests using fallout radionuclide tracers. Geomorphology 104:105–116
178. Zhang X, Walling DE (2005) Characterizing land surface erosion from cesium-137 profiles in lake and reservoir sediments. J Environ Qual 34:514–523
179. Owens PN, Walling DE, He Q, Shanahan J, Foster IDL (1997) The use of caesium-137 measurements to establish a sediment budget for the Start catchment, Devon, UK. Hydrol Sci J 42:405–423
180. Walling DE, Collins AL, Sichingabula HM, Leeks GJL (2001) Integrated assessment of catchment sediment budgets. Land Degrad Dev 12:387–415
181. Walling DE, Collins AL, Jones PA, Leeks GJL, Old G (2006) Establishing fine-grained sediment budgets for the Pang and Lambourn LOCAR catchments. J Hydrol 330:126–141
182. Walling DE, Collins AL (2008) The catchment sediment budget as a management tool. Environ Sci Policy 11:136–143

Books and Reviews

Carroll J, Lerche I (2003) Sedimentation processes: quantification using radionuclides. Elsevier, Amsterdam
Froehlich K (ed) (2010) Environmental radionuclides: tracers and timers of terrestrial processes. Elsevier, Amsterdam
Garcia MH (ed) (2008) Sedimentation engineering: processes, measurements, modelling and practice. American Society of Civil Engineers, Reston
Montgomery DR (2007) Dirt: the erosion of civilisations. University of California Press, Berkeley/Los Angeles
Morgan RPC (2005) Soil erosion and conservation. Wiley-Blackwell, Oxford
Owens PN (ed) (2008) Sustainable management of sediment resources: sediment management at the river basin scale, vol 4. Elsevier, Amsterdam
Owens PN, Collins AJ (eds) (2006) Soil erosion and sediment redistribution in river catchments. CABI, Wallingford
Zapata F, Nguyen M-L (2009) Soil erosion and sedimentation studies using environmental radionuclides. In: Froehlich K (ed) Environmental radionuclides: tracers and timers of terrestrial processes. Elsevier, Amsterdam

Fertilizer Science and Technology

J. F. Angus
CSIRO Plant Industry, Canberra, ACT, Australia

Article Outline

Glossary
Definition of the Subject
Introduction
Mining and Manufacture of Fertilizers
Fertilizer Distribution, Marketing, and Price
Fertilizer Effects on Agricultural Productivity
Fertilizer Recommendations and Decision Support
Fertilizers and Precision Agriculture
Fertilizers in Organic Farming
Environmental Benefits of Fertilizers
Pollution of Surface Water and Groundwater
Greenhouse Gas and Ammonia Emissions
Soil Acidification
Does N Fertilizer Deplete Soil Organic Matter (SOM)?
Nutrient Transfer from Farmland to Natural Terrestrial Environments
Human Health

Resource Availability
Future Directions
Acknowledgments
Bibliography

Glossary

Essential nutrients There are 16 mineral elements that are essential for plant growth. They are referred to here by their symbols: nitrogen, N; phosphorus, P; potassium, K; calcium, Ca; magnesium, Mg; sulfur, S; boron, B; iron, Fe; manganese, Mn; copper, Cu; zinc, Zn; molybdenum, Mo; sodium, Na; chlorine, Cl; silicon, Si; nickel, Ni.

Fertilizer efficiency This refers to the additional grain or other agricultural product produced per unit of additional nutrient applied in fertilizer. A related concept is Fertilizer Recovery, which is the additional mass of a nutrient in the aboveground parts of a crop expressed as a proportion of the additional nutrient applied in fertilizer.

Macronutrients N, P, and K.

Micronutrients Cl, Fe, Mn, B, Zn, Cu, Mo, and Ni.

Soil microbial processes These include mineralization, which is oxidation of organic matter and the release of mineral nutrients; immobilization, which is the reverse process of incorporating mineral nutrients into organic matter; and nitrification, which is conversion of ammonium to nitrate.

Definition of the Subject

Fertilizers are compounds or mixtures delivered as solids, liquids or gases, that supply essential nutrients to crops in soluble forms that are convenient and safe to handle. Fertilizers may be applied to the soil or directly to foliage. All nutrients except N are manufactured by concentrating and refining ores extracted from mines. N fertilizers are manufactured from ammonia, which is synthesized from N_2 and H_2. Science contributes to fertilizer use with improved products and methods to increase fertilizer efficiency, profitability of nutrient used, and reducing adverse environmental effects. Technology contributes to fertilizer use by improving the efficiency of manufacture and the complex logistics of delivering hundreds of million tons of products to farms safely, economically, and on time. Fertilizers can be both inorganic and organic, but this contribution refers mostly to inorganic or manufactured fertilizers, since these provide most of the nutrients now added to soil and crops.

Introduction

Fertilizers are indispensable because nutrient supplies from the soil are normally inadequate for the high-yielding crops needed to supply food and fiber for the growing human population. Fertilizers replenish nutrients removed by previous crops and supplement the supply of nutrients from the soil to a level that will produce the farmer's target yield. Fertilizer may also improve the quality of human food, stockfeed, and fiber. The nutrients in fertilizer are a nonrenewable resource and, if they escape from the field, can cause environmental damage. This article discusses the sustainability of fertilizer in relation to these issues.

Before the invention of fertilizers, the only ways that farmers could accumulate nutrients on a field was to fallow before growing a crop, or to transfer animal manure from grasslands and barns to cropped land, either directly or by grazing livestock on grassland by day and enclosing them by night in a field prior to cropping. An additional source of N has been, and still is, the residues of previous legume crops, pastures, and green manures. With these natural nutrient sources, land is temporarily taken out of crop production. Fertilizer allows land to be used for continuous production.

The consumption of the macronutrients in fertilizer, N, P and, K has grown rapidly since the middle of the twentieth century and has increased the food supply more rapidly than the growth of the human population (Table 1). The increase in fertilizer supply has been even more rapid than the food supply. It is difficult to overstate the importance of fertilizers in sustaining humanity: Stewart et al. [1] concluded from the results of experiments that production of 30–50% of the world's food is a result of commercial fertilizers and Smil [2] calculated from nutrient balances that that nourishment of 40% of the world's population depended on N fertilizers.

The use of the macronutrients is uneven around the world, as shown in Fig. 1. On all continents, fertilizer provides relatively more N than P or K. The usage of all

Fertilizer Science and Technology. Table 1 Growth in world population, cereal production, and consumption of nutrients in fertilizer during the second half of the twentieth century

	Annual growth (%)
Human population[a]	1.8
Cereals[a]	
Maize	2.7
Rice	2.4
Wheat	2.3
Fertilizer[b]	
N	7.1
P	4.6
K	3.7

[a]1961–2001 [3]
[b]1960–1988 [4]

three nutrients in Europe and North America most closely approaches crop requirement while usage in Asia and Africa is relatively high in N. The K applications are negligible in Oceania and Africa probably because soil levels of K tend to be relatively high in dry regions.

This article discusses the sustainability of fertilizers from the perspectives of resources and logistics involved in supplying fertilizer to the farm, the on-farm effects on productivity, and on-site and off-site environmental effects.

Mining and Manufacture of Fertilizers

The raw materials for fertilizer manufacture, apart from N, are mined from ore deposits. In the century before 1920, most fertilizer N was also extracted from mines and, before that, from accumulations of nitrate in soil where farm animals had been housed for long periods. Much of this nitrate was used to manufacture gunpowder and other explosives as well as for fertilizer. The increasing demand for explosives and N fertilizer in the nineteenth century led to brutal mining industries that extracted guano (vitrified fecal deposits from sea birds, mostly on tropical islands) and nitrates, a sorry history told by Bown [7].

In modern mining industries, the nutrient compounds in the ore are concentrated by chemical or physical processes into fertilizers that are stable and available for plant uptake. In some cases, two or more nutrient elements are combined, by chemical reaction or physical mixing, into compound fertilizers. Most fertilizers are applied as solids, and single-element and compound fertilizers are normally manufactured as relatively homogeneous granules, which flow freely, minimize water absorption, produce little dust, and which can be transferred efficiently between storages and applied to the soil using machinery or by hand. Most nutrients are available as several different chemical compounds. Examples of these compounds and the manufacturing processes are described by Tisdale et al. [8].

Nitrogen fertilizers are produced from ammonia, which is synthesized by the Haber-Bosch process under conditions of high temperature and pressure using N_2 and H_2 [2]. The usual source of H_2 is natural gas, and the price of N fertilizer is closely linked to the natural gas price (Fig. 2).

Many highly productive farming systems directly inject anhydrous ammonia into the soil. The advantage of ammonia is its high N concentration (82%) and hence low transport cost. Offsetting this is the need for expensive containment vessels, typically made from thick steel, and other costs of ensuring safety. The use of ammonia is confined to application at or before the time of sowing because of toxicity to growing plants. Applications of a large N amount at these times can cause yield reductions, as discussed below.

Ammonia is used to produce many forms of N fertilizer. The most common is urea, which has the advantages that it contains a relatively large percentage of N (46% N) and is safe to handle, unlike ammonium nitrate (34% N), which can be made to explode, and anhydrous ammonia, which is toxic to humans and animals at low concentrations in the atmosphere. Other common N-containing fertilizers are the solid ammonium phosphates (10–20% N) and the solution of urea-ammonium nitrate (28–32% N).

Fertilizer Distribution, Marketing, and Price

Most fertilizer in developing countries is granular and is sold in 40–50 kg bags and broadcast by hand, apart from

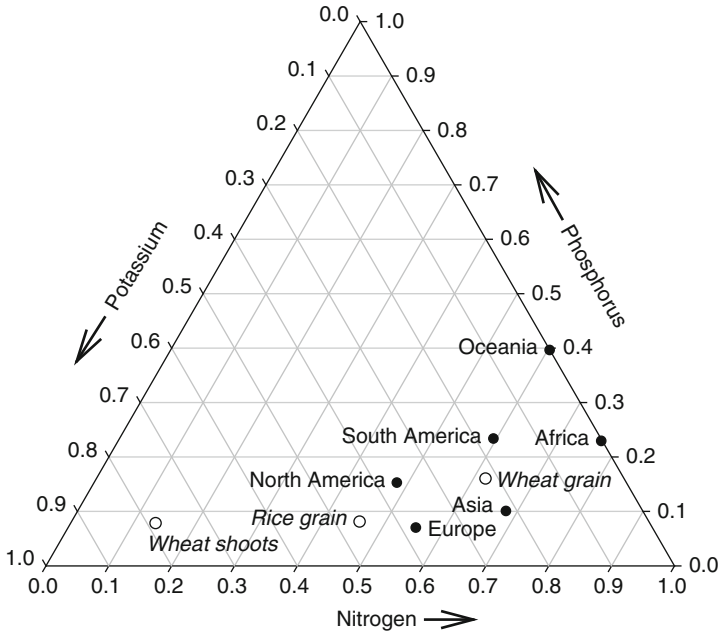

Fertilizer Science and Technology. Figure 1
Variation between continents in the proportions of N, P, and K used in fertilizer, and some examples of the proportions of these nutrients contained in whole crops (fertilizer data from FAOstats, rice data from Dobermann and Fairhurst [5], and wheat data from Bar-Tal et al. [6])

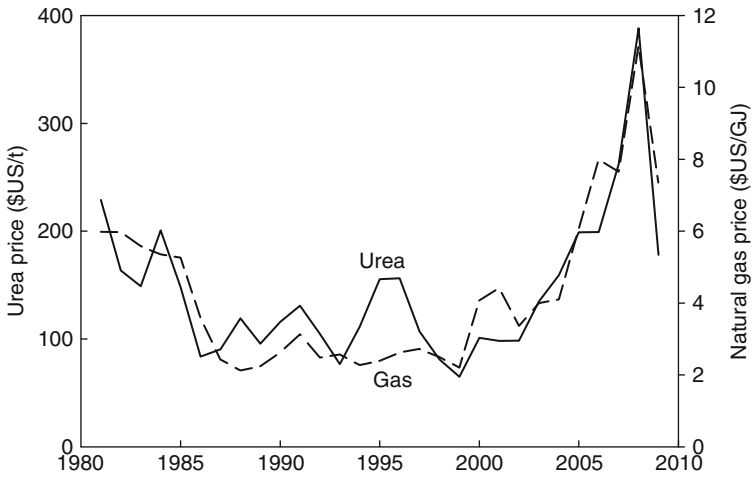

Fertilizer Science and Technology. Figure 2
The price of urea generally follows the price of natural gas, which represents the main production cost [9]

a small but increasing amount applied by machine at the time of sowing. In developed countries, most of the solid fertilizer is supplied in bulk and increasing amounts of liquid fertilizer are used because of the convenience of pumping the product between vessels during transport and application. These advantages can compensate for the additional cost of transporting the water in which the nutrients are dissolved. Most of the advantages of

liquid are for on-farm handling, so an efficient system is for fertilizers to be delivered as solids from the manufacturer to the reseller who then dissolves the solids just before delivery to the farm. The advantages of liquid fertilizer (and gaseous anhydrous ammonia) are greatest for highly productive regions where farms are close to resellers and where it is possible to grow two or more crops each year and spread the cost of specialized equipment for mixing and applying fertilizer over a large crop area. Resellers extend the time of distribution by offering discounts for early use, but this can be at the expense of reduced fertilizer efficiency. One of the hazards of liquid fertilizer is soil compaction due to the mass of water and nutrients contained in equipment at the time of sowing or in spray carts for post-sowing applications.

Extensive dryland farming systems in developed countries use solid fertilizers where the transport costs are high. Solid fertilizer has an advantage for topdressing because granules can typically be mechanically thrown up to 10–15 m on each side of an implement, which is consistent with the 10–15-m width of seeders and 20–30-m width of boom sprays used for controlled traffic. The maximum spreading distance of granules may impose limitations as seeders and spray booms continue to get wider.

Some of the largest financial and environmental costs of fertilizer are related to transport. Products with low concentrations of nutrients are necessarily expensive to transport and their use is confined to specialized applications, for example calcium nitrate, which contains only 16% N, for some vegetables. During the second half of the twentieth century, there has been a general increase in nutrient concentrations leading to reduced cost of transport to the farm and handling on the farm. Nevertheless, the weight of fertilizer means that transport is expensive and low-cost transport methods such as ship, barge, and rail are preferable to road transport. Transport costs are minimized when fertilizer is back-loaded on vehicles carrying agricultural produce to cities. Transport makes up a large part of the on-farm cost of fertilizer in rural areas of sub-Saharan Africa and presents a major obstacle to increasing crop yields [10].

The transport cost is even greater for manures and compost than they are for inorganic fertilizer. Dry animal manures typically contain less than 2% N and 0.4% P, so they cannot be economically carried far from the source. Instead, manures tend to be applied in a radius up to tens of kilometers. Where there is a large source of manure, such as a feedlot or large dairy, the available nutrients can overload the capacity for crop uptake, so that nutrients may accumulate in the soil within a few years. Where the manure contains potentially toxic material such as Cu contained in pig manure, nutrient loading of the soil needs to be closely monitored.

Fertilizer represents the main demand for N, P, and K, but for the micronutrients, usage for fertilizer manufacture is much less than for manufacturing industry. In the case of Zn, annual world production is about 20 million tons, but the amount of Zn contained in all cereal grains is less than 0.1 million tons per year.

The use of compound fertilizers has advantages in ease of handling and may be cheaper than single-element fertilizers. For example, the nutrients in ammonium phosphates are generally cheaper to the farmer than when they are purchased separately, for example as urea and triple superphosphate. In such situations, compound fertilizers can be profitable for the farmer, even if one of the nutrients is not particularly deficient. However with some NPK blends, there may be situations where crops do not respond to all nutrients contained in the fertilizer, and where the compound fertilizer is expensive, the whole product may be unprofitable to use. Such a situation applied to many farms in the Philippines where yield of rice did not respond to either P or K in a NPK compound fertilizer [11]. In this situation, application of the NPK was unprofitable on one third of farms and there was no simple way of determining which fields were deficient in which nutrient element. In such situations, the simplest solution is to make single-element fertilizers available so that strip trials conducted by farmers can show which nutrients give profitable responses [12].

The main fertilizers such as urea, MAP (monoammonium phosphate), and DAP (diammonium phosphate) can be regarded as generic and unspecialized commodities that are traded freely. They are sold by manufacturers to distributors on world markets that are generally open and transparent. An insight to the wholesale market is available online [13]. There is little opportunity for manufacturers or distributors to compete other than through price and service. Intense price competition

does not support the extension services offered by many fertilizer companies until the 1980s or 1990s.

Marketing is generally in the hands of agribusiness employees and media campaigns. Increasingly, advice about fertilizers is supplied to farmers at or near the point of sale by fee-for-service agronomists employed by fertilizer vendors. This represents a conflict of interest between the need for agribusiness to maximize sales and minimize carryover of fertilizer inventory, and the need of farmers to apply the fertilizer at an optimum amount and timing. Independent advice to farmers is important since fertilizer usually represents the single greatest cost of crop production.

Since generic fertilizers do not provide large profits, manufacturers or distributors aim to develop unique products that are easy to use or contain additives that increase fertilizer-use efficiency. Examples are additives to N fertilizers that inhibit urea hydrolysis and so limit the potential for ammonia volatilization, or nitrification inhibitors that restrict the production of nitrate and hence loss by leaching and denitrification [14]. The cost of these additives may not necessarily be justified by additional profit, and they need to be assessed on a case-by-case basis [15]. Some urease and nitrification inhibitors are powerful biocides and have effects other than on N relations, for example, the nitrification inhibitor nitrapyrin has fungicidal activity, so any yield benefits may not be due only to effects on N supply to crops [16]. Slowing the release of nutrients from fertilizer by coating granules with a polymer is another possible means of maintaining adequate nutrient levels near the roots [17]. The cost-effectiveness of these products also needs to be assessed on a case-by-case basis. The most promising markets for fertilizer additives are where subsidies are offered to minimize N release into the environment.

World fertilizer prices fluctuate, depending on variations in supply and demand. The fluctuations for particular products can be massive, for example, the urea price spike in the mid-1990s when Chinese fertilizer companies suddenly increased urea imports (Fig. 2). The cost of fertilizers generally can also fluctuate strongly, as in 2008 when fertilizer price increased in tandem with a rise in world grain prices (Fig. 3).

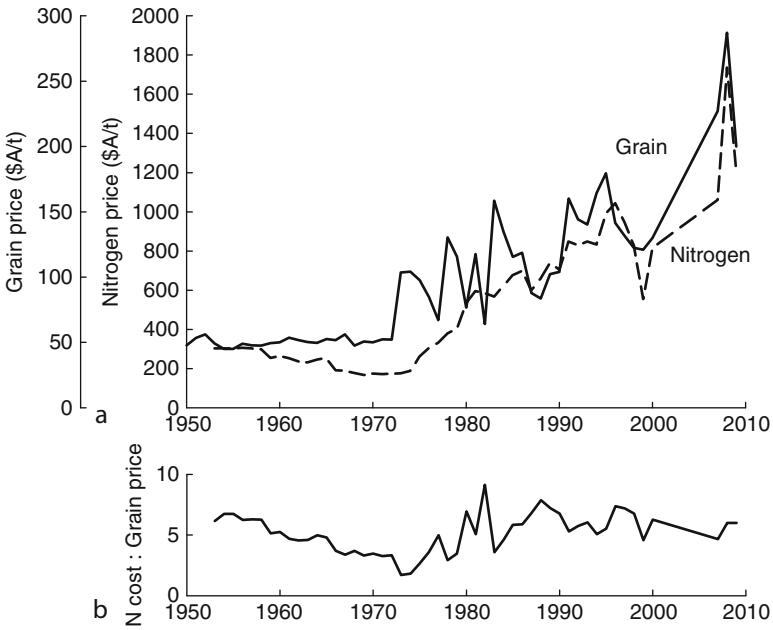

Fertilizer Science and Technology. Figure 3
(**a**) Farm-gate cost of fertilizer N and price of wheat, both expressed in $A and (**b**) the cost to price ratio for N and wheat grain (updated from Angus [18]). Costs and prices are expressed in Australian dollars ($A) since these represent world prices undistorted by subsidies

It is clear from Fig. 3 that the price of grain and cost of fertilizer tend to readjust to maintain a reasonably constant cost:price ratio of about 6, even when grain price or fertilizer cost are disrupted by an external shock.

The price of fertilizer in many markets has been subsidized by governments, generally leading to fertilizer overuse, inefficient methods of application and, in some cases, excess agricultural production that is dumped on world markets. In some countries, the subsidy is through supply of natural gas at less than world price for ammonia production. Fertilizer subsidies have similar effects to subsidies on the price of agricultural production, in that they lead to overproduction because the optimum application rate of fertilizer is affected by the ratio of product price to fertilizer cost. Subsidies on agricultural products and fertilizers have long been criticized because they depress the price of agricultural products in world markets and so reduce the incomes of unsubsidized producers. Criticism is also justified because the overfertilization promoted by subsidies is a major cause of environmental damage [19, 20].

Fertilizer Effects on Agricultural Productivity

In their textbook on plant nutrition, Mengel and Kirkby [21] identify 16 mineral elements as essential for plants. Three of these, Na, Cl, and Si, are normally present in plant tissue at concentrations greater than needed for optimum growth and Ni is rarely or never included in fertilizers. Table 2 lists the remaining 12. A further two, cobalt and selenium, are not essential for plants but are essential animal (and human) nutrients and can be supplied in fertilizer or administered directly to farm animals. The other essential animal and human nutrient, iodine, is not normally supplied through fertilizer.

The concentration of the nutrients in plant tissue varies enormously; for example, N is 100,000 times more concentrated than Mo in cereal grain. The potential yield response to a nutrient, when it is deficient, can be estimated from the inverse of the nutrient concentration. So, for example, if the N concentration in grain is 0.02, as shown in Table 2, a first approximation of potential grain response is 50 kg grain per kg of additional N, assuming that the N concentration of the

Fertilizer Science and Technology. Table 2 Typical concentrations of nutrients in cereal grain, *C*, and the proportion of the aboveground nutrient in the grain [21], called the harvest index for the nutrient (HI). The maximum grain response to the nutrient is given by HI/C. The maximum net financial return is given by [*G*(HI/*C*) − F]/F where *F* is the cost of nutrient in fertilizer and *G* is grain price, assumed here to be $US 0.2/kg

Nutrient	Concentration in grain (*C*)	Proportion in grain (HI)	Maximum fertilizer efficiency (HI/*C*) (kg grain/kg fertilizer)	Nutrient cost ($US/kg)	Maximum net returns ($/$)
N	0.02	0.7	35	1.0	6
P	0.003	0.7	233	5.0	9
K	0.004	0.2	50	0.8	12
Ca	0.005	0.7	140	0.2	140
Mg	0.003	0.5	167	1.1	30
S	0.003	0.4	133	0.2	130
B	0.0001	0.1	1,000	12	15
Fe	0.0002	0.3	1,500	3	100
Mn	0.00002	0.5	25,000	5	1,000
Cu	0.00002	0.5	25,000	5	1,000
Zn	0.00002	0.5	25,000	5	1,000
Mo	0.0000002	0.5	25,000,000	35	150,000

grain is unchanged by the fertilizer. In reality, not all the fertilizer N is present in the grain. In the case of wheat, 0.7 is a reasonable estimate of the proportion of above-ground N contained in mature grain. A better approximation of the maximum grain response to applied N is then $50 \times 0.7 = 35$ kg grain per kg N. Table 2 shows the equivalent calculation for all nutrients. This approach applies only to the first small application of a nutrient and does not account for the diminishing returns of yield to additional applications.

Table 2 also presents estimates of the maximum net financial return calculated from the maximum grain response, the cost of nutrients in fertilizer, and the price of grain. Note again that these are the maximum responses and returns, and real returns are normally much less because not all the fertilizer is recovered by crops. The costs and prices are necessarily assumptions and will vary greatly between markets and between years. However, the differences between nutrients are so great that even with approximations they serve to show some important points.

The maximum responses of additional grain per unit of nutrient applied in fertilizer in Table 2 can serve as benchmarks. When a crop is growing on soil that is believed to be deficient in a nutrient, it should give a yield response comparable with these benchmarks. If it does not it is likely that the nutrient is not seriously deficient or there is a limitation other than the deficiency that is limiting efficient utilization of the nutrient.

The maximum financial crop responses to the micronutrients such as Zn, Cu, and Mo are so large that they are normally applied if there is even a suspicion of deficiency. There are many farming systems where micronutrients still give major grain responses, for example in central Turkey, where widespread Zn deficiency was identified in the 1990s [22]. Continued vigilance is needed in all farming systems in case micronutrients become deficient.

Even for N and P fertilizer, the maximum financial responses are large enough to provide a profit even when the efficiency of recovery is low. In these examples crop recovery of only one sixth of the applied N or one ninth of the applied P gives a break-even return on cost of the fertilizer.

The grain-yield responses to fertilizers are usually much less than these maxima and a great deal of research goes into increasing fertilizer efficiency. Where deficiencies are severe and there is only one nutrient lacking, visual symptoms can be compared with standard illustrations [23]. For less acute deficiencies, a traditional method is to calibrate yield against a soil test and identify the critical nutrient concentration that gives near-maximum yield [8]. The process of soil testing consists of sampling the soil in a field with many cores, combining the samples, and analyzing for nutrient concentration.

Soil tests are not the only methods for determining nutrient status and Table 3 shows examples of methods to estimate N status, including tests related to the nutrient status of vegetative plants. Tests of plant tissue are generally more reliable than soil tests because the volume of soil sampled by plant roots is normally more than the soil volume explored by coring [24, 25].

There are limitations to basing optimum fertilizer application only on tests of soil or plant nutrient status. The approach is suitable for a cropping system in which prices and yields do not vary greatly from year to year, but is less useful where the variation is large. The optimum fertilizer application varies with the ratio of grain price to fertilizer cost, and the optimum fertilizer rate is high when the ratio of grain price is high relative to fertilizer cost.

The optimum fertilizer rate also depends on yield potential, and higher rates are justified by increasing yield potential. Soil and plant tests emphasize the

Fertilizer Science and Technology. Table 3 Tests of N status

Pre-sowing tests	Tests during crop growth
Field history	Tissue N concentration
Total N in the topsoil	Tissue nitrate concentration
Mineral N in the topsoil	Sap nitrate concentration
N released during soil incubation	Shoot density
Previous grain protein	Leaf chlorophyll concentration
	Leaf color compared with standards
	Lower leaf senescence
	Strip trials

Fertilizer Science and Technology. Table 4 Example of a nutrient budget for N fertilizer applied to wheat

Crop N demand	
Target yield	4 t/ha
Target grain protein	12%
N in grain[a]	84 kg/ha
N in aboveground crop[b]	120 kg/ha
Soil N supply	
Soil mineral N at sowing[c]	50 kg/ha
N mineralization during crop growth	80 kg/ha
N available for crop uptake (50%)[d]	65 kg/ha
Fertilizer N requirement	
Additional N required in the crop[e]	55 kg/ha
Fertilizer N required[d]	110 kg/ha

[a]Grain N is the product of yield and grain N, assuming that 1 kg of N = 5.7 kg of grain protein
[b]Assuming grain N is 70% of aboveground N
[c]Soil mineral N sampled to a depth of at least 60 cm
[d]Assuming 50% of soil and fertilizer mineral N is available for crop uptake
[e]Difference between crop demand and soil supply

supply of nutrients but it is important to place equal emphasis on crop nutrient demand. Table 4 shows an example of a nutrient budget, based on a method developed by Myers [26], to illustrate the importance of N supply and demand.

When the quality of the grain is affected by fertilizer, it is necessary to consider the responses of both yield and quality and the ratios of fertilizer cost to the grain price and quality premiums. Angus [27] presents a method to estimate the economic optimum fertilizer for wheat in relation to responses by grain yield and protein.

A well-known but generally erroneous notion about nutrients is the Law of the Minimum, which claims that only one nutrient can limit yield of a particular crop. Where one nutrient is drastically deficient, the Law of the Minimum is a fairly good rule of thumb, for example when a micronutrient such as Zn gives a spectacular yield response. More generally, this Law is deceptive, and crops and cropping systems tend to regulate the quantity of nutrients in the soil by luxury extraction of those that are adequate or surplus, and poor extraction of those that are deficient. The different rates of extraction continue until many nutrients become co-limiting and are required for the yield to reach the biological potential [28].

The weakness of the Law of the Minimum can be seen from the many experiments where fertilization with any one of several nutrients can increase yield (e.g., [11]). Fertilizer management therefore usually needs to consider more than one nutrient. Where several nutrients simultaneously limit yield, the combined effect may be additive, meaning that the yield response of the combined nutrients is the same as the sum of yield responses of the nutrients applied singly. In other situations there may be a positive (or negative) interaction, meaning that the effect of the nutrients when applied together is greater (or less) than the sum of the effects of the individual nutrients. As with many aspects of fertilizer management, there is no alternative to conducting experiments on farms to quantify crop responses to nutrients and their interactions. This rest of this section discusses the macronutrients, N, P, and K, and, as examples of minor and micronutrients, S and Zn.

Nitrogen

Nitrogen is used in greater quantity than other nutrients but the financial returns are often less (Table 1). Nitrogen fertilizer has a reputation for low efficiency and many studies show that a crop typically recovers about half the fertilizer N applied, but the proportion can vary from zero to almost complete recovery [24]. The reasons for incomplete recovery are numerous but often the soil can supply as much N as the crop can take up, and any additional N remains in the soil where it may be lost in several processes. Nitrogen losses include leached nitrate, gaseous ammonia volatilization from urea and ammonia-based fertilizer, and nitrous oxide (N_2O) and N_2 from denitrification. Urea is at particular risk of loss, mainly because the soil becomes alkaline around a dissolving granule, so that any ammonium formed is rapidly converted to ammonia, which volatilizes.

Another cause of low crop recovery is immobilization of fertilizer N by soil microbes. This process is not necessarily a loss, since the N can be present in the soil organic matter (SOM) for one or more seasons, during which it is normally mineralized and taken up by later crops.

Nitrogen is unusual among the nutrients in that excess application often causes a reduction in crop

yield. In wet and high-yielding environments the reasons for yield reductions are lodging, because the crop becomes tall and top-heavy, and because of disease in thick foliage. In dry conditions, excess N stimulates growth, which can lead to exhaustion of soil water before maturity. Another and often more important reason is that high N levels reduce the concentration of water-soluble carbohydrates in the stems, which is an important source of assimilates for grain growth [29]. The time of application of N fertilizer is important in methods to avoid losses. Responses to topdressing N on wheat during the stem elongation phase are comparable to the responses to the same amount of N applied at sowing in both highly productive environments in Europe [30] and in water-limited environments in Australia [31]. Fertilizer N applied at sowing promotes rapid seedling growth, which leads to more risk of lodging, foliar disease, and haying-off than the same amount of N applied at stem elongation or later. Even when growing rapidly, small plants cannot take up large amounts of N, so mineral N in the soil at the time of sowing is at risk of loss from leaching and denitrification.

Mid-season application of N is effective because it coincides with the period of maximum crop uptake and so closely matches supply with demand. Application of N during or after the stem elongation phase in cereals usually increases grain protein more than application at sowing.

The N losses from irrigated rice can be particularly high. De Datta [32] reported that the average recovery of N fertilizer in rice experiments was 35–40%. Extensive research showed that the main pathways for N loss from lowland rice are ammonia volatilization and denitrification when urea is broadcast onto wet soil or shallow water. This research did not show ways to minimize losses and Fujisaka [33] suggested that research should focus more on methods to increase N efficiency rather than quantify the loss pathways. Subsequent agronomic research showed that with suitable methods of application the recovery of N, supplied as urea, can be as high as 75% for tropical rice [34] and 90% for temperate rice at a commercial scale [24].

The most efficient ways to increase N use efficiency (NUE) are different in each region and with each cropping system. Practices that are often effective are injecting fertilizer into the soil rather than broadcasting it on the surface and delaying application of some or all of the fertilizer so that the supply of N is well synchronized with the crop demand. Other ways to increase NUE are to ensure that other factors are not limiting. These limitations can include deficiency of other nutrients, weeds, herbicide damage, and root disease. An example of the importance of overcoming such limitations is apparent in a 40% increase in dryland wheat yield in Australia during the 1990s, which coincided with the adoption of canola break crops and higher applications of N fertilizer. Angus [18] suggested that break crops controlled widespread root disease and provided suitable conditions for a large yield response to N fertilizer.

There have also been reports of improvements of NUE in a single season by classical plant breeding [35] or modification of single genes [36]. Genetic improvements in N use efficiency are promising but it is not yet clear whether they are consistent across environments and seasons, and whether they are as cost effective as the established and reliable improvements in crop management.

There is a widespread and recurring problem of farmers applying more than the economically optimum rate of N fertilizer. The problem was apparent in Europe and the USA from at least the 1970s [20] and the same pattern of overuse emerged in many other countries, including China since the 1980s [37]. N fertilizer applied in excess of crop requirements is sometimes called "insurance nitrogen" [38], implying that farmers are prepared to pay for the excess provided that the yield is maximized. Another explanation lies in the concept of "farming styles" of van der Ploeg [39], which interprets farming practices in relation to farmers' goals. Farmers who want to boast of the highest district yields apply heavy inputs with little regard for input costs and net profit. These competitive individuals are uninterested in the profit-maximizing paradigm of agricultural science. To reverse the pattern of fertilizer overuse, it is important to redirect their competitiveness to efficiency rather than yield.

The reason that overfertilization is more common with N than other nutrients is not clear, but may be related to the rapid and visible response by crops. Within 5–10 days of N application, crops usually become greener and taller, which gratifies farmers, at least when they first observe the response. To this

extent, N fertilizer provides its own advertising. The greener and taller fertilized crops may or may not yield more than those that receive no additional fertilizer. Reasons for a lack of yield response may be that the real yield limitation is not N but some other limitation such as water deficit, disease, deficiency of another nutrient, frost, weeds, or herbicide damage. Since the 1990s, the application rates of N fertilizer have been static or falling in Europe and North America but crop yields have continued to rise [40]. Apparently, farmers and advisers in these regions are learning the lesson that the previous rates were excessive and the time of application was too early.

Phosphorus

Soil contains P as both soluble and insoluble inorganic phosphates and in organic forms including phytates, which make up more than 50% of the soil P. Fertilizer P adds to the soluble pool that can be taken up by crops, but the longer it remains in the soil the more is precipitated as insoluble iron and aluminum compounds in acid soil, or as insoluble calcium compounds in alkaline soil. Soils vary in the speed with which they precipitate soluble P, so soil tests are needed to measure plant-available P and the optimum rate of P fertilizer [8]. Tests of soil P and other nutrients based on ion exchange resins often give closer relations with plant uptake than other extraction methods [41]. Plant P tests are not as useful as plant N tests because P is applied at or before sowing.

Fertilizer management is designed to maximize and prolong P availability to the crop. The most powerful method is to include all the P in a band near the seed so as to maximize plant access before the P becomes unavailable due to precipitation. As with N fertilization, it is important to supply only enough for the crop since some of the excess P is likely to be precipitated. This applies whether the fertilizer is in the solid or liquid form. Liquid forms of P fertilizer are relatively more effective than solid forms on alkaline soils because the precipitated P is still partly available [42].

Most P in the soil is attached to clay particles and is not readily leached from any but the sandiest soils. Because most soil P is close to the surface it is unavailable when the topsoil dries out, so fertilizer injection below the surface can improve the efficiency of uptake in dry environments [43]. Because of the advantages of banding and deep placement, all the P fertilizer needs to be applied at the time of sowing.

Potassium

Crops require a large supply of K but remove little in grain. Most of the K taken up by plants remains in the straw and returns to the soil when the straw decomposes or is burnt, provided the ash that remains after burning is not blown away in the wind. Once in the soil, K is not readily leached because of its positive charge and tends to be used by crops with greater efficiency than N or P. An exception is on soils that contain a large proportion of 2:1 clay minerals, where K is strongly fixed and becomes unavailable to roots.

Other Nutrients

The other nine nutrients commonly applied as fertilizers are not all discussed individually and the reader is referred to nutrient aspects by Mengel and Kirkby [21] and fertilizer aspects by Tisdale et al. [8]. This section discusses S and Zn because of their increasing importance.

Sulfur is present in the soil as sulfate, which as an anion is subject to leaching. Until the later part of the twentieth century, it was inadvertently applied in many regions. One form was in superphosphate, which was used for its P content (9%) but supplied S (11%) as well. The "high analysis" fertilizers, which largely replaced superphosphate, contain relatively small amounts of S. Another source of S for plants was atmospheric deposition as oxides of S from smokestacks, particularly on smelters of metal sulfides. This source of S is also decreasing because smokestacks are being fitted with "scrubbers" to reduce air pollution. Fertilizer S will be increasingly needed to replace these sources.

Zinc is important for not only increasing crop growth, but also as an essential human nutrient that is becoming seriously deficient. Zinc deficiency is widespread in soils and plants, particularly in west and south Asia [44], and methods and products are available in some countries to correct Zn deficiency [23]. Some, but not enough, compound fertilizers in developed countries include Zn but in many developing countries, Zn is available only as zinc sulfate.

Sometimes this expensive compound is diluted by unscrupulous retailers with salts that look similar, such as ammonium sulfate, so the product is an ineffective source of Zn (R.J. Buresh, 2011, personal communication).

Much of the Zn content of plants is transferred from the soil to plant roots by arbuscular mycorrhizal fungi (AMF). The large surface area of AMF filaments increases the ability of plants to explore the soil for immobile nutrients such as Zn. AMF are highly effective in soils with low nutrient status, but the modern farming practices of high levels of P fertilizer and growing brassica break crops tends to reduce AMF activity and increase the need for Zn fertilizer. Breeding plants for increased Zn uptake from soil can be effective in the short term but without supply of Zn fertilizer will exhaust soil reserves and hasten the onset of severe deficiency [45].

Fertilizer Recommendations and Decision Support

Methods for prescribing the fertilizer amount evolved from blanket recommendation provided by advisers, meaning the same practice irrespective of fields or seasons. Soil tests and nutrient budgets, as described earlier, give more differentiated prognoses of response can be used to develop "rules of thumb," which are usually accepted by busy farmers. Computer-based decision support systems can take account of many factors that are known to affect nutrient response but are not as widely adopted as simple systems and rules of thumb. McCown [46] concluded that adoption of decision support systems had not met the promise they offered.

Fertilizers and Precision Agriculture

Precision agriculture is a set of principles that has developed since the 1990s, aimed at managing crops at a scale of several meters rather than as a whole field. It relies on a global positioning system (GPS) that estimates location with precision ranging from 4 to 0.02 m, spatial data about crop production such as maps from a yield monitor, biomass images from a satellite or aircraft, or spatial data about soil conditions such as electrical conductivity [47]. Fertilizer can be managed by precision agriculture by varying the application rate according to the demand by the crop and/or the supply from the soil in different zones in a field. The farmer or adviser first prepares a prescription specifying the fertilizer rate for each zone and programs this in a computer carried in a tractor. This computer continuously determines where the tractor is located relative to the zones in the field, based on signals from the GPS receiver, and controls an actuator on the fertilizer implement that delivers the appropriate rate of fertilizer in each zone.

Yield maps provide useful data for deciding on fertilizer strategies and tactics. If one part of a field is consistently low yielding and it has previously received the same amount of fertilizer as the rest of the field, then it is likely that soil nutrient levels have accumulated. This pattern is common in the case of P fertilizer, and provides evidence to reduce the application rate on low-yielding zones. Variable applications of N fertilizer are a common use of yield maps. An example is in response to natural variation in soil organic matter, with additional N supplied to low-fertility zones [48]. Another example is in response to "unnatural" soil variation due to land leveling, where "cuts" expose subsoil containing low nutrient levels and "fills" consist of additional amounts of topsoil that is relatively fertile.

In these examples, additional fertilizer is designed to compensate for low soil nutrient status. If yield variation is due to soil properties other than nutrient status, then it may be inappropriate to compensate for low yield with more fertilizer and the best strategy is the exact opposite, that is, to apply more fertilizer to zones that consistently give the highest yields. An example of this situation is when spatial yield variation is due to the differences in the available soil water supply. Angus et al. [49] investigated yield and crop response to N across fields that varied in subsoil constraints of salinity, sodicity, and high concentration of boron. They showed that wheat yield and the crop response to N fertilizer were greatest on parts of a field with the least subsoil constraints, and yield responses to applied N were least on zones with the most severe constraints. Even in the absence of subsoil constraints, the soil water-holding capacity can control yield of dryland crops, and the highest rates of N fertilizer should be applied to zones with large water-holding capacity [50]. Spatial soil variation is often best measured by

electromagnetic induction, which directly measures apparent electrical conductivity, which is a proxy for other properties [51].

Where the response of a crop to fertilizer depends on its N status rather than other soil conditions, an optical sensor can provide useful information about a static or on-the-go estimate of crop N status. Optical systems using infrared sensors, such as the Greenseeker [52] and N-Sensor [53], can estimate N status of crops at a scale of about 1 m^2 while mounted on a tractor or fertilizer distributor, and can regulate the fertilizer rate on-the-go. A simple system using a domestic digital camera can provide equivalent information for a single scene [54].

The previous examples applied when the spatial yield patterns are consistent between years. A more complex approach is needed when the fertilizer response is inconsistent between zones and between years. For example in a dry season, N fertilizer may increase yield in low-lying, wet zones of a field but reduce yield in hilly, dry zones. Conversely, in a wet season, N fertilizer may be most effective in the hilly zones. The best response to this situation is not clear. One possibility is to examine yield maps for several years and manage fertilizer for an average season. Another is to delay the decision to apply fertilizer until the seasonal pattern is apparent. It may also be possible to minimize yield variation due to water movement by land-forming and drainage.

Fertilizers in Organic Farming

Many consumers are prepared to pay premiums for organically grown produce and a small proportion of farmers want to supply food produced by one of the organic farming systems. For certification of organic produce, the several organic farming systems generally require nutrients to be applied as manure and unprocessed minerals but not as processed fertilizer. Application of sufficient manure can provide optimum crop nutrition and until recently it was assumed that there were no disadvantages to the nutrient relations of organic farming. Research compiled by Kirchmann and Bergström [55] shows that this assumption is invalid because there is consistently more N leaching under organic than conventional systems, apparently because the soil N supply is not well synchronized with crop N demand. These results suggest that the nutrient relations of organic farms may be less sustainable than conventional farms. Many governments subsidize organic farming systems and thus support unsustainable nutrient management.

In another comparison of organic and conventional farming systems, Fagerberg et al. [56] showed that nutrient levels of the organic part of a split farm remained adequate for several years after conversion from conventional, but that later some nutrients become depleted and productivity fell. The likely reason was that these nutrients had accumulated during several decades of fertilizer application before half the farm was converted to organic farming.

Residual nutrients from previous fertilizer application are not the only source of N in organic farming. In parts of north America and western Europe, the deposition of mineral N from the atmosphere contributes a large part of crop requirement [20]. The sources are ammonia emitted from manure in intensive animal industries and nitrogen oxides emitted from vehicles. Both sources of N originate from industrial operations, so it is difficult to understand how any farming conducted in such regions can be designated as organic.

Some strands of organic farming propose application of plant extracts and microbial preparations to the soil to promote crop growth, and such products have spread in the decades since there was regulation of agricultural chemicals. Reports of the effectiveness of some of these products were reviewed by Edmeades [57], who concluded that they gave no significant yield benefit when used as recommended. A manufacturer of one such product objected to Dr. Edmeades' comments and took legal action against him in New Zealand courts. Dr. Edmeades won the case but effectively lost his scientific career and wasted a year enmeshed in the legal system [58]. It is not clear how reputable science should deal with claims that "alternative" products provide production and environmental benefits out of all proportion to their nutrient composition. Even if one such product is proved to be ineffective and removed from the market, it is likely that others will take its place. A solution may be to strengthen consumer protection laws so that manufacturers can be penalized for making unsubstantiated claims.

Environmental Benefits of Fertilizers

Fertilizers provide environment benefit by increasing soil organic matter in nutrient-deficient soils. For example, superphosphate provided P and S for vast areas of deficient soil in Australia, which provided that trigger for biological nitrogen fixation by pasture legumes [59]. Even more spectacular increases in soil organic matter came when micronutrient deficiencies were corrected with fertilizers in the Western Australian sandplain. These are the only positive environmental effects of fertilizer and other effects are neutral or negative.

Pollution of Surface Water and Groundwater

When there is nitrate in the soil and the water supply from precipitation and irrigation exceeds evaporation, the nitrate will be leached and eventually enter the groundwater. Levels of groundwater nitrate began to increase in the second half of the twentieth century, most notably in Europe and North America, and have stubbornly remained high. For example, Johansson and Gustafson [60] reported that after N-fertilizer application to an arable field in southern Sweden was discontinued, there was a delay of 20 years before the concentration of subsoil nitrate decreased.

The best-known environmental damage from nutrients is water pollution in lakes, rivers, and parts of the ocean. The pollution causes hypoxia, algal blooms, and death of pelagic fish in many water bodies, the largest of which are the Gulf of Mexico [61], the Baltic Sea [62], and the Yellow Sea [63]. The delay in affecting nutrient levels in such water bodies is probably longer than for groundwater, as shown by the constant levels of dissolved N in the Baltic Sea 10 years after N fertilizer usage almost stopped in the eastern Baltic countries after the breakup of the Soviet bloc [62].

Both N and P from fertilizer contribute to pollution of large water bodies but even if N from fertilizer were not present, blue-green algae would be able to obtain their N requirements from biological fixation. Other evidence for the importance of P in water pollution is that the size of the "dead zone" in the Gulf of Mexico is more closely related to the discharge of P than of N [64]. The source of nonpoint P pollution may not be confined to fertilizer, and streambanks disturbed by humans and grazing animals have the potential to release soluble P into water bodies. A promising method to reduce phosphate release into streams is to exclude grazing animals from riparian strips.

Systems to limit nutrient pollution of water have included fertilizer taxes and quantitative limits of nutrient loading from both fertilizer and manure. N fertilizer was taxed in Sweden for many years but there was little change in the rate of N application to crops. In the Netherlands, a system of nutrient accounting of inputs and outputs limits the nutrient balance of farms to reduce nutrient movement into groundwater and streams [65]. A promising method is to define sensitive zones, based on infiltration rate or proximity to streams, where fertilizers are banned, limited, or taxed [66].

Intensive research continues on the nitrogen cascade, a phrase that recognizes a chain of intended and unintended consequences when reactive N moves on land and in the air and water. An example of coordinated research in western Europe is given by Sutton et al. [67].

Greenhouse Gas and Ammonia Emissions

Nitrous oxide (N_2O) and N_2 are released from soil into the atmosphere by the processes of nitrification [68] and denitrification [69]. N_2O absorbs long-wave radiation and remains in the atmosphere for a long time so its greenhouse effect is much greater than that of CO_2. The International Panel on Climate Change estimates the emission of N_2O from agriculture as a percentage of the N fertilizer applied. This approach takes no account of nitrification and denitrification of non-fertilizer sources, mainly from mineralization of organic N. Since fertilizers provide about half of the N used for food production, the contribution of the organic N to N_2O emission is probably underestimated. The most promising strategy to reduce N_2O loss are to minimize waterlogging, since denitrification proceeds most rapidly in anaerobic conditions.

Gaseous loss of NH_3 is greatest when ammonium is on or near the surface of an alkaline soil, or in the floodwater of rice. Windy conditions at the soil surface also contribute to rapid loss. In the worst conditions, the loss of fertilizer N can be up to 10–15% per day [15], but the loss can be reduced or eliminated by injecting ammonia-based fertilizers below the soil surface, or, if topdressing is unavoidable, by applying

fertilizer before forecast rain, so that the granules are dissolved and transported below the soil surface.

Soil Acidification

Ammonia-based fertilizers, including urea, acidify the soil when protons are released during nitrification. Soil pH falls more rapidly in light-textured and poorly buffered soils than in heavy-textured and highly buffered soils, but the process continues irrespective of soil type. The consequence of acidification is reduced plant growth, not because of the protons, but because of increasing concentrations of aluminum and manganese in the soil solution that accompany reduced pH. The most common cure is to apply lime, which represents a deferred and indirect cost of N fertilizers and an environmental cost since the reaction of lime on acid soil releases CO_2. A less common response is to apply nonacidifying fertilizers such as those containing nitrate, but these are more expensive than ammonia-based products.

Does N Fertilizer Deplete Soil Organic Matter (SOM)?

Until recently, there was a general belief that N fertilizer had little or no effect on SOM but this was challenged from analysis of soil data from the Morrow Plots, a long-term experiment at the University of Illinois in Urbana. Khan et al. [70] analyzed soil C and Mulvaney et al. [71] analyzed soil N from these plots and came to the startling conclusion that adding N fertilizer decreased SOM, apparently because the N fertilizer stimulated soil respiration. If true, this conclusion would prove that the modern N fertilizer industry is unsustainable.

Reid [72] and Powlson et al. [73] criticized these interpretations of the Morrow data. Their criticism was that the experiment had been confounded because the plot that received a large N dose from 1965 to 2005 had previously (1904–1966) received large annual doses of manure that had built up SOM to very high levels. After the manuring finished on that plot in 1967, the SOM decreased simply because it was above the equilibrium level for the environment, and not because of N fertilizer. This is a strong argument because there is ample evidence that soil maintains a high level of SOM only if there is a constant input of organic matter to offset soil respiration, and this material contains C, N, P, and S at ratios close to that of SOM. Kirkby et al. [74] surveyed data on SOM content and estimated that the average C:N:P:S ratio of humus was 1000:80:20:14. After manuring stops, the SOM decreases for many decades until it returns to the equilibrium for the environment [73]. The decrease in SOM in the Morrow plots can be explained more by the oxidation of manure than the effect of N fertilizer. The specific criticisms by Reid [72] and Powlson [73] about the confounded treatments have not been challenged after 3 years of debate on the subject [75] so it appears that the concern about N fertilizer depressing SOM was a false alarm.

Nutrient Transfer from Farmland to Natural Terrestrial Environments

It has long been known that nutrients move from farmland to natural environments on land, as well as to freshwater and oceans, as described above. Pathways for nutrient transfer are water, gas, dust, and wild animals [76]. Movement by water is likely to remain in the stream system so is relatively unimportant for transfer to terrestrial environments. The only nutrient moved as gas is ammonia, and the main agricultural source of which is housed animals rather than emissions from fertilizer, although the original source of the nutrients is mostly fertilizer.

Nutrient movement in dust has not been widely discussed in the agricultural literature but is of more interest for earth science. Nutrients move in dust when wind lifts clay particles, which normally contain a large proportion of organic matter [77]. When the wind abates, the particles may land on another agricultural field where the nutrient transfer is relatively unimportant, and in natural environment where the nutrients may cause environmental damage.

The other source of nutrient transfer is through animals. Where farmland is adjacent to natural vegetation, it is common to see wild animals grazing on crops and pastures during the morning and evening and retreating into the cover of bush during the day. Examples are deer in Europe and North America, kangaroos in Australia, and birds almost everywhere. The obvious attraction to animals of the margin between farm and

bushland is access highly nutritious feed on the farms and cover in the natural vegetation. Nutrient transfer occurs through urine and dung deposited in the bushland. A consequence of nutrient enrichment of natural vegetation from all sources is eutrophication of the landscape, analogous to eutrophication of water [78], with weedy annual plants competing with native perennials. Nutrient transfer over short distances could place limits on the development of mosaic farming systems where farming and natural vegetation are distributed through a landscape according to land capability.

Human Health

Heavy metals can enter the human food chain from fertilizer. Cadmium (Cd) is the most toxic and is a contaminant in many phosphatic fertilizers [79]. When Cd is applied to a field it accumulates first in crops, grazing animals, and then in the tissue of people who consume the products. The most promising way of reducing Cd levels in fertilizer is by manufacturing phosphatic fertilizer from sources of rock phosphate that contain low levels of Cd [80].

Another supposed health hazard from fertilizer was nitrate, but the concern turned out to be a false alarm. From the 1940s until the 1990s, nitrate was believed to cause blue-baby syndrome (methemoglobinemia) because some cases of this disease that were associated with groundwater containing high nitrate levels, and this was the main reason for an official limit of 50 mg/L of nitrate in drinking water. Evidence reviewed by Addiscott [20] showed that nitrate at this concentration was harmless and that the original basis for this limit was faulty because water containing high nitrate concentrations also contained bacterial contamination, which was the real culprit for methemoglobinemia.

There are however beneficial effects of fertilizers on human health through micronutrients that are essential for human health. The best example is Zn, which is widely deficient in the human diet. The World Health Organization concluded that human Zn deficiency was one of the most serious causes of poor health [81]. Low levels and low bioavailability of Zn in human food are the cause. Increased use of zinc fertilizer would be a boon to human health, particularly to people who rely on a vegetarian diet, since plant products contain less Zn than meat. In view of the difficulty in correcting Zn deficiency in crops, supplementation of human food with Zn may be more effective [45].

Resource Availability

World food supply relies on increasing amounts of nonrenewable resources to provide fertilizers. In the case of N, the resource involved is energy, and about 1% of the world's supply of fossil fuels is consumed in its production. Production of all the other nutrients depends on mining as well as relatively small amounts of energy used in manufacture and transport.

The energy cost of producing N fertilizer has decreased as technology improved. For example, the amount of natural gas needed to synthesize ammonia in the most efficient plants halved in the last 40 years of the twentieth century, and by 2000 was within about 25% of the highest possible efficiency [2]. With diminishing scope for improved efficiency and exhaustion of natural gas, it is likely that the real cost of N fertilizer will rise.

The nutrient at greatest risk of exhaustion is P. Cordell et al. [82] estimated that "peak phosphorus" had been reached and that reserves would be exhausted by 2030. This conclusion is based on the extrapolation of sigmoid curves of production, similar to those used to predict the exhaustion of crude oil reserves. Alternative approaches reviewed by Cornish [83] comes up with estimates of reserves lasting at least until 2100, based on current rates of extraction and the amounts and quality or known reserves compiled by the US Geological Survey. Whether the reserves will last for 30 or 100 years, there is increasing concern that P will be the most limiting nutrient in the long term. The most promising ways of prolonging supplies is to reduce overuse of P fertilizer and find ways to minimize phosphate fixation in soils. If exhaustion of P is as imminent as the worst predictions, it will be necessary to find ways of recycling at the important points of loss, which are in food preparation and in human urine. Recycling options are discussed by the Global Phosphorus Research Initiative [84].

Reserves of high-quality K fertilizers are likely to outlast those of P and probably N [83]. One concern about K supplies is that they are concentrated in the hands of relatively few producers who could be in

a position to corner the market. Another concern is that the largest reserves of K fertilizer in Canada and Russia are remote from the regions of greatest K deficiency in Asia.

Future Directions

Existing science and technology shows that crops can respond reliably and profitably to fertilizers when used cautiously. This involves applying fertilizer so that the combined supply from fertilizer and the soil is sufficient for, but does not exceed, crop requirement. This principle has not penetrated far into farming systems, and fertilizer management varies from generally inadequate applications in sub-Saharan Africa to excess use of N in East Asia. Many farms in Europe and North America have passed the period of excess N use. However the efficiency of fertilizer use is still generally low and improvement will require incremental research on farms to refine methods to apply fertilizer efficiently and in ways that are compatible with farming systems. As farming systems change, as they inevitably will, fertilizer management will have to change also. The most promising methods are to arrange fertilizer rate, time of application, spacing and depth of placement to synchronize supply with crop demand, and to adjust these parameters in relation to zones in the field and region. The methods will have to be cost effective, so it will be important to continue to develop methods to manage low-cost fertilizers appropriately rather than resorting to high-cost additives, which may have to be supported by subsidies. Science should also critically evaluate and comment on "alternative" fertilizer products and systems that make outrageous claims and will lead to reduced food security if widely used.

More fundamental science should be directed to liberating the large amounts of unavailable soil nutrients, while recognizing that release of these bound nutrients will only delay the need for additional fertilizer. The largest environmental improvements related to nutrient overuse are likely to come from research to increase fertilizer efficiency on farms. The delay between conduct of farm-related research and its benefits on a regional scale can be many decades [85], so well-resourced field research needs to be maintained.

Acknowledgments

Tony Good provided insights into fertilizer technology and John Passioura and Mark Peoples made helpful suggestions about the article.

Bibliography

Primary Literature

1. Stewart WM, Dibb DW, Johnston AE, Smyth TJ (1995) The contribution of commercial fertilizer nutrients to food production. Agron J 97:1–6
2. Smil V (2001) Enriching the earth. Fritz Haber, Carl Bosch, and the transformation of world food production. MIT Press, Cambridge
3. www.fao.org/waicent/portal/statistics_en.asp
4. Bumb BL (1995) World nitrogen supply and demand: an overview. In: Bacon PE (ed) Nitrogen fertilization in the environment. Marcel Dekker, New York, pp 1–40
5. Dobermann A, Fairhurst T (2000) Rice: nutrient disorders and nutrient management. PPI and IRRI, Singapore/Los Baños
6. Bar-Tal A, Yermiyahu U, Beraud J, Keinan M, Rosenberg R, Zohar D, Rosen V, Fine P (2004) Nitrogen, phosphorus, and potassium uptake by wheat and their distribution in soil following successive annual compost applications. J Environ Qual 33:1855–1865
7. Bown SR (2007) A most damnable invention. Dynamite, nitrates and the making of the modern world. Penguin, London
8. Tisdale SL, Nelson WL, Beaton JD, Havlin JL (1993) Soil fertility and fertilizers. Macmillan, New York
9. World Bank (2008) Agriculture for development. World Bank, Washington, DC
10. Sanchez PA (2002) Soil fertility and hunger in Africa. Science 295:2019–2020
11. Angus JF, Fazekas de St. Groth C, Tasic RC (1990) Between-farm variability in yield response to inputs of fertilizers and herbicide applied to rainfed lowland rice. Agric Ecosyst Environ 39:219–234
12. Angus JF, Marquez DA, Tasic RC (2004) Diagnosing variable nutrient deficiencies in rainfed lowland rice using strip trials. In: Fourth international crop science congress, Brisbane. http://www.cropscience.org.au/icsc2004/poster/4/1/2/678_angusjf.htm
13. www.icis.com
14. Freney JR (1997) Strategies to reduce gaseous emissions of nitrogen from irrigated agriculture. Nutr Cycl Agroecosyst 48:155–160
15. Peoples MB, Freney JR, Mosier AR (1995) Minimizing gaseous losses of nitrogen. In: Bacon PE (ed) Nitrogen fertilization in the environment. Marcel Dekker, New York, pp 565–602
16. Martens DA, Bremner JM (1997) Inhibitory effects of fungicides on hydrolysis of urea and nitrification of urea nitrogen in soil. Pesticide Sci 49:344–352
17. Chen D, Freney JR, Rochester I, Constable GA, Mosier AR, Chalk PM (2007) Evaluation of a polyolefin coated urea

(Meister) as a fertilizer for irrigated cotton. Nutr Cycl Agroecosyst 81:245–254
18. Angus JF (2001) Nitrogen supply and demand in Australian agriculture. Aust J Exp Agric 41:277–288
19. Cottrell R (1987) The sacred cow: the folly of Europe's food mountains. Grafton, London
20. Addiscott TM (2005) Nitrate, agriculture and the environment. CABI, Wallingford
21. Mengel K, Kirkby EA (2001) Principles of plant nutrition. Kluwer, Dordrecht
22. Cakmak I, Yilmaz A, Kalayci M, Ekiz H, Torun B, Erenoglu B, Braun HJ (1996) Zinc deficiency as a critical problem in wheat production in central Anatolia. Plant Soil 180:165–172
23. Alloway BJ (2004) Zinc in soils and plant nutrition. International Zinc Association, Brussels, http://www.zinc-crops.org/library_general_zni_publications.html
24. Russell CA, Dunn BW, Batten GD, Williams RL, Angus JF (2006) Soil tests to predict the response of rice to fertiliser nitrogen. Field Crops Res 9:286–301
25. Webster R, Oliver MA (2007) Geostatistics for environmental scientists. Wiley, Chichester
26. Myers RJK (1984) A simple model for estimating the nitrogen fertilizer requirement of a cereal crop. Fertilizer Res 5:95–108
27. Angus JF (1995) Modelling N fertilization requirements for crops and pastures. In: Bacon PE (ed) Nitrogen fertilization and the environment. Marcel Dekker, New York, pp 109–127
28. Sinclair TR, Park WI (1993) Inadequacy of the Liebig limiting-factor paradigm for explaining varying crop yields. Agron J 85:742–746
29. van Herwaarden AF, Farquhar GD, Angus JF, Richards RA, Howe GN (1998) 'Haying-off', the negative grain yield response of dryland wheat to nitrogen fertiliser. I. Biomass, grain yield and water use. Aust J Agric Res 49:1067–1081
30. Ellen J, Spiertz JHJ (1980) Effects of rate and timing of nitrogen dressings on grain yield formation of winter wheat (*T. aestivum* L.). Fertilizer Res 1:177–190
31. Angus JF, Fischer RA (1991) Grain and protein responses to nitrogen applied to wheat growing on a red earth. Aust J Agric Res 42:735–746
32. De Datta SK (1987) Advances in soil fertility research and nitrogen management for lowland rice. In: Efficiency of nitrogen fertilizers for rice. International Rice Research Institute, Los Baños, pp 27–41
33. Fujisaka S (1993) Were farmers wrong in rejecting a recommendation? The case of nitrogen at transplanting for irrigated rice. Agric Syst 43:271–286
34. Peng S, Cassman KG (1998) Upper thresholds of nitrogen uptake rates and associated N fertilizer efficiencies in irrigated rice. Agron J 90:178–185
35. Mi G, Tang L, Zhang F (2000) Is nitrogen uptake after anthesis in wheat regulated by sink size? Field Crops Res 68:183–190
36. Good AG, Johnson SJ, De Pauw M, Carroll RT, Savidov N, Vidmar J, Lu Z, Taylor G, Stroeher V (2007) Engineering nitrogen use efficiency with alanine aminotransferase. Can J Bot 85:252–262
37. Ju X, Liu X, Zhang F, Roelcke M (2004) Nitrogen fertilization, soil nitrate accumulation, and policy recommendations in several agricultural regions of China. Ambio 33:300–305
38. Mitsch WJ, Day JW Jr, Gillliam JW, Groffman PM, Hey DL, Wang N (2001) Reducing nitrogen loading to the Gulf of Mexico from the Mississippi River Basin: strategies to counter a persistent ecological problem. Bioscience 51:373–388
39. van der Ploeg JD (1994) Styles of farming: an introductory note on concepts and methodology. In: van der Ploeg JD, Long A (eds) Born from within: practices and perspectives of endogenous rural development. van Gorcum, Assen, pp 7–30
40. Fischer RA, Byerlee D, Edmeades GO (2009) Can technology deliver on the yield challenge to 2050? FAO, Rome, ftp://ftp.fao.org/docrep/fao/012/ak977e/ak977e00.pdf
41. van Raij B, Quaggio JA, da Silva NM (1986) Extraction of phosphorus, potassium, calcium, and magnesium from soils by an ion-exchange resin procedure. Commun Soil Sci Plant Anal 17:547–566
42. Holloway RE, Bertrand I, Frischke AJ, Brace DM, McLaughlin MJ, Shepperd W (2001) Improving fertilizer efficiency on calcareous and alkaline soils with fluid sources of P, N and Zn. Plant Soil 236:209–219
43. Cornish PS (1987) Effects of direct drilling on the phosphorus uptake and fertilizer requirements of wheat. Aust J Agric Res 38:775–790
44. Sillanpäa M (1990) Micronutrient assessment at the country level: an international study. FAO, Rome
45. Ryan MH, McInerney JK, Record IR, Angus JF (2008) Zinc bioavailability in wheat grain in relation to phosphorus fertilizer, crop sequence and mycorrhizal fungi. J Sci Food Agric 88:1208–1216
46. McCown RL (2002) Changing systems for reporting farmers' decisions: problems, paradigms and prospects. Agric Syst 74:179–220
47. McBratney A, Whelan B, Ancev T, Bouma J (2005) Future directions of precision agriculture. Precision Agric 6:7–23
48. Blackmer AM, White SE (1997) Using precision farming technologies to improve management of soil and fertiliser nitrogen. Aust J Agric Res 49:555–564
49. Angus JF, Norton RM, Pedler JF, Walker CN (2004) Cereal response to N fertiliser in relation to subsoil limitations. In: Proceedings of the fourth international crop science congress, Brisbane. http://www.cropscience.org.au/icsc2004/poster/2/5/1/1170_angusjf.htm
50. Wong MTF, Asseng S (2006) Determining the causes of spatial and temporal variability of wheat yields at sub-field scale using a new method of upscaling a crop model. Plant Soil 283:203–215
51. Sudduth KA, Kitchen NR, Bollero GA, Bullock DG, Wiebold WJ (2003) Comparison of electromagnetic induction and direct sensing of soil electrical conductivity. Agron J 95:472–482
52. Raun WR, Solie JB, Taylor RK, Arnall DB, Mack CJ, Edmonds DE (2008) Ramp calibration strip technology for determining midseason nitrogen rates in corn and wheat. Agron J 100:1088–1093

53. Reusch S, Link A, Lammel J (2002) Tractor-mounted multispectral scanner for remote field investigation. In: Roberts PC (ed) Sixth international conference on precision agriculture. ASA/CSSA/SSSA, Madison, pp 1385–1393
54. Li Y, Chen D, Walker CN, Angus JF (2010) Estimating the nitrogen status of crops using a digital camera. Field Crops Res 118:221–227
55. Kirchmann H, Bergström L (eds) (2008) Organic crop production – ambitions and limitations. Springer, Heidelberg
56. Fagerberg B, Salomon E, Jonsson S (1996) Comparisons between conventional and ecological farming systems at Örjebyn. Nutrient flows and balance. Swed J Agric Res 26:169–180
57. Edmeades DC (2002) The effects of liquid fertilisers derived from natural products on crop, pasture, and animal production: a review. Aust J Agric Res 53:965–976
58. Edmeades DC (2002) Science friction. The Maxicrop case and the aftermath. Fertiliser Information Services, Hamilton
59. Williams CH, Donald CM (1957) Changes in organic matter and pH in a podzolic soil as influenced by subterranean clover and superphosphate. Aust J Agric Res 8:179–189
60. Johansson G, Gustafson A (2004) Discharge and nutrient losses for the agrohydrological year 2002/03 and a long-term review. Swedish University of Agricultural Sciences, Division of Water Quality Management, Uppsala
61. Goolsby DA, Battaglin WA, Lawrence GB, Artz RS, Aulenbach BT, Hooper RP, Keeney DR, Stensland GJ (1999) Flux and sources of nutrients in the Mississippi-Atchafalaya River Basin. NOAA Coastal Ocean Program, Silver Spring, Maryland
62. Wulff FV, Rahm LA, Larsson P (2001) A systems analysis of the Baltic Sea. Springer, Berlin
63. Duan S, Zhang S, Huang H (2000) Transport of dissolved inorganic nitrogen from the major rivers to estuaries in China. Nutr Cycl Agroecosyst 57:13–22
64. Snyder CS (2008) Nutrients and hypoxia in the Gulf of Mexico – an update on progress, 2008. Better Crops 92:16–22
65. Ondersteijn CJM, Beldman ACG, Daatselaar CHG, Giesen GWJ, Huiurne RBM (2002) The Dutch mineral accounting system and the European nitrate directive: implications of N and P management and farm performance agriculture. Ecosyst Environ 92:283–296
66. Wright S, Mallia C (2003) The potential for eco-taxes as instruments of sustainability. J Transdiscipl Environ Stud 2:1–14, www.journal-tes.dk
67. Sutton MA, Howard CM, Erisman JW, Billen G, Bleeker A, Grennfelt P, van Grinsven H, Grizzetti B (2011) The European nitrogen assessment. Cambridge University Press
68. Norton JM (2008) Nitrification in agricultural soils. In: Scheppers JS, Raun WR (eds) Nitrogen in agricultural systems. ASA/CSSA/SSSA, Madison, pp 173–199
69. Coyne MS (2008) Biological denitrification. In: Scheppers JS, Raun WR (eds) Nitrogen in agricultural systems. ASA/CSSA/SSSA, Madison, pp 201–253
70. Khan SA, Mulvaney RL, Ellsworth TR, Boast CW (2007) The myth of nitrogen fertilization for soil carbon sequestration. J Environ Qual 36:1821–1832
71. Mulvaney RL, Khan SA, Ellsworth TR (2009) Synthetic nitrogen fertilizers deplete soil nitrogen: a global dilemma for sustainable cereal production. J Environ Qual 38:2295–2314
72. Reid DK (2008) Comment on "The myth of nitrogen fertilization for soil carbon sequestration". J Environ Qual 37:739
73. Powlson DS, Jenkinson DS, Johnston AE, Poulton PR, Glendining MJ, Goulding KWT (2010) Comments on "Synthetic nitrogen fertilizers deplete soil nitrogen: A global dilemma for sustainable cereal production". J Environ Qual 39:749–752
74. Kirkby CA, Kirkegaard JA, Richardson AE, Wade LJ, Blanchard C, Batten G (2011) Stable soil organic matter: a comparison of C:N:P:S ratios in Australian and other world soils. Geoderma 163:197–208
75. Mulvaney RL, Khan SA, Ellsworth TR (2010) Reply to comments on "Synthetic nitrogen fertilizers deplete soil nitrogen: A global dilemma for sustainable cereal production". J Environ Qual 39:753–756
76. Likens GE, Bormann FH (1974) Linkages between terrestrial and aquatic ecosystems. Bioscience 24:447–456
77. Boon KF, Kiefert L, McTainsh GH (1998) Organic matter content of rural dusts in Australia. Atmos Environ 32: 2817–2823
78. Tilman D, Cassman KG, Matson PA, Naylor R, Polasky S (2002) Agricultural sustainability and intensive production practices. Nature 418:671–677
79. McLaughlin MJ, Tiller KG, Naidu R, Stevens DP (1996) Review: the behaviour and environmental impact of contaminants in fertilizers. Aust J Soil Res 34:1–54
80. Lægreid M, Bøckman OC, Kaarstad O (1999) Agriculture, fertilizers and the environment. CABI, Cambridge
81. WHO (2002) World health report. World Health Organization, Geneva, www.who.int/whr/2002
82. Cordell D, Drangert J-O, White S (2009) The story of phosphorus: global food security and food for thought. Glob Environ Change 19:292–305
83. Cornish P (2010) A postscript to "peak P" - an agronomist's response to diminishing P reserves. Proc. 15th Australian Agronomy Conference. www.regional.org.au/au/pdf/asa/2010/7452_cornish.pdf
84. http://phosphorusfutures.net/
85. Alston JM, Andersen MA, James JS, Pardey PG (2010) Persistence pays: U.S. agricultural productivity growth and the benefits from public R&D spending. Springer, New York

Books and Reviews

Bacon PE (ed) (1995) Nitrogen fertilization in the environment. Marcel Dekker, New York

Hatfield JR (ed) (2005) The farmer's decision. Soil and Water Conservation Society, Ankeny

Marschner H (1995) Mineral nutrition of higher plants. Academic, London

Mosier AR, Syers JK, Freney JR (eds) (2004) Agriculture and the nitrogen cycle. Island Press, Washington

Fission Reactor Physics

Michael Natelson
Retired from the Bettis Atomic Power Laboratory, West Mifflin, PA, USA

Article Outline

Glossary
Definition of Subject
Introduction
Mass–Energy Relationship
Heavy Elements
Fission and Its Products
Cross Sections
Neutron Distributions
Fission Reactor Performance
Future Directions
Bibliography

Glossary

Fissile Fissile isotopes are fissionable by the capture of neutrons of any energy, but are especially easily fissioned by the capture of slow neutrons, for example, U^{233}, U^{235}, Pu^{239}, and Pu^{241}.

Fertile Fertile isotopes may be transmuted into fissile isotopes by neutron capture. The naturally occurring fertile isotopes are Th^{232} and U^{238}.

Critical A critical fission reactor is in a steady state, with its neutron population sustained by a chain reaction.

Reactivity Reactivity is a dimensionless parameter, which characterizes how far from critical a fission reactor is. If zero, the reactor is critical; if positive, the reactor is supercritical and its neutron population is increasing; if negative, the reactor is subcritical.

Microscopic cross section A microscopic cross section is a parameter, with dimensions of area, that is a measure of the probability of a particular reaction resulting from an incident particle on a target nucleus. The *macroscopic cross section* for this "particular" reaction is the microscopic cross section times the number density of the target nucleus.

Definition of Subject

At the end of the nineteenth century and through the first half of the twentieth century, revolutionary discoveries were made in physics, and the laws of physics and our understanding of them were greatly expanded. In addition, tragic historical events led to an unprecedented concentration of intellectual talent and economic resources (the Manhattan Project) that allowed the new physics to be applied to the engineering of nuclear (fission) reactors. This entry will describe the advances in physics, which are key to fission reactor design, and how they enable this engineering practice.

Introduction

In 1900, Lord Kelvin (William Thomson) reportedly told the British Association for the Advancement of Science that "there is nothing new to be discovered in physics now. All that remains is more and more precise measurements." Whether he actually said this or not, it is reasonable to believe that many scientists and engineers of his day would have concurred. Newton's definitions and laws of mechanics and optics had long been successfully applied. Maxwell's equations, Ohm's law, etc. seemed to describe electricity and magnetism. Boltzmann and Gibbs had provided the foundations of statistical mechanics and thermodynamics. And chemists had been busy developing atomic theory, identifying 92 elements, the laws of chemical combination, the weights and sizes of atoms and molecules, and the periodic system.

With hindsight it is clear, however, that in 1900 there were many intriguing questions outstanding in the physical sciences, and there was an historically large cohort of scientists, being produced by the major universities of the day, ready to address them. The questions (and their resolutions) of prime importance to "fission reactor physics" are:

1. Does a theory of relativity apply to Maxwell's equations, and is there a unique frame of reference (ether) for the propagation of light?
2. Why are the heaviest naturally occurring elements unstable, giving off various forms of "radiation" and transmuting to different elements?
3. What does the quantization of electromagnetic radiation (required to describe black body

radiation energy spectra and the photoelectric effect) mean to the laws of physics on the atomic scale?

The resolution of each of these questions will be discussed in this entry, as they are the starting points for the accumulation of knowledge needed to characterize the workings of fission reactors.

Clearly, Einstein's Theory of Relativity addressing question (1), and its identification of mass as a form of energy (1905) would, excuse the bad pun, energize the whole effort. Already in 1914, H. G. Wells in his novel "The World Set Free" envisioned industrial atomic energy and atomic bombs used in a catastrophic world war.

At the end of the nineteenth century, electrochemists looking for heavy elements (heavier than lead and bismuth) found that "radiation" was given off by the materials they were investigating. Becqueral (1896) observed γ rays (penetrating electromagnetic radiation similar to x-rays) from uranium salts. The Curies (1898) observed α and β rays from polonium and radium. Rutherford showed that the positively charged αs were doubly ionized helium atoms. The βs are negatively charged electrons, the same particles as the cathode rays that Thomson characterized and named (1897). These "radiations" proved to be key tools for determining the structure of atoms. The α particle was shown by Rutherford (1911) and his coworkers to scatter from gold foil in a manner inconsistent with the atomic model of the day, Thomson's *raisins* (electrons) *in the pudding* (positive charge medium) model. To explain the α scattering results, an atom's positive charge and its mass, minus that of its electrons, needed to be concentrated in a small nucleus (radius $\sim 10^{-12}$ cm), with its electrons distributed over a much larger volume (radius $\sim 10^{-8}$ cm), that of the whole atom. Niels Bohr, inspired by Rutherford's work, took to determining the *distribution* of atomic electrons. His success, building off Question (3) above, led to quantum mechanics. A complete model for the atom, however, still required an explanation for the mass of the nucleus. Again bombardment of various atoms (elements) with α particles led to the answer. Chadwick (1932) proved that the "rays" produced by αs striking beryllium nuclei were neutral particles with mass slightly greater than the hydrogen nucleus, the proton. These neutral particles are the neutrons that had been hypothesized by Rutherford 12 years earlier. Heisenberg (1932) produced a detailed model of the atomic nucleus where the mass number A is the total number of elementary particles, protons plus neutrons, making up a nucleus, and the nuclear charge is Z, the number of protons. Thus, there can be various *isotopes* for a given element, more than one A for a given Z.

The discovery of the neutron marked the start of furious activity, culminating in the operation of the first fission reactor only 10 years later. Leo Szilard in 1933 recognized that a neutral neutron with modest kinetic energy could penetrate an atomic nucleus and cause a reaction releasing nuclear (mass) energy, and if, as part of the "reaction," additional neutrons were produced, a chain reaction could result. Szilard produced a patent for a reactor based on this idea and assigned it to the British Government in 1936 (before fission was discovered). In 1934, Fermi was using neutron bombardment (with neutrons of various energies) to produce nuclear transformations in many elements. Of special interest was the production of transuranic elements, Z greater than 92. Fermi won the 1938 Nobel Prize for this work. However, unknown at the time, he had also fissioned uranium. This was determined by electrochemical analysis of the products of neutron bombardment of uranium by Hahn and Strassmann. Subsequently, the process was identified as *fission* by Meitner and Frisch. Bohr recognized that the ease with which low energy neutrons could cause fission of uranium was due to the existence of the naturally occurring, but low atom percent (0.72%), isotope ${}_{92}U^{235}$ [1] (Various notations have been used to designate a particular isotope, for example, for uranium with mass number (A) 235; ${}_{92}U^{235}$, U235, and ${}^{235}_{92}U$. The latter is in common use today. For ease of composition and for consistency with most of the references used in this entry the older standard, A as a right superscript, is used.). He and Wheeler, from their Theory of Fission [2], also recognized that the not yet produced isotope ${}_{94}Pu^{239}$, would also be readily fissioned by slow neutrons [3]. This was in early 1939. Bohr still did not think production of a fission bomb to be feasible.

Leo Szilard was, however, not deterred. He persuaded his friend Albert Einstein to write President

Roosevelt (8/2/1939), urging government support of fission research and the stock piling of uranium. This ultimately led to the Manhattan Project. In 1940, Seaborg and McMillan synthesized the readily fissionable isotope of plutonium, $_{94}Pu^{239}$, which is produced by neutron capture in the dominant uranium isotope $_{92}U^{238}$. Wheeler credited Louis Turner [3] with pointing out that kilogram quantities of $_{94}Pu^{239}$ could be produced in a large fission chain reaction reactor. Fermi and Szilard [4] designed and built the prototype for such a reactor, a "pile" of graphite blocks containing an array of natural uranium pellets. It was constructed in a squash court under a grand stand of the University of Chicago's Stagg Field, and went *critical* (sustained a chain reaction) on December 2, 1942. The Manhattan Project built large reactors of this type for weapons material production, and also successfully pursued means of enriching uranium in $_{92}U^{235}$. Enriched uranium allows more compact, higher power density, reactor designs.

The Manhattan Project brought together extraordinary scientific and engineering talent, and immense resources to produce the weapons that ended the Second World War. It also provided the foundation for all fission reactor development that has followed. The subsequent advances in "physics," which have contributed to this development, are principally:

1. The full understanding of the interaction of neutrons with nuclei: scattering (elastic and inelastic), and capture (simple absorption, transmutation, and fission), including measuring the parameters that characterize the probabilities of these "interactions"
2. The formulation of methods to solve the neutron transport (Boltzmann) equation, which governs the behavior of the dilute "gas" of neutrons in a fission reactor

This entry will discuss the topics, pre- and post-Manhattan Project, which encompass the physics of fission reactors.

Mass–Energy Relationship

In his initial paper [5] on the theory of relativity, Einstein confronted the problem of guaranteeing that the laws of electromagnetism (Maxwell's equations) apply in all inertial reference frames, just as the laws of mechanics do. In an inertial reference frame, an object, which is at rest, remains at rest and an object traveling with a particular velocity will maintain that velocity. Einstein asserted that there is no preferred reference frame (like stationary *ether* in space, as postulated years earlier), and that the speed of light c, in vacuum, 2.998×10^8 m/s, is the same in all inertial reference frames. From these assertions, Einstein derived transformations for various variables in the laws of physics from one inertial reference frame to another. This solved the "electromagnetism" problem and provided a firm grounding (theory) for phenomena observed when velocities approach the speed of light. For examples of the latter, see Kaplan, "Nuclear Physics" on the charge-to-mass ratio of the electron as a function velocity, and Mermin, "It's About Time," on the half-life of unstable particles as a function of their velocity. Our interest here is specifically on the relationship between mass and energy resulting from the special (not applying to gravity) theory of relativity. What is meant by the ubiquitous formula.

$$E = Mc^2? \tag{1}$$

For application to fission, an inelastic collision between two particles will be treated for relativistic conditions. The approach presented by Mermin in "It's About Time" will be used.

In an elastic collision, total momentum, $\mathbf{P} = \mathbf{p_1} + \mathbf{p_2}$, mass, $M = m_1 + m_2$, and kinetic energy, $K = k_1 + k_2$ are all conserved, where the mass, m, is an inherent property of a particle and is a measure of how it resists a change in its velocity. In an inelastic collision, only total momentum, **P** needs to be conserved. It needs to be conserved, however, in all inertial frames of reference. For relativistic conditions, one defines a particle's momentum (a vector [in bold face]) as

$$\mathbf{p} = m\mathbf{u}/(1 - \mathbf{u}^2/c^2)^{1/2}, \tag{2}$$

where **u** is the particle velocity. As is required for consistency between relativistic and nonrelativistic laws of mechanics, Eq. 2 is effectively the nonrelativistic definition of momentum for the particle speed, $u << c$. Now to find $\mathbf{p}'$, the particle momentum, in

a frame moving with velocity **v** relative to the frame in which the particle has velocity **u**, one applies the relativistic translation law for velocities:

$$\mathbf{u}' = (\mathbf{u} - \mathbf{v})/(1 - \mathbf{uv}/c^2). \tag{3}$$

Substituting for $\mathbf{u}'$ in the expression for $\mathbf{p}'$ (Eq. 2 with **p** and **u** primed), one obtains the relativistic translation law for momentum

$$\mathbf{p}' = (\mathbf{p} - p^0\mathbf{v})/(1 - \mathbf{v}^2/c^2)^{1/2}, \tag{4}$$

where

$$p^0 = m/(1 - \mathbf{u}^2/c^2)^{1/2}. \tag{5}$$

Now, if total momentum is to be conserved in our two-particle inelastic collision in both the primed and unprimed frames, then $P^0 = p^0{}_1 + p^0{}_2$ must also be conserved. Again, using the relativistic translation law for velocities (Eq. 3) and the definition p^0 (Eq. 5), we find that

$$p^{0'} = (p^0 - \mathbf{pv}/c^2)/(1 - \mathbf{v}^2/c^2)^{1/2}. \tag{6}$$

And so for the *total* quantities we want to be conserved we have

$$\mathbf{P}' = (\mathbf{P} - P^0\mathbf{v})/(1 - \mathbf{v}^2/c^2)^{1/2} \quad \text{and} \tag{7}$$

$$P^{0'} = (P^0 - \mathbf{Pv}/c^2)/(1 - \mathbf{v}^2/c^2)^{1/2}. \tag{8}$$

Examining these expressions, it is clear that if **P** and P^0 are not changed after an inelastic (or elastic) collision, then neither is $\mathbf{P}'$ and $P^{0'}$.

In the limit of the speed u being much smaller than c, the difference between p^0 and m, $(p^0 - m)$, approaches $mu^2/2c^2$. This result leads to a definition of relativistic kinetic energy, k, for a particle

$$k = p^0c^2 - mc^2, \tag{9}$$

which has the required property of reducing to the nonrelativistic form, $mu^2/2$, in the limit of u much smaller than c.

Returning to our two-particle inelastic collision, as **P** is conserved so is P^0c^2 and thus from Eq. 9

$$\Delta Mc^2 = \Delta K, \tag{10}$$

where ΔM is the change in the masses of the inputs and outputs of the collision participants, and ΔK is the change in the kinetic energies of these "inputs and outputs." Thus, Eq. 10 provides insight into the meaning of "$E = Mc^2$" for the fission process. For n + ${}_{92}U^{235}$ ↦ fission products + 202.7 MeV (the ΔK of Eq. 10 in unit of millions of electron volts) the percent change in mass can be estimated by dividing 202.7 MeV by the energy equivalents of the inputs (i.e., 236 amu, where 1 amu = 931.141 MeV). The result is ~0.1%, which may not appear to be large until one makes a comparison with a chemical reaction. For example, $O_2 + C \rightarrow CO_2$ + 4.1 eV. A similar calculation indicates a 1×10^{-8}% conversion of mass to kinetic energy. Since one could not measure such a small change in total input and output masses in chemical reactants, it is not surprising that the full impact of "$E = Mc^2$" had to await demonstration in a nuclear reaction like fission. However, as will be discussed in the next three sections, the large energy release in fission, while conforming to Eq. 10, is due to the strength of the forces that hold a nucleus together and the charge repulsion forces that will accelerate two smaller nuclei as they are formed in the fissioning of a larger "parent" nucleus.

Heavy Elements

The "heavy elements" of particular importance to fission reactors are the radioactive nuclei, which are characterized by systematic chains of decay. In nature, there are three chains (series). In a given series, each nucleus has a *mass number*, A, governed by a simple formula with the variable the integer n (see Table 1), and is identified with its longest lived isotope, that is, Thorium, Uranium, and Actinium (U^{235} had not been discovered when the 4n + 3 series was identified). These *longest half-lives* are not surprisingly comparable to the age of the earth, 4.5×10^9 years. Half-life is one of three related parameters of radioactive decay processes, $T_{1/2}$, λ, and τ. The fundamental equation of radioactive decay is

$$-dN(t)/dt = \lambda N(t), \tag{11}$$

where λ is the *decay constant*, and N(t) is the number of decaying nuclei at time t. The solution of Eq. 11 is

$$N(t) = N(0)e^{-\lambda t}. \tag{12}$$

The time when an original inventory of decaying nuclei, N(0), is halved is

$$T_{1/2} = \ln 2/\lambda = 0.693/\lambda. \quad (13)$$

And as the decay process is statistical the *mean lifetime*, τ, of a decaying nucleus is

$$\tau = (1/N(0)) \int_0^\infty N(0)\lambda t e^{-\lambda t}\, dt = 1/\lambda, \quad (14)$$

the reciprocal of the decay constant.

With the search for transuranic elements through the bombardment of the heaviest natural elements, primarily with neutrons, a fourth decay series was identified, the Neptunium (A = 4n + 1) series whose radioactive members are not found in *nature* (see Table 1).

Of the "heavy elements," the isotope U^{235} is key to fission reactor design. It is the only naturally occurring isotope which readily fissions when bombarded with neutrons of all energies. While its atomic percent abundance, 0.72%, is small, it is large enough to support chain reactions in reactors where neutrons born in fission are slowed down (moderated) by graphite (carbon) or by heavy water (deuterium oxide). When Uranium is enriched in U^{235} (~3–5%), it can fuel reactor designs where ordinary water moderates fission neutrons (today's pressurized water and boiling water reactors). Having U^{235} available as a reactor fuel makes it possible to exploit the two abundant *fertile* "heavy elements," U^{238} and Th^{232}. The term "fertile" refers to the fact that when these elements absorb a neutron they can be transmuted to *fissile* isotopes (Pu^{239} and U^{233} respectively), which like U^{235} readily fission when bombarded by neutrons of all energies. The transmutation processes are shown in Fig. 1. It is important to note that only one neutron capture is required in each of these transmutations. In a reactor design, neutron economy is the key to maintain a chain reaction and, as will be discussed in the section on Future Directions, expending one neutron with a reasonable probability of obtaining an additional fissile nucleus is a winner.

The heavy element radioactive decay series are also important to safety in fission reactor design. Each of the decay processes, α and β^- emissions and associated γs, is favorable to energy release. So any heavy elements, particularly transuranics, in a reactor's fuel system will contribute to the *decay heat* load that must be dissipated when a reactor shuts down. As will be discussed in the next section, the major short-term contributors to decay heat are *fission products*. A power reactor that shuts down following a sustained run at full rating will initially produce ~7% of that rating from decay heat, even if the chain reaction and nearly all fissioning has ceased.

For a full discussion of the radioactive decay series and the particulars of α, β^-, β^+ and γ emission, see Kaplan, and Krane, "Introductory Nuclear Physics."

Fission and Its Products

As noted in the "Introduction," fission was discovered accidentally during the search for transuranic elements. This work by Fermi and others was part of an extensive effort to understand the atomic nucleus and to duplicate the great success of quantum mechanics and the Pauli exclusion principle in providing a fully predictive *Theory* of atomic electron structure. A comparable theory for the nucleus has not been developed, but several models (e.g., shell and liquid drop) provide insight into the trends and correlations found in the data provided by the extensive experimentation performed on the nuclei of the various elements and their isotopes.

Fission Reactor Physics. Table 1 Heavy element decay series

Series name	Type	Final stable nucleus	Longest lived nucleus	Longest half-life (years)
Thorium	4n[a]	Pb^{208}	Th^{232}	1.41×10^{10}
Uranium	4n + 2	Pb^{206}	U^{238}	4.47×10^{9}
Actinium	4n + 3	Pb^{207}	U^{235}	7.04×10^{8}
Neptunium, not in *nature*	4n + 1	Bi^{209}	Np^{237}	2.14×10^{6}

[a]n is an integer

Measurements of atomic mass ($m(X^A)$), and the mass of the electron, proton, and neutron, yields the *binding energy*, B, of a nucleus, ${}_ZX^A$, the work (energy) required to disassemble a nucleus into its neutrons and protons:

$$B = \left\{Zm_p + Nm_n - \left(m(X^A) - Zm_e\right)\right\}c^2, \qquad (15)$$

where Z is the atomic number (the number of protons) and N = A – Z is the number on neutrons. (The binding energy of atomic electrons is ignored as negligible compared to the other factors in Eq. 15.)

Plotting the ratio of measured binding energies B to corresponding mass number A (Fig. 2) immediately makes evident the potential of energy release from fission of heavy element. Note the B/A versus A "curve" has a flat maximum in the middling A range ~50 → ~150, and falls off (decreases) as A increases. Thus, there is a potential energy excess if a heavy element (isotope) can be disassembled and reassembled as two mid-range isotopes (preserving total A, Z, and N). (The behavior of the B/A curve for light elements shows the potential energy release from fusion.) Obviously fission (nor fusion) does not take occur "naturally" on earth today (There is convincing evidence that a naturally occurring chain reaction took place in a uranium deposit in Gabon about 2×10^9 years ago, when the abundance of U^{235} would have been ~3%, high enough for a water-moderated "reactor" to operate. The higher earlier abundance is due to the shorter half-life of U^{235} (7.0×10^8 y) relative to that of U^{238} (4.4×10^9 y). See Krane for an excellent

$$U^{238} + n \rightarrow U^{239} \xrightarrow{23\ \mathrm{min}} Np^{239} + \beta^- + \bar{\nu}$$
$$\searrow\ 2.3d \rightarrow Pu^{239} + \beta^- + \bar{\nu}$$
$$Th^{232} + n \rightarrow Th^{233} \xrightarrow{22\ \mathrm{min}} Pa^{233} + \beta^- + \bar{\nu}$$
$$\searrow\ 27d \rightarrow U^{233} + \beta^- + \bar{\nu}$$

Fission Reactor Physics. Figure 1
Transmutation of fertile to fissile nuclei. ($\bar{\nu}$ is the antineutrino, the chargeless, ~zero mass particle that accompanies $\bar{\beta}$ emission)

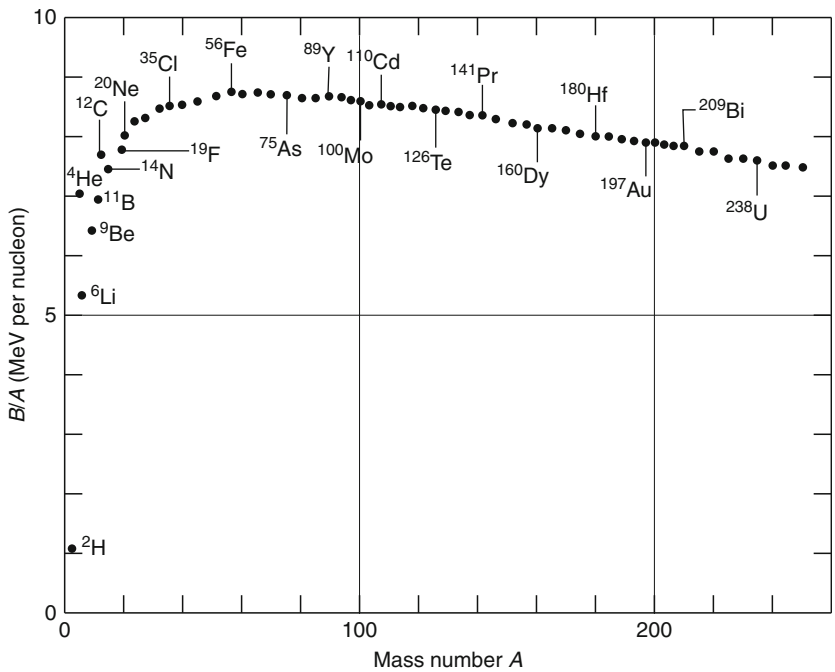

Fission Reactor Physics. Figure 2
Binding energy per nucleon (Krane)

discussion of the Gabon reactor). The remainder of this section is devoted to particular requirements for fission to take place and to the discussion of the resulting fission products and their energies.

Insights provided by examining binding energies, and by additional experiments to determine nucleon–nucleon forces have led to the Shell and Liquid Drop models of the nucleus. Features of these models are incorporated in the *semiempirical mass formula* (Eq. 16). While a thorough discussion of the nuclear models is beyond the scope of this entry (see Kaplan or Krane), the mass formula provides key information on fission, energy release, and the relative likelihood for various nuclei.

In the semiempirical mass formula, the binding energy has five terms, which will be discussed below.

$$m\left({}_{Z}X^{A}\right) = Zm_p + Nm_n - [B_0 + B_1 + B_2 + B_3 + B_4]/c^2. \quad (16)$$

$B_0 = a_vA$ is the volume energy. Note in Fig. 2 that B/A saturates, thus B_0 has a linear dependence on A. The attractive nuclear forces between nucleons (n–n, n–p and p–p) are all equal and short range, smaller than the radius of the nucleus, $r = r_0A^{1/3}$ where $r_0 \sim 1.2 \times 10^{-12}$ cm. If the range were larger, there would be attraction between each nucleon pair and B_0 would depend on A(A – 1).

$B_1 = -a_sA^{2/3}$, is the negative surface decrement. As the nucleon–nucleon forces are "short range," neutrons and protons on the surface of a nucleus are less tightly bound.

$B_2 = -a_cZ(Z-1)/A^{1/3}$, is the coulomb repulsion decrement. While the nuclear forces are strong enough to overcome coulomb forces, the protons in the nucleus do repel and reduce binding energy. Assuming a uniform distribution of protons in a liquid drop model of a spherical nucleus, an electrostatics calculation yields the dependence of B_2 the number of proton pair, Z(Z−1), and a measure of their spacing, $A^{1/3}$.

$B_3 = -a_a|N-Z||N-Z|/A$, is the neutron–proton population asymmetry decrement. As nuclei become heavier, more neutrons than protons are needed to overcome coulomb repulsion. However, as the shell model of the nucleus demonstrates when nucleons, neutrons and/or protons, are added to form heavier elements and their isotopes, they fill *shells* of successively higher energy and are thus less tightly bound. This is analogous to the case of atomic electrons. Neutrons and protons have half-integral spin like the electrons, and therefore no two neutrons (or protons) can occupy the same state in a nucleus in conformance with the Pauli exclusion principle. So B_3 is negative and proportional to the neutron excess and the fraction of the nucleus the excess represents.

$B_4 = +\delta A^{-3/4}$ for even Z even N nuclei, = 0 for odd A nuclei, $= -\delta A^{-3/4}$ for odd Z odd N nuclei, is the pairing energy. As nucleons are added and fill *shells*, they are more tightly bound as spin up and spin down pairs. B_4 is important in determining the relative binding of isotopes of a given element and their propensity to fission.

A set of parameters for B which best fit the B/A curve (Fig. 2) is provided by Krane; a_v = 15.5 MeV, a_s = 16.8 MeV, a_c = 0.72 MeV, a_a = 23 MeV, and δ = 34 MeV.

The potential for, and magnitude of, energy release from fission, whether as spontaneous decay or induced by particle or gamma ray capture, can be assessed with the semiempirical mass formula. As for an estimate of the magnitude of energy release, the B/A curve, as noted earlier, can be used directly. For example, the B/A for U^{238} is ~7.6 MeV. If it fissioned into two approximately equal mass nuclei (A = 119), their B/A would be ~8.5 MeV when in a ground state, and being more tightly bound than their parent (U^{238}) 214 MeV (= 2 × 119 × 8.5 − 238 × 7.6) will be available through conservation of energy as kinetic energy of the daughter nuclei and of other fission products (neutrons, βs, γs, and neutrinos). That this energy is *available* does not mean that there is a significant probability that fission occurs. In this example, which represents spontaneous fission of U^{238}, one finds in nature that this mode of U^{238} decay competes poorly with α decay (Spontaneous fission is a significant mode of decay for some transuranic isotopes found in depleted reactor fuel, particularly Pu^{240} and Pu^{241}.). For fission fragments, daughter nuclei, to separate in spontaneous or induced fission, a potential barrier must be overcome. The height of the barrier relative to the ground state of a fission parent nucleus is called the *fission activation energy* (E_a). It can be estimated with the liquid drop model by calculating the change in the parent nucleus binding energy (B_1 and B_2) between

Fission Reactor Physics. Table 2 Heavy nuclei fission

Target nucleus	Compound nucleus	E_e, Excitation energy (MeV)	E_a, Activation energy (MeV)
U^{233}	$[U^{234}]$	6.6	4.6
U^{235}	$[U^{236}]$	6.4	5.3
Pu^{239}	$[Pu^{240}]$	6.4	4.0
U^{238}	$[U^{239}]$	4.9	5.5
Th^{232}	$[Th^{233}]$	5.1	6.5

the ground-state spherical configuration and a volume-conserving dumbbell configuration (ref. [2] and [6]). Table 2 contains values of E_a for the *compound* nuclei formed by neutron capture in the fissile and fertile isotopes of primary interest in reactor design. These are compared with the *excitation energy* (E_e) provided in forming the compound nucleus.

$$E_e = \left[\left(m\left({}_ZX^A\right) + m_n\right) - m\left({}_ZX^{A+1}\right)\right]c^2. \qquad (17)$$

Note that E_e does not include any kinetic energy contribution from the captured neutron. For the fertile target nuclei (U^{238} and Th^{232}), $E_e < E_a$ and neutron kinetic energy will be required to overcome or quantum mechanically penetrate (with high probability) the potential barrier to fission. For the fissile targets, $E_e > E_a$ and thus "slow" neutrons can initiate fission.

The high values of E_e for the fissile targets are due to the positive "pairing" contribution, B_4, to the binding energy of the compound nucleus ground states. Note ${}_{92}U^{234}$, ${}_{92}U^{236}$, and ${}_{94}Pu^{240}$ are all even Z even N nuclei and the corresponding target nuclei are even Z odd N. So, the second term in Eq. 17 is decreased by $\delta(A + 1)^{-3/4}$, and B_4 is zero in the first term. Thus, an increase in E_e relative to the result if pairing is ignored is achieved. For fertile targets (even Z even N), roles are reversed. It is the first term in Eq. 17 that is decreased and B_4 is zero in the last term. Thus, E_e is lower than if pairing is ignored.

The semiempirical mass formula and the shell and liquid drop models are limited in predicting the fission process. This is best illustrated by the mass distribution of the major fission fragments (see Fig. 3). In the vast majority of cases, fission yields two unstable (having excess neutrons) nuclei, but not of equal mass, as in the example above used to estimate the energy available from spontaneous fission of U^{238}. The two humped curves in Fig. 3 are not predicted by nuclear models. To quote Krane, "surprisingly, a convincing explanation for this mass distribution has not been found."

From the nuclear models, it is not surprising that free (prompt) neutrons are emitted in fission as the daughter nuclei are so rich in neutrons, but the prediction of their number (~2.5 on average) and energy spectrum (the mean ~2 MeV, see Fig. 4) are still an active area of study. The decay chains of the neutron-rich, excited daughter nuclei (fission fragments) are well predicted, including the release of (delayed) neutrons when in some cases neutron decay competes successfully with β-decay. The delayed neutrons are a small fraction of the total neutron emission (0.64% for thermal fission of U^{235}), but as will be discussed in section "Fission Reactor Performance", they are important to reactor control.

Total energy release from the various neutron-induced fissions of interest in reactor design is remarkably consistent with the simple spontaneous U^{238} fission calculation made above. Of course, the constituents are different, as displayed in Table 3.

In a reactor design, the total energy values in Table 3 are not used. First, the contribution from neutrinos is subtracted, as their range before collision is well beyond reactor boundaries. Then, the energy release per fission from neutron captures which produce βs and γs is added. The magnitude of this release is design-dependent as it is a function of the materials used, and the neutron capture rate in these materials. For plant energy balance studies, using 200 MeV/fission is satisfactory.

The problem of *decay heat* was noted in the previous section. From Table 3, it can be seen that fission product decay is the immediate concern when a chain reaction is terminated. Assume full power from U^{235} fissioning, when this ceases, delayed γs and βs are still being released. Thus, ~6.3% ($\simeq 100 \times (6.26 + 6.43)/200$) of rated power, coming from fission product decay, must still be dissipated, along with energy from the decay of transuranic elements present in the reactor, for a total of ~7%.

Over 800 fission fragment nuclei have been identified. Their decay must be tracked to account for *decay*

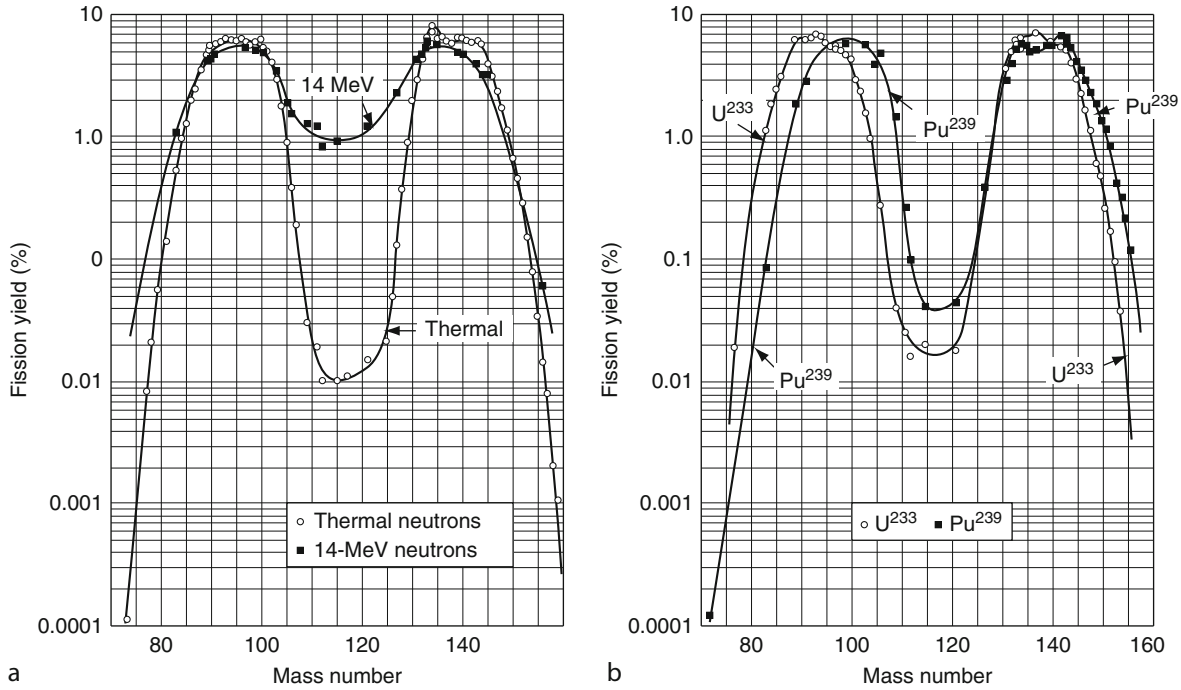

Fission Reactor Physics. Figure 3
Fission yields: (**a**) for U^{235} from fast and thermal neutrons, (**b**) for U^{233} and PU^{239} from thermal neutrons [33]

heat in reactor shut-down safety analysis and for the proper handling and storage of spent fuel (where both energy release and the nature of radiation fields must be known). One hundred and two of these nuclei are delayed neutron precursors. To simplify reactor transient (kinetics) calculations, the precursors are collected into six *effective* groups, where members of a given group have similar decay constants (see Table 4).

The energy spectra for a given delayed group do not vary significantly with fissioning isotope. The spectra are much softer (with lower mean energies, < 1 MeV) than for prompt neutrons [7]. This means that a delayed neutron in a thermal reactor is more *important* than a prompt neutron. It is more likely to reach the low energies (<0.625 eV) where most fission occurs. Delayed neutrons can also result from other reactions, for example, photon capture (γ,n) (The expression (a,b) is shorthand for a nuclear reaction with an input particle "a" and output particle "b", where the target and product nuclei are understood.) and neutron activation (n,p) followed by neutron decay of the product nucleus. If important to a particular reactor design, these delayed neutrons can be included by modifying the effective delayed group structure.

The final aspect of the ~800 fission fragment nuclei that must be dealt with is their impact on neutron balance. Each of them has a probability of capturing neutrons and in some case of causing a transmutation into a nucleus with a particularly large propensity for capturing neutrons. The nuclei of greatest importance to neutron balance are listed in Table 5.

I^{135} is important as it is the direct precursor of Xe^{135}, an especially large absorber of thermal neutrons. The next two isotopes in the table are precursors to a decay chain with three large absorbers, Pm^{147}, Sm^{149}, and Sm^{151}. The final five, with their precursors in parentheses, are large absorbers, but not as sensitive to neutron energy spectrum and power level and history as the others. Clearly, data for the 800 fission fragments must be handled through large computer files [8]. For neutron balance, the fission fragment isotopes, which are not treated explicitly (Table 5), can be lumped into an effective fission product nucleus with

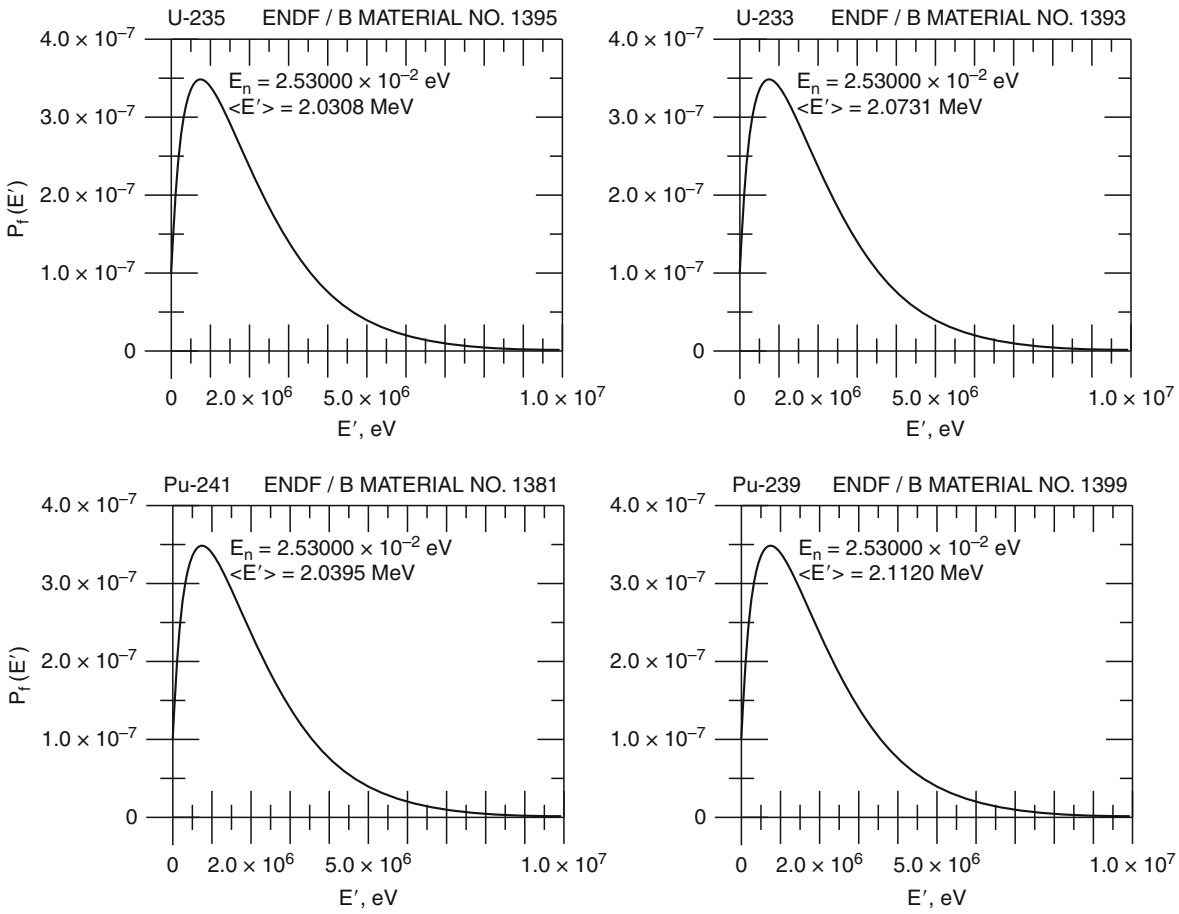

Fission Reactor Physics. Figure 4
Prompt neutron energy spectra where $P_f(E')$ is the probability per unit energy [32]

a yield per fission and *probability* for neutron capture. How one characterizes the *probability* of nuclear reactions is the subject of the next section.

Cross Sections

The nuclear reactions of importance to fission reactor design are by *definition* governed by the postulates of quantum mechanics (i.e., they are on the dimensional scale of the nucleus). And, thus the results of the various reactions are probabilistic in nature. The probability of a particular result is characterized by a parameter, the *microscopic* cross section, σ, with, not surprisingly, the dimensions of area, and which is quoted in units of *barns*. The barn, 10^{-24} cm^2, is a reasonable measure as in some cases σ is nearly the projected area of a target nucleus, $4\pi R^2$, and R is $\sim 10^{-12}$ cm. Thus, envisioning a target foil of area, A, and thickness, dx (where dx is small enough to have negligible shadowing of one nucleus by another in the target foil), the probability that an incident particle in traveling a short distance (i.e., dx) will undergo a specific reaction equals $\sigma\rho A dx/A$, where ρ is the density of target nuclei (#/cm^3) in the foil. It follows that to find the reaction rate in the foil we need the number of impinging particles per second. Given the particles have a density N (#/cm^3) and are monoenergetic and monodirectional (normal to the face of the foil) with speed v, the number impinging per second equals $N \cdot (vdt) \cdot A/dt$. So the total reaction rate in the foil is $(NvA)(\rho\sigma dx)$, and the rate per cm^3 is $vN\rho\sigma$. The parameters that make up this specific rate

Fission Reactor Physics. Table 3 Energy yield in MeV from fission. Thermal neutron fission of fissile isotopes; fertile isotope fission is from neutrons with energy spectrum of a light water-moderated reactor [7, 32]

Energy	Fissile or fertile isotope†					
	^{232}Th	^{238}U	^{235}U	^{233}U	^{239}Pu	^{241}Pu
Fission fragment kinetic energy	162.1 ± 1.5	170.0 ± 0.66	169.6 ± 0.7	168.7 ± 0.7	175.9 ± 0.1	175.5 ± 1.1
Prompt neutron kinetic energy	4.7 ± 0.12	5.51 ± 0.1	4.79 ± 0.07	4.9 ± 0.1	5.9 ± 0.1	5.99 ± 0.13
Delayed neutron kinetic energy	0.024 ± 0.004	0.021 ± 0.003	0.0071 ± 0.0007	0.0014 ± 0.0005	0.001 ± 0.0005	0.0074 ± 0.0015
Prompt γ rays	6.15 ± 1.75	6.28 ± 0.8	6.96 ± 0.7	7.59 ± 0.71	7.74 ± 0.45	7.86 ± 1.8
Delayed γ rays	8.01 ± 0.2	8.04 ± 0.08	6.26 ± 0.05	4.99 ± 0.04	5.16 ± 0.1	6.33 ± 0.07
β particles	8.28 ± 0.21	8.25 ± 0.08	6.43 ± 0.05	5.13 ± 0.04	5.3 ± 0.1	6.51 ± 0.04
Neutrino energy	11.1 ± 0.3	11.14 ± 0.11	8.68 ± 0.06	6.91 ± 0.05	7.15 ± 0.11	8.78 ± 0.09
Total energy yield	200.3 ± 0.5	209.3 ± 0.3	202.7 ± 0.1	198.2 ± 0.1	207.2 ± 0.3	211.0 ± 0.3

Fission Reactor Physics. Table 4 Prompt and delayed neutron data. ν_p is the prompt neutron yield versus initiating neutron energy (ENDF/B-VII.0). ν_d is the total delayed yield, constant for fission initiating neutron energies between 0 and 4 MeV, and above 7 MeV. Between 4 and 7 MeV, ν_d tracks linearly [32]

The relative abundance $\gamma_I = \nu_i/\nu_d$								
Neutron E	^{233}U ν_p		^{235}U ν_p		^{239}Pu ν_p		^{241}Pu ν_p	
0.0253 eV	2.4894		2.4208		2.8724		2.9251	
2 MeV	2.5758		2.6366		3.171		3.1727	
	$\bar{\nu}_d$							
E(MeV)	^{233}U		^{235}U		^{239}Pu		^{241}Pu	
0–4	0.0074		0.0167		0.00645		0.0162	
7	0.0047		0.0090		0.0043		0.0084	
^{233}U			^{235}U		^{239}Pu		^{241}Pu	
Delayed Group	Decay Constant λ_i, s^{-1}	Relative Abundance γ_i	λ_i, s^{-1}	γ_i	λ_i, s^{-1}	γ_i	λ_i, s^{-1}	γ_i
1	0.01258	0.086	0.01272	0.038	0.0129	0.038	0.0128	0.010
2	0.03342	0.274	0.03174	0.213	0.0311	0.280	0.0299	0.229
3	0.131	0.227	0.116	0.188	0.134	0.216	0.124	0.173
4	0.303	0.317	0.311	0.407	0.332	0.328	0.352	0.390
5	1.27	0.073	1.4	0.128	1.26	0.103	1.61	0.182
6	3.14	0.023	3.87	0.026	3.21	0.035	3.47	0.016

Fission Reactor Physics. Table 5 Direct yield fractions (×100) for isotopes in the most important fission product chains [32]

Fission Product	Fissile or fertile isotope[a]				
	^{232}Th	^{238}U	^{235}U	^{233}U	^{239}U
^{135}I	5.238	6.548	6.349	4.860	6.303
^{135}Xe	0.0403	0.0150	0.255	1.337	1.152
^{147}Nd	3.08	2.711	2.271	1.775	2.073
^{149}Pm	0.825	1.765	1.089	0.769	1.261
^{99}Mo (^{99}Tc)	2.965	6.247	6.127	4.957	6.144
^{103}Ru (^{103}Rh)	0.164	6.336	3.137	1.707	6.991
^{131}I (^{131}Xe)	1.481	2.982	2.473	2.352	3.093
^{133}I (^{133}Cs)	3.858	6.356	6.787	5.974	6.923
^{143}Ce (^{143}Nd)	6.619	4.834	5.972	5.881	4.561

[a]The energy of the neutron initiating the fission is in the thermal range for ^{235}U, ^{233}U, and ^{239}Pu. For ^{232}Th and ^{238}U, the yields are due to fissions initiated by neutrons with a spectrum of energies typical of light water-moderated nuclear reactors.

have been reordered to reflect conventional definitions in reactor physics (In the nuclear engineering discipline, *reactor physics* refers to the portion of the field addressed in this entry):

$$vN \equiv \Psi \text{particle } \textit{flux}, \text{ and} \tag{18}$$

$$\rho\sigma \equiv \Sigma \textit{macroscopic } \text{cross section.} \tag{19}$$

The *flux* in our simple foil example is the number of particles per cm^2 per second crossing a plan parallel to the face of the foil. Given the more general representation of particle density (which will be used in the next section):

$N(\mathbf{r},E,\mathbf{\Omega},t)dr^3dEd\Omega \equiv$ no. of particles in dr^3 about $\mathbf{r}$, with kinetic energies in dE about E, and going in the solid angle $d\Omega$ about the unit direction vector $\mathbf{\Omega}$ (see Fig. 5), at time t; then the corresponding definition of *flux*, $\Psi(\mathbf{r},E,\mathbf{\Omega},\mathbf{t})dsdEd\Omega$, is the no. of particles with E in dE going in direction Ω in $d\Omega$ that pass through the surface ds, which is located at $\mathbf{r}$ and is normal to $\mathbf{\Omega}$, per unit time, at time t.

The *macroscopic* cross section is the probability that a particle undergoes a reaction characterized by σ, per unit path (for small paths, dx) traversed by the particle in a homogenous material with target nucleus density, ρ. This definition lends a special significance to $1/\Sigma_T$, where $\Sigma_T = \rho\sigma_T$. σ_T is the *total* microscopic cross section, the sum of the σs for all of the reactions that the initiating particle can undergo with a given target isotope. So the change in flux, where $\mathbf{\Omega}$ is parallel to the x axis of a target material sample, over a small

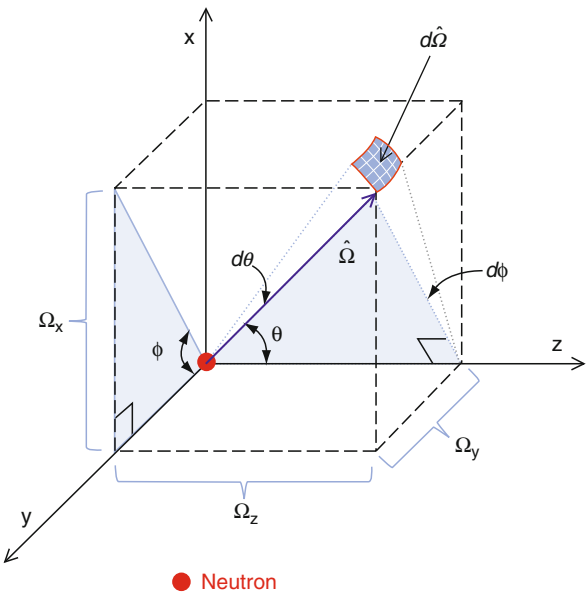

Fission Reactor Physics. Figure 5
The unit direction vector $\mathbf{\Omega}$ associated with neutron velocity and the differential (small) solid angle $d\Omega$ which defines the range of directions

interval dx in the sample is $d\Psi = -\Psi\Sigma_T dx$. And thus, $\Psi(x) = \Psi(0)\ e^{-\Sigma_T x}$, where x is the distance into the "sample" (which has its face in the y – z plane at x = 0). So, the probability of a reaction in dx about x can be expressed as

$$P(x)dx = \Sigma_T dx \bullet (\Psi(x)/\Psi(0)) = \Sigma_T e^{-\Sigma_T x} dx. \tag{20}$$

And thus the *mean free path* of a particle in an incident beam ($\Psi(0)$) before being removed from the beam in a homogeneous target is

$$\overline{x} = \int_0^\infty dx\, xP(x) = 1/\Sigma_T. \tag{21}$$

or generally the *mean free path* is the average distance traveled between successive interactions.

If a homogeneous material is made up of various nuclei (elements/isotopes, indexed by j), then the macroscopic cross section for a reaction, i, is

$$\Sigma_i = \sum_j \rho_j \bullet \sigma_i^j. \tag{22}$$

The reactions of primary interest in fission reactor design are those initiated by neutrons and gammas. Neutron cross sections are key to determining if a chain reaction can be maintained, and that the neutron population can be controlled under various transient conditions (e.g., start-ups and shutdowns, planned and accidental), and, of course, the fission distribution in the reactor. Most of the resulting energy release, from fission fragments, is deposited locally in the fuel elements of a given design. However, gammas, from fission and neutron capture in reactor structures, have large mean free paths, and their distribution and capture rates must be determined, using gamma cross sections, to complete the knowledge of energy deposition. The subsequent engineering problem is to assure that the reactor cooling system can remove the deposited energy under normal and accident conditions. Neutron and gamma cross sections are also required for the shield design of a fission reactor.

Neutron reactions are characterized by their energy balance, the Q factor, as well as microscopic cross sections. For the simple reaction (with the target at rest),

$$n + X \rightarrow Y + y \tag{23}$$

the energy balance is

$$\left(E_n + m_n c^2\right) + M_X c^2 = \left(E_Y + M_Y c^2\right) + \left(E_y + m_y c^2\right), \tag{24}$$

and Q is defined as the difference in the kinetic energies of the inputs (here the neutron) and the outputs:

$$Q = E_Y + E_y - E_n \text{ or } = \left(M_X + m_n - M_Y - m_y\right)c^2. \tag{25}$$

If Q is positive, the reaction is exothermic, if negative, endothermic. For an endothermic reaction to go, for the microscopic cross section to be nonzero, enough kinetic energy must be supplied by the neutron to excite a compound nucleus, X^{A+1}, so it will decay to Y + y. As momentum must be conserved,

$$m_n v_n = (M_X + m_n)V_c \text{ or } V_c = v_n m_n/(M_X + m_n), \tag{26}$$

where V_c is the velocity of the compound nucleus. Then, the neutron energy supplied must be such that

$$-Q = m_n {v_n}^2/2 - (M_X + m_n){V_c}^2/2 \tag{27}$$

and the *threshold energy*, E_{th}, for the reaction is

$$E_{th} = m_n {v_n}^2/2 = (-Q)(1 + m_n/M_X). \tag{28}$$

(n, 2n) is an example of an endothermic reaction whose cross sections will exhibit an energy dependence of zero until the neutron energy E reaches an E_{th}.

The simplest, but very important, neutron reaction to be considered is a form of elastic scattering (Q = 0), where collisions can be treated with classical mechanics as hard sphere, billiard ball, interactions. For the energies of neutrons in fission reactors, 0–10 MeV, elastic scattering cross sections for most nuclei are constant and proportional to the square of the nuclear radius, ~A2/3. Assuming the target nucleus to be at rest and applying conservation of energy and momentum in the center of mass, CM, coordinate system, one determines the probability that the final energy of the scattered neutron, in the laboratory coordinate, LM, system, is E_f in dE_f:

$$\begin{aligned} P(E_i \rightarrow E_f) &= 1/(1-\alpha)E_i, \text{ for } \alpha E_i \le E_f \le E_i \\ &= 0 \text{ otherwise,} \end{aligned} \tag{29}$$

where $\alpha = ((A-1)/(A+1))2$ and E_i is the initial neutron energy. A is the mass number of the target nucleus.

And, scattering is assumed to be isotropic in the CM coordinate system. This is a good assumption for the energy range of interest here, and its basis will be discussed later in this section. A full derivation of Eq. 29 can be found in Duderstadt and Hamilton, "Nuclear Reactor Analysis." Examining $P(E_i \Rightarrow E_f)$ one sees that a neutron scattering off a hydrogen nucleus ($A = 1$) can lose all its energy (as $\alpha = 0$). On average, it loses half its initial energy as

$$\overline{E}_f = \int_{\alpha E_i}^{E_i} dE_f E_f P(E_i \to E_f) = E_i(1+\alpha)/2, \text{and} \quad (30)$$

$$\Delta\overline{E} = E_i \to \overline{E}_f = E_i(1-\alpha)/2. \quad (31)$$

Given $P(E_i \to E_f)$ as in Eq. 29, one defines *differential* microscopic elastic scattering cross sections, $\sigma_{es}{}^j(E_i)P(E_i \to E_f)dE_f$, which are particularly useful in determining how neutrons, born in fission, are slowed down in reactors designed to take advantage of the large fission cross sections of fissile isotopes in what is conventionally defined as the *thermal* neutron energy range, less than 0.625 eV. The superscript "j" of $\sigma_{es}{}^j$ refers to the nuclei of the various *moderators* (hydrogen, deuterium and carbon) that are employed in these thermal reactors.

Once neutrons have slowed to the thermal range the target nuclei can no longer be assumed to be at rest. The interaction frequency will then be

$$|\mathbf{v} - \mathbf{V}|\ \sigma(|\mathbf{v} - \mathbf{V}|)\rho, \quad (32)$$

where $|\mathbf{v} - \mathbf{V}|$ is the relative speed of neutron and target. For elastic scattering, $\sigma(|\mathbf{v} - \mathbf{V}|)$ is still nearly constant and an *average* cross section for *thermal* neutrons with speed v $(=(2E/m_n)1/2)$ is

$$\overline{\sigma}(\mathbf{v}) = (\sigma_{es}/\mathbf{v}\rho) \int d^3\mathbf{V}|\mathbf{v} - \mathbf{V}|\rho(\mathbf{V}), \quad (33)$$

where for many reactor applications the Maxwell–Boltzmann velocity distribution for ideal gases in thermal equilibrium at absolute temperature, T, can be used to represent the targets. Thus,

$$\rho(\mathbf{V}) = \rho \bullet (M/(2\pi kT))^{3/2} \exp(-MV^2/2kT), \quad (34)$$

where M is the mass of the target nucleus and k is the Boltzmann constant (8.6174×10^{-5} eV/K, K is degrees Kelvin).

From Eq. 33, one sees that for $v \gg V$ the *average* cross section is, as expected, σ_{es}. And, as the neutron speed decreases and approaches zero, the *average* cross section goes as one over the neutron speed.

For highly accurate calculations (As part of the process of evaluating nuclear data sets, very accurate calculations of integral experiments are made. Zero power *mockups* of reactors, with carefully recorded dimensions and inventories, are commonly used. Monte Carlo calculations (to be discussed in the next section) of neutron balance in the mockups are made with various data sets (e.g., cross-section libraries) to determine a recommended set. See the CESWG web site for references to such experiments.), more sophisticated treatments of scattering from moderator structures (e.g., molecules in liquids, lattices for solids) are required. The excitation of modes of vibration, and thus energy loss to phonons must be considered. This has been a fertile field of development [9] and double differential scattering cross sections for various moderators have been produced. They are of the form:

$$\sigma_s(E_i \to E_f,\ \Omega_i \to \Omega_f)dE_f d\Omega_f = (1/4\pi kT)(E_f/E_i)^{1/2}\exp(-\beta/2)\sigma_{es}S(\alpha,\beta)dE_f d\Omega_f, \quad (35)$$

where

$$\alpha \equiv (E_i + E_f - 2(E_iE_f)^{1/2})\Omega_i \bullet \Omega_f/kT \text{ and } \beta \equiv (E_i + E_f)/kT. \quad (36)$$

σ_{es} is the scattering cross section of the bound "moderating" nucleus (e.g., proton, deuteron, carbon). $S(\alpha,\beta)$, the *scattering law*, embodies the physics of the influence of the moderator structure on the scattering process. Various formulations of $S(\alpha, \beta)$ are tabulated as part of data files that document *all* the microscopic cross sections that are used in fission reactor design. These files can be found on the web site of the National Nuclear Data Center (currently, nndc.bnl.gov). The most widely used set is ENDF/B, the latest (2009) version is VII.0. In order, however, to produce the differential scattering cross sections (Eq. 35) for design calculations, material temperatures, T, must be identified and supplied with the corresponding ENDF files to NJOY [10], a system of computer programs which produce microscopic cross sections for use in various design programs (which will be discussed in the next section).

The remaining neutron reactions of interest all involve the formation of a compound nucleus, which will be in an excited state, $(X^{A+1})^*$, and will subsequently decay, yielding γ or γ's (neutron capture), n (elastic neutron scattering), n+γ (inelastic scattering), two n's (an (n,2n) reaction), p or α (charged particle production) or fissioning. The probabilities of these various outcomes for a given isotope, j, and incident neutron energy are characterized by the microscopic cross sections: $\sigma_c^j(E)$, $\sigma_s^j(E)$, $\sigma_{in}^j(E)$, $\sigma_{2n}^j(E)$, $\sigma_p^j(E)$, $\sigma_\alpha^j(E)$, and $\sigma_f^j(E)$. As noted above in the discussion of Q factors, for endothermic reactions, $Q < 0$, cross sections will be zero until a threshold value of E for the initiating neutron is reached. This is the case for inelastic scattering, (n,2n) and some (n,α) and (n,p) reactions. There is similar threshold behavior for fertile isotope fission cross sections (see Sect. Fission and Its Products), which when the reactions "go" are exothermic. All neutron capture reactions (n,γ) are exothermic, and thus their cross sections are nonzero over the full range of fission reactor neutron energies.

One can view the "compound nucleus reaction" cross sections as the product of a cross section for compound nucleus formation, σ_C (neutron capture by the target nucleus), times the probability of a particular decay mode of the excited compound nucleus. Both factors of this "product" depend on the nature of the target and compound nuclei, X^A and X^{A+1}, and the energy available to excite the compound nucleus, X^{A+1}. The later is the sum of the reduced mass (i.e., center of mass) kinetic energy of the initiating neutron:

$$E_C = E(M_X/(m_n + M_X)) \cong E(A/(1 + A)), \quad (37)$$

where X^A is assumed to be at rest and momentum is conserved; and the excitation energy, E_e (see Eq. 17), provided by adding a neutron to X^A. E_e is the binding energy of the "added" neutron in the compound nucleus.

The magnitude of σ_C depends on the structure of X^A. First, if neutron number N (=A–Z) is odd, σ_C is larger than its counterpart for neighboring isotopes with even neutron numbers. The opposite is true for N even. This just reflects the binding energy advantage of pairing half-integral spin Fermions in a nucleus (see the discussion of B_4 in Sect. Fission and Its Products). Second, for nuclei of various A's there are *Magic Numbers* for both Z and N (2, 8, 20, 50, 82 and 126) which can be thought of as closing shells of protons and neutrons, analogous to atomic electron shells. The reduction of σ_c for a magic number N nucleus, relative to its N + 1 isotope neighbor's σ_C, is much larger than the pairing effect.

Excited compound nuclei have mean lifetimes, τ (see Eq. 14) of as long as 10^{-14} s (Kaplan), much longer than the transit time for a neutron crossing a target nucleus, $\sim$2R/v. Given the nuclear diameter, $2R \sim 10^{-12}$ cm, the transit time for even a *thermal* neutron is $\sim 10^{-17}$ s (The term *thermal neutron* refers to the most probable energy of the neutrons in thermal equilibrium in a zero-power reactor (e.g., a mockup). At 20°C, this is 0.023 eV, with a corresponding neutron speed of 2,200 M/s.). Thus, the standard assumption is that the decay of an excited compound nucleus is independent of all but the input energy of the initiating neutron. The decay modes of a particular excited state, nuclear level, are characterized by a *level width*

$$\Gamma \equiv h/(2\pi\tau), \quad (38)$$

with dimensions of energy (h is Planck's constant, 4.135667×10^{-15} eV-s), which is based on the Heisenberg uncertainty principle. In a quantum mechanical system like our excited compound nucleus, knowledge of energy and time is governed by

$$\Delta E \Delta t \sim h/2\pi. \quad (39)$$

Thus, Γ can be viewed as the uncertainty in energy of an excited state (level) of a compound nucleus, and τ a measure of the "uncertainty" of the lifetime of the excited state. The microscopic neutron cross sections, which go through the compound nucleus formation process, exhibit resonance behavior (peaking) when the neutron energy and E_e (the added neutron binding energy) produce or nearly produce a well-defined excited state (i.e., having a small Γ). See Fig. 6.

The level width Γ can be thought of as the probability per unit time of decay of an excited state and thus the sum of partial "widths" (probabilities per unit time) for each mode of decay:

$$\Gamma = \Gamma\gamma + \Gamma_n + \Gamma_{n\gamma} + \Gamma_f + \Gamma_{2n} + \Gamma_p + \ldots, \quad (40)$$

(where Γ_n refers to elastic compound scattering and $\Gamma_{n\gamma}$ refers to inelastic scattering, the rest being obvious).

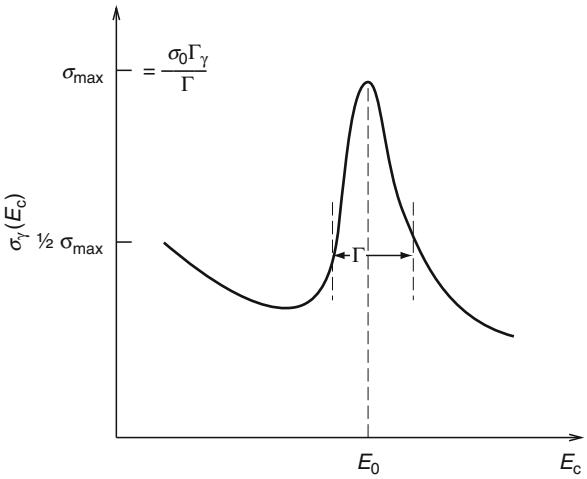

Fission Reactor Physics. Figure 6
A typical neutron capture cross section for an isolated (single) resonance whose width at half maximum is Γ, the total level width. Γ_γ is the partial width for gamma ray emission from the excited state (level). E_c is the center of mass (reduced mass) energy of the initiating neutron (Duderstadt)

Therefore, a "compound nucleus reaction" cross section near an isolated resonance is

$$\sigma(\mathrm{n,i}) = \sigma_C(\mathrm{n})\Gamma_\mathrm{i}/\Gamma, \text{ for } \mathrm{i} = \gamma, \mathrm{n}, (\mathrm{n}\gamma), \mathrm{f}, 2\mathrm{n}, \mathrm{p}, \text{etc.} \tag{41}$$

The functional form of σ (n,i), its dependence on neutron energy, was derived with the principles of quantum mechanics by Briet and Wigner [11] in 1935. Their "formula" for this simple case is

$$\sigma(\mathrm{n,i}) = (\lambda^2/4\pi)\Gamma_\mathrm{n}\Gamma_\mathrm{i}/\left[(\mathrm{E}-\mathrm{E}_0)^2 + (\Gamma/2)^2\right], \tag{42}$$

where λ is the de Broglie wavelength of the neutron, $h/(2m_n\ E)^{1/2}$, and E_0 is the energy of the resonance peak. Figure 6 is an illustration of this "form" for i = γ.

Breit and Wigner' s most impressive derivation is more general than Eq. 42.

First, they considered neutron energies beyond what has been found pertinent to fission reactors. When one accounts for conservation of angular momentum, the initiating neutron has classically a magnitude of angular momentum |L| equal to pb, where p is neutron momentum, $(2m_nE)^{1/2}$, and b is the displacement of the neutron path from a parallel axis running through the center of the target nucleus. In a quantum mechanical treatment,

$$|\mathrm{L}| = (l(l+1))^{1/2}\mathrm{h}/2\pi \text{ where } l = 0, 1, 2, 3, \ldots \tag{43}$$

Then, one can think of "b" as |L| (given by Eq. 43) divided by the neutron momentum, p, and if there is going to be a significant probability of a reaction with the target nucleus, "b" cannot be much larger than the target nucleus radius, $r \cong A^{1/3}(1.28 \pm 0.05) \times 10^{-13}$ cm. For this to be true for a large nucleus, for example, for U^{235}, and for nonzero angular momentum (e.g., $l = 1$), the neutron would have to have kinetic energy ≥ 6.6 MeV. For smaller nuclei the required energy would be greater. Given the spectrum of neutrons in fission reactors, where most neutrons are born at around 2 MeV (see Fig. 4), an assumption of zero angular momentum ($l = 0$) for the vast majority of reactions is good, and thus equation Eq. 42 does not include a factor involving angular momentum or spin quantum numbers. This assumption also means that decay products of an excited compound nucleus will be released isotropically in the center-of-mass coordinate system, which is reflected in the factor of 1/4π in Eq. 42 (the probability that the decay product i (i = n, γ, p) is released dΩ about any **Ω**). The quantum mechanical treatment of angular momentum also accounts for the statement made above that "billiard ball" elastic scattering "can be assumed to be isotropic in the center of coordinate system." This direct elastic scattering is referred to as *potential* scattering so as to be differentiated from resonance (compound nucleus) elastic scattering, that is, i = n in equation Eq. 42.

Second, Breit and Wigner recognized and treated interference between potential and resonance elastic scattering. They found that the total elastic scattering cross section dips at energies right below the resonance peak, E_0.

Finally, as they were aware that there could be multiple possible excited states of a compound nucleus they extended their "formula" to two resonances whose Γs do not over lap.

Since Breit and Wigner's original work, there has been great activity in measuring cross sections, motivated principally the desire to understand the physics

of the nucleus. In the process, however, the basic parameters required for nuclear weapon and reactor design were generated. The neutron cross sections for fission reactor design are summarized in Table 6 [12].

In this table, the distinction is made between resonance cross sections with different densities (spacing) of resonance peaks. With intermediate and heavier nuclei the level structure grows more complex, and the number of possible excited states of a compound nucleus greatly increases. With higher neutron energy more finely spaced excited states can be reached and their level width, Γ's, increasingly overlap until measurement cannot resolve individual resonances.

In parallel with the work of nuclear spectroscopy experimentalists, theoreticians have built on Breit and Wigner's work. Resonance cross-section models [13] are key to creating Evaluated Nuclear Data Files. The Cross Section Evaluation Working Group, a cooperative effort of national laboratories, industry and universities in the United States and Canada (see nndc.bnl.gov), sponsors reviews of the various measurements of a given cross section (target isotope and reaction) and the subsequent determination (As part of the process of evaluating nuclear data sets, very accurate calculations of integral experiments are made. Zero power *mockups* of reactors, with carefully recorded dimensions and inventories, are commonly used. Monte Carlo calculations (to be discussed in the next section) of neutron balance in the mockups are made with various data sets (e.g., cross-section libraries) to determine a recommended set. See the CESWG website for references to such experiments.) of a consensus set of parameters for an appropriate cross-section *model*. These models and their "consensus"

Fission Reactor Physics. Table 6 Types of neutron cross section for various target element/isotope masses pertinent to fission reactor design

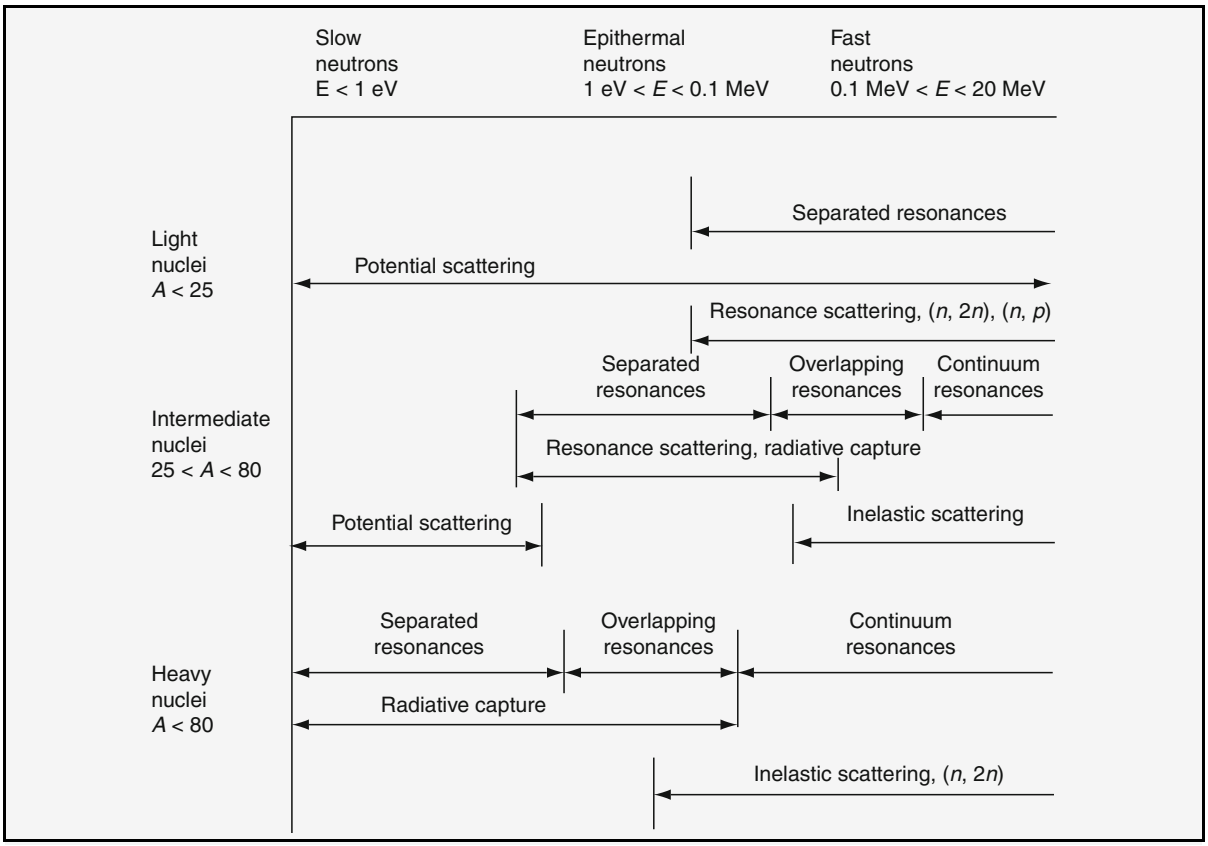

parameters are a large part of the ENDF/B-VII.0 data files. Having the cross sections represented by an analytic model also facilitates dealing with the temperature effect on resonance cross-sections. that is, Doppler shift or broadening. The analytic process of averaging a resonance cross section (i.e., its model), over the velocity distribution of the target nuclei at a given temperature is similar to what was discussed above for reactions initiated by neutrons in thermal energy range. The process is outlined by Duderstadt and Hamilton using the single-level Breit Wigner formula as the resonance model. The effect of increasing temperature is to reduce a resonance peak while broadening its width, thus increasing its Γ. To first order, the area under the resonance is unchanged, which could led one to think that resonance "Doppler" broadening is not an import effect in a reactor application. This is true if the density of the resonance target nuclei is small (i.e., it is very dilute in the reactor), and thus its presence does not change the energy dependence of the reactor's neutron population. However, in most reactor designs, resonance absorbers are concentrated in localized reactor features (e.g., fuel elements, control rods) and there is significant self-shielding at the resonance peak. That is, neutrons with the "peak" energy will most likely be absorbed in the reactor "feature" irrespective of temperature-induced changes in the resonance microscopic cross section. But the story can be different on the wings of a resonance where the cross section is much smaller, and, thus, so is the self-shielding. An increase in temperature of the "feature" can result in a net increase in neutron absorption, with no change at the peak energy, but with increases in the wings. This phenomena can aid in insuring a *negative temperature coefficient* for a fission reactor design (*Temperature coefficients* are collective reactor parameters that reflect how neutron balance is impacted by temperature change through feedback mechanisms, for example, Doppler broadening (or narrowing) of resonances, and moderator density changes. Reactor control will be discussed in Sect. Fission Reactor Performance.). A negative temperature coefficient is a crucial reactor design safety requirement.

Dealing with temperature in producing resonance cross sections for design calculations is handled in a manner similar to the process for thermal energy range cross sections discussed above. The ENDF resonance cross-section models and appropriate material temperatures are input to NJOY, and the output are the broadened cross sections in the model format. How these cross sections are used in design calculations is addressed in the next section.

As noted at the start of this section, gamma ray (photon) cross sections are important in fission reactor design as they are required for the full treatment of energy deposition throughout a reactor (in its fuel bearing *core* and supporting structures). In the order of importance with increasing gamma energy, the mechanisms of attenuation are the photo electric effect (γ,e^-), Compton scattering (γ,γ^*), and pair production (γ, e^-e^+). The photoelectric effect removes a γ when its energy, $h\upsilon$, can eject an atomic electron. Its cross section is approximately proportional to $Z^4/(h\upsilon)^3$, and has discontinuities in energy as the ionization energy of various atomic electron shells are achieved. For higher γ energies, Compton scattering interactions with atomic electrons can be treated as effectively free electron collisions. Conserving momentum and energy relativistically, one can derive expressions for energy loss and change in direction for initiating γs as a function of their incident energy. The magnitude of the cross section is proportional to Z. When γ energies reach a threshold of 1.022 MeV ($2 \times m_e c^2$) and are in the field of a target nucleus, pair production of an electron and positron is possible. The magnitude of the pair production cross section is proportional to Z^2. Of course, in tracking the γ population in a reactor, one recognizes that annihilation of a positron will produce two 0.51 MeV γ's. So pair production can be viewed as a form of inelastic scattering event. Cross sections for these three processes are tabulated in ENDF/B files, and they are described at a thorough but accessible level in the classic text by Robley D. Evans "The Atomic Nucleus."

An example plot of these cross sections for Th^{232} is provided in Fig. 7.

Finally, there are other gamma reactions which can take place in a reactor, for example (γ,f) and (γ,n) (the latter which we noted earlier as a source of delayed neutrons). However, these are threshold reactions for relatively high-energy gammas, and as shown in Table 3 the total energy available from fission from fissile

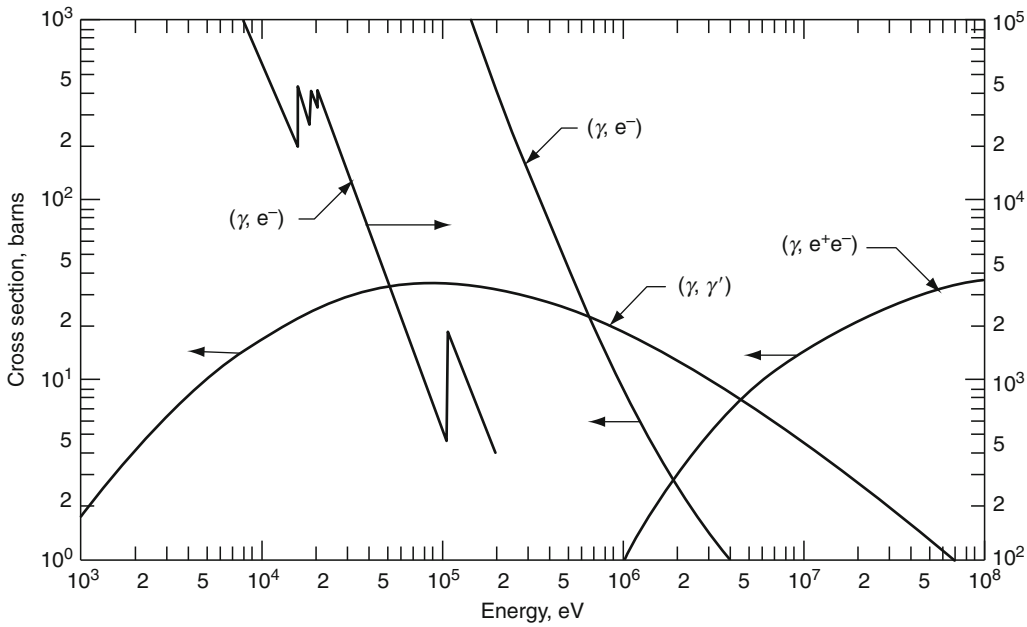

Fission Reactor Physics. Figure 7
Thorium cross section for the photo electric effect (γ,e), for Compton scattering (γ,γ′), and pair production (γ, e + e⁻) [32]

isotopes for gammas is limited: <8 MeV for prompt γ's, and, <6.5 MeV for delayed γ's. Thus, these reactions are not important in determining the overall distribution of gammas in a reactor design.

Neutron Distributions

With the material provided to this point, the primary problem of reactor *theory* can be addressed: that of finding the neutron distribution in phase space ($\mathbf{r}$,E,$\mathbf{\Omega}$), of a reactor design, and subsequently the reactor's power distribution, both throughout the reactor design's lifetime. The first task is to derive the equation for the neutron density, N($\mathbf{r}$,E,$\mathbf{\Omega}$), the neutron transport equation, and auxiliary equations for the atom densities, $\rho_j(\mathbf{r},t)$, of depleting (initial inventory) isotopes and important fission products (Like reactor physics, *reactor theory* is a traditional term in the nuclear engineering discipline. It refers to the study of the neutron transport equation and the means of its solution.). A simple approach to deriving the transport equation is to consider a balance relationship for N($\mathbf{r}$,E,$\mathbf{\Omega}$,t)dEdΩdt for a time invariant volume, V, in configuration space:

$$\begin{aligned} &\mathrm{dEd}\Omega\mathrm{dt}\int_v (\partial \mathrm{N}(\mathrm{r},\mathrm{E},\Omega,\mathrm{t})/\partial \mathrm{t})\mathrm{d}^3\mathrm{r} = \\ &\quad - \text{loss from flow out of V} \\ &\quad + \#\ \text{scattering into dE about E} \\ &\quad \text{and d}\,\Omega\,\text{about}\,\Omega \\ &\quad + \#\ \text{produced by fission} \\ &\quad + \#\ \text{produced by other sources} \end{aligned} \tag{44}$$

For the "flow" term, one defines the neutron angular current $\mathbf{J}(\mathbf{r},\mathrm{E},\mathbf{\Omega},\mathrm{t}) \equiv \mathbf{v}\mathrm{N}(\mathbf{r},\mathrm{E},\mathbf{\Omega},\mathrm{t})$, where $|\mathbf{J}(\mathbf{r},\mathrm{E},\mathbf{\Omega},\mathrm{t})\bullet\mathbf{n}\ \mathrm{dsdEd}\Omega\mathrm{dt}|$ is the no. of neutrons at $\mathbf{r}$, with energies in dE about E, traveling in dΩ about $\mathbf{\Omega}$, which cross an area ds with a unit normal vector $\mathbf{n}$ in dt at t. And thus, net flow out of V, which has a non-reentrant surface S, is:

$$\begin{aligned} &\mathrm{dEd}\Omega\mathrm{dt}\int_s \mathbf{J}(\mathbf{r},\mathrm{E},\Omega,\mathrm{t})\bullet\mathbf{n}\mathrm{ds} \\ &\quad = \mathrm{dEd}\Omega\mathrm{dt}\int_v \mathbf{v}\bullet\nabla\mathrm{N}(\mathbf{r},\mathrm{E},\Omega,\mathrm{t})\mathrm{d}^3\mathbf{r}, \end{aligned} \tag{45}$$

where Gauss' Theorem is applied to transform the surface integral to a volume integral.

The "reactions" in V are simply:

$$\mathrm{dEd\Omega dt}\int_{v} v\Sigma_{\mathrm{T}}(\mathbf{r},\mathrm{E},\mathrm{t})\mathrm{N}(\mathbf{r},\mathrm{E},\mathbf{\Omega},\mathrm{t})\mathrm{d}^3\mathrm{r}, \tag{46}$$

where $\Sigma_T(\mathbf{r},E,t)$ is the total *macroscopic* cross section in V. All scattering cross sections included in Σ_T have been integrated over final energies and directions.

Scattering into V is:

$$\begin{aligned}&\mathrm{dEd\Omega dt}\int_{v} \mathrm{d}^3 r\int_{0}^{\infty}\mathrm{dE}'\int \mathrm{d\Omega}'\\&v'\Sigma_s(\mathbf{r},\mathrm{t},\mathrm{E}'\rightarrow \mathrm{E},\mathbf{\Omega}'\rightarrow\mathbf{\Omega})\mathrm{N}(\mathbf{r},\mathrm{E}',\mathbf{\Omega}',\mathrm{t})\end{aligned} \tag{47}$$

where Σ_s is the double differential *macroscopic* scattering cross section in V (see the definition Eq. 65 for an example of a double differential *microscopic* scattering cross section).

The direct fission source into V is:

$$\begin{aligned}&\mathrm{dEd\Omega dt}\int_{v} \mathrm{d}^3 r\int_{0}^{\infty}\mathrm{dE}'\int \mathrm{d\Omega}''\sum_{\mathrm{i}}\nu_{\mathrm{pi}}(\mathrm{E}'\rightarrow\mathrm{E})\\&\Sigma_{fi}(\mathbf{r},\mathrm{E}',\mathrm{t})v'\mathrm{N}(\mathbf{r},\mathrm{E}',\mathbf{\Omega},\mathrm{t})/4\pi,\end{aligned} \tag{48}$$

where ν_{pi} $(E'\rightarrow E)$ is the number of prompt neutrons emitted in dE about E by a fission of isotope i initiated by neutrons in dE′ about E′: the macroscopic fission cross section for isotope "i" is $\rho_i(\mathbf{r},t)\sigma_{fi}(E')$.

The delayed neutron source into V is:

$$\mathrm{dEd\Omega dt}\sum_{\mathrm{j}}\mathrm{X_{dj}(E)}\frac{\lambda_j}{4\pi}\int_{v}\mathrm{C_j}(\mathbf{r},\mathrm{t})\mathrm{d}^3\mathrm{r}, \tag{49}$$

where $X_{dj}(E)/4\pi$ is the probability that the decay of delayed neutron precursor "j" will produce a neutron in dE about E and $d\Omega$ about Ω, and where λ_j and C_j are, respectively, the decay constant (see the beginning of section "Heavy Elements") and isotope density of precursor "j".

And, finally any source of neutrons in V not produced by a neutron reaction is given by:

$$\mathrm{dEd\Omega dt}\int_{v}\mathrm{d}^3 r\mathrm{S}(\mathbf{r},\mathrm{E},\mathrm{t})/4\pi, \tag{50}$$

where S could characterize a source (e.g., Plutonium (238)-Beryllium(α,n) or Califonium-252 (spontaneous fission)) included in a reactor design to aid in reactor start-up or S might account for decay processes yielding neutrons due to the presence of depleted fuel incorporated from another design.

Now, if the terms on the right side of the "balance relationship," equation Eq. 44, are moved to the left side, and $\mathrm{dEd\Omega dt}$ and the integral operation $\int_{\mathrm{v}}\mathrm{d}^3\mathrm{r}$ is factored out of all the terms, then as the right side is now zero and the small volume V is arbitrary, the collection of expressions under the integral must equal zero. The resulting equation is the *Neutron Transport (or Boltzmann) Equation*:

$$\begin{aligned}\frac{\partial}{\partial \mathrm{t}}\mathrm{N}(\mathbf{r},\mathrm{E},\mathbf{\Omega},\mathrm{t}) = &-\mathbf{v}\bullet\nabla N(\mathbf{r},\mathrm{E},\mathbf{\Omega},\mathrm{t})\\&-\mathbf{v}\Sigma_T(\mathbf{r},\mathrm{E},\mathrm{t})\mathrm{N}(\mathbf{r},\mathrm{E},\mathbf{\Omega},\mathrm{t})\\&+\int_{0}^{\infty}\mathrm{dE}'\int \mathrm{d\Omega}'v'\Sigma_s\\&(\mathbf{r},\mathrm{t},\mathrm{E}'\rightarrow\mathrm{E},\mathbf{\Omega}'\rightarrow\mathbf{\Omega})\mathrm{N}(\mathbf{r},\mathrm{E}',\mathbf{\Omega}',\mathrm{t})\\&+\int_{0}^{\infty}\mathrm{dE}'\int \mathrm{d\Omega}'v'\sum_{\mathrm{i}}\nu_{\mathrm{pi}}(\mathrm{E}'\rightarrow\mathrm{E})\\&\Sigma_{\mathrm{fi}}(\mathbf{r},\mathrm{E}',\mathrm{t})\mathrm{N}(\mathbf{r},\mathrm{E}',\mathbf{\Omega}',\mathrm{t})/4\pi\\&+\sum_{\mathrm{j}}X_{\mathrm{dj}}(\mathrm{E})\lambda_{\mathrm{dj}}\mathrm{C_j}(\mathbf{r},\mathrm{t})/4\pi\\&+S(\mathbf{r},\mathrm{E},\mathbf{\Omega},\mathrm{t}).\end{aligned} \tag{51}$$

The conditions for solutions of this partial-differential-integral equation are the continuity condition:

$N(\mathbf{r}+\alpha\mathbf{\Omega},E,\Omega,t)$ must be a continuous function of α for $\mathbf{r}+\alpha\mathbf{\Omega}$ in the reactor, and the

boundary condition:

$N(\mathbf{r}_s,E,\mathbf{\Omega},t) = 0$, for $\mathbf{\Omega}\bullet\mathbf{n} < 0$, where $\mathbf{n}$ is an outward unit vector normal to a non-reentrant surface chosen to define the extent of the reactor.

The auxiliary equations for number densities of delayed neutron precursors, $C_j(\mathbf{r},t)$, and fission product poisons, depleting fissile isotopes, and *burnable* poisons, $\rho_i(\mathbf{r},t)$s, are simply defined as movement of these isotopes in space can be ignored. *Burnable* poisons are elements with large neutron absorption cross sections (e.g., Boron, Hafnium, Cadmium,

Erbium, Gadolinium) that can be included in reactor designs to maintain neutron balance over design lifetime.

- For delayed neutron precursors:

$$\frac{\partial}{\partial t} C_i(\mathbf{r}, t) = -\lambda_i C_i(\mathbf{r}, t) + \int_0^\infty dE' \int d\Omega' \sum_j \xi_{ij} \nu' \Sigma_{fj}(\mathbf{r}, E', t) N(\mathbf{r}, E', \Omega' t), \quad (52)$$

where ξ_{ij} is the expected number of precursors of type i produced by fission of isotope j.

- For fission product poisons (e.g., Xenon-135 and its precursors Telirium-135 and Iodine-135, and Samarium-149 and its precursors Neodimium-149 and Promethium-149):

$$\frac{\partial}{\partial t} \rho_i(\mathbf{r}, t) = -\lambda_i \rho_i(\mathbf{r}, t) + \lambda_{j \to i} \rho_j(\mathbf{r}, t) - \int_0^\infty dE' \int d\Omega' \rho_i(\mathbf{r}, t) \sigma_{c^i} (E') \nu' N(\mathbf{r}, E', \Omega', t) + \int_0^\infty dE' \int d\Omega' \sum_k \gamma_{ik}(E') \sum_{fk} (\mathbf{r}, E', t) \nu' N(\mathbf{r}, E', \Omega', t), \quad (53)$$

where $\gamma_{ik}(E)$ is the expected number of poison (or poison precursor) nuclei produced by fission of isotope k induced by neutrons of energy E.

- For fissile fuel and burnable poison isotopes:

$$\frac{\partial}{\partial t} \rho_i(\mathbf{r}, t) = -\int_0^\infty dE' \int d\Omega' \rho_i(\mathbf{r}, t) \sigma_{a^i}(E') \nu' N(\mathbf{r}, E', \Omega', t), \quad (54)$$

where the subscript "a" as applied to $\sigma_a{}^i$ conventionally refers to capture plus fission for fissile isotopes. For reactor designs containing fertile isotopes, equation Eq. 54 will have a source term reflecting the transmutation process leading to the fissile isotope "i" (see Fig. 1). Additional "auxiliary" equations may be needed to deal with transmutation of one isotope of a burnable poison to another, which has a significant neutron capture cross section (for example Hafnium, which has four naturally occurring isotopes).

Solving these "auxiliary" equations, irrespective of their number, is not a calculational challenge, given one knows the neutron density, N(**r**.E,**Ω**,t), as they are ordinary differential equations. Obviously, solving the neutron transport equation (Eq. 51) for N(**r**,E,**Ω**,t) is another matter. There are several features of fission reactors, however, that make this task more tractable. First, the density of neutrons needed to produce as much power as can be removed/transferred from various reactor types to do useful work is very small, $\sim 10^7$–10^9 #/cm^3, where as the density of nuclei is many orders of magnitude larger $\sim 10^{23}$ #/cm^3. Therefore, the neutrons can be viewed as a very dilute gas in the matrix of a reactor's nuclei, and thus neutron–neutron collisions can be ignored (they have not been accounted for in Eq. 51) (Another neutron behavior that can be ignored in formulating the transport equation is the finite lifetime of a free neutron. Its mean-life is ~11.5 min. But, as will be discussed in the next section, the lifetime of neutron in a reactor is measured in milliseconds.). Second, in the primary nuclear design calculations, where it is determined if a trial configuration, loading and geometry, of fuel, structure, moderator, coolant, control elements, and poisons, can sustain neutron balance through out the reactors lifetime objective, the time variable "t" in Eq. 51 can be treated in a much simplified manner. Given the initial conditions of a trial reactor configuration, it is a good assumption that the atom densities in the various macroscopic cross sections in Eq. 51 can be treated as nearly constant for a significant time interval, $\Delta t \geq$ minutes. With this assumption, and no neutron–neutron collisions, Eq. 51 is linear in N(**r**,E,**Ω**,t) during Δt, and solution methods for Eq. 51 are greatly simplified. In addition, for the interval, Δt, Eq. 51 can be treated as a time-independent equation. For a *primary nuclear design* calculation, one ignores the source term S(**r**,E,t) (its importance to the start-up problem will be addressed in the next section) and Eq. 51 becomes a linear homogeneous eigenvalue problem:

$$\mathbf{v}\Omega \bullet \nabla \cdot \mathrm{N}(\mathbf{r},\mathrm{E},\Omega) + v\Sigma_{\mathrm{T}}(\mathbf{r},\mathrm{E})\mathrm{N}(\mathbf{r},\mathrm{E},\Omega)$$
$$-\mathrm{v}\int_0^\infty \mathrm{d}E' \int \mathrm{d}\Omega' v'\Sigma_{\mathrm{s}}(\mathbf{r},\mathrm{E}' \to \mathrm{E},\Omega' \to \Omega)\mathrm{N}(\mathbf{r},\mathrm{E}',\Omega')$$
$$= \frac{1}{\mathrm{k}}\int_0^\infty \mathrm{d}E' \int \mathrm{d}\Omega' v' \sum_{\mathrm{j}} \Sigma_{\mathrm{fj}}(\mathbf{r},\mathrm{E}')$$
$$\left\{ v_{\mathrm{pj}}(\mathrm{E}' \to \mathrm{E}) + \sum_{\mathrm{j}} \mathrm{X}_{\mathrm{di}}(E)\xi_{\mathrm{ij}} \right\} \mathrm{N}(\mathbf{r},\mathrm{E}',\Omega')/4\pi, \tag{55}$$

where 1/k is the eigenvalue. It has been customary to use the inverse of "k" as the eigenvalue and to refer to k as the multiplication factor. Note that if Eq. 55 is integrated over the reactor volume and E and $\mathbf{\Omega}$, then k is equal to the ratio of neutron production to neutron loss, this is the origin of its designation as a "multiplication factor." A further simplification in Eq. 55 arising from the assumption of "time independence" during Δt, is that delayed neutron production can just be added to prompt neutron production. As indicated, previously delayed neutrons, though less than a percent of total neutron yield in a fission, are critical to transient reactor behavior, and, therefore, control system design, to be covered in the next section.

Before proceeding with the solution methods for Eq. 55, a description of how the *primary nuclear design* calculation proceeds is required for a basic understanding of reactor design, and to provide perspective on the utility of the various solution methods for the transport equation. Assuming the solution method chosen has yielded a k_i and N_i ($\mathbf{r}$,E,$\mathbf{\Omega}$) for the initial time interval, Δt_i where i = 1, then one proceeds to check design requirements, and make needed modifications to the reactor's initial *trial configuration*. In general, this is an iterative process including other disciplines (i.e., heat transfer and fluid flow, structural analysis). If $k \neq 1$, inventories of fuel/poisons or the positioning of control elements will need to be altered to achieve neutron balance (*Control elements* (sometimes generically called control rods) are structures incorporating highly neutron absorbing isotopes. They have a dual role in fission reactor design: (1) assuring criticality (a controlled steady state chain reaction) throughout a reactor's design lifetime, i.e., compensating for potential excess neutron production from the initial fissile loading which must be large enough to accommodate depletion; and (2) providing safe shut down (termination of the chain reaction) of the reactor in case of an accident condition or during a planned interruption of normal operations (e.g., for plant maintenance or refueling). The same "structures" could accomplish both functions or there could be separate structures (sometimes referred to as "shim" and "shutdown" rods respectively).). The power distribution throughout the reactor must then be determined. As N($\mathbf{r}$,E,$\mathbf{\Omega}$) is the solution to a homogeneous equation, its absolute magnitude is undetermined, but a normalization factor, *p*, can be established from the total thermal power rating, P(MWth), requirement of the design, that is from:

$$\mathbf{P} = p \int_{\mathrm{RVol.}} \mathrm{d}^3 r \int_0^\infty \mathrm{dE} \int \mathrm{d}\Omega v \sum_{\mathrm{j}} \varepsilon_{\mathrm{j}}\, \Sigma_{fj}(\mathbf{r},\mathrm{E})\mathrm{N}(\mathbf{r},\mathrm{E},\Omega), \tag{56}$$

where ε_j is the energy release per fission of isotope j (see Table 3). Now given pN($\mathbf{r}$,E,$\mathbf{\Omega}$), one can calculate the power distribution throughout the reactor

$$\mathbf{P}(\mathbf{r}) = p \int_0^\infty \mathrm{dE} \int \mathrm{d}\Omega v \sum_j \varepsilon_{\mathrm{j}} \Sigma_{fj}(\mathbf{r},\mathrm{E}) N(\mathbf{r},\mathrm{E},\Omega), \tag{57}$$

and determine peak powers in fuel elements, and average and peak heat fluxes into coolant channels. Thus, fuel element and heat removal system limits can be checked. If there are violations, the *trial configuration* must be altered and new results for k and N($\mathbf{r}$,E,$\mathbf{\Omega}$) found. From the power distribution and subsequent thermal analysis, one can also verify the temperatures that were assumed for the *trial configuration*, that is, the temperatures that were needed to define thermal scattering cross sections and Doppler broadened resonance cross sections. Finally, when all conditions are met for the first time interval, Δt_i, where i = 1, the *auxiliary* equations (Eq. 53 and Eq. 54) can be solved to update inventories of fuel and poisons for the next time interval, Δt_2. For a thermal reactor design, where the fission product poisons Samarium-149 and Xenon-135, are important, initial time intervals should be short (minutes) until equilibrium levels of these isotopes are achieved (~hours). Subsequent time intervals can be many hours. From this brief description of the *primary nuclear design process*, it should be clear that

having accurate and efficient solution methods for the time-independent neutron transport equation is key to achieving a successful design.

There are two basic approaches to solving the time independent neutron transport equation, Eq. 55; the probabilistic-statistical Monte Carlo simulation method [14] where individual neutrons are traced through their life experience in a reactor, and analytic methods where the variables, **r,** E, and (sometimes) $\mathbf{\Omega}$, are made discrete, thus transforming Eq. 55 into a matrix equation.

Monte Carlo simulation is in principle well suited for this application because the neutron density is low so the transport equation can be treated as linear. Thus, each "experiment," that is, neutron history, is independent of all others. Initially, a neutron is started at a randomly selected reactor location and with a randomly selected direction, $\mathbf{\Omega}$. Its initial energy is selected by treating a typical prompt neutron energy spectrum as a probability distribution:

$$P(E)dE = v_p(E)dE/\int_{E_{min}}^{E_{max}} dEv_p(E), \tag{58}$$

which is then "sampled" with a random number between 0 and 1. In Monte Carlo computer programs [15, 16] a sequence of random numbers is generated with an algorithm. To provide an example of "sampling," note that in this case, given a random number *n*, the "sampled" starting energy E is found by simply solving the transcendental equation:

$$n = \int_{E_{min}}^{E} dE'P(E')\text{for}E. \tag{59}$$

Now having a speed and direction, one can "sample" (with a new random number) the probability that the neutron travels a distance x before having a collision, using equation Eq. 20. As this probability depends on the total macroscopic cross section, $\Sigma_T(\mathbf{r},E)$, one must keep track of material boundaries. An initial sampling will be for the distance from the starting point of the neutron to the first material boundary it could cross. If the initial sampling results in the boundary being crossed, then there is a new Σ_T and a second sampling is performed to determine if another boundary is crossed. Eventually, either the neutron leaves the reactor or the location of the first collision is established. As the total cross section is the sum of capture, scattering, and possibly fission macroscopic cross sections for the various isotopes present, one can treat the relative magnitudes of the components of the sum as a probability distribution, which when "sampled" leads to the next step in our neutron's history. If capture is the result, the history ends, just as it would end if the neutron leaked (escaped) from the reactor. Either capture or leakage is recorded as a "loss." If fission is the result, the history also ends, but the number of neutrons produced (1, 2, or 3) in the fission of the "selected" isotope j, and the fission location are recorded. The number of fission neutrons is determined by "sampling" the probability distribution for fission yield of isotope j. The mean of the distribution $\overline{\nu}_j(E)$ includes delayed neutrons. The number of neutrons produced by a "history" is counted as "production." If scattering is the result of the collision then the double differential macroscopic cross section is treated as probability distribution and "sampled" to provide a new energy and direction for the neutron. Then, the process of tracking to either escape or the next collision is repeated. Thus, the "history" proceeds until it ends as either "loss" or "production", if "production" a starting point for a subsequent "history" and a location for energy deposition are also provided.

There are various strategies for carrying out Monte Carlo calculations and the evaluation of the statistical nature of the results. A standard approach, in outline, is to run successive groups of "histories" (thousands). Discard the first few groups, which are used to establish a reasonable fission neutron spatial source distribution, and then find the mean and standard deviations of the desired calculational results from the subsequent groups. It is most economical to get good statistics for the eigenvalue k, the multiplication factor, which is just "production" over "loss," quantities which are accumulated over the whole reactor. Energy deposition, that is, power distribution, results are much more costly. Hundreds of groups with millions of histories per group would be required to give good statistics (a five percent 95% confidence interval) for the number of fissions in small reactor volumes (e.g., a 1 cm length of a typical PWR fuel element which has a volume of 0.7 cm^3, out of a reactor volume of 32.8×10^6 cm^3

(for a 3,400 MWth rating)). From this discussion, one can see why, as mentioned in section Cross Sections, Monte Carlo calculations of mock-up experiments are widely used in cross-section data set evaluations, where the results of interest are changes in k, the multiplication factor. Even with the tremendous advances in computing capability which have been made to date, Monte Carlo simulation is not as yet the main line method for primary nuclear design calculations. But, as will be seen in the following description of analytic methods, it can greatly aid in improving the accuracy of the analytic methods.

When the analytic approach of making the neutron density's variables **r,** E and **Ω** discrete is applied, so as to make the computational errors in solving the transport equation comparable to an exhaustive Monte Carlo simulation, the computer resource requirements will challenge today's largest machines (peak speeds of $\sim 2.3 \times 10^{15}$ flops (floating point operations per second) [17]).

This can be demonstrated with the large PWR used in the Monte Carlo discussion: *First*, a spatial mesh of 65.6×10^6 points would result, assuming quarter core radial symmetry, and from using a $1 \times 1 \times 2$ cm^3 cell for averaging cross sections. (The mesh may need to be finer for highly absorbing features, e.g., fixed poisons, control elements, and can be courser in homogeneous regions.) *Second*, the energy variable can be treated with a multigroup approximation where the energy range, $0.0 \rightarrow 10$ MeV is divided into intervals (groups), for example, 24 for thermal neutrons, $0.0 \rightarrow 0.625$ eV, and 57 for the rest of the range, with most of these groups allotted to epithermal neutrons, E = 0.625 eV → 0.1 MeV where there is a concentration of explicit resonance cross sections (see Table 6). A weight function f_g (**r**,E), normalized for E to unity, is required for each interval, *g*. These can be calculated with infinite medium problems representing various portions of the reactor; homogeneous problems with no spatial variables, or an infinite repeating array of cells (e.g., a fuel element and surrounding coolant) with radial spatial variables, but no axial, z, dependence. The power of the multigroup approximation is that it is insensitive to the choice of weight functions and thus simplifying assumptions can be made in selecting and solving the "infinite medium" problems to generate the f_g's. *Finally*, the direction variable, **Ω**, can be dealt with through a discrete ordinate approximation [18]. The unit sphere is divided into segments, the surface areas of which sum to 4π, and a direction vector $\mathbf{\Omega}_n$ is assigned to each segment. The segment surface areas act as weight functions when the transport equation is integrated over a segment to yield an equation for the neutron density going in the direction $\mathbf{\Omega_n}$. There are various schemes for selecting ordinates and weights, the most widely known is the S_n method. All methods, however, can produce *ray effects* if "n" is too small [19]. The channeling of neutrons into a few restricted directions can produce anomalous results in reactor designs with localized neutron source regions, that is, where fissile and fertile fuel predominate in different regions (commonly referred to as seed-blanket designs). For a "highly accurate" treatment, one should let n = 16 in each octant, for a total of 128 ordinates. So for the "large PWR example," the number of unknowns to be solved for in the discretized time-independent transport equation is 170×10^9 (=16.4×10^6 (spatial mesh points) × 81 (energy groups) × 128 (ordinates)). This is clearly a formidable calculational problem. If we view the analytic approach described here as transforming Eq. 55 into a matrix eigenvalue equation, then the simplest solution method of matrix inversion would involve matrices of a billion by a billion. Hence, an iterative method is required [20]. Much effort in reactor *theory* has been devoted to this problem, and to simplifying the analytic approach. Iterative methods for solving matrix equations are beyond the scope of this entry, but to understand how fission reactor design is actually carried out, a description of analytic approach simplifications is needed.

The direction variable, **Ω**, received the earliest attention. Because the neutron population in a reactor can be viewed as a dilute gas, it was natural to assume that the variation of the neutron density in space could be approximated by $\nabla \bullet D(\mathbf{r},E,t)\nabla vN(\mathbf{r},E,t)$ (from Fick's Law of diffusion). When the transport equation, Eq. 51, is integrated over **Ω** and the first term on the right-hand side is replaced by the Fick's Law expression, the result is the time-dependent neutron diffusion equation. Equation 55 can be treated analogously to yield the time-independent neutron diffusion equation. In either case, the limitations of the diffusion approximation

only become apparent in trying to define the diffusion coefficient D(**r**,E,t) (see Henry, Nuclear-Reactor Analysis). The most commonly used expression is

$$D(\mathbf{r}, E, t) \equiv 1/\{3[\Sigma_t(\mathbf{r}, E, t) - \overline{\mu_0}\Sigma_s(\mathbf{r}, E, t)]\}, \tag{60}$$

where $\overline{\mu_0}$ is the average of the average cosine of the scattering angle (in the laboratory coordinate system) of each isotope making up Σ_s(**r**,E,t). This definition (Eq. 60) arises from a low-order spherical harmonics expansion of N(**r**,E,**Ω**,t) in the neutron transport equation. Spherical harmonics are a complete orthonormal set of special functions on the unit sphere defined by **Ω** (the unit vector which is at angle θ from the z axis and projects in the x–y plane at angle φ from the x axis);

$$Y_l^m(\mathbf{\Omega}) = H_l^m \mathbf{P}_l^m(\mu) e^{im\varphi} \text{ for } l = 0, 1, 2, 3..... \quad m = -l \le m \le l, \tag{61}$$

where $H_l^m = \left[\frac{(2l+1)(l-m)!}{4\pi(l+m)!dm}\right]^{1/2}$, $P_l^m(\mu) = \sin^m(\mu)\frac{d^m}{d\mu^m}P_l(\mu)$ is the associated Legendre Polynomial, $P_l(\mu) = \frac{1}{2^l l!}\frac{d^l}{d\mu^l}(\mu^2 - 1)^l$ is the Legendre Polynomial and μ = cosθ. The spherical harmonics are normalized by the relationship:

$$\int_0^{2\pi} d\varphi \int_{-1}^{1} d\mu\, \overline{Y_l^m(\mu,\varphi)}\, Y_{l'}^{m'}(\mu,\varphi) = \delta_{mm'}\delta_{ll'}, \tag{62}$$

where $\overline{Y_l^m}$ is the complex conjugate of Y_l^m and the Kronecker deltas, δ, are 1 for m = m' and $l = l'$ and 0 otherwise.

The "low-order" spherical harmonics expansion, which yields the diffusion approximation, is for $l = 0$ and 1 (also referred to as the P1 approximation). The four functions in the expansion are:

$$Y_0^0 = (1/4\pi)^{1/2}, Y_1^{-1} = (3/4\pi)^{1/2}\sin\theta e^{-i\varphi},$$
$$Y_1^0 = (3/4\pi)^{1/2}\mu \text{ and } Y_1^1 = -(3/4\pi)^{1/2}\sin\theta e^{-i\varphi}. \tag{63}$$

In a Cartesian coordinate system, the expansion coefficients (for simplicity of notation the time-independent case will be treated) are N(x,y,z,E), the neutron density and N_1^{-1} (x,y,z,E), N_1^1 (x,y,z,E) and N_1^0 (x,y,z,E), which when multiplied by v (the speed corresponding to E) are the neutron currents in the x, y, and z directions. Before applying the P1 expansion to Eq. 55, one needs to note that the double differential scattering cross section, Σ_s(E' → E,**Ω'** → **Ω**) in reactor applications (where neutron polarization and Bragg scattering can be ignored) depends on **Ω'•Ω.** Then, given the addition theorem for spherical harmonics,

$$P_1(\Omega' \bullet \Omega) = \sum_{m=-l}^{l} \frac{(l-m)!}{(l+m)!} P_l^m(\mu) P_l^m(\mu') e^{im(\varphi-\varphi')}, \tag{64}$$

Σ_s(**r**,E' → E, **Ω'•Ω**) can be expanded in terms of associated Legendre polynomials. This is done in two steps: first the double differential scattering cross section is expressed as an expansion in ordinary Legendre polynomials (which are a complete orthogonal set of functions)

$$\Sigma_s(\mathbf{r}, E' \to E, \Omega' \bullet \Omega) = \Sigma_s(\mathbf{r}, E) \sum_{l=0}^{\infty} \frac{(2l+1)}{4\pi} F_l(\mathbf{r}, E' \to E)\, \mathbf{P}_l(\Omega' \bullet \Omega), \tag{65}$$

and then Eq. 64 is substituted for P_l(**Ω'•Ω**). (It should be remembered that Σ_s is a macroscopic cross section, and a more complete notation would show a sum over contributions from each isotope present in d^3r about **r**.)

Now when the P1 expansion for N(x,y,z,E,μ,φ) is inserted in Eq. 55 and the resulting equation is, in turn, multiplied by the complex conjugate of each of the four spherical harmonics functions of the P1 expansion (Eq. 63), and integrated over μ (−1 → 1) and φ (0 → 2π), four equations result: The first is

$$\begin{aligned}
&\frac{\partial}{\partial x} vN_1^{-1}(x, y, z, E) + \frac{\partial}{\partial y} vN_1^1(x, y, z, E) \\
&\quad + \frac{\partial}{\partial z} vN_1^0(x, y, z, E) = -v\Sigma_T(x, y, z, E)N(x, y, x, E) \\
&\quad + \int_0^{10Mev} dE' v' \Sigma_s(x, y, z, E')F_0(E' \to E)N(x, y, z, E') \\
&\quad + (\text{the fission term in Eq.55 with } N(\mathbf{r}, E', \Omega') \\
&\quad\quad \text{replaced with } N(x, y, z, E')).
\end{aligned} \tag{66}$$

The remaining three equations are of the same form, one is provided here:

$$\frac{1}{3}\mathbf{v}\frac{\partial}{\partial z}N(x,y,x,E) + v\Sigma_T(x,y,z,E)\,N_1^0(x,y,z,E) = \int_0^{10\text{Mev}} dE'\mathbf{v}\Sigma_s(x,y,z,E')F_1 (E' \to E)N_1^0(x,y,z,E') \tag{67}$$

With these four coupled partial-differential-integral equations, there is still considerable computational complexity. To get to the standard neutron diffusion equation, one additional approximation is made:

$$F_1(E' \to E) \cong \delta(E' - E)\mu(E'), \tag{68}$$

where $\mu(E')$ is the average cosine of the scattering angle in the laboratory coordinate system, and energy loss (or gain) in the non-isotropic component of scattering is ignored. Substituting Eq. 68 in Eq. 67, the relationship between N_1^0 and N is a simple partial differential equation:

$$N_1^0(x,y,z,E) = -\frac{1}{3(\Sigma_T(x,y,x,E) - \mu(E)\Sigma_S(x,y,z,E))}\frac{\partial}{\partial z}N(x,y,z,E), \tag{69}$$

containing the diffusion coefficient D(**r**,E) (see the definition Eq. 60). Given the equations of the same form as Eq. 69 for N_1^1 and N_1^{-1}, and substituting all three into the left-hand side of Eq. 66. The left-hand side becomes the standard Fick's Law expression:

$$-\nabla \bullet D(r,E)\nabla N(r,E) = \ldots. \tag{70}$$

As noted above, this derivation of the diffusion approximation reveals its limitations. The ability of some combination of four low-order spherical harmonic functions, Eq. 63, to describe the true angular distribution of the neutron density throughout a reactor will be limited to regions where the distribution is nearly isotropic, that is away from boundaries and highly absorbing features (control elements and fixed poisons). To address these limitations, special boundary conditions are used, and subsidiary calculations (to be discussed below) are made to provide "fitted" cross sections for highly absorbing features.

To make the diffusion approximation an efficient design tool, additional simplifications have been developed. The differencing of the energy variable as described above for "multigroups" can be extended to a "few group" approximation. Again, weight functions are generated using accurate solutions to small region "cell" problems, which model repeating features of a reactor. But here the weight functions are applied over much larger energy ranges, three or four to cover the energy range of 0 to 10 MeV. Furthermore, one accepts the error associated with the weight functions not perfectly representing the spatial variation of neutron density energy dependence.

The use of "cell problem" auxiliary calculations can be extended. As the core, the central fuel bearing region, of most reactor designs is made up of collections of mostly fuel elements, and possibly some fixed poison and movable control elements, assembled into modules. One can perform highly accurate (e.g., Monte Carlo or multigroup, fine spatial mess, discrete ordinate) calculations for two-dimensional (radial) repeating arrays representations of a core's various modules. Then, for each module type, a series of corresponding few-group diffusion approximation calculations can be carried out, in which key few group cross sections are adjusted ("fitted") to match reaction rates from the "highly accurate" reference calculation. One can the use these fitted cross sections in a full core three-dimensional few group diffusion calculation as part of the *principle design process*.

Of course, with depletion, as inventories of fuel, fission products, and poisons are updated, fitting calculations will have to be repeated. This approach is particularly suited to the design of thermal reactors, that is, PWRs and BWRs, where the proper treatment of epi-thermal and thermal neutrons, including the effects of self-shielding by fuel and poison inventories, is crucial.

In fast reactor design, where most fissions take place at energies above explicit resonances (liquid metals or gasses are coolants, and fissile and fertile densities and inventories are high (no effective moderators are present)) and the mean free path of fission neutrons is large (~10 cm.), the treatment of fuel, structure and

coolant as an homogenized material, in formulating macroscopic cross sections, is a reasonable assumption. Treatment of the energy variable is also simpler as up-scattering is not important. As a result, multigroup, 3D discrete ordinate calculations can be used in the *principle design process* for fast reactors.

Finally, returning to thermal reactor design, there is another analytic calculational approach, which is in wide use, that should be mentioned. The general designation is Nodal Methods. There are a number of variations under this title [21], but they all have as their starting point solving 2D module array problems. One needs to produce few group neutron distributions within each module. Each module (or depending on symmetry each half or quarter module) will be a "node." Then coupling coefficients between nodes, both radially and axially, are generated. (It is predominately in defining coupling coefficients that the various "methods" differ.) The resulting nodal equations can be solved with modest computer resources, but, to obtain power distributions and to update inventories the full reactor neutron distribution must be constructed from the module solutions and the weights found for each node. Nodal Methods have been found to be particularly useful in applying the *primary nuclear design process* to evaluating refueling options for commercial (large scale) PWRs and BWRs, where partially depleted modules are relocated, "shuffled," as new modules are added and fully depleted, "spent" modules removed during periodic refuelings. The computational economy of nodal methods also allows them to be applied to fully time-dependent problems, particularly for accident analyses. The nature of these problems will be discussed in the next section.

Fission Reactor Performance

In the previous section, the focus was the derivation of the neutron transport equation, and how it is solved in carrying out the *primary nuclear design process*. This quasi-static *process* involves a series of time-independent calculations of the neutron density, $N(\mathbf{r},E,\mathbf{\Omega})$, and ultimately results in the configuration and inventories (loadings) that meet design requirements for lifetime (total energy production), and normal operation thermal performance (fuel element burn-up within limits and sufficient coolant flow provided by the design pumping power allocation). There are, however, additional design requirements that involve transients, that is, $N(\mathbf{r},E,\mathbf{\Omega},t)$, which will be the subject here.

The simplest approach to treating transient reactor behavior is through a "point" kinetics model. If one first multiplies the time-dependent transport equation, Eq. 51, by a weight function, $W(\mathbf{r},E,\mathbf{\Omega})$, and integrates over the reactor volume, energy (the full range, $0 \rightarrow 10$ MeV), and direction ($\cos\theta$ from -1 to 1, φ from 0 to 2π); and second, multiplies the time-dependent equation for each delayed neutron precursor, Eq. 52 for $C_i(\mathbf{r},t)$, by $W(\mathbf{r},E,\mathbf{\Omega})X_{di}(E)$ and performs the same integration over reactor volume, energy, and direction, the results are the point kinetics equations:

$$\frac{dT(t)}{dt} - \frac{\rho-\beta}{\Lambda}T(t) + \sum_{l-1}^{l} \lambda_l C_l(t) + Q(t) \tag{71}$$

$$\frac{dC_j(t)}{dt} = \frac{\beta_j}{\Lambda}T(t) - \lambda_j C_j(t) \text{ for } j = 1,2,\ldots I \tag{72}$$

where $T(t)$ is an amplitude function;

$$T(t) \equiv \int_{\text{reactor}} dV \int_0^{10\text{Mev}} dE \int d\Omega W(\mathbf{r},E,\Omega) N(\mathbf{r},E,\Omega,t). \tag{73}$$

In formulating the expressions for the kinetics parameters, $\rho(t)$, $\beta(t)$, and $\Lambda(t)$, it is convenient to factor the neutron density into a product of "shape" and amplitude functions. The shape function is;

$$S(\mathbf{r},E,\Omega,t) \equiv N(\mathbf{r},E,\Omega,t)/T(t). \tag{74}$$

Now the weight function is defined over the same domain (space, energy, and direction) as the neutron density, and thus from the definitions Eq. 73 and Eq. 74 the normalization of S and W follows:

$$\int_{\text{reactor}} dV \int_0^{10\text{Mev}} dE \int d\Omega W(\mathbf{r},E,\Omega) S(\mathbf{r},E,\Omega,t) = 1 \text{ for all t.} \tag{75}$$

In order for the point kinetics equations to provide accurate solutions for small changes in reactor configuration, the weight function, $W(\mathbf{r},E,\mathbf{\Omega})$, is chosen to be the solution the adjoint equation corresponding to the time-independent transport equation, Eq. 55, for the

reactor of interest adjusted to be critical (i.e., the eigenvalue k = 1). In the adjoint of Eq. 55, the variable pairs (E,$\mathbf{\Omega}$) and (E',$\mathbf{\Omega}'$) are interchanged in the scattering and fission terms. The solution, $N^*(\mathbf{r},E,\mathbf{\Omega})$, is referred to as the adjoint neutron density or the importance function. The latter name indicates the physical interpretation of N^*. If the reactor described by Eq. 55 is at zero power (no neutrons) and a neutron is inserted at $\mathbf{r}$ with velocity $\mathbf{v}(E,\mathbf{\Omega})$, the neutron level will increase to a steady-state value (remember the reactor is still critical). This "level" per neutron added at ($\mathbf{r}$,E,$\mathbf{\Omega}$) is $N^*(\mathbf{r},E,\mathbf{\Omega})$. How N^*, acting as a weight function, improves the point kinetics equations will be discussed after ρ, β, and Λ are defined and their physical interpretation given. To simplify notation, the scattering and fission integral operators in Eq. 51 are represented by *A* and *G*:

$$A \equiv \int_0^\infty dE' \int d\Omega' v' \Sigma_S(\mathbf{r}, E' \to E, \Omega' \to \Omega) \bullet, \tag{76}$$

$$G \equiv \int_0^\infty dE' \int d\Omega' v' \sum_i \nu_i(E') \Sigma_{fi}(\mathbf{r}, E') \bullet, \tag{77}$$

where $\nu_i(E')$ is the total number of neutrons (prompt plus delayed) produced by fission of isotope i induced by a neutron with energy E'. In reactor kinetics, delayed neutron yields are expressed in terms of the ratio the number produced with a given half-life (i.e., a member of "delayed group," j, as noted previously, see Table 4) by fission of isotope, i, to the total the total yield, ν_i. These ratios are represented as β_j^i, where normally j = 1,2 . . . 6.

The parameter ρ(t) is the *reactivity* of a reactor and is a measure of how far from criticality (a steady-state chain reaction only from fission neutrons, no other neutron sources present) the reactor is at time t. This can be seen from the expression for ρ(t) that results from the derivation of Eq. 71 from the transport equation (where the functional dependencies on $\mathbf{r}$, E, $\mathbf{\Omega}$, and t are understood for Σ_T, W, and S):

$$\rho(t) \equiv \frac{\int_{\text{reactor}} dV \int_0^\infty dE \int d\Omega W[-v\Omega \bullet \nabla S - v\Sigma_T S + AS + \sum_i X^i(E) GS]}{\int_{\text{reactor}} dV \int_0^\infty dE \int d\Omega W \sum_i X^i(E) GS}, \tag{78}$$

where $X^i(E)$ is the total fission spectrum for isotope i:

$$X^i(E) \equiv X_p^i(E)\{1-\beta^i\} + \sum_{j=1}^{6} X_{dj}(E)\beta_j^i. \tag{79}$$

Now note, if both the numerator and denominator of Eq. 78 are multiplied by the amplitude function T(t), and W is taken as 1, then the numerator is the total neutron production rate minus loss rate for the reactor. (When the first term in the bracket in the numerator is integrated, and Gauss' theorem is applied, it yields the total neutron leakage rate from the reactor.) Similarly, the denominator is the total neutron production rate. Reactivity is a dimensionless parameter whether or not W is unity. If it is zero, the reactor is critical, if negative, subcritical and if positive, supercritical.

β_j in Eq. 72 is the *effective delayed neutron fraction* for the jth precursor group, and β in Eq. 71 is the sum of the βj's:

$$\beta_j \equiv \frac{\int_{\text{reactor}} dV \int_0^\infty dE \int d\Omega W \sum_i X^i(E)\beta_j^i GS}{\int_{\text{reactor}} dV \int_0^\infty dE \int d\Omega W \sum_i X^i(E) GS}. \tag{80}$$

As with the expression for reactivity, multiplying the numerator and denominator of Eq. 80 by T(t) and letting W = 1, one sees that in this case β_j is the fraction of total fission neutrons produced in the reactor by precursor group j.

The parameter Λ is the *prompt neutron lifetime* and is defined as:

$$\Lambda \equiv \frac{\int_{\text{reactor}} dV \int_0^\infty dE \int d\Omega WS}{\int_{\text{reactor}} dV \int_0^\infty dE \int d\Omega W \sum_i X^i(E) GS}. \tag{81}$$

Again multiplying the numerator and denominator by T(t) and taking W = 1, one sees that Λ equals the number of neutrons in the reactor divided by the rate of neutron production by fission. If the reactor is critical, Eq. 81 has the same form as the "fundamental equation of radioactive decay," Eq. 11, and Λ can be thought of as the "mean lifetime" of a neutron born into the reactor. In the point kinetics equations, Λ is the mean *prompt neutron lifetime,* and the timing

of the appearance of delayed neutrons is treated explicitly through the behavior of their precursor, $C_j(t)$ j = 1,2 . . . . I (usually = 6).

The derivation of the point kinetics equations directly from the time-dependent neutron transport equation has been presented here to provide perspective on approximations that are normally made to make the generation of the point kinetics parameters (ρ, β, and Λ) practical. If Eq. 51 and its *auxiliary* equations could be readily solved for $N(\mathbf{r},E,\mathbf{\Omega},t)$, there would be no need for the point kinetics equations. As it turns out, however, "practical" approximations follow from the approaches described in the previous section for solving the time-independent transport equation. Henry in *Nuclear-Reactor Analysis* derives the point kinetics equations starting with the diffusion approximation (with energy a continuous variable). One could just as well start with a few group diffusion approximation which would provide a shape function (a vector) and from the adjoint of the few group diffusion equation, a weight function (also a vector). The advantage of using an adjoint weight function, irrespective of the approximation to the transport equation one starts from, is in calculating reactivity, ρ(t). In transients of interest in design, ρ(t) is the driver. It reflects changes in cross sections with time due to variations in temperature (coolant density, Doppler effects) and configuration (control rod motion). In whatever form Eq. 78 takes, given the neutron transport approximation used, if a changing cross section is represented as a starting value plus a time-varying small delta, $\delta_\Sigma(\mathbf{r},E,t)$, and the shape function is represented as a time-independent function (e.g., from the initial neutron density of the reactor, the same problem that generates the adjoint) plus a time-dependent small delta, $\delta S(\mathbf{r},E,t)$, then the resulting calculation of ρ(t) will to first order in deltas only depend on $\delta_\Sigma(t)$'s. Higher order terms can be ignored, and one does not need to calculate a time-dependent shape function. This is a classic perturbation problem. Henry (chapter 7) provides a detailed derivation.

The time dependence of $\beta_j(t)$ and Λ(t), Eq. 80 and Eq. 81, as used in the point kinetics equations can be ignored in most applications. Measured values of β (and the β_j^i from which it is summed) can be used directly (Table 4). If adjoint weighting is used, the β's will be a bit larger than the physical β's in a thermal reactor due to the increased "importance" of delayed neutrons with their lower initial energies (relative to prompt neutrons). Prompt neutron lifetimes primarily depend on the reactor type; for thermal reactors they are on the order of $\sim 10^{-3}$ s, and for fast reactors as short as 10^{-7} s. They can be measured in zero power reactor mock-up experiments as ratios with β and ρ, or calculated directly from equation Eq. 81 with the approximations for W and S used to obtain ρ. A highly accurate calculation of Λ can be made with a Monte Carlo simulation where neutrons are introduced from the prompt neutron energy spectrum with an S(t = 0) spatial distribution. Each history would be timed and terminated with neutron absorption (capture plus fission) or leakage. The "times" will yield the mean and standard deviation of the prompt neutron lifetime.

One further note on reactivity, if a perturbation of a critical reactor configuration can be viewed as nearly instantaneous, that is, a step change, then a good estimate of reactivity addition or subtraction can be found by solving the eigenvalue (time independent) problem for the perturbed reactor:

$$\rho = 1 - 1/k, \tag{82}$$

and if the initial reactor configuration is subcritical then the reactivity addition from a "step" perturbation can be found by performing two eigenvalue problems, the perturbed case as before, and one for the initial subcritical configuration (ignoring any nonfission source);

$$\rho = 1/k_o - 1/k, \tag{83}$$

where k_o (<1) is the initial subcritical eigenvalue. As reactivity is a dimensionless ratio, it is often given as a percentage or in units of β (as defined by Eq. 80). In the latter case, the "units" are traditionally dollars and cents. If ρ equals β, the reactivity addition is 1 dollar; if ρ equals 0.5β the reactivity addition is 50 cents. If a dollar of reactivity is added to a critical reactor, it is said to be prompt critical (critical on prompt neutrons alone) and delayed neutrons will not mitigate the resulting transient, a condition obviously to be avoided.

The motivation for the description of point kinetics provided here is best provided by Henry:

- "Since mean free paths are fairly long and since the lifetimes of neutrons in a reactor are quite short, the effects of local perturbations on" N(**r**,E,**Ω**,t) "will quickly spread throughout a reactor. The immediate consequences of perturbing a reactor locally (for example by changing a control rod slightly) is thus a readjustment of the shape of the" neutron density. In many cases this readjustment is slight and is completed in a few milliseconds; after that the readjusted shape rises or falls as a whole depending on whether the initial perturbation increases or decreases k_{eff}. For reactors in which transients proceed in this manner, merely being able to predict the change in *level* of the neutron density "is sufficient to permit a very accurate prediction of the consequences of perturbation."

With today's computer capabilities, solving point kinetics problems is not a great challenge, even with time-dependent reactivity reflecting feedback from power changes in the reactor. Henry and Duderstadt provide descriptions of applicable calculational methods (development of which inspired great ingenuity in the past). In any case, to quote Henry again, point kinetics solutions provide "very accurate predictions of the consequences of (reactor) perturbations." Thus, their utility in assuring that a reactor design satisfies fundamental transient requirements. Under normal operating conditions, a reactor must be inherently stable, that is, self-limiting. Reactivity must be reduced with increased temperature; that is, with reduced coolant density, increased mean thermal neutron energy, and Doppler broadening of resonance cross sections. These phenomena are dependent on reactor type. Clearly change in thermal neutron spectra is unimportant in a fast reactor. However, if coolant density decrease results in voiding, reactivity will dramatically decrease in a thermal reactor, but in a liquid metal cooled fast reactor increased leakage must outweigh a higher energy neutron spectrum (and an increased fission to capture ratio in fuel) to assure a negative reactivity effect. Also movement of control rods must reduce reactivity when reactor shutdown is desired. Some movable poisons, power shimming control rods, could be included in a design to flatten (make more uniform) the power distribution throughout life. (Power flattening can reduce coolant pumping power requirements. As coolant flow must meet the heat removal needs of the hottest region of the reactor, minimizing excess flow to cooler regions increases overall power plant efficiency.) But, one must assure that the operating strategy for using such rods does not compromise the speed of reactor shutdown when it is required to deal with an accident condition.

Point kinetics models can also aid in assessing *Xenon override* requirements for thermal reactors. Xe^{135} with its extremely large thermal neutron capture cross section ($\sigma_c = 2.7 \times 10^6$ b at E = 0.023 eV, for comparison $\sigma_f^{U235} = 577$ b at 0.023 eV) is the most important fission product poison. It is produced directly from fission and by decay of its precursor I^{135} (which is a direct fission product and has short-lived precursors, $Sb^{135} \rightarrow Te^{135} \rightarrow I^{135}$). Both Xe^{135} and I^{135} have half-lives measured in hours ($T_{1/2}^{Xe} = 9.14$ h, $T_{1/2}^{I} = 6.58$ h). So, a point kinetics reactor model will show that when a reactor is started up, Xe^{135} and I^{135} build up to equilibrium levels in about 30 h. Their levels, inventories, will depend on power level, that is, neutron density, and the reactor design must have enough excess reactivity (e.g., control rods that can be withdrawn, or for a PWR, a soluble poison in the coolant whose concentration can be reduced) to "override" the negative reactivity perturbation of neutron capture by Xe^{135} (iodine neutron capture can be ignored). In addition, when a thermal reactor is shut down, Xe^{135} builds up as loss by neutron absorption stops and decay of I^{135} continues. The Xe^{135} inventory peaks in about 10 h to approximately three times its equilibrium level and subsequently decays. It is back to its equilibrium level in $\sim$ 40 h (see Fig. 8).

Clearly additional "excess reactivity" is required to deal with a post-shutdown Xenon transient. Eventually, not being able to provide (and control) this excess reactivity can limit the useful lifetime of a thermal reactor design. As a historical aside, it was John Wheeler [3] who recognized the role that Xe^{135} and I^{135} could play in the operation of a thermal reactor. He explained the initial difficulties in operating the first plutonium production reactor at the Hanford Washington site.

While point kinetics can deal with most reactor design transient requirements, there are instances where significant spatial effects must be accounted

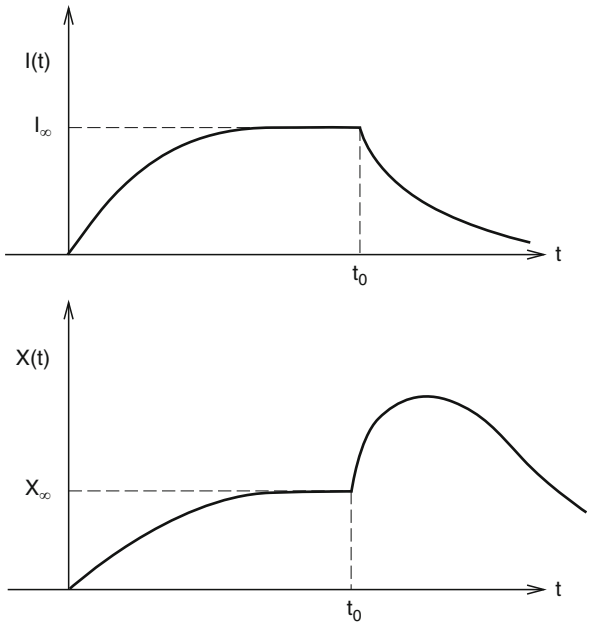

Fission Reactor Physics. Figure 8
Schematic of I^{135} and Xe^{135} inventories following an initial reactor start-up and subsequent shutdown after equilibrium levels have been reached (i.e., at t_0). (Duderstadt)

for. In the normal operation of a large thermal reactor, there is the potential for spatial oscillations of Xenon concentrations, and therefore neutron density and power. These oscillations may not affect criticality and might only be observed by the reactor instrumentation system's ability to measure power distributions in core. The period of these oscillations would be many hours and thus limits on coolant channel performance and fuel temperature could be compromised for extended time intervals. Space-time calculations of neutron density have to be carried out to determine if a particular design has a propensity for these oscillations. If the design is not inherently stable, its instrumentation must provide detection and an operating strategy must be devised to suppress any oscillation initiation. With modern computing capability, few group diffusion approximations to the time-dependent transport equation, Eq. 51 (with explicit spatial mesh or nodal methods), can deal with Xenon oscillation evaluations [22].

There are certain reactor plant accident scenarios, which also require space-time calculations. To deal with these, nodal methods, as described in section "Neutron Distributions", have been incorporated in safety analysis programs (see for example [23]), which model a full power plant; the reactor, its neutronics, fluid mechanics and structural integrity; and the balance of the plant, instrumentation, coolant/working fluid to power conversion, and safety systems (containment, emergency coolant injection and power supply). There are two classes of accidents where space–time effects in the reactor are important. First is "rod ejection," where a single control rod or group of control rods is rapidly withdrawn with a large reactivity addition and neutron distribution change, in no way a small perturbation in the point kinetics sense. Second is a "cold water accident" applicable to a PWR. In this case, in a plant with multiple piping "loops" carrying coolant to the reactor, if one of the loops is not functioning so that water in the loop has cooled below the normal inlet temperature of the reactor, and the loop is reactivated (its pump turned on and isolation valves (if any) opened), while the reactor is critical, there can be large asymmetric reactivity insertion, again, this is not a small perturbation problem.

Finally, there is an additional aspect of reactor neutron time variation, which has interesting *Physics*. The transport equation, derived in section "Neutron Distributions", is for the *mean* neutron density, $N(\mathbf{r},E,\mathbf{\Omega},t)$, but clearly as neutron interactions and production, and fission product decay are inherently probabilistic, there are fluctuations in the neutron population in a reactor (and as there are in delayed neutron precursor populations). These fluctuations were recognized early on in the Manhattan Project and are also referred to as neutron noise [24]. There are several approaches to modeling of the phenomena. The most fundamental is based on the derivation of the neutron transport equation from the quantum Liouville equation (Osborn and Yip [25]). This derivation is extended to produce an equation for the neutron doublet density, $N^{NN}(\mathbf{r},E,\mathbf{\Omega},\mathbf{r}',E',\mathbf{\Omega}',t)$, the expected number of neutrons in d^3r about $\mathbf{r}$, with energies in dE about E, going in the solid angle $d\Omega$ about $\mathbf{\Omega}$ times the expected number in d^3r about $\mathbf{r}'$, and so on for E' and $\mathbf{\Omega}'$, where as in the transport equation neutron–neutron collisions are ignored. Additional equations for neutron–precursor and precursor–precursor doublet densities are produced to complete the set of equations needed to

solve for N^{NN}. One also needs equations for the "mean" (in Osborn's nomenclature, singlet) neutron and precursor densities, which were derived in section "Neutron Distributions" (Eq. 51 and Eq. 52). Being able to solve for N^{NN} is, however, not sufficient to predict the results of neutron "noise" experiments in a reactor. Equations for doublet and singlet densities for events (D) in detectors (e.g., pulse or continuous currents in an ionization chamber) are also needed. With N^{DD} and N^{D} one can predict variance to mean ratios of counts or the power spectral density of the current in a single detector, and the cross power spectral density of currents in two detectors [26]. These experiments are usually performed in a reactor in a steady-state condition (in the mean of course) at zero power, critical or slightly subcritical, to obtain estimates of point kinetics parameters. These experiments have the advantage of verifying expected kinetic performance without putting the reactor into a transient. They are performed at low neutron levels because as power is increased fluctuations become negligible relative to the mean. Detector noise measurements (psd and cpsd) are sometimes made at power in operating reactors to monitor for unplanned mechanical motion, or loose parts. Modeling for these measurements is deterministic.

Fluctuations in neutron populations must be considered in developing initial start-up procedures for a newly constructed reactor (In a reactor design which incorporates fuel (including fission products and transuranics) from a previously operated reactor, natural source levels will most likely be high enough to allow "fluctuations" to be ignored.). The mean neutron density before start-up depends on an external source of neutrons, $S(\mathbf{r},E)$ (not from neutron reactions, Eq. 50) which, as part of the design, could be adjacent or internal to the reactor. At start-up, the reactor is subcritical ($k < 1$) and the mean neutron population, in a point reactor sense, is $N = \Lambda S(k/(1-k))$. In outline, the steps to bring the reactor critical are to pull control rods up (down in most BWR designs) from their fully inserted position so as to insert some precalculated amount of reactivity and then wait for a new steady neutron level to be achieved. The subcritical neutron level is monitored by the reactor's source range detectors. A power reactor is instrumented with detectors for the full range of expected neutron levels. These pull-and-wait steps are repeated until the reactor is slightly super critical, and thus the neutron level is observed to be on a continuously increasing, but easily controlled, trajectory. A pull-and-wait procedure needs to account for neutron level fluctuations because if the observed level, due to a minimizing fluctuation, is below the expected (mean) level when the reactor is actually close to its critical configuration, then the next "pull" might produce an unacceptable rapidly increasing trajectory [27]. The simplest way to avert a problem with a pull-and-wait procedure is to assure that the sources provided in the design (In a reactor design which incorporates fuel (including fission products and transuranics) from a previously operated reactor, natural source levels will most likely be high enough to allow "fluctuations" to be ignored.) are strong enough to render subcritical neutron fluctuations negligible. Of course, one has to understand neutron level fluctuations to make this assessment [28].

Future Directions

Fission reactor development, since its inception, has progressed with advances in computing capability. Early on, analog computers were used for transient analyses, but digital computers have been the primary tool. Design codes have been adapted to advancing digital technology; scalar processing, then vector processing and now massively parallel processing. This is an active field today and should continue to be so, particularly as the drivers for improve computer technology are universal. In section "Neutron Distributions" the two approaches to solving the neutron transport equation, Monte Carlo simulation and analytic methods (differencing variables and solving the resulting matrix equations) were described. Parallel computing would appear to be well suited to Monte Carlo as independent histories can be run on the various (1,000's of) processors simultaneously. There is, of course, the need to provide the reactor configuration (geometry, nuclide inventories, and cross sections) and the Monte Carlo code itself to each processor that runs a history. This challenge is being accepted with considerable success as exemplified by the accomplishments of the Los Alamos National Laboratory group working on the MCNP code [15] and the joint effort at the Knolls and Bettis Atomic Power Laboratories on the MC21 code [29]. Advocates of the analytic approach

have, however, not accepted the ultimate triumph of Monte Carlo. This is clear in the work of a group at the Argonne National Laboratory, which has modestly named their multigroup, discrete ordinate code UNIC, for Ultimate Neutronic Investigation Code [30]. They are demonstrating impressive results for fast reactor designs. Competition in supercomputer development and in attendant codes for nuclear reactor design bodes well for better products in the future.

Physicists in their efforts to understand the atomic nucleus have made myriad measurements and only partially by design these have included the neutron and gamma cross sections, and fission product yields (and their decay mechanisms) needed for the development of fission reactors. Today, work on this reactor-related data is focused on establishing well-founded uncertainty measures. The Cross Section Evaluation Working Group of the National Nuclear Data Center refers to this effort as covariance evaluation [31]. This is particularly appropriate, for as discussed above, one expects calculational methods to improve with computer power and code development. Thus, in assigning error bounds in design, the uncertainty in basic data will become more important relative to the contribution of calculational error (e.g., Monte Carlo statistics or differencing and convergence error in analytic methods). More well-founded and hopefully smaller design error bounds can obviously be taken advantage of in future reactor development. Improving error bounds is also consistent with the approach to overall power plant safety analysis being fostered by many of the world's nuclear regulatory agencies. They favor best estimate analyses plus the assignment of rigorously defined uncertainty factors for various classes of accident conditions. Reactor design error is only a contributor to a safety analysis "uncertainty factor," but for power plant technology to advance, "reactor design" must do its part.

Much of the research for a next generation of fission reactor power plants is focused on higher operating temperatures. Today's thermal reactor plants, PWRs, BWRs, and CANDU (heavy water moderated) have outlet reactor coolant temperatures, T_H, of $\sim 600°F$, and thus thermal (Rankine cycle) efficiencies in the low 30%. Raising T_H would increase cycle efficiency and lower fuel cost, and provide high-temperature process heat (possibly for a catalytic hydrogen production process). Higher operating temperatures in a water (or heavy water) environment present core and structural materials challenges. There likely will be a need for additional resonance cross-section data for some additives (e.g., Manganese and Chrome) to new high-temperature materials. Fast reactors (liquid metal or gas cooled) operate at much higher temperatures than thermal reactors but also require much higher fissile inventories to attain criticality. Experience with design and operation of these reactors is limited (especially for gas cooled reactors) compared to thermal reactors. Their future development with emphasis on the burning of unwanted transuranics as well their traditional mission of efficient conversion of fertile isotopes (U^{238} and Th^{232}) to fissile isotopes (Pu^{239}, Pu^{241} and U^{233}) will stimulate some cross-section work. But, both thermal and fast reactor development will most likely benefit more from advances in branches of physics other than Nuclear, particularly Condensed Matter and Fluid Mechanics. The need for nuclear power, both economic and environmental (if they can be separated?), will drive fission reactor development. While Uranium and Thorium are abundant in the earth's crust, power demand will push reactor development to most efficiently exploit the highest grade ores, which will likely lead to a mix of fast and thermal reactors. In any case, physics as well as engineering will play key roles in this development.

Bibliography

Primary Literature

1. Wheeler JA (1967) Mechanism of fission. Phys Today 20(11): 49–52
2. Bohr N, Wheeler JA (1939) The mechanism of nuclear fission. Phys Rev 56:426
3. Ford KW (2009) Wheeler's work on particles, nuclei, and weapons. Phys Today 62(4):29
4. Fermi E, Szilard L (1955) Neutronic reactor. US Patent 2,708,656, 17 May 1955
5. Einstein A (1905) On the electrodynamics of moving bodies. Ann Phys 17:891–921
6. Frankel S, Metropolis N (1947) Calculations in the liquid-drop model of fission. Phys Rev 72:914
7. Kinsey R (1979) Compiler "ENDF/B Summary Doc." BNL-NCS-17541(ENDF-201), 3rd edn. ENDF/B-V, Brookhaven National Laboratory, Upton
8. England TR, Wilson WB, Stamatelatos MG (1976) Fission product data for thermal reactors. EPRI-NP-356, Los Alamos Scientific Lab., New Mexico

9. Parks DE, Nelkin MS, Wikner NF, Beyster JR (1970) Slow neutron scattering and thermalization with reactor applications. Benjamin, New York
10. MacFarlane RE (1994) The NJOY nuclear data processing system, Version 91, report #LA-12740-M, Los Alamos National Laboratory, New Mexico
11. Breit G, Wigner E (1936) Capture of slow neutrons. Phys Rev 49:519
12. Beckurts KH, Wirtz K (1964) Neutron physics. Springer, Berlin
13. Larson NM (2006) Updated user's guide for SAMMY: multilevel R-matrix fits to neutron data using Bayes' equations, ORNL/TM-9179/R7. Oak Ridge National Lab, OakRidge
14. Spanier J, Gelbard EM (1969, 2008) Monte carlo principles and neutron transport problems, Dover, New York, Addison-Wesley, Reading
15. X-5 Monte Carlo Team (2003) MCNP – A general Monte Carlo N-Particle transport code, Version 5, LA-UR-03-1987, Los Alamos National Laboratory, New Mexico
16. Ondis LA II, Tyburski LJ, Moskowitz BS (2000) RCP01 – a Monte Carlo program for solving neutron and photon transport problems in three dimensional geometry with detailed energy description and depletion capability, B-TM-1638. Bettis Atomic Power Laboratory, West Mifflin
17. TOP 500 Super Computing Sites, www.Top500.org
18. Lathrop KA (1972) Discrete-ordinates methods for the numerical solution of the transport equation. Reactor Technol 15:107
19. Lathrop KA (1971) Remedies for ray effects. Nucl Sci Eng 45(3):355–68
20. Varga RS (2000) Matrix iterative analysis, 2 Revised and Expandedth edn. Springer, Heidelberg
21. Henry A, Dias A, Frances W, Parlos A, Tanker E, Tanker Z (1986) Continued development of nodal methods for nuclear reactor analysis, MIT EL 86-002. Massachusetts Institute of Technology, Cambridge
22. Buslik AJ, Weinreich WA (1967) Variational calculation of complex natural modes of xenon oscillation, WAPD –TM-673 (LWB-LSBR Development Program). Bettis Atomic Power Laboratory, West Mifflin
23. Idaho National Laboratory (2009) RELAP5-D, www.INL.gov
24. Thie JA (1963) Reactor noise (an AEC monograph). Rowman and Littlefield, New York
25. Osborn RK, Yip S (1966) Foundations of neutron transport theory, Monograph series on nuclear technology. Gordon and Breach, New York
26. Natelson M, Osborn RK, Shure S (1966) Space and energy effects in reactor fluctuation experiments. J Nucl Energy Parts A/B 20(7):557–585
27. Hurwitz H Jr, MacMillan DB, Smith JH, Storm ML (1963) Kinetics of low source reactor startups, part I and II. Nucl Sci Eng 15:166
28. Clark WG, Harris DR, Natelson M, Walter JF (1968) Variances and covariances of neutron and precursor populations in time-varying reactors. Nucl Sci Eng 31:440–457
29. Sutton TM et al, Knolls Atomic Power Lab., Griesheimer DP et al, Bettis Atomic Power Lab. (2007) The MC21 Monte Carlo Code, LM-06K144, Proceedings (on CD-ROM) of the joint international topical meeting on M&C and supercomputing applications, Monterey
30. Palmiotti G et al, Argonne National Lab. (April 2007) UNIC Ultimate Neutronic Investigation Code, Proceeding (on CD-ROM) of the joint international topical meeting on M&C and supercomputing applications, Monterey
31. Herman M et al (2008) Covariance evaluation methodology for neutron cross sections, BNL-81525-2008. Brookhaven National Lab, Upton
32. Belle J, Berman RM (eds) (1984) Chapter 2, Natelson M, Nuclear properties of the thorium fuel cycle. In: Thorium dioxide: properties and nuclear applications, Naval Reactors Office, U. S. Department of Energy, Govt. Printing Office, Washington, DC
33. Katcoff S (1958) Fission–Product yields from U, Th and Pu. Nucleonics 16(4):78

Books and Reviews

Duderstadt JJ, Hamilton LJ (1976) Nuclear reactor analysis. Wiley, New York
Evans RD (1955) The atomic nucleus. McGraw-Hill, New York
Henry AF (1975) Nuclear-reactor analysis. MIT Press, Cambridge
Kaplan I (1962) Nuclear physics, 2nd edn. Addison-Wesley, Reading
Krane KS (1988) Introductory nuclear physics. Wiley, New York
Mermin ND (2005) It's about time, understanding Einstein's relativity. Princeton University Press, Princeton

Fly Ash

Mei-In Melissa Chou
Illinois State Geological Survey-Prairie Research Institute and Department of Natural Resources and Environmental Sciences, University of Illinois at Urbana-Champaign, Champaign, IL, USA

Article Outline

Glossary
Definition of the Subject
Introduction
Fly Ash Production and Rate of Utilization
Fly Ash Management
Fly Ash Properties and Classification
Applications
Environmental Impacts and Considerations
Future Directions
Bibliography

Glossary

Cementitious Said of material that has self-cementing properties in the presence of water alone.

Cenospheres Known as "microspheres" that are small, lightweight, inert, hollow spheres filled with air and/or gases, comprised mainly of silica and alumina, produced from coal combustion process like fly ash, and used widely mainly as high-quality, lightweight fillers.

Coal A sedimentary rock of organic origin, consisting mainly of carbonized plant remains and containing some other elements, such as sulfur, hydrogen, and nitrogen, and mineral impurities.

Coal combustion by-products (CCPs) Residues generated from the combustion of pulverized coal, which include fly ash, bottom ash, boiler slag, and flue gas desulfurization (FGD) materials.

Coal mineral matter Material in coal derived from minerals present in the original plant materials that formed the coal, or from external sources such as sediments deposited with the plant remains or precipitates from interstitial water. This mineral matter converts to ash during coal combustion.

Concrete A construction material produced from a mixture consisting primarily of aggregates (sand and crushed stone or gravel), Portland cement, and water. Certain coal ashes can be used as a replacement for a portion of the Portland cement.

Pozzolan Siliceous or aluminosilicate materials in fine powdery form that, in the presence of water, will chemically react with the calcium hydroxide released by hydration of Portland cement to form compounds possessing cementitious properties.

Supplementary cementing material A material that, when used in conjunction with Portland cement, contributes to the properties of hardened cement through its hydraulic or pozzolanic activity, or both.

Definition of the Subject

Fly ash consists of the inorganic matter within coal that has been melted at high temperature during coal combustion, solidified while suspended in the flue gases, and collected by electrostatic precipitators or other devices before the flue gases are released into the atmosphere. Fly ash is the lighter, less dense part of coal ash, consisting of small spherical particles having pozzolanic or some cementitious properties. It is distinguished from the heavier, denser part of coal ash, the bottom ash, which is collected at the bottom of the boilers and consists of coarse nonspherical particles that lack pozzoanic/cementitious properties. Fly ash, also known as pulverized fuel ash (PFA) because of its fine powdery form and pozzolanic and cementitious nature, has many established applications in the production of concrete-related construction and pavement materials.

Introduction

The pulverized coal firing system for electricity generation was developed in early twentieth century in the USA, and since then, the system has been adopted in more than 50 countries. As pulverized-coal-fired generating stations were constructed worldwide, increasing quantities of coal combustion by-products became available. Fly ash is the most abundant coal combustion by-product and the amount generated has increased dramatically during the past few decades. It has become apparent that simply discarding such large quantities of this material would be environmentally unacceptable and methods for its reuse have been developed for years, especially in Europe, the USA, India, and China. Nevertheless, there is a great variation in usage among countries, from total reuse to almost complete disposal. Efficient, environmentally sound, and cost-effective handling of fly ash is a continuing challenge for major fly ash producers, marketers, and regulators worldwide. This entry provides useful resources and a description of the generation, specifications, management, and utilization of fly ash produced by pulverized-coal-fired power plants.

Fly Ash Production and Rate of Utilization

A schematic flow diagram of fly ash production in a typical pulverized-coal-fired power plant equipped with an electrostatic precipitator for fly ash collection is shown in Fig. 1.

In a coal-fired power plant, pulverized coal is burned in a boiler under high temperature and the heat generated converts water to steam for electricity generation. The noncombustible mineral matter in coal (typically 10–25 wt% in US coals and 30–50 wt% in the coals of India) is converted to coal ash. Fly ash,

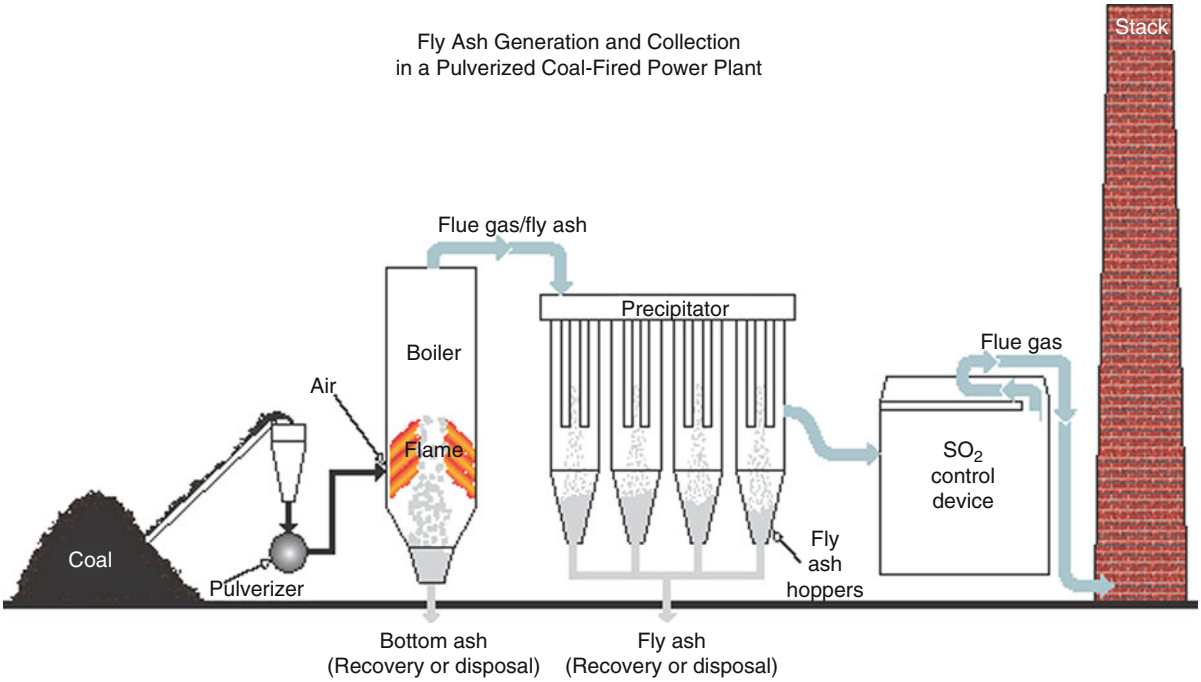

Fly Ash. Figure 1

Fly ash generation in a pulverized-coal-fired power plant equipped with a dry-bottom boiler, an electrostatic precipitator, and a flue gas desulfurization (FGD) device

the lighter part of coal ash, is suspended in the flue gas and is collected before release of flue gas into atmosphere. Fly ash collection systems include electrostatic precipitators, baghouses, fabric filters, or mechanical devices such as cyclones. The electrostatic precipitator is the most common and efficient of these; it can remove about 99.9% of the fly ash in the flue gas. Using a dry-bottom pulverized-coal-fired boiler, fly ash accounts for 75–85% of the total coal ash produced [1] and the remainder is the heavier, denser part, the bottom ash, which is collected at the bottom of the boilers (Fig. 1). The solid waste materials derived from coal combustion are known as "combustion residues" or "coal combustion by-products (CCPs)." If a pulverized-coal-fired power plant is equipped with a flue gas desulfurization (FGD) system for burning high-sulfur coal, another type of CCP, known as FGD residues, is also produced. The amount of all CCPs being generated has increased dramatically around the world during the past few decades as the number of coal-fired power plants increased and as pollution regulations forced plants to reduce their emissions. However, fly ash is the most abundant among these CCPs.

Organizations have been created in many countries, usually with the support, or collaboration of their governments, for the purpose of minimizing landfill and maximizing the utilization of CCPs. They provide information and assistance to those who are interested in developing or using coal combustion by-products in value-added applications. These organizations also collect statistical data, and analyze trends in the production and utilization of CCPs and their disposal practices. These organizations include, but are not limited to, the American Coal Ash Association (ACAA), the European Coal Combustion Products Association (ECOBA), the Ash Development Association of Australia (ADAA), the United Kingdom Quality Ash Association (UKQAA), and the Fly Ash Utilization Program (FAUP) in India. For a more comprehensive list see "Useful Resources" at the end of this entry.

ACAA compiled data on production and usage of CCPs in the USA as early as 1966. They indicate that the fly ash production rate in the USA increased from

about 59.4 million tons in 1996 to about 68.1 million tons in 2001 and to 72.4 million tons in 2008. ACAA's figures use short ton (1 short ton = 2,000 lb = 0.9072 metric tons). The amount of fly ash recycled into commercial products also increased from about 22% in 1996, to about 32% in 2001, to about 42% in 2008. More than half of the remaining fly ash produced in 2008 was still deposited in landfills or storage ponds [2] at a cost to the utility companies and thus to the consumers.

Typical coals in India have ash contents ranging from 30 to 50 wt% [3]. During 1999–2000, the utility industry in India produced about 70 million tons of coal ash per year, but only about 10% of the ash was used in ash dike construction and land filling, about 3% was used in other construction products, and the remainder was disposed of in landfill [4]. In other more developed countries, 80% or more of the fly ash generated was used in manufacturing concrete, bricks, and cellular concrete blocks, in soil-stabilization treatment and land fill applications, in agriculture, in recovery of metals and cenospheres, and in dam construction.

Realizing coal ash posed a significant environmental problem, in 1999, the government of India set up the "Flyash Mission" in New Delhi under its Department of Science & Technology with a goal of coordinating ash utilization efforts and aiming at 100% fly ash utilization [3]. A law was approved by Indian government in 1999 [5] requiring every construction agency engaged in the construction of buildings within a radius of 50 km (amended to 100 km in 2003 [6]) from coal-fired power plants to use only fly ash–containing construction products, and those manufacturing fly ash construction products should contain at least 25 wt% fly ash. During 2004–2005, when the utility industry in India generated about 112 million tons of fly ash per year, the FAUP (Fly Ash Utilization Program) in India has succeeded in increasing fly ash utilization from 1 million tons per year in 1994 to about 42 million tons per year in 2005 [7]. However, the remaining 70 million tons of fly ash still ended up being deposited in ash ponds or lagoons that covered more than 26,000 ac of arable land [8].

In China, there are incentive measures to encourage utilization of fly ash, especially in the concrete and cement industry. For example, the company that produces cement products with more than 30% of fly ash will receive tax deduction. Some areas of China such as Beijing, Shanghai, and Hubei, recycle 100% of their fly ash. The national figures from China Energy Development report indicated that total fly ash production in China increased from 148 million tons in 2000, to 229 million tons in 2004, and is predicted to reach 378 million tons in 2010. The fly ash usage rate also increased from 58% in 2000 to 68% in 2004. Similar to other major fly ash–producing countries, the remaining huge amount ended up in ash ponds [9].

Many individual scientific papers have described the production and usage rates of fly ash from around the world. Dhadse and coworkers published a review paper on fly ash characterization, utilization, and government initiatives in India [10]. In their paper, the fly ash production and usage rates around 2005 in various countries were compared (Table 1), with data from TIFAC (Technology Information, Forecasting and Assessment Council) in India http://www.tifac.org.in. As indicated in Table 1, the US figures differ from those reported by the ACAA, and the figures for China differ widely from those in the China Energy Development report described earlier in this section [9]. The ACAA report indicates that in 2005, the USA produced about 71.1 million (short) tons of fly ash and only about 41% of it was used. Nevertheless, Table 1 provides

Fly Ash. Table 1 Fly ash generation and utilization in different countries (printed with permission of the Journal of Scientific & Industrial Research [10])

Country	Annual ash production, MT	Ash utilization, %
India	112	38
China	100	45
USA	75	65
Germany	40	85
UK	15	50
Australia	10	85
Canada	6	75
France	3	85
Denmark	2	100
Italy	2	100
Netherlands	2	100

a reasonably accurate worldwide comparison in fly ash production and usage. These data indicate that fly ash production in different countries varied from 2 to 112 million tons with the major producers being India, China, and the USA. The fly ash utilization rate varied widely from 38% to 100%, with the total fly ash being recycled in the countries of Denmark, Italy, and the Netherlands.

Worldwide production and consumption of coal for energy has increased dramatically, especially in recent years, in countries such as India and China. This is because the total world reserves for coal (250–1,500 years at current consumption rates) are the most abundant, cheap, and easily produced energy resource, compared to the reserves for natural gas (70–120 years) and crude oil (40–60 years) [11]. The cost of using coal for electricity generation may become more expensive in the future when regulations for green house gas emissions are implemented. Currently, coal provides more than half of the US electricity supply and will continue to be the fuel of choice for worldwide power generation for a couple decades to come [11]. Therefore, managing coal fly ash in an efficient, environmentally sound, and cost-effective manner will remain a continuing worldwide challenge.

Fly Ash Management

Figure 1 shows fly ash produced in a typical pulverized-coal-fired utility boiler and collected by an electrostatic precipitator. There are two commonly used methods for removing the fine powdery fly ash from the fly ash hopper of the precipitator – a wet method or a dry method [12–15].

In the wet method, water is used to flush the fly ash out of the hoppers and the ash slurry is pumped through pipes to large, man-made settling ponds in the vicinity of the power plant. This method was widely used because it was the cheapest method for removing and storing fly ash. Utility companies that use an ash pond for fly ash disposal have three basic options available when the ponds are full: (1) constructing another ash pond nearby; (2) excavating the fly ash from the pond and transporting it to a land fill; and (3) raising the edge of the existing pond by constructing a dike to allow disposal of more fly ash in the pond.

In the dry method, vacuum suction or high-pressure compressed air is used to fluidize and transport the dry fly ash to storage silos, from which it can be either reused or disposed of in a dry or wet form. Most silos are equipped with fluidizing capability for easy discharge of the fly ash through their bottom outlets. Fly ash in a dry form can be directly discharged into enclosed containers, tanks, or wagons [13]. Typically, a little water is added to the dry fly ash to allow stockpiling or transporting in a conditioned form (about 15 to 30% moisture) in trucks or rail cars. The main advantage to conditioning the fly ash is to control the dust that may be released during transporting of the material.

In areas where there is an established fly ash market, coal-fired power plants typically would install a dry fly ash handling system to allow beneficial reuse of the fly ash and avoid disposal in impoundments. In areas, with limited or no markets for fly ash, the expense of installing and operating dry collection systems has been difficult to justify if the space needed for ponding or wet stacking is available near the power plant.

Finding a beneficial application is the preferred method for managing fly ash because it provides a way to convert fly ash from a liability to a value-added raw material. Also, the final products containing fly ash, in general, are more durable and of better quality than their conventional counterparts. Environmentally, use of the fly ash can reduce land disposal requirements and reduce the use of other natural resources, such as the lime or clay that the ash replaces. Economically, recycling can reduce the utility's costs associated with fly ash disposal and may increase revenues for both fly ash producers and users by using fly ash to replace higher cost conventional raw materials. The performance benefits may vary depending on the properties of the fly ash and the type of application. For example, the largest single use of fly ash worldwide is in concrete/cement products (see discussion in section "Applications"), and fly ash–based concrete products or pavements have been found to have better engineering properties and longer service life than conventional concrete products.

Although power companies produce ash at their coal-fired power plants, most power companies do not handle the disposing or marketing of the ash they produce [16]. Commercial ash marketing companies

operating in many countries have been playing increasingly important roles in fly ash management. These companies are able to maintain a product with consistent chemical and physical characteristics, a factor that is extremely important, especially for concrete/cement product applications. Some companies have facilities for research and development, and facilities for fly ash characterization and processing. They can blend different fly ashes, or remove unburned carbon from a high-carbon fly ash to meet concrete specifications. Some companies provide coal-fired power plants with complete on-site ash handling and management, including the installation of dry fly ash collection systems and the environmental and engineering services. Power plants that use ash marketers to sell their fly ash may employ an ash marketing specialist whose responsibility is to monitor ash generation and quality and interface with ash marketing companies or brokers who are under contract to the utility company.

There are about 40–50 commercial ash marketing companies operating throughout the USA, in all states with an exception of Hawaii [16, 17]. Some commercial ash marketing companies are listed in the "Useful Resources" at the end of this entry.

Fly Ash Properties and Classification

Figure 2 shows photos of small quantities of a bituminous coal fly ash (Class F) and a subbituminous coal fly ash (Class C) highlighting their powdery form.

Fly Ash. Figure 2
Photos of small piles of bituminous coal fly ash (Class F) and subbituminous coal fly ash (Class C). Photos courtesy of the Illinois State Geological Survey

Fly ash consists of fine, powdery particles with diameters ranging from <1 to 150 μm. The particles are predominantly spherical in shape and mostly glassy (amorphous, noncrystalline) in nature, because the heat generated during coal combustion is high enough to cause partial melting of many of the minerals present in the coal, and the materials quickly solidify from the molten state while suspended in the flue gas. The color of fly ash can vary from tan to gray to black, depending on the amount of unburned carbon in the fly ash. The darker colors generally indicate greater carbon content. Lignite or subbituminous coal fly ash is typically low in unburned carbon (LOI) content and high in lime (CaO) content (Table 2) and is a light tan to buff color. Most bituminous coal fly ash is typically gray in color, with lighter shades of gray generally indicating a higher quality and lower unburned carbon content fly ash.

Fly ash contains a mixture of crystalline and amorphous materials. Figure 3 shows a typical X-ray spectrogram of a dry and a ponded fly ash sample. The crystalline components include α-quartz (SiO_2) that escaped melting and minerals such as mullite ($3Al_2O_3 \bullet 2SiO_2$), hematite (Fe_2O_3), and magnetite (Fe_3O_4) that formed at high temperature during coal combustion.

Figure 4 shows SEM images, indicating spherical particles, of a bituminous coal fly ash sample at 3,000× magnification (A) and at 6,000× magnification (B). Some fly ashes contain a small proportion of particles that are hollow spheres filled with air/gas that will float on the surface of fly ash ponds. These particles, known as "cenospheres," are collected and used in some specialized applications (see section "Applications").

ASTM (American Society for Testing and Materials) C 618 provides specifications for fly ash and raw or calcined natural pozzolan for use as mineral admixtures in Portland cement concrete [18]. It also specifies two classes for fly ash, F and C, on the basis of their chemical composition, which mostly results from burning different types of coal. As shown in Table 2, the chemical composition of fly ash is generally reported in terms of oxides that include silica (SiO_2), alumina (Al_2O_3), and the oxides of calcium (CaO), iron (Fe_2O_3), magnesium (MgO), sulfur (SO_3), sodium (NaO), and potassium (K_2O). Class F fly ash consists of at least 70% of combined SiO_2, Al_2O_3, and Fe_2O_3, whereas, Class C fly ash must have at least 50% of combined SiO_2, Al_2O_3, and Fe_2O_3.

Fly Ash. Table 2 Chemical compositions (wt%) of typical fly ash from burning coal of different ranks and the requirements of the ASTM C 618 classification

Compound	Bituminous[a]	Subbituminous[b]	Lignite[c]	ASTM C 618 specifications [18]	
	Class F	Class C	Class C	Class F	Class C
Silica (SiO_2)	57.0	34.6	28.9		
Alumina (Al_2O_3)	25.3	17.8	11.1		
Ferric oxide (Fe_2O_3)	5.3	6.1	11.1		
$SiO_2+Al_2O_3+Fe_2O_3$	87.6	58.5	54.1	70.0 min	50.0 min
Lime (CaO)	2.0	27.2	18.9		
Magnesia (MgO)	1.2	5.8	6.0		
Sodium oxide (Na_2O)	0.9	2.3	8.0	1.5 max	1.5 max
Potassium oxide (K_2O)	3.1	0.5	0.9		
Sulfur trioxide (SO_3)	0.2	2.8	6.8	5.0 max	5.0 max
Loss on ignition (LOI)	3.1	0.9	0.4	6.0 max	6.0 max
Moisture content (%)	NV	NV	NV	3.0 max	3.0 max

NV not available
[a]Illinois Basin coal fly ash [19]
[b]Powder River Basin coal fly ash [19]
[c]North Dakota lignite coal fly ash [20]

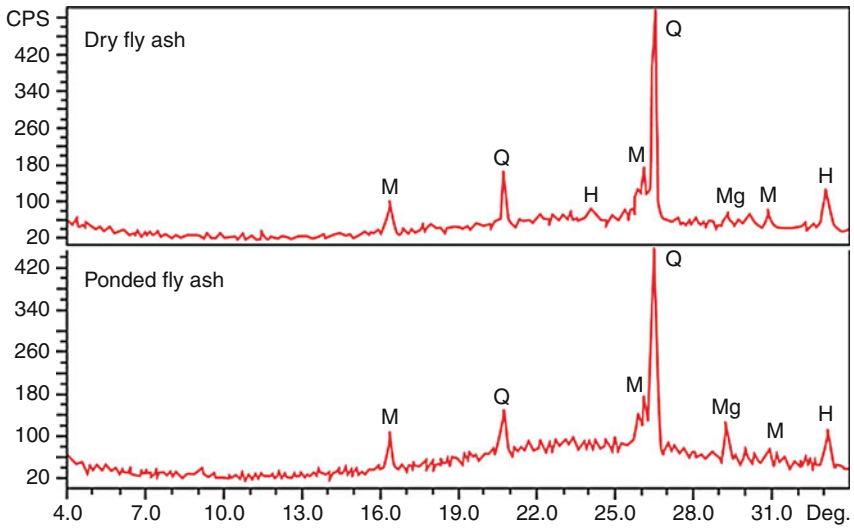

Fly Ash. Figure 3
X-ray spectrogram of a dry fly ash sample and a ponded fly ash sample showing peaks for mullite (M), quartz (Q), hematite (H), and magnetite (Mg). The broad "hump" in the background between about 13° and 30° is due to abundant noncrystalline glass in the samples (printed with permission of the Illinois State Geological Survey) [17]

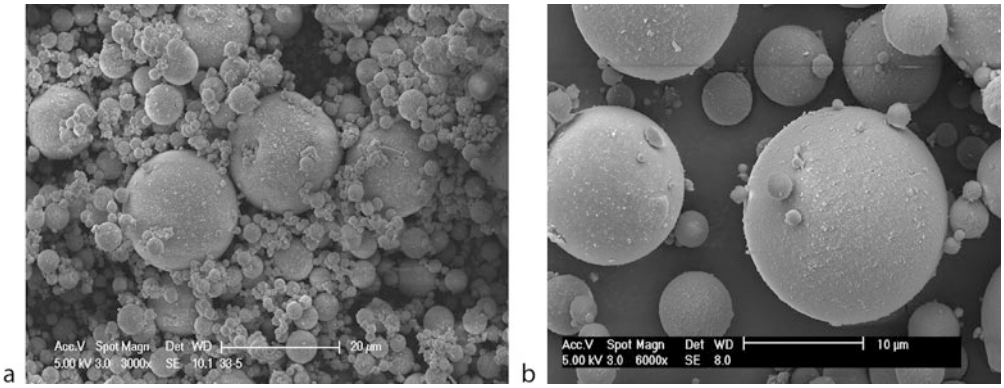

Fly Ash. Figure 4
SEM images of a bituminous coal fly ash sample at 3,000× magnification (**a**) and 6,000× magnification (**b**). Photos courtesy of the Illinois State Geological Survey

It should be noted that the LOI value correlates very well with the unburned carbon content, but it is not an actual measurement of the unburned carbon content in the sample. Burning lignite and subbituminous coals generally produces Class C fly ash that contains more calcium and magnesium and less unburned carbon (LOI) than Class F fly ash, which commonly results from burning bituminous and anthracite coal. Class F fly ash is typically pozzolanic in nature, but not cementitious by itself. Pozzolanic material contains glassy silica and alumina that in itself has little or no cementitious value, but in finely divided form and in the presence of water and free lime, will chemically react with the calcium hydroxide in the lime at ordinary temperatures to produce calcium aluminosilicate hydrates (cementitious compounds). On the other hand, typical Class C fly ash, in addition to having pozzolanic properties, has some cementitious properties, particularly the ability to increase concrete compressive strength in the presence of water alone, because of its higher lime (CaO) content. ASTM C 618 also sets the maximum acceptable LOI value (indicating unburned carbon content) at 6% for both Class F and Class C ash in concrete applications (Table 2) (see section "Concrete (Conventional) and Cement" for more discussion).

For use in Portland cement concrete, fly ash must meet the chemical (Table 2) and physical (Table 3) requirements specified by ASTM C 618. ASTM specification C 311 provides standardized test methods for sampling and testing fly ash or natural pozzolans for use in Portland cement concrete [21].

Specifications have also been established in other countries or by industrial sectors [22–24]. In Canada, for example, specifications for the use of fly ash in concrete are given in CSA A3001 [25], which classifies fly ash further as Types F, CI, and CH based on the calcium oxide content. Type F refers to fly ash with a CaO content less than 8%, Type CI has a CaO content ranging from 8 to 20%, and Type CH fly ash has a CaO content greater than 20%. Higher CaO content generally indicates that the fly ash has higher cementitious properties. Two types of fly ash are produced and used in Canada, Type F and Type CI. Type CH fly ash is imported from the USA and used in concrete applications in Canada [26]. It is important to recognize that not all fly ashes meet the ASTM C 618 specifications. For applications other than concrete, fly ash may not need to meet ASTM C 618 requirements. Specifications of fly ash for other applications have also been developed, such as ASTM D 5239 for soil stabilization [27] and ASTM E 2277 for structural fill applications [28].

Applications

Fly ash, because of its mineralogical composition, fine particle size, and amorphous character, is commonly

Fly Ash. Table 3 Physical requirements of the ASTM C 618 specification [18]

Physical requirements	ASTM C 618 specifications	
	Class F	Class C
Amount retained when wet sieved on 45 μm sieve, max (%)	34	34
Pozzolanic activity index, with Portland cement at 28 days, min (%) of control	75	75
Pozzolanic activity index, with lime at 7 days, min (MPa)	5.5	–
Water requirement, max (%) of control	105	105
Autoclave expansion or contraction, max (%)	0.8	0.8
Specific gravity, max variation from average (%)	5	5
Percentage retained on 45 μm sieve, max variation,% points from average	5	5

pozzolanic and in some cases is also cementitious, whereas, bottom ash is much coarser and is not pozzolanic in nature. Therefore, it is important to distinguish fly ash from bottom ash. In addition, fly ash produced by different power plants commonly has different levels of pozzolanic and cementitious properties; therefore, fly ash must be analyzed and assigned for use in specific applications according to their analysis.

Fly ash has many established applications – mainly as an ingredient in concrete/cement products (see section "Concrete (Conventional) and Cement"), in stabilizing structural fills and embankments [29, 30], and in road bases and subbases [31]. Other uses are as a supplementary cementitious material in grout [32], soil stabilization [27, 33], and inclusion in flowable fill [34].

Fly ash also is used as mineral filler in asphalt concrete [35], roller compacted concrete [36–38], cured blocks, and fired brick products (sections "Autoclaved Aerated Concrete (AAC)" and "Ceramic Brick"), and also in the production of rubber [39, 40], paint [41, 42], and geopolymers [43–45]. It also has been found useful in agriculture [46–50] and in liquid and solid waste management [51, 52].

Another use for fly ash is for the extraction and recovery of high-value metals [53–58] that are minor or trace components of fly ash, such as magnetic iron (Fe), Aluminum (Al), Vanadium (Va), Strontium (Sr), and rare earth metals, such as Gallium (Ga) and Germanium (Ge).

Fly ash generated from some pulverized-coal-fired power plants contains particles of cenospheres (gas-filled glassy spheres that float in water), which can be easily collected from the surface of ash ponds, or separated from dry fly ash using density separation device. Cenospheres have many unique properties including their light weight and hollowness, and almost perfectly spherical shape. They also have high strength compared to ordinary glass, and chemical resistance that enable them to be used in a wide range of commercial and industrial applications. They are especially useful as fillers in materials where their high strength, thermal insulating properties, and resistance to high temperatures are important. For more characteristics, advantages, and applications of cenospheres contact Fillite and Sphere Services, Inc. [59].

Fly ash applications by category and subcategory in various countries from most recent available sources [2, 7, 60–62] are tabulated in Table 4. (Information about such use categorization in China was not found.) The data indicate that the main use of fly ash falls into two categories: (1) concrete/cement products and (2) structural fill, embankments, and road base. In all cases, the use of fly ash as a component in concrete/cement products exceeds any other single application. The proportion of recycled fly ash used in concrete/cement products was 49.0% in India, 52.3% in the USA, 74.5% in the European Union countries, 85.4% in Canada, and 87.0% in Australia.

The governments of major fly ash–producing countries continue to promote use of coal fly ash and other CCPs through mandatory or incentive programs and research funding. Researchers continue to develop new and improved applications that allow fly ash to be used

Fly Ash. Table 4 Fly ash production and application by category and subcategory in various countries

Countries	India		USA		European Union		Canada		Australia	
Year(s) and source	2004–2005 [7]		2008 [2]		2007 [60]		2004 [61]		2008 [62]	
1 short ton = 0.9071 t (metric ton)	million tons		short tons		Kilo t		Kilo t		t	
Total amount produced	112	100%	72,454,230	100%	41,780	100%	4,198	100%	12,549,592	100%
Total used in amount and in percentage	42	37.5%	30,142,274	41.6%	20,015	47.9%	1,300	31.0%	2,018,854	16.1%
Based on total amount used		100.0%		100.0%		100.0%		100.0%		100.0%
Concrete/cement products	21	49.0%	15,766,509	52.3%	14,910	74.5%	1,110	85.4%	1,757,379	87.0%
Blended cement/cement material/clinker	N/A	N/A	3,174,264	10.5%	8,281	41.4%	638	49.1%	N/A	N/A
Concrete/concrete poducts/grout	N/A	N/A	12,592,245	41.8%	6,629	33.1%	472	36.3%	N/A	N/A
Structural fills/ambankments, road base	18	42.0%	9,115,187	30.2%	2,362	11.8%	17	1.3%	252,209[a]	12.5%[a]
Structural fills/embankments	16	38.0%	8,012,825	26.6%	2,071	10.3%	–	–	N/A	N/A
Road base			1,027,568	3.4%	291	1.5%	17	1.3%	N/A	N/A
Flowable fill	–	–	74,794	0.2%	–	–			N/A	N/A
Dike	2	4.0%	–	–	–	–	–	–	N/A	N/A
General engineering fill	–	–	–	–	1,339	6.7%	–	–	–	–
Aerated/non-aerated concrete blocks	–	–	–	–	1,151	5.8%	–	–	–	–
Aerated concrete blocks	–	–	–	–	879	4.4%	–	–	–	–
Non-aerated concrete blocks	–	–	–	–	272	1.4%	–	–	–	–
Bricks + ceramics	1	2.0%	–	–	113	0.6%	–	–	–	–
Waste stabilization/solidification	–	–	2,923,592	9.7%	–	–	–	–	9,266	0.5%
Mining applications	1	2.0%	960,911	3.2%	–	–	89	6.8%		
Miscellaneous/other	3	7.0%	1,376,075	4.6%	140	0.7%	84	6.5%		

[a]Including agriculture and aggregate applications

in greater quantities and in more valuable ways. A brief overview of the most often used and potentially high-volume established construction product applications of fly ash are described below.

Concrete (Conventional) and Cement

Historical background – Ash erupted from nearby volcanoes such as Mounts Etna and Vesuvius was used extensively in the construction of Roman structures. The Pantheon, which was built 2,000 years ago and is still standing today, is a classic example of durability achieved by using volcanic ash (see photo at http://www.acaa-usa.org). Fly ash, which was recognized as possessing pozzolanic properties similar to those of the volcanic ash that made ancient concrete structures durable, was used as an ingredient in concrete as early as 1914 [63]. However, the first comprehensive study of fly ash in concrete was described by R. E. Davis and others in 1937 in the USA [64]. Davis and his coworkers [64–66] studied the effects of the fineness, loss on ignition (LOI), and moisture content of fly ash on the weathering resistance and other properties of concrete and Portland cement. Their work provided a foundation that continues to be developed worldwide into modern specifications and quality assessments of fly ash–based products.

For example, the first British standard for the use of fly ash in concrete was established in 1965 and the first edition of standard BS 3892 [67] was as a fine aggregate (inert filler) and not as supplementary cementing material. During the time that research was underway, several comprehensive research projects were being conducted by the UK power industry to examine how base-load pulverized coal combustion conditions and fly ash collection systems influenced the physical and chemical properties of the fly ash produced and the results of those studies were also published in 1965 [68]. Standard BS 3892 was revised to include fly ash use as a cementitious component in structural concrete in 1982 [69]. Part I required fly ash to have a fineness limit of 12.0% by mass retained on a 45 μm sieve and a LOI of less than 7.0%. This standard was further revised in 1997 with the same general property requirements, but the particle size range was expanded to allow up to 40% of the mass to be retained on a 45 μm sieve [70]. The European fly ash for concrete standard, BS EN 450, was established in 1994–1995 [71] and this standard was further revised into BS EN 450 -1 [72] and BS EN 450 -2 [73] to include definitions, specifications and conformity criteria, and evaluation, with some changes in fly ash categorization.

The construction of the Hungry Horse Dam in the USA completed in 1953, which used about 120,000 metric tons (132,240 short tons) of fly ash in the more than 3 million cubic yards of concrete to build dam, was the first major large-scale project that paved the way for using fly ash in the concrete industry [74, 75]. At least 100 other major locks and dams have been constructed using fly ash–containing concrete under the direction of the US Army Corps of Engineers, the US Bureau of Reclamation, or private engineering firms. Some of the most prestigious construction projects of recent times have relied on concrete containing fly ash, including dams, power stations, offshore platforms, tunnel, walls, highways, airport runways, commercial and residential buildings, bridges, pipelines, and silos. For worldwide examples and photos of some outstanding applications of fly ash in the construction industry see the ECOBA Web site [76] and the ACAA Web site [2].

Benefits – The unique benefit of using fly ash in concrete is that fly ash, like volcanic ash, is capable of reacting with calcium hydroxide (free lime) at ordinary temperature. When fly ash is used in combination with Portland cement, calcium hydroxide librated from the hydration of Portland cement reacts with the aluminosilicates present in the fly ash to form calcium aluminosilicate hydrates (pozzolanic reaction products) possessing cementitious properties. This not only reduces the excess amount of calcium hydroxide (a nondurable by-product from hydration of Portland cement), but, in the pozzolanic reaction process, converts the calcium hydroxide into useful calcium aluminosilicate hydrates, which are the strongest and most durable portion of the paste in concrete. Also, pozzolanic reactions are much slower than cement hydration reaction thus the strength of concrete products is improving continuously.

Fly ash not only has been successfully used worldwide as a mineral admixture in Portland cement concrete for more than half of the past century, but also has been well established as a cement raw material and as a component of blended cement.

Fly ash used in concrete has been shown to have the following benefits: (1) decreases concrete's permeability, thus reducing the rate of penetration and erosion by water and resisting harmful alkali-aggregate and sulfate reactions; (2) increases the concrete mix's cohesiveness, thus reducing segregation and bleeding in the concrete; (3) contributes to long-term strength improvement in concrete; (4) improves the workability of fresh concrete, enabling more thorough compaction, and (5) reduces and delays the onset of heat of hydration in massive concrete structures such as dams and consequently the risks of thermal cracking of the concrete [77–80].

Overall, the greatest benefits in using fly ash in concrete/cement applications are environmental. Fly ash is itself a waste by-product material from coal-fired power plants. In the past, the impoundment and land disposal of raw fly ash has covered millions of acres of valuable land in the major fly ash–producing countries. Utilization of fly ash in valued products will reduce this landfill. Furthermore, when 1 ton of cement is manufactured, 0.85 t of CO_2 (a green house gas) are also produced and released into the atmosphere [81]. Using fly ash as a cement raw material or as a component of blended cement can reduce cement production, and thus reduce green house gas emissions.

Fly ash properties in concrete applications – Fly ash properties may vary depending on the type of coal used and its chemical compositions and the burning conditions at a specific power plant. Class F fly ash, which contains low lime (CaO) content, is typically a result of burning anthracite or bituminous coal, whereas, high-lime Class C fly ash is generally from burning lignite or subbituminous coal. Fineness, loss on ignition (residue unburned carbon content), and chemical composition are the key elements of fly ash affecting its concrete applications. Fine fly ash generally gives resulting concrete high in compressive strength [82, 83]. In many concrete formulations, air bubbles are entrained into the mixture through mechanical agitation and the air bubbles are stabilized by an addition of specialized surfactants known as air-entraining admixtures (AEAs). The presence of small air bubbles increases the workability and cohesion of the concrete mix and improves the resistance of the set material to freeze–thaw cycles. The proper dosage of AEA is critical in generating the desired amount of entrained air and stabilizing the air bubbles during mixing and transportation to the construction site [84]. Since the unburned carbon can adsorb the AEAs that are added to the mixture, the loss on ignition value of fly ash is restricted to no more than 6%. In terms of chemical composition, the fly ash used in concrete applications normally contains less than 10% of lime (CaO). Excessive lime in fly ash lowers the pozzolanic reactivity and affects the volume stability of the concrete. As mentioned in the section "Fly Ash Properties and Classification," fly ash used in Portland cement concrete applications must meet the chemical and physical requirements of ASTM C 618 or the specifications of other jurisdictions. Also, it must be in a dry form and its pozzolanic reactivity and quality consistency must be monitored closely. Those who want detailed information on fly ash for concrete and cement products can find references from Headwaters Resources [85], Turner-Fairbank Highway Research Center's coal fly ash user guide-Portland cement concrete [86], and from the book *Fly Ash in Concrete* by Gordon and Breach Science Publishers [87]. Other publications on the same subject can be obtained from the organizations listed in "Useful Resources" at the end of this entry.

Autoclaved Aerated Concrete (AAC)

Autoclaved aerated concrete (AAC), also known as autoclaved cellular concrete and porous concrete, is a lightweight building material that is made without any coarse aggregate. The manufacturing process of AAC is shown in Fig. 5.

AAC is produced from a mixture of a silica-rich material (such as finely ground sand or fly ash as the major ingredient), lime and/or cement (as a binding agent), water, and very small amount of aluminum powder (as an expansion agent). The mixture is poured into large molds and allowed to expand as bread dough, forming a highly porous, but impermeable cellular structure (see Fig. 6). The cake (green aerated concrete) is separated from the molds and cut into standard size and shape for curing in a pressurized autoclave chamber at a temperature about 375°F. The ingredients combine during steam curing to form calcium silicate hydrates (the minerals typically formed from Portland cement), which give AAC its strength.

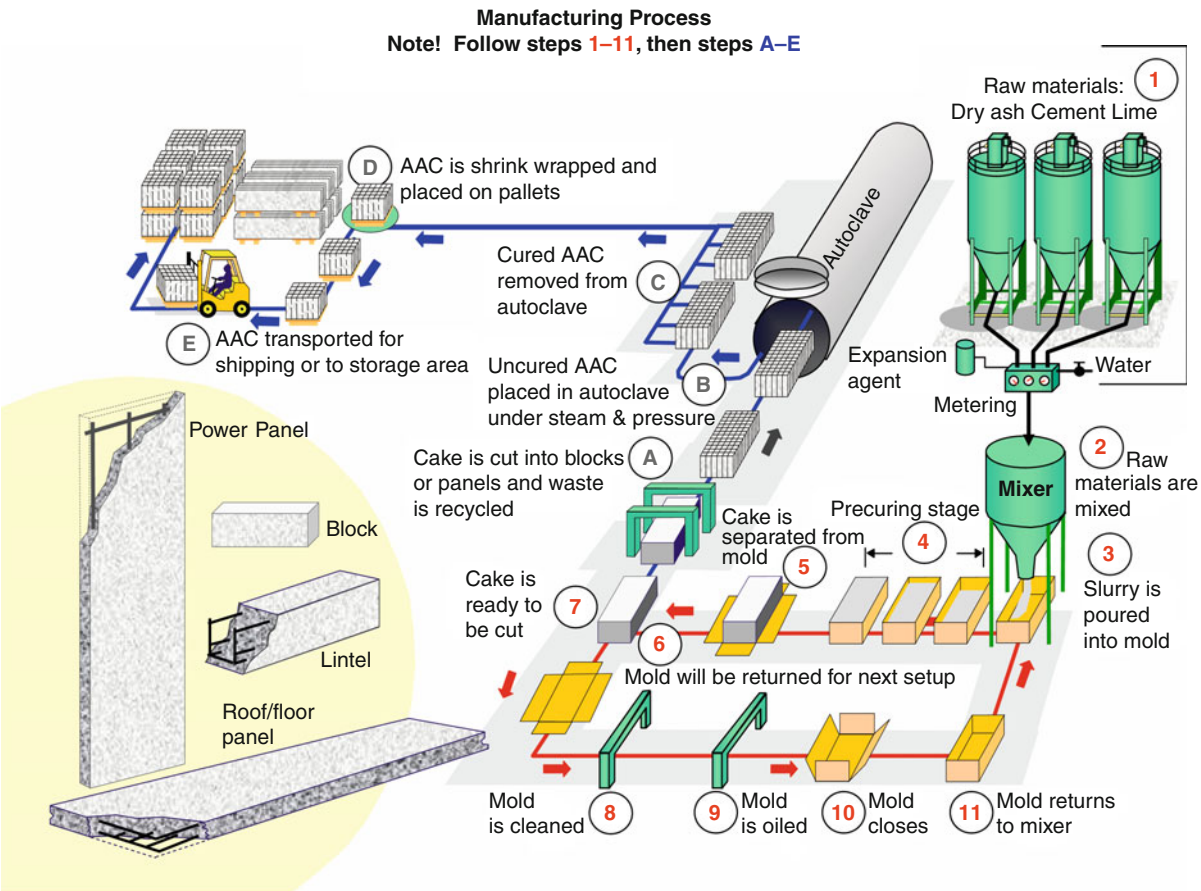

Fly Ash. Figure 5
Typical manufacturing process for producing autoclaved aerated concrete (AAC) (printed with permission of OSA Inc. [88])

Fly Ash. Figure 6
The highly porous structure of two AAC blocks produced at the Illinois State Geological Survey containing 64 wt% fly ash obtained from two different power plants (Photos courtesy of the Illinois State Geological Survey [90])

AAC has been produced in many countries for more than 70 years because it offers considerable advantages over other construction materials [89]. AAC is only one-fourth to one-third the weight of conventional concrete, has excellent thermal and sound insulation properties, is nonflammable, and insect resistant.

Sand-based AAC was developed during the 1920s (patented 1924), when Sweden was enduring an

extreme shortage of wood due to deforestation. In need of an alternative building material, Swedish architect Johan Eriksson developed AAC to meet the growing demand for a product that had wood's workability coupled with excellent thermal insulation, structural strength, and superior fire resistance. To further improve AAC, Hebel invented and patented a method of incorporating steel reinforcements during the manufacturing process in 1945 [89]. Since commercial production of the AAC material began in 1930, AAC has become one of the most commonly used building materials in Europe and its use is rapidly growing in many other countries. Fly ash can be used to substitute for the sand in the mixture, typically at 55–65% by dry weight. During the last decade, fly ash has become a widely used replacement for ground sand for making AAC in many countries.

In 1992, the UK used about 800,000 t of fly ash per year in the manufacture of approximately 1.5 million cubic meters of AAC, produced in ten factories [91]. In Czechoslovakia, six plants produced 2 million cubic meters of AAC, and 70% of this output was produced with fly ash [92]. The use of AAC has grown in recent years because of AAC's excellent thermal insulating properties and other economic and environmental advantages. In some countries, the demand for AAC products has exceeded its rate of production [93]. Currently, there are over 300 AAC manufacturing plants on six continents [94]. However, sand-based AAC production in the USA was not initiated until 1996 when ASTM commercial standards for AAC were established. There are currently three ASTM standards available for AAC – ASTM C1386 for material properties, ASTM C1452 for reinforced AAC panels, and ASTM C1555 for AAC masonry units [95].

In the 1990s, several studies were conducted in an attempt to establish fly ash–based AAC plants in the USA. A collaborative study led by the Electric Power Research Institute (EPRI) was begun in 1993. The project constructed an on-site AAC mobile pilot plant and tested various coal ashes for making AAC at nine utility plants of seven utility companies, including Tennessee Valley Authority (TVA) and Ohio Edison Co. [96]. Another study was initiated in 1997 by Babb International who built an AAC pilot plant in Ringgold, Georgia, [97] for the purpose of conducting test runs for making AAC using coal fly ash. Subsequently during 1998–2000, Babb International built a commercial AAC plant in Indiana for producing fly ash–based AAC. However, both plants were closed in 2003, due in part to the slow acceptance for AAC in the USA [88].

From 1997 to 2005, six sand-based AAC plants were constructed in the USA but, as of 2009, only three of the six remain in limited operation serving a small AAC market. Extensive commercial use of AAC in the USA has not yet been achieved due in part to the low cost of lumber and the resistance of the home and commercial construction industry to switching raw materials and changing construction methods. However, this resistance may soon be overcome when architects, builders, and the public become more aware of the many benefits of using energy-efficient AAC materials. In 2005, OSA Inc. acquired the Ringgold AAC plant and, in collaboration with the Illinois State Geological Survey, developed an economical manufacturing method (2009 patent pending) for fly ash–based AAC production [98]. OSA Inc. is currently working with a local government in producing enough ash-based AAC materials for marketing analysis.

Ceramic Brick

The term "bricks" typically refers to ceramic (fired) bricks, the standard small building units in a rectangular shape, but the term has also been used to refer to unfired small building units in a rectangular shape, such as small concrete blocks, or (aerated or non-aerated) sand-lime bricks [99]. This section mainly considers the use of fly ash in making standard ceramic (fired) bricks.

In the process of manufacturing fired bricks, there are two critical steps – forming firmed green bricks and firing them successfully. Clay and shale are the standard raw materials used in making conventional fired bricks. In general, green bricks are formed by two basic methods – mold-pressing (dry or wet) or extrusion (under vacuum) – and are then dried. Firing of the dried green bricks is done in a kiln or oven with proper temperature control for successful firing. In a typical firing cycle of progressively increasing temperature, the temperature rises fairly rapidly from ambient condition to a temperature of about 1,000°F and then at a slower rate up to about 1,500°F until the carbonaceous matter in clay/shale is oxidized completely [100].

Insufficient oxidation of the carbonaceous matter in the clay/shale mixture results in bricks produced with black or red cores. Also, improper rate of heating would result in defective bricks with cracks or bloating beneath the surface skin, which are commercially unacceptable. Iron oxide in the raw material is the primary cause of the typical redbrick color.

Concrete blocks are manufactured in a much wider range of shapes and sizes than clay bricks and are available with a wider range of treatments. A number of the treatments are used to provide a final size, color, and shape similar to that of fired clay bricks. These small concrete building blocks in a rectangular shape also are referred to as bricks. In this case, the "green" concrete bricks are formed in steel molds by vibration or by compaction with a hydraulic press. When dry, the green bricks rather than being fired are cured under low-pressure steam at ambient temperature to gain strength/hardness and other properties.

Fired brick manufacturing operations in most part of the world are labor- and energy-intensive. Brick manufacturers in developing countries, having cheaper labor, still rely heavily on mold-pressing of green bricks manually or by machine. In comparison, manufacturers in developed countries mainly utilize machine extrusion to form green bricks and tunnel kiln firing. A typical extruder machine produces about 8,000 green bricks per hour, which would take a team of two skilled brick makers 10 days to produce using mold-pressing method [101]. In 1998 in the USA, according to a survey conducted by the Brick Industry Association, 93.2% of total regular clay brick production was formed by extrusion. A machine-molded method was used for making specialty bricks that constituted 5.3% of the total production, and only 1.5% of all the manufactured bricks were produced by the dry-pressing method commonly used in developing countries [102]. Using the extrusion method, as much as 70 wt% of fly ash can be used to substitute for clay or shale; nearly 100% by weight can be substituted when using a mold-pressed method.

Fly ash and bottom ash were used in making ceramic (fired) products such as building bricks, pipes, and roof tiles as early as the 1930s, but the practices used and any valuable technical information gathered, in most cases, were not documented. These early trials generally took place as a result of informal initiatives between a brick company and a local power plant and they had little incentive to preserve or publish results.

A brief historical review of making fired brick using fly ash was first conducted in the UK by Anderson and Jackson of the North Staffordshire Polytechnic in 1987 [103]. Their review indicated that despite successful trials and technical promotion during the late 1950s–1960s, the response by the brick industry to use fly ash in brick production was poor due in part to: (1) the high demand for fired bricks at that time, (2) the low cost of conventional raw materials, (3) the difficulties encountered in some field trials when making bricks containing fly ash, and (4) reservations about the consistency in the quality of the fly ash supply [103].

In 1977, Slonaker experimented with making fired bricks comprised of mainly of Class F fly ash generated from the West Virginia and Pennsylvania coals. He used a dry mold-pressed method to form green bricks, and acceptable bricks were produced from feeds consisting of as much as 72% fly ash, 25% bottom ash, and 3% sodium silicate [104]. However, Slonaker's study did not lead to commercialization. His fly ash bricks did not have conventional redbrick color, and his bricks with a composition of nearly 100% ash probably lacked sufficient plasticity to be extruded well.

In 2005, Freight Pipeline Company (FPC) studied a mold-pressed method for making green bricks composed of almost 100% Class C fly ash. The brick strength, rather than firing, was developed by water-steam curing at room temperature [105]. Commercially available red-colored pigment was used as an additive to give the final brick products the traditional redbrick color. Recently, FPC issued its US patent license to CalStar Cement, a California-based company, for further development.

During 2000, researchers at the Illinois State Geological Survey, University of Illinois, began to experiment with using local Class F fly ash for manufacturing fired bricks. Fly ash was obtained as dry fly ash from hoppers or as ponded fly ash from a power plant pond or a stockpile. A systematic laboratory study on extruded fired bricks containing up to 70 wt% dry fly ash showed that the fired bricks had greater compressive strength (Fig. 7) [106] and lower thermal conductivity [107] than conventional bricks containing no fly ash.

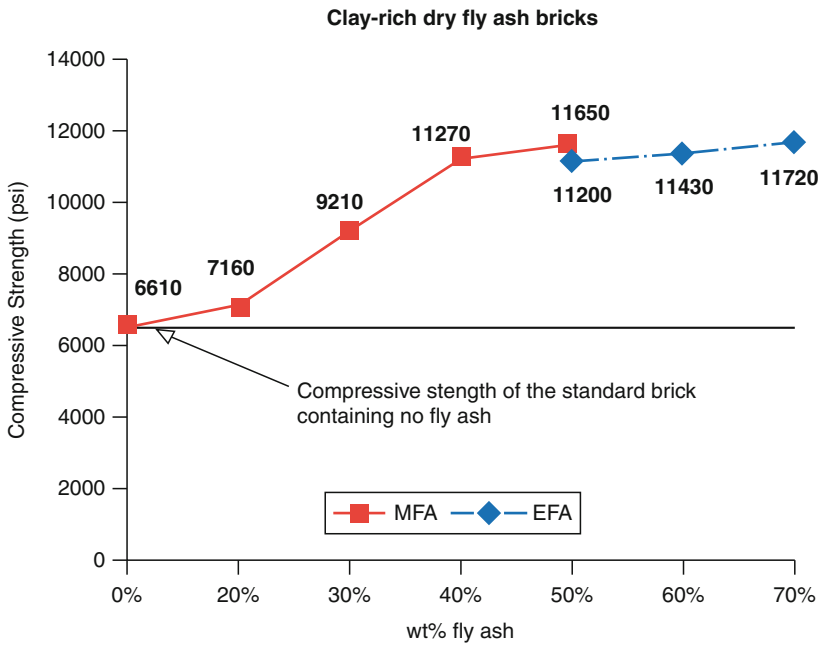

Fly Ash. Figure 7
Compressive strength of fired bricks made with increasing amounts of fly ash in clay brick formulation. MFA, Plant-1 dry fly ash; EFA, Plant-2 dry fly ash. Figure courtesy of the Illinois State Geological Survey [106]

In further studies with industry partners, pilot-scale and commercial-scale tests, formulations, and procedures for producing commercial-size building and paving bricks containing amounts of fly ash were optimized to suit the plant's manufacturing processes. A handful of minor issues encountered in pilot-scale trials were resolved and commercial-scale production runs were successfully completed at three local brick plants [108–110]. Figure 8 shows a photo of an extrusion test run producing three-hole green fly ash building bricks at 8,000 bricks per hour (700 bricks per car). Figure 9 shows four batches of fired bricks successfully produced with fly ash inputs at 0% (E1), 20% (E2), 30% (E3), and 40% (E4) by volume. These studies, supported by state and federal governments, showed that Class F fly ash from Illinois Basin bituminous coals is suitable for fired brick production, especially when wet fly ash from retaining ponds was used. This is because most of the scum is associated with soluble salts in the dry fly ash and has been leached out and removed in the pond water. Thus, the amount of scum-suppressing additive otherwise required can be reduced or completely avoided. Standard commercial-size fired bricks produced with clay/shale mixtures containing 30–40% by volume (28–37% by weight) of ponded fly ash showed color similar to conventional fired bricks and their engineering properties, including results of freeze–thaw tests, met or exceeded the ASTM C 62 commercial specifications [111]. Also, local builders acknowledged that their method for conventional brick construction can be applied directly to the construction of fly ash bricks.

A knee-high wall at the Museum of Science and Industry in Chicago (Fig. 10) was constructed using Illinois fly ash bricks produced from commercial-scale production tests. This was part of the Museum's Clean Coal Technology Exhibition. The economic evaluation of the commercial-scale tests was optimistic [108]. An environmental assessment of fired bricks indicated that the fly ash–containing bricks were fully comparable to regular commercial bricks as environmentally safe construction materials [112].

Participating brick companies are seeking partners for a joint venture to commercially produce bricks containing fly ash. Only a few brick plants in the

Fly Ash. Figure 8
Scale-up extrusion demonstration at a brick plant producing three-hole green fly ash building bricks at 8,000 bricks per hour (700 bricks per car) (photo courtesy of the Illinois State Geological Survey [110])

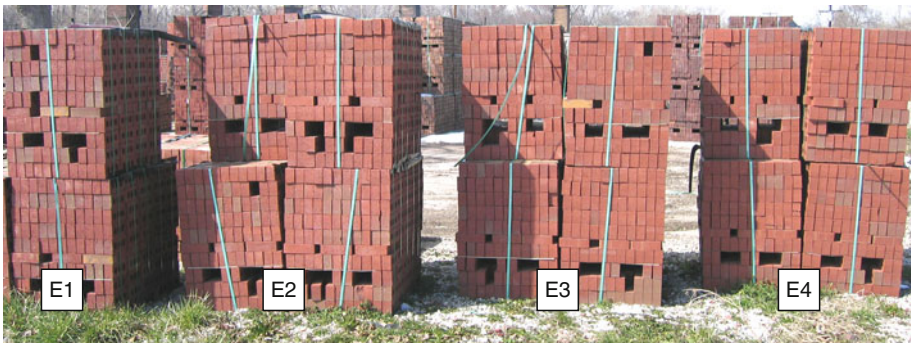

Fly Ash. Figure 9
Four batches of fired building bricks produced from scale-up production test runs with fly ash inputs at 0% (E1), 20% (E2), 30% (E3), and 40% (E4) by volume (photo courtesy of the Illinois State Geological Survey [110])

USA are currently producing bricks containing small amounts (1–5%) of coal ash. In a sustainable world, this rate can be increased manyfold.

Environmental Impacts and Considerations

As mentioned earlier, use of fly ash as a recycled material can have economically and environmentally beneficial results. Use of fly ash as one of the ingredients in concrete to improve durability and service life is important not only to private owners, but also to governmental authorities responsible for the design, construction, maintenance, and repair of buildings, bridges, roads, and infrastructure. The use of fly ash in concrete enhances the recycled material content of a building and is recognized as a beneficial strategy for CO_2 reduction. The use of fly ash in concrete-related products and bricks is an effective and increasingly used environmentally responsible strategy to promote sustainability because it (1) eliminates the need to

Fly Ash. Figure 10
A knee-high wall at the Chicago's Museum of Science and Industry constructed with fly ash bricks produced from commercial-scale production tests. This was part of the museum's Clean Coal Technology Exhibition (photo courtesy of the Illinois State Geological Survey)

dispose of fly ash, a typically industrial waste material; (2) reduces the cement content of concrete, and thus the CO_2 generated from cement manufacturing; (3) reduces the amount of embodied energy in the concrete; and (4) conserves natural resources by replacing the materials that would otherwise have to be mined to make these products. Also, the trace elements in the fly ash are stabilized in the concrete products, reducing the chances for releasing them into the environment [113]. A review on various reports and research papers in the UK regarding the environmental impacts of using fly ash was conducted by Sear and coworkers [114] in 2003. Their conclusion was that coal fly ash is an environmentally harmless material that can be safely used in bound (such as concrete products) and unbound (such as land reclamation) applications.

Potential health issues of using coal ash were also discussed in the Environmental Focus Report issued by the Electric Power Research Institute in 1998. The subjects included ash dust issue, leaching of coal ash from land applications and from products containing fly ash as well as skin contact and radioactivity of coal ash. It concluded that when handled and disposed properly, coal ash does not present a public health or environmental threat [115].

Having advantages in physical, chemical, and mineralogical properties, many fly ashes are marketed for a wide range of engineering applications in construction and other industries. However, large volume of these materials is still remaining for disposal every year in the USA and the other major fly ash–producing countries. The environmental disposal practices of these materials are important issues impacting producers and regulators.

Physically, coal fly ash is a fine powdery material, and in its dry form, just like road dust, it readily becomes airborne even in a mild wind. Initially, coal-fired power plants released their fly ash together with flue gas into the atmosphere. The settlement of noticeable amounts of fly ash dust particles on the land had disturbed ecological systems and degraded agricultural land and soil quality. Health risks for utility workers from long-term exposure to fly ash dust, just like road dust, include diseases such as silicosis, fibrosis of the lungs, and bronchitis. Power plants eventually were mandated to use collection devices such as electrostatic precipitation systems to gather fly ash and keep it from being carried with exhaust gases out the stack. The general public does not now encounter coal ash in quantities that might result in health risks.

During power plant operation, some plant workers may be exposed to appreciable amounts of fly ash, either as suspended particulates or in collected ash piles. Such workers include primarily ash haulers, ash silo operators, truck loaders and drivers, ash system inspectors, and ash collection system personnel. The main sources of ash dust are the ash transfer system and ash loading. Under these circumstances, the precaution measures issued by the health organizations similar to the US Occupational Safety and Health Administration must be followed. However, studies on potential health effects of workers in frequent contact with coal fly ash showed that routine operating activities did not produce hazardous exposures, and occupational health records for these types of workers do not show a higher incidence of respiratory problems than those of power plant workers who do not work as closely with coal ash [115].

Dust control measures are also required at fly ash disposal sites to prevent dust hazard conditions and health risks. For example, transportation of fly ash to the disposal site typically is done in a conditioned form (moisture content about 15–30%) and in covered trucks or rail cars. At the disposal site, as the fly ash dries it forms a crust or clumps and is less easily moved

by the wind. In many cases, soil is applied on top of the fly ash as a cover material. These processes are designed to keep fly ash dust at a low enough level to avoid any expected health impacts.

Chemically, the main components of coal fly ash as indicated in Table 2 are about 60–90% silica, alumina, and iron oxides. Other metals and metal-like elements commonly are present only in trace quantities – arsenic, cadmium, beryllium, thallium, nickel, lead, manganese, chromium, selenium, zinc, and other metals. The primary health concern from the land disposal of fly ash is the potential for the trace elements listed above to enter nearby groundwater. Standardized leaching tests show that small amounts of toxic trace elements (particularly arsenic, selenium, lead, and mercury) may leach from fly ash that is in prolonged contact with ground water, but they do not migrate far from the ash site and are present in small enough concentrations to justify the regulatory classification of fly ash as nonhazardous solid waste [115]. Studies on various animals examining the toxic effects of ingesting fly ash constituents have not found pathological damage that would indicate potential human health problems [115]. The majority of fly ash is not enriched in radioactive elements, nor is it more radioactive, compared to common soils or rocks. Also, radiation in fly ash and in products produced from fly ash is minimal – well below the US Environmental Protection Agency's action standards [115, 116]. However, each fly ash should be analyzed on a case-by-case basis for potential toxins and radioactivity because coals come from many areas. Also, precaution measures should be undertaken when it is required by local governments.

Fly ash is not currently regulated in the USA by the US Environmental Protection Agency (EPA) nor in the other countries as a hazardous waste material; however, it must be handled or disposed of properly to prevent air pollution (irritant dusts) and groundwater contamination. For example, it is important to periodically monitor drinking water wells near fly ash disposal sites to ensure that the concentrations of trace elements remain below the regulatory levels for safe long-term drinking and cooking.

Another precautionary example for ensuring proper disposal of fly ash is evident by the failure of a retaining pond structure on December 22, 2008 at the Kingston power plant of the TVA in the USA. This structural failure led to the release of approximately 5.4 million cubic yards of impounded fly ash onto surrounding land and into the adjacent Emory River. The cost for clean-up is estimated at more than $1 billion, and costs of legal actions and settlement of possible lawsuits may add to this. This incident directly affects citizens/animals living in close proximity to the plant and the TVA, but also indirectly impacts all coal burning utilities and other large coal users throughout the USA. As a result of this incident, the US EPA instructed all power plant operators and companies to conduct on-site assessments to determine the structural integrity of their ash storage ponds, and take whatever measures were needed to ensure the integrity. Eventually, the US EPA may issue more rigorous regulations or may eliminate ash pond disposal altogether [117].

Future Directions

Although the use of nonfossil energy sources such as nuclear or wind is growing, coal will continue to be the major fuel for worldwide power generation for some time to come [118]. While significant progress has been made in terms of reusing fly ash combustion residues in the world, maintaining the quality consistency of a fly ash supply, which is extremely important in many already established applications, would require new strategies. This is because the utility industry starts using new improved coal combustion technologies and using more renewable energy sources, and endures more stringent emissions control regulations. Major developments that would alter fly ash properties and impact the use of fly ash in manufacturing products include, but are not limited to the following.

- The use of mercury reduction and/or NOx reduction technologies (activated-carbon mercury adsorption, low NOx burners, selective catalytic NOx reduction, or selective non-catalytic NOx reduction), would produce fly ash with unacceptably high levels of unburned carbon [119] and, in some cases, adsorbed mercury or ammonia.
- Switching coal sources and/or changing boiler operating conditions in an effort to reduce the cost for electricity generation would result in fly ash with inconsistent properties.
- Co-firing coal with other fuels (such as natural gas, wood, or other biomass) or other combustible wastes (such as petroleum coke, scrap tires,

municipal solid waste) would produce fly ash with inconsistent properties.

- The use of advanced clean coal technologies, such as gasification of coal or burning coal/petroleum coke mixed material, would produce residues, mainly a hard glassy slag, as well as some fly ash with compositions much different from conventional pulverized coal combustion fly ash.

Future developments for fly ash applications will require improved fly ash management strategies that will ensure the quality consistency of fly ash for new and established applications. These may include (1) blending and mixing of ashes for quality consistency, (2) particle size control by classification, grinding, and agglomeration, (3) physical or chemical processing for removal of residual carbon or ammonia, and (4) separation processing, including flotation and electrostatic or magnetic separation [120]. Some fly ash marketing companies have technologies ready for fly ash processing. But when additional treatment is not practical from an economic standpoint, the coal-fired power plant will have no other option other than landfill disposal of the fly ash they produce. Managing fly ash in an efficient, environmentally sound, and cost-effective manner will remain a continuing challenge for the major fly ash producers, marketers, and regulators worldwide.

Bibliography

Primary Literature

1. Joshi RC, Lohita RP (1997) Introduction, p1-4 in Fly ash in concrete: production, properties and uses. In: Malhotra VM (ed) Advances in concrete technology, vol 2. Gordon and Breach Science, Amsterdam
2. American Coal Ash Association (2009) 2008 Coal combustion product (CCP) production & use survey report. 15200 E. Grand Ave. Ste 3050, Aurora, CO 80014. http://www.acaa-usa.org; the data in CCP Production & Use Reports
3. Chikkatur AP, Sagar AD (2007) Cleaner power in India: towards a clean-coal-technology roadmap. Discussion paper 2007–06, Energy technology innovation policy. Belfer Center for Science and International Affairs, Kennedy School of Government, Harvard University, Cambridge
4. Sinha R, Dayal U (2000) Save soil, use flyash. IIT Kanpur, sponsored by Flyash Mission, Department of Science & Technology at New Delhi. http://www.iitk.ac.in/infocell/soil/testing2.htm
5. The Gazette of India (1999) Ministry of Environment and Forests notification, Part II, Section 3, sub-section (ii) *S*.O.763 (E), New Delhi, 14 Sept 1999. http://envfor.nic.in/legis/hsm/so763(e).pdf
6. Ministry of Environment and Forests (2003) Notification S.O. 979 (E): amendment. New Delhi, 27 Aug 2003. http://envfor.nic.in/legis/hsm/so979(e).pdf
7. Kumar V, Mathur M, Sinha SS, Dhatrak S (2005) Fly ash: an environment saviour. Fly Ash Utilization Programme (FAUP), TIFAC, DST, New Delhi, India. http://c-farm.org/001_FLY_ASH_AN_ENVIRONMENT_SAVIOUR.pdf
8. (a) Maiti SK, Jaiswal S (2008) Bioaccumulation and translocation of metals in the natural vegetation growing on fly ash lagoons: a field study from Santaldih thermal power plant, West Bengal, India. Environ Monit Assess 136(1–3):355–370; (b) D'Monte D (2005) Some concrete solutions – recycling fly ash. India Together – the news in proportion, May 4, 2005
9. China Building Material Federation (2010) Introduction on current fly ash research in China. http://www.coalash.org/content/cha_view.asp?id=495&cha_id=38
10. Dhadse S, Kumari P, Bhagia LJ (2008) Fly ash characterization, utilization and government initiatives in India – a review. J Sci Ind Res 67:11–18
11. Vejahati F, Xu Z, Gupta R (2010) Trace elements in coal: associations with coal and minerals and their behavior during coal utilization – a review. Fuel 89:904–911
12. Chou MIM (2000–2008) Communications between Chou MIM and the managers of the utility plants in Central and Midwestern USA
13. (a) DC industrial plant services private limited. http://www.dcips.com/technology.html; (b) FLSmidth Inc. (2005) Pneumatic transport for the fly ash management industry. http://www.flsmidth.com/NR/rdonlyres/610A8705-A482-45E0-9DB1-633F2E0F597C/23644/AshHandling.pdf
14. Charah Inc. (2010) Ash management. http://www.charah.com/AshManagementServices/AshManagement/tabid/76/Default.aspx
15. Turner-Fairbank Highway Research Center (TFHRC) (2010) Coal fly ash – material description. http://www.tfhrc.gov/hnr20/recycle/waste/cfa51.htm. TFHRC, 6300 Georgetown Pike, McLean, VA 22101, USA
16. Manz O, Pflughoeft-Hassett D (2005) Historical perspective of coal ash marketing and promotion in the USA. In: Proceeding: world of coal ash symposium, Lexington, 11–15 Apr 2005. http://www.flyash.info/2005/11man.pdf
17. Chou MIM, Chou SFJ, Chen LM, Stucki JM (2009) Manufacturing bricks with fly ash and advanced coal combustion by-products. Institute of Natural Resource Sustainability, Illinois State Geological Survey, Circular 574, 10 pp
18. ASTM C 618 (2008) Standard specification for fly ash and raw or calcined natural pozzolan for use as mineral admixture in Portland cement concrete. American Society for Testing and Materials, West Conshohocken
19. Unpublished data of Chou MIM. Illinois State Geological Survey
20. The Fly Ash Resource Center – chemistry. http://www.rmajko.com/chemistry.html

21. ASTM C 311 (2007) Standard test methods for sampling and testing fly ash or natural pozzolans for use in Portland cement concrete. American Society for Testing and Materials, West Conshohocken
22. The Fly Ash Resource Center – specification. http://www.rmajko.com/specs.html
23. Recycled Materials Resource Center (2008) Evaluation guidance – standards and specifications. User guidelines for byproducts and secondary use materials in pavement construction, RMRC. http://www.recycledmaterials.org/tools/uguidelines/standards.asp
24. Wang L, Cui Y (2007) The application and development of fly ash in China. Presented at 2007 World Coal Ash (WOCA) conference, Covington, 7–10 May 2007
25. CSA A3001 (2004) Cementitious materials, New Canadian Standard: A3000-03 by Canadian Standards Association
26. Bouzoubaâ N, Foo S (2005) Use of fly ash and slag in concrete: a best practice guide. Final Report – MTL 2004-16 (TR-R) to the Materials Technology Laboratory, Program of Government of Canada Action Plan 2000 on climate change. http://scm-ac.gc.ca/docs/bestpractices.pdf
27. ASTM D 5239 (2004) Standard practice for characterizing fly ash for use in soil stabilization. American Society for Testing and Materials, West Conshohocken
28. ASTM E 2277 (2003) Standard guide for design and construction of coal ash structural fills. American Society for Testing and Materials, West Conshohocken
29. Turner-Fairbank Highway Research Center's coal fly ash user guide on embankment or fill and its references. http://www.fhwa.dot.gov/publications/research/infrastructure/structures/97148/app4.cfm
30. Federal Highway Administration (2006) Fly ash in structural fills/embankments. In: Fly ash facts for highway engineers. U.S. Department of Transportation, Washington, DC (Chap 6). http://www.fhwa.dot.gov/pavement/recycling/fach06.cfm
31. Turner-Fairbank Highway Research Center's coal fly ash user guide – stabilized base and its references. http://www.fhwa.dot.gov/publications/research/infrastructure/structures/97148/cfa55.cfm
32. Dodd WE (2005) Fly ash use in pressurized grout remote backfilling of abandoned underground mines in North Dakota. In: Interstate technical group on abandoned underground mines third biennial workshop. U.S. Department of Transportation, Federal Highway Administration, Kansas City, 25–27 Apr 2000. http://www.fhwa.dot.gov/engineering/geotech/hazards/mine/workshops/kdot/kansas04.cfm
33. Federal Highway Administration (2003) Fly ash in soil improvement. In: Fly ash facts for highway engineers. U.S. Department of Transportation, Washington, DC (Chap 7). http://www.fhwa.dot.gov/pavement/recycling/fach07.cfm
34. Turner-Fairbank Highway Research Center's coal fly ash user guide – flowable fill and its references. http://www.fhwa.dot.gov/publications/research/infrastructure/structures/97148/cfa56.cfm
35. Turner-Fairbank Highway Research Center's coal fly ash user guide – asphalt concrete and its references. http://www.fhwa.dot.gov/publications/research/infrastructure/structures/97148/cfa52.cfm
36. Golden DM, DiGioia AM (2003) Fly ash for highway construction and site development. Environmental Protection Agency (EPA), Coal Combustion Productions Partnership (C2P2), Coal Ash Utilization Case Study 10. http://www.epa.gov/osw/partnerships/c2p2/cases/10-highway2.pdf
37. Nagayama I, Jikan S (2003) 30 years history of roller-compacted concrete dam in Japan. In: Proceedings of the fourth International symposium on Roller Compacted Concrete (RCC) Dam, Madrid, 17–19 Nov 2003. http://www.pwri.go.jp/eng/activity/pdf/reports/nagayama031116.pdf
38. Abdo FY (Nov 2008) Roller-compacted-concrete dams: design and construction trends. Hydro Review, HCI Publications. http://www.cement.org/water/RCC%20Design&Construction.pdf
39. Saowapark T, Sombatsompop N, Sirisinha C (2009) Viscoelastic properties of fly ash-filled natural rubber compounds: Effect of fly ash loading. J Appl Polym Sci 112(4):2552–2558
40. Kruger RA, Hovy M, Wardle D (1999) The use of fly ash fillers in rubber. In: Proceedings of 1999 international ash utilization symposium, Lexington, 18–20 Oct 1999. http://www.flyash.info/1999/newprod/kruger2.pdf
41. Pruett-Schaffer Paint Company. http://www.undeerc.org/carrc/buyersguide/product.asp?prodid=25&catid=33
42. Yamazaki S, Okuda M (2006) Ship bottom paint using coal ash and diatomaceous earth. US Patent 7045788 B2, 23 May 2006
43. Rangan BJ (2008) Fly ash-based geopolymer concrete. In: Sustainable resource use. Your Building. http://www.yourbuilding.org/article/NewsDetail.aspx?p=83&id=1570
44. Louisiana Tech University (2009) Green research results in new geopolymer concrete technology. Science News, ScienceDaily. http://www.sciencedaily.com/releases/2009/09/090929141534.htm
45. Drechsler M (2006) Geopolymers: a new technology for sustainability in mining, construction and hazardous waste industries. Parsons Brinckerhoff PB Netw 62:72–74. http://www.pbworld.com/news_events/publications/network/issue_62/pb%20network%20issue%2062%20-%2025%20-%20geopolymers%20a%20new%20technology%20-%20drechsler.pdf
46. Beaver T (1995) Adding coal ash to the compositing mix. BioCycle 36(3):88–89
47. Renolds K, Kruger R, Rethman N (1999) The manufacture and evaluation of artificial soil (SLASH) prepared from fly ash and sewage sludge. In: 1999 international ash utilization symposium, Paper #1, Center for Applied energy research, University of Kentucky, Lexington, 18–20 Oct 1999
48. Mittra BN, Karmaker S, swain DK, Gosh BC (2003) Fly ash – a potential source of soil amendment and a component of integrated plant nutriment supply. In: 2003 international ash utilization symposium, Center for Applied Energy Research, University of Kentucky, Lexington

49. Smith I (2005) Land uses of coal fly ash – benefits and barriers. International Energy Agency (IEA) Clean Coal Centre Report, CCC/96, London, p 30. ISBN 92-9029-411-6
50. Yunusa IAM, Eamus D, DeSilva DL, Murray BR, Burchett MD, Skilbeck GC, Heidrich C (2006) Fly-ash: an exploitable resource for management of Australian agricultural soils. Fuel 85: 2337–2344
51. Wang S, Viraraghavan T (1997) Wastewater sludge conditioning by fly ash. Waste Manage 17(7):443–450
52. Luna Y, Fernández-Pereira C, Vale JF, Alberca L (2009) Waste stabilization/solidification (S/S) using fly ash-based geopolymers. Influence of carbonation on the S/S of an EAF dust. Presented at 2009 World of Coal Ash (WOCA) conference, Lexington, 4–7 May 2009. http://www.flyash.info/2009/097-fernandez2009.pdf
53. Calzonetti FJ, Elmes GA (1981) Metal recovery from power plant ash: an ecological approach to coal. GeoJournal 3(1):59–70
54. McDowell WJ, Seeley FG (1981) Recovery of aluminum and other metal values from fly ash. US Patent 4252777, 24 Feb 1981
55. Blander M, Wai CM, Nagy Z (1984) Extraction of trace metals from fly ash. US Patent 4475993, 9 Oct 1984
56. Lisowyj B, Hitchcock DC, Epstein H (1987) Process for the recovery of gallium and germanium from coal fly ash. US Patent 4678647, 07 July 1987
57. Tsuboi I, Kasai S, Kunugita E, Komasawa I (1991) Recovery of gallium and vanadium from coal fly ash. J Chem Eng Jpn 24(1):15–20
58. Cao DZ, Selic E, Herbell JD (2008) Utilization of fly ash from coal-fired power plants in China. J Zhejiang Univ Sci A 9(5):681–687
59. Cenospheres services companies: the Fillite http://www.fillite.com/ and the Sphere Services, Inc. http://www.sphereservices.com/
60. European Coal Combustion Products Association (ECOBA) (2009) Production and utilization of CCPs in 2007 in Europe (E15). http://www.ecoba.com/evjm,media/statistics/ECOBA_Stat_2007_EU15.pdf
61. Panagapko D (2006) Cement. Canadian minerals year book 2006. http://www.nrcan.gc.ca/mms-smm/busi-indu/cmy-amc/content/2006/17.pdf
62. The Ash Development Association of Australia (ADAA) (2008) Annual membership survey results. http://www.adaa.asn.au/docs/ADAA_Mship_Report_2008.pdf
63. Anonymous (1914) An investigation of the pozzolanic nature of coal ashes. Eng News 71(24):1334–1335
64. Davis RE, Carlston RW, Kelly JW, Davis HE (1937) Properties of cements and concretes containing fly ash. ACI J 33:577–612
65. Davis RE, Kelly JW, Troxell GE, Davis HE (1935) Proportions of mortars and concretes containing Portland – pozzolan cements. ACI J 33:577–612
66. Davis RE, Davis HE, Kelly JW (1941) Weathering resistance of concretes containing fly-ash cements. ACI J 37:281–296
67. BSI, BS 3892 (1965) Pulverized fuel ash for use in concrete. British Standards Institution, London
68. Sear LKA (2001) UK practice – a review of fly ashes for use in concrete. Proceedings of workshop on novel products from combustion residues, Morella, Spain, 6–8 June 2001
69. BSI, BS 3892 (1982) Part 1: pulverized fuel ash for use as a cementitious component in structural concrete. British Standards Institution, London
70. BSI, BS 3892 (1997) Part 1: specification for pulverized fuel ash for use with Portland cement. British Standards Institution, London
71. BSI, BS EN 450 (1995) Fly ash for concrete – definition, requirements, and quality control. British Standards Institution, London
72. BSI, BS EN 450-1 (2005) Fly ash for concrete – definition, requirements, and conformity criteria. British Standards Institution, London
73. BSI, BS EN 450-2 (2005) Fly ash for concrete – conformity evaluation. British Standards Institution, London
74. FHWA. Infrastructure – materials group, fly ash. Federal Highway Administration, Department of Transportation. http://www.fhwa.dot.gov/infrastructure/materialsgrp/flyash.htm
75. Sutton I (1968) Geographical aspects of construction planning: Hoover Dam revisited. J West 7(3):301–344
76. ECOBA website. http://www.ecoba.com/ecobaccpexs.html
77. Taylor HFW (1997) Cement chemistry, 2nd edn. Thomas Telford, London
78. Papadakis VG (1999) Effect of fly ash on Portland cement systems, Part I. Low-calcium fly ash. Cem Concr Res 29(11):1727–1736
79. Papadakis VG (2000) Effect of fly ash on Portland cement systems, Part II. High-calcium fly ash. Cem Concr Res 30(10):1647–1654
80. Build It Green (2005) Fly ash concrete. http://www.builditgreen.org/attachments/wysiwyg/22/Fly-Ash-Concrete.pdf
81. Van Oss HG, Padovani AC (2003) Cement manufacture and the environment, Part II: environmental challenges and opportunities. J Ind Ecol 7(1):93–126
82. Erdoğdu K, Türker P (1998) Effects of fly ash particle size on strength of Portland cement fly ash mortars. Cem Concr Res 28(9):1217–1222
83. Chindaprasirt P, Jaturapitakkul C, Sinsiri T (2005) Effect of fly ash fineness on compressive strength and pore size of blended cement paste. Cement Concr Compos 27(4): 425–428
84. Gao YM, Shim HS, Hurt RH, Suuberg EM (1997) Effects of carbon on air entrainment in fly ash concrete: the role of soot and carbon black. Energy Fuels 11(2):457–462
85. Headwater Resources. Fly ash for concrete. http://www.flyash.com/data/upimages/press/HWR_brochure_flyash.pdf
86. Turner-Fairbank Highway Research Center's coal fly ash user guide – Portland cement concrete and its references. http://www.fhwa.dot.gov/publications/research/infrastructure/structures/97148/cfa52.cfm

87. Joshi RC, Lohita RP (1997) Fly ash in concrete: production, properties and uses. In: Malhotra VM (ed) Advances in concrete technology, vol 2. Gordon and Breach Science, Amsterdam, pp 269
88. OSA Inc. (2009) Autoclaved aerated concrete, oral presentation at the Tennessee Valley Authority, June 2009
89. Autoclaved Aerated Concrete Products Association (AACPA). AERCON AAC technical manual, introduction. http://www.aacpa.org/; http://www.aerconaac.com/TECHNCAL%20MANUAL/Introduction.pdf
90. Chou SFJ, Chou MIM, Bukowski JM (2003) Manufacturing energy efficient construction products from Illinois coal fly ash, Final technical report to the Illinois Clean Coal Institute. Illinois State Geological Survey
91. Carroll RA, Payne JC (1992) Autoclaved cementitious products using pulverized fuel ash. In: Wittmann FH (ed) Advances in autoclaved aerated concrete. AA Balkema, Rotterdam, pp 297–303
92. Hums D (1992) Ecological aspects for the production and used of autoclaved aerated concrete. In: Wittmann FH (ed) Advances in autoclaved aerated concrete. AA Balkema, Rotterdam, pp 43–49
93. George J (2008) Cement crisis doubles demand for AAC. Article on Emirates Business 24|7, 21 Aug 2008. http://www.business24-7.ae/Articles/2008/8/Pages/08212008_73fd4c-fa6e6744ac80024a2f2a8f6bdd.aspx
94. Masonry Construction (2006) Autoclaved aerated concrete: product offers tremendous business opportunities for the masonry contractor. http://findarticles.com/p/articles/mi_m0NTA/is_3_19/ai_n26815025/
95. (a) ASTM C 1386 (2007) Standard specification for precast Autoclaved Aerated Concrete (AAC) wall construction units. American Society for Testing and Materials, West Conshohocken; (b) ASTM C 1693 (2009) Standard specification for Autoclaved Aerated Concrete (AAC). American Society for Testing and Materials, West Conshohocken; (c) ASTM C 1691 (2009) Standard specification for unreinforced Autoclaved Aerated Concrete (AAC) masonry units. American Society for Testing and Materials, West Conshohocken
96. Horvath ML (1995) Investigation of the use of fly-ash based autoclaved cellular concrete blocks in coal mines for air duct work, 25 Jan 1993–31 Dec 1994. Ohio Edison Company, Final report to the Ohio State Coal Development Office. http://www.ohioairquality.org/ocdo/pdf/d92102.pdf
97. Babb Cellular Concrete/Babb International (1998) News release. The Ringgold micro-plant, Ringgold
98. Chou MIM, Babb RA, Chou SFJ (2009). Concrete manufacturing processes and methods. United States Patent Application No. 12/573,475, University of Illinois at Urbana-Champaign and OSA Inc
99. Cicek T, Tanriverdi M (2007) Lime based steam autoclaved fly ash bricks. Constr Build Mater 21(6):1295–1300
100. Brick Industry Association (2006) Manufacturing of brick. Technical notes on brick construction TN 9, 9 Dec 2006. Brick Industry Association, Virginia
101. Regional Wood Energy Development Program in Asia (1993) Status and development issues of the brick industry in Asia, Report: GCP/RAS/154/NET: sponsored by the Food and Agriculture Organization of the United Nations, 69 pp
102. Brick Industry Association (1998) Manufacturing, classification, and selection of brick. Technical notes on brick construction TN 9, Manufacturing Part 1. Brick Industry Association, Virginia
103. Anderson M, Jackson G (1987) The history of pulverized fuel ash in brickmaking in Britain. Trans J Br Ceram 86(4):107–112
104. Slonaker JF (1977) The role of fly ash brick manufacturing in energy conservation. Report No. 149. Coal Research Bureau, College of Mineral and Energy Resources, West Virginia University, Morgantown, West Virginia, pp 6
105. Liu H (2005) Compacting fly ash to make bricks. Final technical report to National Science Foundation, Mar 2005, 15 pp
106. Chou MIM, Chou SFJ, Patel V, Botha F (2003) Production and testing of fired bricks made with Class F fly ash from two Illinois coal-fired power plants. Preprint and oral presentation at the 15th international symposium on management and use of coal combustion products held by the American Coal Ash Association, St. Petersburg, 27–30 Jan 2003
107. Chou MIM, Patel V, Laird CJ, Ho KK (2001) Chemical and engineering properties of fired bricks containing 50 weight percent of Class F fly ash. Energy Sources 23:665–673
108. Chou MIM, Chou SFJ, Patel V, Stucki JW, and Botha F (2003) Manufacturing commercial bricks with Illinois coal fly ash-a program overview. In: International coal ash utilization symposium, American Coal Ash Association, Lexington, 20–24 Oct 2003
109. Chou MIM, Chou SFJ, Patel V, Stucki JW (2005) Commercial production of fired bricks with Illinois Basin Class F fly ash. Preprint and oral presentation at the international congress on fly ash utilization conference, New Delhi, 4–7 Dec 2005
110. Chou MIM, Chou SFJ, Patel V, Pickering MD, Stucki JW (2006) Manufacturing building bricks with Class F fly ash from Illinois Basin coal, Final Report to US DOE/WVURC-combustion byproducts recycling consortium. Project Number: 02-CBRC-M12. Illinois State Geological Survey
111. ASTM C 62 (2008) Standard specification for building brick (solid masonry units made from clay or shale). American Society for Testing and Materials, West Conshohocken
112. Chou MIM, Chou SFJ, Pickering MD, Stucki JW (2006) An environmental feasibility assessment of fired bricks containing fly ash. Am Chem Soc Div Fuel Chem 51(2):421–422 (Preprint paper)
113. Zhang MH, Blanchette MC, Malhotra MV (2001) Leachability of trace metal elements from fly ash concrete: results from column-leaching and batch-leaching tests. ACI Mater J 98(2):126–136
114. Sear LKA, Weatherley AJ, Dawaon A (2003) The environmental impacts of using fly ash – the UK producers' perspective. In: The 2003 international ash utilization symposium paper

#20, Center for Applied Energy Research, University of Kentucky, Lexington. Paper available at: http://www.flyash.info
115. Electric Power Research Institute (1998) Coal ash: its origin, disposal, use, and potential health issues. Electric Power Research Institute (EPRI) Environmental Focus Report, BR-111026. http://acaa.affiniscape.com/associations/8003/files/epri-coal_ash-origin-disp-use.pdf
116. United States Geological Survey (1997) Radioactive elements in coal and fly ash: abundance, forms, and environmental significance. United States Geological Survey (USGS): USGS Fact Sheet FS-163-97. http://pubs.usgs.gov/fs/1997/fs163-97/FS-163-97.pdf
117. Morford S (2009) EPA study finds dangers in coal ash ponds nationwide. Daily Climate News and Analysis, 1 Sept 2009. http://solveclimate.com/blog/20090901/epa-study-finds-dangers-coal-ash-ponds-nationwide
118. Newell R (2009) U.S. Energy Information Administration – independent statistics and analysis. Annual energy outlook 2010 – reference case. http://www.eia.gov
119. Pedersen KH, Jensen AD, Skjoth-Rasmussen MS, Dam-Johansen K (2008) A review of the interference of carbon containing fly ash with air entrainment in concrete. Prog Energy Combust Sci 34(2):135–154
120. Hall ML, Livingston WR (2002) Fly ash quality, past, present, and future, and the effect of ash on the development of novel products. J Chem Technol Biotechnol 77:234–239

Books and Reviews

Cox M, Nugteren H, Janssen-Jurkovičová M (2008) Combustion residues: current, novel and renewable applications. Wiley, England

Manz OE (1997) Worldwide production of coal ash and utilization in concrete and other products. Fuel 76(8):691–696

Sear LKA (2001) The properties and use of coal fly ash. Thomas Telford, London

Taylor HFW (1997) Cement chemistry, 2nd edn. Thomas Telford, London

Vassilev SV, Vassileva CG (2005) Methods for characterization of composition of fly ashes from coal-fired power stations: a critical overview. Energy Fuels 19(3):1084–1098

Wesche K (1992) Fly ash in concrete: properties and performance. Rilem Report 7, the International Union of Testing and Research Laboratories for Materials and Structures. E & FN SPON, London

Useful Resources

American Coal Ash Association (ACAA). http://www.acaa.org

American Concrete Institute. http://www.aci.org

Ash Development Association of Australia (ADAA). http://www.adaa.asn.au/

Association of Canadian Industries Recycling Coal Ash (CIRCA). http://circainfo.ca/

Boral Material Technologies Inc. (Boral MTI) – a US company. http://www.boralmti.com processing and marketing fly ash

Buyer's guide to coal ash containing products. http://www.undeerc.org/carrc/buyersguide/default.asp

Coal Combustion Products Partnership (C^2P^2) – in the USA. http://www.epa.gov/waste/partnerships/c2p2/index.htm

Electric Power Research Institute – in the USA. http://www.epri.com

European Coal Combustion Products Association (ECOBA) – in Germany. http://www.ecoba.com/

Fly Ash Information Center – in India. http://www.fly-ash-information-center.org.in/

Fly Ash Library http://www.flyash.info/ selected papers from the international ash utilization symposiums held in 1999, 2001, 2003 and world of coal ash conferences held in 2005 and 2007

Fly Ash Utilization Programme (FAUP) – in India. http://flyashindia.tifac.org.in/

Headwaters Resources – fly ash for concrete. http://www.flyash.com/data/upimages/press/HWR_brochure_flyash.pdf

Informational & Analytical Center "Ecology of Power Engineering" of Moscow Power Engineering Institute (IACEE MPEI). http://www.ecopower.ru/index.php?do=cat&category=english

Japan Coal Energy Center. http://www.jcoal.or.jp/index-en.html

KEMA – a commercial service company, owned by several Dutch utilities, but functioning independently. http://www.kema.com/services/consulting/hse/cc-consequences/fly-ash.aspx

Korean Coal Ash Recycling Association. http://coalash.or.kr/en/intro_3.html

National Coal Ash Board, Israel. http://www.coal-ash.co.il/english/index.html

RockTron – a UK company whose mission is to transform fresh and stockpiled fly ash from coal-fired power stations into a sustainable, alternative source of valuable, environmentally-coherent minerals for industrial use. http://rktron.com/

South African Coal Ash Association (SACAA). http://www.coalash.co.za/

The Coal Ash Research Center – at the University of North Dakota, Energy & Environmental Research Center (EERC) is dedicated to improving the technical and economic aspects of by-products management. http://www.undeerc.org/carrc/

Technology Information, Forecasting and Assessment Council (TIFAC) http://www.tifac.org.in (established in 1988 in India)

The Fly Ash Resource Center – in the USA whose mission is to promote knowledge and utilization of fly ash and other coal combustion products. http://www.rmajko.com/flyash.html

United Kingdom Quality Ash Association (UKQAA). http://www.ukqaa.org.uk/

United States Army Corps of Engineers. http://en.wikipedia.org/wiki/United_States_Army_Corps_of_Engineers

United States Bureau of Reclamation. http://www.usbr.gov/

United States Department of Transportation – Federal Highway Administration (FHWA): the Turner-Fairbank Highway Research Center. http://www.tfhrc.gov

United States Geological Survey. http://www.usgs.gov

World Wide Coal Combustion Product Network (WWCCPCN). http://www.wwccpn.org/

Fossil Energy, Introduction

Ripudaman Malhotra
Chemistry and Chemical Engineering Laboratory,
Pure and Applied Physical Sciences Division,
SRI International, Menlo Park, CA, USA

To many in the sustainability community, fossil energy is an anathema. Continued use of fossil resources – oil, coal, and natural gas – poses threats to the environment through the emission of pollutants and greenhouse gases. The fact that they are a limited or exhaustible resource means that in the future we could either run out of them or their extraction will get progressively harder to a point that it takes more energy to extract them than would be derived from their use. Using fossil energy is clearly not sustainable, and the world has to look to renewable resources for long-term survival.

This is an encyclopedia about the science and technology of sustainability. The word, *sustainability* shares its root with *sustenance*. Any discussion of sustainability must therefore include discussions of sustenance, and in the context of modern society, sustenance stems from the use of energy. We derive energy from a number of different sources. Annual global consumption of energy is currently on the order of 500 exajoules (EJ), about 85% of which comes from fossil resources. From 500 EJ/year, the global energy demand is expected to rise to somewhere between 1,000 and 1,500 EJ/year by the middle of this century. The drivers for this increased demand are already in place. Large segments of China, India, and Brazil are poised to increase their standard of living – and the concomitant energy demand – substantially. If the average energy consumption in the Asia-Pacific region were to reach the current global average, which is about half of what is consumed in Europe and Japan, the demand would increase by an amount equal to the total energy consumption in the North America region. The challenge of achieving a sustainable future is in being able to balance the energy requirements for the billions of people so they can lead healthy and productive lives against the need to preserve the environment by not running into its limits in its ability to supply the resources or act as a sink for the waste [1]. The entries in this section examine the current status, assess the resource potential of the various fossil fuels, examine the technologies for using them, and review the environmental impact of their use.

Petroleum and natural gas have similar origin and often occur together in geologic formations, and their global distribution and production is discussed together in the entry by McCabe (► Oil and Natural Gas: Global Resources). This entry makes clear the distinction between reserves and resources. Reserves represent only that fraction of the resource base that can be economically recovered using current technology. These are not fixed quantities as both technology and economics change over time. Global annual production (and consumption) of oil in 2010 was 31 billion barrels and of natural gas was around 120 trillion cubic feet. In energy units, they correspond to 180 EJ of oil and 120 EJ of natural gas [2]. The current reserves are estimated at 1,236 billion barrels of conventional oil (7,500 EJ) and 6,545 tcf of natural gas (6,500 EJ). The current reserves to production ratio (R/P) is about 40 for oil and about 55 for natural gas. The R/P ratio has often been mistakenly taken as the time to exhaustion, but new discoveries as well as advances in technology add to the reserves. In the case of oil, for example, the R/P ratio has stayed around 40–50 years for more than 60 years even with the steadily increasing oil consumption. In addition, there are also unconventional accumulations of these hydrocarbon resources and extracting them requires development of new technologies. In the case of oil, the unconventional resources are oil sands, oil shale, and heavy oil. Unconventional resources of natural gas are coal bed methane, tight gas, shale gas, and gas hydrates. These unconventional resources are vast and have the potential of more than doubling our resource endowment.

Exploration and production of oil from sedimentary deposits and oil sands is the subject of an entry by Speight (► Petroleum and Oil Sands Exploration and Production). The processes for recovering oil could be a simple matter of drilling into the formation with the oil flowing to the surface under its own pressure, or it may require injection of gases, fluids, and surfactants to coax it to flow. In extreme cases, it may even require underground combustion of a portion of the resource to release the oil. Speight describes the chemical and physical factors that govern the flow of oil and the

technology options currently available. In a different entry, Speight (► Petroleum Refining and Environmental Control and Environmental Effects) provides and account of the different processes such as distillation, catalytic cracking, hydrotreating, reforming, and deasphalting used in the refining of crude oil. This entry also deals with environmental effects of the gaseous, liquid, and solid effluents from these processes. Production of oil from shale is principally achieved by retorting of shale, or other thermal processes including in situ pyrolysis. Oja and Suuberg (► Oil Shale Processing, Chemistry and Technology) detail the chemistry and technology of these processes in the entry.

Gas hydrates represent a particularly noteworthy resource and are reviewed in the entry by Patil (► Alaska Gas Hydrate Research and Field Studies). They are naturally occurring ice-like substances in which methane or other light gases are trapped in the cage structures formed by water molecules. They are stable under certain conditions of temperature and pressure, and can be found at many places around the world at depths of several hundred meters below the seabed and in the permafrost in the polar region. Global estimates of gas hydrates are on the order of 500,000 tcf, about a hundred times the proved reserves of natural gas. Apart from being a potentially very important source for energy in the future, the gas hydrates are also important from the perspective of climate change. A general warming could release substantial amounts of methane, which – being a potent greenhouse gas – would reinforce any global warming.

Oil remains the prized fuel. It has a high energy density and as a liquid it is well suited for transportation. The transportation sector relies on oil for over 90% of its energy needs (the remainder being mostly furnished by coal – via electricity) [3]. Given the importance of liquid fuels, there is considerable interest in converting coal and natural gas, the other hydrocarbon resources, into oil. In a pair of entries, Araso and Smith (► Gas to Liquid Technologies and ► Coal to Liquids Technologies) provide an overview of the various processes for converting natural gas and coal to liquids. These reviews cover the basic chemistry and catalytic technologies behind the different approaches. The entry on ► Gas to Liquid Technologies deals with steam reforming of methane, autothermal reforming, and partial oxidation approaches for producing syngas, including strategies for managing the heat and mass transfer through the use of different reactor technologies. The entry next covers the conversion of syngas into liquids by Fischer-Tropsch (FT) synthesis. The entry on ► Coal to Liquids Technologies reviews the different approaches like pyrolysis, direct liquefaction, coprocessing with petroleum, and indirect liquefaction that first converts coal into syngas and then uses FT or other conversion processes to make liquid fuels.

The internal combustion engines that power these vehicles covert only about 20–30% of the energy in the fuel to motive power. Increasing the efficiency of the engines used in transportation represents a significant opportunity to reduce future demand for oil, as well as reduce the carbon footprint of the cars, trucks, and planes. Jacobs (► Internal Combustion Engines, Developments in) provides a detailed account of the thermodynamics of the different kinds of engines and of the various technologies under development for improving the efficiency of the internal combustion engines. These include strategies such as engine downsizing, turbocharging, better controls, variable geometry engines, variable valve timing, homogeneous charge compression engines, and waste heat recovery.

Höök (► Coal and Peat: Global Resources and Future Supply) reviews the global coal and peat resources, which are substantially larger than conventional oil and gas resources. Peat and coal are also distributed more evenly around the globe. The proved reserves of coal are estimated at between 800 billion and a trillion metric tons, representing roughly 20,000 EJ. Most coal is derived from trees and ferns that grew some 250–300 million years ago during the carboniferous period. Aerobic bacteria generally decompose most plant matter into CO_2, but when a tree fell into a swamp and was buried with limited exposure to oxygen, it could be partially preserved. That phenomenon occurs even today and is evidenced in the formation of peat (very young coal) in bogs. Unlike coal, peat has a low calorific content and its commercial use as an energy resource is limited. However, peat is important from global carbon cycle. Peat bogs store vast amounts of carbon, but the product of anaerobic decomposition, methane, contributes to greenhouse gases in the atmosphere such that under steady state conditions they comprise only a slight sink of carbon. The situation changes with

fires as peat bogs become major source of carbon in the atmosphere. Human activities, such as drainage of the area for agriculture, exacerbate the situation, as more peat gets exposed and the swamp is not wet-enough to squelch the fire. Estimates of the amounts of carbon released from peat are on the order of several billion tons, the same order of magnitude as from fuels used in transportation or power production.

As coal resources are vast, they are likely to continue to contribute substantially to global energy mix. However, their use also presents a number of challenges, beginning with mining, and through coal preparation and use. Mining operations result in excavation of billions of tons of earth, and depending on the nature of the waste rock and how it is handled it can lead to contamination of air, water, and soils systems. The wide-ranging nature of environmental impact necessitates a commensurately broad portfolio of technologies for the remediation, restoration and reclamation. Chattopadhyay and Chattopadhyay (► Mining Industries and Their Sustainable Management) provide an overview of the environmental impact of coal mining, and mining processes in general, as well as review the range of the chemical and biochemical strategies to mitigate the impact.

The run-of-mine coal is often laden with noncombustible minerals such as shale and clays that reduce its heating value. Cleaning and washing of coals removes many of these impurities and upgrades the coal into a marketable resource, improve the performance of power plants, and also reduce potential of harmful emissions and dust. Luttrell and Honaker (► Coal Preparation) review these cleaning and preparation operations, and point out the importance of cheap preparation in extending the resource base.

Electricity is one of the most useful forms of energy; its importance to the way we live cannot be over emphasized. It can be used to perform all kinds of useful functions and services that people desire, and at the point of use it produces no pollution. Electricity is a secondary source of energy, as it must be produced from primary sources such as coal, natural gas, oil, nuclear, hydro and, of late, increasingly from wind and solar. In 2010, the global production of energy was 21,325 trillion kWh, which is equivalent to 77 EJ. However, since 68% of electricity is derived from burning fossil fuels at an average efficiency of 38%, the total primary energy the world consumed as electricity amounts to 135 EJ, or roughly 27% of the total energy consumed. Electricity demand in the world is projected to rise at a rate greater than for total energy, and meeting that need for additional sources for producing electricity is critical human welfare.

Several entries in this section are devoted to the production of electrical power. As the fuel with the lowest levelized cost of electricity, coal remains the dominant fuel for producing electricity, and furnishes over half of the electricity. It results in the emission of about 900 g CO_2 per kWh, highest of any fossil resource. The development of coal power in future is going to be constrained by the concerns of CO_2 emissions, and Beer (► CO_2 Reduction and Coal-Based Electricity Generation) discusses the different technology options for increasing the efficiency of coal-fired power plants and reducing the CO_2 emissions. Ultra supercritical steam cycles and combined heat and power applications are relatively straightforward to apply, and have the potential to reduce the largest tonnage of emissions.

Of course, there are other pollutants also that are emitted when coal is used for power productions. Chief among them are oxides of sulfur and nitrogen and toxic metals such as mercury, selenium, and arsenic, as well as carcinogenic PAH-containing soot aerosols. Moyeda (► Pulverized Coal-Fired Boilers and Pollution Control) reviews the technologies for scrubbing the stack gas emissions. The deployment of scrubbers for the nitrogen and sulfur oxides following the Clean Air and Water Act in the 1980s greatly improved the quality of air and water systems.

Natural gas is the other major fuel for producing electric power. When used in a gas-fired combined-cycle mode, it produces only 380 g CO_2/kWh. Smith and Gülen (► Natural Gas Power) review the technology for power generation from natural gas. They discuss the different sources of natural gas, provide a brief history followed by detailed thermodynamics of gas turbines, and modern power plants designs that incorporate combined cycle for maximum overall efficiency. They also review emissions from NGCC plants, notably NO_x, and strategies for minimizing them. The entry concludes with a discussion of power plant economics.

Carbon capture and sequestration (CCS) as a strategy for stabilizing atmospheric CO_2 levels is receiving considerable attention. Friedman (► CO_2 Capture and

Sequestration) provides an overview of the state of technology and the different embodiments of CCS. These cover various strategies for first capturing the CO_2, which may be performed pre- or post-combustion, or from the atmosphere. He discusses the energy requirements under these different scenarios. The entry also reviews the geochemistry of various options for sequestering the captured CO_2, either in deep saline aquifers or in other geological formations.

Bibliography

1. Meadows D, Randers J, Meadows D (2004) Limits to growth, the 30-year update. Chelsea Green Publishing, White River Junction, Vermount
2. BP statistical review of world energy, June 2011 From www.BP.com
3. Energy Information Administration, Annual energy review 2010. http://www.eia.gov/emeu/aer/pecss_diagram.html

Fuel Cell Comparison to Alternate Technologies

Julia Kunze[1,2], Odysseas Paschos[2], Ulrich Stimming[1,2]
[1]Institute for Advanced Study (IAS), Garching, Germany
[2]Department of Physics, Technische Universität München, Garching, Germany

Article Outline

Glossary
Definition of the Subject and Its Importance
Introduction
Classical Heat Engines
Electrochemical Systems
Electromobility: An Example for Combining Key Energy Technologies
Future Directions
Bibliography

Glossary

Fuel cell A fuel cell is an electrochemical cell that can convert the chemical energy stored in a given fuel into electrical energy.

Electrochemical capacitor An electrochemical capacitor (supercapacitor, ultracapacitor or double-layer capacitor) is an electrochemical device that can store and convert energy by charging/discharging the electrochemical double-layer of 2 electrodes with large surface areas and thus large double layer capacitances.

Battery A battery or Voltaic cell consists of one or more electrochemical cells which store and convert chemical energy into electric energy.

Ragone plot A Ragone Plot compares the performances of different energy storing devices by plotting power densities or specific power [W/kg] versus energy densities or specific energy [Wh/kg].

Electromobility Electromobility is a mobility concept in which electric vehicles instead of vehicles powered by internal combustion engines are used.

Definition of the Subject and Its Importance

The actual energy demand and consumption issues make it necessary to critically discuss and compare different energy conversion and storage systems. At present, only one third of the primary energy is converted into end energy, for example, electrical energy. Losses are associated with a high consumption of fossil fuels and large CO_2 emissions. They can be avoided by considering important electrochemical processes for energy conversion, using batteries, fuel cells, supercapacitors and electrochemical photovoltaics and by incorporating energy storage, employing rechargeable batteries, supercapacitors, generation of hydrogen via electrolysis, and generation of methanol.

Fuel cells can offer clean power generation and have the potential to convert fuels directly into electrical energy with high efficiencies. Today, however, they cannot compete with heat engines because of much higher costs, inferior power performance, and insufficient durability and lifetime. As yet, no single electrochemical power source can match the characteristics of the internal combustion engine. A competitive system in comparison to heat engines can be envisioned when available electrochemical power systems are combined. In such hybrid electrochemical power systems, batteries and/or supercapacitors would provide high power and the fuel cells would deliver electricity with high efficiency. The consequence would be to considerably reduce costs of the electrochemical systems.

Moreover, when we compare different systems, we face the genuine problem of geometry and thus the costs related to the space needed for the processes involved. The latter explains the so far success of thermodynamic-based systems (e.g., heat engines) compared to alternative energy technologies (e.g., fuel cells). This is also evident when the power output of a coal power plant which lies in the GW range is compared to the power that a fuel cell can deliver which lies in the MW range. A possible strategy would be to develop highly efficient fuel cell systems that can push their power to larger outputs. Current research is aiming at increasing the power output of a fuel cell without compromising its efficiency; however, the advantages of conventional systems cannot be ignored.

Introduction

Our present situation concerning major (fossil) energy carriers and energy consumption is characterized by limited reserves and resources as well as emission problems, considering crude oil, natural gas, coal, and uranium as primary energy sources. At the same time, the worldwide demand for electrical energy has increased from 8.3 million GWh in 1980 to 18.9 million GWh in 2006 and is estimated to further increase up to 30.7 million GWh in 2030 (see [1] (Fig. 1).

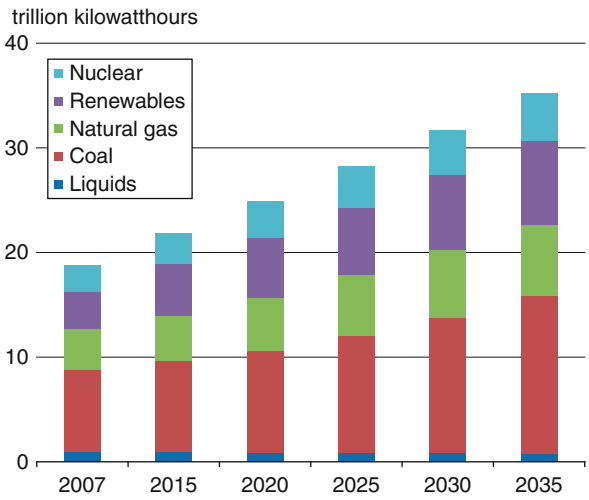

Fuel Cell Comparison to Alternate Technologies. Figure 1
Worldwide demand for electrical energy (From [1])

The problem of the energy management is of a rather complex nature. Increasing contributions of renewable energies such as wind power, solar power, and wave power tend to complicate the grid management. Therefore, generation of electrical energy is only part of the challenge. The management and storage of electrical energy will become essential in order to maintain the present grid quality [2].

Energy conversion processes today are under special consideration because of two issues associated with them:

1. The limited availability of primary energy carriers
2. The emission of pollutants with local and global negative effects on the environment

On average, energy conversion processes aiming at generating electrical power reveal efficiencies not much higher than 30%. This indicates that losses in the form of heat or chemical substances amount to more than two thirds of the primary energy. Conventional processes, for example, those in a heat engine–based power plant, are volume processes such as combustion, which results in mechanical and then in electric energy. By contrast, other technologies such as photovoltaics, batteries, fuel cells, or supercapacitors are based on interfacial transfer of energy and/or charge. In contrast to the performance of heat engines which is limited by the Carnot efficiency, interfacial reactions are usually of much higher thermodynamic efficiency.

Classical Heat Engines

Thermodynamic considerations lead to the first heat engines that were used to generate mechanical or electrical energy. Since the eighteenth century, conventional reciprocating steam engines have served as mechanical power sources, with notable improvements being made by James Watt. The first commercial central electrical generating stations in New York and London, in 1882, used steam engines [3]. These first-generation heat engines are still serving as power plants today.

Further developments lead to the introduction of combined cycle power plants. Here, usually a combination of several cycles, operating at different temperatures yields considerably higher system efficiency. Heat engines are only able to use a portion of

the energy, usually 35–41%. The remaining heat is generally wasted.

In a combined cycle power plant (CCPP), or combined cycle gas turbine (CCGT) plant, a gas turbine generator produces electricity and the waste heat is used to make steam for generating additional electricity via a steam turbine; this last step enhances the efficiency for electricity generation to about 60%, because the temperature difference between the input and output heat levels is higher leading to an increase in the Carnot efficiency. Most modern power plants in Europe and in North America are of this type.

If the waste heat of a conventional thermal power station is utilized for district heating, it is called cogeneration. This heat gives an additional efficiency of about 40–50% which leads to an increase of the overall efficiency to ~90%. The fuels used in these engines comprise black and brown coal and nuclear power.

In contrast to the stationary systems described above, mobile engines are needed in many energy production applications. The best known mobile engines are the four-stroke (Otto), the diesel, and the Stirling engine.

Heat engines have limited efficiencies which are determined by the Carnot cycle. Practical issues reduce the efficiency of steam engines, due to limits of convective heat transfer and viscous flow (friction). There are also mechanical considerations, for example, limitations imposed by the materials such as nonideal properties of the working gas, thermal conductivity, tensile strength, creep, rupture strength, and melting point.

Electrochemical Systems

Energy Conversion and Storage

Alternatively to conventional Carnot-based heat engines, electrochemical systems have the potential to be employed to generate and store energy. Important electrochemical processes for energy conversion are considered in batteries, supercapacitors, electrochemical solar cells, and fuel cells, and energy storage is incorporated by employing rechargeable batteries, supercapacitors, generation of hydrogen *via* electrolysis, and generation of methanol from electrochemically generated hydrogen and CO_2/CO-containing synthetic gas. Electrochemical energy conversion systems are not subject to the Carnot cycle limitations and may operate with much higher efficiencies than combustion engines and related devices. Heat engine cycle processes are volume processes, whereas all electrochemical systems that are used for energy conversion and storage are based on reactions that take place at an interface. This makes them dependent on the surface morphology and its physical and chemical properties.

A *fuel cell* is an electrochemical conversion device. It produces electricity from fuel on the anode side and an oxidant on the cathode side, which react in the presence of an electrolyte. Fuel cells can operate continuously as long as the necessary flows of reactants and reaction products are maintained. They are thus thermodynamically open systems. Many combinations of fuel and oxidant are possible. A hydrogen cell uses hydrogen as fuel and oxygen, usually from air, as oxidant. Other fuels include hydrocarbons and alcohols. Other oxidants include chlorine and chlorine dioxide. The principle of fuel cells is already known for 165 years. In 1838, Christian Friedrich Schönbein discovered that an electrical voltage is measured between two platinum wires in an electrolyte solution surrounded by hydrogen and oxygen. He published these results under the title "On the Voltaic Polarization of Certain Fluid and Solid Substances." Sir William Robert Grove investigated the new effect intensely and was the first to develop useful fuel cells. He connected several elements in series and called these systems "gas batteries." The further development of this concept to a really efficient electrical source proved to be so difficult that it took 100 years until it improved essentially. After the design of the first electrical dynamo by Werner von Siemens in 1867, electrical generators were energy sources that efficiently delivered electricity in almost unlimited amounts. This was the reason why fuel cells were practically replaced completely. *Fuel cells* have the potential for high conversion efficiencies of chemical energy into electrical energy; at the moment the attainable efficiency is up to 65%, depending on fuel and conditions. Fuel cells can substitute other technologies or be operated in synergy, for example, with combustion engines in cogeneration of electricity and of heat and cold, in residential or mobile applications.

Figure 2 shows a comparison of the thermodynamic efficiencies of a hydrogen/oxygen fuel cell and of a Carnot cycle. In the future, fuel cells might be able to convert the used fuels into electrical energy with efficiencies of >70%. The difference between the

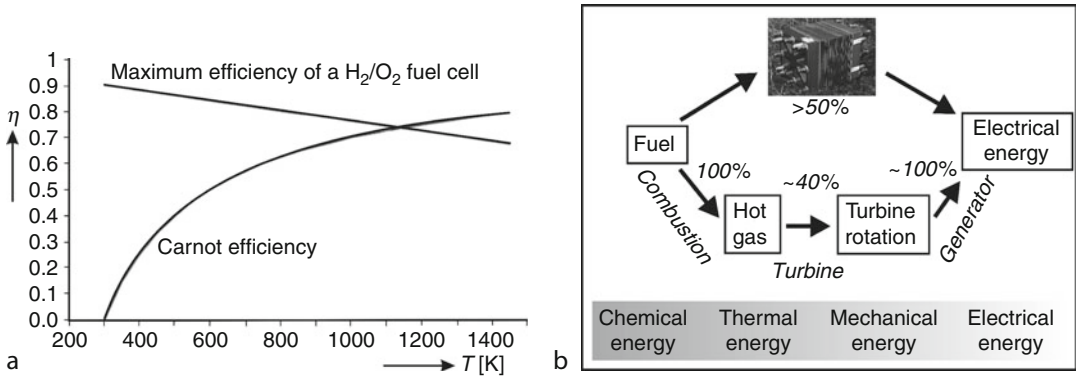

Fuel Cell Comparison to Alternate Technologies. Figure 2
(**a**) Ideal thermodynamic efficiency of polymer electrolyte membrane fuel cells (PEMFCs) compared to that obtained in the Carnot process. (**b**) Comparison of processes in a cogenerated heat engine with fuel cell performance (From [2])

theoretical and practical energy storage capabilities is related to several factors, including (1) inert parts of the system such as conductive diluents, current collectors, containers, etc., that are necessary for its operation, (2) internal resistances within the electrodes and electrolyte and between other cell components, resulting in internal losses, and (3) limited utilization of the active masses, as, for example, parts of the fuel in a fuel cell leave the cell without reaction or as, for example, passivation of electrodes makes them partially electrochemically inactive. Fuel cells offer a very clean power generation. They are quiet in operation and can be located close to the application. They produce much less greenhouse emissions and can be more efficient in conversion of the energy in a fuel into power than gasoline engines or utility thermal power plants. Fuel cells are best utilized as a steady energy source and not as a power source to supply dynamic demands. For applications that require varying power demands, such as automotive propulsion, the use of the fuel cell in a hybrid configuration with a battery or an electrochemical capacitor is envisioned. The fuel cell provides steady power delivery while the battery or the electrochemical capacitor handles the surge for regenerative breaking and acceleration as well as initial start-up. There is a *certain number of fuel cells under development*. Usually fuel cells are classified by the electrolyte that they are using. The electrolyte is a major component of the fuel cell since it determines the operating temperature, fuel, oxidant, poisons, catalysts, electrode design, and system design. According to the type of electrolyte that is used, fuel cells can be classified into six major categories.

The polymer electrolyte membrane fuel cell (PEMFC) uses a solid-type electrolyte that typically cannot withstand high temperatures, and the relatively low operating temperature results in slow reaction rates. The operating temperature of a PEMFC is typically between 50°C and 100°C. The slow reaction rate is overcome by using highly active catalysts such as platinum. The fuel utilized is pure hydrogen and the electrical power that it produces is typically less than 250 kW. The fuel and oxidant must be free of carbon monoxide, which is a poison because it gets strongly adsorbed by the catalyst reducing the active surface area. The main applications for PEMFCs are for small stationary units and as power supplies in vehicles. The direct methanol fuel cell (DMFC) is similar to the PEMFC but methanol is used as a fuel instead of hydrogen. It can be used for portable applications such as laptops, cell phones, and MEMS devices. Maximum power of DMFCs is typically less than 10 kW.

Figure 3 shows a typical polarization curve of a low-temperature PEMFC. The curve is similar for all the other types of fuel cells as same trends are observed. At high operation voltages, the power output of a fuel cell is controlled mainly by the electrocatalytic properties of the catalyst. In this region (>0.8 V), the current density is controlled by the charge transfer and the dissipated heat is minimized. Challenges in fuel cell

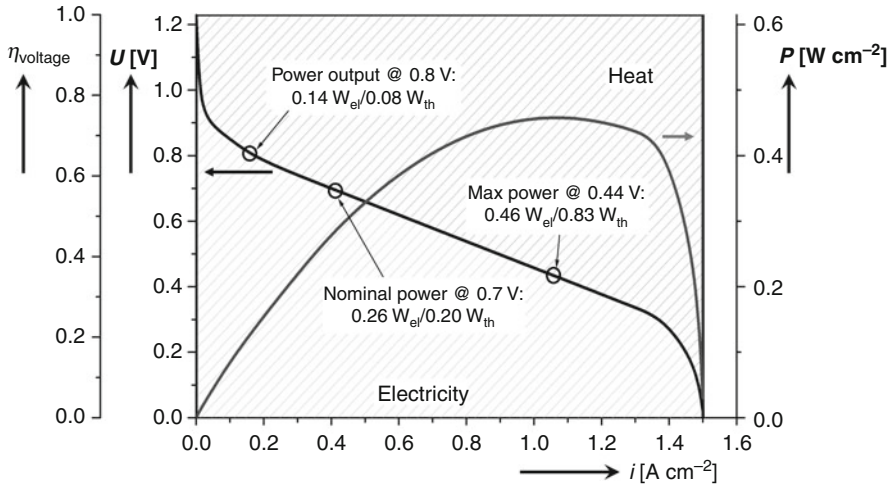

Fuel Cell Comparison to Alternate Technologies. Figure 3
Conversion of chemical energy in fuel cells (voltage efficiency $\eta_{voltage}$ versus current density *i*). *Black line*: cell voltage *U*; *gray line*: power density *P*

catalyst research are to obtain high electric power density, high electric conversion efficiency, and low material costs. At high electric power density, mass transport is the dominant factor affecting the fuel cell operation. This region can be expanded by careful engineering design of the fuel cell system. A general research trend is to obtain as high current densities as possible at high operation voltages.

For *high electric conversion efficiency*, one should aim at the use of less cogenerated heat which would also allow for a simplification of the design and the need of less fuel (hydrogen) for the same electrical energy. To guarantee low material costs, less noble metal should be incorporated, because high catalyst utilization is needed, and highly efficient catalysts are needed for anode and cathode side. The goal in fuel cell research must therefore be a deeper understanding of the parameters controlling electrocatalytic activity which would enable us to propose rational structures for catalysts in fuel cells in the future.

Alkaline fuel cells (AFCs) were used to provide electrical power for many manned spacecrafts. The electrolyte is KOH and the catalysts include silver, nickel, and different metal oxides. AFC catalysts are relatively inexpensive compared to catalysts used for other types of fuel cells. The fuel and oxidant used in an AFC must be completely free of CO_2 since even a small amount reacts strongly with the electrolyte, producing forms of carbonates that poison the ionic conductivity of the electrolyte. Therefore, pure hydrogen and oxygen must be used, limiting the use of the AFC to special applications, like spacecrafts and submarines, where cost of the fuel and oxidant is not a major issue.

The phosphoric acid fuel cell (PAFC) was the first fuel cell to be commercialized and shares some technologies with the PEMFC, such as the porous electrodes and the platinum catalysts. The liquid phosphoric acid allows high operating temperatures, around 200°C. Fuels must be free of carbon monoxide, as with the PEMFCs. With rated power over 50 kW, PAFC systems are used for stationary applications.

Molten carbonate fuel cells (MCFCs) operate at temperatures around 650°C. The electrolyte is a mixture of molten carbonate salts, such as lithium and potassium carbonate. At the operating temperature, the carbonates melt and become conductive to carbonate ions. Due to the high temperature, high reaction rates can be achieved with low-cost catalysts such as nickel. Rated power for MCFC systems is typically greater than 1 MW.

The last fuel cell system is the solid oxide fuel cell (SOFC). Typical operating temperature for the SOFC is between 600°C and 1,000°C. It has the same advantages of the MCFC (high reaction rates, inexpensive catalysts,

and natural gas can be used as a fuel). The electrolyte is in solid form, the most common kind being yttria (Y_2O_3) stabilized with zirconia (ZrO_2), which is a ceramic and therefore makes the fabrication process complex and difficult. The power output can be greater than 200 kW, making the SOFC ideal for large stationary applications, such as power stations.

High-temperature fuel cells such as *molten carbonate fuel cells (MCFC)* or *solid oxide fuel cells (SOFC)* deliver off heat at high temperature level ($T > 600°C$). This can be used in high-temperature fuel cell cogeneration for district heating (heat extraction), for absorption refrigerators and heat pumps. As the energy demand in residential applications is complementary for heating and for cooling over the year, such a combination would be very useful.

A *battery* or voltaic cell consists of one or more electrochemical galvanic cells which store and convert chemical energy into electric energy. Since the invention of the first Voltaic pile in 1800, the battery has become a common power source for many household and industrial applications. The name "battery" was coined by Benjamin Franklin for an arrangement of multiple Leyden jars, an early type of capacitor. There are different types of batteries which comprise non-rechargeable batteries (primary batteries) in which chemical energy is stored internally, the discharging reaction, that takes place at the electrode/electrolyte interface, is irreversible, and rechargeable batteries or accumulators (secondary batteries) having a reversible discharging reaction [4].

In the nineteenth century, no difference was made between *batteries and fuel cells*. Today the *definitions* have been refined: batteries convert and store electrical energy and hence represent a thermodynamically closed system; energy storage and conversion occur in the same compartment. Fuel cells are open systems where the anode and cathode are just charge-transfer media and the active masses undergoing the redox reactions are delivered from outside the cell, either from the environment, for example, oxygen from air, or from a tank, for example, fuels such as hydrogen and hydrocarbons. Energy storage (in the tank) and energy conversion (in the fuel cell) are thus locally separated.

Electrochemical capacitors (EC), also called supercapacitors, store energy using either ion adsorption or fast surface redox reactions. In the first case, they are called *electrochemical double layer capacitors* (*EDLC*), in the second case they are called *pseudocapacitors*. They can complement or replace batteries in electrical energy storage and harvesting applications, when high power delivery or uptake is needed. Several types of ECs can be distinguished, depending on the charge storage mechanism as well as the active materials used. EDLCs, the most common devices at present, use carbon-based active materials with high surface areas. Pseudocapacitors or redox supercapacitors use fast and reversible surface or near-surface reactions for charge storage. Transition metal oxides as well as electrically conducting polymers are examples of pseudocapacitive active materials. Electrochemical capacitors currently fill the gap between batteries and conventional solid state and electrolytic capacitors. They store 100–1,000 times more charge than the latter due to a much larger surface area (1,000–2,000 m^2g^{-1}) available for charge storage in EDLC. They have a lower energy density than batteries, and this limits the optimal discharge time to less than a minute, whereas many applications clearly need more [5]. Since the early days of EC development in the late 1950s, there has not been a good strategy for increasing the energy density; only incremental performance improvements were achieved from the 1960s to 1990s. The increase in performance that has been demonstrated in the past few years is due to the discovery of new electrode materials and improved understanding of ion behavior in small pores, as well as the design of new hybrid systems combining faradic and capacitive electrodes [6].

To compare the power and energy capabilities of fuel cells, batteries, and supercapacitors, a representation known as the *Ragone plot* has been developed. The terms *specific energy* [Wh/kg] and *energy density* [Wh/L] are used to compare the energy contents of a system, whereas the rate capability is expressed as *specific power* [W/kg] and *power density* [W/L]. A simplified Ragone plot (Fig. 4) discloses that fuel cells can be considered to be high-energy systems, whereas supercapacitors are considered to be high-power systems. Batteries have intermediate power and energy characteristics. There is some overlap in energy and power of supercapacitors or fuel cells with batteries. Batteries with thin-film electrodes exhibit power characteristics similar to those of super capacitors.

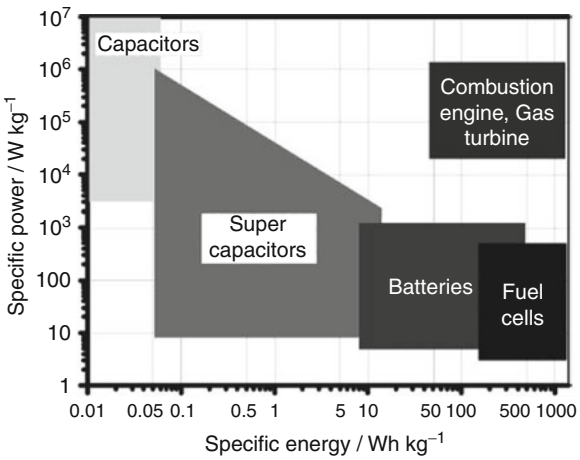

Fuel Cell Comparison to Alternate Technologies.
Figure 4
Simplified Ragone plot of the energy storage domains for the various electrochemical energy conversion systems compared to an internal combustion engine and turbines and conventional capacitors (From [7])

Not all systems can be described using these definitions, since there are also *combined systems* such as metal–air batteries [8–10] which contain a battery electrode (metal anode) and a fuel cell electrode (air cathode), or redox flow batteries [11, 12] which are a form of rechargeable battery in which electrolyte containing one or more dissolved electroactive species flows through an electrochemical cell. Additional electrolyte is stored externally, generally in tanks, and is usually pumped through the cell of the reactor. The best known example is the chromium–iron battery [13]. The active masses are represented by Fe^{3+} and Cr^{2+} ions. In these redox storage devices, the mechanical aging of the accumulator electrodes is prevented. Flow batteries can be rapidly recharged by replacing the electrolyte while simultaneously recovering the spent material. Due to the overlapping properties of batteries and fuel cells, it is nowadays considered to find a definition that recombines the two systems again, to no longer differentiate between batteries and fuel cells like in former times.

In order to bridge the gap between batteries and electrochemical capacitors, a capacitive or pseudocapacitive electrode can be combined with a battery electrode. Batteries exhibit usually high energy densities, while capacitors can deliver high power at the cost of low energy storage. Research efforts have been focused to increase the gravimetric energy of electrochemical capacitor electrodes by using materials with enhanced gravimetric capacitances (gravimetric charge storage per volt) [14]. The latter can be achieved by using carbon subnanometer pores for ion adsorption or by incorporating the pseudocapacitance of nanostructured transition metal oxides. A recent report by S.W. Lee et al. [15] demonstrated that by using a novel class of electrodes for lithium storage high gravimetric energy (200 Wh $kg_{electrode}^{-1}$) was delivered at a high power of 100 kW $kg_{electrode}^{-1}$. Those electrodes were based on functionalized multiwalled carbon nanotubes (MWNTs) that included stable pseudocapacitive functional groups and were assembled using a layer-by-layer technique. Therefore, it was shown that it is possible to benefit from both the capacitor and the battery properties.

A critical parameter of fuel selection is its energy density. The latter should be as high as possible. Additionally, the choice of fuel is also affected by the ease of transportation and storage which in general should be as easy and uncomplicated as possible. The choice of the fuels determines which problems, including environmental problems, will arise.

Figure 5 shows the theoretical specific energies [(kWh)/kg] and energy densities [(kWh)/l] of various rechargeable battery systems in comparison to fuels, such as gasoline, natural gas, and hydrogen. The inferiority of batteries is evident. These values are an indication for the maximum energy content of certain systems. The practical values are significantly lower than the theoretical ones. A rechargeable battery has a practical energy content which is 25% of its theoretical value while a primary battery normally yields more than 50% of its theoretical value. The theoretical efficiencies of fuel cells for the conversion of fuels into electrical energy are higher than 70%. A number of factors influence the observed differences between theoretical and practical energy storage capabilities. The systems contain inert parts such as conductive diluents, current collectors and containers, and internal resistances which results in internal losses and limited utilization of the active masses. Parts of the fuel can, for example, leave the fuel cell without having reacted or partial passivation of the electrodes can make parts of

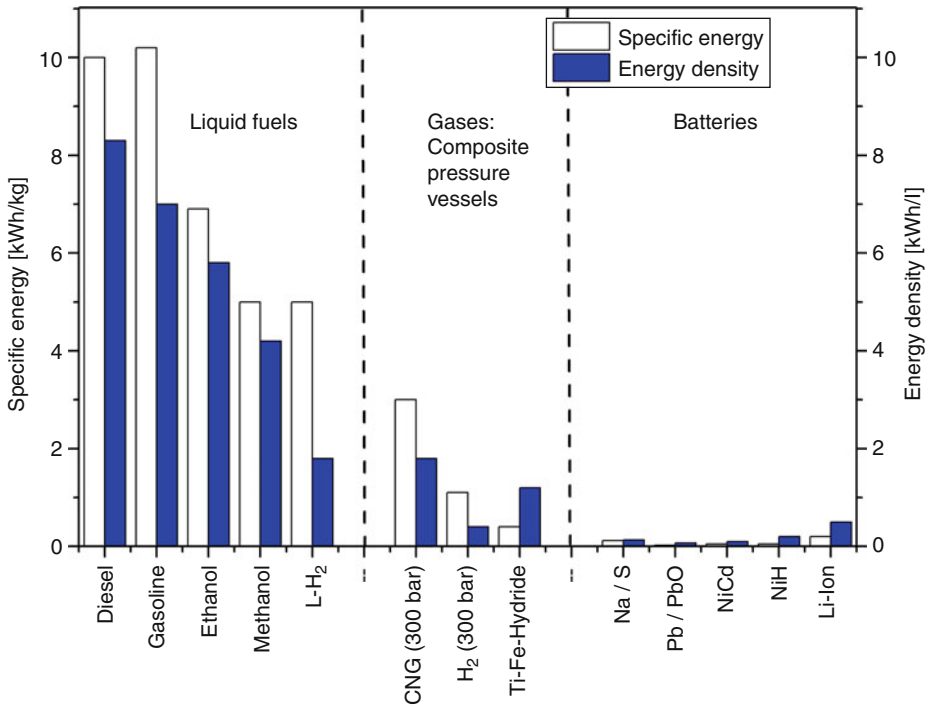

Fuel Cell Comparison to Alternate Technologies. Figure 5
Theoretical specific energies [k Wh/kg] and energy densities [k Wh/l] of various rechargeable battery systems compared to fuels, such as gasoline, natural gas, hydrogen, and alcohols

the surface area inactive. For practical use, however, as batteries and fuel cells are not subject to the Carnot cycle limitations, they may operate with much higher efficiencies than combustion engines and related devices. The efficiencies of PEMFCs, batteries, and supercapacitors are summarized for comparison in Table 1.

Electrochemical photovoltaics are a specific type of photovoltaic systems to convert solar energy, that is, solar radiation into electrical energy. Today, there is a variety of solar cells already on the market. Difference must be made between electrochemical photovoltaic cells and conventional silicon (Si)–based photovoltaic cells; in electrochemical photovoltaic cells two interfaces exist at which charge transport switches from electronic to ionic and back. In photoelectrochemistry a photoactive semiconducting working electrode is used together with a metallic counter electrode. Both are immersed in an electrolyte containing a suitable redox couple. Upon radiation of the semiconductor–electrolyte interface with light having a higher energy than the bandgap of the semiconductor, electron–hole pairs are formed and separated. Photogenerated majority carriers accumulate at the back side of the semiconductor, minority carriers travel to the semiconductor–electrolyte interface. The majority carriers are collected with a charge-collecting substrate and transported to the counter electrode where they

Fuel Cell Comparison to Alternate Technologies.
Table 1 Practical efficiencies of fuel cells, batteries, and supercapacitors

System	Process	Efficiency
PEMFCs	Electrolysis-H_2 storage – FC operation	40%
Batteries	Charging – Discharging	80%
Supercapacitors	Charging – Discharging	95%

electrochemically react with the redox couple in the electrolyte. In the 1970s, wet-type electrochemical photovoltaic cells were discovered [16–18]. Michael Grätzel demonstrated that dye molecules can be adsorbed onto nanocrystalline TiO_2 working electrodes and thus extended the concept to dye-sensitized solar cells (DSSCs) [19–22].

It is noteworthy that electrochemical photovoltaic cells without dyes have working (semiconductor) and counter electrodes that are both immersed in the redox electrolyte. After the formation of electron/hole pairs, specific reactions occur at the semiconductor electrode and at the metal counter electrode. Charge balance is maintained via oxidation and reduction processes, and electrodes are often instable in aqueous media. Photoelectrochemical photovoltaic cells could only replace Si-based photovoltaics if a stable semiconductor material with a band gap of ~1.4 eV is found [23–26]. In dye-sensitized solar cells, a dye-sensitized porous nanocrystalline TiO_2 photoanode with a 1,000-fold surface area compared to flat electrodes has been used. Furthermore, the charge transport of the photogenerated electrons passing through all the particles and grain boundaries is highly efficient [27]. The conversion efficiency of DSSCs has improved to 11.5% [28] since it was first reported with an efficiency of 7.1% [26]. Their efficiencies are now comparable with amorphous silicon solar cells [29] but at a much lower cost.

Electromobility: An Example for Combining Key Energy Technologies

Concerns about global warming and the depletion of petroleum resources demand a shift in automotive transportation from petroleum-based internal combustion engines to electrically driven vehicles (EVs). In the concept of electromobility, all the above-mentioned technologies should be united and combined in order to synergistically provide power to an EV.

Hybrid electric vehicles are a first step, where an internal combustion engine is assisted by a battery-driven electric motor, enabling increased fuel efficiencies when using high-power and low-energy (ca. 1 kWh) batteries. Further reduction or even elimination of petroleum-based fuels can be achieved by successively increasing the onboard stored electrical energy, thus enabling plug-in hybrid electric vehicles, short-range electric vehicles and, ultimately, long-range electric vehicles. Such a development would be the perfect solution to realize electric traction in general.

Together with batteries and supercapacitors, fuel cells are a key component that must be investigated in order to build electric vehicles suitable for continuous use, especially in public transport. Fuel cells have the potential to offer clean power generation, are quiet in operation, and can be located close to the application. They produce much less greenhouse emissions and can be more efficient in conversion of the energy in a fuel into power than gasoline engines or utility thermal power plants. Fuel cells are best utilized as a steady energy source and not as a power source to supply dynamic demands. For applications that require varying power demands, such as automotive propulsion, the use of the fuel cell in a hybrid configuration with a battery or an electrochemical capacitor is required. The fuel cell provides steady power demand while the battery or the electrochemical capacitor handles the surge for regenerative breaking and acceleration as well as initial start-up. This makes fuel cells an essential component for hybrid vehicles with adequate ranges as they are required for public transport and goods traffic.

Fuel cells, batteries, and supercapacitors have a similar configuration, that is, two electrodes separated by an electrolyte. The latter are designed for high power and long life service. Currently nonetheless, the status of batteries, supercaps, and fuel cells does not allow for a satisfactory use in electric vehicles due to tremendous weight and safety issues, too high costs, and too short ranges. Thus, fundamental research is necessary to develop novel battery, supercapacitors, and fuel cell concepts for a new generation of electric vehicles.

Nowadays, also concepts are developed in which photovoltaic cells integrated on the roof or in the windows of EVs can be used to recharge the batteries. It is known from literature that EVs suffer from too short ranges and too high weight [7, 30]. Figure 6 shows typical driving ranges of battery-powered cars compared to ranges of cars powered by modern combustion engines. As it can be seen, for EVs powered with any secondary battery system (i.e., lead acid, nickel metal hydride, sodium sulfur, and lithium ion), the driving ranges that they possess are inferior

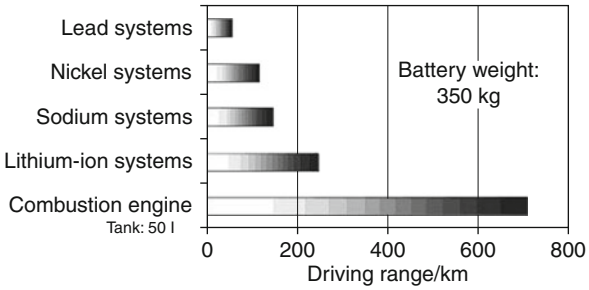

Fuel Cell Comparison to Alternate Technologies.
Figure 6
Comparison of the driving ranges for a vehicle powered by various battery systems or a gasoline-powered combustion engine (From [7])

compared to those of conventional combustion engines. Therefore, it is illustrated clearly why rather fuel cells and not batteries should be considered for replacement of combustion engines.

Fuel cells and batteries can be used to build full electric vehicles and thus provide pure electrification solutions for different mass and usage segments of automotive application. Battery powered EVs based on lithium ion technology will be limited to small-vehicle low-mileage-per-day applications which is due to the low specific energy and long charging times. The required 300 mile range has been reached with hydrogen fuel cell vehicles and the latter have also been proven to be able to operate in all climates. Nevertheless, the costs of the Pt-based catalysts needed in a fuel cell are too high, the hydrogen infrastructure is not present and cost-effective renewable sources of primary energy are not yet efficiently used. Drastic decreases in the amount of Pt used are required which is put into practice via a number of strategies currently under development [30].

A very promising approach to energy conversion in electric vehicles is the use of metal–air batteries, for example, Li–air systems. As was discussed in the earlier section, the metal–air battery combines fuel cells with batteries. In the latter example, substitution of the conventional lithium intercalation cathode with an air cathode is projected to increase the cathode specific capacity by a factor of ~3.5. Additionally, the concept of Li–air systems has another major advantage; it can drastically decrease the weight of the battery pack. Specifically, for the case of short-range EVs (~25 kWh), the total battery would weigh only ~40 kg. For the case of a full-range EV, the projected Li–air battery-pack weight is only 120 kg. This is significantly smaller compared to the minimum weight of 330 kg for a best case Li-ion battery pack. Therefore, the Li–air battery technology would be a very promising and enabling technology for full-range EVs. Li–air batteries give promise of extending the range, but scientists and engineers will have to face many challenges in order to prove the research in this area effective.

The electrical energy required on board to travel a certain range before refueling is provided by the energy storage/generation system and is determined by the total gross energy consumed minus the energy recovered from regenerative braking (Wh_{net}/mile). All loads on board can be major drains of energy since they are powered by the electrical storage/generation system which affects the driving range. Loads that severely affect the driving ranges are heating and cooling devices in the car. The vehicle mass (m) including the mass of the powertrain system and of the passengers, the frontal area (A), the drag coefficient (C_d), and the drive cycle are elements that influence the Wh_{net}/mile requirement to the electric motor the most. Furthermore, the rolling resistance and the ancillary loads mentioned above have strong influence.

An equation has been developed to correlate the different parameters [30]:

$$\text{Energy required} = a_1 \times m + a_2 \times C_d \times A + a_3$$

a_1, a_2, and a_3 are obtained from modeling results. The model is primarily based on the greenhouse gases, regulated emissions, and energy use in transportation (GREET) software developed by the Argonne National Lab [31]. In Table 2 [30], estimates are listed that start from a small subcompact car ($C_d \times A = 0.6\ m^2$) with a total vehicle mass of 1,200 kg for which the energy required to drive the Environmental Protection Agency (EPA) city or highway cycle is 138 or 156 Wh_{net}/mile, respectively. The energy required for a van ($Cd \times A = 1.56\ m^2$) weighing 2,500 kg is 283 or 361 Wh/mile for city or highway cycle, respectively. The energy requirement for driving in the city is lower because the vehicle has less resistance to overcome at lower

Fuel Cell Comparison to Alternate Technologies. Table 2 Electrical energy required as a function of the vehicle type and mass (analysis assumes 70% recovery of braking energy through regenerative braking)

Vehicle type	Mass (kg)[a]	$C_d \times A$ (m^2)	City (Wh_{net}/mile)	Highway (Wh_{net}/mile)
Sub-compact	1,200 (2)	0.60	138	156
Compact car	1,400 (4)	0.64	154	171
Midsize car	1,550 (4)	0.67	166	183
Full-size car	1,700 (5)	0.71	178	194
Minivan	2,200 (7)	0.93	224	250
Van	2,500 (8)	1.56	283	361

Taken from Ref. [30]
[a]The mass includes 65 kg passengers weight shown in parentheses

speed, electricity generation is more efficient at lower loads, and the use of regenerative braking preserves these advantages for the city cycle [30].

The above given examples show that the range problem is the most severe problem of batteries used to power electric vehicles. Fuel cells have the potential to overcome this issue. On one hand, rather cheap materials are used in Li ion batteries, while on the other hand they require a very large surface area of very finely controlled thin layers, interfaces, and separators. Li ion batteries are already mass produced for use in portable electronic devices and thus, many of the opportunities for cost reduction through scale have already been taken. Nowadays, the development and implementation of improved materials must be the way to further reduce costs.

In fuel cells, however, more expensive materials are employed even though their amount can be tremendously reduced. The total geometric surface area of the cells shows a 30-fold decrease due to higher current densities obtained with more conductive fuel cell electrolytes. Fuel cells can be built in a bipolar construction with cells stacked in series with the negative current collector of one cell serving as the positive current collector of the adjacent cell. Fuel cells require a hydrogen tank and an air compressor which makes their balance of plant more complex.

Strong investment is necessary to develop EVs based on the concept of electromobility. The advantages of all available energy conversion and storage technologies need to be utilized in order to achieve efficient full vehicle electrification. It is very likely that both battery and fuel cell technologies will be developed for automotive application, since batteries are well suited for the use in small short-range vehicles and fuel cells are able to deliver electric power for long-range vehicles. Super capacitors can aid with their high power density output whenever it is needed. Photovoltaics integrated in the EV can convert the solar energy and charge the batteries. The main point is that until now no single technology shows the potential to monopolize the implementation into an electrical vehicle. For fuel cells specifically, research needs to focus into identifying novel catalyst materials that can reduce the amount of expensive catalysts currently used (e.g., Pt). Additionally, fuel cell technologies based on alternative fuels other than hydrogen need to be developed. For all suited energy technologies applicable in EVs, the key challenge is their smart combination in order to build long-range vehicles which produce less greenhouse gas emissions than cars powered by combustion engines.

Future Directions

In summary, even though the world is becoming aware of an upcoming energy crisis, according to all statistical data currently available, most of the worldwide energy demand is still delivered via fossil fuels, while renewables unfortunately still account only for a small part. It is a fact that use of fossil fuels results in greenhouse gas emissions to the atmosphere. For this reason, the

industrialized states, under the Kyoto protocol, have committed themselves to reduce their greenhouse gas emissions by a total of 5% in the period of 2008–2012 compared to 1990.

Most of the CO_2 emitted is a result of the inefficient conversion and distribution systems that we use. The current system efficiencies for energy conversion and distribution allow approximately only 30% of the primary energy to be delivered as usable energy. If we manage to increase the system efficiency, CO_2 emissions will be reduced drastically. Therefore, there is the urgent need to develop efficient energy conversion and distribution systems that emit either no or very little CO_2. A technology that has the potential to help in the reduction of CO_2 emissions is fuel cells.

Fuel cells have the potential to efficiently convert chemical energy to electricity. Even though as discussed the concept of fuel cells is not new and research efforts worldwide have been devoted to advance the technology, there are still many ways that need to be covered before bringing them into the market. Some of the key issues related to fuel cells that need to be tackled before even discussing about a broad commercialization of the technology are:

(a) Low efficiency at high power densities
(b) Use of hydrogen which is only a secondary energy carrier
(c) Large amount of noble metal required for widespread applications
(d) Cost and availability of Pt which is commonly used as catalyst
(e) Durability and lifetime of the system

The first issue is the low efficiencies at high power densities of current fuel cell systems. For example in PEMFCs, typical power densities delivered are $\sim$1 $W\,cm^{-2}$ at 0.7 V operating voltage. That accounts for a voltage efficiency of $\sim$56% while the overall system efficiency is even lower. The power output at the high voltage regime is controlled by electrocatalytic properties and suffers from losses attributed mainly to the slow kinetics of the oxygen reduction reaction. In order to achieve a high-power, high-efficiency system, it is necessary to identify and develop highly active catalyst materials that could push the power output to $\sim$1 $W\,cm^{-2}$ at 0.85–0.9 V.

The second issue relates to hydrogen which is the employed fuel for low-temperature fuel cells. The advantage of using hydrogen is that water is the only product. Nonetheless, we need to take into consideration that hydrogen is only a secondary energy carrier which is not freely available and is currently produced by "non-clean" methods, for example, reforming of natural gas. Hydrogen can be produced by regenerative sources but those suffer from low efficiencies. It would be beneficial to fabricate systems that can directly convert alternative fuels such as bio-derived alcohols which have higher energy densities and can be produced efficiently. Direct methanol fuel cells are a starting point but at their current status not a satisfying solution. Bioethanol is a very attractive candidate. It can be produced by cellulosic biomass, has high energy density, is nontoxic, and its liquid form allows using the current fuel infrastructure. Research should also aim at identifying highly active catalysts toward ethanol oxidation and electrolytes with low ethanol permeability that will result in designing an efficient system that will directly convert ethanol to electricity.

The last three issues refer to the current material systems used in fuel cells. Pt supported on carbon (Pt/C) is commonly used in PEMFCs as catalyst and in order to achieve desirable power densities high amounts of noble metal are required. Even though Pt possesses high catalytic activity, it is also associated with limited resources, and high price. Efforts to reduce the metal loading and alloy Pt with other inexpensive and more abundant elements, that is, metals, rare earths have shown improvements, however, there is no system found that would lead PEMFCs to a broader commercialization. Carbon is commonly used as support material in several fuel cell systems since it is inexpensive with high electronic conductivity and high availability. Carbon though is the main reason of the low lifetime since it undergoes corrosion. Efforts to nanostructure carbon, that is, nanotubes, nanofibers, have shown only unsubstantial improvements. Pt and C are materials that have been extensively investigated for many years but have not brought fuel cells to the market. Therefore research should focus to identify novel catalyst/support systems that would replace Pt and C.

Two possible future scenarios for stationary electricity production and road traffic can be envisioned.

For the first scenario small units (<1 MW) based on SOFC with natural gas, biogas, or ethanol could be implemented. In niche markets, electricity storage could be achieved with electrolysis to produce hydrogen that could subsequently be stored and then used in a fuel cell system. For larger units (>10 MW), SOFCs could be used with natural gas, biogas, carbon from biomass. For the latter, a negative CO_2 effect is possible (electricity will decrease CO_2 concentration in the atmosphere). For the second scenario of road traffic, two options are possible. City travel could be handled with battery-operated motor bikes and small cars, possibly in combination with a small (1–5 kW) fuel cell. Long-range travel could be achieved with larger vehicles using mid-temperature (200–300°C) bioethanol fuel cells hybridized with batteries. In both systems, supercapacitors could be employed to handle the high power needs. For both scenarios, all other energy conversion technologies (e.g., solar, wind) can be used in order to convert and subsequently store energy (i.e., battery recharging).

In conclusion, higher targets need to be set for the future and achieved before fuel cells can be a commercially viable technology. There have been numerous efforts to improve fuel cells but all solutions proposed so far are only small steps that address partially only one of the above-mentioned issues. High-risk, high-profit solutions are required that will drastically improve the current fuel cell status and will lead them to their broad commercialization. In fuel cell development, we need to match the available energy source with the application. Hydrogen does not seem to be an option. A direct conversion of an available fuel in a fuel cell would be more desirable. For example, alcohol oxidation at all temperatures and (hydro-) carbons could be used at high temperatures. In all situations, fuel cell research has to acknowledge the fuel problem. Therefore, if one believes that we are close to the end of research for fuel cells and other energy technologies then the reality is different ... we are only at the beginning.

Bibliography

1. DOE/EIA-0484 (2010) National Energy Information Center, EI-30, U.S. Energy Information Administration, Forrestal Building, Washington, DC 20585
2. Kunze J, Stimming U (2009) Electrochemical versus heat engine energy technology: a tribute to Wilhelm Ostwald's visionary statements. Angew Chem Int Ed 48:9230–9237
3. Black WZ, Hartley JG (1985) Thermodynamics. Harper & Row, New York, pp 339–429
4. Armand M, Tarascon J-M (2008) Building better batteries. Nature 45:652–657
5. Kötz R, Carlen M (2000) Principles and applications of electrochemical capacitors. Electrochim Acta 45:2483–2498
6. Simon P, Gogotsi Y (2008) Materials for electrochemical capacitors. Nat Mater 7:845–854
7. Winter M, Brodd RJ (2004) What are batteries, fuel cells, and supercapacitors? Chem Rev 104:4245–4269
8. Jacoby M (2010) Rechargeable metal-air batteries. Chem Eng News 88:29–31
9. Cairns EJ, Albertus P (2010) Batteries for electric and hybrid-electric vehicles. Annu Rev Chem Biomol Eng 1:299–320
10. Girishkumar G, McCloskey B, Luntz AC, Swanson S, Wilcke W (2010) Lithium-air battery: promise and challenges. J Phys Chem Lett 1:2193–2203
11. Zhang HM, Zhang Y, Liu ZH, Wang XL (2009) Redox flow battery technology. Prog Chem 21:2333–2340
12. De Leon CP, Frias-Ferrer A, Gonzalez-Garcia J, Szanto DA, Walsh FC (2006) Redox flow cells for energy conversion. J Power Sources 160:716–732
13. Hagedorn NH (1983) The iron-chromium redox battery. Abstr Pap Am Chem Soc 186:28
14. Chmiola J, Yushin G, Gogotsi Y, Portet C, Simon P, Taberna PL (2006) Anomalous increase in carbon capacitance at pore sizes less than 1 nanometer. Science 313:1760–1763
15. Lee SW, Yabuuchi N, Gallant BM, Chen S, Kim B-S, Hammond PT, Shao-Horn Y (2010) High-power lithium batteries from functionalized carbon-nanotube electrodes. Nat Nanotechnol 5:531–537
16. Gerischer H, Tributsch H (1968) Electrochemische Untersuchungen zur spectraleu sensibilisierung von ZnO-Einkristallen. Ber unsenges Phys Chem 72:437–445
17. Hauffe K, Danzmann HJ, Pusch H, Range J, Volz H (1970) New experiments on the sensitization of zinc oxide by means of the electrochemical cell technique. J Electrochem Soc 117:993–999
18. Myamlin VA, Pleskov YV (1967) Electrochemistry of semiconductors. Plenum, New York
19. Gratzel M (2003) Applied physics: solar cells to dye for. Nature 421:586–587
20. Gratzel M (2004) Conversion of sunlight to electric power by nanocrystalline dye-sensitized solar cells. J Photochem Photobiol A 164:3–14
21. Hagfeldt A, Gratzel M (1995) Light-induced redox reactions in nanocrystalline systems. Chem Rev 95:49–68
22. Hagfeldt A, Gratzel M (2000) Molecular photovoltaics. Acc Chem Res 33:269–277
23. Ellis AB, Kaiser SW, Wrighton MS (1976) Visible light to electrical energy conversion. Stable cadmium sulfide and cadmium selenide photoelectrodes in aqueous electrolytes. J Am Chem Soc 98:1635–1637

24. Ellis AB, Bolts JM, Wrighton MS (1977) Characterization of n-type semiconducting indium phosphide photoelectrodes. J Electrochem Soc 124:1603–1607
25. Hodes G, Manassen J, Cahen D (1976) Photoelectrochemical energy onversion and storage using polycrystalline chalcogenide electrodes. Nature 261:403–404
26. Miller B, Heller A (1976) Semiconductor liquid junction solar cells based on anodic sulfide films. Nature 262:680–681
27. Wurfel U, Peters M, Hinsch A (2008) Detailed experimental and theoretical investigation of the electron transport in a dye solar cell by means of a three-electrode configuration. J Phys Chem C 112:1711–1720
28. Chen C, Wang M, Li J, Pootrakulchote N, Alibabaei L, Ngoc-le C, Decoppet J-D, Tsai J-H, Grätzel C, Wu C-G, Zakeeruddin SM, Grätzel M (2009) Highly efficient light-harvesting ruthenium sensitizer for thin-film dye-sensitized solar cells. ACS Nano 3:3103
29. Gratzel M (2007) Photovoltaic and photoelectrochemical conversion of solar energy. Philos Trans R Soc A 365:993–1005
30. Wagner FT, Lakshmanan B, Mathias MF (2010) Electrochemistry and the future of the automobile. J Phys Chem Lett 1:2204–2219
31. Wang MQ (2007) Greenhouse gases, regulated emissions, and energy use in transportation (GREET). The Argonne National Laboratory, Argonne. http://www.transportation.anl.gov/modeling_simulation/GREET/index.html

Fuel Cell Powered HEV Design and Control

Etim U. Ubong[1], Jim Gover[2]
[1]Center for Fuel Cell Research and Powertrain Integration, Electrical & Computer Eng, Kettering University, Flint, MI, USA
[2]Department of Electrical Engineering, Kettering University, Flint, MI, USA

Article Outline

Glossary
Definition of the Subject
Introduction of Fuel Cells
Candidate Fuel Cells for Hybridization
Hybrid Technology Using Gasoline or Diesel, Fuel Cells, Ultra-Capacitors, and Batteries
Ultra-Capacitors
Conclusion
Bibliography

Glossary

Balance of plant (BOP) Auxiliary components that complement a power unit as a functional or operational unit.

Electric vehicle (EV) A vehicle that uses battery or any other onboard electrical power source to operate the vehicle.

Fuel cell A device that uses fuel and oxidant in an electrochemical reaction to generate direct electricity.

High-temperature proton exchange membrane fuel cell (HT-PEMFC) A PEM fuel cell that operates between 120°C and 200°C.

Hybrid electric vehicle (HEV) A vehicle that uses an auxiliary electrical power source, such as a fuel cell or a battery, along with an internal combustion engine (ICE) for propulsion.

Internal combustion engine (ICE) A device that converts the chemical energy of fuel in a cylinder to mechanical work through the piston, connecting rod and crank shaft mechanisms.

Low-temperature PEM fuel cell (LT-PEMFC) A PEM fuel cell that operates between 50°C and 80°C.

Proton exchange membrane (PEM) A fuel cell that uses either a sulphonated (low temperature) membrane or polybenzimidazole (high temperature) membrane to generate direct electricity.

Reformate A fuel derived from fossil fuel (natural gas) after reformation that is a mixture of hydrogen, carbon monoxide, and carbon monoxide.

Solid polymer fuel cell (SPFC) Same as PEM above.

Definition of the Subject

A hybrid vehicle implies a vehicle that is powered by more than one source of power. It can be an internal combustion engine and a battery, an ICE and fuel cell, and ICE and solar cells or fuel cell and batteries. The current trend of hybridization of internal combustion engines (ICE) is a result of the inefficiency of ICE. Spark ignition internal combustion engine, SI-ICE, is about 25–27% efficient, while compression ignition internal combustion engine, CI-ICE, (diesel) is 34–38% efficient [1, 2]. The remaining percentage of the input energy into ICE is expended in the form of heat loss to the coolant and exhaust, by convection, conduction, and radiation, and by combustion

inefficiency. The electric drive has a higher efficiency around 90%, as such, it is justifiable to incorporate electric drive into the hybridized powertrain. With the increased use of electronics in cars for various applications, such as visual display of GPS, fuel economy, maintenance schedule and diagnostics, voice activation of devices and DVD players, etc., there is a need to use additional power sources to maintain this level of power demand without compromising the power required for ignition, and operate the electronic control unit (ECU), anti-brake systems (ABS), and the fuel injection units.

In the hybridized ICE-powered vehicle, in the series mode of connection, the mechanical drive shaft that transmits power from the crankshaft through the gearbox to the wheels is replaced with a generator and electric wires to the electric motors spinning the wheels. The design configuration of the ICE-battery hybrid presents the base design of other complex hybrid vehicles architecture. The design structure of the fuel cell–powered hybrid electric vehicle includes fuel cell as the primary power source and a battery as a secondary power source for start-up, lighting, and power electronics support. The power transmission shaft reminiscent of the internal combustion engines (ICE)–powered vehicle is absent, rather electric motors spin the four wheels. Fuel cells generate direct electricity that is used to drive the electric motors in hybrid vehicles. As such, reliability is enhanced as there are fewer rotating components. The complexity and maintenance are reduced in electric machinery compared with mechanically driven machinery. The following report will present different types of fuel cells and their electrolytes, sources of fuels for fuel cells, those applicable to the transportation sector and the hybrid vehicle architecture. The ICE hybrid will also be presented as a base model, since its operation is well understood by the general public.

Introduction of Fuel Cells

Fuel cells are electrochemical electricity–generating devices that oxidize the fuel at the anode to electrons and protons and reduce oxygen at the cathode to produce heat and water. The splitting of hydrogen into protons and electrons is done at the catalyst layer (anode). The electrons move across the external circuit generating electricity, while the protons permeate through the PEM to the cathode. The proton exchange membrane fuel cells are of interest in the mobility sector as it is modular (scalable) and, as such, can be built to desirable sizes without compromising the efficiency or performance. Various petroleum and nonpetroleum fuels, chemical compounds, and hydrogen carriers can be used as fuels in fuel cells after preprocessing. However, hydrogen is the most preferred fuel with the end products, in case of the proton exchange membrane (PEM) membrane being water, with the release of heat. Hydrogen is widely used in most fuel cells ranging from the low to the high-temperature PEM to solid oxide fuel cells (SOFCs).

Commonly Used Fuels in Fuel Cells

Fuels commonly used in fuel cells are: hydrogen, methanol, potassium hydroxide; phosphoric acid; methane (natural gas); carbon monoxide; carbonate salts of sodium, lithium, and potassium; and yttrium-stabilized zinc oxide as the electrolyte. Table 1 summarizes various fuels and applicable fuel cells that utilize them.

Low-Temperature and High-Temperature PEMs

The low temperature PEM fuel cell shown in Fig. 2a relies on membrane humidification for ion transport from the anode to the cathode through Grotthuss mechanism or ion-hopping mechanism. If the membrane is not well humidified or is dry, vehicular mechanism is involved in the ion transport. For the high-temperature PEM fuel cell based on polybenzimidazole (PBI) membrane, which is presented in Fig. 2b, the membrane is treated in sulfuric or phosphoric acid. Protons are transported in an acidic medium when the temperature is raised up to 130°C and above. The membrane performs much better at an elevated temperature of 170–200°C. Precautionary measures require that the membrane be raised to above 130°C before the load is applied. Better results are obtained if the cell is allowed to run and equilibrate at a reduced load for about 100 h before readings are taken. This allows the membrane to equilibrate. During the shutdown period, the membrane should be purged

Fuel Cell Powered HEV Design and Control. Table 1 Different types of fuel cells

Parameters	PEM		DMFC	AFC	PAFC	MCFC	SOFC
	LT-PEM	HT-PEM					
Fuels	H_2	H_2, Reformates	Methanol	KOH (H_2)	PO_4 (H_2)	H_2, CO, CH_4	H_2, CO, CH_4
Charge carrier	H^+	H^+	H^+	OH^-	H^+	CO_3^{2-}	O^-
Electrolyte	PEM	PBI	PEM	30–50% conc. KOH in water	100% conc. in PO_4	[a]	[b]
Temperature range	50–80°C	130–200°C	50–80°C	200°C	150–220°C	650°C	650–1,000°C

LT-PEM low-temperature PEM that are made of poly-sulphonated membranes, such as NAFION marketed by Du Pont, GORE membrane, ASAHI glass, 3M, etc.

HT-PEM High temperature membrane, such as polybenzimidazole (PBI) membranes made by BASF (USA), etc.

[a]Liquid molten carbonate salts, such as Na_2CO_3 and Li_2CO_3, in a ceramic matrix of LiAl02

[b]Solid oxide ceramic (Yttrium-stabilized zirconium (ZrO_2/Y_2O_3)

with nitrogen gas till it cools to ambient conditions to avoid leaching of the acid and degrading of the membrane performance [3].

Source of Fuels for Fuel Cell

The current earthquake in Japan and Virginia, USA, is a reminder that the nuclear power–generating plants are very vulnerable to natural disasters. Nuclear plant (prior to the earthquake in Japan) has been projected to be the main source of hydrogen production, as it is cleaner and more efficient. The Chernobyl (1986) nuclear disaster and the Japanese (2011) disaster triggered by an earthquake of 9.0 magnitude on the Richter Scale, clearly drew a line between science, engineering, and nature. Despite the precautions and technological advancement of Japan, it could not contain such magnitude of earthquake. Couple of months after the incident, the levels of radiation at the Japanese nuclear meltdown have been upgraded to level 7, same as the Chernobyl radiation after the disaster. The Virginia quake of summer 2011 rattled Washington D.C., metropolis with a magnitude of 5.8 on the Richter Scale. This spontaneously shutdown the nuclear reactor in Virginia, raising serious concerns of possible nuclear radiation to the atmosphere. These recent incidents pre-suggest that another sustainable source of hydrogen production (and not nuclear power plant) is needed for the hydrogen economy. Following the above Japanese event, Japan, Germany, and Switzerland have frozen proliferation of building further new nuclear reactor plants.

The question now is which is the most environmentally and sustainable way of producing hydrogen for the hydrogen economy? Current pathways of hydrogen production include: steam methane reformation (SMR), partial oxidation (POX) process, and autothermal reformation (ATR) process of fossil fuels. However, the production and availability of fossil fuels are projected to dip after 2020, and as such, a renewable source of hydrogen is required. Electrolysis of water is a viable source; however, energy is required to electrolyze water and compress it to 350 bar (5,000 psi) or 700 bar (10, 000 psi) in order to store enough hydrogen to meet the same driving distance as its gasoline equivalent and package the fuel tank into the available fuel storage space. First, an analysis of the five types of fuel cells will be presented highlighting their potentials for hybrid vehicle propulsion.

In the final analysis, water electrolysis method to obtain hydrogen is a clean technology, but requires energy for the process and storage of the gas under pressure or possibly liquefaction of the fuel. The current technology of steam reformation relies on fossil fuels as feedstocks. Future energy carrier should be sustainable, clean, and renewable. Fuel cells for transportation in hybrid vehicles are feasible with the scalable fuel cell categories, such as PEM, direct methanol fuel cell (DMFC), alkaline fuel cell (AFC), and to a limited extent, with the solid oxide fuel cell (SOFC) as an auxiliary power unit (APU).

Fuel Cell as a Power System

Generally, fuel cells have the following advantages over other power-producing devices:

1. Low to zero emissions, if a reformate or hydrogen is used as fuel, which makes it environmentally very friendly.
2. Performance and efficiency are very high as there are no moving parts (excluding the system's balance of plant, BOP).
3. It is a bridge to hydrogen economy. The bridge may be in the form of electric vehicles (EV) or hybrid electric vehicles (HEV) – in which both fuel cell and a smaller internal combustion engine (ICE) are used for propulsion in the medium and low-power applications.
4. Absence of transmission lines which decreases the complexity of the BOP.
5. Flexible, scalable, and adaptable where remote power systems are required, for example, remote stations, booster stations, traffic and bacon lights, road signs, street lights, etc.
6. For space missions. Fuel cells have long been used for manned space missions, for example, the Apollo Mission of the 1960s and the Shuttle Orbiter.

In the following analysis, much attention is given to PEM because of its potential as the viable candidate fuel cell for use in transportation. It is noteworthy that not all types of fuel cells are suitable for use in the transportation industry because of the power density, type of electrolyte, size, and thermal cycling.

Analysis of Various Fuel Cells

The Proton Exchange Membrane (PEM) Fuel Cell The PEM fuel cell derives its name from the electrolyte used, which is a conducting membrane sandwiched between two catalyst layers, gas diffusion layers and plates. The schematic is shown in Fig. 1. A PEM fuel operates by inducting hydrogen into the anode, where it is oxidized into electrons and protons as per the equation:

$$H_2 \rightarrow 2H^+ + 2e^- \quad (1)$$

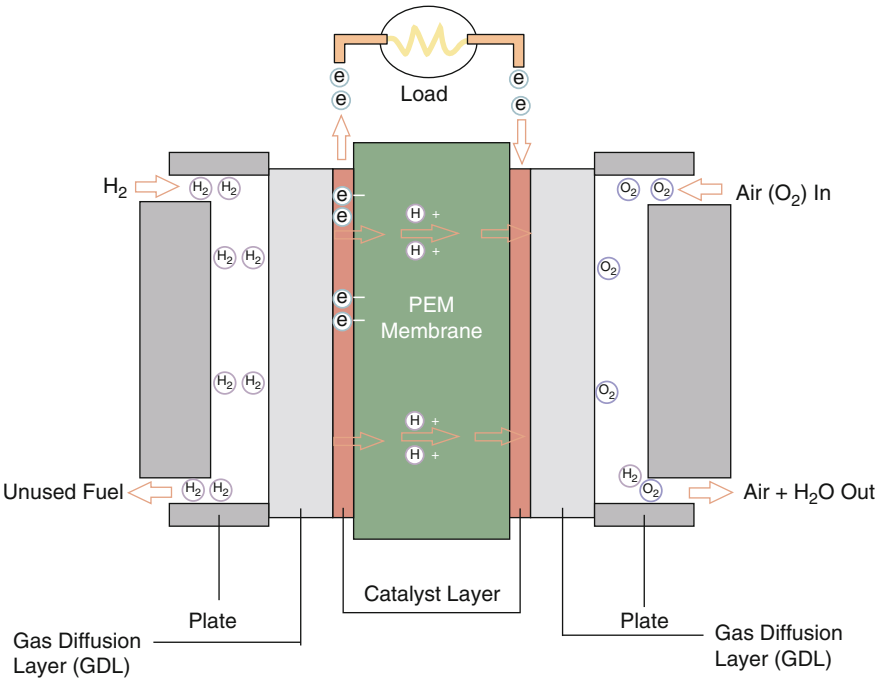

Fuel Cell Powered HEV Design and Control. Figure 1
PEM fuel cell components

The two electrons are not membrane permeable; hence, they travel through the anode electrical interconnect to the load, generating electricity. From there, the electrons travel to the cathode catalyst layer, where they react with the supplied oxygen and the protons that permeate through the membrane to the cathode catalyst layer to form water in a reduction reaction. The process is exothermic.

At the cathode, the reaction is as follows:

$$\tfrac{1}{2}O_2 + 2e^- + 2H^+ \rightarrow H_2O + \text{Heat} \quad (2)$$

Overall reaction:

$$H_2 + \tfrac{1}{2}O_2 \rightarrow H_2O + \text{heat} \quad (3)$$

The schematics of a PEM fuel cell, a 50 cm^2 LT-PEM and HT-PEM fuel cell hardware are shown in Figs. 1, 2a and 2b respectively, while and multi-test station is shown in Fig. 3.

Figure 3 features a SERC (Shartz Energy Research Center) four test station (TS) platform for testing and validation of a single cell to 1 kW stack. The two TS to the left of the computer monitor operate in a dead-end mode and are capable of testing single cells and low-end stacks rated up to 250 W. While TS 3 and 4 are rated up to 1 kWe and operate in a flow-through mode. Low-temperature PEM relies on humidification of the reactants and employs various types of humidifiers. For example, the 4-cell PEM stack on TS 2 has an-inbuilt membrane humidifier while TS 4 has an externally mounted humidifier shown in Fig. 4. That aside, PEM fuel cell stacks require a cooling system which also serves as the medium for maintaining the cell/stack temperature at a constant temperature. The test equipments are designed and sized for testing various output power ranges of cells/stacks. As the power output of the stack increases, the measuring devices ranges and pipe sizes are progressively increased to deliver the desired amount of reactants. Figures 5 and 6 show test equipment for low and high-temperature PEM fuel cell test equipments capable of testing and validating a 5 kW PEM stack.

For the mobility sector, low-temperature PEM requires a complex balance of plant for its smooth operation. That aside, water from the exhaust is an issue of consideration during city driving in winter. It can contribute to slipperiness of the road and can be a hazard to other road users. On the other hand, the high-temperature fuel cells offer an advantage in that vapor exits from the exhaust and can be used for heating the vehicle in winter. However, both low- and high-temperature PEM require heated pads to keep the stacks above 10°C during winter season. Freezing of liquid within the stack's flow field, in the gas diffusion layer and condensates in the exit flow manifold are all unacceptable.

PEM membranes are categorized as low-temperature and high-temperature membranes. A review of both

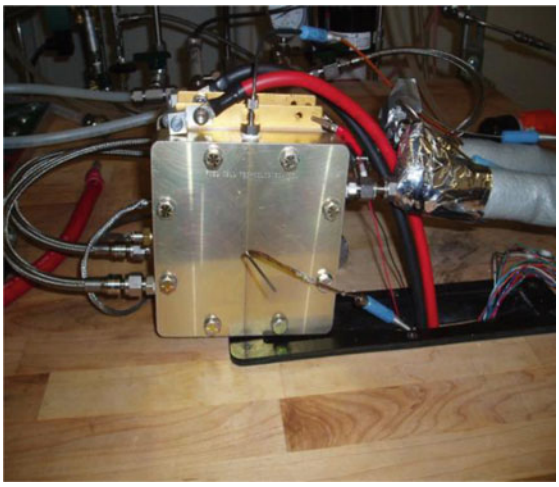

a

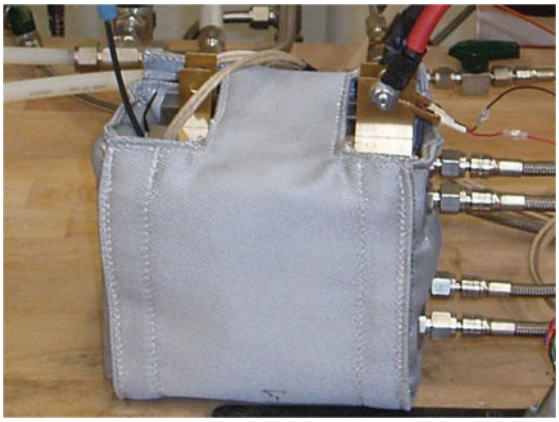

b

Fuel Cell Powered HEV Design and Control. Figure 2 (**a**) LT-PEM single cell of area 50 cm^2 assembled at the Center for Fuel Cell Research, Kettering University, Michigan (Courtesy Kettering PEM Fuel Cell Lab). (**b**) HT-PBI – PEM Single cell of area (Courtesy: Kettering PEM fuel cell research and powertrain integration, laboratory)

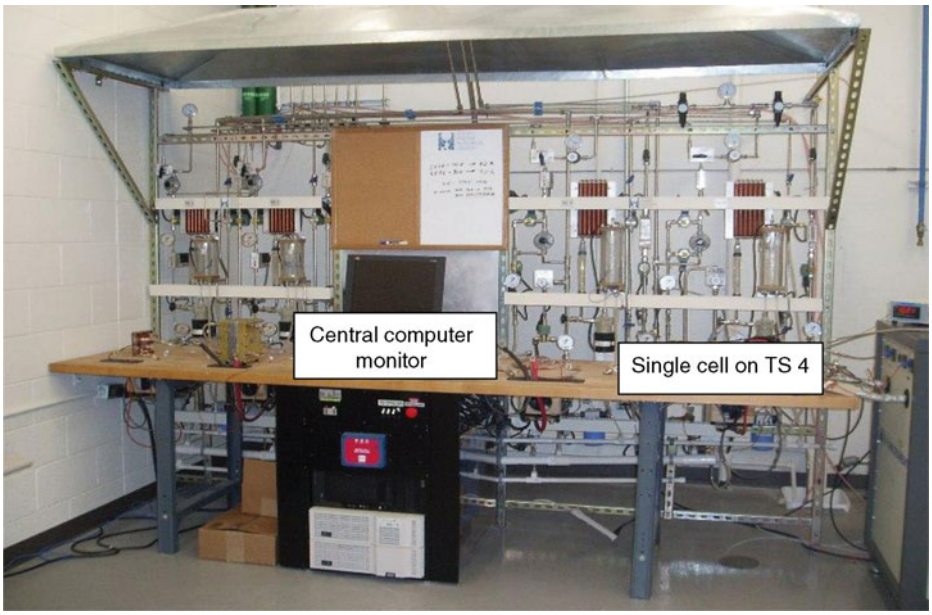

Fuel Cell Powered HEV Design and Control. Figure 3
Multi–test station (TS) for LT- and HT-PEM research

Fuel Cell Powered HEV Design and Control. Figure 4
Humidifier for a LT-PEM fuel cell at Kettering University Center for Fuel Cell Research

types highlights the following advantages and disadvantages: Both are credited with good startability – they start to generate electricity shortly after start-up (LT-PEM from 60°C and HT-PEM at 130°C). Performances of PEM membranes are generally degraded by the presence of carbon monoxide. For LT-PEM, CO concentration above 10 ppm is not recommended, while HT-PEM based on a PBI can tolerate up to 3% CO in the fuel.

Fuel Cell Powered HEV Design and Control. Figure 5
A 5 kW Greenlight low-temperature PEM test equipment at Kettering University Center for Fuel Cell Research

Higher concentrations have been tested up to 8% at a much reduced voltage [3–6]. Operation around 190°C favors higher CO concentration and the loss in performance is reversed if the cell is operated later with pure hydrogen [3].

Both LT and HT-PEM require thermal management systems – LT-PEM uses water as the coolant while HT-PEM uses mineral oil. However, LT-PEM in addition relies on humidification of the membrane for proton transport. The functional humidification range is between 80% and 100% relative humidity (RH). Above 100% RH, the cell floods and impairs the flow of the reactants to the catalyst sites. As a consequence, the cell reaches its mass concentration limit, a point where the flow of reactants to the catalyst sites diminishes and the fuel cell voltage falls off. At a lower RH, the membrane dries up and impairs proton transfer from the anode to the cathode. This inadequacy of the LT-PEM led to the development of a more tolerant membrane, capable of operating without humidification and its complexities. Its electrochemical kinetics are enhanced because of its high-temperature operation; also, the activation overvoltage is reduced. It is more tolerant to a higher CO in the fuel composition.

Future fuels require flexibilities to fuel contaminants. Experience has shown that conventional fuels' dispensing, storage, and transportation systems (trucks, pipelines, etc.) harbor huge deposits of foreign materials that degrade the quality of fuel with time. High-temperature membranes are more resilient and less sensitive to increased CO constituents in the fuel than sulphonated membranes and can tolerate reformates. This enables reformers to be coupled directly to the fuel cell which eliminates the complexity of post-reformation processing of the fuel to obtain hydrogen of 99.997% purity.

Direct Methanol Fuel Cell (DMFC) The direct methanol fuel cell has the same architecture as hydrogen-air PEM fuel cell in that it uses sulphonated membranes. It is a low-temperature fuel cell that operates between 50°C and 80°C. Methanol is fed to the anode while air is fed to the cathode. The anode reaction proceeds as follows:

$$CH_3OH + H_2O \rightarrow +CO_2 + 6H^+ + 6e^- \quad (4)$$

At the cathode, the reactions proceed as:

$$1^1/_2O_2 + 6H^+ + 6e^- \rightarrow 3H_2O \quad (5)$$

Fuel Cell Powered HEV Design and Control. Figure 6 A 5 kW high-temperature PEM fuel cell test stand at Kettering University Center for Fuel Cell Research

The overall reaction is:

$$2CH_3OH + 3O_2 \rightarrow 4H_2O + 2CO_2 \quad (6)$$

The reaction in DMFC is very slow in both electrodes despite its apparent advantages of releasing six electrons. To remedy this, a bi-metal catalyst Pt/Ru is used at the anode with a tenfold increase in catalyst loading compared with hydrogen-air PEM fuel cell [7–10]. The activation overvoltages in both electrodes of DMFC is considered, unlike hydrogen–air PEM where the anode activation overvoltage is ignored because it is by many orders of magnitude smaller than the cathodic activation overvoltage. DMFC is a candidate for portable devices such as cell phones, PDAs, soldier power, laptops, DVD players, iphones, ipads, ipods, kindles, and other portable devices. It works well in remote areas where power is required for a prolonged period such as remote sensing stations, railway crossings, traffic lights, bacon lights, professional cameras, etc. It is one candidate for light HEV application but the technology has not been fully developed for such applications yet. DMFC has a low power density (kW/L); hence, its role as a power source for transportation is diminished.

Alkaline Fuel Cell The AFC uses liquid KOH electrolyte for its operation and it is popular for its past space missions in Apollo Spacecraft in the 1960s and later in the Space Shuttle Orbiter. Due to the renewed interest in the development of solid polymer membranes in the early 1990s, less attention has been given to AFC. The advantage of AFC is overwhelming. The electrolyte is cheap and has a proven technology for the production of KOH. However, the electrolyte is sensitive to the presence of atmospheric CO_2 in the air which combines with the potassium to form an insoluble K_2CO_3 that renders the electrolyte insoluble, hence degrading its performance. AFCs are installed in utility vehicles which operate within a restricted area where pollution by automobiles is restricted. It can be operated as a mobile and stationary power source.

The basic anode reaction

$$2H_2 + 4OH^- \rightarrow 4H_2O + 4e^- \quad (7)$$

At the cathode

$$2H_2O + O_2 + 4e^- \rightarrow 4OH^- \quad (8)$$

Phosphoric Acid Fuel Cell (PAFC) Phosphoric acid fuel cell PAFC derives its name from the type of electrolyte used. It is a medium temperature fuel cell used for stationary power generation. The operational temperature is in the 200–220°C range. It is one of the oldest and matured fuel cells with vast production in the ranges of 200 kW. However, more powerful units ranging in MW have been introduced into service. It finds wide applications as back-up power units in credit card companies' headquarters, police precincts, hospitals, banks, airports, etc. The USA and Japan are the two leading countries in the production and application of PAFCs. Phosphoric acid fuel cell is equally susceptible to CO poisoning as hydrogen-air fuel cell, but can tolerate up to 0.5% or 5,000 ppm of CO [4–7].

Molten Carbonate Fuel Cell (MCFC) Molten carbonate fuel cell is a stationary power generation system that operates around 650°C. It has the advantage of not using noble metals at catalyst as a result of high operational

temperature. It can use multiple fuels, such as methane (CH_4), CO, and hydrogen, as fuel. One advantage of MCFC as well as SOFC is the use of exit gases for cogeneration. That implies using waste heat to operate either steam or gas turbine, thereby bottoming the cycle and increasing the efficiency of the utilized fuel in the entire system. At the exit temperature of 600–650°C, the waste heat is rerouted to the boiler to generate steam to operate a steam turbine. The turbine in turn is connected to a generator or it can be geared to operate several devices of the balance of plant. The final waste heat at a lower enthalpy can be used for heating a facility. This is achieved through routing the city water and the waste heat though a heat exchanger, thereby reducing or eliminating the extra cost of maintaining the facility warm water system.

The common electrolytes used in MCFC are the carbonate salts of sodium, lithium, and potassium. The mobile ion is the CO_3^{-2} that moves from the cathode to the anode [7–10].

The anode reaction using hydrogen as fuel is:

$$2H_2 + 2CO_3^{2-} \rightarrow 2H_2O + 2CO_2 + 4e^- \quad (9)$$

The cathode reaction is:

$$O_2 + 2CO_2 + 4e^- \rightarrow 2CO_3^{2-} \quad (10)$$

The reaction using CO as fuel is as follows:
At the anode, it is:

$$2CO + 2CO_3^{2-} \rightarrow 4CO_2 + 4e^- \quad (11)$$

The cathode reaction is:

$$O_2 + 2CO_2 + 4e^- \rightarrow 2CO_3^{2-} \quad (12)$$

Molten carbonate fuel cell finds a wide application as a stationary power utility plant and is not suitable for hybrid electric vehicles purposes.

The Solid Oxide Fuel Cell (SOFC) The solid oxide fuel cell can be used both as a stationary and auxiliary (for mobile) power unit (APU) depending on its application. Current research favors using it as an auxiliary power unit for inter-state trucks, recreational vehicles, auxiliary power unit, and recharging unit for soldier power, power tools, etc. SOFC uses yttrium-stabilized zinc oxide as the electrolyte [7–10]. The operating temperature is between 650°C and 1,000°C. Due to its high operating temperature, SOFC as of now is not considered a candidate for hybrid electric vehicle applications, but probably for future locomotive or metro-rail transportation systems.

The reaction at the anode using hydrogen as fuel is:

$$2H_2 + 2O^{=} \rightarrow 2H_2O + 4e^- \quad (13)$$

The cathode reaction is:

$$O_2 + 4e^- \rightarrow 2O^{=} \quad (14)$$

The reaction using CO as fuel.
At the anode, the reaction is:

$$2CO + 2O^{=} \rightarrow 2CO_2 + 4e^- \quad (15)$$

The cathode reaction is:

$$O_2 + 4e^- \rightarrow 2O^{=} \quad (16)$$

Candidate Fuel Cells for Hybridization

The above overview shows three fuel cells as candidates for HEV: PEM, DMFC, and AFC in a descending order. Out of these three, AFC is least considered for automotive applications for the following obvious reasons: (1) The electrolyte is easily degraded in the presence of atmospheric CO_2. When potassium carbonate is formed, less OH^- ions are available for ionization, and as such, the performance of the cell is degraded. (2) The fuel cell lacks flexibility in all possible orientations. The advantages are overwhelming: (1) The electrolyte is cheap and easily replaceable. (2) The technology for KOH production is available which makes the fuel source to be sustainable. (3) The absence of bipolar plates reduces the cost and technological process of AFC production [4].

Solid oxide fuel cell SOFC on the other hand can be considered in an auxiliary capacity to support recreation vehicles (RV), large trucks as an APU, but not as the main power unit. The disadvantages are: It requires some hours to bring it up to the operating temperature and shutdown – thermal cycling, and it operates at very high temperatures of 650–1,000°C and, as such, is not suitable for HEV application.

Hybrid Technology Using Gasoline or Diesel, Fuel Cells, Ultra-Capacitors, and Batteries

Hybrid Using Gasoline- or Diesel-Powered Engines

The technology of gasoline and diesel (internal combustion engine) operation is very well understood;

hence, little time will be devoted here for its explanation. Internal combustion engines (ICE) are devices that convert the chemical energy of the fuel (gasoline or diesel) to mechanical work through the piston, connecting rod, and crankshaft mechanisms. The architecture of the gasoline or diesel hybrid consists of an ICE/generator, electric motor, battery, drivetrain, and wheels. The schematic is shown below in Fig. 7

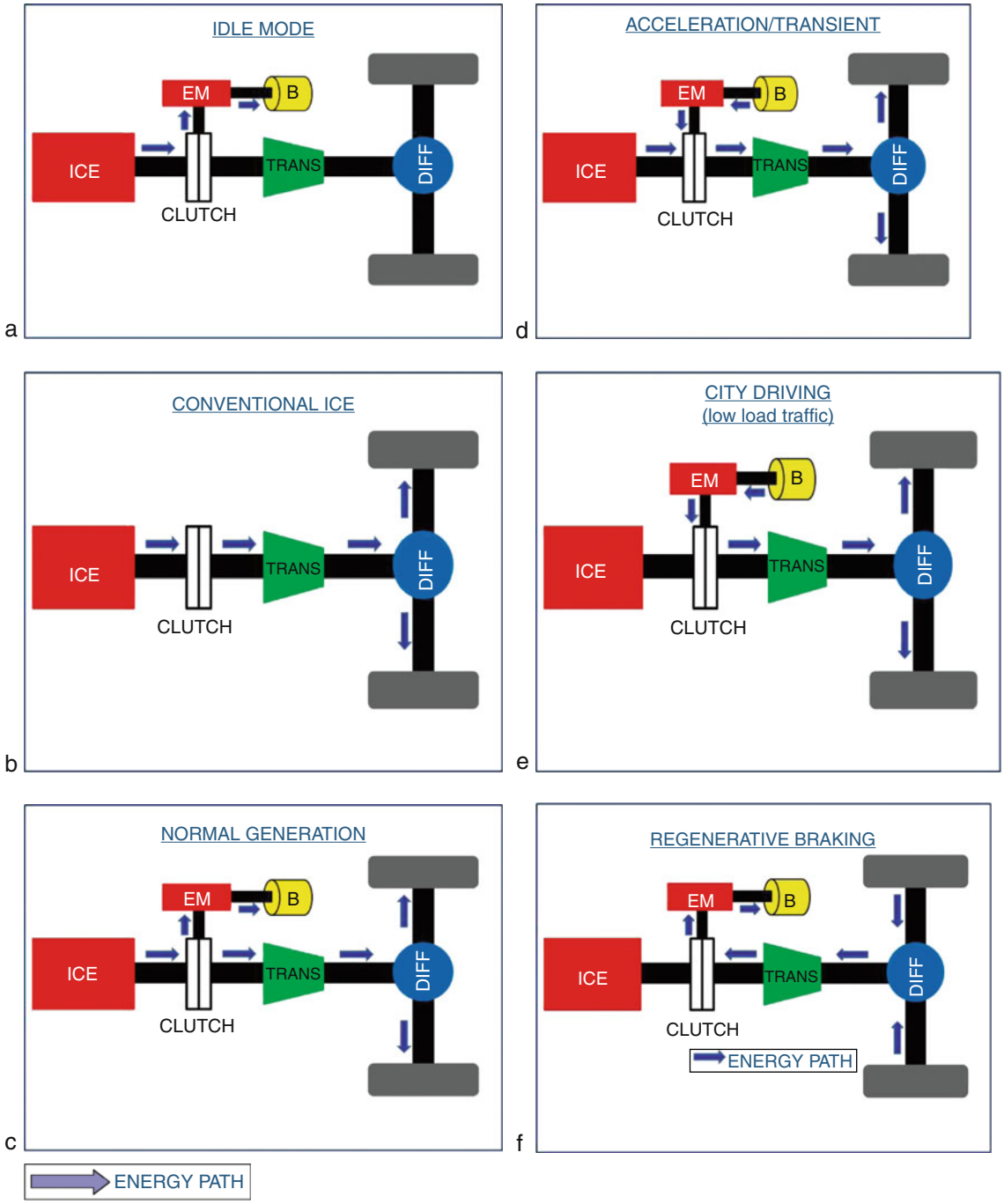

Fuel Cell Powered HEV Design and Control. Figure 7
Hybrid ICE

in which ICE/generator for oversimplification is represented as ICE. The mechanical power from ICE is converted into electrical power through the electric generator connected on the same shaft with the engine. Electric power is transmitted to the motor. Turbo-charged ICE has an immense advantage over its naturally aspirated versions. The exhaust gas energy from the turbine is harnessed by coupling an electric motor generator to the same shaft as the turbo-compressor taking advantage of the exhaust gas energy to generate extra electricity. During acceleration when the vehicle requires more torque/air, the electrical motor is activated with the extra energy from the turbo-generator. When there is excess exhaust energy, that portion would be harnessed to recharge the batteries, thereby bottoming the cycles of the exhaust gas use in hybrid vehicle [11]. The architecture in Fig. 7 shows various modes of ICE hybrid propulsion. Figure 7a presents idle operation where the generated power is used to charge the battery while (b) depicts the normal operation of a conventional ICE. The energy path is indicated with the arrows. Under normal operation, the power from the engine is used both for propulsion and charging the battery as shown in (c) while additional energy is needed during acceleration and transients from the second power source (battery) shown in (d). As an extender, the ICE is turned off during traffic in city driving and the energy from the battery is used for propulsion (e). The concept of regenerative braking involves capturing the kinetic energy during braking and deceleration to charge the batteries (f).

Fuel Cell Hybrid Architecture

The fuel cell hybrid vehicle architecture incorporates PEM fuel cell, onboard compressed hydrogen tank, and power conditioner, batteries, ultra-capacitors, motor and control electronics. A schematic of the PEMFC-powered hybrid vehicle using heavy-duty batteries and ultra-capacitors is presented in Fig. 8. The PEMFC balance of plant includes compressed hydrogen in a storage tank at a pressure of 350 bar (5,000 psi) or 700 bar (10,000 psi); cooling system; humidification system; compressed air system (fan, etc.); and an electronic display panel for controlling the flows into the fuel cell. The steps involved in integrating the entire

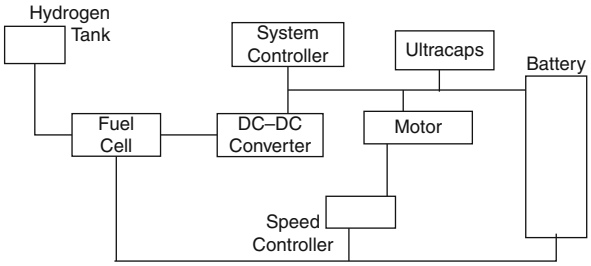

Fuel Cell Powered HEV Design and Control. Figure 8
Fuel cell hybrid architecture

system include sizing the fuel cell to provide average power over the entire operating range [12, 13]. The fuel cell plant has input and output data logging inlets and outlets to monitor the reactants' flow rates, the voltage, current, power, power density, and stoichiometries of reactants. A DC–DC converter is required between the FC and the load. Sets of batteries and ultra-capacitors are also required [12]. Charging of the batteries is done when the vehicle idles, or prior to using the vehicle. The DC–DC converter provides supplementary power for the ultra-capacitor's recharging functions while the ultra-capacitors provide power needs during transients, such as peak loads and transients during acceleration in fuel cell–powered vehicles. Some of the roadblocks in quick implementation of FC-HBVs are hydrogen infrastructure, sub-zero temperature operation, cold start constraints in the colder regions of the country and issues of dealing with fuel cell exhaust water during winter months on the road during city driving.

Ultra-Capacitors

The factor limiting the range and effectiveness of a rechargeable-battery-powered electric vehicle is the battery (or the energy storage system). Ultra-capacitors represent another generation of energy storage devices and are electrochemical double layer capacitors that supply peak energy requirement during transients, such as acceleration and cold start in fuel cell–powered vehicles and other hybrid electric vehicles (HEV). Figure 9 shows Maxwell's 2,600 F ultra-capacitors. Ultra-capacitors are widely accepted in fuel cell vehicles and other HEVs for their quick charge/discharge functions. Some of the advantages are their flexibilities in

Fuel Cell Powered HEV Design and Control. Figure 9
Maxwell ultra-capacitors

charging/recharging. They cannot be overcharged and can be maintained at any voltage above/below the rated value. While rechargeable batteries generally exhibit a very slow charge/response functions with significantly reduced life cycles, ultra-capacitors work best in this condition by recuperating within a few seconds as a result of their low equivalent series resistance (ESR). They possess a high cycle-life with less deterioration when used frequently and infrequently. They respond within a wide temperature range of 65–40°C. They exhibit high columbic efficiency which implies total charge removed over the replenished charge [13–15].

Conclusion

In conclusion, both low- and high-temperature proton exchange membrane fuel cells will be used in fuel cell hybrid vehicles for transportation as they provide overwhelming advantages over the internal combustion engines, such as zero emissions when hydrogen is used as fuel, reduced noise, and higher efficiency.

The use of integrated technologies such as fuel cell, batteries, ultra-capacitors, and other novel techniques will occupy the center stage in fuel cell vehicle development within this decade.

Bibliography

1. Heywood JB (1985) Fundamentals of internal combustion engines. McGraw Hill, New York
2. Ferguson C, Kirkpatrick A (2001) Internal combustion engines and applied thermosciences. Wiley, New York
3. Ubong EU, Shi Z, Wang X (2009) Three dimensioning modeling and experimental study of a high temperature PBI based PEM fuel cell. J Electrochem Soc 156(10):B1276–B1282
4. Ubong EU, Dimitrov B (2010) Regression of the response variable of a high temperature PEMFC-PBI based membrane. J Electrochem Soc 157(7):B1059–B1067
5. Ubong EU (2008) A single cell testing and evaluation of a high temperature PBI based membrane. In: Fuel cell seminar & exposition. Convention Center, Phoenix, 27–30 Oct 2008
6. Ubong E, Das SK, Berry KJ, Antonio R (2008) Experimental performance evaluation of a high temperature PEM fuel cell at different temperatures. In: ASME 6th international fuel cell conference. Denver, 16–18 June 2008
7. Larminie J, Dicks A (2003) Fuel cell systems explained, 2nd edn. Wiley, New York. ISBN 0-470- 84857-X
8. Babir F (2005) PEM fuel cells: theory and practice. Elsevier, Amsterdam/London
9. Mench MM (2008) Fuel cell engines. Wiley, Hoboken
10. O'Hare R, Cha SW, Colella W, Prinz FB (2006) Fuel cell fundamentals. Wiley, New York
11. Sahed SM (2005) The power of turbocharging. Automotive Engineering, International, Sep 2005, SAE
12. Anzicek J, Joel Berry K, Lerner S, Slota G, Thompson M, Ubong E et al (2004) Fuel cell hybrid vehicle at Kettering University.

In: Electrical manufacturing and coil winding conference (EMCWA conference), Indianapolis, 23–25 Sep 2004
13. Ubong EU, Mizell C, Slota G (2005) Ultracapacitors with Ballard Nexa in a GEM vehicle in hybrid mode. In: Electrical manufacturing and coil winding conference) – EMCWA conference, Indianapolis, 20–22 Sep 2005
14. Schneuwly A, Maher B, Auer J. Maxwell Technologies Inc., www.maxwell.com
15. Namisnyk AM, Zhu JG. A survey of electrochemical supercapacitors technology. Faculty of Engineering, University of Technology, Sydney

Fuel Cell Types and Their Electrochemistry

Günther G. Scherer
Paul Scherrer Institut, Electrochemistry Laboratory, Villigen, Switzerland

Article Outline

Glossary
Definition of the Subject
Introduction
What Is a Fuel Cell?
The Role of the Electrolyte
Classification of Fuel Cell Types
The Role of Electrocatalysis and the Electrode/Electrolyte Interface
Fuel Cell Families
Future Directions
Bibliography

Glossary

AFC Alkaline fuel cell.
EC Electrocatalysis.
FC Fuel cell.
GDE Gas diffusion electrode.
GDL Gas diffusion layer.
HOR Hydrogen oxidation reaction.
HT-PEFC High temperature polymer electrolyte fuel cell.
MCFC Molten carbonate fuel cell.
ORR Oxygen reduction reaction.
PAFC Phosphoric acid fuel cell.
PEFC Polymer electrolyte fuel cell.
SOFC Solid oxide fuel cell.

Definition of the Subject

Fuel cells are efficient energy converters, based on electrochemical principles. They convert the chemical energy (heating value) of a fuel directly into electricity, circumventing the various steps of thermal conversion and electricity generation. Fuel cells can be designed and constructed on the basis of a multitude of material combinations for electrolyte and electrodes, opening the choice of different fuels. The electrocatalytic reactions of fuel and oxygen are major challenges to obtain high conversion efficiency. The electrochemical basics of different fuel cell types considered today for technical applications are described in this contribution.

Introduction

Fuel cell technologies have seen a revival in recent years, due to several reasons. Global warming and local air pollution caused by various energy utilization processes have created a multitude of environmental concerns, promoting the development of novel technologies with high conversion efficiencies and low emissions, possibly zero emission, with respect to green house gases and other pollutants [1, 2]. Peak oil is another reason for the renewed interest in fuel cell technologies, in particular for automotive applications [3, 4]. Although this fact is discussed in a highly controversial manner, limitation in crude oil supply is obvious in the long-term perspective. This particular aspect of fossil fuel resources is strongly interlinked to the future perspective of the "oil price" and, hence, its economic competitiveness to other fuels, e.g., fuels from renewable sources. In this context, the installation of new supply infrastructures for alternative fuels, e.g., H_2, is an important additional economical and political factor. Dedicated analysis has clearly shown that energy conversion in fuel cells has to be based on fuels, in particular hydrogen, derived from renewable sources [5]. Further, the geographical distribution of oil reserves causes concerns about the supply security in industrial centers around the world.

Overall, there exist several reasons to ask for novel efficient conversion technologies for mobility (electromobility) and combined heat and power systems (CHP) with independence on fossil fuels, in particular crude oil. Another area of interest in fuel cell technology is portable electric and electronic applications, where the argument of potentially higher energy density as compared to today's available battery technologies, hence, longer time of operation, is of prime interest [6].

Electricity generation via fuel cells is an idea, based on fundamental research carried out by Christian Friedrich Schönbein at the University of Basel in the early nineteenth century. Schönbein's basic investigations of the respective reaction of H_2 gas (oxidation) and O_2 gas (reduction) dissolved in the electrolyte at an electrode/electrolyte interface, representing the fundamental fuel cell reactions, led William Robert Grove to the design and construction of the first operating fuel cell. He utilized H_2 as fuel and O_2 as oxidant at platinum metal electrodes in two separated closed compartments, filled with the respective reactant (hydrogen electrode, oxygen electrode), and joined by sulfuric acid as common electrolyte [7].

As will be shown in this chapter, the basic electrochemistry of a fuel cell, an electrochemical gas battery, is determined by the choice of the electrolyte and the two different electrodes immersed therein. In the course of time since this fundamental work of Schönbein and Grove, many combinations of electrolytes and electrode materials have been tested and fuel cell types derived upon there. This development has also been driven in the past by the choice of available fuel and possible application in view, in particular by space and military applications.

This introductory chapter will give an overview on the basic electrochemistry of some fuel cell types, developed today for dedicated technological applications. The respective electrochemistry will depend on the materials composition of the fuel cell, in particular, on the nature of the electrolyte and the temperature of operation. This further determines the choice of fuel, due to the strong influence of temperature on the mechanism of the respective electrocatalytic processes.

Engineering issues of fuel cell stack and systems design will be dealt with in the following chapters. Hence, issues of, e.g., coflow or counterflow within one cell, stoichiometry and utilization of fuel and oxidant, temperature and current distribution in a fuel cell of technical scale, and, certainly, issues of stacking cells into a bipolar arrangement will not be discussed here.

What Is a Fuel Cell?

A fuel cell is an electrochemical device, converting the chemical energy (Gibbs free energy) stored in a gaseous or liquid fuel, e.g., hydrogen, methane, methanol, ethanol, others, directly into *work of electrical energy* (*direct current electricity*) at constant temperature (Fig. 1). This type of energy conversion process is different from the classical thermomechanical energy conversion process and is not limited by the Carnot principle (see below).

In short, in a fuel cell, the fuel is oxidized at an electrochemical interface (electrode called anode), accepting electrons and donating these electrons at a second electrochemical interface (electrode called cathode, separated from the anode) to an oxidant, e.g., oxygen, which is reduced by accepting these electrons. Both electrochemical interfaces have to belong to a common electrochemical cell and are joined in the cell by a common medium, an ion-conducting electrolyte. Both electrodes have to be connected electronically by an external circuit, containing the electrical device to be operated, in which the electrons, due to the potential difference created by the two electrode reactions, travel from the anode to the cathode delivering electrical work (Fig. 2). Fuel and oxidant are supplied in gas channels of the cell housing (bipolar plate in stacked cells) on the backside of the porous electrodes (not

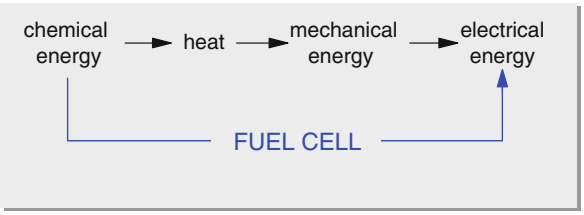

Fuel Cell Types and Their Electrochemistry. Figure 1 Scheme of direct energy conversion in an electrochemical cell as compared to "conventional" thermal conversion

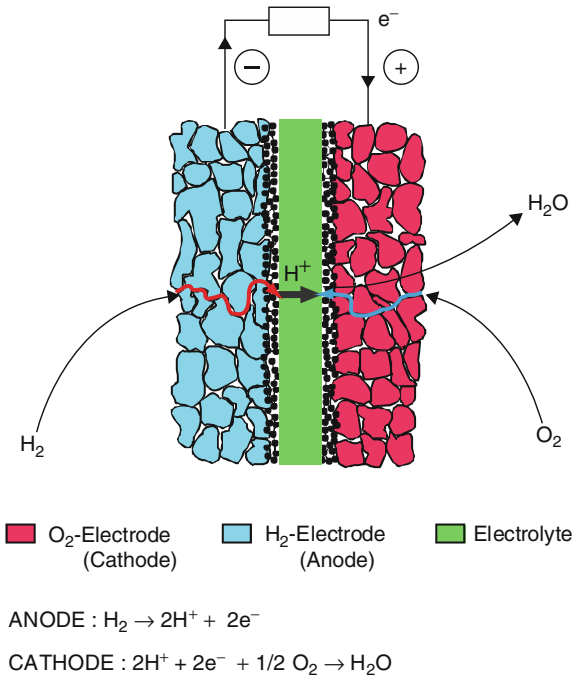

Fuel Cell Types and Their Electrochemistry. Figure 2 Simplified fuel cell scheme with an acidic aqueous electrolyte, e.g., the polymer electrolyte fuel cell (PEFC). Fuel: H_2, oxidant: O_2. Only porous gas diffusion electrodes and electrolyte are shown, cell housing is not shown [8]

displayed in Fig. 2) Both gases have to be transported through the porous gas diffusion layers (GDLs) with pores typically in the micrometer range (blue and red bodies in Fig. 2) to the electroactive catalyst layers (ECLs, black dots in Fig. 2) at the interface to the electrolyte. Colloquially, GDL and ECL together are called gas diffusion electrode (GDE).

The fuel cell and its electrochemically active components, i.e., electrodes, electrolyte, etc., as well as its (electrochemically inert) structure materials, i.e., current collectors, cell housing, etc., should be as invariant as possible, i.e., they should not be consumed and, ideally, not age (corrode) over the time of operation. Hence, as an electrochemical reactor, they provide the electrochemically active interfaces (or interphases, see below) and the necessary pathways for mass transport for educts and products to and from these active interfaces through porous media (active electrode layers, gas diffusion layers, internally corrugated cell housing (flow fields) in bipolar plates) with open porosity at different scales. At the same time, it is a prerequisite that these materials are as conductive as possible because they are responsible for the collection and transmission of the electric current generated at the two interfaces. Hence, ohmic voltage losses in these materials should be as low as possible.

The electrochemistry of the two electrode reactions is exemplified for the simplest and predominant case by the "cold" electrochemical combustion of H_2 with O_2 (pure O_2 or from ambient air) to H_2O (Fig. 2). The overall reaction is split into two partial reactions, occurring at the two different electrodes of the cell:

$$\textbf{Anodic reaction}: \ \mathbf{H_2 = 2H + 2e^-}$$
(hydrogen oxidation reaction, HOR)

$$\textbf{Cathodic reaction}: \ \mathbf{1/2O_2 + 2H^+ + 2e^- = H_2O}$$
(oxygen reduction reaction, ORR)

$$\textbf{Overall reaction}: \mathbf{H_2 + {}^1\!/_2O_2 = H_2O}$$

The reaction product(s) of the individual electrode reactions are constituents of the (aqueous) electrolyte (H^+ in the example of an acidic electrolyte, as displayed in the scheme of Fig. 2), which avoids polarization losses in the electrolyte (see Chapter "► Livestock Somatic Cell Nuclear Transfer").

Each of the two electrode reactions creates a characteristic potential difference across the interface solid electrode/electrolyte, which is different for the two reactions according to the different reactants. The overall cell voltage between the two electrodes, which are joined by the same electrolyte, allows the electrons generated at the anode (HOR) and consumed at the cathode (ORR) to create work in the external circuit. Hence, chemical energy released by the individual electrode reactions at the locally separated electrodes is directly transferred into electrical energy. This pathway is different from the combustion step in the "classical" thermomechanical power generation, where the oxidation of fuel and reduction of oxidant occur in the same volume element, thereby generating heat only.

Generally, the available cell voltage of electrochemical cells depends on the thermodynamics of the two electrode reactions in the prevailing electrolyte, hence the difference in the electrode potentials, and is confined, according to the series of electrochemical potentials, to a few volts [9]. According to the individual

electrode potentials of the H_2/H^+ reaction (by IUPAC standard zero volt in the series of electrochemical potentials, acidic electrolyte, standard conditions of 1 atm and 25 °C or 298K) and the O_2/H_2O reaction (1.23 V, respectively), a cell with H_2 and O_2 as reactants should yield an ideal cell voltage of 1.23 V at these standard conditions. In practice, a lower value in the range of 1 V is observed, due to different implications (side reactions, depolarization of electrodes due to crossover of gases through the electrolyte, etc.).

The free energy ΔG (Gibbs energy at constant pressure) of the fuel cell reaction is related to the cell voltage under open circuit conditions (open circuit voltage, OCV) E^0 and standard conditions according to

$$E^0 = -\Delta G/nF$$

n being the number of electrons transferred in the respective reaction (equal to 2 for the reaction $H_2 + ½O_2 = H_2O$) and F the Faraday constant equal to 96,487 C/mol (electric charge per mol of electrons).

Further, ΔG can be expressed as the difference of the free enthalpy ΔH of the reaction (thermal cell voltage $E_H{}^0$ equivalent to 1.48 V for the H_2/O_2 reaction under standard state conditions) and the term TΔS, (T absolute temperature) expressing entropy losses (or gains) ΔS in the reaction:

$$\mathbf{\Delta G = \Delta H - T\Delta S}$$

Hence, the voltage (thermal) efficiency of a reaction under equilibrium conditions can be written as:

$$\varepsilon_{th} = \frac{\Delta G}{\Delta H} = 1 - \frac{T\Delta S}{\Delta H}$$

The voltage (thermal) efficiency for the electrochemical conversion of the three different fuels H_2, CH_4, and CO reacting with air (oxygen) in dependence of reaction temperature is displayed in Fig. 3. In comparison, also the maximal efficiency $\eta = (T_1 - T_2)/T_1$ for a Carnot process at the respective higher temperature T_1 and the lower temperature T_2 equal to 0 C is included. The different temperature dependence of the three conversion reactions is due to the respective entropy changes, e.g., ΔS = 0 for the reaction $CH_4 + 2O_2 = CO_2 + 2H_2O$ and $\Delta S \neq 0$ for the reactions $2H_2 + O_2 = 2H_2O$ and $2CO + O_2 = 2CO_2$.

Based on thermodynamic arguments only, electrochemical energy conversion offers higher efficiencies

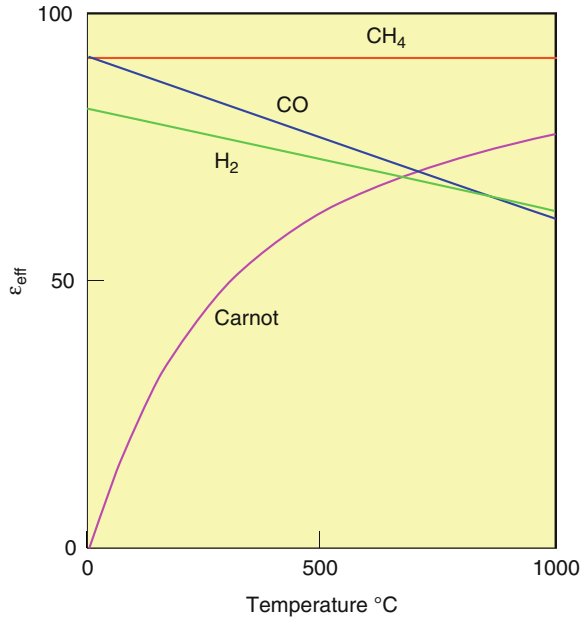

Fuel Cell Types and Their Electrochemistry. Figure 3 Voltage (thermal) efficiency ε_{th} for the electrochemical reaction of H_2, CO, and CH_4 as fuel with oxygen from air under equilibrium versus temperature (°C). In comparison, Carnot efficiency of a thermal process as function of the respective higher temperature in °C and with 0 °C as lower temperature is displayed

within a certain temperature window, depending on the respective reaction.

Introducing Nernst's law for the equilibrium case, the situation when no current (and hence power) is delivered by the cell, the equilibrium cell voltage under nonstandard conditions for a H_2/O_2 cell in dependence of the respective reactant/product concentration (partial pressures) can be expressed as:

$$E^{eq} = -\frac{\Delta G}{n_t F} = E^{eq,c} - E^{eq,a}$$
$$= E^0 + \frac{RT}{2F}\ln\left(\frac{[H_2][O_2]^{1/2}}{[H_2O]}\right)$$

E^{eq} = equilibrium cell potential, $E^{eq,c}$ = equilibrium potential cathode, $E^{eq,a}$ equilibrium potential anode, R gas constant, T absolute temperature, E^0 = equilibrium potential under standard state.

E^{eq} is also called "theoretical" open circuit cell voltage, OCV, in dependence of temperature and reactant,

respectively product concentrations. Practical OCVs may observed to be lower, due to losses (mixed potentials due to side reactions or gas crossover, see practical OCV of H_2/O_2 fuel cell) already occurring at zero current flow.

Under current flow, the kinetics of the electrode reactions comes into effect. The Butler-Volmer equation describes the dependency of the current passing through the electrode interface (current density per unit geometric area) on a small voltage excursion (called overvoltage η) from the respective equilibrium potential E^{eq}.

$$i = i_0[\exp(\alpha nF\eta/RT) - \exp((1-\alpha)nF\eta/RT)]$$

i = current density at overvoltage η, η = overvoltage (excursion from the equilibrium potential, i_0 = exchange current density (at $\eta = 0$), α = symmetry factor, representing the fraction of overvoltage assisting the reaction, n = number of electrons exchanged, F = Faraday constant, R = gas constant, T = absolute temperature.

The exponential dependency points out that small potential excursions cause a larger change in current, while at larger potential excursions, the current follows a linear behavior. This can be described by the Tafel law, which usually is applied when current densities of technical interest, e.g., several 100 mA per cm^2 geometric surface area in a fuel cell, are passing through the cell.

$$\eta = (RT/\alpha nF)\ln i/i_0$$

For the HOR, exhibiting an exchange current density in the range of $i_0 = 10^{-3}$ A/cm^2 with platinum as electrode material [9], only a small overvoltage arises even by drawing a current density of technical interest, e.g., 1 A/cm^2, due to the fact that the H_2 molecule is easily split into two adsorbed H atoms (Tafel reaction), followed by the transfer of one electron per H atom (Volmer reaction) to the electrode generating two hydrated H^+. Alternatively, one electron is transferred to an adsorbed H_2 molecule, followed by a split into a hydrated H^+ and an adsorbed H atom. In a consecutive step, the second H atom is oxidized (Heyrovsky reaction).

In contrast, the exchange current density of the ORR at a platinum electrode is in the range of $i_0 = 10^{-8}$ A/cm^2. Assuming *direct* reduction of the oxygen molecule, the ORR requires four electrons in total, including the four H^+ generated in the HOR at the counterelectrode (see above). As a consequence, ORR generates a major overvoltage and, hence a major contribution to the overall loss.

In addition to the overvoltage losses due to electrode kinetics, one has to take into account the voltage loss in the ion-conducting electrolyte, due to the finite electrolyte conductivity, and (minimized) losses due to the electric resistance of electrode and cell materials, including contact resistances.

This relationship between cell voltage and current density is schematically displayed in Fig. 4. The various voltage losses are deducted from the equilibrium cell voltage (zero current), yielding the available cell voltage E^* at the respective current density i^*. The difference between $E^0{}_H$ and E^* is expressed as (waste) heat. In terms of voltage efficiency, this (heat) loss should be as low as possible; hence, E^* should be as high as possible. On the other side, the current density to be drawn has to be as high as possible to utilize power output values (specific power W/kg or power density W/L) of technical interest.

Further, Fig. 4 points to another advantage of (electrochemical) fuel cell technology: Designing a fuel cell to the maximum or rated power for a certain application (power = cell voltage E times current i), one easily realizes that the voltage efficiency ε_{eff} increases at lower power (lower current but higher voltage). This fact is

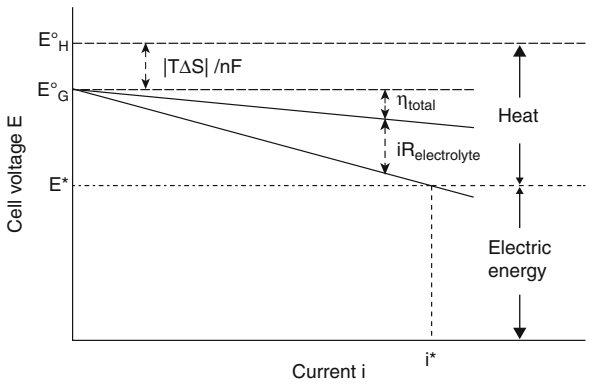

Fuel Cell Types and Their Electrochemistry. Figure 4 Cell voltage *E* versus current *i* of a fuel cell, with $E_H{}^0$ = thermal cell voltage, $E_G{}^0$ = ideal cell voltage based on ΔG, η = sum of overvoltage at anode and cathode, $R_{Electrolyte}$ = electrolyte resistance

particularly important for applications where maximum power (full load) is only required at certain parts of the duty cycle, while in other parts, only part load is necessary. This case is, e.g., exhibited in automotive applications of fuel cell technology.

Generally, the available cell voltage of electrochemical cells depends on the thermodynamics of the two electrode reactions in the prevailing electrolyte, hence the difference in the electrode potentials, and is confined, according to the Electrochemical Series of Standard Potentials, to a few volts. Cells with an aqueous electrolyte exhibit a limitation given by the stability window of water, namely 1.23 V at standard conditions. As stated above, the H_2/O_2 fuel cell allows practical open circuit voltages of around 1.0 V. At cell voltages above 1.23 V, typically around 1.5 V, decomposition of water into H_2 and O_2 occurs.

Hence, to accumulate the necessary voltage for technical applications, e.g., 200–400 V, for an electrical power train in a car, cells must be connected in series. Dedicated bipolar arrangements of cells have been designed and put into operation for serial connection, taking into consideration also the necessary parallel mass flow of fuel and oxidant from a manifold into each individual cell and the respective removal of the product. Such an arrangement of cells is called a fuel cell stack, combining the electrical serial connection of individual cells with a parallel connection for mass flow.

In contrast to batteries, fuel cells are open systems, which convert the chemical energy available in a fuel stored outside the fuel cell, the electrochemical converter. As a consequence, fuel cells need a fuel tank, also a tank for the oxidant, if the oxidant is pure oxygen and not ambient air, and auxiliaries (for temperature, pressure, etc., control) to be operated (Fig. 5).

Mass flow into (reactants) and out of the cell (products) must be allowed and controlled, as well as cooling to remove the waste heat. At a voltage efficiency of 50%, a cell producing 1 kW electric power also generates 1 kW of heat, which has to be removed efficiently not to cause thermal runaway and, hence, degradation of the cell and its components. In summary, this is called a fuel cell system. Engineering issues of mass and heat transfer, current distribution across the active area of a cell, and voltage distribution along the stack, etc., are governing the design of a fuel cell system.

Fuel cells can be operated continuously, as long as they are supplied with fuel and oxidant. Hence, they are not limited by electrical charge–discharge cycles, as batteries are. This fact can be of utmost importance for certain applications, e.g., with respect to refueling time in mobile applications. For mobile or portable applications, the availability of a fuel infrastructure adds another aspect of consideration.

In terms of achievable specific energy (W/kg) and volumetric energy density (W/L), air-fed fuel cells have the advantage that one reaction partner, namely, oxygen, is derived from air, and consequently does not add to the weight and volume of the device. However, ambient air must be processed (cleaned, humidified, etc.), which has to be taken into account.

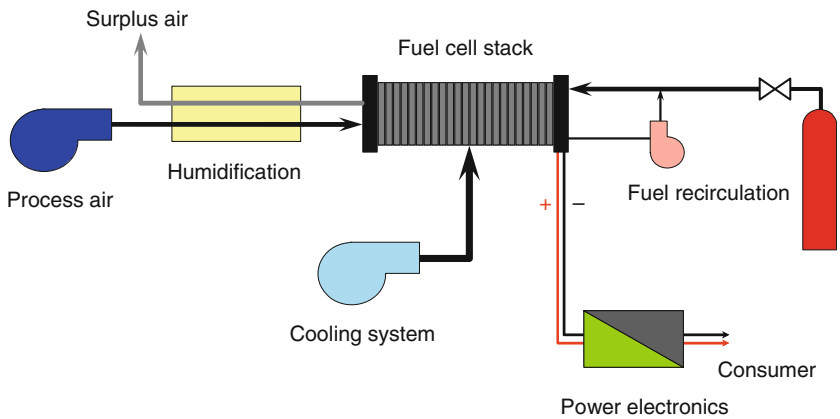

Fuel Cell Types and Their Electrochemistry. Figure 5
Simplified scheme of a fuel cell system (Adapted from L. Gubler, Paul Scherrer Institut)

This advantage is also expressed in the concept of metal air batteries, e.g., the Zn/Air or Al/Air battery, which on the anode (metal) consists as half a battery (closed mass flow) and on the cathode as half a fuel cell (open mass flow).

Next to the multitude of material combinations allowing various fuel cell types to be designed and built, the variety of mobile (transport), stationary, and portable applications provokes a multitude of different cell, stack, and systems designs, guided by the implications of the different fuel cell technologies (see below).

The Role of the Electrolyte

Generally speaking, the ion conduction in the electrolyte contributes to the losses (ohmic losses, see Fig. 3) in the cell voltage. Hence, one of the major tasks in fuel cell development is the reduction of these losses in the ionic circuit part, because the work available in the external electronic circuit should be as high as possible.

The role of the "electrolyte" in a fuel cell is a multiple one:

1. Transport the charge in ionic form from one interface to the other within the cell. To minimize losses in the ionic circuit, the ion conduction should be carried by an ion, which is produced at one electrode and consumed at the other to avoid losses caused by concentration gradients [10]. This majority ion should carry as much charge as possible through the electrolyte, hence its transport number (Hittorf number) should be as high as possible, ideally one. For high power applications with an aqueous electrolyte, the concentration of this respective anion or cation must be high and exclusively responsible for conduction. Typically, a specific ionic conductivity in the range of 100 mS/cm is required, which at a current density of 1 A/cm^2 and an electrolyte gap of 100 µm would yield an ohmic voltage loss in the range of 100 mV. As seen in Fig. 6, the conductivities of various

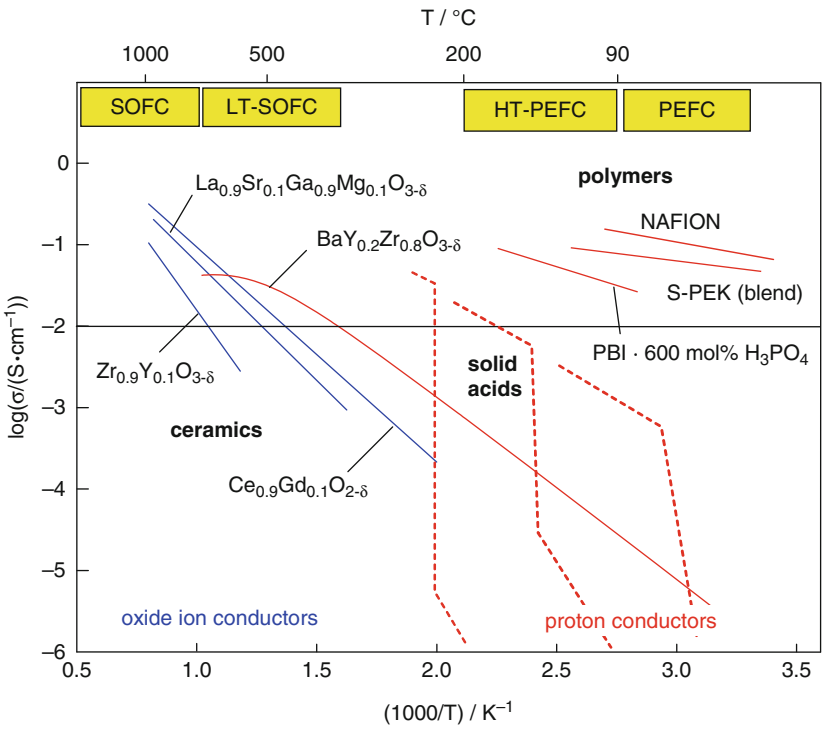

Fuel Cell Types and Their Electrochemistry. Figure 6
Specific conductivity versus temperature of different electrolytes interesting for fuel cell applications (Adapted from K.D. Kreuer)

electrolytes are strongly temperature dependent and cover a wide temperature range, depending on the ion-conducting species in its respective environment (material). Again, electrolytes are of interest, which offer the opportunity that the ionic species is participating in the fuel cell reaction.

2. Act as separator to (1) avoid crossover and, as a consequence, "hot" combustion of the fuel and the oxidant at the respective counterelectrode, and (2) to avoid touching of the electrodes by short circuiting the electronic pathway. Thereby, the electrolyte/separator gap should be as narrow as possible to lower the ohmic contribution to the overall voltage loss. In the case of a liquid electrolyte, it can be absorbed into an inert matrix, providing porosity high enough for an ionic conduction path with low tortuosity for the ion and at the same time a high enough bubble pressure to suppress gas crossover. An ideal concept is the one of a solid electrolyte, which fulfills the dual electrolyte and separator function at the same time, providing a transfer number of one for the current-carrying ionic species, as in the case of solid polymer electrolytes (ion exchange membranes), thereby excluding a contribution of electronic conduction.

One has to emphasize that the electrolyte has to sustain the potential window of the respective fuel cell reaction, given by the Gibbs free energy, at least over the device lifetime, specified for a certain application.

In aqueous acidic electrolytes, the ionic conduction is provided by an H^+ ion, respectively, $H(H_2O)_n{}^+$. As mentioned above, H^+ is created by the anodic oxidation of H_2 as a fuel, and the conducting species is transported to the cathode, where it is consumed in the direct (ideally four electrons) cathodic reduction of molecular oxygen. Hereby, water as the reaction product appears at the cathode side of the cell.

In alkaline solution, the ionic conduction is provided by OH^- ions, created by the ORR at the cathode. Principally, OH^- ions are carriers for the O^{2-} ions, produced as intermediate by the cathodic reduction reaction of molecular O_2 and the follow-up reaction with a water molecule. After conduction, OH^- reacts with the H^+ created at the anode and yields water as a product at the anode side.

Solid polymer electrolytes on the basis of a polymer cation exchange membrane in H^+ form or an anion exchange polymer membrane in OH^- form can be considered as quasi-aqueous electrolytes, whereby the water is absorbed in the phase separated ionic nanomorphology of the respective material. This nanomorphology forms ionic pathways through the polymeric membrane connecting the two fuel cell electrodes.

In cells operated at temperatures below 100 °C, liquid water will be the reaction product. For operation temperatures above the boiling point of water, a cell with an aqueous or quasi-aqueous electrolyte can be operated, however, at the expense of pressurizing it to avoid loss of the water and, as a consequence, concentration and conductivity changes in the electrolyte.

An alternative electrolyte for operating temperatures above 100 °C, which also gained technical relevance, is orthophosphoric acid, H_3PO_4. "Water-free" orthophosphoric acid is a self-ionizing amphoteric system, which yields $H_4PO_4{}^+$ and $H_2PO_4{}^-$. Protons can be passed along pyrophosphate chains at elevated temperatures of around 200 °C, at which product water appears as vapor and can be rejected easily.

Molten salts can also be utilized as electrolytes. Again, the ion responsible for conductivity should be created in one electrode reaction and consumed in the other. However, due to the (1) corrosive nature, (2) the limited thermal stability, and/or (3) the high melting point of many melts, only a few molten salts have been considered. Up to now, the only fuel cell technology based on a molten salt electrolyte has been using a eutectic mixture of alkali metal carbonates, Li_2CO_3 and K_2CO_3, at temperatures of around 650 °C, absorbed in a matrix of $LiAlO_2$. In this molten carbonate fuel cell (MCFC) the ion conducting the current is O^{2-} in the form of $CO_3{}^{2-}$. At the anode, CO_2 is supplied and reacts with O_2 and $4e^-$ to form $CO_3{}^{2-}$, which carries the current to the anode, where it is released in the hydrogen oxidation reaction. As a consequence, MCFC, in addition to the mass flow of fuel and oxidant, needs mass flow management of CO_2.

At even higher temperatures in the range of 800–900 °C, ionic conduction can also be observed in solid oxides. Certain doped metal oxides become O^{2-} conductors; hence, they can be utilized as electrolytes in the solid oxide fuel cell (SOFC). The most

common oxide used is yttria-stabilized cubic zirconia (ZrO_2), called YSZ, with a doping level of 8% Y_2O_3. This material is a ceramic; the thermal expansion coefficient of its thin layers has to be matched with the other fuel cell components.

As indicated by the terminology of fuel cells, e.g., *PEFC, AFC, SOFC, others* (*see below*), *the electrolyte is the decisive cell component, which determines operation temperature, the choice the electrodes* (*electrocatalytic materials*), *and finally the specifics of the electrochemistry of the reactants. This, on the other hand, has consequences for the layout of the fuel cell design* (*balance of plant*) *and possible applications of the respective fuel cell technology, according to the required duty cycle of the application.*

Classification of Fuel Cell Types

Today's fuel cell types under development can be classified in two different ways: either by the temperature range of operation or by the nature of the electrolyte.

The latter classification distinguishes between acidic and alkaline fuel cells. Acidic fuel cells with H^+ conduction require other electrode materials than alkaline with OH^- conduction. Alkaline fuel cells, at least with an aqueous electrolyte, require a CO_2-free fuel, and hence cannot be operated on reformate fuel obtained originally from a C-containing fuel.

The above-described situation displays the fact that there is a temperature gap in the availability of electrolytes between ca. 200 °C and 650 °C. Today, major research efforts are carried out to extend the range of aqueous H^+ and OH^- conduction to temperatures beyond 100 °C, for technological reasons (heat rejection in cars, CO tolerance of platinum-based catalysts). On the other hand, oxide materials are developed with improved O_2^- conductivity al temperatures lower than the operation temperatures of standard SOFCs. Also ceramic proton conductors [11] and proton-conducting salts like CsHSO4 [12] are considered as electrolytes for this temperature regime.

The Role of Electrocatalysis and the Electrode/Electrolyte Interface

Next to the voltage losses due to ionic conduction, voltage losses due to the activation overvoltages of the respective electrode reactions arise, as described by the Butler-Volmer, respectively, the Tafel equation. As stated above, at a certain value of the current density, the overvoltage for the HOR is much smaller than for the ORR, due to the simpler electron transfer kinetics. Overvoltage for an electrochemical reaction shows also a strong temperature dependency, as does activation energy, and decreases with increasing temperature.

For fuel cells with an acidic electrolyte, platinum is the electrocatalyst of choice at temperatures up to 200 °C (e.g., PAFC), due to the stability requirements. High dispersion of the catalyst is required, taking into account its nature as a precious metal, to provide a high surface area to volume ratio. Platinum nanoparticles in the diameter range of a few nanometers, typically 2–5 nm, supported on carbon particles are utilized. Different carbons with different surface areas (up to 800 m^2/g) are used. The amount of platinum in the catalyst powder is specified as wt% per g of carbon and further as mg loading per cm^2 of geometric electrode area.

Platinum is prone to CO adsorption at temperatures of around 100 °C and below. For this reason, care has to be taken with respect to the purity of hydrogen, in particular for hydrogen liberated from a C-containing fuel by a reforming process (steam reforming, partial oxidation, autothermal reforming).

Alkaline electrolytes allow cheaper, non-precious metal catalysts like nickel and its alloys.

High temperature fuel cells, e.g., MCFC or SOFC, require other catalyst materials, which are described in the respective section below.

There is a common problem to all material selections for the different fuel cell types, namely, to generate an optimal electrolyte/electrode interface. One has to realize that gaseous molecular reactants are converted into ionic species, solvated/hydrated in their electrolyte medium, by exchanging electrons with the electrode material. This reaction occurs at the so-called triple phase boundary (triple point), where electron conducting, ion conducting, and gas phase (eventually dissolved in the electrolyte) join to each other. To allow a high surface area for current generation, the electrolyte/electrode interface is extended into a three-dimensional *interphase* with a certain thickness. For a polymer electrolyte fuel cell, this *interphase* is drafted in Fig. 7 for the cathode (oxygen) side.

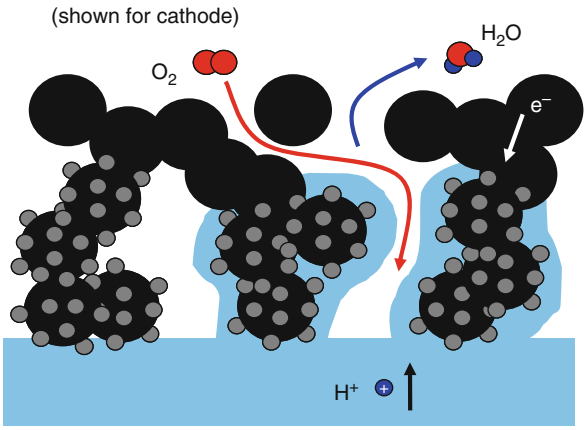

Fuel Cell Types and Their Electrochemistry. Figure 7 Electrode layer (interphase) with three phase boundary (schematic) of a polymer electrolyte fuel cell (cathode side). *Blue*: polymer electrolyte, *black*: carbon particles, *gray*: platinum nanoparticles (Adapted from L. Gubler, Paul Scherrer Institut)

Depending on the respective materials for the different fuel cell types, this three-dimensional inter*ph*ase has to be established by very different preparation/manufacturing procedures. In particular, solid electrolyte materials must be processable to be included into the electrode layer.

Fuel Cell Families

The various fuel cell types considered today having some technical relevance are displayed schematically in Fig. 8. They are arranged according to the nature of electrolyte, acidic or alkaline, and to their temperature of operation.

The polymer electrolyte fuel cell, PEFC, and the phosphoric acid fuel cell, PAFC, are acidic fuel cells; the PEFC operates in the temperature range below and around 100 °C (PEFC), respectively, and the PAFC at around 200 °C. Hydrogen is the preferred fuel for both types. A PEFC can also be fed by liquid or gaseous methanol, called direct methanol fuel cell, DMFC. Other fuels based on alcohols, e.g., the direct ethanol fuel cell, DEFC, are subject to research. Fuel cell types utilizing an acidic aqueous electrolyte will not be considered here.

Most concepts for an alkaline fuel cell in the past have been described with an aqueous alkaline electrolyte. Recently, also anion exchange membranes, alkaline solid polymer electrolytes, have been considered [13].

The molten carbonate fuel cell, MCFC, and the solid oxide fuel cell, SOFC, are high temperature fuel cells, due to their temperatures of operation of around 650 °C, respectively, 800–900 °C. Both can be considered as alkaline fuel cells.

The local appearance of the reaction product is determined by the current-carrying ion. While for acidic fuel cells the reaction product shows up at the cathode (oxidant side), it is the anode (fuel side) for alkaline fuel cells. In case of C-containing fuels, e.g., methanol, a second reaction product containing the oxidized carbon appears at the fuel side. The appearance and hence the removal of the product/s causes consequences for the mass flow engineering of the stack and fuel cell system.

The following ordering of fuel cell types does not reflect the historical development of the various fuel cell technologies.

Polymer Electrolyte Fuel Cell Types

The idea of using a thin ion-conducting polymer membrane, *solid polymer electrolyte*, as electrolyte and separator can lead to different concepts of cells. Firstly, when ionic charges, anions or cations, are chemically bound to the polymer (ionomer) network, the respective countercharge can move freely within the polymer volume, provided a certain volumetric charge density within the polymer exists, which on uptake of, e.g., water leads to phase separation into a hydrophobic polymer (backbone) and a hydrophilic, charge-containing phase [14]. As a consequence, the polymer morphology allows the continuous transport of this ion from one electrode interphase to the other. This concept is normally called polymer electrolyte fuel cell (PEFC).

Depending on the fuel, H_2, MeOH (gas or liquid), or others, the solid polymer electrolyte properties have to be tailored, in particular for their properties toward separation of fuel and oxidant.

Further, non-ionomeric polymers can absorb an electrolyte, e.g., phosphoric acid H_3PO_4, which then renders ion conducting. This concept is realized in the so-called HT-PEFC, high temperature PEFC (ca. 100–200 °C), where a polybenzimidazole film

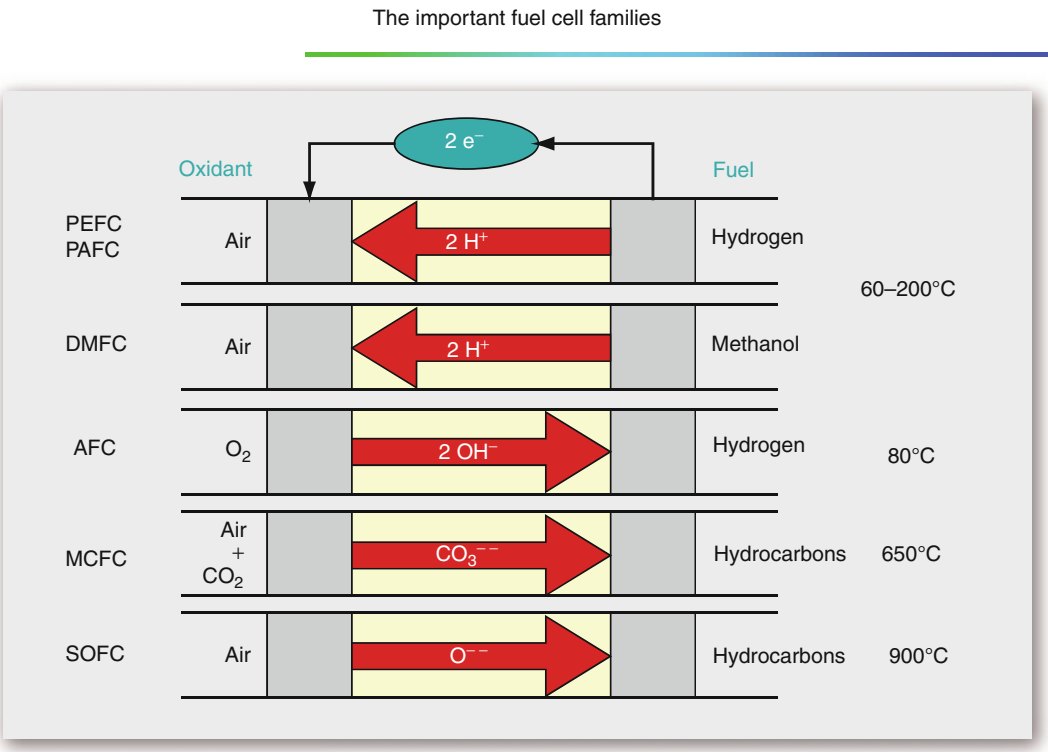

Fuel Cell Types and Their Electrochemistry. Figure 8
The important fuel cell families of today

imbibed with phosphoric acid becomes proton conducting due to the mechanism described above for non-aqueous phosphoric acid (see this book, Chapter Benicewicz).

H_2-Fed PEFC This type of H_2-fed fuel cell, due to its high achievable specific and volumetric power density (in the range of 1 kW/kg and 1 kW/L and above), its cold start behavior, and its fast load following properties, has found interest in the automotive industry and is under development by all major automotive companies.

A thin ion-conducting polymer sheet, typically in the range of 25 μm, is utilized as a solid electrolyte, i.e., electrolyte and separator, in the PEFC (Fig. 1). For thermal stability reasons, only cation exchange membranes in the H^+ form have been considered up to today for technical applications (see also "Alkaline Fuel Cell"). In comparison to cells with liquid electrolyte, this PEFC concept offers the advantage that the "electrolyte" is chemically bound within the polymer matrix and only water as reactant, in addition to the gases, appears in the peripheral system components. Membranes are perfluorinated or partially fluorinated polymers, with side chains ending in pendant acid groups, e.g., the sulfonic acid group $-SO_3H$ (Fig. 9).

Under operation, the membrane has to contain some water, e.g., 15 water molecules per sulfonic acid group, to provide the necessary specific conductivity. This fact causes consequences for some of the system auxiliaries, as the gases, hydrogen and air, have to be humidified before flowing into the cell to sustain the hydration level in the membrane.

The acidic electrolyte requires a precious metal catalyst; hence platinum supported on carbon particles serves as electrocatalyst, with typical Pt loadings of ca. 0.1 mg/cm^2 at the anode side and ca. 0.4 mg/cm^2 at the cathode side. Platinum nanoparticles, typically a few (3–5) nanometers in diameter, are deposited on various carbon substrates (e.g., 20–40%Pt/C) by wet chemical

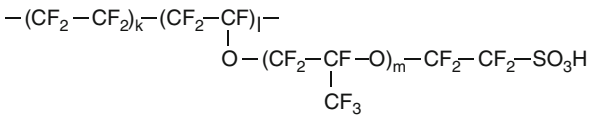

Fuel Cell Types and Their Electrochemistry. Figure 9 Generalized structure formula of Nafion® type membranes (DuPont) with m = 1, l = 1, k = 5–7

processes and then further processed in combination with solubilized ionomer material and binder(s) (PTFE) to yield an ink, which then is applied either to the electrolyte membrane surface (CCM, catalyst-coated membrane) or to the GDL to form the GDE.

Extensive characterization of these electrocatalysts for the fuel cell reactions has shown that the electrocatalytic activity of these nanoparticles is by a factor 10 lower than the activity of a polycrystalline platinum surface for the respective reactions, HOR or ORR [15]. This difference is not fully understood yet.

An interesting proprietary approach has been followed recently by the 3 M Company, creating a continuous electrode area covered by nanoscale Pt whiskers. Reactivity of these electrocatalytic layers is in the range of polycrystalline platinum surfaces [16].

Today, pure hydrogen is considered as the ideal fuel. Due to its CO content, hydrogen derived from C-containing fuels (by steam reforming (SR), partial oxidation (POX), or autothermal reforming (ATR) followed by preferential oxidation (PROX)) would need specific measures in terms of electrocatalysis, e.g., PtRu as bifunctional electrocatalyst, to allow oxidation of CO. As an alternative, purification methods of the anode gas stream prior to entering the cell down to only a few parts per million CO (depending on operation temperature) are necessary.

The electrocatalytic layers are contacted by gas diffusion layers, allowing the gases to be passed to the interphase and the product(s), H_2O with H_2 and O_2 as reactants, which consist of carbon cloth or paper (Fig. 2). This arrangement of membrane, electrocatalytic layers, and gas diffusion layers is colloquially called membrane electrode assembly (MEA).

Most of the applications of this fuel cell type are developed for air operation, taking advantage of utilizing one reactant from the ambient environment. However, there exist also some applications in which pure oxygen is employed as oxidant. Due to the higher partial pressure of oxygen and the absence of electrochemically inert nitrogen as the majority component in the cathodic gas stream, humidification issues of the cell can be strongly simplified [17, 18].

Methanol-Fed Fuel Cell (PEFC Type) The same concept of combination of an acidic solid polymer electrolyte and acid stable precious metal electrocatalysts can also be applied to a methanol-fed fuel cell (direct methanol fuel cell, DMFC). Methanol can be fed in liquid or vapor form, mixed with water. The methanol molecule CH_3OH is electrochemically converted at the anode:

$$\textbf{Anodic reaction}: \mathbf{CH_3OH + H_2O = 6H + 6e^- + CO_2} \quad \text{(methanol oxidation reaction, MOR)}$$

$$\textbf{Cathodic reaction}: \mathbf{O_2 + 4H^+ + 4e^- = 2H_2O} \quad \text{(oxygen reduction reaction, ORR)}$$

$$\textbf{Overall reaction}: \mathbf{CH_3OH + H_2O + O_2 = CO_2 + 3H_2O}$$

As seen above, during MOR, one molecule of water is consumed, which is necessary to oxidize carbon in the CH_3OH molecule to CO_2, while potentially six protons are liberated. The ORR can be formulated the same way as in a hydrogen-fed cell.

The equilibrium potential for the anode reaction is 0.02 V; hence, a theoretical cell voltage close to the H_2/O_2 fuel cell should be observed. In practice, the OCV is lower, for several reasons: Due to the similarity of methanol and water as solvents (e.g., solubility parameter), methanol also penetrates into the water-swollen polymer membrane and passes to the cathode (methanol crossover), causing a mixed potential at a lower value than the oxygen potential. Further, the anode reaction requires a binary or ternary bifunctional catalyst, containing next to platinum one metal component (or two) providing the splitting reaction of the water molecule involved to liberate oxygen for the carbon oxidation at lower potentials as compared to platinum. Examples would be Ru, Sn, Mo, others, or even combinations of two of these together with platinum as the hydrogen-liberating catalyst. Intermediate oxidation species of the methanol molecule, e.g., –COH, may adsorb and poison the platinum catalyst surface, thereby impeding the full oxidation reaction.

These kinetic losses at the anode lead to a high anode overvoltage and, therefore, the cell voltage in

the DMFC is lower at a respective value of current density as compared to a H_2-fed cell, as is the achievable power density.

Direct methanol fuel cell concepts with liquid electrolyte have also been considered in the past. One advantage of circulating liquid electrolytes is the option to cool the cell without additional cooling fluid.

High Temperature PEFC As mentioned above, H_3PO_4 can be absorbed in polybenzimidazole films to yield water-free proton-conducting membranes. The concept is strongly related to the phosphoric acid fuel cell, PAFC. These cells can be operated above 100 °C, typically in the temperature range of 160–180 °C, without humidification, allowing to simplify the balance of plant. Further, due to the higher operation temperature as compared to H_2-fed cells, CO tolerance is drastically increased. Disadvantages are the loss of H_3PO_4 during start-stop cycles, i.e., excursions to temperatures below 100 °C, where liquid product water causes leaching of the ionic component. In addition, achievable power densities are typically lower than with H_2-fed cells, due to the fact that phosphate cations strongly adsorb on platinum even at these temperatures, impeding the ORR. For more detailed information please see chapter "Benicewicz".

Phosphoric Acid Fuel Cell

Looking back at the development of fuel cell technologies, the PAFC technology has been the earliest one to be commercialized. Several 200 kW_e power units for co-generation have been delivered to customers over the past 20 years, mainly by the US company UTC Power [19]. Water-free phosphoric acid is absorbed in an inorganic diaphragm and contacted on both sides by platinum-containing gas diffusion electrodes. Advantages and disadvantages are very similar to the ones of the HT-PEFC.

Alkaline Fuel Cell

Alkaline electrolytes played an important role in the beginning of fuel cell development, due to its less stringent requirements for electrocatalysts. An aqueous solution of NaOH or KOH at higher concentration is absorbed in a matrix, formerly asbestos, today a composite material of an oxide and a polymer binder. The electrochemistry of the respective HOR and ORR can be written the following way:

$$\textbf{Anodic reaction}: \mathbf{H_2 + 2OH^- = 2H_2O + 2e^-} \quad \text{(hydrogen oxidation reaction, HOR)}$$

$$\textbf{Cathodic reaction}: \mathbf{1/2O_2 + 2H_2O + 2e^- = 2OH^-} \quad \text{(oxygen reduction reaction, ORR)}$$

$$\textbf{Overall reaction}: \mathbf{H_2 + {}^1\!/_2O_2 = H_2O}$$

As described above, an alkaline cell generally has to be operated on H_2 and O_2, due to the CO_2 problem. As advantage, a non-precious metal, such as Raney nickel, can serve as electrode material. ORR in alkaline solution shows a lower overpotential loss than in acidic solution; hence, higher specific power densities (mW/cm^2) can be generated in cells.

Recently, some progress in the preparation of anion exchange membranes was reported, leading to the application of the PEFC concept to alkaline fuel cells. However, performance in terms of power output and stability/lifetime is far below the acidic technology [13].

Molten Carbonate Fuel Cell

As a high temperature fuel cell, which operates in the temperature range around 650 °C, the MCFC can use the waste heat of the fuel cell reactions for internal reforming of C-containing fuels (Fig. 10). No further processing of the reformed fuel is necessary. Reformed hydrogen is oxidized at the anode, consisting of a porous nickel electrode, under consumption of the CO_3^{2-} cation, which carries the current through the electrolyte, to H_2O and CO_2. The anode reaction product CO_2 has to be recycled to the cathode compartment, where it is consumed during the ORR at a porous Ni-Oxide cathode to CO_3^{2-} and taken up by the electrolyte melt again, therefore balancing the CO_3^{2-} concentration in the Li_2CO_3/K_2CO_3 eutectic electrolyte, which is absorbed in a $LiAlO_2$ matrix.

MCFC systems in the power range of 250 kW have been delivered for on-site testing, using a variety of fuels, like biogas, reformed natural gas, and others [20].

Solid Oxide Fuel Cell

The electrolyte in a solid oxide fuel cell is a thin ceramic body, which is an O_2-conducting oxide material.

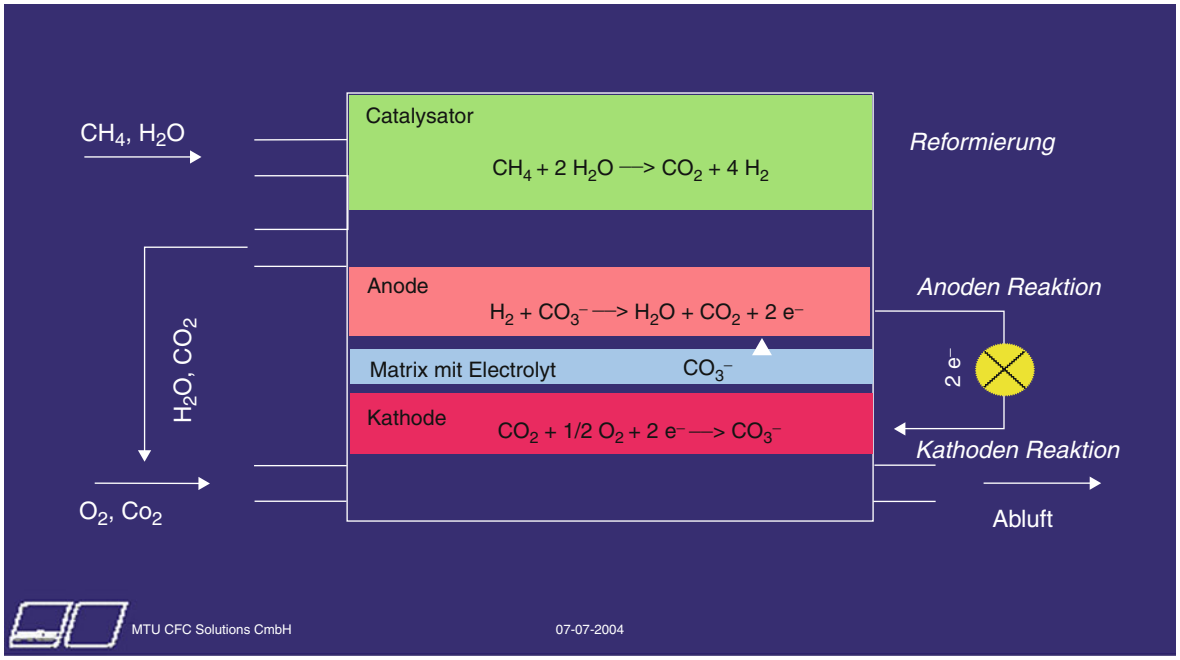

Fuel Cell Types and Their Electrochemistry. Figure 10
Scheme of the molten carbonate fuel cell, MCFC (Adapted from MTU CFC Solutions)

O^{2-} conduction is established by doping a stoichiometric material like ZrO_2 by Y_2O_3, thereby generating O^{2-} vacancies in the lattice. Around 8% of Y_2O_3 are required to stabilize the cubic form of ZrO_2 at temperature of operation. A reasonable specific conductivity for this 8YSZ material is obtained in the range of and above 800 °C (Fig. 11).

Electrode materials consist of a Ni/8YSZ cermet (mixture of ceramic and metal) as anode and $La_xSr_yMnO_3$ (perovskite) as cathode.

Ohmic losses in the electrolyte can be lowered by designing cells with thin electrolyte layers, typically 10 µm thick, supported on one of the electrode structures, instead of utilizing a thicker, free-standing electrolyte layer.

For many years, also a tubular concept had been developed by Siemens Westinghouse, addressing the challenges in matching the thermal expansion coefficients of the different materials, namely for the electrolyte and the electrodes. However, the further development of this concept had been abandoned. SOFC technology development mainly addresses stationary co-generation of power and heat, at a power scale of 100 kWe and more (e.g., Topsoe Fuel Cell, Denmark), as well as small scale (1 kW_e) co-generation for private homes (e.g., Hexis Switzerland).

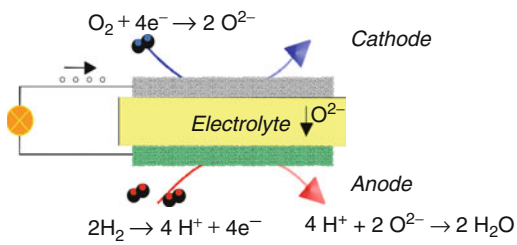

Fuel Cell Types and Their Electrochemistry. Figure 11
Scheme of the planar solid oxide fuel cell, SOFC, and its electrochemistry (Adapted from L. Gauckler, ETH Zürich)

Interestingly, low power application micro-SOFCs are developed as battery alternatives, utilizing materials which allow operation temperatures in the range of 550 °C (One-Bat-Project, ETZ Zürich [21]).

Future Directions

After two decades of intensive fuel cell research and development, some of the described technologies have

come close to the market. This is particularly the case for the PEFC technology developed worldwide by automotive industry. Market introduction is planned, according to various sources, by the year 2015. However, still issues of cost and reliability remain and provide ample space for further research. Unfortunately, other technologies, e.g., the SOFC and MCFC technology, have recently seen some setbacks, due to the fact that some longstanding prominent advocates of fuel cell development have decided not to continue their effort (e.g., SOFC by Siemens, MCFC by Tognum (formerly MCFC solutions), others).

Bibliography

1. International Energy Agency (2011) Clean energy progress report, updated June 2011. International Energy Agency, Paris
2. OECD (2004) Hydrogen and fuel cells, review of National R&D Programs. International Energy Agency/OECD, Paris. ISBN 9789264108837
3. Shell International BV (2011) Shell energy scenarios to 2050, an era of volatile transitions. Shell International BV, The Hague. http://www-static.shell.com/static/aboutshell/downloads/aboutshell/signals_signposts.pdf
4. http://www.peakoil.net/
5. http://www.roads2hy.com/pub_download.asp?PageIndex=1
6. e.g., http://www.sfc.com/en/
7. Bossel U (2000) The birth of the fuel cell. European Fuel Cell Forum, Oberrohrdorf. ISBN 3-905592-06-1
8. Scherer GG (1990) Ber Bunsenges Phys Chem 94:1008
9. Hamman CH, Hamnett A, Vielstich W (1998) Electrochemistry. Wiley, Weinheim
10. Appleby AJ (1994) J Power Sources 49:15
11. Uchida H, Tanaka S, Iwahara H (1985) J Appl Electrochem 15:93
12. Haile SM (2003) Acta Mater 51:5981
13. Merle G, Wessling M, Nijmeijer K (2011) J Membr Sci 377:1
14. Kreuer K-D (2007) Proton conduction in fuel cells. In: Limbach HH, Schowen RL, Hynes JT, Klinman JP (eds) Hydrogen-transfer reactions, vol 1. Wiley, New York, pp 709–736
15. Gasteiger HA, Kocha SS, Sompali B, Wagner FT (2005) Appl Catal B Environ 56:9
16. http://www1.eere.energy.gov/hydrogenandfuelcells//pdfs/merit03/72_3m_mark_debe.pdf
17. http://info.industry.siemens.com/data/presse/docs/m1-isfb07033403e.pdf
18. Büchi FN, Paganelli G, Dietrich P, Laurent D, Tsukada A, Varenne P, Delfino A, Kötz R, Freunberger SA, Magne P-A, Walser D, Olsommer D (2007) Fuel Cells 07:329. doi:dx.doi.org
19. http://www.utcpower.com/products/purecell400
20. http://www.fuelcellenergy.com/
21. http://www.nonmet.mat.ethz.ch/research/onebat

Fuel Cells (SOFC): Alternative Approaches (Electroytes, Electrodes, Fuels)

K. Sasaki[1,2,3], Y. Nojiri[1], Y. Shiratori[1,2,3], S. Taniguchi[1]
[1]International Research Center for Hydrogen Energy, Kyushu University, Fukuoka, Japan
[2]International Institute for Carbon-Neutral Energy Research (WPI), Kyushu University, Fukuoka, Japan
[3]Faculty of Engineering, Kyushu University, Fukuoka, Japan

Article Outline

Glossary
Definition of the Subject
Introduction
Alternative Electrolyte Materials
Alternative Electrode Materials
Alternative Fuels
Future Directions
Acknowledgments
Bibliography

Glossary

Anode Electrode for electrochemical oxidation reactions. In solid oxide fuel cells, hydrogen-containing fuels are oxidized by oxygen ions transported through an electrolyte to form water vapor or CO_2 as the reaction products at this electrode. SOFC anodes may also act as fuel reforming catalysts when hydrocarbon-based fuels are supplied to the anodes.

Cathode Electrode for electrochemical reduction reactions. In solid oxide fuel cells, oxygen in ambient air is reduced to oxygen ions at this electrode.

Electrolyte Ionic conductor with negligible electronic conductivity, used as a membrane between an oxidation atmosphere and a reduction atmosphere. The essential material to construct electrochemical devices including fuel cells.

Fuel flexibility While low-temperature fuel cells (such as polymer electrolyte membrane fuel cells) typically use pure hydrogen gas (or hydrogen gas mixed with CO_2) as the fuel, high-temperature fuel cells

can directly use various kinds of fuels, such as carbon monoxide (CO), which is created by reforming hydrocarbons at the anode to produce hydrogen and carbon monoxide.

Impurity poisoning Even though high-temperature fuel cells have good fuel flexibility with various kinds of fuels, some minor constituents (impurities) coming from, for example, low-purity fuels, raw materials, and system components can also react with electrode materials or can be adsorbed on the electrode reaction sites, hindering electrode reactions. Such poisoning phenomena can lead to fuel cell performance degradation with time.

Mixed ionic electronic conductor Materials with both high ionic conductivity and high electronic conductivity. Such materials are often attractive for electrodes because of extension of electrochemical reaction sites beyond electrode/electrolyte interface.

Oxygen ionic conductor Materials with high oxygen ionic conductivity. Oxides with both high oxygen vacancy (or other charge carrier such as interstitial oxygen atoms) concentration and high oxygen mobility exhibit high ionic conductivities.

Protonic conductor Materials with high protonic conductivity. In the presence of oxygen vacancies, water vapor may be dissolved into oxides forming protons and exhibiting high protonic conductivity.

Definition of the Subject

While we may realize commercialization of SOFC systems in the very near future, continuous challenges will be needed to develop advanced fuel cells with higher efficiency, higher durability, better flexibility, as well as lower production cost. For realizing next-generation SOFCs, we may apply a broad range of knowledge related to (1) electrolyte and (2) electrode materials for cell development as well as (3) explore alternative fuels. This entry gives an overview on possible alternative approaches for these three important aspects to realize advanced high-performance SOFCs in a future generation.

Introduction

Fuel cells, environmentally compatible energy systems using hydrogen-containing fuels [1–5], are strongly desired as promising key technologies to realize a sustainable low-carbon society. Compared to internal combustion, electrochemical energy conversion by fuel cells can achieve much higher efficiency. While the direct electrochemical conversion of chemical energy to electricity using fuel cells has received significant attention for several decades, mass marketing of fuel cell systems is often limited by insufficient performance and/or inadequate durability in service.

While the commercialization of fuel cell technologies has just begun in the form of, for example, stationary cogeneration power units mainly based on polymer electrolyte fuel cells for private houses, a broad variety of other application is strongly desired. Even though solid oxide fuel cells (SOFCs) are the most efficient type of fuel cells, partly due to their higher operational temperature compatible with internal reforming of hydrocarbon-based fuels, their application has often been restricted by the limited operational range of electrolyte and electrode materials [1–3]. Although many current research projects tend to focus on engineering and optimization issues related to cost reduction, durability, and reliability [6–8], in order to take SOFCs closer to full-scale commercialization, breakthroughs in materials and concepts are needed for developing viable fuel cells for broader application. It is therefore essential to consider alternative materials for electrolytes and electrodes and innovative fuel cell concepts including the use of alternative fuels for future-generation fuel cells. For example, alternative electrolyte/electrode materials for lower-temperature SOFCs are needed to improve electrical efficiency in low-power operation, tolerance against thermal cycling, as well as improve longer-term durability. They will help realize alternative fuel cells in real commercial systems. Additionally, morphological control on the nano-scale shows promise in enhancing ionic and electronic transport in nano-ionic systems [9–14], offering an additional degree of freedom in material/device design. A reversing challenge is to harness these effects to the fabrication of practical SOFCs with improved performance.

Alternative device concepts can help realize broader application of SOFCs. SOFCs for automotive applications will enable multi-fuel vehicles capable of being powered by both hydrogen and hydrocarbon fuels. The use of biogas can result in carbon-neutral energy

conversion. The use of hydrocarbon fuels and gasified coal gas fuel for SOFCs will achieve more efficient use of such fossil fuels. Portable SOFCs operating with hydrogen, hydrocarbon fuels [15, 16], and solid carbon [17] are attractive as replacements for batteries. Reversible SOFCs can act as both power units and electrolyzers, efficiently converting excess heat and electricity into hydrogen and vice versa [18–20]. If these technologies with SOFCs are realized, a considerable reduction in CO_2 emissions is possible in household, industrial, and transportation sectors.

It is therefore interesting and essential to consider such material/device issues in SOFC R&D to realize future flexible SOFCs with broader application. In this entry, an overview will be given on alternative approaches to SOFCs related to the following three critical material-related issues: electrolytes, electrodes, and fuels.

Alternative Electrolyte Materials

Electrolyte Materials: General

As the ionic conductivity of solid electrolytes is generally much lower than the electronic conductivity of electrode materials, the ionic conductivity of the solid electrolytes may determine the lowest possible operational temperature of SOFCs. Apart from high ionic conductivity, the following properties are required:

1. High ionic transference number around unity
2. Thermochemical stability in both oxidation and reduction atmospheres
3. Near theoretical density for minimum gas leakage
4. High compatibility with other materials in composite device
5. Match of thermal expansion coefficient with other components with minimal defect-induced chemical expansion

In addition, high mechanical strength and reasonable materials cost are required in the case of electrolyte-supported cells.

There are limited numbers of materials satisfying the above-mentioned criteria. Generally, Y_2O_3-stabilized ZrO_2 (YSZ) is commonly used at high temperatures, that is, $T > 800°C$ to maintain ionic conductance, while thin-film ZrO_2-based electrolytes may be applied for operational temperatures around 700°C. For much lower operational temperatures, alternative electrolyte materials are needed. Ionic conductivity depends strongly on the crystal structure, and oxides with high ionic conductivity have been found among open crystal structures, such as fluorite, pyrochlore, rare-earth, perovskite, and related structures [21, 22].

Oxygen Ionic Conductors

Fluorite-Type Materials

General The fluorite structure is relatively open, and it shows exceptional tolerance for high levels of atomic disorder, which may be introduced either by doping, reduction, or oxidation [23]. Among the binary oxides, CeO_2, Pr_6O_{11}, ThO_2, UO_2, and PuO_2 possess this structure in the pure state in ambient conditions. ZrO_2 and HfO_2 are stabilized in the fluorite structure by doping with divalent or trivalent oxides (Y, Sc, rare-earth oxides) [23–25]. Beyond stabilization, the addition of such dopants gives rise to the creation of oxygen vacancies responsible for the ionic conduction in these oxides.

Several fluorite-type oxides are known to be excellent oxygen ionic conductors, including δ-Bi_2O_3, CeO_2, ZrO_2, ThO_2, and HfO_2. The δ-Bi_2O_3 phase possesses an anion-deficient fluorite structure where one-fourth of the normal fluorite anion sites are vacant. This phase exhibits an order to disorder transition above ~600°C (which can be suppressed to some extent through doping) with a consequent increase in conductivity and has the highest oxygen ionic conductivity so far reported for a solid electrolyte [21, 22]. However, δ-Bi_2O_3 shows poor thermochemical stability, and it is easily reduced at high temperatures. ThO_2 is a radioactive material. HfO_2 has chemical similarity to ZrO_2 but is relatively expensive. Practically available fluorite-type oxides for solid electrolyte are thus limited to ZrO_2 and CeO_2. Most of the rare-earths, as well as Sc, In, and Y, are trivalent and form sesquioxides of various crystal structures with potential for solid electrolyte membranes. Most of them have the cubic C-type structure (Sm_2O_3, Dy_2O_3, Er_2O_3, Sc_2O_3, Y_2O_3, and In_2O_3) which is closely related to the fluorite structure [23], which can be derived from the fluorite structure by removing one-fourth of the oxygen atoms which lie along the four <111> directions [23]. SrO-doped La_2O_3 exhibits

ionic conductivity close to the Y_2O_3-doped ZrO_2 electrolyte [21, 22]. However, most of these sesquioxides are mixed ionic and electronic conductors with a substantial electronic conductivity [23, 26–29].

ZrO_2-Based Oxide Pure ZrO_2 exhibits phase changes from monoclinic to tetragonal and cubic, with increasing temperature. Due to its volume change of ca. 5% in the phase transition from monoclinic to tetragonal, pure ZrO_2 cannot be used as a practical solid electrolyte material. Group 2 elements of the periodic table or rare-earth elements may be added to stabilize the cubic phase at high temperatures and keep this phase stable also at lower temperatures. As for stabilized ZrO_2 with dopants from the group 2 elements, CaO-stabilized ZrO_2 is widely used mainly for Nernst-type oxygen sensors [30], but it is not used for fuel cells because of its relatively low conductivity [31]. On the other hand, stabilized ZrO_2 using dopants from rare-earth elements such as Y_2O_3, Sc_2O_3, Yb_2O_3, In_2O_3, and Er_2O_3 [21, 22, 32, 33] exhibits higher conductivity suitable for SOFC [34–38]. Ionic conductivity (intragrain conductivity) of ZrO_2 doped with (a) Y_2O_3, (b) Yb_2O_3, (c) Er_2O_3, (d) In_2O_3, and (e) Sc_2O_3 measured by impedance spectroscopy is shown in Fig. 1 [33]. In addition, activation energy values for the intragrain ionic conductivity of these doped ZrO_2, $\sigma_{ion}(\mathrm{S/m}) \times T(\mathrm{K}) = \sigma_o(\mathrm{S/m}) \times \exp(-\Delta E_\sigma\ (\mathrm{eV})/kT)$, are compiled in Table 1.

Yttria-stabilized ZrO_2, discovered by Nernst [39], is still one of the state-of-the-art SOFC electrolyte materials which was used to demonstrate the first SOFC (and the first solid "electrolyte" fuel cell) in 1937 at ETH-Zürich [40]. Electronic defect concentrations are negligibly low [41]. As can be observed in Fig. 1, the ionic conductivity of fluorite-type oxides stabilized with hypovalent elements exhibits a maximum at a certain dopant concentration above which defect interactions occur [42–45]. As shown in Fig. 2, it is known that the peak value of the ionic conductivity becomes higher when the ionic radius of the dopant approaches that of Zr^{4+} [35], resulting in minimal distortion of the fluorite lattice. Ionic conductivity is the highest in the case of Sc^{3+}, which is used as a dopant because its ionic radius is almost identical to that of Zr^{4+} [46]. However, Sc_2O_3 is more expensive than Y_2O_3, but Sc_2O_3-stabilized ZrO_2 (ScSZ) has recently become more widely used. In addition, ScSZ with 8 mol% Sc_2O_3 exhibited a high conductivity in the early stages of operation, but the conductivity decreased with operational time due to phase instability [47]. To prevent this decrease in ionic conductivity, ScSZ with 11 mol% Sc_2O_3 was preferably used, but this material had a problem of phase transition in the vicinity of 700°C [35, 48]. Currently, ScSZ with the addition of CeO_2, such as $(ZrO_2)_{0.89}(Sc_2O_3)_{0.1}(CeO_2)_{0.01}$, is widely used to suppress this phase transition [46, 49].

In addition, tetragonal ZrO_2 and partially stabilized ZrO_2 can also be used as an electrolyte due to their better mechanical properties and their lower activation energy for ionic conductivity. Since the grain size of the tetragonal phase is generally much smaller than that of the cubic phase and grain boundaries impede oxide ion migration, the reduction of grain boundary resistivity is important [50]. Stability of the tetragonal phase for longer time periods should be considered to prevent phase transition from the tetragonal phase to the monoclinic phase when applying this material to SOFC systems.

Thin-film technology can also help to realize lower operational temperatures in SOFCs by taking advantage of short transport distance of ions. It is also possible to produce thin-film electrolytes using stabilized ZrO_2, which enables lower-temperature operation of SOFCs because of its stability in both the oxidation and reduction atmospheres, its sinterability, and its high mechanical strength. Ultrathin YSZ electrolyte layers can be prepared on Si or glass ceramic substrates [15, 16, 51], which can realize, for example, lower temperature operation of micro-SOFCs for portable applications. Figure 3 shows an SEM cross-sectional view of a micro-SOFC prepared on a glass ceramic substrate with a YSZ electrolyte thickness of less than 1 μm, as reported by Bieberle–Hütter et al. [51].

Stabilized ZrO_2 exhibits good chemical compatibility with other materials during SOFC operation below 1,000°C. It is possible that stabilized ZrO_2 solid electrolyte reacts with other materials during the cell fabrication processes which often require high temperatures in excess of 1,300°C. YSZ does react with $La_{1-x}Sr_xMnO_{3-\delta}$ (LSM), the state-of-the-art cathode material, to produce $La_2Zr_2O_7$ or $SrZrO_3$ at temperatures above 1,100°C, with a consequential

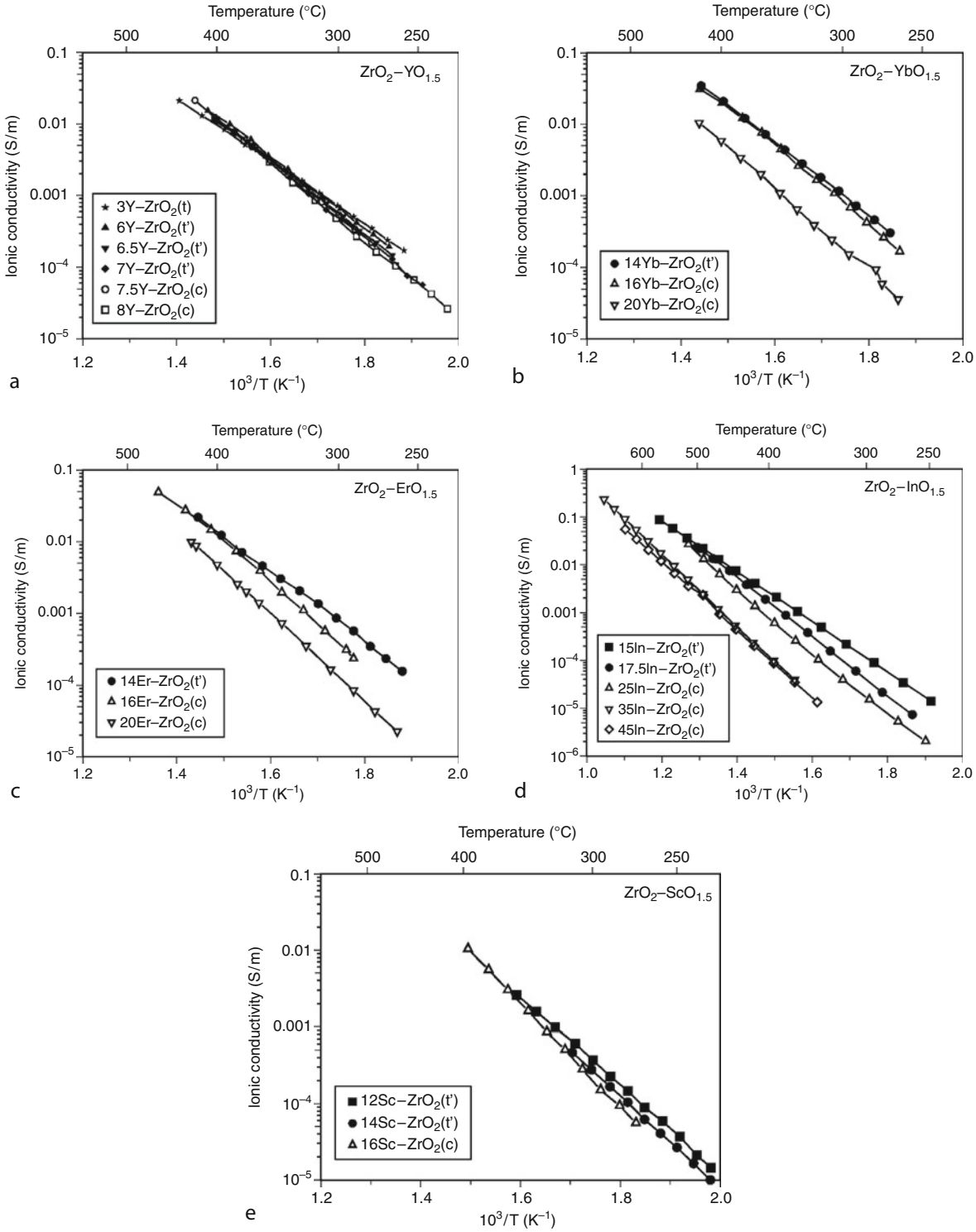

Fuel Cells (SOFC): Alternative Approaches (Electroytes, Electrodes, Fuels). Figure 1
Intragrain conductivity of ZrO_2 doped with (**a**) Y_2O_3, (**b**) Yb_2O_3, (**c**) Er_2O_3, (**d**) In_2O_3, and (**e**) Sc_2O_3 measured by impedance spectroscopy, where t and c denote tetragonal and cubic phases [33]

Fuel Cells (SOFC): Alternative Approaches (Electroytes, Electrodes, Fuels). Table 1 Activation energies and pre-exponential factors of ionic conductivity of ZrO_2 doped with trivalent metal oxides (Y_2O_3, Yb_2O_3, Er_2O_3, In_2O_3, Sc_2O_3) [33], based on the relation $\sigma_{ion}(S/m) \times T(K) = \sigma_o(S/m) \times \exp(-\Delta E_\sigma\ (eV)/kT)$, where t and c denote tetragonal and cubic phases

Dopant	mol%(phase)	Intragrain conductivity	
		ΔEσ(eV)	σ0
$YO_{1.5}$	5.8 (t)^{fc}	0.91	5.11×10^7
	11.2 (t′)	1.04	5.49×10^8
	12.0 (t′)	1.06	6.93×10^8
	12.7 (t′)	1.10	1.34×10^9
	13.5 (c)	1.09	1.20×10^9
	14.3 (c)	1.12	1.69×10^9
$Yb_{1.5}$	14(t′)	1.07	1.43×10^9
	16 (c)	1.13	3.66×10^9
	20 (c)	1.19	3.74×10^9
$ErO_{1.5}$	14 (t′)	1.02	3.86×10^8
	16 (c)	1.20	7.51×10^9
	20 (c)	1.25	7.74×10^9
$InO_{1.5}$	15 (t)	0.80	6.39×10^6
	15 (t′)	1.10	2.99×10^8
	17.5 (t′)	1.28	4.29×10^8
	25 (c)	1.35	7.51×10^9
	25 (c)^{fc}	1.22	5.26×10^9
	35 (c)	1.56	3.47×10^{10}
	35 (c)^{fc}	1.14	1.57×10^8
	45 (c)	1.48	8.22×10^9
	45 (c)^{fc}	1.26	1.83×10^9
$ScO_{1.5}$	12 (t′)	1.20	6.94×10^9
	14 (t′)	1.24	1.20×10^{10}
	16 (c)	1.40	2.44×10^{11}

fc furnace cooling at a rate of 10°C/min. *Others*: air quenching

increase in internal cell resistance [52–54]. In the case of $LaCoO_3$- or $LaFeO_3$-based oxide cathode materials, reaction with stabilized ZrO_2 becomes worse, so that CeO_2-based oxides such as Gd_2O_3-doped CeO_2 are generally used as a buffer layer between the ZrO_2-based

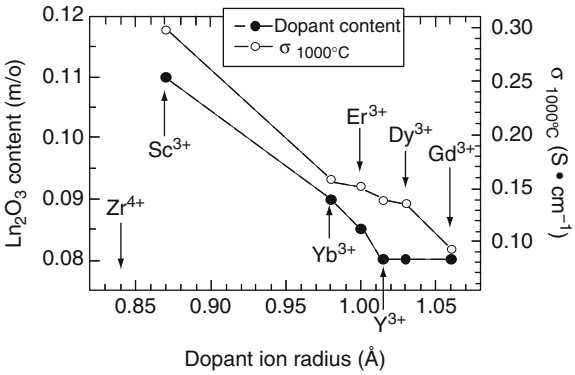

Fuel Cells (SOFC): Alternative Approaches (Electroytes, Electrodes, Fuels). Figure 2
Relation between dopant ionic radius, conductivity, and content of dopant, reported by Arachi et al. [35] (Reproduced by permission of Elsevier)

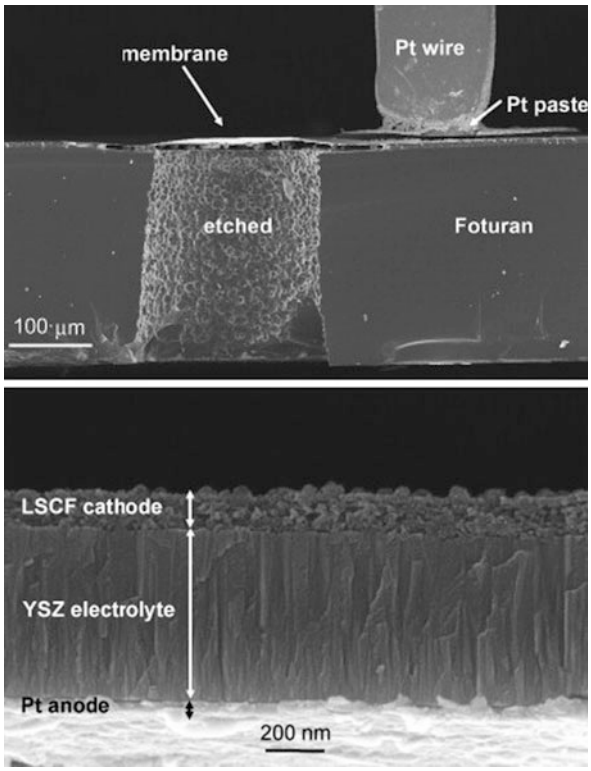

Fuel Cells (SOFC): Alternative Approaches (Electroytes, Electrodes, Fuels). Figure 3
SEM cross-sectional view of a micro-SOFC prepared on a glass ceramic substrate, as reported by Bieberle-Hütter et al. [51] (Reproduced by permission of Elsevier)

electrolyte and such cathode materials to prevent interfacial reactions from forming [3, 55].

CeO_2-Based Oxide CeO_2-based oxide, partially substituted by a hypovalent rare-earth oxide, exhibits high ionic conductivity in a wider range of compositions in comparison to stabilized ZrO_2. This is because even pure CeO_2 has the fluorite-type cubic structure rendering stabilization unnecessary. Like ZrO_2, ionic conductivity of CeO_2 also varies with the substitution of elements. It shows high ionic conductivity when it is partially substituted with alkaline-earth elements such as Ca and Sr [56, 57], and when partially substituted with a rare-earth element, even higher conductivity. As shown in Fig. 4, there is a systematic trend of the conductivity with ionic radius of the substituting element giving the highest conductivity with Sm [58]. Pure Sm_2O_3 has a rare-earth C-type structure, and the similarity of structures between Sm_2O_3 and CeO_2 may lead to high stability. High ionic conductivity can be obtained in a wide range of substitution ratios with Sm_2O_3.

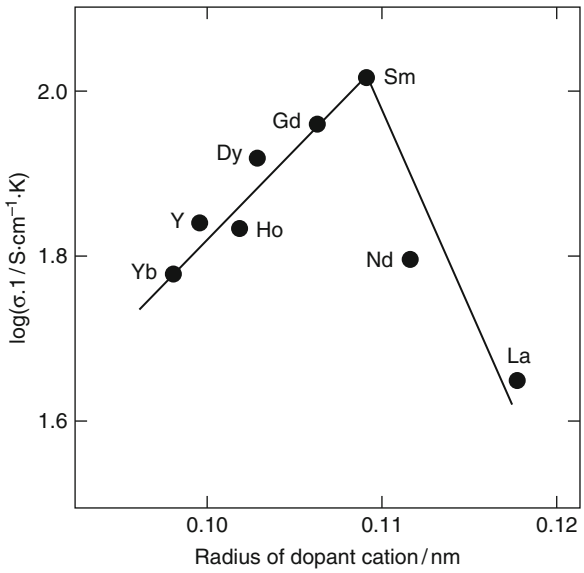

Fuel Cells (SOFC): Alternative Approaches (Electroytes, Electrodes, Fuels). Figure 4
Relationship between the dopant ion radius and the ionic conductivity of doped CeO_2 at 800°C, as reported by Eguchi et al. [58] (Reproduced with permission from Elsevier)

Sm_2O_3-doped CeO_2, usually abbreviated as SDC, with 20 mol% partial substitution of Sm_2O_3, exhibits the highest ionic conductivity. In addition, CeO_2 partially substituted with Gd_2O_3 is also widely used as an electrolyte and, as previously mentioned, interlayer between the stabilized ZrO_2 electrolyte and the cathode, although it shows slightly lower conductivity than SDC [59]. More recently, double doping with Sm and Nd exhibits one of the highest ionic conductivities reported for ceria [60].

When doped CeO_2 is applied as a solid electrolyte for SOFCs, a change in valence state of Ce^{4+} to Ce^{3+} in a reducing atmosphere at the anode results in two main drawbacks. First, it causes n-type electronic conduction in the solid electrolyte which leads to a cell voltage drop. Precisely speaking, when CeO_2 is reduced, both oxygen vacancy and electron are introduced simultaneously. Since the mobility of electrons is much higher than that of oxygen ions, the transference number, that is, the fraction of ionic conductivity from the total, decreases from unity. Second, when lattice oxygen is removed by reduction, the lattice expands, known as chemical expansion. A steep oxygen potential gradient appears in the CeO_2 electrolyte from reducing anode to oxidizing cathode under the operating conditions of SOFCs, and a large mechanical stress in the electrolyte can occur resulting in fracture of the cell [61].

These issues can be overcome partially by using stabilized ZrO_2 as an interlayer between the anode and the electrolyte [62–65]. However, since there is a thermal expansion mismatch between the ZrO_2-based solid electrolyte and the CeO_2-based interlayer, this often causes microscopic fracture [64, 65]. GDC with an addition of Pr ($Ce_{0.8}Gd_{0.18}Pr_{0.02}O_{2-\delta}$) showed enhanced reduction resistance but with the same level of ionic conductivity as SDC [66]. In addition, there have been some attempts to realize lower-temperature operation by fabricating ultrathin membranes of CeO_2 electrolyte materials which contribute to reduce electrical resistance. Electronic conductivity, caused by reduction, decreases with decreasing temperature, but ionic conductivity also decreases simultaneously. Although making thinner solid electrolytes is accompanied with certain difficulties, CeO_2-based electrolytes can be operated at lower temperatures below 600°C, where the influence of electronic conduction caused by the reduction may not be a fatal problem [67].

For example, Oishi et al. [67, 68] have reported stable operation of metal-supported CeO_2-based SOFCs, composed of a porous ferritic stainless steel support, a Ni-$Ce_{0.8}Y_{0.2}O_{1.9}$ anode, a thin $Ce_{0.9}Gd_{0.1}O_{1.95}$ electrolyte, and a $La_{0.6}Sr_{0.4}Co_{0.2}Fe_{0.8}O_3$ cathode, over 1,200 h at 600°C. CeO_2-based electrolyte with a thickness of about 10 μm allows operation of SOFCs at rather low temperatures and selection of ferritic steel as a support material, resulting in enhancement of mechanical strength of cells, improvement of redox stability of cell stacks, and minimization of the use of expensive electrode and electrolyte materials [67, 68]. Considering transport in thin-film CeO_2-based electrolytes, nano-size effects [12] and mixed conduction [62] should be taken into account to tailor transport phenomena in SOFCs.

Pyrochlores and Other Fluorite-Type Oxides (Y, Nb, Zr) $O_{2-\delta}$ Pyrochlore-type oxides have the general formula $A_2^{3+}B_2^{4+}O_7$ in which A is a rare-earth element such as Gd or Y, and B is Ti or Zr. $Gd_2Zr_2O_7$ is the typical composition of pyrochlore-type oxides and can be considered as fluorite-type in which ionic defects are regularly arranged. The defect structure and the mixed conductivity can be controlled by the value of x in, for example, $Gd_2(Zr_xTi_{1-x})_2O_7$, which is abbreviated as GZT [69]. When the ionic radius of rare-earth elements for the A site is larger than that of Gd, the structure changes from highly defective fluorite to pyrochlore [70, 71].

In the $Gd_2Ti_2O_7$ series, relatively high ionic conductivity is obtained at the 20 mol% substitution of Gd sites with Ca [72], though its use as an SOFC solid electrolyte is precluded by its electronic conductivity in air, with an ionic transference number lower than that of YSZ [73]. The thermal expansion coefficient of $Gd_2Ti_2O_7$ (10.4–10.8 $\times$ 10^6 K^{-1}) [73, 74] is close to that of LSGM (10.4 $\times$ 10^6 K^{-1}) [75] and 10ScSZ (10.9 $\times$ 10^6 K^{-1}) [76].

In addition, the solid solution of $Y_4NbO_{8.5}$ and (Y, Nb, Zr)$O_{2-\delta}$ also has the fluorite-related structure, and these materials have stimulated research interest due to their oxide ion conduction [77, 78]. Electrical conductivity of $Y_4NbO_{8.5}$ is independent of the oxygen partial pressure, and it is recognized as an ionic conductor [78]. The ionic conductivity is low, enhancement of conductivity by the addition of Zr was reported, and further improvement of ionic conductivity may be expected [77].

Perovskite-Related Oxides

General Perovskite-type oxides have the general formula ABO_3. The total valence of the A metal and the B metal ions is 6, and various combinations are possible. However, there is a limit to the ionic radius (r) of the constituent metal ions (A and B) and the oxygen ion (O), as the tolerance factor t ($t = \frac{R_A+R_O}{\sqrt{2}\cdot(R_B+R_O)}$) should satisfy $0.75 \leq t \leq 1$ [79, 80]. Oxides related to $LaGaO_3$, $LaAlO_3$, and $Ba_2In_2O_5$ have been well examined as solid electrolyte materials for SOFCs. Takahashi and Iwahara [81] already showed in 1970s that selected perovskite solid solutions exhibited high ionic conductivity around 5×10^{-3} S/m at 800°C [21, 22].

$LaGaO_3$-Based Oxides Oxygen ionic conductivity in perovskite-type-oxide structures has been extensively investigated by Takahashi and Iwahara in their pioneering and detailed studies [81]. High ionic conductivity was observed in the Ti series of perovskite-type oxides. Despite detailed studies, perovskite-type titanate showed poor ionic conductivity compared to that of YSZ. Furthermore, hole conduction was relatively high, so that the ionic transference number was less than unity in oxidizing atmospheres. They also investigated perovskite-type oxides in which trivalent cations were added to both the A site and the B site. $LaCoO_3$ and $LaFeO_3$ are known as such kinds of oxides, but these oxides are mixed conductors with predominately high hole conductivity. However, $LaAlO_3$, with trivalent metal ions on the B site, showed relatively high ionic conductivity [81].

Building on these results, Ishihara et al. [82] attempted to increase lattice cubic volume by applying Ga to the B site which has a slightly larger ionic radius than Al in the La-based perovskite oxides (Fig. 5). They added various dopants, and the highest oxygen ionic conductivity was obtained in the case where 20 mol% of Sr was added to the A site, which has an approximately equal ionic radius to La [82]. As for the dopant on the B site, the highest ionic conductivity was obtained when 20 mol% of Mg was added to the B site ($La_{0.8}Sr_{0.2}Ga_{0.8}Mg_{0.2}O_{2.6}$[83]), since Mg

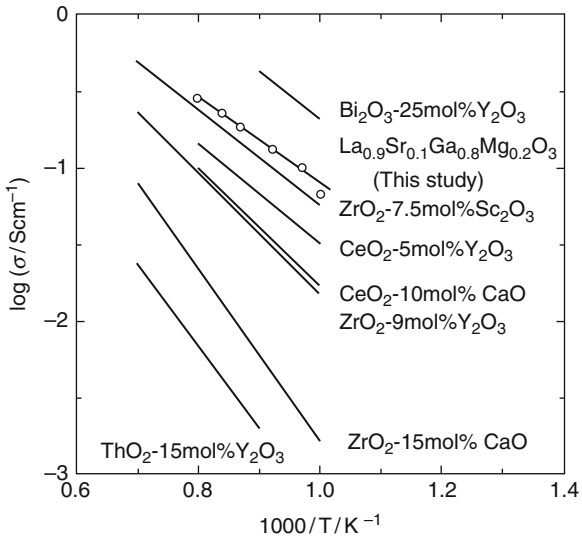

Fuel Cells (SOFC): Alternative Approaches (Electroytes, Electrodes, Fuels). Figure 5
Comparison of the oxygen ionic conductivity of $La_{0.9}Sr_{0.1}Ga_{0.8}Mg_{0.2}O_3$ with conventional oxide ionic conductors with fluorite structures, compiled by Ishihara et al. [82] (Reproduced with permission from American Chemical Society)

is the only element which satisfies the criteria of both ionic radius and low valence number. $La_{0.8}Sr_{0.2}Ga_{0.8}Mg_{0.2}O_{2.6}$ (LSGM) shows the same level of ionic conductivity as GDC at temperatures above 650°C. Electronic conductivity does not become predominant within a wide range of atmospheres from pure oxygen to hydrogen-containing gases [84, 85].

While LSGM exhibits superior properties as an SOFC solid electrolyte, a phase transition from pseudo cubic (monoclinic) to tetragonal was observed at temperatures around 700°C. In order to give high ionic conductivity to this material even below 650°C, the B site was partially substituted with Co, which has a similar ionic radius to Mg ($La_{0.8}Sr_{0.2}Ga_{0.8}Mg_{0.115}Co_{0.085}O_{3-\delta}$, denoted as LSGMC) [84]. The crystalline phase at high temperature was then stabilized, and the phase transition did not occur at temperatures around 700°C, resulting in higher ionic conductivity than that of GDC within a wide temperature range from 500°C to 1,000°C [85]. It was revealed that oxygen ions tend to be trapped around Mg in LSGM [86], and the addition of Co on the B site is effective for preventing such trapping at lower temperatures.

When an $LaGaO_3$-based oxide is applied as a solid electrolyte for SOFCs, reactivity and/or interdiffusion with electrode materials becomes a critical issue. When LSM was used as the cathode material, interdiffusion of Mn into LSGM was observed [87]. When LSCF was used as the cathode material, interdiffusion of Co and Fe into LSGM was also seen [88–90]. A solid-state reaction also occurs at the interface between the Ni-based anode and the LSGM electrolyte due to the similarity of Ni to Co and Mn in the electrolyte materials [91]. There have been some attempts to prevent such solid-state reactions, for example, by optimizing deposition procedures and by applying a CeO_2 interlayer between the LSC cathode and the LSGM electrolyte.

$Ba_2In_2O_5$-Based Oxides The brownmillerite-type oxide has the general formula $A_2B_2O_5$, with the crystal structure presented in Fig. 6. Alkaline-earth metal ions such as Ba occupy the A site, and trivalent typical metal ions such as In occupy the B site [92–99]. At temperatures below 1,140 K, it behaves as a mixed conductor which shows both p-type electronic conductivity and oxygen ionic conductivity due to its oxygen excess [92]. When it is heated to 1,140–1,230 K, ionic conductivity increases, which is associated with the phase transition to the disordered perovskite structure, as shown in Fig. 7 [93]. The ionic transference number also rises drastically to unity.

For example, in the case of $Ba_2In_2O_5$, the typical brownmillerite-type oxide, the disordered perovskite structure can be stabilized, and ionic conductivity in an intermediate-temperature range can be improved by substituting In with another highly charged cation such as Zr, Hf, and Sn [94, 95]. A similar effect can be obtained by the substitution of Ba, as shown in Fig. 8 [93, 96].

$Ba_2In_2O_5$ is stable in the absence of CO_2 but decomposes in the presence of CO_2 in a reducing atmosphere ($p(O_2) = 10^{-9}$–10^{-13} atm), accompanied by the formation of $BaCO_3$. However, in a strongly reducing atmosphere of much lower oxygen partial pressure, In^{3+} is reduced to In^{+}, and the brownmillerite structure cannot be maintained anymore [92, 95, 97–99].

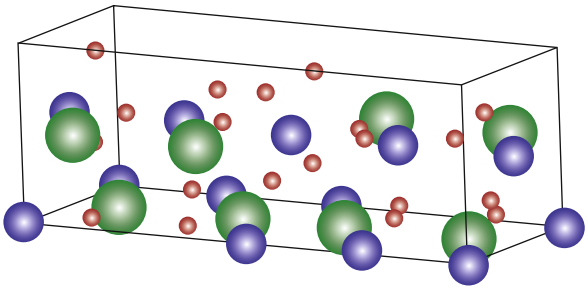

Fuel Cells (SOFC): Alternative Approaches (Electroytes, Electrodes, Fuels). Figure 6
Crystal structure of $Ba_2In_2O_5$ (*Green*: Ba, *Blue*: In, *Red*: O)

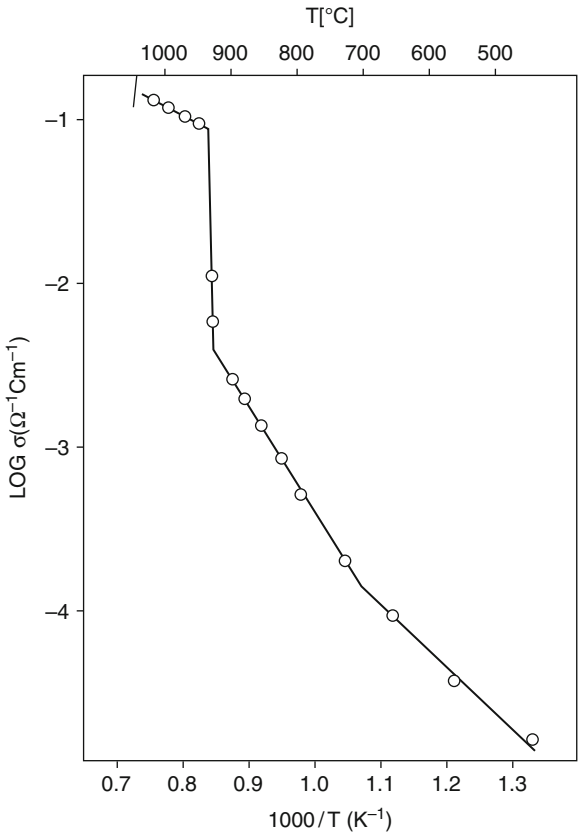

Fuel Cells (SOFC): Alternative Approaches (Electroytes, Electrodes, Fuels). Figure 7
Ionic conductivity of $Ba_2In_2O_5$, reported by Goodenough [93] (Reproduced with permission from Elsevier)

Apatite-Type Oxides

General Apatite is a generic name for minerals with the composition $A_{10}(MO_4)_6X_2$ [100–102]. Generally, the A site can be occupied by alkaline, alkaline-earth, or rare-earth metal ions. The M site can be occupied by elements such as P, Si, and Ge which can have a coordination number of 4. The M site can be partially substituted with transition metal ions. The X site can be occupied by O, OH, F, Cl, and CO_3, etc. Moreover, the A-site cations are divided into two kinds: one occupies the 4f site where the coordination number is 7, and the other occupies the 6h site where the coordination number is 9. Hydroxide apatite $Ca_{10}(PO_4)_6(OH)$ is a typical example. It is the principal ingredient of human bone and is practically used for artificial bone [101–103].

$La_{9.33+x}Si_6O_{26+3x/2}$ (x = 0–0.67) $La_{9.33}Si_6O_{26}$ and $La_{10}Si_6O_{27}$ have often been studied for their crystallographic interest. It is already known that lattice volume will continuously decrease with the ionic radius of lanthanide ions from La to Lu [102, 104]. In the $Re_{9.33+x}Si_6O_{26}$ system, oxides with Re = La-Dy belong to the hexagonal system apatite structure ($P6_3/m$) and oxides with Re = Y-Yb to the monoclinic system apatite structure (I2/a). Specifically, $La_{10}Si_6O_{27}$ is not regarded as the apatite phase. In the case of silicate and germanate, the oxides with the amount of La from 8 to 9.33 exhibit the apatite phase [105].

The crystal structure of this system is shown in Fig. 9. The La 6h site is fully occupied, while the La 4f site is not fully filled. $La_{9.33}Si_6O_{26}$ does not have interstitial oxygen ions, but the conductivity improves by partially substituting the La 4f site or by preparing a slightly La-deficient sample (La = 9.0) to introduce oxygen vacancies into the 2a site [105, 106]. For $x > 0$, oxygen ions are introduced into the interstitial site, and 1 mol of oxygen is introduced into the unit cell at La = 10 (x = 0.67). When the number of interstitial oxygen ions increases, the conductivity also increases [107]. The ionic conductivity in this system is strongly anisotropic, as its crystallographic structure is. A single-crystal conductivity measurement of $Nd_{9.33}Si_6O_{26}$ has revealed that the conductivity along the c-axis is more than 10 times higher than that in the a–b plane [108]. The anisotropy of this conductivity disappears at around 800°C [109].

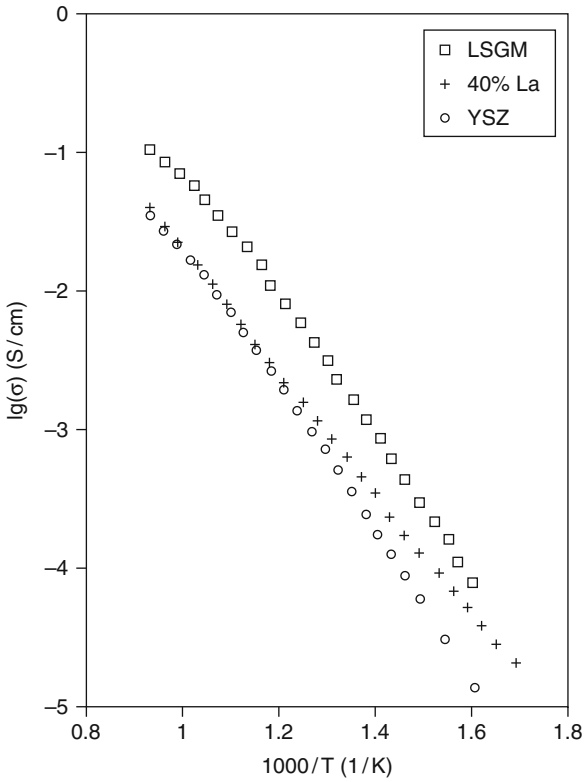

Fuel Cells (SOFC): Alternative Approaches (Electroytes, Electrodes, Fuels). Figure 8
Comparison of the oxygen ionic conductivity of $La_{0.4}Ba_{0.6}InO_{2.7}$ with $La_{0.9}Sr_{0.1}Ga_{0.8}Mg_{0.2}O_{2.85}$ and YSZ, reported by Goodenough [93] (Reproduced with permission from Elsevier)

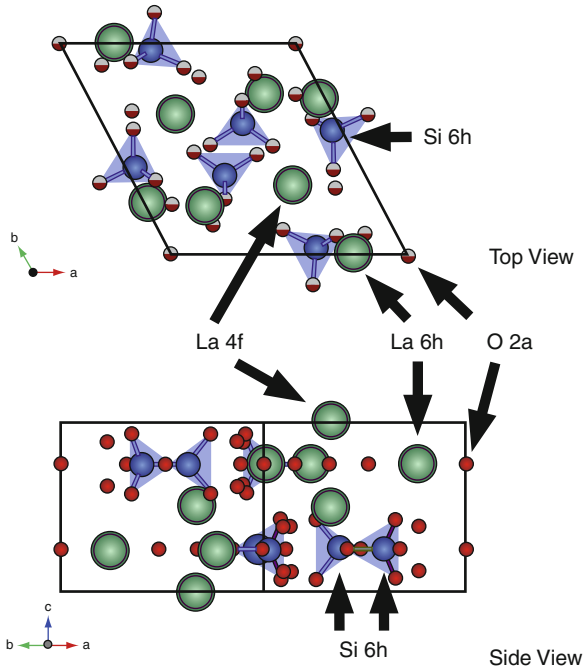

Fuel Cells (SOFC): Alternative Approaches (Electroytes, Electrodes, Fuels). Figure 9
Crystal structure of $La_{10}Si_6O_{27}$ [110] (*Green*: La, *Blue*: Si, *Red*: O) (Reproduced with permission from Elsevier)

As solid electrolytes, the La/Si oxides with La > 9.33 contain interstitial oxygen ions, which can conduct in the channel (2a site) along the c-axis. The conduction mechanism is quite different from that of other oxide electrolytes in which oxygen vacancies are the mobile charge carriers. For example, in $La_{10}Si_6O_{27}$, the activation energy of ionic conductivity via oxygen interstitials is lower than that of YSZ, and the ionic conductivity of this La/Si oxide is higher than that of YSZ at and below 923 K, as described in Fig. 10 [110]. Moreover, it is known that the transference number is unity, and that this material remains stable in humidified hydrogen and in CO_2-containing atmospheres at and below 1,073 K, while p-type conduction can appear at and above 1,173 K [111, 112]. The ionic conductivity decreases, and its activation energy increases with decreasing ionic radius of the rare-earth metal ions in the La site [113, 114]. The substitution sites of dopants should be taken into account in considering ionic conductivities of such materials [106, 107, 110, 115, 116].

These materials are based on inexpensive La_2O_3 and SiO_2 and can be synthesized at relatively low temperatures, but cannot exhibit high conductivity and density without sintering at and above 1,873 K [117]. The thermal expansion coefficient of $La_{10}Si_6O_{27}$ is 9.7–10.3 × 10^{-6} K^{-1}. This value is very close to that of YSZ (10.5 × 10^{-6} K^{-1}) and GDC (11.8 × 10^{-6} K^{-1}) [118, 119], indicating that similar oxide electrodes may be used. There are a few reports on fuel cell electrochemical performance using a $La_{0.9}Sr_{0.1}CoO_{3-\delta}$ cathode with a Ni-SDC cermet anode [110, 116, 119]. The results show 50% better performance than that with Pt electrodes [119]. The interdiffusion of La and Sr in the electrode and in the electrolyte can be technological issues, as observed also in the LSGM-electrolyte-based cells.

$La_{9.33+x}Ge_6O_{26+3x/2}$ (x = 0–2.67) It has been already reported that La/Ge oxides exhibit a phase transition

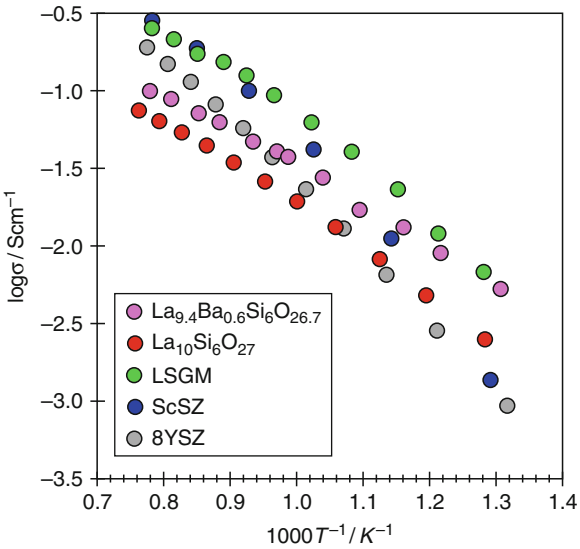

Fuel Cells (SOFC): Alternative Approaches (Electroytes, Electrodes, Fuels). Figure 10
Comparison of the oxygen ionic conductivity of lanthanum silicate with $La_{0.9}Sr_{0.1}Ga_{0.9}Mg_{0.1}O_3$ and oxides with the fluorite structure [110]

from triclinic to hexagonal phase at around 1,000 K [120]. This phase transition disappears by substitution of La by Sr [121]. A similar phase transition is observed in La_2GeO_5 [122]. The ionic conductivity of $La_xGe_6O_{12+1.5x}$ exhibits the highest value in the apatite region, while this result is not the same as in the lanthanum silicates [105, 119, 123]. Due to the volatility of Ge, La_2GeO_5 is difficult to synthesize in the stoichiometric ratio of La/Ge [124].

Protonic Conductors

General In general, most ionic conductors currently used for solid electrolytes in SOFCs are oxygen ionic conductors. However, the use of proton-conducting oxides allowing for lower-temperature operation is anticipated to have a beneficial effect on durability at long-term operation. There are at least two approaches for this aim from the electrolyte materials selection viewpoint. One approach is to increase the oxygen ionic conductivity of the electrolytes, and another approach is to use a proton-conducting oxide which exhibits smaller temperature dependence (i.e., lower activation energy) of the ionic conductivity.

There are many kinds of proton-conducting oxides widely known in the literature, for example, by Kreuer [125]. In a very early study, C. Wagner had already reported the presence of protons in stabilized ZrO_2 [126]. Hydrated oxides such as $WO_3{\cdot}nH_2O$, phosphates such as $Zr(HPO_4)_2$, β-alumina, β″-alumina, zeolites, and heteropoly acid are good examples of proton-conducting oxides [9, 125, 127–130]. Acid salts such as $CsHSO_4$ are also considered as electrolyte materials for fuel cells operating at lower temperatures [131, 132].

Various perovskite-type oxides [133, 134], as well as $Ba_2In_2O_5$ [135–137], and $La_{10}Ge_6O_{27}$ [120, 138, 139] exhibit protonic conductivity. Among these materials, the perovskite-type oxides show outstanding protonic conductivity. To mention a few, SOFCs with $BaCe_{0.8}Y_{0.2}O_{3-\delta}$ solid electrolytes can be operated at low temperatures above 400°C [140, 141], and a power density of 100 mW/cm^2 at 500°C has been achieved (Fig. 11, [141]).

Perovskite-Type Oxides Regarding protonic conduction in perovskite-type oxides (ABO_3), Takahashi and Iwahara [81] discovered the interesting phenomenon that protonic conduction appeared in $SrCeO_3$ at high temperatures, which was associated with the presence of oxygen vacancies [125]. They revealed that $BaCeO_3$ has high hydrogen solubility by using deuterium absorption measurements [142]. This material exhibited mixed conductivity of oxygen ions and protons, which was strongly affected by the Ba/Ce ratio [143, 144]. When the Ba/Ce ratio was more than 1.05, such oxides exhibited high protonic conductivity. When the Ba/Ce ratio was less than 1, it behaved as an oxygen ionic conductor, although the conductivity was relatively low [145]. They also investigated the effect of partial substitution in detail [146–153].

The most important reaction leading to the formation of protonic defects at moderate temperatures is the dissociative absorption of water which requires the presence of oxide ion vacancies $V_O^{\bullet\bullet}$. Those defects may be formed intrinsically by varying the ratio of main constituents (e.g., in $Ba_3Ca_{1+x}Nb_{2-x}O_{3-\delta}$ [154] or $Ba_2YSnO_{5.5}$ [155]), or they may be formed extrinsically to compensate for an acceptor dopant R. In the case of perovskite-type oxides, one generally employs a substitution of up to 25% of the B-site cation by

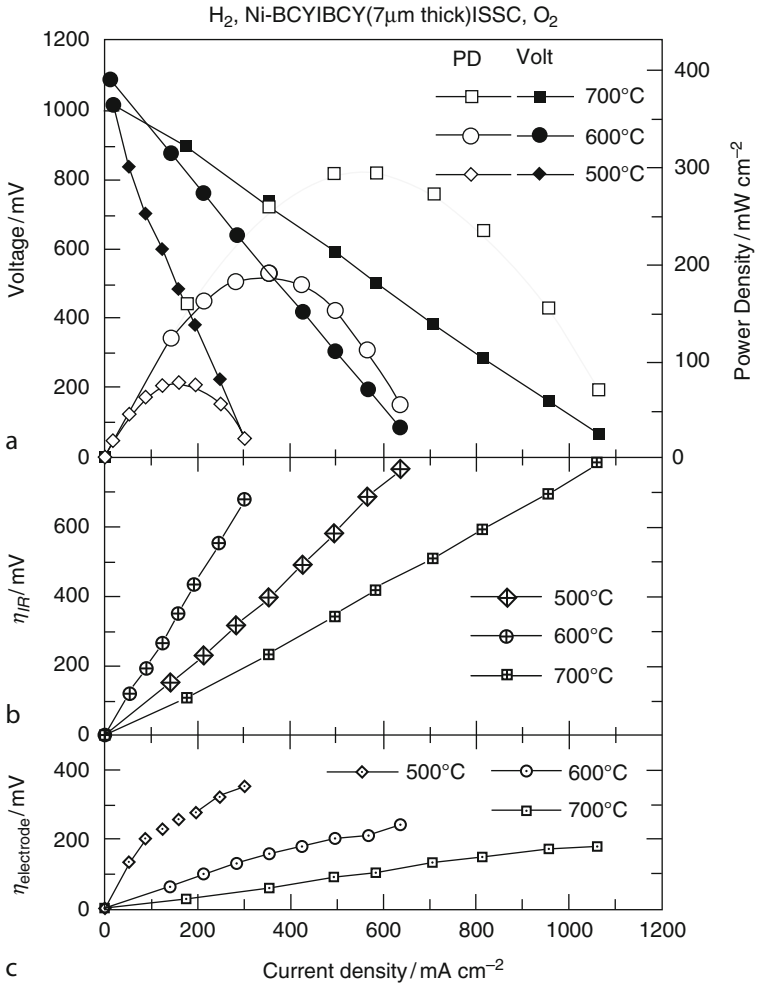

Fuel Cells (SOFC): Alternative Approaches (Electroytes, Electrodes, Fuels). Figure 11
(**a**) *I–V* characteristics (closed symbols) and power density curves (open symbols), (**b**) ohmic loss and (**c**) electrode overpotentials (anode + cathode) of a H_2-O_2 proton conductor thin film SOFC operated at 700–500°C, reported by Matsumoto et al. [141] (Reproduced by permission of Elsevier)

a lower-valence cation (i.e., $A(B_{1-x}R_x)O_{3-\delta}$ in the following denoted $R{:}ABO_3$). In order to form protonic defects, water from the gas phase dissociates into a hydroxide ion filling an oxide ion vacancy and a proton forming a covalent bond with a lattice oxygen. In Kröger–Vink notation, this reaction is written:

$$H_2O + V_O^{\bullet\bullet} + O_O^x \rightleftarrows 2OH_O^{\bullet} \qquad (1)$$

by which two hydroxide ions substituting for oxide ions, that is, two positively charged protonic defects ($OH_O^{\bullet}$), are formed. The hydroxyl ions form dynamical hydrogen bonds with neighboring lattice oxygen, and proton transfer through these hydrogen bonds combined with the rotational diffusion of this defect allows the protonic charge to migrate [156].

For perovskite-type oxides, the proton solubility decreases, but the stability to CO_2 increases as the basicity of B-site ions decreases in the order of Ce → Zr → Sn → Nb → Ti [156]. The best compromise for high proton conductivity and chemical stability is found for Y-doped $BaZrO_3$, but unfortunately, this material exhibits large grain boundary resistance, and it still reacts slightly with CO_2 under certain

conditions [157]. Chemical stability against CO_2 has been demonstrated recently with $BaCe_{0.3}Zr_{0.5}Y_{0.2}O_{3-\delta}$ by Fabbri et al. [158].

Proton concentration is proportional to the solubility of water into oxygen vacancies. Such a protonic conductor tends to lose water at high temperatures, which results in a decrease in the carrier density and also a decrease in conductivity. Figure 12 shows the amount of water dissolution measured by the gravimetric analysis for protonic conductors [156]. The perovskite-type proton-conductive oxides have enough carrier density in the temperature range from ca. 300 to 500°C. On the other hand, mobility changes with temperature according to the Arrhenius equation with activation energy approximately from 0.3 eV to 0.6 eV. As a result, these protonic conductors exhibit their maximum conductivity at certain temperatures as shown in Fig. 13 [156].

It is extremely important that the ionic transference number is high enough to be used as a solid electrolyte in fuel cells. The Ce^{4+} cation has a tendency to be reduced easily, so that electronic conduction caused by the reduction of Ce^{4+} ions becomes a problem in the case of the CeO_2-containing electrolyte. $BaCeO_3$-based oxides contain Ce ions, exhibiting certain electronic conductivity by reduction [157]. Transport parameters including activation enthalpies of hole and proton conduction have been reported [157, 159].

It is commonly believed that this is because the band gaps of the perovskite-type protonic conductors are considerably large, ranging from 4.5 to 5 eV or even larger [160]. On the other hand, hole conduction appears in an oxidizing atmosphere. However, the temperature dependence of the hole conductivity is larger than that of the protonic conductivity. Oxygen vacancies are filled with water dissolved in various oxides, as shown in Fig. 12, at temperatures below 500°C, leading to a high protonic conductivity in an oxidizing atmosphere.

Alternative Electrode Materials

Cathode Materials

Current Cathode Materials The majority of investigations related to SOFC cathode materials have been concentrated on oxides with the perovskite structure [2–4, 161]. The oxides commonly used are SrO-doped $LaMnO_3$ with an A-site deficiency ($(La_{1-x}Sr_x)_{1-y}MnO_{3\pm\delta}$; $x = 0.1–0.5$, $0 \leq y < 0.1$). For example, $La_{0.86}Sr_{0.14}MnO_3$ exhibits an electronic

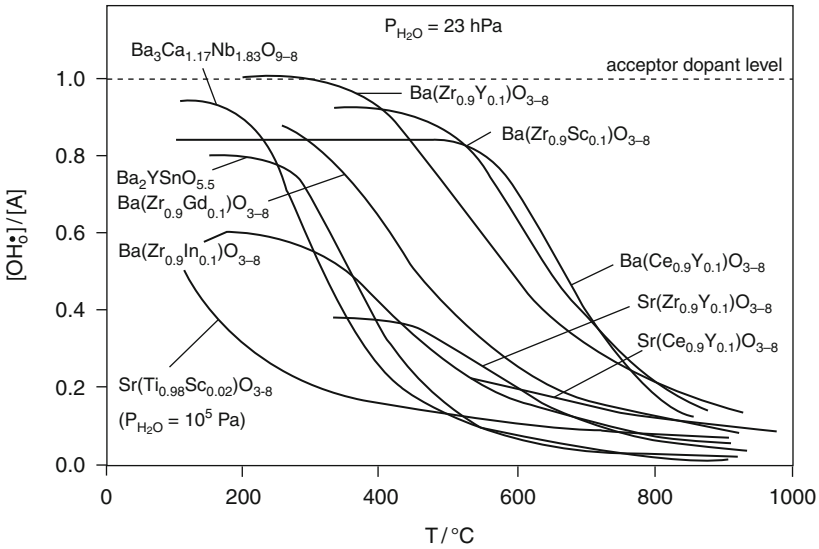

Fuel Cells (SOFC): Alternative Approaches (Electroytes, Electrodes, Fuels). Figure 12
Normalized hydrogen isobars (pH_2O = 23 hPa) for different perovskites, reported by Kreuer [156]. For $BaZrO_3$-based compositions, data for different hypovalent dopants (Y, Sc, Gd, In) are included (Reproduced by permission of Annual Reviews)

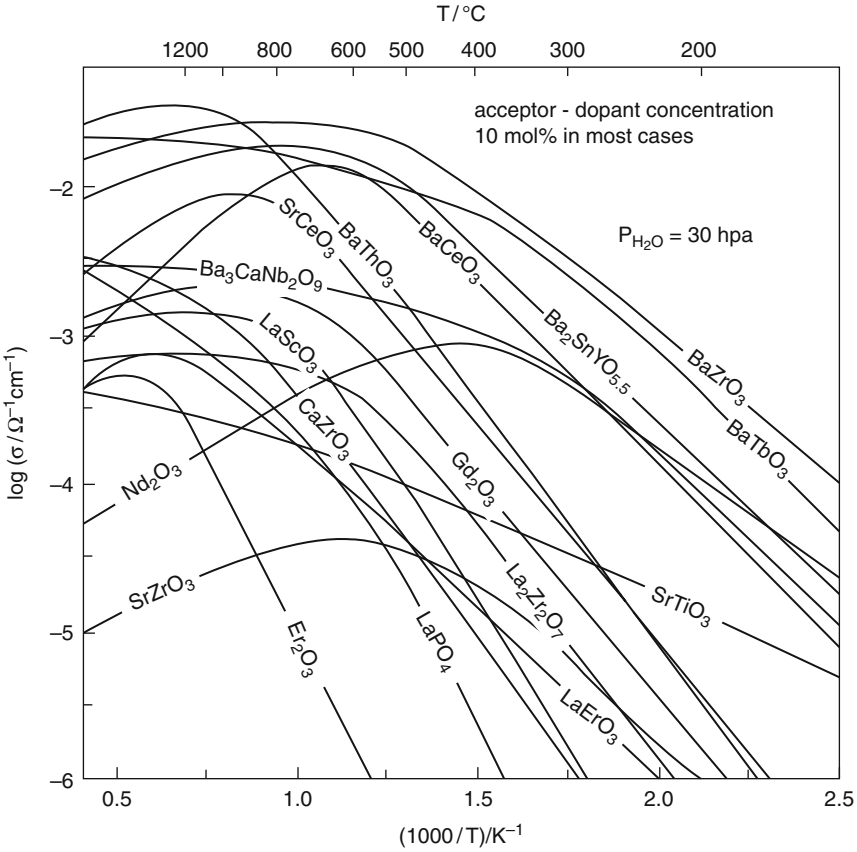

Fuel Cells (SOFC): Alternative Approaches (Electroytes, Electrodes, Fuels). Figure 13
Ionic conductivity of proton-conductive perovskite type oxides, reported by Kreuer [156] (Reproduced by permission of Annual Reviews)

conductivity of 1.4×10^4 S/m at 1,000°C [162]. The electronic conductivity increases with increasing alkaline-earth cation (Sr^{2+}) concentration up to $x \approx 0.5$. The increase in Sr content, however, is accompanied with an increase in thermal expansion coefficient [161–168]. The perovskite structure is very tolerant with changes in the ionic radius of the A- and B-site cations, allowing many possibilities to substitute host cations with various dopants. Related perovskite oxides have also been investigated. The A site in this perovskite can be substituted with other rare-earth oxides (e.g., $Y_{1-x}Ca_xMnO_3$) [169–172] and with other alkaline-earth oxides ($La_{1-x}Ca_xMnO_3$) [173–175]. This structure can also accommodate a high concentration of cation vacancies, particularly on the A site as $(La_{1-x}Sr_x)_{1-y}MnO_3$ [22, 176–179]. By substituting the B site, the electronic conductivity and other properties such as nonstoichiometry, oxygen vacancy concentration, and catalytic activity can be changed considerably [163, 180, 181]. The Mn cation has been substituted with Fe, Co, Ni, and Cu, which enhances the electronic conductivity [180, 182]. Transition metal cations can be substituted on the B site like in $La_{1-x}Sr_xMn_{1-y}Co_yO_3$ or in $La_{1-x}Sr_xFe_{1-y}Co_yO_3$, exhibiting excellent ionic conductivity as well as high electronic conductivity [21, 182–190]. The electronic conductivity of several perovskite oxides is shown in Fig. 14 [180]. Those compounds may be favored for their high electronic conductivity, particularly for planar fuel cell configurations, where in-plane electric current flow is essential in the relatively thin cathode layers. In recent SOFC systems under development,

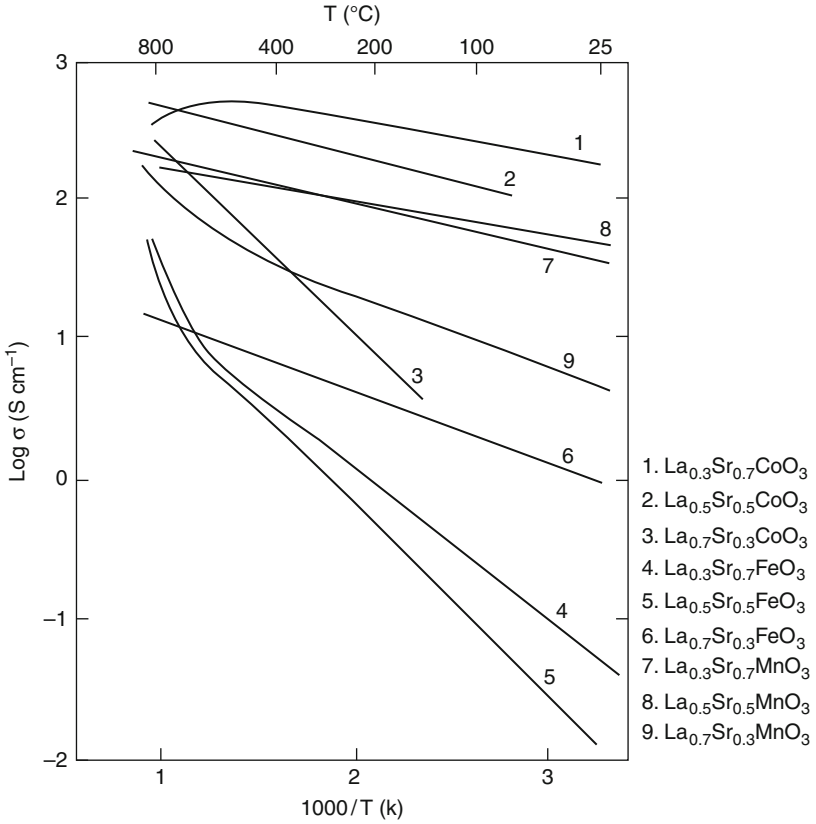

Fuel Cells (SOFC): Alternative Approaches (Electroytes, Electrodes, Fuels). Figure 14
Electronic conductivity of SrO-doped $LaBO_3$ (B = Mn, Co, Fe) after Takeda et al. [180] (Reproduced by permission of ECS-The Electrochemical Society)

Sr-doped $LaMnO_3$ is still widely used as the state-of-the-art cathode material for ZrO_2-based electrolytes [2–4, 161, 191].

In addition, cathode materials with mixed ionic and electronic conductivities can expand the electrode reaction area, leading to a decrease in cathodic overvoltage [2, 161, 192]. The perovskite oxides exhibit excellent electronic conductivity, and in specific compounds and conditions, they possess high ionic conductivity. The ionic conductivity of $La_{0.6}Sr_{0.4}MnO_3$ measured by Steele et al. [193] was 10^{-5} S/m at 900°C in air, which is 6 orders of magnitude lower than the ionic conductivity of 8 mol% Y_2O_3-doped ZrO_2 electrolyte. Therefore, the SrO-doped $LaMnO_3$, the state-of-the-art cathode material, is a poor mixed conductor [193]. However, the oxide becomes a mixed conductor in reduced state (at low oxygen partial pressure) [192, 194], as expected from the defect chemistry [22, 163] and electrocatalytic properties [195].

On the other hand, SrO- or CaO-doped $LaCoO_3$ and $LaFeO_3$ are excellent mixed conductors in ambient atmosphere [22, 180, 186–189, 193], where ionic conduction occurs via the oxygen vacancy mechanism [196]. Teraoka et al. [188] have reported that the $La_{1-x}Sr_xCo_{1-y}Fe_yO_{3-\delta}$ exhibits ionic conductivity ranging from 10 to 10^3 S/m, while the ionic conductivity of doped ZrO_2 electrolyte is around 10 S/m. High ionic conductivity in $La_{0.6}Sr_{0.4}CoO_3$ has been confirmed by Steele et al. to be 80 S/m at 900°C [193]. Ionic conductivity also increases by substituting the B-site cations with cations with a larger number of 3d electrons from Fe to Co and Ni [182], consistent with the increase in oxygen vacancy concentration [163]. The thermal expansion mismatch between the cathode

Fuel Cells (SOFC): Alternative Approaches (Electroytes, Electrodes, Fuels). Table 2 Thermal expansion coefficients of perovskite oxides for SOFC cathode applications [33, 168, 184, 186]

	Materials	Thermal expansion coefficient ($\times 10^{-6}$/K)	Temp. range (°C)
ZrO_2	ZrO_2-8 mol%Y_2O_3	10.5	25–900
LSM	$La_{0.85}Sr_{0.15}MnO_3$	11.7	25–900
	$La_{0.5}Sr_{0.5}MnO_3$	12.6	25–900
	$La_{0.99}MnO_3$	11.2[a]	25–1,000
	$La_{0.94}Sr_{0.05}MnO_3$	11.7[a]	25–1,000
	$La_{0.89}Sr_{0.10}MnO_3$	12.0[a]	25–1,000
	$La_{0.79}Sr_{0.20}MnO_3$	12.4[a]	25–1,000
	$La_{0.69}Sr_{0.30}MnO_3$	12.8[a]	25–1,000
LSC	$La_{0.85}Sr_{0.15}CoO_3$	18.7	25–900
	$La_{0.7}Sr_{0.3}CoO_3$	18.3	25–900
	$La_{0.5}Sr_{0.5}CoO_3$	22.0	25–900
	$La_{0.3}Sr_{0.7}CoO_3$	15.6	25–900
LSCM	$La_{0.85}Sr_{0.15}Mn_{0.8}Co_{0.2}O_3$	11.8	25–900
	$La_{0.85}Sr_{0.15}Mn_{0.5}Co_{0.5}O_3$	14.6	25–900
	$La_{0.5}Sr_{0.5}Mn_{0.5}Co_{0.5}O_3$	14.9	25–900
	$La_{0.8}Sr_{0.2}Mn_{0.8}Co_{0.2}O_3$	11.1[b]	200–800
	$La_{0.8}Sr_{0.2}Mn_{0.6}Co_{0.4}O_3$	13.7[b]	200–800
	$La_{0.8}Sr_{0.2}Mn_{0.4}Co_{0.6}O_3$	16.5[b]	200–800
	$La_{0.8}Sr_{0.2}Mn_{0.2}Co_{0.8}O_3$	17.0[b]	200–800
	$La_{0.8}Sr_{0.2}CoO_3$	17.8[b]	200–800
LSCF	$La_{0.8}Sr_{0.2}Co_{0.8}Fe_{0.2}O_3$	18.4	25–900
	$La_{0.2}Sr_{0.8}Co_{0.8}Fe_{0.2}O_3$	24.0	25–900
	$La_{0.8}Sr_{0.2}CoO_3$	19.7[c]	100–1,000
	$La_{0.8}Sr_{0.2}Co_{0.8}Fe_{0.2}O_3$	20.7[c]	100–1,000
	$La_{0.8}Sr_{0.2}Co_{0.6}Fe_{0.4}O_3$	20.0[c]	100–1,000
	$La_{0.8}Sr_{0.2}Co_{0.4}Fe_{0.6}O_3$	17.7[c]	100–1,000
	$La_{0.8}Sr_{0.2}Co_{0.2}Fe_{0.8}O_3$	15.1[c]	100–1,000
	$La_{0.8}Sr_{0.2}FeO_3$	12.9[c]	100–1,000

[a]See Ref. [168]
[b]See Ref. [184]
[c]See Ref. [186]

and the electrolyte, as compiled in Table 2, leads to insufficient contact and thus the detachment of cathode layers, which limits the SOFC applications of such mixed conducting cathode materials.

Alternative Cathode Materials Perovskite oxides using smaller lanthanide elements than La, such as $Gd_{1-x}Sr_xCoO_3$ [197], $Sm_{1-x}Sr_xCoO_3$ [198], $Pr_{1-x}Sr_xMnO_3$, and $Nd_{1-x}Sr_xMnO_3$ [199] have been investigated as cathode materials in order to decrease reactivity with the YSZ electrolyte. Compatibility with YSZ electrolyte was further improved for $Gd_{1-x}Sr_xCo_{1-y}Mn_yO_3$ [200] by substituting Co with Mn on the B site due to lower reactivity and matching of thermal expansion coefficients. Substitution of Co with Fe on the B site also decreases their thermal expansion coefficient. Perovskite oxides using Co and Fe for the B site, such as $Pr_{1-x}Sr_xCo_{1-y}Fe_yO_{3-\delta}$, $Nd_{1-x}Sr_xCo_{1-y}Fe_yO_{3-\delta}$, and $Gd_{1-x}Sr_xCo_{1-y}Fe_yO_3$, exhibit high electrical conductivity above 600°C as shown in Fig. 15 and exhibit good catalytic activity on

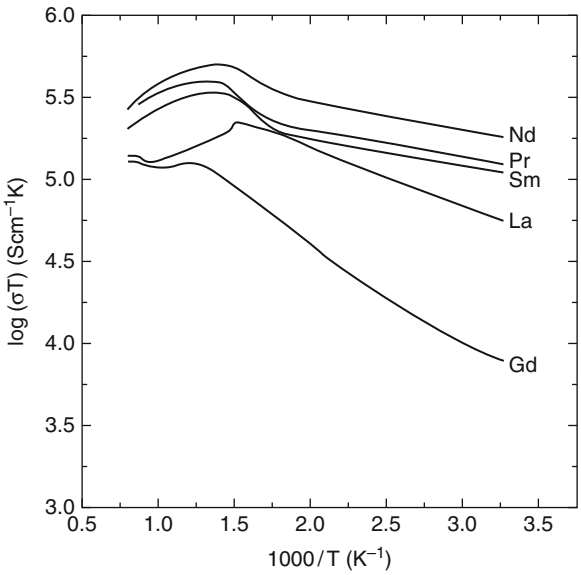

Fuel Cells (SOFC): Alternative Approaches (Electroytes, Electrodes, Fuels). Figure 15 Temperature dependence of the electrical conductivity for $Ln_{0.4}Sr_{0.6}Co_{0.8}Fe_{0.2}O_{3-\delta}$ (Ln = La, Pr, Nd, Sm, Gd), reported by Tu et al. [201] (Reproduced with permission from Elsevier)

GDC electrolytes in the intermediate operational temperature range (600–800°C) [201, 202], as shown in Fig. 16.

$Sm_{0.5}Sr_{0.5}CoO_3$ has been used as a cathode material for the LSGM electrolyte, and a low cathodic overpotential of less than 50 mV at 0.5 A/cm^2 was obtained at 873 K [203]. $BaCoO_3$ was also investigated as a novel cathode material for the LSGM electrolyte. $Ba_{0.6}La_{0.4}CoO_3$ showed a high surface activity for oxygen dissociation and exhibited the same level of cathodic overpotential as $Sm_{0.5}Sr_{0.5}CoO_3$ as shown in Fig. 17 [204].

Perovskite oxides containing Ba in the A site were proposed as cathode materials for a lower-temperature operation. Many of them have been investigated in combination with CeO_2-based electrolytes. High power density of more than 1 W/cm^2 was obtained at 600°C by using $Ba_{0.5}Sr_{0.5}Co_{0.8}Fe_{0.2}O_{3-\delta}$ (BSCF) for the cathode on a thin SDC electrolyte (12–20 μm in thickness) as shown in Fig. 18 [205]. Enhancement of electrical conductivity by an addition of Sm to BSCF was also reported, which resulted in further improvement of cathode performance at low operational temperatures [206]. $Ba_{0.5}Sr_{0.5}Co_{1-y}Fe_yO_{3-\delta}$ possessed low

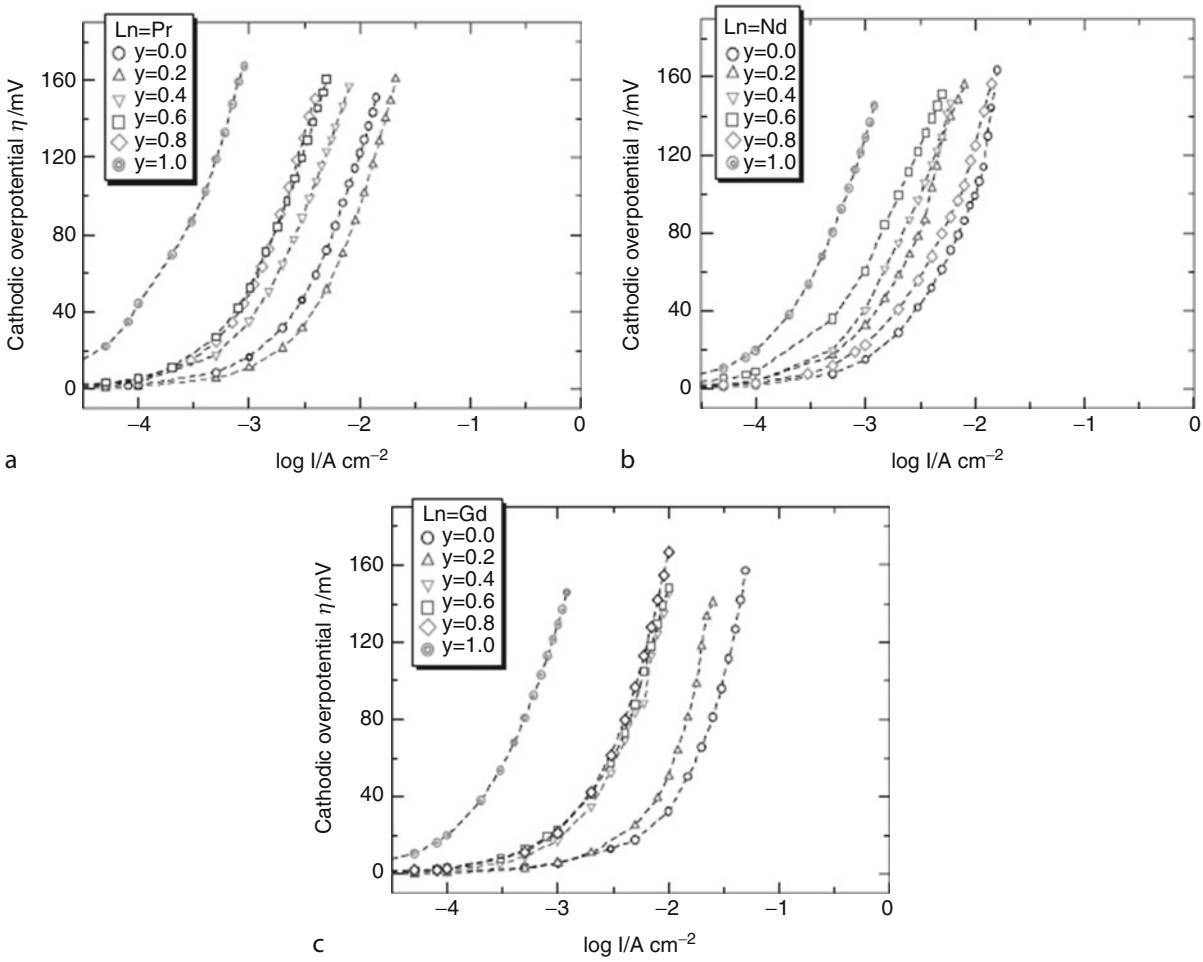

Fuel Cells (SOFC): Alternative Approaches (Electroytes, Electrodes, Fuels). Figure 16
Cathodic polarization curves for $Ln_{0.8}Sr_{0.2}Co_{1-y}Fe_yO_{3-\delta}$ ((**a**) Ln = Pr, (**b**) Ln = Nd, (**c**) Ln = Gd) cathodes on GDC electrolytes at 700°C, reported by Qiu et al. [202] (Reproduced with permission from Elsevier)

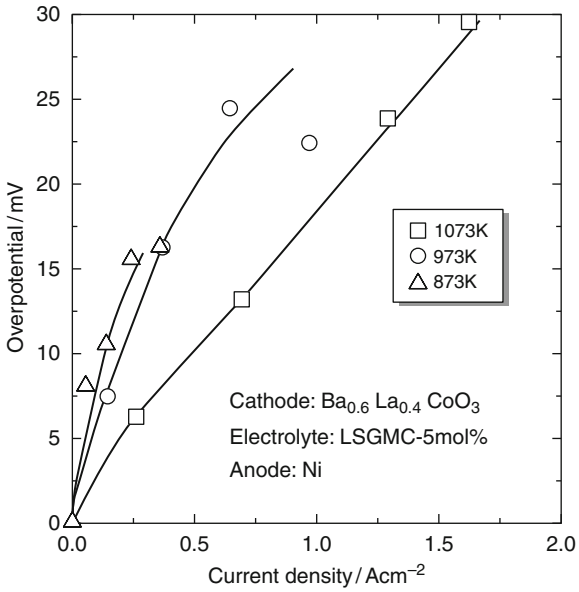

Fuel Cells (SOFC): Alternative Approaches (Electroytes, Electrodes, Fuels). Figure 17
Temperature dependence of cathodic overpotential of the $Ba_{0.6}La_{0.4}CoO_3$ cathode on the LSGMC electrolyte as a function of current density, reported by Ishihara et al. [204] (Reproduced with permission from Elsevier)

vacancy formation energy with low oxygen migration barrier [207]. However, BSCF cathode could degradate in the presence of CO_2 in ambient air, owing to the reaction with alkaline-earth elements, resulting in the formation of Ba and Sr carbonates [208, 209].

Regarding durability of SOFC cathodes, Cr poisoning phenomena of cathode materials have been investigated to better understand long-term cell performance. Taniguchi et al. clarified that not only the vapor pressure of Cr species but also the cathodic overvoltage affects the degradation rate for a cell using $La_{0.9}Sr_{0.1}MnO_3$ [210]. In addition, reaction between the Cr vapor and the cathode material can decrease the vapor pressure and contribute in delaying the beginning of cell performance degradation [211]. Matsuzaki et al. reported that the use of $La_{0.6}Sr_{0.4}Co_{0.2}Fe_{0.8}O_3$ (LSCF) on $Ce_{0.8}Sm_{0.2}O_{1.9}$ electrolyte drastically reduced the Cr poisoning in comparison with $La_{0.85}Sr_{0.15}MnO_3$ [212]. $LaNi_{0.6}Fe_{0.4}O_3$ (LNF) was also proposed as a novel cathode material, exhibiting high tolerance to the Cr poisoning. Chiba et al. have first reported that LNF possesses suitable properties for operating at low temperatures [213]. LNF has shown high electronic conductivity of

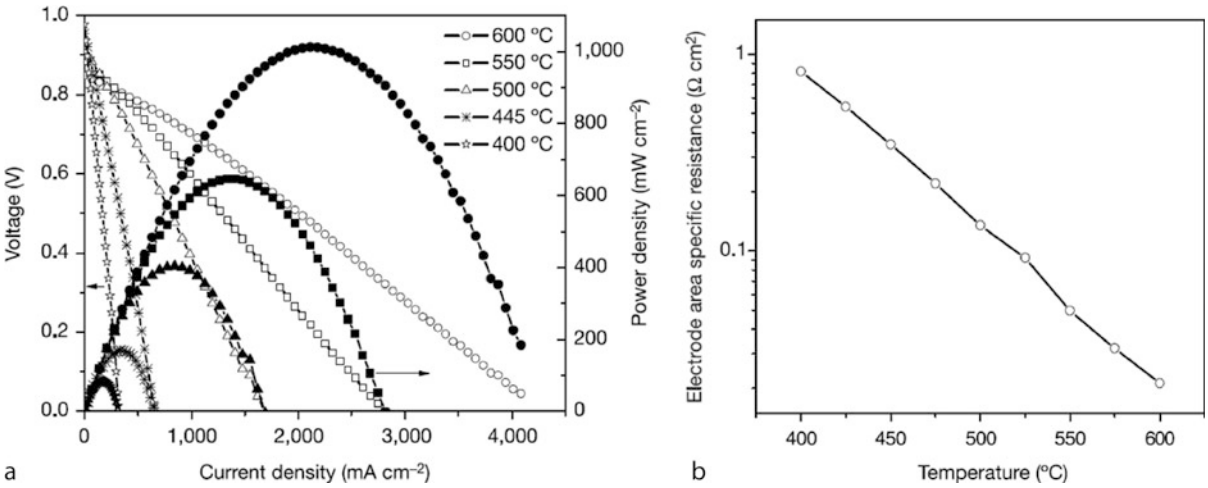

Fuel Cells (SOFC): Alternative Approaches (Electroytes, Electrodes, Fuels). Figure 18
Performance obtained from a $Ba_{0.5}Sr_{0.5}Co_{0.8}Fe_{0.2}O_{3-\delta}$(~20 μm)| $Sm_{0.15}Ce_{0.85}O_{2-\delta}$(~20 μm)| Ni + $Sm_{0.15}Ce_{0.85}O_{2-\delta}$(~700 μm) fuel cell. (**a**) Cell voltage and power density as a function of current density and (**b**) area-specific resistances of the electrodes, reported by Shao and Haile [205] (Reproduced with permission from Nature Publishing Group)

580 S/cm at 800°C and relatively closer thermal expansion coefficient of 11.4 × 10^{-6} K^{-1} (30–1,000°C) to that of YSZ than $La_{0.8}Sr_{0.2}MnO_3$(LSM). Furthermore, it is also revealed that LNF has higher tolerance to Cr poisoning than LSM and LSCF [214]. Figure 19 shows the comparison of cathodic overvoltage by Cr poisoning between LSCF and LNF. Concerning the Cr poisoning phenomena, Jiang et al. [215] explained that the deposition of Cr in the LSM cathode is initiated by the nucleation reaction involving the gaseous Cr species and Mn^{2+}, which are generated by the cathode polarization and regarded as nucleation agents. SrO is identified as a nucleation agent in the case of LSCF. As a result, they concluded that LNF exhibits high tolerance to Cr poisoning because it has no nucleation agent under any electrochemical condition [215]. In terms of electrochemical properties at low temperatures, an electrode resistance of approximately 0.1 Ω cm^2, corresponding to the cathode polarization, was achieved at 700°C in the case of a LNF-YSZ composite cathode which was made by infiltrating LNF into porous YSZ [216].

Another type of oxide with the general formulation of $A_2BO_{4+\delta}$ (e.g., $La_{2-x}Sr_xNiO_{4+\delta}$ [217], $Nd_2NiO_{4+\delta}$ [218, 219], $Pr_{1.4}Sr_{0.6}NiO_4$ [220], and $Sm_{0.5}Sr_{1.5}CoO_{4-\delta}$ [221]) has also been investigated for intermediate-temperature (900–1,000 K) operation. Their K_2NiF_4-type structure allows for some slight oxygen overstoichiometry. Oxygen excess, accommodated by oxygen interstitials rather than cation vacancies, leads to high values of oxygen tracer diffusion coefficient. Current density of 0.5 A cm^{-2} at 0.7 V was obtained at 700°C with an anode-supported half-cell with a $Nd_{1.95}NiO_{4+\delta}$ cathode and a YSZ electrolyte [219].

In order to enhance the catalytic activity of the cathode for oxygen reduction and thus to increase the electrochemical performance, an addition of noble metals has also been investigated [222]. By the addition of silver to a LSCF-CeO_2 composite cathode, an improvement of cathode performance at lower temperatures below 700°C was measured [223, 224]. Consequently, Ag improved the surface exchange step of oxygen from the gas phase into the oxide [223]. Cell performance of more than 500 mW/cm^2 at 0.7 V at 700°C was obtained using anode-supported cells with LSCF-coated Ag cathode and YSZ electrolyte [225]. Generally speaking, Sr-doped $LaMnO_3$ and related materials are suitable for high-temperature operation of SOFCs, while more electrochemically/catalytically active alternative cathode materials may be needed especially for lower operational temperatures.

Anode Materials

Current Anode Materials In state-of-the-art SOFCs, Ni-based cermet anodes are commonly used, which

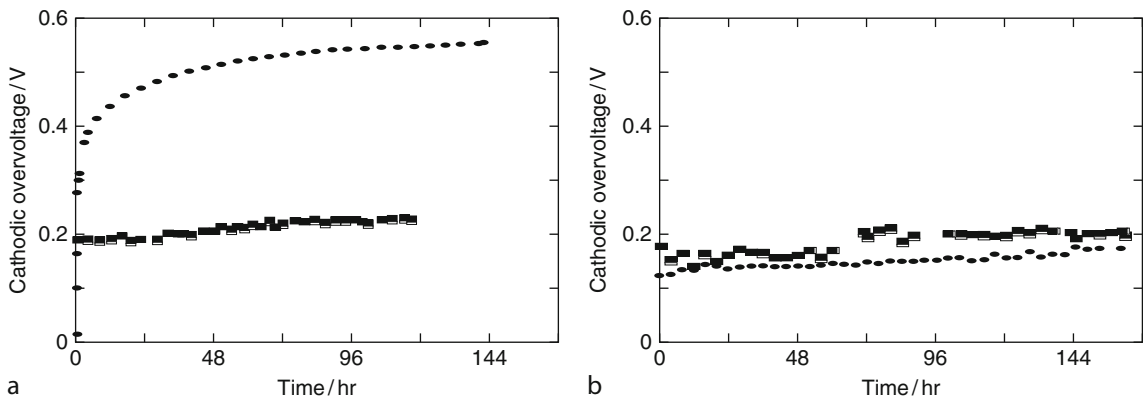

Fuel Cells (SOFC): Alternative Approaches (Electroytes, Electrodes, Fuels). Figure 19
Cathodic overvoltage (IR corrected) for cells using (**a**) LSCF cathode and (**b**) LNF cathode as a function of time: (●) cell with Inconel 600 at 0.7 A cm^{-2} and (■) cell without Inconel 600 at 0.7 A cm^{-2}, reported by Komatsu et al. [214] (Reproduced by permission of Elsevier)

exhibit excellent electrocatalytic activity for anodic electrochemical reactions, fuel oxidation, and internal reforming, as well as sufficient current collection [2–4, 161, 226]. Due to the requirements of operation in reducing environments and high electronic conductivity, pure metallic electrodes are generally used as anodes. Several metals such as Ni, Ru, Pt, and Co have been studied as anode materials [161, 227, 228]. Ni exhibited the lowest anodic overpotentials [161, 227], while Ru could be an excellent anode material [228]. Pure Ni has electronic conductivities of 1.4 $\times 10^5$ Scm^{-1} and 2.6 $\times 10^4$ Scm^{-1} at 298 K and 900 K, respectively; a thermal expansion coefficient of ca. 14.6 $\times 10^6$ K^{-1}; and a melting point of 1,455°C [229]. The transition metals, which show higher activities for the oxidation of hydrogen, tend to change their microstructures at high temperatures under the reducing conditions of the anode, that is, coalescence of metal particles leads to anode densification. To stabilize the anode morphology in terms of porosity and thermal expansion coefficients, in general, cermets are used, where the ceramic component provides a rigid network and hinders the porous anode morphology from coalescence. The ceramic component also ensures to make the thermal expansion coefficient similar to that of the electrolyte materials.

Internal reforming of hydrocarbon-based fuels can also occur on the Ni surface in the cermet anode. In an SOFC cermet anode, substantially long triple phase boundaries (TPB) can be achieved, and given that solid networks of two phases (electronic conductors and ionic conductors) are obtained throughout the anode volume. It has been well accepted that the electrochemical reaction occurs around the TPB, where oxygen ion conductor (electrolyte), electron-conducting metal phase (Ni), and gas phase all meet together [2, 161].

Alternative Anode Materials

General While Ni/YSZ cermet is the most preferred anode material for SOFCs operating with hydrogen-containing fuels, there are several efforts to find alternative materials for the SOFC anode. Many studies on oxide anodes have been made for perovskite-related oxides. $LaCrO_3$ [230–237], $LaFeO_3$ [238], $LaTiO_3$ [239], and $SrTiO_3$ [240–243] systems are considered as possible alternative anode materials.

Perovskite-Type Oxide $LaCrO_3$-based oxides are well known as interconnect materials for SOFCs. They have high durability in reducing atmosphere. The oxygen-deficient perovskite $La_{0.75}Sr_{0.25}Cr_{0.5}Mn_{0.5}O_3$, used as an anode material by Tao et al. [230], is stable in both fuel and air atmospheres and has revealed stable electrode performance, as shown in Fig. 20 [230]. However, this material has a low electronic conductivity in reducing anode atmosphere and is not stable to sulfur impurities in the fuel [231]. Its long-term performance has been proven unsatisfactory [231]. $Sr_2MgM_0O_{6-8}$ exhibited a Sulfur-tolerance up to 50 ppm H_2S [232]. Experimental results on the $La_{0.8}Sr_{0.2}Cr_{0.97}$ $V_{0.03}O_3$ (LSCV)-YSZ composite anode have demonstrated that the electrochemical performance is comparable to that of Ni/YSZ after 48 h operation [233].

Ruiz-Morales et al. [234] demonstrated symmetrical fuel cells (SFCs) using the same material $La_{0.75}Sr_{0.25}Cr_{0.5}Mn_{0.5}O_{3-\delta}$ (LSCM) on both the anode side and the cathode side. Due to its enhanced electrochemical properties under both reducing and oxidizing conditions, LSCM-based SFCs offered sufficient performances, 0.5 and 0.3 Wcm^{-1} at 950°C using H_2 and CH_4 as fuels, respectively [234].

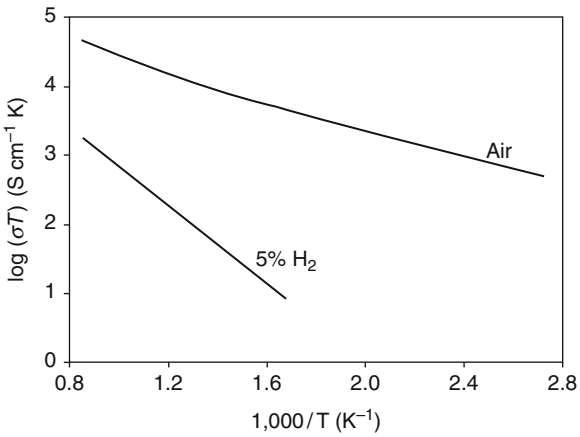

Fuel Cells (SOFC): Alternative Approaches (Electroytes, Electrodes, Fuels). Figure 20
Temperature (*T*) dependence of total conductivity (σ) of $La_{0.75}Sr_{0.25}Cr_{0.5}Mn_{0.5}O_{3-\delta}$ in air and 5% H_2, reported by Tao and Irvine [230] (Reproduced with permission from Nature Publishing Group)

Sauvet et al. [235] have studied the electrochemical properties of $La_{1-x}Sr_xCr_{1-y}Ru_yO_{3-\delta}$ (x = 0.2–0.4, and y = 0.02 and 0.05) for hydrogen and methane fuels at 750 and 850°C. They found the best performances obtained with 30% of Sr doping, and the variation of the ruthenium content, approximately between 0.02 and 0.05, had little influence on the electrochemical results. At 750°C, the polarization resistance was 3.7 Ω cm^2 in hydrogen and 40 Ω cm^2 in methane for the YSZ/CeO_2/graded $La_{0.7}Sr_{0.3}Cr_{0.95}Ru_{0.05}O_3$-YSZ structure [235]. Sauvet et al. also studied $La_{1-x}Sr_xCr_{1-y}Ni_yO_{3-\delta}$ compositions as novel anode materials. They have found that these materials have catalytic activity, but less than that of Ni composites [236, 237].

Lanthanum ferrites have also been investigated as potential anode materials. They are already known for high mixed electronic and ionic conductivity and good oxygen exchange kinetics. However, they have poor stability at lower oxygen partial pressures in the reducing atmosphere. The stability, however, could be improved by mixing with GDC [238].

(La, Sr)TiO_3 has been investigated as alternative SOFC anodes, along with other A-site-deficient lanthanides. Nevertheless, it has poor conductivity than Ni/YSZ cermet [239]. Doped $SrTiO_3$ could be an interesting anode material, and the mixed conductivity of La-doped and Fe-doped $SrTiO_3$ is widely influenced by the chemical composition [240, 244, 245]. $SrTiO_3$ doped with Y [241] and La [242] exhibits increased electrical conductivity. Unfortunately, the high-temperature electrical conductivity of various perovskite anodes is still lower than that of the conventional Ni/YSZ cermet for the use as SOFC anodes [243].

Other Transition Metal Cermets The Cu-based anode cermet has been extensively studied. For example, Park et al. [246, 247] demonstrated that the anode composed of Cu/Sm_2O_3–CeO_2/YSZ was active for direct electrochemical oxidation of alkanes and alkenes, such as methane, ethane, butane, butene, hexane, and toluene, at the operating temperature of 700°C. CeO_2 plays an important role as a primary catalyst material for oxidizing hydrocarbons, and the main role of Cu is to provide electrical conductivity. Zhou et al. [248] reported good performance of CeO_2-Rh anodes for the direct electrochemical oxidation of waste vegetable oil, which led to stable current density of 500 mA cm^{-2} over 100 h under the condition of 0.5 V and 700°C.

Alternative Fuels

Fuel Flexibility

SOFCs are the most flexible fuel cells with respect to the type of fuels [1, 246–255] which can be supplied directly to the anodes. This is partly due to their high operational temperatures suitable for internal reforming within the anodes. Because of their multi-fuel capability, not only hydrogen and carbon monoxide [256] but also various types of fuels such as hydrocarbons, alcohols, and biogas could be used via internal reforming and/or via simple external reforming [246–249, 257–260]. Practical fuels comprise natural gas (consisting mainly of CH_4 with a small amount of other hydrocarbons such as C_2H_6), coal gas (consisting mainly of CO and H_2), liquefied petroleum gas (LPG, consisting mainly of C_3H_8 with C_4H_{10}), naphtha (consisting mainly of C_5 and C_6 hydrocarbons), gasoline (consisting mainly of hydrocarbons with carbon numbers around 8), kerosene (consisting mainly of hydrocarbons with carbon numbers around 12), diesel fuel (consisting mainly of hydrocarbons with carbon numbers around 14–16), alcohols, dimethyl ether, and biogas (consisting mainly of CH_4, CO_2, and H_2O) [251, 252].

In any case, one of the most important issues to be prevented in SOFC systems is carbon deposition (coke formation) from the fuels. Figure 21 shows the equilibrium products for (a) methane- and (b) methanol-based fuels with the steam-to-carbon (S/C) ratio of 1.5 at elevated temperatures [251]. Assuming thermochemical equilibrium, carbon deposition is not expected to occur within a wide temperature range. The calculated results for various other fuels mentioned above have been shown elsewhere [251]. The minimum amounts of H_2O (water vapor) necessary to prevent carbon deposition are shown in Fig. 22 for hydrocarbon fuels. While S/C of 1.5 is enough for CH_4, higher S/C is needed with increasing carbon number of hydrocarbons, especially at lower

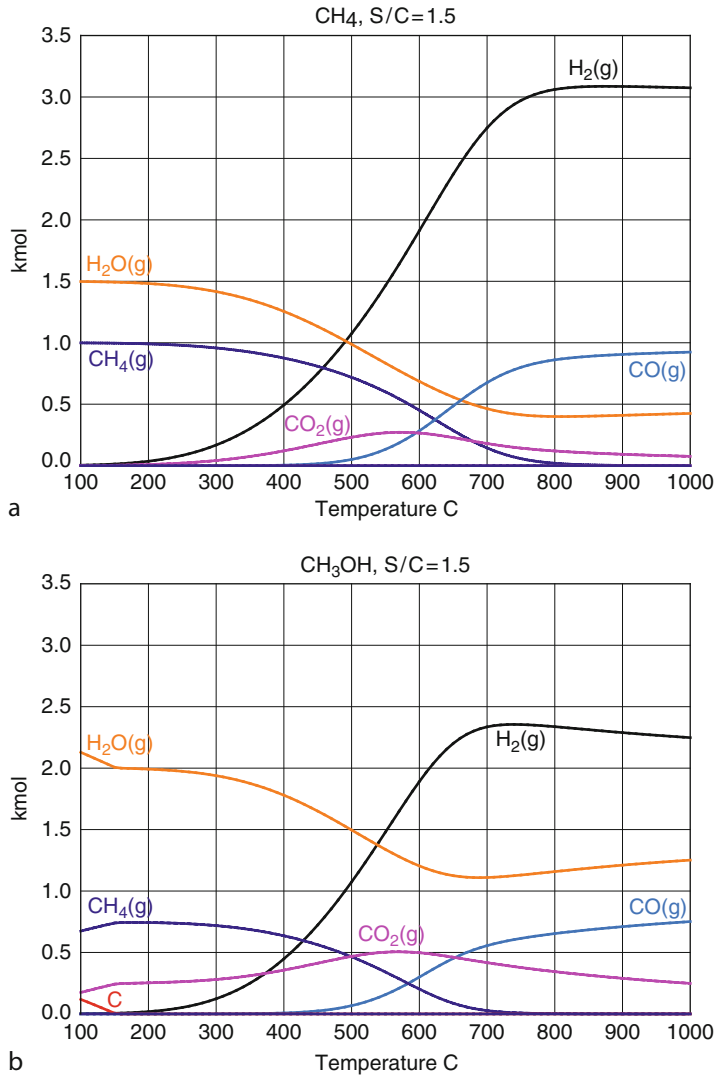

Fuel Cells (SOFC): Alternative Approaches (Electroytes, Electrodes, Fuels). Figure 21
Equilibrium products from (**a**) methane- and (**b**) methanol-based fuels with the steam-to-carbon ratio of 1.5

temperatures. Such dependencies have also been revealed for O_2 (partial oxidation) and CO_2 (CO_2 reforming) [251] to prevent carbon deposition.

It has been found that the major equilibrium constituents in fuel gases are H_2(g), H_2O(g), CO(g), CO_2(g), CH_4(g), and C(s) [251]. Since their equilibrium compositions depend solely on the C–H–O ratio, we can plot, on C–H–O diagrams [252, 253, 255], parameters relevant to optimize operational conditions, including carbon deposition region, gas partial pressures, and electromotive force. Figure 23 shows the positions of various fuel species for fuel cells [252]. Their positions can be shifted by adding H_2O (steam reforming), O_2 (partial oxidation), and/or CO_2 (CO_2 reforming) as co-reactants. Figure 24 shows the carbon deposition limit lines, the carbon-rich side of which corresponds to the carbon deposition region at each temperature. From Figs. 23 and 24, we see that an addition of co-reactants is necessary to prevent carbon formation at SOFC operational temperatures from most fuels shown in Fig. 23. Once the C–H–O ratio is specified, C–H–O ternary diagrams are useful to derive relevant operational parameters without any additional thermochemical calculations [252].

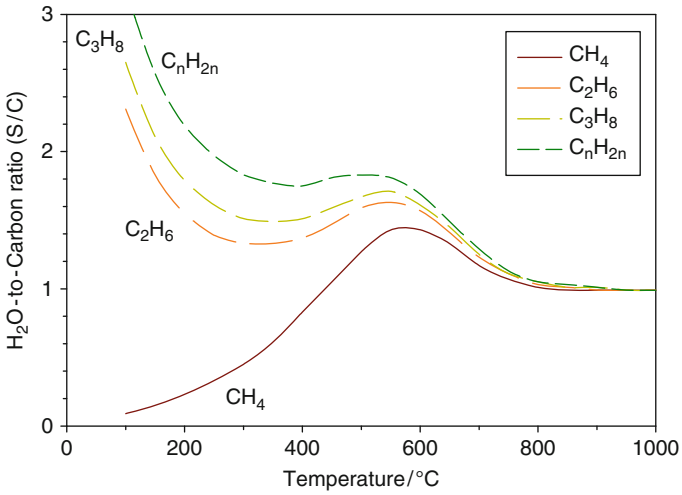

Fuel Cells (SOFC): Alternative Approaches (Electroytes, Electrodes, Fuels). Figure 22
Minimum steam-to-carbon (S/C) ratio needed to prevent carbon deposition in thermodynamic equilibrium for hydrocarbons [251] (Reproduced with permission from ECS – The Electrochemical Society)

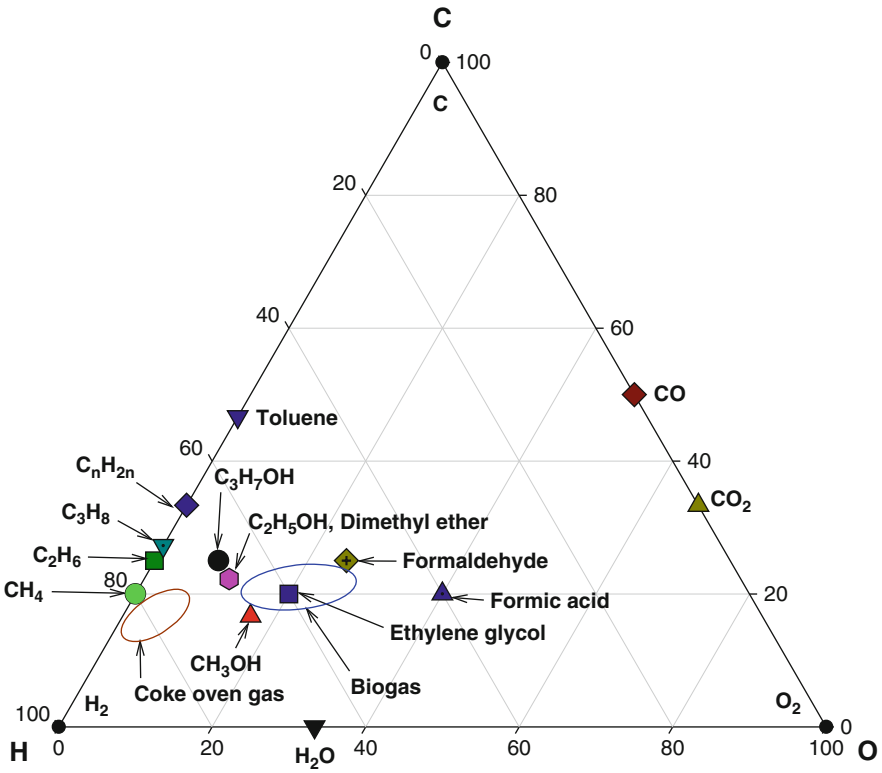

Fuel Cells (SOFC): Alternative Approaches (Electroytes, Electrodes, Fuels). Figure 23
Various hydrocarbons and related species in the C–H–O diagram [252] (Reproduced with permission from ECS – The Electrochemical Society)

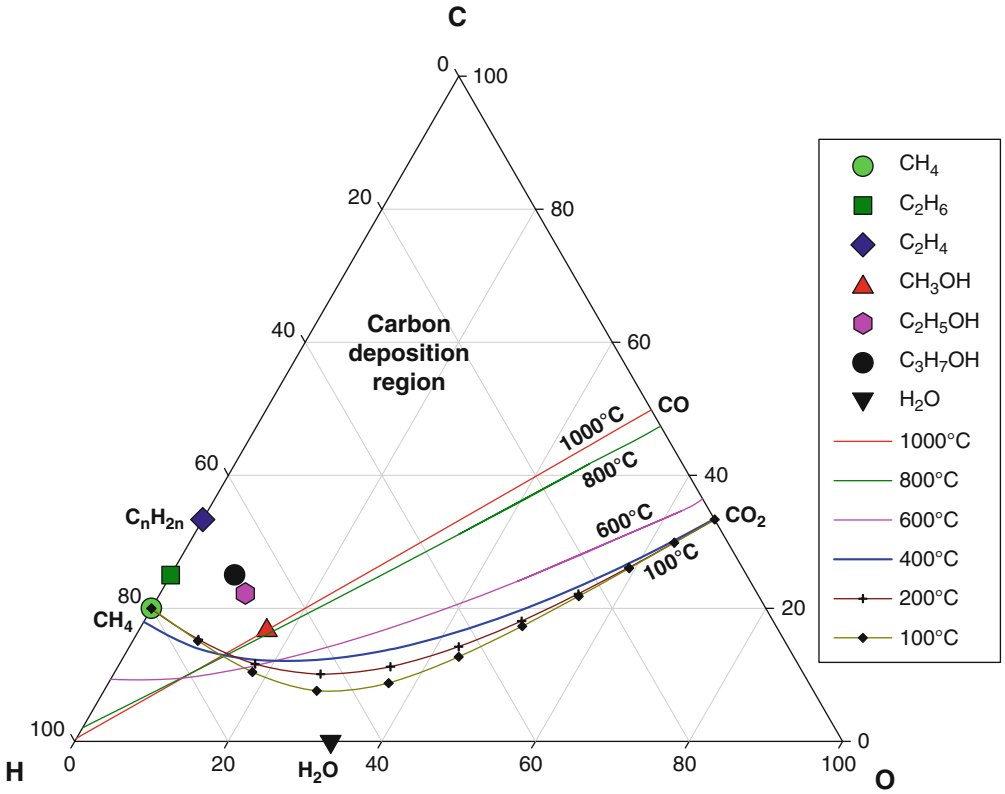

Fuel Cells (SOFC): Alternative Approaches (Electroytes, Electrodes, Fuels). Figure 24
Carbon deposition limit lines at various temperatures in the C–H–O diagram [252] (Reproduced with permission from ECS – The Electrochemical Society)

Apart from such thermochemical processes, also, kinetic phenomena may dominate electrode performance. In the following sections, various practical fuels are experimentally examined, the use of which may enable broader application of SOFCs.

Practical Fuels

City gas (town gas) is used as the state-of-the-art fuel for the first-generation commercial SOFC systems. City gas, consisting mainly of CH_4 from the natural gas, may be partially pre-reformed before supplying to the SOFC systems. Figure 25 shows the comparison of the current-voltage (I–V) characteristics between a H_2-based fuel and a typical SOFC fuel (50% pre-reformed CH_4 with S/C = 2.5) [261]. The cross section of a typical SOFC used for this electrochemical measurement (see Fig. 25) is shown in Fig. 26. This simulated practical SOFC fuel for distributed cogeneration systems consists of the one-to-one mixture of fully reformed CH_4 with S/C = 2.5 and non-reformed CH_4 with S/C = 2.5. While too low S/C may result in carbon deposition, excessive amount of H_2O causes lower OCV and may cause re-oxidation of Ni at high fuel utilization of the SOFC systems.

As practical SOFC fuels may contain a small amount of sulfur as an impurity, H_2S poisoning should be considered with respect to various operational conditions [262–266]. As an example, Fig. 27 shows the cell voltage, anodic polarization, and the ohmic loss on the anode side, measured for 50% pre-reformed CH_4-based fuel with S/C = 2.5 containing 5 ppm H_2S. An initial cell voltage drop followed by a quasi steady-state cell voltage can be observed associated mainly with an increase in anodic polarization and almost constant IR loss, up to 3,000 h [262]. Exactly speaking, cell voltage generally decreased up to ca. 200 h and then remained almost constant but with a slightly higher degradation

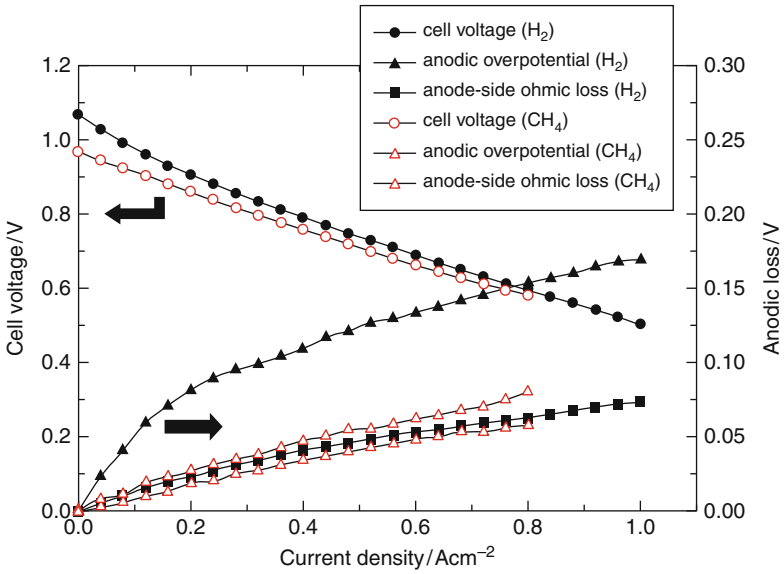

Fuel Cells (SOFC): Alternative Approaches (Electroytes, Electrodes, Fuels). Figure 25
Comparison of the cell voltage and anodic losses in using 3% humidified H_2 and 50% pre-reformed CH_4 (*S/C* = 2.5) as fuels at 800°C. Anodic loss includes anodic overpotential and anode-side ohmic loss [261] (Reproduced with permission from Dr. Kengo Haga)

rate of 0.68%/1,000 h with 5 ppm H_2S, compared to the degradation rate of 0.3%/1,000 h without H_2S impurity [262]. This result clearly shows that SOFC is more tolerant against sulfur poisoning compared to other types of fuel cells, giving more flexibility in practical fuel selection. Even so, it should be noted that carbon deposition phenomena can be affected by the simultaneous presence of sulfur impurities and non-reformed hydrocarbons [262].

Poisoning mechanisms of sulfur, a typical common fuel impurity, have been extensively analyzed for various fuels, including H_2, H_2–CO, CH_4, partially reformed CH_4, and simulated biogas [263–266]. For relatively low concentrations (ppm level) of sulfur, reversible processes associated with adsorption/desorption of sulfur have been considered as the predominant mechanism [263–265]. At higher sulfur concentration and/or lower operational temperature, an irreversible degradation, associated with the oxidation of Ni due to a large anodic polarization, has been observed [263, 264]. Sulfur poisoning to internal reforming reactions is also serious, so that much larger cell voltage drop has been observed in the case where CH_4-rich fuels are supplied [265]. In addition, the C–H–O–Ni–S stability diagram suggests that the formation of Ni_3S_2 (melting point 787°C) could be possible for hydrogen-poor fuels. Possible sulfur poisoning mechanisms are summarized elsewhere [262, 265].

Poisoning phenomena have been analyzed for other impurities, including chlorine, siloxane, phosphorus, and boron on the anode side. Figure 28 shows FESEM micrographs of anodes poisoned by these impurities of ppm levels [266]. Chlorine poisoning is associated with the sublimation of $NiCl_2$ [267], while siloxane poisoning leads to silica deposition [266]. Phosphorus is reactive with Ni to form a eutectic compound [268]. The presence of boron accelerates the grain growth of Ni in the anodes [266].

Various other types of fuels have been examined as possible SOFC fuels. Direct feeding of hydrocarbon fuels has been reported including gaseous fuels such as methane [246, 247, 269], biogas [270], ethane [246, 247], and butane [246, 247], and liquid fuels such as n-decane [271], gasoline [271], synthetic diesel [272], crude and jet fuel oils [273], vegetable oil [248], and biodiesel [274]. Generally speaking, the S/C ratio should be optimized to prevent carbon deposition for

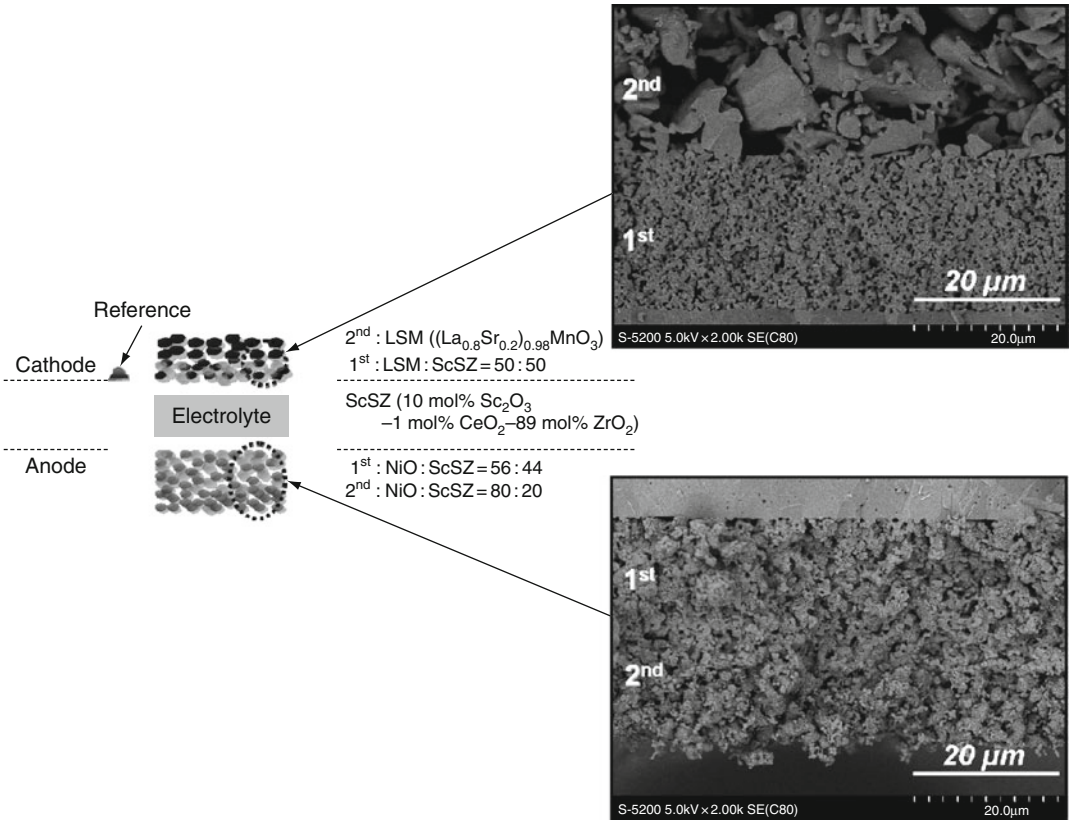

Fuel Cells (SOFC): Alternative Approaches (Electroytes, Electrodes, Fuels). Figure 26
FESEM micrographs of typical cathode and anode. Electrochemical performance of this cell is shown in Fig. 25. The composition of each electrode layer is also shown [261] (Reproduced with permission from Dr. Kengo Haga)

internal steam reforming, and the oxygen-to-carbon (O/C) ratio should be adjusted for internal partial oxidation. Fuel impurities in such practical fuels should also be taken into account to maintain cell performance and durability.

Alcohols

The use of alcohols as SOFC fuels is of technological interest, as alcohols (bioliquids) can be derived from biomass and can be easily reformed. In addition, direct-alcohol SOFCs could be an alternative to direct-methanol fuel cells, typically using polymer electrolytes at a low temperature [4]. Power generation characteristics for alcohol-based fuels and for the simulated reformed gas (consisting mainly of H_2, CO, and H_2O) are shown in Fig. 29 [257]. All these alcohols were premixed with water, so that the C–H–O ratio was fixed to the same value (C:H:O = 9:38:10 for all fuels). It has been demonstrated that direct-alcohol SOFCs are feasible, at least, for alcohols with carbon number up to 4 (butanol) [257, 258]. In case that methanol was directly supplied, the I–V characteristics were similar to those for the simulated reformed gas. However, with increasing carbon number of alcohols, a decrease in cell voltage was observed. From the gas analysis by gas chromatograph, it has been revealed that the compositions of the simulated reformed gas and the methanol-derived fuel gas were almost the same, well explaining the similar I–V characteristics [257]. However, with increasing carbon number of alcohols, a decrease in H_2 and CO concentrations associated with a decrease in cell voltage [257] was observed. Therefore, a higher catalytic activity to reform alcohols at fuel electrodes (or pre-reforming) is necessary to optimize the performance of such direct-alcohol SOFCs.

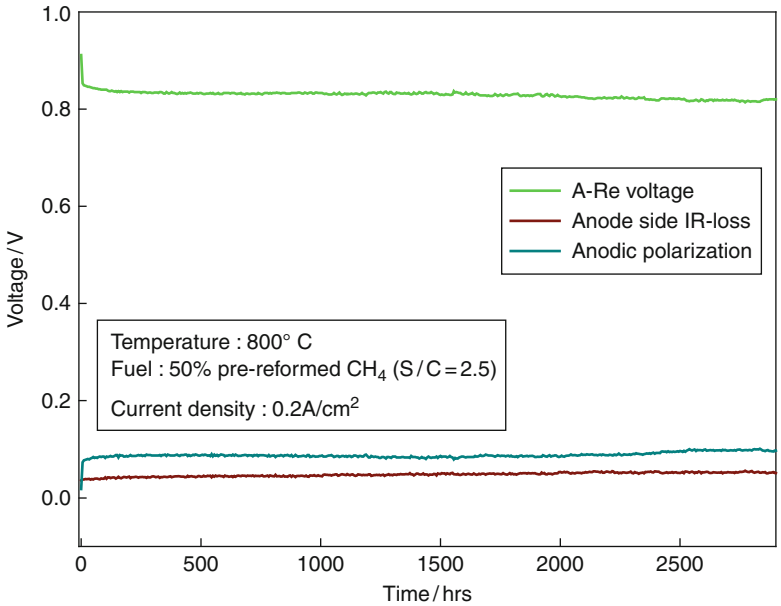

Fuel Cells (SOFC): Alternative Approaches (Electroytes, Electrodes, Fuels). Figure 27
Cell voltage, anodic polarization, and anode-side IR loss, measured at 200 mA/cm^2 during H_2S (5 ppm) poisoning at 800°C for the 50% pre-reformed CH_4 fuel with *S/C* = 2.5

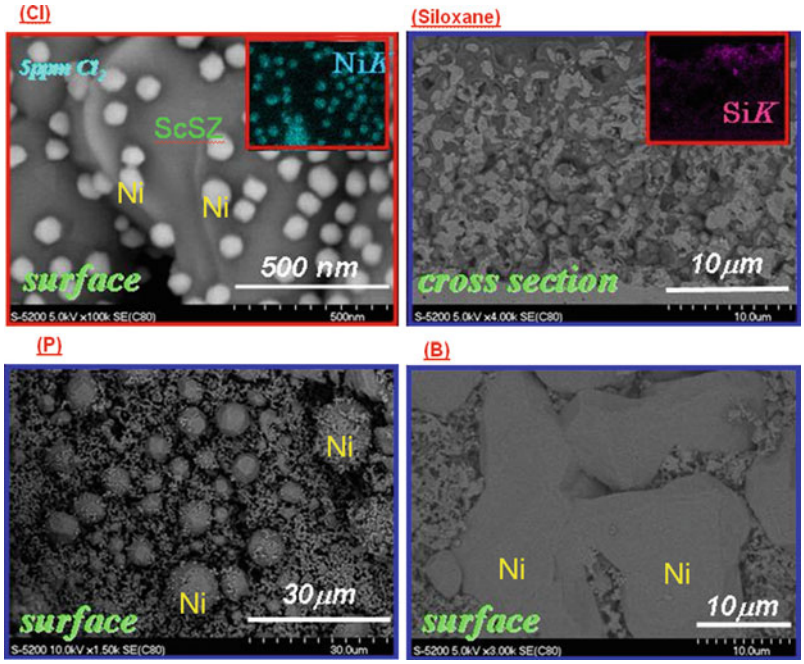

Fuel Cells (SOFC): Alternative Approaches (Electroytes, Electrodes, Fuels). Figure 28
Microstructural change of anodes by various impurities: chlorine, siloxane, phosphorus, and boron. Nanocrystalline Ni precipitates after chlorine poisoning, melted Ni particles after phosphorus poisoning, and grown Ni grains after boron poisoning can be distinguished, while deposited SiO_2 (dark grains) filling the porous Ni-cermet (bright grain) anode can be seen in the cross section of the anode after the siloxane poisoning [262, 266] (Reproduced with permission from Elsevier)

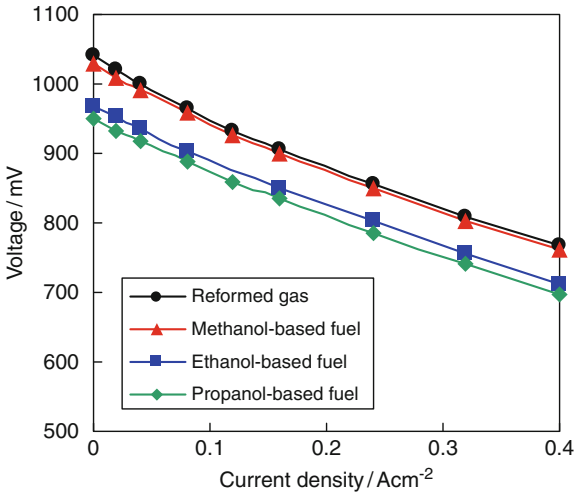

Fuel Cells (SOFC): Alternative Approaches (Electroytes, Electrodes, Fuels). Figure 29
Current-voltage characteristics of SOFCs for alcohol-based fuels at 1,000°C [257] (Reproduced by permission of ECS-The Electrochemical Society)

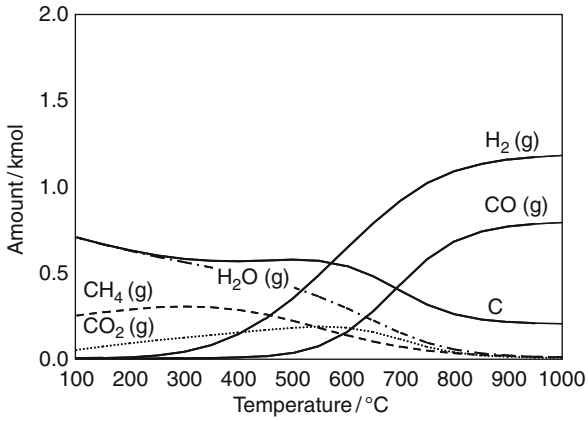

Fuel Cells (SOFC): Alternative Approaches (Electroytes, Electrodes, Fuels). Figure 30
Equilibrium products from biogas (CH_4 60% and CO_2 40%). The calculations are performed by assuming that 1 kmol carbon is supplied

Biogas

The use of biogas as a fuel for SOFCs is of both technological and environmental interest [3, 4, 251, 260, 270, 275–278]. Biogas can be produced from biomass via various procedures such as fermentation and thermal decomposition. Organic municipal wastes (biowastes) are all metabolized by bacteria under anaerobic conditions producing a mixed gas consisting of ca. 60% CH_4 and 40% CO_2. Anaerobic fermentation which proceeds in a reducing atmosphere enables us to extract chemical energy of biowastes as CH_4-rich biogas. Figure 30 shows the equilibrium products from biogas initially consisting of CH_4 and CO_2. High-temperature equilibrium gas from the biogas mainly consists of H_2 and CO, so that a comparable electrochemical performance with hydrogen-based fuels [275, 277] is expected. This figure also indicates that carbon formation is thermochemically expected, so that an addition of H_2O (water vapor) and/or O_2 is needed.

As practical examples, Fig. 31 shows the cell voltages of internal reforming SOFC running on biogas measured at 200 mA cm^{-2} [278]. Simulated biogas with the CH_4/CO_2 ratio of 1.5 had led to stable cell voltage above 0.8 V for 800 h without pre-reformer and humidifier. The degradation rate of only 0.4%/1,000 h

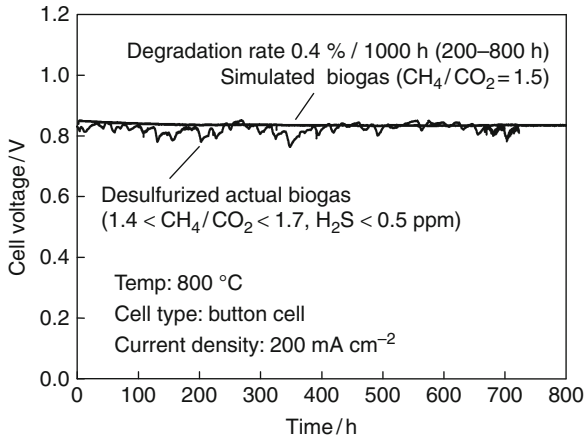

Fuel Cells (SOFC): Alternative Approaches (Electroytes, Electrodes, Fuels). Figure 31
Performance of direct-biogas SOFC: 1 month test of internal reforming SOFC running on simulated and desulfurized actual biogases at 800°C using anode-supported button cells

has proven that the biogas-fueled SOFC can be operated in the internal reforming mode. As for the actual biogas, a rather high voltage comparable to that obtained by simulated biogas was achieved for 1 month. Monitoring of biogas composition simultaneously with the cell voltage has showed that voltage

fluctuation (a maximum of 50 mV level) is related to the fluctuation of the CH_4/CO_2 ratio [270] (Fig. 32). Abrupt decrease in CH_4 concentration (or abrupt increase in CO_2 concentration) induced temporarily lower cell voltage. The CH_4/CO_2 ratio in the actual biogas fluctuated between 1.4 and 1.7, corresponding to a CH_4 concentration ranging between 58 and 63 vol%. Biogas composition is influenced by many factors, for example, kinds of organic wastes, their physical states, and operational conditions of methane fermentation such as temperature and pH of the waste slurry.

It should be noted that carbon deposition was more noticeable for the desulfurized actual biogas compared to simulated biogas. Judging from the result of the gas analysis, carbon deposition is probably triggered by traces of H_2S in the desulfurized biogas which can cause deactivation of Ni catalyst for the dry reforming of methane [270]. Acceleration of carbon deposition in the presence of trace H_2S was also reported for SOFCs operated with partially reformed CH_4-based fuels [262]. Air addition to biogas is effective in preventing carbon deposition [277]. Solid oxide fuel cells could therefore become a core technology in a carbon-neutral zero-emission renewable energy systems, as biogas can be efficiently converted to electricity and heat, while exhaust CO_2 gas may be reused in photosynthesis of biomass using solar energy.

Coal Gas

As one of the most abundant and inexpensive fossil energy resources [279], coal can be used to produce coal gas, with CO and H_2 as main constituents. Coal gas could be applied as a fuel for a combined-cycle power plant with coal gasifier, SOFCs, and gas (and steam) turbine(s) [2, 256, 280–284]. The concentration of water vapor and carrier gas in such a gas depends on the gasification procedures for the partial oxidation of coal by air, oxygen, or water [280]. It is therefore of technological relevance to analyze power generation characteristics of SOFCs operated with mixed H_2 and CO fuel gases, with consideration that coal gas is CO-rich in general.

Figure 33 shows the I-V characteristics of a SOFC at 1,000°C for different H_2-to-CO ratios [256]. The open-circuit voltage increased slightly with decreasing fraction of CO gas, expected from the oxygen partial pressures in thermochemical equilibrium. Figure 33 shows that the I–V characteristics improved, that is, the cell voltage increased for a given current density with decreasing CO concentration of the mixed gas. This change in the I–V characteristics became significant with increasing current density, but this result clearly indicates that the mixture of CO and H_2, the major constituents of coal gas, can be applied as SOFC fuels, provided that fuel impurity effects can be avoided.

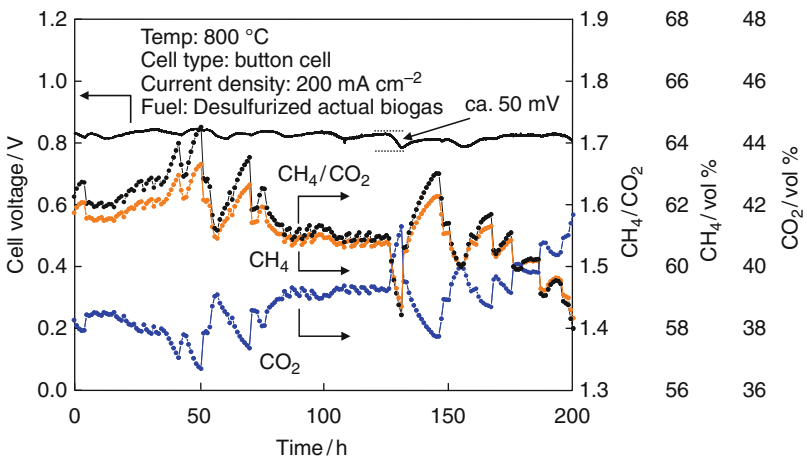

Fuel Cells (SOFC): Alternative Approaches (Electroytes, Electrodes, Fuels). Figure 32
Voltage fluctuation in synchronization with the fluctuation of biogas composition during the long-term test (initial 200 h of Fig. 31 is shown)

It should be noted that raw coal gas contains various kinds of fuel impurities, so that poisoning effects should be carefully examined. Influence of typical fuel impurities in coal gas on electrochemical performance and microstructural stability has been extensively studied and discussed in the literature [262–266, 268, 285–290].

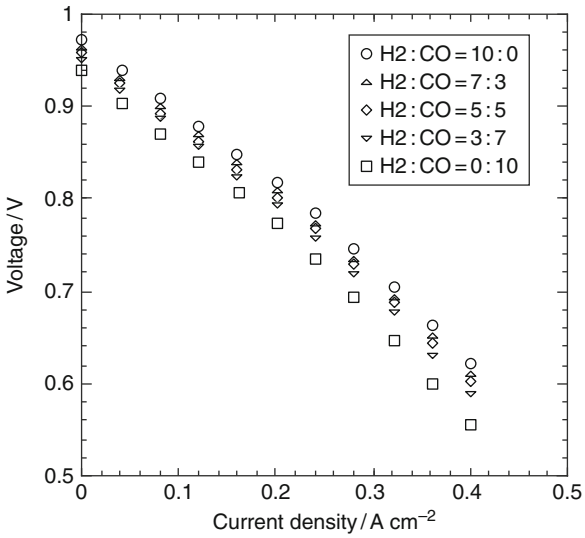

Fuel Cells (SOFC): Alternative Approaches (Electroytes, Electrodes, Fuels). Figure 33
Typical I-V characteristics of SOFCs for different H_2-to-CO ratios at 1,000°C [256] (Reproduced with permission from ECS – The Electrochemical Society)

Future Directions

The first-generation SOFC systems just commercialized are constructed using the most common materials such as stabilized ZrO_2 electrolytes, $La(Sr)MnO_3$ cathodes, and Ni cermets, and applying the most conventional fuels such as city gas. However alternative materials and fuels could expand the future applicability of SOFCs. Table 3 briefly summarizes the state-of-the-art and alternative materials for electrolytes, cathodes, and anodes, as well as possible fuels and applications. Advanced materials may offer alternatives too, for example, high-temperature polymer electrolyte fuel cells, direct-alcohol fuel cells, and portable fuel cells, as well as fuel cells for power generation, cogeneration, and transportation. Advanced fuel electrode materials may realize flexible SOFCs applicable to wide varieties of fuels. Nanostructural design may considerably improve their electrochemical performance, for example, by tailoring nano-size and stress effects, by reducing grain boundary resistivity, as well as by introducing fast ionic/mixed conducting pathways.

While most of the alternative materials and fuels mentioned in this entry have not yet been tested in fuel cell stacks/systems or even as a single cell, they may

Fuel Cells (SOFC): Alternative Approaches (Electroytes, Electrodes, Fuels). Table 3 State-of-the art technologies and typical alternatives of SOFC materials, fuels, and applications

	Electrolyte materials	Cathode materials	Anode materials	Fuels	Possible applications
State-of-the-art technologies	$ZrO_2(Y_2O_3)$ (YSZ) $ZrO_2(Sc_2O_3)$ (ScSZ) $La(Sr)Ga(Mg)O_3$	$La(Sr)MnO_3$ $La(Sr)Co(Fe)O_3$ $Sm(Sr)CoO_3$	Ni/YSZ Ni/ScSZ $Ni/CeO_2(Gd_2O_3)$	City gas, LP gas, H_2	Stational cogenerations, Distributed power units, Combined power plants (SOFC/turbine)
Typical alternatives	$CeO_2(Gd_2O_3)$ $Gd_2(Zr_xTi_{1-x})_2O_7$ $Ba_2In_2O_5$ $La_{9.33}Si_6O_{26}$ $La_{9.33}Ge_6O_{26}$ $BaCe(Y)O_3$ $BaZr(Y)O_3$	$Ba(Sr)Co(Fe)O_3$ $Gd(Sr)CoO_3$ $Sm(Sr)CoO_3$ $La_2(Sr)NiO_4$ Nd_2NiO_4 $Ag\text{-}La(Sr)MnO_3$	$La(Sr)Cr(Mn)O_3$ $La(Sr)Cr(Ru)O_3$ $Sr(La)TiO_3$ $CuYSZ(CeO_2)$	Kerosene, Gasoline, Diesel, Alcohol, Biogas/ biofuel, Coal gas, DME	Automotive APU/power units, Stational applications with kerosene, Coal gas power generation, Portable applications, Direct-alcohol SOFCs, Carbon-neutral power generation using biofuels

have potential for wider varieties of applications in the future. Among others, the following possibilities should be emphasized to consider future directions: (1) High electrical efficiency beyond 50% is attractive to bring about distributed power generation [291], where high ionic conductivity of the electrolyte, low electrode polarization, low contact resistance, as well as sufficient durability are essential. (2) Low-temperature SOFCs may actualize mobile applications of SOFCs where much higher ionic conductance and electrode activities should be tailored [15, 292–297] and more sophisticated materials design at microscopic levels becomes important [9, 13, 298–300]. (3) As the operational temperature of the low-temperature SOFC approaches that of high-temperature PEFCs, we may also learn much from materials and electrochemical research for PEFCs [301–305], which may lead to an integration of materials research between SOFC and PEFC. (4) Fuel-flexible SOFCs may contribute to energy security by using a wide variety of fuels and carbon-neutral power generation by using regenerable energy resources, for which robustness and poisoning tolerance of electrodes may be critical [255, 260, 262]. SOFC researchers should take responsibilities to fulfill their potentials and possibilities via concept demonstrations of operating materials, devices, and systems.

Readers may read references 9, 21, 23, 24, 26, 28, 29, 79, and 100 to understand fundamental materials science related to the topic of this chapter. In order to understand the very early stage of this research field, readers may check references 39, 40, and 126.

Acknowledgments

Financial support by the current NEDO project "Development of System and Elemental Technology on Solid Oxide Fuel Cells (SOFC)" is gratefully acknowledged. We thank Associate Prof. A. Hayashi and WPI Assistant Profs. S. Lyth and S. Bishop in Kyushu University for carefully reading the manuscript and Ms. A. Zaitsu in Kyushu University for her editorial work.

Bibliography

1. Steele BCH, Heinzel A (2001) Materials for fuel-cell technologies. Nature 414:345–352
2. Minh NQ, Takahashi T (1995) Science and technology of ceramic fuel cells. Elsevier, Amsterdam
3. Singhal SC, Kendall K (2003) High-temperature solid oxide fuel cells: fundamentals, design and application. Elsevier, Oxford, UK
4. Larminie J, Dicks A (2003) Fuel cell systems explained, 2nd edn. Wiley, West Sussex, UK
5. Tagawa H (1998) Solid oxide fuel cells and global environment. Agune-Shofudo, Shinjuku, Tokyo (in Japanese)
6. Steinberger-Wilckens R (2009) European SOFC R&D – status and trends. ECS Trans 25(2):3–10
7. Hosoi K, Nakabaru M (2009) Status of national project for SOFC development in Japan. ECS Trans 25(2):11–20
8. Surdoval WA (2009) The status of SOFC programs in USA 2009. ECS Trans 25(2):21–27
9. Maier J (2004) Physical Chemistry of ionic materials: ions and electrons in solids. Wiley, West Sussex, UK
10. Sata N, Eberman K, Eberl K, Maier J (2000) Mesoscopic fast ion conduction in nanometre-scale planar heterostructures. Nature 408:946–949
11. Garcia-Barriocanal J, Rivera-Calzada A, Varela M, Sefrioui Z, Iborra E, Leon C, Pennycook SJ, Santamaria J (2008) Colossal ionic conductivity at interfaces of epitaxial ZrO_2:Y_2O_3/$SrTiO_3$ heterostructures. Science 321(5889):676–680
12. Tuller HL (2000) Ionic conduction in nanocrystalline materials. Solid State Ionics 131(1–2):143–157
13. Maier J (2004) Nano-ionics: more than just a fashionable slogan. J Electroceram 13(1–3):593–598
14. Araki W, Arai Y (2010) Oxygen diffusion in yttria-stabilized zirconia subjected to uniaxial stress. Solid State Ionics 181(8–10):441–446
15. Litzelman SJ, Hertz JL, Jung W, Tuller HL (2008) Opportunities and challenges in materials development for thin film solid oxide fuel cells. Fuel Cells 8(5):294–302
16. Evans A, Bieberle-Hütter A, Rupp JLM, Gauckler LJ (2009) Review on microfabricated micro-solid oxide fuel cell membranes. J Power Sources 194(1):119–129
17. Ihara M, Hasegawa S (2006) Quickly rechargeable direct carbon solid oxide fuel cell with propane for recharging. J Electrochem Soc 153(8):A1544–A1546
18. Hauch A, Jensen SH, Ramousse S, Mogensen M (2006) Performance and durability of solid oxide electrolysis cells. J Electrochem Soc 153(9):A1741–A1747
19. Ishihara T, Kanno T (2010) Steam electrolysis using $LaGaO_3$ based perovskite electrolyte for recovery of unused heat energy. ISIJ Int 50:1291–1295
20. Minh NQ (2010) Operating characteristics of solid oxide fuel cell stacks and systems. ECS Trans 25(2):241–246
21. Steele BCH (1989) Oxygen ion conductors. In: Takahashi T (ed) High conductivity solid ionic conductors. World Scientific, Singapore, pp 402–446
22. Steele BCH (1992) Oxygen ion conductors and their technological applications. In: Balkanski M, Takahashi T, Tuller HL (eds) Solid state ionics. Elsevier, Amsterdam, pp 17–28
23. Nowick AS (1984) Atom transport in oxides of the fluorite structure. In: Diffusion in crystalline solids. Academic, Orlando, pp 143–188

24. Hayes W, Stoneham AM (1985) Defects and defect processes in nonmetallic solids. Wiley, New York
25. Kilner JA, Steele BCH (1981) Mass transport in anion-deficient fluorite oxides. In: Sørensen OT (ed) Nonstoichiometric oxides. Academic, New York, pp 233–269
26. Kofstad P (1972) Nonstoichiometry, diffusion, and electrical conductivity in binary metal oxides. Wiley-Interscience, New York
27. Eyring L (1979) The binary rare earth oxides. In: Gschneidner KA Jr, Eyring L (eds) Handbook on the physics and chemistry of rare earths, vol 3. North-Holland, Amsterdam, pp 337–399, Chap 27
28. Tuller HL (1991) Highly conductive ceramics. In: Buchanan RC (ed) Ceramic materials for electronics. Marcel Dekker, New York, pp 379–433
29. Tuller HL (1981) Mixed conduction in nonstoichiometric oxides. In: Sørensen OT, Sørensen OT (eds) Nonstoichiometric oxides. Academic, New York, pp 271–335
30. Shimizu K, Kashiwagi K, Nishiyama H, Kakimoto S, Sugaya S, Yokoi H, Satsuma A (2008) Impedancemetric gas sensor based on Pt and WO_3 co-loaded TiO_2 and ZrO_2 as total NO_x sensing materials. Sens Actuators B Chem 130:707–712
31. Gong J, Li Y, Tang Z, Zhang Z (2000) Enhancement of the ionic conductivity of mixed calcia/yttria stabilized zirconia. Mater Lett 46:115–119
32. Gauckler LJ, Sasaki K (1994) Ionic and electronic conductivities of homogeneous and heterogeneous materials in the system ZrO_2-In_2O_3. Solid State Ionics 75:203–210
33. Sasaki K (1993) Phase equilibria, electrical conductivity, and electrochemical properties of ZrO_2-In_2O_3. Dissertation, Swiss Federal Institute of Technology, Zürich, Switzerland
34. Stafford RJ, Rothman SJ, Routbort JL (1989) Effect of dopant size on the ionic conductivity of cubic stabilized ZrO_2. Solid State Ionics 37:67–72
35. Arachi Y, Sakai H, Yamamoto O, Takeda Y, Imanishi N (1999) Electrical conductivity of the ZrO_2–Ln_2O_3 (Ln = lanthanides) system. Solid State Ionics 121:133–139
36. Patterson JW (1971) Conduction domains for solid electrolytes. J Electrochem Soc 118:1033–1039
37. Heyne L, Engleson D (1977) The speed of response of solid electrolyte galvanic cells for Gas sensing. J Electrochem Soc 124:727–735
38. Tuller HL, Moon PK (1988) Fast ion conductors: future trends. Mater Sci Eng B1:171–191
39. Nernst W (1899) Über die elektrolytische Leitung fester Körper bei sehr hohen Temperaturen. Z Elektrochem 6(2):41–43
40. Baur E, Preis H (1937) Über Brennstoff-Ketten mit Festleitern. Z Elektrochem 44(9):695–698
41. Sasaki K, Maier J (2000) Re-analysis of defect equilibria and transport properties of Y_2O_3-stabilized ZrO_2 using EPR and optical relaxation. Solid State Ionics 134(3–4):303–321
42. Inaba H, Tagawa H (1996) Ceria-based solid electrolytes. Solid State Ionics 83:1–16
43. Sammes NM, Tompsett GA, Näfe H, Aldinger F (1999) Bismuth based oxide electrolytes-structure and ionic conductivity. J Eur Ceram Soc 19:1801–1826
44. Mogensen M, Sammes NM, Tompsett GA (2000) Physical, chemical and electrochemical properties of pure and doped ceria. Solid State Ionics 129:63–94
45. Yamamoto O, Arachi Y, Sakai H, Takeda Y, Imanishi N, Mizutani Y, Kawai M, Nakamura Y (1998) Zirconia based oxide ion conductors for solid oxide fuel cells. Ionics 4:403–408
46. Arachi Y, Asai T, Yamamoto O, Takeda Y, Imanishi N, Kawate K, Tamakoshi C (2001) Electrical conductivity of ZrO_2-Sc_2O_3 doped with HfO_2, CeO_2, and Ga_2O_3. J Electrochem Soc 148(5):A520–A523
47. Yamamoto O, Arati Y, Takeda Y, Imanishi N, Mizutani Y, Kawai M, Nakamura Y (1995) Electrical conductivity of stabilized zirconia with ytterbia and scandia. Solid State Ionics 79:137–142
48. Tietz F, Fischer W, Hauber Th, Mariotto G (1997) Structural evolution of Sc-containing zirconia electrolytes. Solid State Ionics 100:289–295
49. Wang Z, Cheng M, Bi Z, Dong Y, Zhang H, Zhang J, Feng Z, Li C (2005) Structure and impedance of ZrO_2 doped with Sc_2O_3 and CeO_2. Mater Lett 59:2579–2582
50. Gödickemeier M, Michel B, Orliukas A, Bohac P, Sasaki K, Gauckler LJ, Heinrich H, Schwander P, Kostorz G, Hofmann H, Frei O (1994) Effect of intergranular glass films on the electrical conductivity of 3Y-TZP. J Mater Res 9(5):1228–1240
51. Bieberle-Hütter A, Beckel D, Infortuna A, Muecke UP, Rupp JLM, Gauckler LJ, Rey-Mermet S, Muralt P, Bieri NR, Hotz N, Stutz MJ, Poulikakos D, Heeb P, Müller P, Bernard A, Gmür R, Hocker T (2008) A micro-solid oxide fuel cell system as battery replacement. J Power Sources 177:123–130
52. Ji Y, Kilner JA, Carolan MF (2005) Electrical properties and oxygen diffusion in yttria-stabilised zirconia (YSZ)–$La_{0.8}Sr_{0.2}MnO_{3\pm\delta}$(LSM) composites. Solid State Ionics 176:937–943
53. Ralph JM, Rossignol C, Kumar R (2003) Cathode materials for reduced-temperature SOFCs. J Electrochem Soc 150(11): A1518–A1522
54. Stochniol G, Syskakis E, Naoumidis A (1995) Chemical compatibility between strontium-doped lanthanum manganite and yttria-stabilized zirconia. J Am Ceram Soc 78:929–932
55. Zhao H, Huo I, Sun L, Yu L, Gao S, Zhao J (2004) Preparation, chemical stability and electrochemical properties of LSCF–CBO composite cathodes. Mater Chem Phys 88:160–166
56. Yahiro H, Eguchi K, Arai H (1986) Ionic conduction and microstructure of the ceria-strontia system. Solid State Ionics 21:37–47
57. Thangadurai V, Kopp P (2007) Chemical synthesis of Ca-doped CeO_2 - intermediate temperature oxide ion electrolytes. J Power Sources 168:178–183
58. Eguchi K, Setoguchi T, Inoue T, Arai H (1992) Electrical properties of ceria-based oxides and their application to solid oxide fuel cells. Solid State Ionics 52:165–172
59. Yahiro H, Baba Y, Eguchi Y, Eguchi K, Arai H (1988) High temperature fuel cell with ceria-yttria solid electrolyte. J Electrochem Soc 135:2077–2080
60. Shobit Omar S, Wachsman ED, Nino JC (2008) Higher conductivity Sm^{3+} and Nd^{3+} co-doped ceria-based electrolyte materials. Solid State Ionics 178:1890–1897

61. Bance P, Brandon NP, Girvan B, Holbeche P, O'Dea S, Steele BCH (2004) Spinning-out a fuel cell company from a UK University-2 years of progress at Ceres Power. J Power Sources 131:86–90
62. Göedickemeier M, Gauckler LJ (1998) Engineering of solid oxide fuel cells with ceria-based electrolytes. J Electrochem Soc 145:414–421
63. Atkinson A (1997) Chemically-induced stresses in gadolinium-doped ceria solid oxide fuel cell electrolytes. Solid State Ionics 95:249–258
64. Marques FMB, Navarro LM (1997) Performance of double layer electrolyte cells Part II: GCO/YSZ, a case study. Solid State Ionics 100:29–38
65. Tsoda A, Gupta A, Naoumoidis A, Skarmoutsos D, Nikolopoulos P (1998) Performance of a double-layer CGO/YSZ electrolyte for solid oxide fuel cells. Ionics 4:234–240
66. Kharton VV, Figueiredo FM, Navarro L, Naumovich EN, Kovalevsky AV, Yaremchenko AA, Viskup AP, Carneiro A, Marques FMB, Frade JR (2001) Ceria-based materials for solid oxide fuel cells. J Mater Sci 36:1105–1117
67. Oishi N, Atkinson A, Brandon NP, Kilner JA, Steele BCH (2005) Fabrication of an anode-supported gadolinium-doped ceria solid oxide fuel cell and its operation at 550°C. J Am Ceram Soc 88(6):1394–1396
68. Oishi N, Yoo Y (2010) Evaluation of metal supported ceria based solid oxide fuel cell fabricated by wet powder spray and sintering. J Electrochem Soc 157(1):B125–B129
69. Moon PK, Tuller HL (1990) Evaluation of the $Gd_2(Zr_xTi_{1-x})_2O_7$ pyroclore system as an oxygen Gas sensor. Sens Actuators B Chem 1:199–202
70. Yamamura H, Nishino H, Kakinuma K, Nomura K (2003) Electrical conductivity anomaly around fluorite–pyrochlore phase boundary. Solid State Ionics 158:359–365
71. Moon PK, Tuller HL (1988) Ionic-conduction in the $Gd_2Ti_2O_7$-$Gd_2Zr_2O_7$ system. Solid State Ionics 28–30(1): 470–474
72. Kramer SA, Tuller HL (1995) A novel titanate-based oxygen ion conductor: $Gd_2Ti_2O_7$. Solid State Ionics 82:15–23
73. Kharton VV, Tsipis EV, Yaremechenko AA, Vyshatko NP, Shaula AL, Naumovich EN, Frade JR (2003) Oxygen ionic and electronic transport in $Gd_{2-x}Ca_xTi_2O_{7-\delta}$ pyrochlores. J Solid State Electrochem 7:468–476
74. Mori M, Tompsett GM, Sammes NM, Suda E, Takeda Y (2003) Compatibility of $Gd_xTi_2O_7$ pyrochlores ($1.72 \leq x \leq 2.0$) as electrolytes in high-temperature solid oxide fuel cells. Solid State Ionics 158:79–90
75. Yasuda I, Matsuzaki Y, Yamakawa T, Koyama T (2000) Electrical conductivity and mechanical properties of alumina-dispersed doped lanthanum gallates. Solid State Ionics 135:381–388
76. Tietz F (1999) Thermal expansion of SOFC materials. Ionics 5:129–139
77. Lee JH, Yoshimura M (1999) Phase stability and electrical conductivity of the $Zr_{0.5}Y_{0.5}O_{1.75}$-$Y_{0.75}Nb_{0.25}O_{1.75}$ system. Solid State Ionics 124:185–191
78. Lee JH, Yashima M, Yoshimura M (1998) Ionic conductivity of fluorite-structured solid solution $Y_{0.8}Nb_{0.2}O_{1.7}$. Solid State Ionics 107:47–51
79. West AR (1999) Basic solid state chemistry. Wiley, Chichester
80. Roth RS (1957) Classification of perovskite and other ABO_3-type compounds. J Res Nat Bur Stand 58:75–88
81. Takahashi T, Iwahara H (1971) Ionic conduction in perovskite-type oxide solid solution and its application to the solid electrolyte fuel cell. Energy Convers 11:105–111
82. Ishihara T, Matsuda H, Takita Y (1994) Doped $LaGaO_3$ perovskite type oxide as a new oxide ionic conductor. J Am Chem Soc 116:3801–3803
83. Ishihara T, Matsuda H, Takita Y (1995) Effects of rare earth cations doped for La site on the oxide ionic conductivity of $LaGaO_3$-based perovskite type oxide. Solid State Ionics 79:147–151
84. Ishihara T, Ishikawa S, Yu C, Akbay T, Hosoi K, Nishiguchi H, Takita Y (2003) Oxide ion and electronic conductivity in Co doped $La_{0.8}Sr_{0.2}Ga_{0.8}Mg_{0.2}O_3$ perovskite oxide. Phys Chem Chem Phys 5:2257–2263
85. Ishihara T (2001) Current status of intermediate temperature solid oxide fuel cell (in Japanese). Bull Ceram Soc Jpn 36:483–485
86. Islam MS, Davis RA (2004) Atomistic study of dopant site-selectivity and defect association in the lanthanum gallate perovskite. J Mater Chem 14:86–93
87. Huang K, Feng M, Goodenough JB, Schmerling M (1996) Characterization of Sr-doped $LaMnO_3$ and $LaCoO_3$ as cathode materials for a doped $LaGaO_3$ ceramic fuel cell. J Electrochem Soc 143(11):3630–3636
88. Kostogloudis GC, Ftikos C, Ahmad-Khanlou A, Naoumidis A, Stöver D (2000) Chemical compatibility of alternative perovskite oxide SOFC cathodes with doped lanthanum gallate solid electrolyte. Solid State Ionics 134:127–138
89. Shaula AL, Kharton VV, Marques FMB (2004) Phase interaction and oxygen transport in $La_{0.8}Sr_{0.2}Fe_{0.8}Co_{0.2}O_3$–$(La_{0.9}Sr_{0.1})_{0.98}$ $Ga_{0.8}Mg_{0.2}O_3$ composites. J Eur Ceram Soc 24:2631–2639
90. Sakai N, Horita T, Yamaji K, Brito ME, Yokokawa H, Kawakami A, Matsuoka S, Watanabe N, Ueno A (2006) Interface stability among solid oxide fuel cell materials with perovskite structures. J Electrochem Soc 153(3):A621–A625
91. Joshi AV, Steppan JJ, Taylor DM, Elangovan S (2004) Solid electrolyte materials, devices, and applications. J Electroceram 13:619–625
92. Schober T (1998) Protonic conduction in $BaIn_{0.5}Sn_{0.5}O_{2.75}$. Solid State Ionics 109:1–11
93. Goodenough JB (1997) Ceramic solid electrolytes. Solid State Ionics 94:17–25
94. Goodenough JB, Ruiz-Dias JE, Zhen YS (1990) Oxide-ion conduction in $Ba_2In_2O_5$ and $Ba_3In_2MO_8$ (M = Ce, Hf, or Zr). Solid State Ionics 44:21–31
95. Manthiram A, Kuo JF, Goodenough JB (1993) Characterization of oxygen-deficient perovskites as oxide-ion electrolytes. Solid State Ionics 62:225–234

96. Uchimoto Y, Kinuhata M, Takagi H, Yao T, Inagaki T, Yoshida H (1999) Crystal structure of metal cation-doped $Ba_2In_2O_5$ and its oxide Ion conductivity. In: Proceedings of SOFC VI, Electrochemical Society, Pennington, pp 317–326
97. Schober T, Friedri ch J, Krug F (1997) Phase transition in the oxygen and proton conductor $Ba_2In_2O_5$ in humid atmospheres below 300°C. Solid State Ionics 99:9–13
98. Hashimoto T, Inagaki Y, Kishi A, Dokiya M (2000) Absorption and secession of H_2O and CO_2 on $Ba_2In_2O_5$ and their effects on crystal structure. Solid State Ionics 128:227–231
99. Zhang GB, Smyth DM (1995) Defects and transport of the brownmillerite oxides with high oxygen ion conductivity - $Ba_2In_2O_5$. Solid State Ionics 82:161–172
100. Kingery WD, Bowen HK, Uhlmann DR (1976) Introduction to ceramics, 2nd edn. Wiley, New York
101. Oyane A (2010) Development of apatite-based composites by a biomimetic process for biomedical applications. J Ceram Soc Jpn 118(2):77–81
102. Felsche J (1972) Rare earth silicates with the apatite structure. J Solid State Chem 5:266–275
103. Park J, Lakes RS (2007) Biomaterials: an introduction, 3rd edn. Springer, New York
104. Bonder IA (1982) Rare-earth silicates. Ceramics Int 8(3):83–89
105. Higuchi Y, Sugawara M, Onishi K, Sakamoto M, Nakayama S (2010) Oxide ionic conductivities of apatite-type lanthanum silicates and germanates and their possibilities as an electrolyte of lower temperature operating SOFC. Ceramics Int 36:955–959
106. Panteix PJ, Béchade E, Julien I, Abélard P, Bernache-Assollant D (2008) Influence of anionic vacancies on the ionic conductivity of silicated rare earth apatites. Mater Res Bull 43: 1223–1231
107. Yoshioka H (2006) Oxide ionic conductivity of apatite-type lanthanum silicates. J Alloys Comp 408–412:649–652
108. Higuchi M, Masubuchi Y, Nakayama S, Kikkawa S, Kodaira K (2004) Single crystal growth and oxide ion conductivity of apatite-type rare-earth silicates. Solid State Ionics 174:73–80
109. Masubuchi Y, Higuchi M, Takeda T, Kikkawa S (2006) Preparation of apatite-type $La_{9.33}(SiO_4)_6O_2$ oxide ion conductor by alcoxide-hydrolysis. J Alloys Comp 408–412:641–644
110. Nojiri Y, Tanase S, Iwasa M, Yoshioka H, Matsumura Y, Sakai T (2010) Ionic conductivity of apatite-type solid electrolyte material, $La_{10-X}Ba_XSi_6O_{27-X/2}$ (X = 0–1), and its fuel cell performance. J Power Sources 195:4059–4064
111. Mineshige A, Nakao T, Kobune M, Yazawa T, Yoshioka H (2008) Electrical properties of $La_{10}Si_6O_{27}$-based oxides. Solid State Ionics 179:1009–1012
112. Nakao T, Mineshige A, Kobune M, Yazawa T, Yoshioka H (2008) Chemical stability of $La_{10}Si_6O_{27}$ and its application to electrolytes for solid oxide fuel cells. Solid State Ionics 179:1567–1569
113. Nakayama S, Kageyama T, Aono H, Sadaoka Y (1995) Ionic conductivity of lanthanoid silicates, $Ln_{10}(SiO_4)_6O_3$ (Ln = La, Nd, Sm, Gd, Dy, Y, Ho, Er and Yb). J Mater Chem 5:1801–1805
114. Nakayama S, Sakamoto M (1998) Electrical properties of new type high oxide ionic conductor $RE_{10}Si_6O_{27}$ (RE = La, Pr, Nd, Sm, Gd, Dy). J Euro Ceram Soc 18:1413–1418
115. Yoshioka H (2007) Enhancement of ionic conductivity of apatite-type lanthanum silicates doped with cations. J Am Ceram Soc 90:3099–3105
116. Yoshioka H, Nojiri Y, Tanase S (2008) Ionic conductivity and fuel cell properties of apatite-type lanthanum silicates doped with Mg and containing excess oxide ions. Solid State Ionics 179:2165–2169
117. Li B, Liu W, Pan W (2010) Synthesis and electrical properties of apatite-type $La_{10}Si_6O_{27}$. J Power Sources 195:2196–2201
118. Pivak YV, Kharton VV, Yaremchenko AA, Yakovlev SO, Kovalevsky AV, Frade JR, Marques FMB (2007) Phase relationships and transport in Ti-, Ce- and Zr-substituted lanthanum silicate systems. J Eur Ceram Soc 27:2445–2454
119. Nojiri Y, Chen WF, Tanase S, Iwasa M, Matsumura Y, Sakai T, Tanase S (2008) Lanthanum silicate with apatite-type structure as an electrolyte for intermediate temperature SOFCs and the electrode materials. ITE-IBA Lett 1(6):498–506
120. León-Reina L, Porras-Vázquez JM, Losilla ER, Aranda MAG (2007) Phase transition and mixed oxide-proton conductivity in germanium oxy-apatites. J Solid State Chem 180:1250–1258
121. Arikawa H, Nishiguchi H, Ishihara T, Takita Y (2000) Oxide ion conductivity in Sr-doped $La_{10}Ge_6O_{27}$ apatite oxide. Solid State Ionics 136–137:31–37
122. Ishihara T, Arikawa H, Akbay T, Nishiguchi H, Takita Y (2001) Nonstoichiometric $La_{2-x}GeO_{5-\delta}$ monoclinic oxide as a new fast oxide ion conductor. J Am Chem Soc 123:203–209
123. Nakayama S, Higuchi Y, Kondo Y, Sakamoto M (2004) Effects of cation- or oxide ion-defect on conductivities of apatite-type La–Ge–O system ceramics. Solid State Ionics 170: 219–223
124. Berastegui P, Hull S, García García FJ, Grins J (2002) A structural investigation of $La_2(GeO_4)O$ and alkaline-earth-doped $La_{9.33}(GeO_4)_6O_2$, J. Solid State Chem 168:294–305
125. Kreuer KD (1996) Proton conductivity: materials and applications. Chem Mater 8(3):610–641
126. Wagner C (1968) Die Löslichkeit von Wasserdampf in ZrO_2-Y_2O_3-Mischkristallen, Berichte Bunseng. Phys Chem 72(7):778–781
127. Alberti G, Casciola M (2001) Solid state protonic conductors, present main applications and future prospects. Solid State Ionics 145:3–16
128. Xu ZP, Jin Y, Diniz da Costa JC, Lu GQM (2008) $Zr(HPO_4)_2$ based organic/inorganic nanohybrids as new proton conductors. Solid State Ionics 178:1654–1659
129. Ahmad MI, Zaidi SMJ, Ruhman SU, Ahmed S (2006) Synthesis and proton conductivity of heteropolyacids loaded Y-zeolite as solid proton conductors for fuel cell applications. Miropor Mesopor Mater 91:296–304
130. Norby T (1999) Solid-state protonic conductors: principles, properties, progress and prospects. Solid State Ionics 125:1–11
131. Daiko Y, Nguyen VH, Yazawa T, Muto H, Sakai M, Matsuda A (2010) Phase transition and proton conductivity of

$CsHSO_4$–WPA composites prepared by mechanical milling. Solid State Ionics 181:183–186
132. Sugahara T, Hayashi A, Tadanaga K, Tatsumisago M (2010) Characterization of proton conducting $CsHSO_4$-CsH_2PO_4 ionic glasses prepared by the melt-quenching method. Solid State Ionics 181:190–192
133. Iwahara H, Esaka T, Uchida H, Maeda N (1981) Proton conduction in sintered oxides and its application to steam electrolysis for hydrogen production. Solid State Ionics 3(4):359–363
134. Fukatsu N, Kurita N, Yajima T, Koide K, Ohashi T (1995) Proton conductors of oxide and their application to research into metal-hydrogen systems. J Alloys Comp 231:706–712
135. Schwartz M, Link BF, Sammells AF (1993) New brownmillerite solid electrolytes. J Electrochem Soc 140:L62–L63
136. Zahang GB, Smyth DM (1995) Protonic conduction in $Ba_2In_2O_5$. Solid State Ionics 82:153–160
137. Fisher CSJ, Islam MS (1999) Defect, protons and conductivity in brownmillerite-structured $Ba_2In_2O_5$. Solid State Ionics 118:355–363
138. Orera A, Slater PR (2010) Water incorporation studies in apatite-type rare earth silicates/germinates. Solid State Ionics 181:110–114
139. Marrero-López D, Martín-Sedeño MC, Ruiz-Morales JC, Núñez P, Ramos-Barrado JR (2010) Preparation and characterisation of $La_{10-x}Ge_{5.5}Al_{0.5}O_{26\pm\delta}$ apatites by freeze-drying precursor method. Mater Res Bull 45:409–415
140. Ito N, Iijima M, Kimura K, Iguchi S (2005) New intermediate temperature fuel cell with ultra-thin proton conductor electrolyte. J Power Sources 152:200–203
141. Matsumoto H, Nomura I, Okada S, Ishihara T (2008) Intermediate-temperature solid oxide fuel cells using perovskite-type oxide based on barium cerate. Solid State Ionics 179: 1486–1489
142. Ishigaki T, Yamauchi S, Kishio K, Fueki K, Iwahara H (1986) Dissolution of deuterium into proton conductor $SrCe_{0.95}Yb_{0.05}O_{3-\delta}$. Solid State Ionics 21:239–241
143. Iwahara H, Uchida H, Ono K, Ogaki K (1998) Proton conduction in sintered oxides based on $BaCeO_3$. J Electrochem Soc 135:529–533
144. Bonanos N, Ellis B, Mahmood MN (1991) Construction and operation of fuel cells based on the solid electrolyte $BaCeO_3$: Gd. Solid State Ionics 44:305–311
145. Ma G, Matsumoto H, Iwahara H (1999) Ionic conduction and nonstoichiometry in non-doped $Ba_xCeO_{3-\alpha}$. Solid State Ionics 122:237–247
146. Taniguchi N, Hatoh K, Niikura J, Gamo T, Iwahara H (1992) Proton conductive properties of gadolinium-doped barium cerates at high temperatures. Solid State Ionics 53–56: 998–1003
147. Ma G, Shimura T, Iwahara H (1998) Ionic conduction and nonstoichiometry in $Ba_xCe_{0.90}Y_{0.10}O_{3-\alpha}$. Solid State Ionics 110:103–110
148. Ma G, Shimura T, Iwahara H (1999) Simultaneous doping with La^{3+} and Y^{3+} for Ba^{2+} -and Ce^{4+} -sites in $BaCeO_3$ and the ionic conduction. Solid State Ionics 120:51–60
149. Katahira K, Kohchi Y, Shimura T, Iwahara H (2000) Protonic conduction in Zr-substituted $BaCeO_3$. Solid State Ionics 138:91–98
150. Ranran P, Yan W, Lizhai Y, Zongqiang M (2006) Electrochemical properties of intermediate-temperature SOFCs based on proton conducting Sm-doped $BaCeO_3$ electrolyte thin film. Solid State Ionics 177:389–393
151. Su XT, Yan QZ, Ma YH, Zhang WF, Ge CC (2006) Effect of co-dopant addition on the properties of yttrium and neodymium doped barium cerate electrolyte. Solid State Ionics 177:1041–1045
152. Gorbova E, Zhuravlev BV, Demin AK, Song SQ, Tsiakaras PE (2006) Charge transfer properties of $BaCe_{0.88}Nd_{0.12}O_{3-\delta}$ co-ionic electrolyte. J Power Sources 157:720–723
153. Taherparvar H, Kilner JA, Baker RT, Sahibzada M (2003) Effect of humidification at anode and cathode in proton-conducting SOFCs. Solid State Ionics 162–163:297–303
154. Du Y, Nowick AS (1995) Structural transitions and proton conduction in nonstoichiometric $A_3B'B''_2O_9$ perovskite-type oxides. J Am Ceram Soc 78:3033–3039
155. Murugaraj P, Kreuer KD, He T, Schober T, Maier J (1997) High proton conductivity in barium yttrium stannate $Ba_2YSnO_{5.5}$. Solid State Ionics 98:1–6
156. Kreuer KD (2003) Proton conducting oxides. Ann Rev Mater Res 33:333–359
157. He T, Kreuer KD, Baikov YM, Maier J (1997) Impedance spectroscopic study of thermodynamics and kinetics of Gd-doped $BaCeO_3$ single crystal. Solid State Ionics 95:301–308
158. Fabbri E, D'Epifanio A, Di Bartolomeo E, Licoccia S, Traversa E (2008) Tailoring the chemical stability of $Ba(Ce_{0.8-x}Zr_x)Y_{0.2}O_{3-\delta}$ protonic conductors for intermediate temperature solid oxide fuel cells (IT-SOFCs). Solid State Ionics 179:558–564
159. Kreuer KD (1999) Aspects of the formation and mobility of protonic charge carriers and the stability of perovskite-type oxides. Solid State Ionics 125:285–302
160. He T, Ehrhart P, Meuffels P (1995) Optical band gap and Urbach tail in Y-doped $BaCeO_3$. J Appl Phys 79:3219–3223
161. Minh NQ (1993) Ceramic fuel cells. J Am Ceram Soc 76(3):563–588
162. Mackor A, Koster TPM, Kraaijkamp JG, Gerretsen J, van Eijk JPGM (1991) Influence of La-substitution and -substoichiometry on conductivity, thermal expansion and chemical stability of Ca- or Sr-doped lanthanum manganites as SOFC cathodes. In: Grosz F, Zegers P, Singhal SC, Yamamoto O (eds) Proceedings of the 2nd international symposium of solid oxide fuel cells. Commission of European Communities, Luxembourg, pp 463–471
163. Anderson HU (1992) Review of p-type doped perovskite materials for SOFC and other applications. Solid State Ionics 52:33–41
164. Kuo JH, Anderson HU, Sparlin DM (1989) Oxidation-reduction behavior of undoped and Sr-doped $LaMnO_3$: nonstoichiometry and defect structure. J Solid State Chem 83:52–60
165. Kuo JH, Anderson HU, Sparlin DM (1990) Oxidation-reduction behavior of undoped and Sr-doped $LaMnO_3$: defect

structure, electrical conductivity, and thermoelectric power. J Solid State Chem 87:55–63

166. van Roosmalen JAM, Huijsmans JPP, Cordfunke EHP (1991) Sinter behavior and electrical conductivity of (La,Sr) MnO_3 as a function of Sr-content. In: Grosz F, Zegers P, Singhal SC, Yamamoto O (eds) Proceedings 2nd International symposium on solid oxide fuel cells. Commission of European Communities, Luxemborg, pp 507–516
167. Hammouche A, Siebert E, Hammou A (1989) Crystallographic, thermal and electrochemical properties of the system $La_{1-x}Sr_xMnO_3$ for high temperature solid electrolyte fuel cells. Mater Res Bull 24:367–380
168. Yamada H, Nagamoto H (1993) Thermal expansion coefficient and electrical conductivity of Mn-based perovskite-type oxides. In: Singhal SC, Iwahara H (eds) Proceedings of the 3rd International symposium on solid oxide fuel cells, vol 93–94. The Electrochem Society Inc. Proceedings, Pennington, pp 213–219
169. Nasrallah MM, Anderson HU, Stevenson JW (1991) Defect chemistry and properties of $Y_{1-x}Ca_xMnO_3$. In: Grosz F, Zegers P, Singhal SC, Yamamoto O (eds) Proceedings of the 2nd international symposium on solid oxide fuel cells. Commission of European Communities, Luxembourg, pp 545–552
170. Stevenson JW, Nasrallah MM, Anderson HU, Parlin DMS (1993) Defect structure of $Y_{1-y}Ca_yMnO_3$ and $La_{1-y}Ca_yMnO_3$, I. Electrical properties. J Solid State Chem 102:175–184
171. Stevenson JW, Nasrallah MM, Anderson HU, Sparlin DM (1993) Defect structure of $Y_{1-y}Ca_yMnO_3$ and $La_{1-y}Ca_yMnO_3$ II. Oxidation-reduction behavior. J Solid State Chem 102: 185–197
172. Fu B, Huebner W, Trubelja MF, Stubican VS (1993) $(Y_{1-x}Ca_x)FeO_3$: a potential cathode material for solid oxide fuel cells. In: Singhal SC, Iwahara H (eds) Proceedings of the 3rd international symposium on solid oxide fuel cells. Proceedings, vol 93–4. The Electrochemical Society, Pennington, pp 276–287
173. Yamamoto O, Takeda Y, Imanishi N, Sakaki Y (1993) Electrochemical properties of $La_{1-x}Ca_xMnO_{3-z}$ as cathode in SOFC. In: Singhal SC, Iwahara H (eds) Proceedings of the 3rd international symposium on solid oxide fuel cells. Proceedings, vol 93–4. The Electrochemical Society, Pennington, pp 205–212
174. Mizusaki J, Tagawa H, Katou M, Hirano K, Sawata A, Tsuneyoshi K (1991) Electrochemical properties of some perovskite-type oxides as oxygen gas electrodes on yttria stabilized zirconia. In: Grosz F, Zegers P, Singhal SC, Yamamoto O (eds) Proceedings of the 2nd international symposium on solid oxide fuel cells. Commission of European Communities, Luxembourg, pp 487–494
175. Mizusaki J, Tagawa H, Tsuneyoshi K, Sawata A (1991) Reaction kinetics and microstructure of the solid oxide fuel cells air electrode $La_{0.6}Ca_{0.4}MnO_3$/YSZ. J Electrochem Soc 138(7):1867–1873
176. Dokiya M (1992) A historical review on the SOFC research activity at NCLI, (in Japanese). In: Extended abstracts 1st symposium on solid oxide fuel cells, Japan. Solid Oxide Fuel Cells Society Japan, Tokyo, pp 11–14
177. Yokokawa H, Sakai N, Kawada T, Dokiya M (1991) Chemical thermodynamic compatibility of solid oxide fuel cell materials. In: Grosz F, Zegers P, Singhal SC, Yamamoto O (eds) Proceedings of the 2nd international symposium on solid oxide fuel cells. Commission of European Communities, Luxembourg, pp 663–670
178. Yokokawa H, Sakai N, Kawada T, Dokiya M (1992) Thermodynamic stabilities of perovskite oxides for electrodes and other electrochemical materials. Solid State Ionics 52:43–56
179. Otoshi S, Sasaki H, Ohnishi H, Hase M, Ishimaru K, Ippommatsu M, Higuchi T, Miyayama M, Yanagida H (1991) Changes in the phases and electrical conduction properties of $(La_{1-x}Sr_x)_{1-y}MnO_{3-\delta}$. J Electrochem Soc 138(5):1519–1523
180. Takeda Y, Kanno R, Noda M, Tomida Y, Yamamoto O (1987) Cathodic polarization phenomena of perovskite oxide electrodes with stabilized zirconia. J Electrochem Soc 134(11):2656–2661
181. Mizusaki J (1992) Nonstoichiometry, diffusion, and electrical properties of perovskite-type oxide electrode materials. Solid State Ionics 52:79–91
182. Teraoka Y, Nobunaga T, Okamoto K, Miura N, Yamazoe N (1991) Influence of constituent metal cations in substituted $LaCoO_3$ on mixed conductivity and oxygen permeability. Solid State Ionics 48:207–212
183. Ivers-Tiffée E, Schieβl M, Oel HJ, Wersing W (1993) Investigations of cobalt- containing perovskites in SOFC single cells with respect to interface reactions and cell performance. In: Singhal SC, Iwahara H (eds) Proceedings of the 3rd international symposium on solid oxide fuel cells. Proceedings, vol 93–94. The Electrochemical Society, Pennington, pp 613–622
184. Iberl A, von Philipsborn H, Schieβl M, Ivers-Tiffée E, Wersing W, Zorn G (1991) High-temperature X-ray diffraction measurements of phase transitions and thermal expansion in (La,Sr)(Mn,Co)O_3-cathode materials. In: Grosz F, Zegers P, Singhal SC, Yamamoto O (eds) Proceedings of the 2nd international symposium on solid oxide fuel cells. Commission of European Communities, Luxembourg, pp 527–535
185. Mackor A, Spee CIMA, van der Zouwen-Assink EA, Baptista JL, Schoonman J (1990) Mixed conductivity in perovskite SOFC materials $La_{1-x}M_xMn_{1-y}Co_yO_3$ (M = Ca or Sr). In: Proceedings of the 25th intersociety energy conversion engineering conference, American Institute of Chemical Engineers, vol 3, Aug. pp 251–255
186. Tai LW, Nasrallah MM, Anderson HU (1993) $(La_{1-x}Sr_x)(Co_{1-y}Fe_y)O_3$, A potential cathode for intermediate temperature SOFC applications. In: Singhal SC, Iwahara H (eds) Proceedings of the 3rd international symposium on solid oxide fuel cells. Proceedings, vol 93–4. The Electrochemical Society, Pennington, pp 241–251
187. Chen CC, Nasrallah MM, Anderson HU (1993) Preparation and electrode characteristics of dense $La_{0.6}Sr_{0.4}Co_{0.2}Fe_{0.8}O_3$ thin film by polymetric precursors. In: Singhal SC, Iwahara H (eds)

Proceedings of the 3rd international symposium on solid oxide fuel cells. Proceedings, vol 93–4. The Electrochemical Society Inc., Pennington, pp 252–266

188. Teraoka Y, Zhang HM, Okamoto K, Yamazoe N (1988) Mixed ionic-electronic conductivity of $La_{1-x}Sr_xCo_{1-y}Fe_yO_{3-\delta}$. Mater Res Bull 23:51–58
189. Ftikos C, Carter S, Steele BCH (1993) Mixed electronic/ionic conductivity of the solid solutions $La_{(1-x)}Sr_xCo_{(1-y)}Ni_yO_{3-\delta}$ (x:0.4, 0.5, 0.6 and y:0.2, 0.4, 0.6). J Europ Ceram Soc 12:79–86
190. Inoue T, Seki N, Eguchi K, Arai H (1990) Low-temperature operation of solid electrolyte oxygen sensors using perovskite-type oxide electrodes and cathodic reaction kinetics. J Electrochem Soc 137(8):2523–2527
191. Sasaki K, Wurth JP, Gschwend R, Gödickemeier M, Gauckler LJ (1996) Microstructure-property relations of solid oxide fuel cell cathodes and current collectors: cathodic polarization and ohmic resistance. J Electrochem Soc 143:530–543
192. Kleitz M (1992) Reaction pathways: a new electrode modelling concept. In: McEvoy A (ed) Fundamental barriers to SOFC performance. Swiss Federal Office of Energy, Bern, pp 4–12
193. Steele BCH, Carter S, Kajda J, Kontoulis I, Kilner JA (1991) Optimisation of fuel cell components using $^{18}O/^{16}O$ exchange and dynamic SIMS techniques. In: Grosz F, Zegers P, Singhal SC, Yamamoto O (eds) Proceedings of the 2nd international symposium on solid oxide fuel cells. Commission of European Communities, Luxembourg, pp 517–525
194. Hammou A (1992) Solid oxide fuel cells. In: Gerischer H, Tobias CW (eds) Advances in electrochemical science and engineering, vol 2. VCH-Verlag, Weinheim, pp 87–139
195. Hammouche A, Siebert E, Hammou A, Kleitz M, Caneiro A (1991) Electrocatalytic properties and nonstoichiometry of the high temperature air electrode $La_{1-x}Sr_xMnO_3$. J Electrochem Soc 138(5):1212–1216
196. Ishigaki T, Yamauchi S, Kishio K, Mizusaki J, Fueki K (1988) Diffusion of oxide Ion vacancies in perovskite-type oxides. J Solid State Chem 73:179–187
197. Takeda Y, Ueno H, Imanishi N, Yamamoto O, Sammes N, Phillipps M (1996) $Gd_{1-x}Sr_xCoO_3$ for the electrode of solid oxide fuel cells. Solid State Ionics 86–88:1187–1190
198. Tu H, Takeda Y, Imanishi N, Yamamoto O (1997) $Ln_{1-x}Sr_xCoO_3$ (Ln = Sm, Dy) for the electrode of solid oxide fuel cells. Solid State Ionics 100:283–288
199. Sakaki Y, Takeda Y, Kato A, Imanishi N, Yamamoto O, Hattori M, Iio M, Esaki Y (1999) $Ln_{1-x}Sr_xMnO_3$ (Ln = Pr, Nd, Sm and Gd) as the cathode material for solid oxide fuel cells. Solid State Ionics 118:187–194
200. Phillipps M, Sammes N, Yamamoto O (1999) $Gd_{1-x}A_xCo_{1-y}Mn_yO_3$ (A = Sr, Ca) as a cathode for the SOFC. Solid State Ionics 123:131–138
201. Tu H, Takeda Y, Imanishi N, Yamamoto O (1999) $Ln_{0.4}Sr_{0.6}Co_{0.8}Fe_{0.2}O_{3-\delta}$ (Ln = La, Pr, Nd, Sm, Gd) for the electrode in solid oxide fuel cells. Solid State Ionics 117:277–281
202. Qiu L, Ichikawa T, Hirano A, Imanishi N, Takeda Y (2003) $Ln_{1-x}Sr_xCo_{1-y}Fe_yO_{3-\delta}$(Ln = Pr, Nd, Gd; x = 0.2, 0.3) for the electrodes of solid oxide fuel cells. Solid State Ionics 158:55–65
203. Ishihara T, Honda M, Shibayama T, Nishiguchi H, Takita Y (1998) Intermediate temperature solid oxide fuel cells using a New $LaGaO_3$ based oxide ion conductor. J Electrochem Soc 145:3177–3183
204. Ishihara T, Fukui S, Nishiguchi H, Takita Y (2002) Mixed electronic-oxide ionic conductor of $BaCoO_3$ doped with La for cathode of intermediate-temperature-operating solid oxide fuel cell. Solid State Ionics 152–153:609–613
205. Shao ZP, Haile SM (2004) A high-performance cathode for the next generation of solid-oxide fuel cells. Nature 431: 170–173
206. Li S, Lu Z, Wei B, Huang X, Miao J, Cao G, Zhu R, Su W (2006) A study of $(Ba_{0.5}Sr_{0.5})_{1-x}Sm_xCo_{0.8}Fe_{0.2}O_{3-\delta}$ as a cathode material for IT-SOFCs. J Alloys Comp 426:408–414
207. Kotomin EA, Mastrikov YA, Kuklja MM, Merkle R, Roytburd A, Maier J (2011) First principles calculations of oxygen vacancy formation and migration in mixed conducting $Ba_{0.5}Sr_{0.5}Co_{1-y}Fe_yO_{3-\delta}$ perovskites. Solid State Ionics 188:1–5
208. Yan A, Cheng M, Dong Y, Yang W, Maragou V, Song S, Tsiakaras P (2006) Investigation of a $Ba_{0.5}Sr_{0.5}Co_{0.8}Fe_{0.2}O_{3-\delta}$ based cathode IT-SOFC I. The effect of CO_2 on the cell performance. Appl Catal B Environ 66:64–71
209. Yan A, Yang M, Hou Z, Dong Y, Cheng M (2008) Investigation of $Ba_{1-x}Sr_xCo_{0.8}Fe_{0.2}O_{3-\delta}$ as cathodes for low-temperature solid oxide fuel cells both in the absence and presence of CO_2. J Power Sources 185:76–84
210. Taniguchi S, Kadowaki M, Kawamura H, Yasuo T, Akiyama Y, Miyake Y, Saitoh T (1995) Degradation phenomena in the cathode of a solid oxide fuel cell with an alloy separator. J Power Sources 55:73–79
211. Taniguchi S, Kadowaki M, Yasuo T, Akiyama Y, Itoh Y, Miyake Y, Nishio K (1996) Suppression of chromium diffusion to an SOFC cathode from an alloy separator by a cathode second layer. Denki Kagaku 64(6):568–574
212. Matsuzaki Y, Yasuda I (2001) Dependence of SOFC cathode degradation by chromium-containing alloy on compositions of electrodes and electrolytes. J Electrochem Soc 148(2): A126–A131
213. Chiba R, Yoshimura F, Sakurai Y (1999) An investigation of $LaNi_{1-x}Fe_xO_3$ as a cathode material for solid oxide fuel cells. Solid State Ionics 124:281–288
214. Komatsu T, Chiba R, Arai H, Sato K (2008) Chemical compatibility and electrochemical property of intermediate-temperature SOFC cathodes under Cr poisoning condition. J Power Sources 176:132–137
215. Jiang SP, Zhen Y (2008) Mechanism of Cr deposition and its application in the development of Cr-tolerant cathodes of solid oxide fuel cells. Solid State Ionics 179:1459–1464
216. Lee S, Bevilacqua M, Fornasiero P, Vohs JM, Gorte RJ (2009) Solid oxide fuel cell cathodes prepared by infiltration of $LaNi_{0.6}Fe_{0.4}O_3$ and $La_{0.91}Sr_{0.09}Ni_{0.6}Fe_{0.4}O_3$ in porous yttria-stabilized zirconia. J Power Sources 193:747–753

217. Skinner S, Kilner J (2000) Oxygen diffusion and surface exchange in $La_{2-x}Sr_xNiO_{4+\delta}$. Solid State Ionics 135:709–712
218. Mauvy F, Bassat J, Boehm E, Manaud J, Dordor P, Grenier J (2003) Oxygen electrode reaction on $Nd_2NiO_{4+\delta}$cathode materials: impedance spectroscopy study. Solid State Ionics 158:17–28
219. Lalanne C, Prosperi G, Bassat J, Mauvy F, Fourcade S, Stevens P, Zahid M, Diethelm S, van Herle J, Grenier J (2008) Neodymium-deficient nickelate oxide $Nd_{1.95}NiO_{4+\delta}$ as cathode material for anode-supported intermediate temperature solid oxide fuel cells. J Power Sources 185:1218–1224
220. Nie H, Wen T, Wang S, Wang Y, Guth U, Vashook V (2006) Preparation, thermal expansion, chemical compatibility, electrical conductivity and polarization of $A_{2-\alpha}A'_{\alpha}MO_4$ (A = Pr, Sm; A′ = Sr; M = Mn, Ni; α = 0.3, 0.6) as a new cathode for SOFC. Solid State Ionics 177:1929–1932
221. Wang Y, Nie H, Wang S, Wen T, Guth U, Valshook V (2006) $A_{2-\alpha}A'_{\alpha}BO_4$-type oxides as cathode materials for IT-SOFCs (A = Pr, Sm; A′ = Sr; B = Fe, Co). Mater Lett 60:1174–1178
222. Haanappel V, Rutenbeck D, Mai A, Uhlenbruck S, Sebold D, Wesemeyer H, Röwekamp B, Tropartz C, Tietz F (2004) The influence of noble-metal-containing cathodes on the electrochemical performance of anode-supported SOFCs. J Power Sources 130:119–128
223. Wang S, Kato T, Nagata S, Honda T, Kaneko T, Iwashita N, Dokiya M (2002) Performance of a $La_{0.6}Sr_{0.4}Co_{0.8}Fe_{0.2}O_3$–$Ce_{0.8}Gd_{0.2}O_{1.9}$–Ag cathode for ceria electrolyte SOFCs. Solid State Ionics 146:203–210
224. Zhang J, Ji Y, Gao H, He T, Liu J (2005) Composite cathode $La_{0.6}Sr_{0.4}Co_{0.2}Fe_{0.8}O_3$–$Sm_{0.1}Ce_{0.9}O_{1.95}$–Ag for intermediate-temperature solid oxide fuel cells. J Alloys Compounds 395:322–325
225. Simner S, Anderson MJ, Coleman JS (2006) Performance of a novel La(Sr)Fe(Co)O_3–Ag SOFC cathode. J Power Sources 161:115–122
226. Mogensen M, Lindegaard T, Hansen TU, Mogensen G (1994) Physical properties of mixed conductor solid oxide fuel cell anodes of doped CeO_2. J Electrochem Soc 141(8): 2122–2128
227. Setoguchi T, Okamoto K, Eguchi K, Arai H (1992) Effects of anode material and fuel on anodic reaction of solid oxide fuel cells. J Electrochem Soc 139:2875–2880
228. Sasaki H, Otoshi S, Suzuki M, Sogi T, Kajimura A, Sugiura N, Ippommatsu M (1994) Fabrication of high power density tabular type solid oxide fuel cells. Solid State Ionics 72:253–256
229. Lide DR (2008) CRC handbook of chemistry and physics. CRC Press, Boca Raton
230. Tao SW, Irvine JTS (2003) A redox-stable efficient anode for solid-oxide fuel cells. Nat Mater 2:320–323
231. Zha SW, Tsang P, Cheng Z, Liu ML (2005) Electrical properties and sulfur tolerance of $La_{0.75}Sr_{0.25}Cr_{1-x}Mn_xO_3$ under anodic conditions. J Solid State Chem 178:1844–1850
232. Huang YH, Dass RI, Denyszyn JC, Goodenough JB (2006) - Synthesis and characterization of $Sr_2MgMoO_{6-\delta}$ an anode material for the solid oxide fuel cell. J Electrochem Soc 153: A1266–A1272
233. Vernoux P, Guillodo M, Foulrtier J, Hammou A (2000) Alternative anode material for gradual methane reforming in solid oxide fuel cells. Solid State Ionics 135:425–431
234. Ruiz-morales JC, Canales-Vázquez J, Peña-Martínez J, López DM, Núñez P (2006) On the simultaneous use of $La_{0.75}Sr_{0.25}Cr_{0.5}Mn_{0.5}O_{3-\delta}$ as both anode and cathode material with improved microstructure in solid oxide fuel cells. Electrochim Acta 52:278–284
235. Sauvet AL, Fouletier J (2001) Electrochemical properties of a new type of anode material $La_{1-x}Sr_xCr_{1-y}Ru_yO_{3-\delta}$ for SOFC under hydrogen and methane at intermediate temperatures. Electrochim Acta 47:987–995
236. Sauvet AL, Fouletier J, Gaillard F, Primet M (2002) Surface properties and physicochemical characterizations of a New type of anode material, $La_{1-x}Sr_xC_{r1-y}Ru_yO_{3-\delta}$, for a solid oxide fuel cell under methane at intermediate temperature. J Catal 209:25–34
237. Sauvet AL, Irvine JTS (2004) Catalytic activity for steam methane reforming and physical characterisation of $La_{1-x}Sr_xCr_{1-y}Ni_yO_{3-\delta}$. Solid State Ionics 167:1–8
238. Sin A, Kopnin E, Dubitsky Y, Zaopo A, Aricô AS, Gullo LR, Rosa DL, Antonucci V (2005) Stabilisation of composite LSFCO–CGO based anodes for methane oxidation in solid oxide fuel cells. J Power Sources 145:68–73
239. Lepe FJ, Fernández-Urbán J, Mestres L, Martínez-Sarrión ML (2005) Synthesis and electrical properties of new rare-earth titanium perovskites for SOFC anode applications. J Power Sources 151:74–78
240. Fagg DP, Kharton VV, Kovalevsky AV, Viskup AP, Naumovich EN, Frade JR (2001) The stability and mixed conductivity in La and Fe doped $SrTiO_3$ in the search for potential SOFC anode materials. J Eur Ceram Soc 21:1831–1835
241. Hui S, Petric A (2002) Evaluation of yttrium-doped $SrTiO_3$ as an anode for solid oxide fuel cells. J Eur Ceram Soc 22:1673–1681
242. Moos R, Härdtl KH (1997) Defect chemistry of donor-doped and undoped strontium titanate ceramics between 1000° and 1400°C. J Am Ceram Soc 80(10):2549–2562
243. Hui SQ, Petric A (2001) Conductivity and stability of $SrVO_3$ and mixed perovskites at low oxygen partial pressures. Solid State Ionics 143:275–283
244. Bieger T, Waser MJ, Waser R (1992) Optical investigation of oxygen incorporation in $SrTiO_3$. Solid State Ionics 53–56:578–582
245. Sasaki K, Claus J, Maier J (1999) Defect chemistry of oxides in partially frozen-in states: case studies for $ZrO_2(Y_2O_3)$, $SrZrO_3(Y_2O_3)$, and $SrTiO_3$. Solid State Ionics 121:51–60
246. Park S, Gorte RJ, Vohs JM (2000) Applications of heterogeneous catalysis in the direct oxidation of hydrocarbons in a solid-oxide fuel cell. Appl Catal A Gen 200:55–61
247. Park S, Vohs JM, Gorte RJ (2000) Direct oxidation of hydrocarbons in a solid–oxide fuel cell. Nature 404:265–267

248. Zhou ZF, Kumar R, Thakur ST, Rudnick LR, Schobert H, Lvov SN (2007) Direct oxidation of waste vegetable oil in solid-oxide fuel cells. J Power Sources 171:856–860
249. Craciun R, Park S, Gorte RJ, Vohs JM, Wang C, Worrell WL (1999) A novel method for preparing anode cermets for solid oxide fuel cells. J Electrochem Soc 146:4019–4022
250. Larminie J, Dicks A (2000) Fuel cell systems explained. Wiley, Chichester
251. Sasaki K, Teraoka Y (2003) Equilibria in fuel cell gases I. Equilibrium compositions and reforming conditions. J Electrochem Soc 150(7):A878–A884
252. Sasaki K, Teraoka Y (2003) Equilibria in fuel cell gases II. The C-H-O ternary diagrams. J Electrochem Soc 150(7): A885–A888
253. Sasaki K, Teraoka Y (2003) Equilibria in fuel cell gases. In: Proceedings of the 8th international symposium on solid oxide fuel cells. Proceedings, vol 2003–07. Electrochemical Society, Pennington, pp 1225–1239
254. Sasaki K, Kojo H, Hori Y, Kikuchi R, Eguchi K (2002) Direct-alcohol/hydrocarbon SOFCs: comparison of power generation characteristics for various fuels. Electrochemistry 70(1):18–22
255. Eguchi K, Kojo H, Takeguchi T, Kikuchi R, Sasaki K (2002) Fuel flexibility in power generation by solid oxide fuel cells. Solid State Ionics 152:411–416
256. Sasaki K, Hori Y, Kikuchi R, Eguchi K, Ueno A, Takeuchi H, Aizawa M, Tsujimoto K, Tajiri H, Nishikawa H, Uchida Y (2002) Current-voltage characteristics and impedance analysis of solid oxide fuel cells for mixed H_2 and CO gases. J Electrochem Soc 149(3):A227–A233
257. Sasaki K, Watanabe K, Teraoka Y (2004) Direct-alcohol solid oxide fuel cells: current-voltage characteristics and fuel gas compositions. J Electrochem Soc 151(7):A965–A970
258. Sasaki K, Watanabe K, Shiosaki K, Susuki K, Teraoka Y (2003) Power generation characteristics of SOFCs for alcohols and hydrocarbons. In: Proceedings of the 8th international symposium on solid oxide fuel cells. Proceedings, vol 2003–07. Electrochemical Society, Pennington, pp 1295–1304
259. Kishimoto H, Horita T, Yamaji K, Xiong Y, Sakai N, Brito ME, Yokokawa H (2005) Feasibility of n-Dodecane fuel for solid oxide fuel cell with Ni-ScSZ anode. J Electrochem Soc 152(3): A532–A538
260. Sasaki K, Watanabe K, Shiosaki K, Susuki K, Teraoka Y (2004) Multi-fuel capability of solid oxide fuel cells. J Electroceram 13(1–3):669–675
261. Haga K (2010) Chemical degradation of Ni-based anode materials in solid oxide fuel cells. Dissertation. Kyushu University, Fukuoka Japan
262. Sasaki K, Haga K, Yoshizumi T, Minematsu D, Yuki E, Liu RR, Uryu C, Oshima T, Ogura T, Shiratori Y, Ito K, Koyama M, Yokomoto K (2011) Chemical durability of SOFCs: influence of impurities on long-term performance. J Power Sources 196(22):9130–9140
263. Sasaki K, Susuki K, Iyoshi A, Uchimura M, Imamura N, Kusaba H, Teraoka Y, Fuchino H, Tsujimoto K, Uchida Y, Jingo N (2006) H_2S poisoning of solid oxide fuel cells. J Electrochem Soc 153:A2023–A2029
264. Sasaki K, Susuki K, Iyoshi A, Uchimura M, Imamura N, Kusaba H, Teraoka Y, Fuchino H, Tsujimoto K, Uchida Y, Jingo N (2005) Sulfur tolerance of solid oxide fuel cells. In: Proceedings of the 9th international symposium on solid oxide fuel cells. Proceedings, vol 2005–07. Electrochemical Society, Pennington, pp 1267–1274
265. Sasaki K, Adachi S, Haga K, Uchikawa M, Yamamoto J, Iyoshi A, Chou J-T, Shiratori Y, Itoh K (2007) Fuel impurity tolerance of solid oxide fuel cells. Solid oxide fuel cells 10 (SOFC-10). ECS Trans 7(1):1675–1683
266. Haga K, Adachi S, Shiratori Y, Ito K, Sasaki K (2008) Poisoning of SOFC anodes by various fuel impurities. Solid State Ionics 179(27–32):1427–1431
267. Haga K, Shiratori Y, Ito K, Sasaki K (2008) Chlorine poisoning of SOFC Ni-cermet anodes. J Electrochem Soc 155(12):B1233–B1239
268. Haga K, Shiratori Y, Nojiri Y, Ito K, Sasaki K (2010) Phosphorus poisoning of Ni-cermet anodes in solid oxide fuel cells. J Electrochem Soc 157(11):B1693–B1700
269. Park S, Cracium R, Vohs JM, Gorte RJ (1999) Direct oxidation of hydrocarbons in a solid oxide fuel cell: I. Methane oxidation. J Electrochem Soc 146:3603–3605
270. Shiratori Y, Oshima T, Sasaki K (2008) Feasibility of direct-biogas SOFC. Int J Hydrogen Energ 33:6316–6321
271. Gorte RJ, Kim H, Vohs JM (2002) Novel SOFC anodes for the direct electrochemical oxidation of hydrocarbon. J Power Sources 106:10–15
272. Kim H, Park S, Vohs JM, Gorte RJ (2001) Direct oxidation of liquid fuels in a solid oxide fuel cell. J Electrochem Soc 148: A693–A695
273. Zhou ZF, Gallo C, Pague MB, Schobert H, Lvov SN (2004) Direct oxidation of jet fuels and Pennsylvania crude oil in a solid oxide fuel cell. J Power Sources 133:181–187
274. Shiratori Y, Tran TQ, Takahashi Y, Sasaki K (2011) Application of biofuels to solid oxide fuel cell. ECS Trans 35:2641–2651
275. van Herle J, Maréchal F, Leuenberger S, Membrez Y, Bucheli O, Favrat D (2004) Process flow model of solid oxide fuel cell system supplied with sewage biogas. J Power Sources 131:127–141
276. Girona K, Laurencin J, Petitjean M, Fouletier J, Lefebvre-Joud F (2009) SOFC running on biogas: identification and experimental validation of "safe" operating conditions. ECS Trans 25(2):1041–1050
277. Shiratori Y, Ijichi T, Oshima T, Sasaki K (2010) Internal reforming SOFC running on biogas. Int J Hydrogen Energy 35:7905–7912
278. Shiratori Y, Ijichi T, Oshima T, Sasaki K (2010) Performance of internal reforming SOFC running on biogas. In: Proceedings of 9th European SOFC Forum, Luzern, Switzerland, pp 4-77–4-87
279. Swaine DJ (1990) Trace elements in coal. Butterworths, London

280. Lobachyov K, Richter HJ (1996) Combined cycle gas turbine power plant with coal gasification and solid oxide fuel cell. J Energy Resour Technol 118:285–292
281. Iritani J, Kougami K, Komiyama N, Nagata K, Ikeda K, Tomida K (2001) Pressurized 10kW class module of SOFC. In: Yokokawa H, Singhal SC (eds) Proceedings of the 7th international symposium on solid oxide fuel cells. Proceedings, vol 2001–16. Electrochemical Society, Pennington, pp 63–71
282. Doctor RD, Molburg JC, Thimmapuram PR (1997) Oxygen-blown gasification combined cycle: carbon dioxide recovery, transport, and disposal. Energy Convers Manage 38:S575–S580
283. Timpe RC, Kulas RW, Hauserman WB, Sharma RK, Olson ES, Willson WG (1997) Catalytic gasification of coal for the production of fuel cell feedstock. Int J Hydrogen Energy 22:487–492
284. Sjunnesson L (1998) Utilities and their investments in fuel cells. J Power Sources 71:41–44
285. Cayan FN, Zhi M, Pakalapati SR, Celik I, Wu N, Gemmen RS (2008) Effects of coal syngas impurities on anodes of solid oxide fuel cells. J Power Sources 185:595–602
286. Marina OA, Pederson LR, Coyle CA, Thomsen EC, Coffey GW (2005) Ni/YSZ anode interactions with impurities in coal gas. ECS Trans 25(2):2125–2130
287. Bao JE, Krishnan GN, Jayaweera P, Perez-Mariano J, Sanjurjo A (2009) Effect of various coal contaminants on the performance of solid oxide fuel cells: part I. Accelerated testing. J Power Sources 193:607–616
288. Bao JE, Krishnan GN, Jayaweera P, Lau KH, Sanjurjo A (2009) Effect of various coal contaminants on the performance of solid oxide fuel cells: part II. ppm and sub-ppm level testing. J Power Sources 193:617–624
289. Bao JE, Krishnan GN, Jayaweera P, Sanjurjo A (2010) Effect of various coal gas contaminants on the performance of solid oxide fuel cells: part III. Synergistic effects. J Power Sources 195:1316–1324
290. Trembly JP, Gemmen RS, Bayless DJ (2007) The effect of IGFC warm gas cleanup system conditions on the gas-solid partitioning and form of trace species in coal syngas and their interactions with SOFC anodes. J Power Sources 163:986–996
291. Yoshida S, Kabata T, Nishiura M, Koga S, Tomida K, Miyamoto K, Teramoto Y, Matake N, Tsukuda H, Suemori S, Ando Y, Kobayashi Y (2011) Development of the SOFC-GT combined cycle system with tubular type cell stack. ECS Trans 35(1):105–111
292. Ishihara T (2009) Perovskite oxide for solid oxide fuel cells. Springer, New York
293. Tsuchiya M, Lai BK, Ramanathan S (2011) Scalable nanostructured membranes for solid oxide fuel cells. Nat Nanotechnol 6:282–286
294. Karageorgakis NI, Heel A, Rupp JLM, Aguirre MH, Graule T, Gauckler LJ (2011) Properties of flame sprayed $Ce_{0.8}Gd_{0.2}O_{1.9-\delta}$ electrolyte thin films. Adv Funct Mater 21(3):532–539
295. Bonderer LJ, Chen PW, Kocher P, Gauckler LJ (2010) Free-standing ultrathin ceramic foils. J Am Ceram Soc 93(11):3624–3631
296. Ryll T, Galinski H, Schlagenhauf L, Elser P, Rupp JLM, Bieberle-Hutter A, Gauckler LJ (2011) Microscopic and nanoscopic three-phase-boundaries of platinum thin-film electrodes on YSZ electrolyte. Adv Funct Mater 21(3):565–572
297. Tuller HL, Litzelman SJ, Jung WC (2009) Micro-ionics: next generation power sources. Phys Chem Chem Phys 11:3023–3034
298. Tuller HL, Bishop SR (2011) Point defects in oxides: tailoring materials through defect engineering. Annu Rev Mater Res 41:369–398
299. Sasaki K, Maier J (1999) Low temperature defect chemistry of oxides: I. general aspects and numerical calculations. J Appl Phys 86(10):5422–5433
300. Sasaki K, Maier J (1999) Low temperature defect chemistry of oxides: II. Analytical relations. J Appl Phys 86(10): 5434–5443
301. Matsumoto K, Fujigaya T, Sasaki K, Nakashima N (2011) Bottom-up design of carbon nanotube-based electrocatalysts and their application in high temperature operating polymer electrolyte fuel cells. J Mater Chem 21(4):1187–1190
302. Masao A, Noda Z, Takasaki F, Ito K, Sasaki K (2009) Carbon-free Pt electrocatalysts supported on SnO_2 for polymer electrolyte fuel cells. Electrochem Solid-State Lett 12(9): B119–B122
303. Sasaki K, Takasaki F, Noda Z, Hayashi S, Shiratori Y, Ito K (2010) Alternative electrocatalyst support materials for polymer electrolyte fuel cells. ECS Trans 33(1):473–482
304. Hayashi A, Notsu H, Kimijima K, Miyamoto J, Yagi I (2008) Preparation of Pt/mesoporous carbon (MC) electrode catalyst and its reactivity toward oxygen reduction. Electrochim Acta 53(21):6117–6125
305. Masuda H, Yamamoto A, Sasaki K, Lee S, Ito K (2011) A visualization study on relationship between water-droplet behavior and cell voltage appeared in straight, parallel and serpentine channel pattern cells. J Power Sources 196:5377–5385

Fuel Cells, Introduction

Klaus-Dieter Kreuer
Max-Planck-Institut für Festkörperforschung, Stuttgart, Germany

Article Outline

Acknowledgment
Bibliography

Fuel cells are devices which electrochemically convert the chemical free energy of gaseous or liquid reactants

into electrical energy in a continuous way. As in a battery the reactants are prevented from chemically reacting by separating them with an electrolyte, which is in contact with electro-catalytically active porous electrode structures. Apart from effectively separating the anode and cathode gases and/or liquids, in other words the fuel and air, the electrolyte mediates the electrochemical reactions taking place at the electrodes by conducting a specific ion at very high rates during the operation of the fuel cell. In the simplest case of a fuel cell, operating with hydrogen (fuel) and oxygen (air) as reacting gases, a proton or oxide ion current equivalent to the electronic current passing through the external load is driven through the electrolyte and parts of the heterogeneous electrode structures (Fig. 1).

The driving force of this process is the Gibbs energy (ΔG_r) of the reaction:

$$H_2 + {}^1\!/_2\, O_2 \rightarrow H_2O$$

and the potential difference (electromotive force: emf) forming across the cell simply is:

$$\text{emf} = -\Delta G_r/zF$$

where z is the number of electrons driven through the outer circuit and F is the Faraday constant.

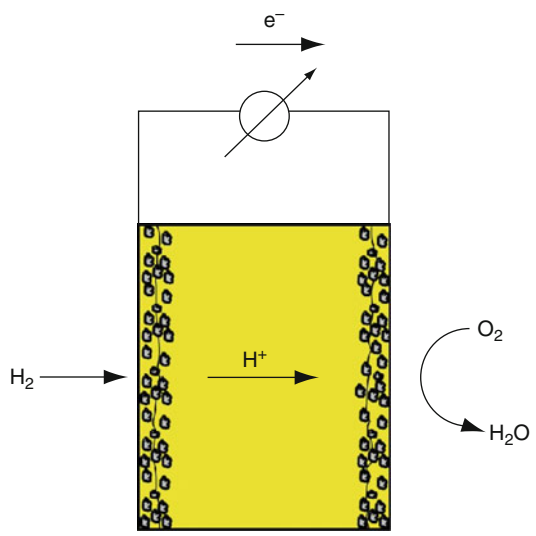

Fuel Cells, Introduction. Figure 1
Schematic illustration of the electrochemical energy conversion process in a fuel cell

The maximum possible electric energy $E_{reversible}$, which can be harvested from such reactions in a fuel cell, is:

$$E_{reversible} = -\Delta G_r$$

and, if the efficiency η is defined as the ratio of the electrical energy taken out of the fuel cell and the reaction enthalpy ΔH_r (heat of reaction), the efficiency limit:

$$\eta_{reversible} = \Delta G_r/\Delta H_r = 1 - (T\Delta S_r/\Delta H_r)$$

can even be higher than unity, provided the reaction entropy ΔS_r is positive (note that ΔH_r is negative for an exothermal reaction) like for the oxidation of carbon-rich fuels, for example:

$$C_3H_8 + 5O_2 \rightarrow 3CO_2 + 4H_2O$$

The first law of thermodynamics is not violated because a fuel cell is a nonadiabatic system exchanging heat with the environment; hence, the missing energy can be taken from the environment by cooling the same.

Looking at fuel cells in such a principle way may lead one to the conclusion that they are perfect energy conversion systems superior to any heat engine, for which the efficiency is strictly limited to this of the Carnot cycle.

However, the issue is more complex, and it is still an open question which role fuel cells will play in future more sustainable energy supply systems.

Following up on above efficiency considerations, it must be mentioned that the thermodynamic efficiency limits of all relevant fuel cell reactions are actually below unity (in the range 80–100%) and that irreversibilities (losses) occur in practically all parts of every fuel cell (e.g., transport losses in the gas diffusion electrodes, over-potentials associated with the electrochemical reactions taking place at the anode and cathode, IR losses across the electrolyte and all interfaces).

Nonetheless, electric efficiencies of more than 50% have been demonstrated experimentally, and, considering the fact that heat engines (e.g., steam turbines) reach such high efficiencies only for very large units, the large fuel efficiency of small fuel cells appears to be a unique feature (Fig. 2).

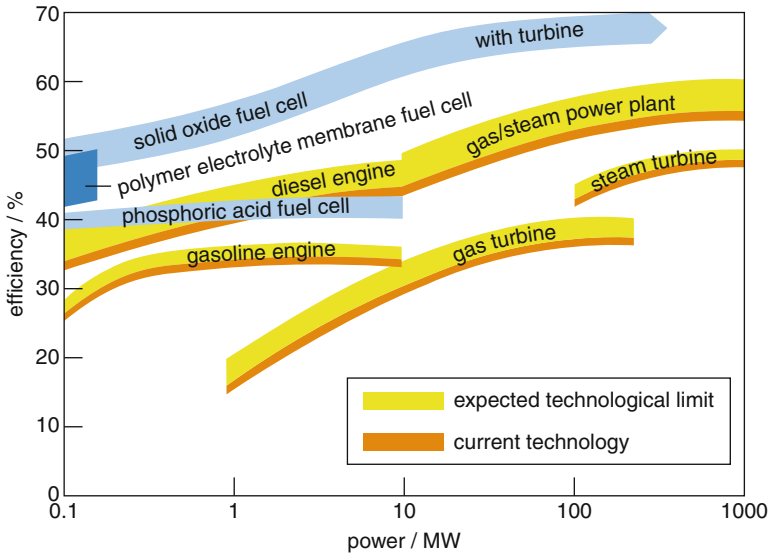

Fuel Cells, Introduction. Figure 2
Efficiency versus power for different fuel cell types compared to other energy conversion technologies

Together with capital cost and operating cost advantages, this is making fuel cells an attractive alternative especially in the sub-10-MW range.

Despite the very demanding conditions in automotive applications and the more than 100 years of optimization of the internal combustion engine, the relatively high fuel efficiency is one of the reasons why fuel cells have a real chance to be applied even in this highly competitive market. For a couple of niche markets (like outdoor, yachting), fuel cells are already well established.

Especially for mass applications such as automotive, a full life cycle assessment (LCA) is absolutely critical. Since there are a lot of embedded resources such as noble metal catalysts and energy for manufacturing fuel cells, LCA very much depends on aspects such as recyclability and lifetime. For the operation period itself, cost, performance, and durability issues are important. But a complete picture must also consider aspects of specific applications including how they are connected in future energy scenarios.

Since fuel cells are just energy conversion devices, also the availability of appropriate fuels is essential for the potential role of fuel cells. The most advanced fuel cell types rely on natural gas (methane) or hydrogen as a fuel.

Due to the high H/C ratio (which gives it some environmental advantage) and availability, methane (CH_4) may play a key role in the broad introduction of fuel cell technology (► Direct Hydrocarbon Solid Oxide Fuel Cells).

Hydrogen can be directly obtained by reforming natural gas, but today it is mainly produced as a by-product only, that is, hydrogen is not being used extensively as an energy carrier. Although, with hydrogen, one can store large amounts of energy which can be distributed in relatively easy ways, the hydrogen storage problem is not fully solved yet. Also the ways of producing hydrogen, including the primary energy used for this, bear a lot of open questions. While some countries are even considering the use of excess nuclear energy (electricity and heat) for producing hydrogen, others want to rely completely on renewables such as wind and solar.

I hope, these few considerations make it clear that the future of fuel cells may heavily depend on severe bifurcations. Heat engines and electrochemical energy storage devices (mainly batteries) existed side by side in the late nineteenth and the early twentieth century, but the abundance of fossil fuels has later driven the development of combustion engines and turbines retarding the development of alternative energy conversion

devices such as batteries and fuel cells. It could well be that the expected end of the "oil age" may also go along with an increasing importance of alternative energy conversion devices, among which fuel cells have the potential to play an important role. Much will depend on the societies driving this development. Their understanding of "Sustainability" will be different depending on the relative importance of its different aspects, such as preservation of natural resources, environmental impact, safety and reliability. Moreover, the temptation to benefit from short-term "economical advantages" may strongly bias the decisions to come.

Making large quantities of hydrogen with sunlight, directly or indirectly, is still far away, but there is no principal physicochemical law preventing this option, which seems to be one of the long-standing driving forces for the many fuel cell activities around the globe.

The entries of the following part on fuel cells will strictly keep out of such aspects which are highly speculative at this stage. They rather focus on the technical issues comprising descriptions of the state of the art and remaining problems, approaches to solve the same, and some speculations about future directions. This volume is meant to provide a solid ground for taking decisions. There is some redundancy and overlap between entries reflecting different points of view which naturally exist even for the technical issues.

Historically, the fuel cell concept is known for more than 170 years. It was Christian Friedrich Schönbein who recognized and described the appearance of "inverse electrolysis" [1], shortly before Sir William Grove, the inventor of the platinum/zinc battery, constructed his first "gas voltaic battery" [2]. Grove already used platinum electrodes and dilute sulfuric acid as a proton conducting electrolyte, and it is worth mentioning that today's low-temperature PEM (polymer electrolyte membrane) fuel cells still make use of related materials (carbon-supported platinum and perfluoro-sulfonic-acid (PFSA)-ionomers). The same is also true for high-temperature fuel cells which are dating back to the 1930s. In an attempt to prove the concept of "Brennstoff-Ketten mit Festleitern" (fuel chains with solid conductors), Emil Baur and Hans Preis tested different solid electrolytes [3], and they came to the conclusion that the "Nernst-Masse ist unübertroffen." At that time "Nernst-Masse" had the composition 85% ZrO_2, 15% Y_2O_3, which is still very close to what is used in current SOFCs (solid oxide fuel cell) as electrolyte material (► Solid Oxide Fuel Cell Materials: Durability, Reliability and Cost). Moreover, they tested "masses" containing ceria (CeO_2), which is still discussed as a base for alternative electrolyte materials (► Fuel Cells (SOFC): Alternative Approaches (Electroytes, Electrodes, Fuels)), and they even discussed power and cost issues of their system which actually used coal as a fuel (power densities of 10 kW/m^3 at a cost of 1,000 Mark/kW were estimated). Although the numbers for both are much higher today, the factor of 4, estimated for the cost disadvantage compared to the cost of conventional technologies seemed to persist over time.

Current R&D work is still focusing on PEM fuels and SOFCs operating at low (sub-freezing to T ~ 90°C) and high temperature (T = 700 to above 1,000°C), but the intermediate temperature range (150–700°C) is progressively attracting more attention. After introducing the most relevant fuel cell types (► Fuel Cell Types and Their Electrochemistry) the remaining entries of this volume are actually ordered by the operation temperature of the considered fuel cells (from high to low T) touching upon various aspects such as material science, engineering, economical issues, and the possible implications for more sustainable energy conversion scenarios.

The high-temperature fuel cell part has a special entry on "Direct Hydrocarbon SOFCs" (► Direct Hydrocarbon Solid Oxide Fuel Cells) which are very interesting as a bridging technology, because they still run fossil fuel (natural gas), but may provide an environmental advantage through a higher efficiency. Since durability and reliability issues are critical for SOFCs they are discussed in a separate entry (► Solid Oxide Fuel Cell Materials: Durability, Reliability and Cost) before introducing alternative approaches with respect to the selection of materials and fuels (► Fuel Cells (SOFC): Alternative Approaches (Electroytes, Electrodes, Fuels)). The subsequent entry is related, additionally discussing devices and configurations and the matter of in situ diagnostics (► Solid Oxide Fuel Cells). Finally, specific SOFC design concepts are described and sustainability aspects including full life cycle analyses (LCA) are discussed (► Solid Oxide Fuel Cells,

Sustainability Aspects) before market issues are addressed (▶ Solid Oxide Fuel Cells, Marketing Issues).

The section on intermediate temperature fuel cells has just one entry on each fuel cell type. With decreasing operation temperature, the "Molten Carbonate Fuel Cell" technology is critically discussed (▶ Molten Carbonate Fuel Cells) before two related systems relying on the unique proton conducting properties of phosphoric acid are described. While the well-established phosphoric acid fuel cell (PAFC) is developed for stationary applications (▶ Phosphoric Acid Fuel Cells for Stationary Applications), polybenzimidazole (used as a matrix for phosphoric acid) fuel cells even have some potential for mobile and small applications (▶ Polybenzimidazole Fuel Cell Technology).

The subsequent part touches upon the various aspects of PEM fuel cells which have seen tremendous progress over the last two decades. But there are still several critical materials issues which are related to the cost and durability requirements especially for automotive applications and which are identified in the first entry (▶ PEM Fuel Cells, Materials and Design Development Challenges). The following entries are discussing specific components which are important, and in most cases also critical, for the function of the PEM fuel cell system. There are three entries on membranes which may be considered to be the "heart" of any PEM fuel cell. In most cases, this is still a PFSA (perfluoro-sulfonic-acid) membrane, but more recently also hydrocarbon membranes have been used, not only because of cost advantages but also because of their distinctly different properties (e.g., lower gas permeation, lower electro-osmotic drag, higher morphological stability). The various aspects of this move are described (▶ Membrane Electrolytes, from Perfluoro Sulfonic Acid (PFSA) to Hydrocarbon Ionomers) before the issue of operation at high temperature and low humidity is addressed (▶ Proton Exchange Membrane Fuel Cells: High-Temperature, Low-Humidity Operation). The latter may help to reduce the system cost especially by reducing the size of the cooling system, the amount of noble-metal catalyst, and the purity requirements for the fuel used (hydrogen). Cost reduction by using non-noble metal catalysts is the motivation for the development of better anion exchange membranes which is described in the following entry (▶ Alkaline Membrane Fuel Cells). The part on electrocatalysts and electrode structures contains an entry on noble metal catalysts (▶ PEM Fuel Cells and Platinum-Based Electrocatalysts), including current attempts to improve both activity and durability, while the following entry presents a radically different approach relying on the activity of some non-noble metals for the oxygen reduction reaction (▶ Polymer Electrolyte Membrane Fuel Cells (PEM-FC) and Non-noble Metal Catalysts for Oxygen Reduction) which may also help to bring cost down. Since PEM fuel cell systems are generally more complex than those of other fuel cell types, this section commences with an entry spanning the bridge from a few fundamentals to the complete fuel cell system including cost and reliability considerations (▶ Polymer Electrolyte (PE) Fuel Cell Systems). The implementation of PEM fuel cells into cars is described in an entry on automotive applications (▶ Polymer Electrolyte Membrane (PEM) Fuel Cells, Automotive Applications). The last entry of this part has some overlap with the first discussing cost, performance, and durability issues of existing systems (▶ PEM Fuel Cell Materials: Costs, Performance and Durability).

The present volume is completed by a critical comparison of fuel cell technologies to other technologies beyond a one-to-one comparison (▶ Fuel Cell Comparison to Alternate Technologies).

Energy conversion by fuel cells has the genuine advantage of high efficiency in a large power range (Fig. 2) which is giving them a high flexibility as part of complex energy conversion and distribution scenarios. The synergetic combination with other technologies (e.g., fuel cells serving as range extenders in electric vehicles) could even help to overcome remaining critical issues such as cost. There has been tremendous progress with respect to cost reduction and increase in power and lifetime which has taken fuel cells into some niche markets (e.g., for military and remote applications), but their widespread use still requires further fundamental research and engineering efforts. This volume provides detailed insight into the current status of the diverse fuel cell technologies and identifies future directions based on critical analyses of the state of the art.

Acknowledgment

I thank Giuliano Gregori and Linas Vilciauskas (both from Max-Planck-Institut für Festkörperforschung) for reading the proofs.

Bibliography

1. Schöenbein CF (1839) X. On the voltaicpolarization of certain solid and fluid substances, Philosophical Magazine Series 3, 14:85, 43–45. http://dx.doi.org/10.1080/14786443908649658
2. Grove WR Esq.M.A.M.R.I. (1839) XLII. On a small voltaic battery of great energy; some observations on voltaic combinations and forms of arrangement; and on the inactivity of a copper positive electrode in nitro-sulphuric acid, Philosophical Magazine Series 3, 15:96, 287–293. http://dx.doi.org/10.1080/14786443908649881
3. Baur E, Preis H (1937) Über Brennstoff-Ketten Mit Festleitern, Ztschr. Elektrochem. Bd. 43, Nr. 9 727–732

G

Gas Expanded Liquids for Sustainable Catalysis

Bala Subramaniam
Department of Chemical and Petroleum Engineering, The Center for Environmentally Beneficial Catalysis, University of Kansas, Lawrence, KS, USA

Article Outline

Glossary
Definition of the Subject
Introduction
Thermodynamic and Physical Properties of GXLs
Catalytic Reactors for Investigating GXLs
Applications in Homogeneous Catalysis
Multiphase Catalysis
An Example of CXL-Based Process Development Including Sustainability (Economic and Environmental Impact) Analyses
Summary and Future Directions
Acknowledgments
Bibliography

Glossary

Carbon selectivity Refers to the fraction of the carbon in a hydrocarbon-based feed that is utilized in making the desired product.

Compressible gas A gas in the vicinity of its critical temperature wherein it is highly compressible with pressure, either condensing or attaining liquid-like densities as the pressure approaches or exceeds its critical pressure. Below the critical temperature, a compressible gas will typically condense at sufficiently high pressures to produce a liquid phase.

Gas-expanded liquids When a liquid such as an organic solvent is pressurized with a compressible gas, the liquid phase will volumetrically expand if the gas dissolves in it. The volumetrically expanded liquid phase is termed as a gas-expanded liquid. When the pressure is released, the dissolved gas will escape from the liquid phase causing the liquid phase to contract to its original volume.

Homogeneous catalysis Refers to a process wherein the reactants, catalyst, and products are soluble in a single phase and the catalytic reaction occurs in that phase.

Multiphase catalysis Refers to a process wherein the reactants, catalyst, and products are present in two or more different immiscible phases separated by phase boundary(ies). The reaction typically occurs at a boundary between two phases.

Renewable feedstock Refers to a feedstock from nature whose use has minimal adverse impact on the ecosystem and that has the ability to manifest itself again in nature in a matter of a few months to a few years rather than in hundreds to thousands of years.

Solvent engineering Exploiting the synergies between catalysis and solvent media for enhancing rates, selectivity, and separations in a sustainable manner.

Supercritical fluid A substance that is above its critical pressure (P_c) and critical temperature (T_c). For applications in catalysis and separations, the near-critical region [0.9–1.2 T_c (in K) and 0.9–2 P_c] wherein small changes in temperature and/or pressure yield relatively large changes (from gas-like to liquid-like values) in density and transport properties, is generally of interest.

Sustainability Sustainability of a catalytic process refers to the long-term environmental, social, and economic viability of the process.

Turnover frequency (TOF) Quantifies the intrinsic activity of a catalyst in converting the reactants to products. It is usually expressed in terms of the rate at which the reactants are converted to products [(moles of substrate converted)/(gram atoms of catalyst used)/(time)].

Robert A. Meyers (ed.), *Encyclopedia of Sustainability Science and Technology*, DOI 10.1007/978-1-4419-0851-3,
© Springer Science+Business Media, LLC 2012

Definition of the Subject

The modern-day chemical industry relies mostly on fossil fuel (such as petroleum, natural gas, and coal)–based feedstock. There are several megaton industrial catalytic processes that produce essential commodities for everyday life but present challenges with respect to reducing environmental footprints and enhancing sustainability. Examples of such processes include the homogeneous hydroformylation of higher olefins, the selective oxidation of light olefins to their corresponding epoxides, and the oxidation of *p*-xylene to produce terephthalic acid. For a targeted product, there are several possible scenarios for developing sustainable alternatives to conventional technologies. These include (a) developing greener process technologies based on existing feedstock, (b) replacement of fossil fuel–based feedstock with renewable ones such as those derived from biomass (which will also entail the development of new chemistries and process technologies), or (c) replacement of the target product itself with alternate candidates from renewable feedstocks. This entry will discuss the potential of gas-expanded liquids (GXLs), a relatively new class of solvents, for developing alternative and more sustainable catalytic processes.

A gas-expanded liquid (GXL) phase is generated by dissolving a compressible gas such as CO_2 or a light olefin into the traditional liquid phase at mild pressures (tens of bar) [1]. When CO_2 is used as the expansion gas, the resulting liquid phase is termed a CO_2-expanded liquid or CXL. GXLs combine the advantages of compressed gases such as CO_2 and of traditional solvents in an optimal manner. GXLs retain the beneficial attributes of the conventional solvent (polarity, catalyst/reactant solubility) but with higher miscibility of permanent gases (O_2, H_2, CO, etc.) compared to organic solvents at ambient conditions and enhanced transport rates compared to liquid solvents [2–5]. The enhanced gas solubilities in GXLs have been exploited to alleviate gas starvation (often encountered in homogeneous catalysis with conventional solvents), resulting in a one to two orders of magnitude greater rates than in neat organic solvent or *sc*CO_2. *Environmental advantages* include substantial replacement of organic solvents with environmentally benign CO_2. *Process advantages* include reduced flammability due to CO_2 presence in the vapor phase and milder process pressures (tens of bar) compared to *sc*CO_2 (hundreds of bar). GXLs thus satisfy many of the attributes of an ideal alternative solvent.

Introduction

Solvent usage has often been linked to waste generation and associated environmental and economic burdens [6, 7]. Within the last two to three decades, many research groups have investigated benign alternate media for performing chemical reactions [8–12]. Examples of such media include supercritical CO_2 (*sc*CO_2) [13–20], water [21–23], gas-expanded liquids (GXLs) [1, 24–27], ionic liquids (ILs) [28–30], and switchable solvents [31–35]. While *sc*CO_2 is "generally regarded as safe," its nonpolar nature renders it unsuitable for most homogeneous catalysis involving polar transition metal complexes. Further, *sc*CO_2 media require operating pressures in excess of 100 bar. The use of either supercritical or near-critical water (P_c = 220.6 bar; T_c = 373.9°C) requires rather harsh operating pressures and temperatures. The use of ionic liquids as tunable media for catalysis either alone or in combination with *sc*CO_2 [36] shows much promise.

The ideal alternative solvent, in addition to being considered green, should typically satisfy the following criteria: (a) retain the beneficial aspects of the conventional solvent (polarity, catalyst/reactant solubility) being replaced, (b) facilitate facile product/catalyst separation, (c) enhance process safety, and (d) operate at mild pressures (tens of bar) for economic viability. The qualitative principles of green chemistry [37] and green engineering [38] provide valuable guidelines for developing greener process alternatives. Some of these principles include the use of renewable and abundant resources as feedstock, nonhazardous reagents as reaction and separation media, inherently safe process design, and process intensification at mild conditions. However, a reliable assessment of overall "greenness" and sustainability requires quantitative comparison with conventional processes using metrics such as atom economy, the E-factor (amount of waste produced/unit of desired product) [6], toxic emissions potential [39], and process economics. Such analyses also provide guidance in identifying potential process

improvement opportunities and establishing performance metrics for sustainability.

For a targeted product from a given feedstock, the basic elements of a catalytic process or system include the catalyst, media, multiphase reactor, and separation. Effective integration of these elements into a sustainable technology requires a multiscale approach [40]. This entry highlights reported examples of catalytic process concepts with gas-expanded liquids and multiscale approaches to develop such processes for large-scale catalytic technologies. The examples include catalytic hydrogenations, hydroformylations, and selective oxidations. Specifically, it is shown how the tunable physicochemical properties of GXLs can be effectively exploited to promote sustainable catalysis. An example of quantitative economic and environmental impact analyses is also presented to show how such an assessment validates and facilitates the design and development of sustainable systems that are also practically viable.

Thermodynamic and Physical Properties of GXLs

A gas in the vicinity of its critical temperature [0.9–1.2 T_c (K)] is highly compressible and attains liquid-like densities when sufficiently compressed to near-critical or supercritical pressures. As an example, consider CO_2 (P_c = 71.8 bar; T_c = 304.1 K) as an expansion gas. At 40°C (313.15 K and T/T_c = 1.03), CO_2 is highly compressible attaining liquid-like densities as its critical pressure is approached. In such a compressed state, CO_2 dissolves in a liquid phase and volumetrically "expands" the liquid phase forming a GXL. When the system pressure is released, the dissolved CO_2 escapes from the liquid phase contracting the liquid phase. Gases whose critical temperatures are far removed from the reaction temperature do not exhibit such compressibility and are generally incapable of expanding solvents.

Liquids expand to different extents in the presence of CO_2 pressure, depending on the ability of the liquids to dissolve CO_2. The equipment and experimental procedures for precise measurements of volumetric expansion and phase equilibria are provided elsewhere [41, 42]. As such, liquids are divided into three general classes [43]. Class I liquids such as water have insufficient ability to dissolve CO_2, and therefore do not expand significantly. Glycerol and other polyols also fall into this class (Fig. 1a).

Class II liquids, such as ethyl acetate, acetonitrile, methanol, and hexane, dissolve large amounts of CO_2 and hence expand appreciably (Fig. 1) undergoing significant changes in physical properties. As shown in Fig. 1, conventional solvents such as acetonitrile and ethyl acetate are volumetrically expanded several fold by compressed CO_2 at 40°C, reaching as high as eight for ethyl acetate at around 70 bar. Regardless of the solvent, the volumetric expansion of class II solvents is strongly dependent on the mole fraction of CO_2

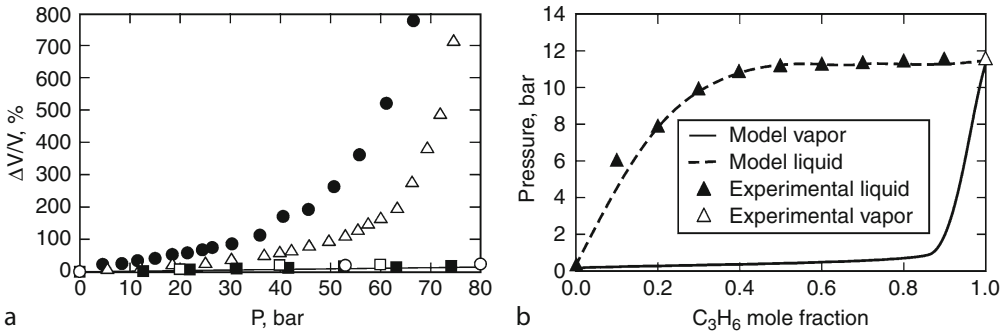

Gas Expanded Liquids for Sustainable Catalysis. Figure 1
(**a**) Expansion of solvents as a function of the pressure of CO_2 at 40°C, for ethyl acetate (•), MeCN (Δ), [1-butyl-3methylimidazolium]BF_4 (filled squares), polypropylene glycol (❑), and polyethylene glycol (O) [1]. (**b**) Vapor–liquid equilibrium for C_3H_6 + MeOH binary system at 21°C [46]

in the liquid phase [41]. Class III liquids, such as ionic liquids and liquid polymers, dissolve relatively smaller amounts of CO_2 and therefore expand only moderately (Fig. 1a, [44]). By using a solvent such as acetonitrile or methanol that exhibits mutual solubility in CO_2 and water, it is possible to create CO_2-expanded ternary systems containing water [45]. Gases such as propylene can also expand organic solvents. Figure 1b shows that for the propylene + methanol binary system, the propylene mole fraction in the liquid phase approaches approximately 30 mol% at 10 bar, implying that compressed propylene at ambient temperatures can cause significant volumetric expansion of the methanol phase. Such behavior has been exploited in epoxidation of light olefins, as explained in a later section.

The expansions of Class II liquids have been successfully modeled by the Peng-Robinson Equation of State (PR-EoS) [47] and by molecular simulations [48, 49]. Gases such as ethane, fluoroform, and other similar compressible gases are also capable of expanding liquids. As discussed in later sections of this entry, gaseous substrates (such as propylene and ethylene) and gaseous oxidants (ozone) have also been exploited as expansion gases to overcome solubility limitations in the liquid phase where reaction occurs [50].

The presence of CO_2 in the liquid phase affects the physicochemical properties. For example, the viscosity of methanol decreases with CO_2 pressure at 40°C, by nearly 80% from pure methanol to CXL methanol at 77 bar CO_2 [51]. This viscosity reduction is especially striking for ionic liquids, which often have higher viscosity than organic solvents [52, 53]. The diffusivity of benzene in CXL methanol at 40°C and 150 bar increases by over 200% on replacing pure methanol with 75% CO_2 [54]. Similarly, the diffusion coefficients of benzonitrile in CO_2-expanded ethanol were observed to increase with increasing CO_2 mole fraction [55].

As regards polarity, Roškar et al. [56] have measured the dielectric constant of methanol with CO_2 at 35°C and found that from ambient conditions to approximately 40 bar of CO_2, the dielectric constant changes very little. However, the dielectric constant significantly decreases by about an order of magnitude at 76 bar of CO_2 pressure. It has been shown that the Kamlet–Taft parameters (for acidity, basicity, and polarizability) for mixed CO_2 + organic solvents are tunable by CO_2 addition [57–59]. This tunability has potential ramifications for the stabilization of charged and polar compounds in CXLs. The following sections provide examples of how GXLs have been systematically exploited to develop greener process concepts that display improved reaction performance with respect to rates, selectivity, and separations.

Catalytic Reactors for Investigating GXLs

Either batch or continuous-flow reactors may be employed for performing catalytic conversion, selectivity, and kinetic studies. In all cases, it is essential to know the phase behavior of the reaction mixture to rationally interpret the results. Equipment must be designed and pressure-tested according to standardized design and testing procedures such as those prescribed by the American Society for Testing Materials. All equipment must incorporate adequate pressure relief and inherent safety measures. For example, in the case of exothermic reactions, the amount of reactants fed should be such that the estimated adiabatic temperature rise at total conversion does not lead to "thermal runaway" conditions and unsafe pressures. Similarly, enough inerts should be added to the vapor phase to avoid the formation of explosive organic vapors in the presence of air. During continuous reactor operation, safety shutdown measures should be incorporated. Described below are examples of batch and continuous reactors reported in the literature.

Batch Reactors

Proof-of-concept batch studies are typically done in 5–10 mL view cells, as shown in Fig. 2, typically rated to operate at 150°C and 200 bar. A schematic drawing of an experimental reactor is shown in Fig. 2. The reactor is a low-volume (10 mL) hollow cylinder with sapphire windows at each end, sealed by o-rings and screw caps. The sapphire windows allow visual inspection of the cell contents and permit in situ spectroscopic studies. The cell body has as many as five ports. Two of the ports are used for introducing reactants such as O_2 or H_2 and the compressed gas medium such as CO_2. Oxygen or hydrogen is typically introduced via a mass flow controller. The third port is used for injecting liquid reactant into the reactor and is connected to a safety head containing a rupture disk. A pressure transducer that continuously monitors the

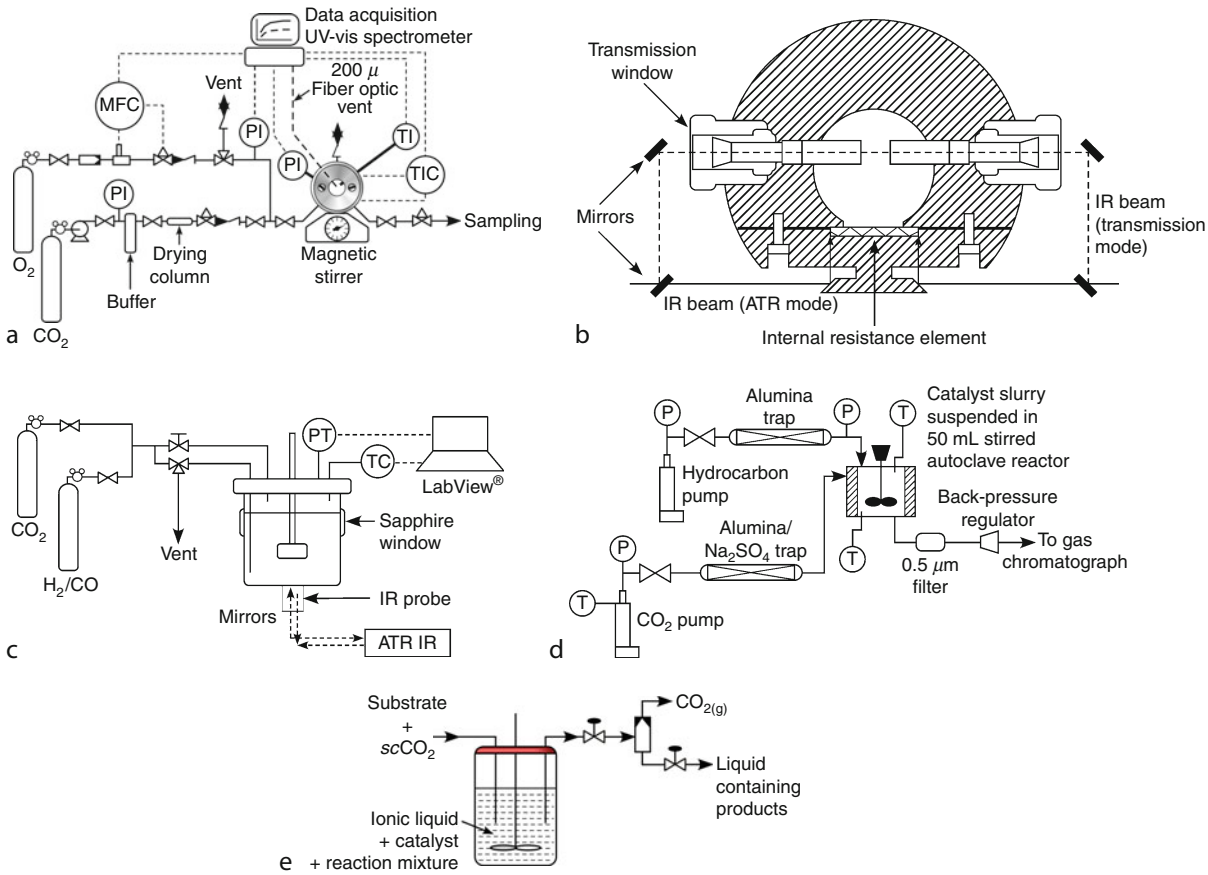

Gas Expanded Liquids for Sustainable Catalysis. Figure 2
Schematics of experimental reactors used for investigations of catalytic reactions in CXLs: (**a**) 5–10 mL view cell; (**b**) ATR-IR view cell; (**c**) 50 mL stirred reactor with ReactIR (*PT* pressure transducer, *TC* thermocouple); (**d**) continuous CXL reactor; (**e**) continuous flow reactor using a supercritical fluid–ionic liquid biphasic system

reactor pressure and a thermocouple that monitors the reactor temperature are connected to the remaining two ports. A magnetic stirrer provides adequate mixing of the reactor contents. Fiber optics may be attached to the sapphire windows and connected to a UV-Vis spectrophotometer. These facilitate temporal in situ monitoring of chemical reactions over broad spectral ranges. At the end of a batch run, the fluid phase cell contents may be depressurized into suitable sample traps for off-line analysis.

Baiker and coworkers [60] employed in situ high-pressure attenuated total reflectance infrared (ATR-IR) spectroscopy to elucidate the molecular interactions between dissolved CO_2 and ionic liquids. This cell, shown in Fig. 2c, consists of a horizontal stainless steel cylinder with sapphire windows on each end, one of which is attached to a piston to control the reactor volume and pressure [61]. It can operate at temperatures up to 100°C and pressures up to 20 bar. The IR beam can be directed by a combination of four mirrors either through the ZnSe internal resistance element for ATR-IR measurements of the dense phase or through cylindrical ZnSe windows for transmission spectroscopy of the upper phase. In addition, the internal resistance element can be coated with a layer of catalyst to measure the interactions between the reactants and the catalyst during the reaction. Thus, the cell can be used to simultaneously provide information about dissolved and adsorbed reacting species and by-products as well as the catalyst itself.

For larger-scale batch investigations, adequate mechanical mixing must be ensured to avoid mass transfer limitations. Mechanically stirred reactors (50–300 mL such as Autoclave and Parr) with stirrer speeds up to 1500 rpm are well suited for this purpose. For example, a 50-cm^3 high-pressure autoclave reactor equipped with an in situ attenuated total reflectance (ATR) IR probe (Mettler Toledo Inc.) was employed to investigate the hydroformylation of 1-octene [62]. Figure 2c shows a schematic of the apparatus (entitled "ReactIR"). Mixing is provided by a magnetic stirrer with a maximum agitation rate of 1700 rpm. Pressure and temperature are monitored by a Labview® data acquisition system and controlled with a Parr 4840 controller. Syngas is introduced from a gas reservoir, which is equipped with a pressure regulator that is used to admit syngas and maintain a constant total pressure in the reactor. The pressure transducer monitors the total pressure in the reservoir. The IR probe, placed at the bottom of the reactor, monitors concentration profiles of various species in the CXL phase. The maximum working pressure of the probe is approximately 140 bar. The temporal IR data are then processed using ConcIRT software to extract the absorbance profiles for each species, based on their characteristic peaks (identified with standards).

Continuous Reactors

For performing heterogeneous catalytic reactions in GXLs, a continuous stirred tank reactor (CSTR) is better suited for isothermal pressure-tuning studies [63]. A schematic is shown is Fig. 2d wherein the experiments are conducted in a 50 mL reactor from Autoclave Engineers, rated to 344 bar and 350°C. Catalyst particles are suspended in the reaction mixture by an impeller operating at 1200 rpm. Reaction pressure is maintained with a dome-loaded back-pressure regulator.

Cole-Hamilton and coworkers [64] demonstrated a continuous reactor system for investigating homogeneous catalytic reactions in IL/*sc*CO_2 systems (Fig. 2e). Here, the IL phase containing dissolved catalyst is retained in the reactor. The *sc*CO_2 is used to transport the soluble substrate into and products from the IL phase continuously. The challenge is to minimize catalyst leaching from the IL phase by the *sc*CO_2 + reaction mixture exiting the reactor.

Applications in Homogeneous Catalysis

Hydrogenations

Hydrogenations have been shown to benefit from CO_2 expansion of the solvent in several ways. For example, CO_2 + H_2 mixtures are just as effective chemically as pure H_2 at the same total pressure, and also desirable from a safety standpoint. Jessop's group [65] showed that the properties of the expanding gas can have a major effect on reaction rate. Investigating the effect of expansion gas on the rate of CO_2 hydrogenation in MeOH/NEt_3 mixture as solvent (Eq. 1), it was found that the turnover frequency was 770 h^{-1} with no expansion gas but 160 h^{-1} with ethane (40 bar) and 910 h^{-1} with CHF_3 (40 bar) as the expansion gas. The addition of liquid hexane produced a similar decrease in the rate. Hence, the low polarity of ethane was implicated for the decreased rate in the ethane-expanded solvent.

$$CO_2 + H_2 \xrightarrow[\substack{50^\circ C \\ NEt_3/MeOH \\ 40\ bar\ H_2,\ 10\ bar\ CO_2 \\ 40\ bar\ expansion\ gas}]{RuCl(OAc)(PMe_3)_4} HCO_2H \quad (1)$$

Solvent expansion as a method to enhance the H_2 availability in the liquid phase of homogeneous catalytic reactions is of interest in asymmetric hydrogenations. Foster's group [66] investigated the asymmetric hydrogenation of 2-(6′-methoxy-2′-naphthyl)acrylic acid, an atropic acid, in CO_2-expanded methanol with $[RuCl_2(BINAP)(cymene)]_2$, finding the reaction faster but less selective than in neat methanol. A subsequent study using $RuCl_2$(BINAP) catalyst reported that the reaction in expanded methanol was slower than in normal methanol [67]. More recently, the asymmetric hydrogenation of methyl acetoacetate to methyl (R)-3-hydroxybutyrate by [(R)-RuCl(binap)(*p*-cymen)]Cl was investigated in methanol-dense CO_2 solvent systems [68]. Although the CO_2-expanded methanol system resulted in a reduction of both reaction rate and

product selectivity, this changed in the presence of water. High selectivities were obtained with the optimized methanol–CO_2–water–halide system.

Contrasting effects are also demonstrated during asymmetric hydrogenations in ionic liquids (ILs). The enantioselectivity during hydrogenation of tiglic acid in [BMIm][PF_6] (where BMIm is L-*n*-butyl-3-methylimidazolium) is superior [H_2 = 5 bar; *ee* = 93%] to that in CO_2-expanded [BMIm][PF_6] (H_2 = 5 bar; CO_2 = 70 bar; *ee* = 79%) wherein the H_2 availability is improved with CO_2 [69]. In contrast, the hydrogenation of atropic acid is greatly improved in selectivity (*ee* increases from 32% to 57%) when the IL is expanded with 50 bar CO_2 [70]. Leitner and coworkers [69] demonstrated that hydrogenation of N-(1-phenylethylidene)aniline proceeded to only 3% conversion in [EMIm][Tf_2N] (1-ethyl-3-methylimidazolium bis(trifluoromethylsulfonyl)imide) and to >99% in CO_2-expanded [EMIm][Tf_2N], in which the H_2 solubility is significantly enhanced with CO_2 pressure (Fig. 3).

Facile hydrogenation of solid substrates such as vinylnaphthalene with a $RhCl(PPh_3)_3$ catalyst was demonstrated by melting the solid with compressed CO_2 and performing the reaction in the melt phase at 33°C, which is well below the normal melting point of the solid [71]. Scurto and Leitner [72] showed that the addition of compressed CO_2 induced a melting point depression of an ionic solid salt (tetrabutylammonium tetrafluoroborate) at greater than 100°C, well below its normal melting point of 156°C. They used this CO_2-induced melting technique to demonstrate hydrogenation, hydroformylation, and hydroboration of vinylnaphthalene using rhodium complexes. Employing homogeneous octene hydrogenation with rhodium complexes as a model system, Scurto and coworkers demonstrated the importance of understanding the phase behavior, mass transfer, and intrinsic kinetics effects for the reliable interpretation and design of hydrogenations in IL + CO_2 media [73].

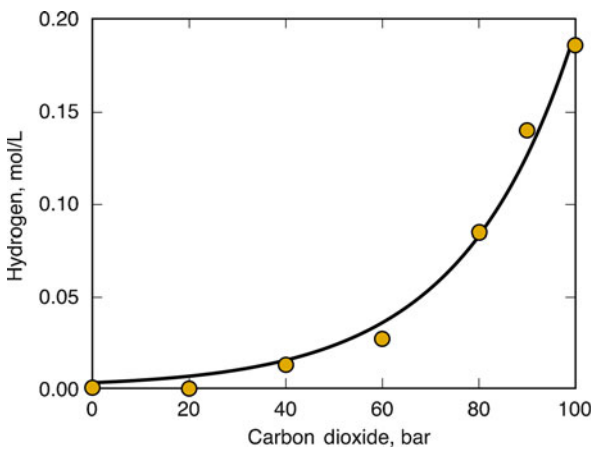

Gas Expanded Liquids for Sustainable Catalysis. Figure 3
Enhancement of H_2 solubility in [EMIm][Tf_2N] by CO_2 pressurization at a constant H_2 partial pressure (30 bar at T = 297 K). Taken from [69]

Hydroformylations

Hydroformylations benefit from CXLs by virtue of the fact that syngas + CO_2 mixtures are more effective than syngas alone at a fixed pressure. The use of CO_2 helps generate CXLs, which enhance both the syngas solubility as well the tunability of the H_2/CO ratio at milder pressures. Jin and Subramaniam [74] demonstrated the advantages of homogeneous hydroformylation of 1-octene in CXLs using an unmodified rhodium catalyst ($Rh(acac)(CO)_2$). The turnover numbers (TONs) in CO_2-expanded acetone were significantly higher than those obtained in either neat acetone or *sc*CO_2. In subsequent reports, the performances of several rhodium catalysts, $Rh(acac)(CO)_2$, $Rh(acac)[P(OPh)_3]_2$, $Rh(acac)(CO)[P(OAr)_3]$, and two phosphorous ligands, PPh_3 and biphephos, were compared in neat organic solvents and in CXLs [75]. For all catalysts, enhanced turnover frequencies (TOFs) were observed in CXLs. For the most active catalyst, $Rh(acac)(CO)_2$ modified by biphephos ligand, the selectivity to aldehyde products was improved from approximately 70% in neat solvent to nearly 95% in CXL media. Such improved catalyst performance for hydroformylation in CO_2-based reaction mixtures were also reported recently for rhodium catalysts modified with triphenylphosphine, triphenyl phosphite, and tris(2,4-di-*tert*-butylphenyl) phosphite [76], with turnover numbers as high as $3(10^4)$ mol aldehyde/(mol Rh)/h. In contrast, the Rh complex-catalyzed hydroformylation of 1-hexene in CO_2-expanded toluene was more rapid than in *sc*CO_2 but slower than in normal toluene [77]. The high CO_2 pressure was believed to

shift some of the 1-hexene out of the liquid phase into the CO_2 phase, thereby lowering the concentration of hexene available to the catalyst.

Ionic liquid + CO_2 media has also been used for hydroformylation [64, 78]. Constant activity for up to 3 days was demonstrated during continuous 1-octene hydroformylation with a Rh-based catalyst in [BMIm][PF_6]/*sc*CO_2 medium. Compared to the industrial cobalt-catalyzed processes, higher TOFs were observed; the selectivity to linear aldehyde (70%) is comparable to those attained in the industrial processes (70–80%). However, the air/moisture sensitivity of the ILs and the ligands may lead to the deactivation and leaching of the rhodium catalyst. Cole-Hamilton and coworkers also reported a solventless homogeneous hydroformylation process using dense CO_2 to transport the reactants into and transfer the products out of the reactor leaving behind the insoluble Rh-based catalyst complex in the reactor solution [79].

Table 1 compares the TOFs, *n*/*i* ratio, and operating conditions (P&T) of some existing industrial processes and recently published work that employ CXLs, supercritical CO_2, and ionic liquids as reaction media [64]. Clearly, hydroformylation in CO_2-expanded octene appears to be promising in terms of both TOF ($\sim$300 h^{-1}) and selectivity ($\sim$90%, $n/i > 10$). In addition, the required operating conditions (60°C and 38 bar) are much milder compared to other processes. The further development of this process, including quantitative sustainability analysis, is provided in a following section.

Another example involves enantioselective hydroformylation of solid vinylnaphthalene with a Rh catalyst in a CO_2-based phase, created by melting the solid with compressed CO_2. This technique is similar to the melt hydrogenation described earlier.

O_2-Based Oxidations

CXLs provide both rate and safety advantages for homogeneous catalytic oxidations. For the homogeneous catalytic O_2-oxidation of 2,6-di-*tert*-butylphenol, DTBP, by Co(salen*) in *sc*CO_2, in CO_2-expanded acetonitrile and in the neat organic solvent [80, 81], it was found that the TOF in the CO_2-expanded acetonitrile is between one and two orders of magnitude greater than in *sc*CO_2. Additionally, the 2,6-di-*tert*-butyl quinine (DTBQ) selectivity is lower in neat acetonitrile, clearly demonstrating that CXLs are optimal media for this reaction. In another example, cyclohexene oxidation by O_2 was investigated with a non-fluorinated iron porphyrin catalyst, (5,10,15,20-tetraphenyl-21*H*,23*H*-porphyrinato)iron(III) chloride, Fe(TPP)Cl, and a fluorinated catalyst (5,10,15,20-tetrakis(pentafluorophenyl)-21*H*,23*H*-porphyrinato) iron(III) chloride, Fe(PFTPP)Cl [80]. While Fe(TPP) Cl is insoluble and displays little activity in *sc*CO_2, it displays high activity and selectivity in CO_2-expanded acetonitrile. The enhanced TOFs in the CXL media were attributed to their tunable polarity compared to *sc*CO_2 and the approximately two orders of magnitude greater O_2 solubility in CO_2-expanded solvents compared to neat solvents at ambient conditions (1 atm and 25°C). These results clearly show that CO_2-expanded solvents advantageously complement *sc*CO_2 as reaction media by broadening the range of conventional catalyst/solvent combinations with which homogeneous oxidations by O_2 can be performed.

Gas Expanded Liquids for Sustainable Catalysis. Table 1 Comparison with commercial processes and other reported work

Process parameters	BASF (Co)	Shell (Co/P)	SCF-IL (Rh/P)	SCF (Rh/P)	CXL (Rh/P)
Substrate	1-octene	1-octene	1-octene	1-octene	1-octene
P, bar	300	80	200	125	38
T, °C	150	200	100	100	60
TOF, h^{-1}	35	20	517	259	316
$S_{n\text{-aldehyde}}$, %	50	80	75	75	89

An important safety aspect when using CXLs is that the dominance of dense CO_2 in the vapor phase reduces the flammability envelope. Brennecke and coworkers showed that either pure O_2 or O_2 + CO_2 mixtures at the same total pressure showed more or less similar O_2 solubilities in pressurized acetonitrile or methanol [2]. Table 2 shows the vapor–liquid equilibrium data for the CO_2/O_2/acetonitrile system at approximately 40°C and pressures between 6 and 83 bar. The CO_2 and O_2 mole fractions are shown in the table, with the balance being acetonitrile. To better understand the effect of CO_2 presence on O_2 solubility in acetonitrile, the authors use the Enhancement Factor (EF), defined as the ratio of the solubility of O_2 in the liquid phase of the ternary mixture to the solubility of pure O_2 in the solvent at the same O_2 fugacity and temperature.

$$EF = \frac{x_{gas}^{mixture}}{x_{gas}^{solvent}}$$

Clearly, EF is >1 implies that the presence of the CO_2 increases the solubility of the O_2. As can be inferred from Table 2, the EF values increase with an increase in pressure and reached values greater than 1 at pressures above 50 bar. EF values >1 can be attributed to the high CO_2 solubility in the liquid phase, which increases free volume in the solution and enhances the solubility of the O_2. If the binary and ternary systems are compared at the same total pressure (rather than the same O_2 fugacity), then the oxygen solubility in the ternary mixture liquid phase is lower than the solubility in the binary system. This finding is significant because it confirms that replacing CO_2 with O_2 in the gas phase does not drastically change the O_2 solubility in the CXL phase but serves to significantly mitigate vapor-phase flammability and thereby to enhance process safety.

The Mid-Century (MC) process for the oxidation of methylbenzenes to carboxylic acids represents an important industrial process for the synthesis of polymer intermediates for producing fibers, resins, and films. For example, terephthalic acid (TPA) is manufactured by homogeneous liquid-phase oxidation of *p*-xylene around 200°C and 20 bar with Co/Mn/Br catalysts in acetic acid medium. The air (source of oxygen) is vigorously sparged into the liquid phase of a stirred tank reactor. The purity of the solid TPA product obtained from this reactor is typically 99.5% pure, the major impurity being 4-carboxybenzaldehyde. For obtaining polymer-grade TPA, further purification is necessary to eliminate the intermediate oxidation products suggesting that the vigorous mixing does not completely overcome the O_2 availability limitations. Recently, the Co/Mn/Br catalyzed oxidation of *p*-xylene

Gas Expanded Liquids for Sustainable Catalysis. Table 2 Vapor–liquid equilibrium for CO_2 (1)–O_2 (2)–acetonitrile (3) [2]

		Liquid-phase composition		Vapor-phase composition				
T (°C)	P_{total} (bar)	x_1	x_2	y_1	y_2	f_{O2} (bar)	x_{O2}, pure gas[a] mole fraction	EF
40.0	13.7	0.03	0.004	0.27	0.68	9.2	0.0046	0.77
40.0	23.7	0.08	0.007	0.35	0.63	14.9	0.0074	0.92
40.0	26.8	0.08	0.009	0.30	0.68	17.9	0.0089	0.98
40.0	48.9	0.15	0.016	0.36	0.62	29.8	0.0148	1.05
40.0	69.4	0.20	0.022	0.37	0.61	41.6	0.0207	1.08
40.0	82.2	0.24	0.028	0.38	0.61	48.6	0.0242	1.18
40.0	6.2	0.02	0.001	0.40	0.52	3.2	0.0016	0.59
40.0	16.7	0.09	0.003	0.55	0.42	7.0	0.0035	0.86
39.8	29.6	0.16	0.005	0.60	0.38	11.1	0.0055	0.99
40.0	52.7	0.29	0.012	0.64	0.34	18.0	0.0089	1.31

[a]Horstmann et al. 2004 [82]

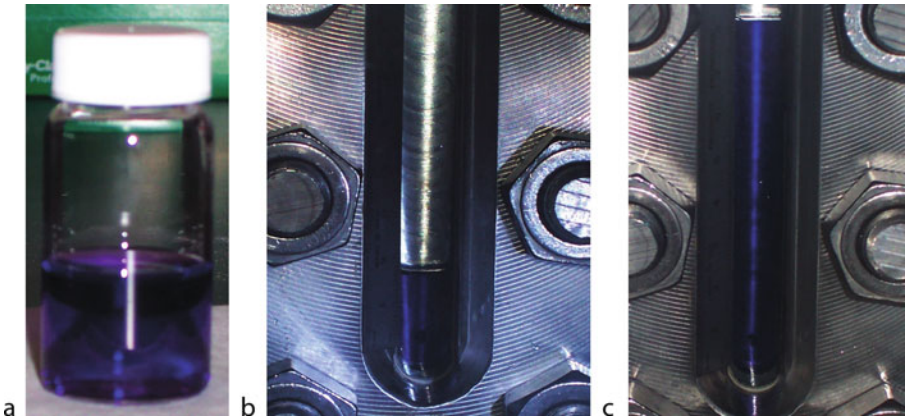

Gas Expanded Liquids for Sustainable Catalysis. Figure 4
Example of CO_2 expansion of a homogenous oxidation catalyst mixture in acetic acid. (**a**) room temperature, (**b**) 120°C with 20 bar N_2 and 18 bar CO_2, (**c**) 120°C with 20 bar N_2 and 159 bar CO_2; [Co] = 60 mM, [Mn] = 1.8 mM, [Br] = 60 mM prior to the expansion

to TPA in CO_2-expanded solvents was demonstrated at temperatures lower than those of the traditional MC process [82]. As inferred from Fig. 4, the acetic acid solution containing the Co/Mn/Br-based catalyst undergoes significant volumetric expansion by CO_2 addition.

As compared with the traditional air (N_2/O_2) oxidation system, the reaction with CO_2/O_2 at 160°C at a pressure of 100 bar increases both the yield of TPA and the purity of solid TPA via a more efficient conversion of the intermediates, 4-carboxybenzaldehyde and *p*-toluic acid. Further, the amount of yellow colored by-products in the solid TPA product is also lessened. Additionally, the burning of the solvent, acetic acid, monitored in terms of the yield of the gaseous products, CO and CO_2, is reduced by approximately 20% based on labeled CO_2 experiments. These findings show that the use of CXLs promotes sustainability by maximizing the utilization of feedstock carbon for desired products while simultaneously reducing carbon emissions.

H_2O_2-Based Oxidations

Many of the current commercial propylene oxide (PO) processes are energy intensive and yield coproducts [83]. They either consume vast amounts of chlorine and lime producing large quantities of wastewater containing HCl and salt, or use expensive reactants that lead to equimolar amounts of coproducts. A novel propylene epoxidation process has been disclosed wherein titanium-substituted silicalite (TS-1) catalysts [84–87] catalyze propylene epoxidation with reasonable efficiency using an O_2/H_2 mixture to generate H_2O_2 in situ. TS-1 catalysts have high catalytic activity and selectivity. However, the catalyst deactivates rapidly and requires high temperatures for regeneration.

Eckert/Liotta and coworkers showed that the reaction between H_2O_2 and dense CO_2 (benign reactants) yields a peroxycarbonic acid species, an oxidant that facilitates olefin epoxidation [88]. Using such a system with NaOH as a base, Beckman and coworkers [89] demonstrated propylene conversion to PO at high selectivity albeit at low conversion (3%). The low conversion is typical of interphase mass transfer limitations between the immiscible aqueous and CO_2 phases. By using a third solvent such as acetonitrile that shows mutual solubility with water and dense CO_2, CO_2-expanded $CH_3CN/H_2O_2/H_2O$ homogeneous mixtures were created. Subramaniam and coworkers [45] showed that olefin epoxidation reactions may be intensified in such a homogeneous phase containing the olefin, CO_2, and H_2O_2 (in aqueous solution). One to two orders of magnitude enhancement in epoxidation rates (compared to the biphasic system without acetonitrile) was achieved with >85% epoxidation selectivity. This is an example of a system where the CO_2 is used as a solvent (for the olefinic

substrate) and as a reactant to generate the peroxy carbonic acid in situ. Recently, a similar concept was proposed for styrene epoxidation in CO_2-based emulsions [90].

Propylene Epoxidation in Propylene-Expanded Liquid Phase Methyltrioxorhenium (CH_3ReO_3, abbreviated as MTO) is known to be an exceptional homogeneous catalyst for alkene epoxidation at relatively mild temperatures using H_2O_2 as the oxidant [91–94]. This catalytic system was recently shown to work elegantly for the industrially significant epoxidations of propylene [95] and ethlyene [96]. As shown in Scheme 1, the light olefin (either propylene or ethlyene) from the gas phase has to first dissolve into the aqueous liquid phase before undergoing reaction. However, the aqueous solubility of the olefins is typically low and limits the epoxidation rate. For example, propylene solubility in water is 1.36 (10^{-4}) M at 1 bar, 21°C [97]. The key to enhancing the reaction rate was to exploit the compressibility of the light olefins at reaction temperatures to enhance their solubilities in the liquid phase. By dissolving a suitable amount of methanol to the liquid phase, the solubility of the light olefins can be substantially enhanced.

For propylene epoxidation, it was found that if a N_2/C_3H_6 mixture at 14 bar was used in the gas phase, remarkably high activity (92% propylene oxide yield in 1 h) was achieved [95]. When pressurizing with N_2 in a closed system at ambient temperatures, C_3H_6 ($P_c = 46.1$ bar; $T_c = 92.5$°C) condenses at 14 bar [98]. In the presence of a solvent such as methanol,

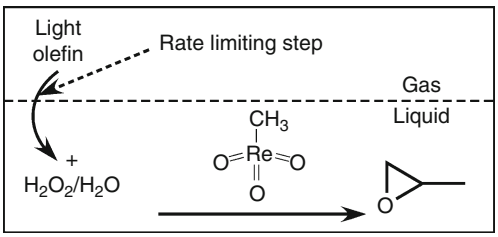

Gas Expanded Liquids for Sustainable Catalysis. Scheme 1
Homogeneous catalytic epoxidation of propylene. The methyltrioxorhenium (MTO) catalyst and oxidant (H_2O_2) are dissolved in the liquid phase and the olefin is supplied from the gas phase

pressurization beyond 10 bar increases the C_3H_6 mole fraction in the liquid phase to >30 mol% [46]. This increased concentration of propylene results in increased epoxidation rates. This is an example of how to utilize a light olefin as the expansion medium and exploit a *substrate-expanded liquid phase* for process intensification.

Table 3 compares the various GXL-based processes with the commercial chlorohydrin and hydroperoxide processes. The pressure-intensified propylene epoxidation process (last entry in Table 3) satisfies the sustainability principles of waste minimization, use of benign reagents, and process intensification at mild conditions. Little or no waste is produced compared to the commercial processes.

Ethylene Epoxidation in Ethylene-Expanded Liquid Phase Conventional ethylene oxide manufacture emits CO_2 as by-product (roughly 18 MM tons/year) from the combustion of both the ethylene (feed) and ethylene oxide (EO) [100]. An alternate technology that is exclusively selective toward EO (eliminating the formation of CO_2) would dramatically reduce the carbon footprint of this large-scale industrial process. It was recently shown that the MTO-based liquid-phase epoxidation process works remarkably well for ethlyene as well. At ambient temperatures, the gaseous ethylene (P_c = 50.6 bar; T_c = 9.5°C) is just above the critical temperature. Hence, by compressing the ethylene gas beyond the critical pressure (>50 bar), it is possible to significantly increase its solubility (by one to two orders of magnitude) in a liquid reaction phase containing methanol or another suitable alcohol [101]. By employing MTO, H_2O_2, and a methanol/water mixture as solvent, a homogeneous catalytic system was demonstrated that eliminates CO_2 formation while producing ethylene oxide at >99% EO selectivity at near-ambient temperatures and EO productivities [~4 g EO/(g Re)/(h)] that are comparable to the conventional EO process (Table 4). *No* CO_2 was detectable in either the liquid or the vapor phases. Furthermore, since H_2O_2 does not decompose at typical reaction temperatures (<40°C), the vapor phase is void of O_2 and the formation of explosive vapors is impeded. In addition to mitigating the carbon footprint of a large-scale industrial process, the demonstrated technology concept is another example of how the

Gas Expanded Liquids for Sustainable Catalysis. Table 3 Comparison with other processes (substrate is propylene in all cases)

Process/reference	Reagents	Conditions	PO yield (Y) or selectivity (S)
Hancu et al. [89]	$CO_2 + H_2O_2 + H_2O$ (Biphasic system), NaOH	–	$Y < 3.0\%$
Danciu et al. [85]	$CO_2 + H_2 + O_2$, Pd/TS-1 catalyst	45°C; 131 bar	$Y \sim 7.3\%$; $S = 77\%$; 4.5 h
Biphasic CXL process, Lee et al. [99]	$CO_2 + CH_3CN + H_2O_2 + H_2O$ (monophasic), pyridine	40°C; 48 bar	$Y = 7.1\%$; 6 h
Chlorohydrin process, Trent [83]	Cl_2, caustic, lime	45–90°C; 1.1–1.9 bar	$S = 88$–95%
Hydroperoxide[a] process, Trent [83]	W, V, Mo	100–130°C; 15–35.2 bar	$Y = 95\%$; $S = 98\%$; 2 h
Pressure-intensified CXL process [95]	CH_3OH–H_2O_2–H_2O, MTO, pyNO	30°C; 17 bar N_2	$Y = +98\%$; $S = 99\%$; 2 h

[a]Isobutane to TBHP: 95 ∼ 150°C; 20.7–55.2 bar; $Y = 20$–30%; $S = 60$–80%

Gas Expanded Liquids for Sustainable Catalysis. Table 4 Comparison of commercial EO process with new GXL-based homogeneous catalytic process

Process	Catalyst, oxidant	Pressure, temperature	EO selectivity	CO_2 selectivity	EO productivity (g/gcat/h)
Shell	Ag/Al_2O_3, air or O_2	10–20 bar, 200–300°C	85–90%	10–15%	3–6
GXL based	MTO, H_2O_2	10–50 bar, 20–40°C	99+%	No CO_2 detected	∼4.5

synergy afforded by the facile compressibility of a substrate such as ethylene and the accompanying enhanced solubility in low molecular weight alcohols can be exploited to enhance selectivity and productivity.

Acid Catalysis

The replacement of mineral acids with benign and less hazardous alternatives has long been a grand challenge in chemicals synthesis. In situ generation of acids by the reaction of CO_2 with alcohols or water is desirable because depressurization leads to self-neutralization [102–104]. The formation of the dimethyl acetal of cyclohexanone is up to 130 times faster in CO_2-expanded methanol than in normal methanol without any added acid. Such in situ acids also catalyze the hydrolysis of β-pinene to terpineol and other alcohols with good selectivity for alcohols rather than hydrocarbons [103].

Addition of CO_2 to pressurized hot water accelerates reactions that can proceed by acid catalysis. CO_2 dissolved in water at 250°C promotes the decarboxylation of benzoic acid [105], the dehydration of cyclohexanol to cyclohexene, and the alkylation of p-cresol to 2-*tert*-butyl-4-methylphenol [106]. The hydration of cyclohexene to cyclohexanol at 300°C showed a fivefold rate increase as the CO_2 pressure was increased from 0 to 55 bar.

Miscellaneous

Ozonolysis Ozone has high oxidation potential ($E^o = 2.075$ V in acid and 1.246 V in base) and has been extensively investigated as a potent oxidant. Though considered toxic, ozone does not persist in the environment eventually decomposing to molecular oxygen. Ozone is effective for the cleavage of carbon–carbon double bonds. This oxidation reaction

is believed to proceed via metastable intermediates that upon further catalytic oxidation or reduction yield products that are suitable as building blocks for chemical synthesis. For example, the ozonolysis of unsaturated fatty acids can yield a range of both monoacids and diacids [107–110]. Ozone attacks most common organic solvents used as reaction media, creating undesirable waste products and consuming the ozone away from the desired reaction. It has been recently shown that ozone can be used effectively in liquid CO_2, in which it is not only stable but also remarkably soluble [111]. At typical ozonolysis temperatures (0–20°C), ozone is sufficiently close to its critical temperature (−12.1°C) such that the ozone density can be increased to liquid-like values by compression beyond its critical pressure (55.6 bar). Conveniently, in the 0–20°C range and beyond 50 bar, the CO_2 ($P_c = 73.8$ bar; $T_c = 31.1$°C) exists as liquid and the O_3 content in this liquid phase is easily tuned with pressure. An order of magnitude increased dissolution of O_3 in liquid CO_2 creates an *O_3-expanded liquid phase*. The O_3 half-life in liquid CO_2 was found to be approximately 6 h at −1.2°C [111]. Further, substrates such as methyl oleate and *trans*-stilbene when dispersed in liquid CO_2 (containing dissolved O_3) undergo complete conversion in minutes to the corresponding aldehyde and acid products (nonanal, nonanoic acid in the case of methyl oleate; and benzaldehyde, benzoic acid in the case of *trans*-stilbene). The foregoing results clearly show that ozonolysis in liquid CO_2 is a facile, clean, and inherently safe oxidation route.

Carbonylations Exploiting the enhanced and tunable CO solubility in CXLs, it was recently shown that selective mono or double carbonylations could be achieved by using CO_2-expanded liquids during [2 + 2 + 1] carbonylative reactions of alkenes or acetylenes with allyl bromides catalyzed by Ni(I) [112].

Polymerizations Catalytic chain transfer polymerizations are free radical polymerizations that use a homogeneous catalyst to terminate one chain and initiate a new one. During the polymerization of methyl methacrylate, the chain transfer step is believed to be a diffusion-controlled reaction in which the Co(II) catalyst abstracts a hydrogen atom from the polymer radical (R•) and transfers it to a monomer to start the growth of a new chain. Zwolak et al. [113] reported that the rate of chain transfer was fourfold greater in CO_2-expanded methyl methacrylate (60 bar, 50°C) than in neat monomer. The improvement was attributed to the lower viscosity of the CO_2-expanded solution.

Biomass Conversions Plant-based biomass has the potential to completely displace fossil fuel–based feedstocks for chemicals production in a sustainable manner. However, new catalytic technologies are needed for the fledgling biorefinery to convert plant-based biomass feedstocks to chemicals and chemical building blocks. Recently, the acid-catalyzed transesterification of soybean flakes in CO_2-expanded methanol containing sulfuric acid was demonstrated for producing fatty acid methyl esters (FAME) [114]. The authors report that the introduction of CO_2 into the system increases the rate of reaction by as much as 2.5 fold in comparison to control reactions without CO_2.

1,2-glycerol carbonate was formed from glycerol and carbon dioxide in methanol using (Bu_2SnO)-Bu-*n* (dibutyltin(IV)oxide, 1) as a catalyst [115]. The yield of 1,2-glycerol carbonate was as high as 35%. The reaction proceeds upon activation of the catalyst by methanol forming dibutyltindimethoxide followed by dibutyltinglycerate, which undergoes CO_2 insertion to ultimately yield glycerol carbonate.

Multiphase Catalysis

The attractive properties of GXLs are also applicable in heterogeneous catalysis. For example, adding CO_2 to an organic liquid phase in a fluid–solid catalytic system should enhance gas solubilities and improve the mass transfer properties of the expanded liquid phase. Reviews of supercritical phase heterogeneous catalysis may be found elsewhere [116–118].

Hydrogenations

Employing dense CO_2 as the solvent medium in a stirred reactor, it was reported that the Pd/Al_2O_3 catalyzed hydrogenation of an unsaturated ketone proceeded faster in CO_2-expanded ketone than in the unswollen ketone [119]. A similar observation was reported during the Pd/C catalyzed hydrogenation of

pinene wherein the reaction rate was higher at lower pressures in a condensed CXL phase compared to single-phase operation at supercritical conditions [120]. Roberts and coworkers reported that the rate constant for the hydrogenation of the aromatic rings in polystyrene (PS) was found to be higher in CO_2-expanded decahydronaphthalene (DHN) than in neat DHN [121]. For the Pt/γ-Al_2O_3 catalyzed hydrogenation of tetralin to decalin, Chan and Tan [122] reported enhanced rates in the presence of a CO_2-expanded toluene phase in a trickle bed reactor. For the Pd/C-catalyzed hydrogenation of CO_2-expanded alpha-methylstyrene, it was shown that the rate-enhancing effect of CO_2 is influenced by two competing factors: solvent strength and reactant concentration [123]. The presence of CO_2 modifies the solvent strength of the liquid phase, resulting in more favorable adsorption equilibrium for the surface reaction. However, the diluting effect of CO_2 leads to reduced reaction rates. Thus, there exists an optimum CO_2 level in the liquid phase that is tunable by reactor pressure.

During the $NiCl_2$-catalyzed reduction of benzonitrile to benzylamine by $NaBH_4$, Xie et al. [124] showed that CO_2 expansion of the reaction mixture converts the primary amine to a carbamate salt, thereby preventing its further reaction to secondary amines. The carbamic species release CO_2 upon gentle heating. Thus, the benzylamine yield was 98% in CO_2-expanded ethanol but <0.01% in normal ethanol.

Heterogeneous catalysis without solvent relies on both the substrate and product being liquids or gases. If the product is a solid at the reaction temperature, then the reaction will not proceed to completion because the reaction mixture will solidify before full conversion is obtained. Normally, this problem is solved by adding a solvent or using an elevated temperature, but a third option is to lower the melting point of the product by expansion with CO_2 [71]. For example, the Pt-catalyzed hydrogenation of oleic acid at 35°C stalls at 90% conversion even with extended reaction times (25 h). However, in the presence of 55 bar CO_2, the reaction proceeds to 97% conversion after only 1 h.

Selective Oxidations

During the Pd/Al_2O_3 catalyzed partial oxidation of octanol, Baiker and coworkers report significantly enhanced oxidation rates at intermediate pressures where a condensed CXL phase probably exists compared to higher pressure where a single supercritical phase exists [125]. The reaction in the condensed phase benefits from increased concentrations of the substrate relative to the single supercritical phase while also enjoying adequate O_2 availability in the liquid phase.

During the O_2-based oxidation of cyclohexene on a MCM-41 encapsulated iron porphyrin chloride complex, conversion and selectivity in CO_2-expanded acetonitrile (~30 mol% CO_2) almost doubled compared to the neat organic solvent [126]. For the oxidation of 2,6-di-*tert*-butylphenol (DTBP) to 2,6-di-*tert*-butyl-1,4-benzoquinone (DTBQ) and 3,5.3',5'-tetra-*tert*-butyl-4,4'-diphenoquinone (TTBDQ), a series of porous materials with immobilized Co(II) complexes were screened as catalysts in neat acetonitrile, supercritical carbon dioxide (*sc*CO_2), and CO_2-expanded acetonitrile [127]. In this case, the highest conversions were found in *sc*CO_2 suggesting that scCO_2, rather than CXL or liquid reaction media, provides the best mass transfer of O_2 and of substrates through the porous catalysts.

Hydroformylation and Carbonylation

Abraham and coworkers [77] investigated 1-hexene hydroformylation over a rhodium–phosphine catalyst immobilized on a silica support and found that the rates in CO_2-expanded toluene and in scCO_2 were comparable but faster than in normal toluene. However, the activity declined with time due to possible catalyst leaching.

Leitner and coworkers have demonstrated that compressed CO_2 can be used to effectively overcome mass transfer limitations encountered during solid-phase organic synthesis with pressurized gaseous reagents [128]. Depending on the relative importance of mass-transfer limitations and catalyst/substrate concentration, CXLs may provide the optimum conditions for both hydroformylation and carbonylation reactions. For example, the catalytic carbonylation of norbornene (Pauson–Khand reaction) supported on a polymer support proceeds nearly quantitatively in CXL media. Here, the CXL medium provides the optimum combination of catalyst concentration and CO availability to maximize the reaction rate.

Solid Acid Catalysis

The acylation of anisole with acetic anhydride was investigated in a continuous slurry reactor over mesoporous-supported solid acid catalysts such as Nafion® (SAC-13) and heteropolyacids [129]. The CXL media gave lower conversion and, surprisingly, faster deactivation compared to a liquid-phase reaction despite the use of polar cosolvents. The deactivation is possibly due to retention of heavy molecules (possibly di- and tri-acylated products) formed by the interaction of acetic anhydride with para-methoxyacetophenone (*p*-MOAP) in the catalyst micropores. The addition of CF_3CO_2H has been shown to catalyze a Friedel–Crafts alkylation of anisole in CO_2-expanded anisole (95°C, 42 bar), but the reaction was no faster than that in normal anisole [130].

An Example of CXL-Based Process Development Including Sustainability (Economic and Environmental Impact) Analyses

For developing sustainable catalytic processes, a multiscale approach involving concurrent catalyst design, solvent engineering, and reactor engineering is essential [40]. An example of such an approach, involving chemists and engineers, is presented in this section for an industrially significant reaction.

For the hydroformylation of higher olefins, cobalt-based catalysts are employed. The cobalt catalysts require rather harsh operating conditions (140–200°C, 50–300 bar) and the catalyst recovery steps involve much solvents, acids, and bases [131]. The challenges for a sustainable technology alternative are to develop a process that operates at milder temperatures (<100°C) and pressures (<100 bar), and requires a simple yet environmentally friendly catalyst recovery method. The use of a Rh catalyst for 1-octene hydroformylation in CXL media provides exceptional TOF ($\sim$316 h^{-1}) and regioselectivity ($n/i \sim 9$) at very mild pressure ($\sim$40 bar) and temperature (30–60°C) compared to conventional Co-based processes [75]. This markedly enhanced regioselectivity in CXLs during homogeneous 1-octene hydroformylation is partly attributed to the beneficial tunability of the H_2/CO ratio in the CXL phase.

It is well known that the concentrations of the syngas components (CO and H_2) in the liquid phase are major determinants of the reaction pathways and therefore the product selectivity. In general, higher H_2 concentrations are needed for catalyst activation and lower CO concentrations are required to achieve higher rates and avoid inhibition effect due to formation of inactive carbonyl species [132]. Because CO is generally more soluble than hydrogen in most conventional solvents [133], the resulting H_2/CO ratio in the liquid phase is less than that in the feed syngas. However, when CO_2 is added to either 1-octene or nonanal (to create a CXL), it was observed that the H_2 is more soluble than CO in the CXLs [5]. This means that the H_2/CO ratio in the liquid phase should be greater in CXLs (based on the organic solvent and extent of CO_2 addition) compared to the ratio in the feed.

Gas solubility measurements showed the presence of CO_2 at hydroformylation conditions (T = 40–80°C and pressures up to 90 bar) enhances the solubilities of both CO and H_2 in the liquid phase. The enhancement factor, defined as the ratio of the gas (CO or H_2) mole fraction in the neat solvent relative to that in the CXL at identical temperature and gas (CO or H_2) fugacities in the vapor phase, is greater for hydrogen (around 1.8) compared to carbon monoxide (around 1.5). This unique tunability of the H_2/CO ratio in CXL media is believed to enhance both the TOF and n/i ratio.

A detailed engineering model that takes into account kinetics, phase equilibrium, and mass transfer effects provided a better understanding of the mass transfer and kinetic effects in the CXL-based media [134]. A plant-scale simulation of the CXL process concept (Fig. 5) was constructed to facilitate economic and environmental impact analyses. Economic analysis revealed that >99.8% rhodium has to be recovered per pass for the CEBC hydroformylation process to be competitive with a simulated Co-based commercial process [135]. Environmental impact analysis revealed that the CEBC process produces half as much waste with lower overall toxicity compared to the simulated conventional process [135].

To develop Rh catalysts that meet the quantitative criterion for economic viability, a soluble polymer-attached, recyclable rhodium(I) catalyst with chelate-capable phosphite functionality, that was used to produce a polymer ligand, was synthesized (Scheme 2). By controlling the molecular weight, the polymer is designed such that it is completely soluble in

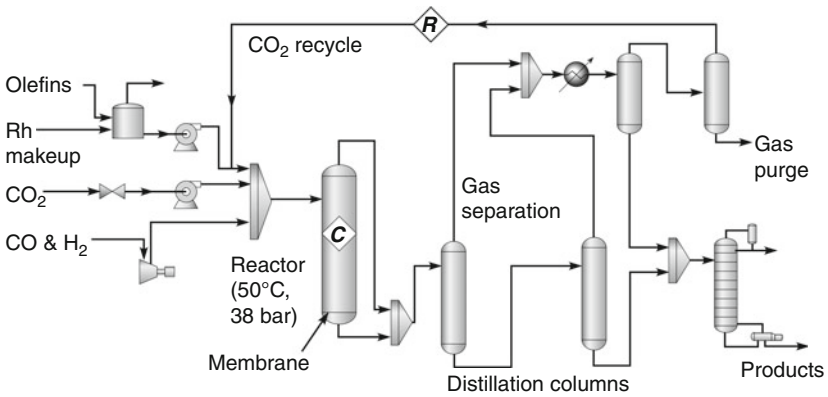

Gas Expanded Liquids for Sustainable Catalysis. Figure 5
Process flow diagram for CXL-based hydroformylation concept

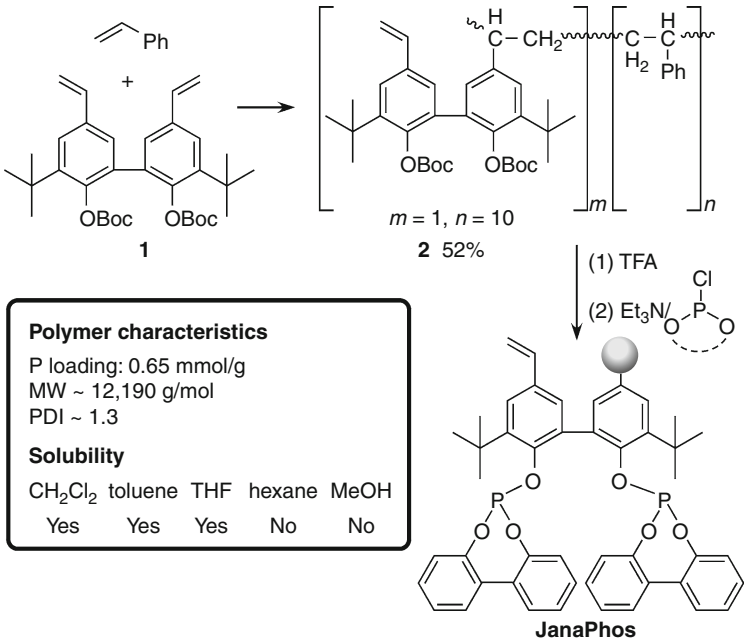

Gas Expanded Liquids for Sustainable Catalysis. Scheme 2
Synthesis of polymer-attached ligand [136]

the hydroformylation reaction medium yet bulky enough to diffuse through a nanofiltration membrane [136, 137]. The polymer support was designed to bind Rh in a bidentate fashion to provide better site isolation for the rhodium catalysts as well as to inhibit decomplexation and subsequent leaching of rhodium from the polymer.

Using the soluble polymer-attached ligand to bind the Rh precursor, a continuous hydroformylation process concept that uses Rh-based homogeneous catalysts and operates at mild pressures (tens of bar) and temperatures less than 100°C has been demonstrated. The reactor schematic is shown in Figure 6. Syngas and compressed CO_2 (to generate CXLs) are

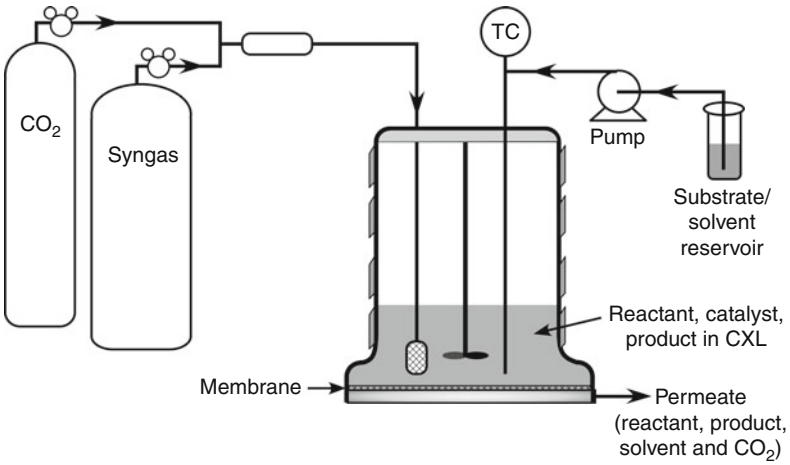

Gas Expanded Liquids for Sustainable Catalysis. Figure 6
Schematic of continuous homogeneous hydroformylation in CXL with catalyst retention by membrane nanofiltration

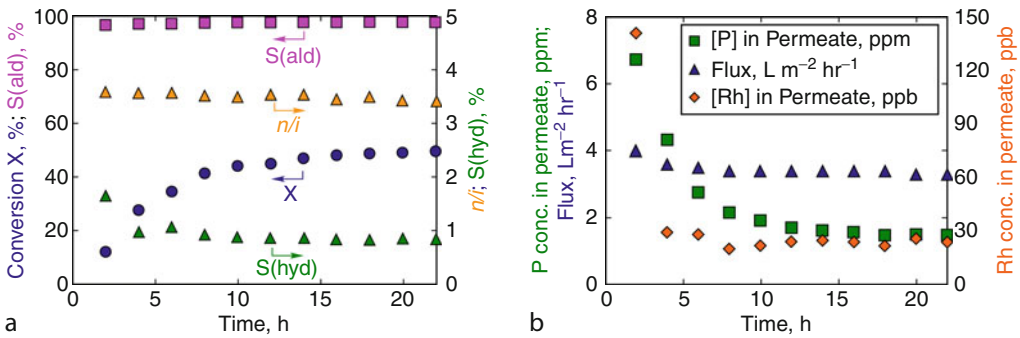

Gas Expanded Liquids for Sustainable Catalysis. Figure 7
Demonstration of a continuous CXL-based homogeneous hydroformylation reactor with effective catalyst retention by membrane nanofiltration. $T = 50°C$, $P_{syngas} = 30$ bar, $CO/H_2 = 1:1$, P/Rh = .6, Oct/Rh = 2200, toluene/1-octene = 70:30 by volume, stirrer speed: 1000 rpm [138]

added to the 1-octene + nonanal reaction mixture in which the polymer-attached rhodium complex is dissolved. The product stream is continuously withdrawn while maintaining the reactor pressure constant.

Continuous operation is characterized by steady membrane flux, constant conversion, and constant product selectivity (Fig. 7a). At steady state, the permeate stream contains the unreacted 1-octene and CO_2 (which is separated by depressurization and may be recycled) products. As seen from Fig. 7b, the Rh and P concentrations in the permeate phase, quantified using ICP analysis, were on the order of a few tens of ppb [138]. The cost of the makeup Rh is 0.4 cent/lb product, which exceeds the economic viability criterion.

The foregoing example represents a systems-based, multiscale research approach developing novel, environmentally beneficial, and economically viable process concepts. A patent pertaining to the CXL-based hydroformylation concept [139] has been licensed to a company for a defined field of use. The demonstrated technology concept, when fully optimized, should find applications in a variety of other applications in

homogeneous catalysis, including hydrogenation and carbonylation of conventional and biomass-based substrates.

Summary and Future Directions

The novel science and technology advances discussed in this entry demonstrate the various unique ways in which GXL media may be exploited to develop greener process concepts for oxidations, hydroformylations, hydrogenations, ozonolysis, and other chemistries. The demonstrated advantages include *process intensification* at mild conditions by increasing dissolution of the limiting reagent in the GXL reaction phase; the *efficient utilization* of feedstock and reactive gases such as O_3 due to the inertness of CO_2, an often used expansion medium; enhancing *inherent safety* of the process by suppression of flammable vapors; and *waste minimization* by suppression of side reactions that generate undesired products such as CO_2 and reduced usage of volatile organic solvents.

The alternative concepts presented herein address chemistries underlying large-scale catalytic technologies, including the homogeneous hydroformylation of higher olefins and the epoxidations of light olefins such as ethylene and propylene. The global capacity of these processes is growing at 4–6% annually. Hence, the deployment of viable alternative technologies for future expansion of these processes (and also as replacement of existing units when needed) would have a significant impact in reducing environmental footprints. For these promising concepts to be developed further and considered for commercialization, continued fundamental investigations that integrate catalysis, phase behavior involving GXL media (for reactions and separations), kinetic and reactor modeling are essential. These investigations must be complemented by ongoing quantitative economic and environmental impact analyses to provide research and process engineering guidance for developing practically viable process concepts.

The use of renewable feedstocks has the potential to completely displace petroleum crude and coal for producing industrial chemicals. Further, reducing the carbon footprint of consumer products will be an important expectation of a majority of next-generation consumers. The deployment of green technologies is also essential for renewable feedstocks in order to fulfill their promise for producing sustainable fuels and chemicals. Renewable feedstocks cannot yet be processed with existing technologies because their chemical structures and compositions (their relative C, H, and O contents) are varied and diverse compared to conventional crude oil. The fledgling biorefinery industry is uniquely positioned to accept new technology concepts. Chemical catalysis is a promising avenue to develop atom-economical and energy-efficient biomass conversion technologies. To address this challenge, multidisciplinary expertise is needed for the design and synthesis of novel metal-based catalysts, high-pressure chemistry, solvent engineering, multiphase reaction engineering, and multiscale modeling. Specifically, the various system elements (i.e., catalysts, solvents, reactors, and separators) should be designed such that when integrated, the resulting system displays enhanced rates and selectivity with reduced environmental footprint.

Acknowledgments

Much of the author's work described in this entry was made possible by NSF ERC Grant EEC-0310689, the Kansas Technology Enterprise Corporation, and the support of the University of Kansas through the Dan F. Servey Distinguished Professorship.

Bibliography

Primary Literature

1. Jessop PG, Subramaniam B (2007) Gas-expanded liquids. Chem Rev 107:2666–2694
2. Lopez-Castillo ZK, Aki SNVK, Stadtherr MA, Brennecke JF (2006) Enhanced solubility of oxygen and carbon monoxide in CO_2-expanded liquids. Ind Eng Chem Res 45:5351–5360
3. Lopez-Castillo ZK, Aki SNVK, Stadtherr MA, Brennecke JF (2008) Enhanced solubility of hydrogen in CO_2-expanded liquids. Ind Eng Chem Res 47:570–576
4. Zevnik L, Levec J (2007) Hydrogen solubility in CO_2-expanded 2-propanol and in propane-expanded 2-propanol determined by an acoustic sensor. J Supercrit Fluids 41:335–342
5. Xie Z, Snavely WK, Scurto AM, Subramaniam B (2009) Solubilities of CO and H_2 in neat and CO_2-expanded hydroformylation reaction mixtures containing 1-octene and nonanal up to 353 K and 9 Mpa. J Chem Eng Data 54:1633–1642
6. Sheldon RA (1994) Consider the environmental quotient. Chem Tech 24:38–47

7. Sheldon RA, Arends IWCE, Hanefeld U (2007) Green chemistry and catalysis. Wiley, Weinheim
8. Tundo AP, Black DS, Breen J, Collins T, Memoli S, Miyamoto J, Poliakoff M, Tumas W (2000) Synthetic pathways and processes in green chemistry: introductory overview. Pure Appl Chem 72:1207–1228
9. DeSimone JM (2002) Practical approaches to green solvents. Science 297:799–803
10. Adams DJ, Dyson PJ, Tavener SJ (2004) Chemistry in alternative reaction media. Wiley, Chichester
11. Eckert CA, Liotta CL, Bush B, Brown JS, Hallett JP (2004) Sustainable reactions in tunable solvents. J Phys Chem B 108:18108–18118
12. Seki T, Baiker A (2009) Catalytic oxidations in dense carbon dioxide. Chem Rev 109:2409–2454
13. Morgenstern DA, LeLacheur RM, Morita DK, Borkowsky SL, Feng S, Brown GH, Luan L, Gross MF, Burk MJ, Tumas W (1996) Supercritical carbon dioxide as a substitute solvent for chemical synthesis and catalysis. In: Anastas PT, Williamson TC (eds) Green chemistry: designing chemistry for the environment, ACS symposium series vol 626. American Chemical Society, Washington, DC, pp 132–151
14. Jessop PG, Leitner W (1999) Chemical synthesis using supercritical fluids. Wiley, Weinheim
15. Amandi R, Hyde J, Poliakoff M (2003) Heterogeneous reactions in supercritical carbon dioxide. In: Aresta M (ed) Carbon dioxide recovery and utilization. Kluwer, Dordrecht, pp 169–180
16. DeSimone JM, Tumas W (2003) Green chemistry using liquid and supercritical carbon dioxide. Oxford University Press, New York
17. Gordon CM, Leitner W (2004) Supercritical fluids as replacements for conventional organic solvents. Chim Oggi 22:39–41
18. Beckman EJ (2002) Using CO_2 to produce chemical products sustainably. Environ Sci Technol 36:347A–353A
19. Licence P, Poliakoff M (2005) Economics and scale-up. In: Cornils B, Hermann WA, Horváth IT, Leitner W, Mecking S, Olivier-Bourbigou H, Vogt D (eds) Multiphase homogeneous catalysis, vol 2. Wiley, Weinheim, pp 734–746
20. Arai M, Fujita SI, Shirai M (2009) Multiphase catalytic reaction in/under dense phase CO_2. J Supercrit Fluids 47:351–356
21. Li CJ, Chan TH (1997) Organic reactions in aqueous media. Wiley, New York
22. Cornils B, Herrmann WA (1998) Aqueous-phase organometallic catalysis. Wiley, Weinheim
23. Savage PE (2009) A perspective on catalysis in sub- and supercritical water. J Supercrit Fluids 47:407–414
24. Musie G, Wei M, Subramaniam B, Busch DH (2001) Catalytic oxidations in carbon dioxide-based reaction media, including novel CO_2-expanded phases. Coord Chem Rev 219–221: 789–820
25. Hutchenson KW, Scurto AM, Subramaniam B (2009) Gas-expanded liquids and near-critical media: green chemistry and engineering, vol 1006, ACS symposium series. American Chemical Society, Washington, DC
26. Akien GR, Poliakoff M (2009) A critical look at reactions in class I and II gas-expanded liquids using CO_2 and other gases. Green Chem 11:1083–1100
27. Scurto AM, Hutchenson KW, Subramaniam B (2009) Gas-expanded liquids (GXLs): fundamentals and applications. In: Hutchenson KW, Scurto AM, Subramaniam B (eds) Gas-expanded liquids and near-critical media: green chemistry and engineering, vol 1006, ACS symposium series. American Chemical Society, Washington, DC, pp 3–37
28. Wasserscheid P, Welton T (2002) Ionic liquids in synthesis. Wiley, Weinheim
29. Rogers RD, Seddon KR, Volkov S (2003) Green industrial applications of ionic liquids. Kluwer, Dordrecht
30. Pârvulescu VI, Hardacre C (2007) Catalysis in ionic liquids. Chem Rev 107:2615–2665
31. Jessop PG, Heldebrant DJ, Xiaowang L, Eckert CA, Liotta CL (2005) Reversible nonpolar-to-polar solvent. Nature 436:1102
32. Liu Y, Jessop PG, Cunningham M, Eckert CA (2006) Liotta CL, switchable sufactants. Science 313:958–960
33. Phan CD, Heldebrant DJ, Huttenhower H, John E, Li X, Pollet P, Wang R, Eckert CA, Liotta CL, Jessop PG (2008) Switchable solvents consisting of amidine/alcohol or guanidine/alcohol mixtures. Ind Eng Chem Res 47:539–545
34. Phan L, Brown H, White J, Hodgson A, Jessop PG (2009) Soybean oil extraction and separation using switchable or expanded solvents. Green Chem 11:53–59
35. Phan L, Jessop PG (2009) Switching the hydrophilicity of a solute. Green Chem 11:307–308
36. Ahosseini A, Ren W, Scurto AM (2009) Understanding biphasic ionic liquid/CO_2 systems for homogeneous catalysis: hydroformylation. Ind Eng Chem Res 48:4254–4265
37. Anastas P, Warner JC (1998) Green chemistry: theory and practice. Oxford University Press, New York
38. Anastas PT, Zimmerman JB (2003) Design through the 12 principles of green engineering. J Environ Sci Technol 37:95A–101A
39. Allen DT, Shonnard DR (2001) Green engineering: environmentally conscious design of chemical processes. Prentice Hall, New York
40. Dudukovic MP (2009) Frontiers in reactor engineering. Science 325:698–701
41. Kordikowski A, Schenk AP, Van Nielen RM, Peters CJ (1995) Volume expansions and vapor-liquid equilibria of binary mixtures of a variety of polar solvents and certain near-critical solvents. J Supercrit Fluids 8:205–216
42. Ren W, Scurto AM (2007) High-Pressure phase equilibria with compressed gases. Rev Sci Instrum 78:125104–125107
43. Heldebrant DJ, Witt H, Walsh S, Ellis T, Rauscher J, Jessop PG (2006) Liquid polymers as solvents for catalytic reductions. Green Chem 8:807–815
44. Ren W, Sensenich B, Scurto AM (2010) High-pressure phase equilibria of carbon dioxide (CO_2) + n-alkyl-imidazolium bis (trifluoromethylsulfonyl)amide ionic liquids. J Chem Thermodyn 42:305–311

45. Rajagopalan B, Wie M, Musie GT, Subramaniam B, Busch DH (2003) Homogeneous catalytic epoxidation of organic substrates in CO_2-expanded solvents in the presence of water soluble oxidants and catalysts. Ind Eng Chem Res 42:6505–6510
46. Ohgaki K, Takata H, Washida T, Katayama T (1988) Phase equilibria of four binary systems containing propylene. Fluid Phase Equilibr 43:105–113
47. Peng DB, Robinson DT (1976) A new two-constant equation of state. Ind Eng Chem Fund 15:59–64
48. Houndonougbo Y, Jin H, Rajagopalan B, Wong K, Kuczera K, Subramaniam B, Laird BB (2006) Phase equilibria in carbon dioxide-expanded solvents: experiment and molecular simulations. J Phys Chem B 110:13195–13202
49. Swalina C, Arzhantsev S, Li HP, Maroncelli M (2008) Solvation and solvatochromism in CO_2-expanded liquids. 3. the dynamics of nonspecific preferential solvation. J Phys Chem B 112:14959–14970
50. Subramaniam B (2010) Gas-expanded liquids for sustainable catalysis and novel materials. Coord Chem Rev 254:1843–1853
51. Sih R, Dehghani F, Foster NR (2007) Viscosity measurements on gas expanded liquid systems-methanol and carbon dioxide. J Supercrit Fluids 41:148–157
52. Kelkar MS, Maginn EJ (2007) Effect of temperature and water content on the shear viscosity of the ionic liquid 1-ethyl-3-methylimidazolium bis(trifluoromethanesulfonyl)imide as studied by atomistic simulations. J Phys Chem B 111:4867–4876
53. Ahosseini A, Ortega E, Sensenich B, Scurto AM (2009) Viscosity of n-alkyl-3-methyl-imidazolium bis(trifluoromethylsulfonyl) amide ionic liquids saturated with compressed CO_2. Fluid Phase Equilibr 286:62–68
54. Maxey NB (2006) Transport and phase-transfer catalysis in gas-expanded liquids. PhD Dissertation, Georgia Institute of Technology, Atlanta
55. Lin IH, Tan CS (2008) Diffusion of benzonitrile in CO_2-expanded ethanol. J Chem Eng Data 53:1886–1891
56. Roškar V, Dombro RA, Prentice GA, Westgate CR, McHugh MA (1992) Comparison of the dielectric behavior of mixtures of methanol with carbon dioxide and ethane in the mixture-critical and liquid regions. Fluid Phase Equilibr 77:241–259
57. Wyatt VT, Bush D, Lu J, Hallett JP, Liotta CL, Eckert CA (2005) Determination of solvatochromic solvent parameters for the characterization of gas-expanded liquids. J Supercrit Fluids 36:16–22
58. Abbott AP, Hope EG, Mistry R, Stuart AM (2009) Probing the structure of gas expanded liquids using relative permittivity, density and polarity measurements. Green Chem 11:1530–1535
59. Ford JW, Janakat ME, Liu J, Liotta CL, Eckert CA (2008) Local polarity in CO_2-expanded acetonitrile: A nucleophilic substitution reaction and solvatochromic probes. J Org Chem 73:3364–3368
60. Seki TJ, Grunwaldt JD, Baiker A (2009) In situ attenuated total reflection infrared spectroscopy of imidazolium-based room-temperature ionic liquids under "supercritical" CO_2. J Phys Chem B 113:114–122
61. Burgi T, Baiker A (2006) Attenuated total reflection infrared spectroscopy of solid catalysts functioning in the presence of liquid-phase reactants. Adv Catal 50:227–283
62. Guha D, Jin H, Dudukovic MP, Ramachandran PA, Subramaniam B (2007) Mass transfer effects during homogeneous 1-octene hydroformylation in CO_2-expanded solvent: modeling and experiments. Chem Eng Sci 62:4967–4975
63. Lyon CJ, Subramaniam B, Pereira CJ (2001) Enhanced isooctane yields for 1-butene/Isobutane alkylation on SiO2-supported Nafion® in supercritical carbon dioxide. In: Spivey JJ, Roberts GW, Davis BH (eds) Catalyst deactivation 2001. Studies in surface science and catalysis, vol 139. Elsevier, Amsterdam, pp 221–228
64. (a) Webb PB, Kunene TE, Cole-Hamilton DJ (2005) Continuous flow homogeneous hydroformylation of alkenes using supercritical fluids. Green Chem 7:373–379; (b) Sellin MF, Webb PB, Cole-Hamilton DJ (2001) Chem Commun 781
65. Thomas CA, Bonilla RJ, Huang Y, Jessop PG (2001) Hydrogenation of carbon dioxide catalysed by ruthenium trimethylphosphine complexes: effect of gas pressure and additives on rate in the liquid phase. Can J Chem 79:719–724
66. Combes GB, Dehghani F, Lucien FP, Dillow AK, Foster NR (2000) Asymmetric catalytic hydrogenation in CO_2 expanded methanol-an application of gas anti-solvent reaction (GASR). In: Abraham MA, Hesketh RP (eds) Reaction engineering for pollution prevention. Elsevier, Amsterdam, pp 173–181
67. Combes G, Coen E, Dehghani F, Foster NR (2005) Dense CO_2 expanded methanol solvent system for synthesis of naproxen via enantioselective hydrogenation. J Supercrit Fluids 36:127–136
68. Floris T, Kluson P, Muldoon MJ, Pelantova H (2010) Notes on the asymmetric hydrogenation of methyl acetoacetate in neoteric solvents. Cat Lett 134:279–287
69. Solinas M, Pfaltz A, Cozzi P, Leitner W (2004) Enantioselective hydrogenation of imines in ionic liquid/carbon dioxide media. J Am Chem Soc 126:16142–16147
70. Jessop PG, Stanley R, Brown RA, Eckert CA, Liotta CL, Ngo TT, Pollet P (2003) Neoteric solvents for asymmetric hydrogenation: supercritical fluids, ionic liquids, and expanded ionic liquids. Green Chem 5:123–128
71. Jessop PG, DeHaai S, Wynne DC, Nakawatase D (2000) Carbon dioxide gas accelerates solventless synthesis. Chem Commun 8:693–694
72. Scurto AM, Leitner W (2006) Melting point depression of organic ionic solids/liquids with carbon dioxide for enhanced catalytic processes. Chem Commun 3681–3683
73. Ahosseini A, Ren W, Scurto AM (2009) Hydrogenation in biphasic ionic liquid/CO_2 systems. In: Hutchenson KW, Scurto AM, Subramaniam B (eds) Gas expanded liquids and near-critical media: green chemistry and engineering, vol 1006, ACS symposium series. American Chemical Society, Washington, DC, pp 218–234

74. Jin H, Subramaniam B (2004) Catalytic hydroformylation of 1-octene in CO_2-expanded solvent media. Chem Eng Sci 59:4887–4893
75. Jin H, Subramaniam B, Ghosh A, Tunge J (2006) Intensification of catalytic olefin hydroformylation in CO_2-expanded media. AIChE J 52:2575–2591
76. Koeken ACJ, Benes NE, van den Broeke LJP, Keurentjes JTF (2009) Efficient hydroformylation in dense carbon dioxide using phosphorus ligands without perfluoroalkyl substituents. Adv Syn Catal 351:1142–1450
77. Hemminger O, Marteel A, Mason MR, Davies JA, Tadd AR, Abraham MA (2002) Hydroformylation of 1-hexene in supercritical carbon dioxide using a heterogeneous rhodium catalyst. 3. Evaluation of solvent effects. Green Chem 4: 507–512
78. Webb PB, Sellin MF, Kunene TE, Williamson S, Slawin AMZ, Cole-Hamilton DJ (2003) Continuous flow hydroformylation of alkenes in supercritical fluid-ionic liquid biphasic systems. J Am Chem Soc 125:15577–15588
79. Frisch AC, Webb PB, Zhao G, Muldoon MJ, Pogorzelec PJ, Cole-Hamilton DJ (2007) Solventless continuous flow homogeneous hydroformylation of 1-octene. Dalton Trans 47:5531–5538
80. Wei M, Musie GT, Busch DH, Subramaniam B (2002) CO_2-expanded solvents: unique and versatile media for performing homogeneous catalytic oxidations. J Am Chem Soc 124: 2513–2517
81. Wei M, Musie GT, Busch DH, Subramaniam B (2004) Autoxidation of 2,6-di-tertbutylphenol with cobalt Schiff base catalysts by oxygen in CO_2-expanded liquids. Green Chem 6:387–393
82. Zuo X, Niu F, Snavely WK, Subramaniam B, Busch DH (2010) Liquid phase oxidation of *p*-xylene to terephthalic acid at medium-high temperatures: multiple benefits of CO_2-expanded liquids. Green Chem 12:260–267
83. Trent DT (1996) Propylene oxide Kirk-Othmer encyclopedia of chemical technology, vol 20, 4th edn. Wiley, New York, pp 271–302
84. Thiele GF, Roland E (1997) Propylene epoxidation with hydrogen peroxide and titanium silicalite catalyst: activity, deactivation and regeneration of the catalyst. J Mol Catal A Chem 117:351–356
85. Danciu T, Beckman EJ, Hancu D, Cochran RN, Grey R, Hajnik DM, Jewson J (2002) Direct synthesis of propylene oxide with CO_2 as the solvent. Angew Chem Int Ed 42:1140–1142
86. Laufer W, Meiers R, Holderich W (1999) Propylene epoxidation with hydrogen peroxide over palladium containing titanium silicalite. J Mol Catal A Chem 141:215–221
87. Jenzer G, Mallat T, Maciejewski M, Eigenmann F, Baiker A (2001) Continuous epoxidation of propylene with oxygen and hydrogen on a Pd-Pt/TS-1 catalyst. Appl Catal A 208:125–133
88. Nolen SA, Lu J, Brown JS, Pollet P, Eason BC, Griffith KN, Glaser R, Bush D, Lamb DR, Liotta CL, Eckert CA, Thiele GF, Bartels KA (2002) Olefin epoxidations using supercritical carbon dioxide and hydrogen peroxide without added metallic catalysts or peroxy ccids. Ind Eng Chem Res 41:316–323
89. Hancu D, Green H, Beckman EJ (2002) H_2O_2 in CO_2/H_2O biphasic systems: green synthesis and epoxidation reactions. Ind Eng Chem Res 41:4466–4474
90. Zha YJ, Zhang JL, Han BX, Hu SQ, Li W (2010) CO_2-controlled reactors: epoxidation in emulsions with droplet size from micron to nanometre scale. Green Chem 12:452–457
91. Herrmann WA, Fischer RW, Marz DW (1991) Methyltrioxorhenium as catalyst for olefin metathesis. Angew Chem Int Ed Engl 30:1636–1638
92. Rudolph J, Reddy KL, Chiang JP, Sharpless KB (1997) Highly efficient epoxidation of olefins using aqueous H_2O_2 and catalytic methyltrioxorhenium/pyridine: pyridine-mediated ligand acceleration. J Am Chem Soc 119:6189–6190
93. Wang WD, Espenson JH (1998) Effects of pyridine and its derivatives on the equilibria and kinetics pertaining to epoxidation reactions catalyzed by methyltrioxorhenium. J Am Chem Soc 120:11335–11341
94. Yin G, Busch DH (2009) Mechanistic details to facilitate applications of an exceptional catalyst, methyltrioxorhenium: encouraging results from oxygen-18 isotopic probes. Catal Lett 130:52–55
95. Lee HJ, Shi TP, Busch DH, Subramaniam B (2007) A greener, pressure intensified propylene epoxidation process with facile product separation. Chem Eng Sci 62:7282–7289
96. Lee HJ, Ghanta M, Busch DH, Subramaniam B (2010) Towards a CO_2-free ethylene oxide process: homogeneous ethylene epoxidation in gas-expanded liquids. Chem Eng Sci 65: 128–134
97. Azarnoosh A, Mcketta JJ (1959) Solubility of propylene in water. J Chem Eng Data 4:211–212
98. Yorizane M, Sadamoto S, Yoshimura S (1968) Low-temperature vapor-liquid equilibriums. Nitrogen-propylene and carbon dioxide-methane systems. Kagaku Kogaku Ronbun 32:257–264
99. Lee HJ, Shi TP, Subramaniam B, Busch DH (2006) Selective oxidation of propylene to propylene oxide in CO_2 expanded liquid system. In: Schmidt SR (ed) Catalysis of organic reactions. CRC Press, Boca Raton, pp 447–451
100. Weissermel K (2003) Industrial organic chemistry, 4th edn. Wiley, Weinheim, pp 145–153
101. Haneda A, Seki T, Kodama D, Kato M (2006) High-pressure phase equilibrium for ethylene + methanol at 278.15 K and 283.65 K. J Chem Eng Data 51:268–271
102. West KN, Wheeler C, McCarney JP, Griffith KN, Bush D, Liotta CL, Eckert CA (2001) In situ formation of alkylcarbonic acids with CO_2. J Phys Chem A 105:3947–3948
103. Chamblee TS, Weikel RR, Nolen SA, Liotta CL, Eckert CA (2004) Reversible *in situ* acid formation for -pinene hydrolysis using CO_2 expanded liquid and hot water. Green Chem 6:382–386
104. Gohres JL, Marin AT, Lu J, Liotta CL, Eckert CA (2009) Spectroscopic investigation of alkylcarbonic acid formation and dissociation in CO_2-expanded alcohols. Ind Eng Chem Res 48:1302–1306

105. Alemán PA, Boix C, Poliakoff M (1999) Hydrolysis and saponification of methyl benzoates. Green Chem 1:65–68
106. Hunter SE, Savage PE (2004) Recent advances in acid- and base-catalyzed organic synthesis in high-temperature liquid water. Chem Eng Sci 59:4903–4909
107. Throckmorton PE, Hansen LI, Christensen RC, Pryde EH (1968) Laboratory optimization of process variables in reductive ozonolysis of methyl soyate. J Am Oil Chem Soc 45:59–62
108. Nickell EC, Albi M, Privett OS (1976) Ozonization products of unsaturated fatty acid methyl esters. Chem Phys Lipids 17:378–388
109. Nishikawa N, Yamada K, Matsutani S, Higo M, Kigawa H, Inagaki T (1995) Structires of ozonolysis products of methyl oleate obtained in a carboxylic acid medium. J Am Oil Chem Soc 72:735–740
110. O'Brien M, Baxendale IR, Ley SV (2010) Flow ozonolysis using a semipermeable Teflon AF-2400 membrane to effect gas-liquid contact. Org Lett 12:1596–1598
111. Subramaniam B, Busch DH, Danby A, Binder TP (2008) Ozonoysis reactions in liquid CO_2 and CO_2-expanded solvents. U. S, Patent Application, 20090118498
112. Del Moral D, Osuna AMB, Cordoba A, Moreto JM, Veciana J, Ricart S, Ventosa N (2009) Versatile chemoselectivity in Ni-catalyzed multiple bond carbonylations and cyclocarbonylations in CO_2-expanded liquids. Chem Commun 31:4723–4725
113. Zwolak G, Jayasinghe NS, Lucien FP (2006) Catalytic chain transfer polymerisation of CO_2-expanded methyl methacrylate. J Supercrit Fluids 38:420–426
114. Wyatt VT, Haas MJ (2009) Production of fatty acid methyl esters via the in situ transesterification of soybean oil in carbon dioxide-expanded methanol. J Am Oil Chem Soc 86:1009–1016
115. George J, Patel Y, Pillai SM, Munshi P (2009) Methanol assisted selective formation of 1, 2-glycerol carbonate from glycerol and carbon dioxide using (Bu2SnO)-Bu-*n* as a catalyst. J Mol Catal A Chem 304:1–7
116. Baiker A (1999) Supercritical fluids in heterogeneous catalysis. Chem Rev 99:453–474
117. Grunwaldt JD, Wandeler R, Baiker A (2003) Supercritical fluids in catalysis: opportunities of in situ spectroscopic studies and monitoring phase behavior. Catal Rev Sci Eng 45:1–96
118. Beckman EJ (2004) Supercritical and near-critical CO_2 in green chemical synthesis and processing. J Supercrit Fluids 28: 121–191
119. Devetta L, Giovanzana A, Canu P, Bertucco A, Minder B (1999) Kinetic experiments and modeling of a three-phase catalytic hydrogenation reaction in supercritical CO_2. Catal Today 48:337–345
120. Chouchi D, Gourgouillon D, Courel M, Vital J, Nunes da Ponte M (2001) The influence of phase behavior on reactions at supercritical conditions: the hydrogenation of α-pinene. Ind Eng Chem Res 40:2551–2554
121. Xu D, Carbonell RG, Kiserow DJ, Roberts GW (2005) Hydrogenation of polystyrene in CO_2-expanded solvents: catalyst poisoning. Ind Eng Chem Res 44:6164–6170
122. Chan JC, Tan CS (2006) Hydrogenation of tetralin over Pt/γ-Al_2O_3 in trickle-bed reactor in the presence of compressed CO_2. Energy Fuels 20:771–777
123. Phiong H-S, Cooper CG, Adesina AA, Lucien FP (2008) Kinetic modelling of the catalytic hydrogenation of CO_2-expanded alpha-methylstyrene. J Supercrit Fluids 46:40–46
124. Xie X, Liotta CL, Eckert CA (2004) CO_2-protected amine formation from nitrile and imine hydrogenation in gas-expanded liquids. Ind Eng Chem Res 43:7907–7911
125. Jenzer G, Schneider MS, Wandeler R, Mallat T, Baiker A (2001) Palladium-catalyzed oxidation of octyl alcohols in "supercritical" carbon dioxide. J Catal 199:141–148
126. Kerler B, Robinson RE, Borovik AS, Subramaniam B (2004) Application of CO_2-expanded solvents in heterogeneous catalysis: a case study. Appl Catal B 49:91–98
127. Sharma S, Kerler B, Subramaniam B, Borovik AS (2006) Immobilized metal complexes in porous hosts: catalytic oxidation of substituted phenols in CO_2 media. Green Chem 8:972–977
128. Stobrawe A, Makarczyk P, Maillet C, Muller JL, Leitner W (2008) Solid-phase organic synthesis in the presence of compressed carbon dioxide. Angew Chem Int Ed 47:6674–6677
129. Sarsani VSR, Lyon CJ, Hutchenson KW, Harmer MA, Subramaniam B (2007) Continuous acylation of anisole by acetic anhydride in mesoporous solid acid catalysts: reaction media effects on catalyst deactivation. J Catal 245:184–190
130. Chateauneuf JE, Nie K (2000) An investigation of a Friedel-Crafts alkylation reaction in homogeneous supercritical CO_2 and under subcritical and splitphase reaction conditions. Adv Environ Res 4:307–312
131. Garton RD, Ritchie JT, Caers RE (2003) Oxo process. PCT International Application, WO 2003/082789 A2
132. Bhanage BM, Divekar SS, Deshpande RM, Chaudhari RV (1997) Kinetics of hydroformylation of 1-dodecene using homogeneous $HRh(CO)(PPh_3)_3$ catalyst. J Mol Catal A Chem 115:247–257
133. Purwanto P, Deshpande RM, Delmas H, Chaudhari RV (1996) Solubility of hydrogen, carbon monoxide, and 1-octene in various solvents and solvent mixtures. J Chem Eng Data 41:1414–1417
134. Guha D, Jin H, Dudukovic MP, Ramachandran PA, Subramaniam B (2007) Mass transfer effects during homogeneous 1-octene hydroformylation in CO_2-expanded solvent: modeling and experiments. Chem Eng Sci 62:4967–4975
135. Fang J, Jin H, Ruddy T, Pennybaker K, Fahey D, Subramaniam B (2007) Economic and environmental impact analyses of catalytic olefin hydroformylation in CO_2-expanded liquid (CXL) media. Ind Eng Chem Res 46:8687–8692
136. Jana R, Tunge JA (2009) A homogeneous, recyclable rhodium (I) catalyst for the hydroarylation of Michael acceptors. Org Lett 11:971–974

137. Wang R, Cai F, Jin H, Xie Z, Subramaniam B, Tunge JA (2009) Hydroformylation in CO_2-expanded media. In: Hutchenson KW, Scurto AM, Subramaniam B (eds) Gas-expanded liquids and near-critical media: green chemistry and engineering, vol 1006, ACS symposium series. American Chemical Society, Washington, DC, pp 202–217
138. Fang J, Jana R, Tunge JA, Subramaniam B (2011) Continuous homogeneous hydroformylation with bulky rhodium catalyst complexes retained by nano-filtration membranes. Appl Catal A: Gen 393:294–301
139. Subramaniam B, Tunge JA, Jin H, Ghosh A (2008) Tuning product selectivity in catalytic hydroformylation reactions with CO_2-expanded liquids. US Patent 7.365,234, 29 Apr 2008
140. Horstmann S, Grybat A, Kato R (2004) Experimental determination and prediction of gas solubility data for oxygen in acetonitrile. J Chem Thermodyn 36:1015–1018

Books and Reviews

Anastas P, Eghbali N (2010) Green chemistry: principles and practice. Chem Soc Rev 39:301–312
McHugh MA, Krukonis VJ (1994) Supercritical fluid extraction: principles & practice. Butterworth-Heinemann, Boston
Muldoon MJ (2010) Modern multiphase catalysis: new developments in the separation of homogeneous catalysts. Dalton Trans 39:337–348
Olivier-Bourbigou H, Magna L, Morvan D (2010) Ionic liquids and catalysis: recent progress from knowledge to applications. Appl Cat A 373:1–56

Gas to Liquid Technologies

Marianna Asaro[1], Ronald M. Smith[2]
[1]SRI International, Menlo Park, CA, USA
[2]SRI Consulting, Menlo Park, CA, USA

Article Outline

Glossary
Definition of the Subject
Introduction
Survey of Specific Gas to Liquids Technologies
Liquefied Natural Gas (LNG)
Methane Reforming in F-T GTL
Methane Reforming for Methanol/DME Synthesis
Fischer–Tropsch Synthesis
F-T Product Upgrading
Methanol
Dimethylether
Methanol to Gasoline and/or Diesel
Methanol to Chemicals
Ammonia
Direct Conversion of Natural Gas to Liquids
Future Directions
Bibliography

Glossary

Autothermal reforming (ATR) The reaction of oxygen and carbon dioxide or steam with methane to form synthesis gas, wherein the exothermic partial oxidation of methane provides energy for the endothermic steam reforming of methane. ATR is also used in reference to the autothermal reformer itself.

bbl Barrels (of oil).

BOE Barrel of oil equivalent.

Btu Also btu, British thermal unit, a measure of energy content.

Catalytic membrane reactor (CMR) A flow-through reactor used to influence an equilibrium-limited reaction to proceed further in the forward direction via selective transport of reactant(s) or product(s) across the membrane.

CPOx Catalytic partial oxidation.

CTL Coal-to-liquids.

DME Dimethylether.

DOE US Department of Energy.

Fischer–Tropsch reaction The catalytic conversion of synthesis gas to primarily hydrocarbons, the discovery being credited to Franz Fischer and Hans Tropsch.

Gas-Heated reforming (GHR) Use of heat available by recycling process gas (tail gas) downstream of an ATR for steam methane reforming, in a heat exchanger type reactor.

Gas to liquids (GTL) The conversion of gas to liquid fuels and/or chemicals.

Heat exchange reforming (HER) See GHR.

kWh Kilowatt hours, a measure of energy.

Light distillate A distillation cut of low molecular weight and low boiling range, obtained from refining of hydrocarbonaceous feedstocks, used to produce liquefied petroleum gas (LPG), gasoline, and naphtha.

Liquefied natural gas (LNG) Natural gas that has been converted to liquid form for transport or storage.

Middle distillate A distillation cut of mid-range boiling point, obtained from refining hydrocarbonaceous feedstocks, containing hydrocarbons ranging from C_5 through about C_{20} or C_{22}. When further distilled, the portion of middle distillates containing C_5 through about C_{15} is often referred to as naphtha, and the portion containing C_{16} through up to C_{22} is referred to as diesel. The naphtha is often distilled further to produce gasoline and kerosene/jet fuel, or can be used as feed for a naphtha cracker unit to make light olefins. (Less commonly, the gasoline cut is initially collected along with the light distillates.)

Natural gas liquids (NGL) The purified and condensed portion of natural gas consisting of gaseous hydrocarbons heavier than methane specifically ethane (C_2H_6), propane (C_3H_8), *n*-butane (n-C_4H_{10}), and isobutane (i-C_4H_{10}).

Partial oxidation (POx) The controlled oxidation of natural gas (primarily CH_4) with oxygen (O_2) such that syngas is formed, rather than forming carbon dioxide (CO_2) via complete combustion.

Pre-reforming The use of an adiabatic, preheating zone upstream of an ATR reactor for the purpose of catalytically converting C_{2+} hydrocarbons to a mixture of methane (CH_4), hydrogen (H_2), carbon monoxide (CO), and carbon dioxide (CO_2), thereby allowing oxygen (O_2) to be used more efficiently in the reformer.

scf Standard cubic feet, a measure of gas volume.

Steam methane reforming (SMR) The high-temperature catalytic reaction of steam with methane to give synthesis gas.

Synthesis gas (syngas) A mixture of primarily hydrogen and carbon monoxide produced by gasification or reforming of hydrocarbonaceous materials, used to synthesize fuels or chemicals.

Water gas shift reaction (WGSR) The gas phase reaction of carbon monoxide (CO) with water to form carbon dioxide (CO_2) and hydrogen (H_2).

Definition of the Subject

Like oil and coal, natural gas is not what first comes to mind when considering sustainable fuel sources. Yet as for other fossil sources, conversion of natural gas to transportation fuel is currently more affordable than conversion of renewable resources such as wind and solar, which are technically far away from availability at even a fraction of the scale required to have significant impact on meeting global demand over the coming decades. Given that global proved natural gas reserves are currently estimated as capable of producing more than 1,100 billion equivalent barrels of oil (the energy equivalent of 42 cubic miles of oil) [1], natural gas is a key contributor when considering a sustainable global fuel supply.

The term "gas to liquids" (GTL) is frequently used in reference to the chemical transformation of natural gas to liquid fuels via the Fischer–Tropsch (F-T) technology. In broader usage, the term "GTL" refers to the transformation of natural gas into any liquid, including other fuels, such as liquefied natural gas (LNG), methanol, dimethylether (DME), methyl-*tert*-butyl ether (MTBE), and chemicals such as ammonia (itself an important feedstock, particularly in the fertilizer industry), light olefins, and methanol and dimethylether intended for chemical use.

For clarity, the term "GTL" is used herein to refer to the chemical conversion of natural gas to liquids. However, a practical discussion of GTL should also include LNG, which is produced from natural gas by a phase change rather than a chemical transformation. Strategists in national governments and energy companies alike weigh all of these options when considering how best to distribute and monetize natural gas.

Modern GTL synthesis technology can produce synthetic fuels (synfuels) that burn more cleanly than conventional fuels derived from petroleum. F-T GTL technology can produce a virtually sulfur-free diesel fuel, much cleaner than conventional diesel – reducing smog and acid rain – and can also produce gasoline, jet fuel, or chemicals. GTL performed at or near the gas well also represents an emerging option to transport large quantities of transportation fuels and chemical feedstocks from natural gas, using commercially available tankers.

Production of liquid fuels and chemicals are lower volume applications compared to use of natural gas for power or as a fuel source for heating. Commercial

application of GTL might increase in magnitude as the ease of oil recovery decreases and its price increases over the next few decades.

Introduction

The methane content of natural gas varies greatly within the range of about 50–99%, typically about 95%. The remainder is a multicomponent mixture including the heavier gaseous hydrocarbons ethane, propane, butane, pentane, and some higher molecular weight hydrocarbons; the acid gases carbon dioxide, hydrogen sulfide; mercaptans such as methanethiol and ethanethiol; water, nitrogen gas; helium gas; liquid hydrocarbons; and trace mercury. Thus the preponderance of species in natural gas are high in energy content, with cleanup of contaminants necessary but greatly simplified compared to that required when using coal. Likewise the CO_2 emissions from combustion of natural gas [2] are considerably less than from oil [3] or coal [4]: 0.40 lb/kWh compared to 0.61 and 0.79 lb/kWh, respectively.

The bulk of natural gas used today goes directly into power generation (32%), residential and commercial heating (27%), and industrial use (22%). Only a small portion, around 5%, is used as a chemical feedstock, and therefore chemical uses have minimal impact on supply and pricing decisions other than in stranded gas regions where the gas is geographically remote from the main end-user markets. Thus in the Middle East, for example, which has large reserves but relatively small local demand, the proportion of natural gas going into feedstocks is higher (around 27%).

Location and transportation are key factors in defining the need for, and choice of, GTL technology. About 40% of known natural gas reserves are of the stranded type [5], including remote gas (located far from existing pipelines) and deeply buried or otherwise inaccessible gas. Remote gas alone accounts for about 16% of the world's proved natural gas reserves [6]. Related factors determine the type of transportation used, and therefore, the type of GTL processing used, including the size of the reserve, how much time is available to monetize the natural gas, the distance to market, and the gas processing requirements. Environmental influences include a growing resistance to the conventional practice of flaring (or reinjecting) gas that otherwise would be released in association with oil recovery operations (i.e., stranded gas that is also associated gas).

Multiple opportunities exist to achieve better value for natural gas than its local fuel value. First, the gas or its gaseous components can be exported to markets having higher fuel values. Exportation can be performed by pipeline, as pressurized gas, or by ocean tanker as liquefied natural gas (LNG, comprised of 99% methane) or natural gas liquids (NGL, comprised of C_2–C_4 alkanes). Second, GTL technologies can be used to chemically convert natural gas to higher value liquid fuels such as naphtha or diesel, using F-T technologies; or to fuel grade methanol, DME (directly or via methanol), MTBE (via methanol), or gasoline (via methanol); or to chemicals.

A flowchart of conceptual routes for chemical conversion of the methane in natural gas to liquids is shown in Fig. 1. All current gas to liquids chemical production processes require that natural gas is first converted to synthesis gas (syngas), a combination of hydrogen and carbon monoxide. The syngas is subsequently converted in a synthesis section to product. GTL processes of today are therefore of the indirect type, in that they proceed first through the intermediate syngas instead of converting methane directly to liquid product. Direct syntheses of fuels from natural gas include oxidative coupling of methane and selective oxidation of natural gas to methanol. These have been investigated in the past but poor economics to date have prevented their commercialization.

The intermediacy of synthesis gas is common when converting various hydrocarbonaceous feedstocks such as natural gas, naphtha, residual oil, petroleum coke, coal, or biomass. The lowest cost routes for syngas production are based on natural gas. There are several different approaches to converting natural gas to syngas, the primary methods being catalytic steam methane reforming (SMR), autothermal reforming (ATR), gas-heated reforming (GHR), partial oxidation (POx), heat exchange reforming, and variants thereof. The ratio of H_2/CO produced varies with the process design as well as the H/C ratio in the feedstock. A process will tend to be most economic if the H_2/CO ratio produced is well matched to the ratio needed in the next step. Exceptions include processes configured to produce more H_2 than needed, because this extra H_2 can be separated and used for power or to augment the syngas

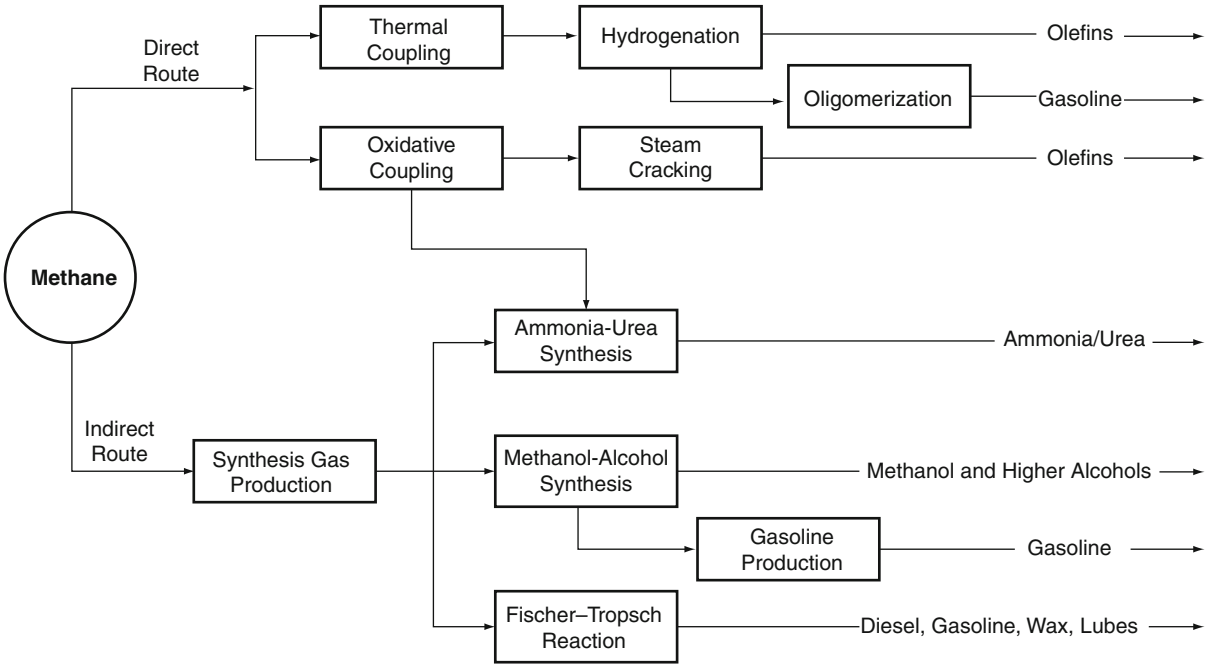

Gas to Liquid Technologies. Figure 1
Conceptual routes for chemical conversion of gas to liquids [7]

ratio of another chemical process. If the H_2/CO ratio is lower than needed, then an additional source of the expensive component H_2 must be supplied. With an H/C ratio of 4, methane is well suited for conversion to syngas when the final product slate will contain saturated hydrocarbons or methanol.

The synthesis of hydrocarbons from CO hydrogenation over transition metals was discovered in 1902 when Sabatier and Sanderens produced CH_4 from H_2 and CO mixtures passed over Ni, Fe, and Co catalysts. In 1923, Fischer and Tropsch reported the use of alkalized Fe catalysts to produce liquid hydrocarbons rich in oxygenated compounds – termed the synthol process. Succeeding these initial discoveries, considerable effort has gone into developing catalysts for the process to produce liquid hydrocarbons. Eventually, a precipitated Co catalyst promoted with ThO_2 and MgO supported by Kieselguhr (diatomateous earth) became known as the standard atmospheric process catalyst. In 1936, Fischer and Pilcher developed the medium pressure (10–15 atm) Fischer–Tropsch synthesis process. Following this development, alkalized Fe catalysts were implemented into this medium pressure process. Collectively the process of converting CO and H_2 mixtures to liquid hydrocarbons over a transition metal catalyst became known as the Fischer–Tropsch synthesis.

Methanol is a commodity chemical, and one of the top ten chemicals produced globally. The long time interest in methanol is due to its potential use as a fuel and as a feedstock to the chemicals industry. In particular, methanol can be used directly or blended with various petroleum products as a clean burning transportation fuel. Methanol is also an important chemical intermediate used to produce formaldehyde, dimethyl ether, methyl tertiary-butyl ether (MTBE), acetic acid, methylamines, and methyl halides among others.

Production of methanol began in the 1800s, with the isolation of wood alcohol from the dry distillation (pyrolysis) of wood. Research and development efforts at the beginning of the twentieth century involving the reaction of syngas to give liquid fuels and chemicals led to the discovery of a methanol synthesis process (concurrently with the development of the Fischer–Tropsch synthesis). Methanol synthesis

is now a well-developed commercial catalytic process with high reaction rate and selectivity (up to 99%). For economic reasons, methanol is produced almost exclusively (over 90%) via the reforming of natural gas.

Survey of Specific Gas to Liquids Technologies

This survey of GTL processes covers the subtopics of liquefied natural gas, natural gas liquids, methane reforming, Fischer–Tropsch GTL, and methanol synthesis from natural gas.

Liquefied Natural Gas (LNG)

Liquefaction of natural gas reduces its volume to about 1/600 the volume of the gas as measured under standard conditions. The most compelling justification for the production of LNG is this volume shrinkage that makes LNG, unlike natural gas itself, practical to both store and transport.

Production of LNG has been commercially practiced since 1960. The two major applications of LNG technology are:

(a) Storage of LNG for use in peak shaving plants with seasonal adjustment (mostly in the USA)
(b) Base load LNG plants for international trade with shipping from remote areas to developed countries via dedicated LNG ocean tankers

The capacities of peak shaving plants are more than an order of magnitude smaller than base load LNG plants.

Construction of pipelines depends on the relative values for gas in the supplying and consuming regions. Plans exist for pipeline delivery of gas from isolated eastern Russian gas fields to consuming markets in Asia (Japan, Korea, and China). Nonetheless shipping tends to be preferred over long-range pipeline construction, because pipeline costs are highly capital intensive: a 621 mile (1,000 km) long pipeline would cost some $1 billion, depending on ground conditions. Exporting LNG to Asia and Europe from distant production fields has become economic as a result of improvements to thermodynamic efficiencies of LNG facilities. However, shipping is still expensive at a cost of at least $15 per bbl to transport from the reservoir to the consumer's storage tanks.

Recent industry trends indicate that tankers to hold as much as 135,000 m^3 (equivalent to 3.2 billion scf of natural gas) have been specially built, with built capacities expected to soon increase to 165,000 m^3. For a shipping distance of 4,000 or 6,600 miles, the shipping requirements for a 1 billion scf/day liquefaction plant can be met by fleets of six or nine tankers, each tanker making 17 or 11 trips per year, respectively. Following transport of the LNG by tanker from the liquefaction site, it is off-loaded at a shore terminal. Vapor generated is compressed for injection into the local distribution pipeline. Independently, a continuous regasification of the LNG from storage tanks is performed, and the amount used for the time period between ships must obviously match the amount unloaded. The LNG pressure is raised by pump to the pressure necessary for it to be vaporized into the distribution pipeline.

Plant Considerations

The liquefaction energy required in a LNG plant typically has been reported as 9–12% of the heat energy in the natural gas, and 9–10% energy shrinkage is a typical number for the modern mega-tonnage capacity plants (without combined cycle systems). Because LNG is stored and delivered at atmospheric pressure and −160°C (−256°F), compression and very deep refrigeration are needed, with associated large consumption of energy. LNG projects have a very high capital cost, in the range of $1.0–1.5 billion for a 3–3.3 million tons per year train on a greenfield site, with 45–60% attributed to off-sites and infrastructure depending particularly on requirements for LNG storage, the marine system, and the heat rejection method. The technology is relatively mature, although economies of scale are being investigated to increase scale size to 4.5–5.5 million tons per year.

The thermal efficiency of LNG plant is determined by two major factors:

(a) Refrigeration cycle efficiency
(b) Power cycle efficiency

Increasing the thermal efficiency of an LNG plant for a given turbine/driver configuration will decrease the cost of production and also minimize both site gas consumption and greenhouse gas emission of CO_2

generated by combustion (0.20 t CO_2/t of LNG at high thermal efficiency, versus 0.25–0.35 t CO_2/t in a typical LNG plant) [8] as well as providing low NOx emission (0.095 kg/t).

The key capital cost elements in LNG facilities are, in descending order:

1. Gas turbines, steam turbines, or motor drivers for refrigeration service
2. Refrigeration compressors, typically over 100,000 kW
3. Steam and power generation including turbines waste heat recovery
4. LNG storage, typically over 250,000 m^3 capacity per tank (equivalent to approximately 112,500 t LNG per tank)
5. LNG loading terminal including jetty or causeway
6. Heat rejection system, in most cases, as suggested, seawater cooling
7. Cold box and prechilling for gas liquefaction
8. Natural gas pretreating for CO_2 removal gas drying and mercury adsorption
9. LPG and natural gasoline recovery as by-products
10. Fuel gas cold recovery and compression

Although heat transfer for chilling (i.e., the cold box) is less important than the capital investment associated with compression, the correct selection of the optimized refrigeration cycle and associated drivers affects both the compression and heat rejection systems and economics.

The most common refrigeration system in LNG plants involves prechilling with propane followed by use of the mixed refrigerant system. Close to 90% of these plants are licensed by Air Products Corporation, Inc. (APCI). The mixed refrigerant liquefaction systems use a mixture of mostly methane and ethane, in about 1.2–2.0:1 molar ratio. Depending on the feed gas composition, up to 3 mol% nitrogen and 6–12 mol% propane may be added to optimize the LNG boiling curve. The refrigerant cooling curve is adjusted to follow closely the feed gas cooling curve in order to achieve maximum thermodynamic efficiency [9].

One significant exception to the propane prechilling, mixed refrigerant approach is the Phillips Kenai Peninsula plant in Alaska, which commenced operation in 1969. This plant produces about 1.5 million tons per year of LNG by a cascade refrigeration system using pure propane, ethylene, and methane refrigeration cycles. The efficiency of this cascade system has been reported as at the lower end of the scale, about 88% [10]. It is reasonable to assume that the adiabatic efficiency of the refrigeration compressors currently operated by ConocoPhillips in Kenai are on the order of 70%, versus adiabatic efficiencies of 80–85% of more modern centrifugal compressors with three-dimensional blades. Even so, the plant has proved reliable and profitable.

Several patents issued to Phillips (now ConocoPhillips) suggest that improvements in cycle efficiency would result from improved refrigeration load distribution, nitrogen stripping (for nitrogen rich gas), open loop methane refrigeration, and LPG recovery [10–12]. The technology appears driven by the desire to distribute load equally among the propane cycle, ethylene cycle, and methane cycle. This is achieved in part by superheating the methane and ethylene refrigerant vapors fed to the compressors, probably to about −46°C (−50°F). Design and construction considerations then allow the use of six identical gas turbines, such as frame 5D (nominal 30,000 kW), to be used. The open loop methane refrigeration appears also to use the methane refrigeration compressor as the fuel gas compressor.

The loads of the propylene compressor are about 47.3%, the refrigeration ethylene compression loads are about 36.4%, and the methane compressor loads are 16.3% of the total refrigeration load. In practice the combined load on the steam turbines may be about 27% of the total motive power in the facility. The estimated power consumption of the Phillips system, for feed gas at 38°C (100°F) and 650 psig, is 371 kWh/t, assuming very lean gas, such as 96 vol% methane, at a heat rejection temperature speculated to be 38°C (100°F) [10]. This estimate probably includes 15 kWh/t of fuel gas compression [13].

A potential drawback of load equalization is use of up to 5% additional refrigeration power and, in case of fixed speed gas turbines, a reduction in production capacity [13]. Further, this could result in a more complex refrigeration cycle where the propane cycle, ethylene cycle, and methane cycles must be more highly

heat integrated [10]. Despite potential drawbacks in power consumption and capacity reduction, the concept of cascade refrigeration may be very sound [14], given the following considerations:

- Even the older, closed loop methane refrigeration as used in Kenai could have an advantage by allowing higher suction pressure to the methane compressor, about 1.7 kg/cm^2 (24 psia) instead of an estimated 1.1 kg/cm^2 (16 psia) for an assumed open loop compressor.
- Modern design methodology would allow the use of conventional carbon steel metallurgy in the compressors.
- Just one electric motor-driven fuel gas compressor is used for two trains.
- In case of outage of the fuel gas compressor, backup is provided by a draw from the feed gas.
- The ethylene refrigeration cycle, aside from superheating the suction to the first stage to about −46°C (−50°F), apparently comprises only a single side load with a probable goal of obtaining the compression in a single casing – potentially without employing superheating of the suction to the ethylene compressors.
- Use of two side loads reduces refrigeration load by 2% and increases production capacity by 2–3% (although using two casings also increases capital investment, possibly by about $5 million).
- On average about 6.2% of the total power is exported as electric power outside the boundary limits. (During times of high ambient temperature, the start-up steam turbine attached to the gas turbine increases its relative steam consumption and electric power export drops to near zero).

Given the pros and cons of cascade versus conventional mixed refrigerant systems, an objective comparative evaluation could be made only on a case-by-case, site-specific basis for LNG production.

Methane Reforming in F-T GTL

Reforming is the means by which natural gas is converted to the synthesis gas used as feed for GTL processes. Syngas for use in Fischer–Tropsch GTL is best characterized by the H_2/CO ratio, which should be about 2.0, after reforming, as per the generic F-T stoichiometry of Eq. 1.

$$2H_2 + CO \leftrightarrows -CH_2- + H_2O \tag{1}$$

There are many process options for reforming technology, used alone or in hybrid reforming approaches, and these are compared in Table 1.

The choice of how syngas is produced depends on several factors, including:

- Match between the H_2/CO ratio produced and the H_2 demand of the overall process
- Plant and process scale
- The need for, or feasibility of, using an air separation unit (ASU) or oxygen enrichment facilities in the overall process
- Scale and logistics of capital equipment, such as compressors and other gas-handling equipment
- Heat integration and gas recycle options

Steam Methane Reforming (SMR)

Steam methane reforming, or steam reforming for short, is a catalytic conversion of natural gas by reaction with steam. The basic chemistry of steam methane reforming is shown in Eqs. 2 and 3.

$$CH_4 + H_2O \leftrightarrows 3H_2 + CO \quad \Delta H_{298} = 206\text{kJ/mol CO} \tag{2}$$

$$CH_4 + 2H_2O \leftrightarrows 4H_2 + CO_2 \quad \Delta H_{298} = 165\text{kJ/mol CO} \tag{3}$$

These reactions are quite endothermic, requiring input of significant transferred heat, and SMR is therefore carried out at high temperature with the catalyst inside tubes within a fired furnace. The amount of steam used is in excess of the reaction stoichiometry requirements, as required to prevent the catalyst from coking.

SMR is the dominant reforming technology used for the production of methanol, ammonia, and other petrochemical products produced from methane at large scale. One reason is that the SMR process is scalable. Another reason is that the high H_2/CO ratio produced in SMR is stoichiometrically suitable for downstream formation of saturated hydrocarbons

Gas to Liquid Technologies. Table 1 Comparison of technologies for syngas generation from natural gas [15]

Technology	Advantages	Disadvantages
Steam methane reforming (SMR)	• Most extensive industrial experience • O_2 not required • Lowest process temperature • (Best H_2/CO ratio if producing H_2)	• H_2/CO ratio higher than typically required for syngas production • Highest air emissions
Gas-heated reforming (GHR), heat exchange reforming (HER)	• Compact size and footprint • Application flexibility offers options for incremental capacity	• Limited commercial experience • Usually best coupled with another syngas generation technology, such as ATR
Two-step reforming (SMR followed by O_2-blown secondary reforming)	• Size of SMR is reduced • Low methane breakthrough favors high purity syngas • Methane content of syngas can be tailored by adjusting secondary reformer outlet temperature	• Increased process complexity • Higher process temperature than SMR • Usually requires O_2
Autothermal reforming (ATR)	• Typical H_2/CO ratio produced is close to stoichiometric for F-T and methanol syntheses • Lower process temperature requirement than Pox • Low methane breakthrough • Methane content of syngas can be tailored by adjusting reformer outlet temperature	• Higher process temperature than SMR • Usually requires O_2
Partial oxidation (Pox)	• Feedstock desulfurization not required • Absence of catalyst permits carbon formation and, therefore operation without steam, significantly lowering syngas CO_2 content • Low methane breakthrough • Low H_2/CO ratio advantageous where ratio < 2.0 is required, such as dimethylether synthesis	• Low H_2/CO ratio disadvantageous where ratio > 2.0 is required • Very high process operating temperatures • Usually requires O_2 • High-temperature heat recovery, and soot formation and handling, add process complexity • Low methane content of syngas not easily modified to meet downstream processing requirements

and oxygenates. The theoretical ratio for H_2/CO of 3:1 is not reached in practice, the maximum practical value being about 2.8, but in the absence of complex recycle schemes, SMR provides the highest H_2/CO ratio available in reforming of natural gas.

Conventional steam reforming catalysts are 10–33 wt% NiO on a mineral support (alumina, cement, or magnesia). Although natural gas usually contains only small amounts of sulfur compounds, generally in the form of H_2S, sulfur compounds are the main poisons of reforming catalysts. Use of uranium oxide or chromium oxide as promoters can impart higher tolerance to sulfur poisoning, but even at a sulfur concentration of 0.1 ppm the catalyst can begin to deactivate and the best practice is to remove sulfur from the raw feed. To maintain a 3-year catalyst lifetime, the sulfur concentration in the reformer feed gas should be less than 0.5 ppm. If the sulfur

concentration in the raw feed gas is greater than 1%, the sulfur must be removed by chemical or physical scrubbing. An upfront desulfurization unit is used to absorb H_2S onto a ZnO bed. Any remaining organic sulfur compounds and carbonyl sulfide are partially cracked and absorbed on the zinc oxide bed.

Recent improvements to catalysts and the reforming process have allowed design for operation of side fired reformers in SMR, at conditions not possible with other reforming methods. The most notable developments are noted below.

- Introduction of new generations of catalysts, suitable for pre-reforming and for reforming of heavy feedstocks

  Pre-reforming catalysis converts higher hydrocarbons (C_{2+}) in the natural gas feed into a mixture of methane, hydrogen, and carbon oxides.
- Commercial application of advanced reforming at low steam/carbon (S/C) ratios down to 1.5, and high outlet temperatures above 950°C

  Low S/C ratios improve energy efficiency.
- Significant increase of heat flux

  Operation at average heat flux above 150,000 kcal/m^3 h has been demonstrated in Haldor Topsøe's Houston, Texas, process development unit (PDU). A high flux unit is now in commercial operation.
- Increase of unit capacity

  Steam reformers can now be constructed for single train reforming units with capacity to provide syngas for a methanol plant of up to 3,000 t/day production.
- Heat exchange reforming

  Heat exchange reforming has been developed and commercialized including with gas-heated option, where the steam reforming reaction is carried out in a unit heated by the product gas from an autothermal reformer.

An obvious advantage of SMR is that it does not need an oxygen plant. However, since steam reformers are more costly than either POx or autothermal reformers, there is a minimal plant size above which the economy of scale of a cryogenic oxygen plant in combination with a POx or autothermal reformer is less expensive than a steam reformer on its own. Use of SMR for Fischer–Tropsch applications does involve recycling of CO_2 and removal of excess hydrogen, by means of pressure swing absorbers or membrane separators, to lower the H_2/CO ratio to a level acceptable to the Fischer–Tropsch stoichiometry. Due to the costs involved with these steps, it is most likely that steam reforming will only be considered for F-T GTL when one or more of the following conditions hold:

- A relatively small GTL plant, with a capacity well below 10,000 bbl/day.
- The additional hydrogen can be used for other applications like methanol or ammonia production.
- The natural gas feed has a high CO_2 content.
- A suitable water supply can be obtained at low cost.

Compact Reforming

Compact reforming represents a novel mechanical design approach to conventional SMR. Under development by BP, it is currently undergoing extended test runs at their new 300 bbl/day GTL demonstration facility in Alaska. The reformer design resembles a conventional shell and tube heat exchanger, and SMR reactions occur tube side of this reactor, with the tubes filled with conventional Ni-based catalyst. Heat for the endothermic SMR reactions is provided shell side, where the tubes are heated by combustion of a fuel and air mixture. Heat transfer is claimed to occur more efficiently in what is described as a highly countercurrent device.

The shell side combustion zone may also be under elevated pressure, leading to more efficient convective heat transfer to the tubes, and this plus a considerably lower catalyst quantity required considerably reduces the size relative to the conventional SMR furnace design configuration – hence the term "compact" reforming coined by BP. The principal advantages claimed for this approach compared to a conventional SMR are a major reduction of capital cost along with an improvement in thermal efficiency. The reduced space requirements are claimed to make this reforming technology more amenable to installation on barges or oceangoing "plantships" for the conversion of relatively small or temporary sources of natural gas. A drawback of the current state of compact reforming technology is that a large number of parallel units would be required for a world-scale GTL plant.

Autothermal Reforming (ATR)

Autothermal reforming (ATR) has been recognized since the mid-1990s as the technology of choice for production of synthesis gas at large scale. Conceptually ATR is similar to catalytic SMR except that ATR includes the use of oxygen, which renders the reaction less endothermic on a per mole basis than SMR. The stoichiometry for ATR is shown in Eq. 4.

$$4CH_4 + O_2 + 2H_2O \leftrightarrows 10H_2 + 4CO \qquad \Delta H_{298} = 85.3\text{kJ/mol CO} \tag{4}$$

In practice the product distribution is strongly affected by the choice of steam/carbon (S/C) ratio. At a S/C ratio of 1.3, the syngas will have a H_2/CO ratio of about 2.5, which is higher than the ratio of about 2.0 needed for Fischer–Tropsch synthesis. The H_2/CO ratio can be controlled by a combination of lowering the S/C ratio and adding CO_2 or CO_2-rich gas to the ATR feed, such as by recycling CO_2 to the reformer. Decreasing the S/C ratio in the feed gas decreases the amount of CO_2 required when adjusting the synthesis gas composition to the desired ratio for F-T synthesis.

A typical ATR process concept for the production of synthesis gas includes the fundamental steps of desulfurization, adiabatic pre-reforming, ATR, and heat recovery. In the desulfurization section, the sulfur present in natural gas feedstock is removed to avoid poisoning the downstream pre-reforming catalyst. Steam, and optionally recycled CO_2, is added to the desulfurized natural gas and, after further heating, the resultant mixture is passed to a pre-reformer. In pre-reforming, preheating of the gas is done in a fired heater upstream of the ATR. The use of a pre-reformer upstream of the ATR unit reduces the oxygen consumption per unit of syngas produced during ATR. The exit gas from the ATR is cooled by high-pressure steam production and boiler feed water preheat, and CO_2 is removed as needed, using methyldiethanolamine (MDEA, N-methyl-diethanolamine) as an absorbent in a CO_2 capture unit. After CO_2 removal, the synthesis gas with a H_2/CO ratio of 2.0 is available for Fischer–Tropsch synthesis. Various process variants are possible, for example, adjustment of synthesis gas composition by recycling CO_2-rich tail gas from the Fischer–Tropsch synthesis.

The result is that ATR offers a reduction in the investment per barrel of product, and the possibility of higher single-line capacity compared to conventional steam reforming. Optimized design in combination with reduction of the S/C ratio can be expected to result in a major increase in the single-line capacity, by more than 25% within the next few years. Currently single train methanol plant units based on ATR can be designed with capacities up to about 7,000 t/day.

The key component of the ATR process is the ATR reactor itself. The ATR reactor has a compact design consisting of a burner, combustion chamber, and a catalyst bed placed in a refractory lined pressure vessel. The pre-reformed natural gas reacts with oxygen and steam in a sub-stoichiometric flame. In the catalyst bed, the gas is equilibrated with respect to the methane steam reforming and shift reactions. Product gas composition is determined by the thermodynamic equilibrium of these reactions at the exit temperature and pressure of the reactor. The exit temperature is determined by the adiabatic heat balance based on the composition and flow of the feed, steam, and oxygen added to the reactor. The product gas is completely free of soot and oxygen.

It is essential that the combined design of burner, catalyst, and reactor ensures that the precursors are destroyed by the catalyst bed to avoid soot formation. The soot limit, that is, the S/C ratio at which soot formation starts, has been investigated by experiment at many combinations of temperature, pressure, so that prediction of acceptable operating conditions for specific feedstocks is now possible.

Additional design parameters of the autothermal syngas generation system that influence cost and thermal efficiency include:

- The preheat temperatures of oxygen and natural gas

  The higher these temperatures are, the less oxygen will be used. The maximum preheat temperatures are determined by safety factors and by the need to prevent soot formation.
- The pressure of the steam generated in the waste heat reboiler

  The higher the steam pressure, the more efficiently can energy be recovered from steam, but the more costly the steam and boiler feed water treatment systems become. The optimum steam pressure will be determined by the relative cost of capital and energy.

The feasibility of soot-free operation of the ATR reactor at very low S/C ratio was demonstrated in Haldor Topsøe's Houston development unit in 1997–1999, with further testing performed since then to explore the limits of the ATR technology with respect to feed gas composition, pressure, and temperatures. Operation at industrial scale at a S/C ratio of 0.6 was demonstrated in a South African plant in 1999 and has been in operation in Europe since the start of 2002 [16]. Two lines have been in operation at Sasolburg since 2004. Haldor Topsøe's ATR technology was also selected for the Oryx plant that Qatar Petroleum and Sasol began operating in 2006 and includes a 6,000 mtd syngas generator; for Chevron Nigeria's Escravos, Nigeria GTL plant scheduled for completion in 2011; and for the methanol portion of Eurochem's gas-to petrochemical complex planned in Lagos State, Nigeria.

Sasol, Syntroleum, and ExxonMobil each have their own proprietary versions of ATR. The most prevalent layout of the syngas production section is a combination of adiabatic pre-reforming and fixed bed ATR. This layout results in high flexibility for variations in natural gas feed and, if needed, in tail gas recycle gas compositions, as well as the ability to reduce oxygen consumption per unit of syngas produced.

ExxonMobil employs a fluidized bed catalytic reformer. Steam-diluted oxygen is fed to the reactor through nozzles, separately from the natural gas. The oxygen reacts exothermically with natural gas in a burning zone near the oxygen inlet. The balance of steam needed in the process is admixed with natural gas and fed at a level below the oxygen inlet to the autothermal reaction zone. A mixture of nickel on alumina catalyst may be combined with a solids diluent (alumina) to form the fluidized bed. The fluidized bed reactor provides superior characteristics of heat and mass transfer for autothermal reforming.

Another ATR approach under consideration is to use slurry bed F-T reactors in series within each train, as the slurry system would facilitate the application of ATR technology at large scale (>10,000 bpd). With this approach, water is removed between stages to enhance the reactant partial pressures in the downstream reactor stage. The removal of other diluents (such as carbon dioxide) between stages may also be considered. This allows lower recycle ratios, increased steam production from the reactor heat removal system, and decreased overall reactor volumes. These advantages will not necessarily compensate for the increased complexity of needing to use reactors in series at larger scale, and detailed studies are required to determine the most cost-effective design approach.

Currently, the most attractive ATR syngas generation technology appears to be oxygen-blown ATR at low S/C ratio. This technology has been chosen for F-T GTL projects that are closest to realization. Extensive testing has proved that technology is ready for application at a large industrial scale with S/C ratios down to 0.6. Application of even lower S/C ratios has been demonstrated at small scale, and the next generation ATR scheme is under development to cut the S/C ratio even lower, to 0.4 or possibly 0.2 [17]. Such low S/C could decrease oxygen requirements and boost the single-line capacity still further.

Two-step reforming is a variant of ATR wherein the exit gas from a fired tubular reformer is further processed in an oxygen-blown, secondary reformer. In both steps, the ATR is carried out in a refractory lined vessel containing a mixer/burner and a catalyst bed. Conditions leading to soot formation are rigorously avoided.

Gas-Heated Reforming/Heat Exchange Reforming (GHR/HER)

Another technology that produces suitable synthesis gas for GTL units is a combination of steam reforming and ATR, performed in separate units, in a process referred to as gas-heated reforming, GHR, or heat exchange reforming, HER. The concept is to use heat available from process gas downstream of the ATR for steam reforming, in a heat exchanger type reactor. The purpose is to reduce oxygen consumption and increase carbon efficiency by optimizing the recycle of tail gas – beyond the range possible with ATR alone – and to achieve this without additional firing that would create an undesired excess of water. The gas-heated reformer is a compact alternative to the fired steam reformer wherein high-grade heat is recycled while the S/C ratio remains below 0.6 [18].

Conventional reformers provide the needed heat by combustion of fuel at atmospheric pressure in a refractory lined duct. Because the convective heat

transfer coefficient of a GHR is considerably higher at the elevated pressures of its hot gas side, unit size reductions claimed can be 10–15 times smaller than conventional tubular steam methane reformers. The absence of combustion flue gases results in an inherently higher thermal efficiency for a GHR, since no combustion heat is lost with the warm flue gases discharged to the atmosphere from the stack. Furthermore, the reduced power consumption, which results from eliminating the need for the associated steam methane reformer air and flue gas blowers, contributes to the overall energy saving of a GHR. Much of this thermal efficiency advantage may be offset, however, by the need to generate additional steam externally in an off-site boiler in order to compensate for the lost waste heat recovery potential of a conventional reformer system.

GHR can be combined with ATR to reduce energy consumption and enable the use of smaller air separation plants, while reducing CO_2 emissions possibly by as much as 50%. In addition, these GHR/ATR schemes allow shrinking of the required high-pressure steam system and reduction in size of steam turbines. Both series and parallel arrangements of GHR with ATR have been studied and are depicted in Fig. 2 [18]. In the series arrangement of HER/GHR, all gas passes through the steam reforming unit and then the ATR. The lower limit for the S/C ratio is typically determined by the steam reforming catalyst [19]. The parallel arrangement allows individual optimization of the S/C ratio by feeding the two reformers independently.

GHR has been employed since the 1980s in some ammonia and methanol plants. In the past, highly efficient GHR was not viewed as an option for high capacity syngas production, mainly because of concerns about metal dusting corrosion. This reformer must operate at higher temperatures in the parallel arrangement than in the series arrangement, to obtain a low methane leakage. Higher operating temperatures may lead to higher cost and more severe conditions, and the main challenge in both series and parallel arrangements is preventing metal dusting corrosion on the shell side of the heat exchange reformer. Mechanical design, including choice of materials of construction, is critical.

A heat exchange reformer designed by Haldor Topsøe for operating in tandem with an ATR at a low S/C ratio was started up at Sasol's facilities in Secunda, South Africa, in early 2003 [16, 20]. The project at Secunda (also referred to as "process gas-heated reforming" or PGR) involved revamping an existing ATR for an increase in syngas production capacity of 30% via GHR.

Engineers at Johnson Matthey have stated that with mechanical design and configuration improvements,

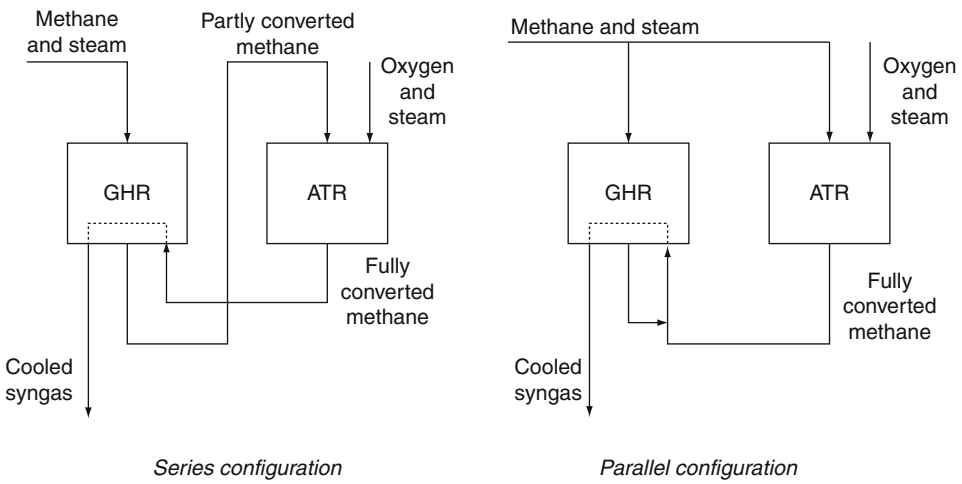

Gas to Liquid Technologies. Figure 2
Series and parallel configuration of the combination of GHR and ATR [18]

GHR/ATR technology is likely to deliver better efficiency and lower operating costs than conventional ATR for F-T GTL plants of the future. In addition, Air Products and Toyo Engineering Corporation have each studied GHR technology. Although commercial F-T GTL plants using ATR/GHR combinations have yet been built, retrofit projects at large-scale methanol and GTL plants are possible, as well as potential applications of ATR/GHR in refinery hydrogen plants.

Air Blown Autothermal Reforming

It is possible to use air instead of purified oxygen as oxidant in autothermal reforming, and an F-T synthesis process based on air blown ATR was developed by Syntroleum Corporation and demonstrated in their plant in Tulsa, Oklahoma, in 2002–2003. In a very similar operation, air blown secondary reforming is used extensively in the production of synthesis gas in ammonia manufacture. The main advantage for air blown processes is that no air separation unit will be required, which could be a strategic advantage for smaller scale, offshore, barge mounted F-T GTL units. For large-scale land-based units, it may present certain restrictions on the energy system configuration of the plant. The savings of eliminating the capital cost of an air separation cost will be offset by the need for compression of incoming air, for example, which will result perhaps in as much as 50% more power required than that required to produce oxygen.

In addition, the increased volumetric flow of nitrogen-diluted syngas will make all downstream equipment through the F-T synthesis reactors larger. Also, the high content of nitrogen in the synthesis gas excludes the use of internal recycle in the F-T synthesis section and external recycle of tail gas from the F-T reactor back to the syngas section of the plant is excluded. This means that all tail gas must be used as fuel, which because of the high nitrogen content will be of poor quality. At a conversion of hydrogen and CO in the synthesis gas of about 70%, the heating value of the tail gas will be so low that it will not burn unassisted. Either supplemental fuel or catalytic combustion will be required if the energy content in the tail gas is converted to power, and a large amount of power will be generated for export. This may be desirable, however, in remote locations where power may be in short supply.

Partial Oxidation (POx) and Catalytic Partial Oxidation (CPOx) Reforming

When the quantity of oxidant (O_2) added to methane is very low and the reaction temperature is raised significantly, uncatalyzed partial combustion of pretreated natural gas occurs. This homogeneous reaction is referred to as gasification or partial oxidation (POx). The resulting syngas is quenched or cooled by steam production, and carbonaceous by-products such as soot are removed by washing. The formation of carbonaceous by-products influences carbon efficiency. For partial oxidation, the syngas H_2/CO ratio produced is slightly below 2.0, which is closest to the optimum needed for the Fischer–Tropsch or methanol syntheses. This low H_2/CO ratio gas results from very little, if any, steam use in the process. Due to the absence of catalyst, the reformer operates at an exit temperature of about 1,300–1,400°C. This high temperature and the absence of catalyst have the following disadvantages as compared to an autothermal reformer.

- Formation of soot and much higher levels of ammonia and HCN appear in the syngas, compared to ATR, which necessitates the use of a scrubber to clean the gas.
- Higher consumption of oxygen.
- Due to the absence of a water gas shift reaction with the POx catalyst, the unconverted methane as well as the methane produced by the Fischer–Tropsch reaction cannot be recycled to the reformer without first removing the CO_2 from the Fischer–Tropsch tail gas.

Depending on the energy needs of the plant, the syngas from the POx reformer can either be cooled by means of a water quench or by the production of steam in a heat exchanger. A quench system is the less costly of the two approaches but is also less thermally efficient. In designing a POx-based GTL plant, the choice between a quench or a waste heat boiler will depend on the relative cost of capital and energy. As mentioned above, CO_2-rich tail gas separated from the syngas may be recycled to the partial oxidation reactor to improve

carbon yield. If recycle is used, the gas production in the POx units must be supplemented by high hydrogen content syngas in an auxiliary steam reformer, as in the Shell process. In Shell's Bintulu GTL plant, each POx unit originally had a capacity rating for production of 3,000 bbl/day of F-T products. Shell has recently scaled up their gasification units to enable production of 10,000 bbl/day of F-T product equivalents.

When a catalyst is employed to assist the partial oxidation, the process is referred to as catalytic partial oxidation (CPOx). The catalyst increases the activity of natural gas conversion and, therefore, provides options for higher throughput, lower operating temperature, or both.

CPOx with no burner (flame) was first practiced on a small scale at low pressures in the 1950s by Haldor Topsøe, and then later with higher pressures by Lurgi. Early versions of CPOx used premixing of hydrocarbon/steam feed and oxygen, with an ignition catalyst placed on top of a fixed bed catalyst, similar to the catalyst used in an ATR-based unit and operating with similar space velocities. Today's CPOx versions feature a combined catalyst system performing both ignition and partial oxidation. The noble metal catalyst operates at very low residence time (very high space velocity). The hydrocarbon feed stream, oxygen, and steam are mixed upstream from the catalytic reactor. All chemical conversion takes place in the reactor and no burner is used. The exit gas composition from CPOx is similar to the exit gas from ATR, given like amount and properties (temperature, pressure, composition) of the inlet streams.

The main potential advantage of catalytic partial oxidation is the smaller size of the reactor. There are also potential disadvantages that will likely outweigh the savings in the cost of the reactor, which is rather modest relative to the total investment in the syngas generation section. The main disadvantages of CPOx relate to the premixing of natural gas hydrocarbon feed and oxygen. The need to premix excludes combinations of CPOx linked in a series arrangement, in particular with pre-reforming or heat exchange reforming, for safety reasons. Premixing hydrocarbon feed with oxygen limits the applicable reactor preheat temperatures to rather low values, kept below the self-ignition temperature of the mixture to maintain control when premixing oxygen and hydrocarbon. A feed gas mixture containing methane and oxygen may spontaneously ignite at temperatures above the autoignition temperature, depending on the actual gas properties, and the industry does not yet have confidence that this issue has been adequately addressed.

When consumption of natural gas and oxygen are compared for CPOx and a combination of pre-reforming and ATR, consumption of both gases are significantly higher for CPOx than for the combination of pre-reforming and ATR. The main reason is that with CPOx operating at a lower inlet temperature than ATR (250–450°C vs. 600°C), a significant part of the hydrocarbon feed is combusted to CO_2 and steam (using the larger amount of oxygen) to generate heat to reach the desired syngas exit temperature of 1,050°C.

Considering that a large portion of the syngas process section of a F-T plant is for the air separation unit, CPOx does not appear to be economical under these conditions. CPOx was being investigated by ConocoPhillips but they have recently discontinued this approach.

An alternative for CPOx could be the use of air as an oxidant. This alternative is being pursued by many as a basis for fuel processing systems for fuel cells. For GTL and similar applications operating at high pressures, however, the issue of safety still remains even with air, although to a lesser extent than with oxygen. Oxygen consumption may be conserved (to an amount about 10% less than the amount required for the ATR reactors) if the inlet temperature can be safely raised to a higher level (about 480°C) with a lower oxygen content in the hydrocarbon/oxygen mix. Additional operational issues with CPOx include concerns about catalyst life, carbon dusting, and combustion "flash back" potential in an integrated F-T GTL process plant.

The combination of POx and conventional steam reforming appears to be the nearest competitor to ATR technology. However, catalytic partial oxidation, either oxygen or air blown, does not appear to offer sufficient advantages to outweigh its limitations with respect to operating conditions and inherent safety concerns. CPOx seems to require an oxygen consumption boost, and it is unclear whether this need can be

adequately diminished. CPOx is not expected to be important in the GTL industry in general, even if successfully developed for commercialization.

Catalytic Membrane Reactors

Catalytic membrane reactors (CMR) are based on the concept that selective transport of reactant(s) or product(s) can influence an equilibrium-limited reaction to proceed further in the forward direction. The combination of SMR and the WGSR is equilibrium limited, and H_2-selective membranes have been used to lower the temperature required for SMR by facilitating the selective removal of H_2 as it forms. Both dense (mostly palladium) and porous (such as silica or alumina) H_2-perselective membranes have been studied [21]. Throughput limitations, membrane stability, and cost combined with the ready availability of several other reforming technologies have thus far hampered commercial development of H_2-permselective membrane reactors for reforming applications.

Another approach to CMR for methane reforming allows a selective passage of reactant oxygen. Nonporous membranes prepared from perovskites or similar ceramic materials allow ionic transport of oxygen from air at low pressure, with up to 100% selectivity for O_2. The selectively transported oxygen moves into a reaction mixture at low partial pressure of oxygen, against a large difference in total pressure.

Process concepts based on the use of O_2-selective CMR eliminate the need for an air separation unit (ASU) and associated large compressors. Successful elimination of the ASU would impart significant economic potential for this technology; however, difficulties with CMR would need to be overcome first. One problem is in mechanical design, including the mechanical integrity of the membranes and also the membrane-to-metal junctions. Significant consortia efforts formed with US DOE funding led to the development of two novel technologies, known as ITM (ion transport membrane) and OTM (oxygen transport membrane).

Because the production of synthesis gas from natural gas by oxygen-blown ATR accounts for about 60% of the total capital cost of the GTL plant, the ATR and cryogenic ASU are the two most capital-intensive components in the syngas generation process section. ITM/ITM Syngas technology aims to lower capital intensity by combining the ASU and ATR units into a single reactor. In the ITM/ITM Syngas process, O_2 in air is selectively reduced and transported across the membrane to the other side, where it partially oxidizes methane to form syngas. The ITM/ITM Syngas concept is particularly attractive for use in locations where space for an ASU would be limited, such as on an offshore platform. The ITM Syngas Team, led by Air Products, has estimated capital cost savings of greater than 30% over a conventional ATR with ASU, as well as an increase in overall fuel efficiency to 61% versus 58% for ATR/ASU, with up to 40% less deck space required [22].

OTM oxygen technology aims to lower capital intensity by replacing cryogenic ASU technology with membrane reactors that allow O_2 to selectively pass through the ceramic membrane to the other side, where it partially oxidizes methane to form syngas. The OTM Alliance team, led by Praxair, focused intensively on materials development [23]. This DOE program ended in 2004 and does not appear to be progressing toward commercialization at this time. The OTM approach also has been studied in combination with electrochemical pumping of O_2 [24] and with CO_2 capture using a solid sorbent [25].

Although membrane materials with satisfactory oxygen permeability at the relevant conditions do exist and progress has been made, the level of oxygen flux in all cases still requires improvement. Concerns persist over mechanical integrity and stability with time. Catalytic membrane reactors are still under development, and it is not possible to predict at this time whether or when CMR will be successfully developed for commercial use. The goal for further development of CMR is to avoid the cost of an oxygen plant.

Pre-reforming and Post-reforming

Additional reforming may be performed upstream or downstream of the main reformer unit, when the main furnace unit has limited heat transfer capability that would otherwise limit overall conversion. The pre-reformer reaction breaks down the heavier hydrocarbons (mostly propane and butane) to methane, upstream of the reformer heater. Post-reforming uses an additional catalyst bed downstream of the main reformer. A down-flow reactor is placed between the outlet transfer line and the steam generator that

recovers excess process heat. Adding a post-reformer raises the effective residence time of the reacting gas and thereby boosts capacity. Pre- and, in particular, post-reforming are often considered as retrofits, which may be complicated by having insufficient space or inadequate metallurgy for the higher heat burden.

Methane Reforming for Methanol/DME Synthesis

Synthesis gas production is best characterized by the generalized stoichiometric ratio M (also referred to as the module), where $M=(H_2–CO_2)/(CO + CO_2)$. Ideally M should be equal to 2.0 for methanol (or for F-T). For kinetic reasons, in order to control by-products formation, a value slightly above 2.0 is normally preferred.

Because about 60% of the capital cost for a methanol plant is in the methane reforming unit, research has aimed at improving reforming processes. Over the years, three process concepts have been considered for preparing syngas targeted for methanol synthesis, described below.

- Single-step tubular reforming
  - Steam/carbon ratio = 2.4.
  - Capacity range up to 2,500 t/day methanol equivalent.
  - Availability of CO_2 increases capacity where single-step tubular reforming is attractive.

  In the past, the methanol industry was dominated by single-step, steam methane reforming without the use of oxygen. Today, single-step reforming is considered mainly for relatively small plants and for cases where CO_2 is present in the natural gas or is available on site or nearby from other sources such as an ammonia plant.
- Two-step reforming
  - Steam/carbon ratio = 1.5–1.8.
  - Capacity range about 1,500–7,000 t/day methanol equivalent.
  - Heavy natural gas makes two-step reforming less attractive compared to single-step tubular reforming.
  - Availability of CO_2 is no advantage with two-step reforming.

  Two-step reforming is a combination of a fired, tubular reformer and an oxygen-blown secondary reformer. This concept was applied by Statoil and Conoco in a 2,400 t/day methanol plant in Tjeldbergodden, Norway, commissioned in 1997. The facility has an annual capacity of about 900,000 t of methanol, which corresponds to 25% of Europe's total production capacity [26].
- ATR
  - Steam/carbon ratio = 0.6–0.8.
  - Capacity range about 5,000–10,000 t/day methanol equivalent.
  - Heavy natural gas makes ATR less attractive.
  - Availability of CO_2 is no advantage.
  - This scheme is most attractive for the production of fuel grade methanol.

  Using ATR, the composition of synthesis gas is raised to have adequate hydrogen content by taking advantage of the WGSR with removal of CO_2.

The main conclusions from early studies were that for relatively small plants (<1,500 t/day methanol equivalent), single-step tubular reforming is advantageous for syntheses gas production. For intermediate scale capacities (corresponding to present world-scale capacities, about 1,500–3,500 t/day methanol), two-step reforming is most attractive. For capacities above about 3,500 t/day, ATR or a combination of ATR and SMR is preferred. For example, the Lurgi-combined reforming process uses a combination of steam and autothermal reforming. Proven single-line capacities for the oxygen plants associated with combined reforming have increased to about 3,000 t/day, corresponding to about 7,000 t/day methanol plant equivalent using two-step reforming, or about 5,000 t/day methanol plant equivalent using ATR alone.

A new process concept for the synthesis loop for methanol has been developed and specially adapted to syngas production by ATR at low steam/carbon ratios. In this scheme, CO_2 removal is not applied. Instead, the gas composition is adjusted by recovery and recycle of hydrogen from the purge gas from the synthesis loop.

Fischer–Tropsch Synthesis

The Fischer–Tropsch (F-T) reaction is a polymerization or oligomerization of carbon monoxide performed catalytically under reducing conditions. As shown in Eq. 5, the F-T reaction is thermodynamically favorable by virtue of high exothermicity. Catalysis, temperature

control, and downstream processing are used to provide a product slate as close to that of target applications as possible.

$$nCO + (2n+1)H_2 \leftrightarrows CH_3 - (C_{n-2}H_{2n-4}) - CH_3 + nH_2O \qquad \Delta H_{298} \approx -159\text{kJ/mol CO} \tag{5}$$

Fischer–Tropsch processes were originally developed for use in coal-to-liquid (CTL) processes and are similar when applied to the syngas derived from natural gas. The reader is referred to the CTL entry in this publication for additional discussion of F-T performance variables, operating regimes, and product distributions.

The primary differences between F-T processes applied for GTL and CTL are the range of operating temperatures used, the type of catalyst used, and the type of reactor used. These differences all relate to differing compositions of F-T syngas feed in GTL versus CTL. The stoichiometry of the F-T reaction to make hydrocarbons is about 2.1/1 in H_2/CO as shown in Eq. 5. Syngas produced by gasification of coal has a H_2/CO ratio of 0.7–1.0 and is therefore stoichiometrically deficient in hydrogen. Use of an iron-based catalyst for the F-T step of CTL is typical because Fe concurrently catalyzes the water gas shift (WGS) reaction, providing makeup hydrogen as per Eq. 6.

$$CO + H_2O \leftrightarrows CO_2 + H_2 \quad \Delta H_{298} = -41.2\text{kJ/mol CO} \tag{6}$$

In contrast, as shown above in Eqs. 2–4, the H_2/CO ratio of syngas produced by reforming methane is at or in excess of the value of 2 required by the stoichiometry of the F-T reaction. Thus iron F-T catalysts are less preferred for use in GTL processes than cobalt F-T catalysts, which do not catalyze the WGS reaction. Cobalt is effective in the low-temperature Fischer–Tropsch (LTFT) regime, operated at about 220°C, and not for high-temperature Fischer–Tropsch (HTFT), operated at about 340°C. At the higher temperatures, Co tends to make methane.

Iron F-T catalysts can be used in GTL processes, performed at low temperature to lessen the contribution of iron-catalyzed WGS reaction. Operating in the LTFT regime, a slurry bed reactor (SBR) is typically preferred for several reasons. One reason is that the slurry bed uses a much lower catalyst loading than either the fixed bed or fluidized bed reactor technologies used in HTFT processes. A second reason is that the slurry bed can remove reaction heat more rapidly, to avoid temperature increases that would result in undesired formation of high levels of methane, light hydrocarbons, and, in the extreme, catalyst deactivation due to coking, sintering, and disintegration. Deposition of carbon by the Boudouard disproportionation reaction, Eq. 7, is to be avoided, and the heat distribution imparted by the slurry bed is advantageous. A third aspect favoring the slurry bed is that the resultant steam to carbon (S/C) ratio is superior.

$$2CO \leftrightarrows C(s) + CO_2 \quad \Delta H_{298} = -83.4\text{kJ/mol CO} \tag{7}$$

Even so, Shell does operate a fixed bed, Co-catalyzed F-T process in its GTL plants in Malaysia and Qatar. Shell commissioned the Bintulu plant prior to the widespread consideration of slurry bubble reactor technology for F-T processes and stands by the fixed bed technology. One advantage of fixed beds over slurry beds is the potential for a lesser degree of catalyst attrition that results from impacts and shear forces in the latter.

Reaction Pathway

Fischer–Tropsch chemistry has long been recognized as in effect a polymerization reaction, wherein the monomeric unit is the methylene group, $-CH_2-$ that is generated in situ from carbon and hydrogen atoms of CO and H_2. The basic steps of the F-T reaction are as follows:

1. Adsorption of reactant, CO, on the catalyst surface
2. Chain initiation, by CO association followed by hydrogenation
3. Chain growth, by insertion of additional CO molecules followed by hydrogenation
4. Chain termination, by reductive elimination of paraffin from catalyst surface or by β-hydride elimination of olefin from catalyst surface
5. Desorption of product, from the catalyst surface

When tested under relatively comparable conditions, Fe and Co catalysts give sufficiently similar carbon number distributions to suggest a common intermediate for the different F-T metals. The predominance of linearity

in F-T products and the formation of terminal, α-olefins suggest that the intermediate responsible for chain growth is a single-carbon unit. For at least the past 50 years, most researchers have agreed that the product distribution observed in F-T is consistent with a single intermediate and chain propagation mechanism for all products (with caveats for C_1 and C_2, vide infra). Research on the mechanism was most defining during the 1960s and 1970s, and experiments and debate continue on the topic of what that single-carbon unit is, and how it derives from the CO or, for iron, the CO or CO_2 present. Candidates include a surface-associated carbon, a metal methylene, a metal hydroxycarbene, a metal alkyl, a metal alkoxide, or a metal carboxylate – a great many choices for a reaction whose mechanism has been under investigation for about a century.

The mechanistic complexity of F-T chemistry is compounded by the use of certain terms, such as carbide or carbene, by different researchers to denote different intermediates. Table 2 shows the steps of the F-T reaction according to various mechanisms currently under consideration in the field, presented as composites that capture the essence of each step. The many descriptors in common use for the mechanistic chemistry and intermediates are also provided.

Formation of C_1 Species The initial reaction of syngas with the F-T metal involves reduction of CO and produces a metal-bound C_1 species CH_2, CHOH, or CH_2OH. Metal-carbides have also been considered for the C1 intermediate, forming by splitting of the C–O bond with formation of water from the O and H_2; however, the formation of carbides as discrete species attached with strong, multiple bonds to the surface has been largely discounted by isotopic tracer studies. Many people do still use the term "carbide" to refer to a more loosely associated metal-C1 species, in what has been referred to as the "modern carbide" mechanism. Surface carbiding of iron has been demonstrated under F-T conditions, but Co does not become carbided unless H_2 is absent. Given that cobalt is a good hydrogenation catalyst, if formed during F-T the carbide would be hydrogenated very quickly.

The intermediacy of immediate C–O bond cleavage and surface carbides need not be invoked if CO itself is hydrogenated prior to C–O bond scission. Devising experiments that would differentiate exactly to what degree the CO is associated with the metal when scission occurs would be difficult under realistic F-T conditions. In addition, work by Davis has shown that CO_2 can initiate chain growth in Fe catalysis (in which case an initial species would be formic acid) [27].

Chain Initiation and Propagation Chain initiation occurs when the first C–C bond of the chain is formed, by coupling of two initial C_1 fragments or by insertion of carbon monoxide into a metal alkyl bond (or possibly a metal alkoxide bond, in the postulated iron case). Propagation occurs by successive insertion of carbene C_1 species into the growing metal-hydrocarbon chain, or by successive cycles of CO insertion and reduction at the metal. The carbene terminology used here is that used by E.O. Fischer in his pioneering discovery of species of this type and refers to any species $M_1C(A_1)(A_2)$ or $M_2(A_1)(A_2)$, where A_1 is hydrogen or carbon and A_2 is hydrogen, carbon, or oxygen. For monometallic M_1, the bonding is formalized as M=C and for bimetallic M_2 the bonding is viewed as M-C-M. These $M{=}CH_2$ or $M{-}CH_2{-}M$ carbenes are highly reactive and are well known to insert into metal–carbon bonds, as required by the F-T product distribution, under milder conditions and more quickly than carbon monoxide does.

Early studies performed by Pettit with ^{13}C labeling strongly supported the intermediacy of $M{=}CH_2$ species [28]. Including ^{14}C labeled alcohols and olefins in the feed, Emmett found that enols of alkoxides can initiate chain growth. Much of this early mechanistic work, as well as the concept that CO_2 can initiate chain growth (Fe catalysis), has been reviewed by Davis [29]. The propagation mechanism also can be considered a carbene mechanism, in that the initial product of CO reaction with a metal alkyl is M–C(=O)R, which has a tautomeric carbene form, $M^{+}{=}C(O^{-})R$. Formation of oxygenates could occur by insertion of CO, to give M–C(=O)alkyl intermediates which are then reduced by H_2. Alternatively the alcohols could form by reductive elimination of metal surface-bound OH and the surface-bound chain.

Chain Termination The typical chain termination reaction is intramolecular, either reductive elimination or β-hydride elimination. Hydrogenation of a metal on which a chain is actively growing allows for reductive

Gas to Liquid Technologies. Table 2 Elements of F-T mechanisms [7]

Formation of C_1 species	*Chemistry*	*Common names for C_1 species*
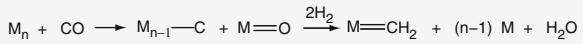	CO dissociation and hydrogenation	Surface-associated carbon (M- – -C), metal carbide (M-C), methylene (CH_2), carbene (M=CH_2), methylidene (M=CH_2), alkylidene (M=CH_2)
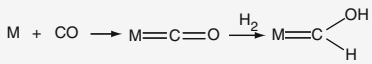	Direct CO hydrogenation	Enol, hydroxycarbene
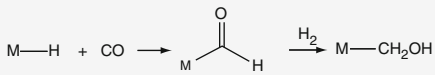	CO insertion and hydrogenation	Hydroxymethylene, alcohol
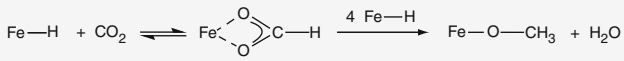	CO_2 insertion and hydrogenation	Oxygenate, metal alkoxide
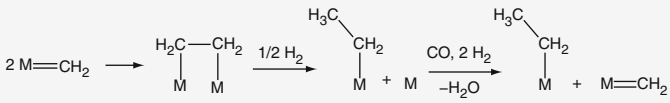	Carbene coupling	Metal alkyl and methylene (CH_2), carbene (M=CH_2), methylidene (M=CH_2), alkylidene (M=CH_2)
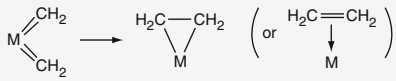	Carbene coupling (intramolecular)	Metallacycle or olefin complex and methylene (CH_2), carbene (M=CH_2), methylidene (M=CH_2), alkylidene (M=CH_2)
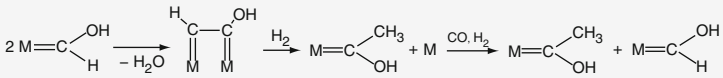	Carbene coupling	Enol or hydroxycarbene
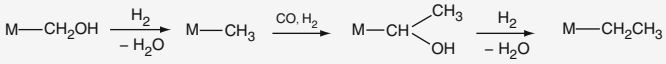	CO insertion and hydrogenation	Metal hydroxyalkyl or metal alkyl
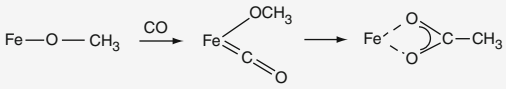	CO insertion	Oxygenate, metal carboxylate
Chain propagation	*Chemistry*	*Common names for propagation species*
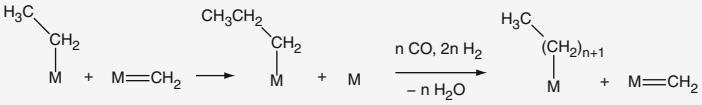	Carbene insertion into metal–alkyl chain	Metal alkyl and methylene (CH_2), carbene (M=CH_2), methylidene (M=CH_2), alkylidene (M=CH_2)

Gas to Liquid Technologies. Table 2 (Continued)

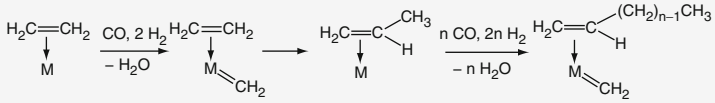	Carbene insertion into metal–olefin chain	Olefin complex and methylene (CH_2), carbene ($M{=}CH_2$), methylidene ($M{=}CH_2$), alkylidene ($M{=}CH_2$)
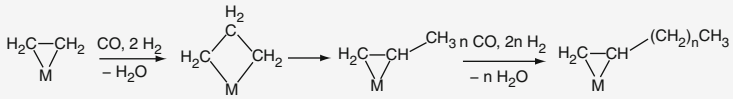	Carbene insertion into metallacyclic chain	Metallacycle or olefin complex and methylene (CH_2), carbene ($M{=}CH_2$), methylidene ($M{=}CH_2$), alkylidene ($M{=}CH_2$)
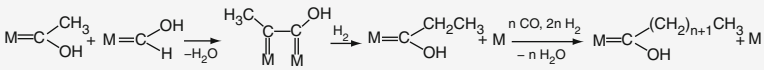	Carbene coupling, or carbene insertion into metal-carbene chain	Enol, hydroxycarbene
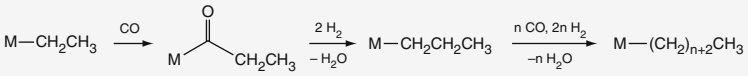	CO insertion and hydrogenation	Metal alkyl
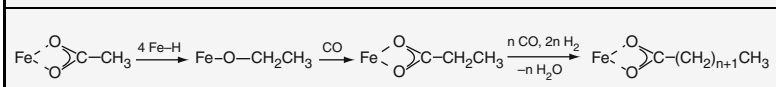	CO insertion and hydrogenation	Oxygenate, metal carboxylate
Examples of chain termination	*Chemistry*	*Comments*
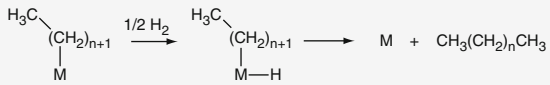	Hydrogenation, reductive elimination	
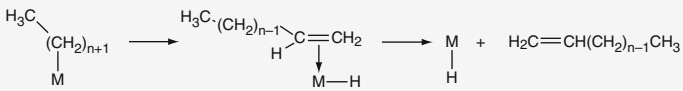	β-elimination, olefin desorption	(The reverse is olefin re-adsorption)
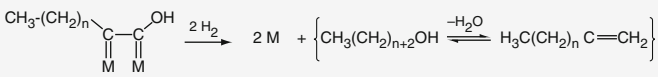	Hydrogenation, dehydration	
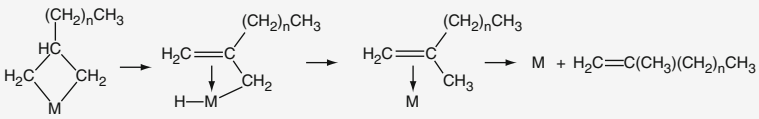	β-elimination, reductive elimination olefin desorption	
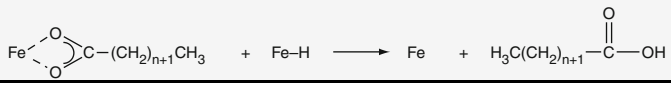	Hydrogenation	

elimination to give the saturated alkane. Loss of an H atom from the beta-position of the chain (the second carbon away from the metal) allows the formation of a metal-hydride and a π-bound olefin, the latter then dissociating easily from the metal center to give an alpha-olefin. The β-elimination is usually quite reversible, and chain growth may resume if an olefin reinserts into the metal-hydride bond.

ASF Distribution For F-T reactions, the number of moles of species with carbon number n decreases exponentially with *n*. The weight fraction of product having carbon number, W_n, is given by the Anderson–Schultz–Flory (ASF) distribution (Eq. 8):

$$W_n = (1-\alpha)^2 n a^{n-1} \tag{8}$$

The parameter *a* is the Schultz–Flory distribution factor and represents the ratio of the rate of chain propagation to the rate of chain propagation plus the rate of chain termination. The parameter α is the chain growth probability, and $1-\alpha$ is the probability of chain termination. Both parameter *a* and parameter α are assumed to be independent of chain length. Either value can be obtained graphically using Eq. 8 in log form, with analytical data for W_n as obtained, for example, using gas chromatography. The α values for oxygenated products appear to be about the same as those for hydrocarbons, which suggests that the products all form by the same or similar chain propagation steps and with similar rates of chain termination, albeit with different chain termination chemistries for the oxygenates, olefins, and paraffins.

The parameter α is used most often to characterize product distribution. Values of $\alpha > 0.9$ are representative of processes producing high amounts of wax, α values of about 0.8 maximize diesel cuts, and α values of about 0.7 are characteristic of naphtha production.

F-T Catalysts

Early studies reported that the level of reaction activities of metal catalysts for the Fischer–Tropsch reaction decline in the order Ru, Ni, Co, and Fe. Later studies indicated that activities declined in the order Ru, Fe, Ni, and Co with alumina as support, and in the order Co, Fe, Ru, and Ni with silica as support. In practice, Ru gives rapid production of high molecular weight wax but this metal is cost-preclusive and supply-limited at plant scale. Nickel gives predominantly methane as product.

Commercially, Co appears to be more active than Fe in that the turnover rates on Co catalysts are about three times higher than on Fe catalysts. In general the observed rates depend on the diffusion rates of reactants and products migrating in and out of the porous catalyst particles, as well as on the intrinsic rate of the F-T reaction at the catalyst surface. The diffusion rates in turn depend on the catalyst's porosity, pore sizes, and particle size, and on whether or not liquid wax is present within the catalyst particles.

The product distribution can be significantly influenced the through use of promoters. The ability of numerous promoters to increase activity with Co catalysts is well documented but their ability to affect selectivity is less clear. In general, any promoter metal that can enhance the even distribution of reduced cobalt on the internal and external surfaces of the catalyst particles could increase the number of active sites available for chain growth and thereby increase the selectivity for wax. Ruthenium appears to do this best, and lanthanum also helps. Rhenium is sometimes used to promote chain growth with cobalt although reports of its efficacy vary.

The traditional industrial support materials for cobalt are alumina, silica, and titania [30]. The choice of support material appears to have little effect on selectivity; however, catalysts using mesoporous supports such as MCM-41 have provided somewhat increased C_{5+} selectivity [31].

The performance of iron catalysts is very dependent on the addition of strong alkali promoters. Oxides of the alkali metals, particularly potassium, promote formation of wax in LTFT catalysis by iron. Use of K_2O also helps keep the iron reduced in carbided form, which may promote the growth of longer chains. Not only is selectivity markedly dependent on the amount of alkali present, but alkali promoters also have a direct effect on the overall rate of reaction. For precipitated iron catalysts, used for LTFT, catalyst activity decreases when the alkali content is raised beyond a threshold level.

Cobalt catalysts produce considerably less CO_2 during F-T synthesis than do iron catalysts.

The partial pressures of water and CO_2 affect selectivity, with the pressure of CO_2 being more relevant for iron than cobalt. Cobalt is a better hydrogenation catalyst than iron, and the products of its F-T reaction tend to have a lower olefin/paraffin ratio than those of iron.

Catalyst Beds and Reactors for F-T Synthesis

Axial temperature gradients, poor heat distribution with carbon deposition, and scale-up limitation mean that multi-tubular reactors are usually not suitable for commercial LTFT synthesis. The slurry bed reactor (SBR) is an attractive alternative to fixed bed reactors. When using precipitated catalysts of identical composition, a SBR system is as active as a fixed bed system despite the much lower catalyst loading of the SBR. Slurry bed reactors have become the technology of choice for companies planning new GTL plants, with the exception of Shell as noted above. Both Sasol and Exxon have operated large demonstration slurry phase F-T units with supported cobalt catalysts. A drawback of SBR technology to date is that additional equipment is required to achieve near complete separation of the finely divided catalyst from liquid wax in slurry systems.

Multi-tubular fixed beds do have advantages as research reactors, because they are easy to operate. No equipment is required to separate the heavy wax product from the catalyst, since the liquid wax simply trickles down the bed and is collected in a downstream knock-out pot. Alternatively, laboratory studies may be performed in high velocity, high recycle stirred tank reactors. By varying the fresh feed gas flow to these units, the partial pressures and the kinetics at different conversion levels (tantamount to different bed depths) can be determined.

Kinetics

Various kinetic equations based on research with laboratory reactors have been generated for the F-T reaction. Equations 9–14 are representative examples of kinetics proposed for Co systems.

$$r = kP_{H_2}{}^2/P_{CO} \tag{9}$$

$$r = aP_{CO}P_{H_2}/(1+bP_{CO})^2 \tag{10}$$

$$r = aP_{CO}P_{H_2O}{}^{0.5}/\left(1 + bP_{CO} + cP_{H_2O}{}^{0.5}\right)^2 \tag{11}$$

$$r = aP_{CO}P_{H_2}{}^2/\left(1 + bP_{CO}P_{H_2}{}^2\right) \tag{12}$$

$$r = c\left(P_{H_2O}{}^{0.5}/P_{CO_2}\right)/(1 + 0.93P_{H_2}/P_{H_2O}) \tag{13}$$

$$r = d(P_{H_2}P_{CO})/P_{CO} + 0.27P_{H_2O}) \tag{14}$$

Equations 15–18 are representative of kinetics proposed or Fe systems.

$$r = kP_{H_2}{}^{0.6}P_{CO}{}^{0.4} - \mathrm{fr}^{0.5}P_{H_2O}{}^{0.5} \tag{15}$$

$$r = mP_{H_2}P_{CO}/(P_{CO} + nP_{H_2O}) \tag{16}$$

$$r = aP_{CO}P_{H_2}{}^2/(P_{CO}P_{H_2} + bP_{H_2O}) \tag{17}$$

$$r = aP_{CO}P_{H_2}/(P_{CO} + bP_{H_2O} + cP_{CO_2}) \tag{18}$$

Equation 10 for Co responds to an increase in pressure: as the pressure increases, the F-T reaction rate decreases. Cobalt is much more resistant to oxidation than iron, whether by oxygen or by water, which could account for the absence of a P_{H_2O} term in kinetic equations for cobalt catalysts. Even so, Co crystals smaller than a certain size (<5 μm) may be oxidized by water vapor and therefore a more detailed kinetic equation for cobalt could include the partial pressure of water.

The kinetics of Fe catalysis are better studied than those for Co. Sasol performed a large number of experiments and measurements in both fixed and fluidized bed reactors to study iron-based catalyst activity in commercial HTFT and LTFT processes. The key findings are as follows:

- Reaction rate is strongly dependent on hydrogen partial pressure. At low conversion levels, reaction rate is solely dependent on hydrogen partial pressure.
- Reaction rate increases with the partial pressure of CO.
- The partial pressure of CO_2 does not appear to have a direct effect on reaction rate. It can, however, affect the partial pressures of other components via the water gas shift reaction and thus may have an indirect effect.
- Reaction rate is markedly depressed by the partial pressure of water.
- The level of hydrocarbon products in the reactor has no apparent effect on F-T reaction rate.

Based on these observations, a satisfactory rate equation for iron-based catalysts is given by Eq. 19:

$$r = mP_{H_2}P_{CO}/(P_{CO} + aP_{H_2O}), \quad \text{where } a = k_{H_2O}/k_{CO} \tag{19}$$

The above kinetic expression is speculative but has been shown to estimate the overall conversion for both HTFT and LTFT reactors. This kinetic equation also predicts that if the total pressure of the gas feed is increased, the rate is increased by the same factor, that is, the residence time in the catalyst bed remains the same and the degree of conversion remains unchanged. This means that the production rate is increased in proportion to the increase in pressure. Pilot plant tests at Sasol for both the fixed bed LTFT and the fluidized bed HTFT operations confirmed these kinetic predictions.

Given that reforming methane gives as much or more H_2 as needed for the F-T reaction, the presence of water gas shift chemistry in the F-T reactor could easily become a liability to efficiency of a GTL process. Using the same reactor under the same operating conditions and feed gas flow, a Co catalyst system will have a much higher syngas conversion than an iron catalyst. With an iron catalyst, after water has been condensed out a larger portion of the tail gas is recycled to the reactor. This means that more reactors are required and there is also a greater need to recycle, both of which increase the total fixed capital and operating costs.

Commercial Activities in the Fischer–Tropsch Synthesis

In 1993, two large-scale F-T plants were built specifically for operation with natural gas (as opposed to coal). Backed with funding from the South African government, Mossgas (now PetroSA) began operating a 22,000 bbl/day plant using Sasol technology. The gas is produced from a South African offshore field. Also that year, Shell built a 10,000 bbl/day plant at Bintulu, Malaysia. The $600 million plant was expanded to 12,500 bbl/day in May 2000, after a fire destroyed the oxygen plant. Also in 1993, a plant designed by Rentech was built in Colorado Springs, Colorado for conversion of landfill gas to liquids. A lack of methane from the landfill shut down the plant.

A joint venture of Qatar Petroleum and Qatar Shell has recently built a GTL plant in Ras Laffan Industrial City, Qatar, using Shells' cobalt-catalyzed, fixed bed technology. The project is referred to as Pearl and is scheduled for the latter part of 2011. At $18+ billion, the cost of Pearl significantly exceeded budget. This may have resulted at least in part from the incorporation of an additional facility, for producing NGL, into the design. Pearl is expected to generate a total of 140,000 bbl/day in two trains operating at full nameplate capacity, making this plant the world's largest GTL project [32]. In addition Pearl has a capacity for 120,000 barrel of oil equivalents total per day of NGL from two trains. Another new GTL plant has been under construction recently in Qatar, by Sasol, and was operating at about 55% of nameplate capacity in 2010.

F-T Product Upgrading

Conversion of syngas through the F-T process leads to a distribution of products essentially consisting of *n*-paraffins (>90%) and smaller percentages of alcohols, olefins, and methane. Typical hydrocarbon product cut weight fractions are shown in Table 3.

A consequence of aliphatic chain growth by one-carbon units is the theoretical impossibility of synthesizing a F-T product having a narrow range of chain length. This wide molecular weight range of the raw F-T product slate means that downstream separations and refining must be used to create fractions for specific end uses. The crude product from the F-T reaction is most commonly separated into a light, relatively low boiling condensate fraction and a heavy, high boiling

Gas to Liquid Technologies. Table 3 Hydrocarbon weight fractions in typical F-T product

Product cut	Carbon No.	wt%
Gas	C_1–C_4	2.5
Naphtha	C_5–C_9	6.7
Diesel	C_{10}–C_{19}	18.5
Soft wax	C_{20}–C_{34}	27.3
Hard wax	C_{35+}	45.0

wax fraction. A typical boiling range cut temperature would be 372°C. The condensate fraction is a liquid that can be shipped from a remote area to a refinery site for upgrading. Condensate containing, for example, C_4–C_{15} products is further separated, into cold separator liquid and hot separator liquid. The cold separator liquid contains C_{5+} in the boiling range of <260°C, retains about 95% of the total oxygenates produced, and has sufficiently low olefin concentration that hydrogenation is unnecessary. The hot separator liquid contains mostly hydrocarbons and has a boiling range of 260–372°C.

Hydrocracking Heavy Paraffins (Wax)

The C_{16+} reactor wax may be upgraded by various hydroconversion reactions including hydrocracking, hydroisomerization, catalytic dewaxing, isodewaxing, or various combinations thereof, to produce middle distillates for use as fuels, lubricants, chemicals, and specialty materials such as nontoxic drilling oils, technical and medicinal grade white oils, chemical raw materials monomers, polymers, emulsions, isoparaffinic solvents, and other specialty products. For example, wax from F-T synthesis is typically first hydrofined, to eliminate alkenes and oxygenated compounds, and then fractionated into different grades of product waxes. The waxes can be sold directly or hydroprocessed by recycle to extinction to yield high quality diesel and kerosene fuels.

Hydrocracking is the most relevant upgrading process, including for maximum production of diesel fuels. Hydrocracking heavy paraffins serves to lower the boiling range of product from that of wax to that of middle distillates, and to improve the cold flow properties of F-T diesel with branched molecules formed during hydrocracking. Because F-T products are predominantly linear, especially those from LTFT, the raw middle distillates have very poor cold flow properties that would hamper their use as transportation fuel unless subjected to hydrocracking.

Another property affected by hydrocracking is the cetane number of diesel. As the pressure of a LTFT reactor increases, the selectivity for wax increases, the degree of branching decreases, and consequently the cetane number of downstream diesel cuts decreases. Subsequent selective hydrocracking of crude wax makes the largest contribution to the final diesel fuel pool. Some chain branching occurs during hydrocracking and thus the cetane number of the diesel fuel produced is somewhat lower than that of straight run F-T diesel. The final diesel pool, however, has a cetane number above 70 – significantly superior to the cetane number for refinery naphtha, which varies from 40 to 50.

Upgrading wax by hydrocracking to middle distillates gives naphtha as the main coproduct. The naphtha fraction may be upgraded to gasoline, via catalytic reforming, or used as a steam cracker feedstock for olefins production. Converting these two naphtha cuts into on-specification gasoline would require a considerable amount of further octane number upgrading. However, this naphtha consists almost entirely of linear alkanes and therefore makes excellent feedstock for production of ethylene by steam cracking, giving much higher selectivity for ethylene than that obtained from steam cracking of naphtha obtained from crude oil.

Feeds derived from LTFT can be hydrocracked under much milder conditions than typical feeds such as vacuum gas oils that are derived from crude oil. In the hydrocracking of crude oil-derived feeds, typically pressures as high as 150 atm are required to prevent coking of the catalyst by aromatic compounds. This is not necessary with paraffinic feeds, wherein LTFT products are hydrocracked at pressures from 35 to 70 atm using commercial hydrocracking catalysts. The relatively low levels of oxygenates, mainly alcohols and lesser amounts of acids or carbonyls, present in F-T waxes are easily and completely hydrodeoxygenated.

The refining of syncrude is often performed in a separate facility from the upstream GTL process. For direct on-site F-T reaction product upgrading, however, the hot separator liquid cut may be combined with F-T wax and processed under much milder conditions than typical crude oil–derived feeds. Conventional hydrocracking of refinery feedstocks is performed in a fixed bed reactor using multiple or single Co/Mo catalyst compositions under operating pressures as high as 2,500 psi, using conventional technologies such as those offered for license by Chevron or UOP. The high operating pressure is required to prevent coking of the catalyst by aromatic compounds contained in the feed. Such high pressures are not

required when hydroprocessing paraffinic feeds from LTFT synthesis, which do not contain aromatics, and lower pressures between 500 and 1,000 psi are used to hydrocrack LTFT products with commercial hydrocracking catalysts. During this process, the oxygenates present in the feed are easily and completely hydrodeoxygenated. Typical hydrocracking conditions for F-T products entail operating temperatures of 320–450°C, pressures of 1,000–1,500 psi, and hydrogen treat rates of 500–5,000 scf/bbl.

The low sulfur content of syngas from natural gas enables consideration of hydrocracking catalysts containing a noble metal component, particularly platinum, instead of the less expensive, conventional sulfur-resistant Co/Mo catalysts. Platinum leads to higher hydroisomerization activity and less severe hydroprocessing conditions, with better low-temperature performance of the resultant diesel fuel. For example, ExxonMobil's hydroisomerization process uses a noble metal catalyst to increase the amount of isoparaffins in the distillate fuel and to help the fuel meet pour point and cloud point specifications without the need for additives. Hydroisomerization may be carried out with a single Pt-based catalyst in a fixed bed reactor. Preferred operating conditions use a temperature range of 260–400°C, a pressure range between 500 and 1,000 psi, and a hydrogen treat rate of 1,000–4,000 scf/bbl, and heavy wax products are recycled to extinction through the hydrocracking process.

The processing pressure is dependent on the hydrogenation capacity of the catalyst. When the hydrogen partial pressure is too low, dehydrocyclization of the paraffins starts to occur with the formation of polynuclear aromatics, which eventually would lead to deactivation of the catalyst due to coking. Lower hydrogen/wax ratios lead to a decrease of conversion rate of the C_{22+} fraction and, after adjustment of reaction conditions to achieve the same conversion levels, an increase of both the isoparaffin content and the selectivity to products lighter than diesel.

Isoparaffin content also increases with operating pressure. The hydrocracking process has to meet the following conditions:

- The chain length of the hydrocracked fragments should be predominantly in the desired product's carbon number range.
- The components above said desired range should be hydrocracked in preference to those that are already within or below the desired range.
- The production of less commercially attractive species, for example, light hydrocarbon gases, should be minimized.

Due to the clean nature of the feed, non-sulfided hydrocracking catalysts containing a noble metal component such as platinum can be considered. The use of noble metal catalysts leads to higher hydroisomerization activity and consequently better low-temperature characteristics for the diesel product. Most probably all C_{14+} material would be treated using such catalysts, due to the enhancement of cold flow properties resulting from simultaneous isomerization and hydrocracking. A high blending cetane value is retained, and very little of the diesel range material in the feed is degraded into naphtha and kerosene. Catalysis using a noble metal on amorphous silica-alumina is likely to be the preferred approach for maximum production of diesel blending material.

There are many technology licensors for hydroconversion processes, including ChevronTexaco, UOP, IFP (Axens), Criterion, and Haldor Topsøe. Catalysts can be obtained from these companies as well as from Akzo Nobel and Sud-Chemie, among others.

Hydrotreating Light Paraffins

Hydrogenation is less costly than hydrocracking. For large-scale plants, a condensate hydrotreater should be used to process hydrocarbons that are already lighter than the desired middle distillates and also for straight run middle distillates if cold flow properties are not an issue. A condensate fractionator may be employed if it is desired to produce linear paraffin products. The condensate fractionator can also serve to remove light gases in order to stabilize the condensate for intermediate storage at atmospheric pressure. If a nearby naphtha cracker is available, then the condensate fractionator will provide a naphtha product that need not be hydrogenated to ensure storage stability. Also, a kerosene fraction can be separated using the condensate fractionator.

If both hydrotreating and hydrocracking are used, they may be operated at the same pressure and use a common hydrogen loop. Alternatively, the

hydrotreater can be operated in a once through mode, at lower pressure, and the hydrogen tail gas then subsequently pressurized and fed to the hydrocracker loop. For a 30,000 bbl/day equivalent product upgrading system comprised of hydrocracking and hydrotreating, the size of the unit is comparable to those used in oil refineries. There are many process configurations possible depending on site-specific factors like plant capacity, available land, and possible integration with other facilities.

While product upgrading schemes center around three fuel products (diesel, LPG, and naphtha), the upgrading plant is quite amenable to different configurations if the market demand so indicates. Even with cracking and hydrotreating, the ASF distribution means that the F-T process and its associated refinery produce other transportation fuel and products beyond middle distillates. Other saleable products may include solvents, kerosene, jet fuel, illuminating paraffins (sold for use in lighting and appliances in South Africa), and base oils (for lubricant products). Maximizing the recovery of the higher boiling jet fuel while maintaining diesel production will tend to increase economic return.

LTFT Naphtha and Blends

Four LTFT naphthas can be produced using process configurations summarized below in Table 4.

The slurry phase distillate (SPD) naphtha is an excellent feed for the production of lower olefins, particularly ethylene, by steam cracking. Such paraffinic naphtha feed demands less feedstock and lower energy consumption in the cracking process than naphthas from other sources. The optimum olefin yields and selectivities obtainable from any naphtha depend on the cracking severity at commercial conditions. The mass ratio of light olefins, propylene/ethylene (P/E), has an inverse relationship to the cracking severity. High P/E values correspond to low severities and also lower coproduction of methane.

Gas to Liquid Technologies. Table 4 Process schemes for production of LTFT naphtha

F-T naphtha		Production scheme
SR	Straight run	Fractionation of F-T condensate
HT SR	Hydrogenated straight run	Fractionating and hydrotreating of F-T condensate
HX	Hydrocracked	Fractionating and hydrocracking of F-T wax
SPD	Slurry phase distillate	Blend of HT SR and HX naphthas

The LTFT naphthas other than SR are essentially entirely paraffinic and therefore have compositions far from those of high-octane naphthas useful in gasoline blends. Even so, the conventional naphthas typically require that the refiner improve cold flow characteristics by changing the boiling point, for compatibility with low-temperature operation. Blends of SPD naphtha with conventional diesels could be used to meet winter grade fuel specifications without decreasing the production volume of diesel and other light products obtained from oil refining. Including F-T naphtha in blends can assist refiners in meeting low sulfur specifications in fuels that have sulfur content near zero (below 1 ppm).

The projected threshold for economic viability of F-T GTL technology, in terms of crude oil price, is now at about $70–75 per BOE. This threshold is based on recycle of reformed NGL (vs. production of NGL for market sales). The investment cost for a modest scale GTL facility producing predominately diesel fuel has been estimated at about $1.1 billion [7]. There are then further opportunities to add value by producing base oils and waxes.

This $1 billion investment value may be taken as a starting point when estimating actual investment costs for a first-of-a-kind plant. There is a substantial gap between such estimate and the final cost of, for example, Pearl. In the Pearl project, the initial configuration was changed to one utilizing NGL for market sales and also the builders experienced escalating capital costs, due to a shortage of major equipment, procurement delays, shortage of skilled engineering labor, and an increased number of reactors from an initially conservative estimate, among other contributing cost factors.

Methanol

General Process Description

Currently the majority of methanol is synthesized from syngas produced from natural gas, using autothermal reforming, steam reforming, or a combination of steam reforming and autothermal reforming. Most existing

commercial plants use steam reforming. Incoming pressurized natural gas feed is preheated and passed through a zinc oxide catalyst bed to remove sulfur compounds that would otherwise poison downstream catalysts. Steam is added to the natural gas stream before it enters the reformer. A typical reformer is a large high-temperature furnace containing a number of vertical tubes that are filled with a nickel catalyst. Once the natural gas is reformed, the resulting synthesis gas is cooled to about 30°C, condensed water is separated from the gas in a process gas separator, and the syngas is compressed using a steam turbine compressor that uses steam generated in an economizer on the syngas outlet from the reformer.

Compressed syngas containing H_2, CO, and CO_2 is fed to a methanol synthesis reactor that uses a copper catalyst. The methanol reactor outlet gas is cooled to about 40°C and then passed to a pressure letdown tank where unreacted synthesis gas is separated from the product methanol and water. A portion of this unreacted syngas stream is purged and burned as fuel, while the majority is compressed by a recirculating compressor and remixed with feed synthesis gas (from the upstream syngas compressor). The unreacted syngas is thus recirculated back to the methanol reactor, resulting in an overall conversion efficiency of 99%.

Crude methanol collected in the letdown tank usually contains up to 18% water plus impurities such as methyl formate, higher alcohols, ketones, ethers, and esters. This is stored at atmospheric pressure in an intermediate storage tank and later fed to a distillation plant. The distillation plant may be configured in a variety of ways. A typical distillation plant consists of a single distillation column that removes the light ends including dissolved gases, dimethyl ether, methyl formate, and acetone that are burned as fuel. Bottoms from the light ends column are sent to a system that consists of two distillation columns, both of which deliver pure methanol overhead and sequentially remove water and heavy ends such as higher alcohols, ketones, and esters (formed by esterification of lower alcohols with formic, acetic, and propionic acids in column bottoms). Water from the bottoms of the first distillation column is discharged to the process sewer system, while heavier ends separated as bottoms in the second methanol recovery column are sent to the reformer furnace fuel system for combustion. The methanol is at least 99.8% pure after this distillation and is transferred from temporary storage to final product storage tanks where it is directly pumped into ships, railcars, or trucks for delivery to customers and distributors.

Reaction Pathway

Chemical reactions considered in methanol synthesis are shown in Eqs. 6, 20, and 21.

$$H_2O + CO \leftrightarrows H_2 + CO_2 \quad \Delta H = -41.2\text{kJ/mol CO} \tag{6}$$

$$\begin{aligned} &CO_2 + 3H_2 \leftrightarrows CH_3OH + H_2O \\ &\Delta H = -\,49.0\text{kJ/mol } CO_2 \end{aligned} \tag{20}$$

$$CO + 2H_2 \leftrightarrows CH_3OH \quad \Delta H = -90.1\ \text{kJ/mol CO} \tag{21}$$

Both CO and CO_2 are reactive in the synthesis. Coupling the methanol synthesis with the water gas shift reaction (Eq. 6) allows a larger quantity of carbon to become available for most efficient synthesis. Although the direct hydrogenation of either CO_2 or CO to methanol is thermodynamically favorable (Eqs. 20 and 21, respectively), the activation energy for direct hydrogenation is apparently too high and instead the reaction proceeds through a different mechanistic pathway.

The reaction of syngas to produce methanol is about 100 times slower if CO_2 is not also present in the mix. Until as recently as the 1990s, the role of CO_2 in methanol synthesis was unclear. The water gas shift activity of Cu catalysts is so high that it was difficult to delineate the roles of CO and CO_2 in methanol synthesis. Isotopic labeling studies have now unequivocally shown that CO_2 is the source of carbon in methanol. The CO undergoes the WGS reaction to make H_2 and CO_2. The CO_2 is thought to keep the catalyst in an intermediate oxidation state, thus preventing the reduction of ZnO followed by the formation of brass.

A long-held mechanism for catalytic methanol synthesis proceeds through a metal-bound formate intermediate, formed by hydrogenation [33, 34]. As depicted in Eqs. 20–24, CO_2 is adsorbed onto the catalyst surface [35], where it reacts with a partially oxidized methane intermediate to form a carbonate, which is then hydrogenated. This intermediate is then

further hydrogenated in the rate-limiting step. The copper catalyst sites have high activity for splitting the first C–O bond of CO_2 that helps maintain the oxidation state of the active copper sites. At high concentrations, however, CO_2 actually decreases catalyst activity and inhibits methanol synthesis. The feed gas composition for methanol synthesis is typically adjusted to contain 4–8% CO_2 for maximum activity and selectivity. Although Cu has water gas shift activity, excessive water causes deactivation by blocking active sites. Site blocking lowers catalyst activity but improves selectivity, with a 50% decrease in by-product formation.

Recent modeling efforts using density functional theory (DFT) suggest that the traditional methanol synthesis mechanism proceeding via CO_2 accounts for only about two third of the methanol produced [36]. The remaining methanol is said to derive from the CO, mostly via direct reduction by H_2. The proposed mechanism is conceptually similar to that for CO_2 reduction to methanol and is shown in Scheme 1. Overall, methanol synthesis appears rate limited by formation of methoxy (CH_3O^*, where * refers to the catalyst surface) at low $CO_2/(CO + CO_2)$ ratios and by CH_3O^* hydrogenation in CO_2-rich feeds. Hydrogenation of CH_3O^* as per Eqs. 20 and 21 is the slow step for both the CO and the CO_2 methanol synthesis routes.

Reactors and Catalysis for Methanol Synthesis

The two main process features considered when designing a methanol synthesis reactor are (a) controlling and dissipating the large reaction heat, and (b) overcoming the equilibrium constraint to maximize per pass conversion efficiency. Methanol synthesis is a version of the classic trade-off between conversion and selectivity. The maximum per pass conversion efficiency of syngas to methanol is limited to about 25%, and catalyst activities generally decrease as the temperature is lowered. At higher temperatures, catalyst activity increases but so does the chance for competing side reactions to form by-products such as dimethyl ether, methyl formate, higher alcohols, and acetone. Catalyst lifetimes are also reduced by continuous high-temperature operation.

Maintaining reaction temperatures below 300°C is the trade-off strategy employed to minimize catalyst sintering while maximizing conversion of syngas to the target product slate. Although the equilibrium conditions favor low temperatures, methanol converters must be operated at temperatures in the range 200–300°C to ensure the catalysts are active and to use the heat of reaction effectively [37].

Removing methanol as it forms is another strategy used for overcoming the thermodynamic limitations and improving the per pass conversion and process efficiency. Methanol is either physically removed or converted to another product, such as dimethyl ether, methyl formate, or acetic acid.

Numerous methanol reactor designs have been commercialized over the years and these can be roughly separated into two categories, namely, adiabatic and isothermal reactors. Adiabatic reactors often contain multiple catalyst beds separated by gas cooling devices, using either direct heat exchange or injection of cooled syngas, either fresh or recycled. Axial temperature profiles often have a saw tooth pattern: dropping down at the point of heat removal and increasing linearly between the heat exchange sections. The isothermal reactors are designed to continuously remove the heat of reaction so they can operate essentially like a heat exchanger with an isothermal axial temperature profile.

Currently all commercial processes produce methanol from syngas in a vapor phase reactor with a synthesis loop. In a gas phase, tubular or packed bed reactor, reaction heat is dissipated in situ by injecting cool, unreacted feed at various points along the reactor length, or by including internal cooling surfaces for heat exchange. Temperature moderation is also achieved by recycling large quantities of gas, with gas cooling in the recycle loop. Even with these heat transfer measures, the CO content of the feed is limited to about 16% as a means of controlling heat content by limiting the conversion.

$$H_2 + CO + 2^* \rightleftharpoons CHO^* + H^*$$
$$CHO^* + H^* \rightleftharpoons HCHO^* + {}^*$$
$$HCHO^* + H_2 + {}^* \rightleftharpoons CH_3OH^* + H^*$$
$$CH_3OH^* + H^* \rightleftharpoons CH_3OH^*$$
$$CH_3OH^* \rightleftharpoons CH_3OH$$

Gas to Liquid Technologies. Scheme 1
Proposed mechanism for reduction of CO to methanol

The design challenge of removing heat while maintaining precise temperature control is significant, because excessive temperatures seriously diminish the lifetime of the catalyst. A liquid process is of interest, wherein nonvolatile mineral oils make up part of the reactor liquid phase and act as a temperature moderator and heat sink. A new approach investigated by Air Products involves bubbling the syngas through a slurry consisting of micrometer-sized methanol synthesis catalyst and mineral oil as reaction medium that transfers heat from the catalyst surface, through the slurry, to boiling water in an internal tubular heat exchanger. Concentrations of CO as high as 50% have been used in the slurry system without damaging the catalyst activity.

A typical commercial methanol synthesis catalyst contains of copper and zinc oxide phases with alumina support, that is, $Cu/ZnO/Al_2O_3$. Recent modifications to catalyst preparation at laboratory scale include specialized coprecipitation methods [38], for a greater synergistic effect between copper and zinc, and the maintaining of a strict control of pH and the temperatures of precipitation and calcination [34]. As shown in Table 5 and Fig. 3, the productivity of commercial catalysts is sensitive to several factors, including conditions used for preconditioning by, for example, aging the catalyst [39, 40].

Activities in Methanol Synthesis

Catalytic methanol synthesis from syngas was classically run as a high temperature, high pressure, exothermic, equilibrium-limited synthesis reaction operated at 320–450°C and 250–350 atm pressure. BASF of Germany introduced the first commercial synthesis of methanol, in 1923, using a zinc/chromium oxide catalyst. New methanol synthesis technologies based on lower reaction pressures (50–100 atm) were introduced in the 1960s. Whereas high-pressure processes require 139,000–146,000 Btu/gal of methanol produced, all modern plants are based on low-pressure technology and are expected to require fewer than 100,000 Btu/gal of methanol produced, on an average yearly basis. Additional advantages of low-pressure processes include lower maintenance costs and reduced downtime.

Johnson Matthey (formerly ICI Chemical Industries) of the United Kingdom and Lurgi of Germany offer the two most widely used technologies for methanol synthesis. The ICI low-pressure process operates at pressures between 50 and 100 atm and temperatures of about 210–290°C. A highly selective copper/zinc alumina catalyst is used in a shot-cooled single or multi-bed reactor. The reaction is quenched on the bed by introducing cold gas through specially designed spargers. Heat recovered from the synthesis loop provides part of the process steam required by the steam reforming furnace.

Lurgi's conventional low-pressure methanol process has a maximum output of 1,830–2,000 t/day. It uses a copper-based catalyst, pressures of 50–100 atm, and temperatures of 230–265°C. Temperature control of the catalyst is achieved by indirect cooling with boiling water. The boiling water in the reactor shell generates 1–1.2 kg of steam/kg of methanol, with a pressure of up to 45 atm. The steam, after moderate superheating, supplies the total energy for driving the recycle gas compressor and is subsequently used for the reboilers in the methanol distillation section. A small quantity of surplus steam is often available for export.

Johnson Matthey, Lurgi, and Haldor Topsøe have been pursuing 10,000 t/day mega-methanol single

Gas to Liquid Technologies. Table 5 Methanol synthesis catalysts prepared under various aging conditions

Catalyst	Metals (molar ratio)	Precipitation parameters	Aging parameters
$Cat_{2\text{-const}}$	Cu/Zn/Al (60/30/10)	pH 7, 70°C	pH 7_{const}, 70°C
Cat_3	Cu/Zn/Al (60/30/10)	pH 8, 70°C	pH 8_{const}, 70°C
$Cat_{2\text{-free}}$	Cu/Zn/Al (60/30/10)	pH 7, 70°C	Free-aged, 70°
$Cat_{Cu/Zn}$	Cu/Zn (70/30)	pH 7, 70°C	pH 7_{const}, 70°C

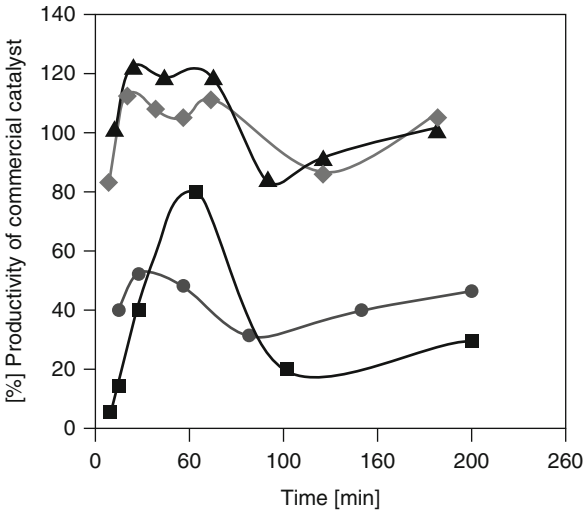

Gas to Liquid Technologies. Figure 3
Methanol productivity as a function of the aging time for selected catalysts: (*triangle*) $Cat_{2\text{-const}}$; (*square*) $Cat_{2\text{-free}}$; (*circle*) $Cat_{Cu/Zn}$; (*diamond*) Cat_3 [39]

train plant designs. Lurgi's MegaMethanol® process can accommodate a single train capacity of at least 5,000 t/day and was developed for capacities larger than one million tons of methanol per annum. A schematic of Lurgi's process is shown in Fig. 4. Lurgi does not use conventional steam reforming to produce syngas, instead employing autothermal reforming with a newer burner system in what is called the MegaSyn process for converting oxygen and natural gas to syngas.

The first plant to use the MegaMethanol® technology was brought on stream in 2004 at Point Lisas in Trinidad. The plant is owned by Atlas Methanol Company, a joint venture between Canada's Methanex and BP Trinidad and Tobago (bpTT). The 1.7 t/year Atlas methanol plant was built adjacent to the existing Titan Plant, which has a methanol production capacity of 850,000 t/year. Average total methanol production from the plants is 2.5 million tons per year, which makes Trinidad and Tobago the world's leading methanol exporter.

The Point Lisas plant has an on-site air separation plant having a production capacity of 2,800 t of pure oxygen per day. Their mega-methanol production process consists of oxygen-blown autothermal reforming at a pressure of about 40 atm, desulfurization and pre-reforming, a two-step Lurgi methanol synthesis in water- and gas-cooled reactors, and adjustment of syngas composition via hydrogen recycle. The reformer outlet temperatures range from about 950°C to 1,050°C. The synthesis gas is then compressed using a single casing gas compressor. An integrated recycler in the compressor generates the pressure for the methanol synthesis.

The methanol reactor contains a fixed number of tube sheets containing the copper-based catalyst. The isothermal reactor enables partial conversion of the syngas to methanol, reduces the by-products produced during the process, and increases the yields at low recycle ratios. The Lurgi-combined converter process employs a gas-cooled reactor and a water-cooled reactor. The gas containing methanol from the first reactor is transferred to a downstream water-cooled reactor where cooling takes place. The purge gas is separated and the cooled crude methanol is processed in a three-column distillation unit through which about 40% of the heating steam is saved.

As smaller, high-cost methanol plants continue to be replaced by mega-methanol plants, the industry's aggregate cash cost curve should drive down price to levels that would still provide adequate profitability at prices below $100 per ton. This price environment creates new business opportunities for methanol to compete with other basic fuel and feedstock options. With combustion, a higher heating value of 9,776 Btu/lb, a $100 per ton methanol fuel has an inherent energy cost of $4.6 per million Btu. This cost is comparable to imported LNG at the receiving/regasification terminal. Since the transportation/distribution cost for methanol as a nonviscous liquid is relatively low, methanol fuel cost at the burner tip can be significantly cheaper than natural gas derived from LNG at the burner tip. Not only can methanol be considered under some economic scenarios as a primary fuel for combustion, its very low sulfur content (even when compared to ultralow sulfur diesel) provides an opportunity for methanol to be used as a backup fuel for utility and commercial power plants.

Research is also underway to convert synthesis gases to methanol in a liquid phase rather than using dry, fixed bed reactors. These technologies aim to avoid the

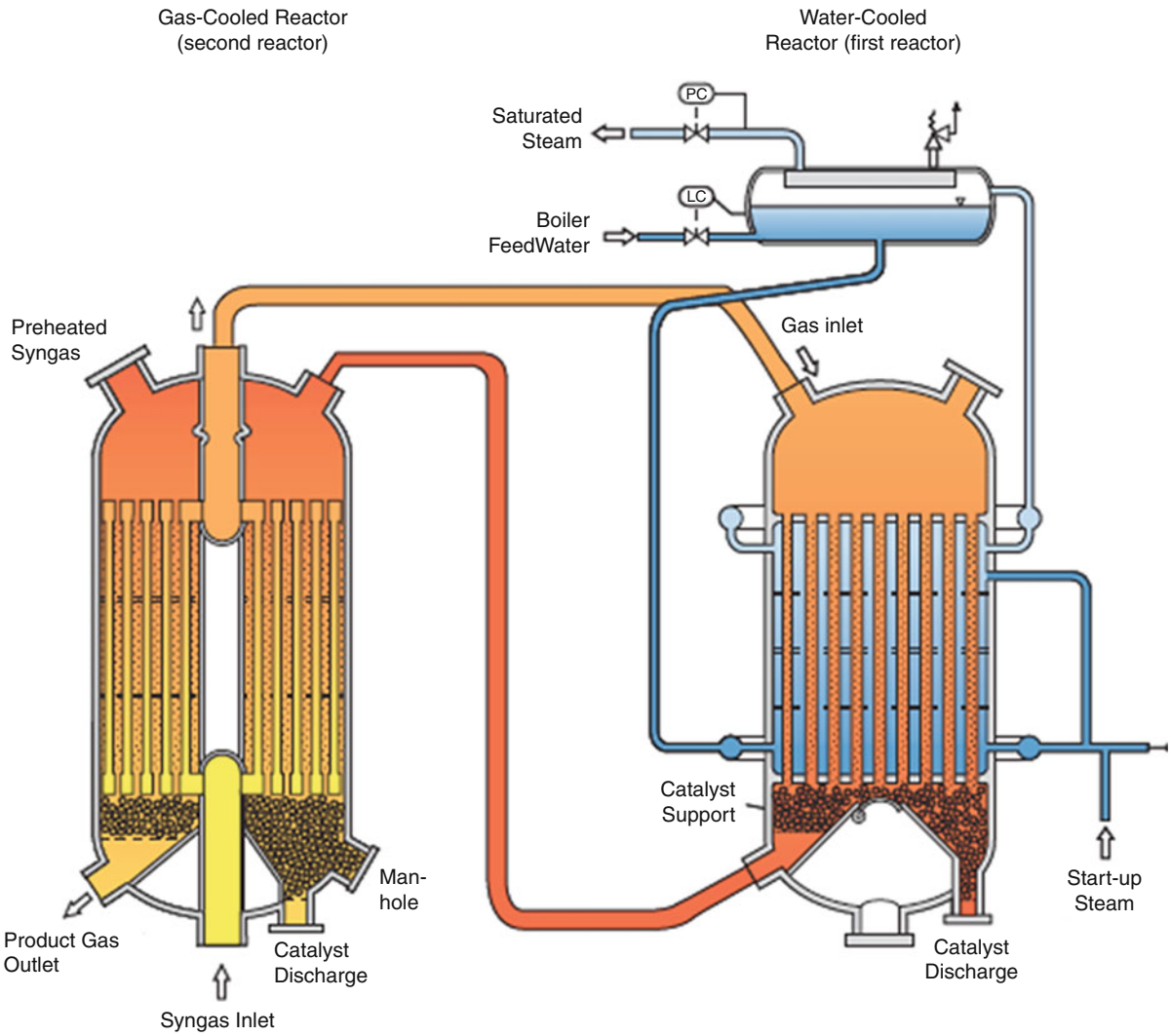

Gas to Liquid Technologies. Figure 4
The Lurgi MegaMethanol® process [41]

problem of low conversion rates and the need for recycling of gases.

Dimethylether

High oil prices and short supplies of LNG and LPG in Asia have led to the construction of many new DME plants, particularly in China. DME is currently industrially important as the starting material in production of the methylating agent dimethyl sulfate. DME has the potential to be used as a diesel or cooking fuel, a refrigerant, or a chemical feedstock. DME is also used as an aerosol propellant.

Reaction Pathway

DME traditionally is formed in a two-step process where methanol is first synthesized and is then dehydrated, over an acid catalyst such as γ-alumina, at methanol synthesis conditions. The dehydration reaction is shown in Eq. 22:

$$2CH_3OH \leftrightarrows CH_3OCH_3 + H_2O \qquad \Delta H = -24.5\ \mathrm{kJ/mol\ DME} \tag{22}$$

Alternatively, DME can be synthesized directly from syngas – without the separate process step

Gas to Liquid Technologies. Table 6 Comparative conversions for DME, methanol, and methanol/DME

Conversion	DME	Methanol	Methanol + DME
Per pass (%)	50	14	18
Total (%)	95	77	85

involving methanol production. Extensive studies have been performed to deduce the stoichiometry of direct DME synthesis from syngas, and the topic is still under debate [42]. Work by Air Products and JFE indicate that the stoichiometry is 1:1 in H_2/CO [43, 44]. The net reaction is shown in Eq. 23:

$$3H_2 + 3CO \leftrightarrows CH_3OCH_3 + CO_2 \qquad \Delta H = -246\ \mathrm{kJ/mol\ DME} \tag{23}$$

Net reaction 23 is a combination of Eqs. 20–22.

Because water produced in the dehydration step is consumed in the WGSR, the conversion of syngas can be higher in DME synthesis than in methanol synthesis. Table 6 shows the conversions obtained for direct processes producing DME, methanol, or a mixture of DME and methanol. The observed optimum ratio for DME synthesis is lower than that for methanol synthesis and ideally should be targeted at about 1.

Interestingly, the use of the methanol synthesis reaction 21 instead of 23 would give a net reaction for direct DME synthesis having H_2/CO stoichiometry of 2:1, which does not agree with experimental observation. Thus the direct synthesis of DME apparently proceeds through a different methanol-producing step than occurs in the production of methanol itself.

Commercial Activities in DME Synthesis

Gas phase reaction in a fixed bed was generally used in the past for DME synthesis from methanol. Development of the direct synthesis of DME in the gas phase with improved fixed bed reactors is also of interest [45]. Other improvements to direct DME production include the use of a slurry reactor for liquid phase, low-pressure DME synthesis.

Commercial production of DME originated as the formation of by-products during high-pressure methanol production. Direct, or single-step, synthesis of DME from synthesis gas was developed in the 1980s, prompted by the high prices and uncertain supply of oil prevailing at the time. The objective of direct synthesis was to produce DME as an intermediate step en route to synthetic gasoline. Interest in non-oil-based fuels waned quickly as the oil supply position eased, until the early 1990s when interest was rekindled – this time on a much wider scale – by the increasing demand in Asia for LPG or the LPG-substitute, DME, and by the growing concern to produce cleaner fuels. The companies currently most actively engaged in the development of an economic DME process at large-scale are JFE (Japan), Haldor Topsøe (Denmark), and Air Products & Chemicals (USA).

Gas Phase DME Production Direct synthesis of DME in the gas phase with fixed bed reactors has been developed most extensively by Haldor Topsøe [45]. For large-scale processes, the reaction may be conducted in a series of three to four reactors with interstage cooling. Each reactor is operated adiabatically. Alternatively, the adiabatic operation may be carried out at low per pass conversion of CO, to keep the reaction exothermal within limits without interstage cooling (although such an option may not be economically attractive) [46].

Haldor Topsøe's process uses natural gas reforming for production of syngas with the ratio $(n_{H_2} - n_{CO_2})/(n_{CO} + n_{CO_2})$ between 2.04 and 2.1, where n is the number of moles. The greatest CO per pass conversion (65%) and the highest selectivity of DME relative to that of methanol (82/18) were observed using CO-rich syngas. With no CO_2, the observed DME selectivity and productivity were substantially higher. Thus in contrast to the synthesis of methanol, described above, the presence of CO_2 in the feed syngas was found to have a major negative impact on the DME formation.

The current DME synthesis catalyst is formulated to catalyze the water gas shift reaction at a minimum level with minimal CO_2 production. The quality of the residual syngas from the reactors is therefore good enough for recycle without the need for a large, dedicated CO_2 removal plant. Ongoing improvements to the gas phase process include the development of bifunctional catalysts to produce DME in a single step in a single reactor [47].

Slurry Phase DME Production Air Products did a substantial body of research toward developing a slurry phase process for the direct synthesis of DME [48–52]. The presence of CO_2 in the feed gas was observed to have a major impact on DME formation, as expected based on the stoichiometry of Eq. 23. In the slurry reactor, syngas is bubbled upward through the solvent, which contains suspended catalyst particles. The catalyst is comprised of alumina particles of about 200 μm average size, with a layer of Zn/Cu oxide methanol synthesis catalyst formed around each alumina particle. The solvent is a light liquid oil (such as Witco-40) or a hydrocarbon such as *n*-hexadecane and acts as both a mass transfer medium for the reaction and a heat transfer medium through which heat from the exothermic reaction is removed by convection [53].

Control of the reaction temperature is even more important in DME synthesis than in methanol synthesis, because the higher equilibrium conversion to DME emits more heat and a hot spot in the reactor could damage the catalyst. In a slurry phase reactor, the heat of reaction is quickly absorbed by the high boiling liquid oil, which has a high heat capacity. Heat is removed from the reactor through immersed internal cooling coils, in which water is vaporized to steam. The temperature within the reactor vessel is well controlled in order to achieve higher conversion with longer catalyst life.

The direct synthesis technology under development by NKK Corporation since 1989 also uses a slurry phase reactor. In this process, natural gas is reformed in an autothermal reformer with oxygen and steam. Carbon dioxide is recycled back from the purification section of the plant to give synthesis gas with a H_2/CO ratio of 1.0. The standard DME synthesis reaction conditions are 260°C and 50 atm pressure. The condensed reactor product is purified in two distillation columns, with CO_2 vapor from the first column returned to the reactor, and the bottoms from the first column distilled in the second column. DME is condensed from the second column overheads, and the by-product methanol in the column bottoms returned to the DME synthesis reactor after water removal. The once through CO conversion is 50%. DME selectivity is more than 90%, and the molar ratio of DME to DME + methanol is 0.91. The coproduction of water is very small, with the molar ratio of (DME/DME + methanol + water) = 0.013. With recycle the total CO conversion reaches 95%. A pilot demonstration plant project of 100 t/day DME capacity was begun by NKK at Hokkaido, Japan, in 2002 [54].

Mitsubishi Gas Chemical (MGC) touts higher single pass conversion for its Superconverter [50] slurry DME reactor system, claiming 70–80% conversion efficiency compared with 50–60% for other processes. MGC claims that DME produced at a remote site with low-cost natural gas feedstock in a 5,000–7,000 t/day plant should beat the delivered cost of both LNG and LPG in Japan. Japan DME (MGC, ITOCHU, and Mitsubishi Heavy Industries) have planned a 1 t/year capacity plant in Papua New Guinea.

One key challenge in the economic design of 7,000 t/day plant is the reactor design configuration and catalyst to enable dehydration using a single reactor vessel, as opposed to multiple serial reactor stages or parallel reactor trains. Another important consideration is the ability to achieve sufficiently high methanol conversions to permit reaction product recovery in a single distillation train.

Another process for scales such as 7,000 t/day is referred to as the Jumbo process and is under development by Toyo Engineering using a dehydration reactor based on radial flow design. The process involves integrated coproduction of methanol from natural gas as an intermediate to DME. DME is produced via the vapor phase dehydration of methanol over a fixed bed of an acid catalyst, typically γ-alumina. Reaction temperatures are typically in the range of 250–400°C, with pressures as high as 250 psig. Gas space velocities have been reported to be in the range of 500–10,000 h^{-1} [56].

Toyo's DME process offers greater flexibility in the methanol/DME product distribution. Since the methanol and DME plants operate independently, the complex could be designed to produce methanol or DME exclusively or in any combination in accordance with market demand. Toyo's design approach would also permit the option of locating their Jumbo DME plant at a different location from that of the methanol plant. The cost of shipping methanol long distances may be less than the cost of shipping an equivalent quantity of DME due to the higher cost of the pressurized refrigerated storage requirements anticipated for oceangoing DME tankers.

Methanol to Gasoline and/or Diesel

The methanol to gasoline (MTG) process developed by Mobil Oil Corporation involves the conversion of methanol to hydrocarbons over a zeolite catalyst. The methanol conversion process occurs in two steps with chemistry as shown in Eqs. 22 and 24 (thermochemistry shown for ethylene as product).

$$2CH_3OH \leftrightarrows CH_3OCH_3 + H_2O \quad \Delta H = -24.5\ \text{kJ/mol DME} \tag{22}$$

$$CH_3OCH_3 \leftrightarrows C_2 - C_5\ \text{olefins} + H_2O \quad \Delta H = -5.5\ \text{kJ/mol DME} \tag{24}$$

Crude methanol (17% water) is superheated to 300°C and partially dehydrated over an alumina catalyst at 27 atm to yield an equilibrium mixture of methanol, diethyl ether, and water (75% conversion of methanol). This effluent is then mixed with heated recycled syngas and introduced into a reactor containing ZSM-5 catalyst at 350–366°C and 19–23 atm to produce hydrocarbons (44%) and water (56%). Because the zeolite has to be regenerated frequently to burn off coke formed during the reaction, the MTG process is rendered continuous by using multiple gasoline conversion reactors operating in parallel with 2–6 week cycles. Mobil's MTG process uses different pressures for syngas production (15–20 atm), methanol synthesis (50–100 atm), and the fixed bed MTG process step (15–25 atm).

The selectivity of Mobil's MTG process to gasoline range hydrocarbons is about 85+%, with the remainder of the product being primarily LPG. Nearly 40% of the gasoline are aromatic hydrocarbons with product distribution of 4% benzene, 26% toluene, 2% ethylbenzene, 43% xylenes, 14% trimethylbenzenes, plus 12% other aromatics. The shape selectivity of the zeolite catalyst results in a relatively high concentration of durene (1,2,4,5-tetramethylbenzene), representing about 3–5% of the gasoline produced. Therefore, MTG gasoline is usually distilled and the heavy fraction is hydroprocessed to reduce the concentration of durene to below 2%. This results in a high quality gasoline with a high-octane number. However, the future of the MTG process remains uncertain because the 1990 Clean Air Act Amendment limits the amount of aromatics in reformulated gasoline.

The first commercial MTG plant came onstream in 1985 in New Zealand (Mobil's Motunui plant), producing 4,500 t/day of methanol and 14,500 bbl/day of high-octane gasoline from natural gas. Gasoline production was later ceased and presently this plant and the nearby methanol plant at Waitara produce 2.43 million tons per year of chemical grade methanol for export [57].

A 100 bbl/day fluidized bed MTG pilot plant was jointly designed and operated near Cologne, Germany, by Mobil (supplying process technology and proprietary catalyst), Union Reinische Brankohlen Kraftstoff AG (acting as the operating agent), and Uhde GmbH (providing engineering services) from 1982 to 1985. Although no commercial plants have been built based on the fluid bed technology, it is considered ready for licensing and/or commercialization [58].

Mobil also developed a methanol to gasoline and diesel process, referred to as the MOGD process. Oligomerization, disproportionation, and aromatization of olefins are the basis for the MOGD process. Selectivity to gasoline and distillate from olefins is greater than 95%. The product slate from MOGD is 3 weight paraffins, 94 wt% olefins, 1 wt% naphthenes, and 2 wt% aromatics [59]. A large-scale test run was performed at a Mobil refinery in 1981. The MOGD process is not currently in commercial practice.

Haldor Topsøe's Integrated Gasoline Synthesis (TIGAS) process was developed to minimize capital and energy costs by integrating methanol synthesis with the MTG step into a single loop (i.e., without isolation of methanol as an intermediate). Whereas Mobil's MTG process uses different pressures for syngas production, methanol synthesis, and the fixed bed MTG process step, the TIGAS process involves catalysts and conditions modified such that the system pressure levels out and separate compression steps are not required. A mixture of methanol and DME is made prior to gasoline synthesis, which results in only one recycle loop from the gasoline synthesis step back to the methanol/DME synthesis step. A 1 t/day demonstration plant was built in Houston, Texas in 1984 and operated for 3 years. The gasoline yield for the TIGAS process (defined as the amount of gasoline produced divided by the amount of natural gas used for feed and as fuel) was 56%. The TIGAS process yields a lower

quality gasoline with a lower octane number compared to MTG, because of a reduced selectivity to gasoline range aromatics.

Methanol to Chemicals

The highest volume chemical processes using methanol as feedstock are formaldehyde, methyl tertiary-butyl ether, and acetic acid. Globally, formaldehyde production is the largest consumer of methanol, followed by methyl tertiary-butyl ether (MTBE) and acetic acid.

Formaldehyde is produced commercially from methanol by three industrial processes:

1. Partial oxidation and dehydrogenation with air in the presence of silver crystals, steam, and excess methanol at a temperature of 680–720°C, otherwise known as the BASF process. The methanol conversion for this process is 97–98%.
2. The same as process 1 except in the presence of crystalline silver or silver gauze at a temperature of 600–650°C. Then, the product is distilled and the unreacted methanol is recycled. The primary methanol conversion for this process is 77–87%.
3. Oxidation with only excess air in the presence of a modified iron/molybdenum/vanadium oxide catalyst at a temperature of 250–400°C, also known as the Formox® process (Perstorp Specialty Chemicals, Sweden). The methanol conversion for this process is 98–99%.

Formaldehyde is used to make resins with phenol, urea, or melamine for the manufacture of various construction board products.

MTBE is produced by reacting isobutene with methanol in the presence of an acidic catalyst. The reaction temperatures and pressures are 30–100°C, and 7–14 atm, respectively, so that the reaction occurs in the liquid phase. Catalysts used are solid acids, including zeolites (H-ZSM-5), and microporous sulfonic acid ion exchange resins such as Amberlyst-15. A molar excess of methanol is used to increase isobutene conversion and inhibit the dimerization and oligomerization of isobutene. At optimum reaction conditions, MTBE yields approaching 90% can be achieved. Currently there are over 140 MTBE plants, with a total installed capacity of about 20 million tons per year, using processes developed by Snamprogetti, Huls (now Oxeno) ARCO, IFP, CDTECH (ABB Lummus Crest and Chemical Research Licensing), DEA (Formerly Duetsche Texaco), Shell (Netherlands), Phillips Petroleum, and Sumitomo.

Greater than 95% of the MTBE produced is used as a fuel additive in the gasoline motor pool. MTBE is also used in the petrochemical industry for the production of isobutene, and it also can be used in a number of chemical reactions including methacrolein, methacrylic acid, or isoprene production.

Acetic acid is produced by methanol carbonylation in the liquid phase using Co, Rh, or Ni catalysts promoted with iodine. The BASF process is initiated by the reaction of methanol with HI to yield methyl iodide. The active catalyst is the metal carbonyl $[Rh_2I_2(CO)_2]$ into which methyl iodide inserts during the rate-limiting step. Acetic acid is formed by the hydrolysis of the eliminated acetyl iodide species CH_3COI that also regenerates HI. The process is run with over 99% selectivity at conditions of 180°C and 30–40 atm.

The Monsanto process is similar to that of BASF but is less severe. All new installed capacity since 1973 is based on the Monsanto process. Even so, the Rh/I catalytic system is very corrosive and requires expensive steels for materials of construction. Complete recovery of the expensive Rh catalyst and recycle of HI are paramount to maintain favorable process economics. The high cost of Rh has lead to the search of other, lower cost metals that could be used as acetic acid process catalysts with similar performance.

Approximately half of the world's production of acetic acid comes from methanol carbonylation and about one third from acetaldehyde oxidation. Methanol carbonylation is the most likely technology of the future. Vinyl acetate, acetic anhydride, and terephthalic acid are all made from acetic acid. Latex emulsion resins for paints, adhesives, paper coatings, and textile finishing agents are made from vinyl acetate. Acetic anhydride is used in making cellulose acetate fibers and cellulosic plastics.

Ammonia

Ammonia is the basic building block of the nitrogen industry worldwide. Almost all ammonia is produced in the anhydrous form (free of water) by a catalytic reaction of nitrogen (from air) with hydrogen from

a hydrocarbon source (usually natural gas). Ammonia is a colorless, pungent, nonflammable gas at normal pressure and temperature and is lighter than air. For storage at atmospheric pressure at sea level, ammonia must be cooled to −33°C and stored as liquid. Lower temperatures are required at higher altitudes. In the usual atmospheric temperature range of 0–40°C, the range of vapor pressure is about 4–15 atm. Approximately 10% of the ammonia produced never reaches the market, because of its volatility and losses, during conversion to other materials and during transportation and storage. Nitrogen fertilizer consumption accounts for more than 85% of the world ammonia market.

General Process Description

The three main steps in producing ammonia are syngas production, syngas purification, and ammonia synthesis. The traditional and current commercial technology for hydrogen production in ammonia production involves steam reforming of natural gas to produce syngas (Eq. 2), and the water gas shift reaction (Eq. 19), both of which occur in the reformer. Steam reforming is by far the least expensive and most popular method of producing hydrogen for ammonia synthesis. Two-step steam reforming or partial oxidation also can be used to generate hydrogen-rich syngas for ammonia production, but these methods are most useful when the feed contains heavier hydrocarbons in addition to methane.

Raw synthesis gas must be purified before being sent to the ammonia synthesis unit. A shift conversion step is used to remove most of the carbon monoxide from the synthesis gas, because CO acts as a poison to the catalyst used in ammonia synthesis. Shift conversion by the WGSR (Eq. 19) also produces more hydrogen. The shift conversion is performed in two stages. In the first stage, called the high-temperature shift (300–450°C), the bulk of the carbon monoxide is oxidized to CO_2 over a chromium-promoted iron oxide catalyst. The second stage is a low-temperature shift (180–270°C) in which the remaining carbon monoxide is oxidized to CO_2 over a copper/zinc catalyst, leaving a few tenths of a percent in the syngas. Typical catalyst lifetimes for both high-temperature and low-temperature shift catalysts are 3–5 years.

Sulfur tolerant ("dirty shift") catalysts also have been developed. These catalysts can handle larger amounts of sulfur. The company ICI makes dirty shift conversion catalysts that consist of cobalt and molybdenum oxides. They operate over a temperature range of 230–500°C. The controlling factors are the ratio of steam to sulfur in the feed gas and the catalyst temperature.

The synthesis gas is then washed with a solvent – such as monoethanolamine or other amine, potassium carbonate, or sulfinol (sulfolane and an alkanolamine) – to remove most of the carbon dioxide. The solvents typically contain an activator to promote mass transfer. Water scrubbing at high pressures was employed in the past to remove CO_2 but is no longer used. Most newer steam reforming plants use methanation to remove residual or trace carbon monoxide and carbon dioxide, by reaction with hydrogen over a nickel catalyst to yield methane and water.

Scrubbing with a liquid nitrogen wash produces a synthesis gas with very low inert gas content. This additional nitrogen is supplied by using air, in excess of the stoichiometric nitrogen requirement, in the secondary reformer or, in the case of plants with no reforming sections such as off-gas plants, by obtaining nitrogen from an associated air separation unit. Older processes involved scrubbing the synthesis gas with copper liquors, such as cuprous ammonium formate, to remove carbon monoxide, and caustic to remove carbon dioxide. Many modern processes include molecular sieve dryers downstream of the methanation step to remove the final traces of water. The synthesis gas is then compressed and finally reaches the ammonia converter, where the contained hydrogen and nitrogen chemically combine over a catalyst into ammonia.

Reaction Pathway

The chemical reaction considered in ammonia synthesis is shown in Eq. 25.

$$N_2 + 3H_2 \leftrightarrows 2NH_3 \qquad \Delta H = -92.2\ \mathrm{kJ/mol\,NH_3} \tag{25}$$

Since the reaction is exothermic, maximum conversion at equilibrium occurs at high pressure and low

temperature. Ammonia synthesis is achieved in catalytic reactors at pressures ranging from 150 to 345 atm, at a minimum temperature of 430–489°C. A maximum temperature of ~500°C results from the balance between increasing reaction kinetics and decreasing the equilibrium ammonia concentration as the temperature increases. Thermodynamics suggest that a low process temperature is favored. However, the kinetics of the reactions dictates that high temperature is required. Nitrogen is usually fed as air, but in some plants (e.g., partial oxidation plants) the N_2 is a purified gas from an associated air separation facility. In terms of the hydrogen source, production methods, product recovery, and overall plant engineering, there are many process variants for ammonia production.

About 50% of the hydrogen in ammonia comes from steam. High temperatures and low pressures favor the highly endothermic methane reforming reaction. Higher pressures tend to lower the methane conversion. In industrial reformers, the reforming and shift reactions result in a product gas composition that closely approaches equilibrium. However, the following side reactions produce carbon in the steam reformer:

Boudouard coking

$$2\,CO \leftrightarrows C(s) + CO_2 \quad \Delta H = -83.3\ \text{kJ/mol CO} \tag{7}$$

CO reduction

$$CO + H_2 \leftrightarrows C(s) + H_2O \quad \Delta H = -125.5\ \text{kJ/mol C} \tag{26}$$

Methane cracking

$$CH_4 \leftrightarrows C(s) + 2H_2 \quad \Delta H = 80.6\ \text{kJ/mol C} \tag{27}$$

The molar steam to carbon ratio in the reformer is usually between 2 and 6, depending on the feedstock and process operating conditions. Excess steam is used to prevent coking in the reformer tubes. The shift reaction is exothermic and favors low temperatures. Since the shift reaction does not approach completion in the reformer (usually there is 10–15 vol% CO, dry basis, in the reformer effluent), further conversion of CO is performed using external shift conversion catalysts.

Reactors and Catalysis for Ammonia Synthesis

The basic design of an ammonia synthesis reactor is a pressure vessel with sections for catalyst beds and heat exchangers. Over the years, there have been many different designs proposed and constructed for commercial operation such that today, ammonia reactors are classified by flow type (radial, axial, or cross flow) and cooling method (quench or indirect) used.

Axial flow reactors are essentially top-to-bottom flow reactors. The design is comparatively simple; however, a fairly large pressure drop develops across the catalyst bed. A radial flow configuration feeds gas into an annular region between the reactor wall and the outer surface of the catalyst bed. Gas flows through the bed and exits out a central collection tube. This design minimizes pressure drop across a shallow bed with a large surface area. Radial flow reactors tend to be tall vessels with relatively small diameters. The cross-flow reactor configuration has a similar principle in that gas is introduced along one side of the reactor and is collected radially across the reactor by a collector on the other side.

Reactant gas is preheated either by circulating it through heat exchangers or by using water to produce steam. However, removing the heat generated from the exothermic synthesis reaction to maintain control of the reaction temperature is a challenge. Quench converters are designed to introduce cool reactant gas at various points along the length of the catalyst bed. Interbed heat exchangers also can be used to remove heat at specific intervals along the bed, effectively separating the bed into multiple synthesis zones, or continuously along the bed with cooling tubes. These indirectly cooled designs allow for efficient recovery of reaction heat that can be used in other parts of the process.

Early designs based on axial flow were easier to build but not as efficient as the more complex radial flow reactors that have more recently been designed. One example of a radial flow design, by Haldor Topsøe, uses two radial beds with quench gas injection between them. A similar radial flow design uses an interbed heat exchanger in the first catalyst bed. Cold ammonia synthesis gas is introduced from the bottom of the reactor through the second catalyst bed, then through the heat exchanger in the first catalyst bed. The cold gas flow

through the second bed also provides indirect heat exchange. An additional heat exchanger is located at the bottom of the reactor to cool the reactor gases.

The Kellogg four-bed axial flow reactor system is a good example of an axial flow reactor design. This quench reactor consists of four catalyst beds held on separate grids. Quench gas is introduced in the spaces between the bed, and a heat exchanger is located at the top of the vessel. Another type of Kellogg reactor is a cross-flow reactor design where gas flows through the catalyst bed perpendicular to the vessel axis. It is available in both quench and indirectly cooled versions.

The ammonia synthesis catalyst is commonly iron, such as magnetite, which may be promoted with aluminum, potassium, and/or calcium. Finely divided iron is pyrophoric, therefore Fe catalysts are reduced to metallic form in situ. Porosity is developed as the catalysts are reduced. During reduction, oxygen is removed from the magnetic crystal lattice without shrinkages. Metallic Fe is formed with essentially the same porous structure as the magnetite precursor. The production and preservation of this highly porous structure during reduction of the ammonia synthesis catalyst precursor leads to highly active catalysts. The addition of structural promoters facilitates the formation of highly porous metallic iron.

Catalyst activity is not directly associated with the Fe surface area but is related to complex interactions of the promoters. Alkali metal promoters in ammonia synthesis catalysts are necessary to attain high activity. Potassium is the most effective alkali promoter, while Li and Na are poor promoters and are not used commercially. Potassium is thought to interact with the Fe crystallites to increase the dissociative sticking probability of N_2 on the Fe sites and thereby increase catalytic activity [60].

The most effective catalysts from a process perspective are those that have the highest rate of conversion at the lowest temperatures. Other catalysts are being developed such as promoted Ru on high surface area graphite supports, and these recently commercialized catalysts offer the possibility of greatly decreasing synthesis temperatures and pressures with improved activity at high ammonia concentrations. The Kellogg Advanced Ammonia Process is based on a Ru catalyst that is claimed to be 40% more effective than Fe catalysts, because synthesis efficiency is increased by lowering the process pressure from 150 to 90 atm.

With effective gas cleanup and conditioning, commercial ammonia synthesis catalyst lifetimes of 5–8 years can be achieved in most cases and potentially up to 14 years. Ammonia formation increases as the process pressure is increased. The optimum H_2/N_2 ratio is near 2 at high-space velocities and approaches 3 at low-space velocities as equilibrium becomes more dominant. Space velocities in commercial ammonia synthesis vary from 12,000/h at 150 atm to 35,000/h at 790 atm.

Per pass conversion on the order of 10–35% is typically achieved. Ammonia is recovered from the synthesis loop by cooling to condense the synthesis gas at process pressures. The liquid ammonia is separated from the gas effluent, which is recycled back through to the reactor. Earlier plant designs used air or water cooling for ammonia recovery. Modern synthesis plants use refrigeration to condense out the ammonia. The ammonia recovery is not extremely efficient so the recycled gas typically contains 4% ammonia plus any inert gasses (Ar, He, CH_4, etc.) that may be in the process stream. Purging some of the gas in the recycle loop before it is recycled minimizes inert gas concentrations, and flashing the liquid ammonia in a pressure letdown step releases any dissolved gases.

Clearly, the ammonia synthesis process consists of many complex unit operations apart from the actual synthesis loop. The way in which these process components are combined with respect to mass and energy flow has a major influence on efficiency and reliability. Many of the differences between various commercial ammonia processes lie in the way in which the above process elements are integrated.

Commercial Activities in Ammonia Synthesis

The entire ammonia industry was originally based on using coal as a feedstock. The industry has now moved toward natural gas as the main hydrocarbon feedstock. By 1990, only 14% of the world ammonia capacity was based on coal or coke. Apart from a few plants operating in India and South Africa, today the majority of coal-based ammonia plants are found in China.

More than 20 commercial ammonia synthesis processes have been described [61].

Commercial technology vendors for ammonia include:

- Johnson Matthey
- Linde
- Kellogg Brown and Root
- Haldor Topsøe
- Ammonia Casale
- Uhde

As a result of a surge of major developments in ammonia process technology beginning in the late 1960s, large 1,000–1,500 t/day capacities became the industry standard for new plant constructions. Plants as large as 2,000 t/day are now common. The main ammonia process contractors have each now developed "mega-ammonia technology," and are offering large plant concepts from 3,000 to 6,000 t/day units. The world's largest ammonia plant, in Al Jubail, Saudi Arabia, is a collaboration between Saudi Basic Industries Corporation (SABIC) and Saudi Arabian Fertilizer Company. The plant, called SAFCO IV, came onstream in 2007 and has a capacity of 3,300 t/day. This huge plant is the first application of a new ammonia process from Uhde, referred to as the Dual Pressure Process, and utilizes Johnson Matthey's KATALCO™ catalysts [62]. A major factor resulting in much lower average production costs has been the switch from electrically driven compression to the use of steam-driven centrifugal compressors powered by waste heat. During the past 30 years, many of the smaller, older, higher-cost plants in the world have been shut down.

Developments to improve energy efficiency or overcome interruptions of natural gas supply have been examined and some are finding application. The recovery of the hydrogen and ammonia from the synthesis purge gas by a cryogenic unit or membrane is now standard and an additional 5% of ammonia can be produced from the same amount of feedstock. The use of computer controls to improve overall plant performance is increasing.

Substantial improvements have been made over the years in the energy efficiency of carbon dioxide removal systems. The first large-scale ammonia plants in the 1960s typically used monoethanolamine as a solvent, with energy input of over 50,000 kcal/kg-mol of carbon dioxide removed, whereas today's modern plants use improvements such as the dual-step methyl diethanolamine process that can reduce the energy input to about 10,000 kcal/kg-mol or lower of carbon dioxide removed. As described above, improvements to efficiency also have been introduced with new ammonia synthesis catalysts.

The current generation of large ammonia plants is much more fuel-efficient than plants constructed 20 or 30 years ago. A typical world-scale plant constructed in the 1970s consumed about 42 million Btu of natural gas per ton of ammonia produced. Retrofitting such a plant to improve fuel efficiency can reduce gas consumption to about 36 million Btu/t; however, the newest generation of ammonia plants use only about 30 million Btu/t of ammonia, are reported to be easier to operate, and have slightly lower conversion costs. Some newer plants also recover more than 1 million Btu/t by generating electricity, used elsewhere in the complex, from waste heat.

An additional minor trend has been to construct an ammonia plant at a location where a hydrogen off-gas stream is available from a nearby methanol or ethylene operation (e.g., Canadian plants at Kitimat, British Columbia, and Joffre, Alberta). Gas consumption at such production sites ranges from 25 to 27 million Btu/t of ammonia, depending on specific circumstances. Perhaps more important, the capital cost of such a plant is only about 50% of the cost of a conventional plant of similar capacity because only the synthesis portion of the plant is required.

Direct Conversion of Natural Gas to Liquids

Substantial capital cost could be avoided if methane could be directly converted to methanol, or other high-volume liquid fuels or chemicals, without the intermediate production of syngas. Several direct processes have been investigated over the years, including methane coupling to produce ethane, which can be oligomerized to give gasoline in a reactor similar to that used in the MTG process. Another consideration has been the direct production of aromatics, using an oxidative coupling membrane. Another option is the selective oxidation of natural gas to produce fuels directly. Direct methods

would need to have a distinct economic advantage over indirect methods, but to date no direct processes have progressed to a commercial stage. Product yields are generally small while operating in the single pass mode, which makes separations difficult and costly.

Oxidative Coupling to Light Hydrocarbons

In the oxidative coupling reaction, methane and oxygen react over a catalyst at elevated temperatures (700°C) and normal pressures to form ethane as a primary product and ethylene as a secondary product. British Petroleum (now BP) has described experiments at higher temperatures (1,100°C) and short residence times, at which conditions methane reacts with oxygen to produce syngas as well as C_{2+} hydrocarbons in addition to syngas. Several catalysts including zirconia gave C_{2+} selectivities of over 50%.

Work on the lower temperature methane coupling reaction has been done by Phillips Petroleum, Texas A&M University, Akzo Chemie, Amoco (now BP), the University of California at Berkeley, the University of Pittsburg, the University of Tokyo, Idmitsu Kosan, and Union Carbide among others. Unfortunately both the methane and the ethylene may react further to produce CO_2, and the single pass combined yield of ethylene and ethane is limited to about 25%. With better catalysts, such as SrO/La_2O_3 and $Mn/Na_2WO_4/SiO_2$, a C_2 selectivity of about 80% can be achieved, but at a low methane conversion of 20%. About half of the C_2 product is ethane and half ethylene. The best C_2 selectivities are almost always achieved under oxygen-limiting conditions. Because the reaction is exothermic, a zone within the catalyst bed may be 150–300°C hotter than the external temperature and heat management is a serious problem. This is complicated by the fact that metals normally used for the construction of reactors catalyze the combustion of methane.

The yield of ethylene can be improved considerably by operating in a recycle mode with continuous removal of ethylene, and by applying various techniques for separating products from reactants including cryogenic, membrane, and adsorptive separations. For economic reasons, either molecular sieve or membrane separation systems are most likely to be employed, both of which have severe mass transport limitations not suitable for scale-up. A variation of this recycle system is to use a zeolite catalytic reactor to convert ethylene to benzene and toluene. In principle, aromatic yields in excess of 70% could be achieved; however, to achieve these yields the conversion of ethane to ethylene must be highly selective.

Selective Oxidation of Natural Gas to Methanol

Selective alkane oxidation by transition metal complexes in solution has been the focus of substantial effort since the 1970s. However, the low activity of alkanes and the typically higher activity of the desired products make this process a great challenge. In 1998, Periana et al. of Catalytica Inc. reported developing an effective catalyst for selective oxidation of CH_4 to CH_3OH in high yield. The initial catalyst was dichloro-(η^2-(2,2′-bipyrimidyl))platinum(II) complex, (bpym) $PtCl_2$. In well-dried sulfuric acid (102%), CH_4 at 3,400 kPa and 220°C was converted to a mixture of CH_3OSO_3H (methyl bisulfate, which presumably would be subsequently hydrolyzed to methanol) and CH_3OH at 72% conversion with selectivity of 81% [63]. Although catalytic in Pt complex, the reaction was very slow and required over half as many moles of catalyst as moles of methane converted. Another catalyst, $(NH_3)_2PtCl_2$, system was more active but less stable. A complete cycle would require the regeneration of concentrated sulfuric acid. The Catalytica process is promising, because it potentially has high yield at relatively low temperatures. On the other hand, it suffers from drawbacks including (1) the catalytic rate is too low; (2) the separation cost is too high; (3) the solvent is too corrosive; (4) reoxidation of SO_2 with regeneration of concentrated sulfuric acid is too expensive; and (5) the catalyst is severely inhibited by water.

Cold flame oxidation is another approach to direct conversion of methane to methanol. A pressurized mixture of methane and oxygen is reacted at moderate temperatures of 350–500°C. The reaction mixture is very fuel rich, with methane to oxygen ratios of about 20:1. The main chemical reaction is the oxidation of methane to methanol. However, further oxidation of methanol to formaldehyde often takes place simultaneously. The University of Manitoba reported 90% selectivity for methanol at a single pass conversion of 7.5% in an isothermal

process. Although this is among the best results reported to date, the yield of methanol from this process is too low to be of commercial interest.

Future Directions

The immediate future of F-T and DME gas to liquids would seem to be in their implementation. Acquisitions and ventures are creating "one stop shops" for commercialization. Johnson Matthey has acquired Davy Process technology and ICI, making the parent company a leader in reforming and methanol GTL technologies. The companies Enichem and IFP/Axens have strong capabilities particularly applicable to F-T GTL. Enichem has skills in catalysis, engineering, and the oil and gas business. IFP/Axens has catalysis expertise, plus basic engineering, process development, licensing, and catalyst manufacturing [64]. The future of methanol may be the status quo, because the technology is already mature. Alternatively, GTL methanol plants may expand in number (and possibly size) given the anticipated increased availability of unconventional gas combined with high oil process.

Bibliography

1. Crane H, Kinderman E, Malhotra R (2010) A cubic mile of oil. Oxford University Press, Oxford
2. United States Environmental Protection Agency (1998) Compilation of emission factors AP-42, v1, 5th edn, Supplement D
3. United States Environmental Protection Agency (2010) Compilation of emission factors AP-42, v1, 5th edn, Supplement E, corrected. Calculation for low-sulfur No. 6 fuel oil
4. United States Environmental Protection Agency (1998) Compilation of emission factors AP-42, v1, 5th ed, Supplement E. Calculation for medium volatile bituminous coal
5. Rajnauth J, Ayeni K, Barrufet M (2008) Gas transportation: present and future. In: CIPC/SPE Gas Technology Symposium 2008 Joint Conference, Calgary, Alberta, 16–19 June 2008
6. Bellussi G, Zennaro R (2007) New developments: energy, transport, sustainability. In: Encyclopaedia of Hydrocarbons, vol III, Chap. 2.6, pp. 161–182, EniChem
7. Smith R, Asaro M (2005) Fuels of the future: technology intelligence for gas to liquids strategies. SRI Consulting, Menlo Park
8. Yost C, DiNapoli R (2003) Benchmarking study compares LNG plant costs. Oil Gas J 101(15):56–59
9. Nielsen R (2001) Fundamentals of mixed refrigerant compared to conventional refrigeration are discussed in "Ethylene Plant Enhancement." PEP Report 29 G, SRI Consulting, Menlo Park
10. Low WR, Andress D, Houser C (1997) Method of load distribution in a cascaded refrigeration process. US 5611216 to Phillips Petroleum Company, 18 Mar 1997
11. Houser C, Yao J, Andress D, Low WR (1997) Efficiency improvement of open-cycle cascaded refrigeration process. US 5669234 to Phillips Petroleum Company, 23 Sept 1997
12. Delong BW (1987) Method for cooling normally gaseous material. US 4680041 to Phillips Petroleum Company, 14 July 1987
13. Netzer D, Nielsen R (2003) Baseload liquefied natural gas by cascade refrigeration. PEP Review 2003–15, SRI Consulting, Menlo Park
14. Smith R, Asaro M (2005) Fuels of the future: technology intelligence for gas to liquids strategies. SRI Consulting, Menlo Park
15. Huffman GP, Feeley III TJ (2000) Fuel science in the Year 2000: where do we stand, where do we go from here? I: Power generation and related environmental concerns – DOE's fine particulate and air toxics research program: responding to the environmental challenges to coal-based power production in the 21st century. Preprints of the Division of Fuel Chemistry of the American Chemical Society, 45(1):108–112, 2000 Spring conference of the American Chemical Society, San Francisco
16. Topsoe_synthesis_g#6D6FFA1.ashx.pdf. Accessed 2 Apr 2011, reprinted from Hydrocarbon Engineering, 2006
17. Christensen TS, Østberg M, Bak Hansen J-H (2001) Process demonstration of autothermal reforming at low steam-to-carbon ratios for production of synthesis gas. In: AIChE Annual Meeting, Reno, 4–9 Nov 2001
18. Wesenberg MH (2006) Gas heated steam reformer modelling. PhD thesis, The Norwegian University of Science and Technology
19. Aasberg-Petersen K, Christensen TS, Charlotte Stub Nielsen CS, Dybkjær I (2003) Recent developments in autothermal reforming and pre-reforming for synthesis gas production in GTL applications. Fuel Process Technol 83(1–3):253–261
20. Loock S, Ernst WS, Thomsen SG, Jensen MF (2005) Improving carbon efficiency in an auto-thermal methane reforming plant with gas heated heat exchange reforming technology. Paper No. O96-001, 7th World Congress of Chemical Engineering, Glasgow
21. Tsuru T, Yamaguchi K, Yoshioka T, Asaeda M (2004) Methane steam reforming by microporous catalytic membrane reactors. AIChE J 50(11):2794–2805
22. Carolan MF, Chen CM, Rynders SW (2003) Development of the ceramic membrane ITM syngas/ITM hydrogen process. Fuel Chem Div Preprints 48(1):344
23. Robinson ET (S), Sirman J, Apte P, Gui X, Bulicz TR, Corgard D, Hemmings J (2005) Development of OTM syngas process and testing of syngas derived ultra-clean fuels in diesel engines and fuel cells. DE-FC26-01NT41096, Final Report
24. Caro J, Wang H, Noack M, Koelsch P, Kapteijn F, Kannelopolous N, Nolan J (2007) Manufacture of composite membranes and their use for selective partial oxidation reactions of hydrocarbons. EP 1847311 to Universität Hannover, Germany
25. Dupont V, Ross AB, Knight E, Hanky I, Twigg MV (2008) Production of hydrogen by unmixed steam reforming of methane. Chem Eng Sci 63(11):2966–2979
26. http://www.statoil.com/en/OurOperations/TerminalsRefining/Tjeldbergodden/Pages/default.aspx. Accessed 11 Jan 2011

27. Davis BH (2001) Fischer–Tropsch synthesis: current mechanism and futuristic needs. Fuel Process Technol 71:157–166
28. Brady RC III, Pettit R (1981) The chain propagation step. J Amer Chem Soc 1981:287–1289
29. Davis BH (2001) Fischer–Tropsch synthesis: current mechanism and futuristic needs. Fuel Process Technol 71:157–166
30. Oukaci R, Singleton AH, Goodwin JG Jr (1999) Comparison of patented Co F–T catalysts using fixed-bed and slurry bubble column reactors. Appl Catal A General 186:129–144
31. Manzer L, Schwarz, S (2002) Fischer–Tropsch processes using catalysts on mesoporous supports. US 2002052289 to Conoco, 2 May 2002
32. http://www.zawya.com/projects/project.cfm/pid210307061231?cc. Accessed 11 Jan 2011
33. Spath PL, Dayton DC (2003) Preliminary screening – technical and economic assessment of synthesis gas to fuels and chemicals with emphasis on the potential for biomass-derived syngas. NREL/TP-510-34929
34. Fisher IA, Bell AT (1998) In situ infrared study of methanol synthesis from H_2/CO over Cu/SiO_2 and Cu/ZrO_2/SiO_2. J Catal 178(1):153–173
35. Chinchen GC, Denny PJ, Parker DG, Spencer MS, Whan DA (1987) Mechanism of methanol synthesis from CO_2/CO/H_2 mixtures over copper/zinc oxide/alumina catalysts: use of ^{14}C-labelled reactants. Appl Catal 30(2):333–338
36. Grabow LC, Mavrikakis M (2011) Mechanism of methanol synthesis on Cu through CO_2 and CO hydrogenation. ACS Catal 1(4):365–384
37. Tijm PJA, Waller FJ, Brown DM (2001) Methanol technology developments for the new millennium. Appl Catal A General 221:275–282
38. Liu J, Wei R, Zhang Y, Xu R, Li Z (2009) Preparation of Cu/ZnO/Al_2O_3 catalysts for methanol synthesis by improved two-step coprecipitation method. Gongye Cuihua 17(7):22–25. C.A. 2009:1625358
39. Baltes C, Vukojevic S, Schüth F (2008) Correlations between synthesis, precursor, and catalyst structure and activity of a large set of CuO/ZnO/Al_2O_3 catalysts for methanol synthesis. J Catal 258(2):334–344
40. Kaluza S, Behrens M, Schiefenhoevel N, Kniep B, Fischer R, Schloegl R, Muhler M (2011) A novel synthesis route for Cu/ZnO/Al_2O_3 catalysts used in methanol synthesis: combining continuous consecutive precipitation with continuous aging of the precipitate. ChemCatChem 3(1):189–199
41. Lurgi brochure 0312e_MegaMethanol.pdf
42. Smith R, Naqvi S, Asaro M (2008) Fuels of the future: technology intelligence for coal to liquids strategies. SRI Consulting, Menlo Park
43. Lewnard JJ, Hsuing TH, White JF, Brown DM (1990) Single-step synthesis of dimethyl ether in a slurry reactor. Chem Eng Sci 45(8):2753–2741
44. Ohno Y, Omiya M (2003) Coal conversion into dimethyl ether as an innovative clean fuel. In: 12th ICCS Coal Conversion in DME, 2–6 Nov 2003
45. Haugaard J, Voss B (2001) Process for the synthesis of a methanol/dimethyl ether mixture from synthesis gas. US 6191175 to Haldor Topsøe, 20 Feb 2001
46. Naqvi S (2002) Dimethyl ether as alternative. Fuel PEP Report 245, SRI Consulting, Menlo Park
47. Kang S-H, Bae JW, Kim H-S, Dhar GM, Jun K-W (2010) Enhanced catalytic performance for dimethyl ether synthesis from syngas with the addition of Zr or Ga on a Cu – ZnO – Al_2O_3/γ-Al_2O_3 bifunctional catalyst. Energy Fuels 24(2):804–810
48. Bhatt BL, Schaub E, Heydorn E (1993) Recent developments in slurry reactor technology at the LaPorte Alternative Fuels Development Unit. In: International Technical Conference on Coal Utilization & Fuel Systems, LaPorte, pp 197–208, 26–29 Apr 1993
49. Peng X-D, Toseland B, Underwood T (1997) A novel mechanism of catalyst deactivation in liquid phase synthesis gas-to-DME reactions. In: Bartholomew C, Fuentes GH (eds) Catalyst deactivation. Elsevier, Amsterdam
50. Peng X-D (2002) Catalyst activity maintenance for the liquid phase synthesis gas-to-dimethyl ether process. Part II: Development of aluminum phosphate as the dehydration catalyst for the single-step liquid phase syngas-to-DME process. DOE contract DE-FC22-94PC93052, Final Report
51. Peng X-D (2002) Kinetic understanding of the syngas-to-DME reaction system and its implications to process and economics. DOE Contract DE-FC22-94 PC93052, Topical Report
52. Tijm PJ (2003) Development of alternative fuels and chemicals from synthesis gas. DOE Contract number FC22-95PC93052, Final Report
53. Smith R (2009) Dimethyl ether (DME) from coal. PEP Report 245B, SRI Consulting, Menlo Park
54. Ogawa T, Inoue N, Shikada T, Ohno Y (2003) Direct dimethyl ether synthesis. J Nat Gas Chem 12:219–227
55. The Ministry of Industry, Energy and Tourism; Orkustofnun/The National Energy Authority, The Innovation Center Iceland; Mitsubishi Heavy Industries, Ltd.; Mitsubishi Corporation; Hekla hf.; NordicBlueEnergy (2010) A feasibility study report for a DME project in Iceland. IDME Project Feasibility Study – 2009. Accessed 4 Apr 2011
56. Pavone T (2003) Jumbo dimethyl ether production process via Toyo technology. PEP Review 2003–9, SRI Consulting, Menlo Park
57. http://www.methanex.com/ourcompany/locations_newzealand.html. Accessed 4 Apr 2011
58. More detailed process design and economics information can be found in Apanel G (1999) Liquid hydrocarbons from synthesis gas. PEP Report 191A, SRI Consulting, Menlo Park
59. Tabak SA, Yurchak S (1990) Conversion of methanol over ZSM-5 to fuels and chemicals. Catal Today 6(3):307–327
60. Spath P, Dayton D (2003) Biopproducts from syngas, Syngas_products.pdf. Accessed 2 Apr 2011
61. Ullmann's Encyclopedia of Industrial Chemistry (2002) "Ammonia" published online 15 Dec 2006, doi: 10.1002/14356007.a02_143.pub2. Accessed 4 Apr 2011

62. Shah J (2007) SAFCO IV: catalyst start-ups in the world's largest ammonia plant. In: 20th AFA International Annual Technical Conference, Tunisia. 5_03 John_BRIGHTLING_ Johnson Matthey Catalysts_ U.K.pdf. Accessed 4 Apr 2011
63. Xu X, Fu G, Goddard III WA, Periana RA (2004) "Selective oxidation of CH_4 to CH_3OH using the Catalytica (bpym)$PtCl_2$ catalyst: a theoretical study" in Studies in surface science and catalysis, Natural gas conversion VII. In: Proceedings of the 7th Natural Gas Conversion Symposium, Dalian, vol 147, pp 499–504
64. Zennaro R, Hugues F, Caprani E (2006) The Eni – IFP/Axens GTL technology: from R&D to a successful scale-up. In: DGMK – SCI conference on synthesis gas chemistry, Dresden

Gasification and Liquefaction Alternatives to Incineration in Japan

Kunio Yoshikawa
Frontier Research Center, Tokyo Institute of Technology, Yokohama, Japan

Article Outline

Glossary
Definition of the Subject and Its Importance
Introduction
EBARA Fluidized Bed Gasification and Ash-Melting Process
The JFE High Temperature Gasifying and Direct Melting Process
The TOSHIBA Process for Liquefaction of Plastic Wastes
Future Directions
Bibliography

Glossary

Gasification Thermal process that involves the reaction of carbonaceous feedstocks with oxygen-containing reagents, usually air, oxygen, steam, or carbon dioxide, generally at temperatures in excess of 800°C
MSW Municipal solid waste
PET Polyethylene terephthalate
PVC Polyvinylchloride
Pyrolysis Thermal process that implies the degradation of the organic materials at temperatures in the range of 400–800°C and in the absence of oxygen or other reagents
RDF Refuse derived fuel
Slag Molten ash
SR Shedder residue

Definition of the Subject and Its Importance

The major technologies used in Japan for energy recovery from municipal solid waste (MSW) are mass burning incinerators combined with landfilling of ash. However, shortage of landfill space along with new regulations for dioxin emission control and the Japanese Containers and Packaging Recycling Law has stimulated active R&D and commercialization of relatively novel thermal treatment processes based on gasification and liquefaction of MSW.

The purpose of this article is to introduce novel gasification and liquefaction processes for MSW that are already commercialized in Japan and are potential future alternatives to mass burning for effective resource recovery from MSW.

Introduction

In Japan, about 40 million tons of municipal solid wastes (MSW) are incinerated each year. Of these, about 20 million tons are used for power generation and in total about 1,000 MW of electric power is produced from MSW. Most of these waste-to-energy (WTE) plants are large-scale plants exceeding 200 t/day scale.

The major technologies used in WTE plants in Japan are stoker-type mass burning of as received MSW, where the final residues such as ash are landfilled. However, shortage of landfill space and also new regulations for detoxifying the fly ash by-product of incineration, as of 2004, has driven many municipalities to accept relatively novel processes such as direct gasification and smelting and, also, rotary kiln or fluidized bed gasification combined with melting of the ash to a vitrified slag.

On the other hand, many municipalities have started to source-separate and collect the plastic materials contained in MSW, under the Japanese Containers and Packaging Recycling Law enacted in 1995. The segregated plastic materials are recycled by three methods: material recycling, chemical recycling, and

production of solid fuel. One of the technologies in the chemical recycling technology is liquefaction of plastic wastes.

There are about 30 Japanese companies engaged in the development of gasification and ash-melting systems, which can be divided into three main types: (1) the vertical shaft types that melt the entire amount of wastes directly, (2) the fluidized bed types that gasify the wastes directly with slagging, and (3) the kiln types that gasify the wastes indirectly with slagging.

This article introduces three novel MSW thermal treatment processes developed and commercialized in Japan: (1) The EBARA Fluidized Bed Gasification and Ash-melting Process, (2) The JFE High Temperature Gasifying and Direct Melting Process, and (3) the TOSHIBA Waste Plastics Liquefaction Process. These processes have the potential to be future alternatives to the existing mass burning processes for maximizing the effective recycling and utilization of MSW.

EBARA Fluidized Bed Gasification and Ash-Melting Process

Process Description

Since the year 2000, EBARA's Fluidized Bed Gasification and Ash-melting process (TwinRec process) is in operation in large commercial installations [1]. It is based on fluidized bed gasification in combination with ash melting. The following description is focused on the core components of the TwinRec system: the fluidized bed gasifier and the cyclonic ash-melting chamber.

Any type of waste can be fed into the gasifier. Only bulky wastes need to be cut to pieces smaller than 30 cm in length. The gasifier is a proprietary internally circulating fluidized bed of compact dimensions, operated at temperatures between 500°C and 600°C. The resulting syngas (fuel gas) and fine particles are entrained into the gas flow leaving the gasifier. The low gasification temperature in the fluidized bed leads to easily controllable process conditions.

The main function of the gasifier is to separate the combustible gases and the dust from the inert and metallic particles of the waste. Metals contained in the waste, such as aluminum, copper, and iron, can be recycled as valuable products from the bottom off-stream of the gasifier as they are neither oxidized nor sintered with other ash components. Together with these metals, larger inert particles are removed from the furnace. Smaller inert particles are returned to the gasifier where they serve as bed material. The fine inerts are blown out of the gasifier and enter the next stage of the process.

Figures 1 and 2 show the operating principle of the gasifier and the ash-melting furnace and the process flowsheet, respectively. The fuel gas and carbonaceous particles that are produced in the gasifier are combusted in the cyclonic ash-melting chamber at temperatures between 1,350°C and 1,400°C by the addition of secondary air. Here, the fine particles are collected on the walls, where they are vitrified and slowly flow downward through the furnace.

The molten slag collected in the furnace is then quenched into a water bath to form a granulate with excellent leaching resistance; this vitrified material meets all regulations for recycling in construction.

The high combustion temperature ensures that the most stringent dioxin emission regulations, below 0.1 ng TEQ/Nm^3 are met by means of minimal air pollution control measures.

The gasifier and the ash-melting furnace operate at atmospheric conditions, without any auxiliary fuels, except for start-up of the process or industrial oxygen. Due to the low excess air ratio that is required for complete combustion, the steam generator, boiler and air pollution control system are very compact. The energy content of the waste is converted into electricity and/or district heat with a high net efficiency.

Recycling and Recovery

The Ebara TwinRec process can treat a wide range of materials generate product streams that match their characteristics and enable optimal resource recovery:

- Metals and alloys are not oxidized in the gasifier and can be recycled.
- Inert mineral materials are free of dust and organic matter and are also suitable for recycling.
- Mineral dust and metal oxide powder are vitrified into slag and can be used as construction materials.
- Any toxic organic substances are completely destroyed and the total organic content is transformed into energy.

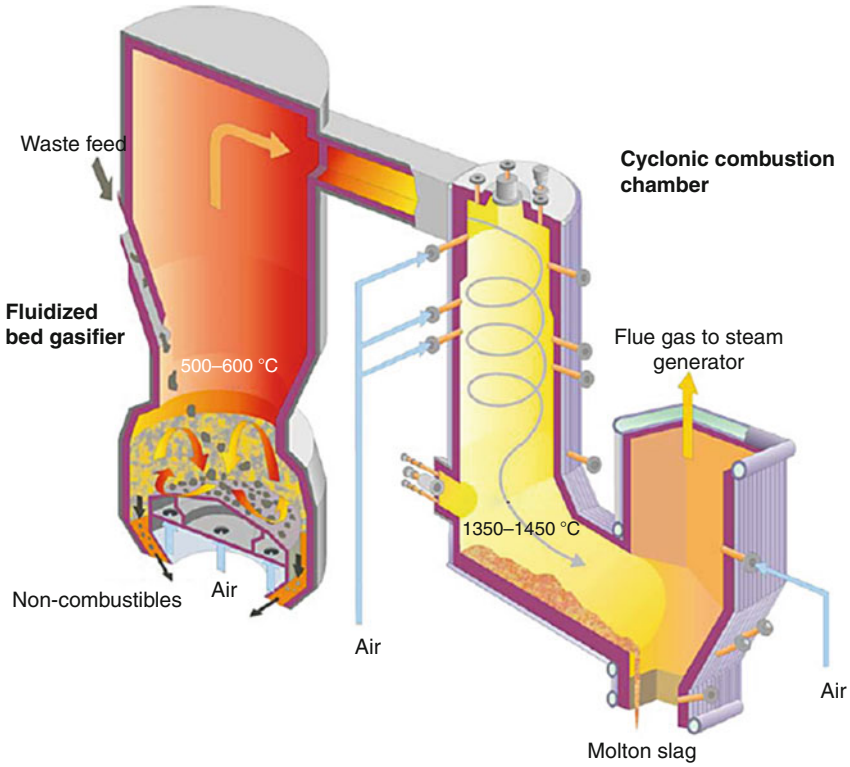

Gasification and Liquefaction Alternatives to Incineration in Japan. Figure 1
The fluidized bed gasifier and the ash melting furnace of EBARA TwinRec process

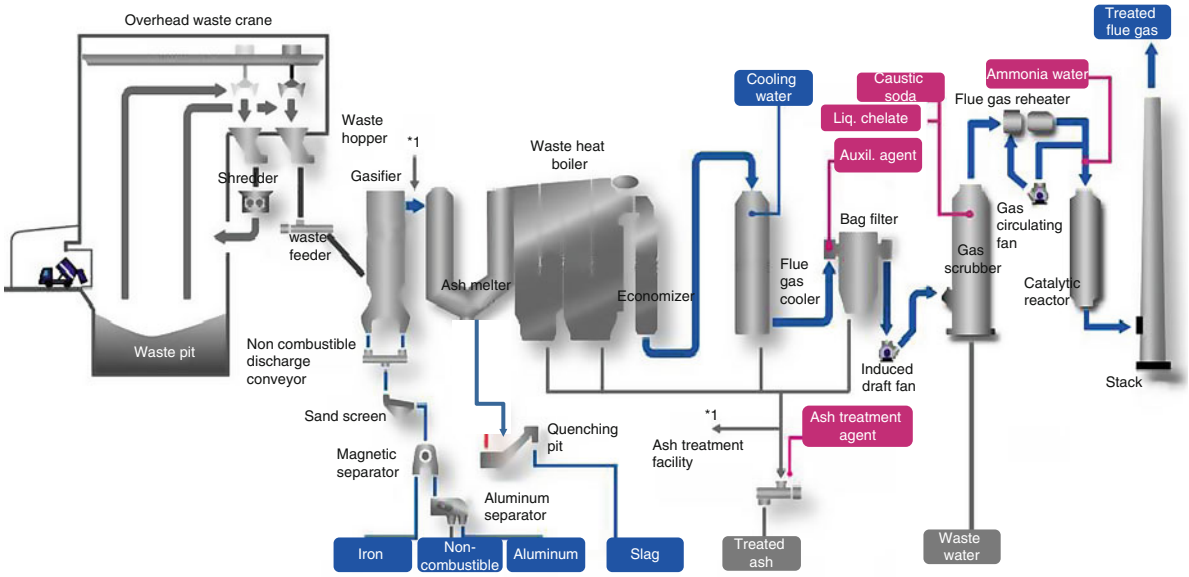

Gasification and Liquefaction Alternatives to Incineration in Japan. Figure 2
Flowsheet of the EBARA TwinRec process

- Volatile metal salts are concentrated into the secondary fly ash and can be used for zinc, lead, and copper recycling in the zinc industry.
- The amount of final residues for landfilling is reduced to very low values.

The energy efficiency of TwinRec is better than the thermal waste treatment processes that require oxygen and therefore internal consumption of electricity. Also, the ash-melting furnace is integrated into the water-steam cycle, making use of the highest temperature level for steam production.

The slag granulate is the largest fraction for recycling. For successful application in the construction industry, it must satisfy technical criteria and pass the respective environmental certification. Technically, the granulate qualifies for various applications, replacing cullet, gravel, or sand. It can be applied as loose bulk material or as filler in combination with inorganic or organic binders. In Japan, the granulate is also used as a filler in asphalt.

Commercial Operational Experience

The first TwinRec commercial plant for MSW was built for Sakata Clean Union. The Sakata plant has a capacity of 2 x 98 t of MSW per day. Since the start-up of the first plant, several other TwinRec plants have been started, resulting in 15 plants in operation to date. Twelve of these plants treat MSW and are listed in Table 1.

Figure 3 shows a photograph of the largest plant at Kawaguchi that treats 420 t of MSW per day in three process lines generating 12 MW. In addition to vitrification of its own ashes, bottom and fly ash of another grate-type incinerator is also vitrified in the ash-melting furnace. Additionally, some of the

Gasification and Liquefaction Alternatives to Incineration in Japan. Table 1 List of operational TwinRec plants

No.	Customer	Location	Capacity	Type	Inst. year	Electricity kw	
Municipal waste							
1	Joetsu Union	Niigata	15.7 t/24 h	TIFG	Mar.2000	45	Night soil sludge
2	Sakata Clean Union	Yamagata	196 t/24 h	TIFG	Mar.2002	1,990	
3	Kawaguchi City	Saitama	420 t/24 h	TIFG	Nov.2002	12,000	
4	Ube City	Yamaguchi	198 t/24 h	TIFG	Nov.2002	4,100	
5	Chuno Union	Gifu	168 t/24 h	TIFG	Mar.2003	1,980	
6	Minami-Shinshu Union	Nagano	93 t/24 h	TIFG	Mar.2003	800	
7	Nagareyama City	Chiba	207 t/24 h	TIFG	Feb.2004	3,000	
8	Chubu Clean Union	Shiga	180 t/24 h	TIFG	Mar.2007	3,000	
9	Dalsung	Korea	70 t/24 h	TIFG	Jun.2008	–	(HEEC license)
10	Eunpyeong	Korea	48 t/24 h	TIFG	Sep.2009	–	(HEEC license)
11	Hwasung	Korea	300 t/24 h	TIFG	Mar.2010	4,400	(HEEC license)
12	Kurahama Clean Union	Okinawa	309 t/24 h	TIFG	Mar.2010	6,000	
Industrial waste							
1	RER aomori renewable energy recycling Co., Ltd.	Aomori	450 t/24 h	TIFG	Nov–02	17,800	Shredder dust, sludge
2	Nikko Mikkaichi recycling Co. Ltd.	Toyama	63 t/24 h	TIFG	Jun–01	–	Shredder dust, waste plastic
3	Tokyo waterfront recycle power Co., Ltd.	Tokyo	550 t/24 h	TIFG	Aug–06	23,000	Industrial waste

Gasification and Liquefaction Alternatives to Incineration in Japan. Figure 3
Photograph of the Kawaguchi plant

secondary fly ash is recirculated and even the inert gasifier bottom ash, after metals separation, is ground and fed back to the ash-melting furnace. In this way, over 97% of the waste input is transformed into energy, metals, and recyclable glass granulate.

Figure 4 shows a photograph of the Tokyo Waterfront Recycle Power plant located in Tokyo Bay area, and treating 22.9 t/h of industrial waste in two process lines. In this plant, industrial wastes (plastic wastes and crushed/separated residue of construction wastes) are received in shredded form. Ash is melted under high temperatures into slag that is granulated and used as construction material. This plant generates 23 MW of electricity by recovering the heat generated in this plant and in another facility, next to this plant, in which medical wastes are treated.

The JFE High-Temperature Gasifying and Direct Melting Process

Process Description

JFE is a new company resulting from the merger of Nippon Kokan (NKK) and Kawasaki Steel. The JFE High-Temperature Gasifying and Direct Melting Process (JFE Process) resembles a small iron blast furnace where wastes are fed through the top of a vertical shaft (Fig. 5).

Air is introduced into the furnace through primary, secondary, and tertiary tuyeres located along the height of the shaft. The primary air, near the bottom of the shaft, is enriched to about 35% oxygen in order to generate the high temperatures required to transform the ash to molten slag and metal. In the gasifying zone, the gas produced in the lower part is partially combusted at approximately 600°C by an air sent through the secondary tuyeres while maintaining a fluidized state. By means of this heat, the wastes charged from the furnace top are preheated and thermally decomposed. Also, the fluidization ensures the downward flow of the bed within the shaft. In the gas reforming zone ("freeboard"), a tertiary air flow is injected to maintain the freeboard outlet temperature at 850°C and decompose organic gases and tar in reducing atmosphere. Ample space in the free board stabilizes the gas flow and reduces the velocity resulting in lower dust carryover in the gas flow. The slag and metal overflow from the furnace are quenched in a water

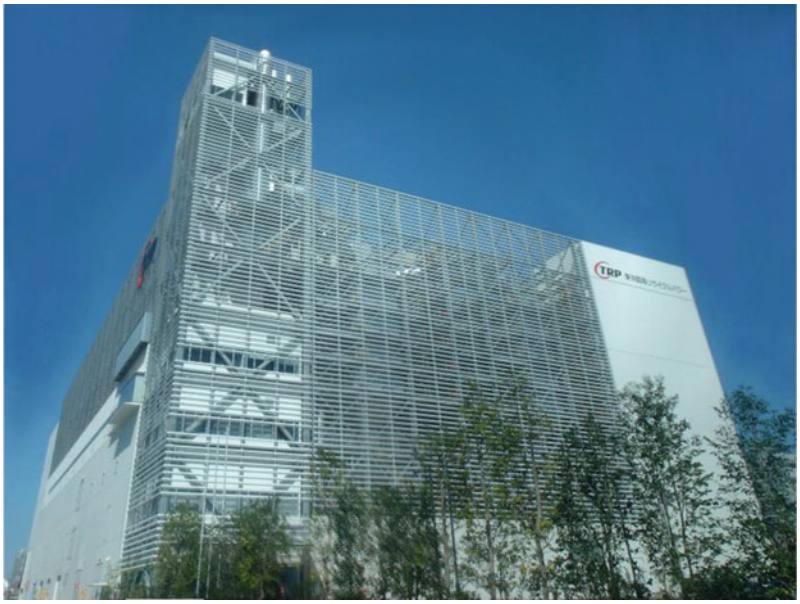

Gasification and Liquefaction Alternatives to Incineration in Japan. Figure 4
Photograph of the Tokyo waterfront recycle power plant

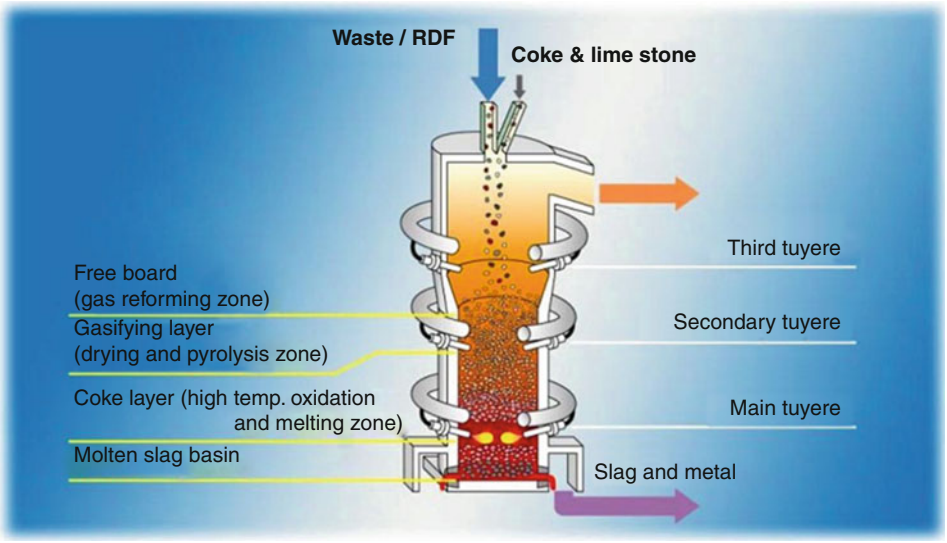

Gasification and Liquefaction Alternatives to Incineration in Japan. Figure 5
JFE High temperature gasifying and direct melting process

tank to form small spherical particles of granulated slag and metal.

The process requires the addition of coke (less than 5% of wastes), which is also added at the top of the shaft along with sufficient lime to form a fluid slag at the bottom of the furnace. The JFE Process produces slag and metal globules that are used beneficially, and fly ash which contains volatile metals and is landfilled.

Commercial Operation Experience

Up to 2010, JFE has delivered ten Direct Smelter plants in Japan, as shown in Table 2 [2]. All of them process as-received MSW except for the Fukuyama plant where RDF is combusted. The most recent plant serves the Chikushino/Ogori/Kiyama association in Fukuoka Prefecture (Kyushu) introduced. This plant is called "Clean-Hill Homan" and will be described in the following sections.

An Example of the Performance of the JFE Direct Melting Process

Figure 6 shows the process flowsheet and Fig. 7 is a photograph of the most recent JFE Direct Smelting plant at Fukuoka.

Table 3 shows the principal components of the Fukuoka plant.

Table 4 shows the mass balance of this plant in 2008. The total weight of MSW treated was 49,348 t and the slag, metal, and fly ash were 11.1%, 0.7%, and 2.3% of the solids feed, respectively. The use of the cyclone shown in Fig. 6 reduced the amount of fly ash significantly. All the slag recovered was utilized as a secondary concrete material or as a sub-base in road construction. The metal and fly ash recovered were also recycled.

Table 5 shows the electric power balance including the power usage in the recycling center of this plant. The 49,000 t of MSW generated 22,000 MWh of electricity of which 9.100 MWh were sold to the grid.

Table 6 shows the exhaust gas emission data along with the national standards. All the emission data were well below the regulation values.

Table 7 compares the results of leachability and concentration tests for various metallic contaminants with the standard values of Japan. It can be seen that in all cases the test data were substantially below the standard values.

Slag Utilization

Japanese government has a policy of encouraging the vitrification of ash ((bottom ash to slag) as part of the hierarchy of waste management and for extending landfill life. Therefore, the production of slag has been increased remarkably during the last 10 years. Slag is standardized by JIS (Japan Industrial Standard) for usage as asphalt and concrete aggregate. As a result, slag utilization is progressing and a considerable

Gasification and Liquefaction Alternatives to Incineration in Japan. Table 2 List of operational JFE process plants

	Municipality/owner	Capacity × Line	Input waste	Completion
1	Kagamihara City, GIFU	192 t/day (64 t/day × 3)	MSW (incl. bulky wastes)	2003.03
2	Amagi/Asakura/Mitsui Association, FUKUOKA	120 t/day (60 t/day × 2)	MSW (incl. bulky wastes)	2003.03
3	Hidaka-chubu Association, HOKKAIDO	38 t/day (19 t/day × 2)	MSW (incl. bulky wastes)	2003.02
4	Morioka/Shiwa Area Association, IWATE	160 t/day (80 t/day × 2)	MSW (incl. bulky wastes)	2003.03
5	Saiki Area Association, OITA	110 t/day (55 t/day × 2)	MSW (incl. bulky wastes)	2003.03
6	Fukuyama Recycle Power Corp., HIROSHIMA	314 t/day (314 t/day × 1)	RDF	2004.02
7	Ibaraki Environment Protection Foundation, IBARAKI	145 t/day (72.5 t/day × 2)	MSW and industrial waste (incl. bottom ash)	2006.03
8	Aki Area Association, KOCHI	80 t/day (40 t/day × 2)	MSW (incl. bulky wastes, landfill-wastes)	2006.03
9	Hamada Area Association, SHIMANE	98 t/day (49 t/day × 2)	MSW (incl. bulky wastes)	2006.11
10	Chikushino/Ogori/Motoyama Association, FUKUOKA	250 t/day (125 t/day × 2)	MSW (incl. bulky wastes, disaster wastes)	2008.03

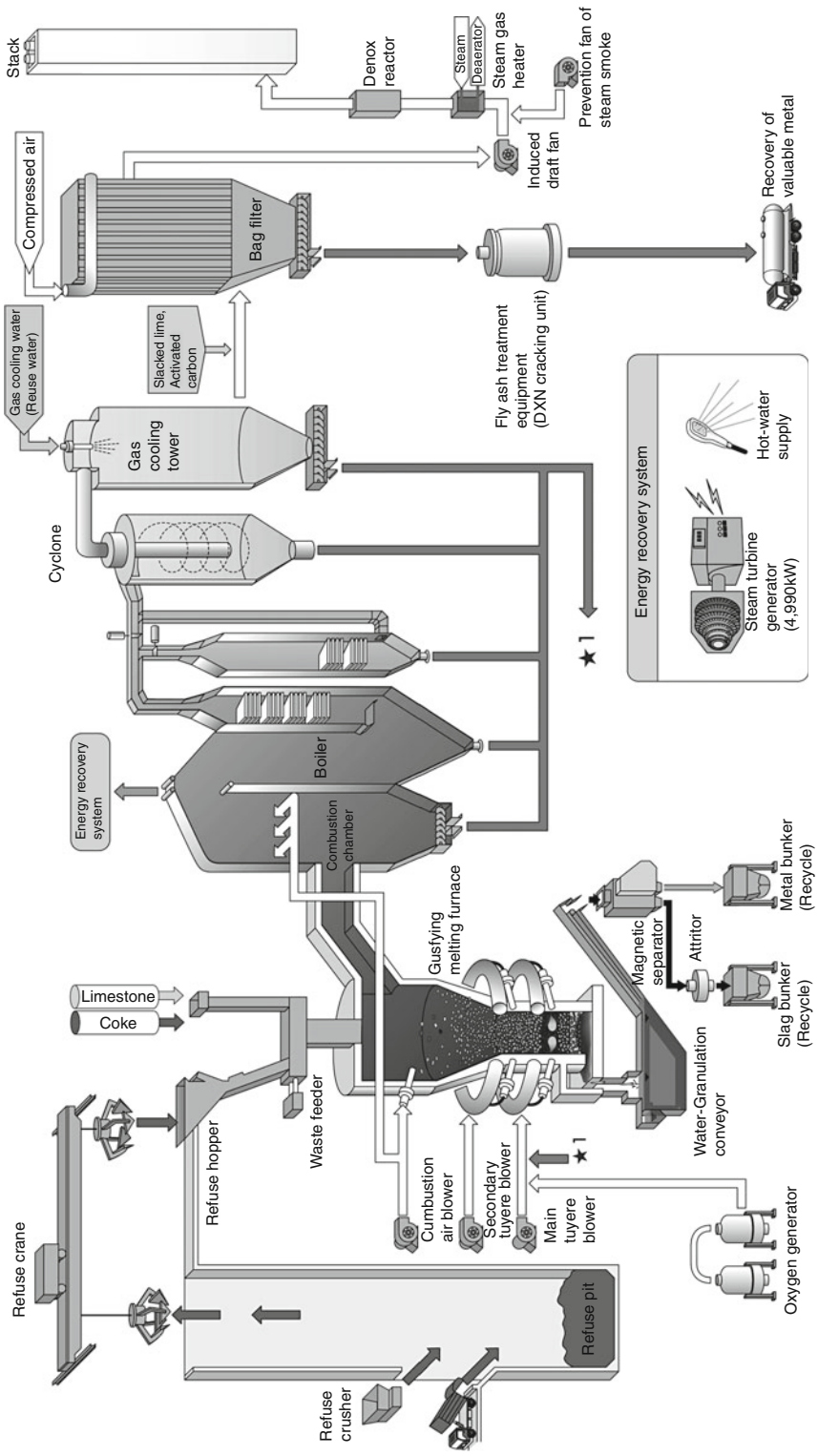

Gasification and Liquefaction Alternatives to Incineration in Japan. Figure 6
Process flowchart of the Clean-Hill Homan plant

Gasification and Liquefaction Alternatives to Incineration in Japan. Figure 7 Photograph of the Clean-Hill Homan plant

Gasification and Liquefaction Alternatives to Incineration in Japan. Table 3 Outline of the clean-hill homan plant

Capacity	250 t/day (125 t/day × 2 Furnaces)
Furnace type	Shaft melting process (high temperature gasifying and direct melting furnace)
Energy recovery system	Boiler 22.0 t/h, 400°C × 3.92 MPa, steam turbine generator (4 990 kW), hot-water supply system
Exhaust gas treatment system	Cyclone, bag filter, Denox reactor
Slag treatment system	Water-granulation conveyor, magnetic separator, attritor
Fly ash treatment system	Dioxins cracking unit

fraction of slag has acquired an economic value. Figure 8 shows the increase in number of ash-melting furnace plants with time. Figure 9 also shows that both the tonnage of slag produced and the slag used beneficially have increased with time.

The various uses to which the slag is put are shown graphically in Fig. 10.

The TOSHIBA Process for Liquefaction of Plastic Wastes

Social Background

The Plastic Waste Management Institute of Japan reported [3, 4] that the domestic plastic waste produced in 2006 had reached a total of 10 million tons, made up of about 5 million tons of household waste and another 5 million tons of industrial waste. Of this waste, 72% (7.21 million tons) was reutilized as materials, fuels, electricity, or heat, among others. However, 28% (2.84 million tons) was incinerated without energy recovery or landfilled. According to the Japan Containers and Packaging Recycling Association [5], the quantity of plastic containers and wrapping, within household plastic wastes was 550,000 t. Of this amount, 23% (130,000 t) was used in materials recycling operations and 46% (250,000 t) in chemical recycling operations, under the Container and Packaging Recycling Law; the remaining 31% was incinerated or landfilled. The breakdown of chemical recycling activities (250,000 t) in 2006 were coke ovens (61%), gasification (22%), blast furnaces (15%), and liquefaction (2%). The waste plastics liquefaction operations of the Sapporo Plastics Recycling Co., Ltd. (SPR) are classified as a chemical recycling technique in Japan. Two plastic

Gasification and Liquefaction Alternatives to Incineration in Japan. Table 4 Mass balance of MSW disposal (total MSW disposal was 49,348 t)

Recovered material	Amount of emergence (t)	Ratio (wt%)
Slag	5,502	11.1
Metal	352	0.7
Fly ash	1,116	2.3

Gasification and Liquefaction Alternatives to Incineration in Japan. Table 5 Electric power balance (Including recycling center)

Item	Electric power (MWh)
Generated	22,349
Purchased	989
Sold	9,070
Consumed	14,268

Gasification and Liquefaction Alternatives to Incineration in Japan. Table 6 Exhaust gas emission data

Item	Regulation value	Analysis value
Dust (g/m^{3}N)	<0.02	<0.005
SOx (ppm)	<50	0.3–6.0
NOx (ppm)	<50	6.0–32.0
HCl (ppm)	<50	<8.6
CO (ppm)	<30	2–7
Dioxins (ng-TEQ/m^{3}N)	<0.05	0.00000009–0.0048

liquefaction facilities have been operating commercially in Japan: the Niigata Plastics Liquefaction Centre (6,000 t/year) and the Sapporo Waste Plastics Liquefaction Plant (14,800 t/year). The waste plastics liquefaction technique is different to other recycling techniques, and, after overcoming initial problems,

Gasification and Liquefaction Alternatives to Incineration in Japan. Table 7 Result of slag measurement (example)

	Elution (standard value, mg/*l*)	Content (standard value, mg/kg)
Cd	<0.005 (<0.01)	<10 (<150)
Pb	<0.005 (<0.01)	<10 (<150)
Cr^{6+}	<0.04 (<0.05)	<10 (<250)
As	<0.005 (<0.01)	<10 (<150)
T-Hg	<0.0005 (<0.005)	<0.1 (<15)
Se	<0.005 (<0.01)	<10 (<150)
F	<0.08 (<0.8)	<150 (<4,000)
B	<0.1 (<1.0)	<150 (<4,000)

SPR process has maintained high levels of safety, stability, and productivity.

Process Description

In 2000, SPR started operating a liquefaction process that includes the unique characteristic of dechlorination of plastic wastes that contain polyvinylchloride chloride (PVC). The flowsheet of the SPR plastic waste liquefaction process is shown in Fig. 11. In the pretreatment stage, bales of compacted waste plastics are shredded and then foreign materials, such as pieces of metal and water are removed, and the remaining plastics are pelletized. The pellets are then fed into the dechlorination process where they are heated electrically to 300–330°C, melted, and the hydrochloric gas resulting from the thermal decomposition of PVC is incinerated at 1,200°C in dechlorinating furnace; scrubbing of this gas yields a solution containing less than 20% HCl which is sold. The molten polymer that is obtained in the dechlorination process is fed into the pyrolysis reactor where it is heated at 400–450°C for about 10 h and separates into a gaseous product that is conveyed to the distillation process and a residue that is fed to the solid fuel production process.

The gaseous product of the pyrolysis reactor is liquefied by spray quenching at 120°C, and the resulting pyrolysis oil is fed into the distillation tower where it is separated into three fractions: light oil at 120°C, "medium" oil at 200°C, and heavy oil at 280°C.

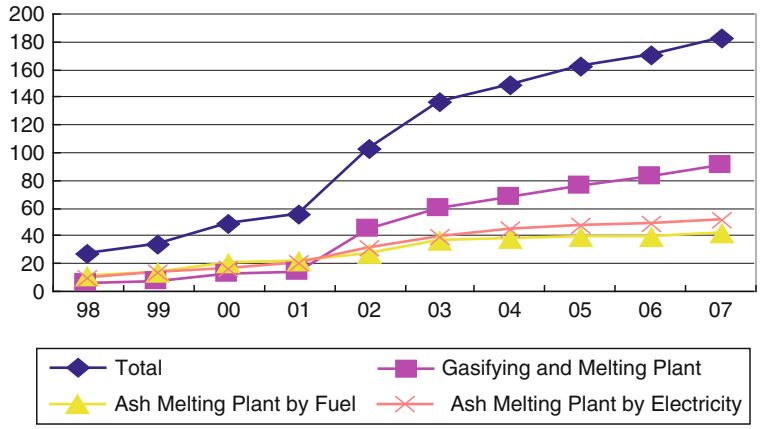

Gasification and Liquefaction Alternatives to Incineration in Japan. Figure 8
Increase in number of ash melting furnace plants

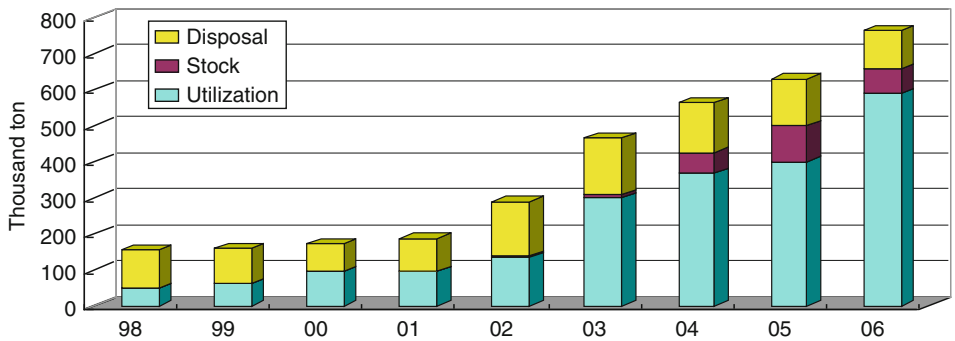

Gasification and Liquefaction Alternatives to Incineration in Japan. Figure 9
Increase of slag production and beneficial use

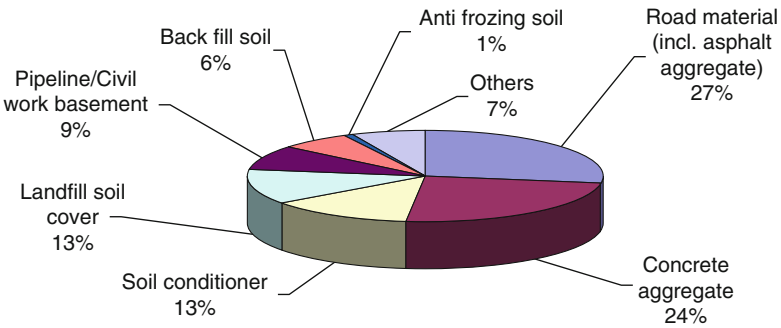

Gasification and Liquefaction Alternatives to Incineration in Japan. Figure 10
Beneficial uses of slag

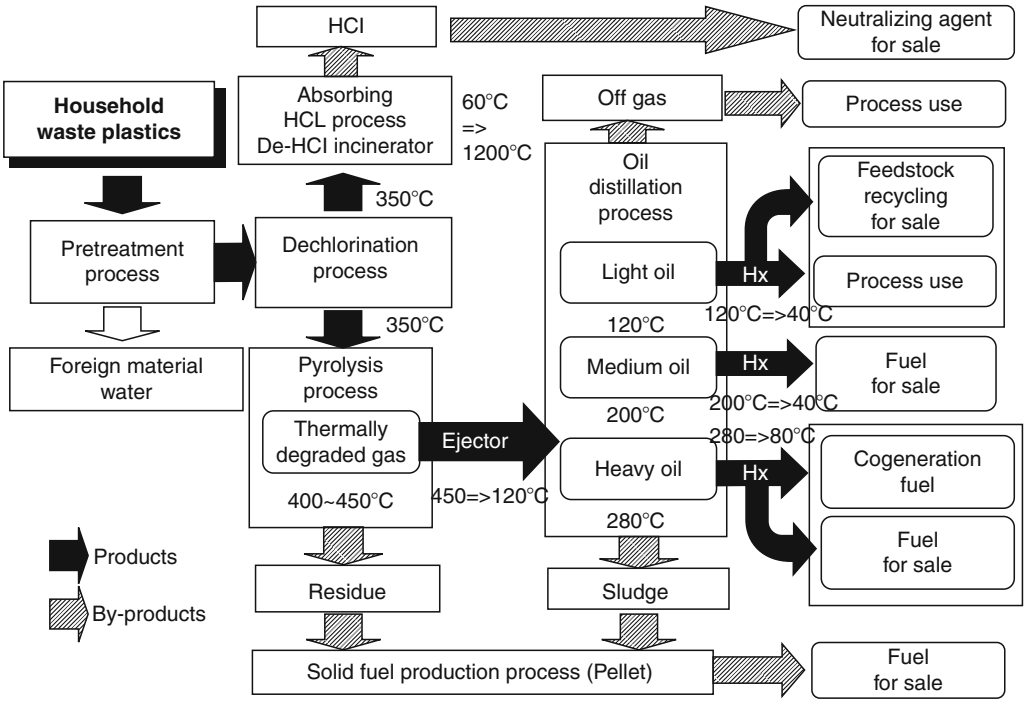

Gasification and Liquefaction Alternatives to Incineration in Japan. Figure 11
Flowsheet of the Sapporo plastics recycling (SPR) plastics liquefaction process. *Hx* Heat exchanger

The remaining volatile hydrocarbon gas is used as fuel in the plant operation. Some of the light oil product is used as a raw material for manufacturing plastic and the rest is used as fuel in the plant. The "medium" oil is sold to local companies and used as boiler fuel. Some of the heavy oil product is provided to local central heating and air-conditioning companies, paper manufacturing companies, and other companies and used as fuel, and the rest is used to power cogeneration diesel engines. The sludge residue derived from the filtering of the heavy oil is mixed with pyrolysis residues and used as a solid fuel. Almost all the plastic, except for the foreign material and water, is being reclaimed. As a result, in 2006, the recycling rate, excluding water contained in the feedstock bales, reached 96%.

Main Technical Challenges

In the first year of operation (2000), it was difficult to maintain normal processing due to corrosion and clogging due to the presence of polyethylene terephthalate (PET) in the plastic waste. The operational problems were due to the formation of benzoic acid (C_6H_5COOH) and terephthalic acid $C_6H_4(COOH)_2$, during the thermal decomposition of PET (Table 8). The cause of the problems was investigated and it was found that the organic acids were mainly formed in the operating temperature range between 170°C and 250°C. This problem was solved by adding hydrated lime [$Ca(OH)_2$] to the plastic waste pellets and plant operation was stabilized.

Composition of Raw Material and Properties of Reclaimed Products

The composition of typical municipal plastic waste is shown in Fig. 12. Polypropylene, polyethylene, and polystyrene (PP/PE/PS:3P), which are easily processed by liquefaction, make up 70–90% of the waste. However, PVC and PET constitute 2–7 t% and 2–15% of the waste, respectively. PVC causes corrosion and quality degradation of the recycled product, and PET can cause corrosion and clogging. Because the problems caused by corrosion and

Gasification and Liquefaction Alternatives to Incineration in Japan. Table 8 Influence of organic acids on the recycling process

	Temperature (°C)		Phase	Concentration (wt%)		Trouble (•; Serious)	
	In	Out		Benzoic acid	Terephthalic acid	Clogging	Corrosion
Heavy oil Hx (upper)	250	170	Liquid	<27	<1	•	None
Heavy oil Hx (lower)	170	80	Liquid	–	–	Minor	None
Fire heater tube	200	300	Liquid			None	•
Distillation tower (upper middle column)	210		Liquid	<90	<2	None	•
Distillation tower (middle column)	220		Liquid	<24	<15	None	•
Distillation tower (bottom column)	270		Liquid	<7	<3	Minor	None

Hx Heat exchanger, *wt%* weight percent

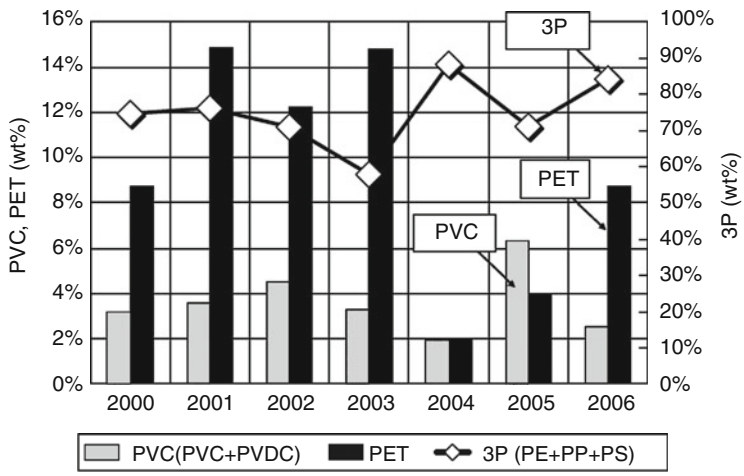

Gasification and Liquefaction Alternatives to Incineration in Japan. Figure 12
Composition of municipal waste plastics. *PET* polyethylene terephthalate, *PVC* polyvinylchloride, *PVDC* polyvinylidene chloride, *PE/PP/PS* polyethylene, propylene, polystyrene

clogging were overcome by the countermeasures mentioned above, the operation of the SPR process is presently stable and safe.

The properties of the reclaimed oil are shown in Table 9. The sulfur, nitrogen, and chlorine contents were below the limit values specified in Japanese Industrial Standards (JIS; technical specification Z 0025 for pyrolytic oil from waste plastics). The SPR reclaimed oil contains 0.003–0.08% sulfur (JIS level: 0.2%), 0.08–0.14% nitrogen (JIS level: 0.2%), and 50–70 ppm chlorine (JIS level: 100 ppm).

The properties of the solid fuel produced from waste plastics are shown in Table 10. Solid fuel pellets are produced from thermally degraded residue and heavy oil sludge. Inorganic chloride levels of 1–4% are found in the solid fuel because $CaCl_2$ is formed by reactions between hydrated lime [$Ca(OH)_2$, tat as noted above is added to the process to mitigate the problems caused by PET] and chlorine. Therefore, this solid fuel is used in a blend with other solid fuels (e.g., wood or coal) at low levels of a few percent (usually below 5%) to minimize environmental problems.

Gasification and Liquefaction Alternatives to Incineration in Japan. Table 9 Properties of the oils recovered in the SPR process

Property		Light oil	Medium oil	Heavy oil	JIS TS Z0025 (Japanese technical standard)
Density	g/cm3 (15°C)	0.814	0.824	0.856	
Flash point	°C	<21	78	114	
Pour point	°C	<−50	−35.0	47.5	
Reaction	pH	Neutral	Neutral	Neutral	
Ash	wt%	<0.001	<0.01	<0.01	≦0.05
Sulfur	wt%	0.002	0.03	0.08	≦0.2
Nitrogen	wt%	0.08	0.14	0.1	≦0.2
Chlorine	wtppm	50	70	60	≦100
Gross heating value	kj/kg	42,070	45,040	45,360	

Gasification and Liquefaction Alternatives to Incineration in Japan. Table 10 Properties of the solid fuel produced in the SPR process

Property	Solid fuel (eco pellet)	Degradation residue	Sludge
Lower heating value (kJ/kg)	15,160	17,570	31,650
Carbon (wt%)	41.8	45.6	67.5
Sulfur (wt%)	0.09	0.06	0.04
Nitrogen (wt%)	0.43	0.4	0.39
Hydrogen (wt%)	5.7	2.6	6.3
Calcium (mg/kg)	88,000	125,000	46,700
Silicon (mg/kg)	12,000	52,300	19,800
Aluminum (mg/kg)	13,000	12,700	940
Total chlorine (wt%)	2.82	4.96	1.42
Inorganic chlorine (wt%)	2.82	4.79	1.42
Bulk specific gravity (kg/l)	0.72	0.389	0.868

The measured results for gas emissions from the SPR off-gas-fired furnace are shown in Table 11. Some of the light oil is used as in-plant furnace fuel and the heavy oil for powering the cogeneration engines. According to periodic analysis of the gaseous emissions of these processes, nitrogen oxides (NOx), sulfur oxides (SOx), dust, dioxins, and HCl levels are below the required standards.

Development of Recycled Products and By-Products

In the SPR process, sludge is separated from the heavy oil by a centrifugal filtering method that was installed after initial operation; this resulted in much better quality of the heavy oil product of this process and, since then, heavy oil has been sold to other companies for use as a fuel. The light oil has been sold to a petrochemical company and is used as raw material for the production of naphtha since 2004. It is also used in the production of plastics. The Japanese recycling law considers only hydrocarbon oil as a recycled product; thermal degradation residue, off-gas (flammable gas), and hydrochloric acid are not considered as recycled products.

The off-gas of the SPR process has been reused as fuel within the plant since 2000. Initially, most of the thermal decomposition residue and oil sludge were discarded as industrial waste, but since 2004 they are supplied to other companies and are used as solid fuel. Hydrochloric acid, after neutralization, was initially discharged into the sewage system, but since 2004, it is also used by other companies as a neutralizer.

The actual recycling rate of the SPR plastics liquefaction plant in 2006 is shown in Fig. 13.

Gasification and Liquefaction Alternatives to Incineration in Japan. Table 11 Properties of gas emitted from the off-gas-fired furnace of the SPR waste plastics liquefaction plant

Periodic survery (twice a year)	Result of measurement	Emission standard	Date
Dust (particulates)	<0.02 g/Nm^3	0.15 g/Nm^3	2007/11/21
Sulfur oxide (SOx)	<0.05 Nm^3/h	3.12 Nm^3/h	2007/11/21
Nitrogen oxide (NOx)	95 vol ppm	150 vol ppm	2007/11/21
Optional survey			
Hydrogen chloride (HCl)	2.3 mg/Nm^3	80 mg/Nm^3	2004/1/13
Dioxin	0.000018 ng-TEQ/Nm^3	0.0006 ng-TEQ/Nm^3	2004/1/20

TEQ Toxicity equivalency quantity, *Nm3* Gas volume at 1 atm and 0°C

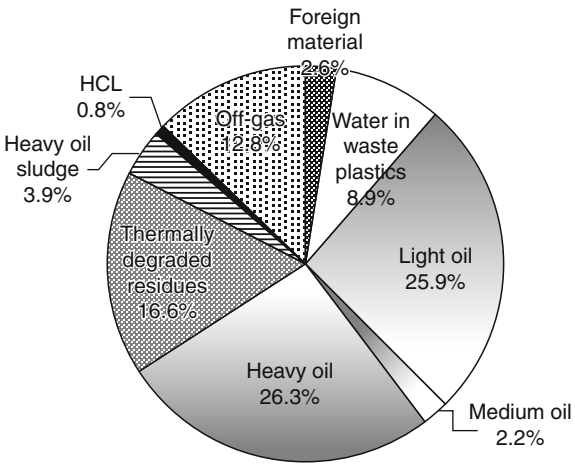

Gasification and Liquefaction Alternatives to Incineration in Japan. Figure 13
Actual recycling rate of the SPR plant in 2006

The recovered hydrocarbon oil amounted to 54.4% of the weight of the initial waste plastic; the gaseous fuel, solid fuel, and the hydrochloric acid products amounted to 35% of the weight of the initial waste plastic. Since SPR recycles almost all of the input waste plastics, except for the water and the foreign materials, a high recycling rate of 96%, excluding the water content, has been achieved (Fig. 13). Also, most of the recovered materials are reused in the local Hokkaido district; as a result, the resource recovery rate for local communities in Hokkaido has reached 93%.

Productivity Improvement

The change in recycling rate and productivity with time of the SPR process are shown in Fig. 14. Productivity is expressed as the total operating cost of electric power, commercial fuel oil, and other supplies, etc.; these costs have decreased by a factor of three since the plant started operations in 2000. The measures that have contributed to productivity improvement are as follows:

- Reduction of hydrocarbon oil consumption during processing
- Reduction of amount of water used by producing and selling hydrochloric acid for use as neutralizer
- Reduction of industrial waste volume by selong solid fuel to others
- Introduction of an energy-saving burning system

Summary

Through its technological improvements and operational know-how, SPR has been able to process municipal waste plastics of almost all quality grades, even those containing PVC and PET. SPR can also process the sorted waste plastics from material recyclers or mechanical recyclers, thus allowing for a more efficient recycling of plastic waste that combines mechanical and chemical recycling. SPR has achieved an extremely high recycling rate (93% in 2006) from mixed plastic wastes and developed a system that allows for the use of the light oil product as a petrochemical raw material.

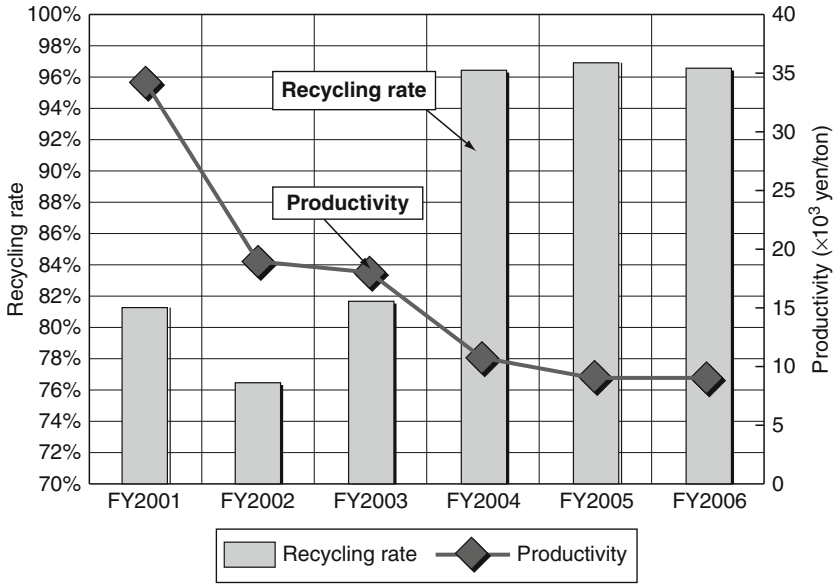

Gasification and Liquefaction Alternatives to Incineration in Japan. Figure 14
Annual trends of actual recycling rate and productivity

Future Directions

In direct comparison with the currently more common stoker grate incineration of MSW, the EBARA TwinRec and the JFE Direct Smetling processes offer a number of advantages: high recovery of metals and inert materials directly from the bottom ash and vitrification of fine ash particles into an inert construction material [1, 3].

These processes are based on gasification and require a lower amount of excess air, resulting in a compact air pollution control system. Also, as shown by the feedstock of the reference plants noted above, these processes are more flexible with regard to feedstock.

The processes described in this entry have demonstrated, through the range of capacity of commercial plants and the use of multiple feedstocks, that gasification of solid wastes is mature, reliable, efficient, and a good solution for current and future waste management applications.

Another approach to enhance the recycling of MSW is to segregate plastic materials and liquefy them, as demonstrated commercially by the SPR process. In the past it was difficult to recycle municipal waste plastics that contained PVC and PET. Thus, material recycling methods have traditionally sorted out only PP/PE/PS from municipal waste plastics and nearly one half were disposed as residue. The SPR commercial liquefaction plant has shown that it is possible to process mixed plastics containing PVC and PET. This plant has attained a very high recycling rate achieved a high recycling rate of 93% of the solids in the feedstock to the process.

Bibliography

1. Selinger A, Steiner Ch, Shin K (2003) TwinRec gasification and ash melting technology – now also established for municipal waste. Presented at 4th international symposium on waste treatment technologies, Sheffield, 29 June–2 July 2003
2. JFE High Temperature Gasifying & Direct Melting System (2010) Operational result of clean-hill homan municipal solid waste treatment center, JFE Technical Report, No. 25, pp 70–71, -(in Japanese)
3. Fukushima M, Shioya M, Wakai K, Ibe H (2009) Toward maximizing the recycling rate in a sapporo waste plastics liquefaction plant. J Mater Cycles Waste Manag 11:11–18
4. Plastic Waste Management Institute http://www.pwmi.or.jp/flow/flame.htm (inJapanese)
5. The Japan Containers and Packaging Recycling Association http://www.jcpra.or.jp/eng/statistics.html

Genetic Engineering of Crops for Insect Resistance

John A. Gatehouse
School of Biological and Biomedical Sciences, Durham University, Durham, UK

Article Outline

Glossary
Definition of the Subject
Introduction
Insecticidal Proteins from *Bacillus thuringiensis*
How Do *Bt* Toxins Work?
Expression of Genes Encoding *Bt* Insecticidal Proteins in Transgenic Plants
Taking Transgenic Plants Expressing *Bt* Toxins into the Field
Developments to "First Generation" Crops Expressing *Bt* Toxins
Exploitation of Endogenous Plant Defensive Mechanisms Against Insect Herbivores
Some Novel Approaches
Insect-Resistant Genetically Engineered Crops and Sustainability
Future Directions
Bibliography

Glossary

Coding sequence The part of a gene which determines the sequence of the protein product

Domain A region of a protein which forms a distinct 3-D structure, and will often form this structure even when separated from the rest of the protein

Genetic engineering Introduction of a specific DNA sequence into an organism by artificial means

Insect orders Lepidoptera = butterflies and moths; diptera = flies; coleoptera = beetles; hemiptera/homoptera = sucking insects such as aphids

Mutagenesis Alteration to a DNA sequence, often resulting in alteration to the sequence of a protein which the DNA specifies

Oligomerization Formation of polymers containing a relatively low number of repeating units

Proteolysis Introduction of breaks in the chain of amino acids making up a protein by a proteinase

Transgenic Organism into which a gene has been introduced by genetic engineering technology

Definition of the Subject

Genetic engineering of crops for insect resistance is the introduction of specific DNA sequences into crop plants to enhance their resistance to insect pests. The DNA sequences used usually encode proteins with insecticidal activity, so that in plants which contain introduced DNA, an insecticidal protein is present. However, other strategies to improve plant defenses against insects have been explored. Genetically engineered crops that are protected against major insect pests by production of insecticidal proteins from a soil bacterium, *Bacillus thuringiensis*, have become widely used in global agriculture since their introduction in 1996.

Introduction

Twenty years have elapsed since the first publications describing transgenic plants, which showed enhanced resistance to insect herbivores, as a result of the expression of a foreign gene encoding *Bacillus thuringiensis* (*Bt*) toxin [1–3]. In the intervening years, crops expressing these toxins have become widely used in global agriculture, and have led to reductions in pesticide usage and lower production costs [4] At the same time, the predictions made by lobby groups supporting "organic" crop production, that irreversible environmental damage would be caused by genetically engineered (GE) crops resistant to insect pests, have not been realized [5]. Despite all the controversy that GE crops have caused in many countries, it is difficult to dispute that the use of this technology to combat insect pests has had a positive impact on global agriculture.

This entry has two aims: first, to provide a summary of how and why *Bt* toxins have become the insect resistance genes of choice for commercial GE crop applications, and to anticipate some further developments of this technology; second, to consider some of the other approaches to engineering insect resistance in plants, and to assess their potential for future development in the development of sustainable agriculture.

Insecticidal Proteins from *Bacillus thuringiensis*

The presence of insecticidal toxins in the soil bacterium *Bacillus thuringiensis* (*Bt*) has enabled both the bacteria themselves, and genes derived from them, to be exploited as plant protectants. The toxicity is almost invariably based on proteins produced during sporulation of the bacteria, which form crystalline deposits associated with the spores. The insecticidal *Bt* proteins are encoded by genes present on plasmids, and the presence of these plasmids is the main feature which distinguishes *Bt* from other spore-forming bacilli [6]. Preparations of *Bt* spores have been used since the 1920s as a conventional, spray insecticide (and, as a "natural" product, are approved for use in organic agriculture), but their efficacy in the field is limited by inactivation and low persistence.

The ecological niche occupied by *Bt* appears to be simple to define. The life cycle starts with a spore and associated crystalline protein body which may be present in the soil. On being eaten by an insect, the protein deposit associated with the spore is dissolved and digested, converting the crystalline protoxin to an active toxin. The insect is then killed, and the carcass provides nutrients for the growing bacteria, which multiply rapidly. When the insect carcass is exhausted, the bacteria sporulate; the spores are dispersed, and the cycle recommences. However, this cycle is clearly too simplistic, as the target insects for *Bt* toxins are only rarely soil dwellers, and the dose of spores required to kill an insect larva is too large for dispersed spores to have much effect. Although *Bt* is widely distributed, levels of the bacterium in soils are generally too low to have any effect on insects, and spraying plants with spores does not result in persistent protection as a result of the establishment of a high bacterial population. The species has been described as an opportunistic pathogen, which has evolved the sporulation mechanism as a "backup" system to ensure its survival under unfavorable conditions [7]. *Bt* is naturally present in the phylloplane, as well as in soil, and has been detected on cabbage foliage [8], and in vegetative form on clover [9] at low levels, without any insecticidal effect. However, the insecticidal characteristic must be of benefit to the bacterium, since most of the insecticidal proteins are encoded by plasmids, and the plasmids are maintained in the *Bt* population as a whole, despite the obvious metabolic costs of producing large quantities of spore-associated proteins. Not only are toxin-encoding plasmids maintained, but there is also a huge reservoir of diversity in the toxins themselves, and much effort has been put into screening bacterial isolates for strains of *Bt* with novel pesticidal activities [10].

Bt toxins are now classified on the basis of amino acid sequence similarity (an earlier classification system based on pesticidal activity has been superseded), in a systematic hierarchical system [11]. For the purposes of this contribution, only the major distinctions need be considered. There are four types of insecticidal proteins produced by *Bt*:

1. Proteins associated with *Bt* spores, usually as crystalline deposits; three domain structure; single toxins; designated by the symbol Cry
2. Proteins associated with *Bt* spores, usually as crystalline deposits; binary toxins and other similar proteins, including truncated versions of three-domain toxins; also designated by the symbol Cry
3. Proteins associated with *Bt* spores, usually as crystalline deposits; single domain structure; cytolytic; single toxins; designated by the symbol Cyt
4. Proteins expressed vegetatively by *Bt*; single chain and binary toxins; designated by the symbol Vip

Each type of toxin is subdivided (on the basis of sequence similarity) into families (number; same number $\geq$45% sequence identity) and then further subdivided using capital letters (same letter $\geq$78% sequence identity), small letters (same letter $\geq$95% sequence identity) and numbers successively. The resulting system yields designations for specific toxins such as Cry1Aa. A single *Bt* strain can produce spores which contain only a single toxin, or a complex mixture, such as the *Bt* subspecies *israelensis*, whose spores contain Cry4Aa, Cry4Ba, Cry10Aa, Cry11Aa, Cyt1Aa, and Cyt2Ba toxins [12].

All four types of proteins have been proposed for use as crop protection agents, although Cyt toxins have not as yet been used in commercial insect-resistant transgenic plants, and three-domain Cry toxins are by far the most commonly used type. Cry and Cyt toxins belong to the class of proteins referred to as bacterial pore-forming toxins, and show structural similarity to the α-helical and β-barrel groups of toxins, respectively

(where α-helical and β-barrel refer to the structures of the membrane-spanning parts of the toxin; reviewed by Parker and Feil [13]).These pore-forming toxins show common features of activity; they are produced as water-soluble proteins, and interact with specific receptors on cell surfaces, often after proteolytic activation by host proteinases. Binding to cell surfaces triggers a conformational change leading to oligomerization, which allows insertion into the cell membrane through promotion of a fluid, partially denatured structure. Insertion of the toxin into the membrane can either cause cell death directly, or result in effects on intracellular metabolism which lead to cell death.

How Do *Bt* Toxins Work?

Three-Domain Cry Toxins

The mechanism of action of the "conventional" three-domain Cry toxins is now well understood, and can be divided into four stages:

1. Solubilization of the protoxin, and proteolytic activation by proteinases in the insect gut to produce active toxin
2. Interaction of the toxin with one or more receptors on cell surfaces in the insect gut epithelium
3. Oligomerization of the toxin
4. Insertion of the oligomerized toxin into cell membranes, leading to the formation of open pores, and cell death (see Fig. 1)

Following the pioneering work of Ellar's group [14] tertiary structures of six different three-domain Cry toxins are known – Cry1Aa [15], Cry2Aa [16], Cry3Aa [14], Cry3Bb [17], Cry4Aa [18], and Cry4Ba [19]; whereas most structures are for the active form, the structure of Cry2Aa includes the N-terminal pro-region. These toxins all show a high degree of structural similarity, and thus the formulation of a general model for their mode of action is justified. The three domains present in the active forms of these proteins are designated I, II, and III, and are normally contained in

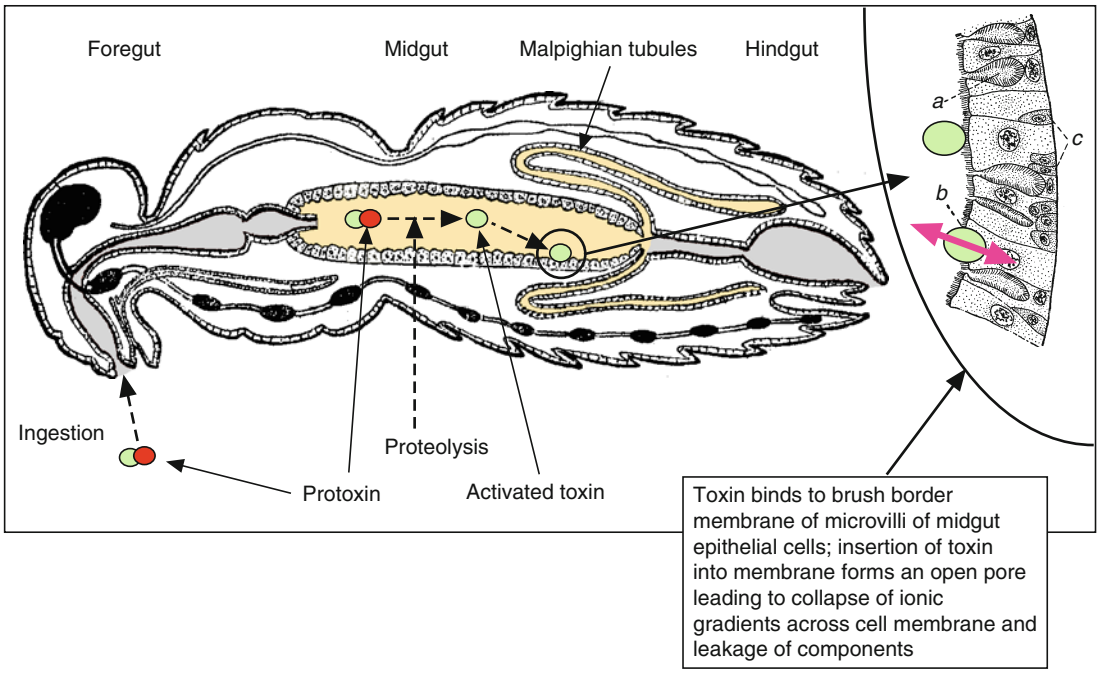

Genetic Engineering of Crops for Insect Resistance. Figure 1
Action of *Bt* toxins on the insect gut epithelium. Death of insect results from disintegration of gut epithelium (due to cell death) and proliferation of gut microflora

a single polypeptide of approximately 600 amino acid residues (in some cases proteolytic cleavages are present within the active three-domain structure as a result of protoxin activation, resulting in multiple polypeptides making up the toxin, but the overall three-domain structure is conserved.). While conservation of structure and sequence is observed in the active forms of three-domain toxins, many toxins are synthesized with C-terminal extensions, which are variable in sequence between *Bt* strains, and in length between Cry families. The presence of C-terminal extensions leads to a large degree of heterogeneity in the size of the protoxins present in bacterial spores, with sizes ranging from approximately 600 amino acids (similar to the active toxin) to approximately 1,200 amino acids. These C-terminal extensions are not required for toxin function, and are removed during toxin activation, although their removal is not sufficient for toxicity to be shown. They are thought to play a role in the formation of crystalline inclusions in the bacterium during the spore-forming process.

The three domains of the active toxin are clearly distinguished in their structures.

1. Domain I, approx. 260 aa, contains seven α-helices, of which six are amphipathic and one hydrophobic. This structure is typical of pore-forming toxins, with the hydrophobic and amphipathic helices being responsible for membrane insertion and pore formation. The hydrophilic sides of the amphipathic helices form the surface lining the pore, so that polar species such as ions are able to cross the membrane.
2. Domain II, approx. 170 aa, forms a "β-prism" structure, with three β-sheets, and exposed loops on its surface.
3. Domain III, approx. 160 aa, has a compact structure with two anti-parallel β-sheets in a "jellyroll" formation, and is structurally similar to carbohydrate-binding domains such as the cellulose-binding domain in cellulases [20]. A general model for three-domain toxins is shown in Fig. 2.

The Proteolytic Activation Process Ingestion of the Cry protoxins by the insect leads to solubilization of the proteins, and exposure to digestive proteinases in the insect gut. Although removal of the C-terminal protoxin region occurs at this stage, the essential step in protoxin activation is the proteolytic cleavage and removal of an N-terminal peptide, which varies from approx. 25–60 amino acids in different Cry proteins. A non-activatable Cry1Ac mutant toxin could not form pores in insect membrane vesicles derived from gut epithelial cells [21], and it is thought that the N-terminal peptide "masks" a region of the toxin involved with interaction with receptors [16]. The activated toxin is fairly resistant to further proteolytic cleavage, which enables it to survive long enough in the gut to reach its site of action, the gut epithelial surface (Fig. 1).

This summary overlooks a number of factors which contribute to toxicity. First, the location of the proteolysis may be important, since many insects, such as diptera (flies), carry out digestion in the foregut, which is chitin-lined and does not contain epithelial surfaces, or even outside the insect altogether, by secreted saliva or regurgitated gut contents. Under these circumstances, the toxin will need to be more resistant to proteolysis, or more effective, since the time between activation and reaching the site of action will be longer. Secondly, gut conditions vary significantly between insects from different orders, or even within orders; in general, larvae of lepidoptera (moths and butterflies) have a highly alkaline midgut environment (pH 10–11 in many major crop pests), whereas larvae of coleoptera (beetles) have an acidic gut environment (pH approx. 5 for many species). These differences in conditions will affect both the activation and survival of the protein, although they may be less relevant to steps taking place at the gut surface, where there is a separation from the gut lumen by the peritrophic membrane (a macroscopic porous chitin-based structure) and by lipids sloughed off from the gut surface. Finally, the nature of the digestive enzymes present in the insect gut differs considerably between different orders; whereas most insects use serine proteinases with an alkaline pH optimum as their major endoproteinases, many coleopteran larvae use cathepsin-type cysteine proteinases with an acidic pH optimum (similar to lysosomal proteinases). On the other hand, protoxin activation does not appear to be very sequence specific. Many lepidopteran-specific Cry proteins can be activated in vitro by mild treatment of the protoxin with bovine trypsin, yielding products that appear to be similar to those

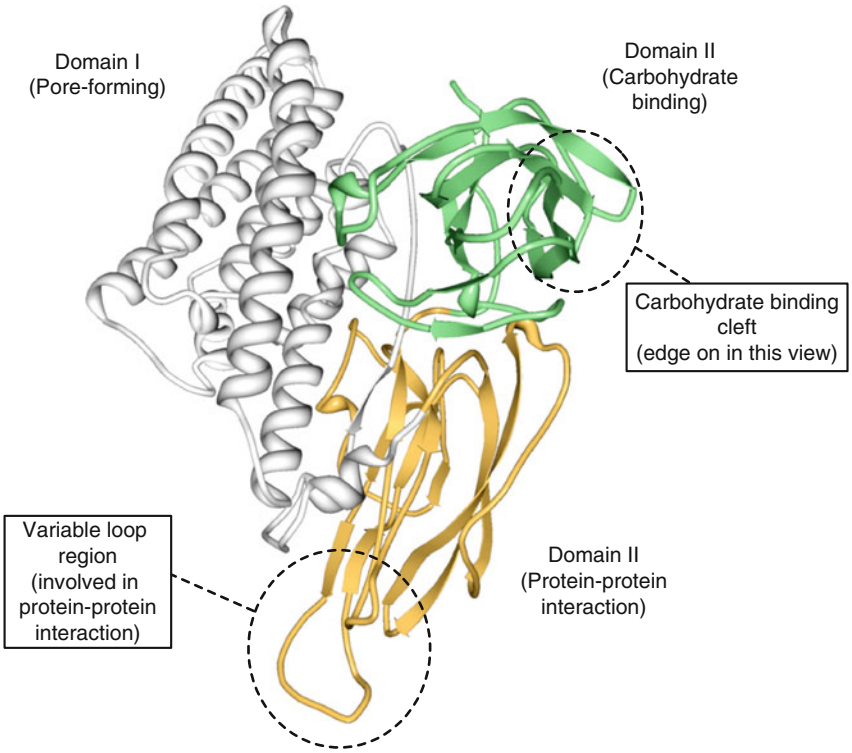

Genetic Engineering of Crops for Insect Resistance. Figure 2
Model structure for three-domain *Bt* toxins. Ribbon diagram showing backbone structure of *Bt* toxin Cry1Aa (PDB 1ciy; [15]); structure of active toxin shown. The three domains are color coded: domain I, silver; domain II, orange, domain III, green. Features as shown on diagram

formed in vivo. This suggests that it is the three-dimensional structure of the protoxin that determines where proteolysis takes place, unless forcing conditions are used.

Interactions with Receptors Proteins to which Cry proteins bind in the insect gut are termed "receptors," although the specificity of interaction is determined by the Cry protein itself, and the ligands to which it binds do not show the properties of receptors as normally understood. Binding takes place on the microvillar membranes of the cells forming the midgut epithelium, and involves interactions with relatively abundant proteins, either attached to the cell membrane by glycosylphosphatidyl-inositol (GPI)-anchors, or integral to the membrane with large extracellular domains. The overall process is summarized in Fig. 3.

Methods for identifying receptors to which Cry proteins bind have largely been based on immunoblotting of proteins prepared from brush border membrane vesicles (BBMV). This method is not a good mimic of conditions in vivo, and may result in interactions with lower affinity, or which are dependent on protein conformations maintained by membranes, not being observed. Nevertheless, the major binding partners for Cry proteins which have been identified show binding when assayed as purified proteins, and as components of BBMVs, with binding constants in the range 1–100 nM.

The initial identification of membrane-anchored aminopeptidase N [23] and an integral membrane cadherin-like protein designated *Bt*-R1 [24] as Cry1A toxin receptors in lepidopteran insects has been supplemented more recently by identification of a 270 kDa glycoprotein [25] and alkaline phosphatase

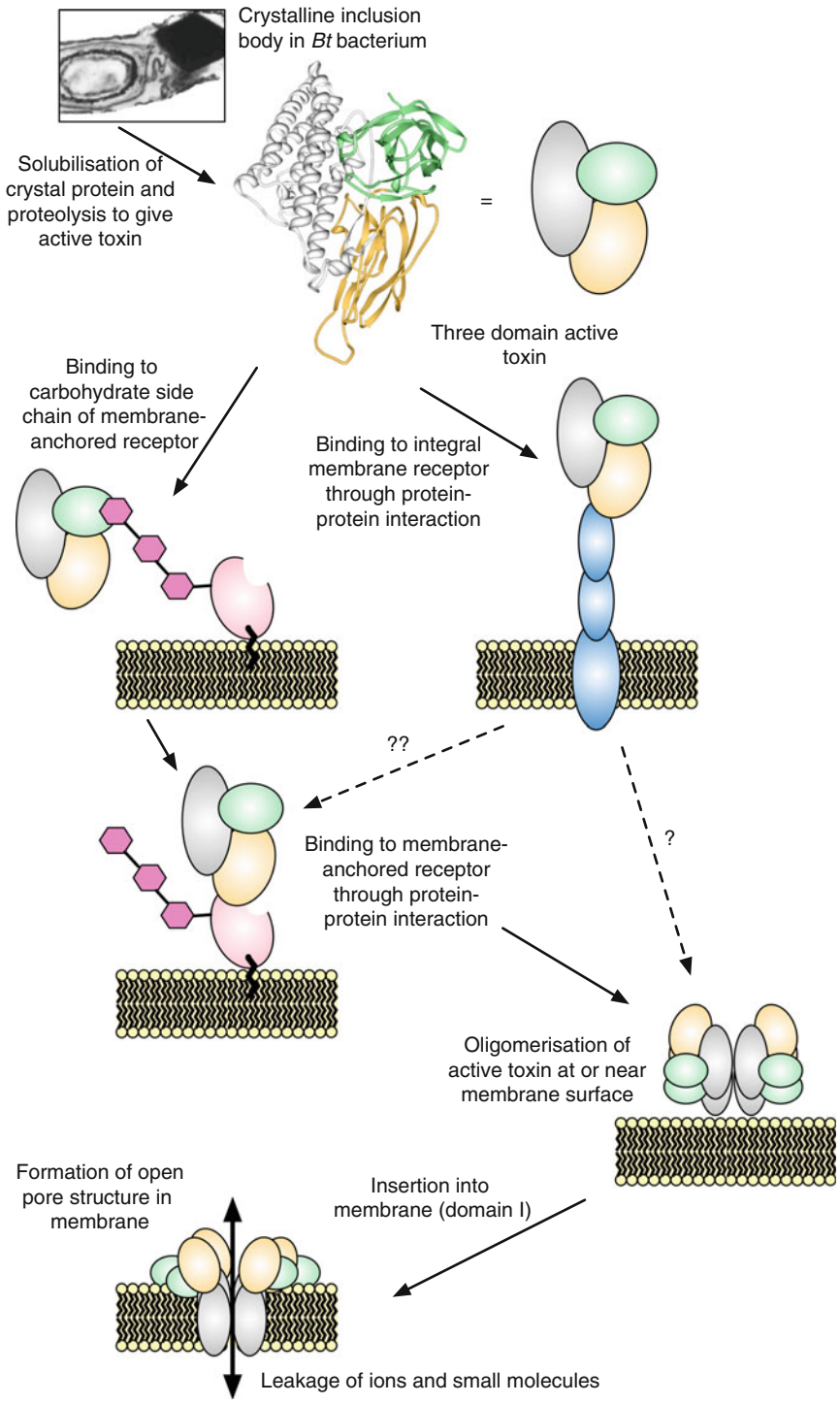

Genetic Engineering of Crops for Insect Resistance. Figure 3

Mechanism of action of three-domain *Bt* toxins. The scheme shown is adapted from the "two-receptor" model [22]

(membrane anchored; [26]) as additional potential receptors. Alkaline phosphatase appears to be the major receptor in mosquitoes [27]. A recent proteomic analysis has identified further potential receptors, such as V-ATP synthase subunit 1 [28]. However, this analysis also showed binding to actin, which could not be present at the cell surface, showing that results from blotting experiments need to be interpreted critically.

Functional roles as "receptors" for aminopeptidase N and cadherin *Bt*-R1 in Cry protein toxicity are supported by numerous studies. Strains of lepidopteran insects resistant to Cry1 toxins have been identified which show mutations in the gene encoding *Bt*-R1, leading to the production of a truncated cadherin lacking the extracellular domains [29, 30]. The correlation with loss of function of cadherin with loss of susceptibility to Cry toxins suggests that binding to the extracellular domains of cadherin is a necessary step for toxicity. Binding of Cry1A toxin to the cadherin extracellular domains has been demonstrated in vitro, and the binding regions have been identified in some detail [31]. Both gain-of-function and loss-of-function assays have been used to provide further evidence for involvement of cadherin in toxicity; when transiently expressed in mammalian cells that were not normally susceptible to Cry toxin, Bt-R1 genes from silkworm conferred sensitivity to Cry1A toxins [32]; whereas suppression of cadherin expression by RNA interference in tobacco hornworm (*Manduca sexta*) decreased sensitivity to Cry1Ab toxin [33]. In the case of aminopeptidase N, similar correlations between resistance to *Bt* toxin and lack of expression of specific isoforms of the protein have been observed [34], but more direct evidence has come from downregulation of aminopeptidase by RNA interference using double-stranded RNA. This technique has been carried out in lepidopteran larvae, giving decreased sensitivity to Cry1C toxin [35], and in lepidopteran cell cultures, giving decreased sensitivity to Cry1Ac [36]. A gain of function experiment in which transgenic fruit flies (*Drosophila*) expressing lepidopteran aminopeptidase N became sensitive to the lepidopteran-specific toxin Cry1Ac [37] showed elegantly and convincingly that this receptor plays a key role in toxicity. Binding to aminopeptidase N involves interaction of Cry toxins with the carbohydrate side-chains of the protein [38, 39], with specificity toward GalNAc residues being shown (this sugar can inhibit binding; [40]). Binding to carbohydrate facilitates subsequent protein–protein interactions, which are thought to be necessary for toxicity [41]. Functional evidence for alkaline phosphatase acting as a Cry toxin receptor has again been provided by correlative observations, in that insect lines resistant to Cry1Ac toxins have lower alkaline phosphatase levels than susceptible lines [26]. Interactions with protein-bound carbohydrate also seem to be involved in the binding of Cry toxins to alkaline phosphatase.

The roles of the different domains of Cry proteins in the interaction with receptors are clearly distinguished. Despite the presence of the N-terminal propeptide which must be removed for activity, domain I plays little or no role in the interaction with receptors, whereas domain II is responsible for most protein–protein interactions (see Fig. 2), and domain III is responsible for binding to carbohydrates. This division of roles is consistent with the observation that a single toxin can interact with more than one type of "receptor"; for example, Cry1Ac interacts with both Bt-R1 and aminopeptidase N [22]. The protein–protein interactions mediated by domain II have been localized to variable loop regions on the surface of the domain, whereas the carbohydrate-binding region of domain III is a typical binding site cleft, which is spatially well-separated from the domain II loops.

Oligomerization Oligomerization is a common feature in bacterial pore-forming toxins, and Cry proteins appear to conform to the model, with the formation of oligomeric structures (probably tetramers) observed for toxins from the Cry1 and Cry3 families. Mutants of the Cry1Ab protein that have impaired oligomerization ability, but bind to the receptor, show much reduced toxicity or no toxicity toward lepidopteran larvae [42]. Similarly, monomeric Cry proteins have much lower intrinsic pore-forming abilities on synthetic membranes than oligomerized preparations [43]. Oligomerization is promoted by binding to a receptor; in the case of Cry1Ab protein binding to the cadherin Bt-R1 receptor, this process involves an additional proteolytic cleavage at the N-terminal end of the protein, in domain I [44]. The proteolytic cleavage, carried out by host enzymes, may aid the oligomerization process. The importance of oligomerization in promoting toxicity has been shown by two

complementary studies. First, a peptide corresponding to the region of cadherin to which Cry1A binds has been shown to act as a synergist, increasing the toxicity of Cry1A toward lepidopteran larvae [45], presumably as a result of the binding between the peptide and Cry1A promoting oligomerization of the toxin prior to interaction with the gut epithelium. Secondly, mutants of Cry1Ab toxin have been produced which contain deletions corresponding to the proteolysis in helix 1 of domain I which occurs on binding to cadherin. These mutated toxins form oligomers in the absence of cadherin binding, and are effective against insects that have cadherin expression suppressed, or which have a cadherin mutation which leads to resistance to unmodified toxin [33]. These results have led to a current view that cadherin is the primary receptor for Cry toxins, since it is necessary to promote oligomerization, with other molecules taking the role of "secondary receptors" [33].

Insertion into the Cell Membrane The oligomeric Cry protein must partially unfold in order for the pore-forming domains (domain I) to insert into the membrane. In the case of bacterial pore-forming toxins active against mammalian cells, this partial denaturation process is stimulated by acidic pH at the cell surface [13]. A similar mechanism could occur with Cry proteins active against lepidopteran insects, although the gut pH is very alkaline; the partial denaturation could still be triggered by a decrease in pH at the cell surface. The pH optimum for aminopeptidase N in lepidopteran larvae (8.0; [46]) is at least 2 pH units less than bulk gut content pH (>10), suggesting that a decrease in pH occurs near the cell surface. The involvement of lipid rafts, microdomains which are less fluid than the membrane as a whole, in pore formation has been suggested [47]. However, membrane-anchored proteins are selectively associated with these lipid rafts, and it is not clear whether lipid rafts are necessary for pore formation, or whether their involvement is a result of the presence of receptors. The trans-membrane cadherin-like *Bt*-R1receptor is not associated with lipid rafts.

A current model for pore formation by Cry1A toxins suggests that interaction with two receptors is necessary; an initial binding step with the cadherin-like *Bt*-R1 receptor leads to toxin oligomerization, followed by interaction of the oligomer with the aminopeptidase N receptor and insertion into the membrane [22, 48]. While this model is plausible, the details of the mechanism of toxicity must differ for different toxins, and a "two-receptor" model should not be assumed to be generally applicable. The gain of function experiments described above show that only one receptor is necessary for toxicity to be shown, and only a few lepidopteran-specific Cry toxins have been shown to interact with cadherin-like proteins [49]. If the major determinant of Cry protein toxicity is the assembly of oligomeric complexes at the surface of cells in the gut epithelium, then this requirement can be met in diverse ways, involving different "receptor" proteins to localize the toxin and promote oligomerization (although the interaction is always likely to involve the most abundant proteins at the cell surface). A "global" diversity of interactions is not inconsistent with specificity when interactions between specific toxins and hosts are considered.

Once the insertion of Cry toxin into the cell membrane leads to pore formation, the gut epithelial cell is unable to maintain its internal solute balance, as the open pore allows free exchange of ions and other small molecules between the gut lumen and the cytoplasm. The cytoplasm of gut cells has markedly different concentrations of ions (including H^+) than the gut lumen; this difference in concentrations is used to drive active transport processes, such as amino acid transport [50]. Free movement of ions thus causes massive disruption to cell physiology, leading to death. The leakage of cell contents also causes proliferation of gut microflora, so that dying insects show massive bacterial infection of collapsing gut tissue. Cry proteins may also produce toxic effects through interference with signaling pathways. Binding of Cry1Ab to the transmembrane *Bt*-R1 receptor has been shown to activate a G-protein-mediated intracellular signaling pathway, resulting in the formation of cAMP by adenylyl cyclase, and activation of protein kinase A [51]. This process led to cytological changes typical of *Bt* toxin activity.

Binary Cry and Vip Toxins

The binary Cry toxins are exemplified by toxins active against corn rootworm [52]. These toxins are only active as a combination of two proteins, designated as

families Cry34 (14 kDa protein) and Cry35 (44 kDa protein). The two proteins are the product of a single operon in the commonly used *Bt* strains. The binary toxin acts on the insect gut epithelium, and leads to swelling and vesicle production from epithelial cells, resulting in the disappearance of microvilli, and extensive disruption of the epithelium. However, it is not clear whether these symptoms are solely a result of open pore formation, or whether other modes of toxicity, such as ADP-ribosylation (see below) are occurring. No structural information on these proteins is available at present. There is evidence that the 44 kDa toxin protein Cry35 is evolutionarily related to an insecticidal toxin from *Bacillus sphaericus* [53]. The *B. sphaericus* toxins have received some attention due to their toxicity toward mosquitoes and other dipteran insects. They also bind to membrane-anchored receptors (α-glucosidase, in the case of the mosquito *Culex pipiens* [54]) and cause disruption of the gut epithelium [55]. However, their detailed mechanism of action is not known. Like Cry34/35, the *B. sphaericus* proteins are binary toxins, although in this case one component does show limited activity in the absence of the other. The designation of the corn rootworm binary *Bt* toxin by the symbol Cry obscures the fact that these toxins have little in common with the three-domain toxins, besides being found in crystalline deposits in *Bt*, and being insecticidal as a result of acting on the insect gut epithelium.

The *Bt* insecticidal Vip1/2 proteins (active against corn rootworm) are also binary toxins with similarity to the *B. sphaericus* toxins [56]. The mechanism of action of Vip1/2 toxins involves ADP-ribosylation by the active component, which disrupts actin polymerization in cellular microfilaments, similar to other bacterial ADP-ribosylating toxins such as botulinum toxin [57]. The inhibition of actin polymerization leads to massive disruption of cellular functions. The Vip1Ac binding component of the binary toxin interacts with membranes to form oligomeric channels, allowing the active component to gain access to the cell cytoplasm [58].

A further class of Vip proteins, Vip3, (active against lepidoptera) has been identified; these protein are single chain toxins which lyse insect gut cells by pore formation in membranes, and have no sequence similarity to Vip1/2 [59, 60]. Vip3 binds to brush border membrane vesicles prepared from target insect gut epithelial cells, but does not bind to the same receptors as Cry1 and Cry2 proteins [61]. Binding to 80 and 100 kDa membrane proteins is observed in ligand binding experiments [62], but these receptors have not been characterized. These proteins are promising candidates for further development; chimeric toxins containing regions from different Vip3 toxins have been produced and show extended ranges of toxicity toward lepidopteran pests [63].

Cyt Toxins

The cytolytic Cyt toxins, also found in crystalline inclusions in some *Bt* strains, are single polypeptides, of approx. 250 amino acids; the N-terminal region contains α-helices which wrap around a C-terminal β-sheet core in the three-dimensional structure [64]. Pore formation results from insertion of the β-sheet region into membranes [65]. Unlike the three-domain Cry toxins, this membrane insertion is not receptor-mediated [66]; the Cyt toxins insert directly into membranes, and are thus cytolytic to a wide range of cells. Like the three-domain Cry toxins, Cyt toxins are synthesized as inactive protoxins which are activated by proteolysis. Activation involves removal of propeptides from both the N- and C-termini of the protoxin; in the case of Cyt2Aa, 32 aa are removed from the N-terminus and 15 aa from the C-terminus to generate active toxin [67]. This process does not require specific proteinases.

The combination of Cry and Cyt toxins found in crystalline inclusions in some *Bt* strains, specifically in the strains of *Bt* subsp. *israelensis* active against mosquito larvae, is highly effective as a toxin due to synergistic interactions between its components. Not only are the three domain Cry protein components in these crystals more effective toxins in the presence of Cyt proteins, but the Cyt proteins also prevent resistance to Cry proteins from developing when insects are exposed to purified protein preparations under laboratory conditions [68]. This synergistic effect could result from the two types of toxin producing complementary disruption of the insect gut epithelial cell membranes, but evidence has been presented that Cry and Cyt toxins can interact directly. Specifically, Cry11Aa and Cyt1Aa bind strongly to each other, both in solution and in a membrane-bound state, and

binding of Cry11Aa to mosquito gut epithelial cell membranes was enhanced by pretreating the membranes with Cyt1Aa [69]. The interaction with Cyt1Aa takes place through the loop region in Cry11Aa involved in protein–protein interactions with its "normal" receptor (membrane GPI-anchored alkaline phosphatase). Insertion of Cyt1Aa into gut cell membranes, which is not dependent on receptor mediation, thus generates additional "receptors" for Cry11Aa, increasing its toxicity, and preventing resistance developing by mutation of the insect-encoded "receptor."

Expression of Genes Encoding *Bt* Insecticidal Proteins in Transgenic Plants

Expression of Three-Domain Cry Toxins from Transgenes in the Nuclear Genome

Almost all the insect-resistant transgenic crops currently in use express three-domain Cry proteins from *Bt* as their protective agent. The initial laboratory-based experiments expressed Cry1 toxins in plants to give protection against lepidopteran larvae, and this has remained the main focus of *Bt* gene utilization up to the present day. However, the three-domain Cry proteins pose a number of problems in terms of expression in plants. The technology involved in achieving sufficient levels of accumulation of these proteins to give adequate levels of protection was initially challenging, but developed rapidly, so that within 5 years of the initial reports of engineered resistance, the methodology for gene manipulation was essentially complete. The slower pace of transfer of this technology into major crop species observed subsequently has had much more to do with technical difficulties in plant transformation (particularly regenerating viable plants), than with any problems at the level of gene constructs. The minimum level of Cry protein expression in leaf tissue to give high levels of mortality of sensitive lepidopteran larvae under laboratory conditions is approximately 0.05% of total protein, but to give effective field protection against species which are less sensitive to *Bt* toxins, and to manage resistance to the toxin in pests (see later), levels of expression an order of magnitude higher (i.e., 0.5% of total protein) are desirable.

Engineering genes encoding three-domain Cry proteins for expression in transgenic plants has been extensively described (the review by Mazier et al. [70], gives a particularly comprehensive survey), but a short summary of the main considerations which had to be taken into account is relevant here. These were:

1. How much of the protein coding sequence should be expressed in plants?
2. Which promoters should be used to drive expression of the Cry protein coding sequence in plants?
3. How should the coding sequence be altered to avoid poor expression?

Protein Coding Sequence The C-terminal part of protoxins for three-domain Cry proteins is variable, and absent in some toxins. Its role in directing the formation of crystalline inclusions in *Bt* sporulation is not required when the proteins are expressed in plants (and might result in disruption of cells unless the protoxin was exported into intracellular spaces). All constructs which result in insecticidal activity have omitted this part of the molecule from the coding sequence expressed in plants. The initial research suggests that a complete protoxin accumulates in plant tissue at levels 10–50-fold less than a protoxin truncated so the C-terminal region is absent [3]. Since removal of the C-terminal region of the protoxin does not result in active toxin being produced, retention of the N-terminal activation peptide ensures that the initial protein product in transgenic plant tissue is not active, and proteolytic activation takes place as normal within the gut of insect herbivores. The coding sequence utilized thus corresponds to the three-domain structure shown in Fig. 2, plus the additional N-terminal propeptide.

Promoters The problems experienced in achieving levels of expression of Cry proteins high enough to confer effective protection meant that the initial use of promoter sequences which only gave low levels of expression, such as those from *Agrobacterium tumefaciens* Ti plasmids, was rapidly superseded by strongly expressed promoters, most of which were based on the Cauliflower Mosaic Virus 35S RNA promoter (CaMV 35S). Constitutive expression of

the Cry protein in all plant tissues does not appear to cause significant problems either in a yield penalty, or deleterious effects due to the accumulated protein. However, tissue-specific promoters have also been used, such as the ribulose-bisphosphate carboxylase small subunit promoter (e.g., [71]) or the phosphoenolpyruvate carboxylase promoter (e.g., [72]), both of which are specific for green tissue. The CaMV 35S promoter was initially considered to be specific for dicots, but further experience showed that it could also be functional in monocots, and, with suitable modification, could be used to direct Cry protein expression (e.g., [73]). However, many researchers have preferred to use promoters derived from constitutively expressed monocot genes in Cry protein expression constructs for use in cereal transformation (e.g., the maize ubiquitin-1 promoter; [74]). Root-expressed promoters have been used in constructs designed to protect cereals against corn rootworm [75].

Considerable research has also been undertaken on the use of promoters whose expression is only induced under specific conditions. The use of wound-induced promoters to direct Cry protein expression has the apparent advantage that production of Cry proteins in transgenic plants is, for the most part, only induced on attack by insect pests. Any potential deleterious effects on phenotype caused by production of the toxin in transgenic plants would therefore be minimized, and toxin residues in plant tissues would be reduced. A wound-inducible maize proteinase inhibitor gene promoter has been used to direct expression of Cry1B in transgenic rice, and has been shown to give effective protection against insect attack (against striped stem borer; [76]). However, the protection afforded by transgene constructs containing wound-inducible promoters is lower than when constitutive promoters are used, both in the laboratory and in the field [77].

While achievement of expression levels of *Bt* toxins sufficient to confer protection in transgenic plants is now considered routine, considerable technical problems may still need to be overcome when specific crop species are considered (e.g., soybean; [78]). These include the construction of the synthetic coding sequence for the toxin, choice of an appropriate promoter for the expression construct, developing protocols for efficient transformation and regeneration of the plant species, and production of homozygous progeny lines containing the transgene.

Engineering the Coding Sequence to Optimize Expression The initial experiments in which Cry toxins were produced in transgenic plants showed that only low levels of Cry protein were accumulated, generally of the order of 0.01% of total protein, or less. Levels of Cry proteins were at least one order of magnitude lower than when plant proteins were expressed using similar promoters in expression constructs, leading to the deduction that the Cry protein coding sequence contained features which decreased protein production as a result of posttranscriptional events. Cry protein coding sequences are generally A-T rich compared to plants (coding%GC in *Bacillus thuringiensis*, 36%; in *Arabidopsis thaliana*, 45%; in *Oryza sativa*, 55%; Codon Usage Database, http://www.kazusa.or.jp/codon/) and codon usages thus differ significantly. Cry protein genes were reengineered, modifying the nucleotide sequence without altering the encoded amino acid sequence, to change the codon usage to one more appropriate for plants, resulting in either partially or wholly synthetic genes (reviewed by Mazier et al. [70]). Codon optimization for both dicots and monocots has been carried out. Codon-optimized synthetic genes show accumulation levels of Cry proteins of up to 1% of total protein in leaf tissue, which is adequate for complete protection of plants against pest insects [79].

The basis for poor expression of Cry proteins in transgenic plants has received comparatively little attention. Evidence suggests that the major problem is not codon usage, but instability of RNA transcripts [80, 81]. Expression of unmodified Cry protein coding sequences leads to accumulation of short, polyadenylated transcripts resulting from incorrect recognition of polyadenylation addition signal sequences within the protein coding sequence [82]. Specific modification of A-T-rich regions within the coding sequence of Cry1Ac toxin putatively responsible for transcription termination and polyadenylation (both AATAAA signal addition sequences and ATTTA upstream motifs) has been shown to lead to increased protein expression in transgenic tobacco [83]. Changing codon usage to increase GC content has eliminated

these A-T-rich regions in synthetic Cry protein genes, which therefore can produce high levels of stable mRNA.

Expression of Three-Domain Cry Toxins from Transgenes in the Chloroplast Genome

The bacterial origin of the chloroplast is reflected in differences in both the genome composition and organization, and the biochemistry of transcription and translation within the organelle, compared to the nuclear genome and transcription and translation in the nucleus and cytoplasm. The bacterial origin of the genes encoding Cry proteins suggests that expression in the plastid, from transgene constructs introduced into the plastid genome, might result in high levels of protein production. This prediction was confirmed in 1995 with a report showing that incorporation of a construct containing a complete coding sequence for the Cry1Ac protoxin protein and the plastid rRNA operon promoter into the genome of tobacco chloroplasts led to accumulation of Cry1Ac protoxin (approx. 130 kDa – i.e., with the C-terminal crystal-forming region intact) in tobacco leaves to levels of 3–5% of total protein [84]. The high level of Cry protein accumulation meant that transformed plants were effectively protected against attack by several major lepidopteran pests, even beet armyworm (*Spodoptera exigua*), a species relatively insensitive to *Bt* toxins.

Despite this highly promising initial report, expression of Cry proteins via plastid transformation has not been widely adopted, and is not used in the current commercial crops. Reasons for this are difficult to pinpoint; there are significant technical problems in achieving stable transformation of plastids, since all of the copies of the plastid genome in the cell (up to 10,000) must be transformed [85], and plastid transformation has been problematic in species other than tobacco [86]. Nevertheless, methods exist to overcome these problems [87]. Cry1, Cry2, and Cry9 proteins have been expressed in plastids of tobacco [88–91], and Cry1Ab has been expressed in soybean plastids [92], all giving high levels of protection against lepidopteran pests to the resulting plants. Overexpression of the Cry2Aa2 operon is particularly effective in giving broad-spectrum protection against a range of pests.

Commercial introduction of transgenic insect-resistant crops based on plastid transformation is almost certainly feasible, but may as yet be restricted by economic considerations, or concern over long-term stability of the transgene phenotype. The maternal inheritance of plastid-encoded characteristics shown by most plants, which means that pollen cannot disperse the transgene to non-transgenic plant stocks, is a further advantage to the method, which could be used to overcome objections to coexistence of transgenic and "organic" agricultural practices by environmental pressure groups.

Expression of Other Genes Encoding Insecticidal *Bt* Toxins

Gene constructs for expression of other *Bt* toxins follow the same principles as those outlined above for three-domain Cry toxins. For example, corn expressing the binary Cry34/35 toxin (for protection against corn rootworm) was transformed with a construct containing a constitutive promoter (maize ubiquitin-1) and synthetic coding sequences for the 44 and 14 kDa polypeptides [52], giving expression levels of up to 0.9% and 0.2% respectively of total soluble proteins in plant tissues. Details of the constructs used for expressing these, and other *Bt* toxins, are apparently not reported in the scientific literature.

Taking Transgenic Plants Expressing *Bt* Toxins into the Field

Dealing with Pest Resistance to *Bt* Toxins

The development of successful strategies for commercial deployment of "first generation" insect-resistant crops expressing a single three-domain Cry toxin has focused on a single major potential problem, the development of resistance to the insecticidal compound by the targeted pest species. Development of resistance to exogenously applied chemical pesticides has occurred in over 500 insect species [93], and field resistance to *Bt* sprays has been observed in the lepidopteran pest diamondback moth (*Plutella xylostella*). Resistance to *Bt* toxins can be produced in the laboratory within a small number of generations of many pests, showing that resistance alleles are present in pest populations at a nonnegligible level, although resistance to high doses

of specific toxins is only shown in individuals homozygous for the resistance allele. This topic has been ably reviewed in the context of the commercialization of *Bt* crops by [94]. The most common mechanism of resistance to Cry toxins in insects is mutation in a toxin receptor, leading to a failure to bind sufficient levels of toxin for lethal effects to be shown; however, the involvement of more than one "receptor" in current models for three-domain Cry toxin mechanisms of toxicity (see above) implies that multiple genetic loci for resistance in the pest are possible. Other mechanisms, such as altered proteolysis of toxins, have been proposed to account for the resistance to multiple toxins which can be produced in the laboratory.

The practical solution to prevent the development of resistance in pest populations, the "high-dose/refuge" strategy, has been extensively reviewed elsewhere [94]. In its simplest form, this strategy couples transgenic plants that are expressing sufficient levels of a specific toxin to kill all pest insects which are homozygous negative, or heterozygous, for a resistance allele, with a reservoir of untransformed plants which maintain a population of pests which have a normal frequency of resistance alleles. It assumes that the frequency of occurrence of resistance alleles is low ($<10^{-3}$). Surviving pests on the transgenic plants will be almost all homozygous positives for the resistance alleles, but will be few in number due to the low frequency of occurrence of these alleles. The non-transformed plants will produce a large number of pest insects, most of which are homozygous negative for resistance alleles. Provided that transgenic and untransformed plants are not spatially separated, mating between resistant insects selected on transgenic plants will be a rare event, and most progeny will be homozygous negative or heterozygous for resistance alleles, and thus susceptible to the insecticidal activity of the transgenic plants. In this way, both the pest population is suppressed, and any increase in the frequency of resistance alleles in the population is minimized by the continuous "diluting out" effect.

This approach has been almost wholly successful in controlling pest resistance to *Bt* toxins in agricultural use of transgenic crops over 10 years. That it has been so successful may be a result of factors other than those originally considered, since the assumption that *Bt* toxin resistance alleles occur at a very low frequency in natural populations has been called into question. Although some insect populations show resistance allele frequencies in the 10^{-3} to 10^{-2} range (e.g., tobacco budworm, *Heliothis virescens* in USA; [95]; *Sesamia nonagrioides* in Spain and Greece; [96]), estimates for pink bollworm (*Pectinophora gossypiella*) in Arizona, USA in 1997 were as high as 0.16 [97]. No evidence for selection for resistance was observed, since the frequency of resistance alleles did not increase over a 3-year monitoring period in which transgenic cotton expressing *Bt* toxins was extensively employed. A subsequent follow-up study [98] confirmed that frequencies of resistance alleles in this insect had not increased over an 8-year monitoring period, with values generally $<10^{-2}$, despite almost continuous exposure to Cry1Ac via transgenic cotton. The possibility that resistance alleles in the insect carry a significant fitness penalty is one additional factor that could account for these observations.

The success of the refuge strategy is dependent on farmers sacrificing part of their crop (untransformed plants) to maintain a pest population. This has been successfully enforced in the industrialized agriculture of developed countries, but may be more difficult to ensure when insect-resistant transgenic crops become available to rural farmers. Although greater agricultural diversity may play the same role as the refuge strategy in maintaining a pest population and decreasing selection pressure, emergence of resistance in pests to *Bt* crops has been delayed, not eliminated, and further strategies to manage it will be necessary.

Pests That Are Not Susceptible to *Bt* Toxins

As described above, most of the *Bt* toxins that have been investigated, and introduced into transgenic crops, are active against lepidopteran or coleopteran insect pests. This is partly a result of the practical requirements of agriculture, since these orders include most of the major pests. However, there are significant insect herbivores which remain outside the range of activity of *Bt* toxins that have been expressed in transgenic plants.

Dipteran pests, such as fruit flies and root flies, are serious pests in many crops, and *Bt* toxins active against diptera have been thoroughly investigated. A major problem with introducing protection against these

pests into plants is that *Bt* strains active against dipteran insects usually contain a mixture of toxins, often including both Cry and Cyt proteins (see above). These toxins act synergistically, and individual components are only of low toxicity. Introduction of genes encoding the mixture of toxins found in a typical dipteran-active *Bt* strain into a transgenic plant has yet to be attempted, although it is not beyond the capacity of existing technology.

The major order of insect herbivores outside the range of *Bt* toxins is Hemiptera, which includes aphids, plant- and leafhoppers, whitefly, and other sap-suckers which feed directly on the contents of phloem and/or xylem vessels, predominantly sucrose and free amino acids. These insects are important pests and virus vectors. No *Bt* toxins with activity against them have been found. The reason for this is not clear; receptors similar to those in other insect orders are present in these insects [99], but generally they contain very low levels of digestive proteolytic activity, as a result of ingesting nitrogen in the form of amino acids rather than protein. This lack of digestive proteolytic activity may interfere with activation of *Bt* toxins, and prevent enough activated toxin to have effects on the insect being present in the gut.

Why Haven't Plants Evolved Their Own *Bt*?

Despite the problems encountered in managing resistance of pests to *Bt* toxins, transgenic plants expressing these insecticidal proteins have proved their value in the field. However, the necessity for resistance management suggests that this solution to defense of plants against insect herbivores may not be viable on an evolutionary timescale. Endogenous expression of *Bt* toxins is not a "natural" method of defense against herbivores, since plants do not produce similar insecticidal proteins themselves. This failure on the part of plants to exploit a viable strategy for protection seems puzzling, and the obvious explanation, that plants lack the capacity to produce *Bt* toxin-like proteins, is not correct. Since introduction of suitably modified *Bt* genes gives adequate levels of protein expression for protection, there is no reason why plants could not have evolved a similar capacity. As discussed in the following section, plants have evolved a diverse array of defensive mechanisms, but make little use of proteins which are highly toxic to insect herbivores. Possibly, this is due to the relative ease with which insects can develop resistance to protein toxins which exert a very strong selection pressure on the population; although alternative hypotheses, such as the balance between investing plant resources into defense versus growth not favoring this strategy, or practical difficulties for a sessile organism in delivering toxins, should also be considered. Unfortunately, the experiments which would enable this issue to be investigated, namely, an evaluation of the "fitness" of *Bt*-expressing plants in a natural ecosystem in competition with varieties relying on endogenous defenses, and the persistence of *Bt* genes in a natural population, are unlikely to be carried out in the near future, due to obvious regulatory issues.

Whatever the reason for plants "in the wild" not using defensive proteins similar to *Bt* toxins, there is no reason to suppose that transgenic plants with engineered insect resistance will not continue to be useful in the artificial growing conditions of agriculture. Manipulation of crop plants by conventional breeding has successfully introduced characteristics such as large seed size, which were not present, and would not be viable, in their wild progenitors. Characteristics introduced into cultivated plants by plant genetic engineering do result from a process that is fundamentally different from selection, but both conventional breeding and genetic engineering are aiming for the same end results, agriculturally desirable phenotypes. Their products should be evaluated by similar criteria.

Developments to "First-Generation" Crops Expressing *Bt* Toxins

Plants Expressing Multiple Toxins ("Pyramiding")

The specificity of a single Cry toxin toward specific target pests can be a problem in the field where a secondary, minor pest species can replace the primary pest and cause serious damage to crops. An obvious method to counter this problem is to add or introduce a second *Bt cry* gene into the crop to extend the range of pests against which protection is afforded. The availability of a wide range of gene constructs encoding Cry toxins has made this a realistic possibility, with crossing singly transformed lines, or repeated transformation,

or transformation with a construct containing two genes as alternative methods for introducing the genes into one line. Monsanto's Bollgard transgenic cotton was improved by introducing a second *Bt* gene as early as 1999. Laboratory trials showed that cotton plants expressing both Cry1Ac and Cry2Ab proteins were more toxic to bollworms (*Helicoverpa zea*) and two species of armyworms (*S. frugiperda* and *S. exigua*) than cotton expressing Cry1Ac alone, even though doses in this trial were sublethal [100]. Subsequent evaluations in greenhouse and field trials [101] confirmed the superior insect resistance of plants expressing both toxins.

A further potential advantage of transgenic plants expressing two Cry proteins with differing specificities, that target different receptors in the insect, is in preventing the appearance of resistance in the pest, since multiple mutations are required to produce the loss of sensitivity to the toxins. This hypothesis was confirmed directly in work reported by [102], in which transgenic broccoli plants expressing either Cry1Ac, or Cry1C, or both proteins were produced. Plants were exposed to a population of diamondback moth (*P. xylostella*) which carried Bt resistance genes at a relatively low frequency in an extended greenhouse experiment, and results showed that selection over 24 generations led to a significant delay in the appearance of resistance in insects exposed to the pyramided two-gene plants. The success of these experiments has led to suggestions that the refuge approach to resistance management may be redundant for crops expressing multiple toxins [103]. However, some care is needed in the selection of genes in relation to potential pests, as resistance to multiple toxins has been observed in several cases. For example, a strain of the lepidopteran cotton pest *H. virescens* which has simultaneous resistance to Cry1Ac and Cry2Aa has been identified, in which the genetic bases of resistance to each toxin are different [104].

Many subsequent programs which have aimed to produce insect-resistant crops expressing *Bt* toxins have adopted the two-gene approach to broaden and improve protection against diverse pests, and to prevent resistance developing in insects (e.g., [105]). Although engineering to produce combinations of different three-domain Cry toxins is the most common approach, other potential resistance genes have been included also, such as those encoding Vip proteins [106], or even proteinase inhibitors (e.g., cowpea trypsin inhibitor; [107]). The "pyramiding" or "stacking" of resistance transgenes has been enthusiastically adopted by commercial organizations, and the recent announcement of a transgenic maize variety containing eight different transgenes by Monsanto and Dow Agrosciences [108] exemplifies this trend. This variety contains insect-resistance genes derived from both companies' research programs, active against corn rootworm and lepidopteran pests (Herculex RW = Cry34Ab1 + Cry35Ab1, Herculex I = Cry1F; YieldGard VT Rootworm/RR2 = modified Cry3Bb1, YieldGard VT PRO = Cry1A.105 + Cry2Ab2), as well as two herbicide tolerance genes (giving resistance against glyphosate and glufosinate-ammonium), and is intended to be a "one-stop" solution to pest and weed problems.

Domain Exchange in Three-Domain Cry Toxins

The separate roles played by the different domains in the process of interaction of three-domain *Bt* toxins with their receptors, and their structural independence, suggested to investigators that hybrid toxins, in which domains from different naturally occurring toxins were grafted together, would be likely to be active, and could show novel specificities in their activity toward insects. This process can be made to occur in vivo in *Bacillus thuringiensis*, using a site-specific recombination vector [109], or can be carried out in vitro using conventional molecular biology techniques, followed by expression in a microbial host. Transfer of domain III between different Cry1 proteins led to identification of this domain as conferring primary specificity to different lepidopteran species, and the generation of hybrids with broader specificity than naturally occurring toxins [110]. Subsequent work generated a Cry1Ab-Cry1C hybrid, which was highly toxic to *S. exigua*, an insect resistant to Cry1A toxins [111], and identified Cry1Ca domain III as sufficient to confer toxicity toward *Spodoptera* in a variety of hybrids [112]. In contrast to the results obtained when exchanging domain III, exchange of domain I between different Cry1 toxins did not yield biologically active proteins [113].

A measure of the potential for improvement in "natural" *Bt* toxins is shown by experiments reported by [114], in which a hybrid Cry protein, constructed by

fusing domains I and III from Cry1Ba with domain II of Cry1Ia, was expressed in transgenic potato. Plants expressing the hybrid toxin at levels up to 0.3% of total soluble protein were produced, and not only showed resistance to the lepidopteran pest potato tuber moth (*Phthorimaea operculella*), but also had a high level of resistance to Colorado potato beetle. The "parental" Cry proteins have high toxicity towards lepidopterans, but only very limited toxicity towards coleopterans such as the potato beetle. The hybrid has effectively created a novel toxicity, which is suggested to be based on interaction with a novel receptor.

Mutagenesis of Three-Domain Cry Toxins

Modification of *Bt* toxins by site-directed mutagenesis to increase toxicity towards target pests has been employed as an alternative to the "domain swap" approach. Most mutagenesis experiments on *Bt* toxins have been carried out to explore structure-function relationships in these proteins (see above; reviewed by Dean et al. [115]), but the accumulated knowledge of which parts of the protein determine specificity of interactions with receptors in the insect have been exploited to produce variants with increased activity toward target pests.

The key role of domain II in three-domain Cry proteins in mediating interactions with insect receptors was shown by a mutagenesis experiment in which altering amino acid residues in the loop regions in this domain of Cry1Ab increased its toxicity toward larvae of gypsy moth (*Lymantria dispar*) by up to 40-fold, with a corresponding increase in binding affinity to brush border membrane vesicles [116]. These results were based on expression of the recombinant protein in microbial hosts. A similar strategy was used to increase the toxicity of Cry3A protein toward target coleopteran pests [117], and of Cry4Ba toxin [118, 119] and Cry19Aa toxin [120] toward mosquito larvae. The level to which rational design of toxins is possible is shown by the engineering of toxicity toward mosquito larvae into the lepidopteran-specific toxin Cry1Aa [121]. Alternatively, a directed evolution system based on phage display technology for producing toxins with improved binding to a receptor, and thus increased toxicity, has been described [122]. Mutagenesis of domain I has also been attempted, with claims that alteration of alpha helix 7 in Cry1Ac to resemble the corresponding helix in diphtheria toxin led to increased toxicity toward cotton bollworm (*Helicoverpa armigera*) larvae [123].

The impressive achievements of toxin engineering at the level of recombinant proteins, have led to the technology being used for gene constructs designed for expression in transgenic plants, although toxins with unmodified amino acid sequences continue to be widely used (largely as they give adequate protection). One example where toxin engineering has been successfully carried out is the current commercial transgenic corn variety with resistance to corn rootworm, MON863, which expresses a modified version of the *Bt* Cry3Bb1 toxin [75]. Unmodified Cry3Bb1 is active against a number of coleopteran species, including Colorado potato beetle and corn rootworm [124], but toxicity toward western corn rootworm (*Diabrotica virgifera virgifera*) was not sufficient to give adequate protection at levels of expression achievable in corn. Modifications to the amino acid sequence increased the toxicity of the protein toward corn rootworm approximately eightfold. The nature of the modifications has not been described in the scientific literature, and is only available through reference to a series of patents (see [75]).

Fusions

As a logical extension to the transformation of plants with separate gene constructs encoding two Cry proteins, some workers have chosen to produce a single construct containing a single translationally fused coding sequence encoding both proteins. This approach has been successfully demonstrated by producing a Cry1Ab-Cry1B translational fusion protein in transgenic maize [125], although there is no apparent advantage over simpler methods for introducing two genes. The Cry1Ab-Cry1B fusion protein has also been expressed in transgenic rice [126], which was fully resistant to yellow stem borer (*Scirpophaga incertulas*).

A more interesting possibility is the introduction of extra functionality into Cry toxins by addition of sequences from other proteins which could lead to binding interactions with more potential receptors in the insect gut, extending the range of toxicity and hindering development of resistance. In work reported

by Mehlo et al. [127], the galactose-binding lectin domain (B-chain) from the ribosome-inactivating protein ricin was fused C-terminally to domain III of Cry1Ac, producing a Cry1Ac-ricin B-chain fusion protein. The fusion protein thus has the ability to bind to galactose residues in side chains of glycoproteins or glycolipids in the insect gut epithelium, as well as *N*-acetyl galactosamine residues which are bound by domain III. The fusion protein was expressed in transgenic maize and rice plants, and was shown to afford a high level of protection to larvae of stemborers (*Chilo suppressalis*) and leaf armyworm (*Spodoptera littoralis*), whereas plants expressing the unmodified Cry1Ac were susceptible to both insects. The transgenic maize plants were also resistant to a homopteran plant pest, the leafhopper *Cicadulina mbila*, although it is possible that this was an effect of the lectin domain in the fusion (see later section Lectins), since *Bt* toxins are not effective against homopteran insects.

The engineering of extended binding properties into three-domain Cry proteins to increase the range of toxicity toward insect pests is clearly possible, but needs to be approached with some caution. There is a risk that the extended range of activity will include mammalian toxicity, which would negate one of the major advantages of these insecticidal proteins.

Exploitation of Endogenous Plant Defensive Mechanisms Against Insect Herbivores

Plants have a range of endogenous mechanisms to defend themselves against insect herbivores, and use both static defense mechanisms based on the accumulation of pre-synthesized insecticidal compounds, and active defense mechanisms in which gene expression is induced as a result of insect damage (response to wounding, and responses to insect secretions), leading to the synthesis of insecticidal compounds [128]. Conventional breeding has sought to exploit endogenous insecticidal genes within a plant species, but the use of transgenic technology allows defensive compounds and mechanisms to be transferred between species, or allows the control of existing defensive systems to be altered to improve their effectiveness. The molecular biology involved in transfer of genes between plant species is technically straightforward, and does not involve the kind of reengineering necessary to make bacterial genes suitable for use in plants. This approach to increasing insect resistance in transgenic plants has almost as long a history as engineering for *Bt* Cry toxin expression, but to date has not resulted in a commercial product, or widescale adoption in agriculture. Some of the reasons for the lack of practical outcomes for this strategy will be discussed below.

Proteinase Inhibitors

Protein proteinase inhibitors (PIs) are ubiquitous in plant species. They are major components of both "static" and "active" defense in that they are accumulated in specific tissues ("static" defense), and are the major end-product in the induced response to wounding ("active" defense). They are generally small proteins, ranging in size from 4 to 25 kDa, with many different sequence families having been identified. They form tightly bound complexes with their target proteinases, which usually involve a "loop" on the inhibitor fitting into the enzyme active site (Fig. 4), blocking the site, and inactivating the enzyme. The observation that most of these inhibitors were active against digestive serine proteinases from higher animals, and not endogenous plant proteinases (where serine proteinases are comparatively rare, and not involved in protein digestion) suggested that they were defensive compounds, and bioassays in which purified PIs were fed in artificial diet confirmed that an antimetabolic effect was exerted on insect herbivores which relied on protein digestion for nitrogen supply, shown as a slower growth rate, retarded development, and increased mortality (reviewed by Garcia-Olmedo et al. and Ryan [130, 131]). Besides a direct effect on digestion of ingested proteins, PIs cause a loss of nitrogen to the insect by preventing the reabsorption of nitrogen used to produce digestive proteinases, which are normally (self)-degraded in the gut rather than excreted. The role of these proteins in induced defense against insects was shown by blocking the normal wounding response in transgenic tobacco plants by suppression of expression of the prosystemin gene, which produces the peptide hormone systemin, using antisense RNA. The transformed plants were unable to synthesize wound-induced PIs and were significantly more susceptible to herbivory by lepidopteran larvae [132]. The importance of the wounding response to

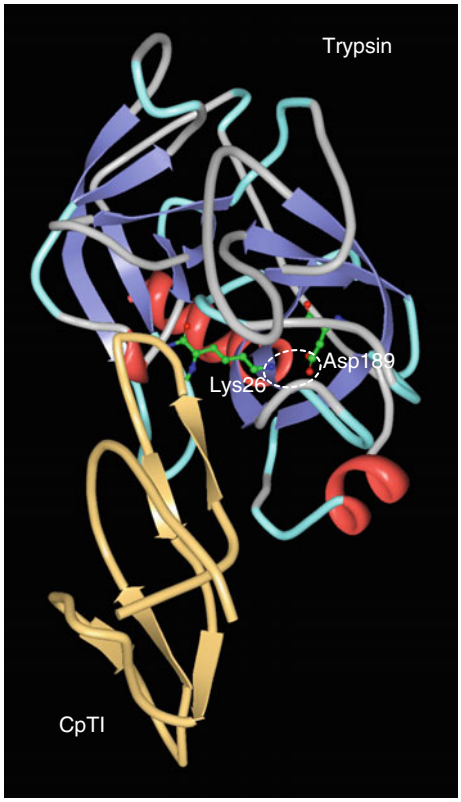

Genetic Engineering of Crops for Insect Resistance. Figure 4
Structure of a complex between a typical plant protein proteinase inhibitor (*PI*) and a target proteinase (from PDB 2g81; [129]). Structure shown in backbone representation is the complex between beta-trypsin (*top*, secondary structure color-coded in red and blue) and a Bowman-Birk PI from cowpea (*Vigna unguiculata*; *bottom*, gold). This inhibitor ("CpTI") has been expressed in transgenic plants to give partial resistance to lepidopteran larvae. The side chains responsible for the specificity-defining ion-pair interaction (dotted ellipse) are shown in ball-and-stick representation; they are Asp189 (S1′) in the substrate binding pocket of the enzyme, and Lys26 (S1) on the active site loop of the inhibitor. Other interactions take place across the contact surface between inhibitor and enzyme to form a tightly bound complex

plant defense in natural ecosystems has been extensively studied by Baldwin's group (reviewed in [133]); this outstanding body of work has established a synthesis of responses in the plant under attack, responses in neighboring plants, and responses of natural enemies of insect herbivores, with communication via volatile signals produced by the plant under attack.

A seed-expressed Bowman-Birk-type serine proteinase inhibitor from cowpea, which contained two inhibitory sites active against bovine trypsin (CpTI) was the first plant PI to be produced in another species [134], using a gene construct containing a CaMV 35S promoter. The resulting transgenic tobacco plants expressed CpTI at up to 1.0% of total soluble protein, and decreased growth and survival of tobacco budworm (*H. virescens*) by up to 50%, with similar effects on other lepidopteran larvae. Subsequent experiments carried out with wound-induced PIs showed that these also had similar effects when constitutively expressed in transgenic plants; for example, the tomato inhibitor II gene, when expressed in tobacco, was also shown to confer insect resistance [135], as did potato PI-II [136]. Both CpTi and PI-II were subsequently expressed in rice, where partial protection against stem borers was observed [137, 138]. The constitutive expression of foreign PIs could be mimicked in transgenic tomato plants by constitutive expression of the prosystemin gene (see above) leading to constitutive expression of wound-induced tomato PIs [139]. Tobacco plants modified in this manner show partial resistance to insect herbivores similar to that produced by expressing foreign PIs [140].

The problem with this strategy for producing insect-resistant plants soon became obvious; in contrast to the expression of Cry proteins, which, when optimized, routinely gave transgenic plants virtually complete protection against susceptible pests (mortality100%, damage minimal) expression of PIs only produced partial resistance. Investigation of the digestive biochemistry showed that exposure to PIs in the diets of lepidopteran and coleopteran herbivores resulted in the appearance of proteinase activities which were insensitive to the inhibitor(s) present [141, 142], or were able to degrade the ingested PIs [143]. These insects contain large families of genes encoding dietary proteinases, whose expression could be up- or downregulated by dietary inhibitors [144]. In effect, these insect herbivores were preadapted to be partially resistant to dietary PIs, as a result of similar or identical compounds being present routinely in their diet. Although expression of resistance to PIs in herbivorous

insects has a fitness penalty, shown by reduced growth on diets to which inhibitors are added, or on plants which are expressing foreign PIs, or over-expressing endogenous PIs (see above), this is not sufficient to cause mortality at a level which affords more than partial protection. In some cases, low levels of expression of a foreign PI in transgenic plants can actually result in improved insect performance, as when tobacco and *Arabidopsis* plants expressing mustard trypsin inhibitor 2 were exposed to larvae of cotton worm (*S. littoralis*; [145]).

A number of investigators have attempted to select PIs for expression in transgenic plants which are optimally active against the dietary proteinases present in specific insect pests. Attempts to develop inhibitors active against specific lepidopteran digestive serine proteinases induced by dietary PIs have not been successful. On the other hand, not all pest insects rely on serine proteinases for digestion. Many herbivorous coleopteran larvae utilize cysteine proteinases, rather than serine proteinases, as their major digestive endoproteinases, and these proteinases can be inhibited by cystatins, a family of proteins present in all kingdoms of organisms. Enzyme assays in vitro were used to characterize digestive proteinases of a coleopteran pest, *Chrysomela tremulae,* as cysteine proteinases, and to show that a cystatin from rice, oryzacystatin, was an effective inhibitor. Transgenic poplar seedlings expressing oryzacystatin were produced, and leaves from these plants were shown to be toxic to larvae of the pest [146]. This promising result does not seem to have been followed up. Expression of oryzacystatin in transgenic potato only gave partial protection against larvae of Colorado potato beetle [147], suggesting preadaptation in this pest, which is known to employ a diverse range of digestive proteinases. In an attempt to use proteinase inhibitors which insects would not be preadapted to, synthetic multidomain cysteine proteinase inhibitors based on domains found in animal and plant sources (kininogen, stefin, cystatin C, potato cystatin, and equistatin) were assembled and expressed in transgenic potato; the plants were deterrent to thrips, and gave partial resistance in greenhouse trials, but complete protection was not observed [148, 149]. Attempts to express the sea anemone cysteine/aspartic proteinase inhibitor equistatin itself in transgenic potato did not give significant levels of resistance to Colorado potato beetle, due to degradation of the inhibitor in the plant [150]. Multiple proteinase inhibitors (potato PI-II and PCI) active against two families of proteinases, serine proteinases and carboxypeptidases, have been expressed in transgenic tomato plants [151], but still only afforded partial protection against lepidopteran larvae due to adaptive mechanisms present in the insects.

In conclusion, the expression of suitable PIs in transgenic plants can give protection against lepidopteran and coleopteran pests, but has not been able to produce results comparable with those achieved by use of *Bt* toxins.

G

Amylase Inhibitors

The widespread occurrence of protein inhibitors of mammalian amylases in plants has become accepted as another defensive mechanism against herbivores (reviewed by Franco et al. [152]). Like proteinase inhibitors, these are generally small proteins, resistant to proteolysis, ranging in size from approx. 8–30 kDa. Although they are also active against insect amylases, it is not clear to what extent these proteins contribute to insect resistance in most cases, since the relatively low nitrogen content of plant tissues compared to insects means that most herbivorous insects are nitrogen limited, not carbon limited, and starch digestion is unlikely to be a limiting factor in growth. However, in the case of coleopteran herbivores whose larvae attack seeds specifically, such as seed weevils (bruchids), there is good evidence for α–amylase inhibitors from legume seeds being highly insecticidal [153], and in being causative factors in the resistance of specific varieties of legumes to bruchids [154]. These proteins belong to a different sequence family than the more common types of α–amylase inhibitors found in cereals, and are similar to legume lectins in sequence [155].

Like proteinase inhibitors, amylase inhibitors form tightly bound complexes with their target amylase (Fig. 5), although the same interaction of a loop on the inhibitor with the active site of the enzyme is not possible, since the enzyme substrate is a polysaccharide, not a polypeptide. The mechanism of toxicity clearly involves inhibition of starch digestion, since bruchid larvae exposed to the α–amylase inhibitor from French

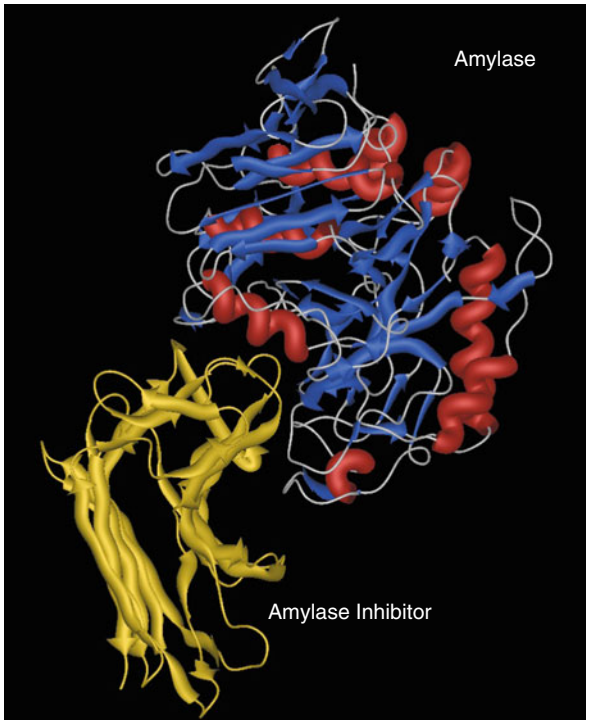

Genetic Engineering of Crops for Insect Resistance. Figure 5
Structure of a complex between a plant protein α-amylase inhibitor and an insect amylase enzyme (from PDB 1viw; [156]). Structures shown in backbone representation; α-amylase from larvae of the coleopteran storage pest *Tenebrio molitor* (yellow mealworm beetle) is shown *top right*, in red and blue (secondary structure color coding); the α-amylase inhibitor from *Phaseolus vulgaris* (French bean) is shown in gold *bottom left*. This inhibitor has been expressed in several transgenic legume species to give resistance to coleopteran pests. The inhibitor shows the typical "all β-sheet" structure of the legume lectin family of proteins. Interaction between the binding loop of the protein and the starch-binding site of the enzyme occurs across the contact surface, sterically blocking access by polysaccharides to the active site

bean (*Phaseolus vulgaris*) show induction of amylase enzymes [157], although other mechanisms of toxicity may also be present, since these proteins can cause 100% mortality in susceptible insect species at levels of <1.0% of total protein. Alternatively, these highly specialized herbivores may lack the adaptive mechanisms to plant defensive proteins shown by species that feed on a wide range of plant foodstuffs [128]. High levels of toxicity toward insects have not been observed in general with amylase inhibitors. For example, α–amylase inhibitors are not strongly toxic to lepidopteran larvae, where the alkaline environment of the gut may interfere with the formation of inhibitor-enzyme complexes. The α–amylase inhibitor from French bean is inactivated by high pH.

The isolation of a lectin-like α–amylase inhibitor gene from *P. vulgaris* [155] stimulated research in this area, and in a ground-breaking series of experiments, this gene was assembled into a construct with a strong seed-specific promoter (from the *P. vulgaris* seed lectin gene), and expressed in seeds of transgenic garden pea. The resulting seeds contained up to 3% of the foreign protein, and were highly resistant to larvae of cowpea and Azuki bean weevils [158], which do not normally attack garden peas in the field, but are stored product pests, and to larvae of the pea weevil *Bruchus pisorum* [159], which is a field pest of garden pea. In all cases larval development from eggs laid on seeds was halted at a very early stage, and damage to the crop was minimal. Subsequent experiments showed that transgenic azuki beans could also be protected against bruchid storage pests [160], and that transgenic garden pea was protected against pea weevil under field conditions [161]. The success of this strategy led to hopes that the *Phaseolus* α–amylase inhibitor gene could be incorporated into a range of crops, particularly other grain legumes such as lentils, mungbean, groundnuts, and chickpeas to give protection against a variety of bruchids. Technical problems with transformation of some of these crop species have delayed this goal being achieved, but transgenic chickpeas expressing high levels of the *Phaseolus* α–amylase inhibitor have been successfully produced [162].

Despite the success of this strategy, full agricultural deployment of transgenic crops expressing the *Phaseolus* α–amylase inhibitor gene has not taken place. Commercial reasons have played a major part in preventing widescale adoption, but safety concerns have also arisen. The protein product of the *Phaseolus* α–amylase inhibitor gene expressed in pea shows minor structural differences to the native product (i.e., expressed in *P. vulgaris*) as a result of differences in posttranslational processing (differences in the extent of glycosylation, and in minor components

resulting from proteolysis). Whereas consumption of the native form of the *Phaseolus* α–amylase inhibitor by mice did not result in immunological responses, consumption of transgenic peas expressing this protein led to the presence of circulating antibodies directed against it, and systemic immunological responses including inflammatory responses (i.e., allergic responses) to inhaled or injected protein [163]. In contrast to some earlier work claiming that consumption of transgenic plant material was harmful, this study has been published in a fully peer-reviewed journal and the quality of the research has not been disputed. Further research will be necessary to identify, and remove, the cause of this increased antigenicity. An additional potential drawback was revealed by feeding trials of transgenic peas expressing *Phaseolus* α–amylase inhibitor with pigs and chickens. These trials did not show immunological effects on animal health, but did show that starch utilization by the animals was significantly decreased due to the presence of the inhibitor in the transgenic peas when compared to non-transgenic peas, consistent with the effect of the protein on higher animal amylases [164, 165]. This factor would limit the utility of transgenic peas as animal feed.

Lectins

Lectins, or carbohydrate-binding proteins, occur throughout the plant kingdom, and in many species are accumulated in plant tissues as defensive proteins, being particularly abundant in seeds and other storage tissues, where they can account for up to 1% or more of total protein (reviewed by Peumans and van Damme and van Damme et al. [166, 167]). They are multimeric proteins containing polypeptides which range from 10 to 35 kDa in size. The insecticidal activity of lectins was first observed in assays with larvae of coleopteran species (e.g., LE QA done [168, 169]), where retardation of development, and in some cases, mortality, was observed when lectins were incorporated into diets at 1–5% of total protein. Lectins have only relatively low antimetabolic effects on lepidopteran larvae when fed in diet [170], possibly as a result of high gut pH inactivating the carbohydrate-binding activity. The mechanism of toxicity of these proteins remains obscure, but is dependent on carbohydrate binding.

Although transgenic tobacco and potato plants expressing lectins from garden pea [171] and snowdrop [172] have been produced by standard transformation techniques, and have been shown to confer partial resistance to lepidopteran larvae (>50% reductions in plant damage, with increased larval mortality and decreased growth), the availability of better insecticidal genes specific for these pests has directed this approach toward different targets. Homopteran plant pests, which are not affected by known *Bt* toxins, were shown to be susceptible to lectin toxicity when the proteins were delivered via artificial diet [173]. Susceptibility varied between species, and between lectins, but LC_{50} values as low as 6 μM have been estimated (for snowdrop lectin fed to rice brown planthopper (*Nilaparvata lugens*); [174]). Expression of the mannose-specific snowdrop lectin (*Galanthus nivalis* agglutinin; GNA) in transgenic rice plants was carried out, using both a phloem-specific (rice sucrose synthase) and a constitutive (maize ubiquitin-1) promoter [175]. The resulting plants were partially resistant to rice brown planthopper, with reductions of up to 50% in survival of immature insects to adulthood, and reduced development and fertility of survivors. Results were confirmed by independent transformations of indica rice varieties [176]. GNA-expressing rice was also resistant to other homopteran plant pests, such as green leafhopper (*Nephotettix virescens*; [177]) and whitebacked planthopper (*Sogatella furcifera*; [178]). Plants expressing both GNA and Cry1Ac were protected against both brown planthopper and striped stem borers (*C. suppressalis*), but no synergistic effects between the two insecticidal proteins was observed [179]. Further progress on this research has been limited, due to concerns about possible adverse consequences to higher animals of ingesting snowdrop lectin. While earlier data must be regarded as unreliable, a recent study found that no adverse effects of consumption of transgenic rice expressing GNA by rats, although significant differences in some parameters to a control group were observed [180]. GNA expression has also been engineered into potato [181] and maize [182], to give partial resistance to peach–potato aphid (*Myzus persicae*) and corn leaf aphid (*Rhopalosiphum maidis*), respectively. However, these insects are insensitive to lectin toxicity, and only marginal effects on fecundity were observed.

Introduction of foreign lectin genes into plants has become established as a potential method for engineering insect resistance, although with the lectins tested at best only partial protection against homopteran pests is conferred, and some species are relatively insensitive to the effects of lectins. As is the case with PIs, it is likely that plant pests are preadapted to the presence of lectins as defensive compounds, and are able to tolerate the toxic effects to varying degrees, although responses induced in insects by ingested lectins have not been characterized. Attempts have been made to select lectins which are the most effective toxins against target insect pests; a mannose-specific lectin expressed specifically in garlic leaves (ASA-L) was observed to show a high level of toxicity toward homopteran pests [183]. A gene encoding this lectin has been engineered into a variety of transgenic plant species, including tobacco [184] and Indian mustard [185], in both cases producing partial resistance to aphid species, with reduced survival and fecundity. Expression of this lectin in transgenic rice using constitutive [186] or phloem-specific promoters [187] gave protection against homopteran pests comparable to, or slightly better than, earlier transformations using gene constructs encoding GNA. The transgenic rice plants expressing ASA-L were shown to decrease transmission of Rice Tungro Virus by its insect vector (green leafhopper), presumably by causing decreased feeding by the pest [188].

Despite these encouraging results, widescale adoption of transgenic crops expressing lectins will probably not occur unless a major commercial company is able to gain exclusive marketing rights, and invests in pushing the transgenic varieties through the regulatory process. This is unlikely to happen, as the technology is not readily protectable by patenting.

Oxidative Enzymes

Induction of polyphenol oxidase (PPO) synthesis is one of the end-results of the plant wounding response [189], and it would seem reasonable to suppose that increased levels of this enzyme would lead to enhanced resistance to insect attack. PPO activity leads to tissue browning, which has been correlated with enhanced insect resistance. The oxidative cross-linking of tannins to proteins catalyzed by PPO decreases protein digestibility, and limits nitrogen availability [190]. However, there is little or no evidence that PPO levels are correlated with insect resistance (e.g., [191]). High-level, constitutive over expression of a poplar PPO gene in transgenic poplar seedlings led to levels of PPO up to 50x higher than normal in plant tissues [192], but these plants had only marginal effects on larvae of the lepidopteran insect pest forest tent caterpillar (*Malacosoma disstria*). No feeding deterrence was observed, and there was no effect on larval growth or survival except under conditions where larval survival was poor on controls. PPO activity was detected in insect gut and frass, so the negative results were not due to enzyme inactivation. The conclusion that herbivorous insects are preadapted to be able to deal with PPO activity, as a result of exposure to the wounding response on an evolutionary timescale (in a similar manner to preadaptation to PIs – see above) is difficult to avoid.

Peroxidase activity is also induced when plants are stressed, or attacked by pathogens, as part of a lignification response, and several attempts have been made to over-express peroxidases in transgenic plants to enhance insect resistance, despite a lack of clear-cut evidence that peroxidase activity in plant tissues is toxic to insect herbivores. Initial results using tobacco as the host plant, with over-expression of tobacco anionic peroxidase, showed only marginal effects [193], although limited broad-range protection against a variety of pests was observed in the field [194]. The limited protection afforded by this technique argues against further development.

Other Plant Proteins

Ribosome inactivating proteins (RIPs) and chitinases have also been viewed as defensive proteins in plants, although it is not clear that they are part of defense against insect herbivores. Both types of proteins have been expressed in transgenic plants, with variable results in conferring insect resistance. Expression of a maize RIP in transgenic tobacco resulted in very low levels of protection against corn earworm (*H. zea*), which were barely statistically significant [195]. Plant chitinases in general show low toxicity toward insects, but a poplar chitinase, designated WIN6, was selected on the basis that its expression was induced by insect attack. Expression of WIN6 in trangenic tomato plants

led to partial protection against larvae of Colorado potato beetle, with retardation of larval development observed [196]. Expression of the chitin-degrading enzyme *N*-acetylhexosaminidase from *Arabidopsis* in various transgenic plant tissues also gave some protective effects against lepidopteran larvae [197], but it is difficult to see what advantages over other strategies this approach could give. Orally ingested insect chitinases are strongly toxic to lepidopteran larvae (e.g., [198]). However, expression in transgenic plants gave only partial protection against insect herbivores [199], or, in one case, increased susceptibility to attack [200]. Expression of chitinase A from baculovirus AcMNPV in transgenic tobacco gave similar results, with only small effects on lepidopteran larvae and aphids [201].

Engineering Secondary Metabolism for Plant Defense

Compounds synthesized as the end-products of secondary metabolism play major roles in both constitutive and induced defense against insect herbivores in many plant species (reviewed by Wittstock and Gershenon [202]). The idea that these compounds could be used as insecticides has been a part of agriculture for thousands of years, and has been exploited successfully by synthetic chemistry in the production of classes of insecticides such as pyrethroids, based on terpenoid esters produced by flowers of pyrethrums (Chrysanthemums). Although the concept of synthesizing a foreign, insecticidal secondary metabolite in a transgenic plant developed concurrently with plant transformation technology, the biosynthesis of most secondary compounds was poorly understood, and the necessity of cloning and introducing a series of genes expressing biosynthetic enzymes to produce a secondary metabolite was considered beyond the techniques available at the time. Anticipation of problems in ensuring controlled co-expression of a series of biosynthetic genes has proved to be over-pessimistic, and plants containing multiple expressing transgenes have been produced without difficulty.

The explosion of knowledge brought about by large-scale cDNA sequencing programs and the *Arabidopsis* genome program has resulted in a much better understanding of secondary metabolism, with many biosynthetic pathways now reasonably well understood, and clones encoding biosynthetic enzymes available. The first successful demonstration that a foreign secondary compound could confer insect resistance in a transgenic plant [203] exploited a biosynthetic pathway for cyanogenic glycosides. The cereal *Sorghum bicolor* produces a cyanogenic glycoside, dhurrin, by a biosynthetic pathway starting from the amino acid tyrosine, a product of primary metabolism. Two oxidation reactions catalyzed by cytochrome P450 oxidases generate *p*-hydroxymandelonitrile, which is then glycosylated by a UDP-glycosyltransferase to form dhurrin. The three sorghum enzymes responsible were cloned and assembled into expression constructs using constitutive (CaMV 35S) promoters [204], and *Arabidopsis* plants were successively transformed with a construct containing both P450 oxidase sequences, and the glycosyl transferase sequence. All the enzymes were localized correctly (to endoplasmic reticulum membranes) and functioned properly. Surprisingly, little disruption to endogenous metabolism was observed in the transgenic plants expressing medium levels of dhurrin, and accumulation of pathway intermediates was not observed. The implication is that the plastic nature of plant metabolism can accommodate and regulate activity in new biosynthetic pathways that are introduced. The resulting plants included individuals producing levels of dhurrin similar to sorghum plants in leaf tissue (up to 4 mg/g fresh weight) and produced hydrogen cyanide on tissue damage (due to the hydrolysis of dhurrin by an endogenous *Arabidopsis* enzyme). The dhurrin-expressing plants showed enhanced resistance to attack by the flea beetle *Phyllotreta nemorum*, a specialist feeder on crucifers; adult beetles avoided feeding on dhurrin-expressing leaves when offered a choice, and larvae under no-choice conditions either failed to initiate feeding, or on initiating feeding showed a significant level of mortality. These initial results clearly imply that production of high levels of dhurrin in transgenic *Arabidopsis* caused phenotypic abnormalities, but subsequent refining of the technology allowed accumulation of dhurrin at up to 4% dry weight in *Arabidopsis* tissues without deleterious effects on plant growth [205]; expression levels of the UPD-glycosyl transferase must be high enough to prevent accumulation of the *p*-hydroxymandelonitrile intermediate.

Although these results represent science of the highest quality, this method is of marginal usefulness for crop protection as it stands, due to the dhurrin end product being toxic to higher organisms, due to the production of hydrogen cyanide when it is hydrolyzed. Worse, many insect herbivores, particularly those which have a polyphagous feeding habit, can detoxify cyanide [206]. However, the feasibility of engineering secondary metabolism in crop plants has now been established. Expression of the cassava cyanogenic glycosides, linamarin and lotaustralin (derived from valine and isoleucine respectively), has also been achieved in *Arabidopsis* [207], and grape vine root cultures have been engineered to produce dhurrin [208], although in this case no protection against root aphids was observed. Other types of secondary metabolites have also been exploited; production of the alkaloid caffeine from its precursor xanthosine in tobacco was achieved by the introduction of three genes encoding *N*-methyl transferases [209]. The resulting plants contained up to 5 μg/g fresh weight caffeine in leaves, and showed a strong feeding deterrent effect toward a generalist lepidopteran herbivore, *Spodoptera litura*. An alternative approach to modifying secondary metabolism was taken by [210], who introduced a gene encoding β-glucosidase from *Aspergillus niger* into tobacco plants, and demonstrated that transgenic plants expressing the enzyme had insecticidal activity toward whiteflies (*Bemisia* spp.) and dipterans (flies), putatively due to hydrolysis of unidentified glycosides in the plant (although the greater density of secretory trichomes observed in transgenic plants may also have been significant). Further developments in this area can be expected.

Besides engineering, secondary metabolism to produce defensive compounds normally present in other plant species, the biosynthetic capacity of plants can be used to produce a variety of volatile secondary compounds used for communication. Better understanding of the terpenoid biosynthesis pathways has led to the production of a number of transgenic plants with altered volatile composition (reviewed by Aharoni et al. [211]). Suppression of expression of a cytochrome P450 oxidase gene expressed in trichomes by RNAi led to transgenic tobacco plants which deterred aphid colonization [212], due to the final step in production of the diterpenoid cembratriene-diol being blocked, resulting in accumulation of the precursor, cembratriene-ol. These compounds are both volatile and components of trichome secretions. Transgenic *Arabidopsis* plants constitutively over-expressing a dual linalool/nerolidol synthase in plastids produced significant amounts of linalool, both as a free alcohol (volatile) and as glycosylated derivatives, and were repellent to aphids (*M. persicae*) when tested in a choice experiment [213]. Modifications to isoprenoid synthesis in *Arabidopsis* have also been shown to attract predatory mites, which could protect plants by destroying pests [214]. This strategy of attracting natural enemies to pests has also been exemplified by transforming *Arabidopsis* with the maize terpene synthase gene TPS10, which is responsible for producing sesquiterpene volatiles emitted by maize. The resulting plants emitted the volatiles normally produced in maize and attracted parasitoid wasps which attack maize pests [215]. A different approach to utilizing terpene production in transgenic plants exploits the activity of the sesquiterpene (E)-β-farnesene as an alarm pheromone in aphids, which causes cessation of feeding and avoidance, as well as acting as an attractant for aphid predators and parasitoids [216]. *Arabidopsis* was transformed with an (E)-β-farnesene synthase gene from mint, under control of a constitutive promoter (CaMV 35S); resulting plants produced (E)-β-farnesene as a volatile. The transgenic plants showed significant levels of aphid deterrence in choice experiments, and were attractive to the aphid parasitoid *Diaeretiella rapae*. Experiments which engineer the volatiles emitted by plants are an exciting area of research at present, which has established the role that volatiles emitted by plants play in the interactions between plants, herbivores, and natural enemies at the tritrophic level. This technology has yet to show that it is a practical method for crop protection in the field, but practical applications look likely to follow.

Some Novel Approaches

Many other approaches to engineering insect resistance in transgenic plants have been proposed, and progressed to varying degrees. The following section gives an overview of some of the most promising of these approaches, which have been taken forward to the stage of demonstrating feasibility by producing insect-resistant plants.

Of necessity, many other interesting ideas have had to be omitted, such as transformation of plants with transcription factors which alter gene expression [217, 218], or the use of transgenic plants expressing potentially toxic proteins from insects [219] or insect peptide hormones [220]. Despite the lack of commercial deployment of any of the insect-resistant transgenic plant other than those expressing proteins derived from *Bt*, this field of research is active and new approaches will continue to be put forward and evaluated.

Photorhabdus luminescens Insecticidal Proteins

Photorhabdus luminescens is an enterobacterial symbiont of entomophagous (insecticidal) nematodes of *Heterorhabditis* species, used for small-scale biological control of insect pests. The bacteria are present in the nematode gut, and when nematodes enter an insect host, bacterial cells are released into the insect circulatory system. The bacterial cells release toxins which cause cell death, leading to a lethal septicemia, providing a substrate for both bacteria and nematodes to grow on [221, 222]. The toxins are present as high-molecular-weight (M_r approx. 10^6) complexes, which are toxic when injected or fed to insects from four major orders of agricultural pests. The complex has been separated into four components, encoded by genetic loci *tca*, *tcb*, *tcc*, and *tcd*; the products of *tca* and *tcd* are toxic individually when fed to lepidopteran larvae. The mechanism of action of the toxins remains unresolved. Subsequent investigation has shown that *Photorhabdus* contains a large number of potentially insecticidal components, some of which are only toxic by injection, whereas others are orally toxic (reviewed by ffrench-Constant [223]); a variety of mechanisms of toxicity, including promotion of apoptosis, seems to be exploited by the bacterium. This presence of a reservoir of redundant insecticidal activities, reminiscent of the situation in *Bacillus thuringiensis*, led to *Photorhabdus* being put forward as a successor to *Bt* as a source of insecticidal genes for expression in transgenic plants.

In order to be able to exploit insecticidal genes, investigators have sought to isolate single toxic proteins from *Photorhabdus*. Two proteins, designated toxin A and toxin B, were isolated from culture supernatant and shown to be orally toxic [224]. They exist as high-molecular-weight complexes (approx. 860 kDa) in solution, and each consist of two polypeptides, 201 and 63 kDa molecular weight. The mature polypeptides are produced from single precursor protoxin polypeptides of 283 kDa by proteolysis by endogenous bacterial proteinases. The 283 kDa protoxin A is the product of a gene designated *tcdA in Photorhabdus,* which has been cloned and assembled into expression constructs for use in transgenic plants. Expression levels of mRNA and protein were improved by adding 5′ and 3′ UTR sequences from a tobacco osmotin gene, but the coding sequence was not reengineered. Expression in transgenic *Arabidopsis* gave plants that contained intact protoxin, with a range of expression levels [225]; expression of toxin A at levels above 0.07% of total soluble protein in leaves gave almost complete protection against larvae of the lepidopteran tobacco hornworm (*M. sexta*). The toxin is not species specific, and leaf extracts were also toxic to the coleopteran corn rootworm (*Diabrotica undecimpunctata*). Commercial development of this technique is highly likely.

Entomophagous nematodes of *Steinernema* species also contain mutualistic bacteria, of *Xenorhabdus* species, which produce insecticidal toxins. These proteins could also be exploited to produce insect resistance in transgenic plants, but have not yet received as much attention as *Photorhabdus* toxins [223].

Cholesterol Oxidase

The identification of a protein from *Streptomyces* that was highly insecticidal to larvae of the coleopteran pest cotton boll weevil (*Anthonomus grandis*) resulted from a screening program assaying culture filtrates of different bacterial species [226]. The protein, which was toxic at levels comparable to a *Bt* three-domain Cry protein, was identified as a cholesterol oxidase. It was able to lyse the midgut epithelium in the insect. The mechanism of action involves the activity of the enzyme, since no activity is seen in lepidopteran larvae where the gut pH is high, and the enzyme has low activity, but may also involve effects on membrane-bound alkaline phosphatase [227]. Oxidation of membrane sterols such as cholesterol in the insect gut epithelium can destabilize membranes, leading to cell lysis as observed. However, expression of this protein in transgenic plants could prove problematic, since

it is equally capable of oxidizing sterols in plant cell membranes. The encoding gene for the cholesterol oxidase was isolated, and assembled into expression constructs containing either the complete coding sequence, the mature protein coding sequence, or the coding sequence fused to a chloroplast targeting peptide from the *Arabidopsis ribulose* bisphosphate carboxylase (RuBisCO) small subunit gene [228]. No codon optimization was carried out. Transgenic tobacco plants were produced by transformation of the nuclear genome, and all constructs were shown to result in synthesis and accumulation of active enzyme. The constructs which omitted the chloroplast targeting peptide caused protein to accumulate in the cytoplasm, and these plants were developmentally abnormal, possibly as a result of interference with plant sterol hormone signaling pathways. Plants in which the enzyme was localized in chloroplasts were phenotypically normal. Leaf tissue from all transgenic plants was toxic to boll weevil larvae when fed as a component of an artificial diet.

This work does not seem to have been progressed beyond the stage of a demonstration of concept, and no further references to it are present in the scientific literature. This gene would seem a good candidate for introduction into the chloroplast genome to engineer insect resistance, although potential effects on chloroplast membrane systems would remain a drawback.

Avidin as an Insecticidal Protein

Exploitation of the biotin-binding properties of the avian egg white protein avidin (and its bacterial functional homologue, streptavidin) in a variety of biochemical techniques has obscured its role as a defensive protein, which is toxic to bacteria. The antibacterial activity is based on its essentially irreversible binding of biotin, leading to this essential enzyme cofactor being unavailable. The insecticidal activity of avidin was recognized in 1993, when assays carried out in artificial diet showed toxicity to coleopteran and lepidopteran larvae at levels as low as 10 ppm in diet (estimated as of the order of 0.01% of total protein), although the level necessary to show toxicity was up to 100x higher for other pest species. The toxic effect was eliminated by addition of biotin to diets, suggesting that the mechanism of avidin insecticidal activity is also through biotin sequestration. Both growth reduction and mortality were observed, and the suggestion was made that gene constructs expressing avidin could provide protection against insect pests in transgenic plants [229]. Subsequent assays confirmed that susceptibility to avidin as an insecticide varies widely between different insect species, and that biotin carried over in the egg between generations had a significant effect on subsequent avidin toxicity [230].

Initial reports of expression of avidin in transgenic maize were focused on producing the protein as a high-value product [231]. An expression construct containing a codon-optimized avidin coding sequence with an N-terminally fused signal peptide from barley α-amylase, driven by the maize ubiquitin-1 promoter, resulted in expression levels of avidin of >2.0% of total protein in seed. Seed from these plants was subsequently bioassayed for resistance to larvae of three different coleopteran storage pests, including red flour beetle (*Tribolium castaneum*), with 100% mortality at avidin levels above 100 ppm of seed (approx. 0.1% of total protein). However, not all pests were as susceptible; larvae of the larger grain borer, *Prostephanus truncatus*, were effectively insensitive to avidin, whether added to artificial diet or expressed in transgenic plant material. The engineered maize was nontoxic to mice over 21 days [232]. Subsequent reports confirmed the insecticidal effects of avidin expressed in transgenic plants: these include protection of tobacco against noctuid lepidopterans [233], using vacuolar targeting sequences from potato proteinase inhibitors to direct avidin accumulation in the vacuole at levels up to 1.5% of total leaf protein [234]; protection of apple against lepidopteran pests [235]; and protection of rice against coleopteran stored grain pests, using a similar approach to that used for maize [236]. Targeting of the foreign protein to vacuolar or similar compartments is important; expression of streptavidin in tomato using plant and bacterial signal peptides and strong promoters led to developmental abnormalities in the plants, which could be corrected by topical application of biotin, suggesting that sequestration of cellular biotin is equally detrimental for plants as well as insects [237].

Despite many promising results, this technology appears to have failed to gain any acceptance for agricultural crops, as illustrated by a recent study in which seed meal from transgenic avidin-expressing maize was tested as an insecticide for topical application to stored maize [238]. Studies have shown that avidin can increase the protection afforded by *Bt* expression in transgenic plants against insect pests which have limited susceptibility to the toxin (e.g., potato expressing Cry3A; [239]), but it is clear that little further development in this area is taking place.

RNA Interference Using Double-Stranded RNA

Downregulation of gene expression by double-stranded RNA (dsRNA) corresponding to part or all of a specific gene transcript has been used as a research technique in insect genetics since 1998. The method has been based on delivery of synthetic dsRNA produced in vitro by injection into insect cells or tissues, which is clearly not practical for applications in crop protection. However, recent results have shown that dsRNA can be introduced into insects as a component of artificial diet, and is effective in downregulating genes normally expressed in gut tissue. This technique has been used to downregulate the production of a gut carboxylesterase in larvae of the lepidopteran *Epiphyas postvittana* (light brown apple moth; [240]), leading to suppression of mRNA in the insect. More significantly, two recent papers show that dsRNA can be delivered to insect pests by expression in plant material, and that this can lead to an insecticidal effect when pests are exposed to plants. Transgenic tobacco and *Arabidopsis* plant material expressing dsRNA directed against a cotton bollworm detoxification enzyme (cytochrome P450 gene CYP6AE14) for gossypol suppressed expression of the gene, and caused the insect to become more sensitive to gossypol in the diet, leading to reduced performance compared to controls [241]. A similar technique was used to suppress expression of a V-type ATPase in larvae of the coleopteran *Diabrotica virgifera virgifera* (Western corn rootworm); transgenic corn plants producing dsRNA directed against this gene showed protection against feeding damage by the insect [242]. The feasibility of using dsRNA in crop protection strategies has thus been demonstrated. This approach holds great promise for future development, as it allows a wide range of potential targets for suppression of gene expression in the insect to be exploited.

Insect-Resistant Genetically Engineered Crops and Sustainability

The success of Bt-expressing crops in the field has been a direct result of taking "sustainability" into account in their introduction, particularly with respect to managing the emergence of pest resistance to the toxins through the refuge strategy, as described earlier. Even organizations hostile to Genetic Engineering technology, such as organic growers in the USA, have reported that *Bt* cotton and corn have reduced insecticide usage significantly (by up to 0.2 kg/ha/year), showing that these crops are compatible with the goals of "sustainable" agriculture [243].

The "sustainability" of transgenic insect-resistant crops has also been examined in terms of potential effects on the wider ecosystem in which the plants are grown. Numerous studies have been carried out to effects on predators and parasites at the third trophic level, and on nontarget insects and other invertebrates. Some initial reports which did report negative effects were based on dubious assumptions, or used experimental designs which had little relevance to field conditions (e.g., the supposed threat to monarch butterflies posed by transgenic *Bt* corn; reviewed by Gatehouse et al. [244]). Nevertheless, it must be the case that if a pest population is decreased as a result of endogenous resistance in crops, then there will be a "knock on" effect to the wider ecosystem, and particularly to predators and parasites of the pest species, when the resistant crop is compared to a nonresistant one that is not treated with pesticide. However, this is not a realistic comparison, since in agricultural practice a crop that does not have endogenous resistance is treated with exogenous insecticides. The use of the refuge strategy allows significant pest populations to be present, and thus can support both beneficial insects which attack the pest, and a wider ecosystem, which would be destroyed by exogenous insecticide application.

Looking to the future, wider use of insect-resistant transgenic crops could contribute positively to "sustainability" in agriculture in general, by further decreasing

insecticide usage and thereby decreasing energy inputs. However, the "sustainability" of the insect-resistant crops themselves is going to come under increasing pressure, as less controlled deployment of insect-resistant plants evades the present compulsory use of the refuge strategy, and use of crop varieties with multiple *Bt* toxins renders the refuge strategy apparently less necessary to prevent pest resistance to *Bt* toxins developing. Field resistance to *Bt* crops has been observed recently (reviewed by Tabashnik et al. [245]), but is manageable using existing practices, or modifications of them. The sustainability of relying on one mechanism of crop protection can be questioned, especially as plants in general have evolved mixed defense strategies [246]. In the longer term, a wider range of strategies for producing insect-resistant plants is going to be necessary, not only to deal with the potential for nonspecific resistance to *Bt* toxins, but to extend the range of crop pests that can be targeted, and further reduce the application of pesticides.

Future Directions

After 20 years, insect-resistant transgenic crops have been a greater success in some ways than the early experiments suggested, but have failed to meet all the hopes that were initially raised. The success is self-evident when the widescale adoption of the technology in certain crops such as cotton and maize is considered, and documented evidence of reductions in damage to human health and the environment as a result of decreases in the use of exogenously applied pesticides. The failure does not lie in any technical shortcomings in the science, although improvements and new strategies are always possible; it lies in a failure to disseminate the technology as widely as should have been the case, so that it remains largely in the hands of commercial organizations, and is limited to the major crops. Is it an unrealistic hope to anticipate that after another 20 years, amateur gardeners in developed countries will be able to choose to buy seed to grow genetically engineered cabbages, which will be resistant to cabbage white butterfly larvae, in their allotments and gardens? Or that rural farmers in developing countries will have free access to engineered rice varieties, suitable for their growth conditions, that are resistant to pests such as stemborers? Both these aims have been scientifically achievable for at least the last 10 years, and it is surely about time that a more rational approach, which cuts through both the largely futile debate about the rights and wrongs of plant genetic engineering, and the protectionism of agrochemical companies, was taken to address the looming problem of producing enough crops to meet humanity's needs.

Bibliography

Primary Literature

1. Barton KA, Whitely HR, Yang N-S (1987) *Bacillus thuringiensis* δ-endotoxin expressed in transgenic *Nicotiana tabacum* provides resistance to Lepidopteran insects. Plant Physiol 85: 1103–1109
2. Fischhoff DA, Bowdish KS, Perlak FJ, Marrone PG, McCormick SH, Niedermeyer JG, Dean DA, Kusano-Kretzmer K, Mayer EJ, Rochester DE, Rogers SG, Fraley RT (1987) Insect tolerant transgenic tomato plants. Bio/Technology 5:807–813
3. Vaeck M, Reynaerts A, Hofte H, Jansens S, De Beuckeleer M, Dean C, Zabeau M, Van Montagu M, Leemans J (1987) Transgenic plants protected from insect attack. Nature (London) 328:33–37
4. Toenniessen GH, O'Toole JC, DeVries J (2003) Advances in plant biotechnology and its adoption in developing countries. Curr Opin Plant Biol 6:191–198
5. Shelton AM, Zhao J-Z, Roush RT (2002) Economic, ecological, food safety, and social consequences of the deployment of *Bt* transgenic plants. Annu Rev Entomol 47:845–881
6. Aronson AI, Shai Y (2001) Why *Bacillus thuringiensis* insecticidal toxins are so effective: unique features of their mode of action. FEMS Microbiol Lett 195:1–8
7. de Maagd RA, Bravo A, Crickmore N (2001) How *Bacillus thuringiensis* has evolved specific toxins to colonize the insect world. Trends Genet 17:193–199
8. Damgaard PH, Hansen BM, Pedersen JC, Eilenberg J (1997) Natural occurrence of *Bacillus thuringiensis* on cabbage foliage and in insects associated with cabbage crops. J Appl Microbiol 82:253–258
9. Bizzarri MF, Bishop AH (2007) Recovery of *Bacillus thuringiensis* in vegetative form from the phylloplane of clover (*Trifolium hybridum*) during a growing season. J Inverteb Pathol 94: 38–47
10. Bernhard K, Jarrett P, Meadows M, Butt J, Ellis DJ, Roberts GM, Pauli S, Rodgers P, Burges HD (1997) Natural isolates of *Bacillus thuringiensis*: worldwide distribution, characterization, and activity against insect pests. J Inverteb Pathol 70:59–68
11. Crickmore N, Zeigler DR, Feitelson J, Schnepf E, Van Rie J, Lereclus D, Baum J, Dean DH (1998) Revision of the nomenclature for the *Bacillus thuringiensis* pesticidal crystal proteins. Microbiol Mol Biol Rev 62:807–813
12. Berry C, O'Neil S, Ben-Dov E, Jones AF, Murphy L, Quail MA, Holden MTG, Harris D, Zaritsky A, Parkhill J (2002) Complete

sequence and organization of pBtoxis, the toxin-coding plasmid of *Bacillus thuringiensis* subsp. *israeliensis*. Appl Environ Microbiol 68:5082–5095
13. Parker MW, Feil SC (2005) Pore-forming protein toxins: from structure to function. Prog Biophys Mol Biol 88:91–142
14. Li J, Carrol J, Ellar DJ (1991) Crystal structure of insecticidal δ-endotoxin from *Bacillus thuringiensis* at 2.5 Å resolution. Nature 353:815–821
15. Grochulski P, Masson L, Borisova S, Pusztai-Carey M, Schwartz JL, Brousseau R, Cygler M (1995) *Bacillus thuringiensis* CryIA(a) insecticidal toxin: crystal structure and channel formation. J Mol Biol 254:447–464
16. Morse RJ, Yamamoto T, Stroud RM (2001) Structure of Cry2Aa suggests an unexpected receptor binding epitope. Structure 9:409–417
17. Galitsky N, Cody V, Wojtczak A, Ghosh D, Luft JR, Pangborn W, English L (2001) Structure of the insecticidal bacterial δ-endotoxin CryBb1 of *Bacillus thuringiensis*. Acta Crystallogr D 57:1101–1109
18. Boonserm P, Mo M, Angsuthanasombat C, Lescar J (2006) Structure of the functional form of the mosquito larvicidal Cry4Aa toxin from *Bacillus thuringiensis* at a 2.8-Angstrom resolution. J Bacteriol 188:3391–3401
19. Boonserm P, Davis P, Ellar DJ, Li J (2005) Crystal structure of the mosquito-larvicidal toxin Cry4Ba and its biological implications. J Mol Biol 348:363–382
20. de Maagd RA, Bravo A, Berry C, Crickmore N, Schnepf HE (2003) Structure, diversity and evolution of protein toxins from spore-forming entomopathogenic bacteria. Annu Rev Genet 37:409–433
21. Bravo A, Sánchez J, Kouskoura T, Crickmore N (2002) N-terminal activation is an essential early step in the mechanism of action of the *B. thuringiensis* Cry1Ac insecticidal toxin. J Biol Chem 277:23985–23987
22. Bravo A, Gill SS, Soberón M (2007) Mode of action of *Bacillus thuringiensis* Cry and Cyt toxins and their potential for insect control. Toxicon 49:423–435
23. Knight P, Crickmore N, Ellar DJ (1994) The receptor for *Bacillus thuringiensis* CryIA(c) delta-endotoxin in the brush border membrane of the lepidopteran *Manduca sexta* is aminopeptidase N. Mol Microbiol 11:429–436
24. Vadlamudi RK, Weber E, Ji I, Ji TH, Bulla LA Jr (1995) Cloning and expression of a receptor for an insecticidal toxin of *Bacillus thuringiensis*. J Biol Chem 270:5490–5494
25. Valaitis AP, Jenkins JL, Lee MK, Dean DH, Garner KJ (2001) Isolation and partial characterization of Gypsy moth BTR-270, an anionic brush border membrane glycoconjugate that binds *Bacillus thuringiensis* Cry1A toxins with high affinity. Arch Insect Biochem Physiol 46:186–200
26. Jurat-Fuentes JL, Adang MJ (2004) Characterization of a Cry1Ac-receptor alkaline phosphatase in susceptible and resistant *Heliothis virescens* larvae. Eur J Biochem 271: 3127–3135
27. Fernández LE, Aimanova KG, Gill SS, Bravo A, Soberón M (2006) A GPI-anchored alkaline phosphatase is a functional midgut receptor of Cry11Aa toxin in *Aedes aegypti* larvae. Biochem J 394:77–84
28. Krishnamoorthy M, Jurat-Fuentes JL, McNall RJ, Andacht T, Adang MJ (2007) Identification of novel CrylAc binding proteins in midgut membranes from *Heliothis virescens* using proteomic analyses. Insect Biochem Mol Biol 37:189–201
29. Gahan LJ, Gould F, Heckel DG (2001) Identification of a gene associated with *Bt* resistance in *Heliothis virescens*. Science 293:857–860
30. Yang YJ, Chen HY, Wu SW, Yang YH, Xu XJ, Wu YD (2006) Identification and molecular detection of a deletion mutation responsible for a truncated cadherin of *Helicoverpa armigera*. Insect Biochem Mol Biol 36:735–740
31. Xie R, Zhuang M, Ross LS, Gómez I, Oltean DI, Bravo A, Soberón M, Gill SS (2005) Single amino acid mutations in the cadherin receptor from *Heliothis virescens* affect its toxin binding ability to Cry1A toxins. J Biol Chem 280:8416–8425
32. Tsuda Y, Nakatani F, Hashimoto K, Ikawa S, Matsuura C, Fukada T, Sugimoto K, Himeno M (2003) Cytotoxic activity of *Bacillus thuringiensis* Cry proteins on mammalian cells transfected with cadherin-like Cry receptor gene of *Bombyx mori* (silkworm). Biochem J 369:697–703
33. Soberón M, Pardo-López L, López I, Gómez I, Tabashnik BE, Bravo A (2007) Engineering modified *Bt* toxins to counter insect resistance. Science 318:1640–1642
34. Herrero S, Gechev T, Bakker PL, Moar WJ, de Maagd RA (2005) *Bacillus thuringiensis* Cry1Ca-resistant *Spodoptera exigua* lacks expression of one of four aminopeptidase N genes. BMC Genomics 6:96
35. Rajagopal R, Sivakumar S, Agrawal N, Malhotra P, Bhatnagar RK (2002) Silencing of midgut aminopeptidase N of *Spodoptera litura* by double-stranded RNA establishes its role as *Bacillus thuringiensis* toxin receptor. J Biol Chem 277: 46849–46851
36. Sivakumar S, Rajagopal R, Venkatesh GR, Srivastava A, Bhatnagar RK (2007) Knockdown of aminopeptidase-N from *Helicoverpa armigera* larvae and in transfected Sf21 cells by RNA interference reveals its functional interaction with *Bacillus thuringiensis* insecticidal protein Cry1Ac. J Biol Chem 282:7312–7319
37. Gill M, Ellar D (2002) Transgenic *Drosophila* reveals a functional *in vivo* receptor for the *Bacillus thuringiensis* toxin Cry1Ac1. Insect Mol Biol 11:619–625
38. Burton SL, Ellar DJ, Li J, Derbyshire DJ (1999) *N*-acetylgalactosamine on the putative insect receptor aminopeptidase N is recognised by a site on the domain III lectin-like fold of a *Bacillus thuringiensis* insecticidal toxin. J Mol Biol 287:1011–1022
39. Knight PJK, Carroll J, Ellar DJ (2004) Analysis of glycan structures on the 120 kDa aminopeptidase N of *Manduca sexta* and their interactions with *Bacillus thuringiensis* CrylAc toxin. Insect Biochem Mol Biol 34:101–112
40. de Maagd RA, Bakker PL, Masson L, Adang MJ, Sangadala S, Stiekema W, Bosch D (1999) Domain III of the *Bacillus thuringiensis* delta-endotoxin Cry1Ac is involved in binding

to *Manduca sexta* brush border membranes and to its purified aminopeptidase N. Mol Microbiol 31:463–471

41. Jenkins JL, Lee MK, Valaitis AP, Curtiss A, Dean DH (2000) Bivalent sequential binding model of a *Bacillus thuringiensis* toxin to gypsy moth aminopeptidase N receptor. J Biol Chem 275: 14423–14431
42. Jimenez-Juarez N, Munoz-Garay C, Gomez I, Saab-Rincon G, Damian-Almazo JY, Gill SS, Soberon M, Bravo A (2007) *Bacillus thuringiensis* Cry1Ab mutants affecting oligomer formation are non-toxic to *Manduca sexta* larvae. J Biol Chem 282:21222–21229
43. Rausell C, García-Robles I, Sánchez J, Muñoz-Garay C, Martínez-Ramírez AC, Real MD, Bravo A (2004) Role of toxin activation on binding and pore formation activity of the *Bacillus thuringiensis* Cry3 toxins in membranes of *Leptinotarsa decemlineata* [Say]. Biochem Biophys Acta 1660:99–105
44. Gómez I, Sánchez J, Miranda R, Bravo A, Soberón M (2002) Cadherin-like receptor binding facilitates proteolytic cleavage of helix a-1 in domain I and oligomer pre-pore formation of *Bacillus thuringiensis* Cry1Ab toxin. FEBS Lett 513:242–246
45. Chen J, Hua G, Jurat-Fuentes JL, Abdullah MA, Adang MJ (2007) Synergism of *Bacillus thuringiensis* toxins by a fragment of a toxin-binding cadherin. Proc Natl Acad Sci USA 104: 13901–13906
46. Parenti P, Morandi P, McGivan JD, Consonnic P, Leonardi G, Giordana B (1997) Properties of the aminopeptidase N from the silkworm midgut (*Bombyx mori*). Insect Biochem Mol Biol 27:397–403
47. Zhuang M, Oltean DI, Gómez I, Pullikuth AK, Soberón M, Bravo A, Gill SS (2002) *Heliothis virescens* and *Manduca sexta* lipid rafts are involved in Cry1A toxin binding to the midgut epithelium and subsequent pore formation. J Biol Chem 277:13863–13872
48. Bravo A, Gómez I, Conde J, Muñoz-Garay C, Sánchez J, Zhuang M, Gill SS, Soberón M (2004) Oligomerization triggers differential binding of a pore-forming toxin to a different receptor leading to efficient interaction with membrane microdomains. Biochem Biophys Acta 1667:38–46
49. Pigott CR, Ellar DJ (2007) Role of receptors in *Bacillus thuringiensis* crystal toxin activity. Microbiol Mol Biol Rev 71:255–281
50. Sacchi VF, Wolfsberger MG (1996) Amino acid absorption. In: Lehane MJ, Billingsley PF (eds) Biology of the insect midgut. Chapman and Hall, London, pp 265–292
51. Zhang X, Candas M, Griko NB, Taussig R, Bulla LA Jr (2006) A mechanism of cell death involving an adenylyl cyclase/PKA signaling pathway is induced by the Cry1Ab toxin of *Bacillus thuringiensis*. Proc Natl Acad Sci USA 103:9897–9902
52. Moellenbeck DJ, Peters ML, Bing JW, Rouse JR, Higgins LS, Sims L, Nevshemal T, Marshall L, Ellis RT, Bystrak PG, Lang BA, Stewart JL, Kouba K, Sondag V, Gustafson V, Nour K, Xu DP, Swenson J, Zhang J, Czapla T, Schwab G, Jayne S, Stockhoff BA, Narva K, Schnepf HE, Stelman SJ, Poutre C, Koziel M, Duck N (2001) Insecticidal proteins from *Bacillus thuringiensis* protect corn from corn rootworms. Nat Biotechnol 19:668–672
53. Ellis RT, Stockhoff BA, Stamp L, Schnepf HE, Schwab GE, Knuth M, Russell J, Cardineau GA, Narva KE (2002) Novel *Bacillus thuringiensis* binary insecticidal crystal proteins active on western corn rootworm, *Diabrotica virgifera virgifera* LeConte. Appl Environ Microbiol 68:1137–1145
54. Darboux I, Nielsen-LeRoux C, Charles JF, Pauron D (2001) The receptor of *Bacillus sphaericus* binary toxin in *Culex pipiens* (Diptera: Culicidae) midgut: molecular cloning and expression. Insect Biochem Mol Biol 31:981–990
55. Charles JF, NielsenLeRoux C, Delecluse A (1996) *Bacillus sphaericus* toxins: molecular biology and mode of action. Annu Rev Entomol 41:451–472
56. Warren GW (1997) Vegetative insecticidal proteins: novel proteins for control of corn pests. In: Carozzi NB, Koziel MG (eds) Advances in insect control: the role of transgenic plants. Taylor & Francis, London, UK, pp 109–121
57. Barth H, Aktories K, Popoff MR, Stiles BG (2004) Binary bacterial toxins: Biochemistry, biology, and applications of common *Clostridium* and *Bacillus* proteins. Microbiol Mol Biol Rev 68:373–402
58. Leuber M, Orlik F, Schiffler B, Sickmann A, Benz R (2006) Vegetative insecticidal protein (Vip1Ac) of *Bacillus thuringiensis* HD201: Evidence for oligomer and channel formation. Biochemistry 45:283–288
59. Estruch JJ, Warren GW, Mullins MA, Nye GJ, Craig JA, Koziel MG (1996) Vip3A, a novel *Bacillus thuringiensis* vegetative insecticidal protein with a wide spectrum of activities against lepidopteran insects. Proc Natl Acad Sci USA 93:5389–5394
60. Yu CG, Mullins MA, Warren GW, Koziel MG, Estruch JJ (1997) The *Bacillus thuringiensis* vegetative insecticidal protein Vip3A lyses midgut epithelium cells of susceptible insects. Appl Environ Microbiol 63:532–536
61. Lee MK, Miles P, Chen JS (2006) Brush border membrane binding properties of *Bacillus thuringiensis* Vip3A toxin to *Heliothis virescens* and *Helicoverpa zea* midguts. Biochem Biophys Res Commun 339:1043–1047
62. Lee MK, Walters FS, Hart H, Palekar N, Chen JS (2003) Mode of action of the *Bacillus thuringiensis* vegetative insecticidal protein Vip3A differs from that of Cry1Ab delta-endotoxin. Appl Environ Microbiol 69:4648–4657
63. Fang J, Xu X, Wang P, Zhao J-Z, Shelton AM, Cheng J, Feng M-G, Shen Z (2007) Characterization of chimeric *Bacillus thuringiensis* Vip3 toxins. Appl Environ Microbiol 73:956–961
64. Li J, Pandelakis AK, Ellar DJ (1996) Structure of the mosquitocidal δ-endotoxin CytB from *Bacillus thuringiensis* sp. *kyushuensis* and implications for membrane pore formation. J Mol Biol 257:129–152
65. Du J, Knowles BH, Li J, Ellar DJ (1999) Biochemical characterization of *Bacillus thuringiensis* cytolytic toxins in association with a phospholipid bilayer. Biochem J 338:185–193
66. Promdonkoy B, Ellar DJ (2003) Investigation of the pore-forming mechanism of a cytolytic δ-endotoxin from *Bacillus thuringiensis*. Biochem J 374:255–259

67. Koni PA, Ellar DJ (1994) Biochemical characterization of *Bacillus thuringiensis* cytolytic δ-endotoxins. Microbiology 140:1869–1880
68. Wirth MC, Georghiou GP, Federeci BA (1997) CytA enables CryIV endotoxins of *Bacillus thuringiensis* to overcome high levels of CryIV resistance in the mosquito, *Culex quinquefasciatus*. Proc Natl Acad Sci USA 94:10536–10540
69. Pérez C, Fernández LE, Sun J, Folch JL, Gill SS, Soberón M, Bravo A (2005) *Bacillus thuringiensis* subsp. *israelensis* Cyt1Aa synergizes Cry11Aa toxin by functioning as a membrane-bound receptor. Proc Natl Acad Sci USA 102:18303–18308
70. Mazier M, Pannetier C, Tourneur J, Jouanin L, Giband M (1997) The expression of *Bacillus thuringiensis* toxin genes in plant cells. Biotechnol Annu Rev 3:313–347
71. Zheng SJ, Henken B, de Maagd RA, Purwito A, Krens FA, Kik C (2005) Two different *Bacillus thuringiensis* toxin genes confer resistance to beet armyworm (*Spodoptera exigua* Hubner) in transgenic *Bt*-shallots (*Allium cepa* L.). Transgenic Res 14: 261–272
72. Fujimoto H, Itoh K, Yamamoto M, Kyozuka J, Shimamoto K (1993) Insect resistant rice generated by introduction of a modified δ–endotoxin gene of *Bacillus thuringiensis*. Bio/Technology 11:194–200
73. Wunn J, Kloti A, Burkhardt PK, Biswas GCG, Launis K, Iglesias VA, Potrykus I (1996) Transgenic Indica rice breeding line IR58 expressing a synthetic cryIA(b) gene from *Bacillus thuringiensis* provides effective insect pest control. Bio/Technology 14:171–176
74. Nayak P, Basu D, Das S, Basu A, Ghosh D, Ramakrishnan NA, Ghosh M, Sen SK (1997) Transgenic elite indica rice plants expressing CryIAc delta-endotoxin of *Bacillus thuringiensis* are resistant against yellow stem borer (*Scirpophaga incertulas*). Proc Natl Acad Sci USA 94:2111–2116
75. Vaughn T, Cavato T, Brar G, Coombe T, DeGooyer T, Ford S, Groth M, Howe A, Johnson S, Kolacz K, Pilcher C, Purcell J, Romano C, English L, Pershing J (2005) A method of controlling corn rootworm feeding using a *Bacillus thuringiensis* protein expressed in transgenic maize. Crop Sci 45:931–938
76. Breitler JC, Cordero MJ, Royer M, Meynard D, San Segundo B, Guiderdoni E (2001) The-689/+197 region of the maize protease inhibitor gene directs high level, wound-inducible expression of the *cry1B* gene which protects transgenic rice plants from stemborer attack. Mol Breed 7:259–274
77. Breitler JC, Vassal JM, Catala MD, Meynard D, Marfa V, Mele E, Royer M, Murillo I, San Segundo B, Guiderdoni E, Messeguer J (2004) Bt rice harbouring *Cry* genes controlled by a constitutive or wound-inducible promoter: protection and transgene expression under Mediterranean field conditions. Plant Biotechnol J 2:417–430
78. Miklos JA, Alibhai MF, Bledig SA, Connor-Ward DC, Gao A-G, Holmes BA, Kolacz KH, Kabuye VT, MacRae TC, Paradise MS, Toedebusch AS, Harrison LA (2007) Characterization of soybean exhibiting high expression of a synthetic *Bacillus thuringiensis cry1A* transgene that confers a high degree of resistance to lepidopteran pests. Crop Sci 47:148–157
79. Perlak FJ, Fuchs RL, Dean DA, McPherson SL, Fischhoff DA (1991) Modification of the coding sequence enhances plant expression of insect controlling protein genes. Proc Natl Acad Sci USA 88:3324–3328
80. De Rocher EJ, Vargo-Gogola TC, Diehn SH, Green PJ (1998) Direct evidence for rapid degradation of *Bacillus thuringiensis* toxin mRNA as a cause of poor expression in plants. Plant Physiol 117:1445–1461
81. Murray EE, Rocheleau T, Eberle M, Stock C, Sekar V, Adang M (1991) Analysis of unstable RNA transcripts of insecticidal crystal protein genes of *Bacillus thuringiensis* in transgenic plants and electroporated protoplasts. Plant Mol Biol 16: 1035–1050
82. Diehn PJ, Chiu SH, De Rocher WL, Green EJ (1998) Premature polyadenylation at multiple sites within a *Bacillus thuringiensis* toxin gene-coding region. Plant Physiol 117:1433–1443
83. Misztal LH, Mostowska A, Skibinska M, Bajsa J, Musial WG, Jarmolowski A (2004) Expression of modified Cry1Ac gene of *Bacillus thuringiensis* in transgenic tobacco plants. Mol Biotechnol 26:17–26
84. McBride KE, Svab Z, Schael DJ, Hogan PS, Stalker KM, Maliga P (1995) Amplification of a chimeric *Bacillus* gene in chloroplasts leads to an extraordinary level of an insecticidal protein in tobacco. Bio/Technology 13:362–365
85. Bock R (2001) Transgenic plastids in basic research and plant biotechnology. J Mol Biol 312:425–438
86. Maliga P (2003) Progress towards commercialization of plastid transformation technology. Trends Biotechnol 21:20–28
87. Daniell H, Khan MS, Allison L (2002) Milestones in chloroplast genetic engineering: an environmentally friendly era in biotechnology. Trends Plant Sci 7:84–91
88. Chakrabarti SK, Lutz KA, Lertwiriyawong B, Svab Z, Maliga P (2006) Expression of the *cry9Aa2 B.t.* gene in tobacco chloroplasts confers resistance to potato tuber moth. Transgenic Res 15:481–488
89. De Cosa B, Moar W, Lee SB, Miller M, Daniell H (2001) Overexpression of the *Bt* cry2Aa2 operon in chloroplasts leads to formation of insecticidal crystals. Nat Biotechnol 19:71–74
90. Kota M, Daniell H, Varma S, Garczynski SF, Gould F, Moar WJ (1999) Overexpression of the *Bacillus thuringiensis* (*Bt*) Cry2Aa2 protein in chloroplasts confers resistance to plants against susceptible and *Bt*-resistant insects. Proc Natl Acad Sci USA 96:1840–1845
91. Reddy VS, Leelavathi S, Selvapandiyan A, Raman R, Giovanni F, Shukla V, Bhatnagar RK (2002) Analysis of chloroplast transformed tobacco plants with *cry1Ia5* under rice *psbA* transcriptional elements reveal high level expression of *Bt* toxin without imposing yield penalty and stable inheritance of transplastome. Mol Breed 9:259–269
92. Dufourmantel N, Tissot G, Goutorbe F, Garcon F, Muhr C, Jansens S, Pelissier B, Peltier G, Dubald M (2005) Generation and analysis of soybean plastid transformants expressing *Bacillus thuringiensis* Cry1Ab protoxin. Plant Mol Biol 58:659–668

93. Chrispeels MJ, Sadava DE (1994) Plants, genes and agriculture. Jones and Bartlett, London
94. Gould F (1998) Sustainability of transgenic insecticidal cultivars: integrating pest genetics and ecology. Annu Rev Entomol 43:701–726
95. Gould F, Anderson A, Jones A, Sumerford D, Heckel DG, Lopez J, Micinski S, Leonard R, Laster M (1997) Initial frequency of alleles for resistance to *Bacillus thuringiensis* toxins in field populations of *Heliothis virescens*. Proc Natl Acad Sci USA 94:3519–3523
96. Andreadis SS, Álvarez-Alfagene A, Sánchez-Ramos I, Stodola TJ, Andow DA, Milonas PG, Savopoulou-Soultani M, Castánera P (2007) Frequency of resistance to *Bacillus thuringiensis* toxin Cry1Ab in Greek and Spanish population of *Sesamia nonagrioides* (Lepidoptera: Noctuidae). J Econ Entomol 100:195–201
97. Tabashnik BE, Patin AL, Dennehy TJ, Liu Y-B, Carrière Y, Sims M, Antilla L (2000) Frequency of resistance to *Bacillus thuringiensis* in field populations of pink bollworm. Proc Natl Acad Sci USA 97:12980–12984
98. Tabashnik BE, Dennehy TJ, Carrière Y (2005) Delayed resistance to transgenic cotton in pink bollworm. Proc Natl Acad Sci USA 102:15389–15393
99. Cristofoletti PT, de Sousa FAM, Rahbe Y, Terra WR (2006) Characterization of a membrane-bound aminopeptidase purified from *Acyrthosiphon pisum* midgut cells. FEBS J 273:5574–5588
100. Stewart SD, Adamczyk JJ, Knighten KS, Davis FM (2001) Impact of *Bt* cottons expressing one or two insecticidal proteins of *Bacillus thuringiensis* Berliner on growth and survival of noctuid (Lepidoptera) larvae. J Econ Entomol 94:752–760
101. Chitkowski RL, Turnipseed SG, Sullivan MJ, Bridges WC (2003) Field and laboratory evaluations of transgenic cottons expressing one or two *Bacillus thuringiensis* var. *kurstaki* Berliner proteins for management of noctuid (Lepidoptera) pests. J Econ Entomol 96:755–762
102. Zhao JZ, Cao J, Li YX, Collins HL, Roush RT, Earle ED, Shelton AM (2003) Transgenic plants expressing two *Bacillus thuringiensis* toxins delay insect resistance evolution. Nat Biotechnol 21:1493–1497
103. Christou P, Capell T, Kohli A, Gatehouse JA, Gatehouse AMR (2006) Recent developments and future prospects in insect pest control in transgenic crops. Trends Plant Sci 11:302–308
104. Gahan LJ, Ma YT, Coble MLM, Gould F, Moar WJ, Heckel DG (2005) Genetic basis of resistance to Cry1Ac and Cry2Aa in *Heliothis virescens* (Lepidoptera: Noctuidae). J Econ Entomol 98:1357–1368
105. Bashir K, Husnain T, Fatima T, Riaz N, Makhdoom R, Riazuddin S (2005) Novel indica basmati line (B-370) expressing two unrelated genes of *Bacillus thuringiensis* is highly resistant to two lepidopteran insects in the field. Crop Prot 24:870–879
106. Dively GP (2005) Impact of transgenic VIP3A x Cry1Ab lepidopteran-resistant field corn on the nontarget arthropod community. Environ Entomol 34:1267–1291
107. Han LZ, Wu KM, Peng YF, Wang F, Guo YY (2006) Evaluation of transgenic rice expressing Cry1Ac and CpTI against *Chilo suppressalis* and intrapopulation variation in susceptibility to Cry1Ac. Environ Entomol 35:1453–1459
108. Grainnet (2007) Monsanto and Dow Agrosciences launch "SmartStax," industry's first-ever eight-gene stacked combination in corn. http://www.grainnet.com/articles/Monsanto_and_Dow_Agrosciences_Launch_SmartStax_Industry_s_First_Ever_Eight_Gene_Stacked_Combination_in_Corn_-48374.html
109. Sanchis V, Agaisse H, Chaufaux J, Lereclus D (1996) Construction of new insecticidal *Bacillus thuringiensis* recombinant strains by using the sporulation non-dependent expression system of *cry*IIIA and a site specific recombination vector. J Biotechnol 48:81–96
110. Bosch D, Schipper B, van der Kleij H, de Maagd R, Stiekema W (1994) Recombinant *Bacillus thuringiensis* crystal proteins with new properties: possibilities for resistance management. Bio/Technology 12:915–919
111. de Maagd RA, Kwa MSG, van der Klei H, Yamamoto T, Schipper B, Vlak JM, Stiekema WJ, Bosch D (1996) Domain III substitution in *Bacillus thuringiensis* delta-endotoxin Cry1A(b) results in superior toxicity for *Spodoptera exigua* and altered membrane protein recognition. Appl Environ Microbiol 62:1537–1543
112. de Maagd RA, Weemen-Hendriks M, Stiekema W, Bosch D (2000) *Bacillus thuringiensis* delta-endotoxin Cry1C domain III can function as a specificity determinant for *Spodoptera exigua* in different, but not all, Cry1-Cry1C hybrids. Appl Environ Microbiol 66:1559–1563
113. Rang C, Vachon V, Coux F, Carret C, Moar WJ, Brousseau R, Schwartz JL, Laprade R, Frutos R (2001) Exchange of domain I from *Bacillus thuringiensis* Cry1 toxins influences protoxin stability and crystal formation. Curr Microbiol 43:1–6
114. Naimov S, Dukiandjiev S, de Maagd RA (2003) A hybrid *Bacillus thuringiensis* delta-endotoxin gives resistance against a coleopteran and a lepidopteran pest in transgenic potato. Plant Biotechnol J 1:51–57
115. Dean DH, Rajamohan F, Lee MK, Wu SJ, Chen XJ, Alcantara E, Hussain SR (1996) Probing the mechanism of action of *Bacillus thuringiensis* insecticidal proteins by site-directed mutagenesis: a minireview. Gene 179:111–117
116. Rajamohan F, Alzate O, Cotrill JA, Curtiss A, Dean DH (1996) Protein engineering of *Bacillus thuringiensis* delta-endotoxin: mutations at domain II of CryIAb enhance receptor affinity and toxicity toward gypsy moth larvae. Proc Natl Acad Sci USA 93:14338–14343
117. Wu SJ, Koller CN, Miller DL, Bauer LS, Dean DH (2000) Enhanced toxicity of *Bacillus thuringiensis* Cry3A delta-endotoxin in coleopterans by mutagenesis in a receptor binding loop. FEBS Lett 473:227–232
118. Abdullah MAF, Alzate O, Mohammad M, McNall RJ, Adang MJ, Dean DH (2003) Introduction of Culex toxicity into *Bacillus thuringiensis* Cry4Ba by protein engineering. Appl Environ Microbiol 69:5343–5353

119. Tuntitippawan T, Boonserm P, Katzenmeier G, Angsuthanasombat C (2005) Targeted mutagenesis of loop residues in the receptor-binding domain of the *Bacillus thuringiensis* Cry4Ba toxin affects larvicidal activity. FEMS Microbiol Lett 242:325–332
120. Abdullah MAF, Dean DH (2004) Enhancement of Cry19Aa mosquitocidal activity against *Aedes aegypti* by mutations in the putative loop regions of domain II. Appl Environ Microbiol 70:3769–3771
121. Liu XS, Dean DH (2006) Redesigning *Bacillus thuringiensis* Cry1Aa toxin into a mosquito toxin. Protein Eng Des Sel 19:107–111
122. Ishikawa H, Hoshino Y, Motoki Y, Kawahara T, Kitajima M, Kitami M, Watanabe A, Bravo A, Soberon M, Honda A, Yaoi K, Sato R (2007) A system for the directed evolution of the insecticidal protein from *Bacillus thuringiensis*. Mol Biotechnol 36:90–101
123. Chandra A, Ghosh P, Mandaokar AD, Bera AK, Sharma RP, Das S, Kumar PA (1999) Amino acid substitution in alpha-helix 7 of Cry1Ac delta-endotoxin of *Bacillus thuringiensis* leads to enhanced toxicity to *Helicoverpa armigera* Hubner. FEBS Lett 458:175–179
124. Rupar MJ, Donovan WP, Groat RG, Slaney AC, Mattison JW, Johnson TB, Charles JF, Dumanior VC, DeBarjac H (1991) Two novel strains of *Bacillus thuringiensis* toxic to coleopterans. Appl Environ Microbiol 57:3337–3344
125. Bohorova N, Frutos R, Royer M, Estanol P, Pacheco M, Rascon Q, McLean S, Hoisington D (2001) Novel synthetic *Bacillus thuringiensis* cry1B gene and the cry1B-cry1Ab translational fusion confer resistance to southwestern corn borer, sugarcane borer and fall armyworm in transgenic tropical maize. Theor Appl Genet 103:817–826
126. Ho NH, Baisakh N, Oliva N, Datta K, Frutos R, Datta SK (2006) Translational fusion hybrid Bt genes confer resistance against yellow stem borer in transgenic elite vietnamese rice (*Oryza sativa* L.) cultivars. Crop Sci 46:781–789
127. Mehlo L, Gahakwa D, Nghia PT, Loc NT, Capell T, Gatehouse JA, Gatehouse AMR, Christou P (2005) An alternative strategy for sustainable pest resistance in genetically enhanced crops. Proc Natl Acad Sci USA 102:7812–7816
128. Gatehouse JA (2002) Plant resistance towards insect herbivores: a dynamic interaction. New Phytol 156:145–169
129. Barbosa JARG, Silva LP, Teles RCL, Esteves GF, Azevedo RB, Ventura MM, Freitas SM (2007) Crystal Structure of the Bowman-Birk inhibitor from *Vigna unguiculata* seeds in complex with beta-trypsin at 1.55 Å resolution and its structural properties in association with proteinases. Biophys J 92: 1638–1650
130. Garcia-Olmedo F, Salmedo G, Sanchez-Monge R, Gomez L, Royo J, Carbonero P (1987) Plant proteinaceous inhibitors of proteinases and α-amylases. Oxf Surv Plant Mol Cell Biol 4: 275–334
131. Ryan CA (1990) Protease inhibitors in plants – genes for improving defenses against insects and pathogens. Annu Rev Phytopathol 28:425–449
132. Orozco-Cardenas M, McGurl B, Ryan CA (1993) Expression of an antisense prosystemin gene in tomato plants reduces resistance toward *Manduca sexta* larvae. Proc Natl Acad Sci USA 90:8273–8276
133. Kessler A, Baldwin IT (2002) Plant responses to insect herbivory: the emerging molecular analysis. Annu Rev Plant Biol 53:299–328
134. Hilder VA, Gatehouse AMR, Sheerman SE, Barker RF, Boulter D (1987) A novel mechanism of insect resistance engineered into tobacco. Nature 330:160–163
135. Johnson R, Narvaez J, An G, Ryan C (1989) Expression of proteinase inhibitors I and II in transgenic tobacco plants: effects on natural defense against *Manduca sexta* larvae. Proc Natl Acad Sci USA 86:9871–9875
136. McManus MT, White DWR, McGregor PG (1994) Accumulation of a chymotrypsin inhibitor in transgenic tobacco can affect the growth of insect pests. Transgenic Res 3:50–58
137. Duan X, Li X, Xue Q, Abo-El-Saad M, Xu D, Wu R (1996) Transgenic rice plants harboring an introduced potato proteinase inhibitor II gene are insect resistant. Nat Biotechnol 14:494–496
138. Xu DP, Xue QZ, McElroy D, Mawal Y, Hilder VA, Wu R (1996) Constitutive expression of a cowpea trypsin-inhibitor gene, CpTI, in transgenic rice plants confers resistance to 2 major rice insect pests. Mol Breed 2:167–173
139. McGurl B, Orozco-Cardenas M, Pearce G, Ryan CA (1994) Overexpression of the prosystemin gene in transgenic tomato plants generates a systemic signal that constitutively induces proteinase inhibitor synthesis. Proc Natl Acad Sci USA 91:9799–9802
140. Ren F, Lu Y-T (2006) Overexpression of tobacco hydroxyproline-rich glycopeptide systemin precursor A gene in transgenic tobacco enhances resistance against *Helicoverpa armigera* larvae. Plant Sci 171:286–292
141. Bolter CJ, Jongsma MA (1995) Colorado potato beetles (*Leptinotarsa decemlineata*) adapt to proteinase inhibitors induced in potato leaves by methyl jasmonate. J Insect Physiol 41:1071–1078
142. Jongsma MA, Bakker PL, Peters J, Bosch D, Stiekma WJ (1995) Adaptations of *Spodoptera exigua* larvae to plant proteinase inhibitors by induction of gut proteinase activity insensitive to inhibition. Proc Natl Acad Sci USA 92:8041–8045
143. Harsulkar AM, Giri AP, Patankar AG, Gupta VS, Sainani MN, Ranjekar PK, Deshpande VV (1999) Successive use of non-host plant proteinase inhibitors required for effective inhibition of *Helicoverpa armigera* gut proteinases and larval growth. Plant Physiol 121:497–506
144. Bown DP, Wilkinson HS, Gatehouse JA (1997) Differentially regulated inhibitor-sensitive and insensitive protease genes from the phytophagous insect pest, *Helicoverpa armigera*, are members of complex multigene families. Insect Biochem Mol Biol 27:625–638
145. De Leo F, Bonade-Bottino MA, Ceci LR, Gallerani R, Jouanin L (1998) Opposite effects on *Spodoptera littoralis* larvae of high

expression level of a trypsin proteinase inhibitor in transgenic plants. Plant Physiol 118:997–1004
146. Leplé JC, Bonade-Bottino M, Augustin S, Pilate G, Letan VD, Delplanque A, Cornu D, Jouanin L (1995) Toxicity to *Chrysomela tremulae* (Coleoptera, Chrysomelidae) of transgenic poplars expressing a cysteine proteinase inhibitor. Mol Breed 1:319–328
147. Lecardonnel A, Chauvin L, Jouanin L, Beaujean A, Prevost G, Sangwan-Norreel B (1999) Effects of rice cystatin I expression in transgenic potato on Colorado potato beetle larvae. Plant Sci 140:71–79
148. Outchkourov NS, de Kogel WJ, Schuurman-de Bruin A, Abrahamson M, Jongsma MA (2004) Specific cysteine protease inhibitors act as deterrents of western flower thrips, *Frankliniella occidentalis* (Pergande), in transgenic potato. Plant Biotechnol J 2:439–448
149. Outchkourov NS, de Kogel WJ, Wiegers GL, Abrahamson M, Jongsma MA (2004) Engineered multidomain cysteine protease inhibitors yield resistance against western flower thrips (*Franklinielia occidentalis*) in greenhouse trials. Plant Biotechnol J 2:449–458
150. Outchkourov NS, Rogelj B, Strukelj B, Jongsma MA (2003) Expression of sea anemone equistatin in potato: effects of plant proteases on heterologous protein production. Plant Physiol 133:379–390
151. Abdeen A, Virgos A, Olivella E, Villanueva J, Aviles X, Gabarra R, Prat S (2005) Multiple insect resistence in transgenic tomato plants over-expressing two families of plant proteinase inhibitors. Plant Mol Biol 57:189–202
152. Franco OL, Rigden DJ, Melo FR, Grossi-de-Sa MF (2002) Plant alpha-amylase inhibitors and their interaction with insect alpha-amylases - structure, function and potential for crop protection. Eur J Biochem 269:397–412
153. Suzuki K, Ishimoto M, Kikuchi F, Kitamura K (1993) Growth-inhibitory effect of an alpha-amylase inhibitor from the wild common bean resistant to the mexican bean weevil (*Zabrotes subfasciatus*). Jpn J Breed 43:257–265
154. Ishimoto M, Kitamura K (1991) Effect of absence of seed alpha-amylase inhibitor on the growth inhibitory activity to azuki bean weevil (*Callosobruchus chinensis*) in common bean (*Phaseolus vulgaris* L.). Jpn J Breed 41:231–240
155. Moreno J, Chrispeels MJ (1989) A lectin gene encodes the $\alpha-$amylase inhibitor of common bean. Proc Natl Acad Sci USA 86:7885–7889
156. Nahoum V, Farisei F, Le-Berre-Anton V, Egloff MP, Rouge P, Poerio E, Payan F (1999) A plant-seed inhibitor of two classes of alpha-amylases: X-ray analysis of *Tenebrio molitor* larvae alpha-amylase in complex with the bean *Phaseolus vulgaris* inhibitor. Acta Crystallogr Sect D 55:360–362
157. Silva CP, Terra WR, de Sa MFG, Samuels RI, Isejima EM, Bifano TD, Almeida JS (2001) Induction of digestive alpha-amylases in larvae of *Zabrotes subfasciatus* (Coleoptera: Bruchidae) in response to ingestion of common bean alpha-amylase inhibitor 1. J Insect Physiol 47:1283–1290
158. Shade RE, Schroeder HE, Pueyo JJ, Tabe LM, Murdock LL, Higgins TJV, Chrispeels MJ (1994) Transgenic pea seeds expressing the alpha-amylase inhibitor of the common bean are resistant to bruchid beetles. Bio/Technology 12: 793–796
159. Schroeder HE, Gollasch S, Moore A, Tabe LM, Craig S, Hardie DC, Chrispeels MJ, Spencer D, Higgins TJV (1995) Bean alpha-amylase inhibitor confers resistance to the pea weevil (*Bruchus pisorum*) in transgenic peas (*Pisum sativum* L). Plant Physiol 107:1233–1239
160. Ishimoto M, Sato T, Chrispeels MJ, Kitamura K (1996) Bruchid resistance of transgenic azuki bean expressing seed alpha-amylase inhibitor of common bean. Entomol Exp Appl 79: 309–315
161. Morton RL, Schroeder HE, Bateman KS, Chrispeels MJ, Armstrong E, Higgins TJV (2000) Bean alpha-amylase inhibitor 1 in transgenic peas (*Pisum sativum*) provides complete protection from pea weevil (*Bruchus pisorum*) under field conditions. Proc Natl Acad Sci USA 97:3820–3825
162. Sarmah BK, Moore A, Tate W, Molvig L, Morton RL, Rees DP, Chiaiese P, Chrispeels MJ, Tabe LM, Higgins TJV (2004) Transgenic chickpea seeds expressing high levels of a bean alpha-amylase inhibitor. Mol Breed 14:73–82
163. Prescott VE, Campbell PM, Moore A, Mattes J, Rothenberg ME, Foster PS, Higgins TJV, Hogan SP (2005) Transgenic expression of bean alpha-amylase inhibitor in peas results in altered structure and immunogenicity. J Agric Food Chem 53: 9023–9030
164. Collins CL, Eason PJ, Dunshea FR, Higgins TJV, King RH (2006) Starch but not protein digestibility is altered in pigs fed transgenic peas containing alpha-amylase inhibitor. J Sci Food Agric 86:1894–1899
165. Li XH, Higgins TJV, Bryden WL (2006) Biological response of broiler chickens fed peas (*Pisum sativum* L.) expressing the bean (*Phaseolus vulgaris* L.) alpha-amylase inhibitor transgene. J Sci Food Agric 86:1900–1907
166. Peumans WJ, van Damme EJM (1995) Lectins as plant defence proteins. Plant Physiol 109:347–352
167. van Damme EJM, Peumans WJ, Barre A, Rougé P (1998) Plant lectins: a composite of several distinct families of structurally and evolutionary related proteins with diverse biological roles. Crit Rev Plant Sci 17:575–692
168. Czalpa TH, Lang BA (1990) Effect of plant lectins on the larval development of European corn borer (Lepidoptera: Pyralidae) and southern corn rootworm (Coleoptera: Chrysomelidae). J Econ Entomol 83:2480–2485
169. Murdock LL, Huesing JE, Nielsen SS, Pratt RC, Shade RE (1990) Biological effects of plant lectins on the cowpea weevil. Phytochemistry 29:85–89
170. Fitches E, Gatehouse AMR, Gatehouse JA (1997) Effects of snowdrop lectin (GNA) delivered via artificial diet and transgenic plants on the development of tomato moth (*Lacanobia oleracea*) larvae in laboratory and glasshouse trials. J Insect Physiol 43:727–739

171. Boulter D, Edwards GA, Gatehouse AMR, Gatehouse JA, Hilder VA (1990) Additive protective effects of incorporating two different higher plant derived insect resistance genes in transgenic tobacco plants. Crop Prot 9:351–354
172. Gatehouse AMR, Davison GM, Newell CA, Merryweather A, Hamilton WDO, Burgess EPJ, Gilbert RJC, Gatehouse JA (1997) Transgenic potato plants with enhanced resistance to the tomato moth, *Lacanobia oleracea*: growth room trials. Mol Breed 3:49–63
173. Powell KS, Gatehouse AMR, Hilder VA, Gatehouse JA (1993) Antimetabolic effects of plant lectins and plant and fungal enzymes on the nymphal stages of two important rice pests, *Nilaparvata lugens* and *Nephotettix cinciteps*. Entomol Exp Appl 66:119–126
174. Powell KS, Gatehouse AMR, Hilder VA, van Damme EJM, Peumans WJ, Boonjawat J, Horsham K, Gatehouse JA (1995) Different antimetabolic effects of related lectins towards nymphal stages of *Nilaparvata lugens*. Entomol Exp Appl 75:61–65
175. Rao KV, Rathore KS, Hodges TK, Fu X, Stoger E, Sudhakar D, Williams S, Christou P, Bharathi M, Bown DP, Powell KS, Spence J, Gatehouse AMR, Gatehouse JA (1998) Expression of snowdrop lectin (GNA) in transgenic rice plants confers resistance to rice brown planthopper. Plant J 15:469–477
176. Nagadhara D, Ramesh S, Pasalu IC, Kondala Rao Y, Krishnaiah NV, Sarma NP, Bown DP, Gatehouse JA, Reddy VD, Rao KV (2003) Transgenic indica rice resistant to sap-sucking insects. Plant Biotechnol 1:231–240
177. Foissac X, Loc NT, Christou P, Gatehouse AMR, Gatehouse JA (2000) Resistance to green leafhopper (*Nephotettix virescens*) and brown planthopper (*Nilaparvata lugens*) in transgenic rice expressing snowdrop lectin (*Galanthus nivalis* agglutinin; GNA). J Insect Physiol 46:573–583
178. Nagadhara D, Ramesh S, Pasalu IC, Rao YK, Sarma NP, Reddy VD, Rao KV (2004) Transgenic rice plants expressing the snowdrop lectin gene (gna) exhibit high-level resistance to the whitebacked planthopper (*Sogatella furcifera*). Theor Appl Genet 109:1399–1405
179. Loc NT, Tinjuangjun P, Gatehouse AMR, Christou P, Gatehouse JA (2002) Linear transgene constructs lacking vector backbone sequences generate transgenic rice plants which accumulate higher levels of proteins conferring insect resistance. Mol Breed 9:231–244
180. Poulsen M, Kroghsbo S, Schroder M, Wilcks A, Jacobsen H, Miller A, Frenzel T, Danier J, Rychlik M, Shu QY, Emami K, Sudhakar D, Gatehouse A, Engel KH, Knudsen I (2007) A 90-day safety study in Wistar rats fed genetically modified rice expressing snowdrop lectin Galanthus nivalis (GNA). Food Chem Toxicol 45:350–363
181. Gatehouse AMR, Down RE, Powell KS, Sauvion N, Rahbe Y, Newell CA, Merryweather A, Hamilton WDO, Gatehouse JA (1996) Transgenic potato plants with enhanced resistance to the peach-potato aphid *Myzus persicae*. Entomol Exp Appl 79:295–307
182. Wang ZY, Zhang KW, Sun XF, Tang KX, Zhang JR (2005) Enhancement of resistance to aphids by introducing the snowdrop lectin gene *gna* into maize plants. J Biosci 30: 627–638
183. Bandyopadhyay S, Roy A, Das S (2001) Binding of garlic (*Allium sativum*) leaf lectin to the gut receptors of homopteran pests is correlated to its insecticidal activity. Plant Sci 161:1025–1033
184. Dutta I, Saha P, Majumder P, Sarkar A, Chakraborti D, Banerjee S, Das S (2005) The efficacy of a novel insecticidal protein, *Allium sativum* leaf lectin (ASAL), against homopteran insects monitored in transgenic tobacco. Plant Biotechnol J 3:601–611
185. Dutta I, Majumder P, Saha P, Ray K, Das S (2005) Constitutive and phloem specific expression of *Allium sativum* leaf agglutinin (ASAL) to engineer aphid (*Lipaphis erysimi*) resistance in transgenic Indian mustard (*Brassica juncea*). Plant Sci 169: 996–1007
186. Saha P, Majumder P, Dutta I, Ray T, Roy SC, Das S (2006) Transgenic rice expressing *Allium sativum* leaf lectin with enhanced resistance against sap-sucking insect pests. Planta 223:1329–1343
187. Saha P, Chakraborti D, Sarkar A, Dutta I, Basu D, Das S (2007) Characterization of vascular-specific *RSs1* and *rolC* promoters for their utilization in engineering plants to develop resistance against hemipteran insect pests. Planta 226:429–442
188. Saha P, Dasgupta I, Das S (2006) A novel approach for developing resistance in rice against phloem limited viruses by antagonizing the phloem feeding hemipteran vectors. Plant Mol Biol 62:735–752
189. Ryan CA (2000) The system in signaling pathway: differential activation of plant defensive genes. Biochim Biophys Acta 1477:112–121
190. Felton GW, Donato KK, Broadway RM, Duffey SS (1992) Impact of oxidized plant phenolics on the nutritional quality of dietary protein to a noctuid herbivore, *Spodoptera exigua*. J Insect Physiol 38:277–285
191. Melo GA, Shimizu MM, Mazzafera P (2006) Polyphenoloxidase activity in coffee leaves and its role in resistance against the coffee leaf miner and coffee leaf rust. Phytochemistry 67: 277–285
192. Wang JH, Constabel CP (2004) Polyphenol oxidase overexpression in transgenic *Populus* enhances resistance to herbivory by forest tent caterpillar (*Malacosoma disstria*). Planta 220:87–96
193. Dowd PF, Lagrimini LM (1997) Examination of different tobacco (*Nicotiana* spp.) types under- and overproducing tobacco anionic peroxidase for their leaf resistance to *Helicoverpa zea*. J Chem Ecol 23:2357–2370
194. Dowd PF, Lagrimini LM (2006) Examination of the biological effects of high anionic peroxidase production in tobacco plants grown under field conditions. I. Insect pest damage. Transgenic Res 15:197–204
195. Dowd PF, Zuo WN, Gillikin JW, Johnson ET, Boston RS (2003) Enhanced resistance to *Helicoverpa zea* in tobacco

expressing an activated form of maize ribosome-inactivating protein. J Agric Food Chem 51:3568–3574
196. Lawrence SD, Novak NG (2006) Expression of poplar chitinase in tomato leads to inhibition of development in Colorado potato beetle. Biotechnol Lett 28:593–599
197. Dowd PF, Johnson ET, Pinkerton TS (2007) Oral toxicity of beta-*N*-acetyl hexosaminidase to insects. J Agric Food Chem 55:3421–3428
198. Fitches E, Wilkinson H, Bell H, Bown DP, Gatehouse JA, Edwards JP (2004) Cloning, expression and functional characterisation of chitinase from larvae of tomato moth (*Lacanobia oleracea*): a demonstration of the insecticidal activity of insect chitinase. Insect Biochem Mol Biol 34:1037–1050
199. Ding XF, Gopalakrishnan B, Johnson LB, White FF, Wang XR, Morgan TD, Kramer KJ, Muthukrishnan S (1998) Insect resistance of transgenic tobacco expressing an insect chitinase gene. Transgenic Res 7:77–84
200. Saguez J, Hainez R, Cherqui A, Van Wuytswinkel O, Jeanpierre H, Lebon G, Noiraud N, Beaujean A, Jouanin L, Laberche JC, Vincent C, Giordanengo P (2005) Unexpected effects of chitinases on the peach-potato aphid (*Myzus persicae* Sulzer) when delivered via transgenic potato plants (*Solanum tuberosum* Linne) and *in vitro*. Transgenic Res 14:57–67
201. Corrado G, Arciello S, Fanti P, Fiandra L, Garonna A, Digilio MC, Lorito M, Giordana B, Pennacchio F, Rao R (2007) The Chitinase A from the baculovirus AcMNPV enhances resistance to both fungi and herbivorous pests in tobacco. *Transgenic Res*. 17:557–571. (published online: DOI: 10.1007/s11248-007-9129-4)
202. Wittstock U, Gershenzon J (2002) Constitutive plant toxins and their role in defense against herbivores and pathogens. Curr Opin Plant Biol 5:300–307
203. Tattersall DB, Bak S, Jones PR, Olsen CE, Nielsen JK, Hansen ML, Hoj PB, Moller BL (2001) Resistance to an herbivore through engineered cyanogenic glucoside synthesis. Science 293:1826–1828
204. Bak S, Olsen CE, Halkier BA, Møller BL (2000) Transgenic tobacco and *Arabidopsis* plants expressing the two multifunctional sorghum cytochrome P450 enzymes, CYP79A1 and CYP71E1, are cyanogenic and accumulate metabolites derived from intermediates in dhurrin biosynthesis. Plant Physiol 123:1437–1448
205. Kristensen C, Morant M, Olsen CE, Ekstrom CT, Galbraith DW, Moller BL, Bak S (2005) Metabolic engineering of dhurrin in transgenic *Arabidopsis* plants with marginal inadvertent effects on the metabolome and transcriptome. Proc Natl Acad Sci USA 102:1779–1784
206. Ogunlabi OO, Agboola FK (2007) A soluble beta-cyanoalanine synthase from the gut of the variegated grasshopper *Zonocerus variegatus* (L.). Insect Biochem Mol Biol 37:72–79
207. Mikkelsen MD, Halkier BA (2003) Metabolic engineering of valine- and isoleucine-derived glucosinolates in *Arabidopsis* expressing CYP79D2 from cassava. Plant Physiol 131:773–779
208. Franks TK, Powell KS, Choimes S, Marsh E, Iocco P, Sinclair BJ, Ford CM, van Heeswijck R (2006) Consequences of transferring three sorghum genes for secondary metabolite (cyanogenic glucoside) biosynthesis to grapevine hairy roots. Transgenic Res 15:181–195
209. Kim YS, Uefuji H, Ogita S, Sano H (2006) Transgenic tobacco plants producing caffeine: a potential new strategy for insect pest control. Transgenic Res 15:667–672
210. Wei S, Semel Y, Bravdo BA, Czosnek H, Shoseyov O (2007) Expression and subcellular compartmentation of *Aspergillus niger* beta-glucosidase in transgenic tobacco result in an increased insecticidal activity on whiteflies (*Bemisia tabaci*). Plant Sci 172:1175–1181
211. Aharoni A, Jongsma MA, Bouwmeester HJ (2005) Volatile science? Metabolic engineering of terpenoids in plants. Trends Plant Sci 10:594–602
212. Wang E, Wang R, DeParasis J, Loughrin JH, Gan S, Wagner GJ (2001) Suppression of a P450 hydroxylase gene in plant trichome glands enhances natural-product-based aphid resistance. Nat Biotechnol 19:371–374
213. Aharoni A, Giri AP, Deuerlein S, Griepink F, de Kogel WJ, Verstappen FWA, Verhoeven HA, Jongsma MA, Schwab W, Bouwmeester HJ (2003) Terpenoid metabolism in wild-type and transgenic *Arabidopsis* plants. Plant Cell 15:2866–2884
214. Kappers IF, Aharoni A, van Herpen TWJM, Luckerhoff LLP, Dicke M, Bouwmeester HJ (2005) Genetic engineering of terpenoid metabolism attracts bodyguards to Arabidopsis. Science 309:2070–2072
215. Schnee C, Kollner TG, Held M, Turlings TCJ, Gershenzon J, Degenhardt J (2006) The products of a single maize sesquiterpene synthase form a volatile defense signal that attracts natural enemies of maize herbivores. Proc Natl Acad Sci USA 103:1129–1134
216. Beale MH, Birkett MA, Bruce TJA, Chamberlain K, Field LM, Huttly AK, Martin JL, Parker R, Phillips AL, Pickett JA, Prosser IM, Shewry PR, Smart LE, Wadhams LJ, Woodcock CM, Zhang YH (2006) Aphid alarm pheromone produced by transgenic plants affects aphid and parasitoid behavior. Proc Natl Acad Sci USA 103:10509–10513
217. Johnson ET, Dowd PF (2004) Differentially enhanced insect resistance, at a cost, in *Arabidopsis thaliana* constitutively expressing a transcription factor of defensive metabolites. J Agric Food Chem 52:5135–5138
218. Johnson ET, Berhow MA, Dowd PF (2007) Expression of a maize Myb transcription factor driven by a putative silk-specific promoter significantly enhances resistance to *Helicoverpa zea* in transgenic maize. J Agric Food Chem 55: 2998–3003
219. Maiti IB, Dey N, Pattanaik S, Dahlman DL, Rana RL, Webb BA (2003) Antibiosis-type insect resistance in transgenic plants expressing a teratocyte secretory protein (TSP14) gene from a hymenopteran endoparasite (*Microplitis croceipes*). Plant Biotechnol J 1:209–219
220. Tortiglione C, Fogliano V, Ferracane R, Fanti P, Pennacchio F, Monti LM, Rao R (2003) An insect peptide engineered into the

tomato prosystemin gene is released in transgenic tobacco plants and exerts biological activity. Plant Mol Biol 53:891–902
221. Bowen DJ, Ensign JC (1998) Purification and characterization of a high-molecular-weight insecticidal protein complex produced by the entomopathogenic bacterium *Photorhabdus luminescens*. Appl Environ Microbiol 64:3029–3035
222. Bowen D, Rocheleau TA, Blackburn M, Andreev O, Golubeva E, Bhartia R, ffrench-Constant RH (1998) Insecticidal toxins from the bacterium *Photorhabdus luminescens*. Science 280: 2129–2132
223. ffrench-Constant RH, Dowling A, Waterfield NR (2007) Insecticidal toxins from *Photorhabdus* bacteria and their potential use in agriculture. Toxicon 49:436–451
224. Guo LN, Fatig RO, Orr GL, Schafer BW, Strickland JA, Sukhapinda K, Woodsworth AT, Petell JK (1999) *Photorhabdus luminescens* W-14 insecticidal activity consists of at least two similar but distinct proteins - purification and characterization of toxin A and toxin B. J Biol Chem 274:9836–9842
225. Liu D, Burton S, Glancy T, Li ZS, Hampton R, Meade T, Merlo DJ (2003) Insect resistance conferred by 283-kDa *Photorhabdus luminescens* protein TcdA in *Arabidopsis thaliana*. Nat Biotechnol 21:1222–1228
226. Purcell JP, Greenplate JT, Jennings MG, Ryerse JS, Pershing JC, Sims SR, Prinsen MJ, Corbin DR, Tran M, Sammons RD, Stonard RJ (1993) Cholesterol oxidase - a potent insecticidal protein active against boll weevil larvae. Biochem Biophys Res Commun 196:1406–1413
227. Shen Z, Corbin DR, Greenplate JT, Grebenok RJ, Galbraith DW, Purcell JP (1997) Studies on the mode of action of cholesterol oxidase on insect midgut membranes. Arch Insect Biochem Physiol 34:429–442
228. Corbin DR, Grebenok RJ, Ohnmeiss TE, Greenplate JT, Purcell JP (2001) Expression and chloroplast targeting of cholesterol oxidase in transgenic tobacco plants. Plant Physiol 126:1116–1128
229. Morgan TD, Oppert B, Czapla TH, Kramer KJ (1993) Avidin and streptavidin as insecticidal and growth-inhibiting dietary proteins. Entomol Exp Appl 69:97–108
230. Markwick NP, Christeller JT, Docherty LC, Lilley CM (2001) Insecticidal activity of avidin and streptavidin against four species of pest Lepidoptera. Entomol Exp Appl 98:59–66
231. Hood EE, Witcher DR, Maddock S, Meyer T, Baszczynski C, Bailey M, Flynn P, Register J, Marshall L, Bond D, Kulisek E, Kusnadi A, Evangelista R, Nikolov Z, Wooge C, Mehigh RJ, Hernan R, Kappel WK, Ritland D, Li CP, Howard JA (1997) Commercial production of avidin from transgenic maize: characterization of transformant, production, processing, extraction and purification. Mol Breed 3:291–306
232. Kramer KJ, Morgan TD, Throne JE, Dowell FE, Bailey M, Howard JA (2000) Transgenic avidin maize is resistant to storage insect pests. Nat Biotechnol 18:670–674
233. Burgess EPJ, Malone LA, Christeller JT, Lester MT, Murray C, Philip BA, Phung MM, Tregidga EL (2002) Avidin expressed in transgenic tobacco leaves confers resistance to two noctuid pests, *Helicoverpa armigera* and *Spodoptera litura*. Transgenic Res 11:185–198
234. Murray C, Sutherland PW, Phung MM, Lester MT, Marshall RK, Christeller JT (2002) Expression of biotin-binding proteins, avidin and streptavidin, in plant tissues using plant vacuolar targeting sequences. Transgenic Res 11:199–214
235. Markwick NP, Docherty LC, Phung MM, Lester MT, Murray C, Yao JL, Mitra DS, Cohen D, Beuning LL, Kutty-Amma S, Christeller JT (2003) Transgenic tobacco and apple plants expressing biotin-binding proteins are resistant to two cosmopolitan insect pests, potato tuber moth and lightbrown apple moth, respectively. Transgenic Res 12:671–681
236. Yoza K, Imamura T, Kramer KJ, Morgan TD, Nakamura S, Akiyama K, Kawasaki S, Takaiwa F, Ohtsubo K (2005) Avidin expressed in transgenic rice confers resistance to the stored-product insect pests *Tribolium confusum* and *Sitotroga cerealella*. Biosci Biotechnol Biochem 69:966–971
237. Ginzberg I, Perl A, Genser M, Wininger S, Nemas C, Kapulnik Y (2004) Expression of streptavidin in tomato resulted in abnormal plant development that could be restored by biotin application. J Plant Physiol 161:611–620
238. Flinn PW, Kramer KJ, Throne JE, Morgan TD (2006) Protection of stored maize from insect pests using a two-component biological control method consisting of a hymenopteran parasitoid, *Theocolax elegans*, and transgenic avidin maize powder. J Stored Prod Res 42:218–225
239. Cooper SG, Douches DS, Grafius EJ (2006) Insecticidal activity of avidin combined with genetically engineered and traditional host plant resistance against Colorado potato beetle (Coleoptera: Chrysomelidae) larvae. J Econ Entomol 99: 527–536
240. Turner CT, Davy MW, MacDiarmid RM, Plummer KM, Birch NP, Newcomb RD (2006) RNA interference in the light brown apple moth, *Epiphyas postvittana* (Walker) induced by double-stranded RNA feeding. Insect Mol Biol 15:383–391
241. Mao Y-B, Cai W-J, Wang J-W, Hong G-J, Tao X-Y, Wang L-J, Huang Y-P, Chen X-Y (2007) Silencing a cotton bollworm P450 monoxygenase gene by plant-mediated RNAi impairs larval tolerance of gossypol. Nat Biotechnol 25:1307–1313
242. Baum JA, Bogaert T, Clinton W, Heck GR, Feldmann P, Ilagan O, Johnson S, Plaetinck G, Munyikwa T, Pleau M, Vaughn T, Roberts J (2007) Control of coleopteran insect pests through RNA interference. Nat Biotechnol 25:1322–1326
243. Benbrook C (2009) Impacts of genetically engineered crops on pesticide use in the United States: The first thirteen years. *The Organic Centre; Critical Issue Report*. http://www.organic-center.org/reportfiles/13Years20091126_FullReport.pdf
244. Gatehouse AMR, Ferry N, Raemaekers RJM (2002) The case of the monarch butterfly: a verdict is returned. Trends Genet 18:249–251
245. Tabashnik BE, Van Rensburg JBJ, Carriere Y (2009) Field-evolved insect resistance to *Bt* crops: Definition, theory, and data. J Econ Entomol 102:2011–2025

246. Nunez-Farfan J, Fornoni J, Luis Valverde P (2007) The evolution of resistance and tolerance to herbivores. Annu Rev Ecol Evol Syst 38:541–566

Books and reviews

Carozzi N, Koziel M, eds. (1997) Advances in Insect Control; The Role of Transgenic Plants. Taylor and Francis, London

Romeis J, Shelton AM, Kennedy G eds. (2008) Integration of Insect-Resistant Genetically Modified Crops within IPM Programs (Progress in Biological Control). Springer

Lemaux PG (2008) Genetically engineered plants and foods: a scientist's analysis of the issues (part I). Annu Rev Plant Biol 59:771–812

Lemaux PG (2009) Genetically engineered plants and foods: a scientist's analysis of the issues (part II). Annu Rev Plant Biol 60:511–559

Park JR, McFarlane I, Phipps RH, Ceddia G (2011) The role of transgenic crops in sustainable development. Plant Biotech J 9:2–21

GEN-IV Reactors

Taek K. Kim
Nuclear Engineering Division, Argonne National Laboratory, Argonne, IL, USA

Article Outline

Glossary
Definition of the Subject
Introduction
GEN-IV Nuclear Systems
Future Directions
Bibliography

Glossary

Breeding ratio Ratio of fission atom production to fissile atom destruction during a certain time interval in a nuclear system.

Closed fuel cycle (full recycle) One of the nuclear fuel cycle options, in which all actinides in the used nuclear fuel are separated and recycled to reduce the radiotoxicity of a geological repository while enhancing uranium utilization.

Energy sustainability Ability to meet the energy needs of the present generation while enhancing the ability of the future generation. In GEN-IV, the sustainability is measured by utilization of uranium resource without creating any weakness in economics and environmental goals.

GFR Gas-cooled Fast Reactor, which features a fast reactor and closed fuel cycle.

GIF Generation IV international forum, which is a cooperative international endeavor organized to carry out the R&D needed to establish the feasibility and performance capabilities of GEN-IV nuclear systems.

LFR Lead-cooled Fast Reactor, which features a fast reactor and closed fuel cycle.

MSR Molten Salt Reactor, which features thermal, epithermal, or fast reactor and closed fuel cycle.

Open fuel cycle (once-through cycle) One of the nuclear fuel cycle options, in which the used nuclear fuel discharged from a nuclear system is stored for some period of time and disposed in a geological repository isolating from environment.

Pyroprocessing The complete set of operations developed in USA. Integral Fast Reactor program based on the pyrometallurgical and electrochemical processes for recovering actinide elements from the used nuclear fuel and recycling them.

SCWR Supercritical Water Reactor, which features either thermal or fast reactor and open or closed fuel cycle.

SFR Sodium-cooled Fast Reactor, which features a fast reactor and closed fuel cycle.

Uranium utilization Ratio of uranium mass used in a nuclear system for energy generation to the uranium mass required by the nuclear system in a nuclear fuel cycle option.

VHTR Very-High-Temperature Reactor, which features a thermal reactor and open fuel cycle.

Definition of the Subject

Generation-IV reactors are a set of nuclear reactors currently being developed under international collaborations targeting sustainability, safety and reliability, high economics, proliferation resistance, and physical protection of nuclear energy. Nuclear systems have been developed over a number of decades and have evolved to the third generation from the first generation of prototypes constructed in 1950s and 1960s,

via the second generation of the commercial reactors operated worldwide after 1970s. While the third generation nuclear systems are currently proposed to the potential customers and under constructions with significant evolutionary in economics and safety based on lessons learnt through plenty reactor operations, nuclear experts from around the world began formulating the requirements for a generation IV of nuclear systems concerning over energy resource availability, climate change, air quality, and energy security. Six systems have been selected for further R&D as generation IV nuclear systems by Generation IV International Forum (GIF), which is a cooperative international endeavor organized to carry out the R&D needed to establish the feasibility and performance capabilities of Generation IV systems. The six systems are Gas-cooled Fast Reactor, Lead-cooled Fast Reactor, Molten Salt Reactor, Sodium-cooled Fast Reactor, Supercritical-Water Reactor, and Very-High-Temperature Reactor.

Introduction

Nuclear energy systems have evolved up to the third generation: a first generation of prototypes constructed in 1950 and 1960; a second generation of commercial nuclear power plants built from 1970, most of which are in operation today; and a third generation of advanced nuclear reactors, called Generation III/III+, which incorporate technical progress based on lessons learnt through more than 10,000 reactor-years of operation. While the generation III/III+ nuclear systems are currently proposed to the potential customers and under constructions with significant evolutionary in economics and safety, nuclear experts from around the world indicated that further advances in nuclear energy systems are required to better meet the rapid growth of environment friendly, highly economic, and secure nuclear energy in both industrialized and developing countries. In particular, it is now globally recognized that the nuclear energy is the practically available massive energy source without greenhouse gas emission among numerous options. To meet these needs, the international nuclear community has engaged in a wide-range discussion on the development of next generation nuclear energy systems known as *Generation IV* (GEN-IV) targeting the deployment around 2030. Figure 1 shows the evolution of the nuclear energy systems.

Nine countries, Argentina, Brazil, Canada, France, Japan, the Republic of Korea, the Republic of South Africa, the UK, and the USA, have initially joined together to form the Generation IV International

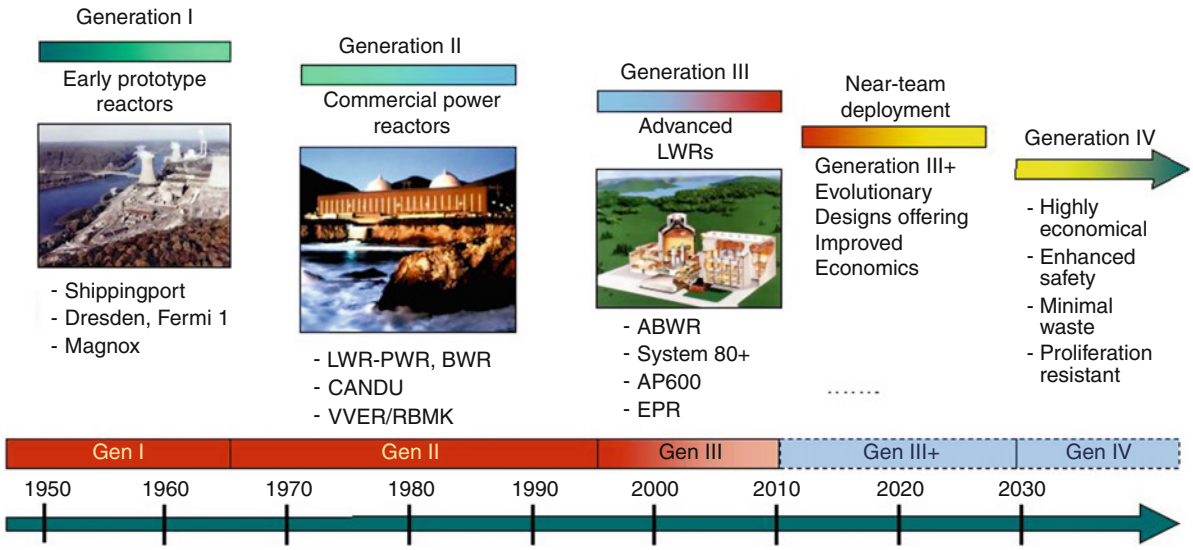

GEN-IV Reactors. Figure 1
Evolution of nuclear systems

Forum (GIF) [1] for developing GEN-IV nuclear systems that can be licensed, constructed, and operated in a manner that will provide competitively priced and reliable energy products while satisfactorily addressing nuclear safety, waste, proliferation, and public perception concerns. Now, the GIF consists of 13 membership countries added by China, Euratom, Russia, and Switzerland, and two permanent observers of International Atomic Energy Agency (IAEA) and the Organization for Economic Cooperation and Development Nuclear Energy Agency (OECD/NEA).

Beginning in 2000, more than 100 of nuclear experts from the countries constituting the GIF began to discuss for development of the GEN-IV technology roadmap in order to select the GEN-IV nuclear systems. As the first effort in the technology roadmap project [2], eight goals for the GEN-IV were defined in the four broad areas as shown in Table 1.

Since the eight goals are all equally important, the promising GEN-IV systems should ideally advance each and not create a weakness in one goal to gain strength in another. Under this central feature of the technical roadmap project, a series of GIF meeting was held in 2002 to conduct the selection process of the GEN-IV nuclear energy systems. The candidate systems were screened by the GIF expert group and six nuclear systems were selected on a consensus of the GIF membership countries such that the systems are the most promising and worthy of collaborative developments. The selected six systems for further R&D are alphabetically

- Gas-cooled Fast Reactor System (GFR),
- Lead-cooled Fast Reactor System (LFR),
- Molten Salt Reactor System (MSR),
- Sodium-cooled Fast Reactor System (SFR),
- Supercritical-water-cooled Reactor System (SCWR),
- Very-High-Temperature Reactor System (VHTR).

GEN-IV Nuclear Systems

In Table 2, the primary characteristics of the GEN-IV nuclear systems are summarized. In the roadmap project, it was recognized that the GIF countries would have perspectives on their priority missions for GEN-IV nuclear systems, which can be summarized as electricity generation, hydrogen production, and

GEN-IV Reactors. Table 1 Goal for generation IV nuclear energy systems

Sustainability 1	Generation IV nuclear energy systems will provide sustainable energy generation that meets clean air objectives and promotes long-term availability of systems and effective fuel utilization for worldwide energy production.
Sustainability 2	Generation IV nuclear energy systems will minimize and manage their nuclear waste and notably reduce the long-term stewardship burden, thereby improving protection for the public health and the environment.
Economics 1	Generation IV nuclear energy systems will have a clear life-cycle cost advantage over other energy sources.
Economics 2	Generation IV nuclear energy systems will have a level of financial risk comparable to other energy projects.
Safety and Reliability 1	Generation IV nuclear energy systems operations will excel in safety and reliability.
Safety and Reliability 2	Generation IV nuclear energy systems will have a very low likelihood and degree of reactor core damage.
Safety and Reliability 3	Generation IV nuclear energy systems will eliminate the need for off-site emergency response.
Proliferation Resistance and Physical Protection 1	Generation IV nuclear energy systems will increase the assurance that they are a very unattractive and the least desirable route for diversion or theft of weapons-usable materials, and provide increased physical protection against acts of terrorism.

GEN-IV Reactors. Table 2 Summary of GEN-IV nuclear systems

	Coolant	Neutron spectrum	Coolant exit temp. (°C)	Fuel cycle	Size (MWe)
GFR	Helium	Fast	850	Closed	1,200
LFR	Lead	Fast	480–800	Closed	50–1,200
MSR	Fluoride salt	Fast/thermal	700–800	Closed	1,000
SFR	Sodium	Fast	550	Closed	30–2,000
SCWR	Water	Thermal/fast	510–625	Open/closed	300–1,500
VHTR	Helium	Thermal	900–1,000	Open	250–300

high-level radioactive material management. All six GEN-IV nuclear systems have electricity applications, while the high temperature and fast neutron spectrum are required for the hydrogen generation and high-level radioactive material management, respectively. The high temperature systems such as VHTR, GFR, LFR, and MSR have potential applications in hydrogen production. By reprocessing and recycling of actinides, the fast reactor systems such as SFR, GFR, and LFR would provide a significant reduction in radiotoxicity of all wastes.

GFR – Gas-cooled Fast Reactor

The Gas-cooled Fast Reactor system features a fast-spectrum helium-cooled reactor and closed fuel cycle. Figure 2 shows the schematic of the GFR, which uses a direct-cycle helium turbine for electricity. Like thermal-spectrum helium-cooled reactors such as the Gas Turbine-Modular Helium Reactor (GT-MHR [3]) and the Pebble Bed Modular Reactor (PBMR [4]), the high outlet temperature of the helium coolant makes it possible to deliver not only electricity, but also process heat for hydrogen production with a high conversion efficiency. Through the combination of a fast-neutron spectrum and closed fuel cycle options, the GFR can manage the high-level radioactive waste isotopes.

The technology base for the GFR includes a number of thermal-spectrum gas reactor plants, as well as a few fast-spectrum gas-cooled reactor designs. Past pilot and demonstration projects include decommissioned reactors such as the Dragon Project [5] built and operated in the UK, the AVR [6] and the Thorium High-Temperature Reactor (THTR [7]) built and operated in Germany, and Peach Bottom and Fort St Vrain [8] built and operated in the USA. Ongoing demonstrations include the High-Temperature engineering Test Reactor (HTTR [9]) in Japan, which reached full power (30 MWth) using prismatic fuel compacts in 1999, and the High-Temperature Gas-cooled Reactor (HTR-10 [10]) in China, which reached 10 MWth in 2002 using pebble fuel.

A 300-MWth pebble bed modular demonstration plant is being designed by PBMR Pty for deployment in South Africa and a consortium of Russian institutes is designing a 300-MWth GT-MHR in cooperation with General Atomics. The design of the PBMR and GT-MHR reactor systems, fuel, and materials are evolutionary advances of the demonstrated technology, except for the Brayton-cycle helium turbine and implementation of modularity in the plant design. The GFR may benefit from development of these technologies, as well as development of innovative fuel and very-high-temperature materials for the VHTR.

Spent fuel treatment for the GFR can be accomplished with aqueous processes similar to those of the SFR but qualified for the unique GFR fuel form. A composite ceramic–ceramic fuel (CERCER) with closely packed, coated (U, Pu)C kernels or fibers is considered as the primary option for fuel development. Alternative fuel options for development include fuel particles with large (U, Pu)C kernels and thin coatings, or ceramic-clad, solid-solution metal (CERMET) fuels. The need for a high density of heavy metal elements in the fuel leads to actinide-carbides as the reference fuel and actinide-nitrides with 99.9% enriched nitrogen as the backup.

The reference material for the structure is reinforced ceramic comprising a silicon carbide composite matrix ceramic. The fuel compound is made of pellets of mixed

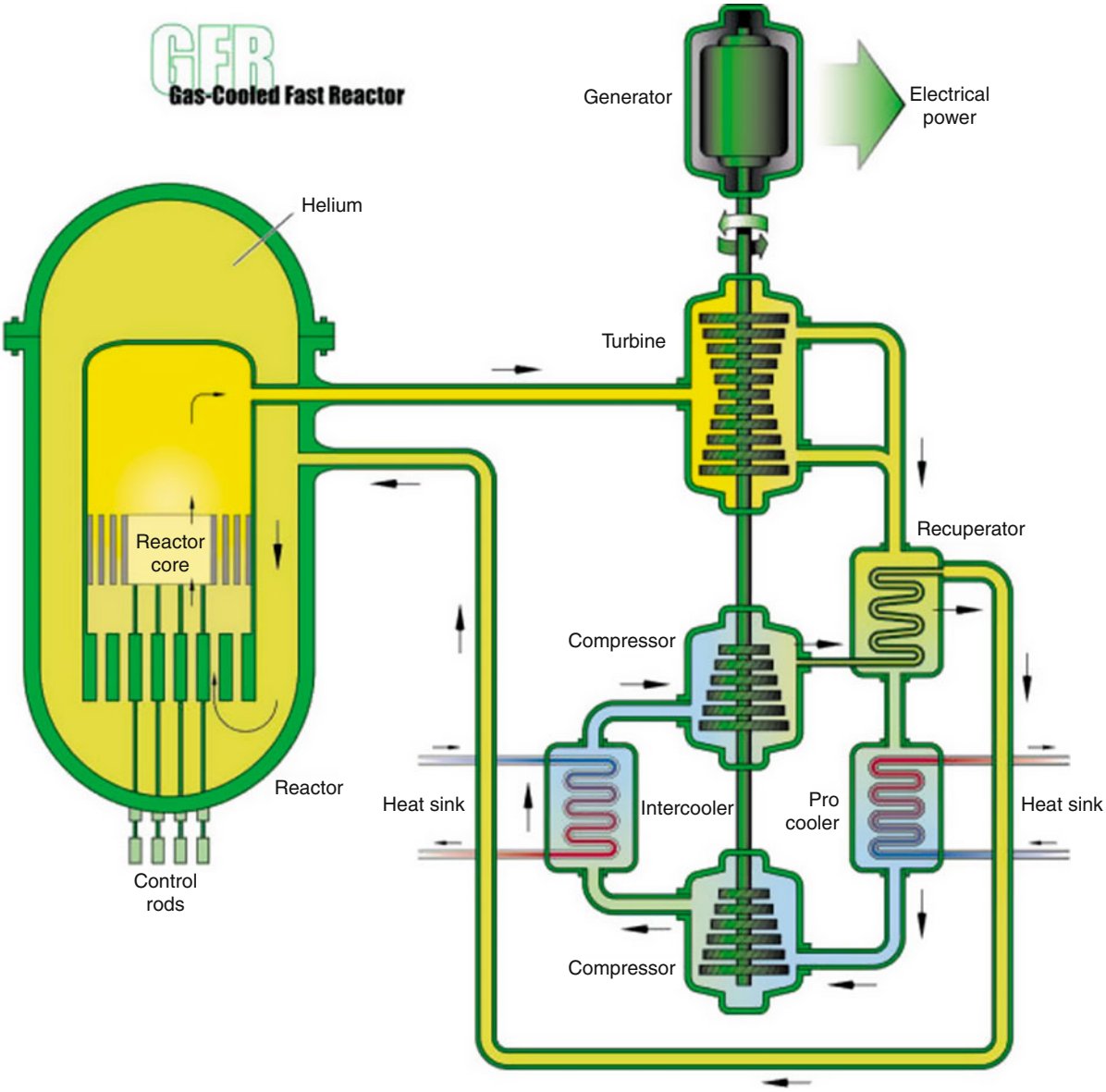

GEN-IV Reactors. Figure 2
Gas-cooled fast reactor

uranium-plutonium-minor actinide carbide. A leaktight barrier made of a refractory metal or of Si-based multilayer ceramics is added to prevent fission products' diffusion through the clad.

Neither experimental reactors nor prototypes of the GFR system have been licensed or built; therefore, the construction and operation of a first experimental reactor – 50 MWth Experimental Technology Demonstration Reactor (ETDR [11]) – is proposed with an extended performance phase to qualify key technologies. A technology demonstration reactor would qualify key technologies and could be put into operation by 2025.

Unlike the VHTR, which uses its considerable thermal mass to limit the rise of core temperature during transients, the GFR requires the development of a number of unique subsystems to provide defense in depth for its considerably higher power density core. These include

a robust decay heat removal system with added provisions for natural circulation heat removal, such as a low-pressure-drop core. The secondary circuit uses a He–N2 gas mixture with an indirect combined (Brayton and bottoming steam) power cycle to achieve more than 45% thermal efficiency.

A gastight envelope acting as additional guard containment is provided to maintain a backup pressure in case of large gas leak from the primary system. It is a metallic vessel, initially filled with nitrogen slightly over the atmospheric pressure to reduce air ingress potential. This unique component limits the consequence of coincident first and second safety barrier rupture (i.e., the fuel cladding and the primary system). Dedicated loops for decay heat removal (in case of emergency) are directly connected to the primary circuit using cross duct piping from the pressure vessel and are equipped with heat exchangers and blowers.

Many of the structural materials and methods are being adopted from the VHTR, including the reactor pressure vessel, hot duct materials, and design approach. The pressure vessel is a thick metallic structure of martensitic chromium steel, ensuring negligible creep at operating temperature. The primary system is comprised of three main loops of 800 MWth, each fitted with compact intermediate heat exchangers and a gas blower enclosed in a single vessel.

As a high-temperature and high-power density system, the GFR gives special attention to safety and materials management for both economics and nonproliferation. During the viability phase that is underway now, there is special interest in examining the use of pin-type fuel with a small diameter, fuel and core performance optimized for a simplified GFR having no minor actinide recycle, but with limited Pu breeding and low fuel burnup, core outlet temperature optimized to balance efficiency with materials limits, and the potential of prestressed concrete vessel technology to replace the guard vessel.

LFR – Lead-cooled Fast Reactor

The Lead-cooled Fast Reactor is similar to the sodium-cooled fast reactor in terms of neutron spectrum, fuel cycles, and the missions, but the coolant materials are changed to lead (Pb) or lead–bismuth (Pb–Bi). The lead coolant exhibits very low parasitic neutron absorption in fast neutron spectral environment, and this enables the sustainability and fuel cycle benefits traditionally associated with SFR. However, lead does not react readily with air, water, or carbon dioxide, which can eliminate the concerns about vigorous exothermic reactions. It has a high boiling temperature. The need to operate under high pressure and the prospect of boiling or flashing in case of pressure reduction are eliminated. Figure 3 shows the schematic of the LFR.

There are several potentials for advances compared to state-of-the-art liquid metal fast reactors. Innovations in heat transport and energy conversion are a central feature of the LFR options. Innovations in heat transport are afforded by natural circulation, lift pumps, in-vessel steam generators, and other features. Innovations in energy conversion are afforded by rising to higher temperatures than liquid sodium allows, and by reaching beyond the traditional superheated Rankine cycle to supercritical Brayton cycle or process heat applications such as hydrogen production and desalination. The favorable neutronics of coolant enable low power density, natural circulation-cooled reactors with fissile self-sufficient core designs that maintain criticality over 15-year refueling interval. For modular and large units, more conventional higher power density, forced circulation, and shorter refueling intervals are used, but these units benefit from the improved heat transport and energy conversion technology. The favorable properties of lead coolant and nitride fuel, combined with high-temperature structural materials can extend the reactor coolant outlet temperature up to 800°C, which is potentially suitable for hydrogen manufacture and other process heat applications.

Two types of LFR reactors were used in Russian submarines of the 1970s with the 155 MWth LFR reactors, OK-550 and BM-440. Recently, Russian joint venture AKME Engineering announced to develop a commercial LFR called SBVR-100 [12]. The core is based on the former LFR reactors used in the submarines and will produce 100 MWe electricity from gross thermal power of 280 MWth, about twice that of the submarine reactors. The coolant is 495°C and 16.5% enriched uranium oxide fuel is used with the refueling schedule of 7–8 years. The small lead-cooled fast reactor concept known as the small secure transportable autonomous reactor (SSTAR [13]) has been under ongoing development as part of the US

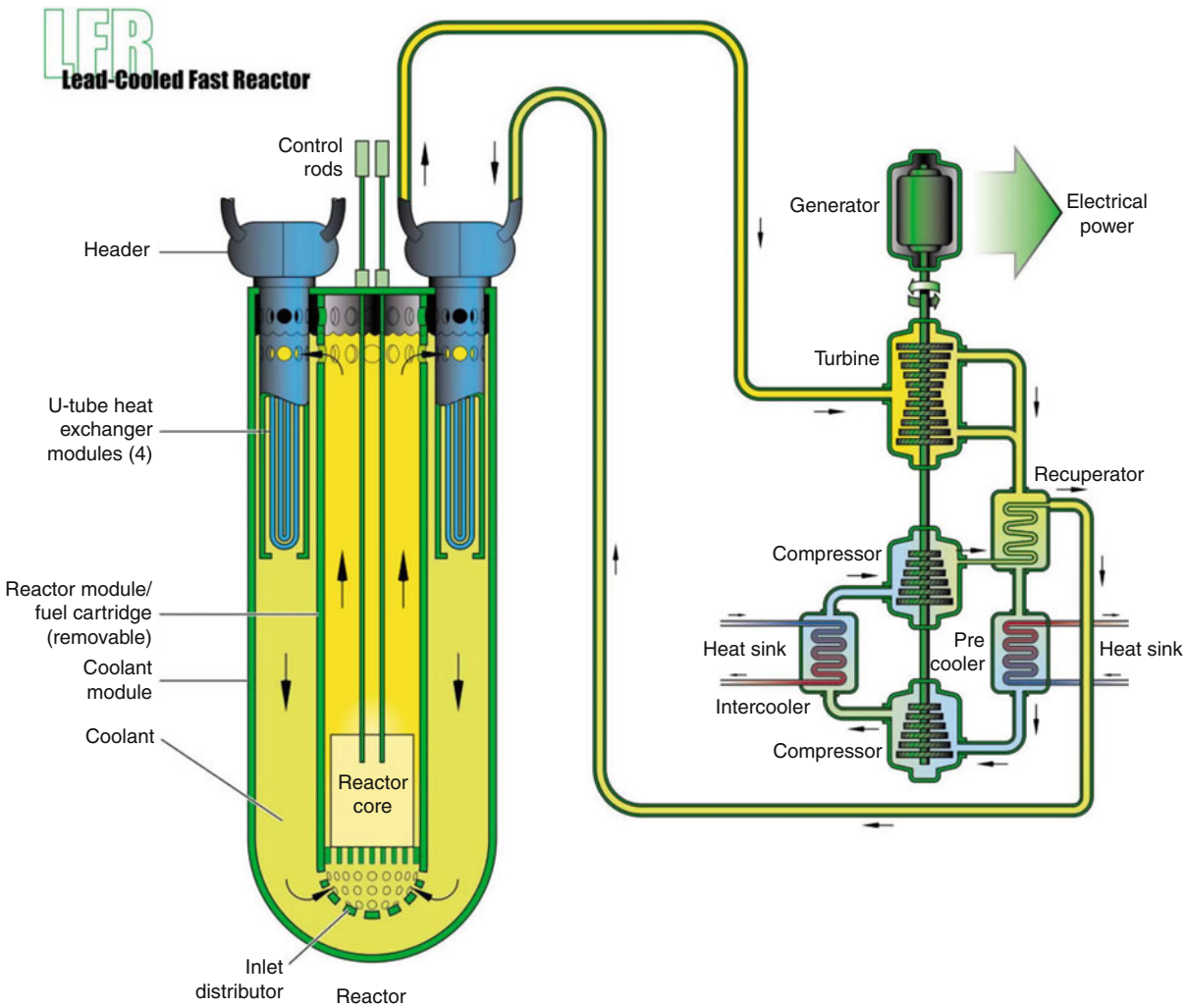

GEN-IV Reactors. Figure 3
Lead-cooled fast reactor

advanced nuclear energy systems programs (see Fig. 4). It is a system designed to provide energy security to developing nations while incorporating features to achieve nonproliferation goals. A 600 MWe European Lead-cooled system (ELSY [14]) has been under development since 2006. The ELSY project aims at the demonstration that it is possible to design a competitive and safe fast power reactor using simple technical engineered features.

The LFR is mainly envisioned for electricity and hydrogen production and high-level radioactive material management. The proposed LFR options include a long refueling interval battery ranging from 50 to 150 MWe, a modular system from 300 to 400 MWe, and a large monolithic plant at 1,200 MWe. The LFR battery option (like SSTAR) is a small factory-built turnkey plant operating on a closed fuel cycle with very long refueling interval (15–20 years) cassette core or replaceable reactor module. Its features are designed to meet market opportunities for electricity production on small grids, and for developing countries that may not wish to deploy an indigenous fuel cycle infrastructure to support their nuclear energy systems. Its small size, reduced cost, and full support fuel cycle services can be attractive for these markets. It had the highest evaluations to the GEN-IV goals among the LFR

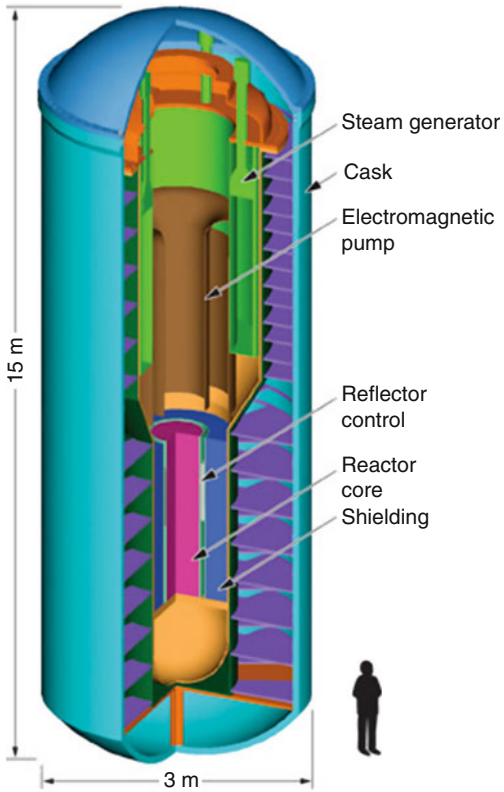

GEN-IV Reactors. Figure 4
SSTAR–A US lead-cooled fast reactor

options, but also the largest R&D needs and longest development time.

The options in the LFR class may provide a time-phased development path: the nearer-term options focus on electricity production and rely on more easily developed fuel, clad, and coolant combinations and their associated fuel recycle and refabrication technologies. The longer-term option seeks to further exploit the inherently safe properties of lead and raise the coolant outlet temperature sufficiently high to enter markets for hydrogen and process heat, possibly as merchant plants.

The technologies employed are extensions of those currently available from the Russian submarine lead-bismuth alloy-cooled reactors, from the Integral Fast Reactor (IFR [15]) metal alloy fuel recycle and refabrication development, and from the Advanced Liquid Metal Reactor (ALMR [16]) passive safety and modular design approach. Existing ferritic stainless steel and metal alloy fuel, which are already significantly developed for sodium fast reactors, are adaptable to lead-bismuth-cooled reactors at reactor outlet temperatures of 550°C.

Corrosion of structural materials in lead is one of the main issues for the LFR. Recent experiments confirm that corrosion of steels strongly depends on the operating temperature and dissolved oxygen. Indeed, at relatively low oxygen concentration, the corrosion mechanism changes from surface oxidation to dissolution of the structural steel. Moreover, relationships between oxidation rate, flow velocity, temperature, and stress conditions of the structural material have been observed as well. The compatibility of ferritic and austenitic steels with lead has been extensively studied and it has been demonstrated that generally below 450°C, and with an adequate oxygen activity in the liquid metal, both types of steels build up an oxide layer which behaves as a corrosion barrier. However, above about 500°C, corrosion protection through the oxide barrier appears to fail and is being addressed with various candidate materials. The prospects for extending much above this temperature are not proven at this time.

MSR – Molten Salt Reactor

The Molten Salt Reactor uses a molten salt mixture as a primary coolant. Systematic analysis of parameters such as reprocessing time, moderation ratio, core size, and content of heavy nuclei in the salt has resulted in several attractive reactor configurations, in thermal, epithermal, or fast neutron spectrum. The use of a molten salt coolant in a solid-fuel system has been investigated, known as the Advanced High-Temperature Reactor (AHTR [17]), which adapts VHTR fuel form and heat exchanger technology. However, in most MSRs, the fuel is dissolved in the molten salt coolant. Thus, the MSR has unique characteristic compared to other GEN-IV systems: i.e., online refueling and reprocessing are allowed without reactor shutdown because the fuel can move. In addition, the MSR have the following characteristics, which may afford advances: good neutron economy and alternatives for actinide burning or conversion, potential for hydrogen production with high operating temperature, low stresses on the vessel and piping with a very low vapor pressure, enhanced safety by fail-safe drainage,

passive cooling, and a low inventory of volatile fission products, etc. Figure 5 shows the schematic of the MSR concept with dissolved fuel.

The MSR was first developed in the late 1940s and 1950s for aircraft propulsion. The Aircraft Reactor Experiment (ARE [18]) was a 2.5 MWth nuclear reactor experiment designed to attain a high-power density for use as an engine in a nuclear powered bomber. One experiment used the molten fluoride salt $NaF\text{-}ZrF_4\text{-}UF_4$ (53-41-6 mol%) as fuel, was moderated by beryllium oxide, used liquid sodium as a secondary coolant, and had a peak temperature of 860°C. It operated for a 1,000 h cycle in 1954. The 8 MWth Molten Salt Reactor Experiment (MSRE [19]) was operated from 1965 to 1969 to demonstrate many features, including lithium/beryllium fluoride salt, graphite moderator, stable performance, off-gas systems, and use of different fuels such as U-233, U-235, and plutonium.

Recently, two MSRs were proposed: Thorium Molten Salt Reactor (TMSR [12]), and FUJI mini-MSR [12]. Figure 6 shows the 1,000 MWe TMSR with graphite moderator. Its operating temperature is 630°C and its thermodynamic efficiency is 40%. The salt used is a binary salt, $LiF\text{-}(HN)F_4$, with the $(HN)F_4$ content set to 22%, corresponding to a melting temperature of 565°C. The U-233 enrichment is about 3%. A graphite radial blanket surrounds the core to improve breeding performance. The reprocessing time of the total salt volume is specified to be 6 months, with external storage of the Pa and complete extraction of the fission products and TRU. It is assumed that the U-233 produced in the blanket is also extracted every 6 months. The FUJI mini-MSR is a 100 MWe molten-salt-fueled thorium fuel cycle

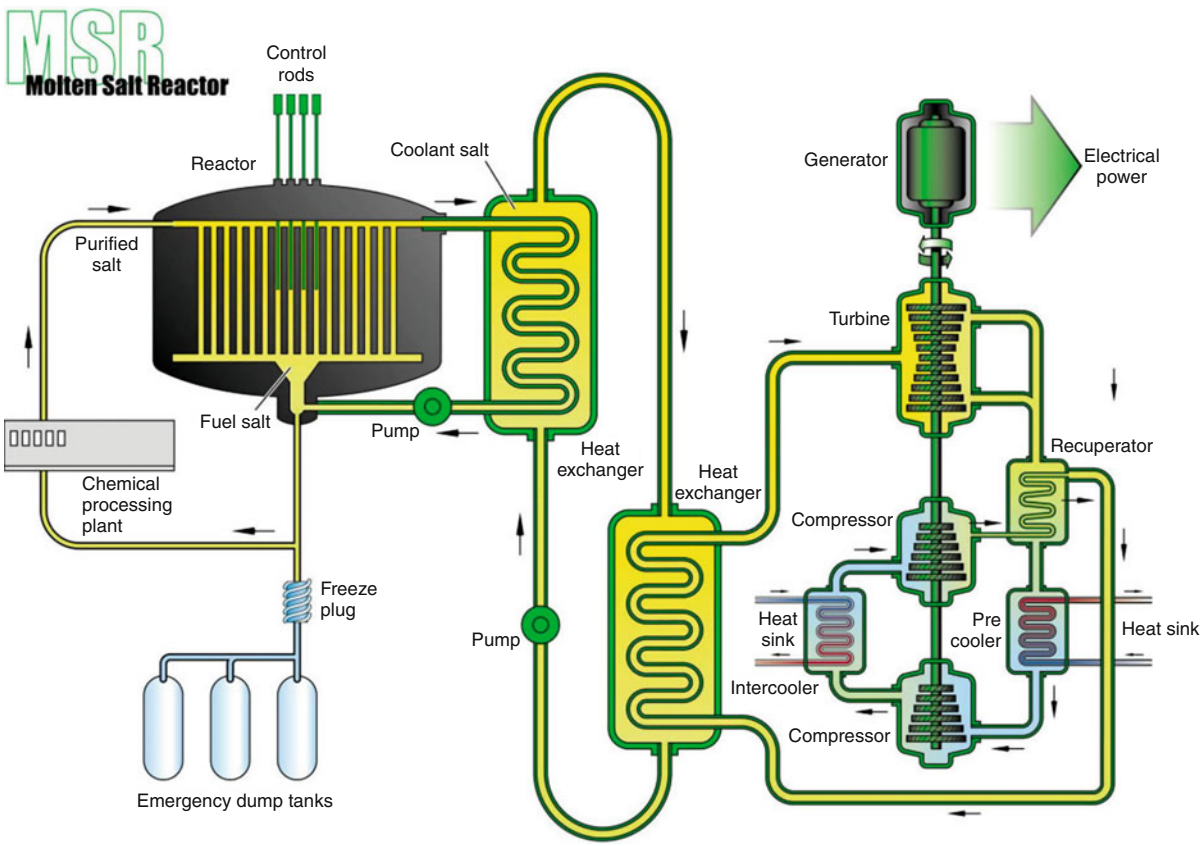

GEN-IV Reactors. Figure 5
Molten salt reactor

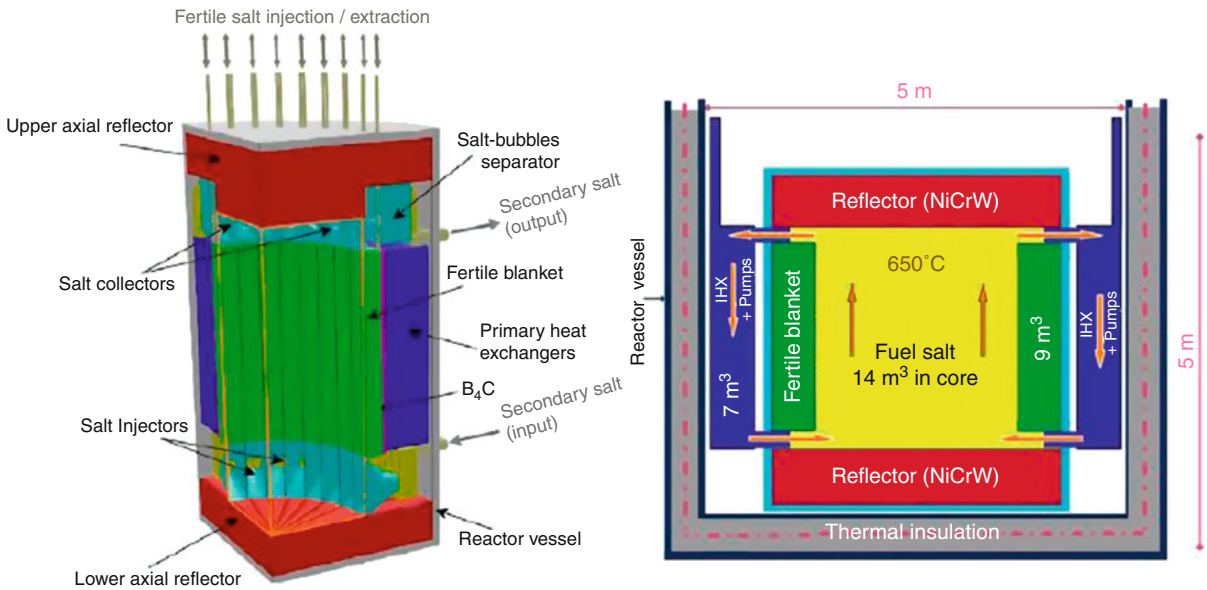

GEN-IV Reactors. Figure 6
Thorium molten salt reactor

thermal breeder reactor being developed internationally by Japanese, Russian and US consortium. Like all molten salt reactors, the core is chemically inert under low pressures to prevent explosions and toxic releases.

There are four fuel cycle options: (1) maximum breeding ratio (up to 1.07) using a Th and U-233 fuel cycle, (2) denatured Th and U-233 converter with minimum inventory of nuclear material suitable for weapons use, (3) denatured once-through actinide burning (Pu and minor actinides) fuel cycle with minimum chemical processing, and (4) actinide burning with continuous recycling. The fourth option with electricity production is favored for the GEN-IV MSR. Fluoride salts with higher solubility for actinides such as NaF/ZrF4 are preferred for this option. Salts with lower potential for tritium production would be preferred if hydrogen production was the objective. Lithium and beryllium fluorides would be preferred if high conversion was the objective. On-line processing of the liquid fuel is only required for high conversion to avoid parasitic neutron loses of Pa-233 that decays to U-233 fuel. Off-line fuel salt processing is acceptable for actinide management and hydrogen or electricity generation missions.

The reactor can use U or Th as a fertile fuel dissolved as fluorides in the molten salt. Due to the thermal or epithermal spectrum of the fluoride MSR, Th achieves the highest conversion factors. However, before sufficient fissile is bred for maintaining the criticality, the MSR requires low-enriched uranium or other fissile materials. The operating temperature ranges from the melting point of eutectic fluorine salts (about 450°C) to below the chemical compatibility temperature of nickel-based alloys (about 800°C).

The R&D will focus on fuel salt cleanup, including pyrochemical separation technologies, extraction of gaseous fission products and noble metals by gas bubbling, tritium speciation and control, and conversion of various waste streams into final waste forms. The research will gradually advance from laboratory scale to larger and more integrated demonstrations. MSR burner and breeder fuel cycles will be evaluated and compared with other nuclear systems. This includes examination of the burning of actinides from other nuclear systems, startup of MSRs on various actinides, avoidance of the generation of most actinides by use of thorium fuel cycles, and alternative breeder reactor fuel cycles.

The MSR also addresses research related to the compatibility of fuel and coolant salts with core and structural materials and challenging MSR subsystem integrity: reactor components and reprocessing unit

regarding mechanical and corrosion resistance. The high temperature, salt reduction-oxidation potential, radiation fluence, and energy spectrum pose a serious challenge for any structural alloy in an MSR. The design of a practical system demands the selection of salt constituents such as LiF, NaF, BeF_2, UF_4, ThF_4, and PuF_3 that are not appreciably reduced by available structural metals and alloys whose component Fe, Ni, and Cr can be in near equilibrium with the salt. Small levels of impurities in the salt may also aggressively corrode the metallics.

Circulating fuel raises challenges within the core such as the loss of delayed neutrons, temperature differences between the salt, reflectors, and moderator, which requires the coupling between neutronics, thermal-hydraulics, salt composition, and properties of the MSR.

SFR – Sodium-cooled Fast Reactor

The Sodium-cooled Fast Reactor features a fast-spectrum reactor and closed fuel-recycle system. Including electricity generation, the primary mission for the SFR could be either enhancement of the uranium resource utilization or high-level radioactive material management, which depends on the SFR designs. Historically, the enhancement of the uranium resource utilization was the primary mission of the SFR by achieving a high breeding ratio, but the mission was recently shifted for consuming transuranics (plutonium and other long-lived radioactive material) in a very low breeding ratio core. The latter has been studied under the Global Nuclear Energy Partnership (GNEP), which was initiated to seek worldwide consensus on enabling expanded use of economical carbon-free nuclear energy to meet growing electivity demand. The GNEP adopted a fully closed nuclear fuel cycle option that enhances energy security while improving proliferation risk management. One of the major goals of the GNEP is to design and demonstrate a SFR for actinide management like the Advanced Burner Reactor (ABR, [20]).

Based on the arrangement of the primary coolant pump and intermediate heat exchanger (IHX), there are two options for the SFR systems: pool type and loop type (see Figs. 7 and 8). The primary pump and IHX are placed inside the reactor vessel in the pool type, while these two components are located outside reactor vessel by connecting them trough pipes. A hybrid option [21] of the pool and loop types has also been proposed.

The experiences on design, construction, and operation provide important input into the design process and have the potential to influence the maturity of the various fast reactor concepts. The greater the number of operating experience years, the greater the opportunity to modify the design based on operating lessons learned. The SFR relies on technologies already developed and demonstrated for sodium-cooled reactors and associated fuel cycles that have successfully been built and operated in worldwide fast reactor programs. Overall, approximately 300 reactor years of operating experience have been logged on SFRs including 200 years on smaller test reactors and 100 years on larger demonstration or prototype reactors. Thus, the technical readiness level, which indicates how soon a system could be deployed, of the SFR is most matured among the six GEN-IV systems.

In the USA, the SFR technology was employed in the 20 MW-electric Experimental Breeder Reactor II (EBR-II [22]) that operated from 1963 to 1994. EBR-II R&D included development and testing of metal fuel and passive safety tests. The 400 MWth Fast Flux Test Facility (FFTF [23]) was completed in 1980 (Fig. 9). The FFTF operated successfully for 10 years with a full core of mixed oxide (MOX) fuel and performed SFR materials, fuels, and component testing. The US SFR development program stalled with cancellation of the Clinch River demonstration reactor in 1983, although US-DOE research for advanced SFR technology continued until 1994. The SFR experience also extends to the commercial sector with the operation of Detroit Edison's FERMI-1 plant from 1963 to 1972.

Significant SFR research and development programs are being conducted in China, France, India, Japan, Russia, and Republic of Korea. The most modern fast reactor construction project was the 280 MWe MONJU (Japan) that was completed in 1990, which will be restarted soon. The construction of 20 MWe Chinese Experimental Fast Reactor (CEFR) and coolant sodium loading was completed in 2009, and the full power operation is expected in 2010. India operates 40 MWth Fast Breeder Test Reactor (FBTR) since 1985 and 500 MWe Prototype Fast Breeder Reactor

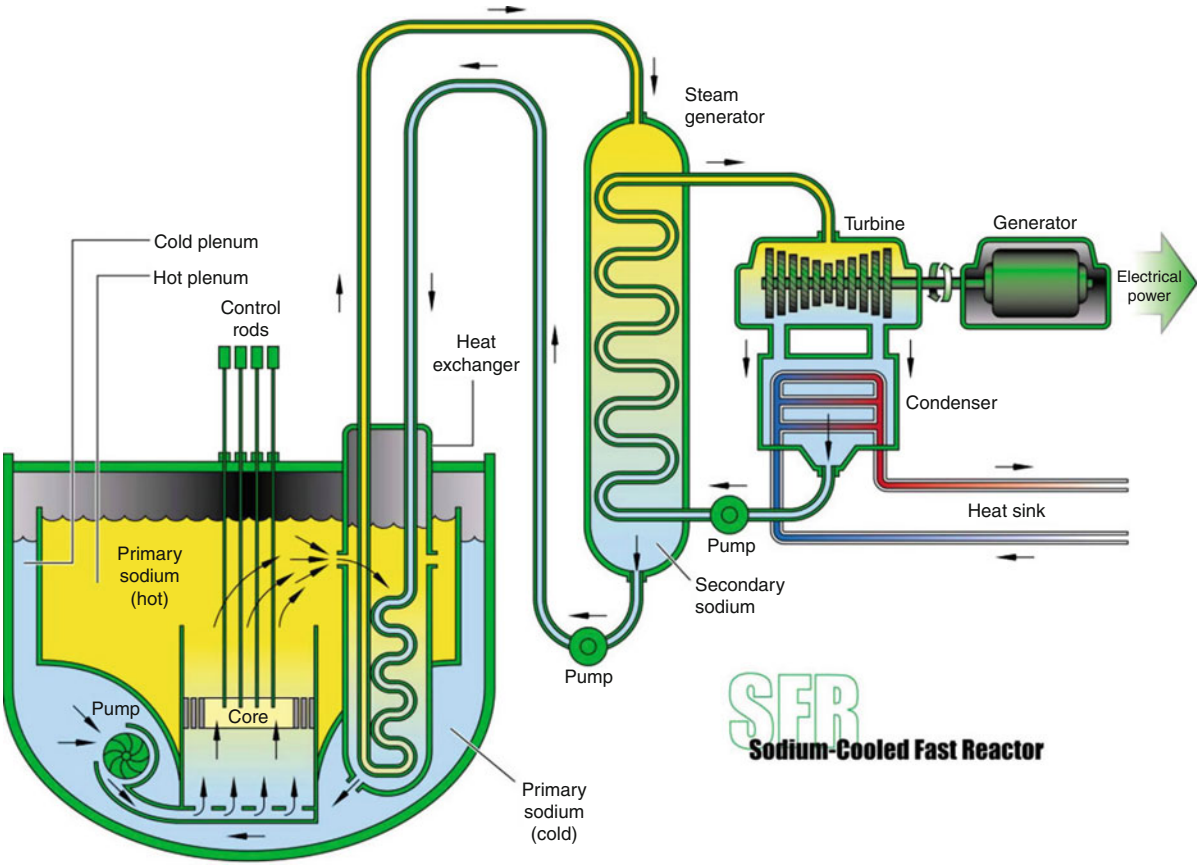

GEN-IV Reactors. Figure 7
Pool-type sodium-cooled fast reactor

(PFBR) is under construction. The only current fast reactor for electrical generation is the Russian BN-600 that has reliably operated since 1980, and the BN-800 is under construction.

A range of plant size options are available for the SFR, ranging from a battery type systems of a hundred MW-thermal to large monolithic reactors of 3,500 MW-thermal. The sodium coolant outlet temperature is limited by the material properties. Coolant outlet temperatures are typically less than 550°C; however, further increase is considered.

A large margin to coolant boiling is achieved by design, and is an important safety feature of these systems. Another major safety feature is that the primary system operates at essentially atmospheric pressure, pressurized only to the extent needed to move fluid. Sodium reacts chemically with air, and with water, and thus the design must limit the potential for such reactions and their consequences. To improve safety, a secondary sodium system acts as a buffer between the radioactive sodium in the primary system and the steam or water that is contained in the conventional Rankine-cycle power plant.

Metallic and oxide fuel forms are available for the SFR. The metallic fuel was originally chosen in the early fast reactor programs because of its high density, compatibility with the liquid metal coolant, relative easiness to fabricate, and excellent thermal conductivity. In the late 1960s, before the full potential of metallic fuels were established, the interest worldwide for fast reactor fuel turned toward the oxide fuel, because the achievable burnup is limited by a large irradiation swelling. However, the development and irradiation test of metallic fuels continued though the 1970s and it was discovered that the metallic fuel can achieve a high burnup by allowing room for fuel to swell. In addition,

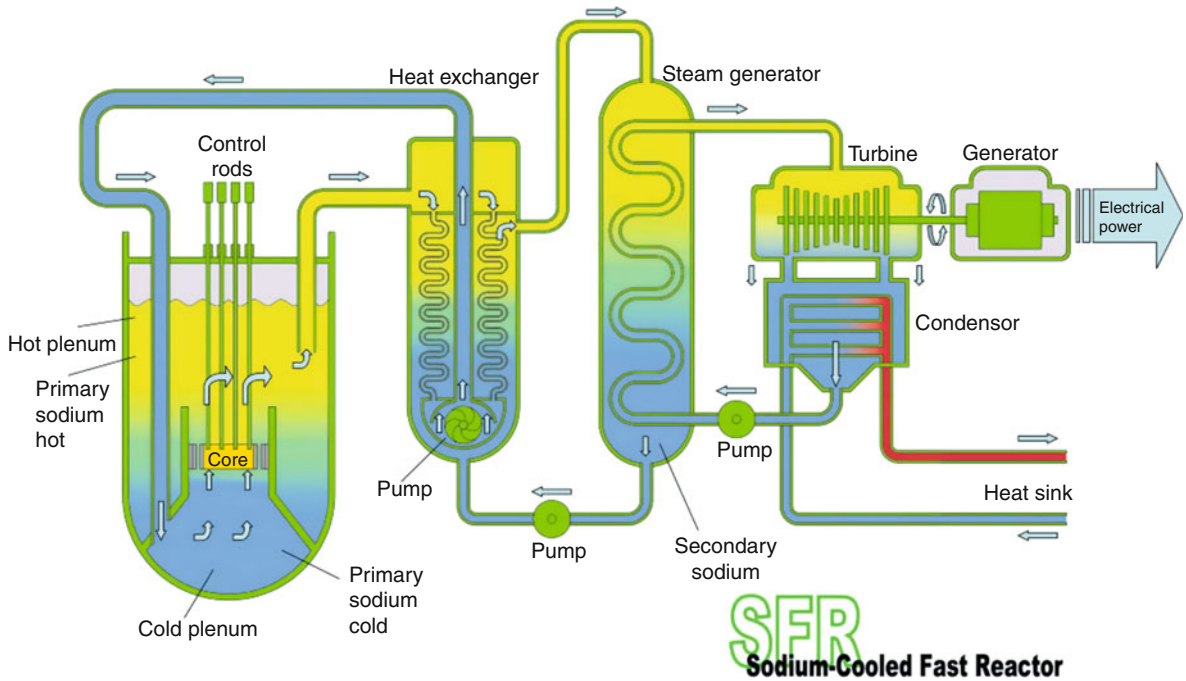

GEN-IV Reactors. Figure 8
Loop-type sodium-cooled fast reactor

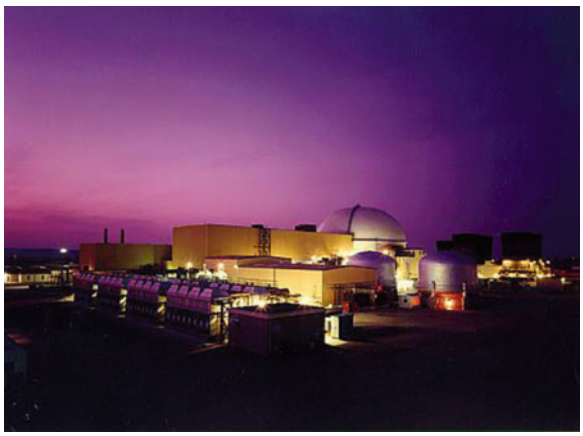

GEN-IV Reactors. Figure 9
Fast Flux Test Facility

the metallic fuel was focused again in the recent fast reactor programs because of its potential passive safety benefits.

The high burnup potential, rich experiences in commercial water-cooled reactors, and the existence of established industry for manufacturing were the critical factors that motivated interest in oxide fuel for the liquid-metal-cooled fast reactors. However, the low heavy metal density and low thermal conductivity are the principal disadvantages of the oxide fuel. The low density is unfavorable to implement a compact core and increase the breeding ratio or cycle length. The low thermal conductivity leads to high temperature gradient from fuel to coolant. As a result, the oxide fuel stores significant amount of Doppler reactivity in the normal operation condition and it provides the unfavorable positive reactivity feedback during an unprotected severe accident.

Recently, the mixed carbide and nitride fuels have been given attention as the alternative fuels for sodium-cooled fast reactor on the basis of their high density, compatibility with sodium coolant, high melting temperature, and excellent thermal conductivity although they are ceramic fuel like a mixed oxide fuel.

The SFR require a closed fuel cycle to enable their advantageous actinide management and fuel utilization features. There are two primary fuel cycle technology options: an advanced aqueous process and the

pyroprocess [15] which derives from the term, pyrometallurgical process. Both processes have similar objectives: recovery and recycle of more than 99.9% of the actinides, inherently low decontamination factor of the product, making it highly radioactive, and never separating plutonium at any stage for nonproliferation. These fuel cycle technologies are adaptable to thermal spectrum fuels in addition to serving the needs of the SFR. Thus, the reactor technology and the fuel cycle technology are strongly linked.

Due to the flexibility of the conversion ratio depending on the core design options, the SFR can be operated in three distinct fuel cycle roles. A conversion ratio less than 1 ("burner") can reduce long-lived radioactive waste. A conversion ratio near 1 can increase the uranium utilization without feeding additional enriched uranium. A conversion ratio greater than 1 ("breeder") affords a net creation of fissile materials. An appropriately designed fast reactor has flexibility to shift between these operating modes; the desired actinide management strategy will depend on a balance of waste management and resource extension considerations.

Regarding economics, the reduction of the plant capital costs is crucial. A number of innovative SFR design features have been proposed: configuration simplifications, improved Operations & Maintenance (O&M) technology, advanced reactor materials, advanced energy conversion systems, fuel handling, etc.

With regard to reactor safety, technology gaps center around two general areas: assurance of passive safety response and techniques for evaluation of bounding events. The advanced SFR designs exploit passive safety measures to increase reliability. The system behavior will vary depending on system size, design features, and fuel type. R&D for passive safety will investigate phenomena such as axial fuel expansion and radial core expansion, and design features such as self-actuated shutdown systems and passive decay heat removal systems. The ability to measure and verify these passive features must be demonstrated. Associated R&D will be required to identify bounding events for specific designs and investigate the fundamental phenomena to mitigate severe accidents.

Finally, the development of SFR technology provides the opportunity to design modern safeguards directly into the planning and building of new nuclear energy systems and fuel cycle facilities. Incorporating safeguards into the design phase for new facilities will facilitate nuclear inspections conducted by the International Atomic Energy Agency (IAEA). The goal of this oversight is to always have an accurate grasp of the current inventory through the utilization of advanced technologies to verify the characteristics of the security system (accountancy, detection, and promptness) and the physical protection characteristics (physical protection measures, the monitoring level, and security measures) and for ensuring robust design to guarantee these characteristics. It is also necessary to maintain transparency and openness in terms of information to more effectively and efficiently monitor and verify nuclear material inventories.

SCWR – Supercritical Water-cooled Reactor

The Supercritical Water-cooled Reactor is a water-cooled reactor like Light Water Reactor (LWR) operated commercially, but the SCWR is operated above the thermodynamic critical point of water (374°C, 22.1 MPa). Figure 10 shows the SCWR system.

The specific heat increases drastically and the water density decreases without boiling of water around the thermodynamic critical point. As a result, the SCWR has unique features that may offer advantages compared to state-of-the-art PWRs: Higher plant thermal efficiency compared to LWRs due to the higher operating temperature. Low density of water without boiling allows the direct cycle like Boiling Water Reactor (BWR), but steam dryers, steam separators, recirculation pumps, and steam generators are not necessary, and as a result, the SCWR can be a simpler plant with fewer major components. Lower-coolant mass flow rate per unit core thermal power results from the high heat capacity of the supercritical water. This offers a reduction in the size of the reactor coolant pumps, piping, and associated equipment, and a reduction in the pumping power. Lower-coolant mass inventory results from the once-through coolant path in the reactor vessel and the lower-coolant density. This opens the possibility of smaller containment buildings. No boiling crisis (i.e., departure from nucleate boiling or dry out) exists due to the lack of a second phase in the reactor, thereby avoiding discontinuous heat transfer regimes within the core during normal operation.

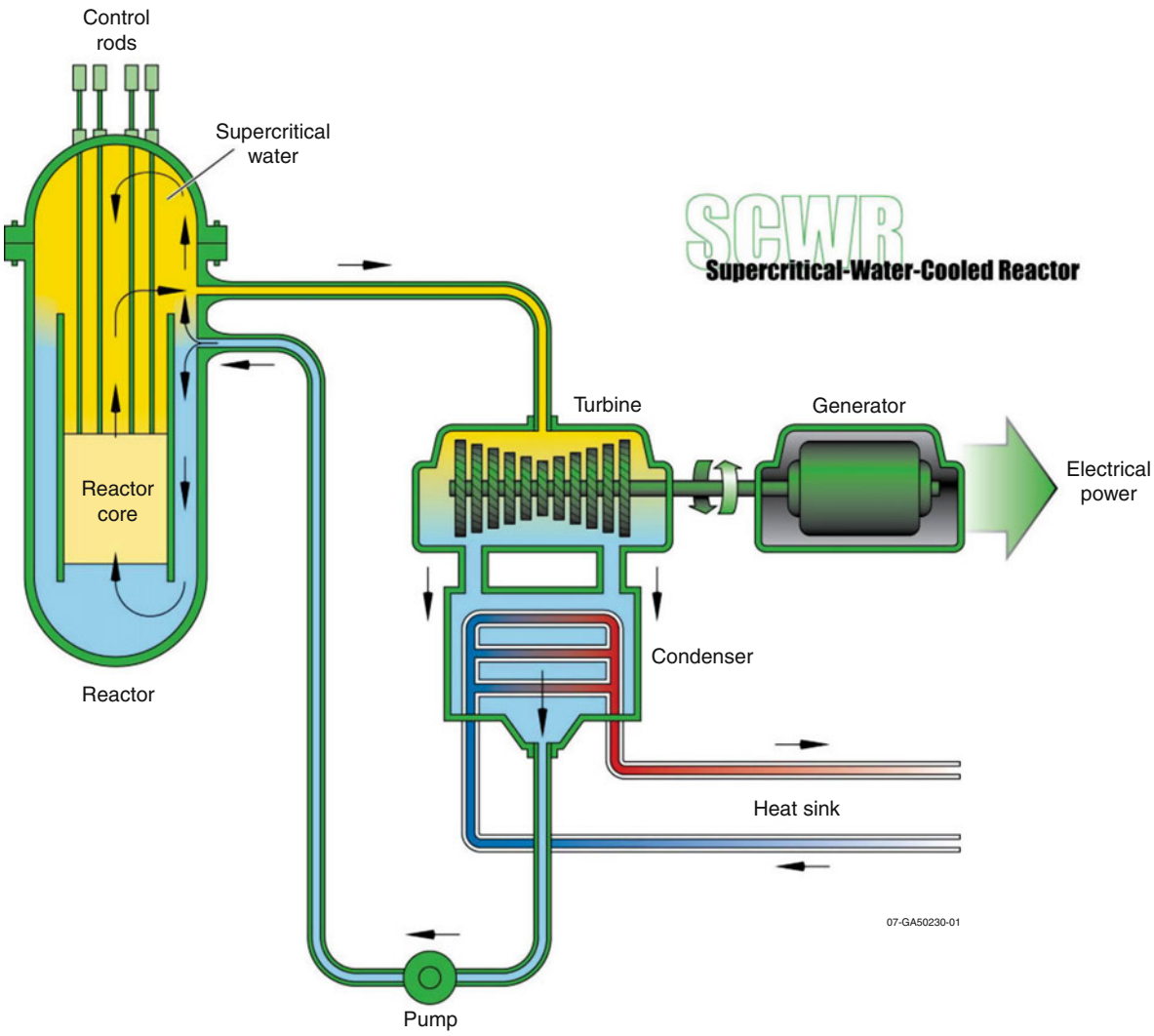

GEN-IV Reactors. Figure 10
Supercritical water-cooled reactor

The SCWR systems may have a thermal [24], fast [25], or mixed-neutron spectrum [26] depending on the core design. The Japanese supercritical light water reactor (SCLWR) with a thermal spectrum has been the subject of the most development work in the last 10–15 years. The SCLWR reactor vessel is similar in design to a PWR vessel (although the primary coolant system is a direct-cycle, BWR-type system). High-pressure (25.0 MPa) coolant enters the vessel at 280°C. The inlet flow splits, partly to a downcomer and partly to a plenum at the top of the core to flow down through the core in special water rods. This strategy provides moderation in the core. The coolant is heated to about 510°C and delivered to a power conversion cycle, which blends LWR and supercritical fossil plant technology; high-, intermediate-, and low-pressure turbines are employed with two reheat cycles.

The SCWR can also be designed to operate as a fast reactor. The difference between thermal and fast versions is primarily the amount of moderator material in the SCWR core. The fast spectrum reactors use no additional moderator material, while the thermal

spectrum reactors need additional moderator material in the core. The mixed-spectrum SCWR was proposed not only to achieve all advantages of SCWR but also the actinide management. The core uses two coolant flow paths: outer zone with high density water and inner zone with low density water (see Fig. 11). Thus, the inner zone features fast neutron spectrum, while the outer zone features thermal spectrum. By recycling TRU in the fast zone, the mixed-spectrum SCWR is capable of keeping all TRU in the reactor.

Much of the technology base for the SCWR can be found in the existing LWRs and in commercial supercritical-water-cooled fossil-fired power plants. However, there are some relatively immature areas. There have been no prototype SCWRs built and tested. For the reactor primary system, there has been very little in-pile research done on potential SCWR materials or designs, although some SCWR in-pile research has been done for defense programs in Russia and the United States. Limited design analysis has been underway over the last decade in Japan, Canada, and Russia. For the balance of plant, there has been development of turbine generators, piping, and other equipment extensively used in supercritical-water-cooled fossil-fired power plants.

The ability to use proven uranium oxide fuel greatly simplifies the application of fuel and fuel cycle technology to the SCWR. However, the supercritical water is known to challenge the corrosion/erosion performance of current cladding technology, and R&D is focused on advanced cladding materials.

There are several unique components needed for the SCWR, including the reactor pressure vessel or pressure tubes and its internal structural components, moderator channels, control rods and drives, the condenser and high-pressure pumps, valves, and seals. The reactor pressure boundary must operate above the high pressure (22.1 MPa) of supercritical water. This may be addressed with thicker sections, and thermal stresses can be avoided with a thermal sleeve for the outlet nozzle.

Zirconium-based alloys, common in water-cooled reactors, may not be a viable material without thermal and/or corrosion-resistant barriers. Based on available data for other alloy classes, there is no single alloy that has received enough study to unequivocally ensure its performance in an SCWR. Another key need of this system will be an enhanced understanding of the chemistry of supercritical water. Water above its critical point is accompanied by dramatic changes in chemical properties. Its behavior and degradation of materials is further accelerated by in-core radiolysis, which preliminary studies suggest is markedly different than what would have been predicted by simplistic extrapolations from conventional reactors.

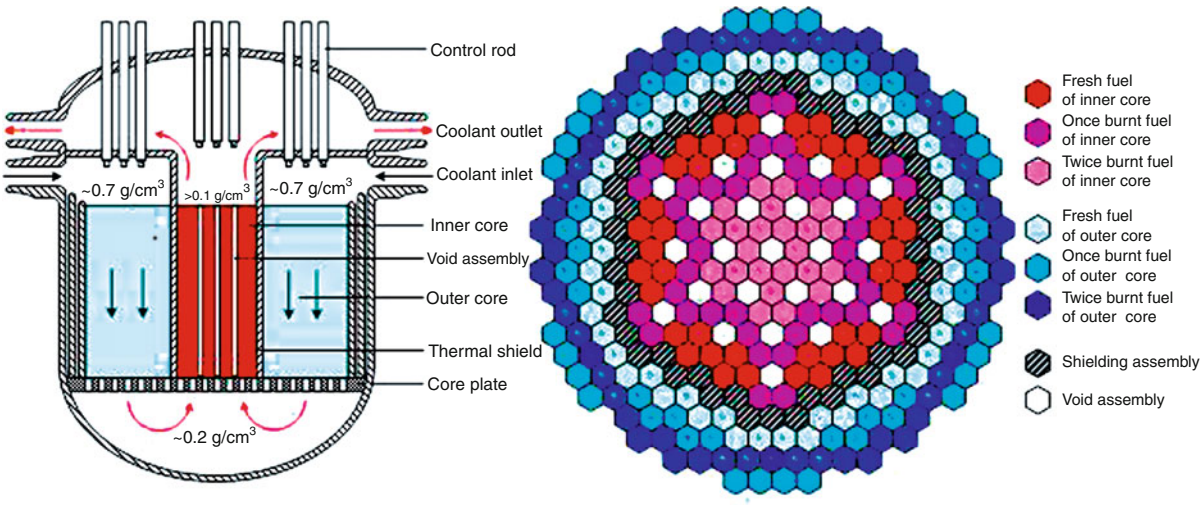

GEN-IV Reactors. Figure 11
Core layout of mixed-spectrum supercritical water reactor

The approach to development of materials and components will build on evaluation of candidate materials with regard to corrosion and stress corrosion cracking, strength, embrittlement and creep resistance, and dimensional and microstructural stability; the potential for water chemistry control to minimize impacts as well as rates of deposition on fuel cladding and turbine blades; and measurement of performance data in an in-pile loop. All of these are critical to establishing viability of the SCWR.

The SCWR leads the way among GEN-IV systems in the development of advanced materials for water coolant. In fact, the diffusion of this technology into current generation light and heavy water reactors seems assured. However, much remains to be done: the thermal-hydraulic performance during normal and off-normal operation, as well as postulated accidents, needs to be addressed both with advances in the design and safety approach as well as the analysis tools. Issues to be addressed include the basic thermal-hydraulic phenomenon of heat transfer and fluid flow of supercritical water in various geometries, critical flow measurements, the strong coupling of neutronic and thermal-hydraulic behavior, leading to concerns about flow stability and transient behavior, validation of computer codes that reflect these phenomena, and definition of the safety and licensing approach as distinct from current water reactors, including the spectrum of postulated accidents, flow instability, etc.

VHTR – Very-high-temperature Reactor

The Very-high-temperature Reactor is a graphite-moderated, helium-cooled reactor like GT-MHR and PBMR capable of generating electricity, but the coolant output temperature is significantly increased up to 1,000°C. In Fig 12, the schematic of the VHTR is depicted. The higher temperatures of this reactor open the door for industrial heat processing opportunities, in particular, for hydrogen production.

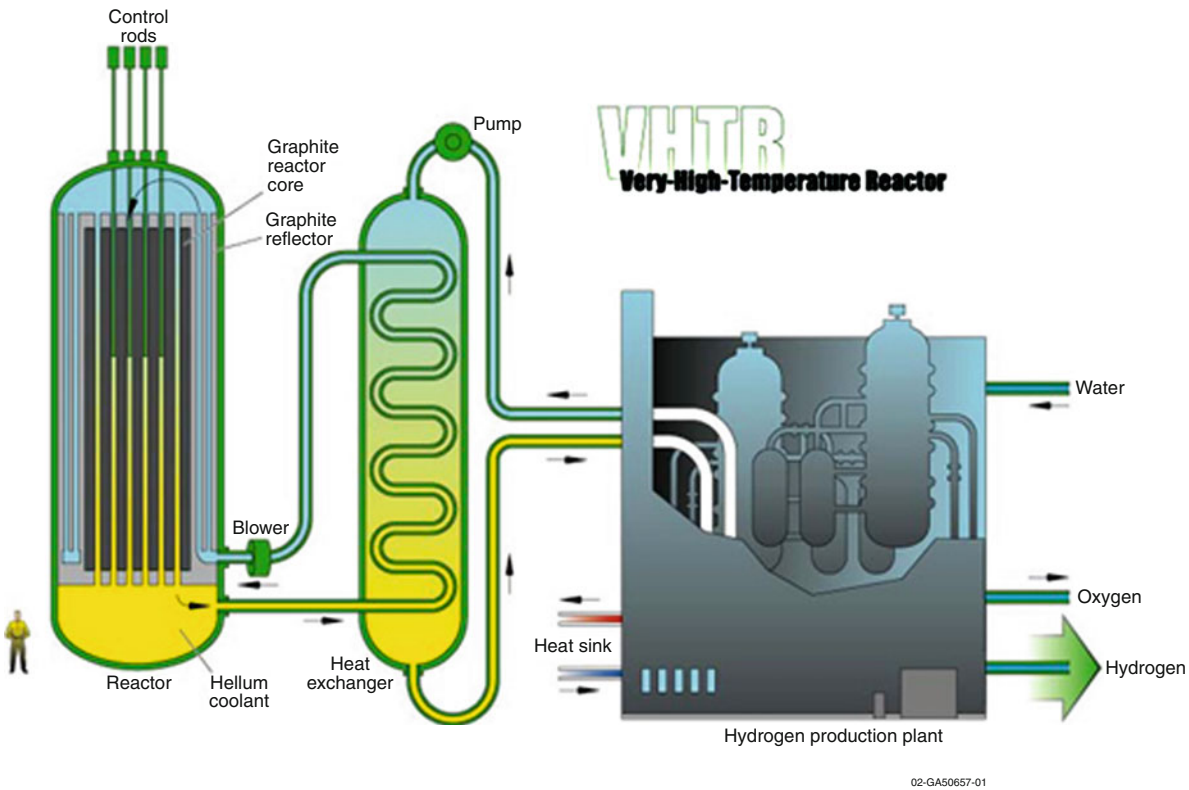

GEN-IV Reactors. Figure 12
Very-high-temperature reactor

The annual US demand for hydrogen is over 12 million tons, and expected to grow to over 30 million tons by 2030. Industry uses hydrogen for fossil fuel refining, treating metals, and food processing. Hydrogen is currently produced primarily from steam methane reforming using fossil fuel as a heat source. Hydrogen can also be produced by various processes using a high-temperature gas-cooled reactor as the primary energy source.

Use of nuclear energy as the heat source of a large-scale hydrogen production operation would result in substantially lower carbon emissions over a natural gas-fired steam methane reforming operation. A 600 MWth VHTR dedicated to hydrogen production can yield over 2 million normal cubic meters per day. The VHTR can also generate electricity with high efficiency, over 50% at 1,000°C.

The VHTR has been evolved from gas-cooled reactor experiences and extensive international databases that can support its development. The basic technology for the VHTR has been well established in former gas-cooled reactors, such as DRAGON, Peach Bottom, AVR, THTR, and Fort St Vrain, and is being advanced in concepts such as the GT-MHR and PBMR. The ongoing 30-MWth HTTR project in Japan is intended to demonstrate the feasibility of reaching outlet temperatures up to 950°C coupled to a heat utilization process, and the HTR-10 in China will demonstrate electricity generation at a power level of 10 MWth. The former projects in Germany and Japan provide data relevant to the VHTR development.

The VHTR core uses TRISO particles to form a pebble bed or prismatic fuel element (see Fig. 13). The TRISO particle, which has a small diameter of less than 1.0 mm, has a fuel kernel in the form of uranium oxide. The enrichment of the uranium is dependent on the core design purposes. The kernel is subsequently coated with a porous carbon layer (to hold fission gases), a dense pyrolytic carbon layer, a silicon carbide layer, and finally another pyrolytic carbon layer. The coatings surrounding the kernel of TRISO particles produce a very robust fuel form by acting as the containment boundary for the radioactive material. These coatings work in much the same way as the massive reinforced concrete structure surrounding the light water reactors currently in service.

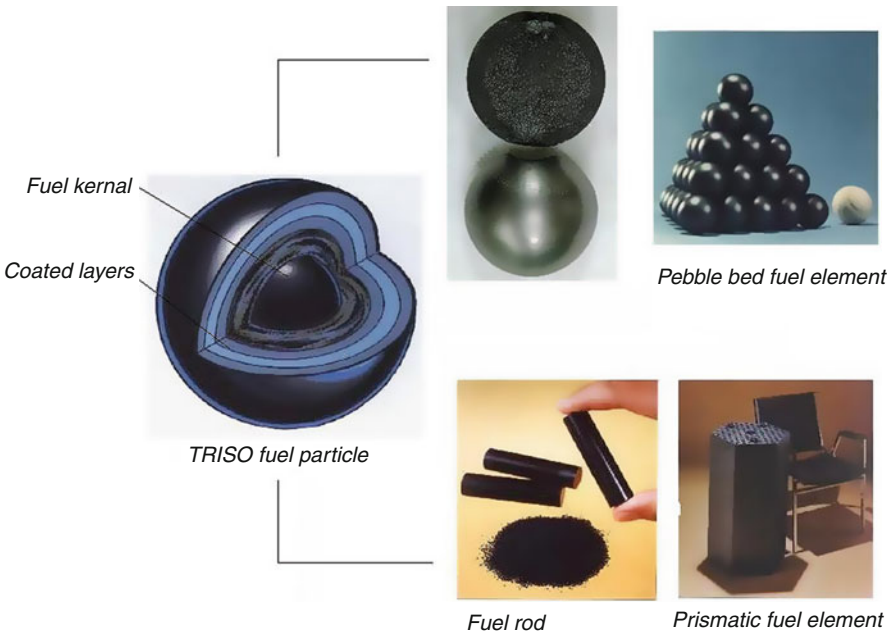

GEN-IV Reactors. Figure 13
VHTR fuel elements

The reactor core type of the VHTR can be a prismatic block core such as GT-MHR and Japanese HTTR, or a pebble-bed core such as PBMR and Chinese HTR-10. Despite of the alternate fuel element designs (pebble bed versus prismatic), the two baselines have many technologies in common that allow for a unified R&D approach. The well-known TRISO particle fuel with a UO_2 kernel and SiC/PyC coating may be used in either, or it may be enhanced with a different fuel kernel form such as UCO or an advanced ZrC coating through additional research. For electricity generation, the helium gas turbine system can be directly set in the primary coolant loop, which is called a direct cycle. For nuclear heat applications such as process heat for refineries, petro-chemistry, metallurgy, and hydrogen production, the heat application process is generally coupled with the reactor through an intermediate heat exchanger (IHX), which is called an indirect cycle.

The fuel cycle will initially be a once-through fuel cycle specified for high burnup (15–20 atom-%) using low enriched uranium. The operation with a closed fuel cycle will be assessed and solutions to better manage the fuel cycle back end will be developed. The possible use of TRU as a fuel will be studied conceptually for actinide management [27].

The primary emphasis in fuel development is on its performance at high burnup, power density, and temperature. The R&D broadly addresses its manufacture and characterization, irradiation performance, and accident behavior. Irradiation tests will provide data on coated particle fuel and fuel element performance under irradiation as necessary to support fabrication process development, to qualify the fuel design, and to support development and validation of models and computer codes on fission product transport. They will also provide irradiated fuel and materials samples for postirradiation and safety testing. The performance expected for the fuel must be verified for all normal, transient, or accident conditions as well as certain severe accident conditions (beyond design basis). A key claim of the fuel is its ability to retain fission products in the fuel particles under a range of postulated accidents with temperatures up to 1,600°C.

Future Directions

The objective for Generation IV nuclear energy systems is to have them available for wide-scale deployment before the year 2030. The anticipated deployment dates for the six GEN-IV systems are provided in Table 3 in terms of R&D phases. The deployment dates of the SFR and VHTR are expected to be earlier than other GEN-IV systems because of their matured technical readiness level.

In the viability R&D phase, the feasibility of key technologies of the GEN-IV systems will be examined. The performance R&D activities undertake the development of performance data and optimization of the system. Assuming the successful completion of viability and performance R&D, the demonstration R&D phase activities involve the licensing, construction, and operation of a prototype or demonstration system in partnership with industry and perhaps other countries.

GEN-IV Reactors. Table 3 Anticipated deployment of GEN-IV systems

System	Deployment timelines		
	Viability phase	Performance phase	Demonstration phase
GFR	2012	2020	2025
LFR	2014	2020	2025
MSR	2013	2020	2025
SFR	2006	2015	2020
SCWR	2014	2020	2025
VHTR	2010	2015	2020

Thus, the detailed design and licensing of the system will be performed during the demonstration phase. The R&D projects and milestones anticipated in each phase were defined in GEN-IV roadmap project [2].

Bibliography

Primary Literature

1. Generation IV International Forum. http://www.gen-4.org
2. US-DOE Nuclear Energy Research Advisory Committee and GIF (2002) A technical roadmap for generation IV nuclear energy systems: ten nations preparing today for tomorrow's energy needs. Generation IV International Forum. http://www.gen-4.org
3. Potter PC (1996) Gas turbine-modular helium reactor (GT-MHR) conceptual design description report. General Atomics GA-910720
4. Koster A, Matzer HD, Nicholsi DR (2003) PBMR design for the future. Nucl Eng Des 222:231–245
5. Simon R (2005) The primary circuit of the DRAGON high temperature reactor experiment. 18th International conference of structural mechanics in reactor technology (SMiRT 18), Beijing
6. Moormann R (2008) A safety re-evaluation of the AVR pebble bed reactor operation and its consequences for future HTR concepts. Institute for Energy Research, Switzerland
7. Wachholz W (1988) The present state of the HTR concept based on experience gained from AVR and THTR. International Working Group on Gas-cooled Reactors International Atomic Energy Agency IWGGCR-19, Vienna
8. Brown JR et al (1987) Physics testing at Fort St. Vrain: a review. Nucl Sci Eng 97:104
9. Yamashita K et al (1996) Nuclear design of the high-temperature engineering test reactor (HTTR). Nucl Sci Eng 122:212
10. Seker V, Colak U (2003) HTR-10 full core first criticality analysis with MCNP. Nucl Eng Des 222:263–270
11. Stainsby R, Peers K, Mitchell C, Poette C, Mikityuk K, Somers J (2009) Gas cooled fast reactor research and development in the European Union. Sci Technol Nucl Installations 2009:1–7
12. IAEA (2007) Status of small reactor designs without on-site refueling. International Atomic Energy Agency IAEA-TECDOC-1536, Vienna
13. Smith C, Halsey WG, Brown NW, Sienicki JJ, Moisseytsev A, Wade DC (2008) SSTAR: the US lead-cooled fast reactor (LFR). J Nucl Mater 376:255–259
14. Cinotti L, Smith CF, Sienicki JJ, Abderrahim HA, Benamati G, Locaelli G, Monti S, Wider H, Stuwe D, Orden A (2007) The potential of LFR and ELSY project. 2007 International congress on advances in nuclear power plants, Nice
15. Hannum WH (1997) The technology of Integral Fast Reactor and its associated fuel cycle. Prog Nucl Energy 31: 1–217
16. Boardman CE (2000) A description of the S-PRISM plant. 8th International conference on nuclear engineering, Baltimore
17. Ingersoll T et al (2004) Status of pre-conceptual design of the Advanced High-Temperature Reactor (AHTR). Oak Ridge National Laboratory, Oak Ridge, ORNL/TM-2004/104
18. Bettis ES, Cottrell WB, Mann ER, Meem JL, Whitman GD (1957) The aircraft reactor experiment: operation. Nucl Sci Eng 2:841–853
19. Haubenreich PN, Engel JR (1970) Experience with the molten-salt reactor experiment. Nucl Appl Technol 8:118–136
20. Kim TK, Yang WS, Grandy C, Hill RN (2009) Core design studies for a 1000 MWt advanced burner reactor. Ann Nucl Energy 36:331–336
21. Zhao H, Zhang H (2007) An innovative hybrid loop-pool design for sodium cooled fast reactor. Idaho National Laboratory INL/CON-07-12657
22. Koch L (2000) Experimental breeder reactor-II. Argonne National Laboratory, Chicago
23. Lash T (1997) Fast flux test facility (FFTF) briefing book 1: summary. Pacific Northwest National Laboratory PNNL-11778
24. Oka Y (2000) Design concept of once-through cycle supercritical pressurized light water reactors. The first International symposium on supercritical water-cooled reactors, SCR-2000, Tokyo
25. Macdonald P (2000) Feasibility study of supercritical light water cooled fast reactor for actinide burning and electric power production. Idaho National Laboratory INEEL/EXT-02-01330
26. Kim TK, Wilson PH, Hu P, Jain R (2004) Feasibility and configuration of a mixed spectrum supercritical water reactor. International topical meeting on the Physics of Fuel Cycles and Advanced Nuclear Systems (PHYSOR-2004), Chicago
27. Kim TK, Taiwo TA, Yang WS, Hill RN, Assessment of deep burnup concept based on graphite moderated gas-cooled thermal reactor. International topical meeting on the Physics of Fuel Cycles and Advanced Nuclear Systems (PHYSOR-2006), Vancouver

Book and Reviews

A Strategy for nuclear energy research and development. Electric Power Research Institute (ERPI)

Bouchard JB (2008) Generation IV advanced nuclear energy systems. Nucl Plant J 26

Kim WJ et al (2006) Supercritical carbon dioxide Brayton power conversion cycle design for optimized battery-type integral reactor system. International congress on advances in nuclear power plants, Reno

MacDonald PE et al (2003) NGNP preliminary point design – results of initial neutronics and thermal-hydraulic assessment. INEEL/EXT-03-00870 Rev. 1. Idaho National Engineering and Environmental Laboratory, September 2003

Sienicki JJ et al (2006) Status report on small secure transportable autonomous reactor (SSTAR)/lead-cooled fast reactor (LFR) and supporting research and development. Argonne National Laboratory ANL-GenIV-089

Schultz RR (2008) Next generation nuclear plant methods research and development technical program plan. Idaho National Laboratory INL/EXT-06-11804

The US Generation IV Implementation Strategy (2003) US Department of Energy office of Nuclear Energy, Science and Technology

The US Generation IV Fast Reactor Strategy (2006) US Department of Energy office of Nuclear Energy

Genotype by Environment Interaction and Adaptation

Ignacio Romagosa[1], Gisela Borràs-Gelonch[1], Gustavo Slafer[1], Fred van Eeuwijk[2]
[1]Department of Crop and Forest Sciences, University of Lleida, Lleida, Spain
[2]Biometris, Wageningen University and Research Centre, Wageningen, The Netherlands

Article Outline

Glossary
Definition
Introduction
Breeding Implications
Traits Determining Adaptation
Statistical Approaches for GE Characterization
Future Directions
Bibliography

Glossary

GE *Genotype by environment interaction* is differential genotypic expression across environments that may cause that a genotype selected among the best in one location to perform poorly in another. GE weakens association between phenotype and genotype, reducing genetic progress in breeding programs. In statistical terms, GE describes a situation in which the simultaneous effect of two classification variables (genotype and environment) on a continuous dependent third one, such as yield, does not follow an additive model.

MET A *multi-environment trial* is a series of trials sampling the target environmental range in which a particular set of genotypes is evaluated.

QTL A *quantitative trait locus* is a region in the genome associated with a particular quantitative phenotypic trait, such as crop yield, resource-use-efficiency, phenology, or height. QTL analysis is a statistical method that links phenotypic data (specific trait measurements on a series of individuals) and genotypic data (usually in the form of molecular markers taken on the same individual) in order to explain the genetic basis of complex traits. QTL number and the variation they explain on the phenotypic trait give clues about the genetic control of that trait, for example, if plant height is controlled by many genes of small effect, or by a few genes of large effect.

QTLxE QTL by environment interaction is differential QTL effect across environments that may cause that a favorable QTL in one environment may become irrelevant, or even unfavorable, in another.

Specific and wide adaptation A genotype is considered stable if it yields well relative to the productive potential of the environments in which is grown. If such concept of stability is shown for a wide agroecological array of environments, a genotype is considered to have general, wide, or broad adaptation. If stability is confined to a limited range, a genotype is said to have specific or narrow adaptation.

Definition

One of the first decisions farmers have to take is the selection of the variety to be grown in their fields based on expectation of economic returns, generally, in the form of the highest attainable yield. This is a critical choice that strongly determines the sustainability of the agricultural system. However, this is by no means trivial as it is very hard to identify the "best" variety across a diverse set of environments subjected to complex biotic and abiotic factors and interactions generally causing significant changes in varietal rank. Therefore, a major objective in plant breeding programs is to determine the potential adaptation of advanced breeding lines across a range of agroecological conditions. William S. Gosset (who signed as "Student [1]"

in a landmark publication introducing the t distribution) wrote at the onset of modern breeding that the ultimate purpose of field experimentation was to determine what varieties pay farmers best. He thought that the design of experiments should aim, not only at determining the average yield, but also at identifying varieties whose yield, being within those of high average value, were relatively less responsive to variation in soil and climate.

Breeding programs normally aim to release cultivars to be successfully grown over a rather large cropping area, varying in soil quality attributes and in average climate, and across several growing seasons, with interannual variations in climatic conditions. The target environment is defined as the set of soil × climatic conditions in which the released cultivars will be grown and to which the cultivars must be adapted. Therefore, a key step in applied plant breeding is the identification of advanced genotypes broadly or narrowly adapted across a wide range of target environments. Breeders focus in the first segregating generations on direct phenotypic selection of highly heritable traits, such as plant architecture and phenology to concentrate in later stages on complex quantitative traits like yield and end-use quality. Marker-assisted selection aims at complementing this phenotypic selection with direct marker screening for, mostly, oligogenic-controlled traits. The traditional approach to estimate the genotypic value in the context of breeding, varietal registration, and recommendation is deployment of extensive field evaluation schemes in a series of sites in which the assessed genotypes could be potentially grown. These collections of trials are generally denominated multi-environment trials (METs) in which a set of genotypes is evaluated in a series of trials that sample the target environmental range. Data from METs are typically summarized in the form of genotype by environment tables of means. Simple inspection of such tables of means will often reveal the presence of genotype by environment interaction (GE) or differences in performance of genotypes that are trial dependent. They also allow for the identification of those genotypes that are partially or generally adapted to the environmental range, showing specific or narrow versus general or wide adaptation, respectively.

The traditional outcome of METs is the identification of "which" cultivar and "where" has performed well. These studies are empirical, based on simple statistical characterizations of genotypic responses across environments and do not provide any physiological insight into the basis of the genotypic response to environmental changes. However, as one wants to move forward toward a *predictive* breeding scenario, the challenge beyond "which" and "where" is "why" narrow or wide adaptation happens, in terms of a thorough understanding of both the environment, the physiological behavior of the different cultivars and, eventually, of the genes responsible for adaptation. Identifying the "why" is not only a matter of satisfying curiosity: It would potentially allow more precise breeding through the direct manipulation of the genes responsible for the different adaptation patterns.

Introduction

Statistical analyses that detect and describe GE have been comprehensively reviewed [2–14]. Means across environments in METs are only adequate estimates of varietal performance in the absence of GE. When GE is significant, average values across environments may hide subsets of environments where genotypes differ markedly in relative performance.

As for any other statistical two-factor model, there are different types of interactions which originate from departure from additivity. In Fig. 1, the average for each of two genotypes, G1 and G2, for the dependent variable of interest, for example yield, is shown for three environments. Figure 1a represents the situation in which differences were detected only between environments. Figure 1b shows an additive model in which differences for both main effects, genotypes and environments, were observed but no GE. Figure 1c shows a quantitative or non-crossover interaction; in this scenario, genotypes with superior means can be recommended for all environments. In plant breeding, the most important GE is of the crossover or qualitative type (Fig. 1d), which implies changes in the rankings of genotypes across environments). In this case, variety G2 may be recommended for environment E1 but not for E2 and E3.

When there are genotypic differences among the varieties tested and the target environments include different soils and variable climate, MET analyses more often than not detect crossover GE (only MET with limited

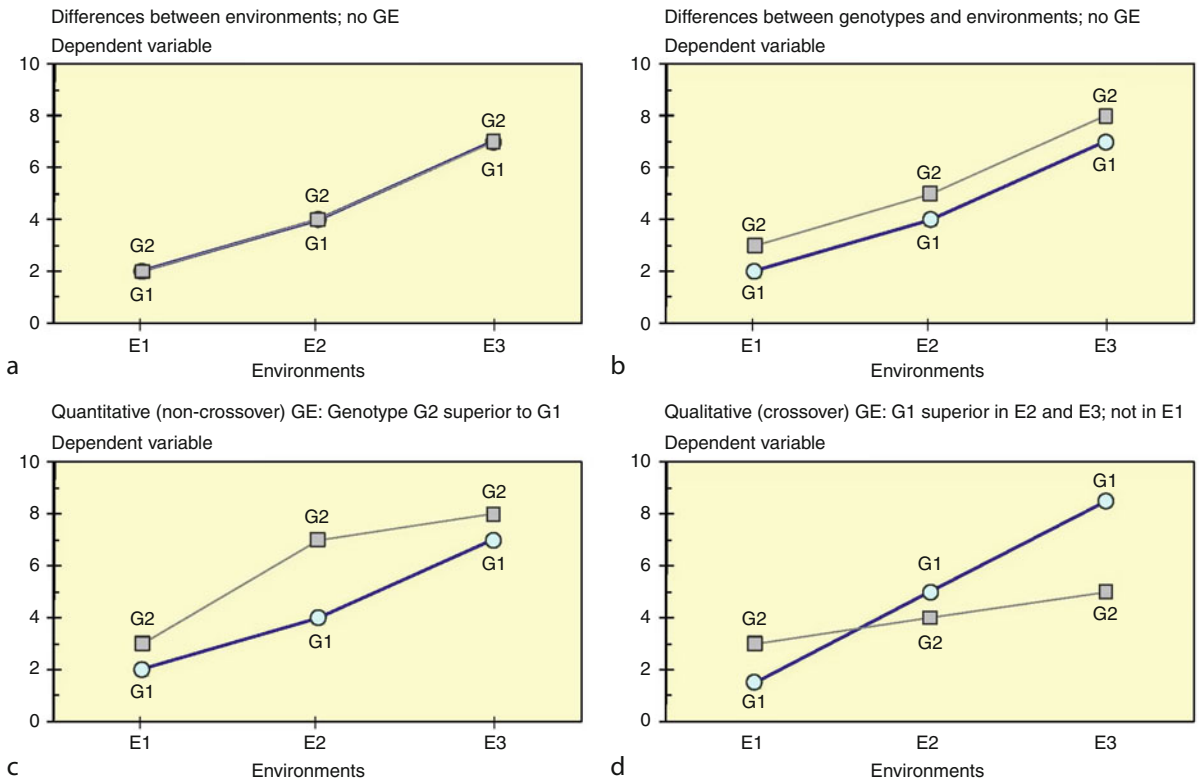

Genotype by Environment Interaction and Adaptation. Figure 1
Performance of two hypothetical genotypes in three environments showing: (**a**) Only environmental differences; (**b**) No GE; (**c**) Quantitative, non-crossover, GE; (**d**) Qualitative, crossover, GE

genotypic and/or narrow environmental diversity might reveal negligible or nonsignificant interaction). Thus, identification of superior genotypes is complicated by qualitative GE and largely depends on extensive field testing conducted over years at different locations. Therefore, there is a strong need to deploy powerful statistical models for MET data taking into account GE and their breeding implications.

Crossover interactions represent a double-edged sword [10]. Whereas they make breeding, testing, selection, and varietal recommendation more difficult, if the underlying ecophysiological grounds of GE are known, identification of genotypes better adapted to certain specific niche conditions, allowing for increased genetic gains, is possible. If the traits conferring adaptation to these specific environments and/or the genes that control them are revealed, direct implementation in breeding may be feasible either by choosing parents for a new cross possessing the adaptive attributes or by directly selecting for the presence of such attributes in the progenies (through direct measurement of the attributes or through genotypic selection, see below).

METs are often carried out over a number of sites and years that are considered to be representative of the target environments. Standard analyses of variance partition the GE term into genotype by locations (GL), genotype by years (GY), and genotype by locations by years (GLY) interactions. The relative size of these terms allow for a statistical assessment of the spatial and temporal components of adaptation. If GL dominates over the other components, then specific adaptation is exploitable by identifying subsets of homogeneous locations for variety release and recommendation. Where GY and GLY terms dominate, as most often happens, no simplification involving spatial subdivision of growing regions is possible. In this

context, specific recommendations may be only possible after counting with robust models trustworthily predicting the main climatic conditions of the growing season in advance to sowing.

Recent efforts have searched for the genetic factors underlying GE and, thus, to describe adaptation patterns. Quantitative trait loci (QTLs) responsible for individual complex traits (see, e.g., [15]), such as yield and adaptation have been reported in several populations for most crop species. QTL related to adaptation show different effects in different environments. The magnitude of individual QTL effects (expressed as the amount of GE variation explained by a particular QTL) varied among populations and across environments. Therefore, implementation of marker-assisted selection strategies for these QTLs in applied breeding programs remains a challenge. Modern GE studies have introduced external environmental, physiological, and/or genetic information to develop statistical models whose parameters relate better to physiological knowledge [16, 17], and therefore offer better possibilities for implementation of QTL selection methodologies in breeding programs.

Breeding Implications

Historically most of the genetic progress in the last decades at the global level, particularly in cereals, has been attained through increases of yield potential and disease resistance. Genetic gains in yield under non-limited growing conditions, i.e., improving yield potential, have often brought about parallel gains in yield under a wide range of more realistic, largely stressful, growing conditions [18–20]; because physiological traits behind improved yield potential may often be constitutive and provide yield advantage over a range of conditions [21]. Thus, improving simultaneously for yield potential (which is directly linked to both attainable and on-farm yields; [22]) and for disease resistance has conferred not only clear progress under high-yielding conditions but also wide adaptation.

Thus, it is critical to further improve yield potential [23]. Lessons from the past allow to optimistically trusting that relatively simple traits might be found that affect yield potential and wide adaptation simultaneously (e.g., [24]). For instance, the incorporation of simple key traits such as reduced height might have such a great impact that may be the basis of a Green Revolution due to its capacity of increasing yield both under potential and most non-potential conditions. Genetically reducing the capacity of the stems to grow through introgression of semidwarfing genes determined firstly an increased partitioning of biomass accumulated during stem elongation to the growing spikes [25, 26]; then the additional availability of resources in the growing spikes allowed floret development to proceed normally in more floret primordia consequently increasing the number of grains [27] and therefore parallel improvements in yield, as cereals are most frequently sink-limited during grain filling even under nonoptimal environments [28, 29]. However, as further reducing height would not keep improving yields [30], it is critical identifying alternative traits that being rather simple were still putatively related to yield across a wide range of conditions. Difficulties in identifying such traits is reflected in the fact that despite continuous breeding efforts in the last decade, current genetic progress in yield potential fall short of both those attained before (see [31] and references therein) and that required to match expected increases in demand [23]. Future improvements in yield potential would largely depend upon the identification of alternative traits that being relatively simple are putatively related to yield in a wide range of conditions representing the target environments of the breeding program. In this context, a thorough examination of GE will be critical both for identifying traits in a top-down approach dissecting yield into physiologically sound traits across conditions representing the target environments, and for determining the stability of the relationship between the identified trait(s) and yield.

In an even more general context, GE has important implications in applied breeding programs [5]. Based on the magnitude and nature of GE, breeders have to decide whether to aim for wide or for specific adaptation. This decision determines the choice of locations for selection, the allocation of limited resources in advanced line testing, and the assessment of the potential trade-off between empirical, molecular, and physiological screening of parents and advanced lines. Related to wide adaptation is the question of breeding sites: Can selection under optimum high-input

environments identify genotypes adapted to more stressed environments? Salvatore Ceccarelli and Stefania Grando at ICARDA have produced a significant number of contributions on the issue of wide versus specific adaptation in barley (see [32] and their own references therein for a review). They have strongly advocated the exploitation of specific adaptation for optimum use of resources particularly in marginal environments, arguing that selection for high yield potential has not increased yield under low-input conditions. However, success of the CIMMYT wheat program aiming at wide adaptation is based on a completely different approach. Rather than focusing on any specific environmental conditions, continuous selection cycles, referred to as shuttle breeding, are carried out in alternative and extremely diverse high yield potential environments differing in altitude, latitude, photoperiod, temperature, rainfall, soil type, and disease spectrum. As a result, CIMMYT wheat genotypes have shown high yield potential and wide adaptation across large geographical regions, perhaps with the exception of very marginal; in fact, poor adaptation of CIMMYT genotypes to specific environments often reflected susceptibility to specific plant diseases.

Field experimentation aims at covering a representative sample of environmental variation. However, the need for adequate resource allocation raises the question of whether multilocation testing in a limited number of years can adequately sample the array of environmental conditions where a variety can be grown. If the MET analysis of variance identifies GY as the most significant term, testing for many crop cycles should be preferred. However, this is not suitable given the increasing pressure to develop new cultivars. Therefore, breeders often substitute temporal for spatial environmental variation, assuming that GL is similar in nature to GY and that GLY is absent. Resource allocation for varietal experimentation schemes depends on the relative magnitude of the variance components for the genotype and GE interaction terms. Given the small number of years available for testing, and the frequently dominant effect of GY and GLY interactions, there is little point in a very extensive series of trials in a given year with a high proportion of genotypes retained throughout. Integrated mixed model analyses for the selected genotypes across the breeding stages can counterweigh for the limited number of years in the later stages of field testing.

A series of papers have suggested the use of reference and probe genotypes to characterize environmental variation and assess GE repeatability [33]. By defining a common reference set of genotypes consistently grown across locations and years, a breeder could define a long-term target environment and weight results from each location in a given year in accordance with its across-year representativeness. Probe genotypes with differential response to known biotic and abiotic conditions could also be used to characterize environments. However, practical application of these two principles is not common. Genetic gains for unidentified biotic and abiotic stresses by direct selection on extensive MET are possible. A more sound approach could be the growing of genotypes in a few key environments with well-characterized levels of the target stress. Manipulation of the breeding environment and selection of key parents for crossing should result in improved genetic gains. However, this second approach requires a clear understanding of the major stress as well as the facilities to reproduce it.

A germplasm strategy is also needed for breeding for wide and specific adaptation. For most crops, there is an important gap between elite and unimproved gene pools as most breeders focus on germplasm reflecting decades of intensive crossing, selection, and recombination [34]. However as genetic gains attained by conventional breeding decrease, more emphasis should be given to the use of new genetic variability both through pre-breeding or through construction of new parent for crosses, incorporating desired traits from local land races and related wild species, or from other unrelated organism through transgenesis.

The first studies on GE were based on standard variety trials across a series of environments. That allowed identification of the wide or narrow adaptation of the checked cultivars, but little could be said on the genetic basis of adaptation. Extensive field testing of biparental crosses (e.g., [35]), either in the form of doubled haploids, or recombinant inbred lines populations, allows for the assessment of the genetic control of plant adaptation based on standard linkage and QTL analyses, but their use is limited by the level of polymorphisms between parents. In contrast, diverse genotypic panels accumulating multiple recombination events provide ample genetic variation for

association studies. However, their main limitation is the high incidence of false-positive associations due to the difficulty to distinguish between true and pseudo linkage between molecular markers and traits of interest, due to population substructure and correlated selection [36]. More recently, other more complex crossing systems have been proposed to exploit the advantages of both linkage analysis and association mapping. This is the case, for example, of the so-called MAGIC (multiparent advanced generation intercross) [37], the nested association mapping (NAM) design based on a huge set of recombinant inbred lines derived from a large number of founder genotypes [38, 39], and AMPRIL (a multiparent recombinant inbred line population) [40].

The use of physiological criteria in analytical breeding is critical for success [41–44]. Breeders develop a deep knowledge of their target environments and of the agroecological adaptation of their genetic materials. However, whereas intensive work is continuously been carried out by crop physiologists in the area of yield potential and adaptation, not many breeders regularly incorporate new physiological criteria in their mainstream-breeding program. In any case, physiological assessment of adaptation is needed to complement breeders' impressions particularly in the first and last stages of a breeding program: selection of parents and assessment of adaptation of new advanced lines. Similarly, despite exciting progress in molecular marker-assisted selection, applied breeding still depends heavily on direct phenotypic selection of advanced genotypes.

In the rest of this entry, two different aspects will be presented: First, an example of the physiological implications of GE through the study of a trait, time to flowering, that has a clear effect on adaptation; second, a series of increasingly complex statistical models to characterize genotypic adaptation, to identify genotypes showing wide or specific adaptation and to dissect the genetic complexity behind this integrative trait. Although these sections may look quite disconnected, a thorough knowledge of crop physiology and/or their genetic control could allow construction of more powerful integrated statistical models incorporating as genetic covariables this information in order to improve the understanding of the nature of GE. Conversely, the statistical models can identify certain genotypes which, if well characterized, could allow for empirical identification of key adaptative traits.

Traits Determining Adaptation

The number of physiological traits with a potential effect in determining yield and adaptation is extraordinarily large. In an excellent *Crop Physiology* manual recently edited by Sadras and Calderini [45], many traits are reviewed and organized according to different criteria from capture and efficiency in the use of resources to crop development and plant architecture. Many trade-off exists between traits that, if ignored, will slow down genetic progress for both potential and actual farmer yields. Araus et al. [43] have also reviewed a number of potentially useful physiological criteria for breeding, particularly, in the framework of C3 cereals under Mediterranean conditions. Crop physiology as a whole is beyond the objectives of this entry. Therefore, the focus is on the single most important crop trait determining plant adaptation, time to flowering, as an example of a key trait to describe the underlying mechanisms and implications for GE.

Time to Flowering

Crop phenology – life cycle as influenced by seasonal variations in climate – has been widely recognized as the most important single factor determining adaptation and thereby crop performance. In determinate species, it allows for matching crop development with availability of resources, avoiding abiotic stresses due to climatic conditions such as late spring frosts and terminal drought. To maximize attainable yield, the most "critical phases" for yield determination have to be match with the most favorable (or least unfavorable) growing conditions. In some cases (Northern Hemisphere), the obvious way to achieve this is sowing cold-tolerant genotypes early enough to have full growth in early spring, but in the warmer Southern Hemisphere similar maximum yields can be achieved sowing in winter with significantly shorter phases, provided the critical phases are ideally timed [46–49]. Crop phenology is, thus, not only a key adaptative trait, but it may also affect yield potential, since different structures are produced throughout the crop cycle, and some of them may be more important than others in determining

yield potential [50]. If the pattern of water deficit in the target region is relatively predictable, manipulation of genes responsible for crop phenology is the most sustainable approach to increase attainable yield and plant adaptation.

The importance of flowering time has been shown, for example, with the fast and diverse shifts in heading time, or in vernalization and photoperiod responses, due to natural selection: When the same bulk population is grown under contrasting environments [51]; when comparing different sowing dates [52]; when studying the contrasting developmental patterns of genotypes adapted to particular regions [53–55]; or in retrospective studies showing changes in heading date over time due to breeding, particularly in areas where the crop was introduced more recently (e.g., bread wheat in Australia; [48]; durum wheat in certain regions of Spain; [56]). Therefore, crop phenology is an important source of GE for yield when testing genotypes from regions differing in climatic conditions [57, 58].

The three major factors determining flowering time are differential responses to photoperiod and vernalization and intrinsic earliness or earliness per se [50]. Further evidence from recent studies in wheat [59–61] support the idea that earliness per se genes represent basically genotypic differences in the response to non-vernalizing temperatures [62, 63]. The wide genotypic differences for these factors are considered as responsible for the spread of winter cereals, worldwide to a wide range of latitudes and altitudes [49, 64].

Genetic Factors Controlling Time to Flowering

At the gene or marker level, the importance of flowering time in crop performance is shown, for example, through the geographical distribution of alleles of major genes such as photoperiod (*Ppd*) and vernalization (*VRN*) responsive genes [49, 64, 65]. The co-location of QTLs for heading with QTLs for yield (e.g., [35, 66–69]), which may help to define an optimal window for heading or combination of alleles in the tested environments [70]. Moreover, in some of these studies, QTLs with strong effects on heading collocated with some of the QTLs for yield that exhibited strongest QTL by environment interactions [35, 69–71]. Recent studies have shown, through factorial regression, that a great part of the effect of these QTLs for heading (underlying QTLxE for yield) can be explained by the different sensitivity of the alleles to environmental conditions such as temperature during different parts of the crop cycle [11, 72].

In the last decade, candidate genes have been identified for major loci controlling flowering time in barley and wheat: The photoperiod responsive gene *Ppd*-H1 in barley and its wheat homologues *Ppd*-D1, *Ppd*-B1, and *Ppd*-A1 are *PRR*-like genes [73, 74]. In both species, the photoperiod-responsive allele accelerates flowering under long-day conditions, but in barley, the greatest differences between sensitive and insensitive alleles are found under long-day conditions or high latitudes, while in wheat, under short day conditions or low latitudes [49, 64, 75, 76]. *HvFT3* is the candidate gene for another gene related to photoperiod in barley, *Ppd*-H2, whose active allele is expressed and accelerates flowering only under short photoperiod or low latitudes [75, 77]. The vernalization genes *VRN*-H1 and its homologues *VRN*-A1, *VRN*-B1, and *VRN*-D1 in wheat are MADS-box transcription factors similar to *APETALA1* in *Arabidopsis* [78–80]. *HvZCCT* and *TaZCCT* are the candidate genes for *VRN*-H2 and its wheat homologue *VRN*-Am2, respectively [81, 82]. The alleles at these loci and their interactions determine the sensitivity to vernalization (e.g., [82, 83]). Finally *VRN*-H3 and its homologues *VRN*-A3, *VRN*-B3, and *VRN*-D3 are *FT*-like genes, which also interact with PPD and VRN genes [77, 84, 85]. Other reported genes that determine differences in heading time are the "earliness per se" loci (*eps*) identified in barley by Laurie et al. [75], the series of "early maturing" (*Eam*) loci [86–89], and the gene HvAP2 [90]. However, except for the latter, no candidate genes have been found yet for them and their role is much less clear.

Figure 2 shows the location of the mentioned loci for barley, as well as for some other genes which are homologues to flowering genes in rice and *Arabidopsis* but whose effect on heading is unknown in barley. In wheat, other less characterized loci have also been identified, as the gene *Eps*-2B on 2BS [91, 92]; *Eps*-Am on 1AL sensitive to temperature [59, 60]; *VRN*-D4 close to the centromere in 5D [93], and other earliness per se genes on 5AL [94]. Additionally other loci have been found to have an effect on heading time in different regions than the loci mentioned above, although

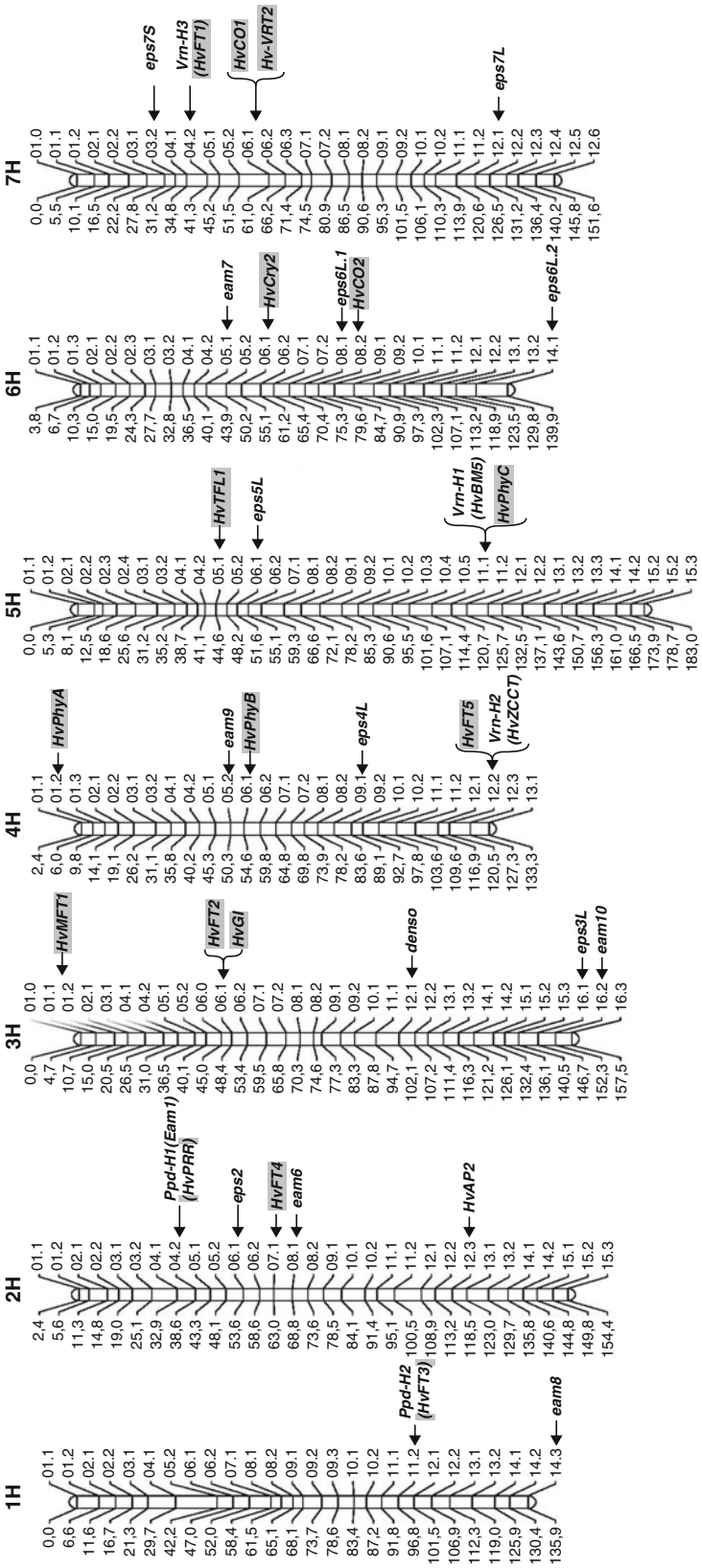

Genotype by Environment Interaction and Adaptation. Figure 2
Barley consensus function map showing the location of the vernalization, photoperiod, and earliness per se loci described in the text, as well as some other genes which are homologues to flowering genes in rice and *Arabidopsis*, whose direct effects on heading are still unknown in barley. Distances are given in Kosambi cM and linkage groups are oriented with short arms at the *top*

most of them with smaller effects: by the use of aneuploids in wheat [49, 95] or through QTL mapping both in barley (e.g., [35, 66–69]) and wheat (e.g., [92, 96–98]). These studies would confirm that heading time is under a strong but complex genetic control [49, 95]. Although particular VRN and PPD alleles may be more frequent in some geographical areas, variation has been found between genotypes within regions, so it is possible finding different combinations of VRN and PPD alleles in successful genotypes well adapted to particular regions, which would reinforce the idea that several other genes may be important in the control of flowering time [64]. As sensitivity to vernalization expresses at earlier stages of development than that to photoperiod, the fact that different combinations of VRN and PPD alleles may confer a similar time to heading or anthesis may also open room for fine-tuning developmental partitioning of a certain time to flowering into different lengths of vegetative and reproductive phases, which might be relevant in improving adaptation (see below).

A very simple quantitative genetic analysis of heading date (HD) for the Steptoe × Morex doubled haploid barley population [35] sown in fall and late winter in 2009 in Spain can be deduced from Fig. 3 which also illustrates alternative types of QTLxE interactions. In the top part of the figure there is, for a MET situation, a whole genome scan according to a composite interval mapping strategy [99] as implemented by Biometris, Wageningen University and Research Center, in GenStat (version 13th, [100]). All markers in the seven barley chromosomes are represented in sequential order on the X-axis. On the Y-axis is the p value, expressed on a minus logarithmic scale, for the successive regression models, including not just the marker or position of interest, but additional markers that act as cofactors. With $-\log_{10}$ (p value) increasing, the evidence for a QTL at that position becomes larger. The bottom part of the figure shows firstly, in green, a one-dimensional summary of the profile in the upper panel, that is, all positions for which the joint null hypothesis of no QTL main effect and QTLxE interaction was rejected. Below the overall test for QTL effects across environments, for each individual environment, in this case defined by fall and late winter planting, an approximate test for environment-specific QTL effects is given in yellow-brown-red (QTL allele second parent increases trait) or light blue-dark blue (QTL allele first parent increases trait). Two major QTLs seem to determine heading date for the genotypes in these two trials, both on the short arm of Chromosome 2H, corresponding to two known genes, Ppd-H1 and Eam6, on Fig. 2. A very strong qualitative or crossover interaction QTLxE interaction is shown for Ppd-H1; the Morex allele (yellow-red) in the late winter sowing (under long-day photoperiod) delays heading, whereas the Steptoe allele at this locus (blue) delays heading under short days on the fall sowing. Non-crossover interaction is shown for Eam6. The presence of the Steptoe allele always delays heading, but more under fall sowing (darker blue effect) than under late winter sowing. Other minor QTLs are shown in chromosomes 1H and 4H.

Genetic Factors Controlling Duration of Subphases of Time to Flowering

The effect of these genes or QTLs may vary not only due to different conditions in temperature and photoperiod, or to epistatic interactions with other genes or QTLs, but also they may have different effects on the different phases of the crop cycle. This may be interesting for improving both adaptability and yield potential. Studying the genetic control of different pre-heading phases could bring about a better understanding of crop development patterns and more tools to fine-tuning it. For example, some adaptative characters, such as the avoidance of late frosts in spring, could be better assessed by knowing the duration of the phase from sowing to terminal spikelet rather than total time to anthesis (e.g., [101]). Moreover extending the duration of stem elongation, without modifying total time to anthesis, which is a key trait for adaptability as shown above, has been proposed as a trait to further increase yield potential [102, 103]. This has been proposed because the stem elongation phase is critical for yield determination, as the number of fertile florets at anthesis, which determines the final number of grains, is set during this phase [104, 105].

Several authors have shown that there is partially independent variability between different pre-heading phases (variability in pre-heading phases between genotypes with similar time to heading), both in wheat [106–108] and barley [109–114]. Other authors have

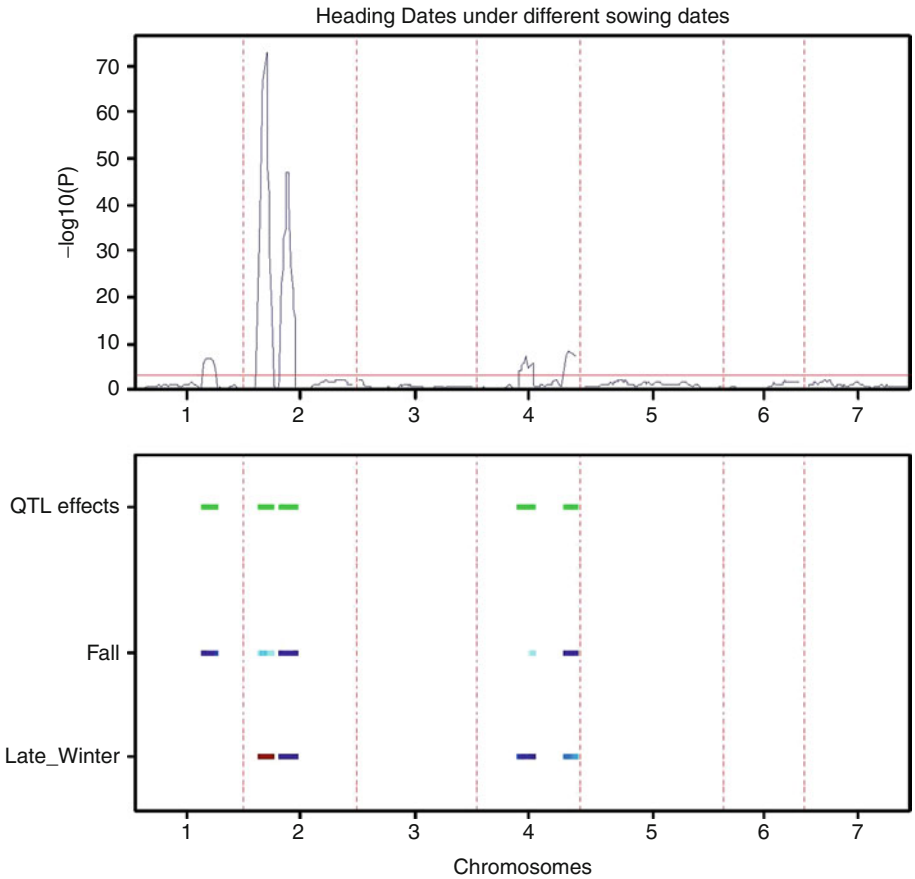

Genotype by Environment Interaction and Adaptation. Figure 3
Genome scan for heading date for the Steptoe × Morex doubled haploid population grown in fall and late winter sowing in Spain in 2009. *Top*: $-\log_{10}$ (*p* values) for the test on QTL+QTL.E effects are shown. The *red horizontal line* indicates the 5% genome-wide significance threshold. *Bottom*: *Upper most line* in *green* gives all genomic positions for which null hypothesis of no QTL+QTL.E is rejected. For the fall and late winter sowing environment, all positions for which there is environment-specific QTL expression are indicated with colors: *blue* showing that the allele from Steptoe delays heading, while *red*/*brown* shows that the Morex allele delays heading

shown that responses to vernalization, photoperiod, and temperature can each differ greatly among genotypes and between phases [50, 62, 115, 116]. In some studies using chromosome substitution lines, near isogenic lines and/or single chromosome recombinant lines, hexaploid wheat Ppd-D1 and Ppd-B1 alleles had different effects on the duration of pre-heading phases and on their response to photoperiod, although results seemed to depend on the genetic background and the environmental conditions of each experiment (see results and review by [117]). Recently Lewis et al. [61] found that alleles of a cultivar and a wild line of *Triticum monoccocum* for Eps-Am had different effects on the leaf initiation and the spikelet initiation phases (due to different sensitivity to temperature), but not on stem elongation, while they had little effect on total time to heading. On the other hand, many of the QTLs responsible for a different genetic control between pre-heading phases had little or no effect on total time to heading, so they may be more difficult to detect when assessing only heading time [111, 118]. Some of these differences in the length of pre- and post-heading phases were maintained under different conditions of photoperiod and temperature [119].

Statistical Approaches for GE Characterization

Means across environments are adequate indicators of genotypic performance only in the absence of crossover GE. When present, the use of means across environments ignores the differential reaction of genotypes to environmental changes. In an analysis of variance, introduction of the GE interaction term, $(GE)_{ij}$ for $i = 1$ to g genotypes and $j = 1$ to e environments, creates as many parameters as there are GE combinations, making predictions of phenotypic responses for environments that were not in the set of trial environments impossible. Most approaches for the study of GE interaction and adaptation depart from ANOVA models with GE interaction terms and are therefore purely empirical descriptions of phenotypic performances of a set of genotypes across a fixed sample of environments. However, if the physiological or environmental underlying causes determining GE interaction can be determined, identification of genotypes better adapted to certain specific environmental conditions would be possible and, thus, larger genetic gains would be achievable. Furthermore, if the traits conferring adaptation and their genetic control are revealed, direct implementation in breeding may be feasible.

This entry reviews three types of statistical approaches used in GE interaction for breeding and variety development: (1) regression on the environmental mean, best known as Finlay–Wilkinson regression, or joint regression analysis; (2) linear-bilinear models, like AMMI and GGE; and (3) factorial regression models (see specific references for these methods below). These methods differ not only on the information they provide, but also in their predictive ability for breeding. A discussion of these three types of models from a common statistical perspective can be found in [120, 121]. The approaches aim at substituting the $(GE)_{ij}$ term by a linear or bilinear approximation using fewer parameters (Table 1). The replacement of double-indexed ANOVA GE interaction parameters by single-indexed regression and bilinear parameters introduces predictive properties.

Regression on the Mean

The most widely used and abused statistical method in breeding programs for characterizing GE has been the regression-on-the-mean analysis first proposed by Yates and Cochran [122] and made popular by Finlay and Wilkinson [123] (FW), and also named joint regression analysis. This method summarizes phenotypic responses to environmental changes as straight lines differing in both intercept (related to genotypic main effect) and slope (which estimates environmental sensitivity); GE interaction is revealed by differences in the slopes of individual genotypes. These straight lines are produced upon regressing individual genotypic means per environment on average site performance across all genotypes in that environment, where the regression is done across the full set of environments.

The rationale behind FW is that in the absence of explicit environmental information, a good estimate of the agronomical value of any environment may be given by the average phenotypic performance of all genotypes in that environment. This method has an important conceptual drawback. Two environments may have a similar low average yield for two completely different agroecological reasons, for example, presence of a disease and an episode of a late spring frost just before flowering. This model assumes the genotypic sensitivity to these two stresses to be approximately the same when the different stresses produce the same environmental means. Therefore, the use of the model is best restricted to those rare cases in which environmental differences are driven by just a single major biotic or abiotic factor; in these cases, the linear regression on the mean model may reflect linear differences in relation to the predominant stress factor. However, if environmental differences are due to a major stress, why not using, rather than the average phenotypic value at every environment, a direct estimate of the genotypic sensitivity to this stress as in the factorial regression method described below?

Regression-on-the-mean models are conceptually simple: The differential genotypic responses are summarized by their slopes, but it is very important to point out that their value and use should depend on the proportion of GE sum of squares that can be described by the differential environmental sensitivities of the genotypes. Figure 4 presents an example for which the Finlay and Wilkinson model should have never been used; however, it has been presented in this entry as similar reports are still too often seen in

Genotype by Environment Interaction and Adaptation. Table 1 Overview of statistical models for GE analyses from two-way genotype by environment table of means derived from MET

General model	Specific model	Model	Data required	Statistical models for $E(Y_{ij}) - \mu$	Key information provided[a]
Reference models	*Additive*	I	Phenotypic data[b]	$G_i + E_j + e_{ij}$	Average cultivar yields
	Full interaction	II	Phenotypic data	$G_i + E_j + (GE)_{ij}$	Departures from additivity for each environment
Regression on the mean	*Finlay and Wilkinson*	III	Phenotypic data	$G_i + E_j + \beta_i E_j + e_{ij}$	Cultivar sensitivity (in form of slopes) to changes in environmental productivity
Bilinear models	*AMMI*	IV	Phenotypic data	$G_i + E_j + \sum_{k=1}^{K} a_{ki} b_{kj} + e_{ij}$	Joint adaptation patterns of genotypes to environments
	GGE	V	Phenotypic data	$E_j + \sum_{k=1}^{K} a'_{ki} b'_{kj} + e_{ij}$	Identification of the "winning genotype" for each uniform subset of environments
Factorial regression models	*Factorial regression model*	VI	Phenotypic and environmental data	$G_i + E_j + \beta_i z_j + e_{ij}$	Cultivar sensitivities (β_i) to changes in any environmental variable z
	Genotypic factorial regression model: QTL.E model	VII	Phenotypic and genotypic (marker information) data	$x_i\rho + E_j + x_i\rho_j + e_{ij}$	Marker (x) potentially associated to QTL and to QTL.E and the corresponding QTL (ρ) and the QTL.E (ρ_j) effects[c]
	Integrated factorial regression model	VIII	Phenotypic, genotypic, and environmental data	$x_i\rho + E_j + x_i(\lambda z_j) + e_{ij}$	QTL sensitivity to changes in environmental variable z[d]

[a]See text for a more detailed discussion of each model

[b]Phenotypic response of the $i = 1\ldots g$ genotype at the $j = 1\ldots e$ environment

[c]In the presence of QTL.E, ρ_j adjusts the average QTL expression across environments, ρ, to a more appropriate level for the individual environment j. This model can be easily extended to x_s markers throughout all the genome

[d]λ is a constant that determines the extent to which a unit change in z, an environmental covariable, influences the effect of a QTL allele substitution. This model can be easily extended to x_s markers and z_t environmental variables

many publications. It summarizes a small MET consisting of seven barley varieties (Var_1 to Var_7) grown at ten Spanish environments according to model III in Table 1. In the part of this figure, there are the simple linear regression models for the seven varieties. If nothing else is shown, it can be wrongly assumed that there are substantial differences among genotypic slopes. This is also shown on the top table that includes regression estimates. When independent simple linear regression analyses are fitted for the seven genotypes, the slopes varied from 0.88 to 1.14 and the individual straight lines were very significant (R^2 from 84% to 98%; p values from 1.8×10^{-04} to 7.1×10^{-08}). However, these R^2s do not mean anything in the GE context. They simply confirm that the genotypic yield increases with the mean environmental yield, which is obvious in the way that this model is built. Based on these estimates, it can be wrongly stated, for example, that Var_3 (slope equal to 1.14) apparently benefits more to improvements in the overall productivity of the environment than Var_6 (1.01) and particularly than Var_2 (0.88) which, with the lowest sensibility,

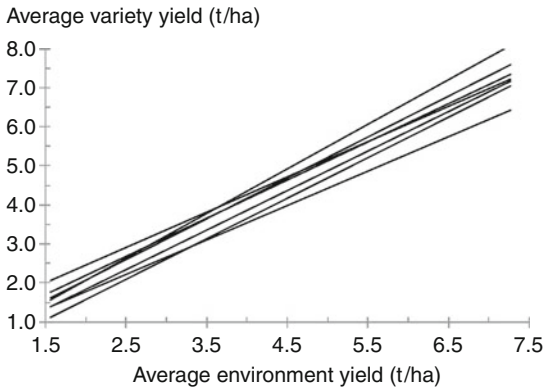

Estimates	Var_1	Var_2	Var_3	Var_4	Var_5	Var_6	Var_7
Mean (t/ha)	4.21	3.6	4.41	4.32	3.71	3.92	4.23
Slope (s.e.)	0.98 (0.08)	0.88 (0.11)	1.14 (0.06)	0.90 (0.14)	1.04 (0.14)	1.01 (0.09)	1.05 (0.08)
R^2	0.95	0.88	0.98	0.84	0.88	0.94	0.95

Source of variation	Degrees of freedom	Sum of Squares	Semipartial R^2 (%)	Mean Squares	F-value	*p*-value
E	9	210.58	89.0	23.40	63.08	<0.0001
G	6	5.97	2.5	1.00	2.68	0.0237
GE	54	20.03	8.5	0.37		
Heterogenity of slopes	*6*	*1.42*	*7.1*	*0.24*	*0.61*	*0.7207*
Residual	*48*	*18.61*	*92.9*	*0.39*		

Genotype by Environment Interaction and Adaptation. Figure 4
Inappropriate use of the Finlay and Wilkinson analysis for a MET consisting of seven barley genotypes grown in ten environments in Spain

does worst than expected. However, this model is completely inadequate for this MET and the previous estimates are useless and misleading and should have never been determined. The standard errors of the slopes, which can be used to assess the significance of the differences among slopes, ranges from 0.06 to 0.14, with an average standard error of the difference equal to 0.16. They are too large for detecting significant differences between genotypic slopes. Furthermore, joint regression analysis of variance table (bottom part of Fig. 4) shows that the observed differences among the genotypic slopes (Heterogeneity of slopes) only explains 7.1% of the GE sum of squares, which is not statistically significant (p value = 0.721).

Bilinear Models (AMMI and GGE)

The usefulness of the integration of ecophysiological and statistical tools in the interpretation of GE interaction is examined based upon the joint application of two multiplicative models for interaction: the additive main effects and multiplicative interaction (AMMI) model [6], and the factorial regression model [120, 124]. Both provide information and insight beyond the classical analysis of variance of two-way genotype by environment tables. AMMI represents an empirical approach (based on yield itself) to analyze GE interaction. Factorial regression attempts to describe interaction by including external genetic, phenotypic, and environmental information (e.g., morphophysiological traits, climatic data, etc.) on the levels of the genotypic and environmental factors. It implies a more analytical approach to the understanding of GE.

The Finlay and Wilkinson model belongs to a wider class of statistical models named linear-bilinear which estimate genotypic sensitivities to one or more environmental characterizations that are just linear functions of the phenotypic data [124–127]. However, the

additive main effects and multiplicative interaction (AMMI) model [128–131] and the GGE models [132, 133] represent more powerful, and thus, useful examples of linear-bilinear models in plant breeding. These two model classes generate for every genotype and for every environment a series of K scores, which summarize the differential sensitivity of the genotypes to the prevalent, and typically unknown, stresses present in the analyzed MET.

The AMMI model successively partitions the $(GE)_{ij}$ interaction term from the basic ANOVA reference model into a series of K multiplicative terms or products of the form $a_{ki}b_{kj}$, where, for the kth term, a_{ki} refers to the genotypic sensitivity of genotype i to an hypothetical environmental variable b_k, which has value b_{kj} in environment j (Table 1, model IV). Alternatively, b_{kj} refers also to the environmental potentiality of environment j to an hypothetical genotypic variable a_k, which takes value a_{ki} for genotype i. The K hypothetical environmental (genotypic) variables have the property of discriminating maximally between genotypes (environments). The number of multiplicative terms to be retained for an appropriate estimate of the GE interaction, K, can be estimated in various ways, see, for example, Gollob [130], Gauch [6], and Cornelius [134]. From a practical point of view, the AMMI model is fitted in two steps. First, an additive ANOVA model is fitted containing the main effects for G and E and then the residuals from the additive model are used to construct the GE interaction matrix. This interaction matrix is then subjected to a singular value decomposition that generates the above-introduced genotypic and environmental scores [128, 130, 131].

Key outputs of the AMMI analysis are the genotypic and environmental scores for the K retained axes, along with the proportions of the interaction sum of squares explained by the multiplicative terms. The output of the $K = 2$ AMMI model, retaining just the first two interaction axes (IPCA1 and IPCA2), can be directly visualized by means of a biplot [5, 128, 135]. If both axes together explain most of the GE interaction, interpretation of the biplot is very simple and potentially extremely useful for understanding GE interaction. The ith genotype is placed in the biplot according to the (a_{1i}, a_{2i}) genotypic scores; similarly, the jth environment is defined by its two IPCA environmental scores (b_{1j}, b_{2j}). Distance of a genotype or environment to the origin is proportional to the GE interaction generated by that genotype or environment, respectively. Genotypes placed close together show similar adaptation patterns. Close environments generate similar GE interactions.

The actual interaction of genotype i in environment j can be estimated by the projection of the genotype position (a_{1i}, a_{2i}) on the jth environmental vector that goes from the origin (0,0) to (b_{1j}, b_{2j}), that is the line that goes through the origin with slope equal to b_{2j}/b_{1j}. The distance between the genotype projection on the line to the origin also provides information about the absolute magnitude of the interaction of genotype i in environment j. Genotype i will be well adapted to environment j, that is, positive interaction, if the projection is in the direction of the environmental vector and negative otherwise. The sign of the interaction of the genotype i in environment j can be estimated by the cosine between the ith genotypic and the jth environmental vector. It will be positive if both vectors form acute (close to 0°) angles, negative if the angle is obtuse (close to 180°), and nonexistent (no interaction) if they form a right angle (close to 90°). In a similar way, two environments whose vectors form an acute angle generate a similar type of GE interaction across genotypes, the environments have positive genetic correlation. If the two environmental vectors form an angle close to 180°, whichever genotype is well adapted in one environment will be poorly adapted to the other, the environments have a negative environmental interaction. Finally if both environmental vectors form a right angle, the genotypic behavior at one environment will be independent of the behavior at the other site, the genetic correlation is zero.

The upper part of Fig. 5 shows an AMMI biplot generated by a set of seven genotypes grown at ten environments. The genotypes are shown by circles and they represent a barley variety Beka, three derived single nonallelic mutants, M01, M02, M03, and the three binary mutant combinations, M12, M13, M23. The environments are shown in the biplot by squares which represent location by year combinations across Spain. Production of these mutants and analysis of these data was presented elsewhere [136, 137]. In this MET, the GE interaction is well described by the AMMI $K = 2$ model, as both axes explain together more than

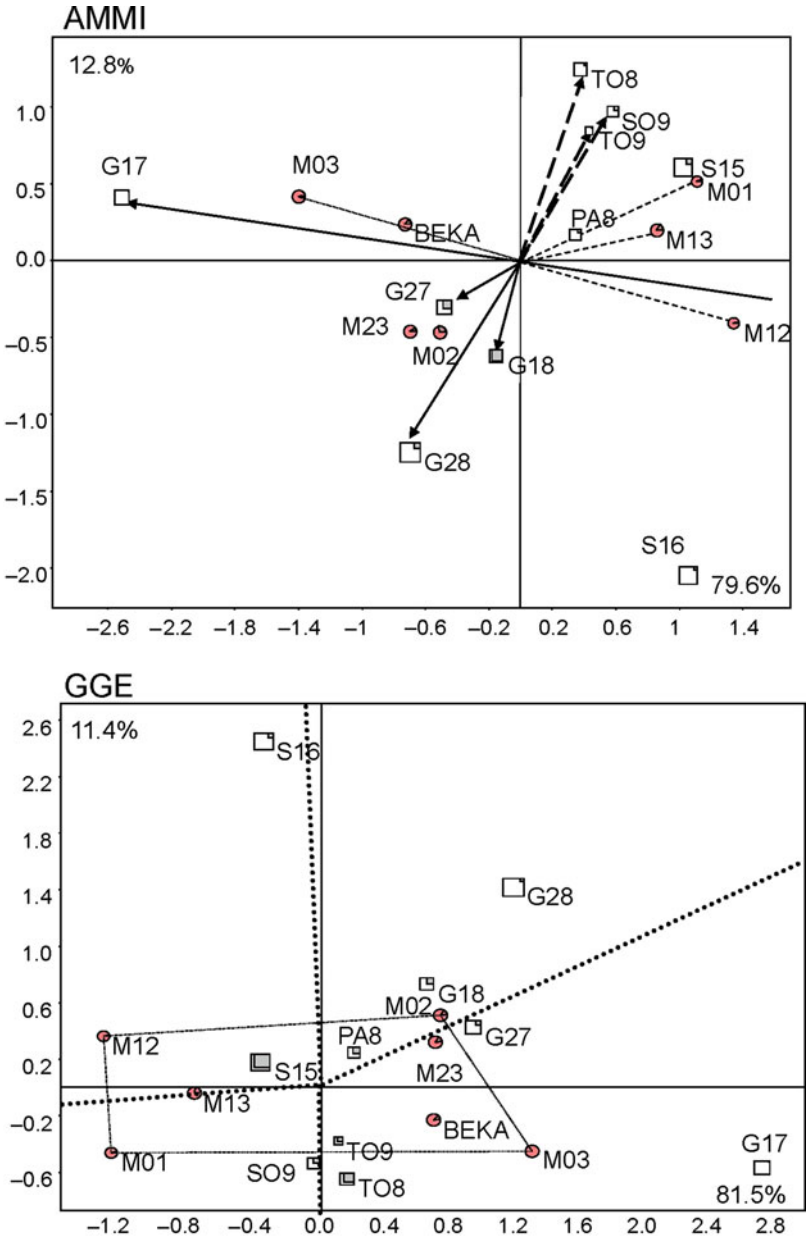

Genotype by Environment Interaction and Adaptation. Figure 5

AMMI and GGE biplots for a MET consisting of seven barley genotypes grown at ten environments in Spain (Data taken from [105]). See text for a detailed description of genotypes and environments

90% of the GE sum of squares. The average yield of each environment and genotype is shown proportional to the area of its corresponding symbol. Within each symbol there is a, generally small, darker sector that represents the proportion of its sum of squares not explained by this model. In this case all environments are well represented except for G27 y G18, which generate GE interactions not correctly described by the

AMMI $K = 2$ model. Beka is placed close to the origin and, thus, it is the genotype that interacts least with the ten environments; on the contrary, M12 and M03 are the two genotypes that interact most with the environments. G17 and S16 are the two environments which showed the largest GE interaction, that is, whose genotypic yields depart most from their averages. PA8, near the origin, produced yields close to the average across all environments.

The relative position of both genotypes and environments can provide some clarification on the nature of the GE interactions in this MET. The first IPCA seems to be associated with differential behavior of genotypes carrying the first mutation, M01, M12, and M13, with positive scores in comparison to the other genotypes. These mutants are particularly poorly adapted to Granada (G in the biplot, especially G17). The second axis, which is quantitatively less important, seems associated with mutant 2 (M02, M12 y M23), which shows negative scores on this axis, whereas the other genotypes have positive scores; the specific adaptation of this mutant to the environments is not as clear.

The angle formed by any two environmental vectors is related to the relative similarity among environments, say, the genetic correlation, as determined by the genotypic yields. In this case, the relative yields of the genotypes in Toledo (TO8 y TO9) seem very similar to Soria (SO8). They all form acute angles with cosine and correlation close to 1. T09, with a smaller size square, had lower yields that the others. By comparing the angle of these three environmental vectors with the vector determined by G28 (very obtuse angle closed to 180° and cosine and correlation close to −1), it can be deduced that those genotypes that behave relatively well in G28 perform poorly in the other three sites and vice versa. The analysis of the genotypic projection on environmental vectors gives clues about specific adaptation patterns. For example for G17, M03 showed a good adaptation to this environment, whereas M12 was particularly poorly adapted there. This AMMI analysis was done on the MET data used for the analysis in Fig. 4. Whereas the Finlay and Wilkinson method was able to explain only 7% of the GE sum of squares, the AMMI model for $K = 2$ retained 90% of the GE sum of squares. Furthermore, as described in the previous paragraphs, the known structure of the seven genotypes developed through artificial mutagenesis, suggested a model with a plausible genetic meaning.

The environmental and genetic scores are simple statistical estimates derived from MET phenotypic data, without any direct physiological meaning. However, these empirical estimates can be associated to physiological processes by correlating the environmental scores to explicit environmental measurements, such as soil or meteorological variables; these correlations can often provide meaningful agroecological information about the nature of GE interactions [11, 14, 138–140].

Another member of the linear-bilinear model class is the GGE model [132, 133], in which single value decomposition is done on the sum of the G and GE components by just subtracting the environmental means (environmental centered) on the two-way table of means (Table 1, model V) rather than on GE interactions alone, as done in AMMI. A GGE biplot for $K = 2$ provides additional information of potential interest to breeders, as it allows for the direct identification of the "winning" genotype in any potentially uniform subset of environments. To do so, the most extreme genotypic scores are connected delimiting an irregular polygon enclosing all other genotypes, that is, a convex hull is constructed. In the previous example (Fig. 5, bottom) this is an irregular quadrilateral defined by M12, M02, M03 y M01. Next, lines perpendicular to each side of the polygon/convex hull are drawn (thicker lines in Fig. 5, bottom) up to the boundaries of the biplot. In this way sectors are created, called mega environments, which contain environments that behave relatively uniform with respect to the genotypes. The "winning genotype" in a mega environment is the genotype that is placed at the vertex of the polygon inside that mega environment. For example, M12 is the best-adapted genotype in the mega environment defined by S15 and, particularly, S16. Mutant M03 is the most productive genotype in G18 and G28. Of course, this interpretation is subjected to the condition that most of G+GE variability is retained in the first two GGE axes.

Factorial Regression Models

Factorial regression models were developed to incorporate additional explicit environmental information

(variable z in Table 1 model VI) into a model [120, 121] for GE interaction and estimate the genotypic sensitivity of each of g genotypes (β_i in Table 1 model VI) to these independent variables (regressors, covariables). The regression on the mean or FW analyses reported before may be seen as a specific case of factorial regression, in which the average yield in each environment is used as an explicit environmental characterization. In the general form, any explicit agroecological variable individually recorded for each environment could be used as independent explanatory variable. Average yield can be a reflection of a certain meteorological variable, such as available soil water. In this situation, this variable recorded for each environment could be used as explanatory independent variable to describe GE interaction (variable z in model VI Table 1). The genotypic slopes will have a more direct physiological meaning when they estimate, for example, sensitivity to changes in available soil water, which is an approximation to water use efficiency. In a triticale MET, GE interaction for grain yield was regressed on soil pH and the genotypic slopes directly assessed the sensitivities to changes in soil pH [141]. Extension to multiple environmental variables and complex response curves is conceptually simple and easily computable using standard statistical packages. As for any multiple regression models, a central question is the choice of variables for description of GE interaction. Continuous monitoring of the environment generates huge numbers of environmental covariables, which will complicate identification of the most relevant ones. Purely statistical selection procedures often lead to physiologically incomprehensible models. Therefore, agroecological insights of genotypes and environments should augment and prevail over purely statistical considerations. A helpful prescreening of environmental covariables can sometimes be done by correlating covariables to scores derived from AMMI or GGE analyses [11].

Factorial Regression Models Incorporating Explicit Genotypic Information Genotypic covariables can also be used to partition the G and GE terms. Molecular markers such as DNA polymorphisms for anonymous sequences or for functional genes are the most useful and readily available genetic covariables. For a codominant marker in a diploid species with potential genotypes *AA*, *Aa*, and *aa*, the number of *A* alleles (2, 1, and 0 to represent genotypes *AA*, *Aa*, and *aa*, respectively) could be used as a genetic covariable, x, in a factorial regression model (Table 1, model VII). If multiple markers across the whole genome are sequentially used, factorial regression has the ability to detect, locate, and estimate QTL main effects and QTL by environment interactions. For marker positions adjacent to a QTL, the ρ slope in model VII (Table 1) estimates directly the effect of a QTL allele substitution. Similarly, the $(GE)_{ij}$ interaction can be further partitioned into a term for differential QTL expression across environments, ρ_j, and a residual GE interaction. For a full genome scan, factorial regression models can be fitted on grid of genomic positions, on markers and in between markers, when necessary. Virtual markers, in between observed markers, can be easily generated from flanking marker information (see [142]). Factorial regression models which include genetic covariables can be potentially used for any set of genotypes for which genetic predictors can be constructed, from standard biparental offspring populations and unrelated diverse association panels, to more complicated intercross systems, such as MAGIC [37], NAM [38, 39], and AMPRIL [40] described before. The QTL.E interaction model shown in model VII (Table 1) is based on application of a simple marker regression to our data. To construct multiple QTL models, a composite interval mapping approach can be followed by incorporating cofactors, or markers that correct for QTL elsewhere, on the genome.

Factorial Regression Models Incorporating Explicit Environmental and Genotypic Information The final goal of any MET is to understand the nature of GE interaction in terms of differential sensitivity of the different QTLs or genes to external environmental variables. This is also possible by means of factorial regression models [11, 13, 72, 92]. Differential QTL expression for environments, ρ_j, can be regressed on any environmental covariable, z, to relate the differential QTL expression directly to key environmental variables responsible for GE. This is done by substituting the QTL.E term, $x_i\rho_j$, with a linear regression $x_i(\lambda z_j)$ and a residual term. λ is a constant that determines the extent to which a unit change in z, the environmental

covariable, influences the effect of a QTL allele substitution. The statistical model used is listed as model VIII in Table 1 which can be easily extended to multiple markers (x_{si}) and various environmental variables (z_{tj}).

Van Eeuwijk et al. [143, 144] and Boer et al. [99] provide examples of differential QTL expression in maize data to environmental variables; by incorporating marker information and environmental covariables describing the environment, these models allow for prediction of differential genotypic sensitivities to environmental changes. An example of the output of these fully integrated genotypic and environmental models is shown in Fig. 6, which shows an analysis for the "Steptoe × Morex" double haploid population data from the North American Barley Genome Project, grown at 12 sites and with environmental covariables at hand. Three main QTLs were responsible of GE interaction [71]. Differential QTL effects across environments could be associated to three different environmental variables related to temperature taken at three different growth periods and according to three alternative models: a simple linear regression model, a second degree response, and a "broken-stick" model (Fig. 6). Furthermore, two out of three QTL.E interactions showed a "crossover" type interaction: The sign of the QTL effect changed according to the value of the environmental external variable. This figure clearly illustrates the importance of QTL.E interaction for complex traits such as grain yield in barley.

The Mixed Model Framework: Modeling Variance-Covariance Structures

Table 1 shows different alternatives for modeling the expected responses of a genotype to environmental changes, without any specific concern about the implicit assumptions of the analyses of variance. Standard linear models take for granted that error terms are independent and have constant variance. However for MET, these assumptions are overly simplistic as variances within environments and correlations between environments tend to be heterogeneous. For the sake of brevity and simplicity, how the mixed model framework also allows for modeling of the variance-covariance component of the data has not been described. However, the optimal statistical modeling for MET data should focus first in finding an adequate variance-covariance model for the random terms and then, as discussed above, search for a parsimonious model for the expected responses. Choice of variance-covariance model can have strong implications. In the case of QTL modeling, QTL may erroneously be declared significant or nonsignificant because of over or under estimation of effect sizes and standard errors [72, 145]. The mixed model framework, which combines modeling of means and variances, provides

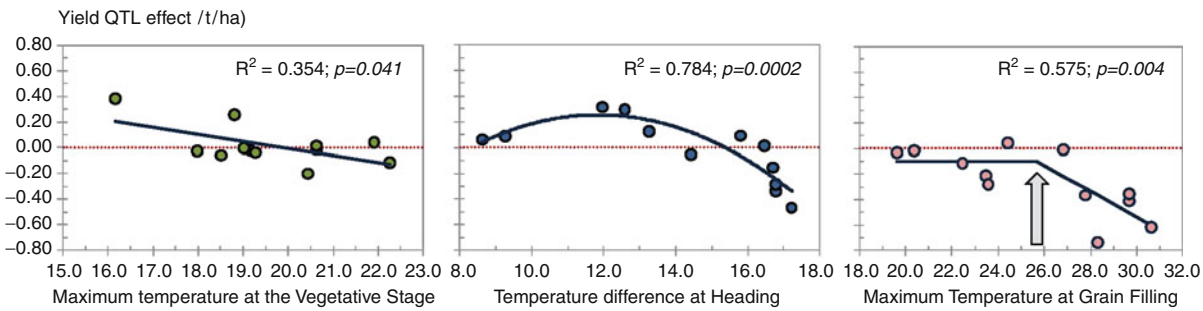

Genotype by Environment Interaction and Adaptation. Figure 6
Differential sensitivities of three major QTLs to temperature, recorded at three different growing periods for the Steptoe × Morex doubled haploid population (Data taken from the North American Barley Genome Project). Twelve sites with environmental characterizations were available. Three different models were used: a straight-line regression model, a second-degree polynomial, and a "broken-stick" factorial regression model

a more appropriate modeling environment for GE and QTL.E interactions offering flexibility with regard to assumptions on heterogeneity of variances and on correlations across environments [17].

Computer Software for GE Analyses

Annicchiarico [3] lists a series of user-friendly computer software available for many GE analyses. CROPSTAT is a freely available package developed by the International Rice Research Institute [146] that has specific modules for FW and AMMI analysis. MATMODEL available in a free version [147] also provides AMMI and joint regression modeling and it is particularly useful for handling missing data. INFOGEN [148] within the INFOSTAT system [149] also includes most described tools for the analysis of MET. At the same time, there are also dedicated commercial softwares, such as GGE BIPLOT [132], useful for joint regression, AMMI, and GGE. Obviously, all general statistical packages can easily be programmed to fit all linear-bilinear models described in this entry in a fixed model context, whereas some like GenStat, ASREML, and SAS also allow fitting mixed bilinear models. SAS instructions for many GE analyses are presented in Kang [100]. GenStat [150] includes specific procedures for FW, AMMI, and GGE analyses. Version 13 of GenStat (2010) also includes dedicated menus for QTL and QTL.E analyses for segregating crosses and for association analyses. GenStat has a policy of free licensing of older versions to institutions in developing countries and for educational purposes in the form of the GenStat Discovery version.

Future Directions

Plant breeding research experiences fast changes. Nowadays, at the genomic side, sequencing and single-nucleotide polymorphism (SNP) technology is becoming increasingly cheap for not only model species, but also for crop species. Besides information at the DNA level, genomic information at RNA, protein, and metabolite level starts to become common. As a consequence, huge amounts of data start to become available for characterizing genotypes at various genomic levels. Similar developments can be observed for monitoring the environment. Environmental characterizations can be stored over the growing season for all environmental factors that are believed to be relevant.

In the past, genotypic and environmental information was the bottleneck; however, the current focus has shifted to access to the right plant material and their correct phenotyping. High-throughput phenotyping techniques are being developed that facilitate monitoring of individual plants at arbitrary small intervals over the growing season. However, high-throughput phenotyping schemes taken in individual cell/tissue/organ/single plant level may not mean anything at the crop level. Up-scaling from processes taking place in a fraction of a second and in a fraction of space to relevant crop traits (produced in a hectare through several months) has consistently failed in the past and remains a challenge. Crop physiology can play a key role in understanding multi-trait interactions for up-scaling from gene to crop.

The strongly increased availability of phenotypic, genomic, and environmental information begs for new statistical techniques that allow the increased information to be used in an effective way. Various requirements can be defined. First, phenotypic information will increasingly concern a wide array of traits that are repeatedly measured over time. Correlations between these traits will need to be explicitly modeled, as will be the correlations between the repeated measurements for the same trait. Information from multiple environments can be treated in the same way as information from multiple traits, although correlations between the same trait in different environments may ask for other models than the correlations between different traits in the same environment and different traits in different environments. Standard mixed model procedures will fail, as too many variances and covariances/correlations will require estimation. A way out may be too regularize the pattern of variances and covariances by inserting biological information in the estimation in the form of alternative statistical tools, such as priors (Bayesian methods) or penalties (penalized multivariate regressions). One popular way of reducing the number of correlation parameters is by imposing network structures on sets of trait by environment combinations, thereby effectively fitting sparse matrices to the inverses of the correlation matrices. The graphical lasso is an example of such an approach [151].

Turning to increased marker numbers and selecting meaningful genotype to phenotype models in the face of 100,000s of SNP markers demand new statistical approaches. As identification of individually contributing SNPs in such conditions is very difficult, an alternative strategy emphasizing prediction from markers above identification of markers is rapidly gaining popularity. In genomic selection, the idea is to use all markers simultaneously for predicting marker-based breeding values that help in ranking individuals on genetic merit [152–154]. Bayesian and penalized regression techniques help to regularize the estimates for individual marker contributions, as it will be evident that with standard regression techniques it is impossible to estimate hundreds of thousands of marker effects. Mixed models can in this context be interpreted as an example of a Bayesian technique in which the prior for the marker effects is a normal distribution. Equivalently, mixed models can be seen as penalized regressions in which the ratios of variance components determine the penalties (shrinkage factors). As an illustration, one may regress a phenotypic trait on a large set of markers, assuming the effects of the markers of individual chromosomes to follow normal distributions with chromosome-specific variances. The predicted values for the genotypes from such a mixed model represent the genomic breeding value. This breeding value can be used for selection purposes. Examples of genomic selection for multiple environments are still hard to find.

The increased information from intensive environmental monitoring can be used to improve prediction of genotypic performance by integrating it with other types of genotype-specific information in crop growth models [16, 17, 155–157]. The environmental information is fed into a suitable crop growth model and when physiological parameters of the crop growth model can be specified at genotype-specific level, the crop growth model can produce predictions for individual genotypes in any environment for which a full environmental characterization is given. An integration of crop growth modeling with genomic selection is possible when the values for the genotype-specific physiological parameters in the crop growth model are inserted from Bayesian or mixed genomic selection models.

The increased amounts of phenotypic, genomic, and environmental data pose strong demands on our statistical ingenuity, but interesting solutions start to appear on the horizon. In this forthcoming scenario, elaborations of mixed models, Bayesian techniques and penalized methods will play a major role in the analysis of GE interactions.

Bibliography

Primary Literature

1. Student (1908) The probable error of a mean. Biometrika 6:1–25
2. Annicchiarico P (2002) Genotype × environment interactions: challenges and opportunities for plant breeding and cultivar recommendations. FAO plant production and protection paper no. 174. FAO, Rome
3. Annicchiarico P (2009) Coping with and exploiting genotype-by-environment interactions. In: Ceccarelli S, Guimaraës EP, Weltzien E (eds) Participatory plant breeding. FAO, Rome, pp 519–564
4. Cooper M, Hammer GL (eds) (1996) Plant adaptation and crop improvement. CAB International, Wallingford
5. Fox PN, Crossa J, Romagosa I (1997) Multi-environment testing and genotype by environment interaction. In: Kempton RA, Fox PN (eds) Statistical methods for plant variety evaluation. Chapman and Hall, London, pp 117–137
6. Gauch HG (1992) Statistical analysis of regional yield trials. Elsevier, Amsterdam
7. Kang MS (1998) Using genotype-by-environment interaction for crop cultivar development. Adv Agron 62:199–252
8. Kang MS, Gauch HG (1996) Genotype by environment interaction: new perspectives. CRC Press, Boca Raton
9. Kempton RA, Fox PN (1997) Statistical methods for plant variety evaluation. Chapman and Hall, London
10. Romagosa I, Fox PN (1993) Genotype-environment interaction and adaptation. In: Hayward MD, Bosemark NO, Romagosa I (eds) Plant breeding, principles and prospects. Chapman and Hall, London, pp 373–390
11. Romagosa I, van Eeuwijk FA, Thomas WTB (2009) Statistical analyses of genotype by environment data. In: Carena M (ed) Handbook of plant breeding, vol 3, Cereals. Springer, New York, pp 291–331
12. van Eeuwijk FA (2006) Genotype by environment interaction: basics and beyond. In: Lamkey K, Lee M (eds) Plant breeding: the Arnell Hallauer international symposium. Blackwell, Oxford, pp 155–170
13. van Eeuwijk FA, Malosetti M, Yin X, Struik PC, Stam P (2005) Statistical models for genotype by environment data: from conventional ANOVA models to eco-physiological QTL models. Aust J Agr Res 56:883–894
14. Voltas J, van Eeuwijk FA, Igartua E, Garcia del Moral LF, Molina-Cano JL, Romagosa I (2002) Genotype by environment interaction and adaptation in barley breeding: basic concepts and methods of analysis. In: Slafer GA, Molina-Cano JL, Savin R,

Araus JL, Romagosa I (eds) Barley science: recent advances from molecular biology to agronomy of yield and quality. Haworth Pres, Binghamton, pp 205–241
15. Paterson AH (1998) Molecular dissection of complex traits. CRC Press, Boca Raton
16. Cooper M, van Eeuwijk FA, Hammer GL, Podlich DW, Messina C (2009) Modeling QTL for complex traits: detection and context for plant breeding. Curr Opin Plant Biol 12:231–240
17. van Eeuwijk FA, Bink MCAM, Chenu K, Chapman SC (2010) Detection and use of QTL for complex traits in multiple environments. Curr Opin Plant Biol 13:193–205
18. Calderini DF, Slafer GA (1999) Has yield stability changed with genetic improvement of wheat yield? Euphytica 107:51–59
19. Foulkes MJ, Sylvester-Bradley R, Weightman R, Snape J (2007) Identifying physiological traits associated with improved drought resistance in winter wheat. Field Crop Res 103:11–24
20. Reynolds MP, Borlaug NE (2006) Impacts of breeding on international collaborative wheat improvement. J Agric Sci 144:3–17, Cambridge
21. Slafer GA, Araus JL (2007) Physiological traits for improving wheat yield under a wide range of conditions. In: Spiertz JHJ, Struik PC, van Laar HH (eds) Scale and complexity in plant systems research: gene-plant-crop relations. Springer, Dordrecht, pp 147–156
22. Fischer RA, Edmeades GO (2010) Breeding and cereal yield progress. Crop Sci 50:S85–S98
23. Reynolds MP, Foulkes J, Slafer GA, Berry P, Parry MJ, Snape JW, Angus WJ (2009) Raising yield potential in wheat. J Exp Bot 60:1899–1918
24. Slafer GA (2003) Genetic basis of yield as viewed from a crop physiologist's perspective. Ann Appl Biol 142:117–128
25. Siddique KHM, Belford RK, Perry MW, Tennant D (1989) Growth, development and light interception of old and modern wheat cultivars in a Mediterranean environment. Aust J Agr Res 40:473–487
26. Slafer GA, Andrade FH (1993) Physiological attributes related to the generation of grain yield in bread wheat cultivars released at different eras. Field Crop Res 31:351–367
27. Miralles DF, Katz SD, Colloca A, Slafer GA (1998) Floret development in near isogenic wheat lines differing in plant height. Field Crop Res 59:21–30
28. Miralles DJ, Slafer GA (1995) Yield, biomass and yield components in dwarf, semidwarf and tall isogenic lines of spring wheat under recommended and late sowing dates. Plant Breed 114:392–396
29. Richards RA (1996) Increasing yield potential in wheat – source and sink limitations. In: Reynolds MP, Rajaram S, McNab A (eds) Increasing yield potential in wheat: breaking the barriers. CIMMYT, Mexico, pp 134–149
30. Foulkes J, Slafer GA, Davies WJ, Berry P, Sylvester-Bradley R, Martre P, Calderini DF, Griffiths S, Reynolds M (2011) Raising yield potential of wheat. III. Optimizing partitioning to grain while maintaining lodging resistance. J Exp Bot 62:469–486
31. Denison RF (2009) Darwinian agriculture: real, imaginary and complex trade-offs as constraints and opportunities. In: Sadras VO, Calderini D (eds) Crop physiology. Applications for genetic improvement and agronomy. Academic, Burlington, pp 215–234
32. Grando S, Ceccarelli S (2009) Breeding for quantitative variables. Part 3: breeding for resistance to abiotic stress. In: Ceccarelli S, Guimaraës EP, Weltzien E (eds) Participatory plant breeding. FAO, Rome, pp 391–417
33. Cooper M, Fox PN (1996) Environmental characterization based on probe and reference genotypes. In: Cooper M, Hammer GL (eds) Plant adaptation and crop improvement. CAB International, Wallingford, pp 529–547
34. Rasmusson DC (1996) Germplasm is paramount. In: Reynolds MP, Rajaram S, McNab A (eds) Increasing yield potential in wheat: breaking the barriers. CIMMYT, Mexico, pp 28–37
35. Hayes PM, Liu BH, Knapp SJ, Chen F, Jones B, Blake T, Franckowiak J, Rasmusson D, Sorrells M, Ullrich SE, Wesenberg D, Kleinhofs A (1993) Quantitative trait locus effects and environmental interaction in a sample of North American barley germplasm. Theor Appl Genet 87:392–401
36. Comadran J, Thomas WTB, van Eeuwijk FA, Ceccarelli S, Grando S, Stanca AM, Pecchioni N, Akar T, Al-Yassin A, Benbelkacem A, Ouabbou H, Bort J, Romagosa I, Hacket CA, Russell JR (2009) Patterns of genetic diversity and linkage disequilibrium in a highly structured Hordeum vulgare association mapping population for the Mediterranean basin. Theor Appl Genet 119:175–187
37. Cavanagh C, Morell M, Mackay I, Powell P (2008) From mutations to MAGIC: resources for gene discovery, validation and delivery in crop plants. Curr Opin Plant Biol 11:215–221
38. Buckler ES, Holland JB, Bradbury PJ et al (2009) The genetic architecture of maize flowering time. Science 325:714–718
39. Yu J, Holland JB, McMullen MD, Buckler ES (2008) Genetic design and statistical power of nested association mapping in maize. Genetics 178:539–551
40. Huang X, Paulo MJ, Boer M, Effgen S, Keizer P, Koornneef M, van Eeuwijk FA (2011) Analysis of natural allelic variation in Arabidopsis using a multiparent recombinant inbred line population. Proc Natl Acad Sci 108:4488–4493
41. Araus JL, Bort J, Steduto P, Villegas D, Royo C (2003) Breeding cereals for Mediterranean conditions: ecophysiological clues for biotechnology application. Ann Appl Biol 142:129–141
42. Araus JL, Slafer GA, Royo C, Serret MD (2008) Breeding for yield potential and stress adaptation in cereals. Crit Rev Plant Sci 27:377–412
43. Araus JL, Slafer GA, Reynolds MO, Royo C (2009) Breeding for quantitative variables. Part 5: breeding for yield potential. In: Ceccarelli S, Guimaraës EP, Weltzien E (eds) Participatory plant breeding. FAO, Rome, pp 449–477
44. Cattivelli L, Ceccarelli S, Romagosa I, Stanca M (2011) Abiotic stresses in barley: problems and solutions. In: Ullrich SE (ed) Barley: improvement, production, and uses. Wiley-Blackwell, Harrisongburg, pp 282–306
45. Sadras VO, Calderini D (2009) Crop physiology. Applications for genetic improvement and agronomy. Academic, Burlington

46. Loss SP, Siddique KHM (1994) Morphological and physiological traits associated with wheat yield increases in Mediterranean environments. Adv Agron 52:229–276
47. Passioura JB (2002) Environmental biology and crop improvement. Funct Plant Biol 29:537–546
48. Richards RA (1991) Crop improvement for temperate Australia, future opportunities. Field Crop Res 26:141–169
49. Worland AJ (1996) The influence of flowering time genes on environmental adaptability in European wheats. Euphytica 89:49–57
50. Slafer GA, Rawson HM (1994) Sensitivity of wheat phasic development to major environmental factors: a re-examination of some assumptions made by physiologists and modellers. Aust J Plant Physiol 21:393–426
51. Goldringer I, Prouin C, Rousset M, Galic N, Bonnin I (2006) Rapid differentiation of experimental populations of wheat for heading time in response to local climatic conditions. Ann Bot 98:805–817
52. Young KJ, Elliott GA (1994) An evaluation of barley accessions for adaptation to the cereal growing regions of western Australia, based on time to ear emergence. Aust J Agr Res 45:75–92
53. Hoogendoorn J (1985) A reciprocal F_1 monosomic analysis of the genetic control of time of ear emergence, number of leaves and number of spikelets in wheat (Triticum aestivum L.). Euphytica 34:545–558
54. Lasa JM, Igartua E, Ciudad FJ, Codesal P, Garcia EV, Gracia MP, Medina B, Romagosa I, Molina-Cano JL, Montoya JL (2001) Morphological and agronomical diversity patterns in the Spanish barley core collection. Hereditas 135:217–225
55. van Oosterom EJ, Acevedo E (1992) Adaptation of barley (Hordeum vulgare L.) to harsh Mediterranean environments. Euphytica 62:15–27
56. Álvaro F, Isidro J, Villegas D, García del Moral LF, Royo C (2008) Breeding effects on grain filling, biomass partitioning, and remobilization in Mediterranean durum wheat. Agron J 100:361–370
57. Jackson PA, Byth DE, Fischer KS, Johnston RP (1994) Genotype × environment interactions in progeny from a barley cross: II. Variation in grain yield, yield components and dry matter production among lines with similar times to anthesis. Field Crop Res 37:11–23
58. Van Oosterom EJ, Kleijn DM, Ceccarelli S, Nachit MM (1993) Genotype-by-environment interactions of Barley in the Mediterranean region. Crop Sci 33:669–674
59. Appendino ML, Slafer GA (2003) Earliness per se and its dependence upon temperature in diploid wheat lines differing in the major gene *Eps-A^{m}1* alleles. J Agric Sci 141:149–154
60. Bullrich L, Appendino ML, Tranquilli G, Lewis S, Dubcovsky J (2002) Mapping of a thermo-sensitive earliness per se gene on *Triticum monococcum* chromosome 1A^m. Theor Appl Genet 105:585–593
61. Lewis S, Faricelli ME, Appendino ML, Valárik M, Dubcovsky J (2008) The chromosome region including the earliness per se locus *Eps-A^{m}1* affects the duration of early developmental phases and spikelet number in diploid wheat. J Exp Bot 59:3595–3607
62. Slafer GA (1996) Differences in phasic development rate amongst wheat cultivars independent of responses to photoperiod and vernalization. A viewpoint of the intrinsic earliness hypothesis. J Agric Sci 126:403–419
63. Slafer GA, Rawson HM (1995) Base and optimum temperatures vary with genotype and stage of development in wheat. Plant Cell Environ 18:671–679
64. Cockram J, Jones H, Leigh FJ, O'Sullivan D, Powell W, Laurie DA, Greenland A (2007) Control of flowering time in temperate cereals, genes, domestication, and sustainable productivity. J Exp Bot 58:1231–1244
65. Eagles HA, Cane K, Vallance N (2009) The flow of alleles of important photoperiod basically and vernalisation genes through Australian wheat. Crop Pasture Sci 60:646–657
66. Baum M, Grando S, Backes G, Jahoor A, Sabbagh A, Ceccarelli S (2003) QTLs for agronomic traits in the Mediterranean environment identified in recombinant inbred lines of the cross 'Arta' × *H. spontaneum* 41-1. Theor Appl Genet 107:1215–1225
67. Bezant J, Laurie D, Pratchett N, Chojecki J, Kearsey M (1996) Marker regression mapping of QTL controlling flowering time and plant height in a spring barley (*Hordeum vulgare* L.) cross. Heredity 77:64–73
68. Li JZ, Huang XQ, Heinrichs F, Ganal MW, Röder MS (2006) Analysis of QTLs for yield components, agronomic traits and disease resistance in an advanced backcross population of spring barley. Genome 49:454–466
69. Tinker NA, Mather DE, Blake TK, Briggs KG, Choo TM, Dahleen L, Dofing SM, Falk DE, Ferguson T, Franckowiak JD, Graf R, Hayes PM, Hoffman D, Irvine RB, Kleinhofs A, Legge W, Rossnagel BG, Saghai Maroof MA, Scoles GJ, Shugar LP, Steffenson B, Ullrich S, Kasha KJ (1996) Regions of the genome that affect agronomic performance in two-row barley. Crop Sci 36:1053–1062
70. Cuesta-Marcos A, Casas AM, Hayes PM, Gracia MP, Lasa JM, Ciudad F, Codesal P, Molina-Cano JL, Igartua E (2009) Yield QTL affected by heading date in Mediterranean grown barley. Plant Breeding 128:46–53
71. Romagosa I, Ullrich SE, Han F, Hayes PM (1996) Use of the AMMI model in QTL mapping for adaptation in barley. Theor Appl Genet 93:30–37
72. Malosetti M, Voltas J, Romagosa I, Ullrich SE, van Eeuwijk FA (2004) Mixed models including environmental variables for studying QTL by environment interaction. Euphytica 137:139–145
73. Beales J, Turner A, Griffiths S, Snape JW, Laurie DA (2007) A *Pseudo-Response Regulator* is misexpressed in the photoperiod insensitive *Ppd-D1a* mutant of wheat (*Triticum aestivum* L.). Theor Appl Genet 115:721–733
74. Wilhelm EP, Turner AS, Laurie DA (2009) Photoperiod insensitive Ppd-A1a mutations in tetraploid wheat (Triticum durum Desf.). Theor Appl Genet 118:285–294
75. Laurie DA, Pratchett N, Bezant JH, Snape JW (1995) RFLP mapping of five major genes and eight quantitative trait loci controlling flowering time in a winter × spring barley (Hordeum vulgare L.) cross. Genome 38:575–585

76. Jones H, Leigh FJ, Mackay I, Bower MA, Smith LMJ, Charles MP, Jones G, Jones MJ, Brown TA, Powell W (2008) Population-based resequencing reveals that the flowering time adaptation of cultivated barley originated East of the Fertile Crescent. Mol Biol Evol 25:2211–2219
77. Faure S, Higgins J, Turner A, Laurie DA (2007) The flowering locus T-like gene family in barley (Hordeum vulgare). Genetics 176:599–609
78. Fu D, Szűcs P, Liuling Y, Helguera M, Skinner JS, Zitzewitz J, Hayes PM, Dubcovsky J (2005) Large deletions within the first intron in *Vrn-1* are associated with spring growth habit in barley and wheat. Mol Genet Genomics 273:54–65
79. Trevaskis B, Bagnall DJ, Ellis MH, Peacock WJ, Dennis ES (2003) MADS box genes control vernalization-induced flowering in cereals. Proc Natl Acad Sci 22:13099–13104
80. Yan L, Loukoianov A, Tranquilli G, Helguera M, Fahima T, Dubcovsky J (2003) Positional cloning of the wheat vernalization gene Vrn1. Proc Natl Acad Sci 100:6263–6268
81. Distelfeld A, Tranquilli G, Chengxia L, Yan L, Dubcovsky J (2009) Genetic and molecular characterization of the Vrn2 loci in tetraploid wheat. Plant Physiol 149:245–257
82. Yan L, Loukoianov A, Blechl A, Tranquilli G, Ramakrishna W, San Miguel P, Bennetzen JL, Echenique V, Dubcovsky J (2004) The wheat *Vrn2* gene, a flowering repressor down-regulated by vernalization. Science 303:1640–1644
83. Casao MC, Igartua E, Karsai I, Bhat PR, Cuadrado N, Gracia MP, Lasa JM, Casas AM (2011) Introgression of an intermediate VRNH1 allele in barley (Hordeum vulgare L.) leads to reduced vernalization requirement without affecting freezing tolerance. Mol Breed. doi:10.1007/s11032-010-9497
84. Bonnin I, Rousset M, Madur D, Sourdille P, Dupuits C, Brunel D, Goldringer I (2008) FT genome A and D polymorphisms are associated with the variation of earliness components in hexaploid wheat. Theor Appl Genet 116:383–394
85. Yan L, Fu D, Li C, Blechl A, Tranquilli G, Bonafede M, Sanchez A, Valarik M, Yasuda S, Dubcovsky J (2006) The wheat and barley vernalization gene *Vrn3* is an orthologue of *FT*. Proc Natl Acad Sci 103:19581–19586
86. Börner A, Buck-Sorlin GH, Hayes PM, Malyshev S, Korzun V (2002) Molecular mapping of major genes and quantitative trait loci determining flowering time in response to photoperiod in barley. Plant Breed 121:129–132
87. Franckowiak JD (1997) Revised linkage maps for morphological markers in barley, *Hordeum vulgare*. Barley Genet Newsl 26:9–21
88. Lundqvist U, Franckowiak JD, Konishi T (1997) New and revised descriptions of barley genes. Barley Genet Newsl 26:22–516
89. Stracke S, Börner A (1998) Molecular mapping of the photoperiod response gene ea7 in barley. Theor Appl Genet 97:797–800
90. Chen A, Baumann U, Fincher GB, Collins NC (2009) Flt-2L, a locus in barley controlling flowering time, spike density, and plant height. Funct Integr Genomics 9:243–254
91. Scarth R, Law CN (1983) The location of the photoperiodic gene, Ppd2, and an additional factor for ear-emergence time on chromosome 2B of wheat. Heredity 51:607–619
92. Shindo C, Tsujimoto H, Sasakuma T (2003) Segregation analysis of heading traits in hexaploid wheat utilizing recombinant inbred lines. Heredity 90:56–63
93. Yoshida T, Nishida H, Zhu J, Nitcher R, Distelfed A, Akashi Y, Kato K, Dubcovsky J (2010) Vrn-D4 is a vernalization gene located on the centromeric region of chromosome 5D in hexaploid wheat. Theor Appl Genet 120:543–552
94. Kato K, Miura H, Sawada S (2002) Characterization of QEet. ocs-5A.1, a quantitative trait locus for ear emergence time on wheat chromosome 5AL. Plant Breed 121:389–393
95. Law CN, Worland AJ (1997) Genetic analysis of some flowering time and adaptative traits in wheat. New Phytol 137:19–28
96. Griffiths S, Simmonds J, Leverington M, Wang Y, Fish L, Sayers L, Alibert L, Orford S, Wingen L, Herry L, Faure S, Laurie D, Bilham L, Snape J (2009) Meta-QTL analysis of the genetic control of ear emergence in elite European winter wheat germplasm. Theor Appl Genet 119:383–395
97. Kuchel H, Hollamby G, Langridge P, Williams K, Jefferies SP (2006) Identification of genetic loci associated with ear-emergence in bread wheat. Theor Appl Genet 113:1103–1112
98. Sourdille P, Snape JW, Charmet G, Nakata N, Bernard S, Bernard M (2000) Detection of QTLs for heading time and photoperiod response in wheat using a doubled-haploid population. Genome 43:487–494
99. Boer M, Wright D, Feng L, Podlich D, Luo L, Cooper M, van Eeuwijk FA (2007) A mixed model QTL analysis for multiple environment trial data using environmental covariables for QTLxE, with an example in maize. Genetics 177:1801–1813
100. Payne RW, Murray DA, Harding SA, Baird DB, Soutar DM (2010) GenStat for windows (13th edition) introduction. VSN International, Hemel Hempstead
101. Limin A, Corey A, Hayes PM, Fowler DB (2007) Low-temperature acclimation of barley cultivars used as parents in mapping populations: response to photoperiod, vernalization and phenological development. Planta 226:139–146
102. Slafer GA, Abeledo LG, Miralles DJ, González FG, Whitechurch EM (2001) Photoperiod sensitivity during stem elongation as an avenue to raise potential yield in wheat. Euphytica 119:191–197
103. Slafer GA, Araus JL, Royo C, García del Moral LF (2005) Promising eco-physiological traits for genetic improvement of cereal yields in Mediterranean environments. Ann Appl Biol 146:61–70
104. Fischer RA (2007) Understanding the physiological basis of yield potential in wheat. J Agric Sci 145:99–113
105. Miralles DJ, Slafer GA (2007) Sink limitations to yield in wheat, how could it be reduced? J Agric Sci 145:139–149
106. Halloran GM, Pennell AL (1982) Duration and rate of development phases in wheat in two environments. Ann Bot 49:115–121
107. Whitechurch EM, Slafer GA, Miralles DJ (2007) Variability in the duration of stem elongation in wheat and barley genotypes. J Agron Crop Sci 193:138–145
108. Borràs-Gelonch G, Rebetzke G, Richards R, Romagosa I (2011b) Genetic control of duration of pre-anthesis phases in wheat (Triticum aestivum L.) and relationships to leaf appearance, tillering and dry matter accumulation. Journal of Experimental Botany, doi: 10.1093/jxb/err230

109. Appleyard M, Kirby EJM, Fellowes G (1982) Relationships between the duration of phases in the pre-anthesis life cycle of spring barley. Aust J Agr Res 33:917–925
110. Borràs G, Romagosa I, van Eeuwijk F, Slafer GA (2009) Genetic variability in the duration of pre-heading phases and relationships with leaf appearance and tillering dynamics in a barley population. Field Crop Res 113:95–104
111. Borràs-Gelonch G, Slafer GA, Casas A, van Eeuwijk F, Romagosa I (2010) Genetic control of pre-heading phases and other traits related to development in a double haploid barley population (Hordeum vulgare L.). Field Crop Res 119:36–47
112. Kernich GC, Halloran GM, Flood RG (1995) Variation in development patterns of wild barley (*Hordeum spontaneum* L) and cultivated barley (*H vulgare* L). Euphytica 82:105–115
113. Kernich GC, Halloran GM, Flood RG (1997) Variation in duration of pre-anthesis phases of development in barley (*Hordeum vulgare*). Aust J Agr Res 48:59–66
114. Kitchen BM, Rasmusson DC (1983) Duration and inheritance of leaf initiation, spike initiation and spike growth in barley. Crop Sci 23:939–943
115. González FG, Slafer GA, Miralles DJ (2002) Vernalization and photoperiod responses in wheat pre-flowering reproductive phases. Field Crop Res 74:183–195
116. Miralles DJ, Richards RA (2000) Responses of leaf and tiller emergence and primordium initiation in wheat and barley to interchanged photoperiod. Ann Bot 85:655–663
117. González FG, Slafer GA, Miralles DJ (2005) Pre-anthesis development and number of fertile florets in wheat as affected by photoperiod sensitivity genes *Ppd-D1* and *Ppd-B1*. Euphytica 146:253–269
118. Zhou Y, Li W, Wu W, Chen Q, Mao D, Worland AJ (2001) Genetic dissection of heading time and its components in rice. Theor Appl Genet 102:1236–1242
119. Borràs-Gelonch G, Denti M, Thomas WTB, Romagosa I (2011a) Genetic control of pre-heading phases in the Steptoe x Morex barley population under different conditions of photoperiod and temperature. Euphytica doi: 10.1007/s10681-011-0526-7
120. Denis JB (1988) Two-way analysis using covariates. Statistics 19:123–132
121. van Eeuwijk FA, Denis JB, Kang MS (1996) Incorporating additional information on genotypes and environments in models for two-way genotype by environment tables. In: Kang MS, Gauch HG (eds) Genotype-by-environment interaction. CRC Press, Boca Raton, pp 15–50
122. Yates F, Cochran WG (1938) The analysis of groups of experiments. J Agric Sci 28:556–580
123. Finlay KW, Wilkinson GN (1963) The analysis of adaptation in a plant breeding programme. Aust J Agr Res 14:742–754
124. van Eeuwijk FA (1995) Linear and bilinear models for the analysis of multi-environment trials: I. An inventory of models. Euphytica 84:1–7
125. Denis JB, Gower JC (1996) Asymptotic confidence regions for biadditive models: interpreting genotype-environment interactions. Appl Stat 45:479–492
126. Gabriel KR (1998) Generalised bilinear regression. Biometrika 85:689–700
127. van Eeuwijk FA (1995) Multiplicative interaction in generalized linear models. Biometrics 51:1017–1032
128. Gabriel KR (1978) Least squares approximation of matrices by additive and multiplicative models. J Roy Stat Soc Ser B 40:186–196
129. Gauch HG (1988) Model selection and validation for yield trials with interaction. Biometrics 44:705–715
130. Gollob HF (1968) A statistical model which combines features of factor analysis and analysis of variance techniques. Psychometrika 33:73–115
131. Mandel J (1969) The partitioning of interaction in analysis of variance. J Res NBS 73B:309–328
132. Yan W, Kang MS (2003) GGE biplot analysis: a graphical tool for breeders, geneticists, and agronomists. CRC Press, Boca Raton
133. Yan W, Hunt LA, Sheng Q, Szlavnics Z (2000) Cultivar evaluation and mega-environment investigation based on the GGE biplot. Crop Sci 40:597–605
134. Cornelius PL (1993) Statistical tests and retention of terms in the additive main effects and multiplicative interaction model for cultivar trials. Crop Sci 33:1186–1193
135. Kempton RA (1984) The use of biplots in interpreting variety by environment interactions. J Agric Sci 103:123–135
136. Molina-Cano JL, García del Moral LF, Ramos JM, García del Moral MB, Romagosa I, Roca de Togores F (1990) Quantitative phenotypical expression of three mutant genes in barley and the basis for defining an ideotype for Merditerranean environments. Theor Appl Genet 80:762–768
137. Romagosa I, Fox PN, del Moral G, Ramos JM, García del Moral B, Roca de Togores F, Molina-Cano JL (1993) Integration of statistical and physiological analyses of adaptation of near-isogenic barley lines. Theor Appl Genet 86:822–826
138. Vargas M, Crossa J, van Eeuwijk FA, Ramírez ME, Sayre K (1999) Using AMMI, factorial regression, and partial least squares regression models for interpreting genotype $\times$ environment interaction. Crop Sci 39:955–967
139. Voltas J, van Eeuwijk FA, Sombrero A, Lafarga A, Igartua E, Romagosa I (1999) Integrating statistical and ecophysiological analysis of genotype by environment interaction for grain filling of barley in Mediterranean areas I. Individual grain weight. Field Crop Res 62:63–74
140. Voltas J, van Eeuwijk FA, Araus JL, Romagosa I (1999) Integrating statistical and ecophysiological analysis of genotype by environment interaction for grain filling of barley in Mediterranean areas II. Grain growth. Field Crop Res 62:75–84
141. Royo C, Rodríguez A, Romagosa I (1993) Differential adaptation of complete and substituted triticale to acid soils. Plant Breed 111:113–119
142. Lynch M, Walsh JB (1998) Genetics and analysis of quantitative traits. Sinauer Associates, Sunderland
143. van Eeuwijk FA, Crossa J, Vargas M, Ribaut JM (2001) Variants of factorial regression for analysing QTL by environment interaction. In: Gallais A, Dillmann C, Goldringer I (eds) Eucarpia, quantitative genetics and breeding methods: the

way ahead, vol 96, INRA Editions Versailles Les Colloques series. INRA, Paris, pp 107–116
144. van Eeuwijk FA, Crossa J, Vargas M, Ribaut JM (2002) Analysing QTL by environment interaction by factorial regression, with an application to the CIMMYT drought and low nitrogen stress programme in maize. In: Kang MS (ed) Quantitative genetics, genomics and plant breeding. CAB International, Wallingford, pp 245–256
145. Piepho HP, Pillen K (2004) Mixed modeling for QTL × environment interaction analysis. Euphytica 137:147–153
146. IRRI (2008) CropStat for windows, version 5. Biometrics and Bioinformatics Unit, International Rice Research Institute, Los Baños, Philippines. http://www.irri.org/science/software/irristat.asp. Accessed 27 Feb 2008
147. Gauch HG (2007) MATMODEL version 3.0: Open source software for AMMI and related analyses. Crop and Soil Sciences, Cornell University, Ithaca. http://www.css.cornell.edu/staff/gauch. Accessed 27 Feb 2008
148. Balzarini MG, Bruno C, Peña A, Teich I, Di Rienzo JA (2010) Estadística en Biotecnología. Aplicaciones en InfoGen. Grupo InfoStat, Facultad de Ciencias Agropecuarias, Universidad Nacional de Córdoba, Argentina
149. Di Rienzo JA, Casanoves F, Balzarini MG, Gonzalez L, Tablada M, Robledo CW (2008) InfoStat, versión 2008. Grupo InfoStat, Facultad de Ciencias Agropecuarias, Universidad Nacional de Córdoba, Argentina
150. Kang MS (2003) Handbook of formulas and software for plant geneticists and breeders. Haworth Press, Binghamton
151. Friedman J, Hastie T, Tibshirani R (2008) Sparse inverse covariance estimation with the graphical lasso. Biostatistics 9:432–441
152. Bernardo R, Yu J (2007) Prospects for genomewide selection for quantitative traits in maize. Crop Sci 47:1082–1090
153. Heffner EL, Sorrells ME, Jannink JL (2009) Genomic selection for crop improvement. Crop Sci 49:1–12
154. Jannink JL, Lorenz AJ, Iwata H (2010) Genomic selection in plant breeding: from theory to practice. Brief Funct Genomics 9:166–177
155. Bertin N, Martre P, Génard M, Quilot B, Salon C (2010) Under what circumstances can process-based simulation models link genotype to phenotype for complex traits? Case-study of fruit and grain quality traits. J Exp Bot 61:955–967
156. Chenu K, Chapman SC, Tardieu F, McLean G, Welcker C, Hammer GL (2009) Simulating the yield impacts of organ-level quantitative trait loci associated with drought response in maize – a 'gene-to-phenotype' modeling approach. Genetics 183:1507–1523
157. Hammer G, Cooper M, Tardieu F, Welch S, Walsh B, van Eeuwijk FA, Chapman S, Podlich D (2006) Models for navigating biological complexity in breeding improved crop plants. Trends Plant Sci 11:587–593

Books and Reviews

Ceccarelli S, Guimaraës EP, Weltzien E (eds) (2009) Participatory plant breeding. FAO, Rome

Geochemical Modeling in Environmental and Geological Studies

Chen Zhu
Department of Geological Sciences, Indiana University, Bloomington, IN, USA

Article Outline

Glossary
Definition of the Subject and Its Importance
Introduction
What Is Geochemical Modeling?
The Part of Three
Future Directions
Acknowledgment
Bibliography

Glossary

Activation energy The energy that must be overcome in order for a chemical reaction to occur.

Mass transport The net movement of mass from one location to another due to hydrological processes such as advection, dynamic dispersion, chemical reactions, and microbial activities.

Rate law A rate law is a statement about how the rate of a reaction depends on the concentrations of the participating species.

Solubility product Equilibrium constants for various kinds of reactions with a solid phase on one side and its constituent ions on the other.

Species A chemical entity distinguishable from other entities by molecular formula and structure, e.g., CO_2 and O_2 in a gas, and HCO_3^-, $H_2CO_3^o{}_{(aq)}$, CO_3^{2-}, $NaHCO_3^o{}_{(aq)}$.

Definition of the Subject and Its Importance

Geochemical modeling uses a set of mathematical expressions thought to represent chemical and transport processes in a particular geological system. The predictions of the model are partially observable or experimentally verifiable. Geochemical modeling has found applications in studies of chemical reactions in geological and

environmental systems because of its utilities for synthesis of data, testing scenarios, and predicting long-term consequences of chemical reactions.

Introduction

Geochemical modeling is a powerful and indispensable tool for research and investigations of environmental sustainability science and technology. It allows quantitative evaluation of complex processes that often have feedback loops and it can predict the extent and consequences of geochemical reactions in the order of thousands to tens of thousands of years, beyond the range of laboratory experiments.

An excellent example of the utility of geochemical modeling in environmental sustainability science and engineering and its unique characteristics is illustrated by geological carbon sequestration – the injection of carbon dioxide (CO_2) into deep geological formations as a climate mitigation tool. Upon injection of CO_2 into a geological formation, CO_2 is dissolved into the native brine. The carbonated brine becomes acidic and corrosive, aggressively reacting with host rocks (e.g., a sandstone or carbonate rocks). Some primary (native) minerals are dissolved and secondary minerals precipitated. These dissolution-precipitation reactions can drastically change the porosity and permeability of the host rocks, and thereby impact the injectivity and storage safety in the long-term.

In the above example, there are many processes that are coupled. The flow of the separate supercritical CO_2 phase transports the CO_2 in the aquifer, determined by the viscosity, density, and the relative permeability of CO_2 in contrast to the brine. CO_2 dissolves into the brine when CO_2 makes contact with it. A brine with dissolved CO_2, probably in the form of HCO_3^-, has higher density than the rest. Density-driven vertical convection can occur, and convection brings about chemical gradients that result in more reactions.

The above example demonstrates that the system is complex and that the chemical reactions are coupled with each other and also coupled to transport processes, such as advection and dispersion. It is difficult to quantitatively evaluate these reactions without a computer model. There may be some ideas about what reactions will occur and how fast they will occur, but by developing a model, ideas can be formulated explicitly and thoughts can be tested quantitatively. Often, ideas are restricted to a particular aspect of chemical reactions, gleaned from specific laboratory experiments or field observations. Whether such ideas are valid when they are examined with measurable or observable consequences of the overall chemical systems is not known. In other words, whether the ideas of a subsystem hold up in the overall scheme of things must be tested. The system of concern often not only involves the coupling of hundreds of reactions, but also to processes like diffusion, advection, and dispersion, biological activities, thermal conduction, mechanical stress, and deformation.

The geological carbon sequestration example also illustrates the necessity of the prediction of chemical reactions for all practical purposes. Although federal or national regulations for safe underground CO_2 storage still need to emerge, it is reasonable to assume that national and local regulations will demand risk assessments of wellbore integrity, well injectivity, and long-term performance in the order of thousands of years. The geology of each injection site differs, and geological heterogeneities at a given site are a fact of life. It is not possible to conduct laboratory experiments either for each possible geochemical system or for durations of more than a few months. Performance assessments necessary at all stages of CO_2 storage operations (site assessment/selection, design, installation, operations and monitoring, and closure/post-closure) have to be partly based on geochemical modeling predictions.

Thus, it is clear that geochemical modeling is an indispensable tool in geochemical research and engineering. This entry introduces the basic concepts of geochemical modeling, provides information for accessing modeling codes and further readings, and shows applications in the field of environmental sustainability sciences and technology.

What Is Geochemical Modeling?

To modify Zhu and Anderson's [1] definition a little bit, a *geochemical model* is "an abstract object, described by a set of mathematical expressions thought to represent chemical and transport processes in a particular system. The predictions of the model are partially observable or experimentally verifiable."

A geochemical model typically includes a *geochemical reaction network*, which means the finite array of reactions in a geochemical system and transport processes for a reactive transport system.

Mathematically, for a geochemical system that has n species, the following ordinary differential equations completely define the geochemical reaction network [2],

$$\frac{dm_i}{dt} = \sum_j \upsilon_{i,j} r_{i,j}, i \in n, \quad (1)$$

where m_i denotes the concentrations of ith species, t the time, υ_j the stoichiometric coefficient for ith species in the jth reaction, and $r_{i,j}$ the production or consumption rate of the ith species in the jth reaction. For a reactive transport system, the geochemical reaction network is defined by the transport equations,

$$\frac{\partial m_i}{\partial t} + L(C_i) = \sum_j v_j r_i \quad (2)$$

where L is the advection, dispersion, diffusion operator [3].

For historic development of geochemical modeling, the readers are referred to Zhu and Anderson [1] and Nordstrom [4]. To develop or apply a geochemical model, the modeler needs three parts: (1) a computer code that solves Eqs. 1 and/or 2; (2) a thermodynamic and kinetics database; (3) an input file that supplies the chemical analysis and the design or conceptual model of the geochemical model. Zhu and Anderson [1] called it "the part of three."

The Part of Three

Numerous computer programs for geochemical modeling have been developed. Without exception, the Newton–Raphson iteration method is used to solve the highly nonlinear Eq. 1. These computer codes include EQ3/6 [5], SOLMINEQ.88 [6], PHREEQC [7], and MINTEQA2 [8]. The codes that are sponsored by government agencies are essentially free of charge and are widely used. With ever more increasing computing power, tremendous advancements have been seen in code developments in the last decade. Zhu [9] pointed out that computer code developments are ahead of underlying science.

Most widely distributed computer codes come with a database of equilibrium constants for chemical reactions. For example, a database called DATA0.DAT was initially developed for EQ3/6 by Tom Wolery [5] and Jim Johnson [10, 11]. This database was later adopted for the program PHREEQC as LLNL.DAT, GWB as THERMO.DAT, and the database in ToughReact. Similarly, thermodynamic databases have been developed for MINTEQA2 as MINTEQA2.DAT for PHREEQC as PHREEQC.DAT.

The compilations of equilibrium constants for chemical reactions draw from the available databases of standard state properties for minerals, such as those from Helgeson et al. [12], Wagman et al. [13], Berman [14, 15], Holland and Powell [16], Nordstrom et al. [17], and Robie and Hemingway [18]. More specialized databases are available for uranium [19]. Because these internally consistent databases only contain a limited number of minerals, while applications of geochemical modeling to a variety of geological and environmental topics require a wider range of minerals and solids, additional minerals are added to these equilibrium constant databases MINTEQA2 and PHREEQC.

For aqueous species, an internally consistent database developed by Harold Helgeson and collaborators, which includes a large number of aqueous species, has been widely used in the field of geochemistry [20–23]. In this database, the temperature and pressure dependences of thermodynamic properties for aqueous species were predicted using the parameters of the revised Helgeson–Kirkham–Flowers (HKF) equations of state for aqueous species [20, 24, 25]. Activity coefficients for the charged aqueous species were calculated from the extended Debye–Hückel equation or B-dot equation fitted to mean salt NaCl activity coefficients [26]. The computer program SUPCRT92 can be used to generate equilibrium constants at elevated temperatures and pressures [11]. Equilibrium constants have been calculated using the standard state properties from this database and compiled into databases that accompany the program EQ3/6 which was then adopted to other programs, e.g., LLNL.DAT in PHREEQC and THERMO.DAT in GWB©.

It has been known for quite some time that the internal consistency of thermodynamic data for modeling calculations is important. Nordstrom and Munoz [27] elaborated on the topic of internal consistency and

readers are urged to consult their writing on the topic. Note that the standard state thermodynamic properties in the mineral databases [12, 14–17] are *internally consistent*, but some added minerals may not necessarily be so. The aqueous species collected in the Helgeson–Sverjensky–Shock compilations are internally consistent, but others collected may not be.

In the deep parts of the subsurface and in the shallow parts where evaporate sediment beds are located, groundwater becomes briny and can have concentrations of dissolved solids up to 300,000 mg/L. In dealing with concentrated solutions, Pitzer's ion interaction approach using virial specific interaction equations is generally preferred over the ion association theory when calculating ionic activities. The Pitzer's model, commonly the Harvie–Moller–Weare (HMW) formulation of it [28], has been incorporated into geochemical modeling codes EQ3/6, PHRQPITZ [29], and TOUGHREACT [30]. Although progress has been made in compiling the Pitzer interaction parameters [31], the lack of Pitzer's activity coefficient parameters at elevated temperatures and for minor or trace elements remains a barrier to accurate calculation of solubility and saturation indices for highly saline fluids.

The input file is where the modeler defines the composition of the chemical system, includes or excludes certain types of chemical reactions, and assigns the boundary and initial conditions. In other words, this is where the modeler translates the conceptual model into recognizable formats by computer programs. The modeler also develops the conceptual model in this way [1].

From the discussion of each of the "part of three," it should be clear that a computer program should always be distinguished from a geochemical model. For example, PHREEQC is a geochemical modeling computer program or code; it is not a geochemical model. It is always true that the modeler, not the computer code, produces a geochemical model. A geochemical modeling code is a utility, e.g., an oven. The oven does not bake the cake. The chef bakes the cake.

Speciation–Solubility Modeling

Speciation modeling calculates the distribution of aqueous species and mineral saturation indices according to the solutions of the mass and charge balance and mass action equations. From the activities of the aqueous species, one can calculate Saturation Indices (*SI*),

$$SI = \log\left(\frac{IAP}{K}\right) \tag{3}$$

where K stands for the equilibrium constant of the dissolution reaction and *IAP* stands for the Ion Activity Product. When $SI = 0$, the mineral is at equilibrium with the aqueous solution. When $SI < 0$, the aqueous solution is undersaturated with respect to the mineral of concern and the mineral will dissolve. When $SI > 0$, the aqueous solution is supersaturated with respect to the mineral and the mineral will precipitate.

Speciation–solubility modeling has become a routine exercise since Garrels and Thompson [32] first calculated the aqueous speciation in seawater and saturation states with respect to mineral solubility. The principles are well known, and the numerical modeling techniques and their tweaking are mature. There are hundreds of computer codes available for this kind of calculation.

The results of speciation and solubility calculations are used for a number of issues in environmental sustainability science and technology. The toxicity of many chemicals is not only related to the total concentrations, but also to the species. Liu et al. [33] measured the total concentrations of antimony (Sb) with valence of V. They then used speciation calculations and found the dominant aqueous Sb species was $Sb(OH)_6^-$. In general, it is assumed that aqueous species in the solution are in mutual equilibrium (homogeneous equilibria). The exception to this rule is redox species, which are well known for not being at equilibrium in surficial water bodies [34, 35].

The calculated saturation indices give directions of chemical reactions. As elaborated in Zhu and Anderson [1] and in numerous books on thermodynamics, saturation indices show the direction of the chemical reactions, as dictated by the second law of thermodynamics, but tell nothing about the rate of reactions. For example, it is well known in geochemistry that natural waters are often supersaturated with respect to crystalline quartz, but the rate of quartz precipitation is too slow for these waters to reach equilibrium with quartz even after thousands of years at low temperatures.

However, reaction direction is the first thing that one must know before one can extract reaction rates (one needs to know which direction the reactions will go before one can estimate how fast or slow they will do it).

One could extend the scope of traditional speciation–solubility modeling to include the equilibrium partitioning of a chemical between the aqueous solution and mineral surfaces (Fig. 1). Many computer codes (e.g., MINTEQA2 and PHREEQC) now allow the calculations of surface adsorption according to the surface complexation theory [35–37]. One can find the details of the surface complexation theories in the textbooks cited above. In terms of modeling, when the total concentration of an ion (e.g., Pb^{2+}) in an aqueous solution is given, the codes can calculate how much Pb^{2+} is partitioned onto the mineral surface(s), how much Pb^{2+} remains in the aqueous solution, what the relative percentage of surface bound Pb^{2+} among different surface species is, and what the dominant aqueous Pb^{2+} species are.

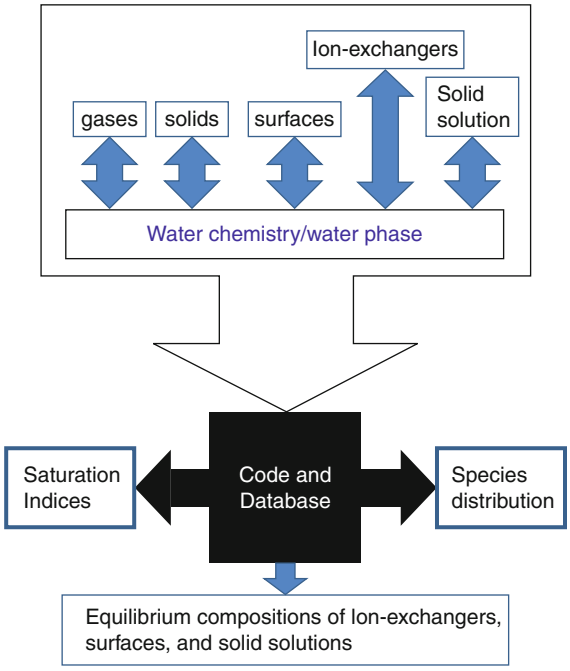

Geochemical Modeling in Environmental and Geological Studies. Figure 1
Schematic configuration of speciation–solubility models

Similarly, one can calculate the equilibrium partitioning of chemicals between an aqueous solution and ion-exchangers. Unlike the surface adsorption and the surface complexation theory that describes it, modeling of ion-exchange reactions lacks both theoretical footing and internally consistent databases [1]. Readers are encouraged to read more in Appelo and Postma [38]. Equally, one can also calculate the equilibrium distribution between an aqueous solution and solid solution phases [49, 50], and gas phases (Fig. 1).

Speciation–solubility modeling provides a "snapshot" of a dynamic system, and the basic building block for more advanced process modeling. The calculated activities of the various ionic and molecular species give the *IAP* for the saturation state evaluation. This type of calculation represents the majority of applications of geochemical modeling to the field of environmental sustainability science and technology. However, despite the maturity of the modeling techniques, a number of challenges exist which make the evaluation of the reaction directions a nontrivial task (cf. [9]).

Reaction Path Modeling

Once the results of aqueous speciation and solubility calculations are obtained (i.e., calculated species distribution and saturation indices) for a given temperature, pressure, and instance of time, processes can be modeled. The simplest next step is *reaction path modeling*, tracing the evolution of aqueous solution composition and speciation and mineral paragenesis through time or the reaction progress as a result of irreversible reactions (e.g., feldspar dissolution) or processes (e.g., titration, mixing, or increase or decrease of temperature or pressure). The modeling is accomplished by applying the principle of mass balance, thermodynamics that govern the equilibrium between species, and kinetics that govern the rate of mass transfer among phases. The concept and mathematical foundation of reaction path modeling was introduced to geochemistry by Harold Helgeson [39]. Numerous articles and books have described this approach [2, 5, 40, 41]. Computer codes EQ3/6, PHREEQC, MINTEQA2, SOLMINEQ.88 and GWB© can all perform these kinds of calculations.

In the past a few years, advancement has been seen in computing powers and development of computer programs, which make it possible to perform reaction path modeling involving complicated reaction networks. This includes incorporation of various forms of rate laws and inclusion of an almost unlimited number of reactions into a single model. Conceptual developments in geochemical reaction networks now allow one to explore the intricacies of feedback mechanisms for complex inorganic geochemical systems [42].

One area that has been rapidly advanced in recent years is the linking of microbial activities with a network of redox and non-redox reactions and the exploration of the complex feedback loops in biogeochemistry. For example, Istok et al. [43] carried out a *biogeochemical reaction path modeling* for simulating an in situ field experiment which investigated the bioreduction of uranium near Oak Ridge National Laboratory in Tennessee, USA. In the field experiment, ethanol was injected into the aquifer to stimulate microbial activities at the field site and the reduction of nitrate, U(VI), Fe(III), Mn(IV), and sulfate were observed to proceed concomitantly.

Historically, microbial mediated reactions were modeled as semiempirical kinetics, decoupled into a whole suit of inorganic geochemical reactions as a consequence of biostimulation or bioremediation [43, 44]. The Monod-type kinetic expressions are used to describe rates of substrate utilization and biomass production. Istok et al. [43] developed a new approach, dubbed as "thermodynamically based." In their approach, the actual microbial community is represented by a synthetic microbial community consisting of a collection of microbial groups, each with a unique growth equation that couples a specific pair of energy yielding redox reactions. Simulations monitored temporal changes of microbial biomass, community composition, aqueous speciation, and oxidation states of multivalent chemicals, as well as the dissolution and precipitation of minerals.

Istok et al.'s [43] modeling results are shown in Fig. 2. Simulations predicted that acetate addition will result in the growth of only 8 of the 25 microbial groups during the experiment. The increasing biomass and changing community composition occurred as increasing amounts of acetate were reacted. Early on in the reaction path, predicted biomass increase was dominated by predicted growth of manganese reducers, iron reducers, and denitrifiers, with much smaller predicted growth of other groups, reflecting the relatively larger initial amounts of Mn(IV)- and Fe(III)-bearing minerals and nitrate compared to oxygen and sulfate. As additional acetate was reacted, growth of other groups was predicted to become energetically favorable, especially sulfate reducers. Predicted patterns of the growth of the various groups resulted in predicted changes in community composition. The results are generally consistent with clone libraries developed from groundwater samples.

While some computer software is fully capable of performing such complex computations, the requirements of modeling parameters for the biogeochemical reactions are daunting [45]. Numerous nonunique interpretations of field data may be possible. However, geochemical modeling can help to integrate processes and reactions in a quantitative manner and provide a more comprehensive understanding of biogeochemical processes than simply providing apparent zeroth-order and first-order rates.

Coupled Reactive Mass Transport Modeling

Geochemical models included in this category all solve the advection-dispersion-reaction (ADR) mass transport equations, typically using the sequential iteration approach. The reaction term is fully coupled to chemical equilibrium and kinetics (and microbial activities). In other words, at each time step and at each node or in each grid cell, reaction path calculations described above are performed. Many transport codes on the market are termed "reactive transport model," but only the partitioning coefficient or K_D approach is used. In the K_D approach, all chemical reactions pertinent to a chemical are described by a single parameter [46]. In this entry, only multiple component mass transport models with the nonlinear mass balance equations for speciation and mass transfer coupled to the ADR equation are called coupled reactive mass transport (CRMT) models. For the fundamentals of the subject, readers are referred to Yeh and Tripathi [47].

Some codes in this category are coupled to fluid flow and also have the capabilities of simulating multiphase flow (air, water, and CO_2), density-dependent flow,

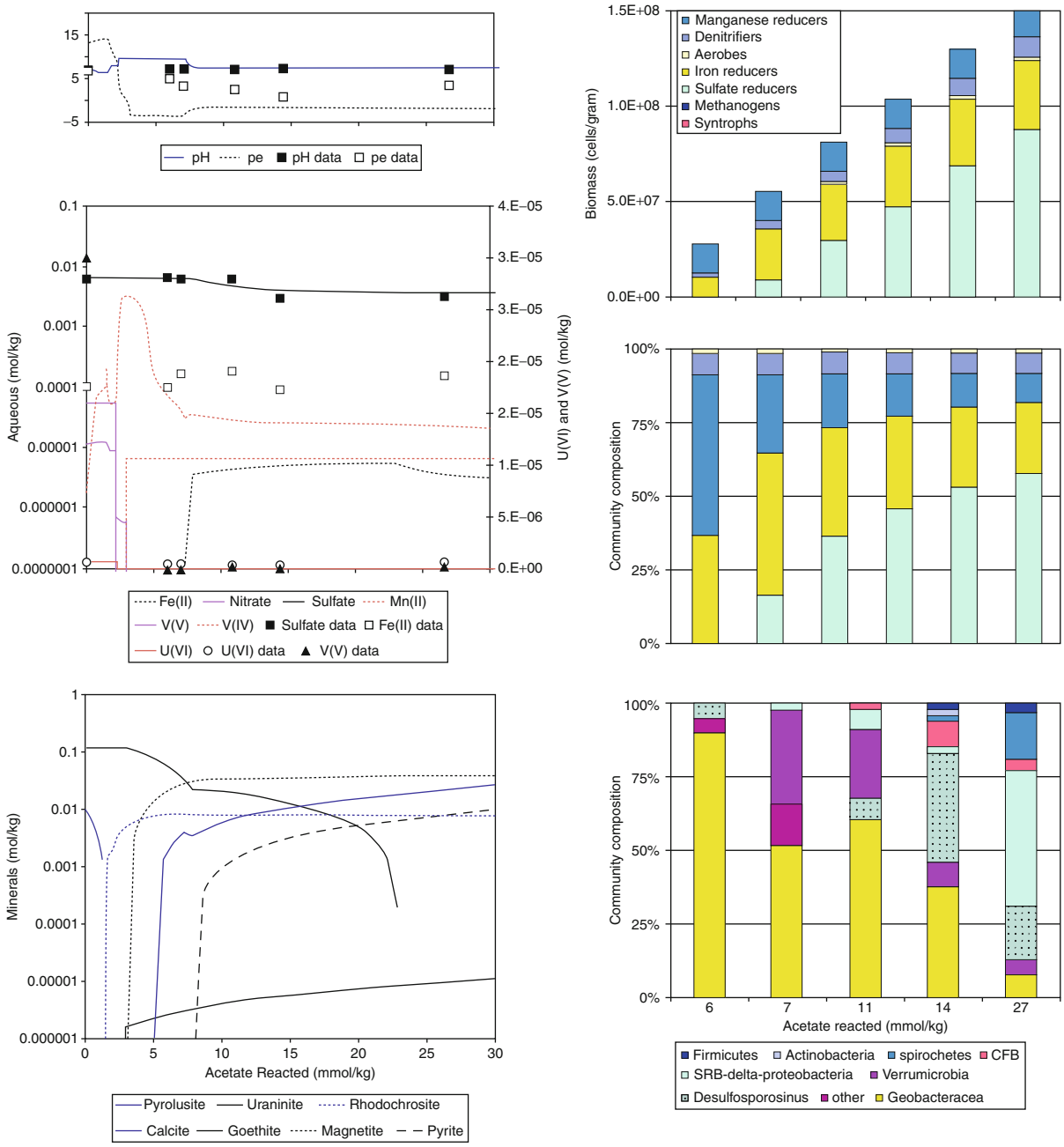

Geochemical Modeling in Environmental and Geological Studies. Figure 2
Comparison of flush simulations with geochemical and clone library data from field natural gradient experiment of Anderson et al. [51]. Figure 3 of Istok et al. [43]

the feedback of dissolution – precipitation reactions and changes of permeability and flow patterns – and thermal and mechanical stress. Applications of CRMT include fate and transport of metal and radionuclides in groundwater systems, geologic carbon sequestration, sediment diagenesis, geothermal energy exploration and production, sea water intrusion, and formation of ore deposits.

As an example, Liu et al. [48] used multiphase reactive flow and transport modeling to simulate large-scale CO_2 injection (a million tons per year for 100 years) into Mt. Simon sandstone, a major candidate saline reservoir in the Midwest of USA. The long-term fate of CO_2 was simulated by extending the modeling period to 10,000 years (the predictive utility of geochemical modeling). The results indicate that most of the injected CO_2 remains within a radius of 3,300 m lateral distribution. Four major trapping mechanisms and their spatial and temporal variations are evaluated in the simulations: hydrodynamic, solubility, residual, and mineral trapping. A strongly acidified zone (pH 3–5) forms in the areas affected by the injected CO_2(0–3,300 m), and consequently causes extensive mineral precipitation and dissolution (Fig. 3).

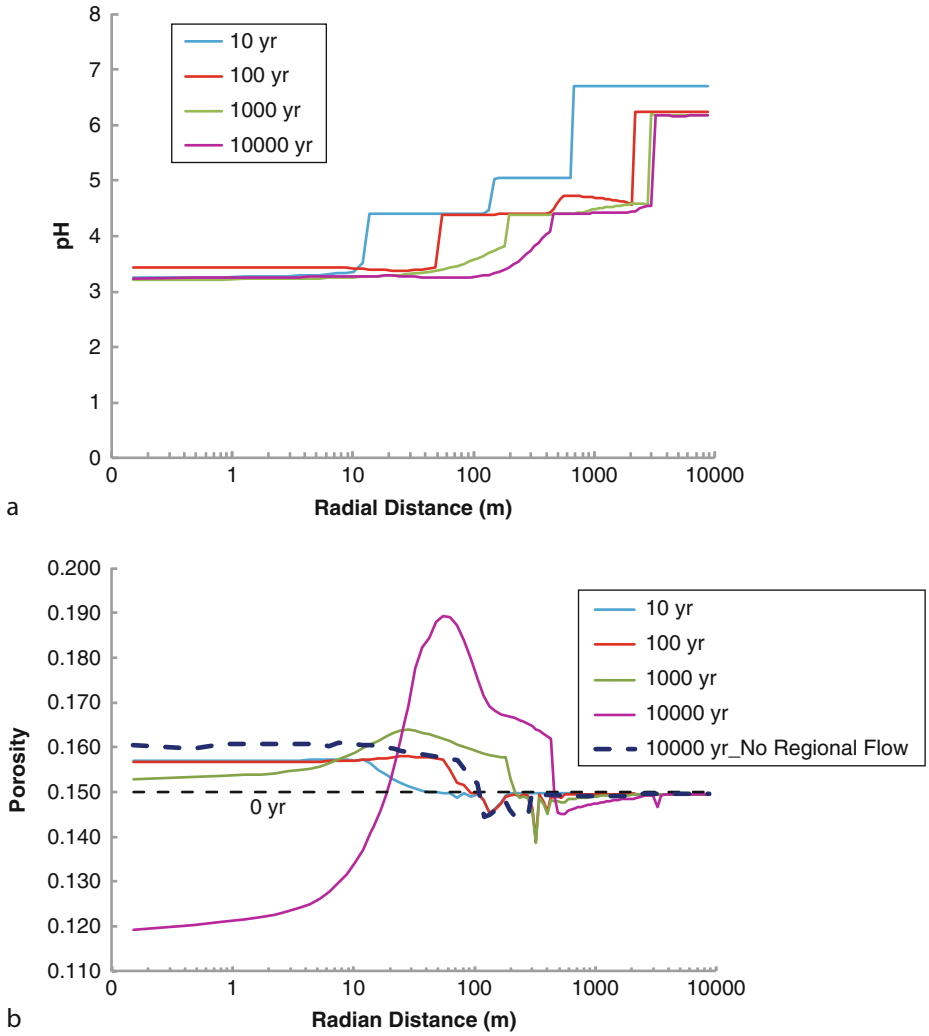

Geochemical Modeling in Environmental and Geological Studies. Figure 3
(**a**) Simulated pH variations as a function of radial distance at year 10, 100, 1,000, and 10,000 with regional flow rate of 0.3 m/year. The initial pore fluids had a pH of 6.9. (**b**) Simulated porosity variations as a function of radial distance at year 10, 100, 1,000, and 10,000 with a regional flow rate of 0.3 m/year, compared at year 10,000 with no regional flow

Coupled reactive mass transport models are great tools to further understand geochemical reaction networks. Typically, CRMT modeling generates a great amount of numerical experimental data. Significant amounts of time and energy are necessary to dissect and distill the information on what reactions have happened and how reactions are coupled.

Future Directions

There is no doubt that geochemical modeling plays an increasingly important role in environmental sustainability sciences and technology, as environmental decisions (carbon dioxide storage, remediation) are made partly based on model predictions. Computer code development has given flexibility to most applications. However, modelers need to have a grasp of the fundamental understanding of the underlying sciences and the limitations of geochemical models.

Zhu [9] gave a list of research needs to model geochemical reactions:

1. Internally consistent standard state thermodynamic properties for minerals, particularly minerals with complex and variable chemical compositions and structures like smectite. More accurate thermodynamic properties for common minerals like feldspars would help to resolve the controversy on the Al-bearing minerals.
2. More experimental data and resolution of ambiguities surrounding the speciation of aqueous elements like that for Al species.
3. Improvements in sampling and filtration of natural and laboratory samples for better saturation state assessments.
4. Solid solution models for feldspar and clay minerals.
5. More measurements of rate – free energy of reaction relations at a variety of temperature and pH conditions, leading to accurate theoretical or empirical correlations.
6. Rates and rate laws for precipitation reactions, and improved understanding of nucleation process.
7. Pitzer activity coefficient parameters for trace elements and for all elements at elevated temperatures.
8. More rigorous treatment of experimental data with statistical analysis.
9. Assessment of error propagations.

Acknowledgment

The writing of this entry was also made possible with continued financial support from the US National Science Foundation (EAR0423971, EAR0509775, EAR 0809903) and the US Department of Energy (DE-FG26-04NT42125, DE-FE0004381). Any opinions, findings, and conclusions or recommendations expressed in this material, however, are those of the authors and do not necessarily reflect the views of the US Government or any agency thereof.

Bibliography

Primary Literature

1. Zhu C, Anderson GM (2002) Environmental applications of geochemical modeling. Cambridge University Press, London, p 304
2. Helgeson HC et al (1970) Calculation of mass transfer in geochemical processes involving aqueous solutions. Geochim Cosmochim Acta 34:569–592
3. Fang YL, Yeh GT, Burgos WD (2003) A general paradigm to model reaction-based biogeochemical processes in batch systems. Water Resour Res 39(4):1083
4. Nordstrom DK (2007) Modeling low-temperature geochemical processes. In: Drever JI (ed) Surface and ground water, weathering and soils, treatise on geochemistry. Elsevier, New York, pp 1–38, online update
5. Wolery TJ (1992) EQ3/6, A software package for geochemical modeling of aqueous systems: package overview and installation guide (Version 7.0). URCL-MA-110662-PT-I, University of California/Lawrence Livermore Laboratory, California/Livermore, p 41
6. Kharaka YK et al (1988) SOLMINEQ.88: a computer program for geochemical modeling of water-rock interactions. Water-resources investigations report 88–4227, US Geological Survey
7. Parkhurst DL, Appello AAJ (1999) User's guide to PHREEQC (Version 2)-a computer program for speciation, batch-reaction, one dimensional transport, and inverse geochemical modeling. Water-resource investigation report, US Geological Survey, p 312
8. Allison JD, Brown DS, Novo-Gradac KJ (1991) MINTEQA2/PRODEFA2, a geochemical assessment model for environmental systems, Version 3.0 user's manual
9. Zhu C (2009) Geochemical modeling of reaction paths and geochemical reaction networks. In: Oelkers EH, Schott J (eds) Thermodynamics and kinetics of water-rock interaction. Mineralogical Society of America, Washington, pp 533–569
10. Johnson JW, Lundeen SR (1994) GEMBOCHS thermodynamic data files for use with the EQ3/6 software package. Lawrence Livermore National Laboratory, p 99
11. Johnson JW, Oelkers EH, Helgeson HC (1992) SUPCRT92 – A software package for calculating the standard molal thermodynamic properties of minerals, gases, aqueous species,

and reactions from 1-bar to 5000-bar and 0°C to 1000°C. Comput & Geosciences 18(7):899–947
12. Helgeson HC et al (1978) Summary and critique of the thermodynamic properties of rock forming minerals. Am J Sci 278A:569–592
13. Wagman DD et al (1982) The NBS tables of chemical thermodynamic properties – selected values for inorganic and C-1 and C-2 organic-substances in SI units. J Phys Chem Ref Data 11(Supplement 2):392
14. Berman RG (1988) Internally-consistent thermodynamic data for minerals in the system Na_2O-K_2O-CaO-MgO-FeO-Fe_2O_3-Al_2O_3-SiO_2-TiO_2-H_2O-CO_2. J Petrol 29(2):445–522
15. Berman RG (1990) Mixing properties of Ca-Mg-Fe-Mn garnets. Am Mineral 75:328–344
16. Holland TJB, Powell R (1998) An internally consistent thermodynamic data set for phases of petrological interest. J Metamorph Geol 16:309–343
17. Nordstrom DK et al (1990) Revised chemical equilibrium data for major water-mineral reactions and their limitations. In: Melchior DC, Bassett RL (eds) Chemical modeling of aqueous systems II. American Chemical Society, Washington, pp 398–413
18. Robie RA, Hemingway BS (1995) Thermodynamic properties of minerals and related substances at 298.15 K and 1 bar (10^5pascals) pressure and at higher temperatures. US Geological Survey Bulletin 2131, p 456
19. Grenthe I et al (1992) The chemical thermodynamics of uranium. Elsevier, New York
20. Helgeson HC, Kirkham DH, Flowers GC (1981) Theoretical prediction of the thermodynamic behavior of aqueous electrolytes at high pressures and temperatures. IV. Calculation of activity coefficients, osmotic coefficients, and apparent molal and standard and relative partial molal properties to 600°C and 5 kb. Am J Sci 281:1249–1516
21. Shock EL, Helgeson HC (1988) Calculation of the thermodynamic and transport properties of aqueous species at high pressures and temperatures: correlation algorithms for ionic species and equation of state predictions to 5 kb and 1000°C. Geochim Cosmochim Acta 52:2009–2036
22. Shock EL, Helgeson HC, Sverjensky DA (1989) Calculations of the thermodynamic and transport properties of aqueous species at high pressures and temperatures: standard partial molal properties of inorganic neutral species. Geochim Cosmochim Acta 53:2157–2183
23. Sverjensky DA, Shock EL, Helgeson HC (1997) Prediction of the thermodynamic properties of aqueous metal complexes to 1000°C and 5 kb. Geochim Cosmochim Acta 61(7):1359–1412
24. Shock EL et al (1992) Calculation of thermodynamic and transport properties of aqueous species at high pressures and temperatures. Effective electrostatic radii, dissociation constants and standard partial molal properties to 1000°C and 5 kb. J Chem Soc London, Faraday Trans 88: 803–826
25. Tanger JC, Helgeson HC (1988) Calculations of the thermodynamic and transport properties of aqueous species at high pressures and temperatures: revised equation of state for the standard partial molal properties of ions and electrolytes. Am J Sci 288:19–98
26. Oelkers EH, Helgeson HC (1990) Triple-ion anions and polynuclear complexing in supercritical electrolyte-solutions. Geochim Cosmochim Acta 54(3):727–738
27. Nordstrom DK, Munoz JL (1994) Geochemical thermodynamics, 2nd edn. Blackwell, Oxford
28. Harvie CE, Moller N, Weare JH (1984) The predication of mineral solubilities in natural waters: the Na-K-Mg-Ca-H-Cl-SO_4-OH-HCO_3-CO_3-CO_2-H_2O system to high ionic strength at 25°C. Geochim Cosmochim Acta 48(4):723–751
29. Plummer LN et al (1988) A computer program incorporating Pitzer's equations for calculation of geochemical reactions in brines. Water resources investigations report 88–4153, US Geological Survey, p 310
30. Xu T et al (2004) TOUGHREACT user's guide: a simulation program for non-isothermal multiphase reactive geochemical transport in variably saturated geologic media (V1.2). Paper LBNL-55460. Lawrence Berkeley National Laboratory
31. Wolery T et al (2004) Pitzer database development: description of the Pitzer geochemical thermodynamic database data0.ypf. Appendix I in In-Drift precipitates/salts model (P. Mariner) report ANL-EBS-MD-000045 REV 02. Bechtel SAIC Company, Las Vegas
32. Garrels RM, Thompson ME (1962) A chemical model for sea water at 25 \degc and one atmospheric pressure. Am J Sci 260:57–66
33. Liu FY et al (2010) Antimony speciation and contamination of waters in Xikuangshan Sb mining and smelting area, China. Environ Geochem Health. doi:10.1007/s10653-010-9284-z
34. Lindberg RD, Runnells DD (1984) Groundwater redox reactions - an analysis of equilibrium state applied to Eh measurements and geochemical modeling. Science 225(4665):925–927
35. Stumm W, Morgan JJ (1996) Aquatic chemistry, chemical equilibria and rates in natural waters. Wiley, New York, p 1022
36. Stumm W (1992) Chemistry of solid-water interfaces: processes at the mineral-water and particle-water interface in natural systems, 1st edn. Wiley, New York
37. Dzombak DD, Morel FMM (1990) Surface complex modeling: hydrous ferric oxide. Wiley, New York, 393
38. Appelo CAJ, Postma D (2005) Geochemistry, groundwater and pollution. A. A. Balkema, Leiden
39. Helgeson HC (1968) Evaluation of irreversible reactions in geochemical processes involving minerals and aqueous solutions-1. Thermodynamic relations. Geochimica et Cosmochimica Acta 32:853–877
40. Helgeson HC (1979) Mass transfer among minerals and hydrothermal solutions. In: Barnes HL (ed) Geochemistry of hydrothermal ore deposits. John Wiley & Sons, New York, pp 568–610
41. Anderson GM, Crerar DA (1993) Thermodynamics in geochemistry: the equilibrium model. Oxford University Press, New York, 588
42. Zhu C et al (2010) Coupled alkali feldspar dissolution and secondary mineral precipitation in batch systems: 4.

Numerical modeling of kinetic reaction paths. Geochimica Et Cosmochimica Acta 74(14):3963–3983
43. Istok JD et al (2010) A thermodynamically-based model for predicting microbial growth and community composition coupled to system geochemistry: application to uranium bioreduction. J Contam Hydrol 112(1–4):1–14
44. Liu C et al (2001) Kinetic analysis of the bacterial reduction of goethite. Environ Sci Technol 35(12):2482–2490
45. Roden EE (2008) Microbiological controls on geochemical kinetics 1: fundamentals and case study on microbial Fe(III) oxide reduction. In: Brantley SL, Kubicki J, White AF (eds) Kinetics of water-rock interaction. Springer, New York, pp 335–415
46. Zhu C (2003) A case against Kd-based transport model: natural attenuation at a mill tailings site. Comput Geosci 29:351–359
47. Yeh GT, Tripathi VS (1989) A critical evaluation of recent development of hydrogeochemical transport models of reactive multi-components. Water Resour Res 25(1):93–108
48. Liu FY et al (2010) Coupled reactive transport modeling of CO_2 Sequestration in the Mt. Simon sandstone formation, Midwest U.S.A. Int J Greenh Gas Con 5:294–307
49. Zhu C (2004) Coprecipitation in the barite isostructural family: 1. Binary mixing properties. Geochimica et Cosmochimica Acta, 68(16):3327–3337
50. Zhu C (2004) Coprecipitation in the barite isostructural family: 2. Binary mixing properties. Geochimica et Cosmochimica Acta, 68(16):3339–3349
51. Anderson TT, Vrionis HA, Ortiz-Bernard I, Resch CT, Long PE, Dayvault R, Karp K, Marutzky S, Metzler DR, Peacock A, White DC, Lowe M, Lovley DR (2003) Stimulating the in situ activity Geobacter species to remove uranium from the groundwater of a uranium-contaminated aquifer. Appl Environ Microb 69:5884–5891

Geoengineering Policy and Governance Issues

Sean Low[1], Nigel Moore[1], Zhewen Chen[1], Keith McManamen[2], Jason J. Blackstock[3]
[1]Centre for International Governance Innovation, Waterloo, ON, Canada
[2]University of Waterloo, Waterloo, ON, Canada
[3]Kennedy School of Government, Cambridge, MA, USA

Article Outline

Glossary
Definition of the Subject
Introduction
History of Weather Modification and Governance Frameworks
Geoengineering Technologies and Governance Challenges
Current Governance Landscape
Future Directions
Bibliography

Glossary

Carbon geoengineering A variant of geoengineering also known as Carbon Dioxide Removal (CDR) concepts aimed at capturing carbon dioxide directly from the atmosphere by either enhancing existing natural sinks or by using chemical engineering technologies.

Geoengineering Also known as "climate engineering" refers to the deliberate and technological manipulation of the climate system to forestall the worst effects of global warming.

Governance The management of political issues and physical systems that relies not only on (traditional) government at state level, but upon a wider range of actors at the international (international organizations, minilateral clubs), substate (provincial and municipal government), and nonstate (industry, civil society, knowledge networks) levels with such management often involving coalitions across multiple levels and actor types.

Solar geoengineering A variant of geoengineering also known as Solar Radiation Management (SRM) concepts aimed at enhancing reflecting incoming sunlight back into space, preventing absorption by Earth's atmosphere, surface or oceans, and thereby reducing global temperatures.

Weather modification An antecedent to climatic geoengineering focused on the manipulation of local atmospheric conditions to induce short-term, bounded changes in weather. Such methods are different from geoengineering methods in that they are smaller in scale and intent of atmospheric modification.

Definition of the Subject

Geoengineering – the deliberate and technological manipulation of the climate system to forestall the worst effects of global warming (*also referred to as*

climate engineering) – has recently emerged as a novel and controversial issue in climate governance. It is sometimes proposed as an insurance policy, should either (a) primary efforts to develop sustainable energy and societal systems prove unable to quickly enough overcome the inertia of current ones, or (b) uncertainty in the climate system lead to unexpectedly large damage to societies and ecosystems [1]. This entry explores the current attempts and future ideas for governing emerging geoengineering research programs and technologies in ways that effectively manage their climatic and societal impacts.

Introduction

The international and national discourses surrounding geoengineering are currently in an early formative stage, bringing together scientific, ethical, legal, and political dimensions, whose details and interlinkages have been at best only preliminarily mapped to date. Given the potential accessibility and proposed utility of various geoengineering techniques, the discussion of geoengineering is expected to expand and evolve significantly as new actors begin to engage with the issue.

As a result, the core challenge of designing governance frameworks for geoengineering technologies, particularly at the international level, stems from uncertainty about the future. On the scientific side, research and deployment is confronted by large constraints in forecasting impacts and in running meaningful field tests. Political contentions include the potentially unequal distribution of technology ownership; risk in field-testing and deployment; the unclear effects of the debate's politicization by a range of states, researchers, private developers of technology, and civil societies; the potential introduction of moral hazard into climate change mitigations efforts; and complex intersections with a number of global governance issues and policy communities. Underlying each of these political contentions are ethical perspectives on how humanity should interface with the natural world.

Hence, the crux of governance is not only to provide guidelines and structure for managing near-term actors and issues, such as scientists and research agendas. It must also set a framework for managing new related issues and interconnections as they evolve. In this context, caution regarding "locking in" governance mechanisms designed to manage only near-term issues is needed, as narrow frameworks might hinder capacity to address future possibilities and issues. Even independent of lock in, any regulation enacted in the near future could clearly have a formative impact on the future governance of geoengineering. However, with the current lack of an institutional forum for discussion, national legal frameworks, or even coherent rules and framings among the actors now driving the debate, projecting what that impact might be is exceedingly difficult. For these reasons, recent initiatives – such as the Solar Radiation Management Governance Initiative (SRM-GI) and Asilomar Conference on Climate Intervention Technologies [2, 3] – aiming to promote the development of responsible governance for emerging geoengineering research and technologies have focused first on expanding the conversation to include greater diversity in the perspectives involved.

The following sections will provide a general overview of the various components of the geoengineering governance debate. For more detail on any of the issues raised, readers are encouraged to examine the references herein in detail. The section on "History of Weather Modification and Governance Frameworks" chronicles historic environmental modification activities as limited antecedents with potential influence on how geoengineering governance may evolve. The section on "Geoengineering Technologies and Governance Challenges" outlines important distinctions between different geoengineering technologies and stages of research, and highlights how these relate to a range of technical and sociopolitical issues that may require governance. The section on "Current Governance Landscape" then provides an overview of the currently emerging governance and policy landscapes, including identifying key actors, institutions, and issues that have shaped and are currently shaping the governance landscape thus far. Finally, as the current landscape remains far from comprehensively developed, the last section on "Future Directions" overviews existing proposals for the future governance and regulation of geoengineering research and technologies.

Given the nascent state of national and international discourses on geoengineering, this entry necessarily focuses as much on speculative future proposals for governance as on existing governance or policy.

This balance highlights the uncertainty – and potential for influencing future developments – that exists within the discourse.

History of Weather Modification and Governance Frameworks

While the current concept of geoengineering is relatively modern, it can be situated within a long tradition of human attempts to influence their environmental surroundings. Throughout history, mankind has imagined and fantasized about weather control; such stories have been found in myths, religious texts, traditional and cultural practices, and science fiction. Granted, the nature of weather control aligns only partially with geoengineering. Yet, its historical treatment has implications for looking at geoengineering from the point of view of antecedent governance efforts.

In practice, the attempt to manipulate atmospheric conditions had its roots in the Enlightenment vision of deconstructing natural processes for the betterment of human society. However, it was not until the nineteenth century that scientific research programs materialized in this capacity. The early weather engineers were rainmakers who proposed various physical, chemical, and electrical approaches to manipulate precipitation.

Prominent figures included James Pollard Espy (1785–1860), a US government appointed meteorologist, who actively promoted the idea of commercial rainmaking by cutting and burning forest woods. Edward Powers and Daniel Ruggles were former US generals who theorized that cloud condensation by explosive agent could lead to rainfall [4]. Other prominent figures of this "concussive" stream included Robert St George Dyrenforth (1844–1910), a lawyer from Washington D.C. who received government funding to lead such experiments, J. B. Atwater, who filed a weather patent to disrupt tornadoes, and Laurice Leroy Brown, who filed a patent application for an "automatic transporter and exploder for explosives aiding rain-fall" [4]. Instead of engaging in serious science, rainmakers of the era often sought to defraud desperate farmers. A famous example was Charles Hatfield, who evaporated chemicals to "coax(ed) rain from the sky" [5]. Projects of the age were backed by poor theory, speculative knowledge, and insufficient financial support; and regulatory frameworks were largely nonexistent.

Whereas agriculture interests were the primary driver for nineteenth-century weather controlling schemes, research into weather control during the two World Wars was supported mostly by military patronage as well as some corporate financial support. Aerial fogs and vapors impeded forward visibility of troops and bombing raids, and the escalation of World War II called for immediate scientific attention. In 1940, Britain created the Petroleum Warfare Department (PWD) and charged it with the task of developing a reliable method of clearing fogs called the Fog Investigation and Dispersal Operation (FIDO), the project brought together scientists, engineers, industrialists, and policy makers under one umbrella. With FIDO, the British and Allied air forces were able to assume normal military activities as the Germans were bound to the ground. Despite its success as a wartime invention, FIDO ultimately proved to be too costly to be commercially viable [4]. However, this complex of interests carried over to the Cold War, with even greater strategic interests of weaponizing weather control techniques.

The scientific foundation began in the General Electric (GE) Research Laboratory, where in 1946, Vincent Schaefer and Irving Langmuir discovered a weather-control technique that used dry ice and silver iodide to "supercool" clouds [4]. Langmuir envisioned that the technology would have the potential to deflect hurricanes, generate large-scale precipitation, and clear the sky for aviation services. The confluence of military interests and GE's concerns over liability threats prompted the transfer of research to a newly established classified cloud-seeding program called Project Cirrus, a collaboration between GE, the US Air Force, the US Army Signal Corps, and the Office Naval Research. Cirrus resulted in more than 250 trials and experiments during 1947–1952, but was canceled due to tort liability lawsuits [4]. Project Stormfury, successor to Cirrus and operational from 1962 to 1983, was another collaboration between the Weather Bureau and the military in exploring cloud-seeding experimentation.

During the Vietnam War, Operation Popeye, a clandestine field trial of cloud seeding was conducted along the Ho Chi Minh Trail to stonewall traffic. With support from the US administration, a much larger scale program known as Operation Motorpool, covering areas over Laos, Cambodia, North and South Vietnam, ran until July 1972 [6]. Similarly, French

forces also attempted artificial rainmaking to impede the movement of Vietnamese troops; not to mention the frequent practice of cloud seeding by Moscow in the 1950s and the 1960s.

The fact that many of the research and trials remained in the domain of military operations shielded them from public criticism and regulatory oversight. Therefore, despite scant court cases on the tort liability of cloud-seeding experiments, no statutory laws were erected to regulate weather modification during the interwar period. However, when a story about the operations in Vietnam broke in the Washington Post in March 1971, it became a public relations disaster that led to pressure from members of the Congress on the Nixon administration to cease the operations. The efforts to ban environmental warfare were led by Senator Claiborne Pell in the Senate and Representative Donald M. Fraser in the House, leading to the passing of numerous bills in 1975 that sought to prevent the weaponization of weather modification [4].

The Soviet Union was quick to respond to the "Watergate of weather warfare." First, it invited the Nixon administration to sign the "Joint Statement Concerning Future Discussion on the Dangers of Environmental Warfare" at the Moscow Summit in 1974 [7]. It then presented the United Nations with a proposal to establish an international convention to outlaw weather modification as a weapon of war. This diplomatic initiative caused the Ford administration to commit the USA to the negotiation and eventual signing of the Convention on the Prohibition of Military or Any Other Hostile Use of environmental Modification Techniques (ENMOD), which banned all militarized environmental modifications with "widespread, long-lasting or severe effects as the means of destruction, damage or injury to any other State Party." ENMOD went into effect in October 1978 with 70 state members. However, the treaty was viewed as deeply flawed: It contained vague texts, established a high threshold for violation, and did not prohibit research and development in the field, which made the treaty almost unusable [4]. Nonetheless, the ENMOD treaty has still been discussed as potentially applicable to certain geoengineering techniques due to the potential for detrimental transboundary impacts [8–11].

Despite limited scientific evidence of success over the past half-century, the turn of the century still witnessed governments in drought-prone countries resort to cloud-seeding techniques to enhance precipitation. During the 2008 Summer Olympics, Beijing deployed over 1,000 rain dispersal rockets to prevent rain during the opening and closing ceremonies [12]. Over the summer months of 2010, the Abu Dhabi government commissioned an $11 M project that used ionizers to generate storms [13].

The boundary between what constitutes weather modification (*a single nation attempting to modify their own weather*) versus geoengineering (*sufficiently large modification of the atmosphere to have significant transboundary impacts*) currently remains ill defined – and, for the moment at least, uncontested. However, the potential for both evolving weather modification and geoengineering experiments to encroach on this boundary points to the importance for effective governance of understanding the above history. In the long tradition of weather modification, human civilization has largely bypassed the ethical, social, and legal dimensions of the issues, rendering much of its governance and legislative aspects unresolved to the present day. Yet, the nature and magnitude of weather modification efforts to date are child's play compared to the potential for some geoengineering technologies to generate impacts over much larger areas and timescales. Thus, the historical incapacity to regulate atmospheric interference causes concerns that geoengineering research will demonstrate a repeat of the same evolutionary pattern.

Geoengineering Technologies and Governance Challenges

Distinguishing Carbon and Solar Geoengineering

Geoengineering is a blanket term that encompasses a suite of very different techniques for intervening in the climate system [14]. In designing effective governance arrangements for different geoengineering technologies and research, it is therefore crucial to take account of the differences between them. Moreover, as these technological constructs will themselves evolve with time, governance frameworks need to be adaptable to addressing their possible evolution as research progresses in climate science and geoengineering. What follows is a basic description of prominent geoengineering methods that have been envisaged to date, including identification of the various technical and social uncertainties surrounding each.

The broadest differentiation of prominent geoengineering technologies is between *carbon* and *solar* geoengineering, which tackle the climate challenge from very different directions. Through removing excess carbon from the atmosphere, carbon geoengineering (*also called carbon dioxide removal or CDR techniques*) aims to treat the *cause* of climate change by removing carbon dioxide already in the atmosphere. Solar geoengineering (*also known as solar radiation management or SRM techniques*), on the other hand, aims to reflect incoming solar radiation before it is absorbed by Earth's atmosphere, surface or oceans. This strategy aims to offset the energy imbalance created in the Earth's climate by greenhouse gasses trapping outgoing infrared radiation, thereby avoiding or reducing the anticipated "global warming" from that imbalance.

The actual technologies being proposed to implement either carbon dioxide removal or solar radiation deflection vary significantly. Carbon geoengineering, for example, can be broken down into two subcategories: engineered and ecosystem. The prominent techniques in these categories differ in ways that would suggest the requirement of very different arrangements for their effective governance. The most studied engineered technique is *direct air capture*, which would utilize machines (the size of large buildings) that draw in ambient air, chemically remove carbon dioxide from it, and store that carbon somewhere for a very long time [15]. On the other hand, the ecosystem carbon geoengineering technique that has garnered the most attention from scientific and environmental governance communities is ocean fertilization, which is premised on the enhancement of a process of CO_2 removal that already exists in nature. With ocean fertilization, nutrients (of which iron is most often discussed) that limit the growth of organisms such as algae and phytoplankton are added to the oceans to stimulate the growth of these species. These organisms require carbon to live and grow which they fix from the atmosphere, and when they die they sink and eventually sequester the carbon in deep ocean sediments [16].

Solar geoengineering tackles the climate challenge from a different direction, focusing instead on attempting to enhance the albedo of the planet. Notable options for achieving this include launching mirrors into space to reflect sunlight before it reaches the atmosphere, brightening clouds by spraying a mist of cloud condensation nuclei (fine particles) into the lower atmosphere, and injecting reflective aerosols such as sulfates [17] – or possibly synthetic variants made of nanoparticles [18] – into the stratosphere. Space mirrors remain presently unfeasible at scale, while the most prominent cloud brightening technique would use globally distributed oceangoing vessels to remove sea salt from the water below them and spray it into the air above [19]. Stratospheric aerosols are perhaps the most plausible solar geoengineering method thus far proposed, in part because they mimic a natural process that is known to cool the planet significantly – large volcanic eruptions which send sulfate aerosols high into the stratosphere for a period of about a year. Delivery methods for distributing aerosols in the stratosphere include balloons, guns fired from ground level, and airplanes [1].

At this early stage of technical research and development, it is important that governance frameworks be developed with recognition that the technicalities of hypothesized geoengineering methods will evolve significantly. To date, most concepts remain largely theoretical, with the technologies for deployment not yet having been developed or demonstrated. Over the coming decades there will assuredly be changes to these proposals. Some may be scrapped and forgotten, and new ideas will emerge. As a result, the early arrangements for governance would best be made flexible to these future developments, whatever they happen to be.

Nonetheless, governance assessments of geoengineering have emphasized that uncertainty about future technologies should not be an excuse for complete inaction today, as there is a great deal of information that can be teased out of prior geoengineering research – and relevant precedents for other evolving technologies – that can guide near-term governance efforts [20]. For one, it has become apparent that some techniques could be extremely inexpensive and yet have the ability to significantly impact climate on a global scale [21]. Take, for example, stratospheric aerosol injection, which may be able to cool the planet by multiple degrees centigrade over a timescale of a few years at a cost of a few billion dollars per year [21]. The technologies necessary to develop this capability are relatively simplistic by modern standards, and more than likely could be developed by a small group of actors [22, 23]. On top of this, deployment has the potential to be carried out

clandestinely given the relatively small amount of aerosol loading required and deployment of this kind would impact the globe, with potentially severe side effects for some human and natural systems. Clearly, with this type of scenario, there is a near-term need for suitably tailored governance.

Despite the negative connotations of geoengineering in the previous example, the large consequences that will likely be faced if climate change is under addressed by insufficient mitigation efforts suggests that geoengineering research may be a prudent investment. If this is the case, there may be a need for near-term governance frameworks for geoengineering research to foster open and collaborative research projects aimed at uncovering whether or not there are techniques that might be worthy of deployment should dangerous climate change appear unavoidable [22].

Research Stages

Research into geoengineering, some of which is already ongoing in the absence of such a governance framework, will follow a predictable set of stages beginning with basic theory and modeling [1]. Understanding stages and categories of research, along with challenges and impacts they may pose, could be a starting point for establishing governance by pointing out which types of activities deserve governance attention, which do not, and therefore at what point in the future a legitimate system of research governance must be put in place . See Table 1 for further detail on different categories of research and the potential governance issues they raise.

The first two stages of research do not involve the release of substances into the environment – they involve strictly lab-based activities. Thus, in the eyes of many, governance of these stages is not warranted – any restriction on these activities would not directly protect the environment or citizens from harm, and likely would be very difficult to enforce because geoengineering research at these stages appears (and could even be disguised as) very similar to other kinds of research such as climate science, meteorology, volcanology, etc. However, other perspectives hold that even these early stages of research will have important path-dependent impact of the types of technologies that evolve and are eventually used, and thus need to be incorporated into broader governance frameworks – even if only through broader discussions of the implications of certain research directions. Moreover, issues of technology ownership and transparency of research activities are directly raised at this stage – both of which are at the core of most evolving geoengineering governance proposals.

The two latter stages of research involve an intentional release of substances into the environment of some kind. Small-scale field studies are defined as having a negligible environmental impact and for this reason there is justification of some reticence regarding strict regulation as these activities would not have transboundary effects, nor would their effects be climatically relevant. Examples might include testing the effectiveness of a nozzle for spraying sulfate particles. To many within the field of geoengineering science, a key governance question is where to define the threshold between negligible and nonnegligible, as this ought to be the point where governance restrictions kick in. Unfortunately, as long as the threshold between negligible and nonnegligible remains difficult to define, this stance toward governance may be problematic to implement.

An alternative viewpoint worthy of mention sees research stages as irrelevant. Proponents of the "slippery-slope" notion hold the view that early stages will increase dramatically the likelihood of eventual deployment and thus are nonnegligible and should themselves be subject to regulation [11]. This argument raises an important set of questions: Is geoengineering research unique? Ought it to be treated like chemical weapons and other kinds of research that have obviously dangerous consequences that make their restriction critical even at early theoretical stages? Can and should geoengineering researchers be trusted? Where in all of this do the widely held value of scientific freedom, and the commitment to the scientific search for truth fit? These are difficult questions that can foster conflict between alternative viewpoints rooted in different ethical perspectives.

Issues

Sociopolitical Linkages Geoengineering requires a highly nuanced governance approach to accommodate the various impacts of research, development, and possible deployment. Unfortunately, thinking of geoengineering in and of itself is not necessarily helpful for governance – in fact, this perspective could be

Geoengineering Policy and Governance Issues. Table 1 Geoengineering research stages

Stage	Description	Challenges	Status	Direct environmental impact
1. Theory and modeling	Publications and computational models studying the anticipated climatic impacts of geoengineering techniques	International cooperation, research funding, and development of more comprehensive models	Studies began more than 20 years ago and continue for both carbon and solar technologies	None
2. Technology development	Design and laboratory development of geoengineering deployment technologies	Emergence of governance issues when technologies are patented or classified. Who has access to and control over new technologies?	Many carbon geoengineering technologies are currently under development	None
3. Subscale field testing	Feasibility testing of geoengineering deployment technologies at levels posing "demonstrably negligible" environmental and transboundary risks	Evaluating risks and modeling uncertainties related to the environmental impacts of field testing	Limited recent tests of atmospheric aerosol injection and ocean iron fertilization have taken place	Small, regional, temporary (negligible)
Difficult to define threshold				
4. Climatic impact testing	Testing the global climate impacts of geoengineering deployment, nominally at scales below actual deployment, but with notable transboundary environmental impacts	Environmental and governance challenges of experiments spread unevenly at local, national, and regional levels. Definition of large scale	A few, limited proposals for this kind of testing to begin soon	Potentially global and large (nonnegligible)

damaging to the design of a successful governance regime because geoengineering is tied inexorably to many other issues. Prudence dictates that these linkages should be accounted for in discussions and deliberations of geoengineering governance challenges.

The climate regime is the most obvious and fundamental decision-making structure with which geoengineering governance must be intimately tied. Further potential need for geoengineering can be seen as proportional to the lag in progress toward mitigation, and related to limited progress toward (or capacity for) adaptation. With their successes and failures, as well as the progression of geoengineering research from theory to practice, the potential future role of geoengineering will become clearer. For this reason it appears important to meaningfully link decision-making structures that dictate responses to climate change – whether they be mitigation, adaptation, or geoengineering based.

Another importantly linked issue is that of the economic and social development of least developed nations. The largest impacts of both climate change and geoengineering are likely to be felt by the poorest communities of the world, leading to an important question of how their needs should be addressed [24]. Another tightly linked issue area is that of international security, as both climate change and geoengineering research or attempts at deployment could have destabilizing geopolitical effects [25]. Such linked issues – also currently including agriculture and food

security – are likely to only grow as geoengineering becomes a more well-defined proposition. Air pollution could also be a future candidate because the injection of sulfates into the stratosphere is one of the prominent techniques proposed. The line between stratospheric and tropospheric sulfate could blur in the future – in fact some people have already begun to examine the dichotomy between costly decreases of sulfur emissions over the oceans from ships which do little to improve human health, yet increase warming through reducing cooling tropospheric sulfate aerosols in ways that may accelerate the danger to societies and ecosystems from climate change [26]. This suggests there may be legitimate reasons to coordinate air pollution and geoengineering governance regimes in some respects as well.

There are additional questions regarding post-deployment governance that while far off, must be agreed upon well in advance of deployment and almost assuredly before any large-scale field-testing is underway. The tough governance questions raised by the prospect of having winners and losers – some nations that benefit more from a geoengineering intervention than others, to the point where some areas could face serious negative side effects while others reap tangible benefits from climate change avoidance – are prime examples of this.

Ethics Those who decide whether or how to utilize geoengineering in response to climate change will wield a tremendous amount of power. The expansive normative and ethical implications of such decisions are the core reasons why geoengineering is such a controversial topic, even in its current formative stage. Though seemingly unwieldy, such far-reaching questions can be teased into a number of more precise ones for understanding the implications for governance of the ethical issues entangled in the prospect of geoengineering our climate.

One example is the question of informed consent. Geoengineering resembles the concept of an experiment being performed on the entire global population [27]. Much like experimental medicine, it would be performed in order to avoid a larger problem; however, there is potential for severe negative side effects that could be very damaging. In medical scenarios, informed consent from the patient is required to carry out treatment. However, in the example of geoengineering, this is impossible: One cannot procure informed consent from everybody on the planet. Implementing geoengineering and large-scale tests of geoengineering methods necessitates a decision-making structure that is remarkably inclusive. Unfortunately, the degree of inclusivity required to make such an experiment ethically acceptable will always be a highly controversial question in and of itself.

There is also the question of liability if something goes wrong. In a scenario where unintended negative side effects are felt by one group of stakeholders, there will certainly be finger-pointing. A successful governance regime will have well-defined courses of action to deal with liability and compensation issues in place well in advance of any large-scale testing [11]. Actors currently engaged in geoengineering discussions today should pay close attention to their personal responsibilities and actions, and how they may be relevant to future liabilities. Scientists in the early stages of research who are pushing for field-testing, as well as those who speak out proposing a ban on all research, should acknowledge the influence that such stances can already have in dictating the future of geoengineering research and development.

These examples are a few of the many ethical issues that arise when geoengineering (both research and potential deployment) is considered. They tend to stem from a small group of high-level concerns. One is the issue of intent. Though humans have been changing our environment for centuries, the scale and intent of this incarnation is different, [28] and intentionality in most moral (and legal) constructs brings with it added responsibility and liability for wrongdoing or negligence. Another issue for many who are skeptical of geoengineering's acceptability is that it is a technologically based fix to a problem caused in large part by the use of other powerful technologies. People with this viewpoint see climate change as a problem requiring behavioral changes – not technical solutions – to ultimately solve. Finally, there is the high-level question of who decides [1]. This brings up issues of informed consent, global participation in the decision-making process, the importance of collaboration, the primacy of the interests of the most vulnerable among us, and many others.

Current Governance Landscape

As the subject of climate intervention technology has gained attention within the scientific community, public debates on the topic have grown in their legitimacy and significance. As a result, the constellation of actors involved has also grown to encompass an array of groups and individuals within the public and private sector, government and NGOs, foundations, private philanthropists, and firms [29]. In spite of the diversity of interests at play, most actors to date have presented arguments somewhere in between the extreme poles of either aiming to have geoengineering implemented in some fashion, or aiming to establish a full moratorium on deployment of the technology.

The recent expansion of attention to geoengineering was nucleated by a landmark 2006 article by Nobel Laureate Paul Crutzen [17]. Within a few years, the emerging attention prompted the UK Royal Society and the US National Research Council to explore geoengineering, and issue reports calling for geoengineering research, and a joint statement by the G8 + 5 nations included a call for an international meeting on geoengineering [30–32]. Policy statements calling for research into climate engineering have also emerged from the American Meteorological Society, the American Geophysical Union, and the UK Institution of Mechanical Engineers [33–35]. Each of these documents emphasized the primacy of reducing GHG emissions, but recommended developing conventions for the scientific community and the blueprints for a formal geoengineering governance framework. The Royal Society concluded:

- Little research has yet been done on most of the geoengineering methods considered, and there have been no major directed programmes of research on the subject. The principal research and development requirements in the short term are for much improved modelling studies and small/medium scale experiments (e.g. laboratory experiments and field trials). Investment in the development of improved Earth system and climate models is needed to enable better assessment of the impacts of geoengineering methods on climate and weather patterns. . .as well as broader impacts on environmental processes [30].

Prompted by the increasing scientific attention to these issues, committees of the UK Parliament and US Congress released their own reports on geoengineering [36]. Both bodies explored related issues in a series of science and technology hearings on the subject, and reached conclusions endorsing increased research into emerging geoengineering technologies. As an important indicator of concern for the international dimensions of geoengineering research and technologies, the UK Parliament and US Congress organized their hearings jointly, allowing testimony, documents, and reports from each other's hearings to be presented in their own. This is the first, and thus far only, time in history that such an arrangement between the UK and US legislative bodies has been used.

Government funding for geoengineering research is currently scarce in the US, where scientists rely primarily on private philanthropy and redirected federal research grants. Some researchers have argued that a delay in establishing a federal program will make it progressively harder for the US government to guide these efforts in the public interest as the dialogue continues to move rapidly forward [37]. Elsewhere, public funding has been gradually forthcoming. Both the UK and the European Union have recently provided preliminary grants to a few moderate research projects [38–40]. Small, government-funded projects using computer models are also underway in Germany, [41] and Russia has already conducted at least one geoengineering field test [41]. Nevertheless, a document from the UK Parliamentary Office of Science and Technology conceded:

- There is currently very little public funding specifically earmarked for geo-engineering. Despite a US Department of Energy White Paper (Unpublished) that in 2001 recommended a $64 M, five-year programme, less than $1M of public money is currently directly funding geoengineering research in the USA. In the UK, the Engineering and Physical Sciences Research Council (EPSRC) has proposed a £3M "Ideas Factory" commencing in 2010. To date, therefore, most research has been either funded using existing climate science grants or has been unfunded, performed in researchers' spare time [42].

The same report posited that an international research program of $100M would significantly increase the scientific and engineering knowledge, as well as provide greater understanding of the risks

associated with altering climate system. (Also in March 2009, the UK's Royal Society proposed that a $200 M international fund be established for research into geoengineering [43].)

Much of the present funding for geoengineering research comes from the private sector. Leading organizations such as Environmental Defense Fund, Novim Group, and Climate Response Fund rely on the philanthropy of private donors. Even billionaires Bill Gates and Richard Branson have also brought money to bear on geoengineering research. (Since 2007, Gates has put at least $4.5 M into the Fund for Innovative Climate and Energy Research [44, 45] and Branson offered a $25 M cash prize rather than a research grant, which went unendowed [46]). To date, despite significant concerns that vested fossil fuel interests may back geoengineering technology development, there remains no evidence that corporations and industries standing to benefit from continued GHG emissions are investing publically in geoengineering research [47, 48].

A group of corporate actors did emerge in the mid-00s with the goal of generating carbon credits to sell from using ocean-fertilization techniques. Ocean fertilization company Planktos' plan to sequester carbon dioxide through a release of iron filings into the Pacific Ocean was blocked by a petition to the EPA by environmental groups invoking the Marine Protection, Research, and Sanctuaries Act (the "Ocean Dumping Act"). Though Planktos attempted to flout the regulation by using a vessel flying under a different national flag, a lack of investors forced the company to abandon the project [49].

As a consequence of such activities, the International Maritime Organization (IMO) became engaged in the governance of iron fertilization projects. (In July 2007, EPA dispatched a memo to the IMO revealing that Planktos intended to proceed with its planned project without the permit required under the Marine Protection, Research, and Sanctuaries Act (the "Ocean Dumping Act"). The document informed IMO that Planktos, opting not to fly a U.S. flag, would be able to avoid U.S. regulations. EPA with no power to regulate advised the member states of the London Convention to carefully evaluate Planktos' plans.) Following an IMO statement issued in 2007 and a report on iron fertilization drafted in 2008, a resolution was made in 2008 at the London Protocol and Convention on the Prevention of Marine Pollution by Dumping of Wastes and Other Matter that "ocean fertilization activities, other than legitimate scientific research... should be considered as contrary to the aims of the Convention and Protocol and do not currently qualify for any exemption from the definition of dumping" [50–52].

To assess the research and governance challenges of geoengineering, the Climate Response Fund (CRF) organized a conference of nearly 200 experts in various scientific and policy disciplines, which gathered at historically resonant Asilomar in 2010 (the site of a prior 1970s conference on genetic recombination). Created in 2009, CRF was established in order to fund geoengineering research projects and work with national and international partners to communicate information about geoengineering research (*referred to as climate intervention research*) to interested groups and the general public. Asilomar conferees set out to develop a set of voluntary guidelines, or best practices, for the least harmful and lowest risk conducting of research and field-testing [53]. The meeting brought together social and natural scientists to deliberate about geoengineering governance, in a tentative first step toward international dialogue between scientists and nonscientists on principles for future research [54, 55].

The Royal Society also maintains a strong leadership role in the continuing climate engineering discourse. Building from its 2009 report, and in partnership with the Academy of Sciences for the Developing World and Environmental Defense Fund, the Royal Society launched the SRM Governance Initiative (SRM-GI) in March 2010. It aims to develop regulatory frameworks and best practices for the research and possible deployment of SRM technology [2]. SRM-GI remains as an advisory body for international organizations and national governments engaging in the debate, bringing together scientific and policy experts to provide guidance for the conduct of research, and incorporating input from a number of civil society stakeholders.

Opponents to geoengineering have also put forth initiatives to try and prohibit or otherwise hinder its advance. The Action Group on Erosion, Technology and Concentration (ETC Group), a Canadian NGO,

has led the organization of the "Hands Off Mother Earth campaign" for a moratorium on real-world geoengineering experiments or deployment (The ETC group turned down it's invitation to the Asilomar Conference on Climate Intervention Technologies and attempted to mobilize opposition against the summit. ETC Group, "Open Letter to the Climate Response Fund and the Scientific Organizing Committee," http://www.etcgroup.org/en/node/5080) [56]. This campaign lobbied the Convention on Biodiversity at its 10th Conference of Parties in 2010, contributing to a decision establishing qualifications on the scope of field tests and deployment [57]. The nonbinding resolution stated that:

- No climate-related geo-engineering activities that may affect biodiversity take place, until there is an adequate scientific basis on which to justify such activities and appropriate consideration of the associated risks for the environment and biodiversity and associated social, economic and cultural impacts, with the exception of small scale scientific research studies that would be conducted in a controlled setting in accordance with Article 3 of the Convention, and only if they are justified by the need to gather specific scientific data and are subject to a thorough prior assessment of the potential impacts on the environment [58].

Meanwhile, the Intergovernmental Panel on Climate Change in 2011 held scoping meetings for the inclusion of geoengineering in its 2013–2014 Fifth Assessment Report (AR5).

Future Directions

The attempts of a nascent landscape of governance actors to assess and regulate geoengineering (see the section on "Geoengineering Technologies and Governance Challenges") faces a complex of ethical, social, and political concerns and the diversity of potential future technological options (see the "Introduction" section). This section outlines a variety of proposed and potential governance options, as well as their capacity and adaptability to confront current and future issues. Some of these proposals – such as the SRM Governance Initiative (SRM-GI) fostering broader international dialogue and decisions at the CBD and London Convention, both discussed above – are already in play, although their longevity and impacts on governance remain uncertain. Most options remain proposals as yet unexplored in depth. Although there are many ways to categorize the range of proposals, most assessments have tended to characterize governance mechanisms primarily by the level and locale of authority [9–11, 59]. Accordingly, discussion of proposed governance frameworks here are divided into the categories of: (1) Nonstate, (2) National and Minilateral, and (3) International, or treaty-based varieties.

Nonstate Frameworks

These tend to emphasize nonbinding guidelines and other forms of soft law, and possess a degree of autonomy from government regulation. They are also intended to engage a transnational range of nonstate actors: researchers and private sector developers of technology, with varying degrees of public participation and feedback. Proposals range in regulatory strength and organizational complexity from an absence of regulation, to informal and ad hoc peer regulation, to professional or institutional codes of conduct. For the lattermost option, it has been suggested that research standards could be cohered by a network of research institutes or an international geoengineering research organization [59].

Variations of self-regulating standards, albeit with broad societal input, have traction among many early proponents of further research, and have also received support from more reserved actors that nonetheless see the need for further exploration of the technology and its attendant issues and impacts. A number of the leading scientific voices driving the development of geoengineering technologies and debate were key participants in the Royal Society's SRM-GI and Asilomar II (David Keith and John Shepherd are two examples pointed out by Banerjee [9] p20). The Royal Society's 2009 report recommends that it should itself partner with international scientific bodies to derive best practices and transparency mechanisms for research [30]. Meanwhile, Asilomar II was itself modeled on the first Asilomar meeting's normative thrust toward self-regulation [53].

Among social scientists, Victor argues that bottom-up norms and assessments formed by the collaborations of international science organizations and research groups actively engaged in the debate represent a more flexible and evolutionary governance mechanism than existing international treaties. Such an option might be "an active geoengineering research programme, possibly including trial deployments, that is highly transparent and engages a wide range of countries that might have (or seek) geoengineering capabilities." Victor adds that "[s]imilar approaches have been followed in other international scientific collaborations that have had potentially hazardous side effects, such as the European Organization for Nuclear Research (CERN) and the Human Genome Project" [59].

The benefits of such codes of conduct center around their relevance to the immediate activities of the geoengineering research community. Most notably, such codes of conduct enable responsible exploration of scientific questions that require significant research in order to guide the development of responsible governance frameworks. Moreover, as they would be driven by a more homogeneous range of actors and could potentially remain free of geopolitical motives, self-derived and imposed codes of conduct for research would likely be much easier to negotiate and swifter to implement through transnational scientific institutions. Finally, soft guidelines may have great flexibility to adapt to evolutions in the debate than rigorously negotiated international agreements [59].

There are, however, drawbacks to this approach. Depending on the extent and severity of the code, a voluntary system raises the important issue of noncompliance, particularly by actors operating outside of publically peer-reviewed scientific literature – such as private actors or clandestine government programs. Moreover, while many researchers support some form of public input, it is uncertain what effect the inclusion of more oppositional civil society groups might have on a code of principles, or on the subsequent desire of researchers and technology developers to be restricted by them. Nonetheless, if research codes forego public participation or government oversight, there may be a backlash that questions the legitimacy of the process. Codes of conduct are also most amenable to the current phase of laboratory research, and potentially – though ambiguously – in small-scale field-testing, when impacts and controversies are limited and more easily defined. However, they will almost certainly prove less effective or relevant to large-scale testing or deployment, as the entry of governmental agendas into governance may render self-regulation obsolete. Finally, there is the basic question of whether some of the actors most in favor of geoengineering should be allowed to formalize the first principles on its regulation.

National and Minilateral Frameworks

The potential for national regulatory frameworks has received the least attention in both academia and policy prescription. Hypothetically, the accepted legal mandate and enforcement capacities (within its own borders) of developed states makes governmental regulation a strong candidate for creating legally binding strictures at all stages of technology development. Besides national-level legislation or regulation, governmental legal frameworks could take a variety of forms. Within federal structures, subnational levels of government (municipal or provincial, with networks thereof) could enact legislation at a level below the state, and might feasibly network across national borders. There is also the possibility for states to cooperate on geoengineering development and regulation on a minilateral basis – a club-based approach that eschews the complications of universal participation in international frameworks.

Few of these options have been discussed in detail, likely because governments have thus far been hesitant to take strong positions on an issue whose controversies – and resulting political blowback – cannot be accurately predicted [47]. SRM-GI and Asilomar II have both noted the need for governments to scope their positions on geoengineering, and the eventual need for state-led oversight mechanisms [60]. Although no governments have formulated a clear position, the initial scoping efforts by the USA and the UK demonstrate the possibility that domestic legal frameworks will be developed. (See, for example, [61]. For example of hearing, see [62] or [63]). Besides

the creation of novel legislation, Hester notes that existing national environmental and air pollution laws and agencies, such as the Clean Air Act and the Environmental Protection Agency in the USA, might be reoriented to regulate the emissions of materials upon which geoengineering initiatives depend (e.g., sulfate aerosols) [49].

A government-focused array of prescriptions could capitalize on the ability of developed states with strong bodies of environmental law and regulatory capacities to create and enforce geoengineering legislation. Such an approach would also uphold the principle of sovereignty, potentially avoiding the problems inherent in determining the extent and form of collective action. Initial actions taken by states also could serve as testing grounds for regulatory measures, societal debate, and building blocks for the negotiation of a more comprehensive framework at the international level. Even if the state proves hesitant to regulate geoengineering, action could also begin at the subnational levels in federal structures.

However, the efficacy of state regulation also relies on the strength and coherence of its own structures. While states of the OECD could legitimately enact strong rulings, it is difficult to forecast how many capacity-deficient states would be able to follow suit. Federalism may be a double-edged sword, as conflicts of interest between the national and subnational levels of government may emerge. Moreover, there are many issues buried in the logic of unilateralism, especially in the development of novel and risky technologies. If states move actively to develop and deploy geoengineering technologies without multilateral consultation, a geoengineering "race" could begin. This could in turn entrench technological know-how, with first-movers maintaining a lead on latecomers. It is possible that an incentive to act early on technology development and to maintain a technological advantage would emerge, and that contestations over intellectual property rights and ownership would follow. Finally, the uncertainty of the transboundary impacts of large-scale field-testing or deployment makes governance options that rely on the good intent of sovereign states, at the least, a controversial prospect [22, 64, 65]. (It is worth, however, noting the arguments of Horton [69], that the dangers of unilateralism are overstated, and that there are rational incentives for states to collaborate on geoengineering development and regulation.)

International Frameworks

Existing analyses of and proposals for international governance of geoengineering have tended to focus on ways existing international environmental agreements (IEAs) and organizations (IOs) might be "co-opted" to address the core governance issues. These explorations have focused particularly on IEAs and IOs whose mandates either regulate materials that are components to forms of geoengineering, or impact geoengineering more broadly.

A number of academic studies have mapped out the potential intersections of geoengineering regulation with the mandates and the governing capacities of numerous IEAs [9, 11, 20, 47, 59, 67]. There is a general consensus that while no single IEA has a direct mandate for geoengineering or could govern it in light of all its stages of development and interdependent issues. On the other hand, many studies name treaties or organizations that could assert a regulatory jurisdiction over some aspect of the technology, or some stage of the research to deployment process. For example, stipulations of the Convention on Long-Range Transboundary Air Pollution and the International Marine Organization on sulfur emissions limits might be used to regulate solar engineering testing or deployment [10, 11]. The Montreal Protocol might be called upon to fulfill a similar function should sulfate be proven to be an ozone-depleting substance. (Tilmes et al. [71] demonstrated with laboratory research that sulphates deplete the ozone layer, but corroborations are ongoing and the item has not made it onto the agenda of the Montreal Protocol.) For carbon engineering, the Law of the Sea convention might similarly be used to regulate ocean fertilization, as the London Convention and Protocol recently did [10, 11].

IOs and regimes that might address geoengineering more generally range from the UNFCCC (*as the default locus of any debate about geoengineering as a supplement to the climate issue*), to the Convention on the Prohibition of Military or Any Other Hostile Use of Environmental Modification Techniques (ENMOD), a treaty of the Cold War era that prohibits environmental

modification for military or hostile purposes. (Lin [66] notes both, with a primary focus on the UNFCCC. Banerjee [8, 9] is in favor of rebooting ENMOD's mandate to ban geoengineering as a reconceptualized form of environmental modification. MacCracken [70], on the other hand, advocates modifying ENMOD to permit certain forms and amounts of geoengineering. A host of other IOs have been cited, some quite obscure: the Outer Space Treaty, the Antarctic Treaty System, etc. See [10, 11, 20].) The Convention on Biological Diversity's 2010 decision on geoengineering field-testing was a seminal event. Although of uncertain legitimacy, efficacy, or longevity, the CBD's actions may set a precedent for other IOs to make decisions on geoengineering, with varying intents and governing capacities.

Although little discussed, a new regime might be able to govern geoengineering as a holistic issue. As a blank slate, a novel mechanism could be specifically tailored to the issues and stages unique to geoengineering. However, the international arena already suffers from a glut of IOs and IEAs [68], and the creation of a new body might create jurisdictional overlaps and competition for visibility with existing ones. Moreover, the creation and implementation of a new regime with broad participation and legitimacy is a gradual process in and of itself. Combined with existing disagreements over the myriad and evolving facets of geoengineering, as well as the near absence of governmental positionings, a drawn-out time lag for creation may make it difficult for a new multilateral body to be a source of strong regulation in the near future.

The benefits of using co-opted regimes stem from leveraging frameworks with strong capacities and legitimacy, where governance – even if it targets only one facet of the geoengineering issue – might be more quickly enacted. On the other hand, a patchwork of co-opted regimes may reveal regulatory gaps that cannot be filled, or overlaps and conflicts that cannot be mediated. A multiplicity of governance forum with no key institutional home could also create an incentive for proponents or opponents of geoengineering to forum shop at the body most amenable to their interests, creating the potential for conflicting bodies of international law. Finally, existing institutions contain established mandates, organizational structures, and political logics that inevitably calcify over time. As such, they may have neither the desire nor flexibility to adjust to an issue as novel and complex as geoengineering [20].

Bibliography

1. Blackstock JJ, Battisti DS, Caldeira K et al (2009) Climate engineering responses to climate emergencies, Novim initial study on geoengineering (Novim Study Group 01, 2009). http://www.novim.org/index.php?option=com_contentview=articleid=31:climate-engineering-responses-to-climate-emergenciescatid=1:recent-papersItemid=2
2. SRM-GI details its mission statements on its website at: http://www.srmgi.org/project-overview/
3. Asilomar Scientific Organizing Committee (ASOC) (2010) The asilomar conference recommendations on principles for research into climate engineering techniques. Climate Institute, Washington, DC, 2006
4. Fleming JR (2010) Fixing the sky: the checkered history of weather and climate control. Columbia University Press, New York
5. Goodell J (2010) How to cool the planet: geoengineering and the audacious quest to fix earth's climate. Houghton Mifflin Harcourt, Boston
6. Fleming JR (2006) The pathological history of weather and climate modification: three cycles of promise and hype. Hist Stud Phys Biol Sci 37(1):3–25
7. Fleming JR (2007) The climate engineers. Wilson Quart 31 (Spring):46–60
8. Banerjee B (2010) ENMOD squad: could an obscure treaty protect developing countries from geoengineering gone wrong?. Slate, 23 Sep 2010
9. Banerjee B (2011) The limitations of geoengineering governance in a world of uncertainty. Stanf J Law Sci Policy IV:15–36
10. Bodansky D (1996) May we engineer the climate? Clim Chang 33(3):309–321
11. Virgoe J (2009) International governance of a possible geoengineering intervention to combat climate change. Clim Chang 95(1–2):103–119
12. Xinhuanet, Beijing disperses rain to dry Olympic night. http://news.xinhuanet.com/english/2008-08/09/content_9079637.htm. Accessed 10 May 2011
13. Leigh K, Abu Dhabi-backed scientists create fake rainstorms in $11m project. http://www.arabianbusiness.com/abu-dhabi-backed-scientists-create-fake-rainstorms-in-11m-project-371038.html. Accessed 10 May 2011
14. Lenton TM, Vaughan NE (2009) The radiative forcing potential of different climate geoengineering options. Atmos Chem Phys Discuss 9(1):2559–2608
15. Keith DW, Heidel K, Cherry R (2009) Capturing CO2 from the atmosphere: rationale and process design considerations. In: Launder B, Thompson MT (eds) Geo-engineering climate change: environmental necessity or Pandora's box?.

Cambridge University Press, Cambridge/New York, pp 107–126
16. Boyd P (2004) Ironing out algal issues in the southern ocean. Science 304(5669):396–397
17. Crutzen PJ (2006) Albedo enhancement by stratospheric sulfur injections: a contribution to resolve a policy dilemma? Clim Chang 77(3–4):211–219
18. Keith DW (2010) Photophoretic levitation of engineered aerosols for geoengineering. Proc Natl Acad Sci USA 107(38):16428–16431
19. Salter S, Sortino G, Latham J (2008) Sea-going hardware for the cloud albedo method of reversing global warming. Philos Trans Roy Soc A Math Phys Eng Sci 366(1882):3989–4006
20. Blackstock J, Ghosh A (2011) "Does geoengineering need a global response- and of what kind?" Working paper of the solar radiation management governance initiative meeting, Kavli, pp 1–35, 21–24 Mar 2011
21. McClellan J, Sisco J et al (2010) Geoengineering cost analysis, contracted engineering cost analysis. Aurora Flight Services, Cambridge. http://people.ucalgary.ca~keith/Misc/AuroraGeoReport.pdf. Accessed 30 Oct 2010
22. Blackstock JJ, Long JCS (2010) The politics of geoengineering. Science 327(5965):527
23. Victor DG, Morgan GM, Apt J, Steinbruner J, Ricke K (2009) The geoengineering option. Foreign Aff 88(2):69–76
24. Suarez P, Blackstock J, Van Aalst M (2010) Towards a people-centered framework for geoengineering governance: a humanitarian perspective. Geoeng Quart 1(1):2–4
25. Cascio J (2008) Battlefield earth. Foreign Policy. http://www.foreignpolicy.com/articles/2008/01/27/battlefield_earth. Accessed 1 July 2011
26. Morton O (2009) The international maritime organisation's plans to warm the world. Heliophage. http://heliophage.wordpress.com/2009/08/20/the-international-maritime-organisations-plans-to-warm-the-world/. Accessed 20 Aug 2009
27. Morrow DR, Kopp RE, Oppenheimer M (2009) Toward ethical norms and institutions for climate engineering research. Environ Res Lett 4(4):045106
28. Keith DW (2000) Geoengineering the climate: history and prospect. Annu Rev Energy Environ 25(1):245–284
29. "Lift Off." *Economist* 4 Nov 2010
30. Shepherd J et al (2009) Geoengineering the climate: science, governance and uncertainty. The Royal Society, London
31. America's Climate Choices: Panel on Advancing the Science of Climate Change (2010) Advancing the science of climate change. The National Academies Press, Washington, DC
32. The National Academies (2008) Joint statement on climate change from G8 + 5 national science academies: climate change adaptation and the transition to a low carbon society. http://www.nationalacademies.org/includes/G8+5energy-climate08.pdf. Accessed 1 July 2011
33. American Meteorological Society Council (2009) AMS policy statement on geoengineering the climate system. http://www.ametsoc.org/policy/2009geoengineeringclimate_amsstatement.pdf. Accessed 1 July 2011
34. American Geophysical Union (2009) Position statement: geoengineering the climate system. http://www.agu.org/sci_pol/positions/geoengineering.shtml. Accessed 1 July 2011
35. Institution of Mechanical Engineers (2009) Geoengineering: giving us the time to act. http://www.imeche.org/Libraries/Key_Themes/IMechEGeoengineeringReport.sflb.ashx. Accessed 1 July 2011
36. Science and Technology Committee (2010) The regulation of geoengineering (House of Commons, 2009–2010); Rep. Bart Gordon, Engineering the climate: research needs and strategies for international coordination (House of Representatives, 2010)
37. Caldeira K, Keith DW (2010) The need for climate engineering research. Issues Sci Technol 26(1):57–62
38. Implications and risks of engineering solar radiation to limit climate change. http://implicc.zmaw.de/. Accessed 1 July 2011
39. Integrated assessment of geoengineering proposals. http://iagp.ac.uk/about-iagp. Accessed 1 July 2011
40. Engineering and Physical Sciences Research Council, "Details of Grant Ep/I-1473x/1." http://gow.epsrc.ac.uk/Viewgrant.aspx?GrantRef = EP/I01473X/1. Accessed 1 July 2011
41. Izrael YA et al (2009) Field experiment on studying solar radiation passing through aerosol layers. Rus Meteorol Hydrol 34(5):265–273
42. Parliamentary Office of Science and Technology (2009) Geoengineering research. http://www.parliament.uk/documents/post/postpn327.pdf,1
43. Royal Society (2009) Geoengineering the climate : science, governance and uncertainty. The UK Royal Society, London. royalsociety.org/Geoengineering-the-climate/
44. Fund for Innovative Climate and Energy Research, http://people.ucalgary.ca/~keith/FICER.html
45. Kintisch E (2010) Bill Gates funding geoengineering research. ScienceInsider, 26 Jan 2010. http://news.sciencemag.org/scienceinsider/2010/01/bill-gates-fund.html
46. Kanter J (2010) Cash prize for environmental help goes unawarded. New York Times, 21 Nov 2010. http://www.nytimes.com/2010/11/22/business/energy-environment/22green.html
47. Reynolds J (2011) The regulation of climate engineering. Law Inn Technol 3(1): 113–136 http://papers.ssrn.com/sol3/papers.cfm?abstract_id=1813965
48. Daly H (2011) Geo-engineering or cosmic protectionism?" Daly news, Centre for the Advancement of the Steady-State Economy http://steadystate.org/geo-engineering-or-cosmic-protectionism. Accessed 31 Aug 2011
49. Hester T (2011) Remaking the world to save it: applying U.S. environmental laws to climate engineering projects, SSRN eLibrary. http://papers.ssrn.com/sol3/papers.cfm?abstract_id=1755203. Accessed 1 July 2011
50. Intergovernmental Oceanographic Commission (2008) Report on the IMO London Convention Scientific Group meeting on ocean fertilization. Intergovernmental Oceanographic Commission (of UNESCO), Paris. http://www.jodc.go.jp/info/ioc_doc/INF/160478e.pdf

51. Resolution LC-LP.1 (2008) see: http://climate-l.iisd.org/news/imo-london-convention-parties-agree-on-moratorium-on-ocean-fertilization/
52. IMO (2010) Assessment framework for scientific research involving ocean fertilization agreed. Press release. http://www.imo.org/mediacentre/pressbriefings/pages/assessment-framework-for-scientific-research-involving-ocean-fertilization-agreed.aspx.
53. Leinen M (2011) The asilomar international conference on climate intervention technologies: background and overview. Stanf J Law Sci Policy IV:1–5. http://www.stanford.edu/group/sjlsp/cgi-bin/users_images/pdfs/61_Leinen%20Intro%20Perspective%20Final.pdf. Accessed 1 July 2011
54. Kintisch E (2010) 'Asilomar 2' takes small steps toward rules for geoengineering. Science 328: 22–23. http://www.sciencemag.org/content/328/5974/22.full. Accessed 1 July 2011
55. Kintisch E (2010) We all want to change the world. Economist 3: 81–82. http://www.economist.com/node/15814427. Accessed 1 July 2011
56. Hands Off Mother Earth, "Organizations". http://www.handsoffmotherearth.org/organisations/. Accessed 1 July 2011
57. ETC Group (2007) ETC, Gambling with GAIA, ETC Communique. http://www.etcgroup.org/upload/publication/pdf_file/ETC_COP10GeoBriefing081010.pdf. Accessed 1 July 2011
58. Convention on Biological Diversity (CBD) (2010) Biodiversity and climate change draft decision submitted by the Chair of Working Group I, conference of the parties to the convention on biological diversity tenth meeting, Nagoya, 18–29 Oct 2010, Agenda item 5.6. www.cbd.int/doc/meet-ings/cop/cop-10/in-session/cop-10-l-08-en.doc
59. Victor DG (2008) On the regulation of geoengineering. Oxford Rev Econ Policy 24(2):325
60. SRMGI report, Asilomar II, Leinert 2011
61. Borenstein S (2009) Obama looks at climate engineering. Associated Press, 8 Apr 2009. www.fas.org/sgp/crs/misc/R41371.pdf
62. Caldeira K (2009) Geoengineering assessing the implications of large scale climate intervention (statement to US House)
63. Lane L (2009) Researching solar radiation management as a climate policy option (statement to US House)
64. Victor DG et al (2009) The geoengineering option: a last resort against global warming? Foreign Aff 88:64–76
65. Robock A (2008) 20 reasons why geoengineering may be a bad idea. Bull At Sci 64:14–17
66. Lin AC (2009) Geoengineering Governance. Issues Leg Scholarsh 8 (3) http://www.bepress.com/ils/vol8/iss3/art2
67. Rayner S (2011) Climate geoengineering governance. Jahrbuch Ökologie in Press, Stuttgart, Germany. http://www.jahrbuch-oekologie.de/aktuelles_rayner.htm
68. Keohane RO, Victor DG (2010) "The regime complex for climate change," Discussion paper 2010–33, Harvard Project on International Climate Agreements, Cambridge, MA, p 5
69. Horton JB (2011) Geoengineering and the myth of unilateralism: pressures and prospects for international cooperation. Stanf J Law Sci Policy IV
70. MacCracken MC (2006) Geoengineering: worthy of cautious evaluation? Clim Change 77(3–4)
71. Tilmes S, Rolf M, Ross S (2008) The sensitivity of polar ozone depletion to proposed geoengineering schemes. Science 320:5880

Geologic Carbon Sequestration: Sustainability and Environmental Risk

Curtis M. Oldenburg
Earth Sciences Division, Lawrence Berkeley National Laboratory, Berkeley, CA, USA

Article Outline

Glossary
Definition of Subject and Its Importance
Introduction
Carbon Dioxide (CO_2) Capture and Storage (CCS): How Does it Work?
Opportunity and Capacity
Potential Impacts
Potential Impacts to Potable Groundwater
Induced Seismicity
Future Directions
Acknowledgments
Bibliography

Glossary

Carbon dioxide capture and storage (CCS) The capture of CO_2 from fossil-fuel power plants and other industrial point sources and its injection through wells into deep geologic formations for permanent storage.

Consequence An impact arising from the occurrence of an event or process. For example, the consequence of high CO_2 concentrations in the atmosphere is global warming.

Geologic carbon sequestration (GCS) = geologic CO_2 storage (GCS) The last step of CCS in which CO_2 is injected through wells into deep subsurface formations for permanent storage.

Hazard A potential impact or consequence of an event or process. For example, high CO_2 emissions are a hazard to climate because CO_2 is a greenhouse gas.

Likelihood The probability or degree of potential for an event or process to occur. For example, the likelihood of CO_2 emissions to increase is very high given population growth and worldwide increases in standard of living.

Risk The product of likelihood and consequence of an event or process. For example, the risk of climate change is very high because both the likelihood and the consequences are high.

Storage Resource (capacity) Physical pore-space volume available for CO_2 storage irrespective of economics or regulations.

Storage Reserve (capacity) Pore-space volume available for CO_2 storage including reductions accounting for economic, legal, environmental, and regulatory factors.

Definition of Subject and Its Importance

Carbon dioxide (CO_2) capture and storage (CCS) is a combination of technologies that addresses climate change by directly reducing the net CO_2 emissions arising from the use of fossil fuels as the main global primary energy source [1]. In CCS as commonly envisioned, CO_2 will be captured from flue gases at point sources such as coal-fired power plants, compressed, transported by pipeline, and injected into deep geologic formations for permanent storage (i.e., geologic sequestration) (Fig. 1).

The capture of CO_2 involves use of liquid sorbents, membranes, or other advanced materials that can extract CO_2 from a mixture of gases associated with power generation or other industrial processes in which CO_2 is often a minor component at relatively low pressure. Few such capture operations exist currently at more than the pilot scale. However, CO_2 occurs in many natural gas (methane, CH_4) fields at concentrations above those required for delivery to customers. Gas processing to remove CO_2 from natural gas has been carried out for decades, and at two gas fields nearly 2 million tons of captured CO_2 are reinjected annually for geologic sequestration [2, 3].

In power-plant capture, extraction of CO_2 can be done after combustion, so-called post-combustion capture, or during precombustion steps, which has the advantage of higher pressures and higher CO_2 concentrations [1]. There are also direct-air capture

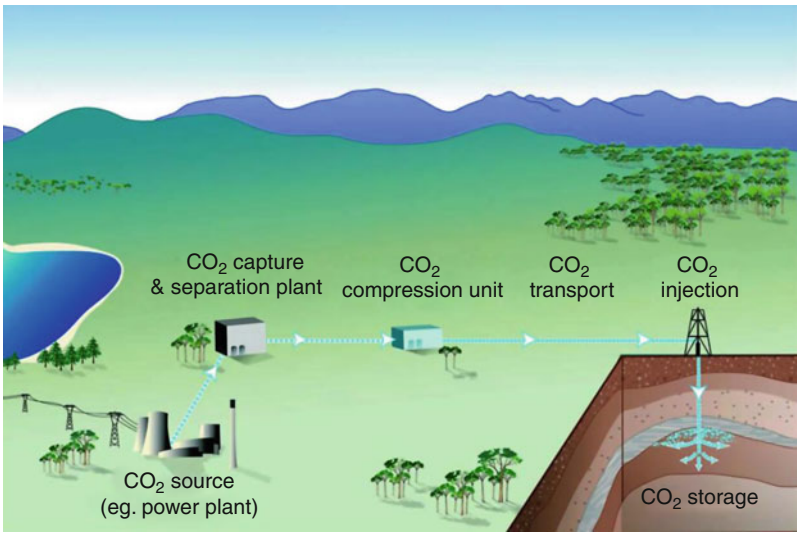

Geologic Carbon Sequestration: Sustainability and Environmental Risk. Figure 1
Schematic of the carbon dioxide capture and storage (CCS) process (CO_2CRC, http://www.co2crc.com.au/aboutccs/)

approaches for CCS that make use of solid sorbents to capture CO_2 from ambient air rather than specifically at point sources [e.g., 4, 5]. Direct-air capture has the advantage that it addresses emissions from all sources, including mobile CO_2 sources such as automobiles and trucks, but also the disadvantages of much lower CO_2 concentration and pressure.

Regardless of how CO_2 capture is accomplished, the process must be capable of providing a stream of CO_2 for compression and transport to sequestration sites. Although direct injection of CO_2 into the deep oceans has received a large amount of attention [e.g., 6], and numerous processes to accelerate uptake of atmospheric CO_2 by the oceans have been discussed [e.g., 7–9], concerns about permanence and impact to marine ecosystems are larger for ocean sequestration than for geologic sequestration [e.g., 10]. This leaves geologic sequestration as the main approach under consideration for isolating from the atmosphere the vast quantities of CO_2 that will need to be captured and stored for CCS to play a role in mitigating climate change.

The extra expense involved in capturing, transporting, and injecting CO_2 in the CCS process can be expressed in terms of an energy penalty, i.e., the amount of energy that must be expended above business-as-usual fossil fuel energy use. Estimates of the energy penalty for CCS vary over a wide range depending on combustion process, age of facility, distance to geologic storage site, etc., but are likely around 40% [1, 11]. Whether stated in terms of dollars or energy penalty, the largest expense in CCS is capture (which also includes compression), currently projected to account for more than 60% of the cost of CCS [12].

Introduction

Fossil fuels are abundant, inexpensive to produce, and are easily converted to usable energy by combustion as demonstrated by mankind's dependence on fossil fuels for over 80% of its primary energy supply [13]. This reliance on fossil fuels comes with the cost of carbon dioxide (CO_2) emissions that exceed the rate at which CO_2 can be absorbed by terrestrial and oceanic systems worldwide resulting in increases in atmospheric CO_2 concentration as recorded by direct measurements over more than five decades [14]. Carbon dioxide is the main greenhouse gas linked to global warming and associated climate change, the impacts of which are currently being observed around the world, and projections of which include alarming consequences such as water and food shortages, sea-level rise, and social disruptions associated with resource scarcity [15]. The current situation of a world that derives the bulk of its energy from fossil fuel in a manner that directly causes climate change equates to an energy–climate crisis.

Although governments around the world have only recently begun to consider policies to avoid the direst projections of climate change and its impacts, sustainable approaches to addressing the crisis are available. The common thread of feasible strategies to the energy–climate crisis is the simultaneous use of multiple approaches based on available technologies [e.g., 16]. Efficiency improvements (e.g., in building energy use), increased use of natural gas relative to coal, and increased development of renewables such as solar, wind, and geothermal, along with nuclear energy, are all available options that will reduce net CO_2 emissions. While improvements in efficiency can be made rapidly and will pay for themselves, the slower pace of change and greater monetary costs associated with increased use of renewables and nuclear energy suggests an additional approach is needed to help bridge the time period between the present and a future when low-carbon energy is considered cheap enough to replace fossil fuels. Carbon dioxide capture and storage (CCS) is one such bridging technology [1].

CCS has been the focus of an increasing amount of research over the last 15–20 years and is the subject of a comprehensive IPCC report that thoroughly covers the subject [1]. CCS is currently being carried out in several countries around the world in conjunction with natural gas extraction [e.g., 2, 3] and enhanced oil recovery [17]. Despite this progress, widespread deployment of CCS remains the subject of research and future plans rather than present action on the scale needed to mitigate emissions from the perspective of climate change. The reasons for delay in deploying CCS more widely are concerns about cost [18], regulatory and legal uncertainty [19], and potential environmental impacts [21].

This entry discusses the long-term (decadal) sustainability and environmental hazards associated with the geologic CO_2 storage (GCS) component of large-scale CCS [e.g., 20]. Discussion here barely touches on capture and transport of CO_2 which will occur above ground and which are similar to existing engineering, chemical processing, and pipeline transport activities and are therefore easier to evaluate with respect to risk assessment and feasibility. The focus of this entry is on the more uncertain part of CCS, namely geologic storage. The primary concern for sustainability of GCS is whether there is sufficient capacity in sedimentary basins worldwide to contain the large of amounts of CO_2 needed to address climate change. But there is also a link between sustainability and environmental impacts. Specifically, if GCS is found to cause unacceptable impacts that are considered worse than its climate change mitigation benefits, the approach will not be widely adopted. Hence, GCS has elements of sustainability insofar as capacity of the subsurface for CO_2 is concerned, and also in terms of whether the associated environmental risks are acceptable or not to the public.

Carbon Dioxide (CO_2) Capture and Storage (CCS): How Does it Work?

In order to understand the main environmental hazards and sustainability issues associated with GCS, the basic principles of CCS must be understood. First, CO_2 gas compresses into a relatively high-density form at the pressures and temperatures encountered below approximately 1 km in the Earth's crust. In this dense form, called its *supercritical* form because it is neither strictly liquid nor strictly gas, a larger amount of CO_2 can be stored per unit volume than if CO_2 is stored as a gas at shallower levels in the crust. The density of CO_2 at depths greater than 1 km in the crust ranges from around 600 to 850 kg/m^3 depending on the geothermal gradient. The maximum depths targeted for GCS are typically in the range of 1–4 km, with the maximum depth dictated by the economics of deep wells and the decreasing permeability of deep sedimentary rock. The density of CO_2 is nearly constant at these depths as the effects on CO_2 density of increasing temperature approximately compensate for increasing pressure in typical sedimentary basins [21]. Although CO_2 is very dense at depth relative to its gaseous form at the ground surface and can therefore be volumetrically sequestered very efficiently in the deep subsurface, it will always be buoyant relative to the native fluids (saline groundwater or brine) in the subsurface and tend to rise up through them if a flow path is available.

Second, global tectonics have created sedimentary basins on all of the continents in which sediment deposition over geologic timescales has produced thick sequences of sedimentary rock capable of storing CO_2 [22]. There is a vast amount of pore space in these sedimentary rocks arising from the imperfect packing of individual rock grains and incomplete cement filling of the space (pores) between the grains. Significant space can also sometimes arise from pervasive fracturing of the rock. In addition, sedimentary rocks commonly exist in alternating sequences of sandstones (relatively coarse-grained, with high porosity and permeability) and shales (fine-grained, with low permeability) making a configuration in which some sedimentary layers are porous and permeable and others are relatively impermeable. The fine-grained and low-permeability formations are the cap rocks that provide the upper seal for the high-porosity and permeability reservoirs into which CO_2 can be injected in the process of GCS.

Four different primary trapping mechanisms are recognized to occur in the deep subsurface to permanently sequester CO_2 [20]. These include:

1. Structural and stratigraphic trapping, which occurs when buoyant CO_2 flows up and becomes trapped against fine-grained and very low-permeability overlying cap rock often in dome-shaped structures. This same mechanism traps oil and natural gas.
2. Residual gas trapping, the process in which CO_2 bubbles are left trapped in the pores of the rock as CO_2 and water flows through the reservoir (e.g., by buoyancy forces) and water in-fills the pores previously occupied by CO_2. This is the same process that occurs in oil reservoirs as water replaces oil and prevents full recovery motivating various enhanced oil recovery approaches.

3. Solubility trapping, the process in which CO_2 dissolves into the saline water or brine in the reservoir rock. This same process of CO_2 dissolution occurs to create both natural and man-made carbonated beverages.
4. Mineral trapping, which occurs as CO_2 dissolved in the native water reacts with minerals and other dissolved constituents to form new carbonate minerals. This is analogous to the precipitation of travertine that forms in some hot (and cold) spring waters after discharge.

CO_2 injected into the deep subsurface will tend to be trapped by all four of these mechanisms in proportions that vary over time. For example, mineral trapping depends on dissolution [e.g., 23] and precipitation of mineral phases that can take on the order of hundreds to thousands of years [24, 25]. Considered together, the fractions of trapping by residual gas and solubility and mineral precipitation processes tend to increase over time, while the fraction of CO_2 trapped by structural and stratigraphic trapping decreases [20]. As sequestered CO_2 progresses over time through the sequence of structural and stratigraphic, residual gas, solubility, and mineral trapping mechanisms, CO_2 storage is considered to become more permanent over time [20].

One process that has similarities to GCS is natural gas storage, carried out at over 450 sites in the USA [26]. In this process, methane (CH_4) produced from natural gas reservoirs in one location is reinjected into depleted natural gas reservoirs or aquifer storage reservoirs for temporary storage until market demand (e.g., a cold or hot spell) exceeds supply at which time extra gas is produced from the storage reservoir. In the USA, the amount of natural gas stored is much smaller than the amount of CO_2 that is produced from fossil-fuel power plants (approximately six times less CH_4 by volume (7.5 Tcf$=1.4\times10^8$ t [27]) is stored overall than there is CO_2 produced at fossil-fuel power plants (47 Tcf$=2.4\times10^9$ t) per year). Furthermore, the natural gas storage industry uses the same reservoir for decades of injection and production cycles, whereas the GCS industry would need to continuously develop new reservoirs. So while the processes are very similar and much can be learned from the natural gas storage industry, the scale of the GCS industry will need to be much larger [e.g., 28, 29] in order for it to have an effect on climate change mitigation.

Opportunity and Capacity

As mentioned above, sedimentary basins in the USA and around the world are the primary targets for large-scale GCS [1, 22]. Shown in Fig. 2 are sedimentary basins (blue) in the USA and Canada with hydrocarbon-producing regions shown in red. As shown, there are large areas of the USA and Canada that are potential sinks for CO_2. Most of the opportunity is in sedimentary basins on the continent, but offshore opportunities are also being pursued [e.g., 30]. Economics and regulatory and environmental considerations will govern the extent to which offshore options are viable. Current efforts in North America are mostly aimed at onshore GCS opportunities, while in Europe primarily offshore opportunities are pursued.

Sustainability and feasibility of GCS are largely dependent on capacity. Evaluations have shown there is more than enough capacity to store point-source CO_2 emissions for hundreds of years or more [e.g., 1]. However, large capacity is a necessary but not sufficient condition for GCS feasibility. First, large capacity does not equate to adequate injectivity, i.e., there may be large porosity in some formations that have low permeability or are highly compartmentalized which would require more wells to inject CO_2 than the economics of a project could support. Second, capacity may not be available in close proximity to large CO_2 sources necessitating long pipeline transport distances and associated extra costs [32]. Some of this transport cost can be accommodated under reasonable projections of CO_2 storage economics, but clearly the closer the sink is to the source, the better. Finally, this discussion points out that there are two different types of capacity, namely, resource and reserve capacity [e.g., 33]. Most evaluations to date have focused on resource capacity, i.e., the total amount of pore space available regardless of where it is located or what it takes to access it. As described in the glossary, reserve capacity is the more practical measure of capacity, because it includes not only economics

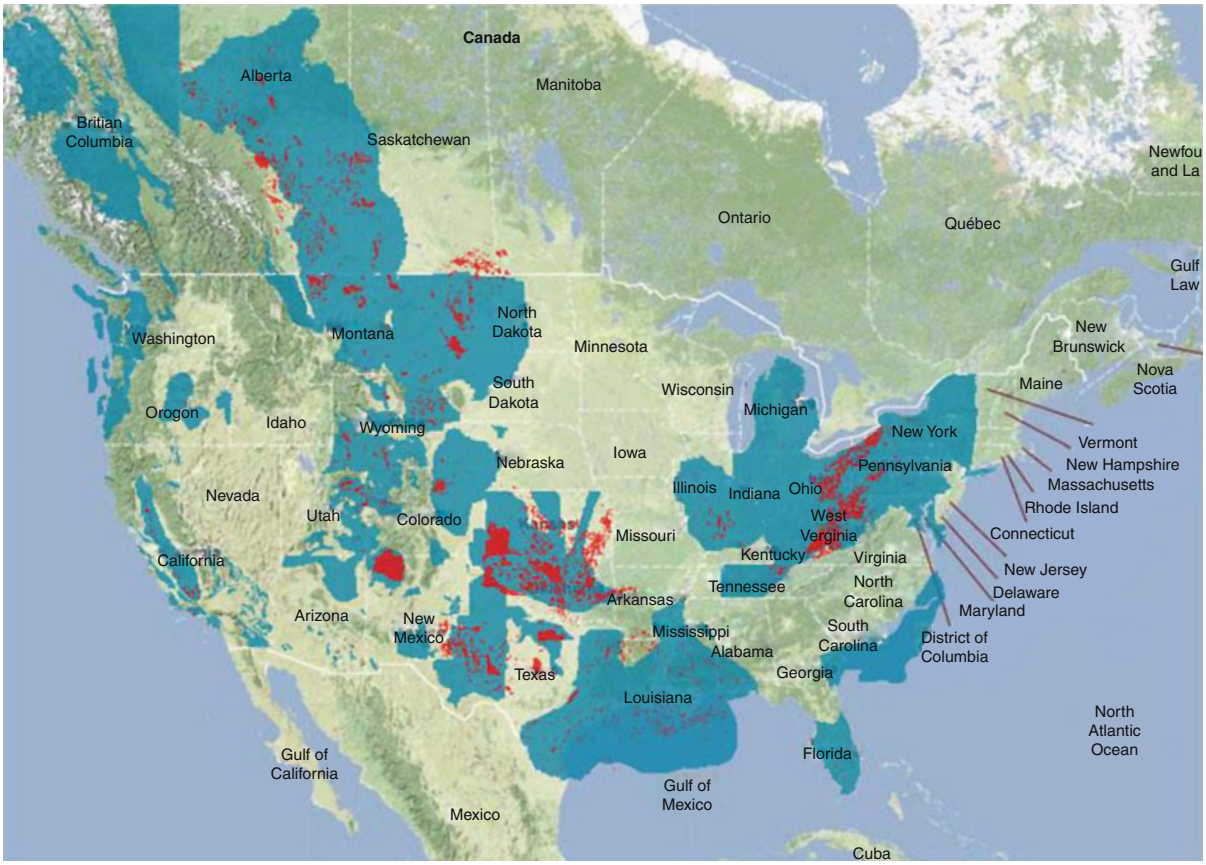

Geologic Carbon Sequestration: Sustainability and Environmental Risk. Figure 2
Sedimentary basins (*blue*) in the USA and Canada considered good targets for potential geologic storage of CO_2, with oil and gas producing regions shown in *red* [31]

but also policy, environmental, and regulatory restrictions and limitations on capacity. By this definition, reserve capacity is a fraction of resource capacity, and reserve capacity can change over time as economics or regulations change.

Although different methods to estimate capacity have led to wide variations in capacity estimates over various regions [e.g., 34], there is no doubt that there is an enormous amount of resource capacity available. In short, resource capacity does not at present appear to limit the long-term (decadal) sustainability of GCS. On the other hand, resource capacity is not the only measure of feasibility. One must take into account potential environmental impacts associated with GCS such as the possibility of groundwater contamination and induced seismicity, since the environmental risks and costs may be unacceptable to the public.

Potential Impacts

The injection of large quantities of CO_2 into the deep subsurface through wells is clearly a large perturbation to the local natural system in terms of changing the composition and pressure of the native fluids. Specifically, CO_2 will partially dissolve into the native saline groundwater or brine while also pushing these native fluids outward away from the well as a relatively fast-moving pressure wave. The deep fluid injection process is very well known and practiced widely for injection of various fluids today [19, 26, 35] – and the reverse, production of

fluids through wells such as oil, gas, and groundwater are similarly practiced widely under regulatory frameworks aimed at protecting against adverse consequences. Nevertheless, the novelty of CCS associated with the large volume of CO_2 that needs to be injected motivates discussion of what can go wrong and what general impacts are possible. This discussion will serve to evaluate which impacts are the most likely and which have the greatest consequences. This in turn will allow focus to be placed on the highest environmental risks so they can be avoided altogether, or assessed and mitigated if unavoidable.

Broadly, impacts of CCS can be broken down into those occurring at depth with no discharge of CO_2 into the atmosphere (i.e., the CO_2 storage objective is achieved even as other consequences occur), and those that involve CO_2 discharging into the atmosphere. Presented in Table 1 are potential impacts of geologic CO_2 storage broken down into these two broad categories.

While the impacts arising from CO_2 leaking upward into the vadose zone, root zone, surface water, and out of the ground may be very serious, such occurrences all require a conduit or flow pathway from the deep injection zone to the near-surface environment, such as an improperly abandoned well or conductive fault. Any GCS project that had moderate to high potential for the leakage scenarios in the upper part of Table 1 would presumably not be undertaken assuming effective risk management, insurance, and regulatory processes are in place. Furthermore, theoretical studies aimed at finding ways that CO_2 could be catastrophically released from CO_2 storage sites leading to the most serious impacts at the ground surface have found self-limiting fluid interference behaviors rather than runaway behaviors [50]. Finally, the impacts described in the upper part of Table 1 are associated with failures of GCS in that CO_2 will enter the atmosphere negating the sequestration objective. Assuming an adequate monitoring program is in place, these leakage events would be relatively obvious and appropriate changes in operations and remedial actions could be carried out.

Geologic Carbon Sequestration: Sustainability and Environmental Risk. Table 1 Shallow (*upper part of table*) and deep (*lower part of table*) processes and potential impacts of geologic CO_2 storage (GCS) (Oldenburg, 2007)

Category	Scenario	Significance	References
CO_2 enters the atmosphere	Root zone impacts	Profound, visible impact on plants, trees, crops	[36, 37]
	Migration in to vadose zone	May include root zone and entry into buildings	[38]
	Bubbling through surface water	Alters water quality (e.g., lowering pH)	[39]
	Accumulation in topographic lows	Very hazardous due to possibility of asphyxiation	[38, 40]
	Seepage into basements and homes	Very hazardous due to possibility of asphyxiation	[41]
	Ground plumes	Very hazardous due to possibility of asphyxiation	[40, 42, 43]
CO_2 may or may not enter atmosphere	Intrusion of CO_2 into potable water	Lowers pH, dissolves minerals potentially releasing heavy metals	[44, 45]
	Intrusion of CO_2 into hydrocarbon, mineral, or geothermal resources	Lowers value of natural gas or mineral resources such as potash	
	Displacement of saline groundwater or brine into potable water by regional pressurization	Saline water intrusion into potable water degrades water quality	[45–47]
	Induced seismicity	CO_2 injection pressure may cause felt earthquakes	[48, 49]

In the exceptional case of the occurrence of an uncontrolled CO_2 leak from a well into the atmosphere, the main consequence of concern is asphyxiation of workers or bystanders. Documented CO_2 well blowouts associated with oil production indicate the asphyxiation hazard is low for blowouts occurring in open environments [e.g., 51, 52]. Modeling studies of open-air scenarios have also found that the area of asphyxiation hazard around a blowout is small because dispersion acts to rapidly decrease concentrations [53].

In contrast to a well blowout or the scenarios in the upper part of Table 1, it may be much more difficult to detect the onset and development of the scenarios listed in the lower part of the table in order to take early action to limit impacts. Although the scenarios listed in the lower part of Table 1 do not involve CO_2 entering the atmosphere and thus do not involve outright failure of GCS, the intrusion of CO_2 or saline groundwater or brine into groundwater resources and injection-induced seismicity are considered the main hazards associated with GCS that are likely enough to warrant risk assessment and related regulatory measures in order to minimize the likelihood of their occurrence and their consequences. These two categories of risk, described in more detail below, must be assessed and managed as part of widespread, long-term, and sustainable GCS deployment.

Potential Impacts to Potable Groundwater

CO_2 that leaks upward out of the storage region through wells [e.g., 54, 55], or faults and fractures [56], can potentially enter potable groundwater resources as shown schematically in Fig. 3a. Degradation of the groundwater quality is possible through indirect contamination. As CO_2 dissolves into groundwater, it partitions into species comprising dissolved inorganic carbon (DIC) as $CO_2(aq)$, HCO_3^-, and CO_3^{2-}, resulting in a decrease in the solution pH. At the same time, alkalinity is controlled by HCO_3^- and CO_3^{2-}, which can increase upon CO_2 dissolution. Control over the geochemical changes in the water is provided by the composition and mineralogy of the mineral grains, coatings, and cements present in the rock. For example,

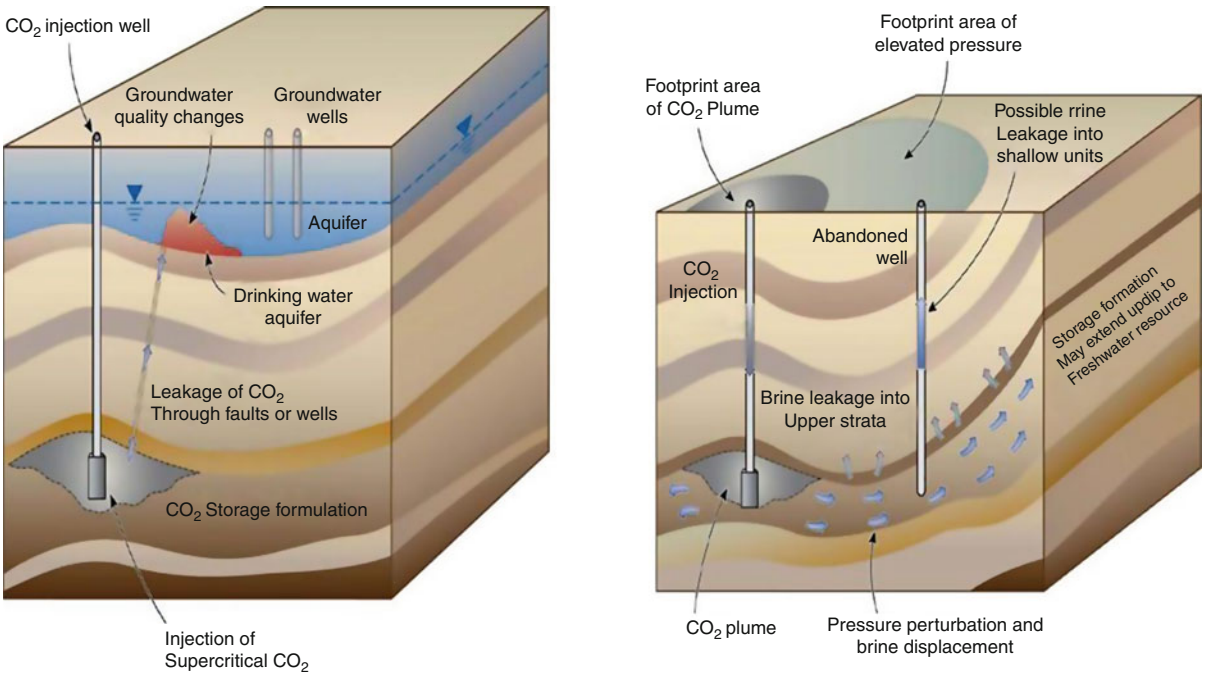

Geologic Carbon Sequestration: Sustainability and Environmental Risk. Figure 3
Potential groundwater impact scenarios. *Left-hand figure* from [45], *right-hand figure* from [47]

a carbonate mineral in the rock such as calcite ($CaCO_3$) will dissolve by the reaction $CO_2 + H_2O + CaCO_3 = Ca^{2+} + 2HCO_3^-$, resulting in the doubling of dissolved inorganic carbon (DIC) (i.e., one mole of CO_2 reacts to produce two moles of HCO_3^-) and a release of Ca^{2+} to solution. Similar reactions are possible involving alteration of biotite, plagioclase, and alkali feldspar, and other common minerals in sedimentary rocks [e.g., 25].

CO_2 or saline groundwater and brine leakage into groundwater aquifers will also give rise to impacts on microbiological communities [57]. Although cell density declines by three to six orders of magnitude from the ground surface to 4 km depth, microbes at the depths of potable groundwater can be affected if CO_2 or brine intrudes into this region. The alteration of minerals such as feldspars by acidic groundwater can release iron which can stimulate Fe^{3+}-reducing communities and result in methanogenesis. Clearly, microbial processes can affect geochemistry and vice versa.

Assuming the reaction kinetics allow it, geochemical reactions can further alter pH, DIC, isotopic composition, and trace element concentrations in solution. For example, trace elements in the minerals, in coatings, or in ion exchange sites in clays (including heavy metals such as lead) may be released into groundwater as biogeochemical conditions change with associated degradation of groundwater quality [44, 58]. Observations of such effects have been made during CO_2 injection experiments at field sites [e.g., 59, 60] and in the laboratory [61]. Recent work has further assessed the potential for such reactions by examining actual groundwater compositions and aquifer mineralogy from across the USA, and found that increases in the concentration of As and Pb could be a concern if widespread CO_2 leakage into groundwater resources were to occur [45]. Buffering reactions may serve to moderate pH decline and may serve to diminish groundwater degradation as observed in a natural analog study in New Mexico [62]. In summary, it is recognized that impacts of CO_2 leakage on potable groundwater may be significant and costly if they occur, and therefore careful monitoring, GCS operations, and site selection [e.g., 63] are essential to reduce groundwater contamination risk.

Another hazard to groundwater resources is the potential intrusion of displaced saline groundwater or brine or CO_2-charged water into potable groundwater as shown in Fig. 3b. In addition to the above biogeochemical impacts arising from the CO_2 itself, there is the first-order degradation arising from the presence of dissolved solids (e.g., NaCl, $CaCl_2$, and KCl) in the saline groundwater or brine along with whatever trace elements it may contain. Potable groundwater in the USA is defined on the basis of total dissolved solids (TDS) content equal to 10,000 mg/L or less. Injection into deep aquifers is regulated in the USA by the Environmental Protection Agency (EPA) under the Underground Injection Control (UIC) program to protect potable groundwater from degradation [e.g., 35, 64]. The hazard arising from GCS is that deep saline water or brine pressurized by CO_2 injection may tend to migrate upward into potable groundwater aquifers, thereby increasing TDS and degrading the resource.

The main reason that saline groundwater or brine intrusion arising from GCS is such a concern is that pressure increases associated with CO_2 injection can occur at great distances (~10–100 km) from the injection site [46, 47, 65, 66]. So while characterization of a given site may have demonstrated that CO_2 will be contained within a well-defined CO_2 storage region, there will generally be a large region of pressure increase in the formation that may not have been characterized to the same degree because of the large distance from the injection site. Because of this, it is possible that the cap rock may not be continuous over these large distances, or may not have the same integrity as the region targeted for CO_2 storage. Nevertheless, in order for upward saline groundwater or brine intrusion to occur, there must be a driving force in addition to the conduit or pathway (e.g., improperly abandoned well, or fault or fracture zone). Although pressure rise is high near the CO_2 injection wells, it falls off rapidly away from the injection wells. In addition, dense brines with high TDS require overpressures to be driven upward into potable groundwater through wells or other conduit (e.g., conductive fault) due to their high density and resistance to flow [67]. Furthermore, once in the potable aquifer, the higher density of the brine will tend to limit the extent of its mixing with potable groundwater [68].

Induced Seismicity

The phenomenon of induced seismicity due to fluid injection has been recognized for approximately 50 years starting with the well-known example of injected fluid waste disposal at the Rocky Mountain

Arsenal in Colorado [69–71]. Induced seismicity is well understood from experience in the fields of injection for deep disposal of liquid waste, and injection for geothermal energy extraction [48, 49, 72]. Induced seismicity is caused by the reduction in effective stress that accompanies an increase in pore pressure. The potential for induced seismicity is determined by the Mohr–Coulomb criterion which quantifies the amount of normal stress beyond that provided by fluid pressure that is needed before shear failure occurs (i.e., reactivation of existing faults or slippage along fractures). The Mohr–Coulomb criterion is given by the relation $\tau = C + \mu\,(\sigma_n - p)$ where τ is the shear strength of the rock, C is the Coulomb criterion, μ is the coefficient of internal friction, σ_n is the normal stress, and p is the fluid pressure [e.g., 73]. When the right-hand side (normal stress) is smaller than the left-hand side (shear strength), the rock is likely to slip along fracture planes of optimal orientation, which releases seismic energy (i.e., causes an earthquake). The Mohr–Coulomb equation shows that injection pressure reduces the effective normal stress in the rock, hence the tendency for injection to cause slippage along existing faults and fractures as shown in Fig. 4a.

A simple graphical representation of pressures as a function of depth helps elucidate the processes active near an injection well. Shown in Fig. 4b are the variations with depth of hydrostatic pressure, so-called fracture pressure (or commonly frac pressure), and lithostatic pressure. As shown, fluid pressure at an injection well must be larger than hydrostatic pressure in order for injection to occur. However, if the pressure exceeds the frac pressure at a given depth, the injection process will tend to fracture the formation. By the Mohr–Coulomb criterion, seismicity can be induced at injection pressures below the frac pressure as effective stress decreases and existing faults are reactivated. Either the generation of new fractures, or slippage along existing faults and fractures, is manifest as induced seismicity.

It is important to note that while the word *earthquake* evokes fear and a certain image of destruction in most people's minds, the term encompasses a wide range of magnitudes, from microseismic earthquakes

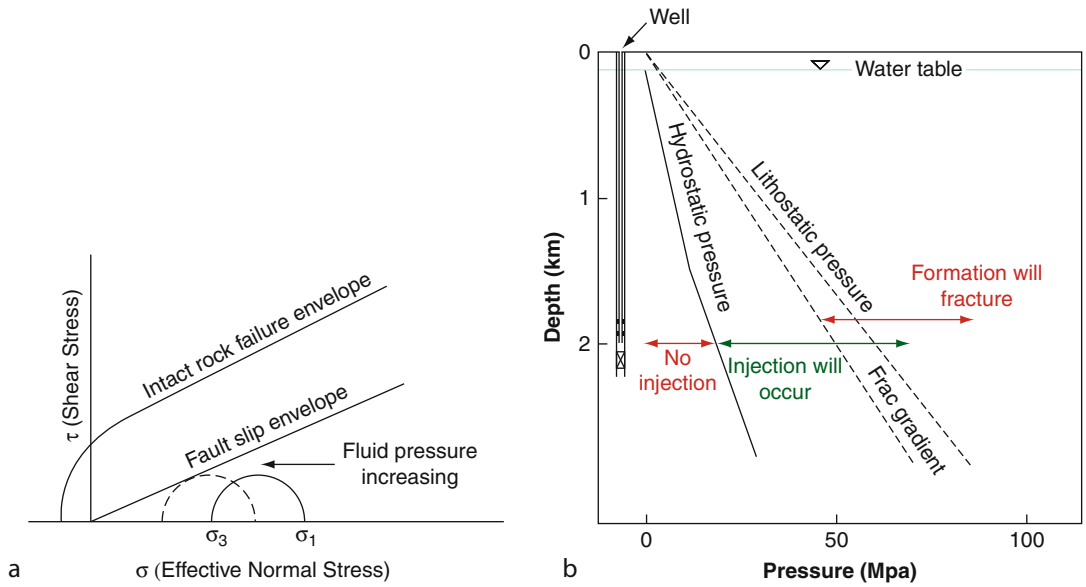

Geologic Carbon Sequestration: Sustainability and Environmental Risk. Figure 4
(**a**) Mohr circle representation of fault slip (induced seismicity) as fluid pressure increases, and (**b**) pressure-depth depiction showing hydrostatic, frac, and lithostatic pressure gradients

that cannot be felt by humans, to great earthquakes that imperil life and damage structures. Earthquakes tend to follow a logarithmic frequency distribution such that very small earthquakes are orders of magnitude more frequent than very large earthquakes [74]. Experience from water injection into geothermal systems shows that the majority of induced seismicity is microseismicity, with felt earthquakes much rarer, and moderate to large earthquakes rarer still [48]. Despite the fact that large earthquakes are not expected to be induced by CO_2 injection in carefully chosen sites [75], the hazard of induced seismicity is looming large at present in the area of public acceptance of GCS.

Aside from the hazard of ground acceleration at the surface, induced seismicity also creates the possibility that a cap rock seal could fracture or a fault could become permeable giving rise to a leakage pathway for CO_2 [e.g., 73, 76]. This is a well-recognized failure mode, and injection regulations are aimed at preventing fracturing from happening. However, induced seismicity of critically stressed rocks on preexisting faults and fractures is still possible even when the frac pressure is not exceeded. The extent to which the risk of induced seismicity, objectively considered to be a small risk, outweighs the benefits in terms of risk reduction of climate change that CCS affords, is one of the questions that must be addressed by the public and decision-makers to guide their acceptance of CCS.

Future Directions

As the discussion here suggests, one approach that can aid in addressing the energy–climate crisis is CCS. There are significant costs to CCS, primarily associated with capture, and CCS also brings with it recognized environmental risks the most uncertain of which are associated with the geologic storage component of the process. The main risks in GCS are threat to potable groundwater and induced seismicity, two areas of active research. Despite the need for greater understanding of these hazards, mitigation measures are available today. For example, if contamination of groundwater were to occur, the water could be treated, or alternate sources could be found if treatment is found impractical [63]. As for induced seismicity, the hazard can be reduced by reducing injection pressure (e.g., through use of more wells for a given CO_2 source), carrying out pressure management through saline groundwater or brine extraction, by careful site selection that avoids heavily faulted and tectonically active areas, and by establishing and enforcing building codes.

The path forward for demonstrating and deploying CCS, as a sustainable part of the portfolio of energy production and use changes that are needed to mitigate the energy–climate crisis, can be described as follows. First, testing and demonstration projects [e.g., 77, 78] that include CO_2 capture from anthropogenic sources need to expand rapidly and by many factors so that the technology can be perfected in different regions and geologic settings. These multiple demonstration projects will show how GCS works, and if GCS continues to perform as envisioned, additional CCS deployments can be added over time. Second, research on capture and alternative combustion approaches that enable more efficient capture should be accelerated. Third, a large program of site characterization and capacity studies [e.g., 79] should be undertaken so that the well-known large basin-scale sites are understood and operational plans can be put in place quickly at the time when large-scale capture facilities come on line and anthropogenic CO_2 streams become available for sequestration. Fourth, research on injection, trapping, migration, long-term fate, leakage impacts, mitigation, monitoring, and modeling should be continued so that GCS can be optimized and related technologies can be commercialized and deployed in a cost-effective manner. Fifth, governments at all levels should promulgate regulatory and economic policies that answer the current questions and uncertainty faced by businesses who foresee the broad outlines of a carbon-constrained future but do not yet have the clear ground rules (e.g., policies on carbon pricing, injection regulations, and legal frameworks) provided by government that are necessary for making the large capital investments required for CCS.

The decision to take on the costs and risks of GCS, with the accompanying promise of contributing to reductions in the extent of climate change, should be made based on an objective comparison against the climate and environmental risks of carrying on business as usual with fossil-fuel use and unabated CO_2 emissions. The public and decision-makers should

keep in mind that the environmental risks of CCS are local to the basin where GCS is carried out, whereas the projected impacts of climate change are global-to-regional in scale and are expected to have profound consequences for the social, physical, and natural systems on Earth. Support for GCS technology will come in the form of policy decisions about carbon pricing, injection regulations, and legal frameworks that encourage commercial applications of CCS. The decision about whether to adopt these policies will ultimately fall on the public or its representatives. The risks to the Earth's environment and social systems of doing nothing about the energy–climate crisis must be communicated effectively to the public and the decision-makers so that they can make an informed decision about acceptable risks and costs of the various options available for avoiding the worst impacts of climate change.

Acknowledgments

This entry greatly benefitted from suggestions and comments by my LBNL colleagues Karsten Pruess, Jens Birkholzer, and Preston Jordan.

Bibliography

Primary Literature

1. Metz B, Davidson O, de Coninck HC, Loos M, Meyer LA (eds) (2005) IPCC special report on carbon dioxide capture and storage. Prepared by working group III of the intergovernmental panel on climate change. Cambridge University Press, Cambridge
2. Torp TA, Gale J (2004) Demonstrating storage of CO_2 in geological reservoirs: the Sleipner and SACS projects. Energy 29(9–10):1361–1369
3. Mathieson A, Midgley J, Dodds K, Wright I, Ringrose P, Saoul N (2010) CO_2 sequestration monitoring and verification technologies applied at Krechba, Algeria. Lead Edge 29(2):216–222
4. Keith DW, Ha-Duong M, Stolaroff JK (2006) Climate strategy with CO_2 capture from the air. Clim Change 74(1–3):17–45
5. Lackner K (2010) Washing carbon out of the air. Sci Am Mag Sci Am 302:66–71. doi:10.1038/scientificamerican0610-66
6. Brewer PG, Friederich G, Peltzer ET, Orr FM Jr (1999) Direct experiments on the ocean disposal of fossil fuel CO_2. Science 284(5416):943–945
7. Caldeira K, Rau GH (2000) Accelerating carbonate dissolution to sequester carbon dioxide in the ocean: geochemical implications. Geophys Res Lett 27(2):225–228
8. Chisholm SW, Falkowski PG, Cullen JJ (2001) Dis-crediting ocean fertilization. Science 294(5541):309–310
9. Buesseler KO, Boyd PW (2003) Will ocean fertilization work? Science 300(5616):67–68
10. Shaffer G (2010) Long-term effectiveness and consequences of carbon dioxide sequestration. Nat Geosci 3:464–467
11. House KZ, Harvey CF, Aziz MJ, Schrag DP (2009) The energy penalty of post-combustion CO_2 capture & storage and itsimplications for retrofitting the U.S. installed base. Energy Environ Sci. doi:10.1039/b811608c
12. McKinsey and Co. (2008) Carbon capture and storage: assessing the economics. McKinsey&Company, New York, NY, p 49
13. IEA, Key World Energy Statistics (2009) International Energy Agency (IEA), Paris, http://www.iea.org/textbase/nppdf/free/2009/key_stats_2009.pdf
14. Keeling RF, Piper SC, Bollenbacher AF, Walker JS (2009) In: Trends A (ed) Compendium of Data on Global Change. Carbon Dioxide Information Analysis Center. Oak Ridge National Laboratory, U.S. Department of Energy, Oak Ridge, Tenn. doi:10.3334/CDIAC/atg.035 (Atmospheric CO_2 records from sites in the SIO air sampling network)
15. Core Writing Team, Pachauri, RK and Reisinger, A (eds) (2007) IPCC, Climate change 2007: synthesis report. Contribution of working groups I, II and III to the fourth assessment report of the intergovernmental panel on climate change. IPCC, Geneva, p 104
16. Pacala S, Socolow R (2004) Stabilization wedges: solving the climate problem for the next 50 years with current technologies. Science 305(5686):968–972
17. Preston C, Monea M, Jazrawi W, Brown K, Whittaker S, White D, Law D, Chalaturnyk R, Rostron B (2005) IEA GHG Weyburn CO_2 monitoring and storage project. Fuel Process Technol 86(14–15):1547–1568
18. Rubin ES, Chen C, Rao AB (2007) Cost and performance of fossil fuel power plants with CO_2 capture and storage. Energy Policy 35(9):4444–4454
19. Wilson EJ, Gerard D (2007) Risk assessment and management for geologic sequestration of carbon dioxide. In: Wilson EJ, Gerard D (eds) Carbon capture and sequestration integrating technology, monitoring, and regulation. Blackwell, Oxford, pp 101–125
20. Benson SM, Cook PJ (eds) (2005) IPCC Special report on CO_2 capture and storage, chap. 5. Cambridge University Press, Cambridge
21. Oldenburg CM (2007) Migration mechanisms and potential impacts of CO_2 leakage and seepage. In: Wilson E, Gerard D (eds) Carbon capture and sequestration integrating technology, monitoring, and regulation. Blackwell, Ames, pp 127–146 (BNL-58872)
22. Bachu S (2003) Screening and ranking of sedimentary basins for sequestration of CO_2 in geological media in response to climate change. Environ Geol 44(3):277–289

23. Spycher N, Ennis-King J, Pruess K (2003) CO_2-H_2O mixtures in the geological sequestration of CO_2. Assessment and calculation of mutual solubilities from 12 C to 100 C and up to 600 bar. Geochemica Cosmochim Acta 67:3015–3031
24. Gunter WD, Bachu S, Benson S (2004) The role of hydrogeological and geochemical trapping in sedimentary basins for secure geological storage of carbon dioxide. Geol Soc Lond Spec Publ 233:129–145
25. Xu T, Apps JA, Pruess K (2005) Mineral sequestration of CO_2 in a sandstone-shale system. Chem Geol 217 (1–4):295–318
26. Benson SM, Hepple R, Apps J, Tsang C-F, Lippmann M (2002) Lessons learned from natural and industrial analogues for storage of carbon dioxide in deep geological formations, E.O. Lawrence Berkeley National Laboratory Report LBNL-51170
27. Katz DL, Tek MR (1981) Overview on underground storage of natural gas. J Petrol Technol 33(6):943–951
28. USGS (2010) http://energy.er.usgs.gov/health_environment/co2_sequestration/co2_illustrations.html. Accessed 6 Oct 2010
29. Haszeldine RS (2009) Carbon capture and storage: how green can black be? Science 325(5948):1647–1652
30. Shrag DP (2009) Storage of carbon dioxide in offshore sediments. Science 325:1658–1659
31. NATCARB (2008) U.S. Department of energy, carbon sequestration Atlas of the United States and Canada, Office of fossil energy, National energy technology laboratory. http://geoportal.kgs.ku.edu/natcarb/atlas08/gsinks.cfm. Accessed 6 Oct 2010
32. McCoy ST, Rubin ES (2008) An engineering-economic model of pipeline transport of CO_2 with application to carbon capture and storage. Int J Greenhouse Gas Control 2(2):219–229
33. Brennan ST, Burruss RC, Merrill MD, Freeman PA, Ruppert LF (2010) A probabilistic assessment methodology for the evaluation of geologic carbon dioxide storage: U.S. Geological survey open-file report 2010–1127, p 31. Available only at http://pubs.usgs.gov/of/2010/1127. Accessed 6 Oct 2010
34. Bradshaw J, Bachu S, Bonijoly D, Burruss R, Holloway S, Christensen NP, Mathiassen OM (2007) CO_2 storage capacity estimation: issues and development of standards. Int J Greenhouse Gas Control 1:62–68
35. USEPA (United States Environmental Protection Agency), Technical program overview, underground injection control regulations, office of water 4606, EPA 816-R-02-025. Revised July 2001. http://www.epa.gov/safewater/uic/index.html. Accessed 10 Oct 2010
36. Qi J, Marshall JD, Matson KG (1994) High soil carbon dioxide concentrations inhibit root respiration of Douglas Fir. New Phytology 128:435–441
37. Farrar CD, Sorey ML, Evans WC, Howie JF, Kerr BD, Kennedy BM, King C-Y, Southon JR (1995) Forest-killing diffuse CO_2 emission at mammoth mountain as a sign of magmatic unrest. Nature 376:675–677
38. Oldenburg CM, Unger AJA (2003) On leakage and seepage from geologic carbon sequestration sites: unsaturated zone attenuation. Vadose Zone J 2(3):287–296
39. Oldenburg CM, Lewicki, JL (2005) Leakage and seepage of CO_2 from geologic carbon sequestration sites: CO_2 migration into surface water, *Lawrence Berkeley National Laboratory Report LBNL-57768*
40. Giggenbach WF, Sano Y, Schmincke HU (1991) CO_2-rich gases from lakes nyos and monoun, cameroon; laacher see, Germany, Dieng, Indonesia, and Mt. Gambier, Australia-variations on a common theme. J Volcanol Geotherm Res 45:311–323
41. Robinson AL, Sextro RG, Riley WJ (1997) Soil-gas entry into houses driven by atmospheric pressure fluctuations–the influence of soil properties. Atmos Environ 31(10):1487–1495
42. Hanna SR, Steinberg KW (2001) Overview of Petroleum Environmental Research Forum (PERF) dense gas dispersion modeling project. Atmos Environ 35:2223–2229
43. Britter RE (1989) Atmospheric dispersion of dense gases. Ann Rev Fluid Mech 21:317–344
44. Wang S, Jaffe PR (2005) Dissolution of a mineral phase in potable aquifers due to CO_2 releases from deep formations; effect of dissolution kinetics. Energy Convers Manage 45:2833–2848
45. Apps JA, Zheng L, Zhang Y, Xu T, Birkholzer JT (2010) Evaluation of potential changes in groundwater quality in response to CO_2 leakage from deep geological storage. Transp Porous Media 82:215–246
46. Birkholzer JT, Zhou Q, Tsang C-F (2009) Large-scale impact of CO_2 storage in deep saline aquifers: a sensitivity study on the pressure response in stratified systems. Int J Greenhouse Gas Control 3(2):181–194
47. Birkholzer JT, Zhou Q (2009) Basin-Scale hydrogeologic impacts of CO_2 storage: capacity and regulatory implications. Int J Greenhouse Gas Control 3(6):745–756
48. Majer EL, Baria R, Stark M, Oates S, Bommer J, Smith B, Asanuma H (2007) Induced seismicity associated with enhanced geothermal systems. Geothermics 36(3):185–222
49. Majer E, Baria R, Stark M (2008) Protocol for induced seismicity associated with enhanced geothermal systems. Report produced in Task D Annex I (, International energy agency-geothermal implementing, agreement (incorporating comments by: Bromley C, Cumming W, Jelacic A and Rybach A) (http://www.iea-gia.org/publications.asp)
50. Pruess K (2005) Numerical studies of fluid leakage from a geologic disposal reservoir for CO_2 show self-limiting feedback between fluid flow and heat transfer. Geophys Res Lett 32(14):L14404
51. Skinner L (2003) CO_2 blowouts: an emerging problem. World Oil 224(1):38–42
52. Gouveia FJ, Johnson M, Leif, RN, Friedmann SJ (2005) Aerometric measurement and modeling of the mass of CO_2 emissions from Crystal Geyser, Utah. NETL 4th Annual carbon capture and sequestration conference. Alexandria, p 2–5

53. Aines RD, Leach MJ, Weisgraber TH, Simpson MD, Friedman SJ, Bruton CJ (2008) Quantifying the potential exposure hazard due to energetic releases from a failed sequestration well. In: *Proceedings of the ninth international conference on greenhouse gas control technologies GHGT-9. Washington, p 16–20*
54. Gasda SE, Bachu S, Celia MA (2004) Spatial characterization of the location of potentially leaky wells penetrating a deep saline aquifer in a mature sedimentary basin. Environ Geol 46:707–720
55. Scherer GW, Celia MA, Prevost J-H, Bachu S, Bruant R, Duguid A, Fuller R, Gasda SE, Radonjic M, Vichit-Vadakan W (2005) Leakage of CO_2 through abandoned wells: role of corrosion of cement. In: Thomas DC, Benson SM (eds) Carbon dioxide capture for storage in deep geologic formations, vol 2. Elsevier, Amsterdam, pp 827–848
56. Shipton ZK, Evans JP, Kirschner D, Kolesar PT, Williams AP, Heath J (2004) Analysis of CO_2 leakage through 'low-permeability' faults from natural reservoirs in the Colorado Plateau, southern Utah. In: Baines SJ, Worden RH (eds) Geological storage of carbon dioxide. Geological society, vol 233. Special Publications, London, pp 43–58
57. Onstott TC (2005) Impact of CO_2 injections on deep subsurface microbial ecosystems and potential ramifications for the surface biosphere. In: Thomas DC, Benson SM (eds) Carbon dioxide capture for storage in deep geologic formations, vol 2. Elsevier, London, pp 1217–1249
58. Schuett H, Wigand M, Spangenberg E (2005) Geophysical and geochemical effects of supercritical CO_2 on sandstones. In: Thomas DC, Benson SM (eds) Carbon dioxide capture for storage in deep geologic formations, vol 2. Elsevier, Amsterdam, pp 767–786
59. Kharaka Y, Cole DR, Hovorka SS, Gunther WD, Knauss KG, Freifield BM (2006) Gas-water-rock interactions in Frio formation following CO_2 injection: implications for the storage of greenhouse gases in sedimentary basins. Geology 34:577–580
60. Kharaka YK, Thordsen JJ, Kakouros E, Ambats G, Herkelrath WN, Birkholzer JT, Apps JA, Spycher NF, Zheng L, Trautz RC, Rauch HW, Gullickson K (2010) Changes in the Chemistry of Shallow Groundwater Related to the 2008 Injection of CO_2 at the ZERT Field, SiteBozeman, Montana. Environ Earth Sci 60:273–284
61. Carroll S (May 2009) Trace metal release from Frio sandstone reacted with CO_2 and 1.5 N NaCl Brine at 60°C. In: Proceedings 8th Annual conference on carbon capture and sequestration. Pittsburgh
62. Keating EH, Fessenden J, Kanjorski N, Koning DJ, Pawar R (2010) The impact of CO_2 on shallow groundwater chemistry: observations at a natural analog site and implications for carbon sequestration. Environ Earth Sci 60(3):521–536
63. Price PN, Oldenburg CM (2009) The consequences of failure should be considered in siting geologic carbon sequestration projects. Int J Greenhouse Gas Control 3(5):658–663
64. Wilson EJ, Johnson TL, Keith DW (2003) Regulating the Ultimate Sink: managing the risks of geologic CO_2 storage. Environ Sci Technol 37(16):3476–3483
65. Nicot J-P (2008) Evaluation of large-scale CO_2 storage on fresh-water sections of aquifers: an example from the Texas Gulf Coast Basin. Int J Greenhouse Gas Control 2(4):582–593
66. Zhou Q, Birkholzer JT, Mehnert E, Lin Y-F, Zhang K (2009) Modeling basin- and plume-Scale Processes of CO_2 storage for full-scale deployment. Ground Water 48(4): 494–514
67. Nicot J-P, Oldenburg CM, Bryant SL, Hovorka SD (2009) Pressure perturbations from geologic carbon sequestration: area-of-review boundaries and borehole leakage driving forces. Energy Procedia 1(1):47–54
68. Oldenburg CM, Rinaldi AP (2011) Buoyancy effects on upward brine displacement caused by CO_2 injection, Transport in Porous Media 87(2):525–540
69. Hollister JC, Weimer RJ (eds) (1968) Geophysical and geological studies of the relationships between the Denver earthquakes and the Rocky Mountain Arsenal well. Q. Colorado School of Mines 63, Golden, p 251
70. Hoover DB, Dietrich JA (1969) Seismic activity during the 1968 test pumping at the Rocky Mountain arsenal disposal well, circular 613, U.S. Geological Survey, Washington
71. Herrmann RB, Park S-K, Wang C-Y (1981) The Denver earthquakes of 1967–1968. Bull Seismol Soc Am 71(3):731–745
72. Cypser DA, Davis SD (1998) Induced seismicity and the potential for liability under U.S. law. Tectonophysics 289(1–3):239–255
73. Rutqvist J, Birkholzer J, Cappa F, Tsang C-F (2007) Estimating maximum sustainable injection pressure during geological sequestration of CO_2 using coupled fluid flow and geomechanical fault-slip analysis. Energy Convers Manage 48(6):1798–1807
74. Gutenberg B, Richter CF (1944) Frequency of earthquakes in California. Bull Seismol Soc Am 17:185–188
75. Sminchak J, Gupta N, Byrer C, Bergman P (2003) Aspects of induced seismic activity and deep-well sequestration of carbon dioxide. Environ Geosci 10(2):81–89
76. Wiprut D, Zoback M (2000) Fault reactivation and fluid flow along a previously dormant normal fault in the northern North Sea. Geology 28(7):595–598
77. Hovorka SD, Benson SM, Doughty C, Freifeld BM, Sakurai S, Daley TM, Kharaka YK, Holtz MH, Trautz RC, Nance HS, Myer LR, Knauss KG (2006) Measuring permanence of CO_2 storage in saline formations: the Frio experiment. Environ Geosci 13(2):105–121
78. Litynski J, Plasynski S, McIlvried HG, Mahoney C, Srivastava RD (2008) The United States department of energy's regional carbon sequestration partnerships program validation phase. Environ Int 34(1):127–138
79. Friedmann SJ, Dooley JJ, Held H, Edenhof O (2006) The low cost of geological assessment for underground CO_2 storage: policy and economic implications. Energy Convers Manage 47(13–14):1894–1901

Books and Reviews

Baines SJ, Worden RH (eds) (2004) Geologic storage of carbon dioxide, geological society, vol 233. Special Publications, London, pp 1–247

Eide LI (2009) Carbon dioxide capture for storage in deep geological formations, vol 3. CPL Press/BP, Newbury, Berkshire

Thomas DC, Benson SM (eds) (2007) Carbon dioxide capture for storage in deep geologic formations-results from the CO_2 capture project, vol 2. Elsevier, Kidlington, Oxford

Wilson EJ, Gerard D (eds) (2007) Carbon capture and sequestration integrating technology, monitoring, and regulation, Blackwell Publishing, Ames, Iowa

Geothermal Conditioning: Critical Sources for Sustainability

Nina Baird
Center for Building Performance & Diagnostics, Carnegie Mellon University, Pittsburgh, PA, USA

Article of Outline

Glossary
Definition of the Subject
Introduction
The Earth's Thermal Energy Sources and Ground Temperature Distribution
Geothermal Conditioning Principles and Approaches
Installed Capacity and Annual Energy Use
Future Directions
Bibliography

Glossary

Closed loop system A continuous, sealed, underground or submerged heat exchanger through which a heat transfer fluid passes to and returns from building conditioning equipment.

Geothermal direct use Use of thermal energy in the earth or earth-coupled fluid as a heat source and heat transfer reservoir for heating or cooling, without further conversion such as electric power generation.

Geothermal heat pump A conditioning device that uses the ground or ground-coupled fluid as the heat source and heat sink in the heat pump's process of extracting heat from a low-temperature source and transferring it to sink at a higher temperature by adding the work of a refrigerant, usually with a vapor compression-expansion cycle.

Low-Exergy System Heating and/or cooling system that uses energy at a temperature close to room temperature for efficient utilization of low-grade energy sources.

Open Loop System A system designed to use groundwater or surface water for the purpose of extracting or rejecting heat for building conditioning.

Underground Thermal Energy Storage (UTES) A subsurface system for storing heat and/or cold using groundwater and/or the ground in natural or constructed media.

Definition of the Subject

Geothermal conditioning is use of the earth's thermal energy and storage capacity for heating, cooling, and ventilation. These types of conditioning strategies can transfer heat to the indoor environment using the ground, groundwater, or surface water – resources that are abundant and ubiquitous – to satisfy some or all of the heating load. They can also capitalize on the heat capacity and thermal inertia of the earth and its waters by transferring excess heat from indoors to outdoors, providing cooling with substantially reduced energy consumption from conventional cooling and negligible thermal impact on the outdoor environment.

Geothermal conditioning, like solar conditioning, includes passive and active strategies. Both have a long history. Passive earth sheltering has been used by plant and animal species throughout time. Active geothermal conditioning as defined here for heating, cooling, and ventilation was not broadly tracked until 1995 when geothermal heat pumps were added to global reports of geothermal direct use installations [1]. However, frequently cited early examples are the district heating system installed in Boise, Idaho (USA) in 1892 to heat 400 homes [2] and a residential geothermal steam heat system in Tuscany, Italy, introduced between 1910 and 1940 [3]. In present times, the Paleiskwartier district geothermal system in 's Hertogenbosch, the Netherlands, includes a large pond and aquifer thermal energy storage (ATES) coupled with heat pumps to condition a mixed-use development of 1,200 housing

units and more than 135,000 m^2 of office space, retail, and entertainment [4].

Accessible geothermal energy includes ground temperatures in excess of 150°C, hot enough to generate electricity and higher than temperatures that can be used directly for building conditioning. In such situations, building conditioning can be linked to geothermal power production through energy cascades, but the cost and complexity of power production processes substantially exceed those for building conditioning alone. In addition, access to geothermal resources that support electricity generation is far more limited. For those reasons, this entry will focus on direct use geothermal conditioning. References that address geothermal power production and geothermal energy cascades are provided in the Future Directions and Books and Reviews sections.

Introduction

In 1973, an Icelandic engineer, Baldur Lindal, listed current and potential uses of geothermal energy for conditioning and industrial processes and their temperature requirements. That list became known as the Lindal diagram, shown in Fig. 1 with conditioning processes highlighted. Since that time, substantial improvements in the availability and use of insulation products have allowed well-designed building enclosures to manage an increasing portion of the conditioning loads. When that occurs, heating and cooling can be provided at temperatures much closer to the human comfort range, no longer needing to overcome extreme heat loss or gain at the perimeter. Sustainably designed buildings can satisfy occupant comfort requirements with smaller mechanical equipment that operates at lower supply temperatures, supporting low-exergy systems (see Fig. 2). This puts building conditioning squarely in the geothermal "sweet spot," a temperature range available to almost every building in contact with the earth. Increased use of geothermal conditioning strategies will significantly lower conventional energy consumption, peak demand, and the corresponding carbon emissions, if done with understanding of these systems and their interaction with the environment.

This entry begins with a discussion of the earth's thermal energy and its ability to supply and store heat. The range of geothermal conditioning approaches are then described and illustrated with pertinent examples. Available data on global use of geothermal conditioning are presented and likely future developments in the design and application of geothermal conditioning technology are discussed. Finally, printed and electronic sources of additional information about geothermal conditioning are enumerated.

The Earth's Thermal Energy Sources and Ground Temperature Distribution

The European Union succinctly defines geothermal energy as *the energy stored in the form of heat beneath the surface of the solid earth* (RES Directive 2009/28/EC). Nothing in that definition, however, suggests the dynamic nature of the heat storage processes. Some of the short wave solar radiation incident on the surface is absorbed and conducted into soil and rock. Precipitation, either rain or snow melt that percolates into the subsurface, can transport this thermal energy substantially farther into underlying aquifers and the soil and rock surrounding them. Thermal energy is also created within the earth through the decay of radioactive isotopes such as U^{238} and Th^{232} in granite and basalt in the earth's crust, and through earthquake friction and the formation of new crust. These types of heat energy, in addition to thermal energy stored when the earth was formed, are transferred via conduction and convection from the interior of the earth to its surface. At the surface, long wave radiation and convective flow to the atmosphere balance the thermal energy inputs. The earth's total heat energy content is estimated to be 12–24 10^{30} J [5].

Within the earth's internal energy reservoir, temperatures are estimated to reach 5,000°C (see Table 1). However, because the earth has been drilled only to a depth of 12,262 km, less than 1% of the earth's diameter [6], and the present limit of economic drilling is approximately 4 km, the practical maximum temperature of geothermal energy is now <1,000°C. Constraining that range to temperatures effective for direct use geothermal conditioning, the range is approximately 4−150°C. An even smaller range, roughly 4–27°C, is sufficient for energy-effective building conditioning (see Fig. 2). In many areas around the world, solar radiation supplies the thermal energy for

Temperature (C)	Application	
200		
190		
180	Evaporation of highly concentrated solutions, Refrigeration by ammonia absorption, Digestion in paper pulp (Kraft)	
170	Heavy water via hydrogen-sulfide process Drying of diatomaceous earth	Conventional power production
160	Drying of fish meal Drying of lumber	
150	Alumina via Bayer's process	
140	Drying farm products at high rates Canning of food	
130	Evaporation in sugar refining. Extraction of salts by evaporation and crystallization, Fresh water by distillation	
120	Most multi-effect evaporation. Concentration of saline solutions.	
110	Drying and curing of light aggregate cement slabs	
100	Drying of organic materials, seaweeds, grass, vegetables, etc. Washing and drying of wool	
90	Drying of stock fish Intense de-icing operations	
80	Space heating (buildings and greenhouses)	
70	Refrigeration (low temperature limit)	
60	Animal husbandry Greenhouses by combined space and hotbed heating	
50	Mushroom growing Baleonology	
40	Soil warming	
30	Swimming pools, biodegradation, fermentations, Warm water for year-round mining in cold climates, De-icing	
20	Hatching of fish. Fish farming	
10		
5		
0		

Geothermal Conditioning: Critical Sources for Sustainability. Figure 1
Original Lindal diagram: geothermal energy uses

most of that temperature range in the top 20 m of the earth's surface.

Solar Energy Input: When the sun strikes the earth's surface, the radiation must be reflected from the surface, absorbed by the surface, or transmitted through the surface to material below. For most ground surfaces, the radiation is either reflected or absorbed; some transmission occurs through snow and ice. In approximate percentages, of the total solar radiation that enters the earth's atmosphere, roughly 55% reaches the earth's surface where 4% is immediately reflected to the atmosphere and 51% is absorbed (see Fig. 3).

The thermal impact of that absorbed radiation can be affected by dynamic processes such as wind and rain, but the static properties of the surface soil, water, and underlying rock are typically used to calculate how solar radiation affects ground temperature. The thermal *conductivity* of a material, expressed as k or λ in units of W/m/K, indicates how readily heat is transferred within a material by rapidly colliding molecules.

°C	Low Range of Conditioning Technology/Process
100	
90	
80	Cogeneration supply for district heating system
70	
60	Conventional boiler supply temperature
50	Fan coil heating water supply, Forced air furnace, Radiator water supply
40	
30	Floor heating, Ceiling panel heating, Wall panel heating
20	
10	Ceiling panel cooling water supply Sewer water supply temperature
0	District cooling Fan coil cooling water supply, Earth sheltering, Earth tube supply air Extended range heat pump entering water temperature: cooling
–10	Extended range heat pump entering water temperature: heating

Geothermal Conditioning: Critical Sources for Sustainability. Figure 2
Low-temperature/low-exergy conditioning

Geothermal Conditioning: Critical Sources for Sustainability. Table 1 Earth temperature profile [7]

Earth layer	Depth (km)	Temperature (°C)
Near-surface solar zone	0–0.02	Similar to mean annual air temperature
Earth's crust	0–30	Up to 1,000
Earth's mantle	Up to 3,000	1,000–3,000
Earth's core	Up to 6,370	3,000–5,000

It is an important mode of heat transfer in solids although most soils and rock are relatively poor conductors. The *specific heat* of a material, expressed as c_p in units of J/kg/K, indicates how much thermal energy a material can absorb for a given change in temperature. A material's specific heat and its *density* (ρ) in kg/m^3 determine its *volumetric heat capacity*, expressed as ρc in units of MJ/m^3/K. Volumetric heat capacity is the specific heat per unit volume and indicates the ability of a substance to store energy without undergoing a phase change. Soil and rock have a very high volumetric heat capacity relative to air and their ability to store heat creates a useful thermal lag. *Thermal diffusivity*, which indicates how quickly a material adjusts to the temperature of its surroundings, is calculated by dividing conductivity by volumetric heat capacity. Thermal diffusivity is expressed as κ in units of m^2/s. A highly conductive material with low volumetric heat capacity will have high thermal diffusivity and readily adjust its temperature, whereas a material with similar conductivity but higher volumetric heat capacity will adjust more slowly. In contrast to high thermal diffusivity, a material with high *thermal inertia* will store heat and give it off slowly, resisting diurnal and seasonal temperature changes. Thermal inertia is the square root of the thermal conductivity, density,

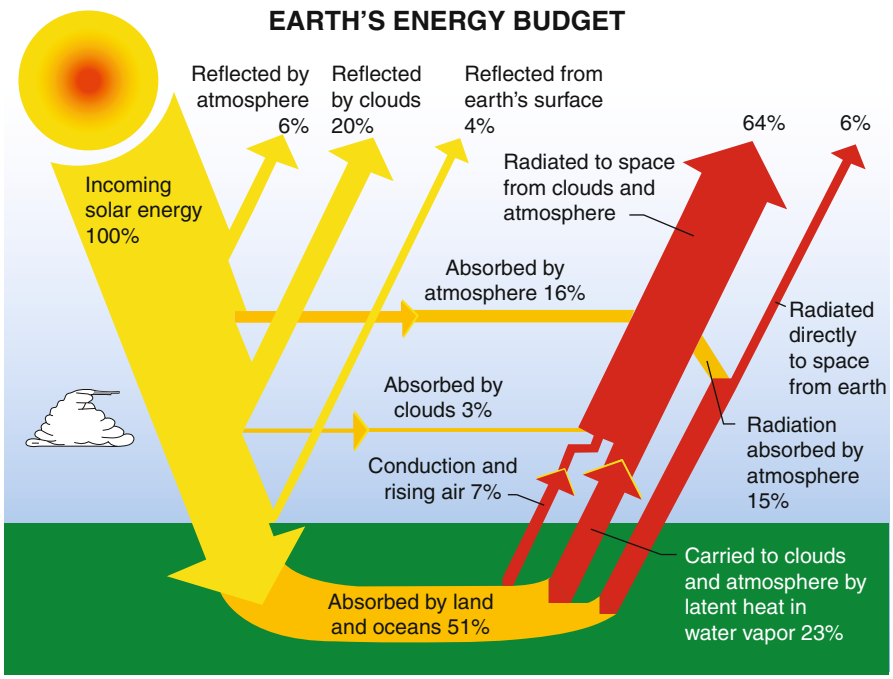

Geothermal Conditioning: Critical Sources for Sustainability. Figure 3
Absorbed and reflected solar radiation

and specific heat capacity expressed as I with units of J m^{-2} K^{-1} $s^{-½}$. Table 2 summarizes these properties and Table 3 shows representative values for air, water, soil, and rock.

Table 3 highlights the benefits of ground- or groundwater-based conditioning compared to air-based strategies. The thermal inertia of water, soil, and rock is high. Surface temperature fluctuations diminish with depth and the time lag between the surface temperature and the ground temperature increases. Daily fluctuations are dampened within 30 cm of the surface [8]. Annually, surface temperature fluctuations reflect monthly solar cycles and attenuate with increased depth, and the time lag between the surface temperature and ground temperature is more extended with depth on an annual basis. At the depth of *zero annual range* [9] or *the neutral zone* [10], the atmosphere and soil are presumed to achieve long-term thermal equilibrium. Here, no seasonal temperature fluctuations occur and the ground temperature should reflect the long-term average annual air temperature for that particular location. Under these circumstances, the ground temperature is warmer in winter and cooler in summer than the air temperature, which means that the ground can provide heat in winter and absorb excess heat in summer.

Table 3 also shows the impact of subsurface moisture. Saturated soil has substantially greater specific heat, volumetric heat capacity and thermal inertia than dry soil, making it a far better and more stable heat source and sink. If soil moisture varies with precipitation, the ground's thermal properties will reflect that variation. Alternatively, if soil moisture can be controlled to some extent, it may be possible to improve ground performance for geothermal conditioning.

The depth at which the neutral zone is said to occur varies within the literature (14–20 m) [9, 10] and is typically calculated, not measured. This is not surprising since determining the density, conductivity, and specific heat of heterogeneous soil and rock layers is difficult. In fact, the ASHRAE *Handbook of HVAC Applications* acknowledges that long-term field-monitored data are a major missing component in the effort to improve calculations for geothermal system design (greater detail about calculations for

Geothermal Conditioning: Critical Sources for Sustainability. Table 2 Key soil and rock properties for thermal performance

Property	Common symbol	Units	
Density	ρ	kg/m	
Specific heat capacity	c_p	J/kg K	
Thermal conductivity	k or λ	W/m K	
Volumetric heat capacity	ρc	MJ/m^3 K	Specific heat * density
Thermal diffusivity	α or κ	m^2/s	Conductivity/volumetric heat capacity
Thermal inertia	I	J m^{-2} K^{-1} s$^{-½}$	√ density * specific heat * conductivity

Geothermal Conditioning: Critical Sources for Sustainability. Table 3 Surface and ground properties affecting subsurface temperature change

Material	Density (ρ) in kg/m^3	Specific heat capacity (c_p) in J/kg K	Volumetric heat capacity (ρc) in 10^{-6} J/m^3 K	Thermal conductivity (k) in W/m K	Thermal diffusivity (κ) in 10^{-6} m^2/s	Thermal inertia (I) in J m^{-2} K^{-1} s$^{-½}$.
Air (STP)	1.29	1,005	0.0012	0.02	15.43	5.09
Water	1,000	4,186	4.19	0.60	0.14	1,585
Sandy soil (dry)	1,600	800	1.28	0.30	0.23	620
Sandy soil (saturated)	2,000	1,480	2.96	2.20	0.74	2,552
Clay soil (dry)	1,600	890	1.42	0.26	0.18	192
Clay soil (saturated)	2,000	1,550	3.10	0.58	0.19	1,341
Rock (basalt)	2,600	800	2.08	2.50	1.20	2,280

geothermal system design is provided by Kavanaugh and Rafferty) [11]. More important than the specific depth of the neutral zone is its occurrence in the ground temperature profile. Within a few meters from the earth's surface, a zone in which building foundations exist, the ground temperature reaches or approximates long-term thermal equilibrium with the atmosphere due to incident solar radiation. Effective integration of the ground's low-temperature heat supply and heat storage capacity can substantially reduce consumption of nonrenewable energy for building conditioning.

Interior Energy Input: Beyond the neutral zone, the temperature typically rises with depth, following what is called the geothermal gradient, shown in Fig. 4 as a broken line descending from the surface. The temperature rise along the geothermal gradient reflects heat flow from the earth's interior via conduction through solid rock and convection within geothermal fluids. Of the sources of heat energy within the earth, *radiogenic heat*, from the decay of radioactive isotopes, contributes the greatest share, annually estimated as 8.6×10^{20} J [13]. The geothermal gradient can vary substantially by locale and region. Recent research suggests that the gradient can be lowered or reversed, at least to 250 m depth, with increased energy input at the surface. Ongoing monitoring of well temperatures by Majorowicz et al. shows that rising surface air temperatures are increasing the amount of thermal energy stored in the shallow geothermal environment in

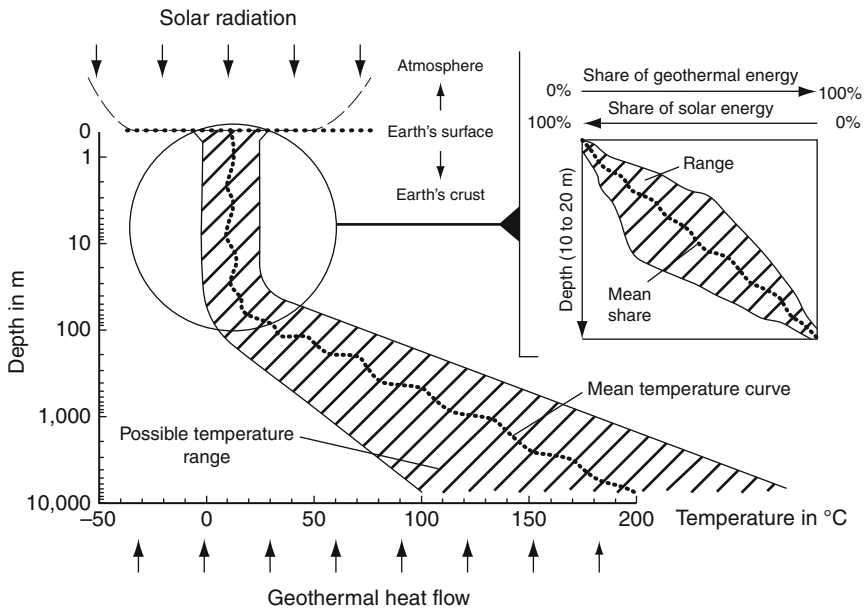

Geothermal Conditioning: Critical Sources for Sustainability. Figure 4
Ground thermal flows and temperature profile [12]

some locations. Their analysis of temperature changes down to 250 m shows that the near-surface heat gain is also creating a null or negative thermal gradient. As a result, drilling below 50 m depth in these locations offers little thermal benefit for heating applications [14]. Their findings also suggest that the ground's near-surface thermal storage (heat sink) capacity may diminish with rising air temperatures.

Globally, the average geothermal gradient ranges from 30 to 60 K/km, but the gradient may be a little as 10 K/km in older crustal areas or as high as 200 K/km in tectonically active areas such as Iceland. The most tectonically active country on earth, Iceland has more than 200 volcanoes. Nearby ground temperatures exceed 200°C at 1 km depth and outside the volcanically active zone, the geothermal gradient is still quite high at 150°C/km. In 2008, 62% of Iceland's primary energy and 24.5% of its electricity came from its geothermal resources [15].

Geothermal Conditioning Principles and Approaches

An essential principle in sustainable building design is to create a building enclosure that manages as much of the heating, cooling, and ventilation loads as possible [see "High Performance Building Facades: Enclosures for Sustainability," V. Hartkopf, A. Aziz and V. Loftness in this volume]. With a high-performance enclosure, the size of the mechanical equipment and its related energy consumption and carbon emissions are reduced. In addition, sustainable building conditioning employs the following general strategies [16].

- Use water as an energy carrier since it carries 3,000× the energy that air carries in an equivalent volume.
- Use low-exergy systems, independently or as part of an energy cascade, to match the energy content of the supply more closely with the need.
- Use distributed rather than central systems, that is, multiple small units distributed throughout the building with commensurate controls rather than a single large central unit to cut transmission losses and to deliver thermal comfort close to building occupants.
- Zone the system to allow equipment to operate at full load efficiency and only when needed to support occupant comfort and health and building durability.
- Use renewable energy and energy recovery wherever possible.

- Design a flexible system that accommodates reconfiguration of interior space over time while maintaining original level of performance.
- Separate the delivery of ventilation air from heating and cooling, and integrate the monitoring of these systems for occupant comfort and energy effectiveness.
- Provide means for occupants to adjust thermal comfort conditions.
- Incorporate sufficient sensors and metering capability so that occupant and building operators can see, assess, and improve conditioning system performance.

Geothermal conditioning lends itself well to the application of these strategies. It provides a renewable source of thermal energy and a heat sink for heating, cooling and ventilation. With the exception of passive earth sheltering and earth tube ventilation systems, geothermal conditioning typically uses water or a water/antifreeze mix as an energy carrier for all or part of the system. Most geothermal conditioning systems are low-temperature/low-exergy systems and those that are not often use energy cascades with energy recovery to make effective use of higher temperature ground resources. The total savings from geothermal conditioning will vary widely depending on the local climate and subsurface temperatures, the conditioning strategy, and its design and operation. Nonetheless, because the ground temperature often approximates the average annual air temperature in a given location, a geothermal approach is likely to save energy wherever the average annual air temperature is closer to the building balance point temperature than the outdoor temperature range.

Discussions of geothermal conditioning often focus on heat pumps as the interior delivery system. One reason for this is that heat pumps operate efficiently at temperatures commonly accessible at and within a few meters below a building foundation. In addition, even when a heat pump's energy consumption is evaluated as source or primary energy rather than site energy, its efficiency usually exceeds 100%. (Note: Primary or source energy is the energy value based on source fuel inputs. For electricity, this is the energy value of the oil, natural gas, coal, or other source fuels used to generate the electricity and is typically 3.0–3.5 times higher than the energy value of the electricity at the building site.) This is because the heat pump can use heat in the ambient air, ground, or water to cause certain refrigerants to vaporize and to reach a much higher temperature when compressed. Low-grade heat coupled with a refrigerant cycle allows the heat pump to supply heat to or absorb heat from a building with a fraction of the energy required by combustion heating or conventional air conditioning.

In the case of a geothermal heat pump, the heat is being transferred from and to the ground or ground-coupled water. In heating mode, a compression heat pump transfers the earth's thermal energy, often in the range of 10–15°C, to a refrigerant that evaporates as the heat is absorbed and becomes a gas. The refrigerant gas then passes through a compressor where it is pressurized. This increases its temperature, generally above 71°C. The heated gas then passes through another heat exchanger, transferring its heat to air or water being used to heat the interior space, often at 38–43°C. As the refrigerant gas loses heat, it condenses back to a liquid, is cooled as it passes through an expansion valve, and is then ready to repeat the cycle (see Fig. 5). A reversing valve allows the heat pump to change the direction of refrigerant flow, causing heat from the indoor space to be transferred to the refrigerant and later to the ground. Compression heat pumps are by far the most common, but absorption and adsorption heat pumps also exist. Like compression heat pumps, absorption heat pumps use low-grade heat to vaporize a refrigerant, but use thermal energy rather than electricity to compress the refrigerant. Adsorption heat pumps, still in development, also use thermal energy to drive the process [17]. Heat pumps and their operation are extensively discussed in several sources [18–20], but their efficiency is a key aspect of their sustainability and is briefly summarized here.

The efficiency of the heat transfer process is the ratio of the energy used to drive the process to the amount of heat transferred. This is called the coefficient of performance or COP. In heating mode, the COP is the ratio of heat supplied to energy used. In cooling mode, the COP is the ratio of heat removed to the energy used [22].

$$\text{COP} = \text{Heat Supplied or Heat Removed (kW)}/\text{Power Input(kW)}:$$

As an example, a geothermal heat pump that provides 12 kW of heat output with 3 kW of electricity has

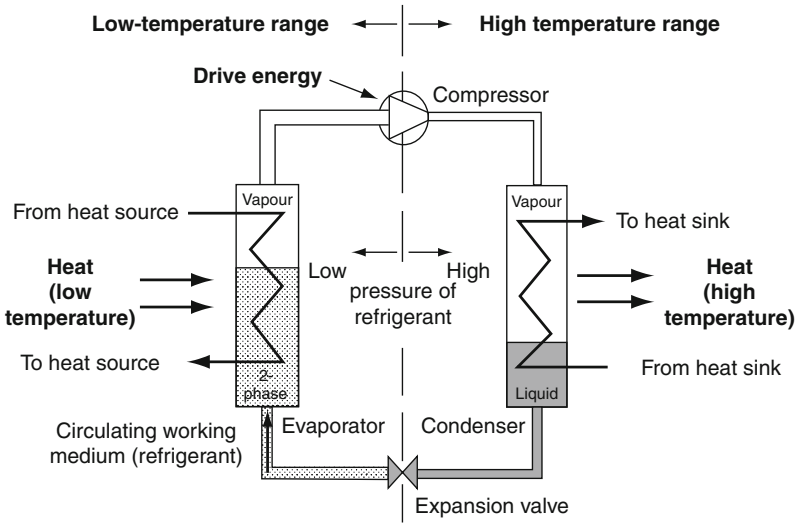

Geothermal Conditioning: Critical Sources for Sustainability. Figure 5
Diagram of vapor compression heat pump in heating mode [21]

a heating COP of 4. This means that one part electrical energy and three parts ground thermal energy supply four parts of usable energy. On a site energy basis, this means that the heat pump efficiency is 400%. When considered from a source or primary energy perspective, and assuming a 30% source to site conversion efficiency for electricity, the source efficiency of this heating process is 120% (30 × 400%). The COP given by the manufacturer is determined under specific operating conditions that usually vary from those on site. Manufacturer COPs typically range from 3 to 6 at present.

The efficiency of heat pumps over the course of a year under actual operating conditions and considering auxiliary system components such as circulation pumps is expressed as the seasonal performance factor (SPF) or average annual COP. The SPF is the ratio of the system's usable energy output to the energy input.

$$\text{SPF} = \text{annual usable energy output (kWh)} / \text{annual energy input (kWh)}$$

This measure more accurately describes system performance and is often lower than the equipment's rated performance for several reasons. Commonly, a heat pump that provides heating and cooling is sized for the dominant load. This may mean that a heat pump with sufficient heating capacity, for example, is oversized for cooling and therefore operates less efficiently in cooling mode. In addition, a system often does not operate at the temperatures at which it is rated but rather under more variable temperatures that decrease its efficiency. Cited SPFs for geothermal heat pumps vary considerably, but may be in the range of 3.3–4.3 [23]. Because a heat pump is able to derive a substantial portion of its heating energy or heat removal capacity from ambient air, the ground, or groundwater, its efficiency generally exceeds that of any other mechanical conditioning equipment powered by nonrenewable energy, even when the source to site conversion efficiency of the power source is much higher than that for electricity, for example, natural gas [24].

A heat pump's ability to heat and cool makes it effective in distributed systems (also known as unitary systems), particularly in mixed-use buildings. In fact, a distributed approach tends to be more energy efficient [25]. In a mixed commercial/residential building with multiple heat pumps connected to a single internal water loop, heat pumps in commercial zones with high internal loads might be in cooling mode while

those in residential zones are heating. Because a heat pump in cooling mode returns warmer water to the internal loop and a heat pump in heating mode returns cooler water to the loop, the temperature of the internal loop will be self-balancing to some extent, remaining in a temperature range favorable for efficient heat pump operation for an extended time period. This reduces the need for heat transfer between the external (ground) loop and internal loop and thus the pumping energy required. Either alone or in combination with other low-exergy equipment such as radiant wall, floor or ceiling panels or fan coil units, heat pumps can be flexibly configured to deliver thermal comfort efficiently and close to the point of use. See Fig. 6 for a geothermal heat pump system design strategy/guideline, developed by Kavanaugh [26].

Heat pumps are not, however, a component of every geothermal conditioning strategy. By focusing on the thermal properties of soil, rock, and water, a host of strategies has been developed to couple building heating and cooling with the ground and ground-coupled fluid. Tables 4 and 5 list many available options. Each capitalizes on the capacity of the ground or ground-coupled water to absorb and supply substantial thermal energy while maintaining a fairly constant temperature year-round. (Note: UTES systems are the exception; they may be designed to concentrate thermal energy for seasonal use, as described later in this section.) The basic components of each approach are (a) the ground coupling through which thermal energy is transferred to and from the ground and (b) the internal system through which thermal energy is distributed from or to the ground for comfort conditioning. Because this entry focuses on the earth's thermal energy for sustainable conditioning, Tables 4 and 5 emphasize ground coupling options. Table 4 lists closed loop systems in subsurface soil and rock and Table 5 lists water-based systems, both open and closed loops. Within the system descriptions and examples, however, internal system options are often discussed.

Like solar conditioning, geothermal conditioning can be passive or active. In essence, every building in contact with the ground exchanges heat with it, intentionally or not. In fact, any ground-based construction, including roads and pavement, alters the ground's thermal profile by changing characteristics such as albedo, reflectivity, and rainwater absorption, and by adding heat transfer surfaces. Passive geothermal conditioning is by far the oldest approach listed, but like passive solar conditioning, it may be overlooked.

Active strategies are more numerous and can be subdivided into approaches that use subsurface soil and rock for their ground coupling and those that use water. The effectiveness of a given approach will depend on site conditions and natural resources, the local geothermal gradient, and many project-specific variables. In recent years, system designers have also developed approaches that derive their thermal stability from a subsurface location (e.g., sewer pipe) while the source of their thermal energy may be other than geothermal, for example, residual heat in building wastewater.

With the exception of earth sheltering and earth tube ventilation systems, geothermal conditioning approaches use a fluid as the energy carrier or heat transfer medium between the outdoor and indoor system components. The interface between the outdoor and indoor components is often a heat exchanger or heat pump, although other types of equipment are possible. Ground sources that provide higher temperature heat (e.g., >30 C) must interface with something other than a heat pump because the maximum input water temperature for a heat pump is approximately 32°C and its efficiency is compromised at these higher temperatures. In open loop water-coupled systems, a heat exchanger is recommended as a buffer between the external water source and the indoor conditioning equipment because of the lively chemistry and/or biology of these water supplies [27].

All of the geothermal conditioning approaches in Tables 4 and 5 take advantage of the earth's stable, low-grade thermal energy and its heat capacity. Most systems use these ground characteristics for energy exchange, to provide a heat source and heat sink for the building. Some approaches target thermal storage only. Given the range of options available and an increasing emphasis on low-exergy conditioning technologies, one or more geothermal conditioning approach is probably feasible in most buildings.

Subsurface Soil and Rock Systems

With the exception of earth sheltering, subsurface soil and rock systems use a fluid enclosed in pipe to transfer

#1 - Building Layout

* Divide floor plan into zones
* Calculate heat loss/gain for each zone
* Group building zones into one central or multiple ground loops

#2 - Select Equipment

* Select heat pumps for each zone based on **capacity and efficiency** at design conditions
* Consider head loss, temperature range, package type, sound, serviceability
* Specify water source water heating and refrigeration equipment if applicable
* Select ventilation air system components—ducting, heat recovery, preconditioning coils, etc.

#3a - For GCHPs

* Determine ground properties (test bores)
* Specify tube type, size, bore separation, backfill
* Calculate required bore
* Design exterior headers
* Design purge system

3b - For GWHPs

* Determine groundwater availability/quality
* Specify required well flow
* Specify water disposal method
* Specify groundwater-to-loop water heat exchanger

3c - For SWHPs

* Find reservoir flows, depth, and temperatures (high/low)
* Specify coil size & type
* Calculate required coil length
* Design exterior headers
* Design purge system

#4 - Design Building Piping Loop

* Weigh advantages of central loop vs. multiple loops
* Route and size piping system for low pressure losses
* Provide on-off flow control through heat pumps and isolation valves
* Specify materials—indoor piping, insulation, antifreeze, inhibitors

#5 - Specify Pump and Control Method

* Weigh advantages of central pump(s) vs. multiple remote pumps
* Select pump(s) to operate near maximum efficiency on pump curve
* Weigh pump control options—no control, on-off, multispeed (or multiple pump), variable speed
* Calculate loop pump power and redesign system if greater than 10% of total demand

#6 - Evaluate Other Alternatives

* Use higher efficiency heat pumps to reduce required ground loop size?
* Use cooling tower or fluid cooler to reduce loop size?
* Increase or decrease bore separation or coil tubing size?
* Look at cost of multiple loops and pumps vs. central loops and pump—**include cost of controls.**

Geothermal Conditioning: Critical Sources for Sustainability. Figure 6
Strategy for geothermal heat pump system design. *GCHPs* ground-coupled heat pumps (soil-based systems), *GWHPs* groundwater heat pumps, *SWHPs* surface water heat pumps

Geothermal Conditioning: Critical Sources for Sustainability. Table 4 Subsurface soil and rock systems (all closed loops)

Passive or active strategy	Exterior equipment/ configuration	Typical depth	Energy carrier	Function	Exterior/interior interface
Passive	Earth berms	At grade or foundation depth	Soil	Insulation, thermal mass, reduced infiltration, reduced solar gain	Building enclosure
Active	Earth tubes	3–5 m	Air	Preheating or cooling of ventilation air	Energy recovery ventilator; possibly UV disinfection
	Horizontal trench with straight pipe or slinky coil	1–2 m	Water–antifreeze mix	Energy exchange for heating and/or cooling	Heat pump
	Direct connection to conditioning equipment	1.2–2 m	Refrigerant		Heat pump
	Building foundation piles (open or closed)	5–30 m	Water or water–antifreeze mix		Heat pump or heat exchanger
	Shallow vertical boreholes with U-tube pipe	30–120 m	Water or water–antifreeze mix		Heat pump
	Deep vertical boreholes with coaxial pipe	1,000–3,000 m	Water		Heating equipment or heat exchanger (typically cooling not attempted with deep systems)
	BTES (borehole thermal energy storage)	20–300 m	Water or water–antifreeze mix	Seasonal hot or cold storage for increased efficiency	Heat pump, heat exchanger, cogeneration power plant, solar hot water system

heat between the building and the outdoors. For earth tubes, that fluid is air and for other systems, refrigerant, water, or a water/antifreeze mix. Under normal operating conditions, there is no direct contact between the fluid and the subsurface environment and this type of sealed subsurface pipe heat exchanger is called a closed loop system.

Design and sizing of the ground heat exchanger is a key aspect of system cost and performance. The characteristics of underlying soils and rock, ground moisture content and water movement are among the variables that affect ground temperature and heat transfer and these can be difficult to model with precision. Research has also shown that in low-temperature systems, the effectiveness of the ground heat exchanger is strongly associated with its heat transfer over time, particularly when multiple heat exchanger pipes are in close proximity [28]. Abundant research focuses on this topic and many sizing calculations, modeling tools, and rules of thumb exist to support this task [13, 29]. It is worth noting, however, that the validity of available sizing methods is still debated by those who design and operate closed loop systems [30]. Data from operating systems are also lacking [31]. Despite these

Geothermal Conditioning: Critical Sources for Sustainability. Table 5 Water-based systems (all active strategies, both closed and open loops)

Water source	Open or closed loop	Exterior equipment/ configuration	Typical depth	Energy carrier	Function	Exterior/ interior interface
Aquifer	Open	Supply well with surface discharge	15–100	Groundwater	Energy exchange for heating and/or cooling	Heat exchanger
		Supply and injection wells, shallow or deep	15+	Groundwater		Heat exchanger, cooling or heating equipment
		Standing column (or coaxial) well	120–375 m	Groundwater		Heat pump
		ATES (aquifer thermal energy storage)	10–400 m	Groundwater	Seasonal hot or cold storage for increased efficiency	Heat exchanger
Surface water (ocean, lake, river)	Open	Supply and reinjection pipe	Varies by water body; ideally at depth where temperature is stable and where reinjection does not affect natural seasonal cycling	Surface water	Energy exchange for heating and/or cooling	Heat exchanger
	Closed or Open	Slinky coil	3–3.5 m minimum; sufficient depth so that supply temperature always $>4°C$	Water or water–antifreeze mix		Heat pump or heat exchanger
Abandoned mine tunnels	Open	Supply and reinjection pipe	Varies with mine	Groundwater	Energy exchange for heating and/or cooling	Heat exchanger, heating or cooling equipment
	Open	CTES (cavern thermal energy storage)	Up to 2,000 m	Groundwater possibly with phase change material	Seasonal hot or cold storage for increased efficiency	
Sewer infrastructure	Closed or Open	Heat exchanger within/around pipe	Standard sewer pipe depth for given location	Water or water–antifreeze mix	Energy exchange for heating and/or cooling	Heat pump
Water treatment infrastructure	Open	Supply and reinjection pipe	Surface or subsurface pipe	Treated wastewater	Energy exchange for heating and/or cooling	Heat exchanger

challenges, the majority of ground-coupled systems now being installed are closed loop systems [32]. Brief descriptions of soil- and rock-based systems and installed examples are offered below.

Earth Sheltering The simplest form of geothermal conditioning is the passive strategy of earth sheltering, also called earth berming or earth integration. Ground temperatures begin to converge on a steady value just 30–50 cm below the surface [8]. An earth-sheltered building enclosure at and below this depth experiences temperatures that vary only a few degrees throughout the year and will generally be warmer in winter and cooler in summer than the outdoor temperature. The constant temperature, together with the reductions in air leakage and in convective and conductive heat loss that accompany earth sheltering, can substantially reduce mechanical conditioning requirements. The effectiveness of earth sheltering is well established, but its use requires careful attention to orientation, structure, waterproofing, daylighting, and egress as well as the standard range of design considerations. Although current enclosure design strategies focus largely on reducing heat transfer at the foundation, there may be substantial room for development or redevelopment of passive geothermal conditioning strategies [33].

Earth Tubes (also called Earth Pipes or Earth-to-Air Heat Exchangers)

Earth tubes are buried pipes through which outdoor air is drawn into the building. The earth's temperature can heat the air in winter and cool it in summer, reducing the energy required to condition ventilation air and in some instances, eliminating the need for additional cooling equipment. Monitoring data for earth tube systems are still limited, but Pfafferott [34] offers a comparative analysis of the performance of systems installed in three buildings in Germany between 1999 and 2001. He found that each system supplied far more heating and cooling energy than the primary energy used by the fans and that the ground characteristics and the impact of the building on ground temperature were as important as the earth tube diameter on thermal efficiency. To avoid unwanted heating in summer and cooling in winter, a control strategy is necessary. In some systems, permeable pipe is used to allow condensation within the tubes to evaporate and UV filtration is used to address mold or bacteria the may be in the air stream. Where radon is a concern, care must also be taken that the earth tubes are not transferring radon gas from the ground into the ventilation system [35].

Horizontal Trench, Pipe, or Slinky Coil Small building loads can be handled with a horizontal ground heat exchanger installed below the frost line (Fig. 7). Since trenching is less expensive than drilling, horizontal installations cost less but require more land area; increased temperature fluctuations at shallower depths (1–2 m) mean that increased pipe length (heat transfer surface area) is required. Because of the land area requirement, horizontal ground heat exchangers typically serve building loads less than 175 kW.

Building Foundation Heat Exchangers (foundation piles, energy piles, slot-die walls): Structural components such as piles, retaining walls, and foundation slabs can be used to exchange thermal energy between

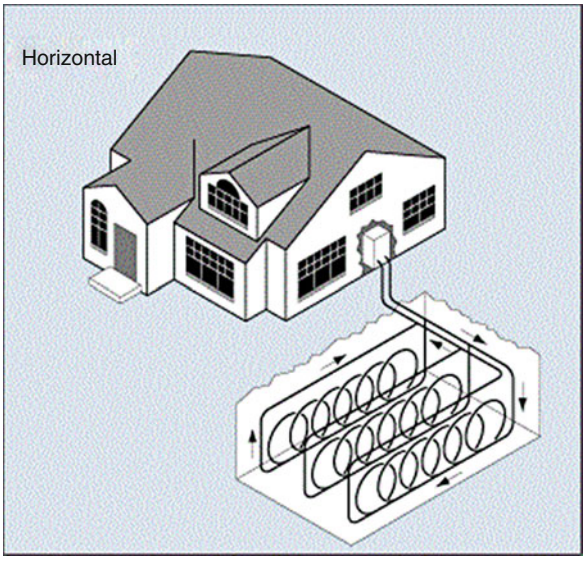

Geothermal Conditioning: Critical Sources for Sustainability. Figure 7
Horizontal ground heat exchanger

the ground and the building. Fluid-filled pipe systems are incorporated inside the foundation elements and serve a purpose similar to vertical borehole exchangers, but within the building's footprint. Relatively new (1990s) as a design strategy, foundation piles may be steel, precast concrete, or cast in place concrete [36]. The piles contain two or more U-tubes (see Fig. 8) that are connected either directly (open) or indirectly (closed) to the building's mechanical system. Pump energy is minimized since the heat exchanger is within the building footprint. Currently, design of these systems is adapted from vertical borehole design and because of uncertainties about the mechanical behavior of the soil over time (thermoelasticity and soil strength with heating and cooling), substantial safety factors are built into these systems, resulting in high costs [37].

Vertical Boreholes, Shallow The most common type of closed loop ground heat exchanger is a shallow vertical borehole system. Borehole diameters vary by pipe size and by construction convention, which differs by country to some extent. In the United States, a typical borehole is about 10–15 cm diameter. The depth may range from 30 to 120 m, depending on several factors such as the conditioning load, available land area, ground conditions and temperature, and drilling costs. A U-tube or ground probe, usually of high-density polyethylene (HDPE) pipe and often 19–25 mm pipe diameter, is inserted into each borehole (see Figs. 9 and 10) and the borehole should be packed and sealed with grout, at least at the surface, to prevent surface contaminants from passing easily down the borehole and into groundwater. (Note: Requirements for grout vary, although the potential for surface contaminants to reach groundwater more easily through a borehole does not. Grouts with improved heat transfer characteristics are available.) The total underground pipe length must provide sufficient heat transfer to satisfy the connected peak block load, which is the maximum cooling or heating load, whichever is greater, imposed on the conditioning equipment during the cooling or heating season. (Note: If the building has good load diversity, the peak block load will be less than the sum of the peak room loads or peak zone loads.) Except where borehole thermal energy storage (BTES) is used, boreholes are often spaced 4.5–6 m apart so that heat transfer with the ground is not compromised by proximity to other boreholes. A radial configuration for shallow boreholes has also been developed [39].

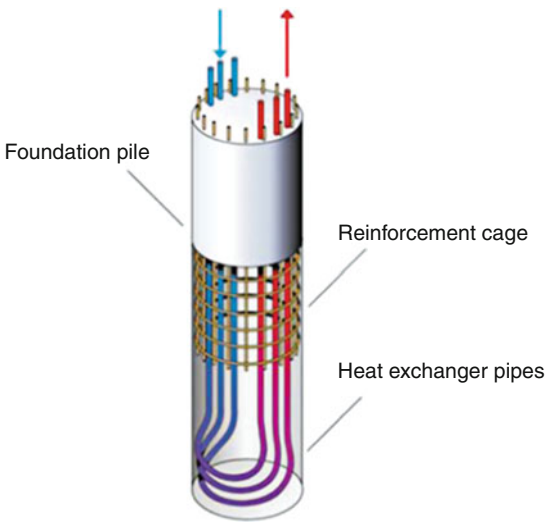

Geothermal Conditioning: Critical Sources for Sustainability. Figure 8
Building foundation pile heat exchanger [38]

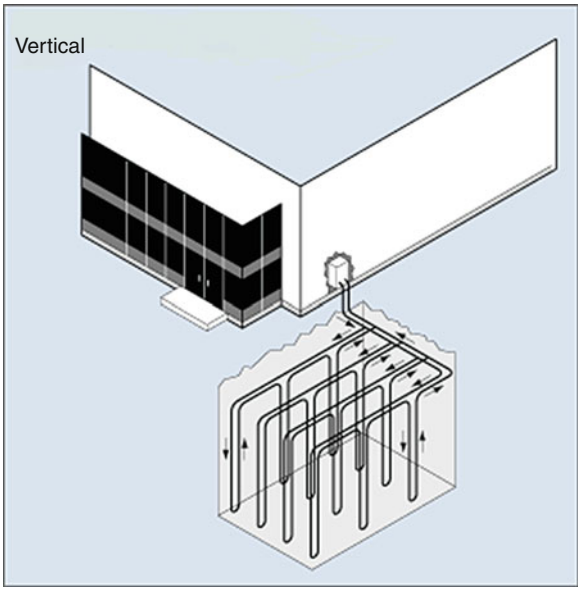

Geothermal Conditioning: Critical Sources for Sustainability. Figure 9
Vertical borehole heat exchanger

Geothermal Conditioning: Critical Sources for Sustainability. Figure 10
HDPE U-tube for vertical borehole [40]

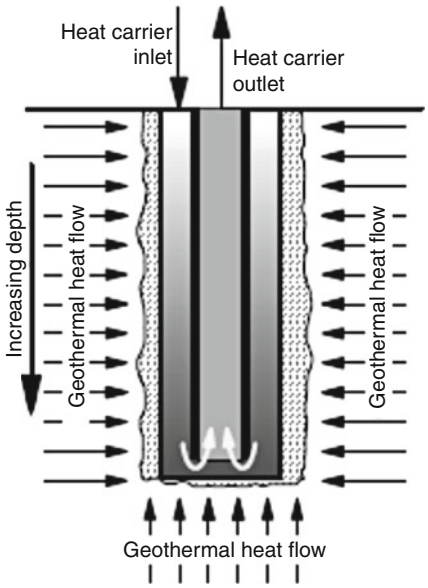

Geothermal Conditioning: Critical Sources for Sustainability. Figure 11
Deep borehole heat exchanger [42]

Vertical Boreholes, Deep Deep borehole systems, 1,000–3,000 m, capitalize on higher ground temperature at depth and so are predominantly used for heating. In this type of system, an insulated production pipe is inserted into a borehole casing sealed at the bottom, providing a concentric pipe configuration. The heat transfer fluid, typically water that may be treated with a corrosion inhibitor, is pumped down the borehole casing, and up through the central production pipe (see Fig. 11). There is no direct contact between the heat transfer fluid and the subsurface soil and rock; the fluid gains heat at depth according to the geothermal gradient. At well exit, the heat transfer fluid passes through a heat exchanger, heat pump, or other heating equipment, depending on the fluid temperature (±40°C). The higher cost of deep borehole systems makes them better suited to serve the base load in systems that have sizable heat demand (see Fig. 12) [41].

Borehole Thermal Energy Storage Borehole thermal energy storage, BTES, is a type of underground thermal energy storage (UTES) system used to concentrate heat and cold for seasonal use. For a BTES, vertical boreholes are placed in close proximity (1.5–3 m apart) to seasonally charge the system with hot or cold fluid. In summer, for example, a heat pump or other mechanical device can transfer heat to the ground for winter heating. In winter, that heat can be extracted and the ground can be charged with cold fluid for summer cooling. For efficiency, different ground areas or depths are often used for hot and cold storage. Although some heat or cold is lost at the system edges and at the ground surface, these systems can be used successfully in existing subsurface rock and soil; constructed storage vessels are not required. From a cost standpoint, underground thermal energy storage systems, including BTES, ATES, and CTES systems, tend to work best for small district systems rather than for single buildings.

Examples of Subsurface Soil and Rock Geothermal Systems *Earth Tubes*: Fraunhofer ISE, Freiburg, Germany: Installed in 2001, the earth-to-air energy exchanger provides cooled or preheated air with a ground temperature of 13.8°C. This open loop system consists of seven polyethylene ducts, 90–100 m long and 250 mm in diameter, buried 4–5 m and

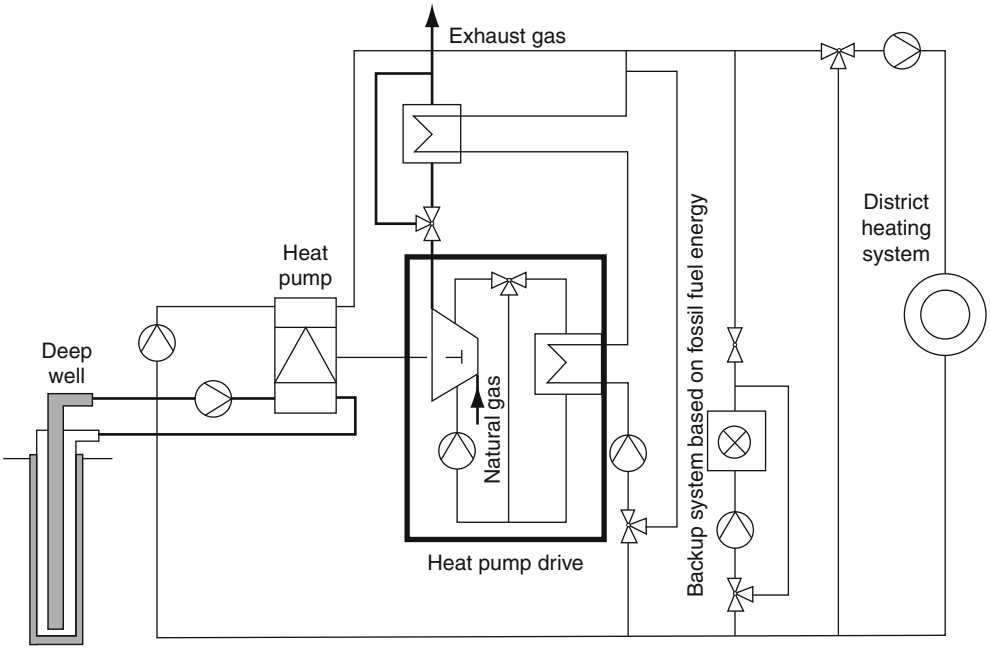

Geothermal Conditioning: Critical Sources for Sustainability. Figure 12
District system served by deep borehole exchanger [41]

partially below the foundation slab. The air speed is 5.6 m/s and mean airflow is 7,000 m^3/h. The system is controlled by air temperature at the inlet and does not operate between 12°C and 16°C. During a 1-year analysis of the system from November 2001 to October 2002, the COP was 29 kWh_{th}/kWh_{mech}, high enough to supply more heating and cooling energy than the primary energy used for fans, with a fan efficiency of 70% [34].

Vertical Borehole Heat Exchanger: In 1993, a 2.2 MW vertical borehole heat exchanger was installed at Richard Stockton College in Pomona, New Jersey (USA) to allow replacement of aging gas-fired heaters and electric compressor type coolers with geothermal heat pumps. A total of 400 boreholes 425 ft (129.54 m) deep and approximately 4.5 m apart were installed under an existing parking lot and adjacent open area. Each 10 cm borehole contains a single 3.25 cm diameter HDPE plastic U-tube pipe and is sealed with clay slurry. Twenty lateral supply and return pipes channel the water circulating through the boreholes to central building where they are combined into 16 in. (40.64 cm) supply and return lines that serve heat pumps (35–123 kW) in campus buildings. The system reduced natural gas consumption approximately 75% and electricity consumption 25%, despite the switch to heat pumps. Since 1993, the college has added substantial geothermal conditioning infrastructure, both closed and open loop systems, and in 2008, an aquifer thermal storage system [43]. Extensive monitoring of system performance and ground/groundwater conditions is conducted.

Building Foundation Piles: The nursing school at Sapporo City University in Japan, completed in 2006, uses steel foundation piles filled with water to provide a ground heat exchanger that supplies the building's base heating and outdoor air cooling loads. For a floor area of 2,800 m^2, 51 piles from 600 to 800 mm diameter were drilled 4 m into the ground. Two U-tubes were inserted in each pile and the pile was filled with 115 m^3 water. The manifold system for the piles feeds a 50 kW heat pump that provides both heating and cooling. Three vertical boreholes 75 m long supplement the system so that the ground heat

exchanger system can meet the base heating load of 50 kW and the base cooling load for outside air. During 2007, the piles extracted 43,929 kWh of heat from the ground in winter and transfer 53,939 kWh of heat into the ground in summer [36].

Borehole Thermal Energy Storage (BTES): The Drake Landing Solar Community in Okotoks, Alberta (Canada) relies on the earth's high volumetric heat capacity to store heat captured with solar hot water systems in summer months and to provide heat throughout Alberta's cold winter. Opened in 2007, the Drake Landing project is a district system serving 52 well-insulated single-family homes. Heat from 800 single-glazed roof-mounted solar hot water panels is fed to a seasonal thermal storage system that consists of 144 vertical boreholes approximately 30 m deep. The borehole field was anticipated to require 5 years to fully charge to 80°C by summer's end, thereby allowing it to supply 90% of the community's heating energy (90% solar fraction). However, 3 years after it began operating, the system reached 80% solar fraction and should be fully charged in 2011. Fan coil units are the terminal heating equipment in each home [44].

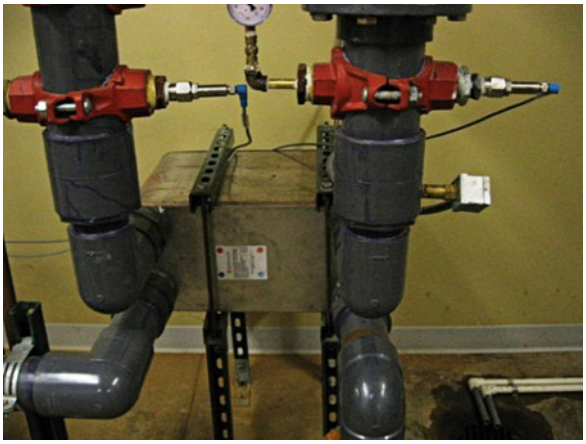

Geothermal Conditioning: Critical Sources for Sustainability. Figure 13
Brazed plate and frame heat exchanger in 4,000 m^2 mixed-use building. Water's remarkable heat capacity allows smaller mechanical system components than those required by air-based systems [47]

Water-Based Systems

Water-based systems use water that originates outside the building – generally groundwater or surface water – as the energy carrier. With a few exceptions, this externally sourced water is piped to the building where it transfers heat in direct contact with some component of the conditioning system: a heat exchanger, heat pump, or other conditioning equipment (see Fig. 13). It is then piped away from the building for release to or near the original water source and usually at a temperature within 6°C of its source temperature. This is called an open loop system. Closed loop water-based systems bring building piping to the external water source such as a pond or lake. Like other closed loop systems, the building piping is filled with a fluid that transfers heat between the building and the outdoors and there is no direct contact between the external water source and the heat transfer medium in the building pipes.

The reason for emphasizing direct contact between an external water supply and the building mechanical equipment, or the lack thereof, is that water is an excellent solvent that "dissolves more substances in greater quantities than any other liquid" [45]. Water will react with pipes and equipment, and natural water such as groundwater or surface water contains minerals and microbes from surrounding soil and rock that can promote those reactions, particularly in the presence of oxygen (see Fig. 15). Whereas equipment connected to the municipal water supply is often treated with chemicals to control chemical and biological activity (e.g., cooling towers), equipment connected to a natural water supply cannot be handled the same way. This characteristic is understood and addressed in water well literature, but underemphasized in building systems literature and should not be ignored in practice when sustainability is the goal [46].

As with subsurface soil and rock systems, the design and sizing of the heat exchange system is a key aspect of overall cost and performance. One obvious prerequisite is the proximity of a suitable water source. Local regulations must also support the use of such systems. In groundwater applications, the water is pumped from an aquifer at stable temperatures similar to the ground temperature at that depth and is discharged either to

surface water or to the same aquifer. Ease of access, water quantity, water quality, and viable discharge options are the limiting factors. In surface water applications, which can be either open or closed loops, water temperature and quantity are essential factors for effective heat exchange. The water temperature must not fall below 4°C and must remain in an efficient range for cooling (preferably <23°C) regardless of solar radiation and other heat transfer to the water. For open loop surface water applications, water quality is also important and can vary seasonally and during storms. Whereas soil- and rock-based heat exchangers are estimated to have a heat output of 20–50 W/m^2, the heat output of groundwater and surface water systems is estimated to be 2,300–4,600 W/m^3/h [18]. Brief descriptions of water-based systems and installed examples are offered below.

Aquifer-Based System Before the development of plastic pipe that could be used for closed loop systems, aquifer-based open loop geothermal systems predominated. Two primary configurations exist: those that reinject the water into the ground, usually into the source aquifer (Fig. 14), and those that discharge to surface water (pump and release or, colloquially, pump and dump systems). Well depths may range from 15 to 100+ m and flow from 1 to 125+ L/s.

Because they require less exterior infrastructure, aquifer-based systems need less land area and have lower first costs. Conventionally, the considerations in choosing an aquifer-based system include proximity to the building site; groundwater availability/quantity, depth and flow rate; water chemistry; the conditioning system temperature drop and load factor; and the groundwater discharge strategy. Today, however, a primary consideration for the sustainability of these and all other groundwater applications may be the protection of drinking water resources. Groundwater is a preferred source of drinking water, but lax or nonexistent groundwater regulation in the past and even at present has allowed contamination and depletion of known aquifers. Population growth compounds these problems. Although some aquifer-based systems have been operating for decades without dropping the groundwater table, ongoing use of aquifer water for any application must consider its impact on future drinking water supplies.

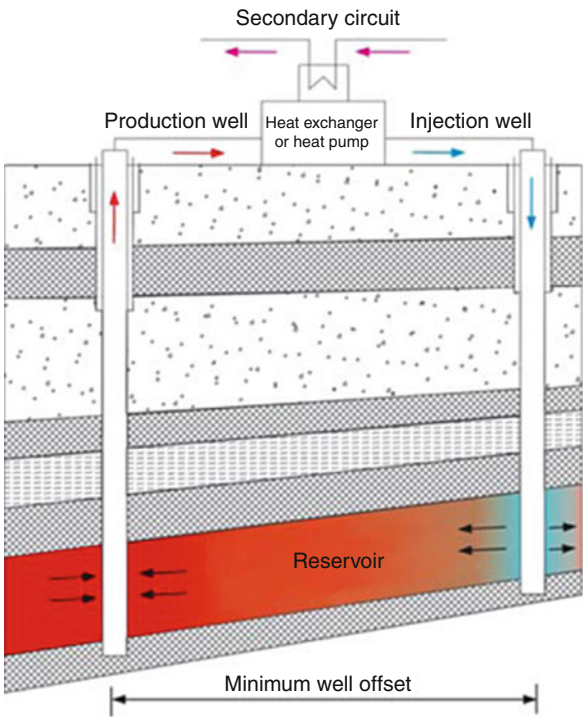

Geothermal Conditioning: Critical Sources for Sustainability. Figure 14
Open loop aquifer system with production and injection well [48]

Standing Column or Coaxial Well A standing column well (SCW) is an open loop system that draws and reinjects to the same well. SCWs are generally used where bedrock is close to the surface. The ground heat exchanger is a vertical well typically 150 mm diameter in bedrock with a 200 mm steel casing in the overlying unconsolidated layer. In shallower wells, the submersible pump is at the bottom of the well with the return near the top. In wells deeper than 150 m, return is generally via a 100 mm PVC dip tube that extends to the well bottom and is perforated for the last 6–18 m. A distinct characteristic of these wells is the practice of "bleeding" the well to control the temperature. Where freezing is possible, the well may be bled, typically with surface disposal, to draw warmer water into the well. Bleeding may also be used if the well is overheating in summer. SCWs connect directly to a geothermal heat pump and in residential systems may also provide domestic water.

Geothermal Conditioning: Critical Sources for Sustainability. Figure 15
Heat exchanger fouling from excessive iron in groundwater [49]. Failure to test groundwater prior to system installation may result in a system too maintenance-intense to operate economically

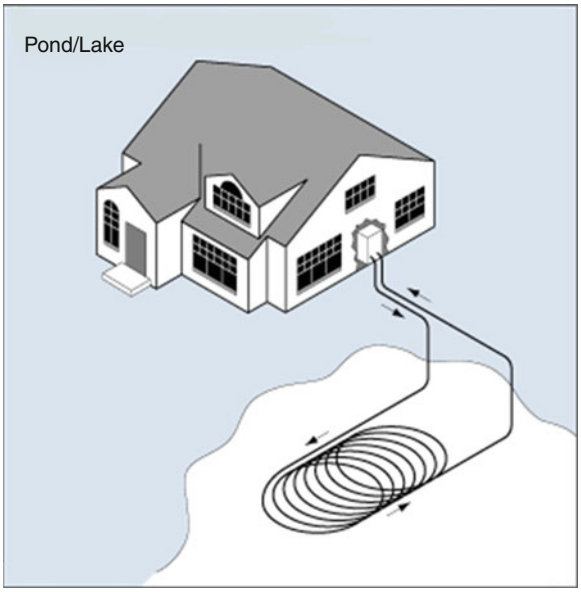

Geothermal Conditioning: Critical Sources for Sustainability. Figure 16
Closed loop surface water exchanger

Surface Water System The diverse thermal profile of surface water bodies results in similarly diverse strategies for surface water geothermal conditioning. Surface water systems can be either open or closed loops. They can be as shallow as a pond and as deep as the ocean (e.g., the Hawaii Gateway Energy Center, described below). In closed loop systems, water or a water/antifreeze mix is pumped through a submerged pipe loop that transfers heat to and from the body of water (see Fig.16). Compared to soil-based closed loop systems, water-based systems have lower excavation costs and usually lower costs for pumping and for overall operation and maintenance. Temperature variations in surface water are typically far greater than those in soil, however, so the system may be less efficient and at greater risk for freezing and other damage if the piping is accessible and/or close to the surface. In open loop systems, the surface water body is often used for a heat sink, similar in function to a cooling tower but without the noise, fan energy, chemical dosing, and maintenance demands. Direct cooling or precooling of ventilation air is also possible by pumping water at 10°C or below through a coil within a return air duct or convector system.

Aquifer Thermal Energy Storage Similar to BTES, aquifer thermal energy storage (ATES) is a means to concentrate heat and cold underground for seasonal use. A series of injection wells is used to inject either heated (13–120°C) or cooled (6–12°C) water for later withdrawal. Heat and cold can be stored at different depths if the underlying geology permits. Withdrawal can occur through the same wells, or through separate ones, in which case the water flows in the aquifer between injection and supply. China began installing large open ATES systems (surface water allowed to infiltrate groundwater) for cold storage in the 1960s [50]. The longest operating high-temperature system was installed at Ultrecht University in the Netherlands in 1991, using residual heat from cogeneration. Estimates of energy savings from ATES are quite high: 80% reduction in cooling costs and 40% reduction in heating costs [51]. Research indicates that a large percentage of land area is underlain by aquifers that could be used for ATES [51].

Abandoned Mine Tunnel/Cavity Systems Abandoned underground mines and tunnels accumulate groundwater. Depending on their size, these cavities can thermally function like an aquifer, providing an

underground reservoir at a stable temperature. Cavity thermal energy storage (CTES) systems typically use supply and injection wells. In some cases, environmental regulation (e.g., in the USA) require that groundwater in mine tunnels be treated for surface discharge. Where this occurs, a water treatment infrastructure system (see below) may be possible.

Sewer and Water Treatment Infrastructure Systems Sewer pipes and municipal or industrial pipes that carry treated water to its discharge point are typically buried and benefit from the ground's thermal stability and capacity. In addition, the processes that serve these pipes add heat energy so that the fluids they carry often have thermal energy content comparable to or higher than groundwater (>10°C). Although water treatment pipes may not be colocated with the buildings they serve, sewer pipes are. With constant and sufficient flow, these pipes and/or the fluids they carry provide a heat source and heat sink for geothermal conditioning without the need for new ground infrastructure. At least one company manufactures concrete sewer pipe with embedded heat exchangers to permit noncontact heat transfer (see Fig. 17) [52].

Examples of Water-Based Geothermal Systems *Aquifer Geothermal System with Surface Discharge*: The Galt House Hotel and Waterfront Plaza Office Towers in Louisville, Kentucky (USA) use a 21 MW open loop heat pump system to condition approximately 185,806 m^2 of hotel, office, and apartment space (see Figs. 18 and 19). The system was initially installed in 1984 and has since expanded to its current capacity. Seven wells approximately 40 m deep supply groundwater at 14°C and approximately 46 L/s to a central network of seven plate and frame heat exchangers. The groundwater discharges to the Ohio River. Distributed heat pump loops serve the buildings' interior. Because the well pumps are close to the ground surface, the groundwater system is shut down when outdoor temperatures fall below 4°C and boilers supply the building loop during cold weather.

Seawater Direct Cooling: The Hawaii Gateway Energy Center (HGEC) visitor center on the south coast of Kona on the Big Island of Hawaii pumps seawater at 7°C from 914 m below the surface to cool the 334 m^2 building. The water is distributed through cooling coils in a subfloor plenum, absorbing heat from air supplied to the plenum through a dedicated air inlet structure. The conditioned air then rises through the building to thermal chimney outlet pipes for exhaust. This open loop seawater cooling system runs continuously throughout the day, providing 10–15 air changes per hour. Cooling

Geothermal Conditioning: Critical Sources for Sustainability. Figure 17
Sewer pipe with embedded heat exchanger [52]

Geothermal Conditioning: Critical Sources for Sustainability. Figure 18
Original Galt House Hotel on *left*; Hotel expansion on *right*, Louisville, KY (USA) [40]

Geothermal Conditioning: Critical Sources for Sustainability. Figure 19
Waterfront Plaza Office Towers, Louisville, KY [40]

Geothermal Conditioning: Critical Sources for Sustainability. Figure 20
Cultural Center: "Gen Coel" in Heerlen – home of mine tunnel geothermal district system [55]

coil condensate is collected and used for irrigation and toilet flushing. No auxiliary cooling equipment is used; only pump energy is consumed. HGEC produces more electricity than it uses (a net energy exporter) and the pump energy is supplied by a PV array.

Aquifer Thermal Energy Storage (*ATES*): At the Reichstag Building in Berlin, Germany, two confined aquifers at different depths are used for thermal separation and storage. The shallower aquifer ranges from 0 to 66 m depth and is served by two sets of five wells. The deeper aquifer lies at 270–370 m depth and is served by two wells 300 m apart. In summer months, residual heat from two combined heat and power (CHP) plants in the building charges the lower aquifer to approximately 70°C. During the winter, this water directly serves heating equipment at the beginning of winter and later, as the storage temperature drops during the heating season to 45°C, its temperature is boosted with an absorption heat pump. Meanwhile, the upper aquifer is charged with ambient cold during winter to a temperature of 10°C. In the summer, cooling needs are met with the cold storage and with an absorption heat pump serving as a chiller [53].

Mine Tunnel Geothermal District System with Cavern Thermal Energy Storage (CTES): In Heerlen, the Netherlands, flooded coal mine tunnels abandoned about 1960 are now part of a district geothermal system that provides conditioning to 350 homes and to businesses (see Figs. 20 and 21). Five wells 700 m deep serve a primary energy grid. Each well can supply almost 80 m^3/h at approximately 32°C. At distributed local "energy stations," heat exchangers transfer energy to the secondary grid that serves district buildings. Heat pumps, combined heat and power (CHP) equipment, and condensing gas boilers are used to add thermal energy for conditioning and domestic hot water, depending on the buildings' requirements. The system supplies low-temperature heating (35–40°C), high-temperature

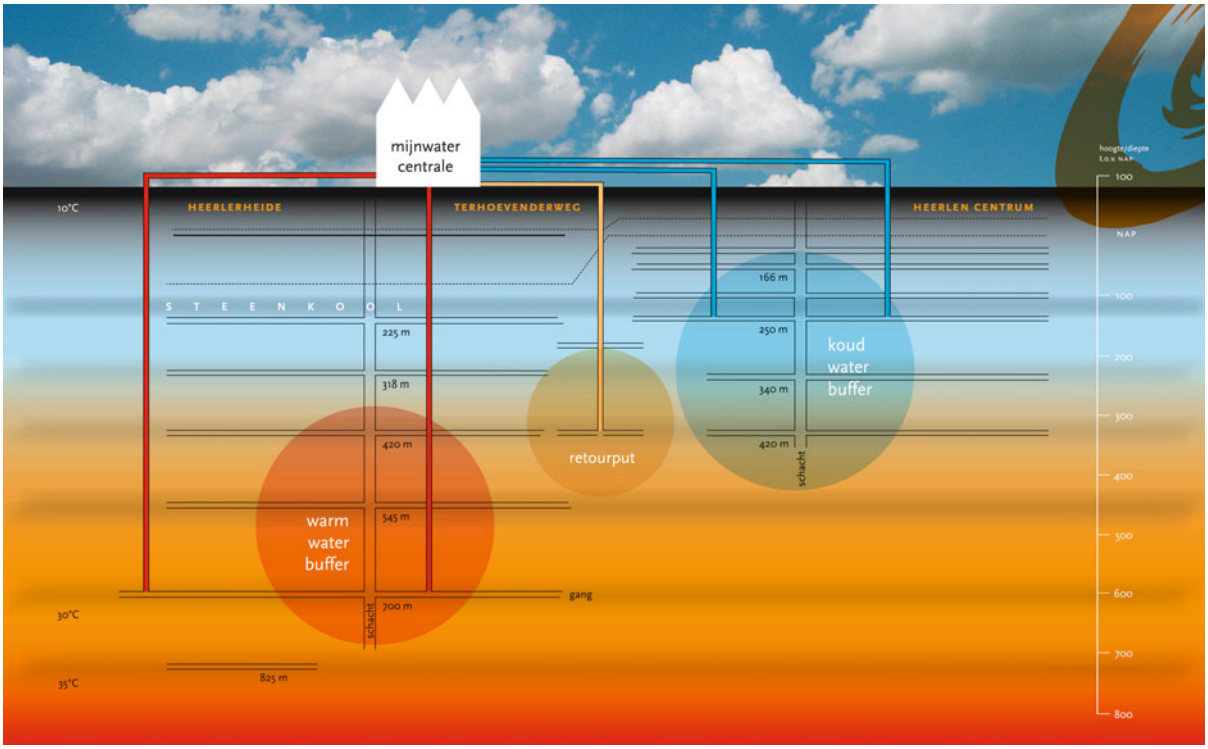

Geothermal Conditioning: Critical Sources for Sustainability. Figure 21
Schematic diagram of Heerlen subsurface system [55]

cooling (16–18°C) supply, and a combined return (20–23°C). The system includes both warm and cool thermal energy storage at 450 and 250 m depth, respectively [54].

Water Treatment Infrastructure: To supply a new geothermal heat pump district system, Oceana Naval Air Station in Dam Neck Annex, Virginia (USA) taps a pipe that carries 113,592 m^3 of 21°C treated wastewater to the ocean daily. The Hampton Roads Sanitary District (HRSD) owns the 1.6 m diameter concrete reinforced pipe that runs above and below ground across Navy property carrying the treated water 2.4 km into the Atlantic Ocean. In a planned conversion from a central steam plant to a 1.6 MW geothermal heat pump coupled with a 14.5 MW cooling water condenser loop, the Navy avoided the installation of a 2,100 vertical borehole ground heat exchanger by using the treated wastewater. Almost 53,000 m^3 of the wastewater flow through four plate and frame heat exchangers daily and are returned to the pipe within 1.7°C of the supply temperature. Sixty-five percent of the base is currently on the new system, which is expandable. In its first year of operation (2009), the system reduced energy consumption for building conditioning by 40%.

Installed Capacity and Annual Energy Use

Global geothermal conditioning capacity including earth sheltering, earth tubes, and ground-based heat exchangers connected to heat pumps or other indoor conditioning equipment is not fully tracked. However, the World Geothermal Congress uses national reports to estimate the total thermal power of direct use geothermal systems. In an analysis of those reports, Lund, Freeston, and Boyd state that installed capacity increased almost sixfold between 1995 and 2010, from 8,664 to 50,583 MWt [56]. Most recent data show that approximately 49% is for

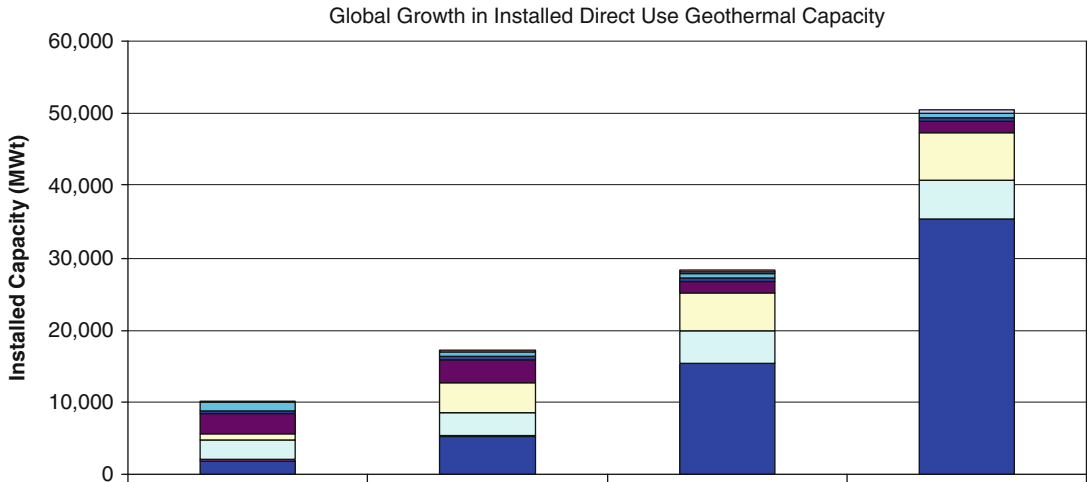

	1995 (MWt)	2000 (MWt)	2005 (MWt)	2010 (MWt)
Agricultural drying	67	74	157	127
Cooling/snow melting	115	114	371	368
Aquacultural pond heating	1,097	605	616	653
Industrial uses	544	474	484	533
Greenhouse heating	2,579	3,263	1,404	1,544
Bathing and swimming	1,085	3,957	5,401	6,689
Space heating	2,579	3,263	4,366	5,391
Other	238	137	86	41
Geothermal heat pumps	1,854	5,275	15,384	35,236

Geothermal Conditioning: Critical Sources for Sustainability. Figure 22
Global growth in installed direct use geothermal capacity

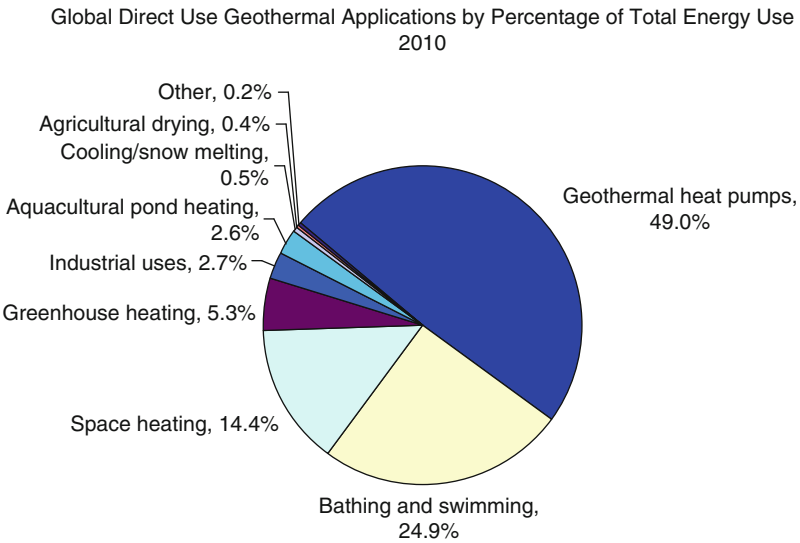

Geothermal Conditioning: Critical Sources for Sustainability. Figure 23
Global direct use geothermal application by percentage of total energy use 2010

conditioning with ground source heat pumps, 25% for bathing and swimming, 14.4% for direct space heating, and the remainder largely for greenhouses, aquaculture, industrial process heating, agricultural drying, space cooling, and snow melting. The annual energy savings from geothermal use based on 2010 data were equivalent to 307.8 million barrels of oil (Figs. 22 and 23).

Four countries accounted for almost 60% of the installed direct use capacity (Fig. 24): the United States (12,611 MWt), China (8,898 MWt), Sweden (4,460 MWt), and Norway (3,300 MWt). The largest increases in installed capacity between 2005 and 2010 occurred in the United Kingdom, South Korea, Ireland, Spain, and the Netherlands, with heat pumps accounting for all capacity additions.

The countries with the greatest geothermal direct use energy consumption per year are China, the United States, Sweden, and Turkey, accounting for 49% of the annual total gigawatt-hours (see Table 6). When energy use per person is calculated, Iceland's geothermal direct use energy per person far exceeds all other countries (see Fig. 25). This results from the prevalence of direct use geothermal systems for space heating (such systems account for 89% of space heating in Iceland [56]) and to high energy content of Iceland's geothermal resources. "Low temperature" wells serving Reykjavik's district heating system, for example, supply water at 62–132°C [57]. Referring back to Fig. 2, the revised

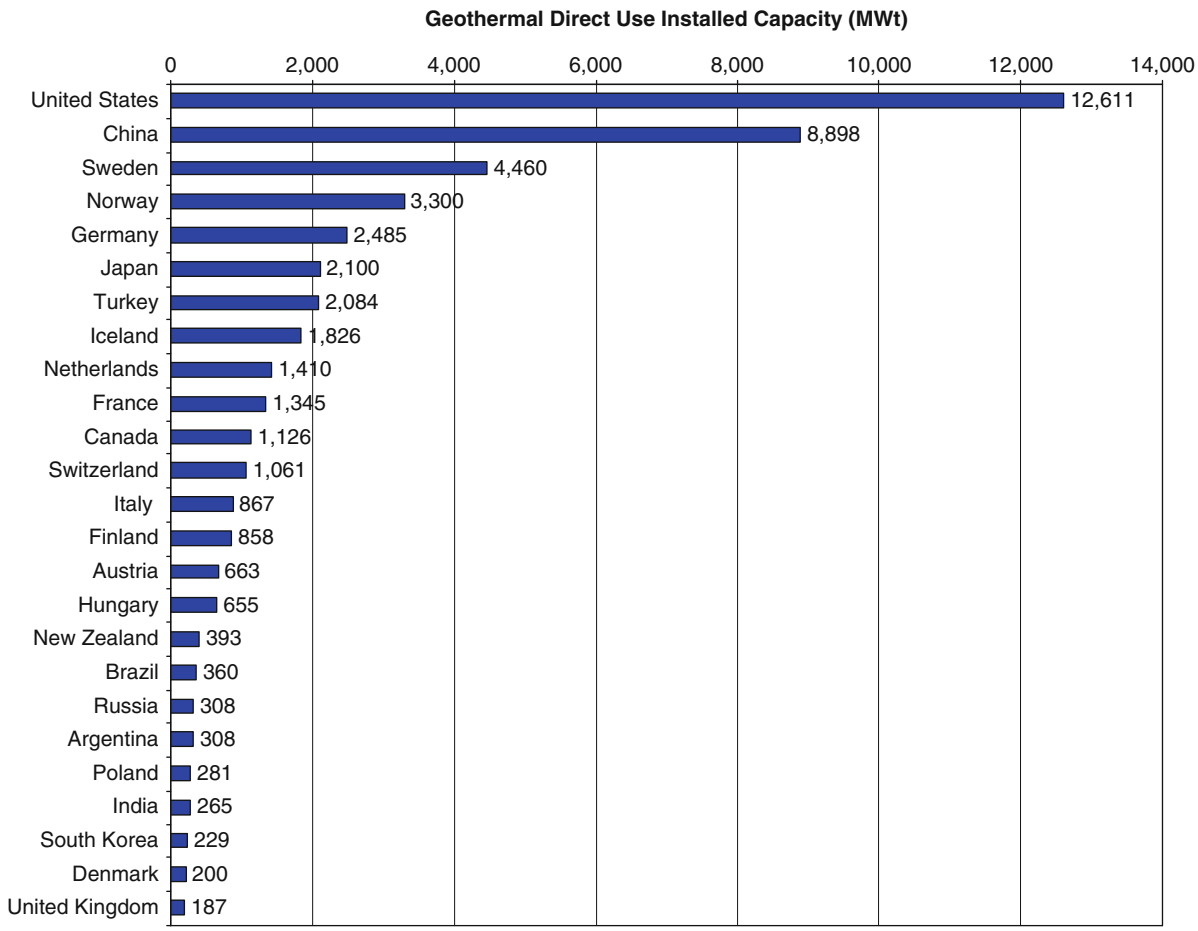

Geothermal Conditioning: Critical Sources for Sustainability. Figure 24
Geothermal direct use installed capacity (MWt)

Geothermal Conditioning: Critical Sources for Sustainability. Table 6 Countries with highest geothermal direct use energy per year

Country	Annual use (GWh/year)
China	20,932
United States	15,710
Sweden	12,585
Turkey	10,247
Japan	7,139
Norway	7,001
Iceland	6,768
France	3,592
Germany	3,546
Netherlands	2,972
Italy	2,762
Hungary	2,713
New Zealand	2,654
Canada	2,465
Finland	2,325
Switzerland	2,143
Brazil	1,840
Russia	1,707
Mexico	1,118
Argentina	1,085
Austria	1,036
Slovak Republic	852
India	707
Denmark	695
Israel	609

Lindal diagram for low-exergy conditioning, it is interesting to note that this temperature range supports cogeneration with ample residual heat for conditioning and cascaded uses such as greenhouse heating.

Future Directions

A study published by Ferguson and Woodbury in 2004 indicated that conductive heat loss from floors and basements of buildings in Winnipeg, Canada was the likely source of a regional groundwater temperature anomaly beneath the city [59]. Just as buildings and their mechanical conditioning systems can generate urban heat islands above the earth's surface, they can also alter the geothermal gradient. Fortunately, a growing emphasis on well-designed building enclosures allows heating and cooling to be provided at temperatures much closer to the human comfort range and to cut extreme heat loss or gain at the perimeter. When occupant comfort requirements can be met with low-exergy systems, building conditioning operates in a range close to the ground temperature and buildings can be coupled with the substantial thermal energy supply and storage capacity the earth offers at the building foundation. The complementary development of high-performance enclosures and geothermal conditioning infrastructure – if accompanied by ongoing monitoring and research – has the potential to appreciably reduce building energy consumption, peak demand, and corresponding carbon emissions while maintaining occupant comfort and supporting environmental health.

To some extent, further development of geothermal conditioning infrastructure is limited by issues of cost, convenience, and property ownership. Nevertheless, there are several technical advances that could further increase its use and sustainability. These developments, some of which are underway, and others that are logical extensions of trends in sustainable building design and operation, may include:

- Increased efficiency of geothermal heat pumps
- Increased use of natural refrigerants such as R-744 (carbon dioxide)
- Improved understanding and modeling of soil mechanical behavior and temperature recovery time periods for ground heat exchangers
- New sustainable approaches to bacteriological and chemical fouling in heat exchangers, piping, and associated equipment
- Improvements in the cost, size, and efficiency of ground heat exchangers
- Increased use of heat recovery from existing underground infrastructure (e.g., sewer pipe, treated wastewater pipe) for building conditioning

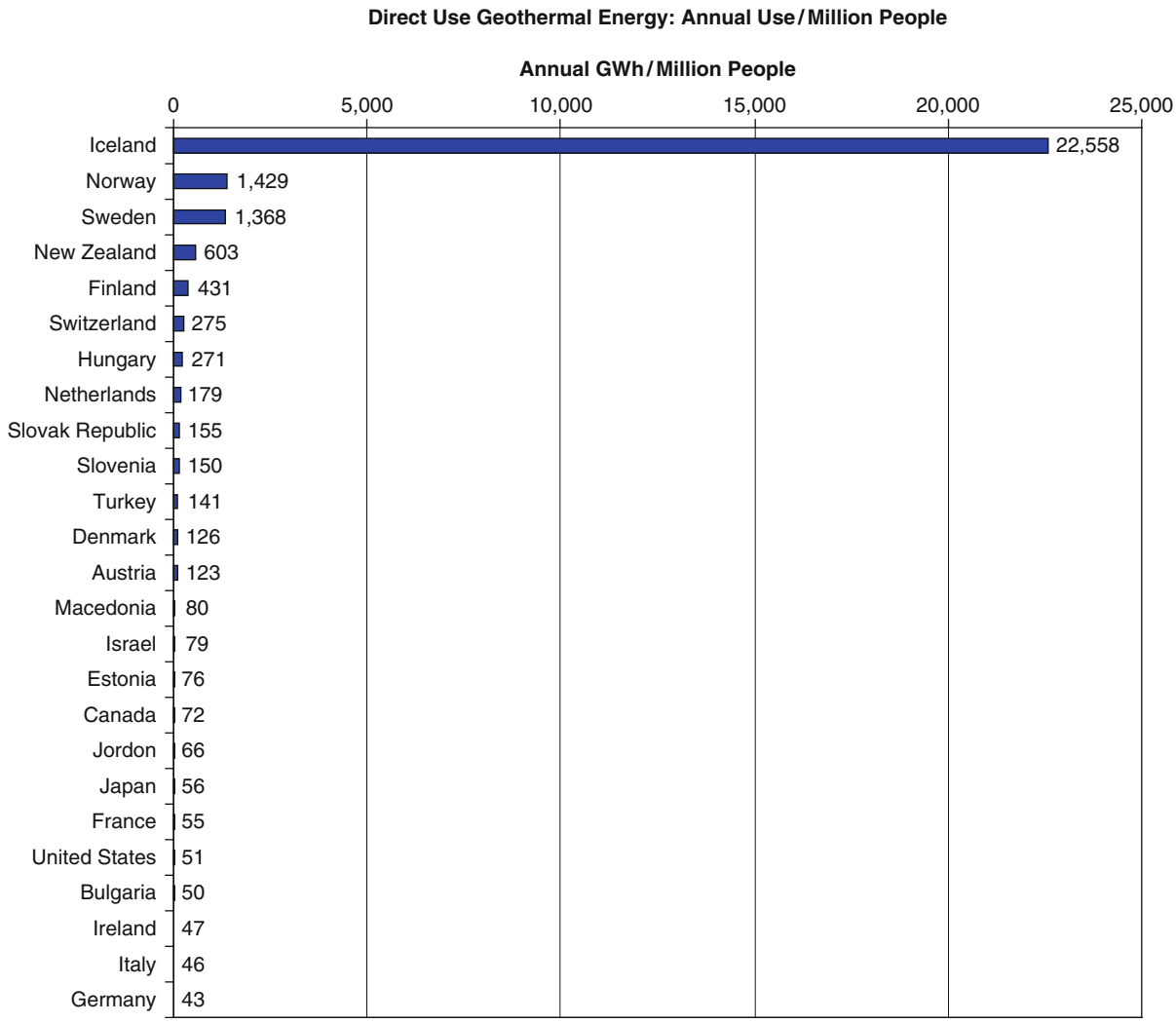

Geothermal Conditioning: Critical Sources for Sustainability. Figure 25
Direct use geothermal energy: annual use/million people [58]

- Improvements in mechanical systems integration and system metering and control
- Increased use of district geothermal and solar/geothermal systems
- Development of vapor compression heat pumps powered by biogas motors or waterpower, or high-temperature gas absorption heat pumps powered by biomass [60, 61]

Expanded geothermal power production will support some of these developments since its scale provides opportunities for district systems and energy cascades. One of the key organizations that conducts and tracks geothermal conditioning research is the International Energy Agency Heat Pump Programme (IEA HPP, www.heatpumpcentre.org). Founded in 1978, HPP current member countries are Austria, Canada, Finland, France, Italy, Germany, Japan, the Netherlands, Norway, South Korea, Sweden, Switzerland, and the United States. Through its web site, news and information about member country activities are available.

The Ground-Reach Project, an international effort supported by the European Commission to evaluate the use of ground source heat pumps in meeting Kyoto targets, maintains a database of 52 GSHP projects in 15 European countries at http://www.groundreach.eu/. In the future, eight demonstration projects from Mediterranean countries and 46 case studies from European projects being field-tested through 2012 will be added to the database. A central source for accessing these case studies and other projects related to geothermal energy research and development is the European Geothermal Energy Council (EGEC) website (http://egec.info/).

Within the United States, the Geo-Heat Center at Oregon Institute of Technology, hosts an online library that emphasizes applied (how-to) engineering of direct use systems http://geoheat.oit.edu/publist.htm. With publication dates ranging from 1975 to 2008, the system details and lessons learned are particularly valuable in this library.

Bibliography

Primary Literature

1. Lund J (2004) Geothermal direct use. In: Encylopedia of energy. Elsevier, New York
2. Lund J (2004) Geothermal direct use. In: Encylopedia of energy. Elsevier, New York, p 863
3. Dickson MH, Fanelli M (2004) What is geothermal energy? Geoscienze Istituto e Georisorse, CNR, Pisa. www.geothermal-energy.org/files-31.html
4. Aparicio E (2008) Urban surface water as energy source & collector. M.Sc. thesis, Delft University of Technology, Delft
5. Kaltshmitt M, Streicher W, Wiese A (2007) Basics of renewable energy supply. In: Renewable energy. Springer, Heidelberg/Berlin, p 92, 23–102
6. Clauser C (2009) Heat transport processes in the Earth's crust. Surv Geophys 30(3):163–191
7. After Table 2.6 in Kaltshmitt M, Streicher W, Wiese A (2007) Basics of renewable energy supply. In Renewable energy: technology, economics and environment. Springer, Heidelberg/Berlin, pp 23–102
8. Short, Nicholas. "Geology, Weather and Climate: A Condensed Primer." http://rst.gsfc.nasa.gov/Sect9/Sect9_4.html
9. Oke TR (1987) Boundary layer climates, 2nd edn. London, Methuen, p 41
10. Kaltshmitt M, Streicher W, Wiese A (2007) Basics of renewable energy supply. In: Renewable energy. Springer, Heidelberg/Berlin, p 98, 23–102
11. Kavanaugh S, Rafferty K (1997) Ground source heat pumps: design of geothermal systems for commercial & institutional buildings. American Society of Heating Refrigerating and Air Conditioning, Atlanta
12. Figure 2.57, p 95, cited as Kaltschmitt M (2006/2007) Renewable energies: lessons. Institute for Environmental Technology and Energy Economics, Hamburg University of Technology, Hamburg
13. Clauser C (2006) Geothermal Energy. In: Heinloth K (ed) Landolt-Börnstein, Group VIII: advanced materials and technologies, vol 3, Energy technologies, Subvol. C: renewable energies. Springer, Heidelberg/Berlin, pp 493–604
14. Majorowicz J, Grasby S, Skinner W (2009) Estimation of shallow geothermal energy resource in Canada: heat gain and heat sink. Nat Resour Res 18(2):95–108
15. Björnsson S (2010) Geothermal development and research in Iceland. Orkustofnun and The National Energy Authority. http://www.nea.is/media/utgafa/GD_loka.pdf
16. Largely developed from work in building systems integration by Vivian Loftness, FAIA, and Volker Hartkopf, Dr. Ing., Dr.h.c., Center for Building Performance & Diagnostics, Department of Architecture, Carnegie Mellon University, Pittsburgh, PA (USA)
17. Quaschning V (2010) Heat pumps – from cold to hot. In: Renewable energy and climate change. Wiley, Hoboken, pp 223–236
18. Laue HJ (2006) Heat pumps. In: Advanced materials and technologies, vol 3, Energy technologies, Subvol. C: renewable energy. Springer, Heidelberg/Berlin
19. American Society of Heating Refrigerating and Air-Conditioning Engineers (2002) Applied heat pump and heat recovery systems. In: ASHRAE handbook: HVAC systems and equipment. American Society of Heating, Refrigerating and Air Conditioning Engineers, Atlanta
20. Kavanaugh S, Rafferty K (1997) Heat pumps for ground source applications. In: American Society of Heating Refrigerating and Air Conditioning Engineers (ed) Ground source heat pumps: design of geothermal systems for commercial and institutional buildings. American Society of Heating Refrigerating and Air Conditioning Engineers, Atlanta
21. Kaltschmitt, Figure 9.1, p 389, cited as Halozan H, Holzapfel K (1987) Heizen mit Wärmepumpen, TÜV Rheinland, Köln
22. Harvey LDD (2006) A handbook on low-energy buildings and district-energy systems: fundamentals, techniques and examples. Earthscan, London. In North America, heat pump cooling efficiency is expressed as an Energy Efficiency Ratio (EER), which is an instantaneous, steady-state ratio of heat removed to the rate of energy used, in BTU/hr per watt
23. Brandl H (2006) Energy foundations and other thermo-active ground structures. Geotechnique 56(2):81–122
24. Nowak T (2009) Heat pumps are renewable – are they not? IEA Heat Pump Centre. http://www.heatpumpcentre.org/en/newsletter/previous/Sidor/default.aspx
25. American Society of Heating Refrigerating and Air-Conditioning Engineers (2007) ASHRAE handbook: HVAC applications, vol 32, Geothermal energy. American Society of Heating, Refrigerating and Air Conditioning Engineers, Atlanta, p 23

26. Kavanaugh S, Rafferty K (1997) Heat pumps for ground source applications. In: Ground source heat pumps: design of geothermal systems for commercial and institutional buildings. American Society of Heating Refrigerating and Air Conditioning Engineers, Atlanta. Reprint of Figure 1.6, Required design steps for GSHPs
27. American Society of Heating Refrigerating and Air-Conditioning Engineers (2007) ASHRAE handbook: HVAC applications, vol 32, Geothermal energy. American Society of Heating, Refrigerating and Air Conditioning Engineers, Atlanta, pp 4–5
28. Kavanaugh S, Rafferty K (1997) Heat pumps for ground source applications. In: American Society of Heating Refrigerating and Air Conditioning Engineers (ed) Ground source heat pumps: design of geothermal systems for commercial and institutional buildings. American Society of Heating Refrigerating and Air Conditioning Engineers, Atlanta, p 22
29. Rafferty K (1998) Heat Exchangers. In: Lund JW, Lienau JP, Lunis B (eds) Geothermal direct use engineering and design guidebook, 3rd edn. Klamath Falls, Geo-Heat Center, Oregon Institute of Technology
30. Canadian GeoExchange Coalition (2010) Codes, standards and regulations in the Canadian GeoExchange industry: report of a national consultation conducted by the Canadian GeoExchange coalition (Summary), p 11. http://www.geo-exchange.ca/en/UserAttachments/news433_Standards%20Consultation%20_%20Final%20Report_Public%20_2010_E.pdf
31. American Society of Heating Refrigerating and Air-Conditioning Engineers (2007) ASHRAE handbook: HVAC applications, vol 32, Geothermal energy. American Society of Heating, Refrigerating and Air Conditioning Engineers, Atlanta, p 13
32. Sanner DB (2007) Geothermal energy – opportunities for industry. In: EMEA environmental health and safety conference, Bruxelles, 13 June 2007. http://www.egec.org/target/bruxelles%20130607%20j&j.pdf
33. Kwok AG, Grondzik WT (2007) The green studio handbook: environmental strategies for schematic design. Architectural Press, Oxford, pp 169–174
34. Pfafferott J, Walker-Hertkorn S, Sanner B (2007) Ground cooling: recent progress. In: Santamouris M (ed) Advances in passive cooling. Earthscan, London, pp 190–227
35. Lechner N (2009) Heating, cooling, lighting: sustainable design methods for architects, 3rd edn. Wiley, Hoboken, p 292
36. Nagano K (2009) GSHP in Japan. IEA Heat Pump Centre Newsletter 27(1). http://www.heatpumpcentre.org/en/newsletter/previous/Documents/HPC-news_1_2009.htm
37. Peron H (2010) Geotechnical design of heat exchanger piles. In: GSHP association research seminar, current and future research into ground source energy. National Energy Centre, Milton Keynes, United Kingdom. http://www.gshp.org.uk/documents/REsearchseminar2010/Herve%20Peron%20Geothechnical%20Design%20of%20Heat%20Ex.pdf
38. Clauser C (2006) Geothermal Energy. In: Heinloth K (ed) Landolt-Börnstein, Group VIII: advanced materials and technologies, vol 3, Energy technologies, Subvol. C: renewable energies. Springer, Heidelberg/Berlin, pp 493–604, Figure 8.31
39. Radial systems are mentioned in Kaltschmitt M (2007) Utilisation of ambient air and shallow geothermal energy. In: Kaltshmitt M, Wolfgang S, Andreas W (eds) Renewable energy: technology, economics and environment. Springer, Heidelberg/Berlin, pp 385–436
40. Baird N (2009) Center for Building Performance & Diagnostics. School of Architecture, Carnegie Mellon University
41. Kaltschmitt M (2007) Utilisation of geothermal energy. In: Kaltshmitt M, Wolfgang S, Andreas W (eds) Renewable energy: technology, economics and environment. Springer, Heidelberg/Berlin, p 465
42. Kaltschmitt M (2007) Utilisation of geothermal energy. In: Kaltshmitt M, Wolfgang S, Andreas W (eds) Renewable energy: technology, economics and environment. Springer, Heidelberg/Berlin, p 463
43. Paksoy, J., A. Snijders and L. Stiles. "Aquifer Thermal Energy Cold Storage System at Richard Stockton College," 2009. http://talon.stockton.edu/eyos/energy_studies/content/docs/effstock09/Session_6_3_ATES_Applications/57.pdf
44. Drake Landing Solar Community. http://www.dlsc.ca/
45. Driscoll FG (1986) Groundwater and wells. St. Paul, Johnson Filtration Systems, p 1, 2 Sub edn
46. Baird N (in progress) Critical guidelines for energy and water performance of open loop geothermal systems for low energy building conditioning. Doctoral dissertation, School of Architecture, Carnegie Mellon University, Pittsburgh
47. Baird N (2008) Center for Building Performance & Diagnostics. School of Architecture, Carnegie Mellon University
48. Clauser C (2006) Geothermal Energy. In: Heinloth K (ed) Landolt-Börnstein, Group VIII: advanced materials and technologies, vol 3, Energy technologies, Subvol. C: renewable energies. Springer, Heidelberg/Berlin, pp 493–604, Figure 8.33
49. Baird N (2010) Center for Building Performance & Diagnostics. School of Architecture, Carnegie Mellon University
50. NL EVD International (2005) China: cold rise (PESP01051). Publication 147970. http://www.evd.nl/cooperation/zoeken/showbouwsteen.asp?bstnum=147970&location=&highlight=
51. Harvey LDD (2006) A handbook on low-energy buildings and district-energy systems: fundamentals, techniques and examples. Earthscan, London, p 587. In North America, heat pump cooling efficiency is expressed as an Energy Efficiency Ratio (EER), which is an instantaneous, steady-state ratio of heat removed to the rate of energy used, in BTU/hr per watt
52. Rabtherm – Energy Systems AG. http://www.rabtherm.com/
53. Sanner B, Kabus F, Seibt P, Bartels J (2005) Underground thermal energy storage for the German parliament in Berlin, system concept and operational experience. In: World geothermal congress 2005, Antalya

54. Roijen E, Op't Veld P, Demollin-Schneiders E (2007) The mine water project Heerlen – low exergy heating and cooling in practice. In: PALENC AIVC 2007. http://www.chri.nl/upload/art.%20minewaterproject.pdf
55. Municipality Heerlen. http://www.heerlen.nl/Pub/Duurzaamheid/Projecten-Stadsplanning-Mijnwaterenergie.html
56. Lund J, Freeston D, Boyd T (2010) Direct utilization of geothermal energy 2010 worldwide review. In: World geothermal congress, Bali
57. Björnsson S (2010) Geothermal development and research in Iceland. Orkustofnun and The National Energy Authority, p 21. http://www.nea.is/media/utgafa/GD_loka.pdf
58. This table was generated using the Lund et al (2010) Worldwide review of geothermal energy use. See Lund J, Freeston D, Boyd T (2010) Direct utilization of geothermal energy 2010 worldwide review. In: World geothermal congress, Bali and population data from http://en.wikipedia.org/wiki/List_of_countries_by_population and http://en.wikipedia.org/wiki/List_of_Caribbean_island_countries_by_population
59. Ferguson G, Woodbury AD (2004) Subsurface heat flow in an urban environment. J Geophys Res 109:B02402
60. Banks D (2008) An introduction to thermogeology: ground source heating and cooling. Wiley-Blackwell, Oxford, p 296
61. European Geothermal Energy Council (2011) Strategic Research Agenda: Geothermal Heating and Cooling. http://egec.info/

Books and Reviews

Carmody J, Sterling R (1983) Underground building design: commercial and institutional structures. Van Nostrand Reinhold, New York

Dickinson JS, Buik N, Matthews MC, Snijders A (2009) Aquifer thermal energy storage: theoretical and operational analysis. Geotechnique 59(3):249–260

Givoni B (1998) Climate considerations in building and urban design. Van Nostrand Reinhold, New York

International Energy Agency (2011) Technology Roadmap: Geothermal Heat and Power. www.iea.org

Lienau P (1998) Geothermal direct use engineering and design guidebook, 3rd edn. Oregon Institute of Technology, Geo-Heat Center, Klamath Falls

Orio CD, Chlasson A, Johnson CN, Deng Z, Rees SJ, Spitler JD (2005) A survey of standing column well installations in North America. Trans Am Soc Heat Refrig Air-Cond Eng (ASHRAE) 111(2):109–121

Powrie W, Preene M (2009) Ground energy systems: from analysis to geotechnical design. Géotechnique 59(3):261–271

Wood CJ, Liu H, Riffat SB (2009) Use of energy piles in a residential building, and effects on ground temperature and heat pump efficiency. Geotechnique 59(3):287–290

Xu X et al (2010) Active pipe-embedded structures in buildings for utilizing low-grade energy sources: a review. Energy Build 42(10):1567–1581

Geothermal Energy Utilization

John W. Lund
Geo-Heat Center, Oregon Institute of Technology, Klamath Falls, OR, USA

Article Outline

Glossary
Definition and Importance of Geothermal Energy
Introduction
Types of Geothermal Resources
Utilization in 2010
Environmental Considerations
Energy Savings
Future Directions
Bibliography

Glossary

Balneology The science of the healing qualities of baths, especially with natural mineral waters; the therapeutic use of natural, warm, or mineral waters.

Binary power plant Used with low-temperature resources (below 150°C or 300°F) where a secondary low boiling point working fluid (normally a hydrocarbon) is vaporized by the geothermal fluid through a heat exchanger to drive a turbine producing electricity. Also referred to as an organic Rankine cycle (ORC) machine.

Caldera A large basin-shaped volcanic depression, circular in form, with a diameter many times greater than the included volcanic vent usually causes by an explosive volcanic eruption that drains the magma chamber resulting in collapse of the volcano.

Calorie The quantity of heat needed to raise the temperature of 1 gram (g) of water by 1 degree centigrade (°C) at 16°C. It is equal to 4.185 J.

Cap rock A comparatively impervious stratum that prevents the circulation of heat or fluid.

Conduction The transfer of heat through a medium or body driven by a temperature gradient and involving no particle motion. The average temperature gradient of the world, caused by conduction is about 25°C/km increasing with depth above the mean annual surface temperature.

Convection A process of mass movements of portions of any fluid medium (liquid or gas) as a consequence of different temperatures in the medium and hence different densities moving the medium and also the heat.

Enhanced (engineered) geothermal systems (EGS) Extracting heat stored in rocks within about 10 km of the surface, from which energy cannot be economically extracted by natural hot water or steam. The system is hydrofractured and water pumped down one well, extracting the heat by flowing through the fractures, and producing hot water or steam through a second well.

Fault A fracture or fracture zone along which there has been displacement of the sides relative to one another parallel to the fracture. The movement can be vertical, horizontal, or a combination of the two.

Flash steam The steam generated when the pressure on hot water (usually above 100°C) is reduced.

Fossil fuel A deposit of organic material containing stored solar energy that can be used as fuel, such as coal, natural gas, and petroleum.

Fumarole A hole or vent from which fumes or vapors issue usually found in volcanic areas.

Geopressured Zones below depths of 1,800–3,000 m, in which sediments in basins are commonly characterized by abnormally high pressure, high temperature, and high salinity.

Geothermal energy The internal energy of the earth, usually from the radioactive decay of potassium, thorium, and uranium, often associated with magma bodies, available to humans as heat from heated rocks, water, or steam.

Geyser A spring that erupts with intermittent jets of heated water or steam.

Heat exchanger A device for transferring heat from one fluid to another. The fluids are usually separated by conducting walls of metal or plastic.

Heat flow Dissipation of heat coming from within the earth by conduction. The worldwide average is about 65 mW/m^2.

Heat pump A device which, by the consumption of work or heat, affects the transport of heat between a lower temperature to a higher temperature source. The useful output is heat in conventional usage. The reverse process is called a refrigerator used for the removal of heat.

Hot Spring A thermal spring whose water has a higher temperature than that of the human body (usually above 40°C).

Hydrothermal An adjective applied to heated or hot aqueous-rich solutions, to the processes of which they are concerned, and to the rocks, ore deposits, and alteration products produced by them.

Joule (J) The SI unit for all forms of energy or work. It is equal to 1 W-s or 0.239 cal.

Lava Hot fluid rock that issues from a volcano or a fissure in the earth's surface coming from subsurface magma.

Magma Molten rock within the earth from which an igneous rock results by cooling, and forms lava when it erupts on the earth's surface.

Permeability The capacity of a rock to transmit fluid, dependent upon the size and shape of the pores and their interconnections.

Seismic Pertaining to an earthquake or earth vibrations, including those that are artificially induced.

Spa A resort using mineral water for bathing, soaking, and drinking along with covering portions of the body with mineral muds for therapeutical purposes. Diet, exercise, and rest can also be part of the spa treatment plan.

Subsidence A sinking of a large part of the earth's crusts, often due to the removal of fluid by pumping.

Volcano A vent in the earth surface through which magma as lava and associated gases, and/or pyroclastic material (rock, cinders, pumice, and ash) erupt.

Watt (W) A unit of power or energy produced over time, equivalent to 1 J/s, or 0.001341 horse power (hp).

Definition and Importance of Geothermal Energy

Geothermal energy is the heat contained within the Earth that generates geological phenomena on a planetary scale. The main sources of this energy are due to the heat flow from the earth's core and mantel generated by the radioactive decay of potassium, thorium, and uranium in the crust or by friction heat generated in subduction zones along continental plate

margins. It may be characterized by surface expression of fumaroles, hot springs, geysers, volcanic eruption, and lava flows. Geothermal energy is often used to indicate that part of the Earth's heat that can, or could, be recovered and exploited by humankind. The resource is large, is renewable in the broad sense, and is available almost everywhere in the world, depending upon the depth to the resource and the economics to produce it. The total estimated thermal energy above surface temperature to a depth of 10 km under the continents, reachable with current drilling technology, is 1.3×10^{27} J (1.3×10^{9} EJ = exajoules). Recovery of geothermal energy utilizes only a portion of the stored thermal energy due to limitations in rock permeability that permit heat extraction through fluid circulation, and to the minimum temperature limits for utilization at a given site. The recovery factor is estimated between 0.5% and 20% [1]; and at the lower rate, this is 6.5×10^{6} EJ, or about 200,000 TW-years (terawatt = 10^{12} W). This is about three times the annual world consumption for all types of energy, and about 130 times at the higher recovery rate.

Geothermal energy can be used over a range of temperature to supply electricity, and heat and cool for the benefit of humankind. The higher temperature (above 175°C) is traditionally used to produce electricity; however with the improvement in the organic Rankine cycle or binary power plants described later, the usable temperature has been reduced to around 100°C. Lower temperatures are used for direct heating and cooling, from industrial process heating, space heating, and cooling including district energy systems, the heating of greenhouses and aquaculture ponds, to heating swimming pools and spas, generally in the range of 40–150°C. Finally the lowest temperatures from 5°C to 30°C, available anywhere in the world at shallow depth (up to 300 m), can utilize geothermal heat pumps for space heating and cooling.

Introduction

Early humans probably used geothermal water that occurred in natural pools and hot springs for cooking, bathing, and to keep warm [2]. There is archeological evidence that the Indians of the Americas occupied sites around these geothermal resources for over 10,000 years to recuperate from battle and take refuge. Many of their oral legends describe these places and other volcanic phenomena. Recorded history shows uses by Romans, Japanese, Turks, Icelanders, Central Europeans, and the Maori of New Zealand for bathing, cooking, and space heating. Baths in the Roman Empire, the middle kingdom of the Chinese, and the Turkish baths of the Ottomans were some of the early uses of balneology, where body health, hygiene, and discussions were the social custom of the day. This custom has been extended to geothermal spas in Japan, Germany, Iceland, and countries of the former Austro-Hungarian Empire, the Americas, and New Zealand. Early industrial applications include chemical extraction from the natural manifestations of steam, pools, and mineral deposits in the Larderello region of Italy, with boric acid being extracted commercially starting in the late 1700s. At Chaudes-Aigues in the heart of France, the world's first geothermal district heating system was started in the fourteenth century and is still going strong. The oldest and still operating geothermal district heating project in the United States is on Warm Springs Avenue in Boise, Idaho, going on line in 1892 and providing space heating for up to 450 homes.

The first use of geothermal energy for electric power production started in Italy with experimental work by Prince Gionori Conti between 1904 and 1905. The first commercial power plant (250 kWe) was commissioned in 1913 at Larderello, Italy. These developments were followed by flash steam plants coming on line in New Zealand at Wairakei in 1958; an experimental plant at Pathe, Mexico, in 1959; and the first commercial plant at The Geysers in the United States in 1960. Japan followed with 23 MWe at Matsukawa in 1966. All of these early plants used steam directly from the earth (dry-steam fields), except for New Zealand, which was the first to use flashed or separated steam for running the turbines. The former USSR produced power from the first true binary power plant, 680 kWe using 81°C water at Paratunka on the Kamchatka peninsula – the lowest temperature ever reported used in the world for power generation from geothermal energy at that time. Iceland first produced power at Namafjall in northern Iceland, from a 3 MWe noncondensing turbine. These were followed by plants in El Salvador, China, Indonesia, Kenya, Turkey, Philippines, Portugal (Azores), Greece, and Nicaragua in the 1970s and 1980s. Later

plants were installed in Thailand, Argentina, Taiwan, Australia, Costa Rica, Austria, Guatemala, Ethiopia, with the latest installations in Germany and Papua New Guinea. Recently in 2006, a 200 kW binary plant was started at Chena Hot Springs in Alaska using geothermal fluids at 74°C, the lowest temperature for electric power generation recorded to date [3].

Types of Geothermal Resources

Geothermal energy comes from the natural heat of the earth primarily due to the decay of the naturally radioactive isotopes of uranium, thorium, and potassium. Because of the internal heat, the Earth's surface heat flow averages 65 mW/m^2 which amounts to a total heat loss of about 44 million megawatts (1,400 EJ/year). The estimated total thermal energy above surface temperature to a depth of 10 km, the limit of the deepest exploration drilling, is 1.3×10^{27} J (1.3×10^9 EJ), equivalent to burning 3.0×10^{17} barrels of oil. Since the global energy consumptions for all types of energy is equivalent to the use of about 100 million barrels of oil per day, the Earth's energy to a depth of 10 km would supply all of humankind's energy needs for six million years [4].

On average, the temperature of the Earth with depth increases about 25°C/km above the surface ambient temperature. Thus, assuming a conductive gradient, the temperature of the earth at 10 km would be over 250°C. However, most geothermal exploration and use occurs where the gradient is higher, and thus where drilling is shallower and less costly. These shallow depth geothermal resources occur due to: (1) intrusion of molten rock (magma) from depth, bringing up great quantities of heat; (2) high surface heat flow, due to a thin crust and high-temperature gradient; (3) ascent of groundwater that has circulated to depths of several kilometers and been heated due to the normal temperature gradient; (4) thermal blanketing or insulation of deep rocks by thick formation of such rocks as shale whose thermal conductivity is low; and (5) anomalous heating of shallow rock by decay of radioactive elements, perhaps augmented by thermal blanketing [4].

Geothermal resources are usually classified as shown in Table 1, modeled after White and Williams [5]. These geothermal resources range from the mean annual ambient temperature of around 20°C to over 300°C. In general, resources above 150°C are used for electric power generation, although power has recently been generated at Chena Hot Springs Resort in Alaska using a 74°C geothermal resource [3]. Resources below 150°C are usually used in direct-use projects for heating and cooling. Ambient temperatures in the 5–30°C range can be used with geothermal (ground-source) heat pumps which provide both heating and cooling.

Convective hydrothermal resources occur where the Earth's heat is carried upward by convective circulation of naturally occurring hot water or steam. Underlying some high-temperature convective hydrothermal resources are temperatures of 500–1,000°C from molten intrusions of recently solidified rocks. The lower temperature resource results from deep circulation of water along fractures. *Vapor-dominated systems* (Fig. 1) produce steam from boiling of deep, saline waters in low permeability rocks. These reservoirs are few in number, with The Geysers in northern California, Larderello in Italy, and Matsukawa in Japan being ones where the steam is exploited to produce electric energy. *Water-dominated systems* (Fig. 2) are produced by ground water circulating to depth and ascending from buoyancy in permeable reservoirs that are a uniform temperature over large volumes. There is typically an upflow zone at the center of each convection cell, an outflow zone or plume of heated water moving laterally away from the center of the system, and a downflow zone where recharge is taking place. Surface manifestations include hot springs, fumaroles, geysers, travertine deposits, chemically altered rocks, or sometimes, no surface manifestations (a blind resource).

Sedimentary basins (Fig. 3) produce higher temperature resources than the surrounding formations due to their low thermal conductivity or high heat flow or both producing geothermal gradients >30°C/km. These generally extend over large areas and are typical of the Madison Formation of North Dakota, South Dakota, Montana, and Wyoming area of the northern United States and the Pannonian Basin of Central Europe where it has been used extensively in Hungary.

Geopressured resources (Fig. 4) occur in basin environments where deeply buried fluids contained in permeable sedimentary rocks warmed in a normal or enhanced geothermal gradient by their great burial

depth. The fluids are tightly confined by surrounding impermeable rock and bear pressure much greater than hydrostatic. Thermal waters under high pressure in sand aquifers are the target for drilling, mainly as they contain dissolved methane. The source of energy available from this type of resources consists of: (1) heat, (2) mechanical energy, and (3) methane. The Texas and Louisiana Gulf Coast in the United States has been tested for the geothermal energy; however, due to the great depths of several kilometers, they have not proved economic, but are currently being evaluated again.

Geothermal Energy Utilization. Table 1 Geothermal resource types

Resource type	Temperature range (°C)
Convective hydrothermal resources	
Vapor dominated	≈240°
Hot water dominated	20° to 350°+
Other hydrothermal resources	
Sedimentary basin	20° to 150°
Geopressured	90° to 200°
Radiogenic	30° to 150°
Hot rock resources	
Solidified (hot dry rock)	90° to 650°
Part still molten (magma)	>600°

Radiogenic resources (Fig. 5) are found where granitic intrusions are near surface heating up the local groundwater from the decay of radioactive thorium, potassium, and uranium. This localized heating increases the normal geothermal gradient providing hot water at economical drilling depths. This type of resource occurs along the eastern United States, but has not been developed commercially.

Hot dry rock resources (Fig. 6) are defined as heat stored in rocks within about 10 km of the surface from which energy cannot be economically extracted by natural hot water or steam. These hot rocks have few pore space or fractures, and therefore, contain little water and little or no interconnected permeability. In order to extract the heat, experimental projects have artificially fractured the rock by hydraulic pressure, followed by circulating cold water down one well to extract the heat from the rocks and then producing from a second well in a closed system. Early experimental projects were undertaken at Fenton Hill (Valdes Caldera) in northern New Mexico and on Cornwall in southwest England; however, both of these projects have been abandoned due to lack of funds and poor results. Projects are currently underway in Soultz-sous-Forêt in the Rhine

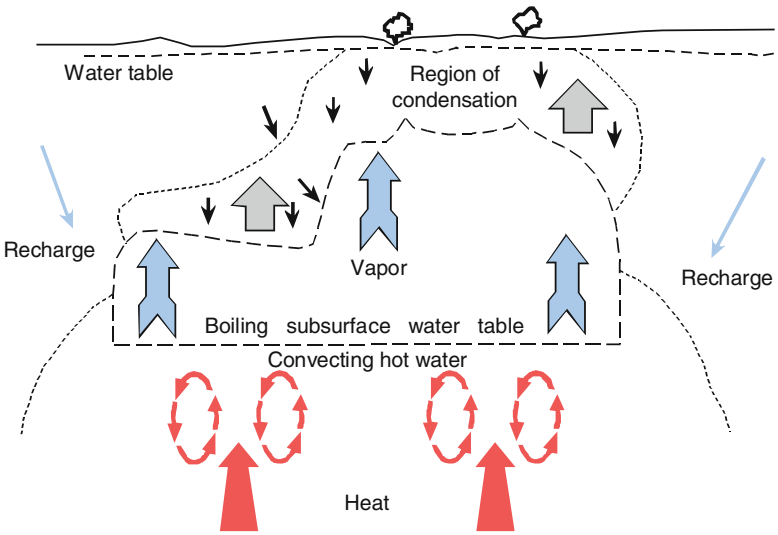

Geothermal Energy Utilization. Figure 1 Vapor-dominated geothermal system

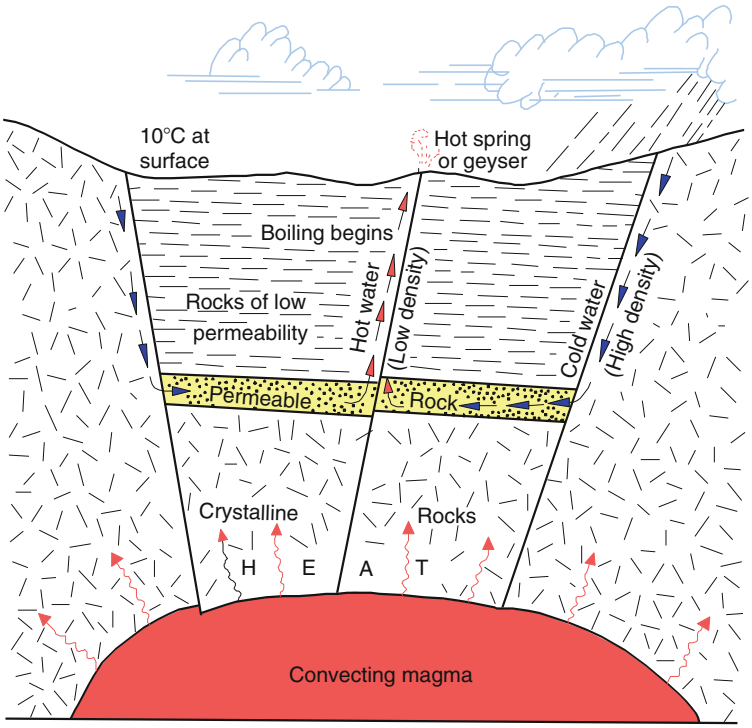

Geothermal Energy Utilization. Figure 2
Hot water–dominated geothermal system

Graben on the French–German border, in Germany at Bad Urach, several locations in Japan, and in the Cooper Basin of Australia [6]. Renewed interest has been generated in the United States for enhanced (engineered) geothermal systems (EGS) based on a recent MIT report [7].

Molten rock or *magma resources* have been drilled in Hawaii experimentally to extract heat energy directly from molten rock. It has been used successfully at Heimaey in Iceland (one of the Westmann Islands) after the 1973 eruption. A heat exchanger constructed on the surface of the lava flow recovered steam resulting from boiling of downward percolation water from the surface. The heat was used in a space-heating system for over 10 years, but is now shutdown due to cooling of the surrounding rock.

Utilization in 2010

Based on 68 country update papers submitted to the World Geothermal Congress 2010 (WGC2010) held in Bali, Indonesia, the following figures on worldwide geothermal electric and direct-use capacity are reported. A total of 78 countries have reported some utilization from WGC2000, WGC2005, and WGC2010 electric, direct use, or both [8–12] (Table 2).

The figures for electric power capacity (MWe) appear to be fairly accurate; however, several of the country's annual generation values (GWh) had to be estimated which amounted to only 0.5% of the total. The direct-use figures are less reliable and probably are understated by as much as 20%. The author is also aware of at least five countries, which utilize geothermal energy for direct-heat applications, but did not submit reports to WGC2010. The details of the present installed electric power capacity and generation, and direct use of geothermal energy can be found in Bertani [12] and Lund et al. [10]. These data are summarized in Table 3.

A review of the above data show that for electric power generation each major continent has approximately the same percentage share of the installed capacity and energy produced with the Americas

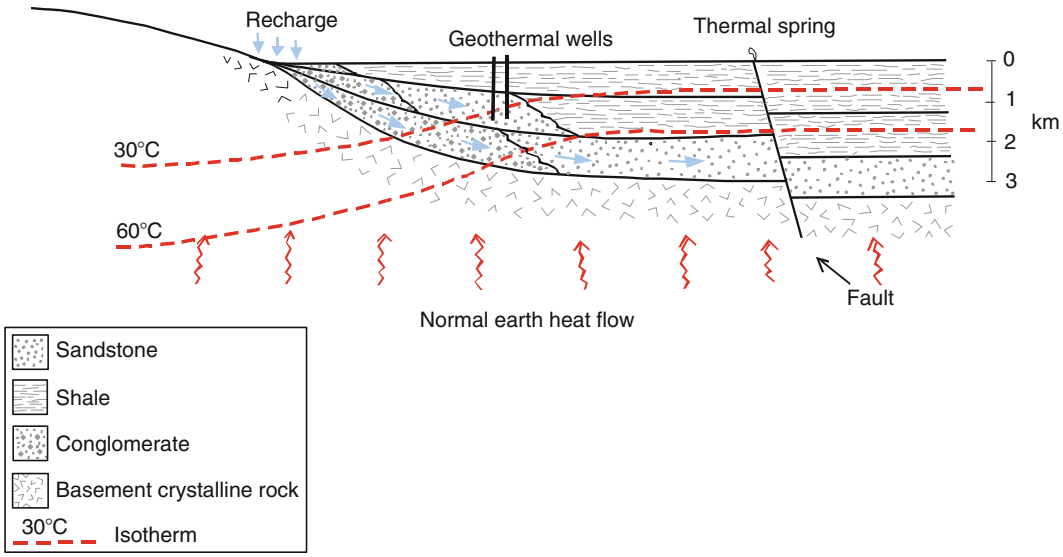

Geothermal Energy Utilization. Figure 3
Sedimentary basin geothermal resource

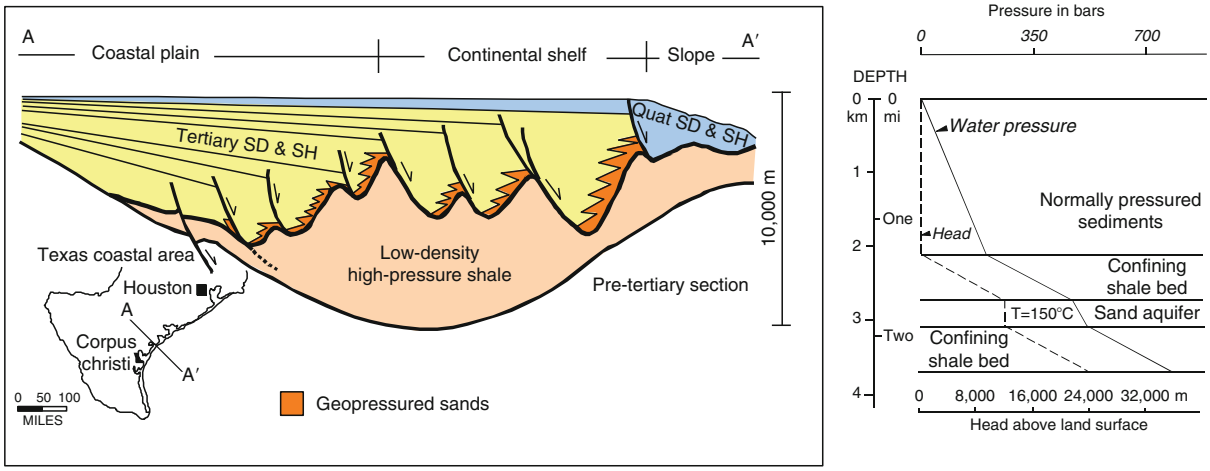

Geothermal Energy Utilization. Figure 4
Geopressured geothermal system

and Asia having over 75% of the total; whereas with the direct-use figures, the percentages drop significantly from installed capacity to energy use for the Americas (28.9–18.4%) due to the high percentage of geothermal heat pumps with low capacity factor for these units in the United States and Canada. On the other hand, the percentages are approximately equal for the remainder of the world due to a lesser reliance on geothermal heat pumps, and the greater number of operating hours per year for these units.

Electric Power Generation

Geothermal power is generated by using steam or a hydrocarbon vapor to turn a turbine-generator set

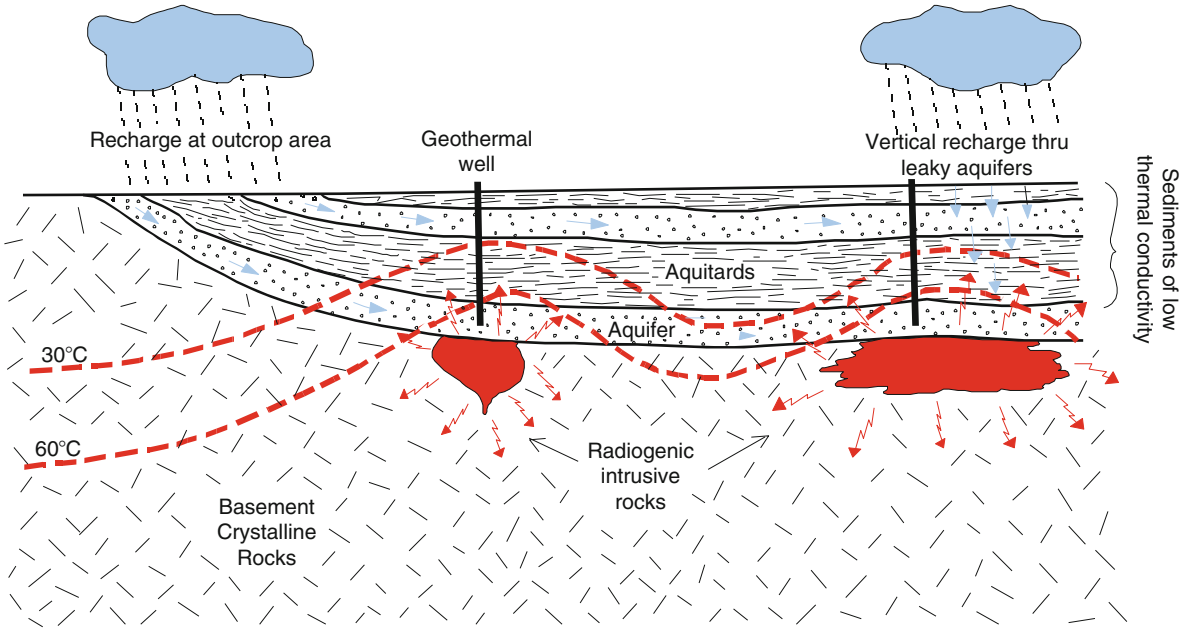

Geothermal Energy Utilization. Figure 5
Radiogenic geothermal system

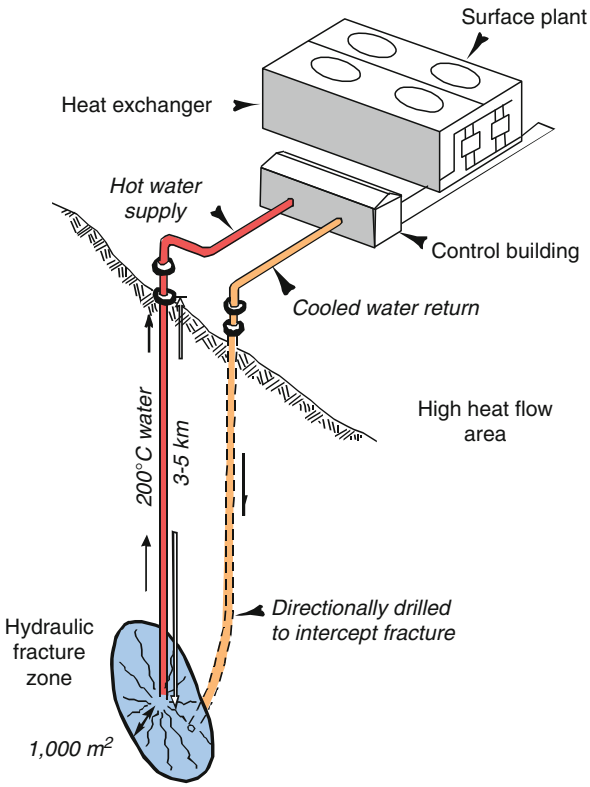

Geothermal Energy Utilization. Figure 6
Hot dry rock exploitation

to produce electrons. A vapor-dominated (dry steam) resource (see Figs. 1 and 7) can be used directly, whereas a hot water resource (see Figs. 2 and 8) needs to be flashed by reducing the pressure to produce steam. In the case of low-temperature resource, generally below 150°C, they require the use of a secondary low boiling point fluid (typically a hydrocarbon) to generate the vapor, in a binary or organic Rankine cycle plant (see Fig. 9). Usually a wet or dry cooling tower is used to condense the vapor after it leaves the turbine to maximize the temperature and pressure drop between the incoming and outgoing vapor and thus increase the efficiency of the operation. The worldwide installed capacity has the following distribution: 27% dry steam, 41% single flash, 22% double flash, 12% binary/combined cycle/hybrid, and 1% backpressure [12].

Electric power has been produced from geothermal energy in 27 countries; however, Greece, Taiwan, and Argentina have shut down their plants due to environmental and economic reasons. Since 2000, the installed capacity in the world has increased almost 3,000 MWe. Since 2000, additional plants have been installed in Costa Rica, France on Guadeloupe in the Caribbean, Iceland, Indonesia, Kenya, Mexico, and Philippines.

In 2004, Germany installed a 210-kWe binary plant at Neustadt Glewe and 56-MWe plants have been installed on Papua New Guinea to generate electricity for a remote mine. Russia has completed a new 50-MWe plant on Kamchatka. More recently, a 200 kW binary plant using 74°C geothermal water and 4°C cooling was installed at Chena Hot Springs Resort in Alaska [3]. The operating capacity in the United States has increased since 1995 due to completion of the two effluent pipelines injecting treated sewage water at The Geysers. In an attempt to bring production back, the Southeast Geysers Effluent Recycling Project is now injecting 340 l/s of treated wastewater through a 48-km long pipeline from Clear Lake, adding 77 MWe. A second, 66-km long pipeline from Santa Rosa was placed on line in 2004, injecting 480 l/s that are projected to add another 100 MWe to The Geyser's capacity. Table 4 lists the leading countries producing electric power.

One of the more significant aspects of geothermal power development is the size of its contribution to national and regional capacity and production of countries. The following countries or regions (Table 5) lead in this contribution with more than 5% of the electrical energy supplied by geothermal power based in data from country update papers from WGC2010 [12].

Geothermal Energy Utilization. Table 2 Total geothermal capacity and use in 2010

Installed annual				
Use	Power (MW)	Energy use (GWh/year)	Capacity factor	Countries reporting
Electric power	10,715	67,246	0.72	24
Direct use	50,583	121,696	0.27	78

Direct Utilization

Direct use of geothermal resources is primarily for direct heat and cooling. The main utilization categories are: (1) swimming, bathing, and balneology; (2) space heating and cooling including district energy systems; (3) agricultural applications such as greenhouse and soil heating; (4) aquaculture application such as pond and raceway water heating; (5) industrial applications such as mineral extraction, food, and grain drying; and (6) geothermal (ground-source) heat pumps, used for both heating and cooling. Direct use of geothermal resources normally uses temperatures below 150°C as illustrated in Fig. 10. The main advantage of using geothermal energy for direct-use projects in this low- to intermediate-temperature range is that these resources are more widespread and exist in at least 80 countries at economic drilling depths. In addition, there are no conversion efficiency losses and projects can use conventional water-well drilling and off-the-shelf heating and cooling equipment (allowing for the temperature and chemistry of the fluid). Most projects can be on line in less than a year. Projects can be on a small scale ("mom and pop operations") such as for an individual home, single greenhouse, or aquaculture pond, but can also be a large-scale operation such as for district heating/cooling, for food and lumber drying, and mineral ore extraction.

Geothermal Energy Utilization. Table 3 Summary of regional geothermal use in 2010

Electric power				Direct use		
Region	%MWe	%GWh/year	#countries	%MWt	%GWh/year	#countries
Africa	1.6	2.1	2	0.1	0.6	7
Americas	42.6	39.9	6	28.9	18.4	15
Asia	34.9	35.1	6	27.5	33.8	16
Europe	14.5	16.2	7	42.5	45.0	37
Oceania	6.4	6.7	3	1.0	2.2	3

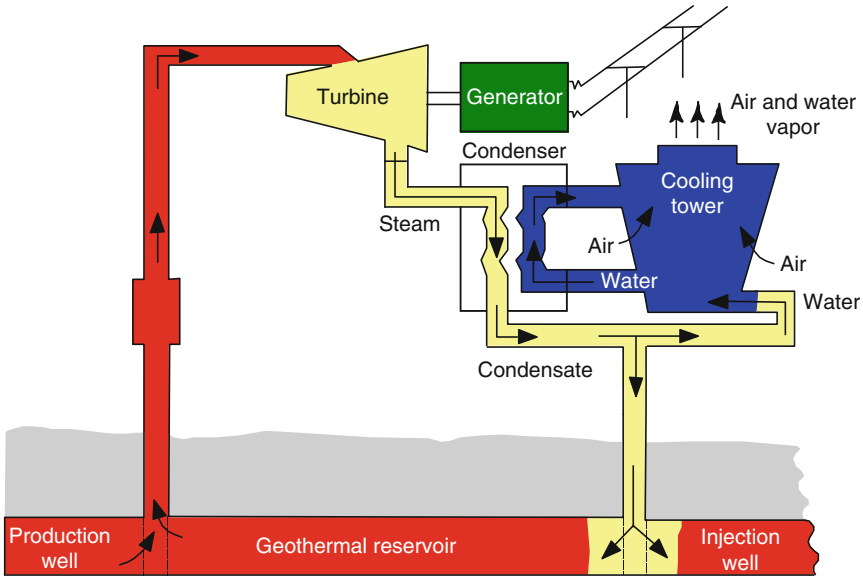

Geothermal Energy Utilization. Figure 7
Steam plant using a vapor- or dry-steam-dominated geothermal resource

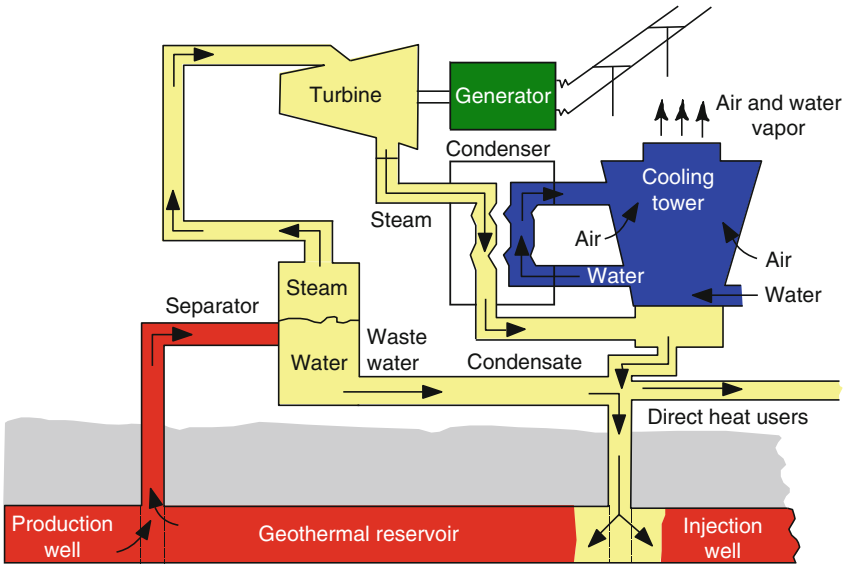

Geothermal Energy Utilization. Figure 8
Flash steam plant using a water-dominated geothermal resource with a separator to produce steam

It is often necessary to isolate the geothermal fluid from the user side to prevent corrosion and scaling. Care must be taken to prevent oxygen from entering the system (geothermal water normally is oxygen free), and dissolved gases and minerals such a boron, arsenic, and hydrogen sulfide must be removed or isolated as they are harmful to plants and animals. On the other hand carbon dioxide, which often occurs

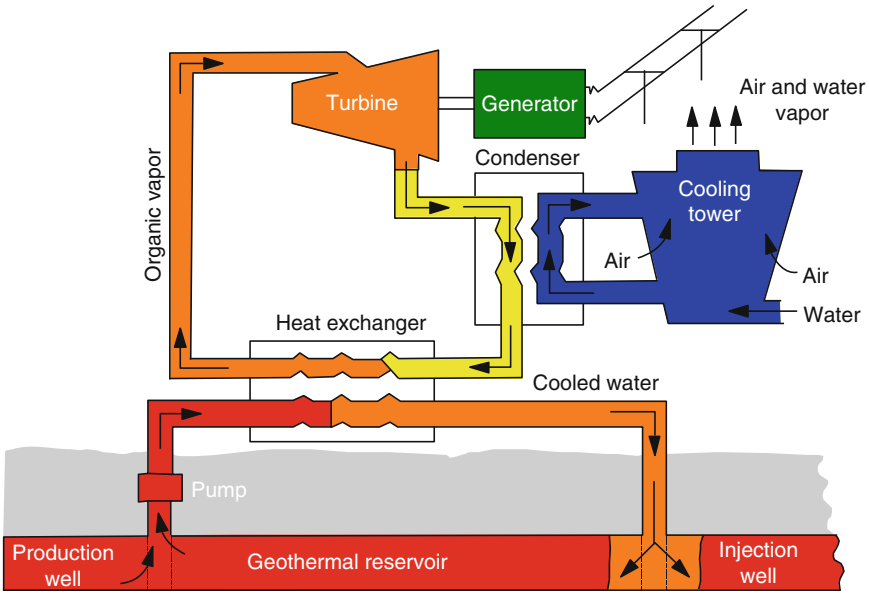

Geothermal Energy Utilization. Figure 9
Binary power or organic Rankin cycle plant using a low-temperature geothermal resource and a secondary fluid of a low boiling point (typically a hydrocarbon)

Geothermal Energy Utilization. Table 4 Leading countries in electric power generation (>100 MWe) [12]

Country	Installed capacity (MWe)	Running capacity[a] (MWe)	Annual energy produced (GWh/year)	Running capacity factor	Number of units operating
United States	3,093	2,024	16,603	0.94	209
Philippines	1,904	1,774	10,311	0.66	56
Indonesia	1,197	1,197	9,600	0.92	22
Mexico	958	958	7,047	0.84	37
Italy	843	843	5,520	0.75	33
New Zealand	628	628	4,055	0.74	43
Iceland	575	575	4,597	0.91	25
Japan	536	422	3,064	0.83	20
El Salvador	204	192	1,422	0.85	7
Kenya	167	167	1,430	0.98	10
Costa Rica	166	166	1,131	0.78	6

[a]Note: Some running capacity figures were not available, and thus were assumed equal to the installed capacity

in geothermal water, can be extracted and used for carbonated beverages or to enhance growth in greenhouses. The typical equipment for a direct-use system is illustrated in Fig. 11, and includes downhole and circulation pumps, heat exchangers (normally the plate type), transmission and distribution lines (normally insulated pipes), heat extraction equipment, peaking or back-up plants (usually fossil fuel fired)

Geothermal Energy Utilization. Table 5 National and regional geothermal power contributions

Country or region	% of national or regional capacity (MWe)	% of national or regional energy (GWh/year)
Lihir Island, Papua New Guinea	75	n/a
Tibet	30	30
San Miguel Island, Azores	25	n/a
Tuscany, Italy	25	25
Iceland	22	27
El Salvador	15	26
Kenya	12	17
Philippines	12	17
Nicaragua	11	10
Guadeloupe (Caribbean)	9	9
Costa Rica	8	12
New Zealand	6	10

to reduce the use of geothermal fluids and reduce the number of wells required, and fluid disposal systems (injection wells). Geothermal energy can usually meet 80 to 90% of the annual heating or cooling demand, yet only sized for 50% of the peak load. Geothermal heat pumps include both open (using groundwater or lake water) and closed-loop (either in horizontal or vertical configuration) systems as illustrated in Fig. 12.

The world direct utilization of geothermal energy is difficult to determine; as, there are many diverse uses of the energy and these are sometimes small and located in remote areas. Finding someone, or even a group of people in a country who are knowledgeable on all the direct uses is difficult. In addition, even if the use can be determined, the flow rates and temperatures are usually not known or reported; thus, the capacity and energy use can only be estimated. This is especially true of geothermal waters used for swimming pools, bathing, and balneology.

One of the significant changes for WGC2010 was the increase in the number of countries reporting use. Six countries were added to the list in the current report as compared to 2005. In addition, the author is aware of three countries (Malaysia, Mozambique, and Zambia) that have geothermal direct uses, but did not provide a report for WGC2010. Thus, there are at least 81 countries with some form of direct utilization of geothermal energy.

Another significant change from 2005 is the large increase in geothermal (ground-source) heat pump installations. They increased by 229% (18% annual growth) in capacity and 245% (20% annual growth) in annual energy produced over the 5-year period to the year 2010. At present (2010), they are the largest portion of the installed capacity (69.7%) and 49.0% of the annual energy use. The equivalent number of 12-kWt units installed (the average size) is approximately 3,000,000 in 43 countries, mostly in the United States, Canada, China, and Europe; however, the data are incomplete. The equivalent number of full-load heating operating hours per year varies from 2,000 in the United States, to over 6,000 in Sweden and Finland, with a worldwide average of 2,200 full-load h/year [10].

A summary of direct-use installed capacity and annual energy use are as follows (excluding geothermal heat pumps at 69.7% and 49.0% respectively of the total); bathing/swimming/spas 43.6% and 48.8%, space heating (including district heating) 35.1% and 28.2%; greenhouse heating 10.1% and 10.4%; aquaculture 4.3% and 5.2%; industrial 3.5% and 5.3%; agricultural drying 0.8% and 0.7%; cooling and snow melting 2.4% and 1.0%; and others 0.2% and 0.4%. District heating is approximately 85% of the space-heating use [10].

In terms of the contribution of geothermal direct use to the national energy budget, two countries stand out: Iceland and Turkey. In Iceland, it provides 89% of the country's space-heating needs, which is important since heating is required almost all year and saves about $100 million in imported oil. Turkey has increased their installed capacity over the past 5 years from 1,495 to 2,084 MWt, most for district heating systems. A summary of some of the significant geothermal direct-use contributions to various countries is shown in Table 6, and the top direct-use countries are listed in Table 7 [10].

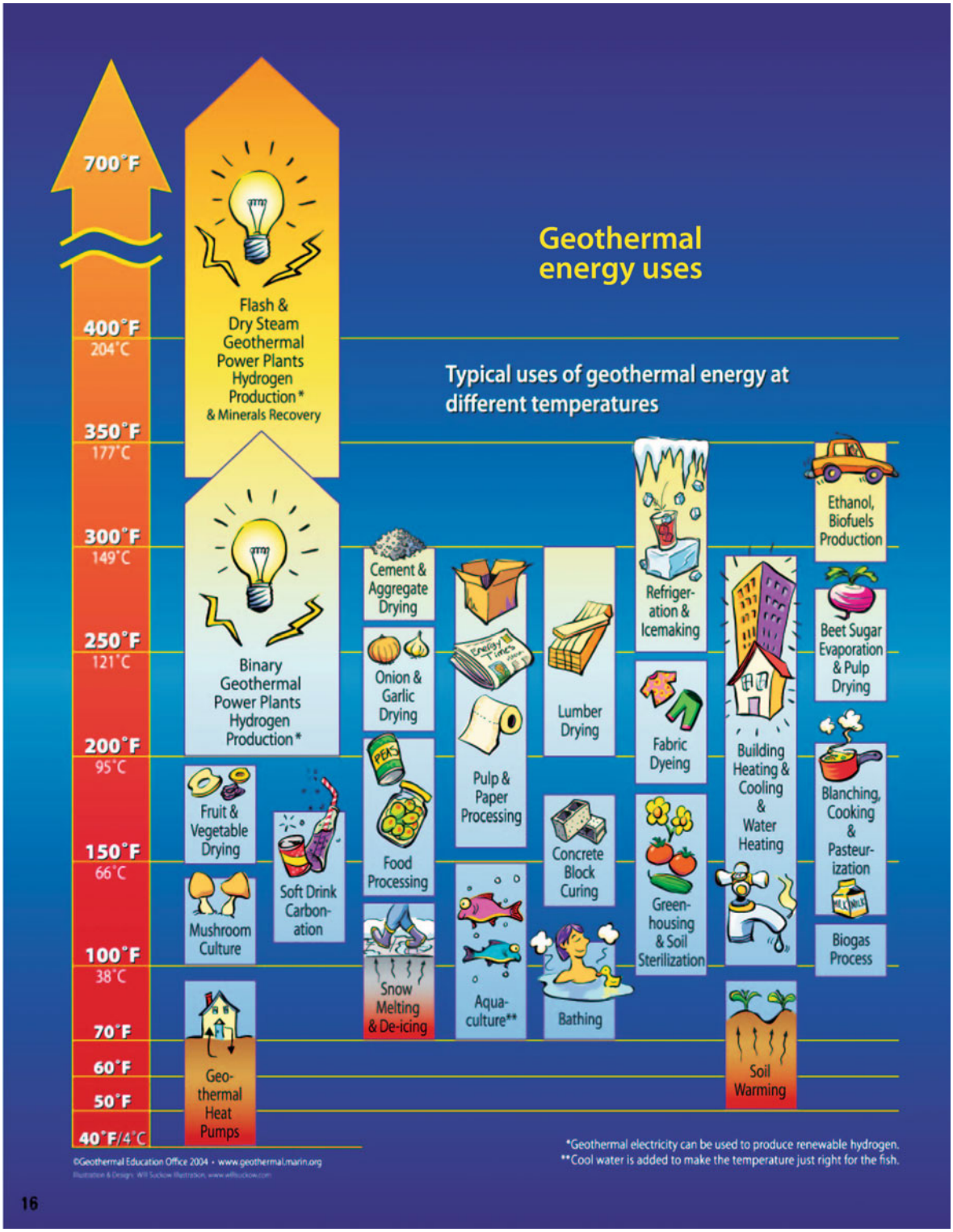

Geothermal Energy Utilization. Figure 10
Geothermal energy uses (Courtesy of the Geothermal Education Office)

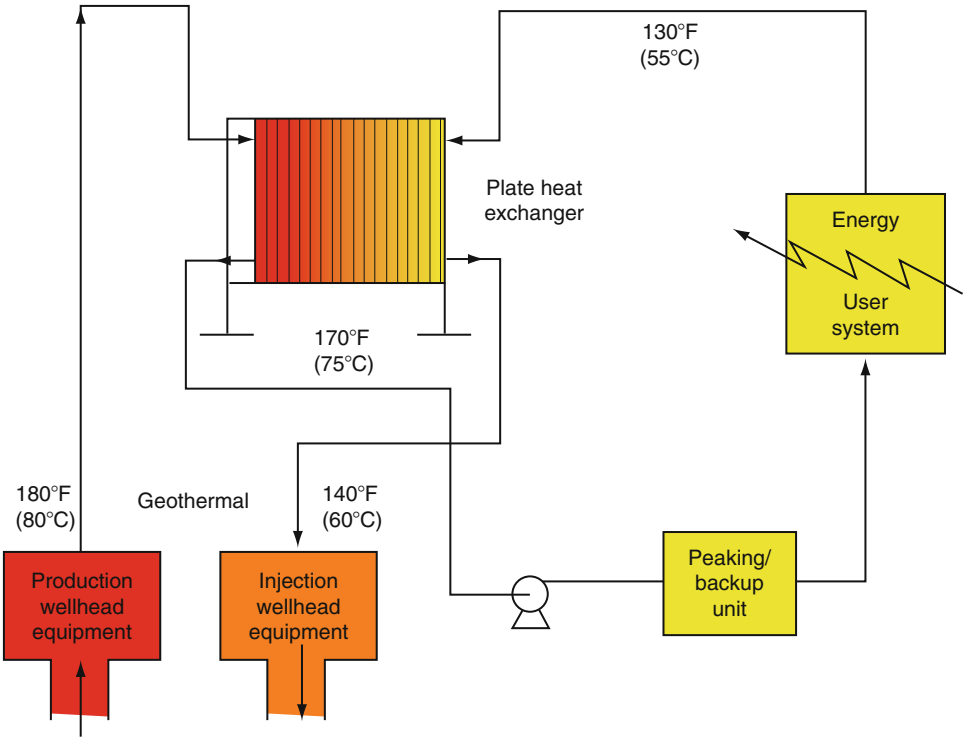

Geothermal Energy Utilization. Figure 11
Typical direct-use geothermal heating system configuration

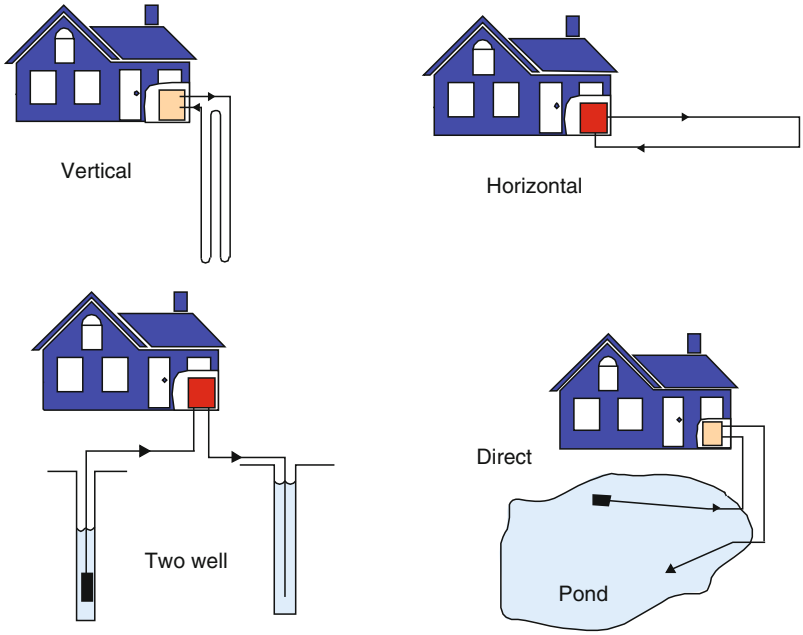

Geothermal Energy Utilization. Figure 12
Examples of common geothermal heat pump installations

Geothermal Energy Utilization. Table 6 National geothermal direct-use contributions

Iceland: provides 89% of country's space-heating needs
Turkey: space heating has increased 40% in the past 5 years, supplying 201,000 equivalent residences and 30% of the country will be heated with geothermal in the future
Tunisia: greenhouse heating has increased from 100 to 194 ha over the past 5 years
Japan: over 2,000 hot spring resorts (onsens), over 5,000 public bath houses, and over 15,000 hotels visited by 15 million quests per years, use natural hot springs
Switzerland: has installed 60,000 geothermal heat pumps = 1/km^2, and 2,000 km of boreholes were drilled in 2009. Drain water from tunnel are used to heat nearby villages and they have also developed several geothermal projects to melt snow and ice on roads
United States: has installed 1,000,000 geothermal heat pump units, mainly in the Midwestern and eastern states, with a 12.5% annual growth. Installation of these units is around 100,000–120,000/year

Geothermal Energy Utilization. Table 7 Top Direct-Use Countries

Country	GWh/year	MWt	Main applications
China	20,932	8,898	Bathing/district heating
United States	15,710	12,611	GHP
Sweden	12,585	4,460	GHP
Turkey	10,247	2,084	District heating
Japan	7,139	2,100	Bathing (onsens)
Iceland	6,768	1,826	District heating
France	3,592	1,345	District heating
Germany	3,546	2,485	Bathing/district heating
Netherlands	2,972	1,410	GHP
Italy	2,762	867	Spas/space heating
Hungary	2,713	655	Spas/greenhouses
New Zealand	2,654	393	Industrial uses
Canada	2,465	1,126	GHP
Switzerland	2,143	1,061	GHP

Environmental Considerations

Geothermal energy is considered a renewable and "green" energy resource; however, there are several environmental impacts that must be considered and are usually mitigated. These are emission of harmful gases, noise pollution, water use and quality, land use, and impact on natural phenomena, wildlife, and vegetation [13].

Emissions: These are usually associated with steam power plant cooling towers that produce water vapor emission (steam), not smoke. The potential gases that can be released, depending upon the reservoir type are carbon dioxide, sulfur dioxide, nitrous oxides, hydrogen sulfide, along with particulate matter. A coal-fired power plant produces the following kilograms of emissions per MWh as compared to a geothermal power plant: 994 vs. up to 40 for carbon dioxide, 4.71 vs. up to 0.16 for sulfur dioxide, 1.95 vs. 0 for nitrogen oxides, 0 vs. 0.08 for hydrogen sulfide (H_2S), and 1.01 vs. 0 for particulate matter. Hydrogen sulfide is routinely treated at geothermal power plants, and converted to elemental sulfur. In comparison, oil-fired power plants produce 814 kg and natural gas fired plants 550 kg of H_2S/MWh. Binary power plants and direct-use projects normally do not produce any pollutants, as the water is injected back into the ground after use without exposing it to the atmosphere.

Noise: The majority of the noise produced at a power plant or direct-use site is during the well-drilling operation, which can shut down at night. The noise from a power plant is not considered an issue of concern, as it is extremely low, unless you are next to or inside the plant. Most of the noise comes from cooling fans and the rotating turbines.

Water use: Geothermal flash steam plants use about 20 l of fresh water/MWh, while binary air-cooled plants use no fresh water, as compared to a coal plant that uses 1,370 l/MWh. Oil plant use is about 15% less and nuclear about 25% more than the coal plant (www.cleanenergy.org). The only change in the fluid during use is to cool it, and usually the fluid is

Geothermal Energy Utilization. Table 8 Energy and greenhouse gas savings from geothermal energy production (electric at 35% efficiency and direct use at 70% efficiency)

	Fuel oil (10^6)		Carbon (10^6 t)			CO_2 (10^6 t)			SO_x (10^6 t)			NO_x (10^3 t)		
	Barrels	Tonnes	NG	Oil	Coal	NG	Oil	Coal	NG	Oil	Coal	NG	Oil	Coal
Electric	114	17	6	15	17	31	49	58	0	0.3	0.4	3.4	10.1	10.1
Direct use	154	23	9	23	27	46	74	88	0	0.5	0.5	4.5	13.6	13.6
Total	268	40	15	38	44	77	123	146	0	0.8	0.9	8.9	23.7	23.7

returned to the same aquifer so it does not mix with the shallow groundwater. At The Geysers facility in northern California, 42 million liters of treated wastewater from Santa Rosa are pumped daily for injection into the geothermal reservoir, reducing surface water pollution in the community and increasing the production of the geothermal field. A similar project supplies waste water (29 million liters daily) from the Clear Lake area on the northeast side of the The Geysers. These projects have increased the capacity of the field by about 200 MWe.

Land use: Geothermal power plants are designed to "blend-in" with the surrounding landscape, and can be located near recreational areas with minimum land and visual impacts. They generally consist of small modular plants under 100 MWe as compared to coal or nuclear plants of around 1,000 MWe. Typically, a geothermal facility uses 404 m^2 of land/GWh compared to a coal facility that uses 3,632 m^2/GWh and a wind farm that uses 1,335 m^2/GWh. Subsidence and induced seismicity are two land use issues that must be considered when withdrawing fluids from the ground. These are usually mitigated by injecting the spent fluid back into the same reservoir. There have been problems with subsidence at the Wairakei geothermal field in New Zealand; however, this has been checked by injection. Induced seismicity is also associated with EGS projects, producing earthquakes of less than 3.4 on the Richter scale. Neither of these potential problems is associated with direct-use projects, as the fluid use is small and well and pipelines are usually hidden. In addition, utilizing geothermal resources eliminates the mining, processing, and transporting required for electricity generation from fossil fuel and nuclear resources.

Impact on natural phenomena, wildlife, and vegetation: Plants are usually prevented from being located near geysers, fumaroles, and hot springs, as the extraction of fluids to run the turbines might impact these thermal manifestations. Most plants are located in areas with no nature surface discharges. If plants are located near these natural phenomena, the fluid extraction depth is planned from a different reservoir to prevent any impact. Designers and operators are especially sensitive about preserving manifestations considered sacred to indigenous people. Any site considered for a geothermal power plant, must be reviewed and considered for the impact on wildlife and vegetation, and if significant, provide a mitigation plan. Direct-use projects are usually small and thus have no significant impact on natural features.

In summary, the use of geothermal energy is reliable, providing base load power; is renewable; has minimum air emission and offsets the high air emissions of fossil fuel-fired plants; has minimum environmental impacts; is combustion free; and is a domestic fuel source.

Energy Savings

Using geothermal energy obviously replaces fossil fuel use and prevents the emission of greenhouse gases. If it is assumed that geothermal energy replaces electricity generation, the conversion efficiency is estimated at 0.35 (35%). These savings using geothermal energy at this efficiency level is summarized in Table 8 [14]. If the replacement energy for direct use is provided by burning the fuel directly, then about half this amount would be saved in heating

systems (35% vs. 70% efficiency), as used in Table 8. Savings in the cooling mode of geothermal heat pumps is also included in the figures in Table 8. The savings in fossil fuel oil is equivalent to about 3 days (1%) of the world's consumption.

It should be noted when considering these savings, that some geothermal plants do emit limited amounts of the various pollutants; however, these are reduced to near zero where gas injection is used and eliminated where binary power is installed for electric power generation. Since most direct-use projects use only hot water and the spent fluid injected, the above pollutants are essentially eliminated.

Future Directions

Geothermal growth and development of electricity generation has increased significantly over the past 40 years approaching 11% annually in the early part of this period, and dropping to 3% annually in the last 10 years due to the low price of competing fuels. Direct use has remained fairly steady over the 40-year period at 10% growth annually. The majority of the increase has been due to geothermal heat pumps. At the start of this 40-year period, only ten countries reported electrical production and/or direct utilization from geothermal energy. By the end of this period, 78 countries reported utilizing geothermal energy. This is almost an eightfold increase in participating countries. At least another ten countries are actively exploring for geothermal resources and should be on line by 2015.

Developments in the future will include greater emphases on combined heat and power plants, especially those using lower temperature fluids down to 100°C. This low-temperature cascaded use will improve the economics and efficiency of these systems, such as shown by those installed in Germany and Austria and at Chena Hot Springs, Alaska. Also, there is increased interest in agriculture crop drying and refrigeration in tropical climates to preserve products that might normally be wasted. Finally, the largest growth will include the installation and use of geothermal heat pumps, as they can be used anywhere in the world, as shown by the large developments in Switzerland, Sweden, Austria, Germany, China, Canada, and the United States.

Bibliography

Primary Literature

1. EPRI (Electric Power Research Institute) (1978) Geothermal energy prospects for the next 50 years. ER-611-SR, Special Report for the World Energy Conference 1978
2. Cataldi R, Hodgson S, Lund J (eds) (1999) Stories from a heated earth – our geothermal Heritage. Geothermal Resources Council, Davis, p 569
3. Lund JW (2006) Chena hot springs. Geo-Heat Center Quart Bull 27(3):2–4, Oregon Institure of Technology, Klamath Falls
4. Wright M (1998) Nature of geothermal resources. In: Lund JW (ed) Geothermal direct-use engineering and design guidebook. Geo-Heat Center, Klamath Falls, pp 27–69
5. White DE, Williams DL (eds) (1975) Assessment of geothermal resources of the United States – 1975. U.S. Geological Survey Circular 727, U.S. Government Printing Office, 155 p
6. Tenzer H (2001) Development of hot dry rock technology. Geo-Heat Center Quart Bull 22(4):14–22, Oregon Institute of Technology, Klamath Falls
7. Tester JW et al (2006) The future of geothermal energy – impacts of enhanced geothermal systems (EGS) on the United States in the 21st century. Massachusetts Institute of Technology, Cambridge, 384 p
8. Lund JW, Freeston DH (2001) World-wide direct uses of geothermal energy 2000. Geothermics 30(1):29–68, Elsevier, Oxford (updated and revised)
9. Lund JW, Freeston DH, Boyd TL (2005) Worldwide direct-uses of geothermal energy 2005. Geothermics 34(6):691–727, Elsevier, Amsterdam, The Netherlands
10. Lund JW, Freeston DH, Boyd TL (2010) Direct utilization of geothermal energy 2010 worldwide review. In: Proceeding, World Geothermal Congress 2010, Bali, Indonesia
11. Bertani R (2005) World geothermal general 2001–2005 – state of the art. Geothermics 34(6), Elsevier, Amsterdam, The Netherlands
12. Bertani R (2010) Geothermal power generation in the World, 2005–2010 update report. In: Proceedings of the World Geothermal Congress 2010, Bali, Indonesia
13. Kagel A, Bates D, Gawell K (2005) A guide to geothermal energy and the environment. Geothermal Energy Association, Washington, DC, 75 p
14. Goddard, W. B. and C. B. Goddard, 1990. "Energy Fuel Sources and Their Contribution to Recent Global Air Pollution Trends." Geothermal Resources Council *Transactions*, v. 14, Davis, CA, pp 643-649

Books and Reviews

Armstead HCH (1983) Geothermal energy, 2nd edn. E. & F.N. Spon, London, 404 p

Dickson MH, Fanelli M (2003) Geothermal energy utilization and technology. Earthscan, London, 205 p

DiPippo R (2008) Geothermal power plants – principles, applications, case studies and environmental impact, 2nd edn. Elsevier, Amsterdam, 493 p

Kavanaugh SP, Rafferty K (1997) Ground-source heat pumps – design of geothermal systems for commercial and institutional buildings. American Society of Heating, Refrigerating and Air-Conditioning Engineers, Inc, Atlanta, 167 p

Lund JW, Lienau PJ, Lunis BC (1998) Geothermal direct-use engineering and design guidebook, 3rd edn. Geo-Heat Center, Klamath Falls, 454 p

Websites

European Geothermal Energy Council, Belgium: www.geothermie.de/egec_geothernet/menu/frameset.htm

Geothermal Education Office, USA: http://geothermal.marin.org

Geothermal Energy Association, USA: http://www.geo-energy.org

Geo-Heat Center, USA: http://geoheat.oit.edu

Geothermal Resources Council, USA: http://www.geothermal.org

IEA (International Energy Agency) Heat Pump Center, Netherlands: www.heatpumpcentre.org

International Geothermal Association: http://www.geothermal-energy.org

International Ground Source Heat Pump Association, USA: http://www.igshpa.okstate.edu

Stanford University Geothermal Program: http://pangea.stanford.edu/ERE/research/geoth/

U.S. Department of Energy, Geothermal Technologies: www.eere.energy.gov/geothermal/

World Geothermal Congress 2010, Indonesia: www.wgc2010.org

Geothermal Energy, Geology and Hydrology of

William E. Glassley
Energy Institute, University of California, Davis, CA, USA
Geologisk Institut, University of Aarhus, Aarhus, Denmark

Article Outline

Glossary
Definition of the Subject
Introduction
Heat Sources in the Earth
Plate Tectonics as the Physical Framework
Heat and Water in the Subsurface
Future Directions
Summary
Bibliography

Glossary

Core The central portion of the Earth that is composed of high density metallic, solid, and liquid components.

Crust The outer layer of the Earth composed of low to moderate density silicates and other minerals and within which the radioactive elements K, Rb, U, and Th are concentrated.

Direct use An application that uses the heat from a geothermal resource to accomplish heating, cooling and drying without converting thermal energy to another energy form.

Enhanced geothermal systems A deep geothermal system in which the porosity and permeability have been artificially enhanced through engineering methods to increase the mass flux of fluid that can be pumped through the reservoir.

Heat flow Strictly, the movement of thermal energy via diffusive conduction. Heat flow, as measured, is also a reflection of advective and convective transport.

Heat pump A device for transferring heat from one location to another.

Hydrology The scientific discipline that studies the flow of fluids in the crust.

Magma Molten rock that is one of the primary means for transferring heat to near-surface environments.

Mantle The interior portion of the Earth between the core and crust within which convective flow of material transfers heat to the crust.

Permeability The measurement or property of a medium that describes the ease with which a fluid will pass through the pores or fractures of the medium.

Plate tectonics The conceptual framework that provides a unifying principle describing the dynamic processes within the Earth.

Definition of the Subject

Geothermal energy is a ubiquitous renewable energy resource that is available virtually anywhere on the Earth. Surface manifestations of this energy resource

are, however, diverse and irregularly distributed. The most obvious and dramatic examples of geothermal energy are volcanoes. Less dramatic but equally unambiguous are geysers, hot springs, and warm pools, all of which are striking by their seemingly endless outflow of warm water from the subsurface. More subtle indications of geothermal energy are measurements in boreholes, mines, and wells that inevitably show that the deeper one goes below the surface, the warmer is the rock. All of these examples unambiguously document that heat is present in the subsurface, and it is this energy resource that geothermal applications utilize.

Access to geothermal resources varies from place to place, reflecting a complex interplay of geological and hydrological processes that have developed over millions of years. As a result, the types of geothermal applications that can be developed also vary from place to place. If high temperature (greater than ~150°C) water can be accessed at depths of a few kilometers, the potential exists for installing a geothermal power plant. Lower temperature waters can be utilized for a broad range of so-called direct-use applications, whereby the thermal energy of the fluid is used for such things as drying timber, drying fruits and vegetables, curing concrete blocks, processing food, or heating buildings. And, virtually anywhere on the planet, at depths of a few meters to a few tens of meters, the constant flow of heat from the Earth's interior provides consistent conditions suitable for the installation of ground source heat pumps for heating and cooling. Evaluating the characteristics and magnitude of a geothermal resource requires unifying information, models, and concepts from a range of disciplines that focus on elucidating the properties of geological systems.

Introduction

Natural hot springs, volcanoes, and geysers are obvious indications that the interior of the Earth is hot. Catastrophic eruptions such as that of Mt. Vesuvius in AD 79 that destroyed the city of Pompeii and of Krakatoa in 1883 that affected weather patterns globally provide compelling evidence that the magnitude of the heat energy is huge. But, the irregular distribution of volcanoes and hot springs over the Earth's surface seems, at first glance, to be enigmatic. If the interior of the Earth is hot, why are some manifestations of that heat restricted to certain regions? What controls the distribution pattern? How large is the resource?

Answers to these questions derive from the evolution of geological processes.

Heat Sources in the Earth

Human awareness of geothermal energy dates back thousands of years [1] although the first uses of geothermal waters remain unknown. However, it was not until the Industrial and Scientific Revolutions in the 1700s and 1800s that investigations of the interior of the Earth began. Mining activities made it apparent that as one went deeper in the Earth temperatures increased [2, 3]. Why that should be so, and how hot the interior of the Earth was remained unknown until the advent of several scientific disciplines that, together, provided an answer to these questions.

The discovery of radioactivity in the late 1890s and early 1900s provided a solution to at least part of the problem. It was eventually recognized that radioactive decay generates heat. The Earth contains a number of radioactive elements, among them potassium (K), rubidium (Rb), uranium (U), and thorium (Th), all of which release heat when radioactive decay occurs. However, it was apparent that these elements could not account for the presence of a hot interior Earth in which there existed a liquid core, a fact that was generally accepted by the end of the 1920s [4]. These elements are concentrated in the crust of the Earth [5], and are of very minor importance in the mantle and core, and therefore they cannot be the exclusive source for the heat that is observed at the surface. This conundrum was resolved when the early accretionary history of the Earth became better understood.

The Earth accreted from the solar nebula about 4.56 billion years ago [6, 7]. The materials that formed the Earth included rocky and metallic bodies as well as icy material from comets. The kinetic energy

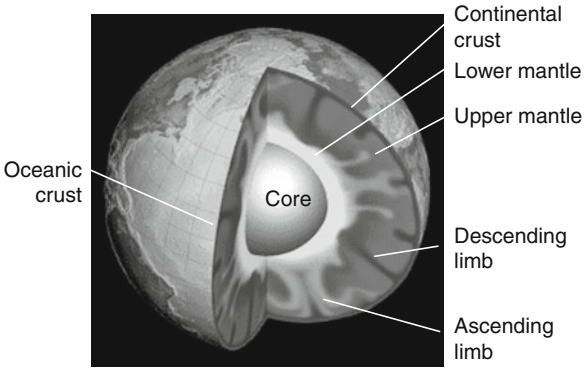

Geothermal Energy, Geology and Hydrology of. Figure 1
A cross section of the Earth showing the main structural divisions. The core, lower mantle, upper mantle, and crust are indicated. Also shown are ascending and descending limbs of convection cells (Source: US Geological Survey, http://geomag.usgs.gov/about.php)

carried by these bodies when they impacted the forming planet was sufficient to heat the Earth substantially. At the same time, during the early life of the solar nebula an abundance of short-lived isotopes were also accumulating in the Earth. Particularly important were specific isotopes of aluminum, hafnium, and manganese (^{26}Al, ^{182}Hf, and ^{53}Mn, respectively). The combination of these heat-generating mechanisms ultimately resulted in the partial melting of the planet. Over a period of about 30 million years [8–13] metallic iron and related compounds became liquid and, because of their high density, settled to the core of the Earth while the remaining silicates stratified into layers (Fig. 1) of different densities. About 40% of the heat energy that is available and used in geothermal applications comes from this early period of differentiation of the Earth [14]. The remaining 60% comes from the decay of the longer-lived isotopes of K, U, Rb, and Th that have concentrated in the crust [15].

Plate Tectonics as the Physical Framework

The materials that make up the Earth are relatively poor thermal conductors. As a result, the heat deep in the Earth is conducted to the surface relatively slowly. The average heat flow at the surface of the Earth is 87 milli-Joules/m^2/s. Since a Watt (W) is a Joule per second (J/s), this heat flow is equivalent to 87 mW/m^2. Deeper in the Earth, near the core–mantle boundary, temperatures are in excess of 3,600°C [16]. The high temperatures in the low thermal conductivity materials that compose the mantle inevitably result in a situation where the lower mantle heats sufficiently to become less dense than the immediately overlying, cooler mantle. This is a gravitationally unstable configuration, and leads to upward flow of the hotter, less dense material. As a result, conditions favorable for development of a convection system become established [17]. The consequence of this condition, over time, is that hot mantle material begins to flow upward toward the Earth's surface [18]. When this ascending mantle material approaches the surface it spreads laterally, eventually descending to complete the pattern characteristic of convection. It is through this mechanism of convection that plate tectonics is driven, providing the resource for geothermal energy.

Plate tectonics describes the features and properties of the global convection system [19, 20]. The surface of the Earth is composed of seven major plates and approximately an equal number of smaller plates. The interior regions of the plates are relatively inactive, forming stable geological environments in which there is little seismic, tectonic, or volcanic activity. The edges of the plates, however, are the regions where seismic and tectonic activity are concentrated. It is mainly in these plate-edge settings where readily accessible, geothermally interesting resources occur. There are, in addition, several other geothermally important geological settings, most notably hot spots, that figure prominently in geothermal efforts. These tectonic environments localize heat in specific ways, providing an explanation for the observation that geothermal regions appear to be constrained to specific regions and zones around the world. Each of these settings is discussed in the following sections. The exceptions to this generalization are "geopressured" resources and "Enhanced Geothermal Systems" (EGS) which are briefly discussed at the end of this chapter and are presented in detail in "► Engineered Geothermal Systems, Development and Sustainability of."

Spreading Centers

When upward ascending limbs of convection cells approach the surface of the Earth, the hot material they are carrying begins to melt as the pressure drops. The melt aggregates into magma bodies that buoyantly rise. When the ascending limb is within about 100 km of the surface it begins to spread laterally, causing the plates on either side of this zone to move away from each other (Fig. 2). Magma in the ascending limb invades this zone, forming new crust at the edges of the diverging plates. Because of these magma bodies, spreading centers have the highest heat flow of any place on the Earth's surface. Theoretically, these zones could have heat flow values approaching 1,000 mW/m^2 [14].

Although of considerable theoretical interest from a geothermal energy perspective, spreading centers are of limited practical value since they are usually found in ocean basins at several kilometers depth and far from population centers. Exceptions to this are the Imperial Valley of California and the East African Rift. Both of these settings are geothermally active. Development of geothermal resources in Africa is underway. Geothermal power production in the Imperial Valley of California, which is currently approximately 2,000 MW [21], provides a significant amount of the renewable energy generated by the state of California.

Subduction Zones

Once crust is formed, it is conveyed away from spreading centers and slowly cools. Since most newly formed crust forms in ocean basins, it interacts with seawater as it migrates away from the spreading centers and ages. This interaction with the seawater results in the formation of mineral phases that commonly contain some water in their structure.

As required by the law of conservation of mass, convecting systems invariable have descending limbs that counter the mass flow from ascending limbs. These zones in plate tectonics are called subduction zones (Fig. 2). Subduction zones are regions where the cooled crust descends back into the mantle. Because they are colder, they have low heat flow where the initial descent into the mantle occurs. In addition, as shown in Fig. 2, isotherms within the mantle are depressed in the immediate vicinity of the descending slab of cooler material.

Nevertheless, the descending crust does heat up as it enters the mantle. As the crust heats, it

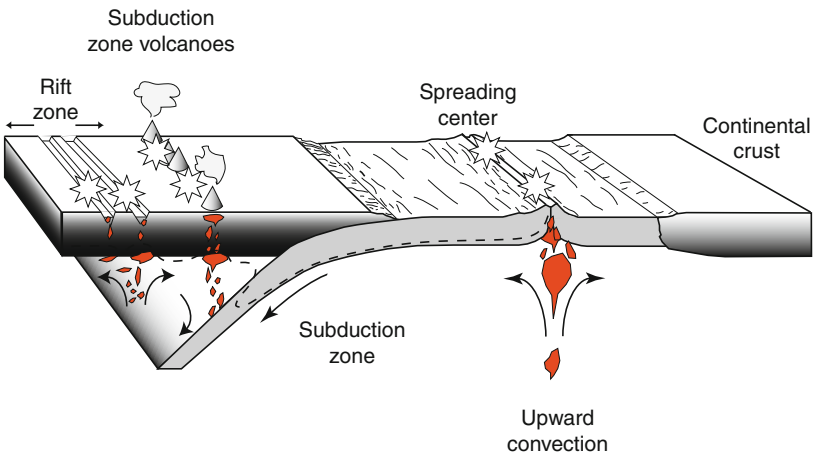

Geothermal Energy, Geology and Hydrology of. Figure 2
Schematic diagram of the main elements in plate tectonic. The *stars* indicate regions where geothermal resources are concentrated. The *dashed line* schematically indicates the general form of isotherms. Magma bodies are indicated by the *red* forms

eventually reaches temperatures sufficient to cause the breakdown of the hydrous minerals that formed when the crust was interacting with seawater. This breakdown of hydrous minerals liberates water. Because of its relatively low density, the released water migrates upward into the overlying warmer mantle where it causes a complex series of reactions, including partial melting. The melts that are generated ascend to the surface, where they form prominent volcanic chains. The so-called Ring of Fire that surrounds the Pacific Ocean formed precisely as a result of this process. This process is, in essence, a heat transfer mechanism whereby the rising magma brings heat to the near-surface environment from the deeper mantle.

The volcanic systems associated with subduction zones are, globally, the most common settings for geothermal power generation and direct use. Geothermal facilities that have utilized the thermal energy in these settings have been built in Chile, Central America, the Cascades in Northern California and Oregon, Japan, the Philippines, and the Mediterranean region, to name a few.

Commonly associated with the volcanic chain that forms above subduction zones are secondary rift systems, or back-arc basins (Fig. 2). These environments are extensional systems somewhat like spreading centers [22]. They appear to develop in response to complex flow dynamics in the mantle above the descending slab [23]. Because they involve the same type of ascending hot mantle flow as found in spreading centers, magma bodies form and ascend to the near surface. As a result, these settings can also be important high temperature zones within which geothermal resources concentrate. An example of this type of environment is the Taupo volcanic zone on the North Island of New Zealand, where occurred the first large-scale development of geothermal power in the world. Although geologically more complex, the Basin and Range Province of the Western United States is, in part, a manifestation of similar processes. Existing and/or planned geothermal facilities in eastern Arizona, California, Colorado, Idaho, Montana, Nevada, and New Mexico, to name a few, utilize geothermal resources in this type of setting.

Transform Faults

The third type of plate boundary is a feature called a transform fault. Transform faults are places where plates move past each other horizontally, forming fault zones in which the rock has been crushed and fragmented. Although transform faults are not intrinsically associated with magma bodies, local geological conditions can result in high heat flow and the development of a geothermal resource. This can occur because such zones provide easy flow paths for warm or hot waters at depth to ascend to shallower levels. The San Andreas fault in California is one example of a transform fault along which warm and hot springs are common and for which there is chemical and isotopic evidence of flow from great depth [24].

Hot Spots

Hot spots are surface manifestations of a persistent heat source deep in the mantle. They are characterized by long-lived volcanic activity and by the fact that they exhibit no specific relationship with any type of plate boundary. Hot spots are found relatively commonly in the interiors of plates. Their cause remains largely unknown. Iceland and the Hawaiian Island–Emperor Seamount chain are two examples of hot spots. In the case of Iceland, the heat and magma source for the hotspot coincides with the spreading center in the Atlantic Ocean. It has persisted at that site for more than 10 million years. The Hawaiian–Emperor chain, by contrast, has traveled over a hot spot that has persisted for more than 50 million years. The only active volcano in this chain is the island of Hawaii. Both of these locations have geothermal facilities, Iceland in particular being a spectacular example of the broad use of geothermal energy resources for both space and district heating and power generation.

Heat and Water in the Subsurface

The above discussion provides a broad conceptual framework for understanding how geothermal heat becomes concentrated in certain regions. Generally,

the responsible processes transport heat to the near surface either through the intrusion of magma or the flow of deep circulating water. The following discussion considers in more detail the specific geological and hydrological conditions that make a heat resource useful for geothermal applications.

Heat Sources

Geothermal power generation uses the heat energy of moderate to high temperature (>140°C) geothermal fluids to power turbines that drive electrical generators (see "► Geothermal Power Conversion Technology"). Direct-use applications, such as aquaculture, food drying, district heating systems, and greenhouses, among others, rely on lower temperature (less than about 150°C) geothermal fluids to directly heat an environment for specific purposes (see entries "► Nuclear Transfer to Produce Transgenic Mammals" and "► Disease-Resistant Transgenic Animals"). Regardless of the technology employed, there are several basic geological and hydrological conditions that determine whether a resource is suitable for its intended use. The key requirements are an adequate resource that can provide the requisite thermal energy for the specific application and whether there is an adequate fluid flow to transfer the thermal energy to power the engineered system.

Cooling magma bodies, or their hot solidified counterparts, are the heat source for many geothermal applications. These bodies can be of many forms and sizes. Shown in Fig. 3 is an example of the kind of irregularity they may have. The main magma body (pluton) can be a few hundred meters to kilometers in size, with offshoots (dikes and sills) a few meters to many tens of meters in size. The magma, when it is liquid, will have temperatures between about 700°C and 1,100°C, depending on its composition.

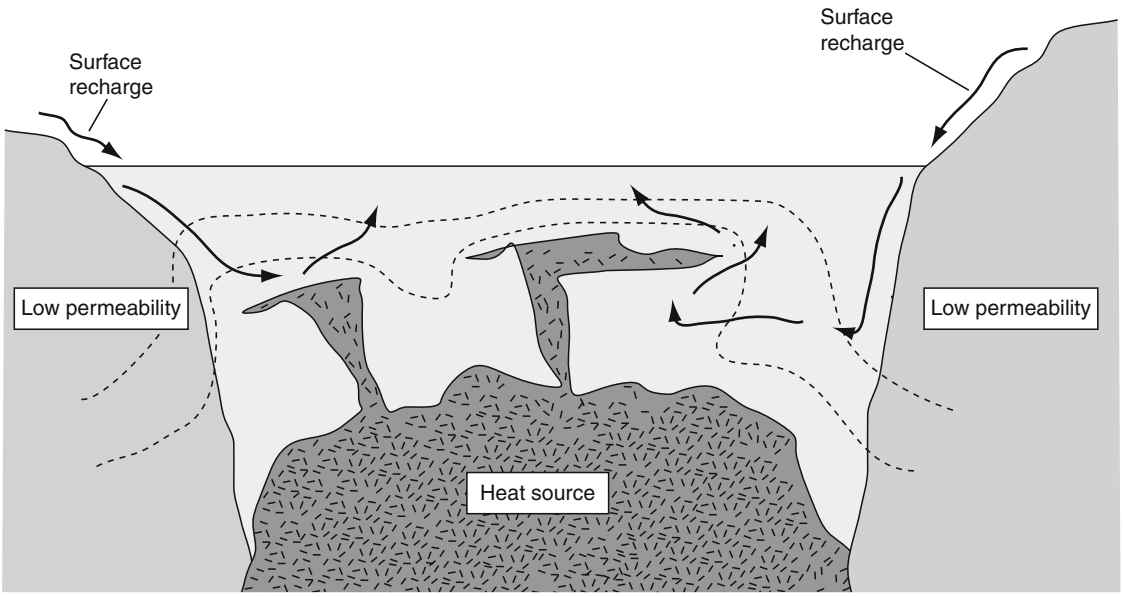

Geothermal Energy, Geology and Hydrology of. Figure 3
Schematic diagram of a high temperature geothermal system. The *arrows* indicate the flow path of water in the subsurface. Hypothetical 250°C and 300°C isotherms are indicated by the *dashed lines*. The *dark gray* body labeled "Heat source" represents a cooling igneous body that once was a magma chamber. The *light gray* pattern indicates porous and permeable rocks into which the magma intruded. The *medium gray* rocks labeled "Low permeability" indicate highland regions that provide recharge of water to the subsurface

The cooling rate for shallow plutons is tens to hundreds of degrees per million years; hence, the lifetime of useful heat output can be quite long. This allows geothermal development of intrusive bodies that are several to ten million years old, depending on the local conditions.

The distribution of heat around these bodies can result in complex isotherm patterns. Shown in Fig. 3 are hypothetical 300°C and 250°C isotherms that might be expected solely from slow cooling of the heat source. The form of the isotherms is influenced by the geometry of the igneous body, as well as the local geology. As will be discussed below, another important factor that influences isotherm form is the extent to which fluid flow transfers heat away from the region. Regardless of the underlying mechanism, the isotherms in such a setting are likely to have an irregular form. It is for this reason that temperature gradient holes are used in exploration efforts to determine the real vs hypothetical subsurface temperature distribution [25]. The importance of acquiring such information is shown in Fig. 4, which depicts measured temperatures in the subsurface in Long Valley caldera in the eastern Sierra Nevada mountains [26]. The Long Valley caldera is a region of geothermal activity and is the site of a 37 MW power generation facility. Linear geothermal gradients are shown for comparison. Note the pronounced departure from linearity. The prominent temperature spikes, as well as the complex variations in temperature over distances of several hundred meters reflect the effects of fluid flow.

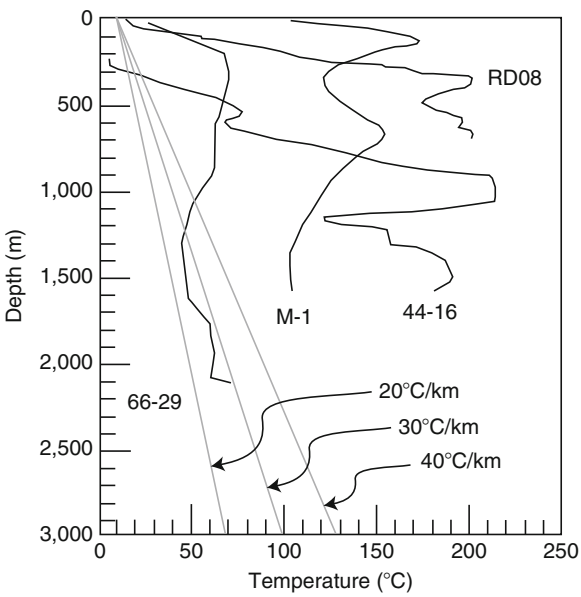

Geothermal Energy, Geology and Hydrology of. Figure 4
Measured temperature profiles in bore holes at Long Valley caldera, California (Data from [26])

The other main source of useful geothermal energy is deep circulation of water in natural aquifer systems. In this instance, meteoric water flows into the subsurface, often along faults or other flow paths. The situation is exactly analogous to the flow field depicted on the right hand side of Fig. 3, except in this case there is no specific heat source present. Instead, the descending water flows to depths of several kilometers where the normal geothermal gradient (10–30°C/km) results in the circulating fluid coming in to contact with rocks in the temperature range of 50–100°C. Deep fault zones that intersect these naturally circulating fluids can allow rapid ascent of the fluid from depth, resulting in the development of warm or hot springs. Although such fluids do not possess sufficient energy to support power generation, they do have sufficient thermal energy for successful development of direct-use applications.

Whether or not a high temperature zone will be useful for geothermal applications depends on whether the heat it possesses can be brought to the surface in sufficient quantity. The fundamental requirement for achieving this is the ability to circulate fluid in sufficient volume to bring the heat to the surface at a rate that matches the demand of the application. The material property that determines whether this criteria can be met is the permeability.

Subsurface Fluid Flow: Porosity and Permeability

Rocks are generally classified as igneous, metamorphic, or sedimentary, depending upon the principal process that controlled their formation. Igneous rocks crystallized from magmas and usually have a very low percentage (usually much less than 10%)

of their volume occupied by pore space (*porosity*). Sedimentary rocks form as the products of erosion and deposition, often in response to the effects of water movement or settling in sedimentary basins. Such rocks have a wide range of porosities, but can be quite porous, with values easily reaching 40% or more. Metamorphic rocks form as a result of changes in temperature and pressure due to burial or other physical effects. As the physical conditions evolve a rock will recrystallize, changing its mineralogy and internal structure. The porosity of metamorphic rocks usually falls somewhere between that of igneous and sedimentary rocks.

All rocks have two related but independent physical properties. One of these properties is porosity (as described above), the other is permeability. Regardless of how solid a rock appears, there will always be some amount of space between mineral grains and/or some cracks and fractures. If the pore space occurs primarily as voids between grains, the porosity is classified *as matrix-dominated porosity*. If most of the void space occurs as fractures, it is termed *fracture-dominated porosity*. The open space between mineral grains can be as small as a micron (i.e., 1 millionth of a meter) or as large as a significant fraction of a centimeter. Fractures can have similar dimensions. Measured values of rock porosity vary from a small fraction of a percent in unfractured crystalline rocks such as granites or some metamorphic rocks, to greater than 40% in some sedimentary sandstones. The porosity determines the instantaneous volume of fluid a rock can possess.

The porosity has an important effect on the thermal and mechanical properties of a rock in the subsurface. The thermal properties of water and minerals are significantly different. At 25°C, for example, the amount of energy it takes to raise the temperature of 1 kg of water 1°C is 4,180 J. On the other hand, it only takes 660 J of energy to raise the temperature of 1 kg of potassium feldspar, a common mineral in granite, 1°C. In other words, the heat capacity of water is quite high compared to the heat capacity of many minerals. Thus, at a given temperature, assuming the porosity is 100% filled by liquid water (i.e., the rock is *saturated*), the heat content of a given volume of potassium feldspar with 1% porosity will be about half that for the case in which the porosity is 20%. Similar results are obtained for most other minerals. Heat capacity varies with mineral, and is a function of temperature. Hence, this specific result *qualitatively* illustrates the relationship between heat content, porosity, and water content (or saturation) for rock systems, but does not *quantitatively* represent the behavior of all rocks under these conditions. When assessing the available thermal energy in a potential geothermal resource, it is important to establish the porosity and degree of saturation of the rock composing the geothermal reservoir. A detailed discussion of resource assessment is provided in later entries in this book.

The ability of fluid to flow through a geothermal reservoir determines the rate at which heat can be extracted. The measure of the ease with which fluid flows through rock is the *permeability*. For an unfractured, porous, saturated rock, if the pores are not interconnected the fluid cannot flow through the rock and the permeability will necessarily be zero. In other words, regardless of the porosity, there would be no fluid flow in this case. For porous rock with interconnected porosity, the ability of fluid to flow will depend on the size of the connections between the pores, the complexity of the flow path (also called the *tortuosity*), the pressure gradient across the flow path, the shape of the pores, and certain physical properties of the fluid. For fractured rocks [27], the important characteristics affecting the permeability include the effective aperture of the fracture, its roughness, the number of fractures per rock volume, and their orientation, as well as the fluid properties.

The concept of permeability was formalized by Henry Darcy in the 1800s. He developed the relationship

$$q = -(\kappa/\mu) \cdot A \cdot \nabla(P)$$

where q is the flux ($m^3/m^2/s$), κ is the permeability (in units of area, m^2), A is the cross-sectional area (m^2), μ is the dynamic viscosity (kg/(m-s)), and $\nabla(P)$ is the gradient in pressure. This relationship strictly applies only to conditions of slow flow in porous media for a single phase [28, 29]. It is often used in more complex situations, but its limitations need to be understood. It is especially important to recognize this limitation in geothermal systems where high flow rates

are often encountered. Note that a standard measure of permeability is the darcy, the conversion for which is 9.869 e^{-13} m^2/darcy.

The relationship between porosity and permeability has been formalized in several ways [30], the most useful of which is the Kozeny–Carmen equation [31–33],

$$\kappa = [n^3/(1-n)^2]/(5 \cdot S_A)^2$$

In this relationship, n is the porosity and S_A is the surface area of the pore spaces per unit volume of rock. This relationship can also be written as

$$\kappa = c_0 \cdot T[n^3/(1-n)^2]/(S_A)^2$$

where T is the tortuosity and c_0 is a constant. The tortuosity is the ratio between the straight path between two points and the actual path length a particle would follow in the flow field. Commonly $c_0 T$ is treated as equivalent to 0.2, making it identical to the Kozeny–Carmen equation.

The ability to obtain sufficient energy for use in geothermal applications usually requires flow rates on the order of several cubic meters per second. Hence, it is important that drilling programs target regions in the subsurface with at least moderate permeability.

Permeability in Geothermal Systems

The physical properties of rocks in real geothermal systems are highly variable. Some geothermal systems extract energy from highly porous sandstones and other sedimentary rocks, while others utilize geothermal resources that occur in fractured crystalline rocks. Björnsson and Bodvarsson [34] compiled porosity and permeability data from operating geothermal power plant locations in various geological settings and documented the high degree of variability such systems possess (Fig. 5). Despite the variability, it is apparent that systems in which the porosity is primarily in the form of matrix pores rather than fractures, a much higher porosity is required to achieve sufficient flow to support power generation. Fracture-dominated systems, on the other hand, can have very low overall porosity and permeability yet support sufficient flow to generate power. This observation suggests that in a fractured rock mass,

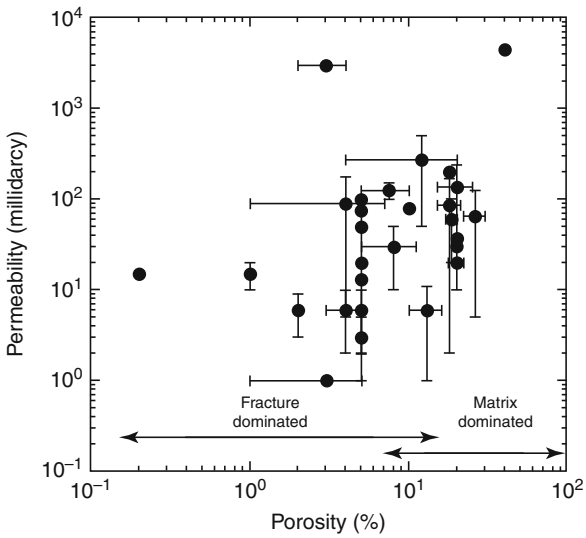

Geothermal Energy, Geology and Hydrology of. Figure 5
Observed porosity vs permeability in geothermal systems used for power generation (Data from [34])

fluid flow may be concentrated in a very small proportion of the overall fracture population [27] and yet still be adequate for supporting power generation. This conclusion is supported by modeling that has recently been reported [35].

Using a fractal model for fracture properties, along with data from well-characterized geothermal systems, Williams [35] demonstrated that the bulk of fluid flow in these geothermal systems occurs in a small fraction of the total porosity. This implies that a few fractures out of a population of many fractures carry most of the fluid flow. These results emphasize the importance of sufficiently characterizing rock properties at a site to establish the likely range of permeability properties. Once established, this information can be used to determine drilling targets and likely production levels.

Future Directions

Basic Geological Principles for Enhanced Geothermal Systems (EGS)

Implicit in the discussion of the driving forces for plate tectonics is the fact that heat is present everywhere in

the subsurface. Geothermal gradients of a few degrees to several tens of degrees per kilometer lead to the conclusion that temperatures greater than 300°C, which are sufficient to generate power, can be obtained at depths between 5 and 15 km virtually anywhere in the world. Pursuit of this resource has a long history [36–38]. Indeed, a recent study [39] concluded that in the United States alone, the amount of thermal energy that could be accessed at depths of less than 10 km is in excess of 13 million exajoules (1 exajoule = 10^{18} J). If only 1.5% of that energy could be accessed it would supply more than 2,000 times the annual electrical power generation needs of the country. Similar conclusions apply for almost every country on the planet.

The challenges faced in accessing this energy are the depths to which drilling must routinely go to tap the resource, and the ability to bring the heat to the surface. The depth to be drilled is determined by the regional geological framework. The interiors of plates often are stable environments that have had little magmatic activity. In the absence of magmatic activity, normal geothermal gradients in the interiors of plates are relatively low, on the order of a few degrees per kilometer to about 20°/km. These conditions would require drilling to depths that approach the limits of current drilling technology. Nevertheless, all plates have large areas in which adequate temperatures can be accessed at depths less than 10 km, and represent potential drilling targets for EGS systems.

The other challenge faced by EGS development is the ability to circulate fluids to depths in sufficient volumes to extract useful quantities of heat. Deep boreholes tend to enter regions where the permeability is low and the volume of subsurface water is small. To overcome these problems, it is possible to enhance the permeability of the rock using standard techniques of hydrofracturing that have been practiced in the oil and gas industry for decades. Hydrofracturing allows development of sufficient fracture permeability to support fluid flow at the volumes required for power generation. For a detailed discussion of EGS technology, see "► Engineered Geothermal Systems, Development and Sustainability of."

Basic Geological Principles for Non-power Producing Applications

Direct-use applications and ground source heat pumps require much lower temperatures than those needed for power generation [40]. As a result, they can usually rely on resources that are in the relatively shallow subsurface. Direct-use applications, such as aquaculture, spas, food processing, lumber drying, etc., often are located where warm or hot water occurs naturally in springs or the immediate subsurface. Such settings mainly rely on high permeability zones, such as local faults or porous and fractured rocks such as some volcanic deposits, for the fluid supply. As a result, most such applications are located in regions where recent volcanic activity has provided a thermal resource.

The use of ground source heat pumps for space heating and cooling [41], on the other hand, is not restricted by location. Ground source heat pumps utilize technology similar to that employed to cool the interior of refrigerators. Using technologically sophisticated but mechanically simple heat pumps, these systems can extract heat from the subsurface and transfer it to a building space (for space heating), or remove heat from a building space and deposit it in the subsurface (for cooling). Because of their high efficiencies, these heat pumps require a thermal resource of only 10–15°C (ca. 50–60°F). Such temperatures are readily accessed within 30–100 m in the subsurface, due to the normal geothermal gradient. These systems can be installed in virtually any geological setting. However, their long-term performance is influenced by the thermal properties of the rock types in a given area, as well as the presence or absence of subsurface water. If an active aquifer is located at the same site, the thermal stability of the system can be influenced by the rate of flow and recharge area of the aquifer. Shallower systems, such as trench installations, are also possible in some areas if suitable space is available and if appropriate soil depths occur.

Summary

Geothermal resources are a reflection of the underlying global and local geological and hydrological framework. The most thermally rich resources tend

to concentrate in environments that have abundant volcanic activity. These tend to be controlled by plate tectonic processes and are, specifically, spreading centers, volcanic chains associated with subduction zones and hot spots. The local geological characteristics that favor useful resources include relatively shallow depths to the resource, high permeability in the rocks surrounding the resource, and adequate fluids. These conditions apply for all applications except those utilizing ground source heat pumps. For these systems, virtually any setting is suitable, since the normal flow of heat from the Earth is adequate to assure a thermal resource of a 10–20°C within a few tens to a few hundreds of meters in the subsurface.

Bibliography

Primary Literature

1. Cataldi R (1993) Review of historiographic aspects of geothermal energy in the Mediterranean and Mesoamerican areas prior to the modern age. Geoth Heat Cent Bull 15:13–16
2. Buffon GL (1778) Histoire naturelle, générale et particulière. Imprimerie Royale, Paris
3. Dickson MH, Fanelli M (2006) Geothermal background. In: Dickson MH, Fanelli M (eds) Geothermal energy: utilization and technology. Earthscan, London
4. Brush SG (1979) Nineteenth-century debates about the inside of the earth: solid, liquid or gas? Ann Sci 36:225–254
5. Van Schmus WR (1995) Natural radioactivity of the crust and mantle. In: Ahrens TJ (ed) Global earth physics. American Geophysical Union, Washington, DC, pp 283–291
6. Göpel C, Manhés G, Allégre CJ (1994) U-Pb systematics of phosphates from equilibrated ordinary chondrites. Earth Planet Sci Lett 121:153–171
7. Allégre CJ, Manhés G, Göpel C (1995) The age of the Earth. Geochim Cosmochim Acta 59:1445–1456
8. Wetherill GW (1990) Formation of the Earth. Annu Rev Earth Planet Sci 18:205–256
9. Canup RM, Agnor C (2001) In: Canup RM, Righter K (eds) Origin of Earth and moon. Cambridge University Press, Cambridge, pp 1839–1848
10. Chambers JE (2001) Making more terrestrial planets. Icarus 152:205–224
11. Kortenkamp SJ, Wetherill GW, Inaba S (2001) Runaway growth of planetary embryos facilitated by massive bodies in a protoplanetary disk. Science 293:1127–1129
12. Kleine T, Münker C, Mezger K, Palme H (2002) Rapid accretion and early core formation on asteroids and the terrestrial planets from Hf-W chronometry. Nature 418:952–955
13. Yin Q, Jacobsen SB, Yamashita K, Blichert-Toft J, Te'louk P, Albarede F (2002) A short timescale for terrestrial planet formation from Hf–W chronometry of meteorites. Nature 418:949–952
14. Stein CA (1995) Heat flow in the Earth. In: Ahrens TJ (ed) Global earth physics. American Geophysical Union, Washington, DC, pp 144–158
15. Shih K-G (1971) Temperature production in the continental crust due to radioactive heat production. Pure Appl Geophys 90:115–125
16. Alfé D, Gillian MJ, Price GD (2007) Temperature and composition of the Earth's core. Contemp Phys 48:63–80
17. Anderson DL (1989) Theory of the Earth. Blackwell, Boston
18. Yamazaki D, Karato S-I (2001) Some mineral physics constraints on the rheology and geothermal structure of Earth's lower mantle. Am Mineralog 86:385–391
19. Isacks B, Oliver J, Sykes LR (1968) Seismology and the new global tectonics. J Geophys Res 73:5855–5899
20. Glen W (1982) The road to Jaramillo: critical years of the revolution in earth science. Stanford University Press, Stanford
21. CGEC (California Geothermal Energy Collaborative) (2006) California geothermal fields and existing power plants, Fact Sheet
22. Hart SR, Glassley WE, Karig DE (1972) Basalts and sea-floor spreading behind the Mariana island arc. Earth Planet Sci Lett 15:12–18
23. Hirth G, Kohlstedt D (2003) Rheology of the upper mantle and the mantle wedge: a view from the experimentalists. Geophys Monograph 138:83–105, American Geophysical Union, Washington, DC
24. Kennedy BM, Kharaka YK, Evans WC, Ellwood A, DePaolo DJ, Thordsen J, Ambats G, Mariner RH (1997) Mantle fluids in the San Andreas fault system, California. Science 278:1278–1281
25. Lachenbruch AH (1968) Preliminary geothermal model of the Sierra Nevada. J Geophys Res 73:6977–6989
26. Farrar CD, Sorey ML, Roeloffs E, Galloway DL, Howle JF, Jacobson R (2003) Inferences on the hydrothermal system beneath the resurgent dome in Long Valley Caldera, east-central California, USA, from recent pumping tests and geochemical sampling. J Volcanol Geoth Res 127:305–328
27. Bear J (1993) Modeling flow and contaminant transport in fractured rocks. In: Bear J, Tsang C-F, de Marsily G (eds) Flow and contaminant transport in fractured rock. Academic, New York
28. Bear J (1979) Hydraulics of groundwater. McGraw-Hill, New York
29. Batu V (1998) Aquifer hydraulics. Wiley, New York

30. Lee CH, Farmer IW (1990) A simple method of estimating rock mass porosity and permeability. Int J Min Geol Eng 8:57–65
31. Kozeny J (1927) Über kapillare Leitung des Wassers im Boden. Sitzungsber. Akad Wissenschaft Wien 136: 271–306
32. Carman PC (1937) Fluid flow through a granular bed. Trans Inst Chem Eng Lond 15:150–156
33. Carman PC (1956) Flow of gases through porous media. Butterworths, London
34. Björnsson G, Bodvarsson G (1990) A survey of geothermal reservoir properties. Geothermics 19:17–27
35. Williams CF (2007) Updated methods for estimating recovery factors for geothermal resources. In: Proceedings of the 32nd Workshop on Geothermal Reservoir Engineering, Stanford University, Stanford, California
36. Smith MC (1983) A history of hot dry rock geothermal energy systems. J Volcanol Geoth Res 15:1–20
37. Tester JW, Brown DW, Potter RM (1989) Hot dry rock geothermal energy – a new energy agenda for the 21st Century. Los Alamos National Laboratory report LA-11514-MS
38. Duchane D, Brown D (2002) Hot dry rock (HDR) geothermal energy research and development at Fenton Hill, New Mexico. Geo-Heat Center Bull 23(4):13–19
39. Tester JW, Anderson BJ, Batchelor AS, Blackwell DD, DiPippio R, Drake EM, Garnish J, Livesay B, Moore MC, Nichols K, Petty S, Toksoz MN, Veatch RW Jr (2006) The future of geothermal energy. MIT Press, Boston
40. Lund JW, Freeston DH, Boyd TL (2005) Direct application of geothermal energy. 2005 worldwide review. Geothermics 34:690–727
41. Ochsner K (2008) Geothermal heat pumps. Earthscan, London

Books and Reviews

DiPippo R (2008) Geothermal power plants, 2nd edn. Elsevier, Amsterdam
Duffield WA, Sass JH (2003) Geothermal energy – clean power from the Earth's heat. U.S. Geological Survey Circular 1249
Glassley WE (2010) Geothermal energy: renewable energy and the environment. Taylor and Francis, Boca Raton
Krauskopf KB, Bird DK (2003) Introduction to geochemistry, 3rd edn. McGraw-Hill, New York
Reynolds JM (1997) An introduction to applied and environmental geophysics. Wiley, New York
Ryback L, Muffler LJP (1979) Geothermal systems: principles and case histories. Wiley, New York
Williams CF, Reed MJ, Mariner RH (2008) A review of methods by the U.S. Geological Survey in the assessment of identified geothermal resources. U.S. Geological Survey Open File Report 2008-1296

Geothermal Energy, Nature, Use, and Expectations

Barry Goldstein[1], Gerardo Hiriart[2], Jeff Tester[3], Luis Gutierrez-Negrin[4], Ruggero Bertani[5], Christopher Bromley[6], Ernst Huenges[7], Arni Ragnarsson[8], Mike Mongillo[6], John W. Lund[9], Ladislaus Rybach[10], Vladimir Zui[11], Hirofumi Muraoka[12]
[1]Pirsa Petroleum Group, Adelaide, SA, Australia
[2]Energías Alternas, Estudios y Proyectos, Mexico
[3]Energy Institute, Cornell University, Ithaca, NY, USA
[4]Mexican Geothermal Association, Mexico
[5]Enel, Rome, Italy
[6]GNS Science, Wairakei Research Centre, Taupo, New Zealand
[7]GFZ-Potsdam, Germany
[8]Iceland GeoSurvey, Reykjavík, Iceland
[9]Geo-Heat Center, Oregon Institute of Technology, Klamath Falls, OR, USA
[10]Geowatt AG, Switzerland
[11]Belarusian Research Geological Prospecting Institute, Belarus
[12]National Institute of Advanced Industrial Science and Technology, Institute for Geo-Resources and Environment (GREEN), Tsukuba, Ibaraki, Japan

Article Outline

Glossary
Definition of Geothermal Energy
Introduction
Geothermal Resources, Reserves, and Supplies
Future Directions for Geothermal Energy Technologies
Expectations for Geothermal Energy Use
Key Points
Acknowledgments
Bibliography

Glossary

Base-load demand Continuous demand for electricity. Power generation plants with high-capacity factors combine as a practical source of continuous base-load supplies.

Capacity factor The energy generated in a span of time divided by the maximum energy that could have been generated at full (name plate) power of the plant during that period of time, most often expressed as a percentage of 1 year of plant operation. The maximum amount of power a plant can generate is its name plate capacity.

Conduction-dominated systems Earth systems of heat transfer in which heat flow is principally via the contact of rocks (and pore- and fracture-filling fluids and gasses in rocks) with a capacity to transfer thermal energy from higher to lower temperature conditions. Non-volcanic (amagmatic) geothermal systems tend to become conduction-dominated systems.

Convection-dominated systems Earth systems of heat transfer in which heat flow is principally via flow of gasses, fluids, and molten rock (magma) from higher to lower temperature conditions. Volcanic geothermal systems tend to become convection-dominated systems.

Dispatchable electricity Power generation systems that can quickly shift from nil to full generation capacity and balance electricity supply and demand within safe technical limits of transmission grids.

Engineered (or enhanced) geothermal systems (EGS) Geothermal reservoirs in which technologies enable economic utilization of low permeability conductive dry rocks or low productivity convective water-bearing systems by creating fluid connectivity through hydraulic, thermal, or chemical stimulation methods or advanced well configurations. EGS also refer to activities to increase the permeability in a targeted subsurface volume via injecting and withdrawing fluids into and from the rock formations that are intended to increase the ability to extract energy from a subsurface heat source.

Geothermal energy Accessible thermal energy stored in the Earth's interior, in rock, gasses, and fluids usable for the generation of electricity and to supply heat for direct use. Continuous radiation from the natural decay of elements and residual energy from the earth's formation are the main sources of geothermal energy.

Ground source heat pumps Equipment that circulates fluids or gasses from lower to higher temperature conditions, or the reverse to heat or cool buildings or industrial processes. Ground source heat pumps (GSHPs) are most commonly used to heat in winter and cool in summer.

Hot sedimentary aquifers Any geologic reservoir that has a capacity to flow fluids at a rate and a temperature sufficient to meet a market for power generation and the direct use of thermal energy. The most accessible and the most prospective hot sedimentary aquifers (HSA) are naturally highly permeable, are overlain by rocks that act as thermal insulators, and are underlain by an effective source of heat energy (magma or high-heat-producing rocks such as granite plutons rich in uranium).

Definition of Geothermal Energy

Geothermal energy is the terrestrial generated heat stored in, or discharged from rocks and fluids (water, brines, gasses) saturated pore space, fractures, and cavities and is widely harnessed in two ways: for power (electricity) generation and for direct use, e.g., heating, cooling, aquaculture, horticulture, spas, and a variety of industrial processes, including drying. Thermal energy is used by taking heat from geothermal reservoirs replenished by natural recharge. Reservoirs that are naturally sufficiently hot and permeable are called hydrothermal reservoirs, whereas reservoirs that are sufficiently hot but require artificial improvement of a rock permeability are called engineered (enhanced) geothermal systems (EGS). Geothermal energy can be used to generate electricity or directly for processes that need thermal energy. Geothermal energy can be used to provide dispatchable, base-load electricity power plants.

Introduction

Geothermal energy systems have a modest environmental footprint, will not be impacted by climate change, and have potential to become the world's lowest cost source of sustainable thermal fuel for zero emission, base-load direct use, and power generation. Displacement of more emissive fossil energy supplies with geothermal energy can also be expected to play a key role in climate change mitigation strategies.

The use of energy extracted from temperatures of the Earth at shallow depth by means of ground source heat pumps (GSHP) is a common form of geothermal energy use. The direct uses of natural flows of

geothermally heated waters to surface have been practiced at least since the Middle Paleolithic [1], and industrial utilization began in Italy by exploiting boric acid from the geothermal zone of Larderello, where in 1904 the first kilowatts of electric energy (kWe) were generated and in 1913 the first 250-kWe commercial geothermal power plant was installed [2].

Where very high-temperature fluids (>180°C) flow naturally to surface (e.g., where heat transfer by convection dominates), geothermal resources are the manifestation of two factors:

- A geologic heat source to replenish thermal energy outflow
- A hydrothermal reservoir that can be tapped to produce geothermal fluids for its direct use and/or for generating electricity

Elsewhere, a third geologic factor, the insulating capacity of rocks (acting as a thermal blanket) is an additional necessary natural ingredient in the process of accumulating usable, stored heat energy in geologic reservoirs that can be tapped to flow heat energy and replenished by convective and conductive *heat flow* from sources of geothermal energy.

Usable geothermal systems occur in a variety of geological settings. These are frequently categorized as follows:

1. High-temperature (>180°C) systems at depths above (approximately) 3.5 km are generally associated with recent volcanic activity and mantle hot spot anomalies. Other high-temperature geothermal systems below (approximately) 3.5 km are associated with anomalously high-heat-producing crustal rocks, mostly granites.
2. Intermediate-temperature systems (100–180°C).
3. Low-temperature (<100°C) systems.

Both intermediate- and low-temperature systems are also found in continental settings, formed by above normal heat production through radioactive isotope decay; they include aquifers charged by water heated through circulation along deeply penetrating fault zones. However, there are several notable exceptions to these temperature-defined categories, and under appropriate conditions, high-, intermediate-, and low-temperature geothermal fields can be utilized for both power generation and the direct use of heat. Offshore geothermal resources are also sometimes included in lists of ocean energy systems [3].

Geothermal systems can also be classified as: *convection-dominated systems*, which include liquid-and vapor-dominated hydrothermal systems; *conduction-dominated systems* which include hot rocks; and *hybrid systems* that are sourced from convection, conduction, and high-heat-producing source rocks. Geologic aquifers that overlie radiating sources of heat and gain heat via convection and/or conduction are sometimes called *hot sedimentary aquifer systems*.

The most widely recognized manifestations of geothermal energy are related to convective heat flow, including: hot springs and geysers (e.g., the movement of hot water to land surface); volcanoes (e.g., the movement of magma to land surface and sea floors); and certain forms of economically significant minerals deposits resulting from their recovery from the injection of geothermally heated fluids into lower temperature levels where minerals crystallize and are accumulated.

Geothermal wells produce naturally hot fluids contained in hydrothermal reservoirs from a continuous spectrum of natural high to low permeability and porosity (including natural fractures). The capacity of geothermal reservoirs to flow hot fluids can be enhanced with hydraulic fracture stimulation and chemical treatment (ex. acidization), creating artificial fluid pathways in *enhanced or engineered geothermal systems* (EGS) as well described in detail in Reference [4]. Once at surface, heated fluids can be used to generate electric energy in a thermal power plant, or used in other applications requiring heat, as heating and cooling of buildings, district heating systems, aquaculture, agriculture, balneology, industrial processes, and mineral drying. Space heating and cooling can also be achieved with GHP systems.

The number, depth, and diameter of geothermal energy production wells vary with local requirements for direct use and electricity power plants. Higher temperatures and higher flow rates result in more thermal energy production per well. Wells drilled to depths down to 3.5 km in volcanic areas frequently produce high-temperature (>180°C) fluids to surface. Indeed, temperatures above 1,000°C can occur at less than 10 km depth in areas of magma intrusion. Given the global average land area surface temperature of (about) 15°C and an approximate global geothermal

gradient for land areas outside volcanic settings of (about) 30°C/km, the same high temperature (>180°C) can be reached (on average) at a depth of about 5.5 to 10 km below ground level.

Electricity Generation

The main types of geothermal power plants use direct steam (often called dry steam), flashed steam, and binary cycles.

Power plants that use dry and/or flashed steam to spin turbines are the most commonly deployed form of geothermal electricity generation. These plants use the heat energy contained in water and steam flowed from geothermal wells to spin turbines, converting thermal and kinetic energy to electrical energy.

Organic Rankine power plants employing secondary working fluids are increasingly being used for geothermal power generation. These so-called binary closed-loop power plants do not flow produced geothermal fluids directly into turbines. Thermal energy contained in water and/or steam produced from geothermal wells is transferred to a secondary working fluid using a heat exchanger (hence the term binary closed loop). Organic compounds with lower boiling points than water (such as isopentane that boils at atmospheric pressure at about 28°C) are often used as working fluids. The heat energy in the geothermal fluid boils the working fluid changing it from a liquid to a pressurized organic vapor within the closed loop, which can then be expanded in a turbine to spin a generator. The exhausted working fluid is cooled, condensed back into a liquid, pressurized, and then recycled into the heat exchanger to complete the cycle.

Direct Use

Direct use provides heating and cooling for buildings including district heating, fish ponds, greenhouses, bathing, wellness and swimming pools, water purification/desalination, and industrial and process heat for agricultural products and mineral extraction and drying.

For space heating, two basic types of systems are used: open or closed loop. Open loop (single pipe) systems utilize directly the geothermal water extracted from a well to circulate through radiators. Closed loop (double pipe) systems use heat exchangers to transfer heat from the geothermal water to a closed loop that circulates heated freshwater through the radiators. This system is commonly used because of the chemical composition of the geothermal water. In both cases the spent geothermal water is disposed of into injection wells and a conventional backup boiler may be provided to meet peak demand.

Transmission pipelines for the direct use of geothermal energy consist mostly of steel insulated by rock wool (surface pipes) or polyurethane (subsurface). However, several small villages and farming communities have successfully used plastic pipes (polybutylene) with polyurethane insulation as transmission pipes in Iceland. It is for your consideration, as Iceland is mentioned below. The temperature drop is insignificant in large-diameter pipes with a high flow rate, as observed in Iceland where geothermal water is transported up to 63 km from the geothermal fields to towns.

It is debatable whether geothermal heat pumps (GHP), also called ground source heat pumps (GSHP), are purely an application of geothermal energy or also partially use stored solar energy. GHP technology is based on the relatively constant ground or groundwater temperature ranging from 4°C to 30°C to provide space heating, cooling, and domestic hot water for all types of buildings. Extracting energy during heating periods cools the ground locally. This effect can be minimized by dimensioning the number and depth of probes in order to avoid harmful impacts on the ground. These impacts are also reduced by storing heat underground during cooling periods in the summer months.

There are two main types of GHP systems: closed loop and open loop. In ground-coupled systems, a closed loop of plastic pipe is placed into the ground, either horizontally at 1–2 m depth or vertically in a borehole down to 50–250 m depth. A water-antifreeze solution is circulated through the pipe. Heat is collected from the ground in the winter and reinjected to the ground in the summer. An open-loop system uses groundwater or lake water directly as a heat source in a heat exchanger and then discharges it into another well or into the same water reservoir [5].

Heat pumps operate similarly to vapor-compression refrigeration units with heat rejected in the condenser for heating or extracted in the evaporator used for cooling. GHP efficiency is described by a coefficient of performance (COP) which scales the heating or cooling

output to the electrical energy input. GHPs typically exhibit between three and five COP [5, 6]. The seasonal performance factor (SPF) provides a metric of the overall annual efficiency of a GHP system. It is the ratio of useful heat to the consumed driving energy (both in kilowatt hour per year), and it is slightly lower than the COP.

Comparative Advantages of Geothermal Energy Use

Geothermal energy use has several comparative advantages in competitive energy markets.

- Geothermal plants have low-emission to emission-free operations and relatively modest land footprints. The average direct emissions yield of partially open cycle, hydrothermal flash, and direct steam electric power plants yield is about 120 g CO_2/kWhe. This is the weighted average of 85% of the world's power plant capacity, according to References [7, 8]. Current binary cycle plants with total reinjection yield less than 1 g CO_2/kWhe in direct emissions. Emissions from direct use applications are even lower [9]. Over its full life cycle (including the manufacture and transport of materials and equipment), CO_2 equivalent emissions range from 23 to 80 g/kWhe for binary plants (based on References [10, 11]) and from 14 to 202 g/kWht for district heating systems and GHPs (based on Reference [12]). This means geothermal resources are environmentally advantageous and the net energy supplied more than offsets the environmental impacts of human, energy, and material inputs.
- Geothermal electric power plants have characteristically high-capacity factors; the average for power generation in 2009 is 74.5% (67,246 $GWh_{electrical}$ used from installed capacity of 10.340 $GW_{electrical}$ in December 2008 based on Reference [13]), and modern geothermal power plants exhibit capacity factors greater than 90%. This makes geothermal energy well suited for base-load (24/7), dispatchable energy use.
- The average estimated 27.5% capacity factor for direct use in 2009 (121.7 $TWh_{thermal}$ used from installed capacity of 50.6 $GW_{thermal}$ based on Reference [14]) can be improved with smart grids (as for domestic and industrial solar energy generation) by employing combined heat and power systems, by using geothermal heat absorptive and vapor-compression cooling technology, and by expanding the distributed use of geothermal (ground source) heat pump for both heating and cooling applications, and
- Properly managed geothermal reservoir systems are sustainable for very long-term operation, comparable to or exceeding the foreseeable design life of associated surface plant and equipment.
- Displacement of more emissive fossil energy supplies with geothermal energy can also be expected to play a key role in climate change mitigation strategies.

Geothermal Resources, Reserves, and Supplies

The theoretical global geothermal resource base corresponds to the thermal energy stored in the Earth's crust (heat in place). The technical (prospective) global geothermal resource is the fraction of the earth's stored heat that is accessible and extractable for use with foreseeable technologies, without regard to economics. Technical resources can be subdivided into three categories in order of increasing geological confidence: inferred, indicated, and measured [15] with measured geothermal resources evidenced with subsurface information to demonstrate its usability. Geothermal reserves are the portion of geothermal resources that can confidently be used for economic purposes. Geothermal reserves developed and connected to markets are energy supplies and global supplies.

Geothermal Supplies

At year-end 2010, geothermal energy supplies were used to generate base-load electricity in 24 countries with an installed capacity of nearly 11 GW of electricity and a global average capacity factor of nearly 75%, with newer installations above 90%, providing 10–30% of their electricity demand in six countries [13]. Figure 1 provides the geothermal electricity generation capacity by country and the mapped (estimated) distribution of global heat flow in milliwatts per square meter (mW/m^2).

At year-end 2010, geothermal energy supplies are also used for direct use applications in 78 countries, accounting for 50 $GW_{thermal}$ including district (space) heating and cooling and geothermal (ground source) heat pumps, which have achieved significant market

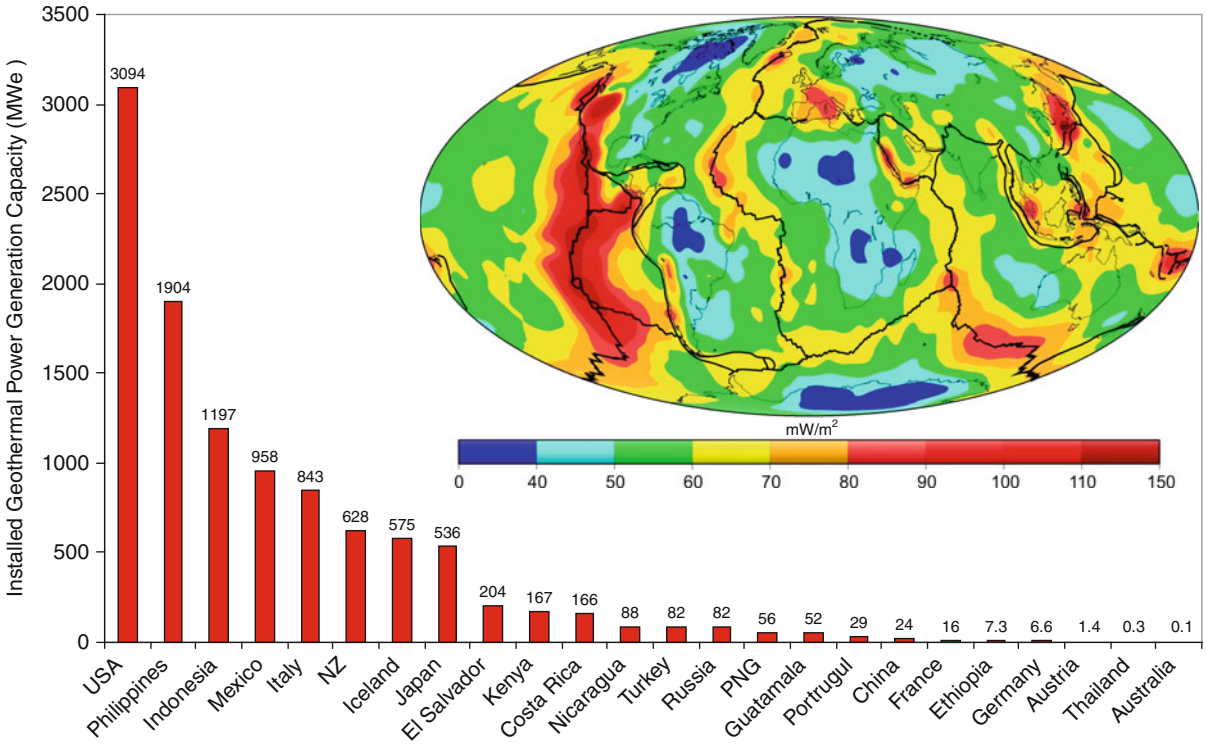

Geothermal Energy, Nature, Use, and Expectations. Figure 1
Geothermal electric installed capacity by country in 2009. This figure also depicts global average heat flow in milliwatts per square meter and tectonic plate boundaries (*black lines*) (Illustration adapted from a figure in Reference [16] with data from Reference [13]). This map of heat flow does not reconcile all geothermal information. The delineation of geothermal resources will be improved by integrating temperature gradient, heat flow, and reservoir data

penetration worldwide [14]. Geothermal electric installed capacity by country in 2009. In the 40-year term 1970–2009, the average annual growth of geothermal electric installed capacity is 7% per annum; and in the 35-year term 1975–2009, the average annual growth for geothermal direct use is 11% per annum [13, 14, 17–19].

Geothermal Resources and Reserves

The total thermal energy contained in the Earth is on the order of 12.6×10^{12} EJ and that of the crust is on the order of 5.4×10^{9} EJ to depths of up to 50 km [20]. The main sources of this energy are due to the heat flow from the earth's core and mantle and that generated by the continuous decay of radioactive isotopes in the crust itself. Heat is transferred from the interior toward the surface, mostly by conduction, at an average of 0.065 W/m^2 on continents and 0.101 W/m^2 through the ocean floor. The result is a global terrestrial heat flow rate of around 1,400 EJ/year. Considering that continents cover ~30% of the earth's surface and their lower average heat flow, the terrestrial heat flow under continents has been estimated at 315 EJ/year [21].

Under continents, the stored thermal energy within 50, 10, 5, and 3 km depth (all depths reachable with the current drilling technology) has been estimated as presented as the theoretical usable geothermal energy in Fig. 2. For the Australian continent alone, Reference [24] estimated that recovery of just 1% of the stored geothermal energy above 150°C to 5 km in the Australian continental crust corresponds to 190,000 EJ. Based on these estimates, the theoretically available resource is enormous and clearly not a limiting factor for global geothermal deployment.

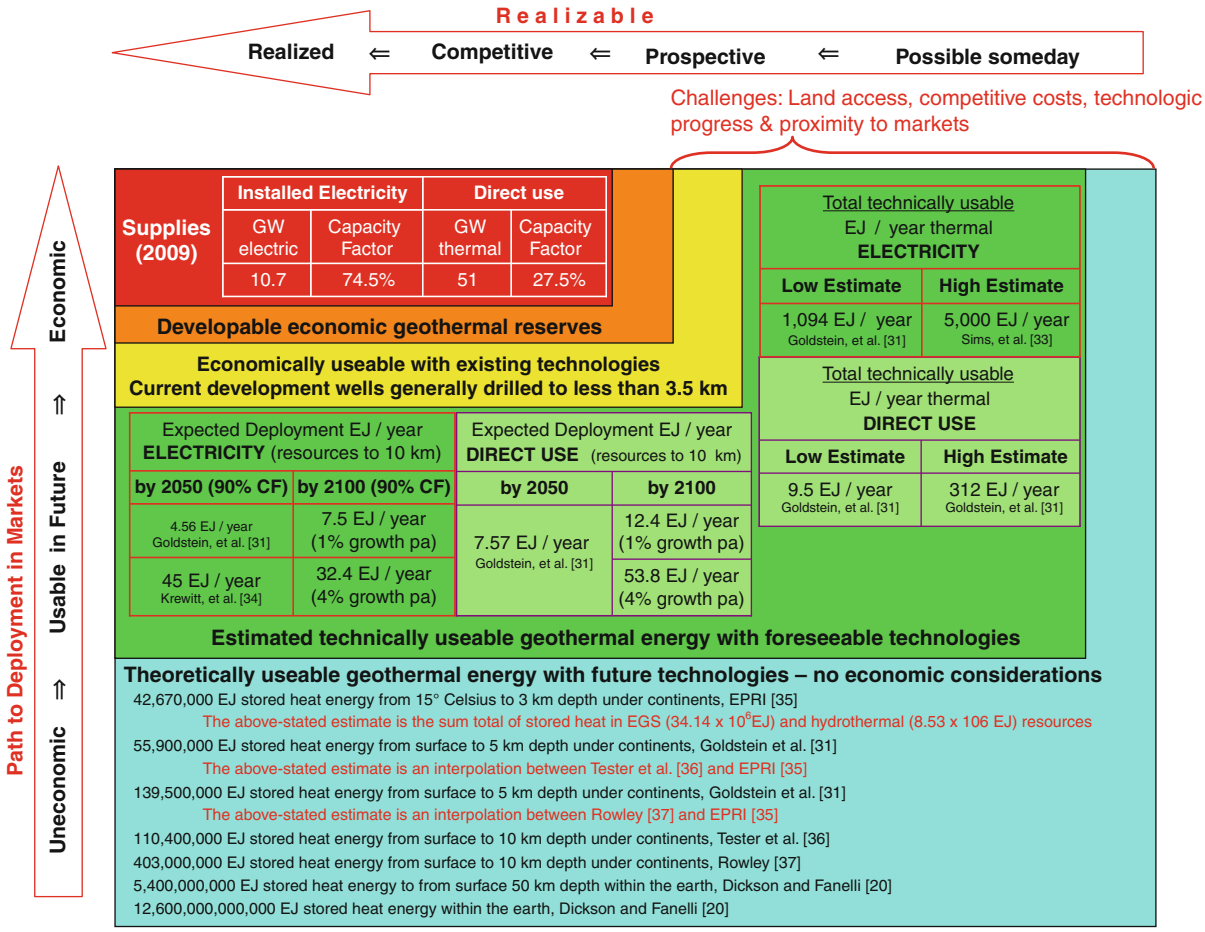

Geothermal Energy, Nature, Use, and Expectations. Figure 2
Potential geothermal energy resources split into categories, e.g., theoretical, technical, economic, developable, and existing supplies for power generation and direct use. All categories for power generation assume a 74.5% capacity factor and 8.1% average efficiency for converting thermal into electrical energy, though both factors will likely improve (increase) in future. All direct use estimates for the future assume an average 31% capacity factor, somewhat higher than the average (27.5%) in 2009 (Adapted from Fig. 1 in Reference [22] and the presentation by L. Rybach published in Reference [23])

Geothermal energy is a renewable resource. As thermal energy is extracted from the active reservoir, it creates locally cooler regions temporarily. Geothermal projects are typically operated at production rates that cause local declines in pressure and/or in temperature over the economic lifetime of the installed facilities. These cooler and lower pressure zones in the reservoir lead to gradients that result in continuous recharge by conduction from hotter rock and convection and advection of fluid from surrounding regions. Detailed modeling studies [25, 26] have shown that resource exploitation can be economically feasible and still be renewable on a reasonable timescale when nonproductive recovery periods are considered.

Future Directions for Geothermal Energy Technologies

Challenges

Geothermal resources contain thermal energy that can be produced, stored, and exchanged (flowed) in rock,

gas (steam), and liquids (mostly water) in the subsurface of the earth.

With proper management practice, geothermal resources are sustainable and renewable over reasonable time periods. As stored thermal energy is extracted from local regions in an active reservoir, it is continuously restored by natural conduction and convection from surrounding hotter regions, and the extracted geothermal fluids are replenished by natural recharge and by reinjection of the exhausted fluids.

The obvious generalized impediments to massive, global geothermal energy use are:

- Currently insufficiently predictable reliability of geothermal reservoir performance (and in particular, the predicable reliability of engineered geothermal system reservoirs)
- Current costs of geothermal well deliverability (and, in particular, fluid production levels from stimulated engineered geothermal systems and the high costs of drilling deep wells)

Hence, the overarching common and well-justified objectives of global government initiatives are to stimulate technologic and learn-while-doing breakthroughs that will lead to a point where the cost of geothermal energy use is reliably cost competitive and comparatively advantageous within markets.

Priorities to Wider Use of Geothermal Energy

Improved, evermore reliable, cost-effective methods to enhance the productivity of geothermal systems will be essential to the competitiveness of geothermal resource in energy markets. In particular, the commercialization of fracture and/or chemical stimulation methods to reliably create engineered geothermal systems (EGS) independent of site conditions will be one key milestone on the road to great expectations for widespread economic use of geothermal energy. Table 1 results from a scan of the objectives of international geothermal energy fora and defines the top 20 priorities for advancing efficiency and competitiveness in geothermal energy use. This is an update of the priorities presented in Reference [27].

Geothermal Energy, Nature, Use, and Expectations.

Table 1 Top 20 research and development priorities for advancing efficiency and competitiveness in geothermal energy use

Openness to cooperation to engender complementary research and the sharing of knowledge	Informing industry, governments, and the public of technologic advances and the merits of using geothermal energy through presentations, publications, websites, submissions to enquiries, and the convening of conferences, workshops, and courses
Creating effective standards for reporting geothermal operations, resources, and reserves	For EGS, improved hard rock drill equipment
Predictive reservoir performance modeling	Improved multiple zone isolation for high-temperature and high-pressure geothermal reservoirs
Predictive stress field characterization	For deep geothermal reservoirs, reliable submersible pumps
For EGS, mitigate induced seismicity	Longevity of well cementing and casing
Condensers for high ambient surface temperatures	For EGS, optimum fracture stimulation methods
Use of CO_2 as a circulating fluid	High temperature logging tools and sensors
Improve power plant design	High temperature flow survey tools
Technologies and methods to minimize water use	High temperature fluid flow tracers
Predict heat flow and reservoirs ahead of the drill bit	Mitigation of formation damage, scale, and corrosion

Expectations for Geothermal Energy Use

The extent or accessibility of geothermal resources will not be a limiting factor for deployment. The key determining factor in the growth in deployment will be the

Geothermal Energy, Nature, Use, and Expectations. Table 2 Global forecasts of: installed capacity for geothermal power generation (GWe), installed capacity to deliver thermal energy for direct use (GWt), geothermal power use (TWh_e/year), and geothermal direct uses (TWh_t/year)

Expected world use	2020		2030		2050		2100	
	Direct (GWt)	Electric (GWe)	Direct (GWt)	Electric (GWe)	Direct (GWt)	Electric (GWe)	Direct (GWt)	Electric (GWe)
Capacity	160.5	25.9	455.9	51.0	800	160.6	1,316–5,685	264–1,141
Expected global use	**TWh_t/year**	**TWh_e/year**	**TWh_t/year**	**TWh_e/year**	**TWh_t/year**	**TWh_e/year**	**TWh_t/year**	**TWh_e/year**
	421.9	181.8	1,998.8	380.0	2102.2	1266.4	3,457–14,940	2,083–9,000
	EJ/year	**EJ/year**	**EJ/year**	**EJ/year**	**EJ/year**	**EJ/year**	**EJ/year**	**EJ/year**
	1.52	0.65	4.41	1.37	7.57	4.56	12.4 to 53.8	7.5 to 32.4

Geothermal Energy, Nature, Use, and Expectations. Table 3 Actual (from 1995 to 2010) and expected (from 2015 to 2100) growth in the use of geothermal energy

Year	Installed capacity actual or mean forecast (GWe)	Electricity production actual or mean forecast (GWh/year)	Capacity factor (%)
1995	6.8	38,035	64
2000	8.0	49,261	71
2005	8.9	56,786	73
2010	10.7	67,246	75
2015	18.5	121,600	77
2020	25.9	181,800	80
2030	51.0	380,000	85
2040	90.5	698,000	88
2050	160.6	1,266,400	90
2100	264–1,141	2,082,762–8,999,904	90+

competitiveness of geothermal energy use within local, regional, national, and trade zone markets. The authors have drawn conclusions in regard to future growth in the use of geothermal energy through 2010. The following table (Table 2) provides those global long-term forecasts of installed capacity for geothermal power and direct uses (heat) and of electric and direct uses (heat) generation. Earlier estimates for deployment beyond 2010 that were considered in developing forecasts include References [13, 28–30].

The above-listed forecasts assume improvements in capacity factors power generation from the current average 74.5–90% by 2050, a level already attained in efficient, existing geothermal power generation plants. A more detailed account of actual and expected growth in the use of geothermal energy follows (Table 3). The statistics for installed capacity to generate electricity from geothermal energy, electricity production from those geothermal plants, and capacity factors for geothermal power plants are from the Reference [29] for the term 1995–2005; Reference [13] for 2010 and the Reference [31] for the term 2015–2100. The expressed forecasts for growth from 2050 are based on 1% and 4% average annual growth for the 50 years to 2100.

Next Steps in Global Resource Assessments

A further global geothermal resource assessment is planned under an existing IEA Geothermal Implementing Agreement research annex. This will include a probabilistic range of estimates, e.g., assuming that a log-normal distribution adequately describes the range of recovery of stored heat from a minimum of 0.5% at a 99% probability to a maximum of 40% of stored heat at a 1% probability. This implies: a low-side recovery of 1.34% of stored heat (90% probability), a mid-range recovery of 4.47% of stored heat

(50% probability), a Swanson's mean recovery of 6.68% of stored heat, and a high-side recovery of 14.95% of stored heat (10% probability). (Swanson's mean is the weighted approximation for a log-normal distribution equal to the summation of 30% of the 90% probability value, 30% of the 10% probability value, and 40% of the 50% probability value, e.g., (P90 × 0.3) + (P10 × 0.3) + (P50 × 0.4) equals the Swanson's mean value.)

Key Points

- With its natural thermal storage capacity, geothermal is especially suitable for supplying both base-load electric power generation and for fully dispatchable heating and cooling applications in buildings, and thus is uniquely positioned to play a key role in climate change mitigation strategies [32].
- Direct use of geothermal energy for heating and cooling, including geothermal heat pumps (GHPs), is expected to increase to 7.86 EJ/year (~815 GWt) by 2050 and between 12.9 EJ/year (with 1% growth per year) and 55.9 EJ/year (with 4% growth per year) by 2100. Marketing and multiple internationally competitive supply chains will underpin this growth. This expectation is supported information published by Reference [6].
- Power generation with binary plants and total reinjection will become commonplace in countries without high-temperature resources.
- Geothermal energy utilization from conventional hydrothermal resources continues to accelerate, and the advent of EGS is expected to rapidly increase growth after 10–15 years putting geothermal on the path to provide an expected generation global supply of 4.56 EJ/year (~160 GWe) by 2050 and between 7.5 EJ/year (with 1% growth per year) and 32.4 EJ/year (with 4% growth per year) by 2100.
- Geothermal energy is expected to meet between 2.5% and 4.1% of the total global demand for electricity by 2050 and potentially more than 10% by 2100. It is also expected to provide about 5% of the global demand for heating and cooling by 2050 and, potentially, more than 10% by 2100. Geothermal energy will be a dominant source of base-load renewable energy in many countries in the next century.
- In addition to the widespread deployment of EGS, the practicality of using supercritical temperatures and offshore resources is expected to be tested with experimental deployment of one or both a possibility by 2100.

Acknowledgments

The authors thank their international colleagues who have contributed so much of their professional lives and time to provide improved understanding of geothermal systems. We are especially grateful to Ken Williamson, David Newell, Trevor Demayo, Arthur Lee, Subir Sanyal, Roland Horne, David Blackwell, Greame Beardsmore, and Doone Wyborn.

Bibliography

Primary Literature

1. Cataldi R (1999) The year zero of geothermics. In: Cataldi R, Hodgson S, Lund JW (eds) Stories from a heated earth. Geothermal Resources Council, Sacramento, pp 7–17. ISBN 0934412197
2. Burgassi PD (1999) Historical outline of geothermal technology in the Larderello region to the middle of the 20th century. In: Cataldi R, Hodgson S, Lund JW (eds) Stories from a heated earth. Geothermal Resources Council, Sacramento, pp 195–219. ISBN 0934412197
3. Hiriart G, Prol-Ledesma RM, Alcocer S, Espíndola G (2010) Submarine geothermics: hydrothermal vents and electricity generation. In: Proceedings world geothermal congress 2010, Bali, Indonesia, 25–29 April 2010
4. Tester JW, Anderson BJ, Batchelor AS, Blackwell DD, DiPippo R, Drake EM (eds) (2006) The future of geothermal energy impact of enhanced geothermal systems on the United States in the 21st century. Prepared by the Massachusetts Institute of Technology, under Idaho National Laboratory subcontract no. 63 00019 for the U.S. Department of Energy, Assistant Secretary for Energy Efficiency and Renewable Energy, Office of Geothermal Technologies, p 358. ISBN-10: 0486477711, ISBN-13: 978–0486477718
5. Lund JW, Sanner B, Rybach L, Curtis R, Hellström G (2003) Ground-source heat pumps – A world overview. Renew Energ World 6(l4):218–227, ISSN 1462–6381
6. Rybach L (2005) The advance of geothermal heat pumps world-wide. IEA Heat Pump Centre Newsletter 23, pp 13–18. ISSN: 0724–7028
7. Bertani R, Thain I (2002) Geothermal power generating plant CO_2 emission survey. *IGA News* 49, pp 1–3. ISSN: 0160–7782

8. Bloomfield KK, Moore JN, Neilson RN (2003) Geothermal energy reduces greenhouse gases. Geoth Res Counc Bull 32(2):77–79, ISSN 01607782
9. Fridleifsson IB, Bertani R, Huenges E, Lund JW, Ragnarsson A, Rybach L (2008) The possible role and contribution of geothermal energy to the mitigation of climate change. In: IPCC scoping meeting on renewable energy sources, Luebeck, Germany, 21–25 Jan 2008, p 36. Available at: http://www.ipcc.ch/pdf/supporting-material/proc-renewables-lubeck.pdf
10. Frick S, Schröder G, Kaltschmitt M (2010) Life cycle analysis of geothermal binary power plants using enhanced low temperature reservoirs. Energy 35(5):2281–2294, ISSN: 0360–5442
11. Nill M (2004) Die zukünftige Entwicklung von Stromerzeugungstechniken, Eine ökologische Analyse vor dem Hintergrund technischer und ökonomischer Zusammenhänge, Fortschritt-Berichte VDI Nr. 518. VDI, Düsseldorf, p346, ISSN: 0178–9414
12. Kaltschmitt M (2000) Environmental effects of heat provision from geothermal energy in comparison to other resources of energy. In: Proceedings world geothermal congress 2000, Kyushu-Tohoku, Japan, 28 May–10 Jun 2000. ISBN: 0473068117
13. Bertani R (2010) World update on geothermal electric power generation 2005–2009. In: Proceedings world geothermal congress 2010, Bali, Indonesia, 25–30 Apr 2010
14. Lund JW, Freeston DH, Boyd TL (2010) Direct utilization of geothermal energy 2010 worldwide review. In: Proceedings world geothermal congress 2010, Bali, Indonesia, 25–30 Apr 2010
15. AGEG-AGEA (2009) Australian code for reporting of exploration results, geothermal resources and geothermal reserves, prepared by the Australian Geothermal Code Committee – A committee of the Australian Geothermal Energy Group (AGEG) and the Australian Geothermal Energy Association (AGEA). Download from: http://www.pir.sa.gov.au/geothermal/ageg/geothermal_reporting_code
16. Hamza VM, Cardoso R, Ponte Neto C (2008) Spherical harmonic analysis of earth's conductive heat flow. International Journal of Earth Sciences 97(2):205–226, (22), Springer
17. Lund JW, Freeston DH, Boyd TL (2005) Direct application of geothermal energy: 2005 worldwide review. Geothermics 34:691–727, ISSN 0375–6505
18. Garwell K, Greenberg G (2007) 2007 Interim report. Update on world geothermal development. Publication of the Geothermal Energy Association. Available at the GEA website: http://www.geo-energy.org/reports/GEA%20World%20Update%202007.pdf
19. Fridleifsson IB, Ragnarsson A (2007) Geothermal energy. In: 2007 survey of energy resources, World Energy Council 2007, pp 427–437. ISBN: 0946121 26 5. Available at: http://www.worldenergy.org/documents/ser2007_final_online_version_1.pdf
20. Dickson MH, Fanelli M (2003) Geothermal energy: utilization and technology. UNESCO, Renewable Energy Series, New York, p 206. ISBN 978-92-3-103915-7
21. Stefansson V (2005) World geothermal assessment. In: Proceedings world geothermal congress 2005, Antalya, Turkey, 24–29 April 2005. ISBN: 9759833204
22. Rybach L (2010) "The future of geothermal energy" and its challenges. In: Proceedings world geothermal congress 2010, Bali, Indonesia, 25–29 Apr 2010
23. Mongillo MA (2010) Proceedings of the Joint GIA-IGA workshop – Geothermal energy global development potential and contribution to mitigation of climate change, Madrid, Spain, 5–6 May 2009. Download from: http://www.iea-gia.org/documents/ProcGIA_IGAWorkshopMadridFinalprepress22Mar10_000.pdf
24. Budd AR, Holgate FL, Gerner E, Ayling BF, Barnicoat A (2008) Pre-competitive geoscience for geothermal exploration and development in Australia: geoscience Australia's onshore energy security program and the geothermal energy project. In: Gurgenci H, Budd AR (eds) Proceedings of the Sir Mark Oliphant international frontiers of science and technology Australian geothermal energy conference, Geoscience Australia, Record 2008/18. ISBN: 9781921498190
25. Pritchett R (1998) Modeling post-abandonment electrical capacity recovery for a two-phase geothermal reservoir. Trans Geoth Resour Counc 22:521–528, ISSN: 0193–5933
26. O'Sullivan M, Mannington W (2005) Renewability of the Wairakei-Tauhara geothermal resource. In: Proceedings world geothermal congress 2005, Antalya, Turkey, 24–29 April 2005. ISBN: 9759833204
27. Goldstein BA, Hill AJ, Long A, Budd AR, Holgate F, Malavazos M (2009) Hot rock geothermal energy plays in Australia. Proceedings of the 34th workshop on geothermal reservoir engineering, Stanford University, Stanford, California, 9–11 Feb 2009, SGP-TR-187
28. IPCC (2007) Climate change 2007, fourth assessment report of the intergovernmental panel on climate change, working group III: mitigation of climate change, chapter 4 – Geothermal, section 4.3.3.4
29. International Energy Agency (IEA) (2008) World energy outlook 2008. Download from: http://www.iea.org/textbase/nppdf/free/2008/weo2008.pdf
30. European Renewable Energy Council (EREC) and Greenpeace International (GPI) (2008) Energy [R]evolution – A sustainable global energy outlook (EREC-GPI-08). Download from: http://www.greenpeace.org/raw/content/international/press/reports/energyrevolutionreport.pdf
31. Goldstein BA, Hiriart G, Tester JW, Bertani R, Bromley CJ, Gutiérrez-Negrín LC, Huenges E, Ragnarsson A, Mongillo MA, Muraoka H, Zui VI (2011) Great expectations for geothermal energy to 2100. In: 36th Stanford workshop of geothermal reservoir engineering
32. Bromley CJ, Mongillo MA, Goldstein B, Hiriart G, Bertani R, Huenges E, Muraoka H, Ragnarsson A, Tester J, Zui V (2010) IPCC renewable energy report: the potential contribution of geothermal energy to climate change mitigation. In: Proceedings world geothermal congress 2010, Bali, Indonesia, 25–30 Apr 2010
33. Sims REH, Schock RN, Adegbululgbe A, Fenhann J, Konstantinaviciute I, Moomaw W, Nimir HB, Schlamadinger B, Torres-Martínez J, Turner C, Uchiyama Y, Vuori SJV, Wamukonya N,

Zhang X (2007) Energy supply. In: B Metz, OR Davidson, PR Bosch, R Dave, LA Meyer (eds) Climate change 2007: mitigation. Contribution of working group III to the fourth assessment report of the intergovernmental panel on climate change. Cambridge University Press, Cambridge/New York. ISBN-13: 9780521705981

34. Krewitt W, Nienhaus K, Klebmann C, Capone C, Stricker E, Grauss W, Hoggwijk M, Supersberger N, Von Winterfeld U, Samadi S (2009) Role and potential of renewable energy and energy efficiency for global energy supply. Climate change, 18 Dec 2009, p 344. ISSN: 1862–4359
35. Electric Power Research Institute (EPRI) (1978) Geothermal energy prospects for the next 50 years. ER-611-SR, Special report for the world energy conference 1978
36. Tester JW, Drake EM, Golay MW, Driscoll MJ, Peters WA (2005) Sustainable energy – Choosing among options. MIT Press, Cambridge, MA, p 850
37. Rowley JC (1982) Worldwide geothermal resources. In: Edwards LM et al (eds) Handbook of geothermal energy. Gulf Publishing, Houston, pp 44–176, Chapter 2. ISBN 0-87201-322-7

Websites, Books and Reviews

Beardsmore GR, Cull JP (2001) Crustal heat flow: a guide to measurement and modelling. Cambridge University Press, Cambridge/New York

DiPippo R (2008) Geothermal power plants. Principles, applications, case studies and environmental impact, 2nd edn. Elsevier, Burlington

Huenges E (2010) Geothermal energy systems: exploration, development, and utilization. Wiley-VCH, Weinheim

Enhanced Geothermal Innovative Network for Europe (ENGINE), http://engine.brgm.fr/

European Energy Research Alliance Joint Programme on Geothermal Energy (EERA JPGE), http://www.eera-set.eu/index.php?index=36

European Geothermal Energy Council (EGEC), http://www.egec.org/

Geo-Heat Center (GHC), http://geoheat.oit.edu/

Geothermal Education Office (GEO), http://geothermal.marin.org/

Geothermal Engineering Integrating Mitigation of Induced Seismicity in Reservoirs (GEISER), http://www.geiser-fp7.eu/default.aspx

Geothermal Resource Association (GEA), http://www.geo-energy.org/

Geothermal Resource Council (GRC) and its annual conference in particular, http://www.geothermal.org/

International Energy Agency's Geothermal Implementing Agreement (IEA GIA), http://www.iea-gia.org/

International Geothermal Association (IGA) and its World Geothermal Congress (WGC) [(a)], http://www.geothermal-energy.org/

International Panel for Climate Change (IPCC). Working group III – Special report on renewable energy (and in particular Chapter 4 – Geothermal), http://www.ipcc-wg3.de/publications/special-reports/special-report-renewable-energy-sources

International Partnership for Geothermal Technologies (IPGT) [(a)], http://internationalgeothermal.org/

Stanford University Geothermal Workshops, http://pangea.stanford.edu/ERE/research/geoth/conference/workshop.html

US Department of Energy, http://www.energy.gov/energysources/geothermal.htm

Geothermal Field and Reservoir Monitoring

Trevor M. Hunt
GNS Science, Wairakei Geothermal Research Centre, Taupo, New Zealand

G

Article Outline

Glossary
Definition of the Subject and Its importance
Introduction
Purposes and Principles of Monitoring
Down-Hole Monitoring
Surface Monitoring
Future Directions
Bibliography

Glossary

Anchor grouting Concrete pumped into the rocks around the upper part of the well to anchor the well and well cellar to the near-surface rock formations.

Aquiclude A geological formation (or formations) which will not transmit water; a barrier to vertical movement of geothermal fluid.

Aquifer A geological formation (or formations) which contains water or geothermal fluid and will allow fluid movement.

Baseline Data set acquired before exploitation begins, against which any future measurements are compared.

Benchmark Permanent survey mark, often consisting of a stainless steel pin set in a concrete block or in the concrete base of a pipeline support.

Bleed A well that is throttled back to a minimum flow is said to be "on bleed." It is often risky to completely shut down a geothermal production well because it may be difficult to restart. Bleeding also keeps the wellbore heated which minimizes corrosion.

Deep liquid level Boundary between the two-phase and deep liquid zones.

Deep liquid zone Region of single phase liquid conditions below a two-phase (liquid and vapor) zone.

Developer Company or organization which locates or uses geothermal energy for domestic or industrial purposes.

Dryout The process whereby liquid saturation in the pores decreases and the vapor saturation increases, as a result of a decrease in pressure.

Epicenter The point on the Earth's surface directly above the hypocenter or focus of an earthquake.

Geothermal system A body of hot water and rock within the Earth.

Go-devil A tool for determining wellbore clearances or for scraping out obstructions from a well or pipeline.

Groundwater Water, generally cold and of meteoric origin, which resides in near-surface aquifers and is often used for domestic and industrial purposes.

High-temperature system A geothermal system, or part thereof, containing fluid having a temperature greater than 150°C; c.f. *low-temperature system* in which the temperature is less than 150°C. Note, however, that this temperature value is arbitrary and that different authorities adopt different values, or divide the range into low, intermediate, and high temperature.

Hypocenter The focus or focal point of an earthquake (x, y, z) c.f. epicenter (x, y).

Injection (syn. reinjection) The process of returning waste water from a geothermal power station or industrial process back into the ground. This generally occurs around the edges of the field and may not be into the production aquifer from which fluid is drawn off to the power station.

Injection aquifer The formation into which injected fluid is put. Generally this has high porosity and permeability.

Liquid-dominated system A geothermal system, or part thereof, in which the pressure is hydrostatically controlled; c.f. *steam (vapor)-dominated system*, where the pressure is steam-static.

Make-up well Well drilled to replace production lost from an existing production well, due to decreases in fluid temperature or pressure.

Perched aquifer An aquifer of limited lateral extent which is separated from an underlying body of groundwater by unsaturated rock.

Permeability A measure of the capacity of a geological rock formation to transmit a fluid.

Production zone That region (depth) of the geothermal reservoir from which most of the production of fluid occurs.

Reservoir The region of a geothermal system from which geothermal fluid is withdrawn, or is capable of being withdrawn.

Residual (liquid) saturation The amount of liquid that remains in the pores (as % of pore volume) which decreases in pressure will not vaporize. The liquid saturation level below which vaporization of liquid will not occur.

Steam zone A region of the reservoir in which steam (vapor) is the pressure-controlling phase.

Trigger point A measured value at which it is considered action needs to be taken to prevent or avoid some detrimental occurrence happening, or exceeding some predetermined limit.

Two (2)-phase zone A region where the liquid and vapor (steam) phases of water coexist in pores or fractures.

Vadose zone The region of unsaturated rock and soil between the ground surface and the shallow groundwater level.

Waste water Geothermal water from which energy has been extracted and is no longer required. This may be separated water, or steam which has passed through turbines or a binary plant and been condensed.

Definition of the Subject and Its Importance

Geothermal systems are dynamic entities in which the liquid and vapor phases of water are the main mobile constituents. In their natural state these are generally in a quasi steady-state condition, when considered over a long period of time (>1,000 years). However, when fluid is withdrawn for the purpose of extracting energy then changes may occur within the system. These changes can result in a variety of environmental effects some of which are undesirable and so to manage the extraction of energy in a sustainable and environmentally responsible way it is necessary to monitor the

changes. By monitoring the changes with time it is possible to understand and model the effects these changes may have on the environment and take steps to minimize any undesirable effects in a timely manner. Changes may also have engineering implications for a geothermal development, especially for a power station. One example is a decrease in the pressure of steam supplied to the station that may necessitate replacement of the original turbines by those designed to operate at lower pressures. At the start of production at Wairakei (New Zealand) in 1958, the high-pressure (HP) turbine inlet pressure was 1.25 MPa, but by the late 1970s the pressure had fallen to about 0.7 MPa, and the HP turbines were taken offline and the wells derated to intermediate pressure [1]. Another example is a change in enthalpy due to a change in the steam-water ratio that may affect the efficiency of a modular binary plant designed for a specific steam-water mixture.

Introduction

In a typical high-temperature geothermal system used for electrical power generation, a large mass of hot water is withdrawn from an area and the cooler, waste water is injected in a different location, and this can give rise to significant changes within the system and at the surface. However, in low-temperature systems or where only heat (no mass) is extracted, the changes may be small and negligible.

Purposes and Principles of Monitoring

Purposes of Monitoring

Where significant changes occur, or it is anticipated they might occur, a developed geothermal system will be monitored to:

1. Obtain data on which rational and informed resource management decisions can be made by developers and regulatory authorities.
2. Verify that management decisions are having the desired outcomes.
3. Enable the public to have confidence in the environmental management process.
4. Assist in building up knowledge of geothermal systems and how to develop them in a sustainable and environmentally responsible way.

Basic Principles

Ideally, monitoring begins before development starts so that a good baseline is obtained. It is not possible to go back in time, so many different eventualities need to be considered and a fully integrated monitoring program needs to be developed and begun before large-scale productions starts.

Monitoring should be conducted at a frequency sufficient to enable natural variations to be distinguished from exploitation-induced changes.

The data collected needs to be interpreted and regularly compared with predetermined "trigger points." No change may be as important as some change, and is not a valid reason for stopping monitoring, although the frequency of measurement may be reduced after a long period of no change.

Data need to be reliable. Equipment should be calibrated regularly and operated by a competent person. Since monitoring may continue over a long period of time, it is important that the same techniques are used such that a valid comparison can be made between early and recent data.

Monitoring Program Planning

A geothermal monitoring program is likely to extend for several decades, therefore all observations and measurements need to be carefully documented in a suitable archive. During this time there will probably be staff changes and therefore there needs to be a written set of instructions about how and when measurements will be made, so that measurements at different times are compatible with each other. Monitoring sites need to be clearly marked and monitoring facilities (e.g., groundwater monitor wells) need to be maintained. Experience has shown that large-scale geothermal developments often start as a small development and increase in size incrementally. Furthermore, as production wells decline new wells are drilled to maintain steam quantities deliverable to the power station. These engineering activities may result in monitoring sites being altered or destroyed, so it is important that the baseline data set has sufficient redundancy to allow for such loss without seriously compromising its integrity.

Interpretation of Monitoring Data

Generally the process of collecting monitoring data is relatively easy, however, correct interpretation of the results may be difficult. Often the first problem in interpretation is separating natural variations from those induced by utilization of the field. Further complexities may be introduced by other human activities, for example, pumping of water supply wells for irrigation or drinking water for animals, and diversion or damming of rivers may cause groundwater level changes. The effects of some anthropogenic changes may be difficult to measure or even estimate. Another significant problem is that what is measured inside a drillhole may not represent what is occurring in the rock outside the drillhole, because as fluid passes from the rock into the hole it may change in character.

Down-Hole Monitoring

A variety of down-hole monitoring techniques have been developed, many originating from the oil industry, to determine reservoir changes. Ideally, down-hole monitoring is undertaken in nonproducing wells, or production wells that are shut down or on "bleed." However, making the measurements is the simplest part of the process because often the casing configuration of the well can strongly influence the data obtained and needs to be taken into account. Furthermore, there is a problem in that conditions within a wellbore may be different from those in the rock outside the wellbore.

Pressure

Changes in fluid pressure with depth and time are key indicators of reservoir changes, especially in high-temperature liquid-dominated systems. In their natural, predevelopment state the reservoirs in such systems contain boiling liquid water, with pockets of 2-phase conditions in the upper part. Pressures are near boiling point for depth. Extraction of fluid, and the concomitant decrease in pressure, generally causes these pockets of 2-phase conditions to coalesce into a continuous 2-phase zone and then expand (both horizontally and vertically). As the pressures fall the liquid saturation in the pores and fissures decreases, and eventually steam becomes the pressure-controlling phase in the upper part of the zone, giving rise to a steam zone in which there is negligible change in pressure with depth (Fig. 1). Continued pressure decreases (e.g., Fig. 2) may lead to cool inflows which resaturate the pores in the 2-phase zone, resulting in a rise in the deep liquid level and an increase in pressure in the deep liquid zone (although pressures may continue to decrease in the overlying steam and 2-phase zones).

A continuous vertical profile of pressure variation with depth is made using high-pressure high-temperature (HPHT) wire line equipment, now generally using quartz pressure transducers.

Temperature

Changes in fluid temperature within the geothermal reservoir are of vital importance in managing and guiding future development of a geothermal field. After drilling and output testing, a geothermal well is generally left for several weeks for the temperatures of the wellbore fluid to stabilize and achieve thermal equilibrium with the surrounding rock formations. A profile of temperature variation with depth is then made using HPHT wire line equipment, and repeated at intervals of time. For production wells this temperature logging can only be done when it is possible to shut the well down for enough time for thermal equilibrium to occur.

Initial temperature logs of deep geothermal wells rarely show a consistent increase of temperature with depth: regions of cooler values (reversals) reveal cool inflows and regions of hotter values reveal feed zones (Fig. 3). When interpreting temperature logs it is important to take into account the casing pattern; in uncased regions or zones of slotted casing, there may be flows within the wellbore between different formations (see below) that result in the measured temperatures being different from the rock outside the wellbore.

Some production wells may experience significant decreases in feed temperatures with time as a result of cold downflows, lateral inflows of cooler water, or changes in the relative amounts of contribution from feed zones of different temperature (Figs. 4 and 5). Lateral inflows of cooler water may be associated with the return of cooler injected water along high permeability paths. Temperature and chemistry monitoring can detect such returns and so guide the location of drilling of make-up wells.

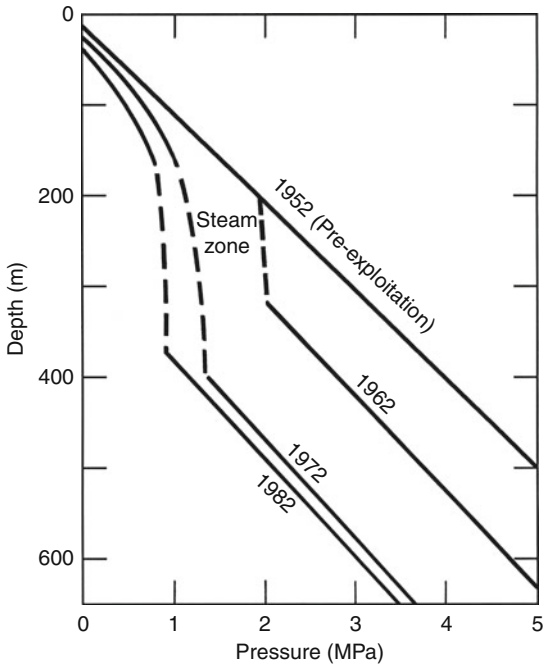

Geothermal Field and Reservoir Monitoring. Figure 1 Sketch showing the variation of pressure with depth at different times during early development of the Wairakei geothermal field, New Zealand (Taken from [2]). Note increase in thickness of the steam zone (1962, 1972) followed by slight decrease (1982)

Flow

Changes in fluid mass and volumetric flow rate, and the proportion of vapor (steam) to liquid (water), for individual production wells are also important for managing and guiding the development of a liquid-dominated geothermal field. Measuring the mass and volumetric flow in a well or pipeline is not easy, especially two-phase flow, and accuracies can vary [4]. One modern method, a vortex mass flowmeter, is based on the phenomenon of vortex shedding. A non-streamlined body, called a "shedder bar," inside the pipeline causes an alternating series of vortices to be shed from each side of the body. The distance between successive vortices on each side is related to the fluid velocity, and is measured by a sensor behind the shedder bar. From the velocity measurement, and simultaneously measured temperature and pressure values, the volumetric and mass flow rates can be calculated. Flow rates within a well can be measured using a spinner type or hot-wire flowmeter. Generally these measurements are made at low flow rates or when the well is shut down and the instrument is passed through a gland at the wellhead. Another type of flowmeter used is the Coriolis or Inertial flowmeter which directly measures the mass flow rate [5]. It has one or more bent, straight, or U-shaped vibrating tubes in the fluid stream, and as the fluid passes through the tubes, they twist. The amount of tube twisting is directly proportional to mass flow. This meter can also be used for heat measurement of low-pressure, superheated steam. The chief advantage of a Coriolis flowmeter is in providing highly accurate measurements of mass flow rate without flow conditioning or accessory devices such as pressure or temperature measurement.

Fluid flow within a wellbore may be complex. In a flowing production well there may be several feed zones at different depths, each contributing to the total flow measured at the wellhead. In a non-flowing geothermal well, the high aspect ratio of the cased part of the wellbore precludes thermally generated fluid movement. However, in an open (uncased) or slotted region of the well there may be fluid movement between formations having different temperatures and physical properties; fluid may exit from one aquifer, travel up or down the wellbore, and enter another (thief zone). Repeated wire line flowmeter measurements may be made to detect changes in flow from the different feed zones over time, or before and after maintenance on a well, and for finding holes in casing that have developed due to corrosion.

Fluid flow within the rock matrix can be measured using chemical tracers introduced into a well and their arrival time and concentration measured in other wells (see below).

Generally, for a high-temperature geothermal field the mass flow rates will decline, and (for liquid-dominated wells) the enthalpy will increase over time, unless injection returns cause an increase in mass flow and decline in enthalpy.

Casing Integrity

Over a period of time, steel well casing and piping, and concrete anchor grouting can become damaged as a result of corrosion (stress or fatigue), scaling, or

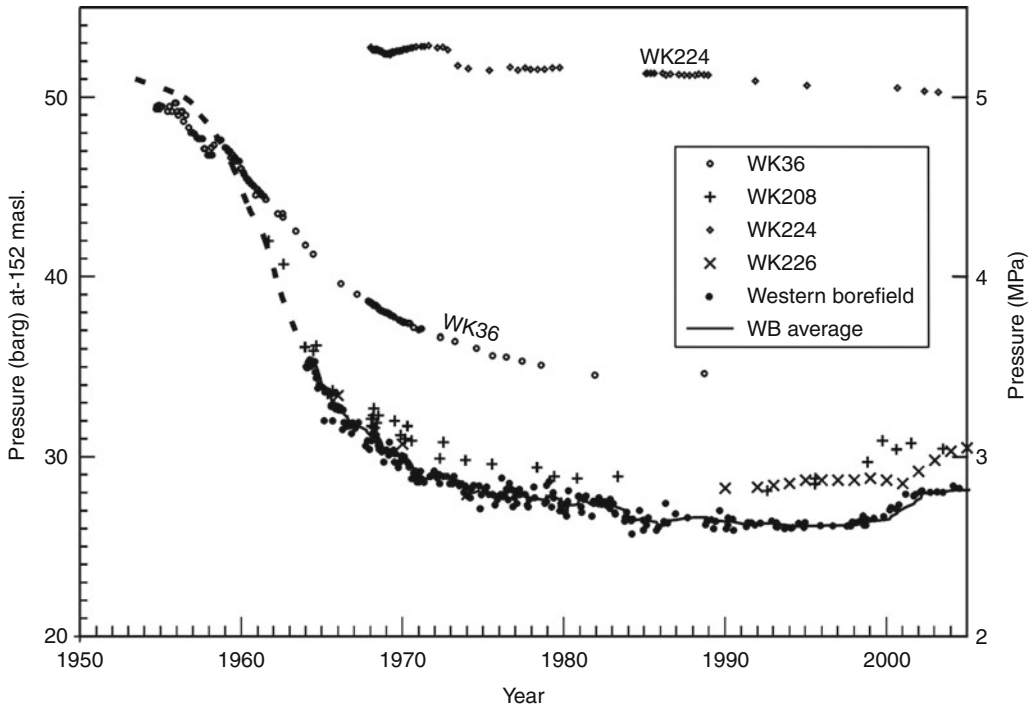

Geothermal Field and Reservoir Monitoring. Figure 2
Changes in deep liquid pressure with time in Wairakei geothermal field (Taken from [3]). Pressure: 1 bar = 0.1 MPa. Testing of exploration wells began in the early 1950s and production started in 1958. Well WK224 (top) lies outside the field

ground deformation. Corrosion may occur on the inner surface of the casing as a result of acidic fluids flowing up from deep feed zones, or it may occur on the outer surface of the casing and attack grouting as a result of acidic fluids being present in a formation through which the well passes [6, 7]. Corrosion is present in most geothermal wells, even low-temperature and low-enthalpy wells, but is generally more of a problem in deep, high-temperature, and high-enthalpy wells tapping CO_2-rich and acidic fluids. Mechanical deformation (breaks, buckling) may occur in wells subject to significant ground deformation [8].

Casing damage is detected by running a mechanical caliper tool with flexible fingers up and down the hole, or by running a "Go-devil" tool down the hole. Detailed determination of the damage may then be investigated using a video camera or a sonic borehole televiewer. Damage to near-surface (<10 m depth) casing can be repaired by excavating a pit around the well and replacing the damaged casing. To repair deeper damage it may be necessary to run new liner of smaller diameter inside the damaged production casing, apply casing patches or install expandable casing.

Fluid Chemistry

The chemical composition of geothermal production fluids may change with time due to dilution and cooling of the reservoir fluids, resulting mainly from the invasion of cool and less-mineralized waters (Fig. 6). Regular measurement of the chemistry of liquid and vapor samples of fluids from selected wells provides information about changes in the reservoir. The data are also used to examine the need for and effectiveness of chemical dosing to prevent corrosion, and to monitor mineral deposition in the wells and pipework. However, interpretation of chemical changes is not necessarily straightforward because the chemistry of production fluids may vary between wells, and as the relative amounts of production from each well change with time (due to supply requirements) so the total chemistry may appear to change.

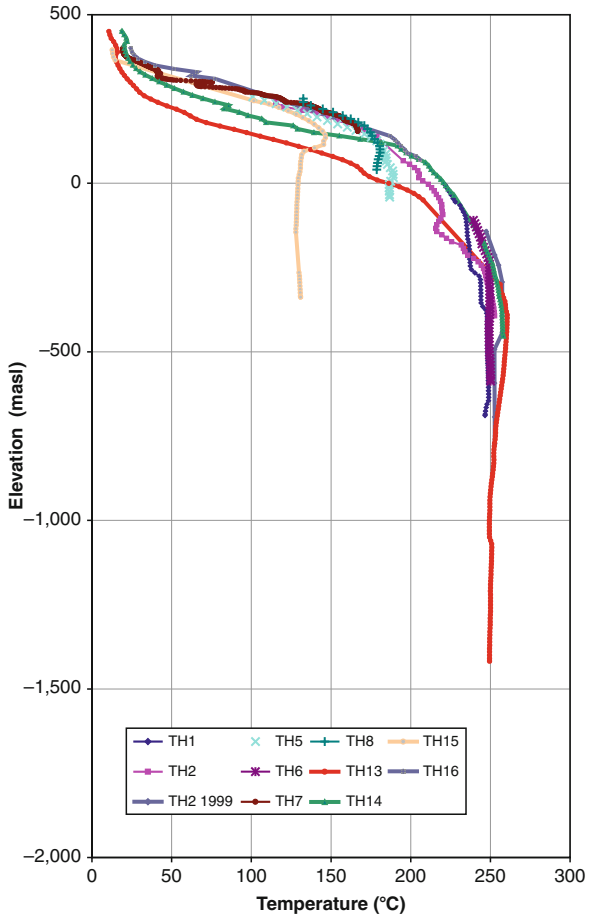

Geothermal Field and Reservoir Monitoring. Figure 3 Variation of temperature with depth in exploration drillholes in Tauhara geothermal field, New Zealand. Note the differences between wells and that in some wells (especially TH2, between −100 and −200 m) there are temperature reversals due to cool inflows

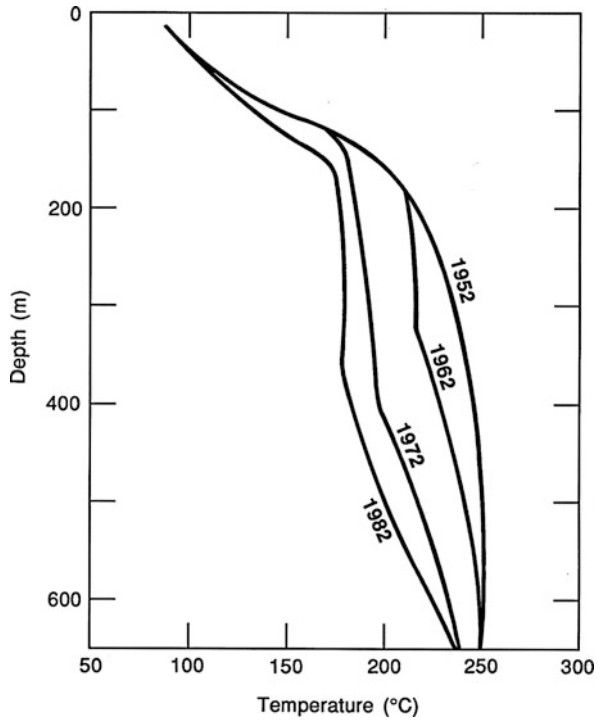

Geothermal Field and Reservoir Monitoring. Figure 4 Sketch showing variation of temperature with depth in some wells (Eastern borefield), at different times during early development of the Wairakei geothermal field, New Zealand (Taken from [2])

Samples of geothermal fluid may be taken either from within the wellbore (i.e., down-hole) or at the surface. Down-hole samples are taken using a special sampling device that captures the geothermal fluid in its in situ, undisturbed state; i.e., before phase separation, irreversible thermal cycles, or chemical reactions have occurred [10, 11]. Samples are usually taken at different depths in a well to determine the changes that occur as the fluid ascends the well. At the surface, a small sample of the two-phase geothermal fluid is drawn off from the flowing well and passed through a small separator which separates the liquid (water) from the vapor (steam). The liquid (water) fraction is then cooled by passing it through a water-cooled coil and analyzed by standard techniques. The vapor (steam) fraction is passed into an evacuated glass flask containing a caustic solution to absorb acidic gases (carbon dioxide, hydrogen sulfide); the solution is then analyzed by titration. Trace gases (Ar, He, N) remain in the top of the flask and are removed and analyzed using a gas chromatograph [12].

In high-temperature liquid-dominated geothermal systems, chloride is a major chemical species and an important indicator of changes in the reservoir fluid. A decrease in the chloride content may indicate dilution due to an influx of cold groundwater (Fig. 7), and an increase may indicate injection returns.

In fields where the geothermal fluid resides or passes through limestone, the fluid may become saturated in calcium carbonate ($CaCO_3$), which precipitates as calcite in the wellbores and pipelines as temperatures and pressures decline. This precipitate, known as scaling, is a serious problem because it

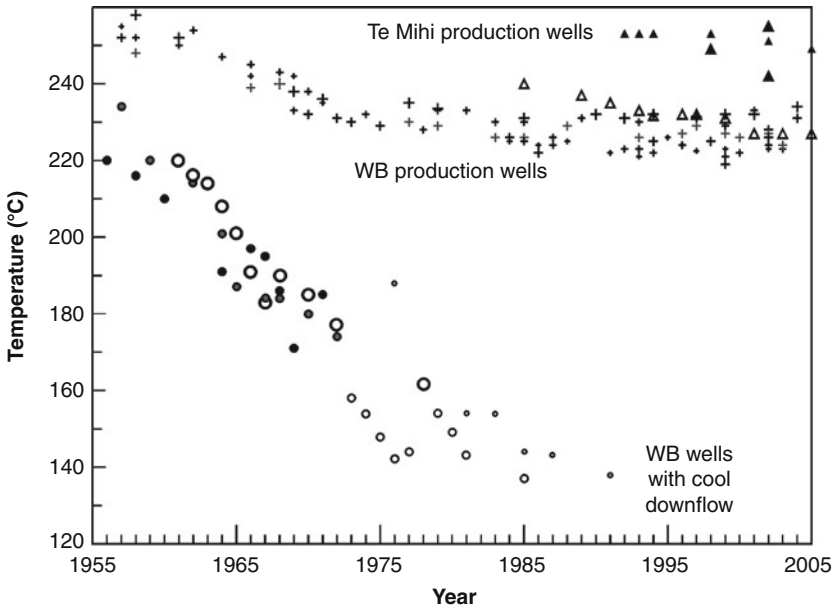

Geothermal Field and Reservoir Monitoring. Figure 5
Changes in production temperatures with time in Wairakei geothermal field (Taken from [3]). WB: Western Borefield. Note the large decrease in temperature of fluid from wells having cool downflows, whereas other production wells have experienced only a small temperature decline and temperatures have remained near constant since about 1975

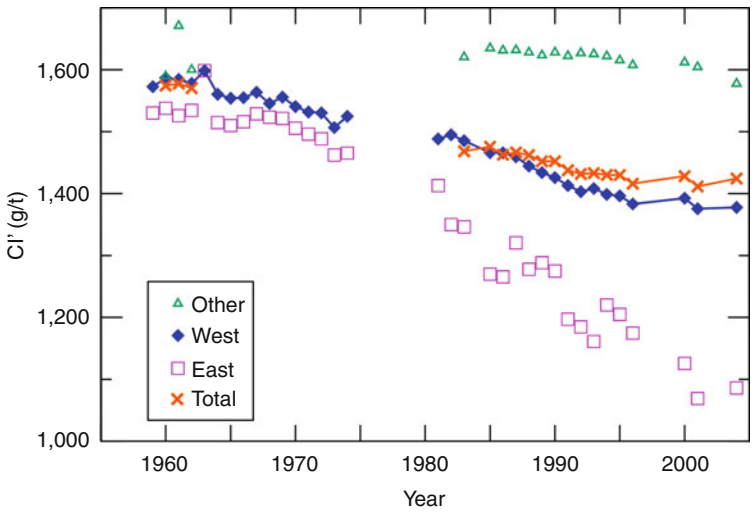

Geothermal Field and Reservoir Monitoring. Figure 6
Changes with time in average chloride content (corrected for aquifer steam loss) of production fluid from different parts of Wairakei geothermal field (Taken from [9]). "West" and "East" refer to Western and Eastern borefields, respectively; "other" refers to the Te Mihi borefield, from where production began in the early 1980s

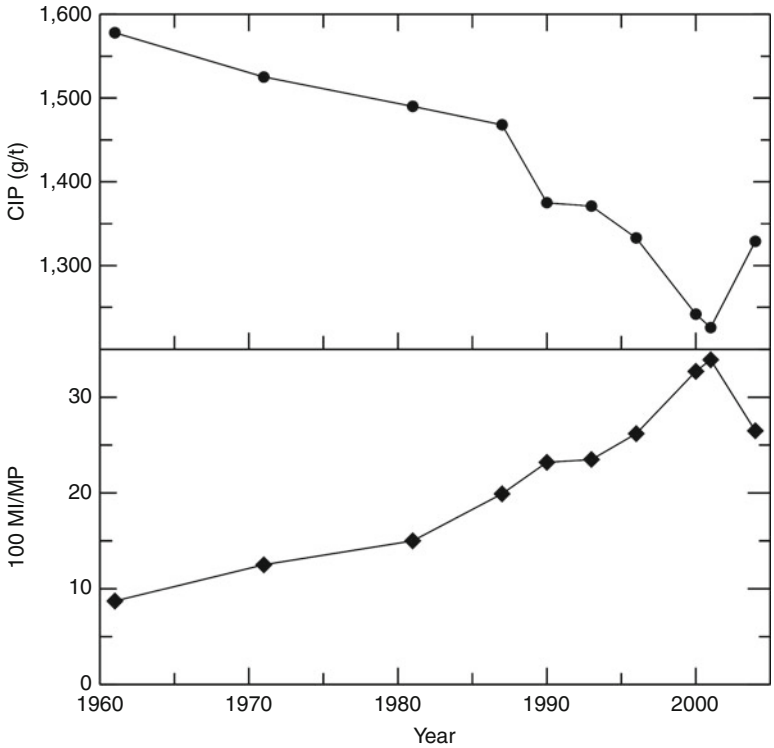

Geothermal Field and Reservoir Monitoring. Figure 7
Changes with time of the average chloride content of production well fluid (ClP) at Wairakei (upper) and in the amount of cold inflow (%) into the production zone computed from the chloride changes (lower) (Taken from [9]). The increase in the chloride value after 2000 is attributed to a larger proportion of deep water coming from a new production area (Te Mihi) and to more injected water (beginning 1995) reaching the production wells

reduces the fluid flow and particles of precipitate may flake off and enter the turbines causing damage. Monitoring of the carbonate helps identify problem wells and enable scaling rates to be determined.

Tracer Tests

Although primarily used for reservoir characterization purposes, tracer tests [13–15] may be used for reservoir management, particularly if major changes are made in the development of a field. A tracer test involves inserting a finite slug of a chemical or radioactive material ("tracer") into an injection well and measuring the time for it to appear, and its concentration, in production and monitoring wells. Tracer tests to evaluate the flow patterns between injection and producing wells are common practice in oil and gas field operations. A wide variety of chemical tracers have been used including: hydrofluorocarbons (tetrafluoroethane, trifluoromethane), naphthalene disulfonate, noble gases (neon, xenon), potassium halides (KBr, KI), rhodamine WT, and fluorescein. Fluorescein is the most commonly used tracer in liquid-dominated geothermal reservoirs because it is sufficiently stable to be used in reservoirs as hot as 250°C; it has a detection limit of approximately ten parts per trillion using conventional spectrofluorimetry; and can be detected using a simple, inexpensive, and easily operated filter fluorometer. Iodine 131 has been used as a radioactive tracer [16]. Some tracers travel preferentially in the vapor (steam) phase, others in the liquid (water) phase. By repeating tracer tests it may be possible to determine changes in fluid flow paths, particularly "short circuiting" of injected fluids from new injection wells directly to production wells.

Surface Monitoring

Flow Rate

Monitoring fluid flow rates at the wellhead of production and injection wells is a basic monitoring tool which can indicate changes in the performance of individual wells and of total field performance. Sudden unexpected changes in flow rate from an individual well may indicate damage to the well casing. Gradual decreases in flow rate may indicate a fall in reservoir pressure in the vicinity of the well feed zone(s), or a change in the relative contributions of supply from different feed zones.

Ground Surface Movements

In a few geothermal fields, notably some of those in New Zealand, there have been significant ground subsidence (up to 15 m) and horizontal deformation (up to 2 m) associated with production.

At Wairakei field (New Zealand), deformation was originally noticed when concrete drains became broken, and subsequently pipework has been mounted on roller supports to accommodate movement, although from time to time it has been necessary to remove and insert sections of pipe. Vertical deformation is measured by repeat surveys using an optical level to measure changes in elevation between permanent reference points such as benchmarks, referenced to a stable point outside the field. The frequency of surveys depends on the rate of subsidence and the location of the subsidence area. At Wairakei, the main steam lines are leveled every 2 years, and the whole field about every 4 years. In some fields, where there are not extensive amounts of surface vegetation, it has been possible to determine subsidence using interferometric synthetic

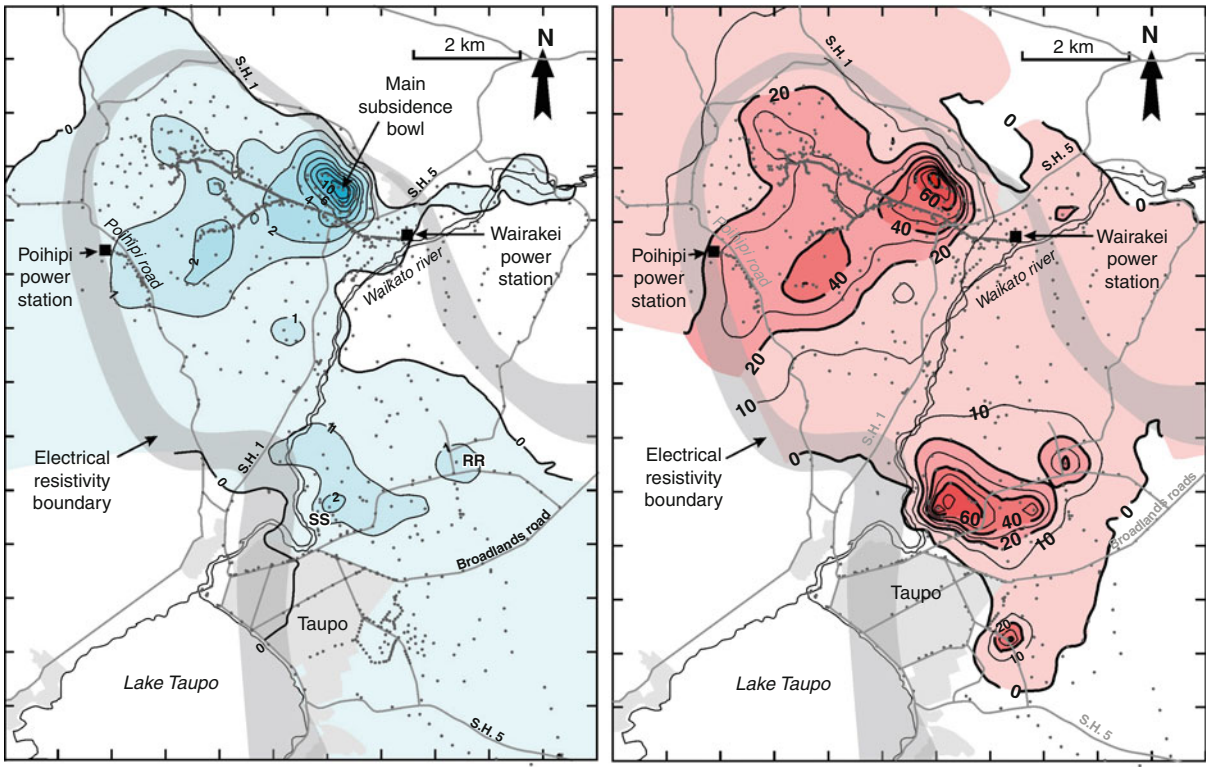

Geothermal Field and Reservoir Monitoring. Figure 8
Ground subsidence (left; m) and subsidence rates (right; mm/year for 2001–2005) at Wairakei-Tauhara geothermal field, New Zealand (Taken from [21]). *Dots* indicate survey points. Note that the intense subsidence is confined to several isolated subsidence bowls: Main; SS Spa Sights; RR Rakanui Road

aperture radar (InSAR) [17–20]. At Wairakei-Tauhara field (New Zealand) there have been small areas of intense subsidence within the field since measurements began shortly after production started in 1958 [21]. In this field the subsidence has occurred mainly in about four localized "subsidence bowls," but over the remainder of the field the subsidence has been less than 1 m (Fig. 8). At the center of the main subsidence bowl the rate of subsidence increased to a maximum of over 450 mm/year in the late 1970s but has since decreased to about 50 mm/year (Fig. 8). The location of the bowls and their centers does not correspond to areas of maximum production; the center of the main subsidence bowl lies about 500 m from the original area of production. The cause of the subsidence at Wairakei-Tauhara and Ohaaki is associated with draining, and consequent compaction, of rocks of locally high compressibility within formations above the reservoir, due to a decrease in pressure within the steam zone in the upper part of the reservoir. Casing deformation indicates these rocks lie at about 100–300 m depth. However, the reason for the localized distribution of high compressibility in these rocks remains a puzzle; other parts of the same formations do not have high compressibility. At Mokai field (New Zealand), there has been subsidence of up to 0.20 m around the injection wells, associated with cooling and thermal contraction of rocks in the injection aquifer.

Horizontal deformation is measured using theodolites or Geodimeters to measure changes in angles or distances between permanent reference points, or using global positioning system (GPS) techniques. Generally the reference points are permanent markers specifically installed for the purpose. At Ohaaki field (New Zealand), these consist of a concrete post made from a drainage pipe (approximately 600 mm diameter), mounted vertically, set in a concrete pad, and filled with concrete. A threaded pipe is set in the upper surface of the post to allow a theodolite, Geodimeter, or a target to be mounted on the post. At Wairakei-Tauhara field (New Zealand), the largest horizontal movement rates have been 25–30 mm/year and have occurred at the edges of the main subsidence bowl where the lateral changes in subsidence (tilt) have been the greatest [21]. The horizontal movement vectors generally point toward the center of the subsidence bowls (Fig. 9). The overall

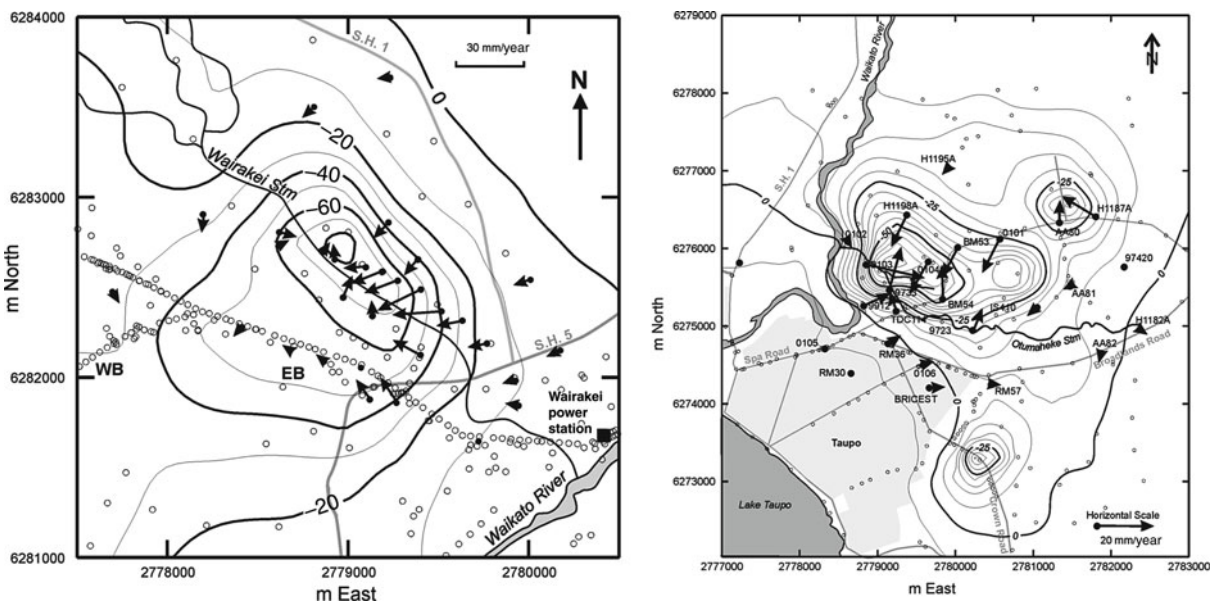

Geothermal Field and Reservoir Monitoring. Figure 9

Horizontal deformation vectors (*arrows*) at subsidence bowls in the Wairakei-Tauhara geothermal field (Taken from [21]). Solid contours indicate rates of ground subsidence (mm/year) determined at benchmarks (*open circles*). Note the vectors point to the center of the subsidence bowl, and have greatest amplitude on the flanks of the bowl

pattern of horizontal movement has not changed greatly with time, but the rates of movement have declined as the subsidence rates have decreased.

Groundwater

Near the ground surface above most geothermal reservoirs there is generally a complex sequence of groundwater aquifers containing cold or warm waters (and in places hot water and steam) which are often a source of potable water or used for industrial and domestic purposes (heating, cleaning). The aquifers are usually separated from each other by aquicludes.

These shallow aquifers can be affected by production from the deeper geothermal reservoir and hence many regulatory authorities require water levels, water chemistry, and temperatures in the aquifers to be monitored periodically. Monitoring is usually done using shallow wells drilled specifically for the purpose. These holes are generally about 3–5 cm diameter and are generally drilled vertically using a small truck-mounted auger. The holes usually have solid casing in the Vadose Zone and slotted or screened casing from the water table to the bottom. Where several groundwater aquifers are present several monitor holes are drilled and care is taken in each to adopt a casing pattern that monitors a specific aquifer and ensures that the well does not result in interaction between separate aquifers, i.e., draining of an upper into a lower aquifer. In places where the ground temperature is less than about 50°C, plastic (PVC or ABS) casing is used, but for ground temperatures greater than this value steel casing is used. The open area of the screened casing should approximate the natural porosity of the rock formation, and the slots should widen inward to minimize plugging of the slots by fine formation material. Over a long period of time, fine silt and debris migrate through the screened casing and are deposited at the bottom of the hole; so the hole is generally drilled 5–10 m deeper than the natural water table.

Water levels are measured using a simple electric circuit device lowered down the well; this is powered by a small battery and contact with the water closes the circuit. Alternatively, a water level recorder can be installed which is comprised of a pressure transducer

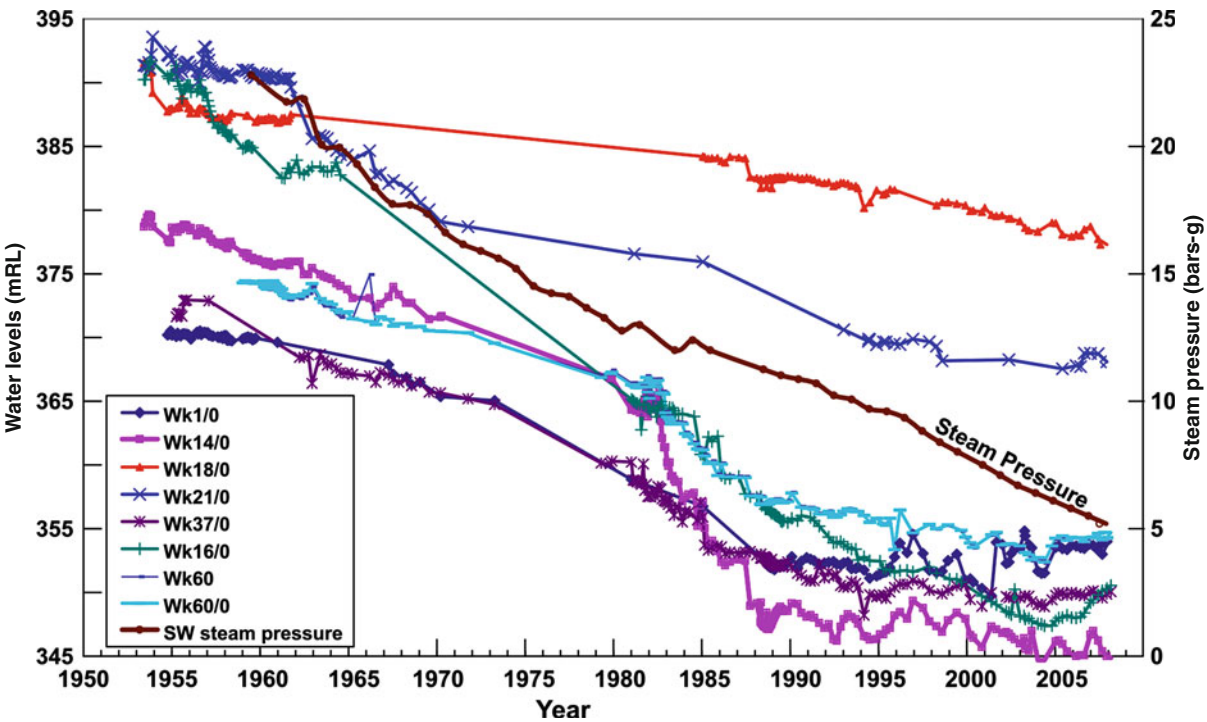

Geothermal Field and Reservoir Monitoring. Figure 10
Changes in shallow groundwater level with time in the Eastern Borefield at Wairakei geothermal field (Taken from [22])

coupled to a data logger. Measurements are generally made at set times during the year to determine and correct for seasonal variations.

Changes in groundwater level (piezometric surface) can occur as a result of pressure declines in the deep geothermal reservoir. At Wairakei (New Zealand), decreases in groundwater level of up to 30 m have been recorded in the Eastern Borefield, an area where thermal features were fed by conduits from the deep reservoir [22] (Fig. 10). As pressures in the upper part of the reservoir decreased, the flow of geothermal fluid up conduits to the surface declined and eventually ceased. This allowed shallow groundwater to drain down the conduits, resulting in local regions of depression of the groundwater surface (Fig. 11). In some cases, where the near-surface geology is complex, these changes can be localized, especially where perched groundwater aquifers are present [23].

The temperature of groundwater is measured in shallow monitor holes using a digital thermometer and probe. Sometimes the temperature is measured not only at the water surface but also deeper in the monitor hole, to enable a temperature profile in the water to be obtained.

Samples for chemical analysis are obtained from groundwater monitor holes after water level and temperature measurements have been made. However, care must be taken not to sample stagnant water in these holes; only after five to ten wellbore volumes of water have been removed and naturally replaced should a sample be collected. Removal of stagnant water and collection of the samples is generally done using a small portable electric pump. Parameters that are usually measured are: pH, chloride, lithium, sodium, potassium, magnesium, sulfate (SO_4), total silica (SiO_2), total bicarbonate (HCO_3),

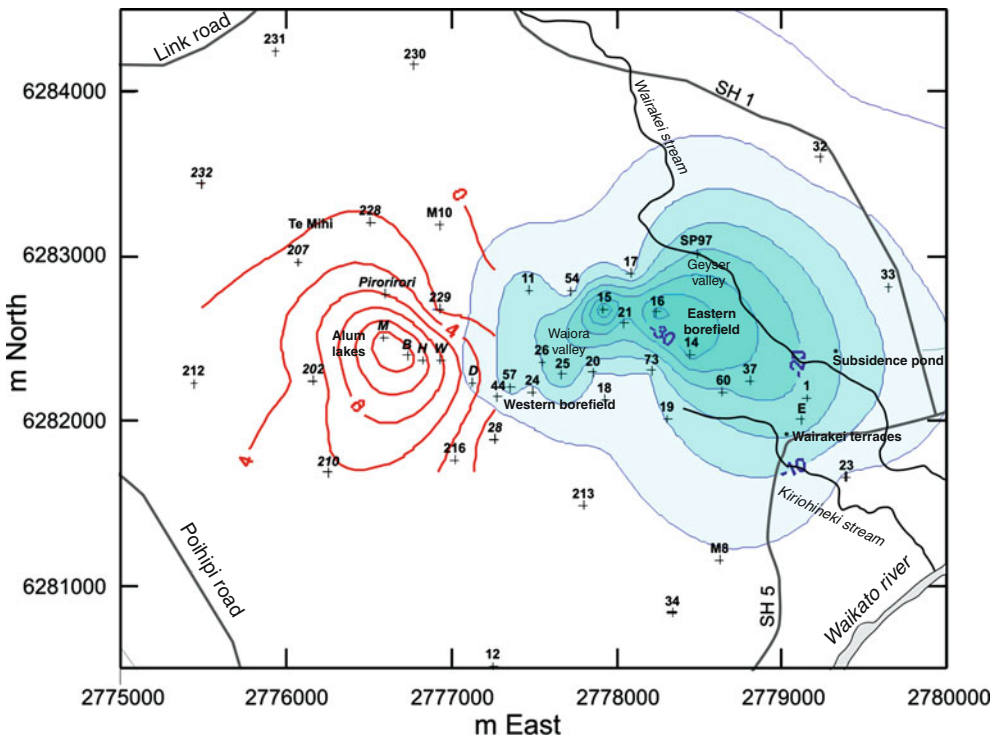

Geothermal Field and Reservoir Monitoring. Figure 11
Changes in shallow groundwater level (m) in at Wairakei geothermal field (Taken from [22]). Changes in the Eastern Borefield (blue contours) are for the period 1956–1995; changes in the Alum Lakes area (red contours) are for the period 1999–2006. Crosses indicate monitor wells; labels indicate well numbers (see Fig. 9); letters in the Alum Lakes area indicate thermal pools

and fluoride. In addition, measurements of stable isotopes $\delta_{18}O$, δ_2H, and tritium are sometimes made.

Microgravity

Exploitation of high-temperature geothermal resources usually involves withdrawing fluid from one area (production area) and, after using it to generate electricity or provide heat, injecting the liquid back into the ground in another area (injection area). This generally results in changes in mass (and corresponding density changes) in these areas, and hence small changes in the force of gravity at the surface (Figs. 12 and 13). The amount of gravity change in the production area will be related mainly to the amount of recharge, and to changes in the proportions of liquid water and steam in the production zone.

The changes in gravity are measured at permanent reference points such as survey benchmarks throughout and beyond the field boundaries using a portable gravity meter. Generally a relative type of gravity meter is used which measures differences in gravity from a stable, reference point outside the geothermal field, although in some instances absolute gravity meters have been employed. Measurement precision is generally 5–10 μGal ($5–10 \times 10^{-8}$ m/s^2). A baseline survey is made at 50–150 points prior to exploitation, and the survey repeated at intervals of 2–5 years afterward. Within each survey, corrections are made for the gravitational effects of changes in the position of the Moon and Sun (Earth tide) and for tares (jumps in zero point of the meter resulting from knocks). In determining the gravity differences between surveys (gravity changes) the data are corrected for the gravitational effects of ground elevation changes (subsidence), gravity changes at the reference point, and changes in groundwater level and temperature.

From the gravity changes it is possible to determine a field-wide value for recharge by numerical integration of the changes and application of Gauss's Theorem [25]. This method is completely independent of any

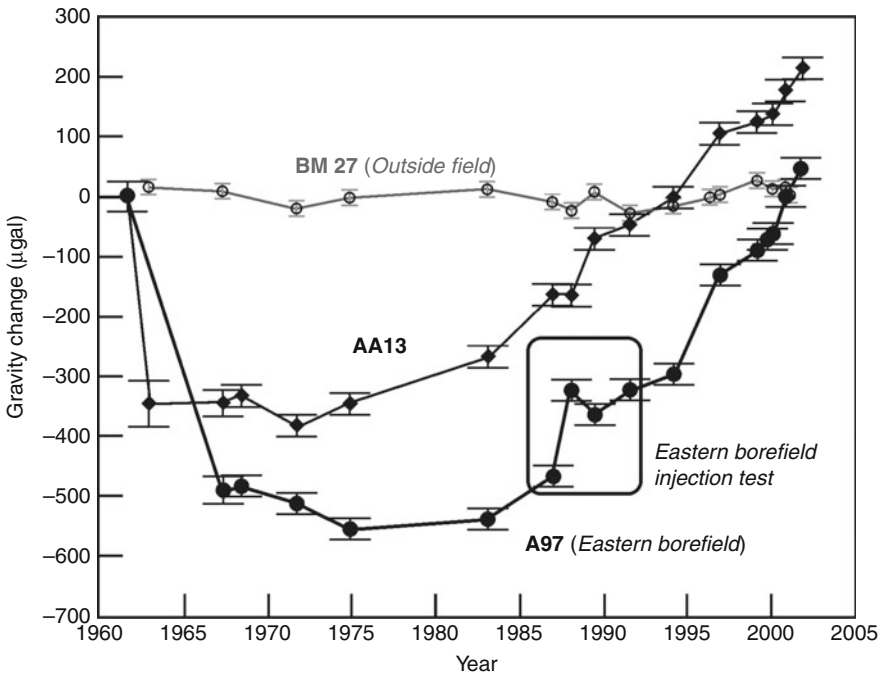

Geothermal Field and Reservoir Monitoring. Figure 12
Changes in gravity (μgal) associated with production at Wairakei geothermal field, New Zealand. Benchmarks A97 and AA13 lie in the Eastern borefield from which most production was obtained between 1958 and the 1980s. Note the increase in gravity since the late 1970s, associated with resaturation of the production aquifer (Taken from [24])

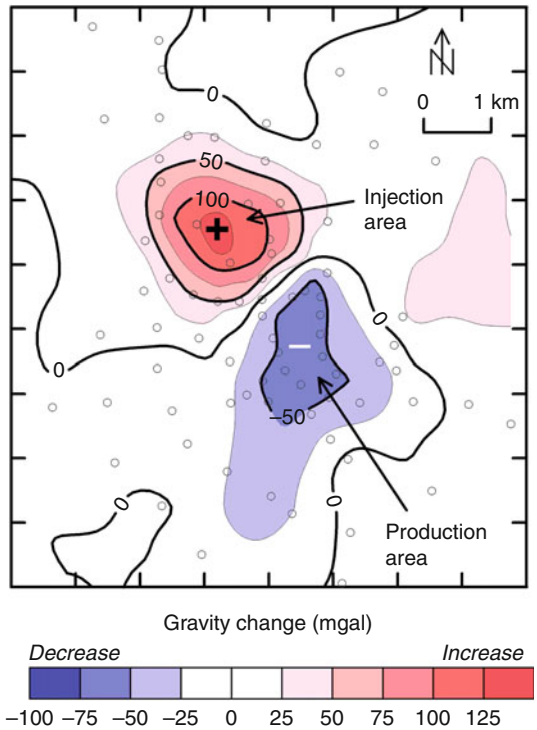

Geothermal Field and Reservoir Monitoring. Figure 13 Gravity changes at Mokai geothermal field, New Zealand, between 1997 and 2004. *Open circles* indicate measurement points; contour interval 25 μgal (25×10^{-8} m/s^2). Data has been corrected for the effects of small amounts of ground subsidence

assumptions about fluid density, depth of production, permeability, or porosity; its accuracy is limited only by the precision of the gravity measurements, and errors inherent in the integration of the data. Gravity change measurements also may provide: field-wide and local values for recharge of fluid into a geothermal system; information about changes in saturation in different parts of the two-phase zone; a test of complex, three-dimensional, numerical reservoir simulation models for exploitation of a field [26, 27]; information about the location and movement of injected fluid [28]; and estimates of reservoir parameters such as permeability (k), permeability-thickness (kh), and storativity (φch) [29].

Gravity change data can also be used to discriminate between two (or more) numerical reservoir simulation models for exploitation of a field. Such models are important in guiding development of a field. The models for high-temperature liquid-dominated fields predict the development and extension of 2-phase conditions and subsequent changes in saturation (and hence density and gravity changes) which involve assumptions about the geometry of the field, various reservoir properties, and behavior of the field during exploitation. Discrepancies between the theoretical (model-derived) and measured gravity changes may indicate that assumptions made in setting up the models are wrong.

Another important use of gravity change data is to track the path of injected water. If the waste liquid water is injected into a region of 2-phase conditions the liquid is cooler, and hence denser than the fluids present, and tends to sink toward the bottom of the zone. If the rocks do not have isotropic permeability the liquid will move more rapidly along paths of high permeability and in response to any pressure gradients that might be present; this movement being reflected by the gravity changes.

Electrical Resistivity

Most high-temperature geothermal fields, particularly liquid-dominated fields, are delineated by a boundary zone in which the electrical resistivity increases from low values (1–50 Ωm) inside the field to high values (>200 Ωm) outside the field. If production from the field causes significant decreases in fluid pressure in the upper part of the reservoir, there may be an influx of cool water from outside the field. If such an influx is large enough and at shallow depth then there may be an apparent lateral shift in the electrical resistivity boundary zone where this influx is occurring. Such a shift may be detected, before the cool water reaches production wells, by repeating electrical resistivity surveys across the boundary zone. Another situation where repeating electrical resistivity surveys may be useful is where hot saline waste water is injected into cold water aquifers outside the field.

Induced Seismicity

In many high-temperature geothermal fields exploitation can result in an increase (above the normal background) in the number of small magnitude earthquakes (micro-earthquakes) within the field (Fig. 14) [30]. Induced seismicity occurs in both liquid- and

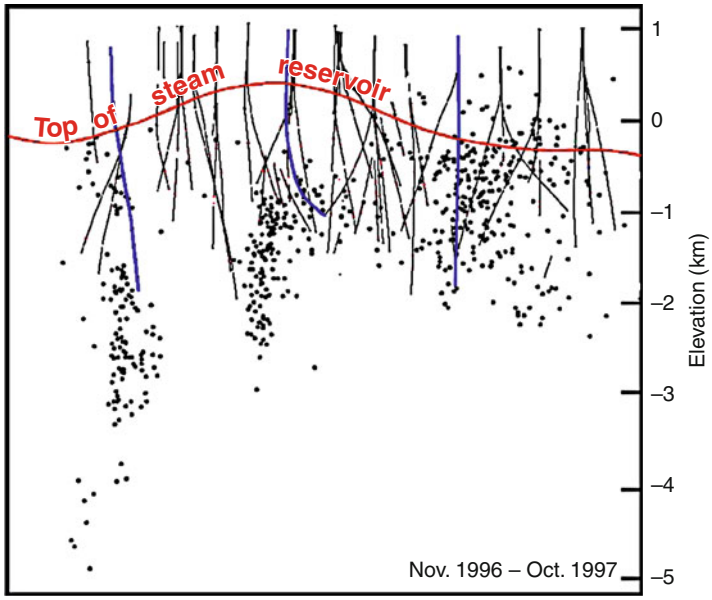

Geothermal Field and Reservoir Monitoring. Figure 14
Cross section through The Geysers field (California, USA) showing locations of earthquakes (*black dots*) during a 12-month period. Injection wells are shown in blue. Earthquake hypocenters and wells within 2,000 ft (600 m) of the section line have been projected onto the cross section. Note that the earthquake hypocenters extend to depths greatly below the bottom of some injection wells (Taken from [34])

vapor-dominated high-temperature fields, and in enhanced geothermal systems, but has rarely been observed in low-temperature fields. The increase is caused mainly by injection because when injection starts or is increased the number of local micro-earthquakes increases, and when injection decreases or is stopped the number of small earthquakes decreases [30, 31]. The main cause of the micro-earthquakes is high wellhead injection pressures that increase the pore pressure at depth, particularly in existing fractures, which allows movement to suddenly release stress and generate an earthquake. Thermal stress associated with the injection of cool waste water into a hot fluid aquifer may also trigger earthquakes in the vicinity of the injection wells.

The micro-seismicity is generally monitored by an array of seismometers (vertical- or three-component) placed in shallow drillholes (to minimize the effects of anthropogenic "noise"). Usually the signals from each seismometer are telemetered in real time to a central recording apparatus – this ensures consistent relative timing of the signals which is critical for determining the location (hypocenter and epicenter) of the earthquake. The hypocenter of each seismic event is then computed from the relative time differences of the arrival of the shock wave at each seismometer, assuming a specific local seismic velocity model [32]. The seismic velocity model is calculated either by inverting the seismic data collected over a period of time [33], or from explosions set off in drillholes. The magnitudes of the micro-earthquakes within the geothermal field are determined by comparison with the magnitudes of large local events as determined by national or regional seismic networks.

During a 4½ year period in which the mass of water injected at The Geysers field increased and decreased (due to seasonal power loading), the number of events measured by a detailed seismic network (Fig. 15) appeared to be related more closely to the injection rates rather than (steam) production rates [34].

Real-time monitoring of micro-seismicity can be used to minimize the felt intensity of shaking by

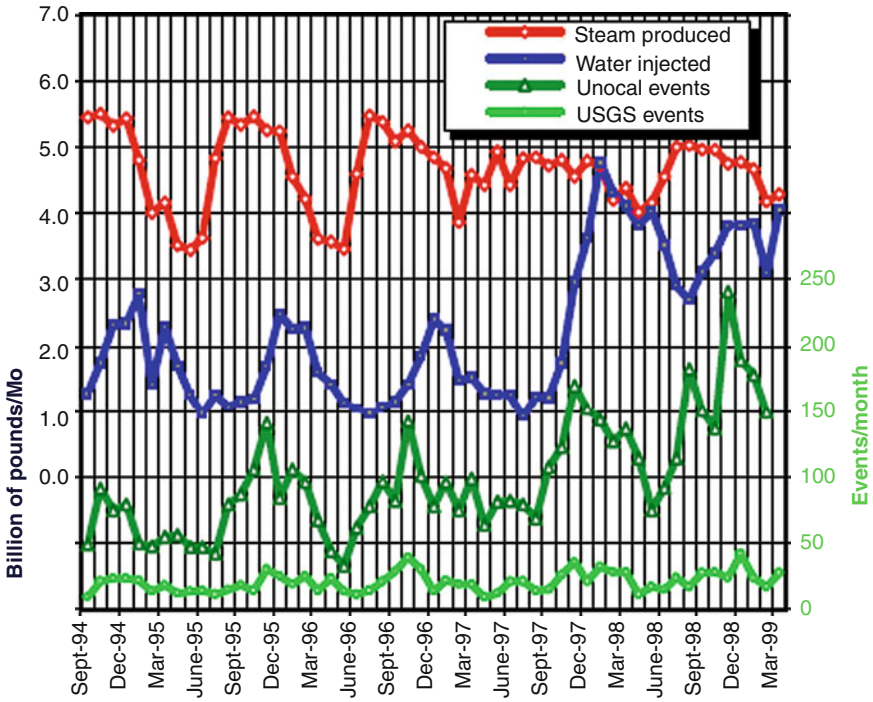

Geothermal Field and Reservoir Monitoring. Figure 15
Comparison of changes in the number of seismic events detected with variation in the amount of injection at The Geysers field, USA (Graph taken from [34])

reducing or stopping injection if the number of events exceeds certain predetermined thresholds – this is known as "traffic light control" of injection [30, 35].

Thermal Features

Many geothermal fields, especially high-temperature liquid-dominated fields, are manifested at the surface by natural thermal features such as geysers, hot pools, hot springs, mud pools, fumaroles, and areas of thermal ground. Changes in these features with time during production from the field can indicate changes in the geothermal reservoir from which fluid is being withdrawn, although in some cases it may be difficult to separate natural changes from production-induced changes. A wide variety of thermal features can be monitored, however, the most sensitive and easiest to monitor are geysers, hot pools, and hot springs.

Geysers Geysers occur in high-temperature geothermal fields. They are the most spectacular and the most valued of natural thermal features (for cultural and economic reasons) and are the most sensitive to production-induced changes in a geothermal system. Geysers are generally monitored by measuring changes in the eruption period (time between the start of successive eruptions), usually by a simple device that continuously measures the temperature of water in a channel leading from the geyser. Increases in the eruption period of geysers may be indicative of pressure decreases in the reservoir: increases in the eruption period of two geysers at Wairakei field were measured (Fig. 16) prior to their demise during the time of preproduction well testing (test discharge period) [36].

It is difficult to measure the volume of erupted water because of flashing to steam during the eruption, and evaporation from or absorption into the rocks surrounding the vent after the erupted water has fallen to the ground. If the geyser erupts frequently, it is

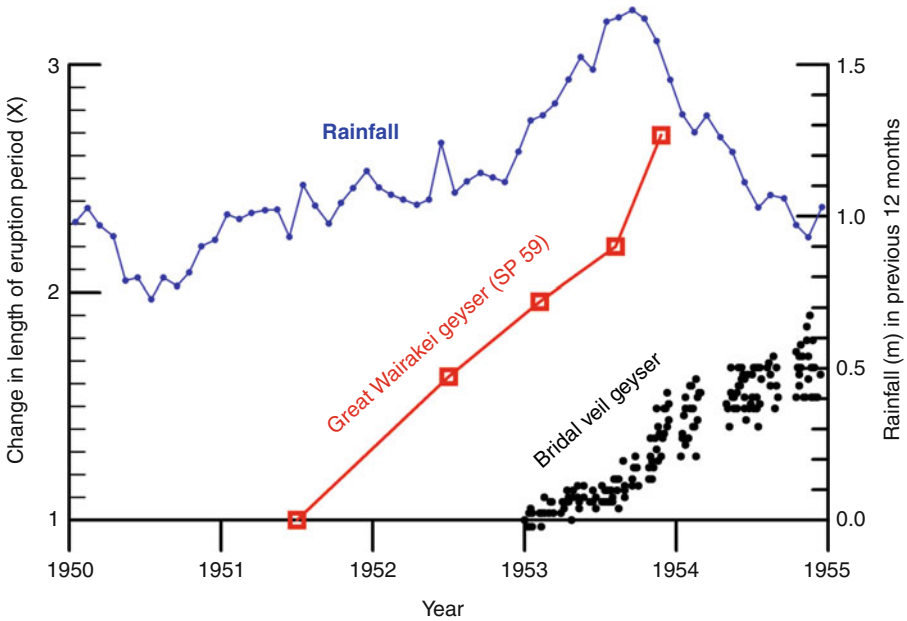

Geothermal Field and Reservoir Monitoring. Figure 16
Changes in length of eruption period (T/T_0) of two geysers in Geyser Valley at Wairakei geothermal field (New Zealand) during the time of preproduction test discharges. Eruption periods are normalized to T_0 = 12.5 h for the Great Wairakei Geyser, and T_0 = 39 min for the Bridal Veil Geyser. Rainfall data are monthly running totals of rainfall in the previous 12 months. Note the steady increase in length of eruption period with time (Taken from [36])

feasible to measure eruption height by using a video camera; however, the volume and height of geyser eruptions often vary naturally due to wind gusts and to seasonal changes in rainfall.

Springs and Hot Pools Hot springs and hot pools are also associated mainly with high-temperature geothermal fields and have important cultural and economic value [37]. Regular or continuous monitoring of the temperature, chemistry and flow rate of hot springs, and the temperature and water level in hot pools are generally made. Decreases in these parameters are also indicative of changes which may lead to the demise of these features.

The temperature of water emerging from the ground in hot springs and in pools is measured using a variety of commercially available devices employing thermistors or thermocouples. The temperature data are often measured continuously and captured in a data logger. The flow rate of springs and the rate of outflow from hot pools are generally measured by constructing a channel to take all the water from the feature and pass it through a V-notch weir. The basic principle is that flow rate is directly related to the water depth above the bottom of the V. The V-notch design causes small changes in flow rate to have a large change in depth allowing more accurate measurement than with a rectangular weir. From the measurement of the height of the water flowing through the V-notch and the angle of the V, the flow rate can be calculated. However, the value obtained may need to be adjusted to take into account rainfall and evaporation from the surface of the pool and channel before the water reaches the V-notch. To monitor changes in the chemistry of the water, samples are taken and analyzed in a laboratory; usually chloride content is the main chemical species measured. If flow into a hot pool decreases sufficiently such that evaporation exceeds inflow, then the water level in the pool may fall below the overflow and the water level may temporarily or permanently fall. A difficulty in interpreting temperature and flow rate data is separating natural changes from production-induced changes; this can be minimized by taking the measurements at a frequency

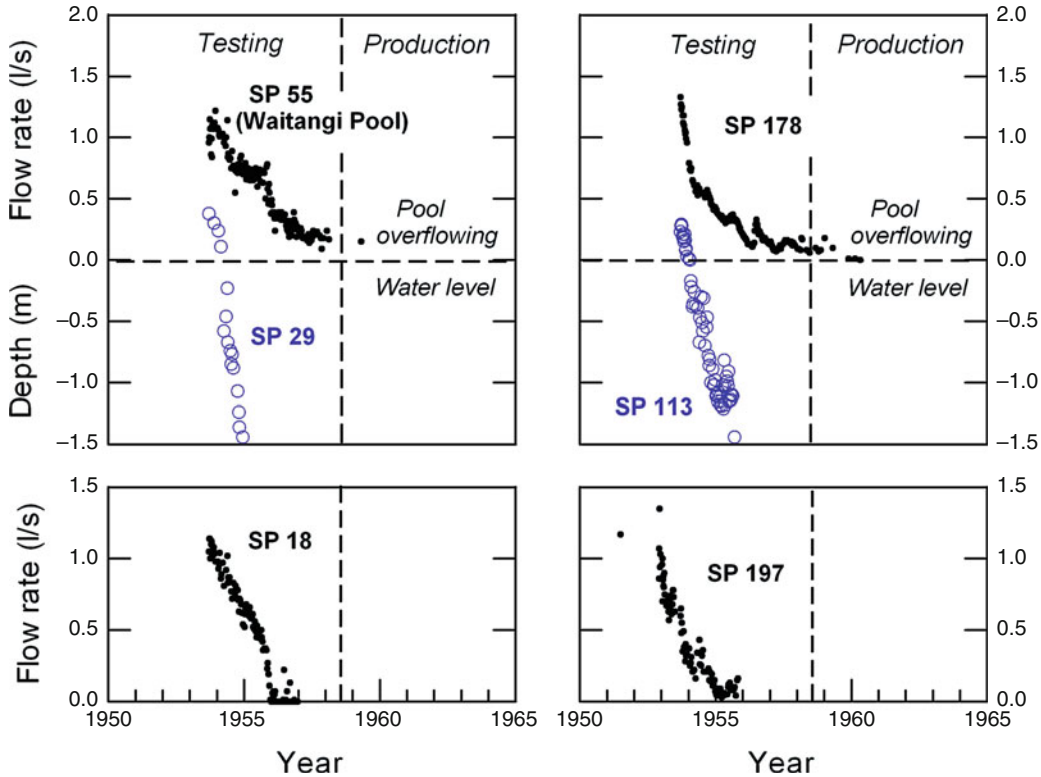

Geothermal Field and Reservoir Monitoring. Figure 17
Changes in outflow rate and water level with time in some hot pools at Geyser Valley, Wairakei (Taken from [36]). Note how, as well testing proceeded, the outflow rates declined and the springs stopped flowing. In the pools associated with springs SP 29 and SP 113, the water level dropped below the outlet until water stopped flowing and they dried up

sufficient to determine natural changes caused by changes in rainfall and groundwater level.

At Wairakei geothermal field, the flow rate from hot springs in Geyser Valley declined (Fig. 17) during the time of preproduction test discharges of exploration wells in the Waiora Valley [36]. Initially, the changes were small and isolated and were thought to be caused by natural climatic variations. It was not until much later that it was recognized that the changes to the hot springs were associated with changes in the deep reservoir resulting from fluid withdrawal some distance away. A decline in thermal features in producing high-temperature geothermal fields appears to be associated mainly with a decline in reservoir pressure. As the pressure declines, so also does the amount of geothermal fluid reaching the surface and hence the thermal features decline in size and vigor. If pressures fall further then the features may die and the flow may reverse, with cold groundwater flowing down into the reservoir; once this situation has occurred it may take a long time to resurrect the features. Monitoring of changes to hot springs and hot pools may enable declines to be recognized quickly and remedial action taken.

Future Directions

Reservoir monitoring will probably expand in scope and increase in frequency in the future because regulatory authorities are generally becoming more concerned about environmental effects. There are also commercial and economic effects which may result in more monitoring. Monitoring data help improve numerical simulation models which developers use to identify the potential effects of changes in production and injection. The modeling is not only for planning and operational

purposes but also to help secure loan funding for future expansion at the most favorable interest rates because bankers seek to reduce risk, and monitoring and modeling help in the reduction of risk.

Significant improvements in monitoring are likely to be the development of down-hole instrumentation capable of withstanding high temperatures for long periods of time. However, the problem of relating what is measured in a drillhole to what is occurring in the rock outside the hole will still remain.

Bibliography

Primary Literature

1. Thain IA, Carey BS (2009) Fifty years of geothermal power generation at Wairakei. Geothermics 38(1):48–63
2. Allis RG, Hunt TM (1986) Analysis of exploitation induced gravity changes at Wairakei geothermal field. Geophysics 51:1647–1660
3. Bixley PF, Clotworthy AW, Mannington WI (2009) Evolution of the Wairakei geothermal reservoir during 50 years of production. Geothermics 38(1):145–154
4. Yoder JL (1998) Using meters to measure steam flow. http://www.flowresearch.com/articles/Plant_Engineering_0498.pdf
5. Mattar WM (2005) Advances in Coriolis technology resolve tough pipeline flow measurement challenges. Pipeline Gas J, July 2005. http://www.pipelineandgasjournal.com
6. Bixley PF, Wilson DM (1985) Rapid casing corrosion in high temperature liquid dominated geothermal fields. In: Proceedings of the 10th Workshop on Geothermal Reservoir Engineering, Stanford, pp 35–40
7. Bowyer D, Bignall G, Hunt T (2008) Formation and neutralization of corrosive fluids in the shallow injection aquifer, Rotokawa geothermal field, New Zealand. GRC Trans 32:201–205
8. Bixley PF, Hattersley SD (1983) Long term casing performance of Wairakei production wells. In: Proceedings of the 5th NZ Geothermal Workshop, Auckland, pp 257–263
9. Glover RB, Mroczek EK (2009) Chemical changes in natural features and well discharges in response to production at Wairakei, New Zealand. Geothermics 38(1):117–133
10. Klyen LE (1973) A vessel for collecting subsurface water samples from geothermal drillholes. Geothermics 2:57–60
11. Arnórsson S, Bjarnason JÖ, Giroud N, Gunnarsson I, Stefánsson A (2006) Sampling and analysis of geothermal fluids. Geofluids 6(3):203–216
12. Grob RL, Barry EF (2004) Modern practice of gas chromatography, 4th edn. Wiley-Interscience, New York, 1064 pp. ISBN-10: 0471229830, ISBN-13: 978-0471229834
13. Rose PE, Apperson KD, Johnson SD, Adams MC (1997) Numerical simulation of a tracer test at Dixie Valley, Nevada. In: Proceedings of the 22nd Workshop on Geothermal Reservoir Engineering, Stanford, pp 169–176
14. Adams MC, Beall JJ, Enedy SL, Hirtz PN, Kilbourn P, Koenig BA, Kunzman R, Smith JL (2001) Hydrofluorocarbons as geothermal vapor-phase tracers. Geothermics 30(6):747–775
15. Hirtz PN, Kunzman RJ, Broaddus MK, Barbitta JA (2001) Developments in tracer flow testing for geothermal production engineering. Geothermics 30(6):727–745
16. McCabe WJ, Barry BJ, Manning MR (1983) Radioactive tracers in geothermal underground water flow studies. Geothermics 12:83–110
17. Massonnet D, Holzer T, Vadon H (1997) Land subsidence caused by the East Mesa geothermal field, California, observed using SAR interferometry. Geophys Res Lett 24:901–904
18. Massonnet D, Feigl KL (1998) Radar interferometry and its application to changes in the earth's surface. Rev Geophys 36:441–500
19. Hsing-Chung C, Linlin G, Rizos C (2005) InSAR and mathematical modelling for measuring surface deformation due to geothermal water extraction in New Zealand. In: Proceedings of the 2005 IEEE International Geoscience and Remote Sensing Symposium, vol 3, pp 1587–1589
20. Hole JK, Bromley CJ, Stevens NF, Wadge G (2007) Subsidence in the geothermal fields of the Taupo Volcanic Zone, New Zealand from 1996 to 2005 measured by InSAR. J Volcanol Geoth Res 166:125–146
21. Allis RG, Bromley CJ, Currie S (2009) Update on subsidence at the Wairakei-Tauhara geothermal system. Geothermics 38(1): 169–180
22. Bromley CJ (2009) Groundwater changes in the Wairakei-Tauhara geothermal system. Geothermics 38(1):134–144
23. Bromley CJ, Hunt TM, Morris C (1993) Cold downflows of groundwater at Ohaaki Geothermal Field; preliminary results. In: Proceedings of the 15th New Zealand Geothermal Workshop, Auckland, pp 181–186
24. Hunt TM, Bromley CJ, Risk GF, Sherburn S, Soengkono S (2009) Geophysical investigations of the Wairakei Field. Geothermics 38(1):85–97
25. Hunt TM (1970) Gravity changes at Wairakei Geothermal Field, New Zealand. Geol Soc Am Bull 81:529–536
26. Atkinson PG, Pedersen JR (1988) Using precision gravity data in geothermal reservoir engineering modelling studies. In: Proceedings of the 13th Workshop on Geothermal Reservoir Engineering, Stanford, pp 35–40
27. Hunt TM, Allis RG, Blakely MR, O'Sullivan MJ (1990) Testing reservoir simulation models for the Broadlands Geothermal Field using precision gravity data. Geoth Resour Counc Trans 14:1287–1294
28. Hunt TM (2005) Using repeat microgravity measurements to track reinjection in a liquid-dominated field. In: Proceedings of the World Geothermal Congress 2005 (CD). Paper No. 1117
29. Hunt TM, Kissling WM (1994) Determination of reservoir properties at Wairakei Geothermal Field using gravity change measurements. J Volcanol Geoth Res 63:129–143
30. Majer EL, Baria R, Stark M, Oates S, Bommer J, Smith B, Asanuma H (2007) Induced seismicity associated with Enhanced Geothermal Systems. Geothermics 36:185–222

31. Sherburn S, Allis RG, Clotworthy A (1990) Microseismic activity at Wairakei and Ohaaki geothermal fields. In: Proceedings of the 12th NZ Geothermal Workshop, Auckland, pp 51–55
32. Stein S, Wysession M (2002) An Introduction to seismology, earthquakes, and earth structure. Wiley-Blackwell, Oxford, 512 pp. ISBN: 978-0-86542-078-6
33. Zuccaa JJ, Hutchingsa LJ, Kasameyera PW (1994) Seismic velocity and attenuation structure of the Geysers geothermal field, California. Geothermics 23(2):111–126
34. Bommer JJ, Oates S, Cepeda JM, Lindholm C, Bird J, Torres R, Marroquín G, Rivas J (2006) Control of hazard due to seismicity induced by a hot fractured rock geothermal project. Eng Geol 83:287–306
35. Smith B, Beall J, Stark M (2000) Induced seismicity in the SE Geysers field, California, USA. In: Proceedings of the World Geothermal Congress 2000, Kyushu-Tohuku, Japan, pp 2887–2892
36. White PA, Hunt TM (1996) Simple modelling of the effects of exploitation on hot springs, Geyser Valley, Wairakei, New Zealand. Geothermics 34:184–204
37. Cataldi R, Hodgson SF, Lund JW (1999) Stories from a heated Earth. Geothermal Resources Council and the International Geothermal Association, Sacramento, California, 569 pp. ISBN 0-934412-19-7

Books and Reviews

Armstead HCH (1980) Geothermal energy: its past, present and future contributions to the energy needs of man. E & F.N. Spon, London

Dickson MH, Fanelli M (2003) Geothermal energy utilization and technology. UNESCO Publishing, Paris, 205 pp. ISBN 92-3-103915-6

DiPippo R (2008) Geothermal power plants: principles, applications, case studies and environmental impact, 2nd edn. Butterworth-Heinemann, Oxford, 520 pp. ISBN: 978-0-7506-8620-4

Ellis AJ, Mahon WAJ (1977) Chemistry and geothermal systems. Academic, New York, 392 pp. ISBN: 0-12-237450-9

Grant MA, Donaldson IG, Bixley PF (1982) Geothermal reservoir engineering. Academic, New York, 369 pp. ISBN: 0-12-295620-6

Hunt TM (2001) Five lectures on environmental effects of geothermal utilization. Report 2000-1, United Nations University, Reykjavik, Iceland, 109 pp. ISBN-9979-68-070-9
http://os.is/Apps/WebObjects/Orkustofnun.woa/swdocument/2056/Trevor03.pdf

Kruger P, Otte C (1973) Geothermal energy: resources, production, stimulation. Stanford University Press, California, 360 pp

Rybach L, Muffler LJP (1981) Geothermal systems: principles and case histories. Wiley, New York

Thorhallsson S (2003) Geothermal well operation and maintenance. IGC2003 – Short Course September 2003:195–217. http://unugtp.is/Apps/WebObjects/Orkustofnun.woa/swdocument/539/13Sverrir.pdf

Geothermal Power Capacity, Sustainability and Renewability of

Subir K. Sanyal
GeothermEx, Inc., Richmond, CA, USA

Article Outline

Glossary
Definition of the Subject and Its Importance
Introduction
Concepts of Sustainability and Renewability
Relation Between Renewable and Sustainable Capacities
Estimation of Renewable, Sustainable and Commercial Capacities
An Illustrated Case History
Future Directions
Bibliography

Glossary

Discharge A measure of the flow rate of steam, water, or heat discharged at or near the ground surface from a subsurface geothermal reservoir.

Geothermal The naturally occurring heat found beneath the surface of the Earth, ultimately originating from the internal magmatic processes of the Earth's core. A geothermal energy project utilizes the hot water or steam found within certain large bodies of rock, referred to as a geothermal reservoir.

Power capacity The amount of energy produced per unit time, or the amount of the electric power capacity that a power generation facility is designed to produce.

Recharge Natural influx of hot fluids into a geothermal system.

Renewable A natural energy resource that is inexhaustible or can replenish itself over time.

Specific heat The amount of heat required, in calories, to raise the temperature of 1 g of a substance by 1°C.

Sustainable A natural energy resource which, if managed carefully, will provide the needs of a community or society indefinitely, without depriving future generations of their needs.

Thermal anomaly A departure from the normal or expected temperature in the subsurface as distinguished by geological, geophysical or geochemical means, which is different from the general surroundings.

Thermal conductivity A measure of the ability of a material to conduct heat.

Definition of the Subject and Its Importance

Geothermal energy is the heat energy of the earth, produced through wells as hot water or steam. Geothermal power capacity is this energy extraction rate (whether as thermal energy or equivalent electrical energy produced per unit time), expressed in Watt or an equivalent unit. The vast content of heat energy within the earth is limitless for all practical purposes, but the geothermal power capacity available from the earth is constrained by various technological and economic limits to the utilization of this energy. Given a geothermal power generation scheme (for example, a district heating scheme using geothermal water or an electric power operation using geothermal water or steam), the issue is how sustainable, technically and economically, the scheme would be and to what extent this energy supply is naturally renewable.

For the purposes of this entry, sustainability is defined as the ability to economically maintain an installed power capacity, over the amortized life of a power plant, by taking practical steps, such as, drilling "make-up" wells as needed to compensate for resource degradation (pressure decline, well productivity decline, or cooling of the produced hot water or steam). Renewability is defined here as the ability to maintain an installed power capacity indefinitely without encountering any resource degradation; this renewable power capacity at a geothermal site is generally too small for commercial development of electrical power capacity, but may be adequate for district heating or other direct uses of the geothermal energy.

Introduction

As per above definitions, it is argued below that only a portion of the sustainable geothermal power capacity at a site is renewable; yet, geothermal energy is widely believed to be entirely renewable. Therefore, it is important to objectively review the concepts of sustainability and renewability of geothermal power capacity and their quantification. These issues are addressed below.

Concepts of Sustainability and Renewability

Many articles have been published on the renewability and sustainability of geothermal energy [1–7]. However, no universally accepted definitions of the words "renewability" and "sustainability" as regards geothermal power seem to exist and definitions used often have ambiguities. For example, Axelsson et al. [3] defines "renewable" generation capacity (Fig. 1) as:

- The energy extracted from a renewable energy source is always replaced in a natural way by an additional amount of energy, and the replacement takes place on a similar time scale as that of the extraction.

And Axelsson et al. [3] define "sustainable" generation capacity as follows (Fig. 1):

- For each geothermal system, and for each mode of production, there exists a certain level of maximum energy production, $\mathbf{E_0}$, below which it will be possible to maintain constant energy production from the system for a very long time (100–300) years. If the production rate is greater than $\mathbf{E_0}$ it cannot be maintained for this length of time. Geothermal energy production below, or equal to $\mathbf{E_0}$ is termed **sustainable production**, while production greater than $\mathbf{E_0}$ is termed **excessive production**.

An objective review of the above definitions is presented below, extracted largely from an earlier paper by the author.

The above definition of renewability essentially equates renewable capacity to the natural heat recharge rate (conductive plus convective) into a geothermal reservoir, which remains constant over geologic time (that is, tens of thousands of years) in the natural state. This recharge rate can be estimated for an actual reservoir by numerical simulation of the natural, steady-state heat flow, and measured temperature and pressure distributions, within the system. The renewable capacity is, however, frequently too small for commercial development because of the unfavorable economy of scale in capital and operation costs and relatively high cost of infrastructure development

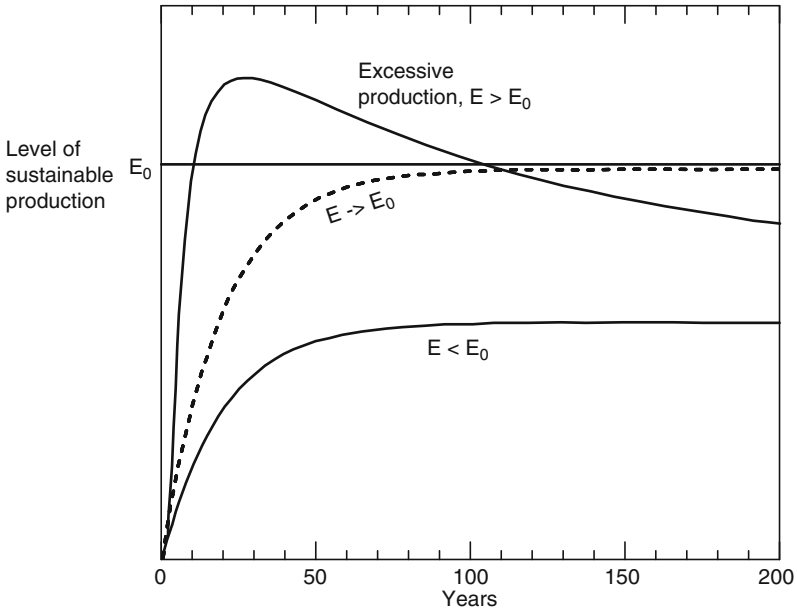

Geothermal Power Capacity, Sustainability and Renewability of. Figure 1
Illustration of the definition of sustainable and excessive production levels [3]

associated with a small power project. The above definition of sustainability may perhaps be acceptable for non-electrical uses of geothermal energy (such as district heating), which are of relatively low intensity and are not capital-intensive, but the definition has inherent ambiguities and limitations for practical applications to the electric power industry. The difference between renewability and sustainability as defined above is a matter primarily of the time scale; as discussed later in connection with a case history presented below, an exploitation level that can be sustained for 100–300 years can most likely be sustained indefinitely. Therefore, for most fields, the above two definitions are essentially identical.

A constant energy production rate over a time span of 100–300 years is reasonable for defining renewability but not sustainability. A power plant can be sustained over a typical amortized life of 20–30 years at a capacity level much higher than the renewable capacity level by make-up well drilling or taking other steps to mitigate resource degradation. Numerical simulation consistently shows that any resource degradation caused over a typical plant life of 20–30 years would essentially disappear within a 100–300-year time frame after the project is shut down; the pressure would return to the original level in about 20–30 years and the temperature within 100–300 years, the actual time taken being dependent on the natural convective heat recharge rate at the site (see, for example, [8]). Therefore, over a 100–300-year time span, commercial exploitation for 20–30 years at the sustainable level should not leave any permanent impact on the resource base. On the other hand, it is likely that producing the reservoir at a level higher than the renewable capacity estimated from natural-state modeling would actually cause an increase in the natural recharge rate of hot water into the reservoir. This has frequently been the author's experience from monitoring many producing geothermal fields; the case history discussed later illustrates this point. Therefore, estimate of renewable or sustainable power capacity from the simulation of the natural state of a geothermal reservoir is conservative; substantial production history is needed to estimate these capacities with any confidence. On the other hand, unless these capacities can be determined to the satisfaction of financial institutions, it is not possible to obtain long-term financing for a power plant; unless a power plant is installed, accumulation of substantial production history is out of the question. This is a fundamental conundrum of the geothermal power industry.

Geothermal reserves are normally expressed in terms of the installed capacity sustainable for the life of a power plant; empirical experience shows this reserve level to be an order of magnitude higher than the renewable level estimated from the natural state of the reservoir; see, for example, Table 1 (to be discussed later). Therefore, if the definition of sustainability in Fig. 1, which is essentially same as renewability, is to be used, the geothermal resource base worldwide should be considered an order of magnitude smaller than is

Geothermal Power Capacity, Sustainability and Renewability of. Table 1 Empirical data on renewable and sustainable capacities [7]

Field	Location	Renewable capacity (MWe)	Sustainable capacity (MWe)	References
Ahuachapan	El Salvador	24.8	95+	[9]
Beowawe	Nevada	1.3	13+	[10]
Cerro Prieto	Mexico	73.3	720	[11]
Desert Peak	Nevada	14	90+	[12]
Heber	California	1.7	70	[13]
Kakkonda	Japan	26.6	80+	[14]
Kawareu	New Zealand	15.5	230	[15]
Krafla	Iceland	5.3	60	[16]
Mammoth	California	25	90+	[17]
Mindanao	Philippines	9.6	102	[18]
Miravalles	Costa Rica	16.5	168	[19]
Mori	Japan	5.4	50	[20]
Mutnovsky	Russia	9.2	100	[21]
Nesjavellir	Iceland	16.6	160	[22]
Ngawha	New Zealand	2.5	30	[23]
Oguni	Japan	8.2	20+	[24]
Onikobe	Japan	2	25	[25]
Roosevelt Hot Springs	Utah	5.3	50+	[26]
San Emidio	Nevada	1.9	10+	[12]
Sibayak	Indonesia	11	30+	[27]
Soda Lake	Nevada	1.6	15	[12]
Stillwater	Nevada	4	40	[12]
Sumikawa	Japan	4	50+	[28]
Takigami	Japan	3	25	[29]
Uenotai	Japan	2.5	25	[30]
Wairakei	New Zealand	46	220+	[31]
Wasabizawa	Japan	5.6	40+	[32]
Zunil	Guatemala	2.44	25	[33]
		Total: 386	Total: 2,056+	

generally accepted today. In other words, exploitation of geothermal resources would be artificially constrained to an order of magnitude lower than the level at which exploitation is readily possible without any long-term negative impact on the resource base. This would make development of many fields for power generation economically prohibitive. Furthermore, this cannot be a socially responsible position considering that a higher rate of exploitation can only reduce the current fossil fuel usage, thus reducing environmental pollution today and saving fossil fuel resources for future generations. As discussed below, there is social virtue in preserving more of fossil fuel resources for the future, and instead, maximizing the use of power from geothermal resources, which are renewable within the 100–300-year time frame.

While geothermal power has far less environmental impact than power from fossil fuels, it is inevitable that power derived from fossil fuels will become progressively more environmentally benign in the future. Finally, unlike geothermal, fossil fuels also serve as raw material for petrochemicals and coal-based organic chemicals. While future generations may harness hitherto unforeseen sources of energy, fossil fuels will still be needed as raw material for chemicals. Therefore, one can justify a higher rate of geothermal power use today than adhering to a level that is renewable within the 20–30-year lifetime of a power plant.

With respect to electric power capacity, this entry proposes an alternative, and more practical, definition for sustainability, and also defines a purposefully unsustained "commercial" capacity level (Fig. 2). The former is defined as the ability to economically maintain the installed capacity, over the amortized life of a power plant, by taking practical steps (such as, make-up well drilling) to compensate for resource degradation (pressure drawdown, well productivity decline and cooling). The latter can be defined as a capacity level that is initially kept higher than the sustainable level but may be allowed to decline with time once make-up well drilling, or other measures to mitigate resource degradation, becomes uneconomic at some point in project life. In a socially responsible vein, this declining capacity starting above the sustainable level could be considered commercial only if the levelized power cost is calculated to be lower than that from alternative renewable resources. Even if the power cost at such a commercial level proves higher than that from fossil fuels, this higher capacity can displace fossil fuel usage if power from renewable or environmentally benign resources is given adequate tax breaks (such as carbon credit), market access (such as implementation of

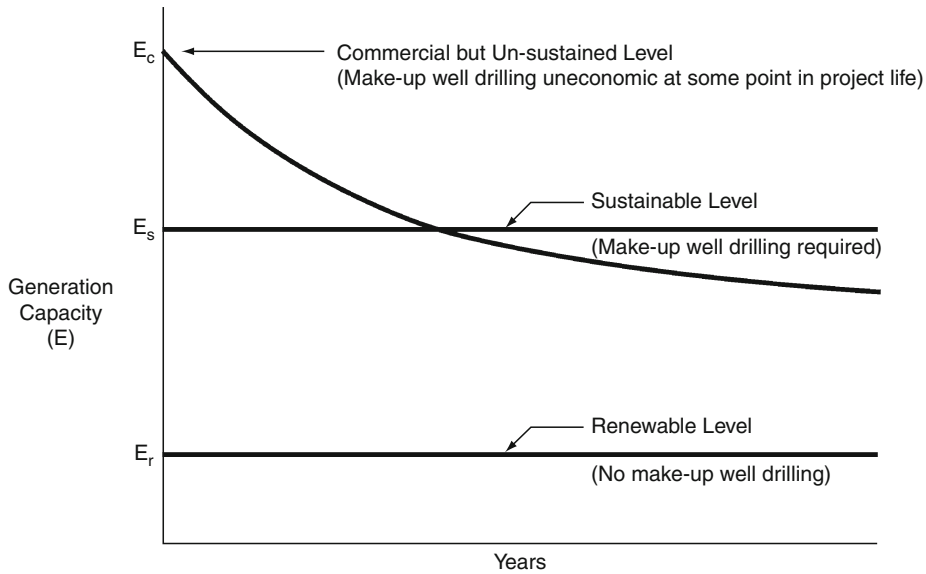

Geothermal Power Capacity, Sustainability and Renewability of. Figure 2
Proposed definitions [7]

"renewable energy portfolio standards"), or price support (such as production tax credit or any direct subsidy) by governments or international agencies.

The appropriate un-sustained but commercial power capacity level can only be arrived at by numerical simulation of the actual production behavior of the reservoir concerned and within the context of the economic realities and market forces. Such a purposefully un-sustained but commercial level is socially beneficial for a market-driven economy because it allows reduction in levelized power cost through accelerated capital recovery while helping to displace the use of fossil fuels. The cumulative energy extraction over the project life at an un-sustained but commercial level need not exceed the cumulative energy that would be extracted at the sustainable level, thus still assuring natural replenishment of the resource base in a 100–300-year time frame. Therefore, such a commercial development level is not only reasonable but also desirable, particularly if one considers the distinct possibility of acceleration of natural recharge of hot water into the reservoir, thus mitigating the impact of a higher initial production rate.

In discussing renewability and sustainability of geothermal energy, interesting analogies have been invoked from time to time by various authors, for example, comparison with mining, management of fisheries, utilization of hydropower, and so on. While all these analogies correspond to some aspects of geothermal energy exploitation, yet another analogy is offered here to elucidate the over-arching concept of sustainability proposed in this entry. A reasonable analogy for renewable capacity would be seasonal harvest of crops while timber harvest would be an appropriate analogy for sustainable capacity, for the timber resource would grow back within a few decades. One could harvest only the annual growth at the tips of the tree branches and keep the forest resource constantly renewable. But is this a reasonable approach to natural resource husbandry? While renewable, annual tree growth can be used as firewood or turned into paper pulp, the forest resource is more valuable to the society if mature trees are harvested for timber and then allowed to grow back. Likewise, constraining geothermal energy exploitation within a continuously renewable level, which is suitable primarily for low-intensity, non-electrical uses, is neither reasonable nor desirable from a socioeconomic viewpoint. In addition, thinning of a forest accelerates tree growth due to the penetration of more sunlight into the forest; this is a convenient metaphor for the increase in natural recharge rate due to exploitation of a geothermal resource above the so-called renewable level.

Relation Between Renewable and Sustainable Capacities

This entry considers only liquid-dominated geothermal fields with capacity for supplying electric power, steam-dominated fields being rare occurrences; only six steam-dominated fields have been exploited to date: The Geysers, California; Lardarello, Italy; Matsukawa, Japan; Kamojang and Darajat; Indonesia; and Los Azufres, Mexico. Based on the experience in monitoring many producing geothermal fields for more than 3 decades and conducting dozens of numerical simulation studies of actual reservoirs, the author has observed that the sustainable capacity of a liquid-dominated field is typically an order of magnitude higher than the renewable capacity. The understanding here is that the renewable capacity of a field corresponds to the power capacity equivalent of the natural heat recharge, conductive plus convective, into the system; and sustainable capacity is supported by "mining" (or "harvesting" if one considers a time frame of centuries) of the stored heat in addition to natural heat recharge. To confirm this empirical observation, a review has been made of both published and unpublished results of numerical simulation and heat flow studies of more than half of the approximately 65 liquid-dominated geothermal fields in the world that have supplied commercial power to date and for which reasonably reliable estimate of the natural heat recharge rate could be made. The heat recharge rate was estimated from either numerical simulation of the reservoir or surface heat flow studies, with the reasonable assumption that the rate of natural heat recharge into the reservoir to be equal to the total rate of heat discharge at the surface over the entire thermal anomaly.

Table 1 lists approximate estimates of the renewable and sustainable capacities of 37 geothermal fields from published sources or various archives. The electrical power equivalent (MWe) was approximated from the estimated thermal power capacity based on First and Second Laws of Thermodynamics assuming a rejection

temperature of 15°C and a utilization factor of 0.45. The sustainable capacity value for a field in Table 1 was taken as the proven exploitation capacity, unless actual reservoir response and/or simulation studies had indicated the sustainable capacity to be higher. As such, the sustainable capacity values in Table 1 should in general be considered minimum estimates. As mentioned before, this table illustrates that renewable capacities are relatively small compared to sustainable capacities, the total for 37 fields being 386 and 2,056+ MWe, respectively. Furthermore, at the renewable level, most fields would not support commercial power development; for example, if 10 MWe were the smallest commercially developable capacity, only 11 of the 37 fields would qualify.

Figure 3 is a cross-plot of the above-listed renewable and sustainable capacities. The points with arrows in the direction of higher sustainable capacity represent fields for which the presently installed capacity appears manifestly smaller than the sustainable capacity but no estimate of the latter is available. This figure confirms the empirical observation that sustainable capacity is typically an order of magnitude higher than renewable capacity. Specifically, sustainable capacity (E_s) is a multiple, Q, of renewable capacity (E_r), where α ranges from about 5–45, with a value of 10 most likely. The author has always observed that α, which can be termed the "Sustainability Factor," tends to be high for a hydrothermal reservoir if the host formation is sedimentary. This is to be expected because having intergranular porosity, a porous sedimentary formation would display better heat transfer characteristics than a fractured non-sedimentary formation.

Wisian et al. [12] concluded from surface heat flow studies of a large number of geothermal fields that the presently installed capacity in most fields is equivalent to no more than ten times the natural heat discharge rate at the surface. Their conclusion at first seems to contradict this entry's assumption that the sustainable capacity is 5–45 times the natural heat discharge rate, 10 times being most likely rather than the maximum. This difference can be explained by the fact that Wisian et al. [12] considered installed plant capacity, which is in general smaller than the maximum sustainable capacity.

Finally, the empirical observation that the sustainable capacity of a reservoir is an order of magnitude higher than the renewable capacity implies that,

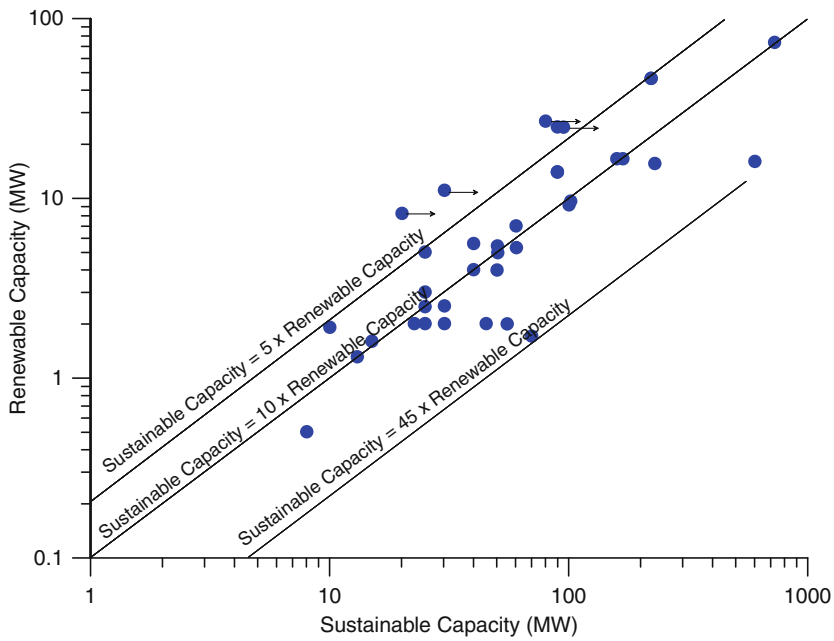

Geothermal Power Capacity, Sustainability and Renewability of. Figure 3
Renewable capacity versus sustainable capacity [7]

following exploitation, the reservoir is expected to take an order of magnitude higher time span compared to the exploitation period for complete natural replenishment. This supports the earlier observation from reservoir simulation that the depletion effects of power production for 20–30 years would require on the order of 100–300 years to completely disappear.

Estimation of Renewable, Sustainable, and Commercial Capacities

The best tool for quantifying renewable capacity is a numerical simulation model that reproduces the natural physical state of the reservoir. But estimating sustainable and commercial capacities requires not only natural-state modeling but also trial-and-error matching of the actual exploitation history of the reservoir, and forecasting its behavior, using a reservoir simulation model. Estimation of an un-sustained commercial capacity also requires market considerations and economic analysis. Assessment of even renewable capacity may require trial-and-error history matching and forecasting if the recharge rate increases with reservoir pressure decline, which is sometimes the case. Obviously, the effective use of such numerical simulation requires adequate data on the natural state of the reservoir and significant production history. For some fields, renewable and sustainable capacities can be approximated by simple, "lumped-parameter" modeling of the production history. For many fields, data may not be available for numerical simulation or even for relatively simple lumped-parameter modeling. For such situations, approximate formulations to quantify these capacities are presented in Sanyal et al. [34] and are reproduced below.

By definition, Renewable Capacity (E_r) is given by [34]:

$$E_r = R = D_{\text{cond}}, \tag{1}$$

where R is heat recharge rate into the reservoir (primarily convective with a small conductive component) and D_{cond} is total heat discharge from the surface over the thermal anomaly; if the entire heat anomaly on the surface is considered, the convective component of heat discharge is usually negligible. Ideally, D_{cond} should be estimated from a comprehensive "heat budget" survey of the anomaly including conductive heat loss at the surface, convective heat discharge (through hot springs, fumaroles and geysers) at surface manifestations, and subsurface convective heat loss to regional aquifers.

Strictly speaking, the small rate of background (regional) heat flow should be subtracted from the estimates of renewable capacity above and sustainable capacity as presented below [34]. However, given the approximate nature of such estimation, this correction is unnecessary in most situations.

Sustainable capacity (E_s), considering both heat mining and heat recharge, is given as [34]:

$$E_s = \left\{ \left(\frac{C_v}{KL} \right) rhd \left(\frac{A_{\text{res}}}{A} \right) + 1 \right\} D_{\text{cond}}, \tag{2}$$

where C_v is volumetric specific heat of fluid-filled rock, K is thermal conductivity of the overburden, L is plant life, r is heat energy recovery factor, h is reservoir thickness, d is depth to the top of the reservoir, A_{res} is reservoir area, and A is the area of the entire thermal anomaly.

A conservative definition of commercial capacity (E_c) would require that $E_c > E_s$ initially, but eventually falls below E_s, such that the total energy recovered over the plant life is same as that would be for production at the sustainable level. With this definition, and "harmonic decline" in well productivity, it can be shown [34]:

$$E_c = \frac{E_s L D_i}{\ln(1 + D_i L)}, \tag{3}$$

where D_i is initial decline rate in well productivity. E_c can be considerably higher than E_s, depending on economic factors. The higher the margin by which E_c exceeds E_s, the higher is D_i.

An actual example, that of the Beowawe geothermal field in the State of Nevada, United States, can be considered. For this field,

$$\left(\frac{A_{\text{res}}}{A} \right) \approx 0.1$$

$$d = 900\,\text{m}, \text{and } h = 1,500\,\text{m}$$

From Butler et al. [10], for this field, R = 1.3 MWe ≈ D_{cond} (ignoring background heat flow).

Therefore, Renewable Capacity = 1.3 MWe

Typical values of the other parameters are: C_v = 2,700 kJ/m^3/°C, K = 3.1 W/m/°C, L = 30 years and r = 0.1.

Therefore, from Eq. 2, Sustainable Capacity ≈18 MWe (ignoring background heat flow).

Most likely reserves for this field, from Klein et al. [35] = 58 MWe.

Therefore, commercial capacity would fall somewhere between 18 and 58 MWe, depending on the economic factors. For example, if no make-up well drilling is contemplated and an initial harmonic productivity decline rate of 10% is economically acceptable, from Eq. 3, $E_c = 40$ MWe.

The above discussion shows that the renewable development level for the Beowawe field is only 1.3 MWe, which is entirely uneconomic. While a sustainable capacity of 18 MWe is commercial, a capacity of 40 MWe may even be more attractive economically, and yet would cause no further cumulative energy withdrawal from the reservoir over a 20–30-year project life, and consequently, the reservoir should still be replenished naturally, in a 100–300-year time frame. It should be noted that a plant capacity of 13 MWe has already been sustained in this field over the past 2 decades.

An Illustrative Case History

This is a case history of estimating renewable and sustainable capacities of a geothermal field (at Wairakei, New Zealand) from its production history using a simple "lumped-parameter" model. The Wairakei field presents a good case history because: (a) it has more than 50 years of production history, longer than that of any other liquid-dominated field in the world; (b) it offers an extensive database that is publicly available (for example, Clotworthy [36]); and (c) since the average temperature of this reservoir has not declined significantly over its long production history, its pressure behavior can be reasonably modeled by considering material balance only (rather than coupled material-and-energy balance).

Numerical simulation and heat flow studies of this field have shown the steady-state recharge rate in the natural state to be about 31 kt/day; in other words, the minimum renewable depletion capacity (E_r) is 31 kt/day. Figure 4 presents a plot of the mass depletion rate (m), defined as production rate minus injection rate, versus time at this field. As of 1956 (2,000 days from the initiation of production in 1950), the reservoir pressure in the deep liquid zone in the Western Borefield (the portion of the field eventually most exploited) was about 52 bar-a, and negligible production had taken place before that time. From material balance consideration, it can be shown [7] that reservoir pressure (p) is given as:

$$p = 52.0 - \frac{(m-31)}{r}\left[1 - e^{-\frac{r}{s}(t-2000)}\right], \qquad (4)$$

where m is assumed constant with time (t, days), r is a recharge coefficient (kt/day/bar), and s is a reservoir storage coefficient (kt/bar).

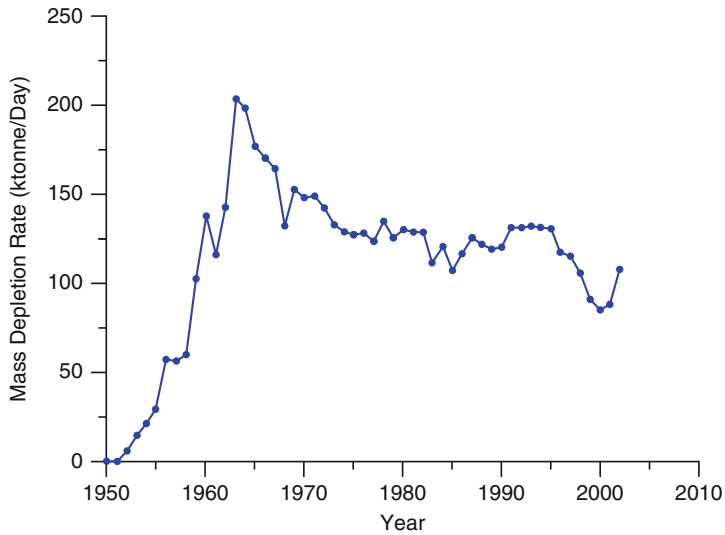

Geothermal Power Capacity, Sustainability and Renewability of. Figure 4
Mass depletion history [7]

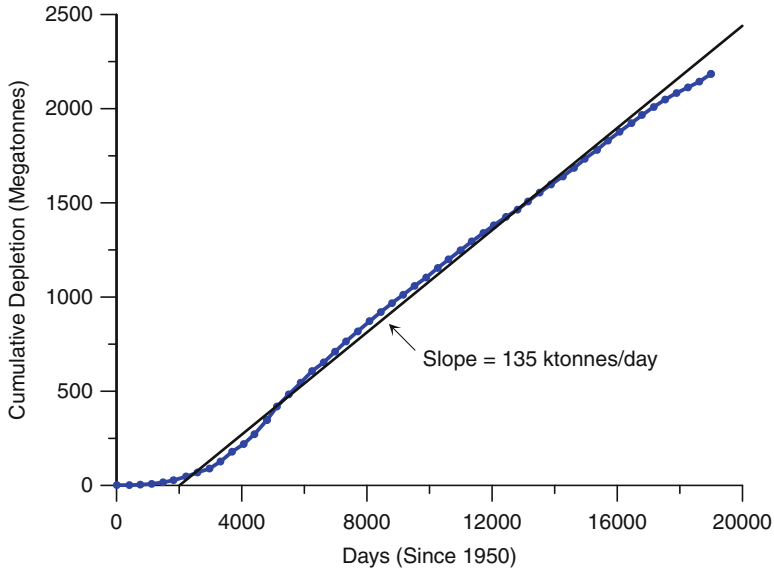

Geothermal Power Capacity, Sustainability and Renewability of. Figure 5
Cumulative depletion history [7]

Figure 5 shows the cumulative depletion history of the field. Between 2,000 days and the present, a reasonably linear trend can be defined with a slope of 135 kt/day. Therefore, one can approximate a constant value of m after 2,000 days as 135 kt/day. The unknowns r and s in Eq. 4 can be estimated by trial-and-error; Fig. 6 shows the best fit the author obtained between the observed pressure (continuous curve) at the deep liquid zone of the Western Borefield and the computed pressures (solid circles) as a function of time; this fit required an s value of 11,000 kt/bar and an r value of 4.2 kt/day/bar. The fit in Fig. 6 is good between 5,000 and 18,000 days, a span of 36 years; a look at Fig. 5 shows that the poor match before and after this period is to be expected as the depletion trend had deviated significantly from the linear in the very early and very recent periods.

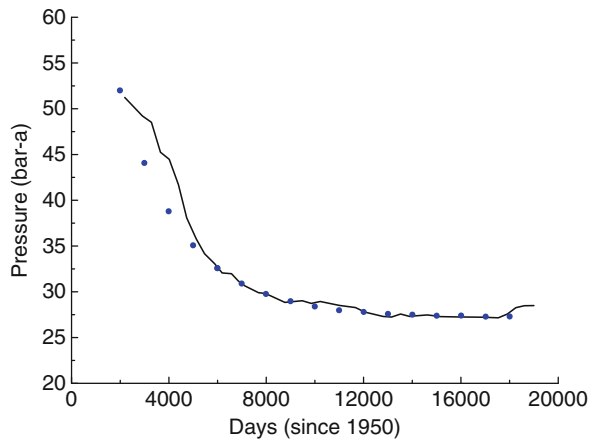

Geothermal Power Capacity, Sustainability and Renewability of. Figure 6
Observed and computed liquid pressures, western borefield [7]

The overall recharge rate at any time is the sum of the steady-state recharge rate (m_{sr}) and the pressure-dependent component of recharge rate (m_r) [7]. Using the r and s values derived above, the historical rate of recharge at Wairakei has been estimated as shown in Fig. 7. Overall, fluid recharge at Wairakei to date appears to have been generally hot because negligible overall cooling of the reservoir has been noted in 50 years, and recharge has steadily increased in response to pressure drawdown (Fig. 7). For this reason, the renewable level of depletion of this reservoir has become steadily higher than the steady-state depletion rate of 31 kt/day derived from natural-state modeling. In fact,

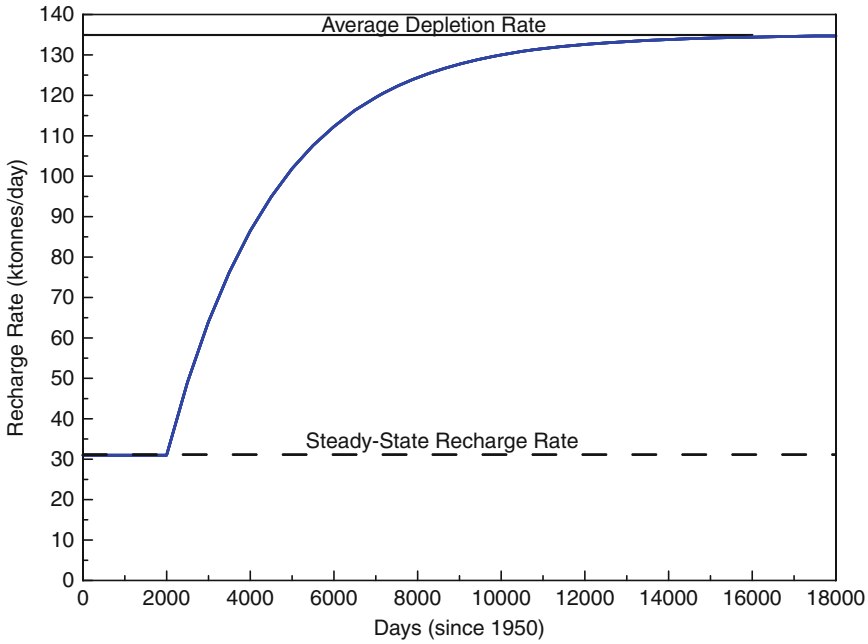

Geothermal Power Capacity, Sustainability and Renewability of. Figure 7
Recharge rate versus time, Wairakei field [7]

the recharge rate by 17,000 days has nearly equaled the depletion rate; if the entire recharge here indeed represents hot fluid entry from depth, then a depletion level of 135 kt/day, rather than 31, can be considered renewable.

Now, what is the sustainable depletion capacity (E_s) of this reservoir? If the minimum static reservoir pressure at which wells in this field can still flow commercially can be estimated, then one can calculate E_s for any assumed project life. Wellbore simulation for wells producing from the deep liquid zone at Wairakei indicates this minimum pressure value to be about 15 bar-a. Therefore, one can calculate the sustainable capacity, assuming only hot recharge, for any assumed project life from Eq. 4.

The above equation gives very similar values of E_s for a 30-year project life or a 300-year project life, 188.8 and 186.5 kt/day, respectively. This relative insensitivity of E_s to project life is due to the very high recharge coefficient and the apparent preponderance to date of hot rather than cool recharge at Wairakei; this latter fact is also supported by numerical simulation. Since recharge rate in most fields is lower than at Wairakei, an assessment was made of how E_s would have changed as a function of project life if the recharge coefficient at Wairakei were smaller. Figure 8 shows the calculated E_s value versus project life for a range of hypothetical recharge coefficients expressed as fractions of the actual recharge coefficient at Wairakei. Figure 8 shows that as the recharge coefficient becomes smaller, so does sustainability and the latter becomes more sensitive to project life. Figure 9 shows the same data as in Fig. 8 represented as sustainable capacity versus recharge coefficient for project lives of both 30 and 300 years. This figure illustrates that the difference between renewable and sustainable capacities for 30- and 300-year project lives becomes less as recharge coefficient increases, for Wairakei this difference (corresponding to an r of 4.2 kt/day) being negligible.

Finally, it should be noted that sustainability factor (α), as defined before, for Wairakei is 188.8/31, or 6.1. Why is this value of sustainability factor at the low end of the range of 5–45 mentioned earlier? The reason is that until recently, there was no injection in this field. Therefore, the above analysis is based on

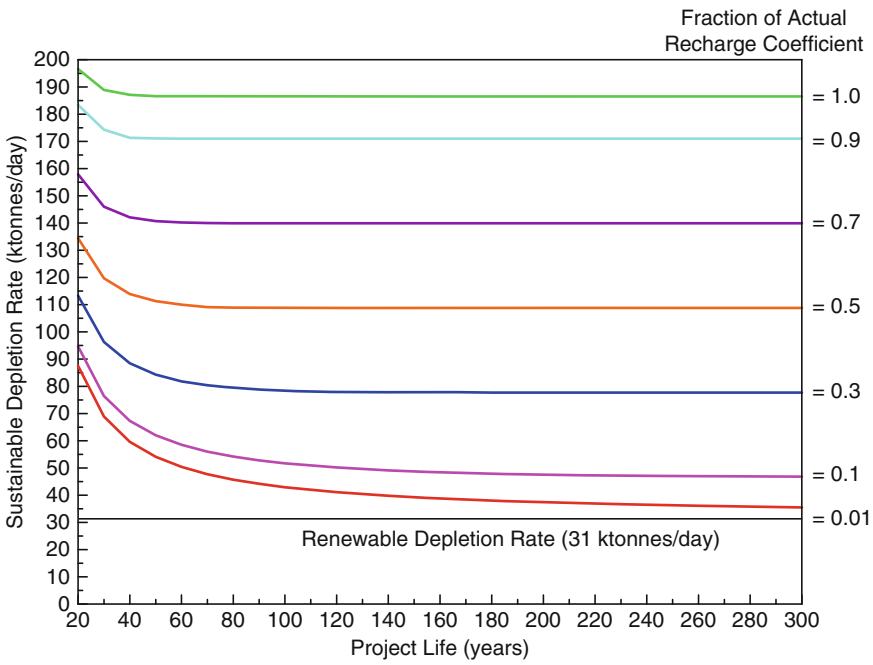

Geothermal Power Capacity, Sustainability and Renewability of. Figure 8
Sustainable depletion rate versus project life, Wairakei field [7]

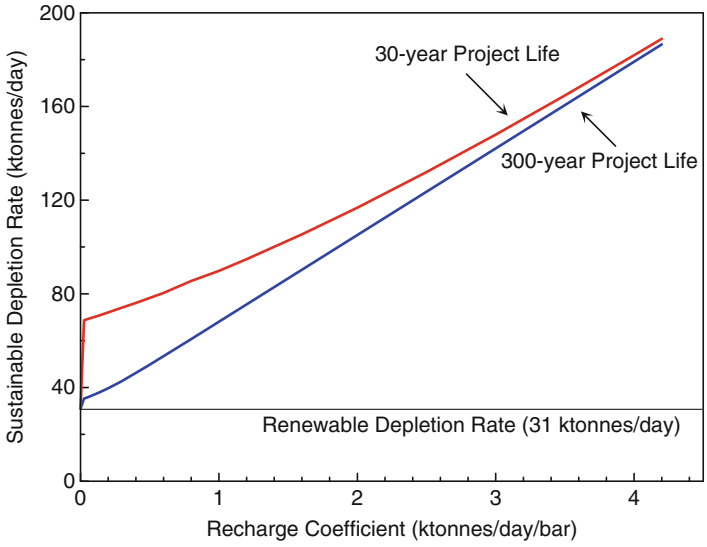

Geothermal Power Capacity, Sustainability and Renewability of. Figure 9
Sustainable capacity versus recharge coefficient [7]

depletion being equal to production. If injection is practiced, the effective depletion rate will be lower than production rate, and therefore, a higher production capacity can be sustained. For example, if 50% of the produced fluid were injected, the sustainable production rate would be double the sustainable depletion rate (188.8 kt/day), that is, 377.6 kt/day, assuming the recharge to be predominately hot.

Therefore, the sustainability factor would be 377.6/31 or 12.2; this sustainable production capacity is an order of magnitude higher than the renewable capacity of 31 kt/day.

Future Directions

The debate over renewability and sustainability of power capacity of a geothermal reservoir still continues for conventional geothermal systems, which are naturally occurring subsurface porous or fractured systems that can be tapped for production by drilling wells. However, in the last decade, considerable hopes have been raised of tapping geothermal energy from enhanced geothermal systems ("EGS") [37]. These are hot subsurface systems with porosity or fracture capacity too low to allow commercial production but can be enhanced by pervasive hydraulic fracturing to enable significant fluid injection and production. In an EGS project, heat is recovered from the artificial reservoir by injecting cool water through a set of wells while producing heated water from another set of wells. Such systems have not yet proven commercial, but research and development toward commercial tapping of EGS systems continue.

If EGS systems can be exploited commercially, the energy reserves in such systems in the USA would be two orders of magnitude larger than the energy contained in the conventional geothermal systems [38]. Even in countries where conventional geothermal systems do not exist, EGS developments would be the theoretically possible, because anywhere on earth adequately hot rock bodies can be reached by drilling wells deep enough and creating an artificial reservoir by hydraulic fracturing of rock.

Renewability and sustainability of EGS systems have not received much attention yet, but in the future, this issue will become important if EGS exploitation becomes a commercial reality. The one major difference between renewability and sustainability of conventional systems and those of an EGS is that an EGS reservoir does not receive natural convective heat recharge; all heat recharge to an EGS reservoir would be conductive which, as discussed earlier, is relatively minor. Furthermore, an abandoned EGS project would not be fully replenished in 100–300 years as expected for conventional systems because of this lack of convective heat recharge.

Bibliography

1. Axelsson G, Stefansson V, Björnsson G (2004) Sustainable utilization of geothermal resources. In: Proceedings of the twenty-ninth workshop on geothermal reservoir engineering, Stanford University, Stanford, pp 26–28
2. Rybach L (2003) Sustainable use of geothermal resources: renewability aspects. In: IGC 2003 short course, UNU Geothermal Training Programme, Iceland
3. Axelsson G, Gudmundsson A, Steingrimsson B, Palmason G, Armannsson H, Tulinius H, Flovenz OG, Bjornsson S, Stefansson V (2001) Sustainable production of geothermal energy: suggested definition. IGA-News Quarterly No. 43:1–2
4. Stefansson V (2000) The renewability of geothermal energy. In: Proceedings World geothermal congress, Kyushu-Tohoku, Japan, 28 May–10 June 2000
5. Rybach L, Mégel T, Eugster WJ (1999) How renewable are geothermal resources? Trans Geotherm Res Council 23:563–566
6. Wright PM (1995) The sustainability of production from geothermal resources. In: Proceedings of the World geothermal congress, Florence, Italy, 18–31 May 1995
7. Sanyal S (2005) Sustainability and renewability of geothermal power capacity. In: Proceedings of the World geothermal congress, Antalya, Turkey, 24–29 Apr 2005
8. Pritchett JW (1998) Modeling post-abandonment electrical capacity recovery for a two-phase geothermal reservoir. Trans Geotherm Res Council 22:521–528
9. Parini M, Cappetti G, Laudiano M, Bertani R, Monterrosa M (1995) Reservoir modeling study modeling study of the Ahuachapan geothermal field (El Salvador) in the frame of a generation stabilization project. In: Proceedings of World geothermal congress, Florence, Italy, 18–31 May 1995
10. Butler SJ, Sanyal SK, Robertson-Tait A, Lovekin JW, Benoit D (2001) A case history of numerical modeling of a fault-controlled geothermal system at Beowawe, Nevada. In: Proceedings of the twenty-sixth workshop on geothermal reservoir engineering, Stanford University, Stanford, 29–31 Jan 2001
11. Butler SJ, Sanyal SK, Henneberger RC, Klein CW, Gutiérrez H, de León JS (2000) Numerical modeling of the Cerro Prieto geothermal field, Mexico. In: Proceedings of the World Geothermal Congress, Kyushu-Tohoku, Japan, 28 May–10 June 2000
12. Wisian KW, Blackwell DD, Richards M (2001) Correlation of surface heat loss and total energy production for geothermal systems. Trans Geotherm Res Council 25:331–336
13. Lippmann MJ, Bodvarsson GS (1985) The Heber geothermal field, California: natural state and exploitation modeling studies. J Geophys Res 90(B1):745–758
14. McGuinness M, White S, Young R, Ishizaki H, Ikeuchi K, Yoshida Y (1995) A model of the Kakkonda geothermal reservoir. Geothermics 24:1–48

15. White SP, Kissling WM, McGuinness MJ (1997) Models of the Kawareu geothermal reservoir. Trans Geotherm Res Council 21:33–39
16. Tulinius H, Sigurdsson O (1989) Two-dimensional simulation of the Krafla-Hvitholar geothermal field, Iceland. In: Proceedings of the fourteenth workshop on geothermal reservoir engineering, Stanford University, Stanford, 24–26 Jan 1989
17. Sorey ML (1985) Evolution and present state of the hydrothermal system in the Long Valley caldera. J Geophys Res 90:11219–11228
18. Esberto MB, Sarmiento ZF (1999) Numerical modeling of the Mt. Apo geothermal reservoir. In: Proceedings of the twenty-fourth workshop on geothermal reservoir engineering, Stanford University, Stanford, 25–27 Jan 1999
19. Haukwa C, Bodvarsson GS, Lippmann MJ, Mainieri A (1992) Preliminary reservoir engineering studies of the Miravalles geothermal field, Costa Rica. In: Proceedings of the seventeenth workshop on geothermal reservoir engineering, Stanford University, Stanford, 29–31 Jan 1991
20. Sakagawa Y, Takahashi M, Hanano M, Ishido T, Demboya N (1994) Numerical simulation of the Mori geothermal field, Japan. In: Nineteenth workshop on geothermal reservoir engineering, Stanford University, Stanford, 18–20 Jan 1994
21. Kiryukhin AV (2004) Modeling study of the Mutnovsky geothermal field (Dachny) in connection with the problem of steam supply for 50 MWe PP. In: Twenty-ninth workshop on geothermal reservoir engineering, Stanford University, Stanford, 26–28 Jan 2004
22. Steingrimsson B, Bodvarsson GS, Gunnlaugsson E, Gislason G, Sigurdsson O (2000) Modeling studies of the Nesjavellir geothermal field, Iceland. In: Proceedings of the World geothermal congress, Kyushu-Tohoku, Japan, 28 May–10 June 2000
23. McGuinness MJ (1998) Ngawha geothermal field – a review. In: Proceedings of the twentieth New Zealand geothermal workshop, University of Auckland, Auckland, New Zealand
24. Yamada M, Iguchi K, Nakanishi S, Todaka N (2000) Reservoir characteristics and development plan of the Oguni geothermal field, Kyushu, Japan. Geothermics 29:151–169
25. Nakanishi S, Nobuyuki I (2000) Reservoir simulation study of the Onikobe geothermal field, Japan. In: Proceedings of the World geothermal congress, Kyushu-Tohoku, Japan, 28 May–10 June 2000
26. Yearsley E (1994) Roosevelt hot springs reservoir model applied to forecasting remaining field potential. Trans Geotherm Res Council 18:617–622
27. Atmojo JP, Itoi R, Fukuda M, Tanaka T, Daud Y, Sudarman S (2001) Numerical modeling study of Sibayak geothermal reservoir, North Sumatra, Indonesia. In: Proceedings of the twenty-sixth workshop on geothermal reservoir engineering, Stanford University, Stanford, 29–31 Jan 2001
28. Pritchett JW, Garg SK, Ariki K, Kawano Y (1991) Numerical simulation of the Sumikawa geothermal field in the natural state. In: Proceedings of the sixteenth workshop on geothermal reservoir engineering, Stanford University, Stanford, 23–25 Jan 1991
29. Furuya S, Aoki M, Gotoh H, Takenaka T (2000) Takigami geothermal system, Northeastern Kyushu, Japan. Geothermics 29:191–211
30. Butler SJ, Sanyal SK, Klein CW, Iwata S, Itoh M (2004) Numerical simulation and performance evaluation of the Uenotai geothermal field, Akita Prefecture. Jpn Trans Geotherm Res Council 28:455–460
31. Bibby HM, Caldwell TG, Davey FJ, Webb TH (1995) Geophysical evidence on the structure of the Taupo volcanic zone and its hydrothermal circulation. J Volcanol Geotherm Res 68:29–58
32. Sanyal SK, Pham M, Iwata S, Suzuki M (2000) Numerical simulation of the Wasabizawa geothermal field, Akita Prefecture. Jpn Trans Geotherm Res Council 24:623–630
33. Menzies AJ, Granados EE, Sanyal SK, Mérida-I L, Caicedo- AA (1991) Numerical modeling of the initial state and matching of well test data from the Zunil geothermal field, Guatemala. In: Proceedings of the sixteenth workshop on geothermal reservoir engineering, Stanford University, Stanford, 23–25 Jan 1991
34. Sanyal SK, Klein CW, Lovekin JW, Henneberger RC (2004) National assessment of U.S. geothermal resources – a perspective. Trans Geotherm Res Council 28:355–362
35. Klein CW, Lovekin JW, Sanyal SK (2004) New geothermal site identification and quantification. In: California energy commission PIER consultant report, P500-04-051
36. Clotworthy A (2000) Response of Wairakei geothermal reservoir to 40 years of production. In: Proceedings of the World geothermal congress, Kyushu-Tohoku, Japan, 28 May–10 June 2000
37. MIT (2006) The future of geothermal energy – impact of enhanced geothermal systems (EGS) on the Unites States in the 21st century. An assessment by an MIT – Led interdisciplinary panel, Massachusetts Institute of Technology, Cambridge
38. Sanyal SK (2010) Future of geothermal energy. In: Proceedings of the thirty-fifth workshop on geothermal reservoir engineering, Stanford University, Stanford, 1–3 Feb 2010, SGP-TR-188

Geothermal Power Conversion Technology

Lucien Y. Bronicki
Ormat Technologies, Inc., Reno, NV, USA

Article Outline

Glossary
Definition of Geothermal Power Conversion Technology
Introduction
Geothermal Project Design and Implementation
Geothermal Resources

Thermodynamic Analysis of the Energy Conversion Process
Main Power Station Components
Choosing the Energy Conversion Systems
Commercial Power Stations
Organic Rankine Cycle Configurations for Geothermal Power Stations
Experimental Power Stations
Future of Geothermal Energy
Acknowledgments
Bibliography

Glossary

Ambient Natural condition of the environment at any given time.

Baseload The lowest level of power production needs during a season or year.

Baseload plants Electricity-generating units that are operated to meet the constant or minimum load on the system. The cost of energy from such units is usually the lowest available to the system.

Binary-cycle power station A geothermal electricity-generating station employing a closed-loop heat exchange system in which the heat of the geothermal fluid (the "primary fluid") is transferred to a different fluid ("motive," "secondary," or "working" fluid), which is thereby vaporized and used to drive a turbine/generator set.

Bi-phase expander A bi-phase expander or bi-phase turbine is a device that produces power by utilizing the energy of two-phase (liquid/vapor) streams. The total energy produced by the brine and the separated steam (in a reduced condition), is expected to be higher than that of the steam turbine alone.

Brine A geothermal solution containing appreciable amounts of sodium chloride or other salts.

Capacity factor A percentage that tells how much of a power station's capacity is used over time. For example, typical station capacity factors range as high as 80% for geothermal and 70% for cogeneration.

Capacity, installed (or Nameplate) The total manufacturer-rated capacities of equipment such as turbines, generators, condensers, transformers, and other system components.

Capacity The amount of electric power delivered or required for which a generator, turbine, transformer, transmission circuit, station, or system is rated by the manufacturer.

Carbon dioxide A colorless, odorless, nonpoisonous gas that is a normal part of the air. Carbon dioxide, also called CO_2, is exhaled by humans and animals and is absorbed by green growing things and by the sea.

CHP Combined heat and power

Condensate Liquid formed by condensation of vapor.

Cooling tower A structure in which process heat is removed to the atmosphere.

Cost The amount paid to acquire resources, such as station and equipment, fuel, or labor services.

Demand The level at which electricity or natural gas is delivered to users at a given point in time. Electric demand is expressed in kilowatts.

Direct use Use of geothermal heat without first converting it to electricity, such as for space heating and cooling, food preparation, industrial processes, etc.

Dispatch The operating control of an integrated electric system to assign generation to specific generating stations and other sources of supply to effect the most reliable and economical supply as the total of the significant area loads rise or fall. Control operations and maintenance of high-voltage lines, substations and equipment, including administration of safety procedures. Operate the interconnection. Schedule energy transactions with other interconnected electric utilities.

Drift eliminator Drift eliminators reduce the amount of drift in the exiting air flow. Drift droplets can be reduced to less than 0.1% by effective use of an eliminator.

Drift Drift droplets are any water droplets and dissolved and suspended solids that are entrained in the air and emitted from the cooling tower stack.

Dry steam Very hot steam that does not occur with liquid.

Efficiency The ratio of the useful energy delivered by a dynamic system (such as a machine, engine, or motor) to the energy supplied to it over the same period or cycle of operation. The ratio is usually determined under specific test conditions.

Effluent Treated wastewater.

EGS Engineered geothermal systems

Emissions standard The maximum amount of a pollutant legally permitted to be discharged from a single source.

Energy efficiency Refers to programs that are aimed at reducing the energy used by specific end-use devices and systems, typically without affecting the services provided. These programs reduce overall electricity consumption (reported in megawatt-hours), often without explicit consideration for the timing of program-induced savings. Such savings are generally achieved by substituting technically more advanced equipment to produce the same level of end-use services (lighting, heating, and motor drive) with less electricity. Examples include high-efficiency appliances, efficient lighting programs, high-efficiency heating, ventilating and air conditioning (HVAC) systems or control modifications, efficient building design, advanced electric motor drives, and heat recovery systems.

Energy source The primary source that provides the power that is converted to electricity through chemical, mechanical, or other means. Energy sources include coal, petroleum and petroleum products, gas, water, uranium, wind, sunlight, and geothermal and other sources.

Energy The capacity for doing work as measured by the capability of doing work (potential energy) or the conversion of this capability to motion (kinetic energy). Energy has several forms, some of which are easily convertible and can be changed to another form useful for work. Most of the world's convertible energy comes from fossil fuels that are burned to produce heat that is then used as a transfer medium to mechanical or other means in order to accomplish tasks. Electrical energy is usually measured in kilowatt-hours, while heat energy is usually measured in British thermal units.

Facility An existing or planned location or site at which prime movers, electric generators, and/or equipment for converting heat into electric energy are situated, or will be situated. A facility may contain more than one generator of either the same or different prime mover type.

Fault A fracture or fracture zone in the Earth's crust along which slippage of adjacent Earth material has occurred at some time.

Flash steam Steam produced when the pressure on a geothermal liquid is reduced. Also called flashing.

Flash tank Vessel in which the geothermal water or brine is flashed into steam by pressure reduction.

Fly ash Particulate matter from coal ash in which the particle diameter is less than 1×10^{-4} m. This is removed from the flue gas using flue gas particulate collectors such as fabric filters and electrostatic precipitators.

Generation (electricity) The process of producing electric energy by transforming other forms of energy also, the amount of electric energy produced, expressed in watt-hours (Wh).

Generator A machine that converts mechanical energy into electrical energy.

Geology Study of the planet Earth, its composition, structure, natural processes, and history.

Geothermal combined cycle An electricity-generating technology in which electricity is produced from the steam exiting from one or more steam turbines at above atmospheric pressure. The exiting steam routed to the evaporator of an ORC station producing electricity. This process reduces the impact of non-condensable gases in the geothermal steam and eliminates the power consumption of the vacuum pumps or ejectors (updated using various sources).

Geothermal energy Natural heat from within the Earth, captured for production of electric power, space (geofluid) heating or industrial steam.

Geothermal fluid Can be steam, water, brine or a mixture of two, may contain noncondensable gases (CO_2, H_2S) and in case of brine, appreciable amounts of sodium chloride, carbonates, and silica.

Geothermal heat pumps Devices that take advantage of the relatively constant temperature of the Earth's interior, using it as a source and sink of heat for both heating and cooling. When cooling, heat is extracted from the space and dissipated into the Earth when heating, heat is extracted from the Earth and pumped into the space.

Geothermal power station A power station in which the prime movers are turbines operated either by steam or organic fluids vapor. The steam is either natural or produced from flashing of hot water. The organic fluid vapor is produced by boiling of the organic fluid using geothermal steam or water.

The natural steam and water derive energy from heat found in rocks or fluids at various depths beneath the surface of the Earth. The energy is extracted by drilling and/or pumping. It includes all the surface facilities including the geothermal fluid gathering and treatment system, but does not include the geothermal wells and pumps.

Geothermal steam Steam drawn from deep within the Earth.

Geothermal Of or relating to the Earth's interior heat.

Geyser A spring mat that shoots jets of hot water and steam into the air.

Geysers, The A large geothermal steam field located approximately 75 miles (121 km) north of the city of San Francisco, California.

Gigawatt (GW) One billion watts.

Gigawatt-hour (GWh) One billion watt-hours.

Greenhouse effect The increasing mean global surface temperature of the Earth caused by gases in the atmosphere (including carbon dioxide, methane, nitrous oxide, ozone, and chlorofluorocarbon). The greenhouse effect allows solar radiation to penetrate but absorbs the infrared radiation returning to space.

Grid The layout of an electrical distribution system.

Heat exchanger A device for transferring thermal energy from one fluid to another.

Hot dry rock (HDR) A geothermal resource created with impermeable, subsurface hot rock structures, typically granite rock below the Earth's surface. The resource is being investigated as a source of energy production.

Hybrid geothermal cycles Cycles in which there are in series or in parallel a steam Rankine cycle and an Organic Rankine cycle.

Hybrid geothermal power stations Stations in which the geothermal heat is supplemented by another heat source.

Hydrothermal resource Underground systems of hot water and/or steam.

Injection The process of returning spent geothermal fluids to the subsurface. Sometimes referred to as reinjection.

Kilowatt (kW) One thousand watts.

Kilowatt-hour (kWh) One thousand watt-hours.

Known geothermal resource area A region identified by the US Geological Survey as containing geothermal resources.

Leaching The removal of readily soluble components, such as chlorides, sulfates, organic matter, and carbonates, from soil by percolating water. The remaining upper layer of leached soil becomes increasingly acidic and deficient in plant nutrients.

Load (electric) The amount of electric power delivered or required at any specific point or points on a system. The requirement originates at the energy-consuming equipment of the consumers.

Magma The molten rock and elements that lie below the Earth's crust. The heat energy can approach 550°C and is generated directly from a shallow molten magma resource and stored in adjacent rock structures. To extract energy from magma resources requires drilling near or directly into a magma chamber and circulating water down the well in a convection-type system.

Megawatt (MW) One thousand kilowatts (1,000 kW) or one million watts (1,000,000 W).

Megawatt-hour (MWh) One million watt-hours.

Muffler It is a device for reducing noise of high-speed steam flow in emergency relief of high-pressure steam from the production well (PW) in the power station. In geothermal applications it not only acts as a silencer but also performs safety and environmental duties. This is because of the high temperature and high salinity of the steam and brine that is released to the atmosphere in case of turbine trip-off or system emergency shutdown.

Noncondensable gases (NCG) Gases present in the steam or dissolved in the brine and liberated in the flash process.

Ormat energy converter (OEC) A unit using Ormat's Organic Rankine Cycle technology, which converts geothermal heat to electric power.

ORC power station A power station operating according to the ORC process.

Organic Rankine cycle (ORC) A Rankine cycle using an organic fluid (updated using various sources).

Outage The period during which a generating unit, transmission line, or other facility is out of service.

Particulate matter (PM) Unburned fuel particles that form smoke or soot and stick to lung tissue when inhaled. A chief component of exhaust emissions from heavy-duty diesel engines

pH The term pH is a measure of acidity or alkalinity and ranges from 0 to 14. A pH measurement of 7 is

regarded as neutral. Measurements below 7 indicate increased acidity, while those above indicate increased alkalinity.

Point source A stationary location or fixed facility from which pollutants are discharged.

Power plant A power station.

Power station A facility at which prime movers electric generators, and auxiliary equipment are located, for converting mechanical, chemical, and/or nuclear energy into electric energy. A station may contain more than one type of prime mover.

Power Electricity for use as energy.

Precipitation Precipitation is the formation of a solid in a solution. The solid formed is called the precipitate, and the liquid remaining above the solid is called the supernate.

Price The amount of money or consideration-in-kind for which a service is bought, sold, or offered for sale.

Purifier Vessel at the turbine in which fine droplets are separated from the vapor.

Regulation The governmental function of controlling or directing economic entities through the process of rulemaking and adjudication.

Reliability Electric system reliability has two components adequacy and security. Adequacy is the ability of the electric system to supply to aggregate electrical demand and energy requirements of the customers at all times, taking into account scheduled and unscheduled outages of system facilities. Security is the ability of the electric system to withstand sudden disturbances, such as electric short circuits or unanticipated loss of system facilities. The degree of reliability may be measured by the frequency, duration, and magnitude of adverse effects on consumer services.

Renewable energy Resources that constantly renew themselves or that are regarded as practically inexhaustible. These include solar, wind, geothermal, hydro, and wood. Although particular geothermal formations can be depleted, the natural heat in the Earth is a virtually inexhaustible reserve of potential energy. Renewable resources also include some experimental or less-developed sources such as tidal power, sea currents, and ocean thermal gradients.

Renewable resources Natural but flow-limited resources that can be replenished. They are virtually inexhaustible in duration but limited in the amount of energy that is available per unit of time. Some (such as geothermal and biomass) may be stock-limited in that stocks are depleted by use, but on a time scale of decades, or perhaps centuries, they can probably be replenished. Renewable energy resources include: biomass, hydro, geothermal, solar, and wind. In the future, they could also include the use of ocean thermal, wave, and tidal action technologies. Utility renewable resource applications include bulk electricity generation, on-site electricity generation, distributed electricity generation, non-grid-connected generation, and demand-reduction (energy efficiency) technologies.

Reservoir A natural underground container of liquids, such as water or steam (or, in the petroleum context, oil or gas).

Revenue The total amount of money received by a firm from sales of its products and/or services, gains from the sales or exchange of assets, interest and dividends earned on investments, and other increases in the owner's equity except those arising from capital adjustments.

Saturation Saturation is the point at which a solution of a substance can dissolve no more of that substance and additional amounts of it will appear as a precipitate. This point of maximum concentration, the saturation point, depends on the temperature of the liquid as well as the chemical nature of the substances involved.

Scaling Scaling is formation of a deposit layer (scale) on a solid surface, i.e., evaporators, pipes, etc.

Screw expander The screw expander is the reverse usage of a screw compressor consisting of two helical rotating wheels compressing gas in between them. When high-pressure gas is introduced to the compressor exit, it expands forcing the screw wheels to rotate backward and produce power.

Scrubber Equipment used to remove sulfur oxides or hydrogen sulfide from the geothermal fluid before discharge to the atmosphere. Chemicals, such as lime, are used as the scrubbing media. The scrubber is also used when fresh water is applied to saline-contaminated steam. The scrubber reduces the steam salinity before it enters the turbine.

Separator A vessel at the wellhead where steam is separated from water or brine. Mostly of centrifugal type.

Solubility Solubility is the property of a solid, liquid, or gaseous chemical substance called solute to dissolve in a liquid solvent to form a homogeneous solution of the solute in the solvent. The solubility of a substance fundamentally depends on the used solvent as well as on temperature and pressure.

Stability The property of a system or element by virtue of which its output will ultimately attain a steady state. The amount of power that can be transferred from one machine to another following a disturbance. The stability of a power system is its ability to develop restoring forces equal to or greater than the disturbing forces so as to maintain a state of equilibrium.

Steam Rankine cycle A Rankine cycle in which water (in liquid and vapor phase) is the motive fluid (updated using various sources).

System (electric) Physically connected generation, transmission, and distribution facilities operated as an integrated unit under one central management, or operating supervision.

System A combination of equipment and/or controls, accessories, interconnecting means, and terminal elements by which energy is transformed to perform a specific function, such as climate control, service water heating, or lighting.

Thermal pollution A reduction in water quality caused by increasing its temperature, often due to disposal of waste heat from industrial, power generation processes, or urban impervious surfaces (such as parking lots). Thermally polluted water can harm the environment because plants and animals may have difficulty adapting to it.

Transmission The movement or transfer of electric energy over an interconnected group of lines and associated equipment between points of supply and points at which it is transformed for delivery to consumers, or is delivered to other electric systems. Transmission is considered to end when the energy is transformed for distribution to the consumer.

Turbine generator A device that uses steam, organic vapor, heated gases, water flow or wind to cause spinning motion that activates electromagnetic forces and generates electricity (updated using various sources).

Turbine A machine for generating rotary mechanical power from the energy of expansion of a stream of fluid (such as water, steam, organic vapor, or hot gas). Turbines convert the kinetic energy of fluids to mechanical energy through the principles of impulse and reaction, or a mixture of the two (updated using various sources).

Utility A regulated entity which exhibits the characteristics of a natural monopoly. For the purposes of electric industry restructuring, "utility" refers to the regulated, vertically integrated electric company. "Transmission utility" refers to the regulated owner/operator of the transmission system only. "Distribution utility" refers to the regulated owner/operator of the distribution system which serves retail customers.

Vapor(or steam)-dominated resources A geothermal reservoir system in which subsurface pressures are controlled by vapor rather than liquid and most of the flow is steam.

Water-dominated resource A resource where the major part of the mass flow is water or brine.

Watt The electrical unit of power. The rate of energy transfer equivalent to 1 A flowing under a pressure of 1 V at unity power factor.

Watt-hour (Wh) An electrical energy unit of measure equal to 1 W of power supplied to, or taken from, an electric circuit steadily for 1 h.

Definition of Geothermal Power Conversion Technology

Geothermal Power Conversion Technology refers to techniques used for the conversion of the heat content of geothermal fluid into mechanical power in order to drive a generator and produce electric power.

The first 1/4 HP reciprocating steam engine unit was installed in 1904 by Prince Piero Ginori Conti in the Larderello geothermal field in Italy. Prior to World War II, there were already 136.8 MW of capacity installed in Larderello area. After the war more wells were drilled and modern power stations were installed in the area. As of December 2009, the current operator, ENEL, had 842 MW of installed geothermal power capacity in the Tuscany area.

The first steam engine–driven generator of 35 kW was installed in the USA in 1921 in The Geysers of California. Only in the 1950s, the region was further developed and today 900 MW are produced in this area.

In Japan, surveys began in 1918 with the first experimental generator installed on the island of Kyushu in 1925. Russia followed in 1941 in Kamchatka. Extensive exploration and installations were performed in the 1950s in Japan, Russia, New Zealand, Iceland, Kenya, the Azores Islands off of Portugal and The Philippines.

In the 1980s, Organic Rankine cycle power conversion was applied to geothermal resources of lower enthalpy and widened the range of exploitable resources to lower temperatures.

Today about 10,700 MW are in operation in 24 countries.

Introduction

Power conversion is the least risky part of a geothermal project. Generally it consists of a straight forward engineering design with work executed by experienced manufacturers, engineering firms and contractors.

The risks and challenges are related to exploration, drilling and managing the resource (see preceding entries). Optimization depends on the choice of adaptation of the power station configuration to the resources available (see section on "Choosing the Energy Conversion Systems").

There are four basic types of resources:

- Vapor dominated
- Water dominated
- Pressurized water
- EGS engineered geothermal systems where water has to be pumped into the hot rock fissures and cavities. These systems are in early development and demonstration phases

Four energy conversion systems for geothermal resources are in commercial operation:

- Steam Rankine Cycle for Dry Steam
- Steam Rankine Cycle for double or triple flash
- Organic Rankine Cycle in Binary stations for moderate resource temperature
- Combined steam and Organic Rankin Cycle for resource of high temperature and non condensable gases.

To widen the range of resources suitable for power generation beyond dry-steam and flashed steam stations. Of the over 10,000 MW of geothermal stations installed worldwide, most use steam turbines operating on dry steam or steam produced by single or double flash by the end of 2009. About 1,000 MW use ORC or geothermal combined cycles.

Operational experience has confirmed the advantages of ORC power stations, not only for low-enthalpy water-dominated resources, but also certain high enthalpy ones where the brine is aggressive or the fluid contains a high percentage of noncondensable gas. The higher installation cost of these systems is often justified by environmental and long-term resource management considerations.

This entry is not a design manual for a power station (for detailed calculations, references are given), a history (see preceding entries), or an inventory of existing geothermal stations or a list of future projects. These subjects are dealt with in the following entries.

This is a review of power conversion configuration based on the author's 30 years' experience of implementing various power systems.

What is attempted here is to give a comprehensive picture of adapting the power conversion to various geothermal resources optimizing the output, minimizing the negative implications, and enhancing the sustainability. The objective is to enable the reader to assess the full picture while relying on experienced consultants and vendors in each discipline.

The most updated and comprehensive data on geothermal energy covering both the resource and power conversion systems can be found in: DiPippo R, "Geothermal Power Plants," 2nd edn. Elsevier and Glassley W, "Geothermal Energy," CRC Press.

Further reading on geothermal energy can be found on the Department of Energy internet site at:

http://www.energy.gov/energysources/index.htm
http://www.energy.gov/energysources/geothermal.htm
http://www1.eere.energy.gov/geothermal/history.html

The MIT publication on the future of geothermal energy can be found at http://geothermal.inel.gov/publications/future_of_geothermal_energy.pdf

The IEA-GIA Website at http://www.iea-gia.org/

The Geothermal Research Council at http://www.geothermal.org/

The Geothermal Energy Association at http://www.geo-energy.org/

Geothermal Project Design and Implementation

General

A geothermal project is composed of two elements very different in nature and risk: a straightforward conversion system, converting heat into electricity, and the heat supply, i.e., the geothermal resource with attributes similar to oil and gas fields.

Using the terminology of the oil industry a geothermal power project is an integration of "upstream" with "downstream," hence its particularity. The "upstream" is handled in the other entries. The "downstream" covers the surface equipment.

The project risk is associated with the primary fuel development and it rests with the Investor (Independent Power Producer (IPP) or Utility) rather than with a supplier of fuel.

The aggregate risk in a geothermal project, in a macro sense is different from fossil fuel plant in that the fuel supply risk and investment are mostly up front. As it is site and location specific, it cannot be monetized and the resource supply or quality cannot be substituted, as fossil fuel can, by finding another source from the market.

An important advantage of geothermal power stations is that after the initial investment is made. The power is supplied at a predictable cost unaffected by price fluctuations.

Overview of Geothermal Station Implementation

Development of a geothermal project typically proceeds in two parallel paths, technical operations, i.e., "work on the ground" and commercial/legal procedures, as shown in the scheme in Table 1.

The process starts with identifying a potential site based on desktop studies and preliminary fieldwork covering known geological data and surface manifestations, indicating the existence of an underground geothermal system (hot springs and fumaroles). Results of previous exploration by other parties (other geothermal developers, state agencies, mining companies, oil and gas companies, etc.), if such data exists. This information is then combined with business information, including the need for power in that area, the expected power prices, the existing and missing infrastructure, namely, a transmission grid and road, environmental/permitting constraints, other business, financial and political risks, etc. A "go/no-go" decision is taken. If a "go" decision is taken, the next steps are as follows:

Obtaining a geothermal concession (when applicable): Since most countries view geothermal resources as a strategic resource owned by the state, obtaining a state geothermal concession is the first step to geothermal development. This concession is typically awarded by winning a state bid. In the USA, the Federal Steam Act basically assigned geothermal rights to the surface owner, be that the Federal Government Bureau of Land and Management, the state, a private owner, etc.

Obtaining a land position: This is done most typically through geothermal leasing, but sometimes also through land acquisition or other business structures.

Initial nonintrusive exploration: typically including basic geology, geochemical sampling, and geophysical surveys, e.g., gravity, magnetic and electric. This phase may require some permitting work, depending on the type of fieldwork and surveys plans and the local regulations.

Permitting for exploration drilling: Exploration drilling, typically starting with shallow temperature gradient holes, moving to medium depth and slim holes and eventually two to three full diameter deep production and injection wells.

Permitting for roads, power lines, power stations, and its operation.

Long-term multi-well flow testing: In order to accurately determine the average temperature and flow, build a reservoir model and estimate the size of the reservoir and the potential electrical generation.

Technical and economical feasibility and final "go/no-go" decision.

Field testing and initial exploration of the site enables the understanding and establishing of the site potential and drawing station layout, initial heat, mass balance and required investment.

This will allow the commercial and legal part to proceed, typically leading to signing of a long-term Power Purchase/Sales Agreement with a local utility.

Although station design will already start during the period of legal and financial negotiations, the completion of design and manufacturing will not

Geothermal Power Conversion Technology. Table 1 Schematic planning of geothermal project implementation

	Prior to kick-off	Year 1				Year 2				Year 3				Year 4				Year 5				Year 6- onwards			
Activity	**Varies**	Q1	Q2	Q3	Q4	Q1	Q2	Q3	Q4	Q1	Q2	Q3	Q4	Q1	Q2	Q3	Q4	Q1	Q2	Q3	Q4	Q1	Q2	Q3	Q4
Resource Identification and Acquisition	■																								
Locating potential sites	■																								
Obtaining surface and subsurface rights	■																								
Power Purchase Agreement (if developer)	■																								
Exploration and Resource Confirmation		■	■	■	■	■	■	■	■	■	■	■													
Non-intrusive exploration		■	■	■	■	■																			
Drilling permitting					■	■	■																		
Temperature gradient drilling							■	■																	
Slim-hole drilling and feasibility									■	■															
Initial full-size deep drilling and resource confirmation											■	■													
Engineering, Procurement, Construction and Field Development													■	■	■	■	■	■	■	■					
Plant design													■												
Plant permitting, including well-field and transmission line													■	■	■	■	■								
Drilling production and injection wells																■	■	■	■	■					
Equipment purchasing and manufacturing													■	■	■	■	■								
Power plant construction																		■	■	■					
Gathering system construction																			■	■					
Transmission line and utility interconnection													■	■	■	■	■	■	■	■					
Commissioning and Start-Up																					■				
Commercial operation																						■	■	■	■

commence before the resource is appraised and sale of electricity secured by, or for a utility. At this stage, an NTP (Notice to proceed) will be issued to the engineering, procurement, and construction (EPC) contractor and all technical operations released. The steps are as follows:

Station design:
Obtaining all necessary station permits, including the well-field and transmission line.
Completion of well-field development and equipment manufacturing.

While equipment is being manufactured, on-site operations continue including wellhead, piping, interfaces to transmission lines, roads, buildings, power house, control room, etc. They are marked as:

Gathering system and station construction.
Transmission and interaction.

Both actions, completion of manufacturing and on-site construction, end approximately 4 to 5 years from obtaining land position and kick-off of initial exploration. The actual timeframe can be as short as 2–3 years or as long as 10 years, depending primarily on the existence of historical exploration data, the complexity and pace of permitting and logistical constraints.

Power Station Costs

Essentially, the costs of a geothermal power station are highly dependent on the resource. Most of the variation in costs is experienced during the drilling phase where initial exploration holes will define the resource, its temperature, flow rates and chemical and mineral content for which assumptions can be made regarding the cost of managing the resource over time.

Overall costs in 2010 US dollars range between US$3,000 and US$5,500 per installed kilowatt depending mainly on the quality of the resource (temperature, geothermal fluid chemistry) which compels the conversion technology (binary, flash, steam). This leads to electricity prices in the range of about US$70–US$100 per megawatt-hour.

Cost Estimates for Megawatt-Hour (MWh) Recent estimates from studies on the costs of developing geothermal power stations provide a range for where actual costs may fall. In September 2008, The US Department of Energy provided a broad range of US $63– US$102 per MWh, assuming resource incentives, such as the Federal Production Tax Credit (US DOE 2008 [1]). Several recent estimates put costs within this range, including the California Energy Commission (CEC 2007 [2]), Emerging Energy Research (EER 2009 [3]) and Glacier Partners (Glacier Partners 2009 [4]), which produce estimates between US$72 and US $100 per MWh. Further evidence for the cost of power comes from recent contracts approved by the Public Utility Commission of Nevada (PUCN [5]) in July 2010 and released to the public ranged between US $86 and US$98 per MWh with resource incentives assumed in the contract price (Source: PUCN 2010 [5]). Internationally, prices may be lower due to economies of scale, but not significantly. The International Energy Agency (IEA) backs this up with a 2010 article that describes costs for new generation is in some countries (such as New Zealand) as highly competitive, ranging from US$50 to US$70 per MWh for "known high-temperature resources." Overall, IEA suggests a wide range of costs, from US$50 per MWh up to US $120 per MWh for flash stations. For binary stations, the range in the USA is US$70 per MWh, up to US$120 per MWh. However, in Europe where some countries, like Germany, are drilling even deeper for low-moderate temperature resources sufficient for power production, costs may be as high as US$200 per MWh (IEA 2010 [6]).

Cost Estimates for Installed Kilowatt (kW) As for installed cost per kilowatt, an August 2009 study by the California Energy Commission estimates costs range between US$2,700 and US$8,000 for geothermal stations (assuming a station built in 2010), with an average cost assumed of US$4,851 for binary stations and US$4,407 for flash stations, although O&M costs are assumed to be higher for flash stations (CEC 2009 [7]). Other recent studies place the range slightly narrower. US DOE, in September 2008, estimated a base cost of US$4,000 per installed kilowatt. Emerging Energy Research assumes a range of US$4,000–US $5,500/kW for projects in the 20–60 MW range (EER 2009 [3]). EER notes that larger projects, "such as those under development in Indonesia, The Philippines, and

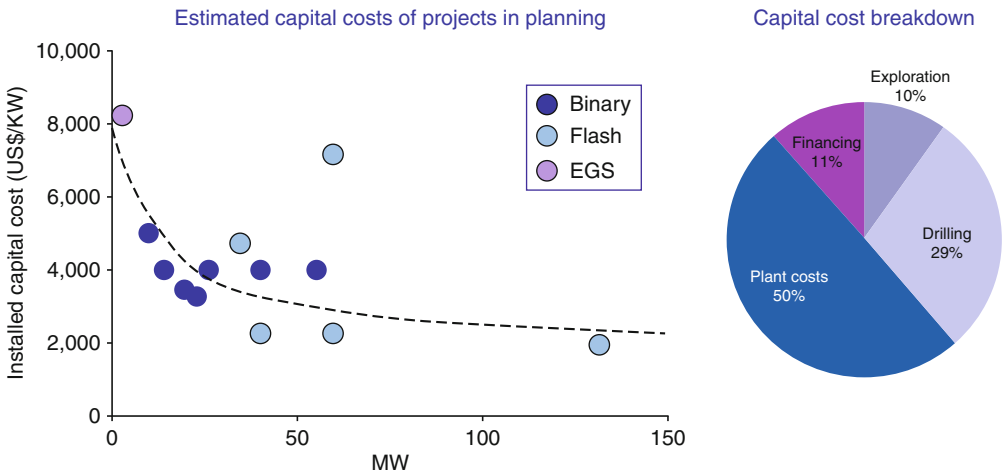

Geothermal Power Conversion Technology. Figure 1
Breakdown of capital costs for a geothermal project (Courtesy of IHS Emerging Energy Research [3], pp. 3–18)

New Zealand, have shown significant advantages of increasing scale, with costs of proposed projects approaching as low as US$2,000/kW" (EER 2009 [3]), refer Fig. 1. According to the International Energy Agency, greenfield flash stations can cost as low as US $2,000 per installed kW and range up to US$4,500, particularly in high-temperature sites which may require fewer wells. They estimate binary power stations, ranging from as low as US$2,400 per installed kW for a productive high-temperature site, suitable for binary technology, to US$5,900 for low-temperature sites, particularly where many wells need to be drilled (IEA 2010 [6]). Currently, most projects in The Philippines are anticipated to be within the 20–60 MW range, as by an announcement of plans by the Energy Development Company (EDC [8]) on July 29, 2010, where upcoming projects sized 20–50 MW where referenced in its portfolio. EDC estimate costs for greenfield sites (sites that are new and not expansions to producing fields) to cost approximately US$3,500 per kilowatt installed (Source: Inquirer.net, July 29, 2010).

Comparison with Other Technologies Typically, the cost of the power station, surface facilities and transmission will constitute approximately half of the total costs of a geothermal station (Source: DOE 2008 [1] and EER 2009 [3]). This reflects the high upfront costs associated with resource assessment. For comparison, the costs to assess solar resources are relatively minor, perhaps even negligible. Yet, materials costs for solar projects are significantly higher on a levelized basis than for fossil fuels or geothermal. Generally more land is needed for economies of scale, which also adds to the costs. For example, in its August 2009 report to the California Energy Commission, KEMA [9] shows that the installed costs for Photovoltaic solar and Parabolic Trough solar technologies are roughly similar in installed cost of geothermal projects overall. However, this recognizes that most of the installed cost is materials, with little of it from actual resource confirmation. Further, capacity factors and annual average production for solar technology are generally much less than for geothermal. Whereas geothermal generally has capacity factors above 90% (CEC 2009 [7]), existing solar technologies have capacity factors between 26% and 29% (CEC 2009 [7] and CPUC 2010 [10]). According to the CEC in its "Renewable Energy Cost of Generation Update," August 2009 (pp. 206, 211, 226, 236) the capacity factor for geothermal projects averages between 90% and 94% depending on technology. On the other hand, solar thermal without storage and solar photovoltaic is between 26% and 28%. Although solar thermal with storage is expected to have much higher capacity factors (60–70%), no advanced solar projects have proposed capacity factors this high. This is reinforced by the California Public Utilities

Commission (CPUC) which in its July 2010 RPS Project Status table identifies contract capacity for projects in operation and projects which have been approved by the Commission. Solar photovoltaic projects in operation and approved by the CPUC average or expect to average 25.7%, while solar thermal projects approved by the CPUC expect to average 28.8%, refer http://www.cpuc.ca.gov/NR/rdonlyres/A5406F32-B0D0-409E-AA92-0EA79E97BECC/0/RPS_Project_Status_Table_2010_July.xls.

Further, for fossil fuels such as natural gas and coal, the risk of resource development falls to the producers of natural gas and coal, and not to the power station operators. Thus, the risk of resource development is spread widely to all natural gas and coal suppliers, creating a price range (per MMBTU for natural gas and per short-ton for coal). The price of the fuel source is thus reflected in O&M, and not the physical construction of the power station, which varies primarily according to cost of materials like metal and steel.

Should a geothermal resource be more difficult to develop or anticipate, this will be born in initial development cost, rather than the O&M, as the operator of a geothermal power station was also the developer who financed the project and incurred upfront risks. Although geothermal resources vary in sustainability and there is a range of O&M costs, much of the risk is borne in the upfront development process.

Levelized Costs For the reasons described above, levelized costs for geothermal are important considerations. The levelized cost of energy includes all the costs over the lifetime of a project. From initial investment (higher for geothermal power than fossil fuels), to construction and materials cost (similar for geothermal and fossil fuels), to operations and maintenance costs (slightly lower for geothermal than fossil fuels) and to cost of fuel (essentially zero for geothermal, whereas a major cost for fossil fuels) (Fig. 2).

Geothermal Resources

For power conversion, the value of a geothermal resource is its enthalpy. All other characteristics, mineral content and noncondensable gases, are almost always a drawback to be dealt with at additional investment and cost. In case of coproduction of geothermal energy from pressurized oil or gas wells, the pressure is also of value but its sustainability is in question and requires further R&D.

Geothermal Resource Characteristics

Conventional drilling techniques are used to reach natural underground reservoirs (aquifers) containing hot water and/or steam. These geothermal fluids are under high temperature/pressure and are at bursting pressure from the well. At lower temperatures the

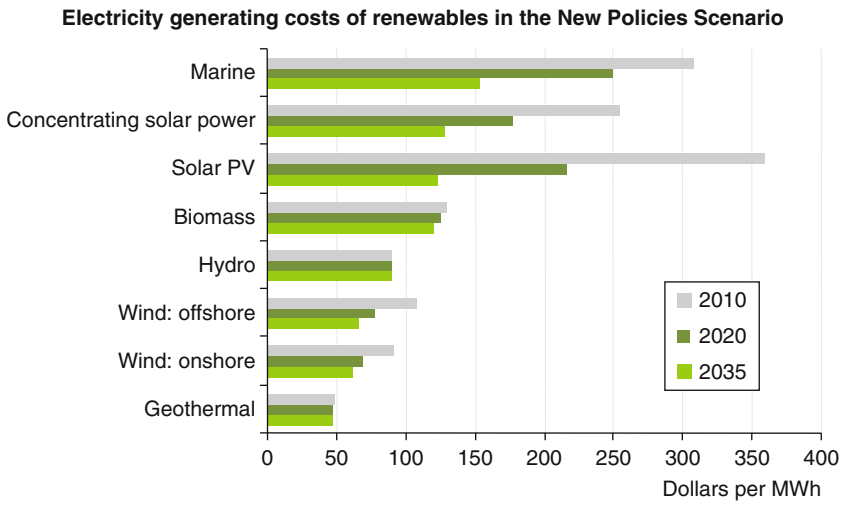

Geothermal Power Conversion Technology. Figure 2
Levelized costs of renewables (IEA World Energy Outlook [6])

geothermal fluid resource has to be pumped to the surface and used to produce electricity via the power conversion system or directly for space or process heating.

While the main aim is to use the heat content for power production, it is essential here to cover all the unwanted source properties (chemical and physical) and the means to mitigate their impact.

Natural geothermal systems can be divided into four categories:

- Dry steam
- Vapor-dominated
- Liquid dominated (superheated water)
- Moderate temperature water (less than 150°C)

In addition, the following are resources in experimental stages:

- Geo-pressured reservoirs
- EGS/HDR
- Lavas and magmas (not dealt with in this entry)

Although dry-steam fields are relatively rare, the Italian fields at Larderello and Mt. Amiata produce about 850 MW [12] and the US field at The Geysers in California, produce about 900 MW (net) of electricity [13, 14]. Vapor-dominated fluids are advantageous for power production as they are usually available at relatively high temperature and pressure. The steam is used to directly drive turbines [15, 16].

The more commonly occurring liquid-dominated systems present a complex utilization problem as reasonably high-pressure vapor must be created for power generation in a conventional turbo-generator unit. The fluid can be partially vaporized by flashing it to a lower pressure, in one or two flashing stages [17]. The vapor then expands in a suitable turbine to produce power [16], or in a binary station using ORC it can heat a secondary fluid vaporizing it at a lower temperature (hydrocarbon). The latter then expands in a turbine, condenses, and is pumped in a continuous closed cycle [16, 17]. A disadvantage of direct steam flashing is that multiple flashing steps are required to attain high conversion efficiencies. Only a fraction of steam is produced with a single-flashing stage. Successive flashing improves efficiency but requires complex turbine design. Furthermore, the relatively high specific volume of steam at these lower temperatures results in large, expensive turbines. Therefore, in most cases only double-flash is used.

Fluid temperatures as high as 300°C have been observed in the Imperial Valley of California, and Russian fields including Kamchatka. Liquid-dominated systems vary widely in terms of the available temperatures and pressures of geothermal fluids. For power production, temperatures above 150°C are desirable when coupled to sink (heat rejection) temperatures of approximately 25°C.

Geothermal pressured reservoirs such as those of the Gulf Coast, contain moderately hot water (150–180°C) under extremely high pressures (250–650 bars) [18]. However, utilization of this resource has been limited by engineering problems associated with drilling into such formations and extracting useful amounts of energy. Lavas and molten magmas are another potentially useful energy source, but controlled energy extraction is only in the formative research stages at this point, mainly in Iceland.

Enhanced (engineered) geothermal systems (EGS) are also under development in Europe, Japan, Australia, and the Western USA. EGS consists of drilling into hot dry rock (HDR) and creating a geothermal reservoir by hydraulically fracturing the rock [19, 20]. Water is then circulated through the fractured zone to remove heat and is pumped to the surface. Additional surface area for underground heat transfer may also be created by thermal stress cracking which will greatly enhance the lifetime of the reservoir. Energy conversion on the surface may utilize direct steam flashing and steam turbine and/or an Organic Rankine power cycle.

Geothermal Fluid Chemistry

Geothermal fluids contain numerous minerals and dissolved gases accumulated in the underground aquifer from its creation. Utilization of the thermal energy of the extracted geothermal fluid changes the fluid's equilibrium properties when the fluid exits the wellhead. Chemical analysis enables the station operator to be prepared for changes in the fluid behavior from changes in temperature and pressure. This parameter is not only required for geothermal power station's (corrosion, scaling, etc.) functional design but also for the station environmental design. Chemical "fingerprints" might adversely affect water quality (domestic,

irrigation, rivers, drainage, etc.). Steam and condensate containing "non-condensable gases" (NCG), e.g., hydrogen sulfide, traces of benzene, toxic (or even only foul-smelling) are handled according to local environmental limitations for such substances.

Reinjection of separated brines, and blow down from cooling towers are common practice in geothermal stations for environmental reasons and for reservoir replenishment.

Noncondensable Gases Two particular ingredients of geothermal fluid production are H_2S and carbon dioxide (CO_2). In most cases, CO_2 outweighs the H_2S concentration and is responsible for relatively low pH of geothermal condensates involved in calcite scaling in production wells. Calcite deposits form more readily in wells with high CO_2. Scaling is not restricted to well casings and may also impact surface piping and heat exchangers.

Hydrogen Sulfide (H_2S) In certain conditions, H_2S creates a protective iron sulfide layer on carbon steel surfaces (limiting their corrosion rate) and stabilizes "deaeration" of geothermal brines (dissolved oxygen in aerated brines dramatically increases corrosion rates). H_2S is toxic foul smelling, corrosive and scale forming with many heavy metals. A specific type of corrosion (sulfide stress cracking or SSC) can occur on high-strength ferrous materials of the steam turbine blades and/or on "high" hardness welds in geothermal fluids at high H_2S partial pressure. This is hydrogen embrittlement cracking where hydrogen is generated by the sulfide corrosion process on the metal surface.

H_2S readily forms heavy metal sulfides on cooling, or when separating steam from brine. In highly saline geothermal fluids, such sulfides may plug wellheads or heat transfer surfaces. Unique sulfide forms may result in less saline brines after cooling (antimony sulfide "stibnite"). Some heavy-metal sulfide precipitates are also suspected of causing pitting corrosion on stainless steels.

NACE standard MR0175 defines a "sour" (high H_2S containing) service, where H_2S partial pressure is above 0.05 psia (0.0003 Mpa) and requires protection of personnel and electrical equipment.

In addition, H_2S is toxic even at low air concentrations and must be mitigated to keep its levels below environmental thresholds.

Calcite Scaling in Production Well Casings One of the common problems in geothermal wells is the deposition of calcium carbonate or calcite, $CaCO_3$, in the well casing starting just above the flash horizon. It is not uncommon for high-temperature geothermal fluids to be close to saturation with respect to calcite as they flow through the formation. The solubility of calcite varies inversely with temperature, so it cannot precipitate from the geothermal fluid because of a decrease in temperature while other factors remain constant. The other properties of the geothermal fluid that influence the solubility are:

- Partial pressure of carbon dioxide CO_2
- pH
- Salinity
- Calcium ion concentration

The first two factors are interrelated. When the geothermal fluid flashes in the well, the released steam carries most of the CO_2. This causes the liquid pH to rise dramatically supersaturating the geothermal fluid (with respect to calcite). Precipitation occurs immediately and can lead to severe narrowing of the wellbore for several meters just above the flash horizon.

The chemical equilibrium reactions controlling the process are:

$$CO_2(aq) \Leftrightarrow CO_2(vap) \quad (1)$$

$$HCO_3^- + H^+ \Leftrightarrow CO_2 + H_2O \quad (2)$$

$$Ca^{++} + 1HCO_3 - CaCO_3 \downarrow + H_2O + CO_2 \uparrow \quad (3)$$

pH Geothermal brines and condensates can exhibit different pH values. There are also variations of measurement results related to environmental conditions at the testing point (i.e., difference between "field" and "lab" pH). At higher temperatures, "neutral" pH value lowers while on steam from water separation (flashing to lower pressure) and pH value rises due to the escape of acidic gases.

The impact of the pH value (after dealing with eventual inaccuracies) is important for design purposes:

- Influence on durability of materials in contact with the fluid. Impact on material selection for its transportation and handling (deleterious influence) on the corrosion resistance of carbon steel and lower pH.

- Influence flow rates and pressure drops by indirect effect of scaling impeding heat transfer due to fouling.
- Design may also need the pH value to adjust to lower values ("pH modification" [21]) as an antiscaling measure (to delay amorphous silica precipitation). Value can be raised to protect carbon steel from corrosion in condensate. pH values in some geothermal brines may be highly buffered by a heavy presence of bicarbonate ions. Therefore the input of pH value alone may suffice to adjust for eventual changes throughout the power station.

Dissolved Solids

Salinity The importance of this parameter is related to geothermal brine characterization. Residual salinities may also be found in separated steam (from carryover of brine). Salinity impacts heavily on scaling problems, corrosion behavior of steel and other alloys, environmental control, etc.

Power station design includes concentrating brines by flashing the steam from them as well as cooling brines, and then mixing the brines and condensates. All this impacts the salinity and solubility of the solids constituting the brine. Some references [22] consider salinity as dissolved "solids" in water.

At geothermal power extraction pressures and temperatures, solids solubility can either increase continuously with temperature (at saturated water vapor) or decrease [22]. Such behaviors are more complex due to pH changes and gas involvement. Design and further operation have to handle solubility issues to avoid scale plugging (resulting in oversaturation of individual salts and their precipitation). Refer to following paragraph (waste brine scale potential).

Scale in Disposed Geothermal Fluid The common problem discussed in literature [21, pp. 124–128] is the "silica" issue. Here the chemistry is problematic as the resource is at higher temperatures. Silica (SiO_2) solubility in the hot reservoir is controlled by the crystalline quartz form. At lower temperatures, solubility is controlled by amorphous silica typical to waste brine. Other forms of silica may be found in geothermal precipitates as shown in Fig. 3.

The dominant scale precipitate is of amorphous silica which at intermediate temperature possesses higher solubility than the quartz (brine is "supersaturated" with quartz but undersaturated with amorphous silica).

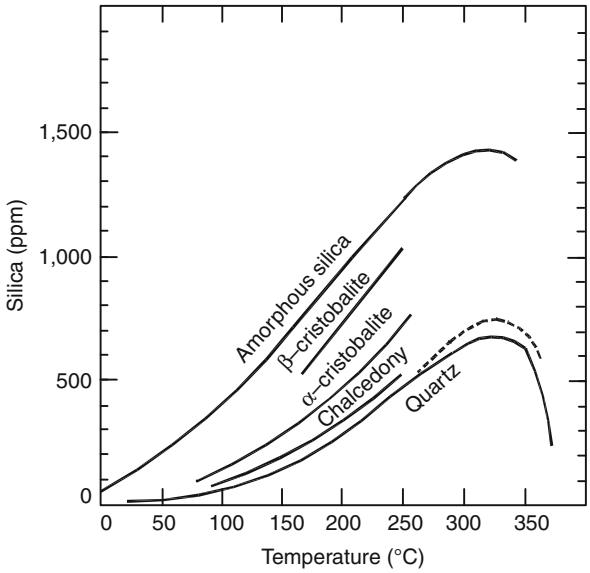

Geothermal Power Conversion Technology. Figure 3 Solubility of various forms of silica in water at saturated water vapor pressures [22, p. 146]

With proper process design it is possible to avoid precipitation of amorphous silica while the fluid is traveling through the station components. It is definitely possible for precipitation to occur in the injection wells or in the reservoir once the waste fluid returns to the formation. This adversely affects the formation permeability, reducing the injectability of the waste fluid. Any reheating of the waste brine in the formation reduces the potential for precipitation in the reservoir [21, p. 124]. Further aspects of silica precipitation see in [21, pp. 125, 126, 128].

The solubility of silica is not only a function of fluid temperature but also of salinity and pH. The figures shown above are for pure water. Qualitatively, for a given temperature and pH of aqueous solutions, the higher the salinity (i.e., higher molarity), the lower the solubility of both quartz and amorphous silica. For a given temperature and salinity, the solubility of amorphous silica is essentially independent of the pH for low (acidic) values, but rises dramatically as pH climbs above neutral, i.e., pH > 7. The effect is more pronounced for fluids with high salinity.

Precipitation kinetics plays a critical role in the scaling potential in geothermal station components. If precipitation can be slowed it may be possible to process the fluid and dispose of it before scaling can occur. Alternatively, if the precipitation can be accelerated, it may be possible to force the fluid to give up its scale-causing minerals in a rapid and controlled manner before it enters the station proper, allowing the purged fluid to be used without fear of further precipitation. Both of these effects have been used at stations near the Salton Sea in the Imperial Valley of the USA where highly mineralized, corrosive brines are present. There are five parameters that influence the kinetics of the silica precipitation (essentially a polymerization process):

- Initial degree of super saturation (i.e., actual SiO_2 concentration – equilibrium concentration)
- Temperature
- Salinity or molarity of the solution
- pH of the solution
- Presence (or absence) of colloidal or particulate siliceous material

The first and second factors can be controlled by proper selection of separator and flash conditions for a given geothermal fluid. The third factor is a fluid characteristic that cannot be controlled. The fourth and fifth factors can be adjusted as the fluid moves through the station from the production wells, through pipes, other components and eventually to the injection wells. When the brine is acidified, the rate of precipitation is very slow and the fluid can be viewed as temporarily stabilized. As the pH is raised, the precipitation rate increases dramatically, reaching a maximum at near-neutral pH values, about 6.0–7.5, and then slowing as pH approaches 9.0–9.5. The rates for pH = 5.3 and pH = 9.0 are roughly the same.

The last factor in the list has been utilized successfully for the Imperial Valley stations. Geothermal fluid is "seeded" with silica particles in large vessels called flash-crystallizers. These provide favorable precipitation sites for the supersaturated solution. After two stages of this process, the precipitated silica is removed, dried, compacted and disposed of. The generated steam is ready for use in turbines and the waste liquid is sufficiently clean for reinjection without fear of clogging the reservoir.

The potential for silica precipitation is mitigated to some degree when binary stations are used as the geothermal fluid is not flashed, but only cooled. Thus, there is no increase in the concentration of silica as the fluid passes through the station. Flow design in binary stations keeps the fluid in the safe region below the amorphous silica equilibrium curve. In comparison to a flash station, this allows the geothermal fluid to be cooled to a lower temperature before silica precipitation occurs.

Entrained Solids Entrained solids consist of sand and clay particles requiring temporary or permanent filters (stand or centrifugal type) to avoid corrosion damage to pipes and heat exchangers as well as clogging of the injection wells.

Material Selection in Geothermal Power Stations This issue was presented and discussed by Kestin in the Source Book on the *Production of Electricity from Geothermal Energy*-Chap. 3 [16], See Table 2.

Different applications within the power station face different requirements which are not only related to mechanical design, but also to durability problems arising from the contact with the complex geothermal environment.

Metallic Materials Most of the construction materials used in such stations are metallic. Performance of metals and alloys in geothermal power stations has

Geothermal Power Conversion Technology. Table 2
Typical turbine element materials [16]

Component	Material
Piping	ASTM A106, Gr B; ASTM A335, GrP11 or P22
H.P. castings	ASTM A356, k Gr I, 6, 9 or 10
L.P. castings	ASTM A285 or A515
Valve bodies	ASTM A216 or A217
Fasteners	ASTM A193 and A194
Rotors	ASTM A470
Blades	AISI 403
Nozzle blades	AISI 403
Bands	AISI 405

long been studied in respect to durability against availability, ease, and cost of fabrication (as in the use of steel and iron base alloys).

Furthermore, mechanical design may reach a conflict with special types of corrosion (sulfide stress cracking) that might occur during the use of some equipment made of high-strength ferrous alloys.

Different types of corrosion and environmentally assisted cracking mostly dictate the materials selection in geothermal power stations. The following corrosion and cracking forms can appear:

- Generalized (or "uniform") corrosion
- Localized corrosion (pitting, "crevice")
- Stress corrosion cracking (mostly induced by chloride ions)
- Sulfide stress cracking
- Fatigue corrosion (synergistic effect of cyclic stress and corrosion)
- Erosion-corrosion (accelerated corrosion by impingement of particles, gas bubbles, droplets, or too high fluid velocity)

Poor operating conditions might impact durability, even after applying a good design and materials selection. Among these conditions:

- "Shutdown corrosion," mostly generating or accelerating uniform and localized attack due to air (oxygen) ingress, water stagnation, corrosion products transformation. This corrosion is caused by frequent or long-term shutdowns without proper preservation actions.
- Bad monitoring or no application of designed corrosion inhibitors added to geothermal fluid.
- Bad or no monitoring of the designed steam quality.
- Unsuitable locally made repairs (like welding).
- Introduction of new geothermal fluid resources.
- Change of flow and temperature conditions.

Geothermal steam turbines are normally fed directly from the production wells, after separation from brine or as slightly superheated steam. Corrosive gases and entrained salts (from brine carryover) impose serious design problems on the turbine, steam transportation system and other ancillary parts. The situation may be more complex due to variations in steam composition (even at the same station).

Geothermal steam turbine manufacturers have established standards for materials selection based on manufacturer experience and material testing:

- For turbine rotors (forgings), some [24] used "low chrome-moly" steel (CrMo steel) and others [16] used "chrome-moly-vanadium" steel or "nickel-chrome-moly-vanadium" steel.
- For moving blades 13 chromium stainless steel.
- For the casings, grey cast iron or carbon steel.
- For steam pipes (large diameter) and silencers, rolled steel.

Sometimes cladding or coating is applied on critical parts:

- Epoxy coating on carbon steel exhaust duct and discharge pipes.
- "Stellite" hard facing on governing valve disc made of cast steel or on check valve made of forged steel [25].
- Austenitic stainless steel type 316L (S.S. 316L) was used as cladding on carbon steel used for condenser shell and for steam separator casing.

Steam turbine equipment also consists of other related parts in contact with steam, separated wet gases and wet air which comprise (partial list):

- Ejectors exhaust and tail pipes (S.S. 316L), condenser spray nozzles (S.S. 316L)

In binary geothermal power stations that are using organic fluids (propane, butane or pentane) there is no corrosion on the motive fluid side. This enables the choice of materials based on mechanical strength only, (i.e., low alloy carbon steel, aluminum or titanium for high speed centripetal expanders) such as low alloy carbon steel, aluminum or titanium for high speed centripetal expanders. The main corrosion issue is encountered in the piping and tubing parts in contact with the geothermal fluid. In most such applications, the use of mild steel benefits from the total deaeration of the geothermal brines which naturally occurs at normal pressurized fluid conditions. Separated brines also benefit from the loss of corrosive CO_2 and H_2S, (of which a high proportion escapes with the separated steam), and of the resulting higher pH. Both factors (oxygen and pH) may contribute to lower corrosion rates and to

reasonable durability of such low-cost material. In some cases, high salinities or high sand content may generate localized corrosion, erosion-corrosion or under-deposit corrosion, requiring different materials such as stainless steel (including duplex) or titanium.

Due to the high presence of corrosive CO_2 in such a fluid, special precautions must be applied on transporting downhole pumped brines inside mild steel piping.

When thin wall tubing (heat exchangers used to evaporate or preheat the working fluid) is applied, stainless steel or even Titanium is selected. Recently, "duplex" stainless steel tubes have been successfully used [23].

Atmospheric Corrosion Geothermal power stations' atmospheric environment might also have an abnormal presence of H_2S and NH_3 gases. These gases together with humidity can attack copper and other metallic materials. This is in addition to carbon steel rusting due to CO_2 presence with steam escaping into the atmosphere.

Galvanized steel, stainless steel, aluminum, and epoxy coatings are preferably used against atmospheric corrosion. Electronic equipment requires special attention, i.e., pressurized shelters, corrosion resistant contacts, and appropriate insulation.

Nonmetallic Materials While nonmetallic materials are not useful in heat transfer equipment (used only for sealing purposes), such materials find use in the transportation of cooled brines or cooling water pipes (made of fiber reinforced plastics (FRP) or polyethylene).

Internally cement-coated steel pipes are used to transport hyper saline geothermal brines. Cements also find large applications in geothermal well completion and civil works.

Thermodynamic Analysis of the Energy Conversion Process

Introduction

For a comprehensive thermodynamic analysis including Energy analysis applied to geothermal power systems from fluid supply to energy conversion including ancillary equipment (separators, cooling towers, etc.) [33].

Available Energy

Energy Conversion Process in Geothermal Power Stations It is assumed that geothermal fluids are utilized in continuous steady state in the energy conversion process. This assumption allows thermodynamic analyses of such systems whether water or steam dominated. The First and Second Law of thermodynamics are used to calculate the maximum available energy and the expected cycle efficiency.

First and Second Law of Thermodynamics The First Law of thermodynamics is the application of the conservation of energy principle to heat and thermodynamic processes.

Maximum Mechanical Energy Available Kestin [26] converting heat into mechanical energy is governed by the Second Law. The maximum mechanical energy which can be obtained from the geothermal fluid provided by a constant temperature (T_H) reservoir is achieved by using an ideal heat engine (the Carnot engine). This produces work and discards heat into a low constant temperature (T_L) reservoir.

The maximum conversion efficiency is expressed by:

$$\eta_C = \frac{T_H - T_L}{T_H} \tag{4}$$

T-Q diagrams are used to allow direct energy analysis of the heat source and heat utilization. A T-Q diagram of the general Carnot cycle of Fig. 4a is given in Fig. 4b. The above is applied to the four different categories of fluids obtained from geothermal sources where T_H and T_L are the absolute temperatures of the heat source and heat sink.

Dry Steam The supply of steam can be considered a constant temperature heat source where the ambient can be considered a constant temperature heat sink.

The relevant T-Q diagram is given in Fig. 5 which is similar to that of Fig. 4b.

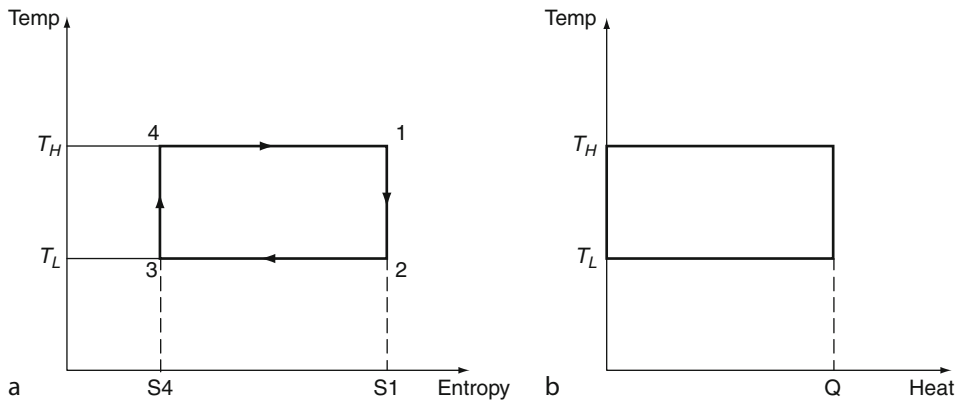

Geothermal Power Conversion Technology. Figure 4
T-S (**a**) and T-Q (**b**) diagrams showing the available mechanical energy

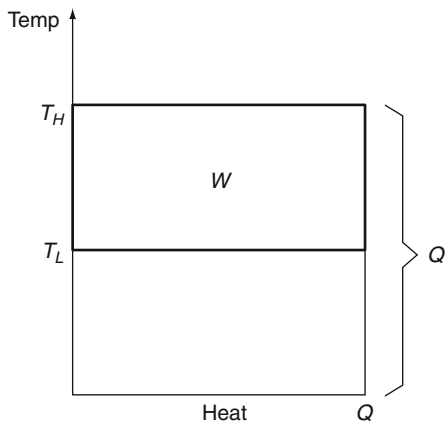

Geothermal Power Conversion Technology. Figure 5
T-Q diagram of dry-steam utilization

$$\eta_C = \frac{T_H - T_L}{T_H} \tag{5}$$

Where Q is the heat source and W, the corresponding work obtained:

$$W = \frac{T_H - T_L}{T_H} Q \tag{6}$$

Pressurized Water In this case, the temperature of the heat being transferred to the cycle by the geothermal water drops during the heat transfer operation and therefore Eq. 5 does not apply here. To calculate maximum efficiency the cycle is represented by a series of infinitesimally narrow Carnot cycles between temperatures T_H and T_L, see Fig. 6a.

Therefore for each engine i:

$$\mathrm{d}W_i = \frac{T_i - T_L}{T_i} \mathrm{d}Q \tag{7}$$

and for the cycle:

$$W = \int_O^Q \frac{T - T_L}{T} \mathrm{d}Q = \left[1 - \frac{1n\frac{T_H}{T_L}}{\frac{T_H}{T_L} - 1}\right] Q \tag{8}$$

The efficiency is:

$$\eta = 1 - \frac{1n\frac{T_H}{T_L}}{\frac{T_H}{T_L} - 1} \tag{9}$$

Steam Dominated:

1. "Dry Steam" (majority of energy in the steam)
2. "Pressurized Water" (majority of energy in the water or sensible heat part) (Fig. 7).

If Q is the total heat constant of the fluid and r is the ratio of the latent heat portion of the total heat. Then the maximum efficiency of mechanical energy available from this source is:

$$W = \left\{ \left(\frac{T_H - T_L}{T_H}\right) r + (1 - r) \left[\frac{1 - \ln\frac{T_H}{T_L}}{\frac{T_H}{T_L} - 1}\right] \right\} Q \tag{10}$$

Liquid Dominated Liquid-dominated case is as in the section on "Steam Dominated" with most of the energy in the water or brine portion. The formula here is the same but the maximum available mechanical energy

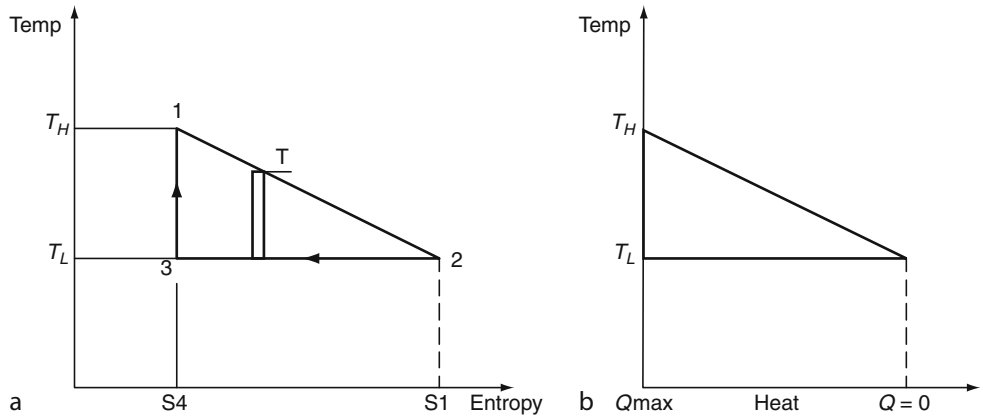

Geothermal Power Conversion Technology. Figure 6
T-S (**a**) and T-Q (**b**) diagrams for pressurized or low-temperature water cycle

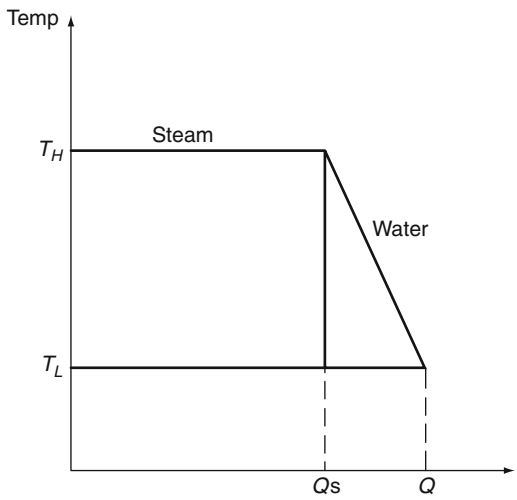

Geothermal Power Conversion Technology. Figure 7
T-Q diagram for steam-dominated cycle

(or efficiency) from the same total heat is smaller due to smaller r (Fig. 8). In both cases above the combined efficiency depends on r and is expressed by:

$$Ws = w\left\{\left(\frac{T_H - T_L}{T_H}\right)r + (1-r)\left[\frac{1-\ln\frac{T_H}{T_L}}{\frac{T_H}{T_L}-1}\right]\right\}Q \tag{11}$$

Maximum Specific Power Using Eq. 11, the maximum specific energy (kW) contained in a unit mass flow (kg/s) of a given heat source, which corresponds to maximum specific power (kW s/kg) is:

$$Ws_{\max} = \dot{W}_{\max}/\dot{m} = h_1 - h_0 - T_0(s_1 - s_0) \tag{12}$$

In Eq. 12, state 1 corresponds to the fluid high-temperature condition and state 0 corresponds to the ambient or heat sink condition.

For a given fluid, a fixed T_0 and reinjection temperature of the geothermal fluid T_{gf}^{out}, having a minimum value of T_0, the maximum work (per unit weight of geothermal fluid) possible from an ideal, reversible process is a function of T_{gf}^{int} only, the geothermal source temperature. Calculations of the relevant curves are given Fig. 9 for both saturated geothermal steam and water. Any real process will have inefficiencies or nonreversible steps that will result in net work less than Ws.

The curves in Fig. 9 allow quick assessment of the maximum power output that can be achieved from a geothermal well producing either water or steam or both. The required parameters are the fluid mass flow rate (in kg/s), fluid mass equilibrium initial temperature, and the ambient temperature or cooling water temperature.

The Temperature Limitation

- The maximum temperature at the inlet to the turbine is T_H, which is the temperature at the well head.

  In practice, the inlet temperature to the turbine is lower because of either the flashing process or the heat transfer in the evaporator.

- The lowest possible temperature T_L of the heat sink (the temperature of condensation at the turbine exhaust) is the ambient temperature T_0.
  - In practice this temperature is higher because of the irreversibility condensers, evaporator, pre-heaters, and cooling towers.

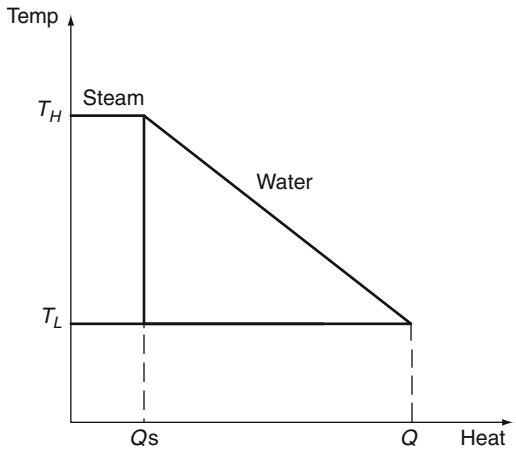

Geothermal Power Conversion Technology. Figure 8
T-QS diagram for liquid-dominated cycle

Power Conversion Processes Cycles

Steam Rankine Cycle Dry-steam power stations were the first type of geothermal power stations to achieve commercial status. The first small steam engine was operated in 1904 at Larderello in the Tuscany region of Italy [12].

Dry-steam power stations are simpler and less expensive than flash-steam or binary power stations as there is no geothermal brine to deal with.

Large dry-steam reservoirs have been discovered only in two areas of the world, Larderello and The Geysers. There are limited dry-steam areas in Japan (Matsukawa), Indonesia (Kamojang), New Zealand (Poihipi Road section of Wairakei) and the USA (Cove Fort, Utah). White [27] estimated that only about 5% of all hydrothermal systems with temperatures greater than 200°C are of the dry-steam type.

The general characteristic of a dry-steam reservoir is that it comprises of porous rocks featuring fissures or fractures, either occluded or interconnected, that are filled with steam. Whereas the steam also contains gases such as carbon dioxide, hydrogen sulfide, methane and others in trace amounts, there is little or no liquid present.

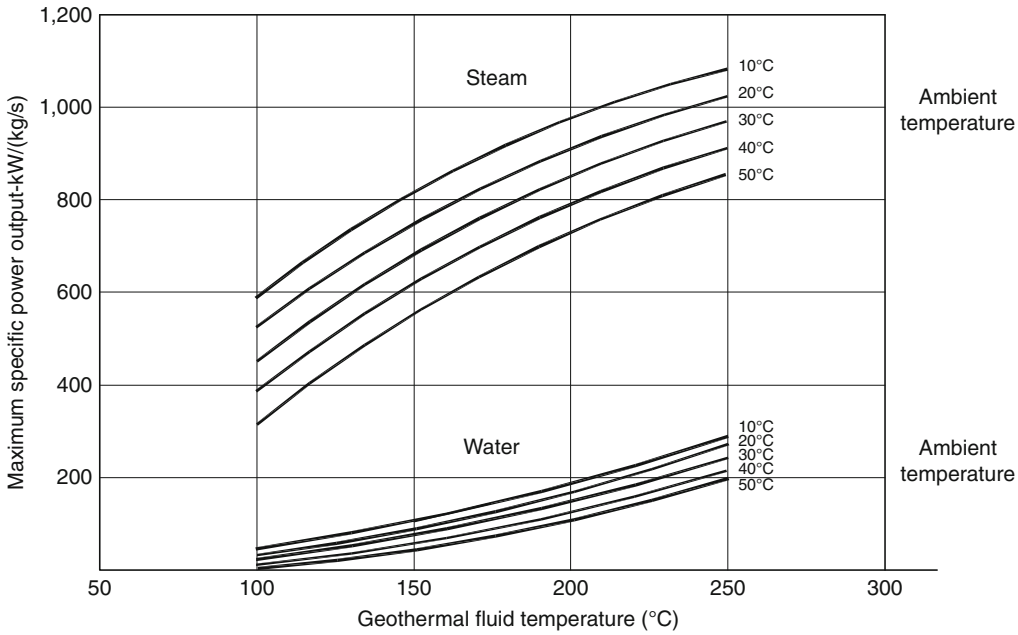

Geothermal Power Conversion Technology. Figure 9
Maximum specific power output as function of geothermal fluid (steam and water) temperature and ambient temperature

The dry steam extracted from the mentioned resources is either saturated or slightly superheated at temperatures near 235°C and at a pressure near the maximum saturation in Mollier curve (30.7 bar). Isenthalpic pressure loss in the upper layers explains the superheated condition at the turbine inlet. Steam from dry-steam reservoirs is superheated due to the pressure drop during the flow through the hot rock at constant temperatures. James [28] estimated the superheating of up to 35°C (above the saturation point). Typical dry-steam power conversion system is given in Fig. 10. The steam only needs final purifying before being sent to the turbine with the condensate used as makeup for the cooling tower. The wastewater collected at the bottom of the purifier and the blow-down of the cooling tower are injected to the aquifer. This eliminates environmental problems and helps in renewal of the aquifer liquids balance.

The power conversion section of a single-flash system is similar to that of dry steam except for the steam preparation that requires adequate separation between the steam and water ahead of the steam purifier as given Fig. 11.

Expansion Process Thermodynamic state diagrams are used for easy understanding of the fluid working cycle. A temperature–entropy (T-S) diagram for the single-flash station is shown in Fig. 12. The Mollier h-s diagram that is alongside it may be preferred as the vertical axis shows the exact turbine work $h_4 - h_5$, and it is easily used for efficiency evaluation. The turbine efficiency in the wet zone is lower than in the dry zone mainly due to appearance of small droplets in the expanding steam. To find the turbine efficiency, use a Mollier diagram as in Fig. 12 where $\Delta h_{is} = h_4 - h_{5S}$. Make a first assumption of 0.8 which finds X_{51},

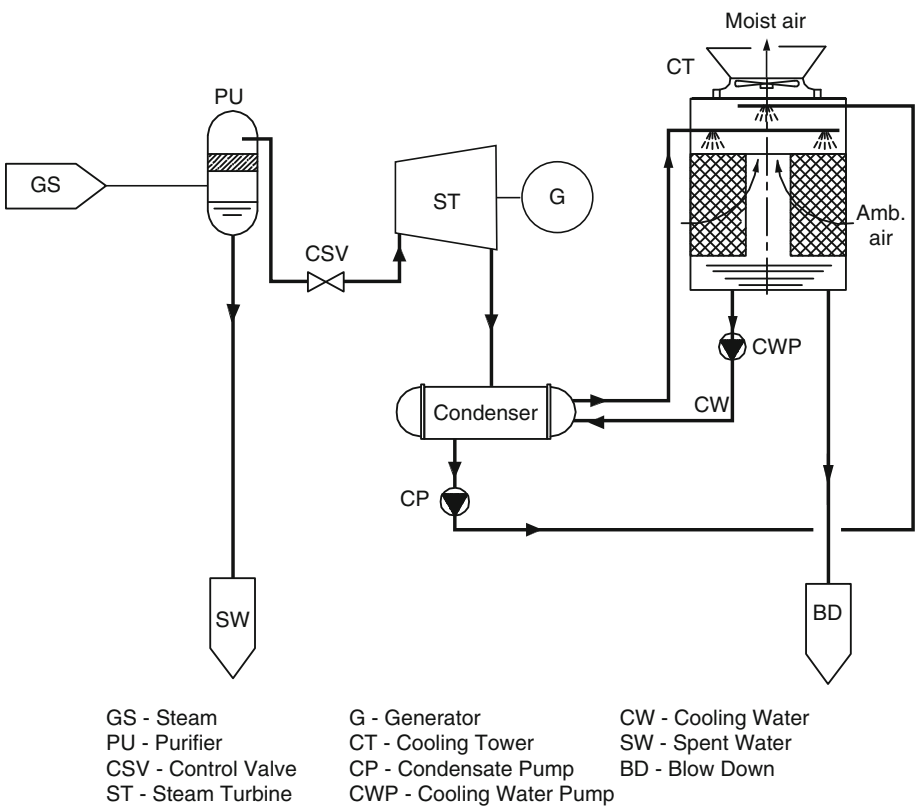

Geothermal Power Conversion Technology. Figure 10
Power conversion system for dry steam

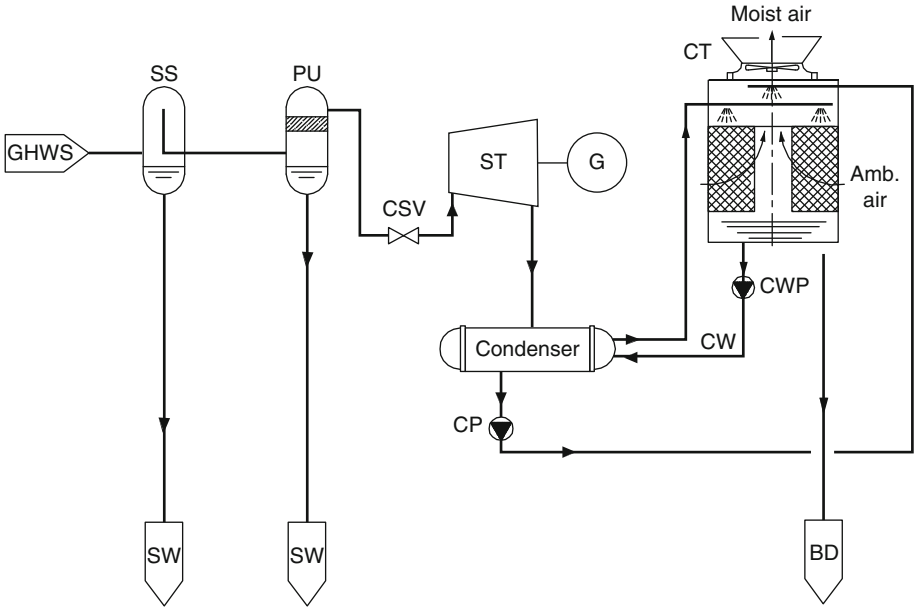

GHWS - Steam and Water
SS - Steam Separator
PU - Purifier
CSV - Control Valve
ST - Steam Turbine
G - Generator
CT - Cooling Tower
CP - Condensate Pump
CWP - Cooling Water Pump
CW - Cooling Water
SW - Spent Water
BD - Blow Down

Geothermal Power Conversion Technology. Figure 11
Power conversion system for single-flash steam supply

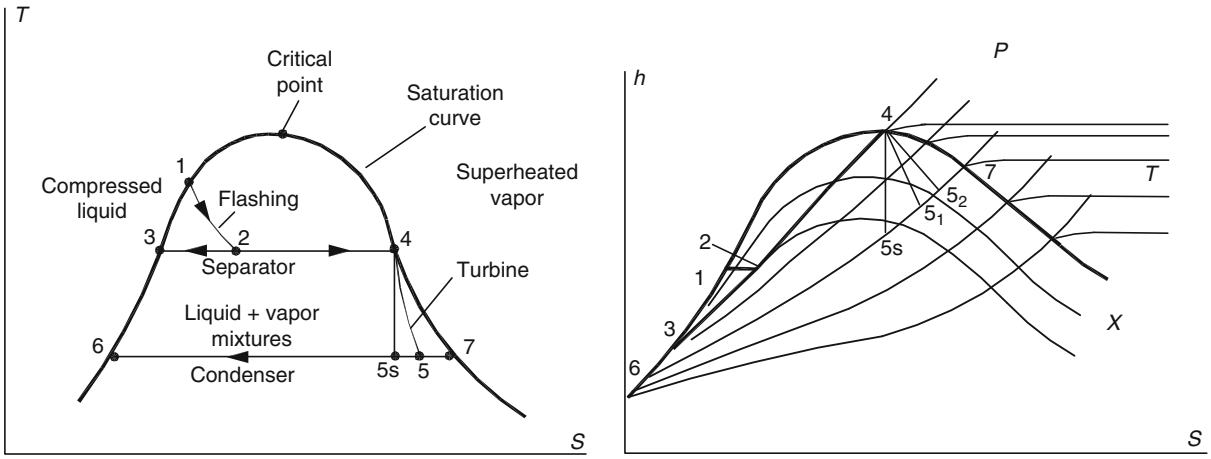

Geothermal Power Conversion Technology. Figure 12
T-S and H-S state diagrams for single-flash stations

(steam dryness at state point 51. The dryness fraction is x = Mass of dry steam/Total mass of wet steam). According to this the turbine efficiency can be found by use of the information on turbine efficiency in the dry and wet zones according to Bauman in [29] or Thermoflow practical assumptions [30].

$$\Delta h_{\text{first}} = h_4 - h_{51} = 0.8^{*}\Delta h_{\text{is}} \rightarrow X_{51} \rightarrow \eta_{\text{isw}} = \eta_t \tag{13}$$

From η_t obtain the final enthalpy drop:

$$\Delta h_{\text{final}} = h_4 - h_{52} = \Delta h_{\text{is}}{}^{*}\eta_t \tag{14}$$

The steam process of a fuel-driven dry-steam station with and without superheating is shown in Fig. 12. Water is pumped to the boiler (1–2), heated (2–3–4), steam is produced that expands from point 4 to 6 in the non-superheated or from 4 to 6 in the superheated case. At the lower pressure the steam is condensed and pumped back to the boiler to complete the cycle (Fig. 13).

In the geothermal dry-steam case the cycle is partial. Since the wells produce saturated steam (or slightly superheated steam), the starting point is located on the saturated vapor curve. The turbine expansion process 1–2 generates less power output than the ideal, isentropic process 1–2s. Heat is rejected to the surroundings in the condenser via the cooling water in process 2–3.

The actual work produced by the turbine per unit mass of steam flowing through it is given by:

$$w_1 = h_1 - h_2 \tag{15}$$

The maximum possible work would be generated if the turbine operated adiabatically and reversibly, i.e., at constant entropy or isentropically. Therefore, the isentropic turbine efficiency η_t, is the ratio of the actual work to the isentropic work, namely:

$$\eta_t = \frac{h_1 - h_2}{h_1 - h_{2s}} \tag{16}$$

The power developed by the turbine is given by:

$$\dot{W}_1 = \dot{m}_s w_1 = \dot{m}_s(h_1 - h_2) = \dot{m}_s \eta_t (h_1 - h_{2s}) \tag{17}$$

The gross electrical power will be equal to the turbine power multiplied by the generator efficiency:

$$\dot{W}_e = \eta_g \dot{W}_1 \tag{18}$$

The net power is further reduced by all parasitic loads including condensate pumping power, cooling tower fan power, etc.

High-Pressure and Low-Pressure Turbine Expansion Processes The processes for the double-flash turbine are shown in Figs. 14 and 15 below. The second flash is of the brine separated by the first steam separator.

Using the assumptions of no heat losses, no change in potential and kinetic energy as in a single-flash system, (refer to "Expansion Process"), the power generated by each separated stage of the turbine can be evaluated.

The expansion work of the HP-stage is expressed by:

$$w_{\text{hpt}} = h_4 - h_5 \tag{19}$$

As in the case of the single flash the efficiency is:

$$\eta_{\text{hpt}} = \frac{h_4 - h_5}{h_4 - h_{5s}} \tag{20}$$

Accordingly, the total work depends on the mass flow:

$$\dot{W}_{\text{hpt}} = \dot{m}_{\text{hps}} w_{\text{hpt}} = x_2 \dot{m}_{\text{total}} w_{\text{hpt}} \tag{21}$$

X_2 is dryness at state 2 (see Fig. 15). The actual outlet state from the high-pressure section of the turbine is found using the Baumann rule [29] and by use of a Mollier $h - s$ steam chart [31, 32].

$$h_5 = \frac{h_4 - A\left[1 - \frac{h_6}{h_7 - h_6}\right]}{1 + \frac{A}{h_7 - h_6}} \tag{22}$$

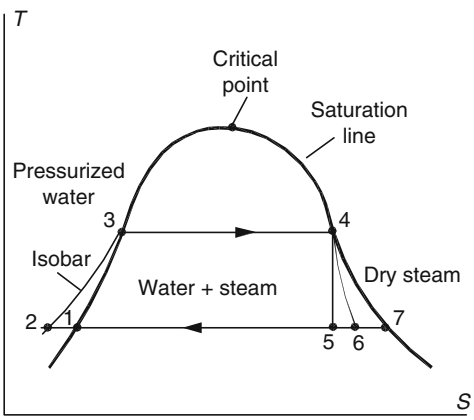

Geothermal Power Conversion Technology. Figure 13 Temperature-entropy diagram for dry-steam power station (steam saturated at the turbine inlet)

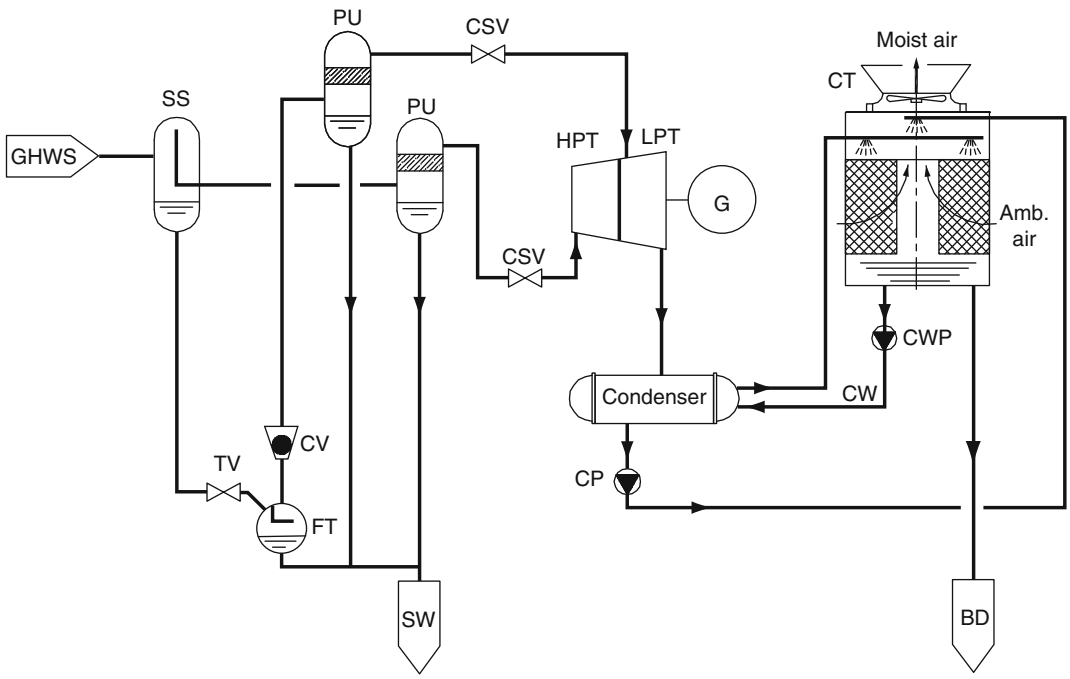

GHWS - Steam and Water
SS - Steam Separator
PU - Purifier
CSV - Control Steam Valve
HPT - High Pressure Turbine
LPT - Low Pressure Turbine
G - Generator
CT - Cooling Tower
CP- Condensate Pump
TV - Throttling Valve
CWP - Cooling Water Pump
CW - Cooling Water
SW - Spent Water
BD - Blow Down
CV - Check Valve
FT - Flash Tank

Geothermal Power Conversion Technology. Figure 14
Double-flash system with dual-pressure turbine

where the factor A is defined as:

$$A = 0.425(h_4 - h_5) \tag{23}$$

The low-pressure steam from the flasher is actually saturated vapor (state 8) which is admitted to the steam path and joins the partially expanded high-pressure steam at state 5. The mixed steam, ready to enter the low-pressure turbine stages is at state 9. The First Law of thermodynamics and conservation of mass allow finding the properties of the mixed state 9:

$$\dot{m}_5 h_5 + \dot{m}_8 h_8 = (\dot{m}_5 + \dot{m}_8) h_9 \tag{24}$$

$$h_9 = \frac{x_2 h_5 + (1 - x_2) x_6 h_8}{x_2 + (1 - x_2) x_6} \tag{25}$$

The low-pressure turbine may now be analyzed as follows:

$$w_{lpt} = h_9 - h_{10} \tag{26}$$

$$\dot{W}_{lpt} = \dot{m}_9 (h_9 - h_{10}) = (\dot{m}_5 + \dot{m}_8)(h_9 - h_{10}) \tag{27}$$

Again, using the Baumann rule [29] and steam Molier chart [31, 32]:

$$h_{10} = \frac{h_9 - A\left[x_9 - \frac{h_{11}}{h_{12} - h_{11}}\right]}{1 + \frac{A}{h_{12} - h_{11}}} \tag{28}$$

$$A = 0.425(h_9 - h_{10s}) \tag{29}$$

$$h_{10s} = h_{11} + [h_{12} - h_{11}] x \left[\frac{s_9 - s_{11}}{s_{12} - s_{11}}\right] \tag{30}$$

$$\eta_{\text{lpt}} = \frac{h_9 - h_{10}}{h_9 - h_{10s}} \tag{31}$$

The total power generated is the sum of the power from each turbine:

$$\dot{W}_{\text{total}} = \dot{W}_{\text{hpt}} + \dot{W}_{\text{lpt}} \tag{32}$$

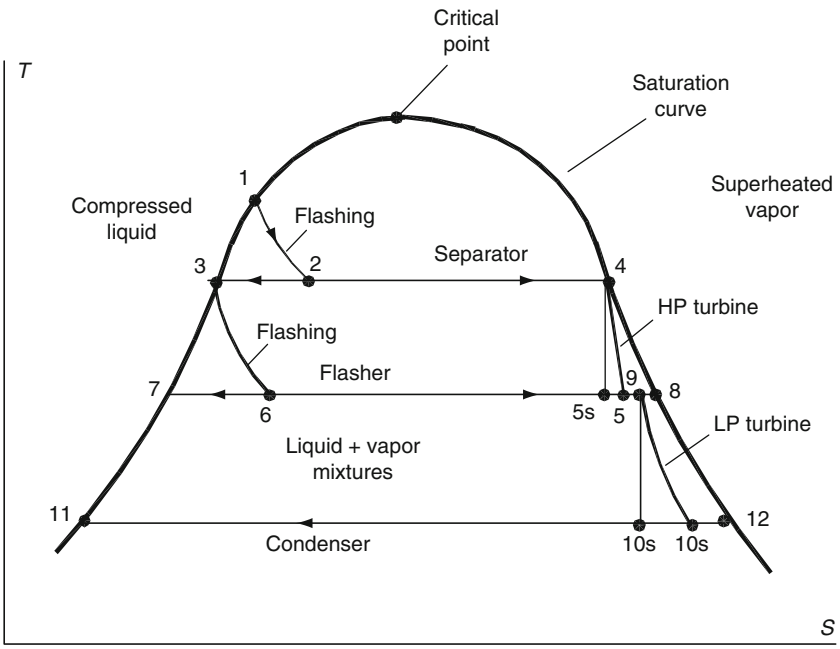

Geothermal Power Conversion Technology. Figure 15
Temperature-entropy process diagram for double-flash station with a dual admission turbine

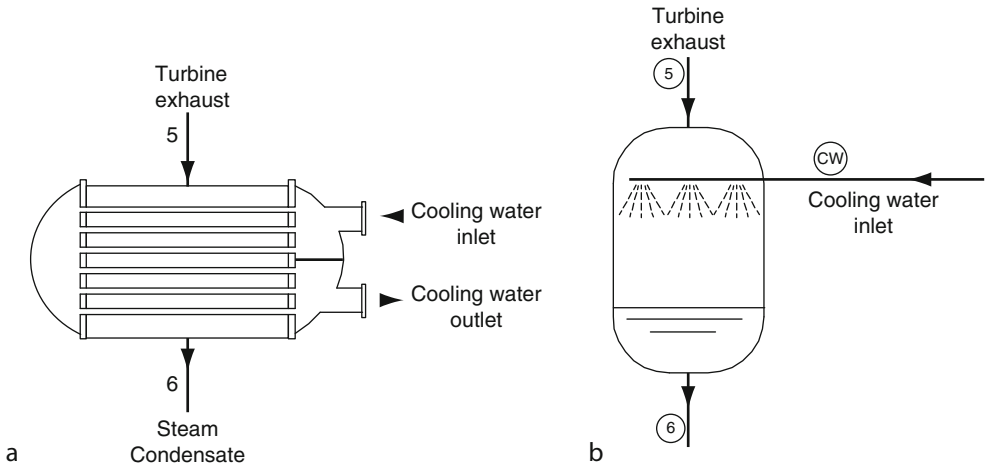

Geothermal Power Conversion Technology. Figure 16
Surface (**a**) and direct contact (**b**) condensers

Finally, the gross electrical power is found from:

$$\dot{W}_{e,\text{gross}} = \eta_g \dot{W}_{\text{total}} \tag{33}$$

Condensing Process In the use of surface-type condenser shown in Fig. 16a, the required flow rate of cooling water $\dot{m}_{\text{cw}}$ related to the steam flow rate $X_2 \dot{m}_{\text{st}}$ is expressed by the First Law of thermodynamics as:

$$\dot{m}_{\text{cw}} = X_2 \dot{m}_{\text{st}} \left[\frac{h_5 - h_6}{\bar{c}\Delta T} \right] \tag{34}$$

where $\bar{c}$ is the assumed constant specific heat of the cooling water (4.2 kJ/kg.K), ΔT is the rise in cooling water temperature at the condenser inlet and outlet and X_5 is the steam dryness stage at the turbine exit.

For a direct-contact condenser (Fig. 16), the equation is:

$$\dot{m}_{cw} = x_2 \dot{m}_{total} \left[\frac{h_5 - h_6}{\bar{c}(T_6 - T_{cw})} \right] \tag{35}$$

Overall Thermal Efficiency The performance of the entire station may be assessed using the Second Law of thermodynamics. This by comparing the actual power output to the maximum theoretical power that could be produced from the given geothermal fluid. This involves determining the rate of energy carried into the station with the incoming geothermal fluid.

The specific maximum energy of a fluid that has a pressure, P, temperature T in the presence of an ambient pressure P_0 and an ambient temperature T_0, is given by:

$$\dot{W}_{max} = h(T, P) - h(T_0, P_0) - T_0[s(T, P) - s(T_0, P_0)] \tag{36}$$

To get the maximum theoretical thermodynamic power, this term is multiplied by the total incoming geothermal fluid mass flow rate:

$$\dot{E} = \dot{m}_{total} \cdot \dot{W}_{max} \tag{37}$$

The ratio of the actual net power to the maximum power is defined [33] as the utilization efficiency or the Second Law efficiency of the station:

$$\eta_u \equiv \frac{\dot{W}_{net}}{\dot{E}} \tag{38}$$

Stations can be designed to maximize η_u when the value of the primary energy is a significant factor in the economics of the operation.

Organic Rankine Cycle Configurations For low-temperature resources, the efficiency of the flash steam cycle led many researchers to propose cycles which enhance the thermal efficiency and utilization of the geofluid energy content. Some of the ideas were executed into working power stations but did not mature into a commercial stage. The systems that are commercial begin with the simple Organic Rankine cycle (using pentane), or super critical cycles (using butane or flouro-carbons), geothermal combined cycle, and other additional similar concepts that will be discussed hereafter. The noncommercial, experimental ideas is included in section on "Experimental Power Stations."

Ideal Organic Rankine Cycle As already mentioned in "Pressurized Water," the hot water or brine is not an isothermal heat source as it cools while transferring heat to the working fluid. A more realistic ideal cycle for a geothermal binary station is a triangular cycle consisting of an isobaric (constant pressure) heat addition process up to the brine inlet temperature T_H, followed by an isentropic expansion and an isothermal heat rejection process at T_L to complete the cycle. See Fig. 17.

The efficiency for such a cycle was expressed in Eq. 9 as:

$$\eta_{TC} = 1 - \frac{T_L}{T_H - T_L} \ln\left(\frac{T_H}{T_L}\right) \tag{39}$$

For the same temperature range of 150°C and 40°C, the triangle cycle yields an efficiency of 14.3% compared with 26% for the constant temperature case.

Organic Rankine Cycle Based Power Generation Process Unlike dry-steam and flash-steam power stations, binary stations do not have condensate to serve as makeup for a water cooling tower. As a result, binary stations need a separate cooling medium, either fresh water or air.

In its simplest form, the binary station follows the schematic flow diagram in Fig. 18 for a water-cooled system [35] and in Fig. 19 for an air-cooled system [36].

The working fluids thermodynamic process are shown in Fig. 20. Due to the inclination of the saturation curve, the vapor expansion extends further into the superheated zone.

The main cycle components will be analyzed later using the state points on Fig. 20.

The supply of heat to the Organic Rankine cycle completes the conversion process and is shown in the two cases. The supply of hot water/brine or supply of steam as shown in Fig. 21. In (a) the sensible heat supply is only by hot water or brine, while in (b) the sensible heat and latent heat are from steam.

Hot geofluid is supplied to the evaporator and from there it flows to the preheater and is then returned to

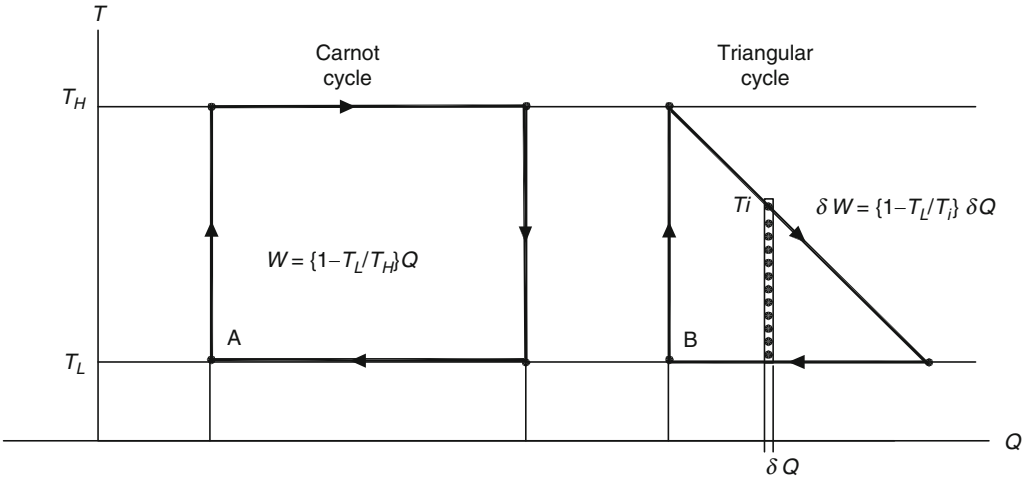

Geothermal Power Conversion Technology. Figure 17
Two ideal thermodynamic cycles: constant temperature and continuous reducing temperature

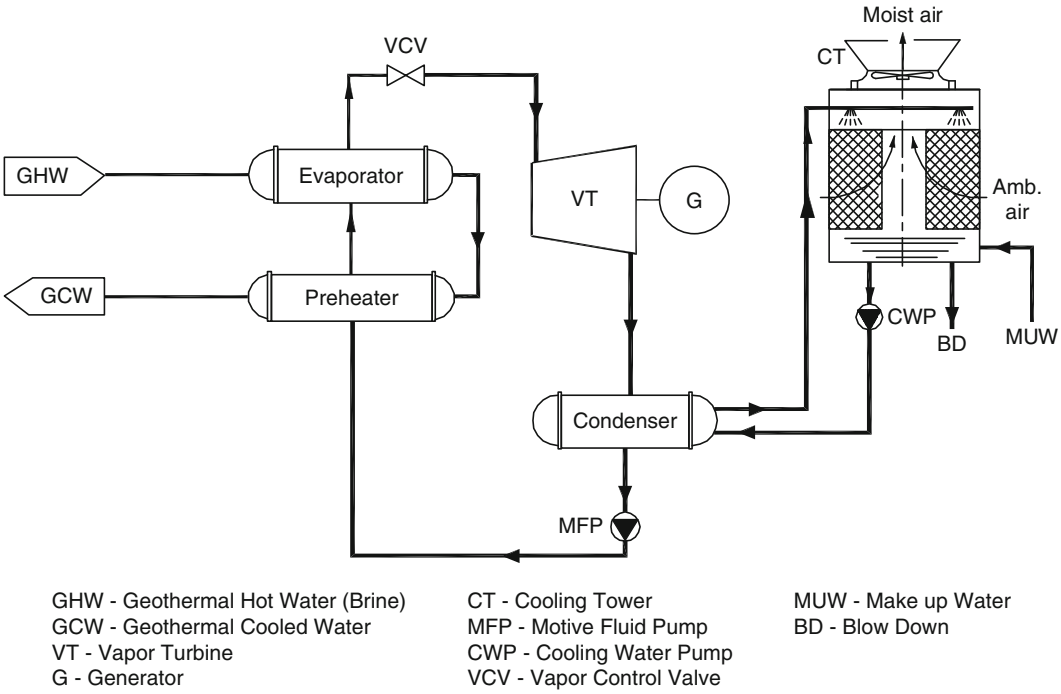

Geothermal Power Conversion Technology. Figure 18
Simplified schematic of a water-cooled binary geothermal power station [35]

the injection well. The working fluid flows through a preheater where it is brought close to its boiling point. It then flows to the evaporator E where it acquires the supplement heat of evaporation. Emerging as a saturated vapor it expands in the turbine, condenses in the condenser and is pumped back to the preheater via a feed pump.

Turbine Analysis The vapor expands in the turbine between points 1 and 2 of Fig. 20.

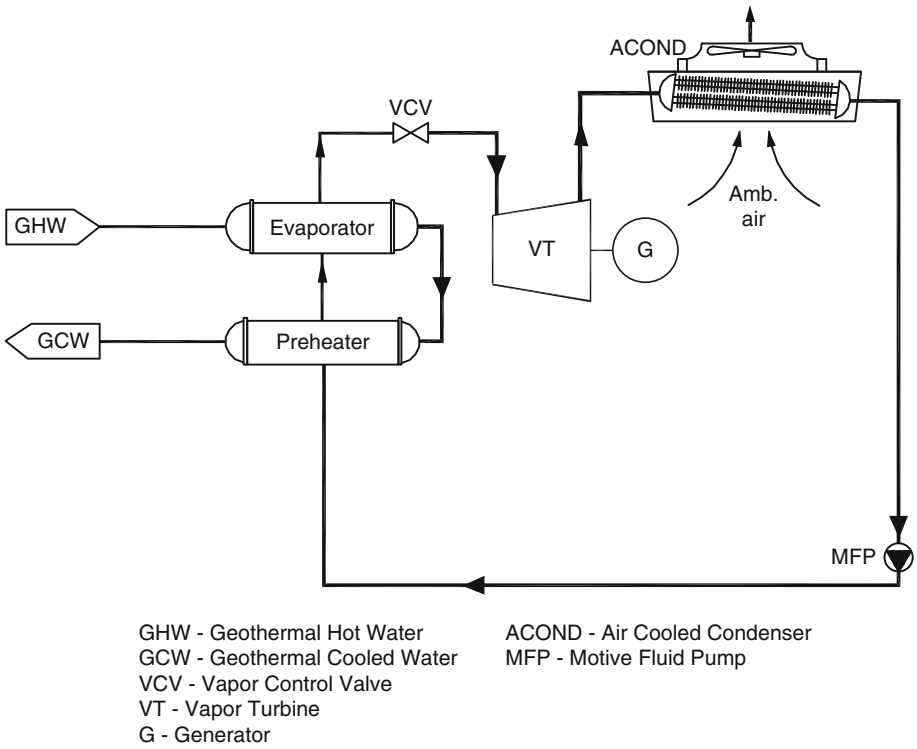

Geothermal Power Conversion Technology. Figure 19
Simplified schematic of an air-cooled binary geothermal power station [36]

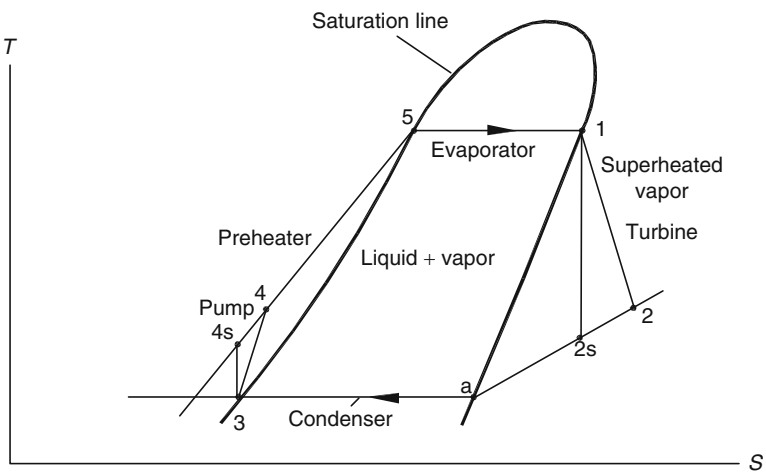

Geothermal Power Conversion Technology. Figure 20
T-S diagram showing a basic Organic Rankine cycle

Assuming the usual of steady adiabatic operation, the power is determined from:

$$\dot{W}_t = \dot{m}_{\mathrm{wf}}(h_1 - h_2) = \dot{m}_{\mathrm{wf}}\eta_t(h_1 - h_{2s}) \qquad (40)$$

where η_t is the isentropic turbine efficiency (known parameter – the organic working fluid $\dot{m}_{\mathrm{wf}}$ expands into the superheated zone). For a given working fluid, the thermodynamic properties can be found from fluid

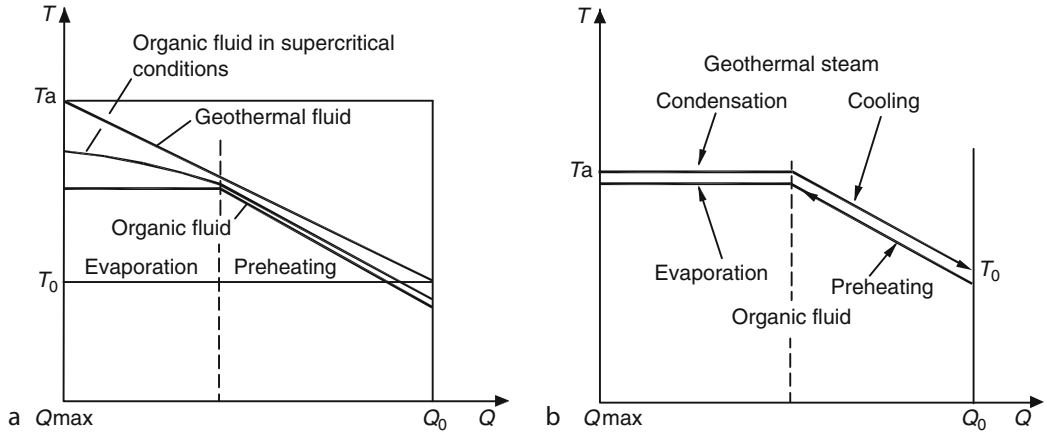

Geothermal Power Conversion Technology. Figure 21
T-Q diagrams of Organic Rankine cycle operated by (**a**) liquid and (**b**) geothermal steam

tables for selected design parameters. Selection of the turbine power output then helps determining the required working fluid mass flow rate.

Feed Pump Analysis Using similar assumptions as for the other components, the power imparted to the working fluid from the feed pump (points 3–4 of Fig. 20) is:

$$\dot{W}_p = m_{\mathrm{wf}}(h_4 - h_3) = \dot{m}_{\mathrm{wf}}(h_{4\mathrm{s}} - h_3)\eta_p \tag{41}$$

where η_p is the isentropic pump efficiency.

Condenser Analysis Condenser heat rejection occurs between points 2 and 3 on the cycle diagram in of Fig. 20).

The heat that must be rejected from the working fluid to the cooling medium, either water (shown here) or air, is given by:

$$Q_c = \dot{m}_{\mathrm{wf}}(h_2 - h_3) \tag{42}$$

The relationship between the flow rates of the working fluid and the cooling water is:

$$\dot{m}_{\mathrm{cw}}(h_{\mathrm{out}} - h_{\mathrm{in}}) = \dot{m}_{\mathrm{wf}}(h_2 - h_3) \tag{43}$$

Assuming a constant specific heat $\bar{c}$ for cooling water temperature between T_{out} and T_{in}, the cooling water mass flow rate can be found from:

$$\dot{m}_{\mathrm{cw}}\bar{c}(T_{\mathrm{out}} - T_{\mathrm{in}}) = m_{\mathrm{wf}}(h_2 - h_3) \tag{44}$$

or

$$\dot{m}_{\mathrm{cw}} = m_{\mathrm{wf}}\frac{(h_2 - h_3)}{\bar{c}(T_{\mathrm{out}} - T_{\mathrm{in}})} \tag{45}$$

Equation 44 will change to:

$$\dot{m}_{\mathrm{cair}}(h_{\mathrm{airout}} - h_{\mathrm{airin}}) = \dot{m}_{\mathrm{wf}}(h_2 - h_3) \tag{46}$$

Assuming constant specific heat Cp for air in the relevant temperature range and neglecting humidity influence then:

$$\dot{m}_{\mathrm{cair}}Cp_{\mathrm{air}}(T_{\mathrm{airout}} - T_{\mathrm{airin}}) = \dot{m}_{\mathrm{wf}}(h_2 - h_3) \tag{47}$$

or

$$\dot{m}_{\mathrm{cair}} = \dot{m}_{\mathrm{wf}}\frac{(h_2 - h_3)}{Cp_{\mathrm{air}}(T_{\mathrm{airout}} - T_{\mathrm{airin}})} \tag{48}$$

Preheater and Evaporator Analysis Heat transfer to the working fluid takes place between points 4 and 1 in Fig. 20. Firstly, there is preheating between points 4 and 5, followed by evaporation up to point 1.

Secondly, on the brine side there is a continuous cooling due to the heat transfer to the organic fluid. Viewing the entire package as the thermodynamic system, the prevailing equation is:

$$\dot{m}_{\mathrm{b}}(h_{\mathrm{a}} - h_{\mathrm{c}}) = \dot{m}_{\mathrm{wf}}(h_1 - h_4) \tag{49}$$

If the brine is considered as liquid only, then the left-hand side of the equation can be replaced by the

average specific heat of the brine $\bar{c}_b$ multiplied with the temperature drop:

$$\dot{m}_b \bar{c}_b (T_a - T_c) = \dot{m}_{wf}(h_1 - h_4) \tag{50}$$

The following equation can be used to find the required brine flow rate for a given set of cycle design parameters:

$$\dot{m}_b = \dot{m}_{wf} \frac{h_1 - h_4}{\bar{c}_b (T_a - T_c)} \tag{51}$$

The total energy transfer between the brine and the organic vapor takes place between clearly between points 4 and 1 shown in Fig. 22. This data is required for the design of the individual heat exchangers. The abscissa represents the total amount of heat passed from the brine to the working fluid and can be presented either in percent or in total heat flow per unit time (kJ/h).

The preheater provides sensible heat to raise the working fluid to its boiling point, state 5. The evaporation occurs from 5 to 1 along an isotherm for a pure working fluid. The point in the heat exchanger where the brine and the working fluid experience the minimum temperature difference is called the pinch-point

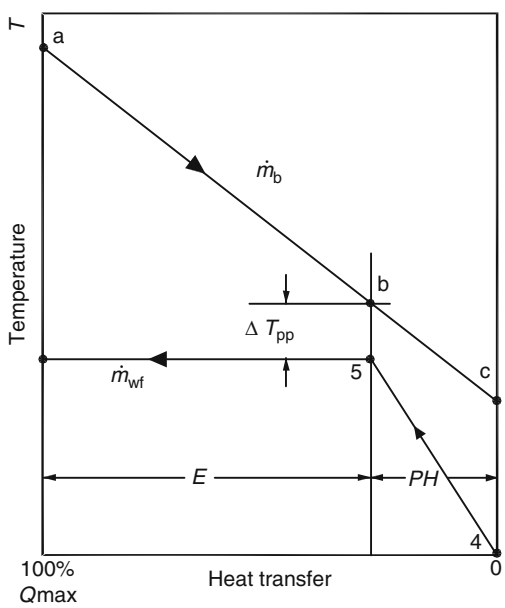

Geothermal Power Conversion Technology. Figure 22 Temperature-heat transfer diagram for preheater and evaporator

and is designated the pinch-point temperature difference ΔT_{pp} (see Fig. 22).

State points 4, 5, and 1 should be known from the cycle specifications. State 4 has the values of the compressed liquid at the outlet from the feed pump, state 5 is a saturated liquid at the boiler pressure, state 1 is a saturated vapor (same as at the turbine inlet condition). The geoliquid transfers heat to the evaporator from point a to point b, with the rest in the preheater down to point c. The two heat exchangers may be analyzed separately as follows:

$$\text{Preheater}: \quad \dot{m}_b \bar{c}_b (T_b - T_c) = \dot{m}_{wf}(h_5 - h_4) \tag{52}$$

$$\text{Evaporator}: \quad \dot{m}_b \bar{c}_b (T_a - T_b) = \dot{m}_{wf}(h_1 - h_5) \tag{53}$$

The brine inlet temperature T_a is always known. The pinch-point temperature difference is known from manufacturer's specifications. This allows T_b to be determined from the known value for T_5.

The evaporator heat transfer surface is between the two fluids A_E, and can be determined from the basic heat transfer relationship:

$$Q_E = \bar{U} A_E LMTD|_E \tag{54}$$

where $\bar{U}$ is the overall heat transfer coefficient and $LMTD|_E$ is the log mean temperature difference.

For detailed calculations see DiPippo [33].

Since heat exchangers can be built in a variety of geometrical arrangements (shell-and-tube, plate, parallel flow, counter flow, etc.), there are correction factors to be used with the equations given above depending on the configuration. Refer to [37], for more details.

Overall Cycle Analysis Organic Rankine cycle performance can be assessed by the First Law using the thermal efficiency:

$$\eta_{th} \equiv \frac{\dot{W}_{net}}{\dot{Q}_{PH+E}} \tag{55}$$

Since the net power of the cycle is the difference between the thermal power input and the rejected thermal energy, this formula can be rewritten as:

$$\eta_{th} = \frac{\dot{Q}_{PH+E} - \dot{Q}_t}{\dot{Q}_{PH+E}} = 1 - \frac{\dot{Q}_c}{\dot{Q}_{PH+E}} = 1 - \frac{h_2 - h_3}{h_1 - h_4} \tag{56}$$

ORC efficiency is low because of low source temperatures and after subtracting all the parasitic loads from the gross power output, the final cycle efficiency may result in about 10%.

Another measure of station performance can be obtained using the Second Law in the form of the utilization efficiency η_u, which is defined (see Eq. 38) as the ratio of the actual net station power to the maximum theoretical power obtainable from the geothermal fluid in the reservoir state:

$$\eta_u = \frac{\dot{W}_{\text{net}}}{\dot{E}_{\text{res}}} = \frac{\dot{W}_{\text{res}}}{\dot{m}_{\text{b}}[(h_{\text{res}} - h_0) - T_0(s_{\text{res}} - s_0)]} \quad (57)$$

where $\dot{E}_{\text{res}}$ is $\dot{W}_{\max}$ defined in the section on "Overall Thermal Efficiency," T_0 is the dead-state temperature (the local wet-bulb temperature if a water cooling tower is used), h_0 and s_0 are the enthalpy and entropy values for the geothermal fluid evaluated at the dead-state pressure and temperature (usually approximated as the saturated liquid values at T_0).

Recuperated Organic Rankine Cycle The efficiency of the Organic Rankine cycle described in the section on "Organic Rankine Cycle–based Power Generation Process" can be improved by recovering part of the heat of the superheated vapor before it enters the condenser (T_2 to T_a in Fig. 20) [53]. This is particularly important when there is limitation in the cooling temperature of the brine and condensate mixture. The silica scaling risk is the limiting factor in most of cases. It is increased as the brine temperature drops. In this case, the recuperator provides some of the preheating heat from the vapor, exiting the turbine.

The recuperator is applicable when the organic fluid is of the "dry expansion" type, where the expansion in the turbine is done in the dry superheated zone and the expanded vapor contains heat that has to be extracted prior to the condensing stage (Figs. 23 and 24). The recuperated Organic Rankine cycle is typically 10–15% more efficient than the simple Organic Rankine cycle described at the beginning of this chapter). This applies also to the two-phase geothermal power station as given in Figs. 25 and 26.

Temperature Cascading Organic Rankine Cycle A cascading system can be used to increase the power output of a binary power station [43]. In a simple cascading method there are two or more evaporators and preheaters, arranged in consecutive structure. The geothermal fluid travels from one pair of units to the

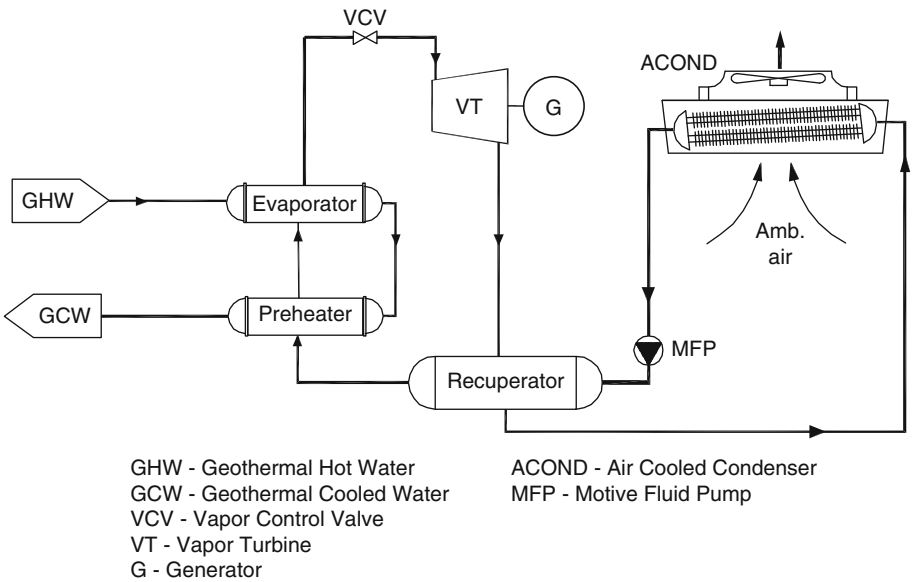

Geothermal Power Conversion Technology. Figure 23
Recuperated Organic Rankine cycle in simple binary power station – schematic

other. The station incorporates three sets of organic systems, each working in different ranges of temperatures. In an improved cascading design, the evaporators are arranged in series while the preheaters all work in the same temperature range [38]. Schematic design is given in Fig. 27.

The T-Q diagram describing this combination is in Fig. 28. Since evaporation is performed at three different temperatures, three turbines are required for such an operation.

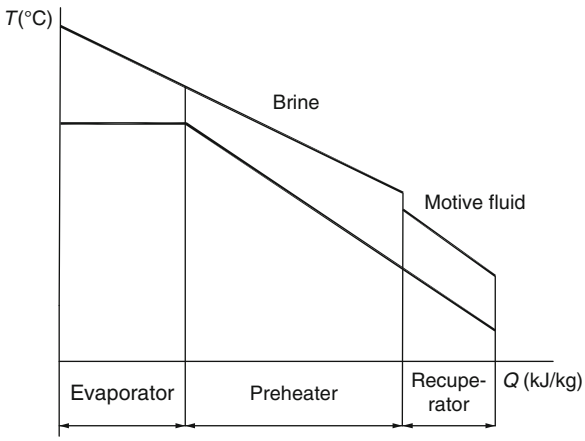

Geothermal Power Conversion Technology. Figure 24
Recuperated Organic Rankine cycle in simple binary power station

Dual-Pressure Organic Rankine Cycle A dual-pressure cycle is designed to reduce the thermodynamic losses incurred in the brine heat exchangers of the basic cycle. These losses are due to the transferring heat across a large temperature difference between the hotter brine and the cooler working fluid, see Fig. 29. By maintaining a closer match between the brine cooling curve and the working fluid heating/boiling curve, these losses can be reduced.

The dual-pressure cycle has a two-stage heating/boiling process that allows the two fluids to achieve a smaller average temperature difference than the one-stage process used in a basic cycle. A dual-pressure station schematic is given in Fig. 29 and the corresponding process diagram is shown in Fig. 30.

A dual-admission turbine is required to allow low-pressure saturated vapor (state 9) to be admitted to the turbine to mix with the partially expanded high-pressure vapor (state 2) to form a slightly superheated vapor (state 3). Given the small size of turbines using organic working fluids, practical considerations may lead to an alternative design using two separate turbines.

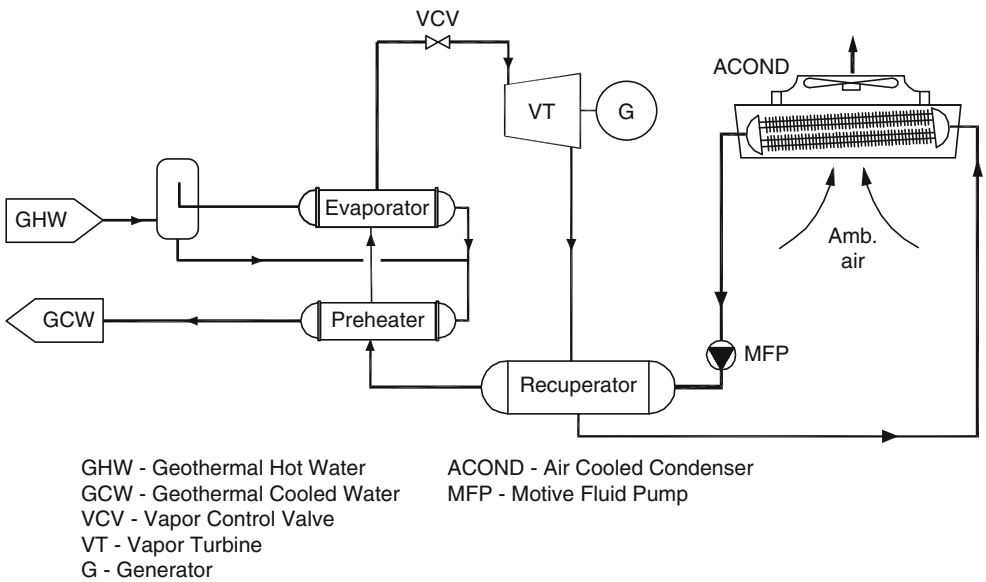

Geothermal Power Conversion Technology. Figure 25
Recuperated ORC in two-phase binary power station – schematic

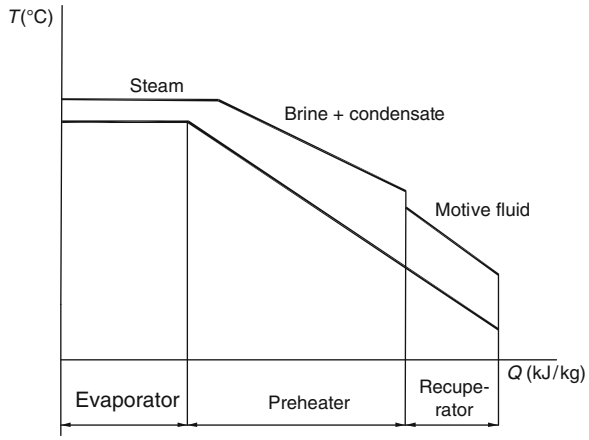

Geothermal Power Conversion Technology. Figure 26 Recuperated ORC in two-phase binary power station

The analysis of a dual-pressure cycle follows the same methodology as a basic cycle but takes more time. A detailed comparison of basic cycles (single-pressure) and the dual-pressure cycles was conducted by Khalifa and Rhodes [39] for two different working fluids. Their results show that in all cases, the thermal efficiency for a dual-pressure cycle is lower than for a basic cycle. However, the utilization efficiency for a dual-pressure cycle is significantly higher than for a basic cycle, ranging from a 6% advantage at the highest brine temperature to 24% advantage at the lowest.

The explanation for this is that thermal efficiency depends on the amount of heat added to the cycle but makes no distinction between resources maximum energy, ignoring the temperature difference between the fluids.

However, the utilization efficiency depends on how effectively the energy of the brine is used. By more closely matching the brine cooling curve to the heating and boiling curves, the average temperature difference between the two fluids is decreased and the irreversiblities are reduced. This allows more energy from the brine to enter the cycle leading to a higher overall utilization efficiency.

The 5 MW Raft River Dual-Boiling station in Idaho, USA, was the first to make use of the dual-pressure concept [40] and was operated as a demonstration station from 1981 to 1982 by the Idaho National Engineering Laboratory for the US Department of Energy.

Supercritical Organic Rankine Cycles As mentioned in section on "Geothermal Resources" and shown in Fig. 21a, an Organic Rankine Cycle where the operating liquid in the supercritical zone follows the heat source cooling curve more closely and the irreversibility losses of heat transfer are reduced as discussed by discussed by Tester and Milora [41] in detail. Four different cycles were examined. The operating fluid selected to illustrate the process is R-115 (C_2ClF_5) having a critical temperature of 80°C and being a suitable working fluid for both subcritical and supercritical operation at a geothermal fluid temperature of l50°C. In all four cases, the vapor was heated to 135°C and condensed at 26.7°C.

The first cycle is performed at 27.5 bar, i.e., subcritical cycle. The cycle efficiency is 9%, utilization efficiency is 46.5% and feed pump pressure ratio is 0.87. There is a quite large temperature gap between the cooling line of the geothermal fluid and the heated fluid. To improve the heat transfer, the second cycle pressure was increased to 39.26 bar which is already in the supercritical zone. This increased the cycle efficiency to 11.2% and utilization efficiency to 56.5% but feed pump pressure ration increased to 1.24. Further increase of the pressure to 80 bar resulted in almost parallel cooling and heating lines. This increased both efficiencies to 11.9% and 63.2% respectively, and feed pump pressure ratio to 2.54. However, additional increase to 114.4 bar dropped cycle efficiency to 10.6% and utilization efficiency to 54.6%, feed pump pressure ratio to 3.62 and accompanied by expansion through the wet zone meaning a possible droplets impingement on the turbine blades.

In summary, the work at supercritical condition has improved the cycle and utilization efficiencies but simultaneously substantially increasing feed-pump work. There is a large pumping power requirement to nearly 50% of the net turbine power. Although the operation in 80 bar seems to achieve the highest cycle efficiency and highest utilization, the question of cost of an 80 bar structure and operation in high pressure against efficiency benefits will influence the final selection of operating conditions.

Nevertheless in more moderate conditions, supercritical cycles have been used, but the cycle efficiency improvement is impaired by the increased cycle pump losses. See the section on "Efficiency and Work Ratio."

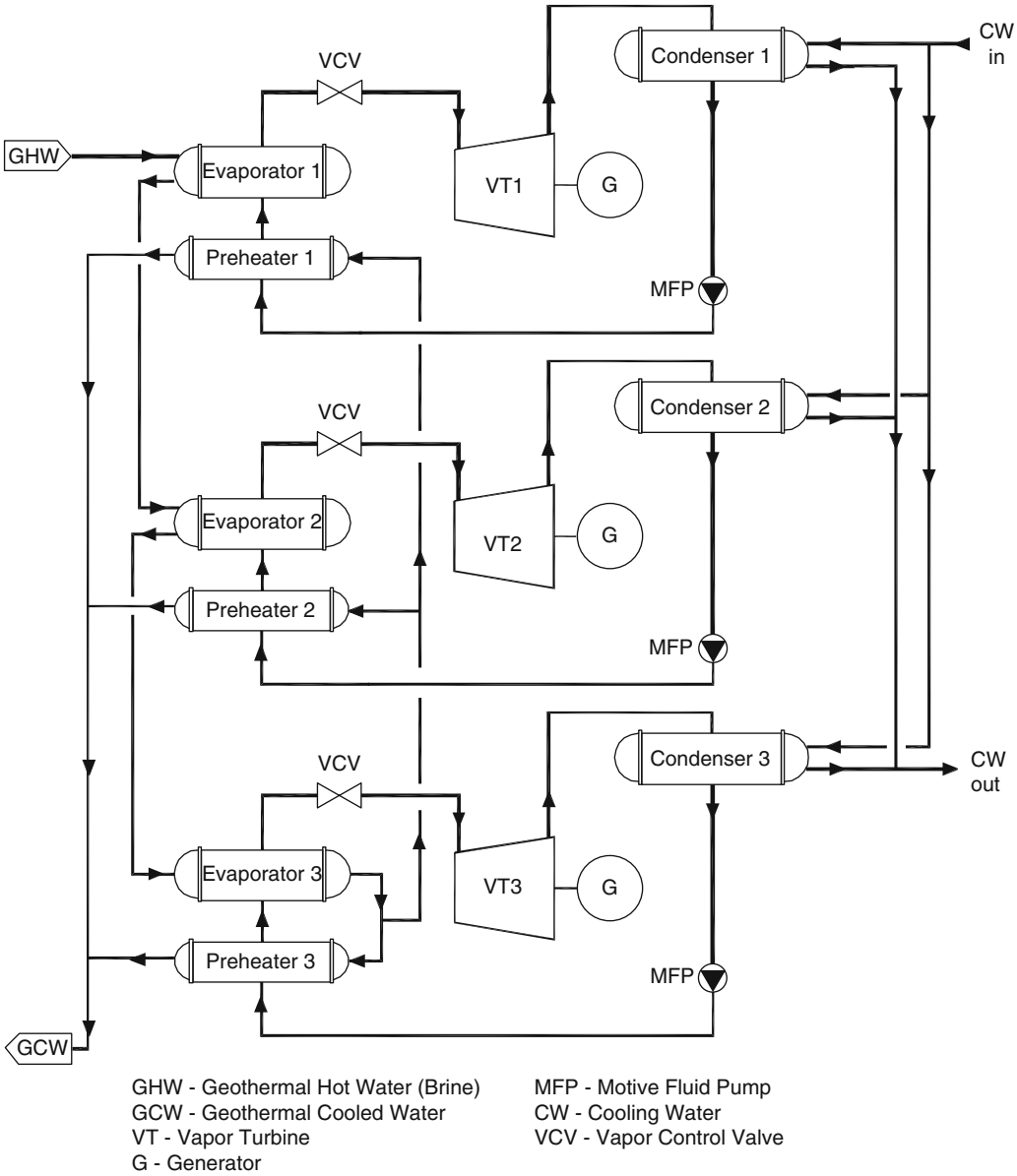

Geothermal Power Conversion Technology. Figure 27
Cascading ORC schematics

Dual-Fluid Organic Rankine Cycle Experimental – see section on "Experimental Power Stations."

Working Fluid Selection Selection of the appropriate working fluid has great bearing on the performance of the Organic Rankine cycle. Considerations should include both thermodynamic properties of the fluids as well as health, safety, and environmental impact [51, 52].

Thermodynamic Properties Table 3 lists some candidate fluids and their relevant thermodynamic properties. Pure water is included for comparison [42]. Clearly all of the candidate fluids have critical temperatures and pressures far below water. Furthermore, since the critical pressures are reasonably low, it is feasible to consider supercritical cycles for the hydrocarbons. As already mentioned in "Supercritical Organic Rankine Cycles," this allows a better match

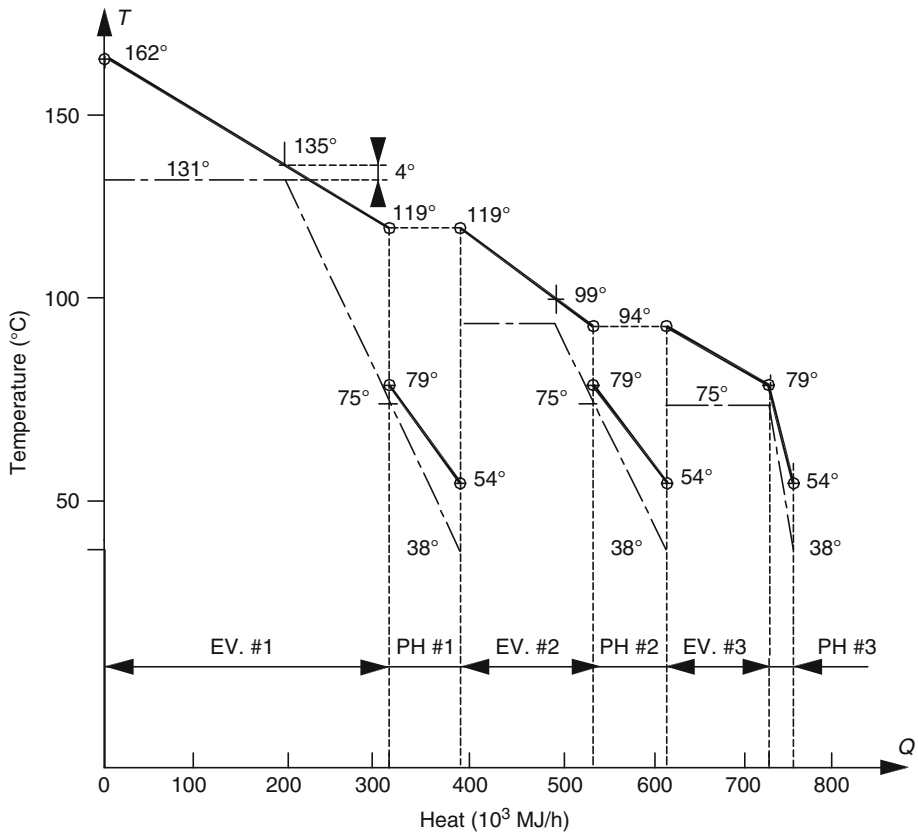

Geothermal Power Conversion Technology. Figure 28
T-Q diagram for cascading ORC

between the brine cooling curve and the working fluid heating-boiling line, reducing the thermodynamic losses in the heat exchangers. However, the net power output may not be higher resulting from the high pumping energy required by the supercritical cycle.

Mixtures of these fluids have been studied for use in geothermal binary stations. In particular, the thermodynamic properties of 90% – C_4H_{10} and 10% i-C_5H_{12} were determined by the National Bureau of Standards (predecessor of NIST) in Washington [43] when it was chosen as the working fluid for the Heber Binary Demonstration station in the 1980s [44]. Mixtures evaporate and condense at variable temperature, unlike pure fluids that change phase at constant temperature. This means that subcritical pressure boilers for mixed fluids can be better matched to the brine curves, similar to, but not exactly like supercritical pure fluids. A practical hurdle in the use of water ammonia (Kalina cycle) mixture is that the differential leaks of the two fluids in various points of the system modify mixture composition over time.

Another important characteristic of candidate fluids is the shape of the saturated vapor curve as viewed in temperature–entropy coordinates, see Fig. 31. This curve for water (thin line) has a negative slope, but certain hydrocarbons and refrigerants show a positive slope for portions of the saturation line. That is, a local minimum in the entropy at some low temperature exists, T_m, and local maximum in entropy at higher temperature, T_M. Retrograde fluids include normal and iso-butane, normal and iso-pentane. These fluids exhibit retrograde behavior over the following temperature ranges, $T_m \rightarrow T_M$. C_4H_{10}, $-3°C \rightarrow 127°C$; i-C_4H_{10}, $-3°C \rightarrow 117°C$; C_5H_{12}, $-3°C \rightarrow 177°C$; and i-C_5H_{12}, $-13°C \rightarrow 177°C$. Since T_m is lower than any temperatures encountered in geothermal binary stations, these fluids can be taken as having saturated vapor lines similar to that shown in Fig. 32 for pratical

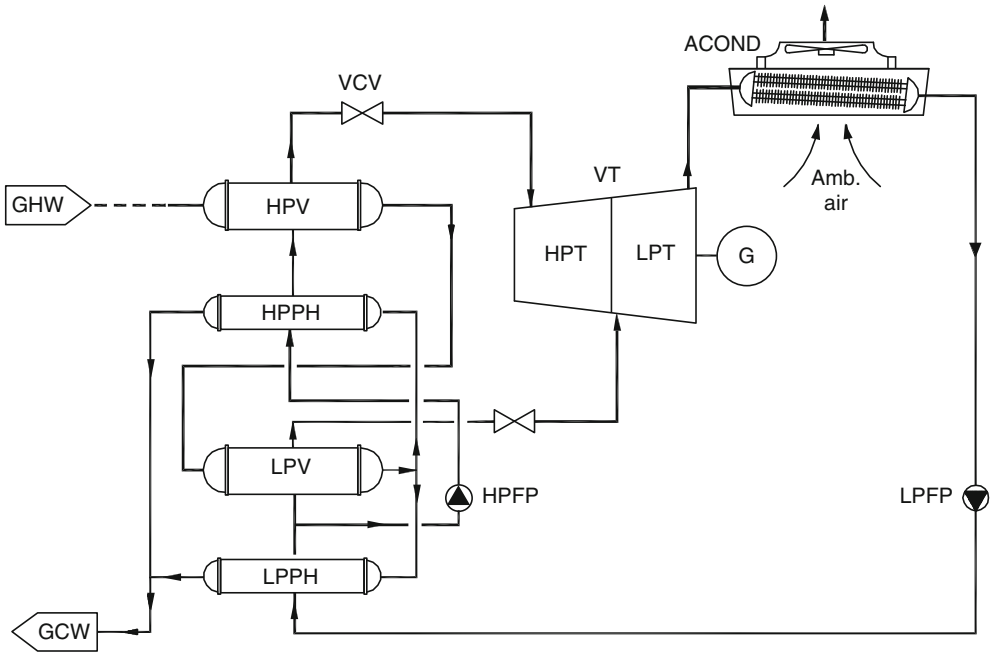

GHW - Geothermal Hot Water (Brine)
GCW - Geothermal Cooled Water
HPV - High Pressure Evaporator
HPPH - High Pressure Preheater
LPV - Low Pressure Evaporator
LPPH - Low Pressure Preheater
VCV - Vapor Control Valve
VT - Vapor Turbine
HPT - High Pressure Turbine
LPT - Low Pressure Turbine
G - Generator
ACOND - Air Cooled Condenser
HPFP - High Pressure Motive Fluid Pump
LPFP - Low Pressure Motive Fluid Pump

Geothermal Power Conversion Technology. Figure 29
Dual-pressure binary station based on single turbine with LP and HP inlets. Simplified flow diagram

purposes. This has major implications for Rankine cycles.

On the one hand, normal fluids such as water require considerable superheating, extending the isobar a–b–c upward to avoid excessive moisture at the turbine exhaust, state g. On the other hand, retrograde (backbend) fluids allow expansion from the saturated vapor line into the superheated region, process b–f, avoiding any moisture during the turbine expansion process. It has been shown [45] that it is possible to run a supercritical cycle where the turbine inlet state lies above the critical point and the expansion line lies inside the wet region for a portion of the process, emerging into the superheated region, without suffering any wetness penalty in efficiency. Apparently, the fluid remains in a metastable vapor state while passing through the wet region by staying on the dry side of the Wilson line [46].

Turbine Size While evaluating the potential working fluid, turbine size and cost must also be considered as part of that task. Milora and Tester [47] compared a line of hydrocarbons that are suitable for use in binary systems (including steam for comparison) on the basis of nondimensional turbine design parameters. They used four basic parameters: turbine blade diameter, turbine rotational speed, enthalpy drop, and volumetric flow rate. Using the factors that build those parameters, they established a "figure of merit" that is influenced by the fluid molecular weight, heat of evaporation (h_{fg}), specific volume, critical pressure, etc. Additional evaluation was made on the exit flow area that is also influenced by the same factors as shown by them [47] and also by DiPippo [33]. The results of both evaluations show that for the same power output and temperature range, systems that use low molecular weight fluids like ammonia (NH_3) result in a smaller turbine than butane or pentane by

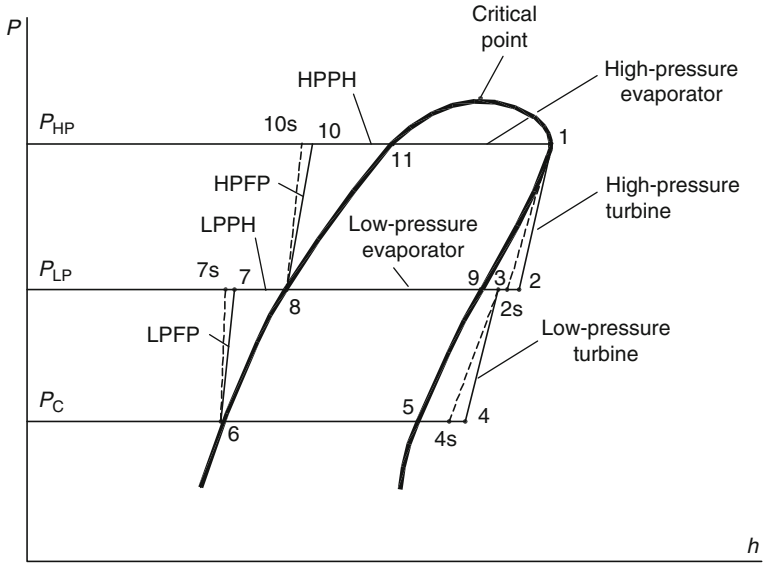

Geothermal Power Conversion Technology. Figure 30
Pressure–Enthalpy (P-h) diagram of a dual-pressure binary station

Geothermal Power Conversion Technology. Table 3 Thermodynamic properties of some candidate working fluids for binary stations

Fluid	Formula	T_c (°C)	P_c (MPa)	P_c (Lbf/in^2)	P_s@ 300 K (MPa)	P_s@ 400 K (MPa)
Propane	C_3H_8	96.95	4.236	614.4	0.9935	n.a.
i-Butane	i-C_4H_{10}	135.92	3.685	534.4	0.3727	3.204
n-Butane	C_4H_{10}	150.8	3.718	539.2	0.2559	2.488
i-Pentane	i-C_5H_{12}	187.8	3.409	494.4	0.09759	1.238
n-Pentane	C_5H_{12}	193.9	3.240	469.9	0.07376	1.036
Ammonia	NH_3	133.65	11.627	1,686.3	1.061	10.3
Water	H_2O	374.14	705.45	3,203.6	0.003536	0.24559

factors of 5 and 12 respectively, and for comparison smaller than steam turbine by factor of 120–150 times due to the large specific volume of steam in low temperatures. These general evaluations do not eliminate the need for particular turbine design for actual operating conditions.

Environmental Safety and Health Considerations The fluids used in the Organic Rankine cycle should comply with local and international health and environmental rules and agreements such as the Copenhagen Amendment of 1994 and Montreal Protocol of 1987 (in comparison with R-12 and R-114 that were banned from use and rated 1 for Ozone Depletion Potential (ODP)). Other potential fluids in Table 4 [48] are acceptable even though they are flammable. The table also compares Global Warming Potential which illustrates main reason for banning R-12 and R-114.

Ancillary Systems

Separation Process The separation process is considered as one at constant pressure, i.e., an isobaric process once the flash has taken place. The quality or

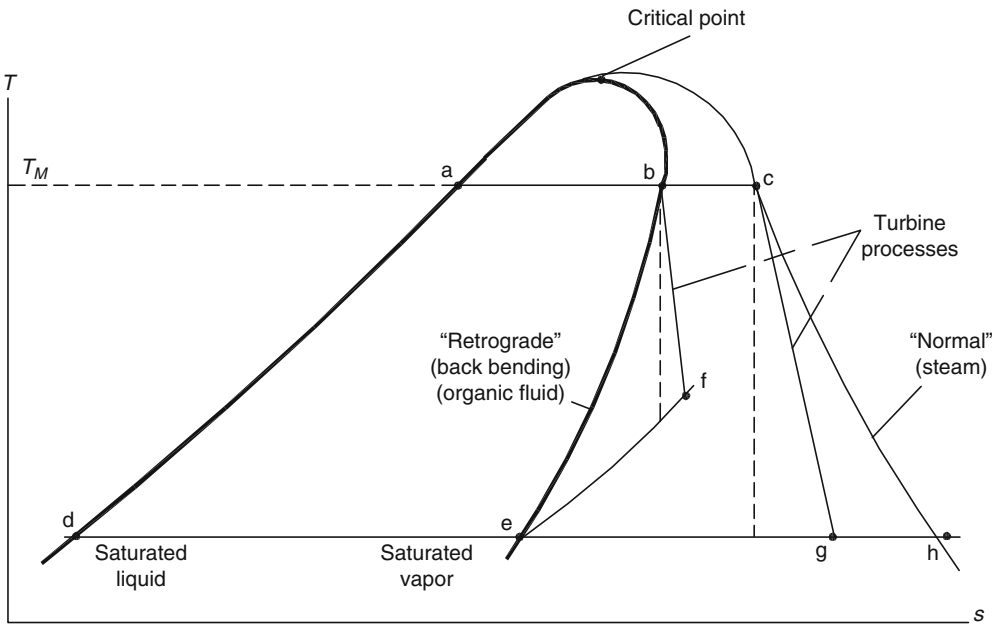

Geothermal Power Conversion Technology. Figure 31
Temperature-entropy diagram contrasting normal and retrograde saturated vapor curves

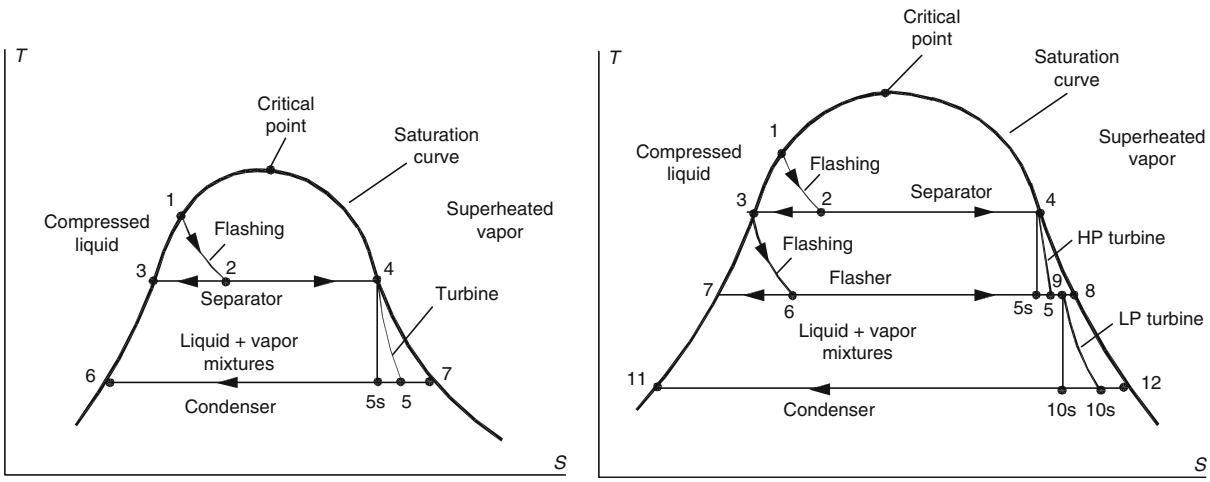

Geothermal Power Conversion Technology. Figure 32
T-S diagrams for single (*left*) and double-flash (*right*) steam cycles

dryness fraction, x, of the mixture that forms after the flash, state 2 (Fig. 32), can be found from:

$$x_2 = \frac{h_2 - h_3}{h_4 - h_3} = \frac{h_1 - h_3}{h_4 - h_3} = \frac{h_1 - h_3}{h_{fg}(T_3, P_3)} \tag{58}$$

(h_{fg} is latent heat of evaporation (B)) by using the "lever" rule between points 3 and 4, the steam mass fraction of the mixture can be found. It specifies the amount of steam flowing to the turbine per unit total mass of flow into the separator.

For the expansion, condensing and cycle analysis refer to the section on "Expansion Process."

Geothermal Power Conversion Technology. Table 4 Environmental and health properties of some candidate working fluids [41]

Fluid	Formula	Toxicity	Flammability	ODP	GWP
R-11	CCl_3F	Nontoxic	Non-flam	1.0	4,000
R-12	CCl_2F_2	Nontoxic	Non-flam	1.0	4,500
R-113	CCl_3CF_3	Nontoxic	Non-flam	0.8	4,800
R-114	$C_2Cl_2F_4$	Nontoxic	Non-flam	0.7	5,850
Propane	C_3H_8	Low	Very high	0	3
i-Butane	i-C_4H_{10}	Low	Very high	0	3
n-Butane	C_4H_{10}	Low	Very high	0	3
i-Pentane	i-C_5H_{12}	Low	Very high	0	3
n-Pentane	C_5H_{l2}	Low	Very high	0	3
Ammonia	NH_3	Toxic	Lower	0	0
Water	H_2O	Nontoxic	Non-flam	0	–
R245fa	$CF_3CH_2CHF_2$	Nontoxic	Non-flam	0	950

Flashing Process The sequence of processes begins with geothermal fluid under pressure at state 1, close to the saturation curve. The flashing process is modeled as one at constant enthalpy, or isenthalpic process as it occurs steadily, spontaneously, essentially adiabatically, and with no work involvement also ignoring any change in the kinetic or potential energy of the fluid as it undergoes the flash, therefore:

$$h = \text{constant} \tag{59}$$

Flash and Separation Processes Referring to Fig. 32b, the two flash processes 1–2 and 3–6 are analyzed the same as the flash process for the single-flash station in Figs. 13 and 32a. Each process generates a fractional amount of steam given by the quality x, of the 2-phase mixture. Each flash is followed by a separation process. The governing equations are as follows:

$$h_1 = h_2 \tag{60}$$

$$x_2 = \frac{h_2 - h_3}{h_4 - h_3} \tag{61}$$

$$h_3 = h_6 \tag{62}$$

$$x_6 = \frac{h_3 - h_7}{h_8 - h_7} \tag{63}$$

The mass flow rates of the steam ($\dot{m}_{hps}$) and liquid (brine) ($\dot{m}_{hpb}$) for the high- and low-pressure stages are found from:

$$\dot{m}_{hps} = x_2 \dot{m}_{total} = \dot{m}_4 = \dot{m}_5 \tag{64}$$

$$\dot{m}_{hpb} = (1 - x_2)\dot{m}_{total} = \dot{m}_3 = \dot{m}_6 \tag{65}$$

$$\dot{m}_{lps} = (1 - x_2)x_6 \dot{m}_{total} = \dot{m}_8 \tag{66}$$

$$\dot{m}_{lpb} = (1 - x_2)(1 - x_6)\dot{m}_{total} = \dot{m}_7 \tag{67}$$

These mass flows will be used to calculate the power generated from the two stages of turbine expansion, the amount of waste liquid to be disposed of and the heat that must be rejected through the condenser and ultimately from the cooling tower.

Optimization

Optimum Wellhead Pressure Once a valve is installed on the well, the pressure at which the power station is to operate must be determined with the wellhead pressure being controlled by a throttling valve. The well productivity curve can be approximated as an elliptical equation in terms of the mass flow rate of steam as a function of the wellhead pressure:

$$\left[\frac{\dot{m}}{\dot{m}_{max}}\right]^2 + \left[\frac{P}{P_{ci}}\right]^2 = 1 \tag{68}$$

where $\dot{m}_{max}$ is the maximum observed mass flow rate at full open valve and P_{ci} is the closed-in wellhead pressure. This function is shown schematically in Fig. 33. Assuming that values for these two parameters are available from well tests, the mass flow rate at any pressure can be calculated by:

$$\dot{m} = \dot{m}_{max}\sqrt{1-(P/P_{ci})^2} \tag{69}$$

Since opening the wellhead valve is a throttling process, the enthalpy of the steam remains the same.

Turbine power is proportional to the product of the steam mass flow rate and the enthalpy drop Δh (shown as an ideal isentropic process), from $h_{ci} = h_1$, down to assumed condenser pressure. The maximum is located somewhere in between.

Compute and solve for the power output per maximum steam flow rate by using Eqs. 15 and 69 as follows:

$$\frac{\dot{W}}{\dot{m}_{max}} = \frac{\dot{W}}{\dot{m}} \times \frac{\dot{m}}{\dot{m}_{max}} = (h_1 - h_2) \times \sqrt{1-(P/P_{ci})^2} \tag{70}$$

where $(h_1 - h_2)$ is the isentropic enthalpy drop across the turbine (Δh in Fig. 34), that can be obtained graphically using a large-scale Mollier diagram, see *Steam Tables* [32].

The work method involves preparing a table of Eq. 70 variables, i.e., h_1, h_2 (for given condenser pressure), $h_1 - h_2$, P/P_{ci} and $\frac{\dot{W}}{\dot{m}_{max}}$ as function of the pressure p changing between closed and open valve position.

DiPippo [33] solved this problem for a non-isentropic turbine for given wellhead data. The result has a parabolic shape with maximum at about 40% of the closed valve pressure.

It should be noted that the curve is relatively flat near the optimum point, i.e., the power output is within 0.2% of the optimum, over a wide range of wellhead pressures. This allows for a wide enough pressure/valve setup range without sacrificing much of the power generation.

The optimization process for a double-flash station is more complicated than for a single-flash station due to the extra degree of freedom in the choice of operating parameters. This results in two maxima, one of which yields the highest power output and the other that has the best specific power output. The results are not identical.

An example of a double-flash optimization was made by DiPippo [49] for the Electric Power Research Institute. The specific and total power outputs reach their respective maxima at different points. The variation results in different second flashing temperatures and a difference of 2.5% in the thermal utilization efficiency. However, in comparison with a single-flash station operating in the same conditions the double-flash generates about 31% more power.

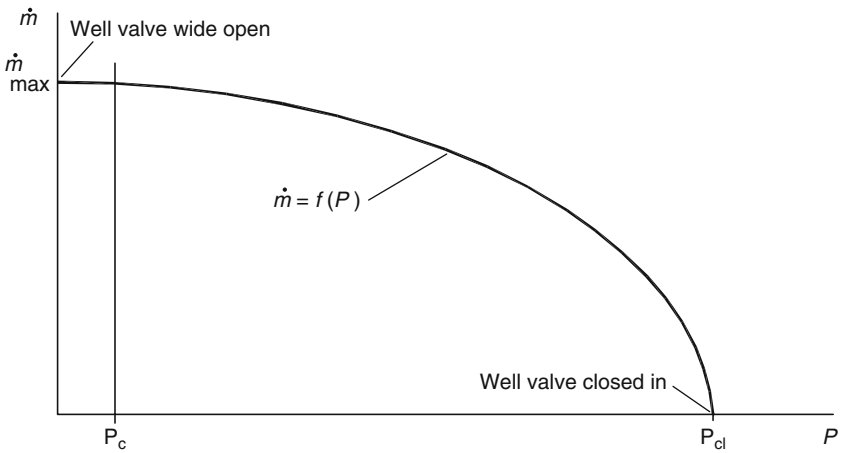

Geothermal Power Conversion Technology. Figure 33
Productivity curve for dry-steam wellhead

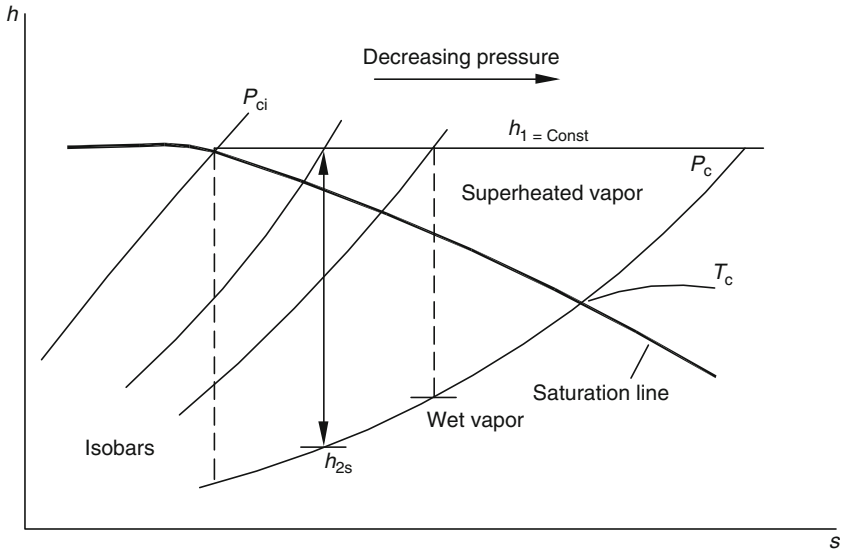

Geothermal Power Conversion Technology. Figure 34
Expansion from variable wellhead pressures (constant enthalpy)

If the rule of "equal temperature split" is used for initial evaluation, then the results for first and second flashing are close to the optimized calculations for maximum power and less accurate for maximum efficiency. This is acceptable for an approximation in view of the optimistic assumptions for the calculation that neglect pressure and thermal losses between the wellhead and the turbine.

Efficiency and Work Ratio The usual definition of thermal efficiency as the ratio between the net work done by the fluid and the total heat input to the cycle can be misleading in assessing the suitability of a given cycle in a heat engine. A concept of paramount importance in evaluating the suitability of a particular cycle for use in a heat engine is that of *work ratio*. This is defined as the ratio of the net work output of the cycle to the total positive (expansion) work of the cycle.

If there is very little negative work, as in a typical subcritical vapor cycle where only liquid of small specific volume has to be pumped at moderate pressure back into the boiler, the work ratio will be high. By contrast, this ratio is lower in a supercritical cycle where because of the high pressure, a larger portion of the positive work of the turbine is used to drive the feed pump [41].

Taking all these practical implications of work ratio, it can be seen that the concept of work ratio into account, it can be seen that the concept of work ratio can be regarded as almost as important as the concept of ideal cycle efficiency in many ways. Refer to Table 5.

Optimizing the Efficiency by Matching the Cycle to the Heat Resource

Single-Phase Water or Brine Resource In Fig. 35, line (a) is a typical T-Q diagram showing the heat exchange between single phase water or brine geothermal fluid and Organic Rankine cycle fluid from the hydrocarbons family of materials. The geothermal fluid cools during the heat transfer operation while there are a few options for heat utilization by the Organic Rankine cycle fluid. The simple case is line (b) that comprises preheating and evaporation of the organic fluid. The optimal case would be a constant temperature difference between the two fluids. This is difficult to achieve, but is almost attained with Organic Rankine cycle fluid operation in a supercritical condition as show in line (c). However, the gain carries penalties. The first penalty is the large pumping power and the second is the high cost of hardware operating at such high pressures. Another option is using the Organic Rankine cycle fluid under the saturation curve applying step heating

Geothermal Power Conversion Technology. Table 5
Comparison of work ratio in supercritical and subcritical ORC

	Supercritical ORC	Cascaded ORC
Gross (kW)	15,900	14,800
Fans (kW)	1,000	1,000
Feed Pump (kW)	2,450	900
Net	12,450	12,900
Work Ratio	78%	87%
For identical heat source and heat sink conditions:		
Heat source (liquid):		
Inlet temperature 170°C		
Outlet temperature 85°C		
Heat sink (air): 25°C		

Geothermal Power Conversion Technology. Table 6
Comparison of power recovered by Ormat and Steam cycles for a 160°C heat source

Cycle comparison based on gross power		
	Steam	Organic
% preheat	9.6%	38%
Optimum Exit Temp	92.5	78
Heat Input	83%	100%
Thermal Efficiency (Gross)	10.7%	11.1%
Power (Gross)	80%	100%
Cycle comparison based on net power		
	Steam	Organic
% preheat	9.6%	38%
Optimum Exit Temp	92.5	78
Heat Input	83%	100%
Thermal Efficiency (Net)	10.6%	10.6%
Power (Net)	85%	100%

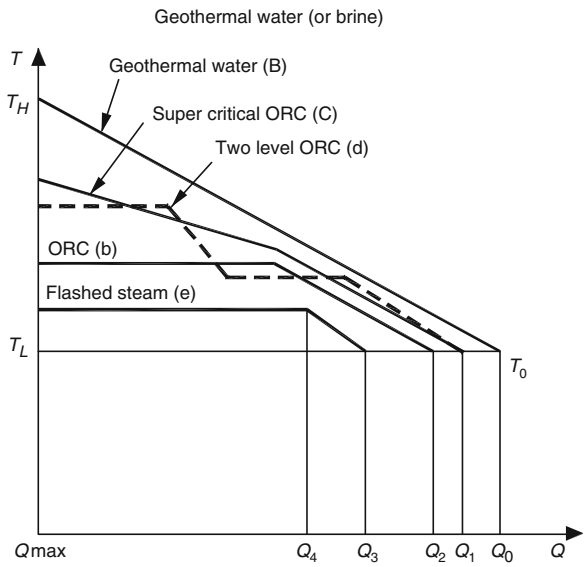

Geothermal Power Conversion Technology. Figure 35
T-Q Diagram comparing of Organic and Flash Steam cycle for 160°C heat source

with one or more evaporation stages – line (d) for two stages or as in a cascading system described in Fig. 35 which gives a better fit.

Figure 35 line (e) illustrates the differences in the temperature drop between a Flash Steam Rankine cycle and an Organic Rankine cycle. Because of the lower heat capacity of organic liquids and their much smaller latent heat of vaporization, these fluids lead to significantly smaller irreversibility losses of availability in the utilization of low or medium temperature predominantly sensible heat streams (Table 6).

Water-Dominated Two-Phase Flow When a substantial portion of the heat content of the geofluid is sensible heat of the liquid phase, the ORC has the advantage that its latent heat of evaporation is smaller than that of steam and therefore the vaporization temperature can be higher than that of a flash plant (Fig. 36). This leads to a higher efficiency and in addition eliminating the parasitic consumption of the condenser vacuum pumps.

Choked Well Flow The selection of separator operating conditions for liquid-dominated well has economical value. Optimization should be made for such evaluation. Two cases for choked and non-choked flows for liquid dominated wells are thoroughly studied by DiPippo [33, p. 98]. In his evaluation, two assumptions are made:

- There are no pressure losses between the wellhead and the turbine.
- Condensation occurs at certain known temperature (site specific).

As detailed in DePippo [33], the flow increases rapidly as the well is opened and the pressure is lowered. However, once the valve position is about 90% open (Fig. 37), the flow rate stabilizes and further opening of the well valve does not raise the total mass flow rate as the flow is "choked."

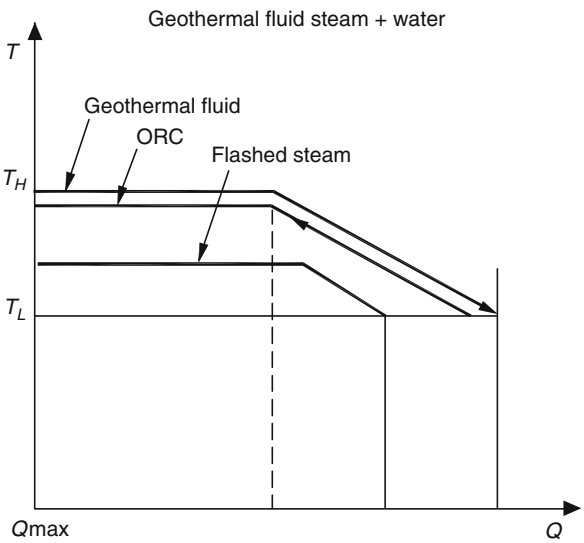

Geothermal Power Conversion Technology. Figure 36
T-Q diagram of binary cycle driven by geothermal steam

The question now is what wellhead pressure should be chosen to maximize the power output from a single-flash station connected to this well.

Eqs. 60–67 and 15–30 and a Mollier chart [32] are used to analyze the flashing, separation and turbine expansion processes. The calculations proceed in two phases:

- Phase 1 to determine the specific power output (measured by enthalpy drop on the Mollier chart) for a range of separator pressures (and equivalently temperatures).
- Phase 2 to find the total power by use of the variations of the total-flow rate as a function of the separator pressure.

Phase 1 calculations may rely on normal Steam Tables [31, 32] since the characteristics of the actual stream are unknown. Using the temperature and pressure of the maximum point, the actual flow rate is found from the productivity curve at that wellhead pressure. When this is multiplied by the corresponding specific power (Eq. 17) the maximum power can be obtained.

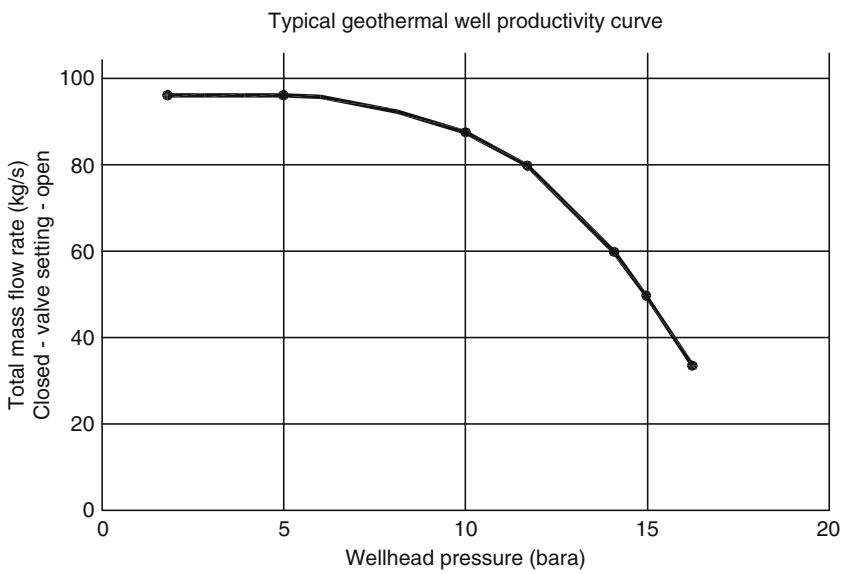

Geothermal Power Conversion Technology. Figure 37
Typical geothermal well productivity curve

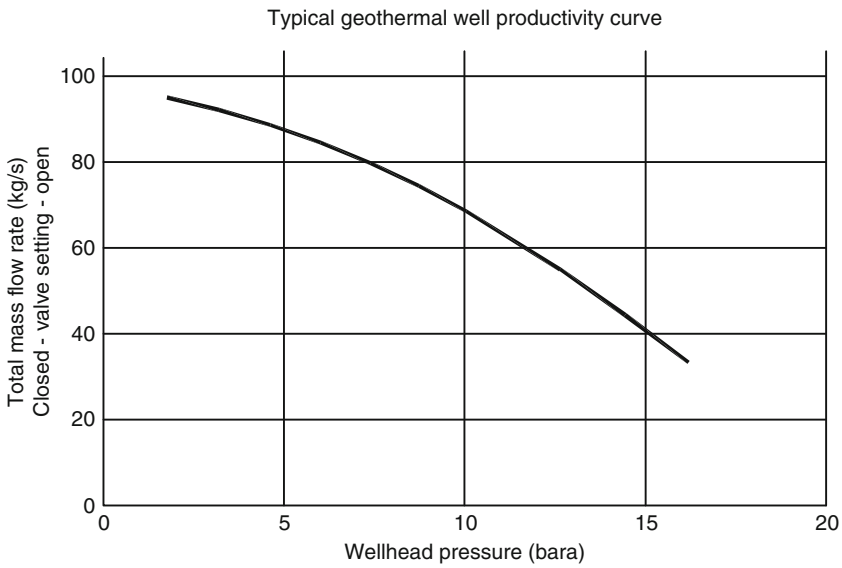

Geothermal Power Conversion Technology. Figure 38
Typical geothermal well productivity curve

Non-Choked Well Flow Many wells do not have a near flat response nearing open valve position. This may be a result of the well bore diameter being to small. The well is characterized by the high slope production data curve as in Fig. 38 meaning a continuously increased flow rate with further opening of the valve on the wellhead.

The results of phase 1 calculations are the same as for the first case. The results of phase 2 calculations are such that the maximum specific power and maximum total power are not at the same temperature. The designer must select the best choice based on economical factors in a particular set of the wells.

An Approximate Formulation for Separation Temperature Along with the previous method described above, DiPippo [33] developed an approximate method that leads to an easy solution for T_3 which is:

$$T_{3,\mathrm{opt}} = \frac{T_1 + T_6}{2} \tag{71}$$

(T_1 is the inlet temperature and T_6 is the condenser temperature)

Since this rule indicates that the temperature range between the reservoir and the condenser is divided into two equal segments, this rule is sometimes called the "equal-temperature-split" rule. This approximate rule applies to all flash stations regardless of the number of flashing steps [50]. The rule is that the temperature difference between the reservoir and the first flash is equal to the temperature difference between the first flash and the second flash, as well as between the second flash and the condenser.

Main Power Station Components

Steam Turbines

General Turbines used in geothermal applications are made of corrosion-resistant materials due to the presence of gases such as hydrogen sulfide which induce stress corrosion and erosion due to droplets and entrained solids.

A dry-steam power station utilizes similar turbines as those used in a fossil fuel power station (Fig. 39).

The turbines are single-pressure units with impulse-reaction blades, either single-flow for smaller units or double-flow for large units above 50 MW as in Fig. 40. The condensers can be either direct-contact (barometric or low-level) or surface-type (shell-and-tube).

Direct Exhaust Steam Turbine Large turbines usually sit over the direct contact condenser maintaining minimum pressure losses at the turbine exit. For small units it is often advantageous to arrange the turbine and condenser side by side, for maintenance reasons.

Turbines for Dry Steam or Single Flash A typical power station flow diagram is detailed in Fig. 41. At each production well (PW), there is equipment to control and monitor geothermal fluid flow from the well to the station. This equipment includes:

- Wellhead valve – WV
- Silencer or rock muffler – S or RM
- Particle remover/purifier – PU
- Emergency relief valve – ERV
- Piping and instrumentation (pressure and temperature gauges)

Geothermal Power Conversion Technology. Figure 39
Dry Steam 35 MW Franco Tossi turbine in Costa Rica (Courtesy of ICE, Costa Rica)

If wellhead separators are used, the cyclone separator, CS is located close to the wellhead on the same pad. Also note that the NCG disposal used in the example below is of the steam ejector type.

The single-flash steam power station is the most common geothermal power industry system. DiPippo states [33] that as of May 2007, there were 159 units of this kind in operation in 18 countries around the world with single-flash stations accounting for about 32% of all geothermal stations, constituting over 42% of the total installed geothermal power capacity in the world. The unit power capacity ranges from 3 to 90 MW, and the average power rating is 25.3 MW per unit.

Turbines for single-flash units are typically rated at 25–50 MW and consist of 4–5 stages of impulse-reaction blades. Both single and double-flow designs are in use. Overall isentropic efficiencies in the high 80% range have been obtained.

For the thermodynamic analysis of the energy conversion process, it is assumed that the geothermal fluid starts as a compressed liquid somewhere in the reservoir. It experiences a flashing process separating the two phases in the cyclone separator. The steam is used to drive a turbine (Fig. 42) and the brine sent for well reinjection [35].

A classic example of a wellhead arrangement showing the valves and separator is given in Fig. 43.

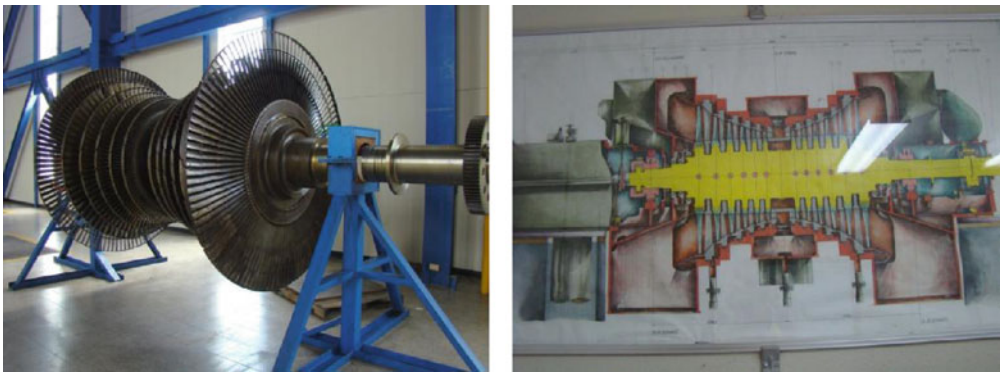

Geothermal Power Conversion Technology. Figure 40
A double-flow turbine rotor and cross section of a double-flow dual-admission steam turbine (Courtesy of ICE Costa Rica)

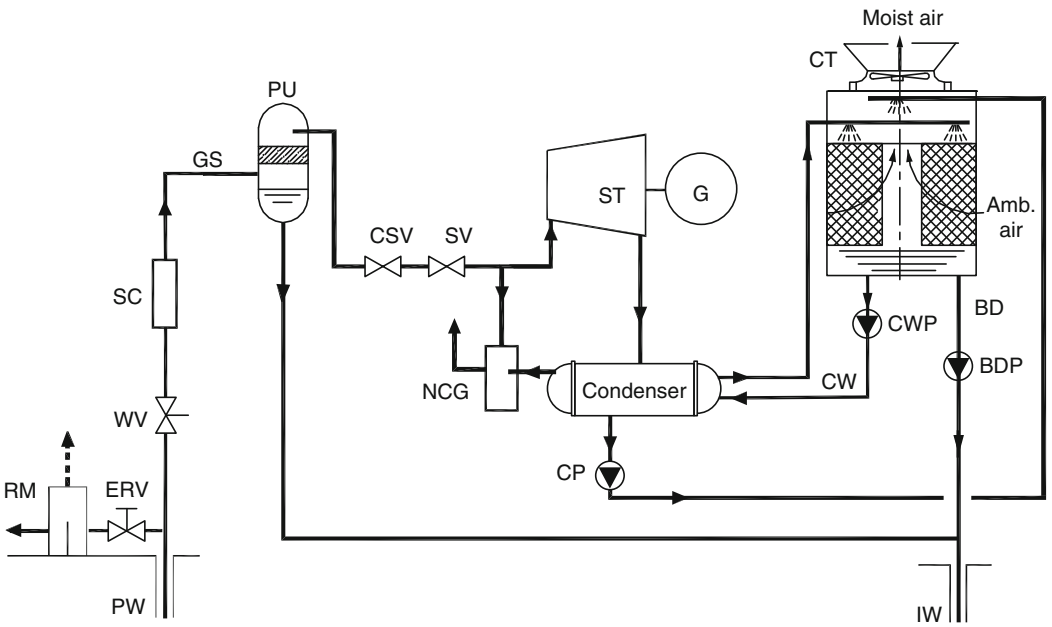

PW - Production Well
IW - Injection Well
GS - Steam
PU - Purifier
CSV - Control Valve
RM - Rock Muffler
WV - Wellhead Valve
SC - Scrubber

ST - Steam Turbine
G - Generator
CT - Cooling Tower
CP - Condensate Pump
CWP - Cooling Water Pump
CW - Cooling Water
SW - Spent Water
BD - Blow Down

BDP - Blow Down Pump
NCG - Non Condensable Gas Disposal (steam ejector type)
SV - Stop Valve

Geothermal Power Conversion Technology. Figure 41
Simplified scheme of a dry-steam power station

The steam from the turbine is condensed by means of either a surface-type condenser (C), as shown in Figs. 16a and 42, or in a direct-contact condenser of either the barometric or low-level type, Fig. 16b.

Turbines for Double-Flash Steam The double-flash steam power station is an improvement on the single-flash design as it can produce 15–25% more power output for the same geothermal fluid conditions. The station is more complex, more costly and requires more maintenance. However, the extra power output often justifies the installation of such stations. According to DiPippo [33], 14% of all geothermal stations are double-flash units as of mid-2007.

Many aspects of a double-flash station are similar to a single-flash station. The fundamental new feature is a second flash process imposed on the separated liquid leaving the primary separator to generate additional steam at a lower pressure than the primary steam.

A schematic diagram of a double-flash station is shown in Fig. 14 [35] and in Fig. 44. The design differs from the single-flash station in Fig. 42 in that the low pressure steam from an additional flasher F flows through a steam line to the turbine in addition to the high-pressure line from the separator.

The turbine must be a dual-admission, single-flow machine to accommodate the high- and low-pressure steam supplies. The low-pressure steam is admitted to the steam path at an appropriate stage to smoothly integrate with the partially expanded high-pressure steam. Other designs are possible e.g., two separate turbines could be used, one for the high-pressure steam and one for the low-pressure steam. In such cases, the turbines could exhaust to a common

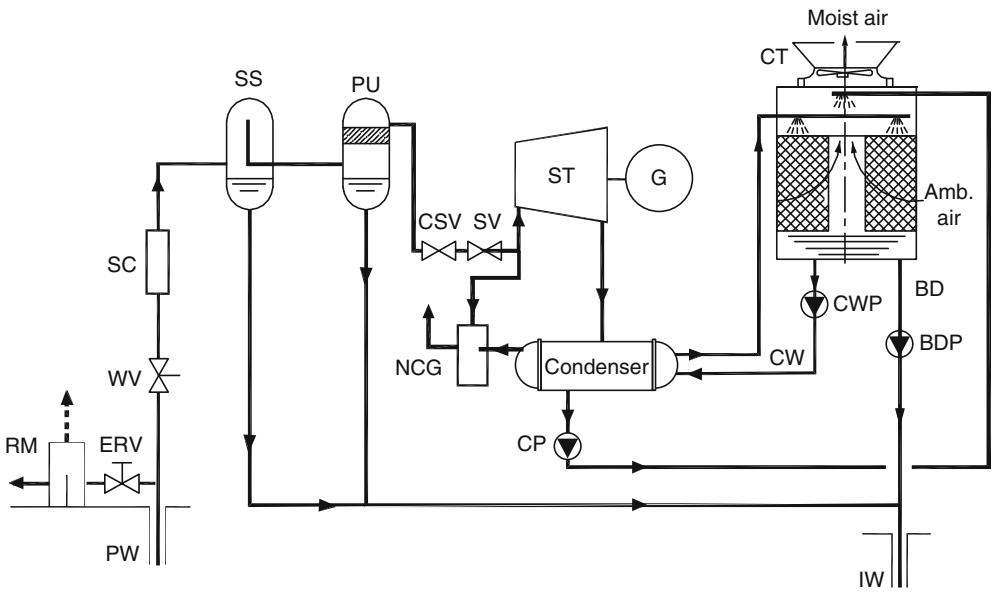

PW - Production Well
IW - Injection Well
PU - Purifier
CSV - Control Valve
RM - Rock Muffler
WV - Wellhead Valve
SC - Scrubber
RV - Release Valve
SS - Steam Separator

G - Generator
ST - Steam turbine
CT - Cooling Tower
CP - Condensate Pump
CWP - Cooling Water Pump
CW - Cooling Water
BD - Blow Down
SV - Stop Valve

BDP - Blow Down Pump
NCG - Non Condensable Gas Disposal

Geothermal Power Conversion Technology. Figure 42
Simplified single-flash power station schematic [56]

Geothermal Power Conversion Technology. Figure 43
Wellhead valve, control valve (*left*), and vertical separators (*right*) (Courtesy of ORMAT)

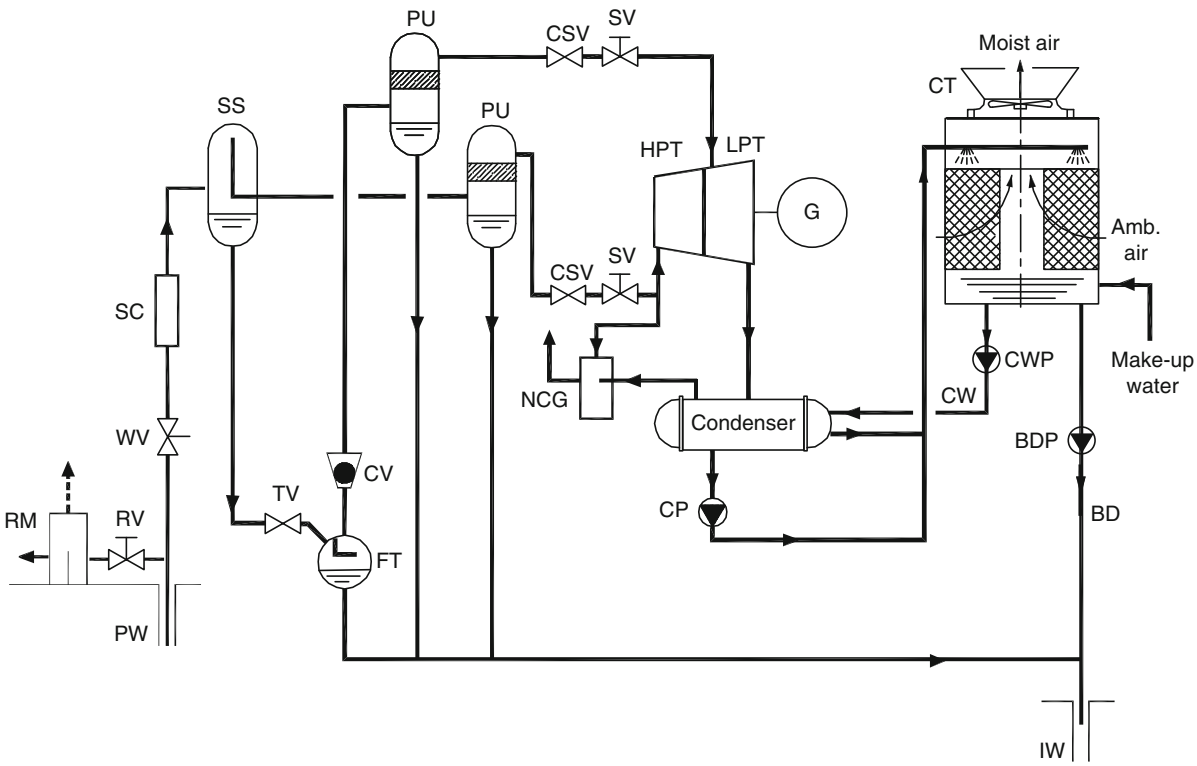

PW - Production Well
IW - Injection Well
GS - Steam
PU - Purifier
CSV - Control Valve
RM - Rock Muffler
WV - Wellhead Valve
SC - Scrubber
TV - Throttling Valve
RV - Release Valve
SS - Steam Separator

G - Generator
HPT - High Pressure Turbine
LPT - Low Pressure Turbine
CT - Cooling Tower
CP - Condensate Pump
CWP - Cooling Water Pump
CW - Cooling Water
BD - Blow Down
SV - Stop Valve
FT - Flash Tank
CV - Check Valve

BDP - Blow Down Pump
NCG - Non Condensable Gas Disposal

Geothermal Power Conversion Technology. Figure 44
Simplified double-flash power station schematic [35]

condenser or to two separate condensers operating at the same or different levels of vacuum. For larger power ratings (50 MW or higher), double-flow turbines are preferred to minimize the height of the last stage blades.

Separators and Purifiers

Particle Separators Particles separators/purifiers are installed on steam lines after the wellhead flow control valve to remove particulates carried by the steam flow. The design is based on filtration by circular flow. Restrictions that create differences in flow velocity help the filtering of the steam-carried particles. To maintain correct separator velocity, more than one separator is installed on a single steam line, see Fig. 45. The collected brine and particles are collected from the bottom exit of the separator.

Separators It is important to separate the two phases efficiently prior to admitting the steam to the turbine. Liquid in the steam can cause scaling and/or erosion of piping and turbine components. Although there are a few designs in use for cyclone separators, the industry has generally settled on the simple Weber-type separator, depicted in Fig. 43 right side and

Geothermal Power Conversion Technology. Figure 45
Particle separators/purifiers (Courtesy of ORMAT)

Geothermal Power Conversion Technology. Figure 46
Scheme and photo of steamboat hills two-phase vertical cyclone separators and accumulators (Courtesy of ORMAT)

Fig. 46. Lazalde-Crabtree [54] published an approach to designing such vessels. The paper presented two variations. One for a primary 1-phase separator and the other for a moisture remover. Their recommended guidelines for separators and moisture removers are summarized in Table 7.

In cases where the separators are situated at a distance from the power building, the steam

Geothermal Power Conversion Technology. Table 7
Separator and moisture remover design guidelines [54]

Parameter	Separator	Moisture remover
Maximum steam velocity at the 2-phase inlet pipe	45 m/s	60 m/s
Recommended range of steam velocity at the 2-phase inlet pipe	25–40 m/s	35–50 m/s
Maximum upward annular steam velocity inside cyclone	4.5 m/s	6 m/s
Recommended range of upward annular steam velocity inside cyclone	2.5–4 m/s	1.2–4 m/s

transmission pipelines are fitted with steam traps (ST) to capture and remove moisture that may form from condensation within the pipes. Prior to being admitted to the turbine, the steam may be scrubbed to remove any fine moisture droplets that may have formed in the transmission pipelines and escaped the steam traps. The moisture remover that is also known as purifier (PU) is usually located directly outside the power building.

Cyclone separators receive incoming two-phase flow via a tangent entry. The incoming stream circulates tangentially at high speed, so that the liquid flows down the separator inner walls and exits to an accumulating tank. The steam (still rotating) remains in the cyclone separator loosing small droplets which exit through a tube on the lower side of the separator, while the steam exits through exterior pipes in the center of the separator. From the accumulator(s) the brine is collected and sent to the reinjection well.

Purifiers Purifiers are needed to protect the turbines blades and structure from corrosion and impingement by removal of residue water droplets. Droplets are either carried by the flowing steam after separation (separation is not 100%), or formed by unintentional condensation on the steam pipe walls. Lazalde and Crabtree [54] recommend a cyclone design similar to the separator but with small water exit due to the smaller water flow load. The basic design parameters are presented in Table 7.

Steam Scrubbing Unit Another method of final steam treatment is scrubbing. To improve the scrubbing, wash water is injected into the pipeline. TDS concentration in the pipeline is reduced by mixing the low TDS wash water with the high TDS brine drops. Refer Fig. 47.

Steam line scrubbing is effective in removing liquid from the steam while maintaining a low TDS concentration in the liquid drops entering the turbine as steam impurities. The water injection system is shown in Fig. 48.

Flash Tank/Flash Chamber Flash chambers are vertical (Fig. 49) or horizontal (Fig. 50) with brine exits at the bottom of the tank. In Brady Power station, vapors from the first flash pass to two separate steam turbines while the brine that goes to the second flash chamber is re-flashed with its flash steam passing to a third steam turbine. A set of silencers is installed behind the flashing chambers in the case of a trip for part or all of the system.

Flash chambers may be installed horizontally above the condenser and vacuum system. The horizontal chamber has a large volume allowing droplets to settle as a result of low steam velocity. This reduces pressure losses.

Condensers

Surface Condensers In the use of surface-type condenser shown in Figs. 51 and 52, the required flow rate of cooling water $\dot{m}_{cw}$ related to the steam flow rate $X_2\dot{m}_{st}$. This is expressed by the First Law of thermodynamics as:

$$\dot{m}_{cw} = X_2\dot{m}_{st}\left[\frac{h_5 - h_6}{\bar{c}\Delta T}\right] \tag{72}$$

where $\bar{c}$ is the assumed constant specific heat of the cooling water (4.2 kJ/kg.K), ΔT is the rise in cooling water temperature at the condenser inlet and outlet and X_2 is the steam dryness stage at the turbine exit.

Direct Contact Condensers For a direct-contact condenser (Fig. 53), the suitable equation is:

$$\dot{m}_{cw} = x_2\dot{m}_{total}\left[\frac{h_5 - h_6}{\bar{c}(T_6 - T_{cw})}\right] \tag{73}$$

The condenser is below the flash chamber, see Fig. 54. The steam returning from the steam turbine is condensed via direct contact with the cooling water.

Geothermal Power Conversion Technology. Figure 47
Amatatilan steam scrubber, horizontal mixer, and vertical purifier (Courtesy of ORMAT)

Because of the open cooling cycle, air and other gases are entrained in the water. The NCG system must remove this air and gas to maintain the designed condensing temperature/pressure.

Air-Cooled Condensers Air-cooled condensers came to solve the problem of water scarcity in many geothermal sites, as well as to answer the environmental ruling against cooling towers plumes, etc. Air-cooled condensers are rarely used with flash steam mainly as they suffer from internal silica buildup. Today they are used in binary cycles despite the fact that the condensing temperature is higher by 15°C with water cooled condensers, but in arid zones it is the only solution. Air-cooled condensers are very sensitive to ambient air (temperature), and it can be controlled to some extent by fan speed control, higher exit shroud and optional water spray into the incoming air at extreme air temperatures. HTRI [55] design and similar software is commonly used for air-cooled condensers design. See Fig. 55 scheme and photo of actual air condensers arrangement.

$$\dot{m}_{\mathrm{cair}}(h_{\mathrm{airout}} - h_{\mathrm{airin}}) = \dot{m}_{\mathrm{wf}}(h_2 - h_3) \tag{74}$$

where h_2 is organic fluid condition at the condenser inlet and h_3 is the condition of the condensed liquid.

Assuming constant Cp for air in the relevant temperature range and neglecting humidity influence:

$$\dot{m}_{\mathrm{cair}} Cp_{\mathrm{air}}(T_{\mathrm{airout}} - T_{\mathrm{airin}}) = \dot{m}_{\mathrm{wf}}(h_2 - h_3) \tag{75}$$

or

$$\dot{m}_{\text{cair}} = \dot{m}_{\text{wf}} \frac{(h_2 - h_3)}{Cp_{\text{air}}(T_{\text{airout}} - T_{\text{airin}})} \tag{76}$$

Cooling Tower The cooling water used for heat rejection in the condenser of steam or binary stations is continuously re-cooled in the cooling tower. Cooling is achieved by evaporation of part of the circulated water into the ambient air. In large cooling towers, cooling be done by natural draft structure while in medium power systems (in geothermal stations), towers usually are equipped with mechanical draft fans.

Geothermal Power Conversion Technology. Figure 48 Mokai 2 – Brine scrubbing on steam line (Courtesy of ORMAT)

The usual temperature difference in mechanical draft towers is about 10°C between the inlet and outlet of the moving air. Cooling water can reach about 25°C depending on the ambient air temperature and humidity. Cooling towers need makeup water to compensate for the evaporation and drift losses and to maintain water quality. The makeup is about 3% of the circulated water depending on ambient air characteristics. In geothermal flash power stations, there is sufficient water quantity collected from the flash steam condensate. In such stations, the condenser is usually of direct contact design which is simpler to design and is more cost effective in production than surface condensers used in binary stations (Fig. 56).

The internal process involves the exchange of both heat and mass between air and water. The following First Law equation describes the overall tower operation, excluding the fan while assuming steady flow and

Geothermal Power Conversion Technology. Figure 49 Brady Double-Flash chambers with back silencers (Courtesy of ORMAT)

Geothermal Power Conversion Technology. Figure 50
GEM horizontal flash chamber (Courtesy of ORMAT)

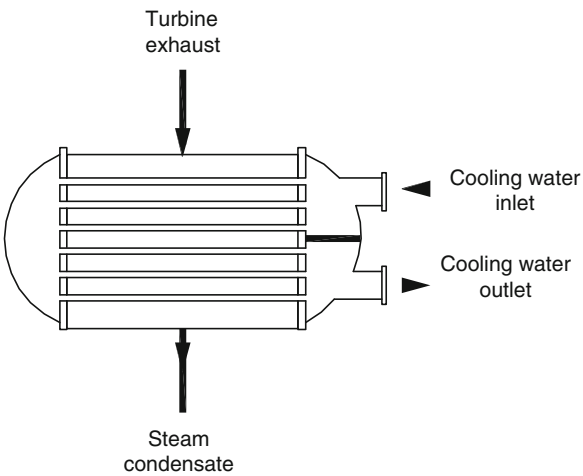

Geothermal Power Conversion Technology. Figure 51
Surface condenser

overall adiabatic conditions for a tower with direct contact condenser:

$$\dot{m}_1 h_1 - \dot{m}_2 h_2 = \dot{m}_{\mathrm{Aout}} h_{\mathrm{Aout}} - \dot{m}_{\mathrm{Ain}} h_{\mathrm{Ain}} + \dot{m}_{BD} h_{BD} \tag{77}$$

$$\dot{m}_1 + \dot{m}_{\mathrm{WAin}} = \dot{m}_2 + \dot{m}_{BD} + \dot{m}_{\mathrm{WAout}} \quad \text{(Conservation of water)} \tag{78}$$

$$\dot{m}_{\mathrm{Aout}} = \dot{m}_{\mathrm{Ain}} \quad \text{(Conservation of dry air)} \tag{79}$$

where the terms $\dot{m}_{\mathrm{wa}}$ and $\dot{m}_{\mathrm{wd}}$ represent water content of the incoming and leaving air streams, respectively. These contents can be determined from the specific humidity, ω, of the air streams:

$$\dot{m}_{\mathrm{WAin}} = \omega_{\mathrm{Ain}} \dot{m}_{\mathrm{Ain}} \tag{80}$$

and

$$\dot{m}_{\mathrm{WAout}} = \omega_{\mathrm{Aout}} \dot{m}_{\mathrm{Aout}} \tag{81}$$

Geothermal Power Conversion Technology. Figure 52
Surface condenser end connections, NCG removal system, and cooling tower (Courtesy of ORMAT)

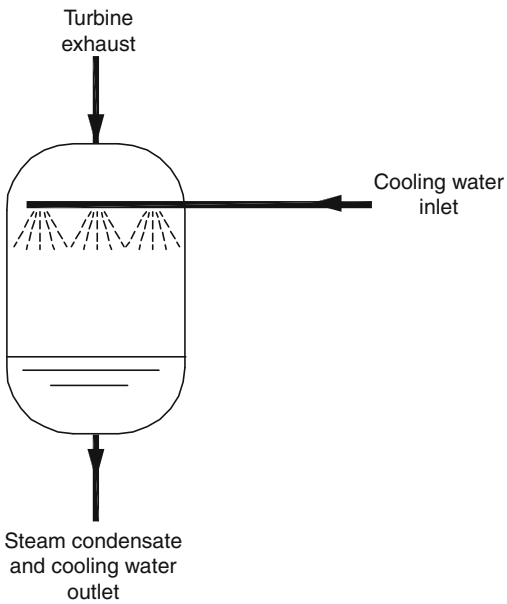

Geothermal Power Conversion Technology. Figure 53
Direct contact condenser

These governing equations are used with the properties of steam, water and moist air, either in tabular, graphic (psychometric chart), electronic form to determine the various flow rates needed for given design conditions.

Cooling towers are characterized by two parameters:

- Range
- Approach

The range is the change in water temperature as it flows through the tower, namely, $T_1 - T_2$.

The approach is the difference between the water outlet temperature and the wet-bulb temperature of the incoming air, namely, $T_2 - T_{\text{wb.Ain}}$. Since the ideal outlet water temperature is the wet-bulb temperature of the incoming air, the approach is a measure of how closely the tower approaches ideal performance, i.e., zero approach or $T_2 = T_{\text{wb.Ain}}$ (Fig. 57).

Pumps

Geothermal Fluid Pumps

Production Pump Production pumps are of multi-stage vertical design. The pump fits the bore diameter of the well casing and has a screen filter before its inlet opening. The motor sits directly on the wellhead, on top of the pump exit pipe. See Fig. 58. Pump pressure

Geothermal Power Conversion Technology. Figure 54
GEM direct contact condenser, hot-well pumps, and vacuum system (Courtesy of ORMAT)

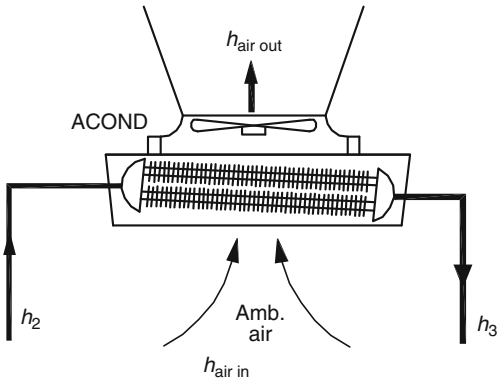

Geothermal Power Conversion Technology. Figure 55
Air-cooled condenser view of the PGV Geothermal combined cycle power station (Courtesy of ORMAT)

should be high enough to overcome all system piping friction while still maintaining pressure above possible precipitation of carbonates as mentioned in section on "Geothermal Resources."

Injection Pump The injection pumps are of horizontal or vertical multistage design to overcome injection well resistance. See Fig. 59 for typical arrangement. The structure must allow quick dismantling for maintenance work.

Condensate Pumps Condensate pumps overcome the subatmospheric pressure at the pump inlet and then lift condensate to the top of the cooling tower, overcoming

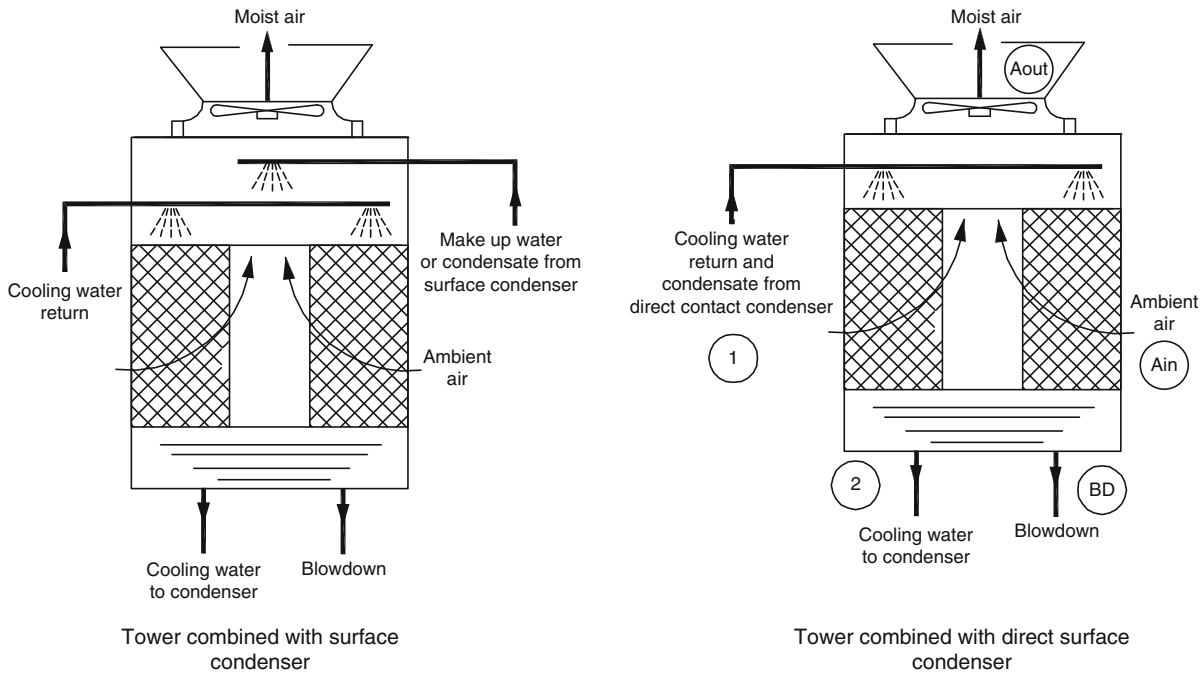

Geothermal Power Conversion Technology. Figure 56
Induced draft cooling towers showing related mass flows

Geothermal Power Conversion Technology. Figure 57
Cooling towers of GEM single-flash power station in East Mesa, California (Courtesy of ORMAT)

distribution system and nozzles resistance. Typical pump is in Fig. 60.

Binary Station Motive Fluid Pump Motive fluid pump is situated below the condenser structure. To eliminate possible inlet vacuum buildup it is usually a vertical with barometric height above its inlet. Typical binary cycle circulation pump is in Fig. 61.

Gathering System

Dry-Steam Gathering The connection between the wells and the power building for a dry-steam power

Geothermal Power Conversion Technology. Figure 58
North Brawly production pump and separator with MCC (Courtesy of ORMAT)

Geothermal Power Conversion Technology. Figure 59
Injection pumps arrangement (Courtesy of ORMAT)

station is relatively simple. At the well, there are the usual valves and a steam purifier. See example in Fig. 62. The purifier is usually an in-line, axial centrifugal separator designed to remove all carried particles from the steam before it enters the piping system. Steam pipes are insulated and include high expansion loops. See example in Fig. 64. Steam traps are sited along the pipes to remove condensate.

At the wellhead, or immediately before the steam approaches the power building, there is an emergency pressure relief valve. This allows for the temporary release of steam in the event of a turbine trip. Before being released to the atmosphere, the steam generally passes through a silencer (Figs. 49 and 63). It has been found preferable to maintain the wells in a steady open mode rather than cycling the wells through open and closed positions. At the power building there is a steam header, a final moisture remover (typically a vertical cyclone separator or a baffled demister), and a venturi meter for accurate steam flow rate measurement.

Water and Brine Piping High-pressure reinjection requirements might require pumps to maintain sufficient injection pressure.

Pressure drop through the pipes due to friction and local losses can be calculated using standard handbooks such as McKetta or similar [56]. The information required includes fluid mass flow rate, fluid density,

Geothermal Power Conversion Technology. Figure 60 Condensate pump (Courtesy of ORMAT)

fluid dynamic and kinematic viscosity, pipe data such as pipe diameter, friction factor and length.

If there is a change in pipe elevation, the gravity contribution must be included.

Pressure loss in a two-phase, steam-liquid pipeline is more complex and less reliable for analytical prediction [57, 58]. Correlations may be used to establish the pressure drop. Field tests are conducted to experimentally determine the exact ΔP. The situation is complex as the two-phase flow in any of several different patterns depends on the pipe orientation and relative amounts of the phases present. See also references [58, 59] for suggested calculation depending on type of flow

Steam Piping There are three types of fluids flowing in the geothermal field piping system:

- Steam
- Water/brine
- Two phase (mixture of steam and water)

One of the main gathering system design concerns is the pressure loss in the steam lines from the wellhead to the power building. The steam pressure drop is a function of the diameter, length, configuration of the steam piping and the density and mass flow rate of the steam. See also Handbooks for fluid systems design such as ref. [56] or similar.

Note that the calculated pressure drop might be higher than the actual values at higher velocities. The central variable is the pipe diameter as pressure drop is inversely proportional to the pipe diameter in the fifth power.

By installing larger diameter pipes pressure loss can be considerably reduced. The extra cost of the larger pipes may be a negative economic factor. A thermodynamic-economic optimization study will determine optimum pipe size.

Single-Flash Gathering System Design Considerations and Piping Layouts When a geothermal field produces a mixture of steam and water, the method used for energy conversion depends on the potential energy available in each of the streams. The curves of maximum available energy for steam and water given in Fig. 8 can be used for the initial analysis. If the separated water stream is not sufficient for power generation, it will be reinjected, while the separated steam is utilized in a single-flash station for conversion to electricity. Each power station comprises a number of production and reinjection wells to assure continuous flow even during maintenance work on any of the wells. A piping system is required between the wells and the installed steam/water separators (usually adjacent to the wells and the power building). There is also a brine piping system leading from the separators and power building to the reinjection wells.

A typical field is usually a few kilometers long with the production wells on one side, injection wells on the other side and with the power building positioned so as to minimize steam side pressure losses.

Double-Flash Gathering System Design Considerations In most cases, the second flashing process is performed near to the first steam separator.

The list of possible arrangements is large and therefore the best choice will be determined by thermodynamic and economic analysis taking site-specific conditions including:

- Temperature, pressure, and chemical nature of the geothermal fluid

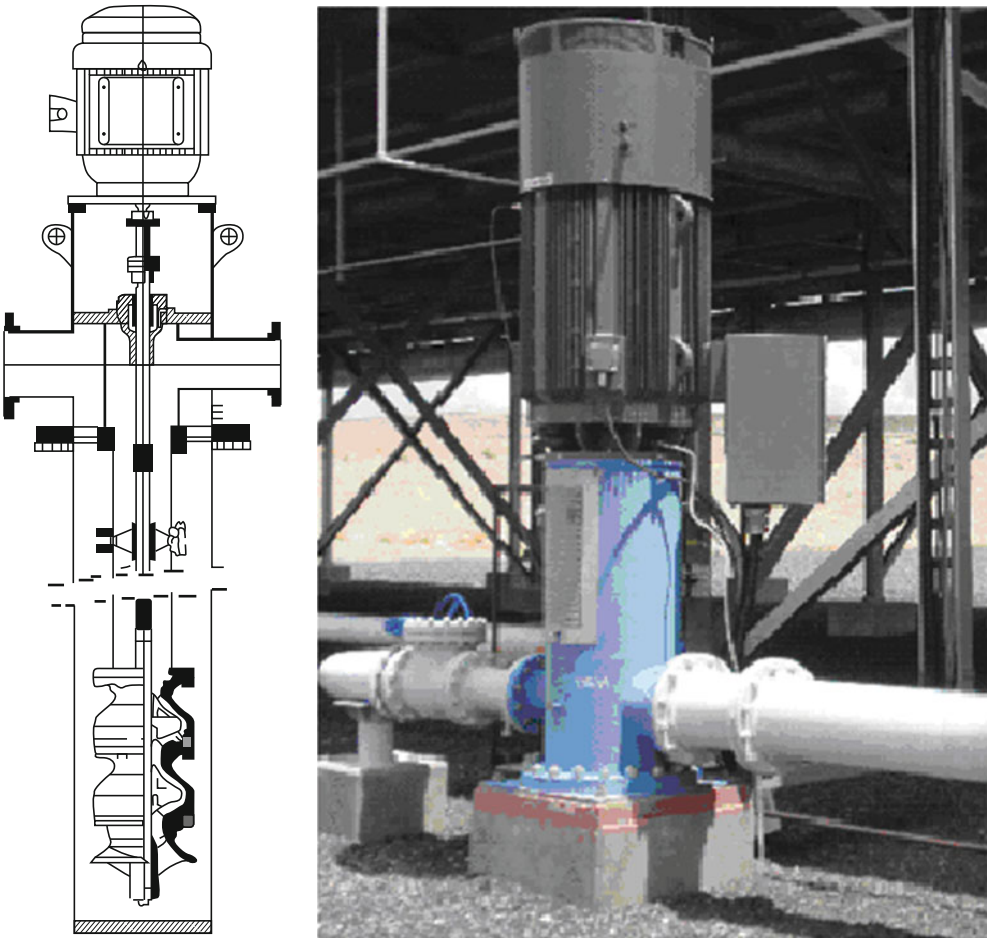

Geothermal Power Conversion Technology. Figure 61
Binary power station – motive fluid circulation pump (Courtesy of ORMAT)

- Location of production and injection wells relative to the power building
- Topography of the site
- Method of fluid disposal, including any required scale-control techniques

For such analysis the pressure drop calculations for the various piping arrangements can use the formulas in "Water and Brine Piping" and "Single-flash Gathering System Design Considerations and Piping Layouts."

Two-Phase Flow The two-phase pipelines can be designed as elements of a geothermal gathering system. Take the correct pressure drop into account as it can be larger than that in single phase steam lines. The presence of unsteady flow patterns such as slug flow can cause excessive vibrations and should be avoided by proper pipe diameter selections. So-called flow pattern "maps" [57] can help the designer with the correct regimes.

Another important aspect concerns the flow of liquid removed from the cyclone separators. The fluid is in a saturated state and any pressure loss can cause it to flash into vapor. This will create a vapor barrier and inhibit the fluid flow down the well. In such cases it may be necessary to bleed the vapor from the wellhead or to install a booster pump upstream of the vapor breakout point. Also, any drop in temperature of the liquid may change the chemical equilibrium and cause precipitation as described in section on "Geothermal Resources."

Geothermal Power Conversion Technology. Figure 62
Production wellhead valve and control valves in PGV station, Hawaii (Courtesy of ORMAT)

Geothermal Power Conversion Technology. Figure 63
Rock Muffler in the station at Brady, Nevada (Courtesy of ORMAT)

Geothermal Power Conversion Technology. Figure 64
Brine line with expansion loop (Courtesy of ORMAT)

Choosing the Energy Conversion Systems

Introduction

Four basic types of geothermal energy conversion systems were covered in the section on "Thermodynamic Analysis of the Energy Conversion Process." There are geothermal resources demanding more sophisticated energy conversion systems than the basics considered until now. Furthermore, energy conversion systems have evolved to fit the needs of specific developing fields by integrating different types of power station into a complex facility described later.

Of the over 10,715 MW of geothermal stations in operation worldwide, most are steam stations operating on dry steam or steam produced by single or double-flash. About 1,000 MW use ORC or steam/ORC combined cycles [60, 61]. Table 8 compares various resources fluids and their temperatures that indicate site potential and recommended configuration.

Operational experience has confirmed the advantages of the ORC stations, not only for the low enthalpy water-dominated resources, but also at high enthalpy with aggressive brine or brine with high noncondensable gas content. The higher installation cost of these systems is often justified by environmental and long-term resource management considerations [62, 63]. The air-cooled ORC stations are particularly well adapted to the engineered geothermal systems (EGS).

Optimization of the Design of the Power Cycle

The optimization of the whole geothermal power station system is accomplished by matching the working cycle and fluid properties to the resource characteristics,when considering not only resulting efficiency and cost, but also the impact on environment, long-term pressure support, requirements for makeup wells and O&M costs.

Resource Considerations Sustainability is defined as the ability to economically maintain the installed capacity over the life of a station [64]. With geothermal power stations, this is controlled by two factors, heat recharge and water recharge.

Sustainable heat flow to the station, beyond the natural heat recharge, is supported by accessing the stored heat through drilling additional wells over the life of the project.

The decline of production in the Larderello, The Geysers, and Wairakei fields has focused attention on the necessity for long-term pressure support by injecting as much of the geothermal fluid as possible back into the aquifer.

In brines rich in carbonates, flashing, as accomplished in conventional steam power stations leads to scaling of injection wells, reducing their life span.

Use of secondary loops and of downhole and booster pumps, as in air-cooled ORC power stations

Geothermal Power Conversion Technology. Table 8 Comparison of basic geothermal energy conversion systems

Resource	Temperature	NCG	Dissolved slides	Configuration
Water	High or medium	Low	Low	Condensing steam (double-flash) *or* ORC
		High	Low	ORC
		Low	High	ORC
	Low	Any	Any	ORC
Water Dominated	High or Medium	Low	Low	Condensing steam double-flash *or* single-flash + ORC
		High	Low	ORC
		Low	High	ORC
	Low	Any	Any	Two-phase ORC
Steam Dominated	High or Medium	Low	Low	Condensing steam (single or double-flash) *or* condensing steam (single-flash) + ORC
		High	Low	Integrated Geothermal Combined Cycle
		Low	High	or Two-phase ORC
	Low	Any	Any	Two-phase ORC
Dry Steam	High or low	Low	Low	Condensing Steam
		High	Low	Geothermal Combined Cycle
		Low	High	Geothermal Combined Cycle
	Very High	Low	Low	Triple Flash Condensing
		High	Low	Geothermal Combined Cycle
		Low	High	Geothermal Combined Cycle

enhance sustainability by assuring complete water recharge while reducing both the fouling of heat exchangers and the scaling of injection wells.

Heat Cycle Considerations When the source is liquid phase only (sensible heat) the-ideal cycle would have a varying source temperature of a succession of infinitesimal Carnot cycles. In a subcritical Rankine cycle the constant temperature of the evaporation leads to a loss of energy, but because of the lower vaporization latent heat this drawback is lower than in a steam cycle.

The objective of attaining to the ideal cycle has been aimed at in proposing the super-critical Organic Rankine cycle, the total-flow regenerative cycle, the cascaded Organic Rankine cycle and the Kalina cycle. When dry steam is available, the most effective way is to use the conventional condensing steam cycle.

When the source is a mixture of steam and brine and/or has a high content of noncondensable gases, the most effective utilization of the resource is achieved through a combined geothermal cycle by firstly expanding the steam in a back-pressure steam turbine. The heat of condensation together with the heat of separated brine is then used to drive a bottoming ORC.

To compare the efficiency of the different systems it is necessary to consider the net output of parasites, such as cycle pumps, production pumps, injection pumps, cooling systems and noncondensable gas extraction power consumption [63].

Work Ratio, Parasitic Losses, and Impact on Total Cost These considerations arise in every design of new power station. These are many options to consider, a few examples follow below. While the technical issues are general, the economic decision is site specific and

depends on the type of financing, interest rate, contracted price of electricity, etc.:

- Condensing temperature
  The heat source temperature is a given factor that cannot be modified. However, the decision on the condensing temperature is negotiable and is a result of technical and economical considerations. Additional heat exchange area to a surface condenser or air-cooled condenser improves the work ratio, but adds cost of hardware. The question is whether the cost of additional kW installed or additional kWh produced per year can be justified economically.
- Single-flash or double-flash steam cycle
  Although the technical advantage of double flashing is understood and is considered to add about 20–30% to the output per well, actual site evaluation is still required. The factors to be considered are source size, heat source temperature, ratio between water and steam, etc. Additional pieces of equipment and different turbines may be required. All this affects the relative cost against the energy gain.
- Subcritical or supercritical operation of binary cycle
  Subcritical operation system is simpler to construct and operate but has limitations in heat transfer between the brine and working fluid. Supercritical cycles improve the heat transfer but require high-pressure operation increasing the pump power.
- Cascading vs. supercritical cycle
  A cascading binary cycle system is a simple solution to heat transfer improvement, while avoiding supercritical cycle limitations. The gain in power output is considered against cost of equipment. Even though multistaging is theoretically the best for gain in efficiency, the practical cost comparison dictates dual- or triple-stage design. Another consideration in cascading systems is the reduced brine temperature that can cause precipitation in the heat exchangers. This is partially compensated for by keeping the brine side under higher pressure (also has some cost impact).

Cooling System Consideration In steam Rankine cycle systems the use of condensate as makeup water is the most cost effective approach.

In areas with no natural water recharge of the geothermal reservoir and no surface water available, air cooling has been used by implementing air-cooled ORC for low-temperature resources or geothermal combined cycle for high-temperature resources. The value of the air-cooled ORC is important in case of EGS which is highly dependent on water recovery ratio.

Environmental Considerations Use of air-cooled ORC reduces the impact on environment by reinjection of:

- Noncondensable gases (mainly H_2S released by the steam)
- Discharged fluids such as the separated brine (carrying heavy metals) and blow-down from the cooling tower (chemicals) and drift from cooling towers.

Commercial Power Stations

Steam Power Stations

Dry-Steam Power Station

General Dry-steam stations were the first type of geothermal power station to achieve commercial status with their history going back 100 years [66].

Dry-steam stations tend to be simpler and less expensive than flash-steam stations in that there is no geothermal brine to contend with. As can be seen, this is a positive issue when it comes to maintaining reservoir performance.

Large dry-steam reservoirs have been discovered only in two areas of the world; Larderello and The Geysers. There are limited dry-steam areas in Japan (Matsukawa), Indonesia (Kamojang), New Zealand (Poihipi Road section of Wairakei) and the USA (The Geysers, California). White [27] estimated that only about 5% of all hydrothermal systems with temperatures greater than 200°C are of the dry-steam type.

The general characteristic of a dry-steam reservoir is that it comprises porous rocks featuring fissures or fractures, either occluded or interconnected, that are filled with steam. Whereas the steam also contains gases such as carbon dioxide, hydrogen sulfide, methane, and others in trace amounts, there is little or no liquid present.

The dry steam extracted from the mentioned resources is either saturated or slightly superheated at

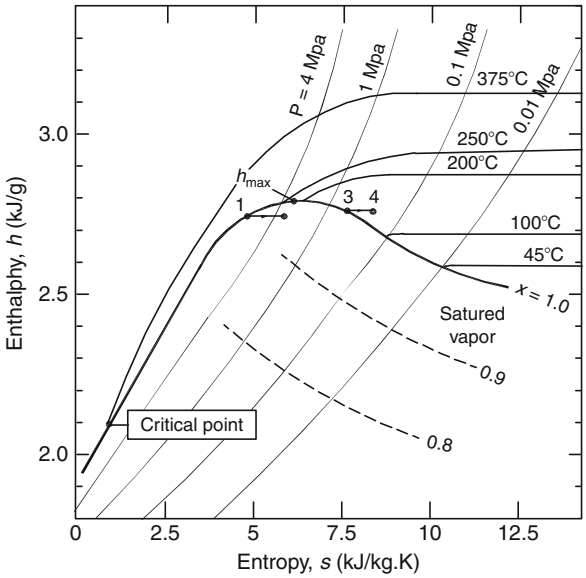

Geothermal Power Conversion Technology. Figure 65 Mollier chart for water (maximum enthalpy at T∼235°C and P∼3.07 MP)

temperatures near 235°C and pressure near the maximum saturation in Molier curve (30.7 bars) as in Fig. 65. Isenthalpic pressure loss in the upper layers (1–2, or 3–4, respectively) explains the superheated condition at the turbine inlet, but does not explain how the steam sometimes remains saturated at the wellhead.

There are over 60 flash or dry-steam commercial stations in operation, each with average power of 40 MW.

Energy Conversion System Once the steam reaches the power building, a dry-steam station is essentially the same as a regular low-temperature boiler steam station. The turbines are single-pressure units with impulse-reaction blading, either single-flow for smaller units or double-flow for large units above 50 MW. The condensers can be either direct-contact (barometric or low-level) or surface-type (shell-and-tube). For small units it is often advantageous to arrange the turbine and condenser side-by-side for maintenance reasons.

A typical dry-steam power station scheme is shown in Fig. 41 and the corresponding steam process is in Fig. 13 (repeated here in Figs. 66 and 67). Since the wells produce saturated steam (or slightly superheated steam), the starting point (state 1) is located on the saturated vapor curve. The turbine expansion process 1–2 generates somewhat less power output than the ideal, isentropic process 1–2s. Heat is discarded to the surroundings in the condenser via the cooling water in process 2–3.

The turbines used in geothermal applications must be made of corrosion-resistant materials owing to the presence of gases such as hydrogen sulfide that can damage ordinary steel.

Single-Flash Power Stations Since single-flash stations have a significant amount of waste liquid from their separators that is still fairly hot (typically 150–170°C), this can be used to generate more power instead of being directly injected. Combined single- and double-flash stations have been built at several fields around the world.

Double- and Triple-Flash Power Stations Double-flash cycles as in Fig. 44 are justified due to the high temperature of the waste brine remaining from the first flash. For such cases the turbines are designed to handle dual-pressure steam. Also, to maintain symmetric axial force on the turbine bearings and shorter blade height they are designed as double-flow machines. See scheme in Fig. 68. In some cases the source temperature and flow-rate justifies triple flashing as in the case of NGA AWA PURA power station in New Zealand shown in Fig. 69. The general station scheme is given in Fig. 70 and the turbine steam flow is given in Fig. 71. The Fuji 120 MW turbine is given in Fig. 72. However, mass flow does not always justify the construction of the special two admittance turbine. This lead to combinations as integrated single and double-flash stations, combined single and double-flash units as will be described later.

Integrated Single and Double-Flash Stations Single-flash units have been built and have been operating for a period of time where the geothermal fluid reservoir temperature is about 220–240°C. The addition of one more flash using the separated brine allows for a lower pressure unit. The arrangement shown in Fig. 73 consists of two single-flash units, Units 1, Unit 2 and Unit 3, added at a later date appears to be simply another single-flash unit. The power station as a whole is an integrated single- and double-flash facility since the

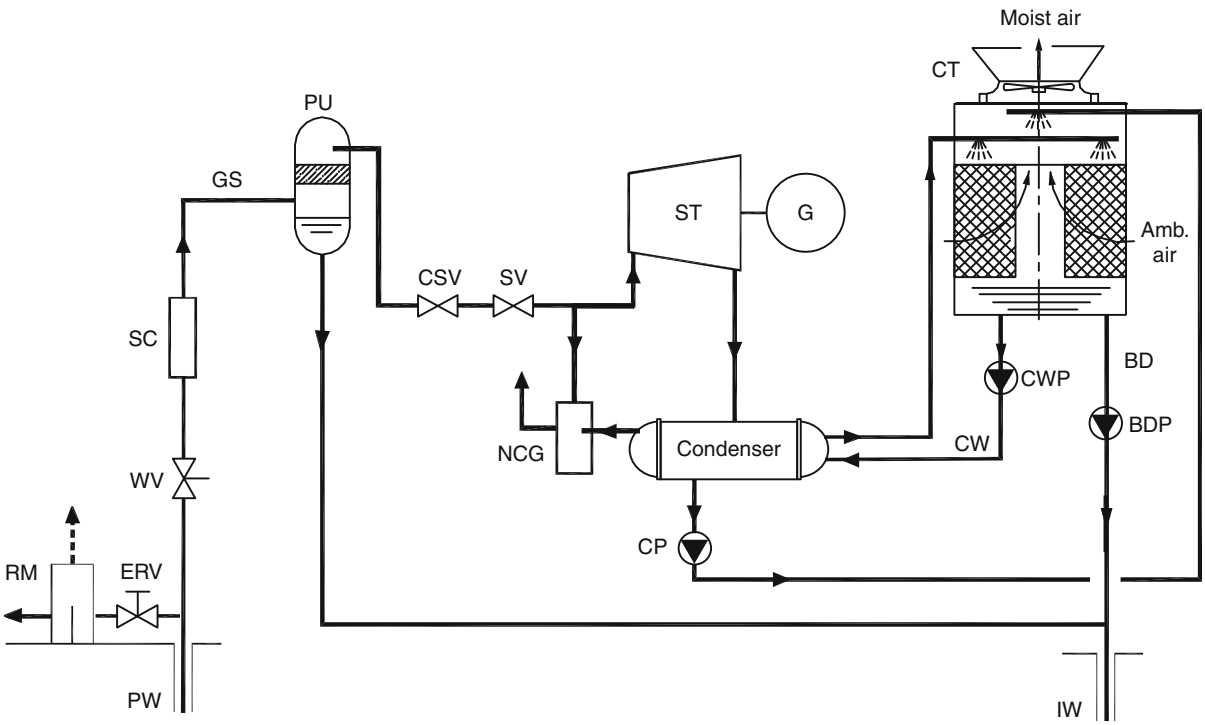

PW - Production Well
IW - Injection Well
GS - Steam
PU - Purifier
CSV - Control Valve
RM - Rock Muffler
WV - Wellhead Valve
SC - Scrubber
ST - Steam Turbine
G - Generator
CT - Cooling Tower
CP - Condensate Pump
CWP - Cooling Water Pump
CW - Cooling Water
SW - Spent Water
BD - Blow Down
BDP - Blow Down Pump
NCG - Non Condensable Gas Disposal
SV - Top Valve

Geothermal Power Conversion Technology. Figure 66
Simplified scheme of a dry-steam power station

original geothermal fluid experiences two stages of flashing [35].

The advantage to this arrangement is that no new wells need to be drilled to supply the third unit. Unit 3 serves as a bottoming unit recovering some of the wasted potential from the still-hot brine. The thermodynamic process diagram is given in Fig. 74.

One possible thermodynamic drawback to this arrangement lies in the selection of the pressure (or equivalently, the temperature) for the second flash process 3–6 in Fig. 74. If the flash temperatures for the first two units (assumed identical) had been optimized, then the addition of the third unit requires not only new optimization but evaluation of possible use of the existing equipment.

Combined Single- and Double-Flash Stations When the resource temperature is equal to or greater than 240°C, it may be possible to augment the single-flash units with a true double-flash bottoming cycle, as in the schematic flow diagram Fig. 75, and in the process diagram Fig. 76. For this case, the waste brine from the first units is subjected to two flashes, resulting in two additional low-pressure steam flows to be utilized in a dual admission turbine. The arrangement can be named as "combined single- and double-flash station" [35].

Although the thermodynamics of this arrangement are favorable, i.e., a higher resource utilization efficiency than for the original single-flash station, there may be problems with chemical scaling. This due to

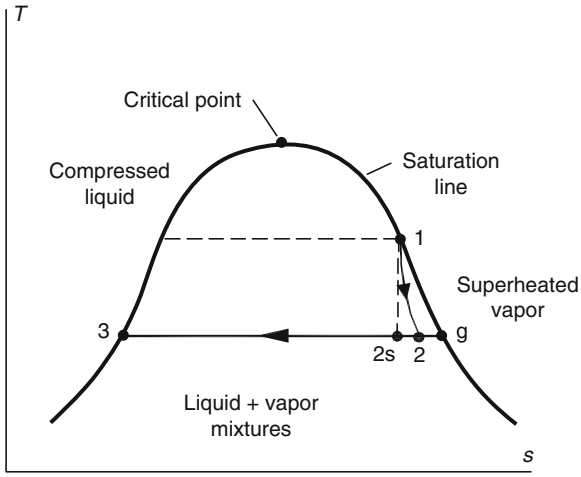

Geothermal Power Conversion Technology. Figure 67 Temperature-entropy diagram for dry-steam station (steam saturated at the turbine inlet)

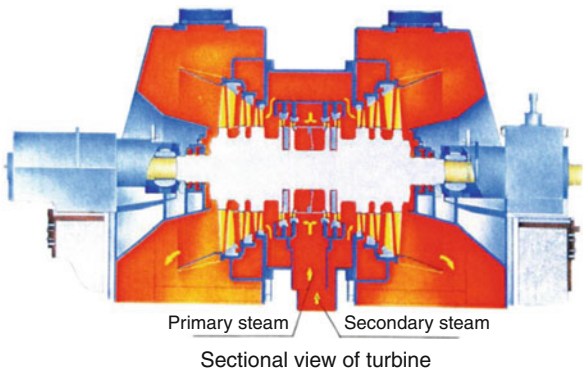

Geothermal Power Conversion Technology. Figure 68 Scheme of double-flow dual-pressure turbine (Courtesy of Mitsubishi)

silica precipitation at low temperatures associated with the last flash as discussed in section on "Geothermal Resources." Therefore few flashes would not be a good choice unless there is no possibility of silica precipitation or if silica treatment is considered as part of the investment.

Power Stations Using Hyper Saline Brines In some geothermal sites, the underground soil formation is comprised of various materials that when dissolved into the hot water cause the water to become acidic and saline. This water can clog a production well or the downstream piping and heat exchangers in a few days, or render surface vessels useless by contamination.

One of the most notorious geothermal resources is located in the Imperial Valley of southern California, near the southeastern shore of the Salton Sea. The resource was recognized in the 1850s when explorers moving west came upon hot pools and mud volcanoes in an otherwise barren desert [67].

Drilling for power production began in the 1960s but the early wells were all plugged and abandoned. Some wells drilled in the 1970s are still in operation today, but the fluids that were produced resisted exploitation for power generation because of severe scaling and corrosion problems. The temperatures were high (up to 360°C), and the total dissolved solids reached as much as 300,000 ppm, placing these fluids in the hyper saline category. The chemical analysis of the fluid produced from the Magmamax No. 1 well drilled in 1972 showed that chlorides, sodium, calcium, and potassium make up about two thirds of the 300,000 TDS in the brine [68].

An extensive research effort began in the 1970s funded by the US Department of Energy, the Electric Power Research Institute and several private companies. Through this effort, techniques were devised that later permitted these fluids to be used for the generation of electricity in a reliable and cost-effective manner [69]. Two approaches for dealing with these aggressive brines have been used with reasonable success, flash-crystallizer, reactor-clarifier (FCRC) and pH modification (pH-Mod) systems. The principles underlying these two methods are detailed below.

Flash-Crystallizer/Reactor-Clarifier (FCRC) Systems In the FCRC approach, clean steam is generated in a train of separators and flash vessels, similar to standard flash-steam power stations, but the separated brine is seeded with material inducing precipitation. A simplified schematic of an FCRC power station is shown in Fig. 77 [69]. The seed material is obtained from the highly concentrated brine waste stream. In this way, the unstable, supersaturated solids precipitate on the seed particles, rather than on the surfaces of the vessels and piping. The particulate matter eventually

Geothermal Power Conversion Technology. Figure 69
Awa Pura Power station in New Zealand (Courtesy of Fuji Electric)

settles in a reactor-clarifier vessel. The slurry from the reactor-clarifier is thickened and a portion of it is recirculated as seed material. The clarified liquid is pumped to a secondary clarifier and then sent to reinjection wells.

The most recent power station to use this approach, Salton Sea Unit 5, has a triple-pressure turbine that receives the high-pressure steam separated at the wellhead separators and expands it through the first four stages of the turbine [70]. This eliminates the throttling loss from the pressure-letdown throttle valve TV shown in Fig. 77.

pH Modification (pH-Mod) Systems Section on "pH" discussed the option of pH control to protect against silica scaling. One approach is to modify the brine pH altering the kinetics of the precipitation process. The technique of acidifying the brine has been used in some Salton Sea stations as an alternative to the FCRC approach. Acids proposed for pH control are Hydrochloric acid HCl [71] and various sulfur-based acids [72]. By reducing the pH of the geothermal fluid the solubility of silica is increased, kinetics of the reaction are slowed and it is possible to avert precipitation, at least until the separated liquid has been processed to generate the flash steam needed for the turbine. A highly simplified flow diagram for a pH-Mod station is shown in Fig. 78 [73].

The addition of hydrochloric acid to the brine requires appropriate corrosion-resistant materials. However, pH-Mod stations are much simpler than FCRC stations in terms of the number of vessels needed and the operating procedures to be followed.

The processing of the discharge waste brine D is omitted from Fig. 78 but treatment may be needed. If the injection faces problems in the pipelines or the injection wells, then the brine pH must be raised. In addition, a reactor-clarifier can be used to remove the silica and assure that the waste brine can be safely injected. Work has been done on the economics of recovered minerals from the brine – which in itself is a by-product [74].

With these two methods for handling Salton Sea brines (FCRC and pH-Mod), it has been possible to construct ten power stations with a total capacity currently generating 327 MW net [75]. It is believed that a significant portion of the ultimate potential of the geothermal field lying offshore beneath the Salton Sea

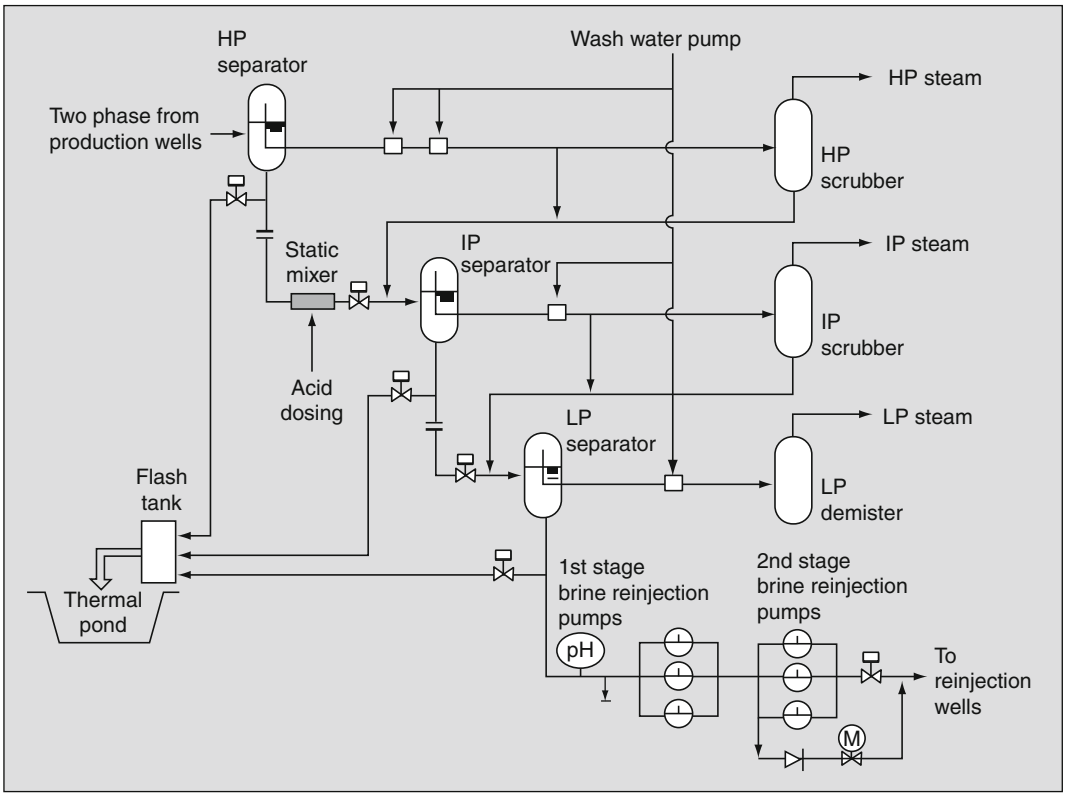

Geothermal Power Conversion Technology. Figure 70
Nga Awa Pura steam separation system overview (Courtesy of Fuji Electric)

is far from being fully exploited. The technologies described in this section should allow this valuable resource to reach its full potential.

Organic Rankine Cycle Configurations for Geothermal Power Stations

Binary Power Stations

Single-Phase ORC In cases where the geothermal fluid temperature is 150°C or less, flash systems require intensive engineering work including large flashing vessels and brine treatment both in the production and reinjection pipes and wells. In addition, in most cases, at such temperatures a production pump is required to maintain continuous geofluid flow and pressure to prevent scaling.

Although the GEM station at East Mesa in the Imperial Valley of California in the USA [34] flashes the compressed liquid as in Fig. 79, it is simpler to pass the geothermal fluid as a compressed liquid through heat exchangers and dispose of it (in the liquid phase) into reinjection wells. By improving the heat transfer across the heat exchangers an economically viable design is obtained. A water-cooled, brine-driven binary cycle is in Fig. 80 [35] and an air-cooled system is given in Fig. 81 [61].

The production wells (PW) are fitted with deep well pumps (P) and are set below flash depth determined by the reservoir properties and the desired flow rate. Sand filters SF are used in most cases to prevent scouring and erosion of the piping and heat exchanger tubes. Typically there are two steps in the process. First the working fluid flows through a preheater PH where it is brought to boiling point, then it flows to the evaporator E acquiring the supplemental heat of evaporation, emerging as a saturated vapor. The working fluid then expands in the turbine, recondenses in the condenser, and is pumped back to the preheater via a feed pump.

The geofluid flows to the evaporator, then the preheater and to the reinjection well. The geothermal fluid is

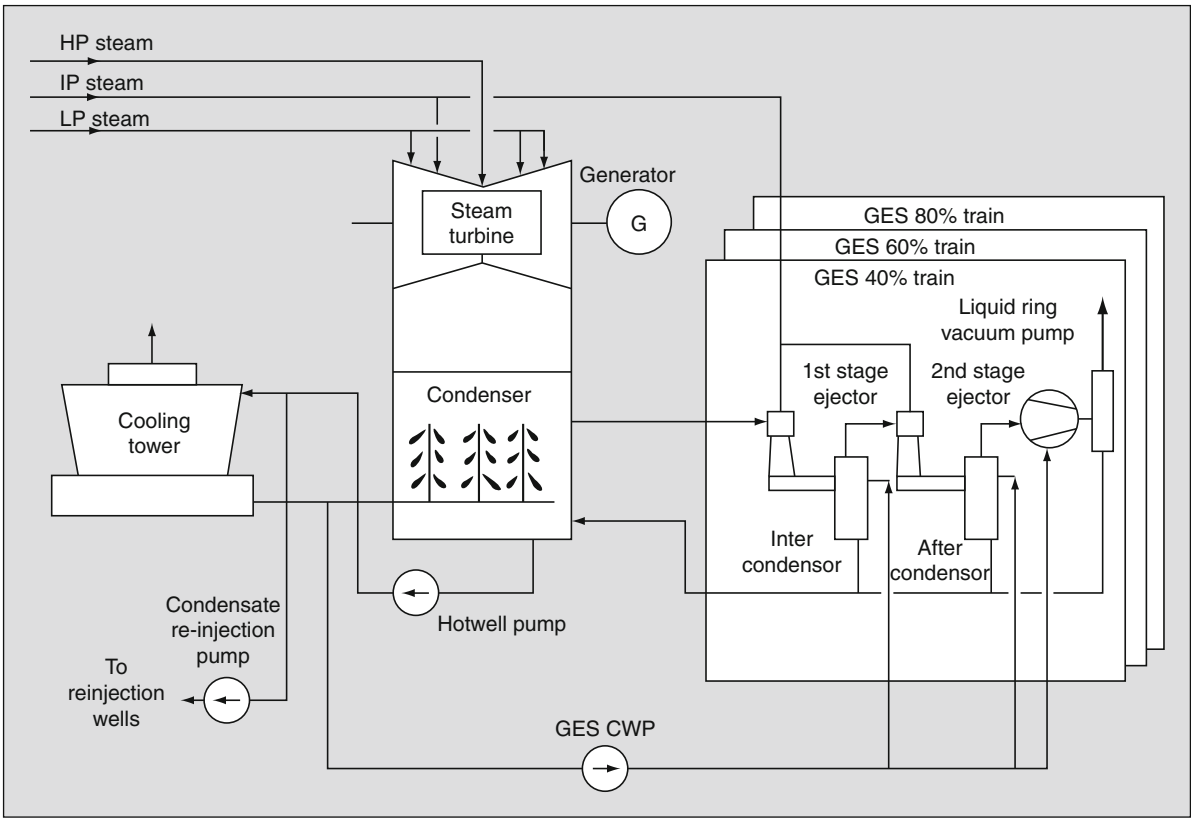

Geothermal Power Conversion Technology. Figure 71
Nga Awa Pura power generation facility overview (Courtesy of Fuji Electric)

always kept at a pressure above its flash point for the fluid temperature to prevent the breakout of steam and noncondensable gases that leads to calcite scaling in the piping. Furthermore, the fluid temperature is not allowed to drop to the point where silica scaling becomes an issue in the preheater, piping, and reinjection wells. Therefore chemical problems mentioned in section on "Geothermal Resources" are eliminated.

Temperature Cascading Organic Rankine Cycle To increase the power output of a binary power station, a cascading system can be used. In a simple cascading method there are two or more evaporators and preheaters, arranged consecutively in consequent structure. The geothermal fluid travels from one pair of units to the next. The station schematic given in Fig. 27 incorporates three levels of organic systems, each working at a different range of temperatures.

All preheaters begin from the same temperature but evaporation is performed at three different temperatures, therefore three turbines are required for such operation, ensuring the cooled brine is better utilized by the preheaters with part of the preheating in the evaporators. A T-Q diagram of the schematic arrangement of this system is given in Fig. 28.

A two-level cascading based on two turbine integrated over one generator was used in Ormat Heber brine station as given in Fig. 82. The brine enters level 1 evaporator then the level 2 evaporator. From this level the brine goes to the preheaters of both levels. The turbines of both levels are connected to single generator. The turbines of each level can be divided into HP and LP turbines, with each pair driving a single generator. Both condensers are water cooled sharing the same cooling water supply line. The station is shown in Fig. 83.

Geothermal Power Conversion Technology. Figure 72
Nga Awa Pura view over turbine generator (Courtesy of Fuji Electric)

Recuperated Organic Rankine Cycle In most actual cases, the perfect match above is not feasible because of limitation of the brine and condensate mixture cooling temperature. In most of the cases the limiting factor is the silica scaling risk, which increases as the brine temperature drops. A method to partially overcome the cooling temperature limit is to add a recuperator which provides some of the preheating heat from the vapor exiting the turbine.

The recuperator is applicable when the organic fluid is of the "dry expansion" type, a fluid where the expansion in the turbine is done in the dry superheated zone and the expanded vapor contains heat that has to be extracted prior to the condensing stage (see [36, 77]). The recuperated Organic Rankine cycle is typically 10–15% more efficient than the simple Organic Rankine cycle described in the beginning of this chapter (Fig. 66 for comparison). This applies to the two-phase geothermal power station in Fig. 84 with its T-Q diagram in Fig. 85.

The recuperated two-phase process is used by Ormat in many geothermal projects around the world, i.e., 20 MW Zunil in Guatemala, 14 MW Ribeira Grande I and II in San Miguel in the Azores (Fig. 86), and 1.8 MW Oserian and 13 MW Olkaria III in Kenya.

Two-Phase Geothermal Power Station In the majority of worldwide geothermal fields, the geothermal fluid is separated in an aboveground separator into a separate stream of brine and steam. In a low to moderate enthalpy resource, the steam quality is 10–30% of the entering fluid quality if comparing enthalpy and separation pressure. The two streams can efficiently be utilized in a two-phase geothermal station as shown in Fig. 87. Separated steam (usually with some percentage of noncondensable gases or NCGs) is introduced in the evaporator to vaporize the organic fluid [81].

The geothermal condensate is mixed with the separated brine to provide the preheating medium of the organic fluid. In the ideal case, presented in the T-Q diagram (Fig. 88), the latent steam heat equals the heat of vaporization of the organic fluid and the sensible heat of the brine plus condensate equals the heat

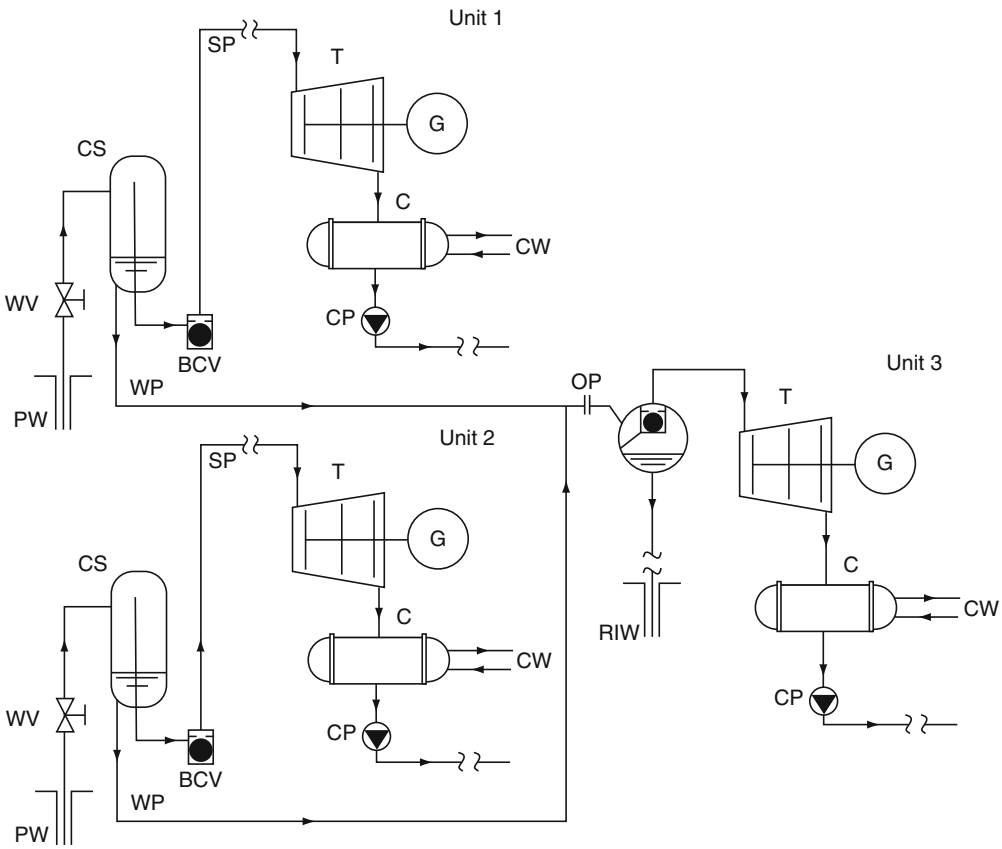

Geothermal Power Conversion Technology. Figure 73
Integrated single- and double-flash power station [35]

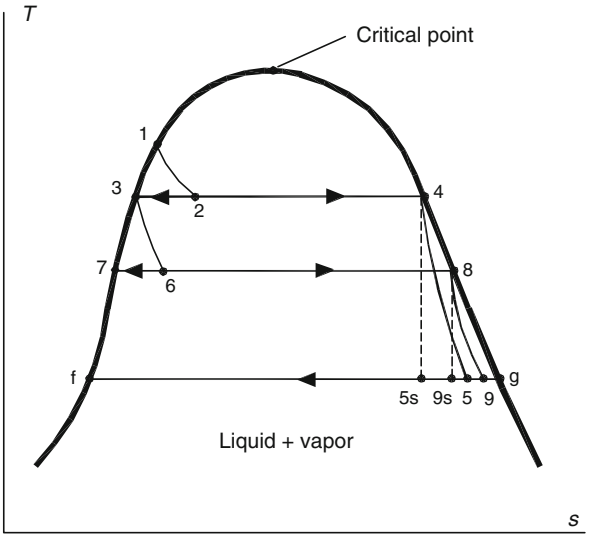

Geothermal Power Conversion Technology. Figure 74
T-S diagram for the integrated single- and double-flash power station in Fig. 73

required to preheat the organic fluid. This "perfect" heat transfer match between the geothermal fluid and the working fluid represents maximum thermodynamic efficiency with minimum losses.

Higher Enthalpy Two-Phase Geothermal Power Station When the resource enthalpy is higher with an increase in proportion of steam in the total fluid, the "perfect match" between the heat source and the working fluid is not maintained. Some of the available heat or available energy is lost for power generation.

To utilize the two-phase heat source in a more efficient manner, a secondary organic loop is used, utilizing the extra steam available. The cycle shown Fig. 89 is feasible when vapor extraction is possible within the expansion phase of the organic cycle. The simplest way to perform the extraction is with two turbines in series. In this case, some vapor is extracted between the high-pressure and the low-pressure

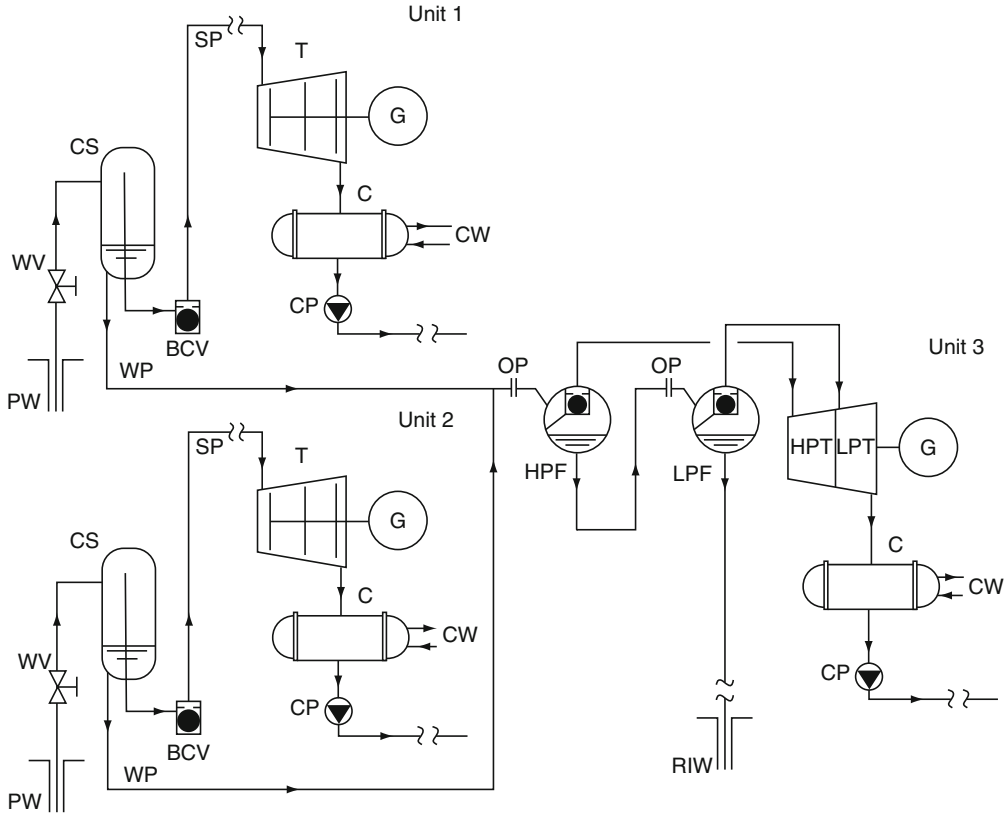

Geothermal Power Conversion Technology. Figure 75
Combined single-and double-flash station [35]

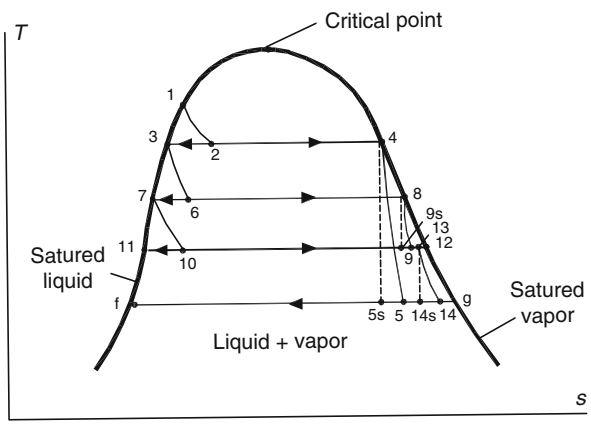

Geothermal Power Conversion Technology. Figure 76
Process diagram for combined single- and double-flash station

turbines and condensed at an intermediate pressure (and temperature).

The condensed vapor preheats the main organic fluid stream as it exits the recuperator. The extracted organic fluid forms a secondary cycle which generates an additional 5–8% electrical power. When there is extra steam compared to brine (higher enthalpy) the above cycle is effective and the cooling temperature of the brine plus condensate is limited.

Figure 90 is a flow temperature diagram of the higher enthalpy cases. Line A is the simple two-phase cycle preheating phase. The significant irreversibility is represented by the large space between the steam and brine lines and line A. Line B shows the preheating phase in a recuperated two-phase cycle. Here irreversibility is reduced and the cycle efficiency is increased accordingly.

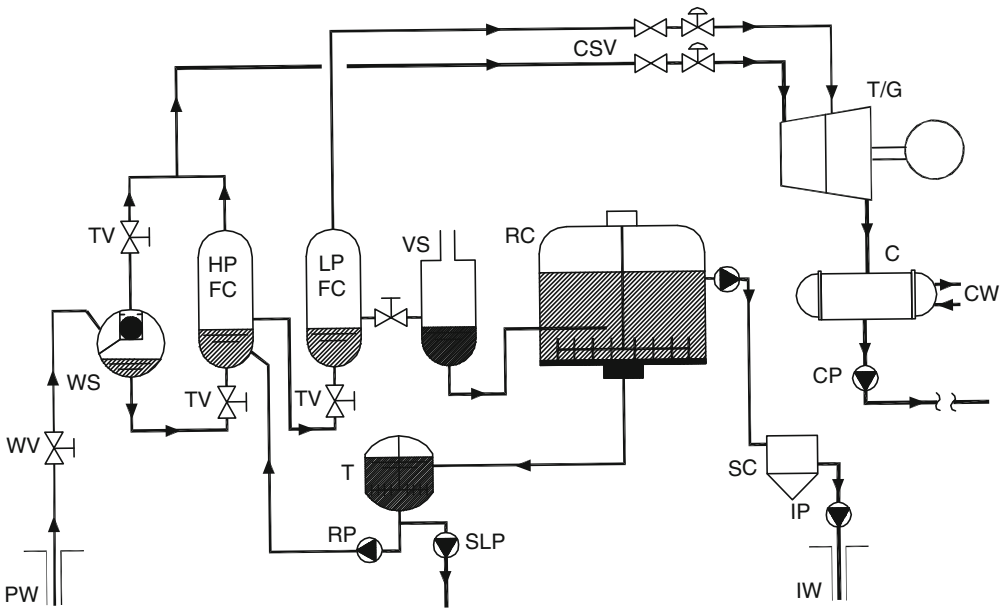

Geothermal Power Conversion Technology. Figure 77
schematic flow diagram for a FCRC power station, after [35, 69]

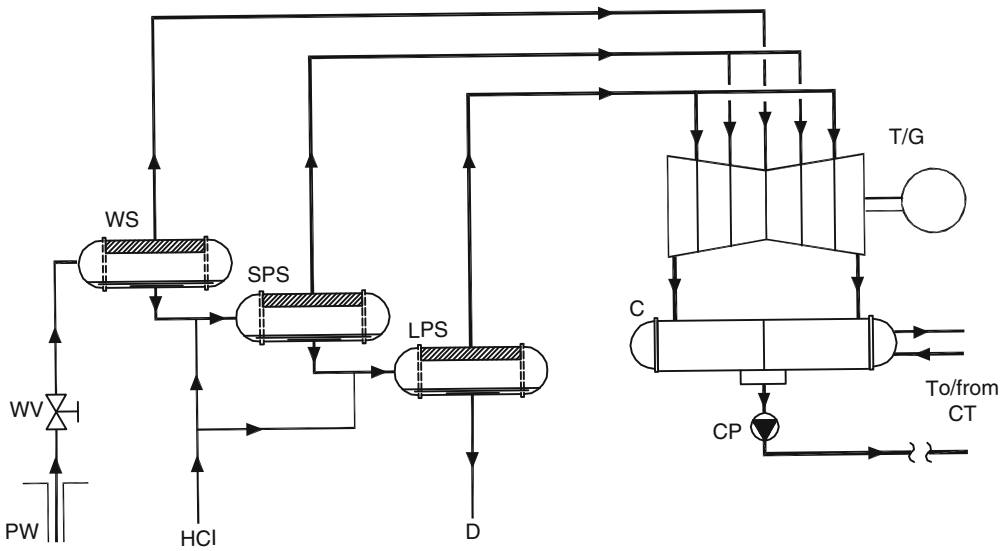

Geothermal Power Conversion Technology. Figure 78
Flow diagram for pH-Mod power station

The third line, C, demonstrates the additional gain in efficiency by using the two-phase/extraction cycle. The line moves further to the right, thus decreasing the gap between the heating line and the working fluid line. Another indication of efficiency increase from cycle A to B and to C, is the increasing heat quantity for heating the working fluid, as presented by points QA, QB, and QC.

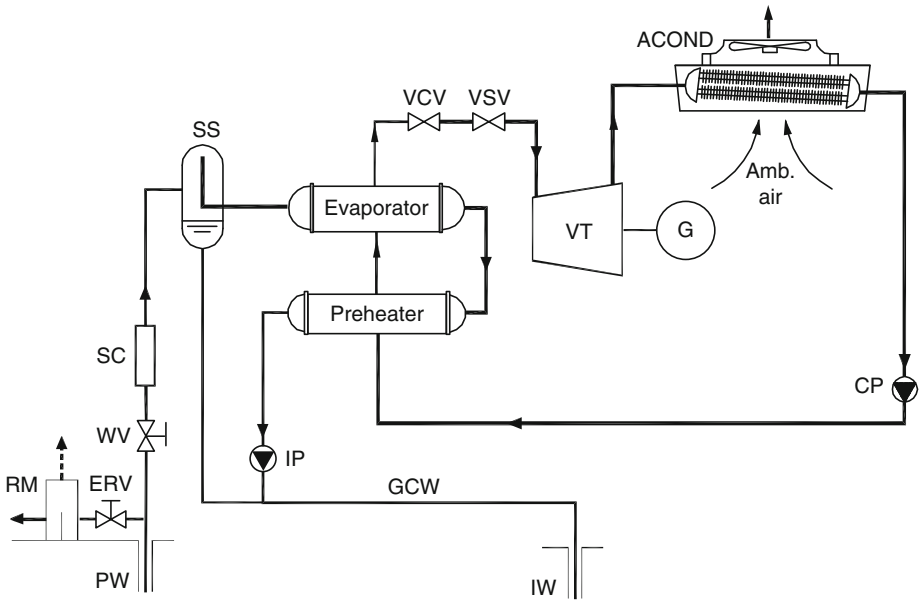

PW - Production Well
IW - Injection Well
RM - Rock Muffler
WV - Wellhead Valve
SS - Steam Separator
SC - Scrubber
VCV - Vapor Control Valve
VSV - Vapor Stop Valve
G - Generator
VT - Vapor Turbine
CP - Condensate Pump
IP - Injection pump
CW - Cooling Water
ACOND - Air Cooled Condenser
GCW - Geothermal Cooled Water

Geothermal Power Conversion Technology. Figure 79
Binary cycle operated by flashed steam

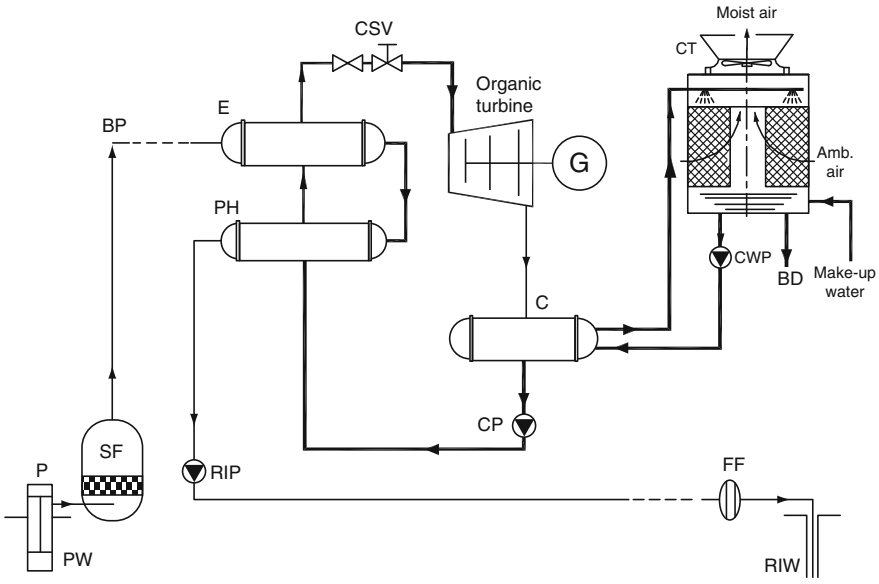

Geothermal Power Conversion Technology. Figure 80
Simplified schematic of a water-cooled binary geothermal power station [35]

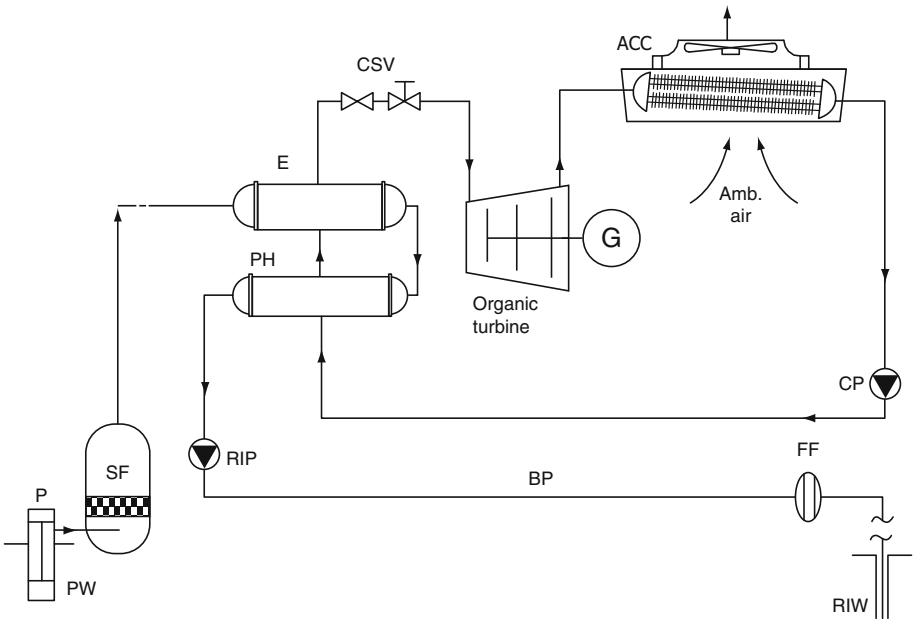

Geothermal Power Conversion Technology. Figure 81
Simplified schematic of an air-cooled binary geothermal power station [61]

Hybrid Geothermal Cycles

The various configurations of hybrid steam and organic Rankine cycles are:
ORC bottoming of flash power stations
Geothermal combined cycle
Integrated geothermal combined cycle
Use of a back pressure steam turbine

ORC Bottoming of Flash Power Stations An elegant alternative to the use of bottoming flash stations at existing single-flash stations is to add a bottoming Organic Rankine cycle. Combined flash-binary stations are in operation at several station sites around the world (see DiPippo [73], Appendix A). A different approach is to design a station, from scratch, as an integrated flash-binary station, thereby taking advantage of the best features of both units.

For this case, assume that a single-flash station has been running for some time (usually a few years), and the reservoir has shown itself capable of sustaining operations for many more years. The power output can be raised by adding a binary unit between the separators and the reinjection wells. A simplified schematic of such an arrangement is given in Fig. 91.

Such modification to the initial field design have been made in Momotombo, Nicaragua. The initial steam-only station comprised of two 35 MW Franco Tosi steam turbines was enhanced by Ormat 9 MW binary bottoming cycle combined with one of the steam turbines as in Figs. 92 and 93. The field suffered from reduced steam production, reduced temperatures, injection difficulties that required more and deeper wells to regain the original field power production allowing the use of the second steam turbine, and possible additional bottoming cycle.

Initially the single-flash station operated alone and waste liquid from the cyclone separators CS was sent directly to the injection wells IW. The Organic Rankine cycle is inserted as shown to tap into the reinjection pipeline where it extracts some heat thereby lowering the temperature of the waste brine prior to injection. The additional power generated by the Organic Rankine cycle is gained without any new production wells.

The thermodynamic process coordinates to facilitate comparison with the cycles in the previous sections. The power units are coupled thermodynamically through the preheater FH and the evaporator E. Using the state points of Fig. 91, the First Law gives the relationship between the brine flow rate $\dot{m}_b$, from the

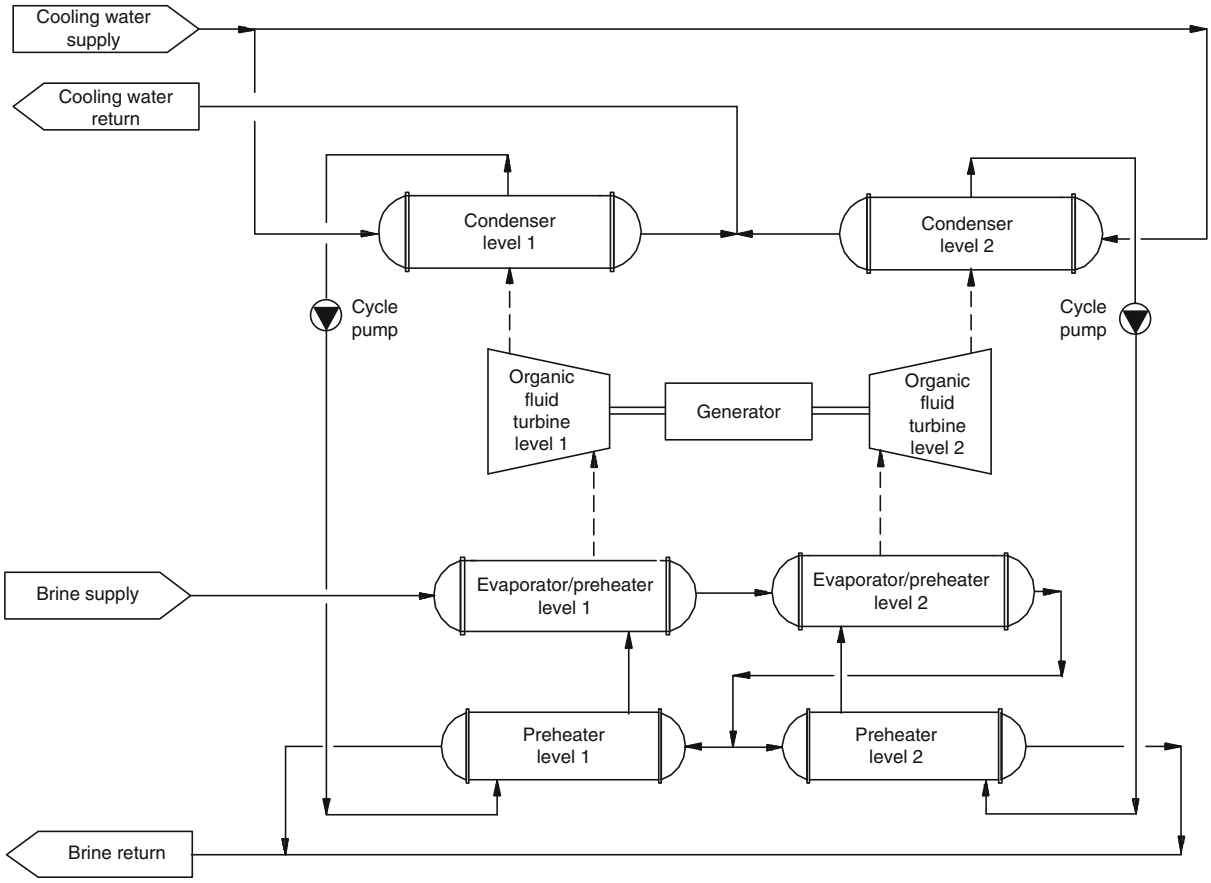

Geothermal Power Conversion Technology. Figure 82
Integrated Two Level (ITLU) Power Station

wells (state 1) and that of the Organic Rankine cycle working fluid $\dot{m}_{wf}$:

$$\dot{m}_b(1 - x_2)c_b(T_3 - T_2) = \dot{m}_{wf}(h_a - h_c) \tag{82}$$

This equation shows that the heat extracted from the waste brine is equal to the heat absorbed by the Organic Rankine cycle working fluid, assuming perfect insulation on the heat exchangers. After solving for the working fluid flow rate it is found:

$$\dot{m}_{wf} = \dot{m}_b(1 - x_2)\left[\frac{c(T_3 - T_2)}{h_a - h_c}\right] \tag{83}$$

Since the state points 1, 2, and 3 for the flash unit are fixed and the new state point 7 is subject to the constraint imposed by silica precipitation, only the Organic Rankine cycle parameters are open for assignment.

Geothermal Combined Cycle Power Stations In case of high enthalpy dry steam or vapor dominated sources the use of condensing steam turbines present a number of disadvantages. First the high humidity in the many stages of the low pressure turbine portions lead to efficiency loss and erosion/corrosion of the blades. Secondly if non-condensable gases are present use of vacuum pumps is necessary to avoid efficiency loss due to back pressure and reduction of the heat transfer coefficient of condensation. Using only the high pressure part of the condensing steam turbine (also called "back pressure steam turbine") and using the exhaust steam as the heat source for the evaporator of an Organic Rankine cycle [82], we get a geothermal combined cycle Fig. 94 which avoids the above drawbacks of condensing steam turbines.

Geothermal Power Conversion Technology. Figure 83
Photo of 40 MW Heber ITLU Power station (Courtesy of ORMAT)

The collected brine at the moisture remover MR exit is dumped (if small quantity), or added to the condensate exit or delivered to the reinjection wells, depending on the quantities and temperatures of the brine.

The T-Q diagram of the Organic Rankine cycle (Fig. 95) will be the same as given before for the two-phase power station.

Geothermal combined cycle configuration avoids both drawbacks: steam expansion in the back pressure steam turbine is smaller limiting the wetness of the steam and its effects while the partial pressure of the non-condensable gases (NCG) is small and so is its effect on the condensation in the condenser/vaporizer of the Organic Rankine portion of the cycle. An additional advantage is that the NCG is above the atmospheric pressure, therefore can be ejected without the need of vacuum pumps or reinjected with the condensate into the injection well. Another advantage is that the use an air-cooled condenser on the ORC is more cost effective than on a condensing steam turbine.

Use of a Back-Pressure Steam Turbine Another approach for a moderate enthalpy two-phase heat source is the use of a back-pressure steam turbine which generates extra power from excess steam not required for the ORC evaporator.

Low-pressure steam exiting the back-pressure steam turbine (Fig. 96) is used to partially preheat the organic fluid.

The gap between the organic fluid steam and the preheating line could be filled more efficiently by a multistage (two or more) back-pressure steam turbine, with steam extraction between the stages. The number of stages takes into account the process trade-off optimization between higher efficiency and the complication (and cost) of the system.

A system based on the above cycle is now operating in the 20 MW Amatitlan geothermal project in Guatemala (station photo is given in Fig. 97 and the station scheme in Fig. 98).

Geothermal Integrated Combined Cycle Power Stations When a bottoming Organic Rankine cycle is integrated with an air-cooled combined cycle, the result is a station with practically zero emissions. An integrated CC single-flash-binary station is shown schematically for water-cooled system in Fig. 99 [73] while Fig. 100 shows the same concept for air-cooled system [78] with three separated turbines. The process diagram is in two parts, the main upper combined cycle

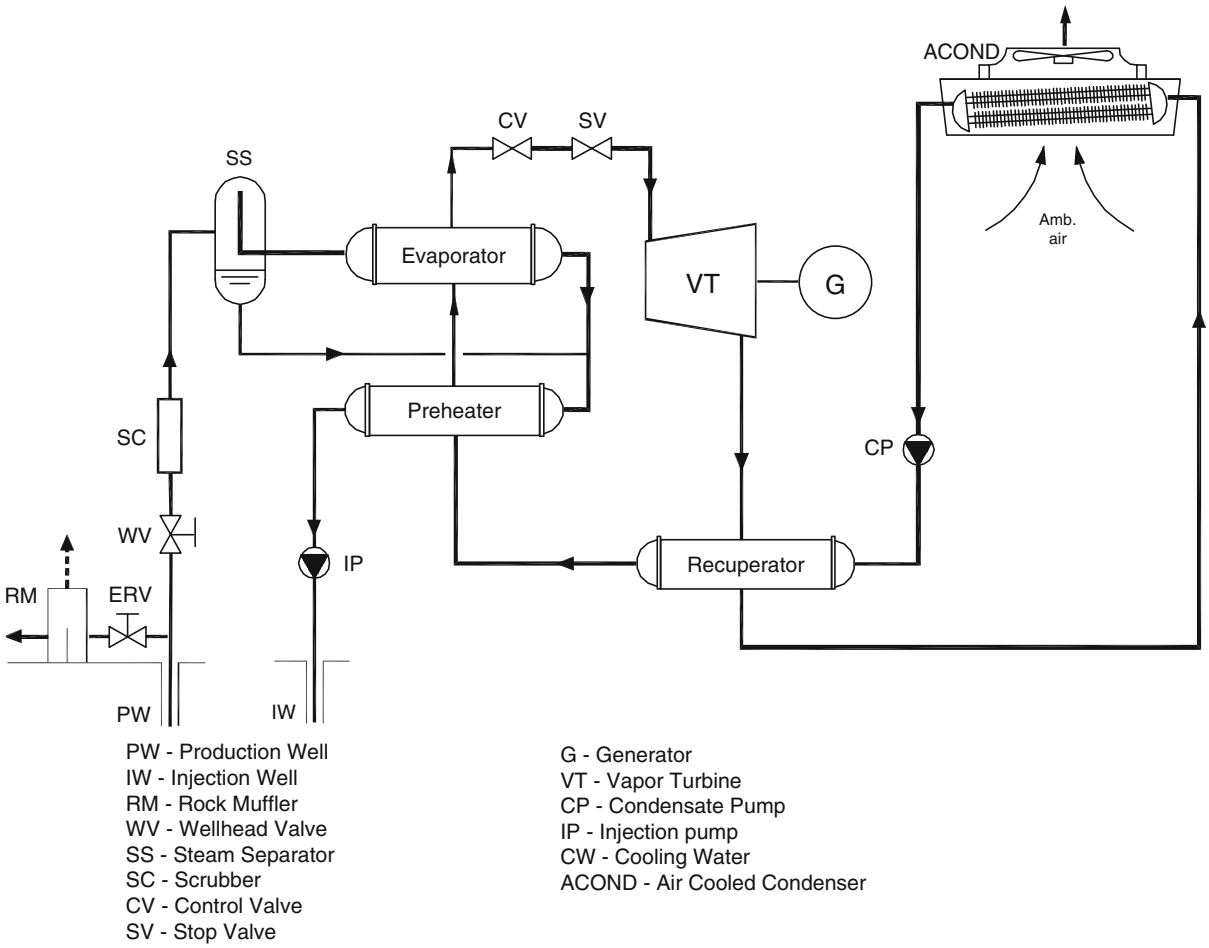

Geothermal Power Conversion Technology. Figure 84
Recuperated Organic Rankine cycle in two-phase binary power station

and the bottoming ORC portion. Geothermal steam first drives the back-pressure steam turbine and then is condensed in the upper ORC evaporator (E in Fig. 99). The two turbines in the upper part of the station may be connected to a common generator.

The separated brine (state 3) is used to preheat and evaporate the working fluid in the bottoming ORC. Noncondensable gases flow with the steam through the steam turbine ST into the evaporator where they are isolated, removed and compressed for recombination with the waste brine prior to reinjection. The brine holding tank (BHT) collects all the steam condensate, waste brine and compressed gases that go back into solution (Fig. 99).

In principle, this station has no emissions to the surroundings. The only environmental impact is the heat rejected to the atmosphere from the Organic Rankine cycle condensers. The scheme shows air-cooled condensers but water-cooling is an option.

This configuration was first used in 1992 in the 30 MW Puna power station in Hawaii, then in the 125 MW Upper Mahiao in the Philippines (Fig. 101), 100 MW Mokai 1 and 2 in New Zealand.

An example for an integrated combined cycle station is given also by DiPippo [73].

Combined Heat and Power

Iceland In most geothermal sites the option for utilization of the residue heat energy contained in the waste brine does not exist. The main reason is the distance from population centers. Iceland is one of

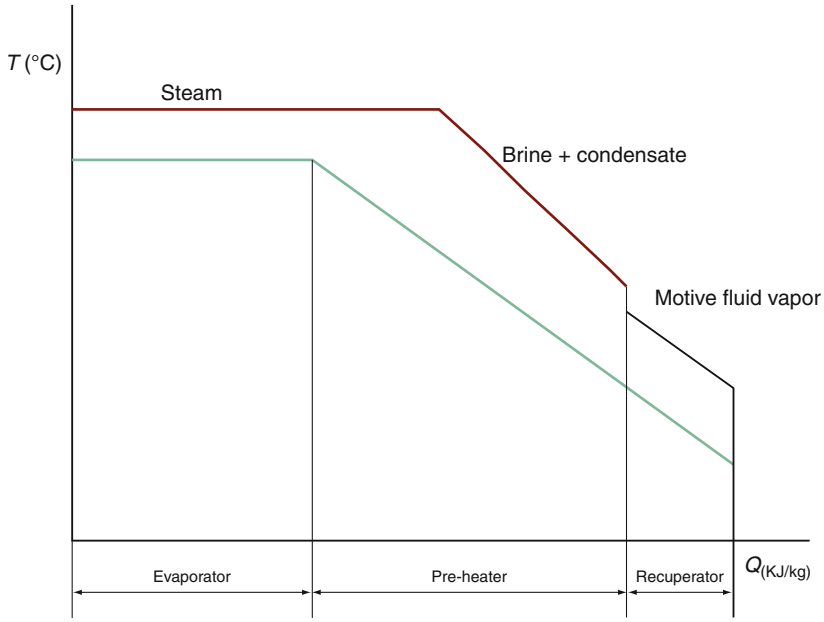

Geothermal Power Conversion Technology. Figure 85
Recuperated ORC in two-phase binary power station

Geothermal Power Conversion Technology. Figure 86
Two-phase 14 MW Ribeira Grande power station in the Azores (Courtesy of ORMAT)

few examples where heat can be used for district heating and similar usage.

The Svartsengi geothermal area is close to the town of Grindavik on the Rekjanes peninsula and is part of an active fissure swarm, lined with crater-rows and open fissures and faults. The high-temperature has an area of 2 km^2 and shows only limited signs of geothermal activity at the surface. The reservoir contains much

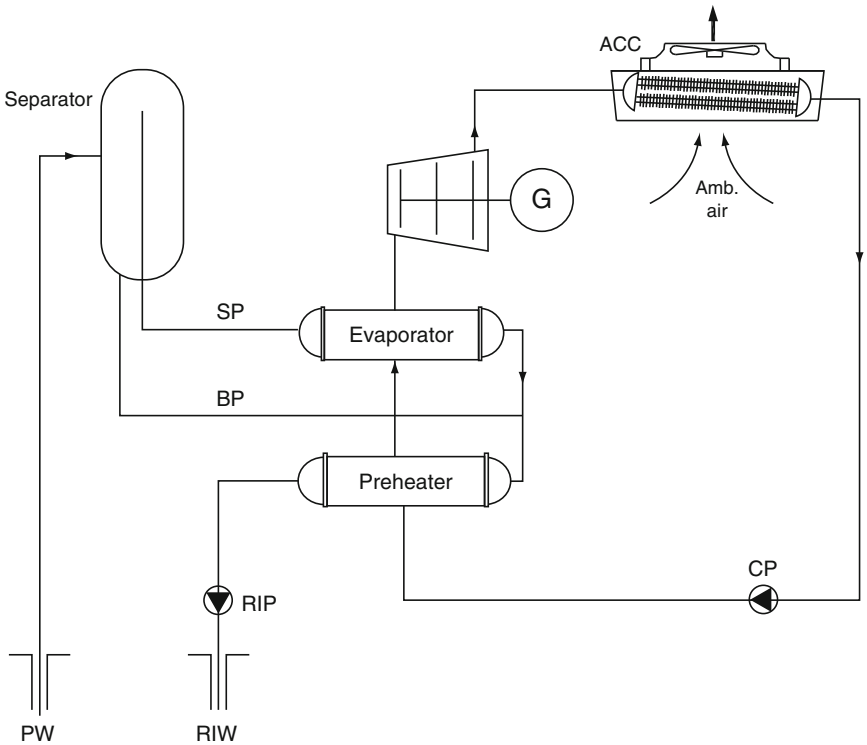

Geothermal Power Conversion Technology. Figure 87
Two-phase binary power station

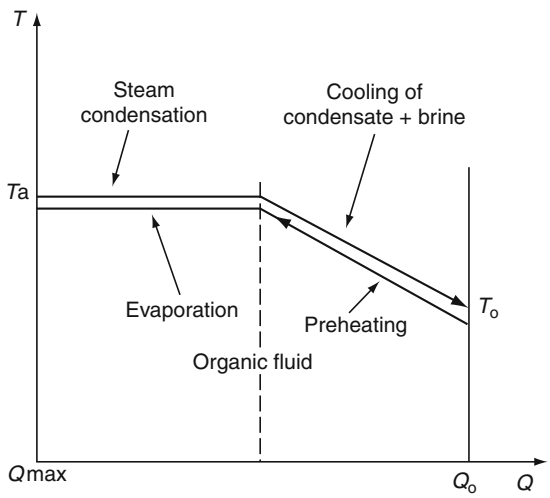

Geothermal Power Conversion Technology. Figure 88
T-Q diagram of a two-phase binary power station

energy with at least 8 wells supplying the Svartsengi Power Stations with steam [79]. The steam is not useable for domestic heating purposes and heat exchangers are used to heat cold groundwater with the steam. Some steam is also used for producing 16.4 MW_e of electrical power, see Fig. 102 bottom. Figure 102 top shows the distribution system piping of hot water to nine towns and the Keflavik International Airport. The effluent brine from the Svartsengi Stations is disposed of into a surface pond, called the Blue Lagoon. This is popular for tourists and people suffering from psoriasis and other forms of eczema seeking therapeutic effects from the silica-rich brine.

In 1969, the Grindavik municipal council decided to do a study of harnessing geothermal energy in the Svartsengi area to heat houses in the village. The wells drilled at that time, 240 and 430 m deep, looked very promising. There was some disappointment as it was revealed that:

- This was a high-temperature geothermal area (i.e., with temperatures rising to more than 200°C at less than 1,000 m depth (to hot for domestic usage).
- The geothermal reservoir contained water with about two thirds of the salinity of the sea.

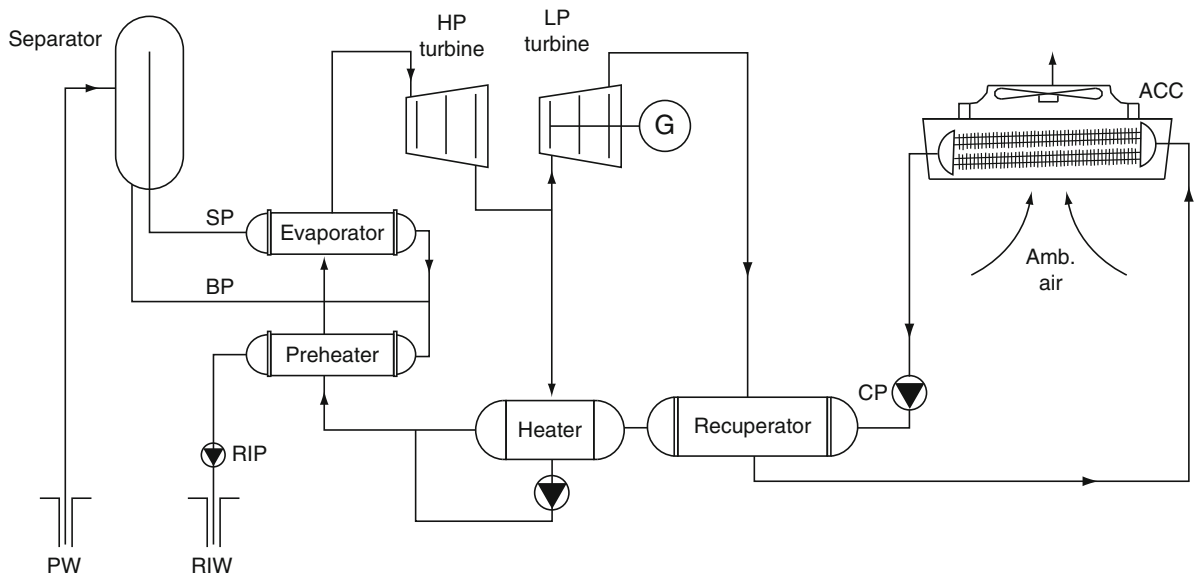

Geothermal Power Conversion Technology. Figure 89
Secondary Organic cycle with LP partial vapor admission

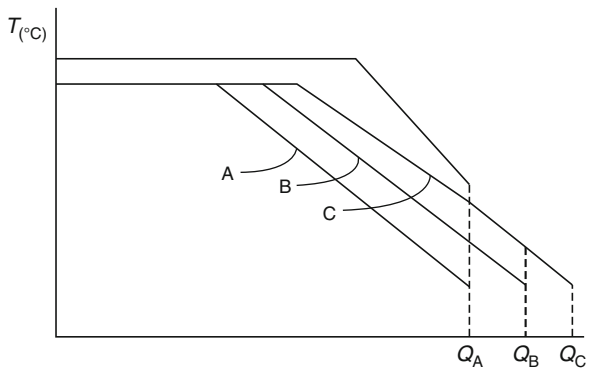

Geothermal Power Conversion Technology. Figure 90
T-Q diagram of the high enthalpy secondary organic cycle

Due to the level of salinity and the high temperature of the water, it was clear that it would not be possible to utilize the geothermal fluid directly as had been the case in Reykjavik and most other places in Iceland. What was needed was the development of a method of heat exchange to facilitate the utilization of the geothermal power.

Rogner Hotel in Austria The 250 kW geothermal project at Bad Blumau is the first geothermal project developed in Austria by the private sector following the deregulation of the electricity industry in this country. Besides its private ownership structure, the project is unique due to its ability to generate electrical power and district heating by using a low-temperature geothermal resource. The unit is shown in Fig. 103.

The air-cooled ORMAT® Energy Converter (OEC) CHP module has been in commercial operation since July 2001. With an annual availability exceeding 99%, the station delivers about 1,300,000 kWh annually to the local grid. The geothermal CHP module utilizes brine at ~110°C available from a 3,000 m deep production well. Exiting the OEC unit at a temperature of ~85°C, the brine is then fed into the district heating system providing heat for the Rogner Bad-Blumau Hotel and Spa. The geothermal brine is returned from the district heating system and injected into a 3,000 m depth well.

The system is a pollution-free, unattended operating power generation module, which averts about 1,000 tons of CO_2 emissions annually.

Experimental Power Stations

Dual-Fluid Organic Rankine Cycle

The first binary station in the USA was the Magmamax station at East Mesa in California's Imperial Valley.

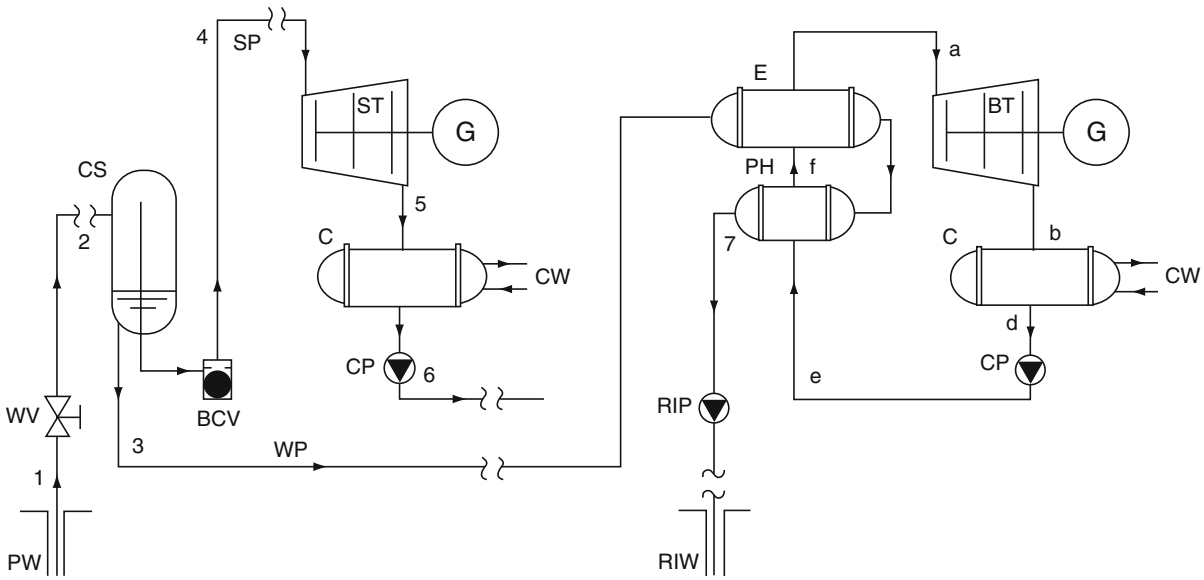

Geothermal Power Conversion Technology. Figure 91
Combined single-flash and ORC station; after [69]

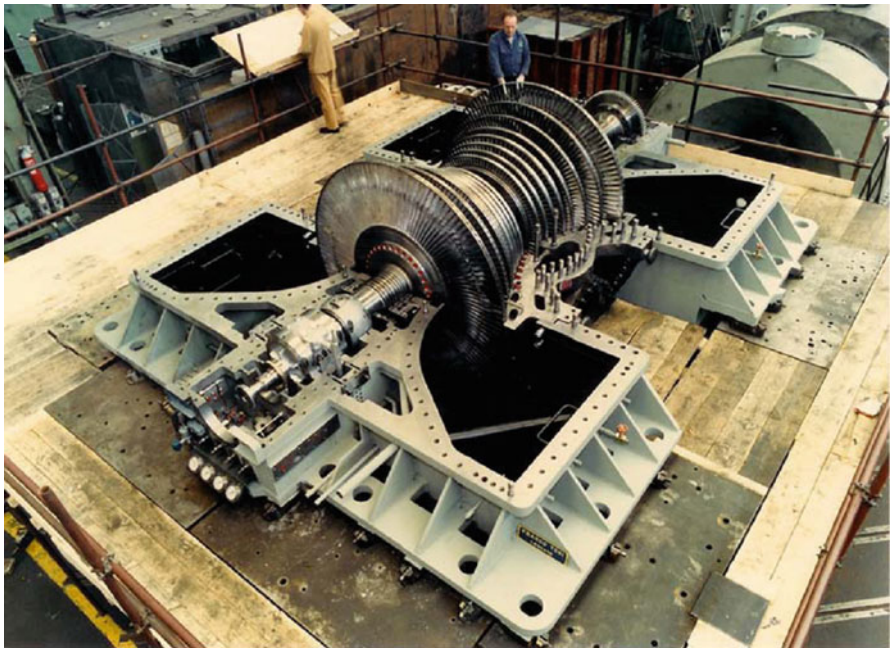

Geothermal Power Conversion Technology. Figure 92
Momotombo Franco Tosi 35 MW steam turbine (Courtesy of Franco Tosi)

The station was a 12.5 MW station that began operation in 1979 using a dual-fluid cycle (two different hydrocarbons were used in interlocking Rankine cycles). One a subcritical cycle and the other a supercritical cycle [83, 84]. The typical dual fluid system is shown in Fig. 104.

Geothermal Power Conversion Technology. Figure 93
Ormat 9 MW ORC bottoming power unit (Courtesy of ORMAT)

As with the dual-pressure cycle, incentive here is to create a good "match" between the brine and the working fluid heating-boiling curves. The temperature-heat transfer diagram Fig. 105, shows this relationship. The discontinuity between state points 5 and 11 arises from the internal heat transfer between the working fluids and does not involve the brine. From the diagram it is seen that the pinch point occurs between state b on the brine cooling curve and state 6, the bubble point for fluid 1. The near-parallelism between the brine and the working fluids in the preheaters means that the thermodynamic irreversibilities will be low, as will the loss of energy during the heat transfer process in those components. Since the average temperature difference in the fluid 1 evaporator is relatively large, it will be associated with a higher energy loss.

If fluid 1 is raised to a supercritical pressure before entering its preheater, the temperature-heat transfer diagram would change dramatically, see Fig. 106.

The sharp corner at state 6 denoting the bubble point for fluid 1 has vanished. Fluid 1 now has a smooth heating curve taking fluid from a cool compressed liquid to a hot supercritical vapor. There will still be a point of closest approach between the two curves, but it is far less pronounced. This allows a good match between the brine and the working fluids which results in lower energy losses and higher utilization efficiency for the cycle.

As already mentioned, the supercritical cycle has higher thermal efficiency. However, the pump work is using greater fraction of the net cycle work and is about 50% higher than for the subcritical cycle.

There are additional practical difficulties with a supercritical cycle. The higher pressures may require change of traditional use of shell and tube heat exchangers in the geothermal application where the brine flows in the tubes and the organic fluid in the shell side. This allows for practical operation of in-tube cleaning as may be required in brine flow during long operation. Also, once it is changed, thicker and more costly tubing in the heat exchangers is required.

In both cases, the heat recovered from the condensation of fluid 1 is used for evaporation of the second fluid in E2. In a T-Q diagram between the two fluids there will be two parallel lines as given in Figs. 105b and 106b.

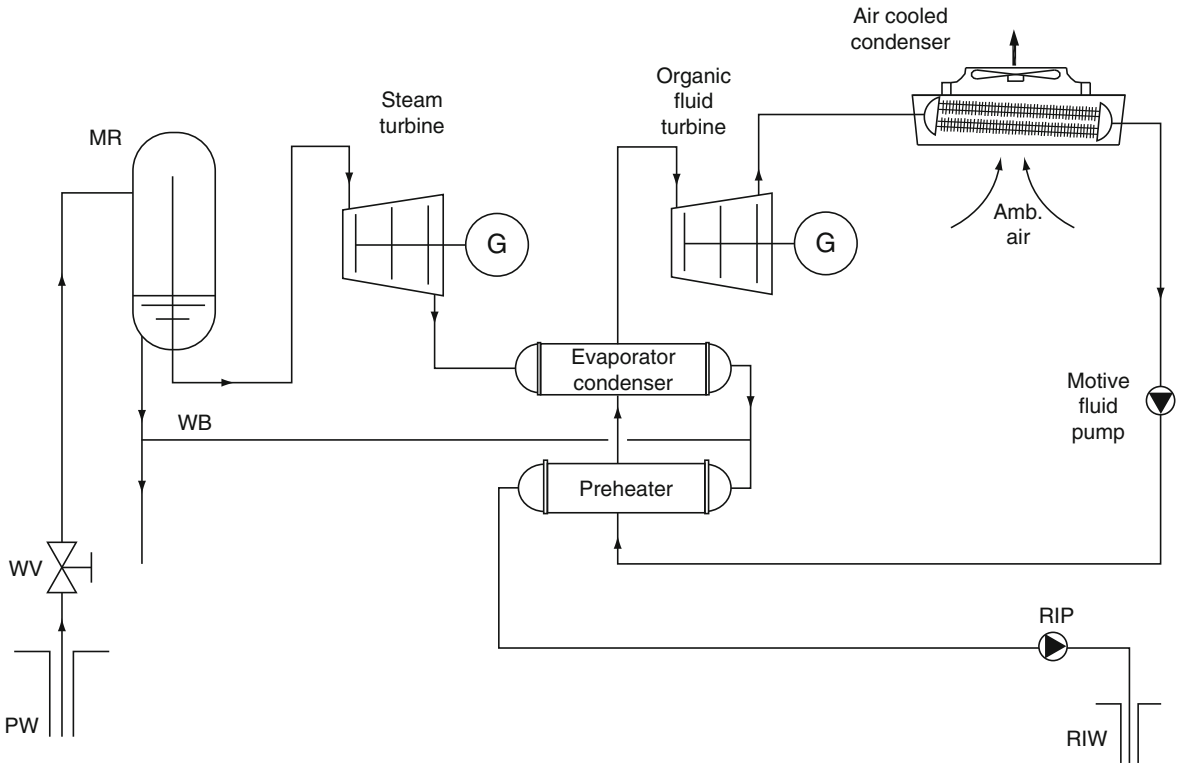

Geothermal Power Conversion Technology. Figure 94
Geothermal Combined cycle (GCC)

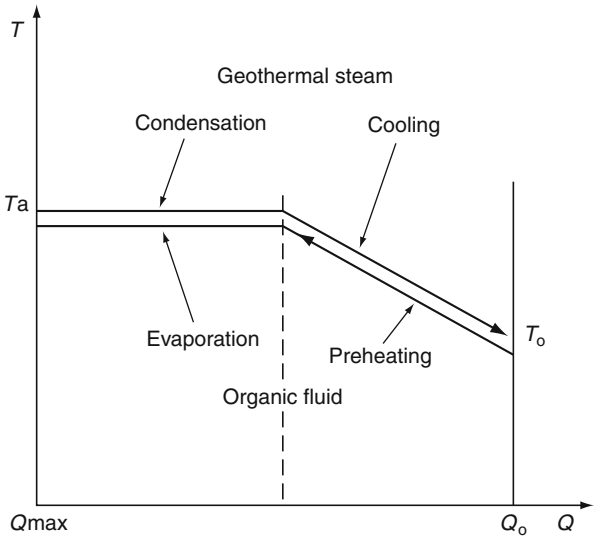

Geothermal Power Conversion Technology. Figure 95
T-Q diagram of the ORC part of the CC

This was one reason why the original Magmamax station [83] placed the supercritical isobutane inside the tubes and the brine on the shell side of the heat exchangers.

Kalina Cycle

Water-ammonia mixtures have long been used in absorption refrigeration cycles [85]. It was not until Kalina patented his Kalina cycle [86] that this working fluid was used for power generation cycles. A typical Kalina cycle, KCS-12, is shown schematically in Fig. 107. The features that distinguish the Kalina cycles (there are several versions) from other Organic Rankine cycles are as follows:

- The working fluid is a binary mixture of H_2O and NH_3.
- Evaporation and condensation occur at variable temperature (requires several heat exchangers).

- Cycle incorporates heat recuperation from turbine exhaust.
- Composition of the mixture may be varied during cycle in some versions.

As a consequence, Kalina cycles show improved thermodynamic performance of heat exchangers by reducing the irreversibilities associated with heat transfer across a finite temperature difference. The heaters are arranged so a better match is maintained between the brine and the mixture at the cold end of the heat transfer process (where improvements in energy preservation are most valuable).

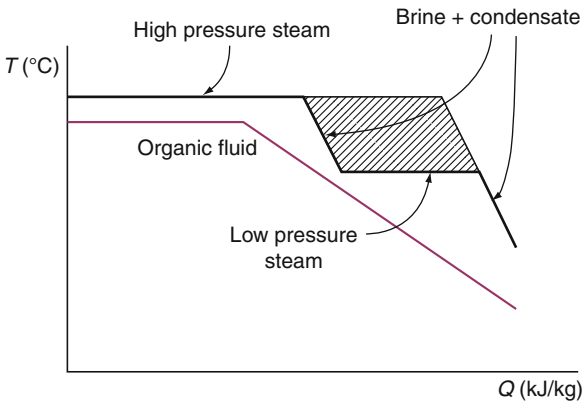

Geothermal Power Conversion Technology. Figure 96
Preheating using exhaust in a back-pressure steam turbine

A reheater is needed because the water-ammonia mixture has a normal saturated vapor line, i.e., $dT/ds < 0$, leading to wet mixtures in the turbine. The station relies on good heat exchangers because more heat is transferred than in a supercritical binary station of the same power output. Bliem and Mines [87] showed that the Kalina cycle of Fig. 107 requires about 25% more heat transfer. A possible advantage to using the recuperative preheaters is that they reduce the heat load on the condenser and cooling tower. The lower capital cost of a smaller condenser and cooling tower must be compared to the extra cost for the recuperators. Over the long haul, the resulting higher efficiency should mean lower operating costs.

The station is more complex than a basic binary station, particularly when a distillation column is used to vary the mixture composition. The simplest configuration of the Kalina cycle with variable working fluid composition is shown in Fig. 108. The separator S allows a saturated vapor rich in ammonia to flow to the turbine, thus permitting a smaller and less costly turbine than for a hydrocarbon working fluid.

Geothermal Power Conversion Technology. Figure 97
20 MW Amatitlan Power Station in Guatemala (Courtesy of ORMAT)

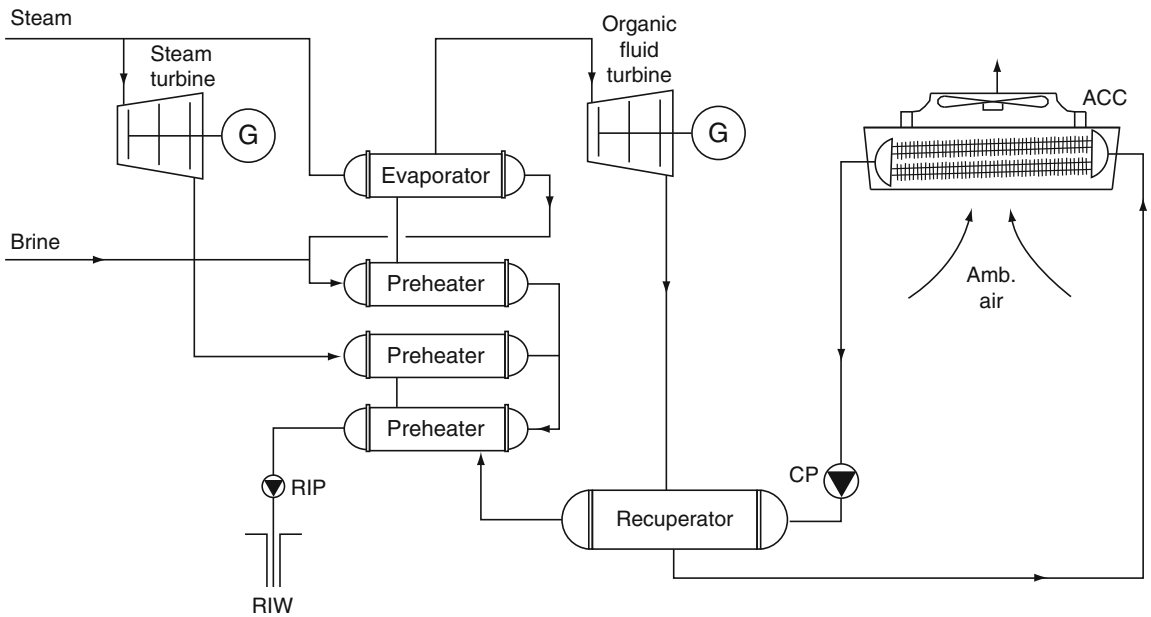

Geothermal Power Conversion Technology. Figure 98
Block diagram of the Amatitlan Power Station

The weak solution (a liquid rich in water), is used in the preheater and is then throttled down to the turbine exhaust pressure before mixing with the strong solution to restore the primary composition. The mixture is then used in a recuperative preheater RPH prior to being fully condensed.

A possible difficulty for the Kalina cycle striving for high efficiency, is maintaining very tight pinch-point temperature differences in the heat exchangers. Also, the advantage of variable-temperature condensation is lessened because the condensing isobars of the ammonia-rich NH_3-H_2O mixtures used in power cycles concave upward, leading to a pinch-point. Thus, there are relatively large temperature differences at the beginning and end of the condensing process.

DePippo compared the Kalina cycle with a simple ORC cycle [88] (Second Law comparison) and concluded that for low temperature brine the Kalina cycle is about 26% more efficient than the ORC cycle. Paola Bombarda [89] compared the Kalina cycle against ORC and found that the dominant factor bringing high efficiency to the Kalina cycle is the system operating pressure.

Kalina cycles operating at pressures lower that 100 bar will have lower efficiency than the ORC system, while those above 100 bar have higher efficiency. This is a disadvantage to the Kalina cycle as high pressure systems are likely to be more expensive in addition to the handling of >100 bar ammonia mixtures.

Geopressured Geothermal Systems

There are deep reservoirs holding geofluids at high pressure and temperature. Those of interest have pressures about 200–300 bar and temperatures ranging between 110°C and 200°C. The water, located at a depth of 3–5 km is high-salinity brine with large amounts of methane dissolved in it.

One location is the Gulf of Mexico, which is known because of the extensive oil/drilling that occasionally ends with water-dominated fluid instead of oil. The high pressurized liquid can drive a hydraulic turbine, then flow through binary unit evaporator and preheater to produce additional power. The solubility of methane depends on pressure, temperature and the salinity of the brine. Extracting the methane after the hydraulic turbine and transferring most of its heat to the organic liquid may give the best results. Test drills along the Louisiana coastline [90] and one actual methane extraction test made by the DOE in Pleasant Bayou

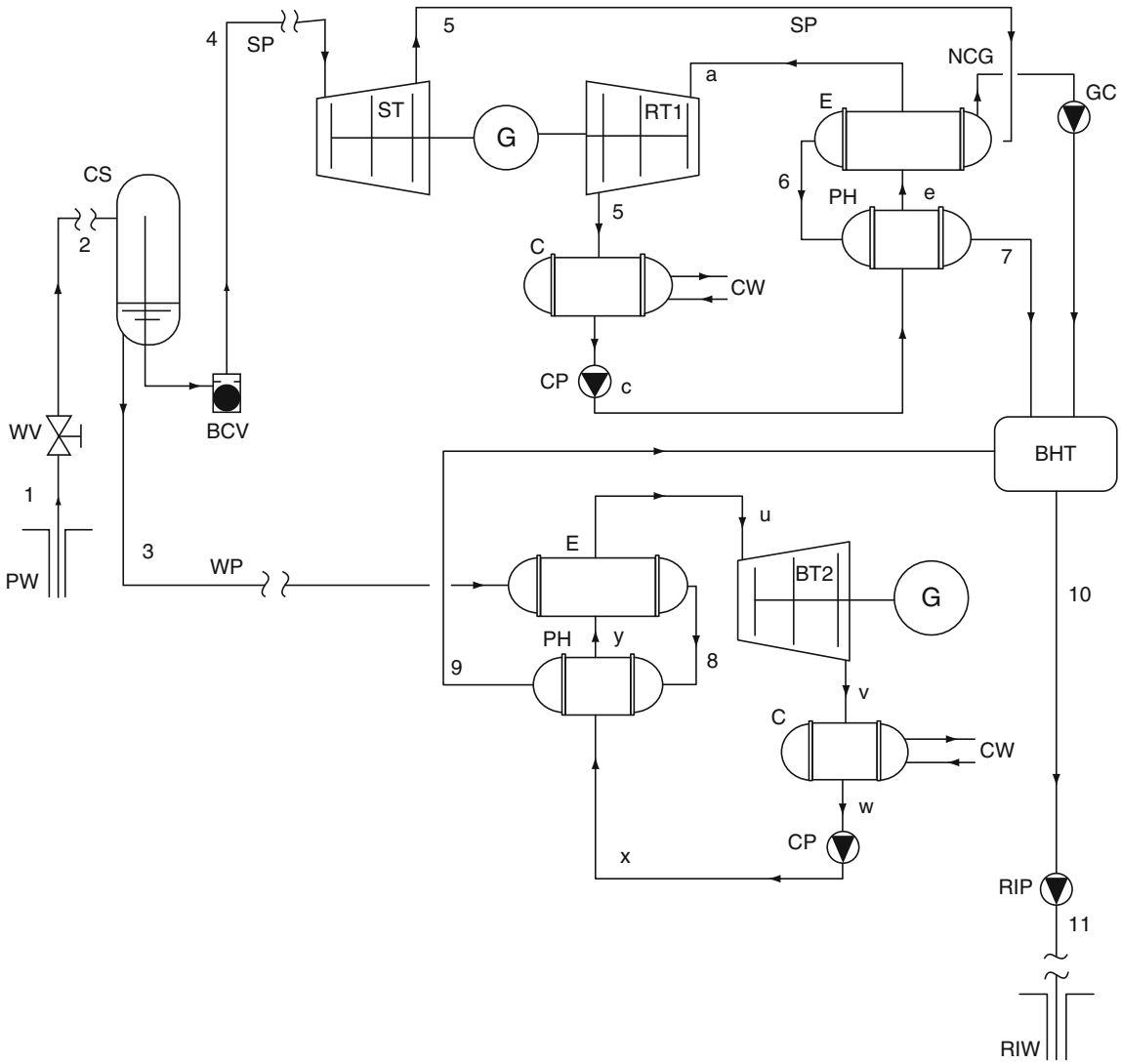

Geothermal Power Conversion Technology. Figure 99
Integrated geothermal combined cycle and bottoming ORC Power Station – water-cooled system

in Texas proved the viability of the gas extraction, even if a hydro-turbine was not used in this case. A comprehensive work by Griggs [91] added valuable information for the utilization of geopressurized aquifers as source of energy. Nitschke and Harris [92] suggested the first use of the geopressurized hot water in a hydro-turbine (Pelton wheel) and then for large-scale water desalination. They suggested an MED desalination station because of its design that allows small temperature difference per effect. Methane is a by-product that may be used on-site but its economic value depends on local energy prices and is not a closed deal. The chemistry of the brine must be followed very carefully for fear of entering the solubility limit. Other locations of geopressured sites are known in Hungary [93] and China [94]. An option for direct utilization of the separated methane is described in section on "Hybrid Fossil Geothermal Systems."

Hybrid Geothermal Power Stations

Hybrid Geothermal Power stations are stations in which the geothermal heat is supplemented by another heat source.

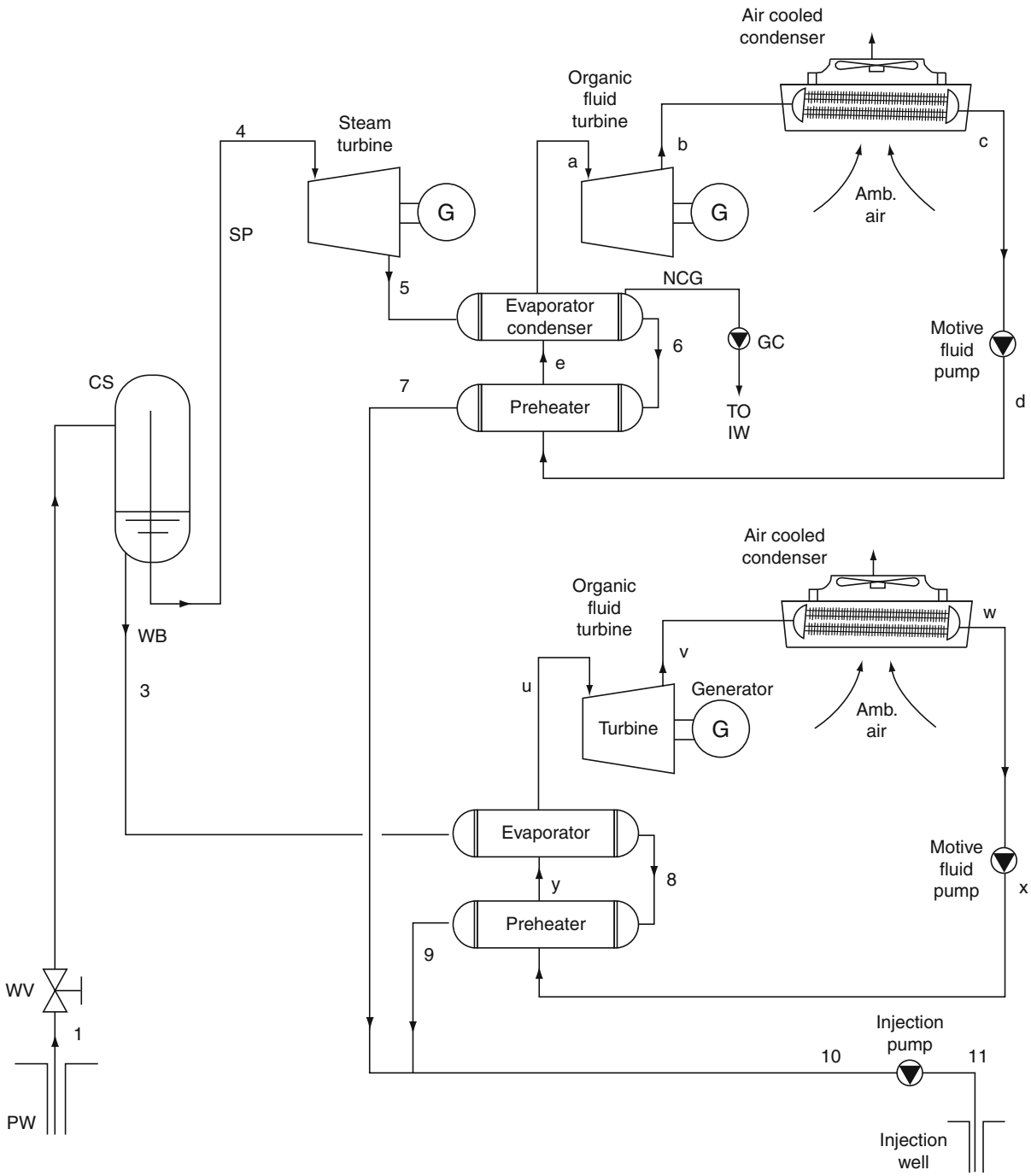

Geothermal Power Conversion Technology. Figure 100
Integrated geothermal combined cycle and bottoming ORC Power Station – air-cooled system

Hybrid Geothermal Fossil Fuel Power Station

Geothermal steam, whether dry or flashed, is bound to expand into the wet zone and therefore its power production is somewhat limited. The idea of using fossil fuels for superheating and to enhance geothermal resources is not a new concept. A paper published in

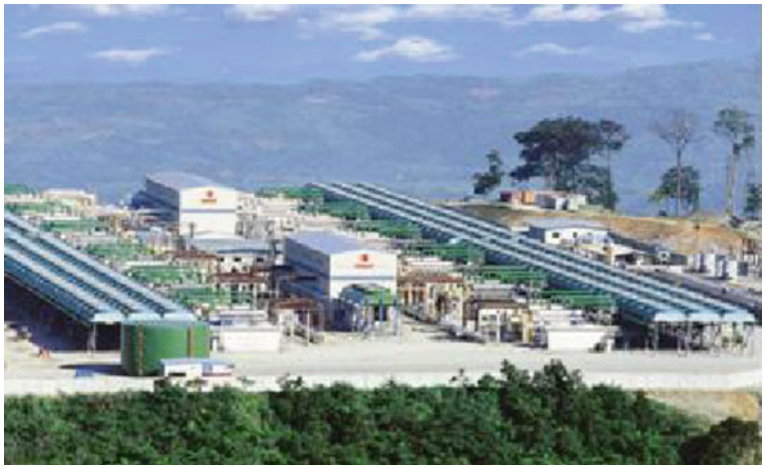

Geothermal Power Conversion Technology. Figure 101
125 MW Upper Mahiao Geothermal Power Station in the Philippines (Courtesy of ORMAT)

1924 indicated that it was already suggested by P. Caufourier [95]. He proposed a hybrid power system in which hot water from a geothermal spring would be successively flashed four times and the generated steam superheated in a fossil fired superheaters prior to being admitted to a multi-pressure turbine. Thermodynamic analysis by DePippo [96] showed that the system which burns fuel for that purpose only is not economical. A different approach suggested usage of heat recovery of a gas-operated gas turbine for superheating of geothermal steam in The Geysers geothermal field [97]. Such a hybrid system would have the highest utilization of fossil fuel as compared with regular GT power generation. For additional information on superheating of geothermal steam see studies by Brown University [98, 99].

In geopressured wells there is usually some natural gas content that is separated before or after usage of the heat energy in binary or flash steam cycles. The gas can be used in a gas engine such as gas turbine and the exhaust heat utilized for the geothermal steam superheating as previously mentioned. Such systems were analyzed by Chang and Williams [100] in a work sponsored by the DOE 1985.

Hybrid Geothermal Biomass Power Station

The concept is similar to the hybridization with fossil fuel, but because of generally lower combustion temperature of biomass, the thermodynamic draw-back is smaller. The geothermal resource is used to preheat the motive fluid while the biomass is used to evaporate the motive fluid. Although the exhaust heat from biomass combustion may provide all the preheating of the motive fluid making the geothermal resource use redundant, however because the high dew point of exhaust gases from biomass combustion there is room for the geothermal heat for preheating. A few such power stations were proposed and it seems that at least one was constructed.

Hybrid Geothermal Solar Power Stations

This hybridization presents three advantages. The first is thermodynamic, by providing all the heat of evaporation from the solar collector, the efficiency of the utilization of the sensible heat of the geothermal reservoir, is improved: see paragraph "Available energy" and Figs. 6 and 7. The second is an improvement of the load following of the station: more power produced during peak hours. Thirdly the economics is improved by a better use of the interconnecting facility and of the personnel. The outline of such a system is shown in Fig. 110.

Power Stations for Enhanced Geothermal Systems (EGS)

MIT report states that the majority of geothermal energy within drilling reach that can be utilized for

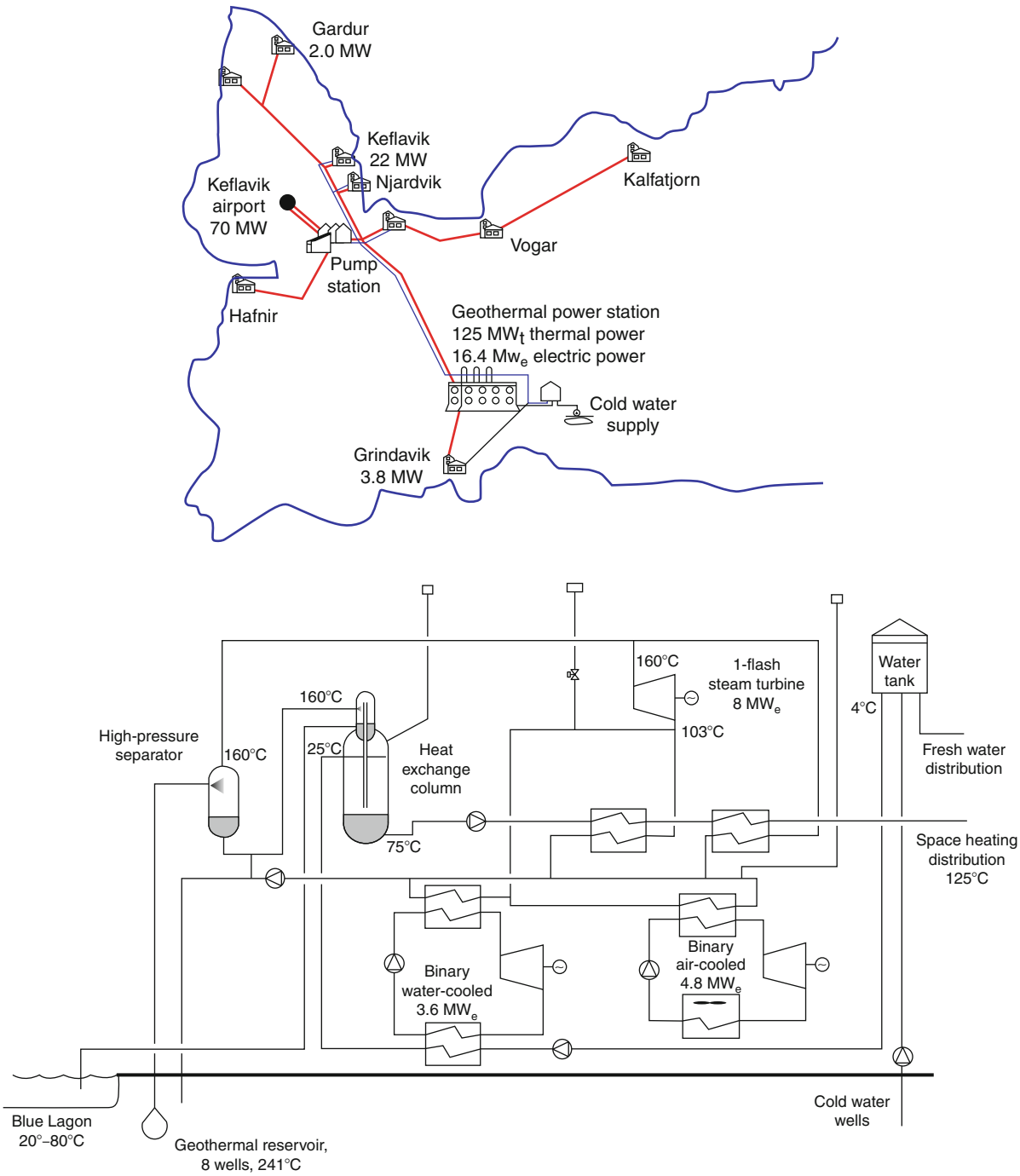

Geothermal Power Conversion Technology. Figure 102
The Sudurnes Regional heating system layout and flow diagram for Svartsengi Power Station

power production is in dry and nonporous rock [101]. Drilling into hot rock formations and creating cavities to accommodate large enough heat transfer area for heating of water are considered as enhanced geothermal systems (EGS). Substantial progress has been made in developing and demonstrating certain components

Geothermal Power Conversion Technology. Figure 103
250 kW Geothermal ORC Power Unit at Rogner Hotel and Spa, Bad Blumau, Austria (Courtesy of ORMAT)

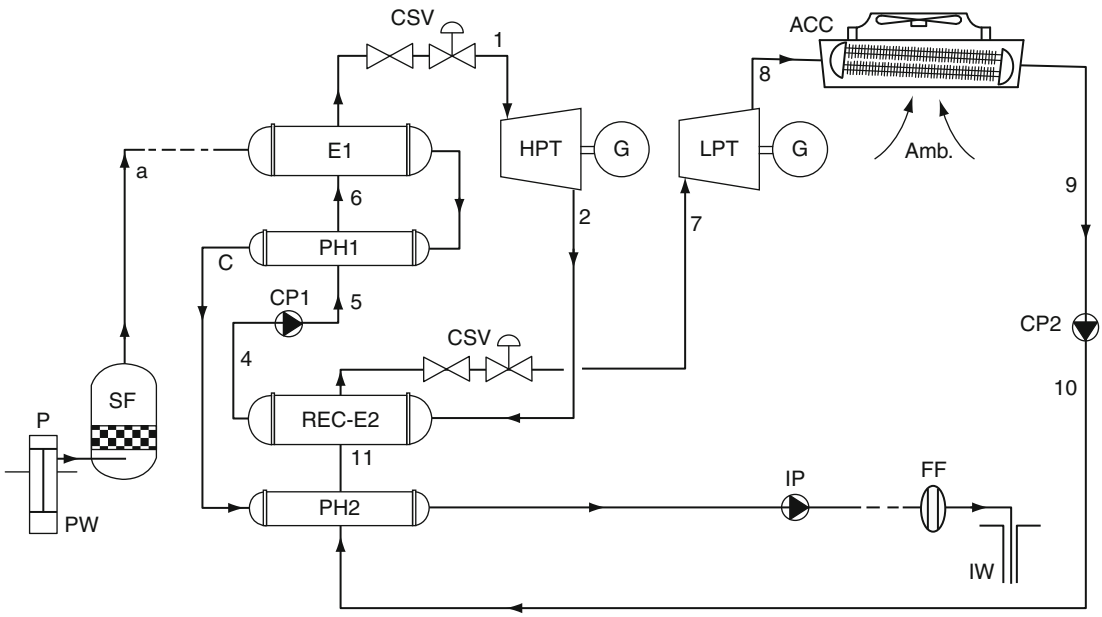

Geothermal Power Conversion Technology. Figure 104
Scheme of dual fluids binary power station

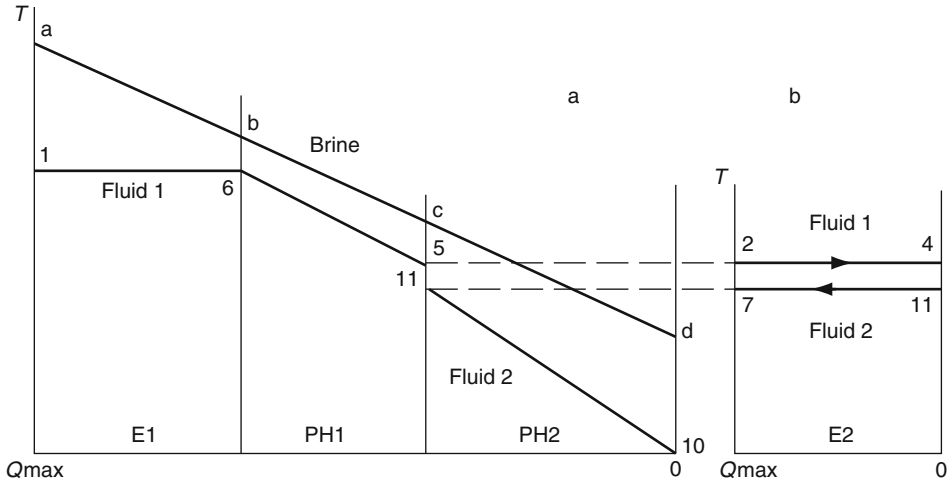

Geothermal Power Conversion Technology. Figure 105
T-Q diagram of dual organic fluids in subcritical condition

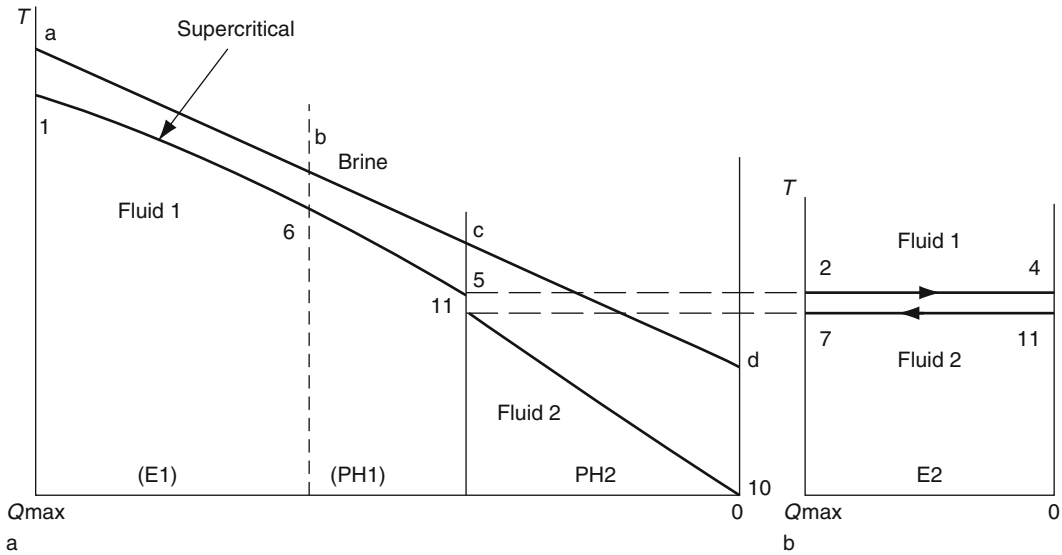

Geothermal Power Conversion Technology. Figure 106
T-Q diagram of dual organic fluids in supercritical condition

of EGS technology in the USA, Europe, Australia and Japan. Further work is needed to establish the commercial viability of EGS for electrical power generation, cogeneration and direct heat supply.

A seperate, specific part of the present publication deals with the resource development, therefore attention is given here to the energy conversion system only.

Assuming that the build-up of the resource has been made. Water travelling through the fractures in the rock captures the rock heat and emerges from the production well accompanied by dissolved solids, large amount of particles and possibly noncondensable gases (NCG). Tests made in Japan [102–105], USA [106], UK [107] and other countries

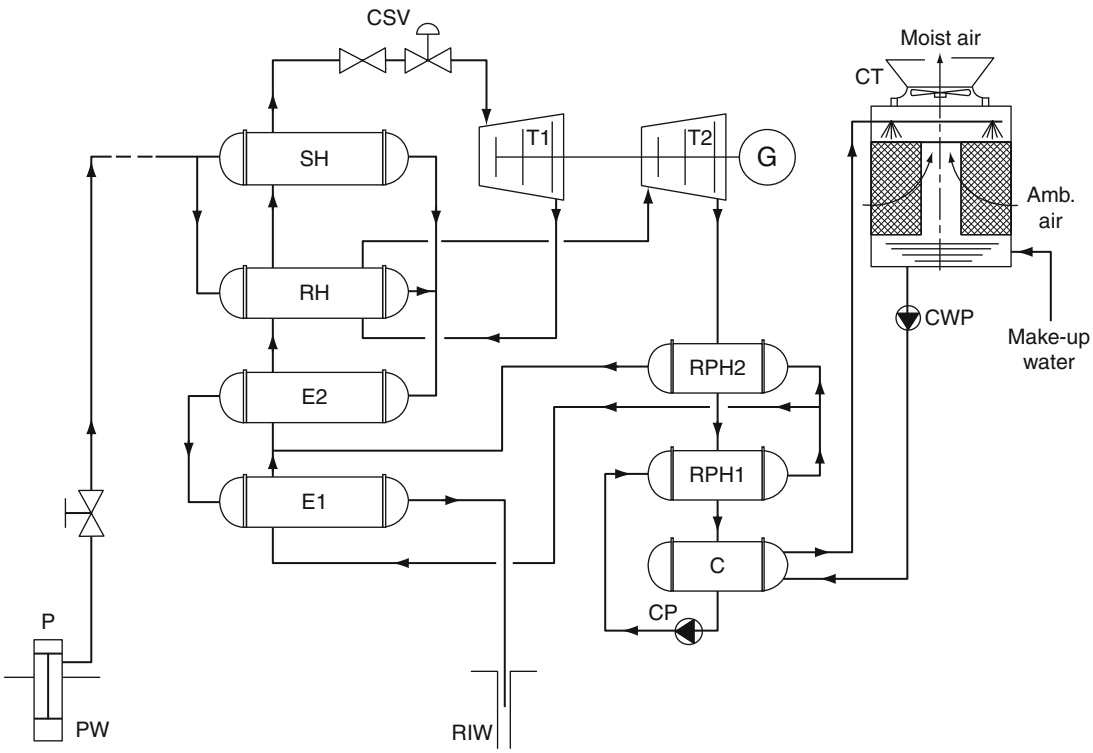

Geothermal Power Conversion Technology. Figure 107
Typical Kalina cycle employing a reheater and two recuperative preheaters

range the out-coming water temperatures between 150°C and 270°C.

The lower-temperature brines are suitable for power generation via binary systems. The higher-temperature brines (above 200°C) are flashed, cured of NCG and particles and then can be directly used in steam turbines providing vapors free of aggressive components. However, due to the NCG problem and since the nature of dissolved materials in the brine may change in time, an indirect utilization by use of ORC binary stations is preferred. The air-cooled ORC stations are particularly well adapted to the EGSs. The somewhat higher installed cost of these systems is justified by environmental and long-term resource management considerations.

Most of the reported EGS stations are experimental with a status between planning, fundraising, drilling and partial operation (see list in [102]. The only partial EGS station in continuous commercial operation is in Landau, Germany using the Organic Rankine cycle [108].

Other Organic Rankine cycle stations are Soultz (France) [109], stations in Australia, Desert Peak and Newberry Oregon in the USA (being planned). The air-cooled ORC stations are particularly well adapted to the HDR/EGS. The fairly higher installed cost of these systems is justified by environmental and long term resource management consideration.

Trilateral Flash Cycle (TFC)

The Trilateral Flash Cycle (TFC) and its more recent "Smith" cycle [110] were developed for efficient utilization of HDR geothermal heat source. Because the work producing process is based on flash expansion of the liquid and the cycle is close to the thermodynamic trilateral ideal, it is a Trilateral Flash Cycle (TFC) system. The main feature as seen in Fig. 109 is to transfer the HDR heat (points A–B) to Organic liquid (points 1–2) and allow expansion in a two-phase expander (points 2–5) instead of the regular evaporator (points 2–3) and dry turbine

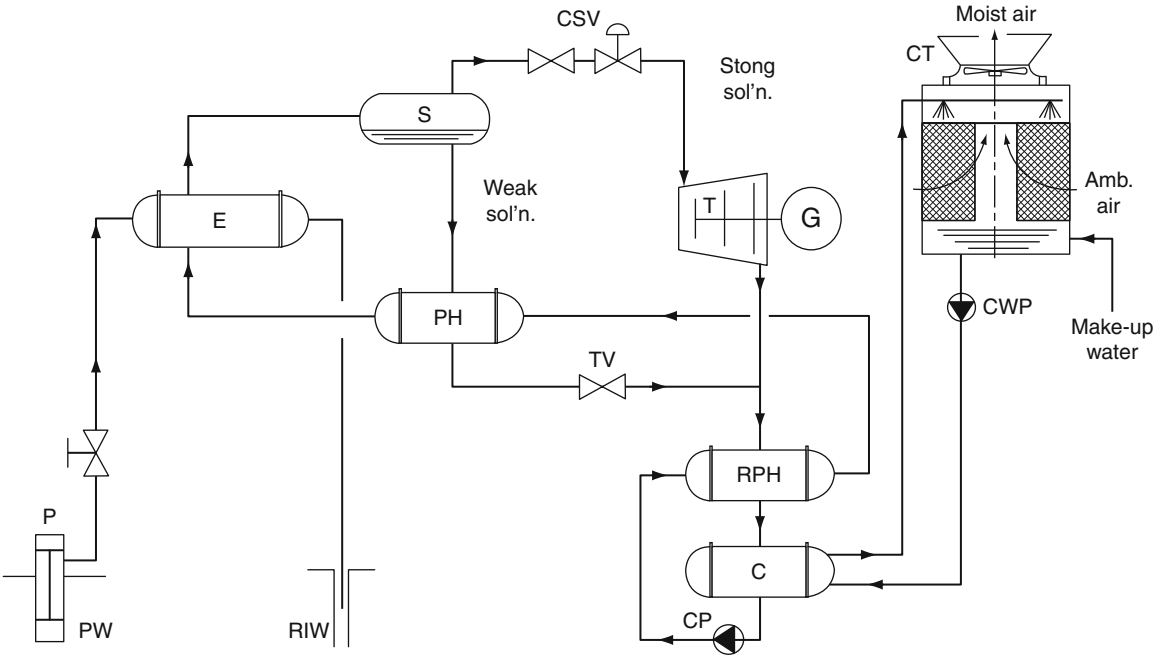

Geothermal Power Conversion Technology. Figure 108
Kalina cycle with variable composition of the water ammonia working fluid

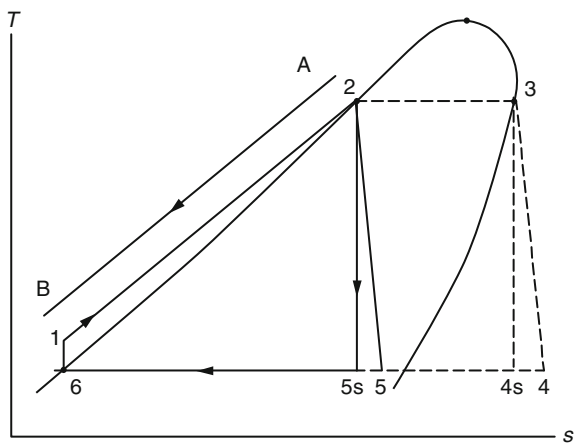

Geothermal Power Conversion Technology. Figure 109
Scheme of the trilateral flash cycle (TFC)

expansion (points 3–4). This is a drawback due to the relative low efficiency of the two-phase expansion resulting from operation deep in the wet zone. The more advanced Smith cycle suggests various options of expansion procedures as the required ratio of expansion is above 100 and this cannot be achieved with the screw expander or even a radial turbine suggested by Smith. There is a two-phase expander in the first stage followed by separation vessel from which the system proceeds in two parallel lines, one a two-phase expander and the other a vapor turbine which expands in the dry zone. Theoretical analyses and cost estimates are optimistic, but the development of a large and still not constructed expander is still required. Few of the expanding devices suggested for this and similar "total-flow" cycles will be described in section on "Total Flow Systems."

Total-Flow Systems

Utilization of the steam or brine geofluids is accompanied by irreversiblities that consume a significant portion of the available energy and include quite large cost of equipment for separation, flashing and expansion. New ideas for direct use of the geofluid are basically directed at the large saving in equipment cost, direct expansion with half of turbine

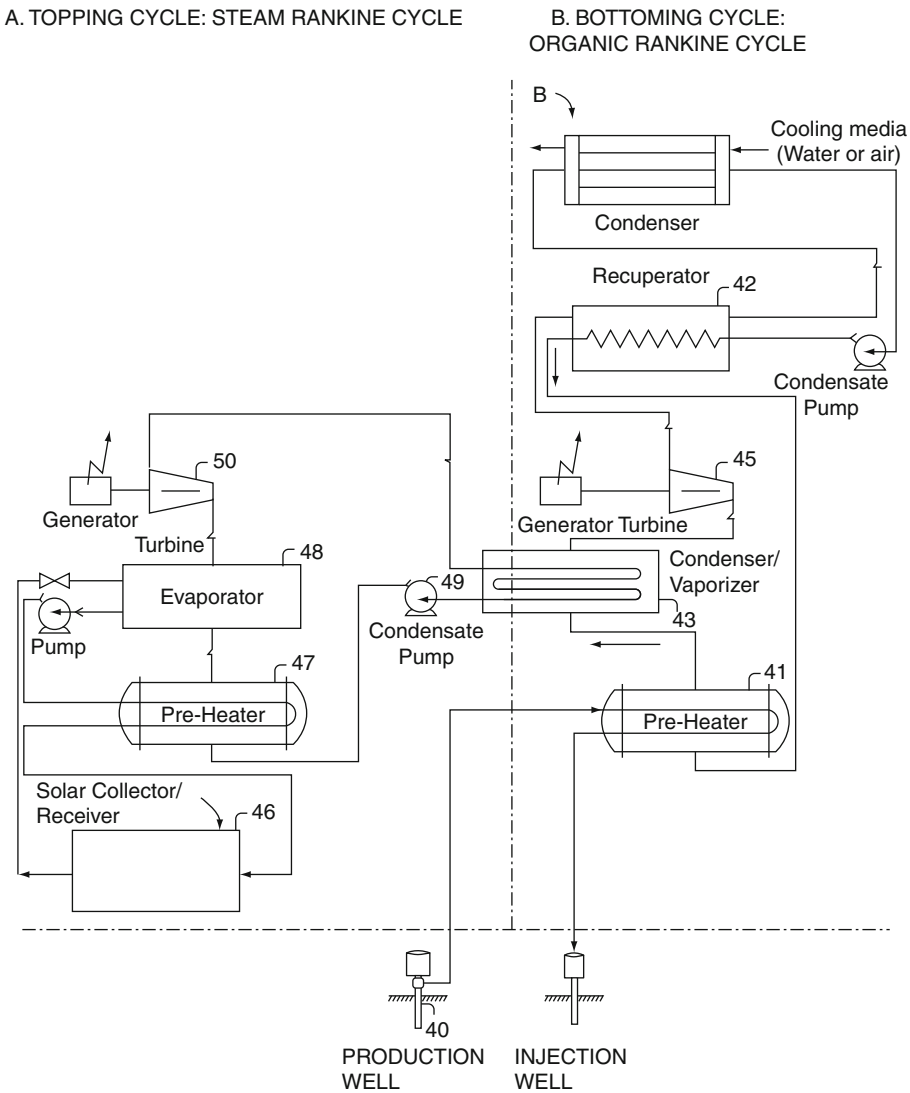

Geothermal Power Conversion Technology. Figure 110
Hybrid Geothermal Solar Power Station (Courtesy of ORMAT)

efficiency but no flashing. The main present directions are:

1. Single-stage impulse turbine [111]
2. Positive-displacement expander (a helical screw expander called also "bi-phase expander" and rotary expander) [112, 113]
3. Rotary separator turbine [114].

Two-Phase Turbine A hybrid geothermal power station comprises in addition to the geothermal heat source a supplementary heat source such as biomass solar or even fuel. In a total-flow turbine the fluid expands from near the liquid line, while with a regular steam turbine the steam expands from near the saturation line. Comparing these two turbine cases between the same given temperatures (fluid high temperature and condensing temperature) it is found [111, 136] that the total-flow turbine efficiency can be about half the steam turbine efficiency for the same power production. Therefore steam turbines efficiency is in the range of 80%, with the best efficiency of single-stage impulse turbine still

at 23%. However, the single stage impulse turbine is remarkably smaller and the system uses all the brine energy compared with only the flashed steam energy.

Positive Displacement: Helical Screw Expander The helical screw machine is usually used as a compressor in refrigeration cycles. It is also used as air compressor in stationary and mobile compression units. Due to the screw shape of the twin rotors, pressure losses are small and high pressure ratio is obtained. If a high-pressure fluid is passed to the "exit" side of such a compressor then the expanding fluid will rotate the screw rotors. Tests with two-phase flow indicated that there are limitations to the rate of expansion caused mainly by the initial liquid content. Pre-flashing and partial flashing that changes the liquid–vapor ratio may diminish this issue. Tests conducted in the Unites States, New Zealand [112, 113] and in 1986 by Sprankle [115] were not continued.

The use of rotary expander used in passenger cars was considered by NEDO in Japan for the same task. A 300 kW prototype was built and tested in 1982, but there is no information on further tests.

Rotary Separator Turbine Here the two-phase flow (steam and brine) is separated in brine-driven primary turbine wheel. The steam is passed to the regular steam turbine for further expansion while the brine is drained from the system. The assumption is that the steam pressure is not significantly reduced by the above separation. The overall energy achieved from the two turbine wheels did not exceed the regular steam turbine. Tests performed in Roosevelt Hot Springs in 1981–1982 by Cerini et al. [114] were unsatisfactory. Additional work was summarized by Hughes [116] in 1986 with no reports in the following years.

Future of Geothermal Energy

Background

The cited papers used in this review do not always agree on the direction of development and forecast of power generation capacity but it is important to bring up and present all views to the reader.

United States

At the Symposium on energy sources for the future, in Oak Ridge, Tennessee, held between July 7–25,1975, M. King Hubbert [117] presented a Survey of World Energy Resources. He was very skeptical about the future of geothermal energy. The total world installed geothermal power capacity in 1975 was approximately 1,500 MW, and in spite of optimistic forecasts by geothermal power enthusiasts, such as Tester and Milora [118] at the same symposium, he forecasted an increase in only "order of magnitude." As injection was hardly used at that time he claimed that in all likelihood most large installations will be comparatively short-lived, perhaps a century or so.

Today however, with deep-well explorations and successful injection programs there is a reassessment of the geothermal potential as reported at the World Geothermal Congress in Bali by Ruggero Bertani [123] in April 2010.

The report indicates that in the USA there are 9 states, all in the West, with operating geothermal power stations, and a total installed capacity of 3,093 MWe. The report estimated that by 2015 up to 5,400 MWe of capacity will be installed in the USA. This assumes conventional hydrothermal resources. The report assumes that known hydrothermal resources in Western USA have a potential to produce 9,000 MWe.

The most comprehensive estimates for the total US recoverable resource were produced by US Geological Survey (USGS) in the late-1970s. In 1978, USGS Circular 790 suggested that the total recoverable resource from identified geothermal prospects is roughly 23,000 MW and the total combined identified/unidentified resource base is as high as 150,000 MW. In 2008, the USGS revised its numbers to reflect lower temperature resources, apply confidence ratios to the numbers and make assertions based on 30 years of results in the field. As such, a new estimate suggested 95% confidence that identified systems can provide 3,675 MWe and 5% confidence that identified systems can provide 16,457 MWe. The new estimate suggested 95% confidence that undiscovered systems can provide 7,917 MWe and 5% confidence that undiscovered systems can provide 73,286 MWe [119].

In January of 2006, a comprehensive assessment was released by the Western Governors' Association (WGA) in its Geothermal Task Force Report. The assessment was performed as part of the WGA's Clean and Diversified Energy Advisory Committee (CDEAC). The report covered 11 western states

(Alaska, Arizona, California, Colorado, Hawaii, Idaho, Nevada, New Mexico, Oregon, Utah, and Washington State) and estimated that there is up to 12,558 MW of recoverable geothermal power by 2025 from identified locations available at a future market at a cost of up to 20 cents per kilowatt-hour (¢/kWh). In the near-term, WGA estimated 5,588 MW of economically developable capacity (5.3–7.9¢/kWh (with the federal production tax credit (PTC) included) by 2015 in these 11 western states [120].

Europe

Simultaneously, in Europe, Bertani [123] in Bali, 2010 reported that Europe accounts for 1,635 MWe of installed geothermal capacity with growth forecasts to 2,125 MWe by 2015. Installation of new binary power stations will increase electricity production over a wide geographical distribution in locations fueled by medium-temperature resources including nonvolcanic sources in interior Eastern and Western Europe. Further, there will be greater development in Geothermal Heat Pump (GHP) installations that can be replicated around the world. As for direct use and GHP, John Lund reported at the Geothermal Resources Council Annual Meeting in October 2010 that European nations represent 10 out of the top 15 nations in utilization of these types of installations, with Sweden in third place behind China and the USA (focused mostly on GHP). Turkey is in fourth place focused mostly on district heating (Lund and Bertani [121]).

Geothermal Resources

Evaluation of the geothermal energy reserves was compiled for the MIT publication "The Future of Geothermal Energy" [122] according to the various types of geothermal systems:

(a) Hydrothermal convective systems
(b) Enhanced geothermal systems ("EGS")
(c) Conductive sedimentary systems
(d) Hot water produced from oil and gas fields
(e) Geopressured systems
(f) Magma bodies

Hydrothermal Convective Systems *Hydrothermal convective systems* to date have seen several decades of commercial exploitation for electric power generation in about 24 countries, but their distribution worldwide is limited. The installed power capacity for such systems totaled 10,715 MW worldwide by the end of the first decade of the twenty-first century, of which 3,000 MW were in the USA. The reserve base for these systems in the USA is estimated to be in the 10,000–30,000 MW range. Technologies involved for power generation from these sources are considered mature. Data sources are in WGC [123] and GEA [124].

Enhanced Geothermal System (EGS) An *enhanced geothermal system (EGS)* implies a man-made reservoir created by hydrofracturing impermeable or very "tight" rock through wells. The creation of an EGS system is performed by injecting water in an artificially fractured reservoir well with production from another well. By using rock heated water it is possible to extract thermal energy. EGS systems are conductive systems with enhanced flow and storage capacity due to hydro fracturing. In theory, EGS can be developed anywhere in the world by drilling deep enough to encounter commercially attractive rock temperatures. However, EGS technology is still experimental and poses a series of technical challenges, such as:

(a) Creating a pervasively fractured large rock volume
(b) Securing commercially attractive well productivity
(c) Minimizing the rate of cooling of the produced water with time
(d) Minimizing the loss of the injected water through fractures
(e) Minimizing any induced seismic effects

Sedimentary Systems Attempts are being made to develop geothermal *projects in sedimentary basins* with high heat flow (particularly in Australia). These systems are neither EGS or convective systems (due to the presence of impermeable shale layers preventing convection). No fracturing is generally needed for such systems as sedimentary rocks have intrinsic porosity and permeability. However, very deep wells are required to exploit such systems and ensure an adequate temperature level (well productivity may not prove adequate). No such systems have been

commercially exploited to date. Developing such systems should be feasible if reservoir temperatures and flow capacities are sufficiently high.

Coproduction with Oil and Gas Wells Another geothermal energy resource presently being considered for exploitation is the heat contained in the water produced from *deep oil and gas wells*. Here the hot water may be coproduced with petroleum production, from existing or abandoned oil or gas wells. While there are no significant challenges to exploiting this energy resource, the cost of this power may not always be attractive due to the relatively low temperature and low production rate of the water.

"Geopressured" Systems "*Geopressured*" *systems* are very restricted geothermal energy resources. These systems are confined sedimentary reservoirs with pressures greatly higher than the local hydrostatic pressure. The high pressure in such systems may allow the exploitation of the kinetic energy of the water produced in addition to its thermal energy. Furthermore, due to the high pressure, such a system may contain attractive amounts of methane gas dissolved in the water which may be used to generate electric power in a gas engine. Therefore, an ideal geopressured well can provide thermal, kinetic and gas-derived energy. No commercial geopressured project has been developed to date and there are several technical challenges to making this energy source commercial.

Magma Bodies Exploitation of geothermal energy directly from a magma body is theoretically possible but faces many technical challenges.

The US reserves of the various geothermal systems discussed above are summarized in Table 1–1 of the MIT report [122].

Of the six basic types of geothermal energy in the USA, the potential from an EGS resource system is three orders of magnitude higher than the other types combined. For additional views see [125, 126]. This conclusion also applies for the rest of the globe.

US View to 2050

Although, as described above, hydrothermal resources retain significant potential, the potential is limited mostly to the Western USA with a smaller contribution possible from coproduced and geopressured systems from oil- and gas-producing states, such as the Gulf Coast. EGS represents a more widely distributed resource base, requiring substantial investment in R&D. An 18-member assessment panel assembled in September 2005 evaluated the technical and economic feasibility of EGS becoming a major supplier of primary energy for US baseload generation capacity by 2050. The MIT report was rediscussed in the DOE Workshop on June 7, 2007 [127], with an intention to recommend DOE action items.

The questions raised were:

1. What is the quality, grade, and distribution of the EGS resource nationally?
2. What is still to be done technically to achieve complete EGS system feasibility?
3. What are the key technical and economic issues that must be resolved for EGS to have national impact in US energy supply by 2050?

The primary goal was to provide an in-depth evaluation of EGS as a major primary energy supplier to the USA. The secondary goal was to provide a framework for informing policy makers of R&D support and policies needed for EGS to have a major impact.

Major impact was defined as enabling 100,000 MWe of an economically viable EGS resource online or as a true reserve by 2050.

Findings were:

1. Large, indigenous, accessible base load power resource – extractable amount of energy that could be recovered is not limited by resource size. EGS can sustain production of $\geq$100,000 MWe of base load electric power.
2. Fits portfolio of sustainable RE options – EGS complements the DOE's RE portfolio and does not hamper the growth of solar, biomass, and wind in their most appropriate domains.
3. Scalable and environmentally friendly –EGS stations have small foot prints and low carbon-free emissions. The stations are inherently modular making them easily scalable from 1+ to 50+ MWe size individual stations, grouping to large base load facilities >1,000 MWe.

4. Technically feasible – much progress in 30+ years of testing worldwide, the major elements of the technology to capture and extract EGS are already in place. Remaining key issue is to establish inter-well connectivity at commercial production rates – only a factor of 2–3 greater than current levels.
5. Economic projections – favorable for high grade areas now with a credible learning path to provide competitive energy from mid-and low-grade resources.
6. Deployment costs low – a modest investment of US$300–US$400 million over 15 years would demonstrate commercial scale EGS technology at several US field sites to reduce risks for private investment and enable the development of 100,000 MWe.
7. Supporting research costs are reasonable – in comparison to other large impact alternative energy programs supported by the US government.

The financial support recommends investing a total of US$600–US$800 million for deployment assistance, research and development over 15 years. This is an average of US$50 M/year.

Refer to the EERE website http://www1.eere.energy.gov/geothermal/ [128] for a follow-up of the DOE Geothermal Technologies Program.

Europe View to 2050

At the Offenburg conference, 2009, Bertani [129], who based his observations largely on Fridleifsson et al. [130], saw a linear increase in direct use of geothermal resources for space heating, greenhouses, etc. Simultaneously the increase of GHP including power generation grew exponentially from about 200,000 TJ/year expected in 2010 to 900,000 TJ/year expected in 2020 to above 4 × 106 TJ/year in 2050. For comparison, the world energy consumption is presently about 420 EJ/year. (1 EJ = 1,018 J, 1 TJ = 1,012 J).

Following the US evaluation, a committee of the Council of Europe met to handle the issue – Geothermal Energy: a solution for the future? A motion for a resolution is found in Doc: 11740 [131].

Presented European and world information proposed that the assembly should focus on geothermal energy and its potential contribution to clean and sustainable energy systems in Europe.

A more in-depth survey followed and was discussed by the Council of Europe in May 2010 as reported in Doc. 12249 [132]. A report of European and world geothermal data was presented at the meeting and summarized in Doc. 12249. The report handles technical data while also noting connected hurdles, technical barriers and seismic problems. Examples of such occurrences were given including Landau, Staufen-im-Brisgau in Germany and a Soultz-type geothermal project launched on a commercial basis in Basel, Switzerland in 2006. This project ceased drilling after the inhabitants reported mini earthquakes around the project site.

The draft resolution detailed the data, stressed the advantages of geothermal energy in urban heating, electric generation and positive impact on the environment. Legislative issues and financial risks were also covered. Resolution No. 9 or the "to-do" recommendations are listed below (from the original):

9.1 Foster the development of geothermal energy operations in their national energy strategies.
9.2 Encourage the use of geothermal energy in all its forms, particularly locally.
9.3 Encourage international cooperation in the transfer of technology and the financing of geothermal development.
9.4 Increase realization and awareness among the general public and potential investors of the advantages of geothermal technologies for a sustainable energy infrastructure.
9.5 Take the necessary steps to set up strategic research programs and encourage the exploitation of geothermal energy resources.
9.6 Foster the introduction of financing and insurance schemes for exploration.
9.7 Encourage the setting up of transfrontier cooperation schemes to finance surface measurements and test drillings.
9.8 Introduce a European training and professional development framework.
9.9 Draw up a map of geothermal energy resources at the European level within the framework of cooperation between the geological research bodies of each country.

For additional information on European data on future plan and research go to [133]. The future of

geothermal development European Geothermal Energy Council (EGEC) Projections www.egec.org, 2010 and [134] European Commission Research – Future prospects, hurdles: http://ec.europa.eu/research/energy/eu/research/geothermal/background/index_en.htm

Global View

Renewable energy including geothermal energy plays an important role in future global policies. In his book, Plan B 4.0 "Mobilization to save the Earth," Brown [135] accounted for the existing and potential geothermal resources in the section on "Choosing the Energy Conversion Systems," which deals with renewable energy. Besides the energy use for power production he details direct usage for domestic heating, heat pumps for heating and cooling. In Germany alone he reports there are 130,000 operating heat pumps with 25,000 being added annually. Leaders for direct use of the above include:

- District heating: Iceland, Hungary, France, and China.
- Pools and spas in Iceland, France, and Japan.
- Greenhouses in Russia, Hungary, Iceland, and USA.
- Aquaculture in China, Israel, and the USA.

The previously mentioned GEA report 2010 [124] summarizes the existing portfolio of power stations and gives a prospect for increase until 2015. Highlights are:

According to the International Geothermal Association in 2005, there was 8,933 MW of installed power capacity in 24 countries, generating 55,709 GWh of green power per year. IGA reports in 2010 that there is 10,715 MW online generating 67,246 GWh. This represents a 20% increase in online geothermal power between 2005 and 2010. IGA projects this will grow to 18,500 MW by 2015, as based on the large number of projects under consideration (Bertani [123]).

Countries which experienced significant increases in installed capacity between 2005 and 2010 included the USA, Indonesia, Iceland, New Zealand and Turkey. These nations expect to have a significant increase by 2015. However, other nations expect to increase generation significantly during that time including Kenya, Russia, the Central American nations of El Salvador, Guatemala, Nicaragua and the South American nation of Chile, which currently has 0 MW of installed capacity (Bertani [123]).

While on-line power increased 20% between 2005 and 2010, countries with projects under development grew at a much faster pace. GEA reported in 2007 that 46 countries were considering geothermal power development. In 2010, an updated report acknowledged 70 countries with projects under development or active consideration, a 52% increase since 2007 (GEA [124]).

Projects under development grew most dramatically in two regions of the world, Europe and Africa. Ten countries in Europe were listed as having geothermal projects under development in 2007, and this has more than doubled in 2010 to 24 countries. Six countries in Africa were identified in 2007 and in 2010, 11 were found to be actively considering geothermal power. It would appear that bodies such as ARGeo and the European Bank for Reconstruction and Development's geothermal initiatives are having a considerable beneficial effect.

However, despite these growth trends, potential of geothermal resources to provide clean energy appears to be underestimated. In 1999, GEA prepared a report that examined geothermal power potential internationally. The report showed that in the vast majority of countries the estimated potential remains undeveloped and largely untapped, even assuming the lowest projections for geothermal resource potential. Moreover, the number of countries with geothermal power potential still not developing their resources is still high. Of the 39 countries identified in 1999 as having the potential to meet 100% of their electricity needs through domestic geothermal resources, significant power production had been developed in only nine – Costa Rica, El Salvador, Guatemala, Iceland, Indonesia, Kenya, Nicaragua, Papua New Guinea and the Philippines. However, this report identified projects under consideration in another 14 of these countries. (For a list of countries identified in the 1999 GEA report which could be 100% geothermal powered, see the Appendix in [124].)

The underlying trend of geothermal power expansion is complemented by the development of projects in entirely new areas. It is interesting to note that there are 24 countries identified with geothermal power projects under development not included in the GEA 1999 study. Most of these countries are in Europe and are accessing resources with new technology developments that allow development of lower-temperature resources. In addition, EGS technologies, or enhanced geothermal systems,

are being developed in a number of countries including Australia, France, Germany, the UK and the USA.

The trends in both the number of new countries developing geothermal energy and the total of new megawatts of power capacity under development appear to continue a growth trend showing a clear reverse from the slowdowns in international markets as seen in the late 1990s. Supported by the development of low-temperature power on the one side and EGS technologies on the other side, the geothermal market appears to be expanding to encompass most of the world's potential geothermal sites.

The report indicates that national and international policies, as well as financial support, are key in realizing the potential for successful geothermal development.

Additional GEA Observations:

- In 2010, global geothermal development is partly being driven by a number of regional institutions which, in addition to financing geothermal projects, are enhancing regional cooperation within an emerging renewable energy sector. Examples include the African Rift Geothermal Energy Development Facility (ARGeo), which underwrites drilling risks in six African nations and is backed by UNEP, the World Bank, and the geothermal initiatives of the European Bank for Reconstruction and Development supported by European Union climate policies.
- Geothermal development appears to be increasingly supported by a global financial market. A growing number of countries, including Australia, China, Germany, Iceland, Italy, Japan, and the USA, are facilitating geothermal development projects around the world. Forms of support other than financing, including technology sharing, training, and geological surveys are also being endorsed by outside governments.
- The growth in geothermal projects under consideration or in development is in part attributable to international and multilateral support for development in new areas. The ongoing question is whether that support will be sustained over time and be adequate to address risks involved in geothermal project development. For example, geothermal resources are abundant in East Africa and support for resource assessment has helped spur interest in project development in several countries. But, new projects will have high associated costs and risk factors. Sustained support for development at this crucial stage is essential to achieving expanded use of geothermal energy in this and other developing areas.
- Geothermal development appears to be trending beyond traditional hydrothermal reserves prevalent along the Pacific Ring of Fire. Lower temperature power systems and EGS technology are allowing a growing and diversified collection of countries to actively pursue geothermal development in areas previously assumed to have little exploitable resource. This is especially true among European countries, notably France, Germany, Latvia, and the UK, all of which are currently exploring and developing local resources by employing EGS. These developments are supported by government policies (such as feed-in tariffs), which make higher-risk and higher-cost projects more feasible. These policies are typically components of broader climate initiatives.
- District heating and direct use of geothermal applications appear to be progressively more commonplace in many countries and are being emphasized in a number of national renewable energy policies as effective measures for curbing greenhouse gas emissions.
- Around the world, villages and tribes are looking to geothermal as a way to utilize land and become energy independent. Warm Springs Indian Reservation in Oregon, the Northwestern Band of Shoshone Nation in Idaho and Utah, and the Jemez Pueblo in New Mexico have all shown interest in developing geothermal energy. Additionally, the Pyramid Lake Paiute Tribe in Nevada is actively developing its geothermal resources and was recently awarded funding from the US DOE. In New Zealand, the Te Arawa Iwi is examining the possibility of geothermal power on Maori land in Rotorua. In The Philippines, 9 of 11 ancestral domain areas consented to the Kalinga geothermal exploration project. A geothermal station is expected to open in the small settlement of Innamincka, Australia, in early 2012.

A country-by-country assessment (both present and forecasted for 2015) is summarized in the WGC report by Bertani [123] and in the GEA report [124] which is arranged by continents considering natural geothermal data and national policies.

Acknowledgments

The author would like to acknowledge with appreciation the valuable contributions of Dr. Uriyel Fisher and Mr. Mike Kanowitz in preparation and typing of the manuscript as well as for the special attention to accuracy and detail.

Bibliography

1. U.S. Department of Energy (2008) The price of geothermal power. Geothermal Tomorrow 2008, pp 19–21. http://www1.eere.energy.gov/geothermal/pdfs/geothermal_tomorrow_2008.pdf
2. California Energy Commission (2007) Comparative costs of California Central Station Electricity Generation Technologies. Document #: CEC-200-2007-011-SF. http://www.energy.ca.gov/2007publications4CEC-200-2007-011/CEC-200-2007-011-SF.pdf
3. Emerging Energy Research (2009) Global geothermal markets and strategies: 2009–2020. Section 3: Geothermal technology and cost trends. http://www.emerging-energy.com/Content/Document-Details/4/Global-Geothermal-Markets-and-Strategies-20092020/280.aspx
4. Glacier Partners (2009) Geothermal economics 101 – economics of a 35 MW binary cycle geothermal plant. http://www.glacierny.com/geothermal.php
5. Public Utilities Commission of Nevada (PUCN) (2010) Docket # 10-02009 "Application of Nevada Power Company d/b/a NV energy for approval of its 2010–2029 triennial integrated resource plan." NV Energy PPA Pricing Info. http://pucweb1.state.nv.us/pucn/DktInfo.aspx?Util=Electric
6. International Energy Agency (IEA) (2010) Renewable energy essentials: geothermal. http://www.iea.org/papers/2010/Geothermal_Essentials.pdf
7. California Energy Commission (2009) Renewable energy cost of generation update. Document #: CEC-500-2009-084. http://www.energy.ca.gov/2009publications/CEC-500-2009-084/CEC-500-2009-084.PDF
8. Remo AR (2010) EDC to put up geothermal plants worth $1B. Philippine Daily Inquirer. http://business.inquirer.net/money/topstories/view/20100729-283909/EDC-to-put-up-geothermal-plants-worth-1B
9. Kema, Inc., California Energy Commission (2009) Renewable energy cost of generation update. Document #: CEC-500-2009-084, pp 52–72; Appendix A, pp 206–215. http://www.energy.ca.gov/2009publications/CEC-500-2009-084/CEC-500-2009-084.PDF
10. California Public Utilities Commission (CPUC) (2010) RPS project status table – July update. http://www.cpuc.ca.gov/NR/rdonlyres/A5406F32-B0D0-409E-AA92-0EA79E97BECC/0/RPS_Project_Status_Table_2010_July.xls
11. Geothermal Energy Association, http://geo-energy.org/geo_basics_plant_cost.aspx
12. Cappetti G et al (2000) Italy country update report 1995–1999. In: Proceedings world geothermal congress 2000, Kyushu – Tohoku, 28 May–10 June 2000
13. Calpine Geothermal, http://www.ncpageo.com/about.htm
14. The Geysers, http://www.geysers.com/
15. Rhinehart JS (1980) Geysers and geothermal energy. Springer, New York
16. Kestin J (1980) Sourcebook on the production of electricity from geothermal energy. DOE, RA/4051-1. US Government Printing Office, Washington, DC
17. Dipippo R (1998) Geothermal power systems, Section 8.2. In: Elliot TC, Chen K, Swanecamp RC (eds) Standard handbook of power plant engineering, 2nd edn. McGraw-Hill, New York
18. Chacko J et al (1998) Gulf coast geopressured-geothermal program summary report compilation. U.S. Department of Energy, Contract no. DE-FG07-95ID 13366
19. Duchane D et al (2002) Hot Dry Rock (HDR) geothermal energy research and development at Fenton Hill, New Mexico. GHC Bulln 13–19
20. Lund JW (2007) Characteristics, development and utilization of geothermal resources. GHC Bull 28:1–9. http://geoheat.oit.edu/bulletin/bull28-2/art1.pdf
21. Dippipo R (2008) Geothermal power plants: principles, applications and case studies, Chapters 6 & 9. Elsevier
22. Ellis AJ, Mahon WAJ (1977) Chemistry and geothermal systems. Academic, New York
23. Grassiani M (1994) Advances in materials selection for geothermal power production application. In: Coutsouradis D et al (eds) Materials for advanced power engineering. Kluwer, Dordrecht, pp 1677–1684
24. Mitsubishi Jukogyo Kabushiki Kaisho (1984) Geothermal power generation, rev edn. Mitsubishi Heavy Industries, Tokyo
25. Fuji brochure (1988) Information data on geothermal power plant. Fuji Electric, Japan
26. Kestin J (1980) Available work in geothermal energy, Chapter 3. In: Sourcebook on the production of electricity from geothermal energy, RA/4051-1. US Government Printing Office, Washington, DC
27. White DE (1973) Characteristics of geothermal resources, Chapter 4. In: Kruger P, Otte C (eds) Geothermal energy: resources, production, stimulation. Stanford University Press, Stanford, pp 69–94
28. James R (1968) Pipeline transmission of steam-water mixtures for geothermal power. NZ Eng 23:55–61
29. Baumann K (1921) Some recent developments in large steam turbine practice. J Inst Electric Eng 59:565
30. http://www.thermoflow.com/ConvSteamCycle_TFX.htm
31. Keenan JH, Keyes EG, Hill PG, Moore JG (1969) Steam tables: thermodynamic properties of water including vapor, liquid, and solid phases (international edition – metric units). Wiley, New York
32. Wagner W, Kretzschmar H-J (2008) International steam tables: properties of water and steam based on industrial formulation IAPWS_IF97. Springer, Berlin

33. DiPippo R (2008) Geothermal power plants: principles, applications, case studies and environmental impact, 2nd edn. Elsevier, Oxford
34. Anonymous (1989) East Mesa 18.5 MW × 2 double flash cycle geothermal power plant. Mitsubishi Heavy Industries, Tokyo
35. DiPippo R (1998) Geothermal power systems, Sect. 8.2. In: Elliott TC, Chen K, Swanekamp RC (eds) Standard handbook of powerplant engineering, 2nd edn. McGraw-Hill, New York, pp 8.27–8.60
36. Bronicki LY (2008) Advanced power cycles for enhancing geothermal sustainability 1,000 MW deployed worldwide. In: IEEE PES general meeting, Pittsburg. McGraw-Hill, New York, pp 8.27–8.60
37. Incropera PP, DeWitt DR (1996) Fundamentals of heat and mass transfer, 4th edn. Wiley, New York
38. Krieger Z et al (1986) Cascaded power plant using low and medium temperature source fluid. US Patent 4,578,953, 01 April 1986
39. Khalifa HE, Rhodes BW (1985) Analysis of power cycles for geothermal wellhead conversion systems, EPRI AP-4070. Electric Power Research Institute, Palo Alto
40. Bliem CJ, Walrath LR (1983) Raft river binary-cycle geothermal pilot power plant final report, EGG-2208. Idaho National Engineering Laboratory, Idaho Falls
41. Tester JW, Milora SL (1976) Geothermal energy as a source of electric power. In: 16th annual symposium, New Mexico Section, American Society o f Mechanical Engineering, Albuquerque, 26–27 Feb 1976
42. Reynolds WC (1979) Thermodynarnic properties in SI: graphs, tables and computational equations for 40 substances. Department of Mechanical Engineering, Stanford University, Stanford
43. Gallagher JS, Linsky D, Morrison G, Levelt Sengers JMH (1987) Thermodynamic properties of a geothermal working fluid; 90% isobutane 10% isopentane, NBS Technical Note 1234. National Bureau of Standards, U.S. Government Printing Office, Washington, DC
44. Berning J et al (1988) Heber binary cycle geothermal demonstration power plant; half load testing. Special report EPRI AP-5787-SR. Electric Power Research Institute, Palo Alto
45. Demuth OJ, Bliem CJ, Mines GL, Swank WD (1975) Supercritical binary geothermal cycle experiments with mixed-hydrocarbon working fluids and a vertical, in-tube, counter-flow condenser, EGG-EP-7076. Idaho National Engineering Laboratory, Idaho Falls
46. IAPWS (2003) Giddeline on the Tabular Taylor Series Expansion (TTSE) method for calculation of thermodynamic properties of water and steam. Applied to IAPWS-95 as an example. International Association for the Properties of Water and Steam, Vejie
47. Milora SL, Tester JW (1976) Geothermal energy as a source of electric power: thermodynamic and economic criteria. MIT Press, Cambridge, MA
48. Anonymous (1997) ASHRAE handbook fundamentals, Chapter 18. American Society of Heating, Refrigeration and Air-Conditioning Engineers, Atlanta
49. DiPippo R (1990) Geothermal power cycle selection guidelines, part 2 of geothermal information series, DCN 90-213-142-02-02. Electric Power Research Institute, Palo Alto
50. Kestin J (Ed. In Chief), DiPippo R, Khalifa HE, Ryley DJ (eds) (1980) Sourcebook on the production of electricity from geothermal energy. U.S. Department of Energy, DOE/RA/4051-1. U.S. Government Printing Office, Washington, DC
51. Tabor H, Bronicki LY (1961) Small turbines for solar energy package. In: United Nations conference on new sources of energy, Rome
52. Tabor H, Bronicki LY (1964) Establishing criteria for fluids for small vapor turbines, SAE Power 931C
53. Tabor H, Bronicki LY (1962) Vapor turbines. US Patent 3,040,528, 26 June 1962
54. Lazalde-Crabtree H (1984) Design approach of steam-water separators and steam dryers for geothermal applications. Geotherm Resour Counc Bull 13(8):11–20
55. http://www.htri.net/articles/htri_xchanger_suite
56. McKetta JJ (1992) Piping design handbook. Marcel Dekker, New York (Originally Encyclopedia of chemical processing and design, 1991)
57. Salomon L (1999) Two-phase flow in complex systems. Wiley, New York
58. Cheremisinoff NP (ed) (1986) Encyclopedia of fluid mechanics, vol 3, Gas-liquid flows. Gulf, Houston
59. Wallis GB (1969) One-dimensional two-phase flow. McGraw-Hill, New York
60. Holm A, Blodgett L, Jennejohn D, Gawell K (2010) Geothermal energy: international market update. GEA, Washington, DC
61. Bronicki LY (1995) Innovative geothermal power plants, fifteen years of experience. In: World geothermal conference, Florence
62. Blaydes PE (1994) Environmental advantages of the binary power plants can enhance development opportunities. Trans Geotherm Resour Counc 18:121–125
63. Flynn T (1997) Geothermal sustainability, heat utilization and advanced Organic Rankine cycle. Trans Geotherm Resour Counc 26(9):224–229. Sept/Oct 1997
64. Sanyal SK (2005) Sustainability and renewalability of geothermal power capacity. In: Prcoceedings world geothermal congress 2005, Anatalya, 24–29 April 2005
65. Wilson SS, Radwanm MS (1977) Appropriate thermodynamics for heat engine analysis & design. Int J Mech Eng 5:68–82
66. History of geothermal energy, http://www1.eere.energy.gov/geothermal/history.html
67. LeConte JL (1855) Account of some volcanic springs in the desert of the Colorado, in Southern California. Am J Sci Art Second Ser 19:1–6
68. Lombard GL (1978) Operational experience at the San Diego gas & electric ERDA Niland geothermal loop experimental

facility. In: Proceedings of the EPRI annual geothermal program project review and workshops EPRI ER-660-SR. Electric Power Research Institute, Palo Alto, pp 3-11–3-16
69. Featherstone J, Butler S, Bonham E (1995) Comparison of crystallizer reactor clarifier and pH mod technologies at the Salton Sea geothermal field. In: Proceedings world geothermal congress 1995, vol 4. International Geothermal Association, pp 2391–2396
70. Anonymous (2001) CalEnergy Company, Inc., U.S.A. Salton Sea Unit 5 Geothermal Power-Plant 1 X 58.32 MW, Brochure GEC 82-14. Fuji Electric, Tokyo
71. Gallup DL (1993) Control of salt precipitation from geothermal brine. US Patent 5,256,301, 26 Oct 1993
72. Kits KR (1997) pH modification of geothermal brine with sulfur-containing acid. US Patent 5,656,172, 12 Aug 1997
73. DiPippo R (2008) Geothermal power plants: principles, applications, case studies and environmental impact, 2nd edn. Elsevier, Oxford, p 225
74. Clutter TJ (2000) Mining economic benefits from geothermal brine. GHC Bull 21:1–3
75. Cal Energy Publication, http://www.calenergy.com/projects2d.aspx
76. Krieger Z, Moritz A (1986) Cascaded power plant using low and medium temperature source fluid. US Patent 4,578,953, 01 April 1986
77. Tabor H, Bronicki L (1962) Vapor turbines. US Patent 3,040,528, 26 June 1962
78. Legman H, Sullivan P (2003) The 30 MW Rotokawa I geothermal project five years of operation, IGC −20034164-2003
79. Lienau PJ (1996) Sudurnes Regional Heating Corporation, Geo-Heat Center. GHC Bull 17(4):14–16
80. Bronicki LY (1981) Practical experience and potential of organic vapor turbines for onsite electricity production from small local energy resources. UNITAR, Los Angeles
81. Kaplan U (1997) Method and apparatus for producing power using geothermal fluid. US Patent 5,664,419, 9 Sept 1997
82. Bronicki LY (1985) Geothermal power plant and method utilizing the same. US Patent 4,542,625, 24 Sept 1985
83. Hinrichs TC, Dambly BW (1980) East mesa magmamax power process geothermal generating plant: a preliminary analysis, EPRI TC-80-907. In: Proceedings fourth annual geothermal conference and workshop, Electric Power Research Institute, Palo Alto, pp 5-1–5-14
84. Hinrichs TC (1984) Magmamax power plant – success at east mesa, EPRI AP-3686. In: Proceedings eighth annual geothermal conference and workshop, Electric Power Research Institute, Palo Alto, pp 6-21–6-30
85. Ferdinand C (1850) http://www.probrewer.com/resources/refrigeration/history.php
86. Kalina A (1986) Method and apparatus for implementing a thermodynamic cycle using a fluid of changing concentration. US Patent 4,586,340, 6 May 1986
87. Bliem CJ, Mines GL (1991) Advanced binary performance power plants: limits of performance, EGG-EP-9207. Idaho National Engineering Laboratory, Idaho Falls
88. DiPippo R (2002) Second low basis for efficient power generation from industrial wasteheat. Report made for Ormat International Inc, Sparks NV
89. Bombarda P et al (2010) Heat recovery from diesel engines: a thermodynamic comparison between Kalina and ORC cycles. Appl Therm Eng 30:212–219
90. Gulf Coast Geopressured-Geothermal program summary report compilation work performed under U.S. Department of Energy Contract No. DE-FG07-95ID 13366
91. Griggs J (2004) A re-evaluation of geopressured-geothermal aquifers as an energy resource. Master's thesis, Louisiana State University, Craft and Hawkins Department of Petroleum Engineering
92. Nitschke GS, Harris JA (1991) Production of fresh water and power from geopressured- geothermal reservoirs. In: Indirect solar, geothermal and nuclear energy. Nova Science, New York
93. Árpási M, Lorberer Á, Pap S (2000) High pressure and temperature (geopressured) geothermal reservoirs in Hungary. In: Proceedings world geothermal congress 2000, International Geothermal Association, pp 2511–2514
94. He L, Xiong L (2000) Extensional model for the formation of geopressured geothermal resources in the Yinggehai Basin, South China Sea. In: Proceedings world geothermal congress 2000, International Geothermal Association, pp 1211–1216
95. Anonymous (1924) Recent developments in the utilization of the earth's heat. Mech Eng 46(8):448–449
96. DiPippo R (1978) An analysis of an early hybrid fossil-geothermal power plant proposal. Geotherm Energy Magazin 6(3):31–36
97. Janes J (1984) Evaluation of a superheater enhanced geothermal steam power plant in the geysers area, Rep. P700-84-003. California Energy Commission, Sitting and Environmental Division
98. Kestin J, DiPippo R, Khalifa HE (1978) Hybrid geothermal-fossil power plants. Mech Eng 100:28–35
99. DiPippo R, Khalifa HE, Correia RJ, Kestin J (1979) Fossil superheating in geothermal steam power plants. Geotherm Energy Magazin 7(1):17–23
100. Chang I, Williams JR (1985) Thermodynamic analysis of a geopressured geothermal hybrid wellhead power system. Final report. DOE/NV/10355-1
101. Future of Geothermal Energy, MIT report. http://geothermal.inel.gov/publications/future_of_geothermal_energy.pdf
102. Vuataz FD (2004) Hijiori hot dry rock project, northern Japan. Swiss Deep Heat Mining Project, Steinmaur. http://www.dhm.ch/imaH00hijiori.html
103. New Energy and Industrial Technology Development Organization (2004) Development of a hot dry rock power generation system, New Energy and Industrial Technology Development Organization, Kanagawa. http://www.nedo.go.jp/chinetsu/hdr/indexe.htm
104. Vuataz FD (2004) Ogachi hot dry rock project, northern Japan, June 2000. Swiss Deep Heat Mining Project. Steinmaur. http://www.dhm.ch/imaOG00ogachi.html

105. Kruger P, Karasawa H, Tenma N, Kitano K (2000) Analysis of heat extraction from the Hijiori and Ogachi HDR geothermal resources in Japan. In: Proceedings world geothermal congress 2000, International Geothermal Association, pp 2677–2682
106. Brown DW (1996) 1995 reservoir flow testing at Fenton Hill, New Mexico. In: Proceeding of the 3rd international HDR forum, Santa Fe, pp 34–37
107. MacDonald P, Stedman A, Symons G (1992) The UK geothermal HDR R&D programme. In: Proceedings seventeenth workshop on geothermal reservoir engineering, SGP-TR-141, Stanford University, Stanford, 29–31 Jan 1992
108. Opportunities in the upper Rhine Valley, http://www.energy-base.org/fileadmin/media/regioner/docs/geothermal-energy-rhine-valley_FINAL.pdf
109. Baria R, Baumgaertner J, Teza D, Michelet S (2005) Reservoir stimulation and testing techniques for EGS systems (Soultz). Presented at EGS workshop, Massachusetts Institute of Technology, Cambridge, MA, 10 Nov 2005
110. Smith IK (1993) Development of the trilateral flash cycle system. Part 1: fundamental considerations. Proc Inst Mech Eng A 207(A3):179–194
111. Austin AL, Lundberg AW (1978) The LLL geothermal energy program: a status report on the development of the total-flow concept, UCRL-500-77. Lawrence Livermore Laboratory, Livermore
112. McKay R (1982) Helical screw expander evaluation project: final report, DOE/ET-28329–1, JPL Pub. 82-5. Jet Propulsion Laboratory, Pasadena
113. Carey B (1983) Total flow power generation from geothermal resources using a helical screw expander. In: Proceeding of the 5th New Zealand geothermal workshop, pp 127–132
114. Cerini DJ, Record J (1983) Rotary separator turbine performance and endurance test results. In: Proceedings of the seventh annual geothermal conference and workshop, EPRI AP-3271. Electric Power Research Institute, Palo Alto, pp 5-75–5-86
115. Sprankle R (1986) Helical screw expander power plant model 76-1 test result analysis. In: Proceedings of a Topical meeting on Small scale geothermal power plants and geothermal power projects, 12–13 Feb 1986. Hydrothermal Power Co., Reno Nevada, pp 39–58
116. Hughes EE (1986) Summary report: rotary separator turbine. Final report, EPRI AP-4718. Electric Power Research Institute, Palo Alto
117. King Hubbert M (1975) Survey of World Energy Resources. In: Symposium on energy sources for the future, Oak Ridge, 7–25 July 1975
118. Tester JW, Milora SL (1975) Geothermal energy. In: Symposium on energy sources for the future, Oak Ridge, 7–25 July 1975
119. Geothermal Energy Association, Geothermal basics potential use. http://www.geo-energy.org/PotentialUse.aspx
120. Western Governors Association (WGA) (2006) Geothermal task force report. http://www.westgov.org/wga/initiatives/cdeac/Geothermal-full.pdf
121. Lund JW, Bertani R (2010) Worldwide geothermal utilization 2010. In: Geothermal resources council annual meeting 2010, Sacramento, 25–27 Oct 2010. GRC transactions, vol 34, pp 195–198
122. The future of geothermal energy, impact of Enhanced Geothermal Systems (EGS) on the United States in the 21st century (2006) MIT Press. http://www1.eere.energy.gov/geothermal/egs_technology.html
123. Bertani R (2010) Geothermal power generation in the world 2005–2010 update report. In: Proceedings world geothermal congress 2010, Bali, 25–29 April 2010
124. Holm A, Blodgett L, Jennejohn D, Gawell K (2010) Geothermal energy: international market update. Geothermal Energy Association, Washington, DC
125. Sanyal SK (2010) Future of geothermal energy. In: Proceedings, thirty-fifth workshop on geothermal reservoir engineering, SGP-TR-188, Stanford University, Stanford, 1–3 Feb 2010
126. Johanson TB, Goldenberg J (2004) World energy assessment overview 2004 update. UNDP 2005, http://www.undp.org/energy/weaover2004.htm
127. Tester J, DiPippo R (2007) The future of geothermal energy structure and outcome of the analysis. In: Presentation at the DOE geothermal program workshop, Washington, DC, 7 June 2007
128. DOE Geothermal Technologies program use EERE website. http://www1.eere.energy.gov/geothermal/
129. Bertani R (2009) Long term projection of geothermal electricity development in the world. In: Geotherm 2009 expo & congress, Offenburg, 5–6 March 2009. http://www.iea-gia.org/documents/LongTermGeothermElecDevelopWorldBertanioffenburg23Feb09.pdf
130. Fridleifsson IB, Bertani R, Huenges E, Lund JW, Ragnarsson A, Ryback L (2008) The possible role and contribution of geothermal energy to the mitigation of climate change. In: IPCC scoping meeting on renewable energy sources, Luebeck, 21–25 Jan 2008
131. Council of Europe, Doc. 11740, 10 October 2008 Geothermal Energy: a solution for the future? Motion for a resolution presented by Mrs Bjarnadottir and others
132. Council of Europe, Doc. 12249, 6 May 2010. Geothermal energy – a local answer to a hot topic? Report by: Mr René ROUQUET, France, Committee on the Environment, Agriculture and Local and Regional Affairs. http://assembly.coe.int/ASP/Doc/DocListingDetails_E.asp?DocID=13060
133. EGEC (2010) The future of geothermal development, European Geothermal Energy Council (EGEC) projections. www.egec.org
134. European Commission Research, Future prospects, hurdles. http://ec.europa.eu/research/energy/eu/research/geothermal/background/index_en.htm
135. Brown LR (2009) Stabilizing climate: shifting to renewable energy, Chapter 5. In: Plan B 4.0: mobilizing to save civilization. W.W. Norton, New York. www.earthpolicy.org/index.php?/books/pb4
136. Hayes L (2011) Demonstration of a variable phase turbine. http://energent.net

Geothermal Power Economics

Subir K. Sanyal
GeothermEx, Inc, Richmond, CA, USA

Article Outline

Glossary
Definition of the Subject and Its Importance
Introduction
Factors That Determine Geothermal Power Cost
Estimating Levelized Power Cost
Sensitivity of Levelized Power Cost
Concluding Remarks
Future Directions
Bibliography

Glossary

Capital cost Capital costs are the one-time costs incurred on project acquisition, drilling, construction, and equipment needed to bring a project to a commercially operable status.

Levelized power cost The present value of the total cost of developing and operating a geothermal power plant over its economic life divided by the total power generated over the same period, costs being levelized in real dollars (i.e., adjusted to remove the impact of inflation).

Make-up well cost Cost of drilling "make-up" wells as needed during project operation.

Operations and maintenance (O&M) Cost Those expenses used for the day-to-day operation of a power facility. The major categories include personnel, general and administrative, insurance, supplies and services, well maintenance, and equipment maintenance costs.

Power capacity The maximum output of power from a power plant, commonly expressed in megawatts (MW).

Definition of the Subject and Its Importance

Geothermal power is the rate of extraction of geothermal energy, whether expressed as heat energy or equivalent electrical energy, and is expressed as Watt or an equivalent unit. The extraction of geothermal energy, and therefore geothermal power capacity, is dependent not only on the technological barriers to this energy extraction but also on the economic barriers. Power generation from geothermal energy, therefore, requires consideration of the economics of geothermal power. This entry considers power cost as the main economic criterion rather than the power price or project profitability because, unlike price or profitability, cost is substantially independent of the corporate culture of the developer and operator, financing mechanism, local market forces, and government policies. The most comprehensive measure of the geothermal power cost is "levelized" power cost, expressed typically as cents per kW-hour power generated over the life of a power plant.

Introduction

The power cost considered here is "levelized" cost (¢/kWh) over the project life, defined here as the cumulative present value of all future costs including annual payments for amortized capital in real dollars (adjusted for inflation) divided by the cumulative power generated [1]. The initial capital cost is amortized over a period of 30 years; make-up well drilling cost is not capitalized and is considered an operating expense. The capital cost includes the cost of money (i.e., the cumulative future interest payments discounted for inflation) but does not include any transmission line cost or any unusually site-specific costs of regulatory compliance or environmental impact mitigation.

Cost calculations in this entry ignore any royalty burden, tax liability, or tax credit. The values of economic parameters assumed in this entry reflect the setting in the USA as of year 2005. However, levelized cost of geothermal power has approximately doubled between 2005 and 2010 because of large increases in drilling cost and commodity prices. Even so, the conclusions arrived at should still be applicable at least qualitatively to geothermal power projects worldwide. In the debate over the relative virtues of various forms of renewable energy, power cost is an objective criterion that should favor geothermal; yet there is considerable difference of opinion as to what it truly is and can be.

The analysis, extracted from Ref. [1], considers a power capacity range of 5–150 MW with 50 MW as

the "base case." Power cost consist of three components: (1) capital cost component (including cost of money), (2) operations and maintenance (O&M) cost component (not counting debt service, which is included under the capital cost component), and (3) make-up well drilling cost component.

Factors That Determine Geothermal Power Cost

These factors can be grouped into four categories: (1) economy of scale, (2) well productivity characteristics, (3) development and operational options, and (4) macroeconomic climate. In general, economy of scale allows both unit capital cost (in US dollars per kilowatts installed) and unit O&M cost (in ¢/kWh) to decline with increasing installed capacity. Based on the data presented by Entingh and McVeigh [2], the unit capital cost (as of 2005) is estimated to vary from \$1,600/kW to \$2,500/kW depending on project size and other project-specific criteria. For the smallest project size of 5 MW considered here, the author has assumed a unit capital cost of \$2,500/kW and for the largest considered project size of 150 MW a cost of \$1,600/kW. A permissive assumption has been made that within the above range of values, unit capital cost declines exponentially with plant capacity. This assumption leads to the following correlation between unit capital cost in \$/kW (c_d) and plant capacity in kW (P):

$$c_d = 2500e^{-0.003\,(P-5)} \tag{1}$$

For the 50 MW base case, the unit capital cost is estimated from Eq. 1 at \$2,184/kW. GeothermEx's experience shows the representative unit O&M cost approximately ranged from 2.0 ¢/kWh for a 5 MW plant to 1.4 ¢/kWh for a 150 MW plant in 2005. Assuming an exponential decline in unit O&M cost in ¢/kWh (c_o) with plant capacity in kW (P):

$$c_o = 2.0e^{-0.0025(P-5)} \tag{2}$$

For the 50 MW base case, the unit O&M cost is estimated from Eq. 2 at 1.79 ¢/kWh.

Well productivity characteristics affect geothermal power cost in mainly two ways:

1. If well productivity is higher, fewer wells are needed to supply a plant, thus reducing power cost.
2. A higher rate of decline in well productivity with time calls for more make-up well drilling, and therefore, leads to higher power cost.

For the purposes of this entry, an average initial productivity of 5 MW per well was assumed; this is a typical value. Geothermal wells generally undergo "harmonic" decline in well productivity with time [3]:

$$W = \frac{W_i}{1 + D_i t} \tag{3}$$

where W_i is initial productivity, D_i is initial annual decline rate in productivity, and W is productivity in year t. The harmonic decline trend implies a decline rate that slows down with time, the annual decline rate (D) in productivity in year t being given by [3]:

$$D = \frac{D_i}{1 + D_i t} \tag{4}$$

If the total production rate from a field is small enough to be entirely compensated by natural recharge or if only a small fraction of the productive reservoir is being exploited, the decline rate in well productivity would be insensitive to increases in plant capacity. These situations are much less common. In most cases, decline rate increases with increasing installed capacity. This sensitivity of productivity decline to installed capacity is too site-specific to be quantified by a generally applicable correlation. Nevertheless, Sanyal et al. [4] attempted an approximate formulation:

$$D_i' = \left(\frac{W_i'}{W_i}\right)\left(\frac{\ln W_i'}{\ln W_i}\right) D_i, \tag{5}$$

where D_i is initial annual harmonic decline rate when total production rate is W_i and D_i' is initial annual harmonic decline rate when total production rate is changed to W_i'. Assuming a typical initial harmonic decline rate of 5% per year for the 50 MW base case, the initial annual harmonic decline rate for any other plant capacity was estimated from Eq. 5.

There are certain resource development and operational options that affect power cost. The developer of a geothermal project has the option to size the power

plant while the operator of the project has the option either to allow generation to decline with time or to maintain generation by make-up well drilling; the operator can also run the plant beyond its amortized life. The sensitivity of power cost to these intertwined options has been studied in this entry. The resource development option has been considered by varying the plant capacity within the range of 5–150 MW. The operational option has been considered by assuming make-up well drilling for various periods of time following plant start-up, and scenarios of plant operation both up to and beyond the amortization period.

While the unit capital cost for a given plant capacity, as given by Eq. 1, includes initial drilling cost, the unit O&M cost given by Eq. 2 does not include make-up well drilling cost. In order to estimate the make-up well drilling cost as a function of time, it is necessary to estimate first the initial number of wells required for a given plant capacity. This estimate was based on a typical initial productivity of 5 MW per well plus the customary need for at least one standby well and a minimum of 10% reserve production capacity at all times. With the above assumptions, it follows that the installed plant capacity can be maintained without any make-up well drilling for up to t_c years following plant start-up, as given by:

$$t_c = \frac{1}{D_i}\left[\frac{W_i N_{wi}}{(1 + r/100)P} - 1\right], \tag{6}$$

where D_i is initial annual harmonic decline rate, W_i is initial productivity per well (MW), N_{wi} is initial number of wells (including at least one standby well), P is plant capacity (MW), and r is minimum production capacity reserve required (%).

Estimating Levelized Power Cost

Figure 1 shows the schematic generation and make-up well drilling histories of a typical power project. Generation can be maintained without make-up well drilling up to year t_c, as given by Eq. 6. Then generation is maintained by make-up well drilling up to year t_d in response to decline in well productivity according to Eq. 3, the initial annual harmonic decline rate being given by Eq. 5. After year t_d, no make-up well is drilled and generation is allowed to decline as per Eqs. 3 and 5.

Given the generation and make-up well drilling histories represented in Fig. 1, the levelized cost of geothermal power ($\bar{c}$) in ¢/kWh is given by [1]:

$$\begin{aligned}\bar{c} = {} & \frac{100D(t_d)}{G\{D(t_d)t_d + \ln[1 + D(t_d)(n - t_d)]\}} \\ & \cdot \left\{\frac{iC(1+i)^n}{(1+i)^n - 1}\right\}\left\{\frac{(1+I)^n - 1}{I(1+I)^{n-1}}\right\} + c_{ov} + \left(\frac{t_d}{n}\right)c_{ofi}, \\ & + \frac{c_{ofi}}{n}\left\{(n - t_d) + \frac{D(t_d)}{2}(n - t_d)^2\right\} \\ & + \frac{100C_{wi}N_{wi}D(t_d)D(t_c)(t_d - t_c)}{G\{D(t_d)t_d + \ln[1 + D(t_d)(n - t_d)]\}}\end{aligned} \tag{7}$$

where $D(t)$ is annual productivity decline rate in year t; G is initial annual generation (kWh); N is power plant life (assumed to be 30 years in base case); C is total capital cost, that is, $c_d \cdot P$ ($); c_o is unit annual O&M cost (¢/kWh); i is annual interest rate (assumed to be 7% in base case); I is annual inflation rate (assumed to be 3% in base case); c_{ofi} is fixed portion of the annual O&M cost at plant start-up divided by initial annual generation (¢/kWh); c_{ov} is variable portion of the annual O&M cost divided by annual generation (¢/kWh); N_{wi} is number of initial production wells; and C_{wi} is drilling cost per initial production well (assumed to be $2 million in the base case).

Capital cost includes exploration cost, power plant cost, gathering and injection system cost, and cost of capital. Annual O&M cost includes personnel cost, general and administrative cost, insurance cost, supplies/consumables/engineering and laboratory services cost, wellfield maintenance cost, generator and turbine maintenance cost, and other equipment and maintenance cost.

The variable portion of the annual O&M cost represents costs that vary with the level of generation, such as, costs of supplies, consumables, etc., which remain proportional to generation; this cost divided by annual generation gives c_{ov}. The fixed portion of the annual O&M cost represents costs that are independent of the generation level; these include costs of personnel, administration, insurance,

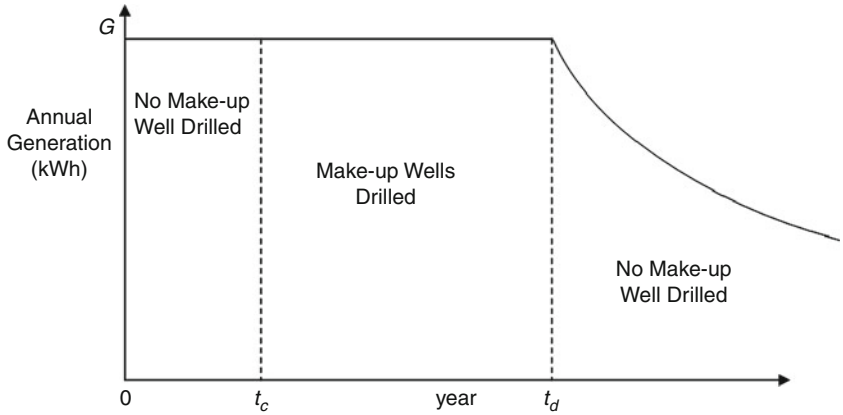

Geothermal Power Economics. Figure 1
Schematic generation and make-up well drilling histories of a project [1]

wellfield maintenance, generator and turbine maintenance, other equipment maintenance, etc., which may not decline in response to any decline in generation. This fixed annual cost divided by annual generation gives c_{of}. For the purposes of this entry, 20% of the annual O&M cost was assumed to vary with generation at plant start-up; however, results are found to be relatively insensitive to the fraction of O&M cost that is variable. As generation declines, c_{ov} remains constant but c_{of} increases from its initial value of c_{ofi}. A typical plant capacity factor of 90% was assumed in estimating annual generation. In Eq. 7, the total capital cost (C) is assumed to be amortized over the plant life of n years at an interest rate i (annual compounding). The calculated power costs in future years are discounted for inflation to arrive at a levelized power cost in present dollars ($\bar{c}$).

Sensitivity of Levelized Power Cost

It should be noted that if there were no economy of scale in capital and O&M costs (i.e., a capital cost of \$2,184/kW and an O&M cost of 1.79 ¢/kWh, as in the base case) and if productivity decline rate were insensitive to installed capacity (remaining at 5% initial annual harmonic rate as in the base case), levelized power cost from Eq. 7 would be 3.6 ¢/kWh irrespective of plant capacity. Table 1 lists all parameters for the range of development scenarios analyzed, assuming the economy of scale in capital and O&M costs as well as the sensitivity of productivity decline to plant capacity.

Figure 2 shows the calculated power cost in ¢/kWh for various levels of installed plant capacity as a function of t_d (i.e., the number of years of make-up well drilling undertaken to maintain plant capacity). This figure takes into account the economy of scale as reflected in Eqs. 1 and 2, as well as acceleration in well productivity decline, as given by Eq. 5, with increased installed capacity. Figure 2 indicates that power cost declines with the number of years of make-up well drilling, the decline rate being steeper for a higher plant capacity. Figure 2 also indicates that if make-up well drilling is discontinued too early (prior to about 10 years), power cost would be higher for a larger plant. This figure also shows that for any plant capacity, a relatively minor reduction in power cost is achieved by continuing make-up well drilling after this period, and continuing make-up well drilling beyond about 20 years may actually increase power cost. Therefore, there is little reason to continue make-up well drilling beyond about 20 years unless the power sales contract imposes significant penalties for any shortfall in plant capacity.

Figure 3 shows the minimum achievable power cost for various plant capacities as read from Fig. 2. This figure shows that the minimum achievable power cost is rather insensitive to plant capacity; it varies from 3.7 ¢/kWh for a 10 MW plant to 3.4 ¢/kWh for a 150 MW plant, a 7.6% decline in power cost for a 1,400% increase in power capacity. Irrespective of the plant capacity and the number of years of make-up well drilling, power cost as of 2005 could not be lowered

Geothermal Power Economics. Table 1 Development scenarios analyzed

Plant capacity (MW)[c]	Capital cost per kW	Total capital cost (million $)	O&M cost (¢/kWh)[b]	Initial harmonic decline rate (%)	No. of initial production wells[a]	Years before make-up well drilling is required (t_c)
5	2,500	12.5	2.0	0.2	2	>30
10	2,463	24.6	1.98	0.6	3	>30
20	2,390	47.8	1.93	1.5	5	9
30	2,319	69.6	1.88	2.6	7	2
50	2,184	109.2	1.79	5.0	11	0
75	2,025	152.0	1.68	8.3	17	0
100	1,880	188.0	1.58	11.8	22	0
125	1,744	218.0	1.48	15.4	28	0
150	1,618	242.7	1.39	19.2	33	0

[a]5 MW per well/minimum of one standby well/minimum of 10% excess capacity
[b]80% of O&M cost varies with capacity
[c]Plant capacity factor=0.9

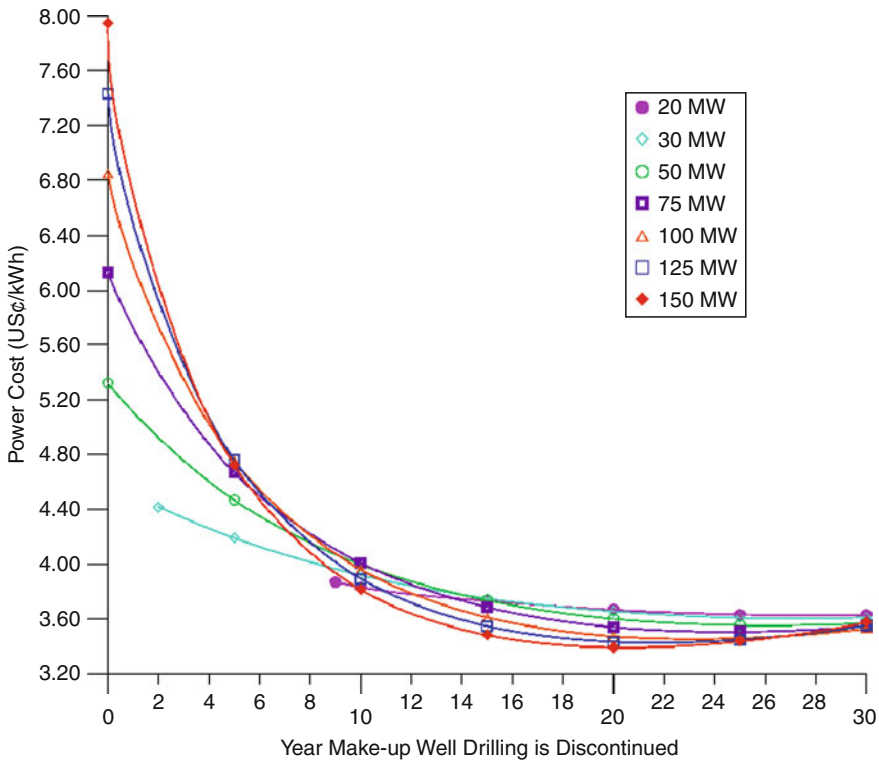

Geothermal Power Economics. Figure 2
Levelized power cost versus the year make-up well drilling is discontinued [1]

significantly below 3.4 ¢/kWh. Figure 4 shows the three components of power cost (capital, O&M, and make-up well drilling) as functions of plant capacity assuming make-up well drilling to be discontinued after 20 years. This figure shows that the capital cost component is approximately equal to the O&M cost component for all plant capacities while the make-up well drilling component assumes greater significance with increasing plant capacity (except for very small capacities). Furthermore, the sum of O&M and make-up well drilling components constitutes the major part of power cost. Capital expenditure is incurred in the first few years of a project, when site-specific knowledge of the resource is still limited; therefore, adequate optimization of capital investment can be a challenge. After plant start-up, little can be done to reduce the capital cost component of power cost, except perhaps refinancing the debt should the interest rate decline. On the other hand, O&M and make-up well drilling costs, being incurred gradually as production continues, should reduce with time due to the "learning curve" effect. As more understanding of the resource characteristics and reservoir performance is gained with operation, O&M and make-up well drilling costs can be reduced, lowering power cost.

Figure 5 is a plot of power cost versus percent deviation in the values of the various independent variables from their base case (50 MW) values. In this figure, a steeper curve through the base case point implies a higher sensitivity of power cost to the variable

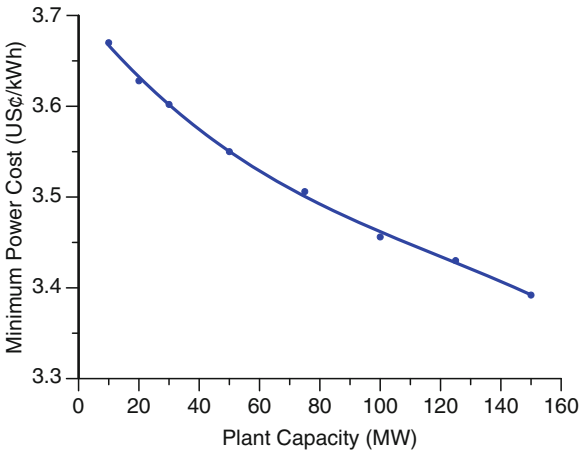

Geothermal Power Economics. Figure 3
Minimum levelized power cost versus plant capacity [1]

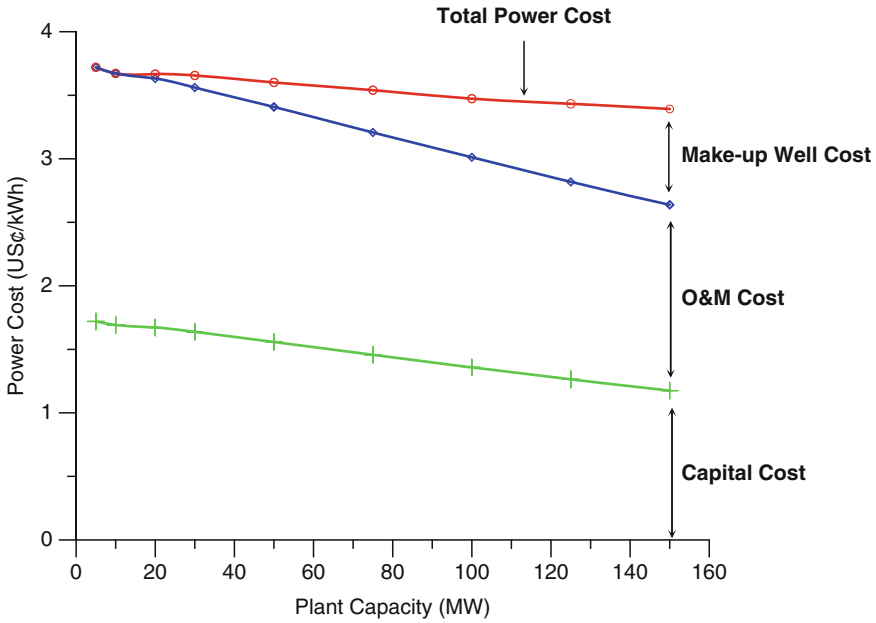

Geothermal Power Economics. Figure 4
Components of levelized power cost versus plant capacity (assuming 20 years of make-up well drilling) [1]

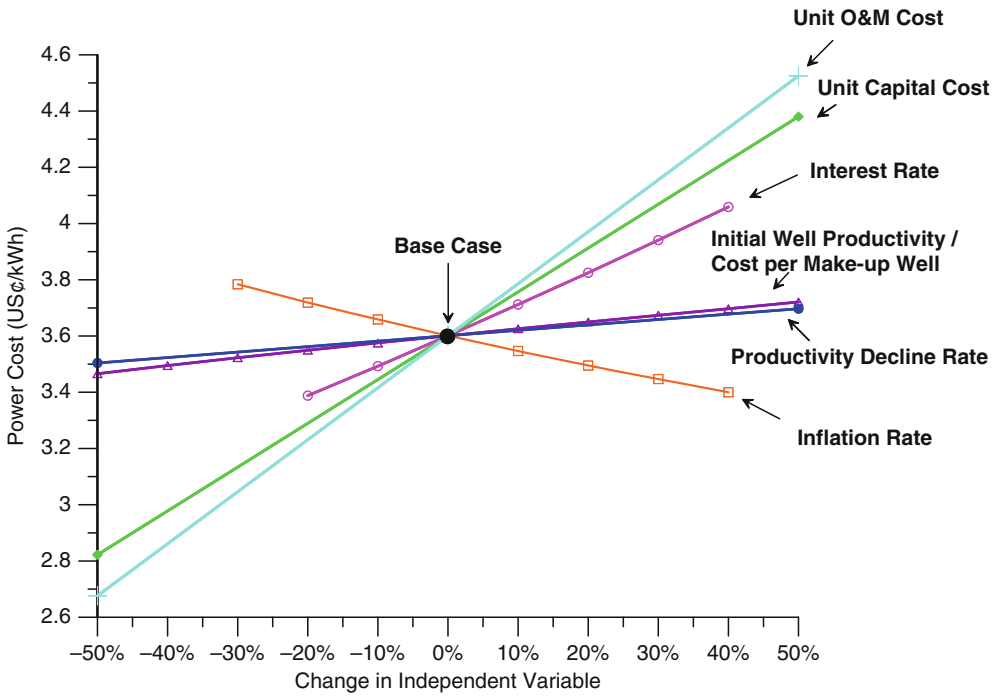

Geothermal Power Economics. Figure 5
Sensitivity of base case power cost to changes in independent variables [1]

represented by the curve. Figure 5 shows that unit O&M cost and unit capital cost have the highest impact on power cost; these two variables are also subject to economy of scale. On the other hand, power cost is relatively insensitive to resource-related variables (such as well productivity, drilling cost per well, and productivity decline rate). Figure 5 indicates a levelized power cost of 3.6 ¢/kWh as of 2005 for a 50 MW plant. However, it should be noted that the author's experience as of 2005 indicated that the estimates of capital cost in the USA as of 2005 based on Ref. [2] was somewhat low. For the base case, the capital cost in the USA as of 2005 was as much as 30% higher than $2,184/kW. Therefore, Figure 5 shows that the levelized power cost for a 50 MW plant in the USA as of 2005 was as high as 4.1 ¢/kWh; in 2010 it is as high as 8 ¢/kWh.

Interestingly, power cost is only modestly sensitive to macroeconomic variables (interest and inflation rates), because interest and inflation rates affect power cost by about the same magnitude but in opposite directions (Fig. 5). Figure 6 shows power cost versus plant capacity for several diverse microeconomic situations: (1) a hyperinflationary environment, (2) a high inflationary environment, (3) the economic environment in the USA as of 2005, and (4) a deflationary environment; appropriate interest rates (i) and inflation rates (I) assumed for the various cases are shown on the figure. Figure 6 implies that, in relative terms, the sensitivity of power cost to the macroeconomic climate is not significant. For example, the variation in power cost over the capacity range of 5–150 MW is of similar magnitude as the variation in power cost in the base case over the extreme range of macroeconomic climates considered.

History of operation of geothermal power plants in Italy, New Zealand, El Salvador, Mexico, Japan, and USA, where some plants have already operated for more than 30 years, indicates that it is possible to continue operating a geothermal plant beyond its typical amortization period of 20–30 years. Can power cost be reduced if a geothermal plant were amortized for 30 years but operated for a longer period? Figure 7 compares power cost versus plant capacity as shown before (for 30 years' operation) and as calculated for

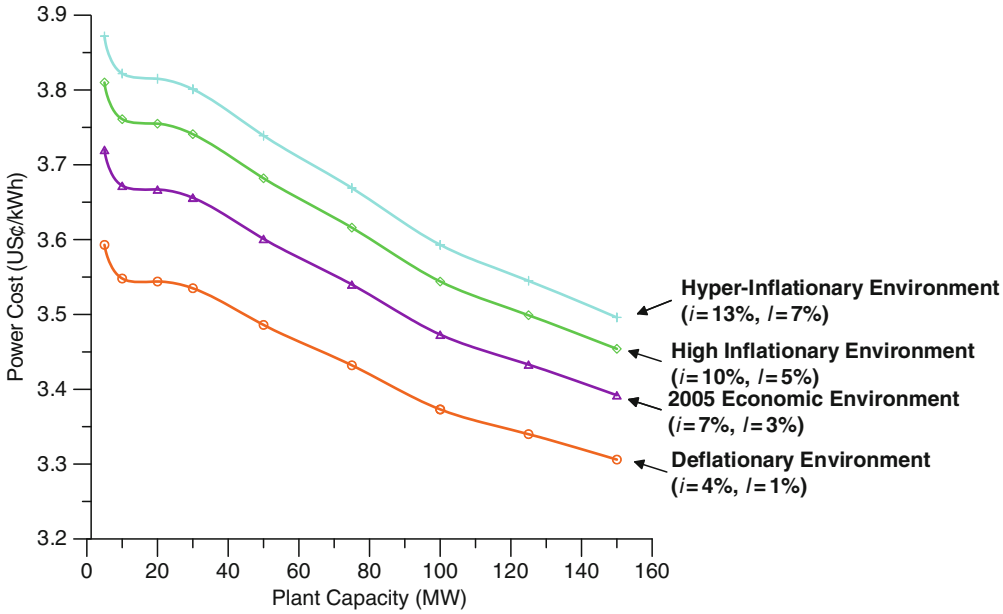

Geothermal Power Economics. Figure 6

Levelized power cost versus plant capacity under various macroeconomic conditions (for 20 years of make-up well drilling) [1]

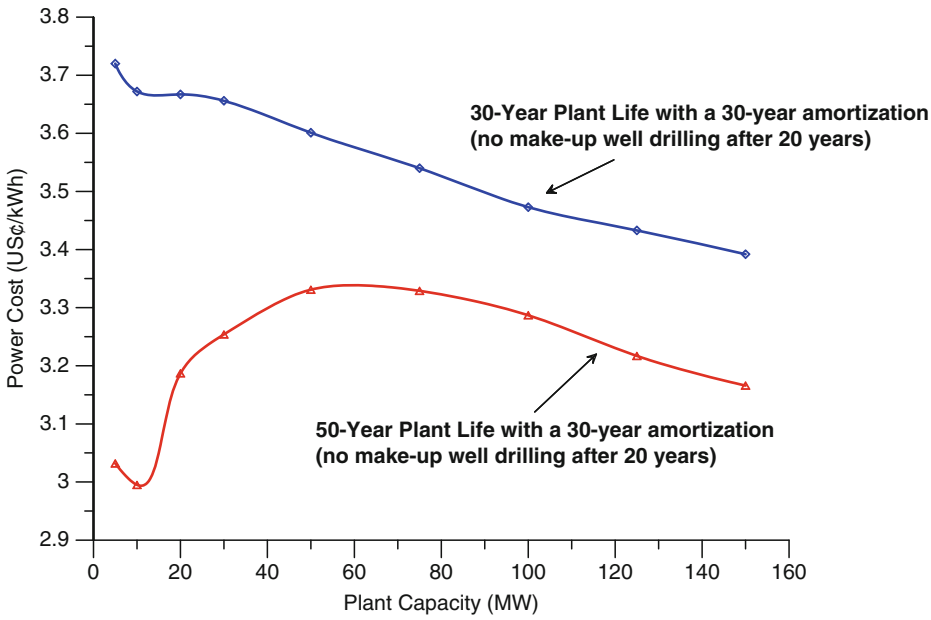

Geothermal Power Economics. Figure 7

Effect of plant life on levelized power cost (20 years of make-up well drilling) [1]

a 50-year operating period, the initial capital cost still being amortized over 30 years. Figure 7 shows that for smaller plants, cost may be reduced significantly, by as much as 20% for plants of 10 MW or smaller capacity. For plants larger than about 50 MW, this reduction in power cost is not significant, particularly considering

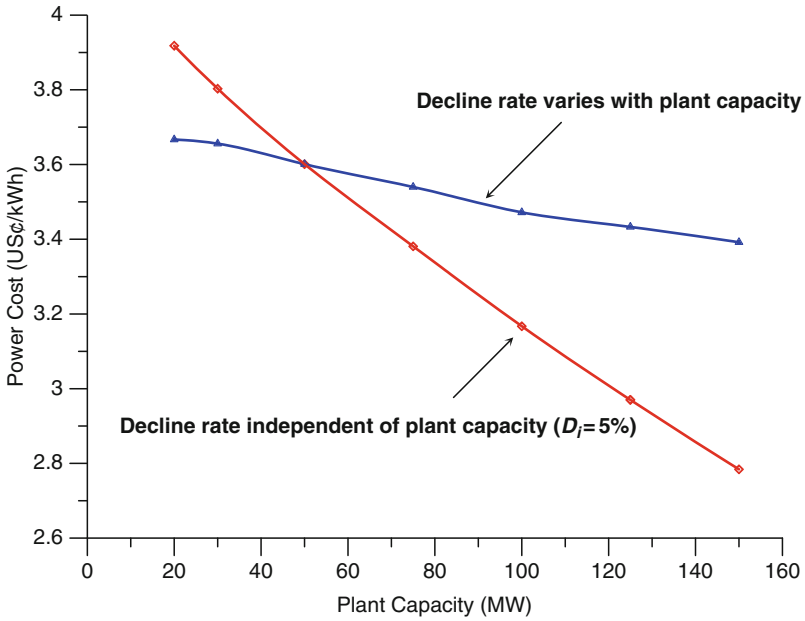

Geothermal Power Economics. Figure 8
Levelized power cost versus plant capacity (for 20 years of make-up well drilling) [1]

the additional risk of operating an aging power plant and pipelines, and possibly deteriorating wells.

The above analysis takes into account the usual acceleration in well productivity decline due to increases in plant capacity. How would the results change in the unusual case of well productivity being insensitive to installed plant capacity? Figure 8 compares levelized power cost as a function of plant capacity, as calculated before, with the case of a constant initial annual harmonic decline rate of 5% irrespective of capacity. Figure 8 shows that if productivity decline rate were insensitive to plant capacity, power cost would decline with plant capacity much more rapidly than in the usual case, the minimum power cost being only 2.8 ¢/kWh (for a 150 MW plant). However, a stand-alone project of a capacity larger than 100 MW is a rarity in the geothermal industry. The existing fields with a generation level greater than 100 MW typically rely on multiple, independent units of up to 100 MW each; as such, the economy of scale enjoyed by these projects would amount to that for a capacity of 100 MW or less. Therefore, if well productivity were insensitive to plant capacity, a power cost of less than 3.2 ¢/kWh (estimated for a 100 MW plant) as of 2005 was unlikely to be realized.

Finally, how would the results change if economy of scale in capital and O&M costs were negligible? One such conceivable situation could be the installation of multiple, modular and infrastructurally independent power plants in the same field. Figure 9 presents power cost versus the number of years of make-up well drilling for various plant capacities ignoring economy of scale. The results in this figure assume that unit capital and O&M costs remain the same as in the base case irrespective of installed capacity, but productivity decline still increases with installed capacity as given by Eq. 5. Figure 9 indicates that if economy of scale were negligible, power price would increase with installed capacity no matter how long one continues make-up well drilling, and power price would be consistently higher than in the usual case with economy of scale. The minimum achievable power cost in this case is still on the order of 3.4 ¢/kWh as of 2005 (estimated for a 20 MW plant).

Concluding Remarks

1. Power cost is sharply reduced by maintaining full generation capacity, by drilling make-up wells, for at least the first 10 years or so following plant

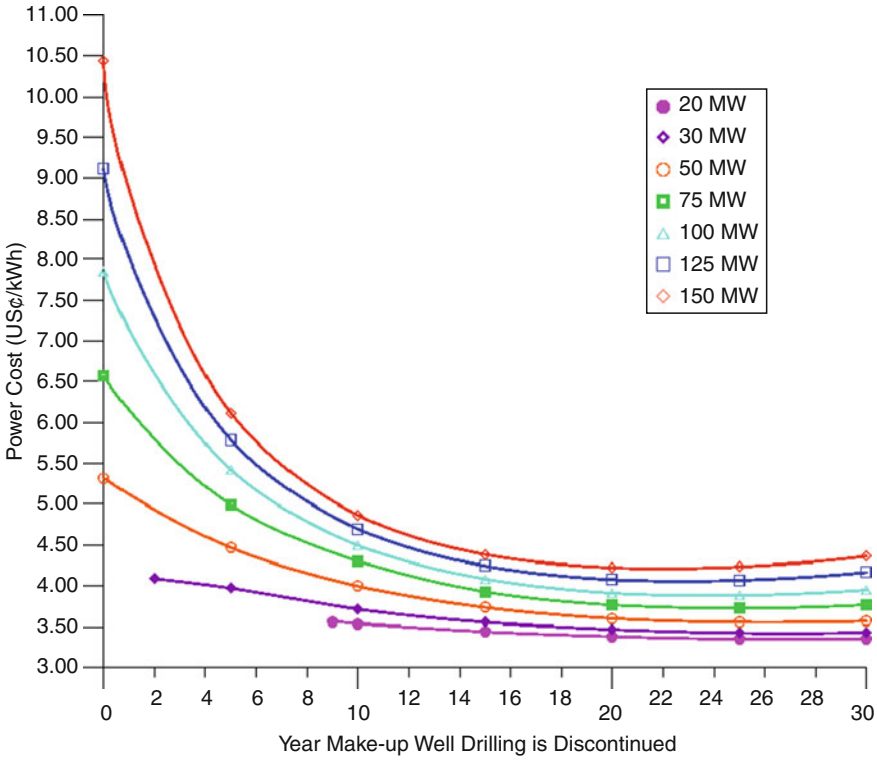

Geothermal Power Economics. Figure 9
Levelized power cost versus the year make-up well drilling is discontinued ("no economy of scale" case) [1]

start-up; continuing make-up well drilling beyond 20 years does not reduce power cost significantly.

2. The minimum achievable power cost is insensitive to plant capacity; as of year 2005, it was on the order of 3.4 ¢/kWh. There are significant opportunities to reduce power cost as site-specific experience is gained in resource management and power plant operation throughout the project life.
3. The levelized cost of power from a 50 MW plant as of 2005 was in the range of 3.6–4.1 ¢/kWh; it is approximately twice as of 2010.
4. Power cost is most sensitive to unit O&M cost followed by unit capital cost, interest rate, and inflation rate in the decreasing order of sensitivity; it is relatively insensitive to well productivity, drilling cost per well, well productivity decline rate, and the macroeconomic climate.
5. Operating small power plants (10 MW or less capacity) beyond their typical amortization period of 30 years can significantly reduce power cost.
6. The minimum achievable power cost does not decline significantly with increasing plant capacity except in the unlikely situation of well productivity decline being insensitive to capacity, when it was as low as 3.2 ¢/kWh as of 2005. In the unusual situation of an absence of economy of scale, power cost increases with plant capacity, the minimum achievable level being 3.4 ¢/kWh. In the very unlikely situation of both well productivity decline as well as unit capital and O&M costs being insensitive to plant capacity, the minimum achievable power cost would be on the order of 3.6 ¢/kWh in 2005 dollars.

Future Directions

This entry analyzes the levelized cost of geothermal power as of 2005. Between 2005 and 2010, this cost has escalated in spurts; today levelized cost is nearly double that in 2005. However, at this time the cost escalation is relatively slow.

While levelized cost of geothermal power has increased over the last 5 years, so has the price available for geothermal power in the USA by a similar ratio. The recent price increases have been driven by a host of new incentives for geothermal power introduced in the USA: (1) the Renewable Portfolio Standard ("RPS"), which requires an utility to derive a minimum fraction (0–33% depending on the State) of its power from renewable resources; (2) a Production Tax Credit ("PTC") of about 2 ¢/kWh for geothermal power; (3) the option to receive an Investment Tax Credit (30% of the capital investment) at the onset of power generation in lieu of PTC; (4) a renewable energy credit ("REC") in the USA or carbon credit worldwide; Geothermal Loan Guaranty, etc. Therefore, it is reasonable to expect that the price of geothermal power will continue to keep pace with, or most likely increase relative to, levelized cost of geothermal power for the near future.

It should be noted that this entry considers the economics of power from conventional geothermal systems, which are naturally occurring subsurface porous or fractured systems that can be tapped for production by drilling wells. However, in the last decade, considerable hopes have been raised of tapping geothermal energy from enhanced geothermal systems ("EGS") [5]. These are hot subsurface systems with porosity or fracture capacity too low to allow commercial production but can be enhanced by pervasive hydraulic fracturing to enable significant fluid injection and production. In an EGS project, heat is recovered from the artificial reservoir by injecting cool water through a set of wells while producing heated water from another set of wells. Such systems have not yet proven commercial, but research and development toward commercial tapping of EGS systems continue. Even in countries where conventional geothermal systems do not exist, EGS developments would be the theoretically possible, because anywhere on earth adequately hot rock bodies can be reached by drilling wells deep enough and creating an artificial reservoir by hydraulic fracturing of rock. Sanyal et al. [6] has presented an analysis of the economics of a prototype EGS project. However, until EGS power proves commercial, its economics would have significant uncertainties.

Bibliography

1. Sanyal SK (2005) Levelized cost of geothermal power – how sensitive it is? Trans Geotherm Res Council 29:459
2. Entingh DJ, McVeigh JF (2003) Historical improvements in geothermal power systems costs. Trans Geotherm Res Council, 533
3. Sanyal SK, Menzies AJ, Brown PJ, Enedy KL, Enedy S (1989) A systematic approach to decline curve analysis for the geysers steam field, California. Trans Geotherm Res Council, Santa Rosa, p 415
4. Sanyal SK, Robertson-Tait A, Klein CW, Butler SJ, Lovekin JW, Brown PJ, Sudarman S, Sulaiman S (2000) Assessment of steam supply for the expansion of generation capacity from 140 to 200 MW, Kamojang Geothermal Field, West Java Indonesia. In: Trans World Geotherm Congress, Beppu and Morioka, Japan, p 2195
5. MIT (2006) The future of geothermal energy – impact of enhanced geothermal systems (EGS) on the United States in the 21st century. An assessment by an MIT – led interdisciplinary panel, Massachusetts Institute of Technololgy, Cambridge
6. Sanyal SK, Morrow JW, Butler SJ, Robertson-Tait A (2007) Is EGS commercially feasible? Trans Geotherm Res Council 31:2007

Geothermal Power Stations, Introduction to

Lucien Y. Bronicki
Ormat Technologies, Inc., Reno, NV, USA

Geothermal energy, contrary to solar and wind, does not depend on weather and is the only one which can supply base-load power. Although not evenly distributed geographically, geothermal energy potential is very important, particularly if the R&D of such advanced systems will be actively pursued.

This section covers the nature of geothermal energy resources, their utilization, conversion technologies as well as its future development (► Geothermal Energy, Nature, Use, and Expectations). The section also highlights the greatest challenge in geothermal development, namely, the geothermal resource. Power conversion is the least uncertain part of a geothermal project, as it consists of a straightforward engineering design with work executed by experienced manufacturers, engineering firms, and contractors.

The risks and challenges are related to exploration, drilling, and managing the resource. Optimization

depends on the choice of adaptation of the power station configuration to the resources available.

When considering different types of resources and uses of geothermal energy, it is important to differentiate between geothermal or ground source heat pumps (GSHP) which utilize the natural insulation of the Earth for heating and cooling, as compared to hydrothermal resources, which are natural flows of geothermal-heated waters associated with underground heat sources or hot rocks.

- The comparative advantages of geothermal energy use include low emissions, high capacity factors, sustainability, and minimal land footprints.
- Hydrothermal sources can be utilized directly for space heating and other direct uses. This source can also be used for power generation if fluids of sufficient temperatures are available at commercial depths.

The distribution of geothermal resources is irregular due to unequal distribution of volcanoes, hot springs, and heat manifestations at specific locations over the Earth's surface (► Geothermal Energy, Geology and Hydrology of). Geothermal resources are a reflection of the underlying global, local geological and hydrological framework. The most thermally rich resources tend to concentrate in environments with abundant volcanic activity and tend to be controlled by plate tectonic processes or spreading centers evident as, volcanic chains associated with subduction zones and hot spots. The local geological characteristics that favor useful resources include relatively shallow resource depths to high permeability in the rocks surrounding the resource, and adequate resource fluids.

Exploration starts with the analysis of available geological information to identify the potential target. Once the target is identified, geochemical studies and core drilling are undertaken. These studies are complemented or sometimes preceded by geophysical surveys including aeromagnetic or resistivity studies and remote infrared and hyperspectral techniques.

Hydrothermal systems have different chemical properties (► Hydrothermal Systems, Geochemistry of). The source of heat is usually a magma chamber a few kilometers below the surface. Less frequently, the source of heat is a crustal site. Fluid origin is meteoric, that is, rainwater which infiltrates the ground to depths of a few kilometers. The permeability and degree of fracturing of this cap rock varies from site-to-site according to the intensity and abundance of the surface hydrothermal systems manifestations (boiling springs, steam vents, hot ponds, and geysers).

In the early stages of a hydrothermal system exploration, when there is only surface evidence, the aim of a geochemical survey is the generation of a model that evaluates the temperature and chemical conditions of the fluid at depth.

Drilling is the process for extracting geothermal energy resources for energy production utilization (► Geothermal Resources, Drilling for). Shallow or intermediate-depth wells may be drilled for the purposes of space heating or direct heat uses; more substantial drilling activities are needed to drill for hotter resources designed for power generation.

Geothermal drilling is a niche within the larger drilling services industry which focuses primarily on oil, gas, and minerals. In particular, deep drilling, required in most exploration programs for geothermal power generation projects, will likely utilize big rigs typical in oil and gas extraction.

There are several aspects unique to geothermal drilling. Mainly, geothermal formations, by nature, involve elevated temperatures which are usually significantly higher than those experienced when drilling for oil and gas. The rock that hosts these formations are typically harder (granite, granodiorite, quartzite, basalt, volcanic tuff), more abrasive, highly fractured, and under-pressured. Caustic elements may be present that can cause corrosion and scaling in the wellbore.

These unique characteristics present challenges in dealing with geothermal wells which, unlike oil and gas wells, do not produce economically until utilized through electric generation or direct uses. For power production, geothermal wells must be of a larger diameter than oil and gas wells to produce necessary flow rates for commercial production. Depths of geothermal wells vary according to location. Some resources are shallow (<1,000 m) and others deep (2,500 m to over 3,000 m).

Reservoir Engineering is the comprehensive integration of all available surface and underground information

regarding geology, geophysics, geochemistry, well drilling-testing, exploitation data, information concerning the geothermal developer and objectives of a geothermal development: market targets, costs, and finance becoming the most powerful tools to evaluate the feasibility (► Reservoir Engineering in Geothermal Fields). As in any scientific or engineering activity, results derived from reservoir engineering depend on the quantity and quality of collected information and the as well as the assimilated handling and in depth comprehension of the collected information. Reservoir engineering is not limited to the final numerical tool, but also includes acquisition information which allows prediction of the impacts on a geothermal resource 20–30 years into the future.

Maintaining the sustainability of a geothermal field through operation requires Monitoring (► Geothermal Field and Reservoir Monitoring). Using techniques such as down-hole monitoring and surface monitoring, the impact of production on the long-term sustainability of a geothermal field can be closely evaluated to ensure that the resource is not prematurely cooling and that any cooling is minimal.

The heat stored in hot dry rock is not accessible via conventional geothermal technology. New methods are being developed and tested to access the huge potential of this type of resources (► Engineered Geothermal Systems, Development and Sustainability of). Commercialization of this technology could unlock many thousands of megawatts of power. For example, the estimate of the Technical Potential for EGS in the USA is estimated at 100 GWe, which is 30 times the total current installed US geothermal capacity from all energy sources. There has been some success, but no actual production from EGS reservoirs as of the end of 2010. Once commercialized, EGS needs to be proved sustainable.

As with any other geothermal energy source, EGS development involves some impact on the environment (► Geothermal Resources, Environmental Aspects of). Geothermal resources are environmentally important as natural thermal features. Typically, the most significant environmental impacts are associated with the exploitation of high-temperature liquid-dominated geothermal systems for electric power generation; however, the majority of these impacts can be avoided or minimized with appropriate techniques. However, as geothermal energy generally offsets use of fossil fuels, the use of geothermal resources are more likely to improve air quality and overall water quality.

The current utilization of geothermal resources worldwide includes direct use of heat and power generation (► Geothermal Energy Utilization). There is a long history of using geothermal heat since the Roman times. The development of geothermal usage began early in the twentieth century in industrial countries with abundant geothermal activity. The list of these countries includes Italy, USA, Japan, New Zealand and Iceland. In addition, developing countries such as the Philippines, Indonesia, Central America and Kenya are also listed as geothermal users.

Applications, such as space heating, agriculture, and other processes, require heat that may otherwise be provided using a fossil fuel (► Geothermal Resources Worldwide, Direct Heat Utilization of). Recent developments in using geothermal sources in large-scale projects include district heating, greenhouse complexes, and major industrial uses. Heat exchangers are also becoming more efficient and better adapted to geothermal projects. This allows the use of lower-temperature water and highly saline fluids. Heat pumps utilizing very low-temperature fluids have extended geothermal developments into traditionally non-geothermal countries such as Canada, France, and Switzerland, as well as areas of the USA.

With the end of 2010, global use of direct geothermal utilization added to approximately 50.5 GW of thermal energy, in 78 countries, displacing over 121 TWh/year of energy consumption.

The techniques used for the conversion of geothermal fluid heat content into mechanical power are similar to those used in fossil-fueled power plants (► Geothermal Power Conversion Technology). Power conversion is the most predictable part of a geothermal project, as it consists of a straightforward engineering design with work executed by experienced manufacturers, engineering firms, and contractors.

The risks and challenges are related to exploration, drilling, and managing the resource. Optimization depends on the adaptation of the power station configuration to the available resources.

Today, 10,000 MW of geothermal power plants are in operation and a majority of them use steam turbines that operate on dry steam or steam produced by single or double flash with about 1,000 MW using Organic Rankine Cycles (ORC) or geothermal combined cycles. However, to widen the range of resources suitable for power generation beyond dry steam and flashed steam plants, ORC cycles have been implemented in the last 30 years, and will probably continue to grow as a common technology driving future development of geothermal resources.

Operational experience confirms the advantages of ORC power stations, not only for low-enthalpy water-dominated resources, but also for certain high-enthalpy sources where the brine is aggressive or the fluid contains a high percentage of non-condensable gas. The higher installation cost of these systems is often justified by environmental and long-term resource management considerations.

In geothermal systems, it is possible to estimate the commercial, sustainable, and renewable capacities of a geothermal system (► Geothermal Power Capacity, Sustainability and Renewability of). Sustainability is defined as the ability to economically maintain an installed power capacity over the amortized life of a power plant. This is done by taking practical steps, such as drilling "make-up" wells as required to compensate for resource degradation. Renewability is defined as the ability to maintain an installed power capacity indefinitely without encountering any resource degradation. Typically, the renewable power capacity at a geothermal site is generally too small for commercial development of electrical power capacity, but may be adequate for district heating or other direct uses of the geothermal energy.

The cost in producing geothermal resources for electric generation is important (► Geothermal Power Economics). In particular, the levelized cost of power is the applicable measurement for the cost of geothermal energy. Unlike fossil fuel power plants, most of the capital costs are incurred upfront in the development of the resource. Power cost is an objective criterion that favors the geothermal solutions compared to other alternative energy sources. However, the costs are heavily tied to the resource and the need for make-up well drilling to maintain full generation capacity.

Geothermal Resources Worldwide, Direct Heat Utilization of

John W. Lund
Geo-Heat Center, Oregon Institute of Technology, Klamath Falls, OR, USA

Article Outline

Glossary
Definition of the Subject
Introduction
Direct-Use Temperature Requirements
Equipment
Economic Considerations
Energy Savings
Future Directions
Bibliography

Glossary

Agribusiness applications In the geothermal context, they are the heating of greenhouses and open ground for various crops, aquaculture ponds and raceways heating for various aquatic species, and the heating of animal pens and houses in an effort to increase production and shorting the growing cycle.

Balneology The science of healing qualities of baths, especially with natural mineral waters and the therapeutic use of natural warm or mineral winters.

District heating Heating of more than one building from a central heating plant with the heated fluid provided through a central distribution systems of pipes.

Heat exchanger A device for transferring heat from one fluid to another. The fluids are usually separated by conducting walls of metal or plastic.

Heat pump A device which, by the consumption of work or heat, effects the transport of heat between a lower temperature to a higher temperature source. The useful output is heat in conventional usage. The reverse process is called a refrigerator used for the removal of heat.

Joule (J) The SI unit for all forms of energy or work. It is equal to 1 W-s or 0.239 cal.

Spa A resort using mineral water for bathing, soaking, and drinking along with covering portions of the body with mineral muds for therapeutic purposes. Diet, exercise, and rest can also be part of the spa treatment plan.

Watt (W) A unit of power or energy produced over time, equivalent to 1 J/s, or 0.001341 horse power (hp).

Definition of the Subject

Direct or non-electric utilization of geothermal energy refers to the immediate use of the heat energy rather than to its conversion to some other form such as electrical energy. The primary forms of direct-use include heating swimming pools and baths, and for balneology (therapeutic use), space heating and cooling including district heating, agriculture (mainly greenhouse heating, crop drying, and some animal husbandry), aquaculture (mainly fish pond and raceway heating), providing heat for industrial processes, and heat pumps (for both heating and cooling). In general, the geothermal fluid temperatures required for direct heat use are lower than those for economic electric power generation, and as a result these resources are available in most countries.

Most direct-use applications use geothermal fluids in the low-to-moderate temperature range between 50°C and 150°C, and in general, the reservoir can be exploited by conventional water well drilling equipment. Low-temperature systems are also more widespread than high-temperature systems (above 150°C), so they are more likely to be located near potential users. In the USA, for example, of the 1,350 known or identified geothermal systems, 5% are above 150°C, and 85% are below 90°C [1]. In fact, almost every country in the world has some low-temperature systems, while only a few have accessible high-temperature systems.

Geothermal energy is a renewable energy since the tapped heat is continuously renovated by natural process of the Earth's interior, and the extracted geothermal fluids are replenished by natural recharge and by reinjection of the exhausted fluids, providing a sustainable development. Using geothermal minimizing the greenhouses gases and particulates that are produced from using fossil fuels, and also provides energy independence since it is a domestic resource. The environmental impact of direct-use of geothermal energy is negligible as in most cases, once the heat is extracted from the fluid, the spent fluid is reinjected back into the ground, thus preventing the release of harmful gasses and particulates.

Introduction

Traditionally, direct use of geothermal energy has been on small scale by individuals. More recent developments involve large-scale projects, such as district heating (Iceland and France), greenhouse complexes (Hungary and Russia), or major industrial use (New Zealand, Iceland, and the USA). Heat exchangers are also becoming more efficient and better adapted to geothermal projects, allowing use of lower temperature water and highly saline fluids. Heat pumps utilizing very low-temperature fluids (5–30°C) have extended geothermal developments into traditionally non-geothermal countries such as Canada, France, Switzerland, and Sweden, as well as areas of the mid-western and eastern USA. Most equipments used in these projects are of standard, off-the-shelf design and need only slight modifications to handle geothermal fluids [2, 3].

Worldwide [4], the installed capacity of direct geothermal utilization is 50,583 MWt, and the energy use is 438,071 TJ/year (121,686 GWh/year), distributed among 78 countries; the leading countries are presented in Table 1. This amounts to saving an equivalent 45.2 million tons of fuel oil per year (TOE) if it replaces electricity . The distribution of the energy use among the various types is listed in Table 2 and shown in Fig. 1 for the worldwide installed capacity, and Fig. 2 for the annual energy use. For comparison, the installed capacity in the USA (2010) is 12,611 MWt, and the annual energy use is 56,552 TJ (15,709 GWh), saving 20.2 million barrels of oils (3.04 million TOE) [5]. Internationally, the largest energy uses are for geothermal heat pumps (GHP) (49%), and swimming, bathing, and balneology (25%); and similar, in the USA, the largest use is for geothermal heat pumps (84%). In comparison, Iceland's largest geothermal energy use is 72% for district heating 17,483 TJ/year (4,857GWh/year) [6]. As can be seen from Tables 1and 2, heat pumps have low load factors (USA), whereas industrial

Geothermal Resources Worldwide, Direct Heat Utilization of. Table 1 The leading direct-use countries (2010)

Country	Energy use		Power MWt	Capacity Factor	Main applications
	TJ/year	GWh/year			
China	75,348	20,932	8,898	0.27	Bathing/district heating
USA	56,552	15,710	12,611	0.14	GHP
Sweden	45,301	12,585	4,460	0.32	GHP
Turkey	36,886	10,247	2,084	0.56	District heating
Japan	25,698	7,139	2,100	0.39	Bathing (onsens)
Iceland	24,361	6,768	1,826	0.42	District heating
France	12,929	3,592	1,345	0.30	District heating
Germany	12,764	3,546	2,485	0.16	Bathing/district heating
The Netherlands	10,699	2,972	1,410	0.24	GHP
Italy	9,941	2,762	867	0.36	Spas/space heating
Hungary	9,767	2,713	655	0.47	Spas/greenhouses
New Zealand	9,552	2,654	393	0.77	Industrial uses
Canada	8,873	2,465	1,126	0.25	GHP
Switzerland	7,715	2,143	1,061	0.23	GHP

Geothermal Resources Worldwide, Direct Heat Utilization of. Table 2 Summary of geothermal direct-use by category (2010)

Category	Utilization		Capacity (MWt)	Capacity factor
	(TJ/year)	(GWh/year)		
Geothermal heat pumps	214,782	59,662	35,236	0.19
Space heating	62,984	17,496	5,391	0.37
Greenhouse heating	23,264	6,462	1,544	0.48
Aquaculture pond heating	11,521	3,200	653	0.56
Agricultural drying	1,662	462	127	0.42
Industrial uses	11,746	3,263	533	0.70
Bathing and swimming	109,032	30,287	6,689	0.52
Cooling/snow melting	2,126	591	368	0.18
Others	956	266	41	0.73
Total	438,071	121,686	50,583	0.27

uses have high load factors (NZ) due to the more continuous annual use in industrial processing.

The Lindal diagram [7], named for Baldur Lindal, the Icelandic engineer who first proposed it, indicates the temperature range suitable for various direct-use activities (Fig. 3). Figure 4 indicates some of the worldwide direct-use applications along with their possible temperature range of use. Typically, the agricultural

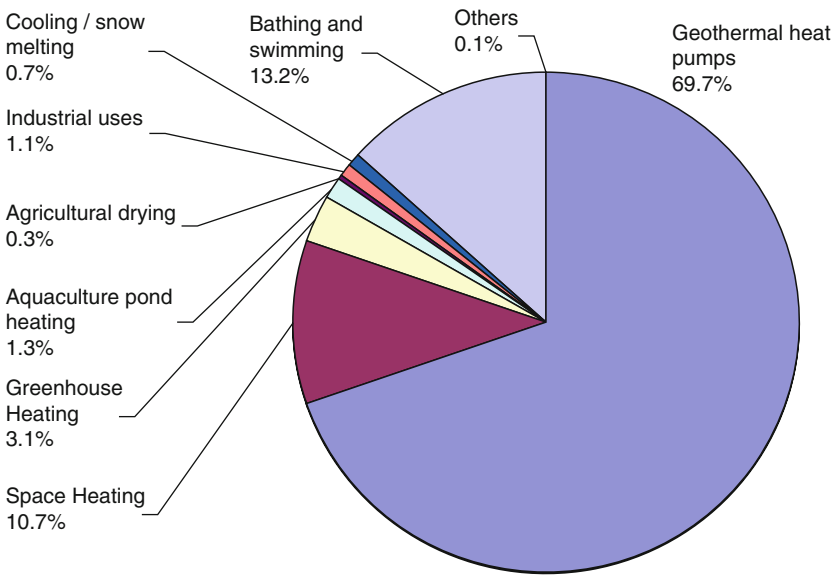

Geothermal Resources Worldwide, Direct Heat Utilization of. Figure 1
Distribution of direct-use installed capacity (MWt) in the world (2010)

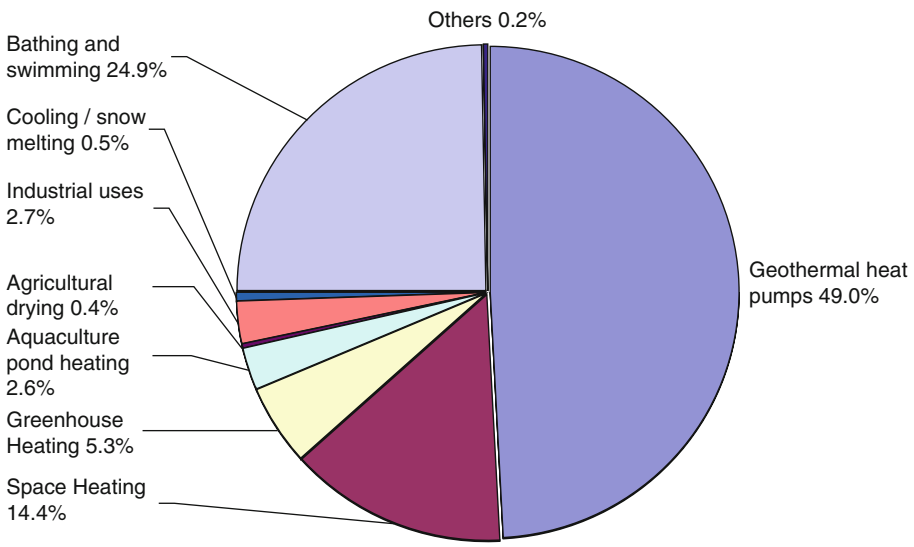

Geothermal Resources Worldwide, Direct Heat Utilization of. Figure 2
Distribution of direct-use annual energy use (TJ/year) in the world (2010)

and aquacultural uses require the lowest temperatures, with values from 25°C to 90°C. The amounts and types of chemicals, such as arsenic and dissolved gases such as boron, are a major problem with plants and animals; thus, heat exchangers are often necessary. Space heating requires temperatures in the range of 50–100°C, with 40°C useful in some marginal cases and ground-source heat pumps extending the range down to 5°C. Cooling and industrial processing normally require temperatures over 100°C. The leading user of geothermal

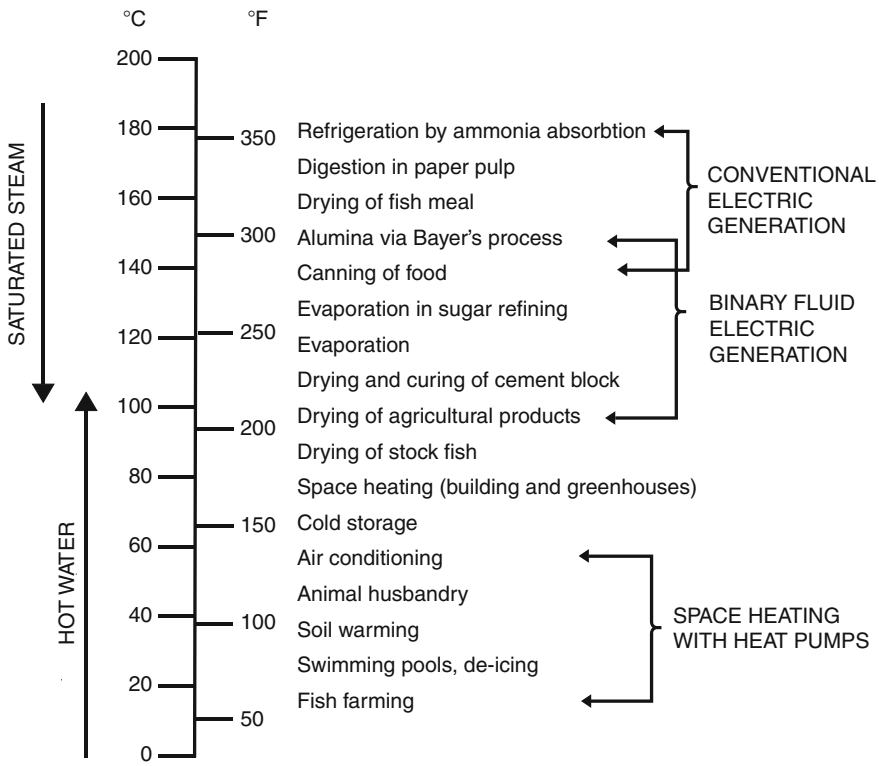

Geothermal Resources Worldwide, Direct Heat Utilization of. Figure 3
Lindal diagram

energy, in terms of market penetration, is Iceland, where more than 89% of the population enjoys geothermal heat in their homes from 30 municipal district heating services, and 54% of the country's total energy use is supplied by direct heat and electrical energy derived from geothermal resources [6].

Swimming, Bathing, and Balneology

People have used geothermal water and mineral waters for bathing and their health for many thousands of years. Balneology, the practice of using natural mineral water for the treatment and cure of disease, also has a long history. A spa originates at a location mainly due to the water from a spring or well. The water, with certain mineral constituents and often warm, give the spa certain unique characteristics that will attract customers. Associated with most spas is the use of muds (peoloids) which either are found at the site or are imported from special locations. Drinking and bathing in the water, and using the muds are thought to give certain health benefits to the user. Swimming pools have desirable temperature at 27°C; however, this will vary from culture to culture by as much as 5°C. If the geothermal water is higher in temperature, then some sort of mixing or cooling by aeration or in a holding pond is required to lower the temperature, or it can first be used for space heating, and then cascaded into the pool. If the geothermal water is used directly in the pool, then a flow-through process is necessary to replace the "used" water on a regular basis. In many cases, the pool water must be treated with chlorine; thus, it is more economical to use a closed loop for the treated water and have the geothermal water provide heat through a heat exchanger [8].

Romans, Chinese, Ottomans, Japanese, and central Europeans have bathed in geothermal waters for centuries. Today, more than 2,200 hot springs resorts in Japan draw 100 million guests every year, and the "return-to-nature" movement in the USA has revitalized many hot spring resorts.

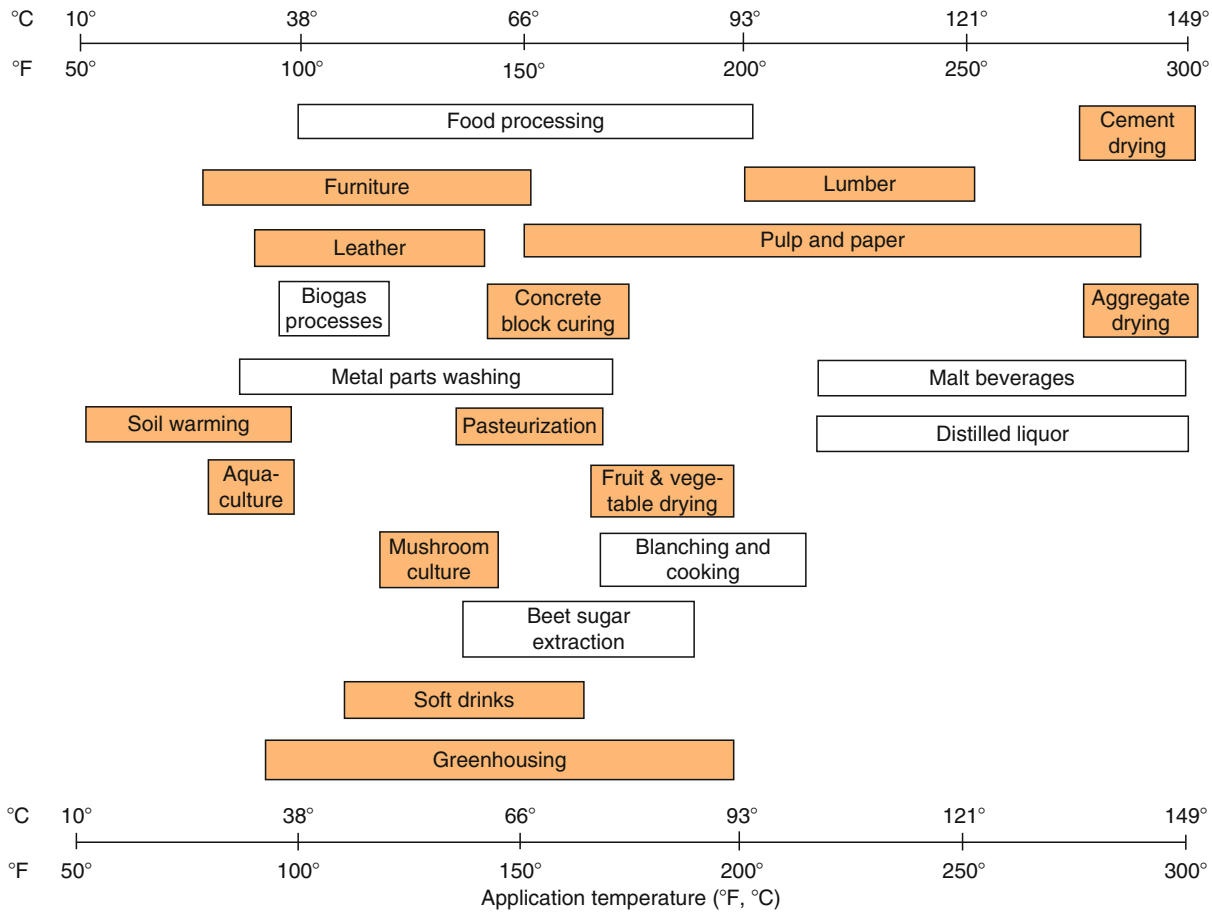

Geothermal Resources Worldwide, Direct Heat Utilization of. Figure 4
Examples of industrial applications of geothermal energy with the colored bars indicating those currently using geothermal energy in the world

The geothermal water at Xiaotangshan Sanitarium, northwest of Beijing, China, has been used for medical purposes for over 500 years. Today, the 50°C water is used to treat high blood pressure, rheumatism, skin disease, diseases of the nervous system, ulcers, and generally for recuperation after surgery. In Rotorua, New Zealand, at the center of the Taupo Volcanic Zone of North Island, the Queen Elizabeth Hospital was built during World War II for US servicemen and later became the national hospital for the treatment of rheumatic disease. The hospital has 200 beds, and outpatient service, and a cerebral palsy unit. Both acidic and basic geothermally heated mud baths treat rheumatic diseases.

In Beppu, on the southern island of Kyushu, Japan, the hot water and steam meet many needs: heating, bathing, cooking, industrial operations, agriculture research, physical therapy, recreational bathing, and even a small zoo [9]. The waters are promoted for "digestive system troubles, nervous troubles, and skin troubles." Many sick and crippled people come to Beppu for rehabilitation and physical therapy. There are also eight Jigokus (hot springs or geysers called "burning hells") in town, showing various geothermal phenomena, used as tourist attractions.

In the former Czechoslovakia, the use of thermal waters has been traced back before the occupation of the Romans and has had a recorded use of almost 1,000 years. Today, there are 60 spa resorts located mainly in Slovakia, visited by 460,000 patients usually for an average of three weeks each. These spas have old

and well-established therapeutic traditions. Depending on the chemical composition of the mineral waters and spring gas, availability of peat and sulfurous mud, and climatic conditions, each sanatorium is designated for the treatment of specific diseases. The therapeutic successes of these spas are based on centuries of healing tradition (balneology), systematically supplemented by the latest discoveries of modern medical science [10].

Bathing and therapeutic sites in the USA include: Saratoga Springs, New York; Warm Springs, Georgia; Hot Springs, Virginia; White Sulfur Springs, West Virginia; Hot Spring, Arkansas; Thermopolis, Wyoming; and Calistoga, California. The original use of these sites was by Indians, where they bathed and recuperated from battle as neutral ground. There are over 115 major geothermal spas in the USA with an annual energy use of 1,500 TJ [8].

Figures for this use are difficult to collect and quantify. Almost every country has spas and resorts that have swimming pools (including balneology), but many allow the water to flow continuously, regardless of use. As a result, the actual usage and capacity figures may be high. Undeveloped natural hot springs have not been included in the data. A total of 67 countries have reported bathing and swimming pool use, amounting to a worldwide installed capacity of 6,689 MWt and energy used of 109,032 TJ/year (30,287 GWh/year) based on data from country update papers from the World Geothermal Congress 2010 (WGC2010) in Bali, Indonesia [4].

Space Conditioning

Space conditioning includes both heating and cooling. Space heating with geothermal energy has widespread application, especially on an individual basis. Buildings heated from individual wells are popular in Klamath Falls, Oregon; Reno, Nevada, USA; and Taupo and Rotorua, New Zealand. Absorption space cooling with geothermal energy has not been popular because of the high-temperature requirements and low efficiency. However, newer units recently placed on the market report to use temperatures below 100°C efficiently. Geothermal heat pumps (groundwater and ground-coupled) have become popular in the USA, Canada, China, and Europe, used for both heating and cooling.

Downhole heat exchangers have been used for heating individual buildings using a closed loop of pipe in a well extracting only heat in Klamath Falls, Oregon, Reno, Nevada, Rotorua, New Zealand, and Izmir, Turkey (see the "Heat Exchanger" section for more details). An example of space heating and cooling with low-to-moderate temperature geothermal energy is the Oregon Institute of Technology in Klamath Falls, Oregon (Fig. 5). Here, 12 buildings (approximately 70,000 m^2 of floor space) are heated with water from three wells at 89°C. Up to 62 L/s of fluid can be provided to the campus, with the average heat utilization rate over 0.53 MWt and the peak at 5.6 MWt. In addition, a 541 kW (154 t) chiller requiring up to 38 L/s of geothermal fluid produces 23 L/s of chilled fluid at 7°C to meet the campus cooling base load (recently decommissioned) [11, 12].

Space heating is reported in 27 countries with an installed capacity of 752 MWt and annual energy use of 9,609 TJ (2,669 GWh) based on data from country update reports presented at WGC2010 in Bali, Indonesia [4].

District Heating

District heating involves the distribution of heat (hot water or steam) from a central location through a network of pipes to individual houses or blocks of buildings. The distinction between a district heating and space heating system is that space heating usually involves one geothermal well per structure, whereas district heating involves serving multiple buildings from a well or well field. The heat is used for space heating and cooling, domestic water heating, and industrial process heat. A geothermal well field is the primary source of heat; however, depending on the temperature, the district may be a hybrid system, which would include fossil fuel and/or heat pump peaking. An important consideration in district heating projects is the thermal load density, or the heat demand divided by the ground area of the district. A high heat density, generally above 1.2 GJ/h/ha or a favorability ratio (heat load available/heat load on the system) of 2.5 GJ/ha/year, is recommended. Often fossil fuel peaking is used to meet the coldest period, rather than drilling additional wells or pumping more fluids, as geothermal can usually meet 50% of the load 80–90% of the time, thus improving the efficiency and economics of the system [13]. Geothermal district heating systems are capital intensive. The principal costs are initial investment costs for production and injection wells,

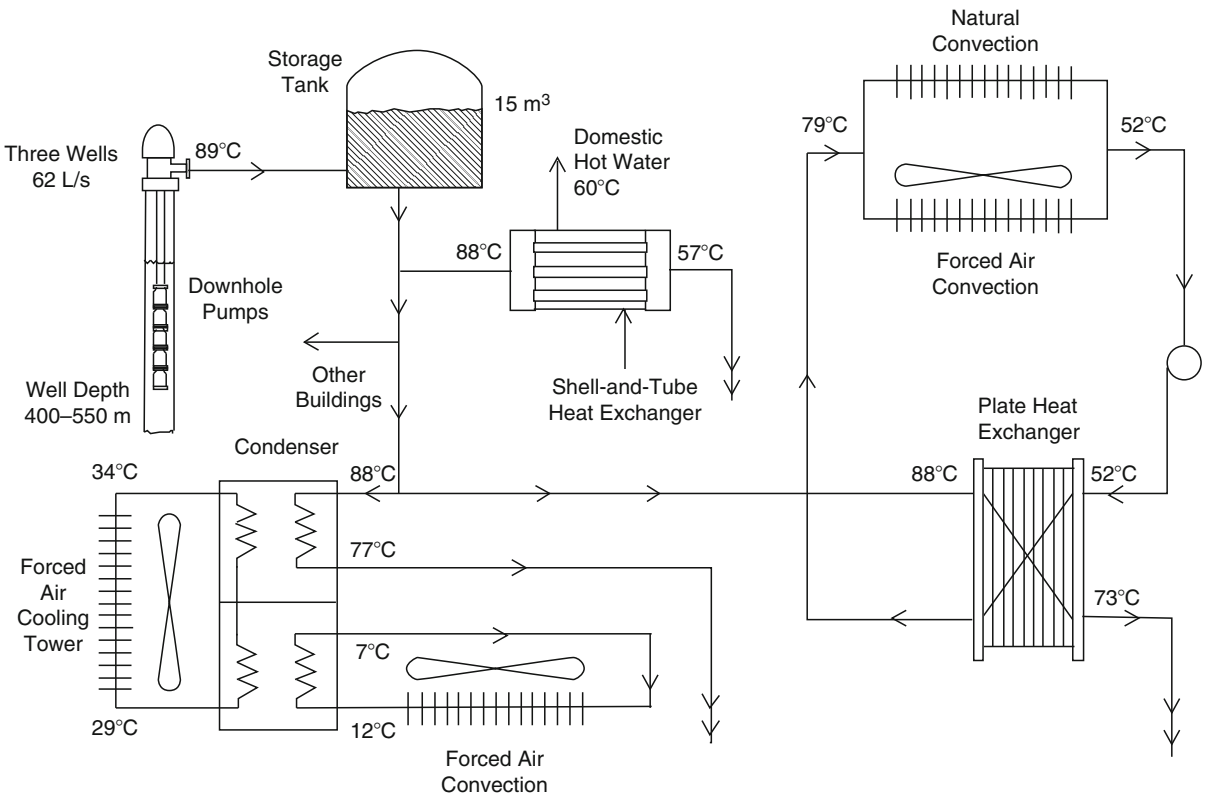

Geothermal Resources Worldwide, Direct Heat Utilization of. Figure 5
Oregon Institute of Technology heating and cooling system

downhole and circulation pumps, heat exchangers, pipelines and distribution network, flow meters, valves and control equipment, and building retrofit. The distribution network may be the largest single capital expense at approximately 35–75% of the entire project cost. Operating expenses, however, are in comparison lower and consists of pumping power, system maintenance, control, and management. The typical savings to consumers range from approximately 30–50% per year of the cost of natural gas.

Geothermal district heating systems are in operation in 24 countries, including large installations in Iceland, France, Poland, Hungary, Turkey, Japan, China, Romania, and the USA. The Warm Springs Avenue project in Boise, Idaho, dating back to 1892 and originally heating more than 400 homes, supplies hot water or steam through a network of pipes to individual dwellings or blocks of buildings [14]. The Reykjavik, Iceland, district heating system (Fig. 6) is probably the most famous [15, 16]. This system supplies heat for a population of around 200,000 people. The installed capacity of 1,240 MWt with peak load of 924 MWt is designed to meet the heating load to about −10°C; however, during colder periods, the increased load is met by large storage tanks and an oil-fired booster station. The total pipeline length is 3,846 km and almost 80 million cubic meters of water are delivered annually [6]. In France, production wells in sedimentary basins provide direct heat to more than 500,000 people in 170,000 dwellings from 34 projects with an installed capacity of 300 MWt and annual energy use of 4,900 TJ/year [17]. These wells provide from 40°C to 100°C water from depths of 1,500–2,000 m. In the Paris basin, a doublet system (one production and one injection well direction drilled from on site) provides 70°C water, with the peak load met by heat pumps and conventional fossil fuel burners (Fig. 7).

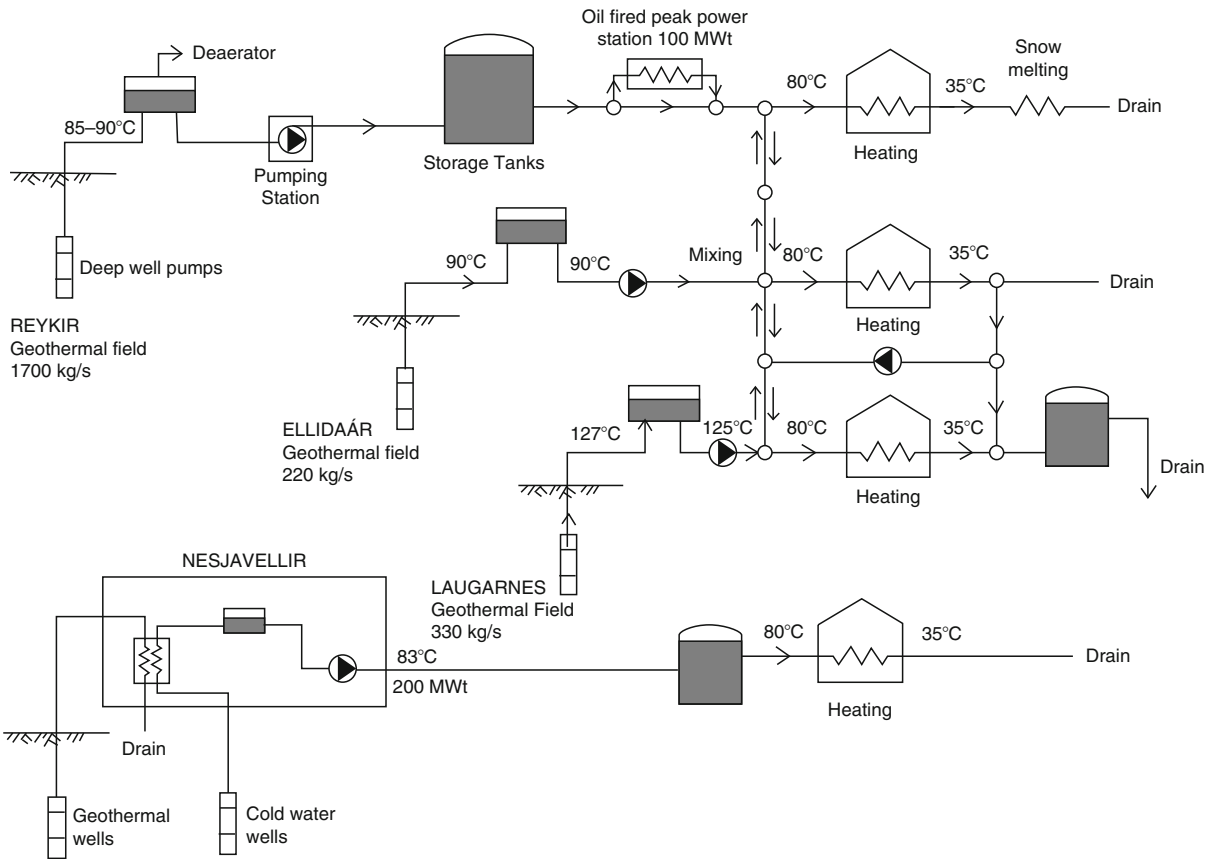

Geothermal Resources Worldwide, Direct Heat Utilization of. Figure 6
Reykjavik district heating system

The total installed capacity for the 24 countries is 4,639 MWt and the annual energy use is 53,375 TJ (12,857 GWh) as reported in WGC2010 [4].

Agribusiness Applications

Agribusiness applications (agriculture and aquaculture) are particularly attractive because they require heating at the lower end of the temperature range where there is an abundance of geothermal resources. Use of waste heat or the cascading of geothermal energy also has excellent possibilities. A number of agribusiness applications can be considered: greenhouse heating, aquaculture and animal husbandry facilities heating, soil warming and irrigation, mushroom culture heating and cooling, and biogas generation.

Numerous commercially marketable crops have been raised in geothermally heated greenhouses in Hungary, Russia, New Zealand, Japan, Iceland, China, Tunisia, and the USA. These include vegetables, such as cucumbers and tomatoes, flowers (both potted and bedded), house plants, tree seedlings, and cacti. Using geothermal energy for heating reduces operating costs (which can account for up to 35% of the product cost) and allows operation in colder climates where commercial greenhouses would not normally be economical.

The use of geothermal energy for raising catfish, shrimp, tilapia, eels, and tropical fish has produced crops faster than by conventional solar heating. Using geothermal heat allows better control of pond temperatures, thus optimizing growth (Fig. 8). Fish breeding has been successful in Japan, China, and the

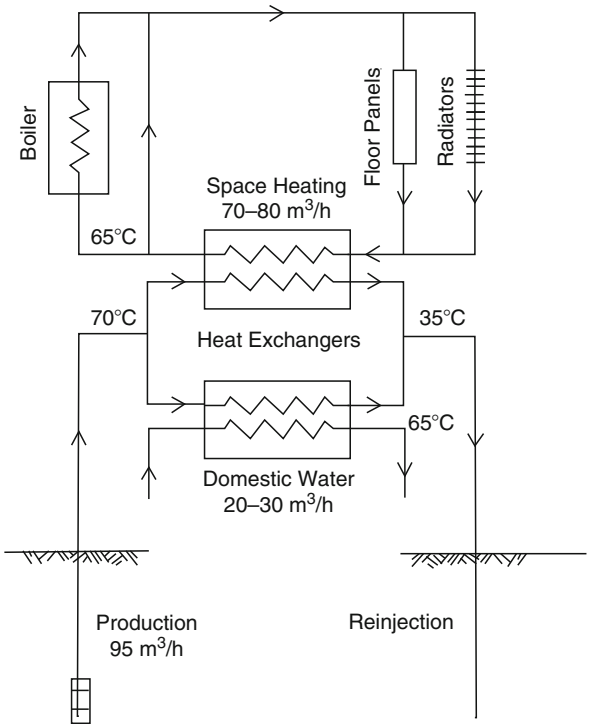

Geothermal Resources Worldwide, Direct Heat Utilization of. Figure 7
Melun l'Almont (Paris) doublet heating system

USA. A very successful prawn raising operation, producing 400 t of Giant Malaysian Freshwater Prawns per year at US $17 to 27/kg has been developed near the Wairakei geothermal field in New Zealand [18]. The most important factors to consider are the quality of the water and disease. If geothermal water is used directly, concentrations of dissolved heavy metals, fluorides, chlorides, arsenic, and boron must be considered, and if necessary, isolated by using a heat exchangers.

Livestock raising facilities can encourage the growth of domestic animals by a controlled heating and cooling environment. An indoor facility can lower mortality rate of newborn, enhance growth rates, control diseases, increase litter size, make waste management and collection easier, and in most cases improve the quality of the product. Geothermal fluids can also be used for cleaning, sanitizing and drying of animal shelters and waste, as well as assisting in the production of biogas from the waste.

Agribusiness uses of geothermal energy are reported in 38 countries with an installed capacity of 2,197 MWt and annual energy use of 34,785 TJ (9,662 GWh) according to WGC2010 reports [4].

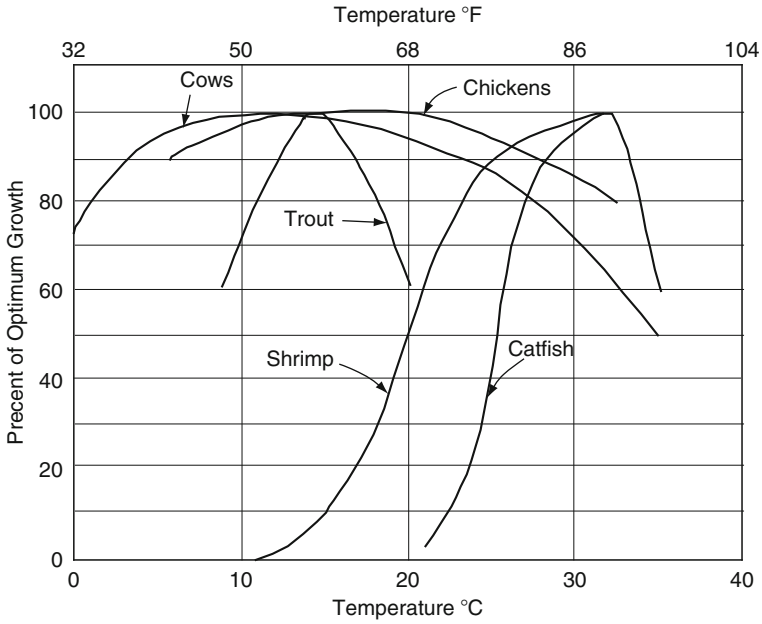

Geothermal Resources Worldwide, Direct Heat Utilization of. Figure 8
Effect of temperature on animal and fish growth

Approximately two thirds of the use is for greenhouse applications, with the remaining in aquaculture production.

Industrial Applications and Agricultural Drying

Although the Lindal diagram and the current direct-use diagram (Figs. 3 and 4) shows many industrial and process applications of geothermal energy, the world's uses are relatively few. The oldest industrial use is at Larderello, Italy, where boric acid and other borate compounds have been extracted from geothermal brines since 1790. Today, the two largest industrial uses are the diatomaceous earth drying plant in northern Iceland and a pulp, paper and, wood processing plant at Kawerau, New Zealand. Notable US examples are two onion dehydration plants in northern Nevada [19], and a sewage digestion facility in San Bernardino, California. Alcohol fuel production has been attempted in the USA; however, the economics were marginal and thus this industry has not been successful. With the recent increase in fossil fuel prices, there has been renewed interest in producing ethanol and biodiesel using geothermal energy [20].

A new development in the use of geothermal fluids is the enhanced heap leaching of precious metals in Nevada by applying heat to the cyanide process [21]. Using geothermal energy increases the efficiency of the process and extends the production into the winter months.

Drying and dehydration are important moderate-temperature uses of geothermal energy. Various vegetable and fruit products are feasible with continuous belt conveyors or batch (truck) dryers with air temperatures from 40°C to 100°C as shown in Fig. 9 [22]. Geothermally drying alfalfa, onions, garlic, pears, apples, and seaweed are examples of this type of direct-use.

An example of a small-scale food dehydrator is one located in northeastern Greece where 4 t of tomatoes are dried annually, using 59°C geothermal water to dry 14 kg/h on racks placed in a long tunnel drier. The tomatoes are then placed in olive oil for shipment and sale. The plant is only operated by three employees. At the other end of the spectrum is the large-scale onion and garlic drying facilities located in western Nevada, USA, employing 75 workers [23]. These continuous belt drier are fed 3,000–4,300 kg/h of onions at a moisture content of around 85%, and after 24 h, produce 500–700 kg/h of dried onions at moisture contents around 4%. These large belt driers are approximately 3.8 m wide and 60 m long.

A total of 20 countries reported industrial and agricultural drying applications from WGC2010 [4], with an installed capacity of 660 MWt and annual energy use of 13,408 TJ (3,724 GWh).

Industrial applications mostly need the higher temperature as compared to space heating, greenhouses, and aquaculture projects. Examples of industrial operations that use geothermal energy are: heap leaching

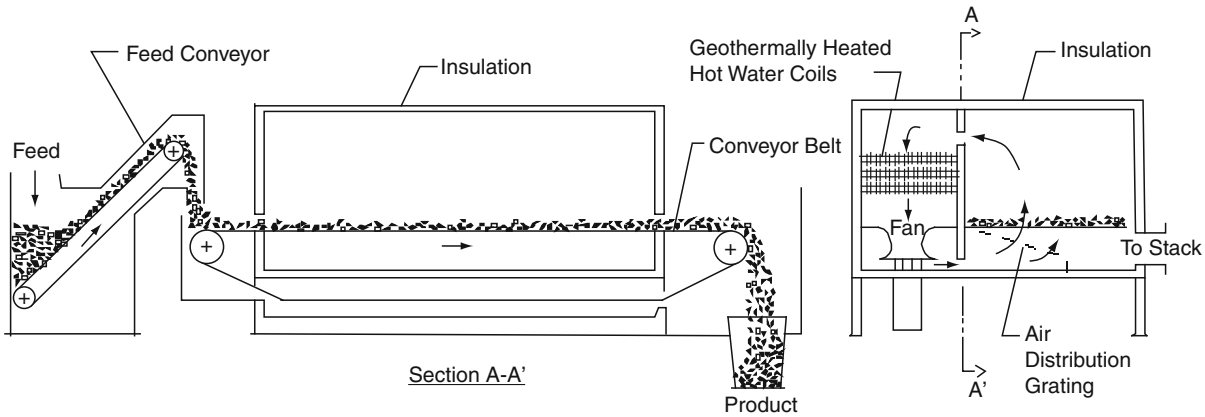

Geothermal Resources Worldwide, Direct Heat Utilization of. Figure 9
Continuous belt dehydration plant, schematic

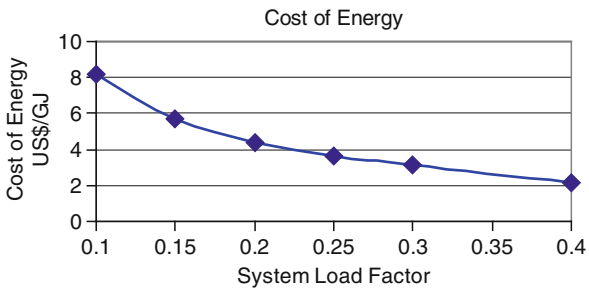

Geothermal Resources Worldwide, Direct Heat Utilization of. Figure 10
Load factor versus cost of energy (Modified from Rafferty [24])

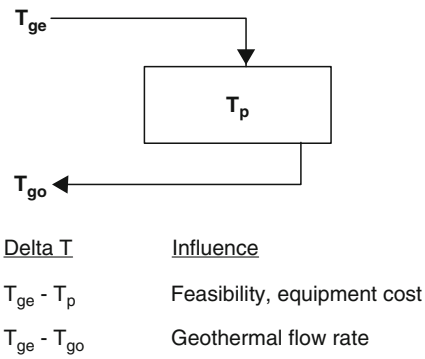

Geothermal Resources Worldwide, Direct Heat Utilization of. Figure 11
Fundamental direct-use temperature differences [25]

operations to extract precious metals in the USA (110°C), dehydration of vegetables in the USA (130°C), diatomaceous earth drying in Iceland (180°C), and pulp and paper processing in New Zealand (205°C). Drying and dehydration may be the two most important process uses of geothermal energy. A variety of vegetable and fruit products can be considered for dehydration at geothermal temperatures, such as onions, garlic, carrots, pears, apples, and dates. Industrial processes also make more efficient use of the geothermal resources as they tend to have high load factors in the range of 0.4–0.7. High load factors reduce the cost per unit of energy used as indicated in Fig. 10 [24].

Direct-Use Temperature Requirements

The design of mechanical systems involving heat transfer, such as direct-use geothermal systems, is heavily influenced by temperature. Temperature difference (delta T or ΔT) is particularly important as it frequently governs feasibility, equipment selection, and flow requirements for the system. Rafferty [25] addresses these issues with several "rules of thumb" that are described below. He introduces the material with the following discussion:

- Two primary temperature differences govern feasibility, flow requirements, and design of direct-use equipment. These are illustrated in a simplified way in Fig. 11. The first is the difference between the geothermal temperature entering the system (T_{ge}) and the process temperature (T_p). This difference determines whether or not the application will be feasible. For a direct-use project, the temperature of the geothermal entering the system must be above the temperature of the process in order to transfer heat out of the geothermal water and into the process (aquaculture pond, building, greenhouse, etc.). Beyond that, it must be sufficiently above the process to allow the system to be constructed with reasonably sized heat-transfer equipment. The greater the temperature difference between the geothermal resource and the process, the lower the cost of heat exchange equipment. The key question is how much above the process temperature does the geothermal need to be for a given application.

  The second temperature difference is the one between the geothermal entering the system and leaving the system (T_{ge} vs T_{go} in Fig. 11). This determines the geothermal flow rate necessary to meet the heat input requirement of the application. The greater the temperature difference between the entering and leaving temperatures, the lower the geothermal flow required. Obviously, the resource temperature is fixed. The process temperature plays a role as well since the leaving geothermal temperature cannot be lower than the process temperature to which it is providing heat. In addition, the specifics of the application and the heat transfer equipment associated with it also influence the temperature required. There are two broad groups of applications with similar characteristics in terms of heat transfer–aquaculture and pools, greenhouses, and building space heating.

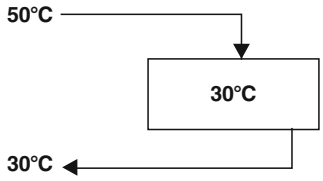

Flow requirement proportional to Tge - Tgo
At 40°C, flow = 2x
At 35°C, flow = 4x
At 32.5°C, flow = 8x

Geothermal Resources Worldwide, Direct Heat Utilization of. Figure 12
Direct pool/pond heating (Modified from Rafferty [25])

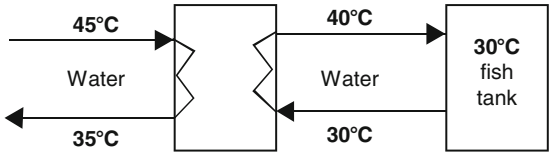

Minimum acceptable supply water temperature = process temp + 10°C
Maximum available supply water temperature = resource temp – 5°C
Minimum achievable geo leaving temp = process temp + 5°C

Geothermal Resources Worldwide, Direct Heat Utilization of. Figure 13
Pond/pool heating with heat exchanger (Modified from Rafferty [25]). Minimum acceptable supply water temperature = space temperature + 15°C. Maximum available supply water temperature = geothermal water temperature −10°C. Minimum achievable geothermal leaving temperature = return air temperature + 10°C

Pool and Aquaculture Pond Heating

Pond and pool heating is one of the simplest geothermal applications as it usually uses the geothermal water directly in the pond/pool to provide the required heat demand. This is illustrated in Fig. 12 [25], where 50°C geothermal water is supplied to heat the pool water to 30°C. Thus, the ΔT is 20°C, and using a flow rate of 10 L/s, the energy supplied would be 837 kW (3.0 GJ/h) (kW = L/s × ΔT × 4,184). If the supply temperature were instead 40°C, the flow rate would have to be doubled to provide the same amount of energy, and four times at 35°C, and eight times at 32.5°C.

If the geothermal water cannot be used directly due to health restrictions, then a heat exchanger is necessary to heat treated water for the pond or pool. Following the "rule of thumb" that the heated water to the pool should be 10°C above the pool temperature, then according to the previous example, 40°C secondary water would have to be provided to the pool. Using a heat exchanger between the geothermal water and the secondary water, an additional ΔT of 5°C is required to accommodate the heat transfer between the geothermal water and the secondary water. Thus, 45°C geothermal water would be required, and on the return side of the heat exchanger, the geothermal reject fluid should be 5°C above the return temperature of the secondary water. Thus, the rule of thumb is "10/5/5" as listed below in Fig. 13.

Greenhouse and Building Space Heating

Heating of greenhouses and building often involves the transfer of heat to the air in the structure using a water-to-air heat exchanger, called a coil, usually consisting of finned copper tubes [25]. The simplest version of this application is shown in Fig. 14. In order to heat the space, heated air should be delivered at least 15°C above the space temperature, 20°C shown in this example. Thus, the air should be delivered at 35°C or above from the water to the coil. The reason for the large difference, 15°C, is to limit the required quantity of air circulated to meet the heating requirements at reasonable levels. Also, as the difference becomes less, the fan and duct sizes become large, and the fan power consumption can be excessive. In addition, occupant comfort is important, as when the air supply drops below the 15°C difference, the temperature of the air approaches human skin temperature, which results in a "drafty" sensation to the occupants, even at the desired air temperature. In addition, the geothermal water delivered to the water-to-air heat exchangers should be at least 10°C above the required air temperature to limit the size and cost of this heat exchanger – usually a coil type. The same ΔT is required between the leaving geothermal water and the return air temperature. Thus, to supply 20°C heat to the room, a geothermal resource temperature would have to be at least 45°C. The "rule of thumb" for this condition is then "15/10/10" as shown in Fig. 14.

The example above assumes that the geothermal water is suitable to flow directly through the

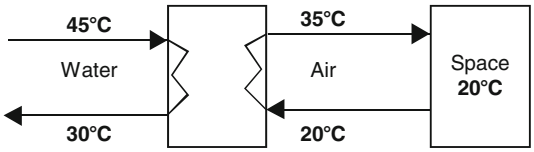

Minimum acceptable supply water temperature = space temp. + 15°C
Maximum available supply water temperature = geo. water temp. – 10°C
Minimum achievable geo. leaving temperature = return air temp. + 10°C

Geothermal Resources Worldwide, Direct Heat Utilization of. Figure 14
Space heating without isolation heat exchanger (Modified from Rafferty [25]). Supply air to space air = 15°C. Supply air to space air = 15°C. Water/air heat exchanger = supply water to supply air of 10°C. Water/water heat exchanger = supply water to supply water of 5°C

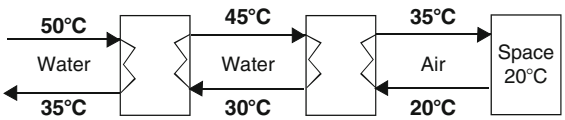

Supply air to space air = 15°C
Water/air heat exchanger = supply water to supply air of 10°C
Water/water heat exchanger = supply water to supply water of 5°C

Geothermal Resources Worldwide, Direct Heat Utilization of. Figure 15
Space heating 15/10/5 rule with geothermal isolation plate heat exchanger (Modified from Rafferty [25])

water-to-air heat exchanger (coil); however, if hydrogen sulfide is present, then this gas will attack copper and solder in the coil and cause leakage and failure to the unit. Thus, in the case where the geothermal must be isolated from the heating system equipment, a plate heat exchanger is normally placed between the two circuits to protect the heating equipment [25]. A plate heat exchanger is then added to the left side of the equipment shown in Fig. 14 and resulting in the configuration shown in Fig. 15. All the temperatures shown in Fig. 14 are still valid; the difference is that the plate heat exchangers will require additional temperature input to maintain the space (home) temperature of 20°C. As in the previous example, a ΔT of 5°C is required between the geothermal supply and the output from the secondary water. Thus, the new geothermal temperature required to meet the needs of the system is 50°C. The return geothermal water can only be cooled to 35°C as a result of the intermediate water loop return temperature of 30°C and the required 5°C ΔT. This then provides of rule of thumb of "15/10/5" as described below Fig. 15.

In summary, the following is provided by Rafferty [25]:

- All of the rules of thumb discussed here are exactly that. It is possible in all cases to "bend the rules," and design systems and equipment for temperatures closer than the guidelines provided above. The values provided here are intended for initial evaluation of applications by those not in the practice of designing heating systems on a regular basis. The guidelines cited apply to new systems using commercially manufactured equipment. Homemade heat exchangers or existing equipment selected for water temperatures well above available geothermal temperature would require additional analysis.

Equipment

Standard equipment is used in most direct-use projects, provided allowances are made for the nature of geothermal water and steam. Temperature is an important consideration, so is water quality. Corrosion and scaling caused by the sometimes unique chemistry of geothermal fluids may lead to operating problems with equipment components exposed to flowing water and steam. In many instances, fluid problems can be designed out of the system. One such example concerns dissolved oxygen, which is absent in most geothermal waters, except perhaps the lowest temperature waters. Care should be taken to prevent atmospheric oxygen from entering district heating waters, for example, by proper design of storage tanks. The isolation of geothermal water by installing a heat exchanger may also solve this and similar water quality–derived problems. In this case, a clean secondary fluid is then circulated through the used side of the system as shown in Fig. 16.

The primary components of most low-temperature direct-use systems are downhole and circulation pumps, transmission and distribution pipelines, peaking or backup plants, and various forms of heat extraction equipment (Fig. 16). Fluid disposal is either surface or subsurface (injection). A peaking system may be

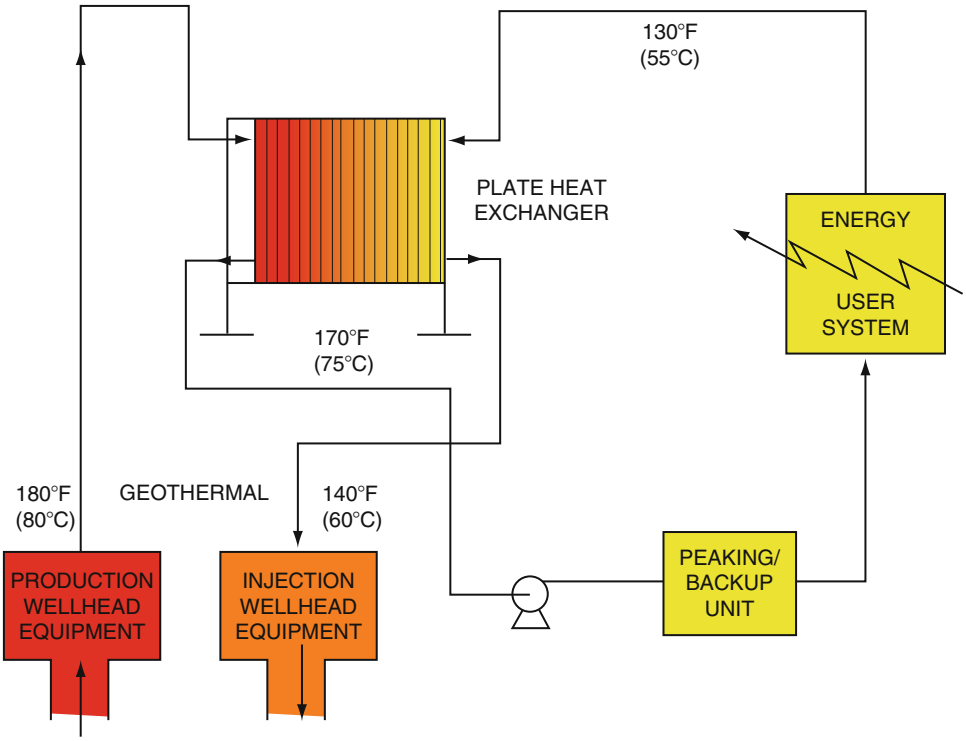

Geothermal Resources Worldwide, Direct Heat Utilization of. Figure 16
Geothermal direct-utilization system using a heat exchanger

necessary to meet maximum load. This can be done by increasing the water temperature or by providing tank storage (such as done in most of the Icelandic district heating systems). Both options mean that fewer wells need to be drilled thus requiring less geothermal fluid. When the geothermal water temperature is warm (below 50°C), heat pumps are often used. The equipment used in direct-use projects represents several units of operations. The major units will now be described in the same order as seen by geothermal waters produced for district heating. Detailed discussion of equipment design and use can be found in Lund et al. [26].

Downhole Pumps

Unless the well is artesian, downhole pumps are needed, especially in large-scale direct utilization system. Downhole pumps may be installed not only to lift fluid to the surface, but also to prevent the release of gas and the resultant scale formation. The two most common types are: lineshaft pump systems and submersible pump systems.

The lineshaft pump system (Fig. 17) consists of a multistage downhole centrifugal pump, a surface mounted motor, and a long driveshaft assembly extending from the motor to the pump bowls. Most are enclosed, with the shaft rotating within a lubrication column which is centered in the production tubing. This assembly allows the bearings to be lubricated by oil as hot water may not provide adequate lubrication. A variable-speed drive set just below the motor on the surface can be used to regulate flow instead of just turning the pump on and off.

The electric submersible pump system (Fig. 18) consists of a multistage downhole centrifugal pump, a downhole motor, and a seal section (also called a protector) between the pump and motor, and electric cable extending from the motor to the surface electricity supply.

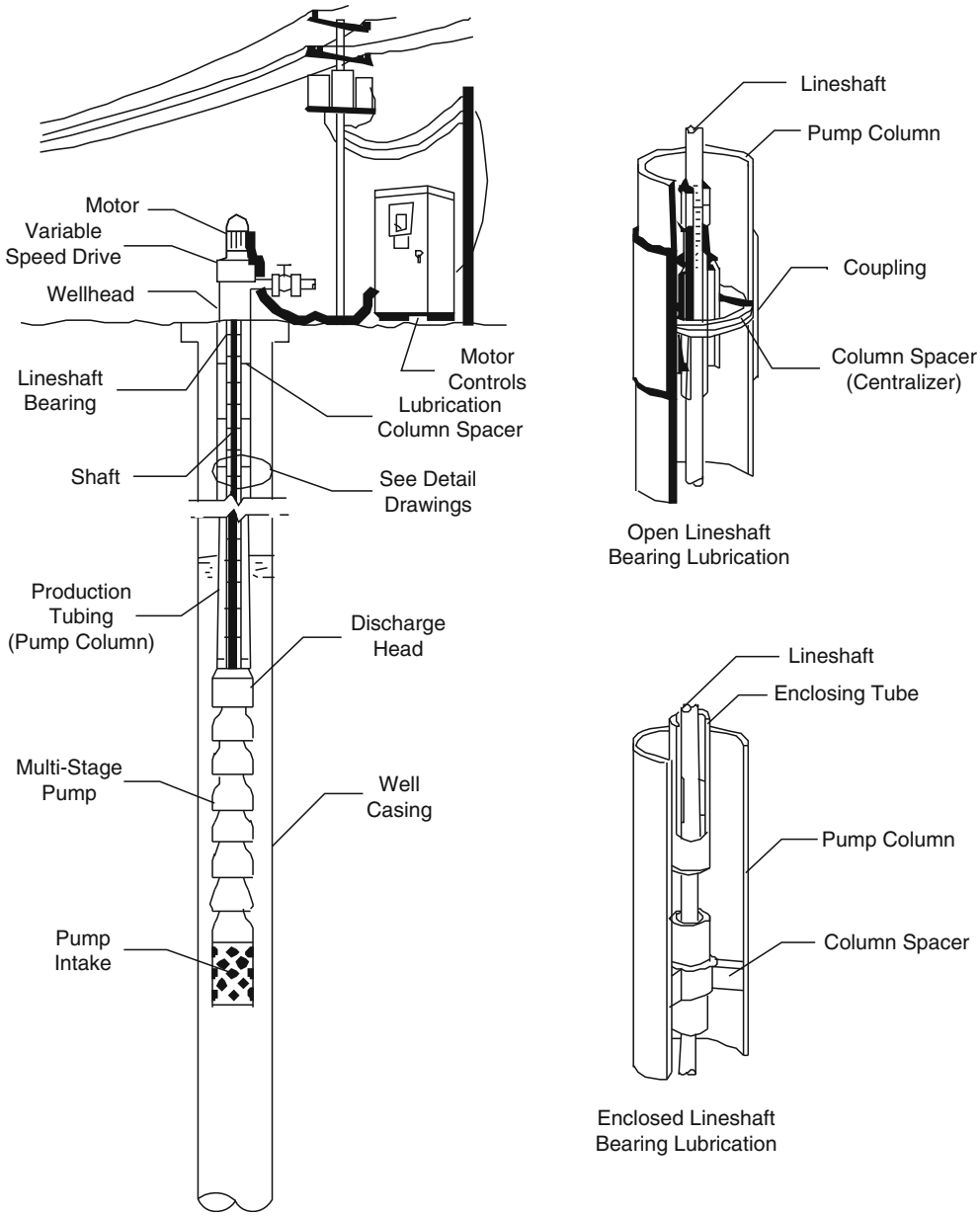

Geothermal Resources Worldwide, Direct Heat Utilization of. Figure 17
Lineshaft pump

Both types of downhole pumps have been used for many years for cold water pumping and more recently in geothermal wells (lineshafts have been used on the Oregon Institute of Technology campus in 89°C water for almost 60 years). If a lineshaft pump is used, special allowances must be made for the thermal expansion of various components and for oil lubrication of the bearings [27]. The lineshaft pumps are preferred over the submersible pump in conventional geothermal applications for two main reasons: the lineshaft pump cost less, and it has a proven track record. However, for setting depths exceeding about 250 m, a submersible pump is required.

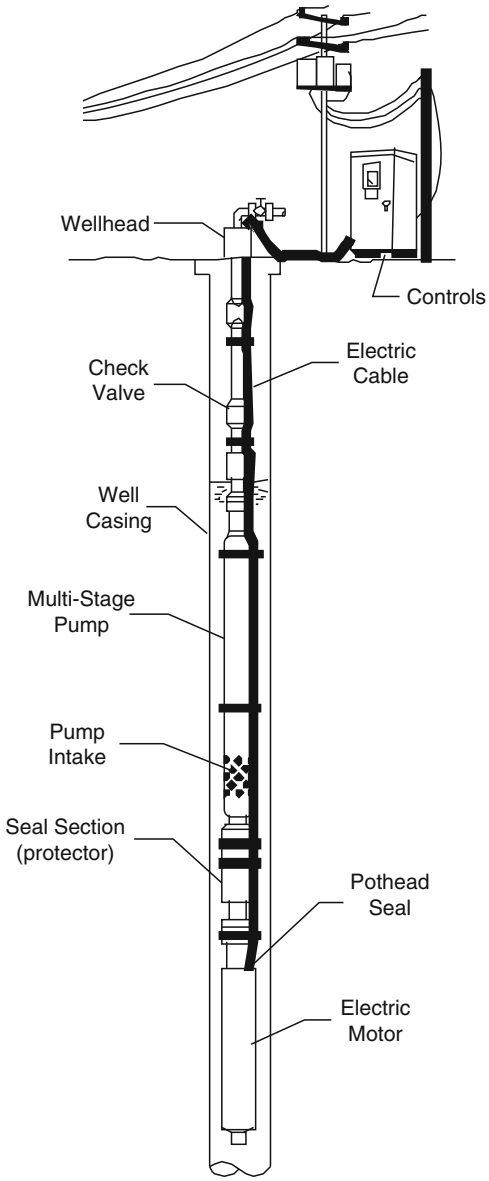

Geothermal Resources Worldwide, Direct Heat Utilization of. Figure 18
Submersible pump

Piping

The fluid state in transmission lines of direct-use projects can be liquid water, steam vapor, or a two-phase mixture. These pipelines carry fluids from the wellhead to either a site of application or a steam-water separator. Thermal expansion of metallic pipelines heated rapidly from ambient to geothermal fluid temperatures (which could vary from 50°C to 200°C) causes stress that must be accommodated by careful engineering design.

The cost of transmission lines and the distribution networks in direct-use projects is significant. This is especially true when the geothermal resource is located at great distance from the main load center; however, transmission distances of up to 60 km have proven economical for hot water (i.e., the Akranes project in Iceland [28], where asbestos cement covered with earth has been successful (see Fig. 20 later).

Carbon steel is now the most widely used material for geothermal transmission lines and distribution networks, especially if the fluid temperature is over 100°C. Other common types of piping material are fiberglass reinforced plastic (FRP) and asbestos cement (AC). The latter material, used widely in the past, cannot be used in many systems today due to environmental concerns; thus, it is no longer available in many locations. Polyvinyl chloride (PVC) piping is often used for the distribution network, and for uninsulated waste disposal lines where temperatures are well below 100°C. Cross-linked polyethylene pipe (PEX) have become popular in recent years as they can tolerate temperatures up to 100°C and still take pressures up to 550 kPa. However, PEX pipe is currently only available in sizes less than 5 cm in diameter. Conventional steel piping requires expansion provisions, either bellows arrangements or by loops. A typical piping installation would have fixed points and expansion points about every 100 m. In addition, the piping would have to be placed on rollers or slip plates between points. When hot water metallic pipelines are buried, they can be subjected to external corrosion from groundwater and electrolysis. They must be protected by coatings and wrappings. Concrete tunnels or trenches have been used to protect steel pipes in many geothermal district heating systems. Although expensive (generally over US $300 per meter of length), tunnels and trenches have the advantage of easing future expansion, providing access for maintenance and a corridor for other utilities such as domestic water, waste water, electrical cables, phone lines, etc.

Supply and distribution systems can consist of either a single-pipe or a two-pipe system. The single-pipe is a once-through system where the fluid is disposed of after use. This distribution system is generally preferred when the geothermal energy is abundant and

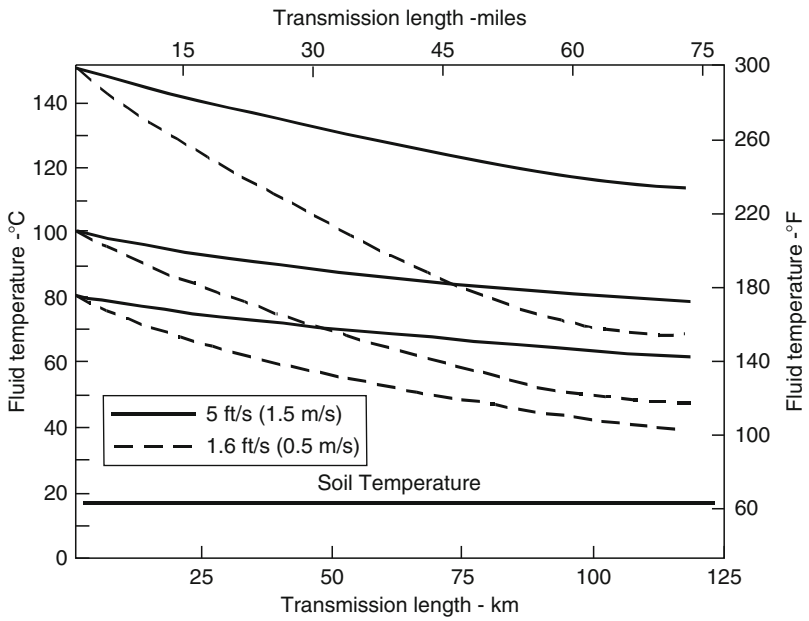

Geothermal Resources Worldwide, Direct Heat Utilization of. Figure 19
Temperature drop in hot water transmission line

the water is pure enough to be circulated through the distribution system. In a two-pipe system, the fluid is recirculated so the fluid and residual heat are conserved. A two-pipe system must be used when mixing of spent fluids is called for, and when the spent cold fluids need to be injected into the reservoir. Two-pipe distribution systems cost typically 20–30% more than single-piped systems.

The quantity of thermal insulation of transmission lines and distribution networks will depend on many factors. In addition to minimize the heat loss of the fluid, the insulation must be waterproof and water tight. Moisture can destroy the value of any thermal insulation and cause rapid external corrosion of metallic pipe. Above ground and overhead pipeline, installations can be considered in special cases. Considerable insulation is achieved by burying hot water pipelines. For example, burying bare steel pipe results in a reduction in heat loss of about one third as compared to aboveground in still air. If the soil around the buried pipe can be kept dry, then the insulation value can be retained. Carbon steel piping can be insulated with polyurethane foam, rock wool, or fiberglass. Belowground, such pipes should be protected with polyvinyl chloride (PVC) jacket; aboveground, aluminium can be used. Generally, 2.5–10 cm of insulation is adequate. In two-pipe systems, the supply and return lines are usually insulated; whereas, in single-pipe systems, only the supply line is insulated.

At flowing conditions, the temperature loss in insulated pipelines is in the range of 0.1–1.0°C/km, and in uninsulated lines, the loss is 2–5°C/km (in the approximate range of 5–15 L/s flow for 15-cm diameter pipe) [29]. It is less for larger diameter pipes. For example, less than 2°C loss is experienced in the new aboveground 29 km long and 80 and 90 cm diameter line (with 10 cm of rock wool insulation) from Nesjavellir to Reykjavik in Iceland. The flow rate is around 560 L/s and takes 7 h to cover the distance. Uninsulated pipe costs about half of insulated pipe, and thus is used where temperature loss is not critical. Pipe material does not have a significant effect on heat loss; however, the flow rate does. At low flow rates (off peak), the heat loss is higher than as greater flows. Figure 18 shows fluid temperatures, as a function of distance, in a 45-cm diameter pipeline, insulated with 50 cm of urethane foam.

Several examples of aboveground and buried pipeline installations are shown in Fig. 20.

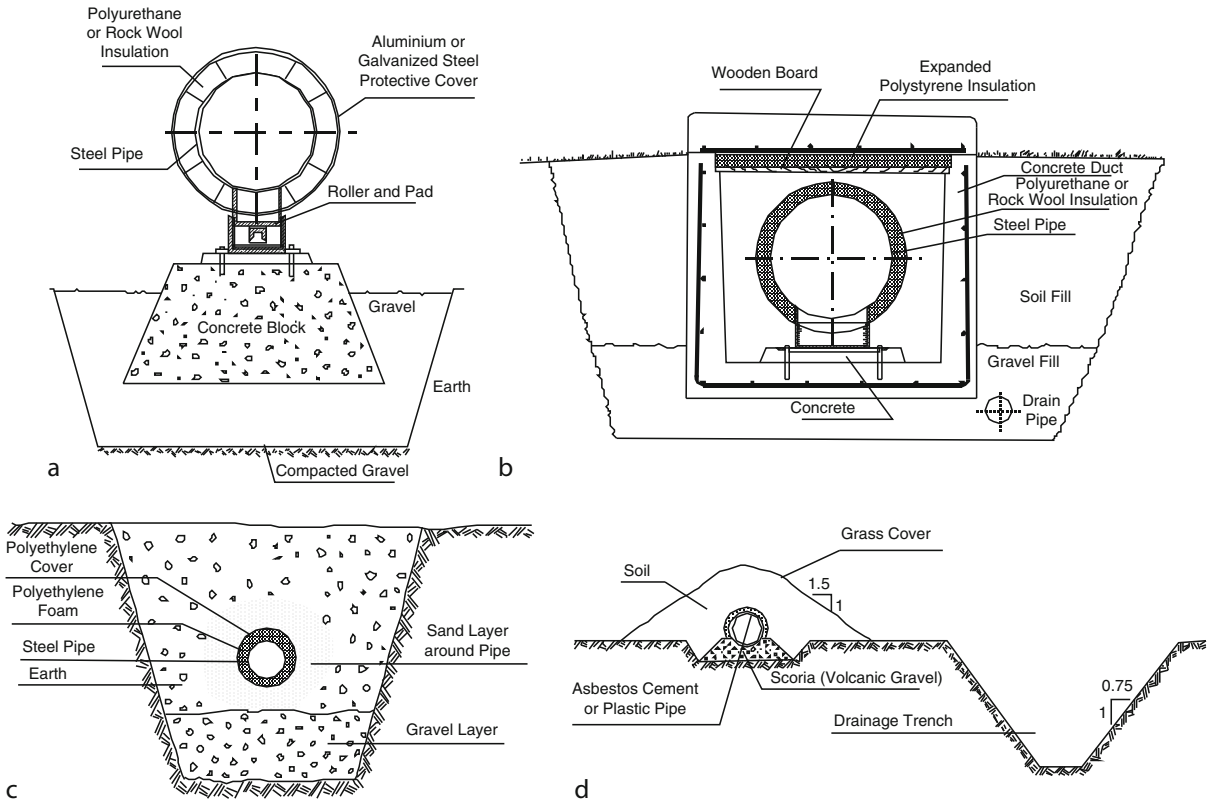

Geothermal Resources Worldwide, Direct Heat Utilization of. Figure 20
Examples of above and below ground pipelines: (**a**) aboveground pipeline with sheet metal cover, (**b**) steel pipe in concrete tunnels, (**c**) steel pipe with polyurethane insulation and polyethylene cover, and (**d**) asbestos cement pipe with earth and grass cover

Steel piping is shown in most case, but FRP or PVC can be used in low-temperature applications. Aboveground pipelines have been used extensively in Iceland, where excavation in lava rock is expensive and difficult; however, in the USA, below ground installations are more common to protect the line from vandalism and to eliminate traffic barriers. A detailed discussion of these various installations can be found in Gudmundsson and Lund [2].

Heat Exchangers

The principal heat exchangers used in geothermal systems are the plate, shell-and-tube, and downhole types. The plate heat exchanger consists of a series of plates with gaskets held in a frame by clamping rods (Fig. 21). The countercurrent flow and high turbulence achieved in plate heat exchangers provide for efficient thermal exchange in a small volume.

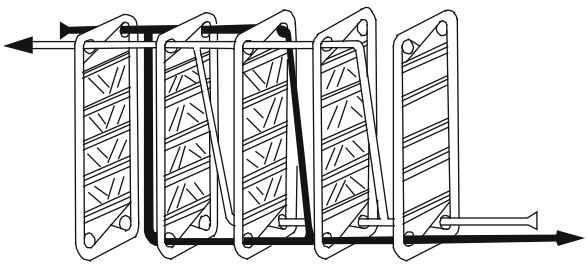

Geothermal Resources Worldwide, Direct Heat Utilization of. Figure 21
Plate heat exchanger

In addition, they have the advantage when compared to shell-and-tube exchangers, of occupying less space, can easily be expanded when addition load is added, and cost 40% less. The plates are usually made of stainless steel; although, titanium is used when the fluids are especially corrosive. Plate heat exchangers are commonly used in geothermal heating situations worldwide.

Shell-and-tube heat exchangers may be used for geothermal applications but are less popular due to problems with fouling, greater approach temperature (difference between incoming and outgoing fluid temperature), and the larger size.

Downhole heat exchangers eliminate the problem of disposal of geothermal fluid since only heat is taken from the well. However, their use is limited to small heating loads such as the heating of individual homes, a small apartment house or business. The exchanger consists of a system of pipes or tubes suspended in the well through which secondary water is pumped or allowed to circulate by natural convection (Fig. 22). In order to obtain maximum output, the well must be

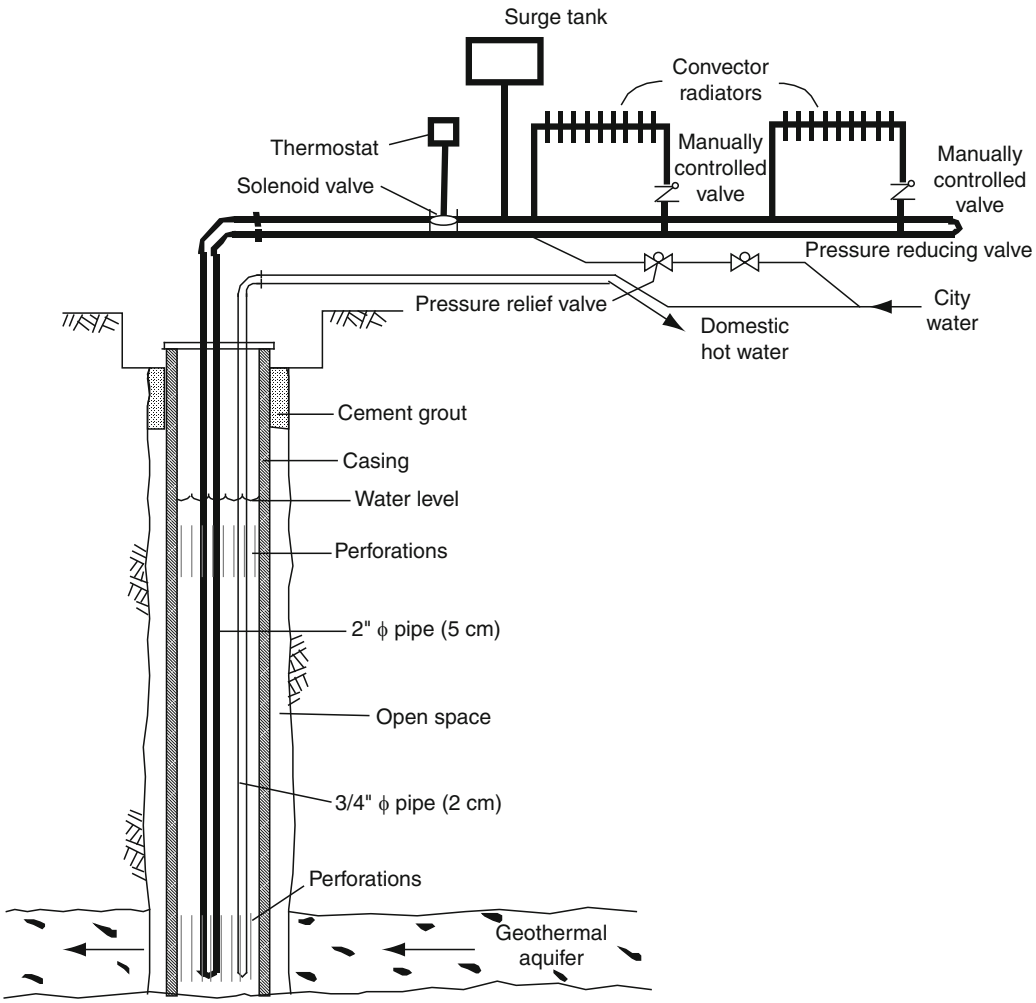

Geothermal Resources Worldwide, Direct Heat Utilization of. Figure 22
Downhole heat exchanger (typical of Klamath Falls, Oregon)

designed to have an open annulus between the wellbore and casing, and perforations above and below the heat exchanger surface. Natural convection circulates the water down inside the casing through the lower perforations, up in the annulus, and back inside the casing through the upper perforations [30, 31]. The use of a separate pipe or promoter has proven successful in older wells in New Zealand to increase the vertical circulation [32].

Heat Pumps

At the present time, ground-coupled and groundwater (often called ground-source or geothermal) heat pump systems are being installed in great numbers in the USA, Canada, Switzerland, Sweden, Austria, and Germany [4, 33]. Groundwater aquifers and soil temperatures in the range of 5–30°C are being used in these systems. Geothermal heat pumps (GHP) utilize groundwater in wells (open loop) or by direct ground coupling (closed loop) with vertical or horizontal heat exchangers. Just about every state in the USA, especially in the midwestern and eastern states are utilizing these systems in part subsidized by public and private utilities. It is estimated that almost 3.0 million units (12 kW) are installed in 43 countries worldwide, with most in Europe, Canada and the USA. Annual growth rates are around 17%, the fastest of all the direct-use applications.

Like refrigerators, heat pumps operate on the basic principle that fluid absorbs heat when it evaporates into a gas, and likewise gives off heat when it condenses back into a liquid. A geothermal heat pump system can be used for both heating and cooling. The types of heat pumps that are adaptable to geothermal energy are the water-to-air and the water-to-water. Heat pumps are available with heating capacities of less than 3 kW to over 1,500 kW.

GHPs use the relatively constant temperature of the earth to provide heating, cooling and domestic hot water for homes, schools, government and commercial buildings. A small amount of electricity input is required to run a compressor; however, the energy output is in the order of four times this input. These "machines" cause heat to flow "uphill" from a lower to higher temperature location – really nothing more than a refrigeration unit that can be reversed. "Pump" is used to described the work done, and the temperature difference called the "lift" – the greater the lift, the greater the energy input. The technology is not new, as Lord Kelvin developed the concept in 1852, which was then modified as a GHP by Robert Webber in the 1940s. They gained commercial popularity in the 1960s and 1970s. See Fig. 23 for diagrams of typical GHP operation.

GHPs come in two basic configurations: ground-coupled (closed loop) which are installed horizontally, and vertically and groundwater (open loop) systems, which are installed in wells and lakes. The type chosen depends upon the soil and rock type at the installation, the land available and/or if a water well can be drilled economically or is already on site. As shown in Fig. 23, a desuperheater can be provided to use reject heat in the summer and some input heat in the winter for the domestic hot water heating.

In the ground-coupled system, a closed loop of pipe, placed either horizontally (1–2 m deep) or vertically (50–100 m deep) is placed in the ground and a water-antifreeze solution is circulated through the plastic pipes (high density polyethylene) to either collect heat from the ground in the winter or reject heat to the ground in the summer [34]. The open loop system uses ground water or lake water directly in the heat exchanger and then discharges it into another well, into a stream or lake, or on the ground (say for irrigation), depending upon local laws.

The efficiency of GHP units are described by the Coefficient of Performance (COP) in the heating mode and the Energy Efficiency Ratio (EER) in the cooling mode (COP_h and COP_c, respectively, in Europe) which is the ratio of the output thermal energy divided by the input energy (electricity for the compressor) and varies from 3 to 6 with present equipment (the higher the number the better the efficiency). Thus a COP of 4 would indicate that the unit produced four units of heating energy for every unit of electrical energy input. In comparison, an air-source heat pump has a COP of around 2 and is dependent upon backup electrical energy to meet peak heating and cooling requirements. In Europe, this ratio is sometimes referred to as the

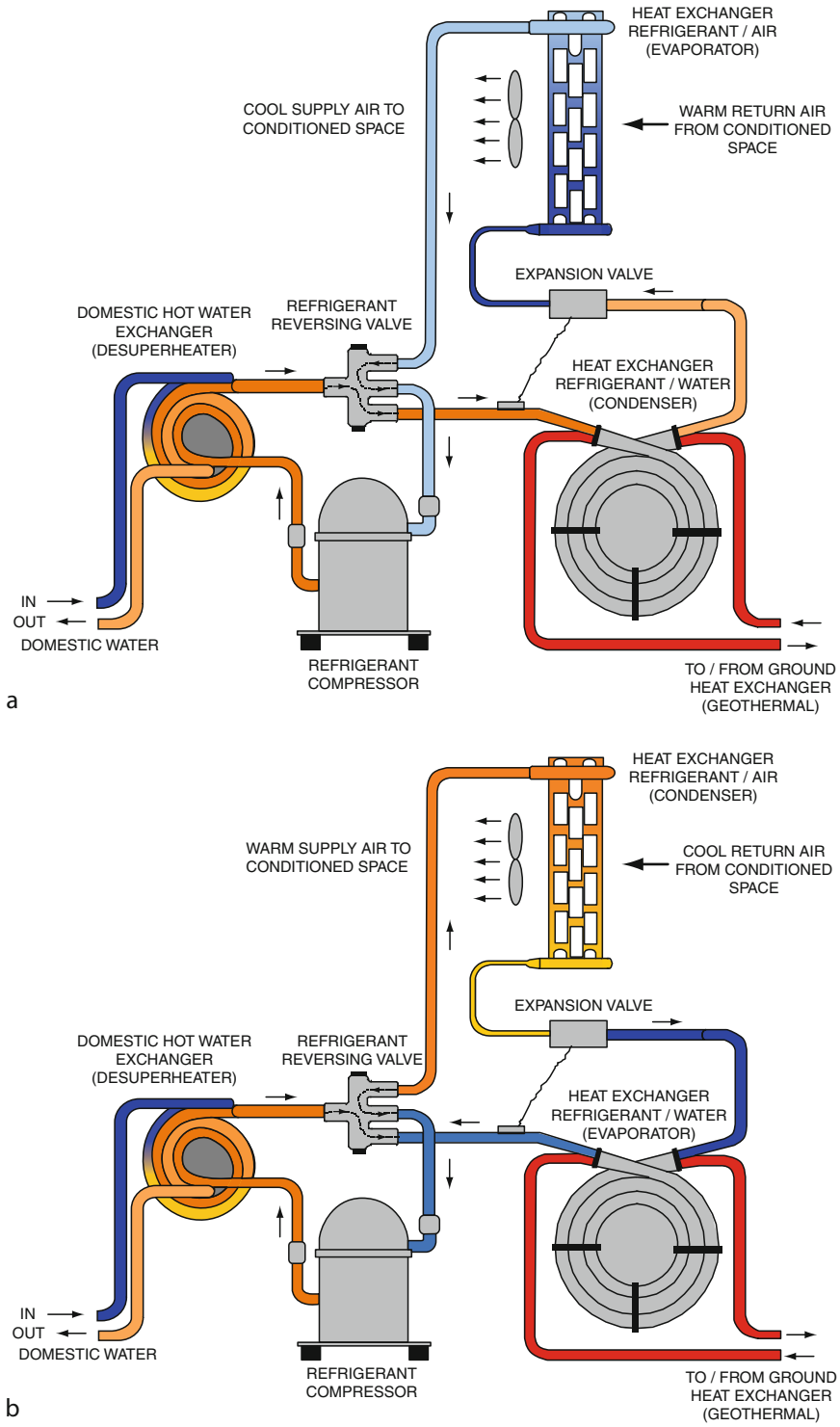

Geothermal Resources Worldwide, Direct Heat Utilization of. Figure 23
(**a**) GHP in the cooling cycle (From Oklahoma State University). (**b**) GHP in the heating cycle (From Oklahoma State University)

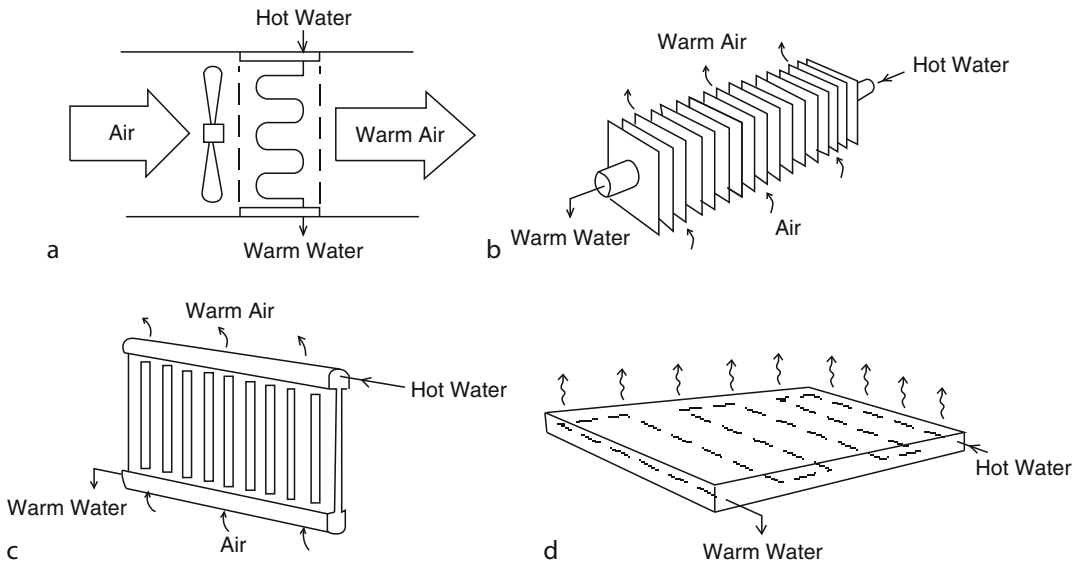

Geothermal Resources Worldwide, Direct Heat Utilization of. Figure 24
Convectors: (**a**) forced air, (**b**) material convection (finned tube), (**c**) natural convection (radiator), and (**d**) floor radiant panel

"Seasonal Performance Factor" ("Jahresarbeitszahl" in German) and is the average COP over the heating and cooling season, respectively, and takes into account system properties (see Curtis et al. [33], Lund et al. [35], and Kavanauagh and Rafferty [36] for more background material).

Convectors

Heating of individual rooms and buildings is achieved by passing geothermal water (or a heated secondary fluid) through heat convectors (or emitters) located in each room [26]. The method is similar to that used in conventional space heating systems. Three major types of heat convectors are used for space heating: (1) forced air, (2) natural air flow using hot water or finned tube radiators, and (3) radiant panels (Fig. 24). All these can be adapted directly to geothermal energy or converted by retrofitting existing systems.

Refrigeration

Cooling can be accomplished from geothermal energy using lithium bromide and ammonia absorption refrigeration systems [26, 37]. The lithium bromide system is the most common because if uses water as the refrigerant. However, it is limited to cooling above the freezing point of water. The major application of lithium bromide units is for the supply of chilled water for space and process cooling. They may be either one- or two-stage units. The two-stage units require higher temperatures (about 160°C); but, they also have high efficiency. The single-stage units can be driven with hot water at temperatures as low as 77°C (such as at Oregon Institute of Technology – see Fig. 5). The lower the temperature of the geothermal water, the higher the flow rate required and the lower the efficiency. Generally, a condensing (cooling) tower is required, which will add to the cost and space requirements.

For geothermally driven refrigeration below the freezing point of water, the ammonia absorption system must be considered. However, these systems are normally applied in very large capacities and have seen limited use. For the lower temperature refrigeration, the driving temperature must be at or above about 120°C for a reasonable performance. Figure 25 illustrates how the geothermal absorption process works.

Economic Considerations

Geothermal projects require a relatively large initial capital investment, with small annual operating costs

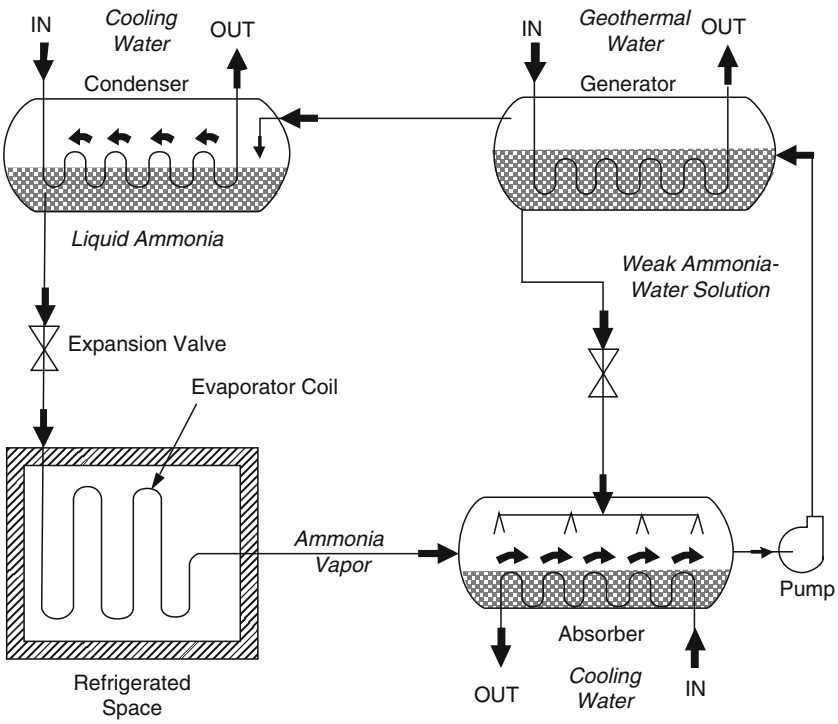

Geothermal Resources Worldwide, Direct Heat Utilization of. Figure 25
Geothermal absorption refrigeration cycle

thereafter. Thus, a district heating project, including production wells, pipelines, heat exchangers, and injection wells, may cost several million dollars. By contrast, the initial investment in a fossil fuel system includes only the cost of a central boiler and distribution lines. The annual operation and maintenance costs for the two systems are similar, except that the fossil fuel system may continue to pay for fuel at an ever-increasing rate while the cost of the geothermal fuel is stable. The two systems, one with a high initial capital cost and the other with high annual costs, must be compared. Table 3 is an attempt to quantify the cost of various direct-use types based on experiences in the USA.

Geothermal resources fill many needs: power generation, space heating, greenhouse heating, industrial processing, and bathing to name a few. Considered individually, however, some of the uses may not promise an attractive return on investment because of the high initial capital cost. Thus, the usage of a geothermal fluid may have to be considered several times to maximize benefits. This multistage utilization, where lower and lower water temperatures are used in successive steps, is called cascading or waste heat utilization. A simple form of cascading employs waste heat from a power plant for direct-use projects referred to as a combined heat and power application (Fig. 19) [38].

Geothermal cascading has been proposed and successfully attempted on a limited scale throughout the world. A generalized example is shown in Fig. 26. In Rotorua, New Zealand, for example, after geothermal water and steam heat a home, the owner will often use the waste heat for a backyard swimming pool and steam cooker. At the Otake geothermal power plant in Japan, about 165 t/h of hot water flows to downstream communities for space heating, greenhouses, baths, and cooking. In Sapporo, Hokkaido, Japan, the waste water from the pavement snow melting system is retained at 65°C and reused for bathing. An example of combined heat and power installation using geothermal waters down to 100°C are installed in Germany and Austria. At Neustadt Glewe in northern Germany, 98°C water from a 2,300 m-deep well at 1,700 L/s provides 11 MW (thermal) for a district

Geothermal Resources Worldwide, Direct Heat Utilization of. Table 3 Average costs of direct-use systems in the USA for 2005

Application	Capital ($/kW)	Cost/year ($/kW/year)	O$M ($/kW/year)	Total ($/kW/year)	Capacity factor	Unit cost (cents/kWh)
Residential space heating[a]	800	71.1	7.1	78.2	0.31	3.08
Comm./inst. Space heating[a]	500	44.4	4.4	48.8	0.25	2.23
District heating	650	57.7	5.8	63.5	0.33	2.42
Greenhouse heating	250	22.2	2.2	24.4	0.26	1.11
Aquaculture pond heating	200	17.8	1.8	19.6	0.69	0.32
Geothermal heat pumps[b]	850	75.5	7.6	83.1	0.13	6.78

Based on 30-year life at 8.0% interest and O&M at 10% of capital cost
The above costs includes a shallow well (<300 m) and no retrofit costs; however, cost can vary by as much as 100% depending on the local geology, hydrology, building construction, and infrastructure
[a]Assumes one production and one injection well for a single building
[b]Heat pump figures are considered only for the heating mode and the capacity factor is a nationwide average

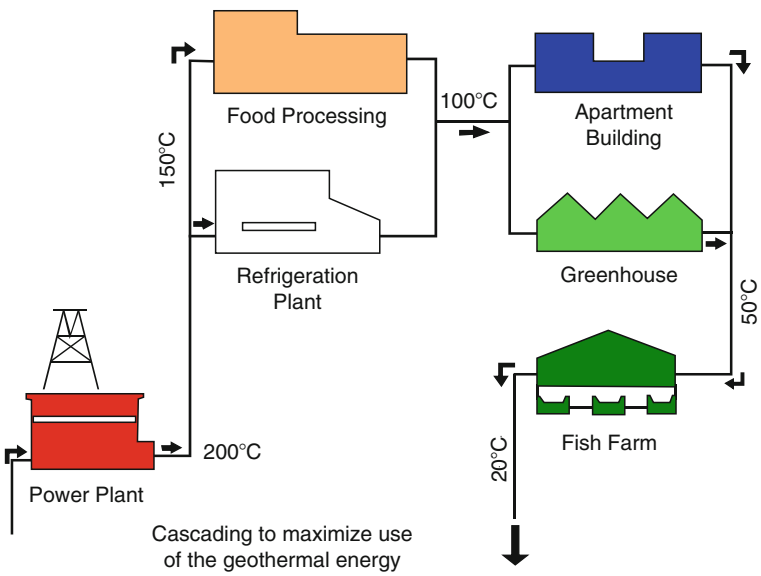

Geothermal Resources Worldwide, Direct Heat Utilization of. Figure 26 An example of cascading

heating network and 210 kW (electric) from a binary power plant meeting the electricity demands for 500 households [39].

Energy Savings

Geothermal, a domestic source of energy, could replace other forms of energy, especially fossil fuels. For many countries, geothermal energy could lead to a reduction in their dependence on imported fuels, and for all countries, it means the elimination of pollutants such as particulates and greenhouse gases. An attempt is made here to quantify the fossil fuel savings, using a 0.35 efficiency factor if the competing energy is used to generate electricity and 0.70 if it is used directly to produce heat, such as in a furnace.

Using the 438,071 TJ/year of energy consumed in direct geothermal applications in 2010 (Table 2), and estimating that a barrel of fuel oil contains 6.06×10^9 J, and that the fuel is used to produce replacement electricity, the savings would be 206.5 million barrels of oil or 31.0 million tons of oil annually. If the oil were used directly to produce energy by burning, then these savings would be halved. The actual savings are most likely somewhere in between these two values.

The carbon savings would be 63 million tons, and the CO_2 emission savings would be 99 million tons based on using oil to produce electricity. If the savings in the cooling mode of geothermal heat pumps is considered, then this is equivalent to an additional annual savings of 101.3 million barrels (15.2 million tons) of fuel oil or 19.2 million tons of carbon pollution from burning fuel oil (see Lund et al. [4] for more details). The total of 308 million barrels (45.2 million tons) corresponds to almost 3 days of worldwide oil consumption.

There appears to be a large potential for the development of low-to-moderate enthalpy geothermal direct-use across the world which is not currently being exploited due to financial constraints and the low price of competing energy sources. Given the right environment, and as gas and oil supplies dwindles and with recent price increases, the use of geothermal energy will provide a competitive, viable, and economic alternative source of renewable energy.

Future Directions

Future development will most likely occur under the following conditions:

1. Collocated resource and uses (within 10 km apart)
2. Sites with high heat and cooling load density (>36 MWt/km^2)
3. Food and grain dehydration (especially in tropical countries where spoilage is common)
4. Greenhouses in colder climates
5. Aquaculture to optimize growth – even in warm climates
6. Ground-coupled and groundwater heat pump installation (both for heating and cooling)
7. Combined heat and power installation using low-temperature resources in a binary power plant

Direct use has grown at an almost 9% annual rate over the past 10 years, and geothermal heat pumps alone has grown at a 17% annual rate over the same period [4]. The recent rise in the cost of oil and natural gas has made geothermal energy more competitive, and along with the environmental benefits associated with this renewable energy, development of this natural "heat from the earth" should accelerate in the future. At the 9% annual growth rate, the geothermal energy use should more than double over the next 10 years.

Bibliography

Primary Literature

1. Muffler LPJ (ed) (1979) Assessment of geothermal resources of the United States – 1978, USGS Circular 790, Arlington, VA, 163 p
2. Gudmundsson JS, Lund JW (1985) Direct uses of earth heat. Int J Energy Res 9:345–375
3. Geo-Heat Center (1997) Quarterly Bulletin 19(1), Geothermal direct-use equipment. Klamath Falls, OR, 38 p. http://geoheat.oit.edu/bulletin/bull19-1/bull19-1.pdf
4. Lund JW, Freeston DH, Boyd TL (2010) Direct utilization of geothermal energy 2010 worldwide review. Proceedings of the World Geothermal Congress 2010, Bali, Indonesia (CD-ROM)
5. Lund JW, Bloomquist RG, Boyd TL, Renner J (2005b) The United States of America country update – 2005. Geothermal Resources Council Transactions, vol. 29, Davis, CA (CD-ROM)
6. Ragnarsson A (2010) Geothermal development in Iceland 2005–2009. Proceedings, World Geothermal Congress 2010, Bali, Indonesia, paper no. 0124
7. Gudmundsson JS, Freeston DH, Lienau PJ (1985) The Lindal diagram. Geothermal Resources Council Transaction 9(1), Davis, CA, 15–19
8. Lund JW (1996) Balneological use of thermal and mineral waters in the USA. Geothermics 25(1), Elsevier, UK, pp 103–148.
9. Taguchi S, Itoi R, Ysa Y (1996) Beppu hot springs. Geo Heat Cent Quart Bull 17(2):1–6
10. Lund JW (1990) Geothermal spas in Czechoslovakia. Geo Heat Cent Quart Bull 12(2):20–24
11. Boyd TL (1999) The Oregon Institute of Technology Geothermal Heating System – then and now. Geo Heat Cent Quart Bull 20(1):10–13
12. Lund JW, Boyd T (2009) Oregon Institute of Technology Geothermal Uses and Projects, past, present and future.

Proceedings, thirty-fourth workshop on geothermal reservoir engineering, Stanford University, Stanford, CA (CD ROM)
13. Bloomquist RG, Nimmons JT, Rafferty K (1987) District heating development guide, vol 1. Washington State Energy Office, Olympia
14. Rafferty K (1992) A century of service: the boise warm springs water district system. Geo Heat Cent Quart Bull 14(2):1–5
15. Frimannsson H (1991) Hitaveita Reykjavikur after 60 years of operation – development and benefits. Geo Heat Cent Quart Bull 13(4):1–7
16. Lund JW (2005) Hitaveita Reykjavikur and the Nesjavellir geothermal co-generation power plant. Geo Heat Cent Quart Bull 26(2):19–24
17. Boissier F, Desplan A, Laplaige P (2010) France country update. Proceeding of the World Geothermal Congress 2010, Bali, Indonesia, paper no.161
18. Lund JW, Klein R (1995) Prawn park – Taupo, New Zealand. Geo Heat Cent Quart Bull 16(4):27–29
19. Lund JW (1995) Onion dehydration. Geothermal Resources Council Transaction, vol. 19, Davis, CA, 69–74
20. Chiasson A (2007) Geothermal energy utilization in ethanol production. Geo Heat Cent Quart Bull 28(1):2–5
21. Trexler DT, Flynn T, Hendrix JW (1990) Heap Leaching. Geo Heat Cent Quart Bull 12(4):1–4
22. Lund JW, Rangel MA (1995) Pilot fruit drier for the Los Azufres geothermal field, Mexico. Proceedings of the World Geothermal Congress 1995, 2335–2338
23. Lund JW, Lienau PJ (1994) Onion dehydration. Geo Heat Cent Quart Bull 15(4):15–18
24. Rafferty K (2003) Industrial process and the potential for geothermal applications. Geo-Heat Center Quart Bull 24(3):7–12
25. Rafferty K (2004) Direct-use temperature requirements: a few rules of thumb. Geo-Heat Center Quart Bull 25(2):1–3
26. Lund JW, Lienau PJ, Lunis BC (eds) (1998) Geothermal direct-use engineering and design guidebook. Geo-Heat Center, Klamath Falls, p 470
27. Rafferty K, Keiffer S (2002) Thermal expansion in enclosed lineshaft pump columns. Geo Heat Cent Quart Bull 23(2): 11–15
28. Ragnarsson A, Hrolfsson I (1998) Akranes and Borgarfjordur district heating system. Geo Heat Cent Quart Bull 19(4): 10–13
29. Ryan GP (1981) Equipment used in direct heat projects. Geothermal Resources Council Transactions, vol. 5, Davis, CA, pp 483–485
30. Culver GG, Reistad GM (1978) Evaluation and design of downhole heat exchangers for direct applications. Geo-Heat Center, Klamath Falls
31. Geo-Heat Center (1999) Downhole heat exchangers. Geo-Heat Center Quart Bull 20(3):28 p. http://geoheat.oit.edu/bulletin/bull20-3/bull20-3.pdf
32. Dunstall MG, Freeston DM (1990) U-tube downhole heat exchanger performance in a 4-in. well, Rotorua, New Zealand. Proceedings of the 12th New Zealand Geothermal Workshop, Auckland, New Zealand, pp 229–232
33. Curtis R, Lund J, Sanner B, Rybach L, Hellström G (2005) Ground source heat pumps – geothermal energy for anyone, anywhere: current worldwide activity. Proceedings of the World Geothermal Congress, 2005 (CD-ROM), International Geothermal Association, Antalya
34. Rafferty K (2008) An Information survival kit for the prospective geothermal heat pump owner. HeatSpring Energy, Cambridge, MA, p 32
35. Lund JW, Sanner B, Rybach L, Curtis R, Hellström G (2003) Ground-source heat pumps – a world overview, Renewable Energy World. James & James, London, pp 218–227
36. Kavanaugh S, Rafferty K (1997) Ground-source design of geothermal systems for commercial and institutional buildings. ASHRAE, Atlanta, p 167
37. Rafferty K (1983) Absorption refrigeration: cooling with hot water. Geo Heat Cent Quart Bull 8(1):17–20
38. Geo-Heat Center (2005) Combined heat and power plant. Geo-Heat Center Quart Bull 26(3):36. http://geoheat.oit.edu/bulletin/bull26-3/bull26-3.pdf
39. Lund JW (complied by) (2005b) Combined heat and power plant, Neustadt-Glewe, Germany. Geo-Heat Center Quart Bull 26(2):31–34

Books and Reviews

Cataldi R, Hodgson SF, Lund JW (eds) (1999) Stories from a heated earth – our geothermal heritage. International Geothermal Association and the Geothermal Resources Council, Davis, p 569

Kavanaugh SP, Rafferty K (1997) Ground-source heat pumps – design of geothermal systems for commercial and institutional buildings. American Society of Heating Refrigerating and Air-Conditioning Engineers, Atlanta, p 167

Lund JW (1996) Lectures on direct utilization of geothermal energy, United Nations University, Geothermal Training Program, Report 1, Orkustofnun, Reykjavik, Iceland, 123 p

Lund JW, Lienau PJ, Lunis BC (eds) (1998) Geothermal direct-use engineering and design guidebook. Geo-Heat Center, Oregon Institute of Technology, Klamath Falls, p 454

Websites

European Geothermal Energy Council, Belgium, www.geothermie.de/egec_geothernet/menu/frameset.htm

Geo-Heat Center, Oregon Institute of Technology, http://geoheat.oit.edu

Geothermal Education Office, USA, http://geothermal.marin.org

IEA (International Energy Agency) Heat Pump Center, The Netherlands, www.heatpumpcentre.org

International Ground Source Heat Pump Association, USA, http://www.igshpa.okstate.edu

Geothermal Resources, Drilling for

John T. Finger
Sandia National Laboratories, retired, Albuquerque, NM, USA

Article Outline

Glossary
Definition of the Subject
Introduction
Well Cost
Planning and Designing the Well
Drilling System Selection Criteria
Drill Bits and Bottom-Hole Assembly
Drilling Fluids
Lost Circulation
Well Control
Completions and Cementing
Instrumentation (Drilling and Mud Logging)
Future Directions
Bibliography

Glossary

Barrel An extremely common unit of volume in the drilling industry, equal to 42 US gallons or 178 l.

BHA (bottom-hole assembly) The assembly of heavy drilling tools at the bottom of the drill string; normally includes bit, reamers, stabilizers, drill collars, heavy-weight drill pipe, jars, and other miscellaneous tools.

Blow out Uncontrolled flow of fluids from a wellhead or wellbore.

BOP (blow-out preventer) One or more devices used to seal the well at the wellhead, preventing uncontrolled escape of gases, liquids, or steam; usually includes annular preventer (an inflatable bladder that seals around drill string or irregularly shaped tools) and rams (pipe rams or blind rams: pipe rams seal around the drill pipe if it is in the hole, blind rams seal against each other if the pipe is not in the hole).

Dewar A double-walled container or heat shield, similar to a vacuum flask, which insulates a piece of equipment from high temperature.

Directional drilling Deliberately drilling on a controlled non-vertical trajectory, usually done to improve productivity.

Drill collars Heavy-walled sections at the bottom of the drill string; provide stiffness, vibration control, and most of the weight on the bit.

Fish Any part of the drill string, or other tools, accidentally left in the hole; also, *fishing* – trying to retrieve a fish.

H_2S (hydrogen sulfide) A poisonous gas sometimes found in geothermal drilling.

LCM (lost-circulation material) Any material used to plug formation fractures to avoid loss of drilling fluid.

Stand More than one joint of drill pipe screwed together; when tripping, pipe is handled in stands to avoid making and breaking every connection – for a coring rig, a typical stand is four 3 m joints (12 m), but for a large rotary rig, a stand is three 10 m joints (30 m).

Sub Generic name for part of the drill string; for example, instrumentation sub carries instruments for navigation or logging; crossover sub allows different threads to be connected; bent sub forms a slight angle between the axis of the drill string and the axis of a downhole motor, allowing directional drilling.

Trip Any event of pulling the drill string out of the hole and returning it.

Twist-off Failure mode in which some element of the drill string parts, leaving at least one portion of the drill string in the hole.

Under-pressured Describes the pore pressure of in situ fluids during drilling as less than the static head of a water column to the same depth in the wellbore.

Washout A hole or leak in the drill string; often caused by fatigue failure, but very dangerous because the flow of high-pressure drilling fluid through the leak will quickly enlarge it to the point of parting the drill string.

Definition of the Subject

The word "geothermal" comes from the combination of the Greek words gê, meaning Earth, and thérm, meaning heat. Quite literally, geothermal energy is the heat of the Earth. Geothermal resources are concentrations of the Earth's heat that can be extracted economically for some useful purposes. All existing applications of geothermal energy use a circulating fluid to carry the heat from depth

to its use at the surface, and this means that holes must be drilled for access to or introduction of these fluids. Drilling, therefore, is a major component of any geothermal project's development.

This entry describes the overall process of drilling, with emphasis on the ways in which geothermal drilling differs from other kinds of drilling, such as that for oil and gas. The entry also focuses on the drilling of relatively large-diameter, high-temperature holes, such as those most often used to supply electrical generating plants, and specifically does not address the following topics: low-temperature drilling for direct-use application, well maintenance and workover, or drilling for geothermal heat-pump installations. The entry should by no means be considered a set of instructions on how to drill a geothermal well, but is intended to illuminate some of the major decisions that will be necessary during that process.

Introduction

Geothermal energy is a growing enterprise. Worldwide electricity production increased from 6,833 MWe (megawatts electric) in 1995 to 9,966 MWe in 2008, and direct use in 2005 displaced more than thirty million barrels of oil [1]. In spite of this growth, geothermal drilling activity is minuscule compared to oil and gas – fewer than 100 geothermal wells were drilled in the USA during 2008, while the total for oil and gas exceeded 50,000 [2]. This means that few service companies or drilling contractors can sustain their business solely within the geothermal industry, and it also leads to a lack of research into tools or techniques specifically aimed at geothermal drilling. A substantial number of deep gas wells, however, now have producing horizons with geothermal-like temperatures (~175°C), so this has brought new interest into high-temperature drilling.

Before describing the aspects that make geothermal drilling unique, however, a brief summary of the fundamental process will be useful. The process of drilling, rather than digging, holes in the ground has been under development for thousands of years, but the techniques we now know as "conventional rotary drilling" began to be developed around the end of the nineteenth century. This technology, with only minor variations, is ubiquitous in the oil, gas, geothermal, water well, and mining industries. There is an extensive literature on the principles and practices of this kind of drilling [3], and a baseline system – a tall, steel derrick supporting a string of pipe which turns a bit to drill the hole – is at least superficially familiar to most readers (Fig. 1).

Basic Drilling Functions

Any drilling system must perform six basic functions:

1. Transmit energy from the surface to the rock face
2. Reduce rock from its more-or-less monolithic state

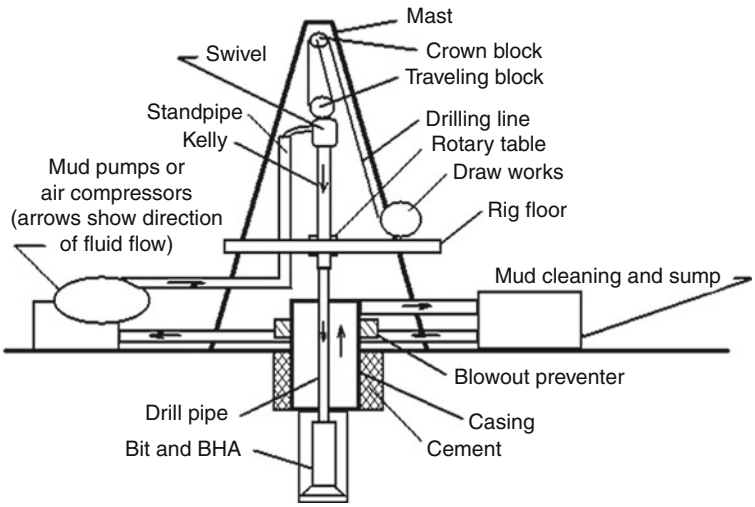

Geothermal Resources, Drilling for. Figure 1
Drill rig diagram

3. Remove the reduced rock from the wellbore
4. Maintain control of any pressures encountered in the wellbore
5. Keep the hole open, stable at some minimum diameter, and on the desired trajectory while drilling
6. Preserve and control the well for some indefinite, but relatively long, time

Each of these functions is described in more detail, with the same numbering reference as above. In the baseline system, all of the equipment necessary for the drilling operation is organized around the derrick, or mast. This is a steel tower, ranging from 16 m to 50 m in height, which supports the drill pipe with the bit and all the other downhole equipment, and which provides a platform for much of the other equipment necessary to drill the hole. Every rig, except for the smallest ones, has a floor just above ground level where most activity required to operate the rig takes place. The driller, who has minute-by-minute control of the rig's operation, has a control console here and most equipment handling (adding a new piece of drill pipe, making and breaking drill string connections, changing bits, etc.) takes place on the floor. In smaller rigs, the mast and the floor are a unit and are simply raised into position in preparation for drilling. Because of larger hole sizes, geothermal wells usually need bigger rigs, which may require 50–60 large truck loads for transportation. These rigs are usually assembled at the drill site, a job which may take several days, even in accessible locations on land.

1. To make the hole, energy must be transmitted from the surface to the rock face at the end of the wellbore. Power supply for drilling has evolved from the early days of steam-driven, mechanically coupled rigs to the current standard of diesel-electric drive. In this configuration, two to four diesel engines (up to 1,500 kW each) drive electric generators, which supply power to individual electric motors driving the rotary table, drawworks, mud pumps, and other equipment. The rotary table is a mechanism, usually inset into the rig floor, which turns the drill string to break rock and advance the hole. (A "drill string" comprises the drill pipe plus the bottom-hole assembly, or BHA. The BHA includes drill collars, stabilizers, bit, and any other specialized tools below the drill pipe.) Torque is applied to the kelly, which is attached to the top of the drill string. The kelly is a section of pipe with a square or hexagonal outside cross section that engages a matching bushing in the rotary table. This bushing lets the rotary table continuously turn the kelly and drill string while they slide downward as the hole advances.

The upper end of the kelly is attached to a "swivel," which is a rotating pressure fitting that allows the drilling fluid to flow from the mud pumps, up the standpipe, through the kelly hose, into the swivel, and finally down the drill pipe as it rotates. The swivel is carried by the hook on the traveling block and it suspends most of the weight of the drill string while drilling.

Moving the drill string into and out of the hole is called tripping. Trips are usually required when the bit or some other piece of downhole equipment must be replaced, or because of some activity such as logging, testing, or running casing. Clearly, trips take longer as the hole grows deeper. Raising or lowering the drill string for a trip is done by the drawworks, which is a large winch. The drawworks reels in or pays out a wire rope (drilling line) that passes over the crown block at the top of the rig's mast and then down to the traveling block which carries the hook, which in turn suspends the drill string or casing. Depending on what mechanical advantage is required, the drilling line is reeved several times between the crown and traveling blocks, as in a block and tackle.

2. Attached to the bottom of the drill string, the bit rotates to break (reduce) the rock from its more-or-less monolithic state into small fragments (usually called "cuttings") and to advance the hole. A tremendous variety of bits is available, and some of the important types are discussed in more detail in the section Drill Bits and Bottom-Hole Assemblies.

3. Once the rock has been reduced to chips and fines, it must be removed from the hole bottom to expose fresh rock surface and to avoid wasting energy by re-grinding these same cuttings. This cleaning is done by a stream of fluid that circulates down the drill pipe, passes through ports (called "jets") in the bit, and returns up the annulus between the wellbore wall and the outside of the drill string, carrying the rock cuttings back to the surface. This fluid is sometimes a gas (air, nitrogen, and natural gas), but is most often a liquid, universally known as "mud" from its origin as a mixture of water and clay.

Air drilling, in which the hole is cleaned by a compressor-driven airstream, generally makes hole faster than mud drilling, but suffers severe issues with well control, hole stability, drill-pipe erosion, and difficulty with handling water influx. Mud drilling uses pumps to circulate the liquid, which not only carries cuttings but stabilizes the wellbore and lubricates the bit and drill string. When mud returns to the surface, it is cleaned to remove most of the rock cuttings and is then recirculated. Pumping mud while drilling, at typical flow rates of 12 to 50 l/s, with pressures up to 20 MPa, can represent more than 75% of the rig's total power consumption. Requirements for drilling fluids and the circulating system are described in more detail in the Section Drilling Fluids.

4. During drilling, the personnel and equipment must be protected against unexpected pressure surges in the wellbore. In oil and gas drilling, these surges can come from hydrocarbon fluids trapped under impermeable rock which holds them at pressures higher than the static head of the fluid column in the wellbore, and in geothermal operations the surges come from hot formations which heat the pore or wellbore fluids above the saturation temperature at the static wellbore pressure. In either case, the first line of control is the weight of the fluid column in the wellbore. With a gas column, this weight is negligible, but with mud the liquid density will range from slightly greater than water (specific gravity $\sim$ 1.05) to almost three times that. In addition to the clays and additives that raise the viscosity of the mud to improve hole cleaning, weighting materials such as barite are often added to increase the mud's density and enable it to control higher downhole pressures. If a pressure surge cannot immediately be controlled with fluid weight, the wellbore can be mechanically sealed at the surface with BOPs, or blow-out preventers. See the Section Well Control for more detailed information on blow-out prevention equipment and well control.

5. Hole stability can be a problem after drilling through some kinds of rock for several reasons: the formation may tend to swell (because it absorbs water) or squeeze (extrude into the wellbore because of overburden pressure), both of which reduce the hole diameter; or chunks of the wellbore wall may cave or slough into the hole. These phenomena can cause problems ranging from minor (the necessity to clean out debris or to ream part of the hole) to major (stuck drill string). With gas drilling, there is no liquid to cause swelling, but there is no fluid pressure to counteract squeezing. With mud, these problems can often be eliminated or mitigated by the pressure of the fluid column or by the mud's chemical composition.

Controlling the hole's trajectory has two major components: keeping it either straight or, in the case of directional drilling, deviating along a relatively smooth curve; and making sure that the hole is advancing in the proper direction. Keeping the hole straight or smoothly curved is necessary to allow the casing to be run easily; getting a string of casing stuck during its deployment can be a serious and expensive problem. If the hole is being directionally drilled, the two principal aspects of hole trajectory are inclination and azimuth. Vertical holes depend mostly on the pendulum effect of gravity to keep the drill string pointed downward, but sometimes the combination of BHA design and formation properties will drive the hole away from verticality.

If the hole trajectory must be changed, either to correct unwanted deviation or to steer it toward a specific target, it is necessary to force the hole into the correct trajectory with directional drilling. Directional drilling is extensively used in the oil and gas industry to increase productivity by keeping the hole in hydrocarbon-bearing strata, and similarly in geothermal reservoirs to intersect more productive fractures. Directional drilling is a complex topic [4] and there are a number of techniques available for performing it, but a complete discussion is far beyond the scope of this entry. One aspect that is relevant to geothermal drilling is that the drilling motors and electronic steering-survey tools are susceptible to high temperature, so the hole trajectory is usually set in the upper, cooler interval of the hole and then efforts are just to keep it straight from there.

6. Once the hole is drilled to the target depth, it must be kept open for testing or production. This is conventionally done by putting steel pipe, or casing, into the hole and cementing it in place. Casing is not done all at once, at the end of drilling, but is placed sequentially in the hole as it reaches increasingly greater depths. As each casing string is placed and cemented, the hole interval below that string must be smaller than the one above, since the new drill bit must pass through the casing just set. The completed hole, then,

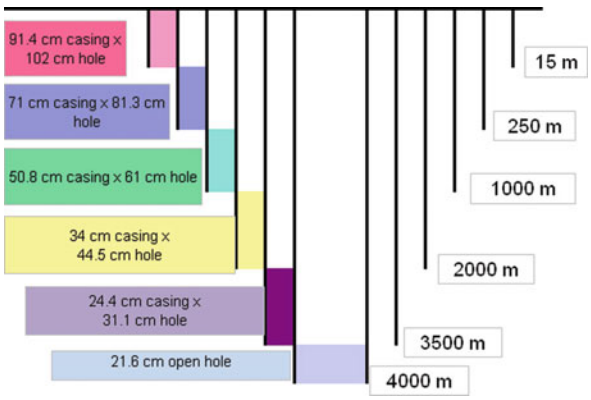

Geothermal Resources, Drilling for. Figure 2
Diagram of typical casing program

will usually have two to four concentric strings of casing cemented in place with an open-hole section at the bottom for production of the desired fluids (Fig. 2).

To complete any given interval of the well, casing (which is several centimeters smaller than the hole diameter at that point) is lowered almost to the bottom of the hole; then cement is pumped down the inside of the casing and displaced with mud up the annulus between the casing and the wellbore wall. Because large volumes of cement must be pumped quickly, and at high pressure because of the density difference between the mud and cement, specialized cementing equipment is used for this job. It is not uncommon for the cost of casing and cement to approach half the total well cost.

Unique Aspects of Geothermal Drilling

Compared to the sedimentary formations of most oil and gas reservoirs, geothermal formations are, by definition, hot (production intervals from 160°C to above 300°C). They are often hard (240^{+} MPa compressive strength), abrasive (quartz content above 50%), highly fractured (fracture apertures of centimeters), and underpressured. They often contain corrosive fluids, and some formation fluids have very high solids content (total dissolved solids in some Imperial Valley brines is above 250,000 ppm). These conditions mean that drilling is usually difficult – rate of penetration and bit life are typically low [5], corrosion is often a problem [6], lost circulation is frequent and severe, and most of these problems are compounded by high temperature.

Lost circulation (loss of drilling fluid into the rock formation) and reservoir damage deserve special mention. Lost circulation is often massive, with complete loss of returns at pumping rates of hundreds of barrels per hour. Geothermal wells have been abandoned because of the inability to get through a loss zone [7], and many more have needed an unplanned string of casing to seal off a problem. Lost-circulation treatment is complicated by the requirement that the treatment of loss zones must not damage the producing formation, but it is often difficult to distinguish between the two.

Finally, geothermal wells produce, relative to oil and gas, a low-value fluid – hot water or steam. For economic viability, then, geothermal flow rates and well diameters must be much larger than comparable oil and gas wells. Oil wells frequently produce through 6 cm tubing, but geothermal wells that supply power plants will generally have production intervals of at least 21.6 cm diameter. Geothermal casing will therefore be larger and more expensive and, also unlike oil and gas, it must be cemented along its complete length, not just anchored at the bottom.

All of these factors will be discussed in more detail below.

Geothermal Rock Formations

With few exceptions, geothermal reservoirs are found in igneous or metamorphic rocks such as granite, granodiorite, quartzite, basalt, and volcanic tuff [8]. Reservoirs in California's Imperial Valley and Mexico's Cerro Prieto fields are among the rare resources in sedimentary formations, and drilling practices in these fields are significantly different from elsewhere. As noted above, these igneous or metamorphic rocks tend to be hard, abrasive, and fractured, which makes drilling difficult, and they are also more variable from one well to another than is the case in a typical oil and gas reservoir. This means that the learning curve in a geothermal reservoir is not as steep as would be the case with hydrocarbons, but experience is still valuable, and each well will have a share of "lessons learned." This variability is a key factor in assessing the variables that drive well cost, as discussed in the next section.

Depth and temperature of geothermal resources vary considerably. Several power plants (e.g., Steamboat Hills, Nevada and Mammoth Lakes, California) operate on

lower temperature fluid (below 200°C) produced from depths of approximately 330 m, but wells in the Geysers produce dry steam (above 240°C) and are typically 2,500–3,000 m deep. In the most extreme cases, an exploratory well with a bottom-hole temperature of 500°C at approximately 3,350 m has been completed in Japan [9], and experimental holes into molten rock (above 980°C) have been drilled both in Hawaii and in Iceland.

Well Cost

Cost of the wells is clearly crucial to the financial viability of a proposed geothermal power project, because the well field – production and injection – can comprise 30–50% of the project's capital cost [10]. Factors that affect well cost are discussed in many places [11], and all of the topics discussed in this entry are related in some measure to the well's cost. It is useful, however, to look specifically at some of the most important cost drivers in geothermal drilling.

Well design: Design of a geothermal well is a "bottom-up" process. Location of the production zone determines the well's overall length, and the required flow rate determines diameter at the bottom of the hole – the well's profile above the production zone is then set by iteration of the successively larger casing strings required by drilling or geological considerations.

Because of the large diameters in geothermal wells, however, casing and cementing costs form a relatively large share of the cost, and the ability to eliminate one string of casing would have a major impact.

The need for directional drilling and the accuracy with which the hole trajectory must be controlled are also important factors in cost, but there is usually less flexibility in those choices as the well is designed.

Trouble: "Trouble" is a generic name for many sorts of unplanned events during drilling, ranging from minor (small amounts of lost circulation) to catastrophic (the BHA is stuck in the hole and the drill string is twisted off). In some cases, experience in the same or similar reservoirs will give a hint that certain types of trouble are likely, but at other times events are completely unexpected. It is difficult, therefore, to estimate a precise budget for trouble, but all well expenditure planning must contain some contingency funds, and this number is often taken to be around 10% of the total budget.

Two kinds of trouble avoidance that have received considerable research effort are lost-circulation treatment and vibration reduction to mitigate bit, BHA, and drill pipe failure. These topics are described in more detail later, but they cannot be dismissed as possible cost drivers.

Rate of penetration (ROP): Many of the costs attributed to drilling are time dependent (primarily related to the rental rate on the rig), so it is clear that anything to speed up the hole advance is beneficial. (Keep in mind, however, that increased ROP at the expense of more trips, or lower tool life, is usually not effective. See the next paragraph.) A tremendous amount of research has been done to improve bit performance, both in terms of drilling speed and life, and there is no doubt that today's bits are far better than those of an earlier generation. Still, even with improved bits it is not always easy to optimize the performance with a new bit design drilling an unfamiliar formation. The three parameters that can be easily changed for any bit/formation combination are rotary speed, weight on bit (WOB), and hydraulics (combination of jet size and flow rate), and it often takes some experimentation to determine the best combination of these factors.

Bit and tool life: Much of the commentary above about ROP applies to bit and tool life. Improved tool life means, of course, that the expense of replacing a bit or other piece of equipment can be avoided or delayed, but there is also a time saving if trips can be eliminated. This becomes more important as the hole gets deeper and the trips take more time.

Comparison: To examine the effect of these factors, the hypothetical well shown in Fig. 3 will have its overall cost calculated with the following changes in the relevant variables. Cost calculations are done with a spreadsheet program that lists and sums the major variables in drilling cost, and are generally in 2009 dollars, although the key point here is not the absolute value of well cost, but the relative effect of the various changes.

- Well design: The first alternative to the "base case" well is a variation designed with one fewer casing strings (this may or may not be realistic, but serves to demonstrate the effect of well design on cost) (Fig. 4).
- Trouble: The base case well is assumed to have a moderate amount of trouble. There are two lost-circulation events, both in the 44.5 cm interval, and

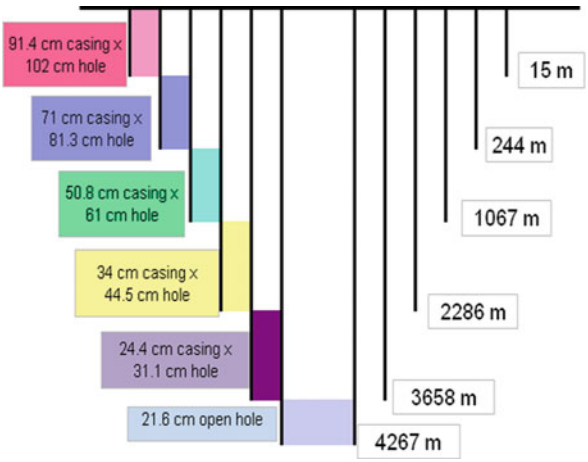

Geothermal Resources, Drilling for. Figure 3
Base case well design

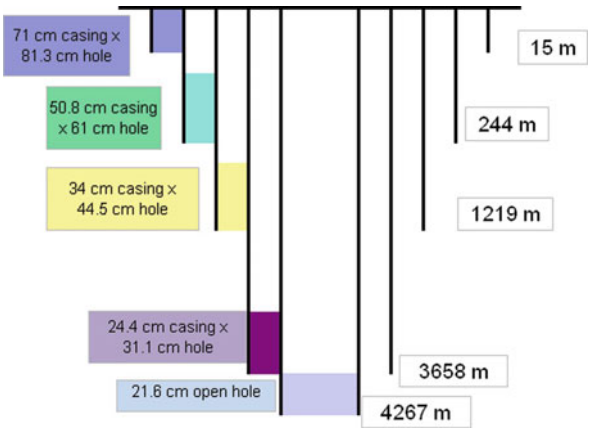

Geothermal Resources, Drilling for. Figure 4
Alternative casing design

one twist-off in the 31.1 cm interval. Each lost-circulation event is treated by pumping 10 m^3 of cement and waiting 12 h on cement to cure, and the twist-off is assumed to require 80 h for fishing and repair.

- Rate of penetration: Base case bit performance is 10 m/h for 44.5 cm bits, 5 m/h for 31.1 cm bits, and 4 m/h for 21.5 cm bits. "Improved" ROPs are 15, 10, and 6 m/h, respectively.
- Tool life: Base case bit life for the sizes above are 100, 80, and 40 h. Improved values are 200, 120, and 80 h, respectively.

Results: The effects of these improvements are shown in Table 1, where the cost savings from various changes are shown in all possible combinations.

Cost reductions that can be attributed to the various individual improvements are

- Redesign casing to eliminate one string – 18.9%
- Improve rate of penetration – 7.2%
- Improve bit life – 1.9%
- Eliminate trouble – 2.0%

From this analysis it is clear that significant cost reductions may be available. If all the postulated improvements were made, total cost would decrease by almost 29%, or more than $3 million. Most important of the improvements considered was redesigning the casing to eliminate one string, with improved rate of penetration a distant second, although still significant. This statement does not imply that either of these improvements is actually possible in every case, but the numbers do give an indication of priorities when considering research into different drilling technologies. The most important factor to remember in considering well cost is that geothermal wells are *extremely* site specific, much more so than oil and gas wells of similar depth, and so these results are not generic.

The numbers above should be taken with some caution, because of this variability in well cost components with location. To give several examples of exceptions, consider the following:

- The trouble postulated for this well was relatively minor, with two cement plugs and a twist-off that could be retrieved by fishing. In at least one case [12], a geothermal well received 20 cement plugs without curing the lost-circulation problem, and the well was abandoned. As for twist-offs, it is often the case that a stuck bottom-hole assembly (BHA) cannot be fished, so that the hole must be side-tracked to go around it – this procedure is much more expensive than simply fishing.
- Differences in site preparation are not included in these spreadsheet calculations, but rugged terrain or an absence of easily available water can have a major impact on well cost.
- Some locations, such as the Imperial Valley in southern California, have extremely corrosive in situ fluids that require titanium casing [13], at a cost exceeding $2 million for the production string.

Geothermal Resources, Drilling for. Table 1 Comparison of well costs, assuming different drilling conditions

	Base case	Improve bit life	Improve ROP	Improve ROP and bit life
Base case	$11,560,857.95	$11,345,822.83	$10,733,021.31	$10,691,820.96
Reduce trouble	$11,335,667.78	$11,120,632.66	$10,507,831.14	$10,466,630.80
Eliminate casing string	$9,372,815.35	$9,151,844.66	$8,624,445.23	$8,461,433.57
Eliminate string, reduce trouble	$9,146,089.76	$8,925,119.08	$8,397,719.65	$8,234,707.98

Geothermal Resources, Drilling for. Table 2 Sample well costs from various geothermal projects

Well location	Depth (m)	Production diameter (cm)	Year drilled	Total cost (US$)
Newberry Caldera, USA [14]	2,927	31.1 hole/24.4 liner	1995	2,895,493
Vale OR, USA [15]	1,755	15.9 hole/12.7 slotted liner	1994	920,325
Habanero-2, S. Australia[a]	4,358	15.2 open hole	2007	6,200,000
GPK-4, Soultz, France[a]	5,260	21.6 open hole	2004	5,000,000

[a]The referenced report "The Future of Geothermal Energy," available online at http://www1.eere.energy.gov/geothermal/future_geothermal.html, has an extensive discussion of well cost variation over periods of several decades, and also goes into much greater detail about the factors that drive well cost

- Bit-life improvements used in the spreadsheet calculations may be unrealistically high, but this only demonstrates the fact that even very large improvements in that area have relatively small effect in the given well design with the stated drilling performance. On the other hand, rock reduction is often the source of trouble cost, so the reduction in drilling time may not be the only cost saving.

In general, cost information on wells drilled by commercial geothermal operators is tightly held and it is difficult to get extensive data on actual drilling costs. In a few cases, however, such data is in the public domain, and a brief sample is given in Table 2.

Even these few examples show the great variability in cost, a significant fraction of which is caused by economic inflation over time.

Finally, if an operator is considering exploratory wells, there are many advantages to drilling "slim holes" – wells with diameters smaller than would be used for production but large enough to be useful in characterizing the reservoir. This would typically mean final diameters of 7–10 cm, compared to common production diameters of 15–24 cm.

Drilling is cheaper for slim holes than for production wells because the rigs, casing and cementing, crews, locations, and drilling fluid requirements are all smaller; because site preparation and road construction in remote areas is significantly reduced, up to and including the use of helicopter-portable rigs; and because it is not necessary to repair lost-circulation zones before drilling ahead. An extensive slimhole-drilling research program [16] showed that slim holes are consistently cheaper than full-size holes in the same locations, and that the slim holes are adequate to characterize the reservoir.

Planning and Designing the Well

There are two separate but closely related parts of preparing for a drilling project – *planning* the well and *designing* the well. "Planning" means to list, define, schedule, and budget for all the multitude of individual activities required to drill the well, and "designing" means to specify all the physical parameters (depth, diameter, etc.) that define the well itself. Detailed instructions on how to complete this process for even one well would need a sizable volume in itself, and so that is well beyond the scope of this entry, but the following discussion will

present a sort of checklist that specifies many of the questions that must be considered during these preparations. (The geographical location of the well can have a major impact on cost, schedule, and even well design, but that choice is a function of exploration for the resource, and so is too variable to be considered as a generic part of well planning.)

Careful planning is critical for any drilling operation. It will not only minimize cost, but will reduce the risk of injury or property damage from unexpected events. A drilling plan should list and define all the activities required to complete the well, with their related costs and times, and should give sufficient descriptions of individual tasks to make clear the sequence in which they must be performed. (A "critical path" approach, showing which operations must be sequential and which can be simultaneous, is often useful. The crux of this technique is that any delay along the chain of sequential operations – the critical path – will cause a delay in project completion, while delay in some other operation may not.) It is also essential that all the contractors and service companies should meet, or at least thoroughly communicate, during the planning stage, so that the plan assigns responsibilities for the various activities and there is no confusion as to what person or company performs each step.

Descriptions in the plan must be relatively detailed. For example, to specify drilling, an interval between two given depths and running casing in it would typically require, at minimum, the following information:

- Bit size and type (include suggested weight on bit and rotary speed, if available)
- Definition of all components of the bottom-hole assembly, and whether downhole motors are to be used
- Expected rate of penetration and bit life (thus, expected time to drill the interval)
- Any directional drilling instructions
- Drilling fluid type and flow rate
- Any required logging during drilling or before casing is run
- Size, weight, and grade of casing
- Proposed cementing program
- Any problems expected in that interval, or special precautions to be taken

A plan can be as simple as a written outline, in list format, of the various activities, or can be quite detailed and in active electronic format. Management software ranges from simple spreadsheets, through freeware available on the Web, to sophisticated planning tools such as Microsoft Project [17]. If one considers commercial planning software specific to drilling, make sure that it can include services that are common in geothermal drilling but not often used in oil and gas, such as mud coolers, high-temperature tools and cement, etc. Clearly, the drilling plan must also be flexible enough to accommodate unexpected events, or trouble, during the project, and there must be a well-defined process to identify the person who is responsible for changes in the plan.

To begin designing the well, a great variety of information is desirable, but it is not always possible to get the complete package. It is worth considerable effort to get as much of it as possible, but sometimes the designer must just go with the best available data. The desirable information includes, but is not limited to, the following parameters.

- Purpose of the well: A given well may serve any one of several different functions – production, injection, exploration, or workover – and the well design will be influenced by its purpose. For example, an exploration well might be of smaller diameter than the one intended for production and, because it might be scheduled for abandonment once the reservoir is characterized, it might also be completed with less attention to the well's longevity (different cement, casing material, or the like). Some considerations for hole diameter in small exploration wells or "slimholes" are described in the section on "Drilling System Selection Criteria".
- Reservoir conditions: It is extremely useful to know as much as possible about the prospective reservoir; such information might come from previous temperature and pressure logs in offset wells, nearby thermal gradient holes, or geophysical information. Clearly, temperature and pressure are crucial, but brine chemistry is also very important because it can have a major impact on casing selection and cost.
- Logistical requirements: It is common that, for reasons including a power sales contract, other

financing requirements, or even weather, a drilling project must be completed on a given schedule. If this is the case, it can complicate planning because of factors ranging from drill rig availability to acquisition of the necessary permits. It is also more or less a standard condition that any lease site will have regulatory stipulations that affect drilling fluid disposal, cuttings disposal, possibly water supply, and even air-quality requirements that will necessitate emissions control on the rig engines. The well planner has little recourse in dealing with these factors, but it is certainly essential to consider them in the planning process.

- Likely problems in drilling: Experience in similar wells or general knowledge of the reservoir can sometimes offer a prediction of what problems may be encountered in drilling the well. If this knowledge is available, it will guide the preparations in many ways: having lost-circulation material (LCM) for under-pressured formations; appropriate drilling fluid additives for corrosive brines or for exceptionally high temperatures; high-temperature logging or steering tools and drilling motors if those tools will be used in a hot hole; and stand-by fishing tools and possibly shock absorbers in the BHA if there is likely to be rough drilling with twist-offs. It may also provide better definition of the best operating envelope (weight on bit, rotary speed, and hydraulics) for the bit in specific formations.
- Casing requirements: The heart of well design is the specification of the casing program, which will be discussed in more detail below. Parameters that determine the casing requirements include the following: nominal production rate from the well and the casing diameter implied by that flow rate, depth of the production zone, expected temperature, brine chemistry, whether the completion will be open hole or slotted liner, well trajectory (vertical, directional, or multi-leg), kick-off point (if directional), need for special casing connections, and the length of individual casing intervals.

In general, the well is designed from the bottom up, that is, the expected depth of the production zone and the expected flow rate will determine the wellbore geometry and casing program and most of the equipment requirements will follow from those criteria. Because geothermal wells produce a relatively low-value fluid – hot water or steam – flow rates must be much higher (often >100,000 kg/h) than for oil and gas wells, and geothermal wells produce directly from the reservoir into the casing, instead of through the production tubing inside casing as in most oil wells. If there is two-phase flow in the wellbore, larger casing diameter where flow is vapor dominated will significantly reduce pressure drop, improving productivity [18]. Finally, many lower-temperature geothermal wells are not self-energized and must be pumped, either with line-shaft pumps driven from the surface or with downhole submersible pumps (and so the well's design must allow for pump removal). All these factors combine to drive geothermal casing diameters much larger than oil and gas wells of comparable depth – typical casing sizes in geothermal production zones are 20–34 cm.

There are three important considerations in designing the casing:

- Because each casing string limits the diameter of the drill bit and successive casing strings that can pass through it, the hole diameter decreases as the well gets deeper.
- Because of casing costs and diameter reduction, it is beneficial to make the intervals between casing points as long as possible.
- The incidence of problems or trouble increases as the wellbore intervals between casing points grow longer.

The two latter points counter each other – it is highly desirable to drill long intervals between running successive casings, but doing so greatly increases the probability of trouble. If a "contingency string" is needed to isolate a troublesome wellbore zone, this imposes a significant cost for the additional casing and cementing. It also implies the necessity of starting with larger diameter casing above the contingency string, to preserve the required bottom-hole diameter, or of completing the well with smaller bottom-hole diameter than was desired, if no provision for the contingency string was included in the plan.

Given a bottom-hole depth and diameter, determination of the casing intervals above that depends on several factors, including rock properties, formation fluids, or even regulatory requirements (some agencies

require that at least 10% of the wellbore always be behind surface casing down to the next casing point, and 1/3 the well behind casing below that). There are many common reasons to set casing in a particular interval:

- Protect an aquifer – regulations require sealing off aquifers to prevent their contamination by wellbore or drilling fluids.
- Isolate troublesome formations – these can be unstable (sloughing, swelling, or unconsolidated) formations, zones with high or incurable lost circulation, or a depleted-pressure zone above the production horizon.
- Fluid pressure control – although more common in oil and gas than in geothermal, drilling fluids often contain additives that bring the specific gravity of the fluid well above that of water, so that the weight of the fluid column will control the downhole pore pressure in the formation. This often leads to the situation in which the higher pressure of the drilling fluid exceeds the fracture gradient of the formation, leading to lost circulation or even loss of well control.
- Define the production zone – geothermal reservoirs can have more than one productive zone and casing is sometimes set to preferentially allow production from the selected zone.

There are many other reasons that casing might be set at a particular depth, but this list gives a flavor of how variable those reasons can be. Once the general casing profile is selected, the casing for each individual interval, or string, is characterized by three basic measurements: diameter, weight, and grade. Diameter is straightforward; it is just the nominal outside diameter for that interval (although this does not include the couplings, which are larger than the casing body and control the smallest possible inside diameter of the next larger string). Weight, expressed in weight units per unit length, is actually a measure of the wall thickness of the casing; heavier casing has smaller inside diameter, since the outside diameter must remain constant for a nominal size. The casing's grade is primarily related to the material's tensile strength, although there are some metallurgical variations aimed to withstand specific effects, such as corrosion, of the wellbore fluid chemistries.

Casing has to withstand different kinds of loading in different situations, and the most common design criteria are for burst pressure, collapse pressure, axial tension, and buckling. Burst pressure and axial tensile strength are a function of the casing grade, but collapse and buckling are more related to the wall thickness, because they are determined by the material's elastic properties as well as its tensile strength.

Although reasonably simple casing designs can be done with hand calculations and manufacturers' handbooks, the general topic can be very complex, and detailed procedures for casing design are well beyond the scope of this entry. Extensive resources are available. All drilling engineering textbooks [19] have sections on casing design, and an Internet search for "casing design software" will indicate the multitude of options to be found among drilling service companies. Although all of these methods are likely to produce satisfactory casing designs, engineering judgment is still important and it is of significant benefit to have a veteran drilling engineer with geothermal experience to at least review a proposed casing program.

Drilling System Selection Criteria

Most of the criteria used to select a drill rig will be derived from well parameters; specifically diameter, depth, and casing design. The process of planning and designing the well will have established the diameter, which is the primary criterion for whether the well is considered a "slimhole" or will be a conventional well and, thus, what kind of rig will be used.

Several factors define the minimum hole diameter, and also bear upon whether a core rig can be used for the hole.

- Logging tools – Typical temperature-pressure-spinner logging tools will fit into almost any reasonable hole size, but if more complex tools, especially imaging tools such as a formation micro-scanner or a borehole televiewer are to be used, the heat-shielding they require at high temperature sometimes defines a minimum hole size.
- Core size – If core is required to validate a geologic model of the reservoir or to assess the fracture dip, density, and aperture, then a coring rig is advantageous, compared with taking core samples with a rotary rig, but the core size must be considered.

Diameter is not too important for fracture data, but sometimes a rock mechanics evaluation will need a minimum core diameter. Larger diameter core also gives better recovery in highly fractured or unconsolidated formation.

- Packers – Inflatable packers are sometimes used to isolate a specific section of the wellbore for injection tests, fluid sampling, or other diagnostics. In general, this means that some kind of logging or sampling tool must be run through the packer into the zone below it, and the size of this tool will determine the minimum size of the packer and thus the hole. Based just on the diameter of the cable head for most logging cables, it would be very difficult to run a pass-through packer in a hole smaller than approximately 100 mm diameter.
- Flow test – If a flow test is expected after drilling, there are two advantages to keeping the hole diameter as large as possible: scaling up for predicted flow in a large-diameter well will be more accurate; and if the combination of depth, pressure, and temperature means that the well's ability to produce is marginal, a larger diameter hole is more likely to flow. The larger-diameter wellbore is particularly important if the flow turns two phase.

If all these factors indicate that a slimhole will satisfy the requirements, then a minerals-type coring rig can often yield significant cost savings for two reasons:

- Smaller casing, tools (bits, reamers, etc.), and cementing volumes
- The ability to drill with complete lost circulation (no returns to the surface)

Coring rigs (see Fig. 5) are fundamentally different from rotary rigs in the way that they retrieve core. A typical coring rig used for minerals exploration stores the core as it is cut in a tube in the lower end of the drill string. At the end of the coring run, a wireline is lowered down the inside of the drill string and is latched into the top of the core tube to retrieve it to the surface. This not only gives a continuous core over the interval of the hole, but is much faster than tripping the drill string to retrieve the core sample as is done in rotary rigs.

If a large-diameter hole is required, then a conventional rotary rig (see Fig. 6) will probably be used and the basic choice to be made is whether it should be a top drive. For many years, as described in the Overview, the drill string was turned by a "rotary table" in the rig floor. A square or hexagonal bushing in this table applies torque to the "kelly" (the topmost part of the drill string), which is square or hexagonal in cross section, so that it can be turned by the table and still slide downward as the hole advances.

Geothermal Resources, Drilling for. Figure 5
Typical coring rig, mast is ~15 m high

In the early 1980s, however, a new system in which the drill string was turned by a motor hanging directly beneath the traveling block gained commercial acceptance (see Fig. 7). This "top drive" technique has at least two critical advantages: instead of adding drill pipe one joint at a time as the hole advances, the driller can work with stands (two or three joints) of pipe,

Geothermal Resources, Drilling for. Figure 6
Rotary drill rig, mast is ~55 m high

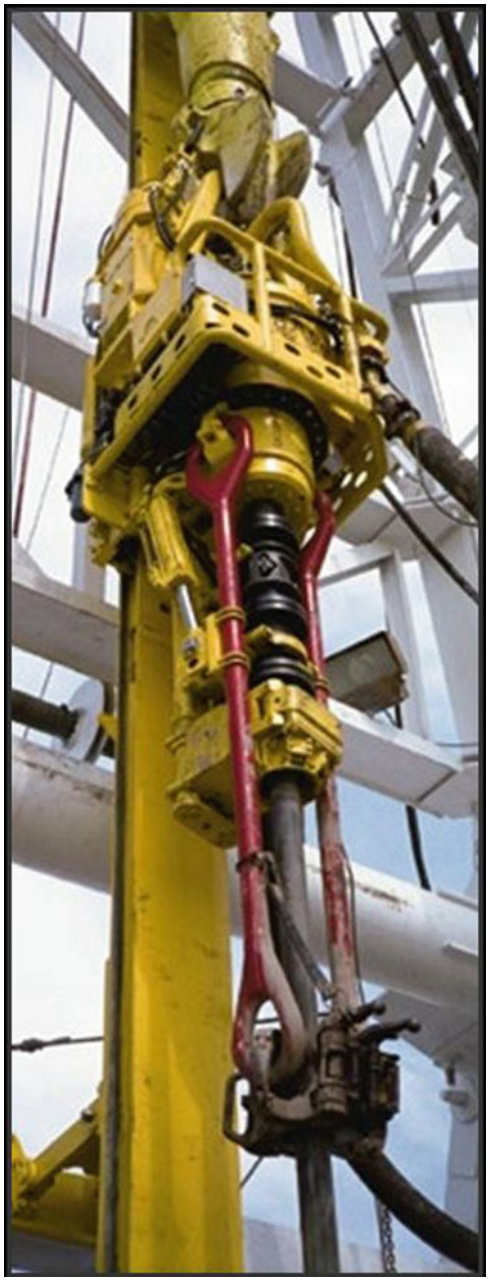

Geothermal Resources, Drilling for. Figure 7
Top drive, photo courtesy of National Oilwell Varco

eliminating time and connections, and the driller can rotate and circulate while tripping. Detailed comparison of operations for one offshore platform [20] showed an 11% decrease in drilling time, and the ability to circulate while tripping is especially important for geothermal wells, because it allows protection of temperature-sensitive tools while tripping into the hole. In one geothermal reservoir [21], it was reported that bit life was improved three- to sixfold by circulating during trips into the hole. The circulation/rotation capability is also useful for avoiding stuck pipe and for working through tight spots during tripping. Top-drive rigs generally cost more in daily rental, but it is often cost effective to use one.

Many considerations will affect the final rig choice but, aside from the purely economic factor of the price quoted by the drilling contractor, the following aspects of the rig should be the minimum list of qualities upon which to make a decision.

Rig capacity: This usually refers to hook load – the weight that can be suspended from the rig's hoisting system. Clearly, the drill string weight, with all the bottom-hole assembly, is an important part of this

requirement, but it should be remembered that the casing is often the heaviest load handled during a drilling project.

Rig footprint: The drilling contractor should provide a dimensioned diagram or map of the rig setup in operating mode. It should clearly show: access points and traffic patterns to various parts of the rig; where different operations (mixing mud, mud logging, etc.) are performed; and the locations where various consumables are stored. If the planned drilling operation includes mud pits, or a water well, those should also be on the map. The contractor's quote will give a cost figure for mobilizing and demobilizing the rig (moving the rig to and from the drilling location) but there should also be an indication of how many truck loads this will entail, and what road clearances are required, in case there are regulatory issues at sensitive locations.

Pump capacity: As discussed under section Drilling Fluids, the pumps must have enough volumetric capacity to give sufficient velocity in the annulus to lift the cuttings. The pumps must also have enough pressure capacity to give the desired pressure drop through the bit jets, and possibly drive a downhole drilling motor, if that is planned or a likely contingency.

Fluid cleaning: These requirements should be defined in consultation with the mud engineer/company, and the rig's shakers, desanders, desilters, and centrifuges should be adequate to the job. There should be some operational consideration of the rig's compatibility with any environmental regulations that affect disposal of the drilling fluid and cuttings, such as the requirement for a closed-loop fluid system with no discharge to the environment.

Drill string and BHA: The bottom-hole assembly design should be defined during planning, so it is clearly important that the rigs have the correct tools, tongs, and fixtures (bit breakers, elevators, etc.) to handle all components of the drill string. It should also be made clear in the contractor's quote whether drill pipe is included in the rig's daily rate. If so, the planner should make certain that it is the correct weight and grade and, if not, the planner should assure that another source of pipe is available.

High-temperature capability: When drilling geothermal wells, it is clearly necessary that any of the rig's downhole or surface equipment that will be exposed to high temperature has that capability. This may be especially noticeable in drilling fluid returns, which will probably be much hotter than in conventional drilling. In most locations, regulatory guidelines will require use of mud coolers when returns exceed a specific temperature, but even with coolers, operating personnel should be aware that hot fluid will create higher-than-normal thermal expansion forces, and that any elastomer seals may become vulnerable to the high temperature.

Rig instrumentation: Complete information about the rig's performance is essential for safe, efficient operation, and the project planner should include an instrumentation list in the rig criteria. Detailed requirements will vary from project to project, but a typical set of desirable measurements includes the following: drilling fluid inflow and outflow rates, drilling fluid inflow and outflow temperatures, standpipe pressure, rotary speed, weight on bit, torque, and kelly height, if available. All these measurements should be digitally recorded on a data logger at reasonably short intervals ($\sim$ every 5 s) so that they can be easily stored and retrieved, but selecting the interval between measurements is not straightforward. For "steady-state" drilling, in which operations are routine, data points every 5–10 s are adequate, but for transient events such as the beginning of a new bit run or the onset of unstable, possibly damaging, drilling conditions, high-resolution data can be extremely valuable. Collecting high-speed data implies very large data files on long drilling projects, which may be a storage problem, but low-speed collection that gives more manageable amounts of data may not give the resolution needed for short-duration events.

Rig instrumentation is often coordinated between the drilling contractor and mud-logging company; see the Instrumentation section below.

Support: In general, rig malfunction or breakdown is one of the less likely kinds of drilling trouble. If the drill site is in an especially remote location, however, it is worth considering how far away the rig's support services may be.

Crew and training: It is not always possible to know in advance who will be working on the rig, but the importance of a well-trained, experienced crew to the project's success cannot be overstated. In the course of evaluating proposals from drilling contractors, every effort should be made to find out the experience and qualifications of the rig crew and supervision.

Like many aspects of drilling, selecting a rig often turns out to be more complicated than it first appears. Keys to a successful choice revolve around having a clear and detailed concept of what is needed for the project. It is frequently very valuable to have an experienced geothermal drilling engineer assigned to the specific task of rig selection, because any extra cost incurred here will almost certainly prove to be well spent.

Drill Bits and Bottom-Hole Assembly

As described in the Overview, the bit is at the lower end of the drill string where, as it rotates, it crushes, gouges, grinds, and cuts the rock to advance the hole. The bottom-hole assembly (BHA) comprises all the components, including the bit, up to the lower end of the drill pipe.

Bits

The bit is usually either a roller cone, which crushes and gouges the rock as the cones turn and their teeth successively come in contact with unbroken areas, or a drag bit, which shears the rock in the same way that a machine tool cuts metal. Because of this shearing action, drag bits are inherently more efficient than roller-cone bits.

The great majority of roller-cone bits today have three cones, with either milled steel teeth (see Fig. 8) that are part of the cone itself or hard-metal (usually tungsten carbide) teeth (see Fig. 9) inserted into the body of the steel cone. Milled-tooth bits are less expensive but are suited only for softer formations. Insert bits are used in medium to harder formations, with the size, shape, and number of inserts varied to fit the specific drilling conditions. The bits are available with either roller or journal bearings, depending on operating conditions, and the bearings, seals, and lubricants should all be specified to withstand high temperatures if the bits are to be used in geothermal drilling. Roller-cone bit technology is very mature – over 100 years since the first patent [22]. Although bit companies still do constant research, and have made significant progress over the last 20 years, the improvements have been incremental. Since the 1950s, R&D for roller-cone bits has alternated between better bearings and more durable cutting structures, depending on which is the dominant failure mode at the time. Roller-cone bits dominate drilling for geothermal resources because of their durability in the hard, fractured rocks that are characteristic of those reservoirs.

Geothermal Resources, Drilling for. Figure 8 Milled tooth roller-cone bit (Photo courtesy of Reed-Hycalog NOV)

Because drag bits reduce rock with a shearing action, they are inherently more efficient than roller-cone bits. Drag bits with polycrystalline-diamond-compact (PDC) cutters (see Fig. 10) began to be widely used in the early 1980s for their ability to drill faster and last longer in soft to medium formations, and they now dominate oil and gas drilling. A particular advantage of drag bits for geothermal drilling is that they do not have any moving parts, so temperature limitations on bearings, seals, and lubricants are not a factor. Unfortunately, PDC bits usually do not have acceptable life in hard or fractured formations, and are not generally used in geothermal drilling. A great deal of work has been done to extend their use to harder rocks [23, 24, 25], and significant progress has been made, but acceptance by the geothermal industry has been minimal. Wider use of these more efficient bits would be a significant technology advance.

Geothermal Resources, Drilling for. Figure 9
Insert roller-cone bit (Photo courtesy of Reed-Hycalog NOV)

Geothermal Resources, Drilling for. Figure 10
PDC drag bit (Photo courtesy of Reed-Hycalog NOV)

If the drilling plan calls for a slimhole to be drilled with a minerals-type core rig, bits are completely different. Much of the rock volume removed from the hole is in the form of core, and the rock cuttings themselves are much smaller, because virtually all hard-rock coring is done with diamond-impregnated bits (see Fig. 11) that grind away the rock.

Principal variations in this kind of bit are the diamond grain size, the diamond grain density, and the hardness of the matrix metal in which the diamond grains are embedded. These bits typically turn at much higher speeds than conventional rotary bits (either roller cone or drag) and have a much lower drilling fluid flow rate because of the smaller annulus between the drill rods and the borehole wall.

Drill Pipe

Choosing the drill pipe specifications can be complicated in some cases, but the primary considerations are the following.

- Strength: The principal requirements are for tensile and torsional strength, so that the pipe can pull the drill string out of the hole (often with some overpull required because of tight spots, or even partially stuck pipe) and can apply the torque needed to rotate the bit. Internal pressure may become an

Geothermal Resources, Drilling for. Figure 11
Diamond-impregnated core bit

issue in some cases, and bending strength is important in directional drilling.

- Size: Given that several different pipe configurations might be strong enough, a major driver for size selection is hydraulics. The internal diameter of the pipe must be large enough to avoid excessive pressure drop in the circulating drilling fluid. It is also necessary that the inside diameter of the pipe be large enough to pass any expected logging tools, and there are sometimes considerations of whether the pipe size is adaptable to fishing tools in the event of trouble. On the other hand, the outside diameter of the drill pipe tool joints must clearly be small enough to pass through the smallest casing to be used, with enough clearance for the same fluid flow on the outside of the pipe.
- Corrosion resistance: Many formation fluids are corrosive; this is especially true in much geothermal drilling. Several special grades of drill pipe are made from alloys designed for corrosive environments.
- Wear resistance: Because many geothermal formations are extremely abrasive, drill pipe tends to wear much faster than in other types of drilling. "Hard banding" (applying layers of wear-resistant material such as tungsten carbide to the outside diameters of the tool joints) is common in geothermal drilling.

Bottom-Hole Assembly (BHA)

A drill string is relatively flexible compared to its length (a scale model, dimensionally, of a 3,000 m drill string is a piece of steel wire, the thickness of a human hair, one meter long). The total weight of the drill string is generally much greater than the desirable force on the bit, so the rig's hoisting capability holds back some of the string weight to control force on the bit. The upper part of the drill string is therefore in tension, while the lower part that applies force to the bit is in compression. Drilling with the relatively thin drill pipe in compression may cause buckling, so it is important that the neutral point (where the drill string stress changes from tensile to compressive) falls within the *drill collars*, which are thick-walled cylinders at the bottom of the drill string. The outside diameter of the collars is controlled by the necessary annulus between the collars and the wellbore, the inside diameter by hydraulic consideration (large enough to prevent excessive pressure drop), and the overall length by that required to provide maximum expected weight on bit. Other components that are often part of the BHA include the following.

- Stabilizers: Because the drill collars and other components must be smaller than the wellbore diameter to provide a path for fluid circulation, they can have major lateral deflections. This can produce serious vibration as well as high fatigue loads in the threaded connections, so stabilizers that have full wellbore diameter on ribs along the outside surface but leave a flow path between the ribs are widely used at multiple points in the bottom-hole assembly.
- Reamers: The outside diameter, or "gauge" of drill bits tends to wear, causing the hole to be smaller than the nominal diameter. When a new bit is tripped in, it has to ream the smaller hole out to the desired diameter, which is time consuming and which causes the new bit to wear prematurely on its own outside diameter. Additional cutting elements, either as fixed cutters or as toothed, cylindrical rollers are often added to the BHA just above the bit, to help maintain the full hole diameter.
- Shock absorbers: When drilling in hard or fractured formations, or those in which soft and hard stringers are interbedded, high vibration loads are common. Shock absorbers, or dampers, are used to attenuate the vibrations transferred to the upper part of the BHA and drill string.
- Jars: If the drill string is stuck in the hole, it can sometimes be released by the impact force produced by jars. These function by suddenly releasing energy stored in the drill string by pulling up on it and stretching it. The two principal types are mechanical jars and hydraulic jars, but both operate on the same principle. Jars are generally used when fishing, but some drillers prefer to have jars already in the drill string during normal drilling.

Directional Drilling

During normal drilling, the pendulum effect of the heavy drill collars tends to keep the hole vertical, but for many of the following reasons it is often necessary to guide or steer the hole's trajectory in a specific direction – institutional, legal, or topographic issues prevent the drill rig from being directly over the geologic target; it is economical

to drill several wells from one prepared site; and, particularly for geothermal wells, it is important for the wellbore to intersect as many formation fractures as possible.

Directional drilling is a relatively complex technology and there are a number of ways to drill a deviated hole, but the most common is to use a downhole motor (hydraulically powered by drilling fluid flowing through it) that turns the drill bit without rotating the drill string. A "bent sub" points the motor and bit at a slight angle to the axis of the drill string or a "bent housing" introduces an angle between the motor and the bit, and since there is no rotation, the bit continues to drill in the direction it is pointed. The difficulties inherent in directional drilling are aggravated in geothermal wells because both the electronic tools used to control and survey the well trajectory and elastomer elements in the motors are susceptible to high temperature. Progress has been made in both of these areas, but it is still often a technical challenge.

Drilling Fluids

Overview

Drilling fluid flows down the drill pipe, through nozzles in the bit, and back up the annulus between the pipe and wellbore wall, carrying the cuttings produced by the bit's action on the formation. (An alternative method, called reverse circulation [26], is sometimes used – the fluid flows in the opposite direction, down the annulus and up the inside of the drill pipe, but it is not common – see the Section Lost Circulation.) Drilling fluids can be either liquid or gas, and liquid-based fluid is universally called "mud" because the first fluids were just a mixture of water and clay.

Drilling mud is made up of three principal components:

- Base liquid: Oil, freshwater, or saltwater can be used as a base liquid in drilling muds, but oil and saltwater are almost totally restricted to hydrocarbon drilling. Freshwater muds are used for geothermal drilling.
- Active solids: Active solids are the clays and polymers added to the water to produce a colloidal suspension. They determine the viscosity of the mud and are known as viscosifiers.
- Inert solids: Inert solids are those added to the mud either by drilling (i.e., particles of the formation) or by using barite as a weighting material. These solids increase the density of the mud without appreciably affecting the viscosity.

Historically, most geothermal drilling fluids have been a fairly simple mixture of freshwater and bentonite clay, possibly with polymer additives [27]. Air drilling is relatively common, especially in areas like the Geysers in northern California, where the reservoir produces dry steam, and air drilling also has advantages in drilling performance because the rate of penetration is usually higher with lighter fluid. Aerated mud has a gas, usually air but sometimes nitrogen if corrosion is serious, injected into it to lighten it, and is also common where lost circulation is a significant problem.

Drilling Fluid Functions

As noted above, the principal function of drilling fluid is to clean the hole of cuttings, but there are several other purposes:

- Cool and clean the bit: keeping the bit cool, especially if it has elastomer seals, is critical to its life.
- Lubricate the drill string: this can be a significant factor in deviated (non-vertical) wells, where the drilling string is lying against the wellbore wall.
- Maintain the stability of the borehole: the proper drilling fluid can help control swelling or sloughing formations, thus lessening the risk of stuck drill pipe. It is also important that the fluid hold the cuttings in suspension when circulation is stopped, so that they do not fall back and pack around the bit and BHA.
- Allow collection of geological information: the cuttings brought back to the surface by the fluid help to identify the formation being drilled.
- Form a semipermeable filter cake to seal the pore spaces in the formations penetrated; this prevents fluid loss from the wellbore.
- Control formation pressures: if high downhole pressures are present or expected, dense material can be added to the drilling fluid to increase its specific gravity, thus resisting the downhole pressure.
- Transmit hydraulic horsepower: this power can be used for driving a drilling motor or for cleaning the hole and/or the bit.

Drilling Fluid System

It should be emphasized that the drilling fluid is part of a *circulating system*, comprising the fluid itself, the mud pumps, and mud-cleaning equipment. The pumps must have sufficient capacity (flow rate and pressure) to provide adequate bottom-hole cleaning, high annular velocity to lift the cuttings, and enough hydraulic horsepower to drive downhole motors and provide the designed pressure drop through the bit jets.

When the cuttings-laden mud returns to the surface, it passes through a series of devices to remove the cuttings. The first of these is usually the shale shakers, which have tilted, vibrating screens that filter out larger cuttings and let them slide off into collection containers; next are usually hydrocyclones, which use fluid inertia to swirl the fluid in a conical chamber, letting the solids drop out the bottom; and finally, centrifuges spin the fluid to extract the finest particles through their density difference. Effective mud cleaning is important for drilling performance as well as cost control. If the fluid has to be discarded because of inadequate cleaning, it is expensive both in material cost and in time loss.

Drilling Fluid Properties

The drilling fluid will be designed to have certain properties, and it is critical to monitor and control these properties at all times. Design and maintenance of drilling fluids is a complex topic, covered in great detail in many sources [28, 29] but primary attributes of fluid for a given well include the following.

- Viscosity: it is vital that the fluid's viscosity be high enough to lift cuttings out of the well as the fluid circulates, and to hold the cuttings more or less in suspension when circulation is stopped.
- Density (or specific gravity): if formation pressures are expected to be high, then the fluid can be weighted to help control them but, as is often the case in geothermal wells, if formation pressures are low, then the fluid should be as light as possible to avoid lost circulation.
- pH: the alkalinity of the fluid is important for corrosion control and for its reaction with certain formation constituents; normal pH is 9.5–10.5, but higher values are not uncommon.
- Filter cake: this is a measure of how well the fluid forms an impermeable layer on the borehole wall to prevent leakage into the formation's natural permeability. (This is typically more important in oil and gas drilling than in geothermal.)
- Solids content: this is a measure of how well the mud is being cleaned, and can also determine when the mud should be discarded or diluted.

There are standard procedures [30] for testing these and other parameters of the drilling fluid, and this testing is normally done at least daily in the field by the drilling fluid specialist or "mud engineer."

Successful mud systems need at least these three attributes:

- Stability: The desired properties of the fluid, once established, should be stable under normal drilling conditions.
- Easy treatment: If the desired fluid properties are lost, treatment should be available to restore them.
- Property testing: Tests and testing equipment should be available to identify fluid properties and indicate any treatment required.

Although the underlying principles of drilling fluids described in the extensive literature are the same for oil/gas and geothermal drilling, high temperatures affect many of the clays and additives used to tailor the fluid properties. Some considerations unique to geothermal drilling are listed below, based heavily on the cited reference [31]:

- Viscosity control: high-quality bentonite clay is the principal vicosifier used in geothermal drilling. Several polymers, available both in liquid and powder form, are also useful but they tend to degrade at high temperatures over long periods of time, so their principal use is for high-viscosity sweeps to clean the hole before cementing, trips, or other activities that require stopping circulation. It is also sometimes necessary to decrease the viscosity, if drilled solids or high-temperature gelation have raised it too high. Proprietary blends of low-molecular-weight polymers and starch derivatives have recently been developed and are effective both in thinning the mud and in inhibiting gelation.
- Solids removal: at high temperatures, the drilled solids tend to take up the available water more

vigorously than at lower temperatures, so effective mud cleaning is even more important than usual to prevent gelation and viscosity increase.

- Filtrate (water loss) control: in the past, geothermal filtrate requirements were often more rigorous than necessary. It is important to analyze the filtrate requirements, not only for each well, but for each interval, so that expensive additives are not used without good cause. Lignite has long been the most common geothermal water-loss reducer, but proprietary polymers are also becoming common.
- Alkalinity: high pH is necessary to control the effect of some wellbore contaminants (CO_2 and H_2S), to reduce corrosion, and to increase the solubility of some mud components (lignite, etc.). Addition of caustic soda (NaOH) has been the traditional method of increasing alkalinity, but caustic potash (KOH) is becoming more common in geothermal drilling because of its benefits to wellbore stability.
- Lubricity: the drill string sometimes needs extra lubrication when directional drilling, and lubrication is very often needed when core drilling, especially when drilling without returns. Hydrocarbon-based lubricants often lose their effectiveness at high temperature, but there are proprietary, environmentally friendly lubricants that offer good performance at sustained high temperature.

Finally, there are instances in which it is desirable to drill with clear water, or clay-free drilling fluids, especially in production zones where conventional clay-based muds create a risk of formation damage. This technique requires a copious water supply, and cannot be used in all wells, but has proven successful in Iceland and in Mexico [32].

Planning the Mud Program

Some general guidelines [33] for planning the drilling fluids program are given below, with a reminder that every well is different and there are very few, if any, generic procedures that can be used without modification. A pre-spud meeting of all operating, drilling, environmental, and service company personnel is highly recommended. Discussions of the drilling plan and contingencies may eliminate trouble later in the program. Once there is agreement on the drilling plan, then the mud program should be planned with the following considerations.

1. Water: Since water is basic to the mud system, it is important to know the quality, quantity, and cost involved with the makeup water. Poor quality makeup water may require chemical treatment prior to its use.
2. Type and thickness of the geologic strata: This is not always known before drilling, but fluid properties must be planned with the best available information about downhole conditions, that is, the reactions between drilling mud and formation.
3. Site accessibility: Make sure that supply trucks have reasonable access to the site and that rig placement in relation to pits, bulk storage, etc., is convenient to reduce handling.
4. Climate: Extremes of heat, cold, and precipitation can affect the mud system and products.
5. Drilling equipment: Make sure that the surface equipment, such as pumps, mixing and circulating tanks, mixing equipment, and solids control capabilities are adequate for the hole size, downhole tools, etc.
6. Environmental considerations: If at all possible, use nontoxic, easily disposed drilling fluids. All personnel should know all regulations pertaining to the job.
7. Manpower: The experience, skill, supervision, and attitude of the rig crews are of paramount importance to a successful drilling program.

This chapter is intended to give some flavor of the complexity of the process that is designing and maintaining a drilling fluid system. It is worth a great deal of attention in preparation for a project, because a high percentage of the problems encountered in drilling are related in some way to the fluids.

Lost Circulation

The most expensive problem routinely encountered in geothermal drilling is lost circulation, which is the loss of drilling fluid to pores or fractures in the rock formations being drilled. In addition to the cost of the drilling fluid itself, the fluid loss and inadequate hole cleaning can create many other drilling problems including stuck drill pipe, damaged bits, slow penetration rates, and collapsed boreholes. Lost circulation represents an average of 10% of total well costs in

mature geothermal areas [34] and often accounts for more than 20% of the costs in exploratory wells and developing fields. Well costs, in turn, represent 35–50% of the total capital costs of a typical geothermal project; therefore, roughly 3.5–10% of the total costs of a geothermal project can be attributable to lost circulation.

Combating lost circulation can be approached in different ways – drill ahead with lost circulation; drill with a lightweight drilling fluid that will have a static head less than the pore pressure in the formation; mix the drilling fluid with fibrous material or particles that will plug the loss apertures in the formation; or pause in the drilling and try to seal the loss zones with some material that can be drilled out as the hole advances.

Drill with Lost Circulation

Under some conditions, it is practical to drill without returns, particularly in the case of core drilling, where the cuttings are very fine and where most of the rock comes out of the hole in the form of core. In many slimhole exploration holes, intervals of hundreds of meters have been drilled with complete lost circulation [16], but this can only be done if the formations are competent enough to remain stable.

Another technology that is useful with lost circulation is dual-tube reverse circulation [35] (DTRC). This method uses a drill string of two concentric tubes, with the drilling fluid passing down the annulus between the inner and outer tubes, circulating out through the bit, and carrying the cuttings back up through the center tube. This means that it is only necessary to maintain fluid around the bit and bottom-hole assembly, so drilling with complete lost circulation is possible. This technique has been used on several geothermal wells [36] and in one case [37] reduced the cost per foot of drilling comparable wells by more than one-third.

Lightweight Fluids

Aerated fluids – liquid with gases injected into it – produce a static head less than the pore pressure and are a common remedy for lost circulation in geothermal drilling. Aqueous (water-based) foam is attractive because of its simplicity, but it is important to use the proper surfactant that has stable properties at high temperature. Considerable modeling was done in the early development of aqueous foam for geothermal drilling [38, 39]. In addition to numerical models of the foam structure and rheology, a laboratory flow loop measured pressure, temperature, and flow rate at different points to allow experimental confirmation of a rheological model.

Aerated drilling is now used extensively in many locations, and recent experience has shown that its use not only avoids problems with lost circulation but may improve the well's productivity after drilling [40].

Lost-Circulation Materials (LCM)

Lost-circulation problems can generally be divided into two regimes, differentiated by whether the fracture aperture is smaller or larger than the bit's nozzle diameter. Clearly, LCM particles that will plug the bit are unacceptable, but for smaller fractures or for matrix permeability, the wellbore can theoretically be sealed by pumping solid or fibrous plugging material mixed with the drilling fluid – this method is much less effective with larger fractures. Very many substances have been used in the oil and gas industry to plug lost-circulation (LC) zones, but most of them have been organic or cellulosic materials that cannot withstand geothermal temperatures. LC zones in oil and gas also tend to be dominated by matrix permeability rather than the much larger fracture apertures common in geothermal reservoirs. Although traditional organic LCM can be used in the upper, cooler, intervals of a well, and several candidate materials that will withstand high temperature have been identified [41], LCM, in general, has often been unsuccessful in geothermal drilling.

Wellbore Sealing

Fractures too large to be plugged by LCM can only be sealed by withdrawing the drill string from the hole and injecting some liquid or viscous material that will enter the fractures, solidify to seal them, and then have its residue removed by resumption of drilling. Conventional lost-circulation treatment practice in geothermal drilling is to position the lower end of an open-end drill pipe (OEDP) near the suspected loss zone and pump a given quantity of cement (typically 10 m^3) downhole. The objective is to emplace enough cement into the loss zone to seal it; however, this does not always occur. Because of its higher density relative to the

wellbore fluid, the cement often channels through the wellbore fluid and settles to the bottom of the wellbore (the larger diameters of geothermal wells aggravate this problem, compared to oil and gas). If the loss zone is not on bottom, the entire wellbore below the loss zone must sometimes be filled with cement before a significant volume of cement flows into the loss zone. Consequently, a large volume of hardened cement must often be drilled to reopen the hole, which wastes time and contaminates the drilling mud with cement fines. Furthermore, because of the relatively small aperture of many loss-zone fractures, the loss zone *may* preferentially accept wellbore fluids, instead of the more viscous cement, into the fractures. This causes dilution of the cement in the loss zone and loss of integrity of the subsequent cement plug. As a result, multiple cement treatments are often required to plug a single loss zone, with each plug incurring significant time and material costs. At least three different approaches have tried to improve this process.

- Cementitious mud: As implied by the name, this is drilling fluid with cement and other materials added to satisfy the criteria: (1) compressive strength above 3.4 MPa after 2 h cure, (2) permeability to water < 10 millidarcies, and (3) volume increase with curing. Brookhaven National Laboratory found that rapid-setting, temperature-driven cement could be formulated by mixing conventional bentonite mud with ammonium polyphosphate, borax, and magnesium oxide [42]. Significant compressive strength was developed by such admixtures in less than 2 h when sufficient concentrations of the magnesium oxide accelerator were used, and the setting time decreased with increased temperature. Furthermore, the material expanded approximately 15% upon setting. These setting characteristics were ideal for plugging major-fracture loss zones, but more control over the setting process was necessary to ensure that the cement would not set up inside drill pipe during field application.
- Better cement placement: Sandia National Laboratories developed a drillable straddle packer (DSP) [43] as a way to improve the effectiveness and reduce the cost of a typical cement treatment by controlling the cement flow into the loss zone and by reducing dilution of the cement caused by other wellbore fluids flowing into the loss zone. An assembly on the end of the drill string carries two fabric bags that straddle the loss zone and provide zonal isolation. The bags are inflated with cement and seal against the wellbore wall, thereby forcing most of the cement to flow into the loss zone. After pumping a specified volume of cement, the straddle packer assembly is disconnected from the drill string and left in the wellbore while the drill string is tripped out of the hole. The packer assembly is constructed of drillable materials: aluminum, fiberglass, and, in some applications, CPVC plastic – after the cement sets, the DSP is drilled out and the operation resumes. This device was successfully tested in a full-scale wellbore and complete design drawings are contained in the reference, but it was never commercialized.
- Polymeric grout: The concept of using polyurethane grout instead of cement to seal fractures was investigated in the 1980s but early efforts were not successful [44]. Recent encouraging laboratory work and the growing use of polyurethane grouting in civil engineering projects [45], however, stimulated new interest in this technology. An opportunity to evaluate polyurethane grout in the field came with a DOE grant to Mt. Wheeler Power that required reopening a well near Rye Patch NV. This well had been temporarily abandoned after 20 cement plugs had failed to cure lost-circulation problems, but a prototype grouting apparatus, combined with DTRC, was successful in sealing a loss zone approximately 6 m in length and allowing the well to be reopened [46]. The polyurethane grout used in the Rye Patch well is not suited for higher geothermal temperatures, but other polymeric grouts have been developed [47] that can withstand 260°C for 8 weeks.

Despite the demonstration of methods described above, familiarity with cementing practice and ready availability of the equipment and materials mean that it is still the dominant method of formation sealing today.

Well Control

Well control, in general, has to do with controlling the flow of drilling fluids and formation fluids out of the

wellbore. If the hole advances into a fractured or permeable stratum where the pore pressure is higher than the static head of the drilling fluid, the formation fluid will flow into the wellbore – this is called a "kick" – and that flow must be controlled. If control of that flow is lost, then the resulting disaster is a "blowout" which, at the least will be very expensive and, at worst, can result in loss of life, equipment, and the drill rig.

The primary method of detecting a kick is to compare measurements of the drilling fluid inflow and outflow; if outflow is greater, there is a kick, if inflow is greater, there is lost circulation. Traditional methods of measuring these flows have been a stroke counter on the mud pumps (a volumetric calculation gives fluid inflow) and a paddle meter on the return line (a flat vane extends into the mud returns such that the angular displacement of the paddle indicates flow rate). Each of these techniques has inaccuracies: pump efficiency (and therefore displacement per stroke) varies with wear and clearances on the pumps, and the paddle meter can be influenced by any number of variables [48]. Development has shown that better methods (magnetic or Doppler flow meters for inflow and rolling float meter for returns) are available [49], and if well control is expected to be an issue, these methods should be investigated.

The apparatus that controls a kick and potential outflow at the wellhead is called the blowout preventer (BOP) or blowout prevention equipment (BOPE). The BOP stack comprises three types of device to shut off the wellbore and prevent fluid flow out of it: annular preventers, pipe rams, and blind rams. The basic function of each is to shut off the wellbore, but they operate in slightly different ways.

- Annular preventer: This is an inflatable bladder that seals around drill pipe, casing, drill collars, or irregularly shaped components of the drill string. It usually has the lowest pressure and temperature ratings of the stack components.
- Pipe rams: These are two sliding gates, each with a semicircular cutout, that come together from each side of the drill pipe. The hole in the center fits and seals around the outside diameter of the drill pipe.
- Blind rams: These are also sliding gates, but there is no hole in the center; they are used when the drill pipe is out of the hole.

Below the BOP stack, two-valved lines (called the choke and kill lines) are connected to the wellhead so that fluids can be either released from or pumped into the wellbore as part of the well-control process. There will usually be detailed regulatory requirements for the BOPE (see the California manual [50], for example, which is also an excellent reference for information on BOPE) but the critical factors are to make sure that the BOP pressure rating is adequate and that all the elastomer seals in the equipment are qualified for high temperature. One of the primary well-control techniques for geothermal drilling is simply to pump cold water down the well, so it is also important to make sure an adequate water supply is available.

In contrast to oil and gas wells, which are often overpressured and where those pressures are controlled by weighted drilling fluids, geothermal wells most often are under-pressured. This means that the formation pressure is *less* than the drilling fluid head, which is the effect that causes lost circulation, as discussed in a previous section. There are exceptions such as wells in Cooper Basin, South Australia, with wellhead pressures of approximately 35 MPa [51] but the principal issues in geothermal well control usually involve unexpected steam flow. This can be caused by drilling into a formation that is at much higher temperature, and circulating the hot fluid up the wellbore, or much higher pressure than predicted, such as an event that occurred in Hawaii [52], or by sudden, major lost circulation. Any of these events, can drop the drilling fluid level to the point that its static head no longer exceeds the saturation pressure at the formation's temperature, and either the drilling fluid or formation fluids flash into steam. Unexpected steam flow in permeable formation that is not completely sealed by casing is particularly dangerous, because steam can begin to flow up the outside of the previous casing string, eventually destroying the casing's integrity and often causing loss of the drill rig [53].

As in many contexts, prevention of a problem is more efficient than a cure. A number of methods are available to estimate the wellbore temperature profile and warn that a problem may be near: comparison of drilling fluid inflow and outflow temperatures, maximum-reading thermometers either run just above the bit or lowered through the drill pipe on a wireline, or onboard logging tools that can transmit temperature

data in real time. Although none of these is guaranteed to provide early warning of a potential kick, it is always important to know as much as possible about the downhole environment.

Having discussed above the problems of steam flow in the wellbore, however, it should be noted that in reservoirs with a dry (superheated) steam resource, such as the Geysers, the production interval is drilled with air to avoid formation damage and plugging [54]. This means that the drilling returns include produced steam from the reservoir. The top of the wellbore is closed by a "rotating head" that seals around the drill pipe, while allowing it to rotate and move downward. The gaseous returns are sent through a manifold called a "banjo box" below the BOP but above a wellhead valve, and then to the "blooie line," which exhausts a distance away from the drill rig and where the returns receive chemical treatment for H_2S abatement. This is very similar to the technique called "managed pressure drilling" in oil and gas reservoirs, where it has been discovered that productivity is much improved if drilling fluid has not been forced into the formation by excessive downhole pressure.

Well control can be a complex topic, but it is clearly critical to a successful drilling operation. Well-control procedures should be part of well planning, so that the proper actions will be established and crews will be familiar with them when drilling begins. It is essential that rig crews be trained to react quickly and appropriately to an unexpected event that might jeopardize the well.

Completions and Cementing

In drilling terminology, a well's *completion* refers to the combination of casing, casing accessories, and cement that allows the well to produce. Casing accessories can refer to perforated or slotted liners in the production zone, internal or external packers, or the hardware necessary for multilateral wells that have more than one leg feeding into the production casing.

Cementing

As described in the Drilling Overview, casing has been traditionally cemented in place by pumping a calculated amount of cement into the casing, placing a movable plug on top of the cement, and then displacing the plug downward with drilling fluid. This forces the cement to flow out the bottom of the casing and up the annulus between the casing and wellbore. In most oil and gas wells, the casing is cemented in place only at the bottom, with a completion fluid between the balance of the casing and the wellbore wall, but geothermal wells must have a complete cement sheath from bottom to surface [55]. This cement has two important functions: to give the casing mechanical support under its sometimes-intense thermal cycling between production and shut-in, and to protect the outside of the casing from corrosion by in situ fluids.

This implies that geothermal cements should have high bond strength to the casing and should be impermeable, but it is also very advantageous for the cement to be lightweight (at least compared to conventional cement, which has a specific gravity of approximately 1.6). Light weight is important because of the oft-encountered lost circulation described above. If the formation's pore pressure will not even support drilling fluids, then it is impossible to lift a column of normal-weight cement back to the surface when casing is cemented in place. One solution to this problem is foam cement, which has gas injected into it, in the same way as drilling fluid is aerated to make it lighter. Recent experience with difficult wells in California [56] and Hawaii [57] has also shown that reverse circulation foam cementing, where the cement is pumped down the annulus and flows back up drill pipe from the bottom of the casing, has several advantages.

If cement returns have not reached the surface in a conventional cement job (i.e., there is an uncemented annulus around the top of the casing), then some method must be used to cement this remaining volume. The most common method is to pump cement, under pressure, into the top of the annulus, which will fracture the formation down to the top of the existing cement. If the cement has reached as high as the top centralizer, then a "top job," which usually means that small-diameter lines (tremie lines) are inserted into the annulus and cement is pumped into them to fill the annular volume, can be performed. The risk in this is that liquid (water or drilling fluid) will be trapped between the upper and lower volumes of cement (see below in *Completions*), so all possible precautions should be taken to avoid

this. If the resources are available, the annulus can be dried with steam [58] to assure the absence of liquid.

Conventional oil well cements are not only too heavy for many geothermal wells, but are susceptible to attack by acids and by CO_2, both of which are common in geothermal reservoirs and both of which degrade the impermeability and strength of the cement. Historically, the major modification to Portland cement for geothermal use is the addition to standard Class G cement of retardants and approximately 40%, or more, silica flour [59], but this does not eliminate the problem of CO_2 and acid attack. Brookhaven National Laboratory carried out a major research program on geothermal cement, intended to mitigate or eliminate these effects. The R&D effort comprised: characterization of cements then used in geothermal environments [60, 61], the extension of hydrothermal cements to higher operating temperatures [62], and the development of new materials such as phosphate-bonded cements [63], polymer cements [64], and other new compositions [65].

BNL worked with cost-sharing industry partners (Halliburton, Unocal, and CalEnergy Operating Company) toward the specific goal of a lightweight cement with outstanding resistance to acid and CO_2 at brine temperatures up to 320°C. Reviews of this work before [66] and after [67] 1997 are provided in detailed reports. BNL succeeded in synthesizing, hydrothermally, two new cements: calcium aluminate phosphate (CaP) cement and sodium silicate-activated slag (SSAS) cement. The CaP cements were designed as CO_2-resistant cements for use in mildly acidic (pH $\sim$ 5.0) CO_2-rich downhole environments. The SSAS cements were designed to resist a hot, strong acid containing a low level of CO_2. Both of these were economical cements because they used inexpensive cement-forming by-products from coal combustion and steel-manufacturing processes. In 1997, Unocal and Halliburton completed four geothermal wells in Sumatra with CaP cement, the first field use of this formulation, and in 1999, Halliburton commercialized it under the name "ThermaLock Cement." SSAS cements have received less attention than CaP, but autoclave experiments in the lab have demonstrated good performance in high-acid environment and, in fact, after undergoing acid damage, the SSAS cement exhibited a self-repairing characteristic. Addition of fly-ash further improved its acid resistance, so SSAS is promising as low-cost geothermal well cement in high-acid conditions up to 200°C.

Completions

Apart from the requirement for a complete cement sheath around the casing, factors that influence completion design include brine chemistry, multibranch completions, and whether the production interval is stable enough to be open hole or must be completed with a slotted liner.

Brine chemistry can cause two major problems: corrosion and scaling. Brine quality varies greatly, ranging from near-potable in moderate-temperature systems to highly corrosive with high dissolved solids in some high-temperature systems. Many techniques – cement-lined casing, exotic alloys, and corrosion-resistant cement – have been applied to the casing corrosion problem, which is especially severe in the Imperial Valley, California. Shallow and hot, CO_2 bearing zones there drive an external corrosion rate approaching 3 mm of carbon steel per year, so the wells must be abandoned after 10–12 years even after well life is extended by cementing in smaller production strings. Most existing production wells in the Imperial Valley have been completed or retrofitted with titanium casing, which has proved to be cost effective in spite of its very high capital investment (approaching US$3,000/m.)

Scaling, the buildup of mineral deposits both inside the casing and in the production interval, is a problem in geothermal plants around the world [68], and can lead to frequent workovers. In severe cases, untreated scaling can reduce the flow area of casing by half in a matter of months. Casing scale can sometimes be removed with high-pressure jets [69], but scaling in the wellbore often seals the formation and must be drilled out with an under-reamer (an expandable bit that can drill a hole below casing that is larger than the inside diameter of the casing). It is highly preferable to inhibit or prevent scale formation than to remove it, and there are many chemical techniques for this, but discussion of those is beyond the scope of this article.

When casing is cemented, it is also critical that no water be trapped between the cement and the casing, especially in intervals where one casing is inside another,

because the water can become hot enough as the well goes on production and heats up that thermal expansion can collapse the inner casing. If the trapped-water location has formation outside it, the fracture gradient is usually low enough to allow the pressure to bleed off into a fracture. These failures can be serious enough that the production casing is imploded and ruptured to the extent that it will reduce production and will provide a path from the formation into the cased hole [70].

Finally, it is necessary to decide whether the production interval of the well is competent enough formation so that it can be left as-drilled (open-hole completion) or whether a slotted liner will be necessary to protect against sloughing or caving into the wellbore. Some indications can be gained from the geologic samples acquired during drilling, or from imaging logs, if available, but this decision is often made based on experience gained from other wells in the same reservoir.

Instrumentation (Drilling and Mud Logging)

This description of instrumentation deals only with those measurements applied to the drilling process, and does not address logging for formation evaluation done during or after drilling. Drilling information comprises both surface measurements – those taken on or around the drill rig – and downhole data retrieved by some type of logging tool that is either lowered into the borehole or forms a part of the BHA.

Surface Measurements

A summary list of desirable measurements for the drill rig was given in the section on rig selection criteria (drilling fluid inflow and outflow rates, drilling fluid inflow and outflow temperatures, standpipe pressure, rotary speed, weight on bit, and torque) but many others exist. The drill rig will have at least a minimum set of instruments that are required for its normal functions, but additional instrumentation and data can be provided by the drilling contractor, the mud-logging company (MLC), or an independent service company. It is most commonly done by the MLC, in conjunction with their primary job of recording the geology of the well, based on the cuttings brought back to surface by the drilling fluid. The MLC also keeps a record of many of the drill rig's operating conditions – a representative MLC, for example, lists all the following measurements as available, so it is the well planner's responsibility to decide which are necessary.

- Depth
- Block height
- Rate of penetration
- Bit depth tracking while tripping
- On bottom/off bottom
- Hook load
- Weight on bit
- Rotary RPM and torque
- Top drive RPM and torque
- Standpipe pressure
- Casing pressure
- Pump stroke rates
- Pump stroke counters
- Totalized pit volumes
- Individual pit volumes
- Trip tank volumes
- Mud gain/loss
- Mud flow rates
- Mud temperature in and out
- Mud weight in and out
- Mud resistivity in and out
- CO_2 and H_2S

Understanding how to use the measurements is clearly important, and should be part of the driller's training. Some comparisons, such as mud flow rates in and out of the wellbore, have been described previously as diagnostics for lost circulation and/or well-control issues. Others, such as a sudden drop in standpipe pressure as an indication of a washout in the drill string, should be part of training. Many of the measurements made by the MLC can be combined electronically in such a way that an alarm will sound if undesirable conditions appear (e.g., the difference in flow rates becomes large). Virtually, all modern MLCs present and record data in digital format, so that it is easily stored, retrieved, and displayed at multiple locations (including a web site, if desired.)

It is also possible to use longer-term data – torque and weight on bit related to rate of penetration, pump efficiency compared to mud flow rate, temperature change as a function of depth – to establish statistical trends that are a measure of drilling performance or downhole conditions. It is also possible, in principle, to combine surface measurements in a way that provides diagnostics for

various drilling conditions and then employs an expert system approach to recommend subsequent action. This has been investigated in the laboratory [71] and some versions of it have been commercialized.

Downhole Measurements

Surface measurements are often ambiguous because there is more than one downhole condition that can produce the same readings at the surface, so downhole measurements are highly valuable in resolving this discrepancy. Downhole measurements can be made in several different ways:

- A sensor package can be lowered into the hole on an electrically conducting cable (wireline), sending back signals in real time as it traverses the wellbore. This method usually requires a specialized wireline truck operated by a logging service company (i.e., this method is relatively expensive and there is some lead time involved unless the truck and crew are on standby at the drill site). Real-time information is advantageous when a very dynamic situation such as drilling is in progress, especially if there is reason to believe that some downhole condition (e.g., pressure, lost circulation, bit dysfunctions) may be harmful, hazardous, or expensive.
- A logging tool with onboard memory can be lowered into the hole on an ordinary cable (slickline), taking readings as it traverses the wellbore, and then brought back to surface where data is downloaded. If real-time data is not required, this method tends to be cheaper and more convenient, because the memory tool can be operated by the rig crew on the rig's hoisting equipment.
- A memory tool can also be part of the BHA, retrieved either when tripping the drill string or by slickline. This method is particularly useful when a slimhole is being drilled with a coring rig, because the memory tool can be part of the core tube and data can be retrieved with every core run.
- An instrumentation package that is part of the BHA can send signals back to the surface through pressure pulses in the drilling fluid. This "mud-pulse telemetry" is most often used for directional drilling, where it provides survey information for steering the hole's trajectory, but it can also send back information on downhole conditions such as pressure and temperature, or on drilling parameters such as shock and vibration. This method provides real-time data from the bottom of the hole, but has a number of disadvantages, in that it is very expensive, is susceptible to high temperature, cannot operate in aerated mud or air, and has a very low data rate (less than 10 baud).
- Signals can also be sent back to surface from a near-bit instrument package through stress waves in the steel drill pipe. This "acoustic telemetry" is reasonably rugged, has a higher data rate than mud pulse (above 20 baud), can operate in any drilling fluid, and has been commercialized by a company in Canada [72].

All of this technology is very mature for the oil and gas industry, but high temperature is a barrier for much geothermal work. Although other parts of a downhole instrumentation package (e.g., seals, the wireline cable head, and sensors) become more difficult in high temperatures, electronic components are the principal challenge. Commercially available electronic components are generally rated at only about 85°C (This is a "guaranteed" operational temperature, although selected components will operate at higher temperatures), unsuitable for use in geothermal environments, so there are three choices: (1) develop electronic components that can withstand higher temperatures, (2) shield conventional components from the high-temperature environment, or (3) use a combination of (1) and (2).

Electronic components can be protected from high temperature by enclosing them in a thermal flask, or Dewar. A Dewar functions like a Thermos bottle, with an evacuated volume between concentric shells providing insulation for the components inside. Like a Thermos bottle, a Dewar in a hot well will eventually (the length of time that the Dewar will protect the electronics is a function of the wellbore temperature, power dissipation requirements of the electronics package, conductivity of the Dewar, and the heat sink inside the package. For typical geothermal applications, the operating envelope is 6–16 h) allow the components inside to heat up to a point at which they may fail. Dewars provide only temporary protection and are expensive and fragile, but even when using high-temperature electronics, they will give the logging tool additional life. Almost all logging tools, both wireline and memory, used in geothermal environments are protected by Dewars.

Electronic components that can operate, unprotected by thermal flasks, at geothermal temperatures, are the ultimate goal. Two technologies – silicon-on-insulator (SOI) and silicon carbide (SiC) – approach that goal. SOI semiconductors can operate virtually indefinitely [73] at 300°C; SiC semiconductors above 450°C – well above existing electronic packaging technology. Some SOI electronic components have been commercially available for several years [74], and a basic suite of SOI-based logging tools is commercially available now.

Of the many measurements that can be made by logging downhole, by far the most useful for drilling purposes is temperature. Apart from the clear necessity to know whether the hole is approaching a geothermal resource, temperature logs can clarify a number of other drilling situations.

- Logs can provide warning if any temperature-limited downhole equipment (including drilling fluid) is approaching its limit.
- If a lost-circulation zone appears during drilling, logs can often define its location (it is not always at the bottom of the hole).
- Logs can guide the amount of retarder to add to cement before cementing casing.
- Because cement has an exothermic reaction as it cures, logs can locate the top of the cement column if returns do not reach the surface.
- For an injection test in a potential production zone, logs can identify fracture locations.
- Logs can usually identify favorable (impermeable) zones for setting packers, if that is part of the test program.

This is only a sample of the applications that logs can have and, for the cases cited above, real-time data is not critical, so memory tools would be quite adequate. These examples indicate the versatility of temperature logs, so having this capability as a standard part of the drilling program is highly useful.

Future Directions

The future direction of geothermal drilling is, in many ways, undefined. This uncertainty stems from the multiple development scenarios that can be envisioned for the industry. It is widely believed that enhanced geothermal systems (the EGS concept is described in detail elsewhere in this encyclopedia but, in general, it means injecting fluid into one well or set of wells, forcing that fluid to gain heat by circulating through fractures in the hot reservoir, and then returning it to the surface through another well or wells. Unlike conventional hydrothermal resources, EGS wells do not produce in situ fluids) (EGS) will provide the bulk of new geothermal capacity, worldwide, but many aspects of EGS development are unresolved. Resource location, reservoir creation, and reservoir management will all be different when applied to EGS than is the case in conventional hydrothermal practice, and these differences could well drive drilling research and development in a new direction compared to past R&D for hydrothermal resources.

Costs and risks may also follow a different pattern with EGS. It is well known that geothermal wells cost more than oil and gas wells of comparable depth, and that drilling costs increase more than linearly with depth. Costs for deep geothermal wells, however, do not increase as rapidly with depth as costs for deep oil and gas wells [36]. There are, in general, four ways to reduce well cost: eliminate "trouble" costs, improve the efficiency of standard operations, introduce new and more efficient operations, or change the well design [75]. Because the "average" EGS well is expected to be considerably deeper than the "average" hydrothermal well, however, the focus of cost reduction may shift among these priorities.

Regardless of the directions that drilling research and EGS development may follow, it is still likely that the geothermal drilling market will remain so small, relative to the oil and gas market, that most innovation in geothermal drilling will derive from technology used in the oil patch. Given that assumption, it is useful to look at several drilling methods and technologies that have gained wide acceptance in the oil and gas industry but have been applied sparingly, if at all, in geothermal wells. The following section describes these technologies, summarizes their advantages (with focus on the geothermal context), and discusses the barriers to their use in geothermal drilling.

Drilling with Casing (DWC)

The casing can be used as the drill string, rotating to turn a bit and advancing with the hole as it gets deeper, so that it is already in place when the hole reaches

desired depth. There are two basic ways that the bit can be attached to the casing: it can be semipermanently mounted, so that it can be dropped off the end of the casing at final depth, or can be drilled through for passage of a subsequent casing string; or it can be mounted on a drilling assembly that is retrieved either by wireline or drill pipe when the bit needs to be changed, or when the hole is at design depth. If a retrievable bit is used, then it must be small enough to pass through the casing's inside diameter; therefore, it must use an under-reamer to cut the diameter that is large enough for the outside of the casing couplings and the annulus for the drilling fluid return flow.

The casing must always be rotated by a top drive unit, and can be connected to the top drive by either screwing into the top coupling of the casing or by a fixture that stabs into the top joint of casing and locks to its inside diameter. The top drive circulates drilling fluid through the casing's inside and back up the outside, just as it would with drill pipe. As in conventional use, the top drive also has the ability to circulate continuously, which can be important in geothermal drilling with heat-sensitive downhole tools.

There are several advantages to this technology, as described in the cited reference [76].

- Eliminate costs, time, and problems related to tripping drill pipe – Time to trip drill pipe and handle the BHA is a significant fraction of total time (and cost) on some wells [77], but it is also the case that many problems of well control and hole stability are associated with trips.
- Reduce lost-circulation problems – Drilling with casing (DWC) systems can continue drilling when lost circulation is encountered. The rock cuttings tend to be washed into the fractures or permeable zones, acting effectively as lost-circulation material. The relatively narrow annulus also means that fluid flow rates can be lower than would be used with conventional drilling in the same size hole.
- Gain casing setting depth – The ability to drill through lost-circulation zones, or other weak formations, means that sometimes the casing can reach a greater depth than would be the case with conventional drilling. It is possible, for some well designs and lithologies, that the casing program could be redesigned to eliminate one string of casing. As shown in Section Well Cost, this is a major saving.
- Improve safety – Handling drill pipe has one of the highest accident incidences in drilling; eliminating this activity means that the crew is exposed to less risk.

Although this technology has been used on hundreds of oil and gas wells, it has seen very limited use for geothermal. There is an issue with retrievable drilling assemblies, because they contain some elastomer components, but the larger factor is hard rock. The cutting structure for most DWC bits uses PDC cutters and, as discussed previously, these cutters have not been notably successful in geothermal formations. Some field experience with hard rock in oil and gas drilling, however, indicates that reasonable performance with roller-cone bits and PDC under-reamers is available [78]. Although a number of questions remain to be answered, this technology appears to have enough potential to warrant further investigation devoted specifically to geothermal drilling.

Expandable Tubulars

As described earlier, casing is installed in successively smaller diameters (see Fig. 3) as the hole gets deeper, so that maintaining the correct diameter in the production zone means having much larger holes and casing at the top of the well. It should also be noted that there is a sizable difference in diameter (10–20 cm) between successive casing strings, so that in the example figure, a 21.6 production interval requires drilling a 102 cm hole at the top. This difference in diameter is required to allow clearance for the couplings on the outside of the inner casing string, to compensate for the fact that the previous casing may not be in a straight hole, and to give sufficient annular area that cement can easily flow through it.

The larger casing sizes and cementing jobs at the top are expensive, however, and drilling larger diameter holes often is slower than drilling a smaller diameter would be. A relatively new technology (first field tested in 1998) makes it possible to run a string of casing with normal clearances and then expand the diameter of the inner string so that the clearance between the two strings is negligible. This diameter increase is implemented by an "expansion cone" in the bottom of the inner casing string (see Fig. 12). Once the hole is drilled, the liner, with the cone assembly in the bottom

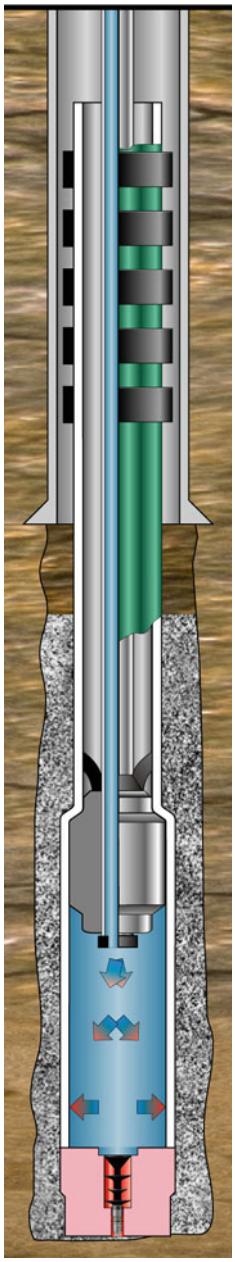

Geothermal Resources, Drilling for. Figure 12 Expandable liner (Diagram courtesy of Enventure Global Technology)

joint, is made up until the desired length is complete. Drill pipe is then screwed into the cone launcher assembly and the liner is run into the hole on the drill pipe. Cement is pumped in the normal way (except less volume than would normally be used) and the cone is forced up the liner by a combination of hydraulic pressure beneath it (delivered through the drill pipe) and pulling with the drill pipe. As the liner expands, it forces the cement upward until the liner annulus is completely cemented.

As shown in Fig. 13, using this system (called SET – solid expandable tubulars – by one manufacturer) means that much less clearance between successive casing strings is necessary and, therefore, the upper casings can be smaller for a given production zone diameter than with conventional casing [79].

When considering this system for geothermal drilling, there at least two potential vulnerabilities: the expandable tubulars depend on elastomer seals in some applications, so the temperature rating of the seals is critical; and the inside of the casing has a proprietary coating to ease the cone's passage through the pipe. It is not clear how this coating would be affected by high temperature, but the system has been used in the field [80] at temperatures above 160°C, and tests are under way to qualify seals for use above 250°C in steam-enhanced oil recovery (SAGD).

Another possible use for expandables is to repair or mitigate lost circulation. A section of casing can be expanded into open hole, rather than into a previous casing string and, if the open hole section has been slightly under-reamed, there will be little, if any, loss of diameter because of the patch. Since no cement is used in this treatment, the casing depends entirely on its external elastomers for zonal isolation, making this component especially important for this application. If it can be shown that all components of expandable tubulars can withstand high temperature, then it appears that there are at least two valuable applications for expandable tubulars in geothermal drilling.

Better Downhole Feedback

Downhole measurements are mentioned in the Instrumentation section, but those were generally measurements related to the state of the wellbore (deviation and trajectory), not real-time data for drilling performance. A few exceptions exist; there is experience with using mud-pulse telemetry to send vibration data uphole [81], but the low mud-pulse data rate limits the applications of these systems. Low data-transmission rates also mean that the downhole sensor package must include a great deal of data processing and, as described

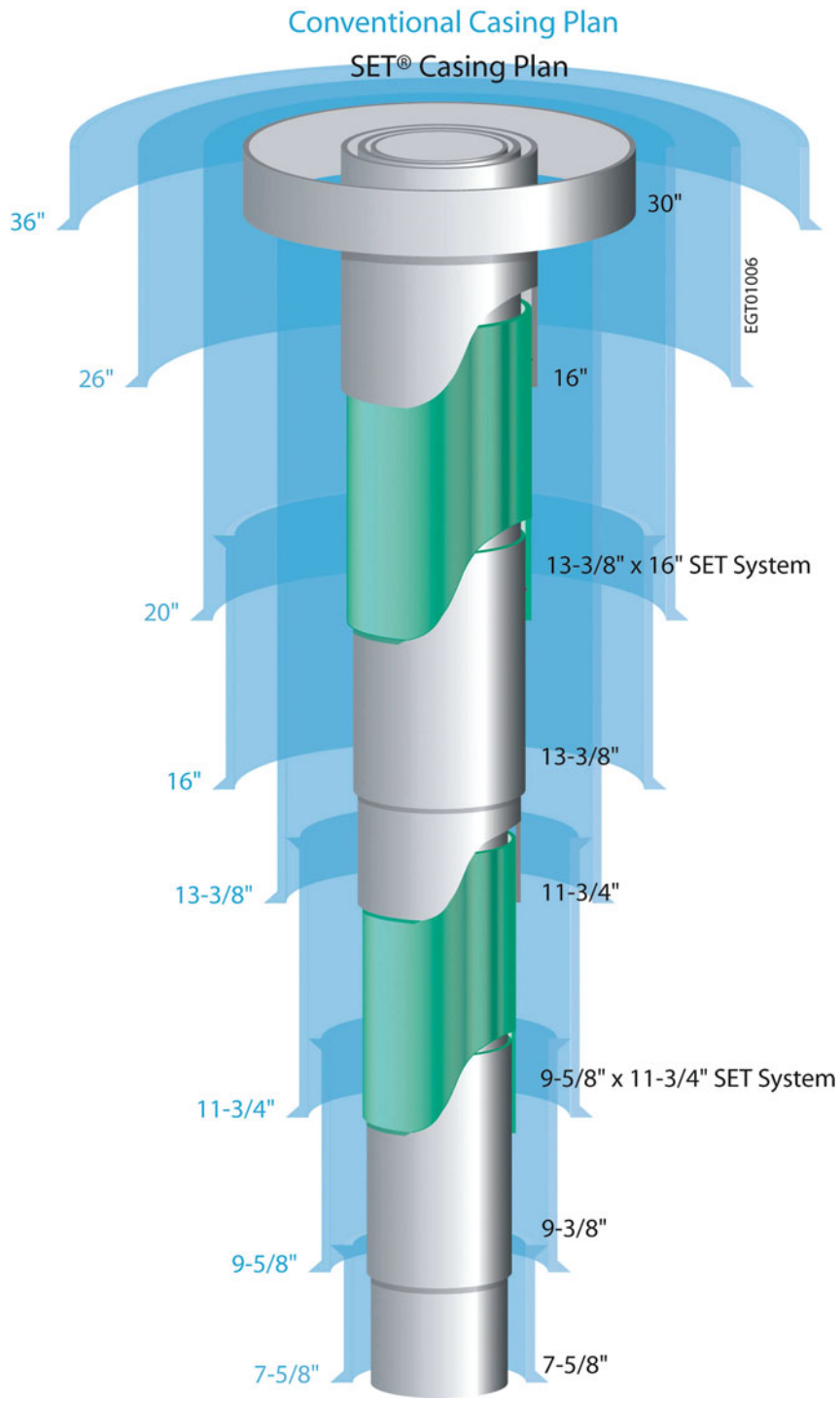

Geothermal Resources, Drilling for. Figure 13
Comparison of casing diameters between SET technology and conventional casing (Diagram courtesy of Enventure Global Technology)

previously, keeping the electronics functional at geothermal temperatures is a challenge.

Better real-time data collection, transmission, and interpretation is a high priority in drilling, corroborated by an industry forum [82] that identified this as the most important technology need for reducing flat time (defined as the time the rig is over the hole, with the hole not advancing). The principal barrier to much of this activity has been the lack of a transmission method with adequate bandwidth. In the last decade, however, drill pipe with built-in instrumentation cable has been developed [83]. This pipe has been used at high bandwidth in the field [84], although not at geothermal conditions, and it offers a very promising opportunity for expanded use of real-time downhole data.

The list of measurements that can be made and transmitted is, of course, very large but they fall into three general categories:

- Improve drilling performance – One of the most common causes for poor bit performance, especially with PDC bits, is excessive shock and vibration. Sandia National Laboratories developed a high-data-rate downhole sensor package to improve PDC performance, and field tests [85] with and without the package demonstrated that it significantly lengthened the life of a PDC bit in hard rock. The primary benefit of the real-time data system was to allow destructive downhole conditions to be immediately recognized and mitigated, but it also showed that surface readings for some parameters (e.g., weight on bit) were much different from the values actually measured near the bit. A later version of this system, modified for high temperature, was run in a geothermal well [86], but it has not been commercialized. Other bit dynamics packages are commercially available, although generally not at high bandwidth.
- Avoid trouble – Aside from the problem of bit failure, many other kinds of trouble (well control, lost circulation, unexpectedly high temperature) can either be avoided or recognized much earlier, allowing more effective treatment, with real-time data.
- Eliminate logging time – With properly configured downhole packages, the well can be logged as it is drilled, eliminating the time (sometimes days) at the end of an interval, or the end of the well, normally required to log it. In some cases, logging could be done with a memory tool rather than with real-time instrumentation, but there is a risk that failure in the logging tool would go undetected until drilling was over.

All of these uses imply high-bandwidth transmission systems and, for geothermal drilling, high-temperature downhole electronics (as well as high-temperature batteries). All of these technologies exist in some form, but they have not yet been put together for geothermal drilling.

For More Information

For more information about the topics in this entry, apart from the extensive references cited, other resources are available. Both the Society of Petroleum Engineers (www.onepetro.org) and the Geothermal Resources Council (www.geothermal.org) provide searchable databases of their own publications that include detailed descriptions of geothermal drilling technology. All of the cited references from *Geothermal Resources Council Transactions* are available through the GRC web site (free to members, nominal charge to nonmembers). Stanford University hosts an annual Geothermal Workshop, and papers from those meetings, as well as from World Geothermal Congress, can be located through http://pangea.stanford.edu/ERE/db/IGAstandard/search.htm. The Office of Science and Technology Information maintains the Department of Energy's Geothermal Technologies Legacy Collection (http://www.osti.gov/geothermal/) and many of the papers cited in this entry are available through that resource. The US Bureau of Land Management provides a summary document describing regulatory requirements for exploration, drilling, production, and abandonment on Federal geothermal leases [87] and The Standards Association of New Zealand has published a 93-page manual that combines regulatory requirements with suggestions on operational practices for drilling, maintenance, repair, and abandonment [88]. Finally, the oil-field service company Schlumberger maintains an online glossary with definitions of many common drilling terms at http://www.glossary.oilfield.slb.com/.

Bibliography

1. International Geothermal Association, Installed Generating Capacity. http://www.geothermal-energy.org/geoworld/geoworld.php?sub=elgen
2. US Department of Energy, Energy Information Administration. http://tonto.eia.doe.gov/dnav/pet/pet_crd_wellend_s1_a.htm
3. Burgoyne AT Jr et al (1986) *Applied drilling engineering*. Society of Petroleum Engineers, Richardson
4. Mitchell RF (ed) (2007) Petroleum engineering handbook, volume II: drilling engineering. Society of Petroleum Engineers, Richardson. ISBN:978-1-55563-114-7
5. Cacini P, Mesini E (1994) Rock-bit wear in ultra-hot holes SPE 28055. SPE/ISRM rock mechanics in petroleum engineering conference, Delft, Netherlands
6. Holligan D et al (1989) Performance of beta titanium in a Salton Sea geothermal production well. SPE 18696, SPE/IADC drilling conference, New Orleans, LA
7. Mansure AJ (2002) Polyurethane grouting geothermal lost circulation zones. SPE 74556 IADC/SPE drilling conference, Dallas TX
8. Renner JL et al (2007) Geothermal engineering. In: Warner HR Jr, (ed) Petroleum engineering handbook, vol. VI: emerging and peripheral technologies. ISBN 978-1-55563-122-2
9. Saito S, Sakuma S (2000) Frontier geothermal drilling operations successful at 500°C BHST, SPE 65104, SPE drilling and completion, September 2000
10. Pierce KG, Livesay BJ (1994) A study of geothermal drilling and the production of electricity from geothermal energy, SAND92-1728, Sandia National Laboratories
11. Pierce KG, Bomber TM, Livesay BJ (1997) Well cost estimates in various geothermal regions. Geothermal Resources Council Transactions, vol. 21
12. Mansure AJ et al (2001) Polyurethane grouting of Rye Patch lost circulation zone. Geothermal Resources Council Transactions, vol. 25
13. Holligan D, Cron CJ, Love WW, Buster JL (1989) Performance of beta titanium in a Salton Sea field geothermal production well source, SPE18696, SPE/IADC Drilling Conference, New Orleans, LA
14. Finger JT, Jacobson RD, Hickox CE (1997) Newberry exploratory slimhole: drilling and testing SAND97-2790, Sandia National Laboratories
15. Finger JT, Jacobson RD, Hickox CE (1996) Vale exploratory slimhole: drilling and testing SAND96-1396, Sandia National Laboratories
16. Finger JT et al (1999) Slimhole handbook: procedures and recommendations for slimhole drilling and testing in geothermal exploration SAND99-1976, Sandia National Laboratories
17. http://office.microsoft.com/en-us/project/default.aspx
18. Combs J, Garg SK, Livesay BJ (2000) Maximum discharge of geothermal fluids from slim holes by optimizing casing designs. Geothermal Resources Council Transactions, vol. 24
19. Mitchell RF (ed) (2007) Petroleum engineering handbook, volume ii: drilling engineering. Society of Petroleum Engineers, Richardson. ISBN:978-1-55563-114-7
20. Cavanaugh, J.M., Adams, D.M., (1988). Top-drive drilling system evaluation. SPE Dril Eng 3(1) 43–49
21. Saito S et al (2003) Advantages of using top-drive system for high temperature geothermal well drilling. Geothermal Resources Council Transactions, vol. 27, pp 183–187
22. US Patent 930,758 "Drill" issued 10 Aug 1909
23. Finger JT, Glowka DA (1989) PDC bit research at Sandia National Laboratories, Sandia Report SAND89-0079, Sandia National Laboratories
24. Wise JL et al (2003) Hard-rock drilling performance of a conventional PDC drag bit operated with, and without, benefit of real-time downhole diagnostics. Geothermal Resources Council Transactions, vol. 27
25. Hareland G et al (2009) Cutting efficiency of a single PDC cutter on hard rock. J Can Pet Technol 48(6):60–65
26. Rickard WM, Johnson B, Mansure AJ, Jacobson RD (2001) Application of dual tube flooded reverse circulation drilling to rye patch lost circulation zone. Geothermal Resources Council Transactions, vol. 24
27. Zilch HE, Otto MJ, Pye DS (1991) The evolution of geothermal drilling fluid in the Imperial Valley SPE21786, Presentation at the SPE Western Regional Meeting, Long Beach, CA
28. Carter TS (ed) (1997) Drilling fluids. Society of Petroleum Engineers, Richardson. ISBN:978-1-55563-069-0
29. Bourgoyne Jr AT, Millheim KK, Chenevert ME & Young Jr FS (1991) Applied Drilling Engineering, Society of Petroleum Engineers,ISBN:978-1-55563-001-0
30. American Petroleum Institute (2003) RP 13B-1/ISO 10414-1, Recommended practice for field testing water-based drilling fluids (includes Errata, July 2004) Product Number: GX13B13
31. Tuttle JD (2005) Drilling fluids for the geothermal industry – recent innovations. Geothermal Resources Council Transactions, vol. 29
32. Jaimes-Maldonado J, Cornejo-Castro S (2006) Case study: underbalanced or mud drilling fluids at Tres Virgenes geothermal field. Geothermal Resources Council Transactions, vol. 30
33. Finger JT, Jacobson RD, Hickox CE, Combs J, Polk G, Goranson C (1999) Slimhole handbook: procedures and recommendations for slimhole drilling and testing in geothermal exploration, Sandia Report SAND99-1976, Sandia National Laboratories
34. Carson CC, Lin YT (1982) the impact of common problems in geothermal drilling and completion. Geothermal Resources Council Transactions, vol. 6
35. Rickard WM et al (2001) Application of dual tube flooded reverse circulation drilling to Rye Patch lost circulation zone. Geothermal Resources Council Transactions, vol. 25
36. Mansure AJ, Bauer SJ (2005) Advances in geothermal drilling technology: reducing cost while improving longevity of the well. Geothermal Resources Council Transactions, vol. 29

37. Petty S et al (2005) Lessons Learned in Drilling DB-1 and DB-2, Blue Mountain NV, Proceedings, thirtieth workshop on geothermal reservoir engineering. Stanford University, CA
38. Drotning WD, Ortega A, Harvey PE (1982) Thermal conductivity of aqueous foam, Sandia Report SAND82-0742, Sandia National Laboratories
39. Rand PB, Montoya O (1983) Evaluation of aqueous foam surfactants for geothermal drilling fluids, Sandia Report SAND83-0584, Sandia National Laboratories
40. Gislason T, Richter B (2008) The aerated drilling experience of icelandic geothermal wells. Geothermal Resources Council, Transactions vol. 32
41. Loeppke G (1986) Evaluating candidate lost circulation materials for geothermal drilling. Geothermal Resources Council Transactions, vol.10
42. Sugama T et al (1986) Bentonite-based ammonium polyphosphate cementitious lost-circulation control materials. J Mater Sci 21
43. Staller GE (1999) Design, development and testing of a drillable straddle packer for lost circulation control in geothermal drilling, Sandia Report SAND99-0819, Sandia National Laboratories
44. Glowka DA et al (1989) Laboratory and field evaluation of polyurethane foam for lost circulation control. Geothermal Resources Council Transactions, vol. 13
45. Mansure AJ, Westmoreland JJ (1999) Chemical grouting lost-circulation zones with polyurethane foam. Geothermal Resources Council Transactions, vol. 23
46. Mansure AJ et al (2001) Polyurethane grouting of rye patch lost circulation zone. Geothermal Resources Council Transactions, vol. 25
47. Mansure AJ et al (2004) Polymer grouts for plugging lost circulation in geothermal wells, Sandia Report SAND2004-5853, Sandia National Laboratories
48. Schafer DM et al (1992) Development and use of a return line flowmeter for lost circulation diagnosis in geothermal drilling. Geothermal Resources Council Transactions, vol. 16
49. Whitlow GL et al (1996) Development and use of rolling float meters and Doppler flow meters to monitor inflow and outflow while drilling geothermal wells. Geothermal Resources Council Transactions, vol. 20
50. Manual M07, California Department of Conservation (2006) Blowout Prevention in California. http://www.conservation.ca.gov/dog/geothermal/pubs_stats/Pages/instruction_manuals.aspx
51. Karner SL (2005) Creating permeable fracture networks for EGS: engineered systems versus nature. Geothermal Resources Council, Transactions, vol. 29
52. New Scientist (1991) Blowout blights future of Hawaii's geothermal power, 20 July 1991, issue 1778
53. Herras EB et al (2004) A geoscientific approach in the design and success of the first relief well at the Leyte geothermal production field. Geothermal Resources Council Transactions, vol. 28
54. Pye DS, Hamblin GM (1991) Drilling geothermal wells at the geysers field. Geothermal Resources Council, Monograph on the Geysers Geothermal Field, Special Report No. 17
55. Nelson EB et al (1981) Evaluation and development of cement systems for geothermal wells SPE10217, Society of Petroleum Engineers
56. Bour DL, Hernandez R (2003) C02 Resistance, improved mechanical durability, and successful placement in a problematic lost circulation interval achieved: reverse circulation of foamed calcium aluminate cement in a geothermal well. Geothermal Resources Council Transactions, vol. 27
57. Spielman P et al (2006) Reverse circulation of foamed cement in geothermal wells. Geothermal Resources Council Transactions, vol. 30
58. Saito S (1994) A new advanced method for top-job casing cementing. Geothermal Resources Council Transactions, vol. 18
59. Koons BE et al (1993) New design guidelines for geothermal cement slurries. Geothermal Resources Council Transactions, vol. 17
60. Nelson EB Development of geothermal well completion systems, final report, Dowell Division, Dow Chemical, USA, DOE Contract DE-ACO2-77ET28324
61. Kalyoncu RS, Snyder MJ (1981) High-temperature cementing materials for completion of geothermal wells, BNL-33127, Brookhaven National Laboratory
62. Curtice DK, Mallow WA (1979) Hydrothermal cements for use in the completion of geothermal wells, Southwest Research Institute, BNL 51183
63. Rockett TJ (1979) Phosphate-bonded glass cements for geothermal wells, University of Rhode Island, BNL 51153
64. Zeldin AN, Kukacka LE (1980) Polymer cement geothermal well-completion materials, final report, Brookhaven National Laboratory, BNL 51287
65. Roy DM et al (1980) New high temperature cementing-materials for geothermal wells: stability and properties, The Pennsylvania State University, BNL 51249
66. Kukacka L (1997) Geothermal materials development at Brookhaven National Laboratory, BNL-64482, Brookhaven National Laboratory
67. Sugama T (2006) Advanced cements for geothermal wells, BNL 77901-2007-IR, Brookhaven National Laboratory
68. Ocampo-Díaz J, Rojas-Bribiesca M (2004) Production problems review of Las Tres Virgenes geothermal field, Mexico. Geothermal Resources Council Transactions, vol. 28
69. Hurtado R, Mercado S (1990) Scale control studies at the Cerro Prieto geothermal plant. Geothermal Resources Council Transactions, vol. 14
70. Southon JNA (2005) Geothermal well design, construction and failures. Proceedings World Geothermal Congress, Antalya, Turkey

71. Harmse JE et al (1997) Automatic detection and diagnosis of problems in drilling geothermal wells. Geothermal Resources Council Transactions, vol. 21
72. Drumheller DS, Kuszmaul SS (2003) Acoustic telemetry, Sandia Report SAND2003-2614, Sandia National Laboratories
73. Normann RA, Henfling JA (2004) Aerospace R & D benefits future geothermal reservoir monitoring. Geothermal Resources Council Transactions, vol. 28
74. Henfling JA, Normann RA (2002) Advancement in HT electronics for geothermal drilling and logging tools. Geothermal Resources Council Transactions, vol. 26
75. Mansure AJ et al (2005) Geothermal well cost analyses 2005. Geothermal Resources Council Transactions, vol. 29
76. Warren TM (2009) Casing while drilling, in advanced drilling and well technology, Society of Petroleum Engineers, ISBN 978-1-55563-145-1
77. Polsky Y (2008) Enhanced geothermal systems (EGS) well construction technology evaluation report, SAND 2008-7866, Sandia National Laboratories
78. Tessari RM, Warren TM (2003) Casing drilling reduces lost circulation problems. Geothermal Resources Council Transactions, vol. 27
79. Tubbs D, Wallace J (2006) Slimming the wellbore design enhances drilling economics in field development, SPE 102929, SPE Annual Conference and Exhibition, San Antonio, TX
80. Nylund J et al (2009) Integrating solid expandables, swellables, and hydra jet perforating for optimized multi-zone fractured wellbores, SPE 125345, Tight Gas Completions Conference, San Antonio, TX
81. Shuttleworth NE et al (1998) Revised drilling practices, VSS-MWD tool successfully addresses catastrophic bit/drillstring vibrations, SPE 39314, SPE/IADC Drilling Conference, Dallas, TX
82. Drilling Engineering Association and Energy Research Clearing House (1999) Flat time reduction opportunities: an industry forum, Houston Advanced Research Center, 21 September 1999, Houston, TX
83. Jellison MJ et al (2003) Telemetry drill pipe: enabling technology for the downhole Internet, SPE 79885, IADC/SPE Drilling Conference, Amsterdam, Netherlands
84. Allen S et al (2009) Step-change improvements with wired-pipe telemetry, SPE 119570, SPE/IADC Drilling Conference, Amsterdam, Netherlands
85. Finger JT et al (2003) Development of a system for diagnostic-while-drilling (DWD), SPE 79884, IADC/SPE drilling conference, Amsterdam, Netherlands
86. Blankenship DA et al (2005) High-temperature diagnostics-while-drilling system. Geothermal Resources Council Transactions, vol. 28
87. 43 CFR Part 3200, Geothermal resources leasing and operations; final rule, Federal Register, vol. 63, No. 189, 30 September 1998
88. Standards Association of New Zealand (1991) New Zealand Standards NZS 2403:1991, Code of practice for deep geothermal wells, 93 pp

Geothermal Resources, Environmental Aspects of

Trevor M. Hunt
GNS Science, Wairakei Geothermal Research Centre, Taupo, New Zealand

Article Outline

Glossary
Definition of the Subject
Introduction
Possible Environmental Impacts and Their Causes
Methods of Avoiding or Minimizing Impacts
Future Directions
Bibliography

Glossary

Aquiclude A geological formation which will not transmit water and is a barrier to vertical movement of geothermal fluid.

Aquifer A geological formation (or formations) which contains water or geothermal fluid and will allow fluid movement.

Downflow Flow of water down a path of high-permeability such as a fracture or a drillhole.

Enhanced geothermal system (EGS) Also called "hot-dry rock". A form of geothermal development in which heat is extracted from rocks that are hot but have low permeability and often low porosity. The rock is artificially fractured by pumping water into it to form a subsurface heat exchanger.

Epicenter The point on the Earth's surface directly above the hypocenter or focus of an earthquake.

Groundwater Water, generally cold and of meteoric origin, which resides in near-surface aquifers and is often used for domestic and industrial purposes.

High-temperature system A geothermal system, or part thereof, containing fluid having a temperature greater than 150°C. c.f. *Low-temperature system* in which the temperature is less than 150°C. It can also be argued that the temperature limit be 180°C, since this is the temperature required for a self-discharging well in a liquid-dominated field.

Hydrothermal eruption An eruption resulting from a localized increase in steam pressure in near-surface

aquifers exceeding the overlying lithostatic pressure, and the overburden is then ejected, generally forming a crater 5–500 m in diameter and up to 500 m in depth (although most are less than 10 m deep).

Hypocenter The point at which an earthquake occurs (i.e., the place of rupture), in three-dimensional coordinates (x, y, z) c.f. epicenter (x, y).

Injection (reinjection) The process of returning waste water from a geothermal power station back into the ground. This is generally around the edges of the field and may not be into the production aquifer from which fluid is drawn off to the power station.

Liquid-dominated system A geothermal system, or part thereof, in which the pressure is hydrostatically controlled. c.f. *Steam (vapor)-dominated system* in which the pressure is steam static.

Non-condensible gas A gas present in geothermal fluid which does not become dissolved in the waste water after the fluid has been condensed.

Reservoir The region of a geothermal system from which geothermal fluid is withdrawn, or is capable of being withdrawn.

Permeability A measure of the ability of a geological formation to transmit a fluid.

Waste water Geothermal water from which energy has been extracted and is no longer required. This may be steam that has passed through turbines or a binary plant and been condensed, or separated water.

Definition of the Subject

The Encyclopedia of Environmental Science considers the environment to be "the sum of all external conditions and influences affecting the life and development of organisms" [1] and the Oxford Dictionary defines it as "the set of circumstances or conditions . . . in which a person or community lives, works, develops, etc., or a thing exists or operates; the external conditions affecting the life of a plant or animal" [2].

The term "environment" is therefore generally used in a broad sense to encompass not only physical conditions, but also the cultural and spiritual conditions of people living nearby.

All sources of energy that are used involve some impact on the environment, either in the process of energy extraction, use or in manufacturing the equipment involved. Key features of the geothermal environment are:

Natural Thermal Features

In many geothermal fields there are beautiful natural thermal features that vary in color and form: geysers, fumaroles, hot springs and pools, silica sinter terraces, mud pools, algal mats, thermophilic plants, and areas of heated ground. They are environmentally important because they are rare on a worldwide basis, and often fragile.

Thermal features are often associated with myths and legends in native peoples culture [3]. For example, the native Maori people of New Zealand have a legend that the thermal areas of NZ were formed when fire gods, summoned from far away and traveling underground, surfaced looking for the person who called them. Many societies that use geothermal energy incorporate it into their ceremonies, for example, in Beppu (Japan) they hold a Hot Spring Festival every year.

Cultural Uses

Bathing in geothermal waters is often claimed to have special medicinal properties, and in New Zealand, geothermal waters are used in the government hospital at Rotorua for the treatment of arthritis and skin diseases. Boiling hot pools are used for cooking: food is placed in a woven basket and lowered into the hot pool – this is still done in Japan and New Zealand, but mainly for tourists. In primitive native societies, red and yellow ochre, formed from hydrothermal alteration of rocks, was used to paint the face and body.

Reasons for Preservation

The most compelling reasons why attempts should be made to preserve the environment are:

Self-respect Most human cultures value their surroundings, even to the extent of significantly modifying them to enhance its beauty or desirability. It is generally recognized that the destruction of beautiful natural thermal features such as geysers, hot springs, and silica terraces is unacceptable. The famous American

philosopher Thoreaux said: "What is the use of a house if you have not got a tolerable planet to put it on?" [4].

Self-preservation Few advanced living organisms will significantly alter or destroy their surroundings because this is likely to threaten their continued existence as a species.

Maintaining Heritage The natural environment is a heritage, inherited from preceding generations, and it is the responsibility of the present generation to pass it undamaged to future generations.

Economic Effects Changing the environment can have negative economic effects. In the case of geothermal development, the destruction, loss, or modification of beautiful natural thermal features can badly affect tourism, which is often a major source of revenue and employment.

To Meet National and International Obligations In most countries, industrial development (including geothermal) is contingent on the developer obtaining a permit (from a regulatory authority) that involves assessing the impact the development may have on the environment and these are difficult to obtain if significant environmental effects are predicted. Preservation of the environment is also of international concern: 21 of 27 Principles proclaimed by the 1992 United Nations Conference on Environment and Development (Earth Summit) refer specifically to the environment.

Introduction

Use of geothermal energy may have some environmental impacts, most of which are associated with the exploitation of high-temperature liquid-dominated geothermal systems for electric power generation. The majority of these impacts, however, can be avoided or minimized with appropriate techniques.

Possible Environmental Impacts and Their Causes

Impact of Access and Field Development Destruction of forests and vegetation resulting from construction of road access to drilling sites can lead to landslides and soil erosion, especially in tropical areas with steep hillsides and high, and occasionally intense, rainfall. The mud resulting from such erosion can choke waterways and inhibit aquatic life. Such effects can extend for large distances downstream, even as far as the coast where fishing industries may be affected.

Effects of Drilling Operations Drilling operations are generally noisy and accompanied by fumes from large diesel engines that drive the drill string and generators that provide electricity to the site. Drilling is generally a continuous (24-h, 7-day) operation, and at night powerful lights are used to illuminate the drill pad area. It may take 1–3 months to drill a deep well (1–5 km deep). The impacts of such operations on people living nearby can be severe, especially at night.

Disposal of Waste Drilling Fluid Drilling involves using a thixotropic fluid ("mud") to provide hydrostatic pressure to prevent formation fluids from entering into the well bore, cooling the drill bit, bringing up drill cuttings, and suspending the drill cuttings, while drilling is paused and the drill string is brought in and out of the hole [5]. The mud is generally a mixture of water and clays such as bentonite, together with additives such as barium sulfate (barite), natural and synthetic polymer, asphalt and gilsonite. Other chemicals (e.g., Potassium formate) are often added to achieve various effects such as controlling viscosity, shale stability, enhancing the drilling rate, and cooling and lubricating the equipment. Deflocculants, such as anionic polyelectrolytes (e.g., acrylates, polyphosphates, lignosulfonates, or tannic acid derivates), are frequently used to reduce viscosity of the drilling fluid. If drilling encounters a highly permeable formation and fluid is lost then bridging agents such as calcium carbonate or ground cellulose are added. If some of these chemical agents are released into natural waterways they can kill aquatic life and result in groundwater contamination.

Mass Withdrawal

Large-scale exploitation of liquid-dominated, high-temperature geothermal systems involves the withdrawal of large volumes (and hence mass) of geothermal fluid from the ground which, if not corrected for, may cause:

Pressure Declines in the Reservoir Withdrawal of large volumes of geothermal fluid are associated mainly with electric power generation. After passing through the power plant the fluid withdrawn (condensed steam and separated water) is usually injected back into the ground, however, the injection wells are generally located away from the production wells to reduce the chances of the cooler-injected water returning to the production wells and reducing the temperature of production fluids. Even if all the waste liquid is injected, there may be mass loss (up to 30% of that withdrawn) associated with evaporation of condensate from ponds where the water is cooled before injection and from the discharge of non-condensible gases into the atmosphere from the power station. A major consequence of the mass loss from parts of the field is often the formation of a two-phase (steam + water) zone in the upper part of the reservoir in the vicinity of the production wells, and as production continues this zone increases in size and the pressures decrease (both in and below this zone). At Wairakei (New Zealand), the deep (liquid phase) pressures declined by about 0.3 MPa (three bar) during discharges associated with exploratory drilling, and a further 2 MPa (20 bar) during the first 10 years of production, although subsequent pressure declines were less than 0.5 MPa (five bar) and pressures have risen since 1997 [6]. Pressure declines in the reservoir, as a result of mass withdrawal and net mass loss, are an important cause of environmental changes at or near the surface.

Degradation of Thermal Features In their natural, unexploited state many high-temperature geothermal systems are manifested at the surface by thermal features such as geysers, fumaroles, hot springs, hot pools, mud pools, sinter terraces, and thermal ground with special plant species (Figs. 1–4). Often these features are of great cultural significance [3], as well as being important tourist attractions. The thermal features result from the (upward) leakage of boiling geothermal fluid from the upper part of the reservoir, through overlying cold groundwater, to the surface.

Historical evidence shows that natural thermal features have been affected, often severely, during the development and initial production stages of most high-temperature geothermal systems. At Wairakei (New Zealand), nearly all the thermal features in the Waiora and Geyser Valleys (including more than 20 geysers) have died or been significantly reduced (Fig. 5, [7]). At Ohaaki (New Zealand), the level and temperature of water in the Ohaaki Pool declined soon after exploration drilling and reservoir testing began, but has been restored by discharging some of the warm waste water from the power plant into the pool [8]. At Tongonan field (Philippines) flow from hot springs decreased after production began [9]. Such effects are not confined to liquid-dominated systems. At Larderello (Italy), where the original natural activity consisted of numerous steam and gas jets, activity has now largely ceased. At The Geysers (USA), there has been a decrease in the flow from hot springs since exploitation began.

Geothermal Resources, Environmental Aspects of. Figure 1
Beehive Geyser, Yellowstone National Park, USA

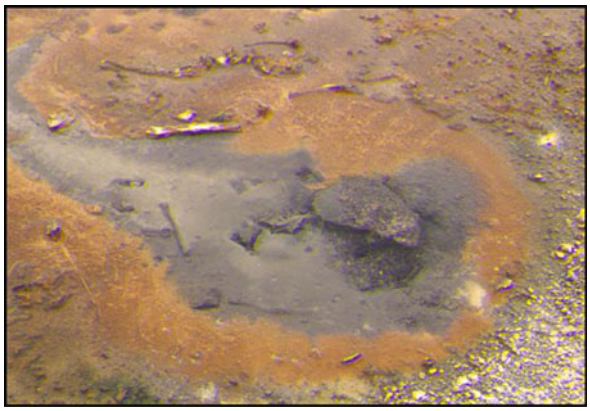

Geothermal Resources, Environmental Aspects of. Figure 2
Hot spring, Norris Geyser Basin, Yellowstone National Park, USA

Geothermal Resources, Environmental Aspects of. Figure 3
Morning Glory hot pool, Yellowstone National Park, USA

Geothermal Resources, Environmental Aspects of. Figure 4
Minerva Terraces, Yellowstone National Park, USA

The decline in thermal features appears to be associated with a decline in reservoir pressure. As the pressure declines, so also does the amount of geothermal fluid reaching the surface and hence the thermal features decline in size and vigor. If pressures fall further then the features may die and the flow may reverse with cold groundwater flowing down into the reservoir; once this situation has occurred it may take a long time to resurrect the features. To reduce the possibility of this occurring, injection is undertaken to keep reservoir pressures as high as possible.

Depletion of Groundwater Most high-temperature geothermal systems are overlain by a cold groundwater zone. If exploitation of the system results in a large pressure drop in the reservoir, this groundwater may be drawn down into the upper part of the reservoir in places where there are suitable high-permeability paths (such as faults). If the lateral permeability of the rocks in the groundwater zone is low then a downflow may result in a drop in the groundwater level. For example, at Wairakei, a localized drop of more than 30 m in groundwater level has occurred associated with an area of cold downflow (Fig. 6, [10]).

Downflows, and resultant groundwater level changes, may also occur as a result of breaks in the casing of disused wells [11]. Such downflows may have flow rates of up to 100–150 t/h.

Ground Deformation Withdrawal of fluid from an underground reservoir can result in a reduction of formation pore pressure which may lead to compaction in rock formations having high compressibility and result in subsidence and horizontal movements at the surface. Such ground movements have also been observed in groundwater reservoirs [12, 13] and petroleum reservoirs [14, 15], and can have serious consequences for the stability of pipelines, drains, and well casings. If the geothermal field is close to a populated area, then subsidence could lead to instability in dwellings and other buildings.

The largest recorded subsidence in a geothermal field (15 m) is in part of the Wairakei-Tauhara field (New Zealand) [16]. Here the subsidence has caused: compressional and tensional strain on pipelines and lined canals, deformation and breaking of drill casing, tilting of buildings and the equipment inside, breaking of sealed road surfaces and alteration of the gradient of streams (Fig. 7, [17]). However, the greatest subsidence rates are confined to small areas (called "bowls") and have decreased since reservoir pressures have stabilized (Fig. 8). In the central part of the bowl there is compressional deformation that may manifest itself as pressure ridges, and on the edges there is tensional deformation that may manifest itself as cracks in the ground (Fig. 9, [16]).

Ground movements have been recorded in other high-temperature geothermal fields in New Zealand (Table 1), at Cerro Prieto (Mexico) [18], Larderello (Italy) [19], and The Geysers (USA) [20, 21].

Ground Temperature Changes The formation and expansion of a two-phase zone, in the early stages of

Geothermal Resources, Environmental Aspects of. Figure 5
Champagne Cauldron in Geyser valley at Wairakei, New Zealand, before (*left*, painting by T. Ryan) and after 20 years of development (*right*). Arrows point to the same rock promontory

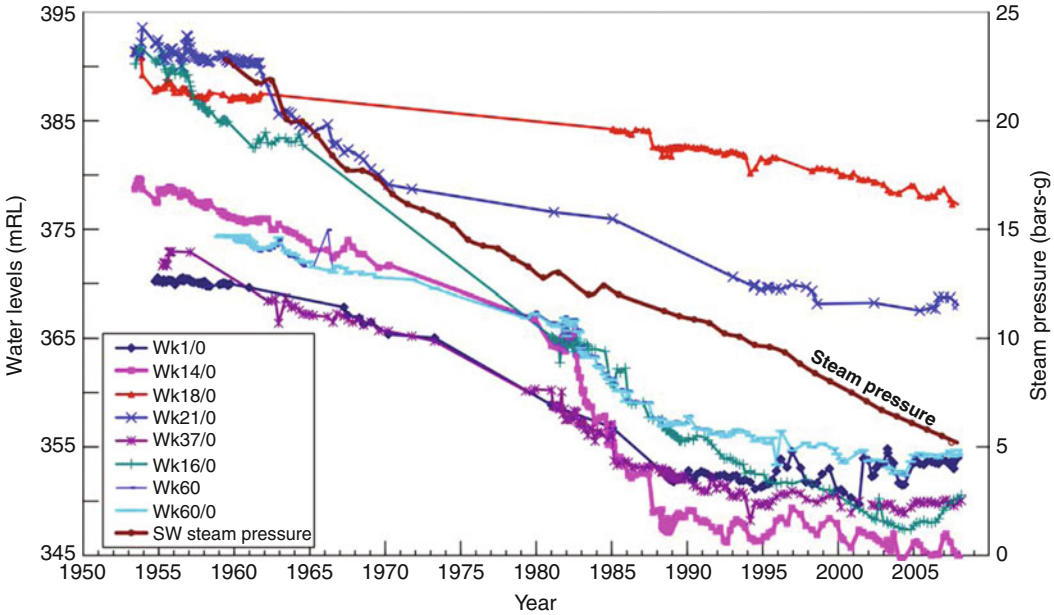

Geothermal Resources, Environmental Aspects of. Figure 6
Changes in level of groundwater in shallow monitor holes at Wairakei (Taken from [10])

Geothermal Resources, Environmental Aspects of. Figure 7
Ponding of the Wairakei Stream near the center of the main subsidence bowl at Wairakei, New Zealand, due to change in the gradient of the stream bed

exploitation of a liquid-dominated geothermal system, can also alter the natural surface heat flow (heat loss). Steam is much more mobile than water; it can move through small fractures that are impervious to water and can move much more quickly through larger fractures. The generation and movement of steam can therefore result in increased heat flow and increased ground temperatures, so that some vegetation may become stressed or killed, generally to be replaced by other, thermally tolerant, species. At Wairakei, heat loss from natural thermal features was about 400 $MW_{thermal}$ prior to the start of exploitation in 1958, increased to a peak of nearly 800 $MW_{thermal}$ by the mid-1960s, and has since declined to about 600 $MW_{thermal}$ (Fig. 10, [27]). Most of this increase was associated with increased thermal activity in the Karapiti Thermal Area, which is situated 3 km south-west of the

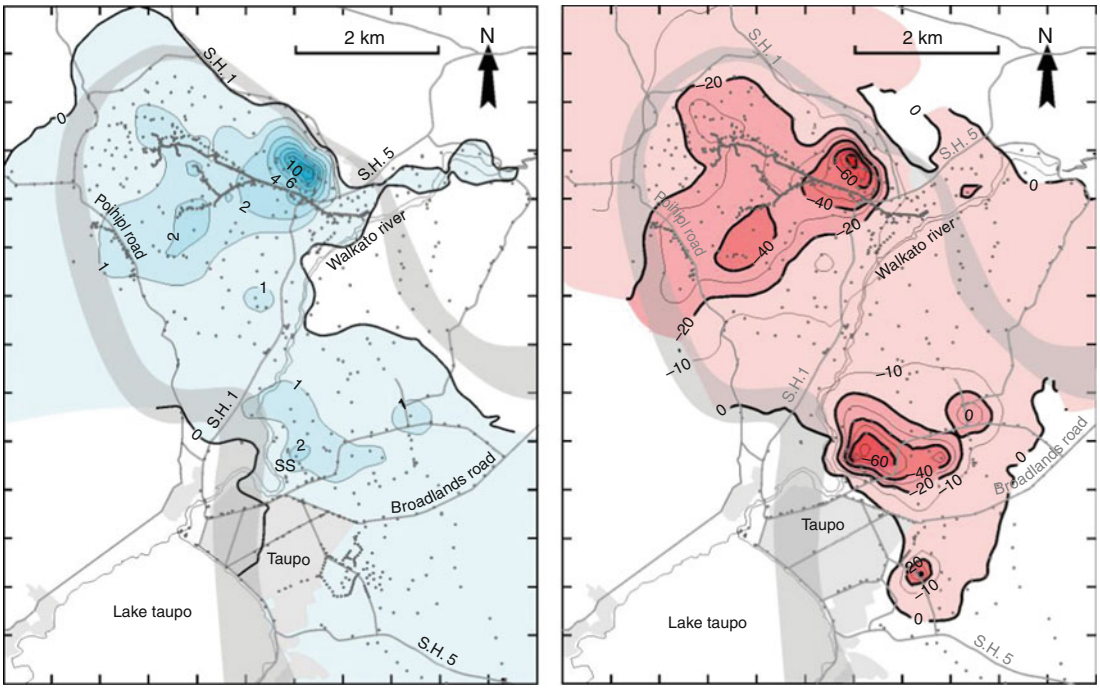

Geothermal Resources, Environmental Aspects of. Figure 8
Maps of ground subsidence and subsidence rate at Wairakei-Tauhara geothermal field, New Zealand. Left hand map shows total subsidence (m) for the period 1953–2005. Right hand map shows subsidence rate (mm/year) for the period 2001–2005. Gray zone indicates electrical resistivity boundary of the field and dots indicate measurement points (Taken from [16]). Note that the greatest subsidence rates are confined to several small parts of the field

Geothermal Resources, Environmental Aspects of. Figure 9
Compressional (*left*) and tensional (*right*) deformation features at Ohaaki geothermal field, New Zealand

Geothermal Resources, Environmental Aspects of. Table 1 Ground subsidence in some producing geothermal fields. Survey dates are the period for which subsidence has been reported; it is not necessarily the whole production period. Note also that the subsidence rate changes with time and location

Field	Country	Survey period	Max. subsidence (m)	Max. rate (mm/year)	Mass change during survey period		Reference
					Withdrawal (Mt/year)	Reinjection (Mt/year)	
Wairakei	NZ	1955–1995	13.5	470	10–74	0	[16]
Ohaaki	NZ	1988–1998	1.3	400	14–17	10–13	[17]
Kawerau	NZ	1970–1996	0.48[a]	30	10	1.7–2.6	[22]
The Geysers	USA	1977–1996	0.90	47	70	21	[20]
Bulalo	Philippines	1980–1999	0.57	32			[23]
Travale	Italy	1973–1991	0.4	25	2.3–3.9		[24]
Takigami	Japan	1992–1998	<0.02	-	11	8.8	[25]
Hatchobaru	Japan	1990–1996	0.015	-	17.7	20	
Cerro Prieto	Mexico	1994–1997	0.5	120	100	1	[18]
Svartsengi	Iceland	1976–99	0.24	14	0–9		[26]

[a]Corrected for vertical displacement caused by the March 1987 Edgecumbe earthquake

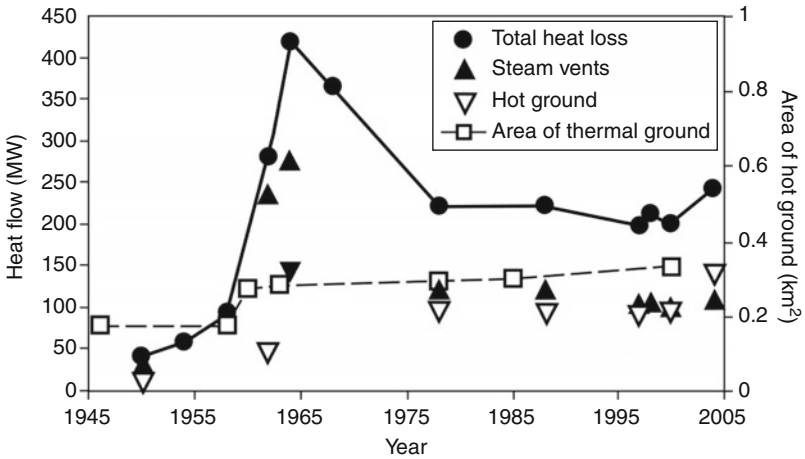

Geothermal Resources, Environmental Aspects of. Figure 10
Changes in heat flow with time at Karapiti thermal area, Wairakei, New Zealand. Note the transient increase in heat flow from steam vents in the early 1960s soon after production began, followed by a decrease and stabilization as steam pressures declined. Figure taken from [27]

main production borefield. The increase has been attributed to steam, associated with lateral expansion of the steam zone resulting from pressure decreases, rising to the surface up narrow fissures that were previously impervious to water. However, the increase in heat flow has resulted in an increased number of fumaroles, which has enhanced the visitor experience of tourists to the area.

Waste Liquid Disposal

Most geothermal energy developments bring fluids containing dissolved minerals to the surface in order to extract some of the heat contained within them. In high-temperature liquid-dominated geothermal fields, the volumes of resultant liquid waste involved may be large: at Wairakei-Tauhara, a medium-sized geothermal power station (156 MW), it is currently about 5,800 m^3/h. For vapor-dominated systems it is less, and for low-temperature systems it is usually much less (e.g., at Chevilly-Larue (France) it is only about 3 m^3/h). After extracting some of the heat, the waste water is generally disposed of by reinjecting it deep into the ground. Surface disposal, such as putting it into waterways or evaporation ponds, may cause more environmental problems than injection because of the dissolved minerals, particularly arsenic, mercury, and boron compounds. The best method of disposal depends on the chemistry of the geothermal fluid. For some high-temperature power plants such as at Nesjavellir (Iceland) the waste water is piped to the city of Reykjavik for district heating and then disposed of into shallow groundwater aquifers, and tests have shown no apparent effects on water chemistry. At Svartsengi power plant the waste water is discharged into the Blue Lagoon, which is a famous tourist attraction in Iceland (Fig. 11). In many cases, the waste water can be used for greenhouse heating, warm water aquaculture, space heating, irrigation swimming pools, and spas before being disposed of at the surface.

Induced Seismicity Most high-temperature geothermal systems lie in tectonically active regions where there are high levels of stress in the upper parts of the crust; this stress is manifested by active faulting and numerous earthquakes resulting from sudden relief of this stress. Studies in many high-temperature geothermal fields have shown that exploitation can result in an increase (above the normal background) in the number of small magnitude earthquakes (micro-earthquakes) within the field [28–30] (Figs. 12 and 13). Induced seismicity occurs in high-temperature fields (both liquid- and vapor-dominated), but has not been observed in low-temperature fields tapping shallow aquifers. Induced seismicity also occurs in Enhanced

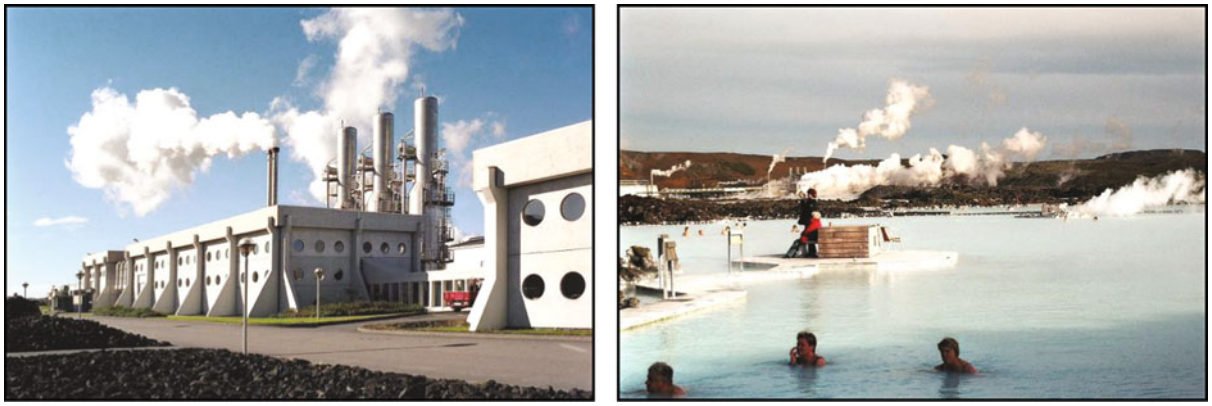

Geothermal Resources, Environmental Aspects of. Figure 11
Svartsengi power plant (*left*) and the Blue Lagoon (*right*)

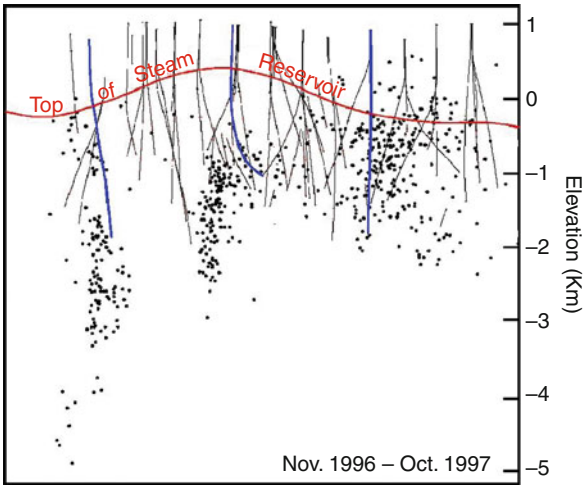

Geothermal Resources, Environmental Aspects of. Figure 12
Cross section through The Geysers field (California, USA) showing locations of earthquakes (*black dots*) during a 12-month period. Injection wells are shown in blue. Earthquake hypocenters and wells within 2000 ft (610 m) of the section line have been projected onto the cross section. Note that the earthquakes may extend to depths greatly below the bottom of some injection wells (Taken from [29])

Geothermal Systems (Fig. 14) where high wellhead injection pressures are used to stimulate production by creating new fractures and extending existing fractures [31]. To date no serious damage has been caused by such earthquakes, but they may result in a temporary shutdown of the power plant. However, the earthquakes can frighten people (especially those in non-tectonic areas who are unaccustomed to earthquakes); this has happened at Soultz in France, Basel in Switzerland, and Landau in Germany.

It is believed the increase is caused mainly by injection because when injection is stopped the number of small earthquakes decreases, and when it is restarted the number increases [28, 31]. High wellhead injection pressures increase the pore pressure at depth, particularly in existing fractures, which allows movement to suddenly release the stress and generate an earthquake. However, there are other, secondary mechanisms for induced earthquakes. Cool injected water can cause contraction of fracture surfaces leading to slight opening of the fractures, reducing static friction and triggering slip on a fracture already near failure. Also, volume changes associated with production and injection may cause perturbation in local stress conditions leading to seismic slip in a similar manner to "rockbursts" in mines as the surrounding rock adjusts to newly created void spaces [31].

Induced earthquakes may number several thousand per year in a geothermal field but few are felt, although a small number of earthquakes may reach (Richter) Magnitude 4. Detailed studies show that the induced micro-earthquakes cluster (in space) around and below the bottom of injection wells, and so the effects at the surface are generally confined to the field [32, 33].

During injection to improve an EGS reservoir at a depth of about 5 km beneath the Swiss city of Basel,

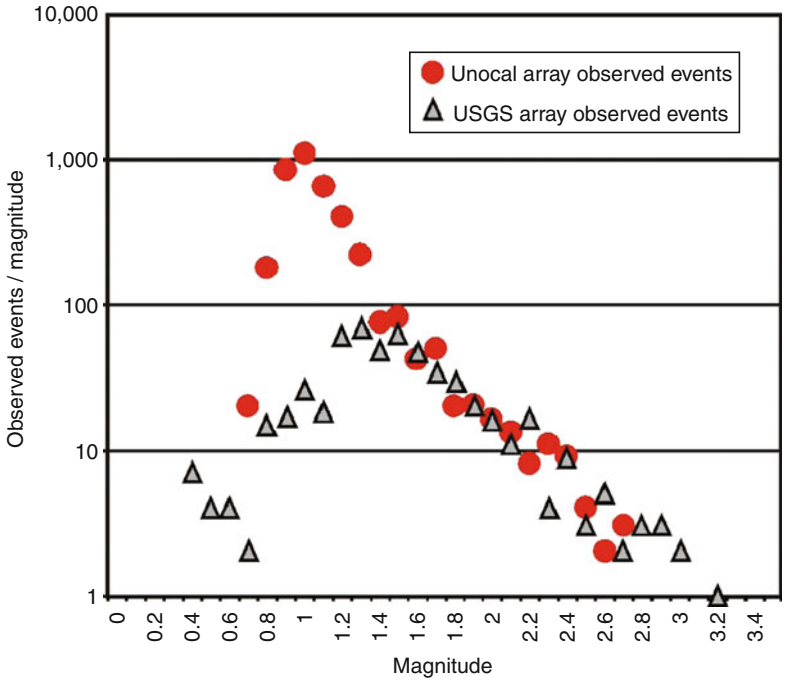

Geothermal Resources, Environmental Aspects of. Figure 13
Plot of frequency against magnitude for microearthquakes in The Geysers field, California, USA for a two-year period (1996–1998). Figure taken from [29]. Note the logarithmic increase in numbers of events as magnitude decreases. The apparent decrease in number of events below about M = 1.3 for the USGS array is because detection of all very small magnitude events (M < 1) was not possible with the equipment used, i.e., M = 1.3 is the effective recording threshold. Similarly for the Unocal array the effective recording threshold is about M = 1.0

an earthquake of magnitude 3.4 was triggered on 8 December 2006. This event caused damage to property, and the developer's insurance paid out damages of about 7 million CHF. Recent probabilistic modeling of the seismic risk [34] (IGA, 2010) has indicated the likelihood of 40 million CHF of property damage and a 15% probability that damages could exceed 600 million CHF if development continued. While the risk of the geothermal project to cause bodily harm is low, that for property damage is considered unacceptable according to Swiss risk criteria and the development has stopped. However, other locations in Switzerland offer a significantly lower seismic risk. The incident at Basel has highlighted the need for thorough evaluation of site-specific seismic risk for future geothermal developments, especially EGS projects in densely inhabited areas.

Effects on Living Organisms If hot geothermal waste water from a standard steam-cycle power station is released directly into an existing natural waterway the localized increase in water temperature may kill fish and aquatic plants near the outlet; therefore, the water is generally passed through cooling ponds and mixed with cold water before being released. Release of untreated mineralized water into a waterway can result in chemical poisoning of fish, and also birds and animals that reside near the water because some of the toxic substances move up the "food chain."

Contamination of Groundwater Release of waste water into cooling ponds or waterways may result in shallow groundwater supplies becoming contaminated and unfit for human use, so care must be taken that the sides and bottoms of such ponds are sealed.

Waste Gas Disposal

Gas discharges from low-temperature systems are minor and do not usually cause significant environmental

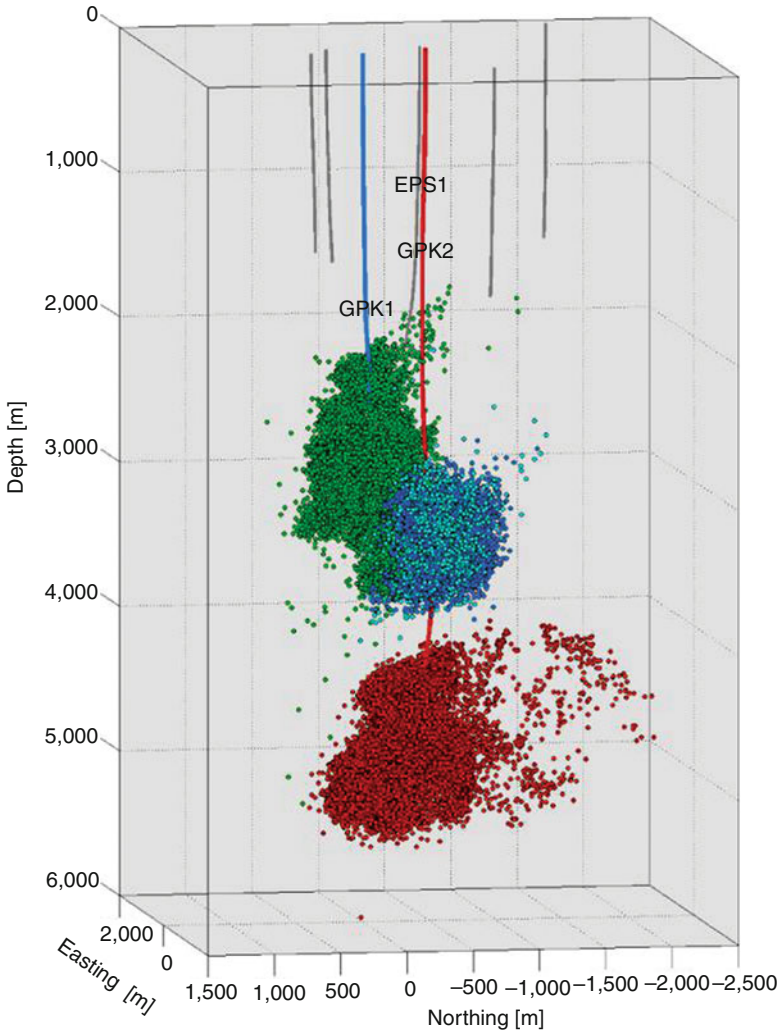

Geothermal Resources, Environmental Aspects of. Figure 14
Clusters of earthquakes resulting from different injection tests at the Soultz EGS, France. Note how the earthquakes cluster around the bottom of the injection wells

impacts. In high-temperature geothermal fields, power generation using a standard steam-cycle or hybrid plant may result in the release of non-condensable gases (NCG) and fine solid particles (particulates) into the atmosphere [35]. In vapor-dominated fields where waste fluids are injected, non-condensable gases in steam will be the most important discharges from an environmental perspective. The NCG emissions are mainly from the gas exhausters of the power station, often discharged through a cooling tower. Gas and particulate discharges during well drilling, bleeding, cleanouts and testing, and from line valves and waste bore water degassing are usually insignificant. The concentration of NCG varies not only between fields but can also vary from well to well within a field, thus changes to the proportion of steam from different wells may cause changes in the amounts of NCG discharged.

Gas concentrations and compositions cover a wide range, but the predominant gases are carbon dioxide (CO_2) and hydrogen sulfide (H_2S), together with small amounts of ammonia, mercury and boron vapor, and hydrocarbons such as methane. In some fields, up to 30% (by weight) of the geothermal fluid is NCG. However, although these amounts appear large they are

relatively small compared with fossil fuel power stations: the amount of H_2S emitted from a geothermal power station (average 0.03 g/kWh) is less than 2% of that from equivalent size coal- and oil-fired power stations (9.23 and 4.95 g/kWh, respectively). In high-temperature geothermal fields, measured direct CO_2 emission from the operation of conventional power or heating plants is widely variable, ranging from 0 to 740 g/kWh, but averages about 120 g/kWh (weighted average of 85% of the world geothermal power plant capacity) [36]. This is much less than that of 915 g/kWh from a coal-fired plant (35% efficiency), 760 g/kWh from an oil-fired plant (35% efficiency), or 315 g/kWh from a combined cycle gas plant (60% efficiency). In Enhanced Geothermal Systems, power plants are likely to be designed as closed-loop circulation systems, with no direct emissions; only if boiling occurs within the loop may some NCG emission occur. Geothermal power plants are also environmentally friendly with regard to the minor NCG: a coal-fired power plant produces the following kilograms of emissions per MWh as compared to a geothermal power plant: 4.71 versus up to 0.16 for sulfur dioxide, 1.95 versus 0 for nitrogen oxides, and 1.01 versus 0 for particulate matter [37]. Hydrogen sulfide is routinely treated at geothermal power plants, and converted to elemental sulfur.

In low-temperature fields (<100°C), direct CO_2 emission from geothermal fluid is about 0–1 g/kWh depending on the carbonate content of the water. If the extracted geothermal fluid is passed through a heat exchanger and then completely re-injected (such as in a closed-loop pumped system), then CO_2 emission is nil to negligible.

Carbon dioxide occurs in all geothermal fluids but is most prevalent in fields in which the reservoir contains sedimentary rocks, and particularly those with limestones. Carbon dioxide is generally the most abundant NCG (>90%). It is colorless and odorless, and is heavier than air so it can accumulate in topographic depressions where there is still air. It is not highly toxic (c.f. hydrogen sulfide) but at high concentrations can be fatal due to alteration of pH in the blood. There is some evidence that in high-temperature fields, the amount of CO_2 discharged (per unit mass withdrawn) decreases with time as a result of de-gassing of the deep reservoir fluid. When examining the CO_2 emissions from geothermal power plants it is necessary to consider what would be emanating from the ground naturally (e.g., from fumaroles) in the vicinity of the plant. A strong case can be made for subtracting the natural background emission rate pre-development from the rate being released by the operation of the geothermal development. This is particularly relevant to the Larderello field in Italy where there has been a noticeable and measurable decrease in the natural release of CO_2 from the ground as a result of the geothermal power development on the field [36].

The main effects of release of non-condensible gases, together with water vapor from the cooling circuits, are local microclimatic effects such as fog. However, CO_2 need not be released directly into the atmosphere. It may be captured, purified of other gases (especially H_2S), and used to enhance plant growth in greenhouses growing vegetables. Studies have shown that as CO_2 concentration is increased from a normal level of 300 ppm to levels of approximately 1,000 ppm, crop yields may increase by up to 15% [38]. Another use of geothermal CO_2 is in carbonated drinks – at Kizildere power plant, Turkey, the NCG is scrubbed of H_2S, and the CO_2 recovered provides around 80% of the CO_2 used by the country's soft drinks industry.

Catastrophic Events

Hydrothermal Eruptions Hydrothermal eruptions have occurred at several high-temperature geothermal fields. These are small, shallow-sourced, steam and soil eruptions that generally result in craters 10–50 m in diameter and 5–20 m deep (Fig. 15). Material ejected from the craters may be deposited up to several hundred meters away. At present they cannot be reliably predicted, however, several causes have been identified that increase the likelihood of an eruption [39]. One mechanism assumes an expanding two-phase zone in the reservoir (due to production) that increases steam flow to the surface. Near the surface, an aquiclude may restrict the flow of steam resulting in an increase in the underlying pressures. Also, it has been noted that at Karapiti Thermal Area (New Zealand) the hydrothermal eruptions sometimes follow a long period of low rainfall. During long dry periods, the amount of water in the near-surface aquifer is reduced and further

Geothermal Resources, Environmental Aspects of. Figure 15
Aerial view of hydrothermal eruption craters at Karapiti thermal area, Wairakei, New Zealand. The white lines are wooden boardwalks that allow tourists to walk over the area safely

increased heating and steam flow occurs. If a period of heavy rainfall then occurs, the permeability of the ground near the surface is quickly reduced by the rain, so that the steam cannot escape and pressures can increase to the point where the overlying rocks cannot contain the pressure and an eruption occurs. Another mechanism involves hydraulic fracturing, allowing a release of non-condensable gases and rapid decrease of the boiling point of hot water close to the surface. A third mechanism is a reduction in the lithostatic pressure by removal of the overburden, either naturally by landslides or by man-made excavations. There are no countermeasures available except to maintain reservoir pressures thus minimizing steam formation and concomitant increase in heat flow, and to refrain from building on or excavating in active thermal ground.

Blowouts During Drilling Drilling a deep well in a high-temperature geothermal field carries the risk of a blowout – an uncontrolled flow of underground fluid to the surface outside of the well. Although now rare, several blowouts have occurred in the past [40–42]. Common causes of blowouts are failure to adequately cement the well casing to the surrounding rock, or damage to the well casing by earth movement. Blowouts are generally brought under control by directionally drilling a relief well from nearby to intersect the original well. This allows cement to be pumped into and around the original well to seal it.

Probably the most spectacular geothermal blowout was during drilling of well WK204 at Wairakei in 1960 [42]. A large and expanding crater, venting steam and rocks, quickly formed near the well, and it was fortunate that the drill rig and associated equipment was able to be removed before they were engulfed. All attempts to control the blowout failed. The crater grew to about 70 m in diameter and 20 m deep, then filled with boiling water that periodically geysered. This activity continued for several years and became a tourist attraction known as "the rogue bore." However during 1973, the temperature and level of water in the crater declined and the feature dried up.

Landslides Many high-temperature geothermal fields are in mountainous regions, and geothermal wells are drilled from well pads carved out from steep slopes. There have been a few instances where landslides, triggered by heavy rainfall or inappropriate engineering works, have broken production wells leading to blowouts [42, 43] or have damaged steam pipelines. The most disastrous has been the landslide of 5 January 1991 in Zunil field, Guatemala, when 23 people were killed [43].

Land Use

Visual Impacts A geothermal plant must be located close to the resource, so there is often little flexibility in siting the plant. Geothermal plants generally have a low profile, and need not have a tall chimney such as coal- and oil-fired power plants. However, their visual impact may still be significant because high-temperature geothermal fields are often situated in areas of outstanding natural beauty and in National Parks (e.g., Japan, USA. and New Zealand). Any associated natural thermal features (e.g., geysers and hot pools) may be a tourist attraction or of historical and cultural significance. Undertaking developments in such areas may cause conflict during the processes for obtaining permits for access and to undertake drilling, and even for access to subsurface resources by directional drilling from outside such parks. Despite good examples of unobtrusive, scenically landscaped developments (e.g., Matsukawa, Japan), and

integrated tourism/energy developments (e.g., Wairakei, New Zealand and Blue Lagoon, Iceland), land use issues still seriously constrain new development options in some countries. Visual impact may be particularly high during drilling due to the presence of tall drill rigs.

Footprint A measure of optimum land use is the "footprint" occupied by geothermal installations. Taking into account surface installations (drilling pads, roads, pipelines, fluid separators, and power stations), the typical footprint of a conventional high-temperature geothermal power scheme is about 900 m^2/GWh/year (for 30 years), or 160 m^2/GWh/year excluding wells. Low-temperature geothermal plants (excluding wells) would require land use of between 1,400 and 2,300 m^2/MW [44] equivalent to 150–300 m^2/GWh per year. Subsurface geothermal resources accessed by directional or vertical boreholes typically occupy an area equivalent to about 10 MW/km^2. Therefore, about 95% of the land above a typical geothermal resource is not needed for surface installations, and can be used for other purposes (e.g., farming, horticulture, and forestry at Mokai and Rotokawa fields in New Zealand, and a game reserve at Olkaria, Kenya).

Methods of Avoiding or Minimizing Impacts

Good Management Practices

Responsibility for protecting the environment rests with the developer, and specifically with the engineers and managers. Some general principles for protecting the environment are: regular monitoring of the environment; reliance on scientists and engineers to recognize problems; acting before scientific consensus is achieved; confronting uncertainty; including human motivation (short-sightedness and greed); taking a precautionary approach and being prepared for worst-case scenarios. These principles can be encouraged by regulators which provide good environmental strategies (such as avoid, remedy, or mitigate) and sound guidelines.

Good Engineering Practices

Site Investigation and Development The impacts of access roads and field development can be minimized by careful planning and construction of access roads and prompt re-planting of vegetation destroyed. Simple and reliable criteria have been developed to assess slope instability and the potential for slope failure in the Philippines [45], and here remediation includes construction of benches to prevent landslides and rigid structural barriers up-slope of and over pipework.

Noise Reduction Noise inevitably occurs during the exploration drilling, construction, and production phases of development. Air drilling is the noisiest (120 dBA) due to the "blow pipe effect" where the gases exit, but suitable muffling can reduce this to around 85 dBA [46]. Mud drilling is quieter at around 80 dBA. Diesel engines operating compressors and electricity generators can also produce a low-frequency resonant sound that carries for long distances; this noise can be constrained, to less than 55 dBA during the day and 45 dBA at night, by suitable muffling and confining noisy operations (such as tripping or cementing) to the daytime hours. Construction of screens of sound-absorbing material, such as vegetation, is also used to reduce the impacts of drilling noise. Following drilling, a well is usually discharged to remove drilling debris. Such vertical discharges are very noisy (up to 120 dBA). After this, there is normally a period of well testing; this can be suitably muffled by the use of silencers, but even then the noise is still significant (70 – 110 dBA). The well is then put on "bleed" where the noise is around 85 dBA reduced to 65 dBA if the "bleed" is led to a rock muffler [46]. Drilling is generally a continuous 24-h/day operation and the effects of using powerful lamps to light the work site at night are reduced by temporary screens and careful placement of the lamps. Modern drilling techniques involve using minimal amounts of fluid and recycling as much as possible.

Injection Changes to thermal features are associated with declines in production reservoir pressures and it appears that the best way to prevent or minimize changes to these features is to minimize any reduction in reservoir pressures by undertaking injection. This will also minimize any changes in groundwater level and temperature, and avoid waste liquid contaminating groundwater. Deep injection also reduces the effects of waste liquid disposal on living organisms. However, it may be necessary to keep injection pressures to a minimum to minimize induced seismicity.

Induced seismicity may be reduced if injection is reduced or halted when the seismicity reaches

pre-determined levels. In 2003, a trial was carried out at Berlin Geothermal Field, located in a tectonically active area, which used pressurized injection in an attempt to improve fracture permeability. A calibrated real-time "traffic light" control system [47] was established to reduce or stop injection operations if the levels of vibration (peak ground velocity) from injection-induced seismicity exceeded acceptable levels (normal background = "green," significant felt events = "orange," and damaging events = "red").

Engineering to Overcome Ground Movements Little can be done to prevent or minimize ground deformation, except to maintain reservoir pressures. Experience suggests that subsidence can be halted, but it is difficult to reverse by increasing reservoir pressure because of the great weight of rock overlying the formation that has compacted. The effects of deformation on pipelines is reduced by mounting the pipelines on rollers, but experience at Wairakei shows that even with such assistance sections of pipe need periodically to be removed or installed to maintain the pipeline network. Equipment that is sensitive to level is generally mounted on an adjustable base.

Plant Design Suitable design of power stations employing active monitoring systems will minimize the effects of non-condensible gas discharges and reduce microclimatic effects (e.g., suitable placement of cooling towers and gas discharge vents). If induced seismicity is likely then all structures in the field should be earthquake resistant.

Regulations

Most geothermal developments are controlled and monitored by independent regulatory authorities, such as central, regional, or local government, and they issue (to developers or users) permits or consents which ensure that the best environmental practices are followed [48–51]. This generally involves preparation of an Environmental Impact Report (EIR) before development begins; consideration of that report by officials, experts, and the public; granting of permits subject to restrictions; setting up of a monitoring program and measurements taken regularly; and periodic review of the monitoring data and renewal of the permits. This is not entirely altruistic because if severe environmental damage occurs it is generally government that has to take ultimate responsibility for the problem.

Economic Measures

Royalties or User Charges One method of encouraging use of a geothermal resource in an efficient and sustainable manner is to charge users for the amount of energy taken. A good example of how implementation of user charges reduced wasteful practices was in Rotorua city, New Zealand [52]. Here, especially during summer, some individual well owners were taking geothermal fluid and not using it, but passing the hot water directly to waste at the surface instead of shutting down their well. Introduction of user charges, and closure of poorly performing wells and equipment, persuaded many of these owners to combine and operate a single well in a sustainable manner, with injection. Since the introduction of the charges the net amount of fluid withdrawn has decreased from about 30 kt/day to less than 10 kt/day, and water levels in the shallow thermal aquifers have risen.

Bonds Another economic measure that can be effectively used to protect the environment and encourage sustainable development is the requirement for a developer to deposit a large refundable bond that is forfeited if environmental damage occurs. Interest on the bond money, less an amount to cover taxes and inflation, may be returned annually to the developer. Although the damage may not be able to be rectified by money, the potential loss of a large amount of money may keep a company more focussed on the environment and the consequences of its actions. Such a system is effective when there is the suspicion that a development company will not be able to meet its obligations either through lack of expertise or financial problems. Bonds are particularly effective with public companies where the profits, share value, and bonuses of the managers may be adversely affected by loss of the bond. However, to date, this approach has not been used in the geothermal industry; it is more common in the mining industry where developers are transient.

Future Directions

The worldwide need for sustainable energy sources means that the exploitation of geothermal energy will

continue and even accelerate in the next few decades. Although a few geothermal developments have had serious environmental effects, such as at Wairakei, most of these cases were before the dynamics of geothermal systems was understood. The causes of most of the environmental effects have since been recognized and countermeasures are employed as part of permitting. International scientific efforts, under the auspices of the International Energy Agency (IEA), to devise methods of extracting geothermal energy with the minimum of environmental effects were started in the late 1990s and will continue.

Bibliography

Primary Literature

1. Parker SP (1980) Encyclopedia of environmental science, 2nd edn. McGraw-Hill, New York
2. Brown L (1993) New shorter oxford english dictionary. Clarendon, Oxford
3. Cataldi R, Hodgson SF, Lund JW (1999) Stories from a heated Earth: our geothermal heritage. Geothermal Resources Council, International Geothermal Association, Sacremento, p 569
4. Thoreaux HD (1860) Letter to Harrison Blake, Written 20 May, 1860. www.walden.org/documents/file/Library/Thoreau/writings/correspondence/Correspondence/1860. Accessed 14 April 2011
5. DiPippo R (2008) Geothermal well drilling. In: DiPippo R (ed) Geothermal power plants, 2nd edn. Elsevier, Amsterdam, pp 39–48
6. Bixley PF, Clotworthy AW, Mannington WI (2009) Evolution of the Wairakei geothermal reservoir during 50 years of production. Geotherm 38:145–154
7. White PA, Hunt TM (2005) Simple modelling of the effects of exploitation on hot springs, Geyser Valley, Wairakei, New Zealand. Geotherm 34:184–204
8. Glover RB, Hunt TM, Severne CM (2000) Impacts of development on a natural thermal feature and their mitigation – Ohaaki Pool, New Zealand. Geotherm 29:509–523
9. Bolanos GT, Parilla EV (2000) Response of the Bao-Banati thermal area to development of the Tongonan geothermal field, Philippines. Geotherm 29:499–508
10. Bromley CJ (2009) Groundwater changes in the Wairakei-Tauhara geothermal system. Geotherm 38:134–144
11. Bixley PF, Hattersley SD (1983) Long term casing performance of Wairakei production wells. In: Proceedings 5th NZ geothermal workshop, Geothermal Institute, Auckland, pp 257–263
12. Lofgren BE, Klausing RL (1969) Land subsidence due to ground-water withdrawal, Tulare-Wasco area, California. US geological survey professional Paper 437-B
13. Holzer TL, Johnson AI (1985) Land subsidence caused by ground water withdrawal in urban areas. GeoJ 11:245–255
14. Mayuga MN, Allen DR (1970) Subsidence in the Wilmington oil field, Long Beach, California, U.S.A. In: Tison LJ (ed) Land subsidence. International Association of Scientific Hydrology, UNESCO, pp 66–79
15. Bruno MS, Bovberg CA (1992) Reservoir compaction and surface subsidence above the Lost Hills Field, California. 33rd US symposium on rock mechanics, Santa Fe, New Mexico, USA, Paper No. 92-0263
16. Allis RG, Bromley CJ, Currie S (2009) Update on subsidence at the Wairakei-Tauhara geothermal system, New Zealand. Geotherm 38:169–180
17. Allis RG, Zhan X (2000) Predicting subsidence at Wairakei and Ohaaki geothermal fields, New Zealand. Geotherm 29:479–497
18. Glowacka E, Sarychikhina O, Nava FA (2005) Subsidence and stress change in the Cerro Prieto geothermal field, B.C., Mexico. Pure Appl Geophys 162:2095–2110
19. Geri G, Marson I, Rossi A, Toro B (1982) Gravity and elevation changes in the Travale geothermal field (Tuscany) Italy. Geotherm 11:153–161
20. Mossop A, Segall P (1997) Subsidence at the Geysers geothermal field, N. California from a comparison of GPS and leveling surveys. Geophys Res Lett 24:1839–1842
21. Gettings P, Allis R, Harris RN, Chapman DS (2001) High-precision gravity and GPS monitoring of The Geysers geothermal system. American Geophysical Union, Fall Meeting, Abstract #G41B-0225
22. Allis RG, Carey B, Darby D, Read SAL, Rosenberg M, Wood CP (1997) Subsidence at Ohaaki field. In: Proceedings of the 19th NZ geothermal workshop, Geothermal Institute, Auckland, pp 9–15
23. Protacio JA, Golla G, Nordquist G, Acuña J, San Andres RB (2000) Gravity and elevation changes in the Bulalo geothermal field, Philippines: independent checks and constraints on numerical simulation. In: Proceedings of the 22nd NZ Geothermal Workshop, Geothermal Institute, Auckland, pp 115–119
24. Di Filippo M, Dini I, Marson I, Palmieri F, Rossi A, Toro B (1995) Subsidence and gravity changes induced by exploitation in the Travale-Radicondoli geothermal field (Tuscany, Italy). In: Proceedings world geothermal congress 1995, Florence, Italy, 3, pp 1945–1949
25. Fujimitsu Y, Nishijima J, Shimosako N, Ehara S, Ikeda K (2000) Reservoir monitoring by repeat gravity measurements at the Takigami geothermal field, central Kyushu, Japan. In: Proceedings world geothermal congress 2000, Japan, pp 573–577
26. Eysteinsson H (2000) Elevation and gravity changes at geothermal fields on the Reykjanes peninsula, SW Iceland. In: Proceedings world geothermal congress 2000, Kyushu – Tohoku, pp 559–564
27. Hunt TM, Bromley CJ, Risk GF, Sherburn S, Soengkono S (2009) Geophysical investigations of the Wairakei field. Geotherm 38:85–97
28. Sherburn S, Allis RG, Clotworthy A (1990) Microseismic activity at Wairakei and Ohaaki geothermal fields. In: Proceedings of the 12th NZ Geothermal Workshop, Geothermal Institute, Auckland, pp 51–55

29. Smith B, Beall J, Stark M (2000) Induced seismicity in the SE Geysers Field, California, USA. In: Proceedings world geothermal congress 2000, pp 2887–2892
30. Rivas JA, Castellón JA, Maravilla JN (2005) Seven years of reservoir seismic monitoring at Berlín geothermal field, Usulután, El Salvador. In: Proceedings world geothermal congress 2005, Antalya, Turkey, 24–29 April 2005, Paper 215 6 pp
31. Majer EL, Baria R, Stark M, Oates S, Bommer J, Smith B, Asanuma H (2007) Induced seismicity associated with enhanced geothermal systems. Geotherm 36:185–222
32. Stark M (1990) Imaging injected water in the Geysers reservoir using microearthquake data. Geoth Resourc Counc Trans 14:1697–1704
33. Baria R, Michelet S, Baumgartner J, Dyer B, Nicholls J, Hettkamp T, Teza D, Soma, N, Asanuma H, Garnish J, Megel T (2005) Creation and mapping of 5000 m deep HDR/HFR reservoir to produce electricity. In: Proceedings world geothermal congress Antalya, Turkey, paper 1627
34. IGA (2010) Seismic risk assessment in Basel. IGA News 79:6–9
35. Webster JG (1995) Chemical impacts of geothermal development. In: Brown KL (convenor) Course on environmental aspects of geothermal development. International Geothermal Association, Pisa, Italy, 145 pp
36. Bertani R, Thain IA (2002) Geothermal power generating plant CO_2 emission survey. IGA News 49:1–3. http://www.geothermal-energy.org/files-39.html. Accessed 13 April 2011
37. Lund JW (2007) Characteristics, development and utilization of geothermal resources. Geo Heat Cent Q Bull 28:1–9
38. Dunstall MG, Graeber G (1997) Geothermal carbon dioxide for use in greenhouses. Geo Heat Cent Q Bull 18(1):8–13
39. Bromley CJ, Mongillo MA (1994) Hydrothermal eruptions – a hazard assessment. In: Proceedings of the 16th NZ Geothermal Workshop, Geothermal Institute, Auckland, pp 45–50
40. Adams N, Thompson JD (1989) How a geothermal blowout was controlled. World Oil 208(6):36–42
41. Anderson I (1991) Blowout blights future of Hawaii's geothermal power. New Sci 1778:17
42. Bolton RS, Hunt TM, King TR, Thompson GEK (2009) Dramatic incidents during drilling at Wairakei geothermal field, New Zealand. Geotherm 38:40–47
43. Goff S, Goff F (1997) Environmental impacts during geothermal development: some examples from Central America. In: Proceedings NEDO international geothermal symposium, 10–14 March 1997, Sendai, Japan, pp 242–250
44. Tester JW (2006) The future of geothermal energy – impact of Enhanced Geothermal Systems (EGS) on the United States in the 21st Century. US Dept Energy, Idaho National Laboratory, Idaho Falls, USA, 372 pp. ISBN 0-615-13438-6. http://geothermal.inel.gov/publications/future_of_geothermal_energy.pdf. Accessed 13 April 2011
45. Leynes RD, Pioquinto WPC, Caranto JA (2005) Landslide hazard assessment and mitigation measures in Philippine geothermal fields. Geotherm 34:205–217
46. Brown KL (1995) Impacts on the physical environment. In: Environmental aspects of geothermal development. IGA pre-congress short course, world geothermal congress Pisa, Italy, May 1995, pp 39–55
47. Bommer JJ, Oates S, Cepeda JM, Lindholm C, Bird J, Torres R, Marroquín G, Rivas J (2006) Control of hazard due to seismicity induced by a hot fractured rock geothermal project. Eng Geol 83:287–306
48. Hietter L (1995) Introduction to geothermal development and regulatory requirements. In: Brown KL (convenor) Course notes on environmental aspects of geothermal development. International Geothermal Association, Pisa, Italy, 18–20 May 1995, 145 pp
49. Goff S (2000) The effective use of environmental impact assessments (EIAs) for geothermal development projects. In: Proceedings world geothermal congress 2000, Japan, 597–603
50. Luketina K (2000) New Zealand geothermal resource management – a regulatory perspective. In: Proceedings World Geothermal Congress 2000, Japan, pp 751–756
51. Daysh S, Chrisp M (2009) Environmental planning and consenting for Wairakei: 1953–2008. Geotherm 38:192–199
52. O'Shaughnessy BW (2000) Use of economic instruments in management of Rotorua geothermal field, New Zealand. Geotherm 29:539–556

Books and Reviews

Dickson MH, Fanelli M (2003) Geothermal energy utilization and technology. UNESCO Publishing, Paris. ISBN 92-3-103915-6

DiPippo R (2008) Geothermal power plants: principles, applications, case studies and environmental impact. Elsevier, Amsterdam

Hunt TM (ed) (2000) Special issue on environmental aspects of geothermal development. Geothermics 29 (4/5), 175 pp

Hunt TM (2001) Five lectures on environmental effects of geothermal utilization. Report 2000-1, United Nations University, Reykjavik, Iceland. 109 pp. ISBN-9979-68-070-9

Hunt TM (ed) (2005) Special issue on environmental aspects of geothermal energy. Geothermics 34(2). ISSN 0375-6505

Rybach L, Muffler LJP (1981) Geothermal systems: principles and case histories. Wiley, New York, 359 pp

Global Economic Impact of Transgenic/Biotech Crops (1996–2008)

Graham Brookes
Agricultural Economist, PG Economics Ltd, Dorset, UK

Article Outline

Glossary
Definition of the Subject
Introduction
Economic Impact of Transgenic/Biotech Crops
Herbicide-Tolerant Soybeans
Herbicide-Tolerant Maize
Herbicide-Tolerant Cotton
Herbicide-Tolerant Canola
GM Herbicide-Tolerant (GM HT) Sugar Beet
GM Insect-Resistant (To Corn-Boring Pests: GM IR) Maize
Insect-Resistant (Bt) Cotton (GM IR)
Other Biotech Crops
Indirect (Nonpecuniary) Farm-Level Economic Impacts
Production Effects of the Technology
Bibliography

Glossary

Direct farm income benefit Improvements in income arising from changes in yield and production levels or associated with cost reductions/productivity enhancements associated with the use of transgenic crops.

Herbicide tolerance Tolerance to a herbicide (e.g., glyphosate) delivered by genetic modification techniques. This allows a crop to be sprayed with the "tolerant herbicide" without harming the crop but providing good weed control.

Insect resistance Resistance to a pest (e.g., corn-boring pests) delivered by genetic modification techniques. This allows a crop to be grown without having to use alternative methods of pest control, notably the use of insecticides.

Nonpecuniary benefit Additional farm-level benefits to direct farm income benefits that are more intangible and difficult to measure in monetary terms (e.g., additional management flexibility).

No tillage agriculture The use of a production technique in which the soil is not tilled/plowed. It is in contrast to traditional plow-based production systems and allows farmers to save on fuel use and contributes to improved soil water retention and reduced soil erosion.

Second crop soybeans The planting of a crop of soybeans after another crop (often wheat) in the same growing season. This allows a farmer to obtain two crops from the same piece of land in one season.

Definition of the Subject

The application of biotechnology to commercial agriculture on a widespread basis has occurred since 1996. The extent of this adoption in terms of crops and (biotechnology) traits is explored and the associated economic impacts for the period 1996–2008 are assessed, to help identify some of the main reasons why farmers have adopted the technology.

Introduction

This article examines specific global socioeconomic impacts on farm income over the 13-year period 1996–2008. It also quantifies the production impact of the technology on the key crops in areas where it has been used. The analysis concentrates on farm income effects because this is a primary driver of adoption among farmers (both large commercial and small-scale subsistence). It also considers more indirect farm income or nonpecuniary benefits, and quantifies the (net) production impact of the technology. More specifically, it covers the following main issues:

- Impact on crop yields
- Effect on key costs of production, notably seed cost and crop protection expenditure
- Impact on other costs such as fuel and labor
- Effect on profitability
- Other impacts such as crop quality, scope for planting a second crop in a season and impacts that are often referred to as intangible impacts such as convenience, risk management, and husbandry flexibility
- Production effects

The contribution is based largely on extensive analysis of existing farm-level impact data for biotech crops. While primary data for impacts of commercial cultivation were not available for every crop, in every year and for each country, a substantial body of representative research and analysis is available and this has been used as the basis for the analysis presented.

As the economic performance and impact of this technology at the farm level varies widely, both between, and within regions/countries (as applies to any technology used in agriculture), the measurement of performance and impact is considered on a case-by-case basis in terms of crop and trait combinations. The analysis presented is based on the average performance and impact recorded in different crops by the studies reviewed; the average performance being the most common way in which the identified literature has reported impact. Where several pieces of relevant research (e.g., on the impact of using a GM trait on the yield of a crop in one country in a particular year) have been identified, the findings used have been largely based on the average of these findings.

This approach may both, overstate, or understate, the real impact of GM technology for some trait, crop and country combinations, especially in cases where the technology has provided yield enhancements. However, as impact data for every trait, crop, location, and year is not available, the authors have had to extrapolate available impact data from identified studies to years for which no data are available. Therefore, the authors acknowledge that this represents a weakness of the research. To reduce the possibilities of over/understating impact, the analysis:

- Directly applies impacts identified from the literature to the years that have been studied. As a result, the impacts used vary in many cases according to the findings of literature covering different years. Hence, the analysis takes into account the variation in the impact of the technology on the yield based on its effectiveness in dealing with (annual) fluctuations in pest and weed infestation levels as identified by research.
- Uses current farm-level crop prices and bases any yield impacts on (adjusted – see below) current average yields. In this way, some degree of dynamic has been introduced into the analysis that would, otherwise, be missing if constant prices and average yields indentified in year-specific studies had been used.
- Includes some changes and updates to the impact assumptions identified in the literature based on consultation with local sources (analysts, industry representatives) so as to better reflect prevailing/changing conditions (e.g., pest and weed pressure, cost of technology).
- Adjusts downward the average base yield (in cases where GM technology has been identified as having delivered yield improvements) on which the yield enhancement has been applied. In this way, the impact on total production is not overstated.

Other aspects of the methodology used to estimate the impact on direct farm income are as follows:

- Impact is quantified at the trait and crop level, including where stacked traits are available to farmers. Where stacked traits have been used, the individual trait components were analyzed separately to ensure estimates of all traits were calculated.
- All values presented are nominal for the year shown and the base currency used is the US dollar. All financial impacts in other currencies have been converted to US dollars at prevailing annual average exchange rates for each year.
- The analysis focuses on the changes in farm income for each year, arising from the impact of GM technology on yields, key costs of production, notably seed cost and crop protection expenditure and also the impact on costs such as fuel and labor (inclusion of impact on these categories of cost are, however, more limited than the impacts on seed and crop protection costs because only a few of the papers reviewed have included consideration of such costs in their analyses). Therefore, in most cases the analysis relates to impact of crop protection and seed cost only.
- Crop quality (e.g., improvements in quality arising from less pest damage or lower levels of weed impurities that result in price premia being obtained from buyers) and the scope for facilitating the planting of a second crop in a season (e.g., second crop soybeans in Argentina following wheat that would, in the absence of the GM herbicide-tolerant

(GM HT) seed, probably not have been planted). Thus, the farm income effect measured is essentially a gross margin impact (impact on gross revenue less variable costs of production) rather than a full net cost of production assessment. Through the inclusion of yield impacts and the application of actual (average) farm prices for each year, the analysis also indirectly takes into account the possible impact of biotech crop adoption on global crop supply and world prices.

This article also examines some of the more intangible (more difficult to quantify) economic impacts of GM technology. The literature in this area is much more limited and in terms of aiming to quantify these impacts, largely restricted to the US-specific studies. The findings of this research (notably relating to the USA, and drawing on Marra and Piggot [1, 2] are summarized and extrapolated to the cumulative biotech crop planted areas in the USA over the period 1996–2008.

Lastly, this article includes estimates of the production impacts of GM technology at the crop level. These have been aggregated to provide the reader with a global perspective of the broader production impact of the technology. These impacts derive from the yield impacts (where identified), but also from the facilitation of additional cropping within a season (notably in relation to soybeans in South America).

Economic Impact of Transgenic/Biotech Crops

The section below is structured on a trait and country basis highlighting the key farm-level impacts.

Herbicide-Tolerant Soybeans

The USA

In 2008, 92% of the total US soybean crop was planted to genetically modified herbicide-tolerant cultivars (GM HT). The farm-level impact of using this technology since 1996 is summarized in Table 1.

The key features are as follows:

- The primary impact has been to reduce the soybean cost of production. In the early years of adoption, these savings were between $25/ha and $34/ha. In recent years, estimates of the cost savings have been in the range of $30–$85/ha (based on a comparison of conventional herbicide regimes in the early 2000s that would be required to deliver a comparable level of weed control to the GM HT soybean system). In 2008, the cost savings declined relative to earlier years because of the significant increase in the global price of glyphosate relative to increases in the price of other herbicides (commonly used on conventional soybeans). The main savings have come from lower herbicide costs (while there were initial cost savings in herbicide expenditure, these increased when glyphosate came off-patent in 2000. Growers of GM HT soybeans initially applied Monsanto's Roundup herbicide but over time, and with the availability of low-cost generic glyphosate alternatives, many growers switched to using these generic alternatives (the price of Roundup also fell significantly post 2000) plus a $6–$10/ha savings in labor and machinery costs.
- Against the background of underlying improvements in average yield levels over the 1996–2008 period (via improvements in plant breeding), the specific yield impact of the GM HT technology used up to 2008 has been neutral (some early studies of the impact of GM HT soybeans in the USA, suggested that GM HT soybeans produced lower yields than conventional soybean varieties. Where this may have occurred, it applied only in early years of adoption when the technology was not present in all leading varieties suitable for all of the main growing regions of the USA. By 1998/1999, the technology was available in leading varieties and no statistically significant average yield differences have been found between GM and conventional soybean varieties.
- The annual total national farm income benefit from using the technology rose from $5 million in 1996 to $1.42 billion in 2007. In 2008, the farm income was about $1.2 billion. The cumulative farm income benefit over the 1996–2008 period (in nominal terms) was $11 billion.
- In added value terms, the increase in farm income in recent years has been equivalent to an annual increase in production of between +5% and +10%.

Argentina

As in the USA, GM HT soybeans were first planted commercially in 1996. Since then, use of the technology

Global Economic Impact of Transgenic/Biotech Crops (1996–2008). Table 1 Farm-level income impact of using GM herbicide-tolerant (GM HT) soybeans in the USA 1996–2008

Year	Cost savings ($/ha)	Net cost saving/increase in gross margins, inclusive of cost of technology ($/ha)	Increase in farm income at a national level ($ millions)	Increase in national farm income as % of farm-level value of national production
1996	25.2	10.39	5.0	0.03
1997	25.2	10.39	33.2	0.19
1998	33.9	19.03	224.1	1.62
1999	33.9	19.03	311.9	2.5
2000	33.9	19.03	346.6	2.69
2001	73.4	58.56	1,298.5	10.11
2002	73.4	58.56	1,421.7	9.53
2003	78.5	61.19	1,574.9	9.57
2004	60.1	40.33	1,096.8	4.57
2005	69.4	44.71	1,201.4	6.87
2006	57.0	32.25	877.1	4.25
2007	85.2	60.48	1,417.2	6.01
2008	68.6	43.88	1,219.5	4.25

Sources and notes:

1. Impact data 1996–1997 based on Marra et al [3], 1998–2000 based on Carpenter and Gianessi [4] and 2001 [5] onward based on Sankala and Blumenthal [6, 7] and Johnson and Strom [8] plus updated 2008 to reflect recent changes in herbicide prices
2. Cost of technology: $14.82/ha 1996–2002, $17.3/ha 2003, $19.77/ha 2004, $24.71/ha 2005 onward
3. The higher values for the cost savings in 2001 onward reflect the methodology used by Sankala and Blumenthal, which was to examine the conventional herbicide regime that would be required to deliver the same level of weed control in a low/reduced till system to that delivered from the GM HT no/reduced till soybean system. This is a more robust methodology than some of the more simplistic alternatives used elsewhere. In earlier years, the cost savings were based on comparisons between GM HT soy growers and/or conventional herbicide regimes that were commonplace prior to commercialization in the mid-1990s when conventional tillage systems were more important

has increased rapidly and almost all soybeans grown in Argentina are GM HT (99%). Not surprisingly, the impact on farm income has been substantial, with farmers deriving important cost saving and farm income benefits both similar and additional to those obtained in the USA (Table 2). More specifically, it covers the following main issues:

- The impact on yield has been neutral (i.e., no positive or negative yield impact).
- The cost of the technology to Argentine farmers has been substantially lower than in the USA (about $1–$4/ha compared to $15–$25/ha in the USA: see Table 1) mainly because the main technology provider (Monsanto) was not able to obtain patent protection for the technology in Argentina. As such, Argentine farmers have been free to save and use biotech seed without paying any technology fees or royalties (on farm-saved seed) for many years and estimates of the proportion of total soybean seed used that derives from a combination of declared saved seed and uncertified seed in 2008 were about 75% (i.e., 25% of the crop was planted to certified seed).
- The savings from reduced expenditure on herbicides, fewer spray runs, and machinery use have been in the range of $24–$30/ha, although in 2008, savings fell back to about $16/ha because of the significant increase in the price of glyphosate relative to other herbicides. Net income gains have been in the range of $21–$29/ha, although in 2008 a lower average level of about $14/ha has occurred.

Global Economic Impact of Transgenic/Biotech Crops (1996–2008). Table 2 Farm-level income impact of using GM HT soybeans in Argentina 1996–2008

Year	Cost savings ($/ha)	Net saving on costs (inclusive of cost of technology ($/ha)	Increase in farm income at a national level ($ millions)	Increase in farm income from facilitating additional second cropping ($ millions)
1996	26.10	22.49	0.9	0
1997	25.32	21.71	42	25
1998	24.71	21.10	115	43
1999	24.41	20.80	152	118
2000	24.31	20.70	205	143
2001	24.31	20.70	250	273
2002	29.00	27.82	372	373
2003	29.00	27.75	400	416
2004	30.00	28.77	436	678
2005	30.20	28.96	471	527
2006	28.72	26.22	465	699
2007	28.61	26.11	429	1,134
2008	16.37	13.87	233	765

Sources and notes:
1. The primary source of information for impact on the costs of production is Qaim and Traxler [9, 10]. This has been updated in recent years to reflect changes in herbicide prices
2. All values for prices and costs denominated in Argentine pesos have been converted to US dollars at the annual average exchange rate in each year
3. The second cropping benefits are based on the gross margin derived from second crop soybeans multiplied by the total area of second crop soybeans (less an assumed area of second crop soybeans that equals the second crop area in 1996 – this was discontinued from 2004 because of the importance farmers attach to the GM HT system in facilitating them remaining in no tillage production systems). The source of gross margin data comes from Grupo CEO
4. Additional information is available in Appendix 1
5. The net savings to costs understate the total gains in recent years because two thirds to 80% of GM HT plantings have been to farm-saved seed on which no seed premium was payable (relative to the $3-$4/ha premium charged for new seed)

- The price received by farmers for GM HT soybeans in the early years of adoption was, on average, marginally higher than for conventionally produced soybeans because of lower levels of weed material and impurities in the crop. This quality premia was equivalent to about 0.5% of the baseline price for soybeans.
- The net income gain from the use of the GM HT technology at a national level was $233 million in 2008. Since 1996, the cumulative benefit (in nominal terms) has been $3.57 billion.
- An additional farm income benefit that many Argentine soybean growers have derived comes from the additional scope for second cropping of soybeans. This has arisen because of the simplicity, ease, and weed management flexibility provided by the (GM) technology, which has been an important factor facilitating the use of no and reduced tillage production systems. In turn, the adoption of low/no tillage production systems has reduced the time required for harvesting and drilling subsequent crops and hence has enabled many Argentine farmers to cultivate two crops (wheat followed by soybeans) in one season. As such, 20% of the total Argentine soybean crop was second crop in 2008 (3.4 million hectares), compared to 8% in 1996. Based on the additional gross margin income derived from second crop soybeans (see Appendix 1), this has contributed a further boost

to national soybean farm income of $765 billion in 2008 and $5.19 billion cumulatively since 1996.

- The total farm income benefit inclusive of the second cropping was $998 million in 2008 and $8.76 billion cumulatively between 1996 and 2008.
- In added value terms, the increase in farm income from the direct use of the GM HT technology (i.e., excluding the second crop benefits) in the last 3 years has been equivalent to an annual increase in production of between +2% and +7%. The additional production from second soybean cropping facilitated by the technology in 2008 was equal to 20% of total output.

Brazil

GM HT soybeans were probably first planted in Brazil in 1997. Since then, the area planted has increased to 62% of the total crop in 2008 (until 2003 all plantings were technically illegal).

The impact of using GM HT soybeans has been similar to that identified in the USA and Argentina. The net savings on herbicide costs have been larger in Brazil due to higher average costs of weed control. Hence, the average cost saving arising from a combination of reduced herbicide use, fewer spray runs, labor and machinery savings were between $30/ha and $81/ha in the period 2003–2008 (Table 3). The net cost saving after deduction of the technology fee (assumed to be about $20/ha in 2008) has been between $9/ha and $61/ha in recent years. At a national level, the adoption of GM HT soybeans increased farm income levels by $592 million in 2008. Cumulatively over the period 1997–2008, farm incomes have risen by $2.74 billion (in nominal terms).

In added value terms, the increase in farm income from the use of the GM HT technology in 2008 was

Global Economic Impact of Transgenic/Biotech Crops (1996–2008). Table 3 Farm-level income impact of using GM HT soybeans in Brazil 1997–2008

Year	Cost savings ($/ha)	Net cost saving after inclusion of technology cost ($/ha)	Impact on farm income at a national level ($ millions)	Increase in national farm income as % of farm-level value of national production
1997	38.8	35.19	3.8	0.06
1998	42.12	38.51	20.5	0.31
1999	38.76	35.15	43.5	0.96
2000	65.32	31.71	43.7	0.85
2001	46.32	42.71	58.7	1.02
2002	40.00	36.39	66.7	1.07
2003	77.00	68.00	214.7	1.62
2004	76.66	61.66	320.9	2.95
2005	73.39	57.23	534.6	5.45
2006	81.09	61.32	730.6	6.32
2007	29.85	8.74	116.3	0.68
2008	64.07	44.44	591.9	2.63

Sources and notes:

1. Impact data based on 2004 comparison data from the Parana Department of Agriculture [11] Cost of production comparison: biotech and conventional soybeans, in USDA GAIN report BR4629 of 11 November 2004. www.fas.usad.gov/gainfiles/200411/146118108.pdf for the period to 2006 [11]. From 2007 based on Galveo [12]
2. Cost of the technology from 2003 is based on the royalty payments officially levied by the technology providers. For years up to 2002, the cost of technology is based on costs of buying new seed in Argentina (the source of the seed). This probably overstates the real cost of the technology and understates the cost savings
3. All values for prices and costs denominated in Brazilian Real have been converted to US dollars at the annual average exchange rate in each year

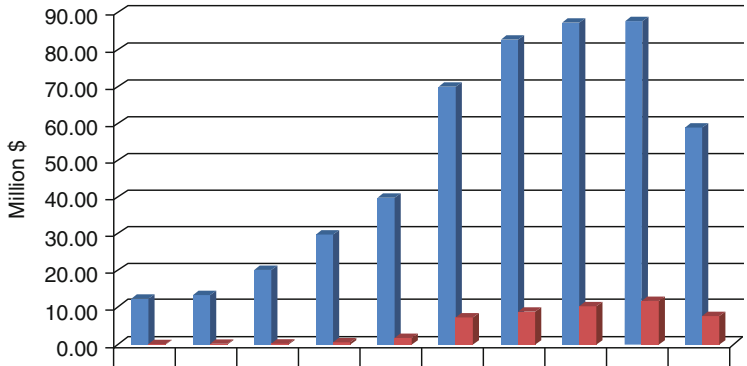

	1999	2000	2001	2002	2003	2004	2005	2006	2007	2008
Paraguay	12.50	13.48	20.42	29.91	40.04	70.06	82.65	87.52	87.80	58.84
Uruguay	0.00	0.06	0.13	0.59	1.80	7.42	9.11	10.49	11.89	7.89

Global Economic Impact of Transgenic/Biotech Crops (1996–2008). Figure 1
National farm income benefit from using GM herbicide-tolerant (GM HT) soybeans in Paraguay and Uruguay 1999–2008 (million $)

equivalent to an annual increase in production of +2.6% (about 1.54 million tons).

Paraguay and Uruguay

GM HT soybeans have been grown since 1999 and 2000 respectively in Paraguay and Uruguay. In 2008, they accounted for 90% of total soybean plantings in Paraguay and 99% of the soybean plantings in Uruguay (as in Argentina, the majority of plantings are to farm saved or uncertified seed). Using the farm-level impact data obtained from the Argentine research [9, 10] – we are not aware of any published country-specific impact research having been conducted in these two countries) and applying this to production in these two countries, Fig. 1 summarizes the national farm-level income benefits that have been derived from using the technology. In 2008, the respective national farm income gains were $58.8 million in Paraguay and $7.9 million in Uruguay.

Canada

GM HT soybeans were first planted in Canada in 1997. In 2008, the share of total plantings accounted for by GM HT soybeans was 73% (0.88 million hectares).

At the farm level, the main impacts of use have been similar to the impacts in the USA. The average farm income benefit has been within a range of $14–$40/ha and the increase in farm income at the national level was $12.6 million in 2008 (Table 4). The cumulative increase in farm income since 1997 has been $116 million (in nominal terms). In added value terms, the increase in farm income from the use of the GM HT technology in 2008 was equivalent to an annual increase in production of about 1% (34,500 tons).

South Africa

In 2001, GM HT soybeans were planted commercially in South Africa. In 2008, 184,000 ha (80%) of total soybean plantings were to varieties containing the GM HT trait. In terms of impact at the farm level, net cost savings of between $5/ha and $9/ha have been achieved through reduced expenditure on herbicides (Table 5), although in 2008, with the significant increase in glyphosate prices relative to other herbicides, this has fallen back to $2/ha. At the national level, the increase in farm income was $0.32 million in 2008. Cumulatively, the farm income gain since 2001 has been $4.13 million.

Romania

In 2008, Romania was not officially permitted to plant GM HT soybeans, having joined the EU at the start of 2007 (the EU has not permitted the growing of GM HT

Global Economic Impact of Transgenic/Biotech Crops (1996–2008). Table 4 Farm-level income impact of using GM HT soybeans in Canada 1997–2008

Year	Cost savings ($/ha)	Net cost saving/increase in gross margin (inclusive of technology cost: $/ha)	Impact on farm income at a national level ($ millions)	Increase in national farm income as % of farm-level value of national production
1997	64.28	41.17	0.041	0.01
1998	56.62	35.05	1.72	0.3
1999	53.17	31.64	6.35	1.29
2000	53.20	31.65	6.71	1.4
2001	49.83	29.17	9.35	3.4
2002	47.78	27.39	11.92	2.79
2003	49.46	14.64	7.65	1.47
2004	51.61	17.48	11.58	1.48
2005	55.65	18.85	13.30	2.26
2006	59.48	23.53	17.99	2.22
2007	61.99	24.52	16.87	1.57
2008	56.59	14.33	12.61	1.03

Sources and notes:
1. Impact data based on George Morris Centre Report [13] and updated in recent years to reflect changes in herbicide prices
2. All values for prices and costs denominated in Canadian dollars have been converted to US dollars at the annual average exchange rate in each year

Global Economic Impact of Transgenic/Biotech Crops (1996–2008). Table 5 Farm-level income impact of using GM HT soybeans in South Africa 2001–2008

Year	Cost savings ($/ha)	Net cost saving/increase in gross margin after inclusion of technology cost ($/ha)	Impact on farm income at a national level ($ millions)
2001	26.72	7.02	0.042
2002	21.82	5.72	0.097
2003	30.40	7.90	0.24
2004	34.94	9.14	0.46
2005	36.17	9.12	1.42
2006	33.96	5.17	0.83
2007	32.95	5.01	0.72
2008	25.38	1.77	0.32

Sources and notes:
1. Impact data (Data source: Monsanto South Africa – data provision not a reference)
2. All values for prices and costs denominated in South African Rand have been converted to US dollars at the annual average exchange rate in each year

soybeans to date). The impact data presented below therefore covers the period 1999–2006.

The growing of GM HT soybeans in Romania had resulted in substantially greater net farm income gains per hectare than any of the other countries using the technology:

- Yield gains of an average of 31% have been recorded [14]. This yield gain has arisen from the substantial improvements in weed control (weed infestation levels, particularly of difficult to control weeds such as Johnson grass have been very high in Romania. This is largely a legacy of the economic transition during the 1990s, which resulted in very low levels of farm income, abandonment of land, and very low levels of weed control. As a result, the weed bank developed substantially and has been subsequently very difficult to control, until the GM HT soybean system became available [glyphosate has been the key to controlling difficult weeds like Johnson grass]). In recent years, as fields have been cleaned up of problem weeds, the average yield gains have decreased and were reported at +13% in 2006 (source: farmer survey conducted in 2006 on behalf of Monsanto Romania).
- The cost of the technology to farmers in Romania tended to be higher than other countries, with seed being sold in conjunction with the herbicide. For example, in the 2002–2006 period, the average cost of seed and herbicide per hectare was $120–$130/ha. This relatively high cost however, did not deter adoption of the technology because of the major yield gains, improvements in the quality of soybeans produced (less weed material in the beans sold to crushers that resulted in price premia being obtained in the early years – no longer relevant post 2005), and cost savings derived.
- The average net increase in gross margin in 2006 was $59/ha (an average of $105/ha over the 8 years of commercial use: Table 6).
- At the national level, the increase in farm income amounted to $7.6 million in 2006. Cumulatively in the period 1999–2006, the increase in farm income was $44.6 million (in nominal terms).
- The yield gains in 2006 were equivalent to an 9% increase in national production (the annual average increase in production over the 8 years was equal to 10.1%).

Global Economic Impact of Transgenic/Biotech Crops (1996–2008). Table 6 Farm-level income impact of using herbicide-tolerant soybeans in Romania 1999–2006

Year	Cost saving ($/ha)	Cost savings net of cost of technology ($/ha)	Net increase in gross margin ($/ha)	Impact on farm income at a national level ($ millions)	Increase in national farm income as % of farm-level value of national production
1999	162.08	2.08	105.18	1.63	4.0
2000	140.30	−19.7	89.14	3.21	8.2
2001	147.33	−0.67	107.17	1.93	10.3
2002	167.80	32.8	157.41	5.19	14.6
2003	206.70	76.7	219.01	8.76	12.7
2004	63.33	8.81	135.86	9.51	13.7
2005	64.54	9.10	76.16	6.69	12.2
2006	64.99	9.10	58.79	7.64	9.3

Sources and notes:

1. Impact data (Sources: Brookes [14] and Monsanto Romania [15]. Average yield increase 31% applied to all years to 2003 and reduced to +25% 2004, +19% 2005 and +13% 2006. Average improvement in price premia from high quality 2% applied to years 1999–2004
2. All values for prices and costs denominated in Romanian Lei have been converted to US dollars at the annual average exchange rate in each year
3. Technology cost includes cost of herbicides
4. The technology was not permitted to be planted from 2007 – due to Romania joining the EU

- In added value terms, the combined effect of higher yields, improved quality of beans, and reduced cost of production on farm income in 2006 was equivalent to an annual increase in production of 9.3% (33,230 tons).

Mexico

GM HT soybeans were first planted commercially in Mexico in 1997 (on a trial basis) and in 2008, a continued trial area of 7,330 ha (out of total plantings of 88,000 ha) were varieties containing the GM HT trait.

At the farm level, the main impacts of use have been a combination of yield increase (+9.1% in 2004 and 2005, +3.64% in 2006, +3.2% 2007, and +2.4% 2008) and (herbicide) cost savings. The average farm income benefit has been within a range of $54–$89/ha (inclusive of yield gain, cost savings, and after payment of the technology fee/seed premium of $34.5/ha) and the increase in farm income at the national level was $0.04 million in 2008 (Table 7). The cumulative increase in farm income since 2004 has been $3.35 million (in nominal terms). In added value terms, the increase in farm income from the use of the GM HT technology in 2008 was equivalent to an annual increase in production of about 0.5%.

Bolivia

GM HT soybeans were officially permitted to be planted in 2008, although "illegal" plantings have occurred for several years. For the purposes of analysis in this section, impacts have been calculated back to 2005, when an estimated 0.3 million hectares of soybeans used GM HT technology. In 2008, an estimated 453,000 ha (63% of total crop) used GM HT technology.

The main impacts of the technology are as follows (Table 8):

- An increase in yield arising from improved yield control. The research work conducted by Fernandez et al. [19] estimated a 30% yield difference between GM HT and conventional soybeans although some of the yield gain reflected the use of poor-quality conventional seed by some farmers. In the analysis presented, a more conservative yield gain of +15% has been used.
- GM HT soybeans are assumed to trade at a price discount to conventional soybeans of −2.7%, reflecting the higher price set for conventional soybeans by the Bolivian government in 2008.
- The cost of the technology to farmers has been about $3.3/ha and the cost savings equal to about $9.3/ha, resulting in a net cost of production change of +$6/ha.
- Overall, in 2008, the average farm income gain from using GM HT soybeans was about $80/ha, resulting in a total farm income gain of $36.3 million. Cumulatively since 2005, the total farm income gain is estimated at $83.4 million.

Global Economic Impact of Transgenic/Biotech Crops (1996–2008). Table 7 Farm-level income impact of using GM HT soybeans in Mexico 2004–2008

Year	Cost savings ($/ha)	Net cost saving/increase in gross margin (inclusive of technology cost and yield gain: $/ha)	Impact on farm income at a national level ($ millions)	Increase in national farm income as % of farm-level value of national production
2004	49.44	82.34	1.18	3.07
2005	51.20	89.41	0.94	2.13
2006	51.20	72.98	0.51	1.05
2007	51.05	66.84	0.33	0.9
2008	33.05	54.13	0.40	0.5

Sources and notes:

1. Impact data based on Monsanto, 2005, 2007, and 2008 [16–18]. Reportes final del programa Soya Solución Faena en Chiapas. Monsanto Comercial
2. All values for prices and costs denominated in Mexican pesos have been converted to US dollars at the annual average exchange rate in each year

Global Economic Impact of Transgenic/Biotech Crops (1996–2008). Table 8 Farm-level income impact of using GM HT soybeans in Bolivia 2005–2008

Year	Cost savings excluding seed cost premium ($/ha)	Net cost saving/increase in gross margin (inclusive of technology cost and yield gain: $/ha)	Impact on farm income at a national level ($ millions)	Increase in national farm income as % of farm-level value of national production
2005	9.28	39.73	12.08	4.09
2006	9.28	36.60	15.55	6.35
2007	9.28	44.40	19.45	7.37
2008	9.28	80.09	36.33	7.24

Sources and notes:
1. Impact data based on Fernandez et al. [19]. Average yield gain assumed +15%, cost of technology $3.32/ha

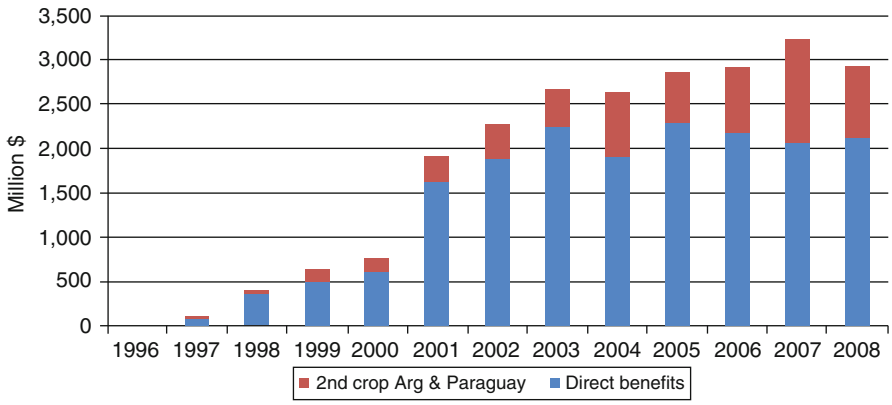

Global Economic Impact of Transgenic/Biotech Crops (1996–2008). Figure 2
Global farm-level income benefits derived from using GM HT soybeans 1996–2008 (million $)

Summary of Global Economic Impact

In global terms, the farm-level impact of using GM HT technology in soybeans was $2.12 billion in 2008 (Fig. 2). If the second crop benefits arising in Argentina are included, this impact rises to $2.92 billion. Cumulatively since 1996, the farm income benefit has been (in nominal terms) $17.9 billion ($23.3 billion if second crop gains in Argentina and Paraguay are included).

In terms of the total value of soybean production from the countries growing GM HT soybeans in 2008, the additional farm income (inclusive of Argentine second crop gains) generated by the technology is equal to a value-added equivalent of 4.3%. Relative to the value of global soybean production in 2008, the farm income benefit added the equivalent of 4.1%.

These economic benefits should be placed within the context of a significant increase in the level of soybean production in the main GM adopting countries since 1996 (a 63% increase in the area planted in the leading soybean producing countries of the USA, Brazil, and Argentina).

These economic benefits mostly derive from cost savings although farmers in Mexico, Bolivia, and Romania also obtained yield gains (from significant improvements in weed control levels relative to levels applicable prior to the introduction of the technology). If it is also assumed that all of the second crop soybean gains are effectively additional production that would not have otherwise occurred without the GM HT technology (the GM HT technology facilitated major expansion of second crop soybeans in Argentina and

to a lesser extent in Paraguay) then these gains are de facto "yield" gains. Under this assumption, of the total cumulative farm income gains from using GM HT soy, $5.56 billion (24%), is due to yield gains/second crop benefits and the balance, 76%, is due to cost savings.

Herbicide-Tolerant Maize

The USA

Herbicide-tolerant maize has been used commercially in the USA since 1997 and in 2008 was planted on 63% of the total US maize crop. The impact of using this technology at the farm level is summarized in Fig. 3. As with herbicide-tolerant soybeans, the main benefit has been to reduce costs, and hence improve profitability levels. Average profitability improved by $20–$25/ha in most years ($17.6/ha in 2008 – affected by the significant increase in glyphosate prices relative to other herbicides). The net gain to farm income in 2008 was $354 million and cumulatively, since 1997 the farm income benefit has been $1.7 billion. In added value terms, the effect of reduced costs of production on farm income in 2008 was equivalent to an annual increase in production of 0.71% (2.17 million tons).

Canada

In Canada, GM HT maize was first planted commercially in 1997. By 2008, the proportion of total plantings accounted for by varieties containing a GM HT trait was 51%. As in the USA, the main benefit has been to reduce costs and to improve profitability levels. Average annual profitability has improved by between $12/ha and $18/ha up to 2007, but fell to about $6/ha in 2008 (due to the higher price increases for glyphosate relative to other herbicides). In 2008, the net increase in farm income was $3.7 million and cumulatively since 1999 the farm income benefit has been $45.8 million. In added value terms, the effect of reduced costs of production on farm income in 2008 was equivalent to an annual increase in production of 0.22% (23,500 tons: Fig. 4).

Argentina

GM HT maize was first planted commercially in Argentina in 2004 and in 2008, varieties containing a GM HT trait were planted on 805,000 ha (35% of the total maize area). It has been adopted in two distinct types of area, the majority (80%) in the traditional "corn production belt" and 20% in newer maize-growing regions, which have been traditionally known as more marginal areas that surround the "Corn Belt." The limited adoption of GM HT technology in Argentina up to 2006 was mainly due to the technology only being available as a single gene, not stacked with the GM IR trait, which most maize growers have also adopted. Hence, faced with an either GM HT or GM IR trait available for use, most farmers have chosen the

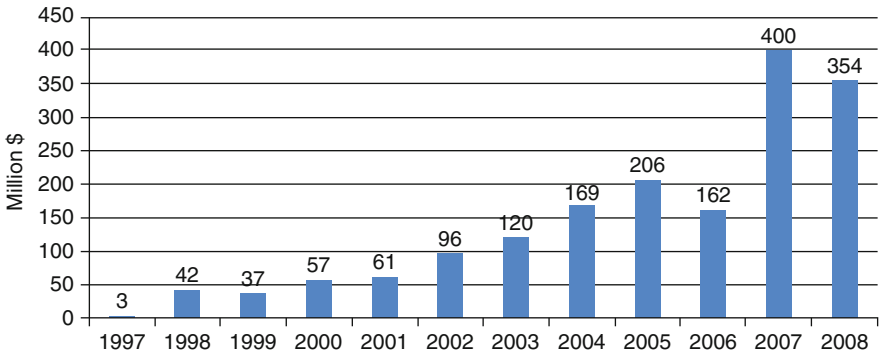

Global Economic Impact of Transgenic/Biotech Crops (1996–2008). Figure 3
National farm income impact of using GM HT maize in the USA 1997–2008 (Source and notes: Impact analysis based on Sankala and Blumenthal [6, 7] and Johnson and Strom [8] and updated for 2008 to reflect changes in herbicide prices. Estimated cost of the technology $14.83/ha in years up to 2004, $17.3/ha in 2005, $24.71/ha 2006 onward. Cost savings (mostly from lower herbicide use) $33.47/ha in 2004, $38.61/ha 2005, $29.27/ha 2006, $42.28/ha 2007, and $40.87/ha 2008)

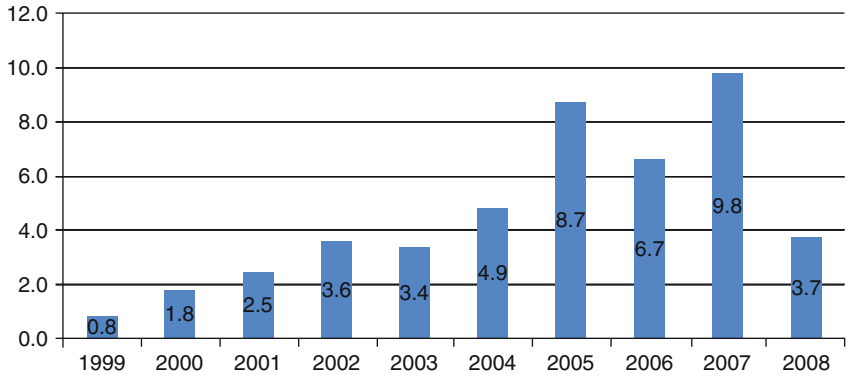

Global Economic Impact of Transgenic/Biotech Crops (1996–2008). Figure 4
National farm income impact of using GM HT maize in Canada 1999–2008 ($ million) (Source and notes: Impact analysis based on data supplied by Monsanto Canada. Estimated cost of the technology $18-$32/ha, cost savings (mostly from lower herbicide use) $31–$45/ha)

GM IR trait because the additional returns derived from adoption have tended to be (on average) greater from the GM IR trait than the GM HT trait (see below for further details of returns from the GM HT trait). Stacked traits became available in 2007 and contributed to the significant increase in the GM HT maize area relative to 2006.

In relation to impact on farm income, the following observations were made:

- In all regions, the cost of the technology (about $20/ha) has been broadly equal to the saving in herbicide costs.
- In the Corn Belt area, use of the technology has resulted in an average 3% yield improvement via improved weed control. In the more marginal areas, the yield impact has been much more significant (+22%) as farmers have been able to significantly improve weed control levels.
- In 2008, the additional farm income at a national level from using GM HT technology has been +$61.6 million, and cumulatively since 2004, the income gain has been $113.8 million.

South Africa

Herbicide-tolerant maize has been grown commercially in South Africa since 2003, and 6,46,000 ha out of total plantings of 2.43 million hectares were herbicide tolerant in 2008. Farmers using the technology have found that small net savings in the cost of production have occurred (i.e., the cost saving from reduced expenditure on herbicides has been greater than the cost of the technology), although in 2008, due to the significant rise in the global price of glyphosate relative to their herbicides, the net farm income balance was negative, at about −$2/ha. This resulted in a total net farm loss arising from using GM HT technology of $1.43 million, though since 2003, there has been a net cumulative income gain of $3.77 million.

Philippines

GM HT maize was first grown commercially in 2006, and 2008 was planted on 270,000 ha. Information about the impact of the technology is limited, although industry sources estimate that, on average farmers using it have derived a 15% increase in yield. Based on a cost of the technology of $24–$27/ha (and assuming no net cost savings), the net national impact on farm income was +$15.9 million in 2008. Cumulatively, since 2006, the total farm income gain has been $27.1 million

Summary of Global Economic Impact

In global terms, the farm-level economic impact of using GM HT technology in maize was $433.5 million in 2008 (82% of which was in the USA). Cumulatively since 1997, the farm income benefit has been

(in nominal terms) $1.9 billion. Of this, 92% has been due to cost savings and 8% to yield gains (from improved weed control relative to the level of weed control achieved by farmers using conventional technology).

In terms of the total value of maize production in the main countries using this technology in 2008, the additional farm income generated by the technology is equal to a value-added equivalent of 0.3% of global maize production.

Herbicide-Tolerant Cotton

The USA

GM HT cotton was first grown commercially in the USA in 1997 and in 2008 was planted on 68% of total cotton plantings.

The farm income impact of using GM HT cotton is summarized in Table 9. The primary benefit has been to reduce costs, and hence improve profitability levels, with annual average profitability increasing by between $21/ha and $49/ha (the only published source that has examined the impact of HT cotton in the USA is the work by Sankala and Blumenthal [6, 7], and Johnson and Strom [8]. In the 2001 study, the costs saved were based on historic patterns of herbicides used on conventional cotton in the mid/late 1990s. The latter studies estimated cost savings on the basis of the conventional herbicide treatment that would be required to deliver the same level of weed control as GM HT cotton. Revised analysis has, however, been conducted for 2008 to reflect changes in the costs of production (notably cost of the technology (in particular "Roundup Ready Flex technology"), higher prices for glyphosate relative to other herbicides in 2008 and additional costs incurred to control weeds resistant to glyphosate in some regions) in the years up to 2004. Since then, net income gains have fallen to between $1/ha and $5/ha. The relatively small positive impact on direct farm income in 2008 (and in the last few years) reflects a combination of reasons, including the higher cost of the technology, significant price increases for glyphosate relative to price increases for other

Global Economic Impact of Transgenic/Biotech Crops (1996–2008). Table 9 Farm-level income impact of using GM HT cotton in the USA 1997–2008

Year	Cost savings ($/ha)	Net cost saving/increase in gross margins, inclusive of cost of technology ($/ha)	Increase in farm income at a national level ($ millions)	Increase in national farm income as % of farm-level value of national production
1997	34.12	21.28	12.56	0.2
1998	34.12	21.28	30.21	0.58
1999	34.12	21.28	53.91	1.29
2000	34.12	21.28	61.46	1.22
2001	65.59	45.27	161.46	4.75
2002	65.59	45.27	153.18	3.49
2003	65.59	45.27	129.75	2.33
2004	83.35	48.80	154.72	2.87
2005	71.12	2.89	9.57	0.18
2006	73.66	3.31	13.29	0.22
2007	76.01	5.40	16.56	0.32
2008	72.76	1.20	2.50	0.08

Source and notes:

1. Impact analysis based on Sankala and Blumenthal [6, 7] and Johnson and Strom [8] and own analysis for 2008
2. Estimated cost of the technology $12.85/ha (1997–2000) and $21.32/ha 2001–2003, $34.55 2004, $68.22/ha 2005, $70.35/ha 2006, $70.61/ha 2007, and £71.56/ha 2008

herbicides, and additional costs incurred for management of weeds resistant to glyphosate (notably *Palmer Amaranth*). Overall, the net direct farm income impact in 2008 is estimated to be $2.5 million (this does not take into consideration any nonpecuniary benefits associated with adoption of the technology: see Section 3.9). Cumulatively, since 1997, there has been a net farm income benefit from using the technology of $799 million.

Other Countries

Australia, Argentina, South Africa, and Mexico are the other countries where GM HT cotton is commercially grown; from 2000 in Australia, 2001 in South Africa, 2002 in Argentina, and 2005 in Mexico. In 2008, 79% (50,460 ha), 38% (124,000 ha), 75% (9,750 ha), and 40% (50,000 ha) respectively of the total Australian, Argentine, South African, and Mexican cotton crops were planted to GM HT cultivars.

We are not aware of any published research into the impact of GM HT cotton in South Africa, Argentina, or Mexico. In Australia, although research has been conducted into the impact of using GM HT cotton (e.g., Doyle et al. [20]) this does not provide quantification of the impact. Drawing on industry source estimates, the main impacts are as follows:

- *Australia*: No yield gain and cost of the technology in the range of $30–$45/ha up to 2007. The cost of the technology increased with the availability of "Roundup Ready Flex" and in 2008 was about $63/ha. The cost savings from the technology (after taking into consideration the cost of the technology have delivered small net gains of $5–$7/ha, although estimates relating to the net average benefits from Roundup Ready Flex are about $25/ha in 2008 [20]. Overall, in 2008, the total farm income from using the technology was about $3 million and cumulatively, since 2000, the total gains have been $8.3 million.
- *Argentina*: No yield gain and a cost of technology in the range of $30–$40/ha, although with the increasing availability of stacked traits in recent years, the "cost" part of the HT technology has fallen to $24/ha. Net farm income gains (after deduction of the cost of the technology) have been $8–$18/ha and in 2008 were just under $10/ha. Overall, in 2008, the total farm income from using GM HT cotton technology was about $7.4 million, and cumulatively since 2002, the farm income gain has been $34.2 million.
- *South Africa*: No yield gain and a cost of technology in the range of $15–$25/ha. Net farm income gains from cost savings (after deduction of the cost of the technology) have been $30–$60/ha. In 2008, the average net gain was $33.6/ha and the total farm income benefit of the technology was $0.37 million. Cumulatively since 2001, the total farm income gain from GM HT cotton has been $2.2 million.
- *Mexico*: Average yield gains of +3.6% from improved weed control have been reported in the first 3 years of use, although no yield gain was recorded in 2008. The average cost of the technology has been in the range of $60–$66/ha and typical net farm income gains of about $80/ha, though in 2008, with no yield gains this fell back to $16/ha. Overall, in 2008, the total farm income gain from using GM HT cotton was about $1.35 million and cumulatively since 2005, the total farm income gain has been $11.7 million.

Summary of Global Economic Impact

Across the five countries using GM HT cotton in 2008, the total farm income impact derived from using GM HT cotton was +$14.6 million. Cumulatively since 1997, there have been net farm income gains of $855.8 million (93% of this benefit has been in the USA). Of this, 96% has been due to cost savings and 4% to yield gains (from improved weed control relative to the level of weed control achieved using conventional technology).

Herbicide-Tolerant Canola

Canada

Canada was the first country to commercially use GM HT canola in 1996. Since then, the area planted to varieties containing GM HT traits has increased significantly, and in 2008 was 83% of the total crop (5.43 million hectares).

The farm-level impact of using GM HT canola in Canada since 1996 is summarized in Table 10. The key features are as follows:

- The primary impact in the early years of adoption was increased yields of almost 11% (e.g., in 2002

Global Economic Impact of Transgenic/Biotech Crops (1996–2008). Table 10 Farm-level income impact of using GM HT canola in Canada 1996–2008

Year	Cost savings ($/ha)	Cost savings inclusive of cost of technology ($/ha)	Net cost saving/ increase in gross margins ($/ha)	Increase in farm income at a national level ($ millions)	Increase in national farm income as % of farm-level value of national production
1996	28.59	−4.13	45.11	6.23	0.4
1997	28.08	−4.05	37.11	21.69	1.17
1998	26.21	−3.78	36.93	70.18	3.43
1999	26.32	−3.79	30.63	90.33	5.09
2000	26.32	−3.79	22.42	59.91	5.08
2001	25.15	−1.62	23.10	53.34	5.69
2002	24.84	−3.59	29.63	61.86	6.17
2003	28.04	−4.05	41.42	132.08	6.69
2004	21.42	+4.44	19.09	70.72	4.48
2005	23.11	+4.50	32.90	148.12	6.56
2006	34.02	+16.93	50.71	233.13	8.09
2007	35.44	+17.46	66.39	341.44	7.54
2008	36.36	+17.56	66.63	364.23	6.35

Sources and notes:

1. Impact data based on Canola Council study [21] to 2003 and Gusta et al. [22]. Includes a 10.7% yield improvement and a 1.27% increase in the price premium earned (cleaner crop with lower levels of weed impurities) until 2003. After 2004, the yield gain has been based on differences between average annual variety trial results for Clearfield and biotech alternatives. The biotech alternatives have also been differentiated into glyphosate tolerant and glufosinate tolerant. This resulted in the following observation: for GM glyphosate-tolerant varieties no yield difference for 2004, 2005, and 2008 and +4% 2006 and 2007. For GM glufosinate-tolerant varieties, the yield differences were +12% 2004 and 2008, +19% 2005, +10% 2006 and 2007
2. Negative values denote a net increase in the cost of production (i.e., the cost of the technology was greater than the other cost (e.g., on herbicides) reductions
3. All values for prices and costs denominated in Canadian dollars have been converted to US dollars at the annual average exchange rate in each year

this yield increase was equivalent to an increase in total Canadian canola production of nearly 7%). In addition, a small additional price premia was achieved from crushers through supplying cleaner crops (lower levels of weed impurities). With the development of hybrid varieties using conventional technology, the yield advantage of GM HT canola relative to conventional alternatives (the main one of which is "Clearfield" conventionally derived herbicide-tolerant varieties. Also, hybrid canolas now account for the majority of plantings (including some GM hybrids) with the hybrid vigor delivered by conventional breeding techniques (even in the GM HT [to glyphosate] varieties) has been eroded. As a result, our analysis has applied the yield advantage of +10.7% associated with the GM HT technology in its early years of adoption (source: Canaola Council study of 2001) to 2003. From 2004, the yield gain has been based on differences between average annual variety trial results for "Clearfield" (conventional herbicide-tolerant varieties) and biotech alternatives. The biotech alternatives have also been differentiated into glyphosate tolerant and glufosinate tolerant. This resulted in the following observation: for GM glyphosate-tolerant varieties no yield difference for 2004, 2005, and 2008 and +4% 2006 and 2007. For GM glufosinate-tolerant varieties, the yield differences

were +12% 2004 and 2008, +19% 2005, +10% 2006 and 2007. The quality premia associated with cleaner crops (see above) has not been included in the analysis from 2004.

- Cost of production (excluding the cost of the technology) has fallen, mainly through reduced expenditure on herbicides and some savings in fuel and labor. These savings have annually been between about $25/ha and $36/ha. The cost of the technology to 2003 was however marginally higher than these savings resulting in a net increase in costs of $3– $5/ha. On the basis of comparing GM HT canola with "Clearfield" HT canola (from 2004), there has been a net cost saving of between $5/ha and $10/ha, although in 2008 this was $17/ha.
- The overall impact on profitability (inclusive of yield improvements and higher quality) has been an increase of between $22/ha and $48/ha up to 2003. On the basis of comparing GM HT canola with "Clearfield" HT canola (from 2004), the net increase in profitability has been between $23/ha and $66/ha.
- The annual total national farm income benefit from using the technology has risen from $6 million in 1996 to $364 million in 2008. The cumulative farm income benefit over the 1996–2008 period (in nominal terms) was $1.64 billion.
- In added value terms, the increase in farm income in 2008 has been equivalent to an annual increase in production of 6.3%.

The USA

GM HT canola has been planted on a commercial basis in the USA since 1999. In 2008, 95% of the US canola crop was GM HT (380,230 ha).

The farm-level impact has been similar to the impact identified in Canada. More specifically, the following observations were noted:

- Average yields increased by about 6% in the initial years of adoption. As in Canada (see above) the availability of high-yielding hybrid conventional varieties has eroded some of this yield gain in recent year relative to conventional alternatives. As a result, the positive yield impacts post 2004 have been applied on the same basis as in Canada (comparison with Clearfields: see Canada above).
- The cost of the technology has been $12–$17/ha for glufosinate-tolerant varieties and $12–$33/ha for glyphosate-tolerant varieties. Cost savings (before inclusion of the technology costs) have been $35–$45/ha ($22/ha in 2008) for glufosinate-tolerant canola and $40–$79/ha for glyphosate-tolerant canola.
- The net impact on gross margins has been between +$22/ha and +$90/ha ($5/ha in 2008) for glufosinate-tolerant canola, and +$28/ha and +$61/ha for glyphosate-tolerant canola.
- At the national level, the total farm income benefit in 2008 was $26.6 million (Fig. 5) and the cumulative benefit since 1999 has been $185 million.

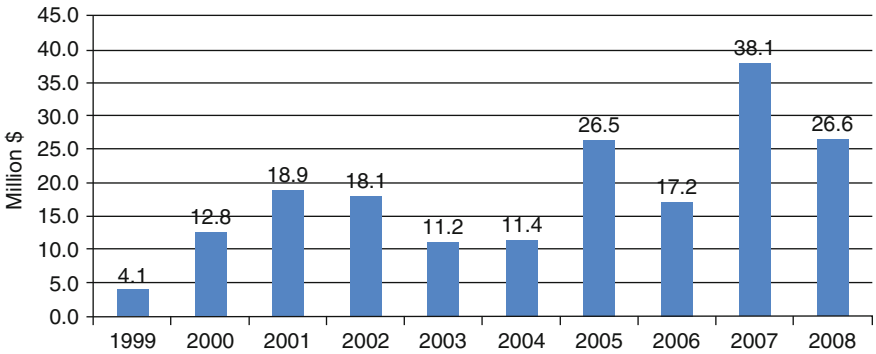

Global Economic Impact of Transgenic/Biotech Crops (1996–2008). Figure 5
National farm income impact of using GM HT canola in the USA 1999–2008 (Source and notes: Impact analysis based on Sankala and Blumenthal [6, 7] and Johnson and Strom [8]. Decrease in total farm income impact 2002–2004 is due to decline in total plantings of canola in the USA (from 612,000 in 2002 to 316,000 ha in 2004). Positive yield impact applied in the same way as Canada from 2004)

- In added value terms, the increase in farm income in 2008 has been equivalent to an annual increase in production of about 10.3%.

Australia

GM HT canola was permitted for commercial use in the two states of Victoria and New South Wales in 2008, and was planted on 10,100 ha in that year (2008/09). Ninety-five percent of these plantings had tolerance to the herbicide glyphosate and the balance were tolerant to glufosinate.

A fairly comprehensive farm survey-based analysis of impact of the glyphosate-tolerant canola was commissioned by Monsanto, which involved interviews with 92 of the 108 farmers using this technology in 2008/09 [23, 24]. Key findings from this survey are as follows:

- The technology was made available in both open-pollinated and hybrid varieties, with the open-pollinated varieties representing the cheaper end of the seed market, where competition was mainly with open-pollinated varieties containing herbicide tolerance (derived conventionally) to herbicides in the triazine (TT) group. The hybrid varieties containing glyphosate tolerance competed with nonherbicide-tolerant conventional hybrid varieties and herbicide-tolerant "Clearfield" hybrids (tolerant to the imidazolinone group of herbicides), although, were used in 2008, all of the 33 farmers in the survey using GM HT hybrids did so mainly in competition and comparison with "Clearfield" varieties.
- The GM HT open-pollinated varieties sold to farmers at a premium of about $Aus3/ha (about $2.5 US/ha) relative to the TT varieties. The GM HT hybrids sold at a seed premium of about $Aus 9/ha ($7.55 US/ha) compared to "Clearfield" hybrids. In addition, farmers using the GM HT technology paid a "technology" fee in two parts; one part was a set fee of $Aus500 per farm plus $Aus 10.2/ton of output of canola. On the basis that there were 108 farmers using GM HT (glyphosate tolerant) technology in 2008, the average "up front" fee paid for the technology was $Aus5.62/ha. On the basis of average yields obtained for the two main types of GM HT seed used, those using open-pollinated varieties paid $11.83/ha (basis: average yield of 1.16 tons/ha) and those using GM HT hybrids paid $Aus12.95/ha (basis: average yield of 1.27 tons/ha). Therefore, the total seed premium and technology fee paid by farmers for the GM HT technology in 2008–2009 was $Aus20.45/ha ($17.16 US/ha) for open-pollinated varieties and $Aus 27.57/ha ($23.13 US/ha) for hybrid varieties. After taking into consideration, the seed premium/technology fees, the GM HT system was marginally more expensive by $Aus3/ha ($2.5 US/ha) and $Aus4/ha ($US 3.36/ha) respectively for weed control than the TT and Clearfield varieties.
- The GM HT varieties delivered higher average yields than their conventional counterparts: +22.11% compared to the TT varieties and +4.96% compared to the "Clearfield" varieties. In addition, the GM HT varieties produced higher oil contents of +2% and +1.8% respectively compared to TT and "Clearfield" varieties.
- The average reduction in weed control costs from using the GM HT system (excluding seed premium/technology fee) was $Aus 17/ha for open-pollinated varieties (competing with TT varieties) and $Aus 24/ha for hybrids (competing with Clearfield varieties).

In the analysis summarized below in Table 11, these research findings have been applied to the total GM HT

Global Economic Impact of Transgenic/Biotech Crops (1996–2008). Table 11 Farm-level income impact of using GM HT canola in Australia 2008 ($US)

Year	Average cost saving ($/ha)	Average cost savings (net after cost of technology ($/ha)	Average net increase in gross margins ($/ha)	Increase in farm income at a national level ($)
2008	19.18	−20.77	93.37	943,054

Source derived from and based on Monsanto survey of license holders 2008

Notes:

1. The average values shown are weighted averages
2. Other weighted average values derive include yield +21.1% and quality (price) premium of 2.1% applied on the basis of this level of increase in average oil content

crop area on a weighted basis in which the results of GM HT open-pollinated varieties that compete with TT varieties were applied to 64% of the total area and the balance of area used the results from the GM HT hybrids competing with "Clearfield" varieties. This weighting reflects the distribution of farms in the survey, in which 59 (64%) of the farmers indicated they grew open-pollinated varieties and 33 (34%) grew hybrids. The findings show an average farm income gain of $US 93/ha and a total farm income gain of $0.93 million in 2008.

Summary of Global Economic Impact

In global terms, the farm-level impact of using GM HT technology in canola in Canada, the USA, and Australia was $392 million in 2008. Cumulatively, since 1996, the farm income benefit has been (in nominal terms) $1.83 billion. Within this, 79% has been due to yield gains and the balance (21%) has been from cost savings.

In terms of the total value of canola production in these three countries in 2008, the additional farm income generated by the technology is equal to a value-added equivalent of 6.9%. Relative to the value of global canola production in 2008, the farm income benefit added the equivalent of 1.5%.

GM Herbicide-Tolerant (GM HT) Sugar Beet

GM HT sugar beet was first grown commercially in the USA in 2007 (under 1,000 ha), although it was 2008 before sufficient quantities of seed were available for widespread commercial cultivation. In 2008, just under 258,000 ha of GM HT sugar beet were planted, equal to about 63.5% of the total US crop. The highest levels of penetration of the technology (85% plus of total crop) occurred in Idaho, Wyoming, Nebraska, and Colorado, with about 50% of the crops in the largest sugar beet growing states of North Dakota and Michigan being GM HT.

Impact of the technology in these early years of adoption has been identified as follows:

(a) *Yield*: Analysis by Kniss [25] covering a limited number of farms in Wyoming (2007) identified positive yield impacts of +8.8% in terms of additional root yield (from better weed control) and +12.6% in terms of sugar content relative to conventional crops (i.e., the GM HT crop had about a 3.8% higher sugar content, which amounts to a 12.8% total sucrose gain relative to conventional sugar beet once the root yield gain was taken into consideration). In contrast, Khan [26] found similar yields reported between conventional and GM HT sugar beet in the Red River Valley region (North Dakota) and Michigan. These contrasting results probably reflect a combination of factors including:
- The sugar beet growing regions in Wyoming can probably be classified as high weed problem areas, and as such, are regions where obtaining effective weed control is difficult using conventional technology (timing of application is key to weed control in sugar beet, with optimal time for application being when weeds are small). Also some weeds (e.g., Kochia) are resistant to some of the commonly used ALS inhibitor herbicides like chlorsulfuron. The availability of GM HT sugar beet with its greater flexibility on application timing has therefore potentially delivered important yield gains for such growers.
- The GM HT trait was not available in all leading varieties suitable in all growing regions in 2008, hence the yield benefits referred to above from better weed control have to some extent been counterbalanced by only being available in poorer performing germ plasm in states like Michigan and North Dakota (notably not being available in 2008 in leading varieties with rhizomania resistance). It should be noted that the authors of the research cited in this section both perceive that yield benefits from using GM HT sugar beet will be a common feature of the technology in most regions once the technology is available in leading varieties.
- The year 2008 was reported to have been, in the leading sugar beet growing states, a reasonable year for controlling weeds through conventional technology (i.e., it was possible to get good levels of weed control through timely applications), hence the similar performance reported between the two systems.

(b) Costs of production
- Kniss's work in Wyoming identified weed control costs (comprising herbicides, application,

cultivation, and hand labor) for conventional beet of $437/ha compared to $84/ha for the GM HT system. After taking into consideration the $131/ha seed premium/technology fee for the GM HT trait, the net cost differences between the two systems was $222/ha in favor of the GM HT system. Kniss did, however, acknowledge that the conventional costs associated with this sample were high relative to most producers (reflecting application of maximum dose rates for herbicides and use of hand labor), with a more typical range of conventional weed control costs being between $171/ha and $319/ha (average $245/ha).

- Khan's analysis puts the typical weed control costs in the Red River region of North Dakota to be about $227/ha for conventional compared to $91/ha for GM HT sugar beet. After taking into consideration the seed premium/technology fee (assumed by Khan to be $158/ha), the total weed control costs were $249/ha for the GM HT system, $22/ha higher than the conventional system. Despite this net increase in average costs of production, most growers in this region used (and planned to continue using), the GM HT system because of the convenience and weed control flexibility benefits associated with it (which research by Marra and Piggot [1]) estimated in the corn, soybean, and cotton sectors to be valued at between $12/ha and $25/ha to US farmers). It is also likely that Khan's analysis may understate the total cost savings from using the technology by not taking into account savings on application costs and labor for hand weeding.

For the purposes of our analysis, we have drawn on both these pieces of work, as summarized in Table 12. This shows a net farm income gain in 2008 of over $21 million to US sugar beet farmers (average gain per hectare of just under $83/ha). With the availability of GM HT technology in more of the leading varieties, it is expected that the farm income gains associated with yield gains will be greater in subsequent years.

GM Insect-Resistant (To Corn-Boring Pests: GM IR) Maize

The USA

GM IR maize was first planted in the USA in 1996 and in 2008, seed containing GM IR traits was planted on 57% (18.14 million hectares) of the total US maize crop.

Global Economic Impact of Transgenic/Biotech Crops (1996–2008). Table 12 Farm-level income impact of using GM HT sugar beet in the USA 2007–2008

Year	Average cost saving ($/ha)	Average cost savings (net after cost of technology ($/ha)	Average net increase in gross margins ($/ha)	Increase in farm income at a national level ($ millions)	Increase in national farm income as % of farm-level value of national production
2007	353.35	222.39	584.00	472,680	0.03
2008	142.50	−8.58	82.88	21,380,290	1.83

Sources derived from and based on Kniss [25] and Khan [26]

Notes:

1. The yield gains identified by Kniss have been applied to the 2007 GM HT plantings in total and to the estimated GM HT plantings in the states of Idaho, Wyoming, Nebraska, and Colorado, where penetration of plantings in 2008 was 85% (these states account for 26% of the total GM HT crop in 2008), and which are perceived to be regions of above average weed problems. For all other regions, no yield gain is assumed. Across the entire GM HT area in 2008, this equates to a net average yield gain of +3.28%

2. The seed premium of $131/ha, average costs of weed control respectively for conventional and GM HT systems of $245/ha and $84/ha, from Kniss were applied to the crop in Idaho, Wyoming, Nebraska, and Colorado. The seed premium of $158/ha, weed control costs of $227/ha and $249/ha respectively for conventional and GM HT sugar beet, identified by Khan were applied to all other regions using the technology. These states account for 26% of the total GM HT crop in 2008. The resulting average values for seed premium/cost of technology across the entire 2008 GM HT crop was therefore $151.08/ha and the average weed control cost saving associated with the GM HT system (before taking into consideration the seed premium) was $142.5/ha

Global Economic Impact of Transgenic/Biotech Crops (1996–2008). Table 13 Farm-level income impact of using GM IR maize in the USA 1996–2008

Year	Cost saving ($/ha)	Cost savings (net after cost of technology ($/ha)	Net increase in gross margins ($/ha)	Increase in farm income at a national level ($ millions)	Increase in national farm income as % of farm-level value of national production
1996	24.71	−9.21	29.20	8.76	0.03
1997	24.71	−9.21	28.81	70.47	0.27
1998	20.30	−4.8	27.04	167.58	0.77
1999	20.30	−4.8	25.51	206.94	1.04
2000	22.24	−6.74	24.32	148.77	0.71
2001	22.24	−6.74	26.76	155.87	0.72
2002	22.24	−6.74	30.74	240.45	0.96
2003	22.24	−6.74	31.54	291.00	1.14
2004	15.88	−6.36	33.82	363.41	1.32
2005	15.88	−1.42	34.52	399.91	1.60
2006	15.88	−1.42	55.78	707.23	1.86
2007	15.88	−1.42	61.22	1,136.21	2.28
2008	24.71	−8.83	67.51	1,224.59	2.40

Sources and notes:
1. Impact data based on a combination of studies including the ISAAA (James) review [27], Marra et al. [3], Sankala and Blumenthal [6, 7], and Johnson and Strom [8], Gianessi and Carpenter [28]
2. Yield impact +5% based on average of findings of above studies
3. Insecticide cost savings based on the above references
4. – (minus) value for net cost savings means the cost of the technology is greater than the other cost savings

The farm-level impact of using GM IR maize in the USA since 1996 is summarized in Table 13:

- The primary impact has been increased average yields of about 5% (in 2008 this additional production is equal to an increase in total US maize production of +2.41%).
- The net impact on cost of production has been a small increase of between $1/ha and $9/ha (additional cost of the technology being higher than the estimated average insecticide cost savings of $15–$16/ha).
- The annual total national farm income benefit from using the technology has risen from $8.76 million in 1996 to $1.22 billion in 2008. The cumulative farm income benefit over the 1996–2008 period (in nominal terms) was $5.12 billion.
- In added value terms, the increase in farm income in 2008 was equivalent to an annual increase in production of 2.4%.

Canada

GM IR maize has also been grown commercially in Canada since 1996. In 2008, it accounted for 62% of the total Canadian maize crop of 1.2 million hectares. The impact of GM IR maize in Canada has been very similar to the impact in the USA (similar yield and cost of production impacts). At the national level, in 2008 the additional farm income generated from the use of GM IR maize was $48.2 million and cumulatively since 1996 the additional farm income (in nominal terms) was $252 million (Fig. 6).

Argentina

In 2008, GM IR maize traits were planted on 75% of the total Argentine maize crop (GM IR varieties were first planted in 1998).

The main impact of using the technology on farm profitability has been via yield increases. Various

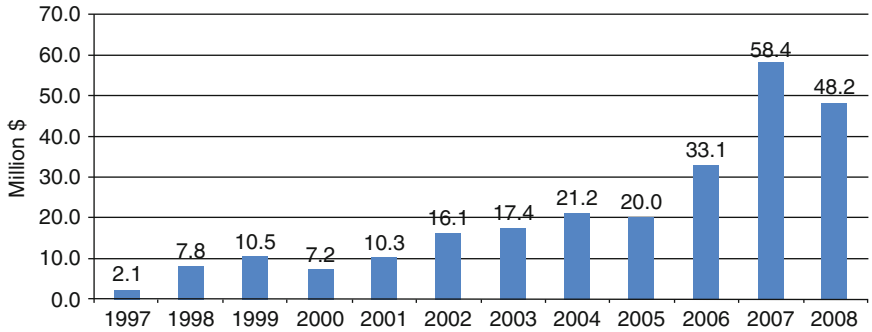

Global Economic Impact of Transgenic/Biotech Crops (1996–2008). Figure 6
National farm income impact of using GM IR maize in Canada 1996–2008
Notes:
1. Yield increase of 5% based on industry assessments (consistent with US analysis). Cost of technology and insecticide cost savings based on US analysis,
2. GM IR area planted in 1996 = 1,000 ha,
3. All values for prices and costs denominated in Canadian dollars have been converted to US dollars at the annual average exchange rate in each year

studies (e.g., see ISAAA review in James [27]) and Trigo and Cap [29] have identified an average yield increase in the region of 8–10%, hence an average of 9% has been used in the analysis up to 2004. More recent trade source estimates provided to the authors put the average yield increased in the last 2–3 years to be between 5% and 6%. Accordingly, our analysis uses a yield increase value of 5.5% for the years from 2004.

No savings in costs of production have arisen for most farmers because very few maize growers in Argentina have traditionally used insecticides as a method of control for corn-boring pests. As such, average costs of production have increased by $20–$22/ha (the cost of the technology).

The net impact on farm profit margins (inclusive of the yield gain) has, in recent years, been an increase of about $20/ha. In 2008, the national level impact on profitability was an increase of $41 million (an added value equal to 2.15% of the total value of production). Cumulatively, the farm income gain since 1997 has been $269.7 million.

South Africa

GM IR maize has been grown commercially in South Africa since 2000. In 2008, 56% of the country's total maize crop of 2.42 million hectares used GM IR cultivars.

The impact on farm profitability is summarized in Table 14. The main impact has been an average yield improvement of between 5% and 32% in the years 2000–2004, with an average of about 15% (used as the basis for analysis 2005–2007). In 2008, the estimated yield impact was +10.6% (source: Van der Weld [33]). The cost of the technology $8–$17/ha has broadly been equal to the average cost savings from no longer applying insecticides to control corn-boring pests.

At the national level, the increase in farm income in 2008 was $117.7 million and cumulatively since 2000 it has been $476 million. In terms of national maize production, the use of GM IR technology on 56% of the planted area has resulted in a net increase in national maize production of 5.9% in 2008. The value of the additional income generated was also equivalent to an annual increase in production of about 5.1%.

Spain

Spain has been commercially growing GM IR maize since 1998 and in 2008, 22% (79,270 ha) of the country's maize crop was planted to varieties containing a GM IR trait.

As in the other countries planting GM IR maize, the main impact on farm profitability has been increased yields (an average increase in yield of 6.3% across farms using the technology in the early years of adoption).

Global Economic Impact of Transgenic/Biotech Crops (1996–2008). Table 14 Farm-level income impact of using GM IR maize in South Africa 2000–2008

Year	Cost savings ($/ha)	Net cost savings inclusive of cost of technology ($/ha)	Net increase in gross margin ($/ha)	Impact on farm income at a national level ($ millions)
2000	13.98	1.87	43.77	3.31
2001	11.27	1.51	34.60	4.46
2002	8.37	0.6	113.98	19.35
2003	12.82	0.4	63.72	14.66
2004	14.73	0.46	20.76	8.43
2005	15.25	0.47	48.66	19.03
2006	14.32	−2.36	63.75	63.05
2007	13.90	0.22	182.90	225.70
2008	11.74	−4.55	87.07	117.73

Sources and notes:
1. Impact data (Sources: Gouse [30–32] and Van der Weld [33])
2. Negative value for the net cost savings = a net increase in costs (i.e., the extra cost of the technology was greater than the other (e.g., less expenditure on insecticides) cost savings
3. All values for prices and costs denominated in South African Rand have been converted to US dollars at the annual average exchange rate in each year

With the availability and widespread adoption of the Mon 810 trait from 2003, the reported average positive yield impact is about +10%. There has also been a net annual average saving on cost of production (from lower insecticide use) of between $37/ha and $61/ha (Table 15). At the national level, these yield gains and cost savings have resulted in farm income being boosted, in 2008 by $17.9 million and cumulatively since 1998 the increase in farm income (in nominal terms) has been $77.9 million.

Relative to national maize production, the yield increases derived from GM IR maize were equivalent to a 2.2% increase in national production (2008). The value of the additional income generated from Bt maize was also equivalent to an annual increase in production of 2.1%.

Other EU countries

A summary of the impact of GM IR technology in other countries of the EU is presented in Table 16. This shows that in 2008, the additional farm income derived from using GM IR technology in these six countries was +$2.5 million, and cumulatively over the 2005–2008 period, the total income gain was $11.1 million.

Other Countries

GM IR maize has been grown commercially in the following countries:

- *The Philippines* since 2003. In 2008, 280,000 ha out of total plantings of 2.6 million (7%) were GM IR. Estimates of the impact of using GM IR (Sources: Gonsalves [36], Yorobe [37], and Ramon [38]) show annual average yield increases in the range of 14.3–34%. Taking the midpoint of this range (+24.15%), coupled with a small average annual insecticide cost saving of about $12–$13/ha and average cost of the technology of about $33/ha, the net impact on farm profitability has been between $37/ha and $109/ha. In 2008, the national farm income benefit derived from using the technology was $33.5 million and cumulative farm income gain since 2003 has been $61.2 million.
- *Uruguay* since 2004, and in 2008, 110,000 ha (73% of the total crop) were GM IR. Using Argentine data as the basis for assessing impact, the cumulative farm income gain over the 3 years has been $3.9 million.
- *Brazil* starting in 2008, when 1.45 million hectares were planted to varieties containing a GM IR trait.

Global Economic Impact of Transgenic/Biotech Crops (1996–2008). Table 15 Farm-level income impact of using GM IR maize in Spain 1998–2008

Year	Cost savings ($/ha)	Net cost savings inclusive of cost of technology ($/ha)	Net increase in gross margin ($/ha)	Impact on farm income at a national level ($ millions)
1998	37.40	3.71	95.16	2.14
1999	44.81	12.80	102.20	2.56
2000	38.81	12.94	89.47	2.24
2001	37.63	21.05	95.63	1.10
2002	39.64	22.18	100.65	2.10
2003	47.50	26.58	121.68	3.93
2004	51.45	28.79	111.93	6.52
2005	52.33	8.72	144.74	7.70
2006	52.70	8.78	204.5	10.97
2007	57.30	9.55	274.59	20.63
2008	61.49	10.25	225.36	17.86

Sources and notes:
1. Impact data (based on Brookes [34] and Brookes [35]). Yield impact +6.3% to 2004 and 10% used thereafter (originally Bt 176, latterly Mon 810). Cost of technology based on €18.5/ha to 2004 and €35/ha from 2005
2. All values for prices and costs denominated in Euros have been converted to US dollars at the annual average exchange rate in each year

Global Economic Impact of Transgenic/Biotech Crops (1996–2008). Table 16 Farm-level income impact of using GM IR maize in other EU countries 2005–2008

	Year first planted GM IR maize	Area 2008 (hectares)	Yield impact (%)	Cost of technology 2008 ($/ha)	Cost savings 2008 (before deduction of cost of technology: $/ha)	Net increase in gross margin 2008 ($/ha)	Impact on farm income at a national level 2008 (million $)
France	2005	Nil	N/p	N/p	N/p	N/p	N/p
Germany	2005	3,173	+4	58.57	73.21	78.64	0.25
Portugal	2005	4,851	+12.5	51.24	0	75.60	0.37
Czech Republic	2005	8,380	+10	51.24	26.35	101.95	0.85
Slovakia	2005	1,930	+12.3	51.24	0	228.31	0.44
Poland	2006	3,000	+12.5	51.24	0	133.08	0.40
Romania	2007	7,146	+7.1	46.85	0	26.59	0.19
Total other EU (excluding Spain)		28,480					2.5

Source and notes:
1. Source: Based on Brookes [35]
2. All values for prices and costs denominated in Euros have been converted to US dollars at the annual average exchange rate in each year
3. N/p – planting not permitted in France in 2008

Based on analysis from Galveo [12], the average yield impact was +4.66%, the cost of the technology was $21.6/ha, insecticide cost savings were $42/ha, and the average improvement to farm income equal to $48.12/ha. Overall, the increase in farm profitability associated with the adoption in 2008 was $69.8 million;

- *Honduras*. Here farm-level "trials" have been permitted since 2003, and in 2008, an estimated 9,000 ha used GM IR traits. Evidence from Falck Zepeda et al. [39] indicated that the primary impact of the technology has been to increase average yields (in 2008 +24%). As insecticides have not traditionally been used by most farmers, no costs of production savings have arisen, coupled with no additional cost for use of the technology (which has been provided free of charge for the trials). In our analysis, we have, however assumed a cost of the technology of $30/ha, and based on this, the estimated farm income benefit derived from the technology was $1.1 million in 2008 and cumulatively since 2003 the income gain has been $2 million.

Summary of Economic Impact

In global terms, the farm-level impact of using GM IR maize was $1.56 billion in 2008. Cumulatively since 1996, the benefit has been (in nominal terms) $6.34 billion. This farm income gain has mostly derived from improved yields (less pest damage) although in some countries farmers have derived a net cost saving associated with reduced expenditure on insecticides.

In terms of the total value of maize production from the countries growing GM IR maize in 2008, the additional farm income generated by the technology is equal to a value-added equivalent of 2.2%. Relative to the value of global maize production in 2008, the farm income benefit added the equivalent of 1.2%.

Insect-Resistant (Bt) Cotton (GM IR)

The USA

GM IR cotton has been grown commercially in the USA since 1996 and by 2008, was used in 63% (1.93 million hectares) of total cotton plantings.

The farm income impact of using GM IR cotton is summarized in Table 17. The primary benefit has been increased yields (by 9–11%), although small net savings in costs of production have also been obtained (reduced expenditure on insecticides being marginally greater than the cost of the technology). Overall, average profitability levels increased by $53–$115/ha with Bollgard I cotton (with a single Bt gene) between 1996 and 2002 and by between $87/ha and $118/ha in 2003–2008 with Bollgard II (containing two Bt genes and offering a broader spectrum of control). This resulted in a net gain to farm income in 2008 of $189 million. Cumulatively, since 1996, the farm income benefit has been $2.44 billion. In added value terms, the effect of the increased yields and reduced costs of production on farm income in 2008 was equivalent to an annual increase in production of 6.3% (165,400 tons).

China

China first planted GM IR cotton in 1997, since when the area planted to GM IR varieties has increased to 64% of the total 5.95 million hectares crop in 2008.

As in the USA, a major farm income impact has been via higher yields of 8–10% on the crops using the technology, although there have also been significant cost savings on insecticides used and the labor previously used to undertake spraying. Overall, annual average costs have fallen by about $145–$200/ha and annual average profitability improved by $123–$472/ha. In 2008, the net national gain to farm income was $859 million (Table 18). Cumulatively, since 1997, the farm income benefit has been $7.6 billion. In added value terms, the effect of the increased yields and reduced costs of production on farm income in 2008 was equivalent to an annual increase in production of 17.1% (1.38 million tons).

Australia

Australia planted 83% of its 2008 cotton crop (total crop of 146,000 ha) to varieties containing GM IR traits (Australia first planted commercial GM IR cotton in 1996).

Unlike the other main countries using GM IR cotton, Australian growers have rarely derived yield gains from using the technology (reflecting the effective use

Global Economic Impact of Transgenic/Biotech Crops (1996–2008). Table 17 Farm-level income impact of using GM IR cotton in the USA 1996–2008

Year	Cost savings (net after cost of technology ($/ha)	Net increase in gross margins ($/ha)	Increase in farm income at a national level ($ millions)	Increase in national farm income as % of farm-level value of national production
1996	4.98	115.32	94.69	1.19
1997	4.98	103.47	87.28	1.30
1998	4.98	88.54	80.62	1.47
1999	4.98	65.47	127.29	2.89
2000	4.98	74.11	162.88	3.10
2001	4.98	53.04	125.22	3.37
2002	4.98	69.47	141.86	3.11
2003	5.78	120.49	239.98	4.27
2004	5.78	107.47	261.23	4.82
2005	24.48	117.81	332.41	5.97
2006	−5.77	86.61	305.17	4.86
2007	−2.71	114.50	296.00	5.49
2008	−2.71	98.22	189.50	5.89

Sources and notes:
1. Impact data based on Gianessi and Carpenter [28], Sankala and Blumenthal [6, 7], Johnson and Strom [8], Marra et al. [3], and Mullins and Hudson [40]
2. Yield impact +9% 1996–2002 Bollgard I and +11% 2003 onward Bollgard II
3. Cost of technology: 1996–2002 Bollgard I $58.27/ha, 2003–2004 Bollgard II $68.32/ha, $49.62/ha 2005, $46.95/ha 2006, $25.7/ha 2007 and 2008
4. Insecticide cost savings $63.26/ha 1996–2002, $74.10/ha 2003–2005, $41.18/ha 2006, $28.4/ha 2007 and 2008

of insecticides for pest control prior to the availability of GM IR cultivars), with the primary farm income benefit being derived from lower costs of production (Table 19). More specifically, the following observations were made:

- In the first 2 years of adoption of the technology (Ingard, single gene Bt cotton), small net income losses were derived, mainly because of the relatively high price charged for the seed. Since this price was lowered in 1998, the net income impact has been positive, with cost saving of between $54/ha and $90/ha, mostly derived from lower insecticide costs (including application) more than offsetting the cost of the technology.
- For the last few years of use, Bollgard II cotton (containing 2 Bt genes) has been available offering effective control of a broader range of cotton pests. Despite the higher costs of this technology, users have continued to make significant net cost savings of $186–$212/ha.
- At the national level in 2008, the net farm income gains were $24.2 million and cumulatively since 1996 the gains have been $214.9 million.
- In added value terms, the effect of the reduced costs of production on farm income in 2008 was equivalent to an annual increase in production of 37% (105,000 tons).

Argentina

GM IR cotton has been planted in Argentina since 1998. In 2008, it accounted for 73% of total cotton plantings.

The main impact in Argentina has been yield gains of 30% (which has resulted in a net increase in total cotton production (2008) of 22%). This has more than

Global Economic Impact of Transgenic/Biotech Crops (1996–2008). Table 18 Farm-level income impact of using GM IR cotton in China 1997–2008

Year	Cost savings (net after cost of technology ($/ha)	Net increase in gross margins ($/ha)	Increase in farm income at a national level ($ millions)	Increase in national farm income as % of farm-level value of national production
1997	194	333	11.33	0.13
1998	194	310	80.97	1.15
1999	200	278	181.67	4.62
2000	−14	123	150.18	2.61
2001	378	472	1,026.26	20.55
2002	194	327	687.27	11.19
2003	194	328	917.00	12.15
2004	194	299	1,105.26	16.89
2005	145	256	845.58	13.57
2006	146	226	792.28	16.86
2007	152	248	942.7	14.46
2008	148	224	858.6	17.14

Sources and notes:

1. Impact data based on Pray et al. [41, 42], which covered the years 1999–2001. Other years based on average of the 3 years, except 2005 onward based on Shachuan (2006) – personal communication
2. Negative cost savings in 2000 reflect a year of high pest pressure (of pests not the target of GM IR technology), which resulted in above average use of insecticides on GM IR using farms
3. Yield impact +8% 1997–1999 and +10% 2000 onward
4. Negative value for the net cost savings in 2000 = a net increase in costs (i.e., the extra cost of the technology was greater than the savings on insecticide expenditure – a year of lower than average bollworm problems
5. All values for prices and costs denominated in Chinese Yuan have been converted to US dollars at the annual average exchange rate in each year

offset the cost of using the technology. In terms of gross margin, cotton farmers have gained annually between $25/ha and $249/ha during the period 1998–2007. At the national level, the annual farm income gains in the last 5 years have been in the range of $2–$27 million (Fig. 7). Cumulatively since 1998, the farm income gain from use of the technology has been $95.4 million. In added value terms, the effect of the yield increases (partially offset by higher costs of production) on farm income in 2008 was equivalent to an annual increase in production of 14.6%.

Mexico

GM IR cotton has been planted commercially in Mexico since 1996. In 2008, GM IR cotton was planted on 70,000 ha (56% of total cotton plantings).

The main farm income impact of using the technology has been yield improvements of between 6% and 9% over the last 6 years. In addition, there have been important savings in the cost of production (lower insecticide costs). Overall, the annual net increase in farm profitability has been within the range of $104/ha and $354/ha between 1996 and 2008 (Table 20). At the national level, the farm income benefit in 2008 was $10.5 million and the impact on total cotton production was an increase of 5.2%. Cumulatively since 1996, the farm income benefit has been $76.4 million. In added value terms, the combined effect of the yield increases and lower cost of production on farm income in 2008 was equivalent to an annual increase in production of 5.4%.

Global Economic Impact of Transgenic/Biotech Crops (1996–2008). Table 19 Farm-level income impact of using GM IR cotton in Australia 1996–2008

Year	Cost of technology ($/ha)	Net increase in gross margins/cost saving after cost of technology ($/ha)	Increase in farm income at a national level ($ millions)	Increase in national farm income as % of farm-level value of national production
1996	−191.7	−41.0	−1.63	−0.59
1997	−191.7	−35.0	−2.04	−0.88
1998	−97.4	91.0	9.06	0.43
1999	−83.9	88.1	11.80	4.91
2000	−89.9	64.9	10.71	4.38
2001	−80.9	57.9	7.87	5.74
2002	−90.7	54.3	3.91	3.43
2003	−119.3	256.1	16.3	11.49
2004	−179.5	185.8	45.7	21.33
2005	−229.2	193.4	47.9	23.75
2006	−225.9	190.7	22.49	26.01
2007	−251.33	212.1	11.73	40.90
2008	−264.26	199.86	24.23	37.40

Sources and notes:
1. Impact data based on Doyle [43], Taylor [44], CSIRO [45] for bollgard II since 2004
2. All values for prices and costs denominated in Australian dollars have been converted to US dollars at the annual average exchange rate in each year

South Africa

In 2008, GM IR cotton (first planted commercially in 1998) was planted on 7,750 ha in South Africa (84% of the total crop).

The main impact on farm incomes has been significantly higher yields (an annual average increase of about 24%). In terms of cost of production, the additional cost of the technology (between $17/ha and $24/ha for Bollgard I and $40–$50/ha for Bollgard II (2006 onward) has been greater than the insecticide cost and labor (for water collection and spraying) savings ($12–$23/ha), resulting in an increase in overall cost of production of $2–$32/ha. Combining the positive yield effect and the increase in cost of production, the net effect on profitability has been an annual increase of between $27/ha and $232/ha.

At the national level, farm incomes, over the last 5 years have annually increased by between $1.2 million and $1.7 million (Fig. 8). Cumulatively since 1998, the farm income benefit has been $21 million. The impact on total cotton production was an increase of 20.1% in 2008. In added value terms, the combined effect of the yield increases and lower costs of production on farm income in 2008 was equivalent to an annual increase in production of 14.5% (based on 2008 production levels).

India

GM IR cotton has been planted commercially in India since 2002. In 2008, 6.97 million hectares were planted to GM IR cotton, which is equal to 77% of total plantings.

The main impact of using GM IR cotton has been major increases in yield [54] found average yield increases of 45% in 2002 and 63% in 2003 (average over the 2 years of 54%) relative to conventionally produced cotton. More recent survey data from Monsanto [16] confirm this high-yield impact (+58% reported in 2004) as do data from IMRB [55], which found an average yield increase of 64% in 2005, and IMRB [56], which found a yield impact of +50% in 2006. With respect to cost of production, the average cost of the

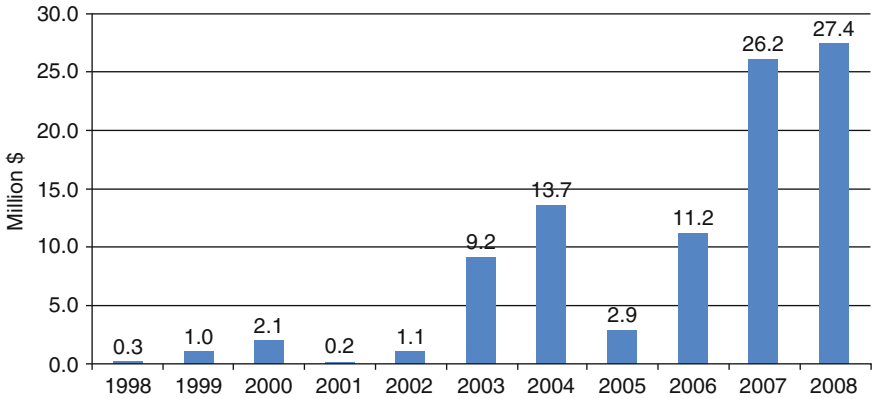

Global Economic Impact of Transgenic/Biotech Crops (1996–2008). Figure 7
National farm income impact of using GM IR cotton in Argentina 1998–2008
Sources and notes:
1. Impact data (Sources: Qaim and De Janvry [46, 47]), Elena [48] and for 2005 and 2006 Monsanto LAP, although cost of technology in 2005 from Monsanto Argentina. Area data: source ArgenBio
2. Yield impact +30%, cost of technology $86/ha ($40/ha 2005), cost savings (reduced insecticide use) $17.47/ha
3. All values for prices and costs denominated in Argentine Pesos have been converted to US dollars at the annual average exchange rate in each year

technology (seed premium: $49–$54/ha) up to 2006 was greater than the average insecticide cost savings of $31–$58/ha resulting in a net increase in costs of production. Following the reduction in the seed premium in 2006 to about $20/ha, farmers have, on average made a net cost saving of about $25/ha. Coupled with the yield gains, important net gains to levels of profitability have been achieved of between $82/ha and $356/ha. At the national level, the farm income gain in 2008 was $1.79 billion and cumulatively since 2002 the farm income gains have been $5.14 billion (Table 21).

The impact on total cotton production was an increase of 31% in 2008 and in added value terms, the combined effect of the yield increases and higher costs of production on farm income in 2008 was equivalent to an annual increase in production of 24% (based on the 2008 production level that is inclusive of the GM IR related yield gains).

Brazil

GM IR cotton was planted commercially in Brazil for the first time in 2006, and in 2008 was planted on 178,000 ha (20% of the total crop). This represents a fall in the share of total plantings relative to 2007, when GM IR traits were planted on 32% of the crop. This decline in plantings largely reflects the relative performance of the seed containing the GM IR traits compared to the leading conventional varieties, in which the GM IR trait has not been available. In 2006, on the basis of industry estimates of impact of GM IR cotton relative to similar varieties, an average yield gains of +6% and a net cost saving (reduced expenditure on insecticides after deduction of the premium paid for using the technology) of about +$25/ha were realized. In 2007 and 2008, however, analysis by Galveo [12] and Monsanto Brazil [57] suggests that the yield performance of the varieties containing GM IR traits has been lower (by −3.6% and −2.7% respectively for 2007 and 2008). As a result, the net farm income of using the technology was (after taking into consideration insecticide cost savings and the seed premium), on average, −$34.5/ha in 2007 and a small net gain of about $2/ha in 2008. At a national level in 2008, GM IR cotton technology delivered a net gain of about $0.35 million (a net loss of $12.3 million in 2007). Cumulatively, the total farm income impact has been positive at about $5 million.

Other Countries

- *Colombia*: GM IR cotton has been grown commercially in Colombia since 2002 (20,000 ha planted in

Global Economic Impact of Transgenic/Biotech Crops (1996–2008). Table 20 Farm-level income impact of using GM IR cotton in Mexico 1996–2008

Year	Cost savings (net after cost of technology ($/ha)	Net increase in gross margins ($/ha)	Increase in farm income at a national level ($ millions)	Increase in national farm income as % of farm-level value of national production
1996	58.1	354.5	0.32	0.1
1997	56.1	103.4	1.72	0.5
1998	38.4	316.4	11.27	2.71
1999	46.5	316.8	5.27	2.84
2000	47.0	262.4	6.85	5.76
2001	47.6	120.6	3.04	3.74
2002	46.1	120.8	1.84	3.81
2003	41.0	127.7	3.33	3.67
2004	39.3	130.4	6.24	4.51
2005	40.8	132.3	10.4	7.64
2006	20.4	124.4	6.44	4.06
2007	20.5	139.7	8.38	4.74
2008	19.9	150.4	10.52	5.44

Sources and notes:
1. Impact data based on Traxler et al. [49] covering the years 1997 and 1998. Yield changes data in other years based on official reports submitted to the Mexican Ministry of Agriculture by Monsanto Comercial (Mexico). Also, Martinez-Carillo and Diaz-Lopez [50]
2. Yield impacts: 1996 +37%, 1997 +3%, 1998 +20%, 1999 +27%, 2000 +17%, 2001 +9%, 2002 +7%, 2003 +6%, 2004 +7.6%, 2005 onward +9.25%
3. All values for prices and costs denominated in Mexican Pesos have been converted to US dollars at the annual average exchange rate in each year

2008 out of a total cotton crop of 40,000 ha). Drawing on recent analysis of impact by Zambrano et al. [58], this shows the main impact has been through a significant improvement in yields of +32%. On the cost impact side, this analysis shows that farmers using GM IR cotton tend to have substantially higher expenditures on pest control than their conventional counterparts, which when taking into consideration the approximate $70/ha cost of the technology results in a net addition to costs of between $200/ha and $280/ha each year (relative to typical expenditures by conventional cotton growers). Nevertheless, after taking into consideration the positive yield effects, the net impact on profitability has been positive. In 2008, the average improvement in profitability was about $33/ha and the total net gain from using the technology was $0.91 million. Cumulatively, since 2002, the net farm income gain has been $13.9 million.

- *Burkino Faso*: GM IR cotton was grown commercially first in 2008. Based on analysis of pre-commercial trials by Vitale et al. [59, 60], the main impact of the technology is improved yields (by +20%) and savings in insecticide expenditure of about $62/ha. Based on a cost of technology of about $42/ha, the net cost savings are about $20/ha, and inclusive of the yield gains, the estimated net income gain in 2008 was $124/ha. The total aggregate farm income gain in 2008 was therefore $1 million.

Summary of Global Impact

In global terms, the farm-level impact of using GM IR cotton was $2.9 billion in 2008. Cumulatively, since

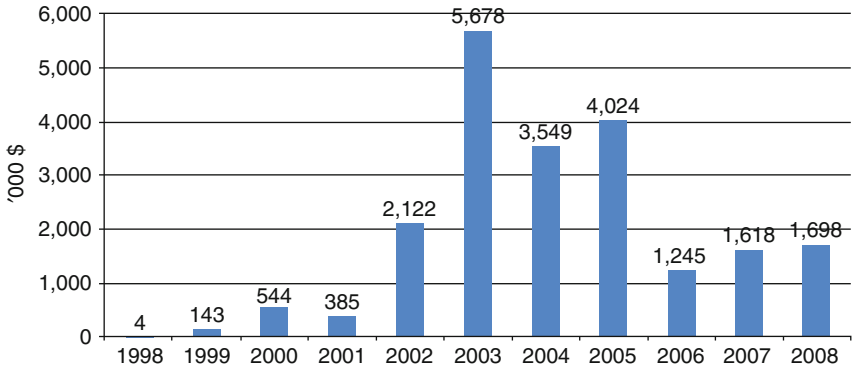

Global Economic Impact of Transgenic/Biotech Crops (1996–2008). Figure 8
National farm income impact of using GM IR cotton in South Africa 1998–2008
Sources and notes:
1. Impact data based on Ismael et al. [51], Kirsten et al. [52], Morse et al. [53]
2. Yield impact +24%, cost of technology $14–$24/ha for Bollgard I and about $50/ha for Bollgard II, cost savings (reduced insecticide use) $12–$23/ha
3. All values for prices and costs denominated in South African Rand have been converted to US dollars at the annual average exchange rate in each year
4. The decline in the total farm income benefit post 2003 relative to earlier years reflects the decline in total cotton plantings. This was caused by relatively low farm-level prices for cotton in 2004 and 2005 (reflecting a combination of relatively low world prices and a strong South African currency). In more recent years, cotton has become less competitive relative to alternatives such as corn because of higher world grain prices

1996, the farm income benefit has been (in nominal terms) $15.61 billion. Within this, 65% of the farm income gain has derived from yield gains (less pest damage) and the balance (35%) from reduced expenditure on crop protection (spraying of insecticides).

In terms of the total value of cotton production from the countries growing GM IR in 2008, the additional farm income generated by the technology is equal to a value-added equivalent of 19.3% (based on the 2008 production level inclusive of the GM IR related yield gains). Relative to the value of global cotton production in 2008, the farm income benefit added the equivalent of 11.1%.

Other Biotech Crops

Maize/Corn Rootworm Resistance

GM rootworm-resistant (CRW) corn has been planted commercially in the USA since 2003. In 2008, there were 13.7 million hectares of CRW corn (43% of the total US crop).

The main farm income impact (Impact data based on Sankala and Blumenthal [6, 7], Johnson and Strom [8], Rice [61]), and Alston et al. [62]) has been higher yields of about 5% relative to conventional corn. The impact on average costs of production has been +$2/ha to −$10/ha (based on an average cost of the technology of $35–$42/ha and an insecticide cost saving of $32–$37/ha). As a result, the net impact on farm profitability has been +$28/ha to +$79/ha.

At the national level, farm incomes increased by $4.6 million in 2003, rising to $1.1 billion in 2008. Cumulatively since 2003, the total farm income gain from the use of CRW technology in the USA corn crop has been $2 billion.

CRW cultivars were also planted commercially for the first time in 2004 in Canada. In 2008, the area planted to CRW-resistant varieties was 119,380 ha. Based on US costs, insecticide cost savings and yield impacts, this has resulted in additional income at the national level of $8.65 million in 2008 (cumulative total since 2004 of $13 million).

At the global level, the extra farm income derived from biotech CRW maize use since 2003 has been just over $2 billion. In 2008, the additional farm income

Global Economic Impact of Transgenic/Biotech Crops (1996–2008). Table 21 Farm-level income impact of using GM IR cotton in India 2002–2008

Year	Cost savings (net after cost of technology ($/ha)	Net increase in gross margins ($/ha)	Increase in farm income at a national level ($ millions)	Increase in national farm income as % of farm-level value of national production
2002	−12.42	82.66	3.69	0.26
2003	−16.2	209.85	20.98	0.47
2004	−13.56	193.36	96.68	1.86
2005	−22.25	255.96	332.74	5.26
2006	3.52	221.02	839.89	14.04
2007	26.41	356.85	2,093.97	22.84
2008	24.28	256.73	1,790.16	24.27

Sources and notes:
1. Impact data based on Bennett et al. [54] and IMRB [55, 56]. As 2008 was reported to be a year of below average pest pressure, the average yield gain used was reduced to +40%
2. All values for prices and costs denominated in Indian Rupees have been converted to US dollars at the annual average exchange rate in each year

generated from use of the technology was equal to 0.9% of the value of the global maize crop.

Virus-Resistant Papaya

Ring spot-resistant papaya has been commercially grown in the USA (State of Hawaii) since 1999, and in 2008 (85% of the state's papaya crop was GM virus resistant (700 ha).

The main farm income impact of this biotech crop has been to significantly increase yields relative to conventional varieties. Compared to the average yield in the last year before the first biotech cultivation (1998), the annual average yield increase of biotech papaya relative to conventional crops has been within a range of +15% to +77% (29% in 2008). At a state level, this is equivalent to a 25% increase in total papaya production in 2008.

In terms of profitability (Impact data based on Sankala and Blumenthal [6, 7] and Johnson and Strom [8]), the net annual impact has been an improvement of between $3,000/ha and $29,000/ha, and in 2008 this amounted to a net farm income gain of $5,790/ha and an aggregate benefit across the state of $4 million. Cumulatively, the farm income benefit since 1999 has been $53.4 million.

Virus-resistant papaya is also reported to have been grown in China in 2008, on 4,500 ha. No impact data on this technology has been identified.

Virus-Resistant Squash

Biotech virus-resistant squash has also been grown in some states of the USA since 2004 and is estimated to have been planted on 2,900 ha in 2008 (17% of the total crop in the USA – mostly found in Georgia and Florida).

Based on analysis from Johnson and Strom [8], the primary farm income impact of using biotech virus-resistant squash has been derived from higher yields, which in 2008, added a net gain to users of $26 million. Cumulatively, the farm income benefit since 2004 has been $107 million.

Insect-Resistant Potatoes

GM insect-resistant potatoes were also grown commercially in the USA between 1996 and 2000 (planted on 4% of the total US potato crop in 1999 (30,000 ha). This technology was withdrawn in 2001 when the technology provider (Monsanto) withdrew from the market to concentrate on GM trait development in

maize, soybeans, cotton, and canola. This commercial decision was also probably influenced by the decision of some leading potato processors and fast-food outlets to stop using GM potatoes because of perceived concerns about this issue from some of their consumers, even though the GM potato provided the producer and the processor with a lower cost, higher yielding, and more consistent product. It also delivered significant reductions in insecticide use Carpenter and Gianessi (2002).

Indirect (Nonpecuniary) Farm-Level Economic Impacts

Apart from the tangible and quantifiable impacts on farm profitability presented above, there are other important, more intangible (difficult to quantify) impacts of an economic nature.

Many of the studies of the impact of biotech crops have identified the following reasons as being important influences for adoption of the technology:

Herbicide-Tolerant Crops

- Increased management flexibility and convenience that comes from a combination of the ease of use associated with broad-spectrum, post-emergent herbicides like glyphosate and the increased/longer time window for spraying. This not only frees up management time for other farming activities but also allows additional scope for undertaking off-farm, income-earning activities.
- In a conventional crop, post-emergent weed control relies on herbicide applications before the weeds and crop are well established. As a result, the crop may suffer "knock-back" to its growth from the effects of the herbicide. In the GM HT crop, this problem is avoided because the crop is both tolerant to the herbicide and spraying can occur at a later stage when the crop is better able to withstand any possible "knock-back" effects.
- Facilitates the adoption of conservation or no tillage systems. This provides for additional cost savings such as reduced labor and fuel costs associated with plowing, additional moisture retention, and reductions in levels of soil erosion.
- Improved weed control has contributed to reduced harvesting costs – cleaner crops have resulted in reduced times for harvesting. It has also improved harvest quality and led to higher levels of quality price bonuses in some regions and years (e.g., HT soybeans and HT canola in the early years of adoption respectively in Romania and Canada).
- Elimination of potential damage caused by soil-incorporated residual herbicides in follow-on crops and less need to apply herbicides in a follow-on crop because of the improved levels of weed control.
- A contribution to the general improvement in human safety (as manifest in greater peace of mind about own and worker safety) from reduced exposure to herbicides and a switch to more environmentally benign products.

Insect-Resistant Crops

- Production risk management/insurance purposes – the technology takes away much of the worry of significant pest damage occurring and is, therefore, highly valued. Piloted in 2008 and more widely operational from 2009, US farmers using stacked corn traits (containing insect resistance and herbicide-tolerant traits) are being offered discounts on crop insurance premiums equal to $7.41/ha.
- A "convenience" benefit derived from having to devote less time to crop walking and/or applying insecticides.
- Savings in energy use – mainly associated with less use of aerial spraying and less tillage.
- Savings in machinery use (for spraying and possibly reduced harvesting times).
- Higher quality of crop. There is a growing body of research evidence relating to the superior quality of GM IR corn relative to conventional and organic corn from the perspective of having lower levels of mycotoxins. Evidence from Europe (as summarized in Brookes [35] has shown a consistent pattern in which GM IR corn exhibits significantly reduced levels of mycotoxins compared to conventional and organic alternatives. In terms of revenue from sales of corn, however, no premia for delivering product with lower levels of mycotoxins have, to date, been reported although where the adoption of the technology has resulted in reduced frequency of

crops failing to meet maximum permissible fumonisin levels in grain maize (e.g., in Spain), this delivers an important economic gain to farmers selling their grain to the food using sector. GM IR corn farmers in the Philippines have also obtained price premia of 10% [37] relative to conventional corn because of better quality, less damage to cobs and lower levels of impurities.

- Improved health and safety for farmers and farm workers (from reduced handling and use of pesticides, especially in developing countries where many apply pesticides with little or no use of protective clothing and equipment).
- Shorter growing season (e.g., for some cotton growers in India), which allows some farmers to plant a second crop (notably maize) in the same season. Also some Indian cotton growers have reported knock on benefits for beekeepers as fewer bees are now lost to insecticide spraying [63].

Some of the economic impact studies have attempted to quantify some of these benefits (e.g., Qaim and Traxler [9] quantified some of these in Argentina (a $3.65/ha saving (−7.8%) in labor costs and a $6.82/ha (−28%) saving in machinery/fuel costs associated with the adoption of GM HT soybeans). Where identified, these cost savings have been included in the analysis presented above. Nevertheless, it is important to recognize that these largely intangible benefits are considered by many farmers as a primary reason for adoption of GM technology, and in some cases farmers have been willing to adopt for these reasons alone, even when the measurable impacts on yield and direct costs of production suggest marginal or no direct economic gain.

Since the early 2000s, a number of farmer-survey based studies in the USA have also attempted to better quantify these nonpecuniary benefits. These studies have usually employed contingent valuation techniques to obtain farmers valuations of nonpecuniary benefits. A summary of these findings is shown in (Table 22).

Global Economic Impact of Transgenic/Biotech Crops (1996–2008). Table 22 Values of nonpecuniary benefits associated with biotech crops in the USA

Survey	Median value ($/ha)
2002 IR (to rootworm) corn growers survey	7.41
2002 soybean (HT) farmers survey	12.35
2003 HT cropping survey (corn, cotton, and soybeans) – North Carolina	24.71
2006 HT (flex) cotton survey	12.35 (relative to first generation HT cotton)

Source: Marra and Piggot 2006 and 2007 [1, 2]

Aggregating the Impact to US Crops 1996–2008

The approach used to estimate the nonpecuniary benefits derived by US farmers from biotech crops over the period 1996–2008 has been to draw on the values identified by Marra and Piggot ([1, 2]: Table 22) and to apply these to the biotech crop planted areas during this 13-year period. Figure 9 summarizes the values for nonpecuniary benefits derived from biotech crops in the USA (1996–2008) and shows an estimated (nominal value) benefit of $855 million in 2008 and a cumulative total benefit (1996–2008) of $5.99 billion. Relative to the value of direct farm income benefits presented above, the nonpecuniary benefits were equal to 21% of the total direct income benefits in 2008 and 25.6% of the total cumulative (1996–2008) direct farm income. This highlights the important contribution this category of benefit has had on biotech trait adoption levels in the USA, especially where the direct farm income benefits have been identified to be relatively small (e.g., HT cotton).

Estimating the Impact in Other Countries

It is evident from the literature review that farmers in other countries, who use GM technology, also value the technology for a variety of nonpecuniary/intangible reasons. The most appropriate methodology for identifying these nonpecuniary benefit valuations in other countries would be to repeat the type of US farmer surveys in other countries. Unfortunately, the authors are not aware of any such studies having been undertaken to date.

Production Effects of the Technology

Based on the yield assumptions used in the direct farm income benefit calculations presented above and taking

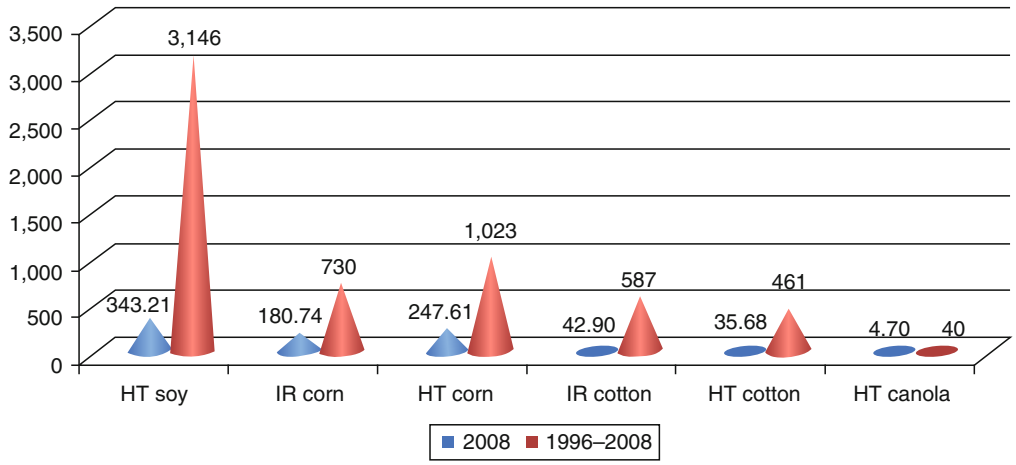

Global Economic Impact of Transgenic/Biotech Crops (1996–2008). Figure 9
Nonpecuniary benefits derived by US farmers 1996–2008 by trait ($ million)

account of the second soybean crop facilitation in South America, biotech crops have added important volumes to global production of corn, cotton, canola, and soybeans since 1996 (Table 23).

The biotech IR traits, used in the corn and cotton sectors, have accounted for 99% of the additional corn production and almost all of the additional cotton production. Positive yield impacts from the use of this technology have occurred in all user countries (except GM IR cotton in Australia: this reflects the levels of *Heliothis* pest control previously obtained with intensive insecticide use. The main benefit and reason for adoption of this technology in Australia has arisen from significant cost savings (on insecticides) and the associated environmental gains from reduced insecticide use) when compared to average yields derived from crops using conventional technology (such as application of insecticides and seed treatments). Since 1996, the average yield impact across the total area planted to these traits over the 12-year period has been +7.1% for corn traits and +14.8% for cotton traits (Fig. 10).

Although the primary impact of biotech HT technology has been to provide more cost-effective (less expensive) and easier weed control versus improving yields from better weed control (relative to weed control obtained from conventional technology), improved weed control has, nevertheless occurred, delivering higher yields in some countries. Specifically, HT soybeans in Romania improved the average yield by over 30% in early adoption years and biotech HT corn in Argentina and the Philippines delivered yield improvements of +9% and +15% respectively.

Global Economic Impact of Transgenic/Biotech Crops (1996–2008). Table 23 Additional crop production arising from positive yield effects of biotech crops

	1996–2008 additional production (million tons)	2008 additional production (million tons)
Soybeans	74.0	10.1
Corn	79.7	17.1
Cotton	8.6	1.8
Canola	4.8	0.6

Biotech HT soybeans have also facilitated the adoption of no tillage production systems, shortening the production cycle. This advantage enables many farmers in South America to plant a crop of soybeans immediately after a wheat crop in the same growing season. This second crop, additional to traditional soybean production, has added 73.5 million tons to soybean production in Argentina and Paraguay between 1996 and 2008 (accounting for 99% of the total biotech-related additional soybean production).

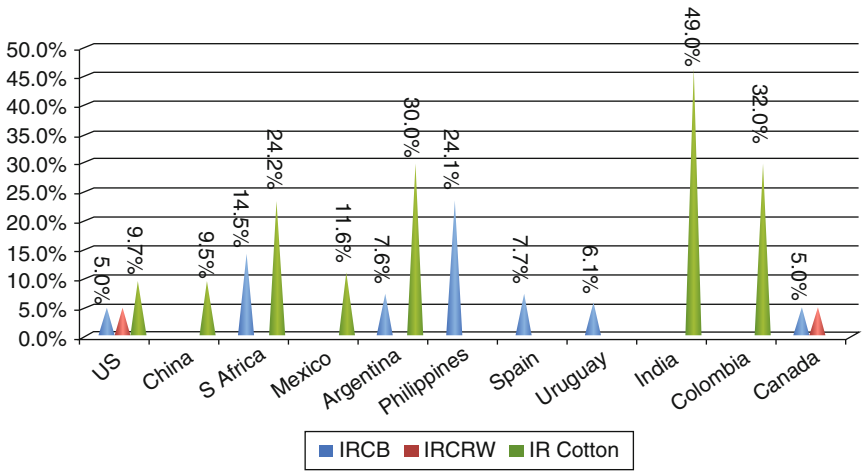

Global Economic Impact of Transgenic/Biotech Crops (1996–2008). Figure 10
Average yield impact of biotech IR traits 1996–2008 by country and trait Notes: IRCB, resistant to corn-boring pests; IRCRW, resistant to corn rootworm

Using the same sensitivity analysis as applied to the farm income estimates presented in the executive summary to the production impacts (one scenario of consistent lower than average pest/weed pressure and one of consistent higher than average pest/weed pressure), Table 24 shows the range of production impacts.

Global Economic Impact of Transgenic/Biotech Crops (1996–2008). Table 24 Additional crop production arising from positive yield effects of biotech crops 1996–2008 under different pest/weed pressure assumptions and impacts of the technology (million tons)

Crop	Consistent below average pest/weed pressure	Average pest/weed pressure (main study analysis)	Consistent above average pest/weed pressure
Soybeans	73.8	74.0	74.3
Corn	48.0	79.7	140.9
Cotton	6.2	8.6	11.8
Canola	3.3	4.8	5.2

Note: No significant change to soybean production under all three scenarios as 99% of production gain due to second cropping facilitation of the technology

Summary of Economic Effects of Transgenic/Biotech Crops

Overall, GM technology has had a significant positive impact on farm income derived from a combination of enhanced productivity and efficiency gains (Table 25). In 2008, the direct global farm income benefit from biotech crops was $9.37 billion. This is equivalent to having added 3.6% to the value of global production of the four main crops of soybeans, maize, canola, and cotton. Since 1996, farm incomes have increased by $52 billion.

The largest gains in farm income have arisen in the soybean sector, largely from cost savings. The $2.93 billion additional income generated by GM herbicide-tolerant (GM HT) soybeans in 2008 has been equivalent to adding 4.3% to the value of the crop in the biotech growing countries, or adding the equivalent of 4.1% to the $71 billion value of the global soybean crop in 2008. These economic benefits should, however be placed within the context of a significant increase in the level of soybean production in the main biotech adopting countries. Since 1996, the soybean area in the leading soybean producing countries of the USA, Brazil, and Argentina increased by 63%.

Substantial gains have also arisen in the cotton sector mainly from the adoption of GM insect-resistant (GM IR) cotton (through a combination of higher yields and lower costs). In 2008, cotton farm income levels in the biotech adopting countries increased by $2.9 billion and

Global Economic Impact of Transgenic/Biotech Crops (1996–2008). Table 25 Global farm income benefits from growing biotech crops 1996–2008: million US $

Trait	Increase in farm income 2008	Increase in farm income 1996–2008	Farm income benefit in 2008 as % of total value of production of these crops in biotech adopting countries	Farm income benefit in 2008 as % of total value of global production of crop
GM herbicide-tolerant soybeans	2,925.7	23,342.0	4.3	4.1
GM herbicide-tolerant maize	433.5	1,896.0	0.6	0.3
GM herbicide-tolerant cotton	14.6	855.8	0.1	0.06
GM herbicide-tolerant canola	391.8	1,829.2	6.9	1.5
GM insect-resistant maize	2,645.5	8,344.2	3.7	2.0
GM insect-resistant cotton	2,904.5	15,612.7	19.3	11.1
Others	51.5	162.1	Not applicable	Not applicable
Totals	9,367.1	52,042.0	5.71	3.65

Notes: All values are nominal. Others = Virus-resistant papaya and squash and herbicide-tolerant sugar beet. Totals for the value shares exclude "other crops" (i.e., relate to the four main crops of soybeans, maize, canola, and cotton). Farm income calculations are net farm income changes after inclusion of impacts on yield, crop quality, and key variable costs of production (e.g., payment of seed premia, impact on crop protection expenditure)

since 1996, the sector has benefited from an additional $15.6 billion. The 2008 income gains are equivalent to adding 19.3% to the value of the cotton crop in these countries, or 11.1% to the $26 billion value of total global cotton production. This is a substantial increase in value-added terms for two new cottonseed technologies.

Significant increases to farm incomes have also resulted in the maize and canola sectors. The combination of GM insect resistant (GM IR) and GM HT technology in maize has boosted farm incomes by $10.24 billion since 1996. In the canola sector (largely North American) an additional $1.83 billion has been generated.

Of the total cumulative farm income benefit, $31.2 billion (60%) has been due to yield gains (and second crop facilitation), with the balance arising from reductions in the cost of production. Within this yield gain component, 76% derives from the GM IR technology and the balance to GM HT crops.

Table 26 summarizes farm income impacts in key biotech adopting countries. This highlights the important farm income benefit arising from GM HT soybeans in South America (Argentina, Brazil, Paraguay, and Uruguay), GM IR cotton in China and India, and a range of GM cultivars in the USA. It also illustrates

Global Economic Impact of Transgenic/Biotech Crops (1996–2008). Table 26 GM crop farm income benefits 1996–2008 selected countries: million US $

	GM HT soybeans	GM HT maize	GM HT cotton	GM HT canola	GM IR maize	GM IR cotton	Total
The USA	11,028	1,705.6	799	185.0	7,107	2,444.1	*23,268.7*
Argentina	8,764.1	113.8	34.2	N/a	269.8	95.4	*9,277.3*
Brazil	2,745.8	N/a	N/a	N/a	69.8	5.0	*2,820.6*
Paraguay	503.2	N/a	N/a	N/a	N/a	N/a	*503.2*
Canada	116.1	45.8	N/a	1,643.2	265.4	N/a	*2,070.5*
South Africa	4.1	3.8	2.2	N/a	475.8	21.0	*506.9*
China	N/a	N/a	N/a	N/a	N/a	7,599	*7,599*
India	N/a	N/a	N/a	N/a	N/a	5,142	*5,142*
Australia	N/a	N/a	8.3	0.9	N/a	214.9	*224.1*
Mexico	3.3	N/a	11.7	N/a	N/a	76.1	*91.1*
The Philippines	N/a	27.1	N/a	N/a	61.2	N/a	*88.3*
Romania	44.6	N/a	N/a	N/a	N/a	N/a	*44.9*
Uruguay	49.4	N/a	N/a	N/a	3.9	N/a	*53.3*
Spain	N/a	N/a	N/a	N/a	77.9	N/a	*77.9*
Other EU	N/a	N/a	N/a	N/a	11.1	N/a	*11.1*
Columbia	N/a	N/a	N/a	N/a	N/a	13.9	*13.9*
Bolivia	83.4	N/a	N/a	N/a	N/a	N/a	*83.4*

Notes: All values are nominal. Farm income calculations are net farm income changes after inclusion of impacts on yield, crop quality, and key variable costs of production (e.g., payment of seed premia, impact on crop protection expenditure). N/a = not applicable. US total figure excludes $182.3 million for other crops/traits

the growing level of farm income benefits obtained in South Africa, the Philippines, and Mexico.

In terms of the division of the economic benefits obtained by farmers in developing countries relative to farmers in developed countries, Table 27 shows that in 2008, 50.5% of the farm income benefits have been earned by developing country farmers. The vast majority of these income gains for developing country farmers have been from GM IR cotton and GM HT soybeans. Over the 13 years, 1996–2008, the cumulative farm income gain derived by developing country farmers was also 50% ($26.2 billion).

Examining the cost farmers pay for accessing GM technology, Table 28 shows that across the four main biotech crops, the total cost in 2008 was equal to 27% of the total technology gains (inclusive of farm income gains plus cost of the technology payable to the seed supply chain: the cost of the technology accrues to the seed supply chain including sellers of seed to farmers, seed multipliers, plant breeders, distributors, and the GM technology providers).

For farmers in developing countries the total cost was equal to 15% of total technology gains, while for farmers in developed countries the cost was 36% of the total technology gains. While circumstances vary between countries, the higher share of total technology gains accounted for by farm income gains in developing countries relative to the farm income share in developed countries reflects factors such as weaker provision and enforcement of intellectual property rights in developing countries and the higher average level of farm income gain on a per hectare

Global Economic Impact of Transgenic/Biotech Crops (1996–2008). Table 27 GM crop farm income benefits 2008: developing versus developed countries: million US $

	Developed	Developing
GM HT soybeans	1,232.1	1,693.6
GM IR maize	2,380.5	265.0
GM HT maize	357.4	76.1
GM IR cotton	213.8	2,690.8
GM HT cotton	5.5	9.1
GM HT canola	391.8	0
GM virus-resistant papaya and squash and GM HT sugar beet	51.5	0
Total	4,632.6	4,734.6

Developing countries = all countries in South America, Mexico, Honduras, Burkino Faso, India, China, the Philippines, and South Africa

basis obtained by farmers in developing countries relative to that obtained by farmers in developed countries.

Concluding Comments

Biotechnology has, to date delivered several specific agronomic traits that have overcome a number of production constraints for many farmers. This has resulted in improved productivity and profitability for the 13.3 million adopting farmers who have applied the technology to 115 million hectares in 2008.

During the last 13 years, this technology has made important positive socioeconomic and environmental contributions. These have arisen even though only a limited range of biotech agronomic traits have so far been commercialized, in a small range of crops.

The biotechnology has delivered economic and environmental gains through a combination of their inherent technical advances and the role of the

Global Economic Impact of Transgenic/Biotech Crops (1996–2008). Table 28 Cost of accessing GM technology (million $) relative to the total farm income benefits 2008

	Cost of technology: all farmers	Farm income gain: all farmers	Total benefit of technology to farmers and seed supply chain	Cost of technology: developing countries	Farm income gain: developing countries	Total benefit of technology to farmers and seed supply chain: developing countries
GM HT soybeans	1,058.2	2,925.7	3,983.9	334.4	1,693.6	2,028.0
GM IR maize	1,045.9	2,645.5	3,691.4	99.7	265.0	364.7
GM HT maize	547.8	433.5	981.3	32.5	76.1	108.6
GM IR cotton	434.6	2,904.5	3,339.1	353.0	2,690.8	3,043.8
GM HT cotton	167.1	14.6	181.7	10.4	9.1	19.5
GM HT canola	109.0	391.8	500.86	N/a	N/a	N/a
Others	41.5	51.5	93.0	N/a	N/a	N/a
Total	3,404.1	9,367.1	12,771.26	830.0	4,734.6	5,564.6

N/a, not applicable. Cost of accessing technology based on the seed premia paid by farmers for using GM technology relative to its conventional equivalents

technology in the facilitation and evolution of more cost-effective and environmentally friendly farming practices. More specifically, it covers the following main issues:

- The gains from the GM IR traits have mostly been delivered directly from the technology (yield improvements, reduced production risk, and decreased the use of insecticides). Thus farmers (mostly in developing countries) have been able to both improve their productivity and economic returns while also practicing more environmentally friendly farming methods.
- The gains from GM HT traits have come from a combination of direct benefits (mostly cost reductions to the farmer) and the facilitation of changes in farming systems. Thus, GM HT technology (especially in soybeans) has played an important role in enabling farmers to capitalize on the availability of a low-cost, broad-spectrum herbicide (glyphosate) and in turn, facilitated the move away from conventional to low/no tillage production systems in both North and South America. This change in production system has made additional positive economic contributions to farmers (and the wider economy) and delivered important environmental benefits, notably reduced levels of GHG emissions (from reduced tractor fuel use and additional soil carbon sequestration).
- Both IR and HT traits have made important contributions to increasing world production levels of soybeans, corn, cotton, and canola.

The impact of GM HT traits has, however contributed to increased reliance on a limited range of herbicides and this has contributed to some limited development of weed resistance to these herbicides. Some degree of reduced effectiveness of glyphosate (and glufosinate) against certain weeds is to be expected and the extent to which this may develop further, will depend on farming practice and behavior relating to mixing, rotation, and sequencing of herbicides. Where resistance has occurred, this has resulted in low-dose rate applications of other herbicides in weed control programs (commonly used in conventional production systems) occurring and hence, has marginally reduced the level of net environmental and economic gains derived from the current use of the biotechnology. Nevertheless, to date, the overall environmental and economic gains arising from the use of biotech crops have been substantial.

Appendix 1: Argentine Second Crop Soybeans

Year	Second crop area (million hectares)	Increase in income linked to GM HT system (million $)	Additional production (million tons)
1996	0.45	Negligible	Negligible
1997	0.65	25.4	0.3
1998	0.8	43.8	0.9
1999	1.4	116.6	2.3
2000	1.6	144.2	2.7
2001	2.4	272.8	5.7
2002	2.7	372.6	6.9
2003	2.8	416.1	7.7
2004	3.0	678.1	6.9
2005	2.3	526.7	6.3
2006	3.2	698.9	11.2
2007	4.9	1,133.6	9.88
2008	3.4	764.6	9.62

Additional gross margin based on data from Grupo CEO

Bibliography

1. Marra M, Piggott N (2006) The value of non pecuniary characteristics of crop biotechnologies: a new look at the evidence, North Carolina State University
2. Marra M, Piggott N (2007) The net gains to cotton farmers of a national refuge plan for Bollgard II cotton. AgBioforum 10(1):1–10 (www.agbioforum.org)
3. Marra M, Pardey P, Alston J (2002) The pay-offs of agricultural biotechnology: an assessment of the evidence. International Food Policy Research Institute, Washington, USA
4. Carpenter J, Gianessi L (1999) Herbicide tolerant soybeans: why growers are adopting roundup ready varieties. AgBioforum 2:65–72
5. Carpenter J (2001) Comparing Roundup ready and conventional soybean yields 1999. National Centre for Food & Agriculture Policy, Washington

6. Sankala S, Blumenthal E (2003) Impacts on US agriculture of biotechnology-derived crops planted in 2003 – an update of eleven case studies. NCFAP, Washington, www.ncfap.org
7. Sankala S, Blumenthal E (2006) Impacts on US agriculture of biotechnology-derived crops planted in 2005 – an update of eleven case studies. NCFAP, Washington, www.ncfap.org
8. Johnson S, Strom S (2008) Quantification of the impacts on US agriculture of biotechnology-derived crops planted in 2006. NCFAP, Washington, www.ncfap.org
9. Qaim M, Traxler G (2002) Roundup ready soybeans in Argentina: farm level, environmental and welfare effects. In: 6th ICABR conference, Ravello, Italy
10. Qaim M, Traxler G (2005) Roundup ready soybeans in Argentina: farm level and aggregate welfare effects. Agric Econ 32(1):73–86
11. Parana Department of Agriculture (2004) Cost of production comparison: biotech and conventional soybeans. In: USDA GAIN report BR4629 of 11 November 2004. www.fas.usad.gov/gainfiles/200411/146118108.pdf
12. Galveo A (2009) Farm survey findings of impact of herbicide tolerant soybeans and insect resistant corn and cotton in Brazil, Celeres, Brazil. www.celeres.co.br
13. George Morris Centre (2004) Economic and environmental impacts of the commercial cultivation of glyphosate tolerant soybeans in Ontario (Unpublished report for Monsanto, Canada)
14. Brookes G (2005) The farm level impact of using roundup ready soybeans in Romania. AgBioforum 8(4) (Also available on www.pgeconomics.co.uk)
15. Monsanto Romania (2007) Roundup ready soybeans: survey growers crops in 2006 and intentions for 2007
16. Monsanto Comercial Mexico (2005) Official report to Mexican Ministry of Agriculture. (Unpublished)
17. Monsanto Comercial Mexico (2007) Official report to Mexican Ministry of Agriculture of the 2006 crop. (Unpublished)
18. Monsanto Comercial Mexico (2008) Official report to Mexican Ministry of Agriculture of the 2008 cotton crop. (Unpublished)
19. Fernandez W et al (2009) GM soybeans in Bolivia. In: Paper presented to the 13th ICABR conference, Ravello, Italy, June 2009
20. Doyle B et al (2003) The Performance of roundup ready cotton 2001–2002 in the Australian cotton sector. University of New England, Armidale, Australia
21. Canola Council of Canada (2001) An agronomic and economic assessment of transgenic canola. Canola Council, Canada, www.canola-council.org
22. Gusta M et al (2009) Economic benefits of GMHT canola for producers, University of Saskatchewan, College of Biotechnology (Working Paper)
23. Monsanto Australia (2009) Survey of herbicide tolerant canola licence holders 2008
24. Fischer J, Tozer P (2009) Evaluation of the environmental and economic impact of roundup ready canola in the Western Australian crop production system. In: Curtin Univeristy of Technology Technical Report 11/2009
25. Kniss A (2009) Farm scale analysis of glyphosate resistant sugar beet in the year of commercial introduction in Wyoming, University of Wyoming
26. Khan M (2008) Roundup ready sugar beet in America. British Sugar Beet Review Winter 2008. 76(4):16–19
27. James C (2003) Global review of commercialized transgenic crops 2002: feature Bt maize, ISAAA No 29
28. Gianessi L, Carpenter J (1999) Agricultural biotechnology insect control benefits. NCFAP, Washington, USA
29. Trigo E, Cap E (2006) Ten years of GM crops in Argentine Agriculture, ArgenBio
30. Gouse M et al (2005) A GM subsistence crop in Africa: the case of Bt white maize in S Africa. Int J Biotechnol 7(1/2/3)
31. Gouse M et al (2006) Three seasons of insect resistant maize in South Africa: have small farmers benefited. AgBioforum 9(1):15–22
32. Gouse M et al (2006) Output and labour effect of GM maize and minimum tillage in a communal area of Kwazulu-Natal. J Dev Perspect 2:2
33. Van der Weld W (2009) Final report on the adoption of GM maize in South Africa for the 2008/09 season. South African Maize Trust
34. Brookes G (2003) The farm level impact of using Bt maize in Spain, ICABR conference paper 2003, Ravello, Italy (Also on www.pgeconomics.co.uk)
35. Brookes G (2008) The benefits of adopting GM insect resistant (Bt) maize in the EU: first results from 1998-2006. Int J Biotechnol 10(2/3):148–166 (www.pgeconomics.co.uk.)
36. Gonsalves D (2005) Harnessing the benefits of biotechnology: the case of Bt corn in the Philippines. ISBN 971-91904-6-9. Strive Foundation, Laguna, Philippines
37. Yorobe J (2004) Economics impact of Bt corn in the Philippines. In: Paper presented to the 45th PAEDA convention, Querzon City, Philippines
38. Ramon G (2005) Acceptability survey on the 80–20 bag in a bag insect resistance management strategy Galveo A (2009) Unpublished (in January 2010) data on first survey findings of impact of insect resistant corn (first crop) in Brazil, Celeres, Brazil. www.celeres.co.br
39. Falck Zepeda J et al (2009) Small 'resource poor' countries taking advantage of the new bio-economy and innovation: the case of insect protected and herbicide tolerant corn in Honduras. In: Paper presented to the 13th ICABR conference, Ravello, Italy
40. Mullins W, Hudson J (2004) Bollgard II versus Bollgard sister line economic comparisons. In: 2004 Beltwide cotton conferences, San Antonio, USA, Jan 2004
41. Pray C et al (2001) Impact of Bt cotton in China. World Dev 29(5):1–34
42. Pray C et al (2002) Five years of Bt cotton in China – the benefits continue. Plant J 31(4): 423–430
43. Doyle B (2005) The performance of Ingard and Bollgard II cotton in Australia during the 2002/2003 and 2003/2004 seasons. University of New England, Armidale, Australia
44. Taylor I (2003) Cotton CRC annual report, UNE, Armidale, Cotton Research Institute, Narrabri, Australia

45. CSIRO (2005) The cotton consultants Australia 2005 Bollgard II comparison report. CSIRO, Australia
46. Qaim M, De Janvry A (2002) Bt cotton in Argentina: analysing adoption and farmers willingness to pay. American Agricultural Economics Association Annual Meeting, California
47. Qaim M, De Janvry A (2005) Bt cotton and pesticide use in Argentina: economic and environmental effects. Environ Dev Econ 10:179–200
48. Elena M (2001) Economic advantages of transgenic cotton in Argentina, INTA. As cited in Trigo and Cap (2006)
49. Traxler G et al (2001) Transgenic cotton in Mexico: economic and environmental impacts. In: ICABR conference, Ravello, Italy
50. Martinez-Carillo J, Diaz-Lopez N (2005) Nine years of transgenic cotton in Mexico: adoption and resistance management. In: Proceedings Beltwide Cotton Conference, Memphis, USA, June 2005
51. Ismael Y et al (2002) A case study of smallholder farmers in the Mahathini flats, South Africa. In: ICABR conference, Ravello Italy 2002
52. Kirsten J et al (2002) Bt cotton in South Africa: adoption and the impact on farm incomes amongst small-scale and large-scale farmers. In: ICABR conference, Ravello, Italy 2002
53. Morse S et al (2004) Why Bt cotton pays for small-scale producers in South Africa. Nat Biotechnol 22(4):379–380
54. Bennett R, Ismael Y, Kambhampati U, Morse S (2004) Economic impact of genetically modified cotton in India. AgBioforum 7(3):96–100
55. IMRB (2006) Socio-economic benefits of Bollgard and product satisfaction (in India). IMRB International, Mumbai, India
56. IMRB (2007) Socio-economic benefits of Bollgard and product satisfaction (in India). IMRB International, Mumbai, India
57. Monsanto Brazil (2008) Farm survey of conventional and Bt cotton growers in Brazil 2007. (Unpublished)
58. Zambrano P et al (2009) Insect resistant cotton in Columbia: impact on farmers. In: Paper presented to the 13th ICABR conference, Ravello, Italy, June 2009
59. Vitale J et al (2006) The Bollgard II field trials in Burkina Faso: measuring how Bt cotton benefits West African farmers. In: Paper presented at the 10th ICABR Conference, Ravello, Italy
60. Vitale J et al (2008) The economic impact of 2nd generation Bt cotton in West Africa: empirical evidence from Burkino Faso. Int J Biotechnol 10(2/3):167–183
61. Rice M (2004) Transgenic rootworm corn: assessing potential agronomic, economic and environmental benefits. Plant Health Progress 10, '094/php-2001-0301-01-RV
62. Alston J et al (2003) An ex-ante analysis of the benefits from adoption of corn rootworm resistant, transgenic corn technology. AgBioforum 5(3), Article 1
63. Manjunath T (2008) Bt cotton in India: remarkable adoption and benefits, Foundation for Biotech Awareness and Education, India. www.fbae.org

Global Wind Power Installations

Thomas Ackermann, Rena Kuwahata
Energynautics GmbH, Langen, Germany

Article Outline

Glossary
Definition of the Subject
Introduction
Current Status
Types of Wind Turbines
Penetration
Costs
Market Forecast (Future Directions)
Conclusions
Bibliography

Glossary

Clean development mechanism Clean development mechanism is the flexible mechanism under Article 12 of the Kyoto Protocol with the purpose to (1) assist non-Annex I Parties in achieving sustainable development, (2) contribute to the ultimate objective of the UNFCCC (United Nations Framework Convention on Climate Change), and (3) assist Parties included in Annex I achieve compliance with their quantified emission limitation and reduction commitments. Annex I Parties refer to industrialized countries that were members of the OECD (Organization for Economic Co-operation and Development) in 1992 plus countries with economies in transition (the EIT Parties), including the Russian Federation, the Baltic States, and several Central and Eastern European States.

Installed capacity Installed capacity is the total MW of operational generation plant of a given technology.

Offshore Wind power plant installed in a marine environment.

Offshore wind developments Offshore wind developments are wind power plants installed in shallow waters off the coast.

Onshore wind developments Onshore wind developments are wind power plants installed on land.

Definition of the Subject

Wind power has been utilized for over 3,000 years to aid with human activities. Although it was predominantly used as mechanical power at the beginning, gradually, with industrialization, the focus shifted to the use as electrical power. With the arrival of the oil price shock in the early 1970s, the use of wind energy as electrical power started to gain more focus, and since the end of the twentieth-century, wind energy has become one of the most important sustainable energy resources. The installation of wind power production capacity is growing at a rapid pace, doubling every 3 years, and is expected to continue growing in the future, providing around 20% of the worlds' power needs by 2030. With strong growth in on- and offshore developments in Europe, and rapid market expansions in the rest of the world, it is imperative that the knowledge which is currently concentrated in a few countries be spread, as implications on research, education, and electric utilities all around the globe are significant. This is the main purpose of this chapter, to present an overview of the relevant areas as well as providing links to further readings and related organizations.

Introduction

The power of the wind has been utilized for at least 3,000 years. Until the early twentieth-century, wind power was used to provide mechanical power for pumping water or for grinding grain. At the beginning of modern industrialization, however, the use of fluctuating energy sources such as wind was gradually replaced by more stable power sources such as fossil-fuel-fired engines and electricity.

With the first oil price shock in the early 1970s, interest in the power of the wind resurfaced. This time, however, the main focus was on wind power providing electrical energy rather than mechanical energy. By converting wind energy into electrical energy, it became possible to provide a reliable and consistent power source, particularly when used with other energy technologies as a backup, via the electrical grid.

The first wind turbines for electricity generation had already been developed at the beginning of the twentieth-century; however, technology started improving step by step since the early 1970s. By the end of the 1990s, wind energy reemerged as one of the most important sustainable energy resources. During the last decade of the twentieth-century, worldwide wind power capacity doubled approximately every 3 years, and in the past decade between 2000 and 2010, it has sustained a compound annual growth rate of over 20% [1]. The cost of wind-generated electricity has fallen by a factor of about 4 during the last 25 years, and some even claim that wind power prices have now converged with the prices of electricity from gas, coal and nuclear plants [2]. Experts in the field predict that the cumulative capacity will be growing worldwide starting off at 27% in 2010 and gradually declining to 5–9% by 2020, supplying up to around 20% of the world's power needs by 2030 [3].

Wind energy technology itself has also moved also very fast toward new dimensions. As can be seen from Table 1, at the end of 1989, a 300-kW wind turbine with a 30-m rotor diameter was state-of-the-art. But only 10 years later, 1,500-kW turbines with a rotor diameter of around 70 m were available from many manufacturers. The first demonstration projects using 2-MW wind turbines with a rotor diameter of 74 m were installed before the turn of the century. 2–5-MW turbines are now in 2010 commercially available, and prototypes of 6–7.5-MW wind turbines are currently being installed. The largest turbine under development is a 15-MW turbine planned for offshore use in 2020 [6].

Global Wind Power Installations. Table 1 Development of wind turbine size between 1985 and 2010

Year	Capacity (kW)	Rotor diameter (m)
1985	50	15
1989	300	30
1992	500	37
1994	600	46
1998	1,500	70
2002	3,000	90
2006	5,000	112
2010	7,000	126
2015	10,000–15,000	150

Source: DEWI [4] and different editions of [5]. 2015 values estimated based on various research proposals

This fast development of the wind energy market as well as of the technology has large implications on research, education, and on professionals working for electric utilities or the wind energy industry. It is important to mention that more than 73% of the worldwide wind capacity is installed in only five countries: USA, China, Germany, Spain, and India. Hence, most of the wind energy knowledge is concentrated in these countries. The use of wind energy technology, however, is fast spreading to other areas in the world. Hence, the available information must also be spread around the world, and this is the main purpose of this chapter. However, despite the fact that wind energy has been already utilized for 3,000 years, it remains a very complex technology. The technology involves a combination of technical disciplines, including aerodynamics, structure-dynamics, mechanical, as well as electrical engineering. Due to the complexity of the wind energy technology, it is not possible to cover all related topics in this chapter in great detail. The chapter aims rather at presenting an overview of the relevant areas as well as providing links to further readings and related organizations.

Current Status

This section will provide a brief overview of the status of wind energy around the world at the end of the first decade of this century. Furthermore, major wind energy support schemes will be presented.

Wind energy statistics are regularly published by various organizations. Regional or countrywide statistics are often compiled and published by the corresponding wind energy associations. For example, The Spanish Wind Energy Association [7], the German Wind Energy Institute [4], the International Economic Platform for Renewable Energies [8], and the Global Wind Energy Council [9] regularly publish worldwide statistics. Up-to date worldwide statistics are published by Windpower Monthly [5] in the January, April, July, and October editions. The Danish wind energy consultant BTM also publishes an annual wind energy development status report with worldwide statistics and forecasts [10]. The latest World Market Update report published in 2010 provides a very good overview of the current status as well as an interesting future scenario of how to meet 10% of the world's electricity demand with wind power by 2020. The World Wind Energy Association's World Wind Energy Report [11] and the IEA Wind Energy Annual Report [12] provide detailed overviews of the research and industry activities and policies in the area of wind energy for various countries.

Global Status

Wind energy has been the fastest growing energy technology since the 1990s in terms of the percentage of yearly growth of installed capacity per technology source. The growth of wind energy, however, is not evenly distributed around the world (see Table 2). By the end of 2010, around 44% of the worldwide wind energy capacity was installed in Europe, a further 31% in Asia and the Pacific, and 23% in North America.

In 2009, more than 38 GW of new wind power capacity was installed around the world (Table 3). This was a surprise for many people in the industry, who expected the financial crisis to put a halt to the record-breaking trend of the growth in wind energy. In fact, the growth rate was 31.7%, the highest rate since 2001. Over a third of the new installations were made

Global Wind Power Installations. Table 2 Operational wind power capacity worldwide

Region	Installed capacity [MW]				
	End-1995	End-2000	End-2005	End-2009	End-2010
Europe	2,518	12,972	40,898	76,152	86,075
North America	1,676	2,695	9,832	38,383	44,189
Latin America	11	103	212	1,274	2,008
Asia and Pacific	626	1,795	7,878	41,831	61,038
Middle East and Africa	13	141	271	865	1,079
Total world wide	4,844	17,706	59,091	158,505	194,390

Source: 1995 and 2001 January editions of [5], 2006 and 2009 editions of [9], and [13]

Global Wind Power Installations. Table 3 Top-ten new installed capacity 2009

Country	MW	%
China	13,803	36.0
USA	9,996	26.1
Spain	2,459	6.4
Germany	1,917	5.0
India	1,271	3.3
Italy	1,114	2.9
France	1,088	2.8
UK	1,077	2.8
Canada	950	2.5
Portugal	673	1.8
Rest of world	3,994	10.4
Total top 10	34,348	89.6
Total world wide	38,342	100.0

Source: 2009 edition of [9]

Global Wind Power Installations. Table 4 Top-ten cumulative installed capacity 2009

Country	MW	%
USA	35,064	22.1
China	25,805	16.3
Germany	25,777	16.3
Spain	19,149	12.1
India	10,926	6.9
Italy	4,850	3.1
France	4,492	2.8
UK	4,051	2.6
Portugal	3,535	2.2
Denmark	3,465	2.2
Rest of world	21,391	13.5
Total top 10	137,114	86.5
Total world wide	158,505	100.0

Source: 2009 edition of [9]

by China, more than doubling its installations compared to the previous year, and catapulting itself to second place in total cumulative installed capacity, just ahead of Germany (Table 4). Almost another third was installed in the USA, who maintains its number one position in total cumulative installations. With over 80 countries using wind energy on a commercial basis in the world, wind energy has become an important player in the world's energy markets. Source: 2009 edition of [11].

The top-ten ranking of wind power plant owners and manufacturers in 2009 is shown in Table 5. Leaders in the development of wind power plants are dominated by European companies such as Vestas, Enercon, and Gamesa, which cover 46.7% of total cumulative installed capacity. However, with rapid developments in China, companies such as Sinovel and Goldwind are now breaking into top ranks of the manufacturing industry.

May 26 (Reuters) – China's wind turbine manufacturers are growing fast, challenging the dominance of players such as Vestas and GE.

According to Danish consultants BTM, three Chinese suppliers now rank among the world's top-ten turbine makers.

Following is a list of the top-ten wind turbine makers and their percentage of the global market.

Europe

Between the end of 2005 and the end of 2010, around 33% of all new grid-connected wind turbines worldwide were installed in Europe (see Table 2). A breakdown of installed capacity per country is shown in Table 6. The main driver in Europe for this development was the creation of fixed feed-in tariffs in countries such as Germany and Spain. Feed-in tariffs are defined by the government as a price per kWh that distribution companies have to pay for electricity that is generated from renewable resources and fed into the local distribution grid. For an overview of tariffs, see [14]. Fixed feed-in tariffs reduce the risk of fluctuating electricity prices and therefore provide a long-term secure income to investors.

In Denmark, a market price and premium is used for onshore wind power plants, and bidding processes are used for offshore wind power plants. For onshore wind power plants, this means that a feed-in premium is paid for a certain number of hours of electricity produced by wind turbines at the installed output, and in addition, a refund of a smaller amount is paid

Global Wind Power Installations. Table 5 Breakdown of global wind turbine manufacturing industry

No.	Company	Country	Newly installed in 2009 (MW)	%	Cumulative (MW)	%
1	Vestas	Denmark	4,766	12.9%	39,705	23.6%
2	GE wind energy	USA	4,741	12.8%	22,931	13.6%
3	Sinovel	China	3,510	9.5%	5,658	3.4%
4	Enercon	Germany	3,221	8.7%	19,738	11.7%
5	Goldwind	China	2,727	7.4%	5,315	3.2%
6	Gamesa	Spain	2,546	6.9%	19,225	11.4%
7	Dongfang electric	China	2,475	6.7%	3,765	2.2%
8	Suzlon	India	2,421	6.5%	9,671	5.7%
9	Siemens wind power	Denmark/Germany	2,265	6.1%	11,213	6.7%
10	REpower	Germany	1,297	3.5%	4,894	2.9%
Total for other companies			7,034	19.0%	26,331	15.6%
Total			37,003	100.0%	168,446	100.0%
Top-ten companies			29,969	81.0%	142,115	84.4%

Source: GWEC, Wind Power (March 2010) and BTM Consult [5, 9, 10]

for balancing costs of electricity. For offshore wind power plants, potential developers are invited to submit offers for building new wind park projects. Developers bid for the amount of financial incentives to be paid for each kWh fed into the grid by renewable energy systems, and the best bidder(s) is awarded their bid feed-in tariff for a predefined period [15].

In the United Kingdom, the approach is based on Fixed Quotas Combined with Green Certificate Trading also known as ROCs (Renewable Obligation Certificates). This scheme enforces fixed quotas for utilities regarding the amount of renewable energy per year they must sell via their transmission or distribution network. At the same time, producers of renewable energy receive certificates for the amount of renewable energy fed into the grid. Utilities must buy these certificates to show that they have fulfilled their obligation of meeting the quota. Similar schemes are used in a number of other European countries, such as Sweden and Norway [1].

No detailed data regarding the average size of the wind turbines installed in Europe is available. However, for single countries such as Germany, data is available as presented in Table 7. This presents the development of the average size of new wind turbine installations in Germany.

The average size of the yearly installed wind turbines in Germany has increased from 20 kW in 1985 to 1,985-kW in 2010. In 2010, in Germany, 14% of the total newly installed wind turbines had a capacity under 2-MW, whereas the share of turbines with 2–2.9-MW was 82.8%. A small 3% of the newly erected wind turbines had a capacity exceeding 3-MW. On a European scale, turbines of 2-MW and larger have become virtually standard since 2005 [1].

Several countries now have operational offshore wind power plants in Europe. These include Denmark, Sweden, the UK, the Netherlands, Belgium, Ireland, and Finland (see Table 8). Although significant development only started in the early twenty-first century, the growth has been steady, and it is starting to have an increasing impact on Europe's wind power development. In 2010, the annual installed capacity more than doubled compared to the previous year, taking the total installed capacity from 2,063 MW at the end of 2009 to 2,964 MW at the end of 2010 [9, 20].

There are significant plans backed by the European Commission to increase production capacity in the North Sea and develop an offshore grid, which is expected to reach up to 40 GW of installed capacity by 2020 (2009 edition of [9]).

Global Wind Power Installations. Table 6 Operational wind power capacity in Europe

Country	Installed capacity (MW)	
	End-2005	End-2010
Germany	18,428	27,214
Denmark	3,128	3,752
Spain	10,028	20,676
Netherlands	1,224	2,237
UK	1,353	5,204
Sweden	509	2,163
Italy	1,718	5,797
Greece	573	1,208
Ireland	495	1,428
Portugal	1,022	3,702
Austria	819	1,011
France	757	5,660
Belgium	167	911
Turkey	20	1,329
Poland	73	1,107
Other[a]	550	2,677
Total	40,898	86,075

Source: 2006 January edition of [9] and [13]
[a]Bulgaria, Croatia, Cyprus, Czech Republic, Estonia, Faroe Islands, Finland, Hungary, Iceland, Latvia, Liechtenstein, Lithuania, Luxembourg, Malta, Norway, Romania, Russia, Slovakia, Slovenia, Switzerland, and Ukraine

Global Wind Power Installations. Table 7 Development of the average turbine size in Germany

Year	Average size of yearly new installed capacity in Germany (kW)
1985	20
1986	45
1987	44.8
1988	66.9
1989	143.4
1990	164.3
1991	168.8
1992	178.6
1993	255.8
1994	370.6
1995	472.2
1996	530.5
1997	628.9
1998	785.6
1999	935,5
2000	1,114
2001	1,278
2002	1,394
2003	1,553
2004	1,696
2005	1,723
2006	1,849
2007	1,888
2008	1,923
2009	2,013
1 HJ 2010	1,985

Source: Various editions of [4] by DEWI

Further offshore projects are planned particularly in the UK (Greater Gabbard: 504 MW; Sheringham Shoal: 315 MW; Walney Phase 1: 184 MW; Ormonde: 150 MW), Germany (Bard 1: 400 MW; Baltic 1: 48 MW), Belgium (Bligh Bank: 165 MW) and Italy (Tricase: 90 MW) [16].

A summary of the offshore wind power plants in Europe in 2010 is shown in Table 8.

North America

After the wind power boom in California during the mid-1980s, development of wind energy slowed down significantly in North America. In the middle of the 1990s, the dismantling of old wind power plants sometimes even exceeded the installations of new wind turbines, which led to a reduction in the overall installed capacity.

In 1998, a second boom started in the USA. This time, wind project developers aimed at installing projects before the federal Production Tax Credit (PTC) expired on the 30 of June 1999. The PTC

Global Wind Power Installations. Table 8 Offshore wind energy projects

Name	Year	Capacity (MW)	Hub height (m)	Distance from shore (km)	Water depth (m)
Nogersund, SE	1991–1998	1*0.22	37.5	0.25	7
Vindeby, Baltic See, DK	1991	11*0.45	37.5	1.5	3–5
Lely, Ijsselmeer, NL	1994	4*0.5	41.5	1	5–10
Tunø Knob, Baltic See, DK	1995	10*0.5	43	6	3–5
Dronten, NL	1996	28*600	50	30	1–2
Bockstigen, Baltic See, SE	1997	5*0.55	41.5	4	5–6
Utgrunden, Baltic See, SE	2000	7*1.425	65	8	7–10
Blyth, North See, UK	2000	2*2	58	1	5–6
Middelgrunden Baltic See, DK	2001	20*2	60	1–3	2–6
Yttre Stengrund, Baltic See, SE	2001	5*2	60	5	8
Horns Rev I, DK	2002	80*2	70	14	6–14
Nysted (Rødsand I)DK	2003	72*2.3	90	6–10	6–0
North Hoyle, UK	2003	30*2	67	3–10	5–12
Samsø, DK	2003	10*2.3		3.5	11–18
Frederikshavn, DK	2003	4*	80	0.8	3
Scroby Sands, UK	2004	30*2	60	2.5	2–10
Arklow Bank, IR	2004	7*3.6	74	10	2.5–5
Enova offshore – Emden, DE	2004	1*4.5	100	<1	–
Kentish Flats, UK	2005	30*3	70	8.5	5
Egmond aan Zee, NL	2006	36*3	70	8–12	19–22
Barrow, UK	2006	30*3	75	7	21–23
Breitling, DE	2006	1*2.5		1	2
Lillgrund, SE	2007	48*2.3	68	10	2.5–9
Beatrice, UK	2007	2*5		25	40
Burbo Bank, UK	2007	25*3.6	84	5.2	10
Lynn and Inner Dowsing, UK	2008	54*3.6	80	5–5.2	10
Princess Amalia, NL	2008	60*2	100	23	19–24
Kemi Ajos I + II, F	2008	10*3	88	<1	3
Hooksiel, DE	2008	1*5	90	0.4	2–8
Thornton Bank I, BE	2008	6*5	94	27–30	12–27
Horns Rev II, DK	2009	90*2.3	68	30	9–17
Rhyl Flats, UK	2009	25*3.6	80	8	4–15
Alpha Ventus, DE	2009	12*5	90	43	30
Storebaelt/Sporgø, DK	2009	7*3		2	6–16

Global Wind Power Installations. Table 8 (Continued)

Name	Year	Capacity (MW)	Hub height (m)	Distance from shore (km)	Water depth (m)
Floating Hywind, NO	2009	1*2.3	65	12	220
Robin Rigg (Solway Firth), UK	2010	60*3	80	9.5	>5
Gunfleet Sands, UK	2010	48*3.6	75	7	2–15
Vänern (Gässlingegrund), SE	2010	10*3	90	4	4–10
Rødsand II, DK	2010	90*2.3	68.5	8.8	6–12
Thanet, UK	2010	100*3	70	12–17.7	14–23
Poseidon, DK	2010	0.011*3			

Source: [16, 17, 18, 19]
SE Sweden, *DK* Denmark, *NL* The Netherlands, *F* Finland, *IR* Ireland, *BE* Belgium, *DE* Germany, *NO* Norway

added $0.016–0.017/kWh to wind power projects for the first 10 years of a wind plant's life. Between the middle of 1998 and June 30, 1999, the final day of PTC, more than 800 MW of new wind power generation was installed in the USA, which included between 120 and 250 MW of "repowering" development at several Californian wind power plants. A similar development took place before the end of 2001, which added 1,600 MW between the middle of 2001 and the end of December 2001. Currently, the USA has over 36 GW of installed wind capacity and is leading as world number one in cumulative installed capacity (Table 4 and Table 9). In addition to Texas, major projects have been carried out in the states of Minnesota, Oregon, Wyoming, and Iowa (Table 10).

The typical wind turbine size installed in North America at the end of the 1990s was between 500 and 1,000 kW. The first megawatt turbines were installed in 1999 and since 2001; many projects have used megawatt turbines. At the end of 2009, the typical size was 1,750 kW (2009 editions of [12] and [21]). In comparison to Europe, however, the overall size of wind power plant projects is usually larger. Typical projects in North America are larger than 50 MW, with some projects of up to 200 MW, whereas, in Europe, projects are usually between 20 and 50 MW. The reason for this is the limited space in Europe due to the high population density, especially in Central Europe. These limitations have led to offshore developments in Europe; however, in North America, offshore projects are not a major topic.

Global Wind Power Installations. Table 9 Operational wind power capacity in North America

Country	Installed capacity (MW)			
	End 1995	End 2001	End 2005	End 2010
USA	1,655	4,275	9,149	40,180
Canada	21	198	683	4,009
Total	1,676	4,473	9,832	44,189

Source: 2005 edition of [9] and [13]

The major driver for further wind energy development in several states in the USA are an extension of the PTC as well as fixed quotas combined with green certificate trading, known as the Renewable Portfolio Standard (RPS) in the USA or Renewable Energy Credits (RECs) in the UK. Other drivers are financial incentives, e.g., offered by the California Energy Commission (CEC), as well as green pricing programs. Green Pricing is a marketing program offered by utilities to provide choices for electricity customers to purchase power from environmentally preferred sources. Customers thereby agree to pay higher tariffs for "Green Electricity" and the utilities guarantee to produce the corresponding amount of electricity by using "Green Energy Sources" such as wind energy.

Considering the immense possibilities its wind resources present, Canada is falling somewhat behind the global development of wind energy. Despite this, 2009 marked the best year for Canada's national wind

Global Wind Power Installations. Table 10 Operational wind power capacity in the USA

State	Installed capacity [MW]	
	End 2001	October 2010
Texas	1,100	9,712
Iowa	332	3,669
California	1,688	2,814
Oregon	199	2,095
Washington	161	2,036
Illinois	0	1,847
Minnesota	311	1,813
New York	19	1,274
Colorado	58	1,248
North Dakota	2	1,222
Indiana	0	1,130
Oklahoma	0	1,130
Wyoming	140	1,101
Kansas	114	1,026
Pennsylvania	34	748
New Mexico	1	597
Missouri	0	457
Wisconsin	53	449
West Virginia	414	414
South Dakota	3	412
Montana	0	386
Utah	0	223
Maine	0	200
Idaho	0	163
Nebraska	3	153
Michigan	1	143
Arizona	0	63
Hawaii	11	63
Tennessee	0	29
New Hampshire	25	25
Massachusetts	1	17
Ohio	0	9
Alaska	1	8
New Jersey	8	8
Vermont	6	6
Delaware	0	2
Rhode Island	1	1
Total	4,688	36,693

Source: 2002 January edition and 2010 edition of [5]

energy market with 950 MW of new capacity being installed. Since 2007, when the ecoENERGY for Renewable Power Program was established, a payment of C$0.01/kWh (before tax) is offered for the first 10 years of a project's life. This program was immensely successful, so much so that the target of reaching 4,000 MW of renewable energy projects by March 31, 2011, was achieved well ahead of schedule. As a consequence, the federal government decided to terminate the program in March 2010, and the future remains uncertain. In addition to the federal scheme, the state of Ontario implemented a feed-in tariff, offering C$0.13/kWh for onshore wind power plants in 2009. With various state governments taking initiative to improve their policy frameworks, substantial growth is expected in the state of Ontario, as well as Quebec, British Colombia, New Brunswick, and Nova Scotia.

Latin America

Despite large wind energy resources in many regions of Latin America, the development of wind-powered electricity is very slow as it can be seen from the figures in Table 11. This is due to the existence of low electricity prices as well as the lack of sufficient wind energy policies. For these reasons, until now, many wind projects in South America have been financially supported by international aid programs.

Argentina, however, introduced a new policy at the end of 1998, which offered financial support to wind energy generation in the form of feed-in tariffs. This initiative triggered a spate of developments until the year 2002, when the economic crisis occurred. With the crisis, most developments stopped, and it was not until 2007 when a new law was established that further development ensued. The federal government in May

Global Wind Power Installations. Table 11 Operational wind power capacity in South and Central America

Country	Installed capacity (MW)		
	End-2001	End-2005	End-2010
Argentina	25.7	27	60
Brazil	20	29	931
Mexico	2.2	3	517
Chile	1.3	2	172
Costa Rica	51	71	123
Other[a]	2.8	80	205
Total	103	212	2,008

Source: 2002 of [5], 2002 edition of [12], 2006 edition of [9], and [13]
[a]Colombia, Chile, and Cuba

2009 announced the intention to revive the former plan for renewable energy development called GENREN, which will serve as a framework to set up a regulation aiming at the promotion of renewable energies. The finalization and efficient application of this plan in conjunction with the National Wind Energy Strategic Plan (PENEE) is expected to reactivate development in the wind industry, with several projects in the range of 20–90 MW already in the pipeline [22].

In Brazil, the government established the "Programa de Incentivo às Fontes Alternativas de Energia Elétrica" (PROINFA) with the objective to increase the share of renewable energy through government incentives, providing feed-in tariffs and 20 year contracts with guaranteed demand. In addition to this, a number of government tax incentives and discounts on transmission tariffs have also been implemented. The PROINFA program has been an important step for establishing a stable platform for growth in the wind industry, accounting for up to 95% of the current wind power installations in Brazil. Since December 2009, a new approach has been adopted, where bids are now based on production, where the quantity of energy delivered annually is divided by 12 months to smooth the monthly income, rather than on a feed-in tariff system [23]. The policies in Brazil has brought about rapid growth in wind-capacity installations from 341 MW to 606 MW in 2009, a 78.5% increase, and manufacturing bases opening on its shores (2009 edition of [9]).

Mexico has also seen a rapid expansion in wind energy development in recent years, particularly in the Isthmus of Tehuantepec. The average turbine size in this region is 1,136 kW (2009 edition of [12]). However, until now, the only incentive to build new projects has been income tax credits which allow some expenses associated with wind installation to be deducted from taxable income streams.

Chile is another country with favorable conditions for wind energy development. Wind energy is considered by the law as a nonconventional energy resource, which has been promoted by the Development Agency of Chile (CORFO) and the National Commission of Energy (CNE) since 2005. The development of wind energy projects, especially grid-connected electricity-generation projects, is supported through financial incentives. The development of wind parks in the country is still at an early stage however, and there are no specific programs or policies for wind energy alone [22].

Until now, the typical size of wind turbines was around 300 kW in Latin America. However, with new manufacturing capacity for larger wind turbines being established in Brazil, further development is envisioned for the future. In other Latin American countries, however, it may still be difficult to install large turbines due to limitations in infrastructure, particularly for larger equipment such as cranes. Offshore wind projects are not planned, but further small to medium-size ($\leq$30 MW) projects are under development onshore.

One of the major incentives for developing wind projects in Latin America is the emission reduction certificate crediting scheme through the Clean Development Mechanism. La Ventosa, for example, the largest wind power plant in Mexico, as well as numerous projects in Chile and Brazil have gained additional income benefits through this scheme.

Asia and Pacific

The Asia-Pacific region contributes to 31% of global installed capacity of wind power (see Table 2), mainly due to the strong growth experienced in India and China. This must be attributed to the rapid growth in demand. Refer to Table 12 for a detailed breakdown of installed capacities in each country.

Global Wind Power Installations. Table 12 Operational wind power capacity in Asia and Pacific

Country	Installed capacity (MW)			
	End-1995	End-2001	End-2005	End-2010
China	44	361	1,266	42,287
India	565	1,426	4,430	13,065
Japan	5	250	1,061	2,304
Australia	10	74	708	1,880
New Zealand	2	37	169	506
Taiwan	0	3	104	519
South Korea	0	8	98	379
Other[a]				98
Total	625	2,162	7,879	61,038

Source: 1997 and 2002 editions of [5], 2006 edition of [9], 2008 edition of [11], and [13]

[a]Phillipines, Thailand, Bangladesh, Indonesia, Sri Lanka, Vietnam, and Pacific Islands

India achieved an impressive growth in wind turbine installation in the middle of the 1990s, in what was called the "Indian Boom." In 1992/1993, the Indian government started to offer special incentives for renewable energy investments by guaranteeing a minimum purchase rate as well as a 100% tax depreciation in the first year of the project. Furthermore, a "power banking" system was introduced, which allowed electricity producers to "bank" their power with the utility and avoid being cut off during times of load shedding. In this scheme, power could be banked for up to 1 year. In addition, some Indian States introduced additional incentives, such as investment subsidies. Development of new installations between 1993 and 1997 were rampant, but it slowed down after 1997 due to uncertainties regarding the future of the incentives (Reference: various editions of [5]). In 2008, the Ministry for New and Renewable Energy (MNRE) announced a national generation-based incentive scheme for grid-connected projects under 49 MW, providing an incentive of 0.5 rupees per kWh (0.7 Euro cents/kWh) in addition to the existing state incentives [24]. This has helped with the development of small- to medium-sized wind power plants, but the tariff is deemed to be too low to have a significant impact on a project's viability. In the absence of a better national framework, some states with Renewable Portfolio Standards or other policies to promote wind generation have introduced feed-in-tariffs for wind generation which are higher than that for conventional electricity.

In China, the wind power industry increased capacity by over 100% in 2009 [25]. Its cumulative installed capacity now ranks second in the world. The main reason for the dramatic increase was due to the new focus of the Chinese government to prioritize wind energy as a measure to diversify its energy mix. A recent study by the China Meteorological Administration showed that the potential for wind power in on- and offshore schemes in China are huge, reaching over 3.5 TW in onshore and 200 GW in offshore [25]. The National Energy Administration of China is currently progressing its plans to capitalize on this resource with targets in six provinces to reach a total of 127.5 GW by 2020, dubbed the "Wind Base" program.

There is also the only offshore wind project outside of Europe in China. The Donghai Bridge Wind Power plant is a 102 MW wind power plant close to the Donghai Bridge in Shanghai constituting 34 Sinovel 3-MW turbines. It started producing and transmitting power to the mainland grid on July 6, 2010, and is the first commercial offshore wind power plant in China [26]. As part of the Wind Base program, the Chinese government is planning the construction of further 7 GW of offshore wind power plants in the province of Jiangsu by the year 2020.

In terms of policies, wind power plants have been eligible for a renewable energy premium which is added to the cost of each kWh of electricity sold since 2006. Furthermore, since 2009 a feed-in tariff has been introduced for wind power, which applies to the entire operation period of a wind power plant. The tariff differs depending on the region's wind resource, and the government is underway to formulate the tariff rate for offshore wind power to be applied to the anticipated growth in the future. Source: 2009 edition of [9].

In Japan, demonstration projects testing different wind turbine technologies dominated the development. At the end of the 1990s, the first commercial wind energy projects started operation on the islands of Hokkaido as well as Okinawa. The interest in wind power is constantly growing in Japan. There also exists

direct financial subsidies aimed at tackling the up-front cost barrier, either for specific equipment or total installed wind system cost.

In Japan and Korea, investment in wind projects are driven by an enhanced feed-in tariff in the form of an explicit monetary reward provided for wind-generated electricity, usually paid by the electricity utility, at a rate per kilowatt-hour somewhat higher than the retail electricity rates being paid by the customer. In addition, these countries employ a form of renewable portfolio standard, which mandates that the electricity utility (often the electricity retailer) source a portion of its electricity supplies from renewable energies.

At the end of the 1990s, the first wind energy projects also materialized in New Zealand and Australia. The main driver for wind energy development in Australia was the Mandatory Renewable Energy Target (MRET) which was introduced in 2001. This scheme requires electricity retailers to source specific proportions of total electricity sales from renewable energy sources according to a fixed timeframe. The national MRET scheme is supported by State-run feed-in-tariff schemes. In addition to the MRET scheme in Australia, there is also a green electricity scheme where customers are given the option to purchase green electricity based on renewable energy from the electric utility at a premium price.

Typical wind turbine sizes installed in the Asia-Pacific region is 1.5–2 MW (Reference: 2009 edition of [12]), and with manufacturing plants based in China and India, further development is anticipated, especially in China.

Middle East and Africa

Wind energy development in Africa is very slow as evident from the figures in Table 13. Most projects require financial support by international aid organizations, as only limited regional support exits. Despite this, an increasing number of African governments are becoming aware of the potential of wind energy in their countries and are beginning to set up the necessary frameworks. An example of this is the setup of the first feed-in tariff in South Africa, which is designed to produce 10 TWh of electricity per year by 2013 from renewable resources [27].

Several projects have been developed in Egypt with the support of the government agency for New and Renewable Energy Authority (NREA). Five hundred and forty-five megawatt of installed capacity had been built near the city of Zafarana by the end of 2010, in addition to 5 MW in the Gulf of Zayt. Significant developments are expected in the order of 3,000 MW in the next years. Furthermore, there is also a buildup of industrial activities in manufacturing of wind turbines. Further projects are planned in Morocco as well as in Kenya, Ethiopia, Namibia, Tunisia, and Cape Verde. Source: 2009 edition of [11], [22] and various editions of [5].

Global Wind Power Installations. Table 13 Operational wind power capacity in Middle East and Africa

Country/ region	Installed capacity (MW)			
	End-1995	End-2001	End-2005	End-2010
Egypt	5	125	145	550
Morocco	0	54	64	286
Tunisia		10	20	114
Other	7	14	42	129
Total	12	203	271	1,079

Source: 1997 and 2002 editions of [5], 2006 edition of [9], 2008 edition of [11], and [13]

[a]Iran, South Africa, Cape Verde, Israel, Lebanon, Nigeria, Jordan, Kenya

The typical wind turbine size used in this region is between 600 and 800 kW. However, in light of the fact that the majority of the African population still has no access to electricity grids, small, decentralized, and stand-alone wind energy systems, in combination with other renewable energies, is expected to play a key role. This process is still in its early stage, however, and the limiting factors remain the lack of access to know-how and to adequate financial resources (2009 edition of [11]).

Types of Wind Turbines

Wind energy conversion systems can be divided into those which depend on aerodynamic drag and those which depend on aerodynamic lift. The early Persian (or Chinese) vertical-axis wind wheels (Fig. 1) utilized the drag principle. Drag devices, however, have a very low power coefficient, with a CP.max of around ≈0.16 [28, 29].

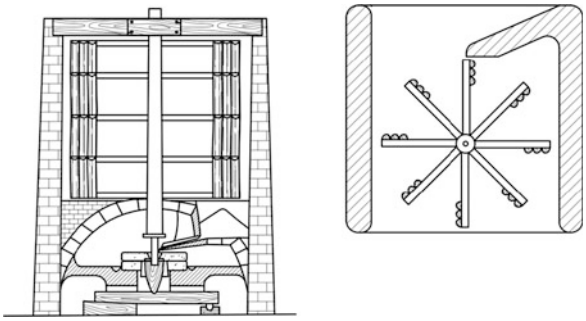

Global Wind Power Installations. Figure 1
Persian-type windmill. (Kaboldy, Wikimedia Commons)

Global Wind Power Installations. Figure 2
Darriues wind power generator near Heroldstatt, Germany. (W.Wacker, Wikimedia Commons)

Modern wind turbines are predominately based on aerodynamic lift. Lift devices use aerofoils (blades) that interact with the incoming wind. The force resulting from the aerofoil body intercepting the air flow does not consist only of a drag force component in direction of the flow, but also of a force component that is perpendicular to the drag: the lift force. The lift force is a multiple of the drag force and therefore the relevant driving power of the rotor. By definition, it is perpendicular to the direction of the air flow that is intercepted by the rotor blade, and via the leverage of the rotor, it causes the necessary driving torque [28–31].

Wind turbines using the aerodynamic lift can be further divided according to the orientation of the spin axis into horizontal axis– and vertical axis–type turbines. Vertical-axis turbines, also known as Darrieus (Fig. 2) after the French engineer who invented it in the 1920s, use vertical, often slightly curved symmetrical aerofoils. Darrieus turbines have the advantage that they operate independently of the wind direction and that the gearbox and generating machinery can be placed at ground level. High torque fluctuations with each revolution, no self-starting capability, as well as limited options for speed regulations in high winds are, however, major disadvantages. Vertical-axis turbines were developed and commercially produced in the 1970s until the end of the 1980s. The largest vertical-axis wind turbine was installed in Canada, the ECOLE C with 4,200 kW. Since the end of the 1980s, however, the research and development of vertical-axis wind turbines has almost stopped worldwide [28, 29, 31, 32].

The horizontal-axis or propeller-type approach dominates the current wind turbine applications. A horizontal-axis wind turbine consists of a tower and a nacelle that is mounted on the top of a tower. The nacelle contains the generator, gearbox, and the rotor. Different mechanisms exist to point the nacelle toward the wind direction or to move the nacelle out of the wind in case of high wind speeds. On small turbines, the rotor and the nacelle are oriented into the wind with a tail vane. On large turbines, the nacelle with rotor is electrically yawed into or out of the wind, in response to a signal from a wind vane.

Horizontal-axis wind turbines typically use a different number of blades, depending on the purpose of the wind turbine. Two or three bladed turbines are usually used for electricity power generation. Turbines with 20 or more blades are used for mechanical water pumping.

The number of rotor blades is indirectly linked to the tip speed ratio, which is the ratio of the blade tip speed and the wind speed. Wind turbines with a high number of blades have a low tip speed ratio but a high starting torque. This high starting torque can be utilized for fully automatically starting water pumping when the wind speed increases. A typical

example for such an application is the water-pumping windmill often seen in the midwest USA. Wind turbines with only two or three blades have a high tip speed ratio, but only a low starting torque. These turbines might need to be started if the wind speed reaches the operation range. But a high tip speed ratio allows the use of a smaller and therefore lighter gearbox to achieve the required high speed at the driving shaft of the power generator [28, 29, 31–33].

Apart from the above discussed wind turbine design philosophies, inventors frequently come up with new designs, using some kind of power augmentation, for instance. However, none of these inventions have given sufficient large-scale performances yet. For the current status of power augmentation wind turbines, see [34] and [35].

The Four Wind Turbine Types

Type-I Type-I wind turbines are fixed-speed wind turbines that were introduced and widely used in the 1980s. It uses a squirrel cage asynchronous generator (SCIG), where the rotor is driven by the turbine and the stator is directly coupled to the grid. The rotation speed of this kind of turbine can vary only slightly, between 1% and 2%; therefore, it is effectively at a "fixed speed." There are single-speed and double-speed versions, but the double-speed version is better at adapting to different wind speeds, producing less noise at low wind speeds. Type-I wind turbines typically have limited voltage control and reactive power control capabilities to support the grid. The stall system is mostly passive stall, inherit to the aerodynamic design of the blades. There are few options for active control besides connecting and disconnecting, especially if there is no blade pitch change mechanism. However, the concept has been continuously improved, for example, in the active stall designs, where the blade pitch angle can be changed toward stall by the control system. Type-I wind turbines make up 15% of the total cumulative European market share and are manufactured by Suzlon, Nordex, Siemens (used to be Bonus), and Ecotecnia [36].

Type-II Type-II wind turbines were commonly used by Vestas in the 1980s and 1990s in Europe and still offered nowadays by Vestas in selected markets as well as by Suzlon. They are equipped with a wound rotor induction generator (WRIG), which has limited variable speed capabilities. Power electronics is used to control the rotor's electrical resistance, which allows both the rotor and the generator to vary their speeds up and down by 10% to cope with wind gusts, to maximize the power quality, and to reduce the mechanical loading on the turbine components, power electronics is also used. Type-II wind turbines also have limited voltage control capabilities to support the grid and are equipped with an active blade pitch control system. Typical Type-II wind turbines are the Vestas models V27, V34, and V47, which make up 5% of the total cumulative European market [36].

Type-III Type-III wind turbines combine the advantages of previous systems with advances in power electronics, producing an improved variable speed capability. It uses a doubly-fed induction generator (DFIG) which has a wound rotor coupled to the grid through a back-to-back voltage source converter that controls the excitation system in order to decouple the mechanical and electrical rotor frequency and to match the grid and rotor frequency. The active and reactive power can be controlled through the use of power electronics, enabling active voltage control. In this type of system, up to approximately 40% of the power output goes directly to the grid, and the window of speed variations is approximately 40% up and down from synchronous speed. Many manufacturers produce Type-III wind generators, including GE, Repower, Vestas, Nordex, Gemasa, Alstom, Acciona Windpower, Suzlon, Bard, and Kenersys. It is the main type of wind turbine in the European market, making up 55% of all installations [36].

Type-IV Type-IV wind turbines are variable speed turbines with full-scale frequency converters that come with the classical drivetrain (geared), in the direct-drive concept (with slow running generator and no gearbox), or in a hybrid version (low step-up gearbox and medium-speed generator). Various types of generators are used for this type of turbine: synchronous generators with wound rotors, permanent magnet generators and squirrel cage induction generators, etc. The stator is connected to the grid via a full-power

electronic converter, and the rotor has excitation windings or permanent magnets. Being completely decoupled from the grid, it can provide an even wider range of operating speeds than the Type-II wind turbine and has a broader range of reactive power and voltage control capacities. Type-IV wind turbines are manufactured by Enercon, MEG (Multibrid), GE, Winwind, Siemens, Leitner, Mtorres and Lagerwey, making up 25% of the total cumulative European market [36].

Penetration

At the end of 2009, electricity produced by wind turbines contributed to only 2% of the global electric energy. However, in some countries and regions of the world, wind has become one of the largest electricity sources. The highest shares are seen in countries such as Denmark (20%), Portugal (15%), Spain (14%), and Germany (9%) [2009 edition of [11].

Costs

Over the past 20 years between 1990 and 2010, the capital cost of producing wind turbines has fallen steadily due to economies of scale created by optimization of manufacturing technologies, mass production, and automation [3]. The cost has fallen by a factor of about 4 during the last 25 years between 1985 and 2010, with the general conclusion that costs decrease by some 20% each time the number of units produced doubles.

However, in the years leading up to 2010, particularly since 2006, increasing commodity prices for raw materials such as copper (used in generators), steel (used for towers, gearboxes and rotors), and concrete (used in foundations), rising energy prices, as well as bottlenecks in certain sub-productions have caused the investment cost per MW to increase for new wind power projects (2009 edition of [21]). Although supply chain pressures can be addressed by building new

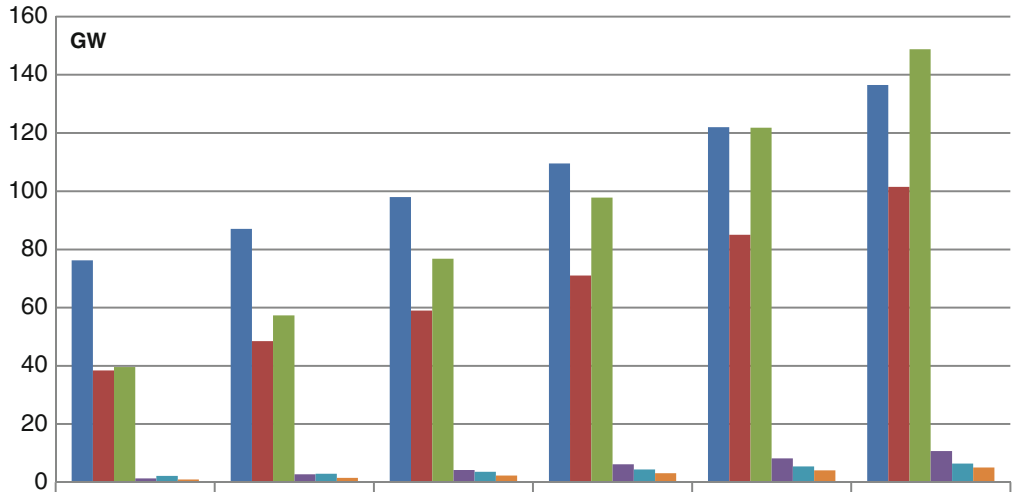

	2009	2010	2011	2012	2013	2014
Europe	76.2	87	98	109.5	122	136.5
North America	38.4	48.5	59	71	85	101.5
Asia	39.6	57.3	76.8	97.8	121.8	148.8
Latin America	1.3	2.7	4.2	6.2	8.2	10.7
Pacific	2.2	2.9	3.6	4.4	5.4	6.4
Middle East and Africa	0.9	1.5	2.3	3.1	4.1	5.1

Global Wind Power Installations. Figure 3
Cumulative market forecast by region 2009–2014 (2009 edition of [9])

production capacity and establishing new manufacturing bases in countries like China, the industry will have to continue battling with the pressure of rising commodity and energy prices.

Despite these challenges, the cost of wind turbine generators has fallen significantly overall, and the industry is recognized as being in the "commercialization phase," as understood in learning curve theory [37].

For example, the average capital cost per kilowatt of installed capacity rose from €1,300 in 2007 to €1,350 in 2009. However, it is assumed that it will then fall steadily from 2010 onward to between €1,240 and €1,172 by 2020 and to between €1,216 and €1,093 by 2030 [21].

Given the high up-front costs of wind power projects, large investments of predominantly private but also public funds are expected to flow into the growing wind power markets. This investment will directly benefit regional development by creating jobs in manufacturing, transportation, construction, project development and operation, and maintenance; providing new revenue sources to local landowners such as a farmers or communities; and increasing the local tax base. The value of investment in the future wind energy markets is thus larger than what is visibly obvious at. Besides these economic benefits, reflected in the economy, wind energy technology also adds value by reducing carbon emission, diversifying fuel supply and providing stable energy production prices. Source: 2009 edition of [12] and [37].

Market Forecast (Future Directions)

2009 saw a 41% market growth in the wind power industry. This was a surprise to many in the field, who expected growth to be staggered by the financial crisis. In particular, growths in the USA and China have been impressive in the past few years, with China single-handedly accounting for one third of the total annual wind-capacity addition in 2009. Although the growth in the USA is expected to stay somewhat flat in the coming years due to the lack of financing and

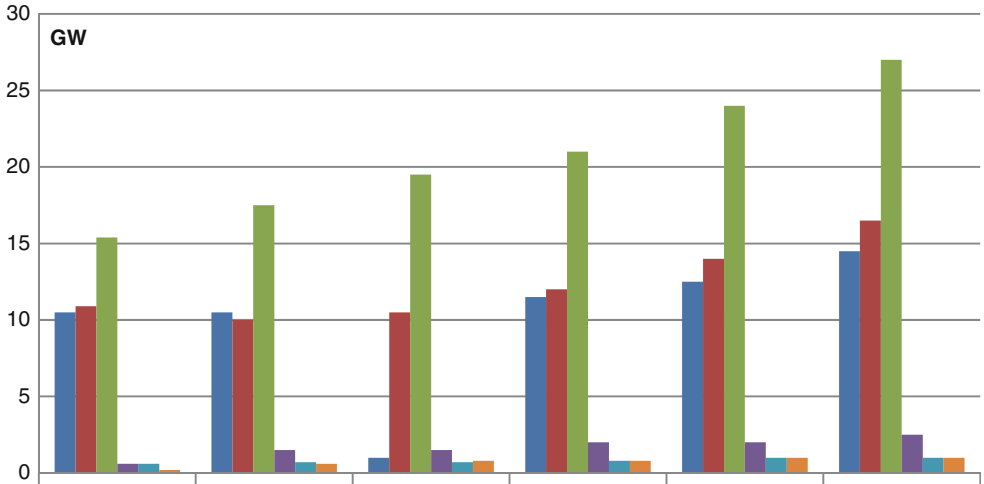

	2009	2010	2011	2012	2013	2014
Europe	10.5	10.5	1	11.5	12.5	14.5
North America	10.9	10	10.5	12	14	16.5
Asia	15.4	17.5	19.5	21	24	27
Latin America	0.6	1.5	1.5	2	2	2.5
Pacific	0.6	0.7	0.7	0.8	1	1
Middle East and Africa	0.2	0.6	0.8	0.8	1	1

Global Wind Power Installations. Figure 4
Annual market forecast by region 2009–2014 (2009 edition of [9])

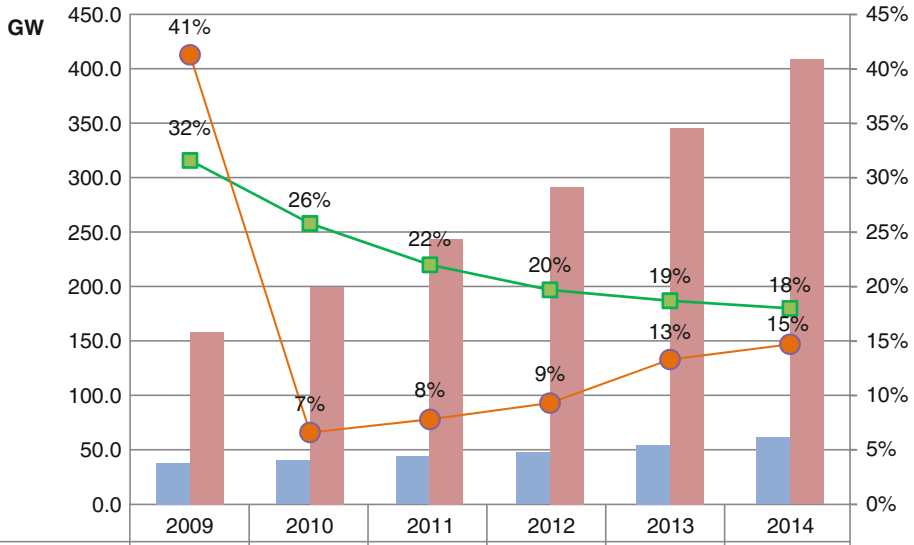

	2009	2010	2011	2012	2013	2014
Annual installed capacity [GW]	38.3	40.8	44.0	48.1	54.5	62.5
Cumulative [GW]	158.5	199.9	243.9	292.0	346.5	409.0
Cumulative capacity growth rate [%]	32%	26%	22%	20%	19%	18%
Annual installed capacity growth rate [%]	41%	7%	8%	9%	13%	15%

Global Wind Power Installations. Figure 5
Market forecast 2010–2014 (2009 edition of [9])

overall economic downturn, the development in China is set to continue at a breath-taking pace, with well over 20 GW of annual additions. Sustained growth is also expected in India, which will increase its capacity by 2 GW each year. Complimented by growth in other Asian markets, including Japan, Taiwan, South Korea, and the Philippines, the market in Asian is expected to nearly double in the next 5 years, reaching 109 GW of new wind capacity. In Europe, continued growth is also expected, however, not at such a dramatic pace. Regardless, it is expected that a total of 60 GW will be installed by 2014, with large developments in the offshore market. While Germany and Spain are expected to remain the leading European markets, growth in Italy, France, the UK, and Portugal is expected to continue, as well as opening for some new markets in Poland and Turkey (Fig. 3).

The market in Latin America has also been growing stronger than previously thought. Encouraging developments are seen in Brazil, Mexico, and Chile; however, due to the lack of favorable policies for wind power development in this region, market development will not reach the heights that would be possible to imagine from the amount of excellent wind resources there is. At the end of 2014, a total of 10.7 GW of installation is expected, increasing from the 1.3 GW in 2009.

In the Pacific region, both Australia and New Zealand seem to be firmly on the track for continued growth at a steady pace, with annual additions of 1 GW by 2014, reaching a total installed capacity of up to 6.4 GW by the end of 2014. Both countries have very good wind resources and a great untapped potential, which is slowly being developed.

In Africa and the Middle East, predictions are less certain, and it is expected that the regions will remain small players in the world's wind market. Substantial plans exist for South Africa however, as well as Kenya, Tanzania, Ethiopia, and Egypt are expected to bring the total capacity up to 5.1 GW by 2014.

As can be seen in Fig. 4 below, in total, it is predicted that in 2014, global wind capacity will stand at 409 GW, with an annual market growth rate of 20.9% being sustained throughout the period in terms of total installed capacity (2009 edition of [9] and [3]) (Fig. 5).

Conclusions

Wind energy has the potential to play an important role in the future energy supply in many areas of the world. Within the last 20 years, wind turbine technology has reached a very reliable and sophisticated level. The growing worldwide market will lead to further improvements, such as large wind turbines or new system applications, including offshore wind power plants. These improvements will lead to further cost reductions and over the medium -erm wind energy will not only be able to compete, but be cheaper than conventional fossil fuel power generation technology. Further research, however, will be required in many areas, for example, regarding the network integration of a high penetration of wind energy.

Bibliography

1. European Wind Energy Association (EWEA) (2009) Wind Energy the Facts, Brussels, Belgium. http://www.wind-energy-the-facts.org/
2. Windpower Monthly (2009) 25th Anniversary special – Generating costs – electricity that gets cheaper and cheaper, 01 July 2009. http://www.windpowermonthly.com/news/972151/25th-Anniversary-Special – Generating-Costs – Electricity-gets-cheaper-cheaper/
3. GWEC (2010) Global wind energy outlook 2010. http://www.gwec.net/fileadmin/documents/Publications/GWEO%202010%20final.pdf
4. DEWI Magazin (1992) published biannually since 1992 by the German Wind Energy Institute (DEWI). http://www.dewi.de/dewi/index.php?id=46
5. Windpower Monthly (1985) Industry magazine, monthly, ISSN 0901–7318. http://www.windpower-monthly.com
6. Gamesa News (2010) Eleven Spanish companies join forces on the Azimut Project to develop a 15-MW offshore wind turbine using 100% Spanish technology. http://www.gamesacorp.com/en/communication/news/eleven-spanish-companies-join-forces-on-the-azimut-project-to-develop-a-15-mw-offshore-wind-turbine-using-100-spanish-technology.html?idCategoria=0&fechaDesde=&especifica=0&texto=&fechaHasta
7. AEE Wind Power, Wind power observatory, Spanish Wind Energy Association (AEE), Madrid, Spain. http://www.aeeolica.es/en/aee_realizado_informes.php
8. IWR International economic platform for renewable energies. http://www.iwr.de/welcomee.html
9. GWEC Global Wind Report, published by the Global Wind Energy Council (GWEC), Brussels, Belgium. http://www.gwec.net/
10. BTM Consult Aps. http://www.btm.dk/
11. WWEA (2010) World Wind Energy Report, World Wind Energy Association (WWEA), Bonn, Germany. http://www.wwindea.org/home/index.php
12. IEA (2009) Wind Energy Annual Report, International Energy Agency (IEA), Paris, France. http://www.ieawind.org/
13. GWEC (2010) Global wind statistics 2010. http://www.gwec.net/fileadmin/documents/Publications/GWEC_PRstats_02-02-2011_final.pdf
14. Energie Verwertungsagentur (1998) Feed-in tariffs and regulations concerning renewable energy electricity generation in European countries, Vienna, Austria. http://www.eva.wsr.ac.at/publ/dl.htm
15. IEA (2009) Global renewable energy policies and measures: feed-in tariffs for renewable power (Promotion of Renewable Energy Act). http://www.iea.org/textbase/pm/?mode=re&action=detail&id=4425
16. EWEA (2009) Operational offshore wind farms in Europe, End 2009. http://www.ewea.org/fileadmin/ewea_documents/documents/statistics/OperationalOffshoreFarms2009.pdf
17. 4 C Offshore, Offshore wind farms data base, http://www.4coffshore.com/
18. Middelgrundens Vindmøllelaug, http://www.middelgrunden.dk
19. Offshore Wind Energy, The Windenergie-Agentur Bremerhaven/Bremen Magazine, Future Energy Supply from Wind at Sea, WAB. http://www.windenergie-agentur.de/english/PDFs/Offshore_Magazin_Eng2007.pdf
20. EWEA (2011) Press release: record 51% growth for EU offshore wind power in 2010. http://www.ewea.org/index.php?id=60&no_cache=1&tx_ttnews[tt_news]=1895&tx_ttnews[backPid]=259&cHash=ccd23cd4806718a5dbcf7dbd9f227997
21. EERE, Wind technologies market report, US Department of Energy, Energy Efficiency and Renewable Energy. http://eetd.lbl.gov/ea/ems/re-pubs.html
22. TERNA-Studie: Energiewirtschaftliche Rahmenbedingungen und Anreizsysteme für netzgekoppelte Stromproduktion aus erneuerbaren Energien. Deutsche Gesellschaft für Technische Zusammenarbeit (GTZ) – German Technical Cooperation, Eschborn, Germany
23. McHugh M (2010) Renewable energy investment, acquisitions and business development: Brazil is set to be the new wind energy powerhouse, but which way does the wind really blow? http://jherrerosdc.typepad.com/jhsdc/2010/10/brazil-is-set-to-be-the-new-wind-energy-powerhouse-but-which-way-does-the-wind-really-blow.html
24. GWEC (2009) Indian wind energy outlook 2009. http://www.indianwindpower.com/pdf/GWEO_A4_2008_India_LowRes.pdf
25. Junfeng L, Pengfei S, Hu G (2010) China wind power outlook 2010. Chinese Renewable Energy Industries Association, GWEC and Greenpeace. http://www.greenpeace.org/raw/content/eastasia/press/reports/wind-power-report-english-2010.pdf
26. Feldman S (2009) Solve climate news: China beats US to offshore wind development. http://solveclimatenews.com/news/20090403/china-beats-us-offshore-wind-development

27. Gipe P (2009) Renewable energy world, news: South Africa introduces aggressive feed-in tariffs. http://www.renewable-energyworld.com/rea/news/article/2009/04/south-africa-introduces-aggressive-feed-in-tariffs
28. Gasch R. Windkraftanlagen. In: Gasch R, Teubner BG (eds) 3 rd edn. Stuttgart, Germany (German version of Wind turbine generators)
29. Gasch R (2002) Wind power plants – fundamentals, design, construction and operation. Solarpraxis, Berlin (Distributed by German Wind Energy Association)
30. Snel H (1998) Review of the present status of rotor aerodynamics. Wind Energy 1(S1):46–69
31. Walker JF, Jenkins N (1997) Wind energy technology. Wiley, Chichester
32. Gipe P (1995) Wind energy comes of age. Wiley, New York
33. Thresher RW, Dodge DM (1998) Trends in the evolution of wind turbine generator configurations and systems. Wind Energy 1(S1):70–85
34. Van Bussel G (1998) Power augmentation principles for wind turbines. Delft University of Technology, Institute for Wind Energy, the Netherlands. http://www.ct.tudelft.nl/windenergy/papers/augment/contents.htm
35. Flay RGJ, Phillips DG, Richards PJ (1999) Development of diffuser augmented wind turbine designs in New Zealand. In: Proceedings of the European wind energy conference, Nice, James & James, London, 1–5 Mar 1999, pp 349–352
36. EWEA (2010) Powering Europe: wind energy and the electricity grid. http://www.ewea.org/fileadmin/ewea_documents/documents/publications/reports/Grids_Report_2010.pdf
37. GWEC (2008) Global wind energy outlook 2008. http://www.gwec.net/fileadmin/images/Logos/Corporate/GWEO_A4_2008_lowres.pdf

GM Crop Risk Debate, Science and Socioeconomics

Klaus Ammann
Botanical Garden, University of Bern, Bern, Switzerland

Article Outline

Introduction
Developments in Risk Handling of GM Crops
The Costs and Lost Benefits of Overregulation
The Dispute Between Scientists and Opponents Today
Debate Improvements: What can we do to Enhance the Situation?
Bibliography

Introduction

The General Strategic Situation of the Debate About Green Biotechnology Today

The aim of this text is to set the framework for a better communication about science and regulation, and production of GM crops. GM stands for Genetic Modification, basically an unfortunate denomination, because actually *all* crops are genetically modified, but it is a worldwide accepted term for genetically engineered crops, including transgenes, auto- and allotransgenes, cis- and infra-genes, and synthetic genes, for details see Beardmore [1]. By including gene stacking of various kinds, the situation is getting even more complex [2]. With the introduction of in Vivo Mutation (with Zink-Finger Technology and the latest transformation method transcription activator-like family of type III effectors [TALEs]) the situation will change even more, the age of a high precision and targeted change of genomes has only begun and will develop rapidly, see section Innovation in Agriculture on All Levels Will Speed Up and Makes it a Necessity to Rethink Regulation Basically and Radically, Most often in the Direction of Lowering the Regulatory Hurdles with details. The term LMOs (Living Modified Organisms), which is generally used in the United Nations Biosafety Protocol (Cartagena Protocol) is nothing but a "Living Proof" that the scientific basis of the Protocol remains questionable, since firstly the term is creating misunderstandings and secondly it is based on an erroneous assumption that GM crops are basically different from conventional crops, as is discussed with detail in the sections Molecular Processes Similar in Natural Mutation and Transgenesis and Dissent over Differences Between GM- and Non-GM Crops Causes Transatlantic Regulatory Divide. More detailed clarification about the terminology of GMOs is given in a text block of the published Statement of the Pontifical Academy of Sciences: [3].

► There are many different terms used to describe the processes involved in plant breeding. All living organisms are made up of cells in which are contained their genes, which give them their distinctive characteristics. The complete set of genes (the genotype) is encoded in DNA and is referred to as the genome; it is the hereditary information that is passed from parent to

offspring. All plant breeding, and indeed all evolution, involves genetic change or modification followed by selection for beneficial characteristics from among the offspring. Most alterations to a plant's phenotype or observable traits (such as its physical structure, development, biochemical and nutritional properties) result from changes to its genotype. Plant breeding traditionally used the random reshuffling of genes among closely-related and sexually compatible species, often with unpredictable consequences and always with the details of the genetic changes unexplored. In the mid-twentieth century this was supplemented by mutagenesis breeding, the equally random treatment of seeds or whole plants with mutagenic chemicals or high-energy radiation in the hope of generating phenotypic improvements; this, too, gave rise to unpredictable and unexplored genetic consequences from which the plant breeder selected the beneficial traits. Most recently, techniques have been developed allowing the transfer of specific, identified and well characterized genes, or small blocks of genes that confer particular traits, accompanied by a precise analysis of the genetic and phenotypic outcomes: this last category is called 'transgenesis' (because genes are transferred from a donor to a recipient) or 'genetic engineering' (abbreviated to GE in this report) but, in truth, this term applies to all breeding procedures.

The strategic situation in the debate on GM crops is difficult, but not desperate, particularly in Europe – this is an evaluation shared by lots of experts of the debate about agricultural biotechnology; in Europe, it is negatively affecting research and researchers [4]. We have reached in Europe the peak of anxiety related to GM-crops since the introduction of the new technologies, and some opponents to transgenic crops have taken advantage of this situation. They have organized themselves in a veritable protest industry, see section The Dispute Between Scientists and Opponents Today. Nevertheless, the next years should lead to reassurance and scientific consolidation on biotechnology views. We encounter the same repeating dynamics as described for previous technology introductions [5]. The Gartner Hype Cycle [6] adds another dimension to technology life cycle models: it characterizes the typical progression of an emerging technology from user and media overenthusiasm through a period of disillusionment to an eventual understanding of the technology's relevance and role in a market or domain (Fig. 1).

In the details of the cycle [6], amended by the author – specified for the technology push in transgenic crop development – it should be noted that there are differences between the development of the technologies in the mind of Linden and Fenn and agricultural technologies, where life sciences, combined with regional and cultural diversity, results in a much more diversified picture, often not following the below described phases.

- **2.1 Technology Trigger.** The Technology Trigger is a technological breakthrough, public demonstration, press release or other event that generates significant publicity and industry interest in an emerging technology. Typically no usable products exist, only research and laboratory prototypes (from the first transgenic plants in the 80ties [7]. Venture capitalists may provide some early funding just after the Trigger, if they expect the technology to be a fast runner.

- **2.2 On the Rise.** On the rise to the Peak of Inflated Expectations, media articles explain the technology and discuss its potential impact on business and society. First-generation products emerge like the Flavr-Savr-Tomato [8], but they usually are highly specialized products or extremely difficult to use or with other hitches in the introductory phase. Products are high margin because vendors are still trying to recover R&D costs, and the technology is expensive compared to its cost of production. For example, in 2002, Bluetooth products such as headsets cost $200, while the final silicon cost of Bluetooth chips likely will be approximately $5. This is a good stage for venture capitalists to enter the market, before evaluations are at their apex. During this phase, some particularly aggressive enterprises may start to pilot the technology, particularly if it contributes to critical business issues. These enterprises work closely with the vendors to create customized solutions for their requirements

- **2.3 At the Peak of Inflated Expectations.** As the Peak crests, the number of vendors offering the technology increases. These vendors are primarily startup companies and small vendors that try to use the increasing amount of hype for their marketing

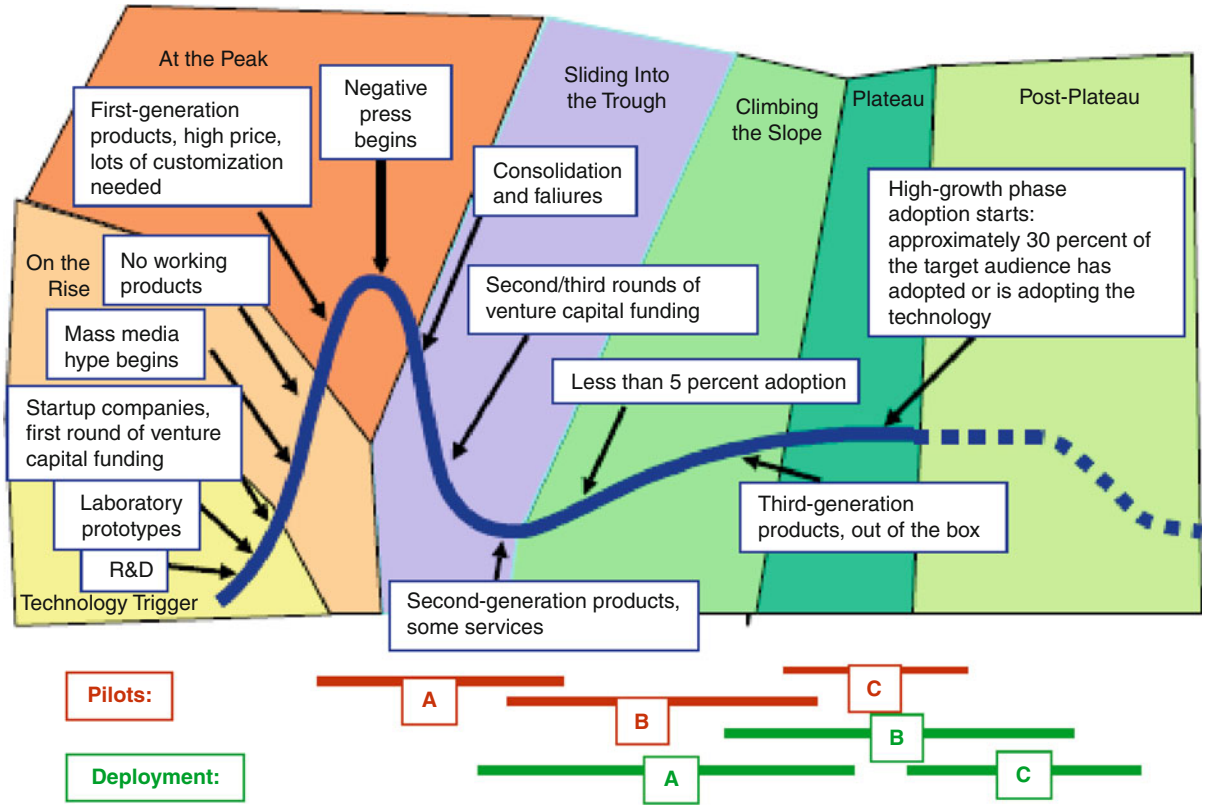

Source: Gartner Research (May 2003)

GM Crop Risk Debate, Science and Socioeconomics. Figure 1
Gartner Hype cycle, extended view from [6] after Fig. 3. Technologically aggressive ("Type A") enterprises are relatively comfortable adopting the technology, and moderately aggressive ("Type B") enterprises start to investigate and pilot the technology. Conservative ("Type C") enterprises remain wary (From [6])

benefit. A growing number of enterprises start to examine how the technology may fit within their business strategies, although most do not take action at this stage. Venture capitalists may be interested in selling some of the startups that they equipped with early funding. As problems with first-generation products become visible (e.g., emerging pest resistance in the Bt cotton regions [9, 10] and the latest success message of Huang et al. [11], often because the technology is pushed to its limits, negative publicity starts to push the technology into the Trough of Disillusionment, often the pertinent publications are pushed for negative statements beyond the limit of scientific rules (for example, Web services in 2002 and biometrics in 2003 and two example from the debate on non-target insects related to Bt crops: a) the case of the monarch butterfly [12] and b) Lovei et al. [13] giving false alarm for ladybirds and its prompt rebuttal by Antony Shelton et al. [14]).

2.4 Sliding into the Trough of Disillusionment. Because the technology does not live up to enterprises' and the media's overinflated expectations, it is rapidly discredited. Some of the early trials end in highly publicized failures. Media interest wanes, except for a few cautionary tales. A significant amount of vendor consolidation and failure occurs. Later-stage investors may be interested in funding vendors during this phase because equity is fairly inexpensive after the "microbubble" at the Peak of Inflated Expectations has burst. However, amid the disillusionment, trials are ongoing and vendors are improving products based on early feedback regarding problems and issues. Some early adopters find some benefit in

adopting the technology. For some slow-moving technologies (for example, biometrics), workable and cost-effective solutions emerge and provide value in niche domains, even while the technology remains in the Trough. The Trough of Disillusionment coincides with the "chasm" in Geoffrey Moore's classic book, "Crossing the Chasm" [15]. During this stage, vendors need to launch their products from a few early adopters to adoption by a majority of enterprises to begin the climb up the Slope of Enlightenment. There is no real parallel in the GM crop history, except that the differences in GM crop regulation and perception between the Americas and Europe caused a deep transatlantic divide [16].

- **2.5 Climbing the Slope of Enlightenment.** Focused experimentation and real-world experience by an increasingly diverse range of enterprises lead to a better understanding of the technology's applicability, risks and benefits. Vendors seek mezzanine or later-round funding for marketing and sales support to pull them-selves up the Slope. Second- and third-generation products are launched by the leading seed companies, and methodologies and tools are added to ease the development process, see the sections under 1.2. The service component declines as a percentage of the sale. Technologically aggressive ("Type A") enterprises are relatively comfortable adopting the technology, and moderately aggressive ("Type B") enterprises start to investigate and pilot the technology. Conservative ("Type C") enterprises remain wary. At the beginning of the slope, the penetration often is significantly less than 5 percent of the potential market segment. This will grow to approximately 30 percent and more as the technology enters the Plateau of Enlightenment. Examples of more or less unexpected enhancements in science and risk assessment of transgenic crops come from a higher precision of gene transfer methods (see sections under 1.2.), also compare to the latest developments in resistance management with a clear success story this year [11].

- **2.6 Entering the Plateau of Productivity.** The Plateau represents the beginning of mainstream adoption, which began in the Americas much earlier from 2000 onwards, when the real-world benefits of the technology are demonstrated and accepted, see the consecutive reports on the world development of transgenic crops on www.isaaa.org. Technologies become increasingly embedded into solutions that increasingly are "out of the box," with decreasing service elements as the technology matures (example conservation tilling). The majority of Type B, then Type C, enterprises adopt the technology. As a high-profile technology matures, an "ecosystem" often evolves around it. The ecosystem supports multiple providers of products and services, and also a market for related products and services that extend or are based on the technology (for example, virtual private networks in 2003 or the growing market for suppliers of molecular laboratories or the growing market for electronic equipment for precision agriculture).

  The final height of the Plateau varies according to whether the technology is broadly applicable or benefits only a niche market, depending heavily on crop and region.

- **2.7 Post-Plateau.** As a technology achieves full maturity and supports thousands of enterprises and millions of users, producers and consumers, its hype typically disappears, as seen in the Americas. Only a few specialist magazines continue coverage of new aspects of implementing and maintaining the technology. Often there may be innovations around this technology that will follow their own Hype Cycles (new crop varieties on stress resistance, on bio-fortification, pharmaceutical crop lines etc.).

- **3.0 The Time-to-Maturity Assessment.** Technologies do not move at a uniform speed through the Hype Cycle. It often takes years for a technology to traverse the Hype Cycle — some technologies like GM crops may take decades, with considerable regional differences. There are three adoption speeds:

  "Fast-track" technologies go through the Hype Cycle within two to four years. This occurs when the performance curve inflects early in the life cycle of a technology. These technologies find themselves adopted without much fanfare, bypassing the Peak of Inflated Expectations and Trough of Disillusionment. Many enterprises are unaware of their sudden maturity and applicability, such as what has happened with instant messaging and Short Message Service.

It is interesting to note that the Showalter "hystories" on the introduction of most new technologies [5]

report no real damage in their subsequent introductory phase, or the benefits were so overwhelming that the debate was soon fading away. This alone demonstrates clearly that it is the sociocultural environment strongly influencing the risk debate [17]. The most recent events seem to hint that Europe finally finds to a more decontracted way of looking at GM crops: The new report of the Royal Society [18] tries to unite conventional and biotechnology approaches for the sake of making progress on agricultural management in developing countries:

- Past debates about agricultural technology have tended to involve different parties arguing for either advanced biotechnology including GM, improved conventional agricultural practice or low-input methods. We do not consider that these approaches are mutually exclusive: improvements to all systems require high-quality science. Global food insecurity is the product of a set of interrelated local problems of food production and consumption. The diversity of these problems needs to be reflected in the diversity of scientific approaches used to tackle them. Rather than focusing on particular scientific tools and techniques, the approaches should be evaluated in terms of their outcomes.

It might well be that we arrive sooner than expected from a period of disillusionment to an eventual understanding of the technology's relevance and role in a market or domain.

Innovation in Agriculture on all Levels will Speed up and Makes it a Necessity to Rethink Regulation Basically and Radically, most Often in the Direction of Lowering the Regulatory Hurdles

Unfortunately, regulatory legislation is in its nature static, needs a long time to be settled in international negotiations, and then, finally, settled and approved with an important number of signatory states as the Cartagena Protocol; therefore, it is nearly impossible to make the necessary changes based on good science. At the time of the establishment of the Cartagena Biosafety Protocol, the similarities between nontransgenic and transgenic organisms on the molecular level were not widely known, although properly published (see latest review with early publications [19]), and a correction about these grave errors (recently called by the author as "Genomic Misconception," publication in preparation) in concept is now nearly impossible – details in section GM- and Non-GM-Crop Differences Over-Estimated, the "Genomic Misconception". But the situation is not getting better: the accelerating speed of scientific progress and discoveries used for new (agricultural) technologies is breathtaking. A short overview is provided in the following sections.

New Biotechnology Approaches in Plant Breeding, Introduction In an early paper, Britt et al. give an overview on many molecular possibilities which will develop for new breeding successes [20], they address the current status of plant gene targeting and what is known about the associated plant DNA repair mechanisms. One of the greatest hurdle that plant biologists face in assigning gene function and in crop improvement is the lack of efficient and robust technologies to generate gene replacements or targeted gene knockouts. They also face an old problem in plant breeding summarized under the complex term of epigenetics [21, 22], a problem corrected in conventional plant breeding by careful and often tedious selection processes. Unfortunately, opponents abuse epigenetics as a seemingly new problem for genetic engineering [23], avoiding the mention of modern molecular insight and its ease to correct such problems in a more targeted way. It is clear that transgenesis will remain a solid technology for breeding, but new approaches will appear – as science is always open for progress and new breakthroughs. Here, we only mention shortly progress from another more holistic perspective of systems biology: the dynamics of Metabolomics [24], and also the growing speed of discovery in proteomics [25], techniques which will increasingly augment more common types of experimentation, especially as they provide the capacity of generating data sets that can be compared across studies and laboratories [26], and because quantitative proteomics data are generated with unprecedented sensitivity, accuracy, and reproducibility. There are many new biotechnologies enhancing the speed of achieving targeted breeding successes such as the high throughput marker finding technology [27, 28], only a few can be mentioned here:

***Cis*- and Intragenic Approaches** A new technology has now proven to be a successful strategy: As Romments describe it, cisgenetics is a welcome way of combining the benefits of traditional breeding with modern biotechnology. It is an understandable enthusiasm of the first researchers using this technology to emphasize the positive sides by also comparing to transgenesis as an "old-fashioned" method with its problems. But things are certainly not so easy: In sections Molecular Processes Similar in Natural Mutation and Transgenesis and Dissent Over Differences Between GM- and Non-GM Crops Causes Transatlantic Regulatory Divide, it is made clear that on the genomic level, particularly on the level of molecular processes, there is no difference between transgenic and nontransgenic crops (supported by an important body of scientific literature), and this is certainly also true to cisgenic and intragenic varieties. This is why it is questionable and based on false grounds to make claims that those new methods in transformation would be safer, as Giddings has made it clear in his letter [29], and his arguments against the views of [30–32] and later publications [33–35] could have been targeted as well: they try to demonstrate that the new cisgenics and intragenics are safer than transgenics, which is not based on any facts, rather it is based on accepting without scientific scrutiny the negative public perception on transgenic crops. It is also wrong to use without clarification the term "alien genes" in view of confirmed and widely accepted universality of DNA and genomic structures.

However, there is nothing to say against the application of such new methods per se, as [33, 34] can demonstrate:

- The classical methods of alien gene transfer by traditional breeding yielded fruitful results. However, modern varieties demand a growing number of combined traits, for which pre-breeding methods with wild species are often needed. Introgression and translocation breeding require time consuming backcrosses and simultaneous selection steps to overcome linkage drag. Breeding of crops using the traditional sources of genetic variation by cisgenesis can speed up the whole process dramatically, along with usage of existing promising varieties. This is specifically the case with complex (allo)polyploids and with heterozygous, vegetative propagated crops. Therefore, we believe that cisgenesis is the basis of the second/ever green revolution needed in traditional plant breeding. For this goal to be achieved, exemption of the GM-regulation of cisgenes is needed.

Reverse Screening Methods: Tilling and Eco-Tilling Two rather independent publications [36, 37] with largely incongruent literature lists promote a new technology of finding useful genes within the genome of the crops involved: They both promote powerful reverse genetic strategies that allow the detection of induced point mutations in individuals of the mutagenized populations, can address the major challenge of linking sequence information to the biological function of genes, and can also identify novel variation for plant breeding [37]. Rigola et al. [36] develop reverse genetics approaches which rely on the detection of sequence alterations in target genes to identify allelic variants among mutant or natural populations. Current (pre-) screening methods such as *tilling* and *eco-tilling* are based on the detection of single base mismatches in heteroduplexes using endonucleases such as CEL 1. However, there are drawbacks in the use of endonucleases due to their relatively poor cleavage efficiency and exonuclease activity. Moreover, prescreening methods do not reveal information about the nature of sequence changes and their possible impact on gene function. Rigola et al. [36] present a *KeyPointTM* technology, a high-throughput mutation/polymorphism discovery technique based on massive parallel sequencing of target genes amplified from mutant or natural populations. Thus, *KeyPointTM* combines multidimensional pooling of large numbers of individual DNA samples and the use of sample identification tags ("sample barcoding") with next-generation sequencing technology. Rigola et al. [36] can demonstrate first successes in tomato breeding by identifying two mutants in the tomato eIF4E gene based on screening more than 3,000 M2 families in a single GS FLX sequencing run, and discovery of six haplotypes of tomato eIF4E gene by re-sequencing three amplicons in a subset of 92 tomato lines from the EU-SOL core collection. This technology will prove to be useful and does not need for its own breakthrough to refer to a scientifically unjustified critique of transgenesis.

Whether the new technology will replace the transgenic "Amflora potato" has still to be proven by further scrutinizing of the results of the equivalent trait [38].

Zinc Finger Targeted Insertion of Transgenes Plant breeding has gone through dynamic developments, from marker-assisted breeding to transgenesis with steadily improved methods to the latest development of the Zink-finger enzyme-assisted targeted insertion of transgenes in complex organisms [39–42]. Zinc-finger nucleases (ZFNs) allow gene editing in live cells by inducing a targeted DNA double-strand break (DSB) at a specific genomic locus. However, strategies for characterizing the genome-wide specificity of ZFNs remain limited. According to [43], comprehensive mapping of ZFN activity in vivo will facilitate the broad application of these reagents in translational research.

The development toward more insertion precision and less genomic disturbance is so rapid that promoters of organic farming will see dwindling one of their pet arguments even more rapidly: Genomic disturbance of modern breeding is certainly less important and will even be negligible compared to the old breeding methods, still promoted stubbornly by the organic plant breeding community [44]: It is very likely that the transcriptomic disturbances will be even smaller in future – compared to the clumsy and tedious methods of conventional breeding, see also the latest developments in sections TALEs: Transformation Method Transcription Activator-like Family of Type III Effectors and Precision Engineering Through DNE Meganucleases below.

TALEs: Transformation Method Transcription Activator-like Family of Type III Effectors The generation of double-strand DNA breaks (DSBs) promotes homologous recombination in eukaryotes and can facilitate gene targeting, additions, deletions, and inactivation. Zinc-finger nucleases have been used to generate DSBs and subsequently for genome editing, but with low efficiency and reproducibility. In contrast, the transcription activator-like family of type III effectors (TALEs) contains a central domain of tandem repeats that could be engineered to bind specific DNA targets. The new method is capable of generating site-specific DNS Breaks and has great potential for site-specific genome modification in plants and eukaryotes in general [45]. See also comments on the newswire CNBS [46] on the discovery:

- Dr. Mahfouz has developed a "repair tool" (molecular scissors) made out of protein that does two things: it finds the exact place on the genome where it is to be cut using a genetic "postcode" and then deletes, adds or edits the gene with great accuracy and precision.

  Dr. Mahfouz's work has the potential for much broader applications including human health. This new technology could enhance the technique that may be used to substitute "good" genes for bad, or to cut out or silence the defective genes that cause disease.

  Commenting on the research, KAUST Provost Stefan Catsicas saw the technology as a scientific breakthrough and, if the patent is eventually successful, having potentially promising revenues. Dr. Nina Fedoroff, Professor of the Life Sciences at Penn State University, said the Mahfouz paper "shows the practicability of creating DNA-cutting enzymes tailored to cut a desired target sequence with very high specificity. This is an excellent step forward toward creating very specific genetic improvements in crop plants, while avoiding the potential risks many are concerned about with more conventional genetic modification strategies. Moreover, the paper gives the first evidence that this particular strategy will work in plants." Professor Fedoroff is "delighted to see such cutting-edge contributions emerging from a university as young as KAUST!".

Precision Engineering Through DNE Meganucleases Engineered DNE meganucleases can be used for cloning and molecular analysis purposes in much the same ways as conventional restriction enzymes. The important difference, of course, is that meganucleases recognize much rarer DNA sequences than restriction enzymes. This makes them particularly well suited to the manipulation of extremely large DNA sequences such as intact genomes. Importantly, DNE meganucleases cleave to leave four base pair 3' overhangs suitable for "sticky-end" cloning. The first application with a new tool called Directed Nuclease Editor™ in plant breeding by Bayer Crop Science http://www.precisionbiosciences.com/ seems promising: The meganucleases have been first

used to do precision work in human gene therapy, but an outlook into various other applications was announced as early as 2003 [47–49].

Synthetic Biology In some 150 laboratories, synthetic biology is intensively researched, and it seems clear that the future will bring here some unexpected revolutions: A new field, synthetic biology, is emerging on the basis of these experiments [50], where chemistry mimics biological processes as complicated as Darwinian evolution. According to [51], the emerging field of synthetic biology is generating insatiable demands for synthetic genes, which far exceed existing gene synthesis capabilities. Tian et al. claim that technologies and trends potentially will lead to breakthroughs in the development of accurate, low-cost, and high-throughput gene synthesis technology – the capability of generating unlimited supplies of DNA molecules of any sequence or size will transform biomedical and any biotechnology research in the near future. And, according to [52], already in 1998 the redesigning of nucleic acids has been judged in an optimistic way, this was confirmed in an important Nature review in 2005 [53].

The real breakthrough came with the synthesis of an organism including its reproduction, achieved after years of research and a firm belief in success, typical of the senior author of the mega project still continuing, [54–57].

A pragmatic view of a new regulatory scheme answering the new biosafety tasks of synthetic biology is proposed by [58] (Fig. 2):

This kind of new regulatory approach will be necessary in order to avoid unnecessary hindering of research progress in synthetic biology, a demand supported with other innovative suggestions for interactive procedures [59]. Another balanced view [60] demonstrates also the new risks arising from synthetic organisms and the accidental (or purposeful) release in the environment. As always, the ethical awareness and behavior has to be developed further, agreeing with [61] not in a way which gives forfeit power to social sciences. What we really need is a new interfaculty, interdisciplinary or, even better, transdisciplinary discursive scheme as proposed in sections Long Term Discourse and Decision Making Processes and The Second Generation Systems Approach as a New Decision Making Process.

What happened some 35 years ago in the US National Institute of Health in the words of Henry I. Miller [62] should be a warning.

> Thirty-five years ago, the US National Institutes of Health adopted overly risk-averse guidelines for research using recombinant DNA, or "genetic engineering," techniques. Those guidelines, based on what has proved to be an idiosyncratic and largely invalid set of assumptions, sent a powerful message that scientists and the federal government were taking seriously speculative, exaggerated risk scenarios – a message that has afflicted the technology's development worldwide ever since.

A final remark: In a way, the artificial altering of genes producing Bt toxins can, strictly spoken, also be summarized under synthetic biology since the specifically altered Bt toxins in order to facilitate resistance management of Bt crops: Bruce Tabashnik, who works on problem solving programs for Bt crops with field research and new concepts of resistance management [63]: Relative to native toxins, the potency of modified toxins was >350-fold higher against resistant strains of *Plutella xylostella* and *Ostrinia nubilalis*. Previous results suggested that the modified toxins would be effective only if resistance was linked with mutations in genes encoding toxin-binding cadherin proteins [64]. Tabashnik et al. report evidence from five major crop pests refuting the Soberon hypothesis.

Illusions and Realities on Educational Effects in the Debate, the Dialogue Between Science and the Public

There is no doubt that there is hope and need to simply start and/or maintain an open dialogue between major stakeholders among young scientists, politicians, industry, and society [65], although there are many obstacles such as asymmetric relationships among the partners, which can render the discourse complex and unpredictable. And it is uncontested here that education on all school levels has its justified place; this has again been shown with empirical results from Spain [66, 67]. Gensuisse should also be mentioned here with educational activities in schools and a popular open day of Genetics in major Swiss cities organized by researchers and institutes every year [68]. And education on biotechnology in the developing world is especially important,

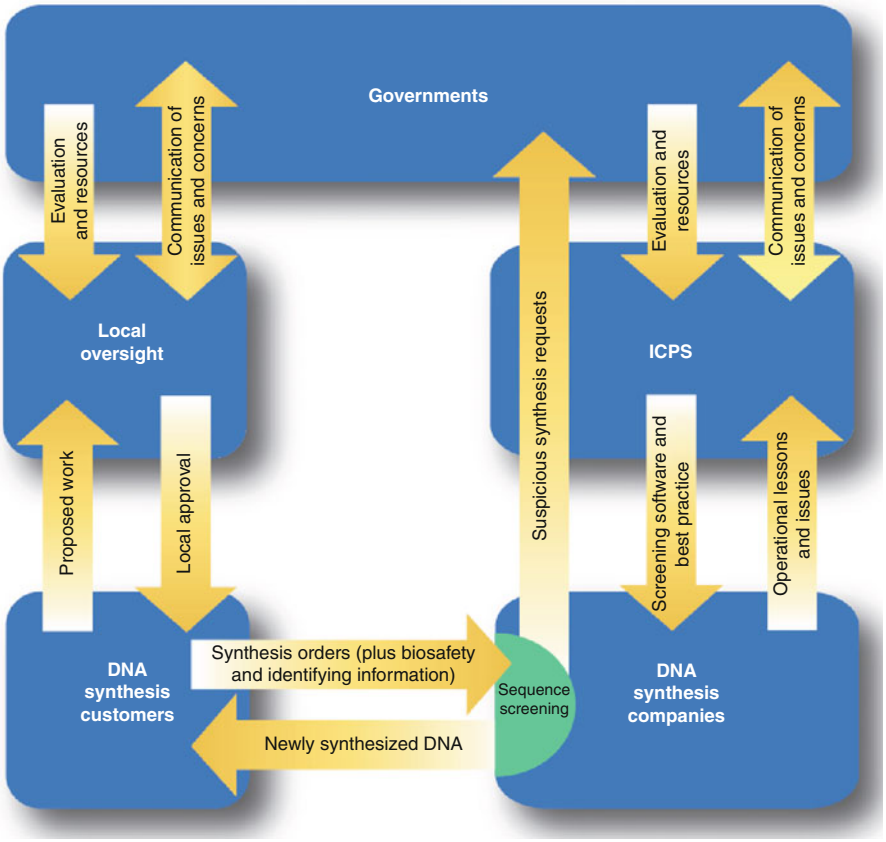

GM Crop Risk Debate, Science and Socioeconomics. Figure 2
Our framework calls for the immediate and systematic implementation of a tiered DNA synthesis order screening process. To promote and establish accountability, individuals who place orders for DNA synthesis would be required to identify themselves, their home organization, and all relevant biosafety information. Next, individual companies would use validated software tools to check synthesis orders against a set of select agents or sequences to help ensure regulatory compliance and flag synthesis orders for further review. Finally, DNA synthesis and synthetic biology companies would work together through the ICPS, and interface with appropriate government agencies (worldwide), to rapidly and continually improve the underlying technologies used to screen orders and identify potentially dangerous sequences, as well as develop a clearly defined process to report behavior that falls outside of the agreed-upon guidelines. ICPS, International Consortium for Polynucleotide Synthesis (From [58])

if done in a participative way, and with proper ramifications in all institutions of communication, science, and regulation: In April 2007, biosafety and biotechnology scientists, regulators, educators, and communicators from Kenya, Tanzania, and Uganda met to examine the status and needs of biosafety training and educational programs in East Africa [69].

Thus, educational efforts on all levels are not in vain, and deplorably there are too few academic institutions active in biotechnology education [70]. The structure of the debate has shifted: Today, the GM crop debate is steered by scientific *and* pseudoscientific arguments. And this also includes an element of hope for the pro-scene: Slowly but surely the pseudoscientific arguments are fading away for the opponents, since there is no serious incident known despite the fact that millions of hectares are grown with GM crops worldwide [71].

There is a widespread mistrust against new technologies where everybody feels it will change their own life,

and this often happens in a phase where the benefits are not yet clearly visible, especially for the consumers/users. But it is not correct to reduce those difficulties to an exclusive criticism of the so-called deficit model [72–74] where the people just have to be educated and then they would refrain from negative emotions. A question mark on the exclusive use of the "deficit model" is justified, but surprising conclusions emerge from the above-mentioned critics themselves: They do not discard altogether the traditional deficit model, rather they propose to combine it with the *contextual approach*, thus emphasizing the complex and interacting nature of the knowledge-attitude interface. This highlights the sophistication and value of lay understandings of science that can exist in the absence of formal scientific knowledge [75, 76]. Surprisingly, positive are results of polls which are conducted by Philip Aerni with more closeness to the real life and careful avoiding of polling mistakes [77], the study concludes:

- The results of our discrete choice analysis show that Swiss consumers treat GM foods just like any other type of novel food. We conclude from our findings that consumers tend to appreciate transparency and freedom of choice even if one of the offered product types is labeled as containing a genetically modified ingredient. Retailers should allow consumers to make their own choice and accept the fact that not all people appear to be afraid of GM food. [77]

There is growing consensus that scientific knowledge extends beyond the simple learning of "facts" that can be straightforwardly defined and measured [78]. From this perspective, privileging formal scientific knowledge as the sole basis of rational preference formation leads us to overlook other knowledge domains that may be equal or even more important determinants of attitudes toward science.

These insights have been condensed into a feasible discursive method of the *Systems Approach* initiated by Churchman [79] and refined by Rittel et al. [80–82]. Details on the methodology are given under sections Long Term Discourse and Decision Making Processes and The Second Generation Systems Approach as a New Decision Making Process, where the *solutions* are discussed.

It is an illusion to solve ill-fated GM-disputes by just adding social and cultural aspects, or that the dispute should, so to say, start from the other end of the controversy ignoring the biosafety science [83] or even worse to primarily appeal to feelings and emotions of the public and indulge in entertaining but ultimately meaningless discussions in order to catch the interest of the public – we should not mimic the strategy of the protest corporations. That said, this does not mean that sociocultural aspects including emotions should be neglected – even the boulevard press sends out strong signals for learning processes. Vaughan's [84] plea is that regulatory officials should engage in an interactive process of information and opinion exchange that is reasonable and effective within vastly different socio-economic and cultural contexts, This is often a challenge to government employees concentrating on office work routine. Patricia Osseweijer [85, 86] offers an interesting compromise: a mix of science, ethics, and emotions with her "Three E-Model" Entertainment (getting attention), Emotion (identification), and Education (information and skills for [future] decision making). It has been developed on the basis of long-term experience and observation of public communication by individuals in the Department of Biotechnology of the Delft University of Technology [87, 88].

Despite all possible refinements and enhancements in the dialogue with the public, we should not underestimate the negative role of the opponents of genetic engineering in plant breeding organized as professional protest corporations, see section The Costs and Loss Benefits of Overregulation.

How the Internet is Influencing the Debate The Internet as a worldwide literacy practice environment is still underestimated, nevertheless it has created a new situation in communication, providing a new dynamic field for research and knowledge accumulation [89]. It has created an Internet-based debate culture with all its ramifications from classic email over blogs and better organized social media to twitter and this not only in nanotechnology [90], but also in other research realms and E-business [91]. The evolution in this kind of debate is still going on with unprecedented dynamics and is not yet fully understood in all its consequences [92], [93], and [94]. The hope is that easier communication through the Internet will invite a *collaborative*

instead of *confronting* modus [95]. Some advice on how to behave in chats and blog debates on the Internet might be useful [96]; compare a list of useful websites and databases on biosafety by DeGrassi et al. [97] and [98]. A list of pertinent websites can be expanded ad libitum, the present state of error of 2011, with all the personal bias in [99].

Informatics and the new ease to access huge amounts of scientific information on the Internet causes a democratization effect on the science debate. But this can only then lead to positive developments if the new flood of information is also well organized and provided people make serious efforts to analyze the available information, so that our understanding of complex scientific knowledge can indeed be improved. As Janetzko (2008) shows, it is not enough to make use of the most common search machines, only professionally organized searches and databases on scientific literature can help and create some limited reliability and sustainability of scientific knowledge. And: clearly, the usual citation clusters among opinion-buddies will not suffice. And it should be emphasized: Electronic ease does not replace the tough job of scholarly reading and understanding. It will be a difficult task for the future to divide up clever knowledge accumulation and genuine thinking work among active scientists. A caveat already signaled by Seneca: Thoughtful Action creates more wisdom than knowledge accumulation, can be interpreted related to social electronic networking in two ways: On one side, the immense intensification of social networking via the Internet creates among other things a new possibility for post-publication reviewing and filtering out the really relevant publications and ideas. On the other hand, it hinders systematically the deepening of your own knowledge in an individual way, and be it only by reading every year a dozen or two really relevant book publications.

This major shift from paper to electronics is also creating new methods of *quantitative* analysis of scientific work: see the Scientometrics Wikipedia: http://en.wikipedia.org/wiki/Scientometrics. Actually, this newly emerging science can provide with caveats and insights into changes in research priorities, reveal citation habits, evaluate journals with new scales, etc. [100–103]. A typical example is given in the analysis of the coming and going of the Frankenfood myth [104], with a somewhat surprisingly early and sharp peak of appearances of the word Frankenfood in websites for 1998, followed by a sharp decline to virtually zero 2 years later (Fig. 3).

This figure is confirmed in [104] with the following statements and figures (Figs. 4 and 5):

The comments in [104]:

- Our interpretation of these results is as follows: the decline of the organizing power of the metaphor was rapid in 1999 and 2000 when the metaphors of 'Frankenfood' and 'Frankenstein food' began to be outdated. Due to its generalized meaning, the metaphor was used increasingly across domains and therefore lost its domain-specificity and the ability to organize distinctions among domains. This might also explain why the NGOs stopped using the metaphor in 2000 (HELLSTEN, 2003). From [104]

Scientometrics can do much more, [105] have shown the potential of a sophisticated statistical analysis combined with modeling of community interactions in the web: Besides tracking just the description-to-acquisition behavior of users, scientometrics can do much more by longer observation periods which offers the chance to make richer inferences about both group and individual user intentions – trends of intruding into human behavior and making conclusions, which are actually beyond Orwell's imagination. Yet we should have no illusions, since a lot of work and application is already going on in the marketing and advertisement scene, which has also an often manifested interest in knowledge accumulation methods [106, 107]. It is somehow amazing to realize that the academic world in most fields of specialization have not yet reached the realms of professional knowledge accumulation and consolidation – not to speak about an efficient way of reaching out from knowledge accumulation to efficient development of new technology. Scientometrics would have the potential to get instrumentalized in research and development, with some good chance to be used also in new peer review processes.

A *qualitative* evaluation of science should involve additional elements – see below under peer review in the section Developments in Risk Handling of GM Crops on regulation.

Deplorably, important networks are often only known in specific reader clusters, these awareness gaps

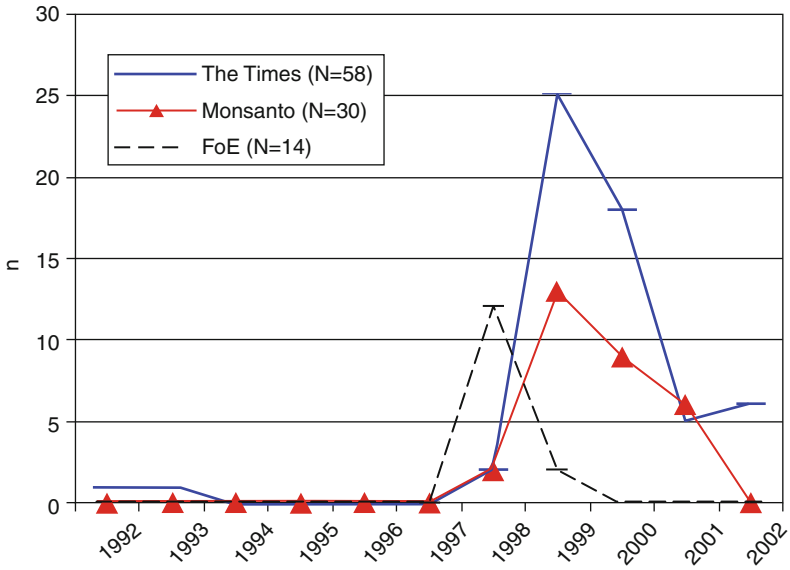

GM Crop Risk Debate, Science and Socioeconomics. Figure 3
Web site pages addressing the "Frankenfood" and "Frankenstein food" issues at Monsanto, the *Times*, and the Friends of the Earth Web sites. jcmc.indiana.edu/vol8/issue4/hellsten.html

should be minimized. We need knowledge exchange, jumping over geographical and ideology fences.

Science Education and New Developments on the Internet In a successful initiative, Ron LaPorte and his group "Supercourse" started in 2002 [108] a new educational Internet-based system: In his view, Journals do not have an exclusive "right" to science. A publication and a scientific presentation do virtually the same thing – they share scientific knowledge. Publication and presentation have been separate but could "morph" into a single entity. This metamorphosis is taking place and is driven by a juggernaut called PowerPoint, Microsoft's graphics and slide presentation software, and today enriched with more media from Twitter over YouTube to all the numerous blog systems, networking enhanced with RSS, etc. More on the Supercourse program in [109–113], also in connection with the Bibliotheca Alexandrina in Egypt: [114] Another possibility on a well-organized collection of Powerpoint slides is offered for free by the University of California by Peggy Lemaux and Barbara Alonso, University of California http://ucbiotech.org/resources/slide_archive/index.html. A series of over 100 slideshows is offered by the bibliography of the author; new slide shows are continuously added, they can be downloaded from [115]. An important new development started 2002 at the Bibliotheca Alexandrina, where a new world center of electronic knowledge is emerging, which is based on thoughtful new structures [116].

On Biosafety Education Biosafety is today a permanent topic on local, national, and international level, and basically, it is good to see educational activity. As demonstrated in this contribution, the topic of biosafety is highly controversial, and so are the views on the various educational activities. The most blatant misunderstandings in biosafety education stem again from the "Genomic Misconception," which forces authors seemingly to focus on transgenic crops alone, which is scientifically unacceptable as we will see in section GM- and Non-GM-crop Differences Overestimated, the "Genomic Misconception". A symptomatic example on the enumeration of risks related to transgenic crops is given by Craig et al. [117]: All risks duly mentioned can be attributed just as well to conventional crops. The only difference between modern and conventional breeds can be found in risk mitigation, which is much easier in the case of the transgenic

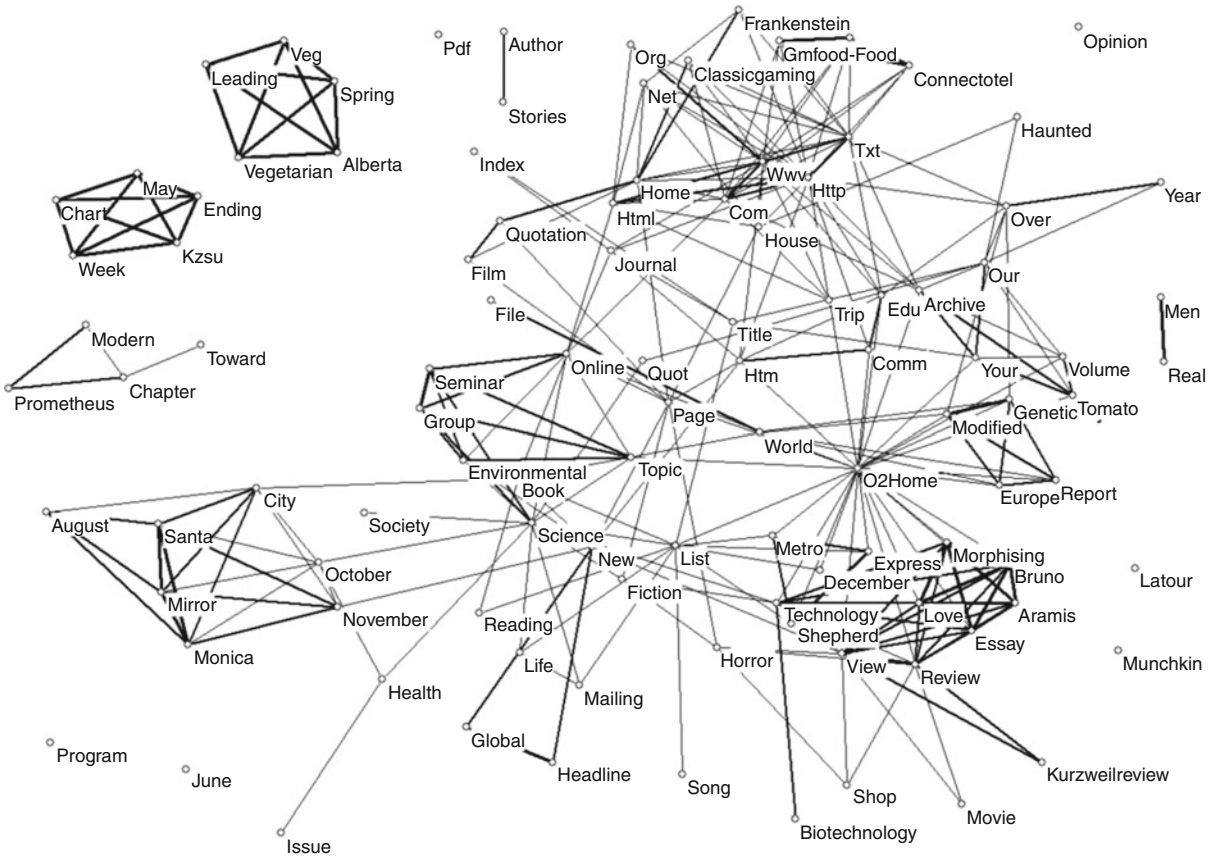

GM Crop Risk Debate, Science and Socioeconomics. Figure 4
The cosine map of 107 words used more than once in the 205 documents on Frankenfoods in 1999 (cosine $\geq$ 0.1) (From [104])

crops. Here, just two recent examples related to the successful prevention of upcoming resistant pest insects (a problem arising in all kinds of agricultural management systems): [63] and [11]. It is deplorable, that most biosafety education is still based on the erroneous "Genomic Misconception," which results automatically into a biosafety risk view focusing on the process of transgenesis instead of working on a product-oriented basis. More about the "Genomic Misconception" is discussed in section GM- and Non-GM-crop Differences Over-estimated, the "Genomic Misconception".

Proposal for a Website of Websites There are simply too many websites (see ASK-FORCE Organization and Related Websites) and not enough coordination, so there is a need for networking structures among the most important websites, a *network of networks* with all the fancy new buttons available like RRS, etc. There should be a place where people see with one glance on the first page what news they can expect on various important sites. It should also not be difficult to add possibilities for an individual choice.

Those website connection activities need professional support with some secretarial/managerial help. We must work out ways in which the broad public can easily reach rebuttals on all the myths, facts, and benefits in the debate on green biotechnology. It will not be difficult to establish a platform for a better communication among the most important websites – in the field of agricultural biotechnology, there are a few very successful ones, but this is not the whole task.

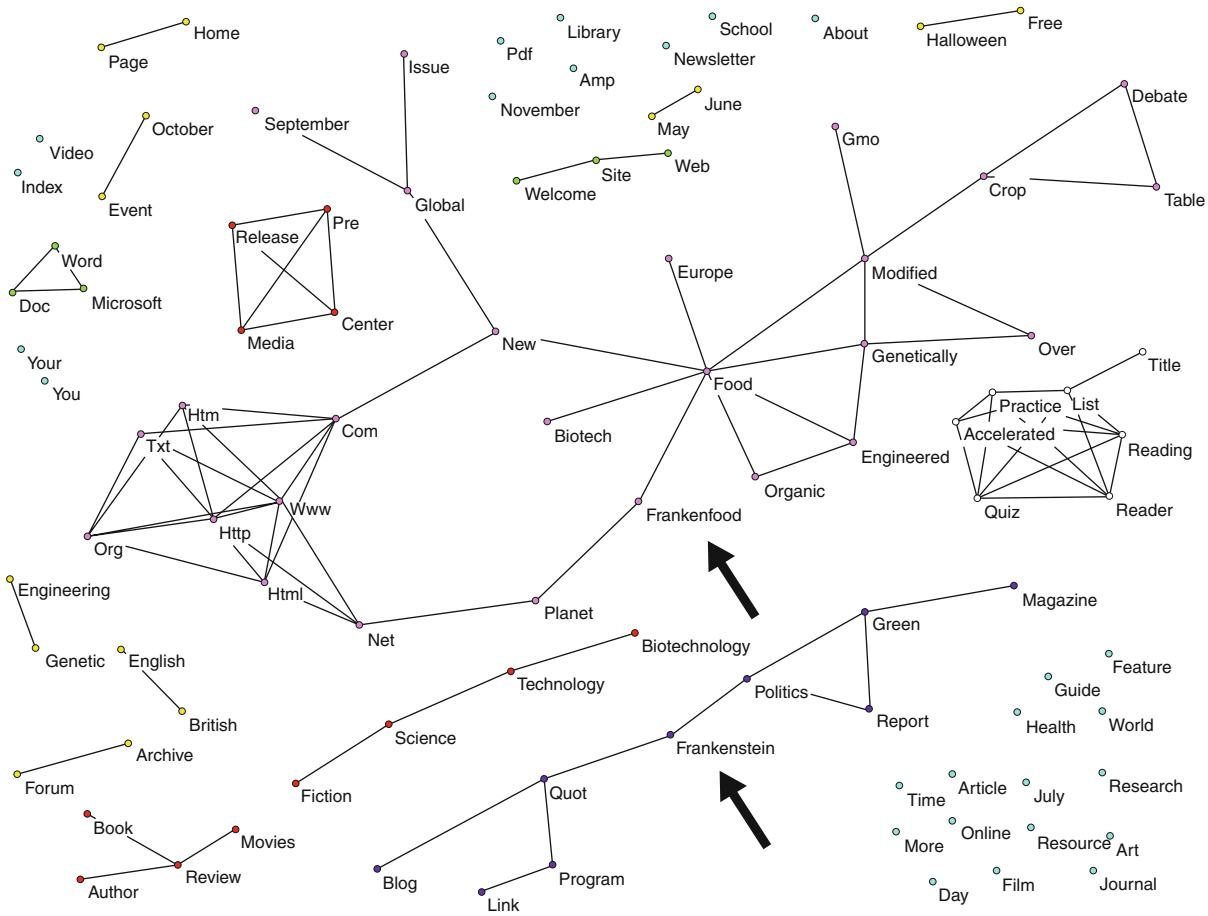

GM Crop Risk Debate, Science and Socioeconomics. Figure 5
The cosine map of 100 words used more than 31 times in the 6,101 documents on Frankenfoods in 2003 (cosine $\geq$ 0.1) (From [104])

We need to look deeper into the theory of networks in order to be really successful; comprehensive reviews demonstrate how complex the networking task really is [118, 119].

As of now, this is just an idea and needs to be discussed with Internet and website specialists. One of the main difficulties will be to establish permanent existence, this is why it would be best to use structures having proofed long years' activities and assured permanence, such as ISAAA, the International Service for the acquisition of Agri-Biotech Applications, www.isaaa.org. After all, the leading webmasters and coordinators agree that it is time to *enhance collaboration through better communication*, see section ASK-FORCE Organization and Related Websites. ASK-FORCE. The task on uniting the most relevant websites and blogs should not be underestimated, see the list already given above [99].

Developments in Risk Handling of GM Crops

General Views on the Dialogue Related to Regulation of GM Crops

The dialogue between scientists and regulators is very complex, as accurately described by Saner [120]. This should be a reminder that it is not about facts alone:

- It should be clear without explanation that each and every rational decision is a combination of facts and values – a decision requires judgment. The agents of judgment are, of course, people, and this leads us to an

entirely different interface – that between scientists and policy-makers.

We should keep this in mind when we concentrate here on the *science* of GM crop regulation. See also the analysis of the debate in The General Strategic Situation of the Debate About Green Biotechnology Today. These philosophical thoughts of Saner are at the basis of the discursive methodology for complex decision-making processes, [121–123]. For details, see below in this contribution in sections Long Term Discourse and Decision Making Processes and The Second Generation Systems Approach as a New Decision Making Process.

A valid overview on the regulatory science and traceability related to GM crops has been published by Gasson and Burke [124, 125], there is no intention to repeat these reviews.

Biotechnology and Economics

How Economics Are Influencing the GM Crop Debate The example of the Flavr Savr Tomato demonstrates that in earlier times, even in Europe, GM food was well received, but several factors just made it clear that economic success was missing [8, 126–128]. And regulation of this pioneer work needs to get a new look; with modern screening methods, the gene silencing on the molecular level revealed some surprises [129].

Economics play a very important role in the process of technology acceptance: This can be illustrated with the present day feed import situation in Europe. First it should be mentioned, that it is the trade policy of Europe still going the wrong way, which causes a lot of difficulties in the transatlantic dialogue: As Graff et al. [130] explain:

> ▶ European policies blocking genetically engineered crops are conventionally attributed to the concerns of European consumers, but they can be attributed to the self-interests of European industry and farmers as well. Biotech policies maintained in the name of consumer interests are helping European chemical firms to slow their losses in the global crop protection market and are helping European farmers differentiate their conventional crops on environmental and safety grounds, maintain their agricultural subsidies and win new non-tariff trade protections.

The recent development in feed supplies, see Lawrence in *The Guardian* [131], in the EU provides argument, and the reports and letters below give excellent examples:

- Food Chain Dossier 2009: http://www.botanischergarten.ch/Feed/Food-Feed-Chain-Dossier-20090616.pdf
- DG AGRI feed report: http://www.botanischergarten.ch/Feed/EC-DG-AGRI-Rep-feed-situation-UnapprovedGMOs-200709.pdf
- EU Report on Pipeline: http://www.botanischergarten.ch/Feed/Stein-EU-Report-GMO pipeline-LLP-2009.pdf
- Letter to the President of the EU Commission Barroso: http://www.botanischergarten.ch/Feed/Letter-big-Producers-Tolerance-Value-Barroso-20090624.pdf

Strict labeling and thus a discrimination of European meat from animals fed with GM crops will soon be impossible as a political goal due to *economic* reasons – as it is also scientifically not justifiable [132, 133].

An interesting thesis with economic arguments is promoted by Paarlberg [134]: Today, Africa's production of GM crops is exported mainly to other African countries, and this might go on this way in the coming years, so the reasoning that Africans would destroy export opportunities to Europe by developing their own GM crops is not really convincing. But in reality, there is growing concern: Commercial fear over potential loss of export sales to Europe and East Asia is also a reason for mounting pressure on biosafety approvals in developing countries. Consumer misgivings toward GM food in rich countries combined with restrictive import and labeling policies are prompting GM-free agricultural production in developing countries. The long-term costs of these negative trends could be enormous [135]. Good arguments for this view are produced with lots of facts on economics and negative labeling effects of European developed countries, published by Gruère et al. [136–138]:

> ▶ In this context, the marketing decision of avoiding GM ingredients in food items rapidly became a quality attribute employed in the competition among the retails chains of Europe, Japan and South Korea. A report by the international NGO, Greenpeace, which

has encouraged companies to adopt GMfree policies, provides evidence of the widespread adoption of such practices in Europe [139] as follows:

- Fourteen of these retailers have a policy of not selling GM-branded products under their company name for all European countries. These include Carrefour, Auchan, Sainsbury's, Safeway, Marks & Spencer, Coop Switzerland, Coop Italia, Migros, Big Food Group, Somerfield, Morrison's, Kesko, Boots, and Co-op UK.
- Seven of these retailers have a non-GM policy for their own branded products for their main markets (mainly in their home countries). These include Tesco, Rewe, Metro Group, Casino, Edeka, Schwarz group, Tengelmann).
- Out of the top 30 European food and drink producers, 22 have a non-GM commitment in Europe, including Nestle, Unilever, Coca Cola, Diageo, Kraft Foods (Altria), Masterfoods (Mars), Heineken, Barilla, Carlsberg, Dr. Oetker, Arla Foods, InBev (Interbrew), Heinz, Chiquita, Cirio del Monte, Orkla, Ferrero, Northern Foods, Eckes Granini, Bonduelle, Kellogg and McCain.
- Thirteen of these 22 multinationals have a company-wide non-GM policy beyond Europe. These include Diageo, Heineken, Barilla, Carlsberg, Arla Foods, Dr. Oetker, Chiquita, Cirio del Monte, Orkla, Ferrero, Northern Foods, Eckes Granini, and Bonduelle [138].

Some companies even go beyond banning processed products derived from GM ingredients to include requirements on GM-free animal feed in animal products. Virtually all supermarkets sell only poultry fed with non-GM feeds, whereas the policies for dairy products, beef, and pork vary. The usual crude Greenpeace mix of facts and interpretation helped efficiently to push the companies for the European market to go GM crop free [139, 140]. The simple fact of labeling allows opponent NGOs to drive a polemic campaign of pompous "contamination" reports, thus delivering junk science "evidence" that there is some risk involved in the numerous events of minute admixtures of transgenes traces.

In India, there is a clear positive trend visible since some years after some difficulties in the beginning because local traits had to be created for the many Indian regions and also because there was right from the beginning a black market with illegal cotton traits developing (which often did better commercially than the legal ones. Presently, there are 38 traits of GM cotton in India [141].

The whole complex story has been recently summarized by [142]:

- On average, Bt-adopting farmers **realize pesticide reductions of roughly 40%, and yield advantages of 30-40%. Profit gains are at a magnitude of US $60 per acre**. These benefits have been sustainable over time. Farmers' satisfaction is reflected in a high willingness to pay for Bt seeds. Nonetheless, in 2006 Indian state governments decided to establish price caps at levels much lower than what companies had charged before. This intervention has further increased farmers' profits, but the impact on aggregate Bt adoption was relatively small. Price controls might have negative long-term implications, as they can severely hamper private sector incentives to invest in new technology. [142]

At the end of the day the profitability of Bt cotton is now uncontested, see comments of Müller-Jung Frankfurter Allgemeine: [143]

Also the old wrong connection between suicides of Indian farmers and the introduction of GM cotton in India has been thoroughly falsified [144, 145]. This does not hinder activists like Vandana Shiva from continuing with cheap propaganda linking GM crops with the sad tradition of farmers' suicides in India, which started decades before the introduction of GM crops and beginning activities of multinational seed companies. Here are two of the many graphs from [145] (Figs. 6 and 7):

- **Abstract.** Bt cotton is accused of being responsible for an increase of farmer suicides in India. In this article, we provide a comprehensive review of evidence on Bt cotton and farmer suicides. Available data show no evidence of a 'resurgence' of farmer suicides. Moreover, Bt cotton technology has been very effective overall in India. Nevertheless, in specific districts and years, Bt cotton may have indirectly contributed to farmer indebtedness, leading to suicides, but its failure was mainly the result of the context or environment in which it was planted [145].

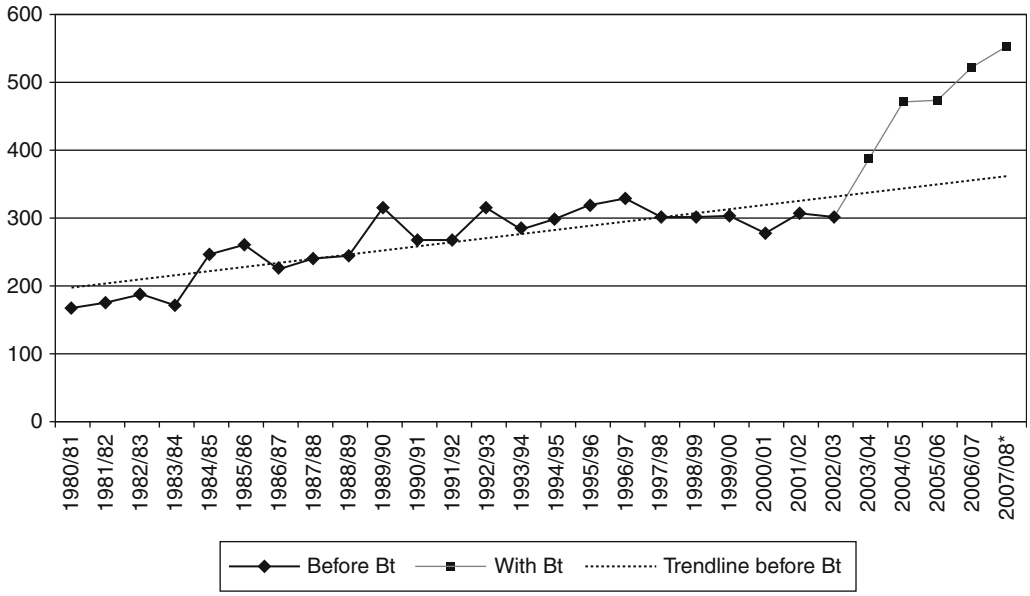

GM Crop Risk Debate, Science and Socioeconomics. Figure 6

Average cotton yields in India (kg/ha), 1980–2007 (Source: International Cotton Advisory Committee (2008). Note: Data for 2007/2008 is an estimate. From [145])

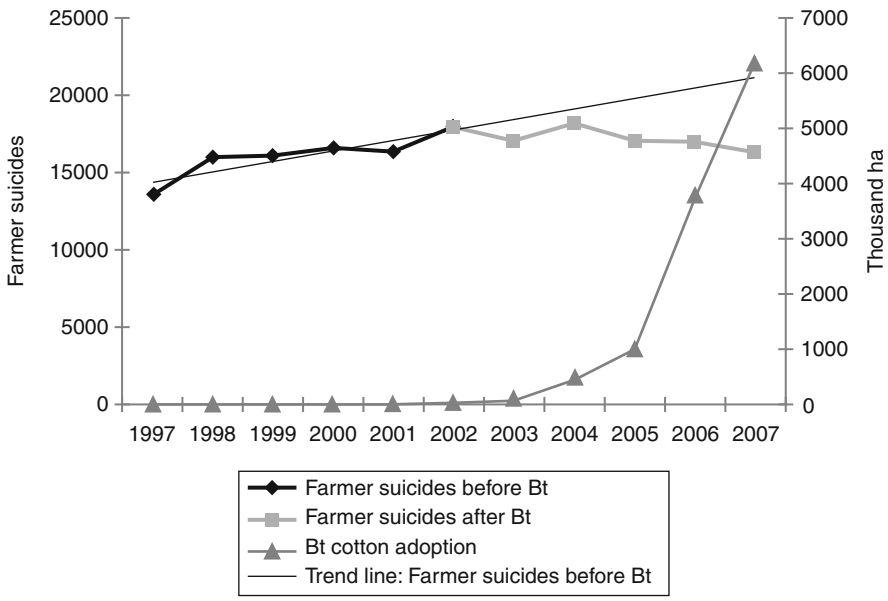

GM Crop Risk Debate, Science and Socioeconomics. Figure 7

Farmer suicides and Bt cotton area in India, 1997–2007 (Source: Combined data from Table 1 and Table 2. From [145])

- **From the discussions.** The absence of irrigation systems in drought-prone areas (especially in Maharashtra), combined with specialisation in high-cost crops, low market and support prices, and the absence or failure of the credit system, is a clear recipe for failure. It is possible, therefore, that under the conditions in which it was introduced, Bt cotton, an expensive technology that has been poorly explained, often misused and initially available in only a few varieties, might have played a role in the overall indebtedness of certain farmers in some of the suicide-prone areas of these two states, particularly in its initial years. But none of these possible links has been explicitly demonstrated with a sufficiently robust analysis. One implication of this study is the critical need to distinguish the effect of Bt cotton as a technology from the context in which it was introduced. Revealed preferences based on farmer adoption rates and official or unofficial data all point toward the overall success it has had in controlling pest damage and therefore raising average yields in India. In particular, the increasing adoption rate in two suicide-prone states, Andhra Pradesh and Maharashtra, indicates that farmers in these states found this technology economically beneficial.

  In contrast, marketing constraints and institutional issues may have played a significant role. Our analysis suggests the need for a better extension system, more controlled seed marketing system, anti-fraud enforcement and better information dissemination among farmers in all regions, before the introduction of any costly new technologies like Bt cotton. Farmers should also be encouraged to diversify their farming and non-farming activities to spread the risks they may incur.

  The second implication is that, as farmer suicides are not new or specific to recent cases or to the introduction of Bt cotton, they point toward the failure of the socioeconomic environment and institutional settings in rural dry areas of India. This has nothing to do with cotton or the use of new technology and would suggest many potential policy changes. In several states, such as Karnataka and Andhra Pradesh, some policy changes have already been proposed. Lastly, much more and better federal and state investment could help prevent the 80 percent or more other cases of suicides.

This does not hinder activists like Vandana Shiva from proclaiming Indian farmers' suicides to be the fault of international corporations: [146] and lately also at a Barilla webinar July 20, 2011 in Milano: http://www.barillacfn.com/en/biotecnologie, she also does not shy away from connecting the sad tradition of farmers suicides in India with the emergence of GM crops, despite hard facts as demonstrated above. In the same picture you can see her pompous literature list she gives in her curriculum of "over 300 scientific publications in important journals" – a quick test in the comprehensive database of the Web of Knowledge http://apps.isiknowledge.com/ reveals some 47 papers, most of them in less important journals and magazines – so much about her scientific achievements.

A new perspective is open since 2006 for the production of cotton seed (oil for human consumption), seed meal for feed, made possible thanks to the detoxification (gossypol) successfully done by modern breeding including genetic engineering [147], see the latest summary on the matter (Fig. 8) [148]:

This latest development will open new doors for the cotton production and marketing.

The Political Economy of Biosafety Regulation in Agriculture An in-depth analysis of how politics is influenced by multiple factors of discursive processes, influenced by economics, has been developed by Graff et al. [149]. They are giving highly differentiated insights in the network of self-interests with some interesting examples of units influencing in their own interest the debate on GM crops: opponents of genetically engineered crops and also industrial units fearing losses in pesticide sales. Often these important socioeconomic elements in the regulatory debate are neglected and it seems to be difficult for all the regulatory analysis to bring together socioeconomic *and* molecular plant breeding aspects.

- This article develops a political-economy framework to analyze the formation of agricultural biotechnology policies. Going beyond accounts, that largely attribute differences between US and European regulatory environments to consumer attitudes, we consider the impact of what amounts to a Schumpeterian process of "creative destruction" across the entire range of relevant economic sectors and interests. **The analysis**

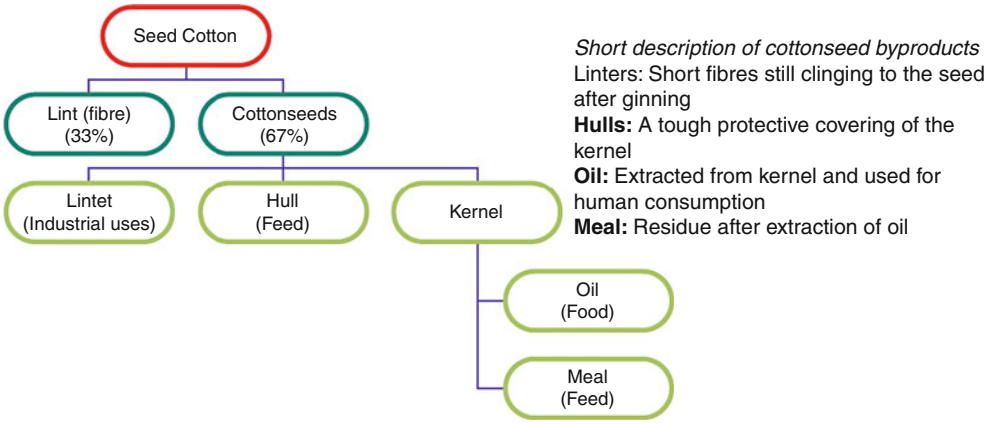

GM Crop Risk Debate, Science and Socioeconomics. Figure 8
Cotton seed byproducts (From [148])

> **suggests that in Europe and in some developing countries a "strange bedfellows" constellation of concentrated economic interests (including incumbent agrochemical manufacturers, certain farm groups, and environmental protest activists)** act in rational self-interest to negatively characterize GM technology in the public arena and to seek regulations that block or slow its introduction. In contrast, those interests most likely to experience welfare gains from biotechnology are the more diffused and less informed – including consumers and small farmers. The most profound implications of overregulation of agricultural biotechnology are (1) delays in the global diffusion of proven technologies, resulting in a lower rate of growth in the global food supply and higher food prices, and (2) disincentives for investing in further R&D, resulting in a slowdown in innovation of second generation technologies anticipated to introduce broad consumer and environmental benefits." [149]

Ayal and Hochman [150], started in some intricate experimental setups working on the cognitive processes underlying choice behavior. With a mix of behavioral actions combined with opinion polls they found that people *do not rely on limited arguments only, but tend to integrate all acquired information into their choice processes*. This could explain the delay in such opinion finding and decision-making processes influencing politics over years, described in the Gartner hype cycles, see The General Strategic Situation of the Debate About Green Biotechnology Today.

Although this would be an epic theme, we shall concentrate here more on the debate of the *Science* of regulation and some discursive elements.

Brazil, A Case Where Politics Positively Influences the Development and Adoption of GM Crops

Studying the biosafety law of Brazil, the similarities with the European legislation cannot be overlooked: Both legislations are process-oriented and obey strict rules on biosafety assessment, including field experimentation:

A closer look at the Brazilian legislation [151] shows the similarities to the European legislation.

- Article 3. Under this Law, it shall be considered:
  V – genetically modified organism – GMOs: an organism the genetic material of which – DNA/RNA has been modified by any genetic engineering technique;

And compare some exclusion rules, typically reducing the safety assessments strictly to the process of genetic engineering.

- Article 4. This Law is not applicable when a genetic modification results from the following techniques, provided they do not imply in using a GMO as the receiver or donator:
  I – mutagenesis;
  I – the formation and use of animal hybridome somatic cells;
  III – cellular fusion, including plant cells protoplasm, which can be produced from traditional culture methods;

IV – the self-cloning of naturally processed non-pathogenic organisms.

The same is the case in the European law:

[152], in the introduction the definition of GMOs is given:

- In order to protect human and animal health, food and feed consisting of, containing or produced from genetically modified organisms (hereinafter referred to as genetically modified food and feed) should undergo a safety assessment through a Community procedure before being placed on the market within the Community.

The intention of this "exclusive" definition is clear in this European Law: it should be restricted to GMOs which are wrongly defined as "genetically modified crops," a scientifically questionable denomination, since in the strict sense of modern genomic science this means to include all crops and horticultural traits having been modified also by conventional breeding. This kind of now false but routine denomination is a symbol for the disregard of proper science in regulation.

A further comparison demonstrates that legislations in Europe and Brazil are both rather strict, the decisive difference is that in Brazil there are clear (political) decision-making rules, whereas these are lacking in Europe. Until lately, the decisions were depending on majority voting rules of the European states, and this caused a lot of confusion and an almost complete stall in decision-making. This is why Commissioner Dalli [153], in July 2010 opened a debate on delegating some important decisions to the national level: Comments from http://www.gmo-compass.org/eng/news/523.docu.html

- (13 July 2010) As expected, the EU Commission decided on 13.07.2010 changes in the legal regulation of green biotechnology. Accordingly, Member States should be able to prohibit the cultivation of genetically modified (GM) crops that have been approved EU-wide. As the next step, the EU Parliament and Council of Ministers must agree.

The outcome will again depend on complex negotiations and it is not sure whether Commissioner Dalli and the EU will come to concrete legislative results. And, except for some modest GMO corn cultivation in Spain, the present day acreage of GM cultivars remains disappointingly low [154].

In contrast to the complex and stalled situation on European GMOs, the case in Brazil documents in the last few years successful regulation of GMOs: Recent reports document steadily growing acres on GMO crops in Brazil: [155, 156]

- The 1st survey on agribiotechnology in Brazi l for the 2010/11 growing season showed there was a substantial growth in the adoption rate of biotech soybeans, corn, and cot ton. The Brazilian farmers are expected to plant 17.2 million hectares with GM soybean cultivars, or 75.6% of the total harvested surface, in 2010/11.

For a general survey of the Brazilian situation, see the recent publication of Mendonca-Hagler et al. [157], where a clearly optimistic picture is developed. The abstract reads:

- Biotechnology is a Brazilian priority, and has been recognized for its potential to promote sustainable development. The Government recently announced an ambitious program for Science and Technology, which includes strategies to develop modern biotechnology, continuing three decades of public investments on capacity building and infrastructure, aimed principally at the development of technologies applied to health, agriculture and the environment (MCT 2008 http://www.mct.gov.br/). Research initiatives have focused on genomics, proteomics, genetically modified organisms (GMOs), gene therapy, stem cells, bio-fuels and nanotechnology, among other biotechnological topics. Research projects in Brazil have been mainly developed in public universities and institutions funded by federal and state agencies, with a minor participation from the private sector [158]. Genomics, an area of considerable success in the country, was launched a decade ago by S. Paulo State Research Foundation (FAPESP), with the organization of a virtual institute, called ONSA, comprising several laboratories with the main task of sequencing the genome of the citrus pathogenic bacterium Xylella fastidiosa [159, 160].

  The success of this genomic network stimulated biotechnology startup companies and projects with

the focus on other genomes, such as sugarcane and coffee, including functional genomics and proteomics. Following in the footsteps of the ONSA network, the Ministry of Science and Technology created a National Genome Project Consortium involving institutions located in the major regions of the country, with the task of sequencing eight microbial and two plant genomes. Recently, they concluded the sequence of Chromobacterium violaceum, a bacterium with exploitable properties, such as the ability to produce a bactericidal purple pigment (violacein) and bioplastics [161]. Later on, several states launched their own genome programs. A group from Rio de Janeiro, part of the Riogene network, recently sequenced the genome of the nitrogen-fixing bacterium Gluconoacetobacter diazotrophicus, a sugarcane endophyte involved in enhancing growth of large crops without the addition of nitrogen fertilizer [162, 163], see also the websites of EMBRAPA http://www.embrapa.br/english and the Ministerio Biotecnologia e Tecnologia http://www.mct.gov.br/.

Agriculture plays an important role in the Brazilian economy, being responsible for ca. 40% of the exports and employing 20% of the active work force. About one third of the Brazilian GDP comes from agribusiness. Traditionally, this country has been competitive in tropical agriculture, supported by strong research programs on conventional and modern technologies. Intense capacity building initiatives resulted in the formation of a critical mass of scientists working in molecular biology and agricultural sciences [158]. Despite these favorable factors, the adoption of GM crops has been delayed due to intense opposition organized by environmental groups and additional difficulties resulting from a conflicting regulatory framework. In this overview, we address the current status of Brazilian biosafety legislation, and discuss the perspectives for the development of molecular biotechnology in Brazil.

This view is confirmed in a recent editorial in *Nature*, [164], interestingly enough with the same emphasis as above on gene sequencing projects which are the basis of independent biotechnological research and development in Brazil.

Also, the latest success of approving regulatory decisions is symptomatic of the positive biotech climate in Brazil: The first fully developed transgenic crop in Brazil has been approved for commercialization, published in 2007: [165]. The press release of the president of AnBio (National Biosafety Association) Leila Oda emphasizes also the socioeconomic importance of this approval: [166].

Without going into a survey on the Brazilian opponent's activities and reports in detail, here just a typical example published by a medical group (not linked in any way with environmental toxicology) [167] on how science is distorted in order to make a negative and totally unfounded point against glyphosate is given. This paper produces negative toxicological effects on clearly doubtful experimental scenarios: experimental Xenopus frog embryos were *injected* with glyphosate, as mentioned in the introduction.

- We show here that sublethal doses are sufficient to induce reproducible malformations in Xenopus and chicken embryos treated with a 1/5000 dilution of a GBH formulation (equivalent to 430 μM of glyphosate) or in frog embryos **injected with glyphosate alone (between 8 and 12 μM per injected cell).** GBH treated or glyphosate injected frog embryos showed very similar phenotypes, including shortening of the trunk, cephalic reduction, microphthalmy, cyclopia, reduction of the neural crest territory at neurula stages, and craniofacial malformations at tadpole stages.

This absurd experiment methodology contradicts all internationally agreed rules on environmental toxicology testing, as described and cited in detail in [168].

But opponents are well organized on an international level, and promptly, the Paganelli paper is cited in many of those reports, here is just one example: [169]. In this extensive report, dozens of papers are cited which do not match the high quality standards of biosafety science; they are cited because they produce negative results related to modern soybean agriculture. The following is an example on how the authors do not even shy away from distorted reporting of published results.

- Very few studies directly examine the effects of GM foods on humans. However, two studies examining possible impacts of GM RR soy on human health found potential problems.

  Simulated digestion trials show that GM DNA in GM RR soy can survive passage through the small intestine

and would therefore be available for uptake by the intestinal bacteria or cells [170]. Another study showed that GM DNA from RR soy had transferred to intestinal bacteria before the experiment began and continued to be biologically active [171]. These studies were not followed up. GM proponents often claim that GM DNA in food is broken down and inactivated in the digestive tract. These studies show that this is false.

Actually, if you read the above Newcastle study properly, you notice that the GM DNA is completely decomposed in the colon, the only traces measurable were found in fresh, undigested stomach probes of human ileostomy patients. Reading the summary alone shows the blatant incorrectness of the comments. Two previous studies, after careful reading, reveal the same results [170, 172]. The conclusion therefore is that the interpretation of [169] is false, as confirmed in the latest publication of the Newcastle research team:

- The transgene did not survive the gastro-intestinal tract of human subjects fed GM soya.

A recently published paper of Zhang is seen as a breakthrough in our knowledge on interkingdom relations between plant and animal genomics: [173]. First data, obtained with modern genomic analysis, demonstrate the surprising finding that exogenous plant miRNAs are present in the sera and tissues of various animals and that these exogenous plant miRNAs are primarily acquired orally, through food intake. MIR168a is abundant in rice and is one of the most highly enriched exogenous plant miRNAs in the sera of Chinese subjects. In addition, these findings demonstrate that exogenous plant miRNAs in food can regulate the expression of specific target genes in mammals.

This could lead to erroneous conclusions that horizontal gene transfer is possible also for the antibiotic resistance genes and even for genes expressing Bt toxins into mammals and humans, and one can see already that opponents to genetic engineering take advantage of the news by clear misinterpretation of the results: They use it as an argument for the unforeseen risks of the technology. See the comments of anonymous scientists in GMwatch [174]:

- The study is yet another nail in the coffin of the already discredited 'safety assessment' process for GM foods in the EU and elsewhere. These assessments do not consider the effects described.

This rather naive statement is typical of the thinking of GM crop opponents: Firstly, they mix up in an unscientific way various categories of transgenes; secondly, they mix up scientific progress and the inevitable adaptation of risk assessment methodology with the present day regulatory rules in place in the laboratories. It is a matter of simple scientific consensus that biosafety assessment has to adapt in methodology with the progress of genetic engineering: on one side, Zink-Finger and TALES methods (details see Zinc Finger Targeted Insertion of Transgenes and TALEs: Transformation Method Transcription Activator-like Family of Type III Effectors.) with all their precision and elegance are prone to simplified risk assessments after detailed studies. On the other hand, technologies using small RNA molecules will undoubtedly force risk assessment researchers to adapt to appropriate methods of analysis, as already proposed by [175]:

- In the future, the predictive ERA process will need to be flexible and adaptable for analysis of the next generation of crops engineered using RNAi and HD-RNAi. As a first step, regulatory agencies and risk analysts need to become familiar with the science of RNAi and its application to plant biotechnology. A concerted effort is needed to develop a pool of expertise to ask the right questions about potential hazards and exposures, to ensure that relevant data are collected and to characterize uncertainty in risk assessments.

  Regulators will have to evaluate the design and implementation of research protocols for laboratory experiments and confined experimental field trials. Scientific questions will need to be answered about off-target effects, non-target effects and the impact of genetic mutations and polymorphisms. Understanding the stability, persistence and half-life of small RNAs in various aquatic and terrestrial ecosystems will be essential for the characterization of exposure pathways. New diagnostic tools will probably be required for the identification and quantification of small RNAs for a range of purposes, including crop identity preservation, monitoring and segregation. Ideally, these tools should have a low detection limit and a high degree of specificity for each RNAi crop, while being relatively inexpensive, functional under field conditions and

operable by individuals with diverse backgrounds and training. With all this in mind, it should be possible for stakeholders, regulators and citizens to develop policies and ERA frameworks for RNAi and HD-RNAi crops. [175]

It is correct that small RNA molecules are considered and used for GM plant improvements, as suggested by [175]. And it is also correct that the risk assessment of GM crops up to now does not specifically include the effects described by Zhang et al., that is, that small miRNAs are obviously passing mammal stomach environments and can be integrated in the organism and even be active genetically. This seems to be routine in the evolution of life (and undoubtedly calls for verification and further studies). And the question arises whether we should *automatically* include in the risk assessment small miRNAs, the answer should be *no*: rather it should be another reason to switch European and UN-Risk assessment to product-oriented mood, following the conclusions drawn in the section on the GM- and Non-GM-crop Differences Overestimated, the "Genomic Misconception".

The above examples of misleading statements and publications of the opponents lead in a logical way to the following section on the quality of scientific papers:

Peer Review in the Biosafety Science Debate on Regulation

Before we start talking about regulation, a word on the science debate shall precede, which depends on the process of peer review, but it may be flawed in many ways, although there is no real good alternative in sight, despite some attempts to change this situation like the proposal to involve respected science journalists. But there are objections: journalists might become part of the system [176] and give up indirectly their strict impartiality and neutrality – which is, maybe, anyway an illusion. Or it might be that they may simply not have the scientific expertise as demonstrated recently in a contribution of a science journalist in Nature [177], extensive critical comments in ASK-FORCE contribution on the Rosi-Marshall publication on aquatic insects, see [178] (more comments about this study are given below). It should also be admitted, that a fresh look of a "greenhorn" might reveal new aspects of the GMO battle.

The quality of biotechnological research is also influenced by the research environment offered to students and is evaluated in a differentiated way for Europe by Reiss et al. [179]. Peer review is a very fragile instrument and needs constant inquiry, as demonstrated also on the Wikipedia website on the subject of peer review http://en.wikipedia.org/wiki/Peer_review. It should also be seriously considered that the present day peer review system is basically "faith based," as described with convincing details by [180].

A trend toward a magazine style is documented for some important journals as *Nature* and others. The facts show that the percentage of externally peer-reviewed articles has dropped dramatically. Facts will be given in a forthcoming publication of R. Laporte, F. Linkov, and K. Ammann.

We should also include a new element in the reviews and evaluation of science as proposed by Lubchenco [181]: the scientific community should formulate a new *Social Contract for science*.

- This contract would more adequately address the problems of the coming century than does our current scientific enterprise. The contract should be predicated upon the assumptions that scientists will (1) address the most urgent needs of society, in proportion to their importance; (2) communicate their knowledge and understanding widely in order to inform decisions of individuals and institutions; and (3) exercise good judgment, wisdom, and humility. The paper concentrates, according to the zeitgeist of the publication date, too much on environmental issues alone, today we should put into the center of our science strategy debates **humanity as a whole – and this means to take care of the most urgent needs, namely to work on the eradication of hunger**.

However, this process should not be mollified on the costs of hard science. The line between science and pseudoscience is often difficult to draw.

An interesting new aspect has been introduced by the Supercourse Group with Faina Linkov and Ron LaPorte: [182]. It is true that quality control of Internet texts need rethinking, and it is also important to analyze in a critical way peer review of print material: Their comments can be summarized as follows: High-quality, Internet-distributed lectures are not basically different

from written science publications, they also must be documented and references properly. A further element could be a method of quality management introduced originally for the industry by Edwards Deming Wikipedia of Edward Deming http://en.wikipedia.org/wiki/W._Edwards_Deming, who very successfully taught management and quality control also in Japan in the 1950s.

Two more initiatives should be mentioned here, they can be summarized under a kind of *post-publication peer review.*

Faculty of 1,000 System With a total of nearly 84,000 articles reviewed by May 2011, the system has accumulated an important body of comments, see http://f1000.com/, the comments, although really critical sentences are not foreseen, the system is now linked to The Scientist and provides helpful orientation about important publications. Some examples have been evaluated by the author [183].

Frontiers of Science Frontiers of Science has been developed over 2 years in consultation with scientists and other faculty, as well as with students and postdoctoral fellows, to address manifest intellectual, logistical, and pedagogical issues, see http://www.sciencecore.columbia.edu/s2.html and http://www.fos-online.org/

Declaration of a New Global Business Ethos as a Barrier Against Undue Influence on the Publication Policy of Scientific Journals On October 6, 2009, Hans Küng, Josef Wieland and Klaus Leisinger presented the Declaration of a NEW GLOBAL BUSINESS ETHOS at the United Nations in New York http://www.novartisstiftung.org/platform/content/element/3177/Newsletter_3-09_2.pdf.

Although coming from a pharmaceutical company like Novartis, multinational seed companies will (or should) most likely join. Such efforts are important, because there is a constant pressure of undue influence on scientific papers, although resisted successfully by most researchers, but the influence of multinational (in this case pharmaceutical) companies can be hidden but nevertheless powerful:

An example of such influence by units sponsoring scientific journals has popped up in Australia: See the debate around the withdrawal of six Australia-based Elsevier "fake" journals sponsored by the pharmaceutical industry, see the statement of Elsevier's CEO Michael Hansen [184] and [185–187]. This kind of influence might still be under control, and peer review is usually functioning in an unbiased way – but the difficulties are deep-rooted, and it is a constant fight for quality, as is summarized comprehensively by Scott [188].

It is a cheap and intellectually intolerable slogan of opponents of genetic engineering in agriculture when they discredit researchers for their relationships with industry, since the great majority of researchers all over the world act as independent persons, although sometimes also funded by industry. The sole quality criteria on science are transparency in applied methods agreed upon by the science community and the reproducibility of the data. For more details see section More on the Quality of Scientific Publications.

In the "dangerous" waters of corporate influence, we need renewed efforts of scientometric analysis, as given earlier in a report of bio-era: [189]. The top part of table 5 reveals the few really successful seed companies in relation to the top universities with agricultural research regarding R&D (Fig. 9):

The calculation rules for the table below:

- The four R&D measures are weighted equally. For example, having 10% of industry patents is just as significant as having 10% of commercialized products. Share of industry R&D output = (share of industry patents + share of industry patent citations + share of industry field trials + share of industry commercialized products)/4 [189].

More on the Quality of Scientific Publications Coming back to the peer review on the quality of scientific papers, all the above statements do not mean to say goodbye to the factual and methodological scrutiny per se – even after a paper is already published. With a focus on the GM food safety research Chassy and Parrott [168] summarize the criterions on how to judge whether a food study is believable or not: (a) Making sure the samples tested are comparable samples. (b) Testing composition to make sure the tests and controls are comparable. (c) The need for an acceptable balanced and nutritious diet. (d) Why the dose is important. (e) What statistics do and do not tell us.

The top 35 R&D orgnizations in agricultural biotechnology

RANK	PARENT ORGANIZATION	SHARE OF INDUSTRY R&D OUTPUT
1.	Monsanto	29.82%
2.	Du Pont / Pioneer	10.98%
3.	Bayer / Aventis	10.14%
4.	Dow	5.81%
5.	Syngenta	5.80%
6.	Savia / Seminis	2.57%
7.	USDA	2.38%
8.	BASF	1.71%
9.	Cornell University	1.25%
10.	Stine Seed Farm Inc	1.15%
11.	Florigene	1.08%
12.	University of California	1.05%
13.	Exelixis	0.98%
14.	Iowa State University	0.91%
15.	Rutgers University	0.83%
16.	University of Guelph	0.79%

GM Crop Risk Debate, Science and Socioeconomics. Figure 9

Table 5, upper part, with a ranking of biotech companies and universities in the USA, from [189], calculation rules above

(f) The importance of peer review and scientific publication. (g) Guidelines for dealing with conflicting information. (h) Ethical considerations. A very important additional point is emphasized by Kostoff [190]: "Multiple technical experts should average out individual bias and subjectivity." Two blatant examples of lack of peer review properly done are, among others, discussed in ASK-FORCE (with some additions related to recent publications, all cited in the renewed blog:

- The case of Bt endotoxins supposedly affecting aquatic organisms by Rosi-Marshall et al. [191]

  See comments in ASK-FORCE blog No. 3 on Rosi-Marshall et al. 2007b: [178] (including also the latest publications of [192]. The study has been criticized heavily by [193] and [194], the main points of critique, summarized in a letter to the editor of PNAS [195]: No indication about the nature of Bt toxin, nor any data about its origin. Unscientific extrapolation from lab to field experiments, suppression of an important result of Fig. 3: low toxicity of normal Bt toxin levels for aquatic organisms etc. It is good to know that the authors of the original study admitted some mistakes and tuned down their alarmist interpretation in the first study:
- The case of the Austrian mice experiments supposedly affecting fertility after some generations [196]. After lots of public and scientific debate, which caused serious and unfounded damage to the image of Bt crops, the study results were distributed on hundreds of websites of GM crop opponents. But critique came up, and since there was no publication in a peer reviewed journal available, the rebuttals were not published in journals either. The whole bitter debate is summarized extensively in two ASK-FORCE blogs: [197].

  The subsequent official retraction done by the Austrian Government itself is hidden in an European Commission Health and Consumers Directorate-General Summary Record of the Standing Committee on the Food Chain and Animal Health from October 19, 2008: European Commission Health and Consumer Directorate-General, Summary Record of the Standing Committee on the Food Chain and Animal Health Held in Brussels October 19, 2008: http://ec.europa.eu/food/committees/regulatory/scfcah/modif_genet/sum_19102009_en.pdf

  See also the published comments of Ammann in [198]:

► Studies that look at non-obvious risks are a welcome addition to the literature, say critics, but poorly conducted studies do more harm than good. "It's just bad science," says Ammann. "There are a lot of scientists producing these studies in a very sloppy way. They bolster public fear yet do nothing to resolve conflicts or move the field forward". And:

But the authors aren't to blame, says Klaus Ammann, emeritus professor at the University of Bern in Switzerland. They are merely the latest victims of what has become the political gerrymandering of science to bolster and support anti-GM sentiment in Europe. "The Austrian government had exhausted all legal avenues to ban cultivation of GM crops," Ammann says.

"The Ministry of Health decided to avoid the peer-review process and announce study results at a conference, hide the data from scientists, and let the activists run amok with the help of uncritical media." Indeed, in the ensuing months the Austrian government has backpedaled. The Ministry of Health responded to a request to interview Zentek or other authors with the following: "We asked the scientists to reevaluate their statistical analysis. Additionally the external evaluation will soon be started. I kindly ask you to wait with your proposal until the reevaluation is completed." [198]

- The case of a review by Dona and Arvanitoyannis [199]. This review would never pass tests designed by Tang et al. [200], which can detect biased filtering of citations and words: According to Tang et al., it is important to distinguish between *subjectivity classification* retrieved from opinionated and factual statements, and combine it with a multiclass *sentiment classification*, and to get a better scale by using neutral training examples. An extensive scientific analysis on [199] has been placed in ASK-FORCE with critical comments: [201]

A caveat at the end of this paragraph on peer review is appropriate. Although it is in principle necessary to ask ethical questions, we should first concentrate on the scientific assessment of a professional peer review strictly following a factual agenda such as [168, 202] are demanding. Only then when this filter has been passed successfully, it is important to go into ethical and socioeconomic questions. But as often, it is the farmers and the market regulating efficiently, and – no surprise – they follow quite naturally socioeconomic principles. It is wrong to mix scientific and ethical questions as de Melo et al. and Interman et al. are asking for [203, 204], the result is then to accept for discussion a paper like the one of [205], which has been seriously and repetitiously criticized on a factual basis by EFSA [206–208]. Such papers should not be seen as a publication which takes also into account a "balanced view," because they are flawed in the first place. Papers from the laboratory of Séralini are then often cited as done by *independent* scientists, which is not very convincing, since digging into the financial support of Séralini and his CRIIGEN lab it is highly interesting to realize that they also receive funds which come from opponents of GMO technology, such as Sevene Pharma, commercializing homeopathic products which claim to detoxify various toxic products [209] and more. CRIIGEN has been created with the financial support of the retailer Carrefour, which has also contributed financially to certain studies of Séralini and his group. Interestingly enough, Carrefour, the second largest food distributor in the world, sells its own brand of "GMO-free" products. . .Source: [210].

- The result of this discussion: it will be necessary to call for new, Internet-based methods to create a more efficient peer review system. A nucleus of such a system is given in Ron LaPorte's supercourse system http://www.pitt.edu/~super1/.

GM- and Non-GM Crop Differences Overestimated, the "Genomic Misconception"

Early Phase of Risk Assessment In the wake of molecular breeding, in particular with the first successes of "gene splicing," the safety debates started soon after the discovery of the DNA structure by Watson & Crick [211–213], followed by the Asilomar Conference [214, 215] – see also some historical accounts [7, 216, 217]. The fascination about the novelty of transgenesis was justified, but also overwhelming, and the many unforeseen scientific breakthroughs following were unprecedented in the history of molecular biology. Unfortunately, the enthusiasm also lashed back in an overacting in risk assessment, when the first GM crops went into production. The debate on how GM crops should be regulated started very early with an emerging divide between regulation in the USA and Great Britain, including later the whole of Europe [218, 219]. Some more traces of early disputes about regulatory decisions in the USA and in Great Britain can be seen in letters to Nature in 1992: [220, 221]. Some support tighter regulation including field biosafety assessments, others fear strangulation of biotechnology research. During the wake of the Cartagena Biosafety Protocol most countries adopted (around 2003) the European way of risk analysis of genetic engineering, emphasizing process-oriented regulation and rejecting product-oriented regulation.

The seemingly absolute novelty of genetic engineering on the molecular level has been contested already in the early days of molecular biology in the 1930s and 1950s with the discovery of cellular systems for genome restructuring discovered with the classic papers of McClintock [222, 223] and with later commentaries of Fedoroff [224, 225], also summarized under "natural genetic engineering" [226, 227].

Molecular Processes Similar in Natural Mutation and Transgenesis Genetic engineering has been brought into evolutionary perspective of natural mutation by authorities such as Werner Arber: his view remains scientifically uncontested that molecular processes in transgenesis and natural mutation are basically similar [228–232]. In a recent paper, Werner Arber [19] reemphasized those similarities on a broader organismal and evolutionary basis; the abstract reads:

- By comparing strategies of genetic alterations introduced in genetic engineering with spontaneously occurring genetic variation, we have come to conclude that both processes depend on several distinct and specific molecular mechanisms. These mechanisms can be attributed, with regard to their evolutionary impact, to three different strategies of genetic variation. These are local nucleotide sequence changes, intragenomic rearrangement of DNA segments and the acquisition of a foreign DNA segment by horizontal gene transfer. Both the strategies followed in genetic engineering and the amounts of DNA sequences thereby involved are identical to, or at least very comparable with, those involved in natural genetic variation.

  Therefore, conjectural risks of genetic engineering must be of the same order as those for natural biological evolution and for conventional breeding methods. These risks are known to be quite low. There is no scientific reason to assume special long-term risks for GM crops.

For future agricultural developments, a road map is designed that can be expected to lead, by a combination of genetic engineering and conventional plant breeding, to crops that can insure food security and eliminate malnutrition and hunger for the entire human population on our planet. Public-private partnerships should be formed with the mission to reach the set goals in the coming decades. "from [19].

The same claim is made with a more organismic view by Hackett [233].

It is therefore no surprise that a natural transgene species has been discovered in a widespread grass genus [234]. An extensive overview on "natural transgenic organisms" is given in the excellent blog of David Tribe GMO pundit on natural transgenics: http://gmopundit2.blogspot.com/2005/12/collected-links-to-scientific.html.

Recent publications demonstrate that transgenesis, for example, has less impact on the transcriptome of the wheat grain than traditional breeding [235–237] (more details see [44, 238]).

One should also take into account that many of the conventional breeding methods such as colchicination [239, 240] and radiation mutation breeding [241] can be obviously more damaging to the genome, and it is, in addition, not possible to clearly define what impact the untargeted process could have caused. Or, on the other hand, as [242] have demonstrated, that irradiation-induced wheat – Aegilops biuncialis intergenomic translocations will facilitate the successful introgression of drought tolerance and other alien traits into bread wheat. In their review, [243] criticized the biased statements of [244, 245] who focus in an unjustified manner on transgenesis alone when describing unwelcome mutations. Still, it has to be admitted that repair mechanisms on the DNA level are powerful [246–248]. It is thus not logical that opposition within organic farming toward genetic engineering is now expanding also to some of those conventional breeding methods, some go even so far as to reject marker-assisted breeding – symptomatic for the organic agriculture scene, this trend is based on the myth of "intrinsic integrity of the genome" [249, 250], for which term it is not possible to find a proper scientific definition, which inevitably should be based on comparisons [44]. The addition of rejected breeding methods would ultimately lead to an absurd situation where most of the modern time traits would have to be rejected and breeding would be forced to virtually start from scratch.

Basically, many of the first-generation GM crops should be today subject to a professional debate on *deregulation*, and there is good and sturdy reason to state that many of these GM crops should not have been treated in such a special way in the first place, they can

be compared in their risk potential to many crops created with traditional methods.

- This should not be misunderstood as a plea for general deregulation of GM crops, rather for a strictly science-based, risk-based regulation and clearly for a shift from process-based regulation toward product-based regulation.

Dissent over Differences Between GM- and non-GM Crops Causes Transatlantic Regulatory Divide This actually includes a critical questioning about some basic rules of the United Nations Convention on Biological Diversity (CBD). Transgenic crops of the first-generation should not have been *generally* subjected to regulation purely based on the *process* of transgenesis alone; rather it would have been wiser to have a close look at the *products* in each case, as John Maddox already proposed in 1992 in an editorial in Nature [251]. This is also the view of Canadian regulators [252–254], where the *novelty* of the crop is the primary trigger for regulation. This transatlantic contrast has been commented by many [16, 218, 255–258], and although for many years a solution and mediation seemed to be too difficult, contrasts can be overcome:

In a letter to the executives of the Convention on Biological Diversity (CBD), the Public Research and Regulation Initiative (PRRI) http://www.pubresreg.org/index.php?option=com_docman&task=doc_download&gid=490 is asking for a scientific discussion in order to exempt a list of GM crops from the expensive regulatory process for approval, here is only the final statement:

- Bearing in mind that the **method of transformation itself is neutral**, *i.e.,* that there are no risks related to process of transformation, PRRI believes that there are several types of LMOs and traits for which - on the basis of the characteristics of the host plant, the functioning of the inserted genes and experience with the resulting GMO - **it can be concluded that they are as safe as its conventional counterpart with respect to potential effects on the environment, taking also into account human health**.

Unfortunately, there was no substantial reaction from the leading Cartagena organizers.

To be quite explicit once more, this does not mean to exempt transgenesis from biosafety assessment as a whole, but it should say that "several types of LMOs and traits, where the inserted genes demonstrate in large scale commercialization (of course after risk assessment done in due course) can be deemed as safe as conventional counterparts according to several years of beneficial agricultural practice, should be exempt under article 7.4 of the Cartagena Protocol for further expensive and time-consuming risk assessment and regulatory procedures. This motion has now officially been repeated by PRRI (Public Research and Regulation Initiative at the occasion of the COP10-MOP5 negotiations in Nagoya, Japan, see the interventions on the website www.pubresreg.org with recent additions.

In a recent paper, an indiscriminate continuation of food biosafety research is questioned on the basis of all the above arguments by Herman et al. [259] with good reason:

- Compositional studies comparing transgenic crops with non-transgenic crops are almost universally required by governmental regulatory bodies to support the safety assessment of new transgenic crops. Here we discuss the assumptions that led to this requirement and lay out **the theoretical and empirical evidence suggesting that such studies are no more necessary for evaluating the safety of transgenic crops than they are for traditionally bred crops.**

Perspectives for Solutions, a Synthesis of Divergent Views in 2.4

These new perspectives create hope that solutions can be found. Even within the difficult and for GMOs totally negative legal environment of the Cartagena Protocol, there are some slim possibilities:

In a first phase some of the widespread transgenic crops like transgenic maize with the Cry1Ab endotoxin could be exempt from regulation. This is indeed possible according to art. 7.4 in the Cartagena Protocol. In COP-MOP5 2010, in Japan (Fifth meeting of the Conference of the Parties serving as the Meeting of the Parties to the Cartagena Protocol on Biosafety (COP-MOP 5), 11–15. 10. 2010 Nagoya, Japan http://bch.cbd.int/protocol/meetings/) it should be possible, to amend

the protocol with the introduction of a dynamics which allows to start the regulatory process with an initial phase focusing on the process of transgenesis, first following procedures proposed for nontarget insects by [260, 261].

Indeed, in COP10-MOP5 in Nagoya October 2010, PRRI www.pubresreg.org has made a request for the exemption of widely adopted Bt maize crops of the endotoxin type of Cry1Ab, see the press release for the context (PRRI press release: http://www.pubresreg.org/index.php?option=com_docman&task=doc_download&gid=586), here the original text as read at the plenary meeting in Nagoya: PRRI Statement on exemptions MOP5: http://www.ask-force.org/web//PRRI-MOP5/PRRI-MOP5-statement-Strategic-Plan-delivered.pdf:

- Third, there is an underlying misperception that there are demonstrated cases of adverse effects. This is incorrect. Over the last 15 years GM crops have been planted over a billion hectares by tens of millions of farmers in the developing and developed world. These crops have been grown in numerous different environments, and they have been consumed in billions of meals. The substantial scientific evidence accumulated shows that there are **no** verifiable reports of any adverse effect to environment or human health.

  The Strategic plan includes an indicator "Number of reports to the BCH on the identification of LMOs or specific traits that may have adverse effects". Such an indicator makes little sense, because it is never possible to rule out that any organisms, LMO or non LMO, may have adverse effects. What is crucial is the question whether they are likely or unlikely to have adverse effects, and PRRI proposes that the strategic plan includes these two questions. PRRI is ready to submit examples of categories of LMOs of which the risk assessments and accumulated evidence indicate that they are unlikely to have more adverse effects on biodiversity or human health than their non modified counterparts, and that consequently those LMOs can be exempted from the AIA procedure on basis of article 7.4 of the Protocol.

In future, it should also be possible to shift eventually the focus on the product, making it possible to abbreviate the regulatory process wherever possible and feasible. The ultimate goal of new regulatory concepts should be to minimize obstacles for new and urgent necessities in crop development, such as Swaminathan and Raven are proposing [262, 263]. The author remains pessimistic, since the whole cumbersome process of legal changes in the Cartagena Protocol is also systematically hindered by a strong anti-GMO lobby, having made its way through the institutions to higher and powerful positions within the Cartagena administration quite successfully, starting from MOP1 all the way up through MOP5, thus influencing negatively all change of regulatory appeasement and lowering regulatory costs. Unfortunately, the recent overview of the European legislation on GM crops does not generate much optimism either: [264].

A second negative trend is triggered by a growing community of risk assessment researchers, who have a vested interest to keep the pot cooking, examples can be downloaded at the website of GENOK www.genok.com and also from the website of the Third World Network http://www.twnside.org.sg/ with its intricate mixture of activist statements and questionable and peer-reviewed scientific contributions. Other similar examples supporting this view can be downloaded over the Freiburger Oekoinstitut http://www.oeko.de/ and on the website of ENSSER, European Network of Scientists for Social and Environmental Responsibility http://www.ensser.org/

A conceptual framework is proposed by IFPRI/ISNAR in 2002, the International Service for National Agricultural Research [265]; a careful evaluation of process-based versus product-based triggers in regulatory action can also lead to a merger of both seemingly so contrasting concepts into a legalized decision-making process on which trigger should be chosen in a case-by-case strategy:

- Process-based triggers are the rule in almost all countries that have developed national biosafety regulatory systems; there are exceptions, however, where the novelty of the trait determines the extent of regulatory oversight and not the process by which the trait was introduced. While such a product-based approach to defining the object of regulation is truest to the scientific principle that biotechnology is not inherently more risky than other technologies that have a long and accepted history of application in agriculture and

food production, it is less prescriptive than process-based regulatory systems.

Many of the debates on those two concepts suffer from a lack of clear-cut definitions, it will be important to have a close look at the Canadian regulatory system and the definition of PNTs (Plants with Novel Traits). In Canada, the trigger for risk assessment is the *novelty* of the plant rather than the *methods* used to produce it. The difficulties start there, where a clear definition of PNTs is needed to come to a decision. It means that plants produced using recombinant DNA techniques, chemical mutagenesis, cell fusion, cisgenics, or any other in vitro technique leading to a novel trait need to undergo risk assessment in the Canadian system. No wonder the Canadian definition of novel traits is rather wordy, but remains broad minded:

- A plant variety/genotype possessing characteristics that demonstrate neither familiarity nor substantial equivalence to those present in a distinct, stable population of a cultivated seed in Canada and that have been intentionally selected, created or introduced into a population of that species through a specific genetic change.

Conclusions: There can be no doubt that product-based regulatory approaches are truest to the scientific principle that biotechnology is not inherently more risky than other technologies that have a long and accepted history of application in agriculture and food production, it is also less prescriptive than process-based systems, see for more details McLean et al. [265].

The Costs and Lost Benefits of Overregulation

The Issue

The Cartagena Protocol on Biosafety (CPB) has now been adopted by 157 parties http://www.cbd.int/biosafety/signinglist.shtml. It still builds on the principle that GM crop plants might bare risks in contrast to the conventional crops, objective of CPB: http://www.cbd.int/biosafety/articles.shtml?a=cpb-01. The huge apparatus on risk assessment based on this protocol is building on the principle that the mechanism of transgenicity is totally artificial and is not found in nature. Modern molecular science insights have proven the contrary, as shown in ASK-FORCE AF-9 [201] on the molecular basis of transgenesis. This results in maintaining the concept of an asymmetric risk assessment of innovation of GM crops. The possible exemption of widespread GM crops in Art. 7.4 (Cartagena Protocol on Biosafety, Article 7: http://www.cbd.int/biosafety/articles.shtml?a=cpb-07) is not even considered officially up to now.

Summary

An excellent summary graph is given in [266] in Fig. 10b: innovations active in the R&D pipeline were growing at an increasing rate during the period before 1998, but declined after 1998. Apart from competition of reasonably close nontransgenic substitutes, the authors consider one regulatory reason to be the main culprit: The halting of regulatory approvals in 1998 in Europe. Although the authors consider the full extent of reasons still to be conjectural, their data suggest that changes in regulatory environment may have been a cause. In a combination of high costs for lost implementation and high costs for regulatory approvals, the present state and operational experience has grown into a major obstacle of modern crop breeding (Fig. 11).

- Commentary from Table 1 in [266]: The primary survey combined records from scientific publications, field trial records, and regulatory filings to identify 558 transgenic plants with quality improvements and determine how far they had progressed through stages of R&D by 2004, including those that had only been published in the scientific literature; those that had reached initial field trials (defined as having completed 1–3 field trials), mid-stage field trials (4–9 field trials) or advanced field trials (>10); those that had entered regulatory filings; and those that were commercialized. The secondary survey canvassed expectations of firms and analysts about the likelihood and time frame for future commercialization of transgenic product quality innovations. Complete one-to-one correspondence between individual observations of the two surveys was not possible.

In a recent publication [267] document the same dramatic negative trend for specialty GM crops is demonstrated:

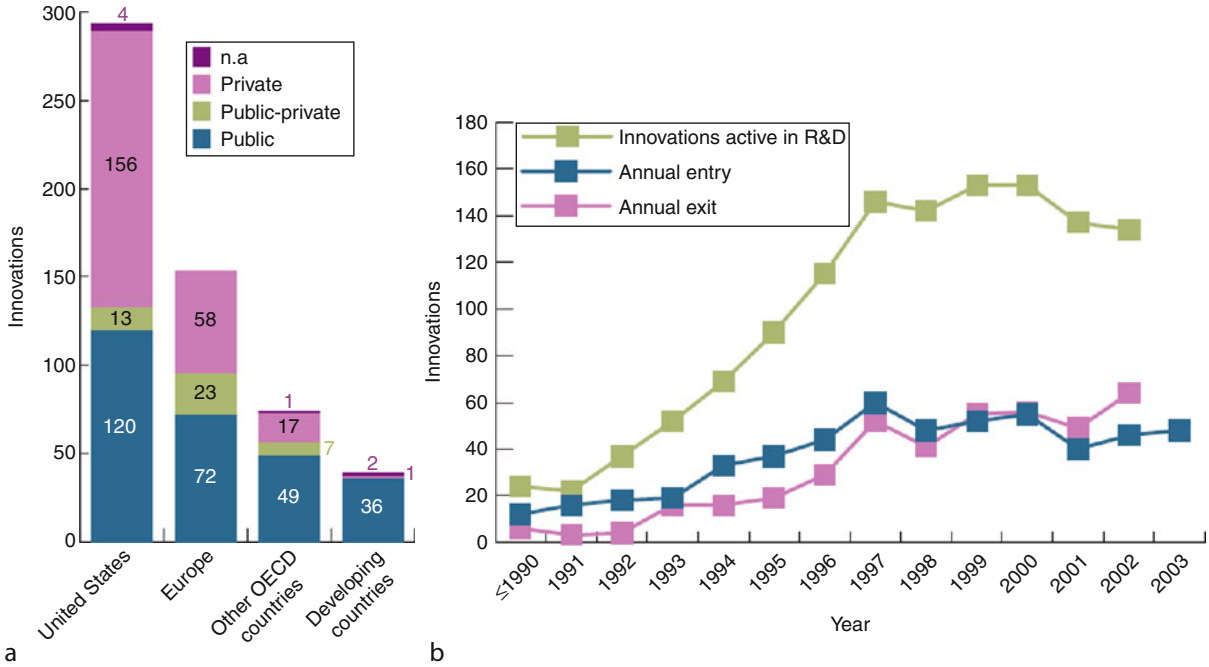

GM Crop Risk Debate, Science and Socioeconomics. Figure 10
Innovation in Ag-Biotech. (**a**) Location and sector of organizations conducting R&D for the 558 transgenic product quality innovations identified. Private sector consists of corporate and privately held firms. Public sector consists of government research laboratories, universities, and nonprofit research institutes. (**b**) Annual entry, exit, and the numbers of innovations active in the R&D pipeline were calculated from observations of the 558 innovations tracked in the primary survey. The number of active innovations stopped growing in 1998, after which those new innovations that entered were more likely to be published and less likely to move toward commercialization. Figure 1 from [266]

Costs and Lost Benefits Worldwide and Europe

An excellent summary graph is given in [266] in Fig. 6 above: innovations active in the R&D pipeline were growing at an increasing rate during the period before 1998, but declined after 1998. Apart from competition of reasonably close nontransgenic substitutes, the authors consider one regulatory reason to be the main culprit: The halting of regulatory approvals in 1998 in Europe. Although the authors consider the full extent of reasons still to be conjectural, their data suggest that changes in regulatory environment may have been a cause.

The full extent of the GM crop development pipeline can be evaluated in websites like the Information Systems for Biotechnology alone from the USA, there are (October 23, 2009) 14,204 notifications with 1,586 full field release permits registered in this Database, ISB: Information Systems of Biotechnology: Field Test Releases in the US: http://www.isb.vt.edu/cfdocs/fieldtests1.cfm

Overall, the present day regulatory regime detains public research in molecular breeding considerably due to enormously high regulation costs. More information about this effect on the development of GM trees is in Strauss and McLean [268, 269]; the abstract reads:

- **Against** the Cartagena Protocol and widespread scientific support for a case-by-case approach to regulation, the Convention on Biological Diversity has become a platform for imposing broad restrictions on research and development of all types of transgenic trees.

Some comprehensive tables on the massive costs of regulation of the major commodity crops are given by Kalaitzandonakes [270]. The compliance costs for herbicide tolerant maize alone have been calculated based on the events in 2006 for the USA. They amount to US

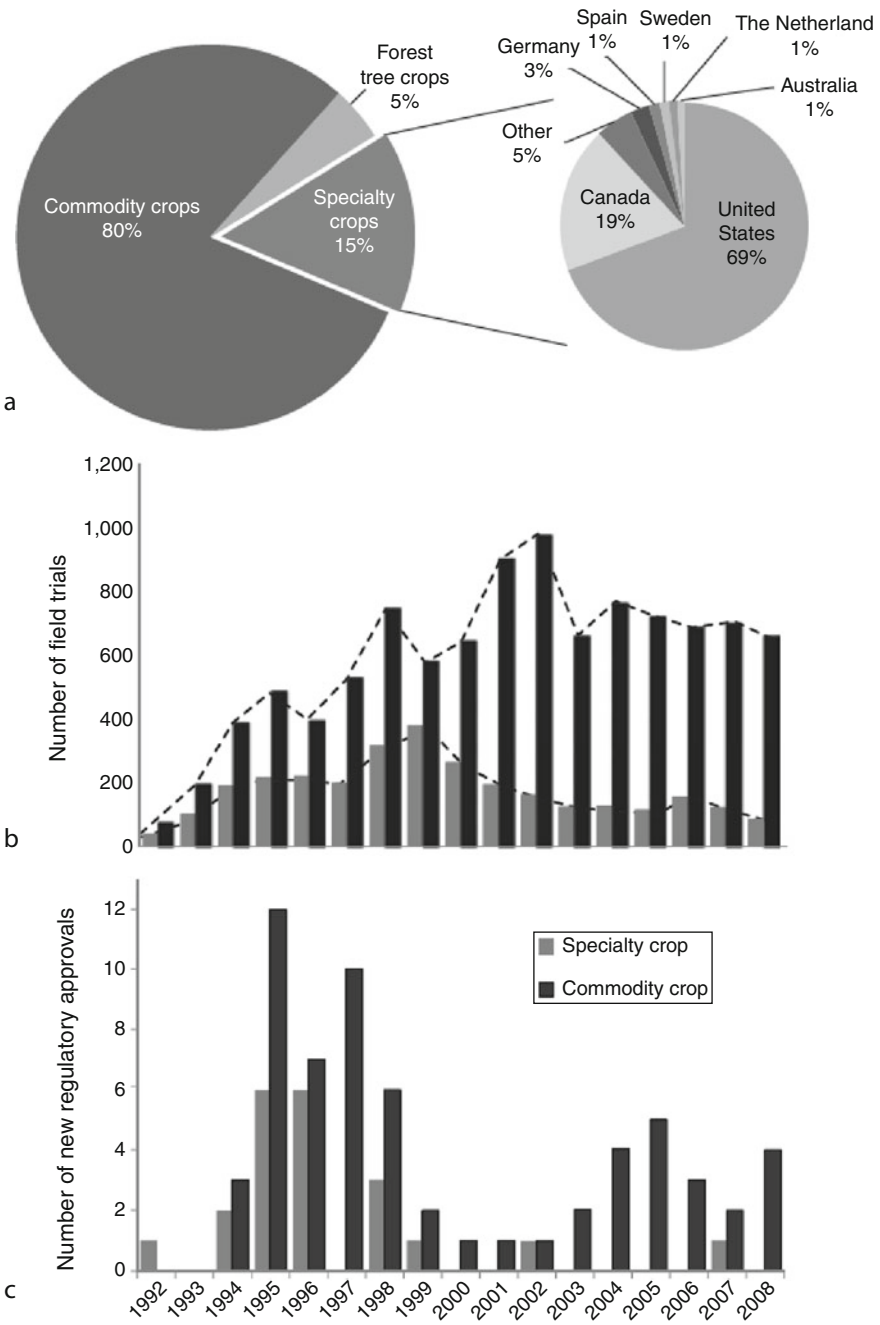

GM Crop Risk Debate, Science and Socioeconomics. Figure 11
Field trials and regulatory approvals. (**a**) Using the UNU-MERIT database, field trials conducted in 24 developed countries between 2003 and 2008 were separated on the basis of commodity, forest tree, or specialty crop. From this, the specialty crops were further subdivided based on the country in which the field trial was conducted. (**b**) The numbers of field trial permits acknowledged or issued in the USA are plotted by year for commodity crops and specialty crops. (**c**) The 84 unique transgenic events that have been granted regulatory approval by one or more countries are plotted by year of approval. If the year of approval varied among countries, the first year of regulatory approval granted by any agency for a given event was used. From [267]

$6,180,000–14,510,000 – a sum most likely to be prohibitive for any trait developed by a public institution.

Another case is reported by Piero Morandini from Italy. A scientific assessment on a field trial on Bt maize is delayed in publication by the Italian Government, although (or because?) it yields very positive results [271, 272].

- The grain yield data (tons/ha, GM crop *vs*. their conventional counterparts) were rather spectacular: 15.9 *vs*. 11.1 and 14.1 *vs*. 11.0, translating into a 43 and 28% yield increases for the P67 and Elgina, respectively. These data have already been released by the INRAN (National Institute for Research on Food and Nutrition, a research institution funded and run by the government) in 2006, albeit without the emphasis they deserved.

  The delay in properly communicating these data can be considered as a very costly omission. In fact, taking into account the total area of maize cultivation in Italy together with yield differences, maize prices and pest pressure, **these data translate into a forfeited value of between roughly € 300 million and € 1 billion a year because Italian farmers are not allowed to plant Bt maize.**

A summary of the Lombardia maize case has also been published in Nature Biotechnology [273]. Unfortunately, the original research report is still not published, it is "resting" in an Italian government drawer. . .

The present day regulatory "cropping apartheid" of high tech farming versus organic farming, large-scale farming against smallholders seriously hampers the development of GM crops, which could foster a more ecological production [44, 274] [275] and [276] – in short, Gene Peace instead of Greenpeace.

Costs and Lost Benefits in Developing Countries

Even more drastically, in the developing world, there is regulatory legislation in place hindering the development of transgenic crop breeding for the benefit of the poor, Driessen, Herring, Paarlberg [277–280].

Doubling agricultural research investment per se (no regulatory costs included in the calculation), would reduce poverty in Sub-Saharan Africa by 9% according to Alene & Coulibaly [281]. But these prospects are seriously hindered and as a result are practically nullified by the exorbitantly high regulatory costs during the implementation phase. Moreover, GM-free private standards set up by food companies and distributors in developed countries have influenced biosafety policymaking in developing countries: Gruère and Sengupta [282] found 29 cases where private importers have affected policy decisions in numerous countries due to irrational fear of export losses. This is based on two generally misleading premises: (1) Europe or Japan represents the only market for exports, and (2) non-GM segregation is too costly. It is amazing to realize, that many of the cases rely on unpublicized lobbying activities, and because of the lack of comprehensive evidence, many cases do not provide straightforward evidence of causality links between importers or traders and policy decisions. There is evidence that development of GM crops in Africa is mainly based on public research, and that the private sector only reluctantly invests in projects for developing countries, although the situation is getting better in the last few years [283, 284].

A blatant case of eco-imperialism is reported from Zambia by Andrew Apel in GMobelus: http://www.gmobelus.com/news.php?viewStory=234, where the Norwegian Government has partly sponsored a $400,000 laboratory, for which GENOK has contributed equipment and training, thus guaranteeing a research policy hostile to GM crops, in accordance with the official policy of the Zambian government, that characterizes GM crops as poisonous. The Norwegian GENOK is a well known anti-biotech NGO, with a very negative attitude toward GM crops, not shying away from spreading myths on allergy caused by pollen of transgenic maize in the Philippines; This is documented in the controversy between GENOK and Rick Roush: http://www.botanischergarten.ch/Allergy/Traavik-Roush-Philippines-controversy-2004.pdf, also supported in favor of Genok without a shred of evidence by John Vidal from the Guardian: http://www.guardian.co.uk/science/2004/feb/27/gm.science. Typically enough, the laboratory's priority will be to detect and search for genetically modified seeds and crops. Former Zambian researcher Ed. Rybicki, now working in Cape Town, said "that the lab would better serve Zambia and the whole region by looking at genuine threats, studying local biodiversity and even making transgenic

crops themselves", as reported by SciDev Net http://www.scidev.net/en/news/zambia-s-molecular-biology-lab-fully-functioning-a.html?utm_source=link&utm_medium=rss&utm_campaign=en_news. Indeed, it is rather ironical that many of the biosafety educational efforts undertaken by organizations, highly critical to transgenesis, are turned into the "contrary": the biotechnological methods introduced in those countries are now also used for research and development of GM crops. A comprehensive report on agricultural biotechnology by Alhassan [285] demonstrates that high regulatory hurdles would hinder a reasonable development of modern agriculture in Africa.

Gruère and Smale [286, 287] report in a carefully calculated assessment that if rice cultures in India, Bangladesh, Indonesia, and the Philippines would be based on present day GM traits, the benefits amount to US$4,331 million. For the USA, an earlier assessment calculates similar sums of benefits related to the introduction of biotechnology in agriculture [288].

There has been much more written about regulatory costs and their negative follow-ups. Here only a small selection of important papers [130, 261, 289–294] is given.

The Golden Rice Development Hampered Through Overregulation. Biofortification as an Ideal Sustainable Way of Foreign Aid in Agriculture

In the case of the Golden Rice this tedious and costly regulation forced upon the regulatory authorities by the CBD solely based on the process of transgenesis has serious ethical consequences as documented in http://www.agbioworld.org/biotech-info/topics/goldenrice/index.html and in [270, 295]. A delay of the introduction of the biofortified rice is directly causing each year hundreds of thousands of children to die or to go blind due to severe vitamin A deficiency. Unreasonable and unscientific regulatory obstacles cause massive delay in approvals, especially in developing countries of S.E. Asia [296–311]. The initiator of the Golden Rice Ingo Potrykus project complains bitterly about the unjustified delays due to overregulation in a Nature article: [312].

Specifically related to the developing world, we should refrain from the old myths that international corporate companies are dominating the field – on the contrary Public Research is responsible for 85% of crop developments, 7% private local companies, and only 1% multinational companies according to figures from Cohen [284], supported by FAO statistics [313]. The myth that patenting rules are seriously hampering the spread of helpful biotech crops in poor countries has been seriously contested [314–316].

As an example, the Golden Rice project will result in biofortified rice traits, which will be distributed to the farmers free of royalties. The Asian farmers will also be able to multiply seeds without paying royalties. The homepage of the project is the main information source http://goldenrice.org/. More about the subject can be found in the important and comprehensive Handbook of Intellectual Property Rights of Krattiger et al. 2007 [317], and more: [318–321].

Biofortification programs are prone to get the highest index numbers in the evaluation system for foreign aid programs of Lempert [322]. Biofortification of indigenous landraces by systematically crossing-in the valuable and royalty free traits to enhance the nutritional value is certainly one of the best ways to sustainably help indigenous people suffering from any kind of malnutrition. In all cases known, the technology transfer is royalty free, secured by contracts.

Use of an indicator to assess the quality and success of developing aid projects defined by [322] reveals that most of the major NGO and UN actors in the field of development are actually providing relief rather than development and are creating dependency by treating symptoms rather than long-term solutions. The indicator points to the specific areas where they need to improve in order to fulfill sustainability criteria including tests of whether aid distorts financial markets and business competition, erodes appropriate government functions, and reverses colonial institutions and ideologies that interfere with sustainable consumption within a resource base.

Estimates in costs for vitamin A capsules are clearly incompatible with the living standard in developing countries; a major distribution campaign would result in millions of dollars. Neidecker-Gonzales [323] produced in their study the following figures:

- Total costs are lowest (roughly US$0.50 per capsule) in Africa, where wages and incomes are lowest, US$1 in developing countries in Asia, and US$1.50 in Latin

America. Overall, this study derives a much higher global estimate of costs of around US$1 per capsule.

A bibliography of publications of the Golden Rice and Biofortification demonstrates the importance of this field of research; out of a general bibliography of 1,640 references a list of over 200 important papers is assembled: http://www.botanischergarten.ch/Golden-Rice/Bibliography-Golden-Rice-WOS-KA-20091008-links-abstracts.pdf.

It should be mentioned that biofortification strategies are also proposed for feed [324]. Straw from harvested crops can be adapted to higher feeding straw quality for cattle.

Conclusions drawn by Ingo Potrykus [325], the creator of the Golden Rice:

- The huge potential of plant biotechnology to produce more, and more nutritive, food for the poor will be lost, if GMO-regulation is not changed from being driven by "extreme precaution" principles to being driven by "science-based" principles.

  Changing societal attitudes, including the regulatory processes involved, is extremely important if we are to save biotechnology, in its broadest applications, for the poor, so that public institutions in developing as well as industrialized countries, can *harness its power for good.*

As a whole, the new, well-documented review paper of Adenle [326] delivers overwhelming evidence that GM crops are urgently needed in the developing world:

- The world needs fast and reliable solutions to fast growing population and the problems of hunger, malnutrition, ravaging diseases, poverty and global warming crisis. One of ideal technological innovations such as GM technology can be part of solutions to these problems. It is imperative to understand that GM technology cannot establish its ground if continuously faced with the baggage of constraints as discussed above. Moreover, it is not surprising to gather from a variety of literatures that most developing countries lack capacity building and still struggling with the establishment of biosafety system that can facilitate GM field trials and commercial release of GM products. Some of the challenges associated with the development of modern biotechnology still boil down to the fact that individual country government and international organisations have not clearly identified a coherent strategy and enabling policy instrument to deal with the problems. While some progress have been made on GM technology in terms of research and development, capacity building, and biosafety regulation in developed countries and a few developing countries, concerted effort is still needed to make it an accessible technology for every country. [326]

The Dispute Between Scientists and Opponents Today

The Role of Some Activist NGOs in the Debate

There is a continuous need for dialogue with regulators, the public, and specifically consumers, since the new technology emerging from modern life science is affecting all aspects of human life, including food, reproduction, etc. We do have an unfortunate trend toward irrational and antiscience argumentation in the GM crop dispute as clearly diagnosed by [327] in his book "The March of Unreason"), see also [328, 329].

This said, we should not create misunderstandings. There is no room for appeasement politics today when it comes to the activist NGOs like Greenpeace and Friends of the Earth, or websites like the Institute of Science in Society (I-SIS) and GM-Watch. Those professional organizations have proven repetitiously not to be interested in peer-reviewed science in a debate on the science and the sociocultural issues. They rather rely on unconfirmed reports in order to follow their own ideological and commercial interests. Any rational discourse with such organizations would be very welcome, but needs to be based on the latest peer-reviewed science. Their usual tactics is to appeal on fear. A good example from Greenpeace has been described on the EFB forum website http://www.efb-central.org/index.php/forums/viewthread/13/ about baseless accusations that 1,600 sheep have died from feeding Bt cotton leaves. A critique on the distorted picture on Indian cotton cultivation by NGOs is given by Herring [330] with lots of figures, facts, and extensive documentation.

Another blatant example of junk science has been launched recently by Greenpeace on You Tube "Genetic engineering: The world's greatest scam?" http://www.youtube.com/watch?v=1H9WZGKQeYg full of misinformation and hatred against multinational seed companies.

We are also confronted with violence – activities clearly documented and justifiably named and pursued as terrorism [331]. Also, in Europe, there are regularly occurring field destructions [332], which hamper seriously biosafety research – what an irony! Eco-terrorism is not confined to Europe, problems of such kind are very real also in the USA [333]:

According to the Federal Bureau of Investigation (FBI), the Earth Liberation Front, together with its sister organization, the Animal Liberation Front (ALF) has committed from 1997 to 2003 more than 600 criminal acts that have resulted in more than $43 million in damages. Moreover, attacks have been perpetrated in virtually every region of the USA against a wide variety of targets.

Recently, Greenpeace destroyed government field research in Australia [334] and defended the act of eco-terrorism with very thin arguments – and promptly lost lots of supporters and sympathy: Even some old friends and supporters of Greenpeace (but not all) distanced themselves from the action: [335]. A list of field destruction actions in Europe has been compiled by Marcel Kuntz [336]. This list, far from being complete, demonstrates that activists have lost their moral compass in recent years: [337, 338].

One of the best rebuttals of cheap anti-GMO propaganda coming in attractive book editions, widely distributed in international events by the author Jeffrey Smith [339, 340] has been published on the Internet by Bruce Chassy http://academicsreview.org/reviewed-content/genetic-roulette/. It is actually a scientific comment, section-by-section, based on the best available peer-reviewed literature.

More chagrin emerges from the mounting pressure from within the academia, where, for instance, German university leaders in Giessen ordered to cease field research on GM crops which is unwelcome in the eyes of the extremists, [341] and there are serious complaints about the difficult atmosphere for biotech researchers in Germany [4].

Another symptomatic row is presently taking place in India, related to the approval of Bt brinjal, where activists are in a desperate attempt to stop the regulatory approval of Bt brinjal with outrageous and completely unfounded rumors like "GM brinjal will render the soil sterile," But contradictions have been posted as well: the most recent and comprehensive summary report published by Kameswara Rao [342], which is a review of massive evidence for the safety of Bt Brinjal and the detrimental heavy use of pesticides for the production of conventional Brinjal. It is ironic that one of the main arguments for proponents of the Bt Brinjal moratorium in India is now seriously questioned. There was the seemingly clear evidence on a crop biodiversity center for Brinjal in India, which called for extra protection of indigenous genomes. But recent extensive genomic analysis has clearly demonstrated that Brinjal is originating in Africa [343].

As an exemplary dispute, you can also follow the exchange of letters between the Public Research and Regulation Initiative (PRRI) and Friends of the Earth (FoE) [344]. Some of those anti-GMO activist groups get hefty funding from governments in the EU, as documented accurately by Andrew Apel and his GMobelus website: Europe's massive funding of world-wide activism. Compare also his recent article on the same subject, focusing on global aspects: [345].

The current set of arguments of GM crop opponents is often a mix of anti-American, antiglobal, postmodern, and even antiscience notions, [346], a strategy which has now been taken over very successfully by NGOs like Greenpeace and Friends of the Earth as global actors. These leading protest forces have helped, particularly in Europe, to build up a postmodern negative picture of biotechnology as a whole [347]. In this light, it is easy to act as "opinion leaders" with pseudoscientific arguments. The feedback mechanisms through the media and a network of citations of all the flawed stories make it possible for the global opponents to maintain confirmation of negation mechanisms. We are in a situation where the opponents already try to claim victory, penetrate highest political levels in governments and international organizations like the United Nations, some produce strikingly flawed reports on GM crops.

An analytical article about media and NGO activities in New Zealand has been published by Motion and Weaver [348]: by attracting media attention through dramatic protests, Greenpeace risks to jeopardize its reputation. The abstract reads:

- The challenges of attracting positive media attention are likened to a contest in which various organizations

attempt to promote and circulate their version of events; however, this is particularly difficult when attempting to circulate less established, unpopular or critical knowledge. Although complying with, and managing, news values is an important starting point, the need to move beyond news values to consider the commercial values and realities of media organizations is highlighted. In this paper, a case study is undertaken of the Greenpeace media relations in New Zealand when a proposed controversial expiry of a moratorium to release genetically modified organisms into the environment. The predicament for Greenpeace is that in attracting media attention through dramatic protests it risks jeopardizing its reputation as a credible news source that can influence the framing of news stories. Insights are offered into the need for organizations to understand and manage the story or knowledge to be circulated and comply with contradictory news values.

Related to this paragraph on NGOs, it is necessary to write a word on the press: Newspapers and other media usually are mirroring what is important in the public debate, and the NGOs are clever in manipulating both the public and the press, after all, it is easy to provoke with fear and scaremongering, and the majority of journalists of all calibers are also committed to their own product, position, and its commercial situation.

A classic example is the coming and going of the Frankenfood Myth, see Fig. 3 and http://en.wikipedia.org/wiki/The_Frankenfood_Myth. Interestingly enough, this myth had its sharp peak in the press statistics around 1998 (see Fig. 3) and since then it has vanished from the headlines [104] as a major buzz word.

Those mechanisms have been precisely described by Burke for the situation in Great Britain some years ago [349]. But it is also clear that in the last 5 years more balanced voices appeared in the press, although there is no room to extend this topic here, just one recent example from the London Financial Times may suffice [350].

The GM Crop Battle, the Dispute Among Scientists, the Use of Strong Language

First, let us not forget some words of Antony Shelton [291], the most important words can translate into a slogan: "Quality of science must back up personal opinions," the abstract reads:

- In agricultural biotechnology there are roles and responsibilities of scientists, scientific journals, the public media, public agencies, and those who oppose or advocate a specific technology and serious consequences for science in general when those roles and responsibilities go awry. Scientists may feel the pressure of competition, especially in an academic setting. Personal views may continue to decide which issues one will work on, but the quality of science must back up those personal opinions. Common sense tells us that scientific inquiry and the publication and reporting of results to the scientific community and general population should be performed with high standards of ethical behavior, regardless of one's personal perspective on agricultural biotechnology.

One of the arising problems is that there has been recently a tendency to mollify peer review for the sake of politically correct so-called critical views of genetic modification of crops, with some blatant examples of flawed pseudocritical papers having passed for publication in highly respected scientific journals – a few examples have been commented by [351]. Some of those papers just passed due to flawed peer review, others passed despite rejection by some peer scientists, obviously for the sake of public debate (and for the promotion of the journal), see as an example the rather thin justifications of the editor in chief of Lancet Richard Horton to go ahead with the publication of Pusztai's rat experiments [352–356]. For more details about this controversy, see in ASK-FORCE on Pusztai [357], it is an anatomy of the case in 46 pages on the Pusztai affair, which had a big influence on the regulatory climate on GM crops in Great Britain and the world.

It is only between 2005 and 2011 that a certain fatigue of new negative arguments against GM crops is developing, and it is interesting to note that opponents, lacking real negative health and environmental effects, now shift their emphasis on negative arguments in socioeconomics. There are hardly any new issues in food safety and environmental impact to be dealt with in the last few years. This might also be the reason why in a desperate routine of repetitious "negative," GM crop stories get into journals, often also on rehashed

events which have been clearly rebutted scientifically many years before. Those "news stories" often pass uncontested and get printed in "news" media due to a mix of short memory effects of uninformed editors and readers of all kind, or worse, they are purposefully repeated by activists counting on short memory of press and public.

A strange effect should also be mentioned that scientists, who defend good science in biosafety research, sometimes get blamed because they use straightforward language when criticizing flawed papers. A paper on such debates has been published by Nature [177], see the comments in a contribution of ASK-FORCE [178] on a paper on aquatic organisms supposedly harmed by Bt toxins of GM maize by Rosi-Marshall [191] and [192]. There are several controversial hints in this Nature story put forward by science journalist Emily Waltz, who is neither specialized nor experienced in the hot scientific regulatory debate on GM crops, suggesting that to criticize flawed papers with "strong language" is detrimental to the progress of scientific research. This statement was supported by interviewed writers such as Ignazio Chapela (famous for starting the controversy of the Mexican gene flow of transgenic maize with a letter to Nature [358], which later turned out containing insufficient evidence for publication [359], see the latest summary in [360]. Another interview Waltz conducted in the cited *Nature* piece with David Schubert, who tries as a pharmacist to give advice in biosafety rules of GM food, and with his strong anti-corporate mood publishes fraud accusations against pro-GMO scientists [361]. Both interviewees Chapela and Schubert defend independent scientific whistle blowing, but themselves they have a proven negative agenda about GM crops, see more controversy papers: [295, 362, 363]. In the meanwhile, several letters to the editor of Nature have been written commenting the feature of Emily Waltz in Nature, they are all cited in [178], the majority is not supporting her thesis.

Incidentally: Strong language has been used before in the history of science, remember some really bitter and hefty disputes about the history of discovery of the double helix structure of DNA between Watson and Crick [216], who later made their peace again.

Other numerous examples of a fight out in the open are documented about evolution when Darwin proposed his revolutionary ideas. Two citations of strong language may suffice: in a debate on natural selection [364] writes on a dispute with William Bateson:

- By these admission almost the last shred of that teleological fustian with which Victorian philosophy loved to clothe the theory of evolution is destroyed. Those who would proclaim that whatever is right will be wise henceforth to base this faith frankly on the impregnable rock of superstition and to abstain from direct appeals to natural fact.

Another clear example of sharp and relentless scientific controversy on evolutionary biology with strong language has been described in detail by Strick [365], among the numerous juicy examples:

- His [Bastian's] tone was sharp in response to Huxley's public accusations that his technique was sloppy (a much more high-powered attack than Huxley ever adopted in private when attempting to correct young scientists). Huxley replied with an equally sharp tone, now saying sweepingly that "what Bastian got out of his tubes was exactly what he put into them," *i.e.* contaminants.

And one last word about strong language: The word "abuse" has been printed by Nature in the Battlefield paper [177] very prominently in the subtitle, when attacking a group of authors including me who criticize flawed papers in the GM crop debate with blunt, but still polite words – what an irony! – And to be quite clear, no complaints from my side. . . .

Negative Effects of Modern Breeding Methods in Food and Environmental Safety do (or Should) not Pass Strict Scientific Procedure Rules and Peer Review or They Are Based on an Unscientific Focusing on Transgenesis Instead on Management Mistakes

If researchers would follow strict procedural rules, the world of scientific biosafety debate would be far less complex, here are a few papers standing for such in fact uncontestable rules: [168, 260, 261, 267, 312, 366–369]. It is a fact that for some years basically no new arguments against agricultural biotechnology (in particular clearly related to transgenesis) on an agronomic base

can be put forward for the most widespread crops, which have run through multiple regulatory processes in many countries.

This does not mean that transgenic crops are completely free of problems, but, in fact, it is that in comparison with conventional crop problems these are minor and manageable in a more efficient way. One of the basic mistakes of GM crop criticism is the unilateral focus on the risks of transgenes inserted, instead of comparing, in a fair and scientific (holistic!) way, with conventional cropping [370].

Still, a growing number of herbicide tolerant weeds are emerging: [371–374]. Powels [375] rightly points to the monotonous fields of glyphosate-resistant soybean landscapes, where the herbicide-tolerant weeds emerge more rapidly:

- Indeed, in spite of longterm use, the evolution of glyphosate-resistant weed populations in non-GRC, burndown systems has been very limited. Thus, functionally competent gene traits endowing glyphosate resistance are relatively rare and not easily enriched in plant populations [376], [377]. This is why glyphosate is a remarkably robust herbicide from a resistance avoidance viewpoint. However, as reviewed above, it is clear that, where there is very intense glyphosate selection without diversity, glyphosate resistant weed populations will evolve. In particular, the evolution of glyphosate-resistant weed populations is a looming threat in areas where transgenic glyphosate-resistant crops dominate the landscape and in which glyphosate selection is intense and without diversity. [375]

But it is also a fact that the emergence of glyphosate-resistant weeds is happening on a much slower pace than that of conventional herbicides [378].

Some critical science journalists question the strategies and behavior of the global opposition players. In a kind of last bid, questionable reviews are published, either containing lots of negative *assumptions* [379] or wrong toxico-analytical concepts resulting in an exaggerated risk assessment for nontarget insects as the lacewings as promoted by Hilbeck et al. [380–382] and contradicted clearly in Romeis [383]. Other examples of questionable eco-toxicological conclusions have been drawn by producing or reviewing flawed data or statistics, or drawing questionable conclusions, see the debate on Ermakova's flawed rat experiments: [384], more details in a contribution to the ASK-FORCE [385]. Typical other examples recognizable on filtered citation lists are Dona et al. and Séralini et al. [199, 386]. Séralini conducted his experiments in disrespect of the internationally approved rules of biosafety experiments established by the OECD [387, 388] and also avoided the citation of certain contradicting peer-reviewed references. Many of those papers have been or will be treated in ASK-FORCE [389], where you can read about new or recently updated ASK-FORCE contributions, for more details see section ASK-FORCE Organization and Related Websites.

It also must be said (remember Saner's statements at the beginning of this section) that vested interests can be spotted with some biosafety researchers, who are in need of research grants and thus paint a negative picture on biosafety; they symptomatically have difficulties to distinguish between the "nice-to knows" and the "need-to knows." Example: see the ASK-FORCE contribution [178] on the publication of [13], a paper which is flawed in several ways. It has been completely rebutted by Shelton et al. [14], the questions asked in the Lovei paper are irrelevant for Bt maize cultivation, since the Bt-toxin-technology is overwhelmingly beneficial for majority of nontarget insects [390–394]. One of the major flaws of the Lovei paper is that they used low quality prey for their laboratory feeding studies. A thorough analysis of risk assessment research has been recently published by Raybould [261]: We need to carefully distinguish between basic ecological research and purposeful and targeted risk assessment research which concentrates on the real agronomic risks and needs [395, 396].

The question and negative answer given in the letter of the Public Research and Regulation Initiative (PRRI) to the Secretariat of CBD [397] is fully justified, *and PRRI stands ready to expand on the points made in this letter.*

- 1. Are there LMOs or traits that have caused adverse effects?

  No. Since the first application of genetic modification in the 80s, many thousands of field trials have been conducted with GM organisms (to date mostly plants), and since 1996 many hundreds of millions of hectares have been planted with GM crops by many millions of farmers and consumed by hundreds of millions of

consumers in developed and developing countries, without any verifiable reports of adverse effects on the environment or human or animal health.

In fact, taking a broader look, experience with those GM crops has shown environmental and socio-economic benefits in terms of increases in yield, significant reductions in use of pesticides, fossil fuels and soil erosion, less mycotoxins in grains, as well as increased farmers health and income.

Final remarks: Coming back to the first statement of Saner [120] given under General Views on the Dialogue Related to Regulation of GM Crops, value-laden scientific activity cannot be avoided, but minimized – if you refrain to work with flawed data, with filtered citation lists, and with reviews pontificating on negative assumptions. The only remedy is to work with high-quality data produced in a methodologically transparent way following international agreement.

It is appropriate to end this rather pessimistic section with a positive note, not free of irony: As Gupta [398] recently stated, there is hope that the introduction of strict biosafety rules in the Cartagena Protocol, originally aiming at a slowing down or even at stopping the transboundary movement (and indirectly development) of GM crops, now seems to turn into its contrary:

- Through analyzing the dynamics of GMO-related information disclosure to the global Biosafety Clearing House (BCH), I argue that the originally intended normative and procedural aims of disclosure in this case to facilitate a GMO-importing country's right to know and right to choose prior to trade in GMOs are not yet being realized, partly because the burden of BCH disclosure currently rests, ironically, on importing countries. As a result, BCH disclosure may even have market-facilitating rather than originally intended market-regulating effects with regard to GMO trade, turning on its head the intended aims of governance by disclosure.

Debate Improvements: What can we do to Enhance the Situation?

Foremost, it is important to *shift from pro-reactive to proactive mode*. This does not automatically mean to filter away negative views on GM crops and to organize a eulogy on the benefits, the pro-active mode should actually engage a new mode of debate, which is more discursive, more structured and definitely concentrates on a solution-oriented decision-making process. It is time for action – as far as a strict scientific view is allowing this. There are several websites working hard on sorting out the strictly science-oriented messages in biotechnology, as mentioned below. We should not, as it often happens, in our struggle against the negative pseudo facts focus on the risk alone and thus trap ourselves in a negativistic perspective.

Rather we should address in a balanced way the obvious (or lost) benefits as well. But this alone will not provoke a turnaround. This shift must be embedded in a discourse with concerned people and organizations and it must clearly oppose untruthful strategies of the global protest corporations and thus also refrain from using the same countertactics. One of the appropriate organizations for this activity will be the two platforms: (1) Public Research and Regulation Initiative PRRI www.pubresreg.org run by public researchers and (2) also the European Federation of Biotechnology http://www.efb-central.org/, so that public science will get a more important place in the international regulatory debate (but also where private seed companies are not fundamentally battled in a naïve neo-Marxist scheme). In many meetings strictly based on science and organized by PRRI, both platforms are well received. The project outline can be described as follows:

ASK-FORCE Organization and Related Websites

There is a flood of papers which cast doubt on the GM crops already regulated in many countries. Most (if not all) of these papers are written in a bad quality, either with flawed methodologies not internationally agreed upon, or with conclusions which are not supported by the data [13], rebutted by [14], details see in [178]. There are also many reviews published in a scientific style, but unfortunately either with a strongly biased set of references or with unsupported assumptions and doubtful conclusions – contradicted by peer-reviewed publications often not cited. In some cases, the flaws are more hidden: Experimental data are achieved on clearly theoretical schemes, working with outdated Bt maize and nontarget butterflies which have in their

biology, in nature, no connection to maize fields: [399]. It is therefore important to set the record straight and to try to rebut at least the most important and blatant cases.

Within an EU project with Marc van Montagu and Piet van der Meer, which has been granted to PRRI, a blog was launched with the name ASK-FORCE on the PRRI website www.pubresreg.org with the secretarial help of Kim Meulenbroeks (until 2008) and presently Zuzana Kulikova. A list of about 130 items [400] has been compiled with international help and will be entered step-by-step in the grid of the following six sections. (1) General (2) Human and Animal Health (3) Environmental Safety (4) Agriculture (5) Public Perception (6) Developing Countries.

Up to now, 11 contributions have been published on the Internet; for links and contributions see [389]. These were reviewed by the experts of the steering committees of Public Research and Regulation Initiative and the European Federation of Biotechnology, some also by the experts united in the blog community of AgBioWorld http://www.agbioworld.org/. All three lists contain some of the best specialists on green biotechnology from all around the world for reviewing and commenting.

In order to become more proactive, we need to develop forward-looking strategies. It is up to the scientists to ask questions to the opposition, and in particular to the professional distorters of the scientific facts. This must escalate into public campaigns if (what is to be expected) those specific questions are ignored. Carefully built contacts with science writers are important here, as a help for networkers a selected list is given here http://www.ask-force.org/web/ASK-FORCE-Summary/Contacts-ASK-FORCE-2011.pdf

Long-Term Discourse and Decision-Making Processes

Let me first be quite clear that I think a dialogue with the professional protest corporations is, as a rule, a waste of time (specifically Greenpeace and Friends of the Earth, not to mention some other organizations). Their only interest is to keep the pot cooking and make sure that the population remains in a state of fear. They should be addressed with a confrontational strategy, which is included in ASK-FORCE. Often such NGOs get the willful help of the press, which acts according to the old proverb (Macbeth, Shakespeare) "evil always fascinates – goodness rarely entertains" [401], see also the arguments produced by Andrew Moore [402]. While some press products concentrate on mirroring public concerns, a press more or less close to boulevard strives to foster its marketing with the help of sensational headlines, creating stories which sell better, but indirectly they are exacerbating the problems. We are also not going to talk about a special discourse, as described by Erjavec [403], related to the politics of the EU commission.

Nevertheless we have to address all segments of the public with its concerns, feelings, and interests. And the discourse we are going to concentrate on is solution oriented. This should be done according to the discursive rules of the management strategies of the second generation, the *Systems Approach* (see under The Second Generation Systems Approach as a New Decision Making Process). As a basic reference with description and citations, see the classic book of Churchman [79]. If we follow some ground rules, this should not be too complicated.

The Second-Generation Systems Approach as a New Decision-Making Process

Instead of making questionable concessions (example: "let's not talk about transgenic crops" as often done by Nestlé and Unilever, with notable exceptions [404] within these two companies!), the dialogue should be organized in an atmosphere of "Active Listening" [405] and understanding in which, apart from the strict rules of scientific argumentation we should send signals that the new technologies also trigger socioeconomic and cultural feedbacks. This will be the key to solve *Wicked Problems* [406], which contain also sociocultural elements besides a set of hard, often contradictory facts [122]. In his usual cynic precision, George Bernard Shaw defined the ultimate problem in the dialogue between scientists and lay people: "Every profession is a conspiracy against the laity."

The new discourse is not about the usual stakeholder meetings; rather it is about instigating modern planning processes of the second generation in evidence based but open ended decision-making processes. This *Systems Approach of the second generation*

contrasts to linear planning with predetermined targets and dominating deontic thinking (e.g., of the industrial corporations and government agencies), it contrasts also to *the Systems Approach of the first generation* (e.g., Apollo moon landing with clear target).

The Rationale of New Management and Decision-Making Processes

- Some problems are so complex that you have to be highly intelligent and well informed just to be undecided about them. Laurence J. Peter [407]

These new strategies should dissolve the traditional stakeholder concept in favor of a much more efficient system respecting *different kinds of knowledge* and other rules (such knowledge differentiation is also known from learning processes, which are related to our decision-making dynamics [408].

There are more practical reasons to employ into the Systems Approach and its concept of different kinds of knowledge, as Zwart [409] rightly emphasizes: Ever since we have realized that the low number of human genes (approximately, 22,500) cannot be interpreted as a narcissistic offence, since organisms are so highly complex, including the emerging consciousness of our human brain, genomics takes us now beyond a genetic deterministic understanding of life, this must have consequences on societal research and debate as well. Policies for self-improvement will increasingly rely on the use of complex interpretation. *Therefore, the emphasis in our discourse must shift from issues such as genetic manipulation and human enhancement to issues involved in governance of novel forms of information.* The same can be said on the side of agriculture. Ikerd [410] develops with the means of the systems approach a more holistic picture of agricultural management.

Fairclough [411] as a linguist gives an in-depth and critical analysis on discourse related to globalization with lots of facets, and again with a totally different set of terminology, he also presents negative examples of discourse. Objectivism treats globalization as simply objective fact, which discourse may either illuminate or obscure, represent or misrepresent. In the Churchman systems approach, there is no such thing as an objective approach, rather it is objectivation. Ideologism focuses upon how particular discourses of globalization systematically contribute to the legitimation of a particular global order which incorporates asymmetrical relations of power such as those between and within countries.

Scoones et al. [412] come to similar conclusions as the Churchman school, but this time related to agricultural policy, the paper explores the national and transnational character of mobilization against GM crops in India, South Africa, and Brazil in the 10-year period up to 2005. The paper argues for a better understanding of national political and economic contexts which must be taken into account, alongside on how the GM debates articulate with other foci for activism and the complex and often fragile nature of alliances that make up activist networks. It is important to understand that the debate about GM crops has become a much wider one: about the future of agriculture and small-scale farmers, about corporate control and property rights, and about the rules of global trade, see also the new report of the Royal Society [18]. In sum, a debate should not just focus on the pros and cons of a particular set of technologies – after all, they have proven safe – it is more about politics and values and the future of agrarian society. Again we see the plea for the complexity of "*wicked problems*" to be solved.

The downside is that those planning processes of the second-generation are time consuming and need a careful and tedious procedure in developing the most important and difficult *zero-step* – before such decision making can be started. It also implies an exchange of knowledge between the parties beforehand, in order to minimize *hidden agendas*. It also must be emphasized that those decision-making processes do not lead necessarily to a predefined goal, they are often *open-ended* and demand flexibility among the discourse participants, who need to remain open-minded.

The more questions we ask the more answers are possible and vice versa. Limitations of technological solutions are always hidden in the open ecological and social systems: Just compare the (in)famous case of DDT sprayings in the past [413–415]. Today, it is clear that with linear planning, DDT has been banned for ecological and health reasons, not considering the wider argument field of malaria prophylaxes. This inconsiderate DDT ban has caused millions of malaria deaths in Africa. Today, reasonable domestic use of DDT has again lowered the malaria threat measurably.

Constraints in possible secondary effects in ecology should be examined carefully. This is well demonstrated in the case of the Monarch larvae being killed by Bt-Maize-Pollen, the result of a laboratory study published in Nature [416] where the subsequent press interpretation got way out of proportion – even though the author Losey himself warned about the limitations of this small lab study. Would researchers have asked the farmers, they would have been able to say that feeding time of the young larvae do rarely overlap with the time of pollen shed of maize, and that the plants the Monarchs are feeding upon are fiercely fought as a weed. Subsequent field studies revealed that there is no problem arising from extensive Bt maize planting for the Monarch larvae [12].

In order to tackle wicked problems, you need to go through *an extensive process of argumentation*, also called objectification, not to be mixed up with an "objective approach" to the problem.

There is rational planning, but there is no way to start to be rational: One should always start a step earlier, since there are important trends and facts which will make straightforward rational thinking and acting in solving wicked problems useless. It is not the theory component, but rather the political component of the knowledge, which determines the vector of the action. This is the *zero-step* so important in the publications of Horst Rittel [121, 122].

As an example: The fact, that experts can be wrong and farmers know better in certain situations in agriculture because they are better observers out in the field and because they are very experienced in traditional knowledge [417].

The knowledge needed in solving wicked planning problems is not concentrated in a single head. It is absolutely essential to let all partners be involved in the problem solution process, which includes part of the population (mainly farmers' organizations and consumer organizations), the Governmental Regulators, the Non-Governmental Organisations, the Life Science Companies, and the Scientists. There is no monopoly of knowledge. Having illustrated the difficulties in solving wicked problems, we need a new approach in problem solving, in order to avoid the pitfalls of ignoring bottom up feedbacks.

You only can keep to this rule if you are also following another important rule. All partners in the planning process have to avoid hidden agendas, which is certainly eased by a minimum amount of respect paid to each other partner. Nobody should be criticized for speaking up in his own interest.

A caveat: It would be naive to just believe in the discursive capacities of the civil society, contrary to what Gerhards [418] has shown – that Habermas' support for the discursive model is based on the assumption that actors of the civil society argue much more discursively and on a higher level of rationality than other collective actors do. But empirical results show that actors of the civil society are, maybe, even less discursive than other actors.

It is primarily the paradox of rationality which has been severely underestimated in the systems approach of the first generation when tackling *wicked problems*.

How to Solve Wicked Problems in Biotechnology and the Environment What we need in such cases is an action-oriented approach. Risk Assessment and Management must be seen as a planning strategy of the second generation in developing a professional framework for *decision making*.

Strategies have to be developed to recognize the consequences of our doing on one side, and to specify our knowledge on the other side. This knowledge has to be gained step by step and case by case. If we want to clearly distinguish our present state knowledge from appropriate decisions to be made *not* based on our views and opinions, we need to go through the following steps:

- What is the problem?
- What do we want?
- What are the alternatives?
- How do we compare them?
- How can we reach the solution?

All participants need to keep in mind that there are *various types of planning knowledge* (arranged according to the five questions asked above).

Examples given here are lumped together as simple keyword illustrations, taken out of their context in real planning examples, and they cannot be regarded as an example of a realistic situation; this would be exactly the task of a planning process of the second generation.

Factual knowledge is the knowledge of what actually happens (quantitative data or empirical, observational

data). Gene flow species by species/region by region/facts about insect resistance in agriculture.

- *Deontic Knowledge*, the very important knowledge of what ought to be. The knowledge about new crops which enhance agricultural production/new agricultural techniques to avoid erosion/new biological approaches to fight insect pests etc.
- *Explanatory Knowledge* explains why things are so or why certain effects will happen. Here, you already start to determine the direction of the solution. The way Bt proteins are acting on specific pest and beneficial insects/what are the main reasons of unwelcome erosion effects/mechanisms of vertical gene flow/mechanisms of resistance development.
- *Instrumental knowledge* on how to steer certain processes, on how to achieve certain goals, knowledge which needs to be balanced against regulation and safety. The way how to build Bt and other genes into crops and how to stabilize them/how to avoid vertical gene flow/how to avoid unwelcome soil erosion/how to avoid early upcoming pest resistance.
- *Conceptual knowledge* which would allow avoiding conflicts before they pop up. This is the knowledge about complex situations, taking into account all previous kinds of knowledge and also weighing them against arguments coming from open ecological and societal systems. Concepts about transgenic crops compatible to the ideas of a sustainable agriculture. Lawyers and judges also may work with this kind of procedural knowledge.

You need to go through an *extensive, time-consuming process of argumentation*, also called objectification, not to be mixed up with an "objective approach" to the problem. The hopes of this process are:

- To forget less, to raise the right issue
- To look at the planning process as a sequence of events
- To stimulate doubt by raising questions, to avoid short-sighted explicitness
- To control the delegation of judgment. Experts have no absolute power; scientific knowledge is important, but always limited.

There is no such thing as "scientific planning."

- Solving practical problems as to develop sustainable transgenic crops cannot be dealt with by "scientification of planning." Dealing with wicked problems is always political because of its deontic premises (means that you have to involve knowledge what ought to be) and because we deal with traditional knowledge. Science only generates factual, instrumental, and in the best case explanatory knowledge.
- The planner (here the manager of an action plan) is not primarily an expert, but a *mid-wife of problem solving*, a teacher more than a doctor. Moderate optimism and careful seasoned disrespect, casting doubt is a virtue, not a disadvantage of an action plan manager.
- The planning process of wicked problems has to be understood as an *argumentative process*, it should be seen as a venture (or even *ad*venture) within a conspiracy framework, where one cannot anticipate all the consequences of plans.
- Systems methods of the *second generation* are trying to make this deliberation explicit, to support it and to find means in order to make this process more powerful and to get it under better control *for all participants*. Methods like the computer-based argument mapping systems of can be helpful [419].
- It helps making such processes more successful if they are conducted in the spirit of the *Symmetry of Ignorance* [420] – this is the secret of the active listening which often leads to acceptable outcomes and trust.

This seems to be a rather theoretical approach with lots of restrictive rules, but actually it is, on the contrary, an opening for much more freedom in dialogue. Also, it is more practical and efficient in creating results and contrasts with the traditional stakeholder concept where hidden agendas prevail in often disguised authoritarian structures. Such discursive processes are described in detail [80, 121–123, 421–425]. A comprehensive and voluminous monograph on risk-related debate methods has been published by Ortwin Renn [426], see especially the texts related to risk communication with essays 7 and 8 and section 8 on risk participation with numerous references, but notably lacking completely the papers on the "Systems Approach" of the Churchman/Rittel/Webber school.

In a French paper, the origin of negatively connoted words in the debate on GM crops like "contamination,"

"pollution," "Frankenfood," etc., Moirand [427] clearly reveals the links to negative events like BSE, dioxin scandals, and of course Tchernobyl, etc., thus explaining new words like "mad soya" and "mad colza" in the media. Moirand concludes that a new type of discourse is needed, but also Renn [426] does not refer to the very pragmatic and promising systems approach of Churchman and Rittel.

There are many more schools promoting discourse and new decision-making processes, also in specialized journals, only a few can be summarized here for space reason: [75, 76, 78, 84, 119, 120, 411, 427–441].

See Patrick Moore's practical examples of decision-making processes solving environmental and sustainability problems in forestry, consult his own website Green Spirit http://www.greenspirit.com/index.cfm. These processes need time. Patrick Moore [442–444] has gone successfully through such processes in the difficult task of reconciliation between the needs of timber production and environmental constraint; he needed months of debate to come to reasonable decisions.

Another good example on how group discourses have good learning effects, has been described by Snyder et al. [258]: Although the US government has assured stakeholders of their safety, the EU continues to be an outspoken opponent. This can largely be attributed to a lack of trust in the regulatory process, and especially a cynical perspective on the underlying science and institutions that govern approval. Such disparities were illustrated in 2003 when the USA donated GM maize to aid African countries stricken by famine. Under purported EU threats, negative propaganda by NGOs, and stressing retaliatory trade sanctions, African officials refused the aid. An examination of this episode contrasts the potential discord between those affected and those who formulate government policy. Using resources from both sides of the debate, this scenario summarizes the pertinent issues regarding EU's refusal to the import of transgenic crops. A group discussion and debate protocol was developed for facilitating small group and entire class consideration of the scenario while strengthening student critical thinking skills.

It helps, if you prepare carefully scenarios before people start the process, a method which has been successfully applied to the reconciliation processes in South Africa after abolishing apartheid by Adam Kahane, one of the principal mediators [445]. He also followed another wise rule: Should only people participate in such processes who are part of the problem. Another excellent example of long-term discourse is described in many aspects by von Grebmer et al. [437]:

- By working collectively the process will be more open, transparent, inclusive and accountable, and sensitive to the normative dimensions of the issues critical to the participants. The themes and processes outlined in this article set the stage for the discussions, internally and between countries, that will shape the policies of agricultural biotechnology in the region. If the dialogue can frame the discussion and be enriched by the information generated from actions taken, it can sustain the interest and commitment of the stakeholders, and more successfully direct biotechnology toward reducing hunger and poverty in the region.

There are too many scientists remaining in the ivory tower, shying away from public debates. They fear losing their independence, a fear which is not just unfounded, but actually it is the contrary: remaining in the academic ivory tower means having lost your independence, since science is not an art per se, it is full of importance for society and humanity. A strong plea in this direction is coming from [446]. Although science should remain at the heart of invention and the drive to make our lives better, scientists should, instead of always having "the answers" ready, should not be afraid to engage in a contradictory evidence-based mode.

In one of the most successful examples of long-term discourse, the author participated as an invited expert in a public hearing in 2000. Strikingly, it was done without the theoretical load described above, but with lots of financial and logistic help from the New Zealand Government, in particular from the Royal Commission on Genetic Modification. A report was finalized after a 14-month inquiry into the risks and benefits of genetic modification. It heard from over 400 experts, including scientists, environmentalists, and ethical specialists. It considered more than 10,000 public submissions and heard the view of many others during a series of public meetings, hui, and workshops around New Zealand.

The Royal Commission's major conclusion was that New Zealand should proceed cautiously with genetic

modification (GM) but not close the door to the opportunities offered by the new technology http://www.mfe.govt.nz/issues/organisms/index.html. The discourse is still continuing. Again, it is visible that the discourse is less confrontational and may lead to innovative solutions in the future [447]:

- The debate about genetic modification (GM) can be seen as characteristic of our time. Environmental groups, in challenging GM, are also challenging modernist faith in progress, and science and technology. In this paper we use the case of New Zealand's Royal Commission on Genetic Modification to explore the application of science discourses as used by environmental groups. We do this by situating the debate in the framework of modernity, discussing the use of science by environmental groups, and deconstructing the science discourses evident within environmental groups' submissions to the Commission. We find science being called into question by the very movement that has relied on it to fight environmental issues for many years. The environmental groups are challenging the traditional boundaries of science, for although they use science they also present it as a culturally embedded activity with no greater epistemological authority than other knowledge systems. Their discourses, like that of the other main actors in the GM debate, are thus part of the constant re-negotiation of the cultural construct of 'science'.

However, this process should not be mollified on the costs of hard science. The line between science and pseudoscience is often difficult to draw.

A Remark About the Psychology of the GMO Debate To be written in the next coming days.

It should also be possible to think and act in relation to the reconciliation of science and spirituality, since it will be an important element besides the ratio of science, the ethics of our societal activities, and the emotional elements in human life. But it will be difficult to separate the cheap esoteric chaff from the precious seeds of true spirituality, as Helmut Reich's writings demonstrate [448]. We must endeavor new fields of thought, as done by Papazova Ammann [449], a Bulgarian-born Swiss philosopher with roots in the schools of Muntjan and Rittel.

- What do we need as visionaries: Progress or Development? This is my question today, as I deal with the topic of Biovisionaries here in the Library of Alexandria. I ask this question because I am convinced that we need to build a new culture of questioning. We need a culture orienting itself by authentic questions. How can we develop taste and the ability to distinguish between those questions which are cognitive, statement-oriented and those which are authentic, close to life and to people? What is more important: cognizance or decision for action? How can we move between Statements and Questions? Statements reflect the need to understand the world. But they are the result of past experience and are often contained in frameworks which are coined by society. They may even protect old routines which hinder innovation. Questions, in contrast to statements¸ can transform our judgements and prejudices. Questions give birth to energy for new orientation, for a more conscious future. This orientation towards the future, towards vision provokes those choice-questions, and they alone will open the way for an urge to change the world. Visions need people who are free! The quality of freedom is inherent in the question. We must strive for this quality through choice-questions. If we cannot befriend these choice-questions with science, it will disengage from the questioners and will not be human science anymore. Thus we need a new humility of thinking – as it has been wonderfully defined by the German philosopher Heidegger: "The question is the devoutness of thinking".

Conclusions Only a multifaceted dialogue over a considerable time span will lead to success. The Internet scene is developing fast and new communication software tools are available now, so careful scrutiny for such a network of networks need to be done first, and the big players like Google and competing networks should be consulted as well.

Personal experience in dialogue with many networkers reveals that sometimes important networks are only known in specific clusters, these lacunas should be closed for many reasons – see section Illusions and Realities on Educational Effects in the Debate, the Dialogue Between Science and the Public. Knowledge exchange, jumping over national fences, and coordination will be a follow-up effect, without

even declaring it to be the goal of such activity. As for now, this is just an idea and needs to be discussed with Internet and website specialists. After all, the leading webmasters and coordinators agree that it is time to *enhance collaboration through better communication*.

ASK-FORCE can contribute to this process in making sure that professional peer-reviewed risk assessment papers are fed into the dialogue processes and are ideally fed into a life decision–making process with relevant participants.

Bibliography

1. Beardmore JA (1997) Transgenics: autotransgenics and allotransgenics. Trans Res 6(1):107–108
2. Taverniers I et al (2008) Gene stacking in transgenic plants: towards compliance between definitions, terminology, and detection within the EU regulatory framework. Environ Biosaf Res 7(4). doi:10.1051/ebr:2008018
3. Potrykus I et al (2010) Transgenic plants for food security in the context of development, statement of the pontifical academy of sciences. New Biotechnol 27(5):443–717
4. Rauschen S (2009) German GM research – a personal account. Nat Biotech 27(4):318–319
5. Showalter E (1997) Hystories. Columbia University Press, New York, 244 pp
6. Linden A, Fenn J (2003) Understanding Gartner's hype cycles. In: Strategic Analysis Report. Gartner Research, p 12
7. Chassy BM (2007) The history and future of GMOs in food and agriculture. Cereal Foods World 52(4):169–172
8. Martineau B (2002) First fruit: the creation of the Flavr savr tomato and the birth of biotech food. McGraw-Hill, New York, 224 pp
9. Carrière Y, Crowder DW, Tabashnik BE (2010) Evolutionary ecology of insect adaptation to Bt crops. Blackwell, Oxford, pp 561–573
10. Ellstrand NC et al (2010) Crops gone wild: evolution of weeds and invasives from domesticated ancestors. Blackwell, Oxford, pp 494–504
11. Huang F, Andow DA, Buschman LL (2011) Success of the high-dose/refuge resistance management strategy after 15 years of Bt crop use in North America. Entomol Experiment Et Appl 140(1):1–16
12. Gatehouse AMR, Ferry N, Raemaekers RJM (2002) The case of the monarch butterfly: a verdict is returned. Trends Genet 18(5):249–251
13. Lovei GL, Andow DA, Arpaia S (2009) Transgenic insecticidal crops and natural enemies: a detailed review of laboratory studies. Environ Entomol 38:293–306
14. Shelton A et al (2009) Setting the record straight: a rebuttal to an erroneous analysis on transgenic insecticidal crops and natural enemies. Trans Res 18(3):317–322
15. Moore GA (2002) Crossing the chasm. Harper Paperbacks, New York, Revised edition 20 Aug 2002, 256 pp
16. Thro AM (2004) Europe on transgenic crops: how public plant breeding and eco-transgenics can help in the transatlantic debate. Commentary. AgBioForum 7:142–148
17. Adams J (1995) Risk. Taylor & Francis, Bristol, 228 pp
18. Royal-Society (2009) Reaping the benefits: science and the sustainable intensification of global agriculture. In: RS Policy document 11/09. Royal Society, London, p 89
19. Arber W (2010) Genetic engineering compared to natural genetic variations. New Biotechnol 27(5):517–521
20. Britt AB, May GD (2003) Re-engineering plant gene targeting. Trends Plant Sci 8(2):90–95
21. Henderson IR, Jacobsen SE (2007) Epigenetic inheritance in plants. Nature 447(7143):418–424
22. Johnson L (2007) The genome strikes back: the evolutionary importance of defence against mobile elements. Evolut Biol 34(3):121–129
23. Moch K, Brauner R, Ott B (2005) Epigenetics, transgenic plants & risk assessment. In: Epigenetics, transgenic plants & risk assessment. 1st Dec 2005, Literaturhaus, Frankfurt am Main, Germany © 2006, Öko-Institut e.V., Box 50 02 40, D-791028 Freiburg, Die Deutsche Bibliothek – CIP Cataloguing-in-Publication-Data, A catalogue record for this publication is available from Die Deutsche Bibliothek
24. Smilde AK et al (2010) Dynamic metabolomic data analysis: a tutorial review. Metabolomics 6(1):3–17
25. Domon B, Aebersold R (2010) Options and considerations when selecting a quantitative proteomics strategy. Nat Biotechnol 28(7):710–721
26. Addona TA et al (2009) Multi-site assessment of the precision and reproducibility of multiple reaction monitoring-based measurements of proteins in plasma. Nat Biotechnol 27(7):633–U85
27. Wittenberg AHJ et al (2005) Validation of the high-throughput marker technology DArT using the model plant Arabidopsis thaliana. Molec Genet Genomics 274(1):30–39
28. Colbert T et al (2001) High-throughput screening for induced point mutations. Plant Physiol 126(2):480–484
29. Giddings VL (2006) "Cisgenic" as a product designation. Nat Biotech 24(11):1329–1329
30. Schouten HJ, Jacobsen E (2007) Are mutations in genetically modified plants dangerous?. J Biomed Biotechnol: 8261, p 2
31. Schouten HJ, Krens FA, Jacobsen E (2006) Do cisgenic plants warrant less stringent oversight? Nat Biotechnol 24(7):753–753
32. Schouten HJ et al (2006) Cisgenic plants are similar to traditionally bred plants – International regulations for genetically modified organisms should be altered to exempt cisgenesis. Embo Reports 7(8):750–753
33. Jacobsen E, Nataraja KN (2008) Cisgenics – Facilitating the second green revolution in India by improved traditional plant breeding. Curr Sci 94(11):1365–1366
34. Jacobsen E, Schouten HJ (2007) Cisgenesis strongly improves introgression breeding and induced translocation breeding of plants. Trends Biotechnol 25(5):219–223
35. Conner AJ et al (2007) Intragenic vectors for gene transfer without foreign DNA. Euphytica 154(3):341–353

36. Rigola D et al (2009) High-throughput detection of induced mutations and natural variation using keypoint (TM) technology. PLoS One 4(3):e4761
37. Parry MAJ et al (2009) Mutation discovery for crop improvement. J Exper Botany 60(10):2817–2825
38. Davies H, Bryan G, Taylor M (2008) Advances in functional genomics and genetic modification of potato. Potato Res 51(3):283–299
39. Townsend JA et al (2009) High-frequency modification of plant genes using engineered zinc-finger nucleases. Nature 459(7245):442–445, advanced online publication
40. Shukla VK et al (2009) Precise genome modification in the crop species Zea mays using zinc-finger nucleases. Nature 459(7245):437–441, advanced online publication
41. Cai C et al (2009) Targeted transgene integration in plant cells using designed zinc finger nucleases. Plant Molec Biol 69(6):699–709
42. Osakabe K, Osakabe Y, Toki S (2010) Site-directed mutagenesis in Arabidopsis using custom-designed zinc finger nucleases. Proc Nat Acad Sci 107(26):12034–12039
43. Gabriel R et al (2011) An unbiased genome-wide analysis of zinc-finger nuclease specificity. Nat Biotech 29(9): 816–823
44. Ammann K (2008) Feature: integrated farming: why organic farmers should use transgenic crops. New Biotechnol 25(2):101–107
45. Mahfouz MM et al (2011) De novo-engineered transcription activator-like effector (TALE) hybrid nuclease with novel DNA binding specificity creates double-strand breaks. Proc Nat Acad Sci 108(6):2623–2628
46. CNBS (2011) Plant genomics "Molecular scissors" developed at KAUST. CNBS, PR newswire. DOI: http://www.cnbc.com/id/41731207/Plant_Genomics_Molecular_Scissors_Developed_at_KAUST and http://www.ask-force.org/web/Genomics/CNBC-Kaust-Genomic-Scissors-2011.PDF
47. Epinat JC et al (2003) A novel engineered meganuclease induces homologous recombination in yeast and mammalian cells. Nucl Acid Res 31(11):2952–2962
48. Paques F, Duchateau P (2007) Meganucleases and DNA double-strand break-induced recombination: perspectives for gene therapy. Curr Gene Ther 7(1):49–66
49. Silva G et al (2011) Meganucleases and other tools for targeted genome engineering: perspectives and challenges for gene therapy. Curr Gene Ther 11(1):11–27
50. Benner SA (2004) Understanding nucleic acids using synthetic chemistry. Acc Chem Res 37(10):784–797
51. Tian JD, Ma KS, Saaem I (2009) Advancing high-throughput gene synthesis technology. Molec Biosyst 5(7):714–722
52. Benner SA et al (1998) Redesigning nucleic acids. Pure Appl Chem 70(2):263–266
53. Benner SA, Sismour AM (2005) Synthetic biology. Nat Rev Genet 6(7):533–543
54. Rusch DB et al (2007) The sorcerer ii global ocean sampling expedition: Northwest Atlantic through Eastern tropical pacific. Plos Biol 5(3):398–431
55. Gibson DG et al (2008) Complete chemical synthesis, assembly, and cloning of a *Mycoplasma genitalium* genome. Science 319(5867):1215–1220
56. Gibson DG et al (2008) One-step assembly in yeast of 25 overlapping DNA fragments to form a complete synthetic Mycoplasma genitalium genome. Proc Nat Acad Sci USA 105(51):20404–20409
57. Gibson DG et al (2010) Creation of a bacterial cell controlled by a chemically synthesized genome. Science 329(5987):52–56. doi:10.1126/science.1190719
58. Bugl H et al (2007) DNA synthesis and biological security. Nat Biotechnol 25:627–629
59. Maurer SM, Lucas KV, Terrell S (2006) From understanding to action: community-based options for improving safety and security in synthetic biology, Draft 1.1, 15 April 2006. University of California, Berkeley, Califorina, p 93
60. Serrano L (2007) Synthetic biology: promises and challenges. Mol Syst Biol 3:158
61. Edmond G, Mercer D (2009) Norms and irony in the biosciences: ameliorating critique in synthetic biology. Law Literat 21(3):445–470
62. Miller HI (2010) Understanding the frankenstein myth. Project Syndicate, a World of Idas. http://www.ask-force.org/web/Genomics/Miller-Understanding-Frankenstein-Tradition-2010.pdf
63. Tabashnik BE et al (2011) Efficacy of genetically modified Bt toxins against insects with different genetic mechanisms of resistance. Nat Biotech, advance online publication
64. Soberon M et al (2007) Engineering modified Bt toxins to counter insect resistance. Science 318(5856):1640–1642
65. Keller D (2009) Start talking to each other!' – dialogue as key to biotechnology's future in Europe. New Biotechnol 25:185, Corrected proof
66. Ramon D, Diamante A, Calvo MD (2008) Food biotechnology and education. Electron J Biotechnol 11(5)
67. Harms U (2002) Biotechnology education in schools. Electron J Biotechnol 5(3):205–211
68. Gensuisse (2011) Themenfocus. Gensuisse Website Forum 2011. Available from: http://www.gensuisse.ch/focus/index.html
69. Sengooba T et al (2009) Biosafety education relevant to genetically engineered crops for academic and non-academic stakeholders in East Africa. Electron J Biotechnol 12(1)
70. McHughen A (2007) Public perceptions of biotechnology. Biotechnol J 2(9):1105–1111
71. James C (2009) Global status of commercialized biotech/GM crops. Brief 39, Executive Summary. ISAAA, p 20
72. Sturgis P, Allum N (2004) Science in society: re-evaluating the deficit model of public attitudes. Public Understand Sci 13(1):55–74
73. Sturgis P, Cooper H, Fife-Schaw C (2005) Attitudes to biotechnology: estimating the opinions of a better-informed public. New Genet Soc 24(1):31–56
74. Sturgis P, Roberts C, Allum N (2005) A different take on the deliberative poll – Information, deliberation, and attitude constraint. Public Opin Quart 69(1):30–65

75. Gaskell G et al (2000) Biotechnology and the European public. Nat Biotechnol 18(9):935–938
76. Schuman H, Presser S (1980) Public-opinion and public ignorance – the fine line between attitudes and non-attitudes. Am J Sociol 85(5):1214–1225
77. Aerni P, Scholderer J, Ermen D (2011) How would Swiss consumers decide if they had freedom of choice? Evidence from a field study with organic, conventional and GM corn bread. Food Policy
78. Irwin A (2006) The politics of talk: coming to terms with the "new" scientific governance. Soc Stud Sci 36(2):299–320
79. Churchman CW (1979) The systems approach and its ennemies and (Commented German transl.: Der Systemansatz und seine "Feinde," with an Introduction by the editor and translator, Werner Ulrich, ed. and transl., Paul Haupt, Bern, 1981). Basic Books, New York
80. Rittel HWJ, Webber MR (2005) Dilemmas in a general theory of planning. Policy Sci 4(2):155–169
81. Rittel H (1992) Planen, entwerfen, design, ausgewählte schriften zu theorie und methodik. In: Reuter Wolf D (ed) Planen, entwerfen, design. Verlag W. Kohlhammer, Berlin, p 432
82. Protzen JP, Harris DW (2010) The universe of design: Horst Rittel's theories of design and planning, 1st edn. Routledge, London/New York, p 264, 19 June 2010
83. Magnan A (2003) Refeudalizing the public sphere: "Manipulated publicity" in the Canadian debate on GM foods. In: Annual meeting of the canadian-sociology-and-anthropology-association (CSAA). University of Alberta, Halifax, Canada
84. Vaughan E (1995) The significance of socioeconomic and ethnic diversity for the risk communication process. Risk Anal 15(2):169–180
85. Osseweijer P (2006) A new model for science communication that takes ethical considerations into account – The three-E model: entertainment, emotion and education. Sci Eng Ethics 12(4):591–593
86. Osseweijer P (2006) Imagine projects with a strong emotional appeal. Nature 444(7118):422–422
87. Osseweijer P (2006) A short history of talking biotech, fifteen years of iterative action research in institutionalising scientists' engagement in public communication. Vrije Universiteit, Amsterdam
88. Osseweijer P, Ammann K, Kinderlerer J (2010) Societal issues in industrial biotechnology. In: Soethaert W, Vandamme EJ (eds) Industrial biotechnology, sustainable growth and economic success, handbook. Wiley, VCH Verlag, Weinheim, pp 457–481, Chapter 14, 522 pp
89. Koutsogiannis D, Mitsikopoulou B (2004) The Internet as a glocal discourse environment – A commentary on "second language socialization in a bilingual chat room" by Wan Shun Eva Lam and "second language cyberhetoric: A study of Chinese L2 writers in an online usenet group" by Joel Bloch. Lang Learn Technol 8(3):83–89
90. Kostoff RN et al (2006) The structure and infrastructure of the global nanotechnology literature. J Nanoparticle Res 8(3–4):301–321
91. Kanter RM (2000) Are you ready to lead the e-cultural revolution? Inc 22(2):43–44
92. Bruns A (2008) Blogs. Wikipedia. Second life and beyond (digital formations). Peter Lang, Bern
93. Reifer D (2002) Ten deadly risks in internet and intranet software development. IEEE Software 19(2):12–14
94. Kalman ME et al (2002) Motivations to resolve communication dilemmas in database-mediated collaboration. Commun Res 29(2):125–154
95. Borland N, Wallace D (1999) Environmentally conscious product design: a collaborative internet-based modeling approach. J Indust Ecol 3(2–3):33–46
96. Dall'Olio GM et al (2011) Ten simple rules for getting help from online scientific communities. PLoS Comput Biol 7(9): e1002202
97. Degrassi G, Alexandrova N, Ripandelli D (2003) Databases on biotechnology and biosafety of GMOs. Environ Biosaf Res 2(3):145–160
98. Burns CG (2011) Biosafety resources on the Internet. J Int Wildlife Law & Policy http://www.jiwlp.com/ 20110801. Available from: http://www.jiwlp.com/contents/biosafety_resources_net.html
99. Ammann K (2011) List of websites related to GM crops and biotechnology. DOI: http://www.ask-force.org/web/Sustainability/Websites-List-Publ.def.pdf
100. Leydesdorff L (2002) Indicators of structural change in the dynamics of science: entropy statistics of the SCI journal citation reports. Scientometrics 53(1):131–159
101. Leydesdorff L (2008) Caveats for the use of citation indicators in research and journal evaluations. J Am Soc Inform Sci Technol 59(2):278–287
102. Leydesdorff L (2009) How are new citation-based journal indicators adding to the bibliometric toolbox? J Am Soc Inform Sci Technol 60(7):1327–1336
103. Leydesdorff L, Wagner C (2009) Macro-level indicators of the relations between research funding and research output. J Informet 3(4):353–362
104. Leydesdorff L, Hellsten I (2006) Measuring the meaning of words in contexts: An automated analysis of controversies about "Monarch butterflies", "Frankenfoods", and "stem cells". Scientometrics 67(2):231–258
105. Aizen J et al (2004) Traffic-based feedback on the web. Proc Nat Acad Sci USA 101(Suppl 1):5254–5260
106. Cavaller V (2009) Scientometrics and patent bibliometrics in RUL analysis: a new approach to valuation of intangible assets. Vine 39:80–91
107. Cavaller V, Aubertin C (2008) Elements of scientometrics and patent bibliometric-analysis for the estimated remaining useful life (RUL) in the valuation of intangible assets. In: Proceedings of the 5th international conference on intellectual capital and knowledge management and organisational learning, New York, pp 87–95
108. Laporte RE et al (2002) Papyrus to powerpoint (P 2 P): metamorphosis of scientific communication. Brit Med J 325(7378):1478–1481

109. Sa ER et al (2003) Open source model for global collaboration in higher education. Int J Med Inform 71(2–3):165–165
110. Linkov F et al (2003) Globallsation of prevention education: a golden lecture. Lancet 362(9395):1586–1587
111. Linkov F, The I (2006) Intemet-based supercourse system. J Public Health Policy 27(4):442–443
112. Laporte RE et al (2002) Infopoints – Whisking research into the classroom. Brit Med J 324(7329):99–99
113. Laporte RE et al (2006) A scientific supercourse. Science 312(5773):526–526
114. Sauer F, Bennett S, Cha M, Linkov F, LaPorte R (2010) Supercourse, Bibliotheca Alexandrina, and the educator as catalyst. Educause Quart 33(3)
115. Ammann K (2011) Presentations for conferences etc. with powerpoint slides. In Audio-Visual Material 20110904, Ammann K, Neuchatel
116. Adly N (2009) Bibliotheca alexandrina: a digital revival. Educause Rev 44(6):8–9
117. Craig W et al (2008) An overview of general features of risk assessments of genetically modified crops. Euphytica 164(3):853–880
118. Leicht EA, Newman MEJ (2008) Community structure in directed networks. Phys Rev Lett 100(11):118703
119. Newman MEJ (2003) The structure and function of complex networks. Siam Rev 45:167–256
120. Saner M (2007) A map of the interface between science & policy, staff papers. Council of Canadian Academies, Ottawa, p 15
121. Rith C, Dubberly H (2007) Horst W. J. Rittel's writings on design: select annotations. Des Issues 23(1):75–77
122. Rittel H, Weber M (1973) Dilemmas in a general theory of planning. Policy Sci 4:155–169
123. Ammann K, Papazova Ammann B (2004) Factors influencing public policy development in agricultural biotechnology. In: Shantaram S (ed) Risk assessment of transgenic crops. Wiley, Hoboken, p 1552
124. Gasson M, Burke D (2001) Scientific perspectives on regulating the safety of genetically modified foods. Nat Rev Genet 2(3):217–222
125. Phillips PWB (2003) Traceability and trade of genetically modified food. Biotechnol Sci Soc Crossroad 5:141–154
126. Sheehy RE, Kramer M, Hiatt WR (1988) Reduction of polygalacturonase activity in tomato fruit by antisense rna. Proc Nat Acad Sci USA 85(23):8805–8809
127. Redenbaugh K et al (1994) Regulatory Assessment of the Flavr-savr tomato. Trends Food Sci Technol 5(4):105–110
128. Kramer MG, Redenbaugh K (1994) Commercialization of a tomato with an antisense polygalacturonase gene – the Flavr Savr(Tm) tomato story. Euphytica 79(3):293–297
129. Krieger EK et al (2008) The Flavr Savr tomato, an early example of RNAi technology. Hortscience 43(3):962–964
130. Graff G, Zilberman D (2004) Explaining Europe's resistance to agricultural biotechnology. Agric Resour Econ 7(5):4
131. Lawrence F (2009) It is too late to shut the door on GM foods consumers said no to the GM farming giants a decade ago, but that didn't stop millions of tonnes of their soya entering the food chain, in The Guardian. The Guardian and Observer, London
132. Flachowsky G et al (2007) Studies on feeds from genetically modified plants (GMP) – Contributions to nutritional and safety assessment. Anim Feed Sci Technol 133(1–2):2–30
133. Aumaitre A (2004) Safety assessment and feeding value for pigs, poultry and ruminant animals of pest protected (Bt) plants and herbicide tolerant (glyphosate, glufosinate) plants: interpretation of experimental results observed worldwide on GM plants. Italian J Anim Sci 3(2):107–121
134. Paarlberg R (2006) Are genetically modified (GM) crops a commercial risk for Africa? Int J Technol Globalisation 2(1–2):81–92
135. Cohen JI, Paarlberg R (2002) Explaining restricted approval and availability of GM crops in developing countries. AgBiotechNet 4:1–6
136. Gruere GP, Carter CA, Farzin YH (2008) What labelling policy for consumer choice? The case of genetically modified food in Canada and Europe. Canad J Econom-Revue Canadienne D Economique 41(4):1472–1497
137. Gruere GP, Rosegrant MW (2008) Assessing the implementation effects of the biosafety protocol's proposed stringent information requirements for genetically modified commodities in countries of the Asia Pacific economic cooperation. Rev Agric Econom 30(2):214–232
138. Gruere GP, Sengupta S (2009) Biosafety decisions and perceived commercial risks, The role of GM-free private standards. In: IFPRI Discussion Paper 00847, Environment and Production Technology Division. FPRI, Washington DC, p 40
139. Greenpeace (2007) Contamination Report 2006, annual review of cases of contamination, illegal planting and negative side effects of genetically modified organisms. Greenpeace International, Amsterdam, p 24
140. Greenpeace (2008) Contamination Report 2007, annual review of cases of contamination, illegal planting and negative side effects of genetically modified organisms. Greenpeace International, Amsterdam, p 48
141. ISAAA (2011) Cotton (*Gossypium hirsutum l.*) events. ISAAA 2011 11. Oct 2011. Available from: http://www.isaaa.org/gmapprovaldatabase/cropevents/default.asp?CropID=6
142. Sadashivappa P, Qaim M (2009) Bt cotton in India: development of benefits and the role of government seed price interventions. AgBioForum 12:172–183
143. Mueller-Jung J (2007) Wie verpackt man eine Kulturrevolution in Watte? How to wrap up a cultural revolution in cotton wool?. In: Frankfurter Allgemeine Zeitung. Frankfurt. p N1
144. Gruere G, Methta-Bhatt P, Sengupta D (2008) Bt cotton and farmer suicides in India, reviewing the evidence. IFPRI-Discussion Paper 2008, 00808
145. Gruere G, Sengupta D (2011) Bt cotton and farmer suicides in India: an evidence-based assessment. J Develop Stud 47(2):316–337
146. Shiva V (2004) The suicide economy of corporate globalisation. Z Net – The spirit of resistance lives 2004. Available from:

http://www.zcommunications.org/the-suicide-economy-of-corporate-globalisation-byvandana2-shiva
147. Sunilkumar G et al (2006) From the cover: engineering cottonseed for use in human nutrition by tissue-specific reduction of toxic gossypol. Proc Natl Acad Sci 103(48):18054–18059. doi:10.1073/pnas.0605389103
148. Choudhary B, Gaur K (2011) Bt cotton in India, a multipurpose crop. In: ISAA (ed) Celebrating 10 years. International Service for the Aquisition of Agri-Biotech Applications, Biotech Information Center, New Delhi, p 6
149. Graff G, Hochman G, Zilberman D (2009) The political economy of agricultural biotechnology policies. AgBioForum 12:1–13, http://www.agbioforum.org/v12n1/v12n1a04-graff.htm and http://www.botanischergarten.ch/Regulation/Graff-Political-Economy-Policies-2009.pdf
150. Ayal S, Hochman G (2009) Ignorance or integration: the cognitive processes underlying choice behavior. J Behav Decis Mak 22(4):455–474
151. Ministerio da Ciencia e Technologia (2005) CTN Bio, Biosafety Law Nº 11.105, of 24 March 2005. Ministerio da Ciencia e Technologia, Brazilia, p 17
152. European Parliament and European Council (2003) Regulation (EC) No 1829/2003. Off J Euro Union L 268(1):1–23, 20030922
153. The European parliament and the council of the European union (2010) EU-Regulation-GMO-free regions, GMOs: Member states to be given full responsibility on cultivation in their territories, IP/10/921. 20100713, The European parliament and the council of the European union, Brussels, p 2
154. James C (2009) Global status of commercialized biotech/GM Crops. In: ISAA (ed) AAA briefs. The International Service for the Acquisition of Agri-biotech Applications (ISAAA), Ithaca
155. Galvao A (2010) Celeres, Biotechnology Report 2010. 20100809, Uberlandia, Matto Grosso, Celeres, p 7
156. Marques R, Neto CGA (2007) The Brazilian system of innovation in biotechnology: a preliminary study. J Technol Manag Innov 2(1):55–63
157. Mendonca-Hagler L et al (2008) Trends in biotechnology and biosafety in Brazil. Environ Biosaf Res 7(3):115–121
158. Silveira JM, Ferreira J, Dal Poz ME, Alssad A (2004) Biotecnologia e recursos genéticos: desafios e oportunidades para o Brasil/Biotechnology and genetic resources: challenges and opportunities for Brazil. Campinas Instituto de Economia, Rio de Janeiro, p 412
159. Frohme M et al (2000) Mapping analysis of the Xylella fastidiosa genome. Nucl Acids Res 28(16):3100–3104
160. Simpson AJG et al (2000) The genome sequence of the plant pathogen *Xylella fastidiosa*. Nature 406(6792):151–157
161. Vasconcelos A (2003) The complete genome sequence of *Chromobacterium violaceum* reveals remarkable and exploitable bacterial adaptability. Proc Nat Acad Sci USA 100(20):11660–11665
162. Magnani GS et al (2010) Diversity of endophytic bacteria in Brazilian sugarcane. Genet Molec Res 9(1):250–258
163. Mendes R et al (2007) Diversity of cultivated endophytic bacteria from sugarcane: Genetic and biochemical characterization of *Burkholderia cepacia* complex isolates. Appl Environ Microbiol 73(22):7259–7267
164. Editorial N (2010) Brazil's biotech boom. Nature 466(7304): 295–295
165. Bonfim K et al (2007) RNAi-mediated resistance to bean golden mosaic virus in genetically engineered common bean (*Phaseolus vulgaris*). Molec Plant Microbe Interact 20(6):717–726
166. Oda L (2011) Approval of Brazilian transgenic beans has social importance, says ANBio in the Sacramento Bee. PRN Newswire, AnBio, Sao Paulo, p 2
167. Paganelli A et al (2010) Glyphosate-based herbicides produce teratogenic effects on vertebrates by impairing retinoic acid signaling. Chem Res Toxicol
168. Chassy B, Parrott W (2009) Is this study believable? Examples from animal studies with GM foods. Agric Biotechnol 9. doi: http://www.agribiotech.info/details and http://www.botanischergarten.ch/Peer-Review/Chassy-Parrott-Believable-2009.doc
169. Antoniou M et al (2010) GM Soy, sustainable?, responsible?, GV-SOJA, Nachhaltig? Verantwortungsbewusst? German, p 11
170. Martin-Orue SM et al (2002) Degradation of transgenic DNA from genetically modified soya and maize in human intestinal simulations. Brit J Nutr 87(6):533–542
171. Netherwood T et al (2004) Assessing the survival of transgenic plant DNA in the human gastrointestinal tract. Nat Biotechnol 22(2):204–209
172. Netherwood T et al (1999) Gene transfer in the gastrointestinal tract. Appl Environ Microbiol 65(11):5139–5141
173. Zhang L et al (2011) Exogenous plant MIR168a specifically targets mammalian LDLRAP1: evidence of cross-kingdom regulation by microRNA. Cell Res
174. GMwatch (20110921) We incorporate genetic information from the food we eat – new study GMwatch website. http://www.gmwatch.org, DOI: http://www.gmwatch.org/index.php?option=com_content&view=article&id=13423:we-incorporate-genetic-information-from-the-food-we-eat-new-study
175. Auer C, Frederick R (2009) Crop improvement using small RNAs: applications and predictive ecological risk assessments. Trends Biotechnol 27(11):644–651
176. Fransen R (2007) Peer review: too much of a good thing? Scientist 21(9):18–18
177. Waltz E (2009) Battlefield, papers suggesting that biotech crops might harm the environment attract a hail of abuse from other scientists, News feature. Nature 461:27–32
178. Ammann K (2011) Review: is the impact of Bt maize on non-target insects significantly negative?. ASK-FORCE contribution AF-8 *AF-8*, 23, 20111002, DOI: http://www.ask-force.org/web/AF-8-Lovei/AF-8-Lovei-Non-Target-20111002-opensource.pdf
179. Reiss T, Lacasa ID (2007) Benchmarking national biotechnology policy across Europe: a systems approach using quantitative and qualitative indicators. Res Eval 16(4):331–339

180. Linkov F, Lovalekar M, LaPorte R (2006) Scientific journals are "faith based": is there science behind peer review? J Roy Soc Med 99(12):596–598
181. Lubchenco J (1998) Entering the century of the environment: a new social contract for science. Science 279(5350):491–497
182. Linkov F, Lovalekar M, LaPorte R (2007) Quality control of epidemiological lectures online: scientific evaluation of peer review. Croatian Med J 48(2):249–255
183. Ammann K (2007) Evaluations faculty of 1000, manuscript and links. p 3
184. Hansen M (2009) Statement from Michael Hansen, CEO of Elsevier's health sciences division, regarding Australia based sponsored journal practices between 2000 and 2005. Elsevier Website 7 May 2009, doi: http://www.elsevier.com/wps/find/authored_newsitem.cws_home/companynews05_01203 and http://www.ask-force.org/web/Peer-Review/Hansen-Statement-ELSEVIER-2009.pdf
185. Goldacre B (2009) Peer review is flawed but the best we've got. In: The Guardian.
186. Smith R (2005) Medical journals are an extension of the marketing arm of pharmaceutical companies. Plos Med 2(5):364–366
187. Smith R (2003) Medical journals and pharmaceutical companies: uneasy bedfellows. Brit Med J 326(7400):1202–1205
188. Scott A (2007) Peer review and the relevance of science. Futures 39(7):827–845
189. Graff GD, Newcomb J (2003) Agricultural biotechnology at the crossroads, Part 1: the changing structure of the industry. Bio-era, p 26
190. Kostoff R (2002) Citation analysis of research performer quality. Scientometrics 53(1):49–71
191. Rosi-Marshall EJ et al (2007) Toxins in transgenic crop byproducts may affect headwater stream ecosystems. Proc Nat Acad Sci USA 104:16204–16208
192. Tank JL et al (2010) Occurrence of maize detritus and a transgenic insecticidal protein (Cry1Ab) within the stream network of an agricultural landscape. Proc Nat Acad Sci
193. Beachy RN et al (2008) The burden of proof: a response to Rosi-Marshall et al. Proc Nat Acad Sci 105:16204–16208
194. Parrott W (2008) Study of Bt impact on caddisflies overstates its conclusions: response to Rosi-Marshall et al. Proc Nat Acad Sci 105: E10
195. McHughen A et al (2007) Letter to the editor of PNAS, related to the publication of Rosi-Marshall, E. PNAS, Washington
196. Velimirov A et al (2008) Biological effects of transgenic maize NK603xMON810 fed in long term reproduction studies in mice, Report, in Forschungsberichte der Sektion IV Band 3/2008, Bundesministerium für Gesundheit Familie und Jugend Sektion IV (ed) Herausgeber, Medieninhaber und Hersteller: Bundesministerium für Gesundheit, Familie und Jugend, Sektion IV Radetzkystraße 2, 1031 Wien, p 109
197. Ammann K (20100407) Review: the Austrian experiment with mice fed with a hybrid GM maize from Monsanto, Part 1: background and Part 2: experiment. ASK-FORCE contribution AF-5 **AF-5**, Experiment: 19p and Background 8p doi: http://www.ask-force.org/web/AF-5-Austrian-Micestudy/AF-5-Austrian-Experiment-20100407-opensource.pdf, http://www.ask-force.org/web/AF-5-Austrian-Micestudy/AF-5-Austrian-Experiment-20100407-web.doc, http://www.ask-force.org/web/AF-5-Austrian-Micestudy/AF-5-Austrian-Exp-Background-20090807-opensource.pdf, http://www.ask-force.org/web/AF-5-Austrian-Micestudy/AF-5-Austrian-Exp-Background-20090828-web.pdf
198. Sinha G (2009) Up in arms. Nat Biotechnol 27(7):592–594
199. Dona A, Arvanitoyannis IS (2009) Health risks of genetically modified foods. Crit Rev Food Sci Nutr 49(2):164–175
200. Tang H, Tan S, Cheng X (2009) A survey on sentiment detection of reviews. Exp Syst Appl 36:10760–10773
201. Ammann K (20090828) Review: genomic misconception of transgenesis, The difference between GM- and non-GM-crops on the level of molecular processes has been overestimated. ASK-FORCE contribution AF-7 AF-7, 57 DOI: http://www.ask-force.org/web/AF-7-Dona-rebuttal/AF-7-Dona-20090828-opensource.pdf
202. Chassy BM (2009) Global regulation of transgenic crops. In: Kriz AL, Larkins BA (eds) Molecular genetic approaches to maize improvement. Springer, Berlin, pp 107–124
203. Intemann KK, de Melo-Martin I (2008) Regulating scientific research: should scientists be left alone? Faseb J 22(3): 654–658
204. de Melo-Martin I, Meghani Z (2008) Beyond risk – A more realistic risk - benefit analysis of agricultural biotechnologies. Embo Reports 9(4):302–306
205. Seralini GE, Cellier D, de Vendomois JS (2007) New analysis of a rat feeding study with a genetically modified maize reveals signs of hepatorenal toxicity. Arch Environ Contamin Toxicol:596–602
206. EFSA (2007) Safety and nutritional assessment of GM plants and derived food and feed: the role of animal feeding trials. Food Chem Toxical 46(Suppl 1):S2–S70
207. EFSA (2007) Statement of the scientific panel on genetically modified organisms on the analysis of data from a 90-day rat feeding study with MON 863 maize. European Food Safety Authority, p 5
208. EFSA (2007) Press release: EFSA reaffirms its risk assessment of genetically modified maize MON 863 maize. European Food Safety Authority, p 5
209. Imposteurs. Tout (ou presque) sur le CRIIGEN 2011 (cited 12. Oct 2011. Available from: http://imposteurs.over-blog.com/pages/Tout_ou_presque_sur_le_CRIIGEN-4536267.html
210. Kuntz M (2011) Seralini critique: the latest opus of "parallel science" of Criigen from March 2011. Parallel Science (Website) 2011 (cited 12 Oct 2011). Available from: http://ddata.over-blog.com/xxxyyy/1/39/38/37/Critical_views_on_Seralini_20110710.pdf
211. Watson JD, Crick FHC (1953) Genetical implications of the structure of deoxyribonucleic acid. Nature 171(4361):964–967
212. Watson JD, Crick FHC (1953) Molecular structure of nucleic acids - a structure for deoxyribose nucleic acid. Nature 171(4356):737–738

213. Wilkins MHF et al (1953) Helical structure of crystalline deoxypentose nucleic acid. Nature 172(4382):759–762
214. Berg P et al (1975) Summary statement of asilomar conference on recombinant DNA-molecules. Proc Nat Acad Sci USA 72(6):1981–1984
215. Berg P, Singer M (1995) The recombinant-DNA controversy - 20 years later. Bio-Technol 13(10):1132–1134
216. Friedberg EC (2007) The writing life of James D. Watson. Adler Museum Bull 33(2):3–16
217. Klug A (2004) The discovery of the DNA double helix. J Molec Biol 335(1):3–26
218. Bennett D, Glasner P, Travis D (1986) The politics of uncertainty. Routledge and Kegan Paul plc, London, p 218
219. NRC (National-Research-Council) (1989) Field testing genetically modified organism. Framework for decisions. In: National Research Council (ed) Committee on scientific evaluation of the introduction of genetically modified microorganisms and plants into the environment, NAO Sciences. The National Academy Press, Washington, DC, p 184
220. Lehrman S (1992) Overregulation could damage united-states biotechnology, says report. Nature 359(6396):569–569
221. Mundell I (1992) Britain wrestles with EC rule on modified organisms. Nature 359(6396):569–569
222. McClintock B (1930) A cytological demonstration of the location of an interchange between two non-homologous chromosomes of Zea mays. Proc Nat Acad Sci USA 16: 791–796
223. McClintock B (1953) Induction of instability at selected loci in Maize. Genetics 38(6):579–599
224. Fedoroff N (1994) Mcclintock, Barbara (June 16, 1902 September 2, 1992). Proc Am Philos Soc 138(3):431–445
225. Fedoroff N, Schlappi M, Raina R (1995) Epigenetic regulation of the maize Spm transposon. Bioessays 17(4):291–297
226. Shapiro JA (1997) Genome organization, natural genetic engineering and adaptive mutation. Trends Genet 13(3): 98–104
227. Lewin R (1983) A naturalist of the genome. Science 222(4622):402–405
228. Arber W (2000) Genetic variation: molecular mechanisms and impact on microbial evolution. Fems Microbiol Rev 24(1):1–7
229. Arber W (2002) Roots, strategies and prospects of functional genomics. Curr Sci 83(7):826–828
230. Arber W (2003) Elements for a theory of molecular evolution. Gene 317(1–2):3–11
231. Arber W (2004) Biological evolution: lessons to be learned from microbial population biology and genetics. Res Microbiol 155(5):297–300
232. Arber W (1994) Molecular evolution: comparison of natural and engineered genetic variations. Pontifical Acad Sci Scripta Varia 103:90–101
233. Hackett P (2002) Genetic engineering: what are we fearing? Trans Res 11(2):97–99
234. Ghatnekar L, Jaarola M, Bengtsson BO (2006) The introgression of a functional nuclear gene from Poa to Festuca ovina. Proc Biol Sci 273(1585):395–399
235. Baudo MM et al (2006) Transgenesis has less impact on the transcriptome of wheat grain than conventional breeding. Plant Biotechnol J 4(4):369–380
236. Batista R et al (2008) Microarray analyses reveal that plant mutagenesis may induce more transcriptomic changes than transgene insertion. Proc Nat Acad Sci USA 105(9):3640–3645
237. Shewry PR et al (2007) Are GM and conventionally bred cereals really different? Trends Food Sci Technol 18(4): 201–209
238. Ammann K (2009) Feature: why farming with high tech methods should integrate elements of organic agriculture. New Biotechnol 25:378–388
239. Barnabás B, Obert B, Kovács G (1999) Colchicine, an efficient genome-doubling agent for maize (Zea mays L.) microspores cultured in anthero. Plant Cell Reports 18(10):858–862
240. Awoleye F et al (1994) Nuclear-DNA content and in-vitro induced somatic polyploidization cassava (*Manihot-Esculenta* crantz) breeding. Euphytica 76(3):195–202
241. Reynolds MP, van Ginkel M, Ribaut JM (2000) Avenues for genetic modification of radiation use efficiency in wheat. J Exp Botany 51:459–473
242. Molnar I, Benavente E, Molnar-Lang M (2009) Detection of intergenomic chromosome rearrangements in irradiated *Triticum aestivum – Aegilops biuncialis* amphiploids by multicolour genomic in situ hybridization. Genome 52(2):156–165
243. Schouten HJ, Jacobsen E (2007) Are mutations in genetically modified plants dangerous? J Biomed Biotechnol
244. Latham JR, Wilson AK, Steinbrecher RA (2006) The mutational consequences of plant transformation. J Biomed Biotechnol 2006:1–7
245. Wilson A, Latham J, Steinbrecher R (2006) Transformation-induced mutations in transgenic plants: analysis and biosafety implications. Biotechnol Genet Eng Rev 23(11):1–26
246. Baarends WM, van der Laan R, Grootegoed JA (2001) DNA repair mechanisms and gametogenesis. Reproduction 121(1):31–39
247. Dong CM, Whitford R, Langridge P (2002) A DNA mismatch repair gene links to the Ph2 locus in wheat. Genome 45(1):116–124
248. Morikawa K, Shirakawa M (2001) Three-dimensional structural views of damaged-DNA recognition: T4 endonuclease V, E coli Vsr protein, and human nucleotide excision repair factor XPA (vol 460, pg 257, 2000). Mutation Res DNA Repair 485(3):267–268
249. Lammerts van Bueren ET, Struik PC, Jacobsen E (2002) Ecological concepts in organic farming and their consequences for an organic crop ideotype. Netherlands J Agric Sci 50(1):1–26
250. Lammerts van Bueren ET, Struik PC, Jacobsen E (2003) Organic propagation of seed and planting material: an overview of problems and challenges for research. Njas-Wageningen J Sci 51(3):263–277
251. Anonymous P (1992) Pose no special risks just because of the processes used to make them. Nature 356(6364):1–2

252. Andree P (2002) The biopolitics of genetically modified organisms in Canada. J Canad Stud Revue D Etudes Canadiennes 37(3):162–191
253. Berwald D, Carter CA, Gruere GP (2006) Rejecting new technology: the case of genetically modified wheat. Am J Agric Econ 88(2):432–447
254. Macdonald P, Yarrow S (2002) Regulation of Bt crops in Canada. In: 8th international colloquium on invertebrate pathology and microbial control/35th annual meeting of the SIP/6th international conference on Bacillus Thuringiensis. Academic Press Inc Elsevier Science, Iguassu Falls, Brazil
255. Ramjoue C (2007) The transatlantic rift in genetically modified food policy. J Agric Environ Ethics 20(5):419–436
256. Ramjoue C (2007) The transatlantic rift in genetically modified food policy. Thesis presented to the Faculty of Arts. University of Zurich, Zurich, p 263
257. Kalaitzandonakes N, Marks L, Vickner SS (2005) Sentiments and acts towards genetically modified foods. Int J Biotechnol 7(1–3):161–177
258. Snyder LU et al (2008) European union's moratorium impact on food biotechnology: a discussion-based scenario. J Nat Resour Life Sci Educ 37:27–31
259. Herman RA, Chassy BM, Parrott W (2009) Compositional assessment of transgenic crops: an idea whose time has passed. Trends Biotechnol 27(10):555–557, Corrected proof
260. Romeis J et al (2008) Assessment of risk of insect-resistant transgenic crops to nontarget arthropods. Nat Biotechnol 26(2):203–208
261. Raybould AF (2010) Reducing uncertainty in regulatory decision-making for transgenic crops: more ecological research or shrewder environmental risk assessment? GM crops 1(1):1–7
262. Raven P et al (2006) Where next for genome sequencing? Science 311(5760):468–468
263. Kesavan PC, Swaminathan MS (2008) Strategies and models for agricultural sustainability in developing Asian countries. Philos Trans Roy Soc B-Biol Sci 363:877–891
264. Plan D, van den Eede G (2010) The EU legislation on GMOs. JRC Scientific and Technical Reports. European Commission Joint Research Denter, JRC, and Institute for Health and Consumer Protection IHCP. Publications Office of the European Union, © European Union, Luxembourg
265. McLean MA et al (2002) A conceptual framework for implementing biosafety: linking policy, capacity, and regulation. In: ISNAR briefing papers. ISNAR, International Service for National Agricultural Research, Washington DC, pp 1–12
266. Graff GD, Zilberman D, Bennett AB (2009) The contraction of agbiotech product quality innovation. Nat Biotechnol 27(8):702–704
267. Miller JK, Bradford KJ (2010) The regulatory bottleneck for biotech specialty crops. Nat Biotechnol 28(10):1012–1014
268. Strauss SH et al (2009) Strangled at birth? Forest biotech and the convention on biological diversity. Nat Biotech 27(6):519–527
269. McLean MA, Charest PJ (2000) The regulation of transgenic trees in North America. Silvae Genetica 49(6):233–239
270. Kalaitzandonakes N, Alston JM, Bradford KJ (2007) Compliance costs for regulatory approval of new biotech crops. Nat Biotechnol 25(5):509–511
271. Morandini P (2007) (20071211) A serious cover up story unveiled in Italy concerning a GM crop field trial, Press release. DOI: http://www.botanischergarten.ch/ASK-FORCE-NEWS-Maize-Lombardia/Morandini-press-release-20071211.pdf
272. Morandini P (2008) Al contadino non far sapere. Espansione n. 5–41, Polenta, May 2008, p 3
273. Marshall A (2007) Another inconvenient truth. In Europe, no one apparently wants to listen if you have good news about genetically modified organisms (GMOs). Nat Biotechnol 25(12):1330
274. Ammann K (2009) Biodiversity and GM crops. In: Ferry N, Gatehouse AMR (eds) Environmental impact of genetically modified/novel crops, released in March, 423p. CAB International, Wallingford, p 28
275. Ronald PC, Adamchak RW (2008) Tomorrow's table: organic farming, genetics, and the future of food. Oxford University Press, Oxford, p 232
276. deRenobales-Scheifler M (2009) More sustainable food: genetically modified seeds in organic farming. Junta General del Principado de Asturias Sociedad Internacional de Bioética (SIBI), Gijon, p 119
277. Paarlberg R (2009) The ethics of modern agriculture. Society 46(1):4–8
278. Herring RJ (2007) The genomics revolution and development studies: science, poverty and politics. J Develop Stud 43(1):1–30
279. Paarlberg RL (2002) The real threat to GM crops in poor countries: consumer and policy resistance to GM foods in rich countries. Food Policy 27(3):247–250
280. Driessen PL (2006) Eco-imperialism: green power–black death. Academic Foundation, New Delhi
281. Alene AD, Coulibaly O (2009) The impact of agricultural research on productivity and poverty in sub-Saharan Africa. Food Policy 34(2):198–209
282. Gruère G, Sengupta D (2009) GM-free private standards and their effects on biosafety decision-making in developing countries. Food Policy 34(5):399–406
283. Spielman DJ, Cohen JI, Zambrano P (2007) Are developing-country policies and investments promoting research and research partnerships in agricultural biotechnology? Int J Biotechnol 9(6): ISSN 0963-6048(print)|1741-5020(electronic)
284. Cohen JI (2005) Poorer nations turn to publicly developed GM crops. Nat Biotechnol 23(1):27–33
285. Alhassan WS (2002) Agrobiotechnology application in West and Central Africa (2002 Survey outcome). CORAF/WECARD–IITA International Institute of Tropical Agriculture, Ibadan, p 107
286. Gruere G, Bouët A, Mevel S (2007) Genetically modified food and international trade: the case of India, Bangladesh,

Indonesia and the Philippines. In: IFPRI Discussion Paper 00740. IFPRI, Washington, p 60
287. Smale M et al (2008) The economic impact of transgenic crops in developing countries: a note on the methods. Int J Biotechnol 10(6):519–555
288. Falck-Zepeda JB, Traxler G, Nelson RG (2000) Surplus distribution from the introduction of a biotechnology innovation. Am J Agric Econ 82(2):360–369
289. Pray CE et al (2006) Costs and enforcement of biosafety regulations in India and China. Int J Technol Globalisation 2(1–2):137–57
290. Antle JM (1999) Benefits and costs of food safety regulation. Food Policy 24(6):605–623
291. Shelton AM (2003) Considerations for conducting research in agricultural biotechnology. J Invertebr Pathol 83(2):110–112
292. Kochetkova T (2006) The transatlantic conflict over GM food: cultural background. In: Kaiser M, Lien M (eds) Ethics and the politics of food. Wageningen Academic, Wageningen, pp 325–329
293. Laget P, Cantley M (2001) European responses to biotechnology: research, regulation, and dialogue. Issues Sci Technol 17(4):37–42
294. Ramessar K et al (2010) Going to ridiculous lengths (mdash) European coexistence regulations for GM crops. Nat Biotech 28(2):133–136
295. Bradford KJ et al (2005) Regulating transgenic crops sensibly: lessons from plant breeding, biotechnology and genomics. Nat Biotechnol 23(4):439–444
296. Stein AJ et al (2007) Plant breeding to control zinc deficiency in India: how cost-effective is biofortification? Public Health Nutr 10(5):492–501
297. Stein AJ, Qaim M (2007) The human and economic cost of hidden hunger. Food Nutr Bull 28(2):125–134
298. Stein AJ, Sachdev HPS, Qaim M (2007) What we know and don't know about golden rice. Nat Biotechnol 25(6):624–624
299. Humphrey JH et al (1998) Neonatal vitamin A supplementation: effect on development and growth at 3 y of age. Am J Clin Nutr 68(1):109–117
300. Humphrey JH, West KP, Sommer A (1992) Vitamin-a-deficiency and attributable mortality among under-5-year-olds. Bull World Health Organization 70(2):225–232
301. Depee S et al (1995) Lack of improvement in vitamin-a status with increased consumption of dark-green leafy vegetables. Lancet 346(8967):75–81
302. Mayer JE, Pfeiffer WH, Beyer P (2008) Biofortified crops to alleviate micronutrient malnutrition**.** Genome studies Molec Genet edited by Juliette de Meaux and Maarten Koornneef/ Plant Biotechnol, edited by Andy Greenland and Jan Leach 11(2):166–170
303. Miller HI (2009) A golden opportunity, squandered. Trends Biotechnol 27(3):129–130
304. Potrykus I (2003) Nutritionally enhanced rice to combat malnutrition disorders of the poor. Nutr Rev 61(6):S101–S104
305. Stein AJ et al (2008) Potential impacts of iron biofortification in India. Soc Sci Med 66(8):1797–1808
306. Stein AJ, Sachdev HPS, Qaim M (2006) Potential impact and cost-effectiveness of Golden Rice. Nat Biotechnol 24(10):1200–1201
307. Qaim M, Stein AJ (2008) Economic consequences of Golden Rice. In: Invited presentation at the fourth conference of the European plant science organisation. Toulon (Cote d'Azur), France
308. Qaim M, Stein AJ, Meenakshi JV (2007) Economics of biofortification. In: Otsuka K, Kalirajan K (eds) Contributions of agricultural economics to critical policy issues. Blackwell, Malden, pp 119–133
309. Qaim M, Pray CE, Zilberman D (2008) Economic and social considerations in the adoption of Bt crops. In: Romeis J, Shelton AM, Kennedy GG (eds) Integration of insect-resistant genetically modified crops within IPM programs. Springer, Dordrect, pp 329–356
310. Bouis HE (2007) The potential of genetically modified food crops to improve human nutrition in developing countries. J Develop Stud 43(1):79–96
311. Atanassov AB, Brink A, Burachik J, Cohen M, Dhawan JI, Ebora V, Falck-Zepeda RV, Herrera-Estrella J, Komen L, Low J, Omaliko FC, Odhiambo E, Quemada B, Peng H, Sampaio Y, Sithole-Niang MJ, Sittenfeld I, Smale A, Sutrisno M, Valyasevi R, Zafar Y, Zambrano P (2004) To reach the poor: results from the ISNAR-IFPRI next harvest study on genetically modified crops, in EPTD Discussion Paper No. 116. 2004, ISNAR-IFPRI, International Food Policy Research Institute, Washington DC
312. Potrykus I (2010) Regulation must be revolutionized. Nature 466(7306):561–561
313. Dhlamini Z et al (2005) Status of research and application of crop technologies in developing countries, preliminary assessment. In: FAO (ed) FAO Reports, FAO, Rome, p 62
314. Krattiger A, Mahoney RT (2006) Intellectual property and public health. Bull World Health Organization 84(5):340–340
315. Atkinson RC et al (2003) Public sector collaboration for agricultural IP management including corrigendum of fig. on front page of text, vol. 302, 5648, pp 1152–1152. Science 301(5630):174–175
316. Beachy R et al (2002) Divergent perspectives on GM food. Nat Biotechnol 20(12):1195–1196
317. Krattiger A, Mahoney RTL, Nelsen L, Thompson GA, Bennett AB, Satyanarayana K, Graff GD, Fernandez C, Kowalsky SP (2007) Intellectual property management in health and agricultural innovation a handbook of best practice. MIHR/PIPRA, Oxford/Davis, pp 1539–1559
318. Singh A, Hallihosur S, Rangan L (2009) Changing landscape in biotechnology patenting. World Patent Information, pp 219–225
319. Wright B (2008) Plant genetic engineering and intellectual property protection. Agricultural Biotechnology in California Series Publication, no. 8186
320. Lawson C (2004) Patents and the CGIAR system of international agricultural research centres' germplasm collections under the International Treaty on Plant Genetic resources for food and agriculture. Aust J Agric Res 55(3):307–313

321. Delmer DP et al (2003) Intellectual property resources for international development in agriculture. Plant Physiol 133(4):1666–1670
322. Lempert DH (2009) A dependency in development indicator for NGOs and international organizations.Global Jurist 9(2): Article 6
323. Neidecker-Gonzales O, Nestel P, Bouis H (2007) Estimating the global costs of vitamin A capsule supplementation: a review of the literature. Food Nutr Bull 28:307–316
324. Gressel J, Zilberstein A (2003) Let them eat (GM) straw. Trends Biotechnol 21(12):525–530
325. Potrykus I (2010) Constraints to biotechnology introduction for poverty alleviation. New Biotechnol 27(5):447–448
326. Ademola AA (2011) Global capture of crop biotechnology in developing world over a decade. J Genet Eng Biotechnol (in press)
327. Taverne D (2007) The March of unreason. Oxford University Press, Oxford, p 320
328. Durant J (2005) The march of unreason: science, democracy, and the new fundamentalism. Nature 435(7040):277–278
329. Taverne D (2005) The new fundamentalism, Commentary. Nat Biotechnol 23(4):415–416
330. Herring RJ (2008) Whose numbers count? Probing discrepant evidence on transgenic cotton in the Warangal district of India. Int J Mult Res Approach 2:145–159
331. Marris E (2006) Environmental activism: in the name of nature. Nature 443(7111):498–501
332. Atkinson HJ, Urwin PE (2008) Europe needs to protect its transgenic crop research. Nature 453(7198):979–979
333. Leader SH, Probst P (2003) The earth liberation front and environmental terrorism. Terrorism Polit Violence 15(4):37–58
334. Finkel E (2011) Vandals attack transgenic wheat test plot. Science Insider, July 2011
335. Bettles C (2011) Scientist distances himself from activists. Farm online. DOI: http://sl.farmonline.com.au/news/nationalrural/grains-andcropping/cereal/scientist-distances-himself-from-activists/2239218.aspx?storypage=0 and http://www.ask-force.org/web/Field-Destruction/Bettles-Scientist-Distances-Schubert-20110728.pdf
336. Kuntz M (2011) Academic and governmental research on GMOs has been the target of numerous acts of vandalism in Europe. OGM, environnement, santé et politique. DOI: http://www.marcel-kuntz-ogm.fr/article-news-55055856.html, news in English, French and Spanish and http://ddata.over-blog.com/xxxyyy/1/39/38/37/public-research-vandalized.pdf and http://www.marcel-kuntz-ogm.fr/article-news-55055856.html and http://www.ask-force.org/web/Field-Destruction/Kuntz-Public-Government-Research-Vandalism-Europe-2011.pdf
337. Da Silva W (2011) In focus: the sad, sad demise of Greenpeace in cosmos. About Luna Media Pty Ltd, the boutique publishing company behind COSMOS. Sidney, Australia
338. Gough M (2011) Greenpeace destroys CSIRO wheat GM trial in Cosmos. About Luna Media Pty Ltd, the boutique publishing company behind COSMOS. Sidney, Australia
339. Smith J (2003) Seeds of deception. Yes! Books, Lowa, p 304
340. Smith J (2007) Genetic roulette, the documented health risks of genetically engineered foods. YES ! Books and Chelsea Green, Fairfield Iowa, p 319, second printing edn
341. Miller H (2008) Auf wiedersehen, academic freedom. Wall Street J Europe. p 3
342. Rao CK (2010) Moratorium on Bt Brinjal, a review of the order of the Minister of Environment and Forests, Government of India. Foundation for biotechnology awareness and education, Bangalore, p 74
343. Weese TL, Bohs L (2010) Eggplant origins: out of Africa, into the orient. Taxon 59(1):49–56
344. PRRI (2006) Correspondence between PRRI (Public Research and Regulation Initiative) and FoE (Friends of the Earth). www.pubresreg.org. DOI: http://www.ask-force.org/web/PRRI-FoE/PRRI-FoE-Corresp-Letter-to-FoE-20060629.pdf and http://www.ask-force.org/web/PRRI-FoE/PRRI-FoE-Corresp-Answer-to-FoE-20060926.pdf and http://www.ask-force.org/web/PRRI-FoE/PRRI-FoE-Corresp-Answer-FoE-to-PRRI-20060703.pdf
345. Apel A (2010) The costly benefits of opposing agricultural biotechnology. New Biotechnol 27(5):635–640
346. Borlaug NE (2000) Ending world hunger. The promise of biotechnology and the threat of antiscience zealotry. Plant Physiol 124(2):487–490
347. Hemming D (2006) Swiss vote encourages Austria's anti-GM stance. Outlook Agric 35(1):82–82
348. Motion J, Weaver CK (2005) The epistemic struggle for credibility: rethinking media relations. J Commun Manag 9(3):246–255
349. Burke D (2004) GM food and crops: what went wrong in the UK? Many of the public's concerns have little to do with science. Embo Reports 5(5):432–436
350. Blas X (2009) Bill Gates shifts focus to fighting hunger. Financial Times, London, p 1
351. Miller H, Morandini P, Ammann K (2008) Is biotechnology a victim of anti-science bias in scientific journals? Trends Biotechnol 26(3):122–125, Electronic Prepublication 17 Feb 2008, Hardcopy available in March
352. Horton R (1999) Secret society – Scientific peer review and Pusztai's potatoes. Tls-the Times Literary Suppl 5046:8–9
353. Horton R (1999) GM food debate – Editors reply. The Lancet 354(9191):1729–1729
354. Horton R (1999) Genetically modified foods: "absurd" concern or welcome dialogue? The Lancet 354(9187):1314–1315
355. Horton R (1999) Health risks of genetically modified foods, editorial, reply to Mitchell and Bradbury, Lancet, p. 1769. The Lancet 353(9167):1811–1811
356. Horton R (1999) Scientific misconduct: exaggerated fear but still real and requiring a proportionate response. The Lancet 354(9172):7–8
357. Ammann K (20110111) Review: Arpad Pusztai's feeding experiments of GM potatoes with lectins to rats: anatomy of a controversy 1998–2009. ASK-FORCE contribution AF-2 AF-2, 46. DOI: http://www.ask-force.org/web/AF-2-Pusztai/AF-2-Pusztai-Food-Safety-20110111.opensource.pdf

358. Quist D, Chapela IH (2001) Transgenic DNA introgressed into traditional maize landraces in Oaxaca, Mexico. Nature 414(6863):541–543
359. Campbell P (2002) Quist-chapela paper: editorial note 2. Nature 417(6892):897–897, 27 June 2002
360. Pineyro-Nelson A et al (2009) Transgenes in Mexican maize: molecular evidence and methodological considerations for GMO detection in landrace populations. Molec Ecol 18(4): 750–761
361. Schubert D, Tribe D. comments (2006) Three faces of science fraud. GMO Pundit, DOI: http://gmopundit.blogspot.com/2006/02/david-schubert-alleges-systematic.html.
362. Bradford KJ et al (2005) Regulatory regimes for transgenic crops – Response. Nat Biotechnol 23(7):787–789
363. Schubert D (2005) Regulatory regimes for transgenic crops. Nat Biotechnol 23(7):785–787
364. Punnett RC (1928) Scientific papers of William Bateson. Cambridge University Press, Cambridge
365. Strick J (1999) Darwinism and the origin of life: the role of H.C. Bastian in the British spontaneous generation debates, 1868–1873. J History Biol 32(1):51–92
366. Chassy BN (2002) Food safety evaluation of crops produced through biotechnology. J Am Coll Nutr 21(3):166S–173S
367. Chassy B et al (2007) Nutritional and safety assessments of foods and feeds nutritionally improved through biotechnology: case studies. J Food Sci 72:R131–R137
368. Shelton AM et al (2009) Appropriate analytical methods are necessary to assess nontarget effects of insecticidal proteins in GM crops through meta-analysis (Response to Andow et al. 2009). Environ Entomol 38(6):1533–1538
369. Duan JJ et al (2010) Extrapolating non-target risk of Bt crops from laboratory to field. Biol Lett 6(1):74–77
370. Broer I et al (2011) Response to the criticism by Taube et al. in ESE 23:1, 2011, on the booklet "Green Genetic Engineering". German Research Foundation (DFG), Environmental Sciences Europe, vol 23, issue 1, p 16
371. Green JM, Owen MDK (2010) Herbicide-resistant crops: utilities and limitations for herbicide-resistant weed management J Agric Food Chem
372. Johnson WG et al (2009) Influence of glyphosate-resistant cropping systems on weed species shifts and glyphosate-resistant weed populations. Euro J Agron 31(3):162–172
373. Duke SO, Powles S (2009) Glyphosate-resistant crops and weeds: now and in the future. AgBioForum 12(3&4):346–357
374. Vila-Aiub MM et al (2008) Glyphosate-resistant weeds of South American cropping systems: an overview. Pest Manag Sci 64(4):366–371
375. Powles SB (2008) Evolved glyphosate-resistant weeds around the world: lessons to be learnt. Pest Manag Sci 64(4):360–365
376. Powles SB, Preston C (2006) Evolved glyphosate resistance in plants: biochemical and genetic basis of resistance. Weed Technol 20(2):282–289
377. Neve P (2008) Simulation modelling to understand the evolution and management of glyphosate resistant in weeds. Pest Manag Sci 64(4):392–401
378. Mikulka J, Chodova D (2000) Long-term study on the occurrence of weeds resistant to herbicides in the Czech Republic. (Zeitschrift Fur Pflanzenkrankheiten Und Pflanzenschutz) J Plant Dis Protect 107:373–376
379. Hilbeck A, Schmidt JEU (2006) Another view on Bt proteins – how specific are they and what else might they do? Biopest Int 2(1):1–50
380. Hilbeck A, Meier M, Raps A (2000) Review on non-target organisms and Bt-plants. Ecostrat GmbH, Ecological Technology Assessment Consulting, Amsterdam, p 80
381. Hilbeck A et al (1998) Toxicity of *Bacillus thuringiensis* Cry1Ab toxin to the predator *Chrysoperla carnea* (Neuroptera: Chrysopidae). Environ Entomol 27(5):1255–1263
382. Hilbeck A et al (1999) Prey-mediated effects of Cry1Ab toxin and protoxin and Cry2A protoxin on the predator Chrysoperla carnea. Entomol Exper Et Applicata 91(2): 305–316
383. Romeis J, Dutton A, Bigler F (2004) Bacillus thuringiensis toxin (Cry1Ab) has no direct effect on larvae of the green lacewing Chrysoperla carnea (Stephens) (Neuroptera: Chrysopidae). J Insect Physiol 50(2–3):175–183
384. Marshall A (2007) GM soybeans and health safety – a controversy reexamined, additional texts. Nat Biotechnol 25(9):981–987
385. Ammann K (2009) Review web version: are rat organs damaged after feeding on GM soybeans? The Ermakova Case. ASK-FORCE contribution No. 4, 20, 20090801. DOI: http://www.ask-force.org/web/AF-4-Ermakova/AF-4-Ermakova-20090828-web.pdf
386. Seralini GE, Cellier D, de Vendomois JS (2007) New analysis of a rat feeding study with a genetically modified maize reveals signs of hepatorenal toxicity. Arch Environ Contamin Toxicol 52:596–602
387. OECD (1998) 408 repeated dose 90-day oral toxicity study in rodents (Updated Guideline, Adopted 21st Sept 1998)
388. OECD (1998) 407 repeated dose 28-day oral toxicity study in rodents, Adopted by the Council on 27th July 1995, in OECD Guideline for the testing of chemicals
389. Ammann K (20110921) Summary of 11 ASK-FORCE contributions on biosafety of biotechnology crops. ASK-FORCE contributions AF summary, 69. DOI: http://www.ask-force.org/web/ASK-FORCE-Summary/ASK-FORCE-Summary.pdf
390. Candolfi MP et al (2004) A faunistic approach to assess potential side-effects of genetically modified Bt-corn on non-target arthropods under field conditions. Biocontrol Sci Technol 14(2):129–170
391. Marvier M et al (2007) A meta-analysis of effects of Bt cotton and maize on nontarget invertebrates. Science 316(5830):1475–1477. doi:10.1126/science.1139208
392. Wolfenbarger LL et al (2008) Bt crop effects on functional guilds of non-target arthropods: a meta-analysis. PLoS ONE 3(5):e2118
393. Naranjo SE (2009) Impacts of Bt crops on non-target invertebrates and insecticide use patterns. CAB Rev Perspect Agric Veterinary Sci, Nutr Nat Resour 4:11–23

394. Duan JJ et al (2008) A meta-analysis of effects of Bt crops on honey bees (Hymenoptera: Apidae). PLoS ONE 3(1):e1415
395. Ammann Ki et al (2004) Biosafety in agriculture: is it justified to compare directly with natural habitats? Frontiers in Ecology, Forum: GM crops: balancing predictions of promise and peril, vol 2, pp 54–160
396. Ammann K (2005) Effects of biotechnology on biodiversity: herbicide-tolerant and insect-resistant GM crops. Trends Biotechnol 23(8):388–394
397. PRRI Public Research and Regulation Initiative(2009) Letter to CBD: LMOs that are likely to have adverse environmental impacts. 20090914, Downloads of PRRI www.pubresreg.org, 3 DOI: http://www.pubresreg.org/index.php?option=com_docman&task=doc_download&gid=490
398. Gupta A (2010) Transparency to what end? Governing by disclosure through the biosafety clearing house. Environ Plann C-Govern Policy 28(1):128–144
399. Felke M et al (2010) Effect of Bt-176 maize pollen on first instar larvae of the Peacock butterfly (Inachis io) (Lepidoptera; Nymphalidae). Environ Biosafety Res 9(1):5–12, Received: 20 November 2008, Accepted: 5 December 2009, online publication 28. October 2010
400. Ammann K (20090911) ASK-FORCE structure and possible contributions. ASK-FORCE contributions, 12 DOI: http://www.botanischergarten.ch/ASK-FORCE-Strategy/ASK-FORCE-General-List-20090911.pdf
401. Freeland C A hard-pressed trade. In: Financial times, 20070504. Financial Times, London
402. Moore A (2006) Bad science in the headlines – Who takes responsibility when science is distorted in the mass media? Embo Reports 7(12):1193–1196
403. Erjavec K, Erjavec E (2009) Changing EU agricultural policy discourses? The discourse analysis of Commissioner's speeches 2000–2007. Food Policy 34(2):218–226
404. Brabeck-Lemathe P (2008) Nestlé Chairman calls on European policymakers to reconsider opposition to genetically modified (GM) crops; Says 10,000 liters of water required to produce as little as one to two liters of biodiesel. In: Finfacts Business and Finace Portal. Finfacts, Irland, 6 pp. http://www.ask-force.org/web/Nestle/Brabeck-Finfact-Irland-Interview-2009.pdf
405. Rogers C, Farson RE (2007) Active listening, excerpt 1957. University of Chicago Industrial Relations Center, Gordon Training International, Chicago
406. Conklin J (2005) Wicked problems and social complexity. In: Conklin J (ed) Dialogue mapping: building shared understanding of wicked problems. Wiley, Chichester, p 20
407. Peter LJ, Hull R (2009) The Peter principle, why things always go wrong. HarperCollins, New York, 192 pp
408. Blackmore C (2007) What kinds of knowledge, knowing and learning are required for addressing resource dilemmas?: a theoretical overview. Environ Sci Policy 10(6):512–525
409. Zwart NH (2007) Genomics and self-knowledge: implications for societal research and debate. New Genet Soc 26(2):181–202
410. Ikerd JE (1993) The need for a system approach to sustainable agriculture. Agric Ecosyst Environ 46(1–4):147–160
411. Fairclough N (2009) Language and globalization. Semiotica 173(1–4):317–342
412. Scoones I (2008) Mobilizing against GM crops in India, South Africa and Brazil. J Agrarian Change 8(2–3):315–344
413. Weissmann G (2006) DDT is back: let us spray! Faseb J 20:2427–2429
414. WHO (2005) WHO position on DDT use. In: WHO (ed) Disease vector control under the stockholm convention on persistent organic pollutants. WHO, Geneva, p 2
415. Tren R, Bate R (2001) Malaria and the DDT story. In: T.I.o.E.A (ed) The Institute of Economic Affairs, London, 112 pp
416. Losey JE, Raynor LS, Carter ME (1999) Transgenic pollen harms Monarch larvae. Nature 399:214
417. Ammann K (2007) Reconciling traditional knowledge with modern agriculture: a guide for building bridges. In: Krattiger A, Mahoney RTL, Nelsen L, Thompson GA, Bennett AB, Satyanarayana K, Graff GD, Fernandez C, Kowalsky SP (eds) Intellectual property management in health and agricultural innovation a handbook of best practices, Chapter 16.7. MIHR, PIPRA, Oxford/Davis, pp 1539–1559
418. Gerhards J (1997) The discursive versus the liberal public sphere: an empirical critique of Jurgen Haberma' concept of the public sphere. Kolner Zeitschrift Fur Soziologie Und Sozialpsychologie 49(1):1–34
419. Conklin J (2003) Wicked problems and fragmentation. (cited 2003; White Papers, This paper is Chapter 2 in Dialog mapping: making sense of project fragmentation Conklin J, forthcoming). Available from: http://www.cognexus.org/id29.htm
420. Fischer G (2000) Symmetry of ignorance, social creativity, and meta-design. Knowledge-Based Syst 13(7–8):527–537
421. Ammann K (2004) The role of science in the application of the precautionary approach. In: Fischer R, Schillberg S (eds) Molecular farming, Plant-made Pharmaceuticals and Technical Proteins. Wiley-VCH Verlag GmbH & Co KGaA, Weinheim, pp 291–302
422. Rittel H (1984) Second generation design methods. In: Cross N (ed) Developments in design methodology. Wiley, New York, pp 317–327
423. Rith C, Dubberly H (2007) Why Horst W. J. Rittel Matters. Des Issues 23(1):72–74
424. Rith C et al (2007) Bibliography of Horst W.J. Rittel. Des Issues 23(1):78–88
425. Schmidt I et al (2004) SEEbalance reg – managing sustainability of products and processes with the socio-eco-efficiency analysis by BASF. Greener Manag Int 45:79–94
426. Renn O (2008) Risk Governance, coping with uncertainty in a complex world. Earthscan, London
427. Moirand S (2003) Communicative and cognitive dimensions of discourse on science in the French mass media. Discourse Stud 5(2):175–206
428. Chiapello E, Fairclough N (2002) Understanding the new management ideology: a transdisciplinary contribution from critical discourse analysis and new sociology of capitalism. Discourse Soc 13(2):185–208
429. Motion J, Leitch S (1996) A discursive perspective from New Zealand: another world view. Public Relat Rev 22(3):297–309

430. Clark CE (2000) Differences between public relations and corporate social responsibility: an analysis. Public Relat Rev 26(3):363–380
431. Galtung J, Ruge MH (1965) The structure of foreign-news – the presentation of the congo, cuba and cyprus crises in 4 norwegian newspapers. J Peace Res 2(1):64–91
432. Renn O (2006) Risk communication – consumers between information and irritation. J Risk Res 9(8):833–849
433. Chen GKC (1975) What is systems-approach. Interfaces 6(1):32–37
434. Priest SH, Bonfadelli H, Rusanen M (2003) The "trust gap" hypothesis: predicting support for biotechnology across national cultures as a function of trust in actors. Risk Anal 23(4):751–766
435. Iyengar S et al (2009) "Dark areas of ignorance" revisited comparing international affairs knowledge in Switzerland and the United States. Commun Res 36(3):341–358
436. Bonfadelli H, Dahinden U, Leonarz M (2002) Biotechnology in Switzerland: high on the public agenda, but only moderate support. Public Understand Sci 11(2):113–130
437. von Grebmer K, Omamo SW (2007) Options for a rational dialogue on the acceptance of biotechnology. Biotechnol J 2(9):1121–1128
438. Huang JC, Newell S (2003) Knowledge integration processes and dynamics within the context of cross-functional projects. Int J Project Manag 21(3):167–176
439. Beer S (2004) Reflections of a cybernetician on the practice of planning. Kybernetes 33(3–4):767–773
440. Feldman M, Lowe N (2008) Consensus from controversy: Cambridge's biosafety ordinance and the anchoring of the biotech industry. Euro Plann Stud 16(3):395–410
441. Bogner A (2010) Participation as a laboratory experiment paradoxes of deliberation on technology issues by lay people. Zeitschrift Fur Soziologie 39(2):87–105
442. Moore P (2000) Trees are the answer. Forest Prod J 50(10):12–19
443. Moore P (2000) A challenge: protect biodiversity and produce wood. J Forestry 98(8):A2–A3
444. Moore P (2002) Communication through participation, getting it right, environmentalism for the 21st Century. In: Ammann K, Papazova AB (eds) 1st dialogue on science. Academia Engelberg, Engelberg
445. Kahane A (2004) Solving Tough Problems: An Open Way of Talking, Listening, and Creating New Realities. In: Baetz BW (ed) Berrett-Koehler Publishers, San Francisco, 150 pp
446. Schenkel R (2010) The challenge of feeding scientific advice into policy-making. Science 330(6012):1749–1751
447. Rogers-Hayden T, Campbell JR (2003) Re-negotiating science in environmentalists' submissions to New Zealand's royal commission on genetic modification. Environ Values 12:515–534
448. Reich KH (2008) Science-and-religion/spirituality/theology dialogue: what for and by whom? Zygon 43(3):705–718
449. Papazova AB (2010) What do we need as visionaries: progress or development? abstract biovision 2010. Biovision 2010, DOI: http://www.bibalex.org/bva2010/speakers/SpeakerDetails.aspx?m=1&sp=XOHvrH47wZRXTXP5lzyEvA

Grain Quality in Oil and Cereal Crops

Déborah P. Rondanini[1,2], Lucas Borrás[2,3], Roxana Savin[4]
[1]Department of Crop Production, University of Buenos Aires, Buenos Aires, Argentina
[2]CONICET, National Council of Scientific and Technical Research, Buenos Aires, Argentina
[3]Departamento de Producción Vegetal, Universidad Nacional de Rosario, Zavalla, Santa Fe, Argentina
[4]Department of Crop and Forest Sciences, University of Lleida, Lleida, Spain

Article Outline

Glossary
Definition of the Subject
Grain Quality: Concept and Importance
Grain Structure
Grain Growth and Source–Sink Balance
Synthesis of Major Components
Main Factors Affecting Grain Quality
Future Directions
Bibliography

Glossary

Cereals Monocotyledon plant grains that accumulate starch as the main storage substance for subsequent germination. Two types have been distinguished – cereals that contain gluten and are used for bread-making (wheat, oats, barley, rye) and cereals that do not contain gluten (rice, maize).

Genotype × environment interaction Relative changes in genotype performance when grown under different environments.

Grain development Structural and functional changes that occur in the fertilized flower producing a mature grain capable of germinating.

Grain growth Irreversible increase in grain weight and size caused by cell division, expansion, and reserves accumulation.

Grain quality Group of grain characteristics and measurable attributes (objectively or subjectively) to meet the clients' requirements (i.e., customer, industry, consumers).

Oilseeds Dicotyledon plant grains that accumulate oil as the main storage substance for subsequent germination. Oilseed crop seeds (sunflower, rapeseed, ground pea) are composed of 40–50% oil and 20–30% protein while proteo-oil crop seeds (soybean, lupine) comprise 15–30% oil and 30–40% protein.

Photoassimilates Carbohydrates (sugars, starch, or fructans, depending on the species) synthesized by the green plant parts and translocated to actively growing organs, like grains. Photoassimilates may originate from current photosynthesis or reserve remobilization.

Source–sink balance Quantitative relationship between plant photosynthetic capacity (source) and number of organs under active growth (sink) that are sustained by the former.

Plant stress Changes in plant metabolism in response to environments that endanger plant survival or hinder reaching maximum reproductive capacity.

Definition of the Subject

Grain quality is frequently regarded by agronomists and breeders to be as important as yield. Quality characteristics are the reason why only few plant species are used to satisfy most human requirements for food and fiber [1]. Grain quality comprises a group of characteristics that collectively determine the usefulness of the harvested grains for a particular end use. Therefore, to breed and manage grain crops to achieve a specific quality standard and to be able to predict the quality of a particular crop in a particular growing environment is rather important. Achieving this objective is dependent upon the knowledge of the factors modifying grain composition, and consequently grain quality.

As grain markets have become more specialized, there is a growing pressure on farmers to produce grains with greater uniformity and with certain characteristics [2]. Appropriate husbandry to obtain grains with high and stable "quality" will likely be of increasing importance in achieving economic benefits. It is well known that grain quality is modified by the environment and the crop management practices used by farmers. However, the strategies and tools required to produce grains with certain quality characteristics are not as well established as the ones for achieving high yields. In this context, improving the understanding of the factors that determine grain quality has become increasingly important.

Grain Quality: Concept and Importance

In field crops, the quality of the end product is related to the composition and structure of the seed at harvest maturity. Seed composition and structure at harvest are determined by the genotype, the environment, and the crop management practices used during the crop growing cycle. It is not possible to propose a unique grain quality definition for any specie because it changes depending on the product end use. There is a proper criterion on the concept of quality for each specific end use and for each stage of the commercial chain in every crop (i.e., from harvest in the field, through grain dealers to the industry, Fig. 1). In this context, quality will be considered in relation to the criteria used by those involved in the various aspects of growth and utilization of the grain. As an example, for wheat and barley (Fig. 1), grain quality at the moment of harvest in the field is related to grain size (and weight) and the carbohydrates and protein composition. When the grain is sold to the grain dealer, seed purity, test weight, grain moisture, and protein percentage are the main characteristics that are taken into account for the prize (Fig. 1). After this stage, other attributes may be relevant and they will depend on the involved industry. For baking industry, flour yield and dough strength will be of maximum importance in wheat, while barley for producing beer will take into account the screening percentage, malt extract, and diastatic power, which in turn is related with nitrogen content.

This article aims to summarize key elements of grain structure, grain growth, and synthesis of major grains components in field crops in order to highlight the main attributes which modify grain quality.

Grain Structure

Harvested cereal and oilseed organs may comprise true seeds (soybeans, rapeseed) or fruits (seeds and maternal-accompanying structures, like sunflower achenes or wheat, barley, rice, maize, and sorghum caryopses). Seeds develop from fertilized ovules and consist of three genetically different tissues: (a) the embryo

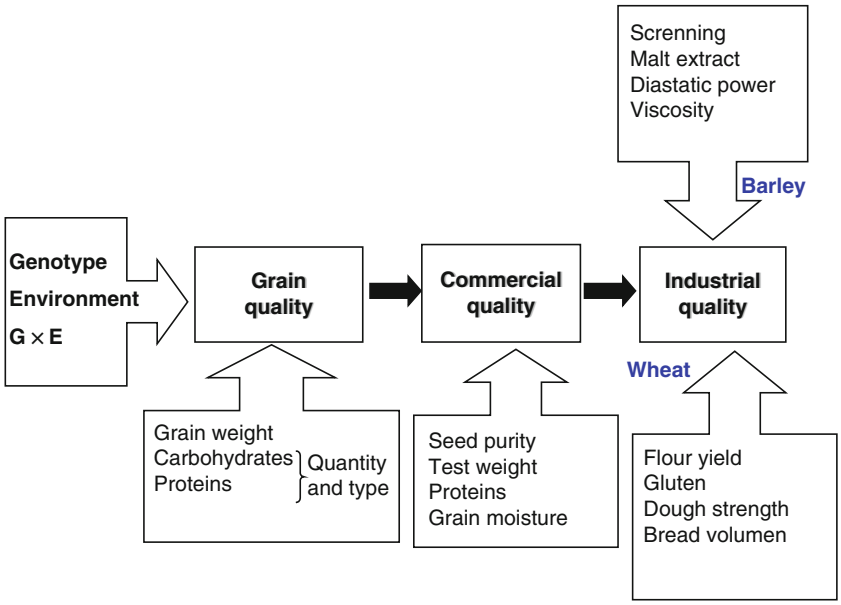

Grain Quality in Oil and Cereal Crops. Figure 1
Schematic postharvest processing and storage of wheat and barley production and main quality attributes in each step

developed from a zygote (diploid, representing the next generation), (b) the endosperm (usually triploid), and (c) the seed coat formed out by integuments, representing the maternal tissues of the ovule [3]. The proportion of these three components differs in mature seeds of cereals and oilseeds; endosperm is preponderant in cereals while the embryo prevails in oilseeds. With a few exceptions, the development of the endosperm always precedes that of the embryo; and the seed coat development precedes both. These genetically different parts interact closely during development and germination, and recent studies demonstrate the complexity of the connections and regulations among the different seed tissues [4, 5]. After fertilization and seed setting, grains are the primary sink in the plant. Grain filling requires important amounts of photoassimilates supplied by the mother plant through actual photosynthesis and/or the remobilization of stored carbohydrates from vegetative structures. No vascular connection exists between the mother plant and the developing embryo [5, 6] so grain growth is therefore sustained by water and solute movement through cell membranes regulated by both mother plant and seed.

Seed-attached structures include coats (testa and tegmen) and other diverse maternal-originated structures, like the lemma and palea in cereals, pods in soybeans, siliques in rapeseed, and hull (ovary wall attached to the floral receptacle) in sunflower. These structures can greatly influence grain quality appreciation. The seed coat color in different types of beans (*Phaseolus*) impacts consumers differently according to the region, causing rejection of some genotypes albeit their good nutritional properties. Sorghum caryopsis with or without tannins are another example of the importance of grain coats affecting seed quality. Some seed coats can provide nutrients, like the B-group vitamins and micronutrients in cereal brans. In addition, they contribute to other important biological and technological functions, protecting the seed from mechanical damage in postharvest, or by affecting the industrial grain processing (wheat grinding, barley malting, rice parboiling). Seed coats can also impact seed dormancy and germination processes [7]. During recent years, seed-attached structures have received special attention as influencing the potential grain size and volume [8–11].

Seeds store carbohydrates (starch, oil) and proteins (soluble and insoluble). The places where these reserves are accumulated vary widely between cereals and oilseeds. In cereals, the tissue that specializes in storing

starch and protein is the endosperm. In contrast, oil seeds do not have a specialized storage tissue; oil and protein accumulate in embryo and cotyledon cells. The well-developed starchy endosperm of cereals, with an outer aleurone layer, can comprise as much as 80% of the dry weight of the mature seed. The mature endosperm consists of dead cells packed with starch granules embedded in a protein matrix. The embryo is relatively small, accounting for only about 1–2% of the seed dry weight in wheat, and is usually located on one side of the seed near the point of attachment of the seed to the mother plant [3, 6]. The non-endospermic true seed of oilseeds consists of a large embryo with two cotyledons and the embryo axis. The majority of the reserve materials are stored in the cotyledons, which make up as much as 70% (sunflower) to 90% (soybean, rapeseed) of the total seed dry weight [6].

Grain structure is important since it determines grain and industrial processing quality. Cereal endosperm structure is defined by the number, shape, and size of the starch granules, together with the quantity and type of proteins in the protein matrix. Endosperm structure is used to classify wheat according to its hardness (soft, hard), thus affecting its industrial processing quality (milling capacity and flour yield). In addition, endosperm structure is used to separate dent and flint maize according to the quantity and partitioning of the floury and horny endosperm (greater proportion of horny endosperm in flint maize). Other endosperm structure characteristics that affect grain quality are vitreousness and color, both important for maize, rice, and bread and pasta wheat. Grain structure is also important for defining oilseed quality. In sunflower, the proportion of hull and embryo is an important attribute that defines oil yield, since the hull does not store oil and therefore reduces the oil concentration in the embryo. In the past 30 years, genetic improvement has reduced the hull proportion of sunflower oilseed, increasing the oil percentage on the whole seed [12]. However, thin hulls are usually harder to remove during industrial processing, so other improvement strategies are needed to increase the percentage of sunflower oil in the future. Grain structure has, therefore, a strong impact on the commercial and industrial quality of the grain, and for this reason its attributes are present in grain marketing regulations worldwide.

Grain Growth and Source–Sink Balance

Seed Biomass During grain filling, the pollinated flower undergoes cell division and differentiation and forms a mature grain (development), which increases in size and weight (growth), reaching mature grain dry weights of 30–50 mg (wheat-barley), 250–400 mg (maize), 20–25 mg (rice), 30–50 mg (sunflower), 150–400 mg (soybeans), and 2–5 mg (rapeseed). Growth and development dynamics can be described by analyzing the rate and time period of grain growth (Fig. 2). The latter are useful tools to explain changes in the final grain weight due to genotypic and environmental factors. Species differ in their biomass per seed, and ample intra-specific differences are also observed [6]. Commercial genotypes used by farmers in maize, wheat, and soybean show differences in seed size, and this variability is even larger when exotic material is considered.

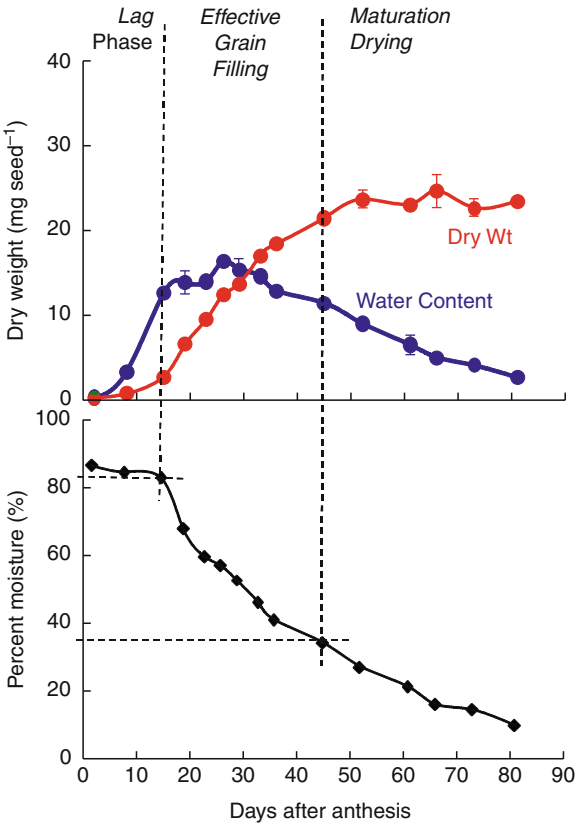

Grain Quality in Oil and Cereal Crops. Figure 2 Dynamics of individual seed dry weight (Dry Wt), water content per seed, and seed moisture of wheat seed

Seed biomass accumulation is commonly partitioned into three phases: the lag phase, the effective seed-filling period, and the maturation drying phase (Fig. 2). The lag phase is a period of active cell division. It is characterized by a rapid increase in water content with almost no dry matter accumulation. Following the lag phase, cells within the seed enter a differentiation and maturation phase, and a period of rapid dry matter accumulation resulting from the deposition of seed reserves. This phase is generally referred to as the effective seed-filling period. As in the lag phase, water content continues to increase rapidly and eventually establishes the maximum volume of the seed. Species vary considerably as to when maximum seed water content is achieved during seed filling [13]. In maize kernels, maximum water content occurs near mid seed filling [14], while in soybean seeds maximum water content is achieved at a later stage, when 70–80% of the final seed size has been achieved [15] and conversely, sunflower reaches it earlier with only 30% of final grain dry weight [10]. During the third phase of development, seeds loose water content, reach "physiological maturity" (maximum dry matter accumulation), and enter a quiescent state [3]. Seed water concentration declines throughout the three stages of seed development (Fig. 2). This decline is most obvious after seeds reach physiological maturity, but it also occurs during rapid seed filling as water is displaced by reserves [14–16].

The progress of dry matter accumulation in developing seeds and the concurrent loss of water are closely related phenomena. Studies with maize, wheat, soybean, and sunflower [17–20] have shown that final seed size is achieved at, or near, a minimum water concentration. Also, results from several studies have shown that seed water concentration accurately predicts the percent of maximum seed size achieved at any moment during seed filling in wheat, soybean, maize, and sunflower [17–20]. Such results support the notion that the duration of seed filling is determined by the interaction between reserve deposition and declining cellular water content, where deposition of reserves such as starch, protein, or lipids replace water until a critical minimum water concentration is reached [6, 20, 21]. Species differ in the seed water concentration when they achieve maximum seed biomass [13]. For example, soybean seeds reach maturity at ~62%, maize seeds at ~36%, and wheat seeds at ~37% moisture. Although minor compared to differences across species, it has been shown that when an ample set of cultivars within a species is analyzed, variability for this trait can also be observed [22].

The rate of seed growth during the effective seed filling is highly dependent upon the number of sites for reserve deposition. The usual estimate of seed sink capacity is the number of differentiated cells during the lag phase. In maize, wheat, and other cereals, the number of endosperm cells is highly related to the rate of seed growth during rapid seed filling. In legumes such as soybean or pea, the number of cotyledon cells is highly related to the rate of seed growth. Thus, rate and duration of grain filling are important to define the final grain weight, an important attribute of grain quality.

Source–Sink Balance In higher plants, nutrients from assimilation sites (sources) are delivered to sites of nutrient utilization (sinks) through an interconnected network of sieve elements. Partitioning of phloem-delivered nutrients between competing sinks is governed by their relative ability to unload major osmotic species from the importing phloem sieve elements [23]. This process depends upon a set of intercellular (post-sieve element) transport events which are integrated with growth or storage functions of the recipient sink tissues [24].

Species differ on the seed size at maturity [25], and this interspecific variability is more related the amount of assimilates available per seed during the early lag phase than during the effective seed-filling period [21]. At flowering, plants adjust the number of seeds and the potential seed size to the growth environment [21], and species differ in how they distribute available assimilates into more seeds or more potential seed size at around the period when seed number is being determined [26]. Seed size is mainly determined by the genotype, although the environment can affect the final size as well. Water availability and temperature are two environmental conditions that can create important changes in the size of the seeds at maturity.

The amount of assimilates available per seed is usually referred as the source–sink balance, and is used to describe the relation between the total amount of available assimilates and the sink number. This ratio is used

to simplify the idea of assimilate availability per sink, and the way the source–sink ratio has been estimated can vary widely. Different researchers have used plant growth per seed, green leaf area per seed, sucrose availability per seed, and alternative approaches including plant growth per day per unit of sink growth per day. The source–sink balance that the seeds experience during their growth is adjusted at around flowering, when plants are setting the number of seeds.

Because plants grow in a nonuniform environmental condition, the source–sink balance during the period when seeds are accumulating biomass can change. An example can be a defoliation caused by an insect eating leaves attacking the crop at mid grain filling (which would reduce the source–sink balance of the crop) or a drought stress reducing plant growth (also reducing the source–sink balance). The source–sink balance becomes relevant because not all seed components vary to the same degree when assimilate availability per seed is altered, so the seed composition and quality may change [27–29].

Jenner and coworkers developed a theoretical model to understand how changes in the amount of assimilates available per seed can affect seed composition [28]. Their model is based on the idea that each one of the seed components can be more or less affected by changes in the level of precursors available for the growing seed because not all components are receiving from the mother plant the same level of precursors needed for their deposition within the seed. An example is illustrated in Fig. 3, where changes in the level of precursors will most surely not affect the starch content of the seed but changes in the level of precursors needed for protein synthesis will affect the protein content and the final protein concentration. This model helps explain why changes in plant growth (that affect the precursor levels) will most surely not affect starch content but will surely affect the protein content of the seed. Recent studies conducted on soybean [30] and maize compositions [27, 31] agree with this model.

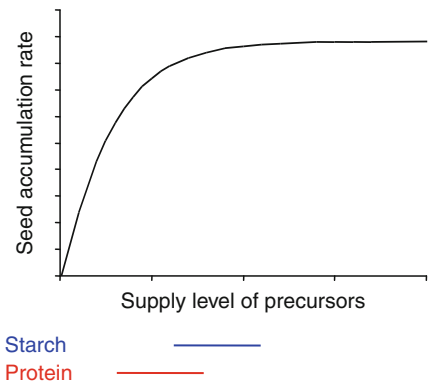

Grain Quality in Oil and Cereal Crops. Figure 3 Level of precursors available per seed to synthesis of different components of seeds (Adapted from [28])

Synthesis of Major Components

Grain growth involves growth processes of various structures (seed coats, embryo, endosperm) and accumulation of different substances (starch, oil, protein). Grain components are not synthesized simultaneously nor do they occur at the same rate; thus, physical and chemical grain composition varies during grain filling. This is an important aspect when dealing with industrial and nutritional grain quality.

As an example, the different parts of a wheat grain and the main components synthesized during grain filling are shown in Fig. 4. Starch is the main component in wheat, comprising 70–80% of the final grain weight. Different types of starch granules of varying numbers, shapes, and sizes are synthesized into the endosperm cells. The A-type granules are bigger and quantitatively more important than the succeeding B- and C-type granules. Starch is composed of amylose and amylopectin at a 3:1 ratio, except in waxy genotypes where amylopectin is more abundant.

In wheat bread, proteins comprise 5–20% of the final grain dry weight and include albumins and globulins (30–40%); gliadins and glutenins (60–70%). Albumins and globulins have enzymatic and metabolic functions and are located in the embryo and aleurone layer; gliadins and glutenins form the gluten and are reserve proteins, confined in the endosperm [32]. During grain filling, metabolic proteins are synthesized first and predominate until 10–15 days after anthesis. Reserve proteins accumulate during the effective filling phase; gliadins are the first to be detected (10–15 days after anthesis) while glutenins are deposited later (15–20 days after anthesis). Gliadins give viscosity to the mass while the glutenins confer elasticity, and both result in viscoelastic gluten appropriate for a good loaf volume. Since the gliadins:glutenins ratio changes

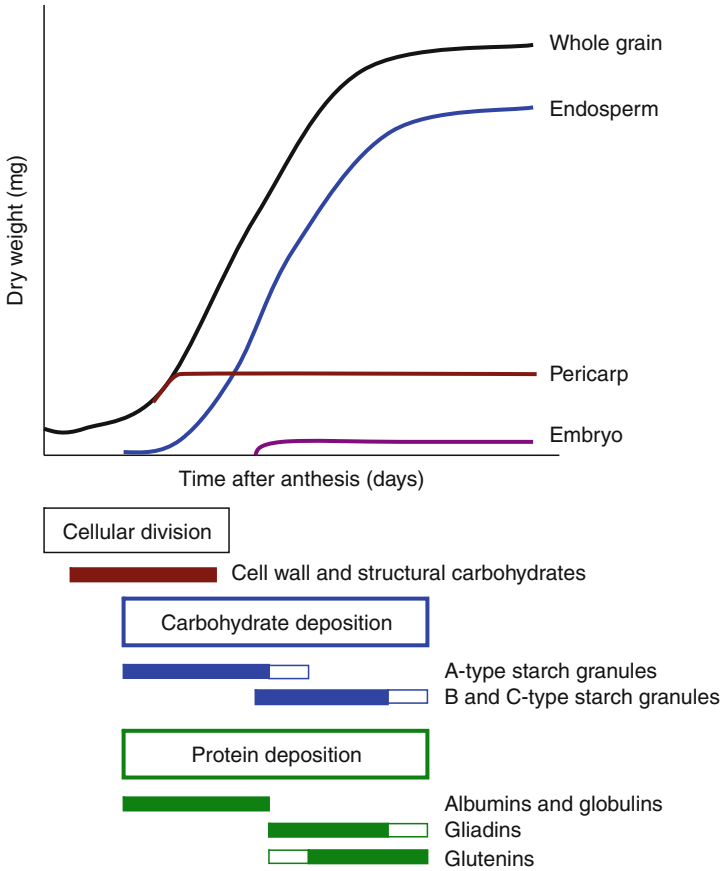

Grain Quality in Oil and Cereal Crops. Figure 4
Grain filling dynamics of a cereal (wheat) and synthesis of major grain components (Adapted from [29])

during grain filling, crop exposure to stressful conditions (i.e., high temperature, water stress) during this phase will modify the total protein mass and the gliadins:glutenins ratio, affecting baking quality.

Grains from other species have different grain component synthesis patterns. For example, in maize there is only one type of starch granule and although starch is synthesized through the entire effective filling phase amylose accumulation occurs after amylopectin. Reserve proteins (5–14% of the final grain weight) are accumulated during the entire effective filling period as well, forming protein bodies in the endosperm cells. Oil accumulation (3–15% of the final grain weight) takes place at the end of the filling phase and most of the oil is found in the embryo. In oilseeds, oil and protein are the main reserve substances; carbohydrates are scarcely accumulated (<20%). Sunflower seeds contain 40–55% oil and 10–20% protein, while soybean seeds contain greater protein percentages (35–50%) and lower oil percentages (10–25%). Both protein and oil are deposited in the embryo cells during the linear grain filling phase. Oil deposits form oleosomes or lipid bodies of spherical shapes, while reserve proteins form dense and irregular protein bodies [33, 34].

During grain filling oilseeds, protein synthesis usually occurs after oil synthesis. Oil is formed by triglycerides, which are composed of one glycerol molecule combined with three fatty acids. Fatty acids differ in the number of carbon atoms (typically between 14 and 22 in vegetable oils) and the number of double bonds between carbon atoms. The different proportions of fatty acids modify the physicochemical and industrial properties of oils. Oils with high saturated fatty acid percentages (without double bonds; like palmitic and stearic acids) are semisolid at room temperature, with a high melting point and a higher resistance to

oxidation (fat degradation due to oxygen presence). However, consumption of these oils (especially palmitic acid) increases cholesterol levels in the bloodstream. On the contrary, oils with high proportions of monounsaturated fatty acids (like oleic acid) and polyunsaturated fatty acids (like linoleic and linolenic acids with two and three double bonds, respectively) are liquid at room temperature, have a lower melting point, and a higher susceptibility to oxidation as the number of double bonds increase; these oils are healthier than saturated fatty acids. During grain filling, the proportion of fatty acids varies according to the species and crop varieties. In traditional sunflower genotypes, the oleic:linoleic ratio decreases during grain filling while total oil accumulation increases. In contrast, in "high oleic" sunflowers, the oleic proportion is high and constant during grain filling due to the low activity of the enzyme responsible for the linoleic synthesis deriving from oleic acid [35, 36]. Oil final composition varies greatly among oilseed species, and genetic improvement has achieved a wide variety of fatty acid compositions within the same species resulting from physical and chemical mutagenesis that affect specific enzyme functions responsible for the presence of double bonds in fatty acids [37, 38]. These enzymes are also affected by the environment, producing changes in grain oil content and composition.

Main Factors Affecting Grain Quality

Genotypic Effects

Some few grain attributes are mainly driven by the genotype, and the environment has relatively low influence. For example, the color of the wheat grain (white, yellow) is strongly determined by the ability of genotype to accumulate lutein, and the character "high oleic" in oilseed genotypes is associated with genetic mutations defective for the enzyme that desaturates oleic acid. Genotypes within the same species can present large differences in grain composition. For example, in commercial genotypes of soybean, the difference in protein percentage can easily vary from 33% to 42% [39]. This variability can be observed for any seed component in any species [40–42], as ample natural variation is common (Table 1).

Grain Quality in Oil and Cereal Crops. Table 1 Grain composition ranges reported in different species

Species	Grain composition range	Source
Soybean	33–42% protein	[35]
Sunflower	20–30% oil (confectionary type)	[33, 38]
	40–55% oil (oil type)	
Wheat bread	5–20% protein	[40]
Corn	5–14% protein	[31]
	8–12% protein (pop corn type)	[41]
	5–10% oil (high oil content)	[42]

Earlier studies working on understanding the genetic basis of genotypic differences in seed composition were based on the use of mutants, and these usually yielded qualitative differences in seed composition. For example, a commercial genotype of maize usually contains ~40% amylopectin and ~60% amylose, and a waxy mutant contains 100% amylopectin and no amylose. At present time, a large number of mutants have been discovered and used within any species as specialty quality genotypes.

The modification of the fatty acid profile of oil seeds has been one of the main tasks faced by oilseed breeders over the past 40 years. Success in this field has been of paramount importance for the worldwide expansion of some oilseed crops. The elimination of erucic acid (a harmful fatty acid) from rapeseed oil was the first step toward the development of canola (zero-erucic, low-glucosinolate rapeseed) as one of the major sources of vegetable oil in the world. Other landmarks in oilseed breeding for seed oil quality have been the development of high oleic, low linolenic acid canola, low linolenic acid linseed and soybean, high oleic acid sunflower, high saturated sunflower, and sunflower lines with modified tocopherol (antioxidant compounds) composition. Most of these traits defining seed oil quality have been found to be governed by a reduced number of genes (one to three major genes, with several alleles for each locus in most cases), and this fact implies that the practical management of single quality traits in breeding programs is relatively easy if compared with polygenic traits (as grain yield, grain weight or protein and oil content). Additionally, the fatty acid composition of the seed oil is determined by the genotype of the developing embryo (not the whole plant), so mutagenesis and selection can be

carried out at a single-seed level, using the half-seed technique.

In wheat, improving yield potential without negatively affecting grain quality is difficult, mainly because increases in grain yield are generally accompanied by a decrease in grain protein content, which is strongly associated with bread-making quality. Wheat breeders give grain quality the same level of importance as yield potential and disease resistance. In contrast to the low heritability of protein content, grain hardness and yellow pigment are highly heritable and can be readily improved through conventional breeding. Plant breeders select at least one parent with the desired quality when designing their crossing strategies, particularly as end-use requirements frequently determine the fate of potential new cultivars, but the stage in the breeding process at which quality determination takes place will influence which tests (micro or macro tests) are applied, according to the sample size available.

At present, natural variation for seed composition is being studied identifying quantitative trait loci (QTLs) for different seed components (oil, protein), as any seed component is a quantitative trait governed by many genes and each one with an individual small effect. The study by Blanco and coworkers can be mentioned as an example, where the authors studied seed protein concentration in wheat where three major QTLs were detected [43]. This methodology is currently becoming very popular and has yielded molecular markers associated with seed component traits that can help understand the genetic bases of the trait and be used by breeders and the industry.

Environmental Effects

As mentioned earlier, the majority of quality traits are greatly modified by the environment and by genotype–environment interactions. Grain weight and protein concentration are found within this group of traits. Environment variables like high temperature, water and nitrogen (N) availabilities have been the most studied modifying grain quality.

The response in grain composition to a particular stress depends mainly on the stress characteristics (i.e., intensity, duration of the stressful period, opportunity of occurrence, and the interaction that this stress may have with other stresses to which the crop is exposed to). The relevance of the intensity and duration of the stress on the magnitude of the change in grain composition is self-explained (the more severe and the longer a stress is, the greater change in composition produced, though not necessarily this implies that the relationship is linear). The timing of occurrence is also critical, as shown in Fig. 4 not all stages are equally critical for the final determination of grain quality: if the stress coincides with critical stages for synthesis and deposition of the components, the changes will result far stronger than that of stresses occurring is less-critical stages. Therefore, the grain composition responses to stressful factors may range from virtual insensitivity (if punctual synthesis reductions are compensated by recovering when no stress occurs) to different ranges of quality reductions to even crop failure to produce a certain quality level.

Seed growth and development are responsive to temperature, but their responses vary with the temperature range considered [44]. As a general rule, the rate of seed development increases as temperature increases, reducing the duration of seed-filling period. At lower temperatures, seed growth rates decrease linearly as temperatures fall below 15°C in wheat, soybean, rice, sunflower, and maize. Seed growth rates increase when temperatures rise from 20°C to 30°C; however, this increase does not offset the linear decrease in seed-filling duration, resulting in lower grain weights [44]. In most cases, moderately high temperatures (20–30°C) prevail during grain filling, although short periods of very high temperatures (>30–32°C) may occur reducing seed growth rate and causing the early end of grain filling period. In addition, the earlier the heat stress, the greater the impact on grain weight [45, 46]. Brief periods of high temperatures can cause reductions in grain weight, but these effects can be overlooked if only the average temperature during post-flowering period is considered. Thus, moderately high temperatures (20–30°C) during the post-flowering period reduced grain weight mainly through shortening the grain filling period, while very high temperatures (>30–32°C) even for a few days can reduce grain weight by reducing grain filling rate and the early cessation of grain growth period. Both aspects of post-flowering temperature should be considered especially because climatic change could bring about high-temperature scenarios

in the next decades, together with an increase in heat-stress events [47, 48].

Grain quality and composition are also affected by temperature. Several experiments suggest that the temperature effects on seed composition are related to dry matter metabolism and accumulation. The timing, intensity, and duration of occurrence of heat stress may alter final grain quality according to the grain component synthesis process involved (carbohydrates, proteins, oils). Interestingly, there are some reports on the possibility of recovery post-stress [49, 50]. In wheat and barley, protein percentage increases with increasing temperatures (15–30°C) because the negative impact of high temperatures on starch synthesis is greater than the impact on protein synthesis, thus decreasing the starch proportion in the grains [28]. High temperatures also affect protein quality, generally increasing gliadin:glutenin ratio, which causes weak dough with a low bread-making quality. The temperature impact on wheat grain quality will therefore depend on the balance between the positive (higher protein) and negative (greater gliadin:glutenin ratio) effects. Temperature also affects oil fatty acid composition in oilseeds [51]. The higher the temperatures during grain filling, the higher the fatty acid saturation (i.e., greater proportions of oleic acids and lower proportions of linoleic and linolenic acids) due to the reduced activity of unsaturation enzymes in grains [52]. Temperatures registered during the night in early grain filling phases have shown to have the best predictive values for modeling the final oil composition in sunflower [53]. Progress in modeling the quality of other grains is underway [54].

In field crops, high-temperature occurrences are commonly associated to water stress, increasing the negative temperature effects. Drought stress produces a shortage of assimilates and often reduced N availability, which cause a reduction in grain growth. In general, a drought episode occurring after flowering has a similar effect as an increase in temperature – the quantity (mg grain^{-1}) of protein per grain remains stable, while starch accumulation in grain is significantly reduced, resulting in smaller grains with a greater protein percentage [55]. In oilseeds, post-flowering droughts decrease grain oil percentages and increase protein percentages [56, 57] indicating that carbon metabolism is affected to a greater extent than N metabolism. Water stress has a smaller impact on fatty acid composition; in general, droughts do not modify the saturation degree in oils except under severe stress conditions which produce an early grain-filling cessation [58].

N availability also affects final cereal and oilseed grain composition. In general, when soil N availability is low, cereal crop yields respond positively to N fertilization. A dilution effect occurs when N taken up by the crop is partitioned in a greater number of grains, which reduces grain protein percentage. If N availability is further increased, both crop yield and grain protein percentage are increased. In addition, the stage of development when N is added is important in defining wheat grain quality. N applications around flowering increase nitrogen availability per grain, increasing protein percentage. It is reported that increases in N availability result in increases of gliadin:glutenin ratio, which in turn produce a weakening of the dough [59]. In oilseeds, a greater soil N availability increases crop yield and grain protein percentage. Consequently, oil percentages in grain decrease due to the negative relationship between oil and protein (expressed as a percentage of the grain weight). Nitrogen application effects on the grain fatty acid composition are smaller and more variable compared to temperature and water stress effects [60, 61]. A greater knowledge on the physiological processes that regulate the responses to these environmental factors is essential to decide the management of the crop to produce grain for a specific end use.

Management Strategies

Although both grain yield and quality are determined throughout the growing season, important decisions that will strongly affect them should be taken before planting [62]. The farmer's choice of genotype and the amount of nitrogen available are central for successfully combining the genotype potential for yield and quality with the environmental availability of resources. As stated earlier, final grain quality is the result of the interaction between the genotype, the natural environment, and the crop management practices [63]. In extensive production systems, it is not possible to provide each stage of the crop cycle with the optimal combination of environmental factors to reach

the highest possible yield and quality, therefore, a trade-off is to make preplanting decisions to ensure that critical crop stages for the definition of yield and quality are given a preferential environment [62]. Nevertheless, knowledge of the effects of environment and G × E interaction is still rather imprecise, so management strategies with the objective of increasing yields, while obtaining high quality, are difficult to design.

There are a number of grain quality attributes that are strongly governed by the genotype and therefore choosing the proper genotype in relation to the final end use of the grain is critical. In several countries, for trading purposes wheat is classified into distinct categories of endosperm hardness (soft, semihard, and hard). Grain hardness is determined by the packing of grain components in the endosperm cells [40] and according to this attribute, the end product can vary from pasta (hard endosperm), biscuits (soft endosperm), to bread (hard endosperm). Usually, this classification can be more detailed and complex [64]. In the case of sunflower, oil fatty acid composition is genetically controlled [65], and the oil composition has been modified mostly by altering the function of major genes through mutagenesis [38].

Addition of nitrogen fertilizer is one of the most frequent management practices for altering grain quality (and of course grain yield). It is difficult a priori to know the effect of adding nitrogen to grain quality as many other factors are intervening and modify the final expected result. In the case of wheat crops, the initial amount of nitrogen in the soil, the specific moment of fertilization, the amount of available water, and rain pattern during the growth cycle as well as plant density at sowing and genotype nitrogen use efficiency are the main factors that interact and may modify the final response in grain quality. In general, it is accepted that regardless of the species, the increase in grain yield leads to a decrease in the protein to starch or oil ratio. This negative relationship between yield and grain N concentration reflects the fact that carbon assimilation and accumulation during the grain filling period is sink-limited [66] while nitrogen accumulation in grains is usually source-limited [67], as a result of dilution effects. The final protein concentration will thus depend on the balance between the source capacity to provide nitrogen and the strength of the sink for accumulating carbohydrates [68].

Future Directions

The compositional requirements for a particular grain vary from one product to the other depending on its end use. In addition, grain quality is a dynamic concept as it changes constantly as new uses can be developed for particular grains. The three major pillars of grain composition are: the genotypes, the environments during grain growth, and their interaction.

On the genetic pillar, the knowledge gained in the recent past has been extraordinary. Based on the molecular tools developed, a number of genes and QTLs involved in the determination of particular grain components (in turn determining grain quality attributes) have been identified and mapped in several crops, and it seems easy to predict that in the near future almost any breeding program in the world will be able to manipulate these genetic factors with certainty.

Regarding the environment during grain filling, important and useful findings have been reported in relation to high temperatures, and in lesser extent in water stress, and nitrogen availability. Few studies have attempted to examine the interactions between these environmental factors on grain quality attributes. It has been recently reported that high-temperature stress effects may be mitigated under high nitrogen availability for wheat and barley [69–71].

Undoubtedly, the challenge for breeders and agronomist is dealing with G × E interactions [72]. Therefore, there is a need for increasing current knowledge on the physiology of quality traits in order to obtain both high yield and high quality through breeding and management strategies. This will also help predict grain composition through a series of genotypes and environments.

Using agronomic simulation models properly calibrated and validated for the target population of environments can be a tool for understanding and predict final grain composition. The incorporation of grain quality modules into crop simulation models is increasing (European Journal of Agronomy 25, 2006). Grain protein content was the first trait incorporated into modeling as well as grain size (grain weight) which is a quality criteria especially valued by millers in the case of cereals but also for oil extraction in oil crops. Recently, more detailed concepts have been incorporated such as

the type of protein [73] and oil quality [74]. It is expected that incorporating genetic data into simulation routines will be done in the near future.

Bibliography

Primary Literature

1. Slafer GA, Satorre EH (1999) Wheat production systems of the Pampas. In: Satorre EH, Slafer GA (eds) Wheat: ecology and physiology of yield determination. Food Product Press, New York, pp 333–343
2. Wrigley CW (1994) Developing better strategies to improve grain quality for wheat. Aust J Agric Res 45:1–7
3. Boesewinkel FD, Bouman F (1995) The seed: structure and function. In: Kigel J, Galili G (eds) Seed development and germination. Marcel Dekker, New York, pp 1–24
4. Berger F, Grini PE, Schnittger A (2006) Endosperm: an integrator of seed growth and development. Curr Opin Plant Biol 9:664–670
5. Meyer CJ, Steudle E, Peterson CA (2007) Patterns and kinetics of water uptake by soybean seeds. J Exp Bot 58:717–732
6. Egli DB (1998) Seed biology and the yield of grain crops. CAB International, New York, 178 p
7. Baskin JM, Baskin CC (2004) A classification system for seed dormancy. Seed Sci Res 14:1–16
8. Millet E, Pinthus MJ (1984) The association between grain volume and grain weight in wheat. J Cereal Sci 2:31–35
9. Calderini DF, Abledo LG, Slafer GA (2000) Physiological maturity in wheat based on kernel water and dry matter. Agron J 92:895–901
10. Rondanini DP, Mantese AI, Savin R, Hall AJ (2009) Water content dynamics of achene, pericarp and embryo in sunflower: associations with achene potential size and dry-down. Eur J Agron 30:53–62
11. Lizana XC, Riegel R, Gomez LD, Herrera J, Isla A, McQueen-Mason SJ, Calderini DF (2010) Expansins expression is associated with grain size dynamics in wheat (*Triticum aestivum* L.). J Exp Bot 61:1147–1157
12. Putt ED (1997) Early history of sunflower. In: Schneiter AA (ed) Sunflower technology and production. American Society of Agronomy, Madison, pp 1–19
13. Egli DB, TeKrony DM (1997) Species differences in seed water status during seed maduration and germination. Seed Sci Res 21:289–294
14. Westgate ME, Boyer JS (1986) Water status and the developing grain of maize. Agron J 78:714–719
15. Egli DB (1990) Seed water relations and the regulation of the duration of seed growth in soybean. J Exp Bot 41:243–248
16. Borrás L, Westgate ME, Otegui ME (2003) Control of kernel weight and kernel water relations by post-flowering source-sink ratio in maize. Ann Bot 91:857–867
17. Borrás L, Westgate ME (2006) Predicting maize kernel sink capacity early in development. Field Crop Res 95: 223–233
18. Swank JC, Egli DB, Pfeiffer TW (1987) Seed growth characteristics of soybean genotypes differing in duration of seed fill. Crop Sci 27:85–89
19. Rondanini DP, Savin R, Hall AJ (2007) Estimation of physiological maturity in sunflower as a function of fruit water concentration. Eur J Agron 26:295–309
20. Schnyder H, Baum U (1992) Growth of the grain of wheat (*Triticum aestivum* L.): the relationship between water content and dry matter accumulation. Eur J Agron 1:51–57
21. Gambín BL, Borrás L (2010) Resource distribution and the trade-off between seed number and weight: a comparison across crop species. Ann Appl Biol 156:91–102
22. Borrás L, Zinselmeier C, Senior ML, Westgate ME, Muszynski MG (2009) Characterization of grain filling patterns in diverse maize germplasm. Crop Sci 49:999–1009
23. Patrick JW (1997) Phloem unloading: sieve element unloading and post-sieve element transport. Annu Rev Plant Biol 48:191–222
24. Patrick JW, Offler CE (2001) Compartmentation of transport and transfer events in developing seeds. J Exp Bot 52:551–564
25. Egli DB (1981) Species differences in seed growth characteristics. Field Crop Res 4:1–12
26. Sadras VO (2007) Evolutionary aspects of the trade-off between seed size and number in crops. Field Crop Res 100:125–138
27. Borrás L, Curá JA, Otegui ME (2002) Maize kernel composition and post-flowering source-sink ratio. Crop Sci 42:781–790
28. Jenner CF, Ugalde TD, Aspinall D (1991) The physiology of starch and protein deposition in the endosperm of wheat. Aust J Plant Physiol 18:211–226
29. Savin R, Molina-Cano JL (2002) Changes in malting quality and its determinants in response to abiotic stress. In: Slafer GA, Molina-Cano JL, Savin R, Araus JL, Romagosa I (eds) Barley science: recent advances from molecular biology to agronomy of yield and quality. Food Product Press, New York, pp 523–544
30. Rotundo JL, Borrás L, Westgate ME, Orf JH (2009) Relationship between assimilates supply per seed and soybean seed composition. Field Crop Res 112:90–96
31. Seebauer JR, Singletary GW, Krumpelman PM, Ruffo ML, Below FE (2010) Relationship of source and sink in determining kernel composition of maize. J Exp Bot 61:511–519
32. Shewry PR, Napier JA, Tatham AS (1995) Seed storage proteins: structures and biosynthesis. Plant Cell 7:945–956
33. Mantese AI, Medan D, Hall AJ (2006) Achene structure, development and lipid accumulation in sunflower cultivars differing in oil content at maturity. Ann Bot 97:999–1010
34. Tanaka W, Mantese AI, Maddonni GA (2009) Pollen source effects on growth of kernel structures and embryo chemical compounds in maize. Ann Bot 104:325–334
35. Garcés R, Mancha M (1989) Oleate desaturation in seeds of two genotypes of sunflower. Phytochemistry 28:2593–2595
36. Ohlrogge J (1997) Regulation of fatty acid synthesis. Annu Rev Plant Physiol Plant Mol Biol 48:109–136
37. Harwood JL (1996) Recent advances in the biosynthesis of plant fatty acids. Biochim Biophys Acta 1301:7–56

38. Velasco L, Perez-Vich B, Fernández-Martínez JM (2004) Grain quality in oil crops. In: Benech-Arnold RL, Sánchez RA (eds) Handbook of seed physiology: applications to agriculture. Food Products Press/The Haworth Press, New York, pp 389–405
39. Rotundo JL, Westgate ME (2009) Meta-analysis of environmental effects on soybean seed composition. Field Crop Res 110:147–156
40. Peña RJ, Trethowan R, Pfeiffer WH, van Ginkel M (2002) Quality (end-use) improvement in wheat compositional, genetic, and environmental factors. J Crop Prod 5:1–37
41. Park D, Allen KGD, Stermitz FR, Maga JA (2000) Chemical composition and physical characteristics of unpopped popcorn hybrids. J Food Comp Anal 13:921–934
42. Thomison PR, Geyer AB (1999) Evaluation of TC-Blend7 used in high oil maize production. Plant Var Seeds 12:99–112
43. Blanco A, Simeone R, Gadaleta A (2006) Detection of QTLs for grain protein content in durum wheat. Theor Appl Genet 112:1195–1204
44. Wardlaw IF, Wrigley C (1994) Heat tolerance in temperate cereals: an overview. Aust J Plant Physiol 21:695–703
45. Savin R, Nicolas M (1999) Effects of timing of heat stress and drought on growth and quality of barley grains. Aust J Agric Res 50:357–364
46. Stone PJ, Nicolas ME (1996) Effect of timing of heat stress during grain filling on two wheat varieties differing in heat tolerance. II. Fractional protein accumulation. Aust J Plant Physiol 23:739–749
47. Easterling D, Horton B, Jones P, Peterson T, Karl T, Parker D, Salinger M, Razuvayev V, Plummer N, Jamason P, Folland C (1997) Maximum and minimum temperature trends for the globe. Science 277:364–367
48. Meehl GA, Tebaldi C (2004) More intense, more frequent, and longer lasting heat waves in the 21st century. Science 305:994–997
49. Hawker JS, Jenner CF (1993) High temperature affects the activity of enzymes in the committed pathway of starch synthesis in developing wheat endosperm. Aust J Plant Physiol 20:197–209
50. Stone PJ, Gras PW, Nicolas ME (1997) The influence of recovery temperature on the effects of a brief heat shock on wheat. III. Grain protein composition and dough properties. J Cereal Sci 25:129–141
51. Canvin D (1965) The effect of temperature on the oil content and fatty acid composition of the oils from several oil seed crops. Can J Exp Bot 43:63–69
52. Garcés R, Mancha M (1991) In vitro oleate desaturase in developing sunflower seeds. Phytochem 30:2127–2130
53. Izquierdo N, Aguirrezábal LAN, Andrade F, Cantarero M (2006) Modeling the response of fatty acid composition to temperature in a traditional sunflower hybrid. Agron J 98:451–461
54. Martre P (2006) Modelling quality traits and their genetic variability for wheat. Eur J Agron 25:75–78
55. Triboï E, Martre P, Triboï-Blondel AM (2003) Environmentally-induced changes in protein composition in developing grains of wheat are related to changes in total protein content. J Exp Bot 54:1731–1742
56. Champolivier L, Merrien A (1996) Evolution de la teneur en huile et de sa composition en acides gras chez deux variétés de tournesol (oléique ou non) sous l'effet de températures différentes pendant la maturation des graines. Oleagineux Corps Gras Lipides 3:140–145
57. Rotundo JL, Westgate ME (2010) Rate and duration of seed component accumulation in water-stressed soybean. Crop Sci 50:676–684
58. Flagella Z, Rotunno T, Tarantino E, Di Caterina R, De Caro A (2002) Changes in seed yield and oil fatty acid composition of high oleic sunflower (*Helianthus annuus* L.) hybrids in relation to the sowing date and the water regime. Eur J Agron 17: 221–230
59. Payne PI, Holt LM, Worland AJ, Law CN (1982) Structural and genetical studies on the high-molecular-weight subunits of wheat glutenin. Theor Appl Genet 63:129–138
60. Steer BT, Seiler GJ (1990) Changes in fatty acid composition of sunflower (*Helianthus annuus*) seeds in response to time of nitrogen application, supply rates and defoliation. J Sci Food Agric 51:11–26
61. Zheljazkov VD, Vick BA, Baldwin BS, Buehring N, Astatkie T, Johnson B (2003) Oil content and saturated fatty acids in sunflower as a function of planting date, nitrogen rate, and hybrid. Agron J 101:1003–1011
62. Calderini DF, Dreccer MF (2002) Choosing genotype, sowing date and plant density for malting quality. In: Slafer GA, Molina-Cano JL, Savin R, Araus JL, Romagosa I (eds) Barley science. Recent advances from molecular biology to agronomy of yield and quality. Food Product Press/The Haworth Press, New York, pp 413–444
63. Gooding MJ, Davies WP (1997) Wheat production and utilization. Systems, quality and the environment. CAB International, Wallingford, 355 p
64. Wrigley CW, Bekes F (2004) Processing quality requirements for wheat and other cereal grains. In: Benech-Arnold R, Sanchez RA (eds) Handbook of seed physiology: applications to agriculture. The Haworth Press, New York, pp 389–405
65. Garcés R, Mancha M (1989) Oleate desaturation in seeds of two genotypes of sunflower. Phytochem 28:2593–2595
66. Borrás L, Slafer GA, Otegui ME (2004) Seed dry weight response to source-sink manipulations in wheat, maize and soybean: a quantitative reappraisal. Field Crop Res 86: 131–146
67. Savin R, Prystupa P, Araus JL (2006) Hordein composition as affected by post-anthesis source-sink ratio under different nitrogen availabilities. J Cereal Sci 44:113–116
68. Stone PJ, Savin R (1999) Grain quality and its physiological determinants. In: Satorre EH, Slafer GA (eds) Wheat: ecology and physiology of yield determination. Food Product Press/ The Haworth Press, New York, pp 85–120
69. Zahedi M, Mc Donald G, Jenner CF (2004) Nitrogen supply to the grain modifies the effects of temperature on starch and

protein accumulation during grain filling in wheat. Aust J Agric Res 55:551–564
70. Dupont FM, Hurkman WJ, Vensel WH, Tanaka C, Kothari KM, Chung OK, Altenbach SB (2006) Protein accumulation and composition in wheat grains: effects of mineral nutrients and high temperature. Eur J Agron 25:96–107
71. Passarella VS, Savin R, Slafer GA (2008) Are temperature effects on weight and quality of barley grains modified by resource availability? Aust J Agric Res 59:510–516
72. Aguirrezábal LAN, Martre P, Pereyra-Irujo G, Izquierdo N, Allard V (2009) Management and breeding strategies for the improvement of grain and oil quality. In: Sadras VO, Calderini DF (eds) Crop physiology: applications for genetic improvement and agronomy. Academic/Elsevier, New York, pp 387–410
73. Martre P, Porter JR, Jamieson PD, Triboï E (2003) Modeling grain nitrogen accumulation and protein composition to understand the sink/source regulations of nitrogen remobilization for wheat. Plant Physiol 133:1959–1967
74. Pereyra-Irujo GA, Aguirrezábal LAN (2007) Sunflower yield and quality interactions and variability: analysis through a simple simulation model. Agr For Meteorol 143:252–265

Books and Reviews

Aguirrezábal LAN, Andrade FH (1998) Calidad de productos agrícolas. Bases ecofisiológicas, genéticas y de manejo agronómico. Unidad Integrada INTA Balcarce, Balcarce, 315 p

Baskin CC, Baskin JM (1998) Seeds: ecology, biogeography, and evolution of dormancy and germination. Academic Press/Elsevier, San Diego, 666 p

Basra AS, Randhawa LS (2002) Quality improvement in field crops. Food Products Press/The Haworth Press, New York, 433 p

Benech-Arnold RL, Sánchez RA (2004) Handbook of seed physiology: aplications to agriculture. Food Products Press/The Haworth Press, New York, 483 p

Bewley JD, Black M (1985) Seeds: physiology of development and germination, 1st edn. Plenum, New York, 125 p

Gunstone FD, Harwood JL, Dijkstra AJ (2007) The lipid handbook with CD-ROM, 3rd edn. CRC Press, Boca Raton, 1472 p

Sadras VO, Calderini DF (2009) Crop physiology: applications for genetic improvement and agronomy. Academic Press/Elsevier, New York, 583 p

Schneiter AA (1997) Sunflower technology and production. ASA, CSSA & SSSA, Madison, 834 p

Simmonds DH (1989) Wheat and wheat quality in Australia. CSIRO, Melbourne, 299 p

Slafer GA, Molina-Cano JL, Savin R, Araus JL, Romagosa I (2002) Barley science: recent advances from molecular biology to agronomy of yield and quality. Food Products Press/The Haworth Press, New York, 551 p

Triboi E, Triboi-Blondel AM (2002) Productivity and grain or seed composition: a new approach to an old problem. Eur J Agron 16:163–186

Gravity Recovery and Climate Experiment (GRACE): Detection of Ice Mass Loss, Terrestrial Mass Changes, and Ocean Mass Gains

Victor Zlotnicki[1], Srinivas Bettadpur[2], Felix W. Landerer[3], Michael M. Watkins[3]
[1]Climate, Oceans and Solid Earth Science Section, Jet Propulsion Laboratory, California Institute of Technology, Pasadena, CA, USA
[2]Center for Space Research, University of Texas-Austin, Austin, TX, USA
[3]Jet Propulsion Laboratory, California Institute of Technology, Pasadena, CA, USA

G

Article Outline

Glossary
Definition of the Subject and Its Importance
Introduction
What Is GRACE
Spherical Harmonics; Equivalent Water Thickness; Mascons; and Spatial Resolution
Background Fields
Ambiguity; Downward Continuation; Data Accuracy
Applications in Land Hydrology
Applications in Cryospheric Studies
Applications in Ocean Studies
Applications in Solid Earth Studies
Future Directions
Acknowledgments
Bibliography

Glossary

Equivalent water thickness Since time changes in the gravity field are caused by time changes in mass distributions, equivalent water thickness ("EWT") is the variable thickness of a thin layer of water (thin relative to both the radius of the Earth and the horizontal scale of the signals) draping the Earth that would correspond to the observed changes in gravity. The conversion from gravitational spherical harmonics to water thickness (and vice versa) is unique and well defined, regardless of what actually causes the gravitational changes. The concept is not

used when studying changes in the solid Earth, such as glacial isostatic adjustment or earthquakes.

Glacial isostatic adjustment (GIA) Also known as postglacial rebound, it is the viscoelastic response of the mantle and lithosphere to the removal of the great ice sheets that covered parts of the Earth and peaked 21,000 years ago [65]. The deglaciation was essentially complete 6,000 years ago. The lithosphere rises where the ice sheets used to be, but sinks in other locations.

Ionosphere A set of layers at altitudes between approximately 80 and 1,000 km above the Earth's surface, with electrons and electrically charged atoms. The ionosphere leads to a delay to electromagnetic radiation, which is frequency-dependent and changes with local time and solar activity. The GRACE KBR system uses two frequencies to correct for this path delay.

KBR K-band microwave ranging system measures the distance between the two GRACE satellites using two frequencies, 24 and 32 GHz.

Mascons Mass concentrations. The term was coined by Muller and Sjogren [60] to describe mass concentrations in the lunar nearside, beneath the center of the surface features termed "mare" (pl. "maria"). Today the term "mascons" refers to an alternative method to solve the GRACE gravity fields in terms of distributed spherical caps or point masses, instead of using the spherical harmonic representation.

Newton's law of gravitation It states that every point mass attracts every other point mass with a force that is directly proportional to the product of their masses and inversely proportional to the square of the distance between them: $F = G.m_1.m_2/r^2$, where m_1 and m_2 are the masses, r is the distance between them, and G is the universal gravitational constant, $G \approx 6.6738 \times 10^{-11}$ $m^3/kg/s^2$. This law is at the heart of the GRACE measurements, since any specific mass on the Earth is in general at a different distance from the two spacecrafts, causing a slight difference in the gravitational acceleration they impart to the spacecraft, and thus causing a slight but measurable relative acceleration between the spacecrafts.

Satellite Is an object, natural (like the Moon) or artificial (each GRACE satellite) that orbits around another large object, in this case the Earth. "Orbits" means that the centripetal acceleration due to the speed of the satellite equals the gravitational acceleration between the satellite and the larger object it orbits around; in this manner the satellite neither falls toward Earth, nor escapes its gravitational pull. In practice, the GRACE satellites do fall slightly toward the Earth while they orbit around it, whereas the Moon slowly increases its distance to the Earth.

Spherical harmonics Are a set of functions of latitude and longitude that form an infinite, orthogonal, normalized set of basis functions whose sum, with appropriate scale coefficients, completely describes any other function defined in terms of spherical coordinates. Spherical harmonics satisfy Laplace's equation, as does the gravitational potential outside the Earth. Laplace's equation states that the sum of the second derivatives of the gravitational potential with respect to each of the three directions of space at a point must add up to zero if there are no masses at that point.

Definition of the Subject and Its Importance

The gravity field of the Earth, caused by the distribution of masses inside and on the surface of the Earth, changes in time due to the redistribution of mass. Such mass fluxes can be due both to natural processes (such as the seasonal water cycle, ocean dynamics, or atmospheric variations), as well as due to human actions, such as the systematic withdrawal of groundwater for human consumption. The ability to measure such changes globally is of great significance for understanding the environmental dimension of sustainability.

Until the launch of the GRACE satellite pair in 2002, such time changes in mass redistribution could only be measured globally as time changes in the longest wavelengths of the gravity field, on the order of 10,000 km and longer, from the orbit perturbations of artificial Earth satellites, or very locally at individual points on the Earth using long-term gravimeter deployments.

The GRACE satellite pair has provided the first global measurements at horizontal resolutions from 300 km to global, and time scales from 10 days to

interannual. These measurements have been used to assess the mass variability in the oceans, terrestrial water storage, and loss of ice mass in glaciers and ice sheets. Long-term trends, episodic variations such as result from large earthquakes, and seasonal changes have all been measured with unprecedented accuracy and detail.

Introduction

Imagine the ability to weigh Greenland every month over several years: It would tell us whether Greenland is losing ice, how fast, and whether the loss is accelerating. Imagine the ability to weigh the total water content every month over several years in the soil of Northern India, where the groundwater supplies hundreds of millions of people: It would tell us whether that precious resource is being used at a sustainable rate or depleted. Imagine the ability to measure how much water the ocean basins are gaining: It would allow us to separate the two key components of sea-level rise, the addition of mass and the thermal expansion due to increased ocean temperature. As we will see below, these are no longer imaginary possibilities but actual findings using data from a satellite pair called GRACE, or Gravity Recovery and Climate Experiment. The GRACE satellite pair was launched on March 17, 2002 to measure monthly changes in the gravity field of the Earth with exquisite accuracy. It is from these monthly changes in the gravitational attraction of large bodies of water, ice, and rock that we can "weigh" changes from month to month in Greenland, groundwater, and even the oceans. GRACE also yields a very accurate measurement of the time-averaged gravity field, a useful quantity for studies of tectonics and of the time-averaged ocean circulation. There is a well-known inherent ambiguity in interpreting changes in gravity: The data type can localize the changed mass horizontally, but it alone cannot distinguish whether the mass change comes from the surface or deeper layers, from the ocean, or from an earthquake that moved the sea floor. Additional information is needed to identify the source of the mass changes unambiguously. This entry reviews the basis of the GRACE measurements, some technical details that clarify the strengths and limitations of the GRACE data, and provides illustrative examples of the applications in hydrological, cryospheric, oceanic, and geophysical sciences. Given the wide variety of phenomena GRACE can tell us about, this entry cannot be an exhaustive review of the more than 700 peer-reviewed publications on GRACE published through the end of 2010. Also, while the GRACE satellite pair carries global position systems (GPS) antennas and hardware for use in "GPS occultation" soundings of the atmosphere, we focus the discussion on results obtained from the gravity data derived from GRACE.

The measurement of gravity from satellite orbit perturbations (that is, from departures of the satellite's path from a classical Keplerian ellipse) has been in existence for many decades. It started immediately at the dawn of the space age, with measurements of the Earth's pear shape [62]. Tracking satellites from terrestrial observatories or from GPS satellites, using radiometric or laser ranging methods, provided important information on the long-wavelength, static (long-term mean) gravity field through the next 3 decades. Precise measurement of time-variable gravity from those techniques was only possible, however, for the Earth's oblateness parameter (J2). Long-term measurements of the J2 parameter were used [24, 27] to identify and explain a steadily decreasing trend in the flattening of the Earth, due to GIA, and associate the departures from that steady trend with interannual climatic variability, such as the El Nino-Southern Oscillation phenomenon. See also [8, 22, 23]. The advent of the German CHAMP mission in mid-2000 improved the situation; CHAMP determined gravity changes at continental (several thousand kilometers) scales and annual and longer periods. The GRACE mission results provided a true paradigm shift, providing an unprecedented global and accurate measurement to 300-km spatial resolution, continuously since 2002.

What Is GRACE

GRACE, launched on March 17, 2002, is a joint mission of the US and German space agencies, the National Aeronautics and Space Administration (NASA) and the Forschungszentrum der Bundesrepublik Deutschland für Luft- und Raumfahrt (DLR). GRACE was the first mission flown under the NASA Earth System Science Pathfinder (ESSP) Program, with Principal Investigator (PI) from the Center for Space

Research at the University of Texas, and the co-PI from the Helmholtz Center Potsdam, German Research Centre for Geosciences (GFZ) [89]. Mission management and implementation are the responsibility of the NASA Jet Propulsion Laboratory (JPL), a NASA center managed by the California Institute of Technology. Mission operations are performed by DLR, with co-funding by the European Space Agency (ESA). DLR was also responsible for the launch services. JPL led the development of the satellite system in partnership with Astrium GmBH and Space Systems Loral (SS/L). Astrium was the prime contractor for major elements of the two satellites based on the CHAMP (CHAlleng-ing MiniPayload) satellite heritage, while SS/L was the prime contractor for the attitude control system and microwave instrument electronics. JPL also provided the key microwave range-rate sensors between the satellite pair, and the Global Positioning System (GPS) receivers.

Almost all Earth-viewing spaceborne instruments measure electromagnetic radiation, either naturally emitted or reflected by the Earth's surface (passive), or the returns of signals emitted toward the Earth by the instrument itself (active). GRACE is fundamentally different: The satellite pair senses gravity through the changes in the intersatellite distance. The two satellites fly along the same orbit (Fig. 1). Currently (as of July 2011), the pair flies 454 km above the Earth's surface (at launch, it was 502 km), separated by 206 km. Imagine the satellite pair passing over a mountain. As the lead satellite "feels" the increased gravitational attraction of the upcoming mountain, it accelerates toward that mass excess. Due to Newton's law of gravitational attraction (whereby the force acting on a mass is inversely proportional to the squared distance to the attracting mass) that acceleration toward the mountain is larger for the lead satellite than for the trailing one, whose distance to the mountain is larger. As a consequence, the distance between the two satellites increases, if ever so slightly. When the mountain is in-between the satellites, both are attracted toward the mountain, so the intersatellite distance decreases.

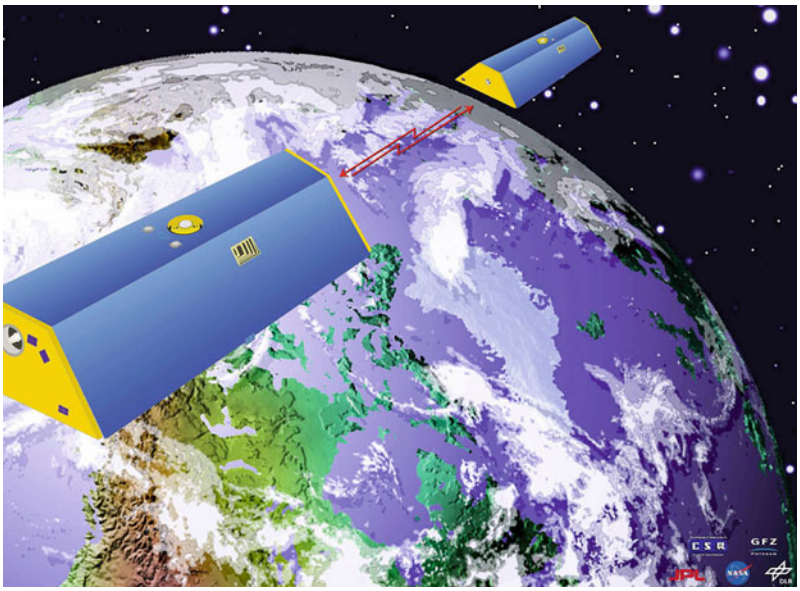

Gravity Recovery and Climate Experiment (GRACE): Detection of Ice Mass Loss, Terrestrial Mass Changes, and Ocean Mass Gains. Figure 1

Artist's conception of the GRACE satellite pair in orbit. In reality, each satellite is 3.123-m long, the distance between the pair ranges between approximately 175 and 230 km, and the altitude has been slowly decaying from 502 km at launch to 454 km currently (July 2011), relative to a distance of 6,378 km from the center of the Earth. The orbital inclination is 89°

A highly precise microwave ranging system (called "KBR," or K-band ranging system) aboard each satellite beams radio signals toward the other satellite and measures those changes in distance: This measurement forms the basis of the computation of the gravitational field. The measurement is so precise that it detects changes of a few microns in range or approximately 0.1 μm/s in velocity every 5 s. To picture that level of accuracy, it is approximately equivalent to measuring the distance between Los Angeles and San Diego to an accuracy of a (fine) human hair's width.

The key science instrument in each GRACE satellite is the microwave K-band ranging instrument. Each satellite transmits signals to the other at two frequencies, (24 and 32 GHz, called "K" and "Ka" bands, respectively) in order to correct for ionospheric path delay. The K-band ranging assembly consists of an ultra-stable oscillator, the microwave electronics, a K-band ranging horn, sampler, and the instrument processing unit (IPU). The ultra-stable oscillator serves as the frequency and clock reference for the GRACE satellites. The K-band ranging horn transmits and receives K-band carrier signals to and from the other GRACE satellite. The IPU is the nerve center for the science instruments in the spacecraft, providing the digital signal processing functions for the K and Ka band signals, as well as for the GPS signals. It also provides various clocks for the satellite operations and performs data processing for the star camera attitude (directions). The K-band ranging system was manufactured by JPL with equipment from Space Systems/Loral and the Applied Physics Laboratory.

The intersatellite range-change measurement must be corrected for the effect of forces other than gravity, such as drag or solar radiation pressure. To do so, both satellites carry accelerometers located very close to each satellite's center of mass. The accelerometers were built by ONERA, the French Aerospace Lab. An approximate orientation of the spacecraft is provided by the star cameras (two aboard each satellite). Used both for science and for attitude and orbit control, they determine each satellite's orientation by tracking their orientation with reference to the stars. They were developed by the Danish Technical University, Copenhagen, Denmark. In order to provide precise synchronization of the ranging data between the two satellites, and in order to geolocate the science data, both satellites carry Global Positioning System (GPS) units developed by JPL. There are three GPS antennas: One is used to collect navigation data, the two other antennas are used for backup navigation and atmospheric occultation data collection. The GPS units provide an additional piece of information essential to the computations: time-tagging events to better than 0.1 ms.

Other instrument assemblies aboard the spacecraft include a Coarse Earth and Sun sensor, used for approximate position and orientation whenever GRACE is in "safe mode" (when a serious anomaly in the satellite cannot be automatically corrected on board, the satellite is put into "safe mode" by the onboard computer, to ensure only the satellite's vital functions remain on, while the failure is being analyzed on the ground); a Center of Mass Trim Assembly, to adjust the satellite's center of mass with respect to the proof mass of the accelerometers; solar cell arrays, covering the outer shell of the satellites to generate power for the electronics, and nickel-hydrogen cell batteries to store and release power as needed; telemetry and telecommand subsystems for the satellites to communicate with Earth via radio systems in the microwave S-band spectrum. Each satellite uses a separate set of S-band frequencies for transmission and reception. Both, the power and telemetry as well as the telecommand subsystems, were supplied by Astrium.

The satellite's "attitude," or orientation and orbit control, is controlled by a system consisting of sensors, actuators, and software. Two kinds of attitude actuators are available. A reaction control system with a set of twelve 10-mN thrusters uses gaseous nitrogen stored in the two tanks along the main satellite axis. Fine corrections of orientation are adjusted using six 30-Amp-m^2 magnetorquers, to minimize the satellite fuel consumption. Each GRACE satellite can adjust its orbit by firing its two orbit-control thrusters (also gaseous nitrogen propellant) mounted on the rear-panel of the satellite, each of which provides 40 mN of thrust. The attitude and orbit-control system was designed by Space Systems Loral and implemented by Astrium and its subcontractors.

Further information on the spacecraft can be found at http://grace.jpl.nasa.gov/files/GRACE_Press_Kit.pdf, and details on the mission, its subsystems, and current operational status are available at the GRACE mission homepage: http://www.csr.utexas.edu/grace/.

Spherical Harmonics; Equivalent Water Thickness; Mascons; and Spatial Resolution

The gravitational potential of the Earth, sensed by a satellite at altitude h, is formally expressed as the sum of spherical harmonic functions [8]

$$T(\theta,\ \varphi) = \frac{GM}{(a+h)} \sum_{l=0}^{\infty} \sum_{m=0}^{l} \left(\frac{a}{a+h}\right)^{l} (C_{lm}\cos(m\phi) + S_{lm}\sin(m\phi))\ P_{lm}\cos(\theta) \tag{1}$$

where T is the "anomalous" potential (the difference between the true potential and a reference value) at colatitude θ, longitude ϕ. The dimensionless C_{lm}'s and S_{lm}'s are called Stokes' coefficients; the P_{lm} are Legendre functions of degree l, order m, m ≤ l, GM is the product of the universal gravitational constant G times the mass of the Earth, M, and a is a mean radius of the Earth. All other quantities (geoid height, gravity acceleration anomaly, or disturbance, etc.) have similar expansions, whose coefficients are related to those in Eq. 1 through functions of the degree l and dimensional constants. The l = 0, m = 0 coefficient in the expansion is exactly 1.0, and accounts for the total mass of the Earth system, conventionally regarded as a constant. The l = 1 terms are zero if the analysis is done in a reference frame where its origin is the instantaneous center of mass of the Earth system. The n = 2, m = 0 term accounts of the Earth's oblateness, and is of order 10^{-3} relative to the central term. All other harmonic coefficients are of order 10^{-6} or smaller. Representation of the geographic features of small spatial extent requires the expansion to be carried to higher degree-l.

The GRACE data analysis problem reduces to the extraction of the Stokes coefficients from residuals of the GRACE tracking data calculated using prior best knowledge of the Earth's gravity field and its variations. A global distribution of the mission data is required before the gravity field parameters can be estimated. It takes approximately 1 month for the GRACE data to provide uniform, global coverage. The Earth's gravity field variations are therefore represented by monthly piece-wise constant spherical harmonic coefficients of the anomalous geopotential, represented to a fixed maximum degree/order. The GRACE mission data products are these Stokes coefficients, delivered monthly for the entire mission lifetime. The long-term mean estimates provide the determination of the static gravity field, and the monthly deviations represent the time-variability of the mass flux at the longer time scales.

However, hydrologists, oceanographers, and cryospheric scientists are less interested in the gravitational C_{lm}'s and S_{lm}'s coefficients, but rather in estimates of time changes in surface mass, or ocean bottom pressure. Let the surface mass density σ be the vertical integral of the density ρ through the Earth's surface layer (containing the atmosphere, the oceans, and the water/snow/ice stored on land), where we assume all time changes are concentrated. Using the above series, with h = 0, σ is

$$\Delta\sigma(\theta,\phi) \approx \frac{a\rho_E}{3} \sum_{l=0}^{l\max} \sum_{m=0}^{l} \frac{(2l+1)}{(1+k_l)} W_l P_{lm}(\cos\theta) \times [\Delta C_{lm}\cos(m\varphi) + \Delta S_{lm}\sin(m\varphi)] \tag{2}$$

where ρ_E is the mean density of the Earth, a is its radius, and the k_l are so-called load Love numbers representing the elastic response of the solid Earth to surface loading [96]. The W_l is an isotropic filter that strongly downweighs high degree l terms, which are often contaminated with noise amplified by the downward continuation effect, discussed below. More general filters, nonisotropic filters and irregular area-averaged filters, are discussed by Swenson and Wahr [84], while a decorrelation filter which removes North–South "striping" from GRACE maps was first discussed by Swenson and Wahr [85], then optimized for ocean studies by Chambers [10]. Equation 2 allows us to convert the C_{lm}, S_{lm} to a surface mass distribution, typically expressed in centimeters of equivalent water thickness ("cm EWT"). In the above formula, the maximum spherical harmonic degree indicated is l_{max}; in practice, there is little signal above spherical harmonic degree 60 in the monthly GRACE fields, although some solutions are given to l_{max} = 120. An order of magnitude estimate for the spatial half-wavelength associated with a particular degree l is given by the approximation 40,000 km/(2l) so l = <60 implies half-wavelengths longer than ~330.

Two sets of coefficients require special handling. The coefficients of degree 1 orders 0 and 1, which

indicate the position of the center of mass of the Earth (which varies in time) relative to an Earth-fixed coordinate origin, are not measured by GRACE. Swenson et al. [87] realized that by assuming that we know the component of n = 1 from an ocean model, it is possible to use the GRACE data and the ocean information to derive degree 1 coefficients. Degree 1 coefficients can also be derived from satellite laser and Doppler ranging data [25]. The coefficients of degree 2 order 0 are poorly determined in the GRACE data, and it is now a standard practice to replace them by coefficients estimated from satellite laser ranging [23]. See also [9].

Another way to describe the gravity field uses "mascons" (mass concentrations, see "Glossary"). In this approach, either small spherical caps or point masses are assumed to cover the Earth's surface, and one solves directly for the mass of each local mascon from the intersatellite range-rate or acceleration data, rather than for the global Stokes coefficients. When the solution is unconstrained, such that no a priori correlation is imposed on neighboring mascons, nor any smoothing is imposed on the Stokes coefficients, there is little difference in the result [79]. However, there are advantages in imposing correlations between neighboring mascons when one knows that, for example, a set is in one hydrological basin and the nearby set is in another one, uncorrelated to the first. In addition, the mascon basis functions more conveniently allow higher spatial resolution at higher latitudes where ground tracks are spaced more densely.

GRACE data products can be obtained from several public sources. Because of small differences in the processing strategy, the results differ in small but significant ways, and it is a good practice to check the results from two centers for a particular application. The GRACE Science Data System consists of three centers, the Center for Space Research (UTCSR) at the University of Texas-Austin [5], the Geoforschungzentrum in Potsdam, Germany, and the Jet Propulsion Laboratory in Pasadena. These three centers provide spherical harmonic solutions through http://podaac.jpl.nasa.gov and a mirror archive at http://isdc.gfz-potsdam.de/; gridded versions of their data, with additional corrections applied (for example, the decorrelation filters of Chambers [10] or Swenson and Wahr [85], can be found at http://grace.jpl.nasa.gov. Additional sources include NASA's Goddard Space Flight Center (GSFC) [79] who supply mascon solutions, the Centre National d'Etudes Spatiales (CNES) in France [7, 46] who supply 10-day SH solutions, the Institut für Geodäsie und Geoinformation at the University of Bonn (ITG-Bonn), Germany who supply both monthly and daily SH solutions [58], and Delft University of Technology, Netherlands [49] who supply monthly SH solutions.

Background Fields

Since the satellite motion is a nonlinear function of the gravitational potential, the derivation of a monthly set of either Stokes coefficients or mascons involves the solution of a very large nonlinear least squares problem. Nongravitational influences are modeled using the data collected by the accelerometer. The satellite orientation is also important because the range-change measurements are made to a reference point displaced from the center of mass of the satellite, to which the dynamical equations of motion refer. To make the solution computationally tractable, one solves not for the full gravity field, but for the difference from an initial guess (a nominal, a priori model). The a priori model is the sum of an earlier estimate of the time-averaged gravity field, plus the disturbances due to the Sun, Moon, and other planets, plus the gravitational effects of solid Earth and ocean tides, plus the time-varying mass of the atmosphere derived from European Center for Medium Range Weather Forecast (ECMWF) model output, plus the time-varying effects of non-tidal ocean mass redistribution derived from a numerical ocean model driven by ECMWF [28], plus a model of the "pole tide" (both Earth and ocean), which is not actually a tide but the result of a perturbation of the Earth's rotation. All the components of the a priori model are collectively called "background models," and the solution depends to some extent on their fidelity. The equations of motion of the satellites are integrated numerically with time steps of a few seconds, the background models are interpolated to those times, the observable position of the satellites and intersatellite range rate are computed from the models and compared to the observed values, and the residual differences are then used in the least squares solutions. These residual differences reflect both the processes not modeled in the background

(e.g., land-surface hydrology, or ice sheet mass changes) as well as processes erroneously modeled in the background (e.g., atmospheric or tidal variability). The residual differences, aggregated over a month, are then used in the least squares solution for the anomalous geopotential for that month. In addition to the desired gravitational model for a month, a large number of instrument- and spacecraft-dependent "nuisance parameters" are adjusted which include biases, bias drifts, clock offsets, orbits of the GRACE satellites and the GPS satellites, etc.

Note that the tides, atmospheric and oceanic mass redistributions, as well as land hydrology, all have energy at periods much shorter than a month, the typical time span of one GRACE gravity solution. The models therefore remove this energy, which could otherwise be aliased into longer period variations in the retrieved gravity fields.

For ocean studies, the monthly averaged ocean model is added back to the solution. At this writing, adding a background model of the land hydrological mass changes, which has been shown to improve the solution, is being considered to become part of the gravity field processing for an upcoming data release.

Ambiguity; Downward Continuation; Data Accuracy

Gravity data provided by in-situ or airborne instruments (called gravimeters) have long been used in both exploration and research geophysics to help define buried structures that exhibit density variations (e.g., ore deposits). Two measurement effects are well known by those practitioners: the ambiguity of interpretation ("nonuniqueness" of a solution), and the problem of "downward continuation" of a measurement taken at some altitude.

Consider a sphere of density ρ_1 and radius r_1 at depth $h_1 > r_1$. This sphere would produce the same gravitational attraction at the surface as another sphere of density ρ_2 and the same radius r_1 but at depth h_2, exactly "under" the first sphere, so long as they satisfied the ratios $\rho_1/\rho_2 = (h_2/h_1)^2$. While this is harder to see in more complex shapes, it illustrates well the ambiguity in the interpretation: It is not possible to assign a mass uniquely to a buried structure without some additional data or constraints [66]. The main assumption to aid the interpretation of GRACE data is that monthly changes in gravitational attraction are produced primarily by movement of water within and among Earth reservoirs: the cryosphere, the oceans, and the soil [96], except in those regions where glacial isostatic adjustment (GIA) and earthquakes produce strong signals. This assumption is generally valid: While large mountain ranges produce large signals in the time-mean gravity field, their effect in the time-varying gravity field over a few years or even decades is negligible (Fig. 2). Indeed, as will be shown below, maps of the time-variable gravity do not show strong signals where the time-averaged gravity field has its stronger signals. In the case of GRACE, ambiguity arises when trends in mass displacements from GIA [due to the lithosphere's slow adjustment to the loss of the ice load that peaked 21,000 calendar years ago [65] and was essentially complete 6,000 years ago] can confound the signals due to trends in present-day ice or hydrological mass changes. Large earthquakes can also cause prominent signals in GRACE data as the lithosphere moves and adjusts following a quake.

To understand downward continuation, consider a simple plane, one-dimensional geometry. The gravity field above the x-axis, due to a mass distribution below the x-axis, satisfies the following equation, a consequence of Laplace's equation which governs the gravity field away from its source masses

$$G(\lambda, z) = G(\lambda, 0)^{*} \exp\left(\frac{-2\pi z}{\lambda}\right) \tag{3}$$

where $G(\lambda, z)$ is the Fourier component of the gravity acceleration distribution $g(x, z)$ with wavelength λ, and z is the altitude above a plane that is (just) above all masses. The exponential in Eq. 3 is the plane equivalent of the factor $(a/(a + h))^l$ in the spherical harmonic expansion (Eq. 1). As a consequence, if we measure $g(x, z)$ at altitude z, short wavelength features of the gravity distribution $g(x, 0)$ are attenuated by the factor $\exp(-2\pi z/\lambda)$; for $\lambda \gg z$, this factor tends to 1 while for $\lambda \ll z$, the factor tends to zero. The "downward continuation" problem arises when we measure at altitude z where short wavelengths are attenuated, but wish to know the signal magnitude at $z = 0$. This would require an exponential amplification of the weak signals, but it would also produce an exponential magnification of

the inevitable noise present in the data. Filter applications to solve or at least mitigate this problem were discussed in section "Spherical Harmonics. Equivalent Water Thickness. Mascons. Spatial Resolution."

The accuracy of GRACE data at a particular point in space and time is the result of several factors: propagation of measurement errors through the processing, loss of signal due to smoothing or destriping which makes the values at a geographical position include "leakage" from neighboring positions (smoothing) and even far away locations (destriping), and the ambiguity associated with the signals of GIA and large earthquakes. The effect of measurement errors depends on latitude (smaller at higher latitudes), and

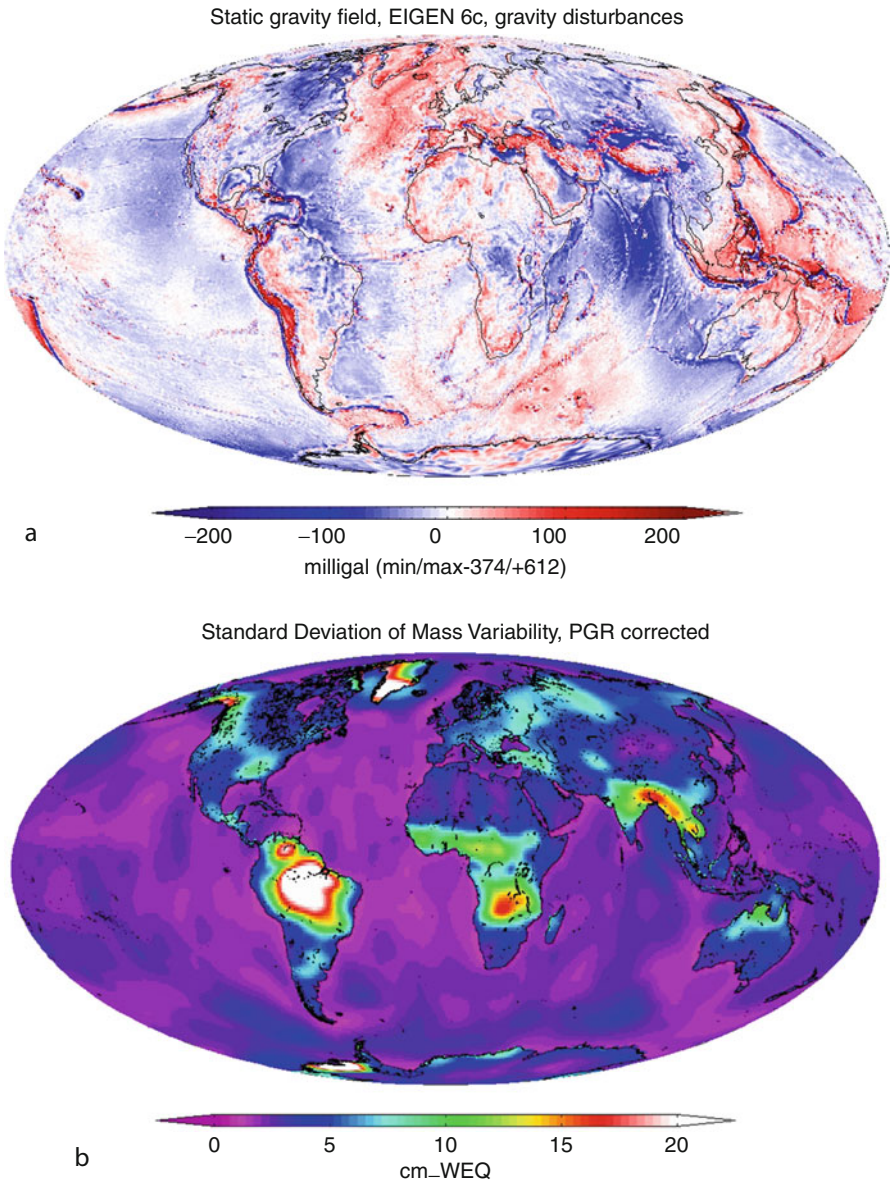

Gravity Recovery and Climate Experiment (GRACE): Detection of Ice Mass Loss, Terrestrial Mass Changes, and Ocean Mass Gains. Figure 2
(Continued)

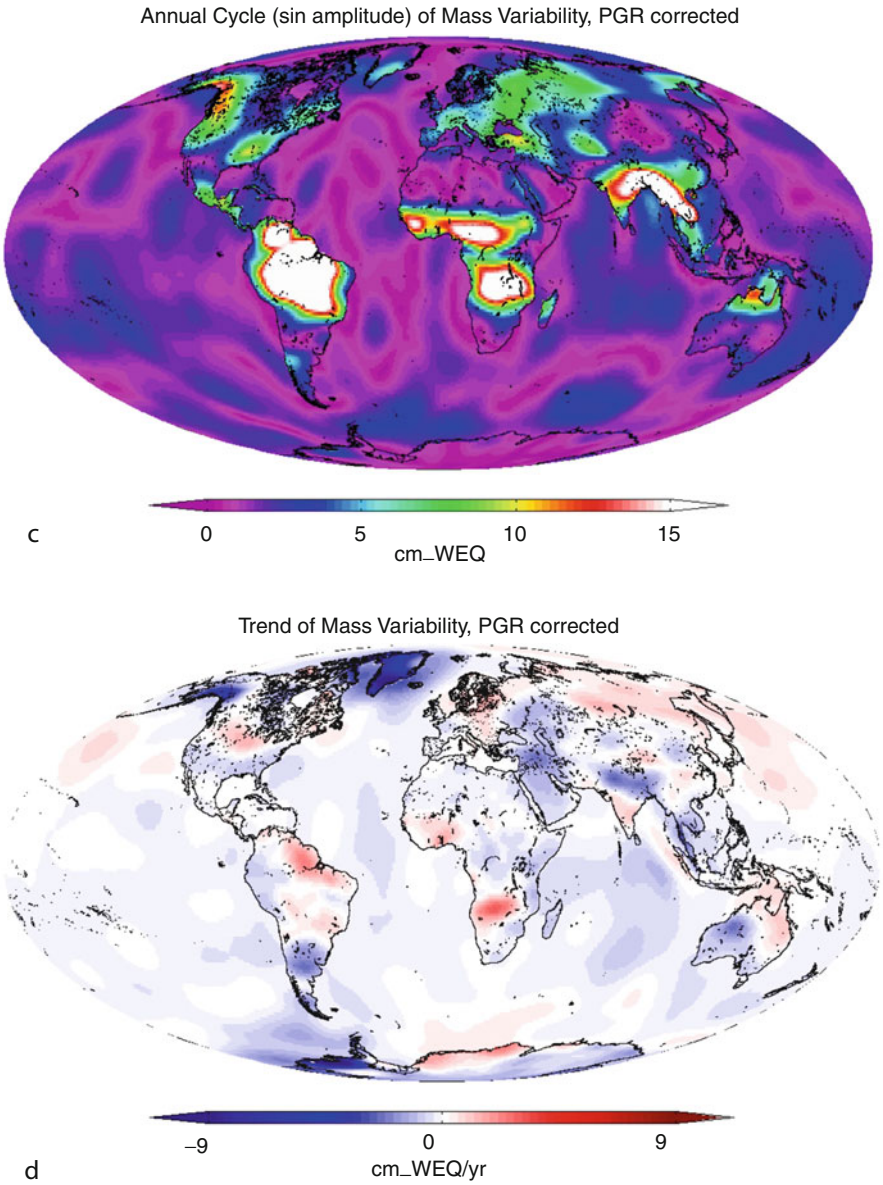

Gravity Recovery and Climate Experiment (GRACE): Detection of Ice Mass Loss, Terrestrial Mass Changes, and Ocean Mass Gains. Figure 2

(**a**) The static gravity field EIGEN6c, which combines GRACE and in situ data. The quantity displayed is the "gravity disturbance," which is the difference between actual gravity acceleration at a point and a reference value, which includes the longest wavelengths of gravity, at the same point. The short length-scale-features in this map are closely related to surface topography, whether on land or at the sea floor. (Data from the International Centre for Global Earth Models, Potsdam, Germany http://icgem.gfz-potsdam.de/ICGEM.) (**b**) The standard deviation of monthly maps of changes of mass which give rise to changes in the gravity field derived from GRACE, expressed in centimeters of equivalent water thickness (see section "Spherical Harmonics. Equivalent Water Thickness. Mascons. Spatial Resolution"; here abbreviated as "WEQ" = "EWT"). Data cover the time period Jan 2003 to Dec 2010. A destriping decorrelation filter has been applied; land data are further smoothed with a 300 km Gauss filter, while ocean data are smoothed with a 500 km Gauss filter. The trends due to glacial isostatic adjustment have been removed from the data using the model of (Paulson et al. [65]). Note that there

smoothing radius (smaller with larger radii); for example, smoothing with a 750 km Gaussian, but not applying any destriping filter, leads to errors in the mass anomalies ranging between 8 mm of equivalent water near the poles to over 28 mm at the Equator [97].

Applications in Land Hydrology

Over land, repeat GRACE gravity data are interpreted as changes in total water stored in groundwater, soil moisture, vegetation, surface water, snow, and ice, a vertical integration over all relevant layers; this quantity is called terrestrial water storage (TWS). The main complicating issue that arises is the effect of destriping and smoothing filters on the hydrological signals. This effect can be estimated by applying the same filters to output of a land-surface hydrology model (LSM), then computing a gain factor as a least squares ratio between the time series of change in TWS of the filtered and unfiltered model outputs [43].

GRACE gravity data in Northern India, interpreted as TWS, revealed a steady, large-scale mass loss beyond the natural variability simulated by a land hydrology model [90], which resulted from the excessive extraction of groundwater (Fig. 3). When the GRACE data were combined with hydrological models to remove natural variability, the authors concluded the region had lost groundwater at a rate of 54 ± 9 km^3/year between April 2002 and June 2008 and noted that continued extraction of groundwater at that rate could lead to a major water crisis (see also [78]). GRACE data also showed groundwater depletion in California: During a drought period that lasted from October 2003 to March 2010, California's Sacramento and San Joaquin River Basins lost water at a rate of 31.0 ± 2.7 mm/year equivalent water height, or a total volume of 30.9 km^3. Adding other data and a hydrological model, the authors concluded that most of the loss, 20.3 km^3, occurred in the Central Valley [30]. While the authors concluded that such a water loss is unsustainable over many years, the most recent data show a return to pre-drought conditions starting in 2009, likely due to significantly increased precipitation.

Australia's recent record droughts motivated many studies using GRACE data. LeBlanc et al. [45] investigated the devastating drought which started in 2001 in the Murray-Darling Basin in southeast Australia. They combined GRACE with in situ and simulated hydrological data to show that groundwater levels continued to decline 6 years after the 2001 onset of the drought, for a total groundwater loss of 104 km^3 between 2001 and 2007; the drought continued even though annual precipitation in the region returned to average during 2007. Combining GRACE data, numerical model output, and various atmospheric datasets, Garcia-Garcia (2011) [31] showed that interannual changes in the seasonal signal in TWS were intricately related both to the El Nino-Southern Oscillation (ENSO) and the Indian Ocean Dipole (IOD) phenomena, with positive phases of the IOD related to anomalously low precipitation in southeastern Australia due to a reduced tropical moisture flux, and that the sustained water storage reduction over central and southern Australia during 2006–2008 was associated with three consecutive positive IOD events. See also [3].

GRACE data over the largest drainage basin in the world, the Amazon, were used to observe two extreme seasons: the very dry 2002–2003 and the extremely wet 2009 seasons, during which (March 2009) TWS in the entire basin was ~624 ± 32 Gt above the 2002–2009 time average [20]; the authors note that this huge TWS excess is roughly equal to the water consumption for 1 year in the USA. Not surprisingly, the GRACE data were consistent with precipitation data from the Global Precipitation Climatology Project. The authors also note the close correlation between these interannual TWS changes in the Amazon and El Nino-Southern

is essentially no correlation between this map and Fig. 2a; by contrast, here the largest signals are at low latitudes, West Antarctica, Greenland, and the Gulf of Alaska, indicating that by and large monthly changes in gravity are indeed associated with changes in the surface water and ice mass redistribution (Data from http://grace.jpl.nasa.gov). (**c**) The amplitude of a (sinusoidal) annual cycle fit to the data of Fig. 2b. Note the differences from Fig. 2b, for example, Antarctica where the annual cycle is almost absent, or Greenland where it is minimal. (**d**) Trend of the data in Fig. 2b. Note that the strongest negative (decreasing mass) trends are in Greenland, West Antarctica, and Alaska

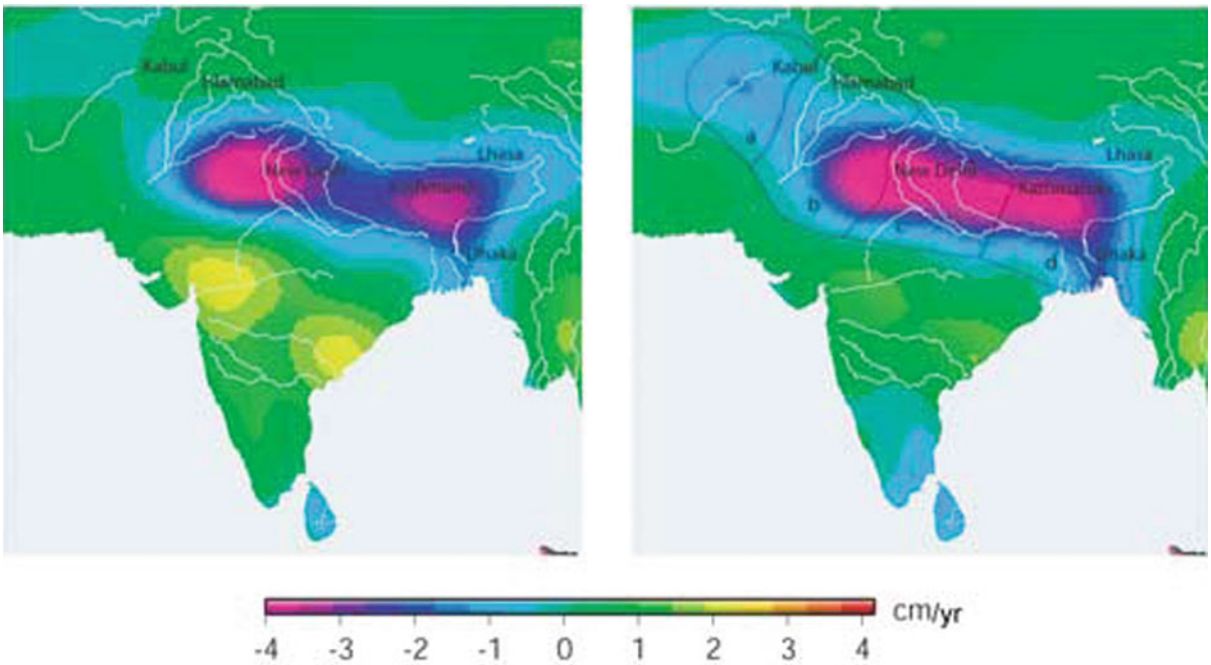

Gravity Recovery and Climate Experiment (GRACE): Detection of Ice Mass Loss, Terrestrial Mass Changes, and Ocean Mass Gains. Figure 3

Left: Mass loss detected by GRACE in Northern India, in centimeter of equivalent water thickness (From [90]). *Right*: after subtracting from the *left* map the prediction of the Community Land Model (*CLM*) hydrology model, a measure of natural variability. Thus, the *right* map depicts the anthropogenic withdrawal of groundwater in the region. See [90] for details

Oscillation (ENSO) events as measured by a widely used ENSO index based on Sea Surface Temperature in the eastern tropical Pacific. The 2002–2003 dry season was tied to 2002–2003 El Niño and the 2009 flood to La Niña conditions. See also [1, 34].

Swenson and Wahr [86] combined GRACE with radar and laser altimetry, scatterometer, and precipitation data to asses water level changes in several lakes in the Great Rift Valley, East Africa, and to separate the effects of climatic variability from those of water resources management at the downstream dams of Lake Victoria. Comparing the water level drops from Lakes Victoria, Tanganyika, and Malawi, the authors concluded that about half of the decrease in Lake Victoria was due to climate forcing, and half to water management; this conclusion for the period 2003–2009 was consistent with previous findings for earlier time periods. See also [2, 4].

An innovative application used GRACE TWS data to evaluate precipitation products from two global analyses – Global Precipitation Climatology Project (GPCP) and Climate Prediction Center Merged Analysis of Precipitation (CMAP) – [83]. Both GPCP and CMAP merge in situ rain gauge data with satellite data. At high latitudes, the uncertainty in these products is significantly higher than at lower latitudes, due to gauge "undercatch," a systematic underestimation by the in situ data, which is empirically corrected for. The authors used GPCP and CMAP to estimate precipitation, and the output of a land hydrology model to estimate evapotranspiration and runoff. They concluded that the gauge undercatch correction used by GPCP may be overestimated and pointed out the usefulness of the GRACE data in assessing precipitation estimates – and their biases – over large regions with sparse in situ gauge data.

The correlation of interannual variability of stored water over land and interannual changes in sea level, corrected for thermal expansion, was found to be ~0.6 [50, 51].

Perhaps the most promising use of GRACE data in land hydrology applications is its rigorous assimilation into numerical land-surface hydrology models (LSMs), together with a variety of other data such as snow water equivalent or soil moisture, and forcing fields such as precipitation. The reason is that the output of such models allows the separation of the various vertical components that add up to the total TWS and can provide information at scales finer than the resolution of GRACE, both in space and time. Zaitchik et al. [101] used an ensemble Kalman filter and smoother applied to the catchment land-surface model (CLSM) to study the Mississippi River basin and its four main subbasins. They found that the model with GRACE data assimilation had improved skill over the model without assimilation; skill was determined by the correlation with measured groundwater and with gauged river flow for the four subbasins and for the overall Mississippi River. They then evaluated model performance for eight smaller watersheds, all smaller than the scale of GRACE observations. In seven of eight cases, GRACE data assimilation increased the correlation between changes in TWS and gauged river flow, evidence of the potential to downscale GRACE data to finer spatial scales in hydrological applications. See also [54, 82].

Applications in Cryospheric Studies

When using the time variability GRACE data to study large glaciers and continental ice sheets, the change in gravity is interpreted as a change in ice mass; the change in equivalent water thickness, integrated over the relevant surface area and multiplied by the density of water, yields the change in Gigatons (Gt) of ice. Two complicating issues arise: glacial isostatic adjustment (GIA) and the effect of GRACE filtering and destriping on the estimates. These same issues certainly arise in hydrological and oceanographic studies, but they are more prominent in cryospheric studies for two reasons: firstly, for most hydrological studies, GIA is a small signal relative to the hydrological trend, or simply, the trend is not the main point of the study but rather interannual changes in the hydrological signal, while in cryospheric studies, the trend is the desired signal; secondly, the effect of the smoothing and destriping filters for hydrological studies can be estimated by applying the same filters to output of a land-surface hydrology model (LSM). No such calculation can be performed for changes in ice mass, since currently no adequate, reliable ice sheet models exist. The GIA correction is relatively small for Greenland, but it is as large as the overall ice mass trend for Antarctica. Therefore, uncertainties in the GIA model propagate directly into uncertainties of the estimated ice loss for Antarctica. The solution to the scaling issue requires having external knowledge about the location of the small regions where ice melt is concentrated. This information could come from the Ice, Cloud, and land Elevation Satellite (ICESat) laser altimeter, or from Interferometric Synthetic Aperture Radar (InSAR), then building a model of spatial ice mass loss based on this information, and finally computing a scaling factor in a similar manner as for hydrological signals. For both the Greenland and Antarctic ice sheets, the mass loss is concentrated in coastal outlet glaciers and ice streams, and this information is used to construct a model of ice loss to which the destriping and smoothing filters are applied to derive necessary gain factors. Needless to say, "whether ice sheets and glaciers are melting, and whether such melting is accelerating" are topics of great scientific and social interest.

GRACE data revealed that Greenland's ice lost mass at an accelerated pace: While 137 Gt/year of ice were lost in 2002–2003, the rate increased to 286 Gt/year in 2006–2009, an acceleration of -30 ± 11 Gt/year^2 in 2002–2009 ([93]; see also [17]). The same study estimated the mass loss from Antarctica to have accelerated from 104 Gt/year in 2002–2006 to 246 Gt/year in 2006–2009, an acceleration of -26 ± 14 Gt/year^2. It is important to note that, while the trends are affected by the accuracy of GIA estimates, the accelerations are not because the GIA process is a trend without notable acceleration over the time periods considered. The Antarctic ice loss is mostly concentrated in West Antarctica. These results were bolstered by another study, which covered the time period 1992–2009 [75], and combined GRACE data over 2002–2009 with the "mass-budget method" (MBM) over the longer time span. In the MBM, Interferometric Synthetic Aperture Radar is used to compute glacier velocities while radio echo sounding is used to compute ice thickness; from this combination, perimeter loss is derived, and the perimeter loss is then differenced from net

accumulation computed from the sum of snowfall minus surface ablation reconstructed from a regional atmospheric model. During the common time period of 2002.9–2009.5, the GRACE data and the MBM results agree within their error bars (Fig. 4). For Greenland, the mass losses estimated from MBM and GRACE differ by ±20 Gt/year, within their respective errors of ±51 Gt/year and ±33 Gt/year, and the accelerations in mass loss agree even better: 19.3 ± 4 Gt/year^2 with MBM and 17.0 ± 8 Gt/year^2 with GRACE. For Antarctica, the mass loss rates differ by ±50 Gt/year, within the error bar of ±150 Gt/year for MBM and ±75 Gt/year for GRACE, while the accelerations are 13.2 ± 10 Gt/year^2 with GRACE data and 15.1 ± 12 Gt/year^2 with MBM (the 18-year MBM estimates of the accelerations are 21.9 ± 1 Gt/year^2 for Greenland and 14.5 ± 2 Gt/year^2 for Antarctica, indicating that the GRACE period is probably too short to estimate long-term accelerations due to strong interannual variability). This study estimates that during 2006, the Antarctic mass loss using the MBM was 200 ± 150 Gt/year, comparable to Greenland's 250 ± 40 Gt/year. The total contribution from both ice sheets amounted to 1.3 ± 0.4 mm/year sea-level rise during 2006. See also [15, 17, 19, 38, 77, 80, 92]. These studies show that most of the Antarctic ice mass loss is concentrated on the West Antarctic Ice Sheet, especially the Peninsula, and that East Antarctica has experienced a small but measurable mass increase during the GRACE years.

Focusing on smaller regions, GRACE data showed that the Greenland ice loss was largest in the southeast at the beginning of the GRACE period, but in the last few years the rates have decreased in this region, while they increased in the northwest [21, 40]. The Canadian Arctic Archipelago, off the northwestern shore of Greenland, was studied using GRACE and two other independent approaches: surface mass-budget modeling plus an estimate of ice discharge and repeat satellite laser altimetry from ICESat [32]. It was found that the three approaches gave comparable results: Between the periods 2004–2006 and 2007–2009, the rate of mass loss increased from 31±8Gt/year to 92 ± 12 Gt/year,

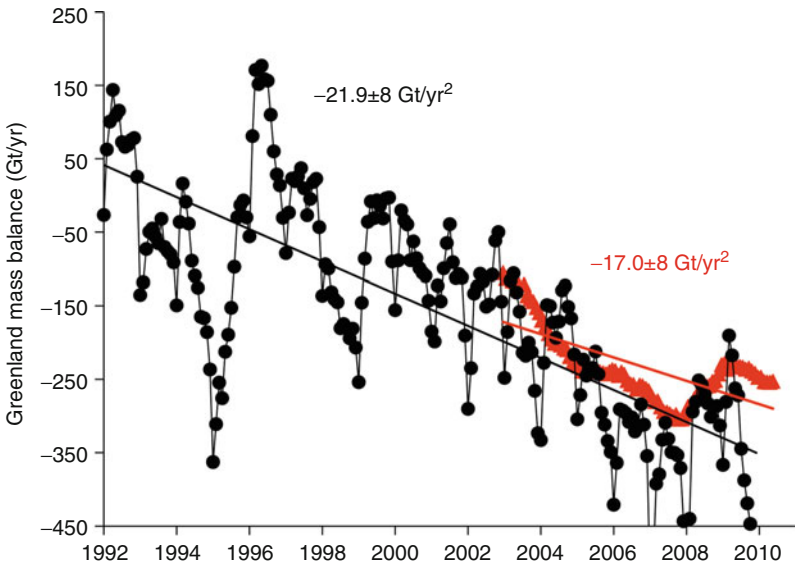

Gravity Recovery and Climate Experiment (GRACE): Detection of Ice Mass Loss, Terrestrial Mass Changes, and Ocean Mass Gains. Figure 4

Decreasing trends in Greenland mass, obtained from two methods: Mass Balance method (*black circles*) and GRACE (*red triangles*). See text in section "Applications in Cryospheric Studies" for details. Note the excellent agreement of these two totally independent methods between 2003 and 2010. Because this plot depicts changes in the trend, the GRACE result is unaffected by uncertainties in modeling GIA, a constant trend (From E. Rignot, 2011, personal communication based on [75])

although the authors recognize that the time series is rather short to establish reliable long-term trends. On even smaller spatial scales, ice mass loss bordering the Gulf of Alaska and northwestern Canada was studied [54] using a mascon approach to localize GRACE signals better. It was found that although there was an overall −84±5Gt/year mass loss (0.23±0.01 mm/year in equivalent sea-level rise) between April 2003 and September 2007, the spatial and temporal variabilities were very large, and choosing another time period (April 2003 to September 2006) gave a very different trend value. See also [16, 19]. Overall, the variability observed with GRACE agrees well with regional patterns of glacier mass loss determined from aircraft altimetry and in situ data. On even smaller spatial scales, large ice mass losses in the Patagonia ice field were documented [18, 39], the latter using a mascon approach. See also [56].

Permafrost regions also received attention. Landerer et al. [44] studied the Eurasian pan-Arctic region during 2003–2009 and concluded that changes in discharge were not due to melting of excess ground ice, but rather to changes in precipitation. However, increases of water storage, while driven by precipitation, were partially co-located with regions of discontinuous permafrost, which has warmed significantly over the last decades and changes in the terrestrial hydrological dynamics are thus likely.

Applications in Ocean Studies

GRACE data for ocean studies have been interpreted in three ways: as the time-averaged geoid, as the time-varying but globally averaged total mass of the oceans, and as the time-varying spatial pattern of ocean bottom pressure (OBP). In many cases, the data have been used together with satellite radar altimetric measurements of sea surface height (SSH). In both cases, the signals are described as changes in centimeters of water height, since 1 millibar of OBP is approximately equal to the weight of 1 cm of water.

Ocean dynamic topography is the difference between an SSH map from radar altimetry and an estimate of the geoid, the equipotential surface of the Earth's gravity field that best approximates mean sea level. Slopes in the dynamic topography imply gravitational forces acting on the ocean, forces that drive surface ocean currents. A mean dynamic topography (MDT) is a multi-year time-averaged dynamic topography, and reflects the stationary component of the surface ocean circulation. GRACE data improved our knowledge about the geoid enormously relative to preexisting models. MDTs based on SSH and GRACE only [94] were used to study the double celled gyre of the South Atlantic ocean. In combination with surface drifter and other in situ data, as well as dynamic constraints imposed by the ocean surface momentum balance [57], these new MDTs were also used to study small scale zonal striations in the ocean; GRACE constrained the longer wavelengths and the drifter data the finer space scales. See also [76]. These MDTs are now being improved with the use of data from the Gravity field and steady-state Ocean Circulation Explorer (GOCE) [42].

Time changes in the total mass of the ocean, and their relation to land-ice melt, are a topic of great climatic and societal interest. SSH increases measured by radar altimeters reflect both increases in ocean mass and thermal expansion due to increased temperatures. In addition to radar altimetry and GRACE, an in situ observing system using Argo floats (www.argo.ucsd.edu) has been measuring temperature and salinity in the upper 1,000–2,000 m of the ocean, with good coverage since 2005. In principle, it is possible to derive the thermal expansion component from Argo, and therefore, the sum of the mass component from GRACE and the thermal expansion component from Argo should add up to the altimetrically observed SSH (assuming that the current thermal expansion is small below 2,000 m). In practice, each observing system has its strengths and weaknesses (for example, GRACE data near land tend to be contaminated by large land hydrological signals; Argo coverage prior to 2005 is spotty). However, the three datasets now agree within error estimates, both on seasonal time scales and in terms of their trend [47, 48]. In fact, a discrepancy in earlier estimates of this balance [53] helped identify a problem in the in situ data [98]. See also [12, 14, 74]. The interannual variability in the spatial distribution of GRACE-derived oceanic mass change and that derived from altimetry minus Argo has also been studied [51].

GRACE data over the oceans have been compared with in situ bottom pressure recorders (BPR). BPR sites are few relative to the vastness of the oceans, they are

seldom occupied for longer than a year or two without changing instruments, and the instruments drift, especially when first installed at the bottom of the ocean. Hence, the comparisons have focused on subannual signals. The general conclusion is that there is good agreement at mid-to-high latitudes where the signal exceeds 1 cm RMS, and poor agreement at tropical and lower latitudes, where the bottom pressure signal is weaker and GRACE errors are larger [55, 59, 64, 73].

Large-scale mass exchanges among the Pacific, Atlantic, and Indian Ocean basins between August 2002 and December 2008 were identified in GRACE data and a numerical ocean model [11]. These exchanges occurred both over seasonal and interannual time scales. Changes in transport of the Antarctic Circumpolar Current were observed through changes in OBP in both GRACE and numerical ocean models [102] and (Fig. 5); an exchange of water between the Southern Ocean and the Pacific was also observed [70].

A declining trend in GRACE-derived OBP in the Arctic was correlated to corresponding changes observed with an in situ bottom pressure gauge and, more importantly, to mass changes due to decreasing upper ocean salinities near the North Pole and in the Makarov Basin [59]. (Data subsequent to the publication of that paper has shown the basin reverting to its previous state.) In addition to this interannual variability, annual oscillations of about 2 cm OBP in the Arctic ocean, with maximum in late summer to early fall, were observed with GRACE and modeled as a response to runoff and precipitation minus evaporation that agrees in phase with the data and is 10% larger [69].

A record increase in OBP (from GRACE) and SSH (from the Jason-2 radar altimeter) was observed in late 2009 to early 2010 over a large mid-latitude region of the South East Pacific, diagnosed as a response to wind stress curl associated with a strong and persistent anticyclone in late 2009, which was likely related to the concurrent Central Pacific El Nino [6]. While all previously described results focused on large regions, a 20 cm seasonal signal in the small Gulf of Thailand was observed with GRACE, altimetric SSH and a nearby tide gage [99].

A promising use of the time-varying spatial distribution of OBP from GRACE is its incorporation into numerical ocean models as a data constraint. Steps in this direction were taken by Siegismund et al. [81] and Quinn and Ponte [71] who compared GRACE with OBP in numerical ocean models in order to assess the errors that should be assigned to the GRACE data in order to assimilate it into a numerical ocean model.

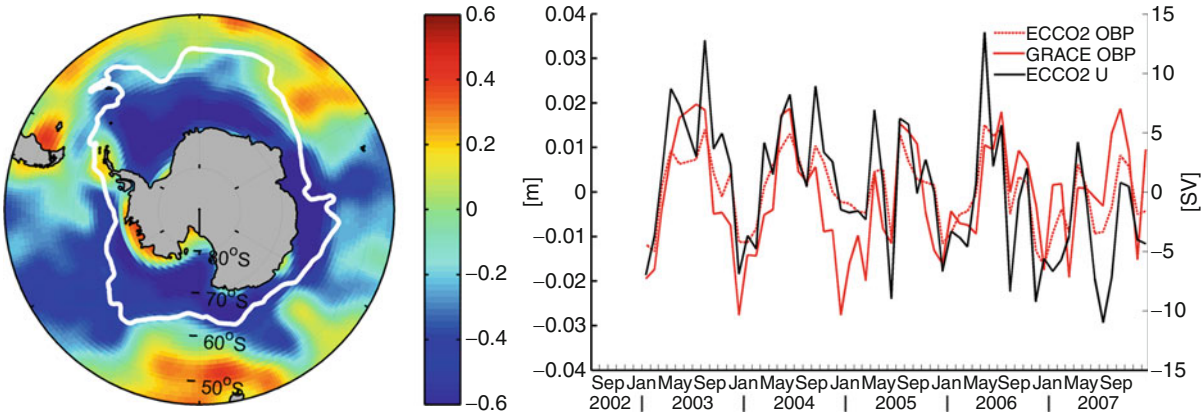

Gravity Recovery and Climate Experiment (GRACE): Detection of Ice Mass Loss, Terrestrial Mass Changes, and Ocean Mass Gains. Figure 5

Left: Correlation of Drake Passage Transport in the ECCO2 numerical ocean model with GRACE-derived ocean bottom pressure (*OBP*). The *white line* indicates the Southern ACC front of the Antarctic Circumpolar Current. *Right*: Time series of Drake transport and OBP averaged along the Southern ACC front, both from ECCO2 and GRACE. Note that the correlation is not only over seasonal time scales but also the interannual variability is captured (Data and plots from Carmen Boening, 2010, personal communication)

The availability of GRACE data made it possible to reevaluate the impact of self-attraction and loading produced by the global redistribution of seawater and land water, as well as in the analysis of tide gage data, which typically disregard these effects (tidal models do include self-attraction and loading) [76]. The authors used continental water mass storage from a hydrological model, Greenland and Antarctica seasonal signals from GRACE, and ocean bottom pressure from a numerical ocean model, and found that the amplitude of the seasonal cycle due to self-attraction and loading at tide gages ranges between 2 and 18 mm. See also [95].

Tides are an area of special interest both as a dealiasing correction to GRACE and radar altimetry data, and more importantly because they have climatic effects; for example, they affect outflows of Antarctic Bottom Water in the Ross Sea by increasing the benthic layer thickness during spring tide [63]. Four global tidal models were assessed in terms of their ability to reduce tidal residuals (identified by their frequency) in the GRACE intersatellite range-rate data [72]; aside from power at the solar semidiurnal tide frequency in low latitudes due to errors in the model of atmospheric tides, the authors found power at the frequencies of nonlinear shallow-water tides indicating areas of needed improvement in global ocean tidal models. Going one step further, Egbert et al. [29] assimilated mass anomalies inferred from GRACE into a hydrodynamic tidal model around Antarctica focused on the M2, S2, and O1 constituents. They showed that after GRACE data assimilation, the model better matched independent tide gage and ICESat laser altimetry data over the Filchner, Ronne and Ross Ice Shelves. See also [36].

Applications in Solid Earth Studies

GRACE time-variable gravity data have been applied in two areas of solid earth science: glacial isostatic adjustment (GIA, also known as postglacial rebound), and large earthquakes. The data processing for these applications is rather different from the previous examples that focus on surface mass changes. In the case of GIA, spatial trends in gravity potential as observed by GRACE are combined with in situ GPS data, ICESat laser altimetry and other data in least squares inversions to separate the contributions to observed surface deformations caused by GIA from those caused by present-day ice mass changes. In the case of large earthquakes, the preferred data type have been the along-track intersatellite range rates, because these can better localize signals with small spatial extent that occur over a short time period.

Tide-gauge, GPS, and GRACE data were combined in a simultaneous inversion for a self-consistent model of GIA and regional sea-level change estimates for the Fennoscandia region [37]; the final models were consistent in peak uplift values (9.5±0.4 mm/year), but located the peak uplift several degrees to the east of previously published results toward the middle of the northern Gulf of Bothnia; this work identified a background uniform gravity rate required for simultaneously fitting the data which could be due either to errors in the GRACE data or to errors in other models used as part of the inversion. A regional study of the Antarctic Peninsula using GRACE mascon and GPS data [38] found that simultaneous solution for ice loss and GIA crustal motions is possible, provided the linear trends in crustal uplift are robustly determined by the GPS stations with adequate spatial coverage of the regions with active GIA uplift and ice loss. A global study [100] combined GRACE and GPS data with ocean bottom pressure from a data-assimilative numerical ocean model to separate the contributions of present-day change (in terms of the thickness of ice and water) from that of GIA; these authors find a measurable GIA uplift signal in Greenland, where GIA models predict a negligible signal. Wu et al.[100] have revised their published estimate of Greenland ice mass loss from 104 Gt/year in their original paper to 140 Gt/year by adding to the inversion more realistic constraints on the ice distribution (X. Wu, 2011, personal communication). See also [13, 41, 68, 91].

Three large earthquakes were studied with GRACE data: (1) the 2004 Sumatra-Andaman earthquake with magnitude M_w 9.2, (2) the somewhat weaker 2010 Maule (Chile) earthquake (M_w 8.8), and (3) the 2011 earthquake off the Pacific coast of Tohoku, Japan (M_w 9.0). At this writing, published results are available for the first two.

The time series (May 2003 to April 2007) of localized gravity changes derived directly from the intersatellite range-rate data, using so-called Slepian

functions every 15 days, allowed [33] to find step-like time behavior (coseismic) and exponential-like time behavior (postseismic relaxation) stemming from the 26 December 2004 Sumatra-Andaman earthquake. The authors used seismic and geodetic data to estimate the coseismic slip and evaluated postseismic relaxation mechanisms that fit the GRACE data with alternate asthenosphere viscosity models. They also observed a prominent positive post-earthquake gravity change around the Nicobar Islands, attributable to seafloor uplift. See also [26]. Small changes in the GRACE satellites' intersatellite range were detected after the Maule, Chile earthquake (Mw 8.8, about 4 times lower energy release than the Sumatra-Andaman earthquake) on February 27, 2010 [35] A gravity anomaly of −5 μGal over 500 km was found east of the epicenter after the earthquake. Based on coseismic models, the long-wavelength negative gravity change is primarily the result of crustal dilatation as well as surface subsidence in the onland region. Finite fault coseismic models predicted a much smaller offshore positive gravity anomaly, due to partial compensation of the gravity changes because of surface uplift and interior deformation. The authors noted that gravity data from GRACE fill in the seldom-observed long-wavelength part of the spectrum of earthquake deformations (for large earthquakes), a complement to surface geodetic measurements and seismic data.

Future Directions

The GRACE mission successfully demonstrated the usefulness of space-based time-varying gravity data in a variety of applications. It is clear that time-varying gravity data can monitor some of the effects and consequences of climate change and anthropogenic activity (ice loss; groundwater loss, the mass component of sea-level rise). Given this utility, it is not surprising that there is much interest in Europe, the USA, and in other countries to launch future missions devoted to measuring time-variable gravity. A mission called e-Motion was proposed to the European Space Agency, but was not selected in 2011. In the USA and Germany, a "follow-on" or "gap-filler" mission, very similar to the first-generation GRACE satellites, has been approved and is scheduled to launch in 2016. Several improvements due to lessons learned from GRACE, as well as an experimental laser link between the two satellites will be implemented. In the USA, the National Research Council's Decadal Survey of Earth Sciences (NRC 2007) recommended a GRACE-II mission, which would be a significant improvement to the GRACE capabilities, and is planned to launch in the 2020 decade. Much discussion for the next decade centers around launching coordinated pairs of satellites, sponsored by different countries, to improve the spatial and temporal resolution of the retrieved signals.

Acknowledgments

This work was performed in part at the Jet Propulsion Laboratory, California Institute of Technology, under contract with the National Aeronautics and Space Administration, and at the Center for Space Research, University of Texas-Austin. Copyright 2011 California Institute of Technology.

Bibliography

Primary Literature

1. Alsdorf D, Han S-C, Bates P, Melack J (2010) Seasonal water storage on the Amazon floodplain measured from satellites. Remote Sens Environ 114:2448–2456
2. Awange JL, Sharifi M, Ogonda G, Wickert J, Grafarend EW, Omulo M (2007) The falling Lake Victoria water levels: GRACE, TRIMM and CHAMP satellite analysis of the lake basin. Water Resources Manage. doi:10.1007/s11269-007-9191-y
3. Awange JL, Sharifi MA, Baur O, Keller W, Featherstone WE, Kuhn M (2009) GRACE hydrological monitoring of Australia: current limitations and future prospects. J Spat Sci 54:23–36
4. Becker M, Llovel W, Cazenave A, Guentner A, Cretaux J-F (2010) Recent hydrological behavior of the East African great lakes region inferred from GRACE, satellite altimetry and rainfall observations. C R Geosci 342:223–233. http://dx.doi.org/10.1016/j.crte.2009.12.010
5. Bettadpur S (2007) CSR Level-2 processing standards document for product release 04 GRACE. The GRACE Project. Center for Space Research, University of Texas at Austin, pp 327–742. http://podaac.jpl.nasa.gov/gravity/grace
6. Boening C, Lee T, Zlotnicki V (2011) A record high ocean bottom pressure in the South Pacific observed by GRACE, J Geophys Res Lett 38:L04602. doi:10.1029/2010GL046013
7. Bruinsma S, Lemoine J-M, Biancale R, Vale's N (2010) CNES/GRGS 10-day gravity field models (release 2) and their evaluation. Adv Space Res 45:587–601. doi:10.1016/j.asr.2009.10.012

8. Cazenave A, Mercier F, Bouille F, Lemoine J-M (1999) Global-scale interactions between the solid Earth and its fluid envelopes at the seasonal time scale. Earth Planet Sci Lett 171:549–559
9. Chambers DP (2006a) Observing seasonal steric sea level variations with GRACE and satellite altimetry. J Geophys Res 111 (C3). doi:10.1029/2005JC002914
10. Chambers DP (2006) Evaluation of new GRACE time-variable gravity data over the ocean. Geophys Res Lett 33(17)
11. Chambers DP, Willis JK (2009) Low-frequency exchange of mass between ocean basins. J Geophys Res 114:C11008. doi:10.1029/2009JC005518
12. Chambers DP, Wahr J, Nerem RS (2004) Preliminary observations of global ocean mass variations with GRACE. Geophys Res Lett 31:L13310. doi:10.1029/2004GL020461
13. Chambers DP, Wahr J, Tamisiea ME, Nerem RS (2010) Ocean mass from GRACE and glacial isostatic adjustment. J Geophys Res 115:B11415. doi:10.1029/2010JB007530
14. Chen JL, Wilson CR, Tapley BD, Famiglietti JS, Rodell M (2005) Seasonal global mean sea level change from satellite altimeter, GRACE, and geophysical models. J Geodesy 79:532–539. doi:10.1007/s00190-005-0005-9
15. Chen JL, Wilson CR, Tapley BD (2006) Satellite gravity measurements confirm accelerated melting of Greenland ice sheet. Science 313. doi:10.1126/science.1129007
16. Chen JL, Tapley BD, Wilson CR (2006) Alaskan mountain glacial melting observed by satellite gravimetry. Earth Planet Sci Lett 248:353–363
17. Chen JL, Wilson CR, Tapley BD (2006) Satellite gravity measurements confirm accelerated melting of Greenland ice sheet. Science 313:1958–1960
18. Chen JL, Wilson CR, Tapley BD, Blankenship DD, Ivins E (2007) Patagonia icefield melting observed by GRACE. Geophys Res Lett 34(22):L22501. doi:10.1029/2007GL031871
19. Chen JL, Wilson CR, Blankenship DD, Tapley BD (2009) Accelerated Antarctic ice loss from satellite gravity measurements. Nat Geosci 2:859–862. doi:10.1038/NGEO694
20. Chen JL, Wilson CR, Tapley BD (2010) The 2009 exceptional Amazon flood and interannual terrestrial water storage change observed by GRACE. Water Resour Res 46:W12526. doi:10.1029/2010WR009383
21. Chen JL, Wilson CR, Tapley BD (2011) Interannual variability of Greenland ice losses from satellite gravimetry. J Geophys Res-Solid Earth 116:B07406. http://dx.doi.org/10.1029/2010JB007789)
22. Cheng M, Tapley B (1999) Seasonal variations in low degree zonal harmonics of the Earth's gravity field from satellite laser ranging observations. J Geophys Res 104(B2):2667–2681
23. Cheng MK, Tapley BD (2004) Variations in the Earth's oblateness during the past 28 yeas. J Geophys Res 109:B09402. doi:10.1029/2004JB003028
24. Cox CM, Chao BF (2002) Detection of a large-scale mass redistribution in the terrestrial system since 1998. Science 297:831–833
25. Cretaux J-F, Soudarin L, Davidson FJM, Gennero M-C, Berge-Nguyen M, Cazenave A (2002) Seasonal and interannual geocenter motion from SLR and DORIS measurements: comparison wit with surface loading data. J Geophys Res 107. doi:10.1029/2002JB001820
26. de Linage C, Rivera L, Hinderer J, Boy J-P, Rochester Y, Lambrotte S, Biancale R (2009) Separation of coseismic and postseismic gravity changes for the 2004 Sumatra-Andaman earthquake from 4.6 yr of GRACE observations and modelling of the coseismic change by normal-modes summation. Geophys J Int 176:695–714
27. Dickey JO, Marcus SL, deViron O, Fukumori I (2002) Recent Earth oblateness variations: unraveling climate and postglacial rebound effects. Science 298:1975–1977
28. Dobslaw H, Thomas M (2007) Simulation and observation of global ocean mass anomalies. J Geophys Res 112:C05040. doi:10.1029/2006JC004035
29. Egbert GD, Erofeeva SY, Han S-C, Luthcke SB, Ray RD (2009) Assimilation of GRACE tide solutions into a numerical hydrodynamic inverse model. Geophys Res Lett 36:L20609. doi:10.1029/2009GL040376
30. Famiglietti JS, Lo M, Ho SL, Bethune J, Anderson KJ, Syed TH, Swenson SC, de Linage CR, Rodell M (2011) Satellites measure recent rates of groundwater depletion in California's central valley. Geophys Res Lett 38:L03403. doi:10.1029/2010GL046442
31. Garcia-Garcia D, Ummenhofer CC, Zlotnicki V (2011) Australian water mass variations from GRACE data linked to Indo-Pacific climate variability. Remote Sens Environ 115:2175–2183. http://dx.doi.org/10.1016/j.rse.2011.04.007
32. Gardner AS, Moholdt G, Wouters B, Wolken GJ, Burgess DO, Sharp MJ, Cogley JG, Braun C, Labine C (2011) Sharply increased mass loss from glaciers and ice caps in the Canadian Arctic Archipelago. Nature 473:357–360. doi:10.1038/nature10089
33. Han S-C, Sauber J, Luthcke SB, Ji C Pollitz FF (2008) Implications of postseismic gravity change following the great 2004 Sumatra-Andaman earthquake from the regional harmonic analysis of GRACE intersatellite tracking data. J Geophys Res 113:B11413. doi:10.1029/2008JB005705
34. Han S-C, Kim H, Yeo I-Y, Yeh P, Oki T, Seo K-W, Alsdorf D, Luthcke SB (2009) Dynamics of surface water storage in the Amazon inferred from measurements of inter-satellite distance change. Geophys Res Lett 36:L09403. http://dx.doi.org/10.1029/2009GL037910
35. Han S-C, Sauber J, Luthcke S (2010) Regional gravity decrease after the 2010 Maule (Chile) earthquake indicates large-scale mass redistribution. Geophys Res Lett 37:L23307. doi:10.1029/2010GL045449
36. Han S-C, Ray RD, Luthcke SB (2010) One centimeter-level observations of diurnal ocean tides from global monthly mean time-variable gravity fields. J Geodyn 84:715–729. doi:10.1007/s00190-010-0405-3
37. Hill EM, Davis JL, Tamisiea ME, Lidberg M (2010) Combination of geodetic observations and models for glacial isostatic adjustment fields in Fennoscandia. J Geophys Res 115: B07403. doi:10.1029/2009JB006967

38. Horwath M, Dietrich R (2009) Signal and error in mass change inferences from GRACE: the case of Antarctica. Geophys J Int 177:849–864. doi:10.1111/j.1365-246X.2009.04139.x
39. Ivins ER, Watkins MM, Yuan D-N, Dietrich R, Casassa G, Rlke A (2011) On-land ice loss and glacial isostatic adjustment at the Drake Passage: 2003–2009. J Geophys Res 116:B02403. doi:10.1029/2010JB007607
40. Khan SA, Wahr J, Bevis M, Velicogna I, Kendrick E (2010) Spread of ice mass loss into northwest Greenland observed by GRACE and GPS. Geophys Res Lett 37:6501. doi:10.1029/2010GL042460
41. King MA, Altamimi Z, Boehm J, Bos M, Dach R et al (2010) Improved constraints on models of glacial isostatic adjustment: a review of the contribution of ground-based geodetic observations. Surv Geophys 31:465–507. http://dx.doi.org/10.1007/s10712-010-9100-4
42. Knudsen P, Bingham R, Andersen O, Rio M-H (2011) A global mean dynamic topography and ocean circulation estimation using a preliminary GOCE gravity model. J Geodesy. doi:10.1007/s00190-011-0485-8
43. Landerer FW, Swenson SC (2011) Accuracy of scaled GRACE terrestrial water storage estimates. Water Resour Res, in press
44. Landerer FW, Dickey JO, Güntner A (2010) Terrestrial water budget of the Eurasian pan-Arctic from GRACE satellite measurements during 2003–2009. J Geophys Res 115:D23115. doi:10.1029/2010JD014584
45. Leblanc MJ, Tregoning P, Ramillien G, Tweed SO, Fakes A (2009) Basin-scale, integrated observations of the early 21st century multiyear drought in southeast Australia. Water Resour Res 45:W04408. doi:10.1029/2008WR007333
46. Lemoine JM, Bruinsma S, Loyer S, Biancale R, Marty JC, Perosanz F, Balmino G (2007) Temporal gravity field models inferred from GRACE data. Adv Space Res 39(10): 1620–1629
47. Leuliette EW, Miller L (2009) Closing the sea level rise budget with altimetry, Argo, and GRACE. Geophys Res Lett 36:L04608. doi:10.1029/2008GL036010
48. Leuliette EW, Willis JK (2011) Balancing the sea level budget. Oceanography 24:122–129. http://dx.doi.org/10.5670/oceanog.2011.32
49. Liu X, Ditmar P, Siemes C, Slobbe DC, Revtova E, Klees R, Riva R, Zhao Q (2010) DEOS Mass Transport model (DMT-1) based on GRACE satellite data: methodology and validation. Geophys J Int 181:769–788. doi:10.1111/j.1365-246X.2010.04533.x
50. Llovel W, Becker M, Cazenave A, Cretaux JF, Ramillien G (2010) Global land water storage change from GRACE over 2002–2009; inference on sea level. CR Geosciences 342:179–188. http://dx.doi.org/10.1016/j.crte.2009.12.004
51. Llovel W, Guinehut S, Cazenave A (2010) Regional and interannual variability in sea level over 2002–2009 based on satellite altimetry Argo float data and GRACE ocean mass. Ocean Dyn 60:1193–1204. doi:10.1007/s10236-010-0324-0
52. Lo M-H, Famiglietti JS, Yeh PJ-F, Syed TH (2010) Improving parameter estimation and water table depth simulation in a land surface model using GRACE water storage and estimated base flow data. Water Resources Res 46:W0551. http://dx.doi.org/10.1029/2009WR007855
53. Lombard A, Garcia D, Ramillien G, Cazenave A, Biancale R, Lemoine JM, Flechtner F, Schmidt R, Ishii M (2007) Estimation of steric sea level variations from combined GRACE and Jason-1 data. Earth Planet Sci Lett 254:194–202. doi:10.1016/j.epsl.2006.11.035
54. Luthcke SB, Arendt AA, Rowlands DD, McCarthy JJ, Larsen CF (2008) Recent glacier mass changes in the Gulf of Alaska region from GRACE mascon solutions. J Glaciol 54(188):767–777. http://dx.doi.org/10.3189/002214308787779933
55. Macrander A, Böning C, Boebel O, Schröter J (2010) Validation of GRACE gravity fields by in-situ data of ocean bottom pressure. In: Flechtner F, Gruber T, Güntner A, Mandea M, Rothacher M, Schöne T, Wickert J (eds) System Earth via geodetic-geophysical space techniques. Springer, Berlin. http://dx.doi.org/10.1007/978-3-642-10228-8_14
56. Matsuo K, Heki K (2010) Time-variable ice loss in Asian high mountains from satellite gravimetry. Earth Planet Sci Lett 290:30–36. doi:10.1016/j.epsl.2009.11.053
57. Maximenko N, Niiler P, Rio M-H, Melnichenko O, Centurioni L, Chambers D, Zlotnicki V, Galperin B (2009) Mean dynamic topography of the ocean derived from satellite and drifting buoy data using three different techniques. J Atmos Ocean Technol. doi:10.1175/2009JTECHO672.1, http://www.springerlink.com/content/r882426635467007/
58. Mayer-Gürr T, Eicker A, Kurtenbach E, Ilk K-H (2010) ITG-GRACE: global static and temporal gravity field models from GRACE data. Adv Technol Earth Sci 2010(Part 2):159–168. doi:10.1007/978-3-642-10228-8_13
59. Morison J, Wahr J, Kwok R, Peralta-Ferriz C (2007) Recent trends in Arctic Ocean mass distribution revealed by GRACE. Geophys Res Lett 34:L07602. doi:10.1029/2006GL029016
60. Muller PM, Sjogren WL (1968) Mascons: lunar mass concentrations. Science 161:680–684
61. Nerem RS, Wahr J (2011) Recent changes in the Earth's oblateness driven by Greenland and Antarctic ice mass loss. Geophys Res Lett 38:L13501. doi:10.1029/2011GL047879
62. O'Keefe JA, Eckels A, Squires RK (1959) The gravitational field of the earth. Astron J 64:245
63. Padman L, Howard SL, Orsi AH, Muench RD (2009) Tides of the northwestern Ross Sea and their impact on dense outflows of Antarctic Bottom Water. Deep-Sea Res Pt II Oceanography 56:818–834. http://dx.doi.org/10.1016/j.dsr2.2008.10.026
64. Park J, Watts DR, Donohue K, Jayne S (2008) A comparison of in situ bottom pressure array measurements with GRACE estimates in the Kuroshio extension. Geophys Res Lett 35:L17601. doi:10.1029/2008GL034778
65. Paulson A, Zhong S, Wahr J (2007) Inference of mantle viscosity from GRACE and relative sea level data. Geophys J Internat 171:497–508
66. Parker RL (1975) Theory of ideal bodies for gravity interpretation. Geophys J Roy Astron Soc 42(2):315–334
67. Peltier WR (2004) Global glacial isostasy and the surface of the ice-age Earth: the ICE-5G (VM2) model and GRACE. Annu

Rev Earth Planet Sci 32:111–149. doi:10.1146/annurev.earth.32.082503.144359
68. Peltier WR, Luthcke SB (2009) On the origins of earth rotation anomalies: New insights on the basis of both "paleogeodetic" data and gravity recovery and climate experiment (GRACE) data. J Geophys Res 114:B11405. doi:10.1029/2009JB006352
69. Peralta-Ferriz C, Morison J (2010) Understanding the annual cycle of the Arctic Ocean bottom pressure. Geophys Res Lett 37:L10603. doi:10.1029/2010GL042827
70. Ponte RM, Quinn KJ (2009) Bottom pressure changes around Antarctica and wind-driven meridional flows. Geophys Res Lett 36:L13604. doi:10.1029/2009GL039060
71. Quinn KJ, Ponte RM (2008) Estimating weights for the use of time-dependent gravity recovery and climate experiment data in constraining ocean models. J Geophys Res 113:C12013. doi:10.1029/2008JC004903
72. Ray RD, Luthcke SB, Boy J-P (2009) Qualitative comparisons of global ocean tide models by analysis of intersatellite ranging data. J Geophys Res 114:C09017. doi:10.1029/2009JC005362
73. Rietbroek R, LeGrand P, Wouters B, Lemoine J-M, Ramillien G, Hughes CW (2006) Comparison of in situ bottom pressure data with GRACE gravimetry in the Crozet-Kerguelen region. Geophys Res Lett 33:L21601. doi:10.1029/2006GL027452
74. Rietbroek R, Brunnabend S-E, Dahle C, Kusche J, Flechtner F, Schröter J, Timmermann R (2009) Changes in total ocean mass derived from GRACE, GPS, and ocean modeling with weekly resolution. J Geophys Res: Oceans 114:C11004. doi:10.1029/2009JC005449
75. Rignot E, Velicogna I, van den Broeke MR, Monaghan A, Lenaerts J (2011) Acceleration of the contribution of the Greenland and Antarctic ice sheets to sea level rise. Geophys Res Lett 38:L05503. doi:10.1029/2011GL046583
76. Rio MH, Guinehut S, Larnicol G (2011) New CNES-CLS09 global mean dynamic topography computed from the combination of GRACE data, altimetry, and in situ measurements. J Geophys Res 116:C07018. doi:10.1029/2010JC006505
77. Riva REM, Gunter BC, Urban TJ, Vermeersen BLA, Lindenbergh RC, Helsen MM, Bamber JL, van de Wal RSW, van den Broeke MR, Schutz BE (2009) Glacial isostatic adjustment over Antarctica from combined ICEsat and GRACE satellite data. Earth Planet Sci Lett 288:516–523. http://dx.doi.org/10.1016/j.epsl.2009.10.013
78. Rodell M, Velicogna I, Famiglietti JS (2009) Satellite-based estimates of groundwater depletion in India. Nature 460:999–1002. http://dx.doi.org/10.1038/nature08238
79. Rowlands DD, Luthcke SB, McCarthy JJ, Klosko SM, Chinn DS, Lemoine FG, Boy J-P, Sabaka TJ (2010) Global mass flux solutions from GRACE: a comparison of parameter estimation strategies—mass concentrations versus stokes coefficients. J Geophys Res 115:B01403. doi:10.1029/2009JB006546
80. Sasgen I, Martinec Z, Bamber J (2010) Combined GRACE and InSAR estimate of West Antarctic ice mass loss. J Geophys Res (Earth Surface) 115:F04010. doi:10.1029/2009JF001525
81. Siegismund F, Romanova V, Köhl A, Stammer D (2011) Ocean bottom pressure variations estimated from gravity, nonsteric sea surface height and hydrodynamic model simulations. J Geophys Res 116:C07021. doi:10.1029/2010JC006727
82. Sun AY, Green R, Rodell M, Swenson S (2010) Inferring aquifer storage parameters using satellite and in situ measurements: estimation under uncertainty. Geophys Res Lett 37:L10401. http://dx.doi.org/10.1029/2010GL043231
83. Swenson S (2010) Assessing high-latitude winter precipitation from global precipitation analyses using GRACE. J Hydrometeorol 11:405–420. doi:10.1175/2009JHM1194.1
84. Swenson S, Wahr J (2002) Methods for inferring regional surface-mass anomalies from gravity recovery and climate experiment (GRACE) measurements of time-variable gravity. J Geophys Res 107(B9):2193. doi:10.1029/2001JB000576
85. Swenson S, Wahr J (2006) Post-processing removal of correlated errors in GRACE data. Geophys Res Lett 33:L08402. doi:10.1029/2005GL025285
86. Swenson S, Wahr J (2009) Monitoring the water balance of Lake Victoria, East Africa, from space. J Hydrol 370(1–4):163–176. doi:10.1016/j.jhydrol.2009.03.008
87. Swenson S, Chambers DP, Wahr J (2008) Estimating geocenter variations from a combination of GRACE and ocean model output. J Geophys Res 113. doi:10.1029/2007JB005338
88. Tamisiea ME, Hill EM, Ponte RM, Davis JL, Velicogna I, Vinogradova NT (2010) Impact of self-attraction and loading on the annual cycle in sea level. J Geophys Res 115:C07004. doi:10.1029/2009JC005687
89. Tapley BD et al (2004) GRACE measurements of mass variability in the Earth system. Science 305:503–505. doi:10.1126/science.1099192
90. Tiwari VM, Wahr J, Swenson S (2009) Dwindling groundwater resources in Northern India, from satellite gravity observations. Geophys Res Lett 36:L18401. doi:10.1029/2009GL039401
91. Tregoning P, Ramillien G, McQueen H, Zwartz D (2009) Glacial isostatic adjustment and nonstationary signals observed by GRACE. J Geophys Res 114:B06406. doi:10.1029/2008JB006161
92. van den Broeke M, Bamber J, Ettema J, Rignot E, Schrama E, van de Berg WJ, van Meijgaard E, Velicogna I, Wouters B (2009) Partitioning recent Greenland mass loss. Science 326:984. doi:10.1126/science.1178176
93. Velicogna I (2009) Increasing rates of ice mass loss from the Greenland and Antarctic ice sheets revealed by GRACE. Geophys Res Lett 36:L19503. doi:10.1029/2009GL040222
94. Vianna ML, Menezes V V (2011) Double-celled subtropical gyre in the South Atlantic Ocean: means, trends, and interannual changes. J Geophys Res 116:C03024. doi:10.1029/2010JC006574
95. Vinogradova NT, Ponte RM, Tamisiea ME, Quinn KJ, Hill EM, Davis JL (2011) Self-attraction and loading effects on ocean mass redistribution at monthly and longer time scales. J Geophys Res-Oceans 116. http://dx.doi.org/10.1029/2011JC007037
96. Wahr J, Molenaar M, Bryan F (1998) Time variability of the Earth's gravity field: hydrological and oceanic effects and their possible detection using GRACE. J Geophys Res 103:30205–30229. doi:10.1029/98JB02844

97. Wahr J, Swenson S, Velicogna I (2006) Accuracy of GRACE mass estimates. Geophys Res Lett 33:L06401. doi:10.1029/2005GL025305
98. Willis JK, Lyman JW, Johnson GC, Gilson J (2008) In situ data biases and recent ocean heat content variability. J Oceanic Atmosph Technol 26:846–852. doi:10.1175/2008JTECHO608.1
99. Wouters B, Chambers DP (2010) Analysis of seasonal ocean bottom pressure variability in the Gulf of Thailand from GRACE. Glob Planet Chang 74:76–81. doi:10.1016/j.gloplacha.2010.08.002
100. Wu X, Heflin MB, Schotman H, Vermeersen BLA, Dong D, Gross RS, Ivins ER, Moore AW, Owen SE (2010) Simultaneous estimation of global present-day water transport and glacial isostatic adjustment. Nat Geosci 3:642–646. doi:10.1038/NGEO938
101. Zaitchik BF, Rodell M, Reichle RH (2008) Assimilation of GRACE terrestrial water storage data into a land surface model: results for the Mississippi river basin. J Hydrometeorol 9:535–548. doi:10.1175/2007JHM951.1
102. Zlotnicki V, Wahr J, Fukumori I, Song Y-T (2007) Antarctic circumpolar current transport variability during 2003–2005 from GRACE. J Physical Oceanog 37(2):230–244

Books and Reviews

Cazenave A, Chen J-L (2010) Time-variable gravity from space and present-day mass redistribution in the Earth system. Earth Planet Sci Lett 298(2010):263–274. doi:10.1016/j.epsl.2010.07.035

Chambers DP, Schröter J (2011) Measuring ocean mass variability from satellite gravimetry. J Geodyn 52:333–343. doi:10.1016/j.jog.2011.04.004

Dickey J et al (1997) Satellite gravity and the geosphere. US National Research Council, National Academy Press, Washington, DC

Green Catalytic Transformations

James H. Clark, James W. Comerford, D. J. Macquarrie
Department of Chemistry, University of York, Heslington, York, UK

Article Outline

Glossary
Definition of the Subject and Its Importance
Introduction
Zeolites
Clays
Supported Reagents
Future Directions
Bibliography

Glossary

Atom economy Calculates the percentage of atoms in the reagents used in the final product.

Chemisorption Where a species is chemically bound to a surface.

Clay A pure material, either synthesized or natural, used as a heterogeneous catalyst or support.

Dehydroxylation Where two isolated silanols condense to form a siloxane bridge, with loss of water.

E-factor A measure of waste produced per quantity of product.

Envirocats™ A series of commercially available catalysts developed by the University of York and Contract Chemicals Ltd.

Heterogeneous Where two species in a reaction, catalyst and reagents, are in a different phase, i.e., solid and vapor phase.

Homogeneous Where species in a reaction are in the same phase.

Ion exchange A process where ions, typically metal cations, are exchanged with other ions on a surface using a suitable solvent.

Physisorption Where a species interacts strongly with a surface through electrostatic interaction, hydrogen bonding.

Support/supported Referring to a species interacting with or bound to a surface.

Zeolite A diverse aluminosilicate structure commonly used in heterogeneous catalysis.

Definition of the Subject and Its Importance

With ever-increasing demand of chemical products on a global scale, as well as poor public image in recent years, there has been increasing pressure for chemistry industry to become more efficient and sustainable. Processes and catalytic cycles on large scales are being scrutinized by companies to enhance efficiency, reduce environmental impact and associated costs using state-of-the-art research and technology. An overwhelming number of new and improved catalytic

transformations are reported in many different fields on a daily basis. However, a catalytic transformation must fulfill a number of criteria to be deemed as "green." The process/catalytic cycle must exhibit a notable improvement on existing syntheses, not only in terms of activity, but as an overall process by assessing waste produced throughout (cradle to grave concept including even the synthesis of the catalyst itself), potential reusability of catalyst, as well as ease of product isolation and potential user risk, where the safety/toxicity of chemicals involved in the process are assessed.

Introduction

The necessitated development of green synthetic procedures has grown from a number of different socio-economic factors over recent decades. Increasing demand of chemical products worldwide has meant that the environmental impact of industry (particularly within the EU), is being assessed more harshly than ever. This has had a distinct effect on the relationship between chemical industry and the environment, and as such green chemistry has received huge attention. The key factor of concern is the quantity and nature of the waste being produced, a number of different strategies have been implemented by the EU and ECHA to reduce waste by restricting the use of hazardous/potentially toxic chemicals on an industrial scale, through either banning the substance completely or imposing substantial tax deterrents on certain chemical wastes (REACH legislation). This provides a financial incentive for companies to employ waste-minimizing techniques for their processes. An excellent overview of waste minimization is given in "Chemistry of Waste Minimization" which gives a detailed insight into how environmental factors are affected by the production and restriction of chemical waste [1]. Focus has been increasingly diverted toward the prevention of waste rather than the treatment, through a combination of replacing homogeneous catalysts with heterogeneous catalysis, utilizing renewable raw materials, and investing in new technologies such as continuous flow.

Homogeneous Versus Heterogeneous

By definition, a heterogeneous catalyst is a catalytically active species that is in a different phase to the reagents within a reaction system, more often than not a solid in either liquid or vapor phase synthesis. There are a number of advantages of using heterogeneous catalysts as opposed to the homogeneous equivalents, detailed below:

- Safety – An important consideration in the practice of green chemistry. Heterogeneous catalysts often tend to be environmentally benign and easy/safe to handle. This is due to the active species being adhered to a support (often forming a powder), essentially reducing its reactivity with the surrounding environment.
- Reusability – Due to the difference in phases, the catalyst is simply filtered off (through centrifugation on industrial scales) and reactivated for reuse many times over. For instance, zeolites used for petroleum refining can be reactivated and reused for many years – sometimes up to a decade – before disposal.
- Activity – In many cases increased activity is observed when supporting an active homogeneous species on a support, due to the complex but unique surface characteristics found with a variety of different supports.
- Selectivity – Heterogeneous catalysts can give an increased degree of selectivity in reaction pathway. This can simply be a consequence of adsorption of substrates and the consequential restricted freedom of movement of the reacting molecules. More famously, the pores of a solid support can cause size and shape restrictions with regard to the substrates, intermediates, and products. For example, the substitution of aromatic rings leads to products with different geometries and bulkier intermediates may be less likely to form and/or bulkier products may not be able to leave the pores leading to orientational selectivity. Shape selectivity can also affect stereoselectivity through control over reaction pathways.

However, there are a handful of disadvantages. The quantity of solid catalyst required is often higher than that of the homogeneous equivalent, due to the lower concentration on the support surface (reusability makes this less of an issue though). Blocking of the pores/support channels can occur with narrow pores sizes and reduce efficiency over time in some liquid phase reactions; nevertheless, this is often twinned with

high stereoselectivity. Despite this, the advantages found with heterogeneous catalysis far outweigh the minor drawbacks.

Green Chemistry Metrics

Green chemistry metrics are important tools in assessing the effectiveness and efficiency of reactions. Increasingly, they are becoming common place in the designing of synthetic routes/chemical syntheses, the main metrics are defined below:

- E-Factor – Developed by Sheldon, the environmental factor determines the quantity of waste (in Kg) produced per Kg of product. This takes into account all waste throughout the synthesis, not only solvents used in reactions, etc., but solvent used for recrystallisation. An E-Factor of 1 is considered ideal.

$$Ef = \frac{Total\ Quantity\ of\ waste\ (Kg)}{Total\ quantity\ of\ product\ (Kg)}$$

- Atom economy – Formulated by Trost, calculates the percentage of atoms in the starting material present in the final product, clean syntheses aim for 100%.

$$Atom\ economy\ (\%) = \frac{Molecular\ weight\ of\ product}{Molecular\ weight\ of\ reagents} \times 100$$

- Reaction mass efficiency – Developed by GSK, similar to atom economy but assesses difference in mass.

$$Mass\ efficiency\ (\%) = \frac{Mass\ product}{Total\ mass\ reagents} \times 100$$

- Carbon efficiency – Developed by GSK, again similar in format, determines difference in carbon mass between reagents and products.

$$Carbon\ efficiency\ (\%) = \frac{Quantity\ of\ carbon\ in\ product}{Quantity\ of\ carbon\ in\ reagents} \times 100$$

Overall, recent research has aimed to reduce the quantity and toxicity of waste produced by industrial processes and substantial focus has been centered on the type of catalysts used. Below is a detailed discussion of heterogeneous catalysts covering structural and mechanistic aspects as well as highlighting applications, interesting developments, and increased green credentials of many "classic" syntheses.

Zeolites

Background

The term "zeolite" was first employed by the Swedish mineralogist Cronstedt in 1756, literally meaning boiling stone in Greek [2]. Natural zeolites have had applications in chemistry over past centuries, such as odor control, gas separation, desiccants, water treatment, agriculture, etc., but the development of synthetic zeolites has been hallmarked as one of the greatest discoveries in science, allowing microporous structures to be "tailored to fit" a huge number of various applications such as extraction, purification, and heterogeneous catalysis. The replication of a natural zeolite was first achieved by Barrer in the early 1940s and further research of entirely synthetic zeolites was continued by Milton at the Union Carbide Linde Division's Research Laboratory in Buffalo, New York, in 1949. The developed Zeolite A and B(P) were used for the separation of gases based on size, in particular air, to produce high purity oxygen for steel mills and other large scale applications [3], although this was not commercialized until the 1970s. Following research by Mobil focused on zeolites for large scale petroleum cracking and dozens of zeolites were produced that were able to act as acid catalysts.

Composition and Structure Zeolites are crystalline three dimensional microporous structures with etrahedral building blocks comprised of $[SiO_4]^{-4}$ and $[AlO_4]^{-5}$. The chemical composition is often represented by $M_{2/n}$ O-Al_2O_3-ySiO_2-wH_2O, where, due to the trivalent aluminum species, the zeolite has a negative charge proportional to each Al and requires either a pentavalent element, such as a neighboring phosphorus (P^{5+}) or a cation to stabilize this. Non-framework cations are found in the porous network and can vary; alkaline metals from group IA and IIA such as Na^+ are often used. The tetrahedral building blocks form structures known as secondary building units, (SBU), of which there is a large variety (around 16). It is these units that form the larger unit cells (cages) which make up the zeolitic framework, commonly used to classify zeolites, although they can be classified through the type of SBU, framework density (the number of T atoms per unit cell), or pore size. For instance, sodalite (SOD), faujasite

(FAU), and zeolite A (LTA) share the same sodalite unit cell, however the SOD cages are of a cubic arrangement, LTA is similar in arrangement but linked together through the 4–4 SBU and FAU comprises of a diamond like structure of sodalite cages, linked together through the hexagonal face [4], Fig. 1. The specific naming of the frameworks is complex and will not be discussed.

Another common classification mentioned above was that of aperature size, referring to the diameter of the rings forming the zeolite channel. Table 1 shows a range of zeolite spanning the typical pore sizes from small to ultralarge, found with common zeolites [1].

Pore sizes up to ~14Å are categorized as microporous in accordance with the IUPAC classification of materials [5]. The size and shape of the zeolite for catalytic applications is crutial, potentially giving exceptional shape size selectivity. Aside from pairing framework with application, it is possible to tune the pore size by changing the Si:Al ratio; a reduction will produce a smaller unit cell, yet require fewer stabilizing

Green Catalytic Transformations. Table 1 Pore sizes of common zeolites

Zeolite	Number of tetrahedral in ring	Diameter of main channels Å
Sodalite	4	very small – <4
Zeolite A	8	Small – 4
ZSM-5	10	Medium – 5.6
Faujasite	12	Large – 7.4
Cloverlite	20	Ultra large – 13.2
MCM-41	>20	Macroporous – 100

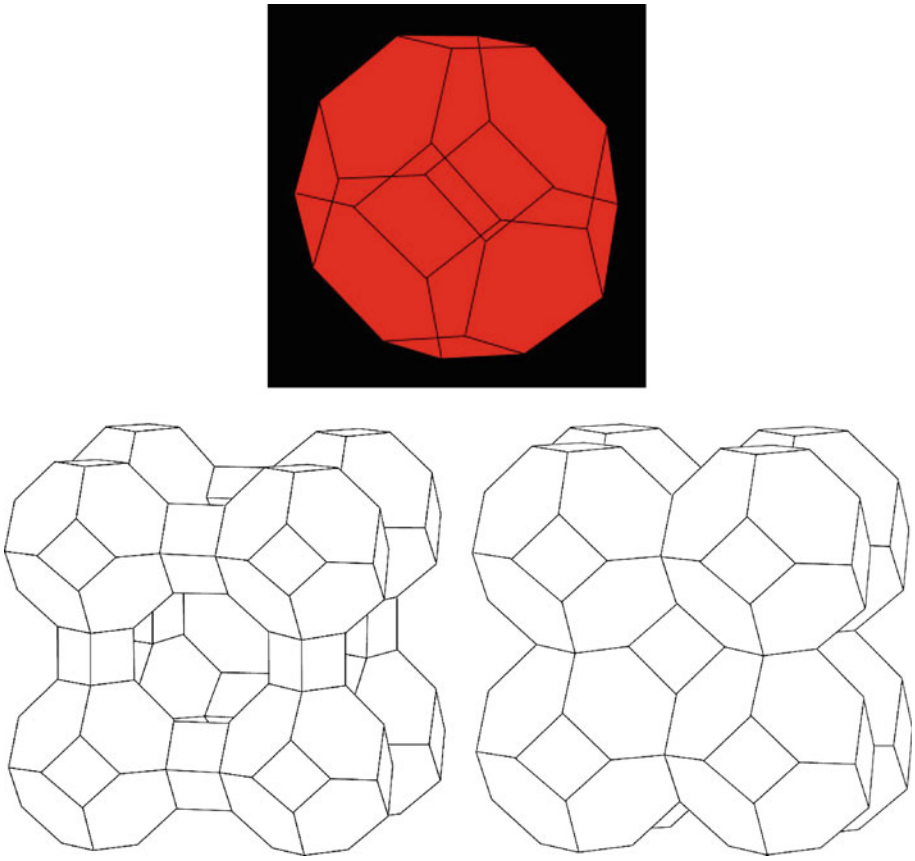

Green Catalytic Transformations. Figure 1
Top – SOD unit cell; *Left* – LTA framework; *Right* – SOD framework

cations, freeing up the zeolite channel. In addition, modification post-synthesis is possible simply through ion exchange, the choice of ions can increase the effective size of the pore opening. Despite the selectivity obtained with smaller pore size zeolites, there can be diffusional and blocking problems in liquid phase reactions. As a result there has been much research into mesoporous zeolites, allowing increased diffusional rates and reduced deactivation.

Synthesis The synthesis of zeolites typically involves mixing a silica and alumina source under basic conditions. Also incorporated into the mixture is a suitable cation of choice, such as either an alkaline metal in an oxide, hydroxide, or salt, with dual function either as counterions in the final material or acting as structure directing templates. Aside from the properties of the mixture, temperature, pressure, and crystallization time are also important variables and vary considerably. Typical syntheses crystallize between room temperature to 200°C under autoclave pressure, the time required ranging from hours to days.

Acidity Counterions within the porous network (Fig. 2a) can be readily exchanged using salt solutions, a process referred to as *ion exchange*. To give the zeolite Bronsted acidity, ammonium salt solution (such as ammonium hydroxide) can be used to exchange the metal ions with ammonium. On heating the material deprotonates giving hydrogen as the stabilizing cation (Fig. 2b). The Bronsted acid strength is dependent on the Si:Al ratio, where a high ratio of silicon to aluminum results in stronger acidity, as well as increased hydrophobicity, i.e., zeolite B150 is a stronger solid acid and more hydrophobic than B25 (with a ratio of Si 25: Al 1). Further heating above 500°C results in the reversible dehydroxylation of the silanol adjacent to the Al site, giving an aluminum Lewis acid site and a charge silicon species (Fig. 2c).

The basicity of zeolite tends to be less well documented. Lewis basicity stems from a negative charge on the oxygen where Bronsted is due to an extraframework cation on the surface [3].

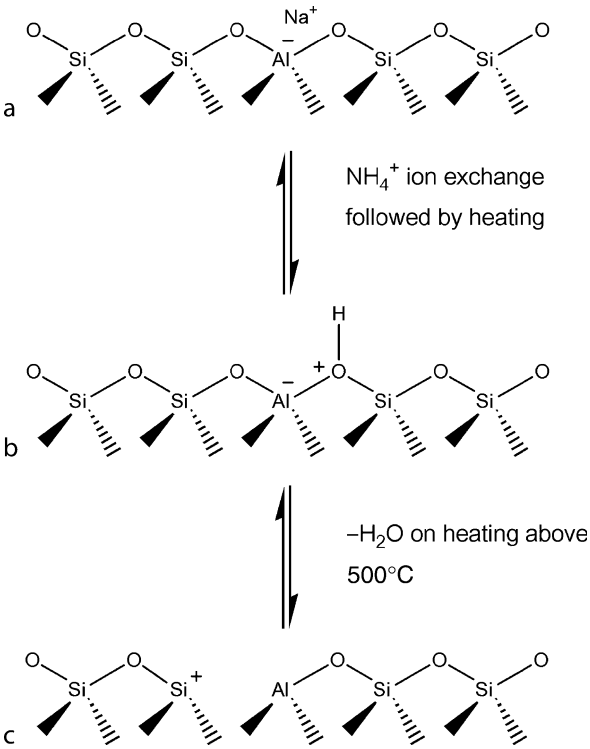

Green Catalytic Transformations. Figure 2
Ion exchanged zeolite and subsequent heating to give Lewis basicity. (**a**) Zeolite as synthesized; (**b**) Bronsted acid zeolite; (**c**) Lewis acid zeolite

Catalysis

There are an overwhelming number of examples of solid zeolite acid, base, and oxidation catalysis throughout the past 60 years. As such, the following section will discuss the most popular applications throughout the decades as well as recently published examples. A common observation with much of the research is the impressive shape selectivity and structural diversity found with zeolitic catalysis.

Catalytic Cracking It has been around 50 years since Mobil first developed the fluid catalytic cracking (FCC) process using zeolite technology and this still remains the dominant catalytic application for zeolites today. Nevertheless, there are many other important transformations using zeolites, of which, a selection are

Green Catalytic Transformations. Table 2 Showing applications and corresponding zeolites

Application	Zeolite	Notes
Catalytic Cracking	HY-high silica zeolite REY Medium pore zeolites	Selectivity and high conversion rate
Hydrocracking	H-ZSM-5, Faujasite (X, Y), metals on Mordenite (Co, Mo, W, Ni) USY, CAMgY	Conversion rate high
Dewaxing	Pt-mordenite, ZSM-5, silicalite, high silica zeolites (ferrierite)	Low pour and cloud points
Hydroisomerisation	Pt-Mordenite	Low octane pentanes and hexanes converted to high octane yields
Aromatization	Pt, K, Ba silicalite, Pt, Ga, Zn-ZSM-5	Aromatization of C3–C8 cuts, aromatization of LPG
Benzene alkylation	ZSM-5	Production of ethylbenzene and styrene with low quantity of by-products
Xylene isomerisation	ZSM-5	High selectivity to para yield
Toluene disproportionation	ZSM-5, Mordenite	Production of xylenes and benzene
Methanol to petroleum	ZSM-5, erionite	High olefin yields (high octane rating) and high petroleum yield
Fischer-Tropsch	Metal-ZSM-5 (Co, Fe)	Natural gas to petroleum

shown in Table 2 [3]. Catalytic cracking typically employs fluidized catalyst bed technology and is simple in concept, but a detailed insight of the process and chemistry is outside the scope of this encyclopedia. As an example take the basics of petroleum refining; the initial feedstock comprises a range of carbons chains/aromatics (paraffins, naphthenic and aromatic hydrocarbons), light being C_{10}–C_{20} and heavy being C_{15}–C_{25}. This is pre-heated to ~370–400°C and mixed with powdered solid catalyst at a ratio of 2:1 oil:catalyst, to give a slurry which is injected into a reaction vessel at ~480–550°C [6]. At this temperature the oil partially evaporates and reacts with the catalyst, after 1–4 s the mixture is separated into catalyst, product for distillation and unreacted product (~20–25% of the starting material). The deactivated catalyst is simply reactivated in a stream of air ~700°C and re introduced back into the process. Impressively, the catalyst can be reused for many years in this highly efficient continuous process. The most utilized catalysts currently used in production consist of type Y faujasite zeolite with a Si:Al ratio of ~2.5 and ZSM-5 with a Si:Al ratio of ~15 to >100, allowing control of activity and selectivity. Typical stabilizing cations consist of H^+, Na^+, Ca^{2+}, Ba^{2+}, NH_4^+, NR_4^+ and various other rare earth metals. Despite some of their advantageous properties to the zeolite structure, Na^+ and particularly K^+ act as a catalyst poisons.

The ZSM-5 catalyst has since in developed in the field of FCC and cationic exchange with phosphorus has been of recent interest [7–13]. Enhanced activity was reported [14] in the cracking of propylene in the presence of phosphorus exchanged ZSM-5 prepared through hydrothermal dispersion. Classic modification techniques such as impregnation and ion exchange result in a material that can easily lose phosphorus, leading to contamination and loss of activity/selectivity. It is thought that the phosphorus compounds interact with bridged OH groups on the surface reducing the zeolites acidity, consequently increasing activity and modifying shape selectivity.

Isomerization Skeletal isomerisation again plays an important role in the refining industry. A well researched transformation is that of n-butene into

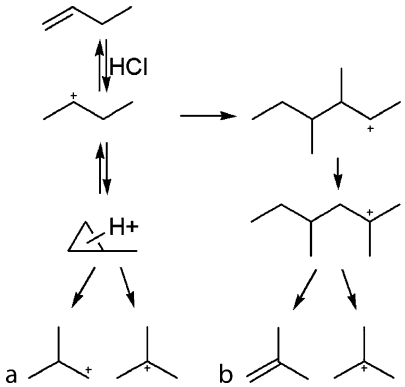

Green Catalytic Transformations. Figure 3
Isomerisation of butene to isobutene. (**a**) Monomolecular mechanism with cyclopropanic intermediate proposed by Brouwer and Hogeveen [15]; (**b**) Bimolecular mechanism proposed by Guisnet et al. [16]

isobutene, an intermediate to methyl-tert butyl ether (MTBE), one of the most important oxygenated additives used in lead free petroleum, Fig. 3. Initially the reaction is thought to be acid catalyzed consisting of a double bond shift to 2-butene, where the second isomerisation step to isobutene requires a stronger acid. Conversely, an increase in acid strength, as found with classic methods employing homogeneous acids such as HCl, also increases quantity of by-products, such as dimerization to octenes, cracking to C_2, C_3, C_5 and C_6 olefins and formation of coke [17]. Potential catalysts, therefore, were of medium acidity to increase selectivity to isobutene and reduced deactivation. As such there has been much research into ferrierite (FER), which shown extremely high selectivity under mild conditions [18–22].

Direct comparison between FER and zeolites of similar acidity (i.e., ZSM-5 – MFI framework) has shown the former to be consistently more selective. This has been ascribed to two main factors; firstly the low number of acid sites (high Si/Al ratio) is thought to prevent undesired bimolecular processes [6] such as aromatization, cyclization, hydrogen transfer and oligomerization, reducing by-products and coke formation (therefore increasing selectivity) and secondly the unique structure of ferrierite. However, despite the high performance of this catalyst, the role of coke formation as well as the precise mechanism in the isomerisation of butane to isobutene is still in debate [19].

Rearrangement The synthesis of ε-caprolactam through the Beckmann rearrangement of cyclohexanone oxime is industrially important in the synthesis of nylon-6 and resins, Fig. 4. Previously, the synthesis would involve the conversion of cyclohexanone with hydroxylamine sulfate or phosphate, to give cyclohexanone oxime. Subsequently, strong acids such as fuming sulphuric were used as an acid catalyst, followed by treatment with ammonia yielding the final ε-caprolactam product. However, large quantities of $(NH_4)_2SO_4$ salt by-product are formed, along with a high reactor corrosion factor and high risk factor (handling large volumes of concentrated acid), making the process environmentally unsound.

As such this has been studied intensely, with a number of developed catalysts being used to varying degrees of success, Table 3. Out these, titanium silicate (TS-1) has shown exceptional activity and selectivity, its development over the past decade gives an excellent example of green synthesis. The old two step process of ammoximation followed by rearrangement has been telescoped into a single continuous flow process [28] and has been used industrially by Sumitomo Chemical Co., Ltd since 2003, (operating on 60,000 tons per year scale!). TS-1 is used to convert cyclohexanone [29] to the oxime giving a conversion of >99% with a selectivity of 98%. This is followed by vapor phase rearrangement of the oxime to the lactam using high silica MFI zeolite, giving a yield on >99% with a selectivity of 95%. The improvement of this reaction can be shown by the increase in atom economy for ammoximation, from 36% using H_2SO_4 + 1.5NH_3 to 100% using TS-1 [11].

Schüth recently reported [30] that by crosslinking the TS-1 structure, both improved catalytic activity and reduced deactivation over time was observed. The preparation of the zeolite uses siloxane linkers, resulting in an increased in mesoporous surface character similar to that of silicalite. Interestingly activity correlates with increased concentration of linkers, as well as Ti concentration. Deactivation of that catalyst was found to be substantially improved compared with standard TS-1, up to 32% increased productivity. The observed effects are thought to be due to both the presence of titanium and siloxane crosslinkage, cooperatively reducing coke formation. The benefits of these heterogeneous catalysts aside from high activity and selectivity include simple

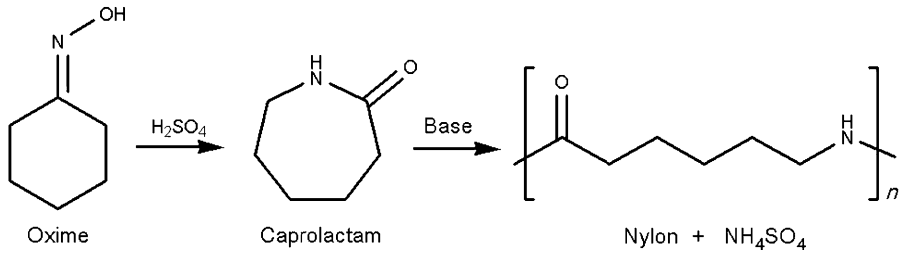

Green Catalytic Transformations. Figure 4
Rearrangement of oxime to give ε-caprolactam and nylon

Green Catalytic Transformations. Table 3 Examples of catalysts reported for the synthesis of ε-caprolactam [23–27]

Catalyst	TOS[a]	Yield (%)	Selectivity (%)
FSM-16	0.5 h	98	49
ZnO/FSM-16	″	99	69
Al2O3/FSM-16	″	98	63
Si-MCM-41	3 h	>99	32
Al-MCM-41(A)[b]	″	>99	48
Al-MCM-41(B)	″	>99	65
Al-MCM-41(C)	″	>99	87
β-MFI	4 h	95	95
H_3BO_3/Hβ	″	>99	80
H-LTL	6 h	>99	97
H-OFF-ERI	″	>99	96
Silicalite-1 MFI	″	77	95
High Si MFI	″	>99	95
H-USY	″	>99	82
H-MOR	″	92	90

[a]Time on stream
[b]Increasing Si:Al ratio

separation of product and any by-products though filtration, recovery, reuse, and low toxicity.

Transformations of Aromatics over Zeolites The production of ethylbenzene from benzene and ethylene is an important step in the synthesis of styrene and subsequently polystyrene [3]. Previously the process used $AlCl_3$ in a Friedel-Crafts alkylation and as with many strong homogeneous Lewis acids, there are

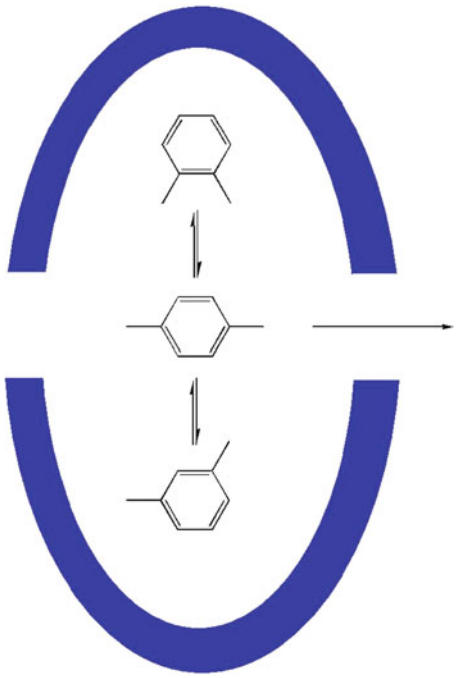

Green Catalytic Transformations. Figure 5
Restrictive ZSM-5 channels

problems with corrosion, waste separation, and contamination. A cleaner, continuous process using fixed beds of ZSM-5 gives high yields. In particular, ZSM-5 is an excellent example of shape selective properties and tuneability available with zeolite catalysis. The alkylation of toluene and methanol, for example, gives p-xylene, industrially important for its use in the manufacture of terephthalic acid and dimethyl terephthalate (starting material for polyester fibers, vitamins and other pharmaceuticals) [1]. The exceptional selectivity observed with ZSM-5 is due to the different diffusional rates of the ortho, meta, and para isomers through the porous zeolite channels, Fig. 5. It has been

demonstrated through variable temperature reactions that the diffusion of p-xylene is around 1,000 times faster than the ortho and meta isomers [31].

Despite this high selectivity, further research into ion exchange of ZSM-5 has produced even more active catalysts. By exchanging ions of different sizes into the porous network the size of the channels can vary, becoming increasingly restrictive with large metal ions. Sotelo [32] discusses ion exchange with magnesium in H-ZSM-5, where para selectivity approaches 100%, with isomer by-products being due to reaction on the external surface of the catalyst.

Zeolites in Fine Synthesis of Speciality Chemicals As well as their application to a number cracking, fuel and polymer reactions, zeolites are also able to catalyze a number of syntheses in fine chemical industry, such as in the synthesis of perfumes, fragrances, flavors, and pharmaceuticals, a few examples are given below.

Fragrances Vanillin propylene glycol acetal and phenylacetaldehyde glycerol acetals are important flavoring compounds with a vanilla and hyacinth fragrance. The propylene glycol acetal of vanillin is often used to imitate vanilla flavors as it causes flavor attenuation, this can easily be reversed through hydration back to the aldehyde, restoring full flavor [33]. Typical homogeneous acid catalysts are often used in the common transformation of the aldehyde to the acetal and suffer similar drawbacks with waste, separation, necessitated neutralization, and expense. A number of zeolites have therefore been applied to many fragrant syntheses, such as Jasminaldehyde (*n*-amylcinnamaldehyde), a violet scent obtained through the condensation of heptanal and benzaldehyde [34] and Fructone (ethyl 3,3-ethylendioxybutyrate), a strong fruity scent of apple/pineapple/wood synthesized thorough the acetalization of ethyl acetoacetate with ethylene glycol [35]. Climent et al. reported of synthesizing 2-benzyl-4-hydroxymethyl-1,3-dioxolane (Fig. 6a) and 2-benzyl-5-hydroxy-1,3-dioxane (Fig. 6b) from the acetalization of glycerol (soon to be a by-product on a million ton/pa scale) and benzaldehyde [33], both give a hyacinth scent.

Out of a number of zeolites investigated (Table 4), USY-2 and beta were particularly active and selective, comparable to p-toluene sulphonic acid. The secondary product (B) is thought to be converted from the acid catalyzed rearrangement of the less stable (A). Interestingly, the ratio of product to by-product is lower for Mordenite and ZSM-5, though overall conversion is low, again demonstrating shape selectivity and narrow pore size of the zeolites. Selectivity is not of huge importance in this case as both are active fragrants and are industrially acceptable, despite A having slightly increased potency than B.

Pharmaceuticals Ibuprofen, [(±)-2-(4-isobutylphenyl)] propionic acid, is a readily available and commonly used nonsteroidal anti-inflammatory/pain killer, able to treat many ailments such as muscular injury, headaches, and cold and flu symptoms (the list goes on). Its synthesis comprises of a six step process first patented by Boots in the 1960s. Typically isobutylbenzene is acylated with acetic anhydride using $AlCl_3$ as a Lewis acid catalyst; this causes problems with waste and to a certain extent selectivity, only isobutyl acting as a directing group to the para position (the ortho and meta are observed less so due to steric and electron effects, respectively). The resulting 2-(4-isobutyl phenyl)-ethanone is then reacted with Propionic acid (1-chloro-ethyl ester) and sodium ethoxide resulting in an epoxide, which, under acid catalysis, eliminates methyl ethanoate to give 2-(4-Isobutyl-phenyl)-propionaldehyde. There has been research into the replacement of $AlCl_3$ with

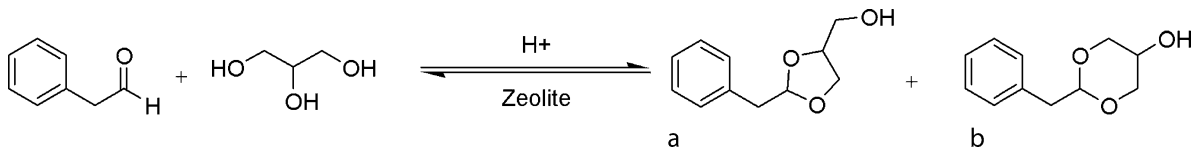

Green Catalytic Transformations. Figure 6
Synthesis of 2-benzyl-4-hydroxymethyl-1,3-dioxolane and 2-benzyl-5-hydroxy-1,3-dioxane

zeolites for synthesis of the intermediate 2-(4-isobutyl phenyl)-ethanone. Beta zeolite is active as an acylation catalyst and interestingly increased surface area through grinding or from formation of small particle sizes gives increased yields to around 20–30% [36, 37]. Higher yields, however, are observed in the synthesis of 2-acetyl-6-methoxynaphthalene ethanone, a precursor to (2-(6-methoxy-2-naphthyl)propionic acid) otherwise known as Naproxen, a similar nonsteroidal anti-inflammatory [38, 39].

Despite the fact that the 1-acetyl-2-methoxynaphthalene (A) Fig. 7 is kinetically favored [40], beta zeolite channels show selectivity toward the 2-acetyl-6-methoxynaphthalene (B). The increased selectivity is generated by the narrow pores, subsequently giving lower yields, potentially due to blocking, Table 5 [36].

After modification (grinding) an increased yield is observed thought to be due to an increase in surface area and accessibility to the acidic sites previously deep within the porous network. However, without the restrictive nature of the pores, selectivity to the 2-acetyl-6-methoxynaphthalene decreases, suggesting that the synthesis of the 1-acetyl-2-methoxynaphthalene largely occurs on the external surface of the zeolite. The incorporation of Ce^{3+} gives higher selectivity thought to be due to increased Lewis acidity.

Green Catalytic Transformations. Table 4 Conversion and selectivity to acetal product using various zeolites

Catalysts	Conversion (%)[a]	Selectivity (%)	
		A	B
USY-2	93	58	35
Beta-2	92	61	31
Mordenite	33	28	5
MCM-41	36	26	10
ZSM-5	54	46	8
PTSA	97	66	31

[a]After 1 h in refluxing toluene

Limitations of Zeolites as Catalysts Despite the numerous advantages found with zeolite catalysis there are still a handful of downsides. Most zeolites tend to have an aperture size between 4 and 8Å which limits application to less bulky substituents, mesoporous zeolites alleviate this for the most part, yet they too have their own disadvantages. The formation of coke (known as coking) as well as the buildup of products/reagents can cause rapid deactivation of the zeolite. The cost of the zeolite is often higher than that of an equivalent homogeneous acid, but as the cost of disposal of toxic chemical waste increases this will become less of an issue.

Clays

Background

Clays are a class of soil <2 μm in diameter primarily composed of fine-grained phyllosilicates (Greek for leaf, "phyllon"and Latin for flint, "silic"), which when wet is generally plastic and sticky in appearance and can be dried out to give a hard, cohesive material [41]. The large majority of applications in the catalytic field are focused on acid catalysis. A particularly helpful book is "The Origin of Clay Minerals in Soils and Weathered Rocks" with a detailed discussion of clay structure and type [42].

Structure of Clays

The subject of clay structure is a complex one [2]; as this chapter is designed to give an overview of clean synthesis, the following discussion will focus on the

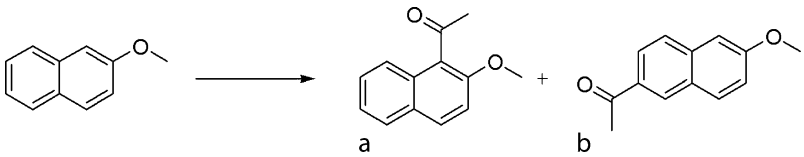

Green Catalytic Transformations. Figure 7
1-acetyl-2-methoxynaphthalene and the 2-acetyl-6-methoxynaphthalene precursors

Green Catalytic Transformations. Table 5 Acylation of isobutylbenzene with acetic anhydride

Catalyst	Yield (%)	Product distribution	
		1-Ac-2-Mn (A)	6-Ac-2-Mn (B)
Beta zeolite	68	30	70
Beta zeolite[a]	75	8	92
Beta zeolite[b]	75	24	76
BZ-1[c]	81	35	65
BZ-1	86	25	75
BZ-2 [d]	82	35	65
Ce^{3+}-BZ-2[e]	88	22	78

[a]Using propionic anhydride
[b]Pre-activation at 750°C
[c]Microcrystalline beta zeolite of particle size 1–10 μm, obtained through mechanical disintegration
[d]Microcrystalline beta zeolite of particle size 10–50 μm obtained through shortening the crystallization time to 48 h instead of one week
[e]Ion exchanged zeolite using 5%wt metal chloride solution

basics. Clay structure consists of sheets, tetrahedral and octahedral, which together can form layers, 1:1 and 2:1. The tetrahedral sheet is made up of $[SiO_4]^{-4}$ groups linked together through three *basal* oxygens, the fourth however is termed apical and points away from the layer toward the adjacent octahedral layer. The basal "structural" oxygens form a hexagonal lattice, characteristic of the tetrahedral layer. It should be noted that through ionic substitution, the Si^{4+} center can be replaced with a cation of similar size, such as Fe^{3+} or Al^{3+}. The octahedral layer comprises of $AlO_4(OH)_2$ units in sixfold coordination (although the cation center can be Al^{3+}, Fe^{3+}, Fe^{2+}, or Mg^{2+} depending on the clay). Depending on the oxidation state of the metal center (2+ or 3+), the structure can fall into a further two categories, dioctahedral or trioctahedral. The former type refers to the state where only two out of a possible three cation sites are filled, as a result of a divalent cation, this is often referred to as a gibbsite sheet (based on the naturally occurring material). Trioctahedral clays have trivalent cations; subsequently all potential cationic sites are filled.

The sheets can form layers in two ways (generally as there are exceptions), 1:1 and 2:1. The former refers to a single tetrahedral sheet bonding with an octahedral, whereas 2:1 refers to an octahedral sheet "sandwiched" between two tetrahedral sheets (Fig. 8).

The sheets bond through the apical oxygen via the interlayer cations, hydrogen bonding, or van der Waals/electrostatic forces. Furthermore, the spatial arrangement of the tetrahedral and octahedral sheets is not directly compatible, creating distortions in either one or both structures (classed as the polytype); however, this level of detail is outside the scope of this encyclopedia. The region between the layers is known as the *interlayer*, (X). This provides access to sites within the clay structure and contains equivalents of stabilizing ions to counteract charge created by isomorphic substitution within the tetrahedral layer, key to the clays activity. Lastly, layers found in various clays can be mixed, in that they contain different octahedral layers, i.e., one layer of chlorite and one of smectite, in regular or irregular quantities. Table 6 shows the structural makeup of some 1:1 and 2:1 clays.

Montmorillonite

Out of the diverse range of clay types available, montmorillonite is the most utilized when applied to organic catalysis. It is comprised of a 2:1 structure of tetrahedral coordinated silicate $[SiO_4]^{-4}$ and octahedrally coordinated gibbsite $[Al_2(OH)_6]$. The material is particularly susceptible to isomorphic exchange, where Al^{3+} replaces Si^{4+} in the tetrahedral sheet and Mg^{2+} replaces Al^{3+} in the octahedral sheet. This creates a negatively charged layer that is compensated by interchangeable cations, such as Na^+ and Ca^{2+}, which are situated between the layers. In fact, large quantities of cations can be "held" or "stored" in the clay depending on the extent of isomorphic exchange. On hydration the clay swells as the layers separate away from each other, allowing easy exchange of stabilizing cations in and out of the clay.

Acidic Properties of Clays

Clays can exhibit both Bronsted and Lewis acidity, the latter being due either to structural cations on the surface of the sheets or ions exchanged in the interlayer region. The Bronsted acidity stems from strong dissociation of intercalated water molecules coordinated to

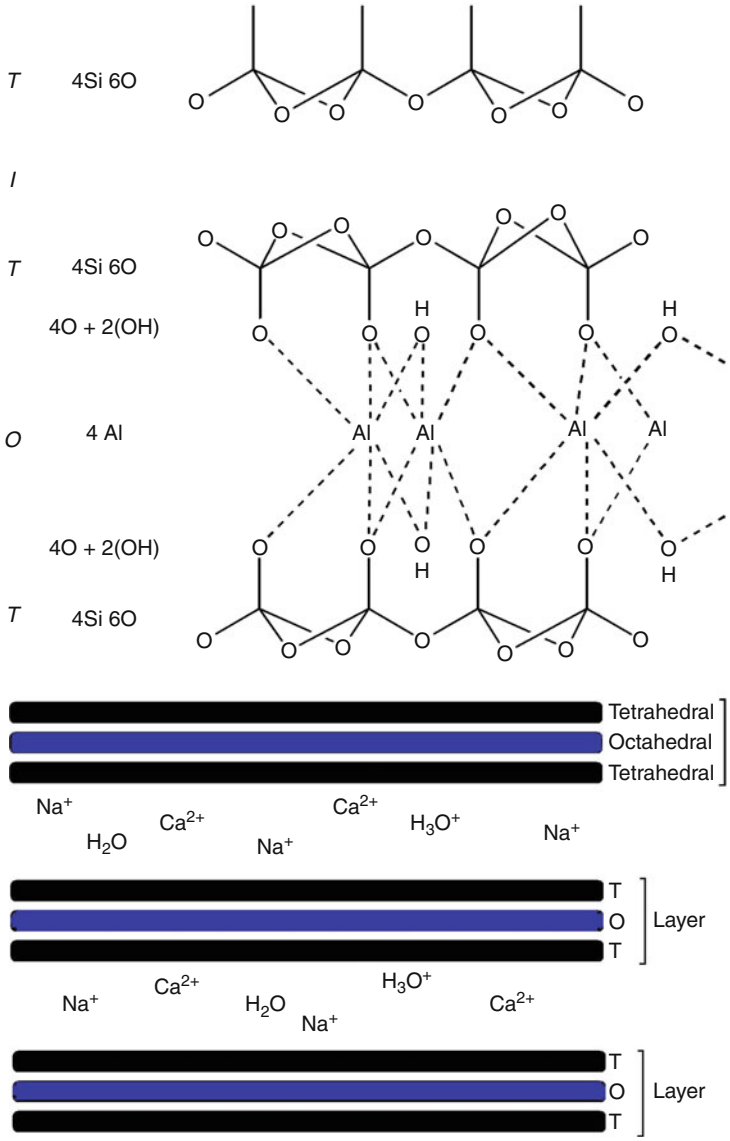

Green Catalytic Transformations. Figure 8
Structure of a 2:1 clay

the Lewis acid center, generating mobile H-bonded protons in a highly polarizing environment, given as,

$$\left[M(H_2O)_6\right]n+ \rightarrow \left[MOH(H_2O)_5\right](n-1)^{+}+H^{+}$$

It follows that the weaker the Lewis acid, i.e., the more electron withdrawing the cation, the more acidic the Bronsted acid [45]. Despite being able to reach acidities close to that of 98% H_2SO_4, increased acidity as well as surface area and hydroxyl group concentration have been researched resulting in a common process, the acid treatment of clays. Typical acid treatment involves using a strong inorganic acid such as HCl, sulphuric, or phosphoric in various quantities. This not only replaces exchangeable cations with hydrogen, but also leaches Al out of the central octahedral layer, producing enhanced surface area and increased acidity [46, 47].

Green Catalytic Transformations. Table 6 Composition of 1:2 and 2:1 clays [43, 44]

Group	Interlayer	Dioctahedral	Trioctahedral
1:1	None or only H_2O	Kaolinite $Al_2Si_2(O_5)(OH)_4$	Serpentine $Mg_3Si_2(O_5)(OH)_4$
2:1	None	Pyrophyllite $Al_2Si_4(O_{10})(OH)_2$	Talc $Mg_3Si_4(O_{10})(OH)_2$
Smectite $0.25 < x < 0.6$	Hydrated exchange-able cations	Montmorillonite $M_x[Al_{2-x}Mg_x](Si_4)O_{10}(OH)_2$	Hectorite $M_x[Mg_{3-x}Li_x](Si_4)O_{10}(OH)_2$
		Beidellite $M_x[Al_2](Si_{4-x}Al_xO(OH)_2$	Saponite $M_x[Mg_3](Si_{4-x}Al_x)O_{10}(OH)_2$
Vermiculite $0.6 < x < 0.9$		Vermiculite (DIO) $M_x[Al_2](Si_{4-x}Al_x)O_{10}(OH)_2$	Vermiculite (TIO) $M_x[Mg_3](Si_{4-x}Al_x)O_{10}(OH)_2$
Mica	Non-hydrated cations	Muscovite $K[Al_2](Si_3Al)O_{10}(OH)_2$	Phlogopite $K[Mg_3](Si_3Al)O_{10}(OH)_2$

Pillared Clays

Despite high acid strength and good surface areas, basic and acid treated clays are still susceptible to thermal degradation; structural collapse of the clay is typically observed upon heating above ~200°C. By *pillaring* the clays increased surface area, concentration of acid site, and thermal stability is achieved, due to a fixed metal oxide pillar. A common pillaring agent is polyoxocation Al_{13}, prepared by mixing a base with aqueous chlorohydrate, $AlCl_3$, or $Al(NO_3)_3$ to give a solution with OH/Al^{3+} ratios of up to 2.5. The polyoxocation complex has been reported to have a tridecamer structure of $[AlO_4Al_{12}(OH)_{24}(H_2O)_{12}]^{7+}$, also known as the Keggin ion [48]. The complex is then mixed with the clay, allowing diffusion of the structure between the layers and ion exchange. Once the clay is then filtered, washed, and calcined between 300°C and 500°C, the cations become bound supporting pillars and are able to release protons, Fig. 9.

Catalysis

As with zeolite, clays have found many applications, due to their high acidity, surface areas, high temperature tolerance (pillar only), and unique swelling properties. Discussed below are a few classic examples as well as more recent developments.

Esterification Organic esters are important in a plethora of applications, from intermediates, pharmaceuticals to fragrances and perfumes to plastisizers (the list goes on). However, there are a number of downsides to conventional esterification process. If using a non-activated carboxylic acid, for instance, the reaction has to be catalyzed with a strong acid in the presence of a large quantity of alcohol, due to the reversible nature of the reaction. It is often the case where the acid is first activated, where electron density is withdrawn from the acid center, usually using thionyl chloride to produce an acid chloride. On reacting the alcohol with the acid chloride a large quantity of HCl waste is produced and a base is often added to the reaction mixture to "mop up" the inorganic acid. Overall the synthesis produces either a large quantity of alcohol or acid waste, or has more than a single step, activation of the acid with a toxic and potent lachrymator, thionyl chloride (PCl_5 has also been used). Avoid the use of these agents not only has a positive environmental impact, but reduces worker risk, and substantially reduces cost. Consequently there has been much research into alternative solid acids and Al^{3+} exchanged montmorillnite clay in particular has shown promising developments. Recent investigation [49, 50] into the synthesis of p-cresyl phenylacetates (industrially used for perfumes, soaps, etc.), using Al^{3+} exchange montmorillonites, has been reported, Table 7. The use of the p-cresyl, and aromatic alcohols in general, is of interest as they are weakly nucleophilic due to lone pair electron delocalisation around the ring, therefore requiring a strong delta positive charge on the acid center.

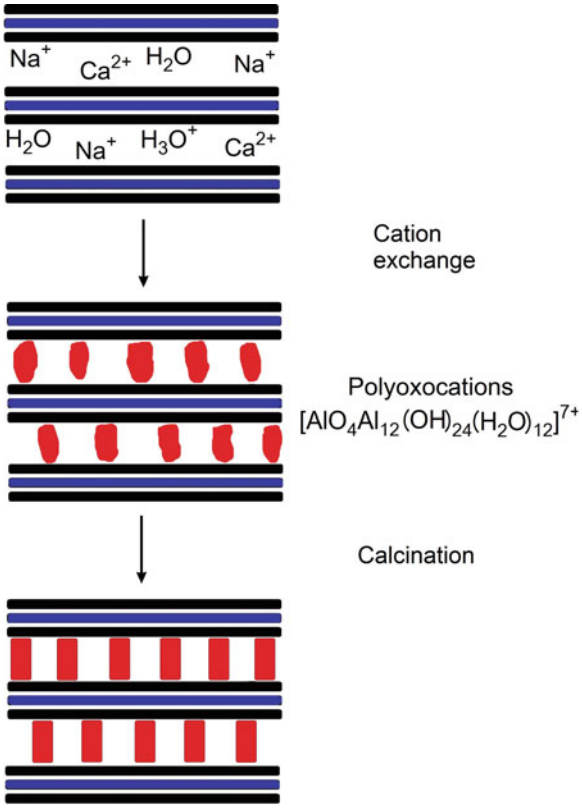

Green Catalytic Transformations. Figure 9
Pillared clays

Green Catalytic Transformations. Table 7 Synthesis of p-cresyl phenylacetate using various montmorillonite catalysts

Catalyst[a]	Calcination temperature (°C)	Reaction time (hours)	Yield (%)
Na^+	100	16	Nil
H^+	100	12	52
Al^{3+}	100	6	67
Al^{3+}	200	12	36
Al^{3+}	400	12	Nil

[a]Ion exchange on montmorillonite clay

Interestingly, the Na^+ exchanged (raw) clay is not active whatsoever and is thought to be attributed to the low electronegativity of the Na+ ions being less able to polarize the interlamellar water and produce strong bronsted acidity. When exchanged with hydrogen, however, increased yields are observed. It is only with

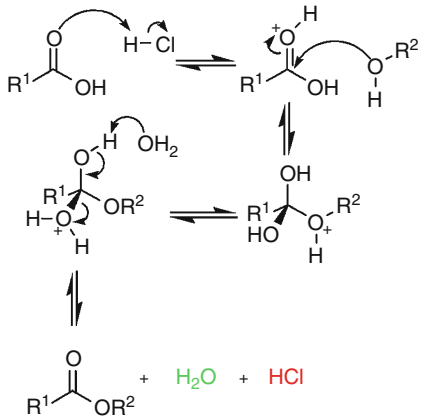

Green Catalytic Transformations. Figure 10
Mechanism of acid catalyzed esterification

the highly polarizing Al^{3+} cation exchange that the highest yields are seen, due to the high acid strength required to protonate and give the oxonium ion intermediate [10], Fig. 10. Increased calcination temperatures cause loss of water from the catalyst surface, converting Bronsted into Lewis acidity, resulting in a loss of activity.

This is an excellent example of a clean synthesis, due to its low molar quantity of alcohol, one part acid to two parts alcohol, the nontoxic by-product (H_2O), as well as the reusability of the catalyst by simply washing with water and heating to 100°C.

Etherification Common ether synthesis typically involves treating an alkoxide anion with an alkyl halide, where a strong homogeneous base such as NaH deprotonates an alcohol giving an alkoxide, which attacks an electrophile such as methyl iodide. A NaOH base will suffice when using alcohols such as phenol and dialkyl sulfates are often used as electrophiles, leaving the sulfate ion in the waste stream. An interesting application recently published looks at transforming the potentially large quantity of glycerol by-product from the biodiesel industry (predicted to reach millions of tons) to useful glycerols ethers [51]. Amberlyst-35, Beta zeolite, Montmorillonite K10, Niobic acid, and p-toluene sulphonic acid (PTSA) were directly compared as acid catalysts, Fig. 11.

The stronger acid catalysts, beta zeolite and amberlyst-35, gave higher yields selectively to the mono benzyl-glycerol ether (around 55% and 38%,

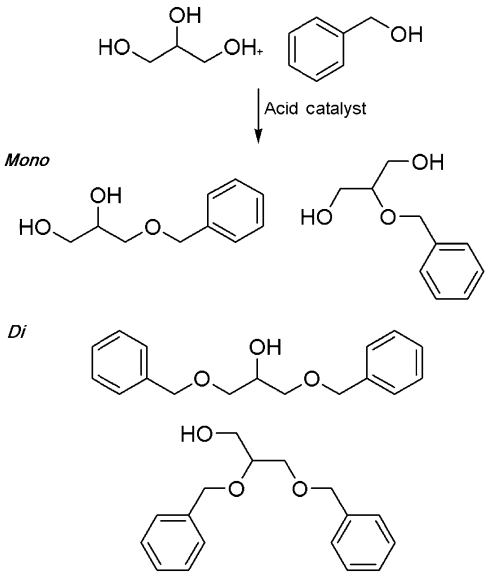

Green Catalytic Transformations. Figure 11 Synthesis of Glycerol ethers

respectively, after only 2 h) due to their narrow porous channels and shape selectivity. Interestingly, montmorillonite K10, gave the overall highest conversion of the di benzyl-glycerol ether, ~56%, and also gave a high conversion of the mono benzyl-glycerol, of around 35%. Overall, the β-zeolite and montmorillonite K10 clay gave similar conversions of opposite selectivity, demonstrating that the observed acidity on the clay surface is only a part of is high activity. With a low stochimetric ratio of benzyl alcohol to glycerol, 3:1, this reaction gives high conversions in short reaction times, allowing easy separation and reuse due to it heterogeneous nature and creates a valuable material from a potentially large future waste stream.

Alkylation The Friedel-Crafts alkylation is problematic when considering the frequency of its use in industry. The alkylation of aromatic rings typically involves reaction of pre-activated alkyl chain, such as 2-chloropropane, with powdered $AlCl_3$ catalyst or liquefied HF, which helps the alkyl halide to polarize, allowing π electrons from the aromatic benzene to attack the carbocation. Many clays have been investigated over past decades [52–54], and early work was focused on increasing the activity thorough ion exchange, (for the most part the base clay does not show appreciable activity). Laszlo and Mathy [55] reported increased activity with exchanged clays when applied to various reactions such as the alkylation of aromatics with alkyl halides, alcohols, and alkenes. The test reaction was that of benzyl chloride and benzene, activity of the metal exchanged clays followed the following reactivity series [56], $Fe^{3+} > Zn^{2+} > Cu^{2+} > Zr^{4+}$, $Ti^{4+} > Ta^{5+} > Al^{3+} > Co^{2+} > K10 > Nb^{5+}$. This not only showed an excellent alternative for alkylation catalysis, but more importantly demonstrated how support surfaces, whether clay, zeolite, or amorphous oxide, provide a very different environments for reacting species when compared to that of homogeneous solutions. For instance, the activity displayed by Zn is much higher than that of Al, where the opposite is true for the homogeneous chloride salt equivalents [19]. The range in activity is thought to be related to water coordinating to the metal center in a highly polarizing environment, exhibiting varying degrees of Bronsted acidity. A number of examples of solid acid catalysts and subsequent reactants/reagents are shown in Table 8 [57]. By far one of the greatest breakthroughs was that of the clayzic catalyst for benzylations, this will be discussed later in the supported reagents section.

Sulfonylations Use of SO_3/R_2SO with H_2SO_4 is commonly in the synthesis of sulfones. These are often used in pharmaceuticals, polymers, and agrochemicals. Aside from the typical drawbacks associated with homogeneous acid catalysis, there can be problems with selectivity between para/ortho isomer in the sulfonylated of aromatic species. Both bronsted acidic and ion exchanged zeolites [58, 59] and clays have been researched as heterogeneous replacements, of which Fe^{+3} exchanged montmorillonite clay has shown high activity toward this type of transformation [60]. The activity of exchanged metals on montmorillonite follows $Fe^{3+} > Zn^{2+} > Cu^{2+} > Al^{3+} > K10$ in the sulfonylation of m-xylene and toluene-p-sulfonic anhydride [61]. A screen of various reagents using beta zeolite and Fe^{3+} montmorillonite can be seen in Table 9. The selectivity in the methanesulfonation of toluene parallels that of $AlCl_3$, achieving 33% selectivity toward the para position, 99% para selectivity is observed in the arenesulfonylation (TsCl). The activity

Green Catalytic Transformations. Table 8 Application of solid acids to alkylations

Reaction type	Catalyst	Reactant	Reagent
Alkylation of aromatic hydrocarbons with	Wyoming montmorillonite expanded with $AlCl_3$ and/or silanized with $(EtO)_4Si$	Benzene	Ethane
i) Olefins	H-ZSM-5	Toluene	Ethane
ii) Saturated hydrocarbons	$FeCl_3$ doped montmorillonite K10	Benzene	Admantane
iii) Alcohols	$ZnCl_2$ clay, Al_2O_3 expanded smectite clay	Benzene, toluene naphthalene	Aliphatic alcohols cyclopentanol
	H-ZSM-5	Benzene	Ethanol
	Pillared montmorillonite, piller saponite, H-ZSM-5, HY	Toluene	Methanol
	H-ZSM-5	Naphthalene, methyl naphthalene	Methanol
iv) Halide	Transition metal salt deposited on montmorillonite K10	Benzene	Benzyl chloride
Alkylation of phenols	Activated clay	Phenol	Isobutene
	Bentonite		Oleic acid
	Supported/mixed oxides		Methanol
Alkylation of aromatic amines	Bentonite and Triton B	Diphenylamine	Styrene

Green Catalytic Transformations. Table 9 Sulfonylation of various species using zeolite and montmorillonite

Catalyst	Sulfonylating agent	Yield (%)	Selectivity		
			O	*M*	*P*
Fe^{3+} montmorillonite	Ms_2O	81	47	19	34
Fe^{3+} montmorillonite	$PhSO_2Cl$	84	5	0	95
Fe^{3+} montmorillonite	TsCl	86	1	0	99
Fe^{3+} montmorillonite	TsOH	42	13	7	80
Fe^{3+} montmorillonite	Ts_2OH	84	11	6	83
Beta Zeolite	Ms_2O	78	42	21	37
Beta Zeolite	$PhSO_2Cl$	72	11	3	86
Beta Zeolite	TsCl	53	1	0	99
Beta Zeolite	TsOH[a]	50	12	5	83
Beta Zeolite	Ts_2OH	88	14	6	80

[a]Standard reaction time 6 h, TsOH reaction time 24 h in refluxing toluene

of the catalysts is thought to be to the mixed of Lewis and Bronsted acid catalysis. Reusability of the catalysts is found to be greater in systems that do not use Cl as an activating agent.

Aldol Condensation The use of clays for acid catalyzed reactions is well researched; however, little investigation (in comparison) is focused on their applications as a base. This largely stems from the

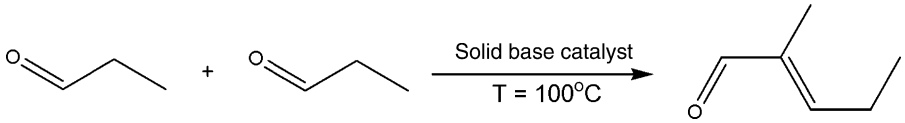

Green Catalytic Transformations. Figure 12
Synthesis of 2-methylpentanal

Green Catalytic Transformations. Table 10 Conversion of 2-methylpentanal

Catalyst	Conversion (%)	Selectivity (%)		
		2-methylpentanal	3-Hydroxy-2-methylpentanal	3-Pentanone
HT (1.5)	44	68	30	2
HT (2.0)	47	83	17	-
HT (2.5)	80	92	8	-
HT (3.0)	86	96	4	-
HT (3.5)	97	99	-	1

components looking to be replaced, in that, typically homogeneous acids, $AlCl_3$, HCl, H_2SO_4, tend to be more of a problem than, say, NaOH or KOH. Nevertheless similar problems still remain with stoichiomeric quantities of waste twinned with disposal cost, as well as difficulty of product/reagent separation. A good example of utilizing basic properties of zeolites is given in the solvent free aldol condensation of propanol to 2-methylpentanal [62], Fig. 12. Propanol itself tends to be limited to solvent applications; alternatively, 2-methylpentenal has commercial importance in pharmaceuticals, fragrances, flavors, and cosmetics. With optimum reaction conditions using a homogeneous base such as NaOH, a high yield of 99% is obtained yet only a selectivity of 86% is achieved. As such, a number of solid bases have been investigated with hydrotalcite showing enhanced selectivity.

Unlike other materials, hydrotalcite (HT) has a typical composition of $Mg_6Al_2(OH)_{16}(CO_3)4(H_2O)$, its name based on its resemblance to talc and high water content. The activity of the HT is found to vary with Mg:Al ratio, from 1.5–3.5, directly proportional to the basicity of the material, Table 10. It is thought that two types of basic site exist in hydrotalcite, firstly a weak OH- Bronsted and secondly a stronger O^- Lewis base [63].

Limitations There are few limitations of modern clay catalysis, most acid-treated clays show enhanced acidity in comparison to untreated and thermal decomposition of the clay structure can be avoided by pillaring the sheets. Increased selectivity is often seen and the ability of clay to ion exchange a variety of metals and make clay catalysis an efficient and green alternative to homogeneous activating agents.

Supported Reagents

Introduction

A supported reagent can be defined as a species that is supported, through either chemisorption or physisorption, onto an organic (such as ion exchange resin/carbon) or inorganic material. Typically supporting materials range from clays, to amorphous and structured silicas, alumina, and zeolites. Often the supported species is inorganic, such as precious metals, although there are a number of organic examples. These offer many advantages over their homogeneous equivalents:

- Reduced or nonexistent toxicity, leading to easier and safer handling
- Reusability

- Enhanced activity due to surface characteristic and active site distribution
- Increased selectivity though structural characteristic of supporting material
- Enantioselective potential

It should be noted, however, that complications related to poor diffusion, blocked pores due to substrates, potential poisoning of active species, and physical use on a large scale (fine silt and powders) sometimes create a few drawbacks.

Types of Support

Different supports have very different properties; however, for the majority of applications high surface areas of >100 m^2 g^{-1} are considered advantageous, as this typically parallels concentration of active species. Depending on the reaction, in particular, the properties of supports can be tailored to suit, such as the acidity/basicity of the surface (the majority of applications utilized an acidic surface), pore size, and channel regularity. This can range from around 4 Å for zeolitic supports to >150 Å for structured silicas, temperature stability from ~200°C for standard acid-treated clays to ~800°C for amorphous silica (high temperature catalysts are often preferred for obvious reasons). Shape selectivity is often acquired with small/restrictive pores found in microporous silicas, zeolites, and pillared clays; however, diffusional problems and blockages can cause loss of activity over time. To overcome this problem many different species are supported on mesoporous supports, such as large pore SBAs, where pore size can reach around 200 Å (some macroporous carbons can be above 500 Å), although shape selectivity is nearly always lost at this size. Table 11 shows commonly used supports and corresponding surface areas [64]. Choice of support is an important consideration when designing clean synthetic routes. For instance, the acid properties of one support may destroy reagents whereas another may stabilize important intermediate species on the surface.

Green Catalytic Transformations. Table 11 Typical surface areas of commonly used supports

Support	Surface area m^2/g	Notes
Amorphous Silica Gel	300–600	Weakly acid surface due to isolated silanols, although is available in neutral and basic forms. Pores sizes typically range from 4 to 10 nm
Amorphous Alumina	100–300	Weakly basic, but through treatment and variation of surface groups can be acidic or neutral. Pore sizes similar to silica
Acid treated montmorillonites	50–300	K10 commonly used, give enhanced acid character compared with untreated montmorillonite clay. Able to swell and ion exchange with suitable solvent
Pillared montmorillonites	200–500	Stable at higher temperatures and can give enhanced shape selectivity
Structured Silica (HMS, SBA)	300–800	A wide choice of pore shapes and sizes available, allowing the supported to be tailored to fit certain syntheses. High temperature tolerance, easy to functionalise surface though SiOH silanols
Zeolites	300–600	Highly selective crystalline microporous materials. Able to exchanges ions to tune acidity type and strength

Preparation of Supported Species

Prior to loading active species on a support, certain pretreatments are commonly performed. Dehydration of the surface at around 120°C upward under vacuum, avoids hydrolysis complications and competitive adsorptions onto binding sites. In the synthesis of $AlCl_3$-Al_2O_3, for example, $AlCl_3$ is readily hydrolysed unless the alumina is dried at least 550°C before impregnation. Another common technique used increases the number of available surface hydroxyls able to react on silica supports (often using HCl), effectively increasing the concentration of active species able to bind to the surface, Fig. 13. A number of preparation methods exist, depending on the end use of the catalysts, different methods are more suited than others.

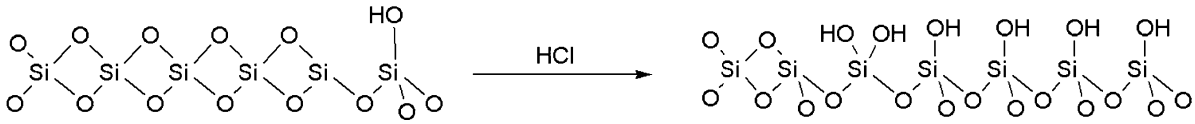

Green Catalytic Transformations. Figure 13
Hydrolysis of siloxane bridges to give increased silanol quantity

Wet impregnation/Evaporation is a commonly used technique for loading species onto a support, due to its suitability for a wide range of reagents and supports. The method is based on dissolving the species of choice in a solvent of reasonable volatility, i.e., DCM, acetone, ethanol and stirring the solution with the support (typically 1–2 h). Once even wetting and diffusion into the pores has occurred the solvent can be evaporated *slowly*, ensuring even distribution of the species on the surface, deep in the porous network of the material. Post-treatment often involves calcining the resulting material, (anything from 200°C to 600°C), allowing chemisorption of the species onto the surface, referred to as thermal activation. *Precipitation* is generally used when there are issues with solubility, often with of metal salts. Deposition of the active species on the surface is achieved through either reaction with a second species to form an insoluble salt, cooling a hot solution containing the solute, or addition of cosolvent in which the active species is insoluble. *Adsorption* methodology simply involves stirring the support and reagent together (sometimes under reflux), yet requires a strong interaction between the surface and supporting species, aiming to achieve chemisorption if possible. After adsorption, suitable post treatment ensures the species is bound to the surface. Other methods have also been used such as *mixing/grinding* support and reagent together, in situ supporting (where the two solids are introduced directly into the reaction and the supported reagent is formed and reacts as the reaction proceeds) and ultrasound, these tend to be used less often.

Aside from post-modification, it is possible to synthesize materials with a species of choice available and evenly dispersed on the surface, known as sol-gel synthesis. The technique allows organic functionality to be incorporated into the structure and gives high surface area materials with high ratios of active species per gram. This methodology uses soluble (generally monomeric) precursors to the "support" and the supported component, polymerising them together, often round templates to give highly structured materials. In addition, the organic species can often be reacted with many other substituents to tailor the functionality, amino functionalized silicas are particularly good at this.

Loading the Support

The dispersion of the active species becomes an important variable when physisorbing/chemisorbing a reactive species, such as a sulphonic acid or metal halide onto a surface. It should be noted that in other cases such as ion exchange of various cations with clays and zeolites, there are a defined number of sites that cannot be exceeded. Correct ratios of support to reagent can be estimated from the surface area and porosity of the material, optimal loadings tend to be between 0.5 and 2 mg per gram of support, aiming to achieve monolayer coverage. Porosimetry using N_2 adsorption onto the surface gives useful information when predicting potential concentration/loadings; however, problems can arise when using microporous supports, often is the case that N_2 can diffuse into pores that reagents cannot. As such, the exact requirement for various supports, active species and reactions, needs detailed investigation to achieve high efficiency. Overloading and underloading a support equally create a number of problems. Overloading can cause agglomerisation of reagents leading to blocked pores, reducing the overall surface area available for catalysis and hindering diffusion. After monolayer dispersion is achieved, a second (bi-layer) can form, diluting the unique surface-reagent properties, where second and third layer species tend toward homogeneous characteristics. Contrastingly, underloading the support can cause lower catalytic activity, therefore requires increase quantities of the catalyst. With a lower concentration of active species, an increase in exposed surface is observed, which can be reactive enough to catalyze by-product formation.

Catalysis

There has been extensive research into supporting Bronsted and Lewis acids on different supports, resulting in many different catalyst properties and applications. Below is a sample out of a number of examples, showing the effect of different supports, supported species, and reactions, giving a much generalized view of the area. As with reactions previously discussed, through supporting active homogeneous species, the production of waste, risk factor, and cost is substantially reduced, giving high efficiency reactions with minimal impact on the environment and resources.

Bronsted Acid Catalysis

The acidity of supports, i.e., isolated silanols and alumina hydroxyls, tend to parallel organic acids, achieving a pKa of around 4–6. This is of little use for the majority of acid catalyzed reactions and as such often requires a species of stronger acidity to be bound to the surface. Typically there are several types of Bronsted acidity observed in relation to supports, the original acidity from mixed oxides (silica and alumina hydroxyls), zeolitic acidity, activated/dissociated H_2O molecules usually coordinated with a Lewis acid metal on the surface and homogeneous Bronsted acids tethered or chemisorbed onto the support. The latter allows very high acid strength species to become reusable and safe to handle, below are a few examples.

Sulphonic Acid on Silica The hazards of using fuming acids on a large scale (as well as the subsequent tax deterrents on chemical waste) are well known and as a result there has been much investigation into supporting them on a variety of different media. One of the more "straight forward" supported acids is that of sulphuric acid/sulphonic acids supported on silica, demonstrating high activity and selectivity in a number of transformations [65–73]. Jérôme et al. have shown that sulphonic acid supported on hexagonal mesoporous silica (HMS) gives selective esterification of multifunctional carboxylic acids with glycerol (a by-product of the biodiesel process) [74]. The reaction choice relates to its poor selectivity and rapid polymerisation to many undesired products, for instance the use of homogeneous p-toluene sulfonic acid in the esterification of glycerol with 16-hydroxyhexadecanoic acid gives a low yield of the amphiphilic monomer, only 35%. By anchoring the sulphonic species to HMS and SBA-15, an impressive increase in selectivity to 98% was observed, due to the restrictive nature of the pores. On application to other, more complex acids, high activity and selectivity remain consistent, Fig. 14.

Other examples of sulphonic acids on silica gel include the synthesis of mono and disubstituted oxadiazoles from acyl hydrazides and orthoesters at room temperature [75]. Heterocycles are an important class of biologically active compounds often used as pharmaceutical intermediates. Out of a number of different solid acids investigated, sulphuric acid on silica gave high yields in as little as 10 min, Table 12. Interestingly, enhance activity was seen when compared to homogeneous H_2SO_4, showing how supported materials are often much more than the sum of their parts. Reuse of the catalyst showed that activity remained high even after five uses.

Shaabani [76] has also recently reported high yields using silica-H_2SO_4 in the synthesis of trisubstituted imidazoles by the one pot condensation of benzyl, benzoin, or benzylmonoxime with a substituted benzaldehyde and ammonium acetate. The synthesis used water as a solvent, whereas previously solvents such as methanol, ethanol, acetic acid, and DMSO were typically used. Excessive water in acid catalyzed reactions is known to deactivate acid centers; nevertheless yields of ~70% are achieved after 4–6 h.

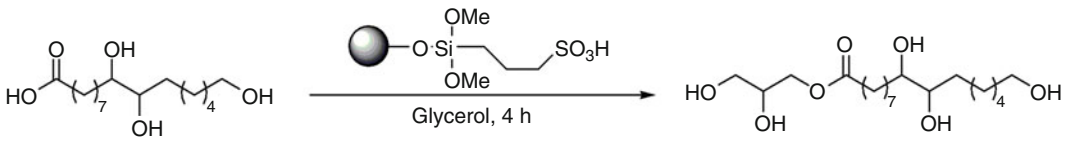

Green Catalytic Transformations. Figure 14
Esterification using sulphonic acid on HMS

Green Catalytic Transformations. Table 12 Synthesis of 2-(4-Chloro-phenyl)-5-propyl-[1,3,4]oxadiazole [1]

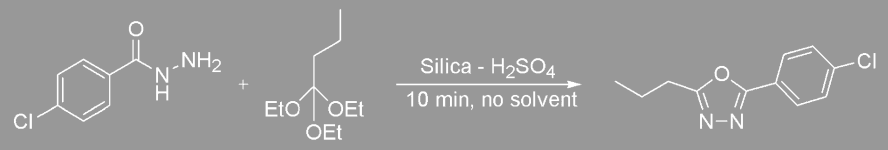

Catalyst	Yield (%)
p-TsOH	42
$NaHSO_4$	33
$NaHSO_3$	28
H_2SO_4	25
Montmorillonite K10	48
Silica sulphuric acid	94

Sulphated Zirconia Zirconia as a support has received attention in recent years due to its high activity toward hydrocarbon conversions. In particular, sulphated zirconia (SZ, SO_4^{2-} – ZrO_2) has shown catalytic potential toward light alkane isomerisation, as well as acylation, alkylation, cracking, and ring opening reactions [77–81]. As well as the many applications of mesoporous SZ to liquid phase reactions, standard microporous SZ is well suited to a number of vapor phase synthesis. It had previously been thought that the high activity of sulphated zirconia had been due to its super acidic properties, with an acid strength 1,000 times greater than homogeneous sulphuric acid [82]; however, more recent literature has shown that this is not the case [83]. FTIR spectroscopic titration with pyridine shows that surfaces activated between 500 and 600°C comprise of Bronsted acidity only [84], thought to be due to rapid adsorption of water, converting any Lewis acidity to Bronsted. Ratnam et al. recently reported of using SZ to catalyze the acylation of alcohols/phenols and amines, typically achieving yields of ~90% in 10 min [85].

Silica Gel as a Catalyst The use of silica as a support has been widely published, yet there has been little report of using silica gel alone as an acid catalyst. Amide synthesis has been a consistent problem area in green chemistry for many years. The majority of the problems stem from the used of stoichiometric quantities of activating agents used to create a δ positive center on carboxylic acids, allowing nucleophilic attack from an amine. It should be noted that there are other type of reagents used for the synthesis of amides, such as nitriles, but the direct condensation of acid and amine is advantageous, due to their relatively low toxicity and by-product formation of water. The use of activating agent creates an equivalent of waste, for instance if an acid is activated to an anhydride, the second "low cost" acid is lost in the waste stream, excluding the proportion that has reacted with the amine, resulting in the formation of side products. There have been attempts at developing homogeneous catalysts, such as Yamamoto's functionalised 3,4,5-trifluorophenyl boronic acid catalysts, though these are often limited to simple reactions, cannot be recovered and their synthesis is not straightforward. However, Clark et al. recently demonstrated the activity of calcined silica gel in the direct synthesis from carboxylic acids and amines [86]. Initially a number of supported metals, $FeCl_3$ and $ZnCl_2$ on silica and montmorillonite clay were investigated, but it was found that the silica gel alone gave the best activity. Unactivated, silica gel is a mild desiccant and does not typically display any catalytic activity towards organic reactions. On heating, a number of surface changes occur, around 120–200°C physisorbed water is lost, above this temperature the silanols start to dehydroxylated to give siloxane bridges up to around 1,000°C (when all of the surface silanols are lost to give quartz). It was found that activation at 700°C gave a hydrophobic

Green Catalytic Transformations. Table 13 Synthesis of amides using thermally activated silica gel

R^1 [c]	R^2	Uncatalysed yield	Isolated yield (%)[a]
C_6H_5	C_6H_5	0	47[b]
$C_6H_5CH_2$	C_6H_5	10	81
$CH(CH_3)C_6H_5$	C_6H_5	4	72[b]
$CHClCH_3$	C_6H_5	4	70
$OCH_2C_6H_4Cl$	C_6H_5	0	73
$CH_2C_6H_5$	C_6H_4Cl	0	48
$CH_2C_6H_5$	$C_6H_4(CH_3)_2$	0	38[b]
$CH_2C_6H_5$	C_4H_8	2	89
CH_2CH_3	$CH_2CH_2CH_2CH_3$	89[c]	98[d]

[a]After 24 h reflux in toluene, 20%wt silica
[b]Using 50% wt silica
[c]After 12 h
[d]After 24 h

surface with mild Bronsted acidity and high activity toward amidation. A number of different reactions are shown below, Table 13.

Despite the use of high loadings of silica with particularly difficult syntheses, such as benzoic acid and aniline, the initial low cost, low toxicity and simple preparation and use makes the synthesis a substantial improvement on previous catalysts. Multiple reuse with reactivation (burning out organic buildup) is possible, without loss of activity. With a high atom economy of 93% and an E-factor of less than 1, the synthesis allows high conversions without the use of toxic and highly corrosive activating agents.

Lewis Acid Catalysis

Lewis acidity is often based on integrated surface cations acting as acid centers, where the strength largely depends on the surrounding environment. However, as previously discussed with zeolites and clays, water can coordinate to these acid centers and give Bronsted acidity, effectively "diluting" the Lewis acid effect. By tethering homogeneous species such as $ZnCl_2$ and $FeCl_3$ to various supports, increased Lewis acidity is observed. An excellent example of this is in the development and use of Envirocats^{TM}.

Envirocats^{TM} Designed as a series of commercially available clay and alumina-based catalysts, Envirocats^{TM} were developed by collaboration between the University of York and Contract Chemicals Ltd. (CCL). They comprise of a metal salt supported on a high surface area inorganic support and have a range of applications, Table 14. Although they are often term "simple" in that the species being supported is not a complicated structure, the mechanism by which they catalyze many different reactions is complex [87].

A good example of their enhanced activity is of the benzylation of benzene and benzylchloride with EPZ10, also known as clayzic, Fig. 15. The diphenylmethane product is often used as a precursor to many pharmaceuticals, making this particular reaction of commercial interest. As with many Lewis acid catalyzed reactions, $AlCl_3$ was formerly the homogeneous catalyst of choice, exhibiting little selectivity and giving high ratios of polybenzylated product, unless very large excesses of benzene are used. Clayzic, on

Green Catalytic Transformations. Table 14 Envirocats™ and common uses

Catalyst	Supported species	Type of reactions	Acidity
EPZG	Iron/Clay[a]	Friedel-Crafts Benzoylations, some acylations such as etherification	Contains both Bronsted and Lewis acid sites
EPZ10	$ZnCl_2$/K10 Clay	Friedel-Crafts alkylation of aromatics, Benzylations	Very strong Lewis acid, few weakly Bronsted acidic sites
EPZE	$ZnCl_2$/Clay	Friedel-Crafts Sulfonylations and some Benzoylations	Prodominatly strong Lewis acid with some strong Bronsted acids. Different preparation method to EPZ10
EPIC	Phosphoric acid/Clay	Esterifications, general Bronsted acid catalyzed reactions	Exclusively strong Bronsted acidity
EPAD	Cr(VI)/ alumina	Oxidations	Cr(VI) oxidant center, not suitable for used with peroxide – causes leaching of the metal

[a]Acid treated montmorillonite clay

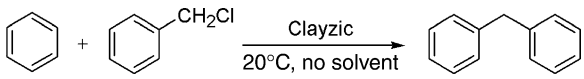

Green Catalytic Transformations. Figure 15 Benzylation of benzene and benzylchloride

the other hand, can be used in similar conditions to $AlCl_3$, yet gives extraordinarily high yields of ~75% after 4 h at room temperature, even with a minimal excess of benzene. In addition, the catalyst can be simply filtered off, washed and reused many times over, showing an excellent example of green chemistry being integrated into industry.

$AlCl_3$ on Silica Aluminum chloride is a widely used strong, in expensive homogeneous Lewis acid. There are, however, many problems associated with its use, including the necessitated destruction of the acid with water to aid separation of products, resulting high volumes of corrosive and toxic waste and formation of by-products due to its inherent activity. There have been a number of reports detailing the immobilization of aluminum chloride on a variety of supports to overcome these problems. Typical procedures involve dissolving the $AlCl_3$ in an organic solvent and slowly reacting this with the silica surface, theoretically creating a $SiOAlCl_2$ species capable of both Bronsted and Lewis acidity [86]. The resulting material has been applied to a range of reactions with success, early syntheses focus on the Fridel-Crafts acylation. Li et al. discusses the use of $AlCl_2$-silica in a one pot, three component Mannich type reaction, Table 15 [88]. Activating agents such as HCl, $InCl_3$, $Y(OTf)_3$, $Zn(BF_4)_2$, $Bi(OTf)_3$, PS-SO_3H, phosphorodiamidic acid, dodecylbenzene sulfonic acid have been reported, suffering from the usual homogeneous drawbacks. Interestingly, the reaction of aniline, benzaldehyde, and acetophenone to give a β-aminocarbonyl (used in numerous pharmaceutical syntheses and natural products) showed that homogeneous $AlCl_3$ gave lower yields when compared with the supported species. The optimum reaction conditions also add to the green credentials of this synthesis, the best solvent out of a range including, MeCN, CH_2Cl_2, THF, and toluene has been found to be ethanol, with a reaction temperature of ~25°C.

Supported Lewis Acids in Acylation Freidel-Crafts reactions are a key target for green chemistry due to their frequent use in chemical industry and large volumes of waste produced. Two main problems areas of the synthesis are the initial activation to an acyl chloride, with subsequent generation of HCl and the use of a strong Lewis acid to cleave the Cl from the acyl chloride to produce an acylium ion, enabling nucleophilic attack from π electrons on the aromatic ring. Early developments focused on the direct replacement of the Lewis acid with a heterogeneous equivalent, examples include Ga_2O_3 and In_2O_3 supported on Si-MCM-41 [89, 90] and $InCl_2$, $GaCl_3$ and $ZnCl_2$ supported on both montmorillonite clay and Si-MCM-41 [91, 92]. Despite high yields, the catalyst

Green Catalytic Transformations. Table 15 Mannich type synthesis using aniline, acetophenone, and benzaldehyde

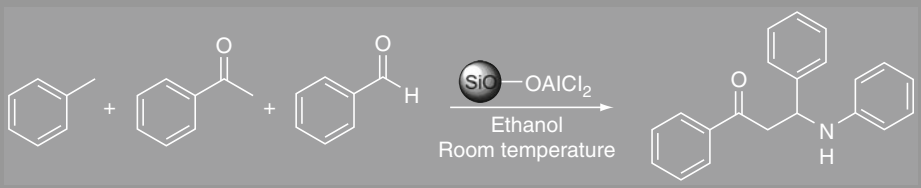

Catalyst	Time (hours)	Yield (%)
$FeCl_3 - SiO_2$	20	0
$ZnCl_2 - SiO_2$	20	0
$AlCl_3$	20	0
SiO_2	20	0
$AlCl_3/SiO_2$ dry mix	5	74
$AlCl_2 - SiO_2$	5	93

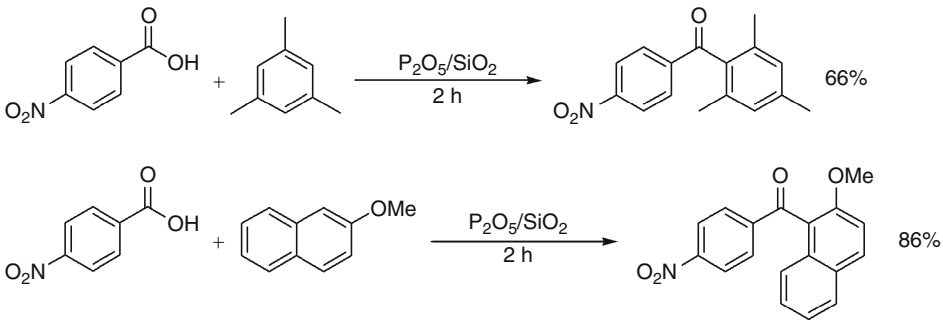

Green Catalytic Transformations. Figure 16
Acylation using P_2O_5/SiO_2. (*Where solvent is 1,2-dichloroethane under reflux, % given is conversion)

required pre-activation to the acyl chloride, creating stoichiometric quantities of HCl waste. Further improvements have developed allowing anhydrides to be used as starting materials, still creating equivalents of waste, yet not as corrosive as previous mineral acid waste [36, 93–96]. However, recent publications discuss the ideal scenario, use of carboxylic acid staring material producing only water as a by-product [97, 98], P_2O_5/SiO_2 in particular has shown potential. Application to a range of aromatic acylations has given high yields (Fig. 16), on average ~20% higher when compared to the homogeneous P_2O_5 alone [99].

The inexpensive nature of the catalyst, simple preparation, and ease of handling, as well as the use of unactivated carboxylic acids, producing only water by-product, make this synthesis improved over previous homogeneous species, as well as a number of heterogeneous catalysts.

Solid Base Catalysis

As mentioned before, the push for research into "clean" and reusable heterogeneous base catalysts has not been as pronounced as that for solid acids; however there is still a wide range of basic catalysts available. Many supporting materials can be thermally treated to exhibit basic properties (alumina), though they are weak and often species with increased basicity are supported. The basicity is usually the result of basic

Green Catalytic Transformations. Table 16 Supported basic species [64]

Solid base	Notes
Alumina – Na	Superbasic
Alumina – KOH	Widely used for many years
Alumina – KF	Widely used with variable basicity
Alumina – CsF	Little advantage over cheaper alumina-KF
Alumina – $AlPO_4$	Used in solventless reactions
Silica – Na	Superbasic
Silica – K	Superbasic
Silica – NaOH	Simplest form of basic silica
Zeolite-M^+	Can be very basic depending on alkali metal
Xonotlite-KO*t*Bu	Unusual supports – similar to alumina-KF
MgO-K/Na	Lower surface area than alumina and silica

hydroxyl groups, oxygen ions bound to the surface or basic ions bound to the surface. Table 16 gives an overview of commonly used solid bases.

Basic Species Supported on Alumina (KF/Alumina) First discussed by Clark [100], potassium fluoride supported on alumina (KF/Alumina) has been acknowledged as an extremely useful catalyst able to promote a variety of base catalyzed reactions [101]. The strength and nature of the basic sites on the surface has been a subject of much discussion over the years, but it has been widely accepted that the basic strength can vary from weak-moderate to superbasic depending on the preparation (drying condition of alumina post impregnation) and subsequent exposure to CO_2, for example. The active species is thought to relate to the "hard" fluoride anion as opposed to oxygen anions. It has been observed that when K_2CO_3 and KOH are supported on alumina, the resulting activity is much lower than that of KF and K_3AlF_6 species (formed at high loadings of KF, itself exhibiting no activity) on the alumina surface, suggesting that the presence of fluorine is essential to its activity [102]. Interestingly, unlike other fluoride ions sources, there has never been any report of KF-alumina exhibiting any nucleophilicity, even in simple substitutions. Another peculiarity of the material is that high activity is increasingly observed when KF loadings are higher than a monolayer equivalent, at low loadings no crystallinity can be observed through X-ray diffraction. Further identification of the F-species has been researched using [21] F NMR, yet the results have proved somewhat controversial [103]. KF-alumina remains one of the most important base catalysts due to its wide range of applications to many syntheses such as, isomerisations [103–105], condensations [102], Knoevenagel [106], cyclization [107], as well as C-N [108], C-O [109–111], S-C [112–114] and Si-O [115, 116] bond forming reactions. In particular, its application to Michael additions has received much attention [117–127], a typical example of this is in the addition of nitroalkanes to electron deficient alkenes [128]. The use of homogeneous catalysts (such as DBU) is often problematic due to the nitro acting as a leaving group, yielding nitric acid and unsaturated alkene. In addition, withdrawing groups on the α, β positions of the alkene make this a poor nucleophile. However, the use of KF-alumina as a catalyst gives impressive results compared to a range of alternative basic catalysts, Table 17.

Temperature control allows high selectivity between potential products, where room temperature conversions give the Michael addition adduct. A high E:Z stereoselective ratio of 95:5, is consistently found for the formation of the unsaturated 1,4 dicarbonyl derivatives from primary nitroalkanes. Overall the high activity, reusability, selectivity, and solvent-less nature of reactions utilizing KF/Alumina make it an excellent alternative to classic homogeneous bases.

Basic Amine Species Supported on Silica Aside from basic metals, there are a range of supported organic species able to provide basicity, of which amine functionality has attracted much interest [129]. The amines in particular vary widely, from imines, phenolates [130] to dialkylaminopyridine type species [131]. Hagiwara et al. discusses the use of amino functionalised silica gel in the Knoevenagel reaction [132]. Out of a range of different silicas of varying morphology, (i.e., pellets/powders) as well as different amines, 3-Aminopropyl supported on powdered silica

Green Catalytic Transformations. Table 17 Michael addition of methyl 4-nitrobutanoate with dimethyl maleate [102]

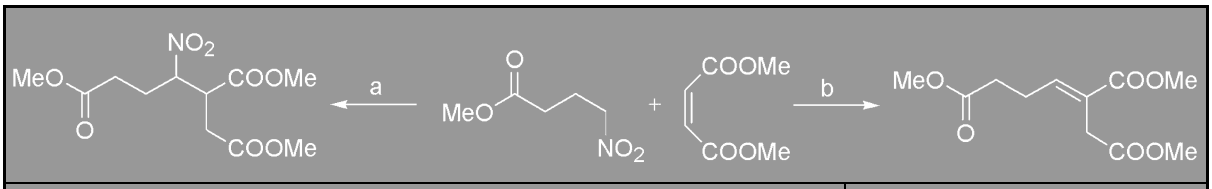

Catalyst	Yield of route A[c] (%)
KF/Basic Alumina	80
KF/Basic Alumina	79[d]
KF/Neutral Alumina	71
Basic Alumina	4
Hydrotalcite MG 70	7
Hydrotalcite MG 50	6
Amberlyst A-21	25
Amberlyst A-27	21
Silica supported-1,5,7-triazabicyclo-[4.4.0]dec-5-ene (TBD)	36
N,N-Diethylpropylamine supported on amorphous silica (KG-60-NEt_2)	19

[a]Catalysed with KF/Alumina at 55°C
[b]Catalysed using KF/Alumina at room temperature
[c]After 7 h, solventless reaction conditions
[d]Yield of route B

has been found to be the most active. Typical yields of a range of different functionalized benzaldehydes reacted with ethyl cyanoacetate are in the region 90–99% in between 2–5 h. In addition, water is able to be used as a solvent, thought to allow both substrates to achieve close proximity to each other on the reverse phase silica gel, increasing reaction efficiency. This demonstrates how organic functionalized solid bases have many advantages over their inorganic equivalents. Often they are mild in reactivity, reducing potential side product formation, have high reproducibility, with flexibility in design allowing the catalyst to be "tailored to fit" a wide range of applications.

Future Directions

The value of catalysis in chemistry has been well known for many years with application in larger scale, petrochemistry especially important and well established in industry. This was emphasized by the emergence in the second half of the twentieth century of more selective, typically zeolitic catalysts in continuous vapor phase processes that helped establish the petrochemical and commodity chemical industries as the engines of the great manufacturing industries of the world. An increasing awareness of the need to reduce the environmental impact of chemical manufacturing has caused a much wider range of industrial sectors to seek process improvements in chemical, pharmaceutical and polymer manufacturing. More efficient and selective processes that give less waste and greater resource efficiency and the avoidance of large quantities of often hazardous traditional reagents including acids, bases, and stoichiometric oxidants are important goals. Here, the transfer of long lifetime, selective, and reusable catalytic technologies from large-scale petrochemical processes to smaller scale, fine, and speciality (including pharmaceutical) chemical manufacturing has become and continues to be very important. It is needed to quickly move away from old, admittedly reliable but often dangerous and almost always very wasteful chemistry in all sectors of manufacturing.

In research, it is required to work ever harder to find effective replacements for the great reagents of the twentieth century – aluminum chloride, chromic acid, hydrogen fluoride, caustic soda, and many others – all cheap, versatile in numerous reactions, and readily available yet also all hazardous, unselective, and leading to more waste than product especially after work-up; progress to date has been limited and most processes continue little changed from decades in the past. The use of heterogeneous catalysts is required to extend the use of continuous production and intensive processing so as to get away from inefficient and inherently risky batch manufacturing. Catalysis should be the norm in all chemical manufacturing and not the exception, and the catalysts themselves must have verifiably sound lifecycles and low environmental footprints including ease of recovery and reuse especially when precious metals are employed.

Bibliography

1. Clark JH (1995) Chemistry of waste minimization. Chapman and Hall, Cambridge
2. Clark JH, Rhodes CN (2000) Clean synthesis using porous inorganic solid catalysts and supported reagents. Royal Society of Chemistry, Cambridge
3. Rabo JA, Schoonover MW (2001) Early discoveries in zeolite chemistry and catalysis at Union Carbide and follow-up in industrial catalysis. Appl Catal A 222:261
4. Nagy JB, Bodart P, Hannus I, Kirics I (1998) Synthesis, characterisation and use of zeolitic materials. DecaGen Ltd., Hungary, p165
5. Sing KSW, Everett DH, Haul RAW, Moscou L, Pierotti RA, Rouquérol J, Siemieniewska T (1985) Reporting physisorption data for gas/solid systems with special reference to the determination of surface area and porosity. Pure Appl Chem 57:603
6. Kissin YV (2001) Chemical mechanisms of catalytic cracking over solid acidic catalysts: alkanes and alkenes. Catal Rev 43(1):85
7. Zhuang JQ et al (2004) Solid-state MAS NMR studies on the hydrothermal stability of the zeolite catalysts for residual oil selective catalytic cracking. J Catal 228(1):234
8. Caeiro G, Magnoux P, Lopes JM, Ribeiro FR, Menezes SMC, Costa AF, Cerqueira HS (2006) Stabilization effect of phosphorus on steamed H-MFI zeolites. Appl Catal A 314(2):160
9. Bao X et al (2005) Enhancement on the hydrothermal stability of ZSM-5 zeolites by the cooperation effect of exchanged lanthanum and phosphoric species. J Mol Struct 737(2–3):271
10. Blasco T, Corma A, Martínez-Triguero J (2006) Hydrothermal stabilization of ZSM-5 catalytic-cracking additives by phosphorus addition. J Catal 237(2):267
11. Ding W et al (2007) Understanding the enhancement of catalytic performance for olefin cracking: hydrothermally stable acids in P/HZSM-5. J Catal 248(1):20
12. Barros ZS, Zotin FMZ, Henriques CA (2007) Conversion of natural gas to higher valued products: light olefins production from methanol over ZSM-5 zeolites. Stud Surf Sci Catal 167:255
13. Lu R, Cao Z, Liu X (2008) Catalytic activity of phosphorus and steam modified HZSM-5 and the theoretical selection of phosphorus grafting model. J Nat Gas Chem 17(2):142
14. Gao X et al (2009) Modification of ZSM-5 zeolite for maximizing propylene in fluid catalytic cracking reaction. Catal Commun 10(14):1787
15. Brouwer DM, Hogeveen H (1972) Electrophilic substitutions at alkanes and in alkylcarbonium ions. Prog Phys Org Chem 9:179
16. Guisnet M, Andy P, Boucheffa Y, Gnep NS, Travers C, Benazzi E (1998) Selective isomerization of n-butenes into isobutene over aged H-ferrierite catalyst: nature of the active species. Catal Lett 50:159
17. Santacesaria E, Di Serio M, Cozzolino M, Tesser R (2004) DGMK-conference C4/C5-hydrocarbons: routes to higher value-added products, Munich
18. Seo G et al (1996) Skeletal isomerization of 1-butene over ferrierite and ZSM-5 zeolites: influence of zeolite acidity. Catal Lett 36(3–4):249
19. Mériaudeau P, Tuan VA, Le NH, Szabo G (1997) Selective isomerization of n-Butene into isobutene over deactivated H–Ferrierite catalyst: further investigations. J Catal 169(1):397
20. Asensi MA, Martínez A (1999) Selective isomerization of n-butenes to isobutene on high Si/Al ratio ferrierite in the absence of coke deposits: implications on the reaction mechanism. Appl Catal A 183:155
21. Wichterlova B et al (1999) Effect of bronsted and lewis sites in ferrierites on skeletal isomerization of n-butenes. Appl Catal A 182(2):297
22. Auerbach SM, Carrado KA, Dutta PK (2003) Handbook of zeolite science and technology. Marcel Dekker, p 481
23. Shouro D et al (2000) Mesoporous silica FSM-16 catalysts modified with various oxides for the vapor-phase Beckmann rearrangement of cyclohexanone oxime. Appl Catal A 198(1):275–282
24. Chaudhari K et al (2002) Beckmann rearrangement of cyclohexanone oxime over mesoporous Si-MCM-41 and Al-MCM-41 molecular sieves. J Mol Catal A Chem 177(2):247
25. Zhang Y et al (2005) Beckmann rearrangement of cyclohexanone oxime over Hβ zeolite and Hβ zeolite-supported boride. Catal Commun 6:53
26. Dai LX et al (1997) Development of advanced zeolite catalysts for the vapor phase Beckmann rearrangement of cyclohexanone oxime. Appl Surf Sci 121/122: 335
27. Misono M, Inui T (1999) New catalytic technologies in Japan. Catal Today 51:369
28. Izumi Y et al (2007) Development and Industrialization of the Vapor-Phase Beckmann Rearrangement Process. Bull Chem Soc Jpn 80(7):1280–1287

29. Roffia P, Leofanti G, Cesana A, Mantegazza M, Padovan M, Petrini G, Tonti S, Gervasutti P (1990) Cyclohexanone ammoximation: a break through in the 6-caprolactam production process. Stud Surf Sci Catal 55:43
30. Palkovits R, Schmidt W, Ilhan Y, Erdem-S_enatalar A, Schüth F (2009) Crosslinked TS-1 as stable catalyst for the Beckmann rearrangement of cyclohexanone oxime. Microporous Mesoporous Mater 117:228
31. Kumar R, Rao GN, Ratnasamy P (1989) Influence of the pore geometry of medium pore zeolites ZSM-5, -22, -23, -48 and -50 on shape selectivity in reactions of aromatic hydrocarbons. Stud Surf Sci Catal 49:1141
32. Sotelo JL, Uguina MA, Valverde JL, Serrano DP (1993) Kinetics of toluene alkylation with methanol over magnesium-modified ZSM-5. Ind Eng Chem Res 32:2548
33. Climent MJ, Corma A, Velty A (2004) Synthesis of hyacinth, vanilla, and blossom orange fragrances: the benefit of using zeolites and delaminated zeolites as catalysts. Appl Catal A 263(2):155
34. Climent MJ, Corma A, Garcia H, Guil-Lopez R, Iborra S, Fornés V (2001) Acid–base bifunctional catalysts for the preparation of fine chemicals: synthesis of jasminaldehyde. J Catal 197(2):385
35. Climent MJ, Corma A, Velty A, Susarte M (2000) Zeolites for the production of fine chemicals: synthesis of the fructone fragrancy. J Catal 196(2):345
36. Kantam ML et al (2005) Friedel–Crafts acylation of aromatics and heteroaromatics by beta zeolite. J Mol Catal A Chem 225(1):15
37. Andy et al (2000) Acylation of 2-methoxynaphthalene and isobutylbenzene over zeolite beta. J Catal 192(1):215
38. Heinichen HK, Holderich WF (1999) Acylation of 2-methoxynaphthalene in the presence of modified zeolite HBEA. J Catal 185(2):408
39. Casagrande M, Storaro L, Lenarda M, Ganzerla R (2000) Highly selective Friedel–Crafts acylation of 2-methoxynaphthlene catalyzed by H-BEA zeolite. Appl Catal A 201(2):263
40. Bejblova M, Zilkova N, Cejka J (2008) Transformations of aromatic hydrocarbons over zeolites. Res Chem Intermed 34(5–7):439
41. Guggenheim S, Martin RT (1995) Definition of clay and clay mineral: joint report of the aipea nomenclature and CMS nomenclature committees. Clays Clay Miner 43(2):255
42. Velde B, Meunier A (2008) The origin of clay minerals in soils and weathered rocks. Springer, Berlin Heidelberg, Chapter 1
43. Clark JH, RhodesCN (2000) Clean synthesis using porous inorganic solid catalysts and supported reagents. R Soc Chem, Chapter 3 clay materials, p 38
44. Duc M et al (2005) Sensitivity of the acid–base properties of clays to the methods of preparation and measurement: 1. Literature review. J Colloid Interface Sci 289:139
45. Brown DR, Rhodes CN (1997) Bronsted and lewis acid catalysis with ion-exchange clays. Catal Lett 45(1–2):35
46. Ravichandran J, Lakshmanan CM, Sivasankar B (1996) Acid activated montmorillonite and vermiculite clays as dehydration and cracking catalysts. React Kinet Catal Lett 59(2):301
47. Ravichandran J, Sivasankar B (1997) Properties and catalytic activity of acid-modified montmorillonite and vermiculite. Clays Clay Miner 45(6):854
48. Kloprogge JT, Duong LV, Frost RL (2005) A review of the synthesis and characterization of pillared clays and related porous materials for cracking of vegetable oil to produce biofuels. Environ Geol 47:967
49. Reddy CR et al (2007) Surface acidity study of Mn+−montmorillonite clay catalysts by FT-IR spectroscopy: correlation with esterification activity. Catal Commun 8:241
50. Reddy CR et al (2004) Synthesis of phenylacetates using aluminium-exchanged montmorillonite clay catalyst. J Mol Catal A Chem 223(1):117
51. da Silva et al (2009) Etherification of glycerol with benzyl alcohol catalyzed by solid acids. J Braz Chem Soc. 20(2):201
52. Salmon M, Zavala N, Martinez M, Miranda R, Cruz R, Cardenas J, Gavino R, Cabrera A (1994) Cyclic and linear oligomerization reaction of 3, 4, 5-trimethoxybenzyl alcohol with a bentonite-clay. Tetrahedron Lett 35(32):5797
53. Sabu KR, Sukumar R, Lalithambika M (1993) Acidic properties and catalytic activity of natural kaolinitic clays for Friedel–Crafts alkylation. Bull Chem Soc Jpn 66:3535
54. Okada S, Tanaka K, Nakadaira Y, Nakagawa N (1992) Selective Friedel–Crafts alkylation on a vermiculite, a highly active natural clay mineral with Lewis acid sites. Bull Chem Soc Jpn 65:2833
55. Laszlo P, Mathy A (1987) Catalysis of Friedel-Crafts alkylation by a montmorillonite doped with transition-metal cations. Helv Chim Acta 70(3):577
56. Clark JH, Macquarrie DJ (1997) Heterogeneous catalysis in liquid phase transformations of importance in the industrial preparation of fine chemicals. Org Process Res Dev 1:149
57. Narayanan S, Deshpande K (2000) Aniline alkylation over solid acid catalysts. Appl Catal A 199(1):1
58. Smith K, Ewart GM, El-Hiti GA, Randlesb KR (2004) Study of regioselective methanesulfonylation of simple aromatics with methanesulfonic anhydride in the presence of zeolite catalysts. Org Bimol Chem 2:3150
59. Laidlawa P, Bethell D, Brown SM, Watson G, Willock DJ, Hutchings GJ (2002) Sulfonylation of substituted benzenes using Zn-exchanged zeolites. J Mol Catal A Chem 178(1):205
60. Choudary BM, Chowdari NS, Kantam ML, Kannan R (1999) Fe (III) exchanged montmorillonite: a mild and ecofriendly catalyst for sulfonylation of aromatics. Tetrahedron Lett 40:2859
61. Choudary BM, Chowdari NS, Kantam ML (2000) Friedel–Crafts sulfonylation of aromatics catalysed by solid acids: an eco-friendly route for sulfone synthesis. J Chem Soc Perkin Trans 1:2689
62. Sharma SK, Parikh PA, Jasra RV (2007) Solvent free aldol condensation of propanal to 2-methylpentenal using solid base catalysts. J Mol Catal A Chem 278(1):135

63. Cavani F, Trifiro F, Vaccari A (1991) Hydrotalcite-type anionic clays: preparation, properties and applications. Catal Today 11:173
64. Clark JH (1994) Catalysis of organic reactions by supported inorganic reagents. VCH Publishers Inc, New York
65. Salehi P, Ali Zolfigol M, Shirini F, Baghbanzadeh M (2006) Silica sulfuric acid and silica chloride as efficient reagents for organic reactions. Curr Org Chem 10(17):2171
66. Li Z, Liu J, Gong X, Mao X, Sun X, Zhao Z (2008) Silica sulfuric acid-catalyzed expeditious environment-friendly hydrolysis of carboxylic acid esters under microwave irradiation. Chem Pap 62(6):630
67. Mobinikhaledi A, Foroughifar N, Fard MAB, Moghanian H, Ebrahimi S, Kalhor M (2009) Efficient one-pot synthesis of polyhydroquinoline derivatives using silica sulfuric acid as a heterogeneous and reusable catalyst under conventional heating and energy-saving microwave irradiation. Synth Commun 39:1166
68. Zarei A, Hajipour AR, Khazdooz L, Mirjalili BF, Chermahini AN (2009) Rapid and efficient diazotization and diazo coupling reactions on silica sulfuric acid under solvent-free conditions. Dyes Pigm 81(1):240
69. Chen X, She J, Shang Z, Wu J, Zhang P (2009) Room-temperature synthesis of pyrazoles, diazepines, β-enaminones, and β-enamino esters using silica-supported sulfuric acid as a reusable catalyst under solvent-free conditions. Synth Commun 39:947
70. Wang Y, Yuan Y, Guo S (2009) Silica sulfuric acid promotes aza-Michael addition reactions under solvent-free condition as a heterogeneous and reusable catalyst. Molecules 14:4779
71. Shobha D, Chari MA, Mukkanti K, Ahn KH (2009) Silica gel-supported sulfuric acid catalyzed synthesis of 1, 5-benzodiazepine derivatives. J Heterocycl Chem 46(5):1028
72. Li J, Meng X, Bai B, Sun M (2010) An efficient deprotection of oximes to carbonyls catalyzed by silica sulfuric acid in water under ultrasound irradiation. Ultrason Sonochem 17:14
73. Yang J, Dang N, Chang Y (2009) Silica sulfuric acid as a recyclable catalyst for a one-pot synthesis of α-aminophosphonates in solvent-free conditions. Lett Org Chem 6(6):470
74. Karam A, Gu Y, Jérôme F, Douliezb J, Barrault J (2007) Significant enhancement on selectivity in silica supported sulfonic acids catalyzed reactions. Chem Comm 22:2222
75. Dabiri M et al (2007) Silica sulfuric acid: an efficient and versatile acidic catalyst for the rapid and ecofriendly synthesis of 1,3,4-oxadiazoles at ambient temperature. Synth Commun 37:1201
76. Shaabani A, Rahmati A (2006) Silica sulfuric acid as an efficient and recoverable catalyst for the synthesis of trisubstituted imidazoles. J Mol Catal A Chem 249(1):246
77. Reddy BM, Patil MK (2009) Organic syntheses and transformations catalyzed by sulfated zirconia. Chem Rev 109(6):2185
78. Reddy BM, Sreekanth PM, Lakshmanan P (2005) Sulfated zirconia as an efficient catalyst for organic synthesis and transformation reactions. J Mol Catal A Chem 237(1):93
79. Deutsch J, Trunschke A, Müller D, Quaschning V, Kemnitz E, Lieske H (2004) Acetylation and benzoylation of various aromatics on sulfated zirconia. J Mol Catal A Chem 207(1):51
80. Deutsch J, Prescott HA, Müller D, Kemnitz E, Lieske H (2005) Acylation of naphthalenes and anthracene on sulfated zirconia. J Catal 231(2):269
81. Zane F, Melada S, Signoretto M, Pinna F (2006) Active and recyclable sulphated zirconia catalysts for the acylation of aromatic compounds. Appl Catal A 299:137
82. Hino M, Arata K (1980) Synthesis of solid superacid catalyst with acid strength of H_0?−16.04. J Chem Soc, Chem Commun (18):851
83. Paukshtis EA, Shmachkova VP, Kotsarenko NS (2000) Acidic properties of sulfated zirconia. React Kinet Catal Lett 71(2):385
84. Clark JH (2002) Solid acids for green chemistry. Acc Chem Res 35:791
85. Ratnama KJ, Reddya RS, Sekhar NS, Kantama ML, Figueras F (2007) Sulphated zirconia catalyzed acylation of phenols, alcohols and amines under solvent free conditions. J Mol Catal A Chem 276(1):230
86. Comerford JW, Clark JH, Macquarrie DJ, Breeden SW (2009) Clean, reusable and low cost heterogeneous catalyst for amide synthesis. Chem Commun 14(18):2562
87. Clark JH, Macquarrie DJ (2002) Handbook of green chemistry and technology. Blackwell Science Ltd, Chapter 13, Green Catalysts for Industry
88. Li Z et al (2007) Silica-supported aluminum chloride: a recyclable and reusable catalyst for one-pot three-component Mannich-type reactions. J Mol Catal A Chem 272(1):132
89. Choudhary VR, Jana SK, Kiran BR (2000) Highly active Si-MCM-41-supported Ga_2O_3 and In_2O_3 catalysts for friedel-crafts-type benzylation and acylation reactions in the presence or absence of moisture. J Catal 192(2):257
90. Choudhary VR, Jana SK (2002) Acylation of aromatic compounds using moisture insensitive mesoporous Si-MCM-41 supported Ga_2O_3 catalyst. Synth Commun 32(18):2843
91. Choudhary VR, Jana SK, Patil NS (2001) Acylation of benzene over clay and mesoporous Si-MCM-41 supported $InCl_3$, $GaCl_3$ and $ZnCl_2$ catalysts. Catal Lett 76(3):235
92. Choudhary VR, Patil KY, Jana SK (2004) Acylation of aromatic alcohols and phenols over $InCl_3$/montmorillonite K-10 catalysts. J Chem Sci 116(3):175
93. Derouane EG, Dillon CJ, Bethell D, Derouane-Abd Hamid SB (1999) Zeolite catalysts as solid solvents in fine chemicals synthesis: 1. catalyst deactivation in the Friedel–Crafts acetylation of anisole. J Catal 187(1):209
94. Derouane EG, Crehan G, Dillon CJ, Bethell D, He H, Derouane-Abd Hamid SB (2000) Zeolite catalysts as solid solvents in fine chemicals synthesis: 2. competitive adsorption of the reactants and products in the Friedel–Crafts acetylations of anisole and toluene. J Catal 194(2):410
95. Yadav GD, George G (2006) Friedel–Crafts acylation of anisole with propionic anhydride over mesoporous superacid catalyst UDCaT-5. Microporous Mesoporous Mater 96(1–3):36

96. Ishitani H, Naito H, Iwamoto M (2008) Fridel-Crafts acylation of anisole with carboxylic anhydrides of large molecular sizes on mesoporous silica catalyst. Catal Lett 120(1–2):14
97. Sarvari MH, Sharghi H (2005) Solvent-free catalytic Friedel-Crafts acylation of aromatic compounds with carboxylic acids by using a novel heterogeneous catalyst system: p-toluenesulfonic acid/graphite. Helv Chim Acta 88:2282
98. Wagholikar SG, Niphadkar PS, Mayadevi S, Sivasanker S (2007) Acylation of anisole with long-chain carboxylic acids over wide pore zeolites. Appl Catal A 317(2):250
99. Zarei A, Hajipour AR, Khazdooz L (2008) Friedel–Crafts acylation of aromatic compounds with carboxylic acids in the presence of P_2O_5/SiO_2 under heterogeneous conditions. Tetrahedron Lett 49:6715
100. Clark JH (1980) Fluoride ion as a base in organic synthesis. Chem Rev 80:429
101. Blass BE (2002) KF/Al_2O_3 mediated organic synthesis. Tetrahedron 58:9301
102. Handa H, Baba T, Sugisawa H, Ono Y (1998) Highly efficient self-condensation of benzaldehyde to benzyl benzoate over KF-loaded alumina. J Mol Catal A Chem 134(1–3):171
103. Kabashima H, Tsuji H, Nakatab S, Tanaka Y, Hattori H (2000) Activity for base-catalyzed reactions and characterization of alumina-supported KF catalysts. Appl Catal A 194–195:227
104. Tsuji H, Kabashima H, Kita H, Hattori H (1995) Thermal activation of KF/alumina catalyst for double bond isomerization and Michael addition. React Kinet Catal Lett 56(2):363
105. Kochkar H, Clacens JM, Figueras F (2002) Isomerization of styrene epoxide on basic solids. Catal Lett 78(1–4):91
106. Nakano Y, Niki S, Kinouchi S, Miyamae H, Igarashi M (1992) Knoevenagel reaction of malononitrile with acetone followed by double cyclization catalyzed by KF-coated alumina in aqueous solution. Bull Chem Soc Jpn 65(11):2934
107. Wang WC, Wang D, Forray C, Vaysse PJJ, Brancheko TA, Gluchowski C (1994) A convenient synthesis of 2-amino-2-oxazolines and their pharmacological evaluation at cloned human α adrenergic receptors. Bioorg Med Chem Lett 4(19):2317
108. Yamawaki J, Ando T, Hanafusa T (1981) N-Alkylation of amides and N-heterocycles with potassium fluoride on alumina. Chem Lett 1143–1146
109. Yamawaki J, Ando T (1980) Potassium fluoride on alumina as a base for crown ether synthesis. Chem Lett 9(5):533–536
110. Sawyer JS, Schmittling EA (1993) Synthesis of diaryl ethers, diaryl thioethers, and diarylamines mediated by potassium fluoride-alumina and 18-crown-6. J Org Chem 58(12):3229
111. Yadav VK, Kapoor KK (1996) KF adsorbed on alumina effectively promotes the epoxidation of electron deficient alkenes by anhydrous t-BuOOH. Tetrahedron 52:3659
112. Moghaddam FM, Bardajee GR, Veranlou ROC (2005) KF/Al_2O_3-mediated Michael addition of thiols to electron-deficient olefins. Synth Commun 35(18):2427
113. Villemin D, Alloum AB (1992) Potassium fluoride on alumina: an easy synthesis of 4-alkylidene-2-thione-1, 3-oxathiolanes from α-acetylenic alcohols. Synth Commun 22:1351
114. Villemin D, Hachemi M, Lalaoui M (1996) Potassium fluoride on alumina: synthesis of O-aryl N, N-dimethylthiocarbamates and their rearrangement into S-aryl N, N-dimethylthiocarbamates under microwave irradiation. Synth Commun 26(13):2461
115. Kawanami Y, Yuasa H, Toriyama F, Yoshida S, Baba T (2003) Addition of silanes to benzaldehyde catalyzed by KF loaded on alumina. Catal Commun 4:455
116. Baba T, Kato A, Yuasa H, Toriyama F, Handa H, Ono Y (1998) New Si-C bond forming reactions over solid-base catalysts. Catal Today 44:271
117. Clark JH, Cork DG, Robertson MS (1983) Fluoride ion catalysed Michael reactions. Chem Lett 12(8):1145
118. Campelo JM, Climent MS, Marinas JM (1992) Michael addition of nitromethane to 3-buten-2-one catalyzed by potassium fluoride supported on Al_2O_3, ZnO, SnO_2, sepiolite, $AlPO_4$, $AlPO_4-Al_2O_3$ and $AlPO_4-ZnO$. React Kinet Catal Lett 47:7
119. Kabashima H, Tsuji H, Shibuya T, Hattori H (2000) Michael addition of nitromethane to α, β-unsaturated carbonyl compounds over solid base catalysts. J Mol Catal A Chem 155(1–2):23
120. Wang SH, Wang XS, Shi DQ, Tu SJ (2003) Michael addition reaction of dimedone and chalcone catalyzed by KF/Al_2O_3. Chin J Org Chem 23(10):1146
121. Figueras F et al (2004) Effect of the support on the basic and catalytic properties of KF. J Catal 221(2):483
122. Tian DB, Zhu J, Zhu JF, Shi YX, Wang JT (2004) Michael addition of alkyl amine to α, β-unsaturated carbonyl compounds catalyzed by KF/Al2O3. Chin Chem Lett 15(8):883
123. Moghaddam FM, Bardajee GR, Taimoory SMD (2006) KF/Al_2O_3 mediated aza-Michael addition of indoles to electron-deficient olefins. Lett Org Chem 3(2):157
124. Wang X, Quan Z, Wang JK, Zhanga Z, Wang M (2006) A practical and green approach toward synthesis of N3-substituted dihydropyrimidinones: using Aza-Michael addition reaction catalyzed by KF/Al_2O_3. Bioorg Med Chem Lett 16(17):4592
125. Lenardão EJ, Ferreira PC, Jacob RG, Perin G, Leiteb FPL (2007) Solvent-free conjugated addition of thiols to citral using KF/alumina: preparation of 3-thioorganylcitronellals, potential antimicrobial agents. Tetrahedron Lett 48:6763
126. Lenardão EJ, Trecha DO, Ferreira PC, Jacob RG, Perin G (2009) Green Michael addition of thiols to electron deficient alkenes using KF/alumina and recyclable solvent or solvent-free conditions. J Braz Chem Soc 20(1):93
127. Clark JH, Farmer TJ, Macquarrie DJ (2009) The derivatization of bioplatform molecules by using KF/Alumina catalysis. ChemSusChem 2(11):1025
128. Ballinia R, Palmieri A (2006) Potassium fluoride/basic alumina as far superior heterogeneous catalyst for the chemoselective conjugate addition of nitroalkanes to electron-poor alkenes having two electron withdrawing groups in α- and β-positions. Adv Synth Catal 348(10):1154
129. Macquarrie DJ (2009) Organically modified micelle templated silicas in green chemistry. Top Catal 52(12):1640

130. Utting KA, Macquarri DJ (2000) Silica-supported imines as mild, efficient base catalysts. New J Chem 24:591
131. Motokura K, Tomita M, Tada M, Iwasawa Y (2009) Michael reactions catalyzed by basic alkylamines and dialkylamino-pyridine immobilized on acidic silica-alumina surfaces. Top Catal 52:579
132. Isobe K, Hoshi T, Suzuki T, Hagiwara H (2005) Knoevenagel reaction in water catalyzed by amine supported on silica gel. Mol Divers 9(4):317

Green Chemistry and Chemical Engineering, Introduction

The goal of Green Chemistry and Chemical Engineering is to minimize waste, totally eliminate the toxicity of waste, minimize energy use, and utilize green energy (solar thermal, solar electric, wind, geothermal, etc.) – that is, non fossil fuel. Clearly, fossil fuels have their own waste and toxicity problems even though usually remote from the site of chemical production.

The objective in preparing this section is to provide a significant sampling of the scientific and engineering basis of green chemistry and engineering with specific processes as examples. There are nine detailed entries written at a level for use by university students through practicing professionals. For ease of use by students, each entry begins with a glossary of terms, while at an average length of 20 print pages each, sufficient detail is presented for utilization by professionals in government, universities, and industry. The reader is also directed to closely related sections in our *Encyclopedia*: *Solar Thermal Energy* (see the entry, ► Solar Energy in Thermochemical Processing); *Hydrogen Production Science and Technology* (see the entry, ► Photo-catalytic Hydrogen Production and also ► Hydrogen via Direct Solar Production); *Solar Radiation* (see the entry on ► Photosynthetically Active Radiation: Measurement and Modeling); *Geothermal Power Stations*; and the section on *Batteries*.

Each of the entries is summarized below.

► Gas Expanded Liquids for Sustainable Catalysis – A gas-expanded liquid (GXL) phase is generated by dissolving a compressible gas such as CO_2 or a light olefin into the traditional liquid phase at mild pressures (tens of bar) (). When CO_2 is used as the expansion gas, the resulting liquid phase is termed a CO_2-expanded liquid or CXL. GXLs combine the advantages of compressed gases such as CO_2 and of traditional solvents in an optimal manner. GXLs retain the beneficial attributes of the conventional solvent (polarity, catalyst/reactant solubility) but with higher miscibility of permanent gases (O_2, H_2, CO, etc.) compared to organic solvents at ambient conditions and enhanced transport rates compared to liquid solvents (ii, iii, iv, v). The enhanced gas solubility's in GXLs have been exploited to alleviate gas starvation (often encountered in homogeneous catalysis with conventional solvents), resulting in a 1–2 orders of magnitude greater rates than in neat organic solvent or *sc*CO_2. *Environmental advantages* include substantial replacement of organic solvents with environmentally benign CO_2. *Process advantages* include reduced flammability due to CO_2 presence in the vapor phase and milder process pressures (tens of bar) compared to *sc*CO_2 (hundreds of bar). GXLs thus satisfy many of the attributes of an ideal alternative solvent.

► Green Catalytic Transformations – A heterogeneous catalyst is a catalytically active species that is in a different phase to the reagents within a reaction system, more often than not a solid in either liquid or vapor phase synthesis. There are a number of green chemistry related advantages of using heterogeneous catalysts as opposed to the homogeneous equivalents: Safety – An important consideration in the practice of green chemistry. Heterogeneous catalysts often tend to be environmentally benign and easy/safe to handle. This is due to the active species being adhered to a support, (often forming a powder) essentially reducing its reactivity with the surrounding environment; Reusability – Due to the difference in phases, the catalyst is simply filtered off (through centrifugation on industrial scales) and reactivated for reuse many times over; Activity – In many cases increased activity is observed when supporting an active homogeneous species on a support, due to the complex but unique surface characteristics found with a variety of different supports; and Selectivity – heterogeneous catalysts can give an increased degree of selectivity in reaction pathway. This can simply be a consequence of adsorption of substrates and the consequential restricted freedom of movement of the reacting molecules. However, there are a handful of disadvantages. The quantity of solid catalyst required is often higher than that of the

homogeneous equivalent, due to the lower concentration on the support surface, (reusability makes this less of an issue though). Blocking of the pores/support channels can occur with narrow pores sizes and reduce efficiency over time in some liquid phase reactions; nevertheless, this is often twinned with high stereoselectivity.

► Green Chemistry Metrics: Material Efficiency and Strategic Synthesis Design – Application of green metrics forces the precise itemization of what constitutes waste so that targeted reductions of these components can be made. The mass of waste of any chemical reaction is the sum of the masses of unreacted starting materials, byproducts produced as a mechanistic consequence of making the desired target product, side products produced from competing side reactions other than the intended reaction, reaction solvent, all work-up materials, and all purification materials used. Simple first generation waste reduction strategies target the last three items in the list since they contributed the bulk of the overall mass of waste. Waste reduction strategies targeting the first three items are based on synthesis design and are necessarily more challenging to implement. The connecting green metrics are atom economy (AE), environmental E-factor (E), and reaction mass efficiency (RME). These metrics and applications are described in detail in this entry.

► Green Chemistry with Microwave Energy – An alternative heating technique using microwaves is useful for targeted energy introduction directly into polar reactants in chemical syntheses and transformations. This entry summarizes noteworthy greener methods that use microwaves that have resulted in the development of sustainable synthetic protocols for drugs and fine chemicals. Microwave assisted organic transformations are presented such as: solid-supported reagents based processes; greener reaction media including aqueous, ionic liquid, and solvent-free for the synthesis of various heterocycles; and oxidation-reduction and also coupling reactions.

► Nanotoxicology in Green Nanoscience – The unique properties that make nanomaterials an attractive technology (surface chemistry, surface area, size, shape, core material functionalization, aggregation, etc.) may also contribute to novel biological effects as a result of nanomaterial exposure. Toxicology will play an important role in elucidating the mechanisms of those interactions. This entry contains an exploration of the role of toxicology in implementing green nanoscience, the methodology of incorporating nanotoxicology in order to directly and indirectly address the principles of green chemistry in green nanoscience, and the importance of utilizing robust models for nanotoxicity testing.

► Organic Batteries – Development of sustainable processes for energy storage and supply is one of the most important worldwide concerns today. Primary batteries, such as alkaline manganese and silver oxide batteries produce electric current by a one-way chemical reaction and are not rechargeable and hence useless for reversible electricity storage. Portable electronic equipment, electric vehicles, and robots require rechargeable secondary batteries. Li-ion, lead acid, and nickel-metal hydride batteries are generally used at the present to power them. Solar cells and wind-power generators expect a parallel use of rechargeable batteries for leveling and preserving their generated electricity. Ubiquitous electronic devices such as integrated circuit smart cards and active radio-frequency identification tags need rechargeable batteries that are bendable or flexible and environmentally benign for durability in daily use. Designing of soft portable electronic equipment, such as rollup displays and wearable devices, also require the development of flexible batteries. It is essential to find new, low-cost, and environmentally benign electroactive materials based on less-limited resource for electric energy storage and supply.[1] Reversible storage materials of electric energy or charge that are currently under use in electrodes of rechargeable batteries are entirely inorganic materials, such as Li ion-containing cobalt oxide, lead acid, and nickel-metal hydride.

► Oxidation Catalysts for Green Chemistry – Catalysis is at the heart of Green Chemistry as it is the means to increase efficiency and efficacy of chemical and energy resources while promoting environmental friendliness and intensifying time and cost savings in chemical synthesis. A catalyst's function simply is to provide a pathway for chemicals (reactants) to combine in a more effective manner than in its absence. In the absence of a catalyst, heat is usually the way to overcome the energy barrier but this increases energy consumption and often results in unwanted side

reactions. A catalyst cannot make an energetically unfavorable reaction occur or change the chemical equilibrium of a reaction because the catalyzed rate of both the forward and the reverse reactions are equally affected. Oxidation processes are used for odor control, bleaching of pulp for paper production, wastewater treatment, disinfection, bulk and specialty chemical production, aquatics and pools, food and beverage processing, cooling towers, agriculture/farming, and many others. There are a great many oxidation reactions that are catalytically driven. Such reactions are presented in this entry with emphasis on implementation of green strategies.

► New Polymers, Renewables as Raw Materials – Recent advances in genetic engineering, composite science, and natural fiber development offer significant opportunities for developing new, improved materials from renewable resources that can biodegrade or be recycled, enhancing global sustainability. A wide range of high-performance, low-cost materials can be made using plant oils, natural fibers, and lignin. These materials have economic and environmental advantages that make them attractive alternatives to petroleum-based materials.

► Supercritical Carbon Dioxide (CO_2) as Green Solvent – A supercritical fluid (SCF) is created when the temperature and pressure are higher than its critical values. Therefore, CO_2 becomes supercritical when its temperature and pressure are higher than 31.1°C (critical temperature, *Tc*) and pressure 7.38 MPa (critical pressure, P_c). SCFs have many unique properties, such as strong solvation power for different solutes, large diffusion coefficient comparing with liquids, zero surface tension, and their physical properties can be turned continuously by varying the pressure and temperature because the isothermal compressibility of SCFs is very large, especially in the critical region. These unique properties of SCFs lead to great potential for the development of innovative technologies. Besides these common advantages of SCFs, supercritical CO_2 ($scCO_2$) has some other advantages, such as nontoxic, nonflammable, chemically stable, readily available, cheap, and easily recyclable, and it has easily accessible critical parameters. Therefore, $scCO_2$ can be used as green solvent in different fields. The basic properties of $scCO_2$ and its applications in extraction and fractionation, chemical reactions, polymeric synthesis, material science, supercritical chromatography, painting, dyeing and cleaning, and emulsions related with CO_2, are discussed in this entry.

Green Chemistry Metrics: Material Efficiency and Strategic Synthesis Design

John Andraos
Department of Chemistry, York University, Toronto, ON, Canada

Article Outline

Glossary
Definition of the Subject and Its Importance
Introduction
Overview of Algorithms
Strategy Metrics
An Example: Sertaline Plans
Summary of Optimization
Thresholds and Probabilities
Future Directions
Bibliography

Glossary

Atom economy Ratio of molecular weight of target molecule to sum of molecular weights of reactants assuming a balanced chemical equation.

B/M Ratio of sum of number of target bonds made in a synthesis plan to total number of reaction steps.

By-product of a reaction A product formed in a reaction between reagents as a direct mechanistic consequence of producing the target product assuming a balanced chemical equation that accounts for the production of that target product.

Degree of asymmetry A parameter determined from the shape of a synthesis tree diagram for a synthesis plan that describes the degree of skewness of a triangle whose vertices are the target product node, the origin, and the node for the last reagent along the ordinate axis.

Degree of convergence A parameter determined from the shape of a synthesis tree diagram for a

synthesis plan that describes the ratio of the angle subtended at the actual product node vertex to that at a product node vertex corresponding to the hypothetical case of all reaction substrates in a plan reacting in a single step.

E-factor with respect to molecular weight (E_{mw}) Ratio of sum of molecular weights of by-products in a reaction to molecular weight of target product in a given reaction or synthesis plan.

E-factor with respect to mass (E_m) The ratio of mass of total waste from all sources to mass of target product collected in a given reaction or synthesis plan.

E_{kernel} Contribution to the total or overall E-factor with respect to mass from reaction by-products, reaction side products, and unreacted starting materials.

E_{excess} Contribution to the total or overall E-factor with respect to mass from excess reagents.

$E_{auxiliaries}$ Contribution to the total or overall E-factor with respect to mass from auxiliary materials such as reaction solvents, work-up, and purification materials.

$E_{overall}$ (or E_m) Ratio of mass of total waste generated from all sources to mass of target product collected for a given reaction or synthesis plan.

f^* Fractional kernel waste contribution from target bond forming reactions.

f(sac) Molecular weight fraction of reagents that absolutely do not end up in the final target molecule structure.

f(nb) Fraction of number of reaction stages that do not form target bonds.

Hypsicity index A parameter that tracks the oxidation numbers of atoms in target bond forming reactions over the course of a synthesis plan relative to their values in the target molecule.

I Number of input materials in a synthesis plan.

Kernel mass of waste Mass of all reagents used in a synthesis reaction or plan minus the mass of target product collected.

Kernel reaction mass efficiency The ratio of the mass of target product collected to the sum of the stoichiometric masses of all reagents used in a chemical reaction or synthesis plan.

μ_1, First molecular weight moment Parameter that describes the degree of building up going on from the reagent molecules toward the target molecule over the course of a synthesis plan.

Mass intensity Ratio of mass of all materials used to mass of target product collected in a given chemical reaction or synthesis plan.

Material recovery parameter A parameter that describes the mass consumption of all solvents and auxiliary materials used in carrying out a given chemical reaction that may be potentially recoverable by recycling.

M Number of reaction steps in a synthesis plan.

N Number of reaction stages in a synthesis plan.

Radial hexagon A diagram that depicts the overall atom economy, overall reaction yield along the longest branch, overall kernel reaction mass efficiency, molecular weight fraction of reagents in whole or in part that end up in the target molecule, fraction of the kernel waste contribution from target bond forming reactions, and the degree of convergence for a given synthesis plan as a hexagon for easy visualization of the synthesis performance.

Radial pentagon A diagram that depicts the reaction yield, atom economy, stoichiometric factor, material recovery parameter, and overall reaction mass efficiency for a given chemical reaction as a pentagon for easy visualization of the reaction performance.

Raw material cost Sum of the costs of all reagents in a synthesis plan calculated using the basis scale in moles of the target product, assuming balanced chemical equations for all reactions in the plan and taking account of excess reagent consumption.

Reaction step Refers to interval between a given isolated intermediate and the next consecutive isolated intermediate in a synthesis plan.

Reaction yield Ratio of moles of target product to moles of limiting reagent for a given balanced chemical equation.

Sacrificial reactions Nonproductive reactions in a synthesis plan that do not form target bonds appearing in the target product structure.

Side product of a reaction A product formed in a reaction between reagents, usually undesired, that arises from a competing reaction pathway other than the one that produces the intended target product and its associated by-products.

Stoichiometric factor (SF) A parameter that describes the total amount of excess reagents used in a given chemical reaction relative to the amounts prescribed by its stoichiometrically balanced chemical equation.

Stoichiometric coefficient An integer appearing before the chemical formula for a reagent in a balanced chemical equation.

Synthesis tree A diagram that describes all features of a synthesis plan, including number of steps, number of stages, number of branches, number of intermediates, number of reagents used, and molecular weights of all chemical species.

Target bond map A chemical structure drawing of the target product of a synthesis plan showing the target bonds made, the step numbers of each target bond, and the set of atoms that correlate directly with the corresponding reagents that ended up in the target molecule.

Target bond forming reactions Productive reactions in a synthesis plan that result in the formation of bonds that appear in the structure of the target molecule.

Total (overall) mass of waste The sum of all masses of materials used in synthesis plan minus the mass of the target product collected.

Total (overall) reaction mass efficiency The ratio of the mass of target product collected to the sum of the masses of all reagents, solvents, and auxiliaries used in a given reaction or synthesis plan.

|*UD*| A parameter that tracks the "oxidation length" traversed over the course of a synthesis plan equal to the sum of all the "ups" and "downs" in a hypsicity profile or bar graph beginning with the zeroth reaction stage.

Definition of the Subject and Its Importance

Over the last 2 decades, the topic of "green metrics" has grown rapidly in conjunction with the field of green chemistry. Green metrics promise to provide a rigorous, thorough, and quantitative understanding of material, energy, and cost efficiencies for individual chemical reactions and synthesis plans. Indeed, before the advent of green chemistry, good synthetic strategy and elegance were ill-defined, yet intuitive concepts couched less in quantitative terms and more by subjective ones. The quest for a reliable method of measuring material efficiency or "greenness" of a chemical reaction, synthesis, or process is of fundamental importance in the field of organic synthesis when various routes to a given target molecule are considered for selection. Such a method should be robust in its application to any kind of reaction or plan regardless of complexity. It should standardize the ranking of efficiencies of synthesis plans in an unambiguous and unbiased way. It should be used as a powerful tool in weeding out bad-performing plans quickly and identifying promising candidate plans at the drawing board stage guided by thorough literature investigations even before embarking on any experiment in the laboratory. Above all, it should facilitate the decision-making process for both chemists and non-chemists by allowing on-the-spot precise identification of potential bottlenecks in plans from easy-to-read graphics and by pointing chemists in the right direction for further optimization with confidence. In the long term, with enough examples and pattern recognition among as many plans as possible, it should be possible to understand why "good" plans are good and offer insights into what good strategy entails and how to parameterize it. *The key take home message is that optimization is an iterative exercise that compares the performances of a set of plans to a common target according to some criteria and that true optimization is achieved when the best possible values of material efficiency and synthetic elegance metrics coincide in the same plan.*

Introduction

In the period 2005–2007, algorithms were introduced to assess the material efficiencies of any reaction and any synthesis plan, and they delivered on all of the points mentioned above [1–6]. Their first and most important triumph was that they provided simple connecting relationships between key green metrics that previously were considered as independent entities. The basis of this discovery was the long forgotten law of conservation of mass pronounced by Antoine Lavoisier in 1775 that allows one to write out complete balanced chemical equations for every reaction in a synthesis plan with appropriate stoichiometric coefficients for all reactants and *all* by-products in addition to the target product of interest. The skill of balancing chemical equations has been resurrected after a long period of dormancy in the field of synthetic organic

chemistry by the need to precisely identify waste composition and quantify waste production, which are essential if any real progress can be made in the newly emerging field of green chemistry whose chief aim is to minimize waste. In fact, before the advent of green metrics, waste was considered as one big lump of unwanted material, which was calculated simply as the difference between the mass of all input materials used and the mass of the desired output material. Application of green metrics forces the precise itemization of what constitutes waste so that targeted reductions of these components can be made. The mass of waste of any chemical reaction is the sum of the masses of unreacted starting materials, by-products produced as a mechanistic consequence of making the desired target product, side products produced from competing side reactions other than the intended reaction, reaction solvent, all work-up materials, and all purification materials used. Simple first-generation waste reduction strategies target the last three items in the list since they contributed the bulk of the overall mass of waste. Waste reduction strategies targeting the first three items are based on synthesis design and are necessarily more challenging to implement. The connecting green metrics are atom economy (AE) [7–9], environmental E-factor (E) [10–12], and reaction mass efficiency (RME) [13, 14]. All other metrics appearing in the literature [15–21] that pertain to material efficiency can be expressed in terms of these three and are therefore redundant. RME and E describe identically the same thing from the positive and negative points of view, respectively. Experimental atom economy for a reaction is just another synonym for the kernel RME (reaction yield times atom economy), mass intensity (MI) is just E + 1, and mass index is the reciprocal of RME. Prior arguments that AE had a lower usefulness than RME and E were dispelled by the simple algebraic connecting relationships found; namely, $AE = 1/(1 + E_{mw})$ and $RME = 1/(1 + E)$, where E_{mw} and E are the E-factors based on reagent molecular weight and mass, respectively. In fact, AE is of fundamental importance in the molecular design phase of synthesis planning even before carrying out any experiments as it describes the intrinsic waste produced in a reaction or plan due to by-products arising out of the nature of the chemical reaction in question. If significant by-products are known to result from reactions in a plan at the outset, then it is inevitable that this will have an additive and cumulative effect on the production of overall waste.

This chapter summarizes the salient features of these algorithms, one for individual reactions and the other for synthesis plans. The reader is referred to prior references by the author for derivations. Numerical computations are greatly facilitated using spreadsheet programs which have been disclosed previously in a detailed investigation of the material efficiencies of the synthesis plans for oseltamivir phosphate a neuraminidase inhibitor used to treat influenza, particularly H5N1 and H1N1 [22]. Here, we illustrate how these algorithms may be implemented by showing complete worked out examples for the analysis of seven literature synthesis plans for the antidepressant pharmaceutical sertraline [23–29]. This compound is unique because its published plans show a steady progression in optimization over the period 1984–2006. This is a very rare situation in the literature where the timeline of publications shows a steady upward rise in synthesis efficiency.

Overview of Algorithms

The main theme and sequence of algorithms used in carrying out green metrics calculations on a given synthesis plan are shown in Fig. 1. The first thing is to access the best available literature procedures that disclose the experimental write-ups for the recipes for each reaction in the synthesis plans to the target compound of interest. Next, fully balanced chemical equations for all reactions are written down where all by-products arising from the intended mechanisms are identified and stoichiometric coefficients for all reactants and products are assigned. From these data, radial pentagons are constructed according to the method described in [5] to obtain diagrams that show the AE, reaction yield, stoichiometric factor (SF), and material recovery parameter (i.e., reaction solvent, work-up, and purification material demand) for each reaction according to the master equation given by Eq. 1:

$$\mathrm{RME} = (\varepsilon)(\mathrm{AE})\left(\frac{1}{\mathrm{SF}}\right)(\mathrm{MRP}) \tag{1}$$

where

ε is the reaction yield with respect to the limiting reagent in a reaction given by the mole ratio of the target product collected and of the limiting reagent.

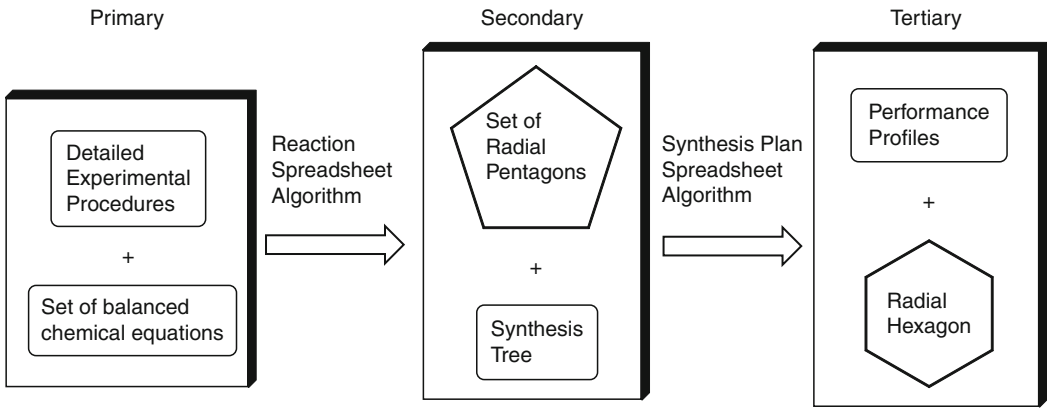

Green Chemistry Metrics: Material Efficiency and Strategic Synthesis Design. Figure 1
Paradigm flowchart for determining green metrics for any synthesis plan

AE is the reaction atom economy given by the ratio of the molecular weight of the target product to the sum of molecular weights of all reagents in the balanced chemical equation.

SF is the stoichiometric factor, taking into account the use of excess reagents, and is given by

$$\mathrm{SF} = 1 + \frac{\sum \mathrm{excess-masses-of-all-reagents}}{\sum \mathrm{stoichiometric-masses-of-all-reagents}} \tag{2}$$

MRP is the material recovery parameter, taking into account the use of auxiliary materials, and is given by

$$\mathrm{MRP} = \frac{1}{1 + \frac{(\varepsilon)(\mathrm{AE})(c + s + \omega)}{m_p(\mathrm{SF})}} \tag{3}$$

where m_p is the mass of the collected target product, c is the mass of catalyst used, s is the mass of reaction solvent, and ω is the mass of all other auxiliary materials used in the work-up and purification phases of the reaction.

For ease of computation, the four factors in Eq. 1 are written as fractions between 0 and 1 instead of as percentages. Eq. 1 basically shows how RME is factored or partitioned into its four constituent contributors. The corresponding radial pentagon gives a clear visual representation of Eq. 1 and tells a chemist which of the parameters may be the bottlenecks in attenuating the RME value for a given reaction. The MRP factor is the strongest attenuator because the total mass of auxiliary materials far outweighs the masses of all reagents used. Hence, this was the area that was targeted in first-generation waste reduction when the 12 principles of green chemistry were announced. The radial pentagon algorithm incorporates two check calculations, one for RME using Eq. 1 and by simply dividing the mass of collected target product by the sum of the masses of all the input materials used in the procedure, and the other for SF using Eq. 2 and from SF = (ε)(AE)/(RME) where RME, in this case, refers to the reaction mass efficiency calculated when all auxiliary materials are assumed to be recovered, that is, not committed to waste so that MRP is set to 1.

A huge bonus from the radial pentagon analysis is that it picks up all errors that appear in literature procedures. The most common are incorrect reporting of reaction yields, masses of ingredients, and moles of ingredients. Unfortunately, there is less care in the reporting of these key parameters by authors in experimental sections of research papers than expected. Moreover, reviewers and editors of journals do not routinely check for the accuracy of these details, particularly if they are buried in supplementary material, as they naively assume that authors have assumed that responsibility. Patent documents are notorious for such errors as they are often made with intent. Practicing chemists know all too well that such mistakes come to light when someone else embarks on duplicating the reported experiment. The biggest drawback in determining the true RME for a reaction is the lack of full disclosure of all masses of auxiliary materials used in a given

procedure. Of particular note are the amounts of solutions used in work-up washes and extractions, mass of drying agent used, and masses of chromatographic materials (solid supports and eluents). If these problems remain unchecked, the successful wide implementation of green chemistry practices will be severely hindered as only cursory guesses and assumptions can be made in such analyses. With missing data, the best that can be accomplished to is to put upper bounds on RME values and lower bounds on E values.

The key set of parameters from the radial pentagon analysis for each reaction that are used as direct inputs in the second spreadsheet algorithm to assess the material efficiency of the entire synthesis plan are as follows: molecular weights of reagents and by-products, molecular weight of product, reaction yield, stoichiometric factor, total mass of excess reagents, mole scale of limiting reagent, mass of reaction solvent, and masses of all other auxiliaries. The use of the second spreadsheet algorithm is greatly facilitated by the construction of a synthesis tree for the plan according to the treatments described in [3, 5] that gives an exact count of the number of reaction stages, reaction steps, input materials, and branches in the plan. It is an excellent bookkeeping and proofreading tool when reading research papers describing synthesis plans. A great advantage of using synthesis trees is that they give a visual representation of an entire plan in one simple diagram. Of particular note is the ease of analyzing convergent plans with multiple branches. Green metrics are determined from a synthesis tree diagram by reading it in the reverse sense from the target product node toward the input reagent nodes. In this way, the mole scales of all reagents are normalized relative to the target product, which is the basis scale for the entire plan. The method uses a simple connect-the-dots approach to determine the appropriate chain of reaction yields required to determine the mole scale of each reagent in a plan originating from any branch. It makes sense to follow the reverse approach since the target product node is the only one that is common to all branches in the tree diagram.

The algorithm for the computation of overall AE, RME, and E for any synthesis plan of any degree of complexity is given by a sequence of computations beginning with the last step ($j = n$) and working toward the first step ($j = 1$) and is described elsewhere [22]. The overall E-factor may be partitioned into its three components as shown explicitly below:

$$\mathrm{E_{total}} = \mathrm{E_{kernel}} + \mathrm{E_{excess}} + \mathrm{E_{auxiliaries}} \tag{4}$$

where,

$$\mathrm{E_{kernel}} = \frac{1}{p_n}\sum_j \left(\frac{1}{\prod_k^{n\to j} \varepsilon_k}\right)\left(\frac{p_j}{(\mathrm{AE})_j}\right)\left[1 - \varepsilon_j(\mathrm{AE})_j\right] \tag{5}$$

$$\mathrm{E_{excess}} = \frac{1}{p_n}\sum_j \left(\frac{1}{\prod_k^{n\to j} \varepsilon_k}\right)\left(\frac{p_j}{(\mathrm{AE})_j}\right)\left[(\mathrm{SF})_j - 1\right] \tag{6}$$

$$\mathrm{E_{auxiliaries}} = \frac{1}{p_n}\sum_j \left(\frac{1}{\prod_k^{n\to j} \varepsilon_k}\right)\left(\frac{c_j + s_j + \omega_j}{x_j^*}\right) \tag{7}$$

Symbol definitions:

x is number of moles of target product in synthesis plan, where x is set to 1 mole.

$\prod_k^{n\to j} \varepsilon_k$ is the multiplicative chain of reaction yields connecting the target product node to the reactant nodes for step j as per synthesis tree diagram read from right to left (i.e., in the direction $n \to j$).

p_j is the molecular weight of product of step j.

ε_j is the reaction yield with respect to limiting reagent for step j.

$(\mathrm{AE})_j$ is the atom economy for step j.

$(\mathrm{SF})_j$ is the stoichiometric factor for step j that accounts for excess reagents used in that step.

$(c_j + s_j + \omega_j)$ is the sum of masses of auxiliary materials used in step j, namely the mass of catalyst, mass of reaction solvent, and mass of all other post-reaction materials used in the work-up and purification phases.

x_j^* is the experimental mole scale of limiting reagent in step j as reported in an experimental procedure.

The summation runs over the n reaction steps. A step begins with an isolated intermediate and ends with the following next isolated intermediate.

The relative magnitudes of these three components break down into the following order: $E_{auxiliary} >>> E_{excess} > E_{kernel}$. For synthesis plans, the hierarchy of contributor metrics that control overall material efficiency according to RME and E at the kernel molecular design stage is in descending order of the number of steps (n), reaction yields (ε), and atom economies (AE). When taking into account all materials used, the recovery and/or minimization of auxiliary materials in the work-up and purification phases plays the largest role in minimizing waste and, hence, the true overall magnitude of RME and E for a synthesis plan. Key assumptions implicit in the use of the algorithm described above are that an intermediate product collected in a given step is entirely committed as a reagent in the next step so that a true mass throughput can be assessed, and that reaction yield performances are invariant with mole scale, something that can only be checked by experiment but is a necessary assumption in implementing such an analysis. The results of synthesis plan algorithm are depicted graphically as a radial hexagon by direct analogy to the radial pentagon analysis. The key six parameters chosen are each fractions ranging from 0 to 1. For the material efficiency performance, there is overall AE, overall yield along the longest branch, and overall reaction mass efficiency. For the strategy efficiency performance, there is molecular weight fraction of reagents ending up as part of the structure of the final target product, the fraction of kernel waste arising from target bond reactions, and degree of convergence. The outer perimeter represents a perfectly green plan. The more the resultant actual hexagon is distorted toward the center, the worse is the plan. Again, strengths and weaknesses in a plan may be seen at once. In addition, the algorithm produces bar graphs that depict profiles of percentage of kernel and percentage of true waste distributions, atom economy, reaction yield, kernel reaction mass efficiency, cumulative mass of waste produced, hypsicity (oxidation level tracking), and target bond reactions per reaction stage. Bottlenecks in the plan may be spotted at once and then appropriate action taken to force optimization in the desired direction.

Strategy Metrics

Parameters that describe and track synthesis strategy for a given plan include: (1) target bond structure maps, (2) target bond forming reaction profiles from which the number of target bonds per reaction step is determined, (3) molecular weight fraction of sacrificial reagents used, and (4) hypsicity (oxidation level) index. A target bond structure map is simply a drawing of the target product structure showing which target bonds are made and at what reaction step. A target bond is denoted with a heavy connecting line, and its associated circled reaction step number is given alongside. From such a diagram, it is possible to trace the origin of each atom in the target structure back to the associated atoms in the reagents used. In effect, the set of reagent atoms is mapped onto the set of atoms comprising the target structure. From such a map, it is possible to determine the molecular weight fraction of sacrificial reagents whose atoms never get incorporated in the final target structure according to

$$f(\text{sac}) = 1 - \frac{\sum \text{MW}_{\text{reagents in whole or in part ending up in target product}}}{\sum \text{MW}_{\text{all reagents}}} = 1 - \frac{(\text{AE})_{\text{overall}} \sum \text{MW}_{\text{reagents in whole or in part ending up in target product}}}{\text{MW}_{\text{target product}}}$$

Sacrificial reagents include those that serve as protecting groups, those that change the electronic states of key atoms so that skeletal building bond forming reactions are possible, those that are used to control stereochemistry, those that are used in substitution reactions to switch poor leaving groups into better ones, and those that are reducing or oxidizing agents that are used in *subtractive* redox reactions, that is, where oxygen atoms or hydrogen atoms are *removed* from a structure. The condition concerning redox reactions is important as it is *additive* redox reactions that are desirable to reduce f(sac) since they contribute oxygen or hydrogen atoms to the target structure. It is obvious that the ultimate goal is to minimize the magnitude of f(sac). One can deduce readily from the above equation that when the overall atom economy is unity, that is, when all atoms in all of the reagents used end up in the target structure, the two sums in the first part of the above equation become equal to each other, and hence, f(sac) is equal to zero. Also, from the target structure map, it is possible to construct a bar graph of the number of target bonds made versus the reaction

step count. Gaps in such bar graphs coincide with the use of sacrificial reagents in those steps and bars indicate productive steps. The number of target bonds made per step may be used as an indicator of synthetic efficiency and elegance since good synthesis strategies are characterized by fewer steps and the accomplishment of more target bonds made per step.

The target structure map also provides the set of atoms in the target structure that are involved in bond-making and bond-breaking processes throughout the synthesis. These atoms are precisely the ones connected by the heavy lines in the target structure map. It is possible to trace the oxidation numbers of these atoms from the target structure back to the progenitor reagent used via the intervening intermediate products. In a manner similar to the determination of the molecular weight first moment building up parameter, the difference between the oxidation number of an atom in an intermediate structure and that same atom in the final target product is determined for each atom involved in this special set of atoms as a function of reaction stage. This idea of tracking the changes in oxidation state, or hypsicity, (Gk: *hypsos*, meaning level or height) of key atoms involved in bond-making and bond-breaking steps was introduced by Hendrickson [30]. He proposed that good synthesis plans aim for the *isohypsic* condition, which is characterized by a zero net change in oxidation state of all atoms of starting materials and intermediates involved until the target product is reached. This can be achieved by designing synthesis plans that eliminate redox reactions entirely as it is consistent with the conclusion that such reactions are to be minimized in a plan because they are the most material inefficient class of chemical reaction and therefore contribute to significant attenuations in kernel and global RMEs. If these cannot be avoided due to practical considerations, then the next best thing to achieve the isohypsic condition is to strategically sequence redox reactions in such a way that for every increase in oxidation level of an atom occurring in a step, it is matched by a concomitant decrease in oxidation level of equal magnitude in the next step, or vice versa. This cuts down on the accumulation of excess gains or losses in oxidation level of atoms, as the case may be, in starting materials and intermediates with respect to the oxidation levels of those atoms in the final target molecule over the course of the synthesis. This second option of achieving the isohypsic condition is purely due to an algebraic cancellation of all the "ups" and "downs" in oxidation state changes and, hence, will coincide with appreciably higher kernel E-factor values and lower kernel RME values for such plans since generally redox reactions are least material efficient. The first option, however, will coincide with lower kernel E-factor values and higher kernel RME values since redox reactions would be completely eliminated.

Formally, we may define a hypsicity index, HI, as

$$\mathrm{HI} = \frac{\sum_{\text{stages},j}\left[\sum_{\text{atoms},i}\left[(\mathrm{Ox})^{\text{atom},i}_{\text{stage},j} - (\mathrm{Ox})^{\text{atom},i}_{\text{stage},N}\right]\right]}{N+1} = \frac{\sum_{\text{stages},j}\Delta_j}{N+1}$$

where (Ox) represents the relevant oxidation number of an atom. If HI is zero, then the synthesis is *isohypsic*. If HI is positive valued, then to get to the target molecule a net reduction is required over the course of the synthesis since an accumulated gain in oxidation level has resulted. Such a condition is termed *hyperhypsic*, by analogy with the term *hyperchromic*, which describes increases in intensities of absorption bands in spectroscopy. Conversely, if HI is negative valued, then to get to the target molecule a net oxidation is required over the course of the synthesis since an accumulated loss in oxidation level has resulted. Such a condition is termed *hypohypsic*, again by analogy with the term *hypochromic*. It is important to note that changes in oxidation number can occur for atoms in reactions that are not formally classified as reductions or oxidations with respect to the substrate of interest. A good example of this is the Grignard reaction which is classified as a carbon–carbon bond forming reaction and yet involves a formal oxidation with respect to magnesium in the preparation of the Grignard reagent. Another is electrophilic aromatic substitution, which begins with an oxidation state of −1 for the ArC-H carbon atom, which then increases to +1 when hydrogen is substituted for chlorine, for example. The hypsicity index therefore accounts for all such changes in oxidation numbers of atoms regardless of the reaction type.

The following sequence of steps may be followed to determine HI for a synthesis plan:

1. Enumerate atoms in the target structure that are only involved in the building up process from

corresponding starting materials according to the structure map. This set of atoms defines those that are involved in bonding changes occurring in the relevant reaction steps.

2. Work backwards intermediate by intermediate to trace the oxidation numbers of the above set of atoms back to original starting materials as appropriate following the reaction stages back to the zeroth stage.
3. For each key atom, *i*, in each reaction stage, *j*, determine the difference in oxidation number of that atom with respect to what it is in the final target structure. Hence,

$$(\mathrm{Ox})^{\mathrm{atom},i}_{\mathrm{stage},j} - (\mathrm{Ox})^{\mathrm{atom},i}_{\mathrm{stage},N}$$

4. Sum the differences determined in step (3) over all key atoms in stage *j*. This yields the term $\sum_{\mathrm{atoms},i} \left[(\mathrm{Ox})^{\mathrm{atom},i}_{\mathrm{stage},j} - (\mathrm{Ox})^{\mathrm{atom},i}_{\mathrm{stage},N}\right] = \Delta_j$.
5. Finally, take the sum $\sum_{\mathrm{stages},j} \Delta_j$ over the number of stages and divide by N + 1 accounting for the extra zeroth reaction stage.

From the above discussion, for a material efficient synthesis plan, it is not a sufficient condition to just aim for an HI value of zero. What matters is that as many of the atoms as possible in oxidizing and reducing agents end up in the target structure. These can only arise from oxidation and reduction reactions that are of the *additive* type where oxygen and hydrogen atoms are added to a structure in a reaction and remain there until the final target structure is reached, and not of the *subtractive* types as described earlier in the discussion of sacrificial reagents. So, it is possible to have HI values that are strongly positive or negative and still be material efficient so long as those key atoms are incorporated as part of the final target structure. It is preferable to have a hypsicity profile that exhibits either a steadily increasing or a steadily decreasing oxidation level rather than an undulating one. Increases and decreases in oxidation levels parallel the types of redox reactions employed in a plan. This will of course depend on the oxidation levels of atoms in the selected reagents used throughout the synthesis. Hence, careful correlation of HI values and overall AE, kernel RME, and f(sac) values need to be made to understand the synergy between material efficiency and oxidation level changes. It is impossible to make inferences solely on the basis of the magnitude of the HI. One needs to examine the shape or distribution of the bar graph that tracks the changes in oxidation level as function of reaction stage for a given synthesis plan.

An Example: Sertaline Plans

Seven synthesis plans for sertraline were examined – four industrial (Pfizer G1, Pfizer G2, Pfizer G3, and Gedeon Richter) and three academic (Buchwald, Lautens, and Zhao). Table 1 summarizes the material efficiency metric performances, Table 2 summarizes the E-factor breakdown, and Table 3 summarizes the strategy efficiency metric performances. From these data, it appears that the overall best material efficient synthesis plan is that of Zhao since it has the highest overall yield, atom economy, and overall kernel RME. Consequently, it produces the least kernel and overall masses of waste. It also uses the least number of input materials. The Pfizer plans show a nice progression from G1 to G3 with a sevenfold decrease in overall E-factor from G1 to G2 and a further 2.5-fold decrease from G2 to G3. The Zhao, Pfizer G3, Gedeon Richter, and Buchwald have the least number of steps at five. The Buchwald and Pfizer G3 plans have all of their kernel waste coming from target bond forming reactions; whereas, the Lautens plan has most of its kernel waste coming from sacrificial reactions. The Lautens plan also has the worst overall atom economy. In terms of E-factor contributors, the Zhao plan has the least E-auxiliary whereas the Pfizer G3 plan has the least E_{kernel} and the Gedeon Richter plan has the least E_{excess} contributions. The overall most wasteful Pfizer G1 plan has the highest contributors in all three categories. From a strategy perspective, it is less clear-cut to decide the overall best plan. The Pfizer G3, Buchwald, and Zhao plans show the greatest degree of building up from starting materials toward product throughout the course of their syntheses. The Gedeon Richter plan has the least degree of asymmetry. The Pfizer G3 plan has the highest degree of convergence. The Pfizer G3 plan has highest number of target bonds made per reaction stage. The Pfizer G3 and Buchwald plans have all reaction stages producing at least one target bond; whereas, almost half the reaction stages in the Lautens plan do

Green Chemistry Metrics: Material Efficiency and Strategic Synthesis Design. Table 1 Summary of material efficiency metrics for the seven plans to produce sertraline ranked in descending order according to percentage of kernel reaction mass efficiency

Plan	Type	N[a]	n[b]	I[c]	f*[d]	Overall yield (%)	AE (%)	Kernel RME (%)
Zhao[e]	linear	5	5	9	0.541	35.0	43.0	18.1
Pfizer G3[f]	linear	5	5	14	1	25.0	39.0	11.2
Gedeon Richter[f]	linear	5	5	11	0.639	20.5	36.6	9.4
Buchwald[e]	linear	5	5	12	1	19.2	38.9	8.6
Pfizer G2[f]	linear	8	8	17	0.894	8.7	34.9	4.3
Lautens[e]	convergent	11	13	28	0.389	14.1	7.1	1.9
Pfizer G1[f]	linear	10	10	18	0.731	1.8	26.7	1

[a]Number of reaction stages
[b]Number of reaction steps
[c]Number of input reagents
[d]Fractional kernel waste contribution from target bond forming reactions
[e]Target is (+)-sertraline
[f]Target is (+)-sertraline hydrochloride

Green Chemistry Metrics: Material Efficiency and Strategic Synthesis Design. Table 2 Summary of mass of waste and E-factor breakdown for seven plans to produce sertraline ranked in ascending order[a]

Plan	E_{kernel}	E_{excess}	$E_{auxiliary}$	E_{total}	Kernel mass of waste (kg)	Total mass of waste (kg)
Zhao[b]	4.54	89.21	64.64	158.38	1.4	48.4
Pfizer G3[c]	7.92	55.21	226.23	289.76	2.7	99.2
Gedeon Richter[c]	9.59	42.07	339.53	391.19	3.3	133.9
Buchwald[b]	10.56	90.25	352.24	453.05	3.2	138.6
Pfizer G2[c]	22.34	163.56	539.67	725.56	7.6	248.4
Lautens[b]	51.99	114.58	2424.98	2591.55	15.9	792.8
Pfizer G1[c]	103.95	350.30	4536.58	4990.82	35.6	1708.6

[a]Basis is 1 mole target product
[b]Target is (+)-sertraline
[c]Target is (+)-sertraline hydrochloride

not produce target bonds. The Zhao and Gedeon Richter plans have the least number of oxidation changes throughout the course of their synthesis plans, whereas, the Lautens plan has the most.

Figures 2 and 3 show the synthesis schemes for the best overall performing Zhao and Pfizer G3 plans. The Zhao plan involves a Friedel–Crafts alkylation in step 1 to give a racemic product, an asymmetric ketone reduction in step 2 with a chiral proline organocatalyst to give an optically active trans-tetralol intermediate, alcohol oxidation in step 3, imination in step 4, and catalytic hydrogenation in step 5. The Pfizer G3 plan involves a Friedel–Crafts acylation in step 1, a tandem reduction-lactonization sequence in step 2, a tandem lactone ring opening Friedel–Crafts acylation in step 3 to create the 1-tetralone ring system, a telescoped

Green Chemistry Metrics: Material Efficiency and Strategic Synthesis Design. Table 3 Summary of strategy efficiency metrics for the seven plans to produce sertraline

Plan	μ1 (g/mol)	β	δ	f(sac)	HI	B/M	f(nb)	|UD|
Zhao[a]	−60.98	0.738	0.435	0.495	+1	1.20	0.33	8
Pfizer G3[b]	−96.77	0.781	0.508	0.540	+2	1.60	0	12
Gedeon Richter[b]	−58.69	0.734	0.476	0.521	+1.33	1.40	0.20	8
Buchwald[a]	−85.98	0.760	0.486	0.358	+2.33	1.40	0	12
Pfizer G2[b]	−72.83	0.839	0.426	0.562	+1.56	1.00	0.25	12
Lautens[a]	−15.81	0.776	0.471	0.764	+1	0.92	0.45	24
Pfizer G1[b]	−50.04	0.848	0.389	0.579	+1.64	0.90	0.30	10

[a]Target is (+)-sertraline
[b]Target is (+)-sertraline hydrochloride

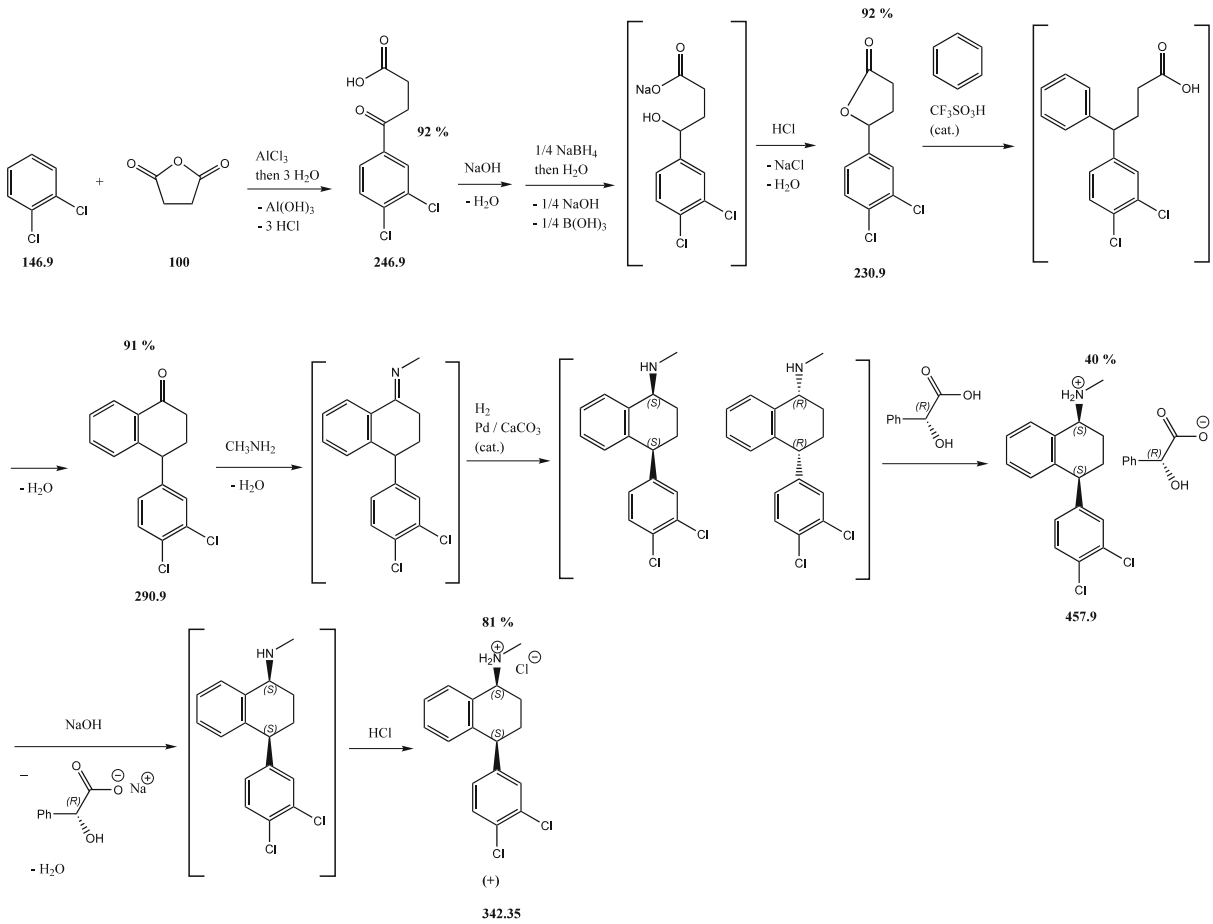

Green Chemistry Metrics: Material Efficiency and Strategic Synthesis Design. Figure 2 Pfizer G3 synthesis plan

imination-hydrogenation-diastereomeric salt resolution sequence in step 4, and, finally, isolation of the hydrochloride salt of the correct *cis*-amine product in step 5. The corresponding synthesis tree diagrams are shown in Fig. 4. Both plans are linear.

Figures 5 and 6 show the radial pentagons for each reaction in the Zhao and Pfizer G3 plans. For the Zhao plan, the bottlenecks are the low atom economy in step 1, the low yield in step 2, the excess reagent usage in steps 1, 2, and 4, and the high auxiliary material usage in steps 1, 3, and 4. For the Pfizer G3 plan, the bottlenecks are the low atom economy in step 1, the low yield in step 4, the high excess reagent usage in steps 1 to 3, and the high auxiliary material consumption in steps 3 to 5.

The numerical data presented in Tables 1–3 are conveniently displayed graphically in Fig. 7, which shows the radial hexagons for all seven plans. It is easily observed that the overall best performing Zhao plan has the least distorted hexagon with the largest area compared to the other plans. The Lautens plan has the least area. Figures 8 and 9 show the kernel and total waste distribution profiles for each plan. The kernel waste distributions account for wastes coming from reaction by-products, side products, unreacted starting materials, and excess reagents. The total waste distributions add on the contributions from auxiliary materials. Reaction steps producing significant amounts of waste from auxiliary materials may be directly correlated with their corresponding MRP performances from their radial pentagons. On comparing both kinds of distributions for each plan, it is observed that the Zhao plan is the only one that has consistently the same shape. Every synthesis plan is made up of reactions that either make target bonds found in the final product or not. In terms of optimization, the goal is to minimize both the global waste and the proportion arising from sacrificial nonproductive reactions at the

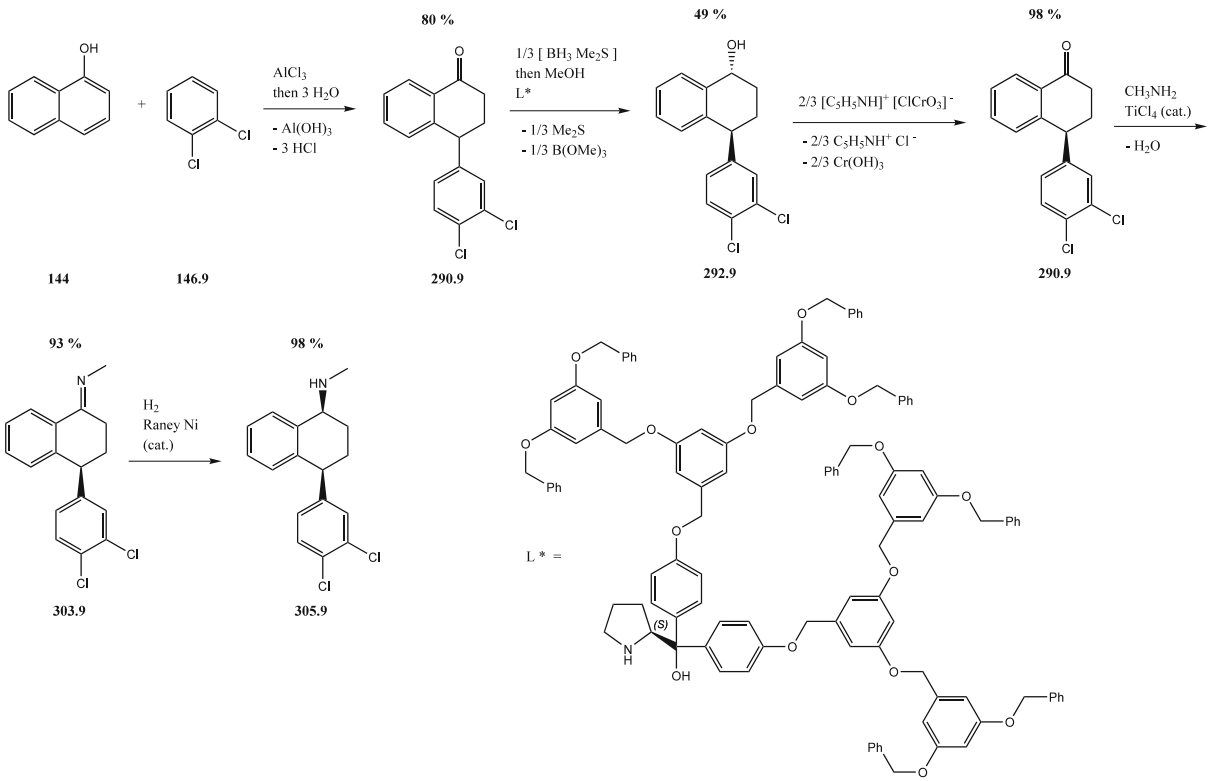

Green Chemistry Metrics: Material Efficiency and Strategic Synthesis Design. Figure 3
Zhao synthesis plan

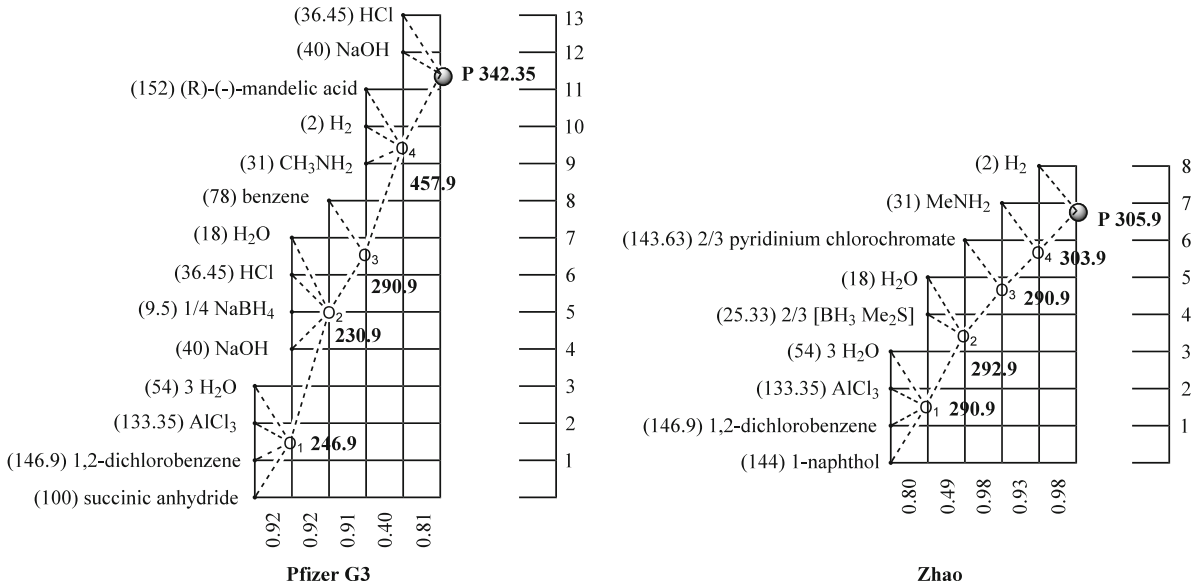

Green Chemistry Metrics: Material Efficiency and Strategic Synthesis Design. Figure 4
Synthesis trees for Pfizer G3 and Zhao plans

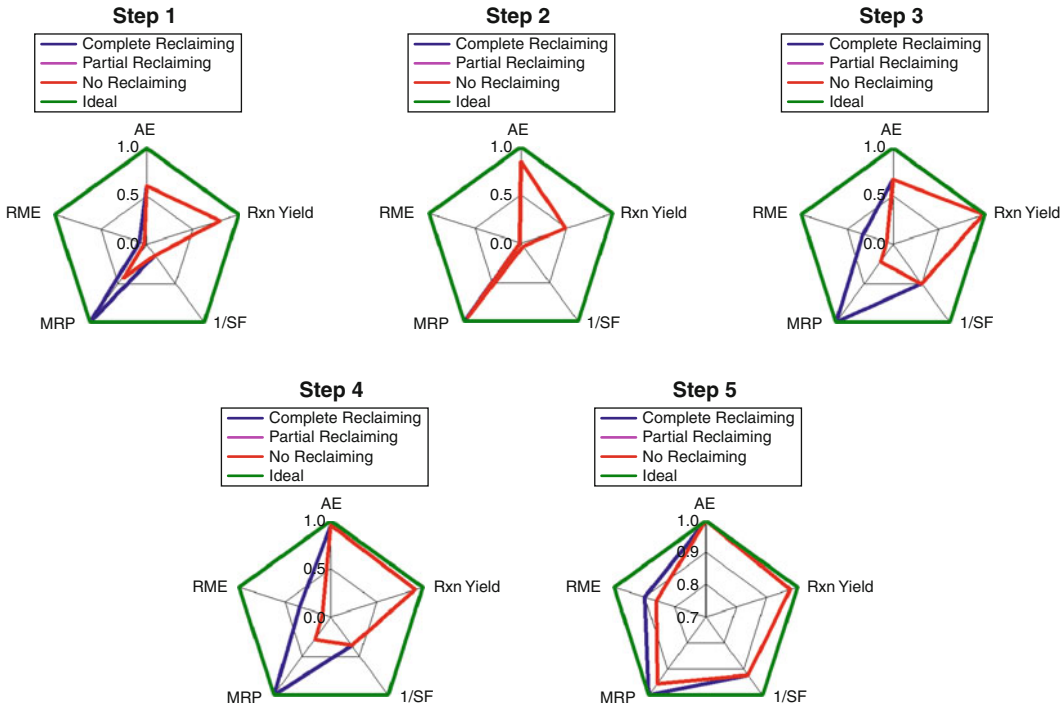

Green Chemistry Metrics: Material Efficiency and Strategic Synthesis Design. Figure 5
Radial pentagons for Zhao plan

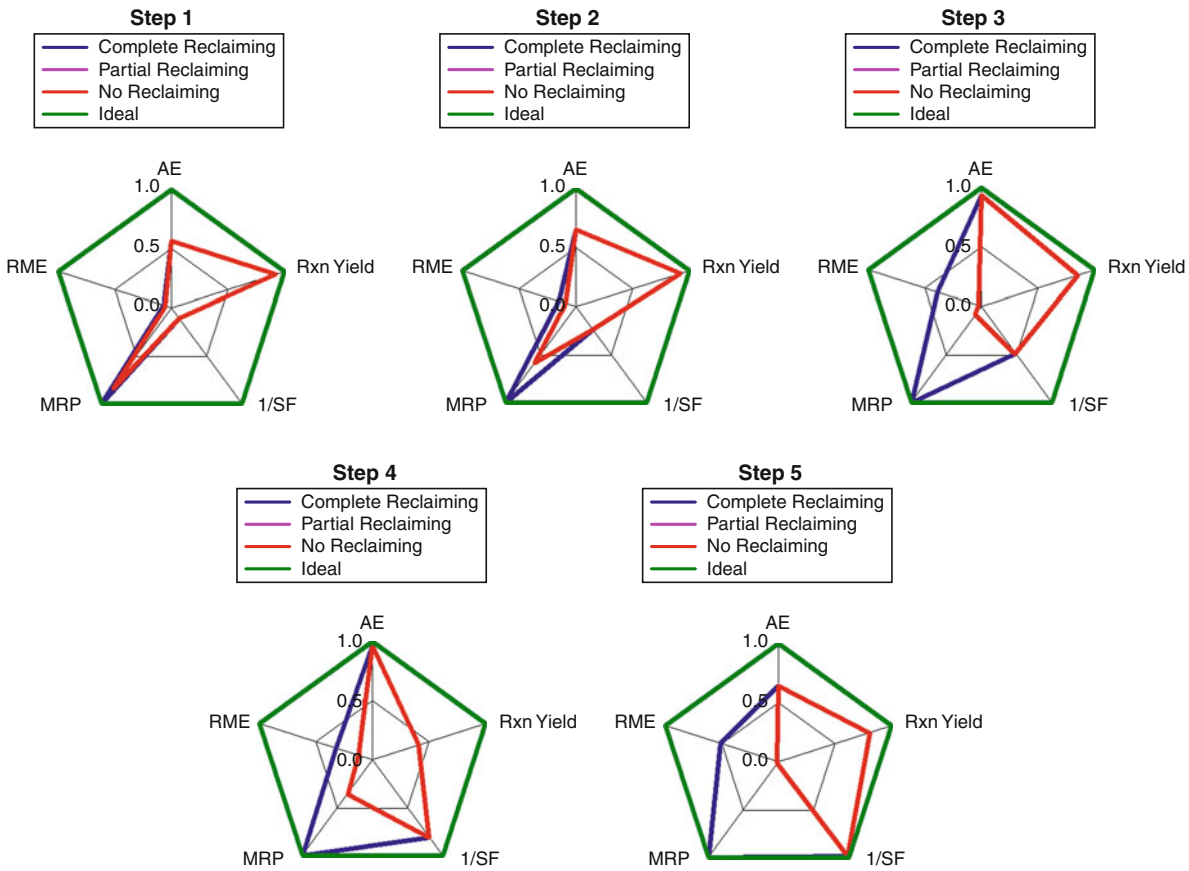

Green Chemistry Metrics: Material Efficiency and Strategic Synthesis Design. Figure 6
Radial pentagons for Pfizer G3 plan

same time. A disastrous situation to avoid is coming up with a synthesis plan that produces a lot of waste, most of which originating from sacrificial reactions such as redox adjustments and excessive use of protecting groups. Figure 10 shows the kernel mass of waste profile for all sertaline plans as a function of the global waste produced and the waste contributions from target bond forming and sacrificial reactions. The lengths of the bars correlate directly with the overall kernel E-factors and each bar, in turn, is subdivided into these two broad groups of reactions. The molecular weight building up profiles are given in Fig. 11. It is easily observed that the Buchwald and Zhao plans exhibit a high degree of building up since no intermediate along their reaction sequences has a molecular weight exceeding that of the target product sertraline. From the hypsicity profiles shown in Fig. 12, it is observed that the Buchwald, Pfizer G2, and Pfizer G3 are hyperhypsic with steadily decreasing oxidation steps which is consistent with the additive reduction reactions employed in their plans. It is obvious that the Lautens plan has the most oxidation number changes compared to the other plans. The target bond profiles and maps for all plans are shown in Figs. 13 and 14. These profiles confirm the conciseness and, therefore, the strategic efficiencies of the Buchwald and Pfizer G3 plans since there are no gaps in their respective bar graphs. From Fig. 14, it is observed that the plans break down into four distinct strategies in constructing the 1,2,3,4-tetrahydro-naphthalene ring system: (1) the Pfizer G2, Pfizer G3, and Buchwald plans involve [4 + 2] cycloadditions via Friedel–Crafts acylations; (2) the Gedeon Richter and Zhao plans begin with 1-naphthol as starting material so the ring frame is

Green Chemistry Metrics: Material Efficiency and Strategic Synthesis Design. Figure 7
Radial hexagons for seven synthesis plans of sertraline

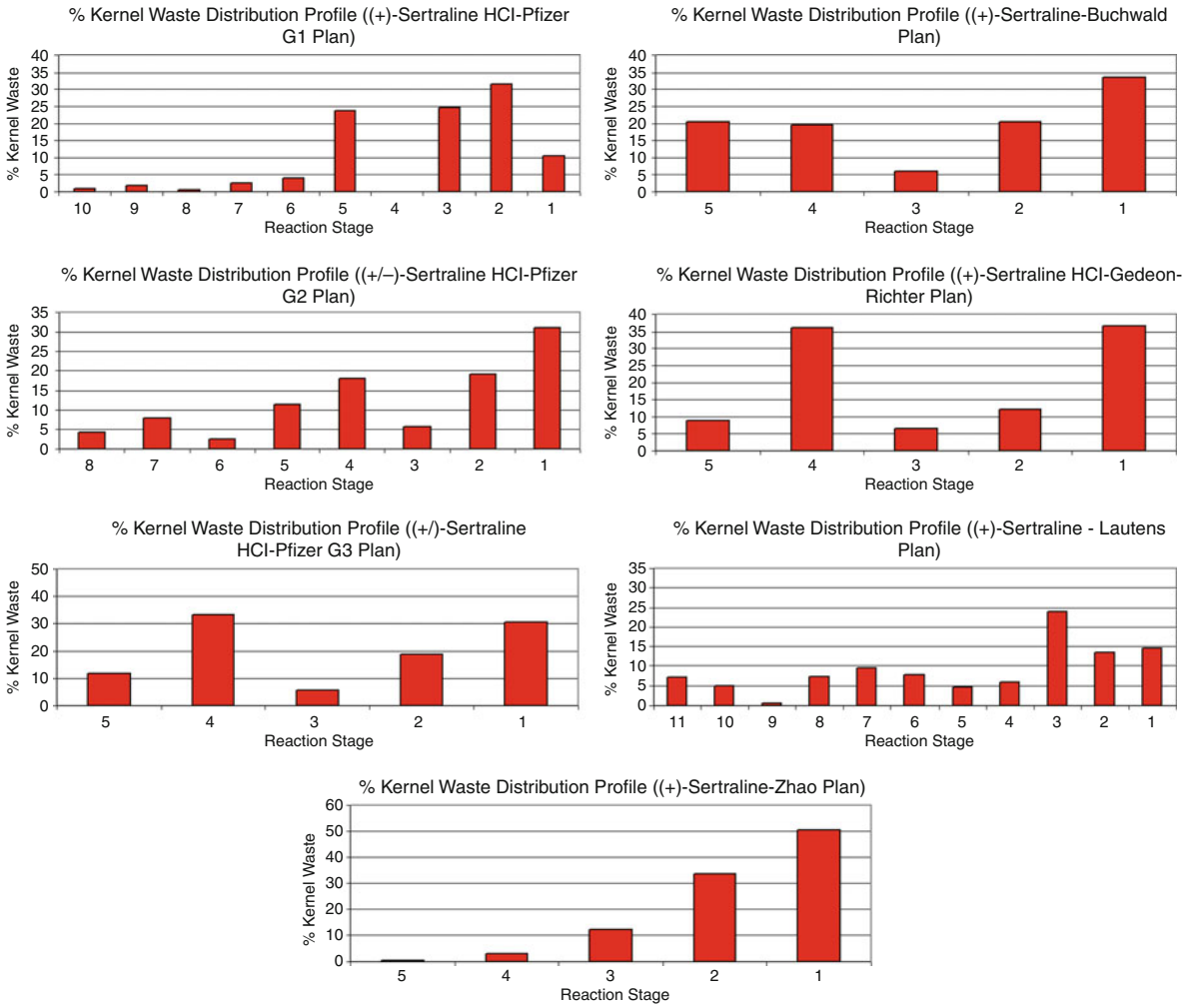

Green Chemistry Metrics: Material Efficiency and Strategic Synthesis Design. Figure 8
Kernel waste distribution profiles for synthesis plans of sertraline

already set; (3) the Pfizer G1 plan involves building up the saturated ring by chain extension in step 2 via an aldol condensation and then a [6 + 0] ring closure in step 5 via an intramolecular Friedel–Crafts acylation; and (4) the Lautens plan involves a unique ring-constructing sequence via a Diels–Alder [2.2.1] adduct, which then undergoes ring opening via an asymmetric reduction as shown in Fig. 15. Though the Lautens strategy clearly demonstrates ingenuity and novelty, it unfortunately failed to translate this attribute into an overall material efficient plan that could compete with the other industrial plans beginning from the third-generation feedstock 1-naphthol available in two steps from the coal tar product naphthalene. The main reasons for this are the high number of reaction steps (11 versus 5) and the high proportion of sacrificial nontarget bond forming reactions involved (see Table 1). This ugly mismatch between demonstration

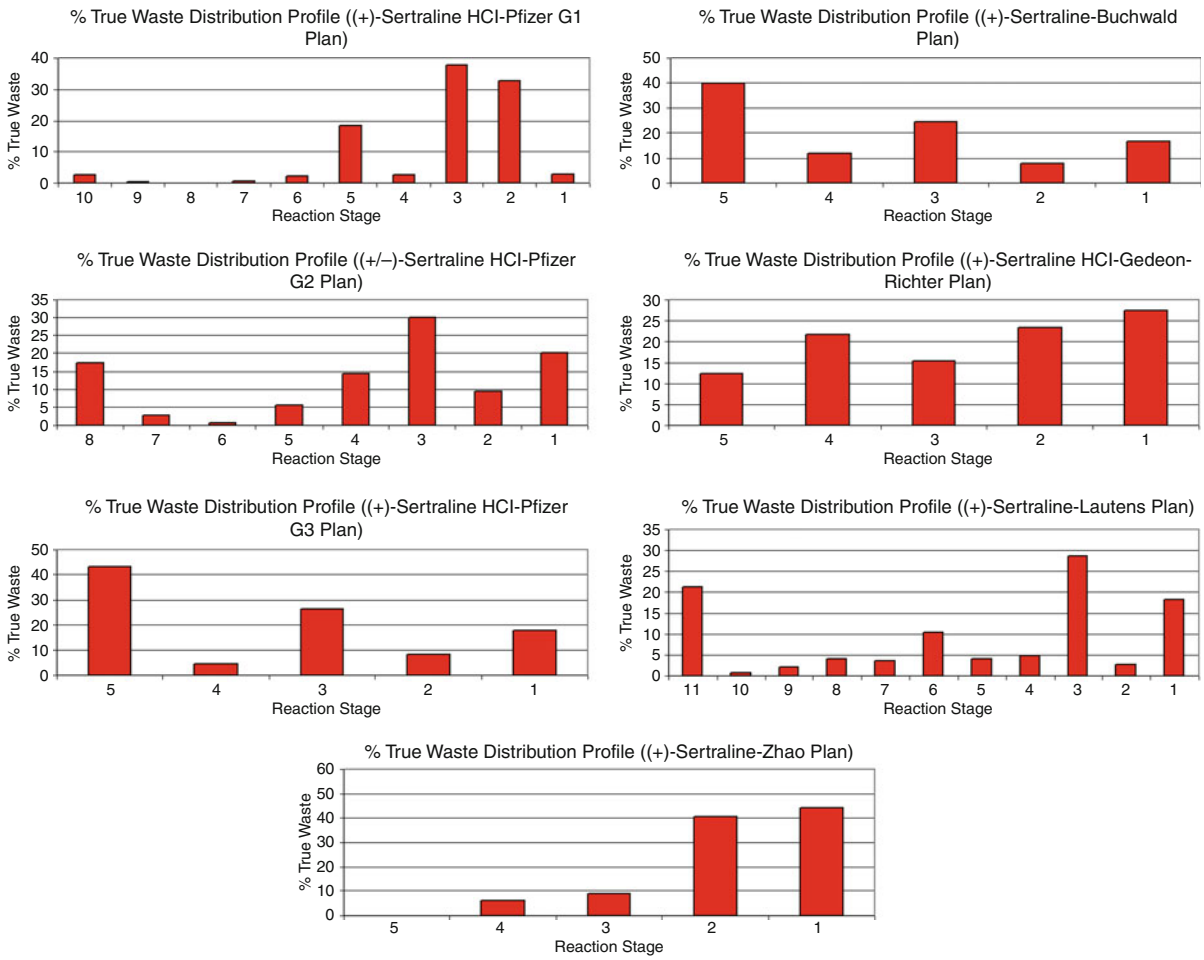

Green Chemistry Metrics: Material Efficiency and Strategic Synthesis Design. Figure 9
Total waste distribution profiles for synthesis plans of sertraline

of novelty in a few steps and overall low-material-efficiency performance in a plan occurs unfortunately all too often. Hence, the achievement of an optimum synergy between the two is indeed hard to achieve within the context of realizing a truly global "green" and hence cost-effective synthesis plan. However, fruitful opportunities for making new reaction discoveries and linking existing reactions in new combinations always exist and will help to make this goal a reality as synthetic organic chemistry continues to expand (Fig. 16).

Summary of Optimization

Characteristics of a "good" synthesis plan that merge both optimum material and strategy efficiencies are given below.

Material Efficiency

1. Minimize overall waste by first identifying major waste contributors such as solvent, work-up, and purification materials used and then minimizing them where possible.
2. Waste contribution from target bond forming reactions should exceed that from sacrificial reactions.
3. Maximize overall reaction yield along longest branch.
4. Maximize overall reaction mass efficiency so that kernel RME $\geq$ 60% for each reaction in a synthesis plan.
5. Maintain SF as close to one as far as possible to reduce impact of excess reagent consumption.

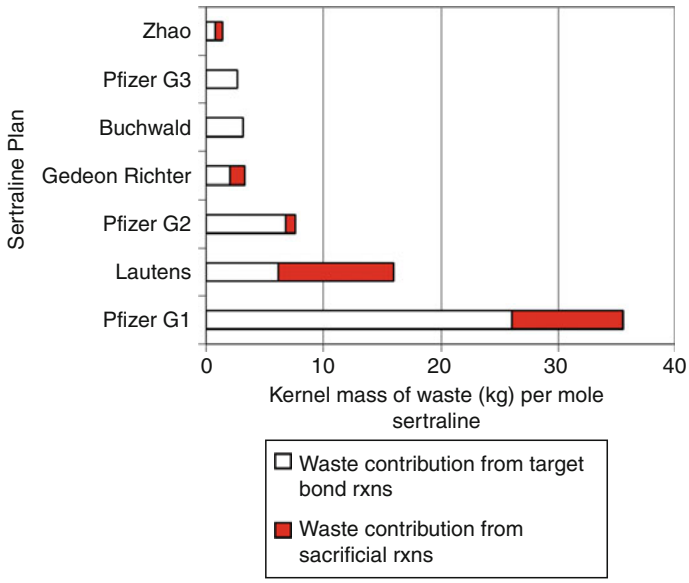

Green Chemistry Metrics: Material Efficiency and Strategic Synthesis Design. Figure 10
Kernel mass of waste profile for synthesis plans showing contributions from target bond reactions and sacrificial reactions

Strategy Efficiency

1. Number of reaction steps that form target bonds should exceed number of reaction steps that are sacrificial reactions.
2. Minimize overall number of reaction steps.
3. Maximize overall atom economy so that AE $\geq$ 60% for each reaction in a synthesis plan.
4. Maximize degree of convergence.
5. Maximize the number of direct synthesis–type reactions such as carbon–carbon and non-carbon–carbon bond forming reactions, additive redox reactions, multicomponent, tandem, domino, or cascade reactions, strategic rearrangements particularly with respect to ring constructions, and non-sacrificial substitution reactions.
6. Minimize the number of indirect synthesis–type reactions such as eliminations or fragmentations, subtractive redox reactions, and nonstrategic rearrangements.
7. Minimize fractional contribution of sacrificial reagents.
8. Minimize degree of asymmetry.
9. Design plans with large negative molecular weight first moments so that plans begin from low molecular weight starting materials and progressively build up toward the molecular weight of the target molecule with minimal overshoots above the molecular weight of the target product.
10. With respect to redox economy: aim for HI = 0 by eliminating all redox reactions, or aim for HI $>$ 0 with a steadily decreasing hypsicity profile using additive-type reduction reactions, or aim for HI $<$ 0 with a steadily increasing hypsicity profile using additive-type oxidation reactions.

Thresholds and Probabilities

From the connecting relationships $\mathrm{RME} = \frac{1}{1+\mathrm{E}}$ and $\mathrm{AE} = \frac{1}{1+\mathrm{E_{mw}}}$, it is possible to set a threshold for "greenness" for individual reactions at the kernel level (excluding all auxiliary materials) as AE $\geq$ 0.618 so that AE $\geq$ $\mathrm{E_{mw}}$, and RME $\geq$ 0.618 so that RME $\geq$ E, respectively. This threshold which exactly corresponds to the golden ratio equal to $\phi = \frac{\sqrt{5}-1}{2}$ is found by equating RME and E in the former expression and AE and $\mathrm{E_{mw}}$ in the latter. This is the justification for putting a 60% minimum cutoff for both AE and RME in the optimization

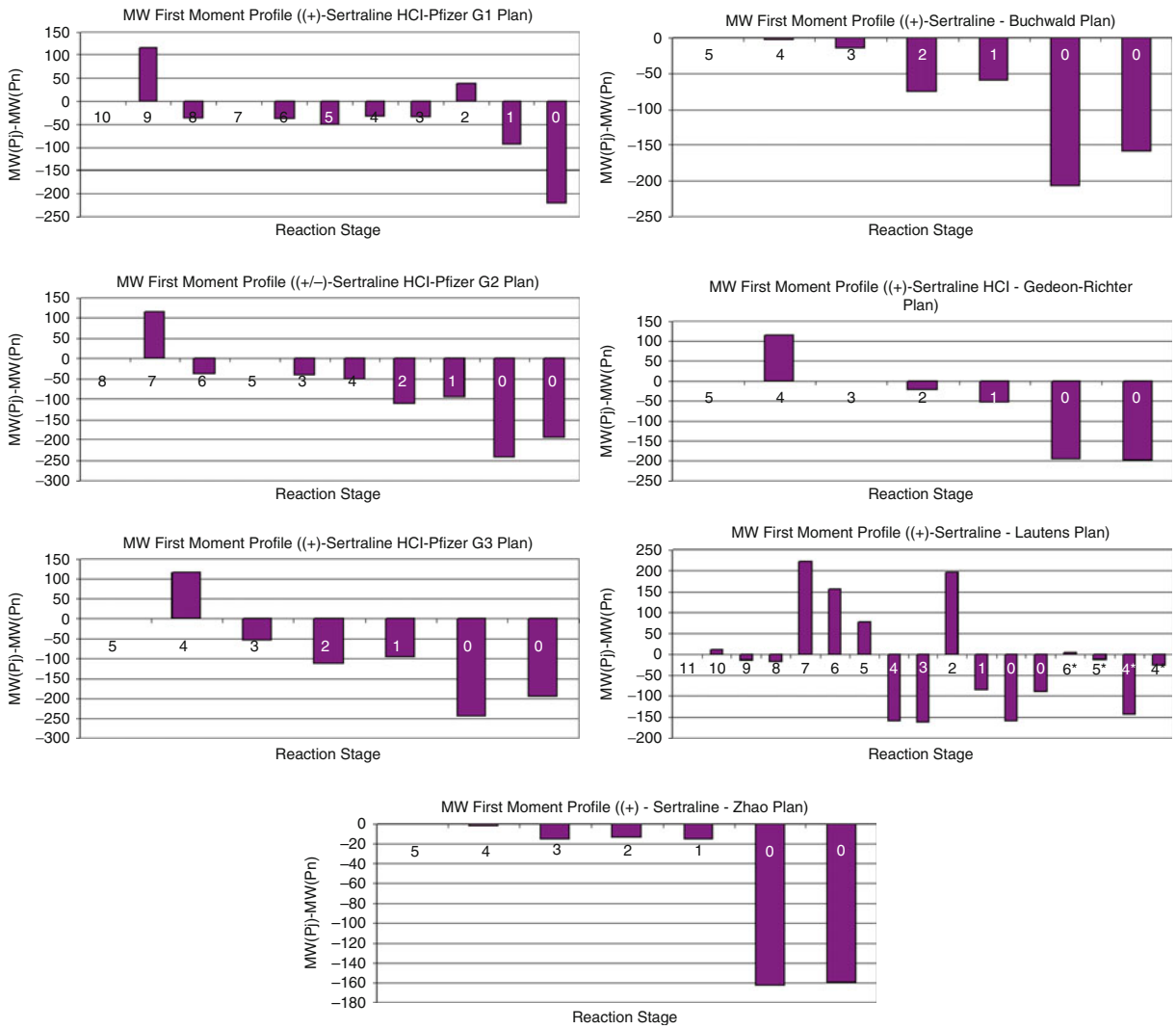

Green Chemistry Metrics: Material Efficiency and Strategic Synthesis Design. Figure 11
Molecular weight first moment profiles for synthesis plans of sertraline

recommendations given in section 6. The implication of this from a marketing point of view is that aiming for "green" chemistry is really aiming for "golden" chemistry. If individual reactions fail to meet this criterion at the kernel level, then there is no hope that they will meet it when all auxiliary materials are taken into account.

For an individual reaction, the kernel RME is given by $\mathrm{RME} = (\varepsilon)(\mathrm{AE})$, which is a reduced form of Eq. 1 when SF = 1 (no excess reagents) and MRP = 1 (all auxiliaries recovered or eliminated). If a threshold value of ϕ is set for the kernel RME, then it is possible to define the probability of achieving this target RME given a reaction's AE and range of possible reaction yield performances. For any given chemical reaction, the magnitude of AE is fixed while the reaction yield is in principle variable over the full range 0–100%. Applying the inequality $\mathrm{RME} = (\varepsilon)(\mathrm{AE}) \geq 0.618$ implies that $(\mathrm{AE}) \geq \frac{0.618}{\varepsilon}$. Figure 17 shows plots of AE versus reaction yield under two scenarios, depending on

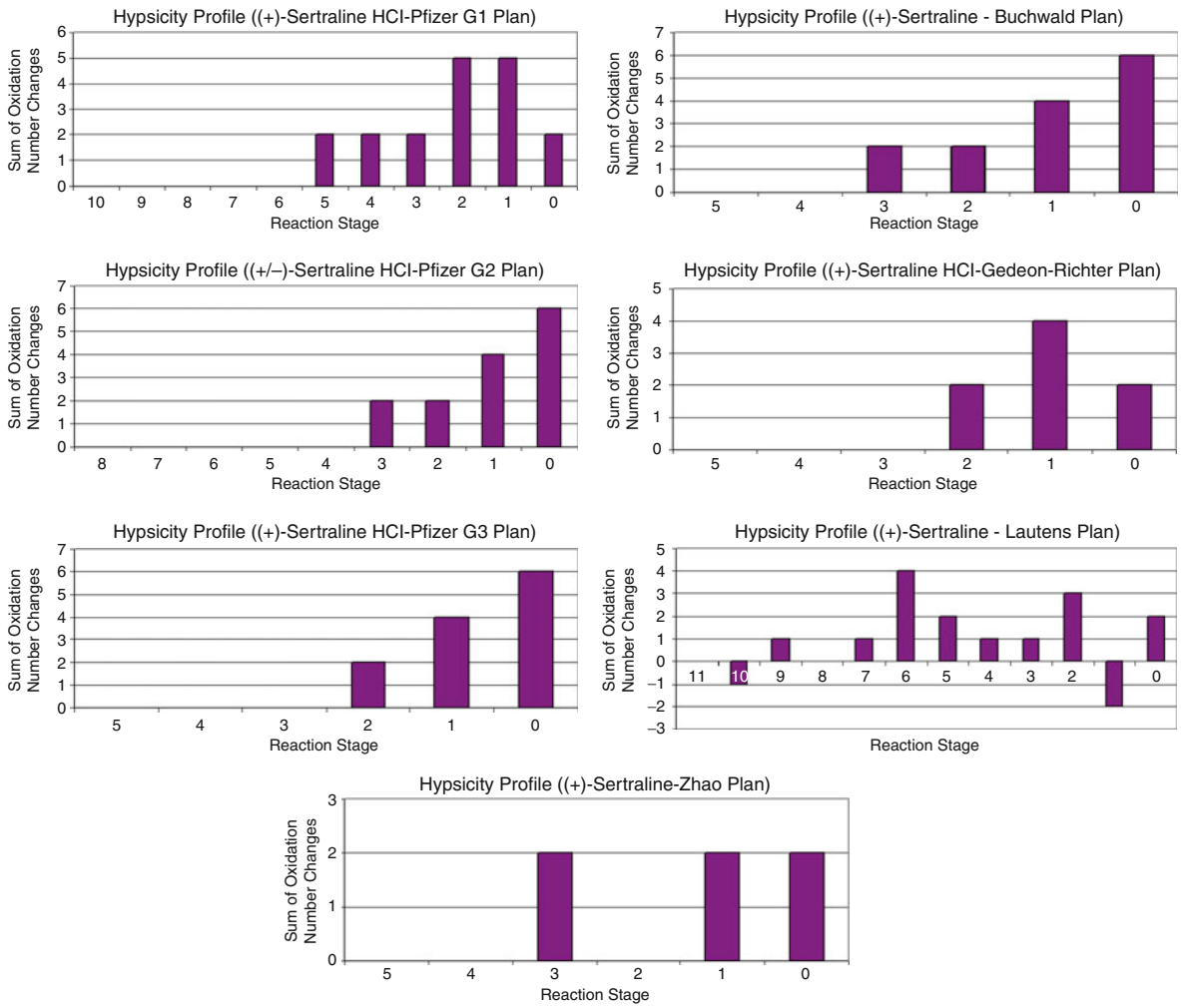

Green Chemistry Metrics: Material Efficiency and Strategic Synthesis Design. Figure 12
Hypsicity profiles for synthesis plans of sertraline

whether a reaction's atom economy, $(\mathrm{AE})^*$, is below or above the threshold value of 0.618. The curved line represents the equation $\mathrm{AE} = \frac{0.618}{\varepsilon}$. The region above this line satisfies the condition $\mathrm{RME} > 0.618$, and the region below the line satisfies the condition $\mathrm{RME} < 0.618$. If a reaction's AE is below 0.618, then the probability of it achieving an RME above 0.618 is zero no matter how high the reaction yield is. This is obvious because the horizontal line does not intersect the curve $\mathrm{AE} = \frac{0.618}{\varepsilon}$. However, if a reaction's AE is above 0.618, then the probability of it achieving this goal is given by the length of the bolded line segment, or $p = 1 - \frac{0.618}{(\mathrm{AE})*}$. So, for example, if a reaction has $(\mathrm{AE})^* = 0.8$, then $p = 0.23$ or 23%. The best possible scenario would yield a probability of only $p = 38\%$ for a reaction with 100% AE. This low probability may be amplified considerably if we consider a minimum cutoff for the reaction yield as well that is better than 0%. This means case II shown in Fig. 17 may be further subdivided into two scenarios given by the conditions $0 < \varepsilon_{\min} < \frac{0.618}{(\mathrm{AE})*}$ and $\frac{0.618}{(\mathrm{AE})*} < \varepsilon_{\min} \leq 1$ as shown in Fig. 18. In the former case, $p = \left(1 - \frac{0.618}{(\mathrm{AE})*}\right)/(1 - \varepsilon_{\min})$ and in the latter, $p = 1$. So, if a reaction proceeds with a minimum yield of 70% and it has an AE of 80%, then the probability of

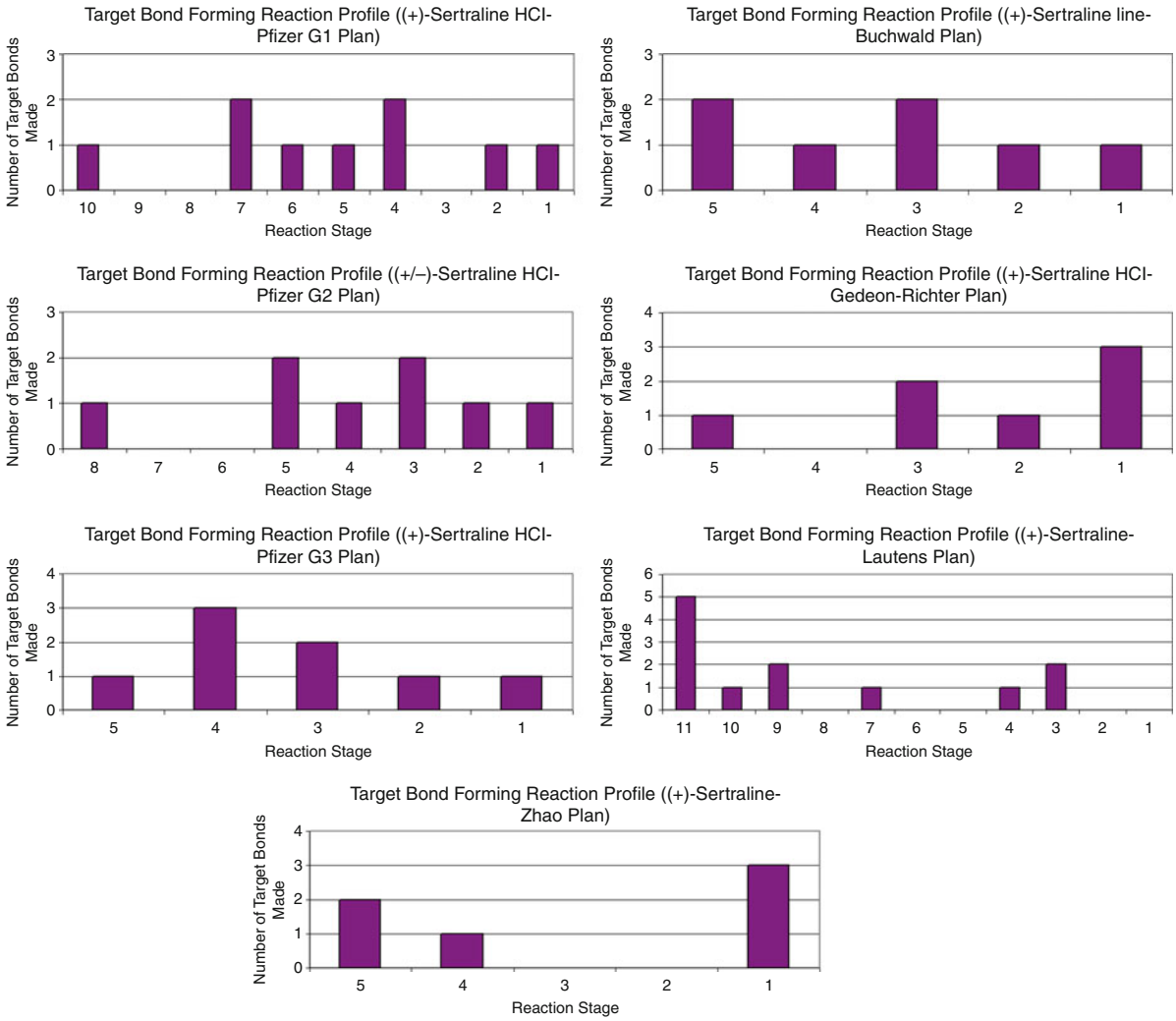

Green Chemistry Metrics: Material Efficiency and Strategic Synthesis Design. Figure 13
Target bond profiles for synthesis plans of sertraline

achieving an RME of 0.618 improves over threefold from $p = 0.23$ to $p = 0.76$. If the minimum yield is no worse than 0.618/0.8 = 0.77 (or 77%), then it is certain that the goal condition is attainable. These simple calculations clearly illustrate the importance of achieving both atom economies and reaction yields as high as possible in order to increase the chances of achieving even a modest target threshold RME of 61.8%. In a nutshell, synthesis plans composed of reactions with high atom economies and high yields working together have the best chance of achieving high kernel reaction mass efficiencies.

Future Directions

The future success of applying green chemistry thinking and metrics to synthesis design and optimization will depend on:

1. Making use of multicomponent and tandem one-pot reactions as central theme reactions in synthesis planning
2. Disclosing all material and energy consumption parameters for each reaction in a given plan (especially masses of chromatographic solvents, drying agents, work-up wash solutions, and reactant

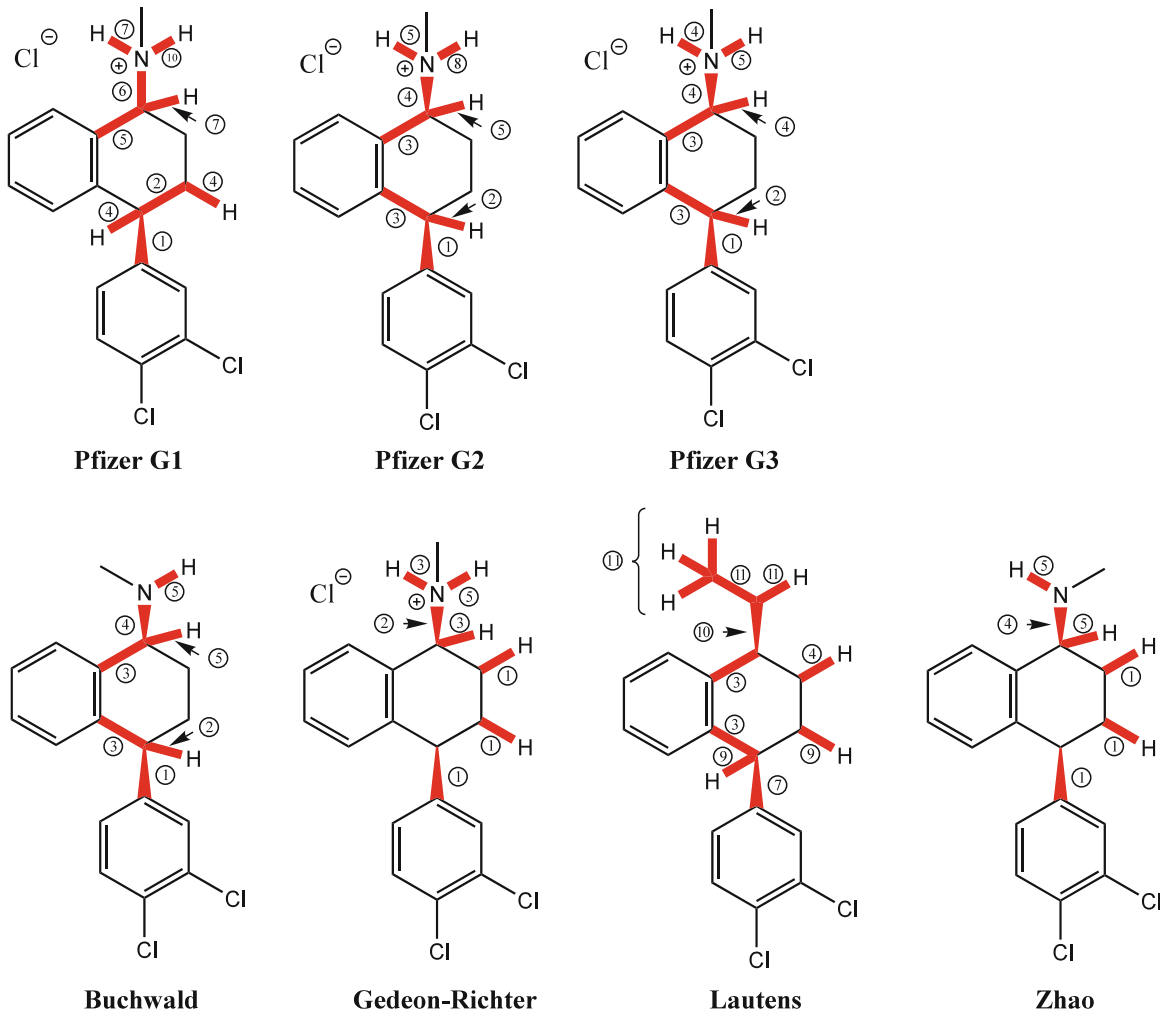

Green Chemistry Metrics: Material Efficiency and Strategic Synthesis Design. Figure 14
Target bond maps for synthesis plans of sertraline

gases) and clamping down on careless and intentional errors in publications, particularly experimental sections and supplementary materials of journal articles, with respect to mass and mole amounts of materials used and reaction yields so that true assessments of RME and E-factors can be made

3. Implementing the radial pentagon spreadsheet algorithm as a standard proofreading tool for reviewers of synthesis papers to trap errors described in (2) and help authors in improving the standard and reliability of their reported procedures
4. Mandating the reporting of green metrics as proof of greenness and part of the standard protocol in reports of synthesis plans in the literature, especially if plans are advertised as "green-er" than prior published plans and hence reduce false claims of "greenness"
5. Accepting that optimization is a continuous ongoing iterative exercise and that ranking of plans is the inevitable consequence of metrics analysis
6. Accepting that optimization is a multivariable problem and that claims of achievements of optimization to a given target molecule are legitimate

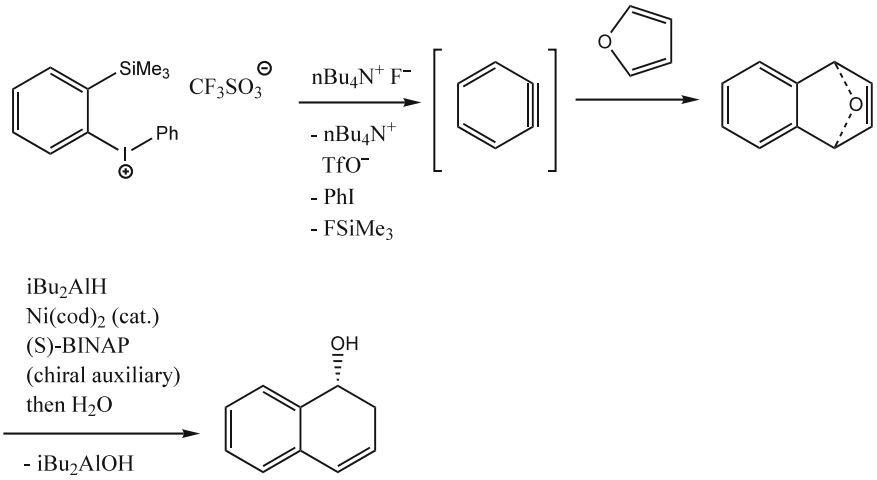

Green Chemistry Metrics: Material Efficiency and Strategic Synthesis Design. Figure 15
Lautens ring construction strategy

when the magnitudes of all variables in the set of plans considered are appropriately maximized and minimized and appear in the same plan

7. Realizing that when a new target molecule is desired to be made with no prior published guidance available, it is necessary to go through poor performing plans before hitting on the "right" one
8. Realizing that quantitative assessment of synthesis plans has an important role in deciding which may be good candidate plans to pursue
9. Changing the well-worn paradigm of designing synthesis plans around a fixed type of reaction just because of its novelty or because it honors the discoverer of that reaction to one that uses material and synthetic efficiency as the uppermost constraints in the choice of the set of reactions ultimately selected for a plan
10. Reaching a consensus on defining the set of first- and second-generation feedstock compounds that form a common basis of starting materials for all synthetic target molecules so that synthesis plans to any given target may be traced back to these and then ranked in an unbiased way
11. Ceasing to divorce the goals of green chemistry from those of elegant synthesis design and cost-efficient process chemistry
12. Creating a searchable structure database based on target bond mapping so that ring construction strategies may be encoded and as an aid to ensure novelty in planning a synthesis to a given target using retrosynthetic analysis

Some caveats to bear in mind when carrying out green metrics analyses include:

1. Generalizations about relative efficiencies of linear versus convergent routes, short plans versus longer ones, or stereoselective versus racemic with resolution must be taken with caution as there exist plenty of examples in the literature when counterintuitive results occur because gains made in one set of parameters are lost in others.
2. The synthesis plans of specialized catalysts or solvents used, such as chiral catalysts, ligands, and ionic liquids, must also be worked out using separate synthesis tree diagrams with appropriate mole-scaling factors as part of the overall assessment of material efficiency to a given target molecule.
3. When using the radial pentagon analysis for single reactions, one must be aware of determining correct mole amounts for reagents that are reported in procedures as solutions given in terms of weight percent and properly assigning the role of each material used in the right place in the template spreadsheet.
4. No claims of greenness can be made if only one plan exists for a given target molecule.

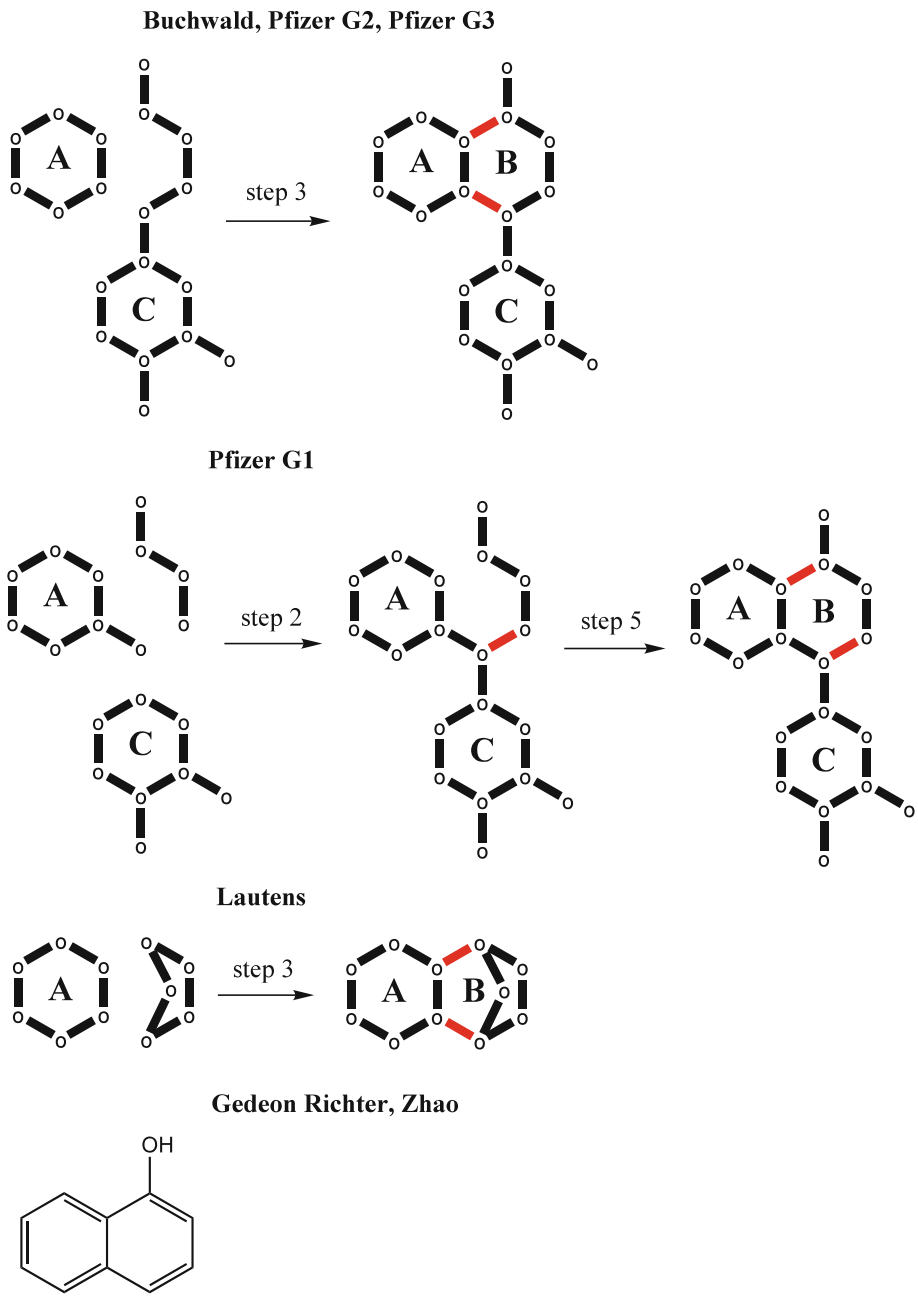

Green Chemistry Metrics: Material Efficiency and Strategic Synthesis Design. Figure 16
Graphs showing ring construction strategies

5. Claims of greenness cannot be made based on one criterion, such as the use of a "green" solvent for example.
6. Once green metrics analyses are done on a set of literature procedures to a given target molecule and it is found in the ranking process that optimized parameters are scattered over a number of plans, it is imperative that the next disclosed plan should demonstrate improvements over the best reported prior plan.

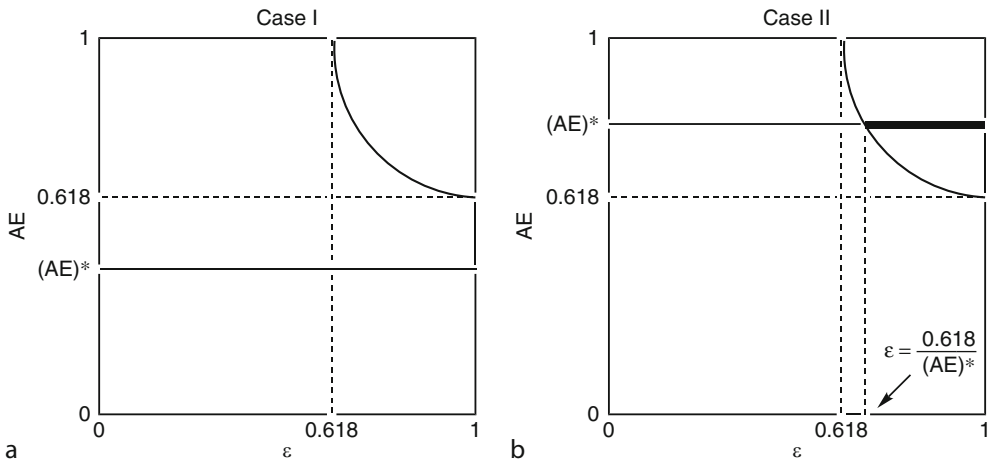

Green Chemistry Metrics: Material Efficiency and Strategic Synthesis Design. Figure 17
Plots of AE versus reaction yield according to AE $= \phi/\varepsilon = 0.618/\varepsilon$ showing the two possible cases: (**a**) when (AE)* ≤ 0.618 and $0 < \varepsilon_{\text{min}} \leq 1$; and (**b**) when $0.618 <$ (AE)* ≤ 1 and $0 < \varepsilon_{\text{min}} \leq 1$

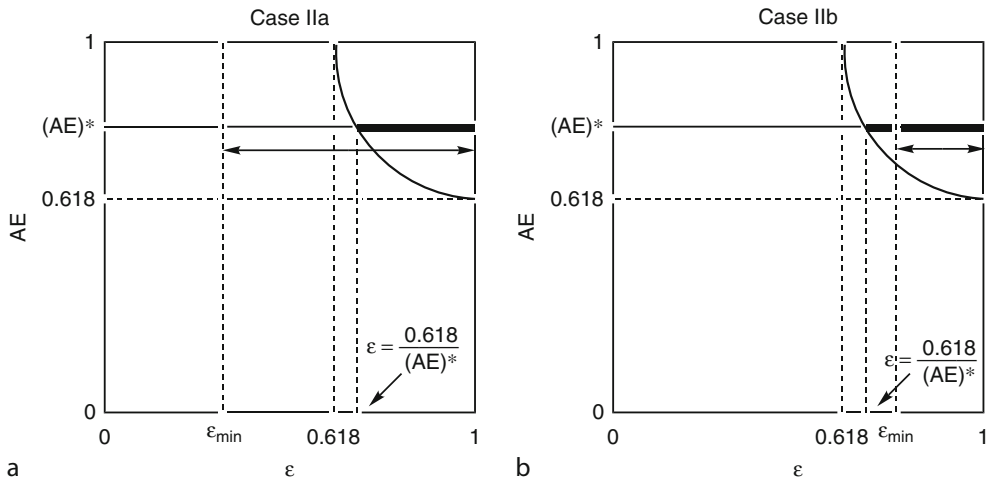

Green Chemistry Metrics: Material Efficiency and Strategic Synthesis Design. Figure 18
Plots of AE versus reaction yield according to AE $= \phi/\varepsilon = 0.618/\varepsilon$ showing the two possible cases: (**a**) $0.618 <$ (AE)* ≤ 1 and $0 < \varepsilon_{\text{min}} < \frac{0.618}{(\text{AE})*}$; and (**b**) when $0.618 <$ (AE)* ≤ 1 and $\frac{0.618}{(\text{AE})*} < \varepsilon_{\text{min}} \leq 1$

Bibliography

Primary Literature

1. Andraos J (2005) Unification of reaction metrics for green chemistry: applications to reaction analysis. Org Process Res Dev 9:149–163
2. Andraos J (2005) Unification of reaction metrics for green chemistry II: evaluation of named organic reactions and application to reaction discovery. Org Process Res Dev 9:404–431
3. Andraos J (2005) On using tree analysis to quantify the material, input energy, and cost throughput efficiencies of simple and complex synthesis plans and networks: towards a blueprint for quantitative total synthesis and green chemistry. Org Process Res Dev 10:212–240
4. Andraos J, Izhakova J (2006) Perspectives on the application of green chemistry principles to total synthesis design. Chimica Oggi/The Int J Ind Chem 24(6, Suppl.):31–36
5. Andraos J, Sayed M (2007) On the use of "green" metrics in the undergraduate organic chemistry lecture and laboratory to

assess the mass efficiency of organic reactions. J Chem Educ 84:1004–1010
6. Andraos J (2007) Gauging material efficiency. Can Chem News 59(4):14–17
7. Trost BM (1991) The atom economy – a search for synthetic efficiency. Science 254:1471–1477
8. Trost BM (2002) On inventing reactions for atom economy. Acc Chem Res 35:695–705
9. Trost BM (1995) Atom economy. A challenge for organic synthesis - homogeneous catalysis leads the way. Angew Chem Int Ed 34:259–281
10. Sheldon RA (1994) Consider the environmental quotient. Chem Tech 24(3):38–47
11. Sheldon RA (2000) Atom utilisation, E factors and the catalytic solution. CR Acad Sci Paris Sér IIc Chim 3:541–551
12. Sheldon RA (2001) Atom efficiency and catalysis in organic synthesis. Pure Appl Chem 72:1233–1246
13. Curzons AD, Constable DJC, Mortimer DN, Cunningham VL (2001) So you think your process is green, how do you know? – using principles of sustainability to determine what is green - a corporate perspective. Green Chem 3:1–6
14. Constable DJC, Curzons AD, Freitas dos Santos LM, Geen GR, Hannah RE, Hayler JD, Kitteringham J, McGuire MA, Richardson JE, Smith P, Webb RL, Yu M (2001) Green chemistry measures for process research and development. Green Chem 3:7–9
15. Steinbach A, Winkenbach R (2000) Choose processes for their productivity. Chem Eng April: 94–104
16. Constable DJC, Curzons AD, Cunningham VL (2002) Metrics to "green" chemistry – which are the best? Green Chem 4:521–527
17. Eissen M, Metzger JO (2002) Environmental performance metrics for daily use in synthetic chemistry. Chem Eur J 8:3580–3585
18. Eissen M, Hungerbühler K, Dirks S, Metzger J (2003) Mass efficiency as metric for the effectiveness of catalysts. Green Chem 5:G25–G27
19. Metzger JO, Eissen M (2004) Concepts on the contribution of chemistry to a sustainable development - renewable raw materials. CR Acad Sci Paris Sér IIc Chim 7:569–581
20. Eissen M, Mazur R, Quebbemann HG, Pennemann KH (2004) Atom economy and yield of synthesis sequences. Helv Chim Acta 87:524–535
21. van Aken K, Strekowski L, Patiny L (2006) EcoScale, a semi-quantitative tool to select an organic preparation based on economical and ecological parameters. Beilstein J Org Chem 2. doi:10.1186/1860-5397-2-3
22. Andraos J (2009) Global green chemistry metrics analysis algorithm and spreadsheets: evaluation of the material efficiency performances of synthesis plans for oseltamivir phosphate (Tamiflu) as a test case. Org Process Res Dev 13:161–185
23. Welch WM, Kraska AR, Sarges R, Koe BK (1984) Nontricyclic antidepressant agents derived from cis- and trans-1-amino-4-aryltetraline. J Med Chem 27:1508–1515
24. Quallich GJ, Williams MT, Friedmann RC (1999) Friedel-Crafts synthesis of 4-(3, 4-dichlorophenyl)-3, 4-dihydro-1(2 H)-naphthalenone, a key intermediate in the preparation of the antidepressant sertraline. J Org Chem 55:4971–4973
25. Lautens M, Rovis T (1999) Selective functionalization of 1, 2-dihydronaphthalenols leads to a concise, stereoselective synthesis of sertraline. Tetrahedron 55:8967–8976
26. Yun J, Buchwald SL (2000) Efficient kinetic resolution in the asymmetric hydrosilylation of imines of 3-substituted indanones and 4-substituted tetralones. J Org Chem 65:767–774
27. Vukics K, Fodor T, Fischer J, Fellegvári I, Lévai S (2002) Improved industrial synthesis of antidepressant sertraline. Org Process Res Dev 6:82–85
28. Taber GP, Pfisterer DM, Colberg JC (2004) A new and simplified process for preparing N-[4-(3, 4-dichlorophenyl)-3, 4-dihydro-1(2 H)-naphthalenylidene]methanamine and a telescoped process for the synthesis of (1 S-cis)-4-(3, 4-dichlorophenol)-1, 2, 3, 4-tetrahydro-N-methyl-1-naphthalenamine mandelate: key intermediates in the synthesis of sertaline hydrochloride. Org Process Res Dev 8:385–388
29. Wang G, Zheng C, Zhao G (2006) Asymmetric reduction of substituted indanones and tetralones catalyzed by chiral dendrimer and its application to the synthesis of (+)-sertraline. Tetrahedron Asymm 17:2074–2081
30. Hendrickson JB (1971) A systematic characterization of structures and reactions for use in organic synthesis. J Am Chem Soc 93:6847–6854

Books and Reviews

Abdel-Magid FA (2004) Chemical process research: the art of practical organic synthesis. American Chemical Society, Washington

Anastas PT, Warner JC (1998) Green chemistry: theory and practice. Oxford University Press, Oxford

Anderson NG (2000) Practical process research and development. Academic, San Diego

Baran PS, Maimone TJ, Richter JM (2007) Total synthesis of marine natural products without using protecting groups. Nature 446:404–408

Bertz SH, Sommer TJ (1993) Applications of graph theory to synthesis planning: complexity, reflexivity, and vulnerability. In: Hudlicky T (ed) Organic synthesis: theory and applications, vol 2, JAI Press. Greenwich, CT, pp 67–92

Burns NZ, Baran PS, Hoffmann RW (2009) Redox economy in organic synthesis. Angew Chem Int Ed 48:2854–2867

Calvo-Flores FG (2009) Sustainable chemistry metrics. ChemSusChem 2:905–919

Carey JS, Laffan D, Thomson C, Williams MT (2006) Analysis of the reactions used for the preparation of drug candidate molecules. Org Biomol Chem 4:2337–2347

Carlson R (1992) Design and optimization in organic synthesis. Elsevier, Amsterdam

Cornforth JW (1993) The trouble with synthesis. Aust J Chem 46:157–170

Eissen M (2001) Bewertung der Umweltverträglichkeit organisch-chemischer Synthesen. PhD thesis, Universität Oldenburg

Fuchs PL (2001) Increase in intricacy – a tool for evaluating organic synthesis. Tetrahedron 57:6855–6875
Hendrickson JB (1977) Systematic synthesis design. 6. Yield analysis and convergency. J Am Chem Soc 99:5439–5450
Hoffmann RW (2006) Protecting-group-free synthesis. Synlett 3531–3541
Lapkin A, Constable DJC (2008) Green chemistry metrics: measuring and monitoring sustainable processes. Wiley, Chichester
Lee S, Robinson G (1995) Process development: fine chemicals from grams to kilograms. Oxford University Press, Oxford
Newhouse T, Baran PS, Hoffmann RW (2009) The economies of synthesis. Chem Soc Rev 38:3010–3021
Nicolaou KC, Vourloumis D, Winssinger N, Baran PS (2000) The art and science of total synthesis at the dawn of the twenty-first century. Angew Chem Int Ed 39:44–122
Nicolaou KC (2003) Perspectives in total synthesis: a personal account. Tetrahedron 59:6683–6738
Nicolaou KC, Snyder SA (2004) The essence of total synthesis. Proc Nat Acad Sci USA 101:11929–11936
Nicolaou KC, Edmonds DJ, Bulger PG (2006) Cascade reactions in total synthesis. Angew Chem Int Ed 45:7134–7186
Orru RVA, de Greef M (2003) Recent advances in solution-phase multicomponent methodology for the synthesis of heterocyclic compounds. Synthesis 1471–1499
Posner GH (1986) Multicomponent one-pot annulations forming three to six bonds. Chem Rev 86:831–844
Qiu F (2008) Strategic efficiency – the new thrust for synthetic organic chemists. Can J Chem 86:903–906
Seebach D (1990) Organic synthesis –where now? Angew Chem Int Ed 29:1320–1367
Serratosa F (1990) Organic chemistry in action: the design of organic synthesis. Elsevier, Amsterdam
Sheldon RA (1997) The E factor: fifteen years on. Green Chem 9:1273–1283
Sheldon RA (2008) E factors, green chemistry and catalysis: an odyssey. Chem Commun 3352–3365
Smit WA, Bochkov AF, Caple R (1998) Organic synthesis: the science behind the art. Royal Society of Chemistry, Cambridge
Snieckus V (1999) Optimization in organic synthesis. Med Res Rev 19:342–347
Tietze LF (1996) Domino reactions in organic synthesis. Chem Rev 96:115–136
Tietze LF, Modi A (2000) Multicomponent domino reactions for the synthesis of biologically active natural products and drugs. Med Chem Rev 20:304–322
Ugi I, Dömling A, Hörl W (1994) Multicomponent reactions in organic chemistry. Endeavour New Ser 18(3):115–122
Ugi I, Dömling A, Werner B (2000) Since 1995 the new chemistry of multicomponent reactions and their libraries, including their heterocyclic chemistry. J Heterocycl Chem 37:647–658
Ugi I (2001) Recent progress in the chemistry of multicomponent reactions. Pure Appl Chem 73:187–191
Weber L, Illgen K, Almstetter M (1999) Discovery of new multicomponent reactions with combinatorial methods. Synlett 366–374
Weber L (2002) Multi-component reactions and evolutionary chemistry. Drug Discov Today 7:143–147
Weber L (2002) The application of multi-component reactions in drug discovery. Curr Med Chem 9:1241–1253
Wender P, Miller BL (1993) Toward the ideal synthesis: connectivity analysis and multibond-forming processes. In: Hudlicky T (ed) Organic synthesis: theory and applications, vol 2, JAI Press. Greenwich, Connecticut, pp 27–65
Zhang TY (2006) Process chemistry: the science, business, logic, and logistics. Chem Rev 106:2583–2595
Zhu J, Bienyamé H (2005) Multicomponent reactions. Wiley, Weinheim

Green Chemistry with Microwave Energy

Rajender S. Varma
Sustainable Technology Division, National Risk Management Research Laboratory, U.S. Environmental Protection Agency, Cincinnati, OH, USA

Article Outline

Glossary
Definition of the Subject
Introduction
Reactions Under Solvent-Free Conditions (With or Without Any Support)
Reactions in Aqueous Medium
Future Directions
Disclaimer
Bibliography

Glossary

Green chemistry Green chemistry is the broad discipline that encompasses the design of chemical processes and products that eliminate or reduce the generation and use of hazardous substances. It applies across the life cycle, including the design, manufacture, and use of a chemical product.

Microwaves Microwaves (0.3–300 GHz) lie in the electromagnetic radiation spectrum between radiowave (Rf) and infrared (IR) frequencies with relatively large wavelengths and are a form of energy and not heat. This nonionizing radiation, incapable of breaking chemical bonds, is a form of energy that

manifests itself as heat through interaction with the polar medium.

Sustainability Literally meaning to "maintain," "support," or "endure" the concept of sustainability calls for policies and strategies that meet society's present needs without compromising the ability of future generations to meet their own needs.

Definition of the Subject

Green chemistry utilizes a set of 12 principles that reduces or eliminates the use or generation of hazardous substances in the design, manufacture, and applications of chemical products [1]. This newer chemical approach protects the environment by inventing safer and eco-friendly chemical processes that prevent pollution "at source" rather than cleaning up "end-of-the-pipe" by-products and pollutants generated by traditional synthesis. The diverse nature of our chemical universe promotes a need for various greener strategic pathways in our quest to attain sustainability. The synthetic chemical community has been under increased pressure to produce, in an environmentally benign fashion, the myriad of chemical entities required by society in relatively short spans of time. This is especially true for the pharmaceutical and fine chemical industries. Among others, one of the best options is to accelerate these synthetic processes by using microwave (MW)-assisted chemistry techniques in conjunction with safer reaction media. The efficient use of the MW heating approach for the synthesis of a wide variety of organics and nanomaterials in aqueous and solvent-free media is discussed in this entry, including the sustainable application of recyclable and reusable nano-catalysts.

Introduction

The emerging area of green chemistry emphasizes minimum hazard as the performance criteria while designing new chemical processes. Rather than remediation, which involves cleaning up of waste after it has been produced, the main objective is to avoid waste generation in the first place. The desired approach requires new environmentally benign syntheses, catalytic methods, and chemical products that are "benign by design" [1]. One of the thrust areas for achieving this target is to explore alternative expeditious reaction conditions and eco-friendly reaction media to accomplish the desired chemical transformations with minimized by-products or waste as well as eliminating the use of conventional organic solvents. Consequently, several newer strategies have appeared, such as solvent-free (dry media) reactions with [2, 3] and without microwave irradiation [4].

The nonclassical heating technique using microwaves, termed as the "Bunsen burner of the 21st century," is rapidly becoming popular for expeditious chemical syntheses and transformations [5]. This entry summarizes noteworthy greener methods that use MWs that have resulted in the development of sustainable synthetic protocols for drugs and fine chemicals. A brief account of the author's own experiences in MW-assisted organic transformations involving benign alternatives, such as solid-supported reagents [2, 4], and greener reaction media, such as aqueous, ionic liquid, and solvent-free, for the synthesis of various heterocycles [3], oxidation-reduction reactions, coupling reactions, and some name reactions is included [5–9].

Microwaves are a nonionizing form of radiation energy that are not strong enough to break chemical bonds but transfer energy selectively to various substances. Some materials (such as hydrocarbons, glass, and ceramics) are nearly transparent to microwaves and therefore behave as good insulators in a MW oven since they are heated only to a very limited extent. Metals reflect MW; molecules with dipole moment (many types of organic compounds) and salts absorb MW energy directly. Microwaves couple directly with molecules in the reaction mixture with rapid rise in temperature; dipole rotation and ionic conduction are the two most important fundamental mechanisms for transfer of energy from microwaves to the molecules being heated. Polar molecules try to align themselves with the rapidly changing electric field of the MW and the coupling ability is determined by the polarity of the molecules. Therefore, there are some significant differences in terms of thermal gradient between the conventional chemical reactions in the liquid phase and the same reactions conducted under MW irradiation.

When a liquid reaction mixture is subjected to conventional heating, the walls of the vessel are directly heated but the reaction mixture receives thermal energy by conduction/convection. The temperature of the

reaction mixture cannot be higher than the temperature of the vessel walls. In contrast, MW energy permeates through glass vessels directly and is available for absorption by molecules in the reaction mixture. Consequently, it is possible for these molecules to be at higher energy levels and the contents of the flask to be at a higher bulk temperature in a few minutes. Another important feature of microwaves is that they penetrate several centimeters into a liquid; in contrast, radiant heat (e.g., from infrared rays) raises the temperature of only the surface layer. A reaction mixture under MW irradiation is therefore at a higher temperature in the middle than at the surface. Accordingly, the temperature profile of the reaction mixture can be quite different depending on whether there is conventional heating or MW-induced energy transfer.

Reactions Under Solvent-Free Conditions (With or Without Any Support)

Although the initial surface-mediated chemical transformation dates back to 1924 [10], it was not until almost half a century later that the technique received well-deserved attention as attested by several books [11, 12, 13], reviews, and account articles [14, 15]. Heterogeneous reactions facilitated by supported reagents on inorganic oxide surfaces have received special attention in recent years. The use of MW irradiation techniques for the acceleration of organic reactions had a profound impact on these heterogeneous reactions since the appearance of initial reports on the application of microwaves for chemical synthesis in polar solvents [16, 17]. The approach has now matured into a useful technique for a variety of applications in organic synthesis and functional group transformations, as is testified by a large number of books [18, 19] and review articles on this theme [2–5, 20–23].

The reactions appear to occur at relatively low bulk temperature although higher localized temperatures may be reached during MW irradiation. Unfortunately, accurate recording of temperature has not been made in the majority of such studies. The situation has now improved as a result of the availability of commercial MW systems. The recyclability of some of these solid mineral supports renders them into environmentally friendlier "green" protocols.

Since the initial report [24], a large number of MW-promoted solvent-free protocols have been illustrated for a wide variety of useful chemical transformations, such as cleavage (protection/deprotection), condensation, rearrangement reactions, oxidation, reduction, and the synthesis of several heterocyclic compounds on mineral supports [2–5, 20–23]. A range of industrially significant chemical precursors, such as enones, imines, enamines, nitroalkenes, and heterocyclic compounds, has been obtained in a relatively environmentally friendlier manner [2–5, 20–23]. A vast majority of these solvent-free reactions has been performed using an unmodified household MW oven or commercial MW equipment usually operating at 2,450 MHz in open glass containers with neat reactants. The general procedure involves simple mixing of neat reactants with the catalyst, their adsorption on mineral or "doped" supports, and subjecting the reaction mixture to MW irradiation.

It is clear that this solventless approach addresses the problems associated with waste disposal of solvents that are used severalfold in chemical reactions, thus minimizing or avoiding the excess use of chemicals and solvents.

Protection–Deprotection Reactions

Although inherently wasteful, protection–deprotection reaction sequences constitute an integral part of organic syntheses, such as the preparation of monomers, fine chemicals, and precursors for pharmaceuticals. These reactions often involve the use of acidic, basic, or hazardous reagents, and toxic metal salts [25]. The solventless MW-accelerated cleavage of functional groups provides an attractive alternative to conventional deprotection reactions.

Deacylation Reactions The utility of recyclable alumina as a viable support surface for deacylation reaction was reported by Varma and his colleagues wherein the orthogonal deprotection of alcohols [26] and regeneration of aryladehydes from the corresponding diacetates [27] is possible under solvent-free conditions on neutral alumina surface using MW irradiation (Scheme 1).

Debenzylation of Carboxylic Esters An efficient solvent-free debenzylation process for the cleavage of

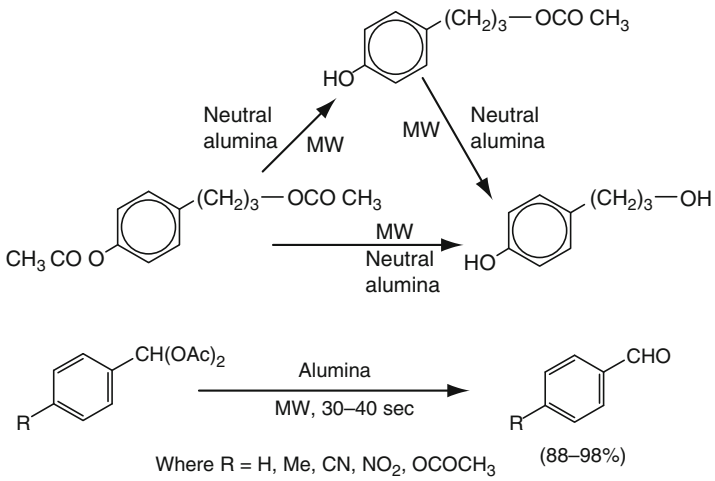

Green Chemistry with Microwave Energy. Scheme 1
Deacylation of protected alcohols and phenols and regeneration of aldehydes from aldehyde diacetates on neutral alumina

carboxylic esters on alumina surface was developed by Varma and coworkers [28]. By changing the surface characteristics of the solid support from neutral to acidic, the cleavage of 9-fluorenylmethoxycarbonyl (Fmoc) group and related protected amines was achieved. The cleavage of *N*-protected moieties, however, required the use of basic alumina and a MW irradiation time of 12–13 min at ~130–140°C.

Desilylation Reactions *Tertiary*-butyldimethylsilyl (TBDMS) ether derivatives of alcohols can be rapidly cleaved to regenerate the corresponding hydroxy compounds on alumina using MW irradiation [29]. This approach circumvents the use of corrosive fluoride ions that is normally employed for cleaving such silyl protecting groups.

Thionation Reactions: Thioketones, Thiolactones, Thioamides, Thionoesters, and Thioflavonoids The conversion of carbonyl compounds to the corresponding thio analogues is especially useful under solventless conditions and circumvents the use of conventional phosphorous pentasulfide under basic conditions, hydrogen sulfide in the presence of acid, or Lawesson's reagent. Using the MW approach, no acidic or basic medium is used and the carbonyl compounds are simply admixed with neat Lawesson's reagent (0.5 equiv.). This benign approach is general and is applicable to the high yield conversion of ketones, flavones, isoflavones, lactones, amides, and esters to the corresponding thio analogs (Scheme 2). The protocol uses comparatively a much smaller amount of Lawesson's reagent and avoids the use of large excesses of dry hydrocarbon solvents, such as benzene, xylene, triethylamine, or pyridine, that are conventionally used [30].

Dethioacetalization Thio acetals and ketals derived from aldehydes and ketones were rapidly deprotected by clayfen within seconds under solvent-free conditions (Scheme 3), thus avoiding the use of excess solvents and toxic oxidants commonly employed in the dethioacetalization process [31].

Oxidation Reactions

Oxidation of Alcohols The oxidation of alcohols to carbonyl compounds is an important transformation in organic synthesis. The use of supported reagents has gained popularity because of the improved selectivity, reactivity, and associated ease of manipulation. Alcohols can be rapidly and selectively oxidized to the corresponding carbonyl compounds by silica-supported active manganese dioxide (Scheme 4) under solvent-free conditions using microwaves [32].

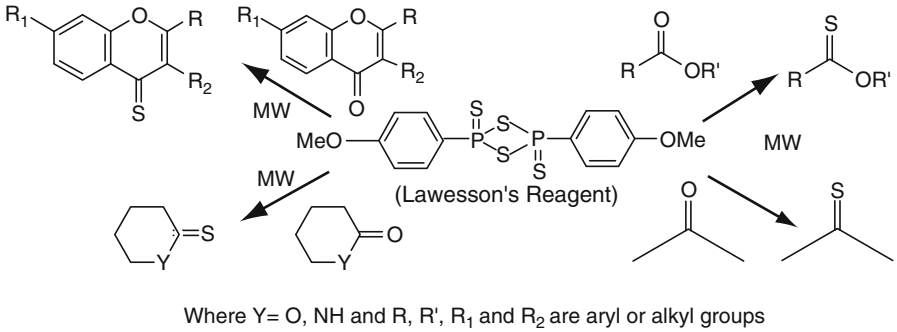

Green Chemistry with Microwave Energy. Scheme 2
Solvent-free synthesis of thioketones, thiolactones, thioamides, and thionoesters by Lawesson's reagent. From Varma and Kumar (Ref. [30])

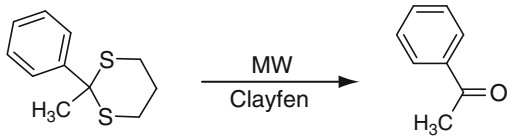

Green Chemistry with Microwave Energy. Scheme 3
Clayfen-catalyzed dethioacetalization

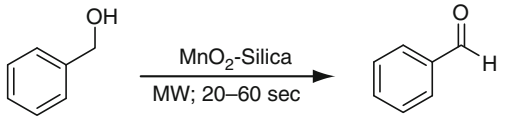

Green Chemistry with Microwave Energy. Scheme 4
MnO_2-silica-catalyzed oxidation of alcohols

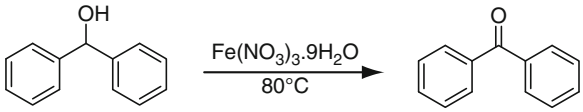

Green Chemistry with Microwave Energy. Scheme 5
Solventless oxidation of alcohols to carbonyl compounds

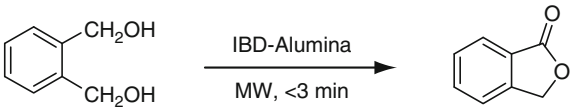

Green Chemistry with Microwave Energy. Scheme 6
IBD-alumina catalyzed oxyhyperiodination of alcohols

This oxidation protocol can also be catalyzed by ferric nitrate under solvent-free conditions [33], without any solid support (Scheme 5).

The nonmetallic oxidant, iodobenzene diacetate (IBD) on alumina, accomplished the oxidation of alcohols under solvent-free MW irradiation conditions and entails only the mixing of the neat alcohols with 1.1 equivalents of IBD doped on neutral alumina (Scheme 6); this rapid procedure avoids the over-oxidation of alcohols to carboxylic acids [34].

The solid-state oxidation of α-hydroxyketones to generate vicinal ketones (benzils) is possible using Oxone® supported on wet alumina (Scheme 7). The protocol circumvents the major limitations of Oxone®, namely, the low solubility in organic solvents and the inherent danger of combustibility upon heating with solvents [35].

Oxidation of Sulfides Selective oxidation of sulfides to sulfoxides and sulfones is possible [36] using wet silica-supported sodium periodate under MW irradiation (Scheme 8). A unique feature of this protocol is its applicability to long-chain aliphatic sulfides which are usually insoluble in polar solvents and are difficult to oxidize.

Oxidation of Dihydropyridines Solventless oxidation of 1,4-dihydropyridines to pyridines was effected by phenyliodine(III) bis(trifluoroacetate) (PIFA) at room temperature or elemental sulfur under MW irradiation conditions (Scheme 9). Dealkylation at the 4-position in the cases of ethyl, isopropyl, and

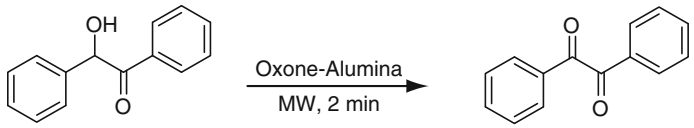

Green Chemistry with Microwave Energy. Scheme 7
Oxone-alumina catalyzed oxidation of benzoin

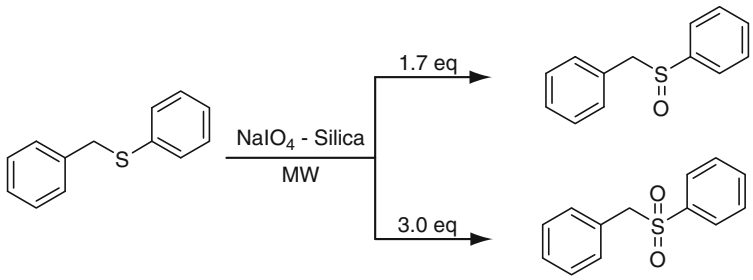

Green Chemistry with Microwave Energy. Scheme 8
$NaIO_4$-silica catalyzed selective oxidation of sulfides

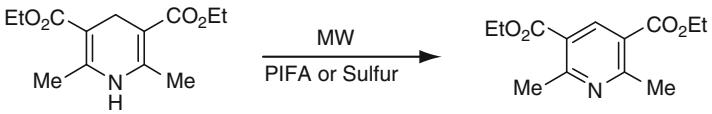

Green Chemistry with Microwave Energy. Scheme 9
PIFA or sulfur-catalyzed oxidation of 1,4-dihydropyridines

benzyl-substituted dihydropyridine derivatives with PIFA was circumvented by an alternative general procedure using elemental sulfur which provides pyridines in good yields [37].

Reduction Reactions

Reduction of Carbonyl Compounds A manipulatively simple and rapid method for the reduction of carbonyl compounds was developed [38] by Varma et al. under solvent-free conditions using $NaBH_4$-Alumina and MW irradiation (Scheme 10a). When sodium borohydride on wet clay was used as support, the reductive-amination of carbonyl compounds was efficiently accomplished under MW irradiation (Scheme 10b) [39]. The reactions involving Schiff's bases generated from cyclohexanone and aniline and aliphatic aldehydes and amines, however, require a relatively longer time for completion.

Reduction of Nitro Compounds Varma and coworkers developed a solvent-free MW reduction protocol that leads to a facile preparation of aromatic amines from the corresponding nitro compounds [40] with hydrazine hydrate supported on solid materials such as alumina, silica gel, and clays (Scheme 11).

Similarly, hydroxylamine supported on clay can convert arylaldehydes into nitriles (Scheme 12) [41].

MW-Assisted Synthesis of Ionic Liquids and Their Application as Catalysts

Ionic liquids (ILs) have been the focus of attention due to their potential in a variety of commercial applications, such as electrochemistry, heavy metal ion extraction, phase transfer catalysis, and polymerization, and as substitutes for conventional volatile organic solvents (Rogers and Seddon 2002) [42, 43]. Additional environmentally friendly attributes of these ILs include

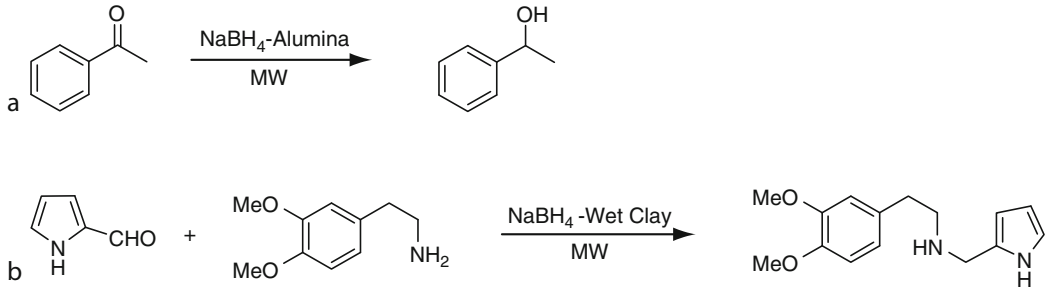

Green Chemistry with Microwave Energy. Scheme 10
(**a**) $NaBH_4$-catalyzed reduction of carbonyl compounds and (**b**) Reductive-amination of carbonyl compounds

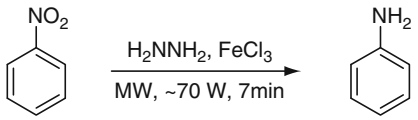

Green Chemistry with Microwave Energy. Scheme 11
Reduction of nitro compounds to amines

negligible vapor pressure, potential for recycling, compatibility with various organic compounds and organometallic catalysts, and ease of separation of products from reactions.

Solvent-Free Synthesis of Ionic Liquids Ionic liquids, being polar and ionic in character, couple with MW irradiation very efficiently and are, therefore, ideal MW-absorbing candidates for enhancing chemical reactions. The first efficient preparation of 1,3-dialkylimidazolium halides via MW irradiation was developed by Varma et al. (Scheme 13) [44, 45]. The reaction time was reduced to minutes and the method avoids the excessive use of organic solvents as the reaction medium. These syntheses can also be ideally carried out using ultrasound under solvent-free conditions [46].

Metal-bearing classes of ILs, [Rmim][$InCl_4$] and [bmim][$GaCl_4$], were prepared using a solvent-free MW procedure (Scheme 14) and utilized as catalysts [47, 48]. This approach is much faster, efficient, and eco-friendly as it does not use any organic solvent.

Synthetic Application of ILs as Catalysts Ionic liquids have emerged as a new class of green solvents for chemical processes and transformations (Rogers and Seddon 2002). Their polarity renders them good solvents for various organic reactions and catalyzes, including the dissolutions of renewable materials such as cellulose [49].

1-Butyl-3-methylimidazolium tetrachlorogallate, [bmim][$GaCl_4$], has been used as an active catalyst for the efficient acetalization of aldehydes (Scheme 15) [48].

Imidazolium-based tetrachloroaluminates ([Rmim][$AlCl_4$]) [50] and tetrachloroindate ([Rmim][$InlCl_4$]) [47] have been used as recyclable catalysts for the efficient protection of alcohols to form tetrahydropyranyl (THP) derivatives (Scheme 16).

The coupling reaction of carbon dioxide (CO_2) with epoxides generates the five-membered cyclic carbonates which are precursors for polymeric materials such as polyurethanes and polycarbonates, serve as aprotic polar solvents, and are utilized as intermediates in the production of pharmaceutical and fine chemicals. The catalytic amounts of tetrahaloindate (III)-based ILs are found to exhibit the highest catalytic activities for the synthesis of cyclic carbonates (Scheme 17) [51].

Reactions in Aqueous Medium

Solvent-free reactions undoubtedly minimize the environmental impacts resulting from the use of solvents in chemical production but there are limitations in view of the poorly understood heat- and mass-transfer issues under these conditions [2]. Fluorous solvents, ionic liquids [52], aqueous systems [7], and supercritical carbon dioxide have emerged as alternatives in this movement. Water, which is naturally abundant and can

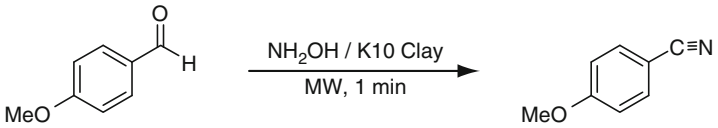

Green Chemistry with Microwave Energy. Scheme 12
Hydroxylamine-clay-catalyzed synthesis of aromatic nitriles

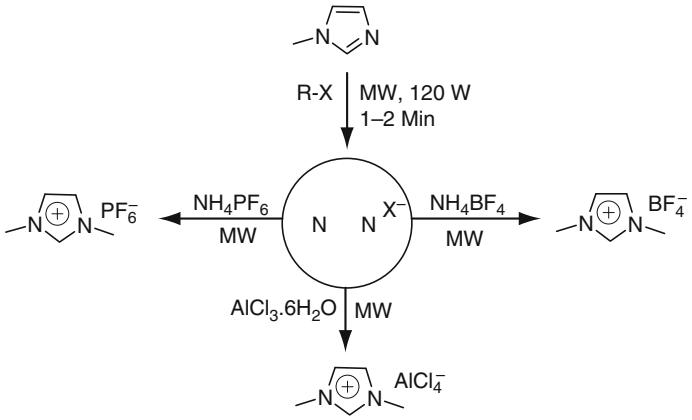

Green Chemistry with Microwave Energy. Scheme 13
MW-assisted synthesis of ionic liquids

Green Chemistry with Microwave Energy. Scheme 14
MW-assisted synthesis of In and Ga containing ionic liquids

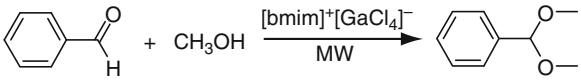

Green Chemistry with Microwave Energy. Scheme 15
Ionic liquid-catalyzed protection of carbonyl compounds

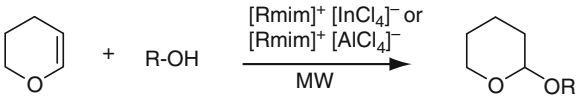

Green Chemistry with Microwave Energy. Scheme 16
Ionic liquid-catalyzed THP-protection of alcohols

be contained because of its relatively higher vapor pressure, appears to be a sustainable alternative because of its nontoxic, noncorrosive, and nonflammable nature [6–8].

In addition to the isolation of products from the aqueous medium, the insolubility of most of the organic substrates in water is a challenge. However, some of these issues can be overcome by using the MW heating technique wherein water is rapidly heated to high temperatures enabling it to act like a pseudo-organic solvent. Two key mechanisms, namely, dipolar polarization and ionic conduction of water molecules (Fig. 1), come into play upon irradiation of a reaction

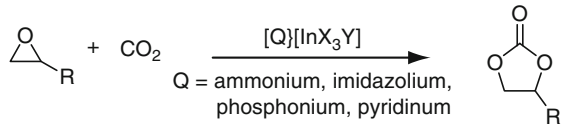

Green Chemistry with Microwave Energy. Scheme 17 Synthesis of cyclic carbonates catalyzed by tetrahaloindate (III)-based ionic liquids

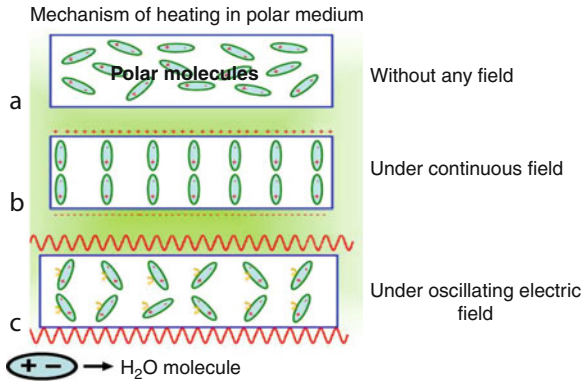

Green Chemistry with Microwave Energy. Figure 1 Effect of microwaves on the reaction mixture in polar medium

mixture in an aqueous medium by microwaves, invoking two distinguishing effects:

(a) *Specific microwave effect*: the dipole–dipole-type interaction of the dipolar water molecules and reactants with the electric field component of MW (Fig. 1b), resulting in what is described by some as a specific MW (nonthermal) effect which is a controversial and debatable issue among chemists. Kappe et al. have shown that this effect is mainly due to thermal phenomenon and is thus not nonthermal [53].

(b) *Thermal effect*: the dielectric heating that ensues from the tendency of dipoles of water molecules and reactants to follow the rapidly alternating electric fields and induce energy dissipation in the form of heat through molecular friction and dielectric loss (Fig. 1c).

It has been observed that various organic reactions can be conducted in an aqueous medium using MW irradiation without using any phase-transfer catalyst (PTC). This is because water at higher temperature behaves as a pseudo-organic solvent, as the dielectric constant decreases substantially and an ionic product increases the solvating power toward organic molecules to be similar to that of acetone or ethanol [9].

Although MW-assisted reactions in organic solvents have developed rapidly for a variety of applications in drug discovery [54] and organic synthesis [7], the focus has now shifted to the more environmentally benign methods, which use greener solvents such as polyethylene glycol (PEG) [55] and water [6–8]. Some illustrative recent synthetic reactions in aqueous reaction medium using MW irradiation are summarized below.

Coupling Reactions (Suzuki, Heck, and Sonogashira)

Among the heterogeneous palladium (Pd)-catalyzed reaction systems, MW-assisted coupling reaction in aqueous medium is a "greener" choice by chemists. Suzuki reaction has been studied in aqueous medium using MW irradiation (Scheme 18) for the preparation of various biaryl derivatives [1] from aryl halide and phenylboronic acid [56] in presence of tetra butyl ammonium bromide (TBAB); the poor yield for aryl chlorides as compared to other halides could be improved by conducting the reaction using simultaneous cooling technique in conjugation with MW heating.

The versatility of aqueous MW-assisted Suzuki reaction has also been demonstrated in the synthesis of natural products and heterocyclic compounds [57].

5-Aryltriazole acyclonucleosides [2] bearing aromatic groups on the triazole ring have been synthesized via the Suzuki coupling reaction in aqueous solution (Scheme 19) [58]. This high-yield coupling method directly afforded the product and involved no protection and deprotection steps, thus providing a convenient one-step procedure for 5-aryltriazole acyclonucleosides.

Benzothiazole-based Pd(II) complexes 3 and 4 have been found to be highly active catalysts in Suzuki and Heck cross-coupling reactions of aryl chlorides and bromides with olefins and arylboronic acids under aqueous MW irradiation conditions. The immobilized catalyst 4 was found to have higher durability compared with its mobilized counterpart 3 (Scheme 20) [59].

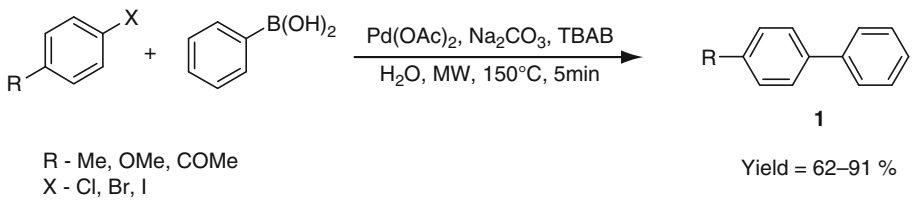

Green Chemistry with Microwave Energy. Scheme 18
Aqueous MW-assisted Suzuki reaction

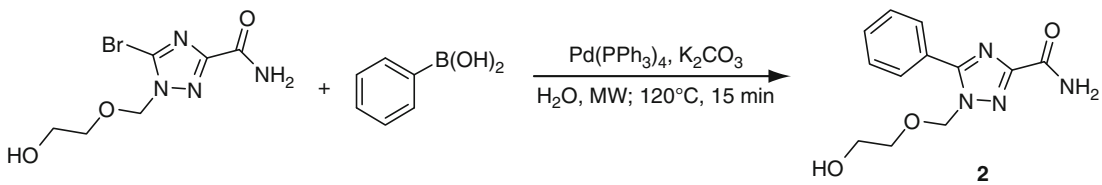

Green Chemistry with Microwave Energy. Scheme 19
Aqueous MW-assisted Suzuki reaction of triazole

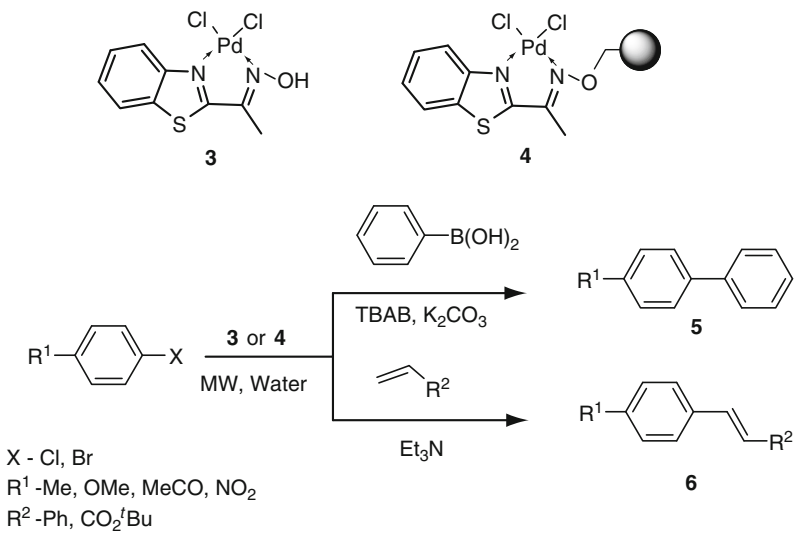

Green Chemistry with Microwave Energy. Scheme 20
Aqueous MW Suzuki and Heck reactions using benzothiazole-based Pd(II) complexes

Arvela and Leadbeater performed the Heck coupling reaction in water using MW heating (Scheme 21), with Pd catalyst concentrations as low as 500 ppb [60].

Larhed et al. have recently reported highly regioselective and fast Pd(0)-catalyzed internal R-arylation of ethylene glycol vinyl ether with aryl halides in aqueous medium (Scheme 22) in presence of 1,3-bis (diphenylphosphino)propane (dppp) [61].

Aryl bromides and iodides were efficiently converted to corresponding acetophenones [7] in high yields in water using ethylene glycol vinyl ether as the olefin and

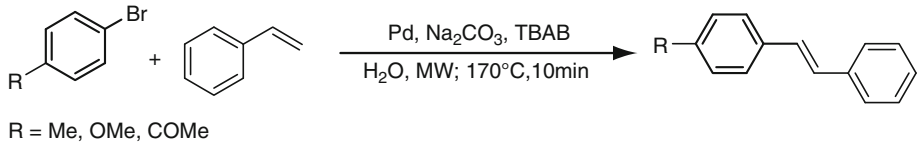

Green Chemistry with Microwave Energy. Scheme 21
Aqueous MW-assisted Heck reaction

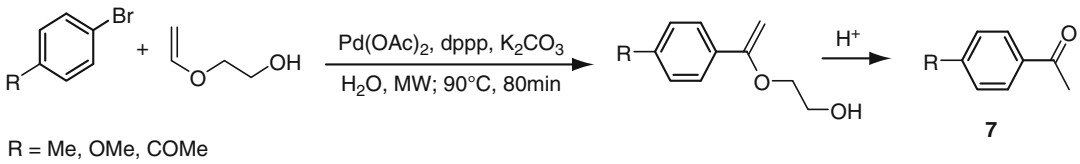

Green Chemistry with Microwave Energy. Scheme 22
Aqueous MW-expedited internal Heck reaction

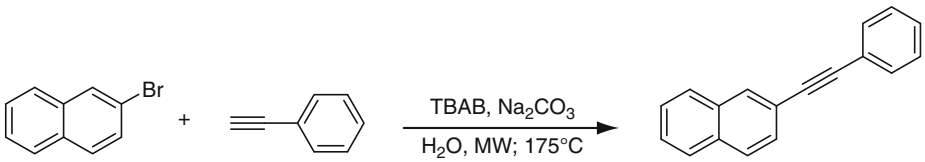

Green Chemistry with Microwave Energy. Scheme 23
Aqueous MW-assisted Sonogashira reaction

potassium carbonate as the base. This Pd(0)-catalyzed method is advantageous as no heavy metal additives or ionic liquids are necessary. The reaction proceeded cleanly without any noticeable byproduct formation and avoided the need for inert atmosphere. MW irradiation has proven to be beneficial in activation of aryl chlorides toward the internal Heck arylation.

An aqueous Sonogashira coupling reaction was reported by Eycken et al. under MW irradiation (Scheme 23). This reaction precludes the need for copper(I) or any transition-metal phosphane complex, thus overcoming the problem of toxicity and air sensitivity of transition-metal complexes, as well as the use of expensive phosphane ligands [62].

Hiyama Cross-Coupling Reaction

The relatively benign and stable organosilanes have emerged as useful entities for cross-coupling reactions. This is exemplified by the Hiyama cross-coupling reactions between vinylalkoxysilanes and aryl halides which were promoted by aqueous sodium hydroxide under fluoride-free conditions and carried out using MW irradiation in aqueous medium (Scheme 24) [63].

Stille Reaction

Stille reaction between organo-tin and aryl halide was achieved using aqueous MW chemistry by van der Eycken et al. (Scheme 25) [64].

Transformation of Amines to Ketones

Although the selective transformation of amines to ketones is a common biological process, conversion of amines to ketones by chemical means are rather limited. A retro-reductive, MW-assisted, Pd-catalyzed amination reaction for direct conversion of amines to

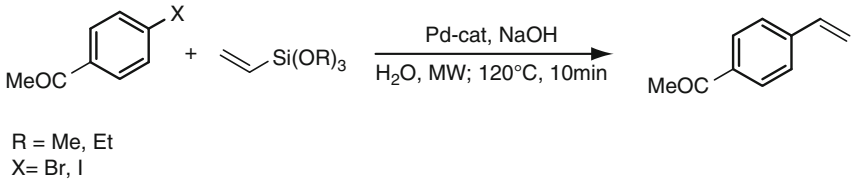

Green Chemistry with Microwave Energy. Scheme 24
Aqueous MW-assisted Hiyama reaction

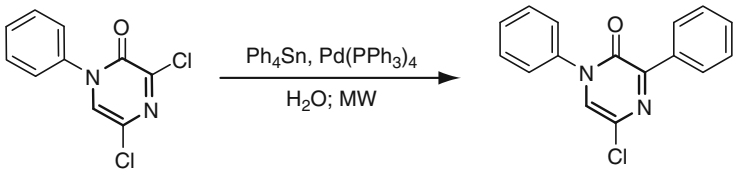

Green Chemistry with Microwave Energy. Scheme 25
Aqueous MW-assisted Stille reaction

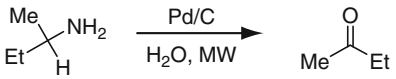

Green Chemistry with Microwave Energy. Scheme 26
MW-assisted aqueous retro-reductive amination reaction

ketones in water was accomplished by Olah et al. (Scheme 26). This expeditious reaction proceeds smoothly without any heavy metal–based oxidant or volatile organic solvents [65].

Decarboxylation of Cinnamic Acids

A metal-free protocol for decarboxylation of substituted α-phenylcinnamic acid derivatives in aqueous media was developed by Sinha et al. [66], wherein a catalytic amount of methylimidazole in aqueous $NaHCO_3$ in polyethylene glycol (PEG) under MW irradiation conditions furnished the corresponding para/ortho hydroxylated (E)-stilbenes (Scheme 27). This is clearly a clean alternative to the conventional multistep methods that often involve the use of toxic quinoline and a copper salt combination. The critical role of water in facilitating the decarboxylation highlights the synthetic utility of water-mediated organic transformations.

Reactions in Near-Critical Water

Dallinger and Kappe examined several MW-assisted organic reactions in near-critical water (NCW) in the temperature range of 270–300°C. The hydrolysis of esters or amides, the hydration of alkynes, Diels–Alder cycloadditions, pinacol rearrangements, and the Fischer indole synthesis were successfully performed in MW-generated NCW without the addition of an acid or base catalyst [67]. This study demonstrated that it is technically feasible to perform MW synthesis in water on scales from 15 to 400 ml at temperatures of up to 300°C and 80 bars of pressure in a multimode MW reactor.

Synthesis of Heterocycles

Heterocyclic compounds are a special class among pharmaceutically significant natural products and synthetic compounds [68, 69]. The remarkable ability of heterocyclic nuclei to serve both as biomimetics and reactive pharmacophores has provided a unique value as traditional key elements for numerous drugs. Conventional organic synthesis is too slow to satisfy the demand for generation of small molecules and this void has been filled by combinatorial and automated chemistry to meet the increasing requirement of new

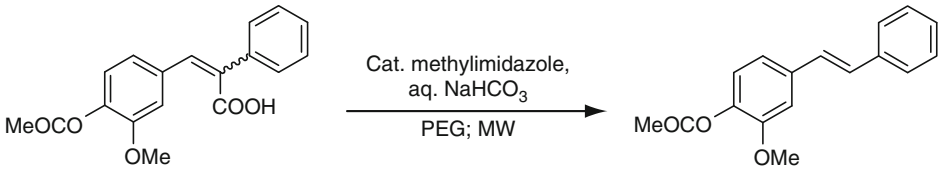

Green Chemistry with Microwave Energy. Scheme 27
Decarboxylation of cinnamic acid in aqueous medium using microwaves

compounds for drug discovery, expediently [70]. The efficiency of MW flash-heating has resulted in dramatic reductions in reaction times from days and hours to minutes and seconds [5, 6, 9, 71–73].

Nitrogen Heterocycles Nitrogen heterocycles are abundant in nature and are of great significance to life because their structural subunits exist in many natural products such as vitamins, hormones, antibiotics, and alkaloids, as well as herbicides, dyes, and pharmaceuticals [68].

An expedient *N*-alkylation of nitrogen heterocycles was reported in aqueous media under MW irradiation conditions (Scheme 28) [74].

The double *N*-alkylation of primary amines and hydrazine derivatives (Scheme 29) in carbonated water using microwaves provided access to the synthesis of nitrogen-containing heterocycles, namely, substituted azetidines, pyrrolidines, piperidines, azepanes, *N*-substituted 2,3-dihydro-1H-isoindoles, 4,5-dihydropyrazoles, pyrazolidines, and 1,2-dihydrophthalazines. The readily available alkyl dihalides (or ditosylates) thus provide a facile entry to important classes of building blocks in natural products and pharmaceuticals [75–77].

This MW-accelerated general approach shortened the reaction time significantly and utilized readily available amines and hydrazines with alkyl dihalides or ditosylates to assemble two C–N bonds in a simple S_N2-like sequential heterocyclization experimental protocol which has never been fully realized under conventional reaction conditions. The strategy avoids multistep reactions, functional group protection/deprotection sequences, and eliminates the use of expensive phase transfer and transition metal catalysts. The experimental observations are consistent with the mechanistic postulation

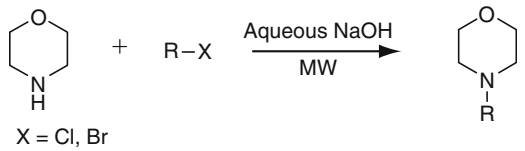

Green Chemistry with Microwave Energy. Scheme 28
N-Alkylation in basic water using MW irradiation

wherein the polar transition state of the reaction is favored by MW irradiation with respect to the dielectric polarization nature of MW energy transfer. In large-scale experiments, the phase separation of the desired product in either solid or liquid form from the aqueous media can facilitate product purification by simple filtration or decantation instead of tedious column chromatography, distillation, or extraction processes, which reduces the usage of volatile organic solvents [77].

A direct Grignard type of addition of alkynes to in situ generated imines, from aldehyde and amines, was catalyzed by CuBr and provides a rapid and solvent-free approach access to propargylamines in excellent yields (Scheme 30) [78].

Direct synthesis of these cyclic ureas using a MW-assisted protocol that proceeds rapidly in the presence of ZnO were reported (Scheme 31) [79].

The imidazo[1,2-a] annulated nitrogen heterocycles bearing pyridine, pyrazine, and pyrimidine moities constitute a class of biologically active compounds that can be assembled via atom-economic, one-pot condensation of aldehydes, amines, and isocyanides (three-component Ugi reaction) using a MW approach (Scheme 32) in the presence of recyclable montmorillonite K-10 clay under solvent-free conditions [80].

Dihydropyrimidinones are an important class of biologically active organic compounds that were synthesized under solvent-free conditions [81] or by an

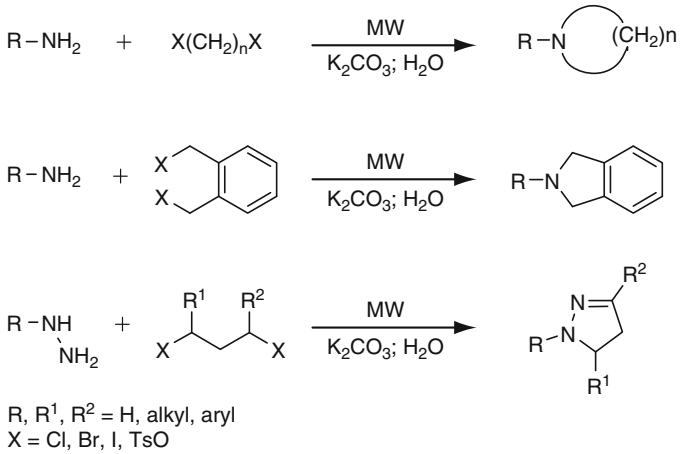

Green Chemistry with Microwave Energy. Scheme 29
Synthesis of *N*-heterocycles in aqueous media using MW irradiation

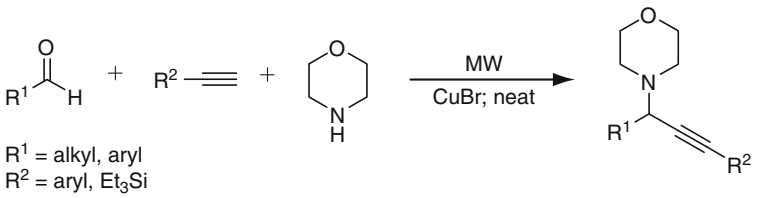

Green Chemistry with Microwave Energy. Scheme 30
CuBr-catalyzed solvent-free synthesis of propargylamines

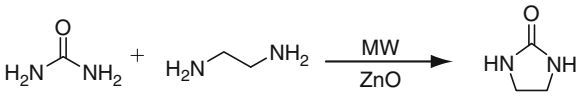

Green Chemistry with Microwave Energy. Scheme 31
ZnO-catalyzed MW synthesis of imidazolidine-2-one

environmentally benign Biginelli protocol using polystyrene sulfonic acid (PSSA) as a catalyst (Scheme 33). A very simple eco-friendly isolation procedure entails the filtration of the precipitated products [82].

Oxygen-Heterocycles Heterocycles bearing oxygen atom are important classes of building blocks in organic synthesis and have attracted the attention of medicinal chemists over the years [69].

The solvent-free synthesis of 2-aminosubstituted isoflav-3-enes was developed, which can be carried out in one pot using microwaves via the in situ generation of enamines and their subsequent reactions with salicylaldehydes (Scheme 34) [83]. This environmentally friendly procedure does not require azeotropic removal of water using large excesses of aromatic hydrocarbon solvents for the generation of enamines or the activation of the catalyst.

The expeditious solvent-free syntheses of 2-aroylbenzo[*b*]furans were developed from readily accessible α-tosyloxyketones and mineral oxides in processes that are accelerated by exposure to microwaves (Scheme 35) [84].

Dioxane rings, common structural motifs in numerous bioactive molecules, can be assembled via tandem bis-aldol reaction of ketones with paraformaldehyde in aqueous media catalyzed by PSSA under MW irradiation conditions to produce 1,3-dioxanes (Scheme 36) [85].

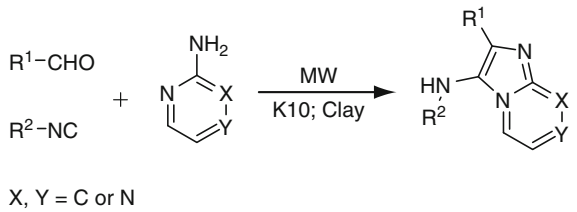

Green Chemistry with Microwave Energy. Scheme 32
Clay-catalyzed solvent-free synthesis of annulated *N*-heterocycles

Heterocyclic Hydrazones The first example of a reaction between two solids, under solvent-free and catalyst-free environment, was accomplished by Varma et al. The reaction of neat 5- or 8-oxobenzopyran-2(1H)-ones with a variety of aromatic and heteroaromatic hydrazines provides rapid access to several synthetically useful heterocyclic hydrazones (Scheme 37) [86].

An aqueous protocol for the synthesis of heterocyclic hydrazones using PSSA as a catalyst was also devel-

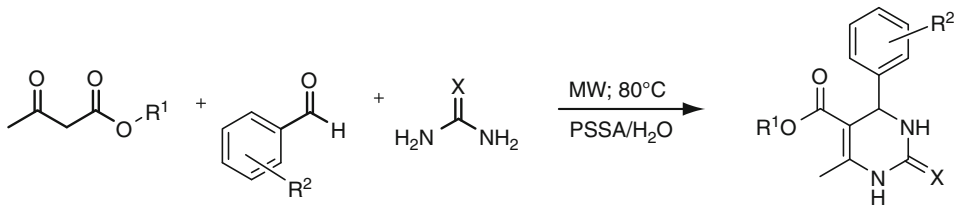

Green Chemistry with Microwave Energy. Scheme 33
Biginelli reaction using microwaves in aqueous medium

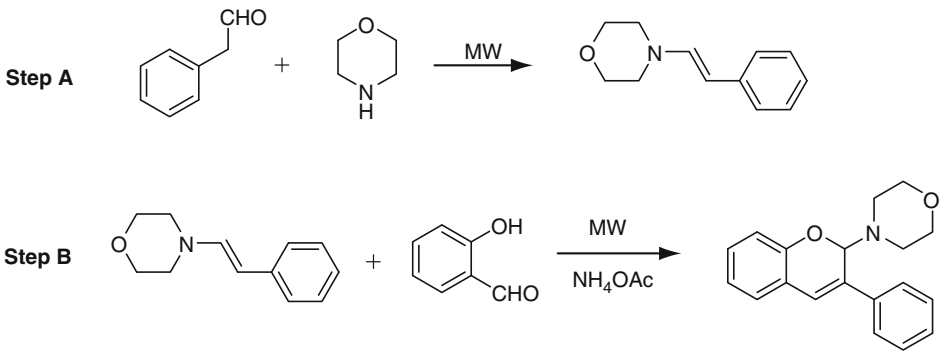

Green Chemistry with Microwave Energy. Scheme 34
One-pot solventless synthesis of isoflav-3-enes

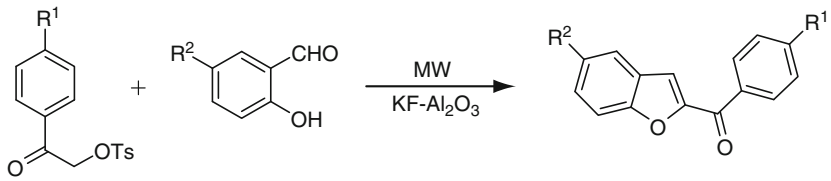

Green Chemistry with Microwave Energy. Scheme 35
MW assisted synthesis of 2-aroylbenzo[*b*]furans

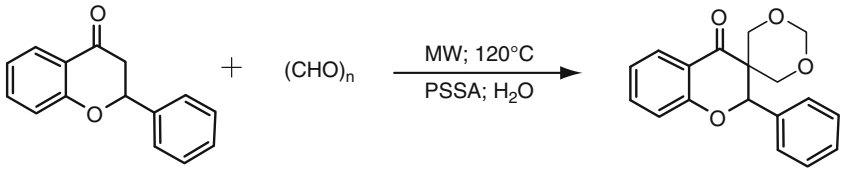

Green Chemistry with Microwave Energy. Scheme 36
PSSA-catalyzed synthesis of 1,3-dioxanes in aqueous media

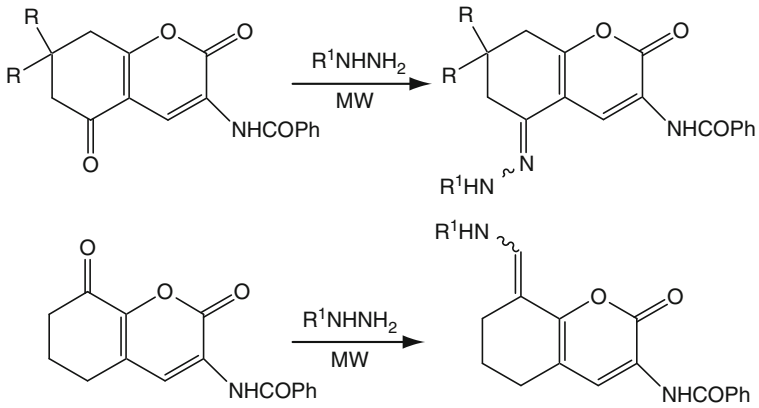

Green Chemistry with Microwave Energy. Scheme 37
Synthesis of heterocyclic hydrazones under solvent-free conditions (Ref. [85])

oped by this group recently (Scheme 38). The protocol entails the simple filtration as the product isolation step in a reaction that proceeds in the absence of any organic solvent under MW irradiation [87].

Sulfur Heterocycles Synthesis of thiazoles often involves utilization of lachrymatory starting materials, phenacyl halides, and hazardous reagents under drastic conditions. Varma and coworkers accomplished the synthesis of 1,3-thiazoles (which are not easily accessible under classical heating conditions) in excellent yields [83] from thioamides and α-tosyloxyketones catalyzed by montmorillonite K-10 clay, (Scheme 39).

The strategy was extended to a concise synthesis of bridgehead 3-aryl-5,6-dihydroimidazo[2,1-*b*][1,3]thiazoles [8], which are difficult to obtain, requiring heating over an extended period of time, and uses α-haloketones or α-tosyloxyketones under strongly acidic conditions. The solventless mixing of α-tosyloxyketones with thioamides in the presence of montmorillonite K-10 clay and exposing the reactants to MW irradiation for 3 min affords the substituted bridgehead thiazoles (Scheme 40) [83].

A novel one-pot solventless synthesis of 1,3,4-oxadiazoles and 1,3,4-thiadiazoles via condensation of acid hydrazide and triethyl orthoalkanates under MW irradiation was recently developed (Scheme 41) [88].

Synthesis of Nanomaterials

The use of MW irradiation as an efficient, environmentally friendly, and economically viable heating method for the production of nanomaterials has increased in recent years. Synthesis of gold (Au) nanoparticles with various morphologies using sugar as reducing agent under MW heating was reported by Nadagouda and Varma [89]. The authors reported the synthesis of nanoparticles (Fig. 2), prism, hexagons, and rods using a wide variety of sugars (D-glucose, sucrose, mannose, etc.) as reducing agents. The highly dispersed

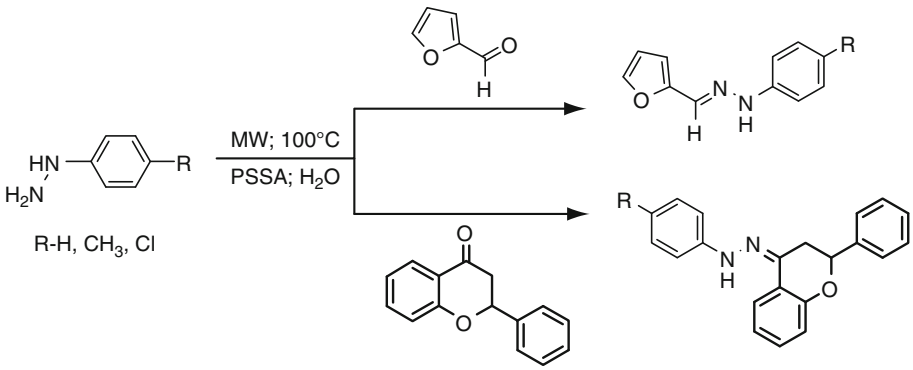

Green Chemistry with Microwave Energy. Scheme 38
Synthesis of hydrazone derivatives of furaldehyde and flavanone in water

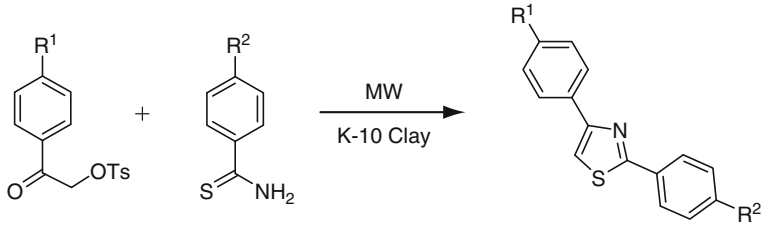

Green Chemistry with Microwave Energy. Scheme 39
MW-assisted solventless synthesis of 1,3-thiazoles

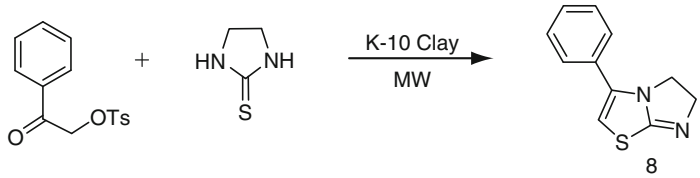

Green Chemistry with Microwave Energy. Scheme 40
MW-assisted solventless synthesis of bridgehead-thiazoles

nanoparticles are produced in the size range of 10–20 nm in less than a minute. When low concentration of sugar is used, hexagonal, triangular, and rod-shaped particles with submicron sizes are obtained.

Baruwati and Varma [90] reported the MW-assisted synthesis of Au nanoparticles along with other noble metal nanoparticles using red wine and red grape pomace extract as a single source of reducing and capping agent; highly dispersed nanoparticles are produced in the size range 5–20 nm (Fig. 3) and only 45–60 s reaction time is required. This general method produces silver (Ag), Pd, platinum (Pt), and iron (Fe)

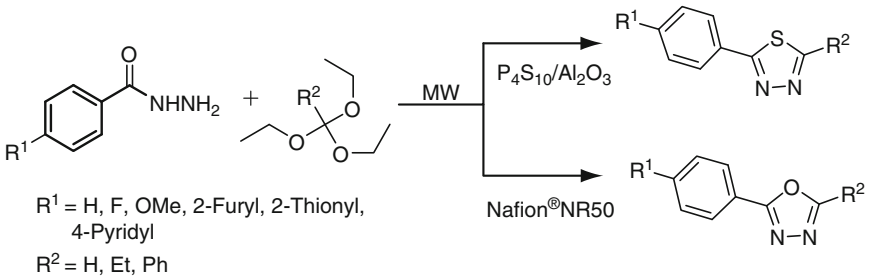

Green Chemistry with Microwave Energy. Scheme 41
One-pot solventless synthesis of 1,3,4-oxadiazoles and 1,3,4-thiadiazoles

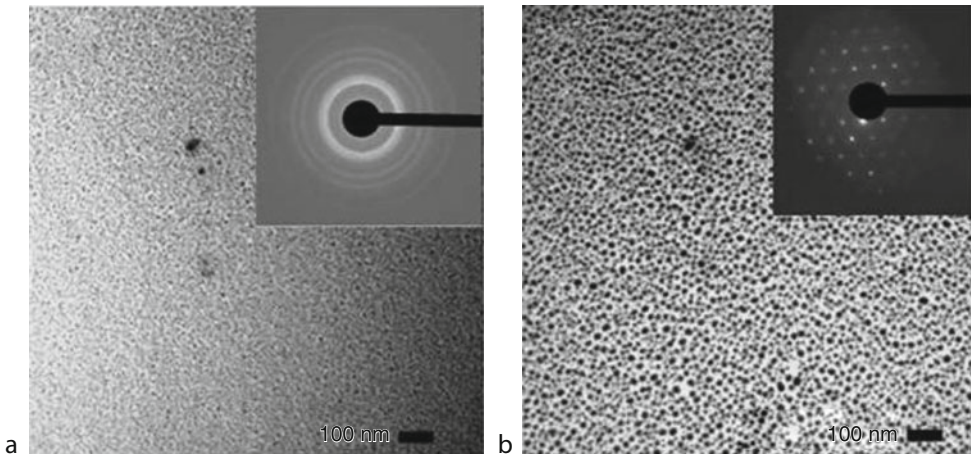

Green Chemistry with Microwave Energy. Figure 2
Au nanoparticles synthesized with (**a**) glucose and (**b**) sucrose under MW irradiation conditions (Ref. [88])

in the particle range 5–20 nm. In contrast, white wine produces highly agglomerated nanoparticles because of lack of polyphenolics which are present in red grape pomace as well as in red wine.

Highly dispersed Ag nanoparticles in the size range 5–10 nm were prepared by Varma et al. [91] using aqueous MW approach within a minute utilizing a completely benign and ubiquitous tripeptide, glutathione (Structure 1). Normally, crystalline Ag nanoparticles (Fig. 4) are obtained and the effect of MW power on the morphology of ensuing Ag nanoparticles has also been investigated for this green and sustainable procedure which is adaptable for the synthesis of Pd, Pt, and Au nanoparticles

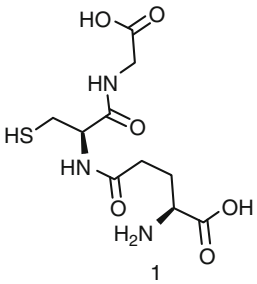

1

Chemical structure of tripeptide, Glutathione

Greener Synthesis of Nanomaterials The development of solution-based controlled synthesis of nanomaterials via a bottom-up approach often uses

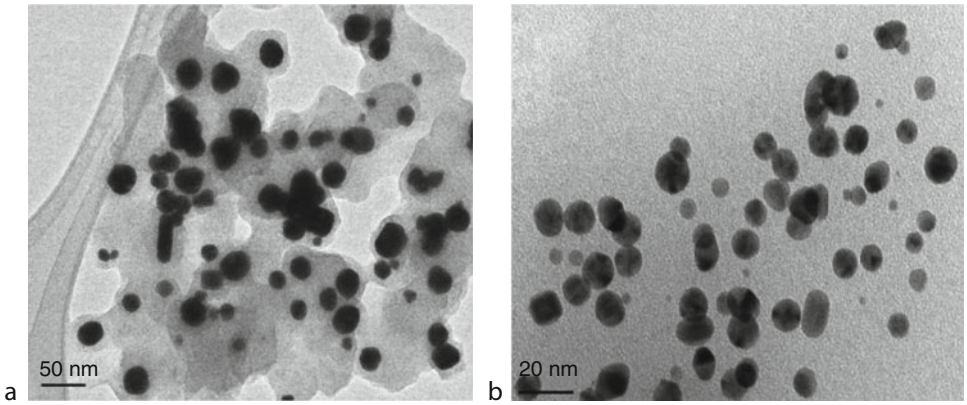

Green Chemistry with Microwave Energy. Figure 3
Au nanoparticles synthesized using (**a**) red wine and (**b**) red grape pomace at MW power level 50 W, time 1 min (Ref. [89])

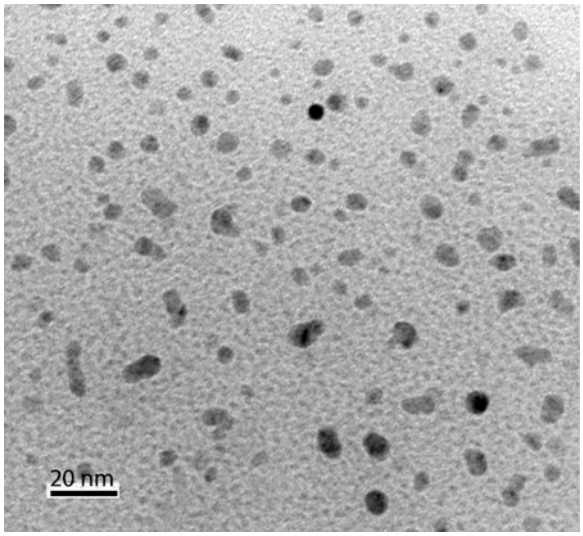

Green Chemistry with Microwave Energy. Figure 4
TEM micrograph of Ag nanoparticles at MW power level of 50 W for 1 min (Ref. [90])

toxic reducing and capping agents and some dispersants. Greener alternatives, especially using a biomimetic approach, are now possible wherein benign entities such as vitamin B_1 [92], vitamin B_2 [93], vitamin C [94], tea polyphenols [95], simple sugars [89], and PEG [96] can generate nanoparticles. These nanoparticles can be cross-linked under the influence of microwaves to form nanocomposites with cellulose [97] or polyvinyl alcohol (PVA) [98].

Vitamin B_1 was used for one-step synthesize of Pd nanobelts, nanoplates, and nanotrees without using any special capping agents (Fig. 5) [92]. Depending upon the Pd concentration, Pd nanoparticles crystallized in various shapes and sizes. At lower Pd concentration, plate-like shape was obtained. The Pd plates were grown on a single Pd nanorod backbone mimicking the leaf-like structures. However with increase in Pd concentration, formation of tree-like structures was observed. Upon further increase in concentration, Pd nanoplates become thicker by vertically aligning themselves to form ball-like shape and this general protocol can be extended to prepare other noble nanomaterials such as Au and Pt. The Pd nanoparticles showed excellent catalytic activity for several C–C bond-forming reactions such as Suzuki, Heck, and Sonogashira reactions under MW irradiation conditions [92].

The control of the size and morphology of nanostructures to tailor the physical and chemical properties is an important aspect in nanoscience. Recently, Varma et al. designed a convenient method for the synthesis of metal oxides with 3D nanostructures [99, 100] which are obtainable from hydrolysis of inexpensive starting materials in water without using any reducing or capping reagent. This economical and environmentally sustainable synthetic concept could ultimately enable the fine-tuning of material responses to magnetic, electrical, optical, and mechanical stimuli. Well-defined morphologies, including octahedron, sphere, triangular rod, pine, and

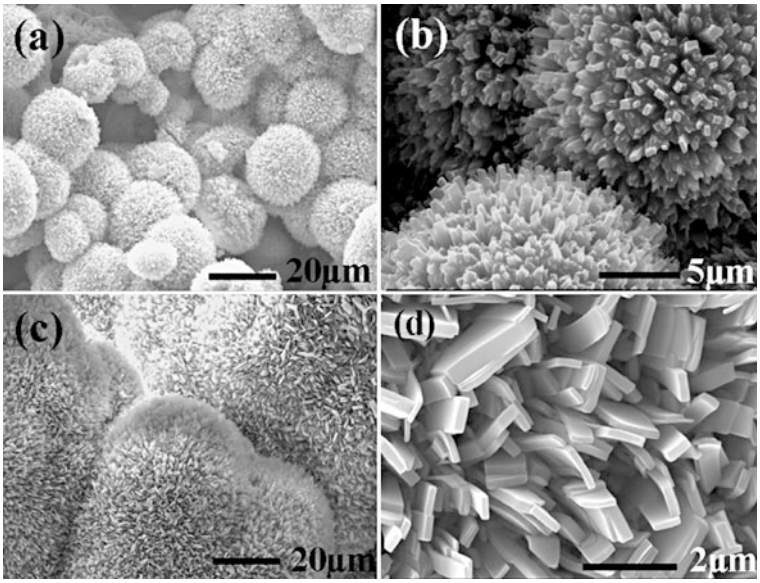

Green Chemistry with Microwave Energy. Figure 5
SEM images of Pd nanoparticles generated using vitamin B_1 (Ref. [91])

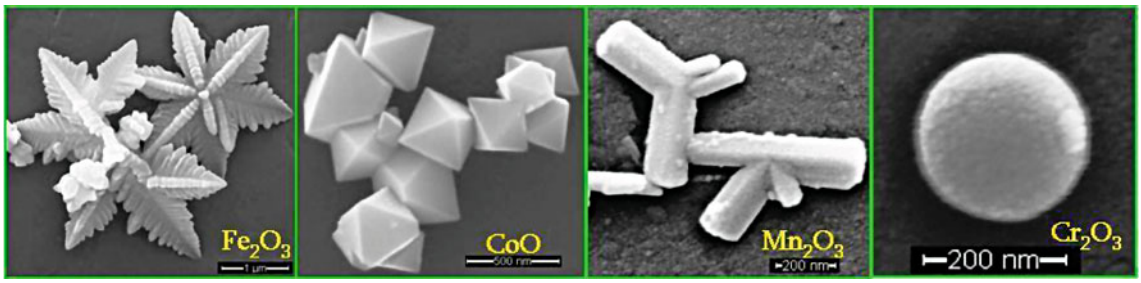

Green Chemistry with Microwave Energy. Figure 6
MW-assisted synthesis of metal oxides with well-defined morphologies (Ref. [99])

hexagonal snowflake with particles in the size range of 100–500 nm were obtained (Fig. 6). Nano-ferrites were then functionalized and coated with Pd metal, which catalyzed various C–C coupling and hydrogenation reactions with high yields. In addition, the effortless recovery and increased efficiency, combined with the inherent stability of this catalyst, rendered the method sustainable [99, 100]. In view of these unique morphologies, synthesized nanomaterials will have significant applications in biomedical science and catalysis.

MW-Assisted Synthesis of Quantum Dots (QD) in Aqueous Medium During the last decade, synthesis of high-quality semiconductor nanocrystals popularly referred to as quantum dots, QD, has been a subject of intense research because of their size-dependent properties. These colloidal semiconductor nanoparticles are much superior compared to the conventional dye molecules in terms of flexible photoexcitation, sharp photoemission, and superb resistance to photobleaching [101]. Their optical properties could be manipulated by changing the size and composition to meet specific wavelength requirements [102] and they have found application in quantum-dot lasers, optoelectronics, nonlinear optical devices, solar cells, and bio-tagging [103–108]. Synthesis of water-soluble ZnSe nanocrystals in

aqueous medium under MW conditions has been reported by Qian et al. [109]. These nanocrystals are water soluble, have high crystallinity, and their photoluminescence (PL) quantum yield ranges up to 17%. These properties are marked improvements when compared to ZnSe QDs prepared by conventional aqueous synthesis method. The method has eliminated the use of expensive, environmentally unfriendly reagents such as trioctylphosphine (TOP), tributylphosphine (TBP), and trioctylphosphine oxide (TOPO).

ZnS nanoballs were synthesized in saturated water solutions under MW irradiation conditions by Zhao et al. [110] under ambient air; the ensuing products were highly crystalline and about 300 nm in diameter. CdSe, PbSe, and Cu_2-*x*Se nanoparticles were prepared under MW irradiation conditions by Zhu et al. [111] wherein $CdSO_4$, $Pb(Ac)_2$, and $CuSO_4$ reacted with Na_2SeSO_3 in water in the presence of complexing agents: potassium nitrilotriacetate ($N(CH_2\text{-}COOK)_3$-NTA) for CdSe and PbSe or triethanol amine for Cu_2-*x*Se in a MW refluxing system. Although the method is simple and adequate for producing CdSe nanoparticles in 4–5 nm range, PbSe, and Cu_2-*x*Se nanoparticles were found to be bigger in size in the range 30–80 nm and often agglomerated. The method also describes how different phases of CdSe could be obtained by varying the MW heating times. A 10 min irradiation led to the formation of CdSe in the cubic (sphalerite) phase, while after 30 min, CdSe obtained is in the hexagonal cadmoselite phase.

A one-pot synthetic method for the synthesis of CdSe/ZnS core/shell QDs using MW radiation was reported by Schumacher et al. [112] and is based on the addition of a water-soluble Zn^{2+} complex, $Zn(NH_3)_4^{2+}$ to a solution containing CdSe initial nanocrystals and 3-mercaptopropionic acid (MPA). Subsequent MW heating for less than 2 h generated high-quality CdSe/ZnS-based QDs possessing good photoluminescent quantum yield (13%) and biocompatibility.

A seed-mediated approach for rapid synthesis of high-quality alloyed quantum dots (CdSe–CdS) in aqueous phase by MW irradiation was reported by Qian et al. [113]. Initially, CdSe seeds were first formed by the reaction of NaHSe and Cd^{2+}, and then alloyed quantum dots (CdSe–CdS) were rapidly generated by the release of sulfide ions from 3-mercaptopropionic acid as sulfide source with MW irradiation.

Magnetic Nanoparticles Recently, magnetic nanoparticles have emerged as viable alternatives to conventional materials, as a readily available, robust, high-surface-area heterogeneous catalyst support [114]. Post-synthetic surface modification of magnetic nanoparticles controls desirable chemical functionality and enables the generation of catalytic sites on the surfaces of resulting nano-catalyst. Their insoluble character together with paramagnetic nature enables effortless separation of these nano-catalysts from the reaction mixture using an external magnet, which eliminates the necessity of catalyst filtration. These novel nano-catalysts bridge the gap between homogeneous and heterogeneous catalysis, thus preserving the desirable attributes of both the systems.

This concept was recently explored for the development of other metal catalysts [99, 100, 115–119]. Varma and coworkers developed a convenient synthesis of nano-ferrite-supported Pd catalyst from inexpensive starting materials in water (Scheme 42) [115, 116]. This catalyst catalyzes the oxidation of alcohols and olefins with high turnover numbers and excellent selectivity. Also, being magnetically separable, this approach eliminates the requirement of catalyst filtration after completion of the reaction, which is an additional sustainable attribute of this oxidation protocol.

MW-Assisted Nano-Catalysis in Water Chemists have been under intense pressure to develop newer methods, which are expeditious and environmentally benign. One of the better alternatives is the use of nano-catalysis in conjunction with MW heating technology. The efficiency of MW heating has resulted in dramatic reductions in reaction times, reduced from days to minutes, which is very significant in process chemistry for the expedient generation of organics and nanomaterials [5, 6, 121–125].

Naturally abundant water is a good alternative because of its nonflammable, nontoxic, and noncorrosive nature, which may help reduce the dependence of chemists on hazardous solvents [6–8, 67, 74–77, 85, 126, 127]. Additionally, water can be contained because of its relatively lower vapor pressure when compared to organic solvents, thus rendering it a sustainable alternative. Interestingly, the combination of MW and aqueous medium has shown excellent benefits such as shorter reaction times, homogeneous

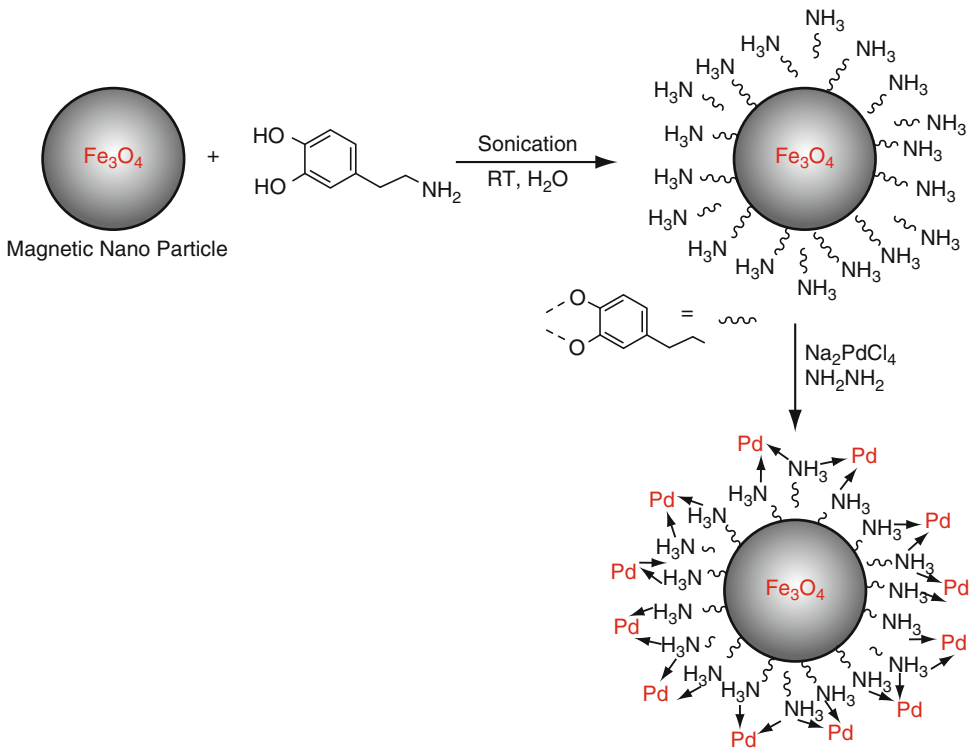

Green Chemistry with Microwave Energy. Scheme 42
Dopamine functionalized nanoferrite-Pd-catalyst. From Polshettiwar and Varma (Ref. [119])

in-core heating, and enhanced yields and selectivity [6–8, 67, 74–77]. In addition to these microwave "thermal effects" and "nonthermal effects" [128], there are additional benefits of using microwaves for nano-catalyzed aqueous protocols as described below:

1. Selectivity toward water

   Microwave heating depends on the composition and structure of molecules (i.e., their dielectric properties) and this property can facilitate selective heating. Microwaves initiate the rapid and intense heating of polar molecules such as water, while nonpolar molecules do not absorb the radiation and are not heated. Loupy and Varma [121], Strauss [122], and Larhed [129] demonstrated that this selective heating can be exploited to develop a high yield rapid MW protocol using a two phase (polar–nonpolar) solvent system. The advantageous use of water in the MW-assisted processes, especially without the use of phase-transfer catalysts [121], has been well demonstrated [6–8, 67, 74–77].

2. Selectivity toward catalyst

   Selective heating can be exploited in heterogeneous catalysis methods as demonstrated in MW-assisted rapid molybdenum-catalyzed allylic reactions by Larhead and his coworkers [130] and in the case of oxidation of alcohol using Magtrieve™ by Bogdal et al. [131]. These authors established that the polar catalyst absorbed extra energy and heated at a higher temperature than the overall reaction temperature, thus making the process more energy efficient.

3. Nano-catalysts serve as susceptors

   Susceptors are materials that efficiently absorb MW irradiation and transfer the generated thermal energy to molecules in the vicinity that are weak MW absorbers. Although transmission of the energy occurs through conventional mechanisms, MW heating is more rapid than conventional heating. Kappe [132] and Leadbeater [133] used silicon carbide and ionic liquid, respectively, as susceptors and established that addition of these

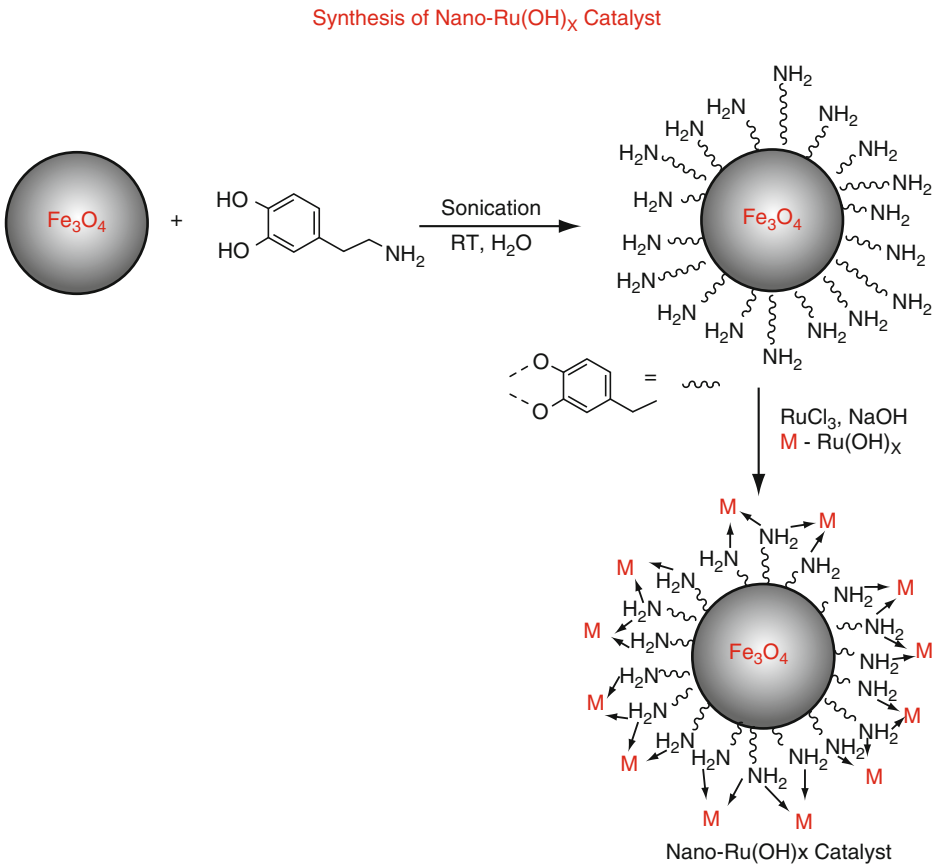

Green Chemistry with Microwave Energy. Scheme 43
Magnetically separable nano-Ru(OH)$_x$ catalyst. From Polshettiwar and Varma (Ref. [119])

materials in the reaction mixture enhanced its overall capacity to absorb microwaves and significantly reduced the required MW energy. The use of these materials as susceptors in the reaction mixture, however, adds to the overall cost of the protocol. Ideally, if suitably designed nanomaterials can play a dual role of catalyst and susceptor, then the advantageous attributes can be enjoyed without the need of any additional material as a susceptor.

4. Nano-catalyst stability

MW-assisted reactions are often fast and consequently the residence time of nano-catalysts at this elevated temperature is kept to a minimum. Catalytic processes with short reaction times thus safeguard the catalyst from deactivation and decomposition, thereby increasing the overall efficiency of the catalyst and the entire method.

It appears that this approach of unifying MW technique with nano-catalysis and benign water (as a reaction medium) can offer an extraordinary synergistic effect with greater potential than these three individual components in isolation. To illustrate the concept of this green and sustainable approach, some representative protocols are presented below.

Ruthenium Hydroxide Nano-Catalyst in MW-Assisted Hydration of Nitriles in Water Amides have been generally prepared by the hydration of nitriles, with catalysis by strong acids and bases which produces several by-products including carboxylic acids. Under the influence of strong reagents and harsh conditions, however, sensitive functional groups on molecules could not be kept intact, thus decreasing the selectivity of the reaction protocol. Heterogeneous

catalyst systems have been developed to overcome these drawbacks associated with homogeneous processes. The limited turnover numbers of these protocols and reusability of the catalyst are continuing challenges. A hydration method in pure water improved the reaction conditions and product yield [134], but it used expensive ruthenium (Ru) complexes as catalysts and required traditional workup using volatile organic solvents for isolation purposes. A green and sustainable pathway was developed using ruthenium hydroxide nano-catalyst under aqueous MW conditions [135] wherein nano-$Ru(OH)_x$ was prepared in two steps. Magnetic nanoparticles were functionalized post-synthetically [100, 117] via sonication of nano-ferrites with dopamine in aqueous medium, followed by the addition of ruthenium (Ru) chloride and subsequent hydrolysis using sodium hydroxide solution (Scheme 43).

The nano-$Ru(OH)_x$ catalyst exhibited high activity for hydration of a range of activated, inactivated, and heterocyclic nitriles in water medium and the reactions rates were not influenced by the nature of the substituents on the benzonitrile molecules. This protocol with high catalytic activity displayed excellent chemoselectively and neither an electronic effect nor the position of the substituents influenced the reaction rate. In the hydration of the benzonitrile-containing dioxole ring, the reaction proceeded only at the cyano group to afford the corresponding amide, while keeping the ring intact (Scheme 44). Therefore, this protocol could be very useful in the total synthesis of drug molecules, where the selective hydration of a nitrile group to an amide is a requirement, without influencing other sensitive functional groups.

After completion of the reaction and when the stirring is stopped, the reaction mixture turns clear and catalyst is deposited on the magnetic bar because of the paramagnetic nature of the nano-$Ru(OH)_x$. The catalyst is conveniently removed using an external magnet, thus avoiding even a filtration step. After separation of catalyst, the clear reaction mixture is cooled slowly and crystals of benzamides with acceptable purity are precipitated. The complete operation is conducted in pure aqueous medium and no organic solvents are used during the reaction or in the workup steps.

Glutathione-Based Nano-organocatalyst for Aqueous MW-Assisted Synthesis of Heterocycles Organocatalysis has been a very active area of research during the past decade and this metal-free approach has attracted universal interest. Although a wide range of reactions has been successfully introduced using this strategy, most of these transformations are generally conducted in organic solvents. In aqueous protocols, it was observed that the addition of water often accelerated the organocatalyst-mediated reaction, making the overall protocol efficient and eco-friendly [136–138]. However, most of these methods use small amounts of water as reaction medium and excessive amounts of volatile organic solvents are used during the workup, which unfortunately defeats the central idea of

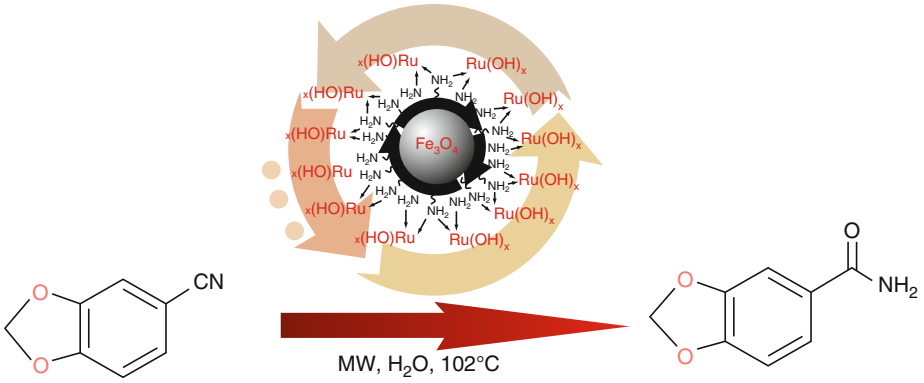

Green Chemistry with Microwave Energy. Scheme 44
Hydration of nitrile using nano-$Ru(OH)_x$ catalyst. From Polshettiwar and Varma (Ref. [119])

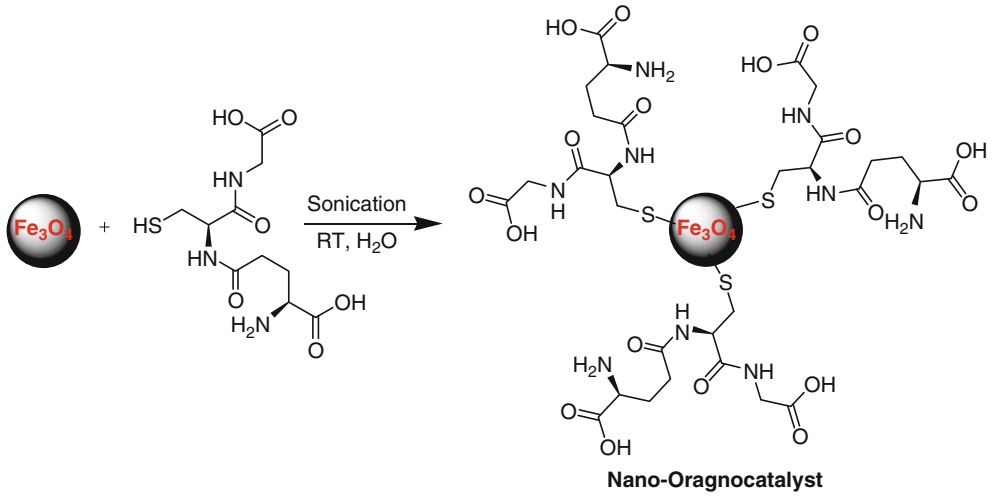

Green Chemistry with Microwave Energy. Scheme 45
Nano-ferrite functionalization using glutathione. From Polshettiwar and Varma (Ref. [119])

reducing the environmental burden of organic contaminants [139].

These drawbacks were successfully circumvented in a green and sustainable manner using glutathione-based nano-organocatalyst under aqueous MW conditions [140–142]. Glutathione, a tripeptide consisting of glutamic acid, cysteine, and glycine units, is a ubiquitous antioxidant present in human and plant cells. The use of glutathione as an active catalytic moiety is preferred due to its benign nature as well as the presence of the highly active thiol group, which can be used for attachment to solid support (ferrites). The catalyst is conveniently prepared by sono-chemical covalent anchoring of glutathione molecules via coupling of its thiol group with the free hydroxyl groups of ferrite surfaces (Scheme 45).

The successful use of this glutathione-based nano-organocatalyst approach was demonstrated by Varma et al. for the synthesis of a series of pyrrole heterocycles by Paal–Knorr reaction under aqueous MW conditions. It showed excellent catalytic activity and several amines reacted with tetrahydro-2,5-dimethoxyfuran to produce the respective pyrrole derivatives in good yields (Scheme 46) [140–142].

Using this strategy, various hydrazines and hydrazides were found to react efficiently with 1,3-diketones thus affording the desired pyrazoles in good yields (Scheme 47) [140–141]. All these reactions proceed efficiently in aqueous medium and get completed in less than 20 min under MW irradiation conditions. This general approach has recently been extended to the homocoupling of boronic acids in aqueous medium under the influence of microwaves [142].

Separation of the catalyst and final product from the reaction mixture is one of the most vital aspects of synthetic protocols. Catalyst recovery occurs generally via filtration or extractive isolation of products, both of which require excessive amounts of organic solvents. However, in the aforementioned protocols, within a few seconds after stirring is stopped, catalyst gets deposited on the magnetic bar and can be easily removed using an external magnet. In most of the experiments, after completion of the reactions, the phase separation of the desired product from the aqueous medium occurs; this facilitates the isolation of synthesized heterocycles by simple decantation, without using any volatile organic solvents during the reaction or during product workup (Schemes 46, 47).

Future Directions

The use of various alternative pathways in green chemistry domain such as solvent-free synthesis and transformations [143–145], mechanochemical reactions by grinding [146–149], reactions in benign solvents like

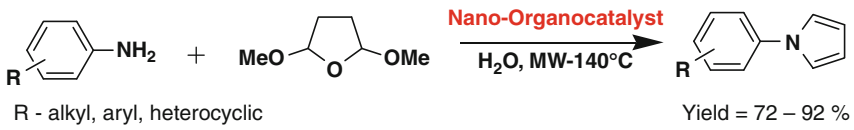

Green Chemistry with Microwave Energy. Scheme 46
Paal–Knorr reactions using nano-organocatalyst. From Polshettiwar and Varma (Ref. [119])

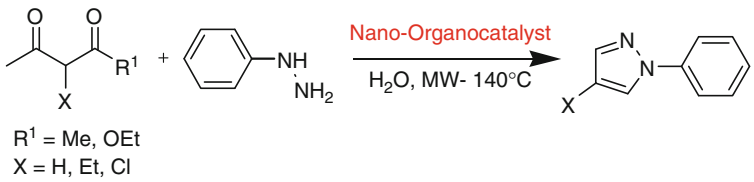

Green Chemistry with Microwave Energy. Scheme 47
Synthesis of pyrazoles using nano-organocatalyst. From Polshettiwar and Varma (Ref. [119])

water [150–153], polyethylene glycol (PEG) [154, 155], and eco-friendly generated ionic liquids [44–48] and their utility in catalysis [156–161] can be augmented nicely by the use of microwave irradiation heating technique.

The "greener" production of nanoparticles [162] with relatively attractive toxicological profile [163, 164] and their enhanced utility in catalysis [115, 116, 135, 140–142] and environmental remediation [165–167] is garnering attention.

Nano-catalysts mimic homogeneous (easily accessible, high surface area) as well as heterogeneous (stable, easy to handle and isolate) catalyst systems. Nano-catalysts possessing a paramagnetic core thus allow rapid and selective chemical transformations with excellent product yield coupled with the ease of catalyst separation and recovery. Among these options, nanocatalyst-catalyzed transformations in aqueous reaction medium are one of the ideal solutions for the development of green and sustainable protocols. However, execution of many organic reactions in water is not simple due to the inherent limitation of solubility of nonpolar reactants in polar aqueous medium, which can be assisted by using MW irradiation conditions. Thus, a combination of benign water medium, nonconventional MW heating, and nano-catalyst seems to be the optimum pathway to develop the next generation of highly efficient processes [120].

Disclaimer

The views expressed in this article are those of the author and do not necessarily reflect the views and policies of the US Environmental Protection Agency. The use of trade names does not imply endorsement by the US Government.

Bibliography

Primary Literature

1. Anastas PT, Warner JC (2000) Green chemistry: theory and practice. Oxford University Press, Oxford
2. Varma RS (1999) Solvent-free organic syntheses using supported reagents and microwave irradiation. Green Chem 1:43–55
3. Varma RS (1999) Solvent-free syntheses of heterocycles using microwave irradiation. J Heterocyclic Chem 36:1565–1571
4. Varma RS (2000) Clay and clay-supported reagents in organic synthesis. Tetrahedron 58:1235–1255
5. Polshettiwar V, Varma RS (2008) Microwave-assisted organic synthesis and transformations using benign reaction media. Acc Chem Res 41:629–639
6. Polshettiwar V, Varma RS (2008) Aqueous microwave chemistry: a clean and green synthetic tool for rapid drug discovery. Chem Soc Rev 37:1546–1557
7. Li C-J, Chen L (2006) Organic chemistry in water. Chem Soc Rev 35:68–82
8. Varma RS (2007) Clean chemical synthesis in water. Org Chem Highlight. http://www.organic-chemistry.org/Highlights/2007/01February.shtm

9. Strauss CR, Trainor RW (1995) Developments in microwave-assisted organic chemistry. Aust J Chem 48:1665–1692
10. Anonymous (1924) Using chemical reagents on porous carriers. Akt –Ges Fur Chemiewerte Brit Pat 231: 901 [Chem Abst (1925) 19: 3571]
11. Laszlo P (1987) Preparative chemistry using supported reagents. Academic, San Diego
12. Smith K (1992) Solid supports and catalyst in organic synthesis. Ellis Hardwood, Chichester
13. Clark JH (1994) Catalysis of organic reactions by supported inorganic reagents. VCH, New York
14. McKillop A, Young KW (1979) Organic synthesis using supported reagents – Part I & Part II. Synthesis 401–422 and 481–500
15. Cornelis A, Laszlo P (1985) Clay-supported copper(II) and iron (III) nitrates: novel multi-purpose reagents for organic synthesis. Synthesis 100:909–918
16. Gedye R, Smith F, Westaway K, Humera A, Baldisera L, Laberge L, Rousell J (1986) The use of microwave ovens for rapid organic synthesis. Tetrahedron Lett 27:279–282
17. Giguere RJ, Bray TL, Duncan SM, Majetich G (1986) Application of commercial microwave ovens to organic synthesis. Tetrahedron Lett 27:4945–4948
18. Varma RS (2002) Advances in green chemistry: chemical syntheses using microwave irradiation. AstraZeneca Research Foundation India, Bangalore [85 Reaction schemes, ~300 references]
19. Varma RS (2002) Organic synthesis using microwaves and supported reagents. In: Loupy A (ed) Microwaves in organic synthesis, Chapter 6. Wiley-VCH, New York, pp 181–218
20. Pillai UR, Sahle-Demessie E, Varma RS (2002) Environmentally friendlier organic transformations on mineral supports under non-traditional conditions. J Mater Chem 12:3199–3207
21. Varma RS (2001) Solvent-free accelerated organic syntheses using microwaves. Pure Appl Chem 73:193–198
22. Perreux L, Loupy A (2001) A tentative rationalization of microwave effects in organic synthesis according to the reaction medium, and mechanistic considerations. Tetrahedron 57:9199–9223
23. Loupy A, Petit A, Hamelin J, Texier-Boullet F, Jacquault P, Mathe D (1998) New solvent-free organic synthesis using focused microwaves. Synthesis 1998:1213–1234
24. Gutierrez E, Loupy A, Bram G, Ruiz-Hitzky E (1989) Inorganic solids in "dry media" an efficient way for developing microwave irradiation activated organic reactions. Tetrahedron Lett 30:945–948
25. Greene TW, Wuts PGM (1991) Protective groups in organic synthesis, 2nd edn. Wiley, New York
26. Varma RS, Varma M, Chatterjee AK (1993) Microwave-assisted deacetylation on alumina: a simple deprotection method. J Chem Soc Perkin Trans −1 999–1000
27. Varma RS, Chatterjee AK, Varma M (1993) Alumina-mediated deacetylation of benzaldehyde diacetates. A simple deprotection method. Tetrahedron Lett 34:3207–3210
28. Varma RS, Chatterjee AK, Varma M (1993) Alumina-mediated microwave thermolysis: a new approach to deprotection of benzyl esters. Tetrahedron Lett 34:4603–4606
29. Varma RS, Lamture JB, Varma M (1993) Alumina-mediated cleavage of *t*-butyldimethylsilyl ethers. Tetrahedron Lett 34:3029–3032
30. Varma RS, Kumar D (1999) Microwave-accelerated solvent-free synthesis of thioketones, thiolactones, thioamides thionoesters and thioflavonoids. Org Lett 1:697–700
31. Varma RS, Saini RK (1997) Solid state dethioacetalization using clayfen. Tetrahedron Lett 38:2623–2624
32. Varma RS, Saini RK, Dahiya R (1997) Active manganese dioxide on silica: oxidation of alcohols under solvent-free conditions using microwaves. Tetrahedron Lett 38:7823–7824
33. Namboodiri VV, Polshettiwar V, Varma RS (2007) Expeditious oxidation of alcohols to carbonyl compounds using iron (III) nitrate. Tetrahedron Lett 48:8839–8842
34. Varma RS, Dahiya R, Saini RK (1997) Iodobenzene diacetate on alumina: rapid oxidation of alcohols to carbonyl compounds in solventless system using microwaves. Tetrahedron Lett 38:7029–7032
35. Varma RS, Dahiya R, Kumar D (1998) Solvent-free oxidation of benzoins using oxone® on wet alumina under microwave irradiation. Molecules Online 2:82–85
36. Varma RS, Saini RK, Meshram HM (1997) Selective oxidation of sulfides to sulfoxides and sulfones by microwave thermolysis on wet silica-supported sodium periodate. Tetrahedron Lett 38:6525–6528
37. Varma RS, Kumar D (1999) Solid state oxidation of 1,4-dihydropyridines to pyridines using phenyliodine(III) bis (trifluoroacetate) or elemental sulfur. J Chem Soc Perkin Trans −1 1755–1757
38. Varma RS, Saini RK (1997) Microwave-assisted reduction of carbonyl compounds in solid state using sodium borohydride supported on alumina. Tetrahedron Lett 38:4337–4338
39. Varma RS, Dahiya R (1998) Sodium borohydride on wet clay: solvent-free reductive amination of carbonyl compounds using microwaves. Tetrahedron 54:6293–6298
40. Vass A, Dudas J, Toth J, Varma RS (2001) Solvent-free reduction of aromatic nitro compounds with alumina-supported hydrazine under microwave irradiation. Tetrahedron Lett 42:5347–5349
41. Varma RS, Naicker KP (1998) Hydroxylamine on clay: a direct synthesis of nitriles from aromatic aldehydes using microwaves under solvent-free conditions. Molecules Online 2: 94–96
42. Welton T (2004) Ionic liquids in catalysis. Coord Chem Rev 248:2459–2477
43. Rogers RD, Seddon KN, Volkove S (2002) Green Industrial applications of ionic liquids. NOTO science, series
44. Varma RS, Namboodiri, VV (2001) An expeditious solvent-free route to ionic liquids using microwaves. Chem. Commun 643–644
45. Namboodiri VV, Varma RS (2002) An improved preparation of 1, 3-dialkylimidazolium tetrafluoroborate ionic liquids using microwaves. Tetrahedron Lett 43:5381–5383
46. Namboodiri VV, Varma RS (2002) Solvent-free sonochemical preparation of ionic liquids. Org Lett 4:3161–3163

47. Kim YJ, Varma RS (2005) Microwave-assisted preparation of imidazolium-based tetrachloroindate (III) and their application in the tetrahydropyranylation of alcohols. Tetrahedron Lett 46:1467–1469
48. Kim YJ, Varma RS (2005) Microwave-assisted preparation of 1-butyl-3-methylimidazolium tetrachlorogallate and its catalytic use in acetal formation under mild conditions. Tetrahedron Lett 46:7447–7449
49. Swatloski RP, Spear SK, Holbrey JD, Rogers RD (2002) Dissolution of cellulose with ionic liquids. J Am Chem Soc 124:4974–4975
50. Varma RS, Namboodiri VV (2002) Microwave-assisted preparation of dialkylimidazolium tetrachloroaluminates and their use as catalysts in the solvent-free tetrahydropyranylation of alcohols and phenols. Chem Commun 342–343
51. Kim YJ, Varma RS (2005) Tetrahaloindate(III)-based ionic liquids in the coupling reaction of carbon dioxide and epoxides to generate cyclic carbonates: H-bonding and mechanistic studies. J Org Chem 70:7882–7891
52. Plechkova NV, Seddon KR (2008) Applications of ionic liquids in the chemical industry. Chem Soc Rev 37:123–150
53. Herrero MA, Kremsner JM, Kappe CO (2008) Nonthermal microwave effects revisited – on the importance of internal temperature monitoring and agitation in microwave chemistry. J Org Chem 73:36–47
54. Polshettiwar V, Varma RS (2007) Greener and sustainable approaches to the synthesis of pharmaceutically active heterocycles. Curr Opin Drug Discov Devel 10:723–737
55. Chen J, Spear SK, Huddleston JG, Rogers RD (2005) Polyethylene glycol and solutions of polyethylene glycol as green reaction media. Green Chem 7:64–82
56. Leadbeater NE, Marco M (2003) Rapid and amenable Suzuki coupling reaction in water using microwave and conventional heating. J Org Chem 68:888–892
57. Crozet MD, Castera-Ducros C, Vanelle P (2006) An efficient microwave-assisted Suzuki cross-coupling reaction of imidazo [1, 2-a] pyridines in aqueous medium. Tetrahedron Lett 47:7061–7065
58. Zhu R, Qu F, Queleverb G, Peng L (2007) Direct synthesis of 5-aryltriazole acyclonucleosides via Suzuki coupling in aqueous solution. Tetrahedron Lett 48:2389–2393
59. Dawood KM (2007) Microwave-assisted Suzuki–Miyaura and Heck–Mizoroki cross-coupling reactions of aryl chlorides and bromides in water using stable benzothiazole-based palladium (II) precatalysts. Tetrahedron 63:9642–9651
60. Arvela RK, Leadbeater NE (2005) Microwave-promoted Heck coupling using ultralow metal catalyst concentrations. J Org Chem 70:1786–1790
61. Arvela RK, Pasquini S, Larhed M (2007) Highly regioselective internal Heck arylation of hydroxyalkyl vinyl ethers by aryl halides in neat water. J Org Chem 72:6390–6396
62. Appukkuttan P, Dehaen W, der Eycken EV (2003) Transition-metal-free Sonogashira-type coupling reactions in water. Eur J Org Chem 2003:4713–4716
63. Alcida E, Najera C (2006) The first fluoride-free Hiyama reaction of vinylsiloxanes promoted by sodium hydroxide in water. Adv Synth Catal 348:2085–2091
64. Kaval N, Bisztray K, Dehaen W, Kappe CO, der Eycken EV (2003) Microwave-enhanced transition metal-catalyzed decoration of 2(1H)-pyrazinone scaffolds. Mol Divers 7:125–133
65. Miyazawa A, Tanaka K, Sakakura T, Tashiro M, Tashiro H, Surya Prakash GK, Olah GA (2005) Microwave-assisted direct transformation of amines to ketones using water as an oxygen source. Chem Commun 2104–2106
66. Kumar V, Sharma A, Sharma A, Sinha AK (2007) Remarkable synergism in methylimidazole-promoted decarboxylation of substituted cinnamic acid derivatives in basic water medium under microwave irradiation: a clean synthesis of hydroxylated (*E*)-stilbenes. Tetrahedron 63:7640–7646
67. Dallinger D, Kappe CO (2007) Microwave-assisted synthesis in water as solvent. Chem Rev 107:2563–2591
68. Garuti L, Roberti M, Pizzirani D (2007) Nitrogen-containing heterocyclic quinones: a class of potential selective antitumor agents. Mini Rev Med Chem 7:481–489
69. Sperry JB, Wright DL Furans (2005) Thiophenes and related heterocycles in drug discovery. Curr Opin Drug Discov Devel 8:723–740
70. Kappe CO (2002) High-speed combinatorial synthetics utilizing microwave irradiation. Curr Opin Chem Biol 6:314–320
71. Polshettiwar V, Varma RS (2008) Greener and expeditious synthesis of bio-active heterocycles using microwave irradiation. Pure Appl Chem 80:777–790
72. Roberts BA, Strauss CR (2005) Toward rapid, "green", predictable microwave-assisted synthesis. Acc Chem Res 38:653–661
73. Kappe CO (2004) Controlled microwave heating in modern organic synthesis. Angew Chem Int Ed 43:6250–6284
74. Ju Y, Varma RS (2004) Aqueous *N*-alkylation of amines using alkyl halides: direct generation of tertiary amines under microwave irradiation. Green Chem 6:219–221
75. Ju Y, Varma RS (2005) An efficient and simple aqueous *N*-heterocyclization of aniline derivatives: microwave-assisted synthesis of *N*-aryl azacycloalkanes. Org Lett 7:2409–2411
76. Ju Y, Varma RS (2005) Microwave-assisted cyclocondensation of hydrazine derivatives with alkyl dihalides or ditosylates in aqueous media: syntheses of pyrazole, pyrazolidine and phthalazine derivatives. Tetrahedron Lett 46:6011–6014
77. Ju Y, Varma RS (2006) Aqueous *N*-heterocyclization of primary amines and hydrazines with dihalides: microwave-assisted syntheses of *N*-azacycloalkanes, isoindole, pyrazole, pyrazolidine, and phthalazine derivatives. J Org Chem 71:135–141
78. Ju Y, Li C-J, Varma RS (2004) Microwave-assisted Cu (I) catalyzed solvent-free three component coupling of aldehyde, alkyne and amine. QSAR Comb Sci 23:891–894
79. Kim YJ, Varma RS (2004) Microwave-assisted preparation of cyclic ureas from diamines in the presence of ZnO. Tetrahedron Lett 45:7205–7208
80. Varma RS, Kumar D (1999) Microwave-accelerated three-component condensation reaction on clay: solvent-free synthesis of imidazo [1, 2-a] annulated pyridines, pyrazines and pyrimidones. Tetrahedron Lett 40:7665–7669
81. Kappe CO, Kumar D, Varma RS (1999) Microwave-assisted high-speed parallel synthesis of 4-aryl-3,

4-dihydropyrimidin-2(1H)-ones using a solventless Biginelli condensation protocol. Synthesis 10:1799–1803
82. Polshettiwar V, Varma RS (2007) Biginelli reaction in aqueous medium: a greener and sustainable approach to substituted 3, 4-dihydropyrimidin-2(1H)-ones. Tetrahedron Lett 48: 7343–7346
83. Varma RS, Dahiya R (1998) An expeditious and solvent-free synthesis of 2-amino-substituted isoflav-3-enes using microwave irradiation. J Org Chem 63:8038–8041
84. Varma RS, Kumar D, Liesen PJ (1998) Solid state synthesis of 2-aroylbenzo[b]furans, 1,3-thiazoles and 3-aryl-5,6-dihydroimidazo [2,1-b][1,3] thiazoles from α-tosyloxyketones using microwave irradiation. J Chem Soc Perkin Trans −1 4093–4096
85. Polshettiwar V, Varma RS (2007) Tandem bis-aldol reaction of ketones: a facile one pot synthesis of 1, 3-dioxanes in aqueous medium. J Org Chem 72:7420–7422
86. Jeselnik M, Varma RS, Polanc S, Kocevar M (2001) Catalyst-free reactions under solvent-free conditions: microwave-assisted synthesis of heterocyclic hydrazones below the melting points of neat reactants. Chem Commun 1716–1717
87. Polshettiwar V, Varma RS (2007) Polystyrene sulfonic acid catalyzed greener synthesis of hydrazones in aqueous medium using microwaves. Tetrahedron Lett 48:5649–5652
88. Polshettiwar V, Varma RS (2008) Rapid access to bio-active heterocycles: one-pot solvent-free synthesis of 1, 3, 4-oxadiazoles and 1, 3, 4-thiadiazoles. Tetrahedron Lett 49:879–883
89. Nadagouda MN, Varma RS (2007) Microwave-assisted shape-controlled bulk synthesis of noble nanocrystals and their catalytic properties. Cryst Growth Des 7:686–690
90. Baruwati B, Varma RS (2009) High value products from waste: grape pomace extract – a three-in-one package for the synthesis of metal nanoparticles. ChemSusChem 2:1041–1044
91. Baruwati B, Polshettiwar V, Varma RS (2009) Glutathione promoted expeditious green synthesis of silver nanoparticles in water using microwaves. Green Chem 11:926–930
92. Nadagouda MN, Polshettiwar V, Varma RS (2009) Self-assembly of palladium nanoparticles: synthesis of nanobelts, nanoplates and nanotrees using vitamin B_1 and their application in carbon-carbon coupling reactions. J Mater Chem 19:2026–2031
93. Nadagouda MN, Varma RS (2006) Green and controlled synthesis of gold and platinum nanomaterials using vitamin B_2: density-assisted self-assembly of nanospheres, wires and rods. Green Chem 8:516–518
94. Nadagouda MN, Varma RS (2007) A greener synthesis of core (Fe, Cu)-shell (Au, Pt, Pd and Ag) nanocrystals using aqueous vitamin C. Cryst Growth Des 7:2582–2587
95. Nadagouda MN, Varma RS (2008) Green synthesis of silver and palladium nanoparticles at room temperature using coffee and tea extract. Green Chem 10:859–862
96. Nadagouda MN, Varma RS (2008) Microwave-assisted shape controlled bulk synthesis of Ag and Fe nanorods in poly (ethylene glycol) solutions. Cryst Growth Des 8:291–295
97. Nadagouda MN, Varma RS (2007) Synthesis of thermally stable carboxymethyl cellulose/metal biodegradable nanocomposite films for potential biological applications. Biomacromolecules 8:2762–2767
98. Nadagouda MN, Varma RS (2007) Microwave-assisted synthesis of cross-Linked poly (vinyl alcohol) nanocomposites comprising single-wall carbon nanotubes (SWNT), multi-wall carbon nanotubes (MWNT) and buckminsterfullerene (C-60). Macromol Rapid Commun 28:842–847
99. Polshettiwar V, Nadagouda MN, Varma RS (2007) Synthesis and applications of micro-pine structured nano-catalyst. Chem Commun 6318–6320
100. Polshettiwar V, Baruwati B, Varma RS (2009) Self-assembly of metal oxides into three-dimensional nanostructures: synthesis and application in catalysis. ACS Nano 3:728–736
101. Mamedov AA, Belov A, Giersig M, Mamedova NN, Kotov NA (2001) Nanorainbows: graded semiconductor films from quantum dots. J Am Chem Soc 123:7738–7739
102. Alivisatos P (1996) Semiconductor clusters, nanocrystals, and quantum dots. Science 271:933–937
103. Klimov VI, Mikhailovsky AA, Xu S, Malko A, Hollingsworth JA, Leatherdale CA, Eisler H-J, Bawendi MG (2000) Optical gain and stimulated emission in nanocrystal quantum dots. Science 290:314–317
104. Sundar VC, Eisler H-J, Bawendi MG (2002) Room-temperature, tunable gain media from novel II-VI nanocrystal-titania composite matrices. Adv Mater 14:739–743
105. Bruchez M, Moronne M, Gin P, Weiss S, Alivisatos AP (1998) Semiconductor nanocrystals as fluorescent biological labels. Science 281:2013–2016
106. Chan WCW, Nie S (1998) Quantum dot bioconjugates for ultrasensitive nonisotopic detection. Science 281:2016–2018
107. Michalet X, Pinaud FF, Bentolila LA, Tsay JM, Doose S, Li JJ, Sundaresan G, Wu AM, Gambhir SS, Weiss S (2005) Quantum dots for live cells, in vivo imaging, and diagnostics. Science 307:538–544
108. Murray CB, Norris DJ, Bawendi MG (1993) Synthesis and characterization of nearly monodisperse CdE (E=sulfur, selenium, tellurium) semiconductor nanocrystallites. J Am Chem Soc 115:8706–8715
109. Qian H, Qiu X, Li L, Ren J (2006) Microwave-assisted aqueous synthesis: a rapid approach to prepare highly luminescent ZnSe(S) alloyed quantum dots. J Phys Chem B 110:9034–9040
110. Zhao Y, Hong J-M, Zhu J-J (2004) Microwave-assisted self-assembled ZnS nanoballs. J Cryst Growth 270:438–445
111. Zhu J, Palchik O, Chen S, Gedanken A (2000) Microwave assisted preparation of CdSe, PbSe, and $Cu_{2-x}Se$ nanoparticles. J Phys Chem B 104:7344–7347
112. Schumacher W, Nagy A, Waldman WJ, Dutta PK (2009) Direct synthesis of aqueous CdSe/ZnS-based quantum dots using microwave irradiation. J Phys Chem C 113:12132–12139
113. Qian H, Li L, Ren J (2005) One-step and rapid synthesis of high quality alloyed quantum dots (CdSe–CdS) in aqueous phase by microwave irradiation with controllable temperature. Mater Res Bull 40:1726–1736

114. Lu A-H, Salabas EL, Schuth F (2007) Magnetic nanoparticles: synthesis, protection, functionalization, and application. Angew Chem Int Ed 46:1222–1244
115. Polshettiwar V, Varma RS (2009) Nanoparticle-supported and magnetically recoverable palladium (Pd) catalyst: a selective and sustainable oxidation protocol with high turnover number. Org Biomol Chem 7:37–40
116. Polshettiwar V, Baruwati B, Varma RS (2009) Nanoparticle-supported and magnetically recoverable nickel catalyst: a robust and economic hydrogenation and transfer hydrogenation protocol. Green Chem 11:127–131
117. Polshettiwar V, Nadagouda MN, Varma RS (2008) Synthesis and applications of micro-pine structured nano-catalyst. Chem. Commun 6318–6320
118. Baruwati B, Guin D, Manorama SV (2007) Pd on surface-modified $NiFe_2O_4$ nanoparticles: a magnetically recoverable catalyst for Suzuki and Heck reactions. Org Lett 9:5377–5380
119. Guin D, Baruwati B, Manorama SV (2007) Pd on amine-terminated ferrite nanoparticles: a complete magnetically recoverable facile catalyst for hydrogenation reactions. Org Lett 9:1419–1421
120. Polshettiwar V, Varma RS (2010) Green chemistry by nano-catalysis. Green Chem 12:743–754
121. Loupy A, Varma RS (2006) Microwave effects in organic synthesis: mechanistic and reaction medium considerations. Chim Oggi 24:36–40
122. Strauss CR, Varma RS (2006) Microwaves in green and sustainable chemistry. Top Curr Chem 266:199–231
123. Kappe CO, Dallinger D (2009) Controlled microwave heating in modern organic synthesis: highlights from the 2004–2008 literature. Mol Divers 13:71–193
124. Polshettiwar V, Nadagouda MN, Varma RS (2009) Microwave-assisted chemistry: a rapid and sustainable route to synthesis of organics and nanomaterials. Aust J Chem 62:16–26
125. Gabriel C, Gabriel S, Grant EH, Halstead BSJ, Mingos DMP (1998) Dielectric parameters relevant to microwave dielectric heating. Chem Soc Rev 27:213–224
126. Poliokoff M, Licence P (2007) Sustainable technology: green chemistry. Nature 450:810–812
127. Polshettiwar V, Varma RS (2008) Olefin ring closing metathesis and hydrosilylation reaction in aqueous medium by Grubbs second generation ruthenium catalyst. J Org Chem 73:7417–7419
128. Hoz A, Diaz-Ortiz A, Moreno A (2005) Microwaves in organic synthesis. Thermal and non-thermal microwave effects. Chem Soc Rev 34:164–178
129. Nilsson P, Larhed M, Hallberg A (2001) Highly regioselective, sequential, and multiple palladium- catalyzed arylations of vinyl ethers carrying a coordinating auxiliary: an example of a Heck triarylation process. J Am Chem Soc 123:8217–8225
130. Kaiser NFK, Bremberg U, Larhed M, Moberg C, Hallberg A (2000) Fast, convenient, and efficient molybdenum-catalyzed asymmetric allylic alkylation under noninert conditions: an example of microwave-promoted fast chemistry. Angew Chem Int Ed 39:3596–3598
131. Bogdal D, Lukasiewicz M, Pielichowski J, Miciak A, Sz B (2003) Microwave-assisted oxidation of alcohols using Magtrieve™. Tetrahedron 59:649–653
132. Razzak T, Kremser JM, Kappe CO (2008) Investigating the existence of nonthermal/specific microwave affects using silicon carbide heating elements as power modulators. J Org Chem 73:6321–6329
133. Leadbeater NE, Torrenius HM (2002) A study of the ionic liquid mediated microwave heating of organic solvents. J Org Chem 67:3145–3148
134. Cadierno V, Francos J, Gimeno J (2008) Selective ruthenium-catalyzed hydration of nitriles to amides in pure aqueous medium under neutral conditions. Chem Eur J 14:6601–6605
135. Polshettiwar V, Varma RS (2009) Nanoparticle-supported and magnetically recoverable ruthenium hydroxide catalyst: effcient hydration of nitriles to amides in aqueous medium. Chem Eur J 15:1582–1586
136. Brogan AP, Dickerson TJ, Janda KD (2006) Enamine-based aldol organocatalysis in water: are they really all wet? Angew Chem Int Ed 45:8100–8102
137. Hayashi Y, Samanta S, Gotoh H, Ishikawa H (2008) Asymmetric Diels-Alder reactions of,-unsaturated aldehydes catalyzed by a diarylprolinol silyl ether salt in the presence of water. Angew Chem Int Ed 47:6634–6637
138. Huang J, Zhang X, Armstrong DW (2007) Highly efficient asymmetric direct stoichiometric aldol reactions on/in water. Angew Chem Int Ed 46:9073–9077
139. Blackmond DG, Armstrong A, Coombe V, Wells A (2007) Water in organocatalytic processes: debunking the myths. Angew Chem Int Ed 46:3798–3800
140. Polshettiwar V, Baruwati B, Varma RS (2009) Magnetic nanoparticle-supported glutathione: a conceptually sustainable organocatalyst. Chem Commun 1837–1839
141. Polshettiwar V, Varma RS (2010) Nano-organocatalyst: magnetically retrievable ferrite-anchored glutathione for microwave-assisted Paal-Knorr reaction, aza-Michael addition and pyrazole synthesis. Tetrahedron 66:1091–1097
142. Luque R, Baruwati B, Varma RS (2010) Magnetically separable nanoferrite-anchored glutathione: aqueous homocoupling of arylboronic acids under microwave irradiation. Green Chem 12:1540–1543. doi:10.1039/C0GC00083C
143. Polshettiwar V, Varma RS (2008) Ring-fused aminals: catalyst and solvent-free microwave-assisted α-amination of nitrogen heterocycles. Tetrahedron Lett 49:7165–7167
144. Varma RS, Naicker KP, Liesen PJ (1998) Microwave-accelerated crossed Cannizzaro reaction using barium hydroxide under solvent-free conditions. Tetrahedron Lett 3:8437–8440
145. Pillai UR, Sahle-Demessie E, Namboodiri VV, Varma RS (2002) An efficient and ecofriendly oxidation of alkenes using iron nitrate and molecular oxygen. Green Chem 4:495–497
146. Kumar D, Chandra Sekhar KVG, Dhillon H, Rao VS, Varma RS (2004) An expeditious synthesis of 1-aryl-4-methyl-1, 2, 4-triazolo [4, 3-a] quinoxalines under solvent-free conditions using iodobenzene diacetate. Green Chem 6:156–157

147. Kumar D, Sundaree MS, Patel G, Rao VS, Varma RS (2006) Solvent-free facile synthesis of novel α-tosyloxy β-keto sulfones using [hydroxy(tosyloxy)iodo] benzene. Tetrahedron Lett 47:8239–8241
148. Kumar D, Sundaree MS, Rao VS, Varma RS (2006) A facile one-pot synthesis of β-keto sulfones from ketones under solvent-free conditions. Tetrahedron Lett 47:4197–4199
149. Varma RS (2008) Chemical activation by mechanochemical mixing, microwave, and ultrasonic irradiation. Green Chem 10:1129–1130
150. Polshettiwar V, Varma RS (2007) Tandem bis-aza-Michael addition reaction of amines in aqueous medium promoted by polystyrenesulfonic acid. Tetrahedron Lett 48:8735–8738
151. Kumar D, Reddy VB, Mishra BG, Rana RK, Nadagouda MN, Varma RS (2007) Nanosized magnesium oxide as catalyst for the rapid and green synthesis of substituted 2-amino-2-chromenes. Tetrahedron 63:3093–3097
152. Skouta R, Varma RS, Li CJ (2005) Efficient Trost's γ-addition catalyzed by reusable polymer-supported triphenylphosphine in aqueous media. Green Chem 7:571–575
153. Ju Y, Kumar D, Varma RS (2006) Revisiting nucleophilic substitution reactions: microwave-assisted synthesis of azides, thiocyanates, and sulfones in an aqueous medium. J Org Chem 71:6697–6700
154. Namboodiri VV, Varma RS (2001) Microwave-accelerated Suzuki cross-coupling reaction in polyethylene glycol (PEG). Green Chem 3:146–148
155. Kumar D, Patel G, Mishra BG, Varma RS (2008) Ecofriendly polyethylene glycol (PEG)-promoted Michael addition reactions of α, β-unsaturated compounds. Tetrahedron Lett 49:6974–6976
156. Keh CCK, Namboodiri VV, Varma RS, Li C-J (2002) Direct formation of tetrahydropyranols via catalysis in ionic liquid. Tetrahedron Lett 43:4993–4996
157. Li Z, Wei C, Varma RS, Li C-J (2004) Three-component coupling of aldehyde, alkyne, and amine catalyzed by silver in ionic liquid. Tetrahedron Lett 45:2443–2446
158. Yang X-F, Wang M, Varma RS, Li C-J (2003) Aldol- and Mannich-type reactions via in situ olefin migration in ionic liquid. Org Lett 5:657–660
159. Yang X-F, Wang M, Varma RS, Li C-J (2004) Ruthenium-catalyzed tandem olefin migration aldol and Mannich-type reactions in ionic liquid. J Mol Catal A Chem 214:147–154
160. Yoo K, Namboodiri VV, Varma RS, Smirniotis PG (2004) Ionic liquid-catalyzed alkylation of isobutane with 2-butene. J Catal 222:511–519
161. Namboodiri VV, Varma RS, Sahle-Demessie E, Pillai UR (2002) Selective oxidation of styrene to acetophenone in the presence of ionic liquids. Green Chem 4:170–173
162. Nadagouda MN, Hoag GE, Collins JB, Varma RS (2009) Green synthesis of Au nanostructures at room temperature using biodegradable plant surfactants. Cryst Growth Des 9:4979–4983
163. Nadagouda MN, Castle A, Murdock RC, Hussain SM, Varma RS (2010) In vitro biocompatibility of nanoscale zerovalent iron particles (nZVI) synthesized using tea polyphenols. Green Chem 12:114–122
164. Moulton MC, Braydich-Stolle LK, Nadagouda MN, Kunzelman S, Hussain SM, Varma RS (2010) Synthesis, characterization and biocompatibility of "green" synthesized silver nanoparticles using tea polyphenols. Nanoscale 2:763–770
165. Hoag GE, Collins JB, Holcomb JL, Hoag JR, Nadagouda MN, Varma RS (2009) Degradation of bromothymol blue by 'greener' nano-scale zerovalent iron synthesized using tea polyphenols. J Mater Chem 19:8671–8677
166. Virkutyte J, Varma RS (2010) Fabrication and visible-light photocatalytic activity of novel $Ag/TiO_{2-x}N_x$ photocatalyst. New J Chem 34:1094–1096
167. Virkutyte J, Baruwati B, Varma RS (2010) Visible light induced photobleaching of methylene blue over melamine doped TiO_2 nanocatalyst. Nanoscale 2(7):1109–1111

Books and Reviews

Ahluwalia VK, Varma RS (2008) Alternative energy processes in chemical synthesis microwave, ultrasound and photo activation. Narosa Publishing House, New Delhi. ISBN 978-81-7319-848-9

Ahluwalia VK, Varma RS (2009) Green solvents for organic synthesis. Narosa Publishing House, New Delhi. ISBN 978-81-7319-964-6

Clark JH, Macquarrie D (2002) Handbook of green chemistry and technology. Blackwell Science, Oxford

Kappe CO, Stadler A (2005) Microwaves in organic and medicinal chemistry. Wiley-VCH, Weinheim, p 410

Kappe CO, Dallinger D, Murphree SS (2009) Practical microwave synthesis for organic chemists – strategies, instruments, and protocols. Wiley-VCH, Weinheim, p 296

Matlack AS (2001) Introduction to green chemistry. Marcel Deckers, New York

Nadagouda MN, Varma RS (2009) Risk reduction via greener synthesis of noble metal nanostructures and nanocomposites. In: Linkov I, Steevens J (eds) Nanomaterials: risks and benefits-proceedings of the NATO advanced workshop. Springer, Faro, pp 209–218

Polshettiwar V, Varma RS (2009) Environmentally benign chemical synthesis via mechanochemical mixing and microwave irradiation. In: Ballini R (ed) Eco-friendly synthesis of fine chemicals, RSC green chemistry book series. RSC, Cambridge, England, pp 275–292

Polshettiwar V, Varma RS (2009) Non-conventional energy sources for green synthesis in water (microwave, ultrasound, and photo). In: Li C-J, Anastas PT (eds) Handbook series, Handbook of green chemistry, Vol. 5: reactions in water. Wiley-VCH, Weinheim. ISBN 978-3-527-31574-1

Polshettiwar V, Varma RS (eds) (2010) Aqueous microwave chemistry: synthesis and applications, vol 7, RSC green chemistry series. Royal Society Chemistry, Cambridge, UK

Strauss CR, Varma RS (2006) Microwaves in green and sustainable chemistry. In: Larhed M, Olofsson K (eds) Microwave methods

in organic synthesis, vol 266, Series in topics in current chemistry. Springer, Heidelberg, pp 199–231
Varma RS (2000) Environmentally benign organic transformations using microwave irradiation under solvent-free conditions. In: Anastas PT, Tundo P (eds) Green chemistry: challenging perspectives. Oxford University Press, Oxford, pp 221–244
Varma RS (2000) Expeditious solvent-free organic syntheses using microwave irradiation. In: Anastas PT, Heine L, Williamson T (eds) Green chemical syntheses and processes, Chapter 23, vol 767, ACS symposium series. American Chemical Society, Washington, DC, pp 292–312
Varma RS (2001) Microwave organic synthesis. In: Geller E (ed) McGraw-Hill Yearbook of Science and Technology 2002. McGraw-Hill, New York, pp 223–225
Varma RS (2006) Microwave technology: chemical synthesis applications. In: Seidel A (ed) Kirk-Othmer on-line encyclopedia of chemical technology, vol 16, 5th edn. Wiley, Hoboken, pp 538–594
Varma RS, Ju Y (2005) Microwaves in organic synthesis. In: Afonso CAM, Crespo JG (eds) Solventless reactions (SLR), Chapter 2.2. Wiley-VCH, Weinheim, pp 53–87
Varma RS, Ju Y (2006) Organic synthesis using microwaves and supported reagents. In: Loupy A (ed) Microwaves in organic sSynthesis, Chapter 8, 2nd edn. Wiley-VCH, Weinheim, pp 362–415

Green Infrastructure and Climate Change

Stephan Pauleit[1], Ole Fryd[2], Antje Backhaus[2], Marina Bergen Jensen[2]
[1]Center of Life and Food Sciences Weihenstephan, Technical University of Munich, Freising, Germany
[2]Forest and Landscape Denmark, University of Copenhagen, Frederiksberg C, Denmark

Article Outline

Glossary
Definition of the Subject
Introduction
The Role of Green Infrastructure for Adaptation of Cities to Climate Change
The Potential of Green Infrastructure to Mitigate Climate Change
Vulnerability of the Green Infrastructure to Climate Change Impacts
Future Directions
Bibliography

Glossary

Adaptation (with respect to climate change) The adjusting of systems, natural or human, in response to actual or expected impacts of climate change, such as sea level rise, to reduce vulnerability or increase resilience in response to observed or expected changes in climate and associated extreme events [1, p. 869]. A distinction has been made between planned adaptation (e.g., urban planning), which is the focus of this chapter, and autonomous adaptation (e.g., by individual action such as improving housing insulation, installing air-conditioning, etc.) [2].

Ecosystem services Are "the benefits people obtain from ecosystems" [3]. "These include provisioning services such as food, water, timber, and fiber; regulating services that affect climate, floods, disease, wastes, and water quality; cultural services that provide recreational, aesthetic, and spiritual benefits; and supporting services such as soil formation, photosynthesis, and nutrient cycling" (3, Preface: V). In urban areas, ecosystem services are clearly related to land use and land cover. Therefore, spatial planning and regulations that influence the spatial pattern and intensity of land use, and in particular the provision and quality of green spaces, can have huge implications for the ecology of cities [4, 5].

Evapotranspiration The sum of evaporation of water from surfaces and the transpiration of water by plants and animals. According to US Geological Survey [6], transpiration from plants accounts for approximately 10% of air moisture. A large oak has been estimated to transpire up to 151,000 l water per year. This would account for more than 400 l/day. More modest figures are given by other sources, for example, 200 l per day for a single, fully grown beech [7]. However, generally, these figures need to be considered with great caution as they are based on rough estimates and will greatly vary between trees depending on stand and site conditions, tree condition, as well as climatic conditions.

Green infrastructure The term "Green infrastructure" was first introduced in the USA at the end of the 1990s – it has been defined as an

"interconnected network of protected land and water that supports native species, maintains natural ecological processes, sustains air and water resources and contributes to the health and quality of life for America's communities and people" [8]. "Urban green infrastructure" is the network of green areas in cities. The term makes reference to other types of urban infrastructures (e.g., the road system). This interpretation of green infrastructure relates to a fine-scale urban application where hybrid infrastructures of green spaces and built systems are planned and designed to support multiple ecosystem services. It has been argued that planning of an urban green infrastructure should promote multifunctionality and connectivity of urban green space. It can integrate both public and private green space. It should be based on a long-term vision and a communicative and socially inclusive approach to its planning and management [9, 10].

Mitigation (with respect to climate change) Reducing greenhouse gas emissions and enhancing sinks.

Resilience Is the ability of a system to adapt and adjust to changing internal or external processes [11, 12]. Resilience is the flip side of vulnerability – a resilient system or population is not sensitive to climate variability and change and has the capacity to adapt [13].

Sustainable urban drainage systems Sequence of management practices utilizing urban green areas for storage, infiltration, evaporation, and conveyance of stormwater runoff.

Urban heat-island effect Significantly higher temperatures experienced in cities compared to the rural surroundings as a result of changed solar reflection in the built environment, less evapotranspiration, and anthropogenic heat from combustion engines, heating of buildings, and other use of energy.

Vulnerability (with respect to climate change) Is the degree to which a system is susceptible to, and unable to cope with, adverse effects of climate change, including climate variability and extremes. Vulnerability is a function of the character, magnitude, and rate of climate change and variation to which a system is exposed, its sensitivity, and its adaptive capacity [1, p. 883].

Definition of the Subject

By 2050, two-thirds of the world's population will live in cities. Already today, cities of the developed world are a major source of greenhouse gas emissions. Therefore, cities need to make serious efforts to mitigate climate change. Urban planning can play a major role in this respect by designing compact, low footprint cities. However, climate change will also make a severe impact on cities mostly by intensification of the heat-island effect, increase of surface runoff from more frequent and intense rainstorms, and by coastal and riverine flooding. Urban planning will play an important role for development and implementation of integrated strategies for climate change mitigation and adaptation. Notably, "green infrastructure" can assist in adapting cities to climate change by reducing the urban heat-island effect and by managing stormwater runoff. Urban greening, such as planting of shade trees and roof greening, can also reduce the energy demand for house heating and cooling. Therefore, the design of the urban landscape will have a direct influence on mitigating climate change and the impact of climate change on people's livelihoods and assets.

Introduction

Urbanization and climate change are closely related. At present, more than half of the world's population lives in cities. Over the next 40 years, the world's urban population is projected to increase by more than three billion people [14]. This will almost double the current urban population and lead to massive land-use changes in and around current urban settlements.

The urban built-up areas are expected to increase by 250% and cover about one million square kilometers by 2030 [15]. This corresponds to the development of more than four hectares of new urban land every minute in the next 20 years. Ninety percent of the future urban expansion is expected to take place in Asia and Africa [14]. New urbanization is primarily an issue in developing countries whereas already 70–90% of the population of the developed world lives in urban settlements. Therefore, climate change mitigation and adaptation is an equally important issue in the developed as well as the developing world.

It has been estimated that 78% of carbon emissions from fossil fuel burning and cement manufacturing [16] and 85% of the anthropogenic emissions of carbon dioxide, chlorine-fluorine-carbons, and tropospheric ozone stem from urban areas [17]. While these and similar figures have been debated [18], there can be little doubt that urban areas, particularly in the developed world and in the transition countries, need to play a major role in climate change mitigation. According to recent reviews, this message has come through as the abatement of greenhouse gas emissions is rising on the political agenda of many cities, particularly in the developed world [19, 20]. Greenhouse gas emissions can be reduced in many different ways by all sectors and at all levels of organization of human society. The overall urban form also plays a role. The "compact city" model has gained wide acceptance as a way to achieve more resource-efficient cities. It is based on the notion that urban density is related to energy consumption, as denser cities consume less energy per capita. This applies especially for car-based travel [21]. This relationship has been used as a powerful argument against urban sprawl, that is, the extension of urban areas through low-density developments. For instance, European cities have on average expanded by 78% in area since the mid-1950s while their population increased by only 33% [22]. Large urban regions have developed, which spread far into the previous countryside and can be delimited by patterns of daily commuting [23]. Sprawl has even been observed in city regions with a decreasing population where people move out from declining inner cities to live in fringe locations [24].

While city governments rightly have given much and still-increasing attention to reducing greenhouse gas emissions, adaptation to climate change has been of much less concern until recently (see reviews in [19, 20, 25]). Moreover, activities are still mostly focusing on certain sectors such as increasing the capacity of the water supply and the sewer systems.

Following Crichton [26] (Fig. 1), the climate change-related risks of urban areas are a function of the (1) hazards, (2) exposure of the urban system to these hazards, and (3) its inherent vulnerability:

1. *Hazards*: By 2100, the average global surface temperatures are projected to rise by 1.1–6.4°C and the sea level is expected to rise by 0.18–0.59 m. Annual precipitation levels will increase in high latitudes and decrease in most subtropical land regions. Hot extremes, heat waves, and heavy rain events are

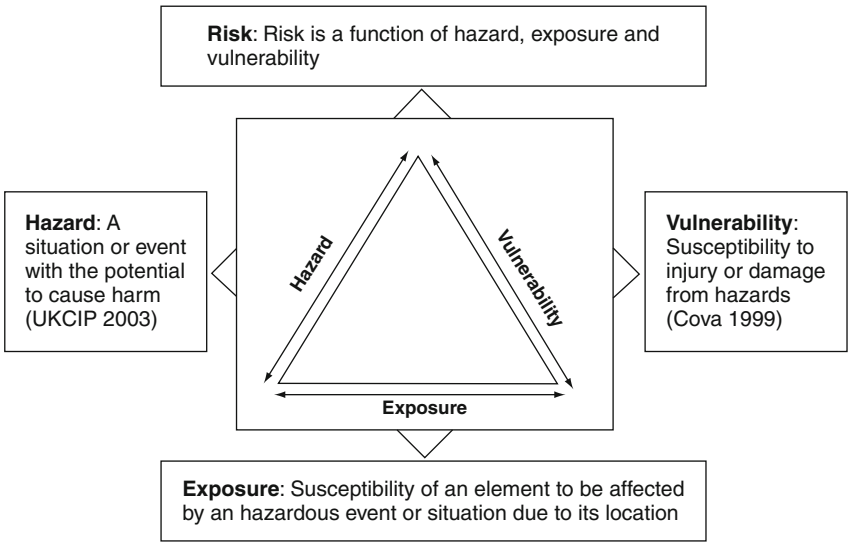

Green Infrastructure and Climate Change. Figure 1
Illustration of risk as a function of hazard, exposure, and vulnerability [26] (Adapted from [26] by [116] with permission from author)

expected to increase, while storms and cyclones will intensify [1]. Regions most vulnerable and/or exposed to climate change include the Arctic (high rate of warming), Africa (low adaptive capacity), small islands (exposure to sea level rise and storms), and the Asian and African "megadeltas" (dense populations combined with exposure to sea level rise, storm surges, and river flooding). Overall, three effects of climate change are of particular concern for urban areas:

- Sea level rise and increase of storm surges caused by tropical storms
- Temperature rise, which intensifies the urban heat island
- Changing amounts and patterns of precipitation, which increase the risk of drought, on the one hand, and pluvial and sewer flooding and landslides from rainstorms, on the other hand

Taking Europe as an example (Fig. 2), temperatures will increase in particular in the North and the South but in more moderate ways in Central and North West Europe. In the North, temperatures and precipitation will particularly rise in wintertime, while the South will be affected by hotter and drier summers. Not all of these changes will be negative to living in the city. For instance, human winter mortality and heating demands are expected to decrease in northerly areas. Also, the summer half year will become more beneficial for outdoor activities in the north. Yet, even for countries such as Sweden, it has been estimated that these beneficial effects are outweighed by increased mortality due to heat waves and increased energy demands for cooling during summertime [27]. In particular, it needs to be highlighted that it is less the general change of temperature and precipitation patterns that are of concern but the increasing frequency and intensity of extreme events such as hot spells of weather and droughts, more frequent thunderstorms that bring large quantities of rainfall in a short time, and perhaps also a higher likelihood of heavy storms, although this is far less certain. For instance, it has been predicted that the number of so-called tropical nights will rise. Tropical nights are nights where the air temperature does not drop below 20°C. Under the IPCC scenario A2, it is predicted that the night temperatures in central Europe in 2080 will be similar to current levels in Spain [28].

2. *Exposure*: Urban areas are often located in zones particularly exposed to climate change hazards such as storm surges, river floods, and landslides. As an example, 13% of the world's urban population live in the low-elevation coastal zone (<10 m above sea level) [29]. Almost two-thirds of urban settlements with a population greater than five million are located in this zone, including the densely populated deltas of Ganges-Brahmaputra (Kolkata, Dhaka), the Nile (Cairo), and the Yangtze River (Shanghai). These areas are at particular risk from flooding when high tides combine with storm surge and/or higher river flows. Yet, not all areas within coastal cities are equally at risk. In a developing world context, particularly the informal settlements of the urban poor are exposed to flooding.

3. *Vulnerability*: Urban vulnerability to climate change is multifaceted and related to the physical, social, economic, and environmental characteristics of urban areas. Various concepts of vulnerability have been proposed by the research community on climate change and disasters [30, 31]. The emphasis is thereby either placed on vulnerability, mainly as a result of physical factors, for example, location and layout of the city ("outcome vulnerability") or of its social makeup, that is, the condition of people that enables a hazard to become a disaster ("context vulnerability"). Adoption of either one of the concepts has consequences for the measures to be taken to reduce urban vulnerability.

An obvious reason for the vulnerability of urban areas to climate change is the concentration of people, infrastructures, and economy. Further, the urbanization process per se increases the vulnerability. Urbanization fundamentally alters the earth's surface by replacing vegetated or otherwise open land with built land, and urban areas may be characterized as open ecological systems with a high throughput of energy and matter. Consequently, ecosystem processes are strongly impacted, such as modification of local and regional climates, air quality, hydrology, soils, and flora and fauna [32]. Annual average air temperatures in big cities are already 1–3°C higher than in the surrounding countryside. Thus, already today, climatic conditions in urban areas may correspond to anticipated climate change. However, urban areas' climate will be further modified by climate change and stormwater runoff will strongly increase [25].

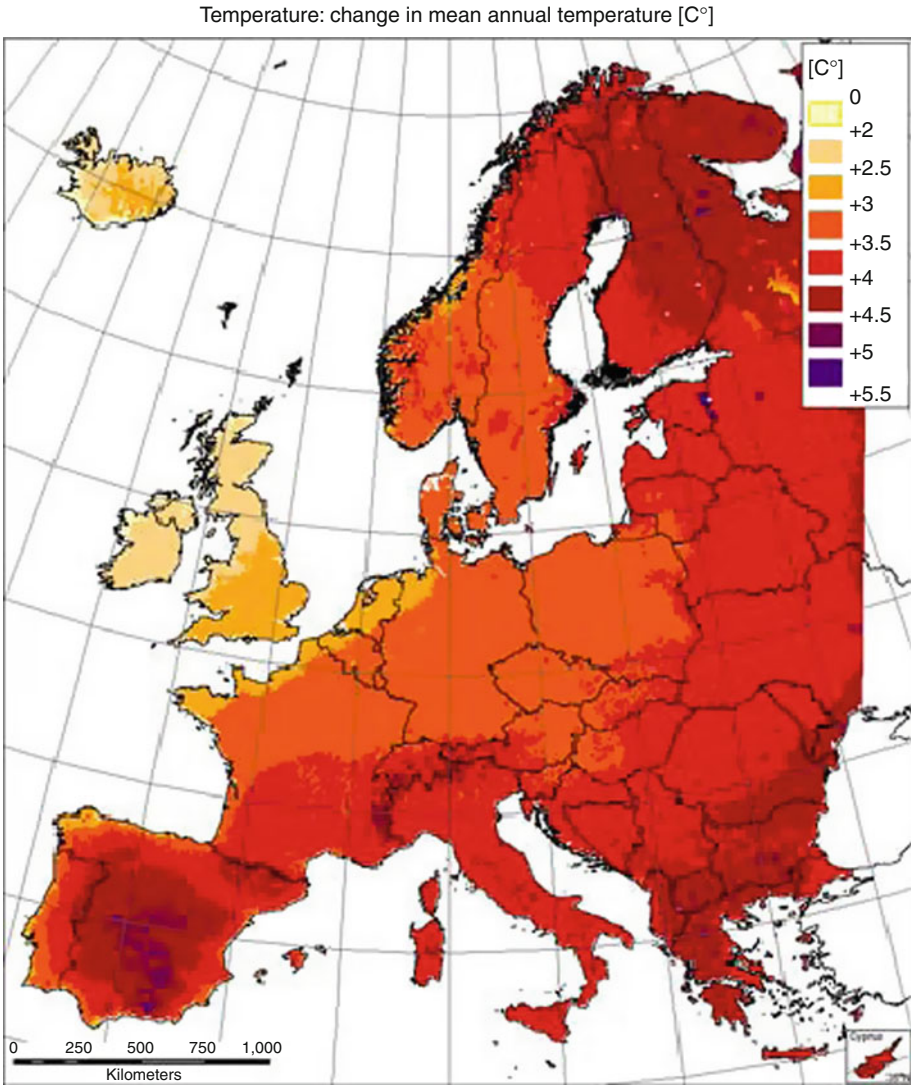

Green Infrastructure and Climate Change. Figure 2
IPCC scenario A2 for Europe [117]. Absolute change in mean annual temperature between control periods 1961–1990 and 2071–2100, under the IPCC SRES scenario A2. The maps are based on PRUDENCE data (http://prudence.dmi.dk), and processed by the European Commission's Joint Research Centre, Institute for Prospective Technological Studies, within the PESETA study (http://peseta.jrc.es). ©European Union, http://eur-lex.europa.eu/

Planning: The critical role of land-use planning and management in climate change mitigation and adaptation has been recognized by the Intergovernmental Panel for Climate Change [1].

Urban planning and land management can mitigate the severity of hazards and reduce the levels of exposure and vulnerability [33]. Land-use planning can reduce transport demands and building regulations can reduce the need for house heating or cooling [20]. Directing urban development away from floodplains can greatly reduce the risks of being affected by increasingly frequent and severe floods. As will be argued in the following sections, planning can increase the resilience or capacity of urban areas to cope with climate change by strategic planning of a green infrastructure. As Lindley et al. observe, "different scales of planning

from macro-scale land-use planning to micro scale urban design are both important to this process, responding to the different scales over which risk and vulnerability are expressed" [33, 34]. Integration of climate change-induced risks in urban planning is, however, only beginning to emerge [35, 36].

Urban areas are densely built, densely populated, have high land costs, and must support multiple functions. This calls for innovative solutions to the design of urban areas that are inclusive and synergetic. It is a challenge that can, at least partly, be addressed by transferring landscape design principles into the design of the city.

There is ample evidence of the beneficial role of urban green space in providing ecosystem services [37–39]. Green space can mitigate the urban heat-island effect and reduce stormwater runoff [40, 41]. Trees and shrubs also sequester carbon, and if the amount of living biomass in a city is permanently enlarged, the overall carbon balance of urban areas will be improved [42]; however, the contribution is likely to be only of marginal importance. The question that remains to be answered is to what extent cities can adapt to the expected large alterations of the environment driven by climate change through planning and design of an urban green infrastructure? Green infrastructure is an emerging concept increasingly gaining acceptance in the fields of urban planning and design as a way to promote multiple ecological and cultural processes in the city [9, 10]. Infrastructures facilitate multiple functions in the city including transportation, communication, energy, and water services. Most existing infrastructures are "grey infrastructures" such as roads and sewers. The "green infrastructure" complements these infrastructures by providing essential ecosystem services such as climate regulation, stormwater management, biodiversity, and social services such as recreation and aesthetics [9, 10]. Has green infrastructure, similar to other infrastructures such as transport and supply infrastructures, the ability to maintain the viability of the city as such by the provision of ecosystem services and increased resilience [10]?

The Role of Green Infrastructure for Adaptation of Cities to Climate Change

Adaptation of cities to climate change refers to the implementation of means to reduce the impact of climate change. By timely preparing the city to face the impact of a changing climate, economic and social costs and potential damage costs can be reduced while synergies can be realized, for instance by developing more attractive and livable cities [43]. Development of the green infrastructure is an effective strategy both for adaptation to and mitigation of climate change.

Adaptation to Rising Temperatures – The Heat-Island Effect

The local climate in urban areas differs from the surrounding open land [44]. Of particular relevance in the context of climate change is the increase of air temperatures in urban areas by 1–3°C on annual average compared to the surrounding open land. On warm summer days, the difference can be up to 5–12°C [45]. This is commonly referred to as the urban heat-island effect. The intensity of the heat-island effect is dependent on the size of the city: the larger the city the stronger the heat-island effect. This is relevant as many urban areas in the world are strongly growing, and the resulting increase of air temperatures in inner cities may be stronger than that caused by global climate change. However, climate change is expected to further intensify the heat-island effect. For instance, a modeling study predicted intensification of the heat-island effect for London by 0.5°C by the 2050s [25].

In warmer cities, it will be more difficult to work and sleep properly without cooling and ventilation systems. This will increase energy demands; it will cost money and cooling systems are only available to people who can afford it. In the USA, peak urban electric demands were estimated to rise by 2–4% for each 1°C rise in daily maximum temperature. The additional use of air-conditioning is responsible for 5–10% of urban peak electric demand in the USA, at a direct cost of several billion dollars annually [46].

Increased temperatures in urban areas can have negative consequences for human health and well-being. In particular, small children and elderly people as well as persons suffering from cardiovascular diseases are at risk from hot spells of weather. An example is the extreme summer of 2003 in Europe where more than 70,000 deaths in excess have been reported [47]. Most casualties occurred in urban areas where most people live and the heat-island effect intensifies.

As outlined above, such hot summers with extreme heat waves will become more frequent and intense in the future [28]. In addition to direct impacts through raised temperatures, the heat-island effect also deteriorates air quality. For instance, the heat-island effect in Los Angeles, California, has been estimated to increase ozone concentrations by 10–15 [48]. It should be noted, however, that climate change impacts on urban areas will play out very differently according to location and type of city and a decline of winter mortality can be expected in urban areas in colder climates.

The heat-island effect is a result of the altered climatic balance in urban areas and it is caused by a number of factors, such as the reflection, storage, and convection of solar energy and emission of heat from anthropogenic process (Fig. 3, [41, 45, 49, 50]). The main reason, however, is the replacement of vegetated, evaporating surfaces by built and paved surfaces. Vegetation consumes much of the solar energy for evaporating water. This imbalance is fortified by the fact that buildings, roads, and pavements are made of materials with a higher capacity to accumulate and store heat than living tissues. Measurements show surface temperatures do not decrease continuously along urban to rural transects but vary strongly within the urban area depending on the physical characteristics of the different land uses along this gradient (Fig. 4). Temperature peaks can be observed in densely built parts of the city, while temperatures are considerably lower in well-greened areas. Therefore, there is not one heat island but in reality a city consists of a small-scale archipelago of heat and cool islands which corresponds well to patterns of urban form.

Although air and surface temperatures can be lower in green spaces than in the surrounding built areas, the effect varies depending not only on the location, size, and design of the green space but also their management (e.g., whether lawns are irrigated). In a large park, annual average air temperatures may be 1–2°C lower than the surroundings. During clear windless nights, temperature differences can be as big as 5–6°C. Moreover, heat is trapped in narrow street canyons of densely built areas. However, parks must have a certain size to develop a distinct climate. According to measurements

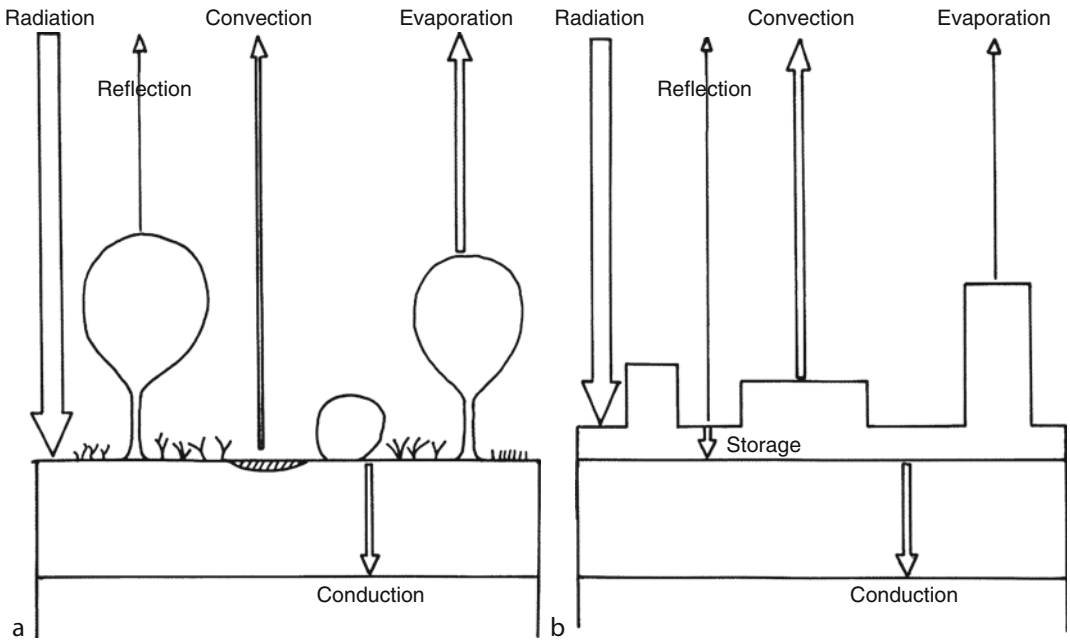

Green Infrastructure and Climate Change. Figure 3
Energy transfers contributing to the urban heat-island effect: (**a**) the situation in the open land, (**b**) the situation in densely built-up areas [40] (Reprinted from [40]. Copyright (2001), with permission from Elsevier)

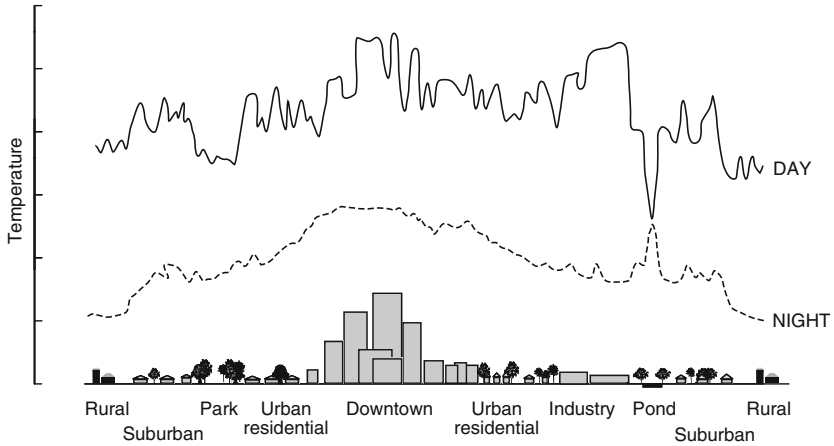

Green Infrastructure and Climate Change. Figure 4
Variations of surface temperatures in urban transect. (Modified from [118] with permission from Actionbioscience.org the author)

in public green spaces in Berlin, temperature differences could only be found when the park was bigger than approximately 3.5 ha [51].

Larger parks can also moderate air temperatures in adjacent built areas. The study on green spaces in Berlin (Germany) established that very large parks such as Tiergarten (212 ha) can lower air temperatures on clear summer days with low wind speeds (<2 m/s) up to 1,300 in lee and up to 200 m windward [51]. Yet, while these figures may be impressive, the effect is much less for smaller green spaces where effects may be limited to distances of 100–200 m. The cooling effect also depends on the surrounding built structures. Corridors in the main wind direction may lead cool air from the park into adjacent built areas whereas closed built structures around the park block the cool air [52]. Therefore, mitigation of the urban heat island cannot rely on single large green spaces. Instead, a dense network of green spaces should permeate the built fabric. Moreover, greening of the urban matrix is crucial to provide for comfortable climatic conditions close to where people live and work. Air temperatures clearly differ between urban land uses dependent on the degree of greening. Even in very densely built areas, shade trees can be planted in streets to control climates at site levels while roof and wall greening reduce the heating up of built surfaces and heat storage. Trees are particularly effective in cooling the city as they have a shading effect. Therefore, parks with a high provision of trees and urban forests are usually the coolest outdoor areas during daytime.

While there is ample evidence from urban climate studies to establish the relationships between urban form, green space, and climates at various scales – from city to streets – research on the likely consequences of climate change on urban climates and the potential of green infrastructure to mitigate these effects are still scarce. One of the few exceptions is a study undertaken in Greater Manchester, UK. In the project "Adaptation Strategies for Climate Change in the Urban Environment" (ASCCUE) [53, 54], a modeling approach was employed to explore the impacts of climate change on urban temperature patterns and establish the relationships with urban form. In Greater Manchester, a large conurbation of approximately 2.5 million inhabitants on a surface area of approximately 1,300 km^2 was selected as it suitably represents the different forms of built and open spaces that are typical for large urban areas in the UK. Greater Manchester is also an interesting case as it undergoes a rapid process of transformation from a former industrial to a postindustrial city where land-use dynamics are high. It also offers opportunities for development of a green infrastructure for climate change mitigation and adaptation.

In the ASCCUE project, the researchers developed an approach for the assessment of climate-related risks

with reference to three exposure units: built, green space, and human comfort. However, only the results from research on urban green space will be reported. This study consisted of three main steps:

1. Characterization of the urban environment based on mapping of urban morphology types from aerial photographs [55]: Overall, the area was classified into 29 "urban morphology types" (Fig. 5). These were further characterized by nine land cover attributes, including cover of built, paved, and vegetated areas by interpretation of aerial photographs. For the latter, detailed estimates were derived for trees, shrubs, rough grasslands, lawns, and arable land.
2. Modeling surface temperatures (and stormwater runoff, which will not be reported here) based on an energy exchange model [40, 54]: Surface temperatures are a useful climate indicator for urban planning as information can be derived from remote sensed imagery or – as was the case here – from models with complete spatial, highly resolved coverage of urban areas whereas measurement of air temperatures is confined to point data or transects from where it is difficult to spatially extrapolate. Moreover, surface temperatures can be taken as a proxy for mean radiant temperatures, which have a strong influence on human comfort and health in outdoor environments, especially on hot days with little wind [56]. For instance, impacts of the heat waves in 2003 in Paris showed that increased levels of human mortality were closely related to heat islands of surface temperature derived from remote sensed data [57]. In the Manchester study, the surface temperature model's main input were land cover data, on the one hand, and climate data from the local weather station, on the other. Climate data were obtained from a parallel project, where climate scenarios were derived for the weather station of Manchester airport for 2020, 2050, and the 2080s [58, 59]. Only results for the most extreme emissions scenario called "2080 high" will be reported here.
3. Urban development scenarios to compare the impacts of "green" versus "densification" strategies under climate change until 2080: In the green strategy, cover of vegetated and water surfaces would be increased by 10% in terms of surface cover while the densification strategy would lead to a reduction in cover of evapotranspiring surfaces by 10%.

The share of green space varies between urban morphology types. In the inner urban areas, the share of green space is usually low (less than 20%); in single-family housing estates, the provision of green space is 50–60%. Overall, formal and informal green spaces (including woodlands) cover approximately 10% of the city surface; another 10% is covered by vegetated areas on derelict land of former industrial sites. Yet the largest green space resources are residential areas where approximately 40% of all vegetated areas can be found. Large differences, however, could be observed between densely built-up residential areas (e.g., terraced houses), and the medium- and low-density types. These differences generally coincide well with the socioeconomic status of the areas with deprived areas being at the lower end of green space provision. Moreover, they often lack in mature trees with large crowns, which are particularly effective in reducing surface and air temperatures via their shading effect.

Surface temperatures greatly differ between the urban morphology types on hot summer days, and these differences are clearly related to the cover of green space (Fig. 6). The highest surface temperatures were identified in the inner city, where buildings, roads, and pavements predominate and where the provision of parks, trees, and other types of vegetation is lowest. Temperatures were also very high in densely built residential areas and industrial and commercial estates. In well-greened neighborhoods with single-family houses, the temperature is considerably lower, whereas woodlands offered the coolest places. The study measured 32.1°C in the urban center, while the temperature in a large park was only 18.4°C.

In the Manchester study, climate scenarios for the year 2080 predicted a rise of air temperatures of more than 4°C during heat waves. The rise in temperature is significantly lower in areas with a high provision of green spaces. While surface temperatures would increase by 4.3°C in the city centers, they would only rise by 3.1°C in low-density residential areas. This shows that the cover of vegetated areas has potential to buffer the effects of climate change to some degree. These results compare favorably with the predicted intensification of the heat island in London mentioned before [25].

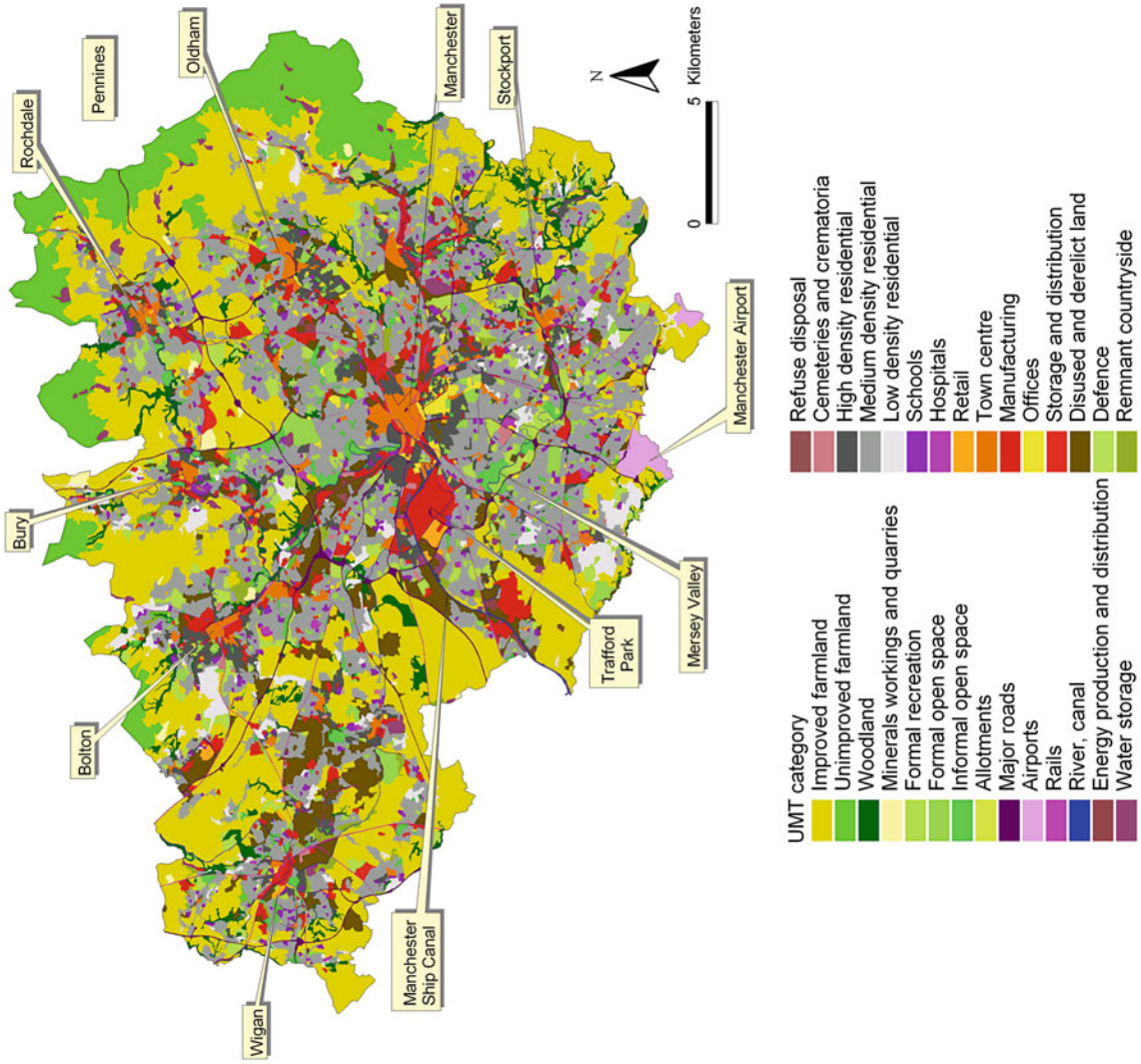

Green Infrastructure and Climate Change. Figure 5
Map of Greater Manchester divided into 29 urban morphology types (Reprinted from [55]. Copyright 2008, with permission from Elsevier)

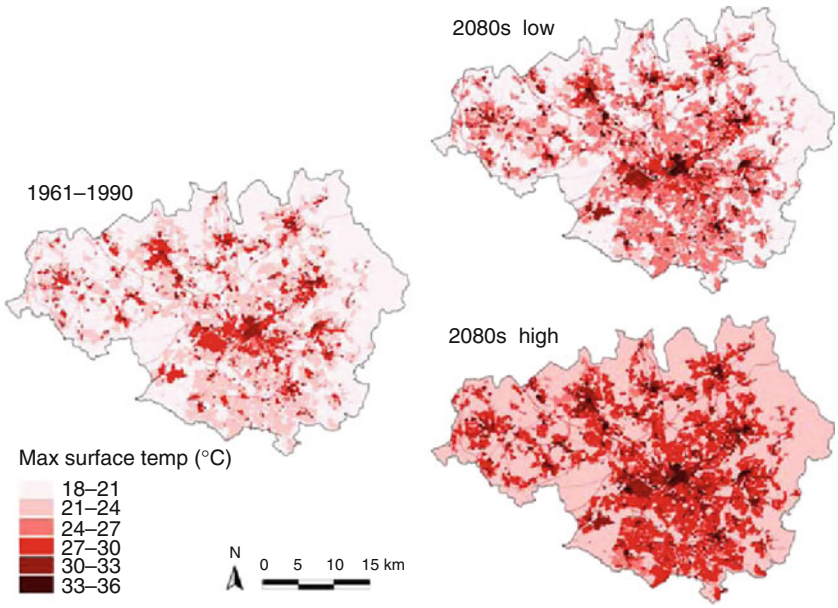

Green Infrastructure and Climate Change. Figure 6
Maximum surface temperatures in Greater Manchester on a hot summer day in 1961–1990 and the 2080s low- and high-emission scenarios [54] (Reprinted from [54]. Copyright (2007), with permission from Alexandrine Press)

The climate scenarios for 2080: the "green strategy," where the provision of green space in the densely built town centers was increased by 10%, and the "grey strategy," where the provision of green space was reduced by 10%, resulted in further support for the important role of green space to increase the coping capacity of urban areas to climate change. It was estimated that 10% more green space would almost compensate for the rising temperatures expected to result from global warming by 2080 even in the worst scenario. In contrast, by reducing the provision of vegetated areas by 10%, the temperature in dense urban areas would rise by 8.2°C (Fig. 7).

It will be very challenging, though, to introduce more green space into densely built urban centers. However, the dynamics of urban areas should not be underestimated: current uses become obsolete, buildings are demolished, and entire neighborhoods are renewed. This may give opportunities for development of a green infrastructure if strategies are clearly defined and supportive to the wider agenda of urban renewal. In particular, this may be feasible in cities with a shrinking population [24] where creation of green spaces can also increase quality of life and thus help to reverse the tendency of decline. In the city of Leipzig, the potential of developing urban woodlands on derelict inner urban sites is currently explored [60]. The project revealed that overall there are more than 500 sites within the built area covering over 1,100 ha. Many sites are located in deprived areas where there is a lack of green space and environmental quality is poor. Therefore, these derelict areas offer a great potential to improve quality of life in these areas. Moreover, they would allow developing a network of strategically placed "cool islands" in otherwise still densely built areas for climate change adaptation.

Where pressure on the land is high, and urban densification rather than urban sprawl is sought, it may be more difficult to develop a green infrastructure and other strategies need to be adopted. Even there, opportunities may exist. For instance, in the city centers of Manchester, about 37% of the city is covered by buildings but 40% by paved spaces of roads, car parks, etc. Thus, it is not the lack of space as such but the intensive use and in particular the occupation by car-based transport which is problematic. Evidently, it is difficult to change this situation but adaptation to climate change will require more radical measures to

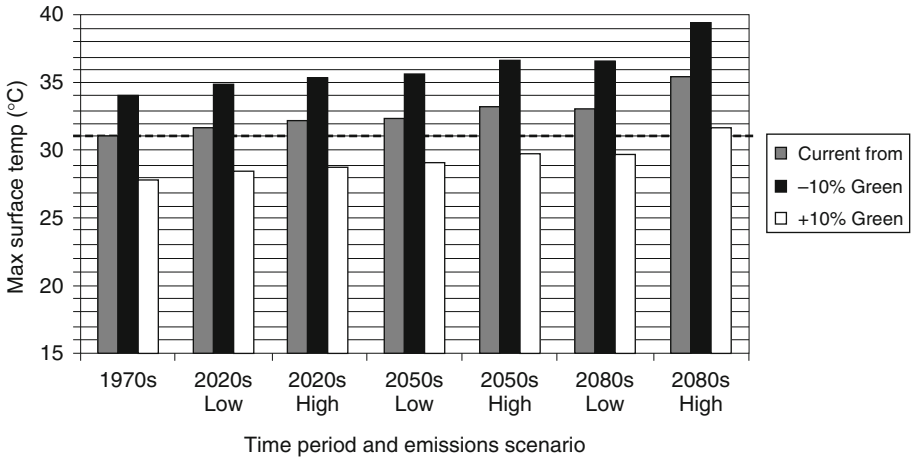

Green Infrastructure and Climate Change. Figure 7
Maximum surface temperature for a hot summer day in inner city areas of Manchester, with current form and when 10% green cover is added or removed [54] (Reprinted from [54]. Copyright (2007), with permission from Alexandrine Press)

be taken for the reorganization of transport in city centers in order to create the space necessary for green space. Here, synergies with climate mitigation are obvious. In addition, green roofs and walls or implementing vegetated permeable pavements should be promoted.

Stormwater Management – From Sewer-Based to Landscape-Based Systems

The ongoing sealing of surfaces due to buildings, roads, and other infrastructure in urban areas leads to a change in the water cycle (Fig. 8). Instead of naturally high transpiration rates and water infiltration for groundwater recharge, large amounts of the precipitation become surface runoff. In natural environments, about 10% of precipitation will run off on the surface and 50% infiltrate, whereas figures are reversed in dense urban settings with about 50% surface runoff and 10% infiltration – of course very much dependent on the specific degree of surface sealing [4]. This leads to a higher and more rapid peak discharge in urban areas, which needs to be handled by the existing sewer systems.

Due to fast urban development and the aging of the systems, already today many existing sewer systems have insufficient capacity. Increase of water-impervious surfaces has been dramatic in urban areas of the Western world. For instance, a study of 26 cities across Europe revealed that the size of urban areas increased by 78% on average between 1950 and 1990 while population increased only by 33% [22]. This low-density development has greatly enlarged the area of water-impervious surfaces for buildings and roads. In addition, densification of existing built areas increases the amount of water-impervious surfaces. Such densification may take different forms, from building over derelict or other non-built areas, infill development, for example, by building houses on vacant land or subdividing large gardens into several smaller parcels. Paving of front gardens to create parking spaces can lead to significant increase of water-impervious surfaces. Research in 11 residential areas in the Liverpool conurbation revealed that approximately 5% of the surface area was converted from vegetated to paved, between 1975 and 2000. The runoff from a 10 mm rainstorm event was modeled to increase on average by 4% [61]. While these changes may appear to be small, they can lead to significant problems for the sewage system when accumulated over an entire sewer catchment. In another UK-based study, increase of water-impervious surfaces due to conversion of front gardens was even bigger: A 13% increase in water-impervious surfaces was detected in a 1.16 km^2 suburban area of Leeds in northern England over the 33-year study period between 1971 and 2004 [62].

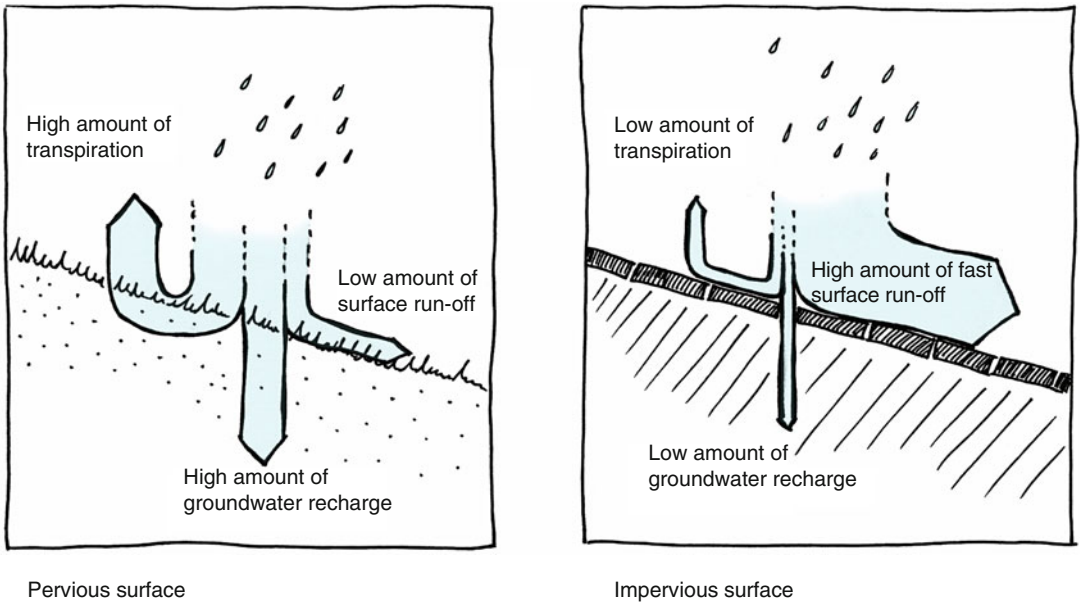

Green Infrastructure and Climate Change. Figure 8
The water cycle in natural and sealed areas. (Adapted after [119] with permission from the author)

An increase of stormwater runoff by 12% was modeled as a consequence.

The increase of stormwater runoff leads more and more often to sewer overflows. This can either be uncontrolled, resulting in the flooding of urban areas, or the overflow happens controlled into nearby streams and other receiving water bodies. In this case, the ecological consequences can be dramatic.

Climate change will strongly exacerbate these problems. In the Manchester study, it was predicted that the amount of precipitation from rainstorm events will increase by 56% until 2080 in the high-emissions scenario. This would lead to 82% more runoff because of limited water retention and infiltration capacity of the soils [54]. Protection of green space on soils with a high infiltration capacity such as sandy soils will be a major task for urban planning to avoid a further dramatic deterioration of this situation. An increase of green space cover by 10% – as explored in the case of heat-island mitigation above – would reduce surface runoff during a rainstorm event by approximately 4%, and thus not suffice to solve the problem. However, implementing on-site retention and infiltration techniques can be a way out, as will be explored in the following section.

The northern European country Denmark will be taken as an example. Comparing regional precipitation data from 1979 to 1997 with 1997–2005 suggests a 10% increase in rain intensity for a 10-year design storm [63]. Model simulations project that extreme rain events will further increase by 20% or more during the next 100 years [64]. To comply with more intensive rainstorms, the drainage capacity needs to be increased by approximately 30% in a 100-year time perspective [65]. Including uncertainties related to urban drainage modeling and urban densification processes, the expansion of drainage capacity is estimated to be 78% higher than present level [65]. This is only to maintain the same flood risk as today, that is, surcharge accepted every tenth year in combined sewers collecting stormwater runoff and wastewater from households and industries in the same pipe system. For the country as a whole, the cost of increasing drainage capacity by conventional means (i.e., installing bigger and more sewers, basins, and pumps) is estimated to be $2.7 billion USD in a 30-year time perspective [66]. Combined with sewer rehabilitation works resulting from aging infrastructures, the total cost accounts to $14.6 billion USD [66]. With a total urban population of 4.5 million people, this corresponds to investment needs in

the range of $3200USD per urban capita. Still, there is no certainty that the predicted level of climate changes are reliable and that the one-off investments in new pipes (relying on long depreciation periods) will provide sufficient drainage capacity in the future. If no action is taken, the risk of floods will increase, which will impact people's assets and livelihoods.

Large challenges lie ahead in adapting cities to more extreme rain events. Conventional solutions are costly and possibly unsustainable long term [67, 68]. Another solution is to imitate the natural water cycle with delay, infiltration, or evaporation of the stormwater as close to where it falls as possible. Single measures for such on-site stormwater management are elements like green roofs, permeable pavement, swales, ponds, and infiltration trenches. This strategy is also referred to as landscape-based stormwater management, Sustainable Drainage Systems or Sustainable Urban Drainage Systems (SUDS), Best Management Practices for Stormwater (BMPs), Low Impact Development (LID), or Water Sensitive Urban Design (WSUD) [69, 70].

Sustainable urban drainage systems (SUDS) can be used as a full stand-alone solution typically employed in new urban developments or retrofitted into the existing city to provide more drainage capacity in the area, in which case it is more likely to be complementary to the existing sewer system. SUDS further provide the opportunity for comprehensive solutions to suspend recreational and spatial utilization of the water as well as increased biological diversity and well-functioning urban drainage systems that contribute to increased groundwater recharge. This type of solution is expected to include economical, environmental, and recreational advantages.

SUDS have been implemented on various places in the world and can include a wide range of different measures. Concepts of on-site stormwater management have growing acceptance in Australia [71], Germany [72], the Netherlands [73], and the UK [74] though still not widely and commonly applied in all settings.

A range of studies show the positive impact that a new stormwater management approach can have on cities. One such example can be found in Malmö in Sweden [75], where a combined green roof and pond system is retrofitted into the Augustenborg neighborhood. Green roofs are one measure out of a wide range of possibilities for stormwater management. For instance, Bengtson [76] established that extensive green sedum roofs with a 3 cm thick substrate layer are expected to retain 10 mm of rain before discharging water. Models run in parts of the Augustenborg neighborhood indicated that a 31% extensive green roof cover in a certain area can reduce the peak flow by 64% for a rain event statistically happening twice a year, and 27% for a rain event reoccurring once in 5 years. In addition, the runoff volume is reduced by 52% and 18%, respectively, for the same return periods [77].

The implementation of SUDS is expected to improve the quality of life in the cities and has furthermore a range of technical as well as ecological advantages. It leads to an improved performance of the wastewater treatment plants, as the wastewater is less diluted, to a reduction of energy demand for wastewater treatment and furthermore to a decrease of combined sewer overflows. Stormwater can be harvested for supply purposes, such as laundry and toilet flushing, and thus reduce the strain on other freshwater sources.

Moreover, infiltration of stormwater can contribute to recharge and maintain groundwater sources in urban areas. Infiltration of stormwater in soil layers that are hydraulically linked to local streams can support the stream's base flow. A lower peak flow reduces the risk of flooding, erosion, and uncontrolled pollution of receiving water bodies. In cities, the groundwater level is commonly lowered as a result of extraction of groundwater for supply purposes, drainage of natural wetlands, and little stormwater infiltration due to few permeable surfaces. A general decrease in the groundwater in an area can result in a lower water table in surrounding wetlands and negatively affect the flora and fauna. It should be noted that climate change is predicted to increase the overall amount of precipitation, which would in general increase groundwater levels in Northern European countries such as Denmark.

Finally, SUDS support the use of rainwater as an asset benefiting city life. People are attracted to water whether it is children playing in a puddle or adults who are happy to pay more for a house with a view to waterfronts than other places. Water increases the attraction of the environment and can contribute to a greener and richer plant and animal life.

Apart from the advantages, the implementation of SUDS bears also some risks, such as groundwater pollution from polluted soils or infiltration of runoff from heavily trafficked areas, or the unwanted flooding of low-lying areas or basements. These risks need to be known by planners and engineers and proper avoidance strategies and monitoring needs to be implemented together with the SUDS.

SUDS are a relatively new concept and not as many experiences exist as goes for conventional sewers. Some of the major aspects that emphasize the difference between conventional systems and on-site stormwater management systems are, for example, the dimensioning, the work across scales, the context dependence and the need for new collaborations, and a new way of thinking.

Regarding urban drainage systems, a good solution must cover and respond to different conditions. It must be suitable for the everyday functionality of the city and appropriately manage the risk of flooding, for example, by redirecting water to areas where the damages and negative impacts are smallest.

Furthermore, stormwater management planning is closely linked to environmental management for entire watersheds. Up to now, most projects have been implemented only at site level with little connection to the surrounding landscape [78]. Little knowledge has been developed regarding large-scale landscape-based stormwater management systems and their potential positive and negative impacts on other aspects of urban land use and possible integration with other urban development goals. An interdisciplinary case study with the goal to develop a suitable strategy for large-scale SUDS retrofit in the eastern parts of Copenhagen (Denmark) [79] suggested that there is a need to place small-scale projects for on-site stormwater management within the context of larger-scale planning for entire watershelds. As an aim, a system of point measurements should be connected by linear elements and zones, and by this create a new green and blue water infrastructure network. Such a system design of connected disconnections would support the capacity of the single sites across special and temporal scales. Single site measures would treat the stormwater independently on a daily basis, while in case of an extreme storm event, streets and green corridors function as emergency overflow systems. Figure 9 is developed as part of the study in Copenhagen and illustrates an interconnected system of SUDS elements covering site-level, district-level, and city-level measures. It points toward the potential of urban green infrastructure to support the planning and design of large-scale landscape-based stormwater management systems, as integrated sites for retention, infiltration and evapotranspiration, and/or conveyance of excess runoff that can be linked to the planning of gardens, parks, and green corridors.

Such a citywide water system requires close collaboration between the different stakeholders. Green space management and sewer management must merge to ensure successful SUDS implementation, and as water does not know administrative borders, a planning system that brings all stakeholders to the table is required.

Flood Management

Sea level rise will challenge many coastal urban areas. In addition, increased runoff will raise river water levels and increase flood risks. More impervious urban areas and more intensive rain events will exacerbate the situation. The conventional way is to manage rivers by means of channelization, raising the dikes and

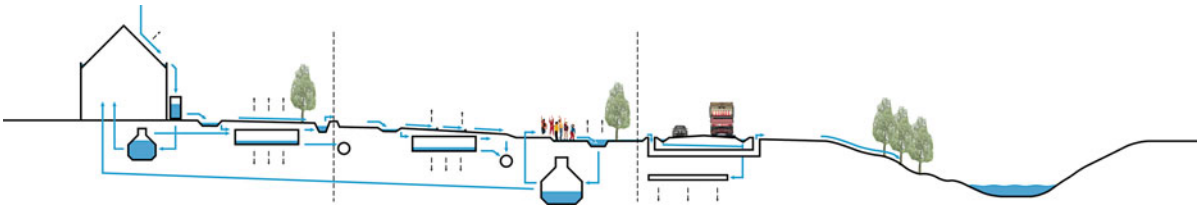

Green Infrastructure and Climate Change. Figure 9
Sketch of an interconnected system of SUDS elements (illustration: O. Fryd)

installing dams. A landscape-based approach to coastal and river flood management is an emerging concept currently being explored in countries like China [80], Germany [81], India [82], the Netherlands [83], Singapore [84], and the USA [85].

In quite many cities, projects of river restoration have been implemented in the last decades, for example, revitalization of the Los Angeles River (USA) [86], Cheonggyecheon Linear Park, Seoul (South Korea) [87], Akerselva, Oslo (Norway) [88], the Aarhus River (Denmark) [89], and the river Isar in Munich (Germany) [90]. Climate change may not yet have been a strong political driver of these projects, but the outcomes are certainly highly relevant for adaptation of cities to climate change via the green infrastructure. As an example, the restoration of the river Isar within the built area of Munich will be briefly presented here. Munich is a city of some 1.3 million inhabitants located on the banks of the river Isar. The river originates in the Alps, and the city's history has been closely connected to the river as a source of water, energy, and a transport route, and the Isar is just as iconic to the city as the Alps nearby or the Oktoberfest. While the medieval city kept a respectful distance to the wild river, the Isar was channelized from the nineteenth century onward for flood prevention and energy use. The floodplains were partly built over. Still, the river is the backbone of the city's green structure with famous parks in the former floodplain.

In the 1990s, a major flood almost caused a catastrophe with river boards being filled to the brink. This, together with new regulations whereby safety thresholds for flooding were increased, caused a radical rethinking of the approach to flood management. It was realized that flood problems could not be solved alone by further increasing the height of the river dams. Moreover, this would have caused major negative impacts on green spaces along the river which are highly valued for recreation and therefore, it would have been difficult to get political and public support for a hard engineering solution. Instead, a strategy was adopted whereby the river bed was broadened where this was still possible to provide more space for the water. The riverbanks were remodeled to enhance access to the river for recreational purposes (water quality has been improved due to new sewage treatment systems of municipalities upstream) and to promote habitats for wildlife (Fig. 10). The river Isar restoration can therefore be considered as an example where a politically contentious situation was turned

Green Infrastructure and Climate Change. Figure 10
River Isar in Munich during a flood after restoration (photo: S. Pauleit)

into a win-win solution by adopting a multifunctional strategy. It should be noted that this was possible due a number of preconditions that had paved the way. Among these was a long history of steadily aggravating problems with the river ecosystem that necessitated taking measures along the entire river, the outstanding role of the river for city image, a society campaigning for the protection of the river that existed for more than 100 years, possibility to renegotiate the use of the river water for power generation due to expiry of contracts, and construction of sewage plants in municipalities upstream, which improved water to bathing quality. Opening of this window of opportunities was essential for realization of the project.

The examples of river Isar and others show that landscape-based flood management systems along coasts and rivers can be fully or partly developed as part of the urban green infrastructure. Landscape-based flood management systems reflect some of the same principles as SUDS by using hydrology as generator of sustainable urban form by specifically addressing flood risks, seasonal flow patterns, and tidal water dynamics as defining factors for integrated design. Much focus seems to be on the edges between cities and their water bodies, that is, a transition from hard edges to softer and more dynamic edges. This is characterized by a change from channelization and embankment to a focus (at least partly) on temporarily wet and dry transition zones. From an ecological perspective, such zones are expected to perform well as marshes, wetlands, mangroves, and riverbanks provide some of the most diverse natural ecosystems. However, they must be designed to also comply with urban needs such as public health and accessibility. Therefore, a multifunctional strategy is prerequisite to successfully developing the green infrastructure.

The Potential of Green Infrastructure to Mitigate Climate Change

Climate change mitigation relates to the reduction of greenhouse gas emissions. For this purpose cities have a series of potentials, for example, by reducing energy consumption rates, exchanging non-renewable by renewable energy sources, and densifying cities so the need for transportation is reduced. As an example, Melbourne, Australia, aims to be CO_2 neutral by 2020 [91]. Many other cities throughout the world are currently launching initiatives to reduce CO_2 emissions and to promote a more climate-friendly development.

To some extent, green infrastructure can mitigate greenhouse gas emissions, either by directly capturing and storing CO_2 or by reducing energy consumption of nearby buildings. It should be stressed, however, that the literature is sparse and that the mitigation potential of urban green infrastructure is not well documented. The chapter heavily, but not solely draws on Nowak [42], where the potential of urban trees to modify the urban environment has been reviewed.

CO_2 Sequestration and Storage

Trees and other types of vegetation take up CO_2 when they grow. A large, old tree can store about 3 t of carbon in the stem, branches, and roots [42]. This corresponds roughly to the amount of CO_2 emitted from driving 18,000 km in a medium-sized car (based on the assumption that a car emits on average 164 gCO_2/km) [92]. As such, the uptake in urban trees is very modest compared to the total CO_2 emission deriving from a city. For Chicago, it was estimated that the yearly sequestration of CO_2 in all the urban trees totaled approximately 140,000 t, corresponding to the CO_2 emissions of all car-based traffic from 1 week [42]. Further, the improvement is only permanent if the trees, when cut or dead, are replaced by new plantings and the dead biomass is used to replace fossil fuel. Simple decay will release the entire amount of stored CO_2 back into the atmosphere. In the balance of biomass CO_2 sequestration, the emissions of CO_2 from decay processes should also be subtracted.

Increasing the amount of green in a city will only marginally meet the mitigation challenge. The main task is still to reduce greenhouse gas emissions. Still, it can be reasonable to include urban trees in a climate plan and as part of the citywide CO_2 strategy as it might serve as part of a city-branding strategy. New York City has launched the "Million Trees Programme" to increase the amount of trees in the city by 20% as a means of carbon sequestration. At present, the urban trees in New York take up 42,000 t of carbon every year and stores a total of 1.35 million t of carbon [93].

Large tree size, longevity, and high growth rates are factors that have a positive influence on trees capacity

to sequester and store carbon. However, trees can only fulfill these functions when they are healthy and growing. In particular, street trees suffer from many stresses, and the average age of such trees has been estimated to be as short as 10–15 years in some cases [94, 95]. Moreover, recently planted trees often die due to bad site conditions and lack of or improper care [96]. Exact figures are rare but for instance, for Liverpool (UK) it was estimated that 39% of all newly planted street trees died within 5 years after establishment [97]. Yet, as a modeling study highlighted, street trees need to grow for at least 5–10 years before trees start to have a positive carbon balance because of the amount of carbon spent on their raising and management [98].

Urban trees are not the only way of greening the city. Lawns, shrubs, green roofs, and grass swales comprise some of the other options. Still, CO_2 storage capacity varies a lot and is mostly dependent on biomass stored in trees. A study of four residential neighborhoods in Liverpool showed a variation in carbon storage from less than 1 t per hectare to 17 t per hectare, with corresponding annual carbon sequestration rates from close to zero to 130 $kgCO_2$/ha [40].

CO_2 sequestration and storage in vegetation has a potential as an "image" of sustainability, but the impact of mitigating climate change is very modest in actual figures. To obtain larger reductions in CO_2 emission rates, urban greening can be used as a strategic tool to reduce energy demands, as presented below.

Reduction of Energy Demand for House Heating and Cooling

Hot weather in the summer period in presently temperate areas will increase the demand for air-conditioning in office buildings as well as in private houses. Yet, air-conditioning is energy demanding and expensive. Green infrastructure can potentially serve as a passive system, which can reduce energy demands for house heating and cooling.

Shading walls in summer time reduces the thermal load on buildings and hence the need for air-conditioning in warm climates. Trees should be best planted on the side where the afternoon sun hits the buildings (the southwestern side on the northern hemisphere). Deciduous trees are better than evergreen trees as the latter block the sun in winter when it warms up the building. Placing evergreen trees at the side of prevailing cold winds during wintertime can also shelter buildings and thus reduce energy loss [42]. These are significant factors in particular when insulation of buildings is not at high standards. For the homes in the US it was estimated that energy use in house can be 20–25% lower with an optimum planting of trees around them [99]. Yet, when badly placed, trees may even increase domestic energy consumption.

Other model calculations from the USA showed that 10% more tree cover can reduce energy consumption rates for cooling by 24% in Sacramento and 12% in Phoenix [100]. Most of the cooling energy savings were attributed to the effect of evapotranspiration and only 10% to the direct effect of shading and wind shielding. In the more northern city of Chicago, which has an 8 month heating season, an increase in the tree cover by 11% in an urban block would potentially reduce annual energy demands for house heating and cooling by up to 3.8% [101]. Here, the wind shielding effect was most important to reduce energy needs.

A field experiment in Sacramento where 16 trees were planted to the southeast and southwest of two houses and where indoor and outdoor temperatures, roof and wall surface temperatures, wind speed, and air-conditioning electricity use was measured during June–October resulted in an estimated cooling energy savings of 29% during the season for the two houses. Peak demand savings for the same houses were estimated to be 47% and 26%, respectively [102].

Roof and wall greening have the potential to decrease energy consumption of buildings for cooling buildings by improving insulation and reducing thermal loadings. In hot climates, reduced heat load during summertime is of significant importance. As an example, cooling load for a two-story nursery school building in Athens (Greece) was reduced by 6–49% during the summer for the whole building and by 12–87% for the top floor [103]. A study of an eight-story building in Madrid in Spain identified that a green roof reduced the building energy demand by 1% annually and 6% during the summer [104]. In a peak hot weather situation, the cooling load was reduced by 25% for the floor below the green roof. This indicates that green roofs have the greatest effect on energy consumption for buildings with a large roof area compared to the height of the wall, such as single-family houses, warehouses, and big box stores.

This way of reducing energy by tree planting, roof and wall greening has the spin-off of greening the city. However, potential conflicts with modern "green architecture" [105, 106] may also arise as, for instance, trees, wall and roof greening may be an obstacle for collecting solar energy by photovoltaics. This is certainly an important area for cooperation between architects and landscape architects to solve emerging conflicts and create synergies in the integrated design of the green infrastructure and green architecture.

Finally, vegetation, and in particular trees and shrubs have also the capacity to capture air pollutants [42]. More green may offset to some degree the potential increase of air pollution caused by intensification of the heat island. However, as with carbon sequestration, few data indicate that this effect will be quite limited [42]. Therefore, planting more trees and shrubs is not to be considered as an effective means solve the problem of emission of carbon dioxide and air pollutants.

Vulnerability of the Green Infrastructure to Climate Change Impacts

Green infrastructure has a series of potentials in terms of climate change mitigation and adaptation in urban areas. At the same time, green infrastructure is vulnerable to the impacts of climate change. Plantings, habitats, and species are challenged by higher temperatures and changing precipitation patterns, and the thermal benefits of evapotranspiration rely on lush vegetation. Furthermore, as Wilby and Perry [107] state in a review, there may be increased competition from exotic species, disease and pests may spread, and sea level rise can threaten rare coastal habitats: "Earlier springs, longer frost-free seasons, and reduced snowfall could further affect the dates of egg-laying, as well as the emergence, first flowering and health of leafing or flowering plants. Small birds and naturalized species could thrive in the warmer winters associated with the combined effect of regional climate change and enhanced urban heat island."

However, the database is very limited at the moment to establish, with any certainty, the impacts of climate change on the urban green infrastructure and to its ecosystem services. In the following, information from the ASCCUE project will be presented to discuss potential consequences of climate change on the capacity of green space to mitigate the heat-island effect.

Based on the climate scenarios used in the ASCCUE project, it was estimated that periods without water content available to plants in the upper 30 cm of the soil layer would increase from currently less than 1 month during summertime to up to 4–5 month in the inner city of Manchester (UK) in the high-emissions scenario. As a consequence, grassland would dry out and loose its capacity to evapotranspire water. Certainly, reliability of these estimates is low, in particular, as regional soil maps had to be used due to lack of better information on urban soils, which are known to be highly variable [108]. Nevertheless, the figures indicate the potential challenges that may arise for management of the green infrastructure under a changed climate.

Temperature differences with and without the provision of evapotranspiring grassland for 29 urban morphology types in Manchester are shown in Fig. 11. On a hot summer day, surface temperatures would be up to 70% higher on dried-out vegetation than on lush vegetation. In particular, areas with large expanses of lawn such as public parks, playing fields, and also schools would suffer. This points to the increasing need for proper water management to ensure well-growing vegetation or the choice of drought-tolerant vegetation. As concerns the former, mechanisms of water storage for irrigation during times when there is abundant rainfall need to be conceived. Reducing the amount of lawns in favor of trees and shrubs, which can access the water in deeper layers of soil with their roots, should also be considered where possible. However, trees require sufficient space for their roots.

Taking street trees as an example, water stress already occurs as a result of limited soil volume and small rooting space in planting pits combined with soil compaction and generally limited stormwater infiltration in built-up urban areas [109, 110]. Longer dry periods and rising temperatures will increase water stress and result in street trees dying if no proper management regime is installed. For instance, studies from Copenhagen (Denmark) indicated that larger planting pits in combination with improved soil substrates and irrigation can significantly improve growth conditions for street trees [109]. However, taking water for irrigation from the water supply system will become

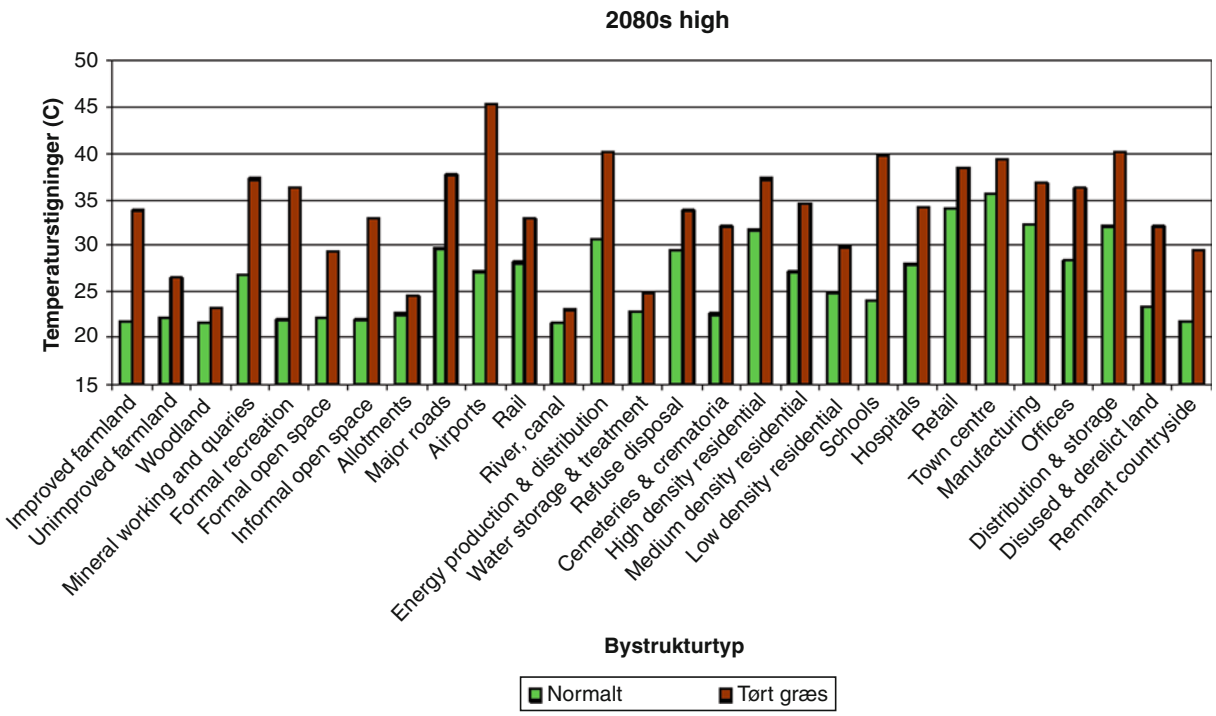

Green Infrastructure and Climate Change. Figure 11
Surface temperatures on a hot summer day in a 2080s high scenario with lush vegetation and dried-out vegetation ([120] with permission from author)

increasingly problematic under climate change. Another option is to combine irrigation needs with stormwater management, for example by discharging stormwater runoff from pavements to street trees. Such systems are, for example currently tested in the City of Stockholm, Sweden [111].

With changing precipitation patterns, higher temperatures, and later spring frost, the appropriate selection of species is an equally important approach to reduce the vulnerability of green infrastructure to the impacts of climate change. To address the challenge and to raise a discussion on the issue a Climate-Species-Matrix was developed for urban trees in Central Europe [110]. The study identified current regions analogous to the expected future climate in cities in Central Europe (i.e., less than 500 mm precipitation per year and average minimum temperatures between −17.8°C and −23.3°C). It resulted in a list of species with an increased focus on species originating from continental Central Asia and the continental northeastern parts of North America. Here, native species have evolved under conditions that may be similar to those experienced in urban areas in North and Central Europe in the future.

Future Directions

Climate change will imply significant consequences for the urban climate and the urban hydrology. The urban heat-island effect will increase if no action is taken. But by increasing the provision of urban green space, the temperature rise resulting from global warming can be mitigated. More intensive rain storms resulting from climate change will challenge the capacity of existing urban drainage systems and increase the risk of flooding. Implementing additional landscape-based stormwater detention, infiltration, evapotranspiration, and conveyance measures can compensate for changing precipitation patterns. By promoting urban green infrastructure, a network of green spaces can be implemented in the city to mitigate climate change and to adapt cities to the impact of climate change. A green infrastructure, which is multi-scale,

multifunctional, interconnected, and reflecting hydrology, is a major generator of sustainable urban form. Yet, the green infrastructure needs to be robust to cope with climate change. This has implications for the design of green spaces, including preparation of planting sites and species selection.

Landscape design to face climate change is an emerging concept, which can assist in sustaining cities in an increasingly urbanizing global context. It calls for continuous loops of collaboration, knowledge exchange, experiments, and learning by doing.

A recent symposium with 40 leading European experts [112] led to the development of a framework for research on urban green space. A total of 35 research questions were specified regarding the physicality, experience, valuation, management, and governance of urban green space. At least five of the research questions were directly related to the future role and capacity of urban green infrastructure in the light of climate change. These were primarily related to the physicality of urban green space and included the desired documentation of the "*direct and indirect effects of the climate changes on urban green spaces and how these changes impact people's well-being in urban areas*," "*how resilient current green space designs are to climate change and how resilience can be improved*," and "*how the resilience and adaptability of urban areas can be enhanced to future economic, housing and environmental demands through appropriate design and management of urban green spaces*." Additionally, 15 research questions were related to aspects of ecological functions, the public goods, and market benefits of urban green infrastructure, interdisciplinarity, and the management and governance of green areas, all addressing appropriate next steps in the exploration, analysis, and understanding of the potential of urban green infrastructure as a tool to face the global challenges of climate change and urbanization.

Adoption of a multidisciplinary approach to the development of the multifunctional green infrastructure is needed, including not only landscape architects and urban planners but also traffic engineers, hydrologists, biologists, sociologists, and economists. Importantly, urban green infrastructure calls for a participatory, socially inclusive approach to its planning and implementation as it will go across public and private land and affect all citizens in different ways. This challenges the sector-based distribution of work and responsibility areas currently prevalent in most public administrations. Multi-scale approach also involves interinstitutional collaboration and close cooperation between local, regional, and national authorities. Research in the field is emerging in Australia [113], the Netherlands [114], and the USA [115]. The examples from Copenhagen and Munich in this paper have shown that there is increasing potential for such an approach as disciplines realize the limitations of sectoral approaches.

Bibliography

Primary Literature

1. IPCC (Intergovernmental Panel on Climate Change) (2007) Climate change 2007: synthesis report. Contribution of working groups I, II and III to the fourth assessment report of the intergovernmental panel on climate change [Core Writing Team, Pachauri RK, Reisinger A (eds)]. IPCC, Geneva, Switzerland, p 104
2. Parry M, Carter T (1998) Climate impact and adaptation assessment. Earthscan, London
3. MEA (Millenium Ecosystem Assessment) (2005) Ecosystems and human well-being: synthesis. Island, London. http://www.millenniumassessment.org/documents/document.356.aspx.pdf. Accessed 4 Nov 2010
4. Alberti M (2008) Advances in urban ecology. Springer, New York
5. Pauleit S, Breuste JH (2011) Land use and surface cover as urban ecological indicators. In: Niemelä J (ed) Handbook of urban ecology. Oxford University Press, Oxford, pp 19–30
6. US Geological Survey (2010) The water cycle: evapotranspiration. http://ga.water.usgs.gov/edu/watercycleevapotranspiration.html. Accessed 6 May 2010
7. Lyr H, Fiedler H-J, Tranquilini W (1992) Physiologie und Ökologie der Gehölze. G. Fischer Verlag, Jena & Stuttgart
8. Benedict MA, McMahon ET (2006) Green infrastructure: linking landscapes and communities. Island, Washington, DC
9. Ahern J (2007) Green infrastructure for cities: the spatial dimension. In: Brown P, Novotny V (eds) Cities of the future: towards integrated sustainable water and landscape management. IWA Publishers, London, pp 267–283
10. Pauleit S, Liu L, Ahern J, Kazmierczak A (2011) Multifunctional green infrastructure planning to promote ecological services in the city. In: Niemelä J (ed) Handbook of urban ecology. Oxford University Press, Oxford, pp 272–285
11. Holling CS (1973) Resilience and stability of ecological systems. Annu Rev Ecol Syst 4:1–23
12. Gunderson LH, Holling CS, Light SS (1995) Barriers broken and bridges built: a synthesis. In: Gunderson LH (ed) Barriers and bridges to the renewal of ecosystems and institutions. Columbia University Press, New York, pp 489–532
13. IPCC (Intergovernmental Panel on Climate Change) (2001) Climate change 2001. Overview of impacts, adaptation, and vulnerability to climate change. Working group II contribution

to the third assessment report of the intergovernmental panel on climate change. IPCC, Geneva, Switzerland, p 89
14. United Nations (2008) World urbanization prospects: the 2007 revision. United Nations Department of Economic and Social Affairs/Population Division, New York
15. Angel S, Sheppard SC, Civco DL (2005) The dynamics of global urban expansion. Transport and urban development department. The World Bank, Washington, DC
16. O'Meara M (1999) Reinventing cities for people and the planet, Worldwatch Paper, 147. Worldwatch Institute, Washington, DC, p 94
17. Oke TR (1997) Urban climates and global change. In: Perry A, Thompson R (eds) Applied climatology: principles and practice. Routledge, London, pp 273–287
18. Satterthwaite D (2008) Cities' contribution to global warming: notes on the allocation of greenhouse gas emissions. Environment and Urbanization 20:539–549
19. Hunt A, Watkiss P (2007) Literature review on climate change impacts on urban city centres: initial findings. OECD Working Paper ENV/EPOC/GSP(2007)10/FINAL. http://www.oecd.org/dataoecd/52/50/39760257.pdf. Accessed 31 May 2010
20. Blanco H, Alberti M (2009) Building capacity to adapt to climate change through planning. In: Blanco H, Alberti M, Forsyth A, Krizek KJ, Rodrıguez DA, Talen E, Ellis C (eds) Hot, congested, crowded and diverse: emerging research agendas in planning. Prog Plan 71:158–169
21. Newman P, Kenworthy JR (1989) Sustainability and cities: overcoming automobile dependence. Island, Washington, DC
22. EEA (European Environment Agency) (2006) Urban sprawl in Europe. The ignored challenge. EEA Report No 10/2006. Office for Official Publications of the European Communities, Luxembourg
23. Nilsson K, Nielsen TS, Pauleit S (2008) Integrated European research on sustainable development and peri-urban landuse relationships. Urbanistica 138:106–109
24. Haase D (2011) Processes and impacts of urban shrinkage and response by planning. In: Encyclopedia of sustainability science and technology. Springer, Berlin
25. Wilby RL (2007) A review of climate change impacts on the built environment. Built Environ 33(1):31–45
26. Crichton D (2001) The implications of climate change for the insurance industry – an update and outlook to 2020. BRE, Watford
27. SoU (Swedish Commission on Climate and Vulnerability) (2007) Sweden facing climate change – threats and opportunities. Swedish Government Official Reports SOU 2007:60. Swedish Commission on Climate and Vulnerability, Stockholm
28. EEA (European Environment Agency) (2008) Impacts of Europe's changing climate – 2008 indicator-based assessment. EEA Report No 4/2008. Office for Official Publications of the European Communities, Luxembourg
29. McGranahan G, Balk D, Anderson B (2007) The rising tide: assessing the risks of climate change and human settlements in low elevation coastal zones. Environment and Urbanization 19(1):17–37
30. O'Brien K, Eriksen S, Sygna L, Nygaard L (2007) Why different interpretations of vulnerability matter in climate change discourses. Clim Policy 7:73–88
31. Kelly PM, Adger WN (2000) Theory and practice in assessing vulnerability to climate change and facilitating adaptation. Clim Change 47:325–352
32. Bridgeman H, Warner R, Dodson J (1995) Urban biophysical environments. Oxford University Press, Oxford
33. Lindley SJ, Handley JF, Theuray N, Peet E, Mcevoy D (2006) Adaptation strategies for climate change in the urban environment: assessing climate change related risk in UK urban areas. J Risk Res 9(5):543–568
34. O'Brien K, Sygna L, Haugen JE (2004) Vulnerable or resilient a multi-scale assessment of climate impacts and vulnerability in Norway. Clim Change 64:193–225
35. Mehrotra S, Natenzon CE, Omojola A, Folorunsho R, Gilbride J, Rosenzweig C (2009) Framework for city climate risk assessment. In: Fifth urban research symposium 2009, Marseille, June 28–30, 2009. http://siteresources.worldbank.org/INTURBANDEVELOPMENT/Resources/336387-1256566800920/6505269-1268260567624/Rosenzweig.pdf. Accessed 31 May 2010
36. Blanco H, Alberti M, Forsyth A, Krizek KJ, Rodrıguez DA, Talen E, Ellis C (2009) Hot, congested, crowded and diverse: emerging research agendas in planning. Prog Plan 71: 153–205
37. Chiesura A (2004) The role of urban parks for the sustainable city. Landscape Urban Plan 68:129–138
38. Tyrväinen L, Pauleit S, Seeland K, de Vries S (2005) Benefits and uses of urban forests and trees: a European perspective. In: Konijnendijk CC, Nilsson K, Randrup TB, Schipperijn J (eds) Urban forests and trees in Europe – a reference book. Springer, Berlin, pp 81–114
39. Tzoulas K, Korpela K, Venn S, Yli-Pelkonen V, Kazmierczak A, Niemela J, James P (2007) Promoting ecosystem and human health in urban areas using green infrastructure: a literature review. Landscape Urban Plan 81(3):167–178
40. Whitford V, Ennos AR, Handley JF (2001) "City form and natural process" – indicators for the ecological performance of urban areas and their application to Merseyside, UK. Landscape Urban Plan 57(2):91–103
41. Gartland L (2008) Heat islands. Understanding and mitigating heat islands in urban areas. Earthscan, London
42. Nowak DJ (2002) The effects of urban forests on the physical environment. In: Randrup TB, Konijnendijk CC, Christophersen T, Nilsson K (eds) COST action E12 urban forests and urban trees. Proceedings No. 1. Office for Official Publications of the European Communities, Luxembourg, pp 22–42
43. Girardet H (2004) Cities people planet: liveable cities for a sustainable world. Wiley, Chichester
44. Landsberg HE (1981) The urban climate. Academic, New York
45. Oke TR (1987) Boundary layer climates, 2nd edn. Routledge, London, New York
46. Akbari H, Pomerantz M, Taha H (2001) Cool surfaces and shade trees to reduce energy use and improve air quality in urban areas. Sol Energy 70(3):295–310

47. Robine JM, Cheung SL, Le Roy S, Van Oyen H, Herrmann SR (2008) Report on excess mortality in Europe during summer 2003. EU Community Action Programme for Public Health, Grant Agreement 2005114. http://ec.europa.eu/health/ph_projects/2005/action1/docs/action1_2005_a2_15_en.pdf. Accessed 27 Jan 10
48. USEPA (United States Environmental Protection Agency) (2001) Inside the greenhouse: a state and local resource on global warming. USEPA (United States Environmental Protection Agency), Washington, DC
49. Robel F, Hoffmann U, Riekert A (1978) Daten und Aussagen zum Stadtklima von Stuttgart auf der Grundlage der Infrarot-Thermographie. Beiträge zur Stadtentwicklung Nr. 15. Landeshauptstadt Stuttgart
50. Taha H (1997) Urban climates and heat islands: albedo, evapotranspiration, and anthropogenic heat. Energy Build 25(2): 99–103
51. von Stülpnagel A (1987) Klimatische Veränderungen in Ballungsgebieten unter besonderer Berücksichtigung der Ausgleichswirkung von Grünflächen, dargestellt am Beispiel von Berlin (West). Unpublished PhD thesis, TU Berlin, Berlin
52. Eliasson I, Upmanis H (2000) Nocturnal air flow from urban parks – implications for city ventilation. Theor Appl Climatol 66:95–107
53. Handley J (2006) Adaptation strategies for climate change in the urban environment (ASCCUE). In: Walsh CL, Hall JW, Street RB, Blanksby J, Cassar M, Ekins P, Glendinning S, Goodess CM, Handley J, Noland R, Watson SJ (eds) Building knowledge for a changing climate: collaborative research to understand and adapt to the impacts of climate change on infrastructure, the built environment and utilities. Newcastle University, March 2007, pp 44–53. http://www.ukcip.org.uk/images/stories/Pub_pdfs/BKCC-Results.pdf. Accessed 11 April 2010
54. Gill S, Handley J, Ennos R, Pauleit S (2007) Adapting cities for climate change: the role of the green infrastructure. Built Environ 30(1):97–115
55. Gill S, Handley J, Pauleit S, Ennos R, Theuray N, Lindley S (2008) Characterising the urban environment of UK cities and towns: a template for landscape planning in a changing climate. Landscape Urban Plan 87:210–222
56. Matzarakis A, Mayer H, Iziomon M (1999) Applications of a universal thermal index: physiological equivalent temperature. Int J Biometeorol 43:76–84
57. Dousset B, Gourmelon F, Laaidi K, Zeghnoun A, Giraudet E, Bretin P, Vandentorren S (2009) Satellite monitoring of summertime heat waves in the Paris metropolitan area. In: The seventh international conference on urban climate, 29 June – 3 July 2009, Yokohama, Japan. http://www.ide.titech.ac.jp/~icuc7/extended_abstracts/pdf/384388-1-090518140731-002.pdf. Accessed 31 May 2010
58. BETWIXT (2005) Built EnviromenT: weather scenarios for investigation of impacts and eXTremes. Daily time-series output and figures from the CRU weather generator [online].http://www.cru.uea.ac.uk/cru/projects/betwixt/cruwg_daily/. Accessed 30 June 2008
59. Watts M, Goodess CM, Jones PD (2004) The CRU daily weather generator. Climatic Research Unit, University of East Anglia, Norwich
60. Burkhardt I, Dietrich R, Hoffmann H, Leschnar J, Lohmann K, Schoder F, Schultz A (2008) Urbane Wälder. Bundesamt für Naturschutz (eds), Naturschutz und Biologische Vielfalt, 63. Bonn-Bad Godesberg, pp 214
61. Pauleit S, Golding Y, Ennos R (2005) Modeling the environmental impacts of urban land use and land cover change – a study in Merseyside, UK. Landscape Urban Plan 71(2–4):295–310
62. Perry T, Nawaz R (2008) An investigation into the extent and impacts of hard surfacing of domestic gardens in an area of Leeds, United Kingdom. Landscape Urban Plan 86:1–13
63. Madsen H, Arnbjerg-Nielsen K, Mikkelsen PS (2009) Update of regional intensity–duration–frequency curves in Denmark: tendency towards increased storm intensities. Atmos Res 92(3):343–349
64. DMI (Danish Meteorological Institute) (2007) Klimaet i Danmark i 2100 i forhold til 1990 for A2- og B2-scenarierne. http://www.dmi.dk/dmi/index/klima/fremtidens_klima-2/aendringer_i_danmark.htm. Accessed 11 April 2010 (in Danish)
65. Arnbjerg-Nielsen K (2008) Forventede ændringer i ekstremregn som følge af klimaændringer. Spildevandskomiteen, Skrift nr. 29, IDA Spildevandskomiteen, Danish Society of Engineers, Copenhagen (in Danish)
66. Rambøll (2008) Kommunernes investeringsbehov i forbindelse med klimatilpasning og veje. Local Government Denmark, Copenhagen. http://www.ramboll-management.dk/news/~/media/Images/RM/RM%20DK%20and%20RM%20Group/PDF/Publications/2009/KommunernesInvesteringsbehovIforbindelseMedKlimatilpasningOgVeje.ashx. Accessed 11 April 2010 (in Danish)
67. Butler D, Parkinson J (1997) Towards sustainable urban drainage. Water Sci Technol 35(9):53–63
68. Chocat B, Ashley R, Marsalek J, Matos MR, Rauch W, Schilling W, Urbonas B (2007) Toward the sustainable management of urban storm-water. Indoor Built Environ 16(3):273–285
69. Marsalek J, Chocat B (2002) International report: stormwater management. Water Sci Technol 46(6–7):1–17
70. Coombes PJ, Argue JR, Kuczera G (2000) Figtree place: a case study in water sensitive urban development (WSUD). Urban Water 1(4):335–343
71. Wong THF (2006) An overview of water sensitive urban design practices in Australia. Water Pract Technol 1(1)
72. Geiger WF, Dreiseitl H (1995) Neue Wege für das Regenwasser. R. Oldenbourg Verlag, Munich
73. Beenen T, Boogaard FC (2007) Lessons from 10 years storm water infiltration in the Dutch Delta. In: Proceedings of the 6th international conference on sustainable techniques and strategies in urban water management, Novatech 2007, June 25–28 2007, Lyon, pp 1139–1146
74. Scholz M (2006) Best management practice: a sustainable urban drainage system management case study. Water Int 31(3):310–319

75. Stahre P (2006) Sustainability in urban storm drainage: planning and examples. Svenskt Vatten, Stockholm
76. Bengtsson L (2002) Avrinning från gröna tak (runoff from greenroofs). Vatten 58:245–250
77. Villarreal EL, Semadeni-Davies A, Bengtsson L (2004) Inner city stormwater control using a combination of best management practices. Ecol Eng 22:279–298
78. Beneke G (2003) Regenwasser in Stadt und Landschaft – Vom Stückwerk zur Raumentwicklung – Plädoyer für eine Umorientierung. Beiträge zur Rümlichen Planung – Schriftenreihe des Fachbereichs Landschaftsarchitektur und Umweltentwicklung der Universität Hannover Heft 70
79. Fryd O, Backhaus A, Jeppesen J, Ingvertsen ST, Birch H, Bergman M, Petersen TEP, Fratini C (2009) Koblede afkoblinger. http://www.2bg.dk/Internal_Workshop/2009-12-03-KE/2BG_HarrestrupAa_Booklet_web.pdf. Accessed 11 April 2010 (in Danish)
80. Turenscape (2004) Yongning river park, Taizhou city. http://www.turenscape.com/English/projects/projectphp?id=323. Accessed 6 June 2010
81. Stokman A, von Seggern H, Rabe S, Schmidt A, Werne J, Zeller S (2008) Wasseratlas: Wasserland-Topologien für die Hamburger Elbinsel. Jovis Verlag, Berlin
82. Mathur A, da Cunha D (2009) SOAK – Mumbai in an estuary. Rupa, New Delhi
83. van Nieuwenhuijze L (2006) (Hoog)water als uitdaging Meervoudig gebruik van de dijk en het buitendijkse gebied: wie durft? Report developed by H + N + S Landscape Architects, Utrecht. (in Dutch). http://www.hns-land.nl/images/stories/Publicaties/hoogwaterstrategie72dpi.pdf. Accessed 6 June 2010
84. Dreiseitl H (2009) Bishan park, Singapore. http://www.dreiseitl.net/index.php?id= 525&lang = en&choice = 58&ansicht = text. Accessed 05 June 2010
85. Mathur A, de Cunha D (2001) Mississippi floods: designing a shifting landscape. Yale University Press, New Haven
86. City of Los Angeles (2007) Los Angeles river revitalization master plan. http://www.lariverrmp.org/CommunityOutreach/masterplan_download.htm. Accessed 11 April 2010
87. Rinaldi BM (2007) Landscapes of metropolitan hedonism. The cheonggyecheon linear park in Seoul. J Landscape Archit 2007:60–73
88. Nyhuus S (2005) Oslo. In: Werquin AC, Duhem B, Lindholm G, Oppermann B, Pauleit S, Tjallingii S (eds) Green structure and urban planning. Final report. COST Action C11, European Commission, Brussels, pp 184–191. http://www.greenstructureplanning.eu/COSTC11-book/. Accessed 11 April 2010
89. Attwell K (2005) Green planning as a prerequisite for urban development in Aarhus, Denmark. In: Werquin AC, Duhem B, Lindholm G, Oppermann B, Pauleit S, Tjallingii S (eds) Green structure and urban planning. Final report. COST Action C11, European Commission, Brussels, pp 345–351. http://www.greenstructureplanning.eu/COSTC11-book/. Accessed 11 April 2010
90. Oppermann B (2005) Redesign of the river Isar in Munich, Germany. Getting coherent quality for green structures through competitive process design? In: Werquin AC, Duhem B, Lindholm G, Oppermann B, Pauleit S, Tjallingii S (eds) Green structure and urban planning. Final report. COST Action C11, European Commission, Brussels, pp 372–378. http://www.greenstructureplanning.eu/COSTC11-book/. Accessed 11 April 2010
91. City of Melbourne (2009) Zero net emissions by 2020 – update 2008. http://www.melbourne.vic.gov.au/Environment/WhatCouncilisDoing/Documents/zero_net_e-missions_2020.pdf. Accessed 11 April 2010
92. Kågeson P (2005) Reducing CO_2 emissions from new cars. European federation for transport and environment, Brussels, p 10. http://www.gronabilister.se/grafik/dynamiskapdf/20050124210807.pdf. Accessed 11 April 2010
93. New York City (2010) Million trees NYC. New York City Department of Parks & Recreation and New York Restoration Project. http://www.milliontreesnyc.org/html/urban_forest/urban_forest_benefits.shtml. Accessed 11 April 2010
94. Morse SC (1978) Trees in the town environment. J Arboric 4:1–6
95. Foster R, Blaine J (1978) Urban trees survival: trees in the sidewalk. J Arboric 4:14–17
96. Pauleit S, Jones N, Garcia-Marin G, Garcia-Valdecantos J-L, Rivière LM, Vidal-Beaudet L, Bodson M, Randrup TB (2002) Tree establishment practice in towns and cities – results from a European survey. Urban Forestry and Urban Greening 1(2):83–96
97. Bradshaw A, Hunt B, Walmsley T (1995) Trees in the urban landscape. Principles and Practice, Spon, London
98. Nowak DJ, Stevens JC, Sisinni SM, Luley CJ (2002) Effects of urban tree management and species selection on atmospheric carbon dioxide. J Arboric 28(3):113–122
99. Heisler G (1986) Energy savings with trees. J Arboric 12(5):113–125
100. Huang J, Ritschard R, Sampson N, Taha H (1992) The benefits of urban trees. In: Akbari H, Davis S, Dorsano S, Huang J, Winnett S (eds) Cooling our communities. US Environmental Protection Agency, Washington, DC, pp 27–42
101. Jo HK, McPherson EG (2001) Indirect carbon reduction by residential vegetation and planting strategies in Chicago, USA. J Environ Manage 61:165–177
102. Akbari H, Kurn DM, Bretz SE, Hanford JW (1997) Peak power and cooling energy savings of shade trees. Energy Build 25:139–148
103. Santamouris M, Pavloua C, Doukasa P, Mihalakakoub G, Synnefaa A, Hatzibirosa A, Patargias P (2007) Investigating and analysing the energy and environmental performance of an experimental green roof system installed in a nursery school building in Athens, Greece. Energy 32(9):1781–1788
104. Saiz S, Kennedy C, Bass B, Pressnail K (2006) Comparative life cycle assessment of standard and green roofs. Environ Sci Technol 40:4312–4316

105. Brown DE, Fox M, Pelletier MR (eds) (2001) Sustainable architecture white papers. Earth Pledge Foundation, New York
106. Jodidio P (2009) Green architecture now! Taschen, Cologne
107. Wilby RL, Perry GLW (2006) Climate change, biodiversity and the urban environment: a critical review based on London, UK. Prog Phys Geogr 30(1):73–98
108. Sauerwein M (2011) Urban soils – characterization, pollution and relevance in urban ecosystems. In: Niemelä J (ed) Handbook of urban ecology. Oxford University Press, Oxford, pp 45–58
109. Bühler O, Nielsen CN, Kristoffersen P (2006) Growth and phenology of established *Tilia cordata* street trees in response to different irrigation regimes. Arboriculture & Urban Forestry 32(1):3–9
110. Roloff A, Korn S, Gillner S (2009) The climate-species-matrix to select tree species for urban habitats considering climate change. Urban Forestry and Urban Greening 8:295–308
111. Alvem B-M, Bennerscheidt C (2009) Baumstandortoptimierung und Regenwasserbewirtschaftung – Chancen für ein gemeinsames Vorgehen. In: Dujesiefken D (ed) Jahrbuch der Baumpflege 2009. Taspo Fachbuchservice, Braunschweig, pp 70–78
112. James P, Tzoulas K, Adams MD, Annett P, Barber A, Box J, Breuste J, Cooper I, Curwell SR, Elmqvist T, Flood T, Frith M, Gledhill DG, Goode D, Gordon C, Greening KL, Handley J, Harding S, Haworth S, Hesketh F, Home R, Johnston M, Kazmierczak AE, Korpela K, Leeks G, Leeks G, Morley E, Nail S, Niemelä J, Moretti M, Stein N, Pauleit S, Powell JA, Radford KG, Richardson D, Roe MH, Sadler JP, Selman P, Scott AV, Snep R, Stern N, Timmermans W, Ward-Thompson C (2009) Urban green – towards an integrated understanding of greenspace in the built environment. Urban Forestry and Urban Greening 8(2):65–76
113. Brown RR, Farrelly MA (2009) Challenges ahead – social and institutional factors influencing sustainable urban stormwater management in Australia. Water Sci Technol 59(4):653–660
114. van der Brugge R (2009) Transition dynamics in social-ecological systems: the case of Dutch water management. PhD thesis, Erasmus University, Rotterdam
115. Roy AE, Wenger SJ, Fletcher TD, Walsh CJ, Ladson AR, Shuster WD, Thurston HW, Brown RR (2008) Impediments and solutions to sustainable, watershed-scale urban stormwater management: lessons from Australia and the United States. Environ Manage 42(2):344–359
116. Handley J (2007) Planning for climate change. Unpubl. Presentation given at the "Future of Cities" 51st international federation for housing programmes (IFHP), World Congress, Copenhagen, Sept 22–26 2007
117. CEC (Commission of the European Communities) (2007) Green paper on adapting to climate change in Europe – options for EU action. Brussels, 29.6.2007. COM(2007) 354 final
118. Voogt JA (2004) Urban heat islands: hotter cities. ActionBioscience.org, American Institute of Biological Sciences. http://www.actionbioscience.org/environment/voogt.html. Accessed 07 May 2010
119. Sieker F (Hrsg) (1998) Naturnahe Regenwasserbewirtschaftung, Reihe Stadtökologie, Bd. 1, Analytica Verlagsgesellschaft, Berlin
120. Gill S (2006) Climate change and urban greenspace. Unpublished PhD thesis, School of Environment and Development, University of Manchester, Manchester

Books and Reviews

Akbari H, Davis S, Dorsano S, Huang J, Winnett S (eds) (1992) Cooling our communities – a guidebook on tree planting and light-colored painting. US Environmental Protection Agency, Washington, DC

Woods-Ballard B, Kellagher R, Martin P, Jefferies C, Bray R, Shaffer P, Kellagher R (2007) The SUDS manual (C697). Construction Industry Research & Information Association (CIRIA), London

Green Roof Infrastructures in Urban Areas

Manfred Köhler[1], Andrew Michael Clements[2]
[1]University of Applied Sciences, Neubrandenburg, Germany
[2]Green Roof Greece, Athens, Greece

Article Outline

Glossary
Definition of the Subject and Its Importance
Introduction
Acknowledgment
Bibliography

Glossary

FLL The Landscape Research and Development Society (FLL) nonprofit organization was founded in 1975. Its mission is to research, produce, and disseminate all the various landscape development principles, guidelines, and specifications for the assurance of environmental quality [1].

FBB The Green Infrastructure Association (FBB) is a specialized group that was founded by some members of FLL to focus more specifically on green building. The FBB is the German counterpart

to the American industry association Green roofs for Healthy Cities (GRHC) and one of the founding members of the World Green Infrastructure Network (WGIN). The German Word "Bauwerksbegrünung" has no translation in English – Green infrastructure in the sense of FBB is focused on all forms of urban green.

Extensive green roofs (EGR) Also called natural green roofs, eco-roofs, and oikosteges in Greece are vegetated roof constructions that require low to no maintenance. Drought-adapted plant species are used to create a self-sustaining vegetated surface suitable for nearly all types of buildings. Growing media is usually less than 10 cm, or 3 in. deep [2]. The term "Natural Green Roof" or oikostegi, coined by the authors, denotes a green roof where the main interest is in maximizing natural endemic biodiversity on vegetated roofs. These systems can incorporate irrigated areas with rain or gray water. Natural green roofs are designed, engineered green roof systems which enlist the help of the natural environment. Natural green roofs may also be engineered in such a way to include intensive green roofs on occasion.

Intensive green roofs (IGR) Also known as roof gardens are garden structures on top of buildings and other artificial urban surfaces. In most cases, the growing media is more than 20 cm deep; for trees it can be more than 1 m. IGRs, with structures including lawns, planter boxes, shrubs, and small trees, require the same maintenance as traditional gardens; therefore, some question their environmental value.

Stormwater runoff Rainwater running off impervious surfaces.

Green infrastructure Overall phrase in North America for all types of green roof technology and other types of greenery on buildings, like vertical greening, living walls, and indoor greening systems. Green infrastructure in a wider sense includes photovoltaic technology and rainwater management.

Growing media Engineered substrate for green roof purposes. Green roof substrates typically have low nutrient content and high drainage rates. Typical materials are expanded slate, shale, pumice, or recycled construction material such as broken ceramic tiles.

Green infrastructure Broad term in the North America for all types of green roof technology and other types of greenery on buildings, like vertical greening, living walls, and indoor greening systems. Green infrastructure in a wider sense includes photovoltaic technology and rainwater management. This term also describes the range of materials and technologies used to enhance urban environments. In addition to green roofs, this term also encompasses other related systems such as vegetated facades with climbers or living wall systems, indoor greening systems, rain gardens, photovoltaic systems, and other technologies. Roof greening can be combined with living walls, indoor plants, and ecological landscaping to enhance the built environment. The USEPA refers to structures specifically intended to manage wet weather as green infrastructure.

Leadership in Energy and Environmental Design (LEED) This is a US-based rating system by the US Green Building Council (USGBC). Benchmarks focus on energy savings, water efficiency, CO_2 emissions reduction, improved indoor environmental quality, and stewardship. The categories of achievement are silver, gold, or platinum. In Australia, a similar rating system uses "stars." After an extensive debate about the merits of such certification systems, Germany set one up in 2009. Certification can be an effective type of marketing; however one critique of existing systems is that there is not enough weight placed on vegetation.

Low-impact development (LID) A storm water management and site-design technique to mimic the situation before construction. Water usage, evaporation, cooling, and water storage and drainage are such benefits of green roof infrastructures.

Definition of the Subject and Its Importance

Definition

Green roofs are engineered constructions that include environments suitable for well-adapted plant species. In most cases, these types of roofing have a longer life span than conventional roofing surfaces. The following elements are built on top of the roof structure (from the bottom to the top, see Fig. 1):

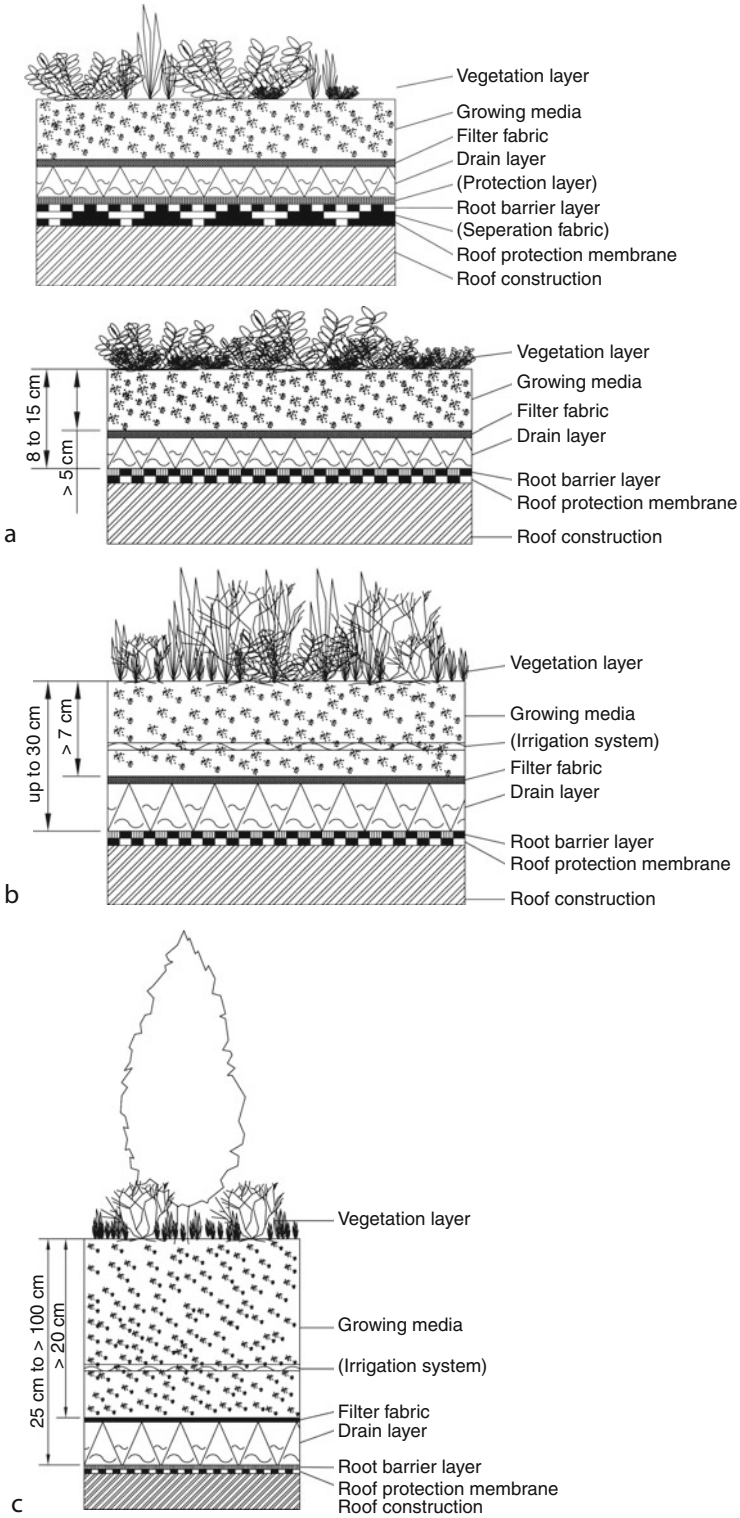

Green Roof Infrastructures in Urban Areas. Figure 1 (Continued)

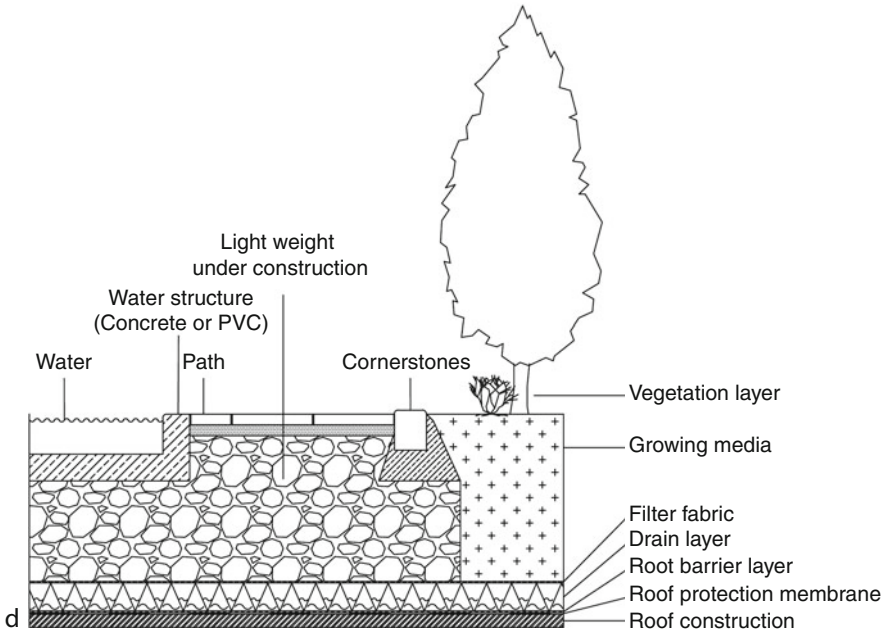

Green Roof Infrastructures in Urban Areas. Figure 1
The first schematic cross section illustrates the principles of green roof structures. (**a**) Details the one-layer solution without drainage components. This could be difficult in a damp, wet climate. (**a1**) is a multiple layer solution, typical construction from various suppliers. (**b**) Semi-extensive means, irrigation is included. (**c**) Intensive roof garden. (**d**) Plaza deck construction on garages and similar structures with high load capacity

- The underlying protective layer is made of an impervious material such as bitumen, rubber, polystyrene, or other similarly adequate technical materials, in short, roof protection membranes.
- Additional, root barrier layers are available to prevent the root penetration of lower layers. These are known as separation fabrics or geotextiles.
- This is commonly followed by a separate water-retaining layer, which could be a natural porous stone material or an artificial retention mat; in short, this is a drainage layer.
- On top of this layer, a filter fabric separates the retention layer from the next layer: the growing media.
- The growing media is, in most cases, a specially mixed lightweight soil material with carefully selected ingredients for storing rainwater. Growing media are mixed for different purposes (for example, extensive green roof growing media differs from roof garden media in nutrient and humus content). Intensive roof garden growing media differs in that in the upper levels there is a higher content of humus and on the lower levels lower humus content.
- The vegetation layer can range from a shallow layer with mosses and only a few taller plants all the way up to full-blown roof gardens. As such, green roof maintenance requirements can be as little as an annual inspection or as much as is usual for ordinary gardens. The success of the vegetation layer depends on the careful selection of the other green roof layers. For example, if the goal is to plant trees on roof tops, a special combination of all these components is necessary (After [3]).

The maximum weight of the construction must be calculated carefully. On average, it varies between 40 kg/m^2 (this is about 8.33 lb/ft^2) and can rise upward to about 350 kg/m^2 (71.7 lb/ft^2, for conversion factors, see [4] on roof gardens, including the weight associated with water storage. Extensive green roofs should be able to store a minimum of at least 20 L/m^2 of water.

Compared to this load, the weight of all the plant components is relatively small.

The longevity of green roofs depends on whether they can be easily accessed with the basic equipment needed for the success of the project as well as repairs. Maintenance and repairs must be planned carefully. Certain areas of the roof like, edges and places around roof fixtures like skylights or climate control systems can be prone to structural damage. Architects often want to install green roofs on very steep roof inclinations and on very tall buildings. These technical and biological limits challenge green roof professionals. It is the duty of green roof specialists to assess the limits which are set. Uncontrollable aspects of local climate, like wind, temperature, and the intensity of storm events and solar exposure can set limits to what is feasible from an architectural design perspective and ideas about developing living surfaces on roofs and facades.

In Germany [1], two main types of vegetated green roofs are observed:

- Extensive green roofs are large lightweight constructions. Most consist of a layer of under 10 cm deep covered by drought tolerant plant species including mosses, sedum sp, other succulents, wild flowers, aromatic herbs, and a plethora of pioneer species. Commonly, no irrigation is installed, particularly in temperate climate experienced in Central and Northern Europe and North America and only one annual maintenance visit occurs. These structures are possible on nearly all types of flat buildings covered with gravel protection layers; gravel has nearly the same weight as green roof materials but gravel has relatively no environmental value.
- Intensive green roofs, synonymous with roof gardens, are fully maintained with garden structures similar to those on the ground level. The first step in planning such constructions is a careful calculation of the loading capacity.

Recently, [1] a third type, called "simple intensive green" has been developed. These are green roof constructions with a little irrigation on demand, a wider range of plant species, and a little maintenance. Shrubs and garden plant species are suitable for such green roofs. Another difference is the need for maintenance. Extensive green roofs usually only need one inspection a year. The simple intensive green roofs or roof gardens do need maintenance, and are thus more similar to ground-level gardens.

The phrase "grass or sod roofs" is used to describe extensive green roofs in the Northern European region, while "Living roofs" is the most commonly used term for green roofs in the UK. They distinguish between "green roofs" and "biodiverse green roofs," which are characterized by a wider range of growing media types at various depths. This creates a wider range of microhabitats. Furthermore, green roof researchers in the UK also talk about "brown roofs" or roofs with shallow layers of growing media and a sparse vegetation cover, mostly developed for insects and nesting birds. The presence of birds like the Black Redstart on green roofs is a key indicator of success about which people in the UK have become especially emotional. Observations like these help to promote green roofs. In Greece, there is growing interest in another form of extreme natural green roof called an Oikostegi (from the Greek "οικος" meaning home, abode, living quarters, and "στέγη" meaning roof, shelter, protection, den). Oikosteges/οικοστέγες/ are designed for the most extreme built environments on Earth, namely, earthquake zones, which permit only ultra-lightweight building greening systems. In addition, oikosteges are designed to be low to zero maintenance and low to no irrigation in extremely hot, dry, windswept, so-called urban canyons like Athens. This is green infrastructure at its hardest core and at its most extreme.

Installations at prestigious locations such as the Greek Treasury, in Constitution Square, opposite The Greek Parliament in Athens have been acclaimed with rave review by specialists, academia, and the media. Countless species of butterfly, spider, and other insects like honey bees and ladybirds attract numerous species of song birds, which have begun to nest in the center of this sprawling metropolis. This ecosystem has been named the "Meadow of Constitution Square" a touching acknowledgment that nature has begun to establish a foothold in the once barren, windswept capital which was the birthplace of democracy, the rule of law, politics, philosophy, Western medicine, logic, science, the Olympic games to name just a few of the contributions that Greece has made to humanity.

It should be also noted here that Greece has the richest biodiversity in Europe boasting fully one third

of all indigenous species on the European continent. The growth of cities like Athens had all but banished this abundant natural wealth from its home. Oikosteges represent a hopeful sign that Athens and Greece as a whole with its rich natural environment is now reestablishing itself to take the place it deserves as an inspiration and testament to the world of what is possible.

Green roofs are also characterized by their technical structure. The non-ventilated flat or "warm roof" is constructed with the insulation under the waterproofing layer. In contrast, on "inverted roofs" the insulation layer is installed on top of the waterproofing layer. These inverted roofs have received a lot of attention because this layering can protect the waterproofing and also be used to prevent leaks. However, there are also some disadvantages, like, for example, reduced insulation function if the thermal insulation is exposed to water. An open debate about such details of building physics must take place between the roofer and the landscaper executing the green roof. Surface sealing, either with an artificial layer or with liquid sealing components must be selected carefully. There are regional differences in such construction materials. All layers must be qualified as "root resistant" and be secure against aggressive roots. Such layers contain, in many cases, components to prevent root penetration [2]. It should be obvious that these layers should not include poisonous substances. These components could be washed out into the sewer systems or could be a problem for the roof vegetation.

Green roof technology has become internationally renowned in the past few years. The books recommended at the end of this chapter offer a wide range of basic information from various regions in the world.

Introduction

Introduction – Worldwide Historic Roots of Green Roofs

Like many other ground-breaking ideas, the basics of green roofs are simple and some historical examples date back more than 2,000 years [3]. A water barrier layer and an additional layer of growing media make it possible to cover a building with plant material. This coverage protects the building and stabilizes temperature fluctuations. That is why green roofs can be found worldwide from the hot and dry climates of the African desert zones where there are examples in places like Uganda, to the Northern European zones with long cold frost periods, such as the Iceland sod homes. These prototypes are the predecessors of extensive green roofs.

Roof gardens or intensive Green roofs may have originated from the "hanging gardens" of Semiramis (Babylon). Intensive green roofs can only be built on flat roofs and are quite similar in structure and form to a ground-level garden. In some Mediterranean countries, flat roofs were traditionally used as recreational space for spending time at home in the evening breeze.

Roofs do not necessarily have to be flat in order to be greened; it is also possible to have green sloped or pitched roofs. The grass-covered tombs in the ancient City of Pamukkale (Turkey) are examples of this. Water tanks with a grass roof structure are common in some countries in Southern Europe. On North European pitched rural farmhouse, green roofs are found in many regions. Roof gardens became especially widely distributed [4], creating green islands in urban environments in the 1920s with a peak of interest in the 1970s. Roof gardens as recreational areas on shopping malls and hotels have also become fashionable.

The first emergence of modern green roofs was observed in the 1860s. During this period of industrialization, roofers developed methods of covering their housing tenements with a gravel layer and turf to avoid the risk of fire. Between 1860 and 1920, similar ideas grew in many German Cities. These older green roofs were a cheap way to protect the sensitive layer of tarred cardboard used for roofing at the time [5]. Vegetable gardens were also planted in these first roofs. All these green roofs were erected above a wooden support construction [6].

In the 1920s, several roof garden projects were documented in the literature of the historic garden library; (see the online Databank of the Technical University of Berlin, (http://freitext.ub.tu-berlin.de/gartenkunst.html) using the German word "Dachgarten" as a search word. At the time of writing (April 2010), 130 titles are available dating from the beginning of twentieth century concerning green roofs.

Since the beginning of the twentieth century architects, like Le Corbusier and Oscar Niemeyer have

included roof gardens in their designs. Some of these early modern roof gardens still exist today. One of the most famous is the roof garden on the Rockefeller Center. Other examples like the roof gardens at "The Bund" in Shanghai were also built at that time. In the late 1930s, LeCobusier, Oscar Niemeyer, Lucio Costa, and Roberto Burle Marx created roof gardens as part of a workshop at the Ministry of labor and work in Rio de Janeiro, which can still be seen today. The landscape Architect Burle Marx completed nearly 100 roof garden projects mostly in South and North America, but also in some other countries of the world.

Flat and green roofs were the preferred style in "Bauhaus" architecture. Planners in the 1920s were fascinated by the open amenity spaces on the roof tops of modern Cities. In 1929, the storehouse Karstadt at Berlin-Hermannplatz was one such famous building. It was well publicized, and *the* place to stay at that time [4]. In its first year, in 1929, the young Roberto Burle Marx began a 1 year stay with his family in Berlin, studying vegetation in the Botanical Garden and Art. Burle Marx is regarded as being as the landscape Architect of the Bauhaus team, newer publications describe him as this [7, 8]. He is considered to be one of the most innovative landscape architects in the twentieth Century and a pioneer of roof garden technology since the 1940s all over the world. Modern examples are documented as award-winning projects in the USA [9, 10].

Maintenance of these early roof gardens was similar to that of gardens. They were high-quality recreational spaces where the affluent could spend their leisure time. No publications discussing maintenance or issues of ecology are mentioned from this era.

It can be deduced from the painting by Carl Spitzweg, called "The poor poet" 1837, that living in a roof apartment entailed long periods of poor living conditions. In the winter time, it was too cold and in summer it was too hot. This is still the case in countries like Greece. Additional insulation provided by rooftop greenery created better living conditions in the top floor of buildings. This idea, to take advantage of additional insulation while bringing nature back into cities, gained popularity in the years following World War II.

The second emergence of green roof technology in Germany occurred in the late 1970s. A movement of urban environmentalists tried to bring nature back into Cities. A key thinker at that time was the Garden stylist LeRoy who had ideas about "natural gardens." People began to reevaluate urban areas [11]. The first ecological studies of green roofs began during this time. Among the pioneers in Germany was, for example, the Architect Minke in Kassel. His focus was the energetic performance of affordable housing. He learned from ancient African architecture and designed simple, modern solutions for "green architecture" in hot climates [12].

Famous artists at that time Friedensreich Hundertwasser and Ben Wargin promoted the concept of more natural cities and especially nature on buildings. But they were not architects. It was a challenge during the following years to materialize these concepts [13].

The Green Roof Movement in Germany

Roof gardens are a well-established technology in many countries. Hotels, holiday resorts, plaza decks, and similar institutions are covered with green roofs in various countries [4]. The main difference between the early stages of the roof garden movement and today is the current focus on ecological function, local plant species selection, and environmentally friendly construction technology.

A water storage and drainage layer can be installed underneath a roof garden, which can then be used as a recreational space for the users, citizens of the entire building. That is the position today. Lots of these older roof gardens failed over the years. Materials knowledge and maintenance techniques have grown over the years. Knowledge has been accumulated over the decades, which means that nowadays green roof technology is vastly superior to earlier attempts.

In the 1970s the so-called "National Nature conservation act" was updated in Germany. Urban areas were included as areas where wildlife should be protected. Local indigenous wildlife was targeted in this act. Naturally occurring urban plants were considered worthy of protection. A new urbanism shifted away from erecting of new neighborhoods on the outskirts of the city, and began to rethink quality of life in urban areas while searching for different places to construct more new apartments. Roofs, which had hitherto been used to dry washing, presented an ideal space to develop green roofs and then develop quality apartments in those buildings.

The Nature Conservation foundation in Berlin "Stiftung Naturschutz", an interdisciplinary cooperation of architects, planner, and ecologists started to erect such Eco – Roofscapes in Berlin. In many other Germany Cities similar activities started to enhance the quality of life in inner cities using greenery. Community projects such as backyard greening, green facades, and roof greenery were important. The use of local plant species was also a focus. Less emphasis was placed on roof gardens.

The FLL guidelines, which focus on plaza decks and green roofs, integrate both stages. The first FLL guidelines came out in 1982. They addressed all green roof varieties from the extensive to the roof garden types. The first English version was printed in 2002 and then updated in 2008 with the second edition [1].

Disseminating the Ideas of the Modern Green Roof Technology

The idea behind green roofs is basically simple; combine a waterproofing barrier, a water storage and drainage layer, a designed growing media (not typical garden soil), and the initial vegetation – that's all.

Looking in more detail, there are several concerns related to warranty that must be acknowledged. German homeowners expect their green roofs to be guaranteed for as long as in minimum warranty periods for traditional pitched tile roofs last. If the vegetation cover is not sufficient, wind and storm water erosion can present an increasing problem over the years. An annual inspection should be made to identify any problems. A good quality green roof should have plant coverage of more than 60%. This means that there will be a minimum amount of weeding necessary [14].

The German model has also been successful because of the cooperation between researchers, manufacturers, and planners, under the FLL guideline group. Green roof technology was executed according to certain norms in order to deliver secure, basic, brand-independent solutions. The FLL-approved structures can occasionally be copied, in part, in other countries with similar building codes and climates as Germany. In countries with radically different building conditions and climates, application of such guidelines is disastrous, to say the least. Many aspects of green roofing which are country or region specific due to the different building codes in different countries and other factors like climate, which affect green roof design and implementation make application of standards established in Germany rather impractical. Despite this, at the European Union level, a CEN Standard working group has started to work on an attempt at a European guideline; this will take time and is probably not practical (please see the discussion about "Green Roof Incentive Programs" below). The results of these studies may be, in part, used to help form the starting point for attempts at drafting potential national regulations. In the USA, similar activities are also underway to set up standards at the national level. The first standards have been prepared and published [15, 16].

Germany is a mature market where more than 10 million square meters of new green roofs are built each year. In neighboring countries, like France, about 0.5 million square meters are now being built each year. The movement exists in about ten European countries.

Green roof activities started to increase in North America around 2000. Since 2003, the North American Association "Green roofs for healthy Cities" hosts annual conferences to disseminate the green roof concept in North America and the world. In many Asian countries, especially Japan, Korea, and Singapore, many green roofs have been constructed in the last 10 years. In contrast to the Western world, these activities are not organized by private corporations. For example, there are incentive programs to support green roof activities in about 50 cities of Japan. In China, many green roofs are part of new city concepts. In addition, Shanghai pledged to erect about 100,000 m^2 of new green roofs in 2009. This figure was achieved in the middle of 2009. In Thailand, preliminary green roof studies have been conducted, and more are planned. The majority of the Asian projects are focused on roof gardens to offer additional city recreational space in the mega-metropolitan areas. Extensive green roofs are increasingly used to cover bus shelters and other such structures. The number of hot summer days in sprawling Asian Cities has increased in the last decade. The cooling potential of green roofs as well as reductions of the peak storm water runoff is important benefits for these regions.

In Scandinavia, especially in Norway, grass roofs are a typical construction on old farmhouses. Such structures are not very exportable to other countries for a number of reasons, but they are regionally adapted to this climate. A resurgence of construction of these types of roofs, for summer homes, has experienced a renaissance in recent years. A few cities, like Oslo, and others have been slow to set up general guidelines for green roof projects. They are focused more on architectural design competitions to promote such environmental friendly roofing technologies.

Other countries, like, Spain, Italy, and Greece have also made strides with several new green roof projects in recent years. These consist of both roof gardens and extensive green roofs. In Spain and Italy, about 500,000 m^2 of green roofs have been installed recently. In the other Mediterranean countries, like Greece, where flat roofs are typical, and the potential benefits of green roofs great, roof greening was seen as unrealistic in the past for various reasons .This changed in 2000 when a team of researchers worked for 5 years to design a Greek roof greening solution, which is adapted to the Greek building code and severe Greek climate. As noted earlier this system is called "oikosteges" and was installed on The Greek Treasury, which is located opposite the Greek Parliament, in the summer of 2008. This installation has been studied twice by the National Metsovio Technical University of Athens by Drs. Rogdakis and Koronaki. These studies concluded that oikostegi significantly effects the thermodynamics of the Treasury leading to appreciable reductions in energy requirement. Photographs of this project can be seen at http://oikosteges.gr/index.php/photogallery.

On behalf of the European Association of Green Buildings (EFB), a move was made to set up a European standard for green roof technology in Europe. Such a law would have to focus on the basics of the technology. In this proposal, each country is then requested to adapt this framework law to their specific national needs. For Germany, this would be a step backward since the current FLL guidelines were updated in 2008 [1].

Green roof projects have been registered in more than 40 countries in 2010; see www.worldgreen roof.org). The focus differs among the various climates and regions, but the benefits are quantifiable in all countries.

The main benefits of green roofs are as follows – First of all, green roof structures last longer than non-green roofs. The longer life span and decreased maintenance cost of the roof is one of the first ways that economic benefit is achieved through implementation of these structures. Different calculation programs demonstrate such benefits. For some examples, refer to Table 1. One current interactive system is the Green roof calculator [17].

Green Roof Incentive Programs

In Germany, in the 1980s, most cities set up programs to encourage urban greening. The basis for these measures was the Environmental nature protection law, updated in the late 1970s, which stated that all regions of Germany had to work on implement urban greening plans. Not only did the regions have to set up specific laws, but the cities also had to set up rules for incentives and tax breaks. An overview of all these different regulations was collected in three rounds of questionnaires distributed by the FBB; see lists on www.fbb.de.

In conclusion, it can be seen that government incentive programs resulted in the development of backyard greenery, green facades, and green roofs in the 1980s. Later on, in 1990, one of the most successful pieces of incentive legislation was implemented whereby homeowners could receive storm water amelioration tax breaks for installing green roofs.

Storm water taxes penalize runoff created by built surfaces, such as roofs, because it burdens the public sewer system. In Germany, such a tax is about €1/m^2 of built surface. Locally, legislation varies between no rebates for roof greening right up to a 100% storm water tax exemption. On average, in Germany, across the board, this equals about €0.50/m^2 of green roof [25].

Today, in late 2009, the implementation of green roofs is well established and is included in about one third of all German building plans for permit submission. In Berlin, there is a government department that is responsible for guiding public building projects, monitoring selected key projects, and publishing basic information and guidelines for public housing and public construction sites (see: http://www.stadtentwicklung.berlin.de/bauen/oekologisches_bauen/index.shtml).

Green Roof Policy in Other European Countries In all other European countries, roof greening legislation is more recent than the laws found in Germany. In the

Green Roof Infrastructures in Urban Areas. Table 1 Selected economic studies about the green roof benefits

Type of study	Source	Results	Comments
National survey of extensive green roof cost – benefits in Germany	[18]	Costs: Extensive green structure (m^2): €17, Maintenance 40 Years €17 additional static. €10–44 costs. Benefit: Costs – longer lifespan (up to €37) – reduce rain tax (up to €32) = profit of about: 25€/m^2	Until 2002 no calculation of energy savings had been completed
			Costs are based on German rates in 2002 which are close to those in 2009
Phillips Eco-Enterprise Center – case study – Warehouse after LEED criteria USA	[19]	Costs of the extensive roof $78,000 ROI, annual return – $1,000	Not calculated energy savings, study not complete
US case study for an affordable neighborhood in NYC – USA	[20]	Break even point after 15 years/return on investment	Calculation investment, energy savings etc.
National comparison Germany, Brazil, USA	[21]	Over the lifespan of 90 years, the profit of a roof garden is the highest: plus $1,200/$m^2$. Extensive roofs lost value ($180/$m^2$) as did Bitumen/gravel roof (minus about $300/$m^2$	Various differences in traditions, technology, and level of salaries
City Study Toronto: (CA)	[22]	If 50% of the roofs of the city of Toronto were extensively greened, there would be annual cost savings: $37 million	See full study on internet as pdf on the web page of city of Toronto. The results are a summary of the Toronto action plan
Portland City Study – USA	[23]	If flat roofs in a warehouse district of Portland were greened, the cost savings of the reduced storm water entering the sewage system is enough to pay for all these green roofs and reap long-term benefits	These results were integrated City of Portland action plans
Life cycle assessment of Green roof systems in Hong Kong	[24]	In tropical climate, green roofs double the life span of roof materials, reduces energy costs for air conditioning systems. Green roofs are an economically viable solution for investors	Available on web page of University of Hong Kong

1980s, Austria, Switzerland, The Netherlands, and Hungary began to follow Germany's lead. The focus was different and simplified. In Austria, roof gardens were the focus of interest. In Austria, recreational space in Vienna and other large Austrian Cities was at a premium. The focus of the green roof movement in Switzerland is on the biodiversity of extensive green roofs. Similar tendencies, among other trends, can be found today in the UK and Sweden.

Regulations at the national government level are foreseen for other countries by late 2009. Some cities are forging ahead. In the UK, London has set up a green roof city policy for the coming years. Many green roof related themes can be found on the official city of Greater London web site (http://search.london.gov.uk/search, key words living roofs). In June, 2009, an internet search returned about 1,620 related links. Other British cities are behind London, but advocacy groups are forming in many British cities. In Ireland, in 2007, thanks to the Dun Laoghaire Authority, the first seminar to promote green roofs was held.

Worldwide Distribution Over the last 10 years, many other countries have begun to write green roof policies. This has led to the growth of roof greening around the world (Table 2). In the USA, about

1,000,000 m^2 of green roofs were installed in 2008. Between 2008 and 2009, an increase of 25% of square meter age was calculated by the national trade association (survey, done by Green Roofs for healthy Cities www.greenroofs.org). In Mexico City, in 2007, 10,000 m^2 and in 2008 8,000 m^2 green roofs were constructed with incentives given by the metropolitan Mexico City government and the current number of Extensive Green Roofs (EGR) constructed with the support of City administration incentives are now about 25,000 m^2. (Welcoming remarks Marcelo Ebrad, Mayor of Mexico City, "Congresso Mundial del Azoteas Verdes", October 7s. 2010) (Tanya Müller and Amenamex personal communication).

In Asia, Singapore started a green roof policy to promote roof gardens in the1980s. Since about 2002, it has been part of national environmental policy to set up and test extensive green roofs. A special department, called CUGE was founded to promote all types of environmental friendly building and construction technologies [26].

The other mega cities in Asia are also getting on board. Hong Kong has conducted a city-wide study, which reviewed the potential of the technology [27]. Bangkok is just starting with an academic research group and demonstration roofs. All these cities already have roof gardens for recreational purposes. The newer ones integrate rainwater retention technology.

Seoul, in South Korea, is an example of an Asian city which adapted the idea of "Biotope area factor" from Berlin http://www.stadtentwicklung.berlin.de/umwelt/landschaftsplanung/bff/index_en.shtml). A green roof with a growing media more than 90 cm has a thermal insulation value of 0.7, a green roof with more than 20 cm has 0.6, and a green roof less than 20 cm has 0.5. Also, a planted wall has a value of 0.4. By 2012, the city hopes to vegetate 600 roofs. Fifty percent of the costs are borne by the state. In 2009, more than

Green Roof Infrastructures in Urban Areas. Table 2 Fact Block, selected numbers on green developments around world

Numbers	Locality	Description	Source
7.5%	Berlin	Calculation of the total percentage of green roofs in Berlin City. This is the number calculated counted only for the quarter Berlin – Kreuzberg	B
32%	USA	Growth of the Green roof market between 2007 and 2008	A
8,000 m^2	Mexico City	An area of public green roofs, officially opened by the lord mayor of Mexico City in 2008	C
53,000 m^2	Chicago	Chicago is the number 1 green roof builder in the USA. The total number of green roof projects presently installed are 84	A
100,000 m^2	Shanghai	Green roof area pledged for installation by 2008, the goal was achieved. Since the beginning of the campaign in 2003, 500,000 m^2 have now been installed	D
600,000 m^2	Beijing	Total area of green roofs installed in the city as of 2006	G
310,000 m^2	USA/ Canada	The total area of new green roofs installed in 2008	A
1,000,000 m^2	France	The total green roof area expected annually	E
11,000,000 m^2	Germany	This is the rough estimate of new green roofs built each year in Germany, two third of these are extensive	F

A: Green roofs for Healthy City, 2008 Green roof Industry survey
B: Koehler, own survey in 2008, (prepared for publishing at Cities Alive, 2009)
C: Personal communication, Tanya Mueller, Amenamex in July 2009
D: China Daily [30]
E: Adivet
F: Hämmerle [31]
G: Koshimizu and Lee [32]

300 green roofs have been installed equaling 100,000 m^2 in total. The Women's University in Seoul is a beacon and a prime example of Seoul's earth-covered buildings [28].

Japan supports green roof projects in about 50 cities. Tokyo, for example, provides a tax break of 50% for 5 years after the installation. New buildings larger than 1,000 m^2 must be offset with at least 20% vegetated surface, which can include the roof surface. There is no general guideline for all Japanese cities [29] (Figs. 2 and 3).

Green roof advocates and activists can be found in nearly every Australian city. They organize workshops and seminars. One of the most prestigious projects using green roof technologies in Australia is on the house of Parliament, in Canberra. It was designed in the late 1970s with a Kentucky blue grass turf roof and many roof gardens, for recreational space for employees. In Sydney, green roof regulations were first instituted in 2008. Other Australian cities are following suit. Main issues in Australia are roof gardens, native plants, and "food on the roofs." The idea of green roofs and water savings, as well the question to accept dried out vegetation during droughts is on the very beginning.

It is not easy to provide an overview of African activities. There are ancient green roofs in many African countries, like Tanzania and Uganda. Modern projects are beginning to be seen in South Africa, especially at holiday resorts and fashion retail stores.

In summary, there are examples of green roofs in more than 40 countries worldwide. An interest on the ecological benefits of roof greening is growing. Establishing regulations that focus on the main needs of each country will be the next major challenge for local environmentalists.

Longevity of Green Roofs

The reason green roofs last longer than traditional roofs is the additional layering, which blocks direct exposure to solar radiation Solar exposure causes premature aging of unprotected roof membranes.

The simplest explanation for this benefit is the direct comparison of roof surface temperatures during daytime. Temperatures up to 70°C are possible on a roof

Green Roof Infrastructures in Urban Areas. Figure 2
The grass roof on the Parliament house in Canberra is an semi-extensive green roof, Australia

Green Roof Infrastructures in Urban Areas. Figure 3
Intensive Green roof, one of the roof garden areas for the Australian politicians in the House of Parliament

that has not been greened. Temperatures are reduced on the green roof surface because of the shading that the vegetation layer provides as well as evaporation cooling. On summer nights, the surfaces of black tar roofs are often cooler than green roofs. These extreme temperature ranges experienced by a nonvegetated roof are another reason for their premature aging.

What these effects mean for a building's energy budget depends on the amount of insulation and the thermal flow through the entire roof construction. This can be calculated for the purpose of assessing energy savings. In both hot and cold countries, the thermal insulation properties of green roofs are an important benefit. It can equate to a significant reduction in building energy requirements. Calculations using a data set from a Neubrandenburg roof for 1 year [33] showed that about 100 m^3 less heating gas would be required for a single house with normal insulation when a green roof has been installed.

In terms of cooling, impressive thermal insulation properties have been observed in two studies conducted by the National Metsovio University of Athens. They studied the thermodynamics of the oikostegi green roof installed on the Treasury in Constitution Square, in Athens, opposite the Greek Parliament. They found that total annual heating and cooling energy savings equaled nearly €6,000. They made a number of important observations, which can be summed up by their conclusion "the thermodynamic behavior of the Greek Treasury is being significantly impacted by the oikostegi green roof."

The amount of captured and evaporated water is also an important aspect for determining reductions in summer air conditioning that could be attributed to green roofs. Of course, it is unwise to use savings in energy consumption to irrigate a roof because water is an even more fundamental and important finite resource than energy. Depending on the region, cooling requirement reductions could be more important than heating requirements. The Metsovio Study suggested that it is feasible to approach a reduction of up to 100% in air-conditioning requirements in a building where an oikostegi green roof has been installed.

How to Promote the Idea of "Green Envelopes"

In order to convince clients to install green roofs, practitioners must explain the technology and create demonstration projects to give them a sense of how these structures will look. To convince economists

and legislators, it is important to quantify the economic costs and benefits of green roofs. Most cities start first with incentive programs, for example, the City of Linz (Austria) set up financial support for green projects for a couple of years. Then, after this worked well, they reduced the amount of money provided. Once the technology was established, it took off by itself [34].

In contrast with planting back yards and walls with climbing plants, green roofing technology needs more professional designers and technicians to avoid the potential of waterproofing compromise and other damage to the underlying roofing and construction materials. Berlin has had a long-term program from 1983 to 1994 [13] to incentivize more greenery in the city. This underlying requirement for a professional orientation for green roofs may explain why 466,571 m^2 green backyards have been constructed but only about 63,575 m^2 green roofs.

US Green Roof Policy There is incentive legislation in many US cities, like Washington DC, Boston, Baltimore, Portland, and others [35]. The environmental protection agency (EPA) set up state policy programs to support green roofing. One of the earliest of such, in September 2007, focused on the reduction of the storm water runoff using green roofs. The next steps will be to consolidate these steps and enhance the reach of the legislation to include other benefits such as thermal insulation. Policy programs are fundamental, but these should be supported by demonstration projects which are then studied by independent academic research organizations who can quantify the benefits of green roofs. Many American projects are documented by the proud activists who post their activities on the YouTube internet platform. Nearly 3,000 contributions are posted under the title "Green roofs"; the majority of these are from the USA (improved in January 2010). The German term, "Gründächer" only got two hits. This is a mirror of an expanding environmental awareness in the USA. Knowledge of this may help to reinvigorate the green movement in Europe.

One important benefit of green roofs is the reduction of storm water runoff, which has been documented in Europe for nearly 20 years by several research institutes. Similar studies are now underway in about ten different institutions in the USA such as PennState, and the Lady Bird Johnston Wildflower Center in Austin, Texas. In 2006, the US mayors' assembly passed a green roof resolution at their annual meeting, at which they stated that "green roofs manage storm water naturally, reduce flooding risk and improves air and water quality." For only a little extra cost during roof installation, long-term benefits can be achieved.

Green Roof Growing Media and Plant Species Richness

A green roof begins on the final surface provided by the builder whether that be metal, wood, or concrete. The first layer and one of the most fundamental aspects of a green roof is the waterproofing. There are a number of ways that sound waterproofing can be achieved, and this variation is due to different building conditions and codes in different countries. For example, in Germany, where building codes are very strict, resulting in highly homogenous final roof surfaces, it is common to find single ply PVC membranes being used. In other less developed countries, such waterproofing technologies are not viable and other forms of waterproofing must be tested, proven, and then used. One thing is certain; there must been good communication between the waterproofing industry and the green roof industry to ensure the quality and viability of green roofs. Guarantees must be provided by the water proofer to the client.

Basic Technical Components are Explained in Fig. 1 Growing media choice can affect the roof's water holding capacity, drainage, and nutrient supply. Nutrient availability is higher for roof garden soils than for extensive roof substrates.

For extensive green roofs, some substrate characteristics have been defined:

Suitable materials are lava aggregates between 2 and 16 mm, pumice, expanded clay, crushed bricks or tiles, basalt gravel, tuff gravel, or gravel.

Growing media criteria have also been described. Good water-holding capacity is defined as more than 45%/volume, pH values should be between 6.0 and 8.5, and the organic matter content should be lower than 90.0 g/l, [1].

Growing media should be mixed locally, in order to achieve regional characteristics and meet

production standards. Each of the different substrate brands have their own trade secrets for finding the best mixture within the material framework described above. Delivering the same quality substrates repeatedly is a must for professional producers of growing media. New mixtures must be tested by certified laboratories. There are testing facilities, where studies analogous to the German testing procedures are conducted, in the USA as well. Growing media for different regions must be engineered to specific local requirements.

Various planting techniques are possible. Seeding is possible, if no danger of erosion exists. Dispersing cuttings and shoots of Sedum is a very effective and cost-effective method. For ornamental plantings, mini planters are suitable products. Preproduced turf mats are a well-tested option used in Germany since the 1980s. Similar technologies will be established in the USA and some other countries. Quality criteria for roof plants in Germany follows standards developed by the FLL in Germany and also follow German DIN (Deutschland Industry Norma) standards such as DIN 18916.

If green roofs are to be installed for specific purposes, such as in natural conservation areas where native plants are wanted, more sophisticated standards must be applied.

Suitable vegetation should be selected according to the type and depth of growing media. On shallow layers up to 15 cm in all climates, drought-adapted plant species are the best choice. Succulents are a favorite group in the Northern Hemisphere [36]. Also, in hot humid tropics some succulents, originally from the South African cape region perform well on extensive green roof structures [37]. The reason for this is that these areas may also experience prolonged drought [38]. Xeric gardens with cacti are good choices in the tropics for saving irrigation water. The concept of xeric roof gardens would be choice for dry adapted plant species and an ecological protection layer for the building [39]. The old green roofs in Europe were planted with a type of xeric garden. Environmental education is needed to reeducate the public to understand and appreciate the natural beauty of dry gardens. A public that has come to consider manicured English highly maintained lawn to be the ultimate in visual appeal without realising the obscene damages by the high input of fertilizer and pesticide to the urban ecosystem causes. Dry green roofs like the Greek oikostegi perform well from the view point of energy savings and rainwater retention as already stated.

The genus Sedum is the favorite for many extensive green roof versions. Sedum can survive long periods of drought. In temperate climates, Sedum album is a species that can exist on nearly no growing media. If the roof has a little shade, Sedum album can cover the full roof area. The genus Sedum has representatives in various regions of the Northern Hemisphere (Clausen). Furthermore, many cultivars exist and add to the local flora. There are over 600 species of Sedum growing naturally in every climate on earth. Consequently, Sedum is an ideally suited green roof plant (Figs. 4–7).

Extensive green roofs can be an extension of the surrounding natural ecosystem using endemic local plants. Variation in the depth of the growing media and different types of growing media can be the foundation for a high diversity of plant species and other organisms (Table 3). In order to support plant species which are less competitive, specific maintenance to keep some space on the green roof open is required. Vegetated roofs can also be designed for the specific purposes of some key species of natural flora or fauna [41]. The bird Black redstart is such a key organism for the green roof movement in London. These birds, whose habitat is threatened by urban encroachment, need more habitats to survive and thrive. So-called brown roofs mimic natural environments and provide viable habitat for such birds [42]. Supporting wildlife with specifically designed green roofs is a way to reduce the destructive impact of new developments that encroach on natural habitats.

Green Roofs as Green Corridors in Urban Areas

Green roofs, living walls and back and front yard gardens can become corridors in cities providing pathways of biodiversity. Such green belt systems connect different open urban spaces for plant species and urban animals. The quantity and the quality of these areas should be assessed and modeled in order to enhance future efforts in this direction. In Germany, sites are assigned scores which are called "Biotope area factor" in Berlin or KÖH value in Karlsruhe.

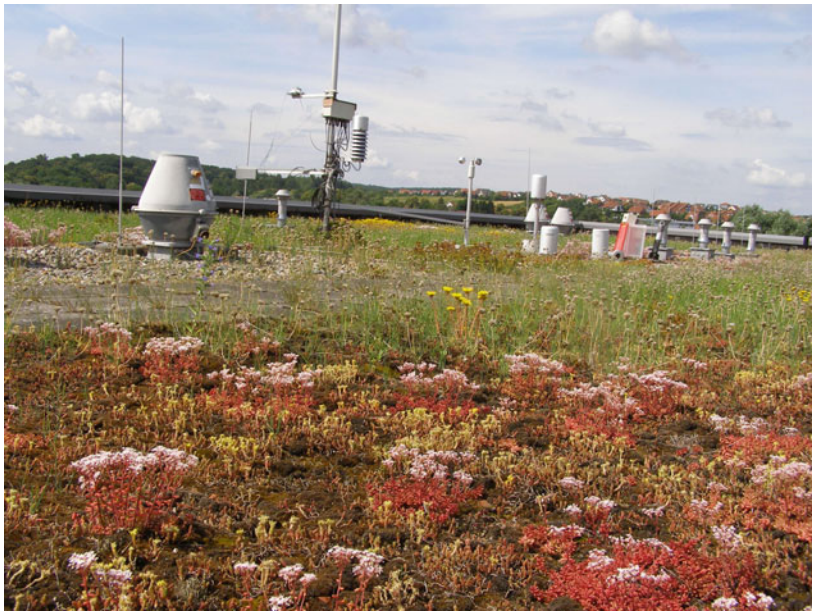

Green Roof Infrastructures in Urban Areas. Figure 4
Sedum album and other Sedum species on the green roof research

Green Roof Infrastructures in Urban Areas. Figure 5
A well-developed multispecies extensive green roof (Neubrandenburg)

In Germany, these scores are the basis for assessing property value and so they are also used to assess measures that can be taken to improve the quality of life in cities.

In Germany, green roofs have become so popular that the percentage of a city that has been greened now can be calculated rather than just talk about the square meter age. Of course, there is still plenty of room for

Green Roof Infrastructures in Urban Areas. Figure 6
Arial view of an ecological neighborhood, all with extensive green roofs, near the lake Constance

Green Roof Infrastructures in Urban Areas. Figure 7
Ecological neighborhood Huckstorf near Rostock with about 50 single and double houses. This is one example of about 180 documented existing ecological settlements in Germany (more: http://www.oekosiedlungen.de/)

Green Roof Infrastructures in Urban Areas. Table 3
Types on vegetation and growing media depth

Depth	Type of vegetation	Description
Lower than 5 cm	Mosses, few annual herbs	In most climate regions, this is not enough growing media for a full plant cover
5–15 cm	Typical depth of a green roof growing media	Within this depth, various plant species are suitable, up to 10 cm in most parts of Europe; Sedum and some herbs are the winners. With more than 10 cm depth grass vegetation dominates [40]
15–50 cm	Suitable for turf, herbs, and shrubs	This is the depth suitable for a wide range of ornamental plant species with irrigation. Without irrigation, several herbs and grasses can survive for a long time.
More than 50 cm	Shrubs, small trees	More than 50 cm with irrigation can support shrub and tree vegetation

even more green roofs. The popularization of roof greening in Germany has been achieved in large part due to carrot and stick legislation and incorporation of green roof technology into building codes in much of the country. In Germany, about two third of all building permits are only given when a green roof is included in the application. The German Association of green buildings (www.FBB.de) has conducted three surveys concerning green roof penetration of all German Cities larger than 10,000 inhabitants. Summarized results of these studies are available [43].

Future Direction: A Simulation of Potential Green Roof Benefits to Urban Areas

Each green roof is unique, but new projects can benefit from well-documented existing ones. Detailed documentation, as a case study of a retrofit project, has been prepared for the green roof on the ASLA headquarters in Washington DC [44]. This project includes roof gardens and extensive green roofs. The project is being monitored to assess the benefits of the installation. This example could be applied around the world. Due to technological advancements, green roofs are now suitable and viable for both retrofit and new buildings [45].

To achieve city-wide benefits, many green roofs must be erected. The potential impact of green roofs on urban environments has been described for Toronto, in a sophisticated study. The aim of the study was to ascertain what the benefits would be derived if all roofs larger than 350 m^2 were greened in Toronto (about 500 ha). The study found that such a move would result in savings of C$46,000,000 from storm water amelioration alone. Annually, cost savings of avoiding beach closures were about C$755,000. An annual reduction in air-conditioning requirements during the summer equaled C$12,000,000 [22]. This equals an air-conditioning requirement reduction of 2.37 kWh/ m^2 year.

The benefits of green roofs for New York have been modeled [46] by measurements of the PennState University. This study suggested that significant reductions in heating requirements particularly during the night would result from the installation of green roofs. Also, the study found similar runoff amelioration benefits to Toronto. These two benefits are driving the implementation of green roofs in NYC. Another oft overlooked benefit of the storm water runoff amelioration impact of green roofs is that smaller bore sewage systems can be used meaning substantial economies to local authorities as they rebuild decaying infrastructure. Many other city authorities are developing a healthy interest in green roof research. For instance Seattle, Vancouver, and Washington are all investigating the benefits of green roofs. Rain harvesting potentials of green roofs is another area of interest to local authorities [47, 48].

A combination of green roof technology with other instruments such as living walls using climbers and other technologies opens a wide range of possibilities for greening in Cities [49].

Acknowledgment

Thanks to Olyssa Sterry, MSU, USA, for proof reading the first draft of this paper. Thanks also go to an endless number of friends and colleagues whose contribution to this paper is much appreciated.

Bibliography

Primary Literature

1. FLL (ed) (2008) Richtlinie für die Planung, Ausführung und Pflege von Dachbegrünungen. Bonn, English version: Guidelines for the Planning, Construction and Maintenance of Green Roofing – Green roofing Guideline, 2008 edition
2. Frank A (2009) Planning principle for Sealing Flat Green Roofs – Roof Technology. In: Ansel W (ed) Proceedings of Green Roofs Appl R, Nuertingen, pp 91–98
3. Köhler M, Barth G, Brandwein T, Gast D, Joger HG, Seitz U, Vowinkel K (1993) Fassaden- und Dachbegrünung. Ulmer, Stuttgart
4. Osmundson T (1999) Roof gardens. Norton, New York
5. Rueber E (1860) Das Rasendach. Cotta, München. (reprint 1998) Hannover
6. Ahrendt J (2007) Historische Gründächer – ihr Entwicklungsgang bis zur Erfindung des Eisenbeton. PhD. Technical University Berlin (downloadable)
7. Siqueira VB (2002) Burle Marx paisagens transversas. Cosaq u Naify, Sao Paulo
8. Nagel W (2009) And compare: the Journal "Häuser", special issue January "Der Schatz der Moderne - Bauhaus", www.haeuser.de
9. Nielsen S (2004) Sky gardens. Schiffer, Atglen, PA
10. Peck S (2008) Award winning Green roof design. Schiffer, Atglen, PA
11. Köhler M, Keeley M (2005) Green roof technology and policy development. In: Hoffmann L (ed) Green roofs. Schiffer, Atglen, pp 108–112
12. Minke G (2006) Building with Earth – design and technology for a sustainable architecture. Birkhäuser, Basel
13. Köhler M, Schmidt M (1997) Hof-, Fassaden und Dachbegrünung – Zentraler Bestandteil der Stadtökologie. Landschaftsentwicklung und Umweltforschung 105:1–177
14. FBB, Bohlen R (ed) (2002) Grundsätze zur Pflege und Wartung von Dachbegrünungen. FBB, Saarbrücken. Download www.fbb.de
15. Standard Guide for Selection, Installation, and Maintenance of Plants for Green Roof Systems (2006) Annual Book of ASTM Standards ASTM, Standard E 2400-06. ASTM International, West Conshohocken, PA
16. Standard Practice for Determination of Dead Loads and Live Loads Associated with Green Roof Systems (2005) Annual Book of ASTM Standards ASTM, Standard E 2397-05. ASTM International, West Conshohocken, PA
17. Velazquez R (2008) Green roof calculator. In: Proceedings of the 6th Conference on Green roofs, Baltimore, MD
18. Hämmerle F (2002) Dachbegrünungen rechnen sich. In: Thalacker (ed) Jhrb. Dachbegrünung, pp 18–19
19. Green Values (ed) (2005) Case studies. Green building, growing assets. Royal Institute of Chartered Surveyors (see: www.riscs.org/greenvalue)
20. Hoffman L, Lossvelt G (2007) Viridian green roofs for multifamily affordable housing: reducing upfront costs and creating financing opportunities. 5th Annual Greening roof top conference, Minneapolis, MN, USA (see: www.greenroofs.org)
21. Köhler M, Porsche U (2003) Life cycle costs of Green Roofs – A comparison of Germany, USA, and Brazil. In: Krauter (ed) Rio3.com: Proceedings of world climate & energy event, Rio de Janeiro, Brazil, 1–5 December 2003, pp 461–467
22. Banting D, Doshi H, Li J, Missios P (2005) Report on the environmental benefits and costs of green roof technology for the city of Toronto. Ryerson University, Toronto, p 88
23. Miller T, Liptan T (2005) Update on portlands integrated cost analysis for widespread green implementation. In: Proceedings of the 3rd Conference on Greening Roof tops, Washington, DC
24. LUI STE (2008) Life cycle assessment of green roof systems in Hong Kong, p 96. Dissertation, University of Hong Kong
25. Köhler M (2009) Green roof policies in Germany: successes and Outlooks. In: Proceedings on Cities alive, Toronto, Oct 2009
26. Tan PJ (2008) Environmental, economics and social benefits in adopting skyrise greenery. In: Proceedings of Regional Seminar CUGE, 22 Oct 2009
27. Townshend D, Duggy A (2007) Study on green roof applications in Hong Kong. Urbis Limited, Hong Kong, pp 1–153
28. Lee UH (2009) Green roof development in Seoul, Korea. In: Proceedings of Cities alive, Toronto, Oct 2009
29. Koshimizu H (2009) Green roofs in Japan. In: Proceedings of Cities alive, Oct 2009 (in press)
30. Chinadaily, posted: 2008-08-12; Shanghai closes in on green roof target. Shanghai Post http://www.chinadaily.com.cn/china/2008-08/12/content_6926333.htm (site visited July10s, 2009
31. Hämmerle F (2002) Der Markt für grüne Dächer wächst weiter. In: Thalacker (ed) Jhrb. Dachbegrünung, pp 11–13
32. Koshimizu H, Lee H (2007) The regulation regarding the rootop greening in the East Asian Cities. In: Proceedings of 5th annual conference on Greening rooftops for sustainable communities, Minneapolis, MN
33. Köhler M, Malorny W (2009) Wärmeschutz durch extensive Gründächer. In: Venzmer H (ed) Europäischer Sanierungskalender 2009, pp 195–212. Beuth, Berlin
34. Maurer E (2009) Successful green roof policies in Linz since 1985. In: IGRA Proceedings, pp 169–172
35. Keeley M (2007) Transatlantic exchange and sustainable urban development: transfering stormwater policies and technologies from Europe to the United States, p 259. PhD, Technical University of Berlin
36. Snodgrass EC, Snodgrass LL (2006) Green roof plants. Timber, Portland
37. Tan PJ, Sia A (2005) A selection of plants for green roofs in Singapore. CUGE, Singapore
38. Tan PY (2009) Understanding the performance of plants on non irrigated Green Roofs in the Tropics using a Biomass yield approach. Nature in Singapore. (http://rmbr.nus.edu.sg/nis

39. Köhler M (2009) How Green should a green roof be. 7th Greening Rooftops for sustainable Communities. Atlanta, 5–7 June 2009
40. Köhler M (2006) Long term vegetation research on two extensive roofs in Berlin. Urban Habitat Urban Habitats 4(1):3–26
41. Brenneisen S (2006) Space for urban wildlife: designing green roofs as habitats in Switzerland. Urban Habitats 4:27–36
42. Gedge D, Newton J, Cradick K, Cooper P, Partington T, Bramfield T, Kendall J (2008) Living roofs and Walls. Technical Report: Supporting London Plan Policy. London 57S
43. Köhler M (2010) Green Roof Policy in German: successes and Outlooks. In: Proceedings on Cities alive congress, Urban policy (in press)
44. Werthmann C (2007) Green roof – a case study. Princeton, New York
45. Weiler SK, Scholz-Barth K (2009) Green roof systems. Wiley, Hoboken
46. Rosenzweig C, Gaffin S, Parshall L (ed) (2006) Green roofs in the New York Metropolitan Region. Research Report Columbia University. http://www.ccsr.columbia.edu/cig/greenroofs/
47. Dunnet N, Clayden A (2007) Rain gardens. Timber press, Portland
48. Dreiseitl H, Grau D (2006) Wasserlandschaften. Birkhäuser, Basel
49. Köhler M (2008) Green facades – a view back and some visions. Urban Ecosyst 11:423–436

Books and Reviews

Dunnet N, Kingsbury N (2008) Planting green roofs and living walls, 2nd edn. Timber, Portland
Ernst W (2005) Dachabdichtung Dachbegrünung. IRB-Fraunhofer Gesellschaft, Stuttgart
Köhler M, Barth G, Brandwein T, Gast D, Joger HG, Seitz U, Vowinkel K (1993) Fassaden- und Dachbegrünung. Ulmer, Stuttgart
Krupka B (1992) Dachbegrünung. Ulmer, Stuttgart
Snodgrass EC, Snodgrass LL (2006) Green roof plants. Timber, Portland
Weiler SK, Scholz-Barth K (2009) Green roof systems. Wiley, Hoboken
Jodidio (2009) Green Architecture now, p 416. Taschen, Hongkong

Recommended and Selected Internet Links

www.worldgreenroof.org
www.greenroofs.org
www.fll.de
www.greenroofs.com
http://www.epa.gov/npdes/pubs/gi_supportstatement.pdf
http://www.usmayors.org/urbanwater/policyres_06c.asp
http://www.ecos.org/content/policy/detail/2861/
http://cfpub.epa.gov/npdes/home.cfm?program_id=298
http://greenvalues.cnt.org/calculator
http://freitext.ub.tu-berlin.de/gartenkunst.html (garden historic documentation on older Green roofs in Journals of the 1920th)
http://www.oekosiedlungen.de/
http://www.oikosteges.gr

Green Roof Planning in Urban Areas

Stephan Brenneisen[1], Dusty Gedge[2]
[1]Life Sciences und Facility Management, Wädenswil, Switzerland
[2]Livingroofs.org Ltd, London, UK

Article Outline

Definition of the Subject and Its Importance
Introduction
The Headline Benefits of Green Roofs to Urban Planning and Climate Change Adaptation
Green Roofs and Pollution Removal from Stormwater Runoff
Role in Urban Planning
Green Roofs in the Rest of the World: A summary
Bibliography

Definition of the Subject and Its Importance

Green roofs are vegetated substrate layers on top of the waterproof membrane of the conventional roof surfaces of buildings. Once the concern that plants could negatively affect plants was overcome, by the use of improved membrane layers that are protected from root penetration, green roofs became more popular, starting in the late 1970s in Germany, Austria, and Switzerland.

As the twenty-first century has been deemed by the UN as the century of the megacity with predictions that nearly 75% (?) of the population of the world will live in cities by the end of the century, urban areas will increasingly need to be planned and developed to take into consideration the ecological and environmental health of the urban climate to ensure cities can cater for people. This is also a pressing matter in as it is recognized that there is a need to adapt cities to the negative effects of climate change. These issues have been central to the work of professionals in the field of green roofs over the last 20 years and increasingly the technologies and approaches of green roofs have been shown to have a positive effect on a number of issues facing cities and mega-cities in terms of ecological and environmental health and in helping cities adapt to climate change, reduction of the urban heat island effect, reduction in localized flash floods, air and

noise pollution and increasing biodiversity in the urban realm. These processes are part of an evolving approach to planning referred variously as green infrastructure or ecosystem services. Urban greening has therefore become an increasingly important approach for planners and is likely to be the one that will predominate in the future.

The Swiss architect Le Corbusier set the installation of green roofs in the form of roof gardens, as one of his five principal requirements in establishing a new architecture in the early twentieth century (Busse 2000). Although his work became well known, it took a long time after Le Corbusier's first steps to the implementation of green roofs as an ecological measure to be absorbed into mainstream urban planning. Green roofs became more popular as a part of ecological construction in the 1970s, and in the early 1980s, a number of cities implemented nascent strategic planning approaches to encourage the uptake of green roofs. Elsewhere a series of pilot projects were initiated to explore the ideas and approaches to green roofs in urban areas. The main drivers for the implementation of green roofs in the 1970s' and 1980s' research also suggested that green roof provided a broad range of environmental benefits, such as energy savings (less winter heating), reduction in storm water runoff, and overheating, but there was also a recognition that green roofs also promoted health and well-being and were an essentially element in an "ecological" approach to construction.

Introduction

Green roofs are vegetated layers that sit on top of the conventional roof surfaces of a building. Usually a distinction is made between "extensive" and "intensive." These terms refer to the degree of maintenance the roofs require. Intensive green roofs are composed of relatively deep substrates and can therefore support a wide range of plant types: trees and shrubs as well as perennials, grasses, and annuals. As a result, they are generally heavy and require specific support from the building. Intensive green roofs (what most people think of as roof gardens) have in the past been rather traditional in their design, simply reproducing what tends to be found on the ground, with lawns, flower beds, and water features. However, more contemporary intensive green roofs can be visually and environmentally exciting, integrating water management systems that process waste water from the building as well as storing surplus rainwater in constructed wetlands. Because of their larger plant material and horticultural diversity, intensive green roofs can require substantial input of maintenance resources – the usual pruning, clipping, watering, and weeding as well as irrigation and fertilization.

Conversely, the green roofs that have received the greatest interest recently are extensive green roofs. They are composed of lightweight layers of free-draining material that support low-growing, tough drought-resistant vegetation. Generally the depth of growing medium is from a few centimeters up to a maximum of around 10 cm. These roof types have great potential for wide application because, being lightweight, they require little or no additional structural support from the building, and because the vegetation is adapted to the extreme roof top environment (high winds, hot sun, drought, and winter cold), they require little in the way of maintenance and resource inputs. Extensive green roofs can be designed into new buildings, or "retrofitted" onto existing buildings.

The Headline Benefits of Green Roofs to Urban Planning and Climate Change Adaptation

Green roofs provide a range of benefits to urban areas. However, there is an increasing interest in three particular headline benefits, namely, amelioration of the urban heat island effect [UHIE]/thermal performance of buildings, reduction in stormwater flows, and providing habitat for wildlife in cities.

The first two are particularly relevant in terms of climate change as there is a recognition especially in temperate and Mediterranean climates that climate change is likely to increase summer temperatures in cities, thus increasing the negative effects of the UHIE (and potential increase in death caused by heat excess) and an increase in the need for air-conditioning (and therefore increase in energy/carbon use). The other prediction is that climate change will lead to increase in intense summer storms leading to flooding in urban areas with a negative effect on both the ecological and economic conditions within urban areas. In many cities, these predictions are actually happening already. Therefore, there

is a pressing need to adapt urban areas to ameliorate both effects and thus ensure the ongoing ecological health and economic well-being of urban areas.

Urban Heat Island and Climate Change Adaption

The benefits green roofs can bring in terms of climate change adaptation can be significant, especially in terms of the urban heat island effect and the energy balance of a given building.

Conventional roofing surfaces, including recreational roofs, absorb sunlight and heat up quickly. The absorption of radiation and the release of the radiation back to the atmosphere during the night is a major factor in UHIE. Where a building has poor insulation and poor ventilation, this can lead to increased use of air-conditioning and therefore increased energy use [1].

Building Energy Balance

The use of vegetation on the roof surface ameliorates the negative effects of conventional roofing surfaces by absorbing heat and using this heat in evapotranspiration. The process of evapotranspiration is an important element in reducing UHIE and provides benefit to the individual building by cooling/insulating the spaces beneath the roof.

Studies have shown that the membrane temperature beneath a green roof can be significantly lower than where the membrane is exposed. Table 1 shows the average temperatures under the membrane of a conventional roof and that of membrane under green roofs in a study undertaken at Nottingham Trent University.

Green Roof Planning in Urban Areas. Table 1 Study of temperatures under membranes of a conventional and a green roof

	Winter	Summer
Mean temperature	0°C	18.4°C
Temperature under membrane of conventional roof	0.2°C	32°C
Temperature under membrane of green roof	4.7°C	17.1°C

www.greenroofs.co.uk

Another study in Ottawa, Canada, by the National Research Council of Canada noted that temperature fluctuations during spring and summer on a conventional green roof were of the order of 45°C while under a green roof the fluctuations were in the order of 6°C [6].

The positive effect on the temperature of the membrane under a green roof not only protects the membrane from the effects of UV, frost, and sunlight, but also moderates the heat flow through a building by shading, insulation, evapotranspiration, and thermal mass.

Urban Heat Island Effect and Indirect Energy Savings

- "Summers by 2050 will be 1.5–3.5°C hotter. . .in central London the urban heat island currently adds 5–6°C to summer night time temperatures and will intensify in the future." *London's Warming. The Impacts of Climate Change on London* www.london.gov.uk

Urban areas have a higher average temperature than surrounding rural areas; this difference in temperatures is called the urban heat-island effect. An increase in the UHIE is likely to lead to increased air pollution and increased use of air-conditioning.

As has been noted already that green roofs do not store heat like conventional roof surfaces but dissipate heat through evapotranspiration. Such a process can have a significant effect on helping to reduce the impact of the UHIE.

A modeling scenario undertaken in New York by the New York Heat Island Initiative determined that providing 50% green roof cover within the metropolitan area would lead to an average 0.1–0.8°C reduction in surface temperatures. It is noted that for every degree reduction in the UHIE roughly 495 million Kilo Watt hour of energy would be saved. The same study also looked at various mitigation strategies other than green roofs, including urban forestry and cool roofs and noted that "living roofs" provided greater benefits than white or "cool" roofs. It was clear from the study that a combination of various mitigation strategies for UHIE including green roofs should be considered by the city. http://ccsr.columbia.edu/cig/greenroofs/index.html www.nyserda.org/programs/environment/emep/project/6681_25/6681_25_project_update.pdf

A study in Toronto estimated that there are 50 million square meters of potential roof space in the city of Toronto that could be greened. Overall it was estimated that the effect of greening the city's roof tops would lead to 0.5–2°C decrease in the UHIE.

A reduction of this magnitude would, the study estimated, lead to indirect energy savings citywide from reduced energy for cooling of $12 million, equivalent to 2.37 kWh/m^2 per year [0.001 CO_2 emissions t/m^2]. http://www.toronto.ca/greenroofs/findings.htm

Energy Savings

Although green roofs do provide potential energy savings by providing building insulation these are often considered difficult to assess due to the varying climatic conditions throughout the winter months, and will be minimal on already well-insulated buildings. However, during summer months, green roofs can have a significant effect on spaces beneath them in terms of cooling.

Studies in Germany have provided various estimates. Figures provided by Zinco estimate that 2 L of fuel oil are saved per square meters per year. A more recent published study on domestic buildings with flat roofs suggests that there is a 3–10% winter saving on fuel bills. The results of the study suggest that there is a maximum saving of 6.8 kWh/m^2 [calculated CO_2 emission tones saving of 1.5 kg/m^2] and a minimum saving of 2.0 kWh/m^2 [calculated CO_2 emission tones saving of 0.44 kg/m^2]. This study did not consider at any summer savings due to cooling [5].

The Toronto study, already referred to above, estimated that the direct energy savings citywide as a consequence of whole scale greening through reduced energy for cooling would be in the order $22 million, equivalent to 4.15 KWh/m^2 per year [0.001 CO_2 emissions t/m^2]. The study also concluded that there would be a reduction in peak demand in the order of 114.6 MW, leading to fossil fuel reductions in the region of 56,300 metric tons per year.

The only information for a building in London suggests that an 850 m^2 retrofitted green roof onto paving in Canary Wharf has seen an estimated reduction of 25,920 kWh in a year, through a reduction in heating and cooling of the spaces below the roof *[per com Livingroofs.org]*.

Green Roofs and Photovoltaic Solar Panels

The combination of green roofs and PV Solar Panels provide multiple benefits. Photovoltaic panels at roof level are known to work more efficiently when installed on a green roof rather than a conventional surface. The green roof element not only saves energy during the summer time [see above] but can increase efficiency of PV by reducing fluctuation of temperatures at roof level and by maintaining a more efficient microclimate around the PV panels. The performance of photovoltaic panels is lowered by 0.5% per °C above or below 25°C. The green roof is better at maintaining the ambient temperature of 25°C [3].

By reducing the temperatures around the PV and by helping reduce the need for air-conditioning in spaces beneath the green roof, the combination of the technologies should be as one of positive interaction and not one of competition in terms of use of roof space [4].

Benefit of Green Roofs to Stormwater Runoff, Flash Floods, and Pollution Removal

Background The combined impact of ongoing development within urban areas and climate change has created higher peak stormwater flows, leading to an increased occurrence of downstream flooding and pollution. Intensive summer storms are becoming, and are likely to become, more prevalent. Such rainfall events, especially in the summertime in temperate zones, can cause the current stormwater system to become overburdened causing localized flooding. The consequence of these events can have both a negative economic and ecological effect. For example a "freak" summer storm in 2005 in West London deposited such a large amount of rainwater that caused raw sewage to be released into the River Thames. This pollution caused large-scale ecological damage to the river's ecosystem, including significant fish mortality. Another series of summer storms in July 2009 in London led to closure of parts of the transport system within the capital causing offices, shops, and businesses to be closed and a reduction in trade/business.

In many parts of the world, sustainable drainage systems (SUDS) are now required to minimize the impact of both new and existing development.

They are designed to both manage the adverse environmental consequences resulting from urban stormwater runoff and also contribute to environmental enhancement wherever possible. The use of green roofs can provide a pivotal role in achieving this as they successfully achieve source control, which is the fundamental concept of SUDS, i.e., the control of rainfall at or as close as possible to its source.

Positive Effect of Green Roofs on Runoff Rates and Volumes of Stormwater

Around 30–40% of rainfall events are sufficiently small that there is no measurable runoff taking place from greenfield areas (it all infiltrates or evaporates). In contrast, runoff from developed areas takes place for virtually every rainfall event. This means that streams and rivers are more subject to overload. In addition, whereas for greenfield areas, small events would be treated through natural filtration processes, development runoff can flush surface pollutants directly into the receiving waters. Where it is possible to provide replication of this natural behavior (described as interception storage) and to prevent runoff of up to 5 mm, this should be provided.

By using green roofs as a source control technique, the volume of surface or underground attenuation storage can be reduced considerably. This can be particularly important in dense urban developments where space for surface level SUDS components such as ponds will be limited. It is also an important consideration when looking at the true cost implications of installing a green roof as the reduction in underground drainage infrastructure must be taken into account as well as the reduced number of downpipes and smaller pipe network, etc.

When rain falls on a green roof, it will first pass into the substrate and possibly pass through until the adsorbancy of the soil is activated (although throughflow will generally be low). It is then absorbed by the substrate (and possibly the drainage layer) and taken up by plants in the same manner as a greenfield site.

For most small storms the rainfall is removed by evapotranspiration. Only when the soil is fully saturated will water percolate through to the underlying drainage layer in significant volumes.

The processes involved in the operation of a green roof are (Tarr 2002):

- Retention of rainwater in substrate and drainage layers
- Uptake of water and release by plants as vapor (transpiration)
- Uptake of water and biochemical incorporation by plants (photosynthesis)
- Evaporation from substrate due to wind and sun

There is a wealth of published information that demonstrates the performance of green roofs in attenuating stormwater runoff by reducing peak flow rates and volumes.

Although there is a variation in performance depending on rainfall patterns, this is no different to other SUDS components such as pervious pavements, or indeed greenfield catchments.

The benefits of a green roof in terms of drainage can be summarized as follows:

1. A green roof will typically intercept the first 5 mm and more of rainfall (provide interception storage).
2. The amount of stormwater stored and evaporated is primarily dependent upon the depth of the growing medium and type of planting. In the summer, a green roof can typically retain between 70% and 80% of the runoff (Livingroofs.org 2004).
3. It has been demonstrated that in Germany between 40% and 100% of rainfall can be retained – depending upon the season (Tarr 2002).
4. Seventy-five percent of rain falling on extensive green roofs can be retained in the short term and up to 20% can be retained for up to 2 months (English Nature 2003).
5. As the rainfall events become longer or more intense, the positive effect of a green roof remains as there is still a significant reduction in peak runoff rates. This increase in the "time of concentration" means that a green roof will be beneficial throughout a wide range of rainfall conditions [2].
6. The above benefits collectively mean that by incorporating a green roof into new development, there will be a reduction in the amount and cost of the overall drainage infrastructure required to serve that development.

Green Roofs and Pollution Removal from Stormwater Runoff

Green roofs retain, bind, and treat contaminants which are introduced to the surface either as dust or suspended/dissolved in rainwater.

The London Ecology Unit (1993) stated that 95% of heavy metals are removed from runoff by green roofs and nitrogen levels can also be reduced. In addition, Auckland Regional Council (2003) advise that green roofs are accepted as removing 75% of total suspended solids.

The roofs showed a reduction in nitrogen (total discharge from green roofs of between 10 and 80 mg/m^3 during the monitoring period) and phosphate was also removed from the runoff (total discharge of between 75 and 100 mg/m^3). The total discharges of nitrogen and phosphate from the conventional roof were 265 and 145 mg/m^3, respectively.

Role in Urban Planning

Examples from

London During the late 1990s, a group of nature conservationists and ecologists were actively in involved in a major regeneration program in South-East London. The Creekside Regeneration Programme was a government-funded program to rejuvenate an economically deprived area of Deptford in the London Boroughs of Lewisham and Greenwich. Part of the preparatory works included an ecological assessment of the value of the area for wildlife. Although a rundown postindustrial landscape the group discovered that, although not the most visually appealing landscape there were a number of interesting species, including one – the black redstart (*Phoenicurus ochruros*), which were of significant ecological value.

Although the use of green roof technology had been tentatively used in the 1970s and a number of innovators had tried to raise the profile of the technology through example projects and a book published by the London Ecology Unit [Building Green], the technology had remained relatively marginal.

However, the work of the group in Deptford pushed developers and planners to consider the use of green roofs as mitigation for wildlife habitat, especially for the aforementioned bird. However, with little information on the value or the technical aspects of green roofs, the process was a hard task. Convincing the relevant professionals, architects, consultants, and planners that this was both technically and an ecologically sound method of roofing was an uphill struggle. In effect, the group was on a process of change, changing people's habitats and assumptions and professional attitudes to vegetation on buildings. Fortunately, in early 2000, the author contacted the Swiss Landscape Department, which led to the first contact with Dr. Stephan Brenneisen and his innovative work on green roofs and biodiversity.

Thus was born the UK+CH green roof partnership. Although the Swiss regulatory process and attitude to green roofs was on a different level at the time, being one of proactive engagement, the Swiss experience has been a major influence on bringing green roofs into the mainstream in London and elsewhere in the UK. The relationship has been one of the major influences in transforming green roofs from a fringe sustainable technology to one that is now incorporated in both strategic policy in London, both at the regional and the local level. Although the agenda for green roofs as moved forward from an initial interest in biodiversity and nature conservation issues, to other themes, such as thermal performance, urban heat island amelioration, and sustainable urban drainage, at its heart the provision of quality green roof habitat for rare invertebrates and birds still remains, and is still a major driver in terms of implementation.

The Black Redstart Although relatively common on the continent and especially in Switzerland, this bird is at the northwesterly edge of its range in the UK. As it is a relatively recent addition to the UK bird fauna, it is vulnerable to competition from more established species, such as the Robin (*Erithacus rubecula*). With less than 100 pairs annually thought to breed in the UK, it is therefore protected under national wildlife legislation. It is relatively unique for a UK protected species as it is found in the main on industrial wastelands and in an urban context. It needs quite sparsely vegetated landscapes, similar to alpine scree slopes and plateaus.

In 1997, a group of ecologists found a number of pairs breeding along Deptford Creek. As the three pairs that were found in the area constitute more than 1% of the national population, there was a degree of pressure, through planning regulation, to ensure development did not have a negative impact on the species. Wherever possible there is an obligation to "enhance or mitigate" development plans for protected species. Thus was born a move to ensure that new developments catered for the black redstart. One of the first projects to be impacted on was the Laban Dance Centre, designed Herzog de Meuron.

The "rubble" roof was the first of many green roofs installed for black redstarts in London. Thirteen years ago this was a real milestone. But now, after much work, green roofs for biodiversity have become embedded.

However, the nature conservationists involved in promoting green roofs had very little knowledge or understanding of the know-how and the technical arguments to pressure developers to deliver habitat at roof level. Most of their thinking was intuitive. Furthermore many professional ecologists viewed the "idea" as unfounded and lacking in any hard and fast data to back up the intuitive reasoning of group. The Swiss connection would change that providing a greater technical understanding of green roofs supported by detailed research.

The Ecological Context While the black redstart started was the starting point for a renaissance in interest in green roofs in London and increasingly across the rest of the UK, a further issue raised its head with the publication of a strategic white paper that set out the vision for development in the UK but which nature conservationists saw as having potentially negative impacts on a swathe of habitats, that, although postindustrial, had become important refuges for a whole swathe of rare and endangered species. In 2000, the UK Government published the Urban White Paper. In the context of this story, the white paper targeted the use of brownfield and postindustrial land as the primary source of land for new development. In London and also in the Thames Gateway Development region, large areas of old factories, dockyards, disused refineries, power stations, and other land become the prime focus for economic regeneration. However, at the same time, these rather ugly and untidy landscapes were increasingly being recognized by urban ecologists as some of the most important sites in the UK for rare invertebrates. Much of this fauna had once been prevalent in well-drained and low-nutrient farmland that had since been improved. In general many postindustrial sites reflect this habitat characteristic. Thus, over time, much of the fauna and flora had colonized these as they were left to nature. In fact one such site in South Essex, Canvey Wick, has been celebrated as "the Amazonian rainforest for rare invertebrates in the UK." Thus was born a conflict between the needs for economic regeneration and an ecology once overlooked but of national importance. At the time of writing a number of other similar sites have become the focus of concern from conservationists, notably the Isle of Grain lorry park (http://www.guardian.co.uk/environment/2011/apr/17/isle-of-grain-wildlife-paradise).

Climate Change: A Shift in Emphasis During the mid-2000s, there was a distinct policy shift as the climate change agenda became more prevalent. Where the London Mayor had previously been concerned with "fuel" poverty a series of extreme hot summers shifted the emphasis to also include concerns regarding "cool" poverty and the likely impacts of increased summer temperatures and the negative effects of the Urban Heat Island. The London Climate Change Partnership stated in 2002 that "Summers by 2050 will be 1.5–3.5°C hotter…in central London the urban heat island currently adds 5–6°C to summer night time temperatures and will intensify in the future" [6].

Thus, green roofs were seen to be a potentially crosscutting technology and multi-beneficial solution that could help the capital meet the challenges of climate change and help the city adapt to the likelihood of higher summer temperatures and increases in intense summer storms [leading to localized flash floods]. These fears have been realized to a certain extent with the exceptionally hot summers of 2005 and 2006 and extensive flash flooding of 2007.

However, London has both a central strategic authority [the Greater London Authority] and also 32 local boroughs [LB] with responsibility for their area. A number of these boroughs, notably city of London,

Islington, Lewisham and Tower Hamlets, were actively promoting and ensuring that green roofs were installed for nature conservation.

The New London Plan In 2007, the author, along with colleagues, was commissioned to write a technical review of green roofs and green walls. This report was to support the change in policy on green roofs from one of "encouragement" to "expectation." The report reviewed all the technical data available for a range of benefits including reduction in the urban heat island, thermal performance, storm water attenuation, biodiversity, and amenity. It also reviewed city policies elsewhere in the world. The technical report, published in late 2007, led to a distinct policy on living roofs and walls in the revised London Plan published in March 2008.

The new London Plan Living roofs and wall [Policy statement 4a 11] states:

The Mayor will and the boroughs should expect all major developments to in corporate living roofs and walls, where feasible and reflect this in Local Development Framework policies. It is expected that this will include roof and wall planting that delivers as many of these objectives as possible:

- Accessible roof space
- Adapting and mitigating for climate change
- Sustainable urban drainage
- Enhancing biodiversity
- Improved appearance

Boroughs should also encourage the use of living roofs in smaller developments and extensions where the opportunity arises [5].

Although it is too early to see what the effect of the new policy, green roofs have been delivered on an increasing scale in the capital over the last 8 years and the new Plan should lead to an increase in delivery.

A London Audit Livingroofs.org undertook an audit of green roofs in London in 2004. The total area of green roofs was no doubt underestimated due to the challenges of accessing information from architects, developers, and companies. The audit estimated that 76,682 m^2 of green roofs had been installed in the Greater London area. Some of these roofs dated back to 1932! In 2008, a further audit was undertaken to assess the amount of green roofs installed between January 2004 and December 2008. This used data provided by a number of green roof companies active in the UK and is estimated that the figures provided represent 80% of the roofs installed during that period. Over 420,00 m^2 were installed by the companies suggesting that near to 500,000 m^2 were actually installed – equivalent to twice the size of Hyde Park and Kensington Gardens combined.

It is important to note that the majority of these green roofs were installed in the central core of the city. Furthermore as the table below highlights that the area with the largest percentage of installed green roofs was the London Borough of Islington. This borough had actively promoted the use of green roofs through its planning department, thus demonstrating that urban planning departments that embrace and promote these activities can have immediate effect in the implementation of green roofs.

This area of green roofs installed between 2004 and 2008 was prior to the publication of the New London Plan, and the positive effect of this strategic planning policy on green roof implementation is yet to be assessed but is likely to augment the delivery of green roofs on new developments in the Capital.

A Green Roof Toolkit Although London now has a distinct policy on green roofs and a large number of green roofs have been installed, there has been limited guidance on how green roofs should be installed in London.

The Environment Agency, a key statutory consultee on new developments, is responsible for flood defense and rivers. Its remit covers flooding, climate change, and biodiversity. In 2008, the Thames region of the Environment Agency commissioned the author to provide a detailed toolkit to guide developers to what the Agency expected green roofs to provide and how. Importantly this work also managed to persuade engineers within the Agency to accept that green roofs do provide significant benefits as a source control mechanism in the sustainable urban drainage train [4].

Greening Existing Building Stock With the new London Policy and activities by the 32 LBs, the argument for green roofs on new developments looks

positive in the London area. However, one of the key concerns for the London Climate Change Partnership [LCCP] is the need to adapt existing buildings to the challenges of climate change. Reduction of the Urban Heat Island is an important element and, as has been recognized elsewhere, there is a need for a 10% increase in urban green spaces in UK cities to combat climate change. In London, especially in the central activity zone [CAZ] where space is limited and the effects of the Urban Heat Island are most pronounced, roofs will be very important in delivering green space.

The Need to Retrofit The implementation of green roofs in new developments within London is now a mainstream ecological construction method as has been outlined above. However, it is also recognized that there is a need to retrofit green roofs on the existing building stock, especially in CAZ. The report published in 2008 by the London Government estimates that 325 of the land area of Central London consists of roofs that could be retrofit with green roofs in the future without additional structural work to facilitate such an approach. Therefore, the area of roofs within 6 km circle centered on Trafalgar Square that could be greened would constitute a total area of 10million square meters.

The burning issue for planners is how to achieve wholescale retrofitting of green roofs on existing buildings. The London Government commissioned a report, economic incentive schemes, for retrofitting London's existing homes for climate change impacts, which outlines how this might be achieved in terms of incentives and the monies that would be needed to achieve. The report also provided detailed figures on how much such a program would cost and the environmental benefits that it would provide:

- "A scheme for four inner city areas – Cannon Street, Oxford Street, Tottenham Court Road, and Canary Wharf – with a green roof area of 226,750 m^2 would cost around £4 million and provide environmental benefits 17 worth £4 million.
- A wider scheme covering the city of London, part of the London Borough of Hackney, part of the London Borough of Tower Hamlets, and part of the
- A scheme in the West End with a green roof area of 3.2 million square meters would cost around £55.5 million and provide environmental benefits worth £55.5 million" (Table 2).

Green Roof Planning in Urban Areas. Table 2

Area	Potential roof area that could be greened (m^2)	NPV of environmental benefits	Size of scheme
Four inner city areas – Cannon Street, Oxford Street, Tottenham Court Road, and Canary Wharf	226,570	£4 million	£4 million
Four larger sample areas – city of London, part of the London Borough of Hackney, part of the London Borough of Tower Hamlets, and part of the West End	3.2 million	£55.5 million	£55.5 million

Economic incentive schemes for retrofitting London's existing homes for climate change impacts www.london.gov.uk/lccp/publications/docs/lccp-eco-incentives.pdf

In a further development since the publication of the report, the idea of retrofitting green infrastructure and in particular green roofs in London is being taken forward by Business Improvement Districts [BID], in particular the Victoria [VBID] area in the South West of the Central Activity Zone. VBID commissioned a report and survey of the inner and outer areas that constitute the BID to assess where and what kinds of green infrastructure could be retrofitted. As has been mentioned early, the driving force for the commission was the effects of climate change. The VBID area was one of the key areas affected by flashfloods in the first week of July 2009 with the closure of Victoria Mainline station and VBID recognizes that this led to a significant loss of business within the zone.

The report highlights the issues of flood management within the BID area:

- One of the key environmental challenges in the Victoria BID is the need to reduce instances of flooding at Victoria Station during periods of heavy rain. These instances are likely to become more frequent, and the UK Climate Impacts program predicts that the average winter rainfall could increase by between 12% and 16% by 2050 and by 16–26% by 2080 (UK Climate Impact Projections website, accessed August 2010: http://ukclimate-projections.defra.gov.uk/content/view/2200/499/). Well-designed GI can alleviate the risk of flooding by retaining water.
- Environment Agency data indicates that extensive areas of Westminster are prone to fluvial and tidal flooding, including many parts of Victoria, as shown in Fig. 1. This includes the area directly outside the entrance to Victoria station, and either side of Bressenden Place. Much of the Victoria BID is identified as a Critical Surface Water Flood Location in the recent Westminster Strategic Flood Risk Assessment (SFRA). The SFRA predicts that this surface water flooding will be exacerbated by the predicted effects of climate change, and will affect an even greater area of the Victoria BID. The Westminster SFRA also indicates that a breach of the Thames Barrier would result in flooding which would extend as far as the eastern part of the Victoria BID.

An audit of the roofs was also under and each roof assessed as to whether it could potentially be greened and what type of green roof in terms of depth could be achieved.

The flat roof audit identified approximately 29 hectares of roof area within both the outer and inner cores of VBID area 4.17. Of these 29 hectares of roof, over 25 hectares had the potential to support a living green roof habitat. Of this 25 hectares, 18% had the potential to support a green roof in keeping with guidelines of biodiversity as outlined in the Environment Agency Green roof toolkit, 55% moderate potential and 42% low potential.

Since the publication of the report, other similar audits are being considered elsewhere in London and also beyond the capital in UK.

Both the London Government's report and VBID report demonstrate the commitment in theory to retrofitting green roofs. However the major task will be to ensure that the theory is put into practice. There are now many examples of green roofs that have been retrofitted in London, most of these have been done through either funding streams associated with biodiversity or where commercial companies have engaged with Livingroofs.org to specifically deliver seminal projects at their own expense, such as the highest green roof in the UK on top of Barlcays Headquarters in Canary Wharf, London. Over the last 4 years a project funded by the SITA NATURE ENHANCED has been ongoing in London. This has led to just under 2,000 m^2 of green roofs being installed on existing buildings throughout the capital for rare invertebrates. One of these projects, 55 Broadway, recently won the Sustain Award for Biodiversity.

A further development that is underway in London is the retrofitting of a number of green roofs as part of the Drain London program (http://www.london.gov.uk/who-runs-london/greater-london-authority/directors-decisions/dd421). The first two will be installed in the summer of 2011. Part of the money allocated for this project is utilized to have the roofs monitored for their positive impact on intense summer storms.

One of the roofs to be funded

The Importance of Policy and refined Planner Tools for green roofs

There is still unfortunately a tendency on designers, whether they be architects or landscape designers, to seek out mechanistic product-based solutions. While most of the

The Future in the UK The development of a unique London green roof policy has been driven by a number of specific factors. Urban ecologists and their issues certainly provided the initial impetus for policy activities and innovations. The climate change agenda and how a large city like London adapts has certainly galvanized the need for a policy. What is needed in the future is a greater understanding and improved planning tools to ensure that good green roofs are installed to meet the cross cutting benefits that a city like London requires. It would be hoped that the Environment Agency Toolkit sets a precedent that at regional level [GLA] and a local [LBs] green roof

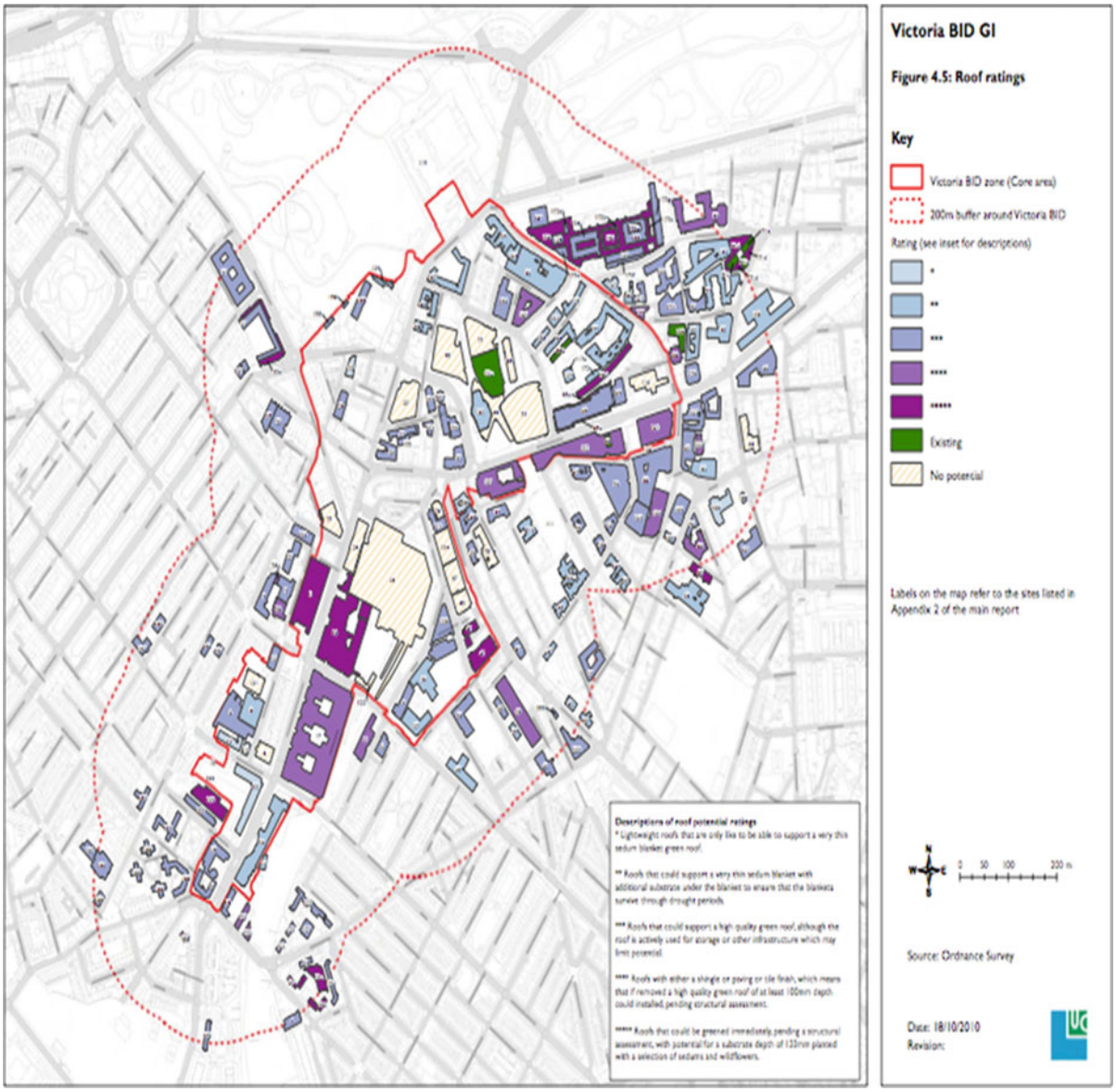

Green Roof Planning in Urban Areas. Figure 1

policies and conditions can be refined to ensure the quality of green roof implementation. There is still unfortunately a tendency on designers, whether they be architects or landscape designers, to seek out mechanistic product-based solutions. While most of the

The implications of green roofs implementation within the capital is having an effect beyond the capital, in particular in the Greater London Watershed – particularly the area known as the Thames Gateway. This area includes much of East London and stretches along the Thames estuary into Kent and Essex. Already there are a number of huge developments, which are under pressure to include green roofs as mitigation and compensation for ecological reasons.

However, there will be a need to constantly refine policy to meet the changing climate and needs of London. Green roofs are certainly no longer a fad but are an ever-growing market and an integral response to

impending climate challenges. The hope is that policy makers and regulators ensure that the roofs that are installed are of the quality needed to meet the capital's diverse and evolving agendas.

Basel In Basel, one of the most important pioneer projects at the time was the construction of an additional tract of the City's University Hospital, which foresaw green roof areas on all new buildings of the hospital complex. Patients should have a more pleasing view over the roof landscape, which in turn would ideally have beneficial effects on their healing process.

Research on sites like the University Hospital focused the potential for urban wildlife based on bird studies. The interesting results showing how black redstarts benefit from green roofs created a link to Dusty Gedge, an urban wild life specialist and planner in London. Dusty Gedge visited Basel in 2000 in regard of Stephan Brenneisen's bird and other studies. The knowledge of the benefits for black redstarts (a national endangered species in UK, with only two populations left in London and UK) by green roofs was the base for Dusty Gedge campaigning green roofs all over UK later.

Energy Saving Fund and the First Green Roof Campaign in Basel To get to the comprehensive green roof research of the University of Basel (later Zurich University of Applied Sciences, Wädenswil) the city of Basel did important contributions. In the early 1990s the city of Basel implemented an ecological mile stone with a new law to support energy saving measures. According to this unique law for Switzerland some 4% of all customers' energy bills are put into the "energy saving fund." Out of this fund campaigns and measures to support energy savings can be financed since then. As one of the benefits of green roofs is improving insulation and reducing energy consumption of buildings, a campaign for green roofs could be launched in 1996 based on the energy saving fund.

Following the "Year of Nature" in 1995 the project called "the improved roof" combined energy saving issues with nature conservation and got a total sum of one million Swiss Francs to subsidize house owners building their own green roofs. Within 18 months, over 120 green roofs were built in Basel, an area equal to 8 football fields. The project was carried out in cooperation with the trade association, which enhanced local know-how in the field. During the campaign, architects, planners, and the contractors installing the green roofs could get good practice and experience in this new technology – an important step to bring the measure into practice later.

Building Code and Wildlife Potential After the first green roofs campaign, Basel Canton passed an amendment to its building code (paragraph 72) in 2002, requiring all new buildings with flat roofs to have green roofs. This amendment was made based on the various benefits and impacts green roofs have for the urban environment and not least in recognition of the potential for green roofs to support biodiversity and species conservation in Basel. It is supported by additional specific guidelines on implementing green roofs in Basel to maximize their nature conservation potential.

The recognition that green roofs provide valuable habitats and support nature conservation objectives was later one of the drivers for Basel's second campaign, which started in 2005. This second campaign funds both green roofs and roof insulation. It was funded in the same way as the first campaign with a total sum of SFr. 1.5Mio.

Quantifying Green Roofs: Urban Heat Island, Climate Change, and Global Warming After the second campaign, again a survey recorded by aerial view photos the actual number and area of green roofs in the city of Basel. As a result 1,711 extensive green roof projects and 218 intensive green roofs (roof gardens) could be registered. So, approximately 23% of Basel's flat roof area is installed with green roofs in 2006 (Figs. 2 and 3). This amount will clearly have an increasing beneficial impact on the city climate. Regarding urban heat island problems accentuated by global warming the green roof policy of Basel could be an example: how to face one of the possible measures with a campaigning strategy getting green roofs from pilot to mainstream successful.

Building Code and Price as Important Drivers for Success The general public in Basel still finds green roofs "special and exciting," but for developers, installing green roofs is now considered routine. The ongoing reduction of the installation prices of green roofs from SFr. 100.-/m^2 (US$90.-) in the 1990s down

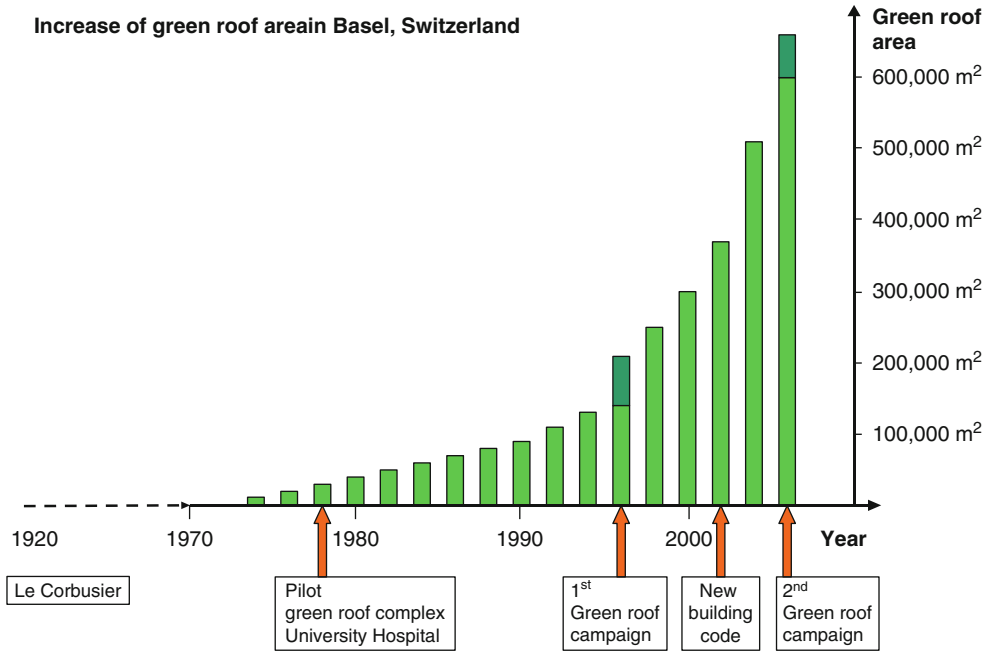

Green Roof Planning in Urban Areas. Figure 2
Increase of green roof area in Basel, Switzerland, from 1970 until 2007

to SFr. 20.- (US$17.-) was an important factor in the inclusion of green roofs into the building code (Fig. 4).

Green Roofs in the Rest of the World: A Summary

Green roofs as an urban planning tool is not becoming more prevalent throughout the world. Although the approach evolved in Germany, Austria, and Switzerland, it is now spreading throughout Europe and North America, and there is increasing interest in South America, Asia, and Australasia.

The oldest green roof policies were derived in Germany and Austria in the early 1980s. Stuttgart in Germany is probably the most renowned of the Germany green roof cities, although green roofs are an integral part of planning in the cities of Munster, Frieburg, Berlin, Dusseldorf, and Munich, to name a few.

In 1985, the municipality of Linz in Austria undertook an assessment of the loss of green areas and the quality of life in the built environment through a unique mapping process, known as the Green Space Plan. Although there were a number of green roofs within the city's boundary, including one of the largest

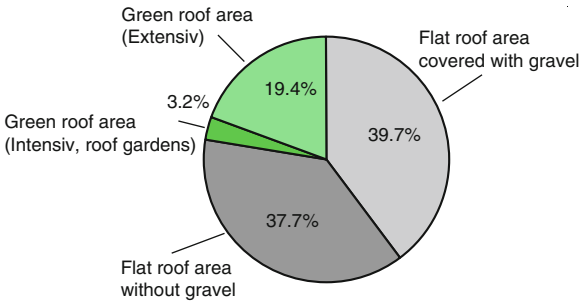

Green Roof Planning in Urban Areas. Figure 3
Percentage of green roof area related to the total flat roof area in Basel, Switzerland

in Austria – the Schachemeyer Factory green roof, this research demonstrated the need for a more direct approach to encourage more uptake of green roofs. The research became the basis for legally binding building plans, which included an obligation for building green roofs.

Green roofs were seen as effective solutions to "greening" in areas of Linz where land use was not compatible with open space development. This was

Green Roof Planning in Urban Areas. Figure 4

particularly important in the city's commercial and industrial zones. As a result, green roof policies were introduced in Linz in 1985 as legally binding and compulsory building plans. The direct impact of this strict measure led to an increase in green roofs, especially in the industrial areas close to the River Danube.

In 1989, the city of Linz instigated a generous financial incentive for building owners, by sponsoring green roofs by up to 30% of their, which was reduced in 2005 to 5%. Over the past 20 years, all these measures have resulted in over 404 green roofs being installed in what is by all accounts a relatively small city. The total area prior to 2007 was 400,000 m^2 (equivalent to 40 football-pitches). About 90% of this area is extensive green roofs and 10% intensive green roofs. However, the recent covering of the main motorway through the city with an intensive green roof (which talk all the city's annual green roof budget increased the total area by at least 40%.

In North America, many cities are now actively promoting the use of green roofs. The first city to undertake this process was the city of Portland followed by Chicago. Other cities include Seattle, Vancouver, Minneapolis, Toronto, Washington DC, and New York.

In Asia, the standard bearer for green roofs has been Singapore, which has been actively promoting green roofs for nearly 10 years and there is increasing interest from China and India in how green roofs can address urban health and environmental issues.

Bibliography

1. Grant G (2006) Green roofs and green facades. BRE, Bracknell
2. Hyder Consulting (2006) Green roofs for eastside outline drainage policy
3. Knaupp W, Staiss F (2000) Photovoltaik – ein leitfaden fur anwender. Fachinformationsentrum karlsruhe
4. Kohler M (2002) Photovoltaic panels and green roofs – positive interaction between elements of sustainable architecture. In: RIO 02 world climate and energy event, Rio de Janeiro
5. Kohler M, Malorny W (2006) Warme –dammeigenschaften von dachsubstraten mit vegetationsschnicht extensiver grundacher. Dach Grun 15(3):8–13
6. Liu K (2002) Energy Efficiency of and Environmental Benefits of a roof top garden. National Research Council Canada, Ottawa. www.professionalroofing.net

Green Roofs, Ecological Functions

Manfred Köhler[1], Andrew Michael Clements[2]
[1]University of Applied Sciences, Neubrandenburg, Germany
[2]Green Roof Greece, Athens, Greece

Article Outline

Glossary
Definition
Introduction
Future Directions
Acknowlegdements
Bibliography

Glossary

FLL The Landscape Research and Development Society (FLL) nonprofit organization was founded in 1975. Its mission is to research, produce, and disseminate all the various landscape development principles, guidelines, and specifications for the assurance of environmental quality [1].

FBB The Green Infrastructure Association (FBB) is a specialized group that was founded by some members of FLL to focus more specifically on green building. The FBB is the German counterpart to the American industry association Green roofs for Healthy Cities (GRHC) and one of the founding members of the World Green roof infrastructure Network (WGRIN). The German Word "Bauwerksbegrünung" has no translation in English – Green infrastructure in the sense of FBB is focused on all forms of urban green.

Extensive green roofs (EGR) also called natural green roofs, or eco-roofs, are vegetated roof constructions that require low maintenance. Drought-adapted plant species are used to create a self-sustaining vegetated surface suitable for nearly all types of buildings. Growing media is about 10-cm, or 3-in. thick [2]. The term "Natural Green Roof" is an own further term, which should set the main focus on enhancing the biodiversity on vegetated roofs. This can include in some regions irrigation with rain or gray water. Natural green roofs means engineered green roof systems under the guidance of nature conservations solutions. This term includes extensive and intensive green roofs.

Intensive green roofs (IGR) also known as roof gardens are garden structures on top of buildings and other artificial urban surfaces. In most cases, the growing media is more than 20 cm deep. For trees, it can be more than 1 m. IGRs, with structures including lawns, planter boxes, shrubs, and small trees, require the same maintenance as traditional gardens.

Storm water runoff Rain water running off impervious surfaces.

Green infrastructure overall phrase in the North America for all types of green roofs technology and other types of greenery on buildings, like vertical greening, living walls, and indoor greening systems. Green infrastructure in a wider sense includes photovoltaic technology and rainwater management.

Growing media engineered substrate for green roof purposes. Green roof substrates typically have low nutrient content and high drainage rates. Typical materials are expanded slate, shale, pumice, or recycled products.

Green infrastructure A term to describe the range of materials and technologies used to enhance urban environments. In addition to green roofs, this term also encompasses other related systems such as vegetated facades with climbers or living wall systems, indoor greening systems, rain gardens, photovoltaic systems, and other technologies. Roof greening can be combined with living walls, indoor plants, and ecological landscaping to enhance the built environment. The USEPA refers to structures specifically intended to manage wet weather as green infrastructure.

Leadership in Energy and Environmental Design (LEED) This is a US-based rating System by the US Green Building Council (USGBC). Benchmarks focus on energy savings, water efficiency, CO_2 emissions reduction, improved indoor environmental quality, and stewardship. The categories of achievement are: silver, gold, or platinum. In Australia, a similar rating system uses "stars." After an extensive debate about the merits of such certification systems, Germany set up one in 2009. Certification can be an effective type of marketing; however, one

critique of existing systems is that there is not enough weight placed on vegetation.

Low impact development (LID) A storm water management and site-design technique to mimic the situation before construction of the settlements. Water usage, evaporation cooling, and water storage and drainage are such benefits of green roof infrastructures.

Definition

Green roofs are engineered constructions that include environments suitable for well-adapted plant species. In most cases, these types of roofing have a longer lifespan than conventional roofing surfaces. The following elements are built on top of the roof structure

- The underlying protective layer is made of an impervious material such as bitumen, rubber, polystyrene, or other similarly adequate technical materials, in short: roof protection membranes.
- Additional, root barrier layers are available to prevent the root penetration of lower layers. These are known as separation fabrics or geotextiles.
- This is commonly followed by a separate water-retaining layer, which could be a natural porous stone material or an artificial retention mat; in short, this is a drainage layer.
- On top of this layer, a filter fabric separates the retention layer from the next layer: the growing media.
- The growing media is, in most cases, a specially mixed lightweight soil material with well-selected components for storing rain water. Growing media are mixed for different purposes (for example, extensive green roof growing media differs from roof garden media in nutrient and humus content). Intensive roof garden growing media differs in that in the upper levels there is a higher content of humus and on the lower levels lower humus content.
- The vegetation layer can range from a shallow layer with mosses and only a few taller plants all the way up to full-blown roof gardens. As such, green roof maintenance requirements can be as little as an annual inspection or as much as is usual for ordinary gardens. The success of the vegetation layer depends on the careful selection of the other green roof layers. For example, if the goal is to plant trees on rooftops, a special combination of all these components is necessary.

The maximum weight of the construction must be calculated carefully. On average, it varies between 40 kg/m^2 (8.33 lb/ft^2) and can rise upward to about 350 kg/m^2 (71.7 lb/ft^2).

The longevity of green roofs depends on whether they can be easily accessed with the basic equipment needed for the success of the project as well as repairs. Maintenance and repairs must be planned carefully. Certain areas of the roof like, edges and places around roof fixtures like skylights or climate control systems can be prone to structural damage. Architects follows design visions, green roofs on "unusual" and for plant development difficult situations. Some times it is too high or to steep for a suitable plant growth or for the needed maintenance work. The technical and biological limits challenge green roof professionals. It is the duty of green roof specialists to figure out the limits, which are stet. Uncontrollable aspects of local climate, such as wind, temperature, and the intensity of storm events, can set limits to what is feasible from an architectural design perspective and ideas about developing living surfaces on roofs and facades.

Green roof technology has become internationally famous in the past few years. The books recommended at the end of this chapter offer a wide range of basic information from various regions in the world.

Introduction

The global human family is currently undergoing a subtle, revolutionary paradigm shift away from an unsustainable, industrialized, mass, homogenized, synchronized society to a sustainable, custom, micro, niche, bio-diverse world. This is seen in every aspect of human life – from the work to entertainment. Gone are the days when work was done 9–5, mass entertainment was enjoyed all together and gone is the factory fortnight in August where all headed for warmer climes for our 2 weeks of holiday. Today it's work and play around the clock telecommuting, working from home, downloading You Tube videos and interacting on Facebook and Skype. This global shift to an information-rich, knowledge society is mirrored in how the urban greening industry worldwide interprets itself.

Once upon a time, not long ago, a green roof predominantly meant an amenity space with garden furniture and well-manicured lawns and water features or maybe at its ecological best mass-produced Sedum mats laid over plastic drainage boards and geotextiles. With deeper movement into a sustainable concept of our lives, this has been replaced by ecological sensitivity, biodiversity concerns, water management and conservation, and other such similar ecological, sustainable ideas. This entry will discuss this shift in detail and what exactly it means.

Green Roofs as Ecosystems

In recent years, there has been a growth in interest in natural green roofs, or eco-roofs, as distinct from roof gardens due to the ecological benefits that may be derived. Roof gardens were traditionally installed in many countries to provide amenity space and for building beautification, in places such as hotels and resorts. The ecological benefits, such as thermal insulation, that were derived were almost an afterthought. Nowadays, in many instances, natural green roofs are installed to become natural ecosystems in urban areas. The benefits achieved by such installations can be measured not only in the building itself but the surrounding urban area as a whole.

Green roofs have been shown to mitigate the urban heat island effect. Two key studies in the hot summer climate of Athens [1–3] concluded that the thermodynamics of both the building and the surrounding area are effected by the natural green roof installation studied on the Greek Treasury in Constitution Square in Athens. In addition, leading natural green roof researchers have compiled a review article, which explains this technology [4]. The concept of natural ecosystem green roofs may have grown out of the idea of just letting pioneer plant species grow on built surfaces in urban areas. Certainly, where this idea originated is a moot point now as it has become an emerging architectural style, which is being used by leading name architects with global reputations.

Natural green roofs are also called bio-mimicry or bio-phillic architecture [5, 6]. Ecologically, natural green roofs can be compared to natural structures such as rocky outcrops or cliffs where harsh weather conditions and shallow layers of substrate are found. It is understandable why cities are sometimes described as being "urban canyons." Many highly specialized ecosystems thrive in such structures [7]. In fact, these ecosystems, in the natural world, have often developed because of these extreme environments.

A number of environmental scientists and thermodynamics researchers are working on quantifying the energy savings, emissions reductions, and water resource management benefits that come from the use of natural green roofs. In addition, research is being conducted to quantify the many other ecological other benefits such as the reestablishment of plant and animal biodiversity in urban areas. Green roofs can be considered as the open ecosystems described by early ecologists [8]; where inputs of water, nutrients, and substrate to such installations occur from precipitation, dust in the urban canyon, and gaseous pollution. Losses to a natural green roof can come from wind erosion and storm water runoff. In terms of ecological productivity, natural green roofs have been compared to desert ecosystems, where there is a similar input/loss situation.

The total phyto-mass of a natural green roof is measured by considering the total shoot/root biomass. This figure varies in Europe between 100 and 500 g/m^2 total dry organic matter [9]. The 500 g/m^2 is an almost fully covered natural green roof, which has been planted with Sedum or similar succulents, Chive (Allium spec.), wildflowers, pioneers, and grasses with about a 95% coverage and about a height of 25 cm. The figure for a south-facing roof with coverage up to 60% is about 100 g biomass/m^2. The gaseous exchange (O_2, CO_2) productivity of such ecosystems is relatively low when compared with richer ecosystems such as forests. A biomass survey found a natural green roof with a 168 g/m^2 above ground biomass and about 107 g/m^2 root system biomass 2 years after installation [10]. These recent dry matter values are similar to the above-mentioned German measurement from the 1980s. If the main aim of the installation of a natural green roof is CO_2 sequestration, annual cutting of the plants is recommended for mulching, followed by allowing the plants to grow back each year. Natural green roofs are also being seriously considered to not only supplement urban agriculture to supply cities, particularly in the third world, but also in the West, as urban agriculture can lead to significant emissions

reductions. This is due to the fact that food can be sourced and consumed locally, reducing the need for transportation from rural areas into cities. There are notable examples of this emerging concept abound, across the world, from New York City to Bangladesh. Urban agriculture is substantially more productive using high-tech hydroponics and other such intensive technologies than it is with natural green roofs. So, green roofs can be used to supplement urban agriculture. In addition, natural green roofs can provide specialist agricultural products such as aromatic herbs for culinary and pharmaceutical use.

Natural green roofs are usually designed to keep vegetation conditions stable over the long term. However, there is a growing belief, particularly among natural green roof pioneers in Greece, that natural biological succession could result in the development of highly successful, bio-diverse, specialist ecosystems, which have adapted to the peculiarities of urban centers. On the whole, human intervention and "maintenance" should be kept to a bare minimum, if not removed altogether. It should be noted that it is advisable that a specialist inspect a natural green roof annually to check the waterproofing and to make sure that the vegetation has not become dangerous in terms of height. Apart from that, nature should be allowed a free reign. It must be noted that natural green roofs are not usually designed as recreational space. Furthermore, safety concerns relating to the height of the vegetation must be addressed. Barriers to prevent falling of material must be installed around natural green roofs.

Natural green roofs, then, can be considered extreme man-started natural habitats on artificial urban surfaces. After the installation annual inspection means that these structures require low to nonexistent human intervention. Environmentalists are becoming increasingly interested in the almost self-sustaining nature of natural green roofs. Overall, researchers are beginning to realize that they may well be able to reduce the anthropogenic impact of urban environments on the biosphere. The level of this impact depends on a plethora of factors, yet, these can be engineered by the design of the structure.

In this entry, three main aspects of natural green roofs will be highlighted. First of all, the benefits of natural green roofs will be discussed. To assess this, a description of natural green roofs as ecosystems will now be made.

Green roofing is currently (2010) practiced in about 40 countries worldwide please see www.worldgreenroof.org. There are organized green roof associations in about 20 countries at the time of writing [11]. Also, about 500 peer-reviewed articles have been published concerning green roofs at the time of writing this article. This would suggest that while green roof technology appears to be quite simple and low tech. the concept, particularly natural green roofs, is in fact complex [12]. Much more research is required and will be conducted going forward.

What is required is a comprehensive picture, based on research, of what exactly are the benefits of natural green roofs. It is certain that all forms of green roofs and green walls will play a fundamental role in terms of thermal insulation for buildings and for mitigation of the urban heat island effect in the future.

It seems certain that the performances of natural green roofs will aid a revised perception of what is aesthetically pleasing toward natural green roofs and away from traditional roof gardens. The new perception will be that bio-phillic is better than manicured human-created gardens [13]. The description of the ecological functions of natural green roofs by pioneers, such as James Todd [14] and his more modern counterparts such as Peck [15] and green roof enthusiasts, campaigners, and activists like Dusty Gedge in the UK (www.livingroos.org), helps to create new paradigm in what a green roof should look like. When the thermal insulation performances of natural green roofs are combined with water conservation and enhanced biodiversity on a massive scale around the world, a technology emerges, which could ameliorate, if not solve, some of the most pressing concerns of our time. This technology may soon become the status quo in architecture.

One of the main challenges of the urban greening industry and its stakeholders now and in the future is to obtain a full and detailed understanding of a natural green roof ecosystem, its energy cycle, and how these systems interact with other green technologies. It must be stated that there are already peer-reviewed articles, which begin to provide insight into this complexity and could make substantial contributions to architectural textbooks in the coming years.

It should be pointed out that roof gardens or intensive green roofs, which are primarily constructed as

amenity and recreational space in towns, could also be used for ecological concerns. For example, if roof garden decks are built with rainwater catchments and rainwater storage systems, there are ecological benefits that can be achieved. The deeper substrates that are used in roof gardens, which often range between 50 cm and 2 m offer enough substrate depth for many species of shrubs and small trees. Of course, safety issues must always be addressed before planting taller plants because at roof level, falling plant is a serious concern. When done properly, urban forestry may be possible on roof top spaces. Susan Weiler's Church project [16] is one example of an attempt to achieve urban forestry. While this project is about traditional horticultural ideas of aesthetics, it does also incorporate the use of trees using forest mimicry. It must be noted, once more, that safety must always be put first when dealing with the urban environment. Which tree species have been considered as suitable for urban forestry? First of all, many common or ornamental plant species have been considered. All phyto-mass-related functions can be delivered. Research about the potential of such forestry structures on rooftops has been conducted and tested in Hong Kong [17].

One conclusion of this entry is that if the load capacity of a building allows greater structural weight, a deeper growing medium opens up a wider range of potential plants species for selection as long as the aforementioned issue of falling has been addressed thoroughly. Consequently, urban forestry becomes possible along with natural green roofs. The challenge for the urban planner is to find appropriate mixes of planting schemes and appropriate safe technologies for particular climatic conditions and building codes. In recent years, forestry structures that have been installed on buildings range from sparse plantings to full earth shelters with copse planting schemes. Greened buildings, then, can have significant thermal performances and also act as natural corridors for the reintroduction of nature into urban areas [18].

Introduction to the Three Main Benefits

Green roofs, and especially roof gardens, offer aesthetic benefits and urban amenity and recreational space for city inhabitants. The measurable ecological and economic benefits that are derived by urban greening make these technologies increasingly attractive to town planners, architects, and civil engineers alike [19]. Roof greening serves both private and public interests. There are also local and global benefits.

Proponents of green roof technologies, such as The World Green Roof Infrastructure Network, (http://worldgreenroof.org) believe that all local and national governments should institute incentives to encourage the implementation of massive scale urban greening. The experience of German roof greening, in the last 30 years, suggests that government incentives to individuals, businesses, and the state lead to significant increases in the implementation of these technologies. This model can be copied around the world. To date, the cities that have taken these technologies most seriously resulting in large-scale implementation are mainly found in Germany. Cities such as Berlin and Stuttgart have high adoption rates, which are measured in percentage points of available city area. It must be noted that cities such as the Austrian city of Linz follow close behind. A full overview of the state of roof greening in Europe was given in a workshop at the World Green roof congress in Nürtingen 2009 [20, 21].

Some European Cites, such as Copenhagen, Malmö, and London, are jumping on the roof greening bandwagon with ambitious plans for roof greening in the coming years. An important next step in the implementation of large-scale greening globally is the mapping and modeling of successful initiatives that are being taken by local and national governments, agencies, and stakeholders.

The three main benefits that are derived by roof greening are the following:

1. The influence on the urban water management cycle
2. The energetic performance of green roofs related to the buildings, the city, and the planet as a whole
3. The development of urban biodiversity, leading to a richness of flora and fauna in urban areas

The Urban Water Management Budget The urban water management budget is stressed by the impervious surfaces of a built environment. In the natural world, storm water runoff forms a small percentage of the total water volume that falls as precipitation. Most of the water that falls as precipitation, in the natural

world, is absorbed by the Earth and becomes ground water. The reverse is true in the urban built environment: Most of the water that falls as precipitation becomes runoff. This causes a number of problems. Athens may be representative of what happens during a storm. The city squares are turned into lakes, and the streets become rivers within minutes of the onset of a storm event. Recent research into urban water management budgets conducted by Göbel et al. [22] suggests that urban landscapes could be transformed using a combination of rainwater catchment and retention areas, use and absorption, which would reduce urban water management costs to a level not much different from water management costs found in the natural world. In this context, green roofs are important as a type of decentralized rain water catchment and retention system. Green roofs and vegetated facades can retain storm water and release excesses over a period of hours, if not days. Green roofs act as a brake on runoff as they absorb and store large percentage of the water that falls as precipitation in a similar method to that which is found in the natural world.

Rainwater management with green roofs can incorporate storage values not only in the growing media but in all other layers in green roof systems. The drainage layer can be used for storage. Surface and subterraneous ponding can be designed to allow further storage. In addition to the defined water capacity of the growing media, drainage/storage layer, ponding, in countries where monsoon and excessively heavy rainfall events are experienced, growing media can be designed and plants selected that can store even larger quantities of water. Again safety issues are an important consideration here because water is heavy, so permissible static loads must be taken into account, particularly in seismic regions of the world. Consequently, it becomes clear how runoff is reduced in quantity and delayed over time by green roofs.

When green roofs are combined with other rainwater catchment and retention technologies, such as rainwater harvesting, re-use, and infiltration, it is possible to create a zero runoff position in a city. The decentralized storm water retention property of green roofs also reduces pressures on wastewater treatment systems that are already overloaded. The peak runoff after a heavy storm event is minimized.

This ability of green roofs to catch and store rainwater also has an impact on the second major benefit of green roofs in their thermodynamic properties. Surface runoff rates and the lack of green spaces can explain why there is almost no evaporation and why urban climates can be hot and dry [23]. With the increasing number of megacities, this climate may contribute to health problems for many citizens [24]. As will be seen in the next section, green roofs are active thermodynamically. This sets them well apart in terms of their thermal performance from conventional forms of thermal insulation using materials like stone wool and polystyrene. This will be discussed further shortly. For now, it can simply be stated that the captured water in a green roof, during a storm event, is evapotranspired by the plants. This actively cools hot cities. This cooling effect reduces air conditioning demands. Reduced air conditioning use further cools the city, leading to a virtuous cycle. This will be discussed later.

In developed countries, in the next few years, sewer systems that are approaching the 100 years of age mark will need to be replaced. The decentralized water management nature of green roofs, which reduces storm water runoff quantities in cities can provide a viable solution to this issue. This has been demonstrated in Berlin [25]. Since the 1980s, numerous projects to reduce storm water runoff, manage water demands, and handle wastewater disposal in cities have been implemented in Berlin; 17 projects were documented, and a list of these projects is downloadable from the official webpage of the Berlin senate [26]. Green roofs and green walls are fundamental components of green building technologies in all of these projects [27].

Increasingly, over the years, peak runoff during heavy storm events as well as the "Urban heat island effect" has become ongoing and challenging problems in inner City water management. Open evaporative surfaces could well become mandatory solutions [28]. In Berlin-Brandenburg, about 80% of the total precipitation that falls is converted to evaporation using various technologies and methods, which include green roofs. This figure could become an achievable target for all cities on Earth. This also links to the third benefit of green roofs, which is the development of natural ecosystems in urban areas.

In Berlin, for example, for each type of inner city habitat, an optimized vegetation value can be

calculated. In Berlin, this value is referred to as the "biotope area factor." These basic strategies must be adapted to suit regional climates with appropriate plants and growing media alternatives and local building codes. A further link between the benefits of green roofs is their effect on the so-called urban heat island effect, which links the water retention benefit with the thermodynamic performance. The urban heat island effect is partly caused by the almost nonexistent property of evapotranspiration in a city. By retaining more water in urban structures in green roofs, the city is cooled in the summer, mitigating this phenomenon. In addition, in an emerging paradigm among climate specialists, water cycles are now considered to have a fundamental causal relationship with man-caused global warming [29].

To develop large-scale vegetation structures on buildings, cooperation between architectural disciplines and green planners, researchers and designers must begin; the conventional so-called black roofers, who use bituminous and plastic membranes, and so-called green roofers, who use water storage/drainage systems, substrates, and plants, must engage in productive dialogue.

Currently, about 5–10% of new buildings in Germany have green roofs. The number of green walls remains, at present, less than 1%. This potentially represents a huge opportunity for environmentally friendly architecture. A paradigm change in architecture is needed to construct not only in terms of energy-efficient designs but also buildings that have zero negative impacts on the environment. This is the challenge for the coming years, and green infrastructure will play a dominant role in assisting cites to achieve this objective [30].

Energy At the dawn of the twenty-first century, humanity faces what could possibly become its defining moment. The choice is becoming ever more obvious, and humanity is going to be forced to make a decision soon, en masse, about whether humanity makes it to the twenty-second century or becomes just another flash in the pan for this planet. The human race potentially faces the horrific possibility of a massive die-off at the very least or extinction at its worst. The reason is quite simple: Mankind has been able to develop modern civilization on the Earth, and achieve the undreamed of standards of living and technologies that it has due to the tremendous subsidy that abundant oil has provided. One liter of oil is the energy equivalent to 100 man-hours of labor. The West has collectively burned or used a large percentage of the oil reserves on Earth during the last 100 years. How much oil has been used and how much is left is open to debate and probably unknowable. More may be found somewhere, sometime. What cannot be debated is the fact that oil is a finite resource, which took millions of years to form, and if only the West continued using it at the rate that it does, it will dry up sooner or later. This is likely to be sooner rather than later because now the rest of the world is developing at rates that make Western industrial development in the late eighteenth and early nineteenth century looks like child's play [31].

In addition, climate change, global warming, the coming ice age, how much influence human activities have on the Earth may be debated endlessly. What cannot be questioned is that continued production of CO_2, CO, and a multitude of other poisonous gases through oil combustion, ongoing quarrying, mining, deforestation, increased urban development, natural ecosystem degradation cannot end well for humanity or for most forms of life. It is inevitable that, again, sooner or later, the human species will have cut down the last tree, used the last drop of water, polluted everything, everywhere, and this is obviously not beneficial for life.

Certain issues require detailed, analytical, scientific study and understanding to attain a deep awareness. This issue can be understood by common sense alone, most effectively. If you keep taking something from a finite source, sooner or later, there will be none left. Moreover, if by using the finite resource taken, degradation of your life-support systems occurs; the end to this scenario does not require much thought to calculate.

So, humanity faces three of what are possibly the greatest challenges any species can face. The first is increasing rates of depletion of ever dwindling energy and natural resource supplies, the second a buildup of toxic waste in its environment, the third exploding population growth. Thankfully, a viable solution to these three scary challenges is available. While it is true that these points may seem exaggerated and the solution simplified. Increasing numbers of highly

acclaimed scientists from around the world are suggesting that the solution comes from the cause of the problem. Nature is the issue, and nature is the solution.

Some activists and campaigners state that there is a need to save the Earth. The Earth has been here, according to most estimates, for 4.5 billion years. In that time, it has survived far greater threats than humanity. Possibly, what humanity needs to do is to save itself. The only savior up to the task is nature itself. This is where urban greening and particularly green roofs really prove their value. Green roofing may well be the ultimate "return to nature" that was much touted by groups in the 1960s and subsequent eco-friendly parties and interests but this is a "return to nature" without having to move anywhere. Cities, can be taken, as there are and transformed into natural ecosystems using green roofs. The impact of this on the challenges would be, to understate it, revolutionary and evolutionary.

Possibly, the most serious and important impact of this would be its effect on human energy requirements. Numerous studies conducted around the world have shown that green roofs significantly reduce heating and particularly cooling requirements in both buildings and whole cities. In the aforementioned thermodynamic study of the oikostegi (natural green roof in Greek) installed at The Greek Treasury in Constitution Square, opposite the Greek Parliament in Athens, Drs. Rogdakis Ph.D., and Koronaki Ph.D., concluded that substantial thermodynamic effects were observed.

Air conditioning requirements were reduced by 50% in the floor directly beneath the green roof installation. This is important when one considers that only 52% of the roof surface is covered by the oikostegi natural green roof. A further important conclusion of the study was the so-called thermal lag effect of the green roof. Peak environmental temperatures were observed at 1 p.m., the building temperature peaked 30 min later where it was not greened, and the area that was greened peaked a full 90 min later at 3 p.m. This is rather important for two reasons. Firstly, due to the fact that only 52% is greened, there are large thermal bridges, which would not be observed had the entire surface been greened. Secondly, this particular building houses government offices and the peak demand for cooling of the building has been delayed by the natural green roof until 3 p.m., at which time the civil servants have already gone home. This means that there are further reductions in air conditioning because it is no longer required. Before the installation, peak requirements were observed 90 min earlier. On the surface, this may not appear substantial but the Treasury has an air conditioned office space that totals nearly 12,500 m^2 http://www.oikosteges.gr/index.php/greenroofs/research.

Another important aspect of the thermodynamics of green roofs is the fact that because air conditioning use is reduced, further reductions in the ambient temperature of the surrounding area are reduced leading to even further reductions in cooling requirements. It was anecdotally stated by a Greek thermodynamics specialist that if all the air conditioning were switched off in Athens for 3 days, Athens would not need air conditioning. The reason for this is simple. The inventor of air conditioning, Carrier, never designed it as a method of cooling. It was designed to condition the air. The way air conditioning works is by taking hot air out of a building and dumping it into the surrounding area. This means that the surrounding area becomes hotter leading to an increased requirement for air conditioning leading to increased dumping, leading to a vicious circle. What green roofs do is to reduce air conditioning requirement, leading to falling ambient temperatures in the city, leading to further reductions in air conditioning requirements in a virtuous circle. Large-scale implementation of green roofs leads to a lowering of peak summer temperatures in cities, which leads to a lowered energy requirement to run air conditioning units and lowered peak ambient temperatures.

A similar story is observed in the winter with heating requirement reductions. This number of reduction depends on various factors, but the values vary between a few percentage up to 20% in roof top level apartments [43]. Reducing energy requirements with green roofs has another important impact, especially in countries like Greece and Germany where lignite is burned to produce electricity by the Public Power Corporations in both countries. Lignite burning produces even greater carbon emissions than oil burning and is much less efficient. Carbon is one of the main greenhouse gases, which are thought to be partially responsible for global warming. Energy efficiencies achieved by green roofs, then directly reduce carbon

emissions, reducing greenhouse gases and slowing down global warming. It must be noted here that green roofs also absorb greenhouse gases, further reducing existing emissions. The full impact of green roofs is still not completely known, and there is room for much research. Having said that there is little doubt that they have a substantially important impact on reducing energy requirements, which has an impact on reducing emissions and heat caused by air conditioning, which has a further impact on reducing energy requirements in a virtuous circle.

In Europe, the goal for fossil fuel consumption reductions stands at 40% by the year 2020. Furthermore, European countries have pledged to reduce carbon emissions by between 10% and 20% by 2020. Greece has ambitious plans to reduce carbon emissions by 30% by 2020. All of these goals become achievable using massive scale urban greening using green roofs. Green roofs can return their installment investment cost many times over in energy requirement reductions and emission reductions very quickly.

It should be stated here that green roofs operate rather differently from other forms of thermal insulation. A green roof is an active cooling and heating device as well as a superior form of thermal insulation. Conventional insulation isolates the environment from the building, keeping heat out of the building in the summer or by trapping heat inside the building in the winter. The way it works is by creating a thermal barrier between the building and the outside environment, which prevents thermal flow. A number of materials are used, including stone wool and polystyrene.

A green roof insulates a building in this way, but it also plays a more active role in the thermodynamics of the building and, in fact, the surrounding environment. First of all, it acts as a thermal pump in the summer. Heat that is in the building is drawn out by the green roof as the green roof temperature is lower than the environment and the building. Also, a green roof lowers ambient temperatures in the surrounding area. So, if green roofs are installed on a large scale, ambient temperatures would fall in the whole city in the summer. The same is not true for conventional thermal insulation. Moreover, as stated earlier, as ambient temperatures fall, air conditioning use falls leading to further falling ambient temperatures. Again, this only applies to green roofs.

Evaporative cooling consumption by green roofs is the name given to these processes. Further improvements to the performance of green roofs can be made if rainwater catchments and green roof irrigation are utilized. This is known as adiabatic cooling, which is a low energetic cooling process in which rainwater can be used.

If roof surfaces are extensively greened, storm water runoff can be detained and retained [28] to irrigate the green roof during the summer to improve the thermal performance still further using evapotranspiration.

So, the evaporation of water in a city is an important component to reduce the heat impact of solar radiation in a city. Lower evaporation rates mean higher surface temperatures and in urban areas a main contributor to the "urban heat island effect." On a global scale, the reduction in evaporation in the built environment is mainly responsible for climate change [29]. Mitigation of global warming by evaporative cooling is one key process, which can be used in the reduction of global warming. A special entry on this was delivered at the climate conference to Copenhagen by Kravčík et al. The conclusion of the entry is that global warming is related to the loss of vegetation worldwide. Green roofs offer new space for vegetation structures and provide the needed evaporation cooling systems.

Biodiversity Urban biodiversity is the third benefit that green roofs provide. The Convention on Biodiversity (compare: http://www.cbd.int/cop9) COP9 Declaration of the Congress in Erfurt in May 2008 demanded that green roof plant selection foster and encourage urban biodiversity. Environmental laws, such as environmental building codes, help to mandate these demands at the national level. Planting trees wherever possible in a city is the first step in solving the issue. This is possible on parking space areas in the commuter zones of cities; tree planting in cities also reduces the air conditioning requirements in cars that have been in the shade, when driving recommences. Parking decks can utilize shade trees to protect cars from direct solar heating. This reduces air conditioning requirements in cars, which again feds into the virtuous circle mentioned earlier. Parking decks are an important source for greenery. In Singapore, for example, there is a government program to set up green roofs in parking areas as an open space resource.

Most natural green roofs (NGRs) are promoted as self-sustaining ecosystems. A plant cover of about 60–75% indicates that a high-quality green roof has been achieved; however, in many cases, the focus is only on few specific types of plant species. NGRs can and should also be designed to encompass a high range of biodiversity. Depending on the type of the project, a focus on regional native plants can be integrated into the design of the installation. To achieve this end, the right selection of plant species, proper design of substrates, and a variety of different methods of ecosystem establishment are important.

The number of plant species on a green roof depends on a number of parameters, such as the manner in which plants are introduced to green roofs. The following is a brief description of the most common methods of plant establishment:

- Seeding (affordable for flat roofs).
- Sedum sprigs (cheap and easy, establishment takes about 1 year).
- Plugs – there are a nurseries, in countries where roof greening is popular, around the world, that specialize in green roof plants.
- Preproduced turf mats. This technology was developed a few decades ago. Most of the turf mats include drought-adapted grasses and also several *Sedum* species. Depending on the local situation, grasses are often the best competitors under shady conditions, and *Sedum* species are usually the winners in the areas with full sun. This method offers a complete vegetation cover from the first day of installation. This is important for pitched green roofs and high-rise buildings with a high wind uplift to avoid the erosion of soil and decline of plant species.

Seasonal changes in the vegetation structure can be observed. The timing of blooming on extensive green roofs is related to the frequency of rain events. In humid and wet summer seasons, more flowering is normal; also more pioneer plants invade spontaneously during wet seasons. The acceptance of unplanned plant species depends on the aims of the project.

Weed Control Some plants are known to be difficult plant species for NGRs. These must be removed as early as possible. An annual inspection and weeding can be helpful. Also, it must added that this is an issue of great debate in the green roof world. Weeds can be defined as plants that grow and are not wanted. Some so-called weeds can be invasive and dominate if they are not controlled, which may or may not be desirable. Another way of looking at a weed is in terms of biological succession. Weeds are really pioneers. They are plants that take over barren desert like environments to begin to nature's slow process back to a climatic ecosystem. Nature is innately wise and so if the building owner, the architect, and the green roofer are aware, then weeds can be viewed as pioneers and a desirable addition to a natural green roof.

Water Management by Green Roofs, an Overview

Approach The most desirable situation in terms of water management, in a city, is to achieve zero runoff and 100% evapotranspiration of precipitation. Green roofs detain and store water by absorbing it in the ways mentioned earlier. This stored watered is then evapotranspired by the plants. The rate of evapotranspiration on a green roof is dependent on the amount of water captured by the NGR.

In order to calculate the various components of the NGR water budget, meteorological data are needed. It is easy to measure precipitation (normally with tipping buckets). Runoff can also be measured quite easily by installing adapted tipping buckets in the downspout. The water content stored in NGR substrates can be measured either with a type of roof lysimeter, or it must be calculated via a typical water budget equation, like HAUDE or others (Figs. 6 and 7).

Currently, about ten research institutions are working on this question to get realistic numbers on the retention rates by measurements on natural green roofs. Such experiments are being conducted globally and on different scales. Scale ranges from the module scale of a small research field, to measurements on small newly constructed test houses of a few square meter, like in PennState State researches in the US or measurements on realistic research roofs, to even larger study areas, like in Neubrandenburg or Berlin [31]. Since 2003, a green roof research facility has been collecting similar data in the British Columbia Institute of Technology (BCIT) in Vancouver [32].

This data about how green roofs perform is a major contribution to "applied ecological research." Other

working groups are using this data to simulate the effects of NGRs at city blocks, neighborhood, and on even larger scales.

To test the performance of green roofs materials, like the drainage layer and growing media, the FLL [34] developed physical test procedures. These tests were carried out in replicate; however, they were only performed on the growing media without a vegetation layer. Research facilities on a real roof situation perform more realistically than test plots at research facilities. Green roof plant species need realistic harsh weather conditions of wind and drying out of growing media [33]. Thus, these values are comparable to but lower than real measurements done on real roofs.

The retention values are counted in different ways [33]. Compared annual retention rates of 12 different research institutions from Germany, Sweden, Belgium, and USA were made. The annual retention rates ranged between 42% and up to 80% on flat NGRs. For sewage calculation, the peak load capacity is the most important value. To count this, a technical report is included in the FLL guideline on how to make replicable measurements [34]. In Germany, all growing media must be certified with this value.

The effect of a pitched roof has no significant influence on the percolation of water, this was another early finding on German test plots situated in Hannover [35].

An Italian group [33] carried this idea further and investigated it in Mediterranean climate over a duration of 18 months' rain events with varying intensities. If the total rain event was less than 10 mm, during periods of good ground coverage (75% +) by the NGR, nearly 100% was retained. During the heaviest rain event of 132 mm in November, only 10% of the precipitation was retained; however, the peak flow reduction was nearly 80%. The time lag from the beginning of the rain of this major rain event and discharge was 148 min compared to almost immediate discharge on an exposed roof. This braking effect of an NGR is most significant for flood control in a city.

An interesting observation is the differing data requirements between professions, such as ecologists and civil engineers, who are responsible for drainage systems of cities.

The debate about NGRs rainwater retention benefits has two aspects:

- How can water be captured by the vegetation structures as well as in a storage tank? Is irrigation also a suitable solution for NGRs? After all, irrigation does help to reduce high temperatures, particularly in the late afternoon hours in summer. How can the evaporative cooling effect be measured?
- The integration of green roofs into a rainwater management strategy to achieve "zero runoff" from a property is desirable. This would also help to reduce mixed sewage overloads of inner city sewer systems. A combination of green roofs, artificial ponds, rainwater harvesting, and infiltration could indeed result in a "zero runoff strategy." Local solutions are needed to achieve this goal for each property and for individual regions. Green roof technology is a "decentralized" technology. Political instruments, like the "runoff tax," in Germany, could be helpful in establishing these strategies in city policies [36, 37].

Evaporation takes place for several days after a rain event on a NGR. The actual evapotranspiration amount depends on the amount of stored water in the substrate, the temperature, the air humidity, solar radiation, and wind speed. The amount of real evapotranspiration water on a NGR in central Europe varies in summer between 0 mm/day (dried out growing media) and 4.5 mm/day in saturated conditions in Neubrandenburg. In most cases, on extensive green roofs in Germany, there are drought conditions [38].

The measured evapotranspiration, by a agricultural field lysimeter station in Berlin, can be up to 8 mm/day. The potential evaporation on green roofs is high due to high solar radiation rates on a roof, high wind speeds, high temperatures, and low humidity in cities.

The full year measurements allow for selection periods with interesting parameters, the following case studies show the range of experiments that have been conducted:

(a) Summer, dry or wet growing media – a light rain event
(b) Summer, dry soil, heavy rain event
(c) Summer, long wet period, effect of rain events
(d) Winter, wet growing media, no frost some rain

(e) Winter, wet growing media, frost, snow layer
(f) Winter, wet growing media, frost, snow melt, more rain

When such periods are selected from the data set, what happens?

(a) In the summer situation, nearly all rain quantities can be retained and be evaporated over the following days.
(b) Surface runoff is lower if the vegetation cover is complete and the green roof is not inclined. On flat roofs, in normal situations, the rainwater will be retained in the coarse structure of the soil and by some ponding on the roof. In experiments, the quantity of the runoff was reduced and the time lag between the rain event and discharge was increased, as already mentioned, when a green roof was installed [39].
(c) The diploma work of Bustorf [40] recorded during a 10-mm precipitation event in the summer in a wet period. A 50% storage capacity in the growing media, with the additional 50%, i.e., 5 mm, being detained for a number of hours and discharged slowly.

Various research groups from Neubrandenburg, Berlin but also in other climate regions have found remarkably similar results.

Figure 1 shows the typical structure of a rain event. Peak intensity is achieved rapidly followed by a much longer duration with lower intensity.

Green roofs arrest discharge for an extended duration, which, in most cases, is as long as 15–20 min after the onset of the rain event. On an exposed roof without a green roof, discharge is instant and complete. If some extra retention technology is incorporated into the green roof system, this time lag can be extended indefinitely. In terms of urban water management, time lag is critical. All impervious services, as is known, and as has been stated, have instant and complete runoff. That is why city streets become flooded during a storm event.

In addition, as already stated, discharge is also arrested and runoff is always much less on a green roof, making it easy for aging urban drainage channels to accommodate the minor amounts of runoff.

Table 1 shows evaporation capacity of NGRs without irrigation in the Northeastern German climate.

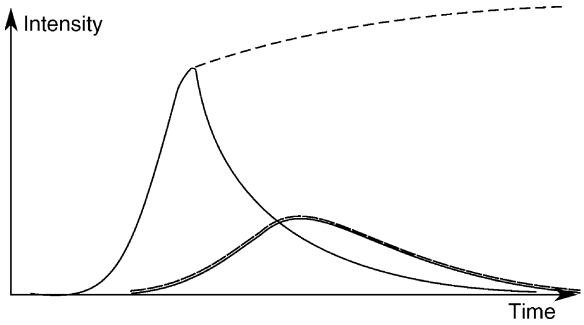

Green Roofs, Ecological Functions. Figure 1
Schematic function of green roof retention values. Typically, peak rain full quantity is achieved shortly after the onset of the rain event followed by decreased rainfall quantities over time as the event develops. In layman's terms, a short downpour is usually followed by subsequent ongoing drizzle in many if not most storm events. Consequently, green roofs are able to absorb the initial peak and then break the subsequent runoff occurring from the ongoing drizzle. In conclusion, the function of a green roof is to absorb initial storm event precipitation, store the water, and break the runoff of subsequent rainfall. The stored water is then evapotranspired over a matter of days and maybe even weeks after the rain event

Green Roofs, Ecological Functions. Table 1 Daily evaporation rates during different seasons (own lysimeter measurements, Neubrandenburg) [41 Koehler 2004, updated)]

Season	Evaporation values in (mm/day)	Growing media saturation
Winter	0.1–0.5	Well saturated, no frost
Spring/autumn	0.6–1.5	Well saturated
Summer, hot	1.5–4.5	Well saturated
Summer, hot	0.0–0.2	Dry substrate

The results of lysimeter measurements demonstrate that evaporation also occurs in winter. Summer evaporation rates depend on the amount of water stored in the growing media. Three millimeters per day of evaporation is the mean under saturated conditions (Fig. 2).

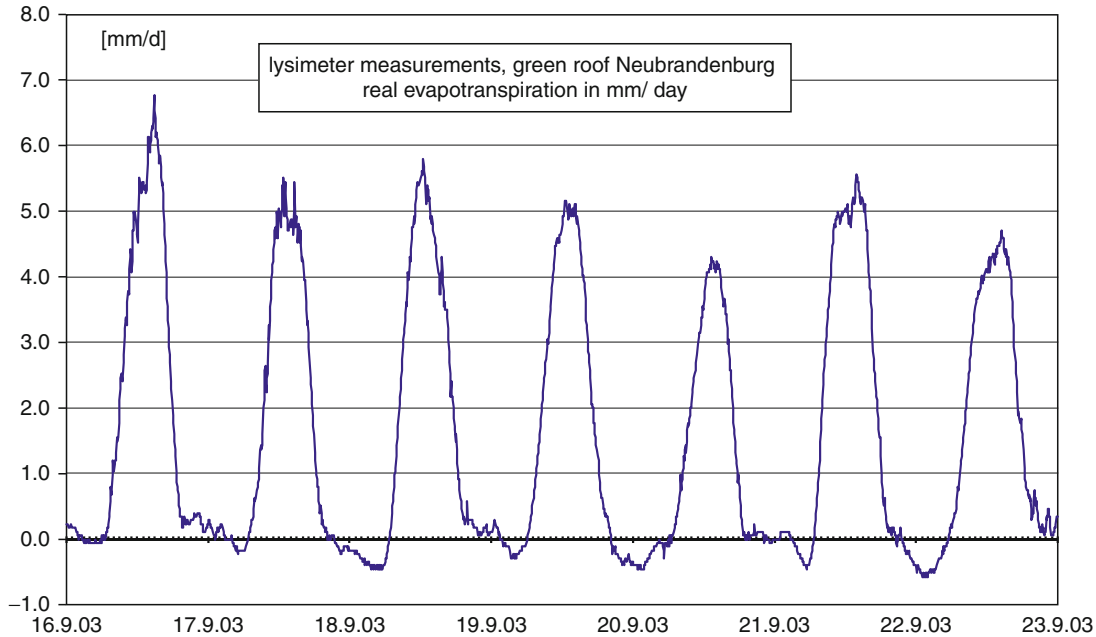

Green Roofs, Ecological Functions. Figure 2
Real evapotranspiration of a green roof in Neubrandenburg under saturated conditions, measured by lysimeters (compare Fig. 7)

The Table 2: shows the real evapotranspiration of a green roof lysimeter in mm/day. At night, the condensation process can also be observed. The evaporation of 1 mm of water means 1 L/m^2 converts 680 Wh of energy into latent heat. The resultant cooling rate of 3 mm/m^2/of evapotranspiration in summer represents 2,040 Wh.

After more than 10 days without rain, green roofs, which have not been designed for extended drought show evidence of stressed conditions due to the lack of water in the system. Specially designed natural green roof systems, such as the Greek oikosteges natural green roof ecosystem, have been able to survive for over 6 months without any inputs of water. So, while the evaporative cooling capacity of a green roof may decrease the dry growing media, it still acts as a thermal insulation layer. This means that the green roof medium provides good insulation but is not always beneficial to the plants unless the whole system is purposely designed for such situations. It is the designer's responsibility to manage this conflict, by installing an irrigation system, accepting drought in the vegetation or designing systems for such situations. Under normal cases, most green roof plants regenerate again, when it rains.

In most models and simulations of the potential daily evaporation rates of NGRs, rates are usually taken from calculations from data provided by standard meteorology stations, which focus on agricultural crop production. The difference with extensive green roofs is the vegetation's ability to survive quite long periods of water stress and regenerate like desert plant species. *Poa compressa* is an example of a plant that has this ability. If the goal is to create a constant cooling system with green roofs, then irrigation is advisable.

Studies measure the long-term retention by an extensive green roof. In Hannover, the effect of distance from the nearest drain to the point of study on retention and discharge rates was studied. The experiment systems studied were designed according to FLL green roof design guidelines. This study showed that discharge rate and discharge volume were dependent on the depth of the growing media, total green roof area, the roof inclination, and the distance to the nearest drain. The discharge values differ between 0.6 for very shallow substrates of about 4 cm and 0.4 for 15–20 cm

Green Roofs, Ecological Functions. Table 2 Energy demands of evaporation of rain water on different roof surfaces mean daily values [38, 41]

Roof surfaces	Net Radiation Wh/m^2/day	Latent heat flux Wh/m^2/day	Sensible heat flux Wh/m^2/day	Bowen ratio[c]
Mean global value	2,463	1,888	575	0.30
Bitumen Roof[a]	1,950	123	1827	14.85
Green roof[a]	2,057	1,185	872	0.74
Gravel roof[b]	2,132	687	1,445	2.10
Green roof[b]	1,800	1,258	542	0.43

[a]UFA-Fabrik Berlin, 4th June until 31st August, 2000. Precipitation 201.4 mm. Mean global radiation 5,354 Wh/m^2/day
[b]Neubrandenburg, 26th April until 8th July 2004. Mean global radiation 4,848 Wh/m^2/day
[c]Bowen ratio: ratio of sensible to latent heat in this context, when the magnitude of this ratio is less than one, a greater proportion of the available energy at the surface is conducted to the atmosphere as latent heat than as sensible heat, and the converse is true for values greater than one

depths under controlled conditions in green houses. The substrates were filled into boxes, which were then fully saturated with water before being subjected to periods of experimental rainfall. This enabled different growing media to be compared. The influence of plant species was not tested by this model.

These measured values can be used to calculate the retention values of typical green roof projects in comparison with standard roofing systems.

In Block 6, in Berlin-Kreuzberg, a system was developed to collect gray water and rainwater from 120 apartments to be treated in a constructed wetland and used to flush toilets. This reduced the demands on potable water by up to 50%. The saved costs for the potable water were almost the same as the installation cost, meaning an instant return on investment [26] (Figs. 8 and 9).

Green roof research suggests retention values of NGRs are better than those quoted in the FLL guidelines. One reason for this is that overload and vegetation of green roofs were not taken into account. Consequently, more research is required here. Bearing that in mind, it should seem obvious that NGRs do have a significant impact on storm water runoff reduction and mitigation. Green roofs are an important part of "green technology." Yet green roofs should be part of a far larger sustainable development plan for the world's cities.

The design and implementation of green roofs specifically focusing on the aspects of rainwater management are a new issue. Green roofs should be standard elements in the calculation of water management in buildings. The data from FLL [34] and other research should be basic elements in programs to model the ecological footprint of buildings. Green roofs must be integrated into policies, regulations, building codes, and other tools for sustainability.

To encourage further understanding of the benefits of green infrastructure on urban water systems, further studies will assist in indentifying regional idiosyncrasies. Green roofs work suitably in temperate and tropic climates, but local research facilities are helpful in identifying site-specific plants and soils. Green roof technology is an interdisciplinary technology for urban water management issues – more research with a focus on civil engineering would be further supportive, like Knoll [42]. Though green roofs do offer long-term benefits, minimum maintenance is required.

A before/after impact mathematical model of an NGR as a retrofit can be seen at, e.g., http://www.sieker.de/modules/wfchannel/index.php?pagenum = 5

In the late 1970s, the German green roof industry's position vis-a-vis the irrigation of extensive green roofs was that green roofs should not be irrigated.

In the 1980s, this position changed as rain water–harvesting concepts and technologies became popular in Germany. Today, green roofs are an integrated technology in the overall rainwater management concept. Evapotranspiration on an NGR, which is irrigated during the summer in a hot country and temperate region alike using water harvested from rainwater provides significant cooling effects in combination with rainwater management. Green roofs can provide an integrated solution to many of the challenges found in the modern built environment. In addition, summer irrigation allows for

greater diversity of plant species on a green roof. Yet, when the third factor of biodiversity is added to tailored solutions, it may be desirable to reduce irrigation (see "Biodiversity and Green Roofs"). What is becoming apparent is that green roofs can provide highly sophisticated solutions to many seemingly intractable problems faced by cities and green roofs are infinitely fine tunable to achieve very specific aims.

Energy Performance of Green Roofs

The thermodynamics and thermal performance of green roofs have been studied extensively since the 1970s. The Fig. 3 explains the typical temperature values of a surface and subsurface temperatures of a gravel roof and a dry extensive green roof on three selected summer days. Remarkable is the attenuation value of the subsurface temperature of the green

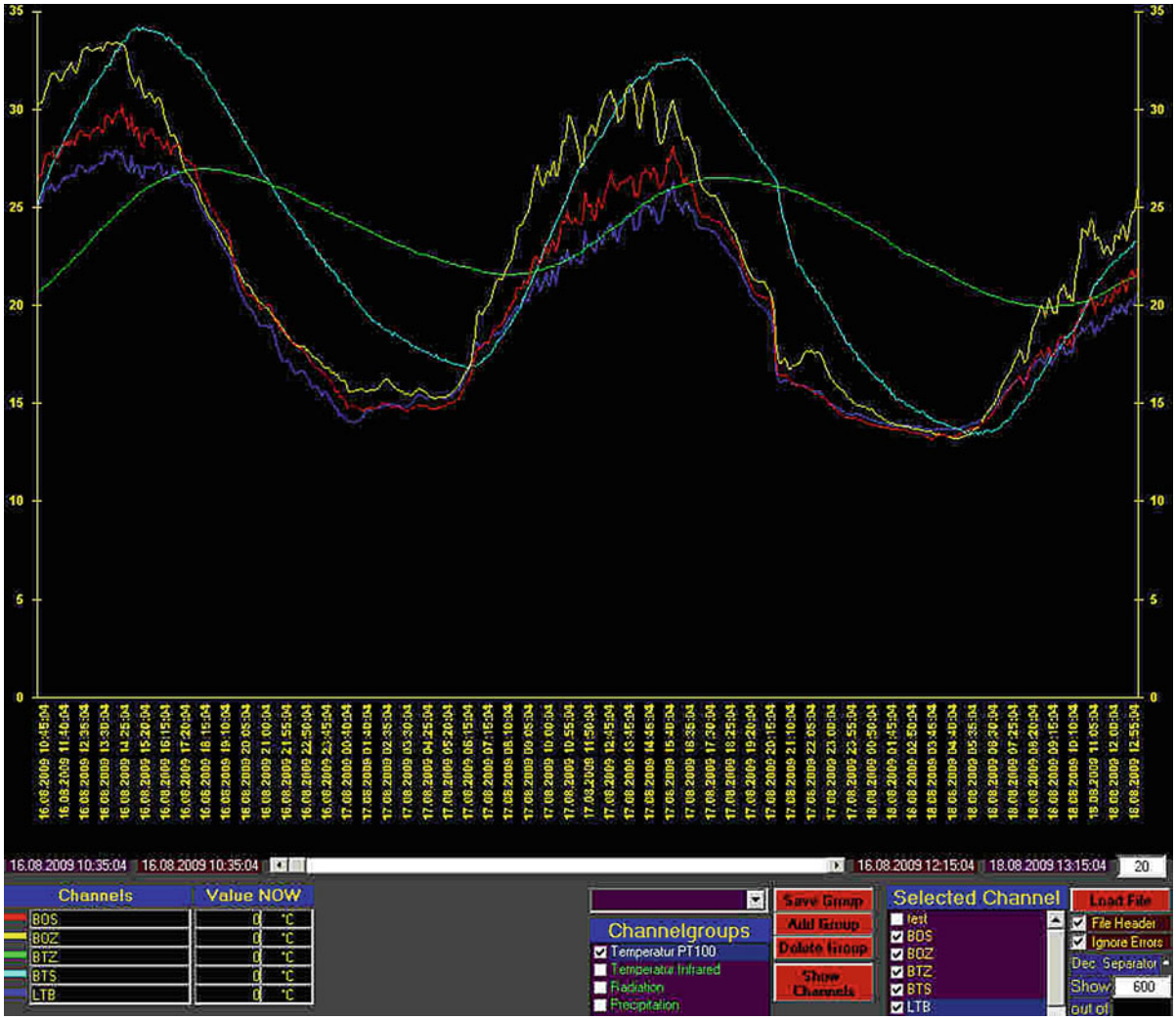

Green Roofs, Ecological Functions. Figure 3
Real summer surface and subsurface temperature performance over 3 days, 16th to 18th of August 2009 (Example of a screenshot of the measurements in Neubrandenburg x-axis: Temperature in 5° steps, from 0°C to 35°C Temperatures: *Green line*: temperature under the substrate *Dark blue line*: Air temperature at 1 m *Light blue*: underneath *Gravel yellow*: Surface *gravel Red*: surface *Green roof*

roof (green line, "BZT", Fig. 3). The surface temperatures of black bitumen roofs have been compared with green roofs structures. A bitumen roof surface can exceed 70°C [43]. The Research roof in Neubrandenburg, see Fig. 3, compares extensive dry green roofs with a gravel layer on non-greened roofs. This facility has a data set from a longitudinal study of about 10 years with thermal values at 5 min intervals. The graph showcases three extremely hot summer days without rain. The green line is the surface temperature underneath the growing media. The red line shows the surface temperature of the green roof. The gravel temperature is shown by the yellow line. It can be seen that the red and yellow lines follow the air temperature. The air temperature, measured in a ventilated shaded shelter, has the same peaks and troughs but at a lower level. If the growing media was damp, these graphs would be almost identical. The light blue (gravel temperature) and the green line (growing media temperature) show the impact of green roofs clearly.

Roof surface building materials are deteriorated and age through exposure to ultra violet and heat. Consequently, it is obvious that a green roof necessarily extends the life expectancy of these materials.

Furthermore, the thermal performance of green roofs in terms of summer cooling and winter insulation, which reduces building energy requirements will obviously become more and more important as the depletion of finite energy resources continues. Germany has instituted strict energy-saving policy in recent decades, and green roofs have spearheaded this drive. [43] calculated the additional insulation effect of a 10-cm layer of growing media. The result was a reduction in energy consumption during winter months in Central Europe, equivalent to that achieved by an extra 1 cm conventional insulation. The thermal impact of green roofs depends on the building being studied. Parameters such as roof/wall juxtaposition are important. A detached house with standard insulation achieves an energy saving equivalent to a "week of free heating." In light of increasing energy prices, this is an important additional benefit [43]. Also in Vancouver, a total heat flow reduction up to 70% was measured for 30 days in a moderate spring [44].

Green roofs really come into their own in the summer in reduced air conditioning requirements. Air conditioning use in Europe is on the rise, so this benefit of green roofs could reverse this trend. The "*Report on Energy Efficiency and Certification of Central Air Conditioners*" [45] of the European commission is a good database concerning the development of the air conditioning market in Europe. In recent years, energy consumption for heating has decreased due to the use of insulation and other energy efficiency strategies. During the same period, the use of air conditioning increased at a rate of 12% per year in Germany. In Germany, an increase in energy consumption for cooling and ventilation of 260% is estimated until the year 2020 [31]. In stark contrast to this, the "climate protection program" of the German government set the target for fossil fuel use reduction at 40%. This ambitious goal is mainly based on the reduction of energy consumption in the building sector.

The poor energy efficiency of air conditioners driven by electricity further contributes to the problem. Cooling a room through electricity releases an even higher amount of energy outside of the building. This approach to cooling contributes to a further increase to the urban heat island effect. However, such an approach is not necessary, because an alternative exists.

On a global scale, evaporation of water is the largest and most important component for the conversion of solar radiation. It is also the largest hydrological component together with precipitation. Only water that evaporates causes rainfall. The evaporation creates a large and small water cycle of condensation and precipitation [31].

Figure 4 shows how global radiation components are converted on the surface of the earth. The data shown represents one square meter. The diagram shows that 328 Wh (7.3%) is reflected, and 1,724 Wh (38%) is directly converted to thermal radiation due to the increase of surface temperatures. The total long-wave or so-called thermal radiation consists of the atmospheric counter-radiation and the thermal radiation of the surface. The net radiation can either be converted into sensible heat or consumed by evaporation, which is the conversion into latent heat. At 1,888 Wh/(m^2d), the energy conversion by evaporation is most important, even more important than the thermal radiation. Additionally, the evaporation influences the thermal radiation due to the change in surface temperatures. The atmospheric counter-radiation of 7,776 Wh is a theoretical component and can be

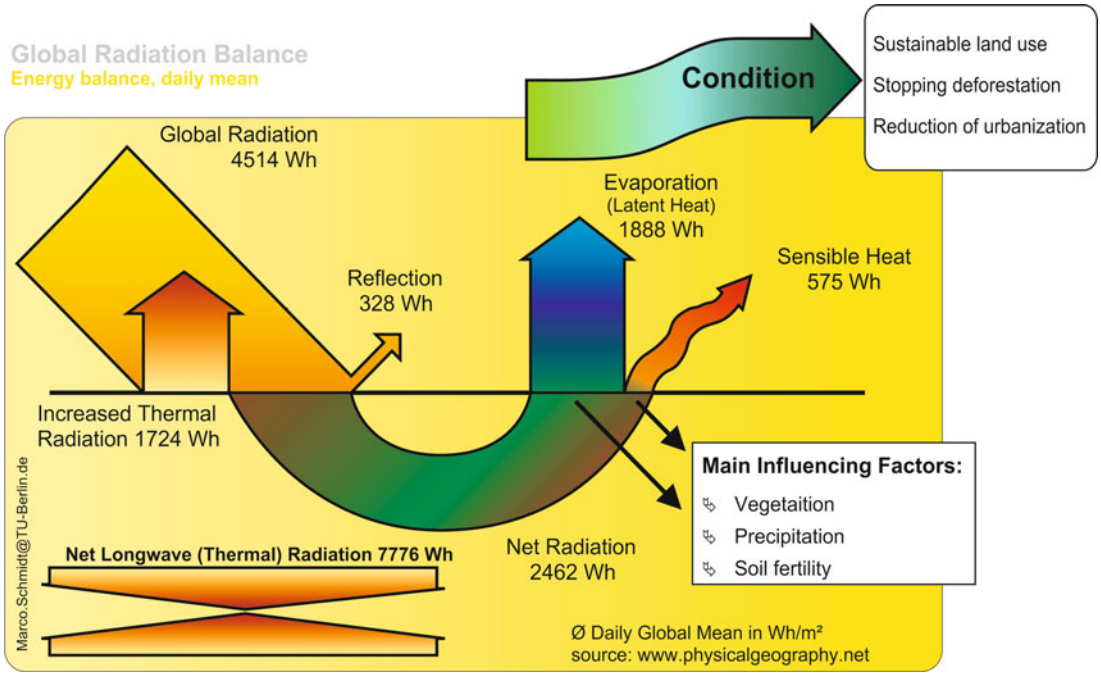

Green Roofs, Ecological Functions. Figure 4
Global daily radiation balance as annual mean [31]

considered as an exchange of long-wave radiation between two surfaces.

Heat flux data were taken at the study green roof in Neubrandenburg. Similar research was conducted by Karen Liu in Canada [44]. Both of these studies show that the heat flux in the summer is greater than in the winter. Consequently, the cooling effect of green roofs in the summer is even more important than the insulation effect in the winter.

When green roofs are irrigated, the evaporation effect results in major cooling, making green roofs natural cooling systems (Figs. 4 and 5).

Conventional non-vegetated roofs have less evapotranspiration in cities. This is the reason for more direct sensible heat causing hotter surfaces at the same time. The deforestation that is occurring worldwide means losses in evaporation and higher temperatures. The two most promising ways of reversing global warming trends are urban greening and reforestation. On the global scale, the reduction in evaporation is what is mainly responsible for climate change [29 (Kravčík et al. 2007; www.waterparadigm.org)]. There is a rise in global temperatures in conjunction with increased CO_2 emissions. Both of these states are caused by reduced vegetation on the Earth and increased human development [46]. The correlation between CO_2 levels and the global temperatures represents the relation between the amount of biomass, i.e., vegetation, the photosynthesis process, and the evapotranspiration of that biomass.

The evaporation of water is the cheapest and most effective way to cool surfaces. If the rate of evaporation can be slowed, the effect is more efficient and longer lasting. This is what a green roof does. Vegetated structures evaporate water and use CO_2. Trees are the most effective cooling systems [47]. Trees must be planted in cities on a massive scale in every available space. Massive implementation of living wall and green roof technology must also be implemented.

The evaporation of one cubic meter of water requires 680 kWh of heat. Green roofs are the most efficient way to cool down a city.

Rainwater harvesting techniques, which focus on evaporation rather than storage could play a key role in further adaptation and mitigation strategies against the urban heat island effect and global warming. Green

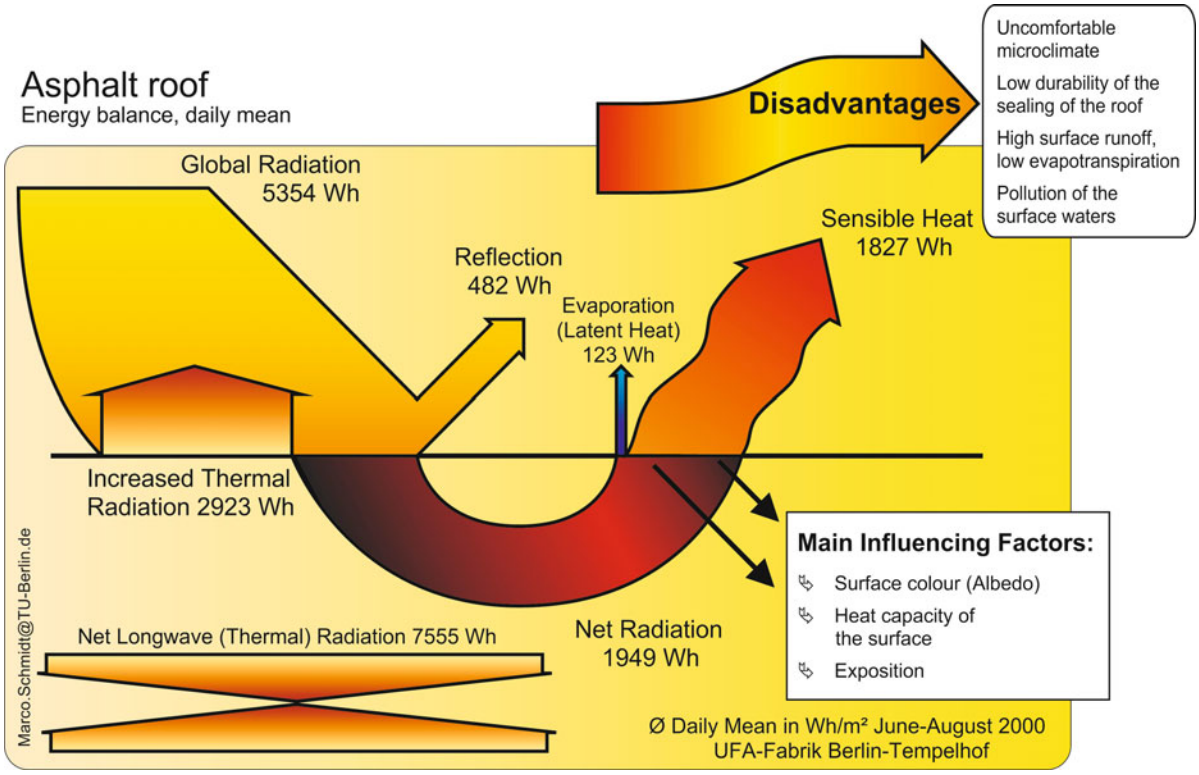

Green Roofs, Ecological Functions. Figure 5
Radiation balance of a black asphalt roof as an example for urban radiation changes [31]

Green Roofs, Ecological Functions. Figure 6
Net Radio meter. Details from the research measurement facilities on a green roof at the University of Applied Sciences, Neubrandenburg, one of the Net – radiometers installed above different roof types to calculate the radiation balance

Green Roofs, Ecological Functions. Figure 7
Lysimeter. Detail of the roof lysimeter installation to measure the real water content of roof growing media and gravel roof

Green Roofs, Ecological Functions. Figure 8
Block 6. Plant sewer system in Berlin with rainwater cleaning facility in the back yard of a residential area of the City Center of Berlin, Details on this project can be seen at: http://www.stadtentwicklung.berlin.de/bauen/oekologisches_bauen/download/modellvorhaben/flyer_block6_engl.pdf

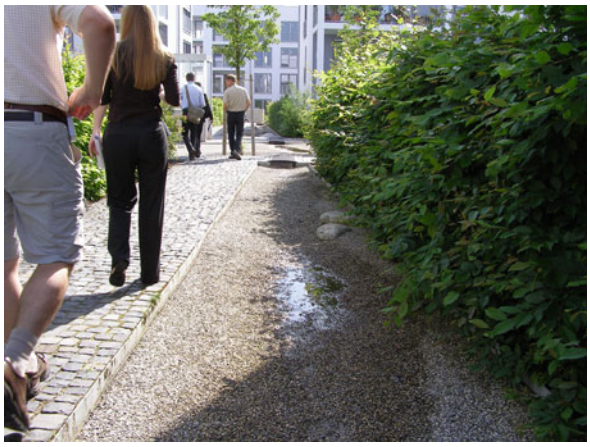

Green Roofs, Ecological Functions. Figure 9
Abb. 4. An example of a rain garden infrastructure on an intensive Green roof/Roof garden in Stuttgart

roofs and green facades have a huge potential for decreasing the environmental impact of urbanization. On a global scale, the reduction in evaporation is main cause of climate change [(see www.waterparadigm.org)]. Simulations of global climate changes still neglect the main driving factor for the global climate: the evapotranspiration of vegetation. Using evaporation, cooling for cooling purposes on green roofs and redirecting the cooling load into the dwellings mean a 41–93 higher efficiency of this energetic process than producing environmental cooling by electricity [48, 49].

Biodiversity and Green Roofs

The conditions on a roof are characterized by higher wind speed, and high direct sun irradiation. To establish vegetation on roofs, it is helpful to have higher parapet walls to protect the plants to establish the plant cover more easily. In addition, pergolas and other supporting structures help the plants grow better.

Roof gardens provide the opportunity to select shrubs and small trees. Roof gardens must be carefully designed with the knowledge of the mature heights and sizes of selected plants along with their maintenance requirements. Plants with aggressive root systems should be avoided. Bamboo is a popular plant, nowadays, which is a disaster on roof gardens because of its aggressive root system, invasive nature, and uncontrollable growth.

Roof gardens or intensive green roofs are known as "urban forestry" in Asia. A wide range of plant species are suitable for roof gardens, which fulfill the design conditions mentioned.

On the other hand, ground cover vegetation species variety is more limited. Research by Tan [49] suggested that succulent plants from South Africa are suitable for green roofs throughout the hot humid tropics. Well-selected dry adapted plant species can survive for about 49 days in the Singapore without water input from precipitation or irrigation, and some plants can go beyond this and although they look dead will recover when water comes [50].

Natural green roofs (EGR) are extreme ecosystems [51]. Many NGRs have low static loads with a shallow layer of artificial growing media of about 5–10 cm in depth. After installation, they are often nearly maintenance-free. Normally, a little irrigation is used in the first year to support and encourage the initial vegetation cover. In subsequent years, only a single annual inspection is necessary to identify any maintenance needs. These needs involve mainly the removal of tree seedlings and erosion control. The vegetation will adapt

to the local climate situation after a short while. It will grow to a nearly full vegetation cover without any additional irrigation and fertilizer for a long time.

Green roofs are completely man made. The negative impact of this urban ecosystem is one of the lowest of all built-up areas in cities.

About 30 years ago, decentralized oven heating emitted so much pollution, which included micro nutrients, such as sulfur and several others, that the EGRs had a good nutrition supply. When "Clean Air Policies" were instituted in cities, a nutrient deficit occurred, and a debate began within the green roof guideline commission in Germany [34] about the need for fertilizing EGRs. Poor nutrient availability is good for extreme plant species. However, added fertilizers could help to achieve a more complete vegetation cover.

The nearly zero maintenance of typical EGRs is good for wildlife as well for establishing plants, which are adapted to poor and extreme climatic conditions found on roofs with higher radiation and higher wind speed. The names for EGRs are different all over Europe, and include the following 'living roofs' 'oikosteges' "Eco roofs," "Sod roofs," or "Grass roofs." In Northern European NGRs, the percentage of grasses is higher; the modern NGR in the last 20 years is dominated by *Sedum* species in Germany.

Only a small number of plant species are suitable for extreme NGRs without any irrigation. Most of the adopted plant species have their origins on sandy dunes or poor soils and wall structures in marginal agricultural land [52]. In normal cases, it is a mixture of mosses and lichens combined with a small number of vascular plants. Succulents are one of the most well suited NGR plants. Consequently, many designers, particularly in Germany and German-influenced regions, use *Sedum* species. Specialized nurseries offer a wide selection of *Sedum* for green roofs [53,54]. But also a number of grasses can dominate such roofs, where the water storage capacity of the growing media becomes important.

The vegetation of the early period of modern green roofs constructed before the World War II was investigated by Kreh et al. [55–57]. These researchers came to the conclusion that a substrate layer of about 10 cm is suitable for a *Poetum compressa* – meadow as the climax vegetation.

Re-building and renovation work can cause damage to the vegetation and what is observed is the arrival of annual plants as biological succession begins again. Urban birds such as pigeons and doves, bring in seed of several pioneers, which will grow there for a while on the roof. The work of Darius and Drepper [57] correlated soil depth in centimeters and the successful establishment of vascular plants. This research concluded that at a depth of less than 10 cm, there will be a cover of mosses and *Sedum* in Germany. Grasses began to become established when substrate depths were 10 cm, and deeper than 20 cm substrate depths can support brown-field-grasses like *Calamagrostis epigejos*. Tree seedlings are in all cases possible, but they can only survive for extended periods if the roots can grow into cracks of the walls for a better water supply in dry seasons. So trees on the roof are, in most cases, a green roof problem as they compromise the waterproofing.

There are some 100 year old + EGRs [58]. Many of these will be removed in the coming years as these buildings are renovated. The potential value of these old green roofs is un-estimable as they are living examples of how a green roof develops and so should be protected in the same way as other natural ecosystems are protected. Research interest in such old German natural green roofs comes from outside Berlin.

At the University of Sheffield irrigation, research was conducted [59] and concluded that plant selection and depth of substrate were the vital characteristics of rich biodiversity and successful natural green roofs in the British climate. The most well suited species the study concluded were a number of Sedum species, *Festuca*, and species such as *Armeria maritima* and *Prunella vulgaris*.

In the more arid climate of Eastern Germany, the last two plant species are not able to survive on an average extensive green roofs. A 20-year longitudinal study concluded that in Berlin, for example, Chive (*Allium schoenoprasum*) was one of the most suitable species [51] (Tables 3 and 4).

To achieve a high value in local biodiversity, some aspects are important, like:

- Location (where is this project located)
- Size of the greened areas of the project

Green Roofs, Ecological Functions. Table 3 Plant species selection for EGR

Endangered Plants, growing well on NGRs (temperate climate of Northern Europe)	*Saxifraga tridactylitis* [55 Kreh]
	Teesdalia nudicaulis
	Poa bulbosa
Some of the fittest in Central Europe	*Sedum album* and many more of the genus *Sedum*
	Cloves, many Fabaceae are good competitors on poor and dry soils
	Grasses, like genus *Festuca, Poa,*
	Allium schoenprasum
Fittest plant species in subtropics and tropics, selected after [49, 50]	*Delosperma cooperi, Cyanotis cristata, Wedelia trilobata, Liriope muscari, Ophiopogon japonicus* (This is a favorite in Germany for indoor living walls, Koehler).
	Bryophyllum "Mother of Thousands" – Crassualceae

Green Roofs, Ecological Functions. Table 4 Groups of plants, considered to be troublesome weeds, which should be removed during the annual maintenance work

		Recommendation
Tree seedlings	*Birch, Prunus, Salix, Hippopohae*	Annual inspection
Grasses	*Agropyron, Calamagrostis*	
Herbs	*Taraxacum,*	
Mosses	Several taxa, removal needed, must be discussed in relation to the project aims.	

- Variation of growing media, and microhabitat
- Plant species sources in the surroundings of the project
- Age of the project, young projects include for the first years a high number of annual plant species, mature projects could have well-established vegetation

Ecological Synergy

A total overview of all ecological benefits of green roofs cannot be described for all regions in the same way. Table 5 summarizes some conclusions from several research projects.

Noise reduction, green roofs are also a good sound proofing technology and for this reason, they are used when there is a lot of noise like Schipol airport in Amsterdam.

Biodiversity: On the research roofs of the University of Neubrandenburg, the plant species richness has been investigated since the installation of the green roof structure in the year 2001. The experimental variables are four orientations (North, South, West, and East), two growing media, two methods of planting (seeds and pre produced lawn mats). The results of this study suggest the following: There are significant differences in vegetation development between the variable "North" and "South." On North, there are more grasses and some interesting herbs. On the South experimental roof, different species of the genus *Sedum* dominate. Grasses are reduced to a very few individuals.

Furthermore, over a period of the first 7 years, a significant difference between the turf mat installation and the *Sedum*-seeded area was observed.

The seeded roof developed higher species richness. The species richness of the preproduced turf mats decreases over this time [65].

Green roofs have become a topic of great research interest by a plethora of disciplines. There are about 500 peer-reviewed publications as of 2010 in various disciplines (a M. Kohler survey with Springerlink and similar data bank systems).

One interesting recent study focused on the topics: Do green roofs affect the quality of the water discharged during a storm event? Can this water be used? [66]. The answer to this question is that it depends on a number of factors. One important conclusion is that the additives used by the construction industry will become scrutinized more carefully in the coming years. Green roofs can remove numerous heavy metals from rainwater.

- The cooling effect of green roof systems must be studied extensively in the various regions of the World. Fang [67] worked on the conditions of Taiwan with climate chamber experiments.

Green Roofs, Ecological Functions. Table 5 Main ecological effects of Green roofs [60, updated]

			Monetary efficiency	Source	Private/ public good
1	Insulation, Winter, Central Europe,	3–10% better than a gravel roof, 100 m^3 gas reduction each year for a single house	40.0 €/Building	Köhler (2009) [60]	Private
	Winter, southern Europe,	Depending on the type of building, no effect	–	[61] Spala	Private
2	Air can substitute summer	Insulation effect and evaporation cooling of about 3 l/m^2	Up to 20% reduction, depending on the climate in upper level of a multistorey house	[62] Alcazar	
3	Urban climate	Cooler surfaces in summer, better insulation	Monetarization, done by Banting et al. in Toronto. A green roof calculator exists on www.greenroof.org under development	[63] Banting	
4	Noise reduction	Test facilities are installed in Vancouver	A reduction of about 5 dB(A), depending on structure, moisture, and some more	[64] Maureen	
5	Biodiversity	Biodiversity depends on various factors	No monetary effect	[65] Kö Baltimore	

The conclusion of this study stated that a thermal reduction of surface temperatures between 20% and 60% was possible depending on the depth of the substrate, its moisture content, and the vegetation type and amount of coverage.

- The thermodynamic performance of NGRs in Greece is now being studied by the Metsovio National Technical University of Athens. They have studied the oikostegi installed on The Greek Treasury in Constitution Square in Athens, opposite the Greek Parliament. They concluded among other things that the oikostegi has significantly altered the thermodynamics of the 10-story building. http://www.oikosteges.gr/index.php/greenroofs/research.
- Binding fine particles is another benefit of green roofs, which is currently being studied. Yang [68] conducted research in Chicago. He concluded that an area of about 20 ha of green roofs can capture about 1,675 kg/m^2 10 particles each year. Gas born emissions, like ozone and NO_x, can be sequestered at of about 27% of total emissions.

Research interest in the subject is growing around the world. Moreover, mathematical and computer modeling algorithms are also improving leading to sound data and conclusions, which can be used to support this exciting emerging technology.

Future Directions

At Climate conferences, like the last one in Copenhagen in November 2009, participants are searching for solutions regarding how to mitigate climate change. There will not be only one strategy. But it is a truth that global deforestation and the ever increasing levels of urbanized land all over the world need strategies to increase the amount of vegetation wherever it is possible. The quality of an "urban forest" in street canyons and on the surface of buildings is not the same. From the perspective of biodiversity, only a selected number of species are able to survive on shallow substrates. So weight must be give to endemic species.

The increasing number of urban surfaces offers opportunities for urban gardening and to establish specific vegetation, in some cases, also for some endangered plant species. Roof vegetation is an engineered system, which offers benefits, as described in this entry. Better insulation against cool and hot temperatures, rainwater management, and longer lasting roof

surfaces all provide monetary benefits for the property owner and all citizens. Finding the best technical solutions requires environmental specialists who understand natural ecosystems in conjunction with construction experts. As this technology grows, developments will be made, which will further improve the benefits [18]. Green roofs organizations and associations are now found in more than 30 countries worldwide. In many of these countries, academics are doing research into green roofs. Green solutions have become the hot subject of the twenty-first century. This is certain to continue as climate change begins to affect our everyday lives. Green roofs offer a way forward, which gives hope that sustainable technology is not only desirable but also very feasible. The further direction is to combine sustainable technologies and materials to enhance the number of plant species and ecological cycles on green roofs. The technical term "Natural Green Roof" will challenge urban planners in coming years. Green roofs are a fixed main and integrative element of sustainable architecture. It is cross-disciplinary subject, which is both simple and at the same time high tech. Much more growing media and plant species are possible. Also many more architectural solutions are possible [69]. It is also a two-way learning opportunity for an exchange between industrial countries and developing countries alike. In this direction, green roofs play an integrative role in rain water savings and management [70]. Green roofs provide a protection layer against temperature extremes, which provide energy-saving opportunities worldwide.

Acknowlegdements

Many thanks to Marco Schmidt for his ongoing support and as a joint researcher in much of the work Manfred has done over the years.

Bibliography

Primary Literature

1. Alexandri E, Jones P (2006) Temperature decreases in an urban canyon due to green walls and green roofs in diverse climates. Build Environ 48(4):480–493
2. Niachou A, Papakonstantinou K, Santamaouris M, Tsangrassoulis A, Mihalakou G (2001) Analysis of the green roof thermal properties and investigation of its energy performance. Energy Build 33:719–729
3. Theodosiou TG (2003) Summer period analysis of the performance of a planted roof as a passive cooling technique. Energ Buildings 35:909–917
4. Oberndorfer E, Lundholm J, Brass B, Coffmann R, Doshi H, Dunnett N, Gaffin S, Köhler M, Liu K, Rowe B (2007) Green roofs as urban ecosystems: ecological structures, functions, and services. Bioscience 57(10):823–833, www.biosciencemag.org
5. Köhler M (2005) The green roof movement – from a botanical idea to a new sustainable style in modern architecture. Proceedings of 1th international landscape education symposium, Shanghai, China, p 168–176. (ISBN 7-112-08650-7) www.china-building.com.cn)
6. Kellert SR, Wilson EO (1993) The biophilia hypothesis. Island Press, Washington
7. Larson D, Matthes U, Kelly PE, Lundholm J, Gerrath J (2004) The urban cliff revolution. Fitzhenry and Whiteside, Markham
8. Odum HT (1994) Ecological and general systems. An introduction to systems ecology. University Press of Colorado, Niwot
9. Köhler M, Barth G, Brandwein T, Gast D, Joger HG, Seitz U, Vowinkel K (1993) Fassaden- und Dachbegrünung. Ulmer, Stuttgart
10. Getter K, Rowe B (2009) Carbon sequestration potential of extensive Green roofs. Proceedings of greening rooftops for sustainable communities. Atlanta
11. Köhler M (2009) Der Gründachmarkt weltweit. Tagungsband 7. Internationales FBB Gründachsymposium 2009, Ditzingen, pp 37–40
12. Yeang K (2008) Ecodesign – a manual for ecological design. Wiley-Academy, Hoboken
13. Kellert SR (2005) Building for life. Island Press, Washington
14. Todd NJ, Todd J (1993) From eco-cities to living machines. North Atlantic books, Berkely
15. Peck S (2008) Green roof designs. A. Schiffer book, Atglen (PA- USA), p 176
16. Weiler SK, Scholz-Barth K (2009) Green roof systems. Wiley, Hoboken
17. Jim CY, Chen WY (2009) External effects of neighbourhood parks and landscape elements on high-rise residential value. Land Use Policy (Elsevier Science, Amsterdam) 27:662–670
18. Jodidio P (2009) Green architecture now. Taschen, Hongkong, p 416
19. Koehler M, Schmidt M, Grimme FW, Laar M, De Assuncao Paiva VL, Tavares S (2002) Green roofs in temperate climates and in the hot-humid Tropics. Environ Health 13(4):382–391
20. Ansel W (2008) A tale of 3 cities – comparative analysis of green roof policies and success factors, Cuge regional seminar. Oct 23th, Singapore
21. Appl R, Meier R, Ansel W (2009) Dachbegrünung in der modernen Architektur. Proceedings of IGRA, Berlin
22. Göbel P, Dierkes C, Kories H, Messner J, Meissner E, Coldewey WG (2007) Einfluss von Gründächern und Regenwassernutzung auf Wasserhaushalt und Grundwasserstand in Siedlungen. Grundwasser – Z. der Fachsektion Hydrogeologie (12):189–200

23. Sukopp H, Wittig R (1997) Stadtökologie. Gustav Fischer Stuttgart, New York
24. Varis O, Biswass AK, Tortajada C, Lundquist J (2006) Mega cities and water management. Water Resource Development 22(2): 377–394
25. Reichmann B, Nolde E, Leithaus J, Vansbotter B (2002) Maßnahmenkatalog Reduzierung der Wasserkosten im öffentlichen Bereich. Berlin, Senatsverwaltung für Stadtenwicklung Berlin. http://www.stadtentwicklung.berlin.de/bauen/oekologisches_bauen/de/downloads/massnahmenkatalog_wasserkosten.pdf. Accessed 26 May 2008
26. Reichmann B, Nolde E, Rüden, H, Vansbotter, E (2007) Innovative water concepts. Service water utilisation in buildings 28 S. http://www.stadtentwicklung.berlin.de/bauen/oekologisches_bauen/de/downloads/betriebswasser_englisch2007.pdf. Accessed 26 May 2008
27. Köhler M (2008) Green facades – a view back and some visions. Urban ecosystems. www.springerlink
28. Centgraf S, Schmidt M (2005) Water management to save energy, a decentralized approach to an integrated sustainable urban development. Proceedings of Rio05, Brasil. Accessed 26 May 2008
29. Kravčík M, Pokorný J, Kohutiar J, Kováč M, Tóth E (2007) "Water for the recovery of the climate – a new water paradigm. Publisher Municipalia. http://www.waterparadigm.org/
30. Köhler M, Schmidt M (2008) London benefits for sustainable water management. World green roof technology. Proceedings of world green roof congress, London, 16–19 Sept
31. Schmidt M, Koehler M (2008) Energetic aspects of green roofs. World green roof technology. Proceedings of world green roof congress, London, 16–19 Sept
32. Connelly M, Liu K (2005) Green roof research in British Columbia – an overview. Proceedings of greening rooftops for sustainable communities, Washington
33. Palla A, Gnecco I, Lanza, LG (2010) Hydrologic restoration in the urban environment using green roofs. Water 2, 1.www.mdpi.com/journal/water . . .
34. FLL (ed) (2008) Richtlinie für die Planung, Ausführung und Pflege von Dachbegrünungen. Bonn, English version: Guidelines for the planning, construction and maintenance of green roofing – green roofing guideline, 2008 edition
35. Liesecke HJ (1998) Das Retentionsverhalten von Dachbegrünungen. Stadt + Grün 47:46–53
36. Köhler M, Keeley M (2005) The green roof tradition in Germany: the example of Berlin. In: Leslie Hoffmann, WMc Donough (eds) Ecological design and construction. Earthpledge, New York, pp 108–112
37. Keeley M (2007) Transatlantic exchange and sustainable Urban development: transfering stormwater policies and technologies from Europe to the United States. Ph.D., Technical University, Berlin, 259 p
38. Köhler M (2004) Energetic Effects of Green roofs on the urban climate near to the ground and to the building surfaces. Proceedings of international green roof conference, Nuertingen, IGRA, S.72–79
39. Köhler M, Schmidt M, Grimme FW, Laar M, De Assuncao Paiva VL, Tavares S (2002) Green roofs in temperate climates and in the hot-humid tropics. Environ Health 13(4):382–391. (UK) ISSN 0956-6163
40. Bustorf J (1999) Simulation of the precipitation/runoff – ratio of greened roofs. Master thesis, Technical University, Berlin, 108 p
41. Köhler M, Schmidt, M (2002) Das Mikroklima extensiver Gründächer. In: Jb. Dachbegrünung 2002: 28–33. Thalacker, Braunschweig
42. Knoll S (2000) Das Abflußverhalten von extensiven Dachbegrünungen. Mitt. Nr. 136 TU-Berlin, Inst. für Wasserbau und Wasserwirtschaft, 115 S
43. Köhler M, Malorny W (2009) Wärmeschutz durch extensive Gründächer. In: Venzmer H (Europäischer Sanierungskalender 2009). Beuth, Berlin, pp 195–212
44. Liu K (2008) Sustainbility matters. U.S. General services administration. See www.Gsa.gov/P100
45. EECCAC (2003) Energy efficiency and certification of central air conditioners. REPORT for the DGTREN of the commission of the E.U, 2001, Volume 1, 52 p
46. Gerlich G, Tscheuschner RD (2007) Falsification of the atmospheric CO2 greenhouse effects within the frame of physics. 114 p. http://arxiv.org/abs/0707.1161; http://arxiv.org/pdf/0707.1161v3; http://www.tsch.de
47. Currie BA, Bass B (2008) Estimates of air pollution mitigation with green plants and green roofs using the UFORE model. Urban Ecosystem 11(4): 335–337, Springer
48. Mankiewicz PS, Spartos P, Dalski E (2009) Green roofs and local temperature: how green roofs partition water, energy, and costs in urban Energy – air conditioning budgets. Proceedings of greening rooftops for sustainable Communities, Atlanta
49. Tan PY (2009) Understanding the performance of plants on non irrigated Green Roofs in the Tropics using a Biomass yield approach. Nature in Singapore. http://rmbr.nus.edu.sg/nis
50. Tan PY, Sia A (2005) A selection of plants for green roofs in Singapore. CUGE Singapore, 117 p
51. Köhler M (2006) Long term vegetation research on two extensive green roofs in Berlin. Urbanhabitats, Brooklyn Bot. Garden (USA) 4(1):3–26. ISSN 1541-7115. http://www.urbanhabitats.org/v04n01/berlin_full.html
52. Darlington A (1981) Ecology of walls. Heinemann, London
53. Stephenson R (1994) Sedum cultivated stonecrops. Timber, Portland
54. Snodgrass EC, Snodgrass LL (2006) Green roof plants. Timber, Portland
55. Kreh W (1945) Die Pflanzenwelt unserer Kiesdächer. Jahresheft des Vereins für Vaterländische Naturkunde in Württemberg 97–101:199–207
56. Bornkamm R (1961) Vegetation und Vegetationsentwicklung auf Kiesdächern. Vegetatio 10:1–24
57. Darius F, Drepper J (1984) Rasendächer in West-Berlin. Das Gartenamt 33:309–315
58. Köhler M, Poll P (2010) Life time performance of selected old green roofs in comparison to extensive green roofs in Berlin. Ecological Engineering 36:722–729

59. Nagase A, Dunnet N (2010) Drought tolerance of different vegetation types in extensive green roofs: effects of watering and diversity. Landscape and Urban Planning 97:318–327
60. Köhler M (2006) Extensive Gründächer – Rechenbare Vorteile in der Eingriffsregelung. Stadt und Grün 9:40–44
61. Spala A, Bagiorgas HS, Assimakopoulos MN, Kalavrouziotis N, Matthopoulos D, Mihalakakou G (2008) On the green roof system. Selection, state of the art and energy potential investigation of a system installed in an office building in Athens, Greece. Renewable Energy 33:173–177
62. Alcazar S, Bass B (2005) Energy performance of green roofs in a multi Storey residential Building in Madrid. Proceedings of 3rd Conference on greening roof tops, Washington
63. Banting D, Doshi H, Li J, Missios P (2005) Report on the environmental benefits and costs of green roof technology for the city of Toronto. (kann auf der Seite der Stadt Toronto als pdf geladen werden. www.toronto.on.ca/greenroofs
64. Connelly M, Hodgson M (2008) Sound transmission loss of green roofs. Sixth Annual Greening rooftops for Sustainable Communities Conference, Baltimore
65. Köhler M (2008) Extensive green roof biodiversity: the influence of growing media, exposition and the methods of establishing. Proceedings of Baltimore green roof for healthy city conference. ISSN 1916-4734, 16 p
66. Berndtsson JC, Bengtsson L, Jinno K (2009) Runoff water quality from intensive and extensive vegetated roofs. Ecol Eng 35:369–380
67. Fang CF (2008) Evaluating the thermal reduction effect of plant layers on rooftops. Energy Build 40:1048–1052
68. Yang J, Yu Q, Gong P (2008) Quantifying air pollution removal by green roofs in Chicago. Atmos Environ 42: 7266–7273
69. Bartoli B (2008) Sostainable dalla A alla Z. Sistemi editoriali. AS 25 Napoli
70. Franken M (2007) Gestion de aguas. Plural editores, La Paz

Books and Reviews

Dunnet N, Kingsbury N (2008) Planting green roofs and living walls, 2nd edn. Timber, Portland
Ernst W (2005) Dachabdichtung Dachbegrünung. IRB-Fraunhofer Gesellschaft Stuttgart
Krupka B (1992) Dachbegrünung. Ulmer, Stuttgart

Recommended Additional Internet Links

http://www.cbd.int/cop9/
http://oikosteges.gr/index.php/studies
http://www.gebaeudekuehlung.de
http://www.a.tu-berlin.de/GtE/forschung/Adlershof
http://www.stadtentwicklung.berlin.de/bauen/oekologisches_bauen
http://www.stadtentwicklung.berlin.de/bauen/oekologisches_bauen/download/modellvorhaben/flyer_block6_engl.pdf
http://www.waterparadigm.org
http://www.evapotranspiration.net
www.worldgreenroof.org
www.livingroofs.org

Greenhouse Gas Emission Reduction by Waste-to-Energy

Bernd Bilitewski, Christoph Wünsch
Institute of Waste Management and Contaminated Site Treatment, Technical University of Dresden, Pirna, Germany

Article Outline

Glossary
Definition of the Subject
Introduction: Importance of Waste Incineration
Release of Greenhouse Gas Emissions by Waste Incineration
Determination Methods for Determining the Fossil-based and Biogenic Carbon Content of MSW
Waste Composition
Fossil Carbon Content of MSW
Global Warming Factors of Different Waste Types in Germany
Reduction of GHG Emissions and Conservation of Fossil Fuels by Means of Energy Recovery from Wastes
Resource Conservation by Savings of Fossil Fuels
Greenhouse Gas Emissions by Landfilling
The Germany Example
Greenhouse Gas Emissions by Waste Incineration in Germany 2007
Reduction of Greenhouse Gas Emissions in Germany by Means of Waste Incineration in 2007
Future Directions
Bibliography

Glossary

Carbon dioxide (CO_2) Is a by-product of the combustion of fossil fuels or organic materials. Carbon dioxide is the principal greenhouse gas (GHG) in earth's atmosphere.

Carbon dioxide equivalents ($CO_{2,eq}$) Greenhouse gases influence the GHG effect in different degrees. Their contribution is calculated in volume (or mole) equivalents to carbon dioxide.

Combined heat and power generation (CHP) Is the simultaneous generation of both electricity and useful heat. Energy at a high temperature level is first converted to electricity and the remaining energy, at a low level, is used to produce heat (e.g., district heating.

Global warming factor (GWF) Expresses the amount of released $CO_{2,eq}$ for a combusted unit of fuel, in Mg $CO_{2,eq}$/Mg of fuel; can be expressed as generated amount of electricity, in Mg $CO_{2,eq}/MWh_{el}$, or heat, in Mg $CO_{2,eq}/MWh_{th}$.

Greenhouse gas (GHG) Gases in the atmosphere that absorb and reemit infrared radiation; they cause the GHG effect that results in heating up of the atmosphere.

Lower heating value(LHV) Also known as net calorific value (CV) of a fuel, defined as the amount of heat released by the combustion of a unit mass of fuel; the LHV assumes that the water produced in combustion is in vapor state and that the latent heat of vaporization is not recovered.

Municipal solid waste (MSW) Predominantly household wastes (domestic wastes) and similar commercial and bulky wastes collected by a municipality. They are in a solid or semisolid form, sludge or liquids are excluded as well as industrial wastes.

Nitrous oxide (N_2O) Also known as laughing gas. Is a major greenhouse gas with a 298 times higher impact factor than carbon dioxide in a 100-year period.

Selective catalytic reduction (SCR) Is the reduction of nitrogen oxides in combustion gases to nitrogen, using a catalyst and anhydrous ammonia, aqueous ammonia, or urea to diatomic nitrogen and water.

Wet weight (ww) Substance in its original state, including combustibles, water, and ash.

Definition of the Subject

Waste management in general plays an important role in the GHG reduction targets of every country. Usually, the generated municipal solid wastes (MSW) are landfilled and in many cases these landfills are not controlled and their emissions are not collected. Collection and treatment of the emissions of regulated landfills can reduce their GHG effect by up to 75%. The reduction of wastes going to landfill and the replacement by a mechanical, biological, and/or thermal treatment lowers the released GHG emissions significantly.

By means of these processes, the contribution of waste management to the GHG emissions of a nation can be reduced from 3.3% to 1.2% (e.g., in Germany [1]). In addition, the use of waste incineration in a modern waste management system produces electrical power and heat from the wastes. This results in a further decrease of GHG emissions.

Introduction: Importance of Waste Incineration

The principal method of disposing MSW worldwide is landfilling. After the initial wastes are covered by other wastes, atmospheric oxygen cannot reach them and under the prevailing anaerobic conditions, the biogenic carbon in MSW is converted to methane (CH_4) and CO_2. If the landfill is not equipped for landfill gas collection, this CH_4 is emitted into the atmosphere. The global warming potential of CH_4, relative to CO_2 and for a time horizon of 100 years, is between 21 and 25 [2].

In developed nations, more and more landfills are equipped with a landfill gas collection system. The collected biogas is then used to generate electricity or heat. This results in reducing GHG emissions, both by reducing the emission of methane and also by the use of fossil fuels substituted by the landfill gas.

Even though modern landfills are secured by ground and surface covers, during operation or if landfill covers are broken after closing the landfill, hazardous substances can be emitted in the environment. The major task of waste incineration plants recovering energy (waste to energy – WtE or energy from waste – EfW) is the environmentally friendly disposal of waste and the destruction of hazardous substances during the combustion process. Modern air pollution control systems clean the flue gas to emission levels below the EU standards. However, the production of the greenhouse gas (GHG) CO_2, resulting from the oxidation of carbon in the MSW, is unavoidable. Also, a small amount of another greenhouse gas, nitrous oxides, is emitted; although this amount is small, as compared to the CO_2 emissions, it has to be assessed, because NO_x has a lifetime of

114 years in the atmosphere and its global warming potential is 298, in a time horizon of 100 years [2].

The thermal energy in the WTE flue gases is transferred to water and steam in a boiler and is used to generate electricity in a steam turbine or for district heating. Overall, the combined effect of WTE, that is, reducing landfill emissions and generating electricity, results in a GHG reduction of 1 t of CO_2 per ton of MSW combusted, for landfills that do not capture landfill gas, or half a ton of CO_2 for those that do (www.wte.org).

Release of Greenhouse Gas Emissions by Waste Incineration

A modern waste incineration plant consists of the combustion chamber where the waste is converted into ash and hot flue gas. The wastes are used as fuel, and an airflow provides the oxygen needed for combustion. The thermal energy of the combustion gases is transferred to steam in the boiler and superheater tubes, and the steam is used to generate electricity and also process steam and district heating. The cooled flue gas is treated in a flue gas purification system, and the clean gas is emitted to the atmosphere – necessary oxygen. A fossil fuel, for example, natural gas or fuel oil, is used only for start-up and shutdown operations. Water is used in the water steam cycle and, in some cases, in the flue gas purification system. The cleaned gas consists of nitrogen, CO_2, water, and oxygen. The residues include the incineration ash and the flue gas purification residues. Figure 1 shows the incoming and outgoing material and energy flows in a waste incineration plant.

For the calculation of GHG emissions, the waste fuels and any use of auxiliary energy are taken into account. Air, water, and auxiliaries do not produce significant GHG emissions. The clean gas containing the GHG and the delivered energy amounts, substituting energy produced and therefore their avoided GHG, need to be considered.

Determination Methods for Determining the Fossil-Based and Biogenic Carbon Content of MSW

In order to estimate the carbon footprint of waste incineration, it is necessary to know the fossil-based carbon content of MSW. The carbon contained in the biogenic fraction of MSW and the corresponding CO_2 emissions are, by definition [4], classified as carbon neutral. The determination of the biogenic and fossil parts of the carbon can be made by means of a direct procedure (determination by the composition of the waste mixture) or an indirect one (determination in the flue gas) as discussed below.

In *manual sorting*, the waste mixture is separated to different waste fractions, and the biogenic and fossil parts in these single fractions are determined.

Selective extraction is a wet chemical procedure where oxidation of biogenic to non-biogenic components is used to identify the biogenic part of the waste mixture.

The ^{14}C *or radio carbon method* is based on the difference in the age of fossil and biogenic materials. Because of the decay of the radioactive carbon isotope ^{14}C, its concentration decreases with time. Because of its age, fossil carbon contains no ^{14}C, whereas biogenic carbon contains a relatively higher ratio of $^{14}C/^{12}C$. Therefore, the biogenic part in the CO_2 of the WTE stack gas is proportional to the ^{14}C content, which can be measured by an instrumental method.

The *balance method* combines a theoretical mass balance with measurable operating data of an incineration plant. Every balance equation is characterized by a specific feature of the waste, for example, ash content, carbon content, etc., and the waste input is theoretically divided into four groups: inert, biogenic, fossil, and water. By solving these mass balance equations and with the help of nonlinear correction calculations, the biogenic carbon content can be determined.

The literature shows that their results are in the same range [5]. The manual sorting method is used in this section. The carbon isotope techniques are discussed in another section of the Encyclopedia.

Waste Composition

The basis of all calculations regarding released GHG emissions of wastes by the manual sorting method is the waste composition. First of all, the aggregate waste has to be separated in their different waste fractions. This is usually done manually. The composition is dependent on the kind of waste

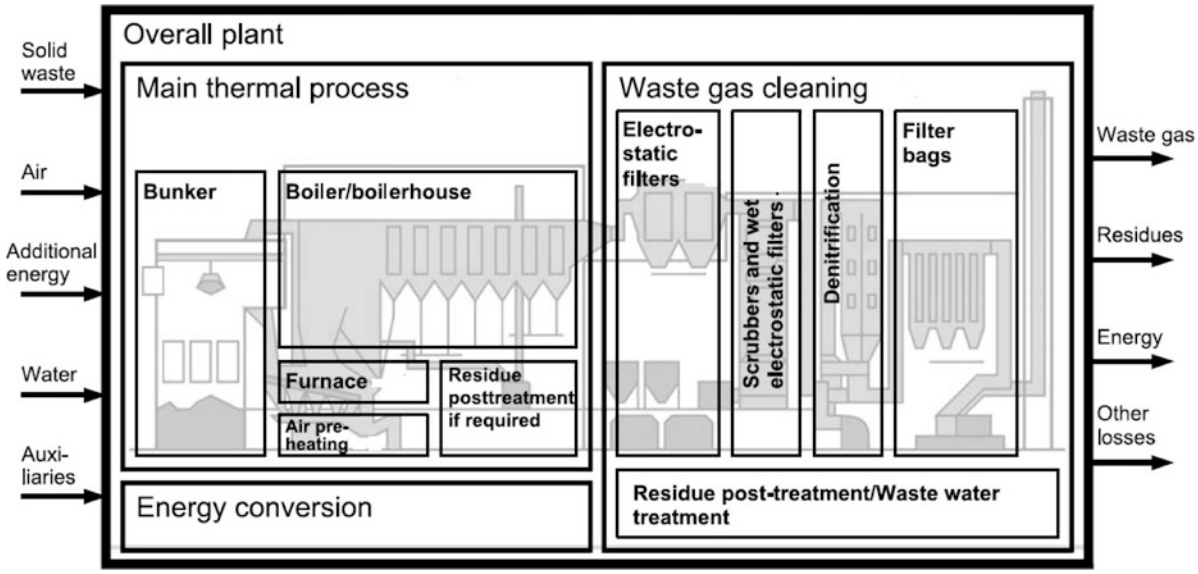

Greenhouse Gas Emission Reduction by Waste-to-Energy. Figure 1
Material and energy flows in a typical waste incineration plant [3]

(municipal solid waste, commercial waste, industrial waste, etc.) and, especially for the municipal solid waste (MSW), on the following:

- Country, region
- Climate
- Settlement structure
- Season
- Economic situation
- Waste collection system

In different countries, rules and laws are existing influencing the waste management and finally the waste composition. As an example, in countries requiring a deposit on several materials like glass, plastic bottles, or cans, people source-separate these materials to get their money back. As a result, only a small part of such materials end up in the MSW. Also, when special bins for organic wastes, glass and paper are provided in a region or country, the amount of these materials in the MSW are reduced appreciably. In regions with hot and dry climate, the generated MSW contains a smaller fraction of organics than in wet climate areas. The reason is that fruits and vegetables grow well in these wet areas and after consumption the residues end up in the MSW.

Organics are often composted, and the compost is used in the gardens of rural areas; thus, this fraction is very small in the MSW. In urban areas, where there is no possibility of composting, the organics remain in the MSW. Another example is the higher amount of minerals and ash in the MSW of communities where coal or wood is used for heating. Also, during the winter season the amount of organic garden waste decreases while in the summer and autumn this fraction increases significantly. Ash residues also disappear in the summer months.

Economic development also results in greater consumption and generation of wastes, such as plastics, cardboard, and other packaging materials. Modern waste collection systems with single collection of glass, paper, cardboard, and plastics, as well as the possibility of sending back the used products to the manufacturers also reduce the amount of MSW and also influence their composition.

MSW is very heterogenic in nature, and no standard methodology exists for defining the waste composition [6]. It is therefore difficult to compare compositions resulting from different types of sorting analysis. Information about MSW composition in different EU countries was compiled by Gentil [7] and is shown in Fig. 2.

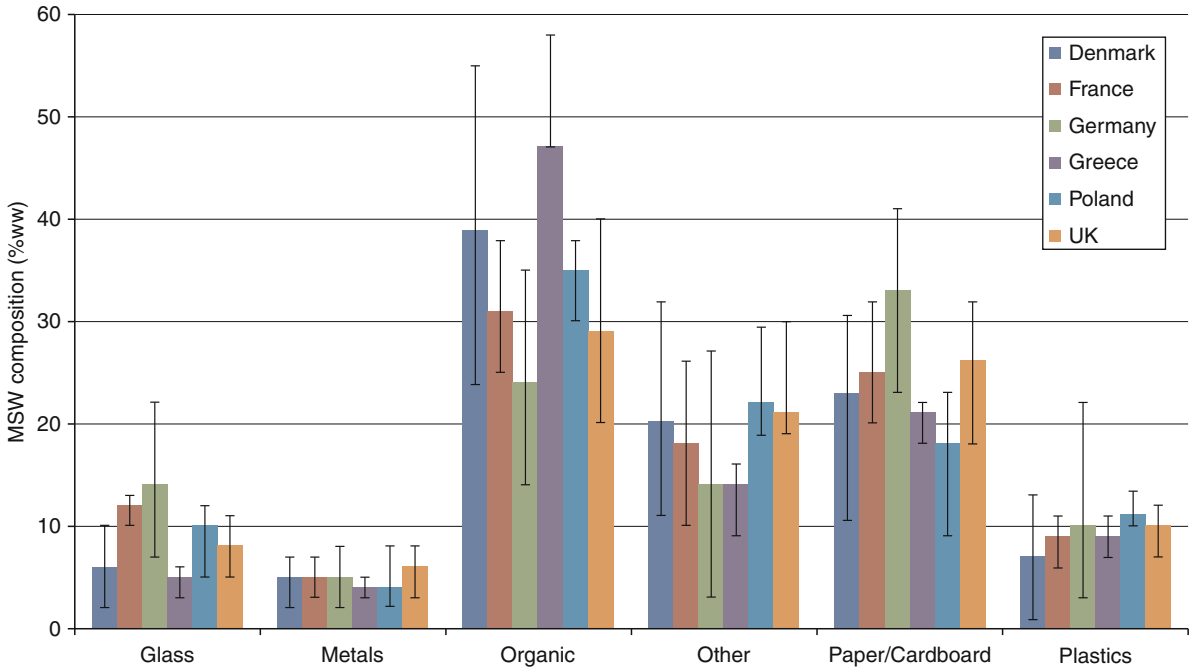

Greenhouse Gas Emission Reduction by Waste-to-Energy. Figure 2
MSW composition in various European nations (Gentil, [7])

As illustrated in Fig. 2, the organic and paper/cardboard fractions constitute about 50% of the wet MSW, as received. Glass and plastics amount to about 10% each, and metals about 5%. "Other" materials (minerals, pollutants, composite materials, textiles, and fines) range from 15% to 20%. The error bars show the minimal and maximum values observed in a particular nation due to seasonal and other conditions.

Fossil Carbon Content of MSW

The total amount of carbon (TC) in MSW is estimated on the basis of the CO_2 released in combustion tests. The biogenic and fossil carbon parts can be estimated from the overall composition of the MSW or by carbon-14/carbon-12 measurements of the WTE stack gas, as described in another section of this Encyclopedia. The only materials containing fossil carbon are composite materials, plastics, and some textiles. Figure 3 shows the measured fraction of fossil carbon in various materials contained in MSW, as reported in the literature [7–13].

Due to the polymeric structure and the low water content of plastic, the concentration of fossil carbon is very high (65–75%). The composite, textile, and fine fractions contain both biogenic and fossil-fixed carbon, and therefore their fossil carbon content is relatively low.

Global Warming Factors of Different Waste Types in Germany

The MSW collected by a municipality consists mostly of household wastes, but also includes bulky wastes, commercial waste that is similar to household wastes. In many communities, there is source-separation and collection of recyclables that are transported to materials recovery facilities (MRF) where they are separated either mechanically or manually to different recyclable streams. Between 2005 and 2007, the Institute of Waste Management and Contaminated Site Treatment of the Technical University of Dresden and the Intecus GmbH carried out an intensive campaign to analyze the waste types of household waste, similar commercial waste, and bulky waste all over Germany. The results of this investigation are shown in Table 1 [10].

Compared to the data that were shown in Fig. 2, Table 1 includes more waste fractions but the values are in the same range. The advantage of more detailed

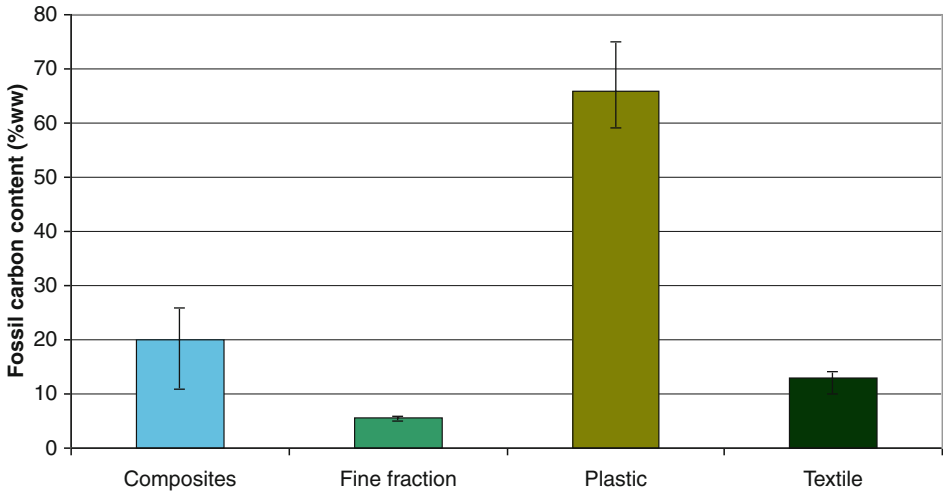

Greenhouse Gas Emission Reduction by Waste-to-Energy. Figure 3
Fossil carbon content of different materials contained in MSW

analysis is in providing a more accurate picture of the fractions of fossil and biogenic carbon. The estimated empirical values of materials of fossil origin are used to provide the estimated fossil carbon content of household, bulky waste, and commercial wastes (Table 2).

As shown in Table 2, textiles in household waste consist mostly of biogenic materials like cotton, and the fossil mass fraction is only 35%. Bulky waste contains a lot of carpets made of synthetic materials, and the fossil carbon fraction is 80%. Table 3 shows the calculated total carbon content of various materials.

There are no significant differences among the total carbon contents of the different waste materials. Thus, the same total carbon content is assumed for all waste types, whereas the total carbon contents vary significantly among the waste fractions as shown in Table 3. The calculated fossil carbon contents of various waste materials and three different types of wastes (household, bulky, and commercial) are shown in Table 4.

The fossil carbon content is 62%; therefore, plastics bring most of the fossil carbon into the MSW. The fossil carbon contents of all other waste fractions are considerably lower and they range from 3% to 36%.

The estimated content of fossil carbon in the waste fraction multiplied by the corresponding wet weighted amount in the waste composition (see Table 1) yields the content of fossil carbon in each waste material of the three types of wastes (Table 5).

Table 5 shows that, in total, 8.8% of the wet household waste consists of fossil carbon, 12.1% of the bulky waste, and 12.4% of the commercial waste that is similar to household waste.

During combustion, the carbon is oxidized to CO_2 and emitted to the atmosphere. A small amount of carbon may not be oxidized and leaves in the incinerator ash. In the literature, the oxidation of carbon, that is, the efficiency of combustion, is reported to be in the range of 95% and 100% [10, 12, 14]. In the following calculations, an oxidation of 97% was assumed for all waste types. Also, the conversion factor from carbon to CO_2, that is, 44/12 on the basis of the respective molecular weights, must be taken into account. On the basis of these data, the CO_2 emission factors for the three types of waste included in MSW are calculated to be as follows:

- Household waste: 0.312 Mg CO_2/Mg waste
- Bulky waste: 0.429 Mg CO_2/Mg waste
- Commercial waste similar to households: 0.443 Mg CO_2/Mg waste

As noted earlier, in addition to CO_2, the other important GHG gas emitted by WTE plants is nitrous oxide (N_2O). N_2O has a long residence time in the atmosphere of 114 years because there appears to be no natural removal processes for this gas [15]. Other GHG trace gases, such as carbon monoxide (CO) that has a global warming potential of 1.9 for a time horizon

Greenhouse Gas Emission Reduction by Waste-to-Energy. Table 1 Composition of different waste types [10]

Waste fraction	Household waste (% ww)	Bulky waste (% ww)	Commercial similar household waste (% ww) (M.-%)
Organic	30.9	0.6	13.2
Wood	1.9	42.6	6.3
Textiles	4.9	5.3	3.0
Minerals	4.6	1.7	4.8
Composite materials	4.7	26.3	8.6
Hazardous materials	0.6	0.1	0
Others	10.6	11.0	7.3
Fine fraction <10 mm	14.7	0.2	17.5
Fe/NE metals	2.7	5.0	3.0
Paper/ cardboard	10.5	2.4	17.1
Glass	4.9	0.1	4.4
Plastic	9.2	4.7	14.8

Greenhouse Gas Emission Reduction by Waste-to-Energy. Table 2 Estimated fossil carbon fraction of materials contained in three types of waste [10]

Waste fraction	Household waste (% ww)	Bulky waste (% ww)	Commercial similar household waste (% ww) (M.-%)
Textiles	35	80	70
Composite materials	70	60	40
Others	20	90	50
Fine fraction <10 mm	40	40	20
Plastic	100	100	100

Greenhouse Gas Emission Reduction by Waste-to-Energy. Table 3 Total carbon content of waste fractions with fossil portions [10]

Waste fraction	Total carbon content (Mg C/Mg of waste material)
Textiles	0.37
Composite materials	0.38
Others	0.19
Fine fraction <10 mm	0.14
Plastic	0.62

Greenhouse Gas Emission Reduction by Waste-to-Energy. Table 4 Fossil carbon content per ton of waste, for different waste materials and type of wastes

Waste fraction	Household waste, Mg C_{fossil}/ Mg waste	Bulky waste, Mg C_{fossil}/ Mg waste	Commercial similar to household waste Mg C_{fossil}/ Mg waste
Textiles	0.13	0.30	0.26
Composite materials	0.26	0.22	0.15
Others	0.36	0.17	0.09
Fine fraction <10 mm	0.06	0.06	0.03
Plastic	0.62	0.62	0.62

of 100 years, are not considered because their contribution to GHG is negligible.

The estimated total GHG emissions for the three types of wastes collected in the MSW stream are shown below:

- Household waste: 0.315 Mg $CO_{2,eq}$/Mg ww
- Bulky waste: 0.432 Mg $CO_{2,eq}$/Mg ww
- Commercial waste similar to households: 0.446 Mg $CO_{2,eq}$/Mg ww

As discussed earlier, the identified global warming factors (GWF) depend on the waste composition and their biogenic and fossil carbon contents. The GWF can

vary considerably from area to area. For household waste in industrial countries, the GWF ranges between 0.253 Mg $CO_{2,eq}$/Mg waste [16] to 0.557 Mg $CO_{2,eq}$/Mg waste [17].

Greenhouse Gas Emission Reduction by Waste-to-Energy. Table 5 Fossil carbon content per ton of *waste type*, for different waste materials and type of wastes

Waste fraction	Household waste, Mg C_{fossil}/ Mg waste type	Bulky waste, Mg C_{fossil}/ Mg waste type	Commercial similar household waste, Mg C_{fossil}/ Mg waste type
Textiles	0.0063	0.0157	0.0077
Composite materials	0.0121	0.0570	0.0130
Others	0.0038	0.0188	0.0069
Fine fraction <10 mm	0.0082	0.0001	0.0049
Plastic	0.0571	0.0291	0.0917
Total	0.0876	0.1207	0.1244

Comparison of Global Warming Factors of MSW with Fossil Fuels

The carbon content of fossil fuels is by definition of fossil origin. Figure 4 compares the calculated global warming factors of three types of wastes in the MSW stream with those of fossil fuels listed in the Global Emission Model for Integrated Systems (GEMIS) [18].

Figure 4 shows that, with the exception of lignite, the global warming factors of MSW are one order of magnitude lower than the various types of fossil fuels used to generate electricity and heat. However, it is also necessary to consider the amount of energy that is generated by the various fuels. Table 6 shows the respective lower heating value (LHV) of the fuels.

The three waste types have a LHV ranging from 2.5 to 3.4 MWh/Mg of waste. The better fossil fuels range in LHV from 7 to 11.8 MWh/Mg of fuel, which is two to three times higher than MSW. The only exception is lignite which, because of its high water content, is in the same range as MSW. The LHV of natural gas is shown in MWh/Nm^3 because at standard conditions (293 K and 101 kPa) it is in the gaseous form. The relation of the global warming factors and the corresponding LHV of the various fuels as used is shown in Fig. 5.

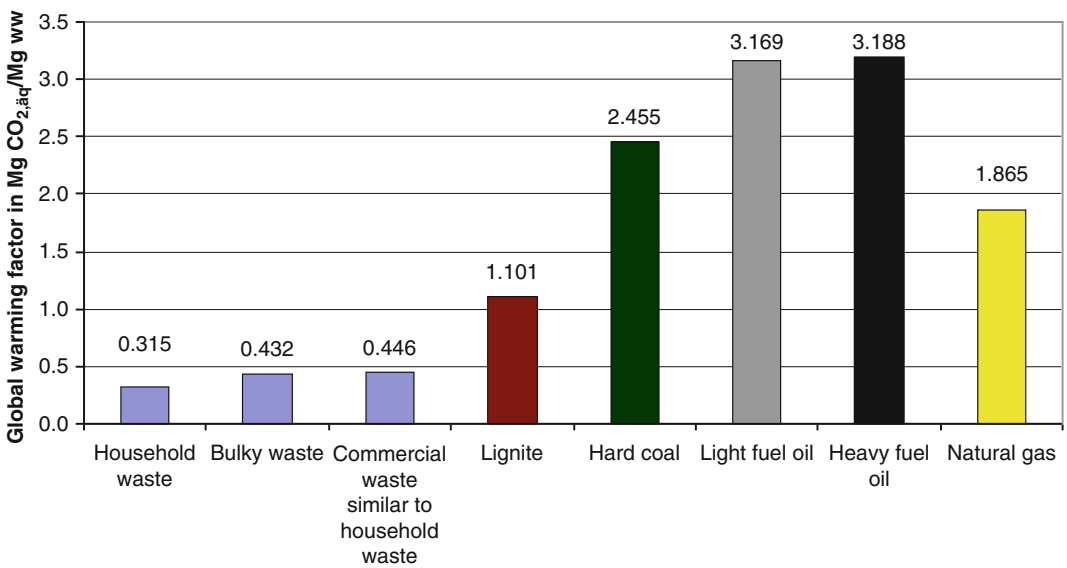

Greenhouse Gas Emission Reduction by Waste-to-Energy. Figure 4
Calculated global warming factors of different waste types and of fossil fuels (per Mg of wet fuel)

Figure 5 shows that the GWF of MSW, per MWh of contained thermal energy, is only one third to one half that of fossil fuels. The main reason is that the biogenic carbon content of MSW has been assigned zero global warming factor, $CO_{2,eq}$/MWh.

The consequence is that when wastes are incinerated with the same energy efficiency like fossil fuels, the corresponding GHG emissions for the same amount of energy delivered is two to three times lower than for fossil fuels. Or, in other words, the released GHG emission for a delivered amount of energy, from waste or from natural gas, would be the same even if the efficiency of energy recovery of waste incineration were to be one half that of natural gas combustion.

Greenhouse Gas Emission Reduction by Waste-to-Energy. Table 6 Estimated LHV of selected fuels [10, 18] and own calculations

Fuel	LHV in MWh/Mg wet weight (MWh/Nm^3 for natural gas)
Household waste	2.468
Bulky waste	4.441
Commercial similar household waste	3.701
Lignite	2.941
Hard coal	6.980
Light fuel oil	11.836
Heavy fuel oil	11.275
Natural gas	9.392

The weighted average *gross* heat efficiency of German WTE plants in 2007 was estimated to be 36.5% [10] and the average weighted *net* heat efficiency was 27.8% [19]. For the 231 European plants that generate both electricity and district heating, an average weighted *gross* heat efficiency of 46% was calculated [20] but the net efficiency was not provided; on the basis of operating experience of WTE plants, it is expected that the average net heat efficiency of these plants is about 35%. The electrical efficiency does not differ significantly between countries because the technology for power generation is everywhere available, and even in developed countries like Germany old incinerators continue to operate.

In the case of heat generation efficiency, a difference between southwest and northern Europe is visible. The gross heat efficiency in southwestern Europe is around 22% and in northern Europe around 83% [21]. The principal reason is the extensive use of WTE plants for district heating in the north. Heat has to be used close

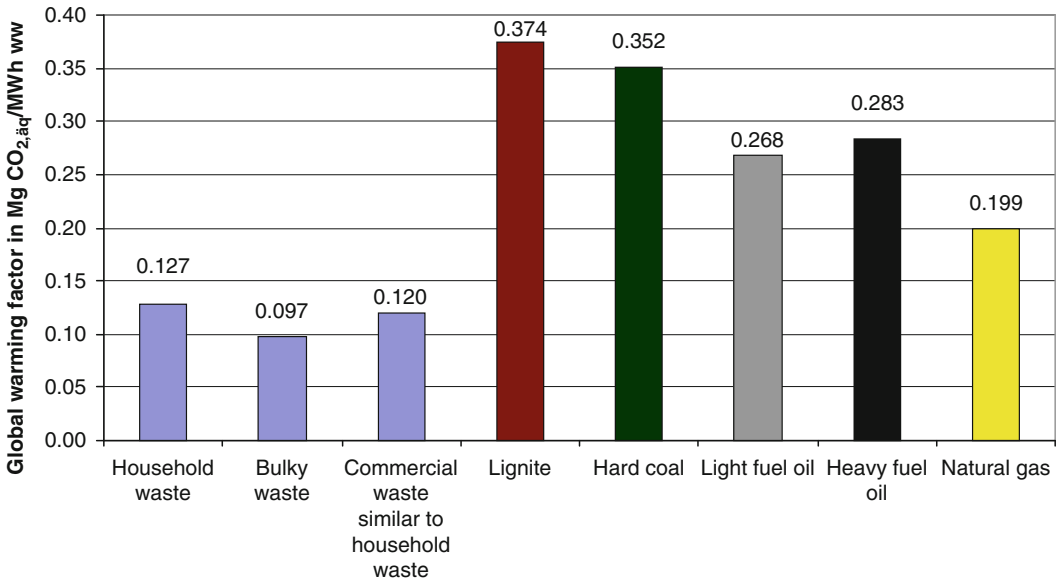

Greenhouse Gas Emission Reduction by Waste-to-Energy. Figure 5
Global warming factors of various types of wastes and fuels expressed as Mg CO_2/MWh of thermal energy

to the place of production because the transfer over higher distances is not economic. If there is no district heating network or industrial plant requiring heat, the low-level thermal energy exiting the turbine is wasted by air or water condensation. Because of their high emissions, decades ago, many incinerators were built far away from settlement structures. Consequently, even in Germany where energy efficiency is an important part in the GHG reduction targets of the government, the heat efficiency of the WTE plants is rather poor.

Another important fact is the climate. In south-western Europe heat is simply not needed because of relatively high temperatures all year round. A conversion from heat by absorption refrigeration to cooling is technically possible, but special cooling networks and cooling energy costumers are necessary. The opposite is in northern Europe. Cold climate and high heat requirements combined with an intelligent energy provision and generation system makes high efficiencies possible. In northern European countries, such as Denmark, WTE plants are positioned close to district heating networks and there is intelligent integration of the WTE plants in the heating system of an area. The simultaneous production of electrical power and heat in a single process of a power plant is called combined heat and power generation (CHP) and ensures maximum efficiency in recovering energy. The very efficient incineration plants in northern Europe are using this technology.

Even when the combined heat and power generation is very efficient is financially supported, as for example in the case of CHP in Germany, most of the large fossil fuel power plants produce exclusively electricity. The electrical net efficiency of lignite power plants is around 36.6%, of hard coal power plants 37.6%, of light and heavy fuel oil around 35%, and of natural gas 43.9% [22]. Usually the produced heat of these power plants is not used, and in the case of lignite, hard coal and natural gas power plants that seek to have a high electrical efficiency, the steam is condensed to relatively low temperatures. This low-level energy cannot be used for district heating.

In comparison, smaller heating plants that are designed to produce only heat have a net heating efficiency of around 91%, using the same fossil fuels [23]. Because of high emissions, heavy fuel oil is not used anymore for power generation in most industrial countries. However, it is still used for fuelling ships and tankers.

Figure 6 shows the global warming factors per unit of energy content, as illustrated in Fig. 5, divided by the

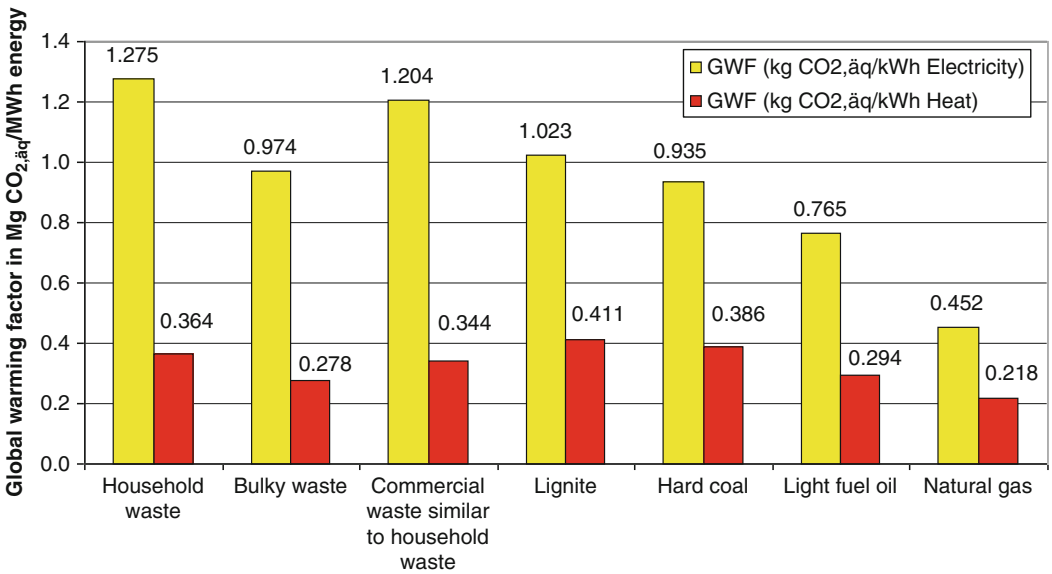

Greenhouse Gas Emission Reduction by Waste-to-Energy. Figure 6
Calculated global warming factors of different waste types and fossil fuels referring a unit of delivered energy

corresponding net efficiencies of the power plants using these fuels. The result of this division yields the amount of released GHG per unit of delivered electrical power or heat.

The low electrical net efficiency of 10% and the heat net efficiency of 35% from WtE plants cause the GWF of around 1 Mg $CO_{2,eq}$/MWh of electricity and about 0.3 Mg $CO_{2,eq}$/MWh of heat from wastes (Fig. 6). The higher net efficiencies of fossil-fired power plants of about 40% for electricity and 90% for heat result in GWF ranging from 0.45 to 1 Mg $CO_{2,eq}$/MWh of electricity and from 0.2 to 0.4 Mg $CO_{2,eq}$/MWh of heat for the most efficient power plants (Fig. 6).

However, it should be noted that the global warming factors for the most efficient WTE facilities are obtained by cogeneration of power and heat. The net efficiencies of 40% for power and 90% for heat for fossil-fired power plants are not possible in the case of cogeneration of electricity and heat.

Reduction of GHG Emissions and Conservation of Fossil Fuels by Means of Energy Recovery from Wastes

The energy released by the combustion in the waste incineration plants is used to produce electricity and/or heat. The effect of this is to decrease the consumption of fossil fuels, thus conserving a nonrenewable resource. The effect of this contribution to the overall mix of power generations differs from country to country. The amount of nuclear energy and renewable energy used, the amount of fossil fuels used, and the degree of cogeneration play an important role. Also, the efficiency of electricity generation from fossil fuels has a big influence on the electricity mix factor. In turn, the electricity mix factor results in the overall GWF (Mg $CO_{2,äq}$/MWh) of a nation. This factor is also affected by the upstream and downstream emissions associated with the mining, processing, and transport of the fuels; the construction and demolition of the energy-producing facilities; and the disposal of by-products, such as coal ash and nuclear wastes.

The electricity mix factors of many countries are calculated every year and are available in the literature. In the EU, the electrical mix factor ranges from 0.007 Mg $CO_{2,äq}$/MWh_{el} for Norway, which uses renewable hydropower, to 1.13 Mg $CO_{2,äq}$/MWh_{el} for Poland, which depends on lignite-fired power plants [24]. Developed industrial economies with a wide mix of nuclear, coal, and renewable energy have GWF of about 0.6 Mg $CO_{2,äq}$/MWh_{el} [24, 25].

The heat mix factors are more difficult to calculate. The big difference between electricity and heat is in the ways that these two kinds of energies are produced and supplied to the users. Electricity is usually produced in a relatively small number of large power plants and is distributed by means of national grids. Heat is generated by a multitude of generating sources, including residential boilers, industrial and municipal boilers, and many other sources. Heat can be produced in cogenerating plants, as a by-product of industrial processes, and also by geothermal or solar energy and is delivered either as steam or warm water. It is therefore much more difficult to compile statistics on the GWF of heat generation than in the case of electricity. For the current 27 countries of the European Union, a weighted heat mix factor of 0.27–0.32 Mg $CO_{2,äq}$/MWh_{th} was estimated by Kreissig and Stoffregen [26] and Skovgaard et al. [27]. The German heat mix factor was calculated to be 0.216 Mg $CO_{2,äq}$/MWh_{th} [22] and for Greece to 0.468 Mg $CO_{2,äq}$/MWh_{th} [7].

As discussed earlier, the biogenic fraction of MSW energy is over 50%, and the energy delivered by waste incineration plants primarily substitutes energy from fossil fuels. Therefore, it is reasonable to calculate electrical and heat mix factors based on the energy provision of fossil fuels, that is, taking out of the energy mix factor of a country nuclear and renewable energy. The German federal environmental energy prefers to use the fossil energy mix factors for calculating the GHG emission savings resulting from MSW and other biomass combustion. In countries like Poland where nearly 100% of the energy is generated from fossil fuels, the fossil energy mix factors are nearly the same as the actual energy mix factors. In the case of Germany, 30% of electricity is generated by lignite, 60% by hard coal, and 10% by natural gas, when nuclear and renewable energy are excluded from the calculation of the energy mix; in this case, the fossil fuel mix factor is 0.886 Mg $CO_{2,äq}$/MWh_{el} versus the actual factor of 0.6 Mg $CO_{2,äq}$/MWh_{el} [22]. The German heat mix factor increases from 0.216 to 0.232 Mg $CO_{2,äq}$/MWh_{th} [22] when heat is exclusively generated by fossil fuels. When a nation obtains most of its energy from

natural gas, the mix factor is about 0.45 Mg $CO_{2,äq}$/MWh for electricity and 0.22 $CO_{2,äq}$/MWh for heat (Fig. 5). When the only fossil fuel is lignite coal, the fossil energy mix factor for electricity is about 1 Mg $CO_{2,äq}$/MWh and for heat 0.4 Mg $CO_{2,äq}$/MWh.

The third scenario is developed to examine the effect of energy provided by WTE as base load operation, that is, on a 24-h basis. Base load plants are primarily nuclear, lignite, and, in some cases, hard coal fired power plants; at times of high demand of electricity, the required peak load power is provided by power plants fired by light oil or natural gas. Waste incineration plants burn waste and provide energy continuously, 24 h a day, and, therefore, are a good base load provider.

In the case of Germany, base load electricity is primarily provided by lignite coal power plants with an electricity factor of 1,088 Mg $CO_{2,äq}/MWh_{el}$ [22]. In Norway or France, where base load electricity is produced by renewable or nuclear energy, the corresponding factor is zero. Because of the difficulties involved in compiling heat generation data, as discussed earlier, it is not possible to calculate the base load heat factor; in this case, the fossil heat mix factor is assumed as the base load factor for generation of heat. The above discussion of GWF is summarized in Table 7.

As an example, in Germany the use of WTE reduces in the fossil energy mix scenario GHG emissions by the factor 0.886 Mg $CO_{2,äq}$/MWh, of electricity provided by the WTE, and 0.232 Mg $CO_{2,äq}$/MWh, for heat generated by the WTE. For the LHV of household waste presented in Table 6 and the power (10%) and heat (35%) net efficiencies of waste incineration plants, 0.247 MWh of power and 0.864 MWh of heat are provided by the combustion of 1 t (1 Mg) of household wastes. Multiplying these amounts of energy by the emission factors of the fossil energy mix scenario yields the factor of 0.419 Mg $CO_{2,äq}$/Mg of household waste combusted. Comparison with the released GHG emissions from the combustion of household waste of 0.315 Mg $CO_{2,äq}$/Mg (Fig. 4) shows that there is a net reduction of 0.104 Mg $CO_{2,äq}$/Mg of MSW. Figure 7 shows the net prevention of GHG emissions for the three waste types and for the three substitution scenarios.

Greenhouse Gas Emission Reduction by Waste-to-Energy. Table 7 Global warming factors for the generation of electricity and heat, under three substitution scenarios in EU

Substitution scenario	Electrical power [Mg $CO_{2,äq}/MWh_{el}$]	Heat [Mg $CO_{2,äq}/MWh_{th}$]
Actual energy mix	0.007–1.13	0.216–0.468
Fossil energy mix	0.45–1.13	0.22–0.5
Base load	0–1.13	0.216–0.468

Figure 7 shows that for Germany, there is a net reduction of GHG emissions, in all three scenarios. The net reduction ranges from 0.02 to 0.14 Mg $CO_{2,äq}$/Mg for household waste to 0.17 to 0.39 Mg $CO_{2,äq}$/Mg for bulky waste. The net reduction is 0.315 for household waste and 0.446 Mg $CO_{2,äq}$/Mg for commercial waste similar to that of households. The difference is due to the higher LHV of the commercial waste.

Resource Conservation by Savings of Fossil Fuels

Each unit of energy produced by WTE conserves a unit of fossil fuel energy. Furthermore, every ton of incinerated waste conserves a certain amount of fossil fuels. Using the LHV of Table 6 and the power and heat net efficiencies mentioned earlier, one can calculate the mass of fossil fuels conserved per ton of MSW combusted (Fig. 8).

In an average WTE plant, between 0.15 Mg of natural gas and 0.55 Mg of lignite can be avoided by the incineration and energy recovery of 1 Mg of household waste (Fig. 8). In the case of heat generation, the amount of avoided fossil fuel per ton of MSW is higher because the energy efficiency of heat-generating WTE is higher than that for electricity. The higher is the LHV of the MSW combusted, the higher will be the reduction in GHG emissions. For example in the case of bulky waste (Table 6), 1 t of waste decreases the use of lignite by about 1 t.

Greenhouse Gas Emissions by Landfilling

As noted earlier, landfilling continues to be the dominant method of disposing MSW worldwide. Under the prevailing anaerobic conditions in a landfill and in the presence of water, the biogenic components of MSW

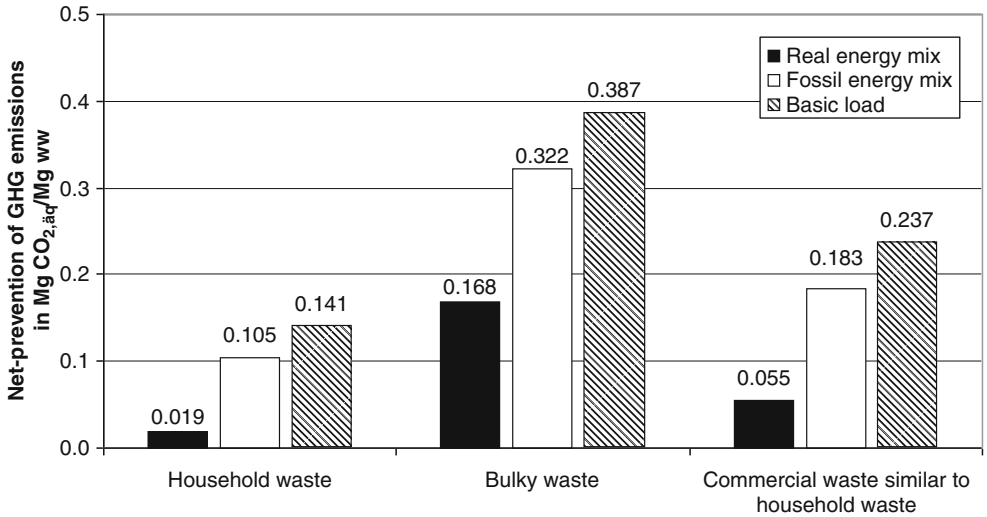

Greenhouse Gas Emission Reduction by Waste-to-Energy. Figure 7
Net reduction of GHG emissions in Germany for the three substitution scenarios and three types of waste

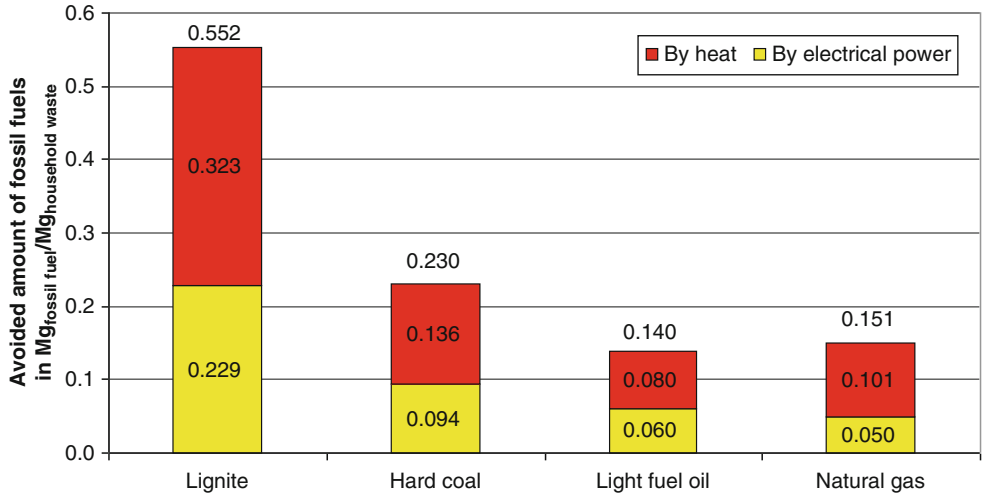

Greenhouse Gas Emission Reduction by Waste-to-Energy. Figure 8
Conserved amount of various fossil fuels by the combustion of 1 t (1 Mg) of MSW in WTE

are converted to methane and carbon dioxide. Figure 9 illustrates that in Phase I, when wastes are first dumped, air can flow through the wastes; under these conditions, aerobic bacteria consume oxygen and break down the long molecular chains of complex proteins, lipids, and carbohydrates. The oxygen concentration decreases, and the concentration of produced carbon dioxide increases. Phase I lasts for days to several months, depending on how loose or compressed the waste is. In Phase II, oxygen is depleted, and carbon dioxide reaches the concentration of over 60%. When anaerobic conditions are reached, methanogenic bacteria produce methane and carbon dioxide and, at the beginning of Phase IV, the generated landfill gas consists of nearly equal volumes of methane and carbon dioxide. It may take a few years until the stable Phase IV

is reached, depending on waste composition, moisture content, temperature within the landfill, and other factors. Phase IV can last several decades with a stable landfill gas composition.

If there is no infiltration of rainwater in the landfill, the production of landfill gas decreases.

Modern, controlled landfills, also called sanitary landfills, are provided with ground sealing and also landfill gas collection systems. However, it may take several years for the landfills to be covered and the gas collection system to start operating. During this time, rainwater can flow through the wastes, and methane gas is formed. The amount of resulting GHG emissions from landfills is primarily dependent on the biogenic carbon and the water content in the wastes. The degradation of the biogenic carbon depends more on the water to solids ratio than on the age of the landfill. In order to calculate the production of landfill gas, one needs to know the amount of biogenic carbon in the different wastes types. The amounts shown below are based on the calculation of the fossil carbon (see section on "Global Warming Factors of different Waste Types in Germany"):

- Household waste: 0.122 Mg C_{bio}/Mg waste
- Bulky waste: 0.232 Mg C_{bio}/Mg waste
- Commercial waste similar to household waste: 0.097 Mg C_{bio}/Mg waste

In practice, the amount of produced landfill gas is calculated by means of mathematical models that describe the decomposition and gas generation processes using mathematically formulated procedures in combination with empirical factors. A commonly used model in Europe was developed by Tabasaran and

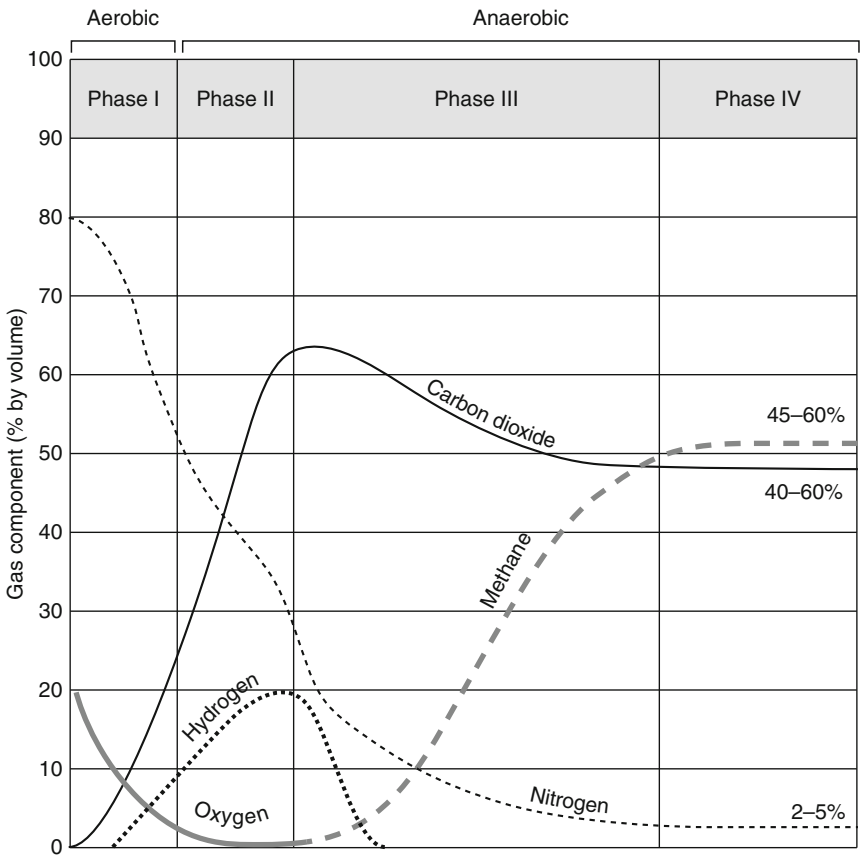

Greenhouse Gas Emission Reduction by Waste-to-Energy. Figure 9
Changes in landfill gas composition with time [28]

Rettenberger on the basis of the following formula [29]:

$$G_t = 1.868 \cdot C_{bio} \cdot (0.014 \cdot T + 0.28) \cdot \left(1 - 10^{-kt}\right)$$

where

G_t = produced amount of landfill gas [m^3/Mg ww]
C_{bio} = biodegradable carbon [Mg C/Mg ww]
T = temperature [°C]
k = degradation constant [a^{-1}]
t = time since deposition [a]

The factor 1.868 indicates the amount of landfill gas (in liters) stoichiometrically produced by 1 g of biogenic carbon. The temperature T in landfills is in the mesophilic range and is assumed to be 30°C. The degradation constant is calculated from the formula by $\ln 2/T_{1/2}$, where the average half-life ($T_{1/2}$) used by the authors is 18 years, and k is calculated to be 0.04. Easily biodegradable material like food wastes have a shorter half-lives than paper and wood that contain lignin; however, to simplify the calculation, the half-life of 18 years is assumed for all waste types. The amount of landfill gas produced annually, using the formula of Tabasaran and Rettenberger, is shown in Fig. 10.

According to Fig. 10, landfill gas production would be nearly finished after 50 years. The accumulated amount of landfill gas over the 50-year period is 158 Nm^3 per Mg of wet weight of household waste, 301 Nm^3 per Mg for bulky waste and 126 Nm^3 per Mg of commercial waste similar to households.

For an assumed distribution of 50% methane by volume and 50% carbon dioxide, the molar mass of methane (16 g/mol) and carbon dioxide (44 g/mol), the molar volume of gases at standard temperature and pressure (22.4 L/mol), and an assumed GWF for methane of 23, the following amounts of GHG emissions are released per ton of waste:

- Household waste: 1.449 Mg $CO_{2,äq}$/Mg waste
- Bulky waste: 2.766 Mg $CO_{2,äq}$/Mg
- Commercial waste similar to household waste: 1.155 Mg $CO_{2,äq}$/Mg

These amounts will be emitted to the atmosphere in landfills that are not provided with gas collection systems. In controlled (sanitary) landfills, over 50% of the total biogas generated can be captured and the rest is emitted to the atmosphere. The following section shows that the amount of GHG emissions from landfills is considerably higher than the GWF associated with the combustion of MSW in WTE.

The Germany Example

Since 2005, landfilling of untreated MSW in Germany is prohibited; the primary reason is to reduce the landfill gas potential of the disposed waste.

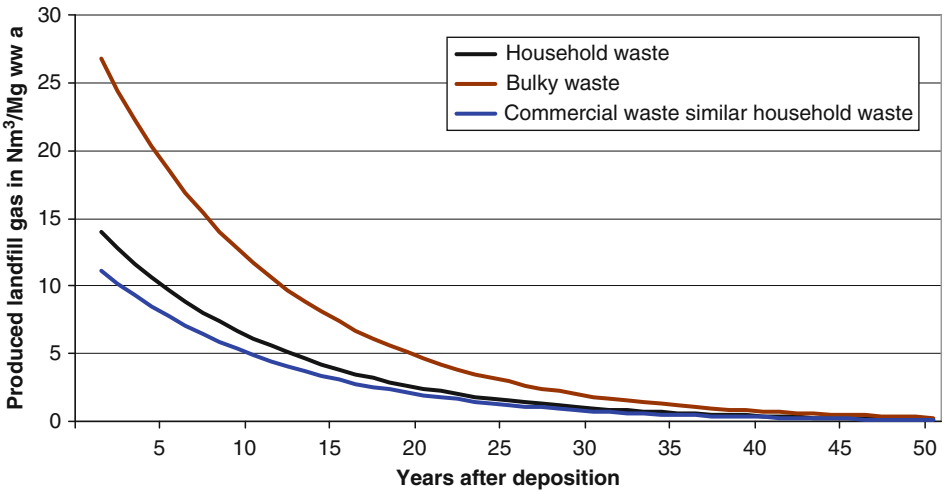

Greenhouse Gas Emission Reduction by Waste-to-Energy. Figure 10
Calculated amount of landfill gas generated annually

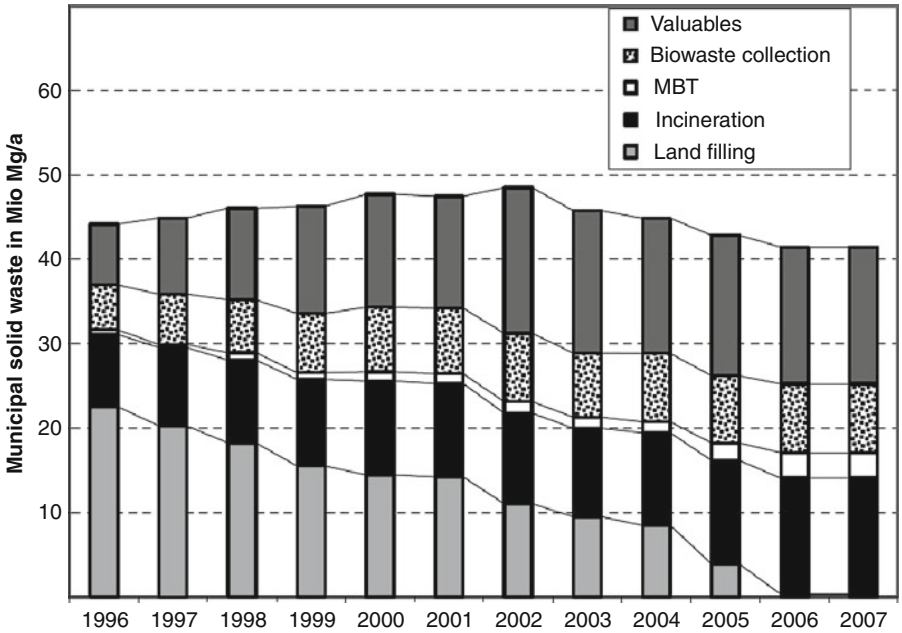

Greenhouse Gas Emission Reduction by Waste-to-Energy. Figure 11
Disposition of MSW collected in Germany [31]

At this time, the post-recycling MSW goes directly to waste incineration or to mechanical and biological treatment (MBT) plants; in 2007, there was no landfilling of untreated MSW. In the MBT plants, some recyclables are recovered, green and food wastes are stabilized, and a high calorific value material is produced that may be used as a solid fuel (SRF or RDF). Figure 11 shows the disposition of municipal solid wastes in Germany, in the years 1996–2007 [30]. It can be seen that only a small fraction goes to BMT, 50% of the post-recycling MCW is combusted in WTE facilities, and in the period 1997–2007 landfilling was reduced from about 23 million tons to zero.

Greenhouse Gas Emissions by Waste Incineration in Germany 2007

In the year 2007, about 17.8 million tons of MSW were incinerated in 66 German waste incineration plants. The waste input composition was in general about 12.5 million Mg of household wastes, 0.5 million Mg of bulky wastes, and 4.8 million Mg of commercial wastes similar to household waste and other materials [10]. As discussed earlier, (see Fig. 4), the annual GHG emissions from household waste were 3.93, for bulky waste 0.22, and for commercial waste similar to household waste 2.14 million Mg $CO_{2,äq}$.

For the calorific value of the waste mix of about 2.8 MWh/Mg [19], the thermal energy generated by the 17.8 million tons of MSW combusted in 2007 was 49.45 million MWh. In addition, an estimated [19] 1.62 million MWh of external energy was used in the form of light fuel oil used for start-up and shutdown operations or as natural gas used for reheating of the flue gas prior to selective catalytic reduction (SCR); Bilitewski [10] determined that 24% of this auxiliary energy was provided by light fuel oil and 76% by natural gas; as stated earlier (Fig. 4), the GWF of light fuel oil is 0.268 Mg $CO_{2,äq}$/MWh and of natural 0.199 Mg $CO_{2,äq}$/Mg. This use of auxiliary fuels resulted in the GHG emission of 0.35 million Mg $CO_{2,äq}$. In total, by waste incineration in Germany in the year 2007 emitted about 6.64 million Mg $CO_{2,äq}$.

Reduction of Greenhouse Gas Emissions in Germany by Means of Waste Incineration in 2007

Table 8 shows the amounts of electricity and thermal energy provided by the 66 German waste incineration plants in 2007.

Greenhouse Gas Emission Reduction by Waste-to-Energy. Table 8 Energy generated by all WTE plants of Germany in 2007 [19]

Type of energy	Amount of energy provided, in million MWh/a
Electrical power	5.16
Heat	13.75
Total	18.91

Since the thermal energy input was estimated earlier to be 49.45 million MWh/a minus the 1.62 million MWh of external fuel, the energy efficiency of delivered electrical power was 10.1% and the energy efficiency of delivered heat 26.9%. The combined efficiency of delivered electrical and thermal energy generation was 37%.

In determining the effect of WTE in substituting fossil energy, three scenarios were considered, same as discussed earlier:

- Actual German energy scenario
  - Power mix: nuclear 23%, natural gas 13%, lignite 23%, hard coal 20%, renewables 15%, others 6%; electricity GWF of 0.596 Mg $CO_{2,äq}/MWh_{el}$ [22]
  - Heat mix (39% hard coal, 42% natural gas, 12% lignite, 6% waste); heat GWF of 0.216 Mg $CO_{2,äq}/MWh_{th}$ [32]
- Fossil fuel scenario
  - Power mix: 60% hard coal, 30% lignite, 10% natural gas; electricity GWF of 0.886 Mg $CO_{2,äq}/MWh_{el}$ [22]
  - Heat mix: 57% natural gas, 40.5% light fuel oil, 2.5% coal; heat GWF of 0.232 Mg $CO_{2,äq}/MWh_{el}$ [22, 33]
- Base load scenario
  - Electricity factor based on lignite coal; GWF of 1.088 Mg $CO_{2,äq}/MWh_{el}$ [22]
  - Heat factor based on the actual German heat mix; heat GWF of 0.216 Mg $CO_{2,äq}/MWh_{th}$ [32]

The actual German power mix consists of a wide range of energy sources, so as to not to be dependent on one source. The future aim is to reduce the nuclear power fraction and replace it by renewable energy. As was shown in Fig. 5, natural gas is the "cleanest" fossil energy with the highest conversion efficiencies. Clean is not only meant in terms of low emission of carbon dioxide; during combustion of natural gas, other emissions such as sulfur oxides, hydrochloric acid, carbon monoxide, and particulates are much lower than from other fossil fuels. For this reason, Germany is making further efforts to increase the use of natural gas by expanding gas pipeline connections to Russia.

As noted earlier, data on industrial heat is hard to obtain; therefore, the above distribution of heat for the actual German energy scenario is based on the provision of district heat. The majority of provided heat is produced by hard coal and natural gas fired power plants, in combined heat and power generation. Actually, nearly 90% of the district heating in Germany is produced in cogeneration with electricity [32]. This cogeneration is financially supported by the German government by implementing high-efficiency technologies and in order to reduce GHG emissions.

The fossil power mix for Germany consists of hard coal and to a lesser degree by lignite and natural gas. The fossil heat mix is based on the energy source share of the German heat market in 2003 [32].

Apart from nuclear power, the base load of electricity in Germany is provided by lignite. Nuclear power has little effect on GHG, so the base load scenario involves substitution of lignite by MSW incineration. For the base load of heat, the actual heat mix factor was used, because the heat requirements change with season rather than time of the day.

Multiplying the amounts of electricity and heat provided by WTE (see Table 8) by the substitution factors of the three scenarios yields the amounts of GHG emissions avoided by substituting MSW incineration for the combustion of fossil fuels (Fig. 12).

The avoided GHG emissions are shown as negative numbers in Fig. 12. The three bars on the left side of Fig. 12 show the effect of WTE in substituting fossil fuels for electricity generation. Substitution of heat energy (three bars in the middle) results in lower avoidance of GHG emissions because heat generation in Germany is very efficient, and the substitution factors lower. The avoided GHG emissions range from 3 and 5.6 million Mg $CO_{2,äq}$/a. In total, the GHG emissions avoided by WTE electrical and thermal energy range from 6 to 8.6 Mio Mg $CO_{2,äq}$ per year. By adding the WTE GHG emissions and the avoided (i.e., negative)

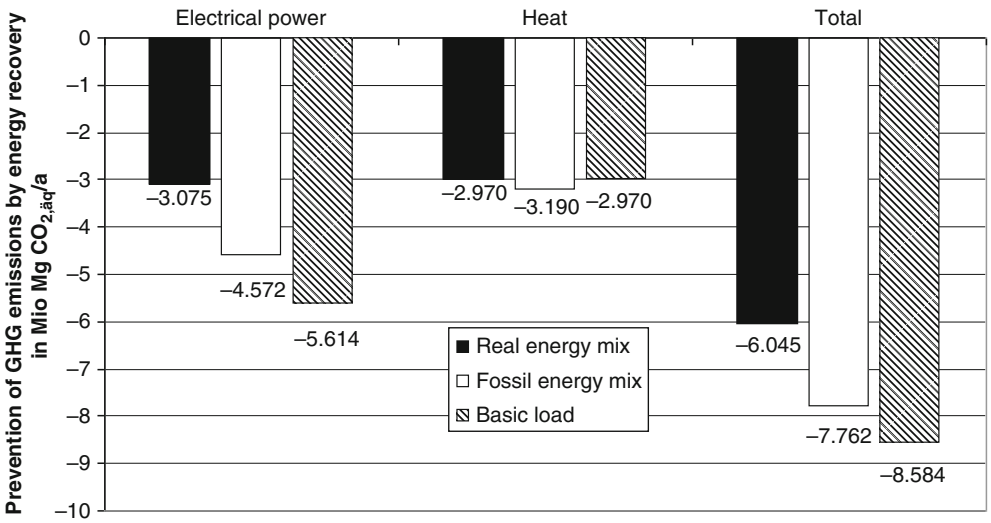

Greenhouse Gas Emission Reduction by Waste-to-Energy. Figure 12
Avoided GHG Emissions in Germany by means of energy recovery in waste incineration plants in 2007, under three energy mix scenarios

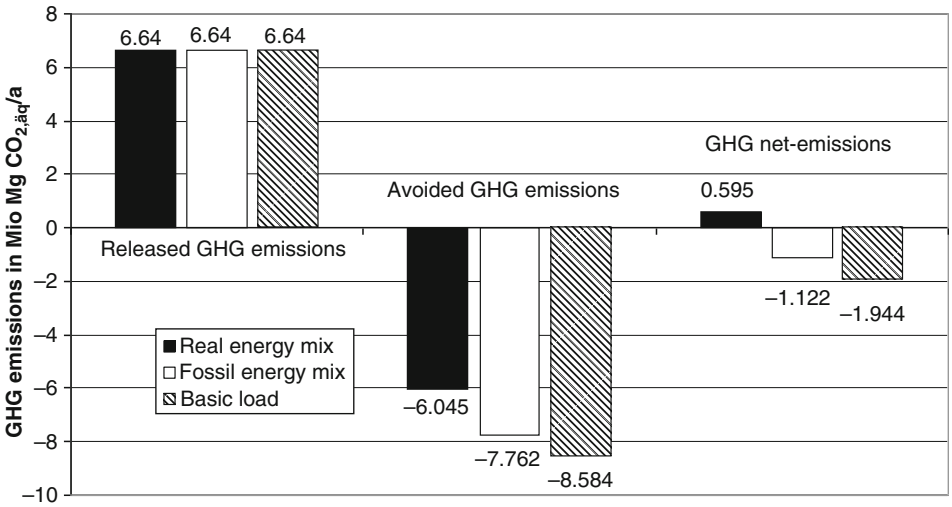

Greenhouse Gas Emission Reduction by Waste-to-Energy. Figure 13
GHG emissions, avoidance of emissions, and net emissions of German waste incineration plants in 2007

emissions of fossil fuels avoided because of the energy generated by WYE (Fig. 12) results in the net GHG emissions shown in Fig. 13 (last three bars).

The German example shows that the scenario chosen for substitution of energy is very important and has a real impact on the GHG balance of WTE plants. In the case of substitution in the actual German energy mix, the GHG net emissions (0.6 million Mg $CO_{2,äq}$/year) is positive. For the substitution of the fossil energy mix and the base load scenarios, the GHG balance is negative, and GHG emissions of 1.1 and 2 million Mg $CO_{2,äq}$/year are avoided.

Comparison to Landfilling

Currently, 95% of all German landfills are equipped with a gas collection system, and the biogas collection efficiency has been estimated at 60% [33]. If it is assumed that the 17.8 million Mg of incinerated MSW were landfilled and using the calculations presented in the section "Greenhouse Gas Emissions by Landfilling", 9.6 million Mg $CO_{2,äq}$ would be directly released. The gas collection systems would capture about 0.4 million Mg of methane. Since the LHV of methane is 13.9 MWh/Mg, the captured gas would provide about 5.6 million MWh that could be used to generate energy in the form of electricity and heat. Usually the landfill gas is burned in slightly modified gasoline engines to produce electricity only. Heat is generally not needed at landfills, and therefore not recovered. The electrical efficiency of the gasoline engines is around 35%. Assumed that all of the captured landfill gas can be used in gasoline engines, about 2 million MWh of electricity would be produced. This electricity would substitute energy produced by other fossil fuels, and thus avoid GHG emissions. On the basis of the substitution scenarios for Germany (see Section Prevention of Greenhouse Gas Emissions by Energy Recovery in German Waste Incineration Plants) between 1.6 and 3 million Mg $CO_{2,äq}$ of fossil fuel emissions would be avoided. Figure 14 shows what would be the effect of landfilling, instead of combusting, 17.8 million Mg on the GHG emissions balance for Germany, for the same three energy mix scenarios.

Figure 14 shows that even if all of the captured methane were used to generate electricity, the GHG net emissions would be between 6.7 and 8 million Mg $CO_{2,äq}$. In comparison to waste incineration (see Fig. 13), the GHG net emissions by land filling would be about 8 million Mg $CO_{2,äq}$, higher than in the case of waste incineration with energy recovery. This amount corresponds to about 0.5 t of carbon dioxide per ton of MSW landfilled rather than combusted. The landfill emissions would be much greater for landfills that do not recover methane or flare the landfill gas instead of using it to generate electricity.

Future Directions

This entry shows clearly that waste incineration results in much lower GHG emissions than landfilling. One of the reasons is that only CO_2 is emitted during incineration, while the landfill gas that is not captured consists of about 50% methane that has a global warming potential that is 23 times higher than the same volume of carbon dioxide. The second reason is that much more energy is generated by the combustion of MSW

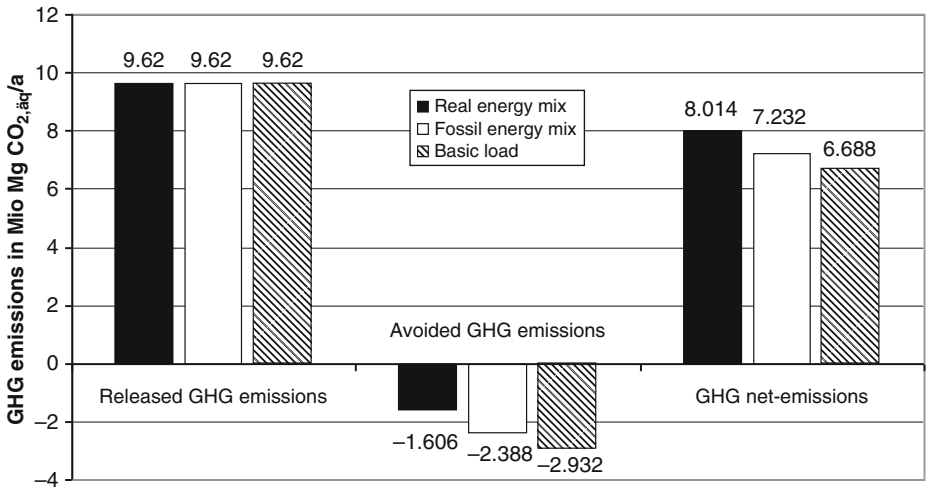

Greenhouse Gas Emission Reduction by Waste-to-Energy. Figure 14
GHG emissions in Germany if 17.8 million tons of MSW were landfilled rather than combusted in 2007

than from the combustion of the methane generated and captured during landfilling.

Many communities have begun to collect biodegradable materials separately. The result is less biogenic fixed carbon in the household wastes and a higher amount of plastics and composite materials with high amounts of fossil-fixed carbon. The result are a lower amount of landfill gas generated during landfilling and a corresponding reduction in GHG emissions. For the waste incineration, removal of organics results in a higher concentration of fossil-based wastes and higher GHG emissions. It also means higher calorific value of the MSW which should result in higher thermal efficiency. In any case, it is necessary for WTE plants to strive to increase their thermal efficiency and energy recovery. This will result in higher amounts of produced and delivered energy and, thus, higher substitution of fossil fuels and increased avoidance of GHG emissions.

Bibliography

Primary Literature

1. National Inventory Report for the German Greenhouse Gas Inventory 1990–2007, Submission under the United Nations Framework Convention on Climate Change and the Kyoto Protocol 2008, Federal Environment Office, Dessau-Roßlau, April 2008, p 47
2. Metz B et al (eds) (2005) Special report on safeguarding the ozone layer and the global climate system: issues related to hydrofluorocarbons and perfluorocarbons. Cambridge University Press, Cambridge/New York
3. Emission control: Energy conversion in thermal solid waste treatment. VDI 3460 Part 2, 2007, issue German/English, ICS 13.030.40, 27.190, p 13
4. Guendehou G, Koch M, Hockstad L, Pipatti R, Yamada M (1997) Incineration and open burning of waste. In: IPCC guidelines for national greenhouse gas inventories, vol 5, chap 5, p 5.5
5. Obermoser M, Fellner J, Rechenberger H (2009) Determination of reliable CO_2 emission factors for Waste-to-energy plants. Waste Manage Res 27(9):407–413, Applied greenhouse gas accounting: methodologies and cases
6. Riber C, Pedersen C, Christensen TH (2009) Chemical composition of material fractions in Danish household waste. Waste Manage 29:1251–1257
7. Gentil E, Clavreul J, Christensen TH (2009) Global warming factor of MSW management in Europe. Waste Manage Res 27(9):850–860, Applied greenhouse gas accounting: methodologies and cases
8. Manfredi S, Scharff HM, Tonini D, Christensen TH (2009) Landfilling of waste: accounting of GHGs and GW contributions. Waste Manage Res 27(8):825–836, Fundamental in greenhouse gas accounting: concepts and mechanisms
9. Astrup T, Moeller J, Fruergaard T (2009) Incineration and co-combustion of waste: accounting GHG and global warming contribution. Waste Manage Res 27(8):789–799, Applied greenhouse gas accounting: methodologies and cases
10. Bilitewski B, Wünsch C, Jager J, Hoffmann M (2010) Energieeffizienzsteigerung und CO_2-Vermeidungspotenziale bei der Müllverbrennung – technische und wirtschaftliche Bewertung. EdDE-Dokumentation 13, Entsorgergemeinschaft der deutschen Entsorgungswirtschaft e.V., April 2010, p 16
11. Roland C, Scheibengraf M (2003) Biologisch abbaubarer Kohlenstoff im Restmüll. Umweltbundesamt, Berichte BE-236. Wien, 2003
12. Pipatti R, Sharma C, Yamada M, Alves J, Gao Q, Guendehou G, Koch M, López Cabrera C, Mareckova K, Oonk H, Scheehle E, Smith A, Svardal P, Vieira S (2006) Waste generation, composition and management data. Solid waste disposal. In: IPCC guidelines for national greenhouse gas inventories, vol 5, chaps 2 and 3
13. Dehoust G, Schüler D, Vogt R, Giegrich J (2010) Klimaschutzpotenziale der Abfallwirtschaft. IFEU und Ökoinstitut e.V, Darmstadt/Heidelberg/Berlin
14. Hiraishi T, Nyenzi B, Miguez J, Alves J, Boeckx P, Brown K, Hoppaus R, Jubb C, Kerr T, Kleffelgaard T, Lucon O, Mauschitz G, Midaglia C, Milton M, Mondshine M, Oonk H, Paradiz B, Steczko K, Teixeira G, Towprayoon S, Yesserkepova I (2001) Waste. In: IPCC good practice guidance and uncertainty management in national greenhouse gas inventories, chap 5, p 5.29
15. Scheutz P, Kjeldsen P, Gentil E (2009) Greenhouse gases, radiative forcing, global warming potential and waste management – an introduction. Waste Manage Res 27(8):716–723, Fundamental in greenhouse gas accounting: concepts and mechanisms
16. Bilitewski B, Schirmer M, Niestroj J, Wagner J (2005) Ökologische Effekte der Müllverbrennung durch Energienutzung, EdDE-Dokumentation 10, Entsorgergemeinschaft der deutschen Entsorgungswirtschaft e.V. Pirna, 2005, p 24
17. Houghton JT et al (eds) (1996) Intergovernmental Panel on Climate Change: climate change 1995: the science of climate change. Contribution of working group I to the second assessment report of the intergovernmental panel on climate change, Cambridge University Press, Cambridge
18. Global Emission Model for Integrated Systems (2009) Version 4.6, Öko-Institut e.V
19. Treder M (2008) Energieerzeugung und Klimarelevanz der W-t-E Anlagen in Deutschland (Kurzfassung vom 16.07.2008), Würzburg
20. Reimann DO (2009) CEWEP Energy Report II (status 2004-2007). CEWEP, Bamberg

21. Fruergaard T, Ekvall T, Astrup T (2009) Energy use and recovery in waste management and implications for accounting of greenhouse gases and global warming contributions. Waste Manage Res 27(8):724–737, Fundamental in greenhouse gas accounting: concepts and mechanisms
22. Staiß F, Linkohr C, Zimmer U, Musiol F, Ottmüller M (2008) Erneuerbare energien in zahlen, nationale und internationale entwicklungen. Bundesministerium für Umwelt, Naturschutz und Reaktorsicherheit (BMU), Berlin, Juni 2008
23. BREF/BAT Waste Incineration for Integrated Pollution Prevention and Control (IPPC) (2005) "Draft Reference Document on the Best Available techniques for Waste Incineration" European Commission, EIPPC Bureau Sevilla, Final Draft, May 2005
24. Dones R, Heck T, Hirschberg S (2004) Greenhouse Gas emissions from energy systems, comparison and overview. In: Cleveland C (ed) Encyclopedia of energy, vol 3. Academic/Elsevier, San Diego, pp 77–95
25. Umweltbundesamt – German Federal Office for Environment, press information 34/2008, Dessau-Rosslau, 16.05.2008, Germany
26. Kressig J, Stoffregen A (2008) Life cycle assessment of waste-to-energy plants in Europe – modeling of thermal treatment of municipal and similar waste to calculate eco-profiles for the European reference life cycle data system (ELCD), Performed for CEWEP by PE International, Leihnfelden-Echterdingen, Germany, 2008
27. Skovgaard M, Hedal N, Valanueva A, Andersen FM, Larsen H (2008) Municipal solid waste management and greenhouse gases, ETC/RWM working paper 2008/1, European Topic Center (ETC) on Resource and Waste Management (RWM), Copenhagen, 2008
28. ATSDR (2001) Landfill gas basic, agency for toxic substances & disease registry. In: Landfill gas primer – an overview for environmental health professionals. Atlanta, chap 2, November 2001
29. Tabasaran O, Rettenberger G (1987) Grundlagen zur Planung von Entgasungsanlagen, Handbuch Müll und Abfall, Kennz. 4547, Lieferung 1/87, E. Schmidt Verlag
30. Abfallbilanz, Umwelt, Statistisches Bundesamt, Wiesbaden, erschienen im Juli 2010
31. National Inventory Report for the German Greenhouse Gas Inventory 1990–2008, Submission under the United Nations Framework Convention on Climate Change and the Kyoto Protocol 2010, Federal Environment Office, Dessau-Roßlau, April 2010
32. Fritsche U, Rausch L (2008) Bestimmung spezifischer Treibhausgas-Emissionsfaktoren für Fernwärme, Bereich Energie & Klimaschutz. Öko-Institut, Büro Darmstadt, Im Auftrag des Umweltbundesamtes, Dessau-Roßlau, Mai
33. Bundesministerium für Wirtschaft und Technologie (Federal Ministry for Economics and Technology) (2006) Energieversorgung für Deutschland, Statusbericht für den Energiegipfel am 3 April 2006. Berlin, March 2006, p 61

Groundwater Impacts of Radioactive Wastes and Associated Environmental Modeling Assessment

Rui Ma[1,3], Chunmiao Zheng[1], Chongxuan Liu[2]
[1]Department of Geological Sciences, University of Alabama, Tuscaloosa, AL, USA
[2]Pacific Northwest National Laboratory, Richland, WA, USA
[3]China University of Geosciences, Wuhan, China

Article Outline

Glossary
Definition of the Subject
Introduction
Overview on Groundwater Impacts of Radioactive Wastes
Controlling Biogeochemical Processes
Environmental Modeling Assessment
Future Directions
Bibliography

Glossary

Absorption The process in which a dissolved substance is incorporated into the interior of a solid grain.

Adsorption The adhesion of a chemical species onto the solid surface.

Contaminant fate and transport The ultimate state of contaminants and the processes by which the contaminants migrate through the subsurface.

Groundwater Water that exists in liquid form beneath the land surface, filling the cracks, voids, and pore spaces in earth materials. The subsurface strata that store and transmit groundwater are referred to as aquifers.

Mass transfer The interaction and exchange of solutes in mobile state with those in immobile state through either physical or chemical processes.

Radioactive Waste A waste product that contains radioactive material. The majority of radioactive waste is "low-level" waste, which has low levels of radioactivity per unit of mass or volume.

Depending on the type and nature of radioactive wastes, it could take hours to thousands of years to diminish their radioactivity.

Reactive transport model The mathematical model that couples hydrogeological, geochemical, and biological processes to simulate and predict the contaminant fate and transport in the subsurface.

Sorption/desorption Sorption is a general term used to describe both adsorption and absorption by which a dissolved substance is attached to the surface or incorporated into the interior of a solid grain. The reverse process from the sorbed phase to the dissolved phase is referred to as desorption.

Definition of the Subject

Ever since the dawn of the nuclear age, especially since the 1970s with the work related to exploration of Yucca Mountain as a potential nuclear waste repository [1] and remediation of former nuclear fuel processing sites such as Hanford [2], there have been significant public concerns over groundwater impacts of radioactive wastes. This is because groundwater is a vital water resource with tremendous values to public water supplies and ecological lives, and because groundwater provides a pathway for potential spread of radioactive contaminants, posing significant risks to human health and ecological systems. Investigation of groundwater impacts of radioactive wastes requires understanding hydrogeological, geochemical, and biological processes that control the fate and transport of radionuclide contaminants. It will also require developing numerical simulators to integrate these processes for future projection under both natural and engineered remediation scenarios. While some sporadic information is available at specific sites, few attempts have been made to integrate scattered information into a coherent framework to answer relevant questions such as what are the most common sources of radioactive contaminants in groundwater and how they are transported and transformed in the aquifer.

Introduction

Radioactive waste contamination in soil and groundwater poses long-term risks to human health and environment. Public awareness on this subject has steadily increased worldwide since the inception of the nuclear age. Significant efforts have been made to understand the fate and transport of radionuclide wastes in environments, and a number of research and remediation programs have been established to remediate contaminated sites in the USA.

The radionuclide fate and transport in groundwater is controlled by hydrologic, microbiologic, and geochemical processes that operate in the subsurface environment. These processes and their coupling control contaminant migration and persistence, and efficiency of remediation technologies. The understanding of the fate and transport of radionuclide contaminants can improve the ability to forecast contaminant destination and select cost-effective remediation technologies such as mobilization, immobilization, or in-ground degradation.

Reactive transport models are important tools to systematically integrate physical, chemical, and biological processes and data that are critical to understand and predict the fate and transport of radionuclide contaminants in the subsurface. Properly designed and calibrated models can describe the interactions of competing processes at a range of spatial and time scales, and hence are helpful for optimizing field operations and designing monitoring systems for remediating contaminated sites.

This entry is intended to provide a review of the major sources of radioactive wastes and their impacts on groundwater contamination, to discuss the major biogeochemical processes that control the transport and fate of radionuclide contaminants in groundwater, and briefly describe the evolution of mathematical models designed to simulate and assess the transport and transformation of radionuclides in groundwater.

Overview on Groundwater Impacts of Radioactive Wastes

Source of Radioactive Wastes

Radioactive wastes were generated primarily from the production of nuclear fuels for the weapons program and electrical energy, development and operation of commercial power reactors, nuclear weapons tests, fuel reprocessing, waste storage and disposal activities, and nuclear accidents. According to the statistics by Ahearne [3], the combined volume of all radioactive

wastes (excluding that in the soil and water) from both the government and commercial sources in the USA is about 5.5 million cubic meters, and the total radioactivity from all anthropogenic sources is about 31 billion Ci. Over the past decades, the uranium mining for production of nuclear fuels has resulted in a large volume of mine and mill tailings, which contain all of the naturally occurring radioactive elements. This has left a legacy of environmental pollution across the countries in the world, such as former Soviet Union, USA, Germany, France, and Eastern European countries [4].

Contamination of Groundwater Caused by Radioactive Waste Release

Radionuclide contaminants have been detected in subsurface sediments and groundwater as a result of intentional and accidental release of radionuclide-containing wastes during storage, processing, and disposal of nuclear materials [5–7] as well as the leaching of uranium mill tailings [8, 9]. Thirty to eighty million cubic meters of soil and 1,800–4,700 million cubic meters of water have been contaminated by radionuclides in USA [10]. Among them, most contamination occurred at US Department of Energy (DOE) sites used for nuclear weapons production, where totally over 5,700 individual contaminant plumes have been detected in subsurface [11]. At DOE sites, the radionuclides (e.g., uranium, cesium, strontium, thorium, and tritium) have been normally co-disposed with chlorinated solvents (e.g., perchloroethylene (PCE) and trichloroethylene (TCE)) and metals (e.g., lead, chromium, and mercury) and thus have been often identified together with these contaminants in groundwater [5]. According to DOE estimation, approximately 38 million cubic meters of groundwater was contaminated from the wastes generated from uranium mill processing or mill tailings [12]. Among the radionuclide contaminants, actinide elements uranium, neptunium, and plutonium are the most problematic [13] because of their long decay half-lives in subsurface sediments and groundwater.

Groundwater Contamination by Radionuclides at Well-Known Sites

Thousands of sites around the world are currently contaminated with radionuclides [7]. In particular, spectacular examples of such sites can be found in the former Soviet Union and USA. Major contaminated areas are often located at or near facilities that reprocessed nuclear fuels from production reactors [6]. In the USA, the major sites are at Hanford in Washington state, Savannah River in South Carolina, and Oak Ridge in Tennessee [5, 6]. The contamination at Oak Ridge was caused by underground injection of cesium and strontium wastes, and at Savannah River resulted from the release of mixed fission product solutions into streams and seepage basins, and at Hanford originated from the discharge of mixed fission wastes into soils and surface ponds [6].

Among the contaminated sites at USA, the Hanford site has been dubbed "the dirtiest place on Earth" [14]. The contamination at the Hanford site, which was divided into three areas, namely, 100 Area, 200 East and West Areas, and 300 Area, has mainly occurred at locations of nuclear fuel fabrication, fuel irradiation, strategic radionuclide separation, and waste storage and disposal for plutonium production [5]. Sixty-seven of the 149 single shell tanks used for storing nuclear wastes were suspected to have released over 1.9 million liters of tank waste to the vadose zone [15]. The tank leaks, combined with discharge of liquid waste through ponds, trenches, pipelines, and cribs, caused a large quantity of radioactivity (through the year 2000: two million Ci) and 100,000–300,000 t of toxic chemicals residing in the vadose zone [2]. Wastes at the site have migrated through the vadose zone, resulting in groundwater contamination including nitrate, chromium, tritium, uranium, strontium-90, technetium-99, iodine, carbon tetrachloride, and others [16–18]. For example, waste disposal in 300 Area resulted in a groundwater plume of uranium (VI) with an area of 0.4–0.5 km^2 that exceeded the drinking water standard of 30 μg/L up to present [19].

For over 30 years, trillions of liters of acidic plating wastes containing high levels of uranium and nitric acid were generated at the Y-12 Facility, Oak Ridge, and Tennessee and were discarded into unlined S-3 Ponds. The wastes were neutralized and denitrified and the area was capped and converted to a parking lot in 1984 [20]. Despite these treatments, radionuclide contaminants continued to migrate from the source along geologic strike and dip to groundwater [21, 22].

The Savannah River Site was established in the early 1950s to produce nuclear materials, primarily tritium and plutonium-239 for nuclear weapon purposes, but also plutonium-238 and various transplutonium radionuclides for medical, industrial, and scientific applications. The production was ended in 1988 [23, 24]. The operations at the Savannah River Site have resulted in the migration of radionuclides (e.g., uranium, cesium, radium, thorium, and tritium) into groundwater at various locations, predominantly in the central areas of the site [24, 25].

Many abandoned mine processing sites were also contaminated with radionuclides during uranium mining activities. Contaminated groundwater at the former uranium mill site located at Naturita, Colorado, which processed uranium and vanadium ores intermittently from 1930s to 1958, occurred in the thin alluvial deposits of the San Miguel River floodplain. High concentrations of uranium were measured in the groundwater below and downgradient of the former tailings pile [26]. The uranium at the Old Rifle UMTRA field experiment site in western Colorado in the aquifer originated at mill tailings (now removed), percolated through a 4 m thick vadose zone to the water table, and was transported laterally through the aquifer via groundwater flow with maximum uranium concentrations of 300 μg/L [27].

Controlling Biogeochemical Processes

The fate and transport of radionuclides in groundwater is controlled by geochemical and biological processes, in addition to the hydrological ones. This section discusses four biogeochemical processes that have been identified to have major effects on the fate and transport of radionuclide contaminants in groundwater.

Adsorption/Desorption

The adsorption to sediment surfaces is a major geochemical process controlling the mobility of radionuclide contaminants in oxic groundwater. This process is regulated by interfacial chemistry of the prevailing mineral surfaces [9, 26, 28–32]. For example, spectroscopic characterization, laboratory transport experiments, and numerical simulations have revealed that adsorption is a primary process controlling uranium transport in the groundwater at Hanford 300 Area [33, 34], at a U(VI) mill located in Naturita, Colorado [26], at the Oak Ridge site in Tennessee [35], and at the Old Rifle UMTRA site in western Colorado [27]. Many experimental studies have also demonstrated that plutonium can be adsorbed onto a variety of minerals and mineral assemblages [36–38].

Sorption of actinides, particularly plutonium, onto submicrometer-sized colloids increases their mobility in groundwater [39]. Certain actinides can be stabilized in natural waters through the formation of actinide pseudo-colloids, in which the actinide sorbs onto aquatic colloids. This process alone can increase the actinide concentrations by many orders of magnitude over the values expected from solubility calculations [24, 39–41]. Colloid-facilitated transport is likely one of major mechanisms for long-distance transport of actinides in groundwater [39].

The kinetic adsorption/desorption behavior of radionuclide contaminants has often been observed in uranium (VI)-contaminated sediments with controlling mechanisms generally not well understood [32, 34, 42–47]. The kinetic uranium (VI) release from the Hanford 300 Area sediments was found to result from diffusional mass transfer from intragrain, intra-coating, and intragrain aggregate regions based on microscopic and spectroscopic characterizations of the sediments [48, 49].

Aqueous Complexation

Uranium (VI) can complex with various ligands such as carbonate in groundwater to form aqueous complexes. The aqueous complexation process stabilizes uranium in aqueous phase and decreases its tendency to bind to mineral surfaces [50]. Fox et al. [51] and Dong et al. [52] found that calcium can have a significant impact on the aqueous speciation of uranium (VI) under neutral to mild alkaline pH conditions through formation of ternary uranium (VI)-calcium-carbonate aqueous species. The aqueous and surface uranium (VI) complexation is sensitive to important groundwater chemical composition including pH, carbonate, and calcium concentrations [9, 26, 51]. Consequently, the hydrogeochemical conditions in groundwater at field sites have a great impact on radionuclide contaminant fate and transport. The groundwater redox conditions have also been found to impact the mobility of other selected radionuclides [53].

Precipitation/Dissolution

Radionuclide fate and transport is also affected by processes, such as precipitation/dissolution reactions [46, 54, 55], co-precipitation with other minerals [56], and microbially induced mineralization [22]. The actinide precipitation/dissolution may occur in intragrain regions where thermodynamic conditions for precipitation/dissolution reactions may significantly differ from bulk solution [46, 54].

Precipitation and co-precipitation processes play an important role in uranium stabilization under both reducing and oxidizing conditions [33, 57–59]. Under oxidizing conditions, radionuclides can react with carbonate and phosphate to form carbonate and phosphate minerals (e.g., autunite, $Ca(UO_2)_2(PO_4)_2$). Under reducing conditions, anaerobic bacteria can reduce uranium (VI) to uranium (IV) to form poorly soluble uraninite [22, 27, 35, 58]. Radium can be sorbed and co-precipitated with Fe–Mn oxyhydroxides, gypsum, barite [4, 60], and amorphous silica [61]. The stability of co-precipitated radionuclides is controlled by the host mineral solubility and stability. For example, microbial reduction of iron minerals can indirectly contribute to radium-226 release in groundwater [60].

All the processes mentioned above can act cooperatively or sequentially to control the transport behavior of radionuclide contaminants in aquifers. For example, a study by Catalano et al. [33] using the sediments collected from the Hanford 300 Area revealed that uranium co-precipitated with calcite in shallow vadoze zone sediments, formed metatorbernite ($Cu(UO_2PO_4)_2{\cdot}8H_2O$) that coexisted with adsorbed species at intermediate depths in the vadose zone, and occurred predominantly as adsorbed onto phyllosilicates in the deeper vadose zone and groundwater.

Bioreduction

Bioreduction has been proposed as a remediation approach to immobilize redox sensitive radionuclides in subsurface environments. Radionuclides can be reduced by various dissimilatory bacteria including metal-reducing bacteria and sulfate-reducing bacteria that use radionuclides as terminal electron acceptors [62, 63]. Microbial reduction of uranium (VI) to insoluble uranium (IV) by the injection of ethanol has been demonstrated at DOE Environmental Remediation Sciences Program (ERSP) Field Research Center in Oak Ridge, Tennessee [64] and Old Rifle UMTRA field site in western Colorado. The results from Wu et al. [22] demonstrated that aqueous uranium concentrations below the USEPA maximum contaminant level (<0.126 μM) can be achieved in situ, that bioreduced/immobilized uranium is stable under anaerobic conditions, and that infiltration of dissolved oxygen into the bioreduced area promotes spatially variable oxidation of uranium (IV) and mobilization of uranium (VI). Studies at Old Rifle UMTRA site demonstrated that the immobilization of uranium (VI) in groundwater can be achieved by iron-reducing bacteria stimulated by acetate amendment at the field scale [27, 65].

However, one major unresolved question in terms of bioreduction as a viable remediation technology is the long-term stability of bioreduced radionuclides such as biogenic uranium (IV). Zhong et al. [66] demonstrated that biogenic uranium (IV) readily oxidizes once groundwater environment returns to oxic condition. Wan et al. [67] presented evidence that bioreduced uranium (IV) was reoxidized under reducing conditions because carbonate accumulation promotes the formation of highly stable carbonato-uranium (VI) complexes under neutral to slightly alkaline conditions. Further researches are needed to enable the bioreduction as a remediation technology.

Environmental Modeling Assessment

Numerical modeling can help scientists and engineers understand and predict the radioactive contaminant fate and transport in the subsurface. Specifically, the modeling can be used to integrate conceptual understanding into a consistent and numerical framework, to test hypotheses on physical and chemical processes under field relevant conditions, to plan for field experiments under uncertainties, to interpret and analyze the field experimental data, and finally to help with the design of remedial alternatives. In an iterative and complementary way, field experiments and modeling activities can work together to enable one to gain new insights and to improve the predictive capabilities on contaminant fate and transport. This section discusses two major types of approaches for modeling radionuclide fate and transport in the subsurface.

Isotherm-Based Transport Modeling

This type of models was based on the simplification that a sorption isotherm involving a single distribution coefficient (Kd) can be used to describe the sorption equilibrium of radioactive contaminants [12]. The Kd based sorption isotherm can be directly incorporated into a hydrological transport equation to simulate the coupled effects of advection, dispersion, and sorption processes [68].

As discussed before, however, the radionuclide adsorption/desorption is controlled by complex geochemical and microbiological conditions at field, and a single Kd value is usually not adequate to represent the sorption behavior over a wide range of geochemical conditions. This is because Kd values are sensitive to geochemical conditions and vary as geochemical conditions change. For example, the Kd value for uranium (VI) can vary by five orders of magnitude over the pH range from 6 to 9 and by four orders of magnitude at pH 8 as the partial pressure of CO_2 gas increases from its value in air to 0.01 atm [9, 26].

In contaminant plumes where the groundwater compositions change spatially and temporally, the Kd values could also have complex spatial patterns and evolve temporally along with the transport processes. Consequently significant errors and uncertainties may be introduced in reactive transport simulations if a constant-Kd modeling approach is used at sites where groundwater chemistry varies temporally and spatially [9, 26, 28–31].

Multi-component Reactive Transport Modeling

Over the last 2 decades, a number of models that couple advective-dispersive-diffusive transport processes with "full" geochemistry, including pH, redox-state, sediment/rock–water interactions have been developed, such as PHT3D [69], MIN3P [70], and PHAST [71]. In these coupled models, the solute transport and chemical reactions are rigorously simulated often in three-dimensional groundwater flow systems. The mechanistic treatment of chemical reactions in the coupled multi-component, multi-species mass transport has obvious advantages over the empirical isotherm-based transport models since the models more realistically account for complex geochemical processes.

In contrast to the constant-Kd modeling approach, the coupled models normally incorporate surface complexation reactions into solute transport models through the mass action equations describing the equlibria between aqueous chemical species and species formed at mineral surfaces to account for the adsorption/desorption [9]. Surface complexation models (SCM) can account for variations in chemical conditions and aqueous speciation, and thus can describe spatial and temporal changes of radionuclide adsorption [26].

There are two major approaches for applying the SCM concept to natural subsurface systems: the Component Additivity (CA) and Generalized Composite (GC) approaches [9]. The CA approach utilizes documented SCMs for well-characterized surfaces and detailed sediment characterization of the study site to determine the quantity of each reactive surface in sediments and then assembles an SCM for the sediment from its basic components [9, 26]. In the GC approach, adsorption is assumed to occur on "generic" surface sites that represent average properties of the sediment surfaces because the surface of the mineral assemblage is considered too complex to be quantified in terms of the contributions of individual phases to adsorption. Adsorption can be described by mass laws written with "generic" surface functional groups, with the stoichiometry and formation constants for each mass law determined by fitting experimental data for the mineral assemblage as a whole [9, 72].

The SCM approach has not been commonly used to describe adsorption in field-scale reactive transport modeling studies because of a poor understanding of the thermodynamics of surface complex formation in natural systems and the lack of field data. However, there is a growing application of SCM in multi-component reactive transport modeling to simulate the radionucide fate and transport in aquifers due to recent advances in computer codes and availability of extensively geochemical characterization data in some filed sites, such as uranium reactive transport models developed at the Naturita site, Colorado [26], the Hanford site [34, 47, 73], the Oak Ridge site [35], and the Old Rifle site [27]. In addition to the models that consider equilibrium-based surface complexation reactions, models that couple kinetic mass transfer processes with surface complexation reactions have also

been developed to simulate the kinetic adsorption and desorption behavior of radionuclides. For example, Liu et al. [34, 47] proposed a multi-rate SCM to consider the effects of diffusive mass transfer on uranium (VI) adsorption/desorption processes, and the approach was evaluated at the Hanford site [73, 74].

The multi-component reactive transport model can also take into account for other biogeochemical reactions including aqueous complexation, precipitation/dissolution of radionuclide-containing minerals, and bioreduction (e.g., references [35, 75]). Thus the multi-component reactive transport model can better describe the transport and fate of radionuclide contaminants in the aquifer. However, obtaining sufficient and accurate field data for properly parameterizing a field-scale multi-component reactive transport model will remain a major challenge.

Future Directions

Future research should be aimed at improving fundamental understanding of radionuclide transport processes in heterogeneous subsurface media and facilitating transfer of knowledge and insights gained from laboratory experiment to field application.

Mass Transfer Processes of Radionuclide Contaminants in Heterogeneous Media

The variability in the physical and chemical properties of subsurface media, such as hydraulic conductivity, porosity, grain size, and reactive surface area, may vary by several orders of magnitude within an aquifer. The heterogeneity of physical and chemical properties causes spatial variations in groundwater flow velocity, reaction rate, and speciation. These variations may be associated with a range of different predominating phenomena such as preferential flow and contaminant migration pathways, hydraulically inaccessible zones into which solutes may only diffuse, and mineral grains by which solutes are selectively sorbed (e.g., references [76–82]). The individual phenomena in turn contribute to a variable extent to the spreading (dispersion) of chemical contamination, emerge and disappear at different time scales, and lead to variable reaction types and rates during solute mass transport.

As a result of physical and chemical heterogeneity, the mass transfer could occur in the subsurface at multiple scales. The release of contaminants including cesium-137, chromium(VI), strontium-90, and uranium from contaminated sediments at the Hanford site to groundwater is found to be controlled by mass transfer in laboratory experiments [46, 55, 83–85]. Mass transfer limitations also occur at increasingly larger (macroscopic) scales in the field (e.g., references [54, 86]) such as between coarse and fine textured zones in a given facies, or between different geologic formations and facies, such as highly conductive and less conductive aquifer layers [87]. Understanding multi-scale mass transfer processes and their implications to contaminant migration and remediation at the field scale is at the forefront of reactive transport science and is a critical need for the remediation of contaminated sites [87].

Upscaling of Radionuclide Transport from Laboratory to Field Scales

Laboratory experiments provide important information on parameters and key insights for contaminant transport processes. Even complex reactive transport models may be reasonably well constrained by measured data at the laboratory scale, where a large number of measurements and observations are available. However, this is generally not the case for field-scale problems where reactive transport may be affected or controlled by strongly chemically and/or physically heterogeneous conditions (e.g., references [74, 88–91]). The heterogeneity at different scales significantly influences and drastically complicates the upscaling of solute transport and its analysis and prediction at larger scales (e.g., references [86, 92–95]). Consequently, important differences can exist between the experimental conditions under which a laboratory model was developed and calibrated, and those present in the field, including the ratios of reaction and transport time scales and variability in reactant properties and distribution.

Without appropriate consideration of the upscaling problem, reliable prediction of reactive transport processes is impossible. Therefore, scale dependence and associated upscaling of transport parameters for porous media have been actively studied for two decades. For the most part, however, the existing research has focused on the development of theoretical or empirical upscaling methods in relatively simple

systems [96–98] and on the investigation of the scale dependence of different transport parameters such as diffusion coefficients, geochemical reaction rates, sorption coefficients, and retardation factors [99] and other factors (e.g., reference [100]) at various scales ranging from pore scale to column experiments, and to field tracer tests. However, very few studies have been reported on upscaling of transport processes of radionuclide contaminants in groundwater [74]. Thus, the unsolved problem is how to systematically upscale the reactive transport process and parameters for reactive transport models involving complex, physically and chemically heterogeneous systems across multi-scales.

Bibliography

1. Bodvarsson GS, Boyle W, Patterson R, Williams D (1999) Overview of scientific investigations at Yucca Mountain – the potential repository for high-level nuclear waste. J Contam Hydrol 38:3–24
2. Gephart RE (2003) Hanford: a conversation about nuclear waste and cleanup. Battelle, Columbus
3. Ahearne JF (1997) Radioactive waste: the size of the problem. Phys Today 50(6):24–29
4. Abdelouas A (2006) Uranium mill tailings: geochemistry, mineralogy, and environmental impact. Elements 2:335–341
5. Riley RG, Zachara JM, Wobber FJ (1992) Chemical contaminants on DOE lands and selection of contaminant mixtures for subsurface science research, DOE/ER-0547T. U.S. Department of Energy, Washington, DC
6. Bradley DJ, Frank CW, Mikerin Y (1996) Nuclear contamination from weapons complexes in the former Soviet Union and the United States. Phys Today 49:40–45
7. Whicker FW, Shaw G, Voigt G, Holm E (1999) Radioactive contamination: state of the science and its application to predictive models. Environ Pollut 100:133–149
8. Abdelouas A, Lutze W, Nuttall HE (1999) Uranium contamination in the subsurface; characterization and remediation. Rev Mineral Geochem 38:433–473
9. Davis JA, Meece DE, Kohler M, Curtis GP (2004) Approaches to surface complexation modeling of uranium (VI) adsorption on aquifer sediments. Geochim Cosmochim Acta 68(18):3621–3641
10. Ewing RC (2004) Environmental impact of the nuclear fuel cycle. In: Gieré R, Stille P (eds) Energy, waste and the environment: a geochemical perspective, geological society special publication 236. The Geological Society, London, pp 7–23
11. Lee D, Walton MR, Megio JL (2005) Biological and chemical interactions with U(VI) during anaerobic enrichment in the presence of iron oxide coated quartz. Water Res 39:4363–4374
12. Zhu C, Anderson G (2002) Environmental applications of geochemical modeling. Cambridge University Press, London
13. Renshaw J, Butchins LJC, Livens FR, May I, Charnock JM, Lloyd JR (2005) Bioreduction of uranium: environmental implications of a pentavalent intermediate. Environ Sci Technol 39:5657–5660
14. Fishlock D (1994) The dirtiest place on earth. New Sci 1913:34–37
15. Zachara JM, Serne J, Freshley M, Mann F, Anderson F, Wood M, Jones T, Myers D (2007) Geochemical processes controlling migration of tank wastes in Hanford's vadose zone. Vadose Zone J 6:985–1003
16. Gee GM, Oostrom M, Freshley MD, Rockhold ML, Zachara JM (2007) Hanford site vadose zone studies: an overview. Vadose Zone J 6:899–905
17. Um W, Serne RJ, Brown CF, Last GV (2007) U(VI) adsorption on aquifer sediments at the Hanford site. J Contam Hydrol 93:255–269
18. Hartman MJ, Morasch LF, Webber WD (2007) Hanford site groundwater monitoring for fiscal year 2006, Pacific Northwest National Laboratory, Richland
19. Hartman MJ, Webber WD, Fluor Hanford Inc (2008) Hanford site groundwater monitoring for fiscal year 2007. DOE/RL-2008-01, Revision 0, Pacific Northwest National Laboratory, Richland
20. Phillips H, Watson DB, Roh Y (2007) Uranium deposition in a weathered fractured saprolite/shale. Environ Sci Technol 41:7653–7660
21. Wu W, Carley J, Fienen M, Mehlhorn T, Lowe K, Nyman J, Luo J, Gentile ME, Rajan R, Wagner D, Hickey RF, Gu B, Watson D, Cirpka O, Kitanidis P, Jardine J, Criddle CS (2006) Pilot-scale in situ bioremediation of uranium in a highly contaminated aquifer. 1. Conditioning of a treatment zone. Environ Sci Technol 40(12):3978–3985
22. Wu W, Carley J, Luo J, Ginder-Vogel MA, Cardenas E, Leigh MB, Hwang C, Kelly SD, Ruan C, Wu L, Nostrand JV, Gentry T, Lowe K, Mehlhorn TL, Caroll S, Luo W, Fields MW, Gu B, Watson D, Kemner K, Marsh T, Tiedje J, Zhou J, Fendorf S, Kitanidis PK, Jardine PM, Criddle C (2007) In situ bioreduction of uranium (VI) to submicromolar levels and reoxidation by dissolved oxygen. Environ Sci Technol 41:5716–5723
23. Carlton WH (1997) Assessment of neptunium, americium, and curium in the Savannah River Site Environment. WSRC-TR-97-00266, Westinghouse Savannah River Co, Aiken
24. Dai M, Kelley JM, Buesseler KO (2002) Sources and migration of plutonium in groundwater at the Savannah River Site. Environ Sci Technol 36:3690–3699
25. Westinghouse Savannah River Co (1998) The Savannah River Site's groundwater monitoring program: third quarter 1997. ESH-EMS-970490, U.S. Department of Energy, Washington, DC
26. Curtis GP, Davis JA, Naftz DL (2006) Simulation of reactive transport of uranium (VI) in groundwater with variable chemical conditions. Water Resour Res 42:W04404. doi:10.1029/2005WR003979
27. Yabusaki SB, Fang Y, Long PE, Resch CT, Peacock AD, Komlos J, Jaffed PR, Morrison SJ, Dayvault RD, White DC, Anderson RT (2007) Uranium removal from groundwater via in situ biostimulation: field-scale modeling of transport and biological processes. J Contam Hydrol 93:216–235

28. Read D, Ross D, Sims RJ (1998) The migration of uranium through Clashach sandstone: the role of low molecular weight organics in enhancing radionuclide transport. J Contam Hydrol 35:235–248
29. Bethke CM, Brady PV (2000) How the Kd approach undermines group water cleanup. Ground Water 38(3):435–443
30. Glynn PD (2003) Modeling Np and Pu transport with a surface complexation model and spatially variant sorption capacities; implications for reactive transport modeling and performance assessments of nuclear waste disposal sites; reactive transport modeling in the geosciences. Comput Geosci 29(3):331–349
31. Zhu C (2003) A case against Kd-based transport models: natural attenuation at a mill tailings site; reactive transport modeling in the geosciences. Comput Geosci 29(3):351–359
32. Bond DL, Davis JA, Zachara JM (2008) Uranium(VI) release from contaminated vadose zone sediments: estimation of potential contributions from dissolution and desorption. In: Barnett MO, Kent DB (eds) Adsorption of metals to geomedia II. chap. 14, Elsevier, Amsterdam, pp 375–416
33. Catalano JG, Mckinley JP, Zachara JM, Heald SM, Smith SC, Brown GE (2006) Changes in uranium speciation through a depth sequence of contaminated Hanford sediments. Environ Sci Technol 40(8):2517–2524
34. Liu C, Zachara JM, Qafoku NP, Wang Z (2008) Scale-dependent desorption of uranium from contaminated subsurface sediments. Water Resour Res 44:W08413. doi:10.1029/2007WR006478
35. Luo J, Weber F, Cirpka OA, Wu W, Nyman JL, Carley J, Jardine PM, Criddle CS, Kitanidis PK (2007) Modeling in-situ uranium (VI) bioreduction by sulfate-reducing bacteria. J Contam Hydrol 92:129–148
36. Keeney-Kennicutt WL, Morse JW (1985) The redox chemistry of $Pu(V)O_2^+$ interaction with common mineral surfaces in dilute solutions and seawater. Geochim Cosmochim Acta 49(12):2577–2588
37. Sanchez AL, Murray JW, Sibley TH (1985) The adsorption of plutonium on goethite. Geochim Cosmochim Acta 49:2297–2307
38. Duff MC, Hunter DB, Triay IR, Bertsch PM, Reed DT, Sutton SR, Shea-McCarthy G, Kitten J, Eng P, Chipera SJ, Vaniman DT (1999) Mineral associations and average oxidation states of sorbed Pu on tuff. Environ Sci Technol 33:2163–2169
39. Novikov P, Kalmykov SN, Utsunomiya S, Ewing RC, Horreard F, Merkulov A, Clark SB, Tkachev VV, Myasoedov BF (2006) Colloid transport of plutonium in the far-field of the mayak production association, Russia. Science 314:638–641
40. Kim JI (1993) The chemical behavior of transuranium elements and barrier functions in natural aquifer systems. Mater Res Soc Symp Proc 294:3–21
41. Kim JI (1994) Actinide colloids in natural aquifer systems. Mater Res Soc Bull 19:47–53
42. Braithwaite A, Livens FR, Richardson S, Howe MT (1997) Kinetically controlled release of uranium from soils. Eur J Soil Sci 48:661–673
43. Barnett MO, Jardine PM, Brooks SC, Selim HM (2000) Adsorption and transport of uranium(VI) in subsurface media. Soil Sci Soc Am J 64:908–917
44. Baik MH, Cho WJ, Hahn PS (2004) Sorption of U(VI) onto granite surfaces: a kinetic approach. J Radioanal Nucl Chem 260:495–502
45. Qafoku NP, Zachara JM, Liu C, Gassman PL, Qafoku OS, Smith SC (2005) Kinetic desorption and sorption of U(VI) during reactive transport in a contaminated Hanford sediment. Environ Sci Technol 39:3157–3165
46. Liu C, Zachara JM, Yantansee W, Majors PD, McKinley JP (2006) Microscopic reactive diffusion of uranium in the contaminated sediments at Hanford, USA. Water Resour Res 42: W12420. doi:10.1029/2006WR005031
47. Liu C, Shi S, Zachara JM (2009) Kinetics of uranium(VI) desorption from contaminated sediments: effect of geochemical conditions and model evaluation. Environ Sci Technol 43(17):6560–6566
48. Arai Y, Marcus MA, Tamura N, Davis JA, Zachara JM (2007) Spectroscopic evidence for uranium bearing precipitates in vadose zone sediments at the Hanford 300-area site. Environ Sci Technol 41:4633–4639
49. Stubbs JE, Veblen LA, Elbert DC, Zachara JM, Davis JA, Veblen DR (2009) Newly recognized hosts for uranium in the Hanford site vadose zone. Geochim Cosmochim Acta 73(6): 1563–1576
50. Waite TD, Davis JA, Payne TE, Waychunas GA, Xu N (1994) Uranium (VI) adsorption to ferrihydrite: application of a surface complexation model. Geochim Cosmochim Acta 58(24):5465–5478
51. Fox PM, Davis JA, Zachara JM (2006) The effect of calcium on aqueous uranium(VI) speciation and adsorption to ferrihydrite and quartz. Geochim Cosmochim Acta 70:1379–1387
52. Dong W, Ball WP, Liu C, Wang Z, Stone AT, Bai J, Zachara JM (2005) Influence of calcite and dissolved calcium on uranium (VI) sorption to a Hanford subsurface sediment. Environ Sci Technol 39:7949–7955
53. Hu QH, Zavarin M, Rose TP (2008) Effect of reducing groundwater on the retardation of redox-sensitive radionuclides. Geochem Trans 9:12. doi:10.1186/1467-4866-9-12
54. Liu C, Zachara JM, Qafoku OS, McKinley JP, Heald SM, Wang Z (2004) Dissolution of uranyl microprecipitates in subsurface sediments at Hanford site, WA. Geochim Cosmochim Acta 68:4519–4537
55. McKinley JP, Zachara JM, Liu C, Heald SM (2006) Microscale controls on the fate of contaminant uranium in the vadose zone, Hanford site, Washington. Geochim Cosmochim Acta 70:1873–1887
56. Gómez P, Garralón A, Buil B, Turrero MJ, Sánchez L, de la Cruz B (2006) Modeling of geochemical processes related to uranium mobilization in the groundwater of a uranium mine. Sci Total Environ 366:295–309
57. Abdelouas A, Lutze W, Nuttall E (1998) Chemical reactions of uranium in ground water at a mill tailings site. J Contam Hydrol 34:343–361

58. Abdelouas A, Lutze W, Gong W, Nuttall EH, Strietelmeier BA, Travis BJ (2000) Biological reduction of uranium in groundwater and subsurface soil. Sci Total Environ 250:21–35
59. Ohnuki T, Kozai N, Samadfam M, Yasuda R, Yamamoto S, Narumi K, Naramoto H, Murakami T (2004) The formation of autunite ($Ca(UO_2)_2(PO_4)_2 \cdot nH_2O$) within the leached layer of dissolving apatite: incorporation mechanism of uranium by apatite. Chem Geol 211:1–14
60. Martin AJ, Crusius J, Jay McNee J, Yanful EK (2003) The mobility of radium-226 and trace metals in pre-oxidized subaqueous uranium mill tailings. Appl Geochem 18:1095–1110
61. Landa ER (2004) Uranium mill tailings: nuclear waste and natural laboratory for geochemical and radioecological investigations. J Environ Radioactiv 77:1–27
62. Lovely DR, Coates JD (1997) Bioremediation of metal contamination. Curr Opin Biotechnol 8:285–289
63. Liu C, Gorby YA, Zachara JM, Fredrickson JK, Brown CF (2002) Reduction Kinetics of Fe(III), Co(III), U(VI), Cr(VI), and Tc (VII) in cultures of dissimilatory metal-reducing bacteria. Biotechnol Bioeng 80(6):637–649
64. Wu W, Carley J, Gentry T, Ginder-Vogel MA, Fienen M, Mehlhorn T, Yan H, Carroll S, Nyman J, Luo J, Gentile ME, Fields MW, Hickey RF, Watson D, Cirpka OA, Fendorf S, Zhou J, Kitanidis P, Jardine PM, Criddle CS (2006) Pilot-scale in situ bioremediation of uranium in a highly contaminated aquifer. 2: U(VI) reduction and geochemical control of U(VI) bioavailability. Environ Sci Technol 40:3986–3995
65. Anderson RT, Vrionis HA, Ortiz-Bernad I, Resch CT, Long PE, Dayvault R, Karp K, Marutzky S, Metzler DR, Peacock A, White DC, Lowe M, Lovley DR (2003) Stimulating the in situ activity of *Geobacter* species to remove uranium from the groundwater of a uranium-contaminated aquifer. Appl Environ Microbiol 69(10):5884–5891
66. Zhong L, Liu C, Zachara JM, Kennedy DW, Szecsody JE, Wood BD (2005) Oxidative remobilization of biogenic uranium (IV) precipitates: effects of Iron (II) and pH. J Environ Qual 34(5):1763–1771
67. Wan J, Tokunaga TK, Brodie E, Wang Z, Zheng Z, Herman D, Hazen T, Firestone MK, Sutton SR (2005) Reoxidation of bioreduced uranium under reducing conditions. Environ Sci Technol 39:6162–6169
68. Zheng C, Wang PP (1999) MT3DMS, a modular three-dimensional multi-species transport model for simulation of advection, dispersion and chemical reactions of contaminants in groundwater systems; documentation and user's guide, U.S. Army Engineer Research and Development Center Contract Report SERDP-99-1, Vicksburg, p 202. http://hydro.geo.ua.edu/mt3d/
69. Prommer H, Barry DA, Zheng C (2003) MODFLOW/MT3DMS based reactive multicomponent transport modeling. Ground Water 41(2):247–257
70. Mayer KU, Frind EO, Blowes DW (2002) Multicomponent reactive transport modeling in variably saturated porous media using a generalized formulation for kinetically controlled reactions. Water Resour Res 38:1174. doi:10:1029/2001WR000862
71. Parkhurst DL, Kipp KL, Engesgaard P, Charlton SC (2004) PHAST – a program for simulating ground-water flow, solute transport and multicomponent geochemical reactions. USGS Tech Meth 6-A8:154
72. Davis JA, Payne TE, Waite TD (2002) Simulating the pH and pCO_2 dependence of uranium(VI) adsorption by a weathered schist with surface complexation models. In: Geochemistry of soil radionuclides. Soil Science Society of America, Madison, pp 61–68
73. Ma R, Zheng C, Prommer H, Greskowiak J, Liu C, Zachara J, Rockhold M (2010) A field-scale reactive transport model for U (VI) migration influenced by coupled multirate mass transfer and surface complexation reactions. Water Resour Res 46: W05509. doi:10.1029/2009WR008168
74. Greskowiak J, Prommer H, Liu C, Post VEA, Ma R, Zheng C, Zachara JM (2010) Comparison of parameter sensitivities between a laboratory and field scale model of uranium transport in a dual domain, distributed-rate reactive system. Water Resour Res 46:W09509. doi:10.1029/2009WR008781
75. Fang Y, Yabusaki SB, Morrison SJ, Amonette JP, Long PE (2009) Multicomponent reactive transport modeling of uranium bioremediation field experiments. Geochim Cosmochim Acta 73:6029–6051
76. Gelhar LW (1986) Stochastic subsurface hydrology – from theory to applications. Water Resour Res 22(9):135S–145S
77. Dagan G (1989) Flow and transport in porous formations. Springer, New York
78. Barber LB (1994) Sorption of chlorobenzenes to Cape Cod aquifer sediments. Environ Sci Technol 28:890–897
79. Friedly JC, Davis JA, Kent DB (1995) Modeling hexavalent chromium reduction in groundwater in field-scale transport and laboratory batch experiments. Water Resour Res 31:2783–2794
80. Kleineidam S, Rugner H, Grathwohl P (1999) Impact of grain scale heterogeneity on slow sorption kinetics. Environ Toxicol Chem 18:1673–1678
81. Allen-King RM, Divine DP, Robin MJL, Alldredge JRG (2006) Spatial distributions of perchloroethylene reactive transport parameters in the Borden aquifer. Water Resour Res 42:W01413. doi:10.1029/2005WR003977
82. Descourvières C, Hartog N, Patterson BM, Oldham C, Prommer H (2010) Geochemical controls on sediment reactivity and buffering processes in a heterogeneous aquifer. Appl Geochem 25:261–275
83. Liu C, Zachara JM, Smith SC, McKinley JP, Ainsworth CC (2003) Desorption kinetics of radiocesium from the subsurface sediments at Hanford site, USA. Geochim Cosmochim Acta 67:2893–2912
84. McKinley JP, Zachara JM, Smith SC, Liu C (2007) Cation exchange reactions controlling desorption of $^{90}Sr^{2+}$ from coarse-grained contaminated sediments from the Hanford formation, Washington. Geochim Cosmochim Acta 71(2):305–325
85. Zachara JM, Ainsworth CC, Brown GE Jr, Catalano JG, McKinley JP, Qafoku O, Smith SC, Szecsody JE, Traina SJ, Warner JA (2004)

Chromium speciation and mobility in a high level nuclear waste vadose zone plume. Geochim Cosmochim Acta 68(1):13–30
86. Zheng C, Gorelick SM (2003) Analysis of solute transport in flow fields influenced by preferential flow paths at the decimeter scale. Ground Water 41(2):142–155
87. Zachara J, Freshley M, Andersen G, DePaolo D, Fredrickson J, Haggerty R, Kent D, Konopka A, Lichtner P, Liu C, McKinley J, Rockhold M, Rubin Y, Szecsody J, Versteeg R, Ward A, Williams B, Zheng C (2007) Integrated field-scale subsurface research challenge, multi-scale mass transfer processes controlling natural attenuation and engineered remediation: an IFC focused on Hanford's 300 area uranium plume. Proposal to the U.S. Department of Energy Office of Biological and Environmental Research LAB 06–16 – Environmental Remediation Science Program
88. Morrison SJ, Tripathi VS, Spangler RR (1995) Coupled reaction/transport of a chemical barrier for controlling U(VI) contamination in groundwater. J Contam Hydrol 17:347–363
89. Zhu C, Hu FQ, Burden DS (2001) Multi-component reactive transport modeling of natural attenuation of an acid groundwater plume at a uranium mill tailings site. J Contam Hydrol 52:85–108
90. Bain JG, Mayer KU, Blowes DW, Frind EO, Molson JWH, Kahnt R, Jenk U (2001) Modeling the closure-related geochemical evolution of groundwater at a former uranium mine. J Contam Hydrol 52:109–135
91. Yabusaki SB, Fang Y, Waichler SR (2008) Building conceptual models of field-scale uranium reactive transport in a dynamic vadose zone-aquifer-river system. Water Resour Res 44: W12403. doi:10.1029/2007WR006617
92. Feehley CE, Zheng C, Molz FJ (2000) A dual-domain mass transfer approach for modeling solute mass transfer in heterogeneous porous media, application to the MADE site. Water Resour Res 36:2501–2515
93. Haggerty R, Harvey CF, von Schwerin CF, Meigs LC (2004) What controls the apparent timescale of solute mass transfer in aquifers and soils? A comparison of experimental results. Water Resour Res 40:W01510. doi:10.1029/2002WR001716
94. Gorelick SM, Liu G, Zheng C (2005) Quantifying mass transfer in permeable media containing conductive dendritic networks. Geophys Res Lett 32:L18402. doi:10.1029/2005GL023512
95. Zheng C, Bianchi M, Gorelick SM (2010) Lessons learned from 25 years of research at the MADE site. Ground Water (in press)
96. Seeboonruang U, Ginn TR (2006) Upscaling heterogeneity in aquifer reactivity via exposure-time concept: forward model. J Contam Hydrol 84:127–154
97. Fernàndez-Garcia D, Llerar-Meza G, Gómez-Hernández JJ (2009) Upscaling transport with mass transfer models: mean behavior and propagation of uncertainty. Water Resour Res 45:W10411. doi:10.1029/2009WR007764
98. Heβe F, Radu FA, Thullner M, Attinger S (2009) Upscaling of the advection–diffusion–reaction equation with monod reaction. Adv Water Resour 32:1336–1351
99. Deng H, Dai Z, Wolfsberg A, Lu Z, Ye M, Reimus P (2010) Upscaling of reactive mass transport in fractured rocks with multimodal reactive mineral facies. Water Resour Res 46:15. doi:10.1029/2009WR008363
100. Wang F, Bright J (2004) Scale effect and calibration of contaminant transport models. Ground Water 42(5):760–766

Groundwater Remediation, Environmental and Economic Assessment

Paul Hardisty[1], Ece Ozdemiroglu[2]
[1]WorleyParsons, Perth, WA, Australia
[2]Economics for the Environment Consultancy (EFTEC), London, UK

Article Outline

Glossary
Definition of the Subject and Its Importance
Introduction
Decision-Making Context
The Economics of Remediation
Case Histories
Discussion and Conclusions
Future Directions
Bibliography

Glossary

CBA Cost benefit analysis – A decision-making tool that compares costs and benefits of a proposed policy or project in monetary terms. The aim is to find the most beneficial (highest net benefit) option of achieving a given objective. Taking no action is also included as an option.

CEA Cost effectiveness analysis – A decision-making tool that compares the costs of a proposed policy or project to a (nonmonetary) measure of its benefits. The aim is to find the option that generates the highest benefit for each unit of money spent.

TEV Total economic value – The economic value of a resource comprised of its use and nonuse values.

Definition of the Subject and Its Importance

As the world's population grows, industrial activities continue to degrade land and water at a faster pace. Under the "polluter pays" principle, increasingly adopted as the fundamental ethical precept for remediation policy, the responsibility for planning, funding, and executing remediation lies with the polluter. And ever present and increasingly vocal and powerful, are the public, the neighbors, the inhabitants of the planet, demanding that their interests be served also, and that the planet's dwindling resources be protected for their future, and the future of their children.

But remediating polluted aquifers can be expensive, technically difficult, and time-consuming [1, 2]. Deciding if and when to remediate, and to what degree, can be regarded in the context of alternative environmentally and socially beneficial actions. What else could be done with the money required to restore a site or aquifer? Which of the many choices available would provide the greatest benefit to society? And then, what are the commercial realities facing those who are called upon to pay for remediation?

Significant amounts of time, effort, and money have already been devoted to remediation of aquifers worldwide. A tremendous diversity of methods and technologies has been applied, in conditions as variable as the individual sites themselves. Along the way, consultants, problem holders, individual professionals, and government institutions have accumulated wide knowledge of the costs of remediation.

Combining and prioritizing the diverse objectives, interests, and constraints of different stakeholders involved requires a multidisciplinary approach to decision-making. Requirements include understanding the objectives, the risks (of taking remediation action and no action), and the environmental and financial costs and benefits of remediation. Combining information and data from different disciplines requires a common unit of value for direct comparison.

Truly sustainable remediation requires moving beyond money and examining which of a variety of options best optimizes overall value to society over the longer term. Given the inherent uncertainty associated with valuing market and nonmarket goods, even in the present, the relative overall long-term performance of remedial options must be evaluated over a wide range of possible future conditions.

Introduction

Until very recently, selecting the least-cost remedial option passed for "economic" analysis [3, 4]. The benefits to the problem holder were sometimes considered; the wider benefits to other parts of society rarely [5]. Borrowing from the wider environmental economics literature [6], the costs and wider economic benefits of remedial alternatives can be compared to select optimal remediation approaches [7]. A critical part of this equation, rarely considered, is the cost of secondary effects or by-products of the remedial action, including the so-called external costs of many common remedial practices, such as excavation and land-filling contaminated soils and materials (discussed below). This entry presents the case for applying an environmental and economic multidisciplinary approach to assessing the costs and benefits of groundwater remediation. This combined approach is termed environmental and economic sustainability assessment (EESA) to remedial decision-making [8]. Environmental approaches within the EESA are used to identify the risks created by contamination and the ability of remediation options to address these risks. Economic approaches are used to quantify the cost to the receptors (the environment itself, users of the environment, water users, and so on) of contamination.

Decision-Making Context

At the outset, it is important to distinguish between the different levels at which remedial decisions need to be made. The current literature makes reference to "remedial approaches," "remedial options," and "remedial technologies," sometimes interchangeably, and often without clear definition. For contaminated groundwater (and indeed for contaminated land sites), the distinctions between objectives, approaches (or strategies) and technologies is vitally important. These are formally defined below [1].

- *Remedial objective* is the overall intent of the remediation. Objectives could include the degree to which groundwater is to be remediated, the

protection of specific receptors, or the elimination or reduction of certain unacceptable risks.

- *Remedial strategy* (or approach) is the way in which the remediation objective is to be reached, and is defined specifically in terms of the pollutant linkage component it addresses: source removal, pathway elimination, source protection/isolation, or a combination thereof.
- *Remedial technologies* are the specific tools which form the components of the remediation strategy. For example, physical containment (a pathway elimination approach) can be achieved through use of slurry walls, sheet pile walls, or liners, often in conjunction with groundwater pumping and treatment. Source removal can be achieved through excavation and on-site treatment of contaminated soils (by a variety of techniques), or through many available in situ mass destruction techniques. A remedial strategy will very often involve the use of several different remedial technologies.

These levels are all interlinked. The remedial objective should be known before detailed design (technology selection) occurs. Designing options to meet the same strategic objective is crucial to ensure a consistent comparison of costs and benefits. The choice of a remedial approach is a critical intermediate step, which can be used both to help set objectives (by considering and comparing various approaches at the conceptual level), and to guide the selection of the technological components that will make up the final design. Each of these three levels of analysis is discussed below.

Contamination issues must be seen in the context of time and space, and are inherently dynamic in nature. This presents a number of challenges for the setting of remedial objectives and assessing the most economic remediation alternative: (1) objectives must be framed in a temporal context; (2) technology changes with time, and (3) regulations change with time. In the same way, the *scale* of a contamination problem is not necessarily fixed. A spill which is initially concentrated in a small area may over time expand and affect a considerable volume, as contaminants migrate laterally and vertically, bringing them into contact with other media and receptors. The scale of a contamination problem may have significant impact on how it is valued by society.

Remedial Objective

The remedial objective is the level at which the benefits of remediation are most readily and fundamentally determined. If a valuable receptor is protected, a benefit to society accrues. If a receptor is not protected, damage (and cost to society) results. Benefits are tied clearly to the fundamental remedial objective, and the basic approach used to achieve it. For a groundwater contamination problem, the choice of whether to achieve the objective using pump-and-treat, a bio-barrier, or natural attenuation, has a direct impact on costs (including any disbenefits associated with the method such as release of off-gases to the atmosphere, for instance), but benefits remain essentially constant.

Choosing a remedial objective can become quite complex when mobile groundwater plumes are involved. Consider, for example, a fixed point source which actively introduces contaminants into groundwater at a mass rate (dm/dt). A conservative solute, such as chloride, will move at the linear advective groundwater velocity. Many organic contaminants, such as benzene for example, will biologically degrade over time, and are also subject to adsorption onto matrix material. As time passes, the plume migrates in groundwater, dispersing laterally and transversely due to the effects of chemical diffusion and mechanical mixing. Early in the plume's evolution, the contaminants may only have migrated a short distance, and might still be quite highly concentrated. Only a relatively small volume of aquifer has been impacted. At this stage, perhaps no receptors of concern have yet been impacted. But as plume migration continues unabated, receptors may become impacted. The further the plume spreads, the greater the likelihood that more distant receptors will be affected. The result is that the number of receptors impacted may increase with time. Depending on the behavior of the contaminant solute (degree of attenuation by adsorption, dispersion, biological and chemical degradation), impacts could also vary with time at a given receptor. In such a situation, risk needs to be described as a function of time and space. As the plume migrates and disperses

with time, various receptors are impacted at different times. For interventions which take place at a given point in time and space ([x, t] coordinates), a remedial cost and benefit (equal to damage avoided if the remediation took place) would be realized. So for the generic case, costs and benefits of remediation vary not only with time, but with the location in space at which the remedial action is implemented. The various remedial objective options can be evaluated within this context.

Remedial objectives might include preventing or reducing the impact to a specific receptor, or preventing contamination from exceeding a given concentration at a specified point. If a receptor has already been impacted by the time the problem is discovered, the objective may be to prevent further exposure, or even attempt reversal of the damage. Remedial objectives may also change with time. An initial evaluation could indicate that net benefits are maximized if a certain noncritical receptor could be sacrificed, and that the situation with respect to a more distant receptor could be reevaluated, given that migration times would be expected to be long and attenuation active. At the reevaluation point, remedial technology options may have broadened, the value of the receptor may have increased, and the degree of attenuation and migration may have turned out to be different from that which was originally predicted. A reanalysis of the costs and benefits could indicate that a change of objectives is warranted. Flexibility based on continuous monitoring of remedial progress is an important part of any remedial strategy.

Remedial Strategy

There exist a staggering number of different remediation technologies available to achieve any specific technical outcome. For example, dissolved volatile organic compounds can be removed from the subsurface by physically pumping out the water and treating it at surface with a variety of methods, can be destroyed in situ by promoting aerobic or anaerobic biodegradation, can be volatilized in situ by introducing air into the saturated zone (air sparging), or can be removed passively with a variety of permeable barrier systems. Available technologies for controlling the migration of contaminants in groundwater include physical barrier systems, funnel-and-gate technology, hydraulic control through pumping and reinjection, and permeable reactive barriers. Sources of ongoing groundwater contamination (often called subsurface sources), including NAPLs (non-aqueous phase liquids), can be removed in a wide variety of ways. Soil remediation is often a critical part of an overall groundwater remediation program. Contaminants can be removed from soil by excavation and treatment using methods such as soil washing, enhanced biological treatment, or chemical oxidation, or with a variety of in situ methods. Often, several different technologies, each designed to achieve a specific technical outcome, will be required to accomplish the remedial objective. Because so many technologies exist, which achieve such different technical outcomes, at such widely varying costs, direct comparison of technologies using EESA is often not practical or useful, without first framing them within a set of remedial strategies [9].

The remedial strategy does not focus on technology per-se, but on ways of breaking the pollutant risk linkage, which causes (or will cause) damage. The list of possible remedial strategies is relatively short: either remove the source, eliminate the pathway, or protect/move/manage the receptor. Consideration of remedial strategy can be very useful in aligning the EESA with current risk-based guidance, and in streamlining the EESA process, since only a limited number of strategies need be considered [8]. Remedial strategy provides a link between remedial objectives, and the hundreds of clean-up technologies available. Also, the degree to which the risk linkage is broken, the timing of the action, and the spatial location at which the action is taken, are all variables which must be considered when choosing a strategy. Constraints analysis can be undertaken to help assess which strategies are realistically achievable. Preliminary high-level costs can be assigned to each strategy which can feasibly achieve the desired objective, and compared to the benefits of achieving the objective. This provides a relatively quick strategic analysis of the costs and benefits of remediation, and a basis for selection of an optimal remedial strategy, before proceeding to detailed technology evaluation and cost analysis.

Remedial Technology

The remedial technology selection level involves choosing the most cost-effective way of implementing

a remedial strategy. This requires detailed comparison of capital and operation and maintenance (O&M) costs for technologies over a projected project life span. The external costs of remediation over the life cycle would also be incorporated into the cost analysis. Application of constraints to remediation helps to reduce the number of viable technologies which can be feasibly applied to the problem. In some cases, different technologies may also realize different benefits (within a given strategy). If these are significant, they should be included in the assessment.

The Economics of Remediation

Introduction to Environmental Economic Analysis

Environmental resources, groundwater included, have economic values that are determined by individuals' preferences for them. Economic values are expressed in relative terms based on individuals' preferences for given *changes* in the quality and/or quantity of resources. The unit used for economic valuation is money – as it is a common unit making the comparison of financial and environmental costs and benefits possible.

Many environmental resources or services they provide are market goods and services. In the context of groundwater, the key market good is water abstracted for public water supply and other uses. The market price at which a good is exchanged reveals some information on its economic value. In particular, for the buyer of a good, the price reveals the amount of money the buyer is at least willing to give up to obtain the good. For the seller, the price reveals the amount of money the seller is at least willing to accept as compensation for giving up the good. Using this unit, preferences are measured in terms of individuals' willingness to pay (WTP) money to avoid an environmental loss or to secure a gain and their willingness to accept (WTA) money as compensation to tolerate an environmental loss or to forgo a gain.

Many resources and services supported by environmental resources are not traded in markets and are consequently "unpriced" or "nonmarket" goods and services. Most groundwater services such as recharging surface waters are nonmarket. These nonmarket goods and services still have economic values.

People have several motivations for having positive WTP and WTA, which are presented in the Total Economic Value (TEV) typology. Total Economic Value is the sum of:

Use values, which involve some interaction with the resource, either directly or indirectly:

- *Direct use value*: The use of groundwater in either a consumptive manner, such as industrial water abstraction or in a nonconsumptive manner such as for recreation (e.g., fishing) from the surface waters supported by groundwater.
- *Indirect use value*: The role of groundwater in providing or supporting key (ecosystem) services, such as nutrient cycling, habitat provision, water regulation and cleaning, etc.
- *Option value*: Not associated with current use of groundwater but the benefit of keeping open the option to make use of groundwater in the future. A related concept is *quasi-option value*, which arises through avoiding or delaying irreversible decisions, where technological and knowledge improvements can alter the optimal management of a natural resource.

Nonuse (or passive use) value is associated with benefits derived simply from the knowledge that the natural resources and aspects of the natural environment are maintained, that is, it is not associated with any use of a resource. For example, individuals place a value to knowing that aquifers will be protected from pollution or over-abstraction even though they have no intention to make any direct or indirect use. Nonuse value can be split into three parts:

- *Altruistic value*: Derived from knowing that contemporaries can enjoy the goods and services provided by groundwater
- *Bequest value*: Associated with the knowledge that groundwater as a resource will be passed on to future generations
- *Existence value:* Derived simply from the satisfaction of knowing that aquifers continue to exist, regardless of use made of it by oneself or others now or in the future

Those who make direct and indirect use of an environmental resource, that is, the users, are likely to hold both use and nonuse values. Those who do not directly or indirectly use the resource but still hold nonuse values are called nonusers. While users are

relatively easy to identify (e.g., owners of the site to be remediated or owners of surrounding properties – see below regarding blight), there is no theoretical definition of nonusers. The definition is an empirical question which can be answered by primary research.

Two types of economic valuation methods are developed to estimate the economic value of the nonmarket goods and services in the absence of price information. The first type is called revealed preference methods. They use price and consumption information from markets that are affected by environmental quality. For example, hedonic property pricing method estimates the premium buyers pay for properties in environmentally high-quality surroundings. Travel cost estimates the economic value of informal (free of direct charge) recreation by analyzing the costs incurred by recreational visitors to travel to and from and at a recreational site. The second type is called stated preference methods, which use questionnaires to elicit individuals' WTP and/or WTA. These methods are potentially applicable to any resource and decision context and the only methods that can estimate nonuse values.

Economic value evidence is used in cost benefit analysis (CBA) as well as other decision-making contexts. CBA is a decision framework that compares the costs and benefits of a policy or project action and nonaction. The costs and benefits have precise meanings. Any change that is likely to increase society's welfare generates a benefit. Any change that is likely to decrease society's welfare generates a cost. An avoided cost (e.g., cost of contamination avoided through remediation) becomes a benefit. Similarly, a foregone benefit (e.g., if remediation does not take place) becomes a cost.

Once each type of cost and benefit is estimated in monetary terms, they are aggregated over different types of costs and benefits, over affected populations, and over time. The comparison of these aggregated costs and benefits is done through two calculations. The first is the Net Present Value (NPV), which is the sum of net benefits (benefits minus costs) each year over time. As the value of a benefit (or a cost) is less in the future for various reasons, the future costs and benefits are discounted. A positive (negative) NPV means that aggregate benefits over time exceed (are less than) aggregate costs over time. CBA recommends options with positive NPV for further consideration. The option with the highest positive NPV is the best option according to the NPV calculation. The second comparison calculation is the Benefit Cost Ratio (BCR), which is the ratio of benefits summed over time (and discounted) to costs summed over time (and discounted). A BCR greater (less) than 1 means that aggregate benefits over time exceed (are less than) aggregate costs over time. CBA recommends options with BCR greater than 1. The option with the highest BCR is the best option according to the NPV calculation. NPV is the preferred calculation when the decision-making context is one of finding the option with the highest positive welfare impact. BCR is the preferred calculation when the decision-making context is one of finding the best (highest welfare) way of spending a given budget.

CBA allows for all options, including not taking action, to be compared so long as all options are set to achieve the same objective. Cost Effectiveness Analysis (CEA), on the other hand, estimates the costs in the same way as CBA but does not quantify the benefits in monetary term. The CEA ratio is then like BCR where benefits are in some physical or other quantity as relevant to the decision-making context. The shortcoming of CEA compared to CBA is that the former cannot judge the cost-effectiveness of taking no action and hence whether it is worthwhile to achieve the given objective at all.

CBA requires a multidisciplinary approach in order to identify and quantify the costs and benefits before their economic (monetary) value can be estimated. Even an extensive CBA is not always able to quantify and monetize all costs and benefits due to lack of data and uncertainties. Therefore, sensitivity analysis for testing different values and parameters is crucial.

Such a multidisciplinary approach has been developed in the context of groundwater remediation. The EESA (environmental and economic sustainability assessment) method employs elements of CBA, risk assessment, and sensitivity analysis, along with a full technical analysis of remedial options, effectiveness, and secondary impacts, to assist in identifying remediation strategies and options, which will result in optimal net benefit to all stakeholders. At the end of the process, it is about comparing possible courses of action, using money as a common unit of measure to

examine necessary trade-offs, but then moving beyond money to examine which options are most robustly superior under the widest range of possible future conditions.

What types of costs and benefits and what rate of discounting applies are discussed below in the specific context of groundwater. Case histories illustrate how to use NPV and BCR.

Economic Analysis in the Context of Groundwater Remediation

An economic assessment framework was specifically developed for groundwater remediation cases in Hardisty and Ozdemiroglu [7]. In this analysis, it is assumed that there is full knowledge that the contamination has occurred, and that damage is occurring. Situations where damage is occurring without the knowledge of the public or regulators are not considered here, though the same method is applicable with added risk/uncertainty.

The main variables in the economic analysis are the timing of remedial action, the spatial context and scope of the action, and the key economic parameters such as discount rate and planning horizon (discussed below). Preventive action could be taken now to avoid future damage, or can be postponed allowing existing damages to continue.

The other variable is spatial – the location at which the avoidance or remediation takes place. For each option being considered, at whatever level of interest, the EESA examines the sum of the benefits of the action over the planning horizon, and compares them with the full-life-cycle environmental, social, and financial costs of remediation. As with any decision-making tool, there is uncertainty surrounding key parameters, which are best addressed by sensitivity analysis. EESA should be run under different assumptions to see what the impacts of different parameters on the results are. The goal is to determine the option that provides an environmental, social, and economic optimum for all stakeholders in the majority of likely combinations of parameters. This process is discussed in more detail below.

The EESA can be used to determine an environmentally, socially, and economically sustainable remedial objective, by considering the costs of remedial alternatives, the benefits of remediation, and the external costs of remediation. Benefits of remediation can be expressed as the value of avoided damage, or prevention of future damages which would have occurred if the remedial action had not been taken [7]. Action which eliminates or reduces damage already incurred is also considered. Each of these elements is discussed in more detail below.

Costs of Remediation

Financial Costs of Remediation The costs of undertaking remediation of contaminated groundwater are well documented and understood, given the decades of activity in this area, particularly in North America and Europe. Remediation costs vary with size of the plume, type of contaminants, and the nature of the geologic and aquifer material and properties. Typically, the later is the intervention, the higher the costs of remediation are likely to be. If the prevention or remedial actions taken produce a secondary impact, it should be included in the analysis as an external cost of remediation (discussed in the following section).

External Costs of Remediation External costs of remediation represent the value of damage done to society and the environment as a result of the remediation process itself. They are "external" in the sense that they are not incurred by the problem holder but by third parties. External costs of remediation can be divided into planned or process-related external costs (which cannot or will not be mitigated against), and unplanned or inadvertent or unforeseen external costs (to which a probability of occurrence can be attached).

Planned external costs may include the landfilling of wastes excavated from contaminated sites, which may result in secondary damage at the new location, and will generate costs to society associated with transporting waste to landfill using heavy goods vehicles by way of increased congestion; impacts on health from air emissions which are produced by remediation systems (such as thermal treatment), noise impacts, and increased probability of accidents [9, 12]. For instance, the external costs of transporting contaminated materials by road in heavy goods vehicles have been estimated at US$0.78/vehicle-kilometers (v-km) [10]. While there are some more up-to-date estimates

for external costs of transport, this estimate is used here for consistency with the case histories presented here. This can add up quickly. For 10,000 vehicle movements, each of 500-km round trip, using the above unit cost estimate, an external cost of US$3.9 million is added to the overall cost of remediation. The relevance of this impact can be seen by considering typical private remediation costs for excavation and landfilling of 10,000 t of contaminated soil. A typical remediation program of this size would cost in the order of US$2 million to US$5 million, depending on location, contaminant type, tipping fees, and the complexity of the dig. In this example, the expected private or internal cost for remediation using "dig-and-dump" was expected to be approximately US$3.2 million. Adding US$0.4 million to reflect the real cost of the remedy represents a 12% overall increase in cost [8]. If clean fill has to be imported to site to fill in the excavation, additional vehicle movements will be required, further boosting the external cost of transport. Furthermore, the other possible external costs of landfilling have not been added, and may be considerable [8].

Examples of other types of planned external costs of remediation are listed in Table 1, below. In general, planned external costs are increasingly being mitigated against. In many jurisdictions, specific regulatory measures are being put in place to ensure that remediation methods which deliberately shift costs from the problem holder to society are reduced or eliminated.

Groundwater Remediation, Environmental and Economic Assessment. Table 1 Examples of planned external costs of remediation

Activity	Secondary effect	Comments
Air stripping of volatile compounds from groundwater, without off-gas treatment	Release of volatile compounds to atmosphere	Still occurs in many jurisdictions, can be mitigated against
Thermal treatment of contaminated soils	Release of CO_2 and other gases to atmosphere	Greenhouse gas emissions
Permanent geo-sequestering of contaminated groundwater (deep well disposal)	Permanent loss of injected groundwater as a resource	Widely used for difficult and recalcitrant contaminants
Excavation of concentrated source of contamination to protect underlying groundwater results in habitat destruction	Habitat in excavated area destroyed	Mitigation "banking" approaches can be used to offset

Based on Hardisty [8].

Accounting for unplanned or unforeseen external costs of remediation is of course problematic. Sometimes, despite best planning and care, remediation activities result in creation of a secondary impact to the environment, or to other stakeholders. If the impact is an unplanned or unforeseen result of remediation, for which mitigation measures have not been provided or have not been successful in countering, then the value of this damage is included as an external cost of remediation. Table 2 provides a list of examples of unplanned external costs.

Accounting for unplanned external costs within an economic evaluation of remedial alternatives is not straightforward. For any given remedial approach being considered, the possibility that its implementation may cause additional external damages must be carefully evaluated. In most situations, experienced remediation engineers and specialists should be able to identify possible secondary damages. In all cases, mitigation measures should be put into place to deal with these possibilities. Whatever probability remains of that damage occurring, after the mitigation measures are applied (and the cost of mitigation is added to the overall cost of remediation), should be applied to the value of the damage anticipated should the event occur. Assigning a probability to an eventuality which is being mitigated against is a matter of professional judgment of the remediation team, and should be based on experience, knowledge of the limitations of remedial technologies, and the mitigation measures themselves.

Benefits of Remediation Traditionally, when examining the "economics" of site remediation, the focus has been placed on cost. This has led to a fixation, in many parts of the industry, at many levels, on least cost solutions. However, there has been little consideration

Groundwater Remediation, Environmental and Economic Assessment. Table 2 Examples of unplanned external costs of remediation

Activity	Secondary effect	Example
Remediation causes LNAPL to revert to DNAPL, due to preferential removal of lighter compounds	NAPL sinks, contaminating a new volume of aquifer, worsening dissolved phase problem	SVE (soil vapor extraction) preferentially removes volatile aromatics from an LNAPL containing less-volatile dense compounds
Bioremediation results in creation of daughter products which are more toxic than parent	Toxicity to receptors increases	TCE (trichloroethene) degrades to VC (vinyl chloride), and VC persists in aquifer
Remediation inadvertently increases mobility of contaminant within the aquifer, through alteration of physiochemical properties	Impact on receptors worsens, either due to further spreading of plume, increased mass flux, or more rapid breakthrough	Surfactant flush greatly increases dissolution and mobility of NAPL, which migrated into previously uncontaminated rock
Remediation inadvertently increases mobility of contaminant within the aquifer, through alteration of properties of the aquifer itself	Impact on receptors worsens, either due to further spreading of plume, increased mass flux, or more rapid breakthrough	In situ fracturing of aquifer to enhance NAPL recovery inadvertently allows increased NAPL mobility toward receptors
Remediation compromises adjacent confining layers or geological features	Contaminant is introduced into a hitherto uncontaminated geologic unit	Pumping wells completed across a confining layer, cross-connecting two groundwater-bearing zones

Based on Hardisty [8].

of whether the lowest cost solutions actually yield commensurate benefit for society. Rational, economically balanced decision-making requires that cost be balanced with benefit – the action must be "worth it." If the lowest cost remedial solution is far greater than the value of achieving the clean-up goal, society is worse off if the remediation is undertaken. Conversely, if there is significant value in achieving a remedial objective, then any method that achieves that clean-up at a cost lower than the benefit which will be realized is a good deal for society. To make such a direct comparison, remedial benefit must be expressed in the same units as the costs of remediation. Without a common unit of measure, decision-makers cannot know definitively if the remediation is actually achieving overall benefit. In the authors' experience, much of the contaminated site remediation done around the world over the last 20 years has likely not produced an increase in overall human welfare. Conversely, much of the remediation that has been undertaken on major issues has likely been underdone, often because insufficient funds were devoted to the effort in relation to the significant social benefit that could have been realized by the right level of remediation. Understanding and quantifying the benefits of remediation is the critical step in allowing a more balanced allocation of resources to remediation, and selection of objectives, strategies, and technologies that optimize outcomes.

Private Benefits If the analysis is undertaken at the company (or problem holder) level, where only the costs and benefits that will accrue to the problem holder are considered, then the analysis is a *financial* analysis. When estimating the financial costs and benefits, market prices are used, including the subsidies or taxes that are included in the market price. Financial analysis does not deal with environmental or other social impacts of an investment unless these have a direct implication for the costs and benefits of the problem holder. In essence, financial analysis is what is traditionally done when evaluating remediation. Table 3 presents a selection of benefit categories that can be used in a financial analysis.

External Benefits If the analysis is undertaken for the whole of society, then the analysis used will be an

Groundwater Remediation, Environmental and Economic Assessment. Table 3 Private benefits of remediation

Private benefit	Comment
Increase in property value	Applies to increase in the value of the property owned by the proponent, which results from the clean-up action. Benefit is the net increase in value over the pre-remediation value. In many instances, this can be a major internal driver to remediate contaminated sites on high-value urban properties
Elimination or reduction of corporate liability	Remediation (and possible sale) of a contaminated site may allow an owner to eliminate a financial liability or provision currently affecting its balance sheet. This can be seen as a direct financial benefit to the owner or company. Contaminated site liability provisions are, depending on the jurisdiction, often based either on guesswork, or on an estimate of remediation cost. On that basis, the net position can often be neutral
Public relations value	Remediation of a contaminated site can result in a reduction in ongoing negative public relations, which may result in improved stakeholder relations, lower cost of capital, or perhaps improved financial performance through customer attraction. In practice, it can be difficult to quantify this benefit
Avoidance of prosecution or fines	If remedial action avoids fines or legal action against the company, the costs avoided are a direct financial benefit to the company. However, when a complete economic analysis is done, these costs are not included as benefits, as they are simply transfer payments (the payments are a cost to the company, but a benefit to society (the government), so they cancel each other out)
Health and safety benefits	If remediation of contamination reduces health and safety impacts on workers of the company, then this will be a direct benefit to the firm, in terms of reduced expenditure on ongoing protective measures, increased workforce productivity, lower absenteeism, and lower medical costs borne by the company. Improvements in the workers' own health, and the benefits the workers themselves realize, are counted as external benefits (see below)
Protection of resources used as production inputs	If remedial action protects the quality or quantity of a resource which the company uses in its production, financial benefits may also be realized. For example, if contamination from the facility is making its way into an aquifer that the company uses as a source of production water, and the company has then to treat that water to allow it to be used, remediation may result in the avoidance of some or all of those ongoing treatment costs

Based on Hardisty [8].

economic (or social) analysis. The EESA method focuses on the wider social analysis (which, of course, includes the financial), to examine the costs and benefits that accrue to society as a whole. External benefits of remediation are those that accrue to the rest of society when a problem holder undertakes remediation. If contaminated sites create damage, either because they are not remediated, or because only some of the effects of the contamination are dealt with, then this damage is an external disbenefit (or cost). Table 4 presents a selection of benefit categories that can be used in an economic (social) analysis.

In practice, only some of the external benefits of remediation can be readily quantified and monetized. The degree to which monetization of benefits is taken depends on the circumstances of the analysis. For more complex, high profile, and serious problems, a greater degree of analysis would be warranted. Wherever benefits can be reliably monetized, they should be. Some of the more important benefit categories listed in Tables 3 and 4, which are particularly important for contaminated sites, are discussed in more detail below.

Remediation of Brownfield Sites: Unlocking Private Benefit As discussed in Tables 3 and 4, one of the most robust ways of examining the economic impact of site contamination is to consider its effects on property value. In many places, the value of property

Groundwater Remediation, Environmental and Economic Assessment. Table 4 External benefits of remediation

Private benefit	Comment
Increase in value of neighboring properties not directly affected by contamination	Increase in the value of neighboring properties which are not physically or directly impacted by the contamination, but are simply affected "by association" with the site, will often results from the clean-up action. Benefit is the net increase in value over the pre-remediation value. The elimination of "blight," which results from proximity to a site, which in some way diminishes people's enjoyment of their property (visual disamenity, odor, concern over health impacts), may all depress property values. This effect is widely observed in the literature and in empirical studies of property value [11]. Reduction in blight through hedonic pricing captures a bundle of benefits accruing to those in the affected properties [12]
Increase in value of neighboring properties directly affected by contamination	If nearby properties are physically affected by the contamination – contaminants have been deposited or have migrated from the site to neighboring properties – then remediation of the site itself may also improve the value of the adjacent properties. If the remediation extends to the nearby properties themselves (the company cleans up the neighboring sites also), then the increase in property value of the nearby properties is also an external benefit of remedial action
Health benefits to neighboring residents	If remedial action improves the health of residents living near the site, an external benefit would result. These benefits are real, and can be measured through reduced medical expenditure, improved productivity, or increased income due to improved work attendance. They are not typically captured in a traditional financial analysis. Care must be taken to ensure that a health component is not also included in the property value benefit (double-counting)
Health and recreational benefits to visitors of the area	Remediation of a contaminated site may reduce the real or perceived health impacts on visitors to an area. This can be valued in the same way as the health benefits to residents of the neighboring area. If the site contamination has been affecting the perceived enjoyment of visitors to a nearby recreational area, either by direct contamination, or by "association," then remedial action can also trigger an increase in wider benefit experienced by the user group
Reduction in ecological damage	In many situations, contaminated land may act as a long-term source of deleterious impact on ecological resources, either within or outside the site. Wetlands, forests, aquatic ecosystems, coastlines, marine habitat, and individual species may be adversely affected by contamination. Elimination of these impacts, and the improvement in the quality and health of the affected ecosystems, can be an important external benefit of remediation, and one which is rarely, if ever, captured in conventional financial analysis
Protection of resources used by others	If remedial action protects the quality of quantity of a resource which is being used (or may be used in the future) by other parties, this would accrue as an external benefit to society. For example, if contamination from the facility is making its way to an aquifer that is used as a source of water for a community, and the community is being affected by that contamination, directly or indirectly, remediation will result in benefits to society. In this example, the benefit could be the elimination of the need for end-of-pipe treatment for the contaminants before distribution of the water to users, or elimination of the need to develop an alternative source of water. For water resources, all elements of the total economic value (TEV) may benefit from remedial action, including nonuse and option values

Based on Hardisty [8].

drives efforts to remediate and then sell on the land. First, there is the value of the site itself. A contaminated property will almost always sell at a discount over the price that could have been fetched if the site were fit for purpose. Groundwater contamination associated with the site can impact on property value in the same way as soil contamination. In many cases, one of the key benefits of remediation to the owner of a contaminated site is the increase in property value achieved. If the increase in value is greater than the costs of remediation, a profit is realized. This can be a powerful impetus to clean up sites. Different

organizations and individuals have different levels of risk tolerance, and so their willingness to pay for liability reduction can be markedly different. Since market prices are often driven at least partially by perceptions of risk, and these perceptions can vary considerably, regulators have a key role to play in brownfield transactions. Regulatory approval of remedial designs and results can be instrumental in creating comfort in the market that remediation has been successful, thus unlocking site value.

Revenue realized by cleaning up a site accrues to the site owner as an internal or "private" benefit. The benefit of remediation is the difference between the value of the site before remediation and the value after remediation. It can be readily and accurately measured in most countries by market techniques, using property value data.

Blight Reduction: An External Benefit When a contaminated site is remediated, it is not only the site owner who benefits. By removing what might have been a potentially dangerous or hazardous condition, the whole neighborhood benefits. Several recent economic studies have shown that people and businesses experience real economic benefit when a neighboring waste site or polluted site is remediated. This is due to the removal of blight (or disamenity) from the properties in the vicinity of the remediated site. Recent research has found substantial negative effects on property values in areas subjected to transshipment of radioactive wastes in the USA [13]. Another study showed a 35% difference between average selling price of homes located within a 2 mile radius of a low-level radioactive waste site in the USA, to those outside a 2 mile radius [14]. Proximity to landfills, active or closed, has also been shown to have a significant depressive effect on property values. In the USA, decreases in property values between 12% and 25% have been recorded, depending on distance from a hazardous waste landfill [15]. A recent study considered the disamenity costs of landfill in Great Britain [12]. The study considered 11,300 landfill sites and over half a million residential property transactions within 2 miles of those landfills, over the period 1991–2000 (inclusive). Residential property prices were found to be negatively affected within 2 miles of landfills. Across Great Britain, property values were found to suffer a 7% reduction within 0.25 miles, decreasing with distance to a 1% reduction between 0.5 and 1 miles from the landfill, and 0.7% between 1 and 2 miles from the landfill. In Scotland, however, impacts on property values were greater, decreasing 41% within 0.25 miles, 3% between 0.5 and 1 miles, and 2.67% between 1 and 2 miles away.

Removal of disamenity by remediation will cause average property prices in the affected area to rise. This increase, multiplied by the number of properties affected, can be used as a direct market valuation of disamenity or blight reduction, and as an estimate of the economic benefit which accrues to those stakeholders involved. This benefit will be greatest in dense urban areas with many neighbors and higher property values [8].

Case Histories

Remediating NAPLs in Fractured Aquifers

The problems associated with NAPLs in fractured aquifers have received significant attention in the technical literature over the last decade [16]. Concerns over the impacts of chlorinated solvents on groundwater have led to a significant body of work examining DNAPLs (dense non-aqueous phase liquid) in the subsurface, including in fractured rocks [17]. More recently, the unique behavior and problems associated with LNAPLs (light non-aqueous phase liquids) in fractured aquifers have been studied [2]. The highly heterogeneous nature of fractured systems, combined with the inherent complexity of multiphase flow, typically make characterization and remediation of NAPLs in fractured systems difficult and expensive.

Because this type of remediation can be so challenging and costly, there is a need to understand clearly the justification for spending large amounts of money. Indeed, the remedial methods that are used to remove or immobilize NAPLs in fractured aquifers tend to be complex, intrusive, and energy intensive. This, in turn, brings the sustainability of such efforts into question. Is that level of effort always warranted, given the other opportunities that may be available, and the value of the damage to society, the economy, and the environment caused by the presence of the contamination? This section examines the

application of EESA in setting an optimal remedial strategy for this difficult problem.

Remediation of LNAPL and DNAPL in fractured aquifers is a complex undertaking. DNAPLs may migrate to significant depths, and if spill volumes are large and fracture interconnectivity high, DNAPL may invade progressively smaller aperture fractures with depth. As NAPL fluid pressures increase, matrix invasion may also occur. The vertical migration of LNAPL in fractured aquifers is constrained by the water table, but significant penetration beneath the water table may occur, and lateral migration may occur in directions independent of the hydraulic gradient [2]. Within fractured aquifers, NAPL movement is governed by the geometry of the fracture network (including fracture orientations, densities, interconnectivity, apertures, and wall roughness), capillary pressure and fluid saturation relationships, and the properties of the NAPL (density, interfacial tension, viscosity). Whether dealing with LNAPL, N-NAPL (neutral-buoyancy NAPLs), or DNAPL, significant challenges exist when contemplating remediation. First, characterization of the distribution and behavior of NAPLs in fractured rock is difficult [18]. To develop a deterministic model, fracture networks need to be characterized, major fracture sets identified in the field, and representative fracture parameters determined. The occurrence of NAPL within these fractures then needs to be ascertained, areally and vertically. For DNAPLs, definitive characterization to depth may be problematic [19]. Rarely in practice is a complete characterization feasible [20]. Next, proven techniques for NAPL removal from fractures are few. Pump-and-treat methods, while effective for containment, have proven disappointing for NAPL removal, even when coupled with targeted NAPL recovery pumping and skimming [21]. Recently, more aggressive in situ NAPL removal methods have been field tested, including high vacuum extraction, thermal heating, and surfactant-assisted aquifer remediation [22]. These relatively expensive methods have shown good results in some cases, but have not yet been widely applied in fractured rock environments. Finally, when the understanding of contaminant distribution is sketchy, even the simplest remediation techniques can prove unsuccessful. The combination of new or unproven remedial techniques, incomplete characterization, and complex aquifer and contaminant distribution conditions makes remediation success uncertain. Within this context, a clear understanding of the financial and broader social, environmental, and economic implications of remediation provides decision makers with the means to select achievable and ultimately valuable remedial objectives [8].

DNAPL in a Fractured Carbonate Aquifer

A variety of chlorinated solvents were disposed of at a site in shallow unlined trenches. The site is situated on a hill, on the outskirts of a small rural town. DNAPL soaked into the surficial layer of fine-grained sediment that covers the site, and in places reached the highly weathered top of the fractured carbonate aquifer below. The groundwater surface at the site is within the bedrock aquifer, which is characterized by low yields and marginal quality from a drinking water perspective. Over 20,000 m^3 of NAPL-contaminated soils were excavated from the site and thermally treated, effectively making the site itself suitable for sale. However, groundwater monitoring revealed low concentrations of TCE moving off-site within the fractured bedrock aquifer, toward a downgradient wetland. As with all similar systems, the complexity of the fracture regime at the site makes detailed characterization of the nature and occurrence of groundwater contamination difficult. TCE may or may not be present in selected fractures a few meters apart. Here, EESA is applied at its most basic level, by examining the problem over a longer term perspective, developing quick estimates of the benefits that occur from remediation, and comparing them to the costs of various overall remedial approaches.

Benefits of Remediation A simple analysis identifies the following benefits, which may accrue from remediation at the site. In each case, benefits estimates are overstated to skew the assessment toward active remediation as an outcome. Benefits examined were:

1. Increase in property value at the site itself. The area is rural, and land values in the area are relatively low. Clean, the site is worth about US$0.50 million.
2. Uplift in the value of surrounding properties through removal of blight. Within a 2 mile radius, the sum of property values is estimated at US$11 million by area realtors. Applying a 10% blight

Groundwater Remediation, Environmental and Economic Assessment. Table 5 Possible remedial benefits summary

Benefit category	Sum of benefits over 20 years (US$ million)
Property value	0.5
Reduction in blight in neighborhood	1.1
Aquifer protection	2.5
Wetland protection	0.1
Total possible benefits	4.2

factor, remediation of the site would result in a one-time benefit of US$1.1 million.

3. Prevention of aquifer damage. Using simple modeling, the presence of the dissolved phase plume at the site effectively eliminates about 200,000 m^3/year of potential abstraction (even though the aquifer is used only sparsely in the area, and not at all for public supply). At 5% discount rate over 20 years, and assuming a value for water of US $1.00/$m^3$, this equates to about US $2.5 m in lost aquifer potential.
4. Value of the wetland, to which dissolved phase contaminants may flow. Given the low concentrations expected under worse case conditions, a nominal value of US$0.1 million is assigned (see the previous example in this entry).

Table 5 provides a summary of the possible benefits of remediation.

Remedial Approach Options Recognizing the difficulties involved in remediating low levels of dissolved phase contamination in the complex fractured rock environment, three main remedial approach options were identified as part of the evaluation process: (1) soil remediation (already completed), with MNA (monitored natural attenuation) for groundwater over 20 years; (2) soil remediation (already completed), with selected in situ treatment of identifiable hotspots in groundwater, and 20 years of MNA; and (3) soil remediation (already completed), with groundwater pump-and-treat to contain and reduce the mass of the dissolved phase plume.

Simple High-Level Environmental and Economic Sustainability Analysis The costs and benefits of each of the three remedial options being examined are provided in Table 6. Although the soil remediation has already been completed, the costs of soil remediation are included in each option to examine how they impact the decision. Nevertheless, none of the options is shown to be economic – they do not result in a net increase in welfare for society. The combination of low property values (small benefits), and a complex and difficult to characterize and remediate aquifer (high costs), produces low BCRs below unity. Even if the value of the aquifer were increased, by raising the value of water from US$1.00/$m^3$ to US$2.00/$m^3$ (which is well above current estimates of the TEV of water in this part of the world), the costs of remediation are so high that all of the options remain uneconomic.

Implications In this case, all options are uneconomic. The high cost of remediation of dissolved phase NAPL constituents in fractured rock exceed the benefits to society stemming from remediation. Even the soil remediation alone, which was accomplished with an energy intensive thermal desorption system, was, in retrospect, too expensive for the benefits created. This is a classic example of remediation driven by numerical concentration-based criteria, in which risks have been significantly overstated. A less expensive soil treatment method may have brought overall costs down enough for the proposition to be economic. However, it is clear that further remediation, by deploying either options (2) or (3), is uneconomic and unsustainable. In this case, a technical impracticability (TI) waiver would be both technically and economically justified, leading to selection of remedial approach (1) [8]. In the USA, TI waivers have been issued by the regulatory authorities in such circumstances. This analysis suggests that, in fact, TI waivers are really economic impracticability waivers. With enough effort and expenditure, using existing technology, it is highly probable that the low levels of VOCs at and off-site could have been dealt with eventually. However, this would have required an unreasonable level of expenditure. It is not technology that limits the efforts in most cases, but the willingness to use scarce resources to achieve levels of remediation,

Groundwater Remediation, Environmental and Economic Assessment. Table 6 Indicative costs and benefits, base case (20 years, 5%)

Remediation approach	PV cost soil (US$ million)	PV cost total (US$ million)	PV benefit (US$ million)	Net benefit (US$ million)	BCR
(1) Soil remediation + MNA	3.0	4.5	2.85	−1.65	0.63
(2) Soil remediation + in situ DNAPL hotspot removal	3.0	9.7	3.6	−6.10	0.37
(3) Soil remediation + pump-and-treat to contain dissolved phase plume	3.0	13.9	4.2	−9.70	0.30

which may not be justified. EESA provides a way of rationally and objectively determining where and to what level remediation is warranted, and where it is not.

Coal Tar Contamination of a Fractured Aquifer

A disused manufactured gas plant facility in the UK is the source of coal tar compounds, including NAPLs, which have contaminated the subsurface. The site lies in the center of a busy town, adjacent a high-value residential neighborhood. The uppermost coarse-grained saturated gravel deposits are extensively contaminated by NAPL, which is very close to neutral density. Groundwater occurs at a depth of about 5 m across the site. A small volume of the NAPL has penetrated a low permeability layer and is present in small aperture fractures within the upper horizon of the underlying carbonate aquifer, to depths of up to 15 m below ground level. The NAPL plume is stable, and occurs mostly as residual saturation. The N-NAPL is composed predominantly of low-solubility PAHs [8].

The aquifer is used for public water supply (PWS), and an operating supply well lies approximately 2 km downgradient of the site. Trace levels of phenolic compounds have been detected at the well over the past several years. Groundwater monitoring and modeling have confirmed that these compounds are migrating from the site in low concentrations. A small culverted river of poor quality runs past the site. The contaminated gravels on-site are in hydraulic connection with the river, but flux of contaminants to the river in the dissolved phase is low, because of the low solubility of the NAPL. The site is derelict, and there is no public access.

Remedial Objective The site owner wishes to remediate the site because of its high value. The regulator and the operator of the PWS well are concerned about contamination of the regional aquifer from contaminants on-site. To date, contaminants detected at the PWS have been at concentrations below drinking water quality standards, and an existing treatment system removes them. However, should the flux of contaminants to the wells increase, there is a risk that the PWS would have to shut down or substantially upgrade the existing treatment system. The objective of the EESA in this example is to: "*select a remedial approach which manages the risks present at the site in the most economic and sustainable way.*" Remediation is to be undertaken sustainably, but what the remediation achieves should also be sustainable in its own right.

Benefits of Remediation The direct financial benefit of remediation to the site owner is the value of the property itself, which can be unlocked if remediation makes the site suitable for hard-covered light commercial use (approximately US$14.0 million). However, other benefits will also accrue to other parties if remediation proceeds, depending on what the remedial design achieves. Sale and redevelopment of the site will immediately trigger an increase in property values around the site, through removal of blight. As discussed above, this is a well-documented and empirically proven effect. If remedial action significantly reduces the mass flux of contaminants reaching the aquifer, this would prevent future damage to the aquifer and to water production from the PWS (currently pumping 1.0 Mm^3/year). Any significant increase in mass flux of contaminants to the well would likely bring it off line. Similarly, removal of NAPL on-site

Groundwater Remediation, Environmental and Economic Assessment. Table 7 Base case benefits summary (5% discount rate)

Benefit category	Sum of benefits over 20 years (2008 US$ million)
Property value	14.0
Reduction in blight in neighborhood (at 5% blight factor)	3.83
Aquifer protection (base case TEV US$ 1/m^3)	12.46
River protection (base case TEV US$ 1/m^3)	3.74
Total Possible Benefits	34.03

would eliminate the source of contamination to the river, whose average annual flow is approximately 0.3 Mm^3/year. For the base case analysis, a replacement value of water of US$1.00/m^3 is used. Later in the sensitivity analysis, TEV of water estimates of up to US$2.00/m^3 are used. A summary of possible benefits realized by remediation is provided in Table 7. If all benefit categories could be realized, total benefits would be approximately US$34 million. However, not all benefits categories will be realized by each remedial approach, as shown below.

Remedial Approach Options Based on the risk assessment discussed above, and understanding the overall social value of preventing damage to the various receptors, and the value of the site itself, a number of remedial approaches were identified to meet the objective. Table 8 lists each option, and describes its basic components and its advantages and disadvantages.

Indicative Remedial Costs Table 9 presents indicative remedial costs for each of the remediation approaches identified above. The remedial approaches are coded to indicate whether they address the risk source (S), or pathway (P) of the problem. Both capital and O&M (operating and maintenance) costs are provided for each approach. External costs of remediation, where applicable, have also been estimated and the basis for those costs are presented (generation of greenhouse gases from thermal treatment, vehicle use, and power consumption). A base case cost of carbon was set at US$52/t CO_2e increasing at 2% per year was used, based on the UK government guidance at the time [23]. External costs of landfill were deemed to be included in the capital costs estimates, where applicable, under the assumption that landfill tax effectively accounts for the external social costs of landfill. The costs of road transport disamenity were also estimated assuming that the landfill was 100 km away from the site, and that the heavy goods vehicles used carry an average of 10 m^3 of material each. Different planning horizons and discount rates are investigated as part of the sensitivity analysis.

Base Case Analysis Table 10 shows the apportionment of benefits among the various remedial approach options. Apportionment of benefits requires careful judgment of the anticipated effectiveness of the techniques assumed to form the basis for the remedial approach. A zero benefit in the table indicates that the remediation approach does not address the damage to that receptor or does not allow that particular type of redevelopment of the site. The basis for apportionment of benefits must however remain consistent and balanced between options. So, for instance, in Table 10, Option S2 is deemed to eliminate 100% of the damage to the aquifer through aggressive removal of the NAPL in fractured bedrock, using concentrated in situ remediation. In contrast, a system that captures contamination in the surficial groundwater and prevents it from reaching the river (option P1) does not protect the fractured aquifer. P1 does protect the river, however, and therefore accrues that benefit.

Figure 1 shows the base case 20 years, 5% discount rate full social NPVs for each option. The S1 option is superior under base case conditions. Note the contrast with Fig. 2, which shows the same base case NPVs over only 5 years. With a shorter term view, S3 is most economic, because the immediate returns to the problem holder from selling the site now dominate the analysis. Other benefits which accrue to society over time, such as protection of river and aquifer, are de-emphasized if only a 5-year horizon is considered. This illustrates the importance of a longer term view, if sustainable outcomes are being sought.

Groundwater Remediation, Environmental and Economic Assessment. Table 8 Remedial approach options

Approach description		Relative cost	Advantages and disadvantages
Source methods			
S1	Partial excavation and removal of main sources. On-site ex-situ treatment. Removal and landfill of remaining material (10,000 m^3). In situ remediation of NAPL in fractured bedrock using chemical oxidation (ISCO) technology	Moderate – High	Pilot trials of ISCO show good success in oxidizing NAPL within fractured rock. On-site treatment focus reduces volume of material for off-site disposal to landfill
S2	Full excavation of contaminants, including into uppermost part of aquifer, use of piling, maximize off-site disposal (40,000 m^3)	High	Quickest and most complete remediation of sources; significant risk of disturbing aquifer during excavation and mobilizing some NAPL into the aquifer, possibly worsening situation at PWS
S3	Partial excavation of NAPL-contaminated materials above water table only (10,000 m^3), leave remaining contaminants in place and monitor	Moderate	Removal of major concentrated sources allows site to be sold with some residual liability; leaves significant mass of contaminant in place
Pathway methods			
P1	Containment in gravels using air-sparge barrier along the downgradient site boundary within gravels.	Moderate	Prevent further off-site migration of contaminants in gravel to River; does not deal with other hazards; perpetual management needed
P2	Hydraulic containment of dissolved phase in bedrock aquifer through installation of a series of capture wells, and operation of a water treatment facility on-site	Moderate	Prevent further off-site migration of contaminants in aquifer to PWS; does not deal with other hazards; perpetual management needed
Receptor methods			
R1	Treat groundwater after abstraction at PWS	Moderate	Directly prevents contaminants from site impacting delivery of water to PWS customers. Treats other contaminants from other sources impacting aquifer also; perpetual management required
Institutional management			
MNA	Monitored natural attenuation. Current data indicate that low levels of dissolved phase contaminants are naturally degrading within the aquifer. No remedial action, monitor groundwater to prove attenuation is occurring.	Low	Does not actively remediate site to any degree; does not eliminate the risk that contaminant flux from the site could increase significantly in future

Based on Hardisty [8].

Remedial approaches MNA and P1 are NPV negative – they do not generate benefits sufficiently large to overcome their costs, even when wider benefits to the whole of society are considered. All of the other remedial approaches generate more benefits overall than they cost to implement. In this example, cost benefit analysis suggests that excavation and treatment of the bulk of contaminated soil, where the vast majority of the contaminant mass exists, is the most economic single remedial approach evaluated. This is driven by

Groundwater Remediation, Environmental and Economic Assessment. Table 9 Indicative costs for selected remedial approach options

Approach	Capital costs (US$ million)	O&M costs (US$ (million)/year)	20 years – 5% PV financial costs (US$ million)	GHG (tCO_2e)	Road transport (v-km)
R1	0.25	0.21	2.87	100/year	–
MNA	0.5	0.10	1.75	10/year	–
P2	3.5	0.35	7.86	200/year	–
P1	3.8	0.40	8.78	100/year	–
P1 – ALT	5.4	0.48	11.38	150/year	–
P1 + P2	6.5	0.55	13.35	300/year	–
S3	9.2	–	7.2	650	200,000
S1	13.9	–	14.4	1,200	480,000
S2	22.0	–	22.0	2,100	800,000

Groundwater Remediation, Environmental and Economic Assessment. Table 10 Base case PV benefits for remedial approaches (US$ million)

Option	Total financial costs	Benefit – land sale (private)	Benefit – elimination of blight to neighboring properties	Benefit – river protection	Benefit – value of aquifer protection	Total PV benefits
R1	2.87	–	–	–	7.48	7.48
MNA	1.75	–	–	–	0.75	0.75
P2	7.86	–	–	3.74	–	3.74
P1	8.78	–	–	–	12.48	12.48
P1 + P2	13.35	–	–	16.21	12.48	28.69
S3	9.2	7.0[a]	3.875	1.25	1.25	13.38
S1	13.9	14.0	3.875	3.74	9.35	30.97
S2	22.0	14.0	3.875	3.74	12.48	34.95

[a]Assumes that site must be sold at a 50% discount due to the presence of residual deeper subsurface contamination. However, commercial redevelopment can take place and so blight is removed.

the relatively high value of the property for commercial development, and the fact that all of the neighbors also benefit by elimination of blight on their property values. Source removal will also benefit both the river and the aquifer to varying degrees by removing a continuing source of contaminants.

Under base case assumption, the river's overall value is too small to justify direct action (using the methods examined) aimed specifically at its protection. In this case, using conservatively high base case valuation parameters for the river, a PV of about US$3.7 million is estimated. Thus, to be considered sustainable, remediation measures aimed specifically at protecting the river should not cost appreciably more than this figure, in PV terms. If appreciably more is spent on this issue alone, then society as a whole is

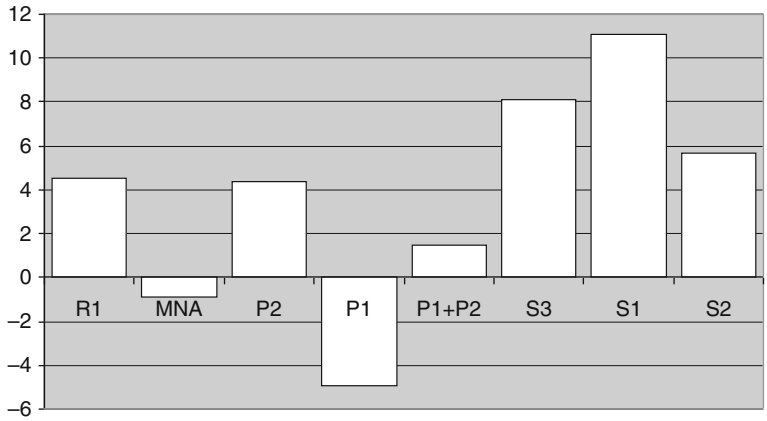

Groundwater Remediation, Environmental and Economic Assessment. Figure 1
NPVs of each option under base case conditions, over a 20 year planning horizon (After Hardisty [8])

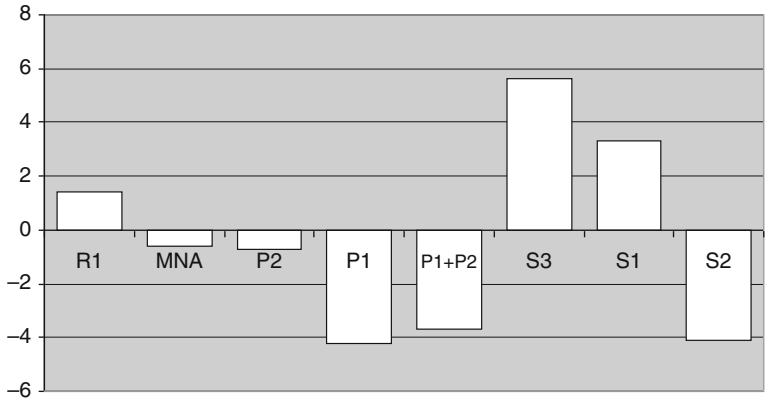

Groundwater Remediation, Environmental and Economic Assessment. Figure 2
Base case NPVs with a 5 year planning horizon (After Hardisty [8])

worse off. Other projects should be sought which provide higher benefits. If combined with measures intended to manage risks to other, more valuable receptors, river protection can be achieved economically and sustainably. This conclusion is, of course, only valid to the extent that the value of the river assumed for the analysis encompasses all of the services it provides, and that value is stable over time. In this example, it is safe to say that both conditions are being violated. The full extent of the services that natural ecosystems provide to mankind are only slowly being revealed, and the inherent value of these ecosystems will increase over time as population growth, resource extraction, development, and pollution reduce their stock and health. This is directly reflected in society's willingness to pay (WTP) for those assets. This is explored in more detail below in the sensitivity analysis section to determine if this kind of variability will affect the overall conclusions.

Sensitivity Analysis and Decision-Making Because of the range of assumptions typically required for this type of analysis, sensitivity analysis is an important tool for testing the robustness of conclusions. EESA uses detailed sensitivity analysis to explore the consequences for decision-making overall, and to help guide an optimal decision. For a more detailed discussion of the EESA as a whole and the EESA equiprobable sensitivity

analysis process in particular, the reader is referred to [8]. Benefit values, particularly, should be varied over the widest possible reasonable range, to test how changes in values will affect decision-making. Table 11 shows the ranges of parameters which are varied for the sensitivity analysis in this example.

Figure 3 shows how the NPVs of the various options vary across the full range of values for TEV of water, with all other factors fixed at base case values. This could reflect, for example, a wider anticipated trend toward an increasing value of water, driven by growing demand, resource degradation, and the impacts of climate change. Higher values for water have a significant impact on the analysis. More aggressive aquifer remediation efforts such as S1, S3, and P2 become increasingly more economic and sustainable. The more water is worth to society, the more remediation action that protects it can be justified.

Option S1, identified as most economic in the base case analysis, fares well, and is superior under the majority of conditions. This is further illustrated in Fig. 4, which shows that S1 is the best choice under 82.5% of all conditions examined, given equiprobable outcomes. S3 is the best option under 14% of conditions, namely, when the value of water is low, and the revenue from property sale dominates the result.

In this example, the site owners could clean up the site at a profit, if no other stakeholder's interests were considered. High property values have driven considerable site remediation over the past decade. However, broader social economic analysis reveals that some of this surplus (profit) could also be used to generate external benefits for the community (and, by extension, the public image of the problem holder). In other words, sustainability in remediation can be identified and justified in an economic context. In this example, several combinations of approaches are in fact possible that would provide wider distribution of the economic benefits of remediation, albeit at higher cost to the problem holder.

Groundwater Remediation, Environmental and Economic Assessment. Table 11 Sensitivity analysis parameter ranges

Parameter	Low value	High value
Property value	US$5 million	US$25 million
Blight factor	0%	20%
Total economic value of water	US$0.50/m^3	US$2.00/m^3
Discount rate	0.03	0.10
GHG external cost	US$52/t$CO_2$e	US$100/t$CO_2$e
External cost of transport	US$0.60/v-km	US$2.40/v-km

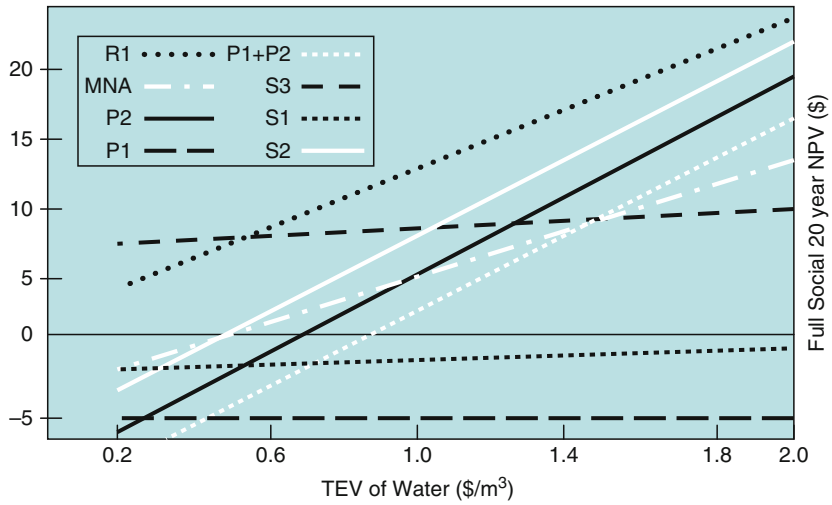

Groundwater Remediation, Environmental and Economic Assessment. Figure 3 Relationship between net present value and total economic value of water (After Hardisty [8])

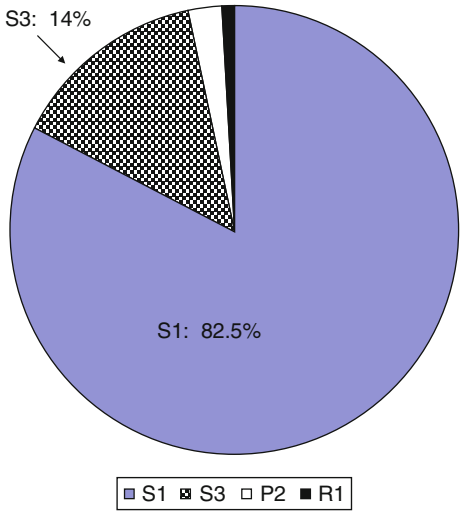

Groundwater Remediation, Environmental and Economic Assessment. Figure 4
Chart showing the proportion of instances where specific options were the most economic. S1 was most economic and sustainable over 82.5% of all conditions tested (After Hardisty [8])

Discussion and Conclusions

The case histories presented herein illustrate the application of EESA at very different contaminated sites. While both involve NAPLs in fractured rock aquifer systems, the results from a decision-making perspective are quite different. At the MGP site, high urban property values combined with the risk of impacts on a major aquifer meant that remediation of NAPL in fractured rock, although very expensive, is economic – it yields overall benefits to society as a whole. In contrast, the rural chlorinated solvent problem involves a poor yield, little-used aquifer, and low concentrations of dissolved phase contamination. Remediation of the low levels of TCE in the fractured aquifer is not economic, and not sustainable. The already-completed soil remediation has removed the continuing source of future dissolved phase contamination, and renders the site suitable for limited commercial use. However, further remediation cannot be justified, based on the benefit to be gained. In both cases, active remediation of NAPL in complex and highly heterogeneous fractured rock is very expensive (over US$4 million and almost US$10 million, respectively). However, the real economics of the two cases are very different, and the optimal decision over a wide range of future possible values for key external assets, reflects this.

In general, active groundwater remediation may be beneficial and warranted if property values are high and are expected to rise, if aquifer use value is high, if alternative water sources are scarce and if important nonuse values are threatened (such as groundwater recharging a sensitive and valued wetland ecosystem), and if ecological assets at risk are unique and valued by society. In many cases, the anticipated benefits of remediation in complex technically challenging environments (such as fractured aquifers) will not justify the level of expenditure required to realize those benefits, with currently available technology.

Future Directions

This approach requires valuation of economic externalities. To allow benefits to be more accurately quantified, studies are required on valuing aquifers, both in the USA and Europe. Supporting this, more quantitative work on establishing estimates of the TEV of water, in various conditions (based on rainfall, population density, demand, and so on) would be very useful. Analysis of the type presented herein also suggests that continued research is needed to bring down the financial costs of groundwater remediation, particularly in more complex subsurface environments.

For too long, decision-making about remediation has been carried out with only half of the required information. Legislation and regulatory standards have driven problem holders to seek the cheapest possible way to meet the applied standards. The real overall benefits of groundwater remediation, however, have been largely ignored. EESA provides a robust way to examine the benefits to all parties from remediation, and compare the overall economic sustainability of a variety of options across a range of possible future conditions to determine an optimal decision that will stand the test of time. Application of this type of approach, however, is in its infancy. Development of improved policy, which mandates a wider perspective on remedial decision-making, would help to avoid the extremes in remediation which destroy value in society: spending too much on a problem that does not warrant it and spending too little when valuable groundwater resources are being seriously damaged.

Bibliography

Primary Literature

1. Hardisty PE, Bracken RA, Knight M (1998) The economics of contaminated site remediation: decision making and technology selection. Geol Soc Eng Geol Sp Pub 14:63–71
2. Hardisty PE, Wheater HS, Johnston PM, Bracken RA (1998) Behaviour of light immiscible liquid contaminants in fractured aquifers. Geotechnique 48(6):747–760
3. Goist TO, Richardson TC (2003) Optimizing cost reductions while achieving long term remediation effectiveness at active and closed wood preserving facilities. In: Proceedings, NGWA conference on remediation: site closure and the total cost of cleanup, New Orleans, Nov 2003
4. Perakami MP, Donovan PB (2003) A remedial-goal driven, media-specific method for conducting a cost benefit analysis of multiple remedial approaches. In: Proceedings, NGWA conference on remediation: site closure and the total cost of cleanup, New Orleans
5. Hardisty PE, Kramer E, Ozdemiroglu E, Brown A (1999) Economic analysis of remedial objective alternatives for an MtBE contaminated aquifer. In: Proceedings of hydrocarbons and organic chemicals in groundwater conference, NGWA, Houston
6. Pearce DW, Warford JJ (1993) World without end. Edward Elgar, London
7. Hardisty PE, Ozdemiroglu E (2005) The economics of groundwater remediation and protection. CRC Press, New York
8. Hardisty PE (2010) Environmental and economic sustainability. CRC Press, New York
9. Hardisty PE, Arch S, Ozdemiroglu E (2008) Sustainable remediation: including the external costs of remediation. Land Contam Reclam 16:4
10. Maddison D, Pearce DW, Johansson O, Calthorp E, Litman T, Verhoef E (1996) The true costs of road transport. Earthscan, London
11. Hardisty PE, Ozdemiroglu E (1999) Costs and benefits associated with remediation of contaminated groundwater: a review of the issues. UK Environment Agency Technical Report P278
12. DEFRA (2003) A study to estimate the disamenity costs of landfill in Great Britain. Final report by Cambridge Econometrics with EFTEC and WRc
13. Gawande K, Jenkins-Smith H (2001) Nuclear waste transport and residential property values: estimating effects of perceived risks. J Environ Econ Manage 42:207–233
14. Payne B, Olshansky S, Segel T (1987) The effects on property values of proximity to a site contaminated with radioactive waste. Nat Resour J 27:579–590
15. Hirshfeld S, Veslind PA, Pas EI (1992) Assessing the true cost of landfills. Water Manage Res 10:471–484
16. Mackay DM, Cherry JA (1989) Groundwater contamination: pump-and-treat remediation. Environ Sci Technol 23:6
17. Cohen RM, Mercer JW (1993) In: Smoley CK (ed) DNAPL site investigation. CRC Press, Boca Raton
18. CL:AIRE (2002) Introduction to an integrated approach to the investigation of fractured rock aquifers contaminated with non-aqueous phase liquids. Technical Bulletin TB1
19. Guswa JH, Benjamin AE, Bridge JR, Schewing LE, Tallon CD, Wills JH, Yates CC, LaPoint EK (2001) Use of FLUTe systems for characterisation of groundwater contamination in fractured bedrock. In: Kueper BH, Novakowski KS, Reynolds DA (eds) Conference proceedings of fractured rock 2001, Toronto
20. Lane JW Jr, Buursink ML, Haeni FP, Versteeg RJ (2000) Evaluation of ground penetrating radar to detect free-phase hydrocarbon in fractured rocks – results of numerical modelling and physical experiments. Ground Water 38:6
21. Schmelling SG, Ross RR (1989) Contaminant transport in fractured media: models for decision makers. EPA Superfund Issue Paper EPA/540/4-89/004
22. Taylor TP, Pennell KD, Abriola LM, Dane JH (2001) Surfactant enhanced recovery of tetrachloroethylene from a porous medium containing low permeability lenses: 1. experimental studies. J Contam Hydrol 48:325–350
23. DEFRA (2007) The social cost of carbon and the shadow price. What they are and how to use them in economic appraisal in the UK. UK Department of Environment, Food and Rural Affairs, London

Books and Reviews

Boardman AE, Greenberg DH, Vining AR, Weimer DL (2010) Cost-benefit analysis: concepts and practice. Pearson, Prentice Hall, Upper Saddle River

Brouwer R, Pearce D (eds) (2005) Cost-benefit analysis and water resources management. Edward Elgar, Cheltenham

Pearce DW, Atkinson G, Mourato S (2006) Cost benefit analysis and the environment – recent developments. OECD, Paris

Tientenberg T (2003) Environmental and natural resource economics. Addison Wesley, London

Groundwater Salinity Due to Urban Growth

J. J. Carrillo-Rivera[1], S. Ouysse[2]

[1]Instituto de Geografía, UNAM, CU México, DF, Mexico

[2]Cadi Ayyad University, Marrakech, Morocco

Article Outline

Glossary

Definition of the Subject and Its Importance

Introduction

Groundwater Movement in Flow Systems
Importance of Groundwater for Urban Development
Groundwater Quality Response
Geological Framework
Climate Framework
Water Quality Response to Groundwater Extraction
Vertical Flow Control to Prevent Water Quality Deterioration
Future Directions
Bibliography

Glossary

Aquifer unit Is a geological formation, part of a formation, or a number of formations that provide water substantially and in adequate quality for the expected usage.

Basin Is often referred to as the drainage basin or the surface area where rainfall is gathered with a common discharge outlet; it is considered to have no additional inflow or outflow.

Flow systems Are manifested by the presence of flows with contrasting hierarchy (local, intermediate, and regional) whose components may be clearly defined from field evidence in conjunction with modeling of groundwater hydraulics, geochemistry, geomorphology, edaphology, as well as on natural vegetation response.

Groundwater vulnerability to contamination Is the tendency or likelihood for a contaminant to reach a specified position in the groundwater system after introduction at some location above the uppermost aquifer.

Hydraulic conductivity Is the rate of water that a unit volume of aquifer material may allow through under a unit hydraulic gradient; such value is a function of its degree of saturation, attaining its maximum at 100% saturation, and is also a function of water density.

Local flow system Is one that is defined traveling a short distance and depth, recharging and discharging in the same valley.

Regional flow System Is generated (recharged) at the highest elevation and then travels along till basement depth and discharges at the lowest position in the region.

Urban sprawl Is a multifaceted concept, which includes the spreading of dwelling construction outward of a city and its suburbs to its outskirts to low-density and becoming an auto-dependant development on rural land, high segregation of uses (e.g., stores and residential), and various design features that encourage car dependency.

Vertical flow Is groundwater traveling downward (as in a recharge area) or upward (as in a discharge) area. This component of flow may be also identified when extraction is carried out at shallow levels and groundwater ascends, induced by extraction.

Water balance As applied to a watershed (basin), is referred to as the application of a lumped parameter approach that lacks consideration of areal variations of precipitation, evaporation, transpiration, recharge, runoff, and change in storage as well as the processes involved.

Water quality change Is the chemical evolution in obtained water quality in borehole with extraction time.

Wellhead protection area Ideally is the entire groundwater inflow area for the well; often, this inflow area is too large to be managed effectively, so a smaller area near around the well is often chosen and delineated by flow lines basically incorporating horizontal flow.

Definition of the Subject and Its Importance

The population of the world is increasing at different rates according to the period of time and geographical position; however, at present, the number of cities that have a population larger than one million are estimated as more than 336, while in the 1950s, 83 cities were in that range. One such urban development has been Mexico City, which has more than 18.6 million population, which could be considered even a larger number (nearly 28 million) if the adjoining urban sprawl is included. Cities have often solved their water supply requirements by means of groundwater extraction. Usually, in ancient times, cities were founded on sites where water was directly available. Water supply works tapped springs and surface water. Later, when the number of inhabitants and economical activities increased, shallow dug wells were the solution to cope with water needs. As historical time went by, the population and economical activities of cities have definitely increased; however, at the turn of the 1900s, many cites experienced a rapid

growth that has evolved to achieve their present size. The consequent need for additional water sources has been met with the assistance of groundwater.

Initially, at the second half of the 1800s, groundwater extraction in Mexico City was made on the surrounding plain by means of boreholes that provided artesian yields with good quality water in sufficient quantities to comply with existing local requirements. However, the limited supply to cope with the continuous increase of water needs led to additional extraction by boreholes. Later, by the end of the first half of the twentieth century, many boreholes were no longer free-flowing artesian waters, so the acquisition of the turbine pump started a new extraction period. At that time, the prevailing view was that water quality would basically remain constant with extraction time due to calculations that included a hydrogeological conceptual model known as the "the water balance," applied in Mexico from the middle of the 1960s. This conceptual model included an important assumption based on the presence of purely radial horizontal flow to the extraction borehole as defined by Theis [23], a condition that was supposed to prevail in existing extraction boreholes.

Initially, boreholes were skunked to shallow depths in the vicinity of 100 m, just touching the top of the full aquifer thickness. At present, deeper boreholes may reach 400 m but are still far from tapping the full thickness of the aquifer, which is estimated to be of more than 3,000 m.

Originally, the deterioration of obtained groundwater quality was solely expected to occur from spillage on the soil surface of foreign substances (i.e., gasoline leaks, leachates from rubbish pits, improper management of sewage water, etc.), not from substances naturally existing in the groundwater. The common prevailing wellhead protection area was considered to be the only source responsible for any negative change in the obtained quality of the groundwater supply. Often, any lack of effect of lateral flow was overcome by the presence of vertical ascending flow from extraction boreholes.

Vertical components of groundwater flow have been overlooked as well as their meaning in producing related environmental impacts [7]. Vertical ascending components of flow become paramount when viewed in the context that usually the screen of the extraction borehole faces less than 1/10 of the full aquifer thickness. Below this extraction depth, groundwater flow systems with different water quality travel below the local flows that were initially captured by the boreholes bottomed at shallow depth. Regional flows with both high temperature and salinity load travel at depth and are represented by a thermal spring reported since pre-Spaniard times: Peñón de los Baños (44°C; Cl, 650 mgL; Li, 1,550 μg/L). Groundwater belonging to regional flows is being slowly but steadily induced to extraction levels, changing the initial water quality. Additionally, there is an increase in the disappearance of springs due to extracting water from boreholes at the spring site. The recognition of the presence of such flow systems is very important. As population and economic activities increase, so will the rate of extraction, which in turn will change the obtained water quality over time.

Introduction

Groundwater may provide feasible alternative solutions to water needs for many growing cities' development worldwide. The definition of groundwater functioning is essential when looking for water accessibility in terms of quantity and quality in both time and space. Such knowledge could assist in providing an adequate definition of water sources to reduce the risk of salinity enhancement of extracted groundwater due to urban growth. Establishment of adequate groundwater management policies needs to be in accordance with the groundwater dynamic in the environment and an understanding of existing flow systems.

The understanding of groundwater functioning is most important in regions where there is an increase in water needs and where shortages in the water supply often affect available infrastructure. The limiting conditions for appropriate development of big cities in many regions could be solved under the discipline of land planning. Proper space planning refers to the methods used by the public sector to influence future distribution of people and economic activities in spaces at various scales. Land-planning processes that are undertaken at local, provincial, and regional levels require covering a broad range of issues, such as housing, commercial and other nonresidential facilities, roads and transportation, schools and utilities, as well as farming. What is meant to be considered proper space planning implies that the proposed land use is in agreement with what the

land "attitude" and its environment could provide without putting in danger its sustainability.

Ideally, socioeconomical and environmental development program should be assisted by an adequate political decision-making to include the definition of the groundwater flow systems. Required actions to increase development involve a responsible and thorough knowledge of the nature of the territory, not only surface elements but also groundwater availability and its underground links with neighboring surface drainage basins. The traditional water availability analysis carried out for additional development in Mexico is related to the "*water balance*" which usually involves hydrological factors that are difficult to obtain through the application of the scientific method. This is due to (1) simplification of natural processes involved; (2) use of estimates of variables not directly measured, such as runoff, precipitation, evapotranspiration, groundwater extraction, infiltration, and groundwater recharge; and (3) presumption of immediate infiltration of local precipitation that is reflected in an ascending water table. Additionally, prevailing geological conditions of Mexico, and in particular those related to the location of Mexico City, imply the presence of aquifer units with thicknesses beyond 3,000 m and with horizontal extent of about 100,000 km^2. Therefore, most surface drainage basins usually have an underground hydraulic connection with near or faraway surface drainage basins [24]. A starting point with most computed water balance carried out on a surface drainage basin generally fails to represent a consistent scenario with groundwater functioning, and as a result, any groundwater extraction program frequently would fail to consider the expected water quality to be obtained by boreholes over time.

From the perspective of safeguarding obtained water quality, the concept of "borehole protection area" (see http://www.state.nj.us/dep/njgs/whpaguide.pdf) in complex hydrogeological systems lacks the required guidance of particular needed measures of protection to preserve obtained water quality and to recommend appropriate monitoring programs for borehole production. Under purely horizontal flow conditions, the sources of water quality variations are solely expected to arrive from the surface and not from beneath the tapped aquifer unit. The concept of groundwater vulnerability to contamination has limited value in protecting existing groundwater supply if every alteration of water quality is solely expected to occur from above ground level, not from beneath the aquifer unit where the water is being tapped.

A different approach is therefore needed to define changes in the obtained groundwater quality over the long term. A better understanding of groundwater functioning will facilitate the process. Additionally, the inclusion of socioeconomic and political variables has an equal importance in preventing effects resulting in extracted water quality deterioration if extraction and demand activities are properly planned in agreement with the groundwater flow regime. A constant increase in extraction yield requires an interdisciplinary understanding to assist decision-makers in reaching a better assessment on how concepts such as a specific land-use planning may change water quality and availability. A particular policy of land planning on a territory with certain water availability could develop a sustainable use according to the knowledge of water sources' functioning and their natural limits. Conversely, without a clear perception of the functioning of water sources, decision-makers are very limited in the understanding of impacts of their decisions regarding specific growth of related cities' needs. In Ref. [7], associated environmental impacts due to a lack of attention to the functioning of groundwater flow systems in México are identified.

In both semiarid and temperate regions, groundwater sources have become crucial to maintain social and economic development [12, 14, 17]. Fresh groundwater is available in many areas as recently infiltrated rainfall manifested in local groundwater flow systems; therefore, it is common sense to improve strategies for its adequate management since it usually remains the lower-cost option for drinking water. This low-cost option is favored not only financially but also environmentally, especially when water transfers among neighboring basins or surface water sources have become polluted. Another alternative often used is to treat the extracted groundwater. However, such a procedure has proved to be inadequate in the case of the control of the continuous inducement of saline waters of Mexico City which exceed local treatment methods and capacity designed to cope with strict levels of salinity. One important issue related to this inefficient rate is linked to water quality changes with extraction time. The quality of the inflow water to the plant will hardly

meet design specifications, and consequently, treatment plants may fail to meet drinking water production standards.

Groundwater Movement in Flow Systems

Groundwater moves in 3-D from its recharge to its discharge area (i.e., river, wetland, lake, spring, sea) in flow systems traveling through paths of different lengths and depths resulting in local- to regional-scale flow systems [25]. The presence of flow systems with contrasting hierarchy may be clearly defined from field evidence in conjunction with modeling of groundwater hydraulics, geochemistry, geomorphology, edaphology, as well as natural vegetation response. Contrasting geomorphological characteristics give groundwater a distinctive flow system with particular physical functioning [25], resulting in specific flow directions: vertical downward in recharge areas, horizontal in transit areas, and vertical upward in discharge areas (Fig. 1). Groundwater flow systems are constantly linked; therefore, it is paramount to understand their functioning to manage them adequately in agreement with their environmental conditions to reduce the impacts of human water usage and land-use changes.

Regions have distinct chemical and physical characters for different flow systems, especially where thick and extensive porous and permeable geological units are present above a basement rock. Usually, different temperature (cold in recharge areas, higher in the discharge area) and chemical conditions (i.e., water with high dissolved oxygen, low pH, and low salinity in recharge areas; and low dissolved oxygen, high pH, and high salinity in discharge areas) are characteristic of existing flow systems. Groundwater flow systems travel in the prevailing geological framework structure along the horizontal and vertical directions including the composition of the geological environment they traveled across. Local flows travel short distances at small depth, while those that initiate their traveling path in a basin and discharge in a neighboring basin containing at least one local flow constitute an intermediate flow (Fig. 1), all of which may be contained by a regional flow. A sketch of the location of Mexico City as related to the prevailing flow systems is represented in Fig. 1 as the current depth of extraction boreholes.

In Mexico, as a result of the thickness and extent of geological formations that constitute the aquifer unit as well as the variability of climatic characteristics, regional flows travel several hundreds of kilometers, often flowing from a temperate climate region to one with arid to semiarid characteristics, where urban growth and related economical development rely on flows of this nature as the city of San Luis Potosí [6]. Such development has been in progress without proper consideration being given to water availability not only in quantity terms but also regarding its quality.

Importance of Groundwater for Urban Development

The Mexico City Case

A large groundwater storage capacity becomes important when urban development exceeds surface water availability. However, the awareness of groundwater functioning is necessary to be understood and to incorporate it in any development plan of megacities as Mexico City (and other major cities worldwide), which is characterized by thick and extensive aquifer units, to avoid inducing inflows of groundwater systems that might deteriorate with time the quality of its originally obtained groundwater supply.

From its establishment, water needed for the development of Mexico City was originally supported from groundwater sources (springs). As time advanced, both development and population increased, and resulted water supply needs were mainly overcome with groundwater. Extraction had a rather stable increase from 1900 to the 1940s (from ≈2 to ≈4.5 m^3/s, respectively); however, from the 1940s, a rampant increase in water needs reached a claimed water supply in excess of 60 m^3/s by the end of the twentieth century, where some 76% was obtained from groundwater sources (Mexico basin ≈67.0% and Lerma basin ≈9.4%) and 23.6% from surface sources (Mexico basin ≈ 2.3% and Cutzamala basin ≈21.3%). This extraction history has produced a drop in water table level from artesian conditions to a depth of more than 50 m; a consequent response of the system to such increase in groundwater extraction is believed to be a key factor to the produced water quality change.

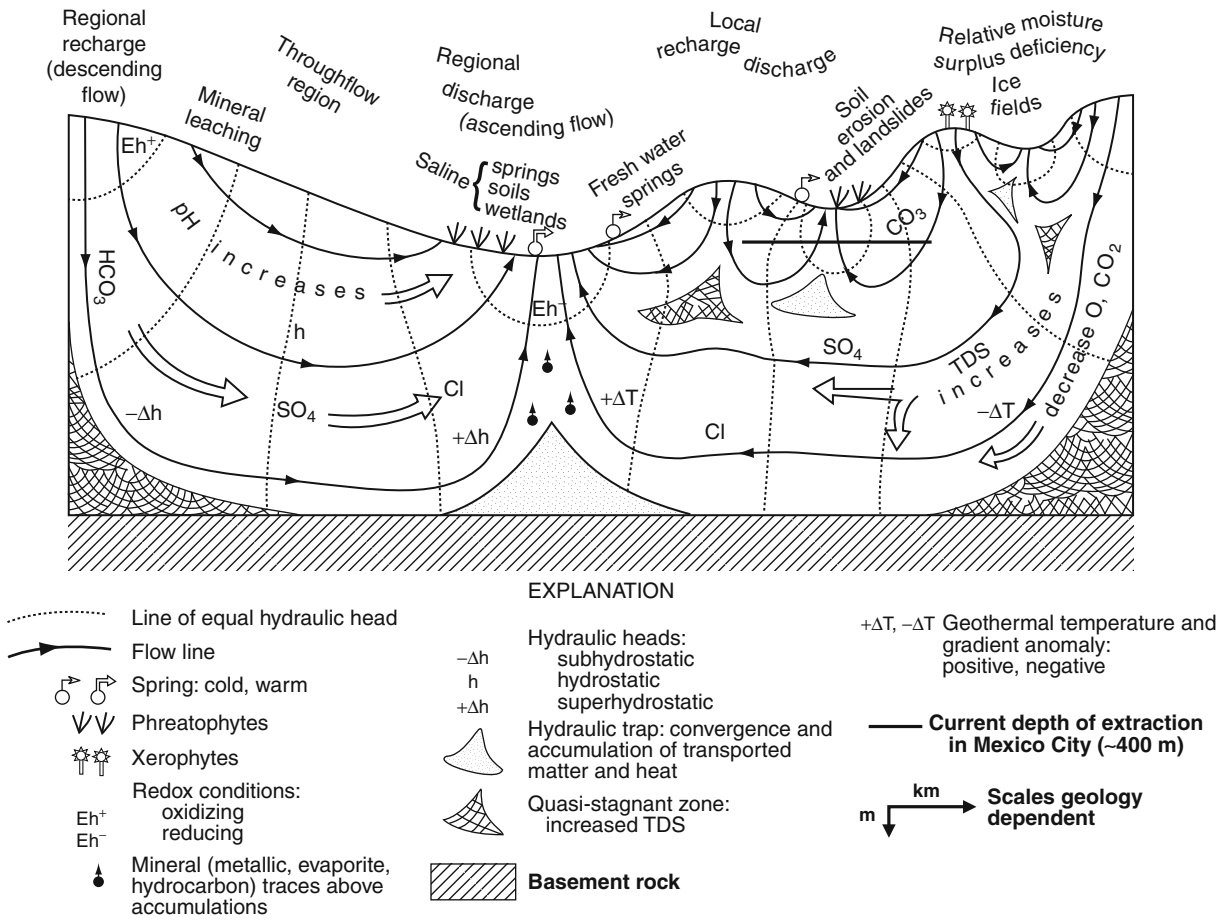

Groundwater Salinity Due to Urban Growth. Figure 1

Gravity groundwater flow systems developed in an unconfined drainage basin defining local, intermediate, and regional flow systems (Adapted from [26]). The location of the groundwater extraction for Mexico City is indicated by the depth of boreholes as related to the full aquifer unit

Groundwater Quality Response

Mexico City is located on a plain within a natural closed basin where its water supply since the beginning of the twenty-first century is about 80% supplied by groundwater. The groundwater supply has been of good quality generally for almost a century, from the late 1840s when the first borehole was constructed to the early 1970s when the extracted water quality drastically changed. Initially, groundwater extraction by artificial means was obtained mainly through artesian boreholes at depths of about 100 m. As technology advanced, construction of deeper boreholes was feasible, and the turbine pump was employed to solve the nonoverflowing conditions; deep boreholes went down to about 400 m, which is their current present depth beneath the foundations of the city. Reported salinity problems from groundwater in the northwest of Mexico City started by 1976, with a reported increase of about 300% in historic salinity; for example, Cl, Fe–Mn, and TDS increased from 32 mg/L, 0.1 mg/L, and 230 mg/L, respectively, to 55 mg/L, 0.45 mg/L, and 750 mg/L, respectively.

An understanding of the response of the chemical groundwater quality under the continuous increase of extraction in the Mexico basin (Fig. 2) may be reached when considering that geological framework and

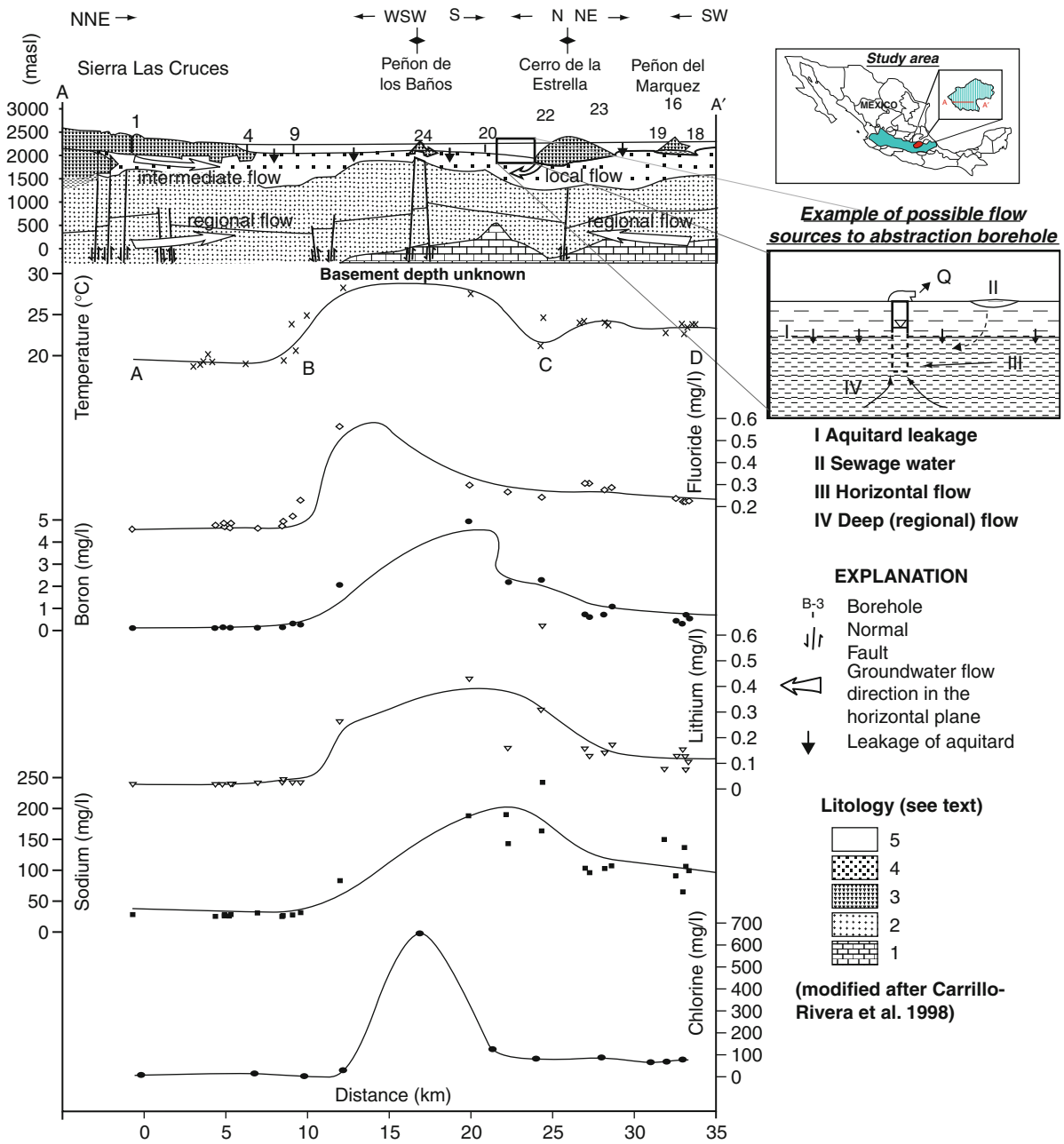

Groundwater Salinity Due to Urban Growth. Figure 2

Groundwater quality evolution along a section located in the south of the Mexico basin. Inset: Location of the basin in the Trans-Mexican Volcanic Belt

current climatic conditions are directly responsible for the presence of contrasting groundwater flows traveling at different depths with different path lengths. Increased extraction with partially penetrated boreholes also contributes.

Geological Framework

Geologically, Mexico City is located on a plain in a closed basin located on a graben structure developed during the Oligocene, where a thick succession of

volcanic and lacustrine materials was deposited. During the Oligocene, the basin drained to the south. This drainage outlet was closed during the Pleistocene from a series of volcanic activities [11] that formed the Chichinautzin Sierra to the south. The closure was part of an intense regional volcanic activity that formed the Trans-Mexican Volcanic Belt, which now covers Central Mexico from east to west with a length of about 1,100 km and some 400 km in width. The Mexico basin is located at its center (Fig. 2). The extrusive events occurred from 700,000 years before present till the Quaternary; during the later stage, volcanism allowed a substantial heterogeneous layer of ash, interbedded with extensive alluvial and lacustrine deposits, to accumulate in the various lakes formed after the closure of the basin. The full volcanic succession consists of a Middle Tertiary volcanic unit that includes clastic material as well as basalt, rhyolite, and andesite rock units with a collective thickness in excess of 3,000 m. These units are partially covered by Lower Pliocene deposits characterized by lacustrine and pyroclastic material with a total thickness of 600 m. These rocks are overlaid by Plio-Quaternary rocks consisting mainly of basaltic andesite, andesite, and pyroclastic material that dominate the highlands and are interstratified with contemporaneous alluvial and lacustrine deposits; their total thickness on the plain is in excess of 1,000 m. Recent volcanic episodes and regional tectonic events have produced an intensive vertical fault structure identified to be crossing beneath the plain [11].

These volcanic rocks overlie a regional Cretaceous sequence of calcareous deposits that consist of limestone, sandstone, and shale outcropping beyond the southern and northern basin limits; this deepest and oldest identified geological unit with a total known thickness is at the center of the basin in excess of 1,500 m. Deep drilling encountered the top of this unit at 1,581 m below ground surface. Karstic and fractured features are reported based on partial and total loss of drilling fluid and the drop of about 8 m of the drilling tools [28].

Recent deposits cover the entire floor of the plain, comprising some 600 m of fluvial and alluvial deposits. A lens of fine material (microfossils, volcanic ash, and, to a minor extent, lacustrine clay interbedded with sand, silt, and occasionally gravel) is included within these deposits; it outcrops in Lake Texcoco, underlying the rest of the plain except at the margins; in general, these deposits contain [19] high Na (up to 9,200 ppm) and Mn (up to 1,920 ppm). Total thickness increases gradually from the edge of the plain to Lake Texcoco, where it attains approximately 300 m. This unit forms a main aquitard saturated with water of heterogeneous quality, which locally acts as confining or semiconfining unit to the aquifer material beneath. This aquifer unit includes the extrusive and sedimentary rocks that extend regionally over Central Mexico with a thickness of more than 4,000 m, and it rests above a basement rock that has not been physically described.

The Mexico basin is one of the largest of a series of closed basins located in the Mexico Trans-volcanic Belt [28]. The basin has a drainage area of about 9,600 km^2; however, the actual area covered by the city proper and its sprawl area incorporates an extent of about 2,400 km^2. The abrupt relief of the surrounding mountains, with altitudes in excess of 5,000 m amsl, slopes toward the flat-lying center of the basin to an altitude of approximately 2,230 m amsl.

Climate Framework

The present climatic conditions where Mexico City is located are those of subtropical but with a significant variation in the mean annual precipitation across the basin. Precipitation ranges from 1,800 mm in the southern Sierra Chichinautzin, 1,100 mm in the west (Sierra Las Cruces), and 1,200 mm in Sierra Nevada, to 600 mm toward the remnant Lake Texcoco toward the center of the basin. The rainy season is mainly in the summer months. The mean annual temperature is from 12° to 14 °C in the sierras of Chichinautzin and Las Cruces and 15 °C in Lake Texcoco site. The potential annual evapotranspiration is around 1,400 mm. Rainfall produces negligible surface runoff in the permeable rocks of the Sierra Chichinautzin to the south of the city. In contrast, substantial runoff is generated in Sierra La Cruces to the west of the city, a condition that has caused severe historical flooding.

Water Quality Response to Groundwater Extraction

Mexico City reportedly extracts more than 50 m^3/s of groundwater from its basin to supply differing water

needs. A plan for actions for positive environmental response resulting from groundwater extraction should rely on an understanding of the flow systems to assist in planning and control of groundwater extraction by defining which particular flow is more vulnerable to intensive local water extraction rates in time and space.

Four real cases of the Mexico City basin [8] are examined; the interference of particular nearby boreholes is not incorporated. The first case presented by borehole 3 in Fig. 3 shows pumping (and recovery test) data that illustrates the local confining characteristics of the geological environment manifested as the classical drawdown–time response; the nature of the horizontal flow is relatively evident by stable values of TDS and temperature of obtained water with extraction time.

The case of borehole 8 shows a response traditionally considered to be the only possibility of chemical water quality change in this basin, portraying the acknowledged leaky effect from the semiconfining unit located above the level of groundwater extraction. There is an inflow of cold water, and withdrawal from this unit produces water with lower temperature. As extraction progresses, inflow water is expected to reach observed previous values (pv) when the borehole was stopped to initiate the test, at about 21°C. Reduction of TDS shows a change in the chemical characteristics of inflow water due to leakage from the semiconfining unit.

Drawdown–time data in borehole 23 would appear to also suggest a standard leaky response where the drawdown rate is diminished along the duration of the test; however, the increase of groundwater temperature may suggest that water is induced from intermediate or regional flows traveling beneath.

The response of the increase in TDS and constant temperature of borehole 12 suggests that obtained water is derived from standard (semi)confined conditions, where aquitard material above and below the tapped aquifer strata provides a steady response in terms of salinity values. Water is derived from the same shallow depth, keeping temperature at a steady value of 21°C.

The overall response of each of these boreholes in terms of obtained water quality results from the combined effect of (1) hydrogeological characteristics of affected aquifer environment (i.e., lack or presence of confined conditions, geological structure, Kv/Kh ratio), (2) discharge yield, (3) effect of drawdown on the local hydraulic potential (i.e., relative thickness among flow systems of different densities), (4) the path length to travel by any flow system to the level of extraction in the particular borehole, (5) borehole construction design as related to the stratigraphic units, and (6) position of the water table. All factors should be further studied to better plan actions to improve the quality of obtained water and to assess possible borehole techniques to better manage flow control. Suggestions on techniques to be applied are proposed in Ref. [8].

As suggested in Fig. 3, the response of borehole 23 is implied to be general to the prevailing long-term extraction yield. The increase over time of groundwater extraction in the basin of Mexico has reached more than 50 m^3/s, with individual boreholes extracting an average of 60 L/s. The effect of the partial penetration of production boreholes is that of radial flow in 3-D; relative shallow extraction level in the Mexico City plain results in ascending flow from a depth beyond current extraction levels. This can be interpreted as confirming the presence of the inflow of water of contrasting chemical quality as well as of higher temperature (Fig. 2). This interpretation appears sound when considering the graph of Fig. 4, where mNa/Cl–log Cl suggests that extracted shallow water (local flow) is evolving to water representing the former thermal spring (end-member) of Peñón de los Baños. The inducement of regional flow with different quality into the extraction level augments the concentration of obtained salinity in the water. The vertical components of ascending flow are important in observed water quality changes. Understanding water quality evolution could enhance better control processes of inducement of deep flowing water and aid in predicting where waters of more desirable quality might be obtained as suggested in Ref. [6].

Vertical Flow Control to Prevent Water Quality Deterioration

The identification and understanding of extracted different quality groundwater from contrasting flow systems entering a pumping borehole is one tool for possible control of obtained water quality [8]. These authors interpreted resulting field tests carried out in partially penetrating boreholes tapping a > 2,000-m fractured volcanic (rhyolitic) rock sequence and

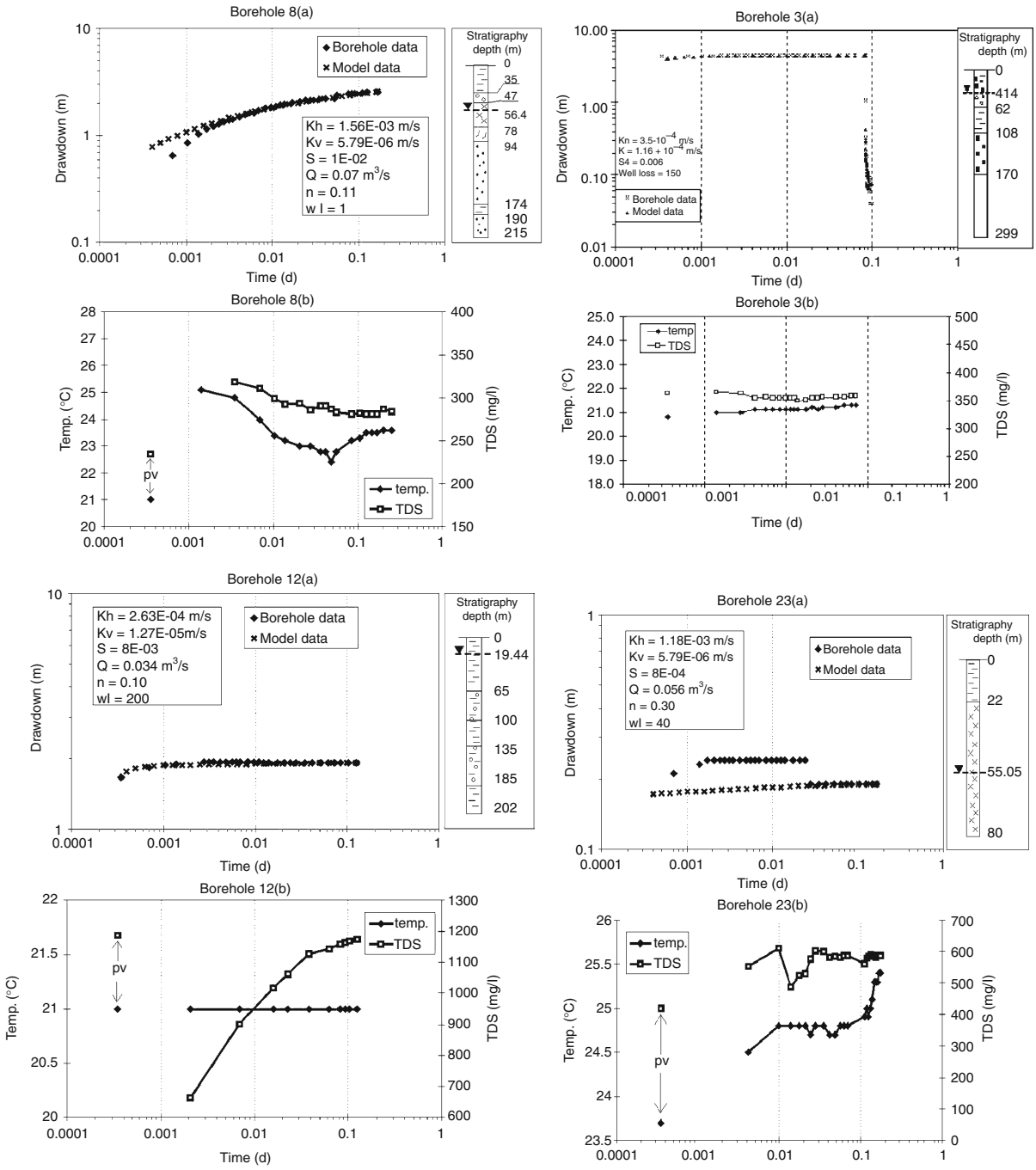

Groundwater Salinity Due to Urban Growth. Figure 3

Different responses to groundwater extraction: case 1 (borehole 3) confined conditions; case 2 (borehole 8) semiconfined conditions; case 3 (borehole 23) ascending groundwater flow; case 4 (borehole 12) leakage effect

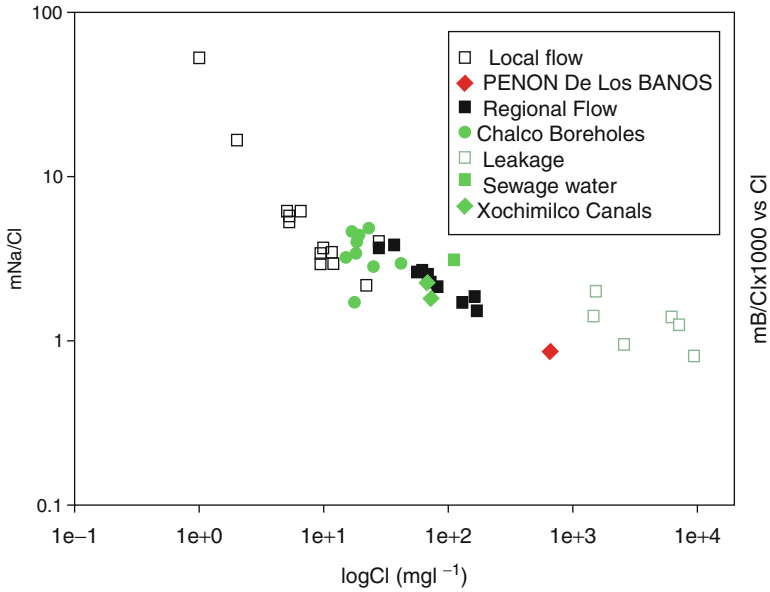

Groundwater Salinity Due to Urban Growth. Figure 4
Relation of the content of mNa/Cl and Cl for selected boreholes tapping local flows and water mixture representing local and regional end-member of former spring of Peñón de los Baños

proposed a technique to induce the production of the required quality water to a particular extraction borehole. The procedure involves the definition of particular response of flow systems' mixture under prevailing local extraction and hydrogeological variables, such as vertical and horizontal hydraulic conductivities, porosity, hydraulic head response between cold and warm flows, and rate and time of extraction. The response is basically defined through long-term aquifer tests (pumping tests) that include measurement of standard drawdown–time (s–t) response plus electrical conductivity (EC) and temperature at the various *t* intervals of the duration of the test. Additional collection of water samples for chemical and isotopic analyses complements obtained results.

Available information on vertical flow in volcanic terrain with large thickness [8] is important in assessing the factors affecting groundwater flow distribution and obtained water quality in the vicinity of the extraction borehole. An extraction yield will present a particular water quality, depending on the design construction of the borehole, lithology, affected flow systems and chemical components, and temperature of the induced flow systems. Obtaining a specific water quality is diverse and difficult to implement; this difficulty may be overcome by understanding the control of obtained water quality related to tests carried out in each particular borehole. Methods include an initial step-drawdown test, followed by a constant extraction-rate aquifer test, both in which temperature and EC measurements may be conducted. The response of the borehole could be further defined and understood when full sampling and water analysis is carried out to define major, minor, and trace elements as well as stable isotopes to differentiate the various components of inflowing groundwater flow systems.

Future Directions

Understanding and defining the groundwater system before planning for extraction is a basic rule that requires further attention, especially when practicing in Mexico as well as other countries. The perception of groundwater behavior achieved in the second half of the twentieth century was obtained mainly on function in shallow, thin aquifer units. This acquired knowledge provides a basis to define groundwater response and propose agreeable solutions for those aquifers.

Such powerful techniques have been applied in growing cities as Mexico City, where the increasing need for

water has produced changes in the flow system regime. The continuous development of an interdisciplinary approach as the Flow System Theory [25] is useful for defining the problem and acquiring solutions to the diversity of parameters involved in extracting water of the desired quality. The application of this theory is a powerful tool as it provides answers that are in agreement among the diverse disciplines involved.

Increase in population and economic activities in large cities relies on developing local groundwater flow systems that are often hydraulically linked to regional flow systems when the lithological sequence has a thickness greater than 1,000 m. An interdisciplinary understanding must be reached where groundwater flows of different chemical compositions and temperatures travel in a stratified mode. Analysis by 3-D modeling is useful for clearly defining a problem and proposing adequate solutions when potential impacts on the development of groundwater in thick aquifer units may induce regional flow. Usually, current analysis carried out is made solely on the horizontal scale; however, vertical components of flow need to be acknowledged. Aquifer tests, as well as other common hydrogeological tools, may define groundwater response and its functioning by incorporating the observation of the quality and temperature of extracted groundwater.

Changes in the obtained groundwater quality due to an increase of extraction rate are reflected by the chemistry and temperature of water flowing from a different level to that of the aquifer unit. Water quality changes could become key factors for density variation identification during water extraction, indicating the presence of semiconfining conditions through the behavior of drawdown with time (s–t) to that of inflow of water from regional systems at depth.

The growth of cities located on thick aquifer units (i.e., >1,000 m), accompanied with increasing water needs, makes the identification of local, intermediate, and regional groundwater flow systems essential. Two main issues arise in the analysis of thick regional aquifers in Central México: (1) the position of basement rock, which in turn implies the coverage of the aquifer unit involved, and (2) effects due to groundwater chemistry change, such as water density variations, affecting actual hydraulic heads and flow direction. These variables become more important in thick aquifer units.

Bibliography

Primary Literature

1. AIC (1995) El Agua y la Ciudad de México. Academia de la Investigación Científica, Academia Nacional de Ingeniería, Academia Nacional de Medicina, National Academy of Sciences (through the National Research Council), 364 pp
2. Ángeles-Serrano G, Perevochtchicova M, Carrillo-Rivera JJ (2008) Posibles controles hidrogeológicos de impacto ambiental por la extracción de agua subterránea en Xochimilco, México. J Lat Am Geogr 7(I):39–56
3. Bouwer H (1978) Groundwater hydrology, McGraw-Hill series in water resources and environmental engineering. McGraw-Hill, Sydney, 480pp
4. Carrillo-Rivera JJ (1998) Monitoring of exploited aquifers resulting in subsidence, example: Mexico City. In: Van Lanen HAJ (ed) Monitoring for groundwater management in (semi-) arid regions, vol 57, Studies and reports in hydrology. UNESCO, Paris, pp 151–165
5. Carrillo-Rivera JJ, Angeles-Serrano G, Hernández GG, Hergt T (2002) Estudio de hidrología subterránea sobre el área de Xochimilco, Distrito Federal. In: Programa rector de manejo del área natural protegida, ejidos de Xochimilco y San Gregorio Atlapulco. Secretaría del Medio Ambiente del Gobierno del Distrito Federal, Distrito Federal
6. Carrillo-Rivera JJ, Cardona A, Edmunds WM (2002) Use of abstraction regime and knowledge of hydrogeological conditions to control high-fluoride concentration in abstracted groundwater: San Luis Potosi basin, Mexico. J Hydrol 261:24–47
7. Carrillo-Rivera JJ, Cardona A, Huizar-Alvarez R, Graniel E (2008) Response of the interaction between groundwater and other components of the environment in Mexico. Environ Geol 2:303–319
8. Carrillo-Rivera JJ, Cardona A (2008) Groundwater flow system response in thick aquifer units: theory and practice in Mexico. Selected Papers, XXXIII-IAH internacional congress, Zacatecas, México, vol 12. Asociación Internacional de Hidrogeólogos, Editorial Balkema, Taylor & Francis, Leiden, pp 25–46
9. CAVM (Comisión De Aguas Del Valle De México) (1966) Datos del Valle de México, Período 1959–1963. Bol Mec Suelos 4
10. Edmunds WM, Carrillo-Rivera JJ, Cardona A (2002) Geochemical evolution of groundwater beneath Mexico City. J Hydrol 258:1–24
11. De Cserna Z, De la Fuente DM, Palacios NM, Triay L, Mitre SLM, Mota PR (1988) Estructura geológica, gravimétrica, sismicidad y relaciones neotectónicas regionales de la Cuenca de México, Institute of Geology, UNAM, México. Boletín 104:71pp (4maps)
12. Foster S, Garduño H, Evans R, Olson D, Yuan T, Zhang W, Han Z (2004) Quaternary aquifer of the North China Plain – assessing and achieving groundwater resource sustainability. Hydrogeol J 12:81–93
13. Freeze A, Cherry J (1979) Groundwater. Prentice, London, 490pp

14. Graniel-Castro D, Morris LB, Carrillo-Rivera JJ (1999) Effects of urbanization on groundwater resources of Mérida, Yucatan. Environ Geol 37(4):303–312
15. Herrera I, Alberro J, León JL, Chen B (1974) Análisis de los asentamientos para construcción de los lagos del Plan Texcoco. UNAM, Instituto de Ingeniería, Internal Report No. 340
16. Huizar-Alvarez R, Carrillo-Rivera JJ, Angeles-Serrano G, Hergt T, Cardona A (2004) Chemical response to groundwater extraction southeast of México City. Hydrogeol J 12:436–450
17. Llamas MR (1999) La inserción de las aguas subterráneas en los sistemas de gestión integrada. Bol Geol Min 110(4):253–370
18. Marsal RJ, Graue R (1969) The subsoil of lake Texcoco. In: Carrillo N (ed) The subsidence of Mexico City and Lake Texcoco project. Secr. de Hacienda y Crédito Publico, México, pp 167–203
19. Mesri G, Rokhsar A, Bohor BF (1975) Composition and compressibility of typical samples of Mexico City clays. Geotechnique 25:527–554
20. Ortega GA, Cherry JA, Rudolph DL (1993) Large-scale aquitard consolidation near Mexico City. Ground Water 31:708–718
21. Rivera A, Ledoux E (1991) Non-linear modelling of groundwater flow and total subsidence in the Mexico City aquifer-aquitard system. In: Proceedings of the fourth international symposium on land subsidence, Houston, May 1991, IAHS Publication No. 200, pp 45–58
22. Rudolph DL, Cherry JA, Farvolden RN (1991) Field investigations and solute transport in a lacustrine aquitard near Mexico City. Water Resour Res 27:2187–2201
23. Theis CV (1935) The relation between the lowering of the piezometric surface and rate and duration of discharge of a well using ground water storage. Trans Am Geophys Union 16:519–524
24. Tóth J (1995) Hydraulic continuity in large sedimentary basins. Hydrogeol J 3:4–16
25. Tóth J (1998) Groundwater as a geological agent: an overview of the causes, processes, and manifestations. Hydrogeol J 7:1–14
26. Tóth J (2008) From the artesian paradigm to basin hydraulics. Eötvös Loránd University. Institute of Geography and Earth Sciences, Budapest
27. Vázquez-Sánchez E (1995) Hidrogeología del Acuífero de la Ciudad de México. M.Sc. thesis en groundwater. UACPyP, Posgrado en Geofísica, Instituto de Geofísica, UNAM
28. Vázquez-Sanchez E, Jaimes-Palomera R (1989) Geología de la Cuenca de México. Geofís Int 28(2):133–190

Books and Reviews

Cardona A, Carrillo-Rivera JJ, Huizar-Alvarez R, Graniel-Castro E (2004) Salinization in coastal aquifers of arid zones: an example from Santo Domingo, Baja California Sur, Mexico. Environ Geol 45(3):350–366

Cardona A, Carrillo-Rivera JJ, Castro-Larragoitia GJ, Graniel-Castro EH (2008) Combined use of indicators to evaluate waste-water contamination to local flow systems in semi-arid regions: San Luis Potosi, Mexico. Selected Papers XXXIII-IAH internacional congress, Zacatecas, México, vol 12. Asociación Internacional Hidrogeólogos, Ed Balkema, Taylor & Francis, Leiden, pp 85–104

Carrillo-Rivera JJ (1988) The Sierra Madre occidental. In: The geology of North America, hydrogeology, vol 0–2. The Geological Society of North America, Boulder, pp 87–88

Carrillo-Rivera JJ (1993) The hydrogeology of the San Luis Potosi area, Mexico. Ground Water J Assoc Ground Water Sci Eng (Abstracts Students Section, Marzo–Abril p 330)

Carrillo-Rivera JJ (1998) Monitoring of exploited aquifers resulting in subsidence, example: Mexico City. In: Monitoring for groundwater management in (semi-)arid regions, vol 57, Studies and reports in hydrology. UNESCO, Paris, pp 151–166

Carrillo-Rivera JJ (2000) Application of the groundwater-balance equation to indicate interbasin and vertical flow in two semi-arid drainage basins, Mexico. Hydrogeol J 8(5):503–520

Carrillo-Rivera JJ (2002) Aquifer evaluation. In: Moore JE (ed) Field hydrogeology. Lewis, Boca Raton, pp 79–87 (Chap 6). ISBN 1-56670-587-8

Carrillo-Rivera JJ (2003) Lack of a conceptual system view of groundwater resources in Mexico, editor's message. Hydrogeol J 11(5):519–520

Carrillo-Rivera JJ (2004) Congreso conjunto: XXXIII asociación internacional de hidrogeológos y 7º asociación Latinoamericana de hidrología subterránea para el desarrollo, Zacatecas, Zac. Méx. Rev Invest Geogr 55:175–177

Carrillo-Rivera JJ, Adrián Ortega G (2008) Special number of environmental geology. In: XXXIII international hydrogeologic congress on groundwater flow understanding from local to regional scales, vol 55. Springer, Berlin, pp 235–464. ISSN 0943-0105

Carrillo-Rivera JJ, Cardona A (2002) Capítulo 14. In: Michael Price (ed) Agua subterránea. Chapman and Hall. Published by Limusa, Noriega Editores, México

Carrillo-Rivera JJ, Cardona A (2008) Groundwater flow system response in thick aquifer units: theory and practice in Mexico. Selected Papers, XXXIII-IAH internacional congress, Zacatecas, México, vol 12. Asociación Internacional de Hidrogeólogos. Editorial Balkema, Taylor & Francis, Leiden, pp 25–46

Carrillo-Rivera JJ, Ortega Guerrero MA (eds) (2008) Groundwater flow understanding: from local to regional scales. Selected Papers, XXXIII-IAH international congress, Zacatecas, México, vol 12. Asociación Internacional de Hidrogeólogos. Editorial Balkema, Taylor & Francis, Leiden, ISBN: 13 978 0 203 94579 7, p 186

Carrillo-Rivera JJ, Clark DI, Fritz P (1992) Investigating recharge of shallow and paleo-groundwater in the Villa de Reyes Basin, SLP, Mexico, with environmental isotopes, applied hydrogeology. Off J Int Assoc Hydrogeol 4/92:35–48

Carrillo-Rivera JJ, Cardona A, Moss D (1996) Importance of the vertical component of groundwater flow: a hydrochemical approach in the valley of San Luis Potosí, Mexico. J Hydrol 185:23–44

Carrillo-Rivera JJ, Cardona A, Hergt T (2001) Inducción de agua termal profunda a zonas someras: Aguascalientes, México. Rev Latinoam Hidrol 1(1):41–53

Carrillo-Rivera JJ, Varsányi I, Kovács LÓ, Cardona A (2007) Tracing groundwater flow systems with hydrogeochemistry in contrasting geological environments. Water Air Soil Pollut 184:77–103

Carrillo-Rivera JJ, Cardona A, Edmunds WM (2007) Groundwater flow functioning in arid zones with thick volcanic aquifer units: North-Central Mexico. In: International symposium on advances in isotope hydrology and its role in sustainable water resources management (HIS-OIEA) Proc, 21–25 May 2007, vol 1, Vienna, pp 199–211

Facundo-Castillo JR, Carrillo-Rivera JJ, Antigüedad-Auzmendi I, González Hernández P, Leláes-Diaz R, Hernández-Diaz R, Cáceres-Govea D, Hernández-Santana JR, Suárez-Muñoz M, Melán-Rodriguez C, Rodríguez-Piña M (2008) Chemical and geological control of spring water in eastern Guaniguanico mountain range, Pinar del Rio, Cuba. Environ Geol 55(2):247–267

Fagundo J, Carrillo-Rivera JJ, Antigüedad I, González P, Peláez R, Suárez M, Melián C, Hernández R, Cáceres D (2005) Caracterización hidrogeoquímica del sistema de flujo local-regional de la Sierra del Rosario (Cuba). Rev Latinoam Hidrol 5:75–90

Gutiérrez de MacGregor MT, Carrillo-Rivera JJ, Valdez-Quijada R (1997) Impact of Mexican and USA policies in urban growth and natural resources in the northern border of Mexico, vol 15, Latin American Studies, Nihon-Burajiru Chou Kyokai, Tokio, pp 49–62

Huizar-Alvarez R, Hernández-García G, Carrillo-Rivera JJ (2009) Simulation of the effects from the groundwater flow on the hydrological balance of the Tecocomulco Lagoon, Central Mexico. Open Environ Sci J 3:1–13

Huizar-Álvarez R, Hernández GG, Carrillo-Martinez M, Carrillo-Rivera JJ, Hergt T, Ángeles-Serrano G (2003) Geologic structure and groundwater flow in the Pachuca–Zumpango sub-basin, central Mexico. Environ Geol 43:385–399

Martinez SE, Carrillo-Rivera JJ (2006) Socio-economic constraints of groundwater in Capital La Rioja, Argentina. Environ Geol 49(6):875–886. doi:10.1007/s00254-006-0183-7

Segovia N, Taméz E, Peña P, Carrillo-Rivera JJ, Acosta E, Armienta MA, Iturbe JL (1999) Groundwater flow system in the valley of Toluca, Mexico: an assay of natural radionuclide specific activities. Appl Radiat Isot 50:589–598

Van-Lanen AJH, Carrillo-Rivera JJ (1998) Framework for groundwater monitoring in (semi-) arid regions. In: Monitoring for groundwater management in (semi-) arid regions, vol 57, Studies and reports in hydrology. UNESCO, Paris, pp 7–20

H

Harmful Algal Blooms

Timothy I. McLean[1], Geoffrey A. Sinclair[2]
[1]Department of Biological Sciences, University of Southern Mississippi, Hattiesburg, MS, USA
[2]DeFelice Marine Center, Louisiana Universities Marine Consortium, Chauvin, LA, USA

Article Outline

Glossary
Definition of the Subject and Its Importance
Introduction
Alexandrium
Karenia brevis
Pseudo-nitzschia
Cyanobacteria
Future Directions
Bibliography

Glossary

Bioaccumulation The retention of substances, various phycotoxins in this context, in the living tissues of organisms at concentrations that are higher than are found in the environment.

Cyanobacteria A phylum of bacteria, once called blue-green algae, that appears in the fossil record as far back as 3.5 billion years all species are photosynthetic, but different species have adapted to aquatic (fresh or marine) or terrestrial (soil, bare rock, or symbiotic associations with plants) environments some species can form colonies, and some colony-forming cells can specialize or differentiate, e.g., to form nitrogen-fixing heterocysts.

Depuration The cleansing or purification of impurities (toxins) from the tissues of the body.

Diatoms A large group of microalgae distinguished by having siliceous cell walls called frustules single cells range in size from 2 μm to over 2 mm and are unicellular, often forming colonies of many cells they contain the pigments chlorophylls a and c, betacarotene, fucoxanthin, diatoxanthin, and diadinoxanthin they constitute the predominant fraction of the phytoplankton community in fresh water and marine environments, found in the water column and in the benthos, being both epiphytic and edaphic.

Dinoflagellates A large group of motile microalgae differentiated from other algal groups by their thecal morphology (cell covering) having either an armored form or a smooth form armored forms contain distinctly ornamented polysaccharide plates they contain two dissimilar flagellae, and species may be exclusively heterotrophic, mixotrophic, or exclusively phototrophic – those that are capable of photosynthesis contain the pigments chlorophylls a and c, dinoxanthin, diadinoxanthin, and either fucoxanthin or peridinin as their major carotenoid, depending upon the species.

Eutrophication The introduction of excessive levels of nutrients such as nitrates and phosphorous into an aquatic ecosystem.

Harmful algae A small fraction of algal species that can have disruptive or devastating effects to an ecosystem, public health, and/or various economies the harmful nature of different species of algae can be manifested in a variety of ways but primarily through the production of one or more phycotoxins.

Phycotoxins Toxic molecules produced by harmful algae collectively, these molecules are chemically diverse and can produce an array of effects in intoxicated organisms ranging from gastrointestinal, neurotoxic, hepatotoxic, carcinogenic, and more.

Trophic transfer The transfer of energy and/or substances, e.g., toxins, from one (trophic) level of a food chain to another, typically higher, (trophic) level within the food chain.

Robert A. Meyers (ed.), *Encyclopedia of Sustainability Science and Technology*, DOI 10.1007/978-1-4419-0851-3,
© Springer Science+Business Media, LLC 2012

Definition of the Subject and Its Importance

Harmful algal blooms (HABs) pose threats to the environment, public health, and a variety of commercial interests and industries. A single bloom can lead to devastating outcomes, including large mortalities of marine organisms (e.g., fish kills); toxic contamination of filter-feeding organisms such as bivalve shellfish that subsequently enter the market for distribution to consumers; economic hardships for fisheries, aquaculture, and recreational- and tourism-related industries; and a compromised quality of life for people living or working along affected shorelines. Depending upon the size of the bloom, its duration, and the number and types of impacts produced, a single bloom can generate multimillion-dollar losses spanning from local to international economies (see ► Oceans and Human Health, Social and Economic Impacts for additional information on HAB-related economic impacts).

As well as a current concern, the issue of HABs will continue to grow in the future, as HABs are being reported at higher frequencies, lasting for longer periods of time, covering larger areas of shoreline or acreage of water, and spreading to regions that historically have not experienced blooms [1–8]. A number of factors have been cited as contributing to this global increase, but each algal species responds to a different set of variables. For many species, degraded water quality is one of the major reasons for the increase in HABs and HAB effects [9, 10]. As eutrophication, urbanization, and climate change continue to escalate, the increasing impact of HABs is a threat to the economic sustainability of many coastal and marine industries, public health, and the health of natural resources.

Introduction

"Algae" is not a true taxonomic designation. Algae are polyphyletic, i.e., species under this umbrella term can be found on numerous branches within the eukaryotic lineage. The diversity of organisms within this assemblage make it difficult to provide a concise definition of algae (reviewed in Ref. [11]), but in general terms algae can be described as simple (i.e., lacking the structures and vasculature characteristic of land plants), mostly aquatic, photosynthetic, and ranging in form from unicellular (microalgae) to multicellular (macroalgae). For historical and physiological reasons, this artificial grouping also includes the prokaryotic cyanobacteria, formerly known as blue-green algae. The inclusion of cyanobacteria is further strengthened in the context of discussions about harmful algae (see below).

Algal blooms denote an increase in the population of a single species of algae within a given area. The increase may be a result of an increased growth rate or the accumulation/aggregation of cells due to, respectively, an infusion of nutrients or physical features such as fronts, a stratified water column, or current entrainment [9, 12, 13]. Algal blooms can form for a multitude of reasons, and the reasons for and the characteristics of a bloom vary by the species. Algal blooms occur worldwide in fresh, brackish, and marine environments. If the cell concentration becomes sufficiently dense, the bloom may discolor the water to produce a "red tide," although, depending on the organism, the water may actually appear green, brown, or gold, instead of red. Although the term red tide has taken on a negative connotation, the majority of red tides occur as natural, seasonal phenomenon that produce beneficial rather than harmful consequences. For example, in the Southern Ocean, successions of blooms produced by different algal species during the spring and early summer months anchor food chains that feed a multitude of organisms from birds to whales [14]and sustains an important fishery that nets >100,000 t of krill per year [15]. Less than a tenth of the 3,400–4,100 identified algal species are known bloom formers, and less than a quarter of those (2% of the total) have the capacity to form a harmful algal bloom [16, 17].

Algal blooms are designated as harmful when they have detrimental effects to other organisms or ecosystem functions either directly or indirectly. In some cases, the mere presence of a high number of cells in the water column increases cell–cell collisions that may damage or kill other planktonic organisms. For example, some microalgae, particularly diatoms with extensive silicate setae, can cause physical trauma when they pierce or tear the cellular structure of other microbes or the gills of fish and crustaceans [1, 18, 19]. Indirectly, harmful effects include changes in resource competition or decreasing ecosystem health by producing biomass whose decomposition fuels the creation of hypoxic or anoxic conditions [20, 21]. Other harmful species may produce allelopathic molecules [22], allelochemicals [23], high amounts of ammonium [24],

or extracellular polymeric secretions that create viscous or mucilaginous barriers in the water [25, 26]. The majority of our attention, however, has been focused on those algae that produce one or more toxic molecules referred to as phycotoxins. Direct contact with, inhalation of, or ingestion of the phycotoxins by humans (or other animals) can cause a range of effects from mild irritation to severe gastrointestinal distress to death. Some of the more hazardous phycotoxins can have hemolytic, hemoagglutinating, neurotoxic, or hepatotoxic effects, or they can promote the formation of tumors, e.g., in the colon (see below for specific examples and references). As described below, these toxins can vector through food webs as they pass from one trophic level to another. During these trophic transfers, toxins may bioaccumulate in tissues or undergo changes in potency. The effects of phycotoxins in the natural environment can lead to massive mortalities of fish, birds, marine mammals, and other less well-characterized marine organisms creating miles of coastline and hectares of water littered with dead animals.

A growing concern about HABs is the real or perceived threat that they are increasing year to year as evidenced by: (1) areas that have historically experienced blooms sporadically, or even rarely, are seeing an increase in frequency; (2) when blooms do occur, they are lasting longer and/or covering larger expanses of coastline; (3) new species of toxic algae are being discovered; (4) species that were previously described as nontoxic are now showing the capacity to be toxic; and (5) the biogeography of certain species is expanding [1–8]. Certainly, our ability and impetus to detect harmful species and their respective toxins has increased over the last 15 years, but the increased awareness and concern about HABs cannot fully explain the explosion in the number and extent of blooms around the world. The most likely culprits, although not for each species, are the introduction of species to new environments through mechanisms such as transport in ballast water and the alteration of the natural environment through mechanisms such as urbanization of our coastlines, diversion of natural water flows, draining of wetlands, introduction of new or increased sources of nutrients from aquaculture practices and runoff of urban and agricultural regions, and climate change. Any of these factors, or combinations of these factors, may produce an environment conducive for HAB species to bloom.

The following sections will highlight four of the better-studied HAB taxa (two genera: *Alexandrium* and *Pseudo-nitzschia*, one species: *Karenia brevis*, and one phylum: cyanobacteria) in terms of why they are harmful, the economic costs and types of impacts associated with each respective bloom, the methods used to detect the cells and/or associated toxin(s), and what is known in regard to what initiates and/or maintains the blooms. For comprehensive overviews of other HAB species or more information about the taxa described herein, refer to recommended readings at the end or the embedded reviews in each section.

Alexandrium

Description

The dinoflagellate genus *Alexandrium* currently contains greater than 30 species [27]. Members of the genus are armored, have a defined cellular and nuclear morphology, occur as either single cells or as chains of two or more cells, and are widely distributed in temperate regions of the Mediterranean and northern and southern Atlantic and Pacific Oceans [27]. Molecular data support the monophyletic grouping of *Alexandrium* spp. [28]. The same data challenge the division of species within the genus, however, as DNA-based assays show that cells tend to cluster based on geography rather than morphospecies designations [29–33]. Twelve *Alexandrium* spp. are confirmed to produce paralytic shellfish toxins ([34] and references therein). Members of the *Alexandrium tamarense* morphospecies complex (*A. tamarense, A. catenella*, and *A. fundyense*) are responsible for the majority of blooms along northeastern and northwestern North American coastlines.

Toxicity

Paralytic shellfish toxins (PSTs) consist of saxitoxins and at least 24 saxitoxin-like congeners (reviewed in Ref. [35]). (It is important to note that, while not discussed here, other dinoflagellates, principally *Gymnodinium catenatum* and *Pyrodinium bahamense* var. *compressum*, and some cyanobacterial species can also produce PSTs (reviewed in Ref. [35]).)

The potency of different PSTs ranges over a scale of one to three orders of magnitude [36], and those with a sulfocarbamoyl group are the most toxic (reviewed in Ref. [35, 37]). The name of this grouping of toxins derives from the syndrome, paralytic shellfish poisoning (PSP), which is produced as a result of consuming seafood, primarily bivalves, containing PSTs. PSTs, such as saxitoxin, bind voltage-gated sodium channels on the membranes of electrically excitable cells such as neurons and block the flow of sodium ions through the channel [38, 39]. The blockage prevents depolarization of the cell [40], which causes a range of gastrointestinal and neurological symptoms that vary with the exact composition of various PSTs and the susceptibility of the individual. Symptoms include tingling around the mouth, numbness of the extremities, weakness, nausea, and vomiting, among others. If a sufficient dose is ingested, neurons will be unable to stimulate muscle contractions. Complete muscle relaxation leads to paralysis, and if the paralysis extends to the muscles controlling breathing, individuals can die from asphyxiation [41].

PSTs can vector through marine food webs, having been found in zooplankton and zooplanktivorous fish (reviewed in Ref. [42]). The bioaccumulation of PSTs in these lower trophic level organisms has been implicated in mortalities of large numbers of fish, oceanic and coastal birds, and marine mammals, including humpback and right whales, which consume whole fish [4, 43–48]. Human intoxication from eating fish is rare since the PSTs accumulate in the viscera, which is typically not eaten by people. The most common route for human intoxication is through consumption of contaminated bivalves (e.g., mussels and clams), although, in rare cases, other organisms (e.g., gastropods, crustaceans, and fish) have served as vectors [49, 50]. Shellfish are indiscriminate filter feeders; they can consume large quantities of microalgae, are relatively immune to the PSTs, and bioaccumulate the toxins in their tissues. Different bivalve species have different tolerances to PSTs, and having a high tolerance allows an organism to accumulate more toxins. An example of an organism with a high tolerance is the blue mussel (*Mytilus edulis*). In Alaskan waters, *M. edulis* can bioaccumulate greater than 20 mg of saxitoxin/100 g mussel tissue – more than enough saxitoxin to kill a person [51]. Typically, 1–2 months after moderate blooms have terminated, the majority of bivalves will have depurated the toxins and will be considered safe for harvest and consumption. By contrast, butter clams bind to saxitoxin with high affinity and can remain toxic for up to 3 years after a bloom has occurred [51]. In some bivalves, PSTs can undergo biotransformation, possibly becoming even more toxic than the original source toxins [52].

Economics

PSTs are heat and acid stable, so cooking not only does not detoxify seafood but also may convert some congeners to more toxic forms. The only way to avoid PSP incidents is to prevent the harvesting of contaminated marine organisms or process them in such a way to reduce or minimize toxicity. For example, adductor muscles of sea scallops, which typically contains very low concentrations of PSTs, are considered safe if separated from the rest of the scallop while at sea before being frozen [53]. If the whole organism is frozen, then PSTs may leech from other tissues into the adductor muscle. For a review of other methods to reduce toxicity in seafood, see [53].

Alternatively, the only mechanism for determining whether to harvest/not harvest or to allow shellfish beds to be open or closed is to monitor for the presence of PSTs in the relevant shellfish tissues. Unlike other HAB species, detection and quantifying of PSP-producing microalgal cells are not sufficient for such management decisions – the collection of tissues and analysis for PSTs is required. These steps add costs to monitoring efforts performed by the relevant agencies. Costs for monitoring can become expensive especially for states with extensive coastlines. Alaska, e.g., only samples random sites and, therefore, discourages recreational harvesting, which leads to a severe underutilization of the endemic shellfish resources [8]. Of course, in a grand economic sense, the lost income and sales are, in part, balanced by reduced monitoring and public health costs.

In terms of economic consequences of PST-producing blooms, only a few case studies have been performed to quantify in dollars how extensive these impacts are. In the Pacific northwest, an *Alexandrium* bloom in 1997 created toxic oysters along the coast of Washington state that resulted in approximately

$9.45 million of lost revenue during a 2- to 3-week industry closure. An extended closure (2 months) of shellfish beds in South Puget Sound resulted in about $27 million in losses (Nosho in Ref. [54]). (Note: All dollar figures throughout this article are represented in 2011 values.) A similar bloom that closed beds along Washington, Oregon, and California state coastlines for a month in 1980 cost oyster growers $2.5 million [55]. During the same year in the northeastern United States, a bloom of *A. tamarense* closed the entire coastline of Maine to shellfish harvesting. The value of the lost harvest was placed at $6.6 million, and the total economic impact was placed at $20 million [56]. In 2005, a massive bloom extended over the majority of the New England coastline, resulting in $3.1 million/week in lost revenue for the affected seafood fisheries [57]. Later analysis determined that the bloom impacted the state of Massachusetts by greater than $20.7 million and at least $2.7 million to the state of Maine [58].

Detection

A number of molecular techniques have been developed to rapidly and correctly identify cells as a particular *Alexandrium* species. The majority of the efforts to differentiate species have focused on molecular sequence data, such as the sequence of the ribosomal RNA gene for either the small or large ribosomal subunit or the internal transcribed spacer [29, 30, 32, 59–61]. Depending upon the marker or technique used, the number of defining ribotypes for *Alexandrium* varies from 5 to 11 [30, 32, 60]. Despite the discrepancy in the number of ribotypes, the results of these assays show that *Alexandrium* cells from the same geographic region are more closely related to each other than to cells from different regions, even if the cells from the different areas are of the same species. The conclusion drawn from the data is that *Alexandrium* is monophyletic, but geographically isolated populations evolved independently subsequent to global dispersion [31].

More effort has gone to developing methods for detecting and quantifying PSTs. The standard assay is the mouse bioassay in which acid extracts of tissue samples from intoxicated organisms are injected into three mice and the average time to death is recorded [62, 63]. The results are converted into a concentration of saxitoxin, or saxitoxin equivalents, which then serves as the basis for determining whether a particular shellfish site stays open or is closed. The current action level in the United States set by the Food and Drug Administration (FDA) is 0.8 ppm (80 μg saxitoxin/100 g tissue) [64]. The action level in other countries may vary slightly and can be found in FAO Marine Biotoxins Paper 80 [65].

Despite monitoring and informing the public of the dangers of PSP, there are still sporadic poisoning incidents from recreational or subsistence harvesting in closed or unmonitored harvest sites [35]. The use of the mouse bioassay has always been fraught with concerns and problems (e.g., poor specificity for different congeners, low sensitivity, high variability, and the sacrifice of a large number of animals), and a number of alternative techniques have been and continue to be developed. Some of these techniques include neuroblastoma tissue culture bioassays [66, 67], a hemolysis assay [68], receptor-binding assays [69–71], enzyme-linked immunosorbent assays (ELISAs) [72, 73], and electrochemical biosensors [74–77]. Most of these techniques have offered improvement in some areas, but they have not been sufficiently developed or tested to replace the mouse bioassay. Of those listed, the ELISAs have received the most attention in terms of lowering the limit of detection and increasing broad-spectrum detection or developing congener-specific antibodies, e.g., [78–82]. An offshoot of the ELISA technique has the development of lateral flow immunochromatography assays [83, 84]. One such assay, the quick (less than 20 min), one-step MIST Alert™ (Jellet Rapid Testing Ltd.), uses a combination of highly specific antibodies to overcome cross-reactivity issues that have plagued immunoassay development. MIST Alert™ has been field tested, and the biggest concern with its use is the high rate of false positives [35, 85, 86]. The US FDA has approved the test kits for use in the field to prescreen samples – negative samples do not need further analysis whereas positives must be confirmed via mouse bioassays [35]. The prescreening will save time, money, and animal lives. A lot of effort has also been expended in regard to developing liquid chromatography-based techniques. Originally developed by the US FDA [87], a number of derivations and modifications have been implemented including tandem linkage to mass

spectrometry and pre- and post-column oxidation of the toxins [75, 76, 88–95]. A particularly useful development was the creation and commercialization of PST standards for use in analyses such as liquid chromatography [96, 97]. Recently, the use of liquid chromatography with post-column oxidation and fluorescence detection has been approved as an official method of analysis by the AOAC [98]. The establishment and validation of this methodology is often a prerequisite for adoption by regulatory agencies and may pave the way for the replacement of the mouse bioassay as the standard assay for detection and quantitation of PSTs.

Origins and Nutrient Interactions

PSP events were reported in Canada over 100 years ago (Ganog in Ref. [99]), but the first documented case in the United States was not until 1958 [100]. In the New England area of the United States, specifically the western Gulf of Maine, PSP events were relatively rare, but they are increasing in frequency and becoming more widespread [101–103]. Similarly, *Alexandrium* and PSP events are now common in historically pristine Pacific waters such as those around Alaska and northern Japan [101]. From these observations, in conjunction with the results from laboratory and field experiments, the spreading of *Alexandrium* blooms and toxifying events can best be explained by examination of cyst deposition and cell transport via storms and currents. A combination of extensive spatial and temporal sampling of cyst seed beds, environmental monitoring and observations, and laboratory experimentation has produced a biophysical model of *Alexandrium* in the Gulf of Maine [57, 104]. The model successfully recreated ("hindcasted") the formation and movement of the 2005 *Alexandrium fundyense* bloom that started in the northern Gulf of Maine and spread southward as far as Long Island, New York [57, 104]. The model has highlighted the role of three factors of particular import for determining bloom impacts to the coastline. First, heavy rainfall and snow melt created substantial freshwater inputs. The inflow provided some nutrients to the coastal ecosystem, but it also helped stratify the water and provided buoyant plumes that helped transport cells in coastal currents. Second, upwelling-favorable winds shifted to become downwelling-favorable, which promoted transport of offshore blooms onshore. Lastly, bloom intensity is directly correlated to the abundance of cysts present in one or both of two seed beds – in the Bay of Fundy or offshore of Penobscot and Casco Bays [57, 104–106]. Cysts are deposited at the end of a bloom where they overwinter (i.e., lie dormant in the sediment) until the spring, at which time the warmer water temperatures and increased light, nutrients, and oxygen will cause the cysts to germinate [107]. Upon germination the resulting vegetative cells rise to the surface, and they can be pushed onshore under downwelling-favorable conditions and transported along the coastline by prevailing winds and currents [57]. As blooms spread to new areas, the seeding of those areas with cysts likely expands the range of blooms [55, 57].

Understanding the role and importance of these variables and the creation of a model provides significant value as a year to year predictor of bloom likelihood and bloom severity. The model has been applied to the bloom seasons since 2006 and has provided guidance for shellfish harvesters, stakeholders, and managers to make more-intelligent decisions about when and where to harvest shellfish, when and where to monitor for toxin, and how best to preserve public health [8]. In light of the importance of cyst seed beds, similar beds are being mapped and monitored in Puget Sound, Washington, as potential initiating sites [8]. The information also provides a warning against indiscriminant dredging activities that may unearth buried, dormant cysts. Almost all cysts (90%) are buried below the surface in anoxic conditions [108] – conditions that sustain their encystment unless resuspended. Dredging may "reawaken" these cysts to form a bloom or enrich a bloom with additional cells the following spring. The transporting and depositing of marine sediment that may contain cysts to new locations must be monitored lest these activities serve to seed new areas and spread the occurrence of *Alexandrium* blooms [102].

Karenia brevis

Description

The harmful dinoflagellate *Karenia brevis* is an athecate dinoflagellate, i.e., it does not possess any armored plates, and it is about 20 μm in diameter. The size of *Karenia brevis* varies over a diel cycle increasing in size

as the day progresses [109]. *Karenia brevis* swims about 250 μm per second or about 1 m an hour. This swimming ability allows *Karenia brevis* to undergo a diel vertical migration, ascending during the day and descending at night [110]. The traditional explanation for this pattern is that cells are maximizing exposure to light during the day to support photosynthesis and maximizing exposure to nutrients at night. *K. brevis* does not, however, undergo a banded migration characterized by synchronous ascent and descent of the entire population, and therefore there appears to be other factors involved in its behavior other than external stimuli.

K. brevis has been intensively studied due to the socioeconomic impacts that blooms have on coastlines throughout the Gulf of Mexico but particularly on the west coast of Florida, where they now occur almost annually [111, 112]. From January to October 2006, Florida red tides killed thousands of fish and numerous manatees and caused incidents of human respiratory distress, which ultimately reduced local tourism. While cell densities of greater than 1×10^5 cells per liter near shore are responsible for these problems, the *K. brevis* populations appear to originate farther offshore in oligotrophic water columns [112, 113].

Toxicity

Karenia brevis produces a suite of cyclic polyether compounds referred to as brevetoxins (PbTxs). Brevetoxins are a type of neurotoxin that disrupts normal neurological processes by binding to voltage-gated sodium channels in nerve cells. Consumption of this toxin results in an illness described as neurotoxic shellfish poisoning [114]. For decades, brevetoxins produced by *K. brevis* have been implicated in animal mortalities throughout the food chain [115, 116]. Blooms not only result in massive fish kills, but brevetoxins also bioaccummulate in fish and result in mortality of bottlenose dolphins that regularly feed on those fish [116, 117]. Other mammals, like the protected manatee, experience mortality either by inhalation of aerosols or by consumption of contaminated sea grasses [115].

Unlike toxins produced by other species, brevetoxins can be aerosolized, affecting the human population along the coast [118, 119]. During a Florida red tide, aerosolized PbTxs produced by *Karenia brevis* cause both immediate and prolonged airway symptoms in humans, especially in those with preexisting airway disease (e.g., asthma). Environmental monitoring indicates that toxins remain airborne for up to four consecutive days. Repeated exposure to PbTx-3 can result in prolonged airway hyperresponsiveness and lung inflammation, and these pathophysiologic responses may contribute to the prolonged respiratory symptoms observed in humans after red tides [120].

Economics

Karenia brevis is a toxic dinoflagellate that is responsible for extensive ecological and socioeconomic impacts from Florida to Texas [121]. Brevetoxins, produced by *K. brevis*, have been implicated in mortalities of marine life including fish, dolphins, and manatees [122, 123], as well as causing respiratory illness in people and affecting local tourism [124–126]. The economic impacts in Florida have been estimated to range from $20 to $34 million per year [127] with losses incurred from restaurant closures to emergency room visits to shellfishery closures [128–131].

Detection

Despite the regularity of impacts of *K. brevis* blooms on the West Florida Shelf (WFS), predicting where and when *K. brevis* blooms occur remains problematic. The difficulty in predicting the occurrence of these populations resides in the phenomenon that dense populations of *K. brevis* (greater than 1×10^5 cells per liter) often appear more quickly than can be explained by growth rates alone [112, 132]. Increases in chlorophyll *a* biomass observed at frontal boundaries through satellite imagery can be tenfold greater over a 1- to 2-day period than can be explained by in situ growth [132]. Such unexplained increases have led to hypotheses of stealthy bloom initiation, defined as persistence of a population near the bottom of the water column [133] and below the first optical depth, therefore undetected by satellites over broad areas of the WFS [134]. Stumpf et al. [132] hypothesized that nutrients derived from the Mississippi River support similar near-bottom populations between the 25- and 50-m isobaths. As winds shift in the fall and promote

upwelling conditions, these populations are subsequently advected onshore to areas of accumulation such as frontal zones [132].

Numerical models of *K. brevis* populations that are transported in the bottom Ekman layers replicate observations of in situ aggregation patterns in frontal zones [135, 136]. These models were based upon an extended Eulerian model of biologically and physically driven *K. brevis* population dynamics [137] and demonstrate the importance of incorporating the behavior and physiology of *K. brevis* into transport models. *K. brevis* undergoes a diel vertical migration (DVM) ascending just before sunrise and descending at night [138]. Recent observations of the diel vertical migration of *K. brevis* in mesocosms suggest that this diel vertical migration is to some degree under metabolic control [133, 139, 140]. Numerous scenarios of a biophysical model suggest that the trapping mechanism at frontal boundaries results from a combination of fluid advection and swimming behavior in response to internal metabolic state and ambient environmental stimuli (such as light and nutrients [135]).

Origins and Nutrient Interactions

Impacts are particularly troublesome in the region between Tampa Bay and Charlotte Harbor, a region that was labeled the red tide epicenter since *K. brevis* blooms were observed in 22 of the last 23 years compared to 5–10 outbreaks north and south of that region [127]. Blooms have been hypothesized to initiate 18–74 km offshore and in oligotrophic water columns [112, 113]. These oligotrophic water columns are characterized by nitrogen and phosphorus concentrations that are commonly about 0.1–0.2 μM within 2–4 km of shore in the Gulf of Mexico [141, 142] and less than 0.01 μM for NO_3^- and NH_4^+ [143]. Nitrate concentrations in both the surface and bottom waters at the 25-m and 50-m isobaths are often at or below 0.1 μM and are not able to sustain large populations of *K. brevis* associated with bloom events [113]. The importance of nutrients to the development and maintenance of bloom events has resulted in numerous hypotheses about potential sources of nutrients that may support populations of *K. brevis* [113, 144]. Potential nutrient sources for *K. brevis* in oligotrophic water columns include aerial deposition [113], N-fixation by *Trichodesmium* sp. blooms [145, 146], water column regeneration from grazers [147], near-bottom regeneration by diatoms responding to upwelling events [113], and regenerated nutrients derived from Mississippi River water [132]. Despite inputs of new nitrogen into the system, nitrate concentrations in both the surface and bottom waters at the 25-m and 50-m isobath are often at or below 0.1 μM [113]. Nutrients in the lower part of the water column, derived either from the sediment or from upwelling plumes below the pycnocline, may also be particularly important in supporting vertically migrating populations [148, 149].

Pseudo-nitzschia

Description

Diatoms are very proficient at utilizing available nutrients and, hence, at forming blooms [12]; however, relatively few diatoms are known to produce harmful blooms, and some species of the genus *Pseudo-nitzschia* are among them. *Pseudo-nitzschia* spp. are cosmopolitan, pennate diatoms found in nearly every major marine and estuarine environment on earth (polar to tropical, coastal to oceanic) [150, 151]. The growth of different *Pseudo-nitzschia* species varies based on each species' optimal ranges to a variety of environmental conditions. So, while *Pseudo-nitzschia* is detectable at the genus level year-round in many locales, the detectability is often a consequence of successions of multiple species in which any one species predominates based on the time of year or the prevailing conditions [152–154]. High levels of inter- and intraspecific variability have been detected at the genetic level [155–159]; this variability is often mirrored in regard to toxicity as well [160]. Twelve of the roughly 30 species of *Pseudo-nitzschia* are capable of producing the neurotoxin domoic acid [161–163]. Domoic acid-producing *Pseudo-nitzschia* species have produced significant blooms along the Pacific Northwestern coastlines of the United States and Canada, and they have recently been responsible for blooms in the Gulf of Mexico.

Toxicity

Domoic acid is structurally similar to glutamic acid, an excitatory neurotransmitter, and mimics its ability to bind to a subclass of the cognate neurotransmitter

receptors at neuronal synapses [163]. Domoic acid not only binds with greater than 20 times the affinity to these receptors as the native glutamic acid [164], but it remains bound to the receptors rather than being recycled. These two characteristics allow domoic acid to create a sustained depolarization of the stimulated neuron. As a consequence, intracellular calcium levels in the stimulated neuron continually increase causing the cell to swell and burst [163]. These effects are particularly pronounced in the hippocampus, the region of brain associated with learning and memory that contains neurons that express high levels of glutamate receptor [165]. For this reason, people who consume sublethal amounts of domoic acid exhibit symptoms of amnesiac shellfish poisoning (ASP), a condition which produces short-term memory loss along with gastrointestinal sickness, vomiting, confusion/disorientation, and convulsions [166, 167]. In some patients, the memory loss lasted as long as 5 years [168].

The first, and so far only, identified ASP event that affected humans was in late 1987 around Prince Edward Island, Canada [162, 169]. Of the many people who got sick, 143 had symptoms befitting ASP and 4 of them died. It was determined that the causative agent was mussels contaminated with domoic acid [162, 167]. Subsequent analysis identified the source of the domoic acid found in the mussels as *Pseudo-nitzschia pungens* f. *multiseris* [169].

Pseudo-nitzschia produces domoic acid, and the toxin can be transferred to higher trophic levels, such as humans, through the consumption of filter-feeding bivalves that bioaccumulate domoic acid in their tissues [169–173]. Alternatively, zooplankton, krill, or planktivorous fish, e.g., anchovy, may consume toxic *Pseudo-nitzschia* spp. directly from the water column. Domoic acid may be biomagnified as secondary consumers, e.g., larger fish, birds, and marine mammals, eat the primary consumers that have digestive tracts full of toxic *Pseudo-nitzschia*. Domoic acid poisoning events have been documented in Monterey Bay that affected pelicans, cormorants, and sea lions [166, 172, 174, 175], in Mexico that affected pelicans [176], in the Gulf of California that affected loons and multiple species of marine mammals [177], and in the central California coast that affected California sea lions [178]. Because humans rarely consume whole fish, the primary and continuing concern is intoxication through consumption of contaminated shellfish or crabs.

Based on the Prince Edward Island incident and domoic acid dosage-response studies with a variety of animal models, it has been determined that acute gastrointestinal symptoms in humans develop within 24 h of ingestion followed by neurological symptoms within another 24 h. Monitoring and sampling have so far prevented additional ASP incidents in humans, so more attention has been devoted to outstanding questions regarding chronic or long-term domoic acid intoxication. Sea lions with chronic exposure to domoic acid exhibit symptoms that are distinct from those of ASP [179], which suggests similar long-term exposure could produce an additional array of detrimental effects in humans. Furthermore, domoic acid can be passed to pups in the breast milk of rodents [180]. If similar passage occurs in humans, what are the possible risks to the mental development of infants who are breast-fed from mothers who eat contaminated shellfish? Epidemiological studies are being conducted on native populations in the Pacific Northwest of the United States and Canada [181]. The diet of these native peoples relies heavily on seafood products, primarily razor clams, which are traditionally vulnerable to being toxified with varying levels of domoic acid. The results of such studies will elucidate what, if any, effects may result from consuming low levels of domoic acid over time [181].

Economics

Like other HAB events, domoic acid poisoning incidents will cause economic impacts if people and animals experience severe illness or even death, or if recreational areas and harvesting sites are closed. Beaches and shellfish-harvesting areas have faced closings in Washington state since 1991 (references within [182]). The first coastal closure in 1991 is estimated to have resulted in $23–28 million and $9 million in lost revenue to razor clam harvesters and Dungeness crab harvesters, respectively [173] (Nosho in Ref. [183]). From 1991 to 2008, about 23% of the potential razor clam fishing days along the Washington coastline have been lost due to closures from high domoic acid detected in shellfish samples (Ayers unpublished data

in [184]). During an extensive domoic acid incident in 1998, the coastal tourism industry is estimated to have lost $15 million (Nosho in Ref. [183]). The first beach closure within Puget Sound occurred in 2003 [185], followed by a second closure in 2007 [182]. Ayers and Reed [186] estimate that the first closure resulted in $11.8 million in lost revenue to the local economy. The potential threat of domoic acid spreading to intracoastal regions and affecting commercial operations could amplify future losses [182]. Dyson and Huppert [184] provided a more detailed estimation of the economic effects stemming from closures of razor clam harvest sites. Based on responses of visitors and razor clam harvesters to a questionnaire, closing four beaches stretching over Grays Harbor and Pacific counties in Washington state during the 2007–2008 season would have resulted in over $25.3 million in lost expenditures. Apart from the recreational aspects of razor clam harvesting, the harvests are important to Native American cultures that rely on the razor clams and other products from the sea, not only for food but also for cultural identity.

In addition to the lost expenditures that result from closures, national, state, and local governments invest in monitoring and detection. Monitoring phytoplankton community composition, correctly identifying and enumerating *Pseudo-nitzschia* species, and measuring levels of domoic acid are all important measures for providing early warning to stakeholders located near possible blooms. Equally important is ongoing sampling of tissues from commercially and recreationally important species to monitor accumulated levels of domoic acid. The majority of methods in use for monitoring and detecting both species and toxin requires expensive equipment and can be costly to perform.

Detection

Species Identification A major hurdle for the study of *Pseudo-nitzschia* is rapid and accurate methods for species determination. Early systematics of *Pseudo-nitzschia* relied on light microscopy to separate the genus into two groups based on the width of the cells [187]. This simple categorization belied significant diversity particularly in terms of toxicity. Later, tunneling and scanning electron microscopies were employed to better resolve species complexes by analyzing such subcellular features as the striae and pore density. These methods are labor intensive, time consuming, require access to and working knowledge of electron microscopes, and still do not always adequately resolve the question of whether a sample contains toxic or nontoxic cells [188–190].

To improve detection and species identification, efforts have been made to develop molecular reagents for use in lectin-binding assays, immunoassays, sandwich hybridization, and PCR. Lectins are glycoproteins that bind sugar molecules, and lectin-binding probes have been developed that recognize species-specific glycosylated proteins on the surface of *Pseudo-nitzschia* cells [191–193]. These probes could discriminate six of seven *Pseudo-nitzschia* species endemic to New Zealand waters [192]. They showed some cross application in testing of samples from Spain and Korea [194, 195], but it was noted that the location of sample isolation and physiological state of cells can confound identification or differences between strains of the same species [196]. DNA-based probes that recognize genetic determinants such as the ribosomal RNA genes and the internal transcribed spacer (ITS) have received the most attention and have been employed in assays such as whole-cell hybridizations, FISH, sandwich hybridization, and PCR [30, 158, 159, 197–207]. Chris Scholin and his group at Monterey Bay Aquarium Research Institute have developed DNA-based probes specific for the large subunit of ribosomal RNA of *Pseudo-nitzschia* species isolated from the west coast of the United States. Similar to the above reagents, the use of these probes has met with mixed results when applied to samples at other geographic locations [203, 208–211]. For example, probes that work for *Pseudo-nitzschia pseudodelicatissima* found on the west coast of the United States did not recognize the same "species" found in the Gulf of Mexico [210], presumably due to high levels of inter- and intraspecific variability. Supporting that conclusion are results based on analyses of microsatellite markers of some *Pseudo-nitzschia* lineages or species that show high level of genetic diversity [155–159]. Additionally, one might be at fault in not identifying or recognizing the relevant markers or characteristics that determine true species differences. The Scholin probes have been further developed for use in sandwich hybridization that has been automated and incorporated into an environmental sample processor (ESP)

for undersea deployment. The ESP samples seawater and quantitates both the concentration of specific harmful algal cells and their corresponding toxin concentration via the sandwich hybridization assay and automated competitive enzyme-linked immunosorbent assay, respectively [212–214]. Autonomous and continual sampling should not only provide an early warning to the presence of toxic cells but also provide important environmental data that may be used to create or enhance models for predicting the presence of such cells and their toxins.

Domoic Acid Detection and Quantitation Immediately following the Prince Edward Island incident, Canada took the lead in developing and implementing food safety standards for domoic acid. In 1989, Health and Welfare Canada instituted an action level at 20 μg domoic acid/g shellfish tissue [64]. That same level has now been adopted by the European Union, New Zealand, the United States, and Australia. One exception to this limit is the United States allows up to 30 μg/g of Dungeness crabs. If tested tissue samples exceed the limit, then the relevant beach/harvest area is closed until the domoic acid can be depurated by the organisms and repeated sampling shows that domoic acid is below the limit.

After the Prince Edward Island incident, Health and Welfare Canada relied on the same mouse bioassays as used for detecting PSTs [215]. For the reasons listed in the previous section, particularly in this case where the detection limit (~40 μg domoic acid/g of tissue) is higher than the action level, other more sensitive and reliable methods have been developed. Some of these alternatives offer one or more advantages to the mouse bioassay but typically at the expense of time, cost, or ease of performance. Different assays also show better efficacy in analyzing domoic acid from particular sources, e.g., a receptor binding assay developed by Van Dolah et al. [216] can analyze domoic acid from shellfish and from seawater extracts of algae. A variety of antibodies have been raised and incorporated into ELISAs and competitive immunoassays for the detection of domoic acid in human body fluids or shellfish extracts [217–220]. The AOAC has a validated ELISA method (AOAC Method 2006.02) for detecting domoic acid in shellfish, and the ELISA method is used in the EU for screening purposes. A variety of modifications to a liquid chromatography (LC) methodology allow for the sensitive detection of domoic acid, but routine detection of domoic acid is often carried out using liquid chromatography coupled with diode-array/UV absorbance or fluorometic detection [221]. An LC-UV method was developed for the routine determination of domoic acid in shellfish [222]. The method was validated in a multi-lab AOAC collaborative study [223] and had an AOAC method established (AOAC Method 991.26), but a number of improvements to the extraction/clean-up procedures, alternative tandem detection systems, or other modifications have been developed and continue to be validated, e.g., [224–226]. The EU Reference Laboratory for Marine Biotoxins has created a standard operating procedure for determining or confirming domoic acid in mollusks using ultraperformance LC-MS [227]. The National Research Council of Canada was also the first to provide certified domoic acid standards for use in calibrating liquid chromatographs [97]. Similar for the detection of PSTs, a promising development is the Jellett Rapid Test or Maritime In Vitro Shellfish Test (MIST™) (Jellett Biotek Ltd.). The immunochromatographic kits can be used quickly and cheaply at sample sites in the field for the detection of domoic acid [228, 229] that must be later confirmed in the laboratory.

It is necessary to individually sample each species of interest since different species of shellfish take up and depurate domoic acid at different rates (reviewed in Ref. [163]). For example, mussels and oysters consume *Pseudo-nitzschia* at higher rates than clams, especially razor clams, but mussels and oysters also depurate much more quickly. Once domoic acid accumulates in razor clams, it can take up to a year for domoic acid levels to fall below the action level [173]. Domoic acid levels in anchovy and sand crabs rise and fall almost contemporaneously (a slight lag) with the initiation and termination of a *Pseudo-nitzschia* bloom. Scallops also depurate slowly, but the only scallop tissue that humans eat is the adductor muscle which has very low levels of domoic acid. Most domoic acid in fish, crabs, and cephalopods is in the viscera, which is typically not consumed by humans. This type of discriminatory feeding behavior is not true for animals in the wild, however, which are more likely to be affected by the presence of domoic acid moving within the food

web. It is also a concern that ground whole fish is used in animal and fish feeds, and those feeds could sicken domesticated animals or fish in aquaculture far from the coasts where blooms have formed.

Origins and Nutrient Interactions

As mentioned above, *Pseudo-nitzschia* is cosmopolitan, and it is capable of taking advantage of nutrients when they are present to grow and form blooms. *Pseudo-nitzschia* has been modeled to bloom under two different scenarios of nutrient introduction. One is upwelling events during early spring and summer that bring water from the bottom up to the surface. The nutrient-rich water coupled with high turbulence from storms are generally conditions that favor diatom growth [12]. The second scenario is rivers carry natural and introduced nutrients from a variety of point and nonpoint sources to the ocean. Corresponding to the second scenario is the detection of *Pseudo-nitzschia* spp. in the Gulf of Mexico. *Pseudo-nitzschia* was considered rare in the Gulf of Mexico prior to 1950, but the numbers of several *Pseudo-nitzschia* species have increased concurrently with elevated nutrient loading into the Gulf from the Mississippi River [230]. Similar connections have been documented in the Yellow and Yangtze rivers and in the South China Sea [153, 154]. Mesocosm experiments corroborate these correlations – *Pseudo-nitzschia* show enhanced growth after pulses of nutrients are added [231].

Off the west coast of the United States, upwelling brings nutrient-rich water in contact with enormous plumes of water exiting the Puget Sound via the Strait of Juan de Fuca. A large gyre, the Juan de Fuca eddy, is formed or enhanced each spring at the junction of these two phenomena. Throughout the summer and into the fall, when it dies back, the gyre is a site of persistent upwelling that acts as a giant bioreactor for many phytoplankton species. The use of drifters to track hydrological movement has enlightened our understanding of the role of the Juan de Fuca eddy, coastal currents, and upwelling versus downwelling conditions in the growth and transport of *Pseudo-nitzschia* to various beaches and coastlines along the Pacific northwest of the United States. Modeled on the movement of drifters, *Pseudo-nitzschia* cells within the Juan de Fuca eddy are believed periodically to spin out into offshore currents. Under upwelling favorable conditions, cells will migrate southward along the Washington and Oregon state coastlines in these offshore currents. A shift to downwelling favorable conditions, such as from a storm or other events leading to a wind reversal, in regions where there is low to no river outflows will cause cells/blooms to move onshore and cause shellfish to become contaminated with domoic acid [183, 232].

The requirements for cell growth are clearly not the same as those for producing domoic acid. While the availability of nutrients is important for growth and increases in cell number, those same factors do not always coincide with domoic acid production. Different toxic species (or even the same toxic species from different geographic regions) will produce or not produce domoic acid in response to different environmental conditions (including the availability of one or more limiting nutrients such as phosphorus or silicate), stages of culture growth (e.g., exponential vs stationary growth phases), and the composition of the associated bacterial community [161, 233–237]. It has also been suggested that iron limitation or copper stress can induce domoic acid to act as either a chelator of iron (to enhance its uptake into the cell) or copper (to alleviate its toxicity) [238]. Iron stimulation experiments in the Southern Ocean show increased *Pseudo-nitzschia* cell abundance, but not a concomitant increase in domoic acid [239, 240]. Axenic cultures of *Pseudo-nitzschia* produce less domoic acid than nonaxenic cultures [241–243] indicating a role for bacteria, although no bacterium has been shown capable of producing domoic acid on its own.

Cyanobacteria

Description

Cyanobacteria, originally classified as "blue-green algae," are prokaryotes capable of photosynthesis (reviewed in Ref. [244]). They underwent a worldwide adaptive radiation that has allowed them to fill a wide range of ecological niches including terrestrial and aquatic systems (both freshwater and marine) as well as forming numerous endo- and ectosymbiotic associations [245]. Their distribution and diversity are likely a function of their ancient origins – it is estimated that they have existed for at least 2 billion years and possibly as long as 3.5 billion

years or more. They may have been one of the first forms of life on Earth (reviewed in Ref. [246]). For this reason, the diversity of cyanobacterial species is also reflected in the wide range of metabolites and secondary molecules that are produced within this phylum. Some of these unique molecules act as toxins, carcinogens, and/or allergens when ingested, inhaled, or contacted by humans and animals. Coupled with the ability of some fresh and marine water species to form blooms, cyanotoxins pose a wide range of threats to human health.

Toxicity

The first recorded deaths from cyanotoxins occurred in Australia in 1878 when livestock drank from a brackish, estuarine lake covered with a *Nodularia spumigena* bloom [247]. Since then, there have been many other reported instances of sickness or death of livestock, pets, and humans attributed to recreational exposure to or ingestion of cyanobacteria-contaminated water (reviewed in Ref. [248–253]). A comprehensive description, or even listing, of all identified or suspected toxic molecules from cyanobacteria is beyond the scope of this article. Listed in Table 1 are a few representative toxins from cyanobacteria.

Hepatotoxins Microcystins are cyclic heptapeptides that include nonprotein amino acids and unique covalent linkages. They are the most frequently found cyanotoxin, and over 70 variants have been described [254]. They are highly stable and water-soluble. Ingestion of microcystins can lead to a rapid symptomatology (within 30 min to 24 h) that may ultimately lead to hemorrhaging in the liver and death [255, 256]. It is also possible that inhalation of microcystins (or other cyanotoxins) could be a route of exposure since microcystins have been detected, albeit at low levels, in aerosol droplets [257]. A major research focus for microcystins, indeed for all the cyanotoxins, is determining what effects low level or chronic exposure may produce. Mounting evidence suggests that microcystins promote tumor growth and certain cancers [258–262]. The World Health Organization has set a provisional consumption limit (for drinking water) of 1 μg/L for the most toxic form of microcystin [263].

Harmful Algal Blooms. Table 1 Representative toxins listed with their genera of origin and toxicity

Toxin	Representative genera[a]	Ecosystem	Toxicity
Microcystins	*Microcystis, Anabaena, Nostoc, Planktothrix*	Fresh water	Hepatotoxin
Nodularins	*Nodularia*	Brackish water	Hepatotoxin
		Marine water	
Cylindrospermopsin	*Cylindrospermopsis, Anabaena*	Fresh water	Hepatotoxin
Anatoxin-a	*Anabaena, Planktothrix*	Fresh water	Neurotoxin
Anatoxin-a(s)	*Anabaena*	Fresh water	Neurotoxin
Saxitoxins	*Anabaena*	Fresh water	Neurotoxin
	Lyngbya	Marine water	
	Cylindrospermopsins	Fresh water	
	Trichodesmium	Marine water	
LPS	All cyanobacteria	All	Endotoxin, Dermatoxin
Aplysiatoxin	*Lyngbya*	Marine water	Dermatoxin, Tumor promoter
	Planktothrix	Fresh water	
Lyngbyatoxin-a	*Lyngbya*	Marine water	Dermatoxin

[a]Not all species within the listed genera necessarily produce the associated toxin, and species in other genera not listed may also produce these toxins

A real concern is the fact that "finished" water from some water treatment facilities has tested above that limit (reviewed in Ref. [264–266]). Microcystin levels can be greater than 24 mg/L in waterbodies with very high cell counts [267], which can pose risks to recreational swimmers based on an average accidental ingestion of 100–200 mL of water. Freshwater-derived microcystins have also been found in marine shellfish located at sites where rivers discharge into marine waters, and these toxins are the implicated source for causing hepatotoxic shellfish poisoning (HSP) that led to the death of 21 southern sea otters in Monterey Bay, California [268]. Microcystins can be bioaccumulated to high levels in the tissue of shellfish that, when coupled with a slow depuration rate [268], poses additional health risks to shellfish consumers, including humans.

To date, nodularins are known to be produced by the single species, *Nodularia spumigena*, a species of cyanobacteria that can form blooms in brackish and marine waters. Nodularins are structurally similar to microcystins (cyclic pentapeptides), and their toxicity and mode of action are similar as well. One distinction between the two classes of hepatotoxins, however, is that nodularins are carcinogenic, i.e., they can initiate tumor formation, as well as act as potent tumor promoters [254].

Cylindrospermopsins primarily produce effects in the liver, but they can also damage other organs. These toxins are guanidine alkaloids that take days, rather than hours, to produce symptoms of intoxication. Additional toxic effects include the inhibition of protein synthesis and genotoxicity [269].

Neurotoxins Saxitoxins have been discussed in a previous section of this article (see "Toxicity" under "*Alexandrium*"). Anatoxin-a and anatoxin-a(s) are structurally unrelated, but both can act swiftly (within minutes to hours) to disrupt the function at nerve synapse leading to muscle paralysis and respiratory arrest [270]. Anatoxin-a can be inhaled, ingested, or absorbed through the skin. The estimated toxic dose for a human adult male is less than 5 mg. Anatoxin-a(s) has only been found in two species of *Anabaena, A. flos-aque* and *A. lemmermannii* [271, 272]. It is the only known natural organophosphate. As such, it acts by inhibiting acetylcholinesterase, and it is ten times more potent than anatoxin-a [272, 273]. Fortunately, the occurrence and concentration of these two toxic molecules are much less than are typically detected for microcystins. While humans will not likely ingest enough cells/neurotoxin(s) in a mouthful of water, some animals that may drink liters at a time may be at risk.

Other Cyanobacterial Toxins Lipopolysaccharides (LPS) are components of the outer membrane of gram-negative bacteria and cyanobacteria. They are capable of forming complexes with several biomolecules to elicit irritant and allergic responses [274]. Cyanobacterial LPS can cause skin irritation, gastroenteritis, and fever, or act as an endotoxin that can kill mice in mouse bioassays or exacerbate the effects of other cyanotoxins [275].

Aplysiatoxin and lyngbyatoxin-a are only produced in marine species of cyanobacteria. Generally, the concern surrounding toxins from marine cyanobacteria is not ingestion from drinking water but either trophic transfer and biomagnifications in fish, shellfish, and other consumables or contact exposure/inhalation from recreating around blooms. Aplysiatoxin and lyngbyatoxin-a can cause severe dermatitis through acute inflammatory reactions [276, 277]. They can also activate protein kinase C, a serine/threonine kinase that is central to diverse signal transduction pathways, to potently promote tumor formation [278, 279]. Sea turtles that consume seaweed overgrown or associated with *Lyngbya*, a genus of marine cyanobacteria, are suspected to bioaccumulate lyngbyatoxins in their tissues, and there has been one potential human death, and other suspected cases, linked to the consumption of sea turtle meat contaminated with lyngbyatoxins [280, 281].

β-*N*-Methylamino-L-Alanine (BMAA) In addition to any of the acute effects listed above, long-term chronic effects, e.g., cancer development, are linked or suspected to several cyanotoxins [258–262]. Additional cyanobacterial metabolites that are receiving attention include unusual amino acids such β-*N*-methylamino-L-alanine (BMAA). BMAA has been proposed as a causative agent of neurotangle diseases, e.g., Parkinson's disease, amyotrophic lateral sclerosis, or Alzheimer's disease. Such a role is controversial, but it

is supported by a number of correlative studies including direct detection of BMAA in brain tissue samples from native individuals from the island of Guam who died from lytico-bodig, a type of neurotangle disease, and a small sampling of Caucasian patients in Canada who died from Alzheimer's disease (reviewed in Ref. [282]). In vitro and in vivo laboratory studies using BMAA support the purported role as a neurotoxin in that BMAA leads to selective motor neuron death, produces behavioral and/or neurological differences, and interferes with learning and memory [283–288].

A second, similar biomagnification mechanism may be responsible for the occurrence of avian vacuolar myelinopathy (AVM) in aquatic and predatory birds. In the southeastern United States, *Hydrilla verticillata*, is an aquatic plant that often contains a BMAA-producing epiphytic cyanobacteria [289, 290]. Herbivorous birds, e.g., ducks and coots, which consume *H. verticillata* (and bald eagles that consume the herbivorous birds), contract high rates of AVM and die [290]. Although the majority of the evidence for vectoring of BMAA to humans and birds is correlative, some direct tests of the hypotheses support the proposed mechanisms (e.g., [291–293]). Also of note, and concern, is the fact that BMAA has been detected in almost all cyanobacteria in all environments worldwide (e.g., [294–298]). Intriguingly, a recent epidemiological study implicates a lake, noted for frequent cyanoblooms, as being responsible for or linked to a 10–25× higher incidence of sporadic ALS, compared to the general US population, in lake-adjacent areas [299].

Economics

In addition to the public health consequences, additional economic and sociocultural impacts caused by cyanoblooms include negative effects to: (1) recreation and tourism due to closure of waterbodies (often at times when recreational use is most desired or when tourism would be at peak, i.e., summer months); (2) aquaculture due to loss of product (death) or production of unwanted, tainted product (some cyanobacterial metabolites can alter the color or taste of the fish) [275]; and (3) the quality of life of people living and working around affected waterbodies due to the reduced aesthetic appeal and/or the unwanted health risks. Few studies have quantified the losses or impacts of cyanobacterial blooms. Tucker et al. [300] estimated that greater than $80 million was lost per year in catfish aquaculture facilities due to cyanobacterial metabolites that produce off-color or off-flavor in the catfish. In addition to toxic effects, cyanobacteria can form nuisance blooms that generate costs associated with cleaning biomass that blocks water intakes used for draining and industrial purposes such as hydroelectric power generation. A conservative estimate of economic costs of all freshwater HABs in the Unites States is $2.2–4.6 billion a year [301].

Where species of known or potential bloom formers are present, monitoring is essential as both a tool for aiding in possible prevention of blooms and to alert the public of existing or impending cyanoblooms. Public guidance should include precautions about avoiding areas of visible algal biomass, about avoiding direct contact with blooms, and to avoid swallowing water containing algae as those interactions are associated the highest risks to human/animal health. A bloom may reach densities of >100,000 cells/mL, but even at lower levels, the concentration of toxic metabolites may be sufficient to cause sickness or death. The WHO had published recommendations for recreational exposure, based in part upon results from [249, 255]: Up to 20,000 cyanobacterial cells/mL requires a warning to visitors but has a low/mild risk to adverse health effects, up to 100,000 cells/mL carries a moderate risk in the short-term as well as potential long-term risks if swallowed, and when a visible bloom forms, then a high risk of inhalation, ingestion, or body contact is likely at that site [302]. Monitoring and public alerts about the presence and dangers of cyanoblooms are recurring costs that state and local agencies will be forced to carry. Atech (2000) (in Ref. [303]) estimated costs related to monitoring for cyanobacteria in Australia at greater than $12 million dollars per year (in 2011 US dollars).

Another significant expense is the detection and removal of cyanotoxins from drinking water sources. It is axiomatic that preventing blooms and/or toxin production should be cheaper, easier, and safer than eliminating or removing cells and/or toxins from the water after a bloom. The primary and essential goal of cyanoHAB management, if not elimination, is identifying the type and source of nutrient loading in order to reduce cyanobacterial proliferation. To remove cells

once a bloom has formed, however, has typically relied on common algaecides such as copper sulfate. Unfortunately, the resulting cell lysis can exacerbate the problems as intracellular cyanotoxins are released into the water, increasing their concentration. Additionally, the indiscriminate or repetitive use of copper-based reagents can cause inadvertent ecological damage and induce copper resistance in surviving algae [304–306]. Other methods for bloom control include destratification, which only works for small waterbodies, and increased flushing, which only works if upstream sources of water are available. Conventional water treatments such as flocculation, coagulation, chlorination, and filtration can remove cells; but not only do they not remove toxins, they also cause cell lysis leading to increased toxin levels in the water [307–312]. While some methods of oxidation, such as chlorination, do not appear effective [307–312], others such as UV disinfection, ozonation, and potassium permanganate treatment are more promising [265, 313]. Pipelines of multiple methodologies, e.g., use of activated charcoal (particularly wood-based, powdered activated carbon), oxidation via ozonation, and nanofiltration (with nominal molecular weight cutoff of 200) appear effective at removing microcystins and anatoxin-a [265, 313]. Titanium dioxide photocatalysis is being developed for both purification and disinfection. This method can destroy microcystins found in concentrations up to 5,000 μg/L [8, 314]. Not all of the methods listed above are universally employed and are absolutely lacking in sources of water such as private wells. Also, these treatments do not protect wildlife from consuming water at natural waterbodies where cyanoblooms may be occurring, all of which argue for preventive management of cyanoblooms rather than reactive management.

Detection

Microscopic inspection of water samples is still primarily used for identification and quantitation of cyanobacterial cells. Assaying for chlorophyll-*a* is a quick alternative to microscopy but may overestimate the amount of cyanobacteria in a sample because chlorophyll-*a* is also present in many other algae [255]. It is also a presumptive indicator of cyanotoxins rather that a direct detection method. Immunoassays [315] following standard practices outlined in Chorus and Bartram [255] have also been developed for these purposes. More recently, genetic identification using polymerase chain reaction and modifications thereof, e.g., quantitative polymerase chain reaction, are being used to detect (and quantify) specific species or toxin-synthesizing genes, e.g., a nodularin synthetase gene in *Nodularia* [316] or a microcystin synthetase gene in *Microcystis* [317], within an environmental sample.

For the detection of cyanotoxins, the mouse bioassay [256] is the official approved method, but a multitude of more-advanced, sensitive, and humane methodologies have been and continue to be developed. Some methods have been adapted to detect more than one type of cyanotoxin, while other methods are specific for one class or variant, e.g., in vitro biological assays such as acetylcholine esterase inhibition (to detect anatoxin-a(s)), protein phosphatase inhibition (to detect microcystins or nodularins), and protein synthesis inhibition (to detect cylindrospermopsins) [318]. Modifications to the standard high-pressure liquid chromatography methodology, e.g., UV detection at the respective absorption maximum of each cyanotoxin, following separation allows for the detection of microcystins, cylindrospermopsins, and anatoxin-a [254]. Liquid chromatography (LC) with post-column oxidation and fluorescence detection is now an official method of analysis by the AOAC for saxitoxins [98]. Similar coupling of LC with tandem mass spectrometry is also useful for detecting anatoxin-a(s) [319]. Antibodies against microcystin, nodularin, saxitoxin, and cylindrospermopsin have been useful for developing ELISAs [72, 320, 321] that show good correlation with HPLC methods. The detection methods have greatly benefited from the creation and commercialization of kits and cyanotoxin standards. Standard hemoagglutination assays, e.g., the Limulus amoebocyte lysate assay, can be used to quantify LPS in aqueous samples [322].

Origins and Nutrient Interactions

Cyanobacteria are ubiquitous [323, 324], and the threat of cyanoblooms is pervasive. Similar to other HAB species, the frequency and geographic distribution of cyanoHABs is increasing worldwide [8, 325]. A 1999–2000 survey in Florida sampled 75 bodies of water and

88/167 samples had cyanotoxins [326]. Eighty percent of the positive samples had levels sufficient to kill a mouse in a mouse bioassay [326]. In a survey of 45 water sources in the United States and Canada between 1996 and 1998, 80% had detectable levels of microcystin – a few above the WHO advisory limit [266]. Other surveys of national or international scope indicate that about 60% of bodies of fresh water contain toxic species of cyanobacteria [266, 297, 327]. The North American Great Lakes and associated water systems are a source of drinking water for ~22 million people, and during late summer months, microcystin sampling routinely exceeds the WHO threshold [328]. Over the long term, e.g., a 75-year lifetime, it has been estimated using the data from Carmichael [266] that cyanotoxin exposure from drinking water is an order of magnitude below the WHO guideline of 1 μg/L [329]. Such a study is somewhat reassuring, but the effects of low-level chronic exposure are still not understood; nor can it be expected that cyanotoxin levels in finished drinking water will not increase unless measures are taken to decrease nutrient loading to decrease bloom formation or methods to more effectively remove cyanotoxins from the water are developed.

Some cyanobacterial blooms occur naturally under specific conditions, but the frequencies are much higher in eutrophic bodies of water [330]. Other significant factors that support bloom formation are warmer temperatures, increased sunlight, and decreased flow/flushing of a waterbody [305]. The induction of bloom formation in stagnant waterbodies or slow-moving, low-flushing systems is clearly linked to nutrient loading, particularly phosphorous [331]. In such systems, gas-filled vesicles allow cyanobacteria to be buoyant and remain suspended near the surface to be exposed to light [332]. Even under conditions of limiting nitrogen or phosphorous, cyanobacteria can outcompete other planktonic organisms due to higher affinities for these nutrients and the capacity to store high amounts of phosphorous inside their cells [333]. In waterbodies that are mixed and/or flushed, factors such as warmer temperatures, high amounts of sunlight, and elevated nutrients will all contribute to different degrees in leading to cyanobloom formation (reviewed in Ref. [255, 333]). The convergence of the optimal conditions for a particular cyanobacterial species will allow it to form a "scum" or surface bloom. Where applicable or possible, efforts by watershed managers to reduce excess nutrient loading, to increase or maintain water flow/flushing rates, and to prevent the removal of grazers have all been effective strategies to reduce cyanoblooms (reviewed in Ref. [305]). The introduction of solar-powered circulation (SPC) devices into nutrient-enriched, cyanobacteria-containing reservoirs has been effective at suppressing the number of cyanobacterial cells and decreasing the need for supplemental copper sulfate (algaecide) applications [334]. Broad-based deployment of such devices would not only decrease the occurrence of cyanoHABs but also do so in an ecologically and environmentally sound manner.

Future Directions

Significant effort has generated a lot of biological and ecological knowledge of selected harmful algae. This knowledge has produced few methods to prevent bloom formation or mitigate the effects of blooms that have formed. Few attempts to control HABs have proven to be practical or free of adverse side effects that would further disrupt ecosystems. The difficulty in preventing HABs is that each species reacts to a different suite of factors; some of these factors can include a complex mixture of biochemical, ecological, geophysical, hydrological, and meteorological conditions. In the majority of cases, any of these conditions may be beyond our control except for one. The one almost universal requirement for any algal blooms is a supply of nutrients. Without nutrients, the likelihood of any species forming a bloom is low, so identifying the source(s) of relevant nutrients and then minimizing those nutrients may be the best strategy for preventing and mitigating harmful algal blooms.

The most advances in HAB research have been in the ability to detect/monitor HAB species and toxins. Despite these advances, continued development of appropriate standards and techniques for regulatory and management practices is imperative, especially because of the continuing discovery of new harmful species. An emerging line of research to aid in detection and modeling cell/bloom behavior is at the molecular level. A lot of new research is beginning to elucidate the genetic composition of these different species and the mechanisms that regulate the genetic responses, and

subsequent physiological responses, to a variety of environmental parameters. These data sets will prove invaluable to refine or develop current or future models, respectfully, that will be useful for predicting bloom formation and behavior.

Bibliography

Primary Literature

1. Hallegraeff GM (1993) A review of harmful algal blooms and their apparent global increase. Phycologia 32:79–99
2. Sandifer P et al (2007) Interagency oceans and human health research implementation plan: a prescription for the future. Joint Subcommittee on Ocean Science and Technology. Interagency Working Group on Harmful Algal Blooms, Hypoxia and Human Health, Washington, DC
3. Smayda TJ (1990) Novel and nuisance phytoplankton blooms in the sea: evidence for a global epidemic. In: Graneli E (ed) Toxic marine phytoplankton. Elsevier, New York, pp 29–40
4. Smayda TJ (1992) Global epidemic of noxious phytoplankton blooms in the sea: evidence for a global epidemic. In: Sherman K, Alexander LM, Gold BD (eds) Food chains: models and management of large marine ecosystems. Westview Press, San Francisco, pp 275–307
5. Smayda TJ, White AW (1990) Has there been a global expansion of algal blooms? If so is there a connection with human activities? In: Graneli E (ed) Toxic marine phytoplankton. Elsevier, New York, pp 516–517
6. Hallegraeff GM (2010) Ocean climate change, phytoplankton community responses, and harmful algal blooms: a formidable predictive challenge. J Phycol 46(2):220–235
7. Ramsdell JS, Anderson DM, Glibert PM (eds) (2005) HARRNESS, Harmful algal research and response: a national environmental science strategy 2005–2015. Ecological Society of America, Washington, DC
8. Lopez CB et al (2008) Scientific assessment of marine harmful algal blooms. Joint Subcommittee on Ocean Science and Technology. Interagency Working Group on Harmful Algal Blooms, Hypoxia and Human Health, Washington, DC
9. Heisler J et al (2008) Eutrophication and harmful algal blooms: a scientific consensus. Harmful Algae 8(1):3–13
10. Anderson DM et al (2008) Harmful algal blooms and eutrophication: examining linkages from selected coastal regions of the United States. Harmful Algae 8(1):39–53
11. Huisman JM, Saunders GW (2007) Phylogeny and classification of the algae. In: McCarthy PM, Orchard AE (eds) Algae of Australia: introduction. Australian Biological Resources Study/CSIRO, Melbourne, pp 66–103
12. Smayda TJ, Reynolds CS (2001) Community assembly in marine phytoplankton: application of recent models to harmful dinoflagellate blooms. J Plankton Res 23(5):447–461
13. Vargo GA et al (2001) The hydrographic regime, nutrient requirements, and transport of a *Gymnodinium breve* Davis red tide on the west Florida shelf. In: Hallegraeff GM et al (eds) Harmful algal blooms 2000. Intergovernmental Oceanographic Commission of UNESCO, Paris, pp 157–159
14. Laws RM (1985) The ecology of the southern ocean. Am Sci 73(1):26–40
15. Croxall JP, Nicol S (2004) Management of southern ocean fisheries: global forces and future sustainability. Antarct Sci 16(4):559–584
16. Smayda TJ, Reynolds CS (2003) Strategies of marine dinoflagellate survival and some rules of assembly. J Sea Res 49(2):95–106
17. Sournia A (1974) Circadian periodicities in natural populations of marine phytoplankton. Mar Biol 12:325–389
18. Kent ML, Whyte JNC, Latrace C (1995) Gill lesions and mortality in seawater pen-reared Atlantic salmon Salmo-Salar associated with dense bloom of *Skeletonema costatum* and *Thalassiora* species. Dis Aquat Organ 22(1):77–81
19. Bell GR (1961) Penetration of spines from a marine diatom into gill tissue of Lingcod (*Ophiodon elongatus*). Nature 192(479):279–280
20. Dagg MJ et al (2007) A review of water column processes influencing hypoxia in the northern Gulf of Mexico. Estuaries Coast 30(5):735–752
21. Rabalais NN et al (2002) Nutrient-enhanced productivity in the northern Gulf of Mexico: past, present and future. Hydrobiologia 475(1):39–63
22. Legrand C et al (2003) Allelopathy in phytoplankton – biochemical, ecological, and evolutionary aspects. Phycologia 42:406–419
23. Kubanek J et al (2005) Does the red tide dinoflagellate *Karenia brevis* use allelopathy to outcompete other phytoplankton? Limnol Oceanogr 50(3):883–895
24. Okaichi T, Nishio S (1976) Identification of ammonia as the toxic principle of red tide of *Noctiluca miliaris*. Bull Plankton Soc Jpn 23:75–80
25. Lancelot C et al (2011) Cost assessment and ecological effectiveness of nutrient reduction options for mitigating Phaeocystis colony blooms in the southern North Sea: an integrated modeling approach. Sci Total Environ 409(11):2179–2191
26. Ciglenecki I et al (2003) Mucopolysaccharide transformation by sulfide in diatom cultures and natural mucilage. Mar Ecol Prog Ser 263:17–27
27. Guiry MD (2011) AlgaeBase. http://www.algaebase.org [cited 10 May 2011]
28. Daugbjerg N et al (2000) Phylogeny of some of the major genera of dinoflagellates based on ultrastructure and partial LSU rDNA sequence data, including the erection of three new genera of unarmoured dinoflagellates. Phycologia 39:302–317
29. Scholin CA, Anderson DM (1994) Identification of group-specific and strain-specific genetic-markers for globally distributed *Alexandrium* (Dinophyceae). 1. RFLP Analysis of SSU ribosomal-RNA genes. J Phycol 30(4):744–754
30. Scholin CA, Anderson DM (1996) LSU rDNA-based RFLP assays for discriminating species and strains of *Alexandrium* (*Dinophyceae*). J Phycol 32(6):1022–1035

31. Scholin CA, Hallegraeff GM, Anderson DM (1995) Molecular evolution of the *Alexandrium tamarense* species complex (Dinophyceae)-dispersal in the North American and West Pacific regions. Phycologia 34:472–485
32. Scholin CA et al (1994) Identification of group-specific and strain-specific genetic-markers for globally distributed *Alexandrium* (Dinophyceae) 2 sequence-analysis of a fragment of the Lsu ribosomal-RNA gene. J Phycol 30(6):999–1011
33. Lilly EL, Halanych KM, Anderson DM (2007) Species boundaries and global biogeography of the *Alexandrium tamarense* complex (Dinophyceae). J Phycol 43:1329–1338
34. Kalaitzis JA et al (2010) Biosynthesis of toxic naturally-occurring seafood contaminants. Toxicon 56:244–258
35. Etheridge SM (2010) Paralytic shellfish poisoning: seafood safety and human health perspectives. Toxicon 56: 108–122
36. Oshima Y, Blackburn SI, Hallegraeff GM (1993) Comparative study on paralytic shellfish toxin profiles of the dinoflagellate *Gymnodinium catenatum* from three different countries. Mar Biol 116:471–476
37. Hall S et al (1990) The saxitoxins: sources, chemistry, and pharmacology. In: Hall S, Strichartz G (eds) Marine toxins: origins, structure, and molecular pharmacology. American Chemical Society, Washington, DC
38. Hille B (1992) Ionic channels of excitable membranes, 2nd edn. Sinauer, Sunderland
39. Ritchie JM, Rogart RB (1977) The binding of saxitoxin and tetrodotoxin to excitable tissue. Rev Physiol Biochem Pharmacol 79:42–50
40. Kao CY et al (1967) Vasomotor and respiratory depressant actions of tetrodotoxin and saxitoxin. Arch Int Pharmacodyn Ther 165:438–450
41. Kao CY (1993) Paralytic shellfish poisoning. In: Falconer IR (ed) Algal toxins in seafood and drinking water. Academic, London, pp 75–86
42. Doucette G et al (2006) Phycotoxin pathways in aquatic food webs: transfer, accumulation, and degradation. In: Graneli E, Turner JT (eds) Ecology of harmful algae. Springer, Berlin/Heidelberg
43. Anderson DM, White AW (1989) Toxic dinoflagellates and marine mammal mortalities. Woods Hole Oceanographic Institution Technical Report. WHOI-89-36 (CRC-89-6). Woods Hole Oceanographic Institution, Woods Hole
44. Geraci JR (1989) Clinical investigations of the 1987–1988 mass mortality of bottlenose dolphins along the US central and south Atlantic coast. In: Final report to the national marine fisheries service. U. S. Navy, Office of Naval Research and Marine Mammal Commission, Ontario Veterinary College, University of Guelph, Guelph, pp 1–63
45. Geraci JR et al (1989) Humpback whales (*Megaptera novaeangliae*) fatally poisoned by dinoflagellate toxin. Can J Fish Aquat Sci 46:1895–1898
46. Shumway SE (1995) Phycotoxin-related shellfish poisoning: bivalve molluscs are not the only vectors. Rev Fish Sci 3:1–31
47. White AW (1981) Marine zooplankton can accumulate and retain dinoflagellate toxins and cause fish kills. Limnol Oceanogr 26:103–109
48. Doucette GJ et al (2006) PSP toxins in North Atlantic right whales (*Eubalaena glacialis*) and their zooplankton prey in the Bay of Fundy. Canada Mar Ecol Prog Ser 306:303–313
49. Deeds JR et al (2008) Non-traditional vectors for paralytic shellfish poisoning. Mar Drugs 6:308–348
50. Shumway SE (1990) A review of the effects of algal blooms on shellfish and aquaculture. J World Aquacul Soc 21:65–104
51. RaLonde R (1996) Paralytic shellfish poisoning: the Alaska problem. In: Alaska's marine resources. Marine Advisory Program, Anchorage
52. Bricelj VM, Lee JH, Cembella AD (1991) Influence of dinoflagellate cell toxicity on uptake and loss of paralytic shellfish toxins in the northern quahog *Mercenaria mercenaria*. Mar Ecol Prog Ser 74:33–46
53. Reboreda A et al (2010) Decrease in marine toxin content in bivalves by industrial processes. Toxicon 55:235–243
54. Trainer VL (2002) Harmful algal blooms on the U.S. west coast. In: Taylor FJ, Trainer VL (eds) Harmful algal blooms in the PICES region of the North Pacific. PICES Scientific Report No. 23. North Pacific Marine Science Organization, Sidney, pp 89–118
55. Nishitani L, Chew KK (1988) PSP toxins in the Pacific coast states: monitoring programs and effects on bivalve industries. J Shellfish Res 7:653–669
56. Anderson DM et al (2000) Estimated annual economic impacts from harmful algal blooms (HABs) in the US. Woods Hole Oceanographic Institute, Woods Hole
57. Anderson DM et al (2005) Initial observation of the 2005 *Alexandrium fundyense* bloom in southern New England: general patterns and mechanisms. Deep Sea Res II 52:2856–2876
58. Jin D, Thunberg E, Hoagland P (2008) Economic impact of the 2005 red tide event on commercial shellfish fisheries in New England. Ocean Coast Manag 51(5):420–429
59. Adachi M, Sako Y, Ishida Y (1996) Analysis of *Alexandrium* (Dinophyceae) species using sequence of the 5.8S ribosomal DNA and internal transcribed spacer regions. J Phycol 32:424–432
60. John U, Fensome RA, Medlin LK (2003) The application of a molecular clock based on molecular sequences and fossil record to explain biogeographic distributions within the *Alexandrium tamarense* "species complex" (Dinophyceae). Mol Biol Evol 20:1015–1027
61. Medlin L et al (1998) Sequence comparison links toxic European isolates of *Alexandrium tamarense* from the Orkney Islands to toxic North American stocks. Eur J Protistol 34:329–335
62. Hollingworth T, Wekell MM (1990) Paralytic shellfish poison biological method. Final action. In: Hellrich K (ed) Official methods of analysis. AOAC, Arlington, pp 881–882
63. AOAC (2000) AOAC official method 959.08 paralytic shellfish poison. In: Horwitz W (ed) Official methods of analysis of AOAC international. AOAC International, Arlington

64. Wekell JC, Hurst J, Lefebvre KA (2004) The origin of the regulatory limits for PSP and ASP toxins in shellfish. J Shellfish Res 23:927–930
65. Food and Agriculture Organization of the United Nations (2004) Marine biotoxins. Paper 80. FAO Food and Nutrition, Rome, pp 5–52
66. Jellet JF et al (1992) Paralytic shellfish poison (saxitoxin family) bioassays: automated endpoint determination and standardization of the in vitro tissue culture bioassay and comparison with the standard mouse bioassay. Toxicon 30: 1143–1156
67. Kogure K et al (1988) A tissue culture assay for the tetrodotoxin, saxitoxin, and related toxins. Toxicon 26:191–197
68. Shimojo RY, Iwaoka WT (2000) A rapid hemolysis assay for the detection of sodium channel-specific marine toxins. Toxicology 154:1–7
69. Davio SR, Fontelo PA (1984) A competitive displacement assay to detect saxitoxin and tetrodotoxin. Anal Biochem 141:199–204
70. Doucette GJ et al (1997) Development and preliminary validation of a microtiter plate-based receptor binding assay for paralytic shellfish poisoning toxins. Toxicon 35(5):625–636
71. Powell CL, Doucette GJ (1999) A receptor binding assay for paralytic shellfish poisoning toxins: recent advances and applications. Nat Toxins 7:393–400
72. Chu FS, Huang X, Wei RD (1990) Enzyme-linked immunosorbent assay for microcystins in blue-green algal blooms. J Assoc Off Anal Chem 73(3):451–456
73. Usleber E, Schnieder E, Terplan G (1991) Direct enzyme immunoassay in microtitration plate and test strip format for the detection of saxitoxin in shellfish. Lett Appl Microbiol 13:275
74. Bergantin JH, Sevilla F III (2010) Quartz crystal microbalance biosensor for saxitoxin based on immobilized sodium channel receptors. Anal Lett 43(3):476–486
75. Metfies K et al (2005) Electrochemical detection of the toxic dinoflagellate *Alexandrium ostenfeldii* with a DNA-biosensor. Biosens Bioelectron 20(7):1349–1357
76. Diercks S, Metfies K, Medlin LK (2008) Development and adaptation of a multiprobe biosensor for the use in a semi-automated device for the detection of toxic algae. Biosens Bioelectron 23:1527–1533
77. Fonfria ES et al (2007) Paralytic shellfish poisoning detection by surface plasmon resonance-based biosensors in shellfish matrixes. Anal Chem 79(16):6303–6311
78. Chu FS et al (1996) Screening of paralytic shellfish poisoning toxins in naturally occurring samples with three different direct competitive enzyme-linked immunosorbent assays. J Agric Food Chem 44(12):4043–4047
79. Garthwaite I et al (2001) Integrated enzyme-linked immunosorbent assay screening system for amnesic, neurotoxic, diarrhetic, and paralytic shellfish poisoning toxins found in New Zealand. J AOAC Int 84:1643–1648
80. Kawatsu K et al (2002) Development and application of an enzyme immunoassay based on a monoclonal antibody against gonyautoxin components of paralytic shellfish poisoning toxins. J Food Prot 65(8):1304–1308
81. Usleber E et al (2001) Immunoassay methods for paralytic shellfish poisoning toxins. J AOAC Int 84:1649–1656
82. Usleber E, Donald M, Straka M (1997) Comparison of enzyme immunoassay and mouse bioassay for determining paralytic shellfish poisoning toxins in shellfish. Food Addit Contam 14(2):193–198
83. Gas F et al (2010) One step immunochromatographic assay for the rapid detection of *Alexandrium minutum*. Biosens Bioelectron 25:1235–1239
84. Jellet JF et al (2002) Detection of paralytic shellfish poisoning (PSP) toxins in shellfish tissue using MIST Alert, a new rapid test, in parallel with the regulatory AOAC mouse bioassay. Toxicon 40(10):1407–1425
85. Costa PR et al (2009) Comparative determination of paralytic shellfish toxins (PSTs) using five different toxin detection methods in shellfish species collected in the Aleutian islands, Alaska. Toxicon 54:313–320
86. Oshiro M et al (2006) Paralytic shellfish poisoning surveillance in California using the Jellett Rapid PSP test. Harmful Algae 5:69–73
87. Sullivan JJ (1988) Methods of analysis for DSP and PSP toxins in shellfish: a review. J Shellfish Res 7:587–595
88. Dell'Aversano C, Hess P, Quilliam MA (2005) Hydrophilic interaction liquid chromatography-mass spectrometry analysis of paralytic shellfish poisoning (PSP) toxins. J Chromatogr A1081:190
89. Oshima Y (1995) Post-column derivation HPLC methods for paralytic shellfish poisons. In: Hallegraeff GM, Anderson DM, Cembella AD (eds) Manual on harmful marine microalgae. IOC of UNESCO, Paris, pp 81–94
90. Rourke WA et al (2008) Rapid postcolumn methodology for determination of paralytic shellfish toxins in shellfish tissue. J AOAC Int 91(3):589–597
91. Thomas K et al (2006) Analysis of PSP toxins by liquid chromatography with postcolumn oxidation and fluorescence detection. In: Henshilwood K et al (eds) Molluscan shellfish safety. The Marine Institute, Galway, pp 132–138
92. Lawrence JF, Menard C (1991) Liquid chromatographic determination of paralytic shellfish poisons in shellfish after prechromatographic oxidation. J Assoc Off Anal Chem 74:1006–1012
93. Lawrence JF et al (1991) A study of ten toxins associated with paralytic shellfish poison using prechromatographic oxidation and liquid chromatography with fluorescence detection. J Assoc Off Anal Chem 74:419–425
94. Lawrence JF, Niedzwiadek B, Menard C (2004) Quantitative determination of paralytic shellfish poisoning toxins in shellfish using prechromatographic oxidation and liquid chromatography with fluorescence detection: interlaboratory study. J AOAC Int 87(1):83–100
95. Quilliam MA, Janecek M, Lawerence JF (1993) Characterization of the oxidation products of paralytic shellfish poisoning toxins by liquid chromatography/mass spectrometry. Rapid Commun Mass Spectrom 6:14–24
96. Laycock MV et al (1994) Isolation and purification procedures for the preparation of paralytic shellfish poisoning toxin standards. Nat Toxins 2:175–183

97. NRC (2003) National Research Council Canada (NRC) – Institute for Marine Biosciences. http://www.nrc-cnrc.gc.ca/eng/ibp/imb.html [cited]
98. Van De Riet, J et al (2011) Liquid chromatography post-column oxidation (PCOX) method for the determination of paralytic shellfish toxins in mussels, clams, oysters, and scallops: collaborative study. J AOAC International 94:1154–1176
99. Anderson DM (1997) Bloom dynamics of toxic *Alexandrium* species in the northeastern US. Limnol Oceanogr 42(5 Pt 2):1009–1022
100. Hurst JW (1975) History of paralytic shellfish poisoning on the Maine coast 1958–1974. In: First international conference on toxic dinoflagellate blooms. Massachusetts Science and Technology Foundation, Wakefield
101. Anderson DM, Glibert PM, Burkholder JM (2002) Harmful algal blooms and eutrophication: nutrient sources, composition, and consequences. Estuaries 25:704–726
102. Boesch DF et al (1997) Harmful algal blooms in coastal waters: options for prevention, control, and mitigation. NOAA Coastal Ocean Program Decision Analysis Series No.10. NOAA Coastal Ocean Office, Silver Spring, 46pp + appendix
103. Mulligan HF (1975) Oceanographic factors associated with New England red tide blooms. In: First international conference on toxic dinoflagellate blooms. Massachusetts Science and Technology Foundation, Wakefield
104. He R et al (2008) Historic 2005 toxic bloom of *Alexandrium fundyense* in the western Gulf of Maine: 2. coupled biophysical numerical modeling. J Geophys Res Oceans 113:C07040–C07042
105. McGillicuddy DJ Jr et al (2005) Mechanisms regulating large-scale seasonal fluctuations in *Alexandrium fundyense* populations in the Gulf of Maine: results from a physical-biological model. Deep Sea Res II 52:2698–2714
106. McGillicuddy DJ Jr et al (2003) A mechanism for offshore initiation of harmful algal blooms in the coastal Gulf of Maine. J Plankton Res 25(9):1131–1138
107. Anderson DM, Taylor CD, Armbrust EV (1987) The effects of darkness and anaerobiosis on dinoflagellate cyst germination. Limnol Oceanogr 32:340–351
108. Anderson DM et al (1982) Vertical and horizontal distributions of dinoflagellates cyst in sediments. Limnol Oceanogr 27:757–765
109. Sinclair GA et al (2006) Nitrate uptake by *Karenia brevis*. I. Influences of prior environmental exposure and biochemical state on diel uptake of nitrate. Mar Ecol Prog Ser 328:117–124
110. Sinclair GA et al (2006) Nitrate uptake by *Karenia brevis*. II. Behavior and uptake physiology in a nitrate-depleted mesocosm with a bottom nutrient source. Mar Ecol Prog Ser 328:125–131
111. Walsh JJ, Steidinger KA (2001) Saharan dust and Florida red tides: the cyanophyte connection. J Geophy Res Oceans 106(C6):11597–11612
112. Tester PA, Steidinger KA (1997) *Gymnodinium breve* red tide blooms: initiation, transport, and consequences of surface circulation. Limnol Oceanogr 42(5):1039–1051
113. Vargo GA et al (2008) Nutrient availability in support of *Karenia brevis* blooms on the central West Florida shelf: what keeps *Karenia* blooming? Cont Shelf Res 28(1):73–98
114. Baden DG, Mende TJ (1982) Toxicity of 2 toxins from the Florida red tide marine dinoflagellate *Ptychodiscus brevis*. Toxicon 20(2):457–461
115. Flewelling LJ et al (2005) Red tides and marine mammal mortalities. Nature 435(7043):755–756
116. Davis CC (1948) *Gymnodinium brevis* sp. nov a cause of discolored water and animal mortality in the Gulf of Mexico. Bot Gaz 109(3):358–360
117. Fire SE et al (2008) Prevalence of brevetoxins in prey fish of bottlenose dolphins in Sarasota Bay, Florida. Mar Ecol Prog Ser 368:283–294
118. Kirkpatrick B et al (2010) Inland transport of aerosolized Florida red tide toxins. Harmful Algae 9(2):186–189
119. Kirkpatrick B et al (2006) Environmental exposures to Florida red tides: effects on emergency room respiratory diagnoses admissions. Harmful Algae 5(5):526–533
120. Zaias J et al (2011) Repeated exposure to aerosolized brevetoxin-3 induces prolonged airway hyperresponsiveness and lung inflammation in sheep. Inhal Toxicol 23(4):205–211
121. Hetland RD, Campbell L (2007) Convergent blooms of *Karenia brevis* along the Texas coast. Geophys Res Lett 34(19):5
122. Flewelling LJ et al (2010) Brevetoxins in sharks and rays (Chondrichthyes, Elasmobranchii) from Florida coastal waters. Mar Biol 157(9):1937–1953
123. Gannon DP et al (2009) Effects of *Karenia brevis* harmful algal blooms on nearshore fish communities in southwest Florida. Mar Ecol Prog Ser 378:171–186
124. Kirkpatrick B et al (2004) Literature review of Florida red tide: implications for human health effects. Harmful Algae 3(2): 99–115
125. Backer LC et al (2003) Recreational exposure to aerosolized brevetoxins during Florida red tide events. Harmful Algae 2(1):19–28
126. Fleming LE et al (2005) Initial evaluation of the effects of aerosolized Florida red tide toxins (Brevetoxins) in persons with asthma. Environ Health Perspect 113(5):650–657
127. Steidinger KA et al (1999) Harmful algal blooms in Florida. Unpublished technical report submitted to the Florida Harmful Algal Bloom Task Force. Florida Marine Research Institute, St. Petersburg, p 63
128. Hoagland P et al (2009) The costs of respiratory illnesses arising from Florida gulf coast *Karenia brevis* blooms. Environ Health Perspect 117(8):1239–1243
129. Morgan KL, Larkin SL, Adams CM (2010) Red tides and participation in marine-based activities: estimating the response of Southwest Florida residents. Harmful Algae 9(3):333–341
130. Morgan KL, Larkin SL, Adams CM (2009) Firm-level economic effects of HABS: a tool for business loss assessment. Harmful Algae 8(2):212–218

131. Plakas SM, Dickey RW (2010) Advances in monitoring and toxicity assessment of brevetoxins in molluscan shellfish. Toxicon 56(2):137–149
132. Stumpf R et al (2008) Hydrodynamic accumulation of *Karenia* on the west coast of Florida. Cont Shelf Res 28:189–213
133. Sinclair G (2008) Environmental, behavioral, and physiological constraints on the persistence of near-bottom populations of *Karenia brevis*. Department of marine, earth, and atmospheric sciences, North Carolina State University, Raleigh, p 181
134. Schofield O et al (1999) Optical monitoring and forecasting systems for harmful algal blooms: possibility or pipe dream? J Phycol 35(6):1477–1496
135. Janowitz GS, Kamykowski D (2006) Modeled *Karenia brevis* accumulation in the vicinity of a coastal nutrient front. Mar Ecol Prog Ser 314:49–59
136. Liu G, Janowitz G, Kamykowski D (2001) Influence of environmental nutrient conditions on *Gymnodinium breve* (Dinophyceae) population dynamics: a numerical study. Mar Ecol Prog Ser 213:13–37
137. Janowitz GS, Kamykowski D (1999) An expanded eularian model of phytoplankton environmental response. Ecol Model 118:237–247
138. Van Dolah FM, Leighfield TA (1999) Diel phasing of the cell-cycle in the Florida red tide dinoflagellate, *Gymnodinium breve*. J Phycol 35(6):1404–1411
139. Kamykowski D, Milligan EJ, Reed RE (1998) Biochemical relationships with the orientation of the autotrophic dinoflagellate *Gymnodinium breve* under nutrient replete conditions. Mar Ecol Prog Ser 167:105–117
140. Kamykowski D, Yamazaki H (1997) A study of metabolism-influence orientation in the diel vertical migration of marine dinoflagellates. Limnol Oceanogr 42(5):1189–1202
141. Dragovich A, Finucane J, Mays B (1961) Counts of red tide organisms, *Gymnodinium breve* and associated oceanographic data from Florida west coast, 1957–1959. In: U.S. Fish and Wildlife Service, Special. Science Report on Fish, Washington, DC, 175p
142. Steidinger KA et al (1998) Bloom dynamics and physiology of *Gymnodinium breve* with emphasis on the Gulf of Mexico. In: Anderson DM, Cembella AD, Hallegraeff GM (eds) Physiological ecology of harmful algal blooms. Springer, Berlin, pp 133–153
143. Masserini RT, Fanning KA (2000) A sensor package for the simultaneous determination of nanomolar concentrations of nitrite, nitrate, and ammonia in seawater by fluorescence detection. Mar Chem 68(4):323–333
144. Hecky RE, Kilham P (1988) Nutrient Limitation of phytoplankton in freshwater and marine environments: a review on the effects of enrichment. Limnol Oceanogr 33(4):796–822
145. Walsh J, Steidinger K (2001) Saharan dust and Florida red tides: the cyanophyte connection. J Geophys Res 106(C6):11,597–11,612
146. Mulholland MR et al (2006) Nitrogen fixation and release of fixed nitrogen by *Trichodesmium* spp. in the Gulf of Mexico. Limnol Oceanogr 51(4):1762–1776
147. Lester KM et al (2008) Zooplankton and *Karenia brevis* in the Gulf of Mexico. Cont Shelf Res 28(1):99–111
148. Sinclair GA, Kamykowski D (2008) Benthic-pelagic coupling in sediment-associated populations of *Karenia brevis*. J Plankton Res 30(7):829–838
149. Janowitz GS, Kamykowski D, Liu G (2008) A three-dimensional wind and behaviorally driven population dynamics model for *Karenia brevis*. Cont Shelf Res 28(1):177–188
150. Hasle GR (2002) Are most of the domoic acid-producing species of the diatom genus *Pseudo-nitzschia* cosmopolites? Harmful Algae 1:137–146
151. Smetacek V et al (2002) Mesoscale distribution of dominant diatom species relative to the hydrographical field along the Antarctic polar front. Deep-Sea Res II 49:3835–3848
152. Fryxell GA, Villac MC, Shapiro LP (1997) The occurrence of the toxic diatom genus *Pseudo-nitzschia* (Bacillariophyceae) on the West Coast of the USA, 1920–1996: a review. Phycologia 36:419–437
153. Qi Y, Wang J, Zheng L (1994) The taxonomy and bloom ecology of Pseudo-nitzschia on the coasts of China. In: IOC-WESTPAC third international scientific symposium, Bali, pp 88–95
154. Zou JZ, Zhou MJ, Zhang C (1993) Ecological features of toxic *Nitzschia pungens* Grunow in Chinese coastal waters. In: Smayda TJ, Shimizu Y (eds) Toxic phytoplankton blooms in the sea. Elsevier, Amsterdam
155. Evans KM et al (2004) Microsatellite marker development and genetic variation in the toxic marine diatom *Pseudo-nitzschia multiseries* (Bacillariophyceae). J Phycol 40(5):911–920
156. Evans KM, Hayes PK (2004) Microsatellite markers for the cosmopolitan marine diatom *Pseudo-nitzschia pungens*. Mol Ecol Notes 4(1):125–126
157. Evans KM, Kuhn SF, Hayes PK (2005) High levels of genetic diversity and low levels of genetic differentiation in North Sea *Pseudo-nitzschia pungens* (Bacillariophyceae) populations. J Phycol 41(3):506–514
158. Hubbard KA, Rocap G, Armbrust EV (2008) Inter- and intra-specific community structure within the diatom genus *Pseudo-nitzschia* (Bacillariophyceae). J Phycol 44:637–649
159. Orsini L et al (2004) Multiple rDNA ITS-types within the diatom *Pseudo-nitzschia delicatissima* (Bacillariophyceae) and their relative abundances across a spring bloom in the Gulf of Naples. Mar Ecol Prog Ser 271:87–98
160. Thessen AE, Bowers HA, Stoecker DK (2009) Intra- and inter-species differences in growth and toxicity of Pseudo-nitzschia while using different nitrogen sources. Harmful Algae 8:792–810
161. Bates SS (2000) Domoic-acid-producing diatoms: another genus added. J Phycol 36:978–985
162. Bates SS et al (1989) Pennate diatom *Nizschia pungens* as the primary source of domoic acid, a toxin in shellfish from eastern Prince Edward Island, Canada. Can J Fish Aquatic Sci 46:1203–1215
163. Lefebvre KA, Robertson A (2010) Domoic acid and human exposure risks: a review. Toxicon 56:218–230

164. Teitelbaum J, Carpenter S, Cashman NR (1990) Neurologic sequelae after ingestion of mussels contaminated with domoic acid. N Engl J Med 323:1632–1633
165. Peng YG et al (1994) Neuroexcitatory and the neurotoxic actions of the amnesic shellfish poison, domoic acid. Neuropharmacol Neurotoxicol 5:981–985
166. Gulland FMD et al (2002) Domoic acid toxicity in California sea lions (*Zalophus californianus*): clinical signs, treatment and survival. Vet Rec 150:475–480
167. Perl TM et al (1990) An outbreak of toxic encephalopathy caused by eating mussels contaminated with domoic acid. N Engl J Med 322:1775–1780
168. Todd ECD (1993) Domoic acid and amnesic shellfish poisoning: a review. J Food Prot 56:69–83
169. Wright JLC et al (1989) Identification of domoic acid, a neuroexcitatory amino acid, in toxic mussels from eastern Prince Edward Island. Can J Chem 67:481–490
170. Garrison DL et al (1992) Confirmation of domoic acid production by *Pseudo-nitzschia australis* (Bacillariophyceae) cultures. J Phycol 28:604–607
171. Lefebvre KA et al (2002) Domoic acid in planktivorous fish in relation to toxic *Pseudo-nitzschia* cell densities. Mar Biol 140:625–631
172. Scholin CA et al (2000) Mortality of sea lions along the central California coast linked to a toxic diatom bloom. Nature 403:80–84
173. Wekell JC et al (1994) Occurrence of domoic acid in Washington state razor clams (*Siliqua patula*) during 1991–1993. Nat Toxins 2:197–205
174. Fritz L et al (1992) An outbreak of domoic acid poisoning attributed to the pennate diatom *Pseudonitzschia australis*. J Phycol 28:439–442
175. Work TM et al (1993) Epidemiology of DA poisoning in brown pelicans (*Pelecanus occidentalis*) and Brandt's cormorants (*Phalacrocarax penicillatus*) in California. J Zoo Wildl Med 24:54–62
176. Sierra-Beltran AP et al (1997) Sea bird mortality at Cabo San Lucas, Mexico: evidence that toxic diatom blooms are spreading. Toxicon 35:447–453
177. Sierra-Beltran AP et al (1998) An overview of the marine food poisoning in Mexico. Toxicon 36:1493–1502
178. Lefebvre KA et al (1999) Detection of domoic acid in northern anchovies and California sea lions associated with an unusual mortality event. Nat Toxins 7(3):85–92
179. Goldstein T et al (2008) Novel symptomatology and changing epidemiology of domoic acid toxicosis in California sea lions (*Zalophus californianus*): an increasing risk to marine mammal health. Proc R Soc Biol Sci Ser B 275:267–276
180. Maucher JM, Ramsdell JS (2005) Domoic acid transfer to milk: evaluation of a potential route of neonatal exposure. Environ Health Perspect 115:1743–1746
181. Grattan LM et al (2007) Domoic acid neurotoxicity in native Americans in the pacific northwest: human health project methods and update. In: Fourth symposium on harmful algae in the US, Woods Hole
182. Trainer VL et al (2007) Recent domoic acid closures of shellfish harvest areas in Washington State inland waters. Harmful Algae 6:449–459
183. Trainer VL, Hickey BM, Horner RA (2002) Biological and physical dynamics of domoic acid production off the Washington coast. Limnol Oceanogr 47:1438–1446
184. Dyson K, Huppert DD (2010) Regional economic impacts of razor clam beach closures due to harmful algal blooms (HABs) on the Pacific coast of Washington. Harmful Algae 9:264–271
185. Bill BD et al (2006) The first closure of shellfish harvesting due to domoic acid in Puget Sound, Washington, USA. Afr J Mar Sci 28:437–442
186. Ayers D, Reed H (2004) Managing important recreational and commercial shellfish fisheries around harmful algal blooms. In: 2003 Georgia Basin/Puget sound research conference, Olympia
187. Hasle GR, Syvertsen EE (1997) *Marine Diatoms*. In: Tomas CR (ed) Identifying marine diatoms and dinoflagellates. Academic, San Diego
188. Hasle GR, Lundholm N (2005) *Pseudo-nitzschia seriata* f. *obtusa* (Bacillariophyceae) raised in rank based on morphological, phylogenetic and distributional data. Phycologia 44:608–619
189. Lundholm N et al (2003) A study of the *Pseudo-nitzschia pseudodelicatissima/cuspidata* complex (Bacillariophyceae): what is *P. pseudodelicatissima*? J Phycol 39:797–813
190. Lundholm N et al (2006) Inter- and intraspecific variation of the *Pseudo-nitzschia delicatissima* complex (Bacillariophyceae) illustrated by rRNA probes, morphological data and phylogenetic analyses. J Phycol 42(2):464–481
191. Fritz L (1992) The use of cellular probes in studying marine phytoplankton. Korean J Phycol 7:319–324
192. Rhodes LL (1998) Identification of potentially toxic *Pseudo-nitzschia* (Bacillariophyceae) in New Zealand coastal waters, using lectins. N Z J Mar Freshw Res 32:537–544
193. Rhodes LL et al (1998) Domoic acid producing *Pseudo-nitzschia* species educed by whole cell DNA probe-based and immunochemical assays. In: Reguera B et al (eds) Harmful algae. Xunta de Galicia and IOC of UNESCO, Santiago de Compostela, pp 274–277
194. Cho ES et al (1999) The rapid differentiation of toxic *Alexandrium* and *Pseudo-nitzschia* species using fluorescent lectin probes. J Korean Soc Oceanogr 35:167–171
195. Fraga S et al (1998) *Pseudo-nitzschia* species isolated from Galician waters: toxicity, DNA content and lectin binding assay. In: Harmful algae: eighth international conference on harmful algae, Vigo, pp 270–273
196. Rhodes L, Scholin C, Garthwaite I (1998) *Pseudo-nitzschia* in New Zealand and the role of DNA probes and immunoassays in refining marine biotoxin monitoring programmes. Nat Toxins 6:105–111
197. Andree KB et al (2011) Quantitative PCR coupled with melt curve analysis for detection of selected *Pseudo-nitzschia* spp. (Bacillariophyceae) from the northwestern Mediterranean Sea. Appl Environ Microbiol 77(5):1651–1659

198. Cho ES, Kodaki Y, Park JG (2001) The comparison of two strains of toxic *Pseudo-nitzschia multiseries* (Hasle) Hasle and non-toxic *Pseudo-nitzschia pungens* (Grunow) Hasle isolated from Chinhae Bay, Korea. Algae 16:275–285
199. Lundholm N et al (2002) Morphology, phylogeny and taxonomy of species within *Pseudo-nitzschia americana* complex (Bacillariophyceae) with descriptions of two new species, *Pseudo-nitzschia brasiliana* and *Pseudo-nitzschia linea*. Phycologia 41:480–497
200. Manhart JR et al (1995) *Pseudo-nitzschia pungens* and *P. multiseries* (Bacillariophyceae): nuclear ribosomal DNA's and species differences. J Phycol 31:421–427
201. McDonald SM, Sarno D, Zingone A (2007) Identifying *Pseudo-nitzschia* species in natural samples using genus-specific PCR primers and clone libraries. Harmful Algae 6(8):849–860
202. Miller P, Scholin CA (1996) Identification of cultured *Pseudo-nitzschia* (Bacillariophyceae) using species specific LSU rRNA-targeted probes. J Phycol 32:646–655
203. Miller P, Scholin CA (1998) Identification and enumeration of cultured and wild *Pseudo-nitzschia* (Bacillariophyceae) using species specific LSU rRNA-targeted fluorescent probes and filter-based whole cell hybridization. J Phycol 34:371–382
204. Scholin CA et al (1996) Identification of *Pseudo-nitzschia australis* (Bacillariophyceae) using rRNA-targeted probes in whole cell and sandwich hybridization formats. Phycologia 35:190–197
205. Scholin CA et al (1999) DNA probes and a receptor-binding assay for detection of *Pseudo-nitzschia* (Bacillariophyceae) species and domoic acid activity in cultured and natural samples. J Phycol 35:1356–1367
206. Scholin CA et al (1997) Detection and quantification of *Pseudo-nitzschia australis* in cultured and natural populations using LSU rRNA-targeted probes. Limnol Oceanogr 42:1265–1272
207. Scholin CA et al (1994) Ribosomal DNA sequences discriminate among toxic and non-toxic *Pseudo-nitzschia* species. Nat Toxins 2:152–165
208. Cho ES et al (2002) Monthly monitoring of domoic acid producer *Pseudo-nitzschia multiseries* (Hasle) Hasle using species-specific DNA probes and WGA lectins and abundance of *Pseudo-nitzschia* species (Bacillariophyceae) from Chinhae Bay, Korea. Bot Mar 45:364–372
209. Orsini L et al (2002) Toxic *Pseudo-nitzschia multistriata* (Bacillariophyceae) from the Gulf of Naples: morphology, toxin analysis and phylogenetic relationships with other *Pseudo-nitzschia* species. Eur J Phycol 37:247–257
210. Parsons ML et al (1999) *Pseudo-nitzschia* species (Bacillariophyceae) in Louisiana coastal waters: molecular probes field trials, genetic variability, and domoic acid analyses. J Phycol 35:1368–1378
211. Vrieling EG et al (1996) Identification of a domoic acid-producing *Pseudo-nitzschia* species (Bacillariophyceae) in the Dutch Wadden sea with electron microscopy and molecular probes. Eur J Phycol 31:333–340
212. Greenfield D et al (2008) Field applications of the second-generation environmental sample processor (ESP) for remote detection of harmful algae: 2006–2007. Limnol Oceanogr Method 6:667–679
213. Greenfield DI et al (2006) Application of the environmental sample processor (ESP) methodology for quantifying *Pseudo-nitzschia australis* using ribosomal RNA-targeted probes in sandwich and fluorescent in situ hybridization. Limnol Oceanogr Method 4:426–435
214. Scholin C et al (2009) Remote detection of marine microbes, small invertebrates, harmful algae and biotoxins using the environmental sample processor (ESP). Oceanography 22:158–167
215. AOAC (1990) Paralytic shellfish poison. Biological method. Final action. In: Hellrich K (ed) Official method of analysis. Association of Official Analytical Chemists (AOAC), Arlington, pp 881–882
216. Van Dolah FM et al (1997) A microplate receptor assay for the amnesic shellfish poisoning toxin, domoic acid, utilizing a cloned glutamate receptor. Anal Biochem 245:102–105
217. Garthwaite I et al (1998) An immunoassay for determination of domoic acid in shellfish and sea water. In: Reguera B et al (eds) Harmful algae. Xunta de Galicia and IOC of UNESCO, Santiago de Compostela, pp 559–562
218. Kawatsu K, Hamano Y, Noguchi T (1999) Production and characterization of a monoclonal antibody against domoic acid and its application to enzyme immunoassay. Toxicon 37:1579–1589
219. Smith DS, Kitts DD (1994) A competitive enzyme-linked immunoassay for domoic acid determination in human body fluids. Food Chem Toxicol 32(12):1147–1154
220. Smith DS, Kitts DD (1995) Enzyme Immunoassay for the determination of domoic acid in mussel extracts. J Agric Food Chem 43:367–371
221. Fernandez ML, Cembella AD (1995) Part B. Mammalian bioassays. In: Hallegraeff GM, Anderson DM, Cembella AD (eds) Manual on harmful marine microalgae. UNESCO, Paris, pp 213–228
222. Lawrence JF et al (1989) Liquid chromatographic determination of domoic acid in shellfish products using the paralytic shellfish extraction procedure of the association of official analytical chemists. J Chromatogr 462:349–356
223. Lawrence JF, Charbonneau CF, Menard C (1991) Liquid chromatographic determination of domoic acid in mussels, using AOAC paralytic shellfish poison extraction procedures: collaborative study. J Assoc Off Anal Chem 74(1):68–72
224. Ciminiello P et al (2005) Hydrophilic interaction liquid chromatography/mass spectrometry for determination of domoic acid in Adriatic shellfish. Rapid Commun Mass Spectrom 19(4):2030–2038
225. Hummert C, Reichelt M, Luckas B (1997) Automatic HPLC-UV determination of domoic acid in mussels and algae. Chromatographia 45:284–288
226. Quilliam MA et al (1989) High-performance liquid-chromatography of domoic acid, a marine neurotoxin, with application to shellfish and plankton. Int J Environ Anal Chem 36:139–154

227. European Union Reference Laboratory for Marine Biotoxins (ed) (2010) Standard operating procedure for determination of domoic acid (ADP toxins) in molluscs by UPLC-MS. European Union Reference Laboratory for Marine Biotoxins/ Agencia Espanola de Seguridad Alimentaria y Nutricion, Vigo
228. Rafuse C et al (2004) Rapid monitoring of toxic phytoplankton and zooplankton with a lateral-flow immunochromatographic assay for ASP and PSP toxins. In: Steidinger KA (ed) Harmful algae. Florida Fish and Wildlife Conservation Commission and Intergovernmental Oceanographic Commission of UNESCO, St. Petersburg
229. Turrell E et al (2008) Detection of *Pseudo-nitzschia* (Bacillariophyceae) species and amnesic shellfish toxins in Scottish coastal waters using oligonucleotide probes and the Jellet rapid test. Harmful Algae 7(4):443–458
230. Parsons ML, Dortch Q, Turner RE (2002) Sedimentological evidence of an increase in *Pseudo-nitzschia* (Bacillariophyceae) abundance in response to coastal eutrophication. Limnol Oceanogr 47(2):551–558
231. Dortch Q et al (2000) *Pseudo-nitzschia* spp. in the northern Gulf of Mexico: overview and response to increasing eutrophication. In: Symposium on harmful marine algae in the U.S. Marine Biological Laboratory, Woods Hole, p 27
232. McFadyen A, Hickey BM, Foreman MGG (2005) Transport of surface waters from the Juan de Fuca eddy region to the Washington coast. Cont Shelf Res 25:2008–2021
233. Bates SS et al (1991) Controls on domoic acid production by the diatom *Nitzschia pungens* f. *multiseries* in culture: nutrient and irradiance. Can J Fish Aquatic Sci 48:1136–1144
234. Pan Y, Subba Rao DV, Mann KH (1996) Changes in domoic acid production and cellular chemical composition of the toxigenic diatom *Pseudo-nitzschia multiseries* under phosphate limitation. J Phycol 32:371–381
235. Pan Y et al (1996) Effects of silicate limitation on production of domoic acid, a neurotoxin, by the diatom *Pseudo-nitzschia multiseries*. I. Batch culture studies. Mar Ecol Prog Ser 131:225–233
236. Pan Y et al (1996) Effects of silicate limitation on production of domoic acid, a neurotoxin, by the diatom *Pseudo-nitzschia multiseries*. II. Continuous culture studies. Mar Ecol Prog Ser 131:235–243
237. Van Apeldoorn ME, van Egmond HP, Speijers GJA (1999) Amnesic shellfish poisoning: a review. In: RIVM report 388802 019. National Institute of Public Health and the Environment, the Netherlands
238. Maldonado MT, Hughes MP, Rue EL (2002) The effects of Fe and Cu on growth and domoic acid production by *Pseudo-nitzschia multiseries* and *Pseudo-nitzschia australis*. Limnol Oceanogr 47:515–526
239. de Baar HJW et al (2005) Synthesis of iron fertilization experiments: from the iron age in the age of enlightenment. J Geophys Res Oceans 110:1–24
240. Marchetti A et al (2008) Identification and assessment of domoic acid production in oceanic *Pseudo-nitzschia* (Bacillariophyceae) from iron-limited waters in the northeast subartic Pacific. J Phycol 44(3):650–661
241. Bates SS et al (1995) Enhancement of domoic acid production by reintroducing bacteria to axenic cultures of the diatom *Pseudo-nitzschia multiseries*. Nat Toxins 3:429–435
242. Bates SS et al (2004) Interaction between bacteria and the domoic-acid-producing diatom *Pseudo-nitzschia multiseries* (Hasle) Hasle; can bacteria produce domoic acid autonomously? Harmful Algae 3:11–20
243. Kaczmarska I et al (2005) Diversity and distribution of epibiotic bacteria on *Pseudo-nitzschia multiseries* (Bacillariophyceae) in culture, and comparison with those on diatoms in native seawater. Harmful Algae 4:725–741
244. Brock TD (1973) Evolutionary and ecological aspects of the cyanophytes. In: Carr NG, Whitton BA (eds) The biology of blue-green algae. University of California Press, Berkeley, pp 487–500
245. Whitton BA, Potts M (eds) (2002) The ecology of cyanobacteria: their diversity in time and space. Academic, New York
246. Schofp JW (2002) The fossil record: tracing the roots of the cyanobacterial lineage. In: Whitton BA, Potts M (eds) The ecology of cyanobacteria: their diversity in time and space. Academic, New York, pp 13–35
247. Francis G (1878) Poisonous Australian lake. Nature 18:11–12
248. Codd GA, Bell SG, Brooks WP (1989) Cyanobacterial toxins in water. Water Sci Technol 21:1–13
249. Pilotto LS et al (1997) Health effects of exposure to cyanobacteria (blue-green algae) due to recreational water-related activities. Aust N Z J Public Health 21:562–566
250. Stewart I (2008) Cyanobacterial poisoning in livestock, wild animals, and birds–an overview. In: Hudnell HK (ed) Cyanobacterial harmful algal blooms: state of the science and research needs. Springer, New York, p 500
251. Teixera MGLC et al (1993) Gastroenteritis epidemic in the area of the Itaparica Dam, Bahia, Brazil. Bull Pan Am Health Organ 27:244–253
252. Tisdale ES (1931) Epidemic of intestinal disorders in Charleston, W.Va., occurring simultaneously with unprecedented water supply conditions. Am J Public Health 21:198–200
253. Turner PC et al (1990) Pneumonia associated with cyanobacteria. Br Med J 300:1440–1441
254. Metcalf JS, Codd GA (2004) Cyanobacterial toxins in the water environment. A review of current knowledge. Foundation for Water Research, Marlow
255. Chorus I, Bartram J (eds) (1999) Toxic cyanobacteria in water. A guide to their public health consequences, monitoring, and management. E & FN Spon, London (on behalf of the World Health Organization)
256. Falconer IR (1993) Measurement of toxins from blue-green algae in water and foodstuffs. In: Falconer IR (ed) Algal toxins in seafood and drinking water. Academic, New York, pp 165–176
257. Cheng YS et al (2007) Characterization of aerosols containing microcystin. Mar Drugs 5:136–150

258. Falconer IR, Buckley TH (1989) Tumour promotion by *Microcystis* sp., a blue-green algae occurring in water supplies. Med J Australia 150:351–352
259. Falconer IR, Humpage AR (1996) Tumour promotion by cyanobacterial toxins. Phycologia 35(Suppl 6):74–79
260. Fujiki H, Sueoka E, Suganuma M (1996) Carcinogenesis of microcystins. In: Watanabe MF et al (eds) Toxic microcystis. CRC Press, Boca Raton, pp 203–232
261. Humpage AR et al (2000) Microcystins (cyanobacterial toxins) in drinking water enhance the growth of aberrant crypt foci in the mouse colon. J Toxicol Environ Health A 61:155–165
262. Zhou L, Yu H, Chen K (2002) Relationship between microcystin in drinking water and colorectal cancer. Biomed Environ Sci 15(2):166–171
263. World Health Organization (2008) Guidelines for drinking-water quality: incorporating the 1st and 2nd addenda. World Health Organization, Geneva
264. Burns J (2008) Toxic cyanobacteria in Florida waters. In: Hudnell HK (ed) Cyanobacterial harmful algal blooms: state of the science and research needs. Springer, New York, p 500
265. Westrick JA (2008) Cyanobacterial toxin removal in drinking water treatment processes and recreational water. In: Hudnell HK (ed) Cyanobacterial harmful algal blooms: state of the science and research needs. Springer, New York, p 500
266. Carmichael WW (2001) Assessment of blue-green algal toxins in raw and finished drinking water. AWWA Research Foundation and American Water Works Association, Denver
267. Chorus I, Fastner F (2001) Recreational exposure to cyanotoxins. In: Chorus I (ed) Cyanotoxins, occurrence, causes, consequences. Springer, Heidelberg, pp 190–199
268. Miller MA et al (2010) Evidence for a novel marine harmful algal bloom: cyanotoxin (microcystin) transfer from land to sea otters. PLoS One 5(9):e12576
269. Wiegand C, Pflugmacher S (2005) Ecotoxicological effects of selected cyanobacterial secondary metabolites a short review. Toxicol Appl Pharmacol 203:201–218
270. Funari E, Testai E (2007) Human health risk assessment related to cyanotoxins exposure. Crit Rev Toxicol 38(2):97–125
271. Henricksen P et al (1997) Detection of an anatoxin-a(s)-like anticholinesterase in natural blooms and cultures of cyanobacteria/blue-green algae from Danish lakes and in the stomach contents of poisoned birds. Toxicon 35(1111):901–913
272. Matsunaga S et al (1989) Anatoxin-a(s), a potent anticholinesterase from *Anabaena flos-aquae*. J Am Chem Soc 111(494):8021–8023
273. Mahmood NA, Carmichael WW (1986) Paralytic shellfish poison produced by the freshwater cyanobacterium *Aphanizomeno flos-aquae* NH-5. Toxicon 24:175–186
274. Stewart I, Schluter PJ, Shaw GR (2006) Cyanobacterial lipopolysaccharides and human health – a review. Environ Health A Global Access Sci Source 5:7
275. Smith JL, Boyer GL, Zimba PV (2008) A review of cyanobacterial odorous and bioactive metabolites: impacts and management alternatives in aquaculture. Aquaculture 280:5–20
276. Fujiki H et al (1985) A blue-green alga from Okinawa contains aplysiatoxins, the third class of tumour promoters. Jpn J Cancer Res 76:257–259
277. Shimizu Y (1996) Microalgal metabolites: a new perspective. Annu Rev Microbiol 50:431–465
278. Fujiki H et al (1990) New tumour promoters from marine natural products. In: Hall S, Strichartz G (eds) Marine toxins. Origin, structure and molecular pharmacology. American Chemical Society, Washington, DC, pp 232–240
279. Gorham PR, Carmichael WW (1988) Hazards of freshwater blue-green algae (cyanobacteria). In: Lembi CA, Waaland JR (eds) Algae and human affairs. Cambridge University Press, New York, pp 404–431
280. Aguirre AA et al (2006) Hazards associated with the consumption of sea turtle meat and eggs: a review for health care workers and the general public. EcoHealth 3(3):141–153
281. Yasumoto Y (1998) Fish poisoning due to toxins of microalgal origins in the Pacific. Toxicon 36:1515–1518
282. Papapetropoulos S (2007) Is there a role for naturally occurring cyanobacterial toxins in neurodegeneration? The beta-*N*-methylamino-*L*-alanine (BMAA) paradigm. Neurochem Int 50:998–1003
283. Wilson JM et al (2002) Behavioral and neurological correlates of ALS-parkinsonian dementia complex in adult mice fed washed cycad flour. Neuromol Med 1:207–221
284. Rao SD et al (2006) BMAA selectively injures motor neurons via AMP/kainate receptor activation. Exp Neurol 201:244–252
285. Lobner D et al (2007) Beta-*N*-methyl-amino-*L*-alanine enhances neurotoxicity through multiple mechanisms. Neurobiol Dis 25(2):360–365
286. Buenz EJ, Howe CL (2007) Beta-methylamino-alanine (BMAA) injures hippocampal neurons in vivo. Neurotoxicology 28(3):702–704
287. Liu XQ et al (2010) Selective death of cholinergic neurons induced by beta-methylamino-L-alanine. Neuroreport 21(1):55–58
288. Karlsson O et al (2009) Selective brain uptake and behavioral effects of the cyanobacterial toxin BMAA (β-*N*-methylamino-*L*-alanine) following neonatal administration to rodents. Toxicol Sci 109(2):286–295
289. Wilde SB et al (2005) Avian vacuolar myelinopathy linked to exotic aquatic plants and a novel cyanobacterial species. Environ Toxicol 20(3):348–353
290. Bidigare RR et al (2009) Cyanobacteria and BMAA: possible linkage with avian vacuolar myelinopathy (AVM) in the southeastern United States. Amyotroph Lateral Scler 10(Suppl 2):71–73
291. Fischer JR, Lewis-Weis LA, Tate CM (2003) Experimental vacuolar myelinopathy in red-tailed hawks. J Wildl Dis 39(2):400–406
292. Birrenkot AH et al (2004) Establishing a food-chain link between aquatic plant material and avian vacuolar myelinopathy in mallards (*Anas plytyrhynchos*). J Wildl Dis 40(3):485–494

293. Murch SJ, Cox PA, Banack SA (2004) A mechanism for slow release of biomagnified cyanobacterial neurotoxins and neurodegenerative disease in Guam. Proc Natl Acad Sci U S A 101:12228–12231
294. Esterhuizen M, Downing TG (2008) Beta-*N*-methylamino-*L*-alanine (BMAA) in novel South African cyanobacterial isolates. Ecotoxicol Environ Saf 71:309–313
295. Johnson HE et al (2008) Cyanobacteria (*Nostoc commune*) used as a dietary item in the Peruvian highlands produces the neurotoxic amino acid BMAA. J Ethnopharmacol 118:159–165
296. Li A et al (2010) Detection of the neurotoxin BMAA within cyanobacteria isolated from freshwater in China. Toxicon 55:947–953
297. Metcalf JS et al (2008) Co-occurrence of beta-*N*-methylamino-*L*-alanine, a neurotoxic amino acid with other cyanobacterial toxins in British waterbodies, 1990–2004. Environ Microbiol 10(3):702–708
298. Cox PA et al (2005) Diverse taxa of cyanobacteria produce beta-*N*-methylamino-*L*-alanine, a neurotoxic amino acid. Proc Natl Acad Sci U S A 102:5074–5078
299. Caller TA et al (2009) A cluster of amyotrophic lateral sclerosis in New Hampshire: a possible role for toxic cyanobacteria blooms. Amyotroph Lateral Scler 10(Suppl 2):101–108
300. Tucker CS (2000) Off-flavor problems in aquaculture. Rev Fish Sci 8(1):45–88
301. Dodds WK et al (2009) Eutrophication of U.S. freshwaters: analysis of potential economic damages. Environ Sci Technol 43:12–19
302. World Health Organization (2003) Guidelines for safe recreational water environments. Volume 1: coastal and fresh waters. World Health Organization, Geneva
303. Steffensen DA (2008) Economic cost of cyanobacterial blooms. In: Hudnell HK (ed) Cyanobacterial harmful algal blooms: state of the science and research needs, vol 619, Advances in experimental medicine and biology. Springer, New York, 500pp
304. Kenefick SL et al (1992) Odorous substances and cyanobacterial toxins in praire drinking water sources. Water Sci Technol 25:147–154
305. Paerl HW (2008) Nutrient and other environmental controls of harmful cyanobacterial blooms along the freshwater-marine continuum. In: Hudnell HK (ed) Cyanobacterial harmful algal blooms: state of the science and research needs, vol 619, Advances in experimental medicine and biology. Springer, New York, 500pp
306. Garcia-Villada L et al (2004) Occurrence of copper resistant mutants in the toxic cyanobacteria *Microcystis aeruginosa*: characterization and future implications in the use of copper sulphate as algaecide. Water Res 38:2207–2213
307. Hitzfeld BC, Hoeger SJ, Dietrich DR (2000) Cyanobacterial Toxins: removal during drinking water treatment, and human risk assessment. Environ Health Perspect 108(6):113–122
308. Hoeger SJ, Hitzfeld BC, Dietrich DR (2005) Occurrence and elimination of cyanobacterial toxins in drinking water treatment plants. Toxicol Appl Pharmacol 203:231–242
309. Hoeger SJ et al (2004) Occurrence and elimination of cyanobacterial toxins in two Australian drinking water treatment plants. Toxicon 43(14248):639–649
310. Jones G, Gurney S, Rocan D (1996) Water quality/toxic algae study interim report: summary of the 1995 field season results. Manitoba Environment, 4 June 1996
311. Lambert TW, Holmes CFB, Hrudey SE (1996) Adsorption of microcystin-LR by activating carbon and removal in full-scale water treatment. Water Res 30(6):1411–1422
312. Wannemacher JRW et al (1993) Treatment for removal of biotoxins from drinking water. US Army Biomedical Research and Development Laboratory, Fort Detrick, Frederick
313. James H, Lloyd A (2002) Blue-green algae and their toxins – Great Britain's perspective. In: Proceedings of the health effects of exposure to cyanobacteria toxins: state of the science, Sarasota
314. Kim S-C, Lee D-K (2005) Inactivation of algal blooms in eutrophic water of drinking water supplies with the photocatalysis of TiO2 thin film on hollow glass beads. Water Sci Technol 52(9):145–152
315. Ueno Y et al (1996) Detection of microcystins, a blue-green algal hepatotoxin, in drinking water sampled in Haimen and Fusui, endemic areas of primary liver cancer in China, by highly sensitive immunoassay. Carcinogenesis 17:1317
316. Koskenniemi K et al (2007) Quantitative real-time PCR detection of toxic *Nodularia* cyanobacteria in the Baltic Sea. Appl Environ Microbiol 73(7):2173–2179
317. Rinta-Kanto JM et al (2005) Quantification of toxic *Microcystis* spp. during the 2003 and 2004 blooms in western Lake Erie using quantitative real-time PCR. Environ Sci Technol 39(11):4198–4205
318. Codd GA et al (2001) Analysis of cyanobacterial toxins by physiochemical and biochemical methods. J AOAC Int 84:1625–1635
319. Dorr FA et al (2010) Methods for detection of anatoxin-a(s) by liquid chromatography coupled to electrospray ionization-tandem mass spectrometry. Toxicon 55:92–99
320. Fischer WJ et al (2001) Congener-independent immunoassay for microcystins and nodularins. Environ Sci Technol 35:4849–4856
321. Metcalf JS, Bell SG, Codd GA (2001) Colorimetric immunoprotein phophatase inhibition assay for specific detection of microcystins and nodularins of cyanobacteria. Appl Environ Microbiol 67:904–909
322. Anderson WB, Slawson RM, Mayfield CI (2002) A review of drinking-water-associated endotoxin, including potential routes of human exposure. Can J Microbiol 48:567–587
323. Carmichael WW (1992) Occurrence of toxic cyanobacteria. US EPA. Agency, Cincinnati, OH, pp 15–26
324. Oberholster PJ, Botha A-M, Grobbelaar JU (2004) Microcystis aeruginosa: source of toxic microcystins in drinking water. African J Biotech 3:159–168
325. Carmichael WW (2008) A world overview one-hundred, twenty-seven years of research on toxic cyanobacteria – where do we go from here? In: Hudnell HK (ed)

Cyanobacterial harmful algal blooms: state of the science and research needs, vol 619, Advances in experimental medicine and biology. Springer, New York, 500 pp
326. Burns J, Williams C, Chapman A (2002) Cyanobacteria and their toxins in Florida surface waters. In: Proceedings of the health effects of exposure to cyanobacteria toxins: state of the science, Sarasota
327. Giddings M et al (2002) Cyanobacterial toxins: the development and evaluation of method to determine microcystin levels in Canadian water supplies. In: Proceedings of the health effects of exposure to cyanobacteria toxins: state of the science, Sarasota
328. Boyer GL (2008) Cyanobacterial toxins in New York and the lower great lakes ecosystems. In: Hudnell HK (ed) Cyanobacterial harmful algal blooms: state of the science and research needs. Springer, New York, p 500
329. Fristachi A et al (2007) A preliminary exposure assessment of microcystins from consumption of drinking water in the United States. Lake Reserv Manag 23(2):203–210
330. Osswald J et al (2007) Toxicology and detection methods of the alkaloid neurotoxin produced by cyanobacteria, anatoxin-a. Environ Int 33:1070–1089
331. Falconer IR (2005) Cyanobacterial toxins of drinking water supplies: cylindrospermopsins and microcystins. CRC Press, Florida
332. Walsby AE, Schanz F, Schmid M (2006) The Burgundy-blood phenomenon: a model of buoyancy change explains autumnal waterblooms by *Planktothrix rubescens* in Lake Zurich. New Phytol 169:109–122
333. Metting B, Pyne JW (1986) Biologically-active compounds from microalgae. Enzyme Microb Technol 8:386–394
334. Sellner KG (1997) Physiology, ecology, and toxic sproperties of marine cyanobacteria blooms. Limnol Oceanogr 42(5 Pt 2): 1089–1104

Books and Reviews

Anderson DM (2009) Approaches to monitoring, control and management of harmful algal blooms (HABs). Ocean Coast Manag 52(7):342–347

Babin M et al (2005) New approaches and technologies for observing harmful algal blooms. Oceanography 18(2):210–227

Bauer M et al (2010) The importance of human dimensions research in managing harmful algal blooms. Front Ecol Environ 8(2):75–83

Fleming LE et al (2011) Review of Florida red tide and human health effects. Harmful Algae 10(2):224–233

Graneli E, Turner JT (eds) (2006) Ecology of harmful algae. Springer, Berlin/Heidelberg

Hoagland P et al (2002) The economic effects of harmful algal blooms in the United States: estimates, assessment issues, and information needs. Estuaries Coast 25(4):819–837

Hudnell HK (ed) (2008) Advances in experimental medicine and biology, vol 619. Springer, New York

Hudnell HK (2010) Harmful algal blooms and natural toxins in fresh and marine waters – exposure, occurrence, detection, toxicity, control, management and policy. Toxicon 55(5):1024–1034

Hudnell HK et al (2010) Freshwater harmful algal bloom (FHAB) suppression with solar powered circulation (SPC). Harmful Algae 9:208–217

Landsberg JH (2002) The effects of harmful algal blooms on aquatic organisms. Rev Fish Sci 10(2):113–390

Lewis RJ, Poli M (2010) Toxins in seafood. Toxicon 56(2):107–258 (Special Issue)

Secher S (2009) Measures to control harmful algal blooms. The Plymouth Student Scientist 2(1):212–227

Shumway S, Rodrick G (eds) (2009) Shellfish safety and quality. Woodhead, Cambridge

Valiela I et al (1997) Macroalgal blooms in shallow estuaries: controls and ecophysiological and ecosystem consequences. Limnol Oceanogr 42(5 Pt 2):1105–1118

Hazardous Materials Characterization and Assessment

Julie M. Schoenung, Carl W. Lam
Department of Chemical Engineering and Materials Science, University of California, Davis, Davis, CA, USA

Article Outline

Glossary
Definition of Subject
Introduction
Hazardous Materials Characterization
Hazardous Materials Assessment Metrics
Future Directions
Bibliography

Glossary

Hazardous materials assessment Systematic review or aggregation methods to consider evidence for material toxicity and hazards to support waste management or pollution prevention priority setting for high-impact substances.

Hazardous materials characterization Identification of environmental, health, and physical hazard traits in materials.

Hazard traits Environmental, health, and physical adverse effects posed by materials to surroundings and living organisms.

Material life cycle The journey a material goes through during its entire life including stages of raw material production, product manufacturing, use, and end-of-life.

Materials selection A design process by which materials are compared and chosen for use according to their functional and environmental attributes.

Definition of the Subject

Some materials can be safely produced with minimal environmental and human health concerns during its use or disposal. Other materials are hazardous to manufacture or use and, when disposed, can contaminate and persist in the environment. These toxicity issues can depend on the chemical traits of the substances, such as polymers, metals and other compounds, in question. Characterization and assessment methods are needed to correctly identify substances of concern and to evaluate in a systematic way the degree of hazard they pose to ecological systems and human health. Building upon toxicological studies, hazardous materials management requires assessment tools that integrate toxicity data to support decision making for the proper handling, treatment, and/or elimination of toxic substances from industrial processes and manufactured products.

Historically, through regulatory or corporate efforts, environmental protection has addressed hazardous materials management primarily as an end-of-pipe treatment step to mitigate emissions and their impacts. Hazardous materials governance with this overarching precedence can potentially distribute the adverse environmental effects across all stages of the products' life cycle including raw material production, manufacturing, use, and end-of-life. As a progressive approach, emerging paradigms of "green engineering" and "green chemistry" seek to eliminate or substitute hazardous materials with inherently safer alternatives during the design of products and processes. Therefore, with the support of hazardous materials characterization and assessment tools, material options can be rigorously compared with consideration of hazard traits during materials selection in the design phase.

Introduction

The number of substances humans can use and synthesize from the natural world is nearly limitless. Ranging from pesticides, catalysts, building materials to electronics, these chemicals and materials help to create the many technological novelties that sustain infrastructure and activities in the modern world. Yet, over the last few decades, despite the clear benefits these new substances offer to improve products and processes in society, there is an increasing awareness of the hazards they pose to humans and natural ecosystems during their life cycles [1, 2]. Current converging trends in international environmental regulations attest to this growing global interest to control and mitigate the toxicity impacts caused by the use of hazardous materials in commercial industries [3].

To address these issues, hazardous materials characterization and assessment frameworks provide a critical first step to identify and compare the multitude of hazard traits that are associated with substances. The communication of material hazard information is essential to highlight and prioritize waste streams for pollution prevention during waste management or remediation and also necessary for achieving safe and sustainable products and processes by design [4]. Clearly, the unwanted dissipation of hazardous materials from use and production increases the chance of pollution and wastes accumulating in environmental media, which can be irreversible. Ecological systems and human populations are threatened in different regions where these materials are mismanaged, making the long-term consequences of unrestrained toxic substances use severe.

An important example of hazardous materials misuse is provided in the context of metallic lead (Pb) in commercial markets. Lead has been one of the most widely used substances worldwide, with applications as a pure metal, an alloy, or as an additive to organic substances, ceramics or glass materials [5]. The human health toxicity of lead has long been recognized and neurological effects can be witnessed even with very low levels in blood, with children being particularly susceptible [6, 7]. Historically, two applications turned lead toxicity into a widespread problem. The first was the use of lead as a brightness enhancer for paints in homes, and second was the use of organo-lead (tetraethyl lead) as a motor fuel antiknock agent [8]. Both have shown to contribute lead into soil and dust contamination and to play a significant role in human exposure [9]. In the U.S., it was not until the late 1970s

when the phase-out of lead additives eventually demonstrated a marked decline of lead blood levels in the population [10]. From a preventative standpoint, this is a clear situation of where appropriate procedures for hazardous materials characterization and assessment at the onset would have promulgated lead's toxicity issues and motivated for reduction in lead exposure and unintended toxicity impact to populations.

At present, there is not a unified consensus on best practices to benchmark and compare materials and chemicals to determine whether a material is "greener" or "safer" than another in terms of its hazards. Fundamentally, the main reason for this nonuniformity is because of the many ways by which substances can be characterized based on their hazard traits. Depending on the substance in question, different hazard criteria may be a focus for consideration.

The aim of this article is to illustrate the multifaceted definition of hazard in materials and how various toxicity data can be aggregated within hazardous materials assessments. The first portion of this article defines what properties make materials hazardous to begin with. Hazard issues from the life cycle perspective of materials are also described. This discussion is followed up with particular examples for plastics and metals. The second portion of this article seeks to provide an overview of currently available assessment metrics and methodologies utilized to compare materials considering the defined hazard traits. Such tools can support decision making during materials selection and priority setting for hazardous materials management.

Hazardous Materials Characterization

Hazard Traits in Materials

Hazardous materials characterization (or identification) is the determination of what type of endpoint adverse effects will be caused by an exposure or release of a substance. Before the discussion on hazardous materials assessment tools, it is necessary to first establish what these hazard traits of materials are.

One of the most prominent hazard trait classification systems is the Globally Harmonized System of Classification and Labeling of Chemicals (GHS) [11]. GHS represents an internationally motivated system with the aim of unifying hazard classification and labeling standards in different nations and regions in the world. Within GHS, classification of hazard criteria falls into three areas:

1. Physical hazards
2. Human health hazards
3. Environmental (or ecosystem) hazards

Figure 1 shows a compilation of the chemical hazard traits for these GHS hazard categories.

Physical hazards are classifications that define the danger posed by a material based on its physical state (gas, liquid, or solid). These hazards can imply many or overlapping endpoints of concern for a substance. These include considerations such as flammability, corrosion, and oxidizing properties of substances and other hazard attributes of a substance that can cause bodily harm or damage to surroundings. An explosive substance is capable of producing gas by chemical reaction at such a temperature, pressure, and speed to cause damage to surroundings. Flammable substances are readily combustible, or may cause or contribute to fire under certain atmospheric conditions. Oxidizing substances refer to materials that if provided oxygen can cause or contribute to the combustion of itself and other materials. Self-reactive substances are thermally unstable substances with the potential to undergo a strongly exothermic reaction even without air. A pyrophoric substance has potential to ignite through contact with air. Self-heating substances have the potential to self-heat by reaction with air and without an energy source. A substance that will materially damage metals is corrosive to metal. More detailed definitions for specific traits in the physical hazard categories can be found in reference [11].

Health hazards, of central importance for hazard classifications, are a series of adverse health effects posed to humans when they are exposed to a toxic substance. Key exposure pathways are inhalation, oral, or dermal routes. These can derive from epidemiological or animal studies. Acute toxicity implies the intrinsic property of a substance to cause adverse effect in humans after short-term exposure. Skin corrosion or irritation refers to substances that can respectively cause irreversible or reversible damage in skin. Likewise, substances reflecting serious eye damage or irritation can cause irreversible or reversible damage in the eye. Respiratory or skin sensitization refers to a substance that induces hypersensitivity of the airways

Physical Hazard

- Explosives
- Flammable gases
- Flammable aerosols
- Oxidizing gases
- Gases under pressure
- Flammable liquids
- Flammable solids
- Self-reactive substances
- Pyrophoric liquids
- Pyrophoric solids
- Self-heating substances
- Substances which, in contact with water, emit flammable gases
- Oxidizing liquids
- Oxidizing solids
- Organic peroxides
- Corrosive to metals

Health Hazard

- Acute toxicity
- Skin corrosion/irritation
- Serious eye damage/eye irritation
- Respiratory or skin sensitization
- Germ cell mutagenicity
- Carcinogenicity
- Reproductive toxicology
- Target organ systemic toxicity – single exposure
- Target organ systemic toxicity – repeated exposure
- Aspiration toxicity

Environmental hazard

- Hazardous to the aquatic environment
  - Acute aquatic toxicity
  - Chronic aquatic toxicity
    - Bioaccumulation potential
    - Rapid degradability

Hazardous Materials Characterization and Assessment. Figure 1
Physical, health, and environmental hazard classifications within GHS [11]

following inhalation or an allergic response following skin contact, respectively. Germ cell mutagenicity classifies substances liable to cause mutations in organisms. Reproductive toxicity implies a substance's potential to adversely affect sexual function and fertility in adults, as well as healthy development in children. Aspiration toxicity refers to substances that can cause acute adverse effects following inhalation. Repeated or single exposure target organ/systemic toxicity refer to substances that can trigger organ specific toxicity effects. Carcinogenicity implies a substance's capability to induce cancer or increase its incidence in humans.

Generally in GHS, each of these health classifications is assigned a "category" number to indicate its damage severity. For example in the acute toxicity category, substances are assigned category 1 (most severe) to 5 (low acute toxicity) classification on the basis of lethal dose or concentration 50% (LD50) (oral, dermal) or LC50 (inhalation) from animal studies. These indicators are defined as the dose or concentration that will be lethal for 50% of tested animals (which are typically rodents). Carcinogens are classified differently according to the categorization scheme provided in Table 1.

Hazardous Materials Characterization and Assessment. Table 1 GHS carcinogenicity categorization scheme [11]

GHS carcinogenicity category	Definition
1A	Known human carcinogen (based on human evidence)
1B	Presumed human carcinogen (based on demonstrated animal carcinogenicity)
2	Suspected carcinogen (limited evidence of human or animal carcinogenicity)

For the environmental hazards category, substances are classified by acute (short term) and chronic (long term) aquatic toxicity data. The basis for acute aquatic toxicity is the median dose of a substance that will likely cause irreversible damage to species (e.g., fish, crustacean, or other aquatic organisms). This is represented by the LC50 or effective concentration for 50% (EC50) in aquatic species. Chronic aquatic toxicity indicators (e.g., chronic EC50s) imply the potential of a substance to cause adverse effect with continuous exposures

throughout the lifecycle of the organism at a specified concentration. Note that for chronic toxicity of substances with lack of rapid degradability, other chemical parameters would be required for classification such as the logarithm of the substance's octanol–water partition coefficient (K_{ow}), to indicate how easily a chemical may be distributed in water bodies [12], and the Bioconcentration Factor (BCF), to characterize the tendency for a chemical to accumulate in organisms [13]. Categorization schemes are also available for environmental hazards in GHS according to Table 2.

Beyond GHS, there are also other international agencies and organizations that provide other hazard trait classifications, particularly in the area of human health hazards. For this, substances are usually described based on their maximum exposure limits and carcinogenic potential to humans. Notable organizations that develop human exposure limit classifications include: the U.S. Occupational Safety and Health Administration (OSHA) who provide Permissible Exposure Limits (PELs) to regulate chemical concentrations in the workplace [14]; the American Conference of Governmental Industrial Hygienists (ACGIH) who develop similar workplace Threshold Limit Values (TLVs) [15]; the U.S. National Institute for Occupational Safety and Health (NIOSH) who provides Recommended Exposure Limits (RELs) which are recommended air concentration limits to protect employees in their working lifetimes [16]; and the German Research Foundation who presents their own maximum occupational exposure limits (MAKs) [17]. Other organizations that identify carcinogenic potential in substances include the International Agency for Research on Cancer (IARC) [18], the European Union (EU) Council [19], and the U.S. National Toxicology Program (NTP) [20].

Historically, there have been limited international organizations that provide threshold concentrations or classifications for ecological toxicity in the natural environment. However, there are a few available that are focused on aquatic impacts. From America, the U.S. Environmental Protection Agency (USEPA) provides values for Total Maximum Daily Load (TMDL) as limits on the amount of a pollutant that a body of water in the natural environment can receive daily while still meeting national water quality standards [21], and the State of California lists maximum freshwater concentrations for inland surface waters and enclosed bays and estuaries [22]. From the EU, the German water pollution classification rating (WGK) represents a substance's potential to be hazardous in water bodies [23].

Life Cycle Contributions to Material Hazards

For some substances, the substance itself does not present inherent hazards. These substances may become of concern, however, when, at some point in the material's life cycle, secondary materials react with them or when their fate and persistence in surrounding environments become problematic. Another issue that cannot be disregarded in hazard characterization is that materials are often manufactured by adding or combining other constituents (e.g., metal alloys), meaning they can exhibit multiple hazard traits deriving from the diverse elemental or molecular groups present. Individually, these substances embody a separate range of physical, health, and environmental hazards. A truly complete

Hazardous Materials Characterization and Assessment. Table 2 Acute and chronic GHS environmental hazards categorization scheme [11]

Acute category I	Acute category II	Acute category III	
EC50 $\leq$ 1.00 mg/l	EC50 $>$ 1.00 but $\leq$ 10.0 mg/l	EC50 $>$ 10.0 but $<$ 100 mg/l	
Chronic category I	Chronic category II	Chronic category III	Chronic category IV
EC50 $\leq$ 1.00 mg/l and log K_{ow} [b] $\geq$ 4 unless BCF[c] $<$ 500	EC50 $>$ 1.00 but $\leq$ 10.0 mg/l and log K_{ow} $\geq$ 4 unless BCF $<$ 500 and unless chronic toxicity $>$ 1 mg/l	EC50 $>$ 10.0 but $\leq$ 100.0 mg/l and log K_{ow} $\geq$ 4 unless BCF $<$ 500 and unless chronic toxicity $>$ 1 mg/l	EC50 $>$ 100 mg/l and log K_{ow} $\geq$ 4 unless BCF $<$ 500 and unless chronic toxicity $>$ 1 mg/l

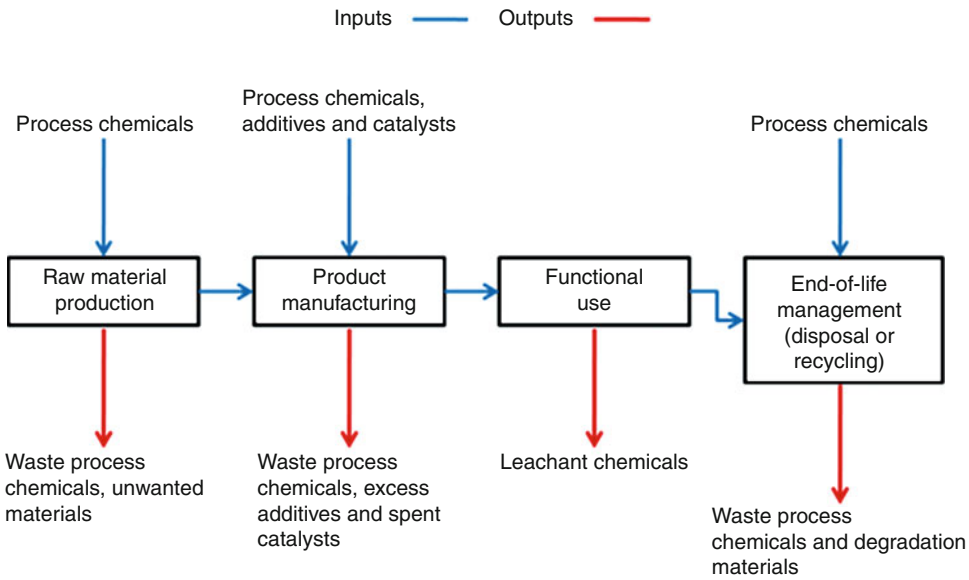

Hazardous Materials Characterization and Assessment. Figure 2
Material life cycle hazard profile from associated inputs and outputs

understanding of hazard traits implied by a material's use requires factoring in these hazard contributions throughout the material life cycle, starting from raw material production to product manufacturing, to use and, ultimately, in end-of-life management.

Figure 2 depicts the potential contributions to the life cycle hazard profile of a material. Different input substances are introduced in separate stages, leading to outputs of potentially hazardous substances. From this viewpoint, the choice of using a particular material requires understanding of the hazards attributed to input and output substances throughout a material's life. Inputs include processing chemicals that are added and utilized to develop a material product. This begins with raw material production and occurs throughout product manufacturing. Some of these additions may not be innocuous and can lead to serious health or environmental concerns if inappropriately managed. Material production of gold, for example, commonly requires the use of cyanide (an acutely toxic chemical) for ore extraction processes [24]. End-of-life materials management can also require using additional chemicals during hazardous waste treatment processes. A common strategy for wastewater treatment is the introduction of hydroxides and sulfides to remove heavy metal contaminants from concentrated solutions through precipitation [25]. Outputs are substances emitted in the material life cycle including waste process chemicals or spent chemicals (e.g., catalysts). Chemicals may leach from the material itself during use or product disposal. Outputs can also be represented as hazardous waste streams emitted during end-of-life disposal, recycling, or other waste management processes.

Ultimately, what this schematic highlights is that, in addition to consideration of the material itself, primary and intermediate chemicals used during manufacturing and, also importantly, chemicals generated at end-of-life, are dynamic contributors to embodied material hazards. Polymers can potentially degrade into their monomer form, which may be more toxic (e.g., polyvinyl chloride to vinyl chloride) [26]. In addition, toxic chemicals can be generated by reaction during waste management processing. For example, natural decomposition of organic materials in landfills can create air pollution such as methane, carbon dioxide, nitrogen, sulfur, and volatile organic compounds [27]. Also, a side effect of waste-to-energy incineration processes for materials is that this can lead to the generation of unwanted toxic substances in fly ash such as heavy metals and other combustion by-products [28]. Although recycling will help to return materials into

the industrial cycle, toxic substances may also be generated through industrial recovery processes.

In order to characterize the hazard attributes of a material, in parallel to what is actually in the material's composition, the related substances that appear throughout the material life cycle also factor into consideration. To provide some examples of these issues in real substances, a general overview of hazard traits is applied to characterize polymers, specifically plastics, and metals in the following section.

Case Study Examples: Hazard Characterization of Plastics and Metals

Plastics Plastics materials, a specific type of polymer utilized ubiquitously in global industries, are macromolecules comprised of covalently bonded repeating subunits (or monomers). Table 3 presents the hazard classifications in alignment with GHS categories [29] for various monomer types including acrylonitrile-butadiene-styrene (ABS), polycarbonate, polyethylene, polyethylene terephthalate, polypropylene, polystyrene, and polyvinyl chloride. This table shows a range of hazard endpoints that can be of concern to environmental and human health as well as physical hazard categories. Of the plastics considered, ABS, polystyrene, and polyvinyl chloride have monomers that are indicated to have carcinogenic potential in GHS categories. ABS, polycarbonate, polyethylene terephthalate, polystyrene, and polyvinyl chloride monomers are classified to be toxic to reproductive systems. In terms of environmental hazard, with the exception of polypropylene due to lack of GHS classification, all of the plastics are categorized to have acute toxicity for aquatic organisms. In addition, physical hazards, as expected for the hydrocarbon-based materials, suggest issues with flammability for some monomers.

The multiple hazard traits posed by monomers used in plastics shown in Table 3 comprise only a segment of the implied life cycle hazards. As suggested by the previous description on hazardous materials characterization, understanding the full impact that plastic materials present requires also understanding the additional input and output substances that occur throughout a material's life cycle.

During production, the majority of plastics are developed from the reaction of petroleum-derived chemicals such as ethylene, benzene, propylene, and butadiene [30]. Additional processing converts primary petrochemicals into intermediate chemicals such as ethylbenzene formed from ethylene and benzene. Then, the monomers are created from the intermediate chemicals such as styrene from ethylbenzene. The plastic (i.e., polystyrene) can then be produced by polymerization reaction of the monomer. In this process, catalysts are often introduced to increase the rate of polymerization.

Some instances of plastic manufacturing require the blending of two independent polymers together (such as polycarbonate and ABS) in order to synthesize a new material (i.e., a copolymer) with different material performance characteristics [31]. Also, chemical additives are often incorporated to modify some mechanical or physical property of the material. These additives may be in the form of flame retardants, ultraviolet and thermal stabilizers, and other processing or functional enhancers [32]. It is not unusual for one type of plastic to contain multiple additives. ABS, for example, can simultaneously utilize ethoxylated fatty alkylamines as an antistatic agent, sulfonyl semicarbazides or azodicarbonamides as foaming aids, calcium stearates as internal lubricants, and fatty amides as a mold release aid, all of which would be in addition to traditional halogenated compounds as flame retardants [32]. The incorporation of all of these substances within the plastic material directly increases the complexity when performing hazard characterization of such plastics [33].

The leaching of residual additives from materials into the environment is a major issue for humans and the ecological systems during use and disposal. Because of this, environmental legislation has emerged to limit toxins (i.e., brominated flame retardants and lead (Pb)) used in commercial materials, which affects the manufacturing of plastics [34]. Of note, however, is that some additives that exhibit toxicity traits have yet to be regulated. Reproductive and developmental toxins such as bisphenol A from polycarbonate bottles [35, 36] and phthalates from polyvinyl chloride plastics are some widely publicized examples [37, 38].

During the end-of-life processing of plastics, in addition to issues posed by monomers and additives that may leach out from these materials, other toxic substances can also be generated due to inappropriate

Hazardous Materials Characterization and Assessment. Table 3 Monomers of common plastic types and their hazard traits in alignment with GHS [29]

Plastic type (monomers marked in parentheses)	Hazard traits of monomers		
Acrylonitrile-butadiene-styrene (acrylonitrile, butadiene, styrene)	Acrylonitrile	Butadiene	Styrene
	Human hazard: Category 2 carcinogenicity Category 2 toxic to reproduction	Human hazard: Category 2 carcinogenicity Category 2 toxic to reproduction	Human hazard: Category 2 carcinogenicity Category 1 toxic to reproduction
	Environmental hazard: Category 3 acute aquatic toxicity	Environmental hazard: Category 3 acute aquatic toxicity	Environmental hazard: Category 1 acute aquatic toxicity
	Physical hazard: Category 2 flammable liquid	Physical hazard: Category 2 flammable liquid	Physical hazard: Category 3 flammable liquid
Polycarbonate (bisphenol A)	Bisphenol A		
	Human hazard: Category 2 toxic to reproduction		
	Environmental hazard: Category 1 acute aquatic toxicity		
	Physical hazard: Not applicable		
Polyethylene (ethylene)	Ethylene		
	Human hazard: Category 3 systemic toxicity (narcotic effects)		
	Environmental hazard: Category 3 acute aquatic toxicity		
	Physical hazard: Category 1 flammable gas		
Polyethylene terephthalate (ethylene terephthalate)	Ethylene	Terephthalate	
	Human hazard: Category 3 systemic toxicity (narcotic effects)	Human hazard: Category 4 acute oral toxicity Category 2 toxic to reproduction	
	Environmental hazard: Category 3 acute aquatic toxicity	Environmental hazard: Category 3 acute aquatic toxicity	
	Physical hazard: Category 1 flammable gas	Physical hazard: Not applicable	
Polypropylene (propylene)	Propylene		
	GHS classification not available		

Hazardous Materials Characterization and Assessment. Table 3 (Continued)

Plastic type (monomers marked in parentheses)	Hazard traits of monomers		
Polystyrene (styrene)	Styrene		
	Human hazard: Category 2 carcinogenicity Category 1 toxic to reproduction		
	Environmental hazard: Category 1 acute aquatic toxicity		
	Physical hazard: Category 3 flammable liquid		
Polyvinyl chloride (vinyl chloride)	Vinyl chloride		
	Human hazard: Category 1 carcinogenicity Category 2 toxic to reproduction		
	Environmental hazard: Category 1 acute aquatic toxicity		
	Physical hazard: Category 1 flammable gas		

hazardous materials management procedures. These substances may also have significant implications on the environmental damage potential of plastic goods. A well-documented case is the generation of dioxins and furans occurring during waste incineration of polyvinyl chloride electronic cables to recover copper [39]. These particular by-product chemicals have been established to be persistent, bioaccumulative, and carcinogenic to exposed populations [40].

From this overall perspective, it is clear that plastics represent a class of materials for which many variations in inputs and outputs during the material life cycle can affect the comprehensive hazard profile. A compilation of hazard traits for the wide range of substances of concern involved during an entire plastic material life cycle has never been generated, but is necessary to comprehensively gauge impacts posed by additives, process chemicals, and degradation behavior of plastics.

Metals A similar high-level discussion on hazard characterization can be presented for metals. From a toxicological standpoint, metals themselves represent an interesting scenario for hazard characterization because at the right concentrations, some metals are essential to living organisms and ecological systems [41]. However, chronic low-dose exposures of others can lead to severe health and environmental effects. Table 4 shows a compilation of metals with an indication of whether they are or are not essential to humans.

In addition, different metals valence states (chemical species) can change the hazard attributes of the metal. There are specific chemical processes that can transform metals from one valence state to another, oftentimes enabling the formation of inorganic and organic substances with different toxicity properties. For instance, chromium can exist in a trivalent state (III), which is essential for proper development in mammals, or a hexavalent state (VI), which is highly toxic to organisms [42, 43]. In general, hazardous metals require special attention because, unlike organic chemicals or polymer materials, they can neither be created nor destroyed by biological or chemical reactions. This may lead to a greater chance for accumulation in various environmental compartments and also in organisms [44].

The metals themselves represent a range of environmental, health, and physical hazard traits. In the human health hazard category, at least six metals (arsenic, cadmium, chromium (VI), beryllium, nickel, and lead)

are accepted or suspected to be human carcinogens in one form or another for particular routes of exposure, according to GHS characterization [29]. For certain metals (e.g., lead and mercury), other human hazard traits such as toxicity to reproduction and development have been demonstrated [29]. With regard to the environmental hazard characterization of metals listed in Table 4, copper, zinc, barium, beryllium, cadmium, and thallium have been classified to have toxicity potential with chronic exposures to aquatic organisms (GHS category 3 or 4) [29]. There is a lack of ecological toxicity data to characterize the ecological hazard traits of other metal species. For the physical hazard category, the majority of metals are not classified in GHS due to the nature of solid metals.

From a life cycle point of view, production of primary metals creates hazardous waste output issues, especially for localities where mining and extraction of metals from ores occur [45]. Chemical pollution (and therefore hazards attributed to outputs) can arise from various routes during mineral processing. A typical large-scale production can leave high metal concentrations such as copper, zinc, lead, cadmium, and arsenic in rivers, groundwater, and sediments [45]. Slag, a necessary by-product of ore-smelting processes, is comprised of metal oxides, elemental metals, and various sulfides that can contaminate soils. Many metal ores are naturally formed as sulfides (e.g., nickel, copper, and lead), which, if exposed to oxygen and water during mining operations, oxidize to create sulfuric acid [46]. In addition, chemicals are often added to ores during mineral processing and these can pollute ecological systems if not properly managed. Examples include the use of concentrated acids for the leaching of copper oxides and other metal oxides [46] or, as mentioned, cyanide for gold. As a whole, these production materials and process chemicals are contributors to the upstream impact of metals.

During manufacturing of metal materials, different metals can be combined to create alloys with modified performance properties. This can be analogous to the case of plastic blends and additives to enhance material functionality. Chromium, for example, is often introduced into various grades of aluminum alloys to improve corrosion resistance [47]. Like plastic additives, these "solute" metals may sometimes be supplemented only in minor quantities to the pure metal to achieve the desired property enhancement. As a whole, these additional metals contribute not only toward manufacturing hazards but also in end-of-life when disposal or recycling operations must manage these different metals simultaneously.

What is seen here is that even with consideration of just the materials themselves, such as plastic monomers and elemental metals, diverse hazard traits can arise under the environmental, human, and physical hazard categories. Factoring in additional considerations for plastics and metals, such as their additives, alloys, and compounds used for production and manufacturing from a life cycle perspective, makes the task of comprehensive hazard characterization of complex materials very challenging. Future efforts in the arena of "green engineering" and "green chemistry" need to include the development of hazardous materials assessment methods to identify and aggregate nonuniform hazards and toxicity information so that decision makers can

Hazardous Materials Characterization and Assessment. Human essential and nonessential metals and their valence states [44]

Essential elements	Nonessential metals	
Cobalt II, III	Aluminum III	Nickel II
Chromium III	Antimony III, V	Niobium V
Copper 0, I, II	Arsenic III, V	Palladium 0, II
Iron II, III	Barium II	Platinum 0, II, IV
Magnesium II	Beryllium II	Rubidium I
Manganese II, IV	Bismuth III, V	Silicon IV
Molybdenum IV, VI	Boron III	Silver 0, I, II
Selenium II, IV, VI	Cadmium II	Strontium II
Zinc II	Cesium I	Tellurium II, IV, VI
	Chromium VI	Thallium I, III
	Gallium III	Tin II, IV
	Germanium IV	Titanium IV
	Gold 0, I, III	Tungsten VI
	Indium III	Uranium IV, VI
	Lead II, IV	Vanadium III, V
	Lithium I	Zirconium IV
	Mercury 0, I, II	

benchmark materials and substances in a systematic way, while accounting for their entire life cycle.

Hazardous Materials Assessment Metrics

A consequence of technology evolution is the creation of increasingly complex waste streams and materials emitted from the industrial society into the natural environment. To this end, hazardous materials assessment metrics are necessary for the comparative evaluation of the hazard traits represented by the many new materials and substances being developed in assorted industry sectors such as energy products, semiconductors, automotive, chemicals, electronics, pharmaceuticals, plastics, and countless others [48]. This is a demanding task because decision making for the proper industrial management of materials can be clouded by the assorted and numerous hazard traits of substances that need to be considered, as discussed above.

The hazardous material assessment tools available today seek to address this issue by providing approaches that consider the available data on hazards so that substances of primary concern can be identified in a transparent and methodical way. Industrial waste stream priority setting is a clear application for these methods since they can help guide environmental decisions for pollution prevention [49–51]. Simultaneously, as a promising new paradigm in the chemical and materials engineering community, these tools can help support the safer design of processes and products by identifying high-impact materials before they are incorporated into a product [52]. Material choices in product design can greatly influence end-of-life waste management as well as implications for hazardous waste generated during manufacturing. Hazardous materials assessment metrics can enable a designer or engineer to evaluate inherent material hazards to humans and ecosystems in lieu of other material properties during product or process design.

Key approaches in this area have been developed to consider hazard information of materials with the objective of standardizing screening of high-impact substances and to streamline comparative evaluation. These tools provide hazard benchmarking for individual agents, but often require hazard and toxicity data collection (characterization) to be performed during the assessment. A summary of established tools, including a comparison of their structure and application, is provided in Table 5. Further details on each method are provided below. Note that because the foundation hazard and toxicity data may vary from one tool to another, clarification of relevant toxicological terminology is provided as needed.

Life Cycle Impact Assessment Tools

Life cycle impact assessment (LCIA) is used in life cycle analysis (LCA) to characterize the impacts of material flows (releases) of processes or products [53]. LCIA involves development of a multimedia and multipathway characterization model to capture the fate, exposure, and potency of a substance in order to determine its contribution to a given impact category (such as potential for ecological or human health toxicity). Commonly, results from these models are reported as "characterization factors" (CFs), which represent a material's impact in a specific category per unit of release (or emission). LCIA is generally conducted by multiplying the amount of release (or emission) by the CFs to quantify the magnitude of impact attributed to the substance. Therefore, impact category contributions from a wide variety of substances can be effectively summed and compared under a standard basis. Two prominent LCIA methods are summarized here.

Tool for the Reduction and Assessment of Chemical and Other Environmental Impacts (TRACI) Version 1.0 Although the Tool for the Reduction of Chemical and Other Environmental Impacts (TRACI) (version 1.0) is originally designed for use in LCIA [54], it has also recently seen wider application as a general pollution prevention and design for environment indicator toolset to quantify environmental impact potential of substances [49, 50, 55–59]. TRACI CFs for particular substances can be used to quantify the major environmental impact effects such as global warming, ozone depletion, acidification, eutrophication, smog formation, ecological toxicity (ecotoxicity), and human health–related effects. For this discussion, only human health and ecotoxicity effects are discussed due to an interest on quantifying toxicity hazards of substances.

TRACI human health CFs are represented by Human Toxicity Potentials (HTPs) [60]. HTPs are

Hazardous Materials Characterization and Assessment. Table 5 Comparison of different aspects of hazardous materials assessment tools

Method		TRACI	USETox™	RSEI	CHEMS-1	TPI	Green Screen
Application		Life cycle impact assessment	Life cycle impact assessment	Population hazard and risk screening	Hazard-based chemical prioritization	Comparative materials selection	Chemicals screening
Complexity for practitioners to apply		High	High	Low	Medium-high	Medium	Medium-high
Quantitative		Yes	Yes	Yes	Yes	Yes	No
		Toxicity data					
Hazard categories	Human health	Yes; human RfC/RfDs for non-carcinogens and cancer potency factors for carcinogens	Yes; ED50 for carcinogens, ED50 extrapolated from NOEL for non-carcinogens	Yes; human RfC/RfDs for non-carcinogens and cancer potency factors for carcinogens	Yes; rodent LD50/LC50, IARC and USEPA carcinogenicity classification	Yes; German MAKs, EU carcinogenic classification	Yes; various
	Environment	Yes; concentration-to-source ratio from CalTOX and impact-to-concentration ratio from PNEC	Yes; aquatic organisms EC50	No	Yes; fish LC50, fish NOEL, rodent LD50	Yes; German water hazard classification	Yes; aquatic organisms LC50/EC50/IC50; GHS categories for chronic and acute aquatic toxicity
	Physical or other safety issues	No	No	No	No	Yes; Risk phrases	Yes; GHS categories for flammability and explosives
	Fate and Exposure	Yes; CalTox for multimedia multi-pathway modeling based on U.S. parameters	Yes; Matrix algebra framework for multimedia multi-pathway modeling	Yes; AERMOD model of air releases	Yes; with indicators to account for	No	Yes; with indicators to account for
				First-order decay model for water releases	(a) Bioaccumulation: BCF		(a) Bioaccumulation: BCF, log k_{ow}
				RSEI makes inherent assumptions on probability of exposure pathways in human populations based on U.S. parameters	(b) Persistence: BOD half-life in water, chemical half-life in water		(b) Persistence: chemical half-life in sediments and water

Hazardous Materials Characterization and Assessment. Table 5 (Continued)

Method		TRACI	USETox™	RSEI	CHEMS-1	TPI	Green Screen
Method to convert to hazard value		Normalized with respect to chemicals such as benzene or toluene (not bounded)	Not normalized (not bounded)	Algorithms to convert chemical toxicity data to toxicity weights (not bounded)	Linear function (0–5 for environmental and health categories; 1–2.5 for fate/exposure categories)	Algorithm to convert to numeric scale (0–100)	Integer scales (1–4)
Method to aggregate hazard categories		Does not aggregate hazard categories	Does not aggregate hazard categories	Uses most sensitive pathway for adverse effect to represent toxicity weight	User choice of weighting factors to aggregate total hazard value	Equivalence between health, environmental, and physical	Benchmark scheme based on: very high, high, moderate, or low classification of hazards
Output of method		Characterization Factors	Characterization Factors	Toxicity weights (hazard-based) Risk scores (risk-based)	Hazard values	TPI scores	Benchmark tiers

RfD reference dose, *RfC* reference concentration, *ED50* effect dose 50%, *NOEL* no observable effect level, *LD50* lethal dose 50%, *LC50* lethal concentration 50%, *MAK* maximum allowed concentrations for workers, *PNEC* predicted no-effects concentration, *EC50* effective concentration 50%, *GHS* Globally Harmonized System, *IC50* inhibitory concentration 50%, *BCF* bioconcentration factor, *BOD* biological oxygen demand, *log* k_{ow} log octanol–water coefficient

cancer and non-cancer (all other adverse health effects) toxicity potentials associated with a chemical's release into select media (i.e., air or water) relative to that associated with the release of a reference chemical. Calculations for HTPs utilize the CalTOX model (Multimedia Total Exposure Model for Hazardous Waste Sites) to determine the pollutant's fate and transport characteristics as a function of the average acceptable daily dose or cancer potency factor for substances [61]. CFs for ecotoxicity potentials are determined by combining two components: (1) a concentration-to-source ratio (CSR) from the CalTOX model and (2) an impact-to-concentration ratio (ICR) from the predicted no-effects concentration (PNEC) (based on fraction of species adversely affected), to estimate potential terrestrial and aquatic toxicity impact relative to a reference chemical's media-specific release [54]. Reference chemicals used to indicate toxicological equivalency in TRACI include benzene for cancer potential, toluene for non-cancer potential, and 2,4-dichlorophenoxyacetic acid (2,4 D) for ecotoxicity potential.

A key distinction of TRACI is that it utilizes input parameters within CalTOX representing average conditions in the U.S., making its application as an international LCIA tool limited. A new methodological development of TRACI (version 2.0) has been recently updated to recommend adopting global characterization factors from another tool known as USETox™ as described below [62].

USETox™: The UNEP-SETAC Toxicity Model The USETox™ method is another LCIA method focused on toxicity hazard characterization. It is unique because its development derives from scientific consensus among international toxicity experts from the United Nations Environment Program (UNEP) and Society for Environmental Toxicology and Chemistry (SETAC) [63]. The objective of this tool is to harmonize the existing LCIA tools and resolve discrepancies between prominent impact analysis models. At its foundation, USETox™ utilizes a matrix algebra approach for multimedia and pathway modeling, reflecting fate, exposure, and effect potency of substances in order to calculate CFs (see Table 5). The tool provides global CFs for substances released to urban air, nonurban air, freshwater, seawater, natural soil, and agricultural soil, for use in LCIA studies.

USETox™ human health toxicity CFs are reported as a change in adverse effect probability due to change in lifetime intake of a pollutant from released quantities (cases/kg). These are also called Comparative Toxicity Units (CTU_h/kg), to highlight the comparative nature of the CFs. Ecological toxicity CFs reflect the change in the Potentially Affected Fraction (PAF) of species due to a change in concentration from released quantities ($PAF^* m^3$/kg or CTU_e/kg). As a further development, USETox™ marks some CFs as "interim" to describe uncertainty in values for substances [64]. The details of the parameters considered for human health and environmental categories are provided in Table 5.

Integrated Screening Tools

The following tools are "screening" approaches developed by separate entities and organizations to simplify the process of aggregating hazard information for chemical assessments. These are different than LCIA tools in that their objective is not to quantify actual impacts of releases but to provide a screening perspective of environmental impact.

Risk-Screening Environmental Indicators (RSEI) Although not a formal risk assessment, USEPA's Risk-Screening Environmental Indicators (RSEI) model utilizes a system in which the toxicity of a given chemical can be quantified by a dimensionless "risk score" to provide a screening-level perspective for comparing chemical emissions' health impacts on human populations [65, 66]. RSEI focuses on releases and is tailored toward evaluation of U.S. Toxics Release Inventory (TRI) data, a national compilation of annual emissions information from manufacturing industries. RSEI is similar to LCIA-type tools in that it incorporates the amount of chemical released, chemical toxicity, fate and transport through the environment, exposure route, and population effects during evaluation (Table 5). The model uses the most potent chronic health endpoint in considering human health impacts due to exposure. "Toxicity weights," calculated from acceptable daily dose values and cancer potency factors, are developed as a chemical-specific toxicity valuation system within RSEI to determine risk scores. As compared to other tools, an important drawback within RSEI is that ecological toxicity is not explicitly addressed.

Toxic Potential Indicator (TPI) by Fraunhofer IZM Based on European-based regulated toxicity and hazards information, the Fraunhofer IZM Toxic Potential Indicator (TPI) method was originally designed to support materials selection for products and processes [67–71].

The computational structure of the TPI method requires three main input variables to reflect environmental, health, and other physical safety considerations for materials:

- Risk phrases (R-phrases)
- Occupational exposure limits based on maximum workplace concentration (MAK) or European Union (EU) carcinogenic classification
- Water hazard classification (WGK)

Risk phrases are defined in the Annex III of European Union (EU) Commission Directive 67/548/EEC: Nature of Special Risks Attributed to Dangerous Substances and Preparations, specifying the multiple hazards and safety issues presented by a material ranging from flammability potential to ecosystem impact potential [72]. Human health hazards are captured with MAK values (maximum concentration of a material allowed in the workplace) and European Union carcinogenic classifications [17, 19]. The German water pollution classification value, WGK, represents impacts posed to the environmental hazard category [23]. Exposure and fate of substances are not captured in TPI.

Because the tool is based on EU regulations, the methodology has also seen limited application on an international basis. However, there has been some ongoing effort to update the TPI method to other nations with case examples of Taiwan and Japan [70, 73].

Chemical Hazard Evaluation for Management Strategies (CHEMS-1) A chemical ranking and scoring method entitled "Chemical Hazard Evaluation for Management Strategies" (CHEMS-1) has been developed as a screening tool to provide a relative comparison of chemical hazards to human health and the environment [74–76]. The purpose of CHEMS-1 is to place chemical release data into perspective by evaluating both the toxic effects of chemicals and the potential exposure to those chemicals. Initially, CHEMS-1 was developed to identify high-impact chemicals within TRI. In principle however, this method can also be extended to support materials decision making in any product and process development.

CHEMS-1 captures human health effects with the use of chronic and acute toxicity data based on animal studies such as LD50s and also carcinogenic classification published by IARC. Environmental hazard effects are derived from rat LD50s for terrestrial toxicity and fish LC50s for aquatic toxicity (Table 5). Exposure potential is captured by persistence and bioaccumulation indicators such as the Bioconcentration Factor (BCF) and hydrolysis half-life. These indicators for various hazard categories are used as input parameters in linear functions to quantify "hazard values" that represent the impacts in the human health, environmental, and exposure categories. The summation of these impacts provides a "total hazard value" for a substance. It is also possible to integrate user weighting preferences for the different impact contributions to calculate for total hazard values.

Green Screen for Safer Chemicals Green Screen for Safer Chemicals is a chemical evaluation tool created by the Clean Production Action [77, 78]. This tool deviates from the others in that it does not try to enumerate hazard scores from hazard traits. The Green Screen approach is very comprehensive in the sense that a wide range of hazard traits is considered including human health, ecological toxicity, and fate as well as physical properties of substances. All of these have been identified through expert judgment and reviews of existing hazard classification schemes, including the GHS, the US EPA's Design for Environment program [79], and other classifications from different regional origins [77]. The resulting criteria include many international qualitative and quantitative thresholds. Within the Green Screen approach, a rubric is provided to help classify the hazard trait information by assigning a level of concern (low, medium, high, very high) for different hazard categories. The tool then considers these levels of concern with additional decision logic to generate an overall substance score in terms of integer "benchmarks." Scores can range from Benchmark 1, meaning a chemical of high concern, to Benchmark 4, a "safer" and preferred substance. Of the aforementioned screening tools presented, only Green Screen captures the degradation of materials, requiring assessments also on those degradation substances.

Case Study Examples: Hazard Assessment for Nickel and Bisphenol A

To provide a sense of the how the outputs of these assessment approaches can differ, nickel and bisphenol A are chosen to exemplify output scores of these tools for a metal and plastic monomer, respectively.

In terms of the LCIA-based tools, Table 6 gives the CF values that derive from TRACI version 1.0 and USETox™ for cancer, non-cancer, and ecotoxicity effects categories due to air emissions. It is not expected that the CFs be comparable between methods and this is confirmed as orders of magnitude differences are observed for the reported values for these substances in the select effect categories shown. In addition to using dissimilar units to represent CFs, these variations can be attributed to differences in methodologies, such as models used to account for fate, exposure, and effect considerations.

Despite these incompatibilities, CFs between methods show a similar trend when comparing the two substances within their respective set. Generally, nickel is expected to rank with a higher impact for all effect categories because it has higher burden to human health and to ecological systems. TRACI and USETox™ human health and ecotoxicity CFs for the substances confirms this. Note that because bisphenol A is a non-carcinogen, its cancer effects CFs are essentially zero for both TRACI and USETox™ methods. CFs for other media releases (such as water and soil) can also be used to quantify impacts attributed to these substances.

In parallel, indicators for nickel and bisphenol A are also provided based on results from the integrated screening assessment tools: RSEI, CHEMS-1, TPI, and Green Screen (Table 7). It is useful to keep in mind that, as described in previous summaries, there are inherent differences by which these screening tools account for hazard traits of substances. These fundamental variabilities are mainly derived from using dissimilar toxicity information, or other safety factors to represent a material's impact during hazard assessment. In addition, each screening tool has its own implicit weighting mechanism to aggregate hazard trait information.

RSEI toxicity weights for these substances, which do not account for fate or exposure considerations and only consider human health effects, show orders of magnitude variation. This is explained by the fact that RSEI uses the most sensitive health endpoint to represent hazard. Nickel is anticipated to be carcinogenic in humans, making its toxicity weight significantly greater in RSEI when compared to bisphenol A. Further use of these toxicity weights in RSEI enables determination of risk scores if population exposure is modeled [65].

CHEMS-1 hazard value results are aggregated into total hazard values and are normalized from 0 to 100

Hazardous Materials Characterization and Assessment. Table 6 TRACI and USETox™ characterization factors for nickel and bisphenol A [54, 63]

	Air – cancer effects		Air – non-cancer effects		Air – ecotoxicity effects	
Chemical	TRACI (kg benzene-equivalents)	USETox™ (CTU_h/kg)	TRACI (kg toulene-equivalents)	USETox™ (CTU_h/kg)	TRACI (kg 2,4 D - equivalents)	USETox™ (CTU_e/kg)
Nickel	3.61	5.18×10^{-5}	8.26×10^{3}	2.91×10^{-6}	1.30×10^{2}	6.08×10^{3}
Bisphenol A	0	0	4.21	2.53×10^{-7}	0	9.37×10^{1}

Hazardous Materials Characterization and Assessment. Table 7 Integrated screening assessment tool hazard indicators for nickel and bisphenol A [65, 74, 77]

Chemical	RSEI (toxicity weights)	CHEMS-1 (normalized total hazard value)	TPI (TPI score)	Green screen
Nickel	930,000	59.0	38.0*	Benchmark 1*
Bisphenol A	20	6.5*	8.7*	Benchmark 1

*Author-determined scores are marked with an asterisk

with respect to the highest attainable value for each hazard category considered [74]. This can most directly compare against the TPI method, which by default presents substance scores with the same range from 0 to 100 [67]. Similar to other indicators, both CHEMS-1 and TPI show again nickel having a higher aggregated human health and environmental impact.

The Green Screen ratings for these substances present an interesting scenario where these two substances are assigned an equivalent Benchmark 1 (highest burden) score. These Green Screen results are caused by separate mechanisms. In the case of nickel, Benchmark 1 is the outcome of the decision logic because it is an anticipated carcinogen. For bisphenol A, it is because the substance is classified as an endocrine disruptor [80]. In Green Screen, these hazard traits effectively shift a substance into the highest level of concern for the human health category according to the method's rubric. Determination of substance scores using the other screening methods (i.e., RSEI, CHEMS-1, and TPI) does not account for endocrine disruption.

Caveats on the Tools

As highlighted in Table 5, different tools have been developed to consider select hazard traits of substances so that substances can be compared on the basis of a defined standard. However, there are key differences when looking at these tools in terms of their application. LCIA tools are designed for application within LCA studies, as they attempt to capture actual effects based on a media release through multimedia and pathway modeling of different chemicals. With the exception of RSEI, the screening tools do not attempt to model fate and exposure behavior. Because LCA-type studies entail the analysis of life cycle substance flows for products, such assessments are generally more complex to conduct. Screening tools are designed to compare individual materials. Depending on the number of hazard traits considered in various environmental, health, and physical hazard categories, they are generally easier to apply. Green Screen is an exception to this since assessments require significant consideration of many toxicity data sources due to its comprehensiveness.

Also, these tools inherently aggregate hazard scores differently. For example, of the methods described, only CHEMS-1 provides a user preference to weigh hazard categories. The LCIA tools essentially provide CFs without a mechanism to weigh contributions from health or ecological toxicity. RSEI simply uses the most potent endpoint for substances in the health category to calculate toxicity weights. Green Screen has its own internal logic system based on decision rules to value hazard traits. The TPI method by default weighs environmental, health, and physical hazards equivalently within its computational structure.

In the end, it is important for designers to recognize these differences and intricacies when applying these tools to identify materials of concern.

Future Directions

There is a clear need to conduct hazardous materials characterization and assessment as a prerequisite in material selection and waste stream prioritization for commercial and industrial applications. For this, there has been significant previous work to assess what makes materials hazardous or "less green" through characterization of the many environmental and health hazard traits they present.

However, even with substantial progress on hazardous materials characterization and assessment frameworks, significant problems with current approaches still remain to be resolved. Of these issues, the first is that, internationally, toxicity data and classification systems on hazard traits are not uniform, leading to diverse methodologies to interpret them. Future efforts should move toward a unified toxicity data system (such as GHS), which can ultimately enable standardization of screening-level and impact-pathway assessments of materials because they will be based upon the same toxicological foundation. This will also help reduce the complexity of gathering data from dissimilar toxicity data sources to be used in hazard assessments. A second issue is that material life cycle hazards are usually not reflected in current hazardous material assessment frameworks. Material selection processes that do not consider implications of downstream and upstream chemicals involved in the production and end-of-life management of the material may not meet the objective of true hazard reduction, which is, in reality, a life cycle consideration. The last, perhaps obvious, problem is that in order to motivate the selection of benign materials for use in industry, these

assessment tools must be put into use by practitioners. Responsible materials use relies on companies to eventually adopt these methods as a fundamental component in the design process. To this extent, hazard assessment tools must be tailored in a way that best fits the needs of the engineer and designer.

As a final note, benchmarking of material hazard traits that can adversely affect environmental and human health is essentially only one factor to consider (albeit a complex one due to the various hazard endpoints in question) when attempting to achieve the overall objective of sustainable materials use. Environmental trade-off considerations outside of the scope of hazardous materials characterization and assessment such as materials embodied energy use, recyclability, and resource depletion potential should be investigated in conjunction to promote sustainable material choices in global industries. At some point in the future, research effort, specifically in the arena of industrial ecology, needs to assimilate material hazard assessment methods into the larger framework of design for environment strategies. This ideology can ultimately help society move toward a more holistic approach to manage hazardous materials [81].

Bibliography

Primary Literature

1. Wilson MP, Schwarzman MR (2009) Toward a new U.S. chemicals policy: rebuilding the foundation to advance new science, green chemistry, and environmental health. Environ Health Perspect 117:1202–1209
2. Christensen FM, Olsen IS (2004) The potential role of life cycle assessment in regulation of chemicals in the European Union. Int J Life Cycle Assess 9:327–332
3. Holzinger K, Knill C, Sommerer T (2008) Environmental policy convergence: the impact of international harmonization, transnational communication, and regulatory competition. Int Organ 62:553–587
4. Graedel TE, Allenby BR (1996) Design for environment. Prentice Hall, New Jersey
5. Schoenung JM (2008) Lead compounds. In: Shackelford J, Doremus R (eds) Ceramic and glass materials. Springer, USA, pp 151–167
6. Centers for Disease Control and Prevention (2007) Toxicological profile for lead. U.S. Department of Health and Human Services, Atlanta, GA
7. Nigg JT, Knottnerus GM, Martel MM, Nikolas M, Cavanagh K, Karmaus W, Rappley MD (2008) Low blood lead levels associated with clinically diagnosed attention-deficit/hyperactivity disorder and mediated by weak cognitive control. Biol Psychiatry 63:325–331
8. Filippelli GM, Laidlaw MA (2010) The elephant in the playground: confronting lead-contaminated soils as an important source of lead burdens to urban populations. Perspect Biol Med 53:31–45
9. Mielke HW, Reagan PL (1998) Soil is an important pathway of human lead exposure. Environ Health Perspect 106:217–229
10. Annest JL, Pirkle JL, Makuc D, Neese JW, Bayse DD, Kovar MC (1983) Chronological trend in blood lead levels between 1976 and 1980. N Engl J Med 308:1373–1377
11. United Nations (2009) Globally harmonized system of classification and labelling of chemicals (GHS), 3rd edn. United Nations Economic Commission for Europe, Geneva
12. Chiou CT, Freed VH, Schmedding DW, Kohnert RL (1977) Partition coefficient and bioaccumulation of selected organic chemicals. Environ Sci Technol 11:475–478
13. Veith GD, DeFoe DL, Bergstedt BV (1979) Measuring and estimating the bioconcentration factor of chemicals in fish. J Fish Res Board Canada 36:1040–1048
14. OSHA (1996) Hazard communication standard 1910.1200. U.S. Department of Labor, Washington, DC
15. ACGIH (2009) Guide to occupational exposure values. ACGIH, Ohio
16. NIOSH (2010) Carcinogen list. U.S. Department of Health and Human Services, Atlanta, GA
17. German Research Foundation (2010) Senate commission for the investigation of health hazards of chemical compounds in the work area. German Research Foundation, Bonn
18. World Health Organization (2010) Agents classified by the IARC monographs, vols 1–100. International Agency for Research on Cancer, Lyon
19. European Council (1967) Commision directive 67/548/EEC: approximation of laws, regulations and administrative provisions relating to the classification, packaging and labeling of dangerous substances. Brussels, Belgium, European Union
20. NTP (2005) 11th report on carcinogens. U.S. Department of Health and Human Services, Atlanta, GA
21. USEPA (1991) Guidance for water quality-based decisions: the TMDL process, 440/4-91-001. U.S. Environmental Protection Agency, Washington, DC
22. Electronic Code of Federal Regulations (2011) Title 40 protection of environment: part 131.38 establishment of numeric criteria for priority toxic pollutants for the State of California. U.S. Government Printing Office, Washington, DC
23. German Institute for Occupational Safety and Health (2010) Database on hazardous substances. German Institute for Occupational Safety and Health, Sankt Augustin
24. Lodgson MJ, Hagelston K, Mudder TI (1999) The management of cyanide in gold extraction. International Council on Metals and the Environment, Ontario
25. Veeken AH, Rulkens WH (2003) Innovative developments in the selective removal and reuse of heavy metals from wastewaters. Water Sci Technol 47:9–18

26. World Health Organization (1997) IARC monographs on the evaluation of carcinogenic risks to humans: 1,3-butadiene, ethylene oxide and vinyl halides (vinyl fluoride, vinyl chloride and vinyl bromide). 97. International Agency for Research on Cancer, Lyon
27. Allen MR, Braithwaite A, Hills CC (1997) Trace organic compounds in landfill gas at seven U.K. waste disposal sites. Environ Sci Technol 31:1054–1061
28. Rushton L (2003) Health hazards and waste management. Br Med Bull 68:183–197
29. Japanese National Institute of Technology and Evaluation (2010) Information about the status of the implementation of GHS in Japan, chemical management field. Japanese National Institute of Technology and Evaluation, Shibuya-ku, Tokyo
30. Brydson J (2000) Plastics materials, 7th edn. Butterworth-Heinemann, MA
31. Harper CA (2000) Modern plastics handbook. McGraw-Hill, New York
32. Zweifel H, Maier RD, Schiller M (2009) Plastics additive handbook, 6th edn. Hanser Publications, New York
33. Clean Production Action (2010) Plastics Scorecard. Clean Production Action, Seattle, WA
34. Cusack P, Perrett T (2006) The EU RoHS directive and its implications for the plastics industry. Plast Addit Compd 8:46–49
35. Krishnan AV, Stathis P, Permuth SF, Tokes L, Feldman D (1993) Bisphenol-A: an estrogenic substance is released from polycarbonate flasks during autoclaving. Endocrinology 132:2279–2286
36. Yamamoto T, Yasuhara A (1999) Quantities of bisphenol A leached from plastic waste samples. Chemosphere 38: 2569–2576
37. Pearson SD, Trissel LA (1993) Leaching of diethylhexyl phthalate from polyvinyl chloride containers by selected drugs and formulation components. Am J Health Syst Pharm 50:1405–1409
38. Jaakkola JJ, Knight TL (2008) The role of exposure to phthalates from polyvinyl chloride products in the development of asthma and allergies: a systematic review and meta-analysis. Environ Health Perspect 116:845–853
39. Menad N, Björkman B, Allain EG (1998) Combustion of plastics contained in electric and electronic scrap. Resour Conserv Recy 24:65–85
40. USEPA (2011) Dioxins and Furans, Persistent Bioaccumulative and Toxic (PBT) Chemical Program. U.S. Environmental Protection Agency, Washington, DC
41. Goyer RA (1997) Toxic and essential metal interactions. Annu Rev Nutr 17:37–50
42. Barnhart J (1997) Chromium chemistry and implications for environmental fate and toxicity. J Soil Contam 6: 561–568
43. World Health Organization (1997) IARC monographs on the evaluation of carcinogenic risks to humans: chromium, nickel and welding 49. International Agency for Research on Cancer, Lyon, France
44. USEPA (2007) Framework for metals risk assessment, 120/R-07/001. U.S. Environmental Protection Agency, Washington, DC
45. Bridge G (2004) Contested terrain: mining and the environment. Annu Rev Environ Resour 29:205–259
46. Moore JN, Luoma SN (1990) Hazardous wastes from large-scale metal extraction: a case study. Environ Sci Technol 24:1278–1285
47. Kendig M, Jeanjaquet S, Addison R, Waldrop J (2008) Role of hexavalent chromium in the inhibition of corrosion of aluminum alloys. Surf Coat Technol 140:58–66
48. Thomas VM, Graedel TE (2003) Research issues in sustainable consumption: toward an analytical framework for materials and the environment. Environ Sci Technol 37:5383–5388
49. Lim SR, Lam CW, Schoenung JM (2010) Quantity-based and toxicity-based evaluation of the U.S. toxics release inventory. J Hazard Mater 178:49–56
50. Lam CW, Lim SR, Schoenung JM (2011) Environmental and risk screening for prioritizing pollution prevention opportunities in the U.S. printed wiring board manufacturing industry. J Hazard Mater 189:315–322
51. Kurk F, Eagan P (2008) The value of adding design-for-the-environment to pollution prevention assistance options. J Clean Prod 16:722–726
52. Kuczenski B, Geyer R (2010) Chemical alternatives analysis: methods, models and tools. California State Department of Toxic Substances Control, Sacramento, California
53. Saur K (1997) Life cycle impact assessment. Int J Life Cycle Assess 2:66–70
54. Bare JC, Norris GA, Pennington DW, McKone TE (2002) The tool for the reduction and assessment of chemical and other environmental impacts. J Ind Ecol 6:49–78
55. Zhou X, Schoenung J (2009) Combining U.S.-based prioritization tools to improve screening level accountability for environmental impact: the case of the chemical manufacturing industry. J Hazard Mater 172:423–431
56. Lim SR, Kang D, Ogunseitan OA, Schoenung JM (2011) Potential environmental impacts of light-emitting diodes (LEDs): metallic resources, toxicity, and hazardous waste classification. Environ Sci Technol 45:320–327
57. Lim SR, Schoenung JM (2010) Toxicity potentials from waste cellular phones, and a waste management policy integrating consumer, corporate, and government responsibilities. Waste Manag 30:1653–1660
58. Lim SR, Schoenung JM (2010) Human health and ecological toxicity potentials due to heavy metal content in waste electronic devices with flat panel displays. J Hazard Mater 177:251–259
59. Thorneloe SA, Weitz K, Jambeck J (2007) Application of US decision support tools for materials and waste management. Waste Manag 27:1006–1020

60. Hertwich EG, Mateles SF, Pease WS, McKone TE (2001) Human toxicity potentials for life-cycle assessment and toxics release inventory risk screening. Environ Toxicol Chem 20:928–939
61. Lawrence Livermore National Lab (1993) CalTOX, a multimedia total exposure model for hazardous-waste sites. UCRL-CR-111456 (I), Livermore, California
62. Bare JC (2011) TRACI 2.0: the tool for the reduction and assessment of chemical and other environmental impacts 2.0. Clean Technologies and Environmental Policy (in press) doi:10.1007/s10098-010-0338-9
63. Rosenbaum RK, Bachmann TM, Gold LS, Huijbregts MA, Jolliet O, Juraske R, Koehler A, Larsen HF, MacLeod M, Margni M, McKone TE, Payet J, Schuhmacher M, van de Meent D, Hauschild MZ (2008) USEtox – the UNEP-SETAC toxicity model: recommended characterisation factors for human toxicity and freshwater ecotoxicity in life cycle impact assessment. Int J Life Cycle Assess 13:532–546
64. Huijbregts MA, Hauschild MZ, Jolliet O, Margni M, McKone TE, van de Meent D (2010) USEtox^{TM} user manual. USEtox^{TM} team
65. USEPA (2010) Risk-screening Environmental Indicators (RSEI) methodology: RSEI version 2.3.0. Washington, DC
66. Toffel MW, Marshall JD (2004) Improving environmental performance assessment: a comparative analysis of weighting methods used to evaluate chemical release inventories. J Ind Ecol 8:143–172
67. Nissen NF, Griese I, Middendorf A, Müller J, Pötter H, Reichl H (1998) An environmental comparison of packaging and interconnection technologies. Proceedings of the 1998 IEEE international symposium electronics and the environment. Institute of Electrical and Electronics Engineers, New York City, NY
68. Middendorf A, Nissen NF, Griese H, Muller J, Potter H, Reichl H, Stobbe I (2000) EE-toolbox-a modular assessment system for the environmental optimization of electronics. Proceedings of the 2000 IEEE international symposium electronics and the environment. Institute of Electrical and Electronics Engineers, New York City, NY
69. Griese H, Müller J, Reichl H, Zuber KH (2006) Sustainable development of microelectronics industry the role of metals in future interconnection technologies. Sust Metals Manag 19:577–592
70. Yen SB, Chen JL (2009) Calculation of a toxic potential indicator via Chinese-language material safety data sheets. J Ind Ecol 13:455–466
71. Schneider F, Salhofer S, Schiffleitner A, Stachura M (2008) The development of an ecodesign product – the ecomouse case study. Prog Ind Ecol 5:102–123
72. European Council (2001) Commission directive 2001/59/EC annex III: nature of special risks attributed to dangerous substances and preparations. Brussels, Belgium, European Union
73. Fujino M, Suga T, Hamano H (2005) Customization of the toxic potential indicator for Japanese regulation. Fourth international symposium on environmentally conscious design and inverse manufacturing. Tokyo, Japan
74. Swanson MB, Davis GA, Kincaid STW, Bartmess JE, Jones SL, George EL (1997) A screening method for ranking and scoring chemicals by potential human health and environmental impacts. Environ Toxicol Chem 16:372–383
75. Greitens TJ, Day E (2007) An alternative way to evaluate the environmental effects of integrated pest management: pesticide risk indicators. Renew Agr Food Syst 22:213–222
76. Dunn A (2009) A relative risk ranking of selected substances on Canada's National Pollutant Release Inventory. Hum Ecol Risk Assess 15:579–603
77. Clean Production Action (2009) The Green Screen for Safer Chemicals version 1.0. Clean Production Action, Seattle, WA
78. Betts KS (2007) Formulating green flame retardants. Environ Sci Technol 41:7201–7202
79. USEPA (2002) Design for the environment program fact sheet, 744-F-00-019
80. Maffini MV, Rubin BS, Sonnenschein C, Soto AM (2006) Endocrine disruptors and reproductive health: the case of bisphenol-A. Mol Cell Endocrinol 254–255:179–186
81. Geiser K (2001) Materials matter. MIT Press, Cambridge, MA

Books and Reviews

Andrady AL (2003) Plastics and the environment. Wiley, New Jersey

Bare JC (2010) Life cycle impact assessment research developments and needs. Clean Technol Environ Policy 12: 341–351

Commoner B (1997) The relation between industrial and ecological systems. J Clean Prod 5:125–129

Graedel TE, Allenby BR (2010) Industrial ecology and sustainable engineering. Prentice Hall, New Jersey

Kuczenski B, Geyer R, Boughton B (2011) Tracking toxicants: toward a life cycle aware risk assessment. Environ Sci Technol 45:45–50

Landner L, Reuther R (2004) Metals in society and in the environment. Kluwer, Dordrecht

Lavoie ET, Heine LG, Holder H, Rossi MS, Lee RE, Connor EA, Vrabel MA, DiFiore DM, Davis CL (2010) Chemical alternatives assessment: enabling substitution to safer chemicals. Environ Sci Technol 44:9244–9249

McDonough W, Braungart M (2002) Cradle to cradle: remaking the way we make things. North Point Press, New York

Pittinger CA, Brennan TH, Badger DA, Hakkinen PJ, Fehrenbacher MC (2003) Aligning chemical assessment tools across the hazard-risk continuum. Risk Anal 23:529–535

Ramani K, Ramanujan D, Bernstein WZ, Zhao F, Sutherland J, Handwerker C, Choi JK, Kim H, Thurston D (2010) Integrated sustainable life cycle design: a review. J Mech Des 132:1–15

Shafer DA (2006) Hazardous materials characterization: evaluation methods, procedures, and considerations. Wiley, New Jersey

Hazardous Waste Incineration Ashes and Their Utilization

L. Reijnders
Institute for Biodiversity and Ecosystem Dynamics, University of Amsterdam, Amsterdam, The Netherlands

Article Outline

Glossary
Definition of the Subject
Introduction
Hazard and Ashes
Utilization of Hazardous Waste Incineration Ashes
Future Directions
Bibliography

Glossary

Ash Solid incineration residue.
Hazard Potential to do harm.
MSWI Municipal solid waste incinerator.
Risk Chance that harm occurs.
WTE incinerator Waste-to-energy incinerator, incinerator also producing useful energy (e.g., electricity).

Definition of the Subject

This chapter deals with hazardous solid residues, usually called ashes, from waste incineration. What is to be considered hazardous in this context shows geographical and temporal variability. Currently, hazardous waste incineration ashes are mostly dumped, or disposed of, in landfills or ash lagoons. There is however also substantial, but geographically variable, utilization of such ashes, mostly in construction, including civil engineering (e.g., in roads and embankments) and there have been proposals for wider utilization. Much research has been done on better and wider utilization of hazardous waste incineration ashes, but little thereof has found its way to actual commercial practice. At the end of the chapter, the matter will be raised whether current waste incineration can be considered sustainable and which changes may lead to a more sustainable management of wastes that are currently incinerated.

Introduction

Wastes are incinerated on a large scale, which in turn generates solid wastes that are often called ashes. There is a wide variety of wastes that are incinerated, partly solid (such as municipal and hospital solid wastes), partly sludges (such as wastewater treatment, paper, and refinery sludges), and partly liquids [1–13]. Most of the wastes that are incinerated are not considered hazardous on the basis of current regulations. Quantitatively most important among incinerated wastes are municipal wastes originating from households, street cleaning, and commercial and industrial sources [1]. Such wastes can be burned in an uncontrolled way or in municipal waste incinerators (MSWIs). When the latter also supply useful energy (e.g., electricity), they may be called waste-to-energy (WTE) installations. In the European Union, the USA and Japan, municipal waste incinerators generated about 25 Mt ($=10^9$ kg)/year of combustion ashes by the year 2000 [2]. In Taiwan, the yearly amount of municipal waste incineration ashes was in 2009 $\sim$1.7 Mt [11], and in China, probably in the order of 2–3 Mt, with fly ashes accounting for 0.5–0.8 Mt [12]. There is also substantial dedicated incineration of nonhazardous industrial solid wastes. Depending on the type of industry, such incineration may lead to ashes with contents of hazardous substances that are different from ashes originating in municipal wastes [10].

Another major type of waste that is not usually categorized as hazardous waste and partly incinerated, is wastewater treatment and sewage sludge [3]. For instance, in Japan, about 90% of wastewater treatment and sewage sludges are incinerated [4], whereas by 2007 in the USA about 22% of these sludges were incinerated and in the European Union about 15%. In the European Union, incineration of wastewater treatment and sewage sludge generated about 2 Mt/year of wastewater treatment and sewage sludge incineration ashes in 2007 [2]. In Japan, the amount of such sludge incineration ash was $\sim$0.5 Mt in 2009 and in Taiwan $>$0.5 Mt in 2010 [11, 13].

In waste incinerators, there are varying degrees of co-firing with fossil fuels to increase incineration temperature. When there is substantial co-firing of coal, which is the case in municipal waste incinerators in large parts of China and in some sewage sludge

incinerators in Europe [14, 15], the composition and characteristics of incineration ashes will be significantly impacted by coal use.

The incineration of "nonhazardous" municipal wastes, wastewater treatment and sewage, and wastewater treatment sludges may generate ashes, which can be considered hazardous according to current regulations [1–3, 5–7, 13]. What is considered hazardous according to these regulations may vary over time and may differ from country to country [1, 7, 16]. The European Union, for instance, currently considers all types of ashes originating in the incineration of "nonhazardous" municipal wastes as "hazardous," contrasting previous practice in several EU countries, whereas in other countries bottom ash from such incinerators may be considered as "nonhazardous" [7].

There is also incineration of wastes that, on the basis of current regulations, are by themselves considered to be hazardous. There is a wide variety of such wastes, ranging from soils heavily contaminated by organic chemicals, several types of discarded preserved wood, and car shredder residues to hospital and radioactive wastes. There are incinerators specializing in burning hazardous wastes, but there is also co-combustion of hazardous waste in power plants and MSWIs. The ashes originating in the incineration of hazardous wastes by specialized incinerators are usually considered hazardous [17, 18], though there also are exceptions. For instance, incineration ashes originating in bone meal and meat from animals suspected to be infected by transmissible bovine spongiform encephalopathy (BSE) are considered to be nonhazardous by the French government [8]. In section Hazard and Ashes of this chapter, the hazard of ashes is considered more closely.

In this chapter, mainly ashes from incinerators that burn wastes in controlled ways will be discussed. Such incinerators may generate a variety of solid wastes. These include grate ash, grate siftings, bottom ash, heat recovery system ash, fly ash, and air pollution control residue. Table 1 gives the definitions of these incineration wastes to the extent that they originate in waste incinerators using grates, energy recovery, and air pollution control systems.

The collection of the various categories of solid incineration wastes mentioned in Table 1 may be different. However, rather often grate ash, grate siftings, and heat recovery system ash are combined and categorized as bottom ash. Fly ash and air pollution control residue may also be combined and categorized together as "air pollution control residues" or "fly ash," comprising all particulates collected from the flue gas of the incinerator before its emission from a smokestack.

The relative amounts of the different categories of solid incinerator wastes outlined in Table 1 can be different. This is illustrated in Table 2 for municipal waste incinerators in the European Union, Japan, and the USA. Table 2 gives ranges for solid incineration wastes per 1,000 kg of incinerated waste.

Publicly available data about the composition and leachability of waste incineration ashes are patchy. Nevertheless, it can be safely stated that the composition of bottom ash, fly ash, and air pollution control residues, as defined in Table 1, may differ much, dependent on the incinerator, including the choice of combustion technology (e.g., rotary kiln, fluidized bed), actual incineration conditions (such as temperature, throughput, waste heterogeneity, and the addition of coal, natural gas, or mineral oil), and the nature of the wastes that are incinerated [6, 19–23]. Large between-incinerator differences occur in the presence of substances relevant to hazard. As (arsenic) concentrations

Hazardous Waste Incineration Ashes and Their Utilization. Table 1 Definitions of solid incineration wastes using grates, energy recovery, and air pollution control systems [3]

Category of solid incineration waste	Definition
Grate ash	Ash collected from grate
Grate siftings	Material collected from underneath the grate
Heat recovery system ash	Ash collected from boiler, superheater, and economizer
Bottom ash	Combination of the previous categories
Air pollution control residues	Particulate material captured from flue gas downstream of air pollution control reagent injection
Fly ash	Particulate matter captured from flue gas prior to the addition of air pollution control reagents

Hazardous Waste Incineration Ashes and Their Utilization. Table 2 Ranges of solid incineration wastes as defined in Table 1 from municipal waste incinerators in kg/1,000 kg waste [140]

Type of solid incineration waste	Bottom ash	Grate siftings	Heat recovery system ash	Air pollution control residues	Fly ash
Amount of solid incineration waste in kg/ 1,000 kg waste	100–250	<1–3	<2–5	10–60	7–25

in bottom ash from municipal waste incinerators may, for instance, vary by over a factor 1,000 and Hg, Pb, Ni, Mo, Cr, and Cd concentrations by over a factor 100 [19]. Differences in chloride and lead concentrations in air pollution control residues, as defined in Table 1, exceed a factor of 10 [23].

Differently from, e.g., a plant manufacturing yogurt, the composition of a specific incineration waste (e.g., bottom ash) from a waste incinerator may vary substantially from day to day. Also, after their generation, waste incineration ashes can undergo major changes due to "aging," which in turn may have a major impact on leachability [2, 5, 24, 25].

Furthermore, there are differences between bottom ash, fly ash, and air pollution control residues originating from the same waste and the same incinerator. Bottom ash is usually enriched in inorganic compounds, which are relatively nonvolatile on incineration, and fly ash and air pollution control residues tend to be enriched in volatile inorganic compounds. It has also been found that bottom ash may be more enriched in adsorbable organohalogens [20] and polycyclic hydrocarbons [18, 26] than fly ash.

In this chapter, the emphasis will be on the utilization of ashes from municipal waste and wastewater treatment and sewage sludge incinerators. Because this encyclopedia deals with sustainability science and technology, in section "Future Directions" the question will be raised whether current waste incineration practices and handling, including utilization of ashes, can be considered sustainable. This raises the contentious matter of intergenerational equity of waste handling [27].

Hazard and Ashes

As pointed out in the introduction, there can be differences between countries as to the categorization of ashes as hazardous. Hazardous may in this context refer to humans and/or organisms in the environment.

When ashes are released to air, as may occur, for instance, in the working environment, and at the end of smoke stacks, the main hazard to humans is linked to fly ash, which contains relatively small particles. The hazard of fly ash particles is related to their size, their surface area, structure, charge, agglomeration, and the presence of specific chemicals [28–30]. Exposure to fly ash adds to the background exposure to small particles in air. In urbanized settings, such background exposure is often associated with substantial risk of cardiovascular and pulmonary disease and exposure to fly ash may increase such risk [28, 29]. Also worker exposure to MSWI fly ash has been associated with increased DNA strand breakage, which may be linked with increased cancer risk [31].

Apart from the emission of ash particles to air, there is substantial agreement that the hazard of ashes is also dependent on the leaching of specific substances.

There have been proposals to use assays measuring the toxicity of leachates to specific organisms ("biotoxicity tests"), which in principle evaluate the complete leachate [32–36]. Such assays may employ strains of bacteria such as *Escherichia coli* [32], *Vibrio fischeri* [15, 33, 34], *Bacillus subtilis* [5], the microcrustacean *Daphnia magna* [15, 35, 36], the alga *Pseudokirchneriella subcapitata* [35, 36], human cell lines [35] and the duckweed *Lemna minor* [36].

A major problem is that there is no proven link between actual risk to humans and/or organisms in the human environment and the outcomes of the proposed biotoxicity tests. This is a common problem with risk assessment of "polluted" materials [37]. Another suggested approach uses an aquatic microcosm, employing a variety of organisms [36, 38]. Though this is more sophisticated than the biotoxicity tests referred to above, the correspondence with effects "in the field," which primarily regards soils, is as yet unknown.

In practice, the hazard of incineration ashes is often regulated on the basis of leaching tests. Usually, a limited number of substances are considered by regulators in this context. These rather often belong to the following categories of substances: relatively toxic elements such as heavy metals and arsenic and the relatively toxic polycyclic and halogenated organic compounds.

A problem is that the substances that are actually leached from ashes may show substantial variations in concentration dependent on conditions such as weathering of ashes, the presence of organic substances such as humic acids and of specific microorganisms, and on factors such as pH, and aerobic or anaerobic ("redox") conditions [6, 39–41].

Standardized leaching tests in the laboratory which underpin estimates of, and regulatory decisions as to, hazard posed by ashes, tend to reflect a limited subset of the conditions as they occur "in the field." This may lead to large differences between leaching as suggested by laboratory tests and actual leaching, which in turn may lead to estimates of hazard and risk that are at variance with actual hazard and risk [2, 40, 42–46].

Whether leached substances should be a matter of concern is dependent on exposure to leached substances and background exposure to the substances involved. For instance, there is evidence that present exposure to metals such as Cd and Pb and to halogenated compounds, such as chlorinated biphenyls, -dioxins, and -benzofurans, and polycyclic hydrocarbons is a health risk to the general human population in industrialized countries [37] and this is a good reason to even consider ashes which leach such substances in very small amounts as hazardous.

Utilization of Hazardous Waste Incineration Ashes

Treatment of Ashes Before Utilization

There has been substantial research into treatment of ashes before utilization. These treatments are aimed at eliminating small metal particles, lowering the amount of hazardous and/or mobile substances and at improving ash performance during utilization in specific applications [2, 42, 47].

A process that has been developed to remove small metal particles (Ag, Cu, Pb, Sn, and Zn), is based on eddy current and magnetic separation [43]. As the particles collected by this process are high-value metals, this treatment may be profitable, depending on actual metal prices.

Other treatments have been developed to improve ash-related product performance during utilization in, or as, building and geotechnical materials. Such treatments include those mentioned in Box 1 [2, 42, 47]:

Many treatments aimed at lowering the amount of hazardous and/or mobile substances have been proposed [2, 42, 47–54]. These can be categorized as indicated in Box 2.

There are also treatments intended to be used prior to utilization, which aim at immobilization of hazardous substances. These include the treatments in Box 3 [2, 10, 11, 17, 24, 43, 49, 54, 55]:

Treatments aiming at immobilization, or lowering the amount, of hazardous substances, may not only precede utilization, but may also serve reduced leaching from landfilled hazardous waste incineration ashes.

There are substantial differences in costs between the pretreatments summarized in Boxes 2 and 3. It would seem that aqueous mobilization techniques tend to be less expensive than thermal mobilization and immobilization technologies [45].

Commercial use of most of the treatments prior to utilization outlined in this section is limited or absent [2, 10, 11, 43, 49]. To the extent that there is treatment, the three treatments in Box 4 are practiced on a large commercial scale. These treatments may be combined [e.g., 11].

Still, much of the utilization of hazardous waste incineration ashes is not preceded by the treatments summarized in Box 4.

Application in or as Building and Geotechnical Materials

To the extent that there is utilization of hazardous waste incineration ashes, most ashes are used in the construction sector, including civil engineering, thus in, or as, building and geotechnical materials [2, 7, 56]. Most of the ashes which are actually applied seem to be bottom ashes, as defined in Table 1, but there is also some application of fly ashes (as defined in Table 1), for instance in asphalt mixtures [2]. Bottom ashes are used in the production of bricks, cement, and

Box 1. Treatments to Improve Ash-Related Product Performance During Utilization in Building and Geotechnical Materials

- Aqueous washing to remove soluble salts
- Oxidation of Al to reduce the generation of H_2 at high pH values
- Thermal treatment to reduce the carbon content of ashes

Box 2. Treatments Aimed at Lowering the Amount of Hazardous and/or Mobile Substances

- Treatments aiming at the destruction of organic (carbonaceous) substances present in ashes. These mainly include thermal, hydrothermal, and thermocatalytic treatment methods. Supercritical fluid treatment to destruct organic substances has also been investigated.
- Treatments aimed at the mobilization of hazardous and/or mobile substances. These include:
  - Aqueous washing to remove easily soluble inorganic compounds such as chlorides and sulfates and fine particulate matter, which is usually characterized by relatively high levels of hazardous substances
  - Supercritical fluid treatment to mobilize heavy metals
  - Electrodialysis for the mobilization of heavy metals, such as Cu, Cr, Zn, and Cd
  - Acid leaching for the mobilization of metals
  - Use of chelating substances for the mobilization of heavy metals
  - Biological mobilization using microorganisms such as *Thiobacillus thiooxidans, Rhodococcus,* and *Aspergillus niger* for the removal of metals
  - Pyrometallurgical or thermochemical mobilization of metals in the presence of excess Cl
  - Use of organic extractants to remove heavy metals

Box 3. Treatments Aiming at Immobilization of Hazardous Substances

- Thermal treatments such as sintering, (co)melting, and calcination.
- Natural weathering including natural carbonation. This results in decrease of pH, mildly reducing conditions, dissolution and precipitation reactions, hydrolysis/hydration, and mineral changes, which reduce leaching of a number of elements (though leaching of some elements (e.g., Cr, Sb) may increase) (see also "Life cycle release of hazardous substances").
- Enhanced or accelerated carbonation.
- Stabilization with phosphate, which may increase the sequestration of metals such as Zn, C, Pb, and Cd.
- Hydrothermal treatment in the presence of additives such as alkaline substances or $FeSO_4$.
- Treatment with supercritical fluids.
- Mechanochemical treatments, such as wet ball milling in the presence of CaO.

Box 4. Treatments of Hazardous Waste Incineration Ash Prior to Potential Utilization, Practiced on a Large Commercial Scale

- Natural weathering.
- Aqueous washing to remove highly soluble and mobile substances and fine particulate fractions that tend to contain relatively high amounts of hazardous substances from ashes [2].
- Melting for immobilization [10, 11, 49]. By the end of 2004, 140 plants melting waste incineration ashes were operational in Japan [49].

cement-derived products such as concrete, in sublayers of roads, cycling tracks, and parking spaces, in covers of landfills, and in embankments and noise insulation works [2, 5]. By the year 2000, in Germany, about 50% of bottom ash from municipal waste incineration was used in this way, in the Netherlands 60% and in Denmark 72% [5]. In China, substantial use of waste incineration ashes in road construction and brick making has been reported [53]. In the USA and

Canada, little actual utilization of hazardous waste incineration ashes seems to occur [5]. The same seems to hold for several other countries [57–60]. There are no good quantitative data regarding the application of hazardous waste incineration ashes per category of building and geotechnical materials, but it would seem that most of the ashes are applied in civil engineering: as or in geotechnical materials.

Utilization of waste incineration ashes can have both positive and negative environmental effects [37]. Utilization of waste incineration ashes in buildings and civil engineering may substitute for virgin resources, which is commonly considered a beneficial environmental effect [61]. On the other hand, hazardous substances may be released. These may be associated with risk and also with detrimental effects on natural resources such as groundwater [61–65]. For instance, in a leaching study of asphalt pavement amended with "waste-to-energy" ash, it was found that aluminum concentrations in leachates were consistently above water quality standards applicable in Florida [64]. In a life cycle assessment study comparing use of "upgraded" bottom ash in Swedish road construction with landfilling of bottom ash, the difference in environmental impact was found to be marginal [61].

It may be noted too, that some types of treatment of incineration ashes before application, are associated with large inputs of energy and/or materials. Such treatment may be a significant determinant of environmental impact [66]. For instance, utilization options involving thermal treatment may be very energy intensive, which may represent a major environmental burden [66].

Life Cycle Release of Hazardous Substances The release of hazardous substances during the life cycle of building and geotechnical materials including hazardous waste incineration ashes has been studied to a limited extent. Firstly, the release of hazardous substances may originate in the production of building materials and the realization of the building or engineering work. There may be leaching from the intact product or civil engineering work, and following wear and tear during the use stage of the life cycle. The latter is for instance prominent in the case of asphalt concrete aggregates applied in areas with rather severe winters such as Scandinavia, Russia, parts of Japan, and the USA, where antiskid materials are applied during the winter. This gives rise to large releases of fine particulate road dust (from which substances may leach) in spring and winter [67]. Leaching may also be impacted by handling after the use stage (e.g., during demolition or reuse) [2].

Knowledge about the release of hazardous substances originating in incineration ashes during the life cycle of buildings and civil engineering work is patchy and mostly concerns ashes that have not been subject to pretreatment [2, 3, 42, 51, 52, 63, 68–71].

Most work on the release of hazardous substances published in peer-reviewed journals has been done on the utilization of ashes in the production of cement and cement clinker. In view of the very high temperature and relatively long residence time involved in clinker production, the input of hazardous waste incineration ashes in cement clinker production can be instrumental in high-efficiency break down of toxic organics [72]. Adequate preventive measures should be taken against *de novo* formation of toxic compounds, such as low scrubber inlet temperatures to prevent the formation of chlorinated dioxins [73]. In actual practice the *de novo* formation of toxics may be significant however. For instance, in Taiwan, it has been estimated that on including hazardous residues in cement production, the emission of chlorinated dioxins may increase from 0.29 ng I-TEQ (international toxic equivalents)/kg clinker produced to 24.34 ng I-TEQ/kg [73]. In the case that ashes are included in cement clinker production, there tend to be significant stack emissions of heavy metals from the cement factory [64]. The incorporation of waste incineration ashes in cement clinker and cement may lead to substantial leaching of hazardous compounds during the life cycle of cement-derived products, including the recycling stage [70]. Hazardous elements present in cement or concrete will not pollute when they remain immobile. Two factors contribute to the immobilization of hazardous elements: high pH and inaccessibility to the solvent. In practice, these protective factors do not allow for complete immobilization of all hazardous elements during the life cycle of building and geotechnical cement-derived products including hazardous waste incineration ashes. Oxyanions such as CrO_4^{2-}, AsO_4^{3-}, MoO_4^{2-}, SeO_4^{2-}, and VO_4^{3-} are mobile at high pH [74]. Actual leaching of these anions from mortars shows

high variability between producers. In a study of 56 cement mortars of worldwide origin, van der Sloot et al. [75] found, for instance, that the leaching of vanadium varied by about two orders of magnitude. The mobility of oxyanions from mortars may have health implications for workers. It has been found that elevated concentrations CrO_4^{2-} in cement that is handled by workers may lead to allergic skin complaints [76]. This has led to legislation, first in the Scandinavian countries [77] and more recently to a Directive of the European Union (EU), which limits the presence of soluble CrO_4^{2-} in cement [78]. Also, CrO_4^{2-} is carcinogenic to humans after inhalation [79]. This is also relevant to the health of workers handling cement [78]. Furthermore leaching of CrO_4^{2-} from cement products may exceed water quality standards [e.g., 65]. One strategy to meet the limitation to soluble Cr^{6+} under EU legislation is to add ferrous sulfate, to reduce Cr^{6+} to Cr^{3+} [76]. This strategy has limited applicability, so there is substantial interest in restricting the input of materials with relatively large concentrations of soluble Cr^{6+} into cement kilns [76]. Metal chlorides may also be incompletely immobilized in cement and cement-derived products [2].

Once incorporated into concrete or other cement-derived products, the long-term fate of hazardous elements present in cement is a matter to consider. Firstly, there is the matter of mobilization from the product during use. Guo [80] has pointed out that use of cement mortar lined pipes for the transport of drinking water may necessitate limits on the presence of chromium and lead in inputs, in view of leaching from the pipes of $CrO4^{2-}$ and Pb. Metal chlorides may be present in high concentration in fly ash from waste incinerators, when there is a high input of materials which generate HCl gas when incinerated, such as polyvinylchloride (PVC) [81]. When clinker is made from such municipal waste incineration ash, substantial leaching of metal chlorides from cement-derived products may occur [82, 83]. The fate of hazardous elements present in cement-derived products during use is dependent on the processes that affect such products and environmental factors. These may include wear and tear, cracking, weathering including carbonation (which lowers pH), leaching, exposure to humic acids (that may increase metal solubility), and microbial activity. Wear and tear, cracking, weathering, and leaching may increase the interaction of solvent with hazardous elements. It has furthermore been shown in laboratory experiments that leaching of elements such as As, Cr, Ni, Sb, and Zn from cement may in the long run increase because of carbonation [83–87]. Microbial activity, according to laboratory experiments, may lead to the mobilization from cement-derived products of Cr [88] and probably also of Pb, Cu, and Zn [89, 90].

It is hard to predict the extent to which processes such as weathering, carbonation, leaching, exposure to humic acids or microorganisms, and wear and tear will lead to actual mobilization of hazardous elements from cement-derived products. As pointed out before, the standard leaching tests as they have been developed for laboratory use do not take account of microbial activity nor of the potential effect of humic acids which may increase mobility. They are also inadequate in representing weathering [2, 40, 42–46, 91–94]. This may lead to predictions of leaching on the basis of tests that are much at variance with actual leaching [40, 42–46, 92, 94]. However, all in all, it may well be that in the long run substantial amounts of hazardous elements will leach from waste-based cement-derived products in actual use.

When concrete structures are demolished at the end of their service life, leaching may become more of a problem. Van der Sloot [95] has shown that, whereas the leachability of Cd, Cr, Mo, and V is low in freshly cured concrete, leaching from construction debris used as an aggregate, e.g., in road stabilization bases, is much increased and may well exceed the statutory leaching limits as they are used in the Netherlands. Serclérat et al. [96] have shown that after incorporation in Portland cement clinker, much CrO_4^{2-} is retained in intact mortar bars leached with demineralized water, but that practically all CrO_4^{2-} is extracted from crushed material, which has a much increased surface area. This implies that without additional containment, much of the CrO_4^{2-} that was meant to be permanently immobilized in concrete may be released into the environment during the life cycle of cement products. A similar fate may apply to other mobile oxyanions of hazardous elements and to metal chlorides.

In view of substantial leaching of hazardous substances from utilized ashes, there would seem to be a case for pretreatments of incineration ash that would lead to the removal of hazardous compounds

[70]. These pretreatments were outlined in Boxes 1 and 2 of section "Treatment of Ashes Before Utilization". Also there would seem to be a case to explore the options for source reduction and separation that would lead to a reduction of leachable hazardous substances. This applies both to hazardous elements and organics, dependent on the processing of ashes. As to the latter, Hunsinger et al. [97–99] have proposed real-time automatic control of primary air supply, grate kinematics and waste feeding rate, and SO_2 recycling to improve burnout, which would lower the concentration of polycyclic aromatics, and to reduce chlorinated dioxin and benzofuran levels in MSWI ashes by about an order of magnitude. The reduction of polychlorobiphenyl levels in MSWI ashes by SO_2 recycling may be more limited than the reduction of chlorinated dioxin levels [100]. As to hazardous elements, for instance, reduced inputs of Pb, As, and Mo in municipal waste incinerators may reduce the potentially leachable amounts of these elements in waste incineration ashes [101, 102]. Similarly, reduced discharges of heavy metals into the sewer system may diminish the presence thereof in ashes originating in the incineration of wastewater treatment and sewage sludges [103]. Lowering the input of heavy metals may in turn, *ceteris paribus,* also lead to lower concentrations of hazardous halogenated compounds in fly ashes [104].

Mobilization of Useful Substances

Waste incineration ashes may contain substantial amounts of useful substances. In this respect attention has been drawn to the presence of substances derived from geochemically scarce natural resources that are formed in slow geological processes. Such substances include phosphate and metals, except Fe and Al. A technology based on eddy current and magnetic separation to collect small particles with geochemically scarce metals has already been referred to in section "Treatment of Ashes Before Utilization". Phosphate has also drawn attention. Sewage and wastewater treatment sludge incineration ashes in European countries have been found to contain 9–21% of P, specified as P_2O_5 [105, 106]. Several methods have been proposed for the extraction of phosphate from such ashes, including extraction with acid [107–109]. Thermochemical treatment leading to the removal of heavy metals and increased biological availability of phosphate present in ashes has also been proposed [105, 106]. The latter ties in with thermochemical or pyrometallurgical treatments in the presence of added chlorine for the winning of heavy metals [50, 105, 106]. This was one of the options mentioned in Box 2 of section "Treatment of Ashes before Utilization", which dealt with the pretreatment of ashes before utilization.

Box 5. Options for the Extraction of Metals from Waste Incineration Ashes

- Supercritical fluid extraction
- Electrodialysis
- Acid leaching
- Use of chelating substances
- Biological mobilization using microorganisms such as *Thiobacillus thiooxidans*, *Rhodococcus,* and *Aspergillus niger*
- Use of organic extractants

Other options to extract metals from waste incineration ashes are in Box 5 [2, 42, 47–51, 110].

There is as yet, no significant commercial exploitation of the technologies for mobilization of phosphate and the extraction of metals by the processes mentioned in Box 5 or pyrometallurgical treatments. However, Germany and Sweden have announced that they will set targets for the recycling of phosphates that currently end up in sewage and wastewater treatment sludges [111]. When recycling targets are implemented, phosphate extraction from ashes will have to compete with phosphate extraction from the original sludges.

Application in Agriculture

There have been proposals for the direct application of wastewater treatment and sewage sludge incineration ashes in agriculture, mainly in view of the presence of phosphate [111, 112]. However, the reason that such sludges are incinerated is usually that they are considered unfit for application in agriculture in view of the presence of substances that can accumulate in soils such as heavy metals [108, 110, 111, 113]. The latter also end up to a large extent in ashes [110, 111, 113]. Moreover, the biological availability of phosphate in

sludge incineration ashes tends to be relatively poor, if compared with the original sludges [106, 107, 109]. No substantial utilization of wastewater treatment and sewage sludge incineration ashes seems to occur as yet.

Also there have been proposals for the application of MSWI ashes in agriculture as soil amendment [112]. This may lead to elevated concentrations of heavy metals such as Pb and Cd in crops cultivated on the amended soil [114–116]. So far, there seems to be no substantial utilization of municipal waste incineration ashes generated in a controlled way, for this purpose.

In urban agriculture in Nigeria, town refuse ash, generated by uncontrolled incineration, is used, which aims at reducing soil acidity and providing for a range of micronutrients [117]. Samples of such ash have been studied to a limited extent. It has been found that their composition is very variable, with some samples being strongly contaminated with heavy metals [118].

Applications in Wastewater Treatment

There have been proposals to apply waste incineration ashes, and products derived from those ashes in wastewater treatment. These include:

- Application in sludge conditioning
- Use as package material for anaerobic filters
- Use of incineration ash and incineration ash-derived materials as adsorbent for removal of substances from wastewater

Sludge Conditioning Wastewater treatment sludges should be dewatered before further processing. Such dewatering may be difficult due to the presence of oil. To facilitate dewatering oily sludge, conditioners can be added. It has been found that fly ash from municipal waste incinerators (at an optimum dosage of 3%) can facilitate dewatering by filtration [119]. In doing so, such ashes may add heavy metals to the discharge of the wastewater treatment plant [119]. So far, there seems to be no substantial utilization of municipal waste incineration fly ash for this purpose.

Material for Filters Yue et al. and Han et al. [120, 121] have proposed the use of ceramic particles made from incinerated sludge in filters used for wastewater treatment. Data about the fate of hazardous components of the sludge-derived ceramic particles or the emission of hazardous substances via the filters are absent from their publications [120, 121].

Use as Adsorbent for Removal of Substances from Wastewater Pan et al. [122] and Bouzid et al. [123] have proposed the use of sewage sludge ash to absorb copper from wastewater. Pan et al. [122] have claimed an efficiency of >98%. Hydrothermally treated paper sludge ash [124] and zeolites produced from paper sludge ash [125] or municipal incinerator fly ash [126], untreated bottom ash from MSWIs [127], and medical waste incinerator fly ash, hydrothermally treated with addition of sodium carbonate [128], have also been proposed as adsorbents for (waste) water treatment. Information about adsorption kinetics and mass transfer in these studies [122–128] is very limited. The papers advocating the use of ashes, and ash-derived materials, as adsorbents [122–128] furthermore do not give data about the net effect of such use on the emission of hazardous substances from wastewater treatment plants.

One would expect that the removal of substances from wastewater by ashes would significantly depend on the presence of residual C and would be variable as the composition of such ashes is also variable [129]. Also one would expect that ash-derived adsorbents would be less effective on a kg basis than high-value absorbents currently available [129] and, in line with section "Introduction", that ash-derived adsorbents would be more variable in performance than current high-value adsorbents. It should furthermore be noted in this context that the utility as adsorbents of sewage sludge incineration ash derivatives is less than that for some other sewage-sludge-derived adsorbents, such as sewage sludges treated with alkali metal hydroxide reagents [130]. In practice, there would seem to be, as yet, no substantial applications of incineration ashes in wastewater treatment.

Other Uses as Adsorbent

Uses of hazardous waste incineration ashes in dry processes have also been suggested. MSWI bottom ash has been proposed as a sorbent for the removal of CO_2 from air [131] and of H_2S and CO_2 from biogas produced from agricultural residues and crops [132]. The utilization of hazardous waste incineration ash,

possibly combined with coke, has also been suggested for the removal of H_2S and mercaptanes from landfill gas [133]. The use of MSWI ashes for the removal of other volatile organics, HCl, NO_x, and $HgCl_2$ in dry processes might also be considered [133–135]. The studies suggesting application of ashes as adsorbent in dry processes have not looked at the fate of hazardous substances beyond the stage of utilization. There seems to be as yet no substantial commercialization of this type of applications of hazardous waste incineration ashes, a phenomenon that may be linked to better removal efficiencies and a more constant performance achieved by current commercial removal technologies.

Future Directions

In the previous sections, the focus has been on the utilization of hazardous waste incineration ashes. From a sustainability perspective, one may wonder, however, whether incineration, from which the ashes discussed here are derived, is actually always a good thing. Here, sustainability is used in line with its original definition, which means that the practice can be continued indefinitely while keeping natural resources in a steady state, without generating pollution that negatively affects future generations and while keeping ecosystem services at their current level [27, 136]. How does current incineration perform in this respect, if compared with its alternatives?

It would seem that only in a very limited number of cases waste incineration is associated with the best environmental performance. Examples thereof probably include the incineration of infectious wastes and of a variety of hazardous organic chemical wastes, such as some organic solvent wastes [137].

However, for many wastes other options than incineration would seem to be preferable. Municipal waste incineration is currently largely fuelled by synthetic polymers, such as plastics. But for these polymers reuse of product or material is often environmentally preferable [138]. State-of-the-art burning of garden and food wastes for electricity production apparently does not displace fossil fuel use in state-of-the-art power plants [139], which is in favor of conversion methods that allow for the recycling of nutrients and carbon compounds to agricultural land and gardens to keep levels of soil carbon compounds and nutrients in a steady state [136].

Source reduction and separation of hazardous substances combined with agricultural application of source-separated nutrients [113] may well be environmentally preferable to current sewerage and wastewater treatment practices, including sludge incineration.

The choice in favor of incineration is often defended on the basis of cost. But, in current calculations of such costs, many costs relevant to sustainability are largely externalized. Such currently externalized costs include replacement costs for depleted natural resources, damage due to pollution associated with incineration and reduction of ecosystem services, assuming a zero discount, as is proper in view of sustainability [136]. Inclusion of such costs may well lead to very different conclusions about the financial benefits of incineration.

Switching to other options of generating and handling what is currently considered waste will have large implications for the "reverse" logistics and handling of what is disposed of. Such a change should not come as a surprise. There is a very large asymmetry between the complicated and sophisticated system of production and handling products and the relatively uncomplicated and often unsophisticated way in which wastes are currently treated.

Bibliography

1. Johannessen KM (1996) The regulation of municipal waste incineration ash: a legal review and update. J Hazard Mater 47:383–393
2. Reijnders L (2005) Disposal, uses and treatments of combustion ashes: a review. Resour Conserv Recycl 43:313–336
3. Cyr M, Coutand M, Clastres PJ (2007) Technological and environmental behavior of sewage sludge ash (SSA) in cement-based materials. Cem Concr Res 37:1278–1289
4. Murakami T, Suzuki Y, Nagasawa H, Yamamoto T, Koseki T, Hirose H, Okamoto S (2009) Combustion characteristics of sewage sludge in an incineration plant to energy recovery. Fuel Process Technol 90:778–783
5. Sawell SE, Chandler AJ, Eighmy TT, Hartlen J, Hjelmar O, Kosson D, van der Sloot HA, Vehlow J (1995) An international perspective on the characterization and management of residues from MSW incinerators. Biomass Bioenergy 9:377–386
6. Römbke J, Moser T, Moser H (2009) Ecotoxicological characterization of 12 incineration ashes using 6 laboratory tests. Waste Manage 29:2475–2482
7. Gidarakos E, Petrantonaki M, Anastasadou K, Schramm K (2009) Characterization and hazard evaluation of bottom ash produced from incinerated hospital waste. J Hazard Mater 172:935–942

8. Coutand M, Cyr M, Deydier E, GR Clastres (2008) Characteristics of industrial and laboratory meat and bone meal ashes and their potential applications. J Hazard Mater 150: 522–532
9. Karamalidis AK, Voudrias EA (2009) Leaching and immobilization behavior of Zn and Cr from cement-based stabilization/solidification of ash produced from incineration of refinery oily sludge. Environ Eng Sci 26:81–96
10. Sakanakura H (2005) Diffusion test of 20 kinds of waste molten slags and competitive materials. J Mater Cycles Waste Manage 7:71–77
11. Chiang K, Hu Y (2010) Water washing effects on metals emission reduction during municipal solid waste incinerator (MSWI) fly ash melting process. Waste Manage. doi:10.1016/j.wasman.2009.12.009
12. Tian S, Yu M, Wang W, Wang Q, Wu Z (2009) Investigating the speciation of copper in secondary fly ash by x-ray absorption spectroscopy. Environ Sci Technol 43:9084–9088
13. Donatello S, Tyrer M, Cheeseman CR (2010) EU landfill waste acceptance criteria and EU hazardous waste directive compliance testing of incinerated sewage sludge ash. Waste Manage 20:63–71
14. Nie Y (2008) Development and prospects of municipal solid waste (MSW) incineration in China. Front Environ Sci Eng Chin 2:1–7
15. Barbosa R, Lapa N, Boavida D, Lopes H, Gulyurtlu I, Mendes B (2009) Co-combustion of coal and sewage sludge: chemical and ecotoxicological properties of ashes. J Hazard Mater 170:902–919
16. Wiles CC (1996) Municipal solid waste combustion ash: state-of-the-knowledge. J Hazard Mater 47:325–346
17. Reich J (2003) Slag from hazardous waste incineration: reduction of heavy metal leaching. Waste Manage Res 21:110–118
18. Zhao I, Zhang F, Chen M, Liu Z, Wu DBJ (2010) Typical pollutants in bottom ashes from a medical waste incinerator. J Hazard Mater 173:181–185
19. Chandler AJ, Eighmy TT, Hartlen J, Hjelmar O, Kosson DS, Sawell SE, van der Sloot HA, Vehlow J (1997) Municipal solid waste incinerator residues. Elsevier, Amsterdam
20. Durnusoglu E, Bakoglu M, Karademir A, Kirli L (2009) Adsorbable organic halogens (AOX) in solid residues from hazardous and clinical waste incineration. J Environ Sci Health A 41:1699–1714
21. Neuer-Etscheidt K, Nordsieck HO, Liu Y, Kettrup A, Zimmermann R (2006) PCDD/F and other micropollutants in MSWI crude gas and ashes during plant start-up and shut down processes. Environ Sci Technol 40:342–349
22. Rubli S, Medilanski E, Belevi H (2000) Characterization of total organic carbon in solid residues provides insight into sludge incineration processes. Environ Sci Technol 34:1772–1777
23. Quina MJ, Bordado JC, Quinta-Ferreira RM (2008) Treatment and use of air pollution control residues from MSW incineration: an overview. Waste Manage 28:2097–2121
24. Freyssinet P, Piantone P, Azaroual M, Itard Y, Clozel-Lecloup B, Guyonnet D, Baubron JC (2002) Chemical changes and leachate mass balance of municipal solid waste bottom ash submitted to weathering. Waste Manage 22:159–172
25. Dugenies S, Combrisson J, Casablanca H, Grenier-Loustalot MF (1999) Municipal solid waste incineration bottom ash: characterization and kinetic studies of organic matter. Environ Sci Technol 33:1110–1115
26. Liu Y, Li Y, Li X, Jiang Y (2008) Leaching behavior of heavy metals and PAHs from MSWI bottom ash in a long-term static immersing experiment. Waste Manage 28:1126–1136
27. Okrent D (1999) On intergenerational equity and its clash with intragenerational equity and on the need for policies to guide regulation of disposal of wastes and other activities posing very long-term risks. Risk Anal 19:877–901
28. Dellinger B, D'Alessio AD, D'Anna AD, Ciajolo A, Gullett B, Henry H, Keener M, Lighty J, Lomicki S, Lucas D, Oberdörster G, Pitea D, Suk W, Sarofim A, Smith KR, Stoeger T, Tolbert P, Wyzga R, Zimmermann R (2008) Combustion byproducts and their health effects. Environ Eng Sci 25:1107–1114
29. Shih S, Wang Y, Chang J, Jang J, Kuo F, Wang L, Chang-Chien G (2006) Comparisons of levels of polychlorinated dibenzo-p-dioxins/benzofurans in the surrounding environment and workplace of two municipal solid waste incinerators. J Hazard Mater B 137:1817–1830
30. Jiang J, Oberdörster G, Biswas P (2009) Characterization of size, surface charge, and agglomeration state on nanoparticle dispersions for toxicological studies. J Nanopart Res 11:77–89
31. Chen H, Chen I, Chia T (2010) Occupational exposure and DNA strand breakage of workers in bottom ash recovery and fly ash treatment plants. J Hazard Mater 174:23–27
32. Lin K, Chen B (2006) Understanding biotoxicity for reusability of municipal solid waste incinerator (MSWI) ash. J Hazard Mater A 138:9–15
33. Chou J, Wey M, Liang H, Chang S (2009) Biotoxicity evaluation of fly ash and bottom ash from different municipal solid waste incinerators. J Hazard Mater 168:197–202
34. Takeuchi M, Kawahata H, Gupta LP, Itouga M, Sakakibara H, Ohta H, Komai T, Ono Y (2009) Chemistry of fly ash and cyclone ash leachate from waste materials and effects of ash leachates on bacterial growth, nitrogen–transformation activity, and metal accumulation. J Hazard Mater 165:967–973
35. Shoji R, Nakayama H, Sakai Y, Mohri S, Yamada M (2008) Evaluation of the ecotoxicity of solid wastes using rapid leaching test and bioassays. J Environ Sci Health A 43:1048–1053
36. Triffault-Bouchet G, Clement B, Blake G (2005) Ecotoxicological assessment of pollutant flux released from bottom ash reused in road construction. Aquat Ecosyst Health Manage 8:405–414
37. Reijnders L (2009) Are soil pollution risks established by governments the same as actual risks? Appl Environ Soil Sci ID 237038:1–7
38. Clement B, Triffault-Bouchet G, Lottmann A, Carbonel J (2005) Are percolates released from solid waste incineration bottom ashes safe for lentic ecosystems? A laboratory ecotoxicological approach based on 100 litre indoor microcosms. Aquat Ecosyst Health Manage 8:427–439

39. Michalzik B, Ilgen G, Hertel F, Hantsch S, Bilitewski B (2007) Emissions of organo-metal compounds via the leachate and gas pathway from two differently pre-treated municipal waste materials – a landfill study. Waste Manage 27:497–509
40. Sabbas T, Poletti A, Pomi R, Astrup T, Hjelmar O, Mostbauer P, Cappai G, Magel G, Salhofer S, Speiser C, Heuss-Ambicher S, Klein R, Lechner P (2003) Management of municipal solid waste incineration residues. Waste Manage 23:61–88
41. Kim Y, Osako M (2004) Effect of adsorption capacity of dissolved humic matter on leachability of dioxins from raw and treated fly ashes of municipal solid waste incinerators. Arch Environ Contam Toxicol 46:8–16
42. Todorovic J, Ecke H (2006) Treatment of MSWI residues for utilization as secondary construction minerals: a review of methods. Miner Energy 20(4–5):45–59
43. Lidelöw S, Lagerkvist A (2007) Evaluation of leachate emissions from crushed rock and municipal solid waste incineration bottom ash used in road construction. Waste Manage 27:1356–1365
44. Apul D, Gardner K, Eighmy T, Linder E, Frizzell T, Roberson R (2005) Probabilistic modeling of one-dimensional water movement and leaching from highway embankments containing secondary materials. Environ Eng Sci 22:156–169
45. Kosson DS, van der Sloot HA, Sanchez F, Garrabrants AC (2002) An integrated framework for evaluating leaching in waste management and utilization of secondary materials. Environ Eng Sci 19:159–204
46. Dabo D, Badreddine R, de Windt L, Drouadaine I (2009) Ten-year chemical evolution of leachate and municipal solid waste incineration bottom ash used in a test road site. J Hazard Mater 172:904–913
47. Reijnders L (2007) Cleaner phosphogypsum, coal combustion ashes and waste incineration ashes for application in building materials: a review. Build Environ 42:1036–1042
48. Aguiar del Toro M, Calmano W, Ecke H (2009) Wet extraction of heavy metals and chloride from MSWI and straw combustion ashes. Waste Manage 29:2494–2499
49. Sakanakura H (2007) Formation and durability of dithiocarbamic metals in stabilized air pollution control residue from municipal solid waste incineration and melting processes. Environ Sci Technol 41:1717–1722
50. Bosshard RP, Bachofen R, Brandl H (1996) Metal leaching from fly ash from municipal waste incineration by *Aspergillus niger*. Environ Sci Technol 30:3066–3071
51. Yang J, Wang QH, Wang Q, Wu TJ (2008) Comparison of one-step and two-step bioleaching for heavy metal removal from municipal solid waste incineration fly ash. Environ Eng Sci 25:783–789
52. Bayuseno A, Schmahl WW, Müllejans T (2009) Hydrothermal processing of MSWI fly ash – towards new stable minerals and fixation of heavy metals. J Hazard Mater 167:250–259
53. Fraissler G, Jollet M, Mattenberger H, Brunner T, Obernberger I (2009) Thermodynamic equilibrium calculations concerning the removal of heavy metals from sewage sludge ash by chlorination. Chem Eng Process 48:152–164
54. Bo D, Zhang F, Zhao L (2009) Influence of supercritical water treatment on heavy metals in medical waste incineration ash. J Hazard Mater 170:66–71
55. Guo X, Xiang D, Duan G, Mou P (2010) A review of mechanochemistry applications in waste management. Waste Manage 30:4–10
56. Siddique R (2008) Waste materials and by-products in concrete. Springer, London
57. Yao J, Li W, Kong Q, Wu Y, He R, Shen D (2010) Content, mobility and transfer behavior of heavy metals in MSWI bottom ash in Zhejang province, China. Fuel 89:616–622
58. Huang C, Yang W, Ma H, Song Y (2006) The potential of recycling and reusing municipal solid waste incinerator ash in Taiwan. Waste Manage 26:979–987
59. Pan JR, Huang C, Kao J, Lin S (2008) Recycling MSWI bottom and fly ash as raw materials in Portland cement. Waste Manage 28:1113–1118
60. Ferreira C, Ribeiro A, Ottosen L (2003) Possible applications for municipal solid waste fly ash. J Hazard Mater B 96:201–216
61. Toller S, Kärrman E, Gustafsson JP, Magnusson Y (2009) Environmental assessment of incinerator residue utilization. Waste Manage 29:2071–2077
62. Francois D, Pierson K (2009) Environmental assessment of a road site built with MSWI residue. Sci Total Environ 407:5945–5960
63. Huang W, Tang H, Lin K, Liao M (2010) An emerging pollutant contributing to cytotoxicity of MSWI ash wastes: strontium. J Hazard Mater 173:597–604
64. Dubey B, Townsend T (2007) Leaching of milled asphalt pavement amended with waste-to-energy ash. Int J Environ Waste Manage 1:145–158
65. Kayhanian M, Vichare A, Green PG, Harvey J (2009) Leachability of dissolved chromium in asphalt and concrete surfacing materials. J Environ Manage 90:3574–3580
66. Birgisdottir H, Bhander G, Hauschild MZ, Christensen TH (2007) Life cycle assessment of disposal of residues from municipal solid waste incineration: recycling bottom ash in road construction or landfilling in Denmark evaluated by the ROAD–RES model. Waste Manage 27:S75–S84
67. Tervahattu H, Kupiainen KJ, Räisänen M, Mäkelä T, Hillamao K (2006) Generation of urban road dust from anti-skid and asphalt concrete aggregates. J Hazard Mater 132:39–46
68. Travat I, Lidelow S, Anderas L, Tham C, Lagerkvist A (2009) Assessing the environmental impact of ashes used as landfill cover construction. Waste Manage 29:1336–1246
69. Beyer C, Konrad W, Rügner H, Bauer S, Liedl R, Grathwohl P (2009) Model-based prediction of long term leaching of contaminants from secondary materials in road constructions and noise protection dams. Waste Manage 29:839–850
70. Reijnders L (2007) The cement industry as a scavenger in industrial ecology and the management of hazardous substances. J Ind Ecol 11(1):15–25
71. Karstensen KH, Kinh NK, Thang LB, Vet PH, Tuan ND, Toi DT, Hung NH, Quan TM, Hanh LB, Thang DH (2006) Environmentally sound destruction of obsolete pesticides in developing countries using cement kilns. Environ Sci Policy 9:577–586

72. Sidhu S, Kast N, Edwards P, Dellinger B (2001) Hazardous air pollutants formation from reactions of raw meal organics in cement kilns. Chemosphere 42:499–506
73. Chen C (2004) The emission inventory of PCDD/PCDF in Taiwan. Chemosphere 54:1413–1420
74. Dermatas CM (2006) Evaluation of ettringite and hydrolumite formation for heavy metal immobilization. J Hazard Mater 136:20–33
75. van der Sloot HA, Seignette P, van Zomeren A, Hoede D, Meeuwsen JCL (2003) Effects of alternative materials, life cycle stages, testing and criteria development. www.ecn.nl
76. Winder C, Carmody M (2002) The dermal toxicity of cement. Toxicol Ind Health 18:321–331
77. Liden C (2001) Legislative and preventive measures related to contact dermatitis. Contact Dermat 44:65–69
78. Lannoye PA (2003) Report on proposed Directive of the European Parliament and Council regarding the limitation of marketing nonylphenol, nonylphenol ethoxylate and cement. European Parliament, Brussels
79. Costa M, Klein CB (2006) Toxicity and carcinogenicity of chromium compounds in humans. Crit Rev Toxicol 36: 155–163
80. Guo Q (1997) Increases of lead and chromium in drinking water from using cement–mortar–lined pipes: initial modeling and assessment. J Hazard Mater 56:181–213
81. Pedersen AJ, Frandsen FJ, Riber C, Astrup T, Thomsen SN, Lundtorp K, Mortensen LF (2009) A full-scale study on the partitioning of trace elements in municipal solid waste incineration – effects of firing different waste types. Energy Fuels 23:3475–3489
82. Alba N, Vazquez E, Gasso S, Baldasano JM (2001) Stabilization/solidification of MSW incineration residues from facilities with different air pollution systems. Durability of matrices versus carbonation. Waste Manage 21:313–324
83. Yvon J, Antenucci D, Lorenzi G, Dutre V, Leclerq D, Nielsen P, Veschkens M (2006) Long term stability in landfills of municipal solid waste incineration fly ashes solidified/stabilized by hydraulic binders. J Geochem Explor 90:143–155
84. Meima JA, Comans RNJ (1998) Reducing Sb leaching from municipal solid waste incineration bottom ash by addition of sorbent materials. J Geochem Explor 62:299–304
85. Valls S, Vazquez E (2001) Accelerated carbonation of sewage sludge–cement–sand mortars and its environmental impact. Cem Concr Res 31:1271–1276
86. Ecke H (2003) Sequestration of metals in carbonated municipal solid waste incineration (MSWI) fly ash. Waste Manage 23:631–640
87. Garrabrants AC, Sanchez F, Kosson DS (2004) Changes in constituent equilibrium leaching and pore water characteristics of a Portland cement mortar as a result of carbonation. Waste Manage 24:19–36
88. Idachaba MA, Nyavor K, Egiebor NO (2003) Microbial stability evaluation of cement based waste forms at different waste to cement ratios. J Hazard Mater B 96:331–340
89. Brombacher C, Bachofen R, Brandl H (1997) Biohydrological processing of solids. A patent review. Appl Microbiol Biotechnol 48:577–587
90. Yang J, Wang Q, Luo Q, Wang Q, Wu T (2009) Biosorption behavior of heavy metals in bioleaching process of MSWI fly ash by *Aspergillus niger*. Biochem Eng J 46:294–299
91. van Zomeren A, Comans RNJ (2009) Carbon speciation in municipal solid waste incinerator (MSWI) bottom ash in relation to facilitated metal leaching. Waste Manage 29:2059–2064
92. Twardowska J, Szczepanska J (2002) Solid waste: terminological and long term environmental risk management problems exemplified in a power plant fly ash study. Sci Total Environ 285:28–51
93. Bayard R, Pestre C, Gourdon R (2009) Aerobic microbial activity in fresh and aged bottom ashes from municipal waste incineration. Int Biodeterior Biodegradation 63: 739–746
94. Aberg A, Kumpiene J, Ecke H (2006) Evaluation and prediction of emissions from a road built with bottom ash from municipal solid waste incinerator (MSWI). Sci Total Environ 355:1–12
95. van der Sloot HA (2000) Comparison of the characteristic leaching behavior of cements using standard EN–196–1 cement mortar and an assessment of their long-term environmental behavior in construction products during service life and recycling. Cem Concr Res 30:1079–1096
96. Serclérat J, Moskowicz P, Pollet B (2000) Retention mechanisms in mortars of trace metals contained in cement clinkers. Waste Manage 20:259–264
97. Hunsinger H, Seifert H, Jay K (2006) An economic process to inhibit PCDD/PCDF formation in MSWI by SO_2. Organohalogen Compd 68:151–156
98. Hunsinger H, Seifert H, Jay K (2007) Reduction of PCDD/F formation in MSWI by a process-integrated SO_2 cycle. Environ Eng Sci 24:1145–1159
99. Hunsinger H, Seifert H, Jay K (2007) Control of PCDD/F formation under conditions of fluctuating combustion performance in MSWI. Organohalogen Compd 69:956–961
100. Ke S, Ianhua Y, Xiaodong L, Shenyong L, Yinglei W, Muxing F (2010) Inhibition of *de novo synthesis of PCDD/Fs by SO_2* in a model system. Chemosphere. doi:10.1016/j.chemosphere.2009.12.043
101. Mast P (1999) Einfluss der Abfallzusammensetzung auf Schadstofgehalt und– Menge der Verbrennuingsrückstaände (Impact of waste composition on the concentration and amount of toxics in combustion residues). TAUW, Berlin
102. Jeong SM, Osako N, Kim Y (2005) Utilizing a database to interpret leaching characteristics of lead from bottom ashes of municipal waste incinerators. Waste Manage 23:694–701
103. Lo S, Tsao Y (1997) Economic analysis of waste minimization for electroplating plants. Water Sci Technol 36:383–390
104. Fujimori T, Takaoka M, Takea N (2009) Influence of Cu, Fe, Pb and Zn chlorides and oxides on formation of chlorinated aromatic compounds in MSWI fly ash. Environ Sci Technol 43:8053–8059

105. Franz M (2008) Phosphate fertilizers from sewage sludge ash (SSA). Waste Manage 28:1809–1818
106. Adam C, Peplinski B, Michaelis M, Kley G, Simon D (2009) Thermochemical treatment of sewage sludge ashes for phosphorous recovery. Waste Manage 29:1122–1128
107. Wzorek Z, Jodko M, Gorazda K, Rzepecki T (2006) Extraction of phosphorus compounds from ashes from thermal processing of sewage sludge. J Loss Prev Process Ind 19:39–50
108. Donatello S, Freeman Pask A, Tyrer M, Cheeseman CR (2010) Effect of milling and acid washing on the pozzolanic activity of incinerator sewage sludge ash. Cement Concr Compos 32:54–61
109. Mattenberger H, Fraissler G, Herk P, Hermann L, Obernberger I (2008) Sewage sludge ash to phosphorus fertilizer: variables influencing heavy metal removal during thermochemical treatment. Waste Manage 28:2709–2722
110. Ottosen LM, Perdersen AJ, Hansen HK, Ribeiro AB (2007) Screening the possibility for removing cadmium and other heavy metals from wastewater sludges and bioashes by an electrodialytic method. Electrochim Acta 52:3420–2426
111. Christen C (2007) Closing the phosphorus loop. Environ Sci Technol 46:2078
112. Zhang F, Yamasaki S, Nazyo M (2001) Application of waste ashes to agricultural land – effect of incineration temperature on chemical characteristics. Sci Total Environ 264: 205–214
113. Lienert J, Larsen TA (2010) High acceptance of urine source separation in seven European countries: a review. Environ Sci Technol 44:556–566
114. Zhang D, Yamaski S, Kimura K (2001) Rare earth element content in various waste ashes and the potential risk to Japanese soils. Environ Int 27:393–398
115. Rosen CJ, Bierman PM, Olson D (1994) Swiss chard and alfalfa responses in soils amended with municipal waste incinerator ash: growth and elemental composition. J Agric Food Chem 42:1361–1368
116. Ferreira C, Ribeiro A, Ottosen L (2003) Possible applications for municipal solid waste fly ash. J Hazard Mater B 93:201–216
117. Pasquini MW (2006) The use of town refuse ash in urban agriculture around Jos, Nigeria: health and environmental risks. Sci Total Environ 354:43–59
118. Passquini MW, Alexander MJ (2004) Chemical properties of urban waste ash produced by open burning on the Jos Plateau: implications for agriculture. Sci Total Environ 319:325–340
119. Hwa TJ, Joyseelan S (1977) Conditioning of oily sludges with municipal solid wastes incineration fly ash. Water Sci Technol 35:231–238
120. Yue Q, Han S, Yue M, Gao B, Li Q, Yu H, Zhao Y, Qi Y (2009) The performance of biological anaerobic filters packed with sludge–fly ash ceramic particles (SPCP) and commercial ceramic particles (CCP) Turing the restart period. Effect of the C/N ratios and filter media. Bioresour Technol 100:5016–5020
121. Han S, Yue Q, Yue M, Gao B, Li Q, Yu H, Zhao Y, Qi Y (2009) The characteristics and application of sludge–fly ash ceramic particles (SCP) as novel filter media. J Hazard Mater 171: 809–814
122. Pan S, Lin C, Tseng D (2003) Reusing sewage sludge as absorbent for copper removal from wastewater. Resour Conserv Recycl 39:79–90
123. Bouzid J, Elouear Z, Ksibi M, Feki M, Montiel A (2008) A study on removal characteristics of copper from aqueous solution by sewage sludge and pomace ashes. J Hazard Mater 152:838–845
124. Okada K, OnoY KY, Nakajima A, MacKenzie KJD (2007) Simultaneous uptake of ammonium and phosphate ions by compounds prepared from paper sludge ash. J Hazard Mater 141:622–629
125. Wajama T, Haga M, Kuzawa K, Ishimoto H, Tamada O, Ito K, Nishiyama T, Downs RT, Rakovan JF (2006) Zeolite synthesis from paper sludge ash at low temperature (90°C) with addition of diatomite. J Hazard Mater B 132:244–252
126. Yang GCC, Yang T (1998) Synthesis of zeolites from municipal incinerator fly ash. J Hazard Mater 62:75–89
127. Shim Y, Kim Y, Kong S, Rhee S, Lee W (2003) The adsorption characteristics of heavy metals by various particle sizes of MSWI bottom ash. Waste Manage 23:851–857
128. Jin J, Chi L, Yan J (2010) Co-disposal of heavy metals containing waste water and medical waste incinerator fly ash by hydrothermal process with addition of sodium carbonate: a case study on Cu(II) removal. Water Air Soil Pollut. doi:10.1007/s 11270-009-0207-5
129. Ahmaruzzaman M (2010) A review on the utilization of fly ash. Prog Energy Combust Sci. doi:10.1016/j.pecs.2009.11.003
130. Smith KM, Fowler GD, Pulket S, Graham NJD (2009) Sewage sludge-based adsorbents: a review of their production, properties and use in water treatment applications. Water Res 43:2569–2594
131. Baciocchi R, Polettini A, Pomi R, Prigiobbe V, von Zedwitz VN, Steinfeld A (2006) Sequestration by direct gas–solid carbonation of air pollution control (APC) residues. Energy Fuels 20:1933–1940
132. Pertl A, Mostbauer P, Obersteiner G (2010) Climate balance of biogas upgrading systems. Waste Manage 30:92–99
133. Ducom G, Radu-Tirnoveanu D, Pascual C, Benadda B, Germain P (166) Biogas-municipal solid waste incinerator bottom ash interactions: sulphur compounds removal. J Hazard Mater 166:1102–1108
134. Wang S, Wu H (2006) Environmental–benign utilization of fly ash as low-cost adsorbents. J Hazard Mater B 136:482–501
135. Karatza D, Lancia A, Musmarra D (1998) Fly ash capture of mercuric chloride vapors from exhaust combustion ash. Environ Sci Technol 32:3999–4004
136. Reijnders L, Huijbregts MAJ (2009) Biofuels for road transport. Springer, London
137. Capello C, Hellweg S, Hungerbühler K (2008) Environmental assessment of waste–solvent treatment options. J Ind Ecol 12:111–127

138. Björklund A, Finnveden G (2005) Recycling revisited – life cycle comparisons of global warming impact and total energy use of waste management strategies. Resour Conserv Recycl 44:309–317
139. Luteijn J (2009) No energy to waste. Thesis, Open University of the Netherlands, Heerlen
140. Vehlow J, Bergfeldt B, Hunsinger H (2006) PCDD/F and related compounds in solid residues from municipal solid waste incineration – a literature review. Waste Manage Res 24:404–420

Hazardous Waste Incinerator Emissions

Montse Mari, José L. Domingo, Martí Nadal, Marta Schuhmacher
Laboratory of Toxicology and Environmental Health, School of Medicine, IISPV, Universitat Rovira i Virgili, Reus, Catalonia, Spain

Article Outline

Glossary
Definition of the Subject
Introduction
Chemicals of Concern
A Review of Scientific Publications on HWI Emissions
Environmental and Human Biological Monitoring of Pollutants
A Case Study: The HWI of Constantí (Catalonia, Spain)
Future Directions
Bibliography

Glossary

Environmental monitoring Control of the environmental status of specific location by means of analyzing the concentration of pollutants in environmental matrices (air, soil, water, or sediments).

Hazardous waste (HW) Materials, usually in solid or liquid form, which are generally produced in industrial processes, and characterized by posing substantial or potential threats to public health or the environment. They must be properly treated and/or conditioned in special HW management plants.

Human health risk assessment Evaluation of the probability that the human exposure to certain substance(s) can derive in adverse health effects to individuals or populations. A differentiation between non-carcinogenic and cancer risks is generally performed.

Incineration Typical process to manage municipal solid waste or hazardous waste consisting on its thermal destruction. Organic matter contained in waste is completely destroyed by combustion in special ovens with the presence of oxygen in excess. Waste is converted into ash, flue gas, and heat. Therefore, incineration is also known as waste-to-energy or energetic valorization.

Polychlorinated dibenzo-*p*-dioxins and dibenzofurans (PCDD/Fs) Simply called "dioxins," PCDD/Fs form a group of chemical substances whose molecular structure presents two benzene rings joined by two oxygen bridges. They include a family of 210 congeners, which are differentiated according to their number and position of chlorine atoms. They were originally included in the Stockholm Convention treaty that aims the elimination/restriction of Persistent Organic Pollutants (POPs). They are characterized by being highly persistent, bioaccumulative and toxic substances, and with a long-range transport capacity. PCDD/Fs are unintentional by-products of combustion processes. Two great groups of sources have been traditionally identified: regulated and nonregulated/diffuse.

Definition of the Subject

This chapter is basically focused on the assessment of emissions from hazardous waste incinerators (HWIs), evaluating specially those pollutants with the greatest interest and concern due their notable toxicity, persistence, and bioaccumulation capacity: polychlorinated dibenzo-*p*-dioxins and dibenzofurans (PCDD/Fs) and heavy metals. The main properties and toxic effects of those chemicals are here summarized. A review of publications on emissions from HWIs indicates that in the last decade significant progresses have been achieved in emission reductions of these facilities as result of very rigorous regulations. The suitability of using environmental (e.g., soils, herbage, etc.) and human biological (e.g., blood, urine, etc.) monitors to

evaluate the impact of the above pollutants is presented together with some results of a case study, a wide survey of a HWI located in Catalonia (Spain). The results indicate that when HWIs are properly designed using the best available techniques (BAT) as well as the best environmental practices (BEP), the emissions are not environmentally significant and, consequently, they do not mean additional risks for the human health.

Introduction

Hazardous waste (HW) is defined as a waste that is dangerous or potentially harmful to human health and/or the environment. HWs include industrial wastes such as organic solvents, waste oil, sludge, rubber, etc. All these wastes contain toxic substances. Therefore, their proper management is crucial to protect the environment and safety of individuals. Currently, there is no estimation about global generation of industrial wastes. However, the rapid increase in volume and types of hazardous waste as a result of the continuous economic growth, urbanization, and industrialization is becoming a burgeoning problem for national, regional, and local governments to ensure effective and sustainable management of waste [1].

Incineration using best available technologies (BAT) in Europe, or maximum achievable control technologies (MACT) in USA, is considered the preferred management option for certain wastes that cannot be recycled or reused, being prevention the first step in the waste management strategy. Combustion is used to destroy hazardous organic constituents and to reduce the volume of waste. However, waste incineration, and specifically HW, generates a great concern on the population because of the toxic substances contained in wastes or other formed during the combustion process, which can be released through the stack, causing potential adverse effects on the environment and the human health of the population living nearby. This chapter is focused on pollutants potentially emitted by incinerators, as well as with the associated environmental and human impacts.

Stack emissions of hazardous waste incinerators (HWIs) contain major contaminants, those at higher concentrations such as nitrogen oxides (NO_x), sulfur dioxide (SO_2), hydrogen chloride (HCl), hydrogen fluoride (HF), particulate matter (PM), and volatile organic compounds (VOCs), including chloroform ($CHCl_3$), carbon tetrachloride (CCl_4), and chlorobenzenes (CLPs). In addition, stack emissions also include minor contaminants, those present in lower concentrations, such as persistent organic pollutants (POPs) and metals. However, because of their characteristics of persistence, toxicity, and capacity of bioaccumulation, POPs and metals are those of major concern. Consequently, these will be considered here in detail.

Some POPs found in stack gas of HWIs are hexachlorobenzene (HCB), polycyclic aromatic hydrocarbons (PAHs), polychlorinated dibenzo-*p*-dioxins and dibenzofurans (PCDD/Fs), polychlorinated biphenyls (PCBs), polychlorinated diphenyl-ethers (PCDEs), and polychlorinated naphthalenes (PCNs) [2]. Among them, PCDD/Fs are the most studied since they were the first ones discovered in the flue gases and fly ash of municipal solid waste incinerators (MSWIs) [3]. The two main methods for controlling PCDD/Fs emissions from waste incinerators are stable combustion and the removal of emitted PCDD/Fs by air pollution control devices (APCDs). The parameters that affect the emissions of PCDD/Fs are those related with the wastes, such as the content of PCDD/Fs or their precursors, or the presence of chlorine in the feed waste, as well as other related to the combustion process, such as retention time, temperature, turbulence in the combustion chamber, and oxygen availability.

The exact mechanism of PCDD/Fs ("dioxins") formation is unknown. However, it is recognized that dioxins generally form from the thermal breakdown of organic materials in the presence of transition metals and chlorinated compounds. Dioxin formation takes place from *de novo* synthesis, as the flue gas from the incineration process cools down from the initial 1,000°C down to about 250°C. Dioxin formation occurs only in the zone of the incinerator where temperature is low and residual particles (fly ash) are present. Fly ash acts as a catalytic surface during the formation process. At those conditions, the components for dioxin formation are carbon, small organic compounds, metal ions, and inorganic chloride [4]. Copper and iron are the metals better catalyzing this reaction [5]. Chlorine may be incorporated into dioxins through elemental Cl_2 or as HCl. As a consequence of this, regulatory efforts have been undertaken in incinerators to avoid PCDD/F formation and

release. For example, incineration of HW with a content of more than 1% of halogenated organic substances, expressed as chlorine, has to accomplish with certain operational conditions in order to destroy as many organic pollutants as possible. Combustion control is based on dioxin destruction at high temperatures, typically over 1,000°C, and residence times of greater than 2 s. Based on remarkable advances in both combustion control and APCD technologies, many countries have established guidelines and regulations for the optimal operation of waste incinerators and for PCDD/Fs control [6].

With respect to metals, a number of studies have shown that elements like antimony (Sb), arsenic (As), cadmium (Cd), cobalt (Co), copper (Cu), chromium (Cr), lead (Pb), manganese (Mn), mercury (Hg), nickel (Ni), thallium (Tl), and vanadium (V) are emitted by industrial, medical, and municipal waste incinerators [7]. After combustion in modern HWIs, metals contained in HW are mainly collected in bottom and fly ash, being only small quantity of metals discharged from the stack as particulate or vapor [8]. Notwithstanding, atmospheric emission of these elements is a matter of concern. Heavy metals emissions from municipal and hazardous waste incinerators are controlled primarily through the use of particulate collection devices (electrostatic precipitators, fabric filters, and wet scrubbers) or acid gas control systems (dry injection, spray dryer absorption, and wet scrubbing). Most metallic compounds are in the vapor phase within the incineration system, where the temperature is around 1,000°C. The metallic compounds tend to condense as the flue gas is cooled and become adsorbed onto fine particulate matter (generally submicron in size, i.e., 0.2–0.7 μm). The major fraction of heavy toxic metals in the flue gas exists as fine particulates, and it is effectively controlled by properly sized electrostatic precipitators or fabric filters. On the other hand, a portion of the more volatile metals such as Hg and Cd may remain in the vapor phase, depending upon temperature conditions, and other technologies are needed to for metal removal from the stream. The additional control for vaporized toxic metals consists on spray dryer absorption systems or wet scrubbers [9].

With regard to the regulations, according to the EU legislation (Directive 2000/76/EC), the distinction between hazardous and nonhazardous waste is based principally on the properties of waste prior to incineration or co-incineration, but not on the differences in emissions. The same emission limit values should be applied to the incineration or co-incineration of hazardous and nonhazardous waste, but different techniques and monitoring measures upon reception of waste should be retained.

The EU has introduced measures to prevent or reduce air, water, and soil pollution caused by the incineration or co-incineration of waste, as well as the resulting risks to human health. These measures specifically require permissions for incineration and co-incineration plants, and emission limits for certain pollutants released to air or to water (Directive 2000/76/EC). This Directive establishes the strictest emission limit for PCDD/Fs, which is set in 0.1 ng International Toxic Equivalents (I-TEQ)/Nm^3. The emission of PCDD/Fs must be measured once or twice yearly under normal good operation conditions, although the periodicity is sometimes increased until obtaining 3-monthly (or even monthly) data. The emission limits established by the Directive of other pollutants such as dust and metals and are summarized in Table 1.

The United States Environmental Protection Agency (US EPA) proposes national emission standards for hazardous air pollutants (NESHAP) in hazardous waste combustors. These combustors include hazardous waste burning incinerators, cement kilns, lightweight aggregate kilns, industrial/commercial/institutional boilers and process heaters, and HCl

Hazardous Waste Incinerator Emissions. Table 1 Emission limits established by the EU Directive 2000/76/CE for some pollutants

Pollutant	Limit
Total dust (mg/m^3)	10
Cd + Tl (mg/m^3)	0.05
Hg (mg/m^3)	0.05
Sn + V + Sb + As + Pb + Cr + Co + Mn + Ni + Cu (mg/m^3)	0.05

The results of the measurements shall be standardized at the following conditions: Temperature 273°K, pressure 101.3 kPa, 10% oxygen, dry gas

production furnaces, known collectively as hazardous waste combustors (HWCs). The US EPA has identified these HWCs as major sources of hazardous air pollutant (HAP) emissions. These proposed standards will, when final, implement section 112(d) of the Clean Air Act (CAA) by requiring HW combustors to meet HAP emission standards reflecting the application of the maximum achievable control technology (MACT). US EPA regulations require sources to demonstrate a destruction and removal efficiency (DRE) for selected principal organic hazardous constituents (POHCs) of at least 99.99%; dioxin listed wastes are required to achieve at least 99.9999% DRE. Similar regulations are being developed in Korea [10], as well as in other countries.

Chemicals of Concern

Among the pollutants emitted by incinerators, dioxins and furans (PCDD/Fs) have traditionally generated the greatest concern because of their important toxicity, persistence, and bioaccumulation capacity. However, other POPs have been also found in HWI emissions. Polychlorinated biphenyls (PCBs) and polychlorinated naphthalenes (PCNs) are organochlorine compounds also formed in combustion processes, with similar characteristics to PCDD/Fs. In addition, incinerators can also emit other organochlorine compounds with toxic properties such as hexachlorobenzene (HCB) or chlorophenols (CLPs). A number of studies have shown that metals are also released in incinerator stacks. Among these, mercury is one of the most remarkable due to its high vapor pressure and high toxicity. A brief description of the sources of these compounds, as well as their behavior and toxicity are next described.

Organic Pollutants

Polychlorinated Dibenzo-*p*-Dioxins and Dibenzofurans (PCDD/Fs) The term polychlorinated dibenzo-*p*-dioxins and dibenzofurans (PCDDs), or simply dioxins, includes a set of 75 congeners, among which the most known and representative is the 2,3,7,8-tetrachlorodibenzo-*p*-dioxin or TCDD (Fig. 1). In turn, polychlorinated dibenzofurans (PCDFs), or simply furans, comprise 135 congeners. PCDDs and PCDFs (or PCDD/Fs) are two of the 12 persistent organic pollutants (POPs) (the "dirty dozen") which were originally included in the Stockholm Convention treaty intended to reduce the environmental levels of POPs.

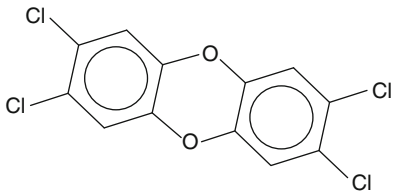

Hazardous Waste Incinerator Emissions. Figure 1 Chemical structure of TCDD

The 75 dioxin congeners mentioned above are due to the different position and/or the number of chlorine atoms in the aromatic rings. This number varies between 1 and 8. On the other hand, polychlorinated dibenzofurans or PCDFs have less symmetry positions, presenting a total of 135 congeners. It is precisely the number and position of chlorine atoms in the molecules of PCDD/Fs what determines the toxicity of the different compounds. Individual toxicity can vary with a relative value of 1,000, which obviously complicates the risk assessment of exposure, since they are commonly found as complex mixtures in the environment.

For this reason, and to simplify the risk evaluation, the concept of toxic equivalency factor (TEF) for each of the congeners that make up the mixtures was defined. The TEF concept, developed in the 1980s, provides a relatively simple method to evaluate the toxicity of complex mixtures of PCDD/Fs [11]. Several systems have been developed to express the total contribution of the 17 most toxic dioxins and furans. The toxicity of each congener is given relative to that of 2,3,7,8-TCDD (called Toxic Equivalency Factor, or TEF). Thus, to calculate the toxicity of the mixture, the concentration of each congener is multiplied by the corresponding TEF value of that congener. When these results are summed, a total TEQ or toxic equivalency of the mixture is obtained.

$$TEQ = \sum (TEF \times concentration)$$

The two most common systems to determine TEQs are based on the TEFs developed by the World Health Organization (WHO-TEF) [12] and the North Atlantic

Treaty Organization (NATO), known as International TEQ (I-TEF) [13]. Most congeners present similar toxicity equivalence factors in both systems, although some differences exist. Table 2 shows the different values of the I-TEFs and WHO-TEFs. The former are more common in North America, while Asia and Europe tends to use the latter.

Dioxins and furans may cause a wide range of biochemical and toxic effects in mammals. Apparently, the different congeners produce the same effects, but with varying degrees of potency. For most of them, the mechanism of action is not clear. However, it seems that the common denominator that mediates the biological effect of PCDD/Fs on cells is the binding of compounds to the aryl receptor hydrocarbon (AHR). Although carcinogenicity studies are still ongoing, one of the PCDD/F congeners, the 2,3,7,8-TCDD has been catalogued as probable human carcinogen by the US EPA, as some human studies have shown an association between this congener and soft tissue sarcomas, lymphomas, and stomach carcinomas. With regard to the non-carcinogenic effects, the most remarkable is the chloracne produced by the acute intoxication to dioxins. Nowadays, the toxicity of TCDD in humans is only partially known and mainly at short term (acute toxicity). The most representative signs and symptoms of acute and subacute exposure are the following:

Skin: chloracne, hyperkeratosis, and hyperpigmentation
Systemic: anorexia and weight loss, mild hepatic fibrosis, digestive problems, aching muscles and joints, pyelonephritis, cystitis hemorrhagic, etc.
Neurological and psychological: sexual dysfunction, visual problems, memory loss, loss of hearing, smell and touch, depression, irritability, sleep disorders
Others: eye irritation and conjunctivitis

Dioxins are not voluntarily produced, but they are formed as by-products in some chemical syntheses involving chlorine (i.e., paper making, manufacture of PVC or herbicides, etc.) and combustion processes (i.e., urban and hospital waste incineration, cement production, metal refining, etc.).

PCDD/Fs are highly persistent in the environment. By increasing the degree of chlorination, both the stability and the lipophilicity (solubility in oil) are enhanced. The octanol/water constant (K_{ow}), which indicates the relative lipid solubility in water, is in an order of one hundred million (log K_{ow} range: 6.5–8.8), which implies a high tendency to move to the fat. The soil microorganisms or animals are not able to effectively break the chlorine in the positions 2,3,7,8 of PCDD/Fs, which makes their elimination very slow.

PCDD/Fs are highly persistent and lipophilic substances. They can be adsorbed very easily by particles present in air, soils, and sediments. There is an increase in its concentration along the food chain. Thus, they are present at highest concentrations in organisms of higher levels in the food chain (birds and mammals), ultimately accumulating in the human body. It is known that these compounds are biomagnifying. Moreover, since dioxins and furans are persistent and semi-volatile, they can be transported long distances by the wind, undergoing what is known as a Long-Range Atmospheric Transport (LRAT). As a consequence, it is sometimes possible to find PCDD/Fs in areas very distant from any known source of emission.

Hazardous Waste Incinerator Emissions. Table 2 Values of I-TEF and WHO-TEF for the 17 most toxic PCDD/F congeners

Congener	I-TEF	WHO- TEF
2,3,7,8-TCDD	1	1
1,2,3,7,8-PeCDD	0.5	1
1,2,3,4,7,8-HxCDD	0.1	0.1
1,2,3,6,7,8-HxCDD	0.1	0.1
1,2,3,7,8,9-HxCDD	0.1	0.1
1,2,3,4,6,7,8-HpCDD	0.01	0.01
OCDD	0.001	0.0003
2,3,7,8-TCDF	0.1	0.1
1,2,3,7,8-PeCDF	0.05	0.03
2,3,4,7,8-PeCDF	0.5	0.3
1,2,3,4,7,8-HxCDF	0.1	0.1
1,2,3,6,7,8-HxCDF	0.1	0.1
1,2,3,7,8,9-HxCDF	0.1	0.1
2,3,4,6,7,8-HxCDF	0.1	0.1
1,2,3,4,6,7,8-HpCDF	0.01	0.01
1,2,3,4,7,8,9-HpCDF	0.01	0.01
OCDF	0.001	0.0003

Polychlorinated Biphenyls

Polychlorinated biphenyls (PCBs) comprise a group of chlorinated aromatic hydrocarbons consisting of 209 congeners. As PCDD/Fs, the number and position of chlorine atoms determines the biological properties and environmental behavior of individual polychlorinated biphenyls (PCBs). As an example, the PCB-28 chemical structure is depicted in Fig. 2.

Commercial mixtures of PCBs have a wide spectrum of toxic effects. Many of these effects are very similar to those caused by 2,3,7,8-TCDD [14]. Some adverse health effects associated with PCBs are chloracne, changes in the immune system, as well as in neurobehavior of adults and children [15]. The United Nations Organization (UNO), through the WHO, has concluded that according to the degree of chlorination and the exposure time, PCBs produce adverse effects such as chloracne, increased eye discharge, swelling, and pain abs (Yushin disease) [16].

Studies in people occupationally exposed to PCBs show that they may cause lung and nasal irritation, as well as liver and hematologic and gastrointestinal disorders, depression, and fatigue [15]. Some PCBs alter thyroid hormone action and/or other endocrine glands that can affect growth, development, and reproduction. PCBs can also cause cancer in mammals [15]. Although it has not been proved that these chemicals cause cancer in humans, both the US EPA and the International Agency for Research on Cancer (IARC) have classified PCBs as probable human carcinogen (category 2A); that is to say, they are considered substances that have little evidence to have causal relationship with cancer in humans, but sufficient evidence presented in studies with laboratory animals [17]. Otherwise, some congeners have carcinogenic effects and may be associated with an increased risk of breast cancer [18].

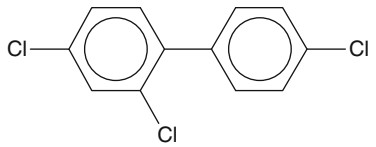

Hazardous Waste Incinerator Emissions. Figure 2 Chemical structure of PCB-28

PCBs are not naturally found in the environment, but they are substances generated in technological processes. PCBs were synthesized in a laboratory for the very first time in 1929 in USA. Their manufacture produces a mixture of compounds, whose properties depend on the degree of chlorination. In general, they present high thermal, chemical, and biological stability with a high dielectric constant. They are insoluble in water and can mix with oils. They are also highly resistant to fire. According to those properties, they were widely used in the past in electrical equipment as insulators such as transformers and thermostats. In addition, they were also used for years in many industrial applications as the manufacture of adhesives, varnishes, plasticizers, and algaecides molusquicides.

Between 1929 and 1977, the total worldwide production of PCBs was around 1,200,000 t. Due to their flameproof characteristics, the majority of dielectric oils with PCBs were used in areas with high fire risk, such as petrochemical and industrial plants [19]. However, in 1977, the manufacture and use of PCBs was banned, as PCBs were noted to cause a major environmental impact because of the properties that made them so useful.

Due to its physical and chemical properties, PCBs tend to be adsorbed on the particles of air, soil, and sediment. Although the air is the compartment where they are degraded more easily, some studies have suggested lifetimes ranging from 2 to 6 years depending on the degree of chlorination [20]. In this compartment, the photodegradation is considered the most important mechanism of elimination [21]. In water, PCBs also adsorbs to particles where they can remain for years [22]. PCBs show a high affinity for soils and sediments that act as reservoirs of these compounds. High lifetimes are observed in this compartment especially for the heavier compounds [23].

PCBs are highly hydrophobic compounds with high lipid solubility, so they tend to accumulate in the adipose tissue. Due to its ability to solubilize lipids and the high persistence and capacity for bioaccumulation, biomagnification occurs along the food chain, increasing their toxicological effects in organisms. Regarding the biological lifetimes, there is a great disagreement on the different congeners of PCBs. It is believed that the lifetimes of commercial mixtures of PCBs in the human body can range from 2 to 6 years [24]. However, if the

lifetimes of different congeners are individually measured, these values can vary greatly. For example, the average life of PCB-153 is estimated in 12.4 years, whereas that of PCB-28 is estimated in 1.4 years [25].

Like PCDD/Fs, PCBs have a great tendency to be adsorbed on the particles of air. Thus, they tend to move up very long distances. As a result, concentrations of PCBs have been detected in air and other compartments in very remote areas like the Arctic mountains, far from any source [26].

Polychlorinated Naphthalenes

Polychlorinated naphthalenes (PCNs) form a family of 75 congeners whose chemical structure is composed by naphthalene with one to eight chlorine atoms. For example, Fig. 3 shows the chemical structure of trichloro-naphthalene. The physical and chemical properties of PCNs are very similar to those of PCBs. They are hydrophobic and present a high chemical and thermal stability. Moreover, they are good electrical insulators and flame retardants [27].

The scientific literature on the toxicity of PCNs is very limited. However, what is known is that, like other POPs, the mechanism of toxicity action is through the aryl hydrocarbon receptor (Ahr) [28]. According to human poisoning episodes, the effects of exposure to PCNs are chloracne, carcinogenesis, teratogenesis, and even mortality [29]. However, the fact that they always appear together with PCBs and PCDD/Fs may have caused an overestimation of the potential adverse effects of PCNs [28]. As in the case of PCDD/Fs and PCBs, PCNs are usually mixtures of different congeners. To characterize the toxicity of PCNs, TEF values have been established for some congeners. The TEFs for PCNs are 3–6 orders of magnitude less toxic than those of PCDD/Fs, while its potency is similar to that of PCBs [30]. Among them, some hexa-congeners are the most potent congeners, with a TEF of 0.002 [28]. Nevertheless, due to lack of sufficiently reliable data, the toxicity of PCNs has been quantified only for a few congeners [31, 32].

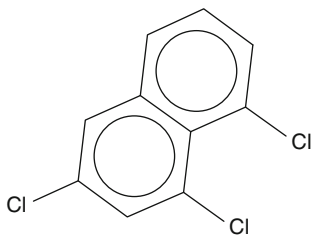

Hazardous Waste Incinerator Emissions. Figure 3 Chemical structure of trichloro-naphthalene

PCNs have been found in the gases and ashes from different incinerators in Sweden, Spain, and Germany [33–35]. In Canada, combustion processes involve the 54% of air releases of PCNs [19]. Chlor-alkali processes have been pointed out as important sources of PCNs [33, 36]. Other sources are technical PCB formulations [37].

Historically, there have been several peaks of PCN wastes according to their degree of chlorination. The highest input of penta- and hexa-CNs occurred before 1944, while the peaks of tetra- and tri-CNS did not occur until the years 50 and 70, respectively [38]. However, a significant increase has been observed for many congeners associated with combustion, which suggests that, nowadays, combustion sources are more important than in the past [38].

The high octanol/water distribution constant (K_{ow}) indicates its capacity for biomagnification. The distribution constant octanol/water is especially significant for hexa- and hepta-CN homologues (log K_{ow} is between 3.90 and 8.3) [39]. Bioaccumulation experiments have focused mainly on determining the bioconcentration factors (BCF) in some aquatic species [40], being some BCF values higher than 20,000 [41]. It is believed that PCNs accumulate along the food chain and eventually accumulate in some human tissues and fluids [42]. Data on residence time of PCNs in water, soils, and sediments are very limited. In fact, lifetimes have been only established for mono-and di-CNS, with values from 38 to 104 days [43]. However, there is still much uncertainty around this issue.

During the preparation of the protocol of the European Convention on Long-Range Transboundary Air Pollution on POPs in the United Nations Economic Commission (UN-ECE-LRTAP POPs Protocol) 1998, the PCNs were not included into the list of the "Dirty Dozen" due to lack of appropriate data [44]. However, scientific knowledge obtained in recent years indicates that PCNs have become candidates to extend the list of chemicals to be restricted [40].

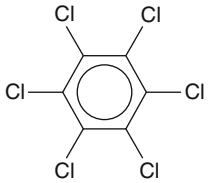

Hazardous Waste Incinerator Emissions. Figure 4
Chemical structure of chlorobenzene

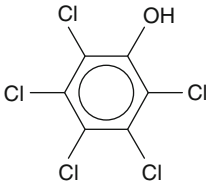

Hazardous Waste Incinerator Emissions. Figure 5
Chemical structure of pentachlorophenol

Hexachlorobenzene

Hexachlorobenzene (HCB) is an organochlorine fungicide introduced for the first time in 1945 (Fig. 4). Many developing countries still use it to spray wheat. Currently, HCB is used as a plasticizer and as an additive for wood preservatives, being an important commodity for the synthesis of chlorinated organic compounds. HCB does not exist naturally in the environment, but it is obtained by chlorination of less chlorinated benzenes, being the basis for the production of pentachlorophenol. It can be also obtained as a by-product in the chlorinated hydrocarbon industry. Therefore, HCB enters in the environment by the burning of chlorine-containing products (e.g., incineration) or through the use of pesticides contaminated with this substance [45, 46].

Hexachlorobenzene is absorbed in the gastrointestinal tract, being slowly metabolized and accumulated in adipose tissue. When adipose tissue is mobilized, HCB is remobilized and then it can be found in all organs. In rats, prolonged exposure to this substance has produced, in some cases, skin diseases, neurological symptoms, and liver injury. In mice, immunotoxic effects were observed as well as viral infections in lungs and liver [47]. The Department of Health and Human Services (DHHS, USA) has determined that HCB could be potentially carcinogenic, since in animal studies liver, kidney, and thyroid cancers have been observed. Therefore, there is strong evidence that it may cause cancer in humans, but mutagenic or teratogenic effects have not been observed.

Chlorophenols

Chlorophenols (CLPs) are a family of 19 different compounds, of which the pentachlorophenol (PCP) is the most important (Fig. 5). Due to the wide spectrum of antimicrobial properties of chlorophenols, they have been used to protect wood, paint, plant fibers, and leather and as disinfectants. They have also been applied as herbicides, fungicides, and insecticides, as well as intermediary agents in the manufacture of pharmaceuticals and dyes.

Most CLPs are obtained by direct chlorination of phenol using chlorine gas. The final product has other isomers of chlorophenol as impurities. Therefore, depending on the conditions of process, chlorophenols can generate heavier polychlorinated phenoxy phenols and low concentrations of PCDD/Fs, being possible the emissions in their manufacture, storage, transport, and application [48].

Chlorophenols can be absorbed by lungs, gastrointestinal tract, and skin. Approximately 80% is expelled by the kidneys without having undergone any transformation. Its toxicity depends on the degree of chlorination, the position of chlorine atoms, and the purity of the sample. At low doses, they can cause irritation in the eyes and airways. Toxic doses produce convulsions, coma, and eventually death. After repeated administration, toxic doses can affect internal organs and bone marrow. Pentachlorophenol exerts a toxic effect on embryos in experimental animals. As a result of studies conducted in animals, which show an increased cancer risk, especially in the liver, the IARC considered that the PCP is a possible human carcinogen.

Heavy Metals

Arsenic Arsenic (As) is an element that is usually classified among metal, although it presents metalloid and nonmetal properties. This element is naturally found in the earth's crust, with levels between 2 and 5 mg/kg [49]. However, anthropogenic sources are usually more important than the natural sources. One of the

main routes of entry of this element in the soil first, and afterward in water is through the use of fertilizers and pesticides in agriculture [50]. The air release is mainly produced by the combustion of coal and timber, mining, smelters, and waste incineration. Arsenic can be found in both inorganic and organic forms. While inorganic forms – As_2O_3, As_2O_5, or AsH_3 – are more toxic, organic arsenic, much less toxic, is originated as a form of detoxification through biotransformation by different organisms [51].

The exposure to As occurs mainly through food intake, especially seafood [52]. Fortunately, the percentage of organic arsenic (usually in the form of arseniobetaina) in foodstuffs is significantly much higher than that of inorganic As [53].

Arsenic compounds have been recognized as carcinogenic to humans (Group 1) based on different evidences [54]. Epidemiological studies have revealed a relationship between high concentrations of As in water and high incidences of skin cancer [55]. It has been also found a positive correlation between inhalation of As and lung cancer. The development of liver cancer, kidney, and bladder has also been associated with exposure to this element [56].

Beryllium Beryllium (Be) is a metal found naturally in rocks, coal, soil, and volcanic dust. The general population is exposed to low levels of Be through air, food, and water. Exposure to high levels of Be (greater than 1,000 mg/m) can produce symptoms similar to pneumonia. In general, however, it is unlikely that the general population develop chronic Be disease because environmental levels of this metal are usually very low (0.00003–0.0002 mg/m^3) [57].

No effects have been reported after ingestion of beryllium in humans because very little Be is absorbed by the stomach and intestines. Contact with skin may cause ulcers [57], while Be has been identified by the US EPA [58] as a probable human carcinogen (Group 2).

Cadmium Cadmium (Cd) is not an essential element from a nutritional point of view. It is released as a byproduct in zinc, copper, or lead smelting. It has excellent corrosion resistance, and therefore, a large percentage of the amount consumed is used to protect other metals (galvanized). A considerable amount is used to prepare pigments for the manufacture of paints and plastics and as a stabilizer of the latter. The mechanical properties of certain copper alloys improve with the addition of cadmium, and its use is widespread in the manufacture of alkaline batteries [59]. The skin absorption is minimal, whereas gastrointestinal absorption is 5% of the amount ingested, reaching up to 20% in case of iron or calcium deficiency. The absorption through inhalation can reach 50% of the total exposure, depending on the size of particles and their solubility [60].

Diet and tobacco play an important role in Cd exposure [61]. Some plants, such as rice or wheat, selectively concentrate cadmium present in soil and water. Thus, environmental pollution can reach the humans through the consumption of contaminated food. One of the greatest episodes of mass poisoning by cadmium was Itai-Itai disease in Japan at the end of World War II, caused by the consumption of rice and contaminated water [62].

The kidney is the organ primarily involved in chronic exposure to cadmium. The effects of inhalation also include pulmonary emphysema, anemia, dysfunction of liver, as well as dysfunctions in calcium, phosphorus, and vitamin D metabolisms. These effects are associated with osteoporosis, osteomalacia, and renal calcium stone formation [63]. On the other hand, the liver is the target organ for cadmium to settle, altering its subclinical hepatic function, and often producing a slight elevation of serum liver enzymes [63].

Finally, numerous epidemiological studies have shown that individuals that have been exposed for long periods to Cd have a higher risk than the general population of contracting prostate, lung, or breast cancer [61]. This element has been classified by the IARC as carcinogenic to humans (Group 1) and probable human carcinogen by the US EPA (Group B1).

Cobalt Cobalt (Co) is naturally found in rocks, soils, water, plants, and animals. Cobalt alloys are used for the manufacture of aircraft engines, magnets, grinding and cutting tools, and artificial knee and hip joints. Co compounds are also used to color glass, ceramics, and paintings to dry enamels and paintings on porcelain. Usually, Co is released to environment from natural sources, when burning coal or oil, or during the production of cobalt alloys. Once in air, cobalt is associated with particles and is finally deposited in a few days.

Cobalt has beneficial (is part of vitamin B12) and harmful effects to human health. Exposure to high levels of cobalt can have effects on lungs and heart [64], as well as it can also cause dermatitis. In animals exposed to high levels of cobalt, effects on liver and lungs have been reported [65]. It has been observed that non-radioactive cobalt does not produce cancer in humans or animals after exposure through food or water. However, cancer has been observed in animals after exposure through inhalation at high levels. Based on laboratory data from the IARC, it has been determined that Co and its compounds are possible carcinogens in humans.

Copper Copper (Cu) is a metal found naturally in rocks, soils, water, and air. Copper is an essential element for animals and plants, and therefore, necessary for life. It is used to manufacture many products such as wire or taps. It is also used in agriculture to treat plant diseases. Once released into the environment, Cu particles adhere to soil organic matter.

High levels of Cu can be harmful to health. Inhalation of high concentrations may cause irritation of the nose and throat. The ingestion of high levels of copper can cause nausea, vomiting, and diarrhea. Very high quantities can damage the liver, kidneys and even cause death [66]. It is not known whether copper can cause cancer in humans. Therefore, the US EPA has determined that copper is not classifiable as carcinogenic in humans [66].

Chromium Chromium (Cr) is found on the surface of rocks, soils, and the sea. This element is widely used in the industry, being its use quite extensive. As metal, it is not basically toxic. However, its oxidation products (chromic acid, chrome dicromats) are very toxic due to the caustic action. The major toxic effects are directly linked to the presence of trivalent chromium and, especially, hexavalent (more toxic) chromium, which are denaturing agents of proteins and nucleic acids, which are slowly eliminated into the urine [67, 68].

The cutaneous manifestations of Cr toxicity consist on skin ulcers and allergic dermatitis. Inflammation of the airways can also occur by inhalation [69]. Based on studies showing sufficient evidence that exposure to Cr (VI) causes lung cancer, the Cr (VI) has been classified by the IARC [70] as carcinogenic to humans (Group 1), while the US EPA has classified the hexavalent form of Cr as a known human carcinogen. Chronic exposure to Cr (VI) can produce non-carcinogenic effects in liver and kidney, as well as in the gastrointestinal and immune systems.

Tin Tin (Sn) metal is not soluble in water. It is present in brass, bronze, and some materials for welding. Tin is used to coat metal cans of food, drinks, and aerosols. Inorganic tin compounds are also used in toothpastes, perfumes, soaps, food additives, and dyes. Organic tin compounds are employed to manufacture plastic packaging for food, plastic pipes, pesticides, paint, and animal repellents. Tin is released into the environment by natural processes and human activities such as mining, oil and coal combustion, and the production and use of tin compounds. In the atmosphere, Sn can exist in vapor form, adhering to dust particles and soils. Organic tin compounds are bioaccumulative, as they can accumulate in animals (including fish) and plants.

Tin metal does not present a high toxicity because only a little part is absorbed from the gastrointestinal tract. Studies in humans have shown that ingestion of large amounts of inorganic tin can cause stomach pain, anemia and alterations in liver and kidneys. Inhalation of organic tin compounds may cause neurotoxic effects. In severe cases, it can cause death [71]. Some organic tin compounds affect the immune system in animals, but their effects in humans have not been accurately evaluated. Animal studies have also shown that tin compounds affect reproduction, although the evidence in humans is not clear. Contact with skin or eyes of organic or inorganic tin compounds can cause irritation [71]. There is no evidence that tin or its compounds may cause cancer in humans. Studies of inorganic compounds in animals have been negative. With respect to this, the IARC and the US EPA have not classified tin metal or its inorganic compounds as carcinogenic [58].

Manganese Manganese (Mn) is an element found naturally in the environment, usually in form of oxides. It is found in soil, air, water, and food. Anthropogenic sources of Mn include cement production plants, power plants, waste incineration, and combustion of fossil fuels [72]. In humans, Mn is an essential element.

Dietary intake is the main route of nonoccupational exposed individuals. Occupational exposure occurs mainly by inhalation of dust. Chronic inhalation of Mn causes effects in the nervous system [73]. There is no data confirming that the Mn causes cancer in humans. Thus, the US EPA does not classify manganese as a carcinogen metal [58].

Mercury Sources of mercury (Hg) are both natural and anthropogenic. Mercury is a liquid metal at room temperature, being the only metal that remains liquid at 0°C. Because of its high volatility and low boiling point, in the atmosphere it is in the gas phase [74]. In combination with elements such as oxygen, sulfur, or chlorine, it forms inorganic compounds. Mercury can be also combined with carbon to form organic mercury compounds. The most common of these is methyl mercury, which is produced by microorganisms in soil and water [75].

Medical and municipal waste incinerators, cement factories, and chlor-alkali plants are causing major concentrations of mercury vapor into the atmosphere [74]. Many occupational exposures occur by inhalation of mercury vapors. Chronic exposures to low concentrations of mercury are common [76].

The most important case of poisoning by methyl mercury was produced by ingestion of contaminated fish in the Minamata Bay, Japan. This episode was so important that the clinic profile caused by this intoxication was named Minamata disease [77]. The effects of mercury are highly dependent on their different chemical forms. The central nervous system is very susceptible to all forms of mercury. Methyl mercury and vapors of metallic mercury are more harmful than other forms because a greater amount of the former can reach the brain. Exposure to high levels of metallic, inorganic, or organic Hg can cause damage to the kidneys, brain, and fetus [75]. The neurological effects of mercury poisoning include involuntary shaking of limbs, lips, and tongue, and psychological disorders such as nervousness, irritability, abnormal reserved behavior (eretisme), mental confusion, and peripheral polyneuropathy, affecting the upper extremities more than the lower [78]. The US EPA has classified both inorganic mercury and methyl mercury within Group C (possible human carcinogens), while metallic mercury is not considered as a human carcinogen (Group D).

Nickel The main uses of nickel (Ni) are industrial. These include the manufacture of steel and other alloys and superalloys. It is used in smaller amounts for the manufacture of cast iron, chemicals, batteries, industrial ceramics, and catalyst. It is also considered an essential element for humans, although the specific deficiency has not been characterized yet.

Most occupational exposure to Ni occurs through inhalation of smoke or dust, or through dermal contact with the skin alloys, salts, or solutions [79]. Among workers of Ni-refining industries, a higher incidence of lung cancer and nasal cavities has been reported. Some studies indicate that these workers may suffer higher risk of getting other types of malignant processes such as cancer of the larynx, stomach, prostate, kidney, and soft tissue sarcoma.

Lead Because of its malleability and low melting point, humans have used lead (Pb) from prehistory in jewelry, manufacture of pipes, and water jars for drinking. Likewise, its salts are appreciated for their bright colors. Currently, it is widely used in industry to manufacture pigments, coatings, containers, ointments, and electric batteries.

The toxic effects of Pb are the same either if it is ingested or inhalated. Lead can affect almost all organs and body systems. In adults, prolonged exposure can impair some functions of the central nervous system [80]. In children, chronic exposure is associated with behavioral problems, learning difficulties and hyperactivity [81]. It can also cause weakness in fingers, wrists, and ankles. Exposure to lead produces an increase in blood pressure and can cause anemia [82] and damage to the kidneys [83]. Lead was classified as a possible carcinogenic in humans (Group 2B) by the IARC [54].

Thallium Thallium (Tl) is a metal found in small quantities in the Earth's crust. It is mainly used for the manufacture of electronic switches and terminals mainly in the semiconductor industry. It is also used in the manufacture of special glass and certain medical procedures. Thallium enters the environment mainly from burning coal and foundries in both cases as a contaminant of raw material. In the environment, Tl bioaccumulates, being absorbed by plants and entering the food chain.

Exposure to high levels of Tl can produce adverse effects on health. In a study in workers exposed for several years to inhalation of thallium, toxic effects were observed in the nervous system [84]. In studies of subjects who have ingested large amounts of thallium over a short period, vomiting, diarrhea, temporary hair loss, and neurological effects, and effects on lungs, heart, liver, and kidneys have been reported [84]. Acute exposure to high amounts of Tl also can cause death. Ingestion of thallium during long periods of time is not well known. Experimental studies with rats exposed to high levels of thallium have indicated developmental alterations. No information is available, either in humans or animals, on the Tl effects in contact with the skin [85]. There are no studies in humans or animals on the carcinogenic effects of inhalation, ingestion, or dermal contact with thallium. Neither the IARC nor the US EPA have classified Tl in terms of carcinogenesis in humans [58].

Vanadium Vanadium (V) and its compounds are present in the earth's crust and rocks, and it is recovered as a by-product in mining of other metals. The main use of this element is in alloys with iron, aluminum, and molybdenum, and to produce bronze and brass. Modest quantities of vanadium are also used as catalysts to make pottery, dyeing processes, insecticides, digital photography, color televisions, and glass production. Oil is relatively rich in this element, and the burning of large masses represents a considerable environmental contribution. Inhalation of dust or fumes, particularly as pentoxides, is the most common form of occupational exposure [86].

Vanadium is mainly absorbed through the respiratory tract and distributed to all tissues through the blood. It is found mainly in bone tissue, as metavanadate. It also binds to liver and lung, being slowly eliminated. The largest amount of vanadium is excreted by the kidney. The classic pattern of response to dust exposure at the working place with high V contents is the irritation of the upper respiratory tract. Depending on the V concentration in the air, symptoms appear within hours of exposure. The specific response includes coughing, forced breathing, eye irritation, nose and throat, bronchitis, chemical pneumonitis, and rarely hemorrhagic. Vanadium has not been implicated in carcinogenic processes [58].

A Review of Scientific Publications on HWI Emissions

Data reported in the scientific literature on emissions from HWIs are rather limited. This section is focused only on the publications from the last decade. The reason is that in the last years significant progresses have been achieved in emission reductions of waste incinerators, as a result of stringent regulations. Most papers discuss measures in combustion control and the performance of different air pollution control devices for POPs and/or metals. Furthermore, advances in the methodologies for stack emissions measurements of PCDD/Fs have been recently reported. Hinshaw and Trenholm [87] compiled data regarding stack emissions from various research and compliance testing programs from HWIs. As expected, it was found that the values for most pollutants considerably vary from incinerator to incinerator, according to operating conditions and feed composition. In relation to the main toxic metals (present in the ppb range), they included lead, chromium, cadmium, and arsenic. Mercury was also frequently found in this range, even though it was present at higher concentrations when emitted by other types of incinerators. Beryllium, if present, was found at lower concentrations in most cases. Naphthalene and other PAHs, as well as phenols, were found generally at higher levels (range 0–10 parts per billion – ppb). With respect to PCDD/Fs, their relative concentrations were the lowest in comparison with all the rest of pollutants. However, PCDD/Fs are especially toxic and bioaccumulative, and therefore one of major concern. van Velzen et al. [88] published a review on mercury and waste incineration, where the efficiency of different processes to remove mercury from flue gases was discussed (i.e., electrostatic precipitators, wet scrubbers, wet scrubbers with conditioning agent, spray absorbers, fabric filters, entrained flow adsorbers, and circulating fluidized bed). In that revision, examples of hazardous waste incinerators achieving good efficiencies were reported through the combination of diverse equipments. In all cases, the mercury outlet concentration was clearly below the limit of 50 μg/Nm^3. Löthgren and van Bavel [89] studied the dynamic behavior of the scrubber installed in a Swedish HWI since high concentrations of PCDD/Fs were found after the scrubber, even though the concentrations before

the scrubber were low. They concluded that the high PCDD/Fs emissions after the installation of the wet scrubber were caused by memory effects due to high formation in the incinerator during the start-up of the plant. These periods with generation of high levels of dioxins during the start-up are not normally recognized since the sampling of PCDD/Fs normally takes place only during stable operating conditions. Consequently, these authors suggested the continuous monitoring of PCDD/Fs in order to cover all modes of operation, including those with elevated dioxin emissions. Gullet et al. [5] had previously emphasized the importance of previous firing conditions on the emissions, resulting in uncertainty regarding the prediction of emissions based solely on the type and rate of co-fired HW. Recently, Choi et al. [6] investigated the PCDD/F concentrations in MSWIs and HWIs from Korea. Different types of wastes and different APCD combinations were evaluated. The range of PCDD/F concentrations was, in general terms, much higher than the regulated upper limit (0.1 ng TEQ/Nm^3). The results indicated that the concentrations of PCDD/Fs and dioxin-like PCBs from small incinerators were notably higher than those from large incinerators. They concluded that a number of incinerators were operating in ways not intended in their original design (for instance, waste composition, shorter operating time, lower combustion temperature, broken APCDs), what was determinant in their emissions. Kim et al. [10] reported the current management practices and emission status from Korean HWIs in order to develop MACT-like guidelines. They studied 3 HWIs, which burned different industrial wastes. The measured air pollutants included dust, heavy metals (Be, Cd, Cr, As, Pb, Ni, Zn, and Hg and its speciation), and VOCs. All the tested HWIs were within the existing Korean limits. The main heavy metals emitted were Ni, Cr, Zn, and Pb. Metal composition in emissions of each one of the HWIs was mainly related to the type of wastes burned, but also to the operating parameters and type of APCDs. Metal removal efficiency of existing APCD was above 99%, excepting mercury for which it was above 30%. All metals sampled were removed within the particulate control devices, with the exception of mercury, which exhibited a higher concentration in the flue gas. Due to its lower boiling point this element escapes the particulate control devices. Benzene, dichloromethane, styrene, ethylbenzene, toluene, *m,p*-xylene, and *o*-xylene were among the VOCs emitted from the stacks of the tested HWIs. The VOC concentrations, as single compounds were low, but in aggregate their contribution was higher. Recently, Van Caneghem et al. [90] compared the amounts of PCDD/Fs and other POPs in the input and the output of three BAT waste incinerators. They developed a methodology to weight the POPs in the input and output of waste incinerators based on minimal risk doses or cancer potency factors. The ratios of the weighed POP input over output clearly depended on the kind of incinerator. The mass balance for PCBs indicated that they were effectively destroyed during incineration in a rotary kiln. This kind of incineration was identified as a weighed POP sink. On the other hand, the grate furnace incinerating MSW was a weighed POP sink or source depending on the POP concentrations in the waste. However, the difference between the output and the input was rather limited. Previously, Kim et al. [91] found that the mean concentration of PCDD/Fs in the stack gas of a HWI in Korea was 1.91 ng I-TEQ/Nm^3. They considered that HWIs were probably the major source of PCDD/F emissions in Korea because of their high emission factors which was due to the poor operation and inadequate maintenance. The congener profiles were characterized by relatively high levels of OCDD, OCDF, 1,2,3,4,6,7,8-HpCDF, and 1,2,3,4,6,7,8-HpCDD. In a recent study, Rivera-Austrui et al. [2] monitored the emissions of a HWI in Spain using a mew methodology that allows measuring PCDD/Fs emitted by the stack in a continued way, instead of punctually. So far, the common practice, which is set by the Directive 200/76/EC, is sampling during periods of 8 h. The new continuous measurement was thought to be a more representative sampling, allowing a more precise assessment of the real emissions and potential impact on the environment. The continuous sampling was carried out on a monthly basis with a total number of 16 samples covering a period of 2 year emissions. In addition, short-term samples were collected in order to compare them with the continuous results. The monthly results varied from 0.11 to 0.077 ng TEQ/Nm^3, resulting in an average of 0.30 ng TEQ/Nm^3. With respect to the short-term sampling performed during the same period of time, the results varied

from 0.007 to 0.021 ng TEQ/Nm^3 (mean 0.012 ng TEQ/Nm^3). The average pattern of both methods was very similar. Nonetheless, subtle differences in the dioxin pattern were identified. The general PCDD/F patterns showed a higher amount of PCDFs than PCDDs in the flue gas. It was concluded that the emission factor for PCDD/F from "state-of-the-art" HWIs is largely overestimated compared with data continuously measured during 2 years.

Environmental and Human Biological Monitoring of Pollutants

As indicated above, few studies have investigated source samples. In contrast, environmental and biological monitoring is often used to evaluate the impact of pollutant sources and the human health risks. Environmental monitoring programs are common tools to control the state of pollution in a particular area or zone [92, 93]. These programs are used to assess the contribution of a potential contaminant source on the surrounding environment. Pollutant levels are determined in environmental matrices like air, water, soil, food, etc. For example, in industrial hygiene, air sampling has become prominent to evaluate workers exposure. For environmental impact, soil and vegetation are two of the most standardized monitors, since they can be easily collected and stored [94–96]. The atmospheric concentrations of environmental pollutants vary according to a number of factors, including the prevailing meteorological conditions. Because emissions of metals and PCDD/Fs from HWIs result in subsequent aerial deposition onto soil and plants, most monitoring programs utilize samples of these monitors. Soil and vegetation have been widely used as matrices of long-term and short-term accumulation, respectively, to environmental pollutants [97, 98]. The combination of different monitors is commonly used to get complementary information regarding punctual emissions (air), emissions during short periods of time (herbage reflects the deposition of pollution during few months), and emissions during long periods of time (soil reflects deposition during years). Environmental monitoring is especially necessary to identify sources of exposure and to facilitate measures for minimizing emissions. On the other hand, human biological monitoring has become an important tool in environmental and occupational medicine for the assessment of the levels of internal exposure to harmful substances taken up from general and occupational environments. Human biological monitoring may be used not only to evaluate the degree of internal exposure to an environmental pollutant of individuals or population groups, but also to evaluate temporal changes in the general population potentially exposed to a defined environmental contaminant [99–101]. It considers all routes of uptake and sources which are relevant. Human biomonitoring allows estimating the dose that is really taken up from the environment (internal dose). The internal doses of the pollutants in the different body tissues depend on their biokinetics and metabolism. The levels of rapidly disappearing biomarkers primarily reflect exposures during the initial hours. Moreover, biomarkers which disappear over the course of several weeks reflect one, several, or numerous exposure incidents occurring anytime during a period of various weeks previous to the measurement. Some toxicants accumulate in one or several tissues and are in dynamic equilibrium with the sites of toxicity. In the case of PCDD/Fs which basically accumulate in fats, the plasma PCDD/F concentrations reflect the amount stored in the body.

According to Angerer et al. [102], the requirements for a proper human biomonitoring of a certain chemical are:

(a) Suitable biomonitoring matrices
(b) Suitable parameters, which can be able to reflect internal exposure
(c) Suitable and reliable analytical methods which are kept under control by quality assurance
(d) Reference and limit values which enable the interpretation of results

Because accuracy is crucial, as trace levels are involved, to determine concentrations of chemicals and metabolites in biological samples require meticulous attention in both sampling process and analytical techniques. Biological monitors include not only blood and urine, the most commonly used biological matrices, but also hair, nails, breast milk, or adipose tissue, among others. The biomarker level has to be correlated with the health effect. One drawback of biological monitoring is that often it means an invasive method, especially when the collection of blood is

required. Blood is the medium which transports chemicals and their metabolites in the body. A chemical in the blood is in dynamic equilibrium with various body tissues. Therefore, most biomarkers present in the body can be found in the blood during some period of time after exposure. Urine is still more readily and available at large volumes, allowing the determination of very low concentrations of chemicals derived from environmental exposure. However, the selection of the most suitable monitor depends on the biokinetics of the pollutant and the kind of exposure (short- or long-term) that it is intended to determine. When the site of critical action for a toxicant is known, the concentration of the biomarker at that site can be a measure of the biologically effective dose.

As aforementioned, blood and urine are the most widely used biological matrices. The advantages of blood are based on the fact that the composition is relatively constant between individuals, avoiding the need to correct the biomarker levels for individual differences. In addition, obtaining samples is straightforward (although it is an invasive procedure). Urine is more suitable for monitoring hydrophilic chemicals, metals, and metabolites than for those chemicals poorly soluble in water. The concentration of the biomarker in urine is usually correlated to its mean plasma level during the period the urine dwells in the bladder. The accuracy of the exposure estimate, using urine monitoring, depends upon the sampling strategy. The most influential factors are the time of collection and urine output. For example, measurements from 24-h specimens are more representative than from spot samples, usually better correlating with the intensity of exposure. However, collection, stabilization, and transportation of 24-h specimens in the field are difficult and often not feasible.

Other frequently used biological monitors are human milk and adipose tissues, which are suitable for assessing exposure to POPs such as PCDD/Fs, PCBs, and polybrominated diphenyl ethers (PBDEs). These contaminants enter humans through environmental and dietary exposure. They reach the adipose tissue, serum, and milk and equilibrate at similar levels on a fat weight basis [103]. With long (5–10 years) half-lives, POPs persist in humans as they do in the environment. On the other hand, hair is used for metal biomonitoring. In this case, exogenous contamination, the kind of hair care, etc., are factors influencing the analytical results.

A Case Study: The HWI of Constantí (Catalonia, Spain)

In this section, the study of the impact of a HWI located in Constantí (Tarragona County, Catalonia, Spain) is widely described. To determine the potential environmental impact and the human health risks derived from emissions of that HWI, environmental and biological monitoring programs were developed for metals and PCDD/Fs before the facility initiated its regular operations. These programs remain still active in order to ensure the proper performance of the facility. Some of the main results, which have been already published in international journals, are here summarized.

In 1999, the new HWI initiated its regular operations. To date, this facility is still the only one of these characteristics in Spain. It is settled in an industrial area (including a big oil refinery, a chlor-alkali plant and other chemical facilities, and a municipal solid waste incinerator). The HWI has a rotator burning furnace that operates at a temperature of 1,100°C and can burn more than 30,000 t of HW per year. The emission control system consists of an electrostatic precipitator, a catalytic converter (selective catalysis reduction) and a humid scrubber. The HWI periodically controls the PCDD/F stack emission concentrations to ensure that the cleaning systems operate properly. Moreover, to determine the potential environmental impact and the human health risks derived from emissions of the HWI, in 1996 (during the construction of the facility), a wide environmental and biological monitoring program ("background") was started and continued since then. Measurements of PCDD/Fs and heavy metals in environmental matrices collected in the vicinity of the facility have been and are being performed. Soil and herbage samples are used to assess environmental pollution, as well as to indirectly estimate the environmental exposure for the population living in the area under potential influence of the emissions of the HWI [104–107]. On the other hand, to assess human health risks, samples of various tissues, hair, plasma, and breast milk had been collected in individuals living in

the vicinity of the facility [52, 108–113]. In addition, organochlorinated compounds and metals have been also monitored in blood and urine of the hypothetically most potentially exposed group of population, the HWI workers [114, 115]. All those monitoring data have been used to establish the temporal trends of PCDD/F and metal concentrations.

For the environmental program, the sampling sites were placed at different distances and wind directions from the HWI, comprehending both urban and rural areas. The concentrations of PCDD/Fs (I-TEQ) in soil and vegetation samples collected from 2003 to 2009 around the HWI of Constantí, as well as those obtained for the baseline (1998 survey; Fig. 6) showed notable fluctuations throughout the time, especially, in some specific sites. However, a general increasing tendency in PCDD/F concentrations in soils and herbage samples was not observed during the study [116]. The variations might have been caused by a number of reasons, such as the meteorological conditions occurring before the annual sampling, or the influence of local point/diffuse emission PCDD/F sources of unknown origin. This is a clear indicator that investigations of temporal trends require data collection from as many different sources as possible. Otherwise, the assessment of limited information (e.g., the use of a single compartment rather than multiple) may lead to significant misinterpretation of the current status. The environmental PCDD/F congener profiles, in both soil and vegetation, were very similar in the course of the campaigns. OCDD was the most important congener, followed by 1,2,3,4,6,7,8-HpCDD, OCDF, and 1,2,3,4,6,7,8-HpCDDF. It indicates similar significant environmental sources, even when the HWI was not operating (background levels in 1998). That entails a low impact of the HWI emissions in the surrounding environment. A particular study of the PCDD/F concentrations in environmental compartments, according to the distance to the HWI (Table 3), indicated that the highest levels of PCDD/Fs were found at the farthest distances

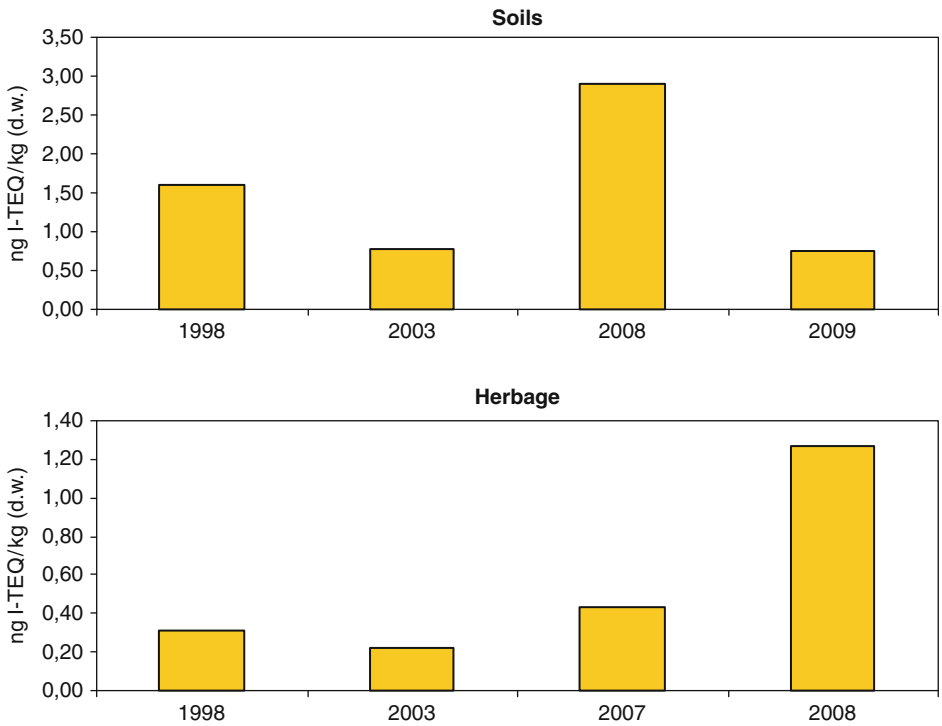

Hazardous Waste Incinerator Emissions. Figure 6
Total PCDD/F concentrations in soils and herbage collected around the HWI of Constantí (Catalonia, Spain) since 1998 (baseline study)

from the facility (>4,000 m), being 1.9- (2009) to 4.0-fold (1998) greater than those collected nearer the HWI (500 m).

With respect to the evaluation of population exposure, concentrations of PCDD/Fs and other organochlorinated compounds were determined in milk of women living in the area under direct influence of the HWI. Since it is well known that the diet is the main pathway of POP exposure for the general population, the influence of the dietary intake of these compounds on their presence in breast milk was also assessed. Milk samples were collected from women living in Tarragona County (Spain) in zones under potential influence of the HWI. The participants in the study were 25–35 years of age, who had lived in Tarragona County for at least the last 5 years. Only healthy primiparae mothers were included in the surveys. All participants completed questionnaires about age, current and former area of residence, as well as dietary habits and lifestyle. Samples were classified according to women living in urban or industrial zones. Detailed information about dietary intake of PCDD/Fs for the 1998, 2002, and 2007 surveys and their concentrations in foodstuffs were obtained from studies of our research group [117, 118]. Food samples included meats of beef (steak, hamburger), pork (loin, sausage), chicken (breast), lamb (steak), and meat products (ham, hot dogs, salami); fish (hake, sardine), shellfish (mussel), and tinned fish (tuna, sardine); vegetables (lettuce, tomato, potato, green beans, cauliflower); fresh fruits (apple, orange, pear); eggs; cow milk (whole, semi-skimmed) and dairy products (yogurt, cheese); cereals (bread, pasta, rice); pulses (lentils, beans); fats (margarine) and oils (olive, sunflower). Composites of 10 individual samples were pooled and analyzed for PCDD/Fs. Average daily food consumption data were obtained from studies carried out in the same area [117]. PCDD/F mean concentrations in the breast milk of women living in the area of

Hazardous Waste Incinerator Emissions. Table 3 Summary of PCDD/F concentrations (ng I-TEQ/kg dry weight) in soil and herbage samples according to the distance from the HWI of Constantí (Spain)

Monitor	Year	500 m	3,000 m	>4,000 m
Soil	1998	0.83 ± 0.41	0.75 ± 0.29	3.36 ± 5.03
	2003	0.59 ± 0.36	0.40 ± 0.30	1.28 ± 1.20
	2008	0.39 ± 0.09	13.2 ± 25.0	1.41 ± 1.73
	2009	0.66 ± 0.78	1.13 ± 1.27	1.23 ± 1.16
Herbage	1998	0.29 ± 0.16	0.21 ± 0.04	0.49 ± 0.58
	2003	0.20 ± 0.06	0.18 ± 0.08	0.22 ± 0.10
	2007	0.27 ± 0.09	0.32 ± 0.15	0.78 ± 0.56
	2008	0.57 ± 0.55	1.45 ± 1.27	1.77 ± 0.77

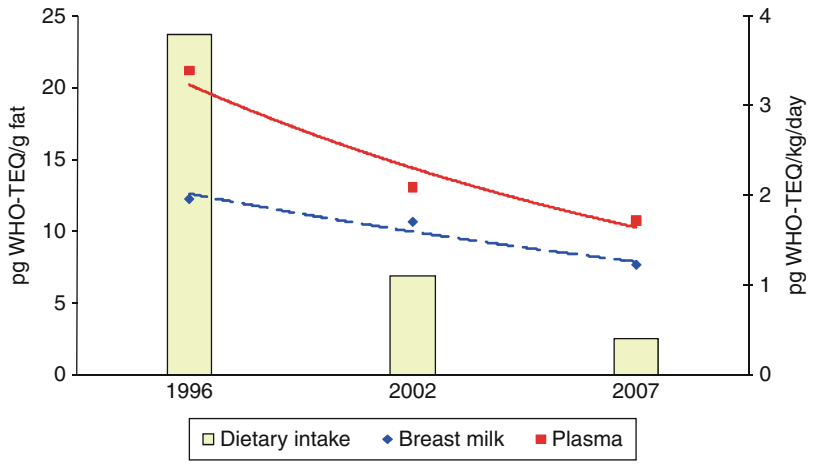

Hazardous Waste Incinerator Emissions. Figure 7
Temporal trends of PCDD/Fs in human plasma and breast milk, as well as comparison with dietary exposure to PCDD/Fs in studies performed in 1998 (baseline), 2002 and 2007

study were 12.2, 10.6, and 7.6 pg WHO-TEQ/g lipid in 1998, 2002, and 2007, respectively (Fig. 7). The historical trend of PCDD/Fs in breast milk of women living in the neighborhood of the HWI was in agreement with the continued decline observed in the emissions and atmospheric concentrations of POPs [119]. The dietary intakes of PCDD/Fs for the adult population were 210 pg I-TEQ/day, 63.80 pg WHO-TEQ/day, and 27.81 pg WHO-TEQ/day in 1998, 2002, and 2007, respectively. Furthermore, the decrease in the dietary intake of these pollutants was higher than the reduction observed in biological tissues (blood and milk), making evident that the effect of the decrease in the dietary intake of PCDD/Fs is not immediately reflected in a reduction of the PCDD/F concentrations in human plasma or milk [103]. Food contamination is primarily caused by airborne POPs that settle on plants and water and accumulate in the food chain, where they are particularly associated with fat. In the program here reported, and taking into account that the HWI is placed in an industrial zone without farms and cattle in the surroundings, it is important to remark that almost all foods consumed in the area come from a diversity of origins, without any direct relationship with the pollutants emitted by the HWI. It is also important to highlight that in recent years, the dietary habits in young women in Spain have changed.

Concerning metals, especially in environmental monitors, the results of a great number of studies, and also in this specific program performed during the last 10 years, show that it is quite usual to find fluctuations in the concentrations of metals through the monitoring period. As a result, if possible, it is important to combine the use of different matrices and maintain the study through a period of time long enough to detect possible changes and trends. It must be taken into account that in addition to combustion processes, environmental levels of metals can be notably influenced by a remarkable number of different emission sources. The HWI is located in an industrial zone, where a considerable number of chemical and petrochemical companies are settled in. Moreover, the area is surrounded by a highway and roads with a heavy traffic. Consequently, the potential impact of other sources must be specially considered. On the other hand, no significant correlation (Pearson) between soil and herbage concentrations was found for any of the analyzed elements. It means that root uptake of heavy metals by plants can be considered negligible. Likewise, the lack of a homogeneous change between soil and vegetation levels also means that other potential emission sources, different from incineration, could be even more important than in principle expected. To assess the influence of the HWI on the

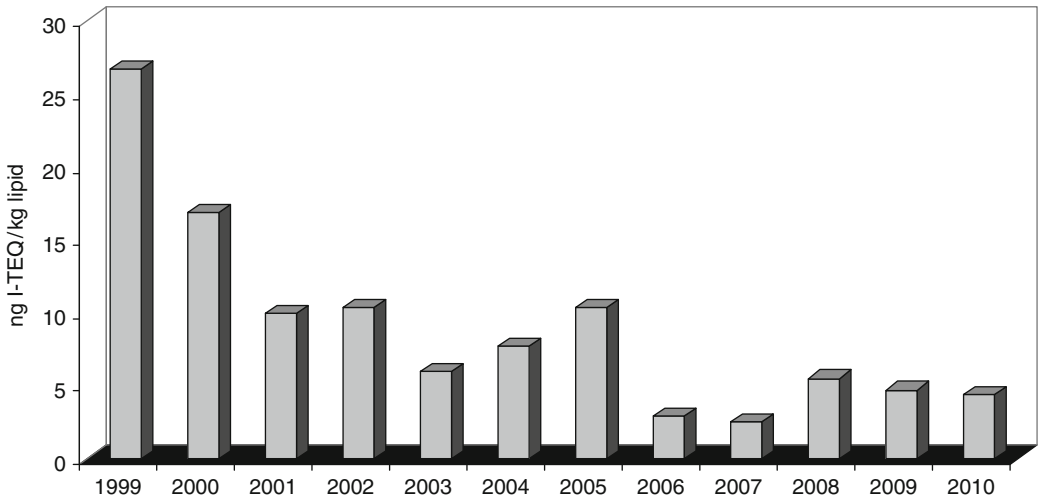

Hazardous Waste Incinerator Emissions. Figure 8
Temporal trends of concentrations of PCDD/Fs in plasma of workers at the HWI of Constantí (Spain) since the plant started its regular operations

area under its direct influence, sampling points collected at different distances and wind directions were grouped and analyzed for clustering. Only significant differences in metal concentrations appeared at distances >1.5 km from the plant, being an indicator that the HWI is not the main contributor of the presence of metals into the environmental area under evaluation. Data fluctuations would be due to the presence of other pollution sources (traffic, industrial activities, etc.) and/or to the environmental variations of these elements in the zone.

With regard to human exposure, the internal exposure of workers of the HWI to a number of organic substances such as PCDD/Fs has been assessed from the beginning of the activity. Information concerning health risks of workers in waste incinerators is rather scarce. In addition, most of these studies are more focused on workers in MSW incinerators (MSWI) than in those working at HWI. Baseline levels of these substances were determined in the future workers of the evaluated HWI during the period of construction of the facility, and since then, they have been annually performed. Figure 8 depicts the temporal trends of PCDD/F concentrations in plasma of the workers of the HWI [120]. A remarkable decrease was noted with respect to the baseline levels. As already commented, it is well established that for nonoccupationally exposed population, the main pathway of exposure to PCDD/Fs is the diet. Therefore, the results observed in the plasma levels of PCDD/Fs of the workers of the HWI indicated that not only the occupational exposure was not significant, but also an important reduction in the dietary intake during the last years, as it has been previously stated.

Future Directions

Hazardous waste incinerators might be a significant source of a wide range of pollutants if stack gases are not properly treated. In fact, in the past, they were a leading source of dioxin emissions to the environment. The composition of the emissions depends on the composition of the materials burned and also on the combustion conditions and air pollution devices used to clean them. Although PCDD/Fs and metals are found at rather low concentrations in comparison with other pollutants, they are among the contaminants that raise more concern for the population and public opinion because of their persistence, toxicity, and capacity of bioaccumulation. When the burning conditions and the APCD used are suitable, pollutant emissions from HWIs are low. However, when incinerators are operating in ways not intended in their original design, emissions may be then significant. Moreover, the emissions of some pollutants, especially PCDD/Fs, vary when operating conditions are not stable (e.g., star up). Legislative regulations indicate that emissions of PCDD/Fs from waste incinerators must be monitored once or twice a year, and when operating conditions are stable. However, that means an underestimation of the real emissions because in unstable conditions emissions are higher. Recent advances in the methodologies for stack emissions measurements of PCDD/Fs already allow measuring their concentrations in continuous. However, few studies have investigated source samples. Instead of that, environmental and biological monitoring is frequently carried out to evaluate the impact of pollutant sources and human health risks. Environmental monitoring programs are common tools to control the state of pollution in a particular area. These programs are used to assess the contribution of a potential contaminant source on the global environment. Chemical pollutants are determined in environmental matrices as air, water, soil, and food. Human biological monitoring has become an important tool in environmental and occupational medicine for assessment of the levels of internal exposure to harmful substances taken up from the environment. The selection of the most suitable biomonitors depends on the biokinetics of the pollutant and the kind of exposure (short- or long- time), which should be determined. Although blood and urine are the most common, others like breast milk, hair, etc., are also commonly used.

The environmental and human impact of the HWI located in Constantí (Spain) has been evaluated since it started to regularly operate in 1999. The concentrations of heavy metals and PCDD/Fs have been determined in environmental monitors around the facility and also in biomonitors of the nearby population, as well as in workers. So far, the results indicate that the emissions of the HWI do not mean a significant source of PCDD/Fs and metal pollution in the area. However, some results, especially those of heavy metals in environmental monitors show sometimes

certain fluctuations. It is a clear indicator that investigations of temporal trends require data collection from as many different sources as possible. Otherwise, the assessment of limited information might lead to significant misinterpretation of the current situation. The global PCDD/F pattern analysis of the environmental and biological samples have shown that the weight of the PCDD/F stack emissions of the HWI on the environmental burden and on exposure of the individuals living in the surroundings of the facility is not significant in relation to the background levels. These results are in agreement with those of other of recent studies where the repercussion of incinerators, especially those in the EU, has been evaluated. These investigations clearly state that waste-to-energy plants using BAT and BEP to meet the stringent emission standards, result in a high reduction in expected risks with respect to older plants with no specific PCDD/F control measures [120]. Therefore, it is clear that if waste incineration plants are equipped with BAT, the presence of these facilities should not mean additional human health risks of exposure to PCDD/Fs (and metals). In the EU, the current Directive 2008/98/EC or Waste Framework Directive (WFD) sets the basic concepts and definitions related to waste management, proposing a hierarchy in the alternatives for waste treatment. In this prioritization, incineration involving the recovery of energy (or waste-to-energy) is enhanced, after prevention, reuse, and recycling of waste. In this context, waste management planning includes the future construction of new incineration plants, some of them for the management of HW. Although this kind of facilities are constrained to follow strict regulations regarding the emissions of chemical pollutants, such as dioxins and mercury, a special control of the air quality around incineration plants must follow through the execution of environmental monitoring programs to assure that their operative activities do not pose a risk for the public health and the environment in a long term.

Bibliography

1. UNEP (2009) Developing integrated solid waste management plan, vol 2: assessment of current waste management system and gaps therein. United Nations Environmental Programme Division of Technology, Industry and Economics International Environmental Technology Centre, Osaka/Shiga
2. Rivera-Austrui J, Borrajo M, Martinez K, Adrados M, Abalos M, Van Bavel B, Rivera J, Abad E (2011) Assessment of polychlorinated dibenzo-p-dioxin and dibenzofuran emissions from a hazardous waste incineration plant using long-term sampling equipment. Chemosphere 82:1343–1349
3. Olie K, Vermeulen PL, Hutzinger O (1977) Chlorodibenzo-*p*-dioxins and chlorodibenzofurans are trace components of fly ash and flue gas of some municipal incinerators in the Netherlands. Chemosphere 8:455–459
4. UNILABS Environmental (2001) Characterisation and estimation of dioxin and furan emissions from waste incineration facilities. www.environment.gov.au/settlements/publications/chemicals/dioxins/dioxinemissions.html
5. Gullett BK, Touati A, Lee C (2000) Formation of chlorinated dioxins and furans in a hazardous-waste-firing industrial boiler. Environ Sci Technol 34:2069–2074
6. Choi K-I, Lee S-H, Lee D-H (2008) Emissions of PCDDs/DFs and dioxin-like PCBs from small waste incinerators in Korea. Atmos Environ 42:940–948
7. Rimmer DL, Vizard CG, Pless-Mulloli T, Singleton I, Air VS, Keatinge ZA (2006) Metal contamination of urban soils in the vicinity of a municipal waste incinerator: one source among many. Sci Total Environ 356:207–216
8. Jung CH, Matsuto T, Tanaka N, Okada, T (2004) Metal distribution in incineration residues of municipal solid waste (MSW) in Japan. Waste Manage 24:381–391
9. Donnelly JR (1992) Metal emissions control technologies for waste incineration. In: Series AS (ed) Clean energy from waste and coal. American Chemical Society, Washington, DC, pp 174–188
10. Kim JH, Seo YC, Pudasainee D, Lee SH, Cho SJ, Jang HN, Park JM, Song GJ, Park KS (2009) Efforts to develop regulations in Korea similar to the US maximum achievable control technology (MACT) regulations for hazardous waste incinerators. J Mat Cycl Waste Manage 11(3):183–190
11. Kutz FW, Barnes DG, Bottimore DP, Greim H, Bretthauer EW (1990) The international toxicity equivalency factor (I-TEF) method of risk assessment for complex mixtures of dioxins and related compounds. Chemosphere 20:751–757
12. Van den Berg M, Birnbaum LS, Denison M, De Vito M, Farland W, Feeley M, Fiedler H, Hakansson H, Hanberg A, Haws L, Rose M, Safe S, Schrenk D, Tohyama C, Tritscher A, Tuomisto J, Tysklind M, Walker N, Peterson RE (2006) The 2005 World Health Organization reevaluation of human and Mammalian toxic equivalency factors for dioxins and dioxin-like compounds. Toxicol Sci 93(2):223–241
13. NATO (1988) International toxicity equivalence factors (I-TEF) method of risk assessment for complex mixtures of dioxins and related compounds. Pilot study on international information exchange on dioxins and related compounds, Report number 176, Aug 1988. North Atlantic Treaty Organisation, Committee on Challenges of Modern Society
14. Kimbrough RD (1995) Polychlorinated biphenyls (PCBs) and human health: an update. Crit Rev Toxicol 25:133–163

15. ATSDR (2000) Polychlorinated biphenyls. Agency for Toxic Substances and Disease Registry, Atlanta
16. Aoki Y (2001) Polychlorinated biphenyls, polychlorinated dibenzo-*p*-dioxins, and polychlorinated dibenzofurans as endocrine disrupters – what we have learned from Yusho disease. Environ Res 86:2–11
17. IARC (1995) Monograph volumes 1972–1994. WHO, Geneva, pp 1–60. www.holgr/medical/nuclear/carcinogen.htm
18. Negri E, Bosetti C, Fattore E, La Vecchia C (2003) Environmental exposure to polychlorinated biphenyls (PCBs) and breast cancer: a systematic review of the epidemiological evidence. Eur J Cancer Prev 12:509–516
19. Helm PA, Bidleman TF (2003) Current combustion-related sources contribute to polychlorinated naphthalene and dioxin-like polychlorinated biphenyl levels and profiles in air in Toronto, Canada. Environ Sci Technol 37:1075–1082
20. Meijer SN, Harner T, Helm PA, Halsall CJ, Johnston AE, Jones KC (2001) Polychlorinated naphthalenes in U.K. soils: time trends, markers of source, and equilibrium status. Environ Sci Technol 35:4205–4213
21. Lin Y, Gupta G, Baker J (1995) Photodegradation of polychlorinated biphenyl congeners using simulated sunlight and diethylamine. Chemosphere 31:3323–3344
22. Gouin T, Cousins I, Mackay D (2004) Comparison of two methods for obtaining degradation half-lives. Chemosphere 56:531–535
23. Sinkkonen S, Paasivirta J (2000) Degradation half-life times of PCDDs, PCDFs and PCBs for environmental fate modeling. Chemosphere 40:943–949
24. Shirai JH, Kissel JC (1996) Uncertainty in estimated half-lives of PCBs in humans: impact on exposure assessment. Sci Total Environ 187:199–210
25. Brown JF (1994) Determination of PCB metabolic, excretion, and accumulation rates for use as indicators of biological response and relative risk. Environ Sci Technol 28:2295–2305
26. Nizzetto L, Cassani C, Di Guardo A (2006) Deposition of PCBs in mountains: the forest filter effect of different forest ecosystem types. Ecotoxicol Environ Safe 63:75–83
27. Falandysz J (1998) Polychlorinated naphthalenes: an environmental update. Environ Pollut 101:77–90
28. Blankenship AL, Kannan K, Villalobos SA, Villeneuve DL, Falandysz J, Imagawa T, Jakobsson E, Giesy JP (2000) Relative potencies of individual polychlorinated naphthalenes and halowax mixtures to induce Ah receptor-mediated responses. Environ Sci Technol 34:3153–3158
29. Hayward D (1998) Identification of bioaccumulating polychlorinated naphthalenes and their toxicological significance. Environ Res 76:1–18
30. Van den Berg M, Peterson RE, Schrenk D (2000) Human risk assessment and TEFs. Food Addit Contam 17:347–358
31. Kannan K, Hilscherova K, Imagawa T, Yamashita N, Williams LL, Giesy JP (2001) Polychlorinated naphthalenes, -biphenyls, -dibenzo-*p*-dioxins, and -dibenzofurans in double-crested cormorants and herring gulls from Michigan waters of the Great Lakes. Environ Sci Technol 35:441–447
32. Eljarrat E, Barcelo D (2003) Priority lists for persistent organic pollutants and emergingcontaminants based on their relative toxic potency in environmental samples. Trend Anal Chem 22:655–665
33. Jarnberg U, Asplund L, De Wit C, Grafstrom AK, Haglund P, Jansson B, Lexen K, Strandell M, Olsson M, Jonsson B (1993) Polychlorinated biphenyls and polychlorinated naphthalenes in Swedish sediment and biota: levels, patterns, and time trends. Environ Sci Technol 27:1364–1374
34. Schneider M, Stieglitz L, Will R, Zwick G (1998) Formation of polychlorinated naphthalenes on fly ash. Chemosphere 37:2055–2070
35. Abad E, Caixach J, Rivera J (1999) Dioxin like compounds from municipal waste incinerator emissions: assessment of the presence of polychlorinated naphthalenes. Chemosphere 38:109–120
36. Kannan K, Imagawa T, Blankenship AL, Giesy JP (1998) Isomer-specific analysis and toxic evaluation of polychlorinated naphthalenes in soil, sediment, and biota collected near the site of a former chlor-alkali plant. Environ Sci Technol 32: 2507–2514
37. Yamashita N, Kannan K, Imagawa T, Miyazaki A, Giesy JP (2000) Concentrations and profiles of polychlorinated naphthalene congeners in eighteen technical polychlorinated biphenyl preparations. Environ Sci Technol 34:4242–4254
38. Meijer SN, Ockenden WA, Steinnes E, Corrigan BP, Jones KC (2003) Spatial and temporal trends of POPs in Norwegian and UK background air: Implications for global cycling. Environ Sci Technol 37:454–461
39. Harner T, Bidleman TF (1998) Measurement of octanol-air partition coefficients for polycyclic aromatic hydrocarbons and polychlorinated naphthalenes. J Chem Eng Data 43: 40–46
40. Domingo JL (2004) Polychlorinated naphthalenes in animal aquatic species and human exposure through the diet: a review. J Chromat A 1054:327–334
41. Opperhuizen A, van der Velde EW, Gobas FAPC, Liem DAK, van der Steen JMD (1985) Relationship between bioconcentration in fish and steric factors of hydrophobic chemicals. Chemosphere 14:1871–1896
42. Hanari N, Horii Y, Taniyasu S, Falandysz J, Bochentin I, Orlikowska A, Puzyn T, Yamashita N (2004) Isomer specific analysis of polychlorinated naphthalenes in pine trees (*Pinus thunbergi* Parl.) and (*Pinus densiflora* Sieb. et Zucc) needles around Tokyo Bay, Japan. Pol J Environ Stud 13:139–151
43. Crookes MJ, Howe PP (1993) Environmental hazard assessment: halogenated naphthalenes. Department of the Environment, Directorate for Air, Climate and Toxic Substances, Toxic Substances Division, Garston
44. Van de Plassche E, Schwegler A, Iestra W (2002) Polychlorinated naphthalenes and the UN-ECE POP protocol. Organohal Compd 58:89–91
45. Breivik K, Alcock R, Li Y-F, Bailey RE, Fierens S, Pacyna JM (2004) Primary sources of selected POPs: regional and global scale emission inventories. Environ Pollut 128:3–16

46. Lönnermark A, Blomqvist P, Marklund S (2008) Emissions from simulated deep-seated fires in domestic waste. Chemosphere 70:626–639
47. ATSDR (2002) Toxicological profile for hexachlorobenzene. U.S. Public Health Services, U.S. Department of Health and Human Services, Atlanta
48. Messerer P, Zober A, Becher H (1998) Blood lipid concentrations of dioxins and furans in a sample of BASF employees included in the IARC registry of workers exposed to phenoxy acid herbicides and/or chlorophenols. Environ Health Perspect 106:733–735
49. ATSDR (2000) Toxicological profile for arsenic. US Department of Health and Human Services, Public Health Service, Agency for Toxic Substances and Disease Registry, Atlanta
50. Basu A, Mahata J, Gupta S, Giri AK (2001) Genetic toxicology of a paradoxical human carcinogen, arsenic: a review. Mutat Res 488:171–194
51. Pongratz R (1998) Arsenic speciation in environmental samples of contaminated soil. Sci Total Environ 224:133–141
52. Nadal M, Perelló G, Schuhmacher M, Cid J, Domingo JL (2008) Concentrations of PCDD/PCDFs in plasma of subjects living in the vicinity of a hazardous waste incinerator: follow-up and modeling validation. Chemosphere 73:901–906
53. Fattorini D, Alonso-Hernandez CM, Diaz-Asencio M, Munoz-Caravaca A, Pannacciulli FG, Tangherlini M, Regoli F (2004) Chemical speciation of arsenic in different marine organisms: Importance in monitoring studies. Marine Environ Res 58:845–850
54. IARC (1987) Overall evaluations of carcinogenicity: an updating of IARC monographs. In: IARC Monographs on the evaluation of carcinogenic risks to humans, vol 1–42(suppl 7). International Agency for Research on Cancer, Lyon
55. Rossman TG, Uddin AN, Burns FJ (2004) Evidence that arsenite acts as a cocarcinogen in skin cancer. Toxicol Appl Pharmacol 198:394–404
56. Huff J, Chan P, Nyska A (2000) Is the human carcinogen arsenic carcinogenic to laboratory animals? Toxicol Sci 55:17–23
57. ATSDR (2002) Toxicological profile for beryllium. Department of Health and Human Services, Atlanta
58. US EPA (2010) Preliminary remediation goals. www.epa.gov/region9/superfund/prg/. Accessed 13 Apr 2011
59. Baldwin DR, Marshall WJ (1999) Heavy metal poisoning and its laboratory investigation. Ann Clin Biochem 36:267–300
60. Robards K, Worsford P (1991) Cadmium: toxicology and analysis. A review. Analyst 116:549–568
61. McElroy JA, Shafer MM, Trentham-Dietz A, Hampton JM, Newcomb PA (2006) Cadmium exposure and breast cancer risk. J Nat Cancer Inst 98:869–873
62. Kasuya MR (2000) Recent epidemiological studies on itai-itai disease as a chronic cadmium poisoning in Japan. Water Sci Technol 42:147–154
63. Satarug S, Moore MR (2004) Adverse health effects of chronic exposure to Low-level cadmium in foodstuffs and cigarette smoke. Environ Health Perspect 112:1099–1103
64. Linna A, Oksa P, Palmroos P, Roto P, Laippala P, Uitti J (2003) Respiratory health of cobalt production workers. Am J Ind Med 44:124–132
65. ATSDR (2004) Toxicological profile for cobalt. Department of Health and Human Services, Atlanta
66. ATSDR (2004) Toxicological profile for copper. Department of Health and Human Services, Atlanta
67. Singh J, Carlisle DL, Pritchard DE, Patierno SR (1998) Chromium-induced genotoxicity and apoptosis: relationship to chromium carcinogenesis (review). Oncol Rep 5:1307–1318
68. Vaglenov A, Nosko M, Georgieva R, Carbonell E, Creus A, Marcos R (1999) Genotoxicity and radioresistance in electroplating workers exposed to chromium. Mutat Res 446(1):23–34
69. ATSDR (2000) Toxicological profile for chromium. US Department of Health and Human Services, Public Health Service, Agency for Toxic Substances and Disease Registry, Atlanta
70. IARC (1990) Chromium and chromium compounds. In: IARC Monographs on the evaluation of carcinogenic risks to humans, vol 49. International Agency for the Research on Cancer, Lyon
71. ATSDR (2005) Toxicological profile for tin. Department of Health and Human Services, Atlanta
72. ATSDR (2000) Toxicological profile for manganese. US Department of Health and Human Services, Public Health Service, Agency for Toxic Substances and Disease Registry, Atlanta
73. Josephs KA, Ahlskog JE, Klos KJ, Kumar N, Fealey RD, Trenerry MR, Cowl CT (2005) Neurologic manifestations in welders with pallidal MRI T1 hyperintensity. Neurology 64:2033–2039
74. ATSDR (1999) Toxicological profile for mercury. US Department of Health and Human Services, Public Health Service, Agency for Toxic Substances and Disease Registry, Atlanta
75. Chang MB, Wu HT, Huang CK (2000) Evaluation on speciation and removal efficiencies of mercury from municipal solid waste incinerators in Taiwan. Sci Total Environ 246:165–173
76. Karimi A, Moniri F, Nasihatkon A, Zarepoor MJ, Alborzi A (2002) Mercury exposure among residents of a building block in Shirz, Iran. Environ Res A 88:41–43
77. Ekino S, Susa M, Ninomiya T, Imamura K, Kitamura T (2007) Minamata disease revisited: an update on the acute and chronic manifestations of methyl mercury poisoning. J Neurol Sci 262:131–144
78. Horng CJ, Tsai JL, Lin SR (1999) Determination of urinary arsenic, mercury, and selenium in steel production workers. Biol Trace Elem Res 70:29–40
79. ATSDR (2005) Toxicological profile for nickel. U.S. Public Health Services, U.S. Department of Health and Human Services, Atlanta
80. Finkelstein Y, Markowitz ME, Rosen JF (1998) Low-level lead-induced neurotoxicity in children: an update on central nervous system effects. Brain Res Rev 27:168–176
81. Torrente M, Colomina MT, Domingo JL (2005) Metal concentrations in hair and cognitive assessment in an adolescent population. Biol Trace Elem Res 104:215–221

82. Navas-Acien A, Schwartz BS, Rothenberg SJ, Hu H, Silbergeld EK, Guallar E (2008) Bone lead levels and blood pressure endpoints: a meta-analysis. Epidemiology 19:496–504
83. dos Santos ACD, Colacciopo S, Dal Bó CMR, dos Santos NAG (1994) Occupational exposure to lead, kidney function tests, and blood pressure. Am J Ind Med 26:635–645
84. Saha A (2005) Thallium toxicity: a growing concern. Indian J Occup Environ Med 9:53–56
85. ATSDR (1992) Toxicological profile for thallium. Department of Health and Human Services, Atlanta
86. ATSDR (1992) Toxicological profile for vanadium. Department of Health and Human Services, Atlanta
87. Hinshaw GD, Trenholm AR (2001) Hazardous waste incineration in perspective. Waste Manage 21:471–475
88. van Velzen D, Langenkamp H, Herb G (2002) Review: mercury in waste incineration. Waste Manage Res 20:556–568
89. Löthgren C-J, van Bavel B (2005) Dioxin emissions after installation of a polishing wet scrubber in a hazardous waste incineration facility. Chemosphere 61(3):405–412
90. Van Caneghem J, Block C, Van Brecht A, Wauters G, Vandecasteele C (2010) Mass balance for POPs in hazardous and municipal solid waste incinerators. Chemosphere 78: 701–708
91. Kim B-H, Lee S-J, Mun S-J, Chang Y-S (2005) A case study of dioxin monitoring in and around an industrial waste incinerator in Korea. Chemosphere 58:1589–1599
92. Morselli L, Passarini F, Bartoli M (2002) The environmental fate of heavy metals arising from a MSW incineration plant. Waste Manage Res 22:875–881
93. Ahammed AKMR, Nixon BM (2006) Environmental impact monitoring in the EIA process of South Australia. Environ Impact Assess Rev 26(5):426–447
94. Klumpp A, Klumpp G, Domingos M (1994) Plants as bioindicators of air pollution at the Serra do Mar near the industrial complex of Cubatao, Brazil. Environ Pollut 85:109–116
95. Moraes RM, Klumpp A, Furlan CM, Klumpp G, Domingos M, Rinaldi MC, Modesto IF (2002) Tropical fruit trees as bioindicators of industrial pollution in southeast Brazil. Environ Int 28:367–374
96. Ho YB, Tai KM (1988) Elevated levels of lead and other metals in roadside soil and grass and their use to monitor aerial metal depositions in Hong Kong. Environ Pollut 49:37–51
97. Meneses M, Llobet JM, Granero S, Schuhmacher M, Domingo JL (1999) Monitoring metals in the vicinity of a municipal waste incinerator: temporal variation in soils and vegetation. Sci Total Environ 226(2–3):157–164
98. Nadal M, Schuhmacher M, Domingo JL (2004) Metal pollution of soils and vegetation in an area with petrochemical industry. Sci Total Environ 321:59–69
99. Ewers U, Krause C, Schulz C, Wilhelm M (1999) Reference values and human biological monitoring values for environmental toxins. Report on the work and recommendations of the commission on human biological monitoring of the German Federal Environmental Agency. Int Arch Occup Environ Health 72:255–260
100. Paustenbach D, Galbraith D (2006) Biomonitoring: is body burden relevant to public health? Regul Toxicol Pharmacol 44:249–261
101. Calafat AM, Ye X, Silva MJ, Kuklenyik Z, Needham LL (2006) Human exposure assessment to environmental chemicals using biomonitoring. Int J Androl 29:166–171
102. Angerer J, Ewers U, Wilhelm M (2007) Human biomonitoring: state of the art. Int J Hyg Environ Health 210:201–228
103. Schuhmacher M, Kiviranta H, Ruokojärvi P, Nadal M, Domingo JL (2009) Concentrations of PCDD/Fs, PCBs and PBDEs in breast milk of women from Catalonia, Spain: a follow-up study. Environ Int 35:607–613
104. Schuhmacher M, Agramunt MC, Rodriguez-Larena MC, Díaz-Ferrero J, Domingo JL (2002) Baseline levels of PCDD/Fs in soil and herbage samples collected in the vicinity of a new hazardous waste incinerator in Catalonia, Spain. Chemosphere 46:1343–1350
105. Schuhmacher M, Rodriguez-Larena MC, Agramunt MC, Diaz-Ferrero J, Domingo JL (2002) Environmental impact of a new hazardous waste incinerator in Catalonia, Spain: PCDD/PCDF levels in herbage samples. Chemosphere 48:187–193
106. Mari M, Nadal M, Ferré-Huguet N, Schuhmacher M, Borrajo M, Domingo JL (2007) Monitoring PCDD/Fs in soil and herbage samples collected near a hazardous waste incinerator. Health risks for the population living nearby. Human Ecol Risk Assess 13:1255–1270
107. Nadal M, Bocio A, Schuhmacher M, Domingo JL (2005) Trends in the levels of metals in soils and vegetation samples collected near a hazardous waste incinerator. Arch Environ Contam Toxicol 49:290–298
108. Nadal M, Domingo JL, García F, Schuhmacher M (2009) Levels of PCDD/F in adipose tissue on non-occupationally exposed subjects living near a hazardous waste incinerator in Catalonia, Spain. Chemosphere 74:1471–1476
109. Nadal M, Espinosa G, Schuhmacher M, Domingo JL (2004) Patterns of PCDDs and PCDFs in human milk and food and their characterization by artificial neural networks. Chemosphere 54:1375–1382
110. Schuhmacher M, Domingo JL, Hagberg J, Lindström G (2004) PCDD/F and non-ortho PCB concentrations in adipose tissue of individuals living in the vicinity of a hazardous waste incinerator. Chemosphere 57:357–364
111. Schuhmacher M, Domingo JL, Llobet JM, Kiviranta H, Vartiainen T (1999) PCDD/F concentrations in milk of nonoccupationally exposed women living in southern Catalonia, Spain. Chemosphere 38:995–1004
112. Schuhmacher M, Domingo JL, Llobet JM, Lindström G, Wingfors H (1999) Dioxin and dibenzofuran concentrations in adipose tissue of a general population from Tarragona, Spain. Chemosphere 38:2475–2487
113. Schuhmacher M, Domingo JL, Llobet JM, Lindström G, Wingfors H (1999) Dioxin and dibenzofuran concentrations in blood of a general population from Tarragona, Spain. Chemosphere 38:1123–1133

114. Mari M, Borrajo MA, Schuhmacher M, Domingo JL (2007) Monitoring PCDD/Fs and other organic substances in workers of a hazardous waste incinerator: a case study. Chemosphere 67:574–581
115. Carmen Agramunt M, Domingo A, Domingo JL, Corbella J (2003) Monitoring internal exposure to metals and organic substances in workers at a hazardous waste incinerator after 3 years of operation. Toxicol Lett 146:83–91
116. Vilavert L, Nadal M, Mari M, Schuhmacher M, Domingo JL (2010) Monitoring temporal trends in environmental levels of polychlorinated dibenzo-*p*-dioxins and dibenzofurans: results from a 10-year surveillance program of a hazardous waste incinerator. Arch Environ Contam Toxicol 59:521–531
117. Martí-Cid R, Bocio A, Domingo JL (2008) Dietary exposure to PCDD/PCDFs by individuals living near a hazardous waste incinerator in Catalonia, Spain: temporal trend. Chemosphere 70:1588–1595
118. Bocio A, Domingo JL (2005) Daily intake of polychlorinated dibenzo-p-dioxins/polychlorinated dibenzofurans (PCDD/PCDFs) in foodstuffs consumed in Tarragona, Spain: a review of recent studies (2001–2003) on human PCDD/PCDF exposure through the diet. Environ Res 97:1–9
119. Hassanin A, Lee RGM, Johnston AE, Jones KC (2006) Reductions and changing patterns of ambient PCDD/Fs in the UK: evidence and implications. Chemosphere 65: 530–539
120. Mari M, Schuhmacher M, Domingo JL (2009) Levels of metals and organic substances in workers at a hazardous waste incinerator: a follow-up study. Int Arch Occup Environ Health 82:519–528

Hazardous Waste, Introduction

Mervin Fingas
Spill Science, Edmonton, AB, Canada

Hazardous waste refers to any waste material that contains toxic or potentially toxic substances. These toxic substances may range from mildly toxic up to highly toxic and may even include highly radioactive materials (see ► Hazardous Materials Characterization and Assessment). The first important definition of a hazardous material mix or stream is an exacting definition of a particular waste stream, its variances and potential contents. The variances in the hazardous content also constitute an important characteristic of the waste. In addition, such waste streams often have measurements such as toxicity testing and other characterization by various testing methods. The hazards considered in hazardous waste are many, including physical hazards such as explosive characteristics, health hazards, and environmental hazards.

Industrial hazardous waste is also a topic here and is often thought of as the true hazardous waste. In reality, this waste is often mixed with domestic waste. Sometimes as well, industrial hazardous waste is treated as a separate waste stream. Industrial wastes are often subject to specific legislation as regards disposal. Often, specific waste streams are subject to detailed legislation regarding disposal. Items of this type include batteries, electronic equipment, mercury-containing products, heavy-metal-containing products, ash from incinerators or crematoriums, refrigerants, etc.

The methods of dealing with hazardous waste are as varied as the waste itself. This section has been divided into incineration methods and non-incineration methods. The incineration methods are very important in terms of low-level hazardous waste, especially that containing municipal waste. Non-incineration methods include landfilling, a method not covered in this encyclopedia, vitrification, solidification/stabilization, specific treatment methodologies, and specific product recycling (► Non-Flame Incineration).

Incineration has developed to a great extent in the past generation. In the past, the problems with incineration, particularly those of the gaseous or stack emissions, and the problems with ash disposal were very limiting to the technology for hazardous waste. Extensive development has led to the better control of these emissions and provided means to deal with incinerator ash. More about this will be discussed later. Incineration is particularly used at this time to deal with organic wastes such as contaminated municipal waste, fuels, and combustible streams.

Related methods include pyrolysis, the heating of materials to high temperatures, without combustion, and thermal desorption. The latter are heating of waste to high temperatures to remove volatiles such as gasoline and diesel fuel. This is now used frequently to deal with soils contaminated with fuels. These methods are still largely under development at this time, however, have specific applicability.

Non-incineration methods include landfilling. Landfilling is the traditional method of dealing with low-level hazardous waste but has rapidly fallen out of favor because of leaching and other problems. The modern use of engineered landfills has changed this somewhat. Engineered landfills include liners to avoid leaching, surface cover to avoid passage of water through the fill, and relief or recovery of gases produced by the decomposing fill.

Of course, among the non-incineration methods is the desirable method of recycling or partial recycling. This is less applicable to hazardous waste than to domestic waste; however, it is increasingly being invoked. Among the materials, solvents, metals, and similar materials are increasingly being recovered.

Another consideration, especially applicable to incineration, is the recovery of energy. Many incineration plants now recover the heat from combustion and convert it to electricity. This is, of course, applicable to hazardous waste that contains sufficient amount of combustible materials. The concept of energy recovery is most often applied to domestic waste which typically contains sufficient caloric value to be economically recovered.

Vitrification is another technology that is useful for dealing with certain types of hazardous materials (► Vitrification of Waste and Reuse of Waste-derived Glass). Amorphous glasses form from the oxides of many materials, especially silica. Vitrification is sometimes applied to metal oxides and radioactive materials. These hazardous waste materials can be added to glasses to form a stable new glass. This material is typically disposed of rather than used in any manner. Such glasses can be stable for millennia.

Incineration continues to be a major disposal mechanism for hazardous wastes (► Incineration Technologies). The issues with incineration continue to be a topic of constant research. These issues include emissions and formation of new compounds. The control factors for incineration include oxygenation, temperature, and residence time. These factors, in turn, strongly influence emission type and amount. Most incinerators include several stages of flue gas cleaning to minimize emissions. Many incinerators have residue or ash conditioning to ensure that these materials can safely be disposed of. There are many types of incinerators, and some are finding increasing utility in the disposal of hazardous materials. Fluidized bed incinerators are very popular and are able to handle many types of wastes. Rotary-kiln incinerators continue to find an important place in hazardous waste destruction. Variants on this include the use of cement kilns to burn organic materials.

Emissions of concern from incinerators are of a wide variety (► Hazardous Waste Incinerator Emissions). The formation of dioxins is certainly a prime topic. Dioxins are toxic chlorinated compounds likely formed from certain specific precursors containing chlorine. Their formation is strongly influenced in incinerators by the temperature. Dioxins partition to particulates in the stack and therefore can be somewhat removed along with the particulates in emission control features such as bag houses. Other POPs or persistent organic pollutants that constitute emission concerns include PCBs or polychlorinated biphenyls (which are also a dioxin precursors), PAHs or polycyclic aromatic hydrocarbons, PCNs or polychlorinated naphthalenes, HCB or hexachlorobenzene, chlorinated phenols, etc.

A prime emission of concern is the metal mercury. Other metals of concern include cadmium, lead, arsenic, and cobalt. Several mechanisms are being investigated to control these emissions.

Gaseous emissions include SO_2, NO_2, HCl, and HF. Incinerators are now often equipped with various flue gas–scrubbing devices which are effective at removing some of these gases, especially SO_2.

The ashes from incinerators also constitute a concern and are a hazardous waste in themselves (► Hazardous Waste Incineration Ashes and their Utilization). Newer technologies are in place to minimize the metal and POP content in ashes. Ashes are currently sometimes used in a variety of ways. One way that is frequent is the use of ashes to produce construction aggregates. Another way is to add to the mix in producing cements such as Portland cement.

There is a strong research interest in reducing and dealing with hazardous waste. Each year produces new and better technologies in this field.

Health Physics

John W. Poston, Sr.
Department of Nuclear Engineering,
Texas A & M University, College Station, TX, USA

Article Outline

Glossary
Definition
Introduction
Early History and Development
The Health Physics Profession
Radiation Exposure to the US Population
Future Directions
Bibliography

Glossary

Absorbed dose The amount of energy deposited by ionizing radiation per unit mass of the material. Usually expressed in the special radiologic unit the rad or in the SI unit the gray (Gy). One Gy equals 1 J/kg or 100 rad.

Dosimeter Any device worn or carried by an individual into a radiation area to establish total exposure, absorbed dose, or equivalent dose (or the rates) in the area or to the individual worker while occupying the area.

Dosimetry The theory and application of principles and techniques associated with the measurement of ionizing radiation.

Epilation Loss of hair due to damage to the follicles in the skin. Temporary epilation occurs for acute exposures in the range of 300 to 500 rad with permanent epilation occurring above about 700 rad.

Equivalent dose (Formally the dose equivalent) The product of the absorbed dose and the radiation-weighting factor (formerly the quality factor) for the type of radiation for which the absorbed dose is measured or calculated. The equivalent dose is used to express the effects of radiation-absorbed dose from many types of ionizing radiation on a common scale. The special radiologic unit is the rem or in the SI unit the sievert (Sv). One Sv is equal to 1 J/kg or 100 rem.

Erythema Reddening of the skin due to exposure to radiation, similar to sunburn or thermal burns depending on the severity of exposure; occurs for acute exposures in the range 600–800 rad.

Exposure A quantity defined as the charge produced in air by photons interacting in a volume of air of known mass. An old quantity that is generally no longer used. Also, a general term used to indicate any situation in which an individual is being irradiated.

Ionization The process of removing one or more electrons from an atom or a molecule. The positively charged atom and the negatively charged electron are called an *ion pair*.

Isotope One of two or more atoms with the same number of protons (same atomic number Z) but a different number of neutrons (N) in their nuclei. A radioisotope is an isotope of a chemical element that is unstable and transforms by emission of nuclear particles and electromagnetic radiation to reach a more stable state. This term is often misused because unless the materials are the same element this term should not be used (see radionuclide below).

Nuclide A general term that indicates an atomic nucleus that is characterized by its atomic number (number of protons), number of neutrons, atomic mass, and energy state.

Radiation Used in this section to mean ionizing radiation. That is, particles or electromagnetic radiation emitted from the nucleus with sufficient energy to cause ionization of atoms and molecules, either directly or indirectly, composing the material with which the radiation is interacting.

Radionuclide A nuclide that is radioactive and upon decaying, emits ionizing radiation.

Definition

Health Physics: The theory and practice of radiation protection [1].

Introduction

The term health physics probably has a large number of definitions because it means many things to many

practitioners of nuclear technology. As indicated above, health physics basically means radiation protection or radiation safety. The term itself has its origins in the Manhattan Engineering District (MED) days during World War II. Dr. Arthur Holly Compton and his deputy, Dr. Robert S. Stone, recognized the need for a group of individuals whose sole responsibilities were to protect the workers from the potential harmful effects of radiation while allowing the MED work to move forward as rapidly as possible. However, such individuals did not exist at the time and the decision was made to select individuals from the medical physics profession, who understood radiation exposures and biological effects of radiation, and those with expertise in measuring low levels of radiation exposure. The former group of individuals was recruited from the ranks of those in hospitals and cancer therapy clinics across the country while the latter group was recruited from cosmic-ray physicists (Compton himself was a cosmic-ray physicist). There was a need to select a name for these individuals and a number were considered. It was important that the name selected did not reveal the work of those involved in the MED activities. Since Dr. Stone was in charge of the Health Division at the Chicago Lab and the members of the group were physicists, the name health physics seemed to come naturally. There was also a clear intent to hide from those without the need to know exactly what was going on at the Lab. Thus, the term health physics was selected with the full intent that it be somewhat nebulous.

Dr. K. Z. Morgan, a cosmic-ray physicist and one of the original eight health physicists, defined health physics as the study and practice of radiation protection [2]. In a lighter moment, he also defined health physics as "what health physicist do." Health physicists are professionals dedicated to the protection of the human race and the environment from the harmful effects of radiation, while recognizing that there are enormous benefits to be derived from the use of nuclear technology [3, 4]. A health physicist is constantly balancing the risk of radiation exposure with the benefit from the use of the nuclear technology. In simple terms, health physicists strive to keep the radiation risk as small as possible and the benefit as large as possible. If one visualizes an old-fashioned balance or scale, the risk would be very small and the benefit would be large. It is not their intent to balance the scale but to have "benefit pan" outweigh the "risk pan" so that the scale is tilted significantly.

Current approaches to health physics (i.e., radiation protection) are based on three principles, summarized in three words: justification, optimization, and limitation. First, there should not be any unnecessary radiation exposures: the benefit must exceed the risk from the exposure. Second, all exposures to radiation should be kept As Low As is Reasonably Achievable (this is called the ALARA principle but, in other countries, this is called "optimization"). Finally, no radiation exposures should exceed the recommended regulatory limits on radiation exposures.

Those facilities licensed by either the US Nuclear Regulatory Commission (USNRC) or by agreement states generally apply an exposure limit of 5 rem/year (0.05 Sv/year) for occupationally exposed workers. But health physicists use the three principles to drive exposures as far below the regulatory limits as is possible. The ALARA principle has not only kept exposures below the regulatory limits, but also has resulted in a significant reduction in the collective doses and average worker doses at nuclear utilities in the United States. The average doses to workers at both pressurized water reactors (PWRs) and boiling water reactors (BWRs) in the United States have been reduced to levels of only a few hundred mrem per worker per year. In 2007, the average dose equivalent to a worker in the US nuclear power plant was 130 mrem [5].

Early History and Development

Even though the terms health physics and health physicist were not used until the early 1940s, the need to protect individuals from harmful radiation exposure dates back to just after the discovery of X-rays by Wilhelm Roentgen in 1885 and natural radioactivity by Henri Becquerel in 1896. With such amazing discoveries, many scientists began to investigate these phenomena for themselves and many were perhaps unnecessarily exposed to radiation. Many researchers took things into their own hands and established exposure guidelines and restrictions for use in their laboratories. However, often these exposure guidelines were based on observable effects such as the production of erythema and even evidence of epilation. Even with these informal and unified guidelines, there were still

individuals who experienced harm from excessive radiation exposures.

In 1899, the British Roentgen Society formed a committee to collect data on the effects of X-rays. These efforts were hampered by the general belief that X-rays were harmless [6]. Later, the British X-ray and Radium Protection Committee adopted recommendations in 1921. It is important to notice the name of this committee because it indicates the limited nature of the early use of radioactivity and radiation-producing machines. In the United States, the American Roentgen Ray Society established a standing committee on radiation protection in 1920 and recommendations of this committee were adopted at the annual meeting of the Society in 1922 [2].

It was not until 1925, at the First International Congress on Radiology, that there was an international effort to begin to control radiation exposure. This effort resulted in the formation of the International Committee on X-ray and Radium Protection in 1928 at Second International Congress held in Stockholm [7]. These efforts resulted in two current organizations, the International Commission on Radiological Protection (ICRP) and the International Commission on Radiation Units and Measurements (ICRU). These international activities were paralleled by similar efforts in the United States. In 1929, the Advisory Committee on X-ray and Radium Protection was formed as an outgrowth of discussions between the American Roentgen Ray Society, the Radiological Society, and the Radium Society. This committee ultimately became the National Council on Radiation Protection and Measurements (NCRP) and was chartered by Congress in 1964 to provide advice and counsel on these matters to the federal government [7]. General overviews of the profession as well as discussion of the early development of the profession can be found in the bibliography provided at the end of this section [8–10].

The International Commission on Radiological Protection (ICRP) is responsible for making general recommendations on approaches to radiation protection. These recommendations are intended to provide the basic framework for radiation protection for those nations with nuclear technology programs, but it is the responsibility of each country to adapt these recommendations to the current state of their nuclear technology program. In the United States, the National Council on Radiation Protection and Measurements (NCRP) reviews the recommendations of the ICRP and provides a set of recommendations that are intended for use in the United States. The Environmental Protection Agency is responsible for establishing the general recommendations for all federal agencies and this guidance is signed into law by the President of the United States. Then, each federal agency is required to promulgate a set of regulations to govern their activities. For example, the USNRC regulations are found in Title 10 Code of Federal Regulations part 20 (10CFR20) and the Department of Energy regulations are in 10CFR835.

But, in the United States, things are not so simple. In the federal government, at least one agency has not revised their recommendations in response to the 1987 EPA guidance and is still functioning under the 1959 version of the Code of Federal Regulations. Most agencies are using the 1977 recommendations of the ICRP in compliance with the EPA guidance. The 35 agreement states in United States have promulgated regulations that are in compliance with the EPA guidance. However, the Department of Energy has instructed their contractors to implement the newer recommendations published by the ICRP in 1990. Even though these recommendations are similar, some significant differences must be recognized and understood. But, the situation in the United States is not currently very simple.

The Health Physics Profession

Health physicists are found in essentially all activities involving the use of ionizing radiation, including research, education, medical uses, industrial applications, consulting services, and state and federal regulatory agencies [3, 4]. Although most health physicists are involved in only one of these areas, it is common for the professional health physicist to become active in many of the above areas. There is always a need to train employees and educate the general public concerning the hazards of radiation and the appropriate methods of protection. A health physicist must ensure that the state and federal regulations regarding radiation exposure are followed and that legal limits are not exceeded. In addition, it is the health physicist's responsibility always to seek better ways of accomplishing tasks so

that exposures to ionizing radiation are kept as low as reasonably achievable, releases to the environment are controlled and appropriate, and all uses of radiation or radioactivity result in a positive benefit.

Health physics is a course of study in a number of universities across the country; both at the baccalaureate and graduate levels. Many universities grant advanced degrees in health physics and related fields (physics, radiobiology, radiochemistry, etc.). The courses of study are found in colleges of engineering, schools of public health, physics departments, biology departments, and chemistry departments. There seems to be no official "home" for these programs. However, this situation provides a certain interdisciplinary flavor to the profession, because each academic program is different and students can find an institution that best satisfies their interests and needs.

Health physics is an exciting, interesting, and challenging profession. Controlling radiation exposures to the lowest possible levels, while allowing the use of nuclear technology for the benefit of society, requires a broad background in a number of technical areas. This broad general understanding includes physics, chemistry, biology, anatomy, physiology, ecology, electronics, and a number of other disciplines. Opportunities for employment exist within a number of allied professional activities, such as medicine, cancer therapy, research, education, and regulatory affairs. Health physics and its related fields present the individual with daily challenges that require the application of sound professional judgment so that other work can proceed safely.

Opportunities within the profession have increased dramatically over the past few years. Projections indicate that the demand for health physicists will exceed to supply for the foreseeable future. Many of the early leaders of the profession have retired and a large number of those active in the profession have more than 30 years of experience. The demands for qualified health physicists will likely stay high for a very long time as the use of nuclear technology continues to increase.

Radiation Exposure to the US Population

Health physicists have the responsibility to protect the general population from unnecessary radiation exposure, just as they do with occupationally exposed workers. A question that often arises is, "what if the average radiation exposure to members of the public?" The NCRP has answered this question in a series of reports over a number of years. In 1987, the NCRP estimated that the average dose equivalent to a member of the US population was 360 mrem/year [11]. A large majority of this exposure was due to naturally occurring radiation sources such as cosmic rays, solar radiation, internally deposited radionuclides, and, especially, radon gas (200 mrem/year). In the most recent NCRP report [12], the average equivalent dose was estimated to be 620 mrem/year (6.2 mSv/year). The significant increase in this average was due to the use of medical technology involving radioactivity (nuclear medicine) and radiation-producing devices used in diagnosis and in cancer therapy (48%). Occupational exposures to radiation were estimated to be $<0.1\%$ of the total average equivalent dose. This is perhaps a testament to the dedication of health physicists to keep these exposures ALARA.

Future Directions

The practice of radiation safety and control (health physics) will continue to evolve as more and more challenges are added to the daily routine of the professionals. Revisions of dose/risk estimates continue to result in lower recommended radiation exposures limits. Some of these may be unjustified but, nevertheless, place an increased burden on those responsible for occupational exposures. One big challenge in the United States is the impact of the use of radiation-producing machines and radioactive materials in medicine. The increase in the average annual exposure to the general population is astounding and is a concern to those dedicated to the profession of health physics and the concept that all exposures should be justified.

Bibliography

1. Poston JW Sr (1987) Health physics. In: Encyclopedia of physics science and technology, vol 6. Academic, New York
2. Morgan KZ, Turner JE (1973) Principles of radiation protection. Robert E. Kreiger, Huntington
3. Health Physics Society, Health physics: a profession of the nuclear age, Health Physics Society, 1313 Dolley Madison Blvd., Suite 402, McLean, VA 22101
4. Health Physics Society, Prospectus, Health Physics Society, 1313 Dolley Madison Blvd., Suite 402, McLean, VA 22101

5. Nuclear Energy Institute (2009) Radiation safety at nuclear power plants, June 2009. http://www.nei.org/keyissues/safetyandsecurity/factsheets/safetystudiespublicworkers. Accessed 20 May 2010
6. Kathren RL, Tarr NE (1974) The origins of the Health Physics Society. Health Phys 27:419–428
7. Taylor LS (1971) Radiation Protection Standards. CRC, Cleveland
8. Taylor LS (1958) Brief history of the National Committee on Radiation Protections and Measurements (NCRP) covering the period 1929–1946. Health Phys 1:3–10
9. Taylor LS (1958) History of the International Commission on Radiological Protections (ICRP). Health Phys 1:97–104
10. Claus WD (1958) What is health physics? Health Phys 1:56–61
11. National Council on Radiation Protection and Measurements (1987) Ionizing radiation exposure of the population of the United States. National Council on Radiation Protection and Measurements, Bethesda
12. National Council on Radiation Protection and Measurements (2009) Ionizing radiation exposure of the population of the United States. National Council on Radiation Protection and Measurements, Bethesda, NCRP Report 160

Heat Content and Temperature of the Ocean

Rui M. Ponte
Atmospheric and Environmental Research, Inc, Lexington, MA, USA

Article Outline

Glossary
Definition of the Subject
Introduction
Brief History of Temperature Observations
From Raw Observations to Scientific Analyses
Spatial and Temporal Patterns of Variability on Climate Scales
Future Directions
Acknowledgments
Bibliography

Glossary

CTD (conductivity-temperature-depth) Instrument used to obtain vertical profiles of salinity, temperature, and pressure in the ocean at resolutions up to 1 m.

Heat content Amount of energy contained in thermal motion associated with any volume of matter, which is proportional to its temperature and specific heat.

Mixed layer Near-surface layer where turbulent mixing primarily induced by atmospheric forcing produces homogeneous conditions of temperature, salinity, and other water properties.

Objective analysis General mathematical procedure by which the value of a variable of interest at a given location and time is derived from similar observations at other times and/or places (also sometimes referred to as optimal interpolation).

Potential temperature Temperature attained by a fluid parcel if measured at a given standard pressure (typically 1,000 hPa corresponding approximately to atmospheric pressure at the ocean surface).

Specific heat Amount of energy per unit mass necessary to change the temperature of a given substance by 1°C, with typical values for seawater around 4,000 J/kg/°C.

Thermistor Sensor that uses known thermal dependences of electrical resistance to determine temperature.

Thermocline Region of enhanced vertical temperature gradients separating well-mixed layers near the surface from the layers with weak thermal stratification found in the deep ocean.

XBT (eXpendable BathyThermograph) Instrument used to obtain essentially continuous recordings of temperature with depth, from the surface to about 700 m, which can be deployed from a ship underway and without having to be retrieved.

Definition of the Subject

The global ocean is a vast body of water covering approximately two thirds of Earth's surface and having an average depth around 4,000 m. Temperatures in the ocean can range from a balmy 30°C in the surface layers of the tropics to an icy cold −2°C in polar regions and at abyssal depths. Apart from the strong spatial variability, water temperatures at a place also change on all time scales, from hours to decades. Variability in surface water temperatures affects air-sea heat exchange and is an important factor determining the nature and strength of ocean–atmosphere coupling. Changes in

ocean temperatures imply expansion or contraction of the water column and can thus have a major impact on sea level. And given the large heat capacity of seawater compared to that of air and the large mass of the oceans compared to that of the atmosphere, relatively small fluctuations in oceanic temperatures imply substantial changes in heat content, which are essential for properly accounting for the planet's energy balance. As such, taking the temperature of the oceans and determining changes in its heat content is an essential diagnostic of the state of Earth's climate and the overall health of our planet.

The task of monitoring seawater temperatures is made very difficult by the vastness of the global oceans and by the remote and harsh environment in which measurements must be taken. Original temperature observations date back at least a few centuries and were made by dropping thermometers in the water, first at the surface and then also at depth. Developments mainly in the second half of the twentieth century have led to a number of different sensor technologies, including continuous vertical profiling instruments deployed on various platforms (ships, moored instruments, autonomous floats), acoustic tomography, as well as space remote sensing techniques. Despite significantly improved data gathering capabilities, considerable challenges remain in observing the oceans globally and at sufficient temporal and spatial resolution. The sampling problem is a daunting one, and the historical temperature database is fraught with other issues as well regarding lack of metadata, unknown instrumental biases, and consistency between shifting technologies. A number of developing observing systems, together with advancements in modeling and data synthesis capabilities, promise to deliver a more accurate chart of ocean temperature and heat content in the years ahead.

Introduction

Measurements of seawater temperatures must have started with the appearance of the first thermometers in the seventeenth century. As early as the eighteenth century, Benjamin Franklin was making use of a thermometer as a rudimentary navigation aid to chart the changes in temperature across the Gulf Stream [1]. With the development of commercial shipping and the birth of well-funded military naval fleets, routine ship measurements of near-surface temperature were well under way in the nineteenth century. Dedicated scientific efforts to sample the oceanic temperature structure, not just at the surface but also at depth, had to wait until the second half of the nineteenth century, however. The global Challenger expeditions in the 1870s [2] and later the Meteor expeditions in the 1920s [3] signaled the birth of oceanography as a science. By this time, the importance of knowing the physical and chemical properties of seawater had become all too clear.

Temperature is a key parameter for determining water density, along with salinity and pressure. As it warms and cools, seawater expands and contracts by an amount determined by its coefficient of thermal expansion, which increases with temperature, pressure, and salinity (e.g., [4]) and can vary significantly from place to place in the ocean. Density changes tend to be more sensitive to temperature at depth, where pressure is largest, and in the tropics, where the waters are warmest. As horizontal differences in density determine pressure gradients and currents, temperature is of crucial dynamical importance when trying to infer the ocean circulation and how it changes in time.

The impact of temperature on density (or correspondingly volume) also means that changes in ocean thermal properties are directly related to changes in sea level. As described in most basic oceanographic texts (e.g., [4]), by knowing the fluctuations in temperature throughout the water column, their integrated effects on volume can be calculated and represent the so-called thermosteric component of sea level variability. (Salinity also affects volume and gives rise to halosteric changes in sea level. Steric sea level signals refer to the combined effects of temperature and salinity.) Interpretation, analysis, and prediction of sea level change are thus tightly related to accurate knowledge of temperatures over all ocean depths.

Last but not least, seawater temperatures give a measure of how much thermal energy or heat content is contained in the ocean. Oceanic heat content is a quantity of major relevance for climate and is a particular focus of this entry. Given the difference in the specific heat of water and air, heating or cooling a given amount of seawater requires approximately four times more energy than for the same mass of air.

More importantly, because the density of water is approximately 1,000 times larger than the density of air, the ocean's heat capacity and thermal inertia are vastly larger than those of the atmosphere. As such, the oceans can serve as a large reservoir of heat in the climate system. Being a dynamic fluid with an active circulation, the oceans continually transport and redistribute heat and participate in important heat exchanges with the atmosphere as well as the cryosphere. Knowledge of oceanic temperature fields can thus hold vital information on the past, present, and future state of Earth's climate.

By the time the classic oceanography text by Sverdrup et al. [5] was published, summarizing much of what was known about the oceans at the time, the crude characteristics of the oceanic temperature structure were beginning to take shape. Apart from the clear decrease of near-surface temperature with latitude away from the tropics, mimicking that of surface air temperatures, other major features, well known to us today and seen in the example of Fig. 1, were already apparent. The presence of a near-surface layer with homogenized temperature and other properties was established early on. This so-called surface mixed layer owed its existence to high turbulence and mixing induced primarily by air-sea fluxes at the upper boundary, and its thickness, which could reach several hundred meters, was very much dependent on location. Below the mixed layer, a region of rapid decrease in temperature with depth was present in most of the oceans. The rapid transition between the warm surface layers and the cold abyss, nominally called the thermocline, exhibited a fairly complex dependence on region and could extend over various thicknesses and up to depths of 1,000 m. Much colder deep and bottom waters beneath the thermocline tended to be less stratified with depth and also more homogeneous in latitude and longitude, without the marked latitudinal dependence of the upper layers.

The initial picture that emerged from the first scientific expeditions in the nineteenth and twentieth centuries was necessarily one of essentially steady conditions, given the paucity of data with a few snapshots taken along a handful of sections. Ever since those original efforts, the quest for determining temperature distributions in space and time over the vast global oceans has been an endeavor with almost epic overtones. In what follows, a brief description of the panoply of instruments and methods used to measure temperature and heat content is attempted within a historical timeline, from the earliest to the most modern period. Such a voyage through the world of instrumentation and data gathering sets the stage for a discussion of what is presently known about ocean temperature and heat content, starting with the near-surface layers and progressing down to the abyssal depths. The main focus is on the thermal structure at large spatial scales (100 km and longer) and its variability on time scales of months to centuries relevant for climate. Although much progress has been achieved in recent decades, considerable challenges remain and some possible pathways for the future are traced at the end.

Brief History of Temperature Observations

Conventional thermometers were the first instruments used to sample oceanic temperatures [5]. The bulk of the data was taken at the surface, either by dropping the thermometers in the water or by using a bucket to collect water for measurement. Some subsurface measurements were obtained by using insulated bottles that would maintain collected water samples at their ambient temperatures, with minimal exchanges of heat with surroundings during ascent. For subsurface sampling, however, most scientific surveys through the first half of the twentieth century were made using reversible thermometers [5], which were set to sample at some predetermined depth levels. The technology was simple and reliable but expensive. Furthermore, only point measurements in time and space were possible with reversible thermometers.

Continuous sampling devices were experimented with early on but their use did not become widespread until the second half of the twentieth century [7]. First thermographs used standard thermometry and various methods for continuous data recording and were mainly deployed in the hulls or intake pipes of ships. Such instruments had no pressure sensors and thus no ability to determine depth, and data gathering was confined mainly to the top few meters of the ocean. The first useful attempts to continuously record temperature and depth are reported by Spilhaus [8, 9]. The original bathythermograph (BT) followed a completely

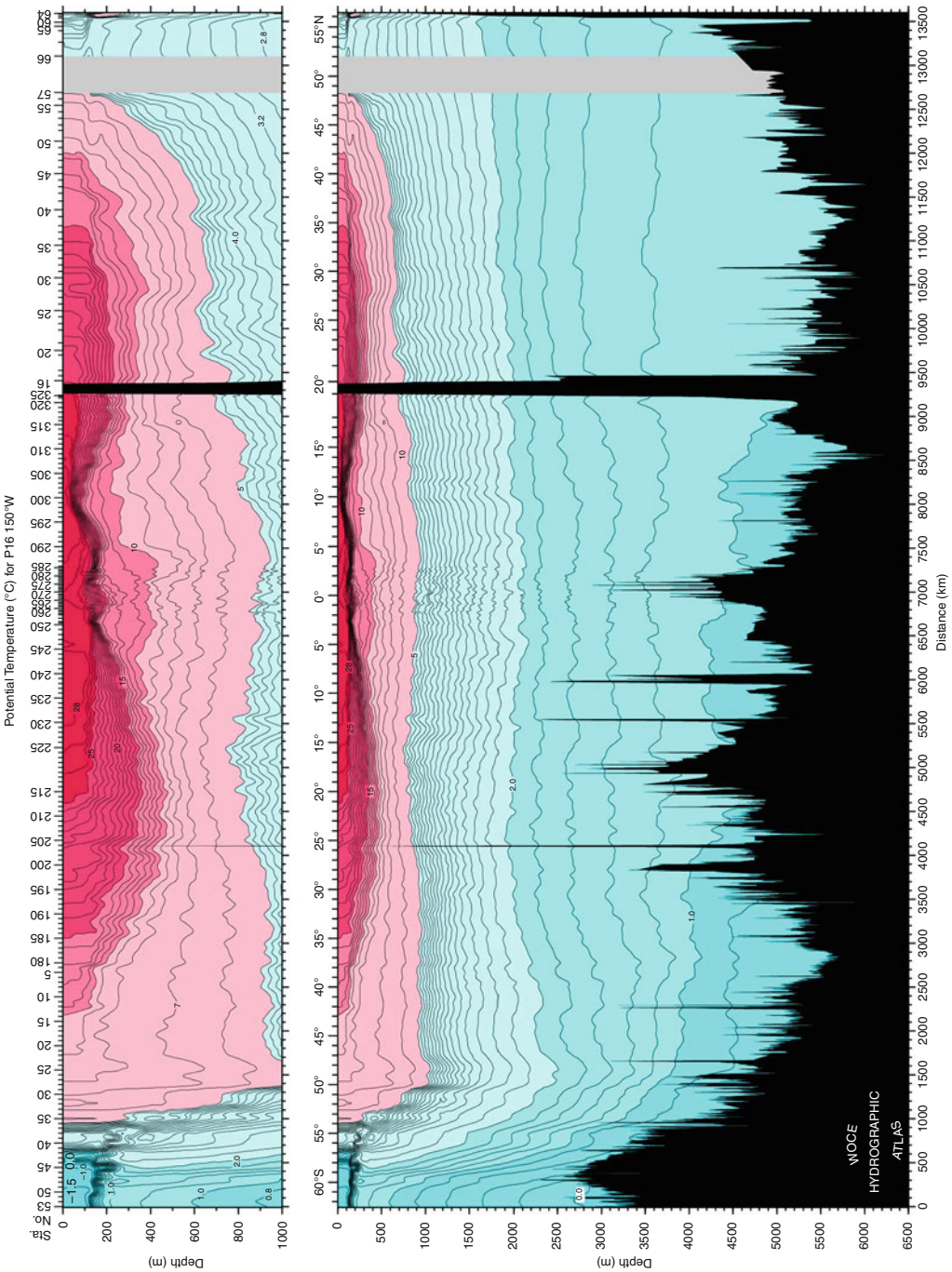

Heat Content and Temperature of the Ocean. Figure 1
Latitude-depth cross-section of potential temperature along approximately 150°W in the Pacific. *Contour lines* are drawn every 1°C (0.2°C) for temperatures warmer (colder) than 5°C. Different *color shading* is shown at intervals of 5°C, with temperatures getting progressively colder from *red* to *blue shades*, and with the *darkest red* representing the range 25–30°C. *Bottom panel* shows the full water column, with the *top panel* focusing on the *upper* 1,000 m for added detail. Bathymetry is shaded in *black*, with the land feature reaching the surface near 20°N being the Hawaiian Islands (Reproduced from Talley [6])

mechanical design and its reliability made it one of the most extensively used instruments for ocean surveying in the 1950s and 1960s [10]. Its depth range was quite limited, however, allowing measurements only in approximately the upper 150 m.

An important development was the appearance of the expendable BT (XBT), which used thermistor technology to measure temperature over approximately the upper 700 m of the ocean [10]. Without a pressure sensor, the depth of measurement was inferred from the elapsed time since deployment and the "known" free fall rates, as established by the manufacturer of the instruments. Because of its relatively low cost and its easy use and operation from a ship underway, the XBT became the workhorse of the in situ observing system for a long time. A great deal of what is known about the upper ocean temperature and heat content variability is owed to millions of XBT profiles carried out mostly from merchant ships and other ship-of-opportunity vessels. As such, XBT sampling tended to be best along most traveled shipping routes, particularly between Europe and North America (see Fig. 2). By any measure, large chunks of ocean were rarely visited by XBT surveys and the deep ocean was totally out of reach. The method of assigning depths to XBT temperature profiles based on instrument free fall rates also led to the introduction of complicated biases, which are still being dealt with to date [12, 13].

In parallel with XBT development, the need for high-accuracy profiling instruments that could sample the ocean all the way to the bottom led to the development of the conductivity-temperature-depth (CTD) sensor. Various different versions were produced mainly in the 1950s and 1960s, and CTD use quickly became the standard in all the major scientific campaigns (e.g., [7]). Compared to XBT deployments, which could be carried out with the ship underway, CTD casts required dedicated ship time, but CTD precisions were significantly better than those possible with XBT sensors, and including pressure sensors ensured an accurate mapping of the thermal structure in the vertical. The CTD instrument has continued to evolve and current versions have accuracies better than 0.001°C and vertical resolutions of about 1 m. (Temperature variability at submeter scales is a topic in its own right and much of the work that led to the CTD sensor has evolved into several instruments capable of measuring thermal microstructure at millimeter scales; interested readers can learn more about microstructure instrumentation by consulting for example [7, 14, 15] and their cited references.)

Traditional CTD surveys, involving basin-wide sections of full-depth casts made at variable horizontal spacings (typically a few tens of kilometers, as in the example of Fig. 1), together with XBT profiles along major shipping lanes, continued to be the main method of observing oceanic thermal structures until the end of the twentieth century. But even as the World Ocean Circulation Experiment (WOCE) became a reality [16], focus was still on obtaining a single realization of the global temperature field. Only a few sections were meant to be sampled repeatedly to assess the full temporal variability. Costs of operating research ships from which CTD casts could be performed continued to be a major impediment for truly global coverage. Even after several decades of XBT and CTD measurement campaigns, extensive oceanic regions, particularly in the Southern Hemisphere, remained severely under-sampled by the end of the twentieth century (Fig. 2).

The march toward a truly global observing system took another major step with the implementation of the Argo system of profiling floats in the last decade [17, 18]. Following years of research and development in autonomous float technology, major international cooperation under the Argo Project led to the seeding of the global ocean with more than 3,000 floats (Fig. 3) with the capability of profiling temperature and other properties between depths of 2,000 m and the surface approximately every 10 days. Measurements are relayed by satellite while the floats are at the surface in between each cycle of ascent and descent. Coverage is almost global, apart from the lack of data in high latitudes and ice-covered regions, where current Argo technology does not work (Fig. 3). Shallow and marginal seas are also not part of the sampling Argo strategy. In a short number of years since their deployment, Argo floats have produced more than 300,000 profiles and have provided more samples than all the data ever collected before in many regions.

Despite all the efforts to measure subsurface temperature, it is at the surface that coverage is most adequate in both space and time (e.g., [19]). A major factor in the density of observations at the surface has

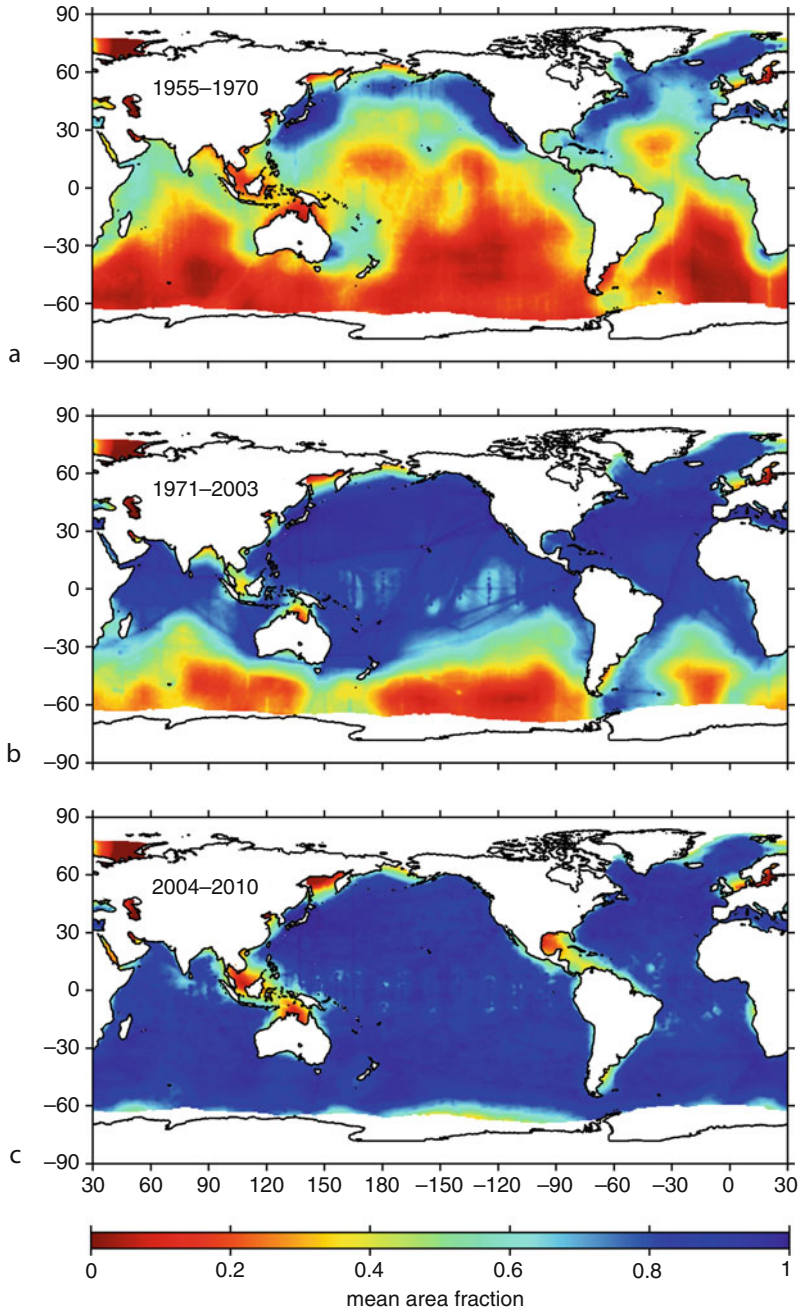

Heat Content and Temperature of the Ocean. Figure 2

Estimate of the annual mean sampling for the *upper* 750 m expressed as the fractional area of data coverage, provided by John Lyman as an update to the results discussed in Lyman and Johnson [11]. (**a**) Coverage prior to 1970 is very poor over most of the global oceans. (**b**) Substantial improvements in the period 1971–2003 come from XBT surveys, mostly in the Northern Hemisphere and along ship routes clearly seen as tracks in the plot. (**c**) The increase in coverage for the most recent period shown (2004–2010) reflects data collected by the Argo system

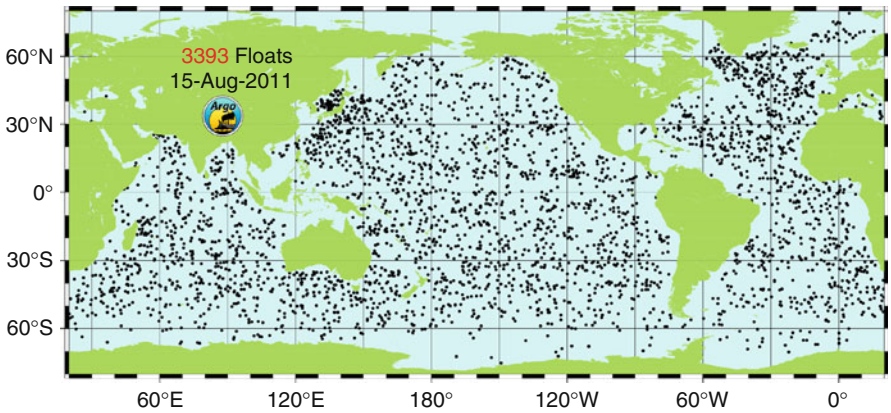

Heat Content and Temperature of the Ocean. Figure 3
Distribution of Argo floats as of August 2011 as estimated by the Argo Project (Reproduced from the Argo Project web site). Global coverage of the oceans involves more than 3,000 floats. High northern and southern latitudes and shallow and marginal seas remain poorly sampled

been the space-based remote sensing techniques established since the 1980s (e.g., [20, 21]). Given the dependence of surface infrared and microwave radiation on sea surface temperature, satellite radiometers measuring at these frequency bands can be used to retrieve sea surface temperature. Many other factors like atmospheric clouds and water vapor impact the radiation reaching the instrument and have to be corrected. For these purposes, increasingly complex validation and calibration methods have been developed over the last 30 years. Many of such efforts rely on in situ measurements from ships, surface buoys, and drifters. However dense in space and time, satellite measurements strictly measure the temperatures right at the surface and their interpretation in terms of near-surface temperatures remains an issue of research [21].

For subsurface thermal information, aside from profiling measurements by XBT, CTD, and Argo instruments, a number of other in situ programs are also useful to mention. Surface and subsurface moorings of various types have been deployed, which usually include thermistor chains. Operational programs are in place in the tropical Pacific and Atlantic [22, 23] with a similar system currently under implementation in the tropical Indian Ocean [24]. Many research projects with local or regional focus provide occasional temperature measurements (e.g., [16, 25]), and a few long-term stations have also been maintained in places like Bermuda and Hawaii [26, 27]. In any case, traditional ship-based XBT and CTD surveys and more recently the Argo floats provide the bulk of information on ocean temperature and heat content over the last decades.

Apart from direct temperature measurements, several other indirect observing methods have been recently developed. Indirect thermometry can make use of the relationship between temperature and any other oceanic variable that can be accurately measured. Such is the case with the strong dependence of sea level on thermosteric height, which is directly related to integrated temperature over the water column. Measuring variability in sea level using satellite altimetry can complement in situ temperature observations in efforts to infer changes in heat content [28, 29]. As with many indirect methods, ancillary observations are needed. As sea level also depends on salinity through changes in halosteric height, measurements of salt content can help in isolating the temperature effects. In addition, changes in sea level can be due to changes in the mass of the water column and the ability to measure the total mass content either using in situ bottom pressure recorders or satellite gravity techniques can lead to improved inferences of heat content based on sea level observations, as discussed by Ponte [30] and Jayne et al. [31].

Temperature has also a strong effect on sound speed. Such dependence is the basis for the acoustic

thermometry ideas proposed by Munk and Forbes [32] and others. Sound travel times can be inverted to estimate variability in averaged temperature and heat content along ray paths connecting any source and receiver pair. Plans to establish acoustic monitoring for the global oceans are revisited in Dushaw et al. [33] but presently current data sets are confined to a few experiments carried out mostly in the North Pacific, between Hawaii and the North American coast [34]. Long-range acoustic thermometry can work over many thousands of kilometers and thus can average noisy mesoscale fields over large oceanic volumes at the expense of lack of horizontal resolution of any temperature or heat content features. Although the vertical resolution is limited, acoustic measurements can provide much needed temperature estimates at depths presently not sampled at all by the Argo system.

From Raw Observations to Scientific Analyses

From a pure observational perspective, the diversity of instruments and observing platforms involved in temperature data gathering at any one time, the shifts in technology throughout many decades of observations, the lack of detailed information about many historical data sets (e.g., types of XBT instruments used, depth at which near-surface temperatures are taken), the various parties involved in collecting observations, among other factors, make archiving and quality controlling the data a laborious and difficult task. Major efforts in the USA have been pursued at NOAA's National Oceanographic Data Center and are well documented in the World Ocean Database series produced by NOAA roughly every 4 years, with the last edition released in 2009 (e.g., [35, 36]). Other more regional compilations are also available (e.g., [37]), and no central archive includes all the collected temperature data. Data processing tasks commonly involve statistical checks for outliers, elimination of duplicate observations, correcting for depth biases, along with many subjective criteria for flagging "suspicious" observations. More restricted data compilations based on specific hydrographic programs like WOCE [38] allow for better quality control and accuracy. In the end, researchers must decide what data to use and to discard (e.g., [38, 39]) and scientific analysis and results can depend on such choices (e.g., [37, 40, 41]).

Apart from data quality issues, the irregular and sparse sampling in both space and time makes quantitative study of temperature and heat content variability for climate inference far from a trivial task. Most studies rely on objective analysis/optimal interpolation methods (e.g., [42, 43]) to fill in data gaps in both space and time and reduce the observations to regularly gridded fields in latitude and longitude at given standard depth levels, which are more prone to scientific analysis. Objective analysis methods require assumptions about the nature of the fields being estimated (e.g., their degree of smoothness in space) and the statistics of the data (e.g., spatial and temporal correlation scales of data noise), which can influence how each data point is weighted to provide an estimated value at places where no data are available. As with data use, subjective choices are often involved and can lead to differences in results, particularly for regions where data are very sparse and estimates become more dependent on the details of the objective analysis method used. The series of World Ocean Atlas from NOAA (e.g., [44]) are a widely used example of a mean and seasonal temperature climatology produced from objective analysis applied to the wide variety of temperature measurements contained in the World Ocean Database [35, 36].

More advanced methods of data interpolation involve the use of ocean general circulation models (GCM), which embody the most complete description of the dynamic relations among all relevant observables (temperature, salinity, velocity, sea level) under strict laws of fluid motion and conservation principles of heat, momentum, and other quantities. Various data assimilation or state estimation techniques (e.g., [43, 45]) allow optimal combination of the information embedded in GCM codes with that contained in observations of all types. The use of such computationally intensive methods for climate analyses has been common practice in meteorology (e.g., [46]) and is becoming more common in oceanography (e.g., [47–49]) after rapid developments in ocean GCMs and data gathering capabilities, as well as in computing power, in the last decade. Most techniques involve minimization of an "objective" function that evaluates model-data misfits and thus require knowledge about data error statistics, which determine how tightly the model is allowed to fit the data. Books by Daley [43], Wunsch [45], and several others discuss the

various basic approaches to data assimilation available. For the purposes of analyzing oceanic temperature and heat content variability in a climate context, it is helpful to use methods that produce temperature evolutions consistent with all the flow fields, air-sea fluxes, and other boundary and initial conditions. As discussed by Wunsch et al. [48], fitting the temperature observations must be achieved if possible through dynamically consistent adjustments in currents, atmospheric forcing, model physics, and other factors, and without introducing unphysical jumps in the temperature evolution, which would imply the violation of basic heat conservation principles.

Estimates of temperature fields, obtained either through objective analysis or model-data synthesis methods of the sort described above, provide the basis for a variety of climate analyses, including studies of air-sea interaction, sea level change, planetary heat balance, and many other topics. In the context of this entry, the focus is on oceanic heat content variability. Changes in heat content per unit area are just proportional to changes in temperature ΔT over a layer of thickness H and given by $\rho C_p H \Delta T$, where ρ is the density of seawater and C_p is its specific heat at constant pressure [4]. For typical values of $\rho \sim 1{,}028$ kg/m^3 and $C_p \sim 4{,}000$ J/kg/°C, increasing the mean temperature of the water column ($\sim$4,000 m) by 1°C implies a change in heat content of around 1.6×10^{10} J/m^2. To achieve such warming over 1 year, an anomalous heat flux of $\sim$500 W/m^2 would have to be applied. By the same token, an error in the annual change in mean temperature of 0.001°C amounts to an error in implied heat flux of 0.5 W/m^2. For comparison, present estimates of the planetary heat flux imbalance under possible global warming scenarios are of the order of 1 W/m^2 [50]. Thus, very small changes in oceanic temperatures can imply large changes in heat content, in terms of Earth's heat balance and climate, and accurate global measurements of ocean temperatures, from the surface to the bottom, and from the tropics to the polar regions, are deemed essential in this context.

Spatial and Temporal Patterns of Variability on Climate Scales

A vast literature documents numerous attempts at describing the temperature and heat content variability in the global oceans, either from straightforward analysis of the temperature observations (e.g., [51]), from objective analysis methods using only temperature or also other types of data (e.g., [29]), or from data-constrained model solutions based on the most sophisticated assimilation methods (e.g., [52]). In this section, a summary of the current state of knowledge on the subject is presented, focusing on the advances made in most recent years. Information on the upper ocean layers is considerably richer in detail than on the deeper layers, as the amount of data quickly dwindles with increasing depth. Temperature and heat content analyses are discussed interchangeably. The simple relation between temperature and heat content discussed in the previous section can be used to approximately convert between the two variables.

Spatial and temporal coverage of the near-surface ocean is far better than at any other depth level, given the early practices of surface measurements from ships and more recently the global daily coverage brought by the advent of the satellite era. These widely different measurement techniques have been combined to produce records of what is commonly called sea surface temperature (SST). What SST values represent is, however, not a trivial issue because of the presence of vertical temperature gradients very near the surface. Much of the in situ data comes without precise information on the depth of measurement, which can be anywhere from near the surface to a few meters below it. In turn, satellite sensors sample the upper few microns or millimeters, depending on whether infrared or microwave instruments are used. As such, satellite values can be influenced by strong diurnal effects affecting the skin layer and can also differ substantially from "bulk" SST properties representing an average of the upper few meters ($\sim$10 m) of the ocean. A detailed account of many of these issues, including various definitions of SST and how in situ and satellite data are being used to improve present and past SST records, can be found in Donlon et al. [21] and references therein.

Despite all the inherent ambiguities, SST records constitute one of the most important oceanic datasets for climate studies. Historical data compilations (e.g., [19]) provide estimates of SST since the middle of the nineteenth century, although the earlier periods have much sparser data coverage (e.g., [53]).

When global mean estimates are attempted, a record of increasing SST over the last century emerges from most studies, consistent with a warming planet [20, 54, 55]. As can be seen in Fig. 4, present global mean SST estimates are almost 1°C warmer than in the early twentieth century. Apart from a long-term warming trend, variability at all time scales is present in the annual mean values. Considerable uncertainties are involved, however. Time-varying instrumental biases are a particular concern (e.g., [56]) and efforts to correct such errors are likely to continue (e.g., [57]).

While global mean SST is an essential climate index, just like surface air temperature, numerous climate variables and processes are related to SST spatial variations, from the intensity and quantity of tropical cyclones, which depend on tropical warm waters to form and grow, to the onset of deep convection in the ocean, which can happen in the presence of cold, dense surface waters at high latitudes. A great deal of effort has thus been devoted to understanding major spatial and temporal patterns of SST variability in relation to air-sea fluxes, ocean and atmosphere dynamics, and their connection to climate variability. Deser et al. [53] review major modes of interannual and multi-decadal variability with clear SST signatures, including the El Niño-Southern Oscillation, the Pacific Decadal Oscillation, the North Atlantic Oscillation, and the Atlantic Multi-Decadal Oscillation. As one parameter controlling air-sea transfers, knowledge of SST is key to making long-range climate forecasts (e.g., [58]). In addition, the existence of century-long time series of SST with some spatial information provides essential surface boundary conditions for atmospheric model simulations of the past climate and allows for model calibration and validation (e.g., [46, 59]).

Depending on region and time of year, SST observations can provide a window on mixed layer temperatures and can thus yield information on heat content in the near-surface layers of the ocean, assuming the mixed layer depth is known. Ultimately, for a full and quantitative description of heat content variability, subsurface temperature observations are needed. Until the implementation of the Argo system, a great majority of temperature profiles were based on XBT casts and confined to the upper 700 m. Multi-decadal analyses of large-scale temperature and heat

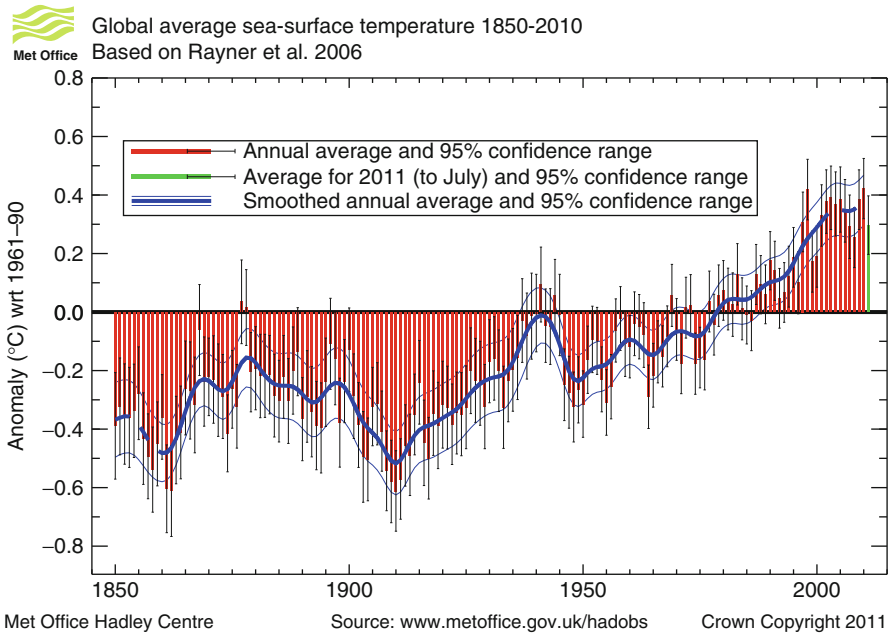

Heat Content and Temperature of the Ocean. Figure 4
Global mean sea surface temperature for the period 1850–2009 (anomalies relative to 1961–1990) based on Rayner et al. [54] and produced by the UK Met Office Hadley Center (http://www.metoffice.gov.uk/hadobs)

content variability have thus focused on these depths. Early observations are, however, quite thin and time series studies are restricted to the period since the 1950s. Apart from the presence of a strong seasonal cycle, which is mainly confined to the upper 100–200 m of the water column (e.g., [60, 61]) and driven by heat exchange with the atmosphere, the main interest has been on determining variability in temperature and heat content at scales of years to decades.

Numerous temperature analyses have produced estimates of mean oceanic heat content anomalies for depths 0–700 m (e.g., [37, 41, 62]). Several such time series, all using mostly the same available data but different processing procedures, are reproduced in Fig. 5 [63]. Most analyses indicate warming and increasing heat content of the upper ocean over the last three decades, in agreement with analyses of SST (see Fig. 4). The long-term warming has been related to anthropogenic influences by several studies (e.g., [64, 65]). Superposed on the general warming are interannual and decadal signals that can be caused by natural climate variability, including the impact of volcanism and variable solar radiation [65–68]. The spread among all series is considerable, however, and this can be an issue particularly if one is interested in studying their year-to-year evolution. Differences in the series can also affect the quantitative determination of long-term trends. Differences are not confined to the period before the 1990s when coverage is sparse (see Fig. 2) and methodologies to fill in data gaps can be influential. Other factors, including quality control and bias correction procedures, can affect the estimates, even over most well-covered periods [41].

Recent discovery of several systematic biases in XBT and Argo data [13, 40, 69] has led to various updates in mean heat content series. The estimates in Fig. 5

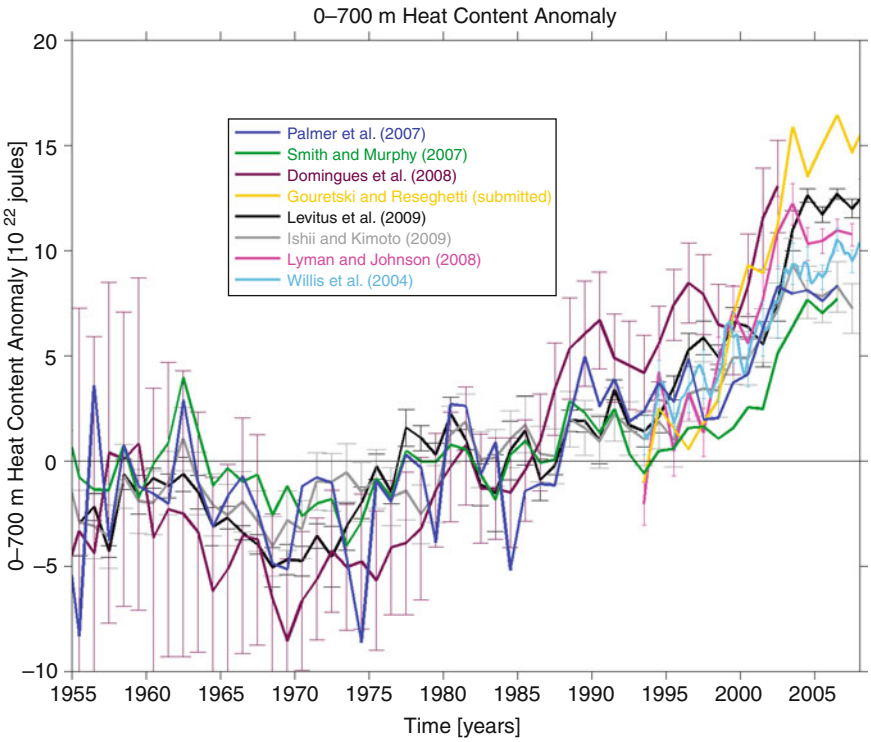

Heat Content and Temperature of the Ocean. Figure 5
Anomalies in upper ocean (0–700 m) heat content relative to the mean over the period 1955–2002. Various curves are from several data-based estimates (Reproduced from Fig. 2 of Palmer et al. [63]). The spread among all the curves is caused by several factors, including the specific data used, the applied bias corrections, and the objective analysis methods for smoothing and interpolation

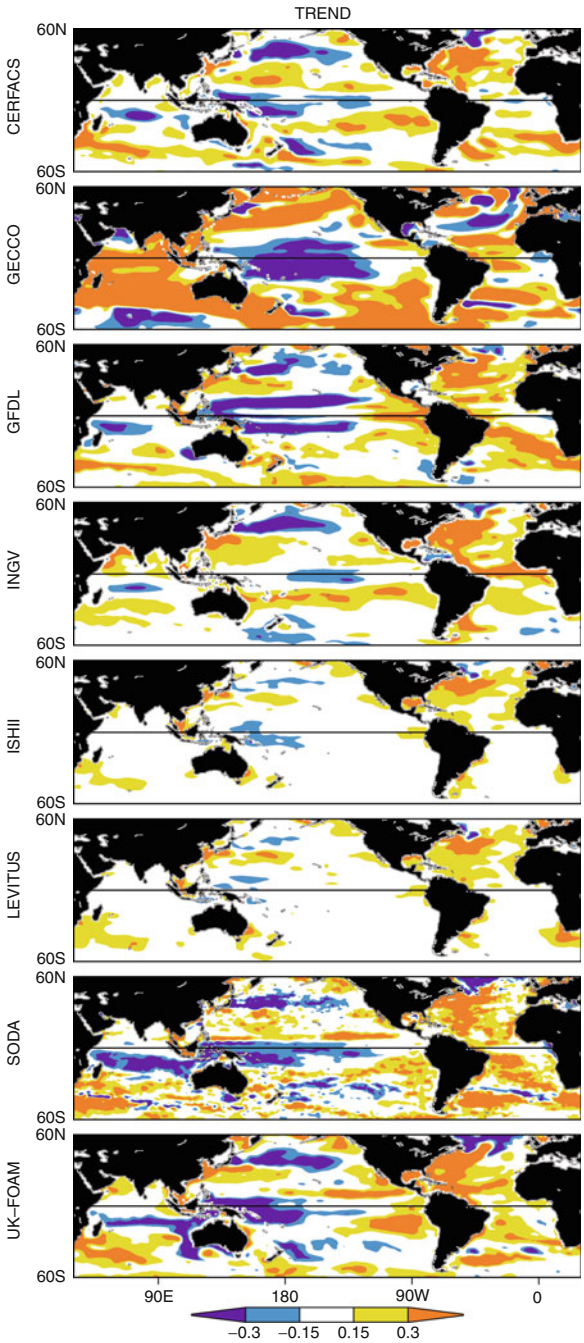

Heat Content and Temperature of the Ocean. Figure 6 Linear trends for heat content in the upper ocean (0–700 m) reproduced from Fig. 2 of Carton and Santorelli [52] and corresponding to several different analyses for approximately the period 1960–2005. Apart from the "Levitus" and "Ishii" fields, which are purely derived from observations, all others involve ocean models and data assimilation schemes. Details of all the analyses are given in Carton and Santorelli [52] and references therein. Coloring represents regions where values are outside the range $\pm 1.5 \times 10^8$ J/m^2/decade

include several of these bias corrections, which imply major differences in temporal evolution with previously published results (e.g., [70]). Efforts to understand the differences in Fig. 5 are ongoing (e.g., [41, 63]) and likely to continue in the foreseeable future. Multi-instrument approaches to estimating heat content, such as combining in situ temperature and altimeter sea level [29] or comparing XBT and CTD temperature estimates [69] can be useful when trying to rid the observing system of systematic errors in the various data streams, which are difficult to detect otherwise. Ultimately the synthesis of all data sets using models and data assimilation can bring out similar benefits (e.g., [52, 71]).

If knowledge of spatial mean temperature and heat content variability, with all the averaging and noise reduction involved, suffers from significant uncertainties, robust information on spatial patterns of variability is even more problematic because of very poor data coverage in extensive areas such as the Southern Ocean (Fig. 2). Even for the more recent Argo period, significant observational gaps are still present in ice-covered regions and marginal seas (Fig. 3). Some of the earliest estimates of variability were based on differences over a few pentadal periods or on time series for whole oceanic basins, to allow for meaningful averages [72, 73]. More recently, state estimation/data assimilation methods have been brought to bear on the problem (e.g., [48, 74]).

Long-term trends in upper ocean heat content (0–700 m), calculated over approximately the last three decades from a number of different analyses and methods summarized in Carton and Santorelli [52], are shown in Fig. 6. Although the warming trend in global mean heat content is clear in Fig. 5, the spatial patterns in Fig. 6 include both places of warming and cooling. Complex spatial and time variability patterns in ocean temperature fields are also evident in the acoustic measurements analyzed by Dushaw et al. [34]. The oceans are far from warming at the same rate everywhere. Despite considerable differences

among all analyses, which can be taken as a crude measure of their uncertainty, there is a general tendency for warming in places like the Atlantic and parts of the south and north Indian Ocean, as well as cooling over the equatorial Pacific and parts of the North Pacific.

The inhomogeneous patterns of warming and cooling in Fig. 6 reflect the complexity of air-sea heat transfers and oceanic heat transports, both in the horizontal and in the vertical. Aside from the long-term (multi-decadal) scales represented in the trends in Fig. 6, heat content variability at all time scales permeates the available records (e.g., [52]). As with SST, some of the spatial patterns in upper ocean heat content can be related to primary modes of natural climate variability reviewed by Deser et al. [53]. Changes in major circulation systems such as the meridional overturning circulation in the North Atlantic [66] or the Antarctic Circumpolar Current in the Southern Ocean [75] can be involved. Achieving a full understanding of the mechanisms responsible for past upper ocean heat content variability is hampered, however, by the poor observational base. As societal focus shifts to the determination and understanding of regional climate variability and how it affects human life at a local level, the need to determine spatial patterns of variability in heat content will only grow in the future. Maintaining some of the recently implemented in situ and satellite observing capabilities is a minimum requirement to be able to monitor heat content variability both at the regional and global level.

As the focus of analysis descends to layers below the XBT maximum sampling depth of 700 m, the amount of historical observations diminishes considerably. Only the most recent period after the implementation of the Argo system, from 2003 onward, provides reasonable near-global coverage up to depths of around 2,000 m. The short record length precludes a comprehensive treatment of variability at all climate scales of interest, but the density and quality of the data provide for good estimates of spatial variability, both horizontally and vertically. Analyses of Argo data by von Schuckmann et al. [61] for the period 2003–2008 and comparisons with mean climatological temperature values confirm long-term warming tendencies, particularly in the North Atlantic, found by Levitus [72], Levitus et al. [76], and Antonov et al. [77] and show that temperature variability on interannual and decadal time scales can reach to 2,000 m and deeper, well below the XBT sampling range. The spatial and time structure of interannual temperature signals is quite complex, however.

Figure 7 reproduced from von Schuckmann et al. [61] shows an example of year-to-year zonally averaged temperature anomalies for the Atlantic Ocean, given as a function of depth and latitude. Typical amplitudes range between $\pm 0.2°C$, alternating sign on relatively long ($\sim$1,000 km) meridional scales. Aside from the long-term warming already noted, other time scales are involved. Spatially, anomalies in Fig. 7 can show vertical coherence, with the same sign extending over most of the sampled water column, or considerable vertical structure including reversals of sign with depth. In addition, strongest anomalies are not always found at the surface, and sizable variability is apparent at all sampled depths, with deepest variability present at mid- and high latitudes. A variety of processes can be related to the temperature signals in Fig. 7, including changes in the position of subtropical and subpolar temperature fronts, strong air-sea interaction and onset of deep convection in the high latitudes, and changes in the strength of the horizontal circulation. von Schuckmann et al. [61] discuss some of the mechanisms behind the variability in Fig. 7 with references to other relevant works. In any case, only now is the observational system becoming dense enough to begin putting together a detailed temporal evolution of the three-dimensional temperature fields. A full understanding of these observations will likely come with the accumulation of good quality data and dedicated modeling and data synthesis efforts in the future (e.g., [49, 78]).

Below the Argo sampling maximum depth of 2,000 m, not even the most recent years are well sampled at all. Yet these very poorly observed layers represent approximately half of the volume of the global oceans. Most of the current knowledge about basin-scale temperature structures and variability in the deep/abyssal oceans comes from high-quality full-depth CTD casts obtained as part of global programs like WOCE [16] and earlier campaigns such as those during the International Geophysical Year in the late 1950s (e.g., [51]). Some attempts at including depths up to 3,000 m in calculations of heat content have been

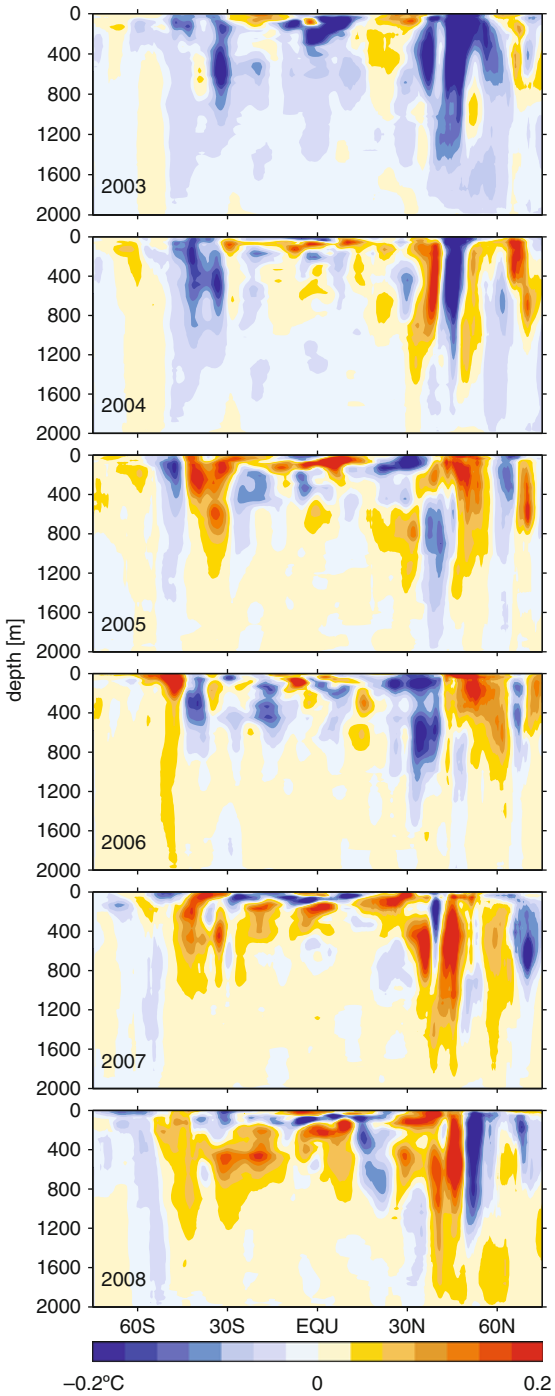

Heat Content and Temperature of the Ocean. Figure 7 Mean annual temperature anomalies for the period 2003–2008, calculated from Argo data as described in detail by von Schuckmann et al. [61]. Values represent zonal averages for the Atlantic basin (Reproduced from Fig. 9 of von Schuckmann et al. [61])

confined to highly averaged estimates in time and space (e.g., [76]). Most analyses, particularly for abyssal layers, tend to examine individual basin sections that have been reoccupied at various times, thus providing snapshots separated by several years to decades (e.g., [51, 79–82]). The observed changes in temperature are then used to infer variability, presumed to be long term and large scale in character, but great care must be taken to properly interpret such sparse observations.

Figure 8 shows an example of decadal temperature changes in the abyssal eastern South Indian Ocean from Johnson et al. [81]. Differences between temperature measurements taken in 1994–1995 and 2007 range between ±0.2°C, with strongest warming observed in latitudes south of 50S. Large variations are seen all the way to the bottom, well below 2,000 m. The warming in the Australian-Antarctic Basin below 3,500 m amounts to a mean change of +0.1°C and is statistically significant and generally consistent with other observational evidence [81]. Such a warming is equivalent to a heat flux imbalance of 0.9 W/m^2, which is substantially larger than values of 0.1 W/m^2 typically associated with geothermal heat flux at the ocean bottom [83]. Causes of the increase in temperature in Fig. 8 are thus likely related to changes in bottom circulation and water mass properties connected to surface processes around Antarctica, where bottom dense waters are formed through strong heat losses to the atmosphere and subsequently descend to great depths before spreading northward.

Abyssal temperature changes similar to those in Fig. 8 have been observed in many other ocean basins. For example, Fukusawa et al. [79], Kawano et al. [84], and Johnson et al. [80] document deep and abyssal warming across several sections of the North and South Pacific. Abyssal changes tend to be larger and decrease in range from south to north, with section mean changes in potential temperature as large as 0.01°C [80]. Similar warming of about 0.04°C is found in the bottom 1,500 m of the Brazil Basin in the South Atlantic [85]. As with the findings in the Indian Ocean shown in Fig. 8, these temperature changes in the abyssal Pacific and Atlantic oceans cannot be explained solely by effects of geothermal heat flux and are likely related to anomalies advected from the south, where sources of bottom water are located [29, 79, 80, 85].

Although changes in abyssal temperatures are relatively small compared to the changes in the upper ocean (cf. Figs. 7 and 8), these changes involve large volumes of water and can amount to substantial signals in global oceanic heat content. Estimates of multi-decadal changes in global mean heat content for depths 0–3,000 m can differ by 25% from those based on the upper 700 m only (e.g., [76]). Contributions from abyssal depths may be smaller but not negligible. For example, if the observed abyssal warming in the western South Atlantic is reflective of global mean changes, it would imply decadal changes in heat content in the abyssal ocean close to 50% of those observed in the upper ocean [85]. Similarly, abyssal temperature changes and corresponding steric height effects could account for significant sea level signals on basin scales. Observed warming in the bottom waters of the South Indian Ocean implies changes in sea level as large as 4 cm over nearly a decade [81]. For comparison, global mean rates of sea level rise have been around 3 cm/decade in recent years (e.g., [86]).

Given that most deep and abyssal observations are confined to a few sections for each basin, the spatial extent of the observed long time scale signals at depths

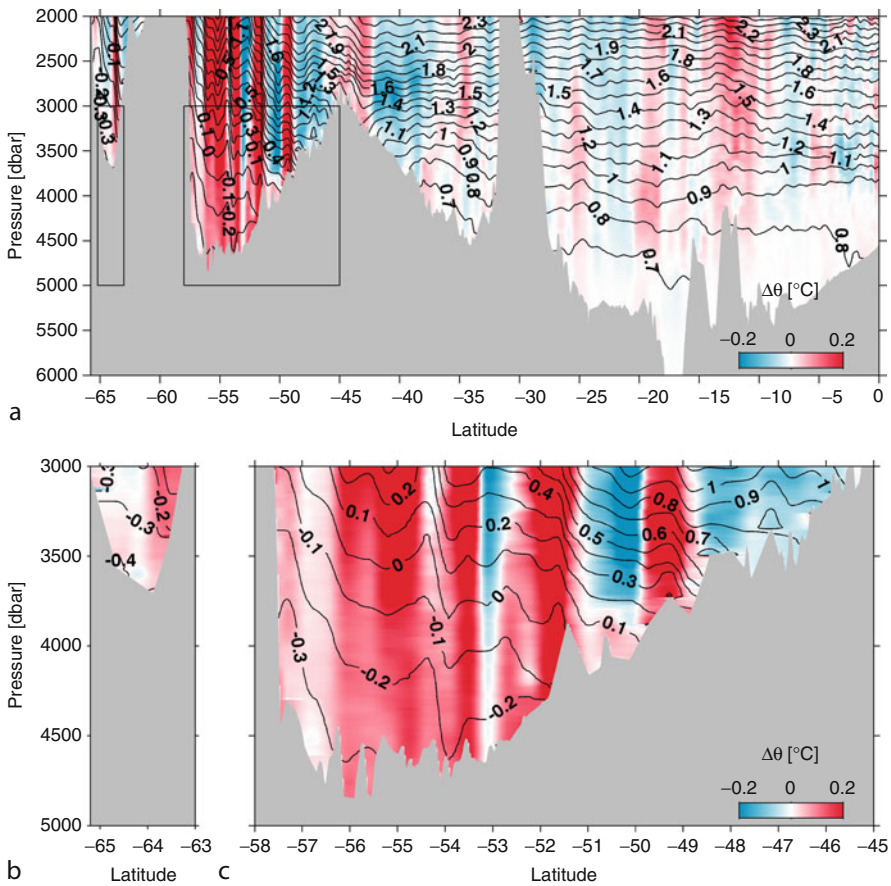

Heat Content and Temperature of the Ocean. Figure 8

Mean values of potential temperature (*contours*) and differences in potential temperature between the periods 1994–1995 and 2007 as a function of latitude and pressure (in decibars, which are approximately equivalent to depth in meters). Section covers most of the Southern Hemisphere, from Antarctica to the equator, at longitudes between 82E and 95E to the west of Australia. Panels (**b**) and (**c**) zoom in on the *boxes* drawn in (**a**) corresponding to abyssal waters in the Princess Elizabeth Trough and the Australian-Antarctic Basin southern most region. Full details are provided in Johnson et al. [81] (Reproduced from Fig. 4 of Johnson et al. [81])

is not known. Thus, global means or even basin means are difficult to estimate [76, 82] and the impact of deep and abyssal temperature changes on large-scale heat content and sea level remains the subject of speculation. Besides the extremely sparse sampling in space, examining snapshots of the temperature field every few years or decades presents other sampling issues. Fluctuations over a range of time scales, from hours to decades, can be present even at depth. As can be seen in the example in Fig. 8, differences of any two temperature sections contain numerous relatively small-scale features, which are generally related to the presence of eddies with time scales of a few months or shorter and with temperature signatures reaching all the way to the bottom. This eddy "noise" is large enough to make much of the differences in Fig. 8 and in many other similar studies statistically insignificant (e.g., [80, 81]). Much denser observations in both space and time are needed to improve statistical robustness and be able to discern whether observed changes are truly long term or the effect of short time scales, which cannot be resolved in the present records. By the same token, for the deep ocean, dynamical interpolations and extrapolations of the data in time and space using model and estimation techniques assume increased importance [48, 49]. These efforts provide the ability to use information from all observations, not just temperature, including data collected at other depths, to provide "best" estimates of the temperature variability in space and time.

Future Directions

Significant investment at the international level will be needed to sustain the current array of in situ and satellite systems (primarily Argo and altimetry) relevant to ocean heat content and temperature monitoring. At the same time, the severe under-sampling of many regions of the global oceans, including the high latitudes covered by sea ice and the deep layers below 2,000 m not sampled by Argo system, continues to be a problem in the quest to achieve truly global measurements of ocean temperatures and heat content at appropriate temporal resolutions for climate monitoring and other purposes. As society grapples with the need to assess current climate conditions and predict their evolution on decadal and longer time scales, future developments in ocean monitoring capabilities gain increased significance. Several paths for action are foreseen, with some of the seeds of an improved observing and estimating system already in place.

The development of float technology promises to extend the capabilities of the Argo system to ice-covered and deep waters [18, 87]. At the same time, efforts are underway to improve sampling of the marginal and coastal seas (e.g., [88, 89]). In all these areas, apart from the use of autonomous Argo-type floats, other observing platforms and technologies are expected to contribute to the collection of temperature data. Programs that use marine mammals for profiling at some high latitude regions (e.g., [90]) could be expanded. Gliders [91, 92] can provide routine profiling with considerably more control on sampling patterns than Argo-type floats and technology improvements could lead to operational glider deployments in many regions in the future. Moored instrumentation at all depths will be involved, as part of calibration programs or monitoring of "choke" points where variability and transports of ocean properties such as heat and freshwater require specific in situ observations.

Besides temperature measurements, other observing systems indirectly relevant for the determination of ocean heat content will see substantial advances over the next decade. High-precision satellite altimetry has reached quasi-operational status with the launch of Jason-2 and the scheduled launch of Jason-3 for 2014. A number of other missions scheduled to fly over the next few years will deliver denser surface height observations in space and time [93]. Potential breakthrough sampling is the goal of the Surface Water and Ocean Topography mission, which is still in the initial stages of planning [94]. Similarly, measurements of the variable gravity field from space with higher accuracies than presently possible should complement developments in altimetry to deliver better estimates of full-depth integrated changes in heat content [31]. In terms of in situ observations, acoustic thermometry [32] has been successfully exploited in the North Pacific [34] and the Arctic [95]. Expanded acoustic measurements discussed by Dushaw et al. [33] promise to deliver much needed coverage of deep layers over basin scales. Such measurements can also contribute to the monitoring of temperature change and heat transport variability across important "choke points" in the ocean, as in the ongoing program in Fram Strait [33].

Within the coming years, concerted and stepped up efforts to create an integrated global observing system will deliver improved measurements of temperature as well as many other oceanic parameters (salinity, velocity, bottom pressure, etc.) which are all indirectly linked to the determination of ocean heat content. Appropriate synthesis of all these diverse measurements, providing interpolation and extrapolation of the observations under rigorous physical conservation principles, can only be achieved with the use of models and state estimation techniques (e.g., [78]). In the future, as is established practice with the atmosphere (e.g., [46]), global estimates of temperature and heat content will come from the implementation of such systems. Similar machinery can be applied to the efficient design of observing systems that maximize collection of relevant information for the purposes of climate monitoring, analysis, and prediction [96]. Glider technologies begin to provide the possibility of adaptive sampling procedures, under which instruments are continuously directed at making measurements at times and places deemed important for determining the evolution of a given parameter of interest.

The combination of developments in observing, modeling, and estimating systems promises to deliver a revolution in the way ocean temperatures and heat content are determined in the near future. The impact on many areas of ocean and climate science will be hard to miss, from making it possible to relate sea level change to increased heat transfer from the atmosphere or melting of ice sheets, to providing better understanding of the variable Earth's radiation balance and hydrological cycle.

Acknowledgments

The author is indebted to J. Carton, G. Johnson, J. Kennedy, J. Lyman, M. Palmer, K. von Schuckmann, and S. Walker for help with the figures reproduced here. The support of NASA and the National Oceanographic Partnership Program is gratefully acknowledged.

Bibliography

Primary Literature

1. Stommel H (1965) The Gulf stream: a physical and dynamical description, 2nd edn. University of California Press, Berkeley, 248 pp
2. Thomson CW (1877) The voyage of the Challenger, vol 2, The Atlantic. Macmillan, London, 396 pp
3. Wüst G, Defant A (1936) Atlas zur Schichtung und Zirkulation des Atlantischen Ozeans. Schnitte und Karten von Temperatur, Salzgehalt und Dichte. In: Wissenschaftliche Ergebnisseder Deutschen Atlantischen Expedition auf dem Forschungs-und Vermessungsschiff "Meteor" 1925–1927, 6: Atlas, 103 plates
4. Gill AE (1982) Atmosphere–ocean dynamics. Academic, New York, 662 pp
5. Sverdrup HU, Johnson MW, Fleming RH (1942) The oceans: their physics, chemistry and general biology. Prentice-Hall, New York
6. Talley LD (2007) In: Sparrow M, Chapman P, Gould J (eds) Hydrographic atlas of the world ocean circulation experiment (WOCE), vol 2, Pacific Ocean. International WOCE Project Office, Southampton
7. Baker DJ Jr (1981) Ocean instruments and experiment design. In: Warren BA, Wunsch C (eds) Evolution of physical oceanography. MIT Press, Cambridge
8. Spilhaus AF (1938) A bathythermograph. J Mar Res 1:95–100
9. Spilhaus AF (1940) A detailed study of the surface layers of the ocean in the neighborhood of the Gulf Stream with the aid of rapid measuring hydrographic instruments. J Mar Res 3:51–75
10. Snodgrass JM (1968) Instrumentation and communications. In: Brahtz JF (ed) Ocean engineering: goals, environment, technology. Wiley, New York, pp 393–477
11. Lyman JM, Johnson GC (2008) Estimating annual global upper-ocean heat content anomalies despite irregular in situ ocean sampling. J Climate 21:5629–5641
12. Hanawa K, Rual P, Bailey R, Sy A, Szabados M (1995) A new depth-time equation for Sippican or TSK T-7, T-6, and T-4 expendable bathythermographs (XBT). Deep-Sea Res I 42:1423–1451
13. Willis JK, Lyman JM, Johnson GC, Gilson J (2009) In situ data biases and recent ocean heat content variability. J Atmos Ocean Tech 26:846–852
14. Gregg MC (1998) Estimation and geography of diapycnal mixing in the stratified ocean. In: Imberger J (ed) Physical processes in lakes and oceans, vol 54. Amer Geophys Union, Washington, DC, pp 305–338
15. Thorpe SA (2004) Recent developments in the study of ocean turbulence. Ann Rev Earth Planet Sci 32:91–109
16. Siedler G, Church J, Gould J (2001) Ocean circulation and climate: observing and modelling the global ocean. Academic, Boston
17. Roemmich D, Johnson GC, Riser GCS, Davis R, Gilson J, Owens WB, Garzoli SL, Schmid C, Ignaszewski M (2009) The argo program: observing the global ocean with profiling floats. Oceanography 22:34–43
18. Freeland, H, Roemmich D, Garzoli S, LeTraon PY, Ravichandran M, Riser S, Thierry V, Wijffels S, Belbéoch M, Gould J, Grant F, Ignazewski M, King B, Klein B, Mork K, Owens B, Pouliquen S, Sterl A, Suga T, Suk M, Sutton P, Troisi A, Vélez-Belchi P, Xu J (2010) Argo – A decade of progress. In: Hall J, Harrison DE, Stammer D (eds) Proceedings of the OceanObs'09: sustained ocean observations and information for society, vol 2, Venice, 21–25 Sep 2009

19. Woodruff SD, Diaz HF, Kent EC, Reynolds RW, Worley SJ (2008) The evolving SST record from ICOADS. In: Brönnimann S, Luterbacher J, Ewen T, Diaz HF, Stolarski RS, Neu U (eds) Climate variability and extremes during the past 100 years, vol 33, Advances in global change research. Springer, Dordrecht, pp 65–83
20. Reynolds RW, Smith TM (1994) Improved sea surface temperature analyses using optimal interpolation. J Climate 7:929–948
21. Donlon C, Robinson IS, Casey KS, Vasquez-Cuervo J, Armstrong E, Arino O, Gentlemann CL, May DA, LeBorgne P, Piolle J, Barton I, Beggs H, Poulter DJS, Merchant CJ, Bingham A, Heinz S, Harris A, Wick GA, Emery B, Minnett PJ, Evans R, Llewellyn-Jones D, Mutlow CT, Reynolds R, Hawamura H, Rayner NA (2007) The global ocean data assimilation experiment high-resolution sea surface temperature pilot project. Bull Am Met Soc 88:1197–1213
22. McPhaden MJ, Busalacchi AJ, Cheney R, Donguy J-R, Gage KS, Halpern D, Ji M, Julian P, Meyers G, Mitchum GT, Niller PP, Picau J, Reynolds RW, Smith N, Takeuchi K (1998) The tropical ocean-global atmosphere (TOGA) observing system: a decade of progress. J Geophys Res 103:14169–14240
23. Bourlès B, Lumpkin R, McPhaden MJ, Hernandez F, Nobre P, Campos E, Yu L, Planton S, Busalacchi A, Moura AD, Servain J, Trotte J (2008) The PIRATA program: history, accomplishments, and future directions. Bull Am Met Soc 89:1111–1125
24. McPhaden MJ, Meyers G, Ando K, Masumoto Y, Murty VSN, Ravichandran M, Syamsudin F, Vialard J, Yu L, Yu W (2009) RAMA: the research moored array for African-Asian-Australian monsoon analysis and prediction. Bull Am Meteorol Soc 90:459–480
25. Send U, Weller RA, Wallace D, Chavez F, Lampitt RL, Dickey T, Honda M, Nittis K, Lukas R, McPhaden M, Feely R (2010) OceanSITES. In: Hall J, Harrison DE, Stammer D (eds) Proceedings of OceanObs'09: sustained ocean observations and information for society, vol 2, Venice, 21–25 Sep 2009. ESA Publication WPP-306, doi:10.5270/OceanObs09.cwp.78
26. Michaels AF, Knap AH (1996) Overview of the U.S. JGOFS BATS and hydrostation S program. Deep-Sea Res 43(2–3):157–198
27. Karl DM, Lukas R (1996) The Hawaii ocean time-series (*HOT*) program: background, rationale, and field implementation. Deep-Sea Res II 43:129–156
28. White WB, Tai C-K (1995) Inferring interannual changes in global upper ocean heat storage from TOPEX altimeter. J Geophys Res 100:24943–24954
29. Willis JK, Roemmich D, Cornuelle B (2004) Interannual variability in upper ocean heat content, temperature, and thermosteric expansion on global scales. J Geophys Res 109:C12036. doi:10.1029/2003JC002260
30. Ponte RM (1999) A preliminary model study of the large-scale seasonal cycle in bottom pressure over the global ocean. J Geophys Res 104:1289–1300
31. Jayne SR, Wahr JM, Bryan FO (2003) Observing ocean heat content using satellite gravity and altimetry. J Geophys Res 108:3031. doi:10.1029/2002JC001619
32. Munk WH, Forbes AMG (1989) Global ocean warming: an acoustic measure? J Phys Oceanogr 19:1765–1778
33. Dushaw B, Au W, Beszczynska-Möller A, Brainard R, Cornuelle B, Duda T, Dzieciuch M, Fahrbach E, Forbes A, Freitag L, Gascard J-C, Gavrilov A, Gould J, Howe B, Jayne S, Johannessen OM, Lynch J, Martin D, Menemenlis D, Mikhalevsky P, Miller JH, Munk WH, Nystuen J, Odom R, Orcutt J, Rossby T, Sagen H, Sandven S, Simmen J, Skarsoulis E, Stephen R, Vinogradov S, Wong KB, Worcester PF, Wunsch C (2010) A global ocean acoustic observing network. In: Hall J, Harrison DE, Stammer D (eds) Proceedings of OceanObs'09: sustained ocean observations and information for society, vol 2, Venice, 21–25 Sep 2009. ESA Publication WPP-306, doi:10.5270/OceanObs09.cwp.25
34. Dushaw BD, Worcester PF, Munk WH, Spindel RC, Mercer JA, Howe BM, Metzger K Jr, Birdsall TG, Andrew RK, Dzieciuch MA, Cornuelle BD, Menemenlis D (2009) A decade of acoustic thermometry in the North Pacific Ocean. J Geophys Res 114: C07021. doi:10.1029/2008JC0051
35. Boyer TP, Antonov JI, Baranova OK, Garcia HE, Johnson DR, Locarnini RA, Mishonov AV, O'Brien TD, Seidov D, Smolyar IV, Zweng MM (2009) World ocean database 2009. In: Levitus S (ed) NOAA atlas NESDIS 66. US Gov Printing Office, Washington, DC, p 219, DVDs
36. Johnson DR, Boyer TP, Garcia HE, Locarnini RA, Baranova OK, Zweng MM (2009) World ocean database 2009 documentation. In: Levitus S (ed) NODC internal report 20. US Government Printing Office, Washington, DC, p 175
37. Ishii M, Kimoto M (2009) Reevaluation of historical ocean heat content variations with time varying XBT and MBT depth bias corrections. J Oceanogr 65:287–299
38. Gouretski VV, Koltermann KP (2004) WOCE global hydrographic climatology [CD-ROM], Ber Bundesamt Seeschiffahrt Hydrogr Rep 35. Bundesamt Seeschiffahrt Hydrogr, Hamburg, pp 52
39. Worthington LV (1981) The water masses of the world ocean: some results of a fine-scale census. In: Warren BA, Wunsch C (eds) Evolution of physical oceanography. MIT Press, Cambridge
40. Gouretski VV, Kolterman KP (2007) How much is the ocean really warming? Geophys Res Lett 34:L01610. doi:10.1029/2006GL027834
41. Lyman JM, Good SA, Gouretski VV, Ishii M, Johnson GC, Palmer MD, Smith DM, Willis JK (2010) Robust warming of the global upper ocean. Nature 465:334–337
42. Bretherton FP, Davis RE, Fandry CB (1976) Technique for objective analysis and design of oceanographic experiments applied to MODE-73. Deep-Sea Res 23:559–582
43. Daley R (1991) Atmospheric data analysis. Cambridge University Press, Cambridge, 457 pp
44. Locarnini RA, Mishonov AV, Antonov JI, Boyer TP, Garcia HE (2010) World ocean atlas 2009, volume 1: Temperature. In: Levitus S (ed) NOAA Atlas NESDIS 68. U.S. Government Printing Office, Washington, DC, pp 184
45. Wunsch C (1996) The ocean circulation inverse problem. Cambridge University Press, Cambridge

46. Kalnay E, Kanamitsu M, Kistler R, Collins W, Deaven D, Gandin L, Iredell M, Saha S, White G, Woollen J, Zhu Y, Leetmaa A, Reynolds R, Chelliah M, Ebisuzaki W, Higgins W, Janowiak J, Mo KC, Ropelewski C, Wang J, Jenne R, Joseph D (1996) The NCEP/NCAR 40-year reanalysis project. Bull Am Meteor Soc 77:437–470
47. Carton JA, Giese BS, Grodsky SA (2005) Sea level rise and the warming of the oceans in the simple ocean data assimilation (SODA) ocean reanalysis. J Geophys Res 110:C09006. doi:10.1029/2004JC002817
48. Wunsch C, Ponte RM, Heimbach P (2007) Decadal trends in sea level patterns: 1993–2004. J Climate 20:5889–5911
49. Köhl A, Stammer D, Cornuelle BD (2007) Interannual to decadal changes in the ECCO global synthesis. J Phys Oceanogr 37:313–337
50. Hansen J, Nazarenko L, Ruedy R, Sato M, Willis J, Del Genio A, Koch D, Lacis A, Lo K, Menon S, Novakov Y, Perlwitz J, Russell G, Schmidt GA, Tausnev N (2005) Earth's energy imbalance: confirmation and implications. Science 308:1431–1435
51. Roemmich D, Wunsch C (1984) Apparent changes in the climatic state of the deep North Atlantic Ocean. Science 307:447–450
52. Carton JA, Santorelli A (2008) Global decadal upper-ocean heat content as viewed in nine analyses. J Climate 21:6015–6035
53. Deser C, Alexander MA, Xie S-P, Phillips AS (2010) Sea surface temperature variability: patterns and mechanism. Annu Rev Mar Sci 2:115–143
54. Rayner NA, Brohan P, Parker DE, Folland CK, Kennedy JJ, Vanicek M, Ansell TJ, Tett SFB (2006) Improved analyses of changes and uncertainties in sea surface temperature measured in situ since the mid-nineteenth century: the HadSST2 dataset. J Climate 19:446–469
55. Smith TM, Reynolds RW, Peterson TC, Lawrimore J (2008) Improvements to NOAA's historical merged land-ocean surface temperature analysis (1880–2006). J Climate 21:2283–2296
56. Thompson DWJ, Kennedy JJ, Wallace JM, Jones PD (2008) A large discontinuity in the mid-twentieth century in observed global-mean surface temperature. Nature 453:646–649
57. Rayner NA, Kaplan A, Kent EC, Reynolds RW, Brohan P, Casey KS, Kennedy, JJ, Woodruff SD, Smith TM, Donlon C, Breivik LA, Eastwood S, Ishii M, Brandon T (2010) Evaluating climate variability and change from modern and historical SST observations. In: Hall J, Harrison DE, Stammer D (eds) Proceedings of OceanObs'09: sustained ocean observations and information for society, vol 2, Venice, 21–25 Sep 2009. ESA Publication WPP-306, doi:10.5270/OceanObs09.cwp.71
58. Chen D, Cane MA, Kaplan A, Zebiak SE, Huang DJ (2004) Predictability of El Niño over the past 148 years. Nature 428:733–736
59. Compo GP, Whitaker JS, Sardeshmukh PD (2006) Feasibility of a 100 year reanalysis using only surface pressure data. Bull Am Met Soc 8:175–190
60. Antonov JI, Levitus S, Boyer TP (2004) Climatological annual cycle of ocean heat content. Geophys Res Lett 31:L04304. doi:10.1029/2003GL018851
61. von Schuckmann K, Galliard F, Le Traon P-Y (2009) Global hydrographic variability patterns during 2003–2008. J Geophys Res 114. doi:10.1029/2008JC005237
62. Levitus S, Antonov JI, Boyer TP, Locarnini RA, Garcia HE, Mishonov AV (2009) Global ocean heat content 1955–2008 in light of recently revealed instrumentation problems. Geophys Res Lett 36:L07608. doi:10.1029/2008GL037155
63. Palmer MD, Antonov J, Barker P, Bindoff N, Boyer T, Carson M, Domingues CM, Gille S, Gleckler P, Good S, Gourtetski V, Guinehut S, Haines K, Harrison DE, Ishii M, Johnson GC, Levitus S, Lozier MS, Lyman JM, Meijers A, von Schuckmann K, Smith D, Wijffels S, Willis J (2010) Future Observations for Monitoring Global Ocean Heat Content. In: Hall J, Harrison DE, Stammer D (eds) Proceedings of OceanObs'09: sustained ocean observations and information for society, vol 2, Venice, 21–25 Sep 2009. ESA Publication WPP-306, doi:10.5270/OceanObs09.cwp.68
64. Levitus S, Antonov JL, Wang J, Delworth TL, Dixon KW, Broccoli AJ (2001) Anthropogenic warming of earth's climate system. Science 292:267–270
65. Barnett TP, Pierce DW, AchutaRao KM, Gleckler PJ, Santer BD, Gregory JM, Washington WM (2005) Penetration of human-induced warming into the world's oceans. Science 309:284–287
66. Lozier MS, Leadbetter S, Williams RG, Roussenov V, Reed MSC, Moore NJ (2008) The spatial pattern and mechanisms of heat content change in the North Atlantic. Science 319:800–803
67. Church JA, White NJ, Arblaster JM (2005) Significant decadal-scale impact of volcanic eruptions on sea level and ocean heat content. Nature 438:74–77
68. White WB, Dettinger MD, Cayan DR (2003) Sources of global warming of the upper ocean on decadal period scales. J Geophys Res 108:3248. doi:10.1029/2002JC001396
69. Wijffels SE, Willis J, Domingues CM, Barker P, White NJ, Gronell A, Ridgway K, Church JA (2008) Changing eXpendable BathyThermograph fallrates and their impact on estimates of thermosteric sea level rise. J Climate 21:5657–5672. doi:10.1175/2008JCLI2290.1
70. Domingues CM, Church JA, White NJ, Gleckler PJ, Wijffels SE, Barker PM, Dunn JR (2008) Improved estimates of upper-ocean warming and multi-decadal sea-level rise. Nature 453:1090–1093. doi:10.1038/nature07080
71. Stammer D, Köhl A, Awaji T, Balmaseda M, Behringer D, Carton J, Ferry N, Fischer A, Fukumori I, Giese B, Haines K, Harrison DE, Heimbach P, Kamachi M, Keppenne C, Lee T, Masina S, Menemenlis D, Ponte R, Remy E, Rienecker M, Rosati A, Schröter J, Smith D, Weaver A, Wunsch C, Xue Y (2010) Multi-model ensemble ocean synthesis in support of climate diagnostics. In: Hall J, Harrison DE, Stammer D (eds) Proceedings of OceanObs'09: sustained ocean observations and information for society, vol 2, Venice, 21–25 Sep 2009. ESA Publication WPP-306, doi:10.5270/OceanObs09.cwp.85
72. Levitus S (1989) Interpentadal variability of temperature and salinity at intermediate depths of the North Atlantic Ocean, 1970–74 versus 1955–59. J Geophys Res 94:6091–6131

73. Levitus S, Antonov J, Boyer TP, Stephens C (2000) Warming of the world ocean. Science 287:2225–2229
74. Köhl A, Stammer D (2008) Decadal sea level changes in the 50-year GECCO ocean synthesis. J Climate 21:1876–1890
75. Böning CW, Dispert A, Visbeck M, Rintoul SR, Schwarzkopf FU (2008) The response of the Antarctic circumpolar current to recent climate change. Nature Geosci 1:864–869
76. Levitus S, Antonov JI, Boyer TP (2005) Warming of the world ocean, 1955–2003. Geophys Res Lett 32:L02604. doi:10.1029/2004GL021592
77. Antonov JI, Levitus S, Boyer TP (2005) Thermosteric sea level rise, 1955–2003. Geophys Res Lett 32:L12602. doi:10.1029/2005GL023112
78. Wunsch C, Heimbach P, Ponte RM, Fukumori I, The ECCO-GODAE Consortium Members (2009) The global general circulation of the ocean estimated by the ECCO-consortium. Oceanography 22:88–103
79. Fukasawa M, Freeland H, Perkin R, Watanabe T, Uchida H, Nishina A (2004) Bottom water warming in the North Pacific Ocean. Nature 427:825–827. doi:10.1038/nature02337
80. Johnson GC, Mecking S, Sloyan BM, Wijffels SE (2007) Recent bottom water warming in the Pacific Ocean. J Climate 20:5365–5375. doi:10.1175/2007JCLI1879.1
81. Johnson GC, Purkey SG, Bullister JL (2008) Warming and freshening in the abyssal southeastern Indian Ocean. J Climate 21:5351–5363. doi:10.1175/2008JCLI2384.1
82. Purkey SG, Johnson GC (2010) Warming of global abyssal and deep Southern Ocean waters between the 1990s and 2000s: contributions to global heat and sea level rise budgets. J Climate 23:6336–6351
83. Stein C, Stein S (1992) A model for the global variation in oceanic depth and heat flow with lithospheric age. Nature 359:123–129
84. Kawano T, Fukasawa M, Kouketsu S, Uchida H, Doi T, Kaneko I, Aoyama M, Schneider W (2006) Bottom water warming along the pathway of lower circumpolar deep water in the Pacific Ocean. Geophys Res Lett 33:L23613. doi:10.1029/2006GL027933
85. Johnson GC, Doney SC (2006) Recent western South Atlantic bottom water warming. Geophys Res Lett 33:L14614. doi:10.1029/2006GL026769
86. Cazenave A, Nerem RS (2004) Present-day sea level change: observations and causes. Rev Geophys 42:RG3001. doi:10.1029/2003RG000139
87. Klatt O, Boebel O, Fahrbach E (2007) A profiling float's sense of ice. J Atmos Ocean Technol 24(7):1301–1308
88. Poulain P, Barbanti R, Font J, Cruzado A, Millot C, Gertman I, Griffa A, Molcard A, Rupolo V, LeBras S, Petit de la Villeon L (2007) MedArgo: a drifting profiler program in the Mediterranean Sea. Ocean Sci 3:379–395
89. Malone T, DiGiacomo P, Muelbert J, Parslow J, Sweijd N, Yanagi T, Yap H, Blanke B (2010) Building a global system of systems for the coastal ocean. In: Hall J, Harrison DE, Stammer D (eds) Proceedings of OceanObs'09: sustained ocean observations and information for society, vol 2, Venice, 21–25 Sep 2009. ESA Publication WPP-306, doi:10.5270/OceanObs09.cwp.59
90. Charrassin JB, Hindell M, Rintoul SR, Foquet F, Sokolov S, Biuw M, Costa D, Boehme L, Lovell P, Colman R, Timmermann R, Meijers A, Meredith M, Park Y-H, Bailleul F, Goebel M, Tremblay Y, Bost C-A, McMahon CR, Field IC, Fedak MA, Guinet C (2008) Southern Ocean frontal structure and sea-ice formation rates revealed by elephant seals. Proc Nat Aca Sci 105:11634–11639. doi:10.1073/pnas/0800790105
91. Rudnick DL, Davis RE, Eriksen CC, Fratantoni DM, Perry MJ (2004) Underwater gliders for ocean research. J Mar Tech Soc 38:73–84
92. Eriksen CC, Perry MJ (2009) The nurturing of seagliders by the National Oceanographic Partnership Program. Oceanography 22:146–157
93. Wilson S, Parisot F, Escudier P, Fellous J-L, Benveniste J, Bonekamp H, Drinkwater M, Fu L, Jacobs G, Lin M, Lindstrom E, Miller L, Sharma R, Thouvenot E (2010) Ocean surface topography constellation: the next 15 years in satellite altimetry. In: Hall J, Harrison DE, Stammer D (eds) Proceedings of OceanObs'09: sustained ocean observations and information for society, vol 2, Venice, 21–25 Sep 2009. ESA Publication WPP-306, doi:10.5270/OceanObs09.cwp.92
94. Durand M, Fu L-L, Lettenmaier DP, Alsdorf DE, Rodríguez E, Esteban-Fernandez D (2010) The surface water and ocean topography mission: observing terrestrial surface water and oceanic submesoscale eddies. Proc IEEE 98(5):766–779
95. Gavrilov AN, Mikhalevsky PN (2006) Low frequency acoustic propagation loss in the Arctic Ocean: results of the arctic climate observations using underwater sound experiment. J Acoust Soc Am 119:3694–3706
96. Heimbach P, Forget G, Ponte RM, Wunsch C, Balmaseda M, Awaji T, Baehr J, Behringer D, Carton J, Ferry N, Fischer A, Fukumori I, Giese B, Haines K, Harrison DE, Hernandez F, Kamachi M, Keppenne C, Köhl A, Lee T, Menemenlis D, Oke P, Remy E, Rienecker M, Rosati A, Smith D, Speer K, Stammer D, Weaver A (2010) Observational requirements for global-scale ocean climate analysis: lessons from ocean state estimation. In: Hall J, Harrison DE, Stammer D (eds) Proceedings of OceanObs'09: sustained ocean observations and information for society, vol 2, Venice, 21–25 Sep 2009, ESA Publication WPP-306, doi:10.5270/OceanObs09.cwp.42

Books and Reviews

Hall J, Harrison DE, Stammer D (eds) (2010) Proceedings of OceanObs'09: sustained ocean observations and information for society, vol 2, Venice, 21–25 Sep 2009. ESA Publication WPP-306

Koblinsky C, Smith N (eds) (2001) Ocean observations for the 21st century. GODAE Office/BoM, Melbourne

Peixoto JP, Oort AH (1992) Physics of climate. American Institute of Physics, New York

Sparrow M, Chapman P, Gould J (2007) The world ocean circulation experiment (WOCE) hydrographic atlas, 4 volumes. International WOCE Project Office, Southampton

Warren BA, Wunsch C (1981) Evolution of physical oceanography. MIT Press, Cambridge

High Speed Rail, Technology Development of

Eda Beyazit, Moshe Givoni
Transport Studies Unit, School of Geography and the Environment, University of Oxford, Oxford, UK

Article Outline

Glossary
Definition of the Subject
Introduction
Technological Development of HSTs
The Spatial Development of HST
Main Planning Principles of HSTs
Economic Costs of HSTs and Financing Strategies
Impacts of HSTs
Future Directions: Future of the High-Speed Train
Bibliography

Glossary

Dedicated lines In transport and telecommunication, dedicated lines are special rail, road infrastructure, cable or other facilities dedicated to a specific application. In transport technology examples can be found in bus, train, and subway systems running on dedicated lines.

Induced traffic/demand Induced traffic (or demand) is the volume of traffic that is drawn to a new road by additional capacity [8]. Induced demand occurs from a number of different sources such as new infrastructure, capacity increase, and infrastructure improvement or land use and location changes.

Shinkansen Shinkansen (new trunk line in Japanese) refers to the high-speed trains in Japan but also to the world's first HSR corridor, Tokaido Shinkansen, which was opened between Tokyo and Osaka in 1964. The main reason for the development of the Shinkansen network was to increase the network capacity between major cities of Japan. Shinkansen runs on dedicated railways designed only for high speed.

TEN Trans-European Network (TEN) Program comprises of a large number of projects in telecommunications, transport, and energy [13]. Trans-European Transport (TEN-T) Network is an important part of this program aiming to establish and develop the key links and interconnections needed to eliminate existing bottlenecks to mobility fill in missing sections and complete the main routes – especially their cross-border sections cross natural barriers and improve interoperability on major routes [33]. TEN-T includes projects such as road, rail, seaport, inland waterway, airport, shipping management, air traffic management and navigation networks. Number of total rail projects makes almost 50% of all transport projects and high-speed rail network is one of the most important projects of TEN-T. With projects such as the PBKAL (Paris-Brussels-Köln-Amsterdam-London) network and Southwest Europe network, high-speed rail lines are expected to create substantial reduction in travel times, increase the capacity and promote alternative transport to air and road transport.

TGV TGV (Train à Grande Vitesse) is the name given to the high-speed trains in France, which later on adopted by other countries using the same technology. French TGV is the first high-speed train in Europe, started to serve between Paris and Lille in 1981. Unlike Shinkansen, TGV operates on conventional tracks as well, thus, it can serve in city centers as well as regions by reducing its speed and this leads to a better connectivity between regional and urban network and significant cost savings. French recorded the highest speed ever reached on *wheel on steel* trains as high as 574 kph in 2007 during test drives [34].

Tunneling Effects A notion brought up by Graham and Marvin [18] referring to the possible effects of transport systems connecting specific areas in a region and bypassing others. This leads to some highly mobile socio-economic groups traveling through these places without even noticing the existence of them. Connecting places via high-speed systems may create adverse impacts as it may push disconnected places to the periphery (see also space-time compression by Harvey [21]).

Definition of the Subject

High-Speed Rail is an advanced railway technology for carrying passengers at high speeds. It can be defined as

the infrastructure capability to support high-speed rolling stocks. In the transport literature, rail (or railway) and train are often used synonymously [15]. In this section of the Encyclopedia of Sustainability the term will be used as High-Speed Train with reference to the technological development of both the vehicle (the train) and the track (the railways) but also with a reference to the *train* as a carrier and high-speed train not as a single element but as a system. Moreover, the main focus is on the passenger transport, although some emphasis will be made on the freight transport. Late twentieth century witnessed the return of the train as an important passenger transport mode and the reason for this is the rapid development of the high-speed rail technology. Twenty-first century is witnessing even a larger impact of train as a transport mode. World's biggest economies are racing with each other to implement high-speed train systems in order to enhance their economies with fast transfer between major centers of business, finance, residential development, and tourism. However, these ambitions come with a price: high-speed train can enhance economies and societies but at the same time it can create environmental, spatial, and socio-economic deprivation. This review evaluates the challenges that the future HST development faces within the context of sustainable development.

Introduction

- Transport technologies seldom make a comeback, save in nostalgia trips for well-heeled tourists. Stagecoaches have not made a reappearance on the Bath Road, nor sedan chairs on the streets of London. But there is a spectacular exception: railways, written off thirty years ago as a Victorian anachronism destined to atrophy before the steady growth of motorway traffic, have suddenly become one of the basic technologies of the twenty-first century.

  The reason of course is the high-speed train. . .
  (Hall and Banister 1993 [19, p. 157])

Speed has been one of the biggest ambitions of the mankind, not only in transport but also in different aspects of life: fast broadband, fast food, fast vehicles, and fast monetary transactions are only a few examples for the desire of a fast life. The reason behind this passion can be explained sociologically and can be attributed to the way in which modernism was shaped around the Fordist ideas of production and daily life in the twentieth century, however, one can discuss that it dates back to pre-Fordism, to the industrial revolution when the train emerged as one of the most important modes of transport of the time. Although rail lost its power over the years, especially after the introduction of the motorcar, in the last 40 years the number of passengers using rail has increased substantially within the European Union (EU15 see [14]) and in Japan. Nevertheless, the situation differs from one country to another. According to the figures of European Commission's 2010 Statistical Pocketbook, the Eastern European countries witnessed a significant decline in the rail use over the years while in the Western European countries the rail use increased significantly within the same period [12]. This might be related to the differences between countries in terms of "investment in rail services, the quality and frequency of services offered, the growth in car ownership, levels of expendable income, and the location of rail services with respect to the population" [14, p. 4].

High-Speed Train development can also be seen as one of the reasons of the differences between rail uses in countries since majority of the Western European countries have HST services, whereas HST development has recently started in Eastern Europe. However, HSTs still do not accommodate the majority of the trips in many countries. In countries where the HST growth took place more effectively, such as France, Germany, Sweden, Spain, and Italy, in 2008 share of HST in total rail transport was 61.9%, 28.5%, 27.2%, 22.9%, and 17.8%, respectively [12]. However, within the European Union, HST network accounts only 23.9% of the EU27 passenger kilometer in 2006 [12]. Although these figures show that the HST use in Europe is only a small fraction of the total rail usage and is mainly applied by the Western European countries, more and more countries are becoming interested in HST systems. By 2025 the HST network around the world will reach more than 40,000 km and one third of the whole network will be in China, a new emerging force in HST development ([36], See Fig. 4, [4]). Moreover, the EU White Paper for 2010 emphasizes the importance of an effective passenger high-speed rail network integrated with the air travel [10]. Recently, in the USA, the government committed $8 billion to

HST projects on 13 corridors across 31 states. All these investments around the globe shows that the governments started to become more aware of the benefits of a HST network as it not only increases the passenger capacity between places but it also can be a driving force of development in many scales from local to regional and national.

However, this fast development of HST network creates new challenges, especially in terms of the goals of sustainability. As discussed earlier, speed is one of the main elements of defining the movement of people and goods and in transport research travel time savings has been one of the main concerns: "[t]ransport appraisal is almost totally (80%) dependent on the user benefits resulting from travel time savings and hence the overwhelming desire to speed up traffic" [2, p. 955]. Since traveling in high speed is very attractive not only for businesses but also for tourism and daily commuting, HST often increases the demand for traveling which is one of the main obstacles of sustainability and one of the main arguments of the sustainable mobility paradigm [1]. In transport literature, the volume of traffic created on a route with new infrastructure or expansion in the current road structure is called the *induced demand*. With the help of the new improvements, cars, passengers, and trucks are drawn from other routes or even new demand is generated with the relief in traffic on some routes. As Cervero [5] states "[...] road improvements, critics charge, provide only ephemeral relief—within a few years, most facilities are back to square 1, just as congested as they were prior to the investment" [5, p. 3]. This phenomenon points out one of the main challenges for HST development in terms of sustainability: "how should the railway take a larger share of the current demand for transport without inducing new demand" [14, p. 1].

Under the light of the discussions above, this review will first give explanation of the meaning of the High-Speed Train and evaluate the technological development of HSTs by demonstrating different HST types. It will then discuss the principles of HSTs briefly and mention the latest debates on the transport, socio-economic, and environmental impacts of HSTs. The review will be finalized with a discussion on the future of High-Speed Train system.

Technological Development of HSTs

The idea of increasing the speed of the railways dates back to as early as 1903 when in Germany test drives achieved 200 kph [9]. Since then and until the inauguration of the modern HST, tests continued in many countries. Minor technological attempts in Germany during 1930s were followed by the achievement of Italian ETR in 1938, reaching up to 203 kph during test drives. However, these tests were interrupted by the Second World War. The attempts took off again in 1955 in France where the highest speed by that time was recorded as 331 kph. Although the first attempts were made in Europe, it was Japan who first succeeded in the commercial operation of HSTs after its success in recording 256 kph in test drives in 1963.

Although much of the reference is to the increased speed while defining High-Speed Trains, the main reason for constructing such a system is to increase the capacity of routes. HST lines can increase the capacity first, by supplementing the existing lines with more capacity and second, by shortening the headway between trains. The latter generates as the frequency between services increases due to high speeds, longer trains and the most up-to-date signaling systems [15]. Higher frequency increases the capacity, therefore makes the HST an attractive investment for countries. For instance, Shinkansen carried 400,000 passengers between Tokyo and Osaka per day in 2010 [34].

It is difficult to talk about a single definition of High-Speed Train (HST), however, "the reference is always to passenger services and not to freight" [15, p. 594]. In order to define HST, one should look at the meaning of high speed: "[h]igh speed can relate to the infrastructure capability to support high speed, the rolling stock capability to achieve high speed and/or the actual operation speed achieved" (ibid. 594). According to the European Union (EU), high speed is 250 kph for dedicated new lines and 200 kph for upgraded lines in respect of the infrastructure capabilities [38]. Therefore, EU describes High-Speed Train as;

- Those built specially for High-Speed travel.
- Those specially upgraded for High-Speed travel. They may include connecting lines, in particular junctions of new lines upgraded for High Speed with town center stations located on them, on which speeds must take account of local conditions.

Thus, high-speed lines would comprise:

- Specially built High-Speed lines equipped for speeds generally equal to or greater than 250 km/h.
- Specially upgraded High-Speed lines equipped for speeds of the order of 200 km/h.
- Specially upgraded High-Speed lines which have special features as a result of topographical, relief or town-planning constraints, on which the speed must be adapted to each case.

Currently, with some HSTs operating at speeds of 350 kph, 200 kph might not seem high speed anymore. "In practice, however, speed has not always been the best indicator, since commercial speed in many services is often limited due to, for example, proximity to densely urbanized areas or the existence of viaducts or tunnels" ([40], p. 20). Thus, speed cannot be regarded as the only determining factor of the HSTs and according to the International Union of Railways there are two important principles composed of different measurements [35]:

- High-Speed Railway is not element but systems. They are in fact very complex system, comprised by state of the art of the following components: Infrastructure, station emplacement, rolling stock, operation rules, signaling systems, marketing, maintenance systems, financing, management, legal aspects
- High speed is not unique and must be adapted to all countries and circumstances: As well as other railway systems, high speed can be considered under different conceptions, regarding commercial aspects, operation aspects, etc.

The differences between countries in terms of geographic and demographic characteristics, needs, and resources have led to the evolution of different types of HSTs [15]. These models which developed in the conditions of different countries then adopted by others, can be grouped into four: The Shinkansen, TGV, The tilting HST and The MAGLEV. However, in the last 10 years these models have been evolved to include each other's features. Examples such as tilting technology adopted by the TGV and Shinkansen trains can be found. Furthermore, MAGLEV technology is still in the first stages of its development and it is not certain whether this technology will be implemented widely in the future or will be completely abandoned due to extremely high construction costs compared to other HST models.

Shinkansen Model: The Bullet Train

Japanese Shinkansen is regarded as the first modern HST in operation [15]. The Tokaido Shinkansen opened in 1964 between Tokyo and Osaka as a celebration of the Olympics hosted by Japan [20]. However, the main reason was to increase the passenger capacity between these cities. Shinkansen travels 552.6 km, connecting Tokyo, Nagoya, and Osaka at a maximum speed of 270 kph in 2 h and 25 min. As of March 2010, approximately 138 million passengers are carried per annum [23] and there are 400,000 passengers on board per day [34]. Remarkably, since its opening no fatal accidents or injuries have been recorded [23].

Due to the unique geographic features of Japan and technical differences between conventional tracks and new gauges, it was not possible to achieve high speeds on the existing narrow gauge lines. Thus, the Shinkansen was built on a new line, dedicated only to high-speed trains. With this feature, Shinkansen differs from other HST models in most of Europe. The need for construction of new lines, high usage of tunnels and high land values within city centers are some of the factors that increase the building costs of Shinkansen [15] (Fig. 1).

High Speed Rail, Technology Development of. Figure 1 Shinkansen (Source: BakaOnigiri, Wikipedia)

The TGV

French TGV (Train à Grande Vitesse) In Europe, where the high-speed system emerged in its modern form in 1970–1980s, the rationality behind building high-speed lines and developing it in such a way that the lines in different countries would connect with each other and other transport networks, was to build up a Trans-European High-Speed Rail Network in the future. TEN-T network comprises of road, rail, air, and water transport networks designed to provide seamless transport within the European Union and High-Speed Rail network has a crucial role in achieving the cohesion goals of the EU. According to Vickerman, the reasons for creating such a network were [37, p. 22]:

- To overcome limited capacity on critical links of the rail network, where some new investment was needed and a completely new alignment appeared the most cost effective solution.
- To increase speeds on particularly slow sections of the trunk network where the developments in rail technology could not be fully exploited.
- To improve the accessibility of more remote regions.

However, it was initially France, within the EU members, where the high-speed lines were developed in a network and later on expanded to connect with other national lines.

Although French began test drives as early as 1950s, it was not until 1980s that they put the first modern HST into service in Europe. The first TGV line opened between Paris and Lyon in 1981. It serves the same purpose as Shinkansen but differs in design due to different features of France. "The most significant difference between the TGV and the Shinkansen is probably the ability of the former to operate on conventional tracks as well, which allows the TGV to use the conventional lines as it enters and leaves the city center, leading to significant cost savings" [15]. This feature of the TGV creates a network extending to regions without HST and allows connections between major cities and small towns where the demand is not high enough to justify the construction of a dedicated line (ibid.). This operational model is an example to the mixed high-speed model [40]. The TGV can reach up to 320 kph for commercial speed. French recorded the highest speed ever reached on *wheel on steel* trains as high as 574 kph in 2007 during test drives [34]. Nevertheless, operating at this speed is not possible at the moment (Fig. 2).

High Speed Rail, Technology Development of. Figure 2 TGV at Gare de Lyon (Source: Sese Ingolstadt, Wikipedia)

Since 1981, the opening of the first TGV line 1,400 million passengers have been carried [34]. Currently the French TGV consists of eight lines [35]: TGV Sud-Est (Paris – Lyon); TGV Rhône-Alpes (Lyon – Valence); TGV Méditerranée (Valence – Marseille); TGV Atlantiqué (Paris – Le Mans & Tours); TGV Interconnexion-Est (east of Paris); TGV-Nord (Paris – Lille –London via Channel Tunnel, Brussels – Amsterdam – Cologne); TGV Est (Paris – Strasbourg); TGV Peripignan Figures (France – Spain). The current network under operation is 1,896 km with a further 210 km under construction and 2,616 km planned (ibid.).

The Tilting Trains

Tilting train is a type of train with a sophisticated computerized mechanism running on conventional lines. The mechanism helps the train to tilt while it is going through the curves so that the train can travel on conventional lines at high speeds and passengers do not feel the discomfort from the centrifugal force. Tilting technology was initially invented in the UK in early 1980s, however, it was later abandoned. Nowadays, Italy is the leading country in tilting train technology with its Pendolino trains. Opposite to the Japanese, French, Spanish, and German HST trains which all use a newly built track on the sections where high speed is achieved (except the German ICE-T), in Italy the tilting

technology is developed on routes where the demand is not high enough to justify the cost of constructing new tracks that allow high-speed operation [15].

The German ICE-T, the Swedish X-2000 and the Virgin Trains in the UK connecting London, Birmingham, Manchester, Liverpool, and Glasgow are the examples of tilting trains adopting the technology from Italy's Pendolino (ETR-450) trains. The Italian Pendolino reaches up to the maximum speed of 250 kph, whereas the Swedish X-2000 and the UK Virgin Trains Pendolino are slightly slower reaching up to 210 kph and 225 kph, respectively. Tilting mechanism is adopted by other HST models such as Shinkansen trains which use this technology to increase their speed.

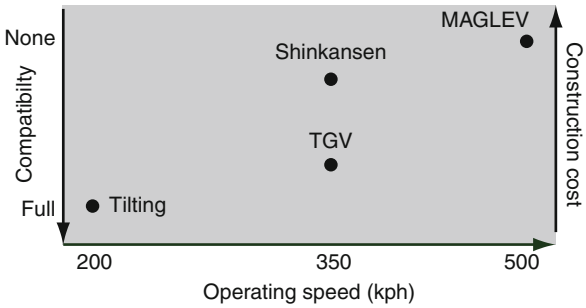

High Speed Rail, Technology Development of. Figure 3 Operating speed, construction cost, and compatibility (with the conventional network) characteristics of the four high-speed train models ([15, p. 509], updated by the authors)

The MAGLEV

The idea of running the train on magnetic plates dates back to as early as 1970s, to the first tests conducted in Germany. "The technology relies on electromagnetic forces to cause the vehicle to hover above the track and move forward at theoretically unlimited speeds" [15, p. 597]. In practice, the aim is for an operation speed of 500 kph (Taniguchi [39] cited in [15, p. 597]. Japan is one of the leading countries in testing the MAGLEV technology. In 1997, tests started on the Yamanashi Maglev Test Line [24]. According to Japanese Railway Technical Research Institute that is responsible of conducting the MAGLEV tests in cooperation with the JR Central, in 2003, a MAGLEV three-car train set attained a maximum speed of 581 kph in a manned vehicle run [29]. In November 2004, two train sets succeeded in passing each other at relative speeds of up to 1,026 kph [29]. Even though the MAGLEV technology has been proved to be successful in the test drives, it has not been put into practice widely due to high construction costs and no compatibility with the existing lines. In Japan, Yamanashi Maglev Test Line has recently been agreed to be extended for another 23 km and is planned to become a part of the Tokaido Shinkansen Bypass, making it the first long-distance MAGLEV line in commercial operation [25]. In China, a short MAGLEV line was opened in December 2003 connecting Shanghai Airport and the city's Pudong financial district with trains running at maximum speed of 430 kph. However, as mentioned earlier, the investment on MAGLEV trains is very small in number compared to the rest of the HST development all around the world.

As explained above, there are differences in principle between the models of HSTs. Givoni [15] compared these models in terms of compatibility, construction costs, and speed (Fig. 3).

The Spatial Development of HST

According to the reports of the International Union of Railways [34], the HST lines in operation and construction cover many of the developed and developing countries. Nowadays there are high-speed train services in 14 countries and planned lines in other ten countries [36]. According to the UIC 2011 report, there is 14,700 km of high-speed line in operation, 9,703 km under construction and 17,594 km planned HST system in the world, that will make 41,997 km of high-speed line in 2025, 17,769 km of which in Europe and 21,460 km in Asia [36] (Fig. 4). However, considering more than 150 countries in the world have railway systems [28]; the number of countries investing in HST system is very low. Thus, it is questionable how much the HSTs can be a part of the solution for the increasing travel demand and whether it is the high costs or lack of planning or else that is making some countries reluctant of investing in this technology.

Europe

Besides France and Italy, HST development takes places in other European countries as well. The Spanish AVE

	SITUATION / COUNTRIES	In operation	Under construction	Planned	Total
EUROPE	Belgium	209			209
	France	1896	210	2616	4722
	Germany	1285	378	670	2333
	Italy	923		395	1318
	The Netherlands	120			120
	Poland			712	712
	Portugal			1006	1006
	Russia			650	650
	Spain	2056	1767	1702	5525
	Sweden			750	750
	Switzerland	35	72		107
	United Kingdom	113		204	317
	Europe Total	**6637**	**2427**	**8705**	**17769**
ASIA	China	4175	6058	2901	13134
	Taiwan-China	345			345
	India			495	495
	Iran			475	475
	Japan	2534	508	583	3625
	Saudi Arabia			550	550
	South Korea	412			412
	Turkey	235	510	1679	2424
	Asia Total	**7701**	**7076**	**6683**	**21460**
Other HST Systems	Morocco		200	480	680
	Argentina			315	315
	Brazil			511	511
	USA	362		900	1262
	Total other HSTs	**362**	**200**	**2206**	**2768**
	WORLD TOTAL	**14700**	**9703**	**17594**	**41997**

High Speed Rail, Technology Development of. Figure 4
The HST lines in operation, under construction and in the planning stage. Based on [36]

(Alta Velocidad Espanola, or Spanish High Speed), opened in 1992, can be seen as another type of TGV as it uses TGV-type rolling stocks in order to create integration with rest of Europe, mainly with France. However, like Shinkansen, "it runs on a dedicated line throughout, because the Spanish conventional network is wider than the standard International Union of Railways (UIC) gauge used across most of Europe" [15, p. 596]. Since it runs on dedicated lines and not compatible with the rest of the domestic network, it is possible to classify AVE in the Shinkansen category. In order to solve the problem of integration within the country, tracks have been developed to have three rails, thus, both types of trains (conventional and AVE) can run on them. The Spanish AVE achieved 350 kph in test drives and runs on 300 kph max speed commercially,

connecting Madrid-Barcelona (689 km) in 2 h 38 m and Madrid – Sevilla (471 km) in 2 h 30 m.

Germany's HST, the ICE (Inter-City Express) that started to operate in 1991, today reaches the speeds of up to 320 kph [7]. Unlike other systems, the initial network was planned for both passenger and freight transport, using a technology deviating from the TGV and Shinkansen models. However, this mixed-use turned out to be a disadvantage due to high construction costs and low utilization of the lines, thus, no other country attempted to replicate it. Today the ICE network consists of different technologies with trains running on both dedicated lines and existing lines using the tilting technology where the demand is high enough to run high-speed train services but not high enough to construct dedicated lines [7]. Five different lines operate between several major European cities including international destinations in Switzerland, Austria, Belgium, and the Netherlands.

Portugal is also one of the leading countries in terms of the extent of the network to be developed. According to UIC [36], 1,006 km of new HST line has been planned to connect major cities with each other and with Spain. Portugal is followed by Sweden, Poland, and Russia that will have, respectively, 750 km, 712 km, and 650 km new high-speed lines in the near future. By the extension of 72 km HST lines in Switzerland and 204 in the UK, the HST lines in Europe (currently 6,637 km) will reach 17,769 km in 2025 [36]. In the UK, currently the only operating dedicated high-speed line is the Channel Tunnel Rail Link (CTRL, nowadays referred to HS1) which connects London to the Channel Tunnel.

Asia (Including Middle-East)

In Asia, following Shinkansen's success, China is aiming to be the new leader in HST development. Currently, there are 4,175 km of high-speed lines in operation which are planned to be extended to 13,161 km by 2025 [36]. When finished, China will have one third of the world's total HST network. Although South Korea (KTX – Korea Train eXpress – 412 km) and Taiwan (345 km) have put the HST lines into operation before China, they have no future plans to develop the network within the next 15 years. With the new lines in India, Iran, Saudi Arabia, and Turkey, the existing 7,701 km HST network in Asia will reach to 21,460 km in total in 2025 [36].

Other High-Speed Systems

In the USA, the only HST line in operation is the Acela Express tilting train running on the North East Corridor line between Boston and Washington, DC. Recently, the USA government announced the eight billion US dollars of state funds to be spent for the development of future HST lines. Currently, only the State of California is planning to develop a HST network between Los Angeles, San Francisco, and Sacramento which will add 900 km of HST line to the existing network [36]. In South America, Brazil, and Argentina planned 511 km and 315 km HST lines, respectively, which are aimed to be completed by 2020. Moreover, Morocco has 200 km of HST lines under construction and a further 480 km planned network [36].

Main Planning Principles of HSTs

As mentioned earlier, the main reason behind developing the high-speed rail technology is to increase the capacity of routes and reduce the travel time. However, increased speed is not solely sufficient to reach these goals; other measures need to be met as well. These are the integration of the HST network with the existing transport system, creating seamless transfer between the different modes of transport system and choosing the location and number of the stations.

First of all, there are three main models of station location: at the city center and in the outskirts (a third model, station at the edge of the city, can be included in either of the two models mentioned. For a detailed analysis and explanation of the subject, see Menéndez et al. [27]). Each option has its own pros and cons, and the balance is always context specific. From an accessibility perspective, the city center station location model might be better than the outskirts model as demand is likely to be higher due to higher population density and/or level of commercial activity. It is also likely to be much better served by public transport including regional and national train services. On the other hand, this model is significantly more costly and more complicated than the outskirts model due to

restricted land for development and high costs of land intake. The outskirts model is likely to be cheaper in terms of land acquisition, simpler to construct and might offer more land for redevelopment and likely better connection opportunities for regional accessibility from a road transport perspective. Therefore, pros of one model become generally the cons of the other. Moreover, as Givoni and Banister mention the design of the stations is as important as the location in terms of allowing "seamless transfer between HST services and other rail (or air) services" [14, p. 9]. The transfer centers need to be designed in order to ease the passenger flows between different modes and also to accommodate different needs of passengers especially in international stations.

The number of stations is another important element in the planning of HSTs. In simple economic terms, the number of stations is a function of a trade-off between reducing the cost of accessing the station by opening an additional station, thus shortening the access journey, and the cost of adding a station which is the cost of providing it (construction) and the cost penalty of stopping the train (longer travel time) [17]. The characteristics of HST suggests it should have very low number of stops between the start and end stations. HSTs are feasible mainly on high-demand routes with stations located in major conurbations with 12–15 million passengers a year [37]. Most cities, except large metropolises like Tokyo and Paris, have one HST station. Increased number of stations means longer travel time, as the train will stop frequently and that would in turn reduce the desirability of the high-speed train. For instance, in France, an important number of trains between Paris and Lyon do not stop for 447 km which is different than the UK Channel Tunnel rail link that has three stops between London and the Channel tunnel which is 109 km apart ([20, 22]). However, there are also negative consequences of limiting the number of stations and planning them only for the major cities. "Since the HST often replaces or supplements an existing conventional railway service, these bypassed cities along the HST line will see substantial reduction in rail services because they will lose the through traffic to the HST and local demand would not support the same level of service. In turn, this reduction in rail accessibility can contribute to economic decline" [14, p. 6]. Thus, in routes where the demand is high enough to run extra services, cautions are taken due to possible negative impacts of HSTs. The different service levels can be found in Japan (see the "Socio-economic Impacts and Spatial Imbalance" section). However, as stated earlier, these measures can be applied in high-demand routes, therefore, for other places with low demand the integration of the HST network with the existing road, rail, and air system is essential.

There are three levels of integration: integration with the urban transport network, the national intercity transport network and the international, long-distance air transport network. The attractiveness of using HST compared to aircraft depends on the ease to get to the station vs. the airport and the time of doing so. Moreover, integration with the regional network is one of the essentials of HST development. Since the spatial spread of HST network is constrained by the station location choice and number of stations, its integration with the regional rail network is crucial for sustaining an increased accessibility from different regions. As Givoni and Banister suggest "the location of the HST stations must consider the entire rail network and not only local demand from cities" in order to spread the accessibility benefits from HST services across the entire network [14, p. 9]. Also, the integration with the rail network is more important than the road network as the latter would not create opportunities for a decrease in the car use due to the efficiency of the car in many ways such as door-to-door travel. Lastly, integration with air travel is another important strategy to spread the benefits of HST network. More emphasis will be made on the integration of air and rail in the next section.

It is those guiding principles for the development of HST that will determine the scope and scale of its impacts. Therefore, they are crucial in the planning of HST systems.

Economic Costs of HSTs and Financing Strategies

Construction costs and financing strategies of HSTs vary between countries and pretty much depend on the type of technology that is used. Different technologies are adopted by countries in order to overcome the restrictions that occur from geographic features or the existing technology of the railways.

The construction costs have been briefly discussed earlier when describing different HST models and

different systems were compared in Fig. 3. However, a more detailed comparison of construction costs requires more information as the costs depend on so many criteria that are mentioned in the previous paragraph. Nevertheless, "the comparison of construction costs between different HSR projects is difficult since the technical solutions adopted in each case to implement these features do not only differ widely (depending on topography and geography), but also evolve over time" ([40], p. 22).

The UIC [41] points out three major types of costs for building a new HST structure. These are planning and land costs, infrastructure building costs, and superstructure costs [41]. According to a study comparing the construction costs of HSTs from different countries by Campos and de Rus [40], the range of costs varies between €9 and €39 million per kilometer (2005 figures). In Europe "France and Spain have slightly lower building costs than Germany, Italy, and Belgium. The HSR construction in Asia, except China, seems to be more expansive than in Europe" (ibid. 23). In addition to the building costs, operation costs are important in planning HST systems. According to Campos and de Rus [40], these costs can be grouped in two: infrastructure operating costs and rolling stock and train operating costs (for a detailed explanation of the operating costs see [40]).

Some of the well-known financing strategies can be discussed here. The TGV was financed by SNCF (Société Nationale des Chemins de fer Français – *French National Railway Corporation)* with expectations of minimum 12% financial rate of return. Unexpectedly, SNCF's investment was fully amortized by the end of 1993 after 12 years of service, proving that it was hugely profitable [37]. In 2010, SNCF's revenue from high-speed train services including TGV was €7.2 billion [30]. The SNCF is considered a state-owned industrial and commercial enterprise under French law [31]. Thus, the investment and operation of the TGV is under the control of the state. In Japan where the Shinkansen was initially constructed using government and World Bank funds the situation is slightly different. The Shinkansen lines were privatized in 1987 making the financing strategy a public-private partnership. The JNR (Japan National Railways) was divided to six passenger and one freight rail companies collectively called Japanese Railways Group (JR Group) that include East Japan Railway Company, West Japan Railway Company, and Central Japan Railway Company, all operating and maintaining different parts of the HST network. The initial investment for the Shinkansen was recovered by 1971, in 7 years of operation. Revenue from the Shinkansen has been an important source for financing local lines. However, these two examples (French TGV ad Shinkansen) are exceptional and the outcomes cannot be attributed to other HST systems.

Recently, in the US, the President Obama announced a spending of nearly $8billion for a new high-speed railway project funded by the Recovery Act in order to move the US in the direction of developing a high-speed rail service in 13 travel corridors covering 31 states all across this country with the goal of making high-speed rail accessible to 80% of Americans within 25 years [6]. In this sense, the financing strategy in the USA is similar to that of in France where the state controls the investment and operations through state-owned companies.

In the UK, the first high-speed line, CTRL, was initially planned as a state investment. However, due to the financial difficulties the governments signed several consortiums until 2010 when a 30-year concession to a consortium of Canadian investors was announced. For the HS2 the government set up an initiative under the name of HS2 Limited Company in 2009 for the design and development of the new HST line.

Impacts of HSTs

Transport Impacts

The main benefit of high-speed train which also fosters other benefits at economic and social levels is the increased route capacity. Here, the attribute is given not to the increased speed but to the reduced headways due to the high speeds. Higher speeds and the up-to-date signaling systems which are prerequisites of high-speed systems create short headway between trains and thus, trains run at higher frequencies [15] and provide more capacity on the routes where the existing network cannot meet the demand. Thus, changes in modal share occur due to the demand shift between transport modes and generation of additional demand. In TGV line between Paris and Lyon the share of the train

journeys increased by 32% within the 3 years of its opening opposite to the decreased aircraft, car, and bus traffic (ibid.) "Paris-Lyon air traffic halved between 1980 and 1984, Paris-Geneve fell by around 20% and Paris-Sud Est in general grew at less than half the rate of other radial routes from Paris" [37, p. 24]. A similar result was seen in Spain after the inauguration of the AVE between Madrid and Seville where the train journeys increased by 35% between 1991 and 1994 [15]. Likewise, in the first 5 years of operation ICE, passengers more than doubled from just over 10 million to nearly 23 million [37]. "The AVE has been remarkably successful in terms of traffic growth and diversion. [. . .] [A]ir traffic has suffered with an estimated 60% reduction. Some 32% of travelers have diverted from air, 25% from car, and 26% were newly generated" (ibid. 30). However, it is important to mention that developing HSTs come at the expense of other railway networks. For instance, in EU 27 the number of passengers traveled by conventional railways showed no significant increase, whereas this increase is notable in HST trips (Fig. 5). This shows the fast increase in HST use while the rail use stays constant.

Apart from modal shift, high-speed lines also create substantial reduction in travel times which makes HSTs an attractive mode of transport. Before the inauguration of the HST in Japan, it took 7 h to travel between Tokyo and Osaka on the conventional line; it was then reduced to 4 h following the inauguration of the Shinkansen (Matsuda, 1993 cited by [15]). The current travel time between Tokyo and Osaka is 2 h 25 min with a maximum speed of 270 kph. Traveling with TGV between Paris and Lyon takes about 2 h at the moment. Likewise, in central and southern China almost 1,000 km is taken in 3 h and in northern China around 120 km is traveled in 30 min by Chinese HST, bringing countries' largest cities closer to each other.

With reductions in travel time and changes in modal share, HSTs become competitors to airline companies. However, rather than competition, cooperation is more beneficial for airlines. "Cooperation between air and HST can take place if the airport is situated on the rail and HST networks allowing airlines to retain connecting traffic from short-haul routes to their more profitable long-haul services, thus giving up flights without compromising their Hub and Spoke

EU-27	HST		RAIL	
YEARS	Thousand million pkm	CHANGE	Thousand million pkm	CHANGE
1990	15,23		400,7	
1995	32,94	116%	350,5	−13%
2000	58,8	79%	370,7	6%
2005	80,11	36%	377	2%
2008	97,6	22%	409,2	9%

High Speed Rail, Technology Development of. Figure 5
Number of passengers transported by HST and conventional railways per km in EU27. Based on [12]

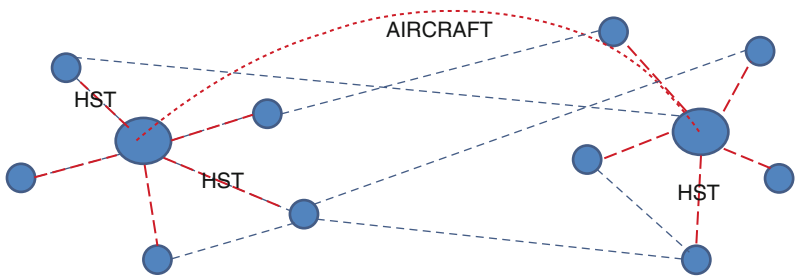

High Speed Rail, Technology Development of. Figure 6
Integration of HST network with airport can reduce short-haul flights

operation" [14, pp. 6–7]. In Europe, Amsterdam Schiphol, Paris Charles de Gaulle, and Frankfurt International are examples where the seamless connection between the airport and high-speed train already exists.

Figure 6 demonstrates the possibility of airline-HST cooperation and integration of the HST network with the existing regional railway network. According to this, rather than providing services between minor cities, airlines can reduce the number of short-haul flights and operate on long-distance routes which are more profitable. The connection of airports with HST network which is also connected to the conventional rail network would not reduce the profits of the airline companies; on the contrary this type of connection would decrease their costs occurring from short-haul flights by keeping the number of long-haul flight passengers steady.

Sustainability Impacts

Socio-economic Impacts and Spatial Imbalance Transport investments that supply fast, affordable, reliable, and secure systems are seen as a condition for economic development either creating new economic areas with the help of agglomeration economies or increasing the size of actual markets (for a detailed understanding of the subject see [3]). "Development opportunities from new networks will occur at locations with good access to the new network and which provide nodal connections to other networks"[37, p. 35].

It is possible to observe this argument in the case of high-speed rail investments as well. Evaluating the previous studies on Shinkansen HST, Banister and Berechman [3] states that there are three conditions needed for growth: high incidence of information exchange industries; sufficient opportunities for higher education; good accessibility to a Shinkansen station [3, p. 279]. At the local level, Shinkansen's impacts occurred differently. The stations located in existing cities barely had any impacts, conversely, new stations at the edge of existing cities boosted the population and employment growth rates. First TGV line between Paris and Lyon created similar impacts in some parts on the route. A new station in Lyon Part-Dieu, close to central Lyon 2 h from Paris by TGV Sud-Est, has been largely affected from the opening of the TGV line especially in terms of the significant increase in the demand for office space (ibid.). Moreover, further local impacts have been observed as the TGV has been extended to the west and north. "Substantial growth has taken place at Le Mans, Nantes, and Vendôme in the TGV Atlantique" (ibid. 281). Also on the TGV-Nord line opened later in 1993 in order to connect Paris, London, and Brussels (northern Europe), a technopole concept, Euralille, was planned (ibid.). Initially, the network was planned strategically that Lille would become "a business bridge-head on the continent for London; city of services for Brussels and an attraction of relocations from Paris" ([42], p. 130). Recently, a major office development has been extended southward in Lille [20]. Likewise in Spain, AVE is known to have created new markets with the help of the shuttle services Ciudad Real and Puertollano around 200 km from Madrid [37].

However, new HST lines do not generate the same economic effects everywhere: "only those centers which are prepared to support it with complementary investment will stand to gain" [37, p. 35]. As seen in the example of The Channel Tunnel, where the stations are not located in major conurbations (but in the Kent countryside), the development potential accrues in other centers (ibid.), having maybe less impact that it would have had they been located in major centers. Nevertheless, a major office development around station, King's Cross and St Pancras after the completion of the CTRL (Channel Tunnel Rail Link) in 2007, can be seen [20].

The accumulation of investments only in major centers might not always have positive influences, especially when the subcenters or minor cities are concerned. As mentioned earlier, HSTs are feasible mainly on high-demand routes. This economic necessity makes it difficult for other areas – minor cities – to connect to the high-speed system which in turn creates economic and social imbalances. According to Graham and Marvin [18], "advanced infrastructure networks targeted on valued parts of the metropolis and drawing them into intense interaction with each other" create "tunnel effects" [18, p. 201]; also mentioned by Plassard, 1991 cited in [37]). In this case, HSTs connecting major cities within and beyond countries can create so-called tunneling effects, changing the proximity of places: making some closer to each other

while pushing others to the periphery. Hall [20] calls this effect "peripheralization of the periphery" emphasizing that the regions which are already in the periphery, due to the lack of economic viability, are even more peripheralized as a result of making investments in other parts of the region. Maps of Europe as a "Shrinking Continent" have been created by Spiekermann and Wegener [32]. According to the time-space maps of rail travel times which are based on a deeper geographical understanding of space and time (see for example, [21] for more detailed understanding of the space-time compression), the core cities are drawn closer in terms of time-distance, while the more distant places which lack high-speed networks are bypassed and thus, become relatively more remote (ibid.). For instance, in a recent study by Martínez Sánchez-Mateos and Givoni [26] where the authors explore possible impacts of London – Birmingham HS2 link, they demonstrate that the towns in Birmingham catchment area will be affected from the construction of the HST stations in different ways. According to the study that explores the possible accessibility changes in the area after the introduction of the HS2 link, the towns that are relatively close to Birmingham and have good access to London will not benefit from the HS2, on the contrary, they might be adversely affected resulting in a decrease in their accessibility to London. Whereas, the settlements on the North of Birmingham that have less accessibility to London will benefit from the HS2 service more than the others. Thus, this would result in changing the geography of the county [26]. This example not only demonstrates the power of transport systems on geography but also shows the importance of station locations and integration between the transport modes.

In order to solve this problem, "in Japan the Shinkansen was deliberately structured on the basis of two service levels, fast (Hikari) serving only main cities and semi-fast (Kodama) serving intermediate cities, and this has been maintained; a super-fast (Nozomi) service was added in 1992" [20, p. 65]. In France and Germany similar measures were taken and additional stations were planned in small cities (ibid.). Likewise, in the UK, the Channel Tunnel Rail Link (HS1) was seen as a tool to regenerate the economy and Ebbsfleet and Stratford stations formed part of the Thames Gateway regeneration project east of London (ibid.). However, these solutions are only possible where the demand is high enough to compensate this investment. Furthermore, since high-speed trains are relatively more expensive compared to conventional trains, network solutions which aim to spread the impacts of HSTs would not be sufficient to make the system socially inclusive as not all socio-economic groups would be able to afford them. Here the crucial question is who benefits from such an expensive system.

Apart from economic and social impacts of HSTs that have been argued above, the safety benefits of HSTs are also important for the society. According to Campos and de Rus [40], "any comparison of accident statistics for the different transport modes immediately confirms that HSR is – together with air transport – the safest mode in terms of passenger fatalities per billion passenger-kilometers" (ibid. 25). As mentioned earlier, no fatal accidents or injuries on Shinkansen lines have been recorded since its opening [23].

Despite the social and economic inequalities that the HSTs might create in some regions, they are still important tools for the social and economic sustainability of the regions as they play an important role in the regeneration of the regions in the longer term and creating safe travel for societies. However, the governments need to be careful in planning these networks as like other transport investments they can be "the maker of some cities, but the breaker of the others" (Clark, 1957 cited in [20]).

Environmental Sustainability The environmental impacts of HSTs are not negligible. Although high-speed train systems are widely perceived to be climate friendly, there are serious environmental costs that they generate both during the construction and the operation. The impacts range from land take, barrier effects, visual intrusion, noise, and air pollution to contribution to global warming ([40]; [15]). The amount of energy used during construction and operation of HSTs, the source of energy and the level emissions created by the HSTs are important determinants of how green the HSTs are. "HSTs are predominantly electric powered and therefore emissions from HST operations are considered to be linearly related to energy consumption and the sources used to generate the electricity" [15, p. 606]. Thus, the cleaner the source of energy, the more climate friendly HSTs are.

In France, the main energy source of the TGV trains is nuclear energy. Nuclear power is seen as an important source of energy as it generates electricity in higher amounts than any other clean energy source. However, nuclear power carries high risks in terms of radioactive elements produced during the energy production process and the problems of radioactive wastes; thus, great attention needs to be paid in planning these systems especially in places where geographical hazards are more likely to happen.

As discussed earlier, the modal shift from cars and aircrafts to HSTs as a result of increased connectivity between major cities is known to be beneficial for the environment. The CO_2 emissions per passenger generated by HSTs are significantly lower than the emissions from aircraft [16]. While the cleanest aircraft produces 56.7 kg of CO2 per passenger between London and Paris, the HST produces 14.4 kg per passenger on the same route (ibid. 80). Thus, it is quite common to speak about CO_2 benefits as a result of HST operations. However, it is not possible to achieve reductions in CO_2 emissions unless HSTs fully replace road and air traffic. According to Givoni and Banister [14] London and Paris route has not experienced such a decline in air traffic after the introduction of HST services. On the contrary, carriers like British Airways and Air-France continue to offer frequent services on this route even though the HST operator captures over 70% of the market [14, p. 6].

Givoni and Banister [14] mention two conditions that are necessary for the HST to reduce air transport impact on the environment. "First, the HST service must be integrated with other aircraft services provided by the airline and thus it must complement it rather than compete with it. Second, the airline (or airport) should not use the freed runway slots for other flights. With the development of the HST network and successful integration of air and rail services (for example, at CDG) the first condition is now being met at a number of airports" [14, p. 7]. However, unless new regulations are introduced to the airway companies, the second necessary condition is unlikely to happen.

Future Directions: Future of the High-Speed Train

The fast development of the modern HST in the last 50 years and the construction of high-speed lines by a growing number of countries all around the world every year show that the HSTs are regarded as crucial elements for the future of the transport systems.

First of all, the HST development needs to be seen as a network development integrated both within and in-between countries rather than single lines connecting major cities, which is often the case. Thus, integration of HSTs with other transport modes is crucial. As discussed earlier, the development of HST lines in Europe under the Trans-European Network is an important step toward achieving a more inclusive network in Europe. However, further development is needed especially in the Eastern European countries. This can be achieved not only in Europe but also in other parts of the world by "adopting a HST technology where the trains can also run on the conventional network (the TGV model) and by designing the HST stations to allow fast and seamless transfer between HST services and other (national and regional) services" [14, p. 17]. Moreover, a global integration of the whole system can be achieved by possible connectivity of HSTs all around the world via airports.

Second, the uneven distribution of HST network is an important obstacle for the regional development and equality. Although it is not possible to build HST lines connecting every single city due to the high construction and operation costs, it is an important task for planners, engineers, and authorities to make the HST service available to the wider community. Thus the question, as the UIC [34] suggests will be "how to reduce the door-to-door travel time when serving large built-up areas?" [34, p. 1]). In this sense, the use of existing rail systems and their integration with the HST lines is crucial.

Third, as discussed earlier, HSTs can help shifting the demand from other modes of transport to rail as they offer reductions in travel time. This might result in reducing the impacts of transport on the environment. However, there is evidence that the HSTs can create new demand [15]. In this case, "the introduction of HST services might be counterproductive to sustainable transport, even when it promotes rail use" [14, p. 6]. In order to overcome this problem there is a need to ensure the development of HST result in modal shift (e.g., from aircraft) and not generation of new travel. Moreover, as integration is a crucial element in creating sustainable transport, technical incompatibilities need

to be solved to integrate the systems fully. Differences in electrical power, safety requirements, track belts, loading gauge sizes are the main technical problems to overcome [20]. Technical standardization has been a major issue for the EU. In order to improve the interlinking and interoperability of the national rail networks as well as access to them, rail interoperability directives have been published [11].

Finally, HSTs can be seen as locomotives of the regional development and can regenerate the economy in regions where the socio-economic deprivation has started as a result of lack of public services and private investment. However, they might also create spatial imbalance and social inequalities. Therefore, introduction of HSTs need to be evaluated within the regional and national socio-economic plans.

In conclusion, High-Speed Train can be considered an important element of sustainable development as it can increase the social integration, act as a catalyst for the economic development and provide greener transport with less energy consumption and high passenger volumes only if the conditions that are discussed in this text are met. Only then it would be possible to discuss the benefits of HSTs not only for a sustainable transport system but also for sustainable local, regional, and national development by all means. It would then be possible to state that the high-speed train marks the second age of the railways.

Bibliography

Primary Literature

1. Banister D (2008) The sustainable mobility paradigm. Transp Policy 15:73–80
2. Banister D (2011) The triology of distance, space and time. J Transp Geogr 19:950–959
3. Banister D, Berechman J (2000) Transport investment and economic development. UCL Press, London
4. Bradsher K (2010) China is eager to bring high-speed rail expertise to the US. NY Times, 7 April 2010
5. Cervero R (2002) Induced travel demand: research design, empirical evidence, and normative policies. J Plan Lit 17(1):3–20
6. Cooper M (2011) Administration pitches big rail projects. NY Times, 8 Feb 2011. www.nytimes.com/2011/02/09/us/09rail.html?ref=highspeedrailprojects
7. Deutche Bahn (2011) The ICE. Deutsche Bahn's fastest train. http://www.bahn.com/i/view/GBR/en/trains/overview/ice.shtml. Accessed 10 Apr 2011
8. Ewing R, Lichtenstein A (2002) Induced traffic and induced development: a literature review, Prepared for the Chester County Planning Commission
9. Ellwanger G, Wilckens M (1994) High speed for Europe. JPN Railway Transp Rev 3:17–25
10. European Commission (2001) White paper, European transport policy for 2010: time to decide. www.ec.europa.eu. Accessed 28 May 2011
11. European Commission (2004) M1 directive of the European parliament and of the council of 19 March 2001 on the interoperability of the conventional rail. www.eur-lex.europa.eu. Accessed 28 May 2011
12. European Commission (2010) EU energy and transport in figures statistical pocketbook 2010. www.ec.europa.eu. Accessed 14 May 2011
13. European Commission (2011) Trans-European networks. www.ec.europa.eu/ten/index. Accessed 12 May 2011
14. Givoni M, Banister D (2008) Reinventing the wheel – planning the rail network to meet mobility needs of the 21st century. TSU working paper, Ref. 1036
15. Givoni M (2006) The development and impact of the modern high speed train. Transp Rev 26(5):593–611
16. Givoni M, Brand C, Watkiss P (2009) Are railways 'climate friendly'? Built Environ 35(1):70–86
17. Givoni M, Rietveld P (2010) Access to rail in urban areas – examination of the number of stations. TSU working paper, Ref. 1044
18. Graham S, Marvin S (2001) Splintering urbanism. Routledge, London
19. Hall P, Banister D (1993) The second railway age. Built Environ 19(3/4):157–162
20. Hall P (2009) Magic carpets and seamless webs: opportunities and constraints for high-speed trains in Europe. Built Environ 35(1):59–69
21. Harvey D (1990) The condition of postmodernity: an enquiry into the origins of cultural change. Blackwell Publishing, Oxford
22. HS1 (2011) Key facts. http://www.highspeed1.com/about/facts/. Accessed 12 May 2011
23. JR-Central (2011) Central Japan Railway Company, about the Shinkansen, safety. http://english.jr-central.co.jp/about/safety.html. Accessed 11 Apr 2011
24. JR-Central (2011) Central Japan Railway Company, company profile. http://english.jr-central.co.jp/company/company/about/history.html. Accessed 11 Apr 2011
25. JR-Central (2011) Central Japan Railway Company, FY2011 key measures and capital investment. Report can be accessed on http://english.jr-central.co.jp/index.html. Accessed 11 Apr 2011
26. Martínez Sánchez-Mateos HS, Givoni M (2009). The accessibility impact of a new high-speed rail line in the UK: a preliminary analysis of winners and losers. TSU working paper series, Ref. 1041
27. Menendez JM, Guirao B, Coronado JM, Rivas A, Rodriguezi FJ, Ribalaygua C, Urefia JM (2002) New high-speed rail lines and small cities: locating the station. In: Brebbia CA, Martin-Duque JF, Wadhwa LC (eds) The sustainable city II. WIT Press, UK

28. Railisa (2011) The UIC statistics database. www.railisa.tsf.it/railisa/ password required and can be obtained from the UIC website
29. RTRI (2011) Japan Railway Technical Research Institute, Overview of MAGLEV R&D. http://www.rtri.or.jp/rd/division/rd77/yamanashi/english/maglev_frame_E.html. Accessed 18 Nov 2011
30. SNCF (2010) Profile and key figures. http://medias.sncf.com/resources/en_EN/medias/MD0006_20100210/file_pdf.pdf. Accessed 11 Apr 2011
31. SNCF (2011) Legal framework. http://www.sncf.com/en_EN/html/media/CH0012-Suppliers/BR1051-Important-laws/MD0005_20100804-Read-article.html
32. Spiekermann K, Wegener M (2008) The Shrinking continent: accessibility, competiveness, and cohesion. In: Faludi A (ed) European spatial research and planning. Lincoln Institute, Cambridge, MA, pp 115–139
33. Tentea (2011) TEN-T projects, Trans-European Transport Network Executive Agency. www.tentea.ec.europa.eu/en/ten-t_projects/. Accessed 11 May 2011
34. UIC (2010) High speed rail: fast track to sustainability. www.uic.org/IMG/pdf/20101124_uic_brochure_high_speed.pdf. Accessed 11 Apr 2011
35. UIC (2011) High speed principles and advantages. http://www.uic.org/spip.php?article443#outil_sommaire_0. 11 Apr 2011
36. UIC (2011b) High speed lines in the world – UIC High Speed Department. http://www.uic.org/spip.php?article573. Accessed 11 Apr 2011
37. Vickerman R (1997) High-speed rail in Europe: experience and issues for future development. Ann Regional Sci 31:21–38
38. European Commission (1996) Council Directive 96/48/EC of 23 July 1996 on the interoperability of the trans-European high-speed rail system. Official Journal of the European Communities, 17 Sep 1996. http://eur-lex.europa.eu/LexUriServ/LexUriServ.do?uri=OJ:L:1996:235:0006:0024:EN:PDF. Accessed 22 Aug 2011
39. Taniguchi M (1993) The Japanese magnetic levitation trains. Built Environ19(3/4):235–243
40. Campos J, de Rus G (2009) Some stylized facts about high-speed rail: A review of HSR experiences around the world. Transp Policy 16:19–28
41. UIC (2005) High Speed Rail's leading asset for customers and society. UIC Publications, Paris. Accessible at: /www.uic.asso.fr cited in Campos J, de Rus G (2009)
42. Ampe F (1995) Technopole development in Euralille. In: Banister D (ed) Transport and urban development. E & F.N. Spon, London, pp 128–135

Books and Reviews

Ampe F (1996) Technopole development in Euralille. In: Banister D (ed) Transport and urban development. E & F.N. Spon, London

Banister D, Goodwin MT (2011) Quantification of the non-transport benefits resulting from rail investment. J Transp Geogr 19(2):212–223

Brons M, Givoni M, Rietveld P (2009) Access to railway stations and its potential in increasing rail use. Transport Res A 43:136–149

Campos J, Gagnepain P (2009) Measuring the intermodal effects of high-speed rail. In: Rus G (ed) Economic analysis of high speed rail in Europe. BBVA Foundation, Madrid

Coto-Milla´n P, Inglada V (2004) Social benefit of investment projects: the case for high-speed rail. In: Coto-Millan P (ed) Essays on microeconomics and industrial organisation. Springer, Berlin

De Rus G, Nombela G (2007) Is the investment in high speed rail socially profitable? J Transp Econ Policy 41(1):3–23

Department for Transport (2010) High speed rail London to the West Midlands and beyond – A report to the government by high speed two limited. www.dft.gov.uk

Garmendia M, Ureña JM, Ribalaygua C, Leal J, Coronado JM (2008) Urban residential development in isolated small cities that are partially integrated in metropolitan areas by high speed train. Eur Urban Reg Stud 15:249–264

Givoni M, Banister D (2006) Airline and railway integration. Transp Policy 13:386–397

Givoni M (2007) Environmental benefits from mode substitution - comparison of the environmental impact from aircraft and high-speed train operation. Int J Sust Trans 1(4):209–230

Givoni M, Holvad T (2009) The prospects for European railways: is the second railway age still here or yet to begin? Built Environ 35(1):5–10

Givoni M, Rietveld P (2007) The access journey to the railway station and its role in passengers' satisfaction with rail travel. Transp Policy 14:357–365

González-Savignat M (2004) Will the high-speed train compete against the private vehicle? Transp Rev 24(3):293–316

Hall P (1999) High-speed train and air: competitive or complementary? Paper presented at the Lake Arrowhead transportation symposium, 25 Oct 1999

Holvad T (2009) Review of railway policy reforms in Europe. Built Environ 35(1):24–42

Mokhtarian PL, Salomon I (2001) How derived is the demand for travel? Some conceptual and measurement considerations. Transport Res A 35:695–719

Murikami J, Cervero R (2010) California high-speed rail and economic development: postindustrial market profiles and public policy implications, symposium, Berkeley, 2–3 Dec 2010

Norman C, Vickerman R (1999) Local and regional implications of trans-European transport networks: the channel tunnel rail link. EnvironPlann A 31:705–718

Preston J (2009) Trends in European railways over the last two decades. Built Environ 35(1):11–23

Rietveld P (2002) Why railway passengers are more polluting in the peak than in the off-peak; environmental effects of capacity management by railway companies under conditions of fluctuating demand. Transport Res D 7(5):347–356

Sánchez-Borràs M, Nash C, Abrantes P, López-Pita A (2010) Rail access charges and the competitiveness of high speed trains. Transp Policy 17:102–109

Sasaki K, Ohashi T, Ando A (1997) High-speed rail transit impact on regional systems: does the Shinkansen contribute to dispersion? Ann Regional Sci 31:77–98
Steer Davies Gleave (2004) High speed rail: international comparisons. Final report for the commission for integrated transport (February). http://cfit.independent.gov.uk/pubs/2004/hsr/research/pdf/hsr.pdf
Takagi R (2005) High speed railways: the last 10 years. JPN Railway Transp Rev 40:4–7
Ureña JM, Menerault P, Garmendia M (2009) The high-speed rail challenge for big intermediate cities: a national regional and local perspective. Cities 26:266–279
Whitelegg J, Hultén S, Flink T (1993) High speed trains: fast tracks to the future? Leading Edge Press, Hawes

High-Occupancy Vehicle and Toll Lanes

Katherine F. Turnbull
Department of Landscape Architecture & Urban Planning, Texas Transportation Institute, College of Architecture – The Texas A&M University System, College Station, TX, USA

Article Outline

Glossary
Definition of the Subject
Introduction
Types of HOV Lanes
Access Treatments
Allowed Vehicles and Vehicle-Occupancy Requirements
Operating Hours
Supporting Facilities and Services
Planning
Design
Enforcement
Public Information and Marketing
Case Studies
Future Directions
Bibliography

Glossary

Buses Vehicles designed to carry multiple passengers. Depending on the size, buses may carry between 12 and 100 passengers.

Carpools Vehicles carrying two or more persons.

High-occupancy toll (HOT) lanes HOV lanes that also allow single-occupant vehicle use through payment of a toll.

High-occupancy vehicle (HOV) lanes Roadway lanes designed and operated for buses, vanpools, and carpools at all times of the day or during specific time periods.

Hybrid vehicles Vehicles which operate under a combination of gasoline and electric power.

Low-emission and energy-efficient vehicles Vehicles which typically use non-gasoline power sources and do not emit high levels of pollutants.

Vanpools Vans organized to carry commuters to and from work.

Definition of the Subject

Traffic congestion continues to be a significant issue in metropolitan areas throughout the country. Transportation agencies at the federal, state, metropolitan, and local levels are using a variety of techniques and approaches to improve traffic flow, enhance mobility, and provide travel options.

High-occupancy vehicle (HOV) and high-occupancy toll (HOT) lanes are being used in some metropolitan areas to ease traffic congestion and enhance mobility. HOV lanes provide travel-time savings and improved trip-time reliability by encouraging travelers to change from driving alone to carpooling, vanpooling, or riding the bus. HOV/HOT lanes expand the allowed user groups to include solo drivers or lower-occupant vehicles, who can access the lanes by paying a fee.

The use of HOV/HOT lanes has evolved since the late 1960s. Today, HOV lanes and HOV/HOT lanes are in operation in 32 metropolitan areas in North America. These facilities represent an important element of the transportation system in these areas, enhancing mobility, managing congestion, and providing travel options.

Introduction

The development and operation of HOV/HOT facilities in the USA have evolved over the past 42 years. The opening of the bus-only lane on the Shirley Highway (I-395) in northern Virginia/Washington, D.C., in 1969,

the contraflow bus lane on the approach to New York-New Jersey's Lincoln Tunnel in 1970, and the El Monte Busway in Los Angeles in 1973 represents the first freeway HOV applications in the country.

Many of the initial HOV lanes were bus-only applications or allowed buses and vanpools. In an effort to maximize use, carpools became the dominant use group on most projects during the 1970s and 1980s. The vehicle-occupancy requirements for carpools have evolved over time. A three-person per vehicle (3+)-occupancy level was initially used on many projects, but most current facilities use a two-person per vehicle (2+) carpool designation.

In the 1990s, a few areas began experimenting with value pricing projects, often called HOT lanes, which were allowed under the Value Pricing program in previous federal legislation. HOV/HOT lanes expand the allowable user groups to include single-occupant or lower-occupant vehicles for a fee, while maintaining free travel to qualifying HOVs. In addition, the introduction of electronic toll collection (ETC) and other advanced technologies provided greater opportunities for pricing applications on HOV lanes. HOV/HOT lanes enhance mobility and travel options in congested corridors.

The Safe, Accountable, Flexible, Efficient Transportation Equity Act: A Legacy for Users (SAFETEA-LU) provides operating agencies with additional flexibility by allowing exempt user groups to use HOV lanes when available capacity exists on an HOV lane. Tolling single-occupant vehicles (SOVs) represents one of the exempt user groups. Low-emission and energy-efficient vehicles, including some types of hybrid vehicles, are allowed to use HOV/HOT lanes in some states.

Today there are some 130 HOV freeway projects in the 32 metropolitan areas in North America. Further, there are12 HOV/HOT lanes in operation in eight metropolitan areas, and more projects in the planning and development stage. Further, 10 states allow low-emission and energy-efficient vehicles to use HOV/HOT lanes.

HOV/HOT lanes involved different designs and operating strategies. Some facilities, such as the I-25 Express Lanes in Denver, are barrier-separated facilities located in the center median of the freeway, with limited access points. Other HOV/HOT lanes are separated from the adjacent general-purpose lanes only by normal paint striping. Access and egress to these facilities may be limited to specific sections or unlimited. The I-394 HOV/HOT lanes in Minneapolis include sections of both types of treatments.

Some facilities are reserved for HOV/HOT vehicles at all times (24/7). Other facilities are reserved for HOV/HOT vehicles only during the morning and afternoon peak periods and are open to all traffic at other times of the day.

Many HOV/HOT projects throughout the country carry more people than the adjacent freeway lane. In addition, they provide trip-time savings and trip-time reliability while enhancing mobility. Further, the revenues from the HOV/HOT lanes in some areas are used to support transit services, improve overall operations, and maintain the facilities.

This article provides an overview of key aspects related to HOV/HOT facilities. The types of HOV facilities and supporting elements are described next. Factors to consider in planning, designing, marketing, and enforcing HOV/HOT lanes are then described. Case studies of the HOV/HOT lanes in Denver, Houston, and Minneapolis are presented. The article concludes with a discussion of future directions for HOV/HOT lanes.

Types of HOV Lanes

There are four general types of HOV lanes or busways in separate rights-of-way – exclusive freeway HOV lanes, concurrent flow freeway HOV lanes, contraflow freeway HOV lanes, and arterial HOV lanes [1–4].

Busways in separate rights-of-way are special lanes in separate rights-of-way reserved for buses only during all operating hours. Busways are in operation in Pittsburgh, Miami, Minneapolis-St. Paul, Boston, and Ottawa, Canada.

Exclusive HOV lanes are separated from general-purpose lanes by barriers or wide painted buffers. Exclusive lanes may be reversible. This approach is more expensive due to separation, but easier to enforce and safety enhanced.

Concurrent flow HOV lanes are lanes in the same direction of travel as the general-purpose lanes separated by paint striping and in some cases a 2–4 ft buffer. Concurrent flow HOV lanes are the most common type of HOV facility found in the USA.

Contraflow HOV lanes use a lane in the off-peak direction of travel for HOVs in the peak direction of travel. They are typically separated from the general-purpose lanes by pylons or moveable barriers. These types of lanes are appropriate when there is available capacity in the off-peak direction of travel. They are typically peak-only operation, and in some cases, only the morning peak period. There are only five contraflow lanes in operation: three in New York/New Jersey, one in Boston, and one in Dallas.

HOV lanes are also in operation on some arterial streets. Most of these are lanes reserved for buses only. Most are also found in downtown areas or on streets approaching downtown areas. There are a few arterial street HOV lanes open to carpools and vanpools.

Access Treatments

A number of different access alternatives may be used with HOV/HOT lanes. These alternatives include continuous access, slip ramp and limited access, direct access, and freeway-to-freeway HOV connections [1].

Continuous access is common with many concurrent flow HOV lanes. Vehicles may move into and out of the HOV lanes at any point. This approach offers more flexibility, but is more difficult to enforce and may cause safety concerns.

Slip ramps or limited access may be used with concurrent flow or exclusive lanes. This approach provides specific locations for access. This approach also limits flexibility for users, but enhanced safety and enforcement.

Direct access uses flyover ramps and other ramp designs to provide direct access to HOV lanes for park-and-ride lots and transit centers. This approach has higher capital costs, but provides additional travel-time savings and is easier to enforce and enhances safety.

A few areas, such as Los Angeles, have connectors from HOV lanes on one freeway to HOV lanes on another freeway. These connectors have high capital costs, but can provide significant travel-time savings to HOVs.

Allowed Vehicles and Vehicle-Occupancy Requirements

Some HOV facilities allow only buses. These include busways and a few freeway lanes, such as the I-495 contraflow lane in New York/New Jersey. A few HOV lanes are restricted to only buses and vanpools. These include the contraflow lanes on the Long Island Expressway and The Gowanus Expressway in New York City. Most HOV lanes allow buses, vanpools, and carpools. SAFETEA-LU also includes requirements for eligible vehicles, and allows operating agencies to allow other types of exempt vehicles, including low-emission and energy-efficient vehicles and some types of hybrid vehicles.

There are three commonly used vehicle-occupancy requirements with HOV lanes. These requirements are three people per vehicle (3+), two people per vehicle (2+), and variable requirements (2+/3+). A three-person per vehicle (3+) requirement is used on the Shirley Highway in northern Virginia and the approach to the Bay Bridge in Oakland. Most HOV lanes that allow carpools use a 2+ requirement. The variable requirements (2+/3+) are used on the El Monte busway in Los Angeles and US 290 HOV lanes in Houston.

Operating Hours

Four different hours of operation commonly used with HOV facilities. Some HOV lanes operated 24 h a day/7 days a week (24/7). Peak-period only – typically morning and afternoon (in the range of 6:30–9:00 a.m. and 3:00–6:00 p.m.) – is found on many HOV lanes. Peak-period only/peak direction, typically morning peak-period only, is found on some HOV lanes. The Houston HOV system is one example of the use of extended hours with operation hours from 5:00 a.m. to 12:00 p.m. in the inbound direction and from 2:00 to 9:00 p.m. in the outbound direction.

Supporting Facilities and Services

Supporting facilities and programs are typically found with HOV lanes to help encourage travelers to change their mode. Examples of supporting facilities and services include new and expanded bus services, park-and-ride and park-and-pool facilities, and transit stations. Newer or expanded express bus routes are often provided with HOV/HOT lanes. Rideshare programs, vanpool programs, and employer-based programs are also key elements of many successful HOV/HOT projects.

Planning

Planning for transportation improvements, including HOV/HOT facilities, usually occurs at different levels. A broad regional planning effort is often undertaken first. This level focuses on the general needs, issues, and opportunities throughout a metropolitan area. The outcome of this process is a long-range regional plan that identifies the general types of facilities anticipated in the major travel corridors and areas. Regional plans may not define the exact type of treatment or design, however.

These more detailed analyses are conducted in the planning process at the corridor and facility level. Planning at this stage is much more detailed, focusing on preliminary alternative design treatments, access options, vehicle-occupancy levels, and other issues. For example, a regional plan may identify the need for an HOV/HOT facility in a specific corridor, but the type of HOV/HOT lane and the preliminary design would be examined in later planning phases.

Planning for HOV/HOT facilities can be thought of as a cascading or funneling process. Planning at the regional scale focuses on identifying an overall system plan and the general types of facilities that may be appropriate. Planning at the corridor and facility level is more detailed, resulting in projects that can be taken forward into the design stage. Different models and analytical tools and techniques are needed at various levels. Sketch planning techniques, travel forecasting models, and more detailed models and methods may be used.

Design

The design of an HOV/HOT lane is similar to the design of a general-purpose traffic lane. There are special elements that should be considered with the design of an HOV/HOT lane, however. Elements that may influence design considerations of an HOV/HOT lane include the separation between the HOV/HOT lane and the general-purpose freeway lanes, access points and the types of access, the toll payment method and the method for HOV declaration or observation, the number and nature of enforcement areas, and signs and markings.

The design of HOV/HOT lanes should follow the standards recommended by the American Association of State Highway and Transportation Officials (AASHTO), the Institute of Transportation Engineers (ITE), and the Transportation Research Board (TRB). The design for different types of HOV facilities have been examined by these organizations and other groups, and are documented in different reports [5–7]. In addition, Texas [8], California [9], Washington [10], and other states have developed design guidelines.

Enforcement

Enforcement is a key component of operating HOV/HOT lanes. The roll of an HOV/HO enforcement program is to ensure that operating requirements, including vehicle-occupancy levels, are maintained to protect HOV travel-time savings, to discourage unauthorized vehicles, and to maintain a safe operating environment. Visible and effective enforcement promotes fairness and maintains the integrity of the HOV facility to help gain acceptance of the project among users and nonusers. Ensuring that tolls are paid is another key element of HOV/HOT enforcement. Key elements of successful enforcement programs are highlighted in this section [1].

First, the appropriate agency must have the legal authority to issue citations for possible violations. The appropriate agency may include the state police, local police, and transit police. Toll authorities involved in HOT projects must also have the legal authority to enforce toll violations.

State legislation or local laws may be needed to ensure that the appropriate agencies and law enforcement personnel have the legal authority to issue citations for various offenses, including vehicle eligibility requirements, vehicle-occupancy requirements, operating regulations (such as entering and exiting an HOV lane at the appropriate places), and not paying tolls. If new user groups (tolled vehicles, low-emission and energy-efficient vehicles) are allowed to use an HOV/HOT lane a check should be made to be sure the legal authority for enforcement exists. Legislative action may be necessary if the legal authority does not exist.

Two elements of HOV enforcement are the type of citation issued for violating the HOV requirements and the level of the fine. Most areas classify occupancy violations and entering and existing the HOV lanes illegally as a moving violation. Some areas include

demerits on a driver's record. Fines in different states for violating occupancy requirements and other operating procedures range from $40 to $500 for repeat offenses. Some areas use a graduated scale, with fines increasing for repeat offenses, and some areas add court costs.

Four general enforcement strategies are typically used with HOV facilities. These strategies are routine enforcement, special enforcement, selective enforcement, and peer-enforcement.

Routine enforcement maintains the normal level of law enforcement in the corridor or freeway, with no extra enforcement designated for the HOV lane. Routine enforcement is used with many HOV facilities around the country during some or all operating hours. Advantages of this approach include no additional funding needed and usually some level of enforcement provided. Disadvantages include the potential for a low level of enforcement, monitoring HOV facility not a priority, and a potential for high violation rates.

Special enforcement includes the dedication of additional law enforcement personnel and resources to the HOV facility. Approaches may include assigning a patrol car or motorcycle to an HOV lane, adding extra patrols in a corridor, or locating enforcement personnel along the lane. Special enforcement may be accomplished by reallocating existing personnel or by adding additional personnel during key periods. Advantages include a more visible police presence, lower violation rates, and enhanced public perceptions. A disadvantage is the costs associated with extra personnel and the need for additional funding.

Selective enforcement provides extra enforcement personnel at specific times or in response to certain situations. These situations may include when a new HOV facility is open, in response to high violation rates, when major operation changes are made, or periodically to reinforce occupancy and other requirements. Advantages include higher visibility, positive public perception, and lower violation rates. Disadvantages include the cost, which requires additional funding and may become too predictable.

The final general enforcement strategy is peer-enforcement, which involves peer-regulation by HOV lane users and motorists in the general-purpose lanes by providing a telephone hotline to report potential violators. Peer-enforcement is typically used in addition to other enforcement methods – not as the only strategy. Peer-enforcement provides a telephone number people can call to report the license plate of a vehicle they feel is violating the HOV requirements. Typically, a letter is sent to the vehicle owner with information on the correct use of the HOV/HOT lane. License plates reported more than once typically receive more strongly worded follow-up correspondence and may be monitored by enforcement personnel in the field. The HERO program in Seattle is the best example of a peer-enforcement program.

Specific enforcement techniques include the use of stationary patrols, roving patrols, team patrols, multipurpose patrols, electronic assistance, and citations or warnings by mail. Stationary patrols are law enforcement personnel located at dedicated enforcement areas or other areas. It is important that these areas provide a safe location for enforcement personnel. The dedicated enforcement area is located just before the exit point of some HOV/HOT lanes.

Roving patrols involve the use of law enforcement cars or motorcycles patrolling the length or a portion of an HOV/HOT facility. A safe area to pull vehicles over is still needed with this approach. These enforcement vehicles may travel in the HOV lane or the adjacent general-purpose lanes. A safe area to pull vehicles over and stop is still needed with this approach.

Team patrols use a combination of stationary and roving patrols. Law enforcement personnel maintain radio contact to identify potential violators, which may be pulled over by downstream enforcement personnel. Multiple enforcement points may also be used.

Multipurpose patrols may provide HOV enforcement as one of many duties. These extra patrols may be located in congested corridors to assist with incident management and other functions.

Closed-circuit television cameras (CCTV), infrared cameras, and photographing license plates may be used to assist in enforcing HOV lanes. To date, no technology is commercially available to detect the number of individuals in a vehicle. Public and institutional acceptance of electronic monitoring may be an issue in some areas.

Legal authority is needed for enforcement personnel to issue warnings or citations for violating HOV/HOT requirements by mail. This approach eliminates

the need to stop a vehicle. At present, no ticketing by mail of HOV/HOT violations is in effect in the USA.

It is important that information on enforcing HOV/HOT facilities, especially the citation and fines for violating requirements, be communicated to motorists and the public. It is also important that the courts and judicial system is informed of the HOV penalties and the importance of the facilities to help ensure that citations are upheld.

Public Information and Marketing

Public involvement is a key element of the transportation planning and project development process, including planning HOV/HOT lanes. The term relates to proactively involving the public in the discussion of transportation plans and projects. There are specific federal and state requirements associated with public involvement, including those contained in the National Environmental Policy Act (NEPA) and SAFETEA-LU.

Public and stakeholder outreach is a key element in the planning, project development, implementation, and operation phases of HOV/HOT projects. Public and stakeholder outreach is focused on building understanding and support for the project with targeted groups. These targeted groups might include members of the state legislature, local elected officials, business organizations, neighborhood groups, and other organizations. Examples of possible techniques include collaborative task forces and advisory committees. Public information represents another key element in the planning, project development, implementation, and operation phases of HOV/HOT projects. Public information focuses on building awareness, understanding, and support for an HOV/HOT project among travelers and the public. Potential techniques include printed and electronic newsletters, press releases, Internet sites, presentations, and meetings and workshops.

Market research is frequently used in the planning and project development stages of HOV/HOT projects. Market research helps test potential concepts, projects, and messages. Examples of market research techniques include focus groups, interviews, and mail, telephone, and Internet surveys. Examples of market research techniques used with HOT projects include focus groups in San Diego and Minneapolis and surveys of bus riders, carpoolers, and HOT lane users in San Diego.

Promotion and marketing is used during the implementation and operation phases of HOV/HOT projects. These efforts and techniques focus on promoting the initial and ongoing use of the HOV/HOT lanes. Possible marketing techniques include paid television and radio advertisements, television and radio public service announcements, paid advertisements in neighborhood and city or regional newspapers, the Internet, direct mail, service centers, and billboards.

A number of elements are typically associated with developing a marketing program for an HOV/HOT project. First, the target markets are identified. Examples of target markets include households in the corridor, commuters in the corridor, and major employers in the corridor. The marketing concepts, messages, and branding of the HOV/HOT project may be tested through the use of the different market research techniques described earlier. Based on the results of the market research, the branding and messages are finalized. The appropriate media and approaches, which were described previously, are identified. Media and approaches are matched with available funding and local perceptions to develop the marketing plan to be implemented.

Three phases are typically associated with marketing HOV/HOT projects. These phases are preopening, opening/initial operation, and ongoing operation. The focus of the marketing program during the preopening phase is on building awareness of the requirements for using the HOV/HOT lanes and promoting individuals to purchase transponders. During the opening and initial operation of an HOV/HOT project, marketing efforts continue to focus on explaining the use requirements and selling transponders. The marketing effort during this phase also promotes the use of the HOV/HOT lane by all groups – toll paying SOVs, carpools and vanpools, and bus riders – and converting travelers violating the toll or vehicle-occupancy provisions into users. Ongoing marketing efforts focus on promoting the use of all options, as well as transponder sales.

A variety of approaches may be used to market HOV/HOT projects. These approaches include Internet sites, direct mail, regional and neighborhood newspaper advertisements, radio and television advertising, radio and television earned media or public service announcements, and customer service centers. Brochures, which may be distributed at meetings,

by direct mail, or at businesses or service centers, represent another marketing approach used with many existing HOV/HOT projects.

Case Studies

Denver

The I-25 HOV lanes were opened in the mid-1990s. Called the Downtown Express, the HOV lanes are 7 miles in length. The barrier-separated facility includes two lanes with shoulders on each side. Access is provided at both ends of the lane. The lanes operate in the inbound direction toward downtown Denver in the morning and in the outbound direction in the afternoon. A 2+ vehicle-occupancy requirement is used.

Although carpool, vanpool, and bus use of the HOV lanes was good, available capacity existed. Consideration of expanding the eligible user groups to include toll paying solo drivers began in the late 1990s. Enabling legislation was approved in 1999 to allow HOT projects in the state.

Implementation of the Express Lanes included adding ETC and new signs along the facility. Drivers entering the Express Lane self-declare as HOV or toll paying vehicles by using the appropriate access lane. In June 2006, toll paying solo drivers were allowed to use the I-25 HOV lanes. The Express Lanes use ETC, with preset variable pricing by time-of-day. The current fees range from a low of $.50 on Saturdays, Sundays, and off-peak periods to a high of $3.25 during peak times.

Solo drivers must obtain a transponder and maintain an active account to use the Express Lanes. The transponders can also be used on the E-470 and the Northwest Parkway toll facilities.

The development and operation of the HOV lanes and the Express Lanes represent the coordinated efforts of the Colorado Department of Transportation (CDOT) and the Regional Transit District (RTD). The Colorado Tolling Enterprise (CTE), a part of CDOT, assumed operating responsibility when the Express Lanes were initiated. The Colorado State Patrol and the E-470 Tollway Authority are responsible for the enforcement of the I-25 Express Lanes. Video enforcement is used to identify vehicles without valid toll tags.

Traffic counts taken in November 2006, 6 months after the implementation of the HOT project, show toll vehicles accounting for between 28% and 32% of the vehicles using the facility. Of the total 1,043 vehicles using the lanes in the afternoon peak hour, 287, or 24%, were tolled vehicles, and 756, or 73%, were HOVs. In the morning peak hour, tolled vehicles represented 32% of the total 899 vehicles, while HOVs accounted for 68%. The travel time for buses and carpools has remained relatively constant [11].

Houston

The Houston metropolitan region is characterized by low-density development, typical of southwestern cities. In response to ongoing concerns related to traffic congestion on the freeway system, limited available right-of-way, and air quality, an initial 9-mile contraflow demonstration project has evolved over an almost 30-year period into a system that encompasses some 100 miles of HOV lanes, numerous direct access ramps, 28 park-and-ride lots, 4 park-and-pool lots, an extensive network of express bus service, and a managed lanes/HOT lane project. This system provides preferential treatment to buses, vanpools, and carpools in the major freeway corridors.

Planning, designing, operating, and enforcing the HOV system elements has been accomplished through the coordinated efforts of the Texas Department of Transportation (TxDOT) and the Metropolitan Transit Authority of Harris County (METRO). Recently, Harris County and the Harris County Toll Road Authority (HCTRA) have joined this partnership to assist with the development and operation of the managed lanes on I-10 West. These efforts have been coordinated with the Houston-Galveston Area Council (HGAC), the metropolitan planning organization (MPO) for the area.

The HOV lanes are primarily one-lane, reversible, barrier-separated facilities, located in the median of six freeways. A short two-lane, two-direction section exists on the Northwest (US 290) Freeway. A two-way facility, with one lane in each direction of travel, is in operation on the Eastex (US 59) Freeway. A concurrent flow HOV lane is in operation on the Katy Freeway, leading to the reversible lane. The design used for the HOV lanes was influenced by a number of factors, including limited right-of-way in the freeway corridors, providing a safer operating environment using barriers, and the directional splits in the corridors.

The lanes operate in the inbound direction from 5:00 a.m. to 12:00 p.m. and in the outbound direction from 2:00 to 9:00 p.m. The lanes are closed from 12:00 to 2:00 p.m. to reverse operations and are closed to all traffic at other times. A 2+ vehicle-occupancy requirement is used on all the HOV facilities, except the Northwest Freeway. This facility has a 3+ occupancy requirement from 6:45 to 8:00 a.m. and 5:00 to 6:00 p.m., due to congestion occurring at the 2+ level. The Quick Ride value pricing project operates on these two lanes, allowing participating 2+ carpools use of the lane for a $2.00 per trip fee.

A total of 28 park-and-ride lots and four park-and-pool lots are located in the six corridors with HOV lanes. The larger park-and-ride lots have direct access to the HOV lanes and transit stations with passenger amenities. There are spaces for between 900 and 2,500 automobiles at 19 of the lots. The number of parking spaces at lots in each corridor range from slightly over 3,000 to almost 7,500.

The park-and-ride lots have transit stations with covered passenger waiting areas and other amenities. Transit centers without park-and-ride lots or with only small lots are located at strategic transfer points.

Direct access ramps connect the major park-and-ride lots and transit stations to the HOV lanes. These ramps provide travel-time savings for buses using the HOV lanes and enhance the safe operation of both the HOV lanes and the freeways. Use of the direct access ramps is restricted to buses, carpools, and vanpools during operating hours. The ramps are closed during nonoperating periods. Carpools and vanpools can access the ramps and the HOV lanes through the lots. The direct access ramps provide significant travel-time savings for buses and other HOVs. The 1990 opening of the direct access ramp linking the Northwest Freeway Station park-and-ride lot with the Northwest Freeway HOV lane provided travel savings of 14 min for vehicles entering and exiting the HOV lane. Prior to the ramp opening, HOVs had to travel local streets, enter the freeway, and merge across the general-purpose lanes to enter the HOV lane. Use levels increased after the ramp opened.

METRO provides a high level of bus service in each corridor, with frequent trips from the major park-and-ride lots. Over-the-road coaches are operated on many routes, as are articulated buses. Although there is no direct evidence linking increased ridership to use of the coaches, surveys of bus riders indicate support for their use and support for frequent service. The HOV lanes and express bus services are oriented primarily in a radial direction, with downtown Houston as the major destination. The express bus system has evolved over the years, however, providing service to major activity centers such as the Texas Medical Center (TMC), Greenway Plaza, and the Post Oak/Galleria area. More recently, reverse commute services have been added in some corridors, taking advantage of buses in the general-purpose lanes deadheading back to park-and-ride lots.

METRO also provides rideshare services in the Houston area. METRO's RideShare program includes a number of elements to help individuals form carpools and vanpools. Rideshare matching services are available by telephone and online through METRO's Internet site. The METROVan program helps commuters form vanpools and provides vans for their use. METROVan is cosponsored by HGAC, allowing METRO to provide vanpools outside the METRO service area. METRO's corporate RideSponsor program focuses on encouraging employees to commute to work by bus, carpools, or vanpools. The program provides computerized ridematching services, vanpools, and employer outreach. Corporate RideSponsors are eligible for discounted bus passes for their employees.

In 2003, some 212,079 passengers used the HOV lanes on a daily basis. Buses carried 43,225 passengers, vanpools accounted for 2,500 riders, carpools had 74,867 occupants, and 407 motorcycles used the lanes daily. Morning peak hour utilization levels range from approximately 1,000 vehicles on the Katy Freeway HOV lane to 1,551 on the Northwest Freeway HOV lanes.

Corresponding person volumes in the morning peak hour average between 3,424 on the Gulf Freeway HOV lane and 4,836 on the Northwest Freeway HOV lane. The HOV lanes account for 40% of the morning peak hour total person movement on three of the freeways. The AM peak hour is defined as the hour with the highest vehicle volumes. As a result, the peak hour may vary by HOV lane.

The HOV lanes and direct access ramps have significantly increased METRO bus operating speeds. The peak hour bus operating speeds have almost doubled,

from 26 to 54 mph, resulting in significant reductions in bus schedule times. Examples of reductions in the morning peak hour schedule time for buses from park-and-ride lots to downtown Houston include from 45 to 24 min from the Addicks park-and-ride lot on the Katy Freeway HOV lane, from 40 to 25 min from the Edgebrook park-and-ride lot on the Gulf Freeway HOV lane, and from 50 to 30 min from the Northwest Freeway Station park-and-ride lot on the Northwest Freeway HOV lane.

The HOV lanes provide travel-time savings for buses, vanpools, and carpools. Morning peak hour travel-time savings range from approximately 2 to 22 min on the different HOV lanes. The Northwest Freeway HOV lane generally provides the largest travel-time savings of about 22 min. The Katy Freeway HOV lane averages between 17 and 20 min, the Northwest Freeway 14 min, and the Gulf Freeway and Southwest Freeway between 4 and 2 min. In addition, the HOV lanes provide more reliable trip times to carpoolers, vanpoolers, and bus riders.

Approximately 32,293 spaces are provided at 28 park-and-ride lots associated with the HOV lanes. An additional 1,377 spaces are located at four park-and-pool lots. METRO buses serve the park-and-ride lots, while the park-and-pool lots provide staging areas for carpools and vanpools. In 2003, the overall occupancy levels at the individual facilities ranged from about 10% at some park-and-pool lots to 100% at well-used park-and-ride lots. From 1980 to 1990, the number of park-and-ride lots doubled from 10 to 20. The number of available spaces increased from 4,070 spaces to 12,626 spaces. Use of the lots grew from 4,070 parked vehicles to 12,626 vehicles. As of 2003, there are 28 park-and-ride lots, with 32,293 spaces. Approximately 54% of the available spaces are used on a daily basis [12].

The travel-time savings and the improved trip-time reliability have influenced commuters to change from driving alone to taking the bus, carpooling, and vanpooling. Periodic surveys of HOV lane users show that between 36% and 45% of current carpoolers formerly drove alone, while 38–46% of bus riders previously drove alone. Surveys conducted in 1988, 1989, and 1990 indicate that the opening of the HOV lanes was very important in their decision to ride a bus for between 54% and 76% of the bus riders using the Houston HOV lanes. Between 22% and 39% of the respondents also indicated that they would not be riding the bus if the HOV lane had not been opened.

The HOV system has resulted in an increase in available vehicle-occupancy (AVO) levels in the corridors with HOV lanes. For example, the morning peak hour AVO increased on the North Freeway from 1.28 in 1978 before the contraflow HOV lane opened to 1.41 in 1996. The morning peak hour AVO increased on the Northwest Freeway from 1.14 in 1987 prior to the opening of the HOV lane to 1.36 in 1996. The 1996 morning AVO for the HOV lanes ranged from 2.6 to 3.65, compared to 1.02 to 1.12 for the general-purpose lanes.

Periodic surveys of HOV lane users and motorists in the general-purpose lanes included questions designed to obtain feedback on the general perception toward the HOV lanes and support for these facilities. Between 40% and 81% of motorists in the general-purpose lanes on freeways with HOV facilities and one freeway without an HOV lane have responded positively to these surveys that the HOV facilities are a good transportation improvement.

A demonstration, called QuickRide, which uses an electronic toll collection system, was implemented at the end of January 1998 on the Katy Freeway. It was later expanded to the Northeast Freeway. Although use levels were modest, the demonstration was successful at allowing an additional user group to use the HOV lanes during the 3+ restricted period. It appeared that many enrollees view having an electronic tag as insurance for the occasional need and opportunity to ensure a quick trip, but cannot use the program on a regular basis.

Plans for expanding the Katy Freeway began in the late 1990s. The 23-mile corridor carries some 280,000 vehicles a day. The existing cross section in the most congested section from SH 6 to I-610 includes three general-purpose lanes in each direction, the HOV lane, and three-lane frontage roads in each direction.

A number of alternatives were examined in the Major Investment Study (MIS), including four special-use lanes in the freeway median. Other options included additional general-purpose lanes and expanding the HOV lanes. The special-use or managed lane option emerged from this study as the preferred alternative. The specific operation of the managed lanes was not defined, but user groups considered including buses, 3+ HOVs, QuickRide HOVs, vanpools, trucks,

and long-distance travelers. Other than QuickRide participants, tolling was not considered as an operational strategy. The cross section for the section between SH 6 and I-610 would include a three-lane frontage road and four main lanes in each direction of travel, and the four managed lanes.

During the environmental impact statement (EIS) process, the Harris County Toll Road Authority (HCTRA) expressed interest in participating in the managed lanes portion of the project. The EIS was modified to include tolling. Additional public involvement activities were conducted, along with a more detailed assessment of potential toll-related issues. The constructed facilities include four general-purpose freeway lanes, two managed lanes in each direction of travel. HCRTA helped fund the construction of the facility and operates the managed lanes. Carpools, vanpools, and buses travel for free in the managed lanes, while SOVs can use the lanes by paying toll.

Minneapolis

Two HOV/HOT lanes are currently in operation in the Minneapolis-St. Paul metropolitan area. HOV/HOT lanes are in operation on I-394 to the west of downtown Minneapolis and on I-35W to the south of downtown Minneapolis. Both facilities were initially implemented as HOV lanes and both were expanded to HOV/HOT lanes to maximize and enhance mobility in the corridors.

I-394 was constructed on the alignment of TH 12, a four-lane signalized arterial. An interim HOV lane, called the Sane Lane, was opened in 1985 at the beginning of the construction process. The Sane Lane was implemented for a number of reasons. First, it helped with traffic management during the almost 7-year construction period. Second, it introduced the HOV lane concept to travelers in the corridor and the metropolitan area as a whole. Third, it helped build transit ridership and carpooling for the completed facility.

The I-394 HOV lanes are approximately 11 miles in length and include two different designs. A 3-mile, two-lane, barrier-separated reversible section is located directly to the west of downtown Minneapolis. To the west of this segment are 7 miles of concurrent flow HOV lanes. The reversible lanes provide direct connections with three downtown parking garages, which include bus stops and passenger waiting areas, reduced parking fees for carpoolers, and links to the downtown skyway pedestrian system.

The complete I-394 HOV system was opened in 1992. Although the HOV lanes were well used, averaging between 900 and 1,000 vehicles in the concurrent flow section during the peak hour, interest in considering HOT applications emerged in the early 2000s to help maximize the use of the lanes.

In 2003, state legislation was approved allowing the HOT project on I-394. A task force, comprised of 22 individuals appointed by the Governor, the Lieutenant Governor, and communities in the corridor, was formed to help oversee the project.

MnPASS was undertaken to meet a number of objectives. These objectives included increasing the efficiency of I-394 by increasing the person and vehicle-carrying capabilities of the HOV lanes, maintaining free-flow speeds for transit and carpools in the HOV lanes, and improving highway and transit in the corridor with project revenues. Other objectives focus on developing ETC and advanced technologies to facilitate dynamic pricing and in-vehicle enforcement.

MnPASS implementation activities included restriping the concurrent flow HOV lanes to change from unlimited to limited access, installation of the ETC and electronic enforcement systems, and marketing the sale of MnPASS transponders, which are available online and at the MnPASS Customer Service Center. The MnPASS operating hours on the concurrent flow segment were initially expanded to 24/7. The hours were changed back to the peak hour, peak direction after the 24/7 operation caused traffic congestion in the off-peak travel direction.

The sale of MnPASS transponders and use of the lanes have grown since 2005. As of September 2011, there are 11,890 active I-394 MnPASS accounts and 15,246 transponders. Some 9,000 transponders have been sold. Traffic counts from mid-2006 recorded 1,756 vehicles using the concurrent flow section in the morning peak hour. HOVs accounted for 63% of the traffic, tolled vehicles comprised 32%, and some 5% were toll violators.

MnPASS allows solo drivers to use the HOV lanes on I-394 for a fee. Dynamic pricing is used, with tolls based on the level of congestion in the HOV lanes. The base toll is $.25 and the maximum toll is $8.00.

MnPASS, which was implemented in 2005, represents the first use of tolling in the Minneapolis-St. Paul metropolitan area. MnPASS also represents the first HOV/HOT project in the country on concurrent flow HOV lanes.

Drivers must have a valid MnPASS transponder displayed on the front windshield to use the lanes without meeting the vehicle-occupancy requirement. MnPASS transponders can be purchased online and at the MnPASS Customer Service Center.

MnPASS represents a partnership of the Minnesota Department of Transportation (Mn/DOT), Metro Transit, the Minnesota State Patrol, and local communities.

HOV lanes on I-35W South were extended to HOT lanes between 2009 and 2010 with funding from the US Department of Transportation Urban Partnership Agreement (UPA) program. With the construction of new HOV/HOT lanes through the Crosstown Commons section and the opening of the Priced Dynamic Shoulder Lane (PDSL) approaching downtown, 16 miles of HOV/HOT lanes are in operation. As of September 2011, there were 6,896 active I-35W MnPASS accounts and 7,836 active transponders. There were between 2,570 and 3,209 daily MnPASS users on I-35 W South in September 2011. Approximately 1,000 MnPASS vehicles were using the HOV/HOT lane during the morning peak period in the northbound lane, along with 1,784 carpools/vanpools, and 54 buses [13].

Future Directions

HOV/HOT facilities will continue to play an important role in major metropolitan areas in North America. The evolution from HOVs to HOV/HOT lanes will continue to progress to the broader managed lanes concept. The use of intelligent transportation systems (ITS) and other advanced technologies will allow for additional innovative approaches for maximizing the use of HOV/HOT facilities.

Bibliography

Primary Literature

1. Texas Transportation Institute, Parsons Brinckerhoff Quade and Douglas, Pacific Rim Resources (1998) NCHRP Report 414, HOV systems manual. Transportation Research Board, National Research Council, Washington, DC
2. Institute of Transportation Engineers (1988) The effectiveness of high-occupancy vehicle facilities. Institute of Transportation Engineers, Washington, DC
3. Transit Cooperative Research Program (2006) TCRP Report 95, Chapter 2 HOV facilities, traveler response to transportation system changes. Transportation Research Board, National Research Council, Washington, DC
4. Turnbull K (1992) An assessment of high-occupancy vehicle facilities in North America. Texas Transportation Institute, College Station
5. American Association of State Highway and Transportation Officials (AASHTO) (1992) Guide for the design of high occupancy vehicle facilities. American Association of State Highway and Transportation Officials, Washington, DC
6. American Association of State Highway and Transportation Officials (1989) Roadway design guide. American Association of State Highway and Transportation Officials, Washington, DC
7. Institute of Transportation Engineers Technical Committee 5 C-11(1992) Design features of high occupancy vehicle lanes. Institute of Transportation Engineers, Washington, DC
8. Mounce J, Stokes R (1985) Manual for planning designing and operating transitway facilities in Texas. Publication No. FHWA/TX-851425-2. Texas Department of Highways and Public Transportation, Austin
9. California Department of Transportation (1991) High occupancy vehicle (HOV) guidelines for planning, design and operations. California Department of Transportation, Sacramento
10. Washington State Department of Transportation, Design Manual – Section 1050, High-Occupancy Vehicle Priority Treatment. Washington State Department of Transportation, Olympia
11. Federal Highway Administration (2007) HOV/HOT lanes. Federal Highway Administration, Washington, DC
12. Federal Highway Administration (2003) Houston managed lanes case study: the evolution of the Houston HOV system. Federal Highway Administration, Washington, DC
13. Cofiroute USA (2011) MnPASS express lanes monthly status report. Cofiroute USA, Golden Valley

Books and Reviews

Arnold E Jr (1987) Changes in travel in the Shirley highway corridor 1983–1986. Virginia Transportation Council, Charlottesville

Beihler A (1996) The Pittsburgh busways. In: Conference proceedings, 8th international conference on high-occupancy vehicle systems, Pittsburgh. Transportation Research Board. Unpublished

Betts S, Jacobson L, Rickman T (1983) I-5 HOV lanes: three month report. Washington State Department of Transportation, Olympia

Bonsall J (1993) Development of the Ottawa transitway system. In: Conference proceedings, 6th national conference on high-occupancy vehicle systems, Ottawa, 25–25 Oct 1993.

Transportation Research Record 409. Transportation Research Board, Washington, DC

Bullard D (1991) An assessment of carpool utilization of the Katy high-occupancy vehicle lane and characteristics of Houston's HOV lane users and non-users. Texas Transportation Institute, College Station

California Department of Transportation (1992) Route 55 status information sheet

Christiansen D, Morris D (1990) The status and effectiveness of the Houston transitway system. Texas Transportation Institute, College Station

Crain & Associates (1978) San Bernardino expressway bus evaluation of mixed-mode operations. Southern California Association of Governments

Curitiba's Surface Metro (1993) The urban transport industries report, pp 53–43

Hultgren L, Kawada K, Lawrence S (1998) San Diego's interstate 15 value pricing project [CDROM]. In: 68th ITE annual meeting, Toronto

Institute of Transportation Engineers (1992) More for Less with HOV, The Benefits of High-Occupancy Vehicle Projects

Klusza R (1989) Route 55 three-year status report. California Department of Transportation, Los Angeles

Lancaster A, Lomax T (1987) Proceedings from the second national conference on high-occupancy vehicles lanes and transitways, Houston

McQueen J, Levinsohn D, Waksman R, Miller G (1975) The Shirley highway express-bus-on-freeway demonstration project: final report. U. S. Department of Transportation, Washington, DC

McQueen J, Levinsohn D, Waksman R, Miller G (1985) The Shirley highway express-bus-on-freeway demonstration project: final report. U. S. Department of Transportation, Washington, DC

Metropolitan Washington Council of Governments (1998) 1997 performance of regional high-occupancy vehicle facilities on interstate highways in the Washington region – an analysis of person and vehicle volumes and vehicle travel times. Metropolitan Washington Council of Governments, Washington, DC

Paiewonsky L (1998) A new approach to HOV entry requirements: MassHighway's 3+/limited 2+ sticker program. TRB Pre-print 981081

Pratt R, Copple J (1981) Traveler response to transportation system changes, 2nd edn. U.S. Department of Transportation

SRF, Inc. (1987) Technical memorandum #3 case study: I-394 HOV lane six month data for I-394 Interim HOV lane, Wayzata

SRF, Inc. (1995) I-394 HOV lane case study: final report. Minnesota Department of Transportation, St. Paul

Stockton B, Daniels G, Hall K, Christiansen D (1997) An evaluation of high-occupancy vehicle lanes in Texas, 1996. Texas Transportation Institute, College Station

Stockton B, McFarland F, Ogden M (1998) Feasibility of priority lane pricing of the Katy HOV lane: feasibility assessment. Texas Transportation Institute, College Station

Sullivan E (1998) Impacts and lessons from value pricing on the California state route 91 express lanes [CDROM]. In: 68th ITE annual meeting, Toronto

Sullivan E, Mastako K (1997) Impact assessment for the California route 91 variable-toll express lanes. Transportation Research Board Preprint No. 971046, Washington, DC

Transcore (1997) I-66 congestion management program monitoring project final report. Prepared for the Virginia Department of Transportation

Turnbull K (1988) Proceedings from the 1988 national HOV facilities conference, Minneapolis

Turnbull K (1990) Proceedings from the 1990 HOV facilities conference, Washington, DC, 10–12 Apr 1990. Transportation Research Board Circular 366. Transportation Research Board, Washington, DC

Turnbull K (1991) HOV Facilities – coming of age: fifth national high-occupancy vehicle (HOV) facilities conference. Transportation Research Board Circular 382. Transportation Research Board, Washington, DC

Turnbull K (1991) HOV Facilities – coming of age: national conference on HOV systems, Seattle. Transportation Research Board Circular 384. Transportation Research Board, Washington, DC

Turnbull K (1992) High-occupancy project case studies: historical trends and project experiences. Texas Transportation Institute, College Station

Turnbull K (1992) Moving into the 21st century. In: Conference proceedings, 6th national conference on highway-occupancy vehicle systems, Ottawa. Transportation Research Board Circular 409. Transportation Research Board, Washington, DC

Turnbull K (1992) An assessment of high-occupancy vehicle facilities in North America: executive report. Texas Transportation Institute, College Station

Turnbull K (1996) International HOV facilities. Transportation Research Record 1360, pp 126–137

Turnbull K (1997) HOV, HOT lanes, congestion pricing in the United States. In: Conference proceedings, 25th European transport forum annual meeting

Turnbull K, Capelle D (1998) Development of an HOV systems manual. National Cooperative Highway Research Program, Washington, DC

Turnbull K, Hubbard S (1994) HOV Systems in a new light. Transportation Research Board Circular 442. Transportation Research Board, Washington, DC

Turnbull K, Hubbard S (1994) HOV Systems in a new light. In: Conference proceedings, 7th national conference on high-occupancy vehicle systems, Los Angeles. Transportation Research Circular 442. Transportation Research Board, Washington, DC

Turnbull K, Hall K, Ringrose M (1994) High-occupancy vehicle treatments on toll facilities. Transportation Research Record 1446, pp 14–24

Ulberg C, Farnsworth G, Etchart D, Turnbull K, Henk R, Schrank D (1992) I-5 north high-occupancy vehicle lane 2+ occupancy requirement demonstration evaluation. Washington State Transportation Center, Seattle

Urbitran, Hayden-Wegman (1997) Evaluation of the high-occupancy vehicle (HOV) lanes on the long island expressway: January 1997 HOV lane user and non-user survey. Urbitran, New York

Van Luven H (1995) Implementation of HOV lanes on I-270: lessons learned. In: Proceedings – 7th national conference on high-occupancy vehicle systems: HOV systems in a new light. Transportation Research Record 442, Washington, DC

Virginia Department of Transportation (1997a) I-66 HOV-2 annual report. Commonwealth of Virginia, Richmond

Virginia Department of Transportation (1997b) I-66 HOV-2 demonstration project final report. Commonwealth of Virginia, Richmond

Washington State Department of Transportation (1985) I-5 HOV lanes: 20-month update, Olympia

Hitachi Zosen Inova Technology

Craig Kedrowski, Peter Chromec
Hitachi Zosen Inova U.S.A. LLC, Norcross, GA, USA

Article Outline

Glossary
Definition of the Subject and Its Importance
Introduction
Description of the Elements of the Hitachi Zosen Inova Energy-from-Waste Technology
Future Directions
Bibliography

Glossary

ACS Auxiliary Control Systems are advanced controls used in addition to the basic CCS in order to better control the combustion, specially with large grates or with inhomogeneous waste.

CEMS Continuous Emission Monitoring System: continuous monitoring of stack emission data, as well storing and transmitting data to environmental authorities.

CFD Computational Fluid Dynamics: mathematical model for calculating velocities, temperatures, concentrations, and properties of fluids flowing for example through a combustion chamber.

CCS Combustion Control System: automated system for controlling the combustion process on the grate including frequency, speed, and stroke of the ram feeder and of each grate module (also called GCS), as well as the flow of underfire air to each grate module, overfire and recirculated airflows.

DCS Distributed control system: automated system for controlling and coordinating all the WTE functions.

ECS Equipment control systems are separate control systems dedicated to control individual equipment functions to assure the desired equipment performance.

EfW Energy from waste (synonym to WTE = Waste to Energy).

FGT Flue Gas Treatment.

HHV Higher heating value or gross calorific value (expressed in kJ/kg or Btu/lb): heat released by a material when completely oxidized (reference temperature: 25°C, approx. 77°F, and assuming that H_2O is in liquid form).

HPS High-Pressure Steam: steam from superheater tubes to steam turbine.

LHV Lower heating value (expressed in kJ/kg or Btu/lb): heat released by a material when completely oxidized (reference temperature: 25°C, approx. 77°F, and assuming that H_2O is in vapor form).

LPS Low-pressure steam: usually from extraction of steam turbine, used for internal or external heating tasks.

LRD Load range diagram (or combustion diagram): shows the operating range of a combustion system in terms of fuel input, on one side, and heat input on the other.

O&M Operation and maintenance.

SCC Secondary combustion chamber: usually the vertical chamber above the grate, where gases and ash released from the fuel are completely combusted. Minimum temperature and residence time requirements often refer to the SCC.

SCR Selective catalytic reduction: process for reducing NO_x (nitrogen oxides) usually by means of reaction with an ammonia-containing reagent and in the presence of a catalyst.

SNCR Selective non-catalytic reduction: process for reducing NO_x (nitrogen oxides) usually by means of reaction with an ammonia-containing in the absence of a catalyst.

TOC Total organic carbon: amount of all non-combusted organic carbon in WTE ash; it is also used to express carbon content in MSW.

VOC Volatile organic carbon: concentration of organic compounds in flue gas.

Definition of the Subject and Its Importance

Traditionally, waste has been landfilled – and still is today, when cost is the main criterion for waste management (Fig. 1). "Out-of-sight, out-of-mind" has been the early concept, before science provided a more complete picture of the effects of landfilling on land, water, and air for a long time after a landfill has been filled [1]. The primary reason for these effects is the continuing decomposition of organic waste compounds into methane and other gases that escape to the air, or to water-soluble compounds that dissolve in rainwater percolating through the waste and may contaminate surface and groundwater.

This is why today's acknowledged hierarchy of waste treatment options considers landfilling as the least desirable option [2]. As shown in Fig. 2, best options are obviously "avoid" and "reuse," both of which reduce the amount of waste to be treated, and then recycle whatever is reasonably possible from the waste stream. However, the best that has been achieved by recycling and composting is about 70% [3]. This still leaves at least 30% of all waste produced to be treated by waste to energy (also called energy from waste) or landfilling. This entry describes the Hitachi Zosen Inova energy from waste (EfW) technology that recovers the energy contained in the waste and reduces municipal solid waste (MSW) to a maximum 10% of its original volume and to a chemically stable form.

Introduction

The Hitachi Zosen Inova energy-from-waste technology is a mass burn technology which treats post-recycling MSW (i.e., after all reuse and recycling efforts), as collected and without any pretreatment. It consists of a grate-fired steam generator followed by an air pollution control system. Steam is converted to electricity in a conventional steam turbine system. One of the most common configurations is shown in Fig. 3. Collection vehicles dump the waste from the *tipping area* into the *waste pit*. A *waste crane*, manually operated from the *crane control cabin*, or automatically operated by the control system, loads waste from the pit into the *feed hopper*. The waste pit and tipping floor area are ventilated by using the building air as the *primary air intake* for combustion so that no odors can escape to the surroundings. From the *feed hopper*, waste descends through a water-cooled chute and on to the horizontal *feeder table*, over which a hydraulically driven *ram feeder* slides back and forth and pushes waste on to the *reciprocating incineration grate*.

The combustion process is regulated by the combustion control system (CCS). It automatically regulates waste feed, grate movement, and airflow and distribution across the length of the grate to ensure efficient combustion and stable steam generation. Bottom ashes are continuously discharged at the end of the grate, along with siftings falling through the small gaps between the grate blocks, into the *bottom ash discharger* where it is quenched in water.

Hitachi Zosen Inova Technology. Figure 1
From landfilling to a modern energy-from-waste plant

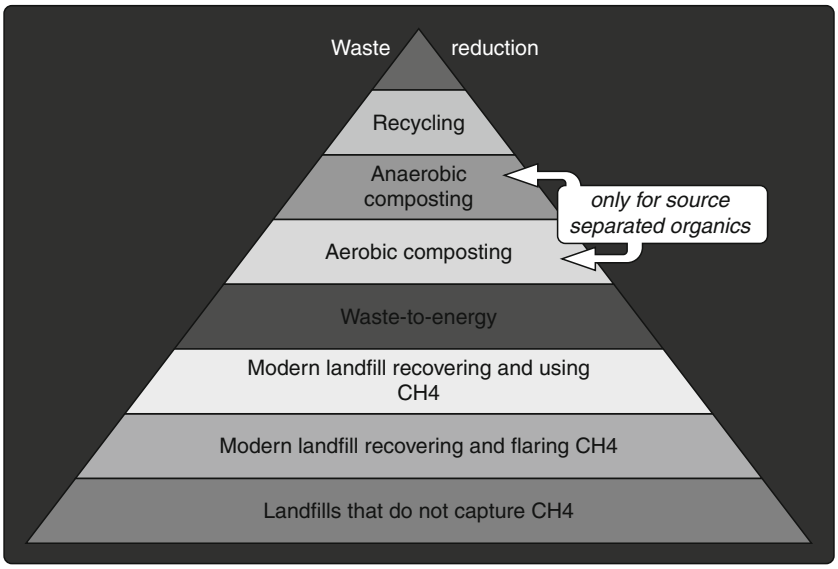

Hitachi Zosen Inova Technology. Figure 2
Waste treatment hierarchy as per Prof. Themelis [2]

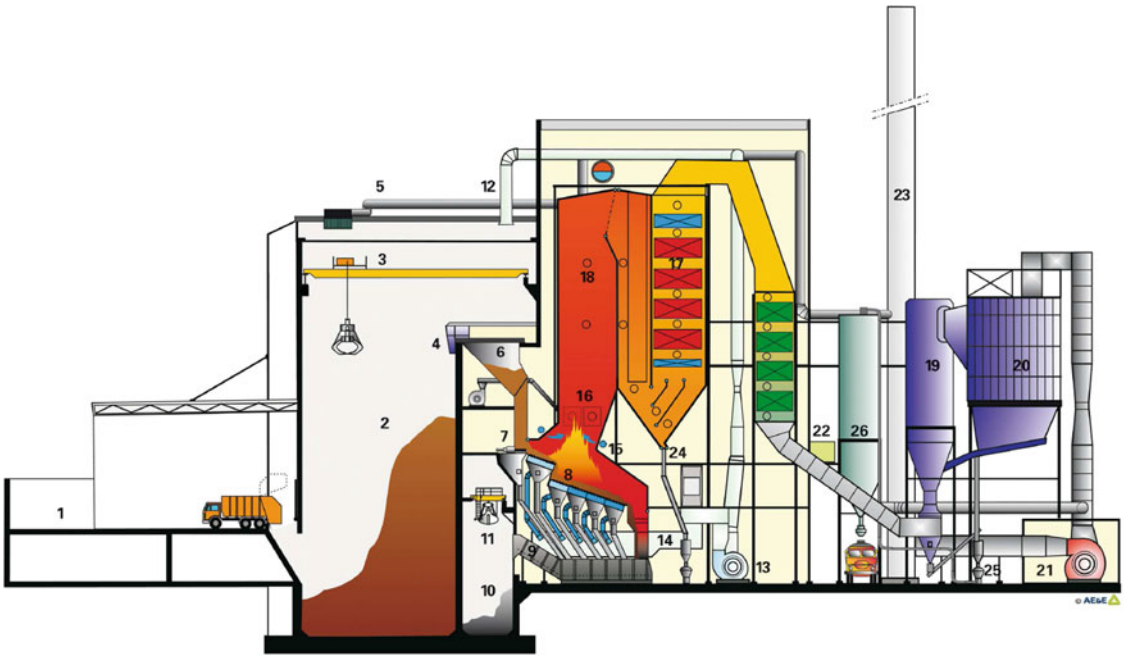

Waste receiving and storage

1 Tripping area
2 Waste pit
3 Waste crane
4 Crane control cabin
5 Waste pit ventilation at plant standstill

Combustion and steam generator

6 Feed hopper
7 Ram feeder
8 Reciprocating incineration grate
9 Bottom ash discharger
10 Bottom ash pit
11 Bottom ash crane
12 Primary air intake
13 Primary air fan
14 Primary air distribution
15 Secondary air injection
16 Start-up burner
17 4-pass steam generator

Flue gas treatment

18 SNCR injection levels
19 Semi-dry reactor
20 Fabric filter
21 Induced draft fan
22 Emission control room
23 Stack

Consumables and residues

24 Ash conveying system
25 Residue conveying system
26 Residue silo

Hitachi Zosen Inova Technology. Figure 3
A typical WTE unit

The ash discharger pushes the bottom ash into the bottom ash pit or alternatively (not shown) into a metal separation system that can recover ferrous and nonferrous metals.

Primary air is injected underneath the grate by the *primary air distribution system*. The *secondary air injection* is right above the grate. At about the same location, a part of the cleaned flue gases is recirculated back into the furnace. Both injections create a swirl in the combustion chamber and assure complete combustion with less excess air and thus a higher efficiency. The *start-up burner* is only needed for start-up and controlled shutdown, as well as to keep temperatures at minimum required levels if wastes with insufficient heat value are treated.

On the way through the *steam generator*, heat from the flue gases is recovered by heat exchangers and used for the production of superheated steam. The heat exchangers consist of membrane walls as well as superheater, evaporator, and economizer tubes. Each of the heat exchangers is designed specifically for the different steam and flue gas temperature ranges and properties. The membrane walls located in the combustion chamber (i.e., first pass) are lined with refractory and/or Inconel cladding to protect against erosion and corrosion. Effective cleaning systems such as sootblowers and water showers are installed to keep fouling of the heat exchanger surfaces within tolerable limits.

The superheated steam produced by the *steam generator* is then piped to a steam turbine / generator which produces electrical energy. A small part of the electricity is used to power the plant. Also, a small part of the low-pressure steam from the turbine is used for heating the plant and preheating combustion air.

The flue gases are cleaned in a multiple-stage flue gas treatment consisting of a selective non-catalytic reduction process (DyNOR®) and a HZ Inova's semidry flue gas treatment process.

The DyNOR® process is based on the principle of selective non-catalytic reduction (SCNR) of nitrogen oxides (NO_x) by injecting ammonia (NH_3) obtained from an aqueous ammonia solution. The *SNCR injection* takes place at the optimum temperature range within the furnace.

After the flue gas has left the boiler, it enters the semidry flue gas treatment process which is designed so that acidic gases are removed by sorption on hydrated lime, while the heavy metal compounds and organic contaminants, such as dioxins and furans, are adsorbed on activated carbon or lignite coke in the same process step. The HZ Inova Semidry FGT process provides intensive contact between the flue gases and the sorbents in a fluidized bed created in the *semidry reactor*. Water is injected to control the temperature in the reactor and to improve the sorption process on the lime. The following *fabric filter* is used for filtering the solid particles from the gases by means of gas-permeable fabric filter bags. A large portion of the filtered solids is recirculated to the semidry reactor in order to improve separation efficiency and sorbent utilization. The rest, generally called fly ash, is transported to the *residue silo* by the *residue conveying system*.

A continuous emission monitoring system (CEMS) is located in the *emissions control room* and monitors continuously the flue gases exiting the air pollution control system. The *induced draft fan* maintains the necessary sub-pressure in the whole plant and assures that the flue gases are conveyed from the furnace to the *stack*.

The above parts of the Hitachi Zosen Inova energy-from-waste technology are described in further detail in the following sections.

Description of the Elements of the Hitachi Zosen Inova Energy-from-Waste Technology

HZ Inova Technology Features

General Grate combustion is the most reliable and proven technology for thermal treatment of municipal and similar wastes. HZ Inova has used this technology for over 70 years and has built over 500 units worldwide. Over this period, the technology has continuously been perfected, supplemented with new developments, and adapted to changing requirements. In the following sections, the HZ Inova EfW technology is presented.

Plant Sizes A single combustion train operates within the range of the load range diagram (LRD) shown in Fig. 4. This diagram shows the waste throughput, in tons per hour (t/h), on the horizontal axis and the thermal load, in megawatts (MW), on the vertical axis for different heating values (here lower heat value

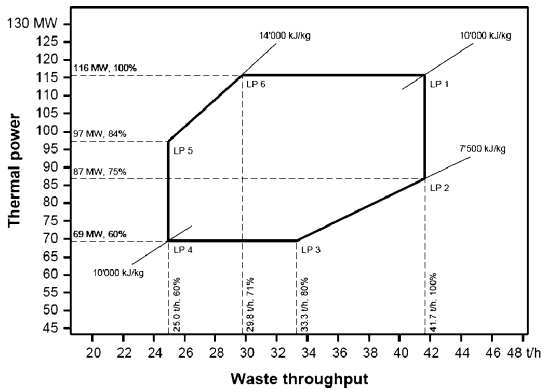

Hitachi Zosen Inova Technology. Figure 4
Typical load range diagram of a 1,000 tpd EfW plant

LHV, in kJ/kg) of the waste. The LRD of an EfW plant defines, for a given waste LHV, how much of that waste can be treated in this plant and how much energy will be released during combustion within the operating range of the unit.

HZ Inova EfW units (or "trains") are typically built within the following size range:

Waste throughput (metric tons)	t/h	4–42	Per combustion unit
	t/day	100–1,000	Per combustion unit
	kt/year	33–330	Per combustion unit
Waste			
LHV	kJ/kg	4,500–18,000	
HHV	Btu/lb	2,500–8,400	
Thermal capacity	MW	15–120	Per combustion unit

Recently, with the proven reliability of the HZ Inova EfW technology, ever more single train plants are planned and built. The main question related to single train plants is if waste can be stored or otherwise diverted as well as if it is acceptable to have no heat and/or power supply during service outages. For larger plants, or if redundancy is important, multiple trains can be combined in one EfW plant as needed.

Technology Requirements The waste management market requires for EfW solutions with highest possible flexibility regarding calorific values and composition of wastes to be treated. With changing consumer habits and waste management strategies, including various recycling schemes, properties of feed streams available for an EfW plant can significantly change. At the same time, EfW solutions must meet the highest environmental standards, high thermal efficiency, and be cost effective. The main objectives of the thermal treatment of waste can be summarized as follows:

- Complete inertization and volume reduction of waste
- Destruction of organic pollutants
- Recovery of metals and other useful products
- Concentration of inorganic pollutants in a usable or inert form
- Highest recovery of energy contained in waste for substitution of primary energy
- Cleaning of flue gases to very stringent environmental standards

These objectives translate into the following requirements for a grate combustion system:

- Continuous and controlled waste feed to achieve a constant thermal output despite inhomogeneous waste properties
- Closely controlled supply of combustion air to the individual combustion zones (drying, gasification, ignition, primary combustion, post-combustion) and minimization of infiltration air to ensure good and efficient combustion
- Controlled and adapted movement and stoking of the waste on the grate through the above combustion zones to ensure good burnout
- Efficient and reliable boiler system in order to minimize scaling, corrosion, and erosion in a very difficult environment
- Effective and economic air pollution control system that is adaptable to special local requirements, such as non-attainment zones

Specific main components that make up the Hitachi Zosen Inova EfW technology and fulfill the above requirements are described below in detail.

Waste Pit and Crane

General The purpose of the waste pit and crane is to receive the waste as delivered by the collection or

transfer vehicles, store the waste, and also blend it and load it into the waste hoppers so that they are always full.

Waste Pit The waste pit is a large concrete bunker for storage of the waste delivered until it is treated. It serves to uncouple the waste delivery from the waste treatment so that the plant can continue to operate during weekends and holidays when waste delivery is interrupted. Also waste delivery can continue while the plant is shutdown for periodic maintenance.

Another important function of the waste pit is to provide the crane operator with the volume needed to mix the waste. To get the highest capacity and to reduce wear and tear of the equipment, the plant should be operated as stably as possible. This can only be done if the incoming waste, where one truckload could contain completely different waste than the next, is mixed within the waste pit.

To prevent the combustible waste from igniting in the pit, infrared cameras are installed. When they detect a hot spot, water cannons are used to cool it down.

To prevent the odors in the waste pit from escaping to the environment, either the entire tipping area is enclosed or the dropshafts are equipped with doors. As noted earlier, air is aspirated from the waste pit and used as primary air for combustion. This assures that when the doors are open, air is drawn into the pit and the odor is contained.

Waste Crane A grapple crane (Fig. 5) is used to move the waste in the waste pit for mixing, stacking, and transferring waste to the feed hopper. A single crane can lift loads of several cubic meters of waste in the grapple.

Scales are integrated into the crane in order to weigh every load which is deposited into the feed hopper. This allows the combustion control system to calculate the operating point, monitor trends of waste composition changes, and adapt operating parameters accordingly.

The crane operation can also be automated for certain periods of time so the operator can follow other duties.

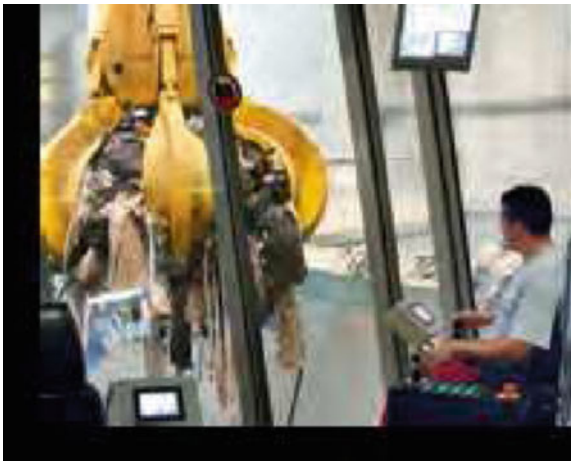

Hitachi Zosen Inova Technology. Figure 5
Crane operator loading waste to feed hopper

Feed Hopper

General The purpose of the feed hopper/feed chute is to receive waste from the waste pit/bunker via the crane and then to convey the waste onto the ram feeder. It also serves the purpose, by means of the compacted waste column in the chute, of forming a seal between the pit bunker and the combustion chamber, which prevents leakage air into the combustion chamber. Alternatively, the feed chute can be shut off by closing its flap gate.

Description Figure 6 shows the complete feed hopper, consisting of hopper, hopper flap gate, feed chute, and support frame. In order to prevent wear, certain key areas are protected with wear-resistant steel sheet. The slope of the hopper walls and the arrangement of the hopper flap gate are designed to prevent arch buildup and, thereby, ensure continuous delivery of waste to the ram feeder table. The hopper rests on the concrete loading deck above the bunker pit and a sufficiently high protection barrier is provided for personnel safety.

The height of the feed chute facilitates a sufficiently high waste column that seals the combustion chamber from the waste bunker during combustion. The feed chute and the support frame are water-cooled to resist any thermal stress that may occur during operation.

The feed hopper flap gates (Fig. 7) are installed in the bottom of the hopper, one for each grate lane.

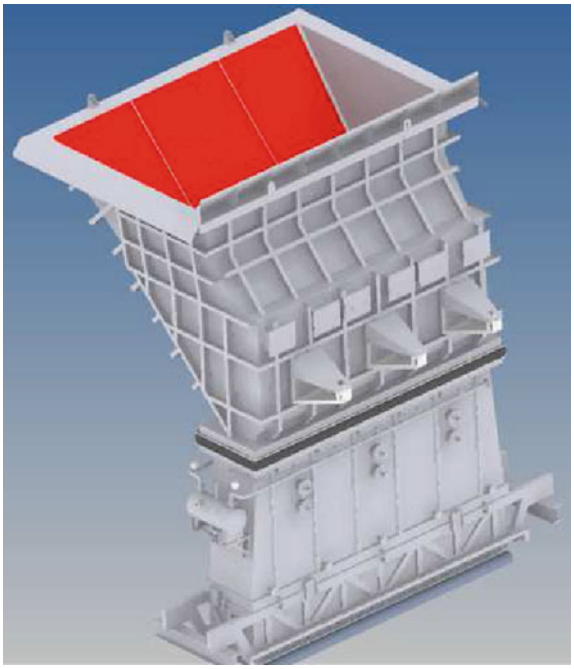

Hitachi Zosen Inova Technology. Figure 6
Feed hopper, chute, and support frame

These gates are hydraulically operated by cylinders powered by the hydraulic station. The hopper flap gates seal the combustion chamber from the bunker prior to waste charging and during system shutdown. An interlock with the combustion chamber temperature ensures that during system start-up the hopper flap gate cannot be opened and waste cannot be charged until the minimum combustion chamber temperature is reached.

In order to monitor the waste height, a reliable, low-maintenance level monitor is installed on the feed chute to provide a low-level alarm. Depending on the requirements for automated operation, one additional level monitor can be installed in the hopper in order to signal to the crane operator to load additional waste. A third-level detector can be installed in order to signal a possible formation of an arch in the feed hopper.

Ram Feeder

General The purpose of the ram feeder (Fig. 8) is to push the waste from the feed chute and distribute it onto the grate at a controlled rate, as required by the combustion control system.

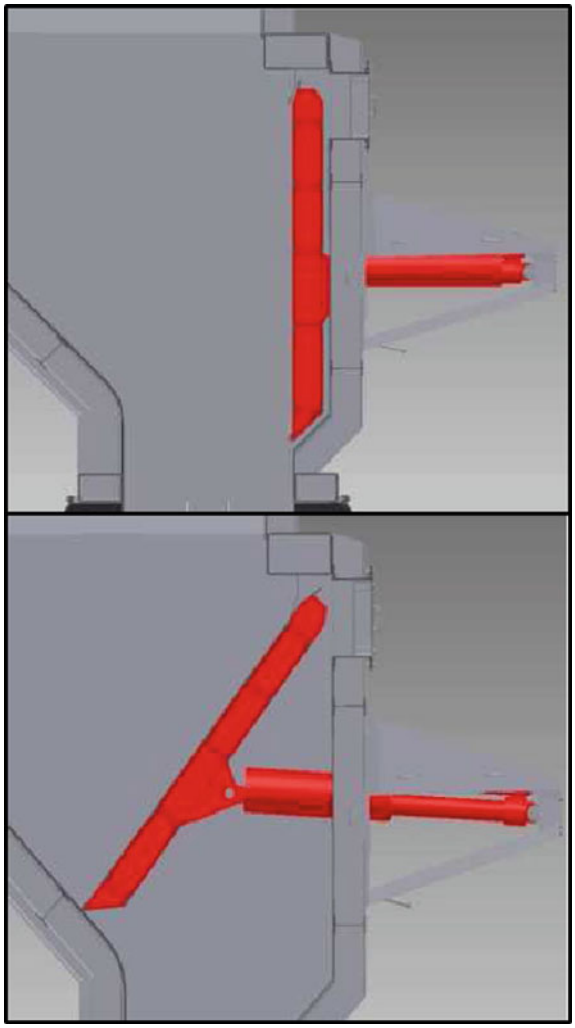

Hitachi Zosen Inova Technology. Figure 7
Feed hopper flap gate

Description The waste descends in the feed chute and falls on to the horizontal feeder table, over which hydraulically driven ram feeders (one for each grate lane) slide. As the feeders slide back, waste falls from the feed chute to the feed table. As the feeders slide forth, waste on the feed table is pushed onto the incineration grate.

The speed and length of the forward stroke can be continuously varied, depending on steam flow demand and waste properties. With each stroke, a defined volumetric quantity of waste is pushed onto the incineration grate. The return stroke is made at full speed. The continuous regulation of the forward stroke allows

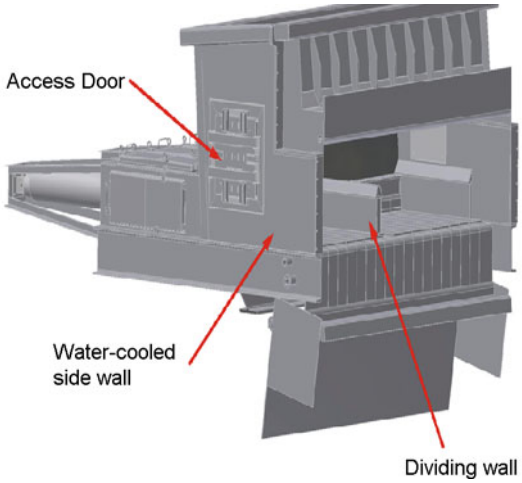

Hitachi Zosen Inova Technology. Figure 8
Ram feeder arrangement

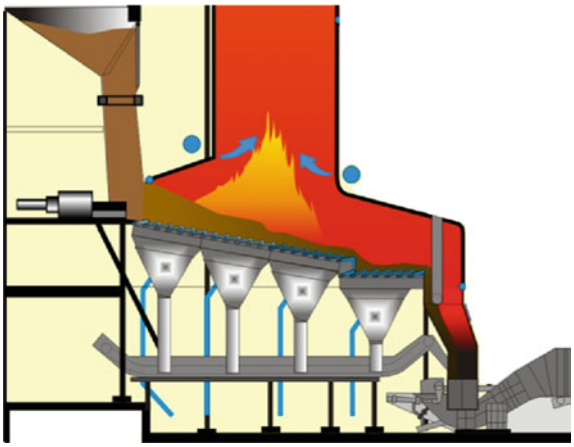

Hitachi Zosen Inova Technology. Figure 9
Four-grate modules in a lane

uniform metering and immediate adjustment of waste required on a specific grate row. The strokes are adjusted by the ram feed controller housed in the grate control cabinet located in the immediate vicinity of the waste-charging area. The ram feeders can also be operated manually from this local control cabinet and monitored by the DCS.

Grate

General The purpose of the grate is to incinerate the waste and to ensure continuous and complete combustion resulting in an adequate burnout of the bottom ash to a level of typically less than 3% TOC (total organic carbon).

Hitachi Zosen Inova Technology. Figure 10
Three-lane grate

Description

Overview The basic component of the combustion grate is the grate module. As can be seen in Fig. 9, the four-grate modules are joined together longitudinally to form one-grate "lane." A grate consists of one to four parallel grate lanes. Figure 10 shows a three-lane grate. The width and the number of grate lanes, and therefore the grate size, are determined by the design throughput and the calorific value of the wastes.

The grate is an inclined forward-feed grate with a slope of 10° to the horizontal. The last grate zone - the burn-out zone - is not inclined, in order to provide for optimal bottom ash quality. The grate, including the riddling hoppers below, is attached to the furnace structure at the feed end by means of a pivot mount which allows it to move. The grate rests on the grate support structure; this allows it to move in response to thermal expansion. The grate cylinders and riddling hoppers move with the grate as it expands and contracts. A boiler-to-grate expansion joint is installed between the grate module and the lower water wall headers.

Each grate module is driven by two hydraulic cylinders. A separate hydraulic control block is provided for each grate element. The stroke acts on the grate carriage located on guide surfaces, thereby cycling the movable grate block rows.

The number, speed, and length of strokes performed by the movable grate block rows can be continuously controlled in response to the process needs and the frequently changing properties of the waste.

Grate Modules Each grate module (Figs. 11 and 12) consists of six grate block rows, alternating between movable and stationary rows. An end piece is bolted onto the last grate module which forms the transition from the grate end to the bottom ash discharge chute.

With the exception of the side plates, the stationary and movable blocks are identical. The grate blocks are supported and mounted on retaining tubes. The block-retaining tubes for the stationary block rows are supported on brackets which rest on the stationary support structure of the grate module. However, the block-retaining tubes for the movable block rows are connected to brackets, which in turn are secured to the supports of the grate carriage that moves in the direction of the waste. The grate carriage is equipped with rollers and guides the movable grate rows. Dual hydraulic cylinders drive the rows back and forth.

The drive cylinder is attached to the grate carriage and secured to the support structure by means of a universal joint. The piston rod acts on the drive carriage attached to it, and thus to the movable grate block rows. The hydraulic cylinders are powered by a hydraulic station.

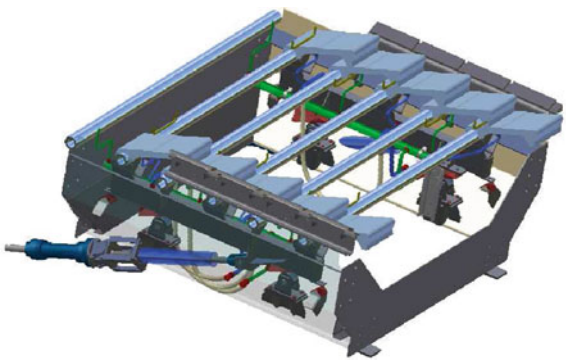

Hitachi Zosen Inova Technology. Figure 11
Grate module

Grate Block Rows All of the six grate block rows per module are made up of either air-cooled or water-cooled grate blocks. The grate blocks are supported on the block-retaining tube as shown in Fig. 13. To minimize the gaps between blocks, they are held together by means of a tension rod. The two-part tension rod is inserted into the outermost grate blocks and tightened in the middle with a turnbuckle. This reduces riddlings and prevents undesirable airflow between the grate blocks and maintains a constant pressure drop across the grate.

Air-Cooled Grate Block The grate blocks support and push the waste through the combustion zone, and thus are exposed to extreme thermal, chemical, and mechanical stress. They are made of cast steel and are surface-machined as required.

The grate blocks are also designed to distribute the primary air evenly through the waste bed. This is done

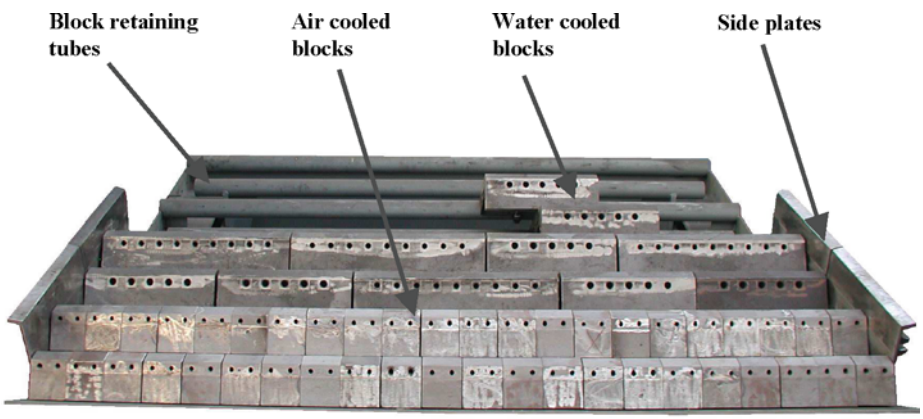

Hitachi Zosen Inova Technology. Figure 12
Rows of grate blocks in a module

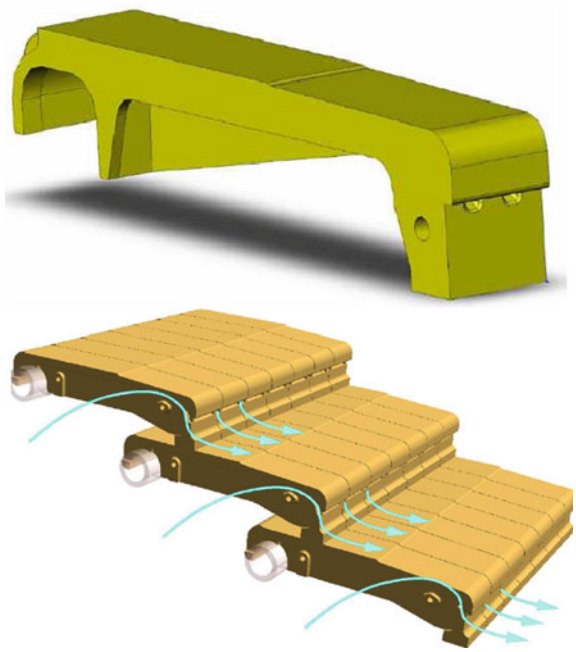

Hitachi Zosen Inova Technology. Figure 13
Air-cooled grate block

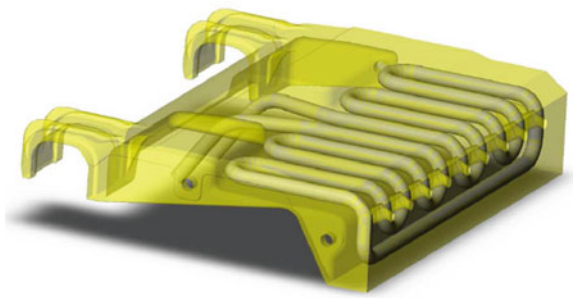

Hitachi Zosen Inova Technology. Figure 14
Aquaroll® water-cooled grate block

by openings at the front of the grate block. These openings are angled downward and protected by a small nose in order to help prevent them from getting fouled or clogged (Fig. 14).

To reduce the thermal stress on the grate block, it has to be cooled as uniformly as possible. This is achieved by the air that is guided through the grate block. The total opening of the air path through the grate blocks is designed such that a minimum pressure drop across the grate is maintained at all operation

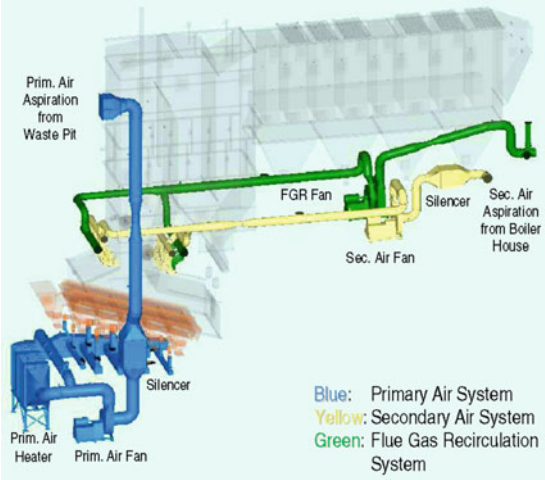

Hitachi Zosen Inova Technology. Figure 15
Combustion air and flue gas recirculation systems

points. This assures an even distribution of the primary air through all grate blocks and reduces the risk of local superheating and associated excessive wear and tear. In addition, good distribution of primary air is essential to prevent excess formation of carbon monoxide and prevents the formation of clinkers on the grate surface.

Water-Cooled Grate Block For high-calorific wastes, the airflow alone does not provide sufficient cooling of the grate blocks. Aquaroll® water-cooled grate blocks as shown in Fig. 14 are used in such applications. Forced water circulation through a cooling tube cast into the grate block assures a low enough surface temperature of the grate block such that wear is drastically reduced.

Combustion Air System

General The main purpose of the primary air system (blue in Fig. 15) is to control and deliver the drying and combustion air to the hoppers underneath the grates at the right flow rate, pressure, and temperature as required for optimum combustion in the individual zones.

The secondary purpose of the primary air system is the ventilation of the tipping and waste pit area such that odors are contained therein.

The purpose of the secondary air system is to control and deliver the secondary combustion air to the

combustion chamber above the grate. It creates the turbulence in the combustion chamber, which assures complete burnout of the flue gases.

Primary Air System

Overview The primary air is drawn in from the waste bunker and delivered separately, by the primary air fan, to the underside of the individual grate zones. The air is sucked from the pit in order to maintain a negative pressure and thus control odors. The system comprises the intake filter/screen, the primary air fan, the primary air preheater (if needed), as well as all associated ducts, dampers, and expansion joints. Distribution headers and ducts as shown in Fig. 16 direct the primary air to the respective grate modules and the combustion zones.

The primary air flow is controlled by the variable speed drive of the primary air fan. The distribution of primary air to each of the four zones is controlled by zone dampers. The flow rate of the primary air is measured in total as well as for each of the four zones to provide feedback to the combustion control system.

In areas where the calorific values of the waste are very low, the primary air is preheated using steam. This improves drying of the waste in the first grate zone and ensures proper burnout.

Hitachi Zosen Inova Technology. Figure 16
Primary air distribution headers and ducts underneath grate

Primary Air Fan The primary air fan is a standard centrifugal, backward inclined blade-type fan with single or double bearing and with direct connection to an electric motor drive. Since the air may contain dust from the waste pit area, the fan is equipped with openings for inspection and cleaning.

Primary Air Preheater For waste with low calorific value, a two- or three-stage air preheater is installed on the discharge side (positive pressure) of the primary air fan. The first stage preheats the air by cooling the condensate formed in the subsequent stage(s). The second stage is a low-pressure steam (LPS) and the third stage is a high-pressure steam (HPS) heater. The LPS stage is typically fed off an extraction from the steam turbine, while the HPS stage is feed off the boiler steam drum. This setup uses internal steam sources and therefore increases the plant's overall energy efficiency.

Since the primary air contains dust from the waste pit area, the open cross-sectional area is largely dimensioned, and the tube arrangements used as heat exchanger surfaces are exclusively in-line. A sufficient number of openings are provided for online inspection and cleaning. A bypass is provided for possible cleaning while the heater is off-line.

Secondary Air System

Overview Volatile components of the waste are released on exposure to heat. Some of them do not immediately combust on the grate because they may react more slowly or because oxygen is missing at that particular location in the waste bed on the grate. It is therefore necessary to provide overfire air and thoroughly mix the air with the flue gases above the grate to assure complete combustion of all volatiles released. This air is delivered via the secondary air system (Fig. 17).

The secondary air is drawn in from the boiler house under the roof in order to recover some energy from the radiant losses of the boiler equipment. It is delivered by the secondary air fan to the secondary air nozzles above the grate (Fig. 18). This system consists of the intake filter/screen, the secondary air fan, the secondary air preheater (if needed), the secondary air nozzles, and associated ducts, dampers, and expansion joints.

The secondary air is injected into the furnace at an angle, so that it causes a swirl flow in the combustion

Hitachi Zosen Inova Technology. Figure 17
Secondary air and recirculated flue gas headers and injection nozzles

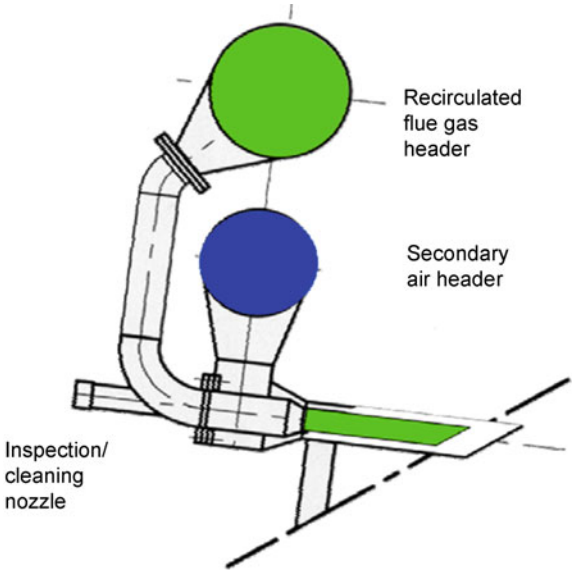

Hitachi Zosen Inova Technology. Figure 18
Secondary air and recirculated flue gas nozzle

chamber. This swirl assures good mixing of the combustion gases and stabilizes the flue gas flow in the furnace.

The secondary airflow is controlled by the variable speed drive of the secondary air fan. Its flow is controlled by locally adjustable dampers in the distribution lines to the secondary air nozzles. These are preset during initial start-up. The flow rate of the secondary air is monitored and controlled by the CCS.

In case the calorific values of the waste are very low, the secondary air is preheated. This ensures that the combustion products are properly burned out without using auxiliary fuel.

Secondary Air Fan The same type of fan can be used as for the primary air system.

Secondary Air Preheater At very low waste heat values, a single-stage air preheater is installed on the discharge side (positive pressure) of the secondary air fan. It uses low-pressure steam. This setup extends the operating range of the furnace without using the auxiliary burners to maintain the furnace temperature. Using internal steam sources increases the plant's overall energy efficiency.

Flue Gas Recirculation System

General The purpose of the flue gas recirculation system (green in Fig. 18) is to supply a portion of the cleaned flue gases back to the combustion chamber, in order to improve mixing and provide additional cooling without the need for more combustion air. This improves the overall energy efficiency of the unit.

Description

Overview Flue gas recirculation reduces the amount of fresh air that has to be injected at the secondary air injection level for cooling and mixing purposes. It controls the combustion chamber temperature without adding air. This reduces the oxygen content in the flue gases as well as carbon monoxide and nitric oxides formation.

The flue gas is diverted downstream of the induced draft fan and is reinjected into the combustion chamber. The system comprises the flue gas recirculation fan as well as all associated ducts, dampers, and expansion joints. The system further has a purge connection for fresh air so the ducts can be purged with ambient air in order to dry them and prevent corrosion during a plant shutdown. The flue gas ducts must be well insulated.

The recirculated flue gases are injected through a central pipe of the secondary air nozzles. The flow rate is controlled by a variable speed drive as calculated by the CCS.

Recirculated Flue Gas Fan The same type of fan can be used as for the primary air system, however, adapted to the higher operating temperature and properly insulated.

Secondary Air/Recirculated Flue Gas Nozzles The nozzles (Fig. 18) are specially designed and placed to provide the impact needed to create a swirl flow pattern in the secondary combustion chamber. The concentric design with the recirculated flue gas in the center tube and clean secondary air in the annular gap minimizes the risk of plugs due to dust possibly present in the flue gases. A poke hole allows cleaning the center tube online.

Flow Optimization with Swirl Injection

General The injection of secondary air and recirculated flue gas as described above has been optimized to achieve best gas burnout. CFD modeling, as shown in Fig. 19, has been used to optimize number, location, and angle of injection points. Tangential injection into the furnace creates a swirl in the combustion chamber. This swirl improves the mixing of the combustion gases and helps maintain a uniform flow pattern.

Description The geometry of the secondary combustion chamber (SCC) is designed for optimal flow conditions. In addition, the arrangement of the secondary air and recirculated flue gas nozzles creates a swirl in the SCC. Due to this swirl, the gas flow is homogenized with respect to temperature, velocity, and concentrations (Fig. 20). This flow configuration results in:

- Improved burnout of flue gas
- Uniform temperature profile across the secondary combustion chamber
- Reduction of CO-concentrations by approx. 70% (Fig. 20)
- Minimize risk of corrosion of unprotected heating surfaces
- Improved burnout of fly ash
- Reduced reformation of dioxins

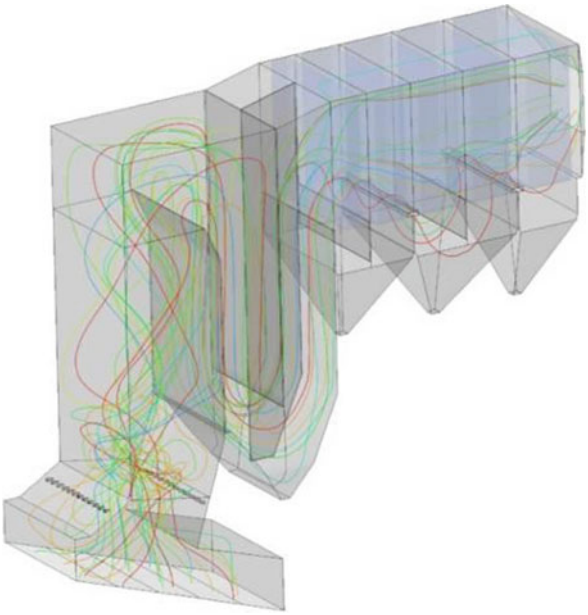

Hitachi Zosen Inova Technology. Figure 19
CFD of swirl injection

Start-up Burners

General Start-up burners are specially designed for use in waste incinerators. They are located in the lower part of the combustion chamber above the secondary air injection area. Their primary purpose is to heat up the furnace gradually and in line with refractory requirements until the temperature is reached where wastes can be burned. The same applies during a controlled shutdown. During normal operation, the burners are switched off. Very seldom, with very low calorific wastes, the burners have to run to assure the minimum combustion temperature in the furnace.

Description A separate burner fan provides the combustion air needed for the burner. The volume of combustion air is controlled by the burner control system and adjusted by the control damper incorporated into the air manifold. A pressure indicator is located in the duct upstream of the air manifold to monitor the operation of the combustion air fan. Since the burner is normally off during operation, it must be protected from the thermal radiation in the furnace. This can be done by a small, cooling air fan as shown on Fig. 21 together with the burner. Alternatively, a refractory-lined guillotine-type damper can be installed, which isolates the auxiliary burner from the furnace.

The burner control system ensures the burner safety and controls the correct fuel/air ratio. It is installed in a control cabinet located near the burner. All burner-operating commands, and the release signal from the system safety network, come from the plant control system. The local control panel can be used to

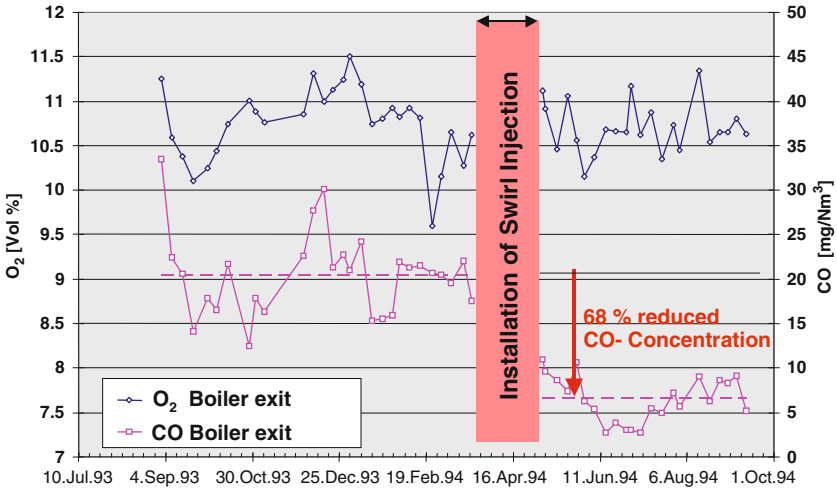

Hitachi Zosen Inova Technology. Figure 20
Average CO levels before and after installation of the swirl injection system

Hitachi Zosen Inova Technology. Figure 21
Typical auxiliary burner with cooling air fan

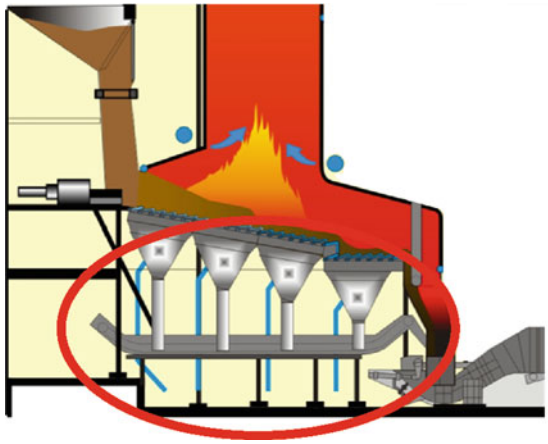

Hitachi Zosen Inova Technology. Figure 22
Riddlings conveyor

commission and optimize burner operation as well as to cancel local error messages during operation.

Conveyor of Grate Siftings/Riddlings

General While all moving parts of the ram feeder and the grate are designed with minimum gaps, the thermal expansion of the materials between ambient and operating temperatures unavoidably lead to small gaps through which small parts in the waste or the ash can fall through. The purpose of the grate siftings/riddlings conveyor (circled in Fig. 22) is to constantly remove these so-called siftings/riddlings while maintaining the air seal to the environment for the primary air system.

Description A wet drag chain conveyor is used for this application. One conveyor can be used for up to two grate lanes. Riddlings are collected from five locations for each lane: four grate modules and the ram feeder. The siftings/riddlings are collected in hoppers underneath these locations and delivered to the conveyor via chutes. The chutes are immersed under the water level inside the conveyor, thus ensuring an air seal between the furnace enclosure and the environment. The wet drag chain conveyor quenches the grate siftings and transports them toward the bottom ash extractor.

The amount of siftings/riddlings delivered varies and can change over the operating years due to wear and tear of the moving equipment. The drag chain conveyor can be adjusted to these conditions. Appropriate openings are installed at various points of the conveyor for inspection and cleaning as needed. The conveyor is a watertight steel construction. The key areas prone to wear are protected using wear-resistant plates.

The conveyor designed for the case that a heavy piece such as a damaged grate block falls into the conveyor. A shear pin protects the conveyor, and a zero-speed switch alarms the control room. The conveyor's water level is maintained using a float valve.

Bottom Ash Extractor

General The purpose of the bottom ash extractor (Fig. 23) is to cool the bottom ashes from the furnace as well as discharge bottom ashes and riddlings while at the same time maintaining the air seal from the furnace to the environment.

Description The bottom ashes remaining at the end of the grate fall into the bottom ash extractor, where they are quenched in a water bath. The grate siftings/riddlings are delivered to the bottom ash extractor via the grate siftings/riddlings conveyor. The bottom ash discharge chute has an airtight connection to the grate, and the water bath in the bottom ash extractor provides an air seal between the furnace and the environment.

The design of the bottom ash chutes and extractor is such that the large pieces of bottom ash can be discharged without difficulty. A hydraulically driven ram pushes the bottom ashes once every few minutes from the bottom of the extractor upward to the sloped chute and toward the outlet. There, the ashes stay until they are further pushed by the next ram stroke. After a few strokes, the ashes reach the edge at the outlet, fall on a belt or vibrating conveyor, and are transported to the ash storage and treatment. During this period, water contained in the ashes drains back to the water bath so that the final moisture content of the bottom ash is typically about 20%.

The hot ashes falling into the water bath cause some of the water to evaporate. This water vapor rises into the combustion chamber through the bottom ash chute. Water vapor is also formed in the outlet chute of the ash expeller since larger ash pieces may still be warm. From there, the vapor is conveyed into the furnace by means of a small fan. A water-level control regulates the feed of water to replace the evaporated water and maintain the water level in the bottom ash extractor.

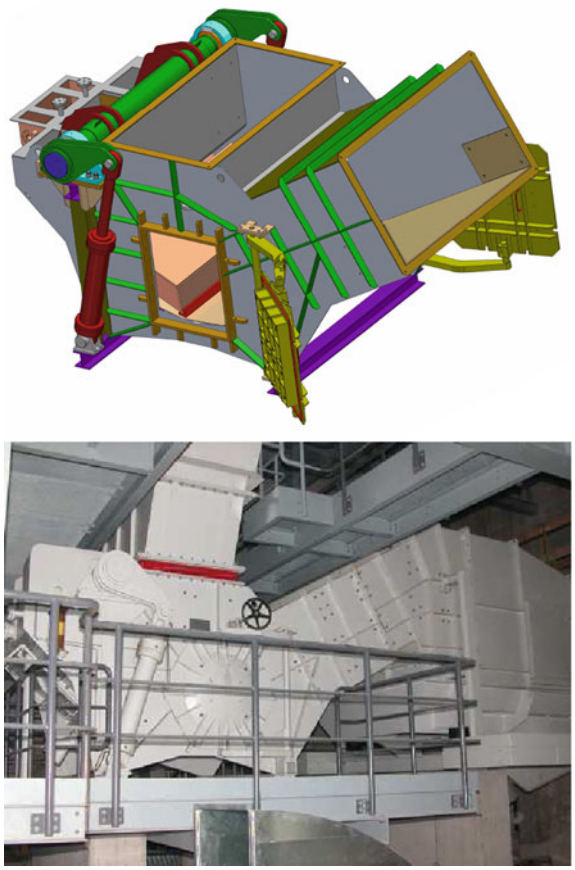

Hitachi Zosen Inova Technology. Figure 23
3D model and picture of bottom ash extractor

The bottom ash extractor is made of reinforced steel plates in a completely welded design. In order to reduce wear, the trough is internally lined with wear plates. The bottom ash discharge chute is a double-walled structure made of steel plate.

Hydraulic Station

General The purpose of the hydraulic station is to power the hydraulic cylinders for the feed hopper, the ram feeder, and the grate and the bottom ash extractor.

Description A single hydraulic station as shown in Fig. 24 is provided for each incineration train. The pumps, tanks, heat exchanger, and valves are all mounted and placed in a secondary containment in an easily accessible location at grade. Hydraulic oil is supplied by a set of hydraulic pumps located on the hydraulic reservoir. Each hydraulic drive has a separate hydraulic control block with electrical control elements.

Two redundant sets are equipped with a pressure-dependent flow rate control system, to perform the respective functions of the feed hopper, the ram feeder and the grate. Each grate module has a separate control block.

A third hydraulic pump is pressure-controlled and is used for the bottom ash extractor. Redundancy is provided by the other two pumps.

A water-cooled heat exchanger is integrated into the return line of the hydraulic circuit.

A pressurized tank is provided for the case of power failure in order to safely close and/or open the necessary cylinders and bring the system into its fail-safe position.

Combustion Control System

General The purpose of the combustion control system (CCS) is to provide a stable steam load in automatic mode. Since waste is a highly variable fuel, this is not a simple task. Various parameters must be monitored and various equipment need to be controlled in a concerted way.

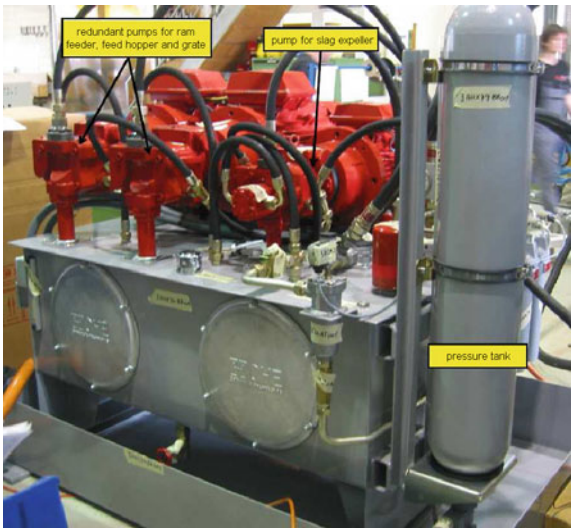

Hitachi Zosen Inova Technology. Figure 24
Typical hydraulic station

Description

Overview Control Functions Figure 25 shows a typical Hitachi Zosen Inova combustion control system (CCS). It allows for largely automatic and secure operation at the requested load. Even at varying waste qualities, compliance with legal operating conditions such as the combustion chamber temperature and the oxygen content in the flue gas as well as an efficient gas and bottom ash burnout are assured because of the automatic control system. Steady control of the combustion conditions minimizes stress to the equipment and reduces fouling in the combustion chamber. Good combustion control includes:

- Keeping the steam flow constant, as preset by the operator
- Keeping the flue gas flow rate constant
- Ensuring an efficient gas burnout by keeping the oxygen content in the flue gas within the desired limits
- Ensuring the fire is in the right position for an efficient bottom ash burnout

All these aspects are interdependent and are heavily influenced by changing waste properties. Thus, a multivariable control system is required. The following parameters are monitored and controlled:

- Steam flow rate
- Oxygen content at the boiler outlet
- Primary airflow rate
- Primary air temperature
- Secondary airflow rate
- Flue gas recirculation flow rate
- Temperature of ceiling above grate end

Also, the following equipment is controlled:

- Ram feeder
- Grate
- Primary air fan
- Primary air dampers per zone
- Primary air heater
- Secondary air fan
- Flue gas recirculation fan

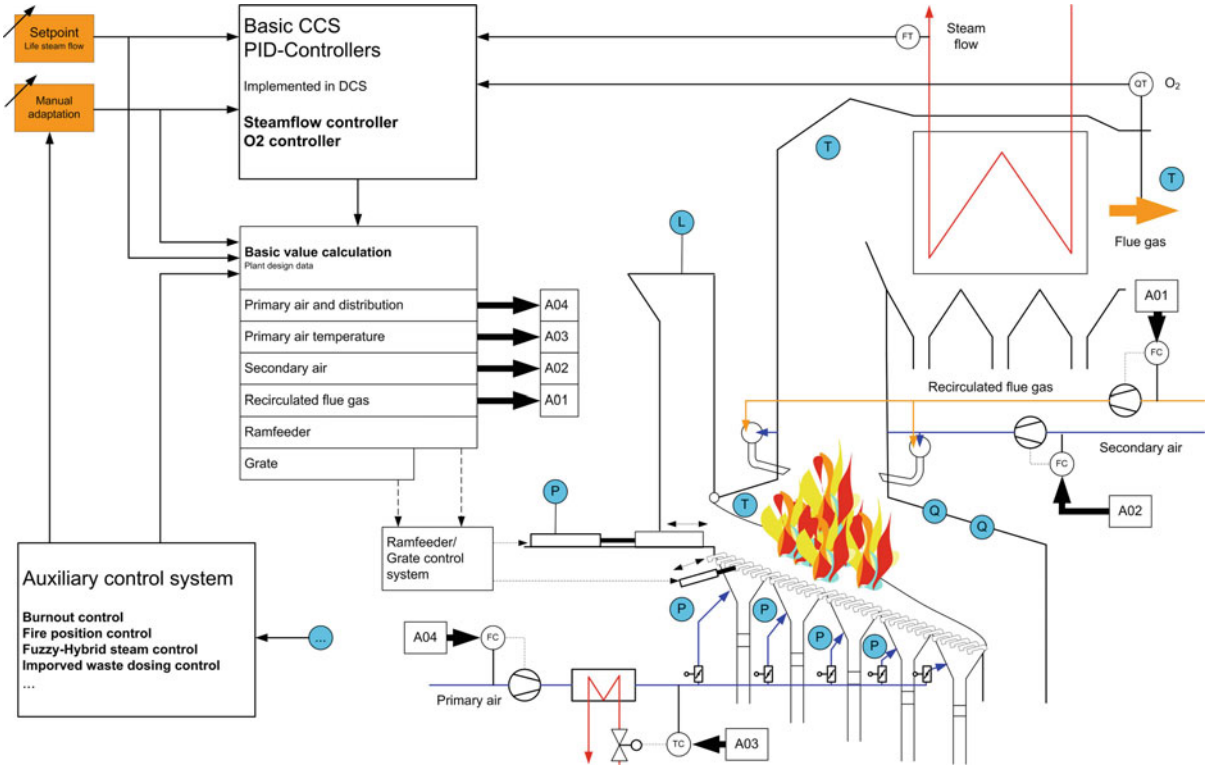

Hitachi Zosen Inova Technology. Figure 25
Overview main combustion control functions

The control structure consists of both parallel connections of different controllers and of serial (cascading) connections of controllers located at various levels in the control system.

Overview Control Systems As shown in Fig. 26, the DCS controls the EfW plant. It contains three main elements: (1) the basic Combustion Control System (CCS) as well as other control systems of the plant such as the controls of the Air Pollution Control System (not shown in the graph). (2) the Sequence Controller, which informs about the state of the plant as well as automatically brings it to the next mode as needed. (3) the Operator Terminals where the plant can be monitored and manually optimized or operated. The DCS receives signals from the plant such equipment status and flowrates or temperatures and it controls the plant through main control variables such as primary air temperatures and flowrates or ram feeder throughput etc. Its parameters and setpoints may not only be determined through the Operator Terminal, but also by Auxiliary Control Systems (ACS) which further improve quality and stability of operation.

The main control variables either directly control certain parameters such as for example the steam flow to the primary air heater such that the correct primary air temperature is reached, or it controls Equipment Control Systems (ECS) which are in turn controlling various individual equipment functions to assure the desired operation. The DCS will for example ask the ECS of the grate and ram feeder to provide more or less waste to keep the steam flow to the turbine constant. But it lets the ECS do the detailed equipment control to feed, move and riddle the waste fuel by setting the stroke of all grate elements in the individual combustion zones. The ideal stroke pattern can be assigned to each individual grate element depending on waste properties and actual combustion profile. The optimum stroke frequency is preset for each grate module. For example, the grate modules in the main combustion zone have a higher stroke rate than those in the

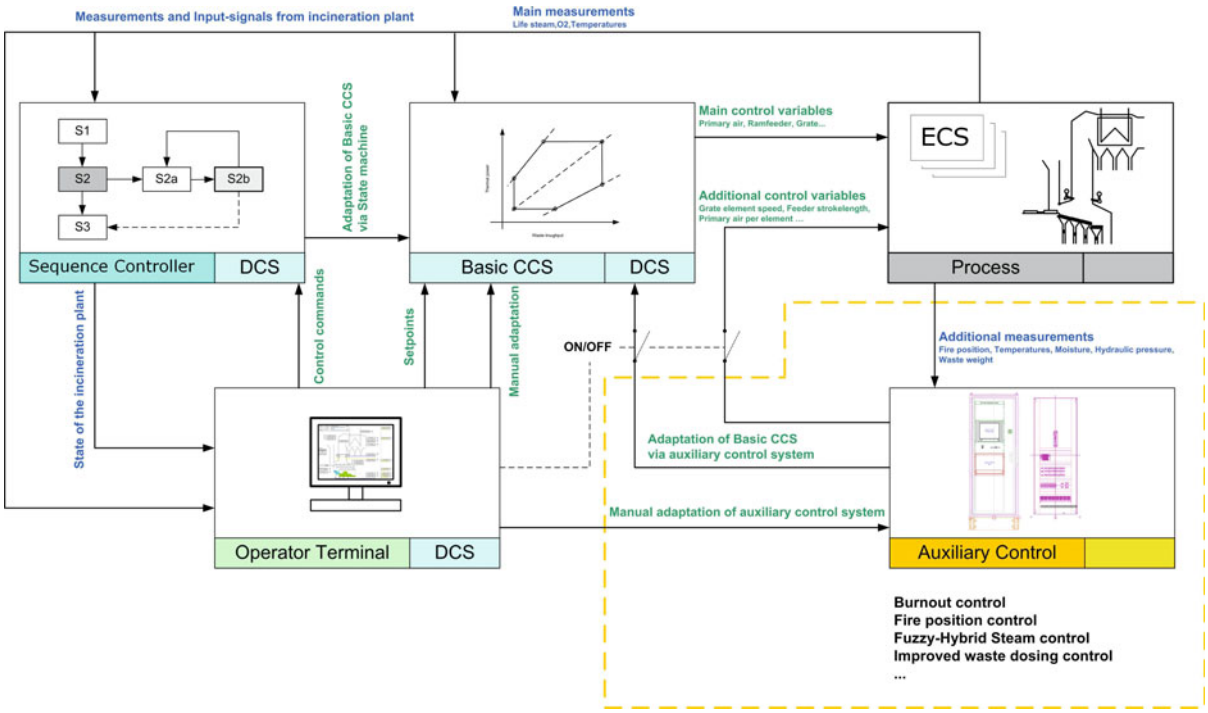

Hitachi Zosen Inova Technology. Figure 26
Main combustion control system architecture

burnout zone. For simple changes of the throughput the stroke rates for the entire grate can be uniformly increased or decreased without changing the relationship between the individual grate modules. If there is a change in calorific value and therefore in the combustion profile on the grate, the specific stroke rate for the individual grate zones can be adjusted by changing the frequency or length of strokes. This affects the travelling speed of the waste on the grate, but also the thickness of the waste layer on the grate, the stoking effect and therefore the combustion profile.

For an even more precise and automatic control of the combustion profile, specially for large grates and very inhomogeneous wastes one or more ACS can be installed. The Burnout Control or the Fire Position Control measure the location of the fire by means of pyro-sensors at various locations across the width and along the length of the grate. This allows to automatically adjust the stroke pattern locally on the grate if the waste properties are different on one side of the grate than on the other side. This further improves the burnout of the waste to even lower values. With the basic CCS one typically can only see that the waste properties have changed after the steam flow has already dropped or increased. An improved waste dosing control and fuzzy-hybrid steam control allow to better anticipate possible changes in the waste composition and to proactively change the control settings such that the steam flow to the turbine and therefore the power production constantly remains at the desired value.

Basic Control Functions The basic settings for the controlled equipment are set during design and adjusted during commissioning. These settings are valid for the desired operation point with mean waste properties. During normal operation, there may be two reasons why these settings have to be changed:

The operator needs to operate at a different operation point because he receives more or less waste or because he wants to deliver more or less electricity or steam.

The operator wants to stay at the same operation point, but the properties of the wastes change with time, for example, because the ratio between industrial and residential wastes changes or because

the waste is wetter due to heavy rain in the past days or similar.

The main parameter to be controlled is the produced steam flow, while keeping other parameters such as the temperatures and the oxygen content in the flue gases within the desired range. When the steam flow is below the desired value at a given load, the primary airflow below the grate is increased; simultaneously, the secondary airflow above the grate is decreased by the same rate. With this intervention, the combustion load is increased at constant total air supply. At the same time, the ram feeder and the grate stroke frequency are increased. As a result, the fire is intensified and more waste is fed to the grate. If the capacity is increased or if the oxygen concentration in the flue gas drops, the total combustion airflow is increased and the recirculated flue gas flow adjusted. In analogy, when the steam flow is higher than desired, the control interventions are reversed.

Hitachi Zosen Inova Navigator The CCS automates the complete combustion process in such a way that the operator has to select only the set point for the desired steam flow rate and an estimation of the calorific value of the present waste (calorific value adjustment). In case of a change of the waste qualities, all basic set points are simultaneously modified by means of the calorific value adjustment so that favorable combustion conditions are always given.

Using measured data and some minor assumptions, the thermal load from waste in the combustion diagram can be calculated (Fig. 27). The measured waste flow, at the crane, is used to calculate the actual calorific value and set the next operating point (short term, 3 h and 8 h average). The navigator screen is permanently updated.

While this screen allows the operator to see the past operating points, there is also a feature called "calorific value adjustment" in the CCS that allows the operator with one simple adjustment to adjust the system for an anticipated change of the future operating point. The CCS then correctly adjusts the many set points of all the relevant subsystems.

Additionally, manual intervention is possible allowing the operator to further optimize the combustion process if necessary. However, the Hitachi Zosen

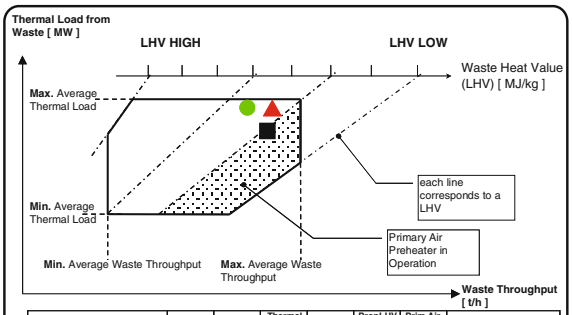

	Waste	Waste	Thermal Load	LHV	PropLHV (S12)	Prim.Air Temp.	
	[t]	[t/H]	[MW]	[MJ/kg]	[%]	[°C]	
▲ = Short Term Average	4,76	11,2	38,5	—	—	—	(not available)
● = 3 Hour - Average	34,7	10,4	39,2	9,4	– 16	164	(not available)
■ = 8 Hour - Average	86,9	10,9	38,0	8,3	– 28	—	(not available)

Hitachi Zosen Inova Technology. Figure 27
Navigator diagram

Inova CCS is designed so that the plant cannot be continuously operated outside the permissible range as defined by the combustion diagram.

Start-up Sequence Also start-up is automated in the CCS. This includes heating up the post-combustion chamber by means of the start-up burners following a given ramp (Fig. 28) until the temperature in the chamber reaches the required minimal temperature. Once this condition is met, the gate in the feed chute is opened to admit the waste onto the grate where it will start to burn immediately.

Shutdown Sequence After the waste feed is stopped, the temperature of the post-combustion chamber is kept above the minimal required temperature using the burners. When the grate is empty, the temperature in the post-combustion chamber is gradually and steadily decreased as shown in Fig. 29, until it is safe to start maintenance work.

Steam Boiler

General The purpose of the steam boiler is to transfer the heat from the flue gas to water and steam. The most frequent case is to produce superheated steam, as required in a steam turbine / generator to produce electricity. In the case where the recovered energy is used for heating only, a boiler can be designed to produce saturated steam only or heat water to be used in district heating.

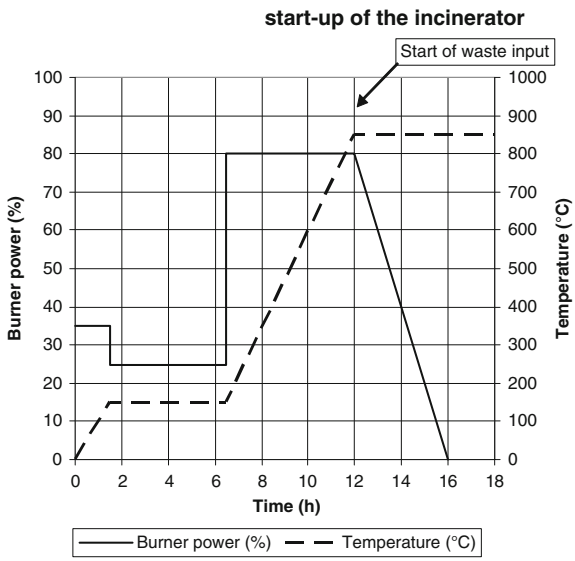

Hitachi Zosen Inova Technology. Figure 28
Typical start-up curve

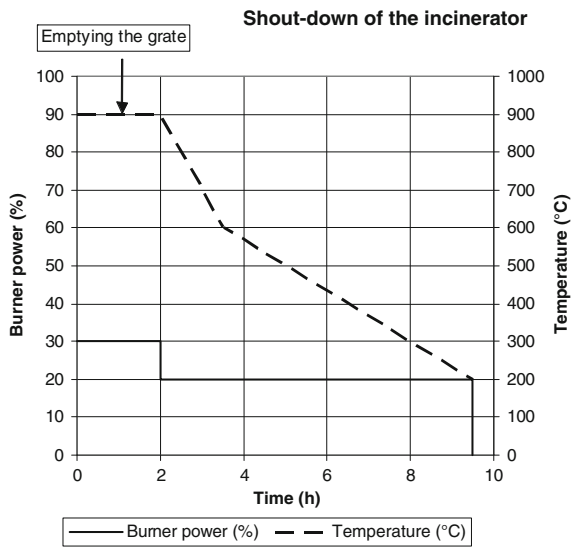

Hitachi Zosen Inova Technology. Figure 29
Typical shutdown curve

Description The Hitachi Zosen Inova steam boiler, in the example of the four-pass vertical boiler shown in Fig. 30, can be described by the following main functions it provides in the water–steam cycle:

- *Economizer* (*green bundles*): In this section, the pressurized feed water is preheated to close to boiling conditions and fed into the steam drum.

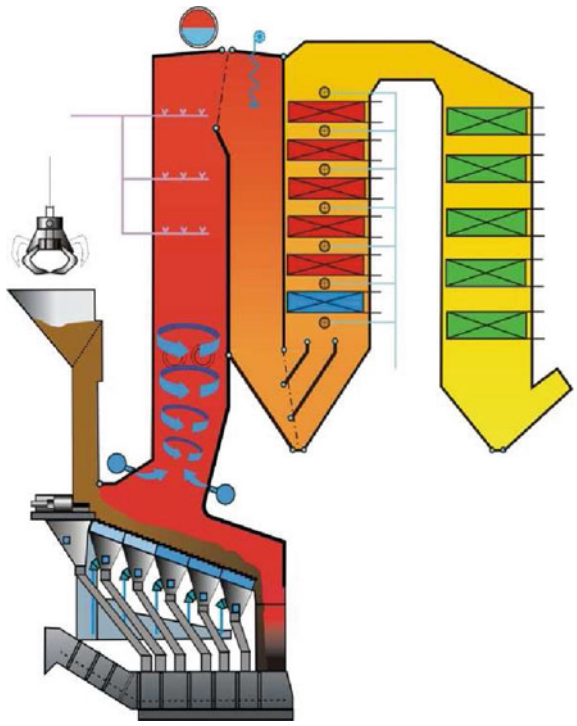

Hitachi Zosen Inova Technology. Figure 30
Typical four-pass steam boiler

- *Evaporator* (*blue bundles and all boiler walls*): In this section, water is recirculated from and to the steam drum. It is heated in the evaporator surfaces such that it partially evaporates. Steam is separated in the steam drum and water is recirculated again.
- *Superheater* (*red bundles*): In this section, the steam separated in the steam drum is further heated to desired conditions.

The steam boiler can also be described by its configuration in terms of the number and arrangement of passes. A pass is a section of the boiler in which the flue gases flow in the same direction. The boiler can be designed in various possible configurations. In the following, a four-pass vertical boiler is described in further detail. It consists of the following passes in which one or more of the above functions are performed:

- *First pass:* Vertical radiation pass made of evaporator membrane walls with refractory lining and/or Inconel cladding on flue gas side.

- *Second pass:* Vertical radiation pass made of evaporator membrane walls and possibly with additional evaporation bundle sections.
- *Third pass:* Vertical convection pass made of evaporator membrane walls as well as with bundles of superheater and evaporator sections.
- *Fourth pass:* Vertical convection pass with steel casing and bundles of economizer sections.

The steam boiler (passes 1–3) can be bottom or mid supported or even suspended. The fourth boiler pass is bottom supported. The steam drum is placed above the first boiler pass on the steel structure.

The first pass is located above the incinerator grate and consists of membrane walls. Since these are exposed to the hottest temperatures and to the fire, they have to be protected by refractory lining or inconel clading. The sidewalls of the boiler extend downward such that the walls on the side of the grate form an integral part of the first pass. The front and back walls of the first pass extend downward to create the sloped roofs above the grate. The differences of thermal expansion between the boiler and the grate as well as between the third and fourth pass are compensated by expansion joints.

Auxiliary Boiler Systems The steam drum is the central part of the steam boiler, where water and steam is separated and the water level and the steam pressure are monitored. It includes a feed water preheater coil as well as separating baffles or cyclones to efficiently separate water from the steam. It is of fusion-welded construction and fabricated from steel plate. It contains a manhole, hinged to open inward, as well as all necessary nozzles, connections, and openings required for operation, maintenance, and testing. All drum nozzles for instruments, valves, fittings, and tubes are welded to the drum.

Since the boiler load may vary and the boiler heating surfaces are subject to scaling, the uncontrolled superheater section may provide more or less superheating depending on load and conditions. To be able to control the superheated steam temperature at all conditions, one or two spray desuperheaters are installed between the various superheater sections. There, feed water is injected in order to accurately adjust the superheater steam temperature.

The superheated steam is collected in an outlet header where a pressure control valve and a stop valve are installed before the live steam pipe is directed toward the steam turbine.

Safety valves are provided on the steam drum and in the live steam pipe to protect the boiler from excessive pressures.

The cleaning of surfaces causes the ash to fall down from refractory, membrane walls or tube bundles. The ash is collected in the ash hoppers below each boiler pass and then removed via double gate or rotary valve to the ash collection system.

All necessary provisions for normal maintenance access are made. Access doors are placed where required on both sides of the boiler. Ample space is provided between each tube bundle for adequate inspection and cleaning. External platforms provide access to each door and all control instruments. Provisions are made so internal platforms can be installed at various boiler levels for inspection, cleaning, and maintenance during outages.

Boiler Cleaning

General A waste incineration boiler is inevitably exposed to high fly ash loads. Hence, the effectiveness of the heat exchanger surface is reduced during the operation time by fouling. The purpose of online cleaning of the heat exchange surfaces is to extend the operating period and reduce maintenance cost. This can be accomplished by various means. The main options are:

- Water shower cleaning
- Sootblowers
- Rappers

Description

Water Shower Cleaning A water shower cleaning system as shown in Fig. 31 can be installed for the online cleaning of the empty boiler pass. It enables an automatic cleaning of the membrane walls by means of water injection. The evaporation of the water on the dust layers results in sudden cooling and contraction of the ash layer which lets the ash layer crack and fall off.

The water shower system is not often used in the beginning of an operation campaign. During that phase, the clean surfaces of the evaporator sections in

pass 1 and 2 take more heat out of the flue gases than in the average. So less heat is available in the superheaters in the third pass and they may not reach the required superheated steam temperature at all conditions.

With proceeding of the operation campaign, it is used more and more often to assure that the flue gas temperatures at the inlet to the superheaters do not exceed design temperatures. This is usually about once per week at the end of the operating campaign. And it is used right before shutdown for manual boiler cleaning which makes the cleaning much easier and faster.

Sootblowers Sootblowers as shown in Fig. 32 are installed in before, after, and between bundles in a vertical boiler pass.

The areas of the tube bundles exposed to the direct sootblower spray are protected by stainless steel tube shields. Various types of sootblowers exist. A typical retractable-type sootblower has two opposite high-performance nozzles and is helically moved in and out of the boiler during a cleaning cycle. Between cycles it is located in a cavity of the boiler wall and cooled with a small air stream to avoid prolonged exposure to the high temperatures.

Sootblowers allow an effective online cleaning of tenacious fouling at heating surface banks with high flue gas temperatures. Sootblowers use superheated steam or compressed hot air as blowing agent because wet and moist steam can cause further caking of the fouling and cold air can cause corrosion if surface temperature of the sprayed area falls locally below the acid dewpoint of the flue gases.

Rappers Rappers are usually used in vertical tube banks installed in a horizontal boiler pass. One rod connected to each of the vertical tube rows penetrates the boiler wall. On the outside of the boiler this rod can

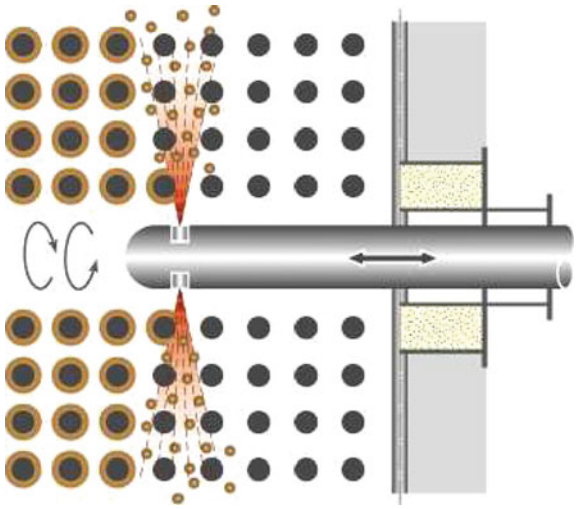

Hitachi Zosen Inova Technology. Figure 32
Retractable sootblower

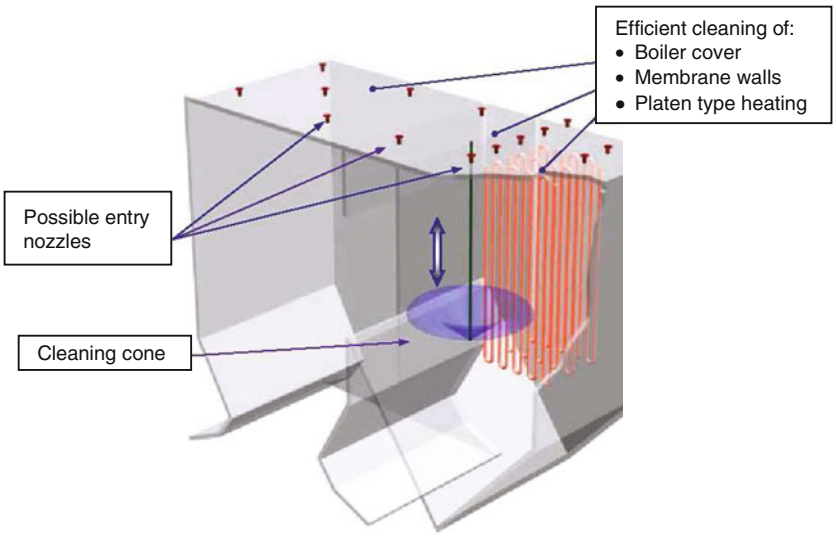

Hitachi Zosen Inova Technology. Figure 31
Typical water shower system

be hit with a hammer from time to time. The rod transmits the impact of the hammer to the heat exchanger tubes and creates a vibration such that the accumulated dust and scaling falls off. The key is to hit the bundle at the right place with the right force to achieve ideal vibrations and acceleration.

The hammering of the many heat exchanger tube rows is automated. Figure 33 shows a traveling rapping system which moves along the boiler and strikes each rod at a given interval and with a defined force.

Boiler Surface Protection

General The purpose is to protect the boiler surfaces from flame impingement and aggressive flue gas and boiler ash conditions. Usually, a combination of refractory lining and Inconel cladding is used.

Refractory Lining The refractory is different in various sections of the furnace (Fig. 34) and is optimized for:

- Proper ignition of waste
- Improved burnout of waste on the grate
- Protection of heating surfaces from furnace erosion
- Protect heating surfaces from high flue gas temperatures (corrosion protection)
- Achievement of high residence time of the flue gases at high temperatures for a complete burnout

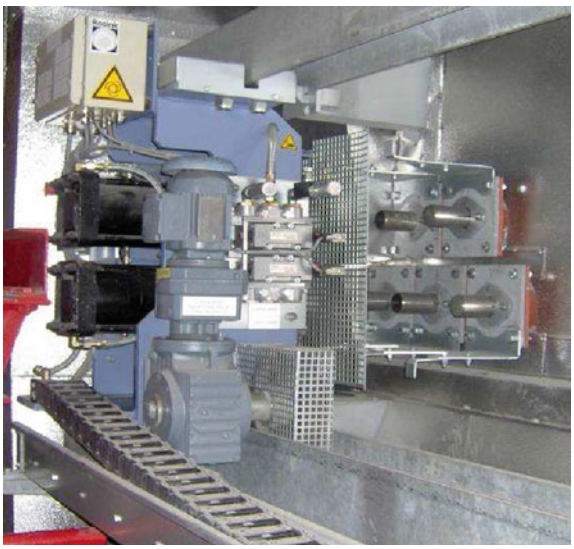

Hitachi Zosen Inova Technology. Figure 33
Automated rapper system

These requirements are satisfied by choosing appropriate materials and thickness of refractory in different zones.

Inconel Cladding Inconel cladding is one option to protect the steel surfaces of the boiler from the corrosive atmosphere of the flue gases after waste combustion. Its biggest advantage is that it protects the boiler tubes without reducing the heat transfer. Its main disadvantage is cost. This is why the design of the surface protection concept is always an optimization which has to be done in view of the waste properties and the plant owner's operation and maintenance philosophy. A welding robot applying an Inconel overlay to a boiler membrane wall is shown in Fig. 35.

Sampling Station

General The purpose of the sampling station is to monitor the water and steam quality at various locations in the boiler system (Fig. 36). Correct sampling

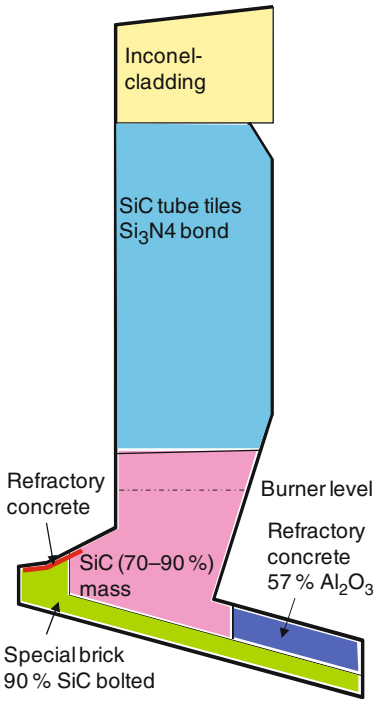

Hitachi Zosen Inova Technology. Figure 34
Surface protection concept in furnace and first boiler pass

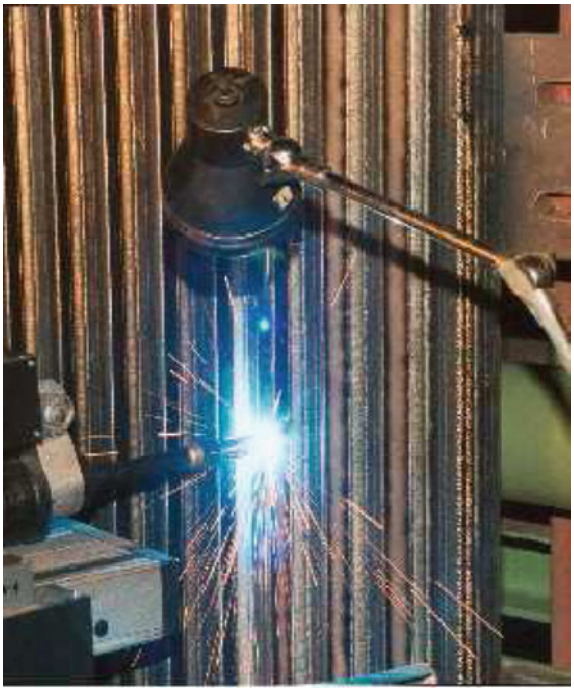

Hitachi Zosen Inova Technology. Figure 35
Welding roboter applying Inconel overlay to boiler tubes

Hitachi Zosen Inova Technology. Figure 36
Sampling station

and possible required adjustments prevent corrosion or other serious malfunction of the water side of the boiler or subsequent equipment.

Description The online sampling of a boiler is typically made to analyze the following fluids and parameters:

- Condensate (pH and conductivity)
- Boiler water (pH and conductivity)
- Steam (conductivity)
- Feed water (oxygen, pH, and conductivity)

To simplify analysis, all fluids are piped to an easily accessible location. Therefore, sampling station equipment contains a lot of piping, valves, and instruments, as well as heat exchangers to cool the fluids to temperatures suitable for handling.

Chemical Dosing

General The purpose of the chemical dosing system is to condition the water–steam cycle by the addition of chemicals such that required water and steam properties are maintained.

Description The water–steam cycle chemistry is controlled in accordance with the requirements in the relevant boiler codes and turbine manufacturers by chemical injection into the feed water, usually of ammonia solution and trisodium phosphate.

Ammonia is fed continuously into the feed water pipe between the feed water tank and the feed water pumps. Trisodium phosphate is fed continuously into the feed water pipe before the economizer of the boiler, but after the connecting pipes for spray water for the cooling of desuperheaters.

Turbine System

General The purpose of the turbine and generator system is to take the superheated steam produced by the boiler and create electrical energy.

Description The turbine system is a standard steam generator turbine package consisting of an extraction turbine, a generator with electrical equipment and

Hitachi Zosen Inova Technology. Figure 37
Typical steam turbine and generator

protection, a lubrication oil system including oil filter and cooler and local control panel (Fig. 37).

The turbine will typically have one or two steam extraction points. The first is typically around 3–5 bars (about 45–75 psi), which will provide steam to various internal, and possibly to external steam consumers via the low-pressure steam (LPS) system. A second extraction point is made if heat is used by a heat consumer at higher temperature. This extraction point is typically around 10–25 bars (150–375 psi), which will provide steam to external and possibly to some internal steam consumers via the medium pressure steam (MPS) system. If there is no second extraction point, any possible internal MPS consumers will be fed with high-pressure steam directly from the boiler. The exhaust steam from the turbine is directed to the condenser at a pressure as low as possible with prevailing ambient conditions.

During normal plant operation, the pressure control in the live-steam header will be performed by the steam turbine's pressure control valve. In case of a trip of the steam turbine, a controlled live-steam release to the condenser via the turbine bypass system will be initiated, in order to prevent the boilers' safety valves from relieving pressure. In the event that the steam turbine's capacity (typically 110% of the nominal load) is exceeded, the turbine bypass system is also activated, which will then take over pressure control in the main steam header. The turbine bypass system is also active during start-up and shutdown of the boiler in order to minimize any water losses. If the controlled live-steam release or the turbine bypass does not work, steam is blown off to the air through safety valves.

Condenser

General The purpose of the condenser is to condense the turbine's exhaust steam during normal operation. However, during start-up, shutdown, and/or upset conditions, the purpose of the condenser is to condensate the entire steam load.

Condenser Types Condensers can typically be one of the following three types:

- Non-evaporative water-cooled condenser
- Evaporative water-cooled condenser
- Air-cooled condenser

The lower the condensation temperature which can be achieved, the higher is the electrical energy efficiency of the turbine and the EfW plant.

A once-through non-evaporative water-cooled condenser will reach the highest efficiency. However, it is rare today to find a large enough body of water which can absorb the cooling needs of a power plant seldom today there is a large enough water carrier close to the EfW plant which is allowed to be heated up for cooling of a power plant. This is why this solution cannot be realized very often.

An evaporative water-cooled condenser reaches average efficiencies of the three proposed solutions. Its downside is the requirement of treated water which is not available everywhere in sufficient amounts and the frequent formation of a vapor plume which is not welcome everywhere.

So an air-cooled condenser as shown in Fig. 38 remains as the least energy-efficient option which however also causes negligible impacts to the environment and the neighborhood.

Description of an Air-Cooled Condenser Large air fans blow ambient air across the steam condenser tubes to cool them.

The condenser is designed both for the maximum steam flow from the turbine in normal operation as well as for the total plant steam flow in the turbine bypass case.

Hitachi Zosen Inova Technology. Figure 38
Air-cooled condenser

Air or other incondensable gases entering the condenser with the steam are extracted from the steam space of the condenser by a two-stage steam jet ejector. The condensed steam is returned to the condensate tank. The air extracted by the ejector is vented to the atmosphere. The driving steam for the ejector is taken from the HPS header.

Cooling System

General The purpose of the cooling system is to adequately cool the turbine and generator's lubrication system.

Description The cooling system is a closed loop cooling system that provides cooling water to the turbine oil cooler, the generator air cooler, the compressor cooling, and the sampling coolers. In an air cooler, the excess heat from the cooling water is transferred to the ambient air supplied by fans. The air cooler consists of different small cooler modules. Each cooler module has a fan with electrical motor.

In case of partial-load operation and/or low ambient air temperatures, the cooling-water outlet temperature can be adjusted by taking some of the cooler modules out of operation. The cooling water is circulated by means of redundant cooling-water circulating pumps. The cooling-water system is filled and/or drained by the cooling-water system filling pump. It is important to keep the pressure constant in the system and this is done by means of a diaphragm pressure-compensating tank equipped with a nitrogen buffer.

Hitachi Zosen Inova Technology. Figure 39
Deaerator and feed water tank

Feed Water System

General The purpose of the feed water system is to provide the boiler and superheaters with the required feed water flow and pressure.

Description The feed water system consists of the deaerator with feed water tank (Fig. 39), the redundant feed water pumps (Fig. 40), and all the associated piping and valves. The feed water tank is sized adequately to provide enough storage volume to provide feed water to the boiler for a defined time.

High-Pressure Steam System

General The purpose of the high-pressure steam (HPS) system is to deliver HPS to the in- and out-of-plant consumers as required.

Description The boiler produces high-pressure superheated steam which is sent to the turbine/generator to create electrical energy during normal operation. In order to compensate for possible variations in load, the steam is first sent to the HPS system. The HPS system typically consists of the live steam piping from the boiler to the HPS header, the HPS header

Hitachi Zosen Inova Technology. Figure 40
Feed water pump

Hitachi Zosen Inova Technology. Figure 41
HP steam header

(Fig. 41), the piping from the HPS header to the turbine, the piping from the HPS header to the air-cooled condenser via steam pressure reduction station of the turbine bypass, the piping from the HPS header to the LPS header via the steam pressure reduction station (HPS/LPS), and the piping from the HPS header to the main and start-up air extraction vacuum pumps. In addition, there may be other HPS consumers as per plant or external steam consumer requirements.

Low-Pressure Steam System

General The purpose of the low-pressure steam (LPS) system is to deliver LPS to the in- and out-of-plant consumers as required.

Hitachi Zosen Inova Technology. Figure 42
LP steam header

Description The LPS system is typically set at approx. 3–5 bars (45–75 psi) pressure. The system supplies steam to the feed water tank with deaerator, to the air preheater and possibly to external LPS consumers, such as a district heating system.

If the turbine is in operation, LP steam is taken from the turbine extraction point to the LPS header. If the turbine is not in operation, the LPS is supplied from the HPS header via the HPS/LPS reduction station. The LPS system consists of an LPS header (Fig. 42), piping from the turbine extraction to the LPS header, piping from the HPS header via the steam pressure reduction station to the LPS header, and piping from the LPS header to the internal users.

Condensate System

General The purpose of the condensate system is to collect and treat all condensates which arise in the plant. The more clean condensates can be recovered, the less demineralized water has to be made up.

Description The condensate system consists of a main condensate tank, the redundant condensate pumps, as well as the connection to all condensate sources. These are typically the main condenser via its condensate pumps, steam ejector condenser, as well as all condensate traps of the internal steam systems and heaters. To recover additional energy contained in the

condensate from HPS systems and heaters, high-pressure condensate is first flashed and the generated LPS is utilized in the plant.

Demineralized Water System

General The purpose of the demineralized water system is to clean the available raw water to obtain the required purity and chemistry required for a steam boiler and turbine system in order to prevent corrosion and equipment damage. Additional water purification steps may be needed if the raw water source for the EfW plant is of low quality.

Description A demineralized water system as shown in Fig. 43 is designed for a continuous supply of demineralized water for the boiler. It is designed with sufficient capacity and redundancy. This includes redundancy of all components with the exception of piping and storage tanks.

The typical demineralized water system consists of a raw water tank, a cation exchanger, an anion exchanger, a regeneration unit, a neutralization unit, a demineralized water storage tank, and demineralized water pumps.

Nitrogen Oxides (NO_x) Reduction Measures

General Nitrogen oxides (NO_x, mainly consisting of NO and NO_2) reduction includes multiple measures with the goal to have lowest concentrations of nitrogen oxides in the flue gases leaving the plant. Nitrogen in the combustion air and even more nitrogen chemically bound in the waste will partially react with the oxygen at combustion temperatures and form NO_x.

Hitachi Zosen Inova Technology. Figure 43
Demineralized waste system equipment

Primary measures have the goal to minimize the formation of NO_x. The flue gas recirculation presented above is a powerful means to achieve this goal. Generally the reduction of the oxygen level in the flue gases and in particular the oxygen level achievable using flue gas recirculation has resulted in uncontrolled NO_x level in Hitachi Zosen Inova's latest plants of only about half the levels of plants built in the 1970s.

Secondary measures have the goal to reduce NO_x which has already been formed during combustion. The most known measures include a reaction of ammonia with the NO_x to form nitrogen and water vapor.

$$2NO + 2NH_3 + O_2 \rightarrow 2N_2 + 3H_2O$$

$$2NO_2 + 4NH_3 + O_2 \rightarrow 3N_2 + 6H_2O$$

This reaction can technically occur at different temperature ranges:

- At high temperatures, as a spontaneous and selective reaction, referred to as the selective non-catalytic reduction (SNCR)
- At lower temperatures, only with the aid of a catalyst, referred to as the selective catalytic reduction (SCR)

Selective Non-catalytic Reduction (SNCR)

Overview The SNCR process is based on the principle of injecting an ammonia-containing reagent into the furnace where the temperature range is between 850°C (1,560°F) and 950°C (1,740°F). The reagent is typically an aqueous ammonia or urea solution. The required temperature range exists in the upper part of the furnace (the first pass of the boiler). However, the actual furnace temperature at any given injection point may vary a lot due to typically varying combustion conditions on the grate caused by highly varying waste properties, by load changes, or by fouling of the boiler walls. If actual temperatures become too low, the reaction is not efficient any more and the ammonia slip at the stack is increased. If actual temperatures become too high, the following secondary reactions become significant and actually

ammonia is decomposed or burned leading to highly increased reagent consumption and NO_x emissions.

$$4NH_3 + 5O_2 \rightarrow 4NO + 6H_2O \text{ at high temperatures}$$

$$4NH_3 + 3O_2 \rightarrow 2N_2 + 6H_2O$$

The key of a good SNCR process is to inject the reagent at exactly the right temperature level and to mix it evenly into the flue gases.

The Dynamic NO_x Reduction (DyNOR®) System

CFD calculations show that flue gases do not mix well perpendicularly to the flow direction [4]. Therefore, the conditions in a vertical segment of the first boiler pass are predominantly defined by what happens on the grate at the bottom of that segment. And since the waste is so inhomogeneous, this can mean that at the same location the short-term temperature changes can be 100°C (180°F) and more.

The main features of the Hitachi Zosen Inova DyNOR® system (Fig. 44) are the following:

- The first boiler pass is divided into several vertical segments, depending on the size of the boiler.

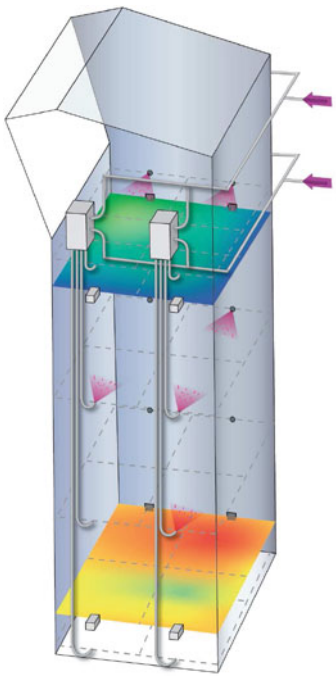

Hitachi Zosen Inova Technology. Figure 44 DyNOR® setup

- Three or four injection levels are determined and on each level one or more injection nozzles are dedicated to each segment.
- In each vertical segment, a fast infrared temperature sensor measures the instantaneous temperature.
- For each vertical segment, the controller calculates the optimum injection level at each point in time.
- For each vertical segment, a fast distributor directs the reagent and the atomizing medium without time lag to the nozzles closest to the optimum injection level.

As with conventional SNCR systems, the configuration of the nozzles is important to cover the entire cross section of the boiler or segment and assure an even distribution of the reagent across the whole cross section. Other measures that improve the performance of the SNCR system are:

- Keeping steady combustion conditions on the grate with a high-quality combustion control system automatically adjusting to the varying qualities of the waste incinerated (see section "Combustion Control System")
- Good distribution and mixing of secondary air and recirculated flue gases which level out oxygen and temperature profiles as achieved by a swirl flow pattern (see section "Flow Optimization with Swirl Injection")
- No unnecessary internals in the SNCR reaction zone which would disturb the flow pattern and therefore compromise the even distribution of reagent

Selective Catalytic Reduction (SCR)

Overview In the SCR method, the conversion of nitrogen oxides is assisted by a catalyst and can take place at temperatures between about 180–350°C (350–650°F). The reaction is up to typically 90% efficient without stoichiometric overconsumption of ammonia, and thus only with minimum ammonia slip at the stack. As a secondary benefit, dioxins and furans are also oxidized on the catalyst. An undesired secondary reaction is the conversion of SO_2 to SO_3, which can then further react with ammonia to form solid ammonium sulfate salts which deactivate the catalyst. The reaction will also happen at lower or higher temperatures, but secondary effects such as

catalyst deactivation and scaling or energy efficiency considerations have practically led to the mentioned temperature range.

At operating temperatures below about 220°C (430°F), the catalyst needs to be periodically regenerated, during operation. In order to evaporate possible salt deposits from the surface of the catalyst modules, the flue gas entering the catalyst is heated up to about 320°C (610°F) over a period of about 6 h.

To implement an SCR process (Fig. 45) in an EfW plant, the following components are typically needed:

Gas–Gas Heat Exchanger A gas–gas heat exchanger is only needed in tail-end configuration. The flue gases entering the catalyst have to be reheated. The most economic way to reheat flue gases is by cooling down flue gases coming from the catalyst by means of a gas–gas heat exchanger. This can be done by a plate or tube-type steel heat exchanger. An external heat source, preferably a steam preheater, then only has to compensate the gas–gas heat exchanger temperature driving force.

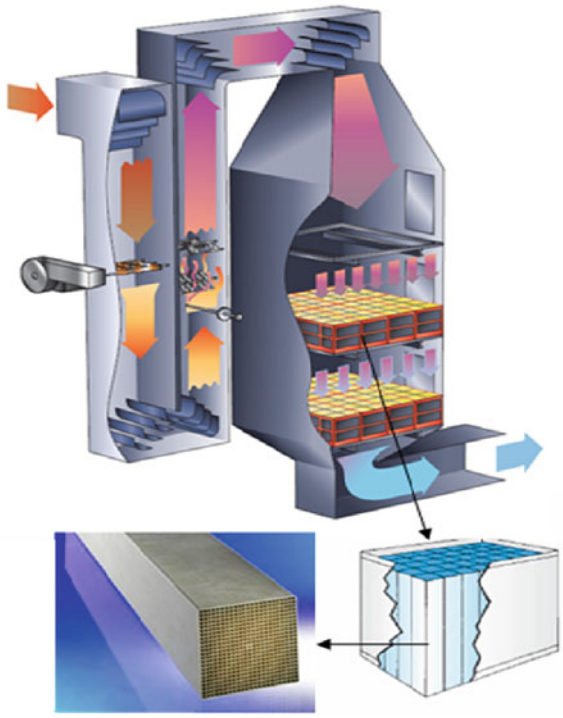

Hitachi Zosen Inova Technology. Figure 45
SCR reactor with layers, catalyst module, and element

If flue gases have to be reheated after a wet scrubber, the cold heat exchanger surfaces have to be protected against corrosion.

Steam Preheater Final preheating can be done with a steam–gas heat exchanger. Steam from the boiler steam drum is typically between 40 and 60 bar (600–900 psi) which allows to heat flue gases to a temperature of about 220–250°C (430–480°F). The steam/gas preheater is a self-supported, flue gas-tight, welded structure made up of sheet-metal sections and equipped with peripheral frame into which the steam bundles can be inserted.

Duct Burner If steam is not available or if the flue gases have to be heated above the temperature range that is practical for a steam preheater, for example, for regeneration, the gas is heated with a duct burner.

Ammonia Injection and Distribution Ammonia-containing gas or solution is injected into flue gas duct upstream of the catalyst. The turbulence generated in a static mixer installed downstream the ammonia injection assures a good distribution of the ammonia in the flue gas and a homogeneous velocity, temperature, and concentration profile. Since in the catalyst there is virtually no further mixing, best reaction efficiency and lowest ammonia slip is heavily dependent on the conditions prior to entering the catalyst.

Catalyst Reactor The reactor is made as a self-supported, flue gas-tight, welded, rectangular steel casing with provisions to hold the catalyst modules. Within the reactor, the catalyst is typically arranged in 1–3 layers and space is provided for a spare layer.

The catalyst modules are ready-to-install steel cases containing the catalyst elements. Depending on the cross section of the reactor, a layer contains several modules. The height of one layer is typically 0.5–1 m (1.5–3 ft). Between the layers there is about 2 m space for access. Depending on the possible dust load in the flue gases, sootblowers are installed upstream of each layer (Fig. 45).

Typically, a plate or honeycomb-type catalyst consisting of TiO_2 (titanium dioxide) support material plus V_2O_5 (vanadium pentoxide) and WO_3 (tungsten trioxide) active substances is used. The channel pitch of a typical SCR catalyst is only a few millimeters and is

one of the important design criteria. The smaller the pitch the more surface there is per catalyst volume, however, the bigger is the risk of plugging.

Acid Gas Removal

General Acid gases such as hydrogen chloride, hydrogen fluoride, sulfur dioxide, and sulfur trioxide are formed when wastes containing chlorine, fluorine, and sulfur are burned. Removal of acid gases involves the use of an alkaline reagent, which reacts with the acid and forms a nonvolatile salt, which in most cases has to be disposed of. With the example of hydrated lime as the reagent, the following simplified reactions take place:

$$Ca(OH)_2 + H_2O + SO_2 = CaSO_3 + 2H_2O$$

$$Ca(OH)_2 + H_2O + SO3 = CaSO_3 + 2H_2O$$

$$CaSO_3 + 1/2O_2 = CaSO_4$$

$$Ca(OH)_2 + 2HCl = CaCl_2 + 2H_2O$$

$$Ca(OH)_2 + 2HF = CaF_2 + 2H_2O$$

$$Ca(OH)_2 + 2HF = CaF_2 + 2H_2O$$

$$Ca(OH)_2 + CO_2 = CaCO_3 + H_2O \text{ (unwanted)}$$

Depending on the physical state in which the reaction takes place, three main types of processes are differentiated:

- Wet: The flue gases are cooled down to saturation temperature in the process and the reaction takes place in an aqueous solution or slurry of the reagent.
- Semi-wet or semidry: Semi-wet means the reagent is injected as an aqueous solution or slurry. Semidry means the reagent is injected as a dry powder, but is subsequently conditioned by a separate water injection. However, in both cases, the water evaporates in the process so the reaction products are removed as a dry powder while the water vapor stays in the flue gases. The flue gas temperature is controlled in the process by the amount of water added.
- Dry: The reagent is injected and the reaction products are removed as a dry powder. Temperature control happens upstream of the process.

While Hitachi Zosen Inova offers all the above processes and even combinations of such processes, the following detailed description focuses on the HZ Inova Semidry FGT process, which is one of the most efficient and widely used acid gas removal processes in the EfW sector.

Description of the HZ Inova Semidry FGT Process

Process The flue gases are brought into intensive contact with the reagents in a fluidized bed reactor. Unused reagents and reaction products entained with the flue gases from the reactor and collected in the downstream fabric filter. A large portion of the solids removed in the filter are recirculated and reinjected into the reactor in order to optimize the utilization of the reagents. A small amount is discharged.

The HZ Inova Semidry FGT process (Fig. 46) has the following advantages:

- Highly efficient reaction due to high turbulence and good mixing in the reactor and conditioning water addition to the reaction zone
- High flexibility relative to load changes and contaminant peaks due to the large amount of reagent in contact with the flue gas at any time
- Optimized use of reagent due to solids recirculation
- High availability due to simple construction and no moving parts

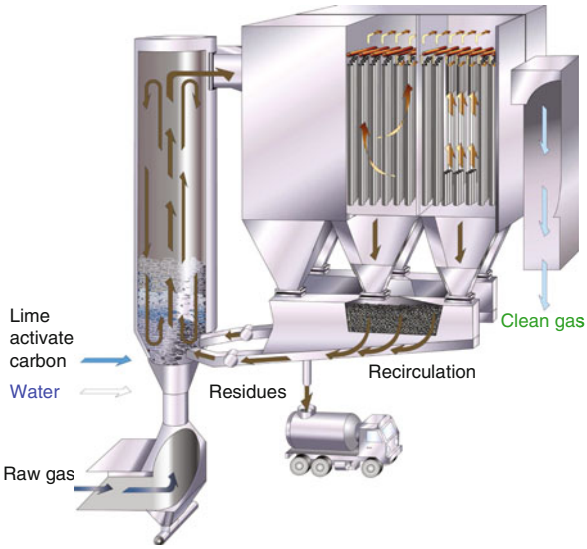

Hitachi Zosen Inova Technology. Figure 46
Hitachi Zosen Semidry FGT process schematic

Process Control The HZ Inova Semidry FGT process has three control loops, which regulate the process to achieve low emissions and minimize the consumption of hydrated lime.

The first loop continuously controls the pressure drop across the fluidized bed and maintains fluidized bed level constant by adjusting the flow of recirculated solids.

The second control loop controls the flue gas temperature at the outlet of the reactor by regulating water injection at the bottom of the fluidized bed (Fig. 47).

The third loop controls the acid gas emissions at the stack by regulating the flow of fresh hydrated lime to the reactor (Fig. 48).

The HZ Inova Semidry FGT process is automatically controlled by the plant DCS including sequences for start-up, normal shutdown, and emergency shutdown.

HZ Inova Semidry Reactor The flue gas enters the reactor centrally from below through a venturi-type restriction. Therein, the flue gas velocity is high enough to ensure that all solids are entrained into the reactor or prevented from falling down against the flue gas flow. The fluidized bed is sustained in the reactor by larger particles that are kept in suspension by the upward flowing flue gas. Smaller particles and the flue gases exit the reactor laterally at top of the reactor. Depending on the flow pattern formed at the top of the reactor, a part of the solids will sink back to the bed along the wall where the velocities are lower. The flue gas has a mean residence time of approx. 3 s in the reactor.

The injection ports for hydrated lime, for other reagents, for the recirculated solids, and for the water are located in the conical inlet of the reactor.

Recirculation Conveyor In order to form a fluidized bed and to fully utilize the reagents, the largest part of the solids separated inside the fabric filter is circulated back to the reactor via a moving bed conveyor as shown in Fig. 49. Fluidizing air from special blowers is injected through the bottom of the conveyors. This ensures the steady flux and keeps the solids in a permanent motion thus preventing the formation of deposits.

Water Injection Lance The water is injected through a lance with a specially developed hydraulic nozzle which atomizes the water to the required droplet size of about 30–100 μm. The nozzles are equipped with an automatic cleaning system consisting of a rubber cap which can be bloated periodically with pressurized air in order to break off possible deposits (Fig. 50).

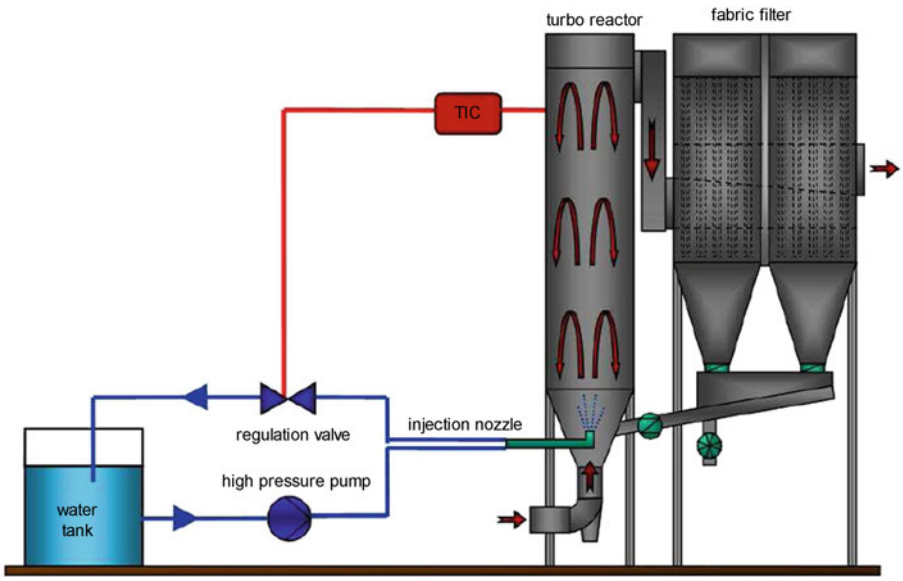

Hitachi Zosen Inova Technology. Figure 47
Temperature control loop

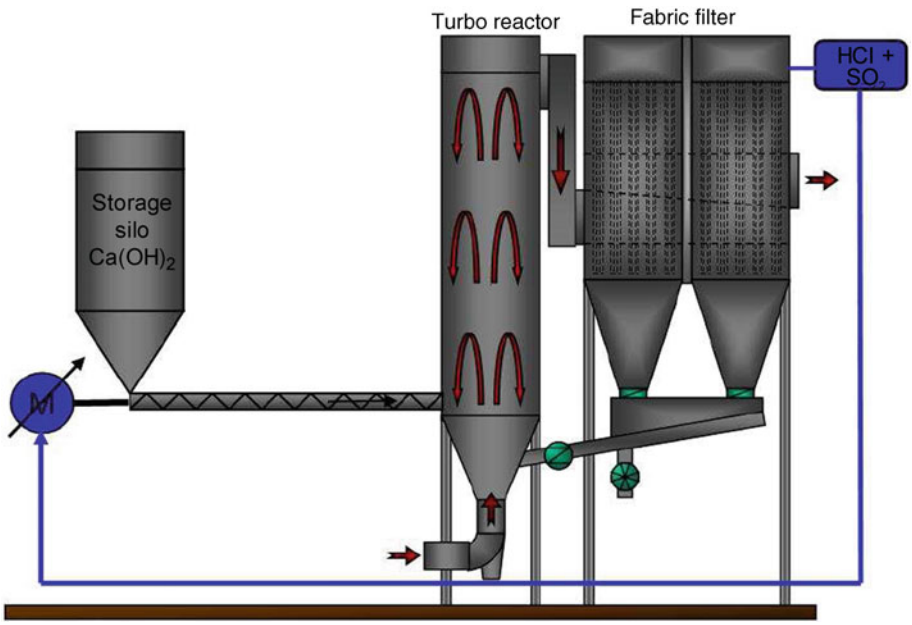

Hitachi Zosen Inova Technology. Figure 48
Emission control loop

Hitachi Zosen Inova Technology. Figure 49
Reagent recirculation conveyor and residue discharge

High-Pressure Water System Water for injection is supplied from the head tank via a high-pressure pump at about 30–40 bar (450–600 psi). An example of the HP water system equipment is shown in Fig. 51. The amount of injected water is controlled by a valve in the return line to the head tank.

As long as the water does not contain solids incompatible with the injection nozzle, any type of water can be injected. This is often used to safely dispose of contact or wash water collected during such operations. This allows EfW plants to be effluent free.

Volatile Heavy Metal and Organic Component Removal in the HZ Inova Semidry FGT Process
Apart from the chemical reactions between the reagent and the acid gases, the immense surface of the large amount of reagent particles also serves to adsorb other contaminants. In order to enhance the adsorption of volatile heavy metals, predominantly mercury, and volatile organics, such as dioxins and furans, activated carbon or lignite coke is also injected into the reactor. Only small amounts of such an additive assure, due to the good mixing and the high solids recirculation rate in the HZ Inova Semidry reactor, that most such contaminants are safely removed.

Fabric Filter

General The purpose of the fabric filter (Fig. 52) is to separate the ash particles in the flue gas as well as the reaction products from the HZ Inova Semidry reactor from the flue gas.

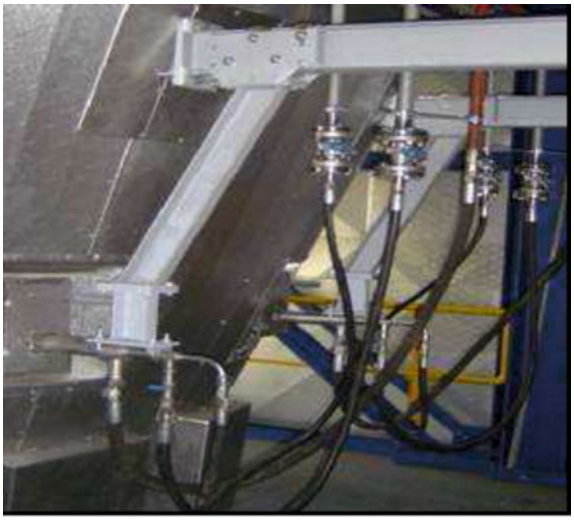

Hitachi Zosen Inova Technology. Figure 51
HP water skid

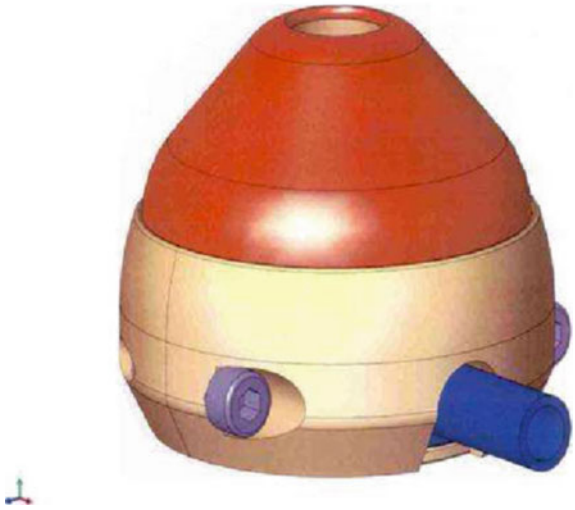

Hitachi Zosen Inova Technology. Figure 50
Water injection lance and nozzle

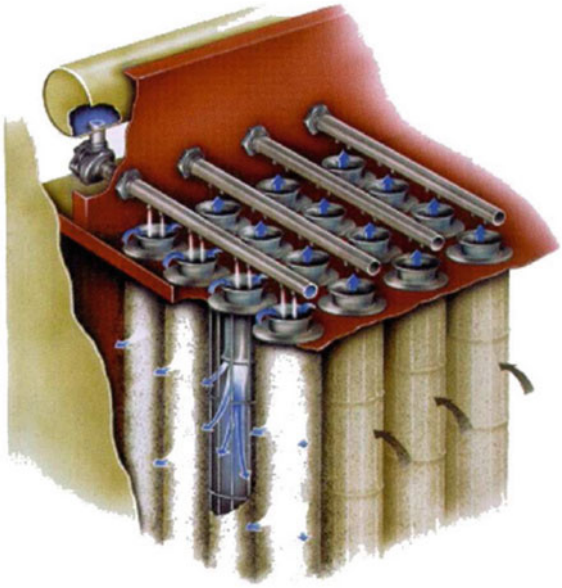

Hitachi Zosen Inova Technology. Figure 52
Filter chamber

Description The fabric filters are used for the separation of solids from gases. The separation is a physical process where the solids are filtered on the surface of a gas-permeable fabric. Due to the intensive contact of the flue gas and the adsorbents in the filter layer, the removal of pollutants from the flue gas is also further improved.

The fabric filter consists of several filter chambers into which the total flue gas stream is divided up. Each chamber can be isolated from the flue gas stream in case of a leakage in the filter material. The flue gases enter into the respective filter chamber and are deflected by a distributor panel to assure a uniform distribution of the gases through the filter and separate a large part of the solids carried with the flue gas. The gases flow around the outside of an array of the filter bags suspended in the chamber. Then they pass through the filter media, which are supported on a wire cage, and are collected from the inside of the filter bags

through the top of the filter chamber into a common clean gas duct.

Due to the flow characteristics induced by the chamber geometry as well as the pressure drop, the flue gas passes uniformly through the filter bags. This causes a uniform deposition of the solids on the outside of each individual filter bag. These need to be cleaned when solids layer on the bags becomes too thick and the pressure drop across the filter becomes too large (Fig. 53). This happens in an automated process. The solids are purged by suddenly inflating the bags with pulses of compressed air from the clean gas side. The filter bags are inflated for a short time which breaks off the solid layer on the outside. These fall down into the hoppers below the filter bags, from where they are transported away by the recirculation conveyor. The hoppers of the fabric filter can be isolated from the pneumatic conveyors by means of manually operated slide gate valves.

The cleaning air is supplied via compressed air reservoirs (one per filter chamber). From there it is distributed by a series of nozzle lances to each row of filter bags.

The fabric filter is equipped with differential pressure, temperature, and level-measuring instruments. The devices assure the supervision of the filter operation and the detection of possible malfunctions.

On top of the clean gas chamber, there is an accessible platform with complete enclosure – the filter penthouse. It is dimensioned such that there is enough room to install and remove bags from the fabric filter via walk-in plenum to the clean gas chamber.

In order to prevent deposits of and corrosion by the hygroscopic and corrosive reaction products at cold temperatures, the fabric filter hoppers are heated with electric heaters during start-up and shutdown.

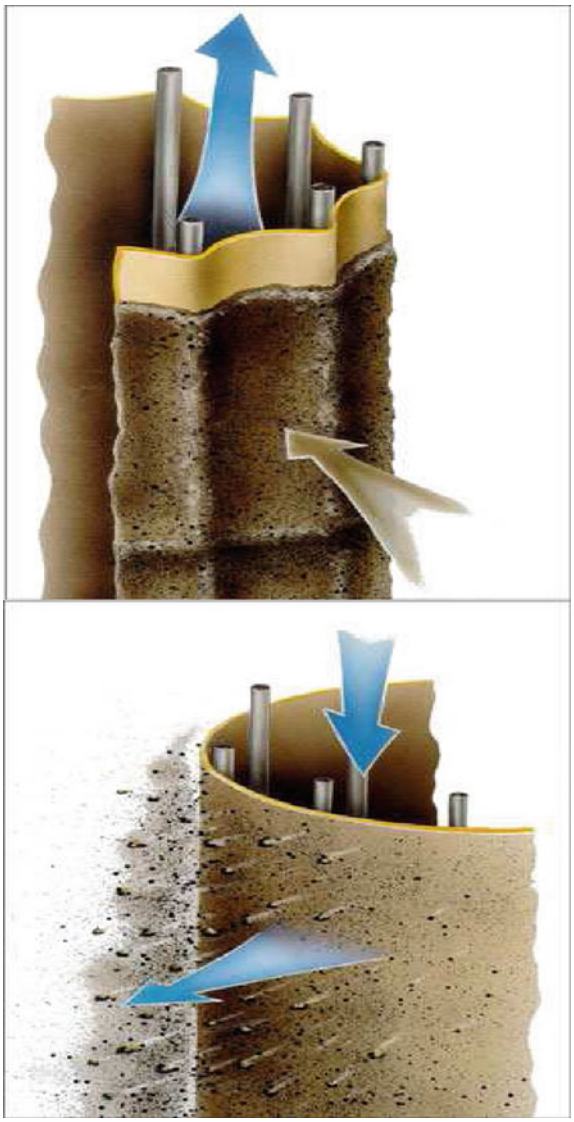

Hitachi Zosen Inova Technology. Figure 53
Filter bag during operation and cleaning

Additive Systems

General The purpose of the additive feed system as shown in Fig. 54 is to store and transport additive (reagents and sorbents) to the HZ Inova Semidry reactor.

Reagent System (Hydrated Lime) The reagent silo typically contains a few days' to a weeks' supply. The discharge from the silo is ensured by a mechanical discharge and dosing system. Then the hydrated lime is conveyed to the reactor pneumatically and injected as dry powder together with the transport air directly into the HZ Inova Semidry reactor. Solids dosing and transport systems are preferably designed redundant since they assure compliance with the plant's emission limits.

The concentrations before and after the flue gas treatment system of the lead acid gas component are used to

Hitachi Zosen Inova Technology. Figure 54
Reagent and residue silos

control the flow of hydrated lime. The hydrated lime dosing and transport system is dimensioned such that also expected peaks of pollutants can be safely treated.

Sorbent System (Activated Carbon) The sorbent storage can be a silo or a big bag, depending on the size of the plant. It typically contains a few days' to a weeks' supply. The discharge from the storage is ensured by a mechanical discharge and dosing system. Then the activated carbon is conveyed to the reactor pneumatically and injected as dry powder together with the transport air directly into the HZ Inova Semi-dry reactor. Solids dosing and transport systems are preferably designed redundant since they assure compliance with the plant's emission limits.

Hitachi Zosen Inova Technology. Figure 55
ID-fan with thermal and noise insulation

The amount of activated carbon to be injected into the reactor depends on the expected concentrations of volatile organics (dioxins/furans) as well as volatile heavy metals (mercury). The quantity of activated carbon per volume of flue gas is set during commissioning and annual emission testing.

Induced Draft Fan

General The purpose of the induced draft fan (ID-fan, Fig. 55) is to maintain a negative draft in the combustion chamber and flue gas cleaning system and then to push the flue gas through the stack.

Description The ID-fan is controlled to keep the furnace pressure constantly a little below atmospheric. Since the ID-fan is the largest electrical consumer in the plant, this is done by means of a variable speed drive which gives the best energy efficiency for this task.

The fan is equipped with openings for inspection and cleaning purposes. The fan and its drive are mounted on a common concrete frame structure designed to absorb and dampen vibrations. Bearing temperature and vibrations are constantly monitored.

Emissions: Continuous Emission Monitoring System

General The purpose of the continuous emission monitoring system (CEMS) is to monitor purity of the flue gas exiting the stack and to provide signals to the various control loops of the air pollution control systems.

Flue Gas Quality The following table shows European and US standard emission limits as well as a range of typical values achieved in various Hitachi Zosen Inova plants (Table 1).

While all legal emission limits can be safely kept, it is also possible to design plants which lead to substantially lower emissions as required by the referenced national limits. However, this is often a factor of the waste composition and of the complexity of the air pollution control equipment – thus of the cost which a region is ready to spend for responsible waste treatment.

Hitachi Zosen Inova Technology. Table 1 Typical Emission Limits and Hitachi Zosen Inova EfW Plant emission data

	EU		USA		Hitachi Zosen INOVA	
	(1) (3)	(2)	(1)	(2) (4)	(1) (13)	(2) (13)
CO	50 mg/Nm^3	56 ppmv	89 mg/Nm^3	100 ppmv	10–50	11–56
TOC (5)	10 mg/Nm^3	13 mg/scm	–	–	1–10	1.3–13
Particulate	10 mg/Nm^3	13 mg/scm	15 mg/Nm^3	20 mg/scm	1–10	1.3–13
HCl (6)	10 mg/Nm^3	8.6 ppmv	29 mg/Nm^3	25 ppmv	1–10	1.3–13
HF	1 mg/Nm^3	0.9 ppmv	–	–	0.1–1	0.09–0.9
SO_2 (7)	50 mg/Nm^3	24.5 ppmv	61 mg/Nm^3	30 ppmv	5–50	2.5–24.5
NO_x as NO_2 (8)	200 mg/Nm^3	136 ppmv	220 mg/Nm^3	150 ppmv	40–200	27–136
NH_3 (8)	10 mg/Nm^3	18.5 ppmv	–	–	1–10	1.8–18
Hg (9)	0.05 mg/Nm^3	0.065 mg/scm	0.038 mg/Nm^3	0.05 mg/scm	<0.038	<0.05
Cd (+Tl) (10)	0.05 mg/Nm^3	0.065 mg/scm	0.008 mg/Nm^3	0.01 mg/scm	<0.008	<0.01
Pb (+HM) (11)	0.5 mg/Nm^3	0.65 mg/scm	0.107 mg/Nm^3	0.14 mg/scm	<0.1	<0.14
PCDD + PCDF	0.1 ng/Nm^3 TEQ		0.1 ng/Nm^3 TEQ	13 ng/scm 12	0.01–0.1	1–10

(1) European emission values are daily average values or average values over a sampling period based on 11% O_2 in dry flue gas standardized at 273K and 101.3 kPa
(2) US emission values are based on 7% O_2 in dry flue gas standardized at
(3) As per EU Directive 2000/76/EC [5]
(4) As per EPA Title 40 Part 60, Subpart Eb [6]
(5) Total organic carbon (TOC)
(6) While the EU value is absolute, the US value can be exceeded if the removal efficiency is at least 95%
(7) While the EU value is absolute, the US value can be exceeded if the removal efficiency is at least 80%
(8) Local air permits in the USA often reduce NO_x and introduce NH_3 emission limits, specially in non-attainment zones
(9) While the EU value is absolute, the US value can be exceeded if the removal efficiency is at least 85%
(10) The EU value includes the sum of Cd + Tl, the US value only Cd, which is however by far the largest portion of the sum
(11) The EU value includes the sum of the following heavy metals Sb + As + Pb + Cr + Co + Cu + Mn + Ni + V, the US value is only for Pb, which is one of the larger portions of the sum
(12) The EU value is based on a toxic equivalence concept which calculates a weighted sum of all different PCDD and PDCF isomers is calculated. The US value uses the sum of all isomers without weighing. For typical mixtures of PCDD and PCDF isomers present in flue gases of EfW plants, these emission limits are similar
(13) Same units as used in preceding columns

Description of the CEMS A separate CEMS monitors the flue gas properties and composition at the stack for each incineration line. Each system mainly consists of:

- Temperature, pressure, and flow rate measurement
- Particulate measurement
- Complete extractive gas analyzer for concentration measurement of typically the following flue gas components: H_2O, O_2, CO, HCl, SO_2, NO_x, NH_3, VOC.
- Computer-based data evaluation and storage system

The instruments are directly installed on either the discharge ductwork between the ID-fan and stack or the stack. The flue gas is extracted through a heated extraction line and conveyed to the analytical instruments installed in the CEMS container.

The emission measurement system is designed to meet the particular requirements of the operating permit for the plant. It complies with the applicable directives for installation and quality assurance and has the possibility to generate direct reports for the supervising Environmental Protection Agency.

Stack

General The purpose of the stack is to expel the clean flue gases to the atmosphere at a high enough point to ensure adequate dispersion (Fig. 56).

Hitachi Zosen Inova Technology. Figure 56
Stack with individual support of single flues (Moerdijk, the Netherlands)

Description The cleaned flue gases enter the stack with a temperature of about 150°C (300°F). In multiple train plants, all flues can be integrated into the same stack structure. The internal flues are made of steel for flue gases above typically 130°C (270°F) or of fiber-reinforced plastic below. The flues are thermally insulated to avoid excessive condensation along the walls. The stack support structure can be steel or concrete.

Underneath the flue gas inlet to the stack, condensed water vapor or rain water is collected on an inclined stack base plate and discharged via a condensate discharge line. The condensate discharge is drained into the contact water storage.

The stack includes a safety ladder to a maintenance and work platform at the top of the stack from where the flues can be monitored and the lightning protection and air traffic lighting systems can be maintained. Depending on the location of emission monitoring nozzles an additional platform may be located in the middle of the stack.

Since the stack is normally the most visible part of an EfW plant, there are ideas how a stack could be converted to a landmark, for example in Fig. 57.

Future Directions

The EfW (or WTE) technology described above has been shown to be reliable, efficient, and proven:

- Reliable means that a large number of plant owners operate their Hitachi Zosen Inova plants in the range of 7,900–8,300 h per year, which corresponds to 90–95% availability.
- Efficient means that all national emission limits can be met, sometimes with a considerable margin. It also means that energy can be efficiently recovered in the form of electricity and/or heat meeting or exceeding the relevant energy efficiency standards [7].
- Proven means that this technology has been developed and has matured with the over 500 reference plants built worldwide since the 1930s.

It is evident that the Hitachi Zosen Inova technology is mature. Technical developments concentrate mainly on the following areas:

- Increase energy efficiency and electricity production og EfW plants

Hitachi Zosen Inova Technology. Figure 57
Stack with combined support of flues and architectural treatment (Osaka, Japan)

- Improve the automated control of the EfW plants in order to further increase average plant capacity and availability.
- Improve monitoring of plant components in order to allow operators to track the plant efficiency and better plan preventive maintenance actions.
- Further improve stack emission limits.
- Further improve bottom ash quality and recycling options for bottom ash (recovery of valuable resources such as copper, aluminium, brass and other metals).

However, since EfW technology in many areas still commercially competes with relatively cheap landfilling or is not available for large economic areas, one goal of development is always concentrated on plant economics:

- Achieve the same performance with less and simpler equipment
- Find less-expensive materials of construction, in terms of investment and maintenance cost
- Further improve the operation flexibility and availability of the plant thus reducing O&M cost

Last but not least, the goal must be to do all that is necessary to make EfW plants politically acceptable and a part of the infrastructure in the densely populated areas. Wastes are created and energy is needed where the people live. EfW plants are an essential part needed to close the loop of the material cycle [3]. Whatever cannot be reused or recycled can be efficiently treated for energy recovery in an EfW plant. An excellent example is the Isséane EfW plant that started operations in 2008 in France:

- It is located in the middle of the Paris metropolitan area about 5 km (3 miles) from the Eiffel Tower along the river Seine.
- It is an integrated part of the city's recycling activities and contains a plastics sorting and recycling facility.
- It serves a population of about one million people all living within a short distance from the plant.
- It provides electricity to the national electrical grid.
- It provides heat to the city's district heating system.
- However, both electricity and heat are consumed in the vicinity of the plant. This concept helps reduce the need for long-distant transport of energy and the associated complexity of energy distribution.
- The EfW plant was designed to fit architecturally into the neighborhood and, in fact, may not even be recognized as an EfW plant.

Although the total cost of the Isséane EfW plant (Fig. 58) is on the high side compared to other modern EfW plants, it is an excellent example of sustainability within the material and energy cycles. Research and development is focusing on all aspects needed to make such a concept available to more and more highly populated areas. This includes emissions and architecture to increase acceptability to the public as well as efficiency, reliability, and total cost in order to increase its affordability to communities in developing nations.

Hitachi Zosen Inova Technology. Figure 58
Isséane energy-from-waste plant, Paris, France

Bibliography

1. Kjeldsen P, Barlaz MA, Rooker AP, Baun A, Ledin A, Christensen TH (2002) Present and long-term composition of MSW landfill leachate: a review. Critical Reviews in Environmental Science and Technology 32(4):297–336
2. Kaufman SM, Themelis NJ (2009) Using a direct method to characterize and measure flows of municipal solid waste in the United States. J Air Waste Manage Assoc 59:1386–1390. doi:10.3155/1047-3289.59.12.1386, ISSN:1047-3289; Copyright 2009 Air & Waste Management Association, Earth Engineering Center, Columbia University, New York
3. European Environment Agency (2007) Sustainable consumption and production. In: State of the environment report no 1/2007 (Chap 6). Office for Official Publications of the European Communities, Luxembourg. http://www.eea.europa.eu/publications/state_of_environment_report_2007_1
4. Sigg F, Halter R, Chromec P (2010) DyNOR® DeNOx performance confirmed in further MSW plants, NAWTEC18-3504. In: Proceedings of the 18th annual North American waste-to-energy conference, Orlando. Copyright 2010 by ASME
5. Directive 2000/76/EC of the European Parliament and of the Council of 4 December 2000 on the Incineration of Waste, 28.12.2000, Official Journal of the European Communities, L 332/91
6. US Electronic Code of Federal Regulations (Title 40, Part 60, Subpart Eb) current as of 29 July 2010
7. Reimann DO (2004–2007) Results of specific data for energy, R1 plant efficiency factor and net calorific value (NCV) of 231 European WtE plants. In: CEWEP Energy Report II (Status 2004–2007). http://www.cewep.eu/studies/climate-protection/index.html

HIV/AIDS Global Epidemic

Phyllis J. Kanki
Department of Immunology and Infectious Diseases, Harvard School of Public Health, Boston, MA, USA

Article Outline

Glossary
Definition of the Problem
Introduction
Basic Virology of HIV

HIV and the Cause of AIDS
Epidemiology of the Global HIV Pandemic
Sub-Saharan Africa
Asia
Eastern Europe and Central Asia
Caribbean
Central and South America
North America and Western and Central Europe
Middle East and North Africa
Oceania
Prevention
Genetic Diversity of HIV
Treatment
Vaccine
Future Directions
Bibliography

Glossary

Acquired immunodeficiency syndrome (AIDS) A clinical syndrome caused by the human immunodeficiency virus (HIV). Its pathogenesis is related to a qualitative and quantitative impairment of the immune system, particularly a reduction of the CD4+ helper T lymphocyte cell count (surrogate marker of the disease). After an average of 10 years, if untreated, HIV + individuals can develop opportunistic diseases (i.e., infections and cancers rarely detected in people with normal immune systems). The natural history of the disease can be dramatically modified with administration of combination therapy composed of antiretroviral (ARV) drugs.

CCR-5 A cell membrane protein expressed on several cell types including peripheral blood-derived dendritic cells, CD34+ hematopoietic progenitor cells, and certain activated/memory Th1 lymphocytes. This receptor is well defined as a major coreceptor in conjunction with CD4+, implicated in susceptibility to HIV-1 infection.

CD4+ A large glycoprotein that is found on the surface of helper T lymphocyte cells, regulatory T cells, monocytes, and dendritic cells. Its natural function is as a coreceptor that assists the T cell receptor (TCR) to activate its T cell following an interaction with an antigen-presenting cell. CD4+ is a primary receptor used by HIV-1 to gain entry into host T cells.

CD4+ T cell An immune cell, lymphocyte (white blood cell) characterized by the CD4+ antigen (protein) on its surface. This is a T lymphocyte considered to have a "helper" function to enhance the cellular immune response. The CD4+ is the primary receptor for the HIV virus, and upon infection, the virus can destroy the CD4+ cell. In HIV-infected people, the drop in CD4+ T lymphocyte cells is a major determinant of the progression of HIV infection to AIDS.

Coreceptor (CCR-5 or CXCR-4) Protein molecules on the surface of lymphocytes or monocytes that bind to the gp120 protein of HIV and facilitate, with CD4, binding, fusion, and entry of the virus into the susceptible cell.

CXCR-4 An alpha-chemokine receptor specific for stromal-derived factor-1 (SDF-1 also called CXCL12), a molecule endowed with potent chemotactic activity for lymphocytes. This coreceptor is one of several chemokine receptors that HIV isolates can use to specifically infect CD4+ T cells.

DNA (deoxyribonucleic acid) A nucleic acid that contains the molecular basis of heredity for all known living organisms and some viruses and is found in the nuclei and mitochondria of eukaryotes. Chemically, DNA consists of two polymer strands of units called nucleotides made up of one of four possible bases plus sugar and phosphate groups. The polymers are joined at the bases by hydrogen bonds to form a double helix structure.

Fusion of virus and cell membranes A merging of cell and virus membranes that permits HIV proteins and nucleic acids to enter the host cell.

Fusion/entry inhibitors A class of ART drugs that interferes with the virus' ability to fuse with the target cell's outer membrane, thereby blocking entry of the HIV into the host cell.

gp120 The major HIV envelope glycoprotein having a molecular weight of 120 that protrudes from the outer surface of the virion. This glycoprotein binds to a CD4+ receptor on a T cell to facilitate entry of the virus into the cell.

Human immunodeficiency virus (HIV) The virus that causes acquired immunodeficiency syndrome (AIDS). It is a lentivirus belonging to *Retroviridae* family and was discovered in 1983 by Robert Gallo

and Luc Montagnier. HIV infects and destroys helper T cells of the immune system causing a marked reduction in their numbers. Loss of CD4 cells leads to generalized failure of the immune system and susceptibility to life-threatening opportunistic infections. It is transmitted mainly through sexual intercourse, exchange of contaminated syringes among intravenous drug users, and contaminated blood transfusion. HIV-1 is the HIV type most frequently detected HIV worldwide and responsible for the global pandemic.

HIV-1 subtypes or clades Genetically related HIV strains that are essentially phylogenetically equidistant, generating a starlike phylogeny. Subtypes A, B, C, D, F, G, H, J, and K are currently known subtypes A, B, C, and D are highly prevalent others have low prevalence and limited geographic distributions.

HIV-2 The second HIV virus discovered in West Africa in 1984, the virus is more closely related to the simian immunodeficiency virus of primates. Although HIV-2 can cause AIDS, it has a distinct epidemiology, lower rate of transmission, and slower progression to disease.

Incidence Rate describing the number of new cases of disease occurring within a given time period, expressed as new cases per person-time.

Integrase An enzyme found in retroviruses including HIV that permits the reverse transcribed viral DNA to be integrated into the infected cell's DNA. Integrase is an enzyme encoded by the polymerase gene of HIV.

Integrase inhibitors A class of ART drugs that blocks the viral integrase the enzyme HIV uses to integrate its genetic material into its target host cell DNA.

Nucleus A membrane-enclosed central compartment of a cell that functions to contain the genomic DNA and to regulate gene expression.

Prevalence Number of cases of disease in a defined population at a specific point in time it is often expressed as a percentage.

Protease An enzyme that hydrolyzes or cleaves the polyproteins into proteins and is important in the final steps of HIV maturation. In HIV, the protease enzyme is encoded by the *polymerase* gene.

Protease inhibitors A class of ART drugs that interferes with the viral protease enzyme of HIV by inhibiting the viral polyproteins from being cleaved, which would allow the individual viral proteins to produce infectious viral particles.

Reverse transcriptase An enzyme found in HIV that creates double-stranded DNA using viral RNA as a template and host tRNA as primers. The reverse transcriptase enzyme is encoded by the *polymerase* gene of HIV.

Reverse transcriptase (RT) inhibitors A class of ART drugs that interfere with the reverse transcription step during the HIV life cycle. During this step, the HIV enzyme RT converts HIV RNA to HIV DNA. There are two main classes of RT inhibitors that are used as ART drugs.

Nucleoside/nucleotide RT inhibitors (NRTI) are faulty DNA building blocks. When these faulty pieces are incorporated into the HIV DNA (during the process when HIV RNA is converted to HIV DNA), the DNA chain cannot be completed, thereby blocking HIV from replicating in a cell.

Nonnucleoside RT inhibitors (NNRTI) bind to RT, interfering with its ability to convert the HIV RNA into HIV DNA.

RNA (ribonucleic acid) A universal form of genetic material typically transcribed from DNA, it differs from DNA in that it contains ribose and uracil as structural components. In retroviruses like HIV, RNA is their primary genetic material and is found in a mature virus particle.

T-lymphotropic A characteristic of a virus that infects and replicates in T lymphocytes, a type of immune cell. This was the descriptor of the human T cell leukemia virus (HTLV), a human retrovirus that causes T cell leukemia and lymphoma and is T-lymphotropic like HIV. HIV was originally called human T-lymphotropic virus type III (HTLV-III) by Gallo and colleagues.

Tuberculosis The infectious disease caused by *Mycobacterium tuberculosis*. It usually involves the lungs (pulmonary tuberculosis) but can also affect other organs (i.e., kidneys, central nervous system, lymph nodes, bones, etc.; extrapulmonary tuberculosis). Pulmonary tuberculosis, which is the most frequent clinical form, can be classified as smear positive or smear negative according to the result of the sputum bacteriological examination. The former is a major public health problem being highly

contagious. Only a few individuals develop tuberculosis after a mycobacterial infection, and most of them soon after infection: it is estimated that the lifetime risk is 5–10% in HIV negatives and 5–15% yearly in HIV positives.

Virion A single and complete extracellular infective form of a virus that consists of an RNA or DNA core and in the case of HIV with a glycoprotein coat or "envelope."

Definition of the Problem

The HIV/AIDS epidemic is now in its third decade since the discovery of the virus responsible for the disease in 1981. While the first cases of AIDS were first recognized in young men who have sex with men in the United States and Europe in the 1980s, it soon became clear that the virus could be spread through contaminated blood products and heterosexual sex. At the time of its discovery, acquired immunodeficiency syndrome (AIDS) was a new disease with high mortality, and the discovery of a new human virus as its cause in 1983 created new challenges for prevention, treatment, and vaccine efforts, many of which remain unmet today. Human immunodeficiency virus type 1 (HIV-1), as the causative agent of AIDS, has been the subject of intense research over the past three decades, in an effort to understand the biological properties of this new virus, its relatedness to other known retroviruses, characterize its epidemiology, and discover drugs and vaccines to control the epidemic.

In the early 1980s, it was recognized that HIV could be spread through blood, blood products, and sexual and perinatal transmission routes. High rates of HIV infection and its accompanying disease began to be recognized throughout the world in the late 1980s as the HIV/AIDS global pandemic became a frightening reality to the international community. The disproportionate burden of infection and disease first recognized in sub-Saharan Africa and then Asia with growing rates of disease and mortality led to estimates of global infections growing in the tens of millions with no magic bullet to end the spread. While global estimates are necessarily fraught with numerous assumptions and subjected to poor reporting, UNAIDS revised down their global estimates in 2007 [1]. Nonetheless, at the end of 2009, an estimated 33.3 million people worldwide were living with HIV; 2.5 million of these were children, with almost two thirds of them in low- and middle-income countries [2]. While stunning in magnitude, these estimates now reflect a continued slowing of the growth trajectory of the pandemic, with lower rates of new infections and mortality, the latter being largely due to the continued scale-up of provision of antiretroviral therapy (ART) that began in 2004.

We are therefore at an important point in the time for the global HIV pandemic; the peak of infections in most countries occurred about a decade ago, and many high-burden countries are seeing a plateau or decrease in HIV prevalence rates. Large-scale treatment programs for low-income countries have succeeded in providing complex and relatively expensive ART drugs to almost one third of patients in need of these life-saving therapies; 5 million of the 15 million in need. Recent strides in identifying new and efficacious methods for prevention have been encouraging as the development of an effective vaccine is still awaited.

Introduction

AIDS was first recognized as a new and distinct clinical entity in 1981 [3–5]. The first cases were recognized because of an unusual clustering of diseases such as Kaposi's sarcoma and *Pneumocystis carinii* pneumonia in young homosexual men. Although such syndromes were occasionally observed in distinct subgroups of the population – such as older men of Mediterranean origin in the case of Kaposi's sarcoma or severely immunosuppressed cancer patients in the case of *Pneumocystis carinii* pneumonia – the occurrence of these diseases in previously healthy young people was unprecedented. Since most of the first cases of this newly defined clinical syndrome involved homosexual men, lifestyle practices were first implicated as the cause of the disease.

AIDS cases were soon reported in other populations as well, including intravenous (IV) drug users [6] and hemophiliacs [7–9]. Hemophiliacs used clotting factor preparations which were prepared from the pooled blood of a huge number of donors, and IV drug users often used needles contaminated with small amounts

of blood from previous users, thereby increasing their exposure to foreign tissue antigens. Asymptomatic hemophiliacs and intravenous drug users were often found to have abnormally low CD4 helper lymphocytes and higher than normal T suppressor cells, similar to the gay men with AIDS. The increase in T suppressor cells was presumably due to frequent antigenic stimulation; the decrease in CD4+ T helper cells was the more direct effect of the yet-to-be-discovered causative agent.

Three new categories of AIDS patients were soon observed: blood transfusion recipients [10, 11], adults from Central Africa [12–14], and infants born to mothers who themselves had AIDS or were IV drug users [15, 16]. The transfusion-associated cases had received blood donated from an AIDS patient at least 3 years before they began showing symptoms [10, 11].

Based on the disparate populations afflicted with this new malady and the emerging epidemiology of the disease, the possible infectious etiology for AIDS was considered [17]. Multiple studies were initiated to determine the possible role of various microorganisms, especially viruses in causing AIDS. These studies measured and compared seroprevalence rates for suspect viruses in AIDS patients and controls. The short list of candidate viruses included cytomegalovirus (CMV), because it was already associated with immunosuppression in kidney transplant patients; Epstein-Barr virus (EBV), presumably because it was a lymphotropic virus; and hepatitis B (HBV), because infection with this virus was known to occur at elevated rates in both homosexual men and recipients of blood or blood products. However, based on the unique clinical syndrome and unusual epidemiology of AIDS, if the etiology was an already known virus, it would presumably have to be a newly mutated or recombinant genetic variant.

Max Essex [18, 19], Bob Gallo [20, 21], and Luc Montagnier, Francoise Barre-Sinoussi, and Jean-Claude Chermain [22] postulated that a variant T-lymphotropic retrovirus (HTLV) might be the etiologic agent of AIDS. Among the most compelling reasons for this hypothesis was that the human T-lymphotropic retrovirus (HTLV), discovered by Gallo and his colleagues [23] in 1980, was the only human virus known to infect T helper lymphocytes at that time. This fit with the new disease where T helper lymphocytes were selectively depleted by the causative agent [24–26]. AIDS patient blood samples were repeatedly cultured in an attempt to find a virus related to HTLV-I or HTLV-II [27]; however, these studies were only partially successful. Although antibodies cross-reactive with HTLV-I and HTLV-related genomic sequences were found in a minority of AIDS patients [18, 21, 22, 28], the reactivity was weak, suggesting either the coinfection of AIDS patients with an HTLV, or that a distant, weakly reactive virus was the causative agent. Proof that the disease was linked to a T-lymphotropic retrovirus was obtained by Gallo and his colleagues [29–31]. Further characterization of the agent – now termed human immunodeficiency virus type 1 (HIV-1) – revealed that it was the same as the isolate detected earlier by Montagnier and his colleagues [22]. Despite controversy over the names and identity of certain isolates, it is now clear that this new and unique human pathogen was not only a distant genetic relative of the known HTLV but also a virus that may have been more recently introduced into the humans from a primate reservoir.

A second HIV was discovered in 1984 based on antibodies from West African commercial sex workers that recognized proteins not only from the simian immunodeficiency virus (SIV) but also from HIV-1 [32, 33]. It is now known that HIV-1 is more closely related to SIVcpz, found mainly in the *Pan troglodytes troglodytes* chimpanzee species [34], while HIV-2 is related to SIVsm found in sooty mangabey monkeys (*Cercocebus atys*) [35]. HIV-2 is the second human immunodeficiency virus and constitutes the closest known human virus related to the prototype AIDS virus, HIV-1. HIV-2 shares many virologic and biologic features with HIV-1; however, its ability to transmit and cause disease is much lower [36–38]. HIV-2 infection is much less prevalent in the world; it is found primarily in West Africa and other parts of the globe with connections to West Africa, such as India, parts of South America, and urban centers with high rates of immigration from West Africa [39, 40].

Basic Virology of HIV

Human immunodeficiency virus types 1 and 2 (HIV-1 and HIV-2) are members of the *Lentivirus* genus of the

Retroviridae family of RNA viruses and are 50% similar at the genetic level. Retroviruses are enveloped viruses that infect a wide range of vertebrate hosts in a species-specific manner [41]. Steps in the HIV replication cycle (Fig. 1) include (1) recognition and binding of the virion to the host cell surface via specific primary and coreceptors and fusion to the host cell membrane; (2) uncoating of the virion and release of the HIV genetic material and other viral proteins including enzymes such as reverse transcriptase, integrase, and

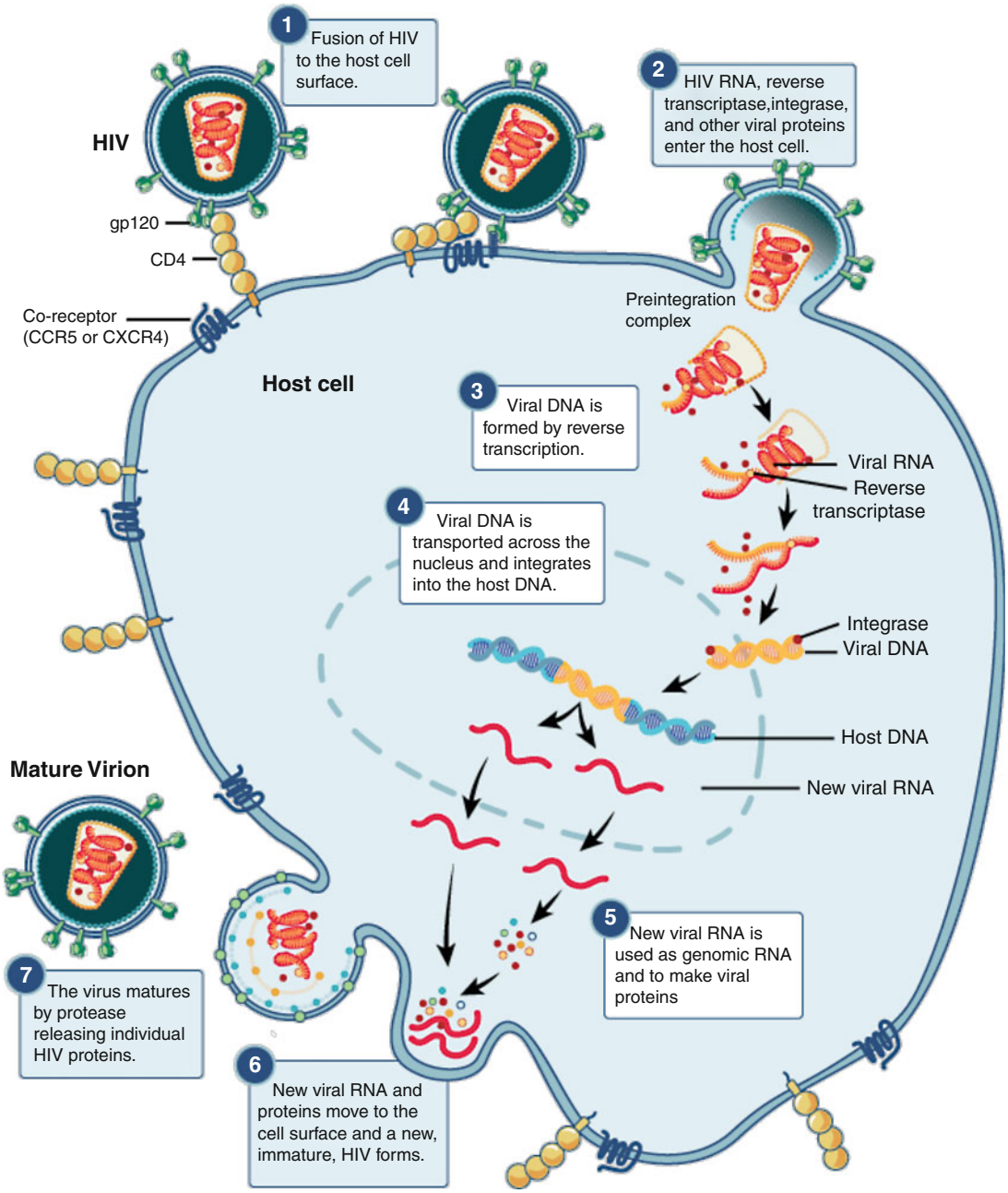

HIV/AIDS Global Epidemic. Figure 1
HIV replication cycle [43]

protease; (3) HIV RNA is reverse transcribed by the enzyme reverse transcriptase to make a double-stranded DNA copy; (4) HIV viral DNA is transported to the cell nucleus, where it integrates into the host cell's DNA, using the HIV viral integrase; (5) a new copy of the HIV viral RNA is produced which will become the genetic material for new HIV virions; (6) new viral RNA and proteins produced by the host cell move to the cell surface, and new, immature virions are packaged; and (7) the viral envelope proteins are inserted into the host cell membrane, and the virions bud from the cell surface, encapsulated by viral envelope, forming a mature HIV virion [42, 43].

Like other retroviruses, HIV's genetic material becomes permanently integrated in the host cell's DNA, resulting in lifelong infection. The enzyme responsible for viral replication and encoded by the *polymerase* gene is the reverse transcriptase, which as an enzyme is error-prone, which results in considerable genetic variation. HIV enters susceptible cells via a primary receptor, the CD4+ on immune cells such as T lymphocytes. However, secondary coreceptors are also required for HIV's entry into a cell [44–47]. These are normal cellular membrane proteins, part of a seven-transmembrane spanning protein family, called chemokine receptors, and involved in the recruitment of chemokines for normal cellular function. CCR-5 and CXCR-4 are chemokine receptors that also serve as major coreceptors for the HIV virus. In conjunction with the primary receptor, CD4 molecule, they allow the virion to fuse with the susceptible host cell and allow virion entry. The CCR-5 coreceptor along with CD4 allows for HIV to infect CCR-5 bearing cells usually of the macrophage/monocyte lineage. The CXCR-4 coreceptor along with CD4 allows for HIV's fusion and entry into T cells [44, 48, 49].

The HIV genome, or genetic makeup, has been characterized and is 9.8 kilobases in length and contains nine different genes, which encode 15 proteins. There are three major classes of proteins: structural, regulatory, and accessory [42]. Three genes, *gag*, *pol*, and *env*, each encode multiple viral structural proteins. The *gag* (group-specific antigen) gene produces a 55-kd precursor protein, which is cleaved during viral maturation into the matrix (MA; p17), capsid (CA; p24), nucleocapsid (NC; p9), p1, p7, and p6 proteins. The *pol* gene (polymerase) encodes the enzymes including protease, reverse transcriptase (RT), and integrase, while the *env* gene (envelope) gives rise to the envelope proteins gp120 and gp41. The regulatory proteins are Tat and Rev, while the accessory proteins include Vpu, Vpr, Vif, and Nef [42].

HIV and the Cause of AIDS

HIV typically enters the body by blood, blood products, or through fluids exchanged in sex or childbirth. The virus infects a large number of CD4+ cells and replicates rapidly. During the acute phase of HIV infection, the blood carries a large number of HIV virus particles, which spread throughout the body, infecting various organs, particularly the lymphoid organs such as the thymus, spleen, and lymph nodes [50, 51]. During this phase, the virus may integrate and hide in the host cell's genetic material. Thus, evading the host's immune system, the virus may remain dormant for an extended period of time. In the acute phase of infection, a significant proportion of people may suffer flu-like symptoms [51, 52] (Fig. 2).

Weeks after exposure to the virus, the immune system responds with killer T cells (CD8+ T cells) and B cell–produced antibodies. At the same time, CD4+ T cell counts rebound. The virus levels may decrease at this point in time perhaps in response to the first host immune response. During this latency phase, a person infected with HIV may not experience HIV-related symptoms for several years despite the fact that the HIV continues to replicate [53]. It is this long course of dormancy that has given the lentiviruses ("lenti" – meaning slow) their name.

The immune system eventually deteriorates to the point that the human body is unable to fight off other infections; the timing and reasons for this are still subject to research. The level of HIV virus in the blood may dramatically increase, while the number of CD4+ T cells drops to dangerously low levels. An HIV-infected person is diagnosed with AIDS when he or she has one or more opportunistic infections, such as

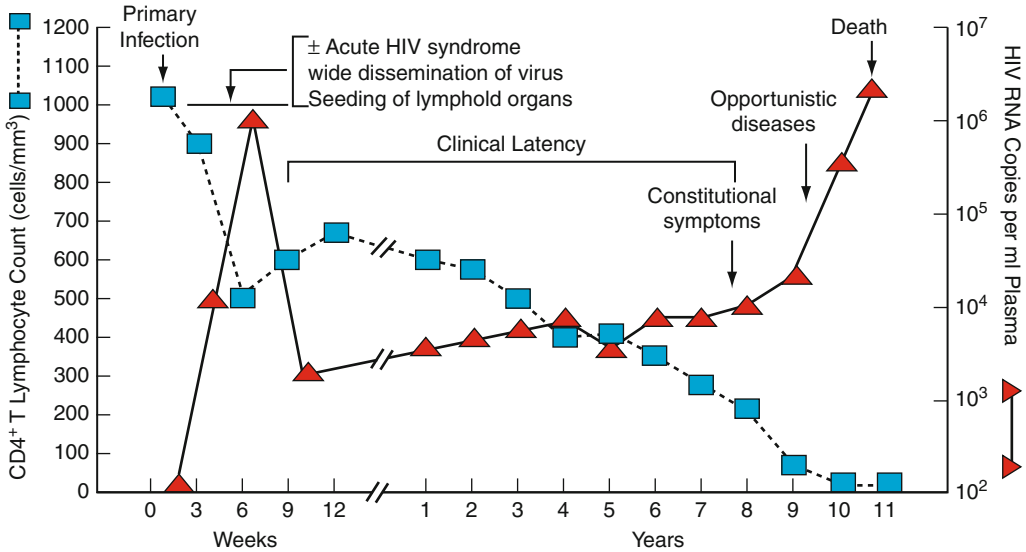

HIV/AIDS Global Epidemic. Figure 2
Clinical progression of HIV infection [52]

tuberculosis, and CD4+ T cells drop below 200 cells per cubic millimeter of blood, where the normal would be ~1,000 CD4+ T cells.

Epidemiology of the Global HIV Pandemic

HIV and AIDS is a global pandemic. Although the means by which the virus can spread between people remains unchanged, the populations that are highly infected in different parts of the world are different. Transmission of the virus by blood and blood products for the treatment of various diseases such as hemophilia was recognized in the early 1980s. Ensuring that blood banks and blood products were free of HIV was accomplished relatively early in the pandemic in high-income countries, but is yet to be perfected in many low-income countries where screening of HIV and the high burden of disease pose distinct challenges to maintaining safe blood banks and blood products.

Spread of HIV infection through intravenous drug use was also recognized in high-income countries early in the epidemic. These often disenfranchised and stigmatized populations were difficult to identify to provide necessary diagnosis, care, and treatment. This continues to be a challenge for prevention efforts throughout the world, most significant in parts of Asia, where the spread of HIV through this mode of transmission is both prevalent and difficult to control.

Sexual transmission of HIV in most of the high-income countries remains a threat to men who have sex with men, where the virus and its disease were first recognized. In contrast, in most middle- and low-income countries, the risk of HIV transmission is predominantly through heterosexual sex. This means that the risk to women and their offspring is more significant in these geographic locations and represents a distinction in the epidemiology of HIV/AIDS in these settings. As a consequence, the risk of mother-to-child transmission in middle- and low- income countries was most severe in nations already burdened with high infant mortality. In 2009, 370,000 (230,000–510,000) children were infected with HIV through mother-to-child transmission [2]. This represents a decrease of 24% from 5 years earlier due to better methods of preventing transmission through identification of infected pregnant women and provision of more effective prophylaxis. Inadequate access to antenatal and postnatal services remains a barrier in providing these methods to all those in need [54].

UNAIDS has just completed their 2010 report which reports on HIV and AIDS statistics from around the globe ending in 2009 [2] (Table 1). Extensive

HIV/AIDS Global Epidemic. Table 1 UNAIDS regional estimates for adults and children living with HIV (Adapted from [2])

Geographic region	People living with HIV	
	2009	2001
Sub-Saharan Africa	22,500,000	20,300,000
Middle East and North Africa	460,000	180,000
South and Southeast Asia	4,100,000	3,800,000
East Asia	770,000	350,000
Oceania	57,000	29,000
Central and South America	1,400,000	1,100,000
Caribbean	240,000	240,000
Eastern Europe and Central Asia	1,400,000	760,000
Western and Central Europe	820,000	630,000
North America	1,500,000	1,200,000

analysis of these current rates and the trends from previous years allows for some cautious optimism on the status of the pandemic. This report continues to support the notion that the peak of new infections occurred in 1999 and rates of new infections continue to decline or plateau [55, 56]. In 2009, an estimated 2.6 million (2.3–2.8 million) people were newly infected with HIV. In 33 countries, most in sub-Saharan Africa, HIV incidence showed significant decreases compared to 2001 [2].

Globally, an estimated 33 million people are infected with HIV. In earlier years treatment was only provided in high-income countries; more recently local governments and international programs supporting antiretroviral therapy in low-income countries have had an impact on the annual death toll. A cumulative total of 24 million people have died from AIDS between 1980 and 2007, and Bongaarts and colleagues project that this will reach 75 million by 2030 [56].

Regional HIV statistics for both 2009 and 2001 are provided in Table 1. These demonstrate the heterogeneity of the global pandemic. It is beyond the scope of this chapter to discuss each of the region's HIV epidemiology in depth. Summarized findings are therefore provided with more emphasis on sub-Saharan Africa where the highest burden of infection and disease is found.

Sub-Saharan Africa

Over 22 million people in sub-Saharan Africa are infected with HIV, although there is considerable variability among nations in rates of infection and disease [2] (Fig. 3). The countries of Southern Africa (Angola, Botswana, Lesotho, Malawi, Mozambique, Namibia, South Africa, Swaziland, Zambia, and Zimbabwe) have over 11 million people currently infected. Thus, this region of the continent alone represents over one third of the global pandemic in terms of adult HIV infections, new HIV infections, and deaths due to HIV. Swaziland, in 2009, reported a prevalence of 25.9%, representing the highest adult HIV prevalence rate for a given country [57]. In South Africa, where over five million people are living with HIV in 2009, AIDS is the major cause of maternal mortality and attributed to cause over one third of deaths in children under the age of 5 years old.

Other large countries, such as Nigeria with a population estimated at 150 million and Ethiopia with a population 82 million, have relatively low HIV prevalence rates below 4%, but still represent a significant portion of the global burden of disease because of their large populations. By contrast, many of the countries of Southern Africa are small, but with high prevalence rates. Thus, the distinct impact of the epidemics in such diverse settings can be appreciated.

As of 2009, the rates of HIV infection in the countries of East Africa have been declining. Uganda's HIV prevalence has been stable in the 6–7% range since 2001. Kenya and Tanzania have shown declining prevalence rates, and Rwanda has been stable at 3% since 2005 [2].

In West and Central Africa, countries have maintained some of the lowest HIV infection rates of the continent. In 2009, 12 countries had rates below 2%; these included: Benin, Burkina Faso, Democratic Republic of the Congo, Gambia, Ghana, Guinea, Liberia, Mali, Mauritania, Niger, Senegal, and Sierra Leone. Nigeria's HIV infection rate has been declining for the past 6 years with the 2009 estimate at 3.6% (3.3–4.0%). The prevalence of HIV is highest in Cameroon at 5.3% (4.9–5.8%); Central African Republic, 4.7% (4.2–5.2%); Côte d'Ivoire, 3.4% (3.1–3.9%); and Gabon, 5.2% (4.2–6.2%) [2].

Asia

HIV infection rates in 2009 for the region are similar to 2004, with an estimated 4.9 million (4.5–5.5 million)

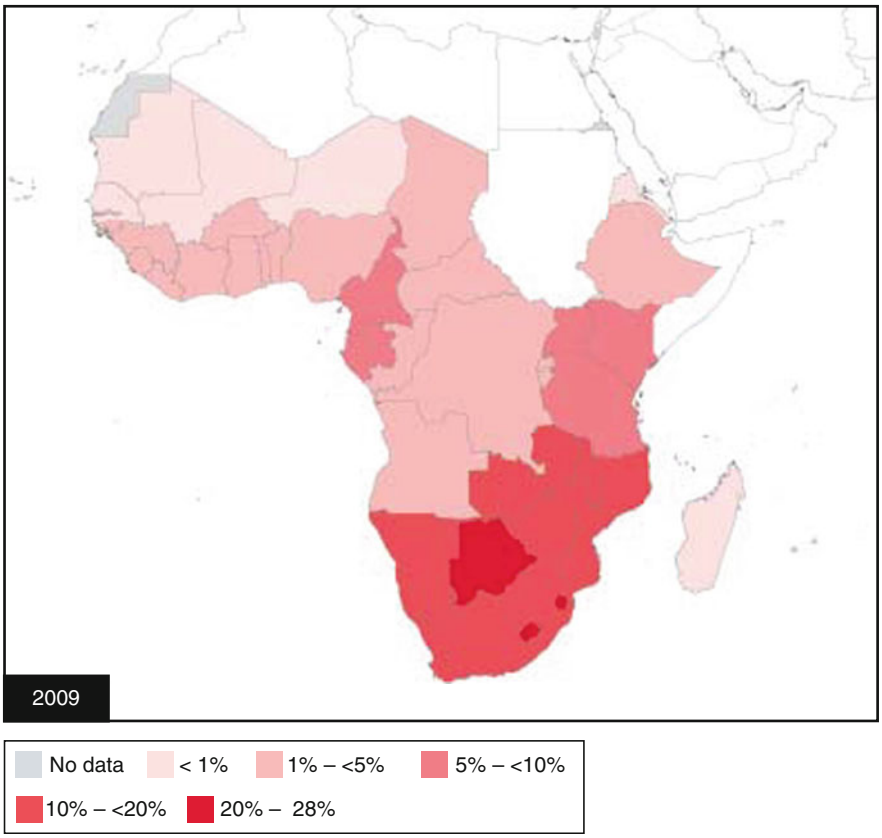

HIV/AIDS Global Epidemic. Figure 3
HIV prevalence rates among adults aged 15–49 years old in sub-Saharan Africa, 2009 (Adapted from [2])

people are currently infected [2]. There is considerable heterogeneity of infection by countries, and some previously low-prevalence countries like Pakistan and Bangladesh are increasing, largely due to transmission in drug-injecting populations. Within countries, there is also considerable variation; for instance, five provinces of a total of 22 in China account for over half of the HIV infections of the country [58, 59]. The epidemic in this region of the world is largely due to significant subpopulations of injecting drug users and men who have sex with men, where rates remain high and often increasing.

Eastern Europe and Central Asia

The largest increases in new HIV infection rates are seen in this region of the world with a burden of 1.4 million people estimated to be living with the virus in 2009 [2]. HIV prevalence exceeds 1% in the Russian Federation and Ukraine. The epidemic is concentrated in high-risk populations that use injection drugs and are involved in sex work and their sexual partners [60].

Caribbean

This region of the world has a relatively low burden of people living with HIV (240,000), yet because of their small population size, their HIV prevalence of ~1% (0.9–1.1%) is still considered high for the region [2]. There is considerable variability between countries and within countries. Haiti has highly variable rates, including 12% in pregnant women from some urban settings [61, 62], whereas Cuba's prevalence is exceptionally low, at 0.1% (0.08–0.13%) [2]. Unprotected paid sex is considered the major mode of HIV transmission, and infection rates in women are over half of those infected with the virus.

Central and South America

The HIV epidemic appears stable in 2009 compared to previous years, and the number of children infected is declining with ~4,000 children newly infected in 2009 [2]. There are 1.4 million people living with the infection in this region, with concentrated infection rates in men who have sex with men and sex workers.

North America and Western and Central Europe

The burden of HIV infection is 2.3 million (2.0–2.7 million) in these higher-income countries, representing a 30% increase from 2001 [2]. It is believed that unprotected sex among men having sex with men is responsible for these disturbing increasing trends in Canada, the USA, and parts of Europe [63]. General decreases are seen in injecting drug user subpopulations overall, but certain countries continue to see this as a driver of the epidemic [64–66]. Immigrant populations and individuals acquiring HIV from more endemic regions are also contributing to the burden of infection particularly in urban centers [67].

Middle East and North Africa

This region of the world has historically had low rates of HIV infection, which may be due to inadequate reporting. In 2009, an estimated 460,000 people are living with HIV, which is a substantial increase from the 2001 reported statistics [2]. Transmission of the virus from contaminated drug-injection equipment is considered the major mode of transmission in the countries of this region.

Oceania

The burden of HIV infection in this region is small at 57,000 (50,000–64,000) but has increased from the 2001 statistics [2]. Papua New Guinea has the largest infection rates in this region, with a national adult HIV prevalence of 0.9% (0.8–1.0%). Unprotected heterosexual sex is more predominant in Papua New Guinea, whereas unprotected sex in men who have sex with men is more common in New Zealand and Australia [68].

Prevention

The optimal biomedical means of preventing infection with an infectious disease pathogen would be the use of an effective vaccine. As efforts to develop such a vaccine are still underway, public health officials around the world have resorted to other methods of preventing HIV transmission [69]. These revolve around the various types of HIV transmission such as men who have sex with men, sex workers, intravenous drug users, and heterosexual adults in places such as Africa. Education on risks of transmission, methods of prevention, and behavior change are at the core of all prevention programs spanning on populations at risk. For many of these subpopulations, stigma, lack of access to services, or even legislation can diminish the potential of prevention programs and messages for behavior change.

Access to HIV testing and counseling is a foundation to all prevention methods, which provides access to comprehensive HIV care. Education and behavior change are critical components of prevention methods, and provision is often most effective when provided by community groups. In the early 1980s in the USA, pioneer groups such as the San Francisco AIDS Foundation, Gay Men's Crisis in New York, and AIDS Project Los Angeles demonstrated the role of education in promoting safer sex practices among gay and bisexual men [70]. Recent increases in new infections in young gay men in North America and Europe are of concern and suggest the need to enhance prevention efforts [2, 63].

Globally, HIV acquired through injecting drug use is estimated to represent 20% of the people living with HIV in 2009 [2]. Efforts to make injecting drug use safer through provision of clean needles have proven efficacy in lowering transmission through this route. UNAIDS reports in 2009 that in Eastern Europe and Central Asia where injecting drug use is a major driver of the HIV epidemic, five of nine countries report that more than 80% of people injecting drugs used sterile injecting equipment at their last injection. Eight of twelve countries in South and Southeast Asia reported the same [2]. However, the various governmental responses across the globe have often prevented the widespread adoption and support of such programs [65]. While provision of clean needles is inexpensive, it is believed that many programs provide inadequate numbers of clean needles to insure optimal prevention [66]. In addition, the substance abuse treatment programs, such as methadone programs, may help curtail

the intravenous drug–using behavior and therefore eliminate the risk of the transmission [64].

Prevention methods directed at commercial sex work are needed worldwide and again represent a targeted high-risk population that is disenfranchised and difficult to reach through conventional health system structures. The prevention methods focus on HIV counseling and testing, safe sex through proper condom use, and concomitant diagnosis and treatment of sexually transmitted infections (STIs), which are known to facilitate HIV transmission [71]. A long-standing program for sex workers in Southern India, called Avahan, provided a combined prevention approach of community outreach, empowerment, condom programming, and STI and HIV testing services over an 8-year period with a decrease in HIV prevalence from 20% to 16% in these high-risk women [71, 72].

In many parts of the resource-limited countries, heterosexual transmission is the major risk factor for HIV acquisition. Testing and access to HIV care is again critical to these populations along with appropriate counseling on behavior change, proper condom use, and STI diagnosis and treatment. Proven prevention measures for this group would include abstinence, mutual monogamy, reduced number of sexual partners, and consistent condom use. For young people, abstinence and older age of sexual debut are considered part of prevention messages [69].

Since 2000, a number of epidemiologic surveys and studies considered the possible benefit of male circumcision (surgical removal of the foreskin) in decreasing HIV transmission [73]. The penile foreskin is thought to be sensitive to epithelial tears, which carry a high density of CD4-bearing cells as targets for virus infection and subsequent replication [74]. In addition, uncircumcised men are at higher risk for STIs, which would facilitate HIV transmission [75–77]. In 2005–2006, randomized clinical trials conducted in South Africa, Kenya, and Uganda demonstrated a 55–76% lower HIV incidence compared to men still on the wait list of circumcision [78–80]. It is still unknown whether male circumcision will decrease male-to-female transmission of the virus, but these studies are underway [80]. There are other health benefits to male circumcision, but the surgical procedure is not without some risk, although serious complications are rare [76]. Nonetheless, for populations where men or boys are not circumcised, such as much of Southern and Eastern Africa, this becomes an important prevention tool [81].

Mother-to-child transmission of HIV is in large part responsible for the 2.5 million children living with HIV worldwide. Prevention of mother-to-child transmission (PMTCT) consists of identification of HIV infection in pregnant women and provision of a short course of antiretroviral drugs in a prophylactic manner (rather than treatment of the mother for her own disease to lower the viral burden in the mother and to decrease the risk of transmission to the baby). In resource-rich countries, most HIV-infected pregnant women would receive full ART (three drugs) as a means of preventing mother-to-child transmission; however, in most resource-limited settings, mono- or bi-therapy ART has been used due to cost and international recommendations at the time [82, 83]. In 2010, WHO revised their PMTCT guidelines based on clinical trial data from Africa, indicating that full ART could virtually eliminate mother-to-child transmission [84]. In settings where breast-feeding is judged to be the safest infant feeding option, ART prophylaxis continued to the mother and baby during this period could severely limit this mode of transmission [82–84]. While access to any PMTCT services remains a problem in a number of resource-limited countries and settings, only 54% access for sub-Saharan Africa, the potential for virtual elimination of mother-to-child transmission as these new guidelines are implemented becomes a real possibility [2, 82].

Postexposure prophylaxis (PEP) was the terminology frequently used to describe the use of short-course ART drugs given after an occupational setting exposure such as needle sticks with potentially HIV-infected blood. Similarly, PEP has been used in rape cases in settings where HIV infection is high and the potential for sexual transmission can be potentially decreased [85, 86]. Preexposure prophylaxis (PrEP) is the use of an ART drug administered to an HIV-negative individual prior to or at the time of the potential transmission event in an effort to decrease the viral inoculum and limit the potential for infection.

A recent study reported from South Africa this past year described the use of tenofovir-based gel as a microbicide to be used once 12 h before sex and

again 12 h after sex as both safe and effective in reducing HIV transmission and STIs [87–89]. PrEP has also been successful in decreasing transmission in men who have sex with men and in heterosexual discordant couple studies [90, 91]. This paves the way for additional biomedical means of preventing infection, which can be coupled with other prevention methods depending on the setting and populations at risks [92, 93]. Further trials are underway to test this new and promising strategy to prevent HIV transmission.

Genetic Diversity of HIV

Early in the history of HIV research, it was recognized that each viral isolate varied from another in its nucleotide sequence, and multiple mechanisms for this genetic variation were considered [42, 94]. Part of the HIV replication cycle requires the reverse transcription of viral RNA by the virus' reverse transcriptase. This enzyme is error-prone, thereby generating approximately 1 error per 10^4 nucleotides, or viral genome. Estimates of HIV replication in people have suggested 10^{10}–10^{12} new viral particles produced per day [95, 96]. Thus, the potential for viral variation is significant even if the immune system, tissue compartmentalization, or antiretroviral therapy does not select for particular viral variants. Genetic variability between viral isolates from different patients [97, 98], frequently termed interisolate or interpatient variability, can vary by up to 5%. And in turn, this was also distinguishable from the genetic variation that was seen at the level of an individual patient, often termed intrapatient variability and variability up to 1% [99]. At the level of the individual patient, a swarm or quasispecies of highly related but distinguishable viral variants has been demonstrated throughout the course of HIV infection [100–102]. Thus, the genetic variation of HIV is hierarchical as depicted in the simplified schematic of subtype variation, interpatient variation, and intrapatient variation (Fig. 4).

Phylogenetic analyses of viruses from various geographic regions were used to identify three distinct groups M, N, and O within HIV-1 [34, 103, 104]. Most HIV-1 sequences belong to group M (major). A divergent subset of viruses identified in Cameroon in 1994, which did not cluster with group M viruses, were classified as group O (outlier) [105], and in 1998, another set of viruses which did not cluster with group

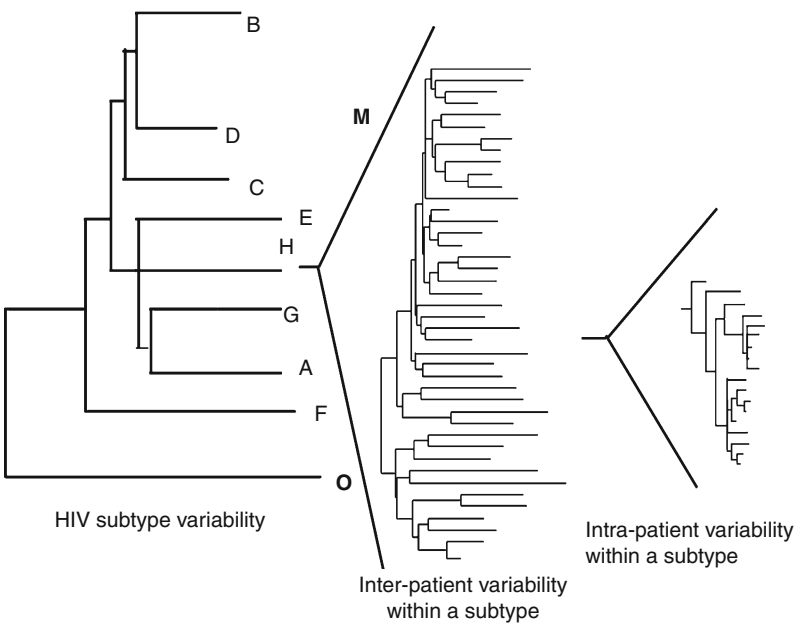

HIV/AIDS Global Epidemic. Figure 4
Phylogenetic trees depict differences between HIV subtypes, variation between viruses from different patients, interpatient variability, and variation between viruses within the same patient, intrapatient variability

M or O viruses were termed group N viruses [106]. A recent virus characterized from a gorilla has been designated group P [107]. It is thought that all virus groups were introduced by independent SIVcpz or SIVgor transmissions into the human population in the early part of the twentieth century [34, 104, 108].

The fruits of international HIV research have provided information of HIV viruses from different parts of the globe [109] (Fig. 5). The HIV-1 group M has been subdivided into genetic subtypes, defined originally on comparison of gag and env sequences of the virus and then later with full-length sequencing of the virus [110, 111]. Within a subtype, the average env genetic variation ranges from 5% to 15%, whereas the average env genetic variation between subtypes ranges from 20% to 30% [112, 113]. Remarkably, all the HIV-1s from the USA and Western Europe have been of a single subtype, B. Most of the diverse subtypes of HIV-1 including circulating recombinant forms (CRFs) and unique recombinant forms (URFS) have been found in sub-Saharan Africa and, to a lesser degree, Asia, now accounting for 20% of the worldwide HIV viruses [109].

In Thailand, HIV-1 subtype B was detected in IV drug users during the mid-1980s. During the late 1980s, subtype E was first detected. By the early to mid-1990s, HIV-1 subtype E (CRF01_AE) had spread very rapidly throughout heterosexuals in Thailand, with the highest rates in the northern regions of the country [114]. Although apparently present earlier in the region, HIV-1 subtype B never spread to cause a major heterosexual epidemic, as did HIV-1 subtype E. Full-length sequencing of subtype E determined that it is actually a circulating recombinant form, consisting of subtypes A and E, now referred to as CRF01_AE [115, 116].

A similar situation occurred in India, with HIV-1 subtypes B and C. While B appeared to be introduced earlier and it expanded among intravenous drug users, this subtype did not appear to spread as rapidly among heterosexuals as did HIV-1 C. Previously associated with

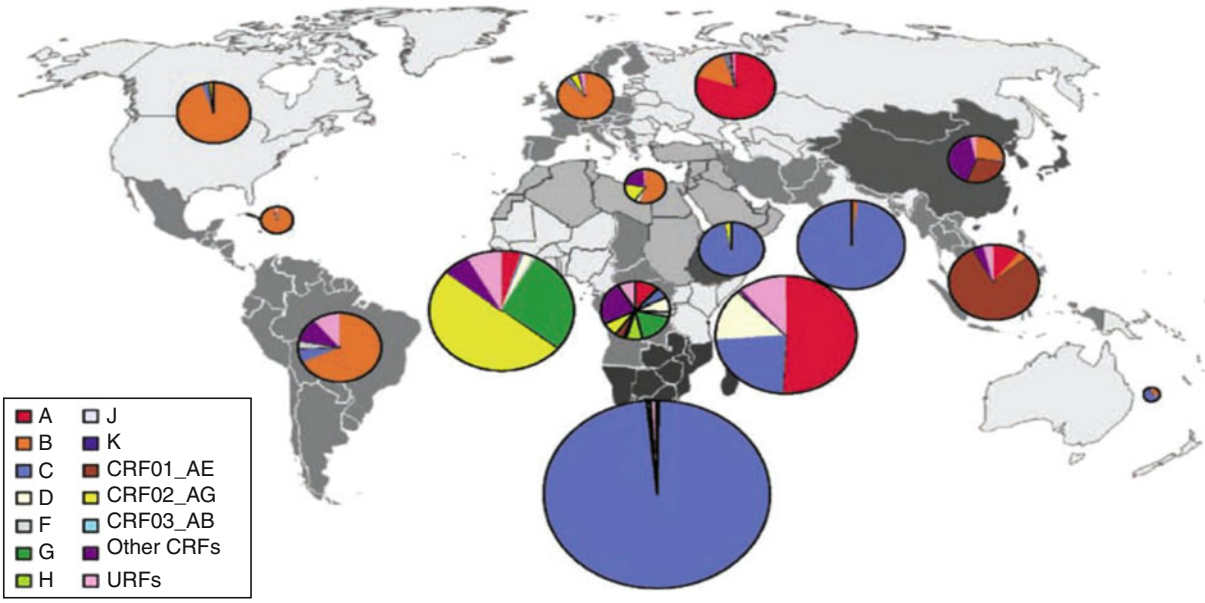

HIV/AIDS Global Epidemic. Figure 5

Regional distribution of HIV-1 subtypes and recombinant viruses, 2004–2007. Fifteen regions of the world are depicted with *pie charts* representing the distribution of HIV-1 subtypes and recombinants from 2004 to 2007. The size of the pie charts corresponds to the relative numbers of people living with HIV in the region. *CRF* circulating recombinant form, *URF*, unique recombinant form (Adapted from [109])

the massive heterosexual epidemic in southeastern Africa, subtype C also caused a rapid heterosexual epidemic in Western India, apparently initially spreading from the Bombay region [114, 117]. The results in Africa and Asia suggest that HIV-1 subtypes A, C, D, and CRF01_AE are well adapted for heterosexual transmission compared to subtype B, perhaps due to differential ability to infect dendritic cells in the sexual mucosa [118].

Various studies have shown associations between viral genotype and biology [119]. There is some evidence suggesting a relationship between subtype and modes of transmission. Studies in Cape Town [120], Finland [121], Thailand [122, 123], and Australia [124] found that most subtype B strains were associated with homosexual transmission while non-B strains were associated with heterosexual transmission. Infection with certain subtypes has also been associated with increased risk of vertical transmission. A study conducted on mother-child pairs in Tanzania revealed that mothers infected with HIV-1 subtype A, subtype C, and intersubtype recombinant were more likely to transmit to their infants than mothers infected with subtype D [125]. In an earlier related study, Renjifo et al. [126] also found that in perinatally transmitted C/D recombinant viruses, the V3 regions (*env*) were always from subtype C and never from subtype D, suggesting that viruses containing subtype D-V3 have a reduced fitness as compared to those with subtype C-V3. Finally, a study of injection drug users in Thailand found a significantly higher transmission probability associated with subtype E (CRF_01 AE) as compared to subtype B [127].

Some studies have also demonstrated significant differences between subtypes with regards to disease progression. Kanki et al. [128] found that women infected with a non-A subtype were eight times more likely to develop AIDS than were those infected with subtype A. Similarly, Kaleebu et al. [129, 130] reported that subjects with subtype A had a slower progression to disease than those with subtype D. Clinical and immunological differences have also been found between subtypes. In Kenya, where subtypes A, C, and D were all cocirculating within the same population, Neilson et al. [131] found that high plasma RNA levels and low CD4 counts were significantly associated with subtype C infection. In a prospective study conducted at a methadone treatment clinic in Thailand, people infected with CRF01_AE were found to have higher viral loads in early infection than those infected with subtype B [132]. However, this difference decreased over time such that the viral loads were similar at 12, 18, and 24 months postseroconversion [132]. Similarly, a study in our laboratory indicated that women infected with CRF02_AG had a significantly higher viral load during the early stage of infection than women not infected with CRF02_AG [133]. Infection with multiple subtypes has also been associated with higher viral load and lower CD4+ T cell counts [134].

Complete sequence analysis of viruses from around the world has further characterized an HIV pandemic that is increasing in complexity with a higher prevalence of recombinant viruses, currently at 20% of all HIV viruses [109]. In West Africa, Asia, and South America, the predominant virus is a circulating recombinant form. The predominant virus of West Africa is CRF02_AG, which appears to represent a recombinant event that occurred early in the divergence of subtypes A and G. In contrast, the BC and BF recombinants of China and South America, respectively, are derived from more recent recombinants between contemporary parental virus lineages [135]. An understanding of the genetic diversity of predominant HIV-1 subtypes, sub-subtypes, and circulating recombinant forms in a given population may be important in designing effective HIV vaccines [136, 137]. Although the importance of matching a vaccine candidate to regional circulating strains is yet unclear, incorporation of local strains might maximize the efficacy of a potential vaccine candidate [137].

Treatment

Antiretroviral therapy (ART) drugs that block or reduce HIV virus replication in the infected patient are used for the treatment of AIDS. The first ART drug was put into use in 1986–1987: zidovudine (AZT), a nucleoside reverse transcriptase inhibitor (NRTI) that because of its chemical similarity to the host's nucleoside, inhibited the growing DNA chain and served as a chain terminator such that virus replication could not occur. Other NRTIs act in a similar

manner, but another class of ART drugs includes nonnucleoside reverse transcriptase inhibitors (NNRTI), which bind to the virus' reverse transcriptase enzyme in a specific position and manner, blocking the enzyme from completing the transcription. NRTI and NNRTIs are often used in combination as the typical first-line regimens for patients with AIDS [138–140]. Since AZT, there has been tremendous progress in developing improved and more efficacious ART drugs and combination regimens for treating AIDS patients in high-income regions of the world; however, the cost of many of these newer drugs has been prohibitive for most middle- and low-income countries despite their disproportionate share of the AIDS burden.

Currently, there are a total of five classes of FDA-approved ART drugs that act on different parts of the HIV virus life cycle: NRTIs and NNRTIs act on the reverse transcription; other drugs act by inhibiting the viral protease, the viral integrase, or blocking virus entry at the level of the coreceptor. ART is typically prescribed in combination with current recommendations requiring at least two active classes of drugs [138–140]. Side effects and toxicities for each of these drugs may be serious and result in significant complications, requiring the patient to switch drug regimens.

The error-prone reverse transcription of HIV replication and its viral dynamics suggest that every possible single point mutation in the HIV genome occurs between 10^4 and 10^5 times per day in an untreated HIV-1-infected individual [141]. Therefore, the propensity for development of drug resistance mutations is high and the reason that strict adherence to taking the prescribed drugs is necessary to maintain viral suppression. In an effort to improve adherence and decrease pill burden to the patients, fixed-dose combination pills are available for most of the typical first-line ART regimens, allowing all drugs to be included in a single pill.

By the late 1990s, treatment for AIDS was widely available in high-income countries, but the vast majority of patients in middle- and low-income countries could not access these expensive drugs. In 2000, at the United Nations Millennium Summit, Kofi Annan declared a call for action to address the gap in treatment and to promote prevention and research in response to the AIDS epidemic [142]. In 2001, the UN General Assembly adopted a Declaration of Commitment on HIV/AIDS, endorsing equitable access to care and treatment as a fundamental component of a comprehensive and effective global HIV response [143]. UNAIDS had reported at the end of 2002 that developing countries had ~300,000 AIDS patients receiving ART with an unmet need estimated at 5.5 million [144]. The international donor community moved toward addressing the goals of equitable access through initiation of large-scale treatment and care programs. The President's Emergency Plan for AIDS Relief (PEPFAR), a program launched in late 2003, authorized over $15 billion dollars in 15 target countries, the largest commitment to a single disease in the history of US government support [145]. Other programs such as the Global Fund to Fight AIDS, Tuberculosis and Malaria [146], the Bill & Melinda Gates Foundation [147], Clinton Foundation [148], World Bank [149], and Medecins Sans Frontieres [150], to name a few, supported this effort with advocacy to country governments, and the rapid scale-up of providing ART to patients in need moved from rhetoric to action.

UNAIDS reported at the end of 2009 that 5.2 million people in low- and middle-income countries received ART, a significant increase from 2008 and unimaginable in 2003 [2]. However, the pandemic has continued, and in these countries, this accomplishment only represents 36% of the 15 million AIDS patients in these countries in need. Children and patients coinfected with TB remain an ART priority in these settings. Many of the original ART drugs developed in the late 1980s went off patent and have now been manufactured in generic form and meet international standards [151]. The Clinton Foundation in mid-2000 helped negotiate important drug cost reductions so that first-line drug per patient approximated $350 per year, rather than the $1,000 per month of the brand name drugs in 2000 [148]. However, the improvement in ART therapy in high-income countries was made possible through newer drugs and new classes of drugs like integrase inhibitors, or entry blockers, which are still cost-prohibited in most middle- and low-income country ART programs. Thus, although patients are receiving ART, the pharmacy of drugs available for toxicities or second- and third-line therapy remains limited in most low-income countries.

ART is not just the provision of pills; the diagnosis of AIDS requires laboratory tests and the clinical management of an AIDS patient entails regular monitoring of immune function, diagnosis, and treatment of comorbidities and measurement of viral load (virus levels in the bloodstream) when possible [142]. These laboratory tests often require sophisticated lab equipment and costs per test that can be quite high, almost the same cost of annual drug costs. In many low-income settings, these diagnostic or monitoring tests were not even available; in some instances where patients were required to pay for clinical tests, the costs were prohibitive to the typical AIDS patient that already had significant economic burdens. In recent years, a major contribution of large-scale care and treatment support from PEPFAR and others has built the infrastructure and provided the training to perform these critical laboratory tests. Provision of laboratory equipment, insuring adequate clean water and electricity to run the equipment and laboratory test specific requirements for cold chain, and short expiration remain challenges for both start-up and sustainability. In some instances, the costs of the tests have been reduced, but there is a critical need for cheaper, efficient, and point-of-care tests that will increase their availability and use for patient management.

Further, the complexity of clinical management and care of HIV infection requires training, infrastructure building, and overall strengthening of the existing health-care system in most developing country settings. Again, the leadership in individual countries coupled with support from the international donor communities has provided the training necessary for the complex administration of HIV care and treatment. However, human resources in many countries are limiting, and further efforts to encourage task-shifting within the medical team and bolstering of the medical education system are important to achieving the provision of ART to the many patients that are still in need.

Vaccine

Since the discovery of the virus and its initial characterization in the early 1980s, the search for an effective vaccine has been the subject of intense research. HIV infection can occur via free virus and/or virus-infected cells. Once infection has occurred with integration of viral genetic material in the target host cell, elimination of the virus by the host's immune mechanisms is not possible. The approach to vaccine design has often sought to mimic the protective immune responses, often identified in animal model systems or in individuals that have demonstrated protection [152, 153]. To date, the correlates of protective immunity from HIV have yet to be identified. Vaccine scientists therefore began with more conventional approaches of seeking to design vaccine candidates that would elicit strong virus-neutralizing antibodies or robust cell-mediated responses or both [154, 155]. The proof of principle has been shown for both of these approaches in nonhuman primate model [156, 157]. However, the model has not been predictive of HIV vaccine efficacy in humans; differences in routes of exposures, strains, and amount of virus are just some of the complexities of this model. Dozens of vaccine candidates have been developed, tested in nonhuman primate models and even early clinical trials in humans [157, 158].

AIDS vaccine candidates are evaluated in a stepwise manner in a series of clinical trials known as phases I, II, and III. Phase I and II trials generally involve a small number of volunteers and provide researchers with critical information about the safety and immunogenicity of the vaccine. The cost of phase III trials can be in hundreds of millions of dollars, and the enrollment for the trial is large, so the AIDS vaccine community moved to an intermediate "test of concept" trial where lower numbers of trial participants were needed; the statistical power of the trial design would allow evaluation of immunogenicity and low ranges of efficacy. It is not until phase III trials that the efficacy of the vaccine is truly assessed.

Candidate HIV vaccines that were tested in phase I and II trials over the past 20 years included inactivated whole virus, or virus particles, subunit HIV envelope vaccines delivered in novel adjuvant or delivery systems, DNA vaccines and live recombinant vector vaccines, and various combination approaches. The results of phase I and II trials indicated that they were safe but did not generate sufficient immune responses to warrant proceeding to phase III trials [157, 159–163].

By 2008, only four candidate HIV vaccines had proceeded to phase IIb and III efficacy trials. Two of the trials were subunit gp120 (envelope) vaccines tested by VaxGen in the USA, Canada, and the Netherlands

with 5,400 volunteers, largely men who have sex with men [164]. A second trial was conducted in 2,545 intravenous drug users in Thailand, using recombinant envelope from subtype B and also CRF01_AE [165, 166]. Although neutralizing antibodies were induced by the vaccine, neither trial showed evidence of protection. Subsequently, two trials assessed vaccine candidates based on the premise that cellular immune responses would be protective; the viral antigens were delivered in an adenovirus 5 vector; in order to enhance the generation of the cellular responses, the candidates were tested in the "Step" and "Phambili" trials conducted by Merck [167–169]. Adenovirus 5 is considered a harmless virus, but it does infect humans, and many populations mount antibodies to this virus, frequently without any signs of disease. Some of the volunteers in the Step and Phambili trials did not have antibodies to adenovirus 5, and in those volunteers, the vaccine showed no effect. However, in volunteers with antibodies to adenovirus 5, the vaccinated group showed higher rates of HIV infection, and thus, the vaccine had increased rather than decreased the chances of HIV infection [167–170]. Both trials were interrupted as a result of these unexpected results.

In 2008, a Summit on HIV Vaccine Research and Development determined that research toward a vaccine needed to place greater emphasis on basic research and slowed the pace of candidates, moving toward expensive clinical trials in people [171, 172].

In late 2009, the results of the US military vaccine group's RV144 trial in Thailand were announced. A phase IIb trial was conducted with a recombinant vector approach using the ALVAC virus (an avian poxvirus) used to express HIV proteins to prime the immune response combined with recombinant gp120 protein; both of these entities alone had been tested in people and shown poor immunogenicity [173]. The RV144 trial conducted in 16,400 men and women in Thailand starting in 2003, nonetheless, showed a modest efficacy of 31% protection after 3.5 years of follow-up; there were 51 infected in the vaccine group compared with 74 in similarly sized placebo group [174]. Further analysis of those protected failed to show significant neutralizing antibodies or even CD8+ T cell responses although more had favorable CD4+ T cell responses. Thus, the trial, while giving some optimism for vaccines, has failed to clearly indicate what specific type of immunity was responsible for the protection seen; further analysis will continue to evaluate the trial in hopes of guiding more improved candidates for the future [175].

While the search for a vaccine continues, the research thus far has given not only the scientific community a deeper understanding of both the HIV virus but also the human immune system and its interaction with this unique virus [157]. This will not only inform vaccine efforts for other infectious diseases but also facilitate the use of novel immunomodulatory entities and delivery systems that have been developed and tested. The development of an effective HIV vaccine will be used in conjunction with the many established methods of prevention that have been described, and new modalities such as male circumcision and ART treatment as prevention, which show great promise for additional preventative benefits [176]. Advances in these areas have now merged the interventions of treatment, vaccine, and prevention, to form a future strategy of combined prevention [69].

Future Directions

Thirty years ago, a mysterious disease affecting men who have sex with men in the USA initiated the world's appreciation of a new human virus with disease-causing potential and global spread that was unprecedented. Since that time, it is estimated that 60 million people have been infected with HIV responsible for over 25 million deaths. The history of HIV's discovery is instructive to our overall outlook on infectious diseases in general. HIV originated in closely related viruses of primates with multiple variants that still resemble close relationship to the viruses of great apes. The virus and its many genetic variants showed distinct differences in its epidemiology based on geographic location, risk groups affected, spread, and disease. In addition, the increasing complexity and higher prevalence of recombinant forms of the HIV epidemic suggests that more vigilant surveillance with improved technologies will be important. The marked dichotomy between the epidemics of high-income versus middle- and low-income countries has challenged public health efforts to address prevention and treatment needs. ART drugs

and laboratory tests developed in high-income countries are high in cost and complexity of use; this continues to be a major obstacle to the largest number of people infected and suffering from HIV and AIDS. In the past decade, an international effort to provide equal access to prevention, care, and treatment has demonstrated that the gap in access can be narrowed. Newer and more efficacious regimens to prevent mother-to-child transmission have just been adopted in the 2010 WHO guidelines and hold the potential of eliminating transmission as the guidelines are rolled out [84]. WHO has also revised the 2010 ART guidelines, which will initiate treatment for patients with less severe disease, CD4+ cell counts below 350, rather than 200 cells per cubic milliliter of blood [177]. While the increased costs and actual implementation of these new guidelines will pose an obstacle for many poor countries of the world, the ultimate realization of these guidelines will further decrease the burden of people living with HIV and increase the longevity of those already on treatment.

The historic and unprecedented support and efforts from the international donor community have made major progress in scaling up prevention and treatment of HIV in areas of the world with the most need. They have begun the difficult task of encouraging national leadership, building up broken or nonexistent health systems, in order to address the pandemic, but the burden of disease is still significant, and efforts must be continued with a perspective of long-term sustainability.

Bibliography

1. UNAIDS (2007) AIDS epidemic update. http://data.unaids.org/pub/epislides/2007/2007_epiupdate_en.pdf
2. UNAIDS (2009) AIDS epidemic update. http://data.unaids.org/pub/Report/2009/JCI700/Epi Update 2009 en.pdf
3. Gottlieb MS, Schroff R, Schanker HM, Weisman JD, Fan PT, Wolf RA, Saxon A (1981) Pneumocystis carinii pneumonia and mucosal candidiasis in previously healthy homosexual men: evidence of a new acquired cellular immunodeficiency. N Engl J Med 305:1425–1431
4. Masur H, Michelis MA, Greene JB, Onorato I, Stouwe RA, Holzman RS, Brettman L, Lange M, Murray HW, Cunningham-Rundles S (1981) An outbreak of community-acquired *Pneumocystis carinii* pneumonia: initial manifestation of cellular immune dysfunction. New Eng J Med 305:1431–1438
5. Siegal FP, Lopez C, Hammer GS, Brown AE, Kornfeld SJ, Gold J, Hassett J, Hirschman SZ, Cunningham-Rundles C, Adelsberg BR et al (1981) Severe acquired immunodeficiency in male homosexuals, manifested by chronic perianal ulcerative herpes simplex lesions. New Eng J Med 305:1439–1444
6. Anonymous (1982) Epidemiologic aspects of the current outbreak of Kaposi's sarcoma and opportunistic infections. New Eng J Med 306:248–252
7. Davis KC, Horsburgh CR Jr, Hasiba U, Schocket AL, Kirkpatrick CH (1983) Acquired immunodeficiency syndrome in a patient with hemophilia. Ann Int Med 98:284–286
8. Poon MC, Landay A, Prasthofer EF, Stagno S (1983) Acquired immunodeficiency syndrome with *Pneumocystis carinii* pneumonia and Mycobacterium avium-intracellulare infection in a previously healthy patient with classic hemophilia. Clinical, immunologic, and virologic findings. Ann Int Med 98:287–290
9. Elliott JL, Hoppes WL, Platt MS, Thomas JG, Patel IP, Gansar A (1983) The acquired immunodeficiency syndrome and Mycobacterium avium-intracellulare bacteremia in a patient with hemophilia. Ann Int Med 98:290–293
10. Curran JW, Lawrence DN, Jaffe H, Kaplan JE, Zyla LD, Chamberland M, Weinstein R, Lui KJ, Schonberger LB, Spira TJ et al (1984) Acquired immunodeficiency syndrome (AIDS) associated with transfusions. New Eng J Med 310: 69–75
11. Jaffe HW, Francis DP, McLane MF, Cabradilla C, Curran JW, Kilbourne BW, Lawrence DN, Haverkos HW, Spira TJ, Dodd RY, Gold J, Armstrong D, Ley A, Groopman J, Mullins JI, Lee TH, Essex M (1984) Transfusion-associated AIDS: serologic evidence of human T-cell leukemia virus infection of donors. Science 223:1309–1312
12. Piot P, Quinn TC, Taelman H, Feinsod FM, Minlangu KB, Wobin O, Mbendi N, Mazebo P, Ndangi K, Stevens W (1984) Acquired immunodeficiency syndrome in a heterosexual population in Zaire. Lancet 2:65–69
13. Van de Perre P, Rouvroy D, Lepage P, Bogaerts J, Kestelyn P, Kayihigi J, Hekker AC, Butzler JP, Clumeck N (1984) Acquired immunodeficiency syndrome in Rwanda. Lancet 2:62–65
14. Clumeck N, Mascart-Lemone F, de Maubeuge J, Brenez D, Marcelis L (1983) Acquired immune deficiency syndrome in Black Africans (letter). Lancet 1:642
15. Oleske J, Minnefor A, Cooper R et al (1983) Immune deficiency syndrome in children. J Am Med Assoc 249:2345–2349
16. Scott GB, Buck BE, Leterman JG et al (1984) Acquired immunodeficiency syndrome in infants. New Eng J Med 310:76–81
17. Francis DP, Curran JW, Essex M (1983) Epidemic acquired immune deficiency syndrome (AIDS): epidemiologic evidence for a transmitted agent. J Natl Cancer Inst 71:1–6
18. Essex M, McLane MF, Lee TH, Falk L, Howe CWS, Mullins J, Cabradilla C, Francis DP (1983) Antibodies to cell membrane antigens associated with human T-cell leukemia virus in patients with AIDS. Science 220:859–862

19. Essex M, McLane MF, Lee TH, Tachibana N, Mullins JI, Kreiss J, Kasper CK, Poon M-C, Landay A, Stein SF, Francis DP, Cabradilla C, Lawrence DN, Evatt BL (1983) Antibodies to human T-cell leukemia virus membrane antigens (HTLV-MA) in hemophiliacs. Science 221:1061–1064
20. Gelmann EP, Franchini G, Manzari V, Wong-Staal F, Gallo RC (1984) Molecular cloning of a unique human T-cell leukemia virus (HTLV-IIMo). Proc Natl Acad Sci USA 81:993–997
21. Gallo RC, Sarin PS, Gelmann EP, Robert-Guroff M, Richardson E, Kalyanaraman VS, Mann D, Sidhu GD, Stahl RE, Zolla-Pazner S, Leibowitch J, Popovic M (1983) Isolation of human T-cell leukemia virus in acquired immune deficiency syndrome (AIDS). Science 220:865–867
22. Barre-Sinoussi F, Chermann J-C, Rey F, Nugeyre MT, Chamaret S, Gruest J, Dauguet C, Axler-Blin C, Vezinet-Brun F, Rouzioux C, Rozenbaum W, Montagnier L (1983) Isolation of T-lymphotropic retrovirus from a patient at risk for acquired immune deficiency syndrome (AIDS). Science 220:868–870
23. Poiesz BJ, Ruscetti FW, Reitz MS, Kalyanaraman VS, Gallo RC (1981) Isolation of a new type C retrovirus (HTLV) in primary uncultured cells of a patient with Sezary T-cell leukaemia. Nature 294:268–271
24. Ammann AJ, Abrams D, Conant M, Chudwin D, Cowan M, Volberding P, Lewis B, Casavant C (1983) Acquired immune dysfunction in homosexual men: immunologic profiles. Clin Immunol Immunopathol 27:315–325
25. Fahey JL, Prince H, Weaver M, Groopman J, Visscher B, Schwartz K, Detels R (1984) Quantitative changes in T helper or T suppressor/cytotoxic lymphocyte subsets that distinguish acquired immune deficiency syndrome from other immune subset disorders. Amer J Med 6:95–100
26. Lane HC, Masur H, Gelmann EP, Longo DL, Steis RG, Chused T, Whalen G, Edgar LC, Fauci AS (1985) Correlation between immunologic function and clinical subpopulations of patients with the acquired immune deficiency syndrome. Am J Med 78:417–422
27. Kalyanaraman VS, Sarngadharan MG, Robert-Guroff M, Miyoshi I, Golde D, Gallo RC (1982) A new subtype of human T-cell leukemia virus (HTLV-II) associated with a T-cell variant of hairy cell leukemia. Science 218:571–573
28. Gelmann EP, Popovic M, Blayney D, Masur H, Sidhu G, Stahl RE, Gallo RC (1983) Proviral DNA of a retrovirus, human T-cell leukemia virus, in two patients with AIDS. Science 220:862–865
29. Popovic M, Sarin PS, Robert GM, Kalyanaraman VS, Mann D, Minowada J, Gallo RC (1983) Isolation and transmission of human retrovirus (human T-cell leukemia virus). Science 219:856–859
30. Schupbach J, Popovic M, Gilden RV, Gonda MA, Sarngadharan MG, Gallo RC (1984) Serological analysis of a subgroup of human T-lymphotropic retroviruses (HTLV-III) associated with AIDS. Science 224:503–505
31. Sarngadharan MG, Popovic M, Bruch L, Schupbach J, Gallo RC (1984) Antibodies reactive with human T-lymphotropic retroviruses (HTLV-III) in the serum of patients with AIDS. Science 224:506–508
32. Barin F, M'Boup S, Denis F, Kanki P, Allan JS, Lee TH, Essex M (1985) Serological evidence for virus related to simian T-lymphotropic retrovirus III in residents of west Africa. Lancet 2:1387–1389
33. Kanki P, Barin F, Mboup S, Allan JS, Romet-Lemonne JL, Marlink R, McLane MF, Lee TH, Arbeille B, Denis F, Essex M (1986) New human T-Lymphotropic retrovirus related to simian T-lymphotropic virus type III (STLV-III_{AGM}). Science 232:238–243
34. Gao F, Bailes E, Robertson DL, Chen Y, Rodenburg CM, Michael SF, Cummins LB, Arthur LO, Peeters M, Shaw GM, Sharp PM, Hahn BH (1999) Origin of HIV-1 in the chimpanzee Pan troglodytes troglodytes (see comments). Nature 397: 436–441
35. Hirsch VM, Olmsted RA, Murphey Corb M, Purcell RH, Johnson PR (1989) An African primate lentivirus (SIVsm) closely related to HIV-2. Nature 339:389–392
36. Marlink R, Kanki P, Thior I, Travers K, Eisen G, Siby T, Traore I, Hsieh SS, Dia MC, Gueye EH, Hellinger J, Gueye NA, Sankalé JL, Ndoye I, Mboup S, Essex M (1994) Reduced rate of disease development with HIV-2 compared to HIV-1. Science 265:1587–1590
37. Kanki PJ, De Cock KM (1994) Epidemiology and natural history of HIV-2. AIDS 8:S1–S9
38. Kanki P, Peeters M, Gueye-NDiaye A (1997) Virology of HIV-1 and HIV-2. AIDS 2(Suppl B):S33–S42
39. Kanki P (1989) HIV-2 infection in West Africa. In: Volberding P, Jacobson M (eds) 1988 AIDS clinical reviews. Marcel Dekker, New York, pp 95–108
40. Kanki P, Meloni S (2009) Biology and variation in HIV-2 and HIV-1. In: Marlink RG, Teitelman S (eds) From the ground up: building comprehensive HIV/AIDS care programs in resource-limited settings. Elizabeth Glaser Pediatric AIDS Foundation, Washington, DC, pp 1–24
41. Katzourakis A, Tristem M, Pybus OG, Gifford RJ (2007) Discovery and analysis of the first endogenous lentivirus. Proc Natl Acad Sci USA 104:6261–6265
42. Wong-Staal F (1990) Human immunodeficiency viruses and their replication. In: Fields DM et al (eds) Virology. Raven, New York, pp 1529–1540
43. NIAID (2011) HIV Replication cycle. http://www.niaid.nih.gov/topics/HIVAIDS/Understanding/Biology/Pages/hivReplicationCycle.aspx
44. Jiang S (1997) HIV-1–co-receptors binding (letter; comment) (published erratum appears in Nat Med 1997 Aug; 3(8):817). Nat Med 3:367–368
45. Feng Y, Broder CC, Kennedy PE, Berger EA (1996) HIV-1 entry cofactor: functional cDNA cloning of a seven-transmembrane G protein-coupled receptor. Science 272: 872–877
46. Deng H, Liu R, Ellmeier W, Choe S, Unutmaz D, Burkhart M, Di Marzio P, Marmon S, Sutton RE, Hill CM, Davis CB, Peiper SC, Schall TJ, Littman DR, Landau NR (1996) Identification of

a major co-receptor for primary isolates of HIV-1. Nature 381:661–666
47. Cocchi F, DeVico AL, Garzino-Demo A, Cara A, Gallo RC, Lusso P (1996) The V3 domain of the HIV-1 gp120 envelope glycoprotein is critical for chemokine-mediated blockade of infection. Nat Med 2:1244–1247
48. Dittmar M, McNight A, Simmons G, Clapham P, Weiss R (1997) HIV-1 tropism and co-receptor use. Nature 385:495–496
49. Moore PS, Boshoff C, Weiss RA, Chang Y (1996) Molecular mimicry of human cytokine and cytokine response pathway genes by KSHV. Science 274:1739–1744
50. Cooper DA, Imrie AA, Penny R (1987) Antibody response to human immunodeficiency virus after primary infection. J Infect Dis 155:1113–1118
51. Loes S, de Saussure P, Saurat JH, Stalder H, Hirschel B, Perrin LH (1993) Symptomatic primary infection due to human immunodeficiency virus type 1: review of 31 Cases. Clin Infect Dis 17:59–65
52. Fauci AS, Pantaleo G, Stanley S, Weissman D (1996) Immunopathogenic mechanisms of HIV infection. Ann Intern Med 124:654–663
53. Pantaleo G, Graziosi C, Demarest JF, Butini L, Montroni M, Fox CH, Orenstein JM, Kotler DP, Fauci AS (1993) HIV infection is active and progressive in lymphoid tissue during the clinically latent stage of disease. Nature 362:355–358
54. Cavarelli M, Scarlatti G (2011) Human immunodeficiency virus type 1 mother-to-child transmission and prevention: successes and controversies. J Intern Med 270(6):561–579
55. Bongaarts J, Sinding S (2011) Population policy in transition in the developing world. Science 333:574–576
56. Bongaarts J, Pelletier F, Gerland P (2010) How many more AIDS deaths? Lancet 375:103–104
57. Root R (2010) Situating experiences of HIV-related stigma in Swaziland. Glob Public Health 5:523–538
58. Wu Z, Sullivan SG, Wang Y, Rotheram-Borus MJ, Detels R (2007) Evolution of China's response to HIV/AIDS. Lancet 369:679–690
59. Wang L (2007) Overview of the HIV/AIDS epidemic, scientific research and government responses in China. AIDS 21(Suppl 8):S3–7
60. UNAIDS (2010) Global report Europe and Central Asia. http://www.unaids.org/en/regionscountries/regions/easterneuropeandcentralasia/
61. Guillard EM, Eustache L (2007) Estimation de la séroprevalence du VIH en Haiti en 2007 selon le milieu de residence urbain et rural pour chacun des 10 départments. United States Agency for International Development, Washington, DC
62. Anonymous (2008) US Virgin Islands and Caribbean HIV epidemic need more attention, researchers say. HIV infection rate is high among sex workers. AIDS Alert 23:42–44
63. Bezemer D, de Wolf F, Boerlijst MC, van Sighem A, Hollingsworth TD, Prins M, Geskus RB, Gras L, Coutinho RA, Fraser C (2008) A resurgent HIV-1 epidemic among men who have sex with men in the era of potent antiretroviral therapy. AIDS 22: 1071–1077
64. Mathers BM, Degenhardt L, Ali H, Wiessing L, Hickman M, Mattick RP, Myers B, Ambekar A, Strathdee SA (2010) HIV prevention, treatment, and care services for people who inject drugs: a systematic review of global, regional, and national coverage. Lancet 375:1014–1028
65. Strathdee SA, Hallett TB, Bobrova N, Rhodes T, Booth R, Abdool R, Hankins CA (2010) HIV and risk environment for injecting drug users: the past, present, and future. Lancet 376:268–284
66. Stockman JK, Strathdee SA (2010) HIV among people who use drugs: a global perspective of populations at risk. J Acquir Immune Def Syn 55(Suppl 1):S17–22
67. de Felipe B, Perez-Romero P, Abad-Fernandez M, Fernandez-Cuenca F, Martinez-Fernandez FJ, Trastoy M, Mata Rdel C, Lopez-Cortes LF, Leal M, Viciana P, Vallejo A (2011) Prevalence and resistance mutations of non-B HIV-1 subtypes among immigrants in Southern Spain along the decade 2000–2010. Virol J 8:416
68. Ryan CE, Gare J, Crowe SM, Wilson K, Reeder JC, Oelrichs RB (2007) The heterosexual HIV type 1 epidemic in Papua New Guinea is dominated by subtype C. AIDS Res Hum Retroviruses 23:941–944
69. Centers for Disease Control and Prevention (2011) High-impact HIV prevention – CDC's approach to reducing HIV infections in the United States. CDC, Atlanta
70. Katoff L, Dunne R (1988) Supporting people with AIDS: the Gay Men's health crisis model. J Palliat Care 4:88–95
71. Laga M, Galavotti C, Sundararaman S, Moodie R (2010) The importance of sex-worker interventions: the case of Avahan in India. Sex Transm Infect 86(Suppl 1):i6–7
72. Verma R, Shekhar A, Khobragade S, Adhikary R, George B, Ramesh BM, Ranebennur V, Mondal S, Patra RK, Srinivasan S, Vijayaraman A, Paul SR, Bohidar N (2010) Scale-up and coverage of Avahan: a large-scale HIV-prevention programme among female sex workers and men who have sex with men in four Indian states. Sex Transm Infect 86(Suppl 1):i76–i82
73. Tobian AA, Gray RH (2011) The medical benefits of male circumcision. J Am Med Assoc 306:1479–1480
74. Kreiss JK, Hopkins SG (1993) The association between circumcision status and human immunodeficiency virus infection among homosexual men. J Infect Dis 168:1404–1408
75. Weiss HA, Quigley MA, Hayes RJ (2000) Male circumcision and risk of HIV infection in sub-Saharan Africa: a systematic review and meta-analysis. AIDS 14:2361–2370
76. Siegfried N, Muller M, Deeks JJ, Volmink J (2009) Male circumcision for prevention of heterosexual acquisition of HIV in men. Cochrane Database Syst Rev: CD003362
77. Weiss HA, Hankins CA, Dickson K (2009) Male circumcision and risk of HIV infection in women: a systematic review and meta-analysis. Lancet Infect Dis 9:669–677
78. Auvert B, Taljaard D, Lagarde E, Sobngwi-Tambekou J, Sitta R, Puren A (2005) Randomized, controlled intervention trial of male circumcision for reduction of HIV infection risk: the ANRS 1265 Trial. PLoS Med 2:e298
79. Gray RH, Kigozi G, Serwadda D, Makumbi F, Watya S, Nalugoda F, Kiwanuka N, Moulton LH, Chaudhary MA, Chen MZ,

Sewankambo NK, Wabwire-Mangen F, Bacon MC, Williams CF, Opendi P, Reynolds SJ, Laeyendecker O, Quinn TC, Wawer MJ (2007) Male circumcision for HIV prevention in men in Rakai, Uganda: a randomised trial. Lancet 369:657–666

80. Wawer MJ, Makumbi F, Kigozi G, Serwadda D, Watya S, Nalugoda F, Buwembo D, Ssempijja V, Kiwanuka N, Moulton LH, Sewankambo NK, Reynolds SJ, Quinn TC, Opendi P, Iga B, Ridzon R, Laeyendecker O, Gray RH (2009) Circumcision in HIV-infected men and its effect on HIV transmission to female partners in Rakai, Uganda: a randomised controlled trial. Lancet 374:229–237
81. WHO/UNAIDS (2007) Announce recommendations about male circumcision as HIV prevention. Strategy should be employed with care. AIDS Alert 22:66–67
82. Shapiro RL, Hughes MD, Ogwu A, Kitch D, Lockman S, Moffat C, Makhema J, Moyo S, Thior I, McIntosh K, van Widenfelt E, Leidner J, Powis K, Asmelash A, Tumbare E, Zwerski S, Sharma U, Handelsman E, Mburu K, Jayeoba O, Moko E, Souda S, Lubega E, Akhtar M, Wester C, Tuomola R, Snowden W, Martinez-Tristani M, Mazhani L, Essex M (2010) Antiretroviral regimens in pregnancy and breast-feeding in Botswana. N Engl J Med 362:2282–2294
83. Chasela CS, Hudgens MG, Jamieson DJ, Kayira D, Hosseinipour MC, Kourtis AP, Martinson F, Tegha G, Knight RJ, Ahmed YI, Kamwendo DD, Hoffman IF, Ellington SR, Kacheche Z, Soko A, Wiener JB, Fiscus SA, Kazembe P, Mofolo IA, Chigwenembe M, Sichali DS, van der Horst CM (2010) Maternal or infant antiretroviral drugs to reduce HIV-1 transmission. N Engl J Med 362:2271–2281
84. World Health Organization (2010) Antiretroviral drugs for treating pregnant woman and preventing HIV infections in infants, Recommendations for a public health approach. 2010 revision.
85. Youle M, Wainberg MA (2003) Pre-exposure chemoprophylaxis (PREP) as an HIV prevention strategy. J Int Assoc Physicians AIDS Care (Chic) 2:102–105
86. Young TN, Arens FJ, Kennedy GE, Laurie JW, Rutherford G (2007) Antiretroviral post-exposure prophylaxis (PEP) for occupational HIV exposure. Cochrane Database Syst Rev:CD002835
87. Karim QA, Kharsany AB, Frohlich JA, Baxter C, Yende N, Mansoor LE, Mlisana KP, Maarschalk S, Arulappan N, Grobler A, Sibeko S, Omar Z, Gengiah TN, Mlotshwa M, Samsunder N, Karim SS (2011) Recruitment of high risk women for HIV prevention trials: baseline HIV prevalence and sexual behavior in the CAPRISA 004 tenofovir gel trial. Trials 12:67
88. Karim QA, Kharsany AB, Naidoo K, Yende N, Gengiah T, Omar Z, Arulappan N, Mlisana KP, Luthuli LR, Karim SS (2011) Co-enrollment in multiple HIV prevention trials – experiences from the CAPRISA 004 Tenofovir gel trial. Contemp Clin Trials 32:333–338
89. Abdool Karim Q, Abdool Karim SS, Frohlich JA, Grobler AC, Baxter C, Mansoor LE, Kharsany AB, Sibeko S, Mlisana KP, Omar Z, Gengiah TN, Maarschalk S, Arulappan N, Mlotshwa M, Morris L, Taylor D (2010) Effectiveness and safety of tenofovir gel, an antiretroviral microbicide, for the prevention of HIV infection in women. Science 329:1168–1174
90. Grant RM, Lama JR, Anderson PL, McMahan V, Liu AY, Vargas L, Goicochea P, Casapia M, Guanira-Carranza JV, Ramirez-Cardich ME, Montoya-Herrera O, Fernandez T, Veloso VG, Buchbinder SP, Chariyalertsak S, Schechter M, Bekker LG, Mayer KH, Kallas EG, Amico KR, Mulligan K, Bushman LR, Hance RJ, Ganoza C, Defechereux P, Postle B, Wang F, McConnell JJ, Zheng JH, Lee J, Rooney JF, Jaffe HS, Martinez AI, Burns DN, Glidden DV (2010) Preexposure chemoprophylaxis for HIV prevention in men who have sex with men. N Engl J Med 363:2587–2599
91. Cohen MS, Chen YQ, McCauley M, Gamble T, Hosseinipour MC, Kumarasamy N, Hakim JG, Kumwenda J, Grinsztejn B, Pilotto JH, Godbole SV, Mehendale S, Chariyalertsak S, Santos BR, Mayer KH, Hoffman IF, Eshleman SH, Piwowar-Manning E, Wang L, Makhema J, Mills LA, de Bruyn G, Sanne I, Eron J, Gallant J, Havlir D, Swindells S, Ribaudo H, Elharrar V, Burns D, Taha TE, Nielsen-Saines K, Celentano D, Essex M, Fleming TR (2011) Prevention of HIV-1 infection with early antiretroviral therapy. N Engl J Med 365:493–505
92. Vissers DC, Voeten HA, Nagelkerke NJ, Habbema JD, de Vlas SJ (2008) The impact of pre-exposure prophylaxis (PrEP) on HIV epidemics in Africa and India: a simulation study. PLoS One 3:e2077
93. Veronese F, Anton P, Fletcher CV, DeGruttola V, McGowan I, Becker S, Zwerski S, Burns D (2011) Implications of HIV PrEP trials results. AIDS Res Hum Retroviruses 27:81–90
94. Alizon M, Wain-Hobson S, Montagnier L, Sonigo P (1986) Genetic variability of the AIDS virus: nucleotide sequence analysis of two isolates from African patients. Cell 46: 63–74
95. Wei X, Ghosh SK, Taylor ME, Johnson VA, Emini EA, Deutsch P, Lifson JD, Bonhoeffer S, Nowak MA, Hahn BH, Saag MS, Shaw GM (1995) Viral dynamics in human immunodeficiency virus type 1 infection. Nature 373:117–122
96. Ho DD, Nuemann AU, Perelson AS, Chen W, Leonard JM, Markovitz M (1995) Rapid turnover of plasma virions and CD4 lymphocytes in HIV-1 infection. Nature 373:123–126
97. Starcich BR, Hahn BH, Shaw GM, McNeely PD, Modrow S, Wolf H, Parks ES, Parks WP, Josephs SF, Gallo RC, Wong-Staal F (1986) Identification and characterization of conserved and variable regions in the envelope gene of HTLV-III/LAV, the retrovirus of AIDS. Cell 45:637–648
98. Wong-Staal F, Gallo RC (1985) Human T-lymphotropic retroviruses. Nature 317:395–403
99. Myers G, Pavlakis GN (1992) Evolutionary potential of complex retroviruses. In: Levy JA (ed) The retroviridae. Plenum, New York, pp 1–37
100. Goodenow M, Huet TH, Saurin W, Kowk S, Sninsky J, Wain-Hobson S (1989) HIV-1 isolates are rapidly evolving quasispecies: evidence for viral mixtures and preferred nucleotide substitutions. J Acquir Immune Def Syn 2: 344–352
101. Wolfs TFW, deJong JJ, van den Berg H, Tijnagel JMGH, Krone WJA, Goudsmit J (1990) Evolution of sequences encoding the principal neutralization epitope of human immunodeficiency

virus type 1 is host dependent, rapid, and continuous. Proc Natl Acad Sci USA 87:9938–9942
102. Balfe P, Simmonds P, Ludlam CA, Bishop JO, Brown AJ (1990) Concurrent evolution of human immunodeficiency virus type 1 in patients infected from the same source: rate of sequence change and low frequency of inactivating mutations. J Virol 64:6221–6233
103. Essex M, Kanki P (1997) Human immunodeficiency virus type 2 (HIV-2). In: Merigan T, Bartlett J, Bologenesi D (eds) Textbook of AIDS medicine, 2nd edn. Williams & Wilkins, Baltimore, pp 873–886
104. Sharp PM, Bailes E, Chaudhuri RR, Rodenburg CM, Santiago MO, Hahn BH (2001) The origins of acquired immune deficiency syndrome viruses: where and when? Philos Trans R Soc Lond B Biol Sci 356:867–876
105. Gurtler LG, Hauser PH, Eberle J, von Brunn A, Knapp S, Zekeng L, Tsague JM, Kaptue L (1994) A new subtype of human immunodeficiency virus type 1 (MVP-5180) from Cameroon. J Virol 68:1581–1585
106. Simon F, Mauclére P, Roques P, Loussert-Ajaka I, Muller-Trutwin MC, Saragosti S, Georges-Courbot MC, Barre-Sinoussi F, Brun-Vezinet F (1998) Identification of a new human immunodeficiency virus type 1 distinct from group M and group O. Nat Med 4:1032–1037
107. Plantier JC, Leoz M, Dickerson JE, De Oliveira F, Cordonnier F, Lemee V, Damond F, Robertson DL, Simon F (2009) A new human immunodeficiency virus derived from gorillas. Nat Med 15:871–872
108. Keele BF, Van Heuverswyn F, Li Y, Bailes E, Takehisa J, Santiago ML, Bibollet-Ruche F, Chen Y, Wain LV, Liegeois F, Loul S, Ngole EM, Bienvenue Y, Delaporte E, Brookfield JF, Sharp PM, Shaw GM, Peeters M, Hahn BH (2006) Chimpanzee reservoirs of pandemic and nonpandemic HIV-1. Science 313:523–526
109. Hemelaar J, Gouws E, Ghys PD, Osmanov S (2011) Global trends in molecular epidemiology of HIV-1 during 2000–2007. AIDS 25:679–689
110. Louwagie J, McCutchan F, Mascola J (1993) Genetic subtypes of HIV-1. AIDS Res Hum Retroviruses 9(Suppl 1): 147s–150s
111. Louwagie J, McCutchan F, Peeters M (1993) Phylogenetic analysis of gag genes from 70 international HIV-1 isolates provides evidence for multiple genotypes. AIDS 7:769–780
112. McCutchan F, Salimen MO, Carr JK, Burke DS (1996) HIV-1 genetic diversity. AIDS 10:S13–S20
113. Burke D, McCutchan F (1997) Global distribution of human immunodeficiency virus-1 clades. In: Vincent T, DeVita J, Hellman S, Rosenberg S (eds) AIDS: biology, diagnosis, treatment and preventions, 4th edn. Lippincott-Raven, Philadelphia, pp 119–126
114. Weniger BG, Takebe Y, Ou C-Y, Yamazaki S (1994) The molecular epidemiology of HIV in Asia. AIDS 8:13s–28s
115. Korber B, Brander C, Moore J, D'Souza P, Walker B, Koup R, Moore J, Haynes B, Myers G (eds) (1996) HIV molecular immunology database 1996. Theoretical Biology and Biophysics Group, Los Alamos National Laboratory, Los Alamos
116. Robertson D, Gao F, Hahn B, Sharp PM (1997) Intersubtype recombinant HIV-1 sequences. In: Korber B, Hahn B, Foley B, Mellors JW, Leitner T, Myers G, McCutchan F, Kuiken C (eds) Human retroviruses and AIDS 1997. Theoretical Biology and Biophysics Group, Los Alamos National Laboratory, Los Alamos, pp III-25-III30
117. Jain MK, John TJ, Keusch GT (1994) Epidemiology of HIV and AIDS in India. AIDS 8:S61–75
118. Soto-Ramirez LE, Renjifo B, McLane MF, Marlink R, O'Hara C, Sutthent R, Wasi C, Vithayasai P, Vithayasai V, Apichartpiyakul C, Auewarakul P, Pena Cruz V, Chui DS, Osathanondh R, Mayer K, Lee TH, Essex M (1996) HIV-1 Langerhans' cell tropism associated with heterosexual transmission of HIV. Science 271:1291–1293
119. Taylor BS, Sobieszczyk ME, McCutchan FE, Hammer SM (2008) The challenge of HIV-1 subtype diversity. N Engl J Med 358:1590–1602
120. Vanharmelen J, Wood R, Lambrick M, Rybicki EP, Williamson AL, Williamson C (1997) An association between HIV-1 subtypes and mode of transmission in Capetown, South Africa. AIDS 11:81–87
121. Liitsola K, Holmstrom P, Laukkanen T, Brummer-Korvenkontio H, Leinikki P, Salminen MO (2000) Analysis of HIV-1 genetic subtypes in Finland reveals good correlation between molecular and epidemiological data. Scand J Infect Dis 32:475–480
122. Kalish ML, Korber BT, Pillai S, Robbins KE, Leo YS, Saekhou A, Verghese I, Gerrish P, Goh CL, Lupo D (2002) The sequential introduction of HIV-1 subtype B and CRF01 in Singapore by sexual transmission: accelerated V3 region evolution in a subpopulation of Asian CRF01 viruses. Virology 304:311–329
123. Ou CY, Takebe Y, Weniger BG, Luo CC, Kalish ML, Auwanit W, Yamazaki S, Gayle HD, Young NL, Schochetman G (1993) Independent introduction of two major HIV-1 genotypes into distinct high-risk populations in Thailand. Lancet 341:1171–1174
124. Herring BL, Ge YC, Wang B, Ratnamohan M, Zheng F, Cunningham AL, Saksena NK, Dwyer DE (2003) Segregation of human immunodeficiency virus type 1 subtypes by risk factor in Australia. J Clin Microbiol 41:4600–4604
125. Renjifo B, Fawzi W, Mwakagile D, Hunter D, Msamanga G, Spiegelman D, Garland M, Kagoma C, Kim A, Chaplin B, Hertzmark E, Essex M (2001) Differences in perinatal transmission among human immunodeficiency virus type 1 genotypes. J Hum Virol 4:16–25
126. Renjifo B, Gilbert P, Chaplin B, Vannberg F, Mwakagile D, Msamanga G, Hunter D, Fawzi W, Essex M (1999) Emerging recombinant human immunodeficiency viruses: uneven representation of the envelope V3 region. AIDS 13: 1613–1621

127. Hudgens MG, Longini IM Jr, Vanichseni S, Hu DJ, Kitayaporn D, Mock PA, Halloran ME, Satten GA, Choopanya K, Mastro TD (2002) Subtype-specific transmission probabilities for human immunodeficiency virus type 1 among injecting drug users in Bangkok, Thailand. Am J Epidemiol 155:159–168
128. Kanki PJ, Hamel DJ, Sankalé JL, Hsieh CC, Thior I, Barin F, Woodcock SA, Guèye-NDiaye A, Zhang E, Montano M, NDoye I, Essex ME, MBoup S (1999) Human immunodeficiency virus type 1 subtypes differ in disease progression. J Infect Dis 179:68–73
129. Kaleebu P, French N, Mahe C, Yirrell D, Watera C, Lyagoba F, Nakiyingi J, Rutebemberwa A, Morgan D, Weber J, Gilks C, Whitworth J (2002) Effect of human immunodeficiency virus (HIV) type 1 envelope subtypes A and D on disease progression in a large cohort of HIV-1-positive persons in Uganda. J Infect Dis 185:1244–1250
130. Kaleebu P, Ross A, Morgan D, Yirrell D, Oram J, Rutebemberwa A, Lyagoba F, Hamilton L, Biryahwaho B, Whitworth J (2001) Relationship between HIV-1 env subtypes A and D and disease progression in a rural Ugandan cohort. AIDS 15:293–299
131. Neilson JR, John GC, Carr JK, Lewis P, Kreiss JK, Jackson S, Nduati RW, Mbori-Ngacha D, Panteleeff DD, Bodrug S, Giachetti C, Bott MA, Richardson BA, Bwayo J, Ndinya-Achola J, Overbaugh J (1999) Subtypes of human immunodeficiency virus type 1and disease stage among women in Nairobi, Kenya. J Virol 73:4393–4403
132. Hu DJ, Vanichseni S, Mastro TD, Raktham S, Young NL, Mock PA, Subbarao S, Parekh BS, Srisuwanvilai L, Sutthent R, Wasi C, Heneine W, Choopanya K (2001) Viral load differences in early infection with two HIV-1 subtypes. AIDS 15:683–691
133. Sarr AD, Eisen G, Gueye-Ndiaye A, Mullins C, Traore I, Dia MC, Sankale JL, Faye D, Mboup S, Kanki P (2005) Viral dynamics of primary HIV-1 infection in Senegal, West Africa. J Infect Dis 191:1460–1467
134. Sagar M, Lavreys L, Baeten JM, Richardson BA, Mandaliya K, Chohan BH, Kreiss JK, Overbaugh J (2003) Infection with multiple human immunodeficiency virus type 1 variants is associated with faster disease progression. J Virol 77:12921–12926
135. Zhang M, Foley B, Schultz AK, Macke JP, Bulla I, Stanke M, Morgenstern B, Korber B, Leitner T (2010) The role of recombination in the emergence of a complex and dynamic HIV epidemic. Retrovirology 7:25–40
136. Ellenberger DL, Li B, Lupo LD, Owen SM, Nkengasong J, Kadio-Morokro MS, Smith J, Robinson H, Ackers M, Greenberg A, Folks T, Butera S (2002) Generation of a consensus sequence from prevalent and incident HIV-1 infections in West Africa to guide AIDS vaccine development. Virology 302:156–163
137. Essex M (2009) The impact of HIV variation on prevention and treatment. In: Kanki PM, Marlink RG (eds) A line drawn in the sand. Harvard University Press, Cambridge, MA, pp 231–242
138. Siegfried N, Uthman OA, Rutherford GW (2010) Optimal time for initiation of antiretroviral therapy in asymptomatic, HIV-infected, treatment-naive adults. Cochrane Database Syst Rev:CD008272
139. Spaulding A, Rutherford GW, Siegfried N (2010) Tenofovir or zidovudine in three-drug combination therapy with one nucleoside reverse transcriptase inhibitor and one non-nucleoside reverse transcriptase inhibitor for initial treatment of HIV infection in antiretroviral-naive individuals. Cochrane Database Syst Rev:CD008740
140. Spaulding A, Rutherford GW, Siegfried N (2010) Stavudine or zidovudine in three-drug combination therapy for initial treatment of HIV infection in antiretroviral-naive individuals. Cochrane Database Syst Rev:CD008651
141. Coffin JM (1996) HIV viral dynamics. AIDS 10:S75–84
142. Kanki P, Marlink RG (2009) A line drawn in the sand: responses to the AIDS treatment crisis in Africa. Harvard University Press, Cambridge, MA
143. United Nations (2001) Secretary-general urges united states business leaders to take concerted action against "Unparalleled Nightmare" of AIDS, U.N. Document
144. UNAIDS (2003) AIDS epidemic. data.unaids.org/publications/inc-pub06/jc943.epiupdate2003_en_pdf
145. PEPFAR (2011) United States President's emergency plan for AIDS relief. http://www.pepfar.gov/about/index.html
146. GFATM (2002) Global fund to fight AIDS, Tuberculosis and Malaria. http://www.theglobalfund.org/en/
147. BMGF (2011) Bill & Melinda Gates Foundation Global Health http://www.gatesfoundation.org/global-health/Pages/overview.aspx
148. CHAI (2011) Clinton Health Access Initiative. http://www.clintonfoundation.org/what-we-do/clinton-health-access-initiative
149. MAP (2011) World Bank Multi-Country HIV/AIDS Program (MAP). http://web.worldbank.org/WBSITE/EXTERNAL/COUNTRIES/AFRICAEXT/EXTAFRHEANUTPOP/EXTAFRREGTOPHIVAIDS/0,,contentMDK:20415735~menuPK:1001234~pagePK:34004173~piPK:34003707~theSitePK:717148,00.html
150. MSF (2011) Medecins sans Frontieres. http://www.msf.org/msf/about-msf/about-msf_home.cfm
151. Holmes C, Coggin W, Jamieson D, Mihm H, Savio P, Hope M, Ryan C, Moloney-Kitts M, Dybul M (2009) Measuring progress in reducing the costs of ARV drugs purchased by the president's emergency plan for AIDS relief, 2005–2007. In: Conference on retroviruses and opportunistic infections. Montreal, Canada
152. Shearer G, Clerici M (2010) Historical perspective on HIV-exposed seronegative individuals: has nature done the experiment for us? J Infect Dis 202(Suppl 3): S329–332
153. O'Brien SJ, Nelson GW (2004) Human genes that limit AIDS. Nat Genet 36:565–574

154. Wu X, Yang ZY, Li Y, Hogerkorp CM, Schief WR, Seaman MS, Zhou T, Schmidt SD, Wu L, Xu L, Longo NS, McKee K, O'Dell S, Louder MK, Wycuff DL, Feng Y, Nason M, Doria-Rose N, Connors M, Kwong PD, Roederer M, Wyatt RT, Nabel GJ, Mascola JR (2010) Rational design of envelope identifies broadly neutralizing human monoclonal antibodies to HIV-1. Science 329:856–861
155. Koup RA, Graham BS, Douek DC (2011) The quest for a T cell-based immune correlate of protection against HIV: a story of trials and errors. Nat Rev Immunol 11:65–70
156. Bradac J, Dieffenbach CW (2009) HIV vaccine development: lessons from the past, informing the future. IDrugs 12:435–439
157. Girard MP, Osmanov S, Assossou OM, Kieny MP (2011) Human immunodeficiency virus (HIV) immunopathogenesis and vaccine development: a review. Vaccine 29:6191–6218
158. Fauci AS, Johnston MI, Dieffenbach CW, Burton DR, Hammer SM, Hoxie JA, Martin M, Overbaugh J, Watkins DI, Mahmoud A, Greene WC (2008) HIV vaccine research: the way forward. Science 321:530–532
159. Corey L, McElrath MJ (2010) HIV vaccines: mosaic approach to virus diversity. Nat Med 16:268–270
160. Caputo A, Gavioli R, Bellino S, Longo O, Tripiciano A, Francavilla V, Sgadari C, Paniccia G, Titti F, Cafaro A, Ferrantelli F, Monini P, Ensoli F, Ensoli B (2009) HIV-1 Tat-based vaccines: an overview and perspectives in the field of HIV/AIDS vaccine development. Int Rev Immunol 28:285–334
161. MacGregor RR, Boyer JD, Ugen KE, Lacy KE, Gluckman SJ, Bagarazzi ML, Chattergoon MA, Baine Y, Higgins TJ, Ciccarelli RB, Coney LR, Ginsberg RS, Weiner DB (1998) First human trial of a DNA-based vaccine for treatment of human immunodeficiency virus type 1 infection: safety and host response. J Infect Dis 178:92–100
162. Pantaleo G, Esteban M, Jacobs B, Tartaglia J (2010) Poxvirus vector-based HIV vaccines. Curr Opin HIV AIDS 5:391–396
163. Graham BS, Koup RA, Roederer M, Bailer RT, Enama ME, Moodie Z, Martin JE, McCluskey MM, Chakrabarti BK, Lamoreaux L, Andrews CA, Gomez PL, Mascola JR, Nabel GJ (2006) Phase 1 safety and immunogenicity evaluation of a multiclade HIV-1 DNA candidate vaccine. J Infect Dis 194:1650–1660
164. Flynn NM, Forthal DN, Harro CD, Judson FN, Mayer KH, Para MF (2005) Placebo-controlled phase 3 trial of a recombinant glycoprotein 120 vaccine to prevent HIV-1 infection. J Infect Dis 191:654–665
165. Gilbert PB, Peterson ML, Follmann D, Hudgens MG, Francis DP, Gurwith M, Heyward WL, Jobes DV, Popovic V, Self SG, Sinangil F, Burke D, Berman PW (2005) Correlation between immunologic responses to a recombinant glycoprotein 120 vaccine and incidence of HIV-1 infection in a phase 3 HIV-1 preventive vaccine trial. J Infect Dis 191:666–677
166. Gilbert PB, Ackers ML, Berman PW, Francis DP, Popovic V, Hu DJ, Heyward WL, Sinangil F, Shepherd BE, Gurwith M (2005) HIV-1 virologic and immunologic progression and initiation of antiretroviral therapy among HIV-1-infected subjects in a trial of the efficacy of recombinant glycoprotein 120 vaccine. J Infect Dis 192:974–983
167. Buchbinder SP, Mehrotra DV, Duerr A, Fitzgerald DW, Mogg R, Li D, Gilbert PB, Lama JR, Marmor M, Del Rio C, McElrath MJ, Casimiro DR, Gottesdiener KM, Chodakewitz JA, Corey L, Robertson MN (2008) Efficacy assessment of a cell-mediated immunity HIV-1 vaccine (the Step Study): a double-blind, randomised, placebo-controlled, test-of-concept trial. Lancet 372:1881–1893
168. McElrath MJ, De Rosa SC, Moodie Z, Dubey S, Kierstead L, Janes H, Defawe OD, Carter DK, Hural J, Akondy R, Buchbinder SP, Robertson MN, Mehrotra DV, Self SG, Corey L, Shiver JW, Casimiro DR (2008) HIV-1 vaccine-induced immunity in the test-of-concept step study: a case-cohort analysis. Lancet 372:1894–1905
169. Gray G, Buchbinder S, Duerr A (2010) Overview of STEP and Phambili trial results: two phase IIb test-of-concept studies investigating the efficacy of MRK adenovirus type 5 gag/pol/nef subtype B HIV vaccine. Curr Opin HIV AIDS 5: 357–361
170. Nicholson O, Dicandilo F, Kublin J, Sun X, Quirk E, Miller M, Gray G, Pape J, Robertson MN, Mehrotra DV, Self S, Turner K, Sanchez J, Pitisuttithum P, Duerr A, Dubey S, Kierstead L, Casimiro D, Hammer SM (2010) Safety and immunogenicity of the MRKAd5 gag HIV type 1 vaccine in a worldwide phase 1 study of healthy adults. AIDS Res Hum Retroviruses 27(5):557–567
171. Voronin Y, Manrique A, Bernstein A (2010) The future of HIV vaccine research and the role of the Global HIV Vaccine Enterprise. Curr Opin HIV AIDS 5:414–420
172. Voronin Y, Phogat S (2010) HIV/AIDS: vaccines and alternate strategies for treatment and prevention. Ann NY Acad Sci 1205(Suppl 1):E1–9
173. Nitayaphan S, Pitisuttithum P, Karnasuta C, Eamsila C, de Souza M, Morgan P, Polonis V, Benenson M, VanCott T, Ratto-Kim S, Kim J, Thapinta D, Garner R, Bussaratid V, Singharaj P, El-Habib R, Gurunathan S, Heyward W, Birx D, McNeil J, Brown AE (2004) Safety and immunogenicity of an HIV subtype B and E prime-boost vaccine combination in HIV-negative Thai adults. J Infect Dis 190:702–706
174. Rerks-Ngarm S, Pitisuttithum P, Nitayaphan S, Kaewkungwal J, Chiu J, Paris R, Premsri N, Namwat C, de Souza M, Adams E, Benenson M, Gurunathan S, Tartaglia J, McNeil JG, Francis DP, Stablein D, Birx DL, Chunsuttiwat S, Khamboonruang C, Thongcharoen P, Robb ML, Michael NL, Kunasol P, Kim JH (2009) Vaccination with ALVAC and AIDSVAX to prevent HIV-1 infection in Thailand. N Engl J Med 361:2209–2220
175. Kresge KJ (2009) Raft of results energizes researchers. IAVI Rep 13:4–5, 7–13, 17
176. Dieffenbach CW, Fauci AS (2011) Thirty years of HIV and AIDS: future challenges and opportunities. Ann Intern Med 154:766–771
177. World Health Organization (2010) Antiretroviral therapy for HIV infection in adults and adolescents: recommendations for a public health approach. 2010 Revision, Geneva

HOT Lanes/Value Pricing: Planning and Evaluation of Multiclass Service

Douglass B. Lee, Jr., Kent M. Hymel
US Department of Transportation, Volpe National Transportation Systems Center, Cambridge, MA, USA

Article Outline

Glossary
Definition of the Subject
Introduction
Characteristics of Managed Lanes
Evaluation of Pricing Alternatives
Future Developments
Note
Bibliography

Glossary

HOT Lane A limited access (expressway) separated highway service that permits qualifying HOVs to travel free, but allows non-HOVs to use the service for a fee (toll) [1]. Also HO/T.

Managed lanes Separated lanes that are operated or controlled actively in a way to limit congestion; charging a toll is one way to manage and an occupancy requirement is another. Other management tools include temporary shoulder use and dynamic signing (see http://ops.fhwa.dot.gov/freewaymgmt/managed_lanes.htm and http://managed-lanes.tamu.edu/).

Congestion pricing A toll or user charge on a facility that varies by time of day in accordance with demand, so as to maintain traffic flow on the facility at a freely flowing speed. Flat tolls that do not vary with demand, i.e., by time of day, do not qualify as pricing, and are not included within the scope of managed lanes.

HOV A high-occupancy vehicle, meaning there is at least one passenger in addition to the driver; the definition or criterion may require a minimum of two passengers (HOV 3+) in order to be eligible to use the HOV reserved lane.

Reserved lane A separated dedicated lane restricted to one or more special purposes for which not all vehicles are eligible. Bus lanes, HOV lanes, HOT lanes, truck lanes, and express lanes are forms of reserved lanes. Heavy vehicles may not be permitted at all on restricted lanes.

Toll Payment by a user vehicle to access a reserved lane; the toll may vary by time of day or with the level of demand so as to manage congestion and may also vary by vehicle type.

Expressway A design standard for multilane divided highways with grade-separated interchanges. HOT lanes are installed on mostly urban expressways.

Express lane A lane that allows some traffic to go faster than the default alternative, by restricting entry or skipping stops. A common usage refers to a tolled lane on an expressway, whether HOVs are discounted or not.

Express toll lanes (ETL) Restricted lanes that are tolled, perhaps with discounts for HOVs; facilities that charge discounted rates for HOVs are also referred to as hybrid systems.

General purpose lanes (GP) Lanes available for unrestricted traffic; also mixed flow lanes.

Slug lines Persons who line up at transit stops offering themselves as passengers to allow autos to meet the criterion for HOV eligibility in the same corridor.

Value pricing Application of the microeconomic theory of efficient pricing to the problem of highway congestion.

ORT Open road tolling, allowing vehicles with transponders to maintain highway speed and change lanes while the toll is collected electronically.

VOT The value of travel time, or the opportunity cost per hour of time spent in traveling, including congestion.

VOR The value of reliability, which is the consistency and predictability of travel times. Both speed and reliability are goals of managed lanes.

VMT Vehicle miles of travel.

Definition of the Subject

Economists have recognized for a long time (and transportation professionals more recently) that congestion on highways indicates that they are being operated inefficiently. The inefficiency stems from a failure to vary the price that drivers face with the level of demand

for vehicle travel on the congested facility. In practice, congestion pricing on a transportation facility or service utilizes tolls that vary either by time of day, or directly with demand. Although there are many tolled highway facilities in the USA, including bridges, tunnels, and turnpikes, (see http://www.fhwa.dot.gov/ohim/tollpage.htm), few currently vary the toll by time of day (see http://ceprofs.tamu.edu/mburris/pricing.htm). One example is the New Jersey Turnpike and another is the Port Authority Hudson River crossings in New York City that have recently introduced a modest variation for peak periods [2].

Pricing one or more lanes of a facility so as to keep traffic on them moving smoothly, while leaving parallel lanes unpriced, is one way to increase the price toward a more efficient level. This strategy for congestion pricing is the dominant paradigm in the USA, and is referred to both as HOT lanes and as value pricing.

In most instances, tolled express lanes were preceded by lanes that were (or would have been) reserved for high-occupancy vehicles (HOVs). HOV lanes were created in an attempt to induce travelers to carpool by offering them a faster trip in return for the willingness to coordinate travel schedules and take only one vehicle. The goal can also be viewed as increasing passenger throughput by getting higher-occupancy vehicles to the head of the queue [3]. Although the utilization of HOV lanes is often well below capacity, reducing the criterion for high occupancy by one passenger may overshoot capacity by allowing too many vehicles. The concept of selling off the extra capacity to single-occupant vehicles (SOVs) was developed in order to "fine-tune" demand and more productively utilize the full capacity of the lanes. Such lanes became high-occupancy/toll lanes, or HOT lanes.

"Value Pricing" is a label that was developed for the purpose of avoiding the term "congestion pricing," thought at the time to create a negative impression. Subsequently, congestion pricing has been adopted as an acceptably neutral term, and value pricing has come to mean providing separated express service for an additional fee, on the same facility as the untolled service. Technically, such a differentiated alternative is a multiclass service, and it is this multiclass attribute that is the defining characteristic of HOT lane service.

Introduction

HOT lanes are the most popular form of road congestion pricing in the USA, but the form occurs rarely outside the USA. Other ways of controlling congestion, such as charging for entry to the downtown area of a city, are found in other countries but not in the USA. Thus HOT lanes should be seen within the context of a range of strategies for managing congestion by varying the price of road use so as to encourage traffic to avoid times and locations where demand is high. The HOT lane strategy is a blending of two strategies that involve offering motorists a choice: (1) the HOV strategy of offering speedier service to vehicles in which there is a minimum number of occupants, and (2) the pricing strategy of setting a toll on a facility that is high enough to maintain free-flowing traffic during peak periods, and lowering the toll at other times.

Each management strategy has its primary features and numerous variations in implementation and detail, and consequently each strategy has its own advantages and disadvantages. Although the general method of raising the price during the peak – congestion pricing – is clearly beneficial (if the cost of imposing the pricing is not too large), the costs and benefits of the various incomplete or partial methods of applying congestion pricing are not so clear. For that reason, the theory and practical methods for evaluating HOT lanes against other strategies for congestion management that use pricing are discussed. The issues are not fully resolved at either the theoretical or the practical levels, despite many strong assertions about the benefits of some of the strategies.

A source of the difficulty of rigorously evaluating HOT lanes is in their nature of offering two alternative "classes" of service for serving the same purpose, namely, a vehicle trip from point A to point B. Users are making several choices simultaneously, primarily, how many persons share the same vehicle, whether to travel during the peak period in the peak direction or avoid peak conditions, and whether to select the faster premium service or the lower-priced unrestricted service.

Because HOT lane management is entangled with the currently unsettled and highly contentious policy decisions of how to manage and pay for roads, the future evolution of HOT lanes and related congestion pricing schemes is uncertain at this time in the USA.

Characteristics of Managed Lanes

The discussion that follows covers three main topics: what are HOT lanes and other "managed" lanes, how can we tell whether they make us better off, and how will they evolve? The first topic – description – outlines the characteristics of managed lanes within the urban transportation context. The second topic – evaluation – explains the economic theory for assessing the benefits of the HOT lane innovation and its alternatives. The third topic – future developments – speculates about the likely outcomes of conflicting current trends.

Distinguishing Features of Priced Lanes

HOV lanes, HOT lanes, and express lanes have been generically called "managed" lanes, implying that certain attributes of the service are controlled by the provider so as to affect the quality of service. The purpose of "lane management" is to reduce or control congestion on the lanes that are managed. Pricing is one mechanism for managing highway lanes, but occupancy requirements and truck-only lanes are also considered to be tools for lane management (Collier and Goodin [4] survey the planning, design, and operation of managed lanes, offering several case studies).

Although pricing is often classified as demand management, express lane management is more accurately viewed as supply management, even to the point of constructing additional lanes. One planning study listed HOV lanes, HOT lanes, express toll lanes, and truck-only toll lanes, and "special use lanes such as express, bus-only, or truck-only" as the full range of "management tools" [5]. To date, the multiclass service strategy for dealing with congestion has been applied almost exclusively in the USA (see, e.g., [6] on European experience).

HOT lanes have been utilized in metropolitan areas on limited access urban expressways. Table 1 lists projects currently in operation; others are under construction or planned. An express lane can be a single lane per direction or several; two lanes per direction is common and also the maximum in practice.

Electronic Toll Collection Electronic toll collection (ETC) on HOT lanes is required in practice, and can be implemented using prepaid accounts, automatic debit accounts, or via video license plate readers [11]. The toll paid to use the express lanes may or may not apply to HOVs, but the price is set on the tolled vehicles so as to maintain free-flowing conditions on the express lanes (the SOV share gets as high as 16% in Minneapolis [12]). Congestion on the remaining general purpose (GP) lanes is left to fall where it may. Users are usually informed of the reserved lane toll near points of

HOT Lanes/Value Pricing: Planning and Evaluation of Multiclass Service. Table 1 Existing HOT/Express lanes in the USA in 2010

Location	Name	Year opened	Length (mile)	Lanes (reversible)
Orange Country, CA	SR-91 Express lanes	1995	10	4
Houston, TX	QuickRide (US 290)	2000	13	1R
Houston, TX	Katy freeway managed lanes	2009	13	1R
Denver, CO	I-25 HOT lanes	2006	7	4
San Diego, CA	I-15 Fastrak	1996	8	4R
Miami, FL	I-95 HOT lanes northbound	2008	21	2
Minneapolis, MN	I-394 MnPASS express lanes	2005	13	2
Minneapolis, MN	I-35 MnPASS express lanes	2010	13	2
Salt Lake City, UT	I-15 HOT lanes	2006	38	2
Seattle, WA	SR-167 HOT lanes pilot	2008	9	2

Sources: [7–10].
The number of lanes and their reversibility often changes from one section of the facility to another

entry, especially when tolls are determined by concurrent congestion levels. Implementation of a HOT lane facility in practice is a demanding task. There are many reports that describe the process of planning, outreach, consensus, physical configuration, barrier separation, access points, operational details, etc. Two extensive guidebooks are Parsons Brinkerhoff [13] and PB Study Team [14].

Facilitating payment by manual toll collection, exact change, credit card, or other procedure that requires the vehicle to come to a full stop is very costly and disruptive. The trend is toward open-road tolling (ORT) in which the toll is collected electronically without any slowing down, and all HOT lanes currently operate as ORT. Mixed toll collection requires that non-ETC payers be segregated from the main travel stream, with enough storage space provided to serve them off-line, and then merged back into the free-speed stream.

Users without transponders can be billed by reading their license plates via video camera and sending a bill to the owner of the plate. The 407 highway around Toronto, Canada, has been primarily ETC for over a decade, with supplemental video tolling for the small share of traffic without transponders [15].

The HOV Lane Precursor Tolled express lanes likely would not have occurred in the USA without the pre-existence of HOV lanes (although the first – SR-91 – was built directly rather than being a conversion). Ironically, perhaps, separate lanes for high-occupancy vehicles was devised as an incentive mechanism that would achieve the behavior objectives of pricing without its deterrent effect.

The concept of giving priority to vehicles having more than one passenger was implemented primarily as a means to encourage bus transit and carpoolers over SOV (single occupant vehicles), and thus reduce the number of vehicles needed to carry the same number of passengers. The physical configurations to create the separate service range from lanes marked with a diamond but no barrier, to concrete barrier separation, to reversible lanes with barriers, queue bypass lanes, and separated bus-only lanes [16]. Lanes may be restricted only during weekday peaks or during all hours and days.

The potential gain from providing HOV lane service is a reduction in the number of vehicles as a result of ridesharing. The magnitude of the benefit is greater if existing carpools are not reduced, if new carpools are formed from existing peak travelers, if bus travelers do not switch to auto, and if the increase in vehicle occupancy is significant. In practice, the sources of additional occupants are same family (75%), work colleagues (20%), and casual carpooling [17]. The last depends heavily on the physical configuration of the corridor and the level of transit service ("slugs" come from transit). Thus the level of actual induced carpooling tends to be low, and not enough to overcome the handicaps of lower capacity overall and particularly on the HOV lane (Poole [18] notes the low effectiveness of occupancy requirements; Poole and Orski [19] describe the historical backlash against HOV lanes and the origins of HOT lanes; Lee [20] describes the loss of capacity). Because not all HOV operators provide data on utilization rates or violation rates, actual HOV performance can be difficult to assess [21].

The number of HOV facilities (roughly 350 in the USA) greatly exceeds the number of HOT lane examples. Some HOV lanes are over 50 miles in length (see [22] for a full HOV inventory and details). The large number of existing HOV lanes indicates that the pool of potential conversions from HOV to HOT lanes is large. Because the user cost of assembling a carpool is a fixed cost, per trip, the incentive is strongest for long commuting trips (over 35 miles, according to [23]). Conditions suitable for conversion of HOV lanes to HOT lanes are analyzed in detail in [24].

Multiclass Service A possible outcome of applying either the microeconomic theory of efficient pricing or of congestion management could be a strategic decision to offer two (or more) types of service whose primary differentiating characteristic is speed. The criteria for eligibility for the higher quality service could be a minimum vehicle occupancy level and/or the payment of a toll that varies with the level of demand.

The success and benefits of such a multiclass strategy depend upon heterogeneity in the values of travel time among the group of users at the time the service is offered. If all vehicles have the same value of travel time (VOT), then multiclass service may not be any better than single class service and could be worse if there are

costs in providing the service. Hence the desirability of offering two-class service depends upon the distribution of the values of (vehicle) time in the traffic stream. Ideally, there would be two relatively distinct groups of vehicles, with respect to time value. The emphasis on valuation at the vehicle rather than the person level is that it is the vehicle that is consuming the scarce resource, and different occupancy levels could provide sufficient distinction among vehicles to warrant multiclass service even if all travelers have the same VOT (see Both Services Priced Efficiently on p. 27).

Eligibility Requirements Use of the special lane is controlled by vehicle occupancy requirements, price, and other user or vehicle characteristics. Usually only one requirement (occupancy or price) needs to be satisfied. Other characteristics (proposals have been made to include low-emission vehicles (LEV) and hybrids as also deserving favorable treatment) are unrelated to congestion management but have taken a significant share of capacity on some facilities.

The effectiveness of HOV (untolled) lanes is difficult to sustain because fluctuations or growth in demand necessitate changes in the required number of vehicle occupants in order to insure free-flow conditions on the reserved lanes. If congestion occurs frequently with a two-person criterion for occupancy, then the criterion can be raised to three persons. But such a discrete change may result in the lanes being underutilized, at least for some period of time. In general, HOV lanes have not been shown to be effective in increasing occupancy or reducing congestion [25], compared to the same number of lanes in GP service. So far, HOV and HOT lanes have been the result of new construction, which inevitably reduces congestion below what it would have been without the added capacity.

Pricing refers to the application of microeconomic concepts for reconciling supply and demand, when normal market responses (changing price and quantity) are nonexistent or too rigid (other than queuing). For a given capacity (i.e., in the short run), price can be set so as to clear the market without resorting to queuing. Microeconomic theory requires setting price equal to marginal cost in order to achieve efficient utilization of the scarce resource (capacity), but "management" can be applied more broadly to achieve other appropriate goals such as a level of service (LOS) standard.

Performance Objectives Because the incentive for inducing vehicles to rideshare or pay the price depends upon a promise of faster and more reliable service, management of multiclass services places a primary emphasis on ensuring that the exclusive service is always superior. HOT lanes are sustainable in the short run and medium run because the price on the express lanes can be adjusted in time increments as short as 3 min, so as to maintain a consistent level of service (LOS) (the 3 min adjustment rate is claimed for the MnPASS express lanes in Minneapolis [12]).

The standard for level of service (LOS) can be defined in several ways, including the ratio of volume to capacity or the average speed for a given type of facility. Liu et al. [9] citing Supernak et al. [26] determine that US HOT lanes are priced to achieve 45 mph 90% of the peak period (approximately LOS C), which is congested but still flowing smoothly (see Transportation Research Board [27]). In practice, HOT lane prices can be adjusted upward and sometimes downward to maintain service standards; for example, tolls on the SR-91 express lanes in southern California were actually lowered in 2009 following a recession-caused decrease in demand [28]. Whether the tolls will be sufficient to maintain and replace the facility over the long run is largely unknown at present because the history of such lanes is still fairly short (see Revenues on p. 15 below).

Additional Costs of Multiclass Service

Creating a two-class (or more) service incurs several costs that can be avoided or lessened if the facility is left in a single class of service.

Safety and Enforcement With separate but unequal services, there is an incentive to take advantage of the faster service if that can be done without paying the price, whether the price is the inconvenience of carpooling or in the form of a toll. The incentive is especially strong if the GP lanes are barely moving while the restricted lanes are underutilized. If there are no barriers between the lanes, then some drivers may be tempted to switch lanes. Because this places fast and slow vehicles in juxtaposition, changing lanes creates a safety problem. If the violation rates are high (15%) for a tolled service, there is an additional

incentive to switch lanes, and there is a revenue loss to the owner. A study found a 15% violation rate on a Phoenix HOV lane that was (as is common) not barrier separated, even with a fine of $350 [29]. Finally, if eligibility includes a minimum number of occupants in the vehicle (or a hybrid gasoline-electric vehicle), enforcement may be more costly because visual verification of the occupancy or vehicle make is required (Poole [18] reviews the technology for occupancy verification and mentions that where HOV2 are eligible for free travel they are a majority of vehicles).

To minimize the cost of enforcement, physical separations of some kind are needed. There is thus a tradeoff between the cost of enforcement and the cost of physical infrastructure. Whatever the optimum balance, the net result is an increase in cost over a single undifferentiated service.

Accidents tend to be higher on HOV/HOT facilities, affected by differing traffic speeds when merging narrower lane width and shoulder width, but not affected by continuous versus limited access [30].

Infrastructure HOV services require shoulders, transition, or merging lanes, breakdown and emergency services, and other features that may be needed above those required for GP service. Some HOV lanes are simply marked with diamonds, with no buffer or barriers or pylons demarcating the lanes. Vehicles can enter or leave at any point.

Transforming HOV into HOT additionally requires toll collection gantries and machines, and back-office functions related to user accounts. Toll administration may or may not impose greater costs than normal ETC.

Electronic signs and other information systems are used to inform users of the toll rate on the express lanes, at the time the user needs to make a choice. Other information may also be conveyed, such as the days or hours of operation.

Loss of Capacity In general, the more lanes moving in the same direction, the greater the capacity per lane. This phenomenon occurs because vehicles can weave across lanes to make use of space in front of slower or less aggressive drivers. Hence, the disruption from entrance and exit ramps is lessened. But with barrier-separated lanes, such opportunities for weaving are diminished, which results in an effective loss of capacity. Rough averages for capacity and speed for different number of contiguous lanes are shown in Table 2. Actual capacities and speeds vary substantially from these upper-bound estimates on capacity and speed ranges. As for usage, many single HOV lanes rarely get above 1,000 vehicles per hour, perhaps as a result of the uneven demand from eligible vehicles.

One or two lanes is the norm for express lanes, whereas GP lanes or full facility pricing can apply across all numbers of lanes. Capacities are often dependent on the sources for inflow (feeder links) and recipients for outflow (exits).

Cassidy et al. [31] argue that carpool lanes can smooth traffic flows at bottlenecks, in all lanes including GP lanes, but these conditions apply when volume is sufficient to a cause breakdown in flow.

Imbalanced Throughput The maximum flow on the facility occurs when all lanes are part of the same flow. When some lanes are allowed to go faster, the total throughput for the two services combined is less than for the same number of lanes without separation. This result is due to the nonlinearity of delay: The marginal delay from adding a vehicle to a congested stream is always greater than the marginal reduction in delay from taking the vehicle from a less congestion stream. While popular intuition is perhaps as often wrong as right, the effect of unbalanced flows per lane is perceived as making throughput worse [32].

HOT Lanes/Value Pricing: Planning and Evaluation of Multiclass Service. Table 2 Estimated capacity and speed by number of lanes in the same direction [27]

Number of lanes	Capacity (vehicles per lane per hour)	Free-flow speed (mph)
1	1,600 [17]	45–55
2	1,800	58 Goodall and Smith [12] claim average speeds as high as 78 mph on a two-lane HOT lane service in Minneapolis
3	2,050	65
4 or more	2,200	70

If the objective is to minimize overall vehicle delay, the optimal result occurs when traffic is distributed equally across all lanes; at that point, the reassignment of any vehicle to another lane increases delay more on that lane than it reduces delay on the lane it left. This is necessarily the case because the second derivative of the delay curve is always positive. As an example, the speed–volume relationship can be represented by a curve of the BPR form

$$S(v) = \frac{F_s}{1 + \alpha\left(\frac{v}{c}\right)^{\gamma}}$$

where $S(v)$ = speed as a function of volume, F_s = free-flow speed, c = capacity, and α and γ are parameters [33]. Travel time is the reciprocal of speed.

This function is used in the illustrative example shown in Fig. 1, with $\alpha = 0.3$ and $\gamma = 7.0$. Consider a two-lane facility with a fixed vehicle flow (one direction), where the problem is how to allocate traffic to each lane to minimize total travel time. Proceeding from left to right in the diagram, as more traffic is added to lane 1 the total time cost declines because the extreme congestion in lane 2 is relieved without heavily impacting lane 1. The lowest curve shows vehicle delay for all vehicles combined. The minimum is reached when half the traffic is assigned to each lane.

Converting time into cost, through vehicle occupancy and the individual value of travel time (VOT), produces the thick solid curve that replicates the time curve (but higher on the graph) so long as both occupancy and VOT are the same for all vehicles.

If the number of occupants and their VOT are not uniform, lower travel cost may be obtained by sorting users into categories of higher occupancy and higher time value, rewarding the latter with faster travel times. Taking the numbers shown in Table 3, and assuming that the occupancy and time values are determined by the lane to which the vehicle is assigned, the time cost by the share assigned to lane 1 is shown by the heavier dashed magenta curve. VOT per person is the same for all travelers, but occupancy is twice as high on lane 2 as on lane 1. The optimum (least total time cost) occurs when about 56% of the traffic is on lane one, and the total cost is slightly lower than the average in part because higher VOT vehicles go faster and in part because there are fewer passengers (56% of the vehicles

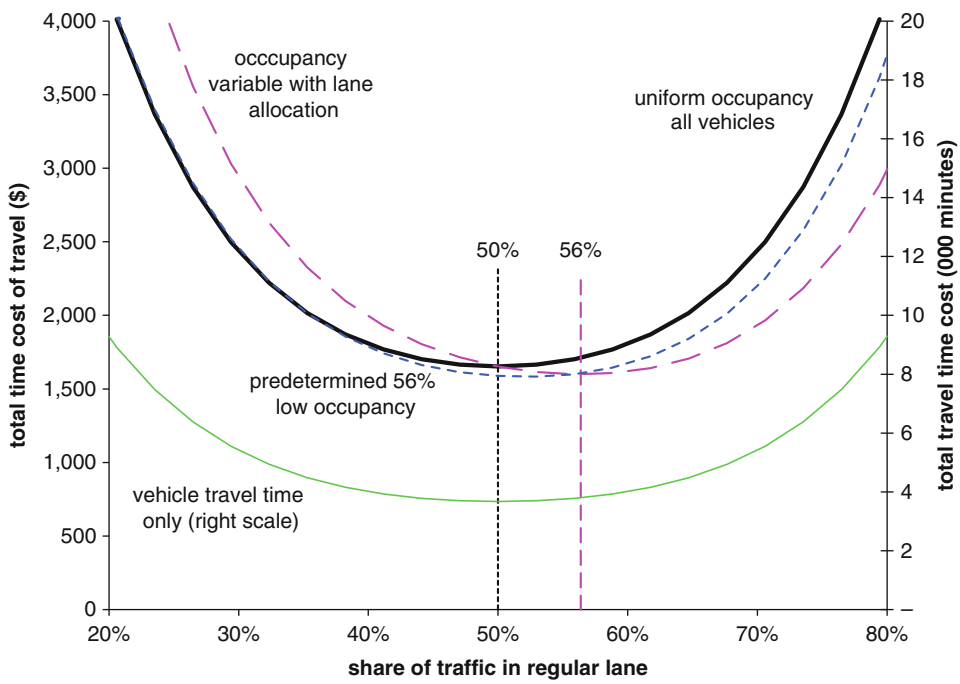

HOT Lanes/Value Pricing: Planning and Evaluation of Multiclass Service. Figure 1
Total travel time cost as a function of traffic share allocated to lane 1

have 1.2 passengers versus 50%). This curve crosses the uniform-traveler (dotted) curve at 50% because at that point they are the same.

If the number of vehicles in each category is determined a priori, such as in the right-hand column of Table 4, in this case at approximately 50%, the cost is shown by the heavy blue curve, which has a minimum between 50% and 56%. At the latter allocation, it is the same as the previous curve in which occupancy depended upon the lane to which the vehicle was assigned. Again, the parameters are the same at that point. Assigning more than 56% to lane 1, however, means assigning high-occupancy vehicles to the slow lane (more people at slower speed), so total cost rises rapidly. To the left of 56%, there are fewer people in the constant-occupancy scenario than the variable occupancy scenario, so costs are a little lower.

Changing VOT has the same effect as occupancy, which is to make the time of some vehicles higher valued than others. For a difference of a factor of 2.0 in the vehicle value of time, the least-cost flow still only varies from the equally balanced flow by less than five percentage points.

The Los Angeles County MTA has announced the intention of converting HOV lanes to HOT without reducing service on the GP lanes, which should not be a problem; the problem occurs if a GP lane is converted directly to HOT. So long as the HOV lane is a new lane, the political backlash is mild compared to taking an existing lane out of service. When the same capacity is split into classes, flow in the GP lanes may exceed the breakdown level, resulting in "hypercongestion," a condition in which capacity is less than what the facility is capable of under ideal conditions. The extent and magnitude of this phenomenon is open to question [34], but at a network level an overloaded system with unbalanced flows appears to be less productive than one that is not unbalanced [35].

HOT Lanes/Value Pricing: Planning and Evaluation of Multiclass Service. Table 3 Assumed average vehicle occupancy (AVO) for regular GP and HOT lanes

Vehicles	Occupancy	VOT	No. veh.
Low occupancy/regular	1.2	$15.00	1,900
High occupancy/HOT	2.4	$15.00	1,500
Average (unweighted)/ total	1.8	$15.00	3,400

HOT Lanes/Value Pricing: Planning and Evaluation of Multiclass Service. Table 4 Seattle SR-167 single lane speed and volume (Lin et al. [9])

Segment No.	% Peak flow <800 vph	% Flow >1,050 vpl %Speed >55 mph	Flow <1,050 vpl
1	82	1	99
2	31	7.2	92
3	9	10	77.4
4	21	11.1	87
5	8	11.2	87.7
6	30	7.5	91.4

Utilization Despite the pricing, HOT lanes may still be underutilized, if there is general resistance to paying tolls. Perhaps unusual, the HOT lanes in the Seattle area appear to be underutilized, despite congestion on the GP lanes. The data in Table 4, inferred from volume and occupancy detectors, indicate difficulty in achieving full utilization of all lanes.

Time savings on SR-167 averaged 9.1 min over 11 miles, but can get as high as 20 min. The express lanes consistently operate over 45 mph, with a mean travel time of 8.5 min and a standard deviation of 26 sec. The HOT service is relatively new, and demand is continuing to grow.

Currently, the existing ten US HOT lane examples are able to effectively manage the level of service on the HOT lanes by changing prices dynamically or by modifying fixed prices based on observation of traffic flows and patterns. Diagnostic guidance on obtaining close to optimum utilization in HOV or HOT lanes is provided in [36].

Demand

It is well known that express lane users do not always choose to pay for the faster service whenever they use the facility [37]. A large share of users pay the toll two or three times a week and use the GP lanes on other

days, making the choice to use the express lanes trip by trip. Hence the value of saving travel time varies considerably for the same individuals from one day to another, as well as among travelers.

Although peak travelers moving in the peak direction on the same facility are relatively affluent compared to the general population, they are far from identical. Occupancy, of course, also makes a difference in the vehicle's willingness to pay for faster speed.

Some demand studies exist for predicting the factors that determine which class of service a driver will select on the basis of traveler attributes, but less work exists that examines how variations in service attributes affect lane choice. Most new HOT lane users were previously SOVs in the GP lanes on the same facility (or HOV2s), at least in the case of conversions from HOV to HOT service [38]. Relative to other peak travelers, express lane users have significantly higher income and education than the average, even of other peak highway users. The small share of lower-income toll payers is likely to be in carpools. For the most part, carpoolers use the express lanes because they are already carpooling; few carpools are formed in order to use the lanes. While there are no surprises here, it may be reassuring that HOT lanes do not cannibalize carpools or transit.

Market Research on Express Lane Users The demand model may be approximated as this: Users estimate the magnitude of the time savings and decide whether the price is right, without changing mode or occupancy. Other reasons as well, however, factor in. Drivers in Minneapolis use the HOT lanes even when there is no time advantage, perhaps by (previous) habit or perhaps to ensure reliability [12].

Zmud et al. [39] find toll willingness to pay is affected by income, age, trip purpose, time of day, trip distance, and time savings (time of day is, of course, a surrogate for demand level).

Burris et al. [40] find that tolling HOVs causes a small but significant reduction in their numbers, while increasing total revenue.

Revealed Preference on Toll Lane Users Aggregate demand tends to grow, due to rising income, population, and economic activity. Liu et al. [9] observe that a higher-than-typical price at a given time may signal to users that the express lanes may be approaching congestion due to high overall demand, hence an indication that the GP lanes are slow. For SR-167 in Seattle, a toll of $1–2.00 for a speed increase from 30 to 60 mph over 11 miles yields a time saving of around 11 min, for an implied vehicle value of time (VOT) of less than $10 per hour. The toll rate is adjusted every 5 min. A good deal of data has been collected on user behavior regarding SR-91, including interview surveys, and these data have been extensively studied [41].

Diversion For HOT lanes, most of the diversion is between the two classes of service. Because the lanes have resulted in additional capacity when the multiclass service was initiated, there has not been much need for concern about diversion to other facilities.

If, however, existing lanes are converted to express or HOT lanes, the overall price on the facility will rise (in dollar terms for the tolled lanes, and in delay on the GP lanes), so diversion to other facilities will need evaluation. Depending upon the substitutability of nearby arterial streets – measured in travel time – tolls may need to be lowered on the express lanes in order to retain enough traffic to prevent arterials from being choked.

This problem is different in kind from the consideration of delay on the GP lanes when tolls are raised on the tolled lanes. If the facility manager is responsible for ameliorating delay on the GP lanes, the level of service on the express lanes may need to be compromised to retain reasonable flow on the GP lanes [42, 43]. This is how the I-95 Express Lanes in Miami are managed, with the project manager coining the term "quality throughput." Pricing both services, of course, would allow for much greater control and less compromise.

Variations in the Value of Travel Time Savings Variation in time values is widely asserted, largely on circumstantial grounds (e.g., toll payers vary from day to day in their choice). Patil et al. [44] use stated preference (SP) to find a 95% confidence range of 41–79% of the wage rate, a fairly broad band. Small, Winston, and Yan [45] use both stated preference and revealed preference data to determine that motorists place high value on travel time and travel time reliability, with considerable heterogeneity in both.

Travel Time Reliability Express lanes offer significantly more reliable travel times, as well as shorter travel times. The general pattern from user surveys and potential user surveys is that most travelers are occasional users who decided each day how urgent their arrival time is [46]. Using data from SR-91 in southern California, Brownstone and Small [47] find high values for both time and reliability. Defining and measuring reliability is a challenging task, and the real or perceived benefits have not been integrated into benefit-cost evaluations [48, 49]. Patil et al. [50] surveyed travelers on the Katy Freeway in Houston regarding their travel on the GPLs and the managed lanes. One area of investigation was the travelers' willingness to pay for a trip on the managed lanes under unusual situations – basically when the traveler was in more of a hurry or pressed for time, for example, running late for a meeting or when they see bad weather that may cause congestion. They found the willingness to pay for travel time savings in those instances was between two and four times as much as regular travel time savings.

Evidence from travelers using the express lanes on I-394 in Minnesota also points to express lane users placing a high premium on travel time reliability. Cho et al. [51] obtained data on travel times for the GPLs and ELs plus toll collection data from every transaction in 2008. Based on these data it was found that approximately 50% of the paying EL users paid for travel time savings of 1 min or less. Mostly due to these small time savings, the average values of time were found to be considerably higher (ranging from $73 to $116 per hour) than what was found in the literature (often around $10–25 per hour). This would indicate a willingness to pay for something other than the travel time savings offered by the lane.

Revenues

A policy that both reduces congestion and raises revenues should be an attractive policy, but that has not made congestion pricing in general widely adopted. While some commentators express the observation that the revenue potential seems to have overshadowed the congestion management benefits, the evolution of the HOT lanes concept from HOV to allowing a few more vehicles to "buy in" to the service does not suggest that revenue raising is the primary motivation.

Nonetheless, tolls do generate revenue, and more under some circumstances than others. Tolls used for congestion management vary with demand and hence by time of day. Flat tolls that do not vary with time of day are primarily if not exclusively for revenue generation to pay for the road. Such tolls may vary by vehicle type to reflect costs of serving heavier or larger vehicles, but the rates are generally not set so as to obtain a particular mix of vehicles.

Monopoly The monopolist in microeconomic theory faces a downward sloping demand curve (unlike a firm in a competitive market) and sets prices that are intended to maximize profit. The monopolist does not necessarily have full control over the market price and does not face totally inelastic demand, but any degree of downward sloping demand for the firm's output conveys some measure of monopoly power. In theory, the monopolist maximizes profit by setting price on the demand curve at the quantity where marginal cost equals marginal revenue.

If profit is positive at any volume (it might not be, depending upon the cost structure), the MC = MR point will yield the highest profit. More generally, the monopolist may not choose to seek the absolute maximum profit in the short run, perhaps lowering the price to increase market share or provide a cushion of loyal customers. Express lanes are typically priced so as to reliably maintain 45 mph speeds during the peak periods, which is normally a higher volume than the profit maximizing volume.

The degree of monopoly power possessed by toll roads or express lanes is controversial. There is inevitably some spatial monopoly, but given the ability of travelers to carpool, switch to transit, take an alternative route or destination, shift to an off-peak time, or forgo the trip, the demand for any single facility is necessarily somewhat elastic.

Exemptions A much more important factor with respect to revenue is the level of exemptions from paying the toll. If two-person carpools go free, it is possible to use all the capacity for HOVs and leave no paying customers. Adding exemptions for electric vehicles and hybrids further erodes the revenue yield. Broadly speaking, as the share of nonpaying vehicles increases, the revenue production of the facility becomes a less viable purpose for the express service [52].

The significance of revenue, then, is whether it can pay for the operation of the facility and the collection of the revenue. Varying the toll according to demand and billing each vehicle separately is more costly than collecting the same revenue through a gas tax, so the question of whether the service is a good idea depends upon the benefits of better congestion management in travel time savings, reliability, and providing the option to avoid the GP lanes, compared to the costs of creating and maintaining a more accurate pricing system.

HOV discounts or exemptions are problematic because compliance is hard to verify. This is true for enforcement of all HOV lanes, but the addition of tolling certain vehicles while others go free greatly complicates the task.

Price Volatility

Express lanes are those which charge all users a toll, perhaps discounted for HOVs, while HOT lanes allow vehicles meeting the HOV criterion to travel free. SR-91 charges HOVs half price. A problem with exempt or discounted vehicles is that it creates uncertainty about the potential revenue stream and amplifies any volatility in the price per trip over the time of day or day of the week. As the share of traffic that is insensitive to price (free or discounted) becomes larger, the remaining price-sensitive traffic has to respond proportionately more to maintain the congestion at LOS C. At the limit, when the share of price-sensitive traffic approaches zero, the fluctuations in price needed to maintain LOS C become infinite. Poole [53] describes an Atlanta planning study in which the HOT facility would generate no revenues in the peak period at some time in the future, because the capacity would be fully used by HOV2+ vehicles and paying vehicles would be entirely excluded. Under such circumstances, the investment of private capital is unlikely without explicit guarantees. The requirements for exemption can be increased (e.g., from 2+ to 3+), causing a sudden drop in the toll for SOVs (and now two-person carpools), but this volatility does not provide confidence in the long-term stability of the operation.

Another possible source of volatility is the misperception by some express lane users that the price is a measure of congestion on the GP lanes, rather than a price based on the number of express lane users. Miami-area HOT lane users, among others, have expressed the belief that the price is an index of congestion on the free lanes [54]. While the perception has a perverse effect on the use of price as a rationing instrument, it indicates that express lane customers are willing to pay a premium for guaranteed higher quality, or more specifically, reliability. Posting the time savings between the two services could serve as a counter to the misperception.

Cost Recovery Because no revenues are collected other than fuel excise taxes, HOV lanes are not held to any financial recovery standard.

If express lanes are to be regarded as a means for financing transportation infrastructure, the tolls will need to be higher than currently, apply to all vehicles, and apply to a large share of daily traffic [55]. There may be some circumstances where the surplus revenue after paying for operation and toll collection is large enough to recover the capital cost of the lane and associated infrastructure (barriers, gantries, buffers). It seems unlikely that express lane revenues will ever be sufficient to pay for the capital costs of the GP lanes as well as the tolled lanes.

Hence it is misleading to propose using the surplus revenues to pay for transit or equity-compensating income transfers when the gross revenue is insufficient to cover the full costs of the highway [56]. This makes the issue of exemptions (as well as multiclass service itself) an important factor in transportation financing, above and beyond the short-run economic efficiency impacts.

With the entire road priced – whether single- or multiclass – the revenues from efficient pricing can more than cover the long-run capital costs of the facility, and the surplus applied to capacity expansion of the highway, improved transit service, or equity transfers. Dividing revenues in thirds to highway capital, transit service, and equity transfers is referred to as the Small rule (Small [57]), as applied to whole-facility pricing. Capacity expansion of the highway will lower the congestion toll rates, by reducing congestion, and the decision to expand should be based on estimated benefits and costs, not on the amount of revenue, although toll revenues are a good indicator of WTP for highway investment.

Some Variations in Configuration and Operation

Numerous variations in design and operation have been tried, for purposes of making a restricted class of service work successfully, which is to say the service is neither underutilized nor overutilized, and customers are not complaining unduly. A few of the most notable variations are described below.

Multiclass Networks If the concept of multiclass service is expanded to the metropolitan area, two broad strategies arise:

1. All potentially congestible expressways offer HOT lanes along with GP lanes, and separation of the services is maintained at interchanges with other expressways.
2. Some portions of the expressway network are fully priced and others are not, in a way that allows users to reach the same destinations via tolled or untolled paths.

The first strategy requires substantial infrastructure to permit all choices of direction to be continuously separated (i.e., express lane users never have to sit in GP lane congestion). Potentially, the costs of such infrastructure may be sufficiently large that they might outweigh the benefits from reduced congestion, especially in places that are not highly congested. The second strategy avoids many of the problems of multiclass service, including the above infrastructure costs, but different locations would be differentially served. Motorists would still have a range of choice, but not as much as when all expressways offer both GP and express services.

Shoulder Used for Travel Lane During Peak By incorporating the shoulder as a travel lane on a temporary basis during peak periods, an increase in capacity can be achieved at low capital costs and an unknown increase in safety costs.

A complementary strategy is to restripe the road for a larger number of narrower lanes. The full 12-ft width is not required for speeds below 50 mph, so more lanes can be squeezed into the same roadway width [58]. Speed limits need to be lower, which actually helps to smooth traffic flows during peak flows but is awkward during off-peak periods.

Discounts for HOVs Most HOT lanes in the USA were previously lanes restricted to high-occupancy vehicles (HOVs), and the tolling strategy was intended to utilize the excess capacity resulting from the discrete nature of carpool lane eligibility criteria (two- vs three-passenger minimums). In these cases, the tendency is to permit the HOVs to continue to use the lanes free or at a discount.

The effectiveness of HOV segregation as a stimulus for reducing peak vehicle trips through higher vehicle occupancy varies with the context. Prearranged carpooling has been in secular decline for several decades, but casual or opportunistic or unscheduled carpooling (e.g., slug lines) have spontaneously appeared when the particular conditions are suitable. Because the HOV concept originated as a substitute for pricing, it could be argued that keeping the HOV preference is both redundant and a move away from efficiency by overencouraging ridesharing. The addition of the ability to pay to use the lanes can also reduce demand for casual carpools. The number of casual carpoolers decreased dramatically on the Katy Freeway once the carpool lanes were opened to paying SOVs. This may be due both to much better travel along the freeway (high time-value drivers no longer need occupants to gain faster travel) and to passengers switching to toll-paying SOV mode (while there is no increased incentive to attract new volunteer passengers).

Number of Priced Lanes

The greatest penalty for reconfiguring an expressway for multiclass service occurs when the priced service consists of a single lane, because of the limited capacity of a single segregated lane (see Loss of Capacity above on p. 10). Two lanes are better because they allow for some weaving and therefore higher flows per lane. This suggests that a minimum of four or five lanes in the same direction is a requirement for creating efficient multiclass service.

Evaluation of Pricing Alternatives

Although there has been a great deal of writing, both theoretical and empirically based, on the performance of HOT lanes, no single analysis has taken in the full welfare consequences of HOT lanes in comparison with the relevant alternatives. Lee [20] urges an evaluation

framework based on welfare measures for applicable alternative uses of the same capacity. Sullivan and Burris [59] made pioneering efforts to differentiate average VOT for toll payers versus non-payers. Light [60] has constructed an abstract framework that addresses the optimal price of one service that is priced, the optimal capacity with an explicit distribution of travel times and no exemptions, and no demand elasticity; he uses a modification of the "two route problem." Agency evaluations tend to focus on utilization and revenue, and seldom attempt to perform benefit-cost analysis [61].

Counterfactual

Many studies that assert benefits of HOV or priced lanes are either vague about what they are being compared to or pick a counterfactual that may not be the economically efficient use of the infrastructure. HOV lanes are judged by the difference in speed between GP lanes and HOV lanes, rather than the change in travel speeds for all users resulting from the dedication of one or more lanes to restricted usage (see for example [14] with respect to HOV lanes).

Within the context of managed lanes and highway pricing, there is a range of alternatives that needs to be made explicit.

	Single-class service	Multiclass service
No tolls	All lanes merged into GP	HOV lanes separated
Express lanes tolled	All lanes pay the same toll	Express lanes pay toll
All lanes tolled		Both services priced but with different toll rates

Efficient Congestion Pricing

To evaluate the performance of priced lanes, it is necessary to review the basic theory of road pricing [62]. Without a compensating adjustment in price, the number of vehicles using a facility when congestion arises is greater than the number that would occur under economic efficiency. The efficiency condition is not met because some number of users value the travel (to themselves) at less than the incremental cost in delay time that they impose on the traffic stream as a whole. The reason they choose to travel anyway is because the user faces the average travel time cost rather than the marginal social time cost. The marginal is always larger than the average because the average rises with additional traffic.

Thus, without correction, the price to users on congested facilities is always lower than the efficient price. The efficient price does not eliminate all congestion, but it should be sufficiently high to permit free-flowing traffic (not necessarily free-flow speed). Maximum capacity is often defined [27] as a density of 45 vehicles per lane per mile. The efficient volume will be somewhere between the maximum flow and the volume that results in free-flow speed.

Any increase in price from the unpriced situation will result in a gain in efficiency, up to the point where traffic speed is higher than what the users would be willing to pay for to deter enough vehicles so that the speed can be maintained. Express lane managers typically seek a minimum speed of 45 mph during the peak period, which is probably close to efficient, depending upon the VOTs of the vehicles in the stream.

The Standard Road Pricing Model The basic theory of efficient pricing of roads applies to a single distinct segment of road or a bridge, with a given demand for vehicle trips (in vehicles per hour). Users bear a group of variable costs, the most significant of which is travel time. The facility has a flow capacity, depending upon the number lanes, curves and grades, and other attributes, measured in passenger car equivalents per hour. As vehicle flow increases and begins to approach capacity, travel speed declines at an accelerating rate, thereby increasing travel time (the reciprocal of speed). The relationships in their most simplified form are displayed in Fig. 2. The vertical axis is the generalized cost or generalized price, in which all variable costs including travel time are translated into dollars [63–65].

It is assumed that the user pays vehicle operating costs and accident risk, and correctly anticipates the average travel time during the period the user is on the facility. There are no user charges or excise taxes, at least of a nature that vary with the amount of use, or else

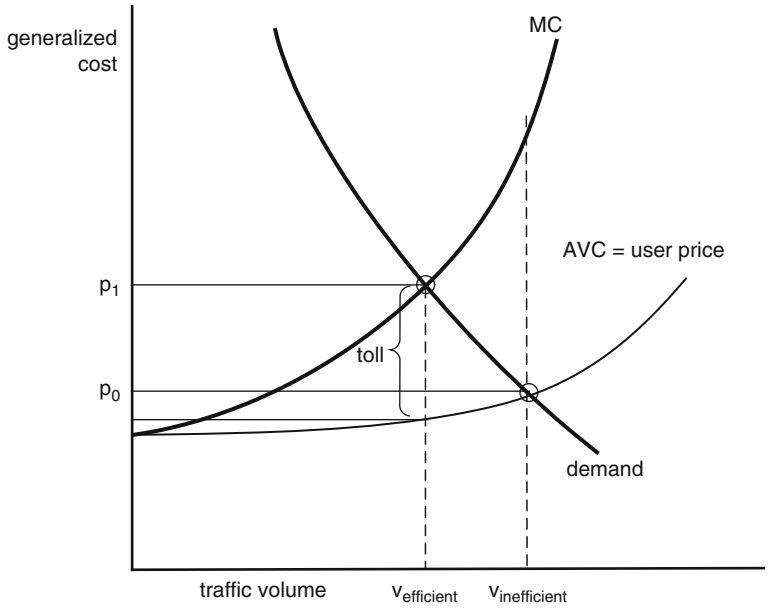

HOT Lanes/Value Pricing: Planning and Evaluation of Multiclass Service. Figure 2
Basic highway congestion tolling

such fees exactly pay for the variable costs of maintaining the road for the particular user (pavement wear, law enforcement). There are no external costs that the user fails to pay for (e.g., pollution), and no external benefits outside of the demand curve. Fixed costs of the highway and the vehicle are not explicitly included in this analysis.

The result of these simplifications is that the price to the user is the same as average variable cost (AVC), whereas the true cost to society of the marginal vehicle is the marginal cost (MC), described heuristically as the AVC plus the delay created for others by the presence of the marginal vehicle. In that sense, each vehicle creates a negative externality in the form of delay to other vehicles. Usage of the facility occurs at an equilibrium volume higher than that which would maximize net benefits to society – that being where price = MC – from the availability of the facility.

The "overusage" is the volume between $V_{\text{inefficient}}$ and $V_{\text{efficient}}$, which results in an increase in costs represented by the area under the marginal cost curve between the two volumes, while the incremental benefit of this traffic is represented by the area under the demand curve (which is the same as the marginal social benefits curve) between the two volumes. The "toll" is a monetary charge levied on the vehicle, calculated to make the price to the user (per mile or per trip) equal to the marginal cost at the efficient equilibrium.

This inefficiency, indicated as a shaded triangular-like area in Fig. 3, consists of two components: an increase in consumer surplus (a positive benefit) from the value placed on the travel by the additional vehicles, above what they actually pay, and an increase in delay for "old" vehicles (those that would be on the facility if it were efficiently priced). In congested conditions the delay greatly exceeds the consumer surplus, the difference being the area of the inefficiency triangle (also called welfare loss). Mathematically,

$$\text{Inefficiency} = \text{delay savings} - \Delta\text{CS}$$

where the "inefficiency" is a loss or net disbenefit and ΔCS = incremental consumer surplus. The data needed to calculate these benefits consist of observed traffic volumes and speeds, estimated delay functions, other variable costs, and the generalized price to the user [66]. Throughput by service and time savings are not sufficient for evaluation, although they may be useful performance indicators. Kidd [67] compares numerous configurations of HOV, HOT, BRT, and light rail modes on performance measures emphasizing

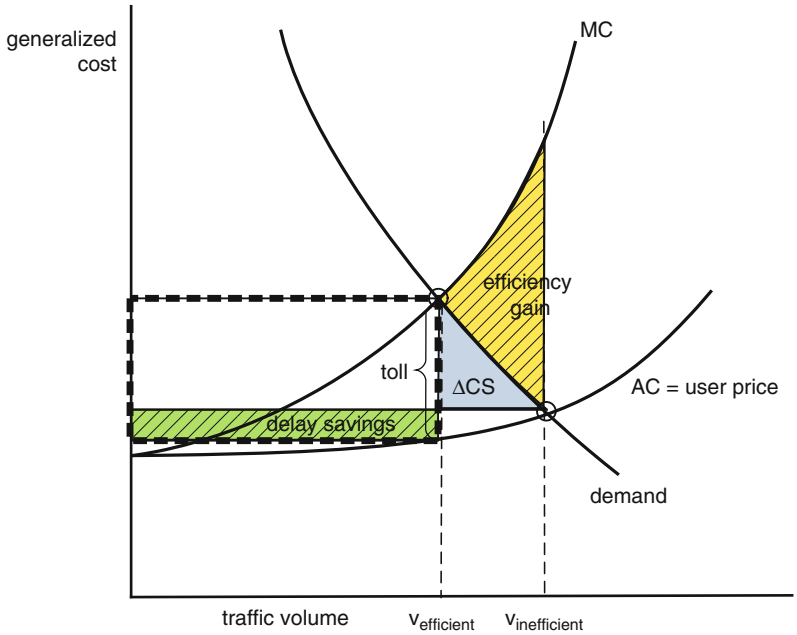

HOT Lanes/Value Pricing: Planning and Evaluation of Multiclass Service. Figure 3
Benefits of congestion pricing

throughput and speed, and recommends HOT lanes, in part for their potential BRT use. Poole [68] also emphasizes this combination.

The standard model also does not represent the possibility for hypercongestion, where capacity is lost by overloading the facility beyond its ideal maximum capacity. Peak pricing can prevent this from happening, even if the toll is well below the efficient price.

Dynamic Demand Schedule

The above assumes a given static demand curve. If demand was always at the same level, the toll would be constant. The nature of the congestion problem is that demand is not constant, but instead has peaks and valleys. A benefit of the congestion toll then becomes the shifting of some users from peak periods into off-peak periods during which the price (toll) is lower or zero. In addition to the previously available user options of higher occupancy (carpool, bus transit), alternative mode (e.g., rail freight or transit), and forgoing the trip, the user can shift the time of the trip to an off-peak period. The more options available to the user, generally the higher (in absolute value) is the demand price elasticity, and hence the smaller the toll required to achieve an efficient equilibrium.

With multiple demand periods, there is an interdependency among them. Specifically, if the price is raised in any period (e.g., the peak), then the demand curve will shift outward in the other periods (e.g., the off-peak). This effect is shown in Fig. 4. An increase in peak price from p_{P1} to p_{P2} shifts the whole demand curve in the off-peak market from D_{OP1} to D_{OP2}; correspondingly, a price decrease causes demand in the related market to shift inward. The magnitude of the shift is measured as a cross-elasticity.

Peak versus off-peak periods illustrate the case of markets too closely related to be treated as separate markets. A similar situation of markets for close substitutes arises with multiclass service. There are a number of elasticities and cross-elasticities that result from changing prices in any one of the several closely related markets. New users will be attracted in each of the markets, at higher or lower occupancy levels, and others may be deterred from the same and other markets. For some simple purposes, the numbers of travelers, vehicles in the corridor, number of carpools, etc., can be approximated as remaining constant, but in general they will

change. For example, when HOT lanes constructed and operated by private concessionaires promised guaranteed speed at all times, bus service was planned to use the expressways; previously the buses avoided the freeways due to unreliability of schedules [69]. How to value such changes makes evaluation of multiclass service difficult.

Nonoptimal Pricing

The standard model makes the convenient assumption that average cost and user price are the same, but in practice this only applies to travel time; for other costs (emissions, vehicle operation) and user charges (fuel taxes, flat tolls), any correspondence between cost and price is coincidental. Because for HOT lane policy it is necessary to analyze tolls separately from costs, a more realistic representation is needed. A general framework for evaluating transportation investment and pricing that recognizes the price function as a separate factor is shown in Fig. 5. In this case, price is shown as lying below AVC. Because both price and AVC include travel time, the two curves tend to have the same shape. In the

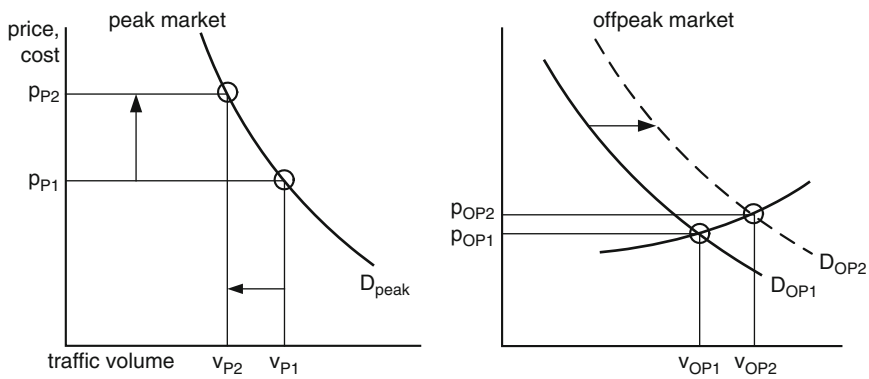

HOT Lanes/Value Pricing: Planning and Evaluation of Multiclass Service. Figure 4
Peak and off-peak demand periods

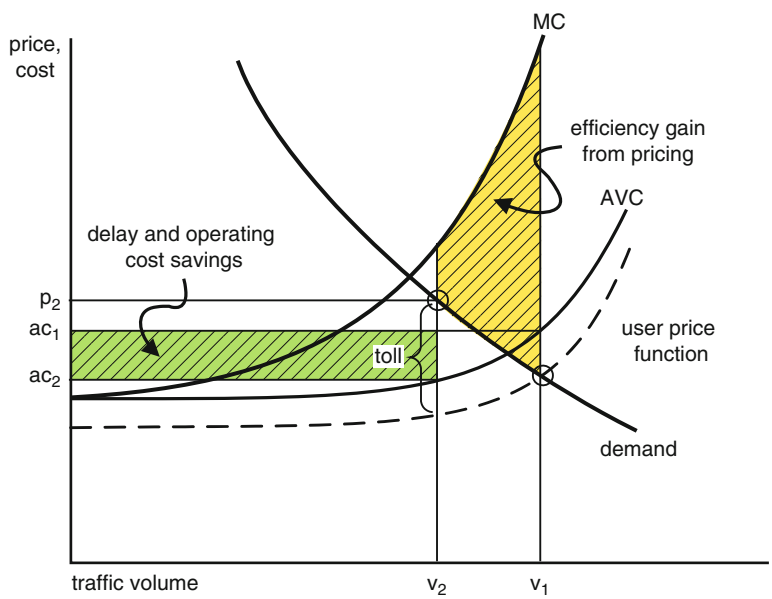

HOT Lanes/Value Pricing: Planning and Evaluation of Multiclass Service. Figure 5
Benefits of pricing when price is not efficient and not equal to AVC

example, the assumption is that external costs in the form of noise and air pollution emissions, plus agency costs for maintenance and administration, outweigh the variable user taxes paid by the vehicle. The intersection of the price function with the demand curve determines the initial volume v_1. The average cost (including social costs) at that volume is marked as ac_1. In reality, the price function might lie either above or below the AVC curve.

The user impact components from Fig. 3 still apply, but they are a little more complicated. In this example, the context is simply two different prices, neither of which is efficient. Although the optimum price is not achieved by the toll, there is an efficiency improvement from reducing volume from v_1 to v_2. The efficiency gain (reduction in the efficiency loss) now consists of three parts:

1. A reduction in excess delay (and operating costs to the extent they increase with congestion), indicated by the shaded rectangle
2. A loss of consumer surplus (not marked in the diagram), which is still a triangular area lying under the demand curve between v_2 and v_1
3. A reduction in net external costs that are above the price curve, represented by a rectangle (not marked) whose height is the difference between price and AVC at v_1 and whose length is v_1 minus v_2

Emissions changes can be estimated by modeling the conditions, which translate into speed change or "drive cycles" that alter the power load on the engine. Congested drive cycles are much different from constant speed cycles, and patterns on tolled lanes are different from GP lanes, but the differences and magnitudes are relatively small compared to time values. Estimating changes in consumer surplus (including the value of delay) is more difficult with multiclass service.

Network Effects

The congestion pricing model in Fig. 2 assumes implicitly that all facilities are optimally priced. The demand interactions considered so far have been between peak demand and off-peak demand. In a more generalized system or network, each link is a separate but interrelated market for travel. Each traveler seeks the minimum path through the network to his/her destination, considering operating costs and the value of time. In the face of an increase in money price on a particular link, the traveler may

- Continue to travel and pay the toll (high time value)
- Divert to another route or path (higher time cost for traveler, increase delay on alternative path)
- Shift to carpool or transit (perhaps offering better service because of reduced congestion)
- Shift time to off-peak (traveler worse off than without the toll, but not as bad as paying the toll)
- Change in location or origin or destination, long run or short run, or combine trips into tours (trip chaining)
- Forgo the trip

Each of these responses represents a valuation by the user of the available alternatives. The benefit of the price changes (whether positive or negative) is the sum of all changes in consumer surplus. Poole [68] has stated the welfare objective in the following way: "... a managed lane that charges all customers the market value of their trips (time plus reliability) maximizes the utility of those customers. The higher the total revenue such a lane produces, the greater the value of the transportation benefits it is providing. By contrast, the goal of maximizing the number of people per lane per hour implicitly values all those trips equally, and at a low value (the extra time and convenience of being in a carpool)."

Related Markets

The concept of a market, with supply and demand, and a resolution, whether a constrained or an unconstrained equilibrium, is an abstraction from the field of economics. Whether the concept can be applied to a given context, how it should be applied, and whether anything useful results depends upon the skill and insights of the analyst.

Inherent in the idea of a market is the understanding that markets are connected to each other: a change in one market affects all other markets, directly or indirectly. Such an understanding would be paralyzing (nothing can be concluded unless all markets are studied) without some principles for

bounding the scope. Three ranges of scope can be considered:

1. Primary Market
   Responses taking place within the market are endogenous, and all relevant factors should be resolved; other markets may be incorporated indirectly via changes in consumer surplus, but are not recognized explicitly.
2. Related Markets
   Markets whose demand or costs are directly affected by the primary market may need to be included, such as peak and off-peak markets, as being not autonomous (e.g., peak and off-peak may share the same capacity).
3. Other Markets
   Related markets that exhibit market failure (monopoly, constrained pricing) may be incorporated into the evaluation, to the extent that their inefficiencies are affected by pricing in the primary market.

All other markets not explicitly included are assumed to adjust efficiently to whatever changes occur in the primary market. When pricing a single facility, it is assumed that all other facilities are "other" markets, which adjust their prices and output (including investment in capacity) to remain efficient. Whether vehicle trips gained or lost in the primary market are the result of diversion, occupancy shifts, or deterred/induced travel is unimportant, or at least ignored. Shifts between peak and off-peak, however, are certainly relevant.

Multiclass service creates two markets that are closely related. Similarly to peak and off-peak demands, an increase in the price of the premium service causes an outward shift in demand for the standard service. If peak and off-peak are also distinguished, then there is a matrix of elasticities connecting the four options. An increase in the price of the premium service in the peak, for example, will increase demand for off-peak premium service and both standard service demand periods.

Evaluation of changes in related markets might be approached by treating the market in which the change occurs as the primary market, and changes in related markets as relevant. Benefits would be as described above for a single facility, plus changes in the magnitude of the efficiency loss in related markets. If all other markets, whether directly related or only indirectly, adjust efficiently, then nothing in those adjustments need be considered in evaluating the changes in the primary market. If, alternatively, related markets are inefficiently priced or constrained, then the change in inefficiency can be regarded as a benefit of the change in the primary market [70].

An increase in price in the express lane market, for example, would cause an increase in demand in the substitute GP market, as shown in Fig. 6. If the related

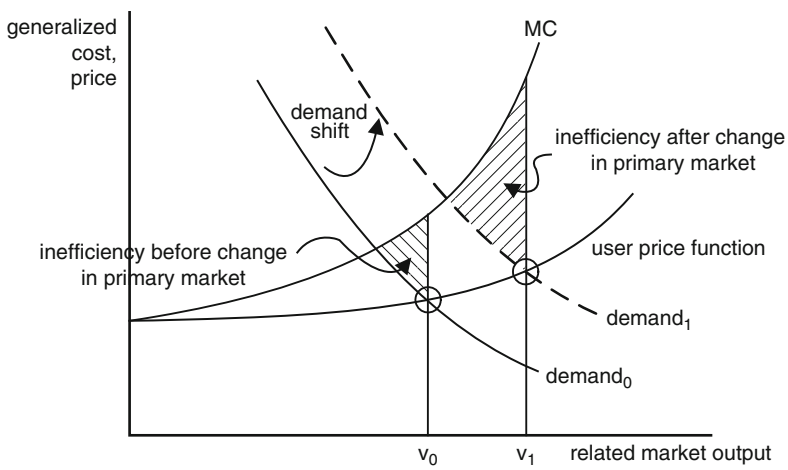

HOT Lanes/Value Pricing: Planning and Evaluation of Multiclass Service. Figure 6
Change in inefficiency in related market

market is priced inefficiently, and the deviation between price and marginal cost is increased by higher output, then the inefficiency is worsened by the price change in the primary market. The change in efficiency (a negative number, in this case) could be added to the benefits of the price change.

Some Lanes Priced

If the theory shown in Fig. 2 is applied to one or several lanes of an urban expressway, but not to all lanes, an improvement in efficiency can be obtained even if the pricing is not optimal, as in Fig. 5. Vehicles tolled off the restricted lanes may take any of the options listed above, including consolidation into more person trips in the remaining vehicles. At least some of the vehicles, however, will choose to not to pay the price but will use the remaining GP lanes. This demand shift in the closely related market, as in Fig. 4, would not be accounted for in the benefits (disbenefits) from pricing.

One could assume that all other markets are efficient and make optimum adjustments to price changes in related markets, but this assumption is clearly violated in practice. The price is fixed at an inefficient level (unlike the stopped clock, it is never correct), and the capacity cannot be varied either. Inevitably, the inefficiency that is (in this case) worsened in the related market needs to be addressed.

If a portion of the traffic is separated from the rest and charged a price to keep it flowing at LOS C, the price on those lanes is higher than without the pricing, and the delay is greater on the GP lanes if the total travel remains the same (more demand is imposed on less capacity). Therefore the average generalized price is greater and the result is that the total traffic volume will be less. Vehicle occupancy is raised by the pricing (and not by congestion), but this reduction in vehicles will less than offset the additional demand directed at the GP lanes. Under a reasonable range of conditions, then, time savings on the express lanes may be more than the increased delay on the GP lanes (because the average user price is higher and some efficiency is gained) or may be less than the delay on the GP lanes because not enough vehicles have been deterred to offset the capacity loss from separation. This assumes, of course, that there is no increase in the total capacity of the facility.

All Lanes Priced Uniformly (Single Service)

The prototypical condition imagined in the standard theory is steady flow on a single uninterrupted facility. In this abstract market, there is a single demand curve and single cost curve. Cost is determined primarily by the relationship between traffic volume and delay. Marginal cost can be derived from the average flow relationship (empirically or analytically) and the optimal toll calculated and imposed. The gains from this congestion pricing is a reduction in delay for the users choosing to the pay the toll, minus the loss of consumer surplus suffered by the deterred vehicles, shown previously in Fig. 3. The number of travelers may stay the same (or even grow) but some of them have been inconvenienced by having to share the same vehicle.

This simplified abstract model does not say anything about the distribution of travel time values among the vehicles along the demand curve. As the price goes up, some users are deterred by the sum of time and money costs, but the trade-off between them will not necessarily be the same at any point along the demand curve. Moving up the demand curve, it is implicitly assumed that the money price is increasing while the delay portion of generalized price is decreasing.

Thus the standard model is robust for the mechanism it uses (a single price for all users), but does not acknowledge that conditions may be considerably more complicated.

Both Services Priced Efficiently

The fundamental question in regard to multiclass service is whether there are market segments with the demand for the service that are sufficiently distinct as to warrant separate tailored services along with the additional costs that differentiation entails. In the case of highway travel, the question is what distribution of travel time values among the vehicles potentially demanding service justifies differentiating the demand into two or more classes and charging different prices. Clearly, charging a price for both services is a gain in benefits over charging for only one service, but are the optimal prices charged for the two classes different enough to justify the loss in capacity?

There seems to be little analysis or evidence on this problem. Many analysts assert that the distribution of

VOTs is wide, but how wide in truth and what width is needed to take the extra step of multiclass service is not yet solved.

To evaluate a multiclass service is to address the problem of allocating a fixed amount of capacity to two classes of users, each with its own demand (reflecting differing preferences for travel time, occupancy, and other attributes) and pricing structure. The resulting equilibrium is then compared to the base case.

First-best evaluation is a comparison of alternatives all of whom are efficiently designed and priced. Second-best evaluation occurs when at least one constraint is imposed on at least one of the alternatives, and the net benefits of one alternative versus another are estimated.

A first-best evaluation of multiclass highway service would compare an efficiently priced single facility to two efficient service alternatives. Total capacity would be fixed, the two services would be designed with demand attributes that maximized the net benefits to users, including pricing at marginal cost. The conclusion as to whether two-class service was better than a single class would derive from the net social benefits (user benefits minus implementation costs) for each alternative.

A hypothetical example is shown in Fig. 7. A single-class service is portrayed on the left, and a two-class service in the two markets on the right. Each market is resolved efficiently at p = MC, and the net benefits of each – the area above the MC curve and below demand, up to the equilibrium volume – are shaded for each service. In the single-class service, a dashed demand line indicates the separation of demand into those who will choose each one when it is offered.

Once the two types of service are offered, each has a separate demand curve (related in that a change in price in one of the markets will shift demand in the other; thus each demand curve is based on a given price in the other market). By separating the two market segments, the attributes of each service can be tailored to its customers. The two demand curves are not necessarily a partition of the single-service demand: new users may be induced by the existence of, especially, the premium service. With differing prices, movements along the demand curves may result in greater or lesser total volume, i.e., the sum of v_1 and v_2 may be larger or smaller than V.

The problem is greatly complicated by the need to distinguish different values of time. The standard efficient pricing diagram assumes that time and monetary costs can be combined on a single scale, implying that the ratio of time to dollars – the value of travel time – is fixed. Thus the two-dimensional diagrams in Fig. 7 are only slices through a three-dimensional space in which demand is represented as a surface that is a function of both time and money. If a third dimension to the diagram is imagined, the standard service is a slice through the low-time-value end of the diagram while the premium service is a slice at the high VOT end. The single market is a slice through the middle, or at average VOT.

In the particular representation in Fig. 7, the generalized price to the user in both markets is below what it was in the combined market because the money price

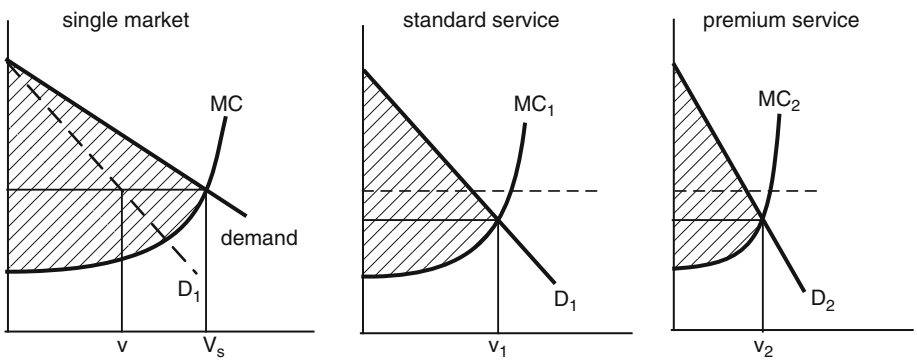

HOT Lanes/Value Pricing: Planning and Evaluation of Multiclass Service. Figure 7
Benefits of two-class service relative to single service

is lower and the time cost is less highly valued. Hence, total net benefits are higher for multiclass than for single service. For the premium service, the price is lower because the higher money price is more than offset by the faster travel. For the GP lanes, travel times are worse than in the combined market, but are valued less highly than the reduced price. These results are not true in general, but occur only if the service characteristics and prices very closely match the demands of each group. Otherwise, the generalized prices combining toll and travel time will be close to the single market price or above it, and the multiclass service will offer no advantage over the efficiently priced single-class service. Keep in mind that all services – combined or separated – are priced efficiently in this comparison.

The provision of two classes of service creates a net benefit if the sum of the benefits for standard and premium services exceeds the benefit of the single service by enough to offset the costs of providing two services. If all travelers are homogeneous in their preferences, then there are no benefits from multiclass service because all users want the same thing. This fact and several other aspects of the problem are addressed by Small and Yan [71]. Thus the two market segments must have distinctly different demand curves, and the service classes must have attributes that separate the demand segments. The benefit of multiple services relative to a single service depends upon how different the market segments are, and how well the service designs appeal to and satisfy those differences. The theoretical basis for this evaluation has been most completely developed by Small et al. [45], but they did not incorporate any penalties for partitioning the facility into service classes.

Empirically, attempting to measure the benefits by valuing the attributes (such as travel time differences) is not likely to be useful, because less easily observed differences are too hard to measure or observe (e.g., the cost of schedule shift, or coordinating a carpool). Revealed preference can show demand quantities and generalized price at equilibrium, but the remainder of the demand curve is a problem, as are the cross-elasticities.

A paper from the operations research literature [72] describes a model for allocating customers to two classes of service according to their willingness to pay for service time. The model determines the capacity given to each service and the profit-maximizing prices charged. Possibly a model of this form could fit the multiclass service optimization problem.

Equity

Any form of pricing of highways raises numerous claims of inequitability. The concept of HOT lanes generates additional objections beyond those that occur in the context of "simple" (single class) tolling and congestion pricing because there is a side-by-side comparison. People observe that, among toll payers, the burden of payment declines as a share of income as income rises, so pricing is regressive. Others observe that middle and higher income users are the majority among payers, so they are getting the benefits, and that is regressive. These both reveal an incomplete understanding of distributional equity.

Lexus Lanes Vertical equity impacts (impacts on the distribution of income) can be addressed objectively and quantitatively, although the data are coarse at best. Among travelers, peak highway users have higher average incomes than both transit users and off-peak users. Where express lanes are available, income levels of toll payers are usually higher than non-payers (Sullivan and Burris [59]; FHWA [73]). As the income of toll payers decreases, vehicle occupancy usually goes up. Hence the accusation that express toll lanes disproportionately benefit higher income users. The counter anecdote to the Lexus lane barb is the observation that working parents use the express lanes to pick up their children from daycare. Despite the expressions of concern, equity discomfort tends to subside after initial reaction to proposed HOT lane conversions, and has not so far been an impediment to implementation [55].

Unlike tax instruments, both the costs and benefits of paying for a market good are borne directly by the buyer. The buyer weighs the costs and benefits to himself/herself and makes a choice. If the consumer chooses to buy, then the benefits outweigh the cost, possibly by a large amount but a magnitude not apparent to the outside observer. If there are no external costs and no subsidies, then the social benefit of the good or service is at least as great as its costs, and neither consumers nor taxpayers are disadvantaged.

The existence of the good may divert consumption from other goods, but there are no inherent equity impacts, i.e., income is not being transferred without compensation. The above notwithstanding, "some argue the HOT lanes unfairly favor those wealthy enough to afford high tolls" [74].

This leaves the only complaint being that the underlying distribution of income is unfair. The solution, then, is a "Robin Hood" income transfer that rearranges income solely according to income, not according to road usage or any other criterion. The poor will then have the wherewithal to purchase peak SOV travel, or use the income for some other purpose.

Perceptions of equity are difficult to address in rational terms. Resentment against those who choose to buy their way out of congestion is not really any different from resentment against those who buy luxury yachts and large mansions, except that the cost of buying out of congestion is far less.

Earned Credits In an effort to improve the public acceptability of tolls, it has been proposed that drivers earn credits by using the unpriced lanes. The credits could then be applied to use of the express lanes [75]. Other proposals have been offered [76]. No projects have so far been implemented.

Generally credits are earned for purchasing something, as opposed to *not* purchasing. Thus credits would be awarded for paying the tolls for some period of time or amount, and a bonus paid to the user. The purpose is to create brand loyalty, which is not relevant here.

Hence the purpose is based on equity concerns. Sometimes it is vertical equity that is of concern, in which case the credits should be awarded to all persons or households solely on the basis of income, and unrelated to whether the recipients actually drive in the peak period or would like to. Rewarding drivers for using the GP lanes does not seem to accomplish any equity goal and is perverse from an efficiency standpoint (it encourages peak usage).

However credits are awarded, they constitute a financial transfer that reduces the net revenues from the tolls. Other losses of revenue include collection costs, operating subsidies for transit, and matched reductions in unrelated taxes such as property taxes. If the proceeds are rebated to users of the facility *because of usage*, they have a negative efficiency impact as well as an equity impact.

Land Use Impacts The rent gradient model of urban form relates the rate of decline in land value with distance from a point of central access to the unit cost of transportation. In this model, a reduction in the price of transportation to the user tends to flatten the rent gradient, causing land use activities to spread out at lower densities. Other things being equal, an increase in capacity reduces the travel time from delay and leads to dispersal of economic activity. Correspondingly, an increase in prices – e.g., through higher prices to users – should result in more compact development. While whole-facility pricing shifts the relative spatial preferences of households, on average the price is higher with efficient pricing. Thus the standard congestion pricing model applied to an urban network will tend to steepen the rent gradient.

HOT lane pricing does not lead to unambiguous results when interpreted via the rent model. While the explicit money price is greater on the tolled lanes, delay is greatly reduced; the net result, however, is an increase in price – for the same capacity. HOT lanes have never, however, been taken from existing capacity. The one attempt to do so – the infamous Santa Monica freeway diamond lane in Los Angeles – was a political disaster sufficiently painful to ensure that removing existing lanes has not been attempted again, and extensive outreach is undertaken before any kind of reserved lane is implemented [77]. Even if the amount of capacity added is less than what would be added by all GP lanes, the result is nonetheless to increase capacity and lower the cost of travel, spreading out the urban area.

Future Developments

Although the mileage of highways in "pure" HOV facilities vastly exceeds the tolled mileage, there are few plans to add HOV-only capacity; treatments being considered include general capacity expansion and tolling [16].

DKS Associates [10] describes activities in ten metro areas, most of which do not have congestion pricing currently, and some that do are not included in the survey. The report also describes how HOT lanes

can be incorporated into the regional planning process, and offers lessons learned regarding implementation from each of the areas.

Demonstration Effect

For at least some analysts, the HOT lane was a way to leverage the perception that HOV lanes were underutilized into a demonstration that pricing works. In this scenario, the mechanism of pricing could substitute for the awkwardness of verifying occupancy, and the occupancy requirement could then be dropped because the pricing would have the same effect. With pricing established as a management tool, all lanes could be priced and the physical separation no longer necessary. All links of the network (or the arterial network) could be readily tolled, and traffic flow greatly improved. With no other evidence of political willingness to try congestion pricing, HOT lanes was the only game.

In this way, the expansion of the concept could encompass all roads, or at least urban highways. Fielding and Klein [78] were early promoters of the spread of congestion pricing by imitation. The next level in this scenario is the congestion pricing of whole facilities in a strategic pattern. The planned pricing of the SR 520 bridge in the Seattle area will be the first example of such whole-facility congestion pricing in the USA, if and when it occurs.

Evolution of Multiclass Networks

Poole [79] has described a scenario in which single-lane HOT lanes phase out the HOV exemption or discount, because the exemptions prevent the revenue streams from being large enough to cover capital costs. These more-or-less fully priced one-lane highways are then successful enough to construct the ramps and flyovers that permit the express service to be continuous when one freeway intersects another. With this success as a model, the one-lane priced highways can be expanded to two lanes in each direction, resulting in a reasonable enough level of capacity and associated throughput to justify the separation.

An alternative scenario has emerged. Travelers are greatly enamored of the freedom to choose between tolled and untolled lanes, and HOT lanes are being extended into separated networks. The expense of the infrastructure for maintaining separation at interchanges has not deterred investment in HOT lanes. Although the benefits in time savings may not warrant the construction costs in many circumstances, such calculations do not seem to have been done and there is not an obvious political market for them.

From HOV to BRT The San Francisco Bay Area plans to evolve from HOV lanes to a single-lane HOT lane network with physical separation at interchanges, and from there to a tolled network that is heavily used by express buses [80]. The region plans to add capacity by utilizing shoulders and relaxing freeway design standards. HOVs will remain free or discounted. Realization of this vision still implies a continuing primary contribution to transportation funding from the federal government.

From HOV to HOT Texas seems to be moving in the direction of two-class service with express lanes having at least two lanes (generally permanent) in each direction on both service classes [41]. This will entail considerable expenditures for physically separated infrastructure, yet HOVs appear to remain free and BRT does not carry a large share of passengers. The Texas DOT has produced plans for public–private partnerships to build and finance major multimodal intercity corridors, but there has been some political backlash from the legislature.

From HOV to Full Facility Tolling The Puget Sound region has an extensive existing HOV network, some of which the region expects to convert to HOT along the way to creating a network of fully tolled expressways with no differentiated classes of service and no exemptions or discounts [81]. While this end state is the most likely to be sustainable in the long run, the path for moving to there from HOVs is not presently spelled out.

From HOV to HOT and Truck Lanes The Reason Foundation has proposed an evolutionary path that leads from express lanes to multiclass service in which all services are priced and truck-only lanes are a candidate service [79]. Poole claims that these characteristics will emerge once federal subsidies are limited to highways of national interest and local regions take responsibility for most of the transportation

infrastructure, including its funding. The resolution will be a system paid for primarily by users.

Inevitably there are limits to the expansion of simple (i.e., unpriced) HOT lanes in metropolitan areas. Swisher et al. [82] portray various longitudinal scenarios showing how express lane viability (i.e., neither too much nor too little traffic) can be retained by pricing selected users, including carpools. The ideal timing for introducing occupancy and pricing policy changes depends upon the growth of demand in the corridor.

At present, the prospects of universal road charges (VMT charges graduated by congestion and other costs) appear uncertain and not imminent, although there are some indications that the eroding contribution of fuel excise taxes and the lack of other revenue sources are improving the climate for tolling [83]. It may be that the inefficiencies of congestion will be tolerated in many locations, as well as the inefficiencies of multiclass services.

Public–Private Partnerships The USA is beginning to explore various arrangements that allow for more flexible management of the highway asset procurement process. Design-build construction and its extension into operation and financing have been used in some instances to create transportation infrastructure. Availability payments can allow the public sector owner to postpone payments to the builder until the facility is in operation.

If a project can cover its operating costs from tolls, then the possibility exists for letting a private firm operate the road and collect the tolls, potentially also setting the toll rates. One of a planned series of HOT lanes in the Washington, DC area is being constructed via a public–private partnership between the State of Virginia, the Federal Highway Administration, and Transurban-Fluor [84, 85]. The first modern era US toll lane facility was financed and constructed by a private firm, although it was eventually necessary for the State of California to buy out the private firm. SR-91 opened in 1995 and was repurchased in 2002 by the Orange County Transportation Authority [86]. The logic of letting some vehicles pay extra for speed creates an opportunity for letting the private sector front the funds to construct the additional lanes. Planned toll lanes in Sacramento may be funded in this way [87].

Using General Revenues The alternative to toll revenues for financing is general fund revenues. Many states and localities have passed referenda to pay for transportation with sales taxes. The federal government has transferred $30 billion into the Highway Trust Fund to keep it solvent. Perhaps because most voters see themselves as highway users, they favor spreading the costs over more payers than just users. This scenario maintains strong controls at the federal level over the raising of revenues and how they are spent, with Congress making decisions based on political balancing.

Whether the path ahead lies through extended multiclass service, private equity, and political devolution, or major general fund support for transportation is subject to conjecture and, we hope, debate.

Note

Information contained in this chapter consists of the judgment of the authors and does not necessarily represent the policy of the Volpe Center or the U.S. DOT.

Bibliography

1. Federal highway administration (2008) Managed lanes: a primer. US DOT/FHWA, Washington, DC. http://ops.fhwa.dot.gov/freewaymgmt/pubs.htm#mngd_lns_hov. Accessed 27 June 2011
2. Port authority of New York and New Jersey (2010) Bridges and tunnels, tolls, PANYNJ. http://www.panynj.gov/bridges-tunnels/tolls.html. Accessed Aug 2010
3. Small KA, Gomez-Ibanez JA (1998) Road pricing for congestion management: the transition from theory to policy. In: Button KJ, Verhoef ET (eds) Road pricing, traffic congestion and the environment: issues of efficiency and social feasibility. Edward Elgar, Cheltenham, pp 213–246
4. Collier T, Goodin G (2004) Managed lanes: a cross-cutting study. Prepared for Federal Highway Administration, Texas Transportation Institute, College Station
5. Sallach M, Vu P, Zhan YJ (2010) Corridor level analysis of potential Managed lanes investment on I-75 South in Atlanta, Georgia. Paper for TRB, Georgia State Road and Tollway Authority, Atlanta
6. Mirshahi M, Obenberger J et al. (2007) Active traffic management: the next step in congestion management. Prepared for DOT/FHWA, US, Washington, DC. http://international.fhwa.dot.gov/pubs/pl07012/. Accessed 27 June 2011
7. Federal highway administration (2010) Value pricing projects involving tolls. US DOT/FHWA. http://ops.fhwa.dot.gov/tolling_pricing/value_pricing/projects/involving_tolls/priced_lanes/index.htm. Accessed Aug 2010

8. Martin PT, Vladisavljevic I, Yusufzyanova D (2007) The I-15 Express lanes evaluation. Prepared for Utah Department of Transportation, Salt Lake City, University of Utah. http://www.udot.utah.gov/expresslanes/dld/U%20of%20U%20Express%20Lanes%20Evaluation%20November%202007.pdf. Accessed 27 June 2011
9. Liu X, Zhang G, Wu YJ, Wang Y (2009) Analyzing system performance for Washington state route 167 high occupancy toll (HOT) operations. Prepared for TRB, University of Washington, Seattle
10. DKS Associates (2009) A domestic scan of congestion pricing and managed lanes. Prepared for Administration, DKS Associates in association with PBSJ and Jack Faucett Associates, Federal Highway, Oakland
11. Federal Highway Administration (2008) Technologies that enable congestion pricing: a primer, US DOT/FHWA, Washington, DC. http://ops.fhwa.dot.gov/tolling_pricing/value_pricing/publications.htm. Accessed 27 June 2011
12. Goodall N, Smith BL (2009) What drives single occupant traveler decisions in HOT lanes? : an investigation using archived traffic and tolling data from the MnPASS Express Lanes. Paper for TRB, University of Virginia, Charlottesville
13. Brinckerhof P (2003) A guide for HOT lane development. Prepared for Federal Highway Administration, Parsons Brinkerhoff with Texas Transportation Institute in partnership with US DOT/FHWA, Washington, DC
14. PB Study Team (2002) HOV performance program: evaluation report, Los Angeles county metropolitan transportation authority, Los Angeles
15. 407 ETR (2010) ETR 407 express toll route, 407 ETR Concession Company Limited, Toronto. http://www5.407etr.com. Accessed 27 June 2011
16. Fuhs C, Obenberger J (2002) HOV facility development: a review of national trends. Prepared for TRB, Parsons Brinkerhoff, Houston
17. Burris MW, Lipnicky K (2009) HOV or general purpose lanes? Public Works Manag Policy 14(2):130–147
18. Poole Jr RW (2008) The HOT topic: enforcement in the fast lanes. Tolltrans, pp 44–49
19. Poole Jr RW, Kenneth Orski C (1999) Building a case for hot lanes: a new approach to reducing urban highway congestion. Reason Public Policy Institute, Los Angeles
20. Lee DB Jr (2008) Toward the evaluation of value pricing. Transport Res Record 2079:71–78
21. Chang M, Wiegmann J, Smith A, Bilotto C (2008) A review of HOV lane performance and policy options in the United States. Prepared for FHWA, Booz Allen & Hamilton and HNTB, McClean
22. Booz Allen Hamilton, and HNTB (2008) A compendium of existing HOV lane facilities in the United States. Prepared for Federal Highway Administration, BAH and HNTB, McClean
23. Cervero R (1999) Reviving HOV lanes. Transport Quart 53(4):67–81
24. Sas M, Carison S, Kim E, Quant M (2007) Considerations for high occupancy vehicle (HOV) to high occupancy toll (HOT) lane conversions guidebook. Prepared for Federal Highway Administration, HNTB/Booz Allen Hamilton, McClean
25. Plotz J, Konduri KC, Pendyala RM (2009) To what extent can HOV lanes reduce vehicle trips and congestion?: An exploratory analysis using national statistics on HOV mode use. Paper for TRB, Arizona State University, Tempe
26. Supernak J, Kaschade C, Steffey D (2003) Dynamic pricing on I-15 in San Diego: impact on travel time and its reliability. Transport Res Record 1839:45–54
27. Transportation Research Board (2000) Highway capacity manual: HCM 2000. TRB, Washington, DC
28. Barboza T (2009) O.C. Toll road price drops to attract commuters. Los Angeles times, 27 Mar 2009
29. Arizona Republic (2007) More Arizona drivers disobeying HOV rules. Arizona Republic, 31 Oct 2007
30. Jang K, Chung K, Ragland DR, Chan CY (2009) Safety performance of high-occupancy-vehicle facilities. Transport Res Record 2099:132–140
31. Cassidy MJ, Daganzo CF, Jang K, Chung K (2006) Empirical reassessment of traffic of traffic operations: freeway Bottlenecks and the case for HOV lanes. Institute of Transportation Studies, Berkeley
32. Anderson T (2007) Car-Pool lanes may be switched to toll lanes. Los Angeles Daily Breeze, 30 Nov 2007
33. AASHTO (2003) A manual of user benefit analysis for highways. American Association of State Highway and Transportation Officials, Washington, DC
34. Cassidy MJ, Bertini RL (1999) Some traffic features at freeway Bottlenecks. Transport Res (B) 33:25–42
35. Jung S, Wunderlich K (2008) Roadway network productivity assessment: system-wide analysis under variant travel demand. Prepared for Federal Highway Administration, Noblis, Falls Church. http://ops.fhwa.dot.gov/tolling_pricing/value_pricing/publications.htm. Accessed 27 June 2011
36. Booz Allen Hamilton, HNTB (2008) Policy options evaluation tool for managed lanes (POET-ML) users guide and methodology description. Prepared for Federal highway Administration, BAH and HNTB, McLean
37. Yan J, Small KA, Sullivan EC (2002) Choice models of route, occupancy, and time of day, with value-priced tolls. Transport Res Record 1812:69–77
38. Burris MW, Goel R (2009) Mode choice due to HOV to HOT conversions. Paper for TRB, Texas A&M University, College Station
39. Zmud J, Bradley M, Douma F, Simek C (2007) Attitudes and willingness to pay for tolled facilities: a panel survey evaluation. Transport Res Record 1996:58–65
40. Burris MW, Ungemah DH, Mahlawat M, Pannu MS (2009) Investigating the impact of tolls on high-occupancy-vehicle lanes using managed lanes. Transport Res Record 2099:113–122
41. Sullivan E (2000) Evaluating the impacts of the SR 91 variable toll express lane facility. Prepared for California Department of Transportation, Cal Poly State University, San Luis Obispo. http://ceenve3.civeng.calpoly.edu/sullivan/SR91/final_rpt/finalrep_full.pdf. Accessed 27 June 2011
42. Regan ED (2010) Pricing trade-offs: revenue vs. traffic management. Presentation to the National Road Pricing Conference,

Houston TX, Wilbur Smith Associates, Atlanta. http://tti.tamu.edu/conferences/nrp10/program/. Accessed 27 June 2011
43. MacGregor ME (2010) How revenue and traffic management are combined in the North Tarrant Expressway (NTE) managed lanes project in Fort Worth, TX. Presentation to the National Road Pricing Conference, Houston TX, Texas Department of Transportation, Dallas. http://tti.tamu.edu/conferences/nrp10/program/. Accessed 27 June 2011
44. Patil S, Burris M, Shaw D (2009) A comparison of survey designs for stated choice models: an application to commuting on managed lanes. Prepared for TRB, Texas A&M University, College Station
45. Small KA, Winston C, Yan J (2006) Differentiated road pricing, express lanes, and carpools: exploiting heterogeneous preferences in policy design. Brookings – Wharton Papers on Urban Affairs, Washington, DC, pp 53–96
46. Weiss E (2008) Will drivers pay to hurry up and wait? Washington Post, 25 Feb 2008
47. Brownstone K, Small KA (2005) Valuing time and reliability: assessing the evidence from road pricing demonstrations. Transport Res (A) 39:279–293
48. Joint Transport Research Centre (2009) Improving reliability on surface transport networks, OECD/International Transport Forum, Paris, France
49. Lam CT, Small KA (2001) The value of time and reliability: measurement from a value pricing experiment. Transport Res (E) 37:231–251
50. Patil S, Burris M, Shaw D, Concas S (2010) The value of travel time savings on managed lanes for urgent situations. Prepared for TRB, Texas A&M University, College Station
51. Cho Y, Goel R, Gupta P, Bogonko G, Burris M (2011) What are I-394 HOT lane drivers paying for?. Prepared for TRB, Texas A&M University, College Station
52. Poole Jr RW (2006) Managed lanes*:* what should we maximize? Surface Transport Innovations, Dec 2006
53. Poole Jr RW (2006) Transportation policy review: competing models of HOT lanes. Public Works Financing, July–Aug 2006, pp 25–26
54. Stone R (2010) High tolls lure drivers to I-95's pay lanes, Miami Herald, 31 Mar 2010
55. Bhatt K, Higgins T, Berg JT (2008) Value pricing pilot program: lessons learned. Prepared for Federal Highway Administration, K.T. Analytics and Cambridge Systematics, Washington, DC. http://ops.fhwa.dot.gov/tolling_pricing/value_pricing/publications.htm. Accessed 27 June 2011
56. Cuff D (2009) MTC approves plan for toll lanes, Contra Costa Times, 23 Apr 2009
57. Small KA (1992) Using the revenues from congestion pricing. Transportation 19(4):313–333
58. Ng CF, Small KA (2008) Tradeoffs among free-flow speeds, capacity, cost, and environmental footprint in highway design. University of California, Irvine
59. Sullivan E, Burris M (2006) Benefit-cost analysis of variable pricing projects: SR-91 express lanes. J Transport Engin 132(3):191–198
60. Light T (2009) Optimal highway design and user welfare under value pricing. J Urban Econ 66(2):116–124
61. Loudon WR, Synn J, Miller H (2010) Consideration of congestion pricing and managed lanes in the metropolitan transportation planning process. Prepared for TRB, DKS Associates, Oakland
62. Federal Highway Administration (2008) Economics: pricing, demand, and economic efficiency, a primer. US DOT/FHWA, Washington, DC
63. Mohring H (1976) Transportation economics. Ballinger, Cambridge, MA
64. Vickrey WS (1963) Pricing in urban and suburban transport. Am Econ Rev 53:452–465
65. Walters AA (1968) The economics of road user charges. International Bank for Reconstruction and Development, Washington, DC
66. Mohring H (2006) Congested roads: an economic analysis with twin cities' illustrations. In: Roth G (ed) Street smart. Transaction Publishers for the Independent Institute, New Brunswick, pp 141–170
67. Kidd B (2006) Multimodal optimization of urban freeway corridors. Prepared for Arizona Department of Transportation, Lee Engineering, Phoenix
68. Poole Jr RW (2010) Managed lanes: networks vs. individual facilities. Prepared for TRB, Reason Foundation, Plantation
69. Craig T (2007) Deals clinched on HOT lanes, Washington Post, 21 Dec 2007
70. Verhoef ET, Nijkamp P, Rietveld P (1996) Second-best congestion pricing. J Urban Econ 40(3):279–302
71. Small KA, Yan J (2001) The value of "value pricing" of roads: second-best pricing and product differentiation. J Urban Econ 49:310–336
72. Celik S, Maglaras C (2005) Dynamic pricing and leadtime quotation for a multi-class make-to-order queue. Columbia University Business School, New York
73. Federal Highway Administration (2008) Income-based equity impacts of congestion pricing: a primer, US DOT/FHWA Washington, DC. http://ops.fhwa.dot.gov/tolling_pricing/value_pricing/publications.htm. Accessed 27 June 2011
74. Cassidy WB (2010) Congestion pricing advances in virginia. J Commerce, May 27. http://www.joc.com/government-regulation/congestion-pricing-advances-northern-virginia
75. Buckeye KR, DeCorla-Souza P, Lari A, Aultman S (2009) User perceptions of fee lane concepts in Minnesota. Minnesota Department of Transportation, St. Paul
76. Gulipalli P, Kalmanje S, Kockelman K (2008) Credit-based congestion pricing: expert expectations and guidelines for application. J Transport Res Forum 47(2):5–20
77. Billheimer JW (1978) The Santa Monica freeway diamond lanes: evaluation overview. Transport Res Record 663:8–16
78. Fielding GJ, Klein DB (1993) "High occupancy/toll lanes: phasing in congestion pricing a lane at a time", Reason Foundation Policy Study 170. Reason Foundation, Santa Barbara
79. Poole Jr RW (2010) Pricing and Fiscal implications of different types of HOT Lanes. Presentation to the National Road

Pricing Conference, Houston TX, Reason Foundation, Santa Monica, CA. http://tti.tamu.edu/conferences/nrp10/program/. Accessed 27 June 2011
80. Klein L (2010) 2010 bay area express lane network. Presentation to the National Road Pricing Conference, Metropolitan Transportation Commission, Houston, Oakland. http://tti.tamu.edu/conferences/nrp10/program/. Accessed 27 June 2011
81. Stone C (2010) SR 520 Lake Washington Project: Seattle's urban partnership agreement. Presentation to the National Road Pricing Conference, Houston, Washington State Department of Transportation, Olympia. http://tti.tamu.edu/conferences/nrp10/program/. Accessed 27 June 2011
82. Swisher M, Eisele WL, Ungemah D, and Goodin GD (2003) Lifecycle graphical representation of Managed HOV lane evolution. In: 11th International HOV conference, Seattle
83. Copeland L (2010) States turn to tolls to fund roads. USA Today, 2 Aug 2010
84. Adams T (2010)Toll concession model for the I-495 beltway HOT lanes. Presentation to the national road pricing conference, Transurban, Houston, Washington, DC 2–4 June 2010. http://tti.tamu.edu/conferences/nrp10/program/). Accessed 27 June 2011
85. Weiss EM (2008) Money spent vs. time saved debated for HOT lanes. Washington Post, Aug 25. http://www.washingtonpost.com/wp-dyn/content/article/2008/08/24/AR2008082402559.html
86. Miles M (2007) Tolling & value pricing: the California experience. In: ITE – Technical Conference 2007, California Department of Transportation, San Diego
87. Turner M (2008) Officials look to toll lanes to solve traffic, funding issues. Sacramento Bus J, Feb 22. http://www.bizjournals.com/sacramento/stories/2008/02/25/story1.html

Human Bacterial Diseases from Ocean

Darrell Jay Grimes[1], Lisa W. Plano[2], Okechukwu Ekenna[3,4]
[1]Department of Coastal Sciences, The University of Southern Mississippi, Ocean Springs, MS, USA
[2]Departments of Pediatrics & Department of Microbiology and Immunology, Miller School of Medicine, University of Miami, Miami, FL, USA
[3]Singing River Health System, Pascagoula, MS, USA
[4]University of South Alabama, Mobile, AL, USA

Article Outline

Glossary
Definition of the Subject and Its Importance
Introduction
Autochthonous Pathogens
Allochthonous Pathogens
General Treatment Principles
Treatment Considerations for Gram-Positive Organisms
Future Directions
Bibliography

Glossary

Allochthonous Exogenous, alien or nonindigenous; arising from another source or medium.

Ambient Being of the surrounding area or environment.

Archaea One of three domains on Earth, including the *Bacteria* and *Eukarya*. *Archaea* are prokaryotes that do not have peptidoglycan cell walls; they lack membrane-bound organelles (e.g., nucleus, mitochondria, endoplasmic reticulum, chloroplasts), possess 70 S ribosomes and have ether-linked lipids in their membranes.

Autochthonous Indigenous, native, arising from within.

Bacteria One of three domains on Earth, including the *Archaea* and *Eukarya*. *Bacteria* are prokaryotes that possess peptidoglycan cell walls; they lack membrane-bound organelles (e.g., nucleus, mitochondria, endoplasmic reticulum, chloroplasts), possess 70 S ribosomes and have ester-linked lipids in their membranes.

Biodiversity The richness or complexity of life forms in an ecosystem, biome or on Earth itself.

Commensal organism An organism participating in a symbiotic relationship in which one species derives some benefit while the other is unaffected.

Ectotherm An organism that controls body temperature through external means.

Endotoxin The lipid component (lipid A) of the outer membrane lipopolysaccharide (LPS) of all gram-negative bacteria. Endotoxin is released into a host or the environment when the cell lyses and its outer membrane breaks up.

Epidemic The incidence of disease above the normal or endemic incidence.

Eukarya One of three domains on Earth, including the *Bacteria* and *Archaea*. *Eukarya* possess

membrane-bound organelles (e.g., nuclei, mitochondria, chloroplasts), histones associated with their DNA and 80 S ribosomes in their cytoplasm. Plants and animals are eukaryotic.

Exotoxin Any toxin that is secreted into the cell's immediate environment. Most exotoxins are proteins, and they are made by both gram-negative and gram-positive bacteria.

Facultative organism An organism that is capable of growth both in the presence and absence of oxygen.

Foodborne disease A disease that is caused by the ingestion of pathogens conveyed by food.

Food intoxication Illness caused by the ingestion of food that contains a toxic substance.

Hemolysin A proteolytic enzyme that lyses red blood cells.

Lysogenic conversion Insertion of bacterial virus (bacteriophage) DNA into the chromosomal DNA of its bacterial host thereby conferring one or more new traits on the host.

Nosocomial Infections (and disease) that are acquired in clinical settings (e.g., hospitals, outpatient clinics, emergency rooms, physician offices).

Opportunistic pathogen Any pathogen that accidently acquires entrance to a host and then only causes disease if one or more risk factors are present in the host.

Pandemic An epidemic of world-wide proportions.

Pathogenesis The production or development of a disease, specifically the cellular reactions and other pathologic mechanisms occurring in the progression of the disease.

Pathogenic The ability of a species to cause disease. However, because pathogenesis is typically caused by one or more than one virulence factors produced by one or more genes, any given pathogenic species will often display different degrees of pathogenesis.

Pathogenicity island A cluster of virulence genes (and sometimes cryptic genes and other small genetic elements) flanked by direct repeats, insertion sequences or tRNA genes such that the clusters are easily transmitted to other bacteria via a process called *horizontal gene transfer*.

Plasmid A circular, double-stranded DNA molecule containing specialty genes that, in general, are not essential for survival of the host bacterium or genes that are cryptic (unknown). Plasmids can replicate autonomously or integrate into and replicate with the chromosome. Plasmids are smaller than the chromosome, on average 5% the size of the chromosome.

Point source A single, identifiable localized source of something.

Quorum sensing A chemical mechanism used by bacteria to measure their population density. When the chemical signals reach a certain level, special genes are expressed.

Sentinel An indicator whose presence is directly related to a particular quality in its environment at a given location.

Sequences The order of nucleotides in a specific length of DNA or RNA.

Virulence The degree of pathogenicity. Virulence is a compilation of toxins, hemolysins, proteases and lipases that may not be possessed by all strains of a pathogenic species.

Waterborne disease A disease that is transmitted by water.

Zoonosis An animal disease transmissible to humans under natural conditions or a human disease transmissible to animals.

Definition of the Subject and Its Importance

Several bacteria that cause human disease can be found in the ocean. The actual incidence of bacterial disease that results from seawater or seafood is not precisely known but is thought to be relatively low in the USA, although some diseases are on the rise. Bacterial disease from the ocean is more prevalent worldwide, especially in developing countries and in countries that derive most of their protein from seafood. Compared to the viruses, bacteria account for a much lower incidence of disease emanating from the ocean, both in the USA and worldwide. However, it is important to understand and mitigate bacterial disease from the ocean, because of such environmental pressures as global warming, antibiotic resistance, pollution, breakdowns in sanitation (e.g., Haiti after the earthquake) and tourism.

Introduction

Myriad bacteria reside in the ocean and most (>99.9%) have not been isolated and are known only by their

unique molecular signatures (e.g., 16 S rRNA sequences) [35, 59]. These bacteria belong to the domain *Bacteria* which exhibits extensive *biodiversity*, only exceeded by the biodiversity within the domain *Archaea* and the viruses. The vast majority of bacteria in the ocean do not cause disease and Archaea are not known to cause any human disease [39]; however, a very small number (percentage) of bacterial species found in the ocean cause *pathogenesis* in plants and animals. Some of these pathogens are indigenous to the ocean and are defined as *autochthonous*. Others (*allochthonous* bacteria) are of exogenous or terrestrial origin and are introduced to the ocean via surface runoff, rivers and streams, atmospheric fallout and ocean disposal of wastes (intentional or accidental); the chapter on enteric viruses (See S.NO.12, J. Woods, Waterborne Diseases of the Ocean, Enteric Viruses, this volume) has a nice discussion of allochthonous sources. This chapter will focus on those allochthonous and autochthonous bacteria that cause *waterborne* and *foodborne* disease in humans. Some also cause disease in marine animals (and a few in marine plants) but nonhuman diseases will not be addressed in this chapter.

Autochthonous human pathogens have evolved in the ocean and for largely unknown reasons have the ability to infect and cause disease in humans. Almost all of these diseases result from ingesting seawater, eating seafood, or broken skin contact (swimming, wading, or working in seawater). The allochthonous human pathogens are transients in the ocean with varying abilities to survive in seawater; all of the allochthonous pathogens infect humans via the same routes as autochthonous pathogens, i.e., contaminated seawater, seafood or broken skin contact. There are a few bacteria that may fit both definitions, and there is no current scientific consensus about the place of these bacteria. Examples of these ubiquitous bacteria include the enterococci [159], *Staphylococcus aureus* (see Allochthonous Pathogens in this chapter) and *Pseudomonas aeruginosa* [114].

In the following pages, allochthonous and autochthonous marine bacteria that cause disease(s) in humans will be discussed in terms of their biology, ecology, pathogenesis, and epidemiology. Disease treatment will also be discussed but not in clinical detail.

Autochthonous Pathogens

Autochthonous pathogens generally cause one or more diseases in marine animals and if the disease(s) is transmissible to humans it is classified as a *zoonosis*. It some cases, humans can transmit disease to marine animals.

Vibrio

Vibrios, and specifically *Vibrio cholerae*, were first observed by Pacini in 1854 and later isolated in pure culture from cholera patients by Robert Koch in 1883 [8, 27]. Today, the Vibrios comprise a large genus (>80 species) and belong to the *Gammaproteobacteria* [47]. They are gram-negative rods, often slightly curved (e.g., *V. cholerae*) and most are motile in liquids by means of one or more polar flagella; on solid surfaces they are motile by means of lateral flagella. Unlike most bacteria, Vibrios possess two circular chromosomes (one large and one small) which are of relevance to this chapter because of the distribution of *virulence* genes on the two chromosomes. The large chromosome is usually referred to as Chromosome 1 (Ch1) and it tends to contain housekeeping genes (DNA replication, transcription, translation, flagellar synthesis, metabolic pathways). Chromosome 2 (Ch2) tends to contain accessory genes (pathogenicity, antibiotic resistance, host defense avoidance, survival in adverse environments). Most of the Vibrios can metabolize a large number of organic compounds, including sugars, amino acids, fatty acids, carbohydrates, proteins, lipids, alcohols, and selected aliphatic and aromatic hydrocarbons. Indeed, prior to the development of molecular biology methods, the Vibrios were largely identified and classified by these diverse and extensive metabolic traits [22].

In addition to metabolic diversity, the pathogenic Vibrios also possess an array of *exotoxins*, proteases, transport proteins, attachment mechanisms, and lipases that act as virulence factors. Since Vibrios are gram-negative, they also possess *endotoxin* which differs in toxicity from strain to strain. Indeed, the Vibrios are well equipped to cause disease in their hosts – accidental or otherwise. In general, the Vibrios are opportunistic pathogens – for both humans and marine animals – and they cause systemic infections, skin lesions and gastroenteritis. In fish, the infections often lead to hemorrhagic skin lesions

(known as vibriosis) and pathology in the liver, spleen, and kidney. In humans, the diseases arise from contamination of cuts and other skin lesions with seawater (and to a lesser extent marine animals, e.g., stingray barbs and barnacles) and from ingestion of raw, undercooked or cooked but re-contaminated seafood and seawater. Depending on the species, skin infections can remain localized or become systemic and ultimately fatal. Oral ingestion of seafood and seawater leads to various degrees of gastroenteritis and, in some cases (e.g., *V. vulnificus)* life-threatening systemic infections. Although 12 *Vibrio* spp. are considered to be human pathogens, the predominant human pathogens are *V. cholerae, V. parahaemolyticus* and *V. vulnificus*. Table 1 presents a recent compilation of *Vibrio* diseases in the USA. In addition to the eight species listed in Table 1, the other human pathogens include *V. cincinnatiensis, Photobacterium damselae* (initially named *V. damsela*), *V. furnissii*, and *V. harveyi*; these four Vibrios, along with *G. hollisae* and *V. metschnikovii*, will not be discussed in this chapter, due to their low incidence of disease in humans.

All of the Vibrios require NaCl to grow properly, although this requirement is minimal for some species, e.g., *V. cholerae* and *V. mimicus*. Most if not all Vibrios use a sodium motive force to drive their polar flagella [94, 157] and at least a few species appear to use a sodium motive force to make ATP [37, 138]. Lateral flagella are produced by Vibrios when they grow on solid surfaces; these flagella are driven by a proton motive force [94] and are responsible for swarming. In addition to a requirement for sodium, most Vibrios are mesophiles and, therefore, do best in warmer waters. Recently, it has been suggested that global warming might increase the incidence of Vibrios worldwide [25, 28]. Interestingly, laboratory-confirmed infections with *Vibrio* spp. began to exceed those from *Salmonella*, Shiga toxin-producing *Escherichia coli* O157, *Campylobacter* and *Listeria* in late 2000 and this US trend has increased through 2008 [17]. In 2009, the overall rate of foodborne disease

Human Bacterial Diseases from Ocean. Table 1 Number of *Vibrio* illnesses (excluding toxigenic *V. cholerae*) in the USA, 2008[a]

Species	Patients	Deaths	Isolates	Specimen[b]
V. alginolyticus	99	1	99	Wound and other[c]
V. cholerae (nontoxic)	50	2	50	Stool and blood
V. fluvialis	29	3	29	Stool and wound
V. hollisae[d]	4	1	4	Stool and wound
V. metschnikovii	1	0	1	Blood
V. mimicus	32	0	32	Stool and other
V. parahaemolyticus	270	4	270	Stool and wound
V. vulnificus	85	24	94	Blood and wound
Species not identified	23	0	24	Stool and other
Multiple species	6	0	13	Wound and stool
Total	**599**	**35**	**616**	**Stool most frequent**

[a]Data reported to the Cholera and Other *Vibrio* Illness Surveillance (COVIS) system maintained by the CDC (see http://www.cdc.gov/nationalsurveillance/PDFs/Jackson_Vibrio_CSTE2008_FINAL.pdf)

[b]The predominant specimen types with the most predominant listed first. Additional specimens, including actual numbers, can be seen in the COVIS report[a]

[c]"Other" consists of ear, sputum urine, and other specimens

[d]Reclassified to *Grimontia hollisae* in 2003 [137]

Human Bacterial Diseases from Ocean. Table 2 Temperature and salinity preferences for the pathogenic Vibrios[a]

Vibrio species	Temperature		Salinity	
	Optimum	Range	Optimum	Range
V. cholerae	25°C [24, 26]	17–40°C [15, 31]	2–14 ppt [26, 31]	<1–60 ppt [15]
V. parahaemolyticus	38°C [27, 33]	8–45°C [16, 33]	17–23 ppt [19, 27, 44]	<1–96 ppt [33]
V. vulnificus	30°C [39]	9–40°C [21, 39, 40, 106]	5–10 ppt [25]	5–35 ppt [25, 40, 106]

[a]Bracketed numbers are supporting citations found in the *Primary Literature*

caused by Vibrios was 0.35 per 100,000 population [18]. The relative rates of the other four pathogens have either remained level (*Salmonella*) or shown a decrease (*Shigella* rates decreased 40% and STEC O157 decreased 25%) while Vibrio rates have increased by 47% [17]. Some have suggested that because this trend began just before the El Niño years 2002–2003 and continued through the El Niño years 2006–2007, it was caused by global warming. Intriguing as it may be, this observation is circumstantial and cannot be confirmed. However, in 1991 there was an outbreak of cholera in Peru, a country that had not seen this disease for over 100 years [136]. The source of the 1991 outbreak was never determined and two more outbreaks occurred in 1993–1995 and 1997–1998. Gil et al. [56] very nicely demonstrated that the Peru outbreaks in summer 1998 correlated (linear regression, $P < 0.001$) with the sea surface temperature peak associated with the strong El Niño that year. Colwell et al. [25] and [28] have made similar observations for the Bay of Bengal. In 2004, an outbreak involving cultured raw oysters and *V. parahaemolyticus* occurred aboard a cruise ship in Prince Edward Sound [96]. Mean water temperatures had been increasing in Prince William Sound (0.21°C per year) since 1997, and in 2004, for the first time, mean daily temperatures in the sound did not drop below 15°C [96]. Johnson et al. [74] reported that when temperatures drop below 15°C *V. parahaemolyticus* and *V. vulnificus* are no longer culturable from water and sediment in Mississippi Sound; similar observations have been reported by others, suggesting that 15°C is a limiting temperature for many of the Vibrios. Clearly, it is beginning to look like increasing ocean temperatures are increasing the incidence of Vibrio disease and as more data become available this Vibrio incidence-climate link may be substantiated. Temperature and sodium preferences for the three principal pathogenic Vibrios are shown in Table 2. Finally, in the past decade, scientists are using remotely-sensed satellite data, including temperature and salinity, to predict human health risks from pathogenic vibrios in water and oysters [90, 117].

Vibrio alginolyticus This *Vibrio* is very common in estuarine and marine waters worldwide; in fact, it is unusual not to isolate *V. alginolyticus* when culturing coastal and estuarine water samples. It is known for its ability to swarm on isolation media [141] and it often overgrows desired isolates. Recently, it was demonstrated that *V. alginolyticus* is capable of quorum sensing and that QS is responsible for biofilm formation (swarming is a prelude to this phenomenon) and development of virulence factors involved with fish disease [64].

The most common disease caused by *V. alginolyticus* in humans is wound infection. Of the 99 infections reported to the CDC in 2008 (Table 1), 64 isolates came from wound infections, 5 from blood, 3 from stools and 27 from other specimens. Most infections are mild and self-limiting, although *V. alginolyticus* has been demonstrated in a few cases of severe necrotizing fasciitis that involved patients at risk because of cirrhosis [66]. Cases of gastroenteritis caused by *V. alginolyticus* are rare [140], as indicated in Table 1. This Vibrio has also caused eye infections [86].

Vibrio cholerae During the early cholera pandemics of the 1800s, *V. cholerae* was responsible for millions of deaths and was feared as the most dangerous waterborne human pathogen known [27, 76]. It still causes several thousand deaths annually [153] and a small number of cases occur in the USA each

year (see COVIS report cited in Table 1). The World Health Organization recently reported that in 2009 the number of cases worldwide (45 countries reporting) was 221,226 with 4,946 deaths (2.24% case fatality rate) [153]. The number of cases in the USA in 2008 was nine and none of these patients died (see COVIS report, Table 1). Although molecular detection is very effective and widely used [102] and the genomes of several strains have been fully sequenced, for documentation and epidemiology purposes isolates are still serogrouped by means of their O antigens. The predominant serogroups causing human disease worldwide are O1 and O139; in the USA, the CDC tests for serogroups O1, O75, O139, and O141 (COVIS report cited in Table 1).

The classic disease caused by *V. cholerae* is a rapidly developing, profuse, watery diarrhea that is usually accompanied by severe dehydration. The cholera diarrhea is often called a "rice-water" stool because as the disease progresses the frequent stools are little more than water containing flecks of mucous abraded from the intestinal mucosa. When death occurs, it is because of the severe dehydration (water loss) and acidic coma (loss of sodium bicarbonate to the diarrhea). Historically, the death rate often exceeded 50% and death could result in as few as 24–36 h after onset of symptoms. As noted above [153] the death rate for cholera is now below 5% and most cases of cholera today are little more than a transient diarrhea. In addition to classic cholera, *V. cholerae* can also cause self-limiting gastroenteritis and wound infections; it has also been implicated in fish disease (eels and ayu). An interesting and illustrative human case occurred after Hurricanes Katrina and Rita and involved a Louisiana couple who consumed properly cooked (boiled) shrimp that had been placed on the ice used by them to transport the raw shrimp. The husband developed a severe case of cholera that caused renal, pulmonary and cardiac failure. He was given ciprofloxacin and aggressive rehydration therapy and he did not die. Of interest is that the husband had a history of common Vibrio risk factors – history of high blood pressure, alcoholism, diabetes, brain tumor, and renal failure that required frequent dialysis. His wife had mild diarrhea and was treated (ciprofloxacin and rehydration) as an outpatient. *V. cholerae* O1, serotype Inaba, biotype El Tor was isolated from both patients [15].

The main virulence factor associated with cholera is an exotoxin known as the cholera toxin (CTX). CTX is not produced by all strains of *V. cholerae*, and it is a protein that is composed of two subunits – one A subunit and five B subunits. The *ctx* genes that encode for these two subunits, *ctx*A and *ctx*B, are actually genes in a virus (a bacteriophage or phage) that infects *V. cholerae* and establishes a lysogenic relationship with its host [148]. The CTX phage that infects *V. cholerae* is a lambdaphage; and instead of producing more phage when it infects its host, this phage inserts its DNA into the chromosome (Ch1) of the host which then allows the host to produce CTX – a process called *lysogenic conversion*.

V. cholerae produces other virulence factors, including the toxin-coregulated pilus (TCP) produced by the *tcp*A gene, repeat-in-toxins (RTXs), and a heat-stable enterotoxin (NAG-ST) that is related to the heat-stable enterotoxin produced by *E. coli* [135]. The TCP is thought to be necessary for intestinal colonization by *V. cholerae* and may also serve as an attachment site for CTX phage [148]. Type 2 secretion systems are present in *V. cholerae*, and these systems provide a physical conduit for the bacteria to secrete toxins into their host cells (see secretion system discussion in "*Vibrio parahaemolyticus*" section).

In closing, prevention and treatment of cholera deserves mention. Cholera has a very low incidence in developed countries, primarily because of good sanitation, but this is not the case in developing countries [68]. In both developed and developing countries, cholera is usually a self-limiting disease requiring minimal treatment other than rehydration and electrolyte replacement; antibiotics are not usually administered. In developing countries where safe drinking water is not readily available, filtration of drinking water is very effective in preventing cholera. A very simple but highly effective filtration procedure was pioneered in Bangladesh [26]. The procedure involves using folded sari cloth (eight layers of old sari) to filter the drinking water; this procedure removes zooplankton to which the cholera bacilli are attached [26].

Cholera in Haiti

In January, 2010 Haiti was ravaged by a major earthquake that had an epicenter approximately 25 km from the capital city of Port-au-Prince. On October 21, 2010 cholera was confirmed in Haiti by the CDC; the causative agent has been identified as *V. cholerae* O1 serotype Ogawa. As of October 14, 2011, the Hatian Public Health Ministry reported that over 473,649 people have been infected and 6,631 patients have died. The disease peaked in early 2011 but cases and deaths continue. Interestingly, Haiti had not reported a cholera case for over a century and the source of the outbreak was, early on, not known. Clearly, the lack of hygiene, safe drinking water and safe food that followed the earthquake and continues to exist has contributed to the onset and continuation of cholera in Haiti. However, recent molecular evidence reported in the CDC journal "Emerging Infectious Diseases" demonstrated that a UN peacekeeping force from Nepal introduced the cholera strain into the Meille River.

Vibrio fluvialis The incidence of disease caused by *V. fluvialis* is thought to be very low, both in the USA (Table 1) and worldwide. This *Vibrio* primarily causes enteric disease but can cause wound infections and, rarely, other extraintestinal infections.

Vibrio mimicus This *Vibrio* is similar to *V. cholerae* in many ways and early on was thought to be an atypical *V. cholerae* – hence the species name "mimicus." The primary disease caused by *V. mimicus* is gastroenteritis and some strains carry *ctx* genes as well as other virulence factors found in *V. cholerae* and other Vibrios.

Vibrio parahaemolyticus First isolated in Japan from a gastroenteritis outbreak traced to the consumption of shirasu, a popular fish product (272 cases and 20 deaths; [54]), *V. parahaemolyticus* is the most common cause of foodborne disease in countries that consume high quantities of seafood [61]; in the USA, it is the most common cause of seafood-borne disease (see Table 1). As is the case with all the Vibrios that cause human disease, *V. parahaemolyticus* causes gastroenteritis and wound infections, and it is the most common cause of Vibrio disease in the USA (Table 1). *V. parahaemolyticus* can be isolated from most forms of seafood but is most commonly associated with shellfish [12].

The first *V. parahaemolyticus* pandemic began in 1996, and it continues to involve three major serotypes – O3:K6, O4:K68, and O1:K untypable [23]. Recent outbreaks are described in Table 3.

All *V. parahaemolyticus* strains possess the *tlh* (thermolabile hemolysin) gene, and this gene is frequently used to rapidly detect and confirm identification of the species. However, *tlh* is not unique to *V. parahaemolyticus*; *V. harveyi*, *V. alginolyticus*, and *V. fischeri* have also been shown to contain a *tlh* homologue or a related hemolysin gene [72, 134, 149].

When first discovered, it was shown that *V. parahaemolyticus* had the ability to hemolyze red

Human Bacterial Diseases from Ocean. Table 3 Recent outbreaks and cases of *V. parahaemolyticus* gastroenteritis

Date	Location (ref.)	Source	Cases/deaths	Serotype	El Niño
1997	Pacific North West [12]	Oysters	209/1	O1, O4, O5	Yes
1998	Gulf of Mexico, NE, Pacific NW [32]	Oysters	416/?	O3:K6	Yes
1998	Chile [62]	Shellfish	~300/?	O3:K6	Yes
1998	Japan [61]	Seafood	12,318/?	O3:K6	Yes
2004 and 2005	Chile [62]	Seafood	~5,100/?	O3:K6	No
2004	Alaska [96]	Oysters	62/0	O6:K18	No
2006	New York, Oregon, Washington [16]	Oysters	177/0	O4:K12	Yes
2006	Chile [62]	Shellfish	900/?	O3:K59	Yes

blood cells in a special culture medium called Watsumaga agar; it was later shown that this hemolysis, called the Kanagawa reaction, was mediated by a hemolysin called thermostable direct hemolysin TDH [67]. Most pathogenic *V. parahaemolyticus* strains possess the *tdh* gene and/or the *trh* (thermostable related hemolysin) gene [73], although some pathogenic strains contain neither *tdh* nor *trh* [98]. The *tdh* genes are located in a *pathogenicity island* on Ch2 [91]. In general, environmental and food isolates do not contain tdh and trh ([73] and [74]).

Gram-negative bacteria possess a fascinating injection apparatus called secretion systems. These allow bacteria to inject various substances into the cells of *Eukarya*. As is the case for many bacterial virulence factors, especially those associated autochthonous pathogens, such as the Vibrios; microbiologists understand how these factors function in human pathogenesis but do not know the function of these factors in the environment. To date, six secretion systems (T1SS, T2SS, T3SS, T4SS, T5SS and T6SS) have been described. In 2003, the sequenced genome of *V. parahaemolyticus* RIMD2210633 was shown to contain two different T3SS genes – T3SS1 and T3SS2 [91]. T3SS1 is located in a pathogenicity island on Ch1, T3SS2 is in a Ch2 pathogenicity island, and it is now known that there are two different T3SS2 – T3SS2α and T3SS2β [103].

Makino et al. [91] identified at least 50 other genes in *V. parahaemolyticus* that may be involved with pathogenesis. Some of these additional virulence factors include urease [112], attachment mechanisms [60, 130], ToxR [30], and RTX toxin [91].

Vibrio vulnificus One of the more recently discovered pathogenic Vibrios [46, 123], *V. vulnificus*, causes serious diseases in humans and is thought by some Vibrio biologists to be the most virulent bacterium now known (death rate >50% in patients at risk [104]; the overall case fatality rate reported by CDC [97] for 1992–1997 was 39%). *V. vulnificus* is thought to cause three human diseases: primary septicemia (caused by the ingestion of raw or undercooked shellfish – especially oysters), gastroenteritis (caused by the ingestion of raw or undercooked shellfish), and wound infections (caused by contact with water, barnacles, fish barbs, and other marine objects). The literature documenting simple gastroenteritis is scant and, accordingly, some experts question this disease having a *V. vulnificus* etiology (J.D. Oliver, personal communication). Primary septicemia is a rapidly developing disease that can result in death in less than 48 h after consuming seafood containing the bacteria. The bacteria move from the intestinal tract into the blood stream and, from there, set up serious infections in tissues, especially the extremities. Wound infections also most frequently involve extremities and will cause bullas (Fig. 1). When the infection progresses into deep tissue and begins to cause death of that tissue, the disease is called necrotizing fasciitis. The infection shown in Fig. 1 did not develop into necrotizing fasciitis but is a good example of what often happens when patients

Human Bacterial Diseases from Ocean. Figure 1
Wound infection of unknown etiology, caused by a minor scratch from a barnacle. Within 36 h the scratch had developed into a bula (**a**). The bula was debrided (**b**) and did not progress into necrotizing fasciitis (Grimes DJ, Ekenna O unpublished data)

are placed on aggressive antibiotic therapy to prevent progression of the infection. In this case, the patient was given three different antibiotics (clindamycin, levafloxacin, and doxycycline) prior to culture of the lesion, and these antibiotics probably caused the etiological agent to become nonculturable, a phenomenon observed and discussed by others [55, 126].

In general, *V. vulnificus* infections in healthy individuals are often not serious, but this is not always the case. Serious and fatal infections can occur in all patients and especially in those at risk; risk factors include: preexisting liver dysfunction or disease, diabetes, alcoholism, poor circulation, and immunosuppressive drug therapy. It is imperative that such individuals at risk are properly counseled about contact with seafood and seawater, so that they do not become infected with any *Vibrio* capable of causing disease in humans.

The virulence factors associated with *V. vulnificus* are not well understood. Known factors include *V. vulnificus* hemolysin (VVH) and RT [104]. There are two genotypes of *V. vulnificus* – clinical (C) and environmental (E) – and only C causes disease in humans. All strains of *V. vulnificus* have powerful iron sequestration ability (siderophores) which allows them to out-compete other species (including humans and fish) for essential iron. Capsular polysaccharide (CPS) formation is important and only encapsulated strains are virulent [104]. In addition, endotoxin (the lipoidal moiety of LPS) is very important and may be the most important cause of shock and death from *V. vulnificus* infections [104]. The complete genomic analysis of *V. vulnificus* YJ016 revealed the presence of RTX genes and they along with siderophore genes are located on Ch2 [21]. Type IV pilins, used as adherence mechanisms by many *Gammaproteobacteria* including *V. cholerae*, are a consistent feature of *V. vulnificus* and function in biofilm formation, attachment to epithelial cells, and possibly in the colonization of oysters [109, 110]. Other putative virulence factors have been described but their role in pathogenesis is unclear.

Aeromonas

Members of the genus *Aeromonas* are primarily freshwater bacteria that cause disease in both humans and aquatic animals. The most common isolates from human clinical specimens are *A. hydrophila, A. caviae, and A. sobria*, with *A. hydrophila* being the most common. Although *Aeromonas* spp. are frequently isolated from estuaries and the coastal ocean, they may not be truly autochthonous, and human disease from *Aeromonas* does not normally result from seawater or seafood. In fact, there is controversy about the ability of *Aeromonas*, a well-known pathogen of fish and amphibians, to cause disease in humans [48]. If one accepts the literature in support of human disease, it is believed that most human disease occurs in the form of gastroenteritis resulting from the ingestion of fish, shellfish, red meats, and contaminated water [48]. *Aeromonas* gastroenteritis presents either as a cholera-like disease with watery stools or a dysenteric-like illness that can include bloody stools [48]. Wound infections can also result from contact with contaminated water, either freshwater, seawater or brackish water [14, 75, 144].

Three recent reports of *Aeromonas* infections are illustrative of this seafood-borne and waterborne pathogen. In the aftermath of the 2004 tsunami that devastated eight countries and caused an estimated 225,000 deaths, the Thai Ministry of Public Health quickly began meeting health care needs in Thailand. From December 26, 2004 (the day of impact) to January 11, 2005, 1,237 cases of acute diarrhea, 356 wound infections, 177 febrile illnesses, and 156 respiratory illnesses were reported to the MOPH; only two deaths (both from aspiration pneumonia) resulted [14]. The most common isolates from the wound infections were *Proteus* spp., *Klebsiella* spp., *Pseudomonas* spp., *Enterobacter* spp. *E. coli*, and *A. hydrophila* (two isolates); surprisingly, no Vibrios were isolated, as was the case with Hurricanes Katrina and Rita.

Eighty-two strains of presumptive *Aeromonas* spp. were isolated from 250 frozen freshwater fish (Tilapia, *Oreochromis niloticus niloticus*) intended for human consumption and purchased in local markets in Mexico City. The isolates were identified with standard molecular techniques (16 S rRNA) and 88.3% were placed in two species – *A. salmonicida* (67.5%) and *A. bestiarum* (20.9%). The remaining isolates were identified as *A. veronii* (5.2%), *A. encheleia* (3.9%), and *A. hydrophila* (2.6%). The authors noted that this was one of the first major *Aeromonas* studies conducted in Mexico, and further noted that their results

demonstrated the need for concern over putative pathogens with antimicrobial resistance and known virulence factors being present in food meant for human consumption [9].

Finally, a study of the prevalence of *A. hydrophila* in marketed seafood (fish and prawns) was conducted in land-locked city in South India by Vivekanandhana et al. [145]. Random samples of seafood (536 fish and 278 prawns) were collected from several vendors in a popular seafood market, and fish showing visible spoilage, injury or disease were avoided. Overall, 180 fish samples (33.6%) and 49 prawn samples (17.6%) contained *A. hydrophila*. The authors attributed the incidence to temperature abuse, fly contamination from a nearby sewage treatment plant, and the ability of *A. hydrophila* to grow at refrigerator temperatures (4–7°C); and they further noted that *A. hydrophila* is a pathogen of emerging importance [145].

Aeromonas Soft-Tissue Wound Infection

In late summer of 2010, a 7-year-old boy suffered a large and complex laceration injury to the right calf while recreational boating on a coastal river. He was brought within 2 h to the hospital, after initial first aid in the field. The wound was thoroughly washed and cleansed at surgery and closed with over 30 fine stitches. He was discharged the next day in stable condition and on oral antibiotics.

He failed to take the prescribed antibiotics because of nausea and vomiting (no diarrhea or fever). On readmission 6 days later, the wound was infected. Wound culture showed a rapid growth of a gram-negative rod (GNR) that was beta-hemolytic on blood agar, and also grew on MacConkey and chocolate agars. It was oxidase positive, mucoid, catalase positive, and motile.

The organism was confirmed to be *Aeromonas hydrophila*. It was found to be sensitive to second and third-generation cephalosoprins, quinolones, tetracycline, trimethoprim/sulfamethoxazole, and aminoglycosides. He responded well to intravenous ceftriaxone (a third-generation cephalosporin), local wound care, and later to applied skin graft to the injured calf. He made a full recovery.

The infection was most likely caused by wound contamination from the freshwater (river), and occurred because of a combination of factors: premature surgical closure of wound, and inability of the patient to take prescribed oral antibiotics to which the organism was sensitive.

Edwardsiella

There are three species of *Edwardsiella*, and the one that causes human disease is the opportunistic pathogen *E. tarda*. *E. tarda* causes a Salmonellosis-type enteritis in humans and typically derives from freshwater and freshwater animals (e.g., pet turtles). Infections from marine sources are unknown. *E. ictaluria* is a serious fish pathogen, often associated with septicemia in catfish (especially in aquaculture of catfish), but it is not known to cause disease in humans or marine fishes.

Yersinia

Several *Yersinia* spp. cause diseases in humans (Bubonic plague or Black Death, pseudotuberculosis, enteritis, extraintestinal complications) and in fish, including marine fish (salmonids). However, none of the marine fish pathogens are known to cause human disease and will therefore not be discussed here.

Brucella

Long known to cause disease in terrestrial animals and humans, these zoonotic bacteria are now known to exist in the ocean. The classic *Brucella* spp., *B. abortus*, *B. melitensis* and *B. suis*, cause brucellosis or undulant fever in humans and domestic animals. In domestic animals, the disease outcome is often abortion because the bacteria prefer to metabolize mesoerythritol which is found in the uterus and fetus of animals but not in humans. In humans, symptoms are general and include fever, chills, malaise, with heavy sweating, and high fever at night.

The three classic *Brucella* species have not been reported in marine mammals. Instead, it appears that marine mammals carry their own *Brucella* spp. [71], and they have caused three naturally acquired cases of human disease. Two cases were reported in Peru in 2003 (Sohn et al. 2003) and one in New Zealand [95]. The three *Brucella* human isolates were characterized with several molecular methods, and all three were

found to share a common genotype with previously reported marine mammal *Brucella* spp. [152]. Representing 173 animals and one human patient were analyzed using a molecular method called multiple loci VNTR (variable number of tandem repeats), and the authors targeted 16 genetic loci (MLVA-16) that had been shown to be highly descriptive for *Brucella* spp. [93]. The study included two new species isolated from marine mammals, *B. ceti* and *B. pinnipedialis*, and concluded that these two species cluster into three distinct clades. Interestingly, the three isolates described by Whatmore et al. [152] did not cluster within the three clades but were, however, closely linked to the three marine mammal groups [93].

Enterococcus

Members of the genus *Enterococcus* are largely commensal colonizing organisms of the gastrointestinal tract of humans and warm-blooded animals and are commonly recovered in their feces [49]. These organisms are gram-positive facultative anaerobes that do not form spores but are capable of survival and growth in a wide variety of environmental conditions. These include tolerance of temperatures ranging from 10°C to 45°C, pH from 4.5 to 9.0 and high sodium chloride concentrations [63]. Although *Enterococcus* species have been found in many different marine and freshwater environments [85, 92, 124, 143, 158] as well as being associated with processed and fresh fish and seafood [31, 70, 99, 116, 154], these organisms are not usual pathogens for fish or marine mammals. *Enterococci* are known to be introduced into these environments by sewage contamination from known point sources, such as sewage treatment plants, and are used as indicator organisms for the probable presence of disease-producing pathogens in marine waters [147]. It is unlikely that point sources are the sole contributor of these organisms to an aquatic environment. Domestic and wild animals, water runoff from storms or agricultural sources, wind-driven sediment resuspension events, and humans utilizing the waters have all been shown to contribute to the presence of *Enterococcus* species in aquatic environments. ([1, 33, 42, 43, 107]; Rebarchik DM, Grimes DJ unpublished data).

The principal pathogenic *Enterococcus* in humans, *Enterococcus feacalis* and *E faecium*, are among the *Enterococcus* species isolated from aquatic environments; however, *Enterococci* found in marine settings have not been linked directly to the onset of human enterococcal infections. In general, these organisms are primarily associated with serious, often fatal, nosocomial infections, including postsurgical wound infections, endocarditis, urinary tract infections, and sepsis; and they are currently emerging common pathogens [49]. Enterococci lack significant virulence factors associated with disease but are intrinsically resistant to many antibiotics currently in use. These bacteria, especially *E. fecium*, are known to easily acquire antibiotic resistance genes from other microorganisms encountered in their environment. In addition to its importance as an indicator organism, the significance of *Enterococcus* in a marine-water setting is the increased likelihood that the organisms will be exposed to other microorganisms from which they might acquire antibiotic resistance genes, thus adding to the difficulty of treating an already challenging infection.

Streptococcus

Numerous species of fish are susceptible to infection by members of the genus *Streptococcus*. Although these infections are not common, when they do occur, it is often in an aquaculture setting and can be responsible for significant mortality and large economic costs. One species that is responsible for such infections, *Streptococcus iniae*, is a primary pathogen for fish that can also infect humans. This organism was first isolated from infected freshwater dolphins in 1996 [113] and has subsequently been associated with sporadic infections in multiple fish species [41, 77, 80, 115]. It was recognized as a human pathogen in the mid-1990s with several documented infections in North America [11, 150], and later in Japan [84]. *S. iniae* infections in humans present as fever and cellulitis, often with bacterimia, and can be treated with intravenous penicillin and gentamicin [84].

S. agalactiae (Lancefield group B) is a significant human pathogen especially in newborn infants where it can cause sepsis, pneumonia, and meningitis; and in pregnant women where it is associated with urinary tract infections. This organism has been linked to

disease outbreaks and some massive kills in several fish species [121]. Investigations performed to type the bacteria isolated from infected fish and environmental samples indicated that sewage contamination was a likely source for the infections in fish [121, 125]. There is no evidence linking fish or a marine environment with human disease.

Listeria

The genus *Listeria* consists of six species including two that are recognized as pathogens. *L. monocytogenes* is an important human pathogen, and *L. ivanovii* is an animal pathogen that may very rarely infect humans but is not associated with marine related infections. *L. monocytogenes* are short, motile, gram-positive rods that may appear as coccobaccili. They are hardy organisms that grow as facultative anaerobes in a wide range of temperatures (from 1°C to 45°C), pH (pH 4.3 to pH 9), and they tolerate high salt concentrations. They are ubiquitous organisms that are commonly found in soil and water, on vegetation, and decaying matter and excreted in feces of humans and animals [89]. *L. monocytogenes* is the causative agent of listeriosis, a serious but rare infection caused by eating food contaminated with the bacteria. Multiple types of food have been associated with *Listeria* infections, classically soft cheeses made from unpasteurized milk, meat and processed meat products, and fish and shell fish [87]. Food may become contaminated before, during, or after preparation; and the usual measures for prevention of growth of contaminating organisms, low temperatures, extremes of pH, and high salt, are ineffective against *Listeria*. Included among the marine sources implicated in food contamination are crab meats and dips, lobster and shell fish, and many varieties of fish, especially those smoked or processed [6, 36, 81–83]. In a recent report from the CDC addressing the incidence of infection with pathogens that are commonly transmitted via a food borne route, of the greater than that 17,000 culture-proven infections, Listeria accounted for less than 1% of cases with an incidence of 0.34 per 100,000 [18].

Listeriosis occurs primarily in pregnant women, newborn infants, elderly patients, and patients who are immunocompromised, and in all but the newborns; the infections result in an initial mild influenza-like illness that may progress to sepsis and meningitis. In pregnant women, there is an increased risk of miscarriage, and in newborns the infection is associated with a high mortality, up to 40%, and long-term side effects [7, 120]. Adults and children acquire the disease after ingestion of contaminated foods, whereas newborns acquire infecting organisms either transplacentally or via an ascending route during labor and delivery. Onset of the disease varies with population and exposure routes, and it may be from days to weeks. The mortality rates for infections in these populations are high, up to 25%. *Listeria* are facultative intracellular pathogens, a characteristic that contributes to the severity of listeriosis. After being phagocytosed, the bacterium utilizes unique virulence factors to spread from cell to cell without an extracellular state, thus evading the humoral immune response. Included among these factors are internalins (inlA, inlB, inlC) that facilitate attachment to the cells. Once inside the cell, listerolysin O and phospholipase C enzymes act to release the bacteria to the cytosol where the bacteria utilizes a protein, ActA, to coordinate the assembly of actin into a "tail" that propels the bacterium across one cell and into the next. *Listeria* infections can be treated with common antibiotics, such as ampicillin, ciprofloxacin, linezolid and azithromicin.

Mycobacterium

The genus *Mycobacterium* consists of numerous aerobic, nonmotile, non-spore-forming, acid-fast rods that occur widely in nature. These bacteria range from soil-dwelling saprophytes to pathogens of humans and animals. Of the greater than 20 human pathogenic *Mycobacterium* species, few have been associated with infections from or in a marine environment [155]. *Mycobacterium marinum* (synonym *M balnei*) is the primary aquatic pathogen and is a free living organism found throughout the world in both fresh and marine water environments. It was first discovered as a pathogen for fish, causing skin nodules and ulcers, in the mid-1920s and has since been recognized as a natural pathogen for other *ectotherms*, such as frogs. Since the early 1950s [88] it has been recognized as a cause of human infections first described as causing

superficial skin lesions, nodules referred to as "swimming pool granulomas," in children who swam in contaminated pools. Like most other human pathogenic Mycobacteria, *M marinum* grows slowly, having a typical incubation period of 2–4 weeks before cutaneous lesions appear, but occasionally may progress rapidly. Unlike other human pathogenic Mycobacteria, it optimally grows at lower temperatures, 30–33°C, and is usually inhibited at 37°C, helping to explain the typical location of the lesions on the extremities and the usual lack of systemic involvement.

Currently *M marinum* is the most common cause of atypical *Mycobacterium* infection in humans with a reported incidence of 0.27 cases per 100,000 adults [128] Infection with these organisms can occur at any age, but it usually occurs in adults who handle fresh- or saltwater fish or fish tanks, and is now rarely associated with swimming pools, as proper construction and chlorination has eliminated this source [40]. Human exposure now primarily comes through inoculation of existing skin abrasions while handling fish or their tanks, or directly through fish bites or puncture wounds from fins. Local trauma is an important factor in establishing *M marinum* infections and their sequelea. Infections obtained after inoculation of an existing abrasion or a direct puncture manifests as a localized nodule or granuloma at the site of bacterial entry that may develop into an ulcer or progress to involve nearby lymph nodes, sporotrichotic lymphangitis. In healthy individuals it rarely progresses to involve bones, joints, or other systemic sites. Immunocompromised states increase the risk for becoming infected and can be associated with more aggressive systemic disease [111, 151]. Diagnosis and treatment are often delayed because of a lack of suspicion for mycobacterial involvement versus more common bacterial pathogens and are contributed to by the long incubation period.

Treatment for *M marinum* is driven by the severity of the infection [122] and ranges from oral monotherapy with minocycline, clarithromycin, doxycycline, ciprofloxacin, and trimethoprim-sulfamethoxazole for superficial cutaneous infections with susceptible organisms to combination therapies for drug resistant strains. Severe infections, including those with a sporotrichoid distribution pattern, generally require combination therapy with rifampicin and ethambutol. Surgical debridement is not usually recommended, however, other alternative topical therapies, such as cryotherapy, X-ray therapy, electrodesiccation, photodynamic therapy, and local hyperthermic therapy can be effective.

Allochthonous Pathogens

Escherichia

The first species of this genus, *Bacterium coli*, was first isolated in the late 1800s and it was proposed as an indicator of fecal contamination of water. The isolate was renamed *Escherichia coli* in 1919 and today remains in use as the fecal indicator recommended by the USEPA for freshwater [142]. Unfortunately, *E.coli* and the enterococci do not correlate with indigenous pathogens such as the vibrios [29] and enteric viruses (see s.no. 12, J. Woods, Waterborne Disease of the Ocean, Enteric Viruses, this volume). In addition to its worldwide use as a fecal indicator, *E. coli* is the most common cause of urinary tract disease in humans (ca. 90% of human UTIs): certain strains cause gastroenteritis of various degrees of severity (e.g., STEC or the Shiga toxin-producing *E. coli* O157 usually derived from meats and produce) and nonpathogenic strains such as *E. coli* K12 that laid the early foundation for much of what is known about metabolism and enzymology.

Despite extensive documentation of *E. coli* causing human disease from the consumption of contaminated raw and undercooked foods, oral–fecal transmission in public facilities such as nurseries and day care centers and contaminated drinking water, transmission from seafood and seawater is rare and does not occur in the USA with great frequency. The overall foodborne STEC O157 incidence in the USA for 2009 was 0.99 per 100,000 population, and the STEC non-O157 incidence was 0.57 [18] for many years. This disease agent will not be further discussed in this chapter, and readers interested in this important pathogen are encouraged to peruse other literature.

Shigella

Shigella spp. cause a significant incidence of foodborne disease worldwide, but they are not often acquired

from the ocean. Some strains produce the powerful Shiga toxin which, like CTX, is a lysogenic conversion product. In the USA, shigellosis (bacillary dysentery) has a fairly high incidence (3.99 per 100,000) as a foodborne agent of disease [18].

Salmonella

The Salmonellae are important pathogens but are much like *E. coli* and *P. aeruginosa*, with regard to their importance as marine pathogens. There are two species of *Salmonella, S. enterica* and S. *bongori*, and these two species are comprised of many serovars and subspecies. Both *Salmonella enterica* serotype Typhi (formerly *S. typhi*) and the other gastroenteritis-causing *Salmonella* spp. are human pathogens that historically were frequently acquired from the ingestion of contaminated seafood (especially filter-feeding bivalves, such as raw or undercooked oysters) and seawater. With the advent of fecal indicator monitoring of seafood and seawater, refrigeration of seafood, sanitary surveys (especially surveys of molluscan shellfish beds), and sewage treatment in developed nations, the origin of these diseases from the ocean declined significantly. Today, diseases caused by Salmonellae are still frequent worldwide, most commonly caused by *S. enterica* subspp. *enterica*, and they are almost always foodborne in both developed and developing countries (see http://www.who.int/mediacentre/factsheets/fs139/en/; [97]). In the USA, CDC reported a Salmonella foodborne disease incidence of 15.9 per 100,000 population; this is the highest incidence of any foodborne disease, but there was no breakdown on food type, i.e., seafood incidence was not given [18].

Non-typhoid salmonellosis in humans is most commonly gastroenteritis although complications, such as septicemia, can occur; deaths are rare if the patients are kept hydrated and placed on appropriate antibiotic treatment. Virulence is largely determined by pathogenicity islands, and the non-typhoid Salmonellae contain at least 12 of these genetically mobile elements [65]. Human salmonellosis is usually acquired from food, although contaminated water can also serve as a vehicle for transmission. The Food and Agriculture Organization (FAO) of the United Nations recently published a report on the control of *Salmonella* in sustainable aquaculture, and it contains a very nice review of occurrence and survival in the aquatic environment [44].

The incidence of salmonellosis deriving from seafood in the USA is low but is probably far underreported. DePaola et al. [34] recently provided evidence that, even though the reported incidence is low, the potential for acquisition in the USA certainly exists. They conducted a 2-year study of market oysters collected twice each month from retail establishments (restaurants and raw bars, seafood markets, wholesale dealers) in nine states. In all, FDA collected 397 samples representing 258 establishments. Salmonella was detected in 8.6% of the market oysters, a rate only exceeded by *V. parahaemolyticus* and *V. vulnificus* [34].

In the FAO report [44], it was noted that many studies have shown *Salmonella* serotype Sneftenberg to be the major serotype in marine environments and raw seafood worldwide. The report further noted that *Salmonella* spp. have been isolated from many marine mammals.

Morganella

Human disease from *Morganella morganii* is common (postoperative and other nosocomial) but these infections rarely emanate from the ocean. However, *M. morganii is* often associated with the decomposition of seafood; and if such seafood is consumed, scombroid fish poisoning can result. Scombroid results from histamine build up (and possibly buildup of other vasoactive amines) in the seafood as a result of histidine decarboxylation during the seafood spoilage process. This disease is a true food poisoning or intoxication, as opposed to a food infection, e.g., Salmonellosis and *Vibrio* gastroenteritis. Scombroid is probably caused by several enteric bacteria, including *Proteus*, spp. *Klebsiella pneumoniae, Hafnia alvei, Enterobacter* spp., *Serratia* spp., and *Citrobacter freundii;* in addition, *V. alginolyticus, Aeromonas* spp., and *Photobacterium* spp. are also histamine formers; and all have been isolated from spoiled fish [139]. The incidence of scombroid in the USA is thought to be common (http://www.fda.gov/Food/FoodSafety/FoodborneIllness/FoodborneIllnessFoodbornePathogensNaturalToxins/BadBugBook/ucm070823.htm), and worldwide incidence is also common. However, because scombroid is not a reportable disease,

documented cases are very low, e.g., only 103 incidents involving 827 people were reported from 1968 to 1980 (see above FDA URL). The most common fish involved with this intoxication are tuna, bonito, mackerel, and *mahi mahi*, and once the amines are formed in the meat, neither cooking, canning, or freezing lowers toxicity. Onset of this intoxication is rapid (often 30 min) and symptoms include a tingling or burning sensation in the mouth, rash on the upper body, and a drop in blood pressure; nausea, vomiting, and diarrhea may also present, and hospitalization may be required.

Pseudomonas

The most common human pathogen in this genus is *Pseudomonas aeruginosa*, and, like the Vibrios, this species is metabolically very diverse. *P. aeruginosa* is a very common cause of death in third-degree burn patients, it is a common nosocomial agent of disease, is frequently resistant to most clinically useful antibiotics, it is a cause of urinary tract infections, and it is a common (and often lethal) complication of cystic fibrosis. There have been numerous reports of human *P. aeruginosa* infections occurring from various types of freshwater contact (e.g., swimming pools, whirlpools, hot tubs, atomizers), but this literature is far too extensive to be summarized here. Although *P. aeruginosa* is frequently isolated from the coastal ocean [58], the authors are not aware of any literature documenting that disease caused by *P. aeruginosa* came from the ocean. It is primarily a freshwater bacterium [114].

Campylobacter

Campylobacter spp. are frequently isolated from healthy cattle, chickens, and birds [48], and they are also associated with several foods (unpasteurized milk, poultry, shellfish, fruits, and vegetables), freshwater ponds, and streams contaminated with fecal material [69]; Campylobacters are not normally isolated from seawater. While a few reports of seawater isolations exist [3, 58], most marine isolates come from shellfish [69]. The association with shellfish is similar to that of *Salmonella*, in that shellfish acquire *Campylobacter* spp., and usually *C. jejuni*, from filter-feeding in water contaminated with fecal material [2]. The incidence of foodborne *Campylobacter* disease in the USA is 13.02 per 100,000, second only to Salmonella [18]. However, seafood-borne disease is rare [2, 69].

Staphylococcus

The genus *Staphylococcus* is made up of at least 40 species of gram-positive, facultative anaerobic organisms that are found throughout the world. Most of these organisms exist as commensal colonizing organisms of animals and humans, but may also be found in soil, on surfaces and in untreated water. They are hardy organisms that grow in the presence of bile salts and NaCl (up to 6.5%), and they can survive on many types of surfaces for extended periods of time making them a challenge to eliminate in public environments, such as gyms, prisons and hospitals. *Staphylococcal* species are differentiated from other important gram-positive organisms by the presence of the enzyme catalase, and they are differentiated amongst themselves by the presence of the enzyme coagulase which is present in the more clinically relevant organisms.

Among the organisms that make up this genus are a large variety of coagulase-negative staphylococci (CoNS) that are the primary commensal colonizers of humans. CoNS are pathogenic primarily for compromised populations only, such as preterm infants or persons with implanted prosthetic devices. *Staphylococcus aureus* is coagulase positive, and this species is the principle pathogen associated with human infection. In humans, *S. aureus* strains are opportunistic pathogens that may colonize, without infecting, up to 40% of the population [24, 79, 146], but may occasionally gain access to the host, evade the immune response, and causes disease [52, 53]. In addition, these organisms have acquired resistance to most of the antibiotics used against them making treatment of infections challenging.

Most infections caused by *S. aureus* are limited to the cutaneous tissues and are caused by a person's own colonizing organisms. However, these bacteria are also capable of causing serious, life threatening systemic disease. In fact, *S. aureus* including the methicillin resistant *S. aureus*, MRSA, are among the leading causes of *nosocomial* infections [10, 78]. Furthermore, MRSA have emerged as significant causes of community as well as hospital-associated infections [38, 78].

The diseases caused by *S. aureus* in humans and animals are often produced through the action of specific toxins or virulence factors that different bacterial isolates can produce. Specific toxins are associated with particular syndromes, such as toxic shock syndrome toxin and scalded skin syndrome. Many *S. aureus* are also capable of producing and secreting toxins responsible for staphylococcal food poisoning, termed enterotoxins, that only need to be ingested to cause intoxication and do not require the continued presence of the bacteria for disease. Consumption of seafood contaminated with *S. aureus* producing enterotoxins leads to staphylococcal food poisoning. Contamination of the food products often comes during processing as is seen in Listeriosis; however, organisms in the water and associated with marine life as seen in Peter the Great Bay, Japan, and Nha Trang Bay, South China, seas may also contribute to human disease [5].

S. aureus including drug resistant MRSA and CoNS have been isolated at recreational beaches, from marine ccc and temperate environments [5, 19, 50, 57, 133]. Adults and toddlers in diapers have been shown to shed *S. aureus* and the indicator organism *Enterococcus* into recreational marine waters and sand [118]. Persons using these recreational beaches may transmit and receive these organisms from the environment [42, 51, 131]. A retrospective epidemiological/microbiological monitoring study performed in Hawaii in subtropical marine waters and beaches found that persons were four times more likely to have staphylococcal skin infections if they had a history of seawater contact [20]. Whether there is a correlation of the microbial load in these environments and increased infections is yet to be verified; however, a recent study performed at a South Florida recreational beach did show a correlation between the average number of bathers in the water and the presence of *S. aureus* [119].

S. aureus and MRSA have also been isolated from marine mammals, including bottlenose dolphins (*Tursiops truncates*), seals, and walruses (blowholes, gastric fluids, fecal and anal cultures), both in captivity and in the wild, and have been associated with both colonization and disease [45, 105, 129]. In marine mammals in captivity, it is likely that the source of *S. aureus* and MRSA are colonized human handlers. The source of these organisms for the non-captive animals is not clear; however, colonized wild mammals were primarily identified in locations associated with human recreational use in the estuarine waters of Charleston, SC and Indian River Lagoon, FL [100, 129]. It has been suggested that some of the marine mammals, such as bottlenose dolphins, might serve as sentinels for transfer of resistant organisms from humans and animals into this environment, or simply indicate that the antibiotics are reaching this environment. To date, there are no confirmed cases of human infection from colonized or infected marine mammals.

Staphylococcus aureus and MRSA at Recreational Beaches

Since the early 1990s, investigators in Hawaii have isolated *S. aureus* from the waters used for recreation and suspected that exposure of bathers to the organisms in this environment might put them at risk for staphylococcal infections. Recent investigations have also isolated *S. aureus* and methicillin resistant, MRSA, from recreational marine beaches at multiple locations, including Hawaii, Puget Sound, California, and South Florida. The sources of the bacteria in these environments are likely multiple and not yet completely appreciated. *S. aureus* are not known to have a marine reservoir; however, humans and other mammals that may be present at the beach are known to be colonized with the bacteria and are potential sources. In fact, humans have been shown to readily shed their colonizing methicillin sensitive *S. aureus* (MSSA) and MRSA into marine waters and sand.

A recent study completed at a South Florida recreational beach collected MSSA and MRSA from ambient water, water nearby bathers and sand and evaluated the bacteria present in these environments for their potential to be associated with infection by determining the virulence factors they could produce. The study showed that 30–37% of water samples had *S. aureus*; however, it was unable to show a correlation between exposure to *S. aureus* and reported illness. The majority, greater than 97%, of *S. aureus* found at this location were MSSA that carried few virulence factors known to be associated with infection. However; the MRSA isolated from this location were similar to the MRSA found in the community that are known to have the potential to cause serious infections. The lack of association

between exposure to *S. aureus* and illness in this study, at this location, and the lack of an adequate number of participants (sample size) to establish an association with an organism that is present in only present 37% of samples overall is explained in part by the low percentage of potentially virulent MRSA. The populations and concentrations of MSSA and MRSA at other more crowded, recreational beaches would likely be as different as the human populations utilizing these beaches. Bathers exposed to greater numbers of more virulent organisms could be at increased risk for infections. Further studies are required to establish the true risk to bathers exposed to MSSA and especially MRSA in these settings.

General Treatment Principles

Many of the marine or ocean-dwelling microorganisms important in human disease are gram-negative bacteria. The diseases caused by these microorganisms run the spectrum, from septicemia (e.g., *V. vulnificus*), to gastroenteritis, wound infections, ear infections, and eye infections. It is not surprising that treatment is also varied from syndrome to syndrome.

Cholera (*V. cholera*) is the classic example of a cause of noninflammatory severe gastroenteritis (rice water stools). In cholera, the diarrhea is toxin induced. The pathogenesis of diarrhea in other organisms may be inflammatory (e.g., *Salmonella, Campylobacter* or *Shigella*). The nature or mechanism of the diarrhea may affect the primary choice of, or decision regarding, treatment.

As a general rule, severe diarrheal diseases require fluid replacement, given either by mouth (oral rehydration) or by intravenous means as the primary mode of treatment, while inflammatory diarrheas require, in addition to fluids, also antimicrobial therapy. The mode of fluid delivery will depend on how sick the patient is, the availability of which treatment, and the capacity or resources available to deliver the fluid replacement to the patient.

Sometimes, antimicrobial treatment may be detrimental in severe diarrhea. A good example is the bloody diarrhea caused by *E. coli* 0157:H7, which may lead to hemolytic-uremic syndrome, especially in children exposed to both the toxin-producing *E. coli*, as well as antibiotic therapy [156]. In such cases, withdrawal of antimicrobial therapy may sometimes help prevent further complications of renal failure [108]. Treatment in this circumstance is entirely supportive.

For toxin-producing diarrheas, antibody binding in situ presents an attractive and elegant option, but this type of therapy has not yet been developed (for all practical purposes) for most diarrheal diseases seen in the clinical setting [101].

Septicemia (e.g., due to *V. vulnificus*) requires aggressive management in the intensive care unit (ICU) setting, surgical debridement where necessary, as well as antimicrobial therapy. Severe wound infections like necrotizing fasciitis require primary surgical debridement, antimicrobial treatment, and sometimes hyperbaric oxygen therapy.

Most patients with severe wound infections or septicemia do not typically die or have other adverse outcomes due to or as a consequence of antimicrobial resistance, but complications result because they present too late to the hospital, have devitalized tissues that were not promptly debrided, or for other host factor reasons.

In our experience, most *Vibrio* organisms seen in clinical practice on the Gulf Coast are sensitive to the third-generation cephalosporins (sometimes also to second generation cephalosporins), quinolones, tetracyclines, and aminoglycosides. The same goes for *Aeromonas hydrophila*, with similar susceptibilities as above, in addition to usual sensitivity to trimethorprim/sulfamethoxazole.

Acute diarrheal illnesses require antimicrobial therapy usually only for a short period (5 days is typically enough); while septicemia (e.g., typhoid fever and *Vibrio* sepsis) would require longer therapy (2 weeks or longer), depending on the complications.

Severe wound infections of the necrotizing fasciitis type often require multiple surgical debridements, in addition to antimicrobial therapy and local wound care. In addition, skin grafting or plastic surgery is often required to cover defective skin or tissue.

The key to successful treatment of all of these disease entities is timeliness in starting treatment. The earlier appropriate therapy is started, the better the clinical outcome. The later treatment is started, the more complications one can expect. Adjustments in antimicrobial therapy can and should be made after in vitro antimicrobial susceptibility studies are

available. However, prompt treatment must be started very early, empirically (best guess or educated guess), before the laboratory susceptibility reports are available.

The Vibrios have predictable antimicrobial susceptibilities, more so than *Salmonella, E. coli*, or *Shigella*. Antimicrobial resistance to enteric pathogens reflects the pattern of use of antibiotics in a given environment, as well as the ease of antimicrobial drug availability and abuse in the area or locale where the infection was acquired. Typically for *Aeromonas*, resistance to ampicillin-like agents and first-generation cephalosporins is common; these agents should therefore not be used to treat infections due to *Aeromonas*.

In general, a gram-negative bacillus found in coastal or ocean water (outside and far away from a sewage drainage site) is likely to be free-living and, therefore, is more likely to be sensitive to multiple antimicrobial agents. Organisms causing disease acquired through human-to-human or foodborne transmission (e.g., *Salmonella*), on the other hand, are more likely to have been previously exposed to antibiotics (e.g., in animals or food products). Infections acquired through such contacts may therefore be more resistant to antimicrobials than free-living ocean, river, or brackish water bacteria [4].

The sensitivity of human-to-human or animal-to-human transmitted gram-negative bacteria (*E. coli, Salmonella, Shigella, Pseudomonas*, etc.) will usually reflect the pattern of local prevailing antimicrobial use in that community. The local hospital's antibiogram should provide the initial guide in the choice of empiric therapy, with necessary adjustments made after in vitro susceptibility studies are available.

Antimicrobial therapy for Brucellosis is often prolonged (up to 6 weeks) in order to prevent relapse. Often, combination therapy that includes a tetracycline plus rifampin, or an aminoglycoside, is required and recommended for complete cure of this debilitating disease [127, 132].

Acute gastroenteritis caused by food poisoning (e.g., staphylococcal preformed heat-stable enterotoxin) is often rapid in onset (within 1–6 h of food ingestion) and is also self-limited. The symptoms of severe nausea and vomiting occur usually within 1–6 h, and are usually over in less than 24 h [13]. Antimicrobial therapy is usually not required.

Treatment Considerations for Gram-Positive Organisms

Enterococci lack significant virulence factors associated with disease but are intrinsically resistant to many antibiotics currently in use. These bacteria are known to easily acquire antibiotic resistance genes from other microorganisms encountered in their environment. Treatment is guided by the determined antibiotic sensitivities of the infecting organisms and may be prolonged.

Streptococcus iniae infections usually present after exposure to fish with fever and cellulitis, often with bacterimia, and can be treated with intravenous penicillin and gentamicin [84]. *S. agalactiae* (Lancefield group B) remains sensitive to penicillin.

Listeria infections can be treated with common antibiotics, such as ampicillin, ciprofloxacin, linezolid and azithromicin. The delivery method of antibiotic is determined by the severity of diease.

Treatment for *Mycobacterium marinum* is driven by the severity of the infection [122] and ranges from oral monotherapy with minocycline, clarithromycin, doxycycline, ciprofloxacin, and trimethoprim-sulfamethoxazole for superficial cutaneous infections with susceptible organisms to combination therapies for drug-resistant strains. Severe infections, including those with a sporotrichoid distribution pattern, generally require combination therapy with rifampicin and ethambutol. Surgical debridement is not usually recommended however other alternative topical therapies such as cryotherapy, X-ray therapy, electrodesiccation, photodynamic therapy, and local hyperthermic therapy can be effective.

The majority of infections by *Staphylococcus aureus* are cutaneous infections limited to skin and soft tissues. Minor skin infections are usually treated with topical antibiotics, such as a nonprescription triple-antibiotic mixture or mupirocin. In some cases, oral antibiotics may be given for more severe skin infections. If abscesses are present, surgical drainage may be required and for smaller abscesses may be curative. More serious and life-threatening systemic infections are treated with intravenous antibiotics. The choice of antibiotic depends on the susceptibility of the particular staphylococcal strains, as determined by culture results in the laboratory. MRSA from the community may be

sensitive to several antibiotics effective against MSSA; however, hospital-associated MRSA are usually resistant multiple antibiotics and may be challenging to treat. Vancomycin remains the drug of choice for multidrug resistant MRSA.

Future Directions

Clearly, most of what is known about waterborne human pathogens is based on laboratory and clinical observations, and this is especially true for autochothonous bacteria. The diseases and metabolic capabilities of these pathogens can be described in great detail, and in many cases the genomes of these bacteria have been completely sequenced. However, until their role or niche in the ocean and in freshwater habitats is fully investigated, it will not be possible to fully understand their ability to cause disease in humans. Accordingly, scientists need to continue asking the question, "how does this microorganism live in the ocean and yet invade humans to cause disease?"

Bibliography

Primary Literature

1. Abdelzaher AM, Wright ME, Ortega C, Solo-Gabriele HM, Miller G, Elmir S, Newman X, Shih P, Bonilla JA, Bonilla TD, Palmer CJ, Scott T, Lukasik J, Harwood VJ, McQuaig S, Sinigalliano C, Gidley M, Plano LR, Zhu X, Wang JD, Fleming LE (2010) Presence of pathogens and indicator microbes at a non-point source subtropical recreational marine beach. Appl Environ Microbiol 76:724–732
2. Abeyta C, Deeter FG, Kaysner CA, Stott RF, Wekell MM (1993) *Campylobacter jejuni* in a Washington state shellfish growing bed associated with illness. J Food Prot 56:323–325
3. Alonso JL, Alonso MA (1993) Presence of *Campylobacter* in marine waters of Valencia, Spain. Water Res 27:1559–1562
4. Baya AM, Brayton PR, Brown VL, Grimes DJ, Russek-Cohen E, Colwell RR (1986) Coincident plasmids and antimicrobial resistance in marine bacteria isolated from polluted and unpolluted Atlantic Ocean samples. Appl Environ Microbiol 51:1285–1292
5. Beleneva IA (2011) Incidence and characteristics of Staphylococcus aureus and Listeria monocytogenes from the Japan and South China seas. Mar Pollut Bull 62(2):382–387
6. Boerlin P, Boerlin-Petzold F et al (1997) Typing Listeria monocytogenes isolates from fish products and human listeriosis cases. Appl Environ Microbiol 63(4):1338–1343
7. Bortolussi R (2008) Listeriosis: a primer. CMAJ 179(8):795–797
8. Brock TD (1999) Robert Koch, a life in medicine and bacteriology. ASM Press, Washington, DC
9. Castro-Escarpulli G, Figuerasb MJ, Aguilera-Arreolaa G, Solerb L, Ferna´ndez-Rendo´na E, Aparicioa GO, Guarrob J, Chaco´n MR (2003) Characterisation of *Aeromonas* spp. isolated from frozen fish intended for human consumption in Mexico. Int J Food Microbiol 84:41–49
10. Centers for Disease Control and Prevention (1999) National Nosocomial Infections Surveillance system report: data from 1997–1999, Atlanta, GA
11. CDC (1996) Invasive infection due to *Streptococcus iniae* – Ontario, 1995–1996. Morb Mortal Wkly Rep 45:650–653
12. CDC (1998) Outbreak of *Vibrio parahaemolyticus* infections associated with eating raw oysters – Pacific Northwest, 1997. MMWR 47:457–462
13. CDC (2001) Diagnosis and management of foodborne illnesses: a primer for physicians. MMWR 50(RR02):1–69
14. CDC (2005) Rapid health response, assessment, and surveillance after a tsunami – Thailand, 2004–2005. MMWR 54:61–64
15. CDCb (2006) Vibrio parahaemolyticus infections associated with consumption of raw shellfish – three states, 2006. MMWR 55:1–2
16. CDCa (2006) Two cases of toxigentic Vibrio cholerage O1 infection after Hurricanes Katrina and Rita – Louisiana, October 2005. MMWR 55(02):31–32
17. CDC (2009) Preliminary FoodNet data on the incidence of infection with pathogens transmitted commonly through food – 10 states, 2008. MMWR 58:333–337
18. CDC (2010) Preliminary foodnet data on the incidence of infection with pathogens transmitted commonly through food – 10 states, 2009. MMWR 59:418–422
19. Charoenca N, Fujioka R (1993) Assessment of staphylococcus bacteria in Hawaii marine recreational waters. Water Sci Technol 27:283–289
20. Charoenca N, Fujioka RS (1995) Association of staphylococcal skin infections and swimming. Water Sci Technol 31:11–17
21. Chen C-Y, Wu K-M, Chang Y-C, Chang C-H, Tsai H-C, Liao T-L, Liu Y-M, Chen H-J, Shen AB-T, Li J-C et al (2003) Comparative genome analysis of *Vibrio vulnificus*, a marine pathogen. Cold Spring Harbor Laboratory Press, pp 2577–2587
22. Colwell RR, West PA, Maneval D, Remmers EF, Elliot EL, Carlson NE (1984) Ecology of the pathogenic vibrios in Chesapeake Bay. In: Colwell RR (ed) Vibrios in the environment. Wiley, New York
23. Chowdhury NR, Chakraborty S, Ramamurthy T, Nishibuchi M, Yamasaki S, Takeda Y, Nair GB (2000) Molecular evidence of clonal Vibrio parahaemolyticus pandemic strains. Emerg Infect Dis 6:631–636
24. Cole AM, Tahk S, Oren A, Yoshioka D, Kim YH, Park A, Ganz T (2001) Determinants of *Staphylococcus aureus* nasal carriage. Clin Diagn Lab Immunol 8:1064–1069
25. Colwell RR (1996) Global climate and infectious disease: the cholera paradigm. Science 274:2025–2031
26. Colwell RR, Huq A, Islam MS, Aziz KMA, Yunus M, Khan NH, Mahmud A, Sack RB, Nair GB, Chakraborty J, Sack DA, Russek-Cohen E (2003) Reduction of cholera in Bangladeshi villages by simple filtration. Proc Natl Acad Sci 100:1051–1055

27. Colwell RR (2006) A global and historical perspective of the genus *Vibrio*. In: Thompson FL, Austin B, Swings J (eds) The biology of Vibrios. ASM Press, Washington, DC, pp 3–11
28. Constantin de Magny G, Murtugudde R, Sapiano MRP, Nizam A, Brown CW, Busalacchi AJ, Yunus M, Nair GB, Gil AI, Lanata CF, Calkins J, Manna B, Rajendran K, Bhattacharya MK, Huq A, Sack RB, Colwell RR (2008) Environmental signatures associated with cholera epidemics. Proc Natl Acad Sci 105:17676–17681
29. Cook DW, Ruple AD (1989) Indicator bacteria and Vibrionaceae multiplication in post-harvest shellstock oysters. J Food Prot 52:343–349
30. Croci L, Suffredini E, Cozzi L, Paniconi M, Ciccaglioni G, Colombo MM (2007) Evaluation of different polymerase chain reaction methods for the identification of *Vibrio parahaemolyticus* strains isolated by cultural methods. J AOAC Int 90:1588–1597
31. Dalgaard P, Vancanneyt M et al (2003) Identification of lactic acid bacteria from spoilage associations of cooked and brined shrimps stored under modified atmosphere between 0 degrees C and 25 degrees C. J Appl Microbiol 94(1):80–89
32. DePaola A, Kaysner CA, Bowers J, Cook DW (2000) Environmental investigations of *Vibrio parahaemolyticus* in oysters after outbreaks in Washington, Texas, and New York (1997 and 1998). Appl Environ Microbiol 66:4649–4654
33. DePaola A, Nordstrom JL, Bowers JC, Wells JG, Cook DW (2003) Seasonal abundance of total and pathogenic *Vibrio parahaemolyticus* in Alabama oysters. Appl Environ Microbiol 69:1521–1526
34. DePaola A, Jones JL, Woods J, Burkhardt W III, Calci KR, Krantz JA, Bowers JC, Kasturi K, Byars RH, Jacobs E, Williams-Hill D, Nabe K (2010) Bacterial and viral pathogens in live oysters: 2007 United States survey. Appl Environ Microbiol 76:2754–2768
35. DeLong EF, Pace NR (2000) Environmental diversity of bacteria and archaea. Syst Biol 50:470–478
36. Destro MT (2000) Incidence and significance of Listeria in fish and fish products from Latin America. Int J Food Microbiol 62(3):191–196
37. Dibrov P (2005) The sodium cycle in *Vibrio cholerae*: riddles in the dark. Biochemistry (Mosc) 70:150–153
38. Diep BA, Carleton HA et al (2006) Roles of 34 virulence genes in the evolution of hospital- and community-associated strains of methicillin-resistant *Staphylococcus aureus*. J Infect Dis 193(11):1495–1503
39. Eckburg PB, Lepp PW, Relman DA (2003) Archaea and their potential role in human disease. Infect Immun 71:591–596
40. Edelstein H (1994) Mycobacterium marinum skin infections. Report of 31 cases and review of the literature. Arch Intern Med 154(12):1359–1364
41. Eldar A, Bejerano Y, Bercovier H (1994) *Streptococcus shiloi* and *Streptococcus difficile*: two new streptococcal species causing a meningoencephalitis in fish. Curr Microbiol 28:139–143
42. Elmir SM, Wright ME, Abdelzaher A, Solo-Gabriele HM, Fleming LE, Miller G, Rybolowik M, Peter Shih MT, Pillai SP, Cooper JA, Quaye EA (2007) Quantitative evaluation of bacteria released by bathers in a marine water. Water Res 41:3–10
43. Elmir SM, Shibata T, Solo-Gabriele HM, Sinigalliano CD, Gidley ML, Miller G, Plano LR, Kish J, Withum K, Fleming LE (2009) Quantitative evaluation of enterococci and Bacteroidales released by adults and toddlers in marine water. Water Res 43:4610–4616
44. FAO (2010) FAO expert workshop on the application of biosecurity measures to control *Salmonella* contamination in sustainable aquaculture. Food and Agriculture Organization of the United Nations, Rome (ISBN 978-92-5-106553-2)
45. Faires MC, Gehring E et al (2009) Methicillin-resistant Staphylococcus aureus in marine mammals. Emerg Infect Dis 15(12):2071–2072
46. Farmer JJ (1980) Revival of the name *Vibrio vulnificus*. Int J Syst Bacteriol 30:656
47. Farmer JJI, Janda M, Brenner FW, Cameron DN, Birkhead KM (2005) Genus 1. *Vibrio*. In: Brenner DJ, Krieg NR, Staley JT, Garrity GM (eds) Bergey's manual of systematic bacteriology, vol 2, The proteobacteria, Part B. The gammaproteobacteria. Springer, New York, pp 494–546
48. FDA (2009) Bad bugs book: foodborne pathogenic microorganisms and natural toxins handbook. http://www.fda.gov/Food/FoodSafety/FoodborneIllness/FoodborneIllnessFoodbornePathogensNaturalToxins/BadBugBook/ucm070523.htm
49. Fisher K, Phillips C (2009) The ecology, epidemiology and virulence of Enterococcus. Microbiology 155(Pt 6): 1749–1757
50. Fleisher JM, Fleming LE et al (2010) The BEACHES Study: health effects and exposures from non-point source microbial contaminants in subtropical recreational marine waters. Int J Epidemiol 39(5):1291–1298
51. Fleming L, Solo Gabriel H et al (2008) Final report on the pilot epidemiologic assessment of microbial indicators for monitoring recreational water quality in marine sub/tropical environments. The NSF NIEHS OHH Center, Rosenstiel School of Marine and Atmospheric Sciences, University of Miami, Miami
52. Foster TJ (2004) The *Staphylococcus aureus* "superbug". J Clin Invest 114(12):1693–1696
53. Foster TJ (2005) Immune evasion by staphylococci. Nat Rev Microbiol 3(12):948–958
54. Fujino T, Okuno Y, Nakada D, Aoyama A, Fukai K, Mukai T, Ueho T (1953) On the bacteriological examination of shirasu-food poisoning. Med J Osaka Univ 4:299–304
55. Gefen O, Mumcuoglu M, Engel G, Balaban NQ (2008) Single-cell protein induction dynamics reveals a period of vulnerability to antibiotics in persister bacteria. Proc Natl Acad Sci 105:6145–6149
56. Gil AL, Louis VR, Rivera ING, Lipp E, Huq A, Lanata CF, Taylor DN, Russek-Cohen E. Choopun N, Sack RB, Colwell RR (2004) Occurance and distribution of *Vibrio cholerae* in the coastal environment of Peru. Environ Microbiol 6:699–706
57. Goodwin KD, Pobuda M (2009) Performance of CHROMagar Staph aureus and CHROMagar MRSA for detection of Staphylococcus aureus in seawater and beach sand–comparison of culture, agglutination, and molecular analyses. Water Res 43:4802–4811

58. Grimes DJ, Singleton FL, Stemmler J, Palmer LM, Brayton P, Colwell RR (1984) Microbiological effects of wastewater effluent discharge into coastal waters of Puerto Rico. Water Res 18:613–619
59. Grimes DJ, Mills AL, Nealson KH (2000) The importance of viable but nonculturable bacteria in biogeochemistry. In: Colwell RR, Grimes DJ (eds) Nonculturable microorganisms in the environment. ASM Press, Washington, DC, pp 209–227
60. Guvener ZT, McCarter LL (2003) Multiple regulators control capsular polysaccharide production in *Vibrio parahaemolyticus*. J Bacteriol 185:5431–5441
61. Hara-Kudo Y, Saito S, Ohtsuka K, Yamasaki S, Yahiro S, Nishio T, Iwade Y, Otomo T, Konuma H, Tanaka H, Nakagawa H, Sugiyama K, Sugita-Konishi Y, Kumagai S (2010) Decreasing *Vibrio parahaemolyticus* infections and analysis of seafood contamination in Japan. Vibrios in the Environment-2010, Biloxi, MS (Abstracts)
62. Harth E, Matsuda L, Hernández C, Rioseco ML, Romero J, González-Escalona N, Martínez-Urtaza J, Espejo RT (2009) Epidemiology of *Vibrio parahaemolyticus* outbreaks, southern Chile. Emerg Infect Dis 15:163–168
63. Harwood VJ, Whitlock J, Withington V (2000) Classification of antibiotic resistance patterns of indicator bacteria by discriminant analysis: use in predicting the source of fecal contamination in subtropical waters. Appl Environ Microbiol 66: 3698–3704
64. He H, Wang Q, Sheng L, Liu Q, Zhang Y (2010) Functional characterization of *Vibrio alginolyticus* twin-arginine translocation system: Its roles in biofilm formation, extracellular protease activity, and virulence towards fish. Curr Microbiol. doi:10.1007/s00284-010-9844-6
65. Hensel M (2004) Evolution of pathogenicity islands of *Salmonella enterica*. Int J Med Microbiol 294:95–102
66. Ho PL, Tang WM, Lo KS, Yuen KY (1998) Necrotizing fasciitis due to *Vibrio alginolyticus* following an injury inflicted by a stingray. Scand J Infect Dis 30:192–193
67. Honda T, Iida T (1993) The pathogenicity of *Vibrio parahaemolyticus* and the role of thermostable direct haemolysin and related haemolysins. Rev Med Microbiol 4:106–113
68. Huq A, Sack RB, Nizam A, Longini IM, Balakrish Nair G, Ali A, Morris JG Jr, Khan MNH, Siddique AK, Yunus M, Albert MJ, Sack DA, Colwell RR (2005) Critical factors influencing the occurrence of *Vibrio cholerae* in the environment of Bangladesh. Appl Environ Microbiol 71:4645–4654
69. Jacobs-Reitsma W (2000) *Campylobacter* in the food supply. In: Nachamkin I, Blaser MJ (eds) Campylobacter, 2nd edn. ASM Press, Washington, DC, pp 467–480
70. Jaffres E, Sohier D et al (2009) Study of the bacterial ecosystem in tropical cooked and peeled shrimps using a polyphasic approach. Int J Food Microbiol 131(1):20–29
71. Jensen AE, Cheville NF, Thoen CO, MacMillan AP, Miller WG (1999) Genomic fingerprinting and development of a dendrogram for *Brucella* spp. isolated from seals, porpoises, and dolphins. J Vet Diagn Invest 11:152–157
72. Jia A, Woo NY, Zhang XH (2010) Expression, purification, and characterization of thermolabile hemolysin (TLH) from *Vibrio alginolyticus*. Dis Aquat Organ 90:121–127
73. Johnson CN, Flowers AR, Young VC, Gonzalez-Escalona N, DePaola A, Grimes DJ (2009) Genetic relatedness among *tdh*$^+$ and *trh*$^+$ *Vibrio parahaemolyticus* cultured from Gulf of Mexico oysters (*Crassostrea virginica*) and surrounding water and sediment. Microb Ecol 57:437–443
74. Johnson CN, Flowers AR, Noriea NF III, Zimmerman AM, Bowers J, DePaola A, Grimes DJ (2010) Relationships between environmental factors and pathogenic vibrios in the northern Gulf of Mexico. Appl Environ Microbiol 76:7076–7084
75. Joseph SW, Daily OP, Hunt WS, Seidler RJ, Allen DA, Colwell RR (1979) *Aeromonas* primary wound infection of a diver in polluted waters. J Clin Microbiol 10:46–49
76. Kaper JB, Morris JG, Levine MM (1995) Cholera. Clin Microbiol Rev 8:48–86
77. Kitao T, Aoki T, Sakoh R (1981) Epizootic caused by beta-hemolytic *Streptococcus* species in cultured freshwater fish. Fish Pathol 19:173–180
78. Klevens RM, Morrison MA, Nadle J, Petit S, Gershman K, Ray S, Harrison LH, Lynfield R, Dumyati G, Townes JM, Craig AS, Zell ER, Fosheim GE, McDougal LK, Carey RB, Fridkin SK (2007) Invasive methicillin-resistant Staphylococcus aureus infections in the United States. JAMA 298:1763–1771
79. Kluytmans J, van Belkum A, Verbrugh H (1997) Nasal carriage of *Staphylococcus aureus*: epidemiology, underlying mechanisms, and associated risks. Clin Microbiol Rev 10:505–520
80. Kusuda R (1992) Bacterial fish diseases in marineculture in Japan with special emphasis on streptococcosis. Isr J Aquacult 44:140
81. Lappi VR, Ho A et al (2004) Prevalence and growth of Listeria on naturally contaminated smoked salmon over 28 days of storage at 4 degrees C. J Food Prot 67(5):1022–1026
82. Lappi VR, Thimothe J et al (2004) Longitudinal studies on Listeria in smoked fish plants: impact of intervention strategies on contamination patterns. J Food Prot 67(11):2500–2514
83. Lappi VR, Thimothe J et al (2004) Impact of intervention strategies on Listeria contamination patterns in crawfish processing plants: a longitudinal study. J Food Prot 67(6):1163–1169
84. Lau SK, Woo PC et al (2003) Invasive Streptococcus iniae infections outside North America. J Clin Microbiol 41(3):1004–1009
85. Lauková A, Juris P (1997) Distribution and characterization of *Enterococcus* species in municipal sewages. Microbios 89:73–80
86. Li XC, Xiang ZY, Xu XM, Yan WH, Ma JM (2009) Endophthalmitis Caused by *Vibrio alginolyticus*. J Clin Microbiol 47:3379–3381
87. Lianou A, Sofos JN (2007) A review of the incidence and transmission of Listeria monocytogenes in ready-to-eat products in retail and food service environments. J Food Prot 70(9):2172–2198

88. Linell F, Norden A (1954) Mycobacterium balnei, a new acid-fast bacillus occurring in swimming pools and capable of producing skin lesions in humans. Acta Tuberc Scand Suppl 33:1–84
89. Liu D (ed) (2008) Handbook of *Listeria monocytogenes*. CRC Press, Boca Raton
90. Louis VR, Russek-Cohen E, Choopun N, Rivera ING, Gangle B, Jiang SC, Rubin A, Patz JA, Huq A, Colwell RR (2003) Predictability of *Vibrio cholerae* in Chesapeake Bay. Appl Environ Microbiol 69:2773–2785
91. Makino K, Oshima K, Kurokawa K, Yokoyama K, Uda T, Tagomori K, Iijima Y, Najima M, Nakano M, Yamashita A, Kubota Y, Kimura S, Yasunaga T, Honda T, Shinagawa H, Hattori M, Iida T (2003) Genome sequence of *Vibrio parahaemolyticus* a pathogenic mechanism distinct from that of *V. cholerae*. Lancet 361:743–749
92. Manero A, Blanch AR (1999) Identification of *Enterococcus* spp. with a biochemical key. Appl Environ Microbiol 65:4425–4430
93. Maquart M, LeFleche P, Foster G, Tryland M, Ramisse F, Djønne B, Al Dahouk S, Jacques I, Neubauer H, Walravens K, Godfroid J, Cloeckaert A, Vergnaud G (2009) MLVA-16 typing of 295 marine mammal *Brucella* isolates from different animal and geographic origins identifies 7 major groups within *Brucella ceti* and *Brucella pinnipedialis*. BMC Microbiol 9:145. doi:10.1186/1471-2180-9-145
94. McCarter LL (2006) Motility and chemotaxis. In: Thompson FL, Austin B, Swings J (eds) The biology of Vibrios. ASM Press, Washington, DC, pp 115–132
95. McDonald WL, Jamaludin R, Mackereth G, Hansen M, Humphrey S, Short P, Taylor T, Swingler J, Dawson CE, Whatmore AM, Stubberfield E, Perrett LL, Simmons G (2006) Characterisation of a *Brucella* sp. strain as a marine-mammal type despite isolation from a patient with spinal osteomyelitis in New Zealand. J Clin Microbiol 44:4363–4370
96. McLaughlin JB, DePaola A, Bopp CA, Martinek KA, Napolilli NP, Allison CG, Murray SL, Thompson EC, Bird MM, Middaugh JP (2005) Outbreak of *Vibrio parahaemolyticus* gastroenteritis associated with Alaskan oysters. N Engl J Med 353:1463–1470
97. Mead PS, Slutsker L, Dietz V, McCaig LF, Bresee JS, Shapiro C, Griffin PM, Tauxe RV (1999) Food-related illness and death in the United States. Emerg Infect Dis 5:607–625
98. Meador CE, Parsons MM, Bopp CA, Gerner-Smidt P, Painter JA, Vora GJ (2007) Virulence gene- and pandemic group-specific marker profiling of clinical *Vibrio parahaemolyticus* isolates. J Clin Microbiol 45:1133–1139
99. Mejlholm O, Kjeldgaard J et al (2008) Microbial changes and growth of Listeria monocytogenes during chilled storage of brined shrimp (Pandalus borealis). Int J Food Microbiol 124(3):250–259
100. Morris PJ, Johnson WR et al (2011) Isolation of culturable microorganisms from free-ranging bottlenose dolphins (*Tursiops truncatus*) from the southeastern United States. Vet Microbiol 148(2–4):440–447
101. Mukherjee J, Chios K, Fishwild D, Hudson D, O'Donnell S, Rich SM, Donohue-Rolf A, Tzipori S (2002) Human Stx2-specific monoclonal antibodies prevent systemic complications of *Escherichia coli* O157:H7 infection. Infect Immun 70(2): 612–619
102. Nishibuchi M (2006) Miscellaneous human pathogens. In: Thompson FL, Austin B, Swings J (eds) The biology of Vibrios. ASM Press, Washington, DC, pp 367–381
103. Noriea NF III, Johnson CN, Griffitt KJ, Grimes DJ (2010) Distribution of type III secretion systems in *Vibrio parahaemolyticus* from the Northern Gulf of Mexico. J Appl Microbiol 109:953–962
104. Oliver JD (2006) *Vibrio vulnificus*. In: Thompson FL, Austin B, Swings J (eds) The biology of Vibrios. ASM Press, Washington, DC, pp 349–366
105. O'Mahony R, Abbott Y et al (2005) Methicillin-resistant Staphylococcus aureus (MRSA) isolated from animals and veterinary personnel in Ireland. Vet Microbiol 109(3–4): 285–296
106. O'Neill KR, Jones SH, Grimes DJ (1992) Seasonal incidence of *Vibrio vulnificus* in the Great Bay Estuary of New Hampshire and Maine. Appl Environ Microbiol 58:3257–3262
107. Oshiro R, Fujioka R (1995) Sand, soil, and pigeon droppings – sources of indicator bacteria in the waters of Hanauma Bay, Oahu, Hawaii. Water Sci Technol 31:251–254
108. Panos GZ, Betsi GI, Falagas ME (2006) Systematic review: are antibiotics detrimental or beneficial for the treatment of patients with *Escherichia coli* O157:H7 infection? Aliment Pharmacol Ther 24(5):731–742
109. Paranjpye RN, Strom MS (2005) A *Vibrio vulnificus* Type IV pilin contributes to biofilm formation, adherence to epithelial cells, and virulence. Infect Immun 73:1411–1422
110. Paranjpye RN, Johnson AB, Baxter AE, Strom MS (2007) Role of Type IV pilins in persistence of *Vibrio vulnificus* in *Crassostrea virginica* oysters. Appl Environ Microbiol 73:5041–5044
111. Parenti DM, Symington JS et al (1995) Mycobacterium kansasii bacteremia in patients infected with human immunodeficiency virus. Clin Infect Dis 21(4):1001–1003
112. Park K-S, Iida T, Yamaichi Y, Oyagi T, Yamamoto K, Honda T (2000) Genetic characterization of DNA region containing the *trh* and *ure* genes of *Vibrio parahaemolyticus*. Infect Immun 68:5742–5748
113. Peir GB, Madin SH (1976) *Streptococcus iniae* sp. nov., a beta-hemolytic streptococcus isolated from an Amazon freshwater dolphin, *Inia geoffrensis*. Int J Syst Bacteriol 26:545–553
114. Pellett S, Bigley DV, Grimes DJ (1983) Distribution of *Pseudomonas aeruginosa* in a riverine ecosystem. Appl Environ Microbiol 45:328–332
115. Perera RP, Johnson SK, Collins MD, Lewis DH (1994) *Streptococcus iniae* associated with mortality of *Tilapia nilotica* and *T. aurea* hybrids. J Aquat Anim Health 6:335–340
116. Petersen A, Dalsgaard A (2003) Species composition and antimicrobial resistance genes of Enterococcus spp, isolated from integrated and traditional fish farms in Thailand. Environ Microbiol 5(5):395–402

117. Phillips AMB, DePaolo A, Bowers J, Ladner S, Grimes DJ (2007) An evaluation of the use of remotely sensed parameters for prediction of incidence and risk associated with *Vibrio parahaemolyticus* in Gulf Coast oysters (*Crassostrea virginica*). J Food Prot 70:879–884
118. Plano LR, Garza AC et al (2011) Shedding of Staphylococcus aureus and methicillin-resistant Staphylococcus aureus from adult and pediatric bathers in marine waters. BMC Microbiol 11(1):5
119. Plano LRW, Shibata T et al (2011) Characterization of *Staphylococcus aureus* and community associated MRSA at a recreational marine beach in South Florida. J Antimicrob Chemother (in review)
120. Posfay-Barbe KM, Wald ER (2009) Listeriosis. Semin Fetal Neonatal Med 14(4):228–233
121. Qasem JA, Sameer A-Z, Salwa A-M, Samee A-A, Ahmed A-M, Al-Sharifi Faisal A-S (2008) Molecular investigation of *Streptococcus agalactiae* isolates from environmental samples and fish specimens during a massive fish kill in Kuwait Bay. Pakistan J Biol Sci 11:2500–2504
122. Rallis E, Koumantaki–Mathioudaki E (2007) Treatment of Mycobacterium marinum cutaneous infections. Expert Opin Pharmacother 8(17):2965–2978
123. Reichelt JL, Bauman P, Bauman L (1979) Study of genetic relationships among marine species *Beneckea* and *Photobacterium* by means of DNA/DNA hybridization. Arch Microbiol 1110:101–120
124. Rice EW, Messer JW et al (1995) Occurrence of high-level aminoglycoside resistance in environmental isolates of enterococci. Appl Environ Microbiol 61(1):374–376
125. Rivas AL, Gonzalez RN, Wiedmann M, Bruce JL, Cole EM et al (1997) Diversity of *Streptococcus agalactiae* and *Staphylococcus aureus* ribotypes recovered from New York dairy herds. Amer J Vet Res 58:482–487
126. Rivers B, Steck TR (2001) Viable but nonculturable uropathogenic bacteria are present in the mouse urinary tract following urinary tract infection and antibiotic therapy. Urol Res 29:60–66
127. Roushan MRH, Mohraz M, Hajiahmadi M, Ramzani A, Valayati AA (2006) Efficacy of Gentamicin plus Doxycycline versus Streptomycin plus Doxycycline in the treatment of Brucellosis in humans. Clin Infect Dis 42:1075–1080
128. Saubolle M (1989) Nontuberculous mycobacteria as agents in human disease in the United States. Clin Microbiol Newslett 11:113–117
129. Schaefer AM, Goldstein JD et al (2009) Antibiotic-resistant organisms cultured from Atlantic bottlenose dolphins (*Tursiops truncatus*) inhabiting estuarine waters of Charleston, SC and Indian River Lagoon, FL. Ecohealth 6(1):33–41
130. Shime-Hattori A et al (2006) Two type IV pili of *Vibrio parahaemolyticus* play different roles in biofilm formation. FEMS Microbiol Lett 264:89–97
131. Sinigalliano CD, Fleisher JM et al (2010) Traditional and molecular analyses for fecal indicator bacteria in non-point source subtropical recreational marine waters. Water Res 44(13):3763–3772
132. Skalsky K, Yahav D, Bishara J, Pitlik S, Leibovici L, Paul M (2008) Treatment of human brucellosis: systematic review and meta-analysis of randomized trials. BMJ 336(7646):701–704
133. Soge OO, Meschke JS, No DB, Roberts MC (2009) Characterization of methicillin resistant Staphylococcus aureus and methicillin-resistant coagulase negative Staphylococcus spp isolated from US West coast public marine beaches. J Antimicrob Chemother 64:1148–1155
134. Sun B, Zhang XH, Tang X, Wang S, Zhong Y, Chen J, Austin B (2007) A single residue change in *Vibrio harveyi* hemolysin results in the loss of phospholipase and hemolytic activities and pathogenicity for turbot (*Scophthalmus maximus*). J Bacteriol 189:2575–2579
135. Takeda T, Peina Y, Ogawa A, Dohi S, Abe H, Nair GB, Pal SC (1991) Detection of heat-stable enterotoxin in a cholera toxin gene-positive strain of *Vibrio cholerae* O1. FEMS Microbiol Lett 64:23–27
136. Tauxe R, Seminario L, Tapia R, Libel M (1994) The Latin American epidemic. In: Wachsmuth IK, Blake PA, Olsvik O (eds) *Vibrio cholerae* and cholera: molecular to global perspectives. American Society for Microbiology, Washington, DC
137. Thompson FL, Hoste B, Vandemeulebroecke K, Swings J (2003) Reclassification of *Vibrio hollisae* as *Grimontia hollisae* gen. nov., comb. Nov. Int J Syst Evol Microbiol 53:1615–1617
138. Tokuda H, Unemoto T (1982) Characterization of the respiration-dependant Na^+ pump in the marine bacterium *Vibrio alginolyticus*. J Biol Chem 257:10007–10014
139. Tsai YH, Kung H-F, Lee T-M, Lin G-T, Hwang D-F (2004) Histamine-related hygienic quantities and bacteria found in popular commercial scombroid fish fillets in Taiwan. J Food Prot 67:407–412
140. Uh Y, Park JS, Hwang GY, Jang IH, Yoon KJ, Park HC, Hwang SO (2001) *Vibrio alginolyticus* acute gastroenteritis: a report of two cases. Clin Microbiol Infect 7:104–106
141. Ulitzer S (1975) The mechanism of swarming of *Vibrio alginolyticus*. Arch Microbiol 104:67–71
142. USEPA (2000) Improved enumeration methods for the recreational water quality indicators: Enterococci and *Escherichia coli*. EPA/821/R-97/004, Washington, DC
143. Valdivia E, Martin-Sanchez I et al (1996) Incidence of antibiotic resistance and sex pheromone response among enterococci isolated from clinical human samples and from municipal waste water. J Appl Bacteriol 81(5):538–544
144. Vally H, Whittle A, Cameron S, Dowse GK, Watson T (2004) Outbreak of *Aeromonas hydrophila* wound infections associated with mud football. Clin Infect Dis 38:1084–1089
145. Vivekanandhana G, Hathab AAM, Lakshmanaperumalsamy P (2005) Prevalence of *Aeromonas hydrophila* in fish and prawns from the seafood market of Coimbatore, South India. Food Microbiol 22:133–137
146. Von Eiff C, Becker K, Machka K, Stammer H, Peters G (2001) Nasal carriage as a source of Staphylococcus aureus bacteremia. Study Group. N Engl J Med 344:11–16

147. Wade TJ, Pai N et al (2003) Do U.S. Environmental Protection Agency water quality guidelines for recreational waters prevent gastrointestinal illness? A systematic review and meta-analysis. Environ Health Perspect 111(8):1102–1109
148. Waldor MK, Mekalanos JJ (1996) Lysogenic conversion by a filamentous phage encoding cholera toxin. Science 272:1910–1914
149. Wang SX, Zhang XH, Zhong YB, Sun BG, Chen JX (2007) Genes encoding the *Vibrio harveyi* haemolysin (VHH)/thermolabile haemolysin (TLH) are widespread in vibrios. Wei Sheng Wu Xue Bao 47:874–881
150. Weinstein MR, Litt M, Kertesz DA, Wyper P, Rose D, Coulter M, McGeer A, Facklam R, Ostach C, Willey BM, Borczyk A, Low DE et al (1997) Invasive infections due to a fish pathogen, Streptococcus iniae. N Engl J Med 337:589–594
151. Wendt JR, Lamm RC et al (1986) An unusually aggressive Mycobacterium marinum hand infection. J Hand Surg Am 11(5):753–755
152. Whatmore AM, Dawson CE, Groussaud P, Koylass MS, King AC, Shankster SJ, Sohn AH, Probert WS, McDonald WL (2008) Marine mammal *Brucella* genotype associated with zoonotic infection. Emerg Infect Dis 14:517–518
153. WHO (World Health Organization) (2010) Cholera, 2009. Wkly Epidemiol Rec 85:293–308
154. Wilson IG, McAfee GG (2002) Vancomycin-resistant enterococci in shellfish, unchlorinated waters, and chicken. Int J Food Microbiol 79(3):143–151
155. Wolinsky E (1992) Mycobacterial diseases other than tuberculosis. Clin Infect Dis 15(1):1–10
156. Wong CS, Jelacic S, Habeeb RL, Watkins SL, Tarr PI (2000) The risk of the hemolytic-uremic syndrome after antibiotic treatment of *Escherichia coli* O157:H7 infections. N Engl J Med 342(26):1930–1936
157. Yakushi T, Maki S, Homma M (2004) Interaction of PomB with the third transmembrane segment of PomA in the Na^+-driven polar flagellum of *Vibrio alginolyticus*. J Bacteriol 186:5281–5291
158. Yamahara KM, Walters SP et al (2009) Growth of enterococci in unaltered, unseeded beach sands subjected to tidal wetting. Appl Environ Microbiol 75(6):1517–1524
159. Zimmerman AM, Rebarchik DM, Flowers AR, Williams JL, Grimes DJ (2009) *Escherichia coli* detection using mTEC agar and fluorescent antibody direct viable counting on coastal recreational water samples. Lett Appl Microbiol 49:478–483

Books and Reviews

Belkin S, Colwell RR (eds) (2005) Pathogenic microorganisms in the sea. Kluwer/Plenum, New York

Colwell RR, Grimes DJ (eds) (2000) Nonculturable microorganisms in the environment. ASM Press, Washington, DC

Walsh PJ, Smith SL, Fleming LE, Solo-Gabriele HM, Gerwick WH (eds) (2008) Oceans and human health: risk and remedies from the sea. Elsevier, St. Louis

Hurricane and Monsoon Tracking with Driftsondes

Philippe Drobinski[1], Philippe Cocquerez[2], A. Doerenbecher[3], Terrence Hock[4], C. Lavaysse[1], D. Parsons[4], J. L. Redelsperger[3]

[1]Institut Pierre Simon Laplace/Laboratoire de Météorologie Dynamique, École Polytechnique/UPMC/ENS/CNRS, Palaiseau, France

[2]Sous-direction Ballon, Centre National d'Études Spatiales, Toulouse, France

[3]Centre National de Recherches Météorologiques, Météo-France/CNRS, Toulouse, France

[4]Atmospheric Technology Division, National Center for Atmospheric Research, Boulder, CO, USA

Article Outline

Glossary
Definition of the Subject
Introduction
The Driftsonde Observations
Analysis of the Driftsonde Trajectories and the Respective Synoptic Environment
Analyses of AEW with the Driftsondes
Conclusion
Future Directions
Acknowledgments
Bibliography

Glossary

African easterly jet (AEJ) Wind jet developing at about 600-hPa pressure level (about 4,200 m) and 5°N latitude over the African continent.

African easterly waves (AEWs) Synoptic scale, westward propagating waves embedded in the AEJ.

AMMA African Monsoon Multidisciplinary Analysis (AMMA) program, initiated in 2002 with an intensive field campaign in 2006, and focusing on the physical changes in the environment of the West African monsoon and their impacts on society.

Boundary layer pressurized balloon (BLPB) Balloon drifting in the atmospheric boundary layer and carrying an instrumented gondola which collects measurements of the typical meteorological variables.

Concordiasi International project of the THORPEX-International Polar Year aiming at a better understanding of the climate of Antarctica.

Driftsonde Stratospheric drifting balloon launching dropsondes over high-impact weather, providing vertical profiles of meteorological data.

Hurricane A hurricane is a tropical cyclone, occurring in the North Atlantic Ocean or the Northeast Pacific Ocean. A tropical cyclone is a storm system characterized by a large low-pressure center and numerous thunderstorms that produce strong winds and heavy rain.

HyMeX Hydrological cycle in the Mediterranean experiment (HyMeX) program aiming at improving the understanding of running-water cycle in the Mediterranean region with a particular focus on the evolution and predictability of hydro-meteorological extreme events in the perspective of climate change.

Mesoscale convective system (MCS) Complex of thunderstorms normally persisting for several hours or more.

Saharan air layer (SAL) Surges of hot, dry air that cascade into the Atlantic from the Sahel region of Africa.

THORPEX Global program of the World Meteorological Organization (WMO) aiming at accelerating improvements in the prediction of high-impact weather.

T-NAWDEX THORPEX-North Atlantic Waveguide and Downstream impact Experiment.

T-PARC THORPEX Pacific Asian Regional Campaign.

West African monsoon Rainy phase of a seasonal change in atmospheric circulation over West Africa. The other major monsoon systems are the Asia-Australian monsoons in the sampled environment.

Definition of the Subject

Tropical cyclones (TCs) are a typical weather threat. The threat can apply to humans, their properties, and activities. Their prediction, particularly their trajectory and intensity, remains difficult. In addition, TCs develop above the tropical oceans where the coverage by in situ observations is poor and within cloud clusters (mesoscale convective systems MCS) that limit the ability of numerical weather prediction (NWP) models to assimilate satellite data [18]. Improved forecast of TCs trajectories is a huge benefit in terms of material costs of evacuations and damage, not being able to quantify saved life.

The deployment of additional observations to improve understanding and forecasting TCs started very early in the USA, from the early 1980s. This approach is called adaptive observation and was initiated by the National Oceanic and Atmospheric Administration (NOAA). The philosophy of adaptive observation is the adjustment of the usual (so-called routine) observing network in order to deal with some particularly threatening weather situations to come. This adaptation aims at improving the numerical weather prediction (NWP) through the deployment of additional observations. When incorporated in the models, thanks to data assimilation procedures, these added observations decrease the uncertainty on the modeled state of the atmosphere (analysis). Subsequent numerical weather forecasts are likely to be improved. This improvement is expressed with respect to the NWP system that would not incorporate the additional data.

Any type of observation can be used. All time and space scales may be considered. Historically, the adaptive observation focused on the synoptic scales, for TCs first, then for mid-latitudes winter storms [15, 22]. The terms "adaptive observation" or "observation targeting" may be used in various senses that may be misleading. Adaptive observation first refers to the observing strategy itself, which is a real-time observation practice in close link with NWP.

An adaptive observing strategy requires a constant monitoring of the weather situation. The typical strategy is implemented following five stages:

- Case identification (weather threat) using forecasts
- Computation of objective targeting guidance to help the decision process (where and when to deploy)
- Design of the deployment and decision making, transmitting the deployment instructions to the observation providers (observing platforms)
- Deployment of additional observations (data collection, transmission)
- Assimilation (this stage is automatic and do not imply any specific effort)
- A posteriori evaluation of the data impact (in research mode, optional, often ignored)

The Hurricane Synoptic Flow was the first regular seasonal TC targeting campaign, conducted by NOAA, on the North Atlantic hurricane basin (1982–1996). The research aircraft P3 deployed dropsondes along a circular navigation around the cyclone [5]. The choice of deployment was essentially subjective, but the campaign was a success. From 1997 to 2011, the NOAA Hurricane Synoptic Surveillance has combined subjectively and objectively guided deployments [1] of dropsondes in the Gulf of Mexico, Eastern Pacific, and Western Atlantic. In Asia, the annual campaigns DOTSTAR [25] that started in 2003 allow the improvement of the observing system in the Western Pacific with dropsondes released from Taiwanese jet aircrafts. Again, the choices of deployments are based on both subjective and objective analyses. From an NWP impact point of view, observations that are deployed in the close TCs' environment produce the best results in terms of TC trajectory prediction [11]. However, this conclusion holds for already formed and named TCs. Another issue is to better monitor tropical environment in which TCs may appear, develop, and strengthen.

Introduction

More recently, in West Africa, drifting balloons launched from Zinder (Niger) (Fig. 1) into the stratosphere (about 50 hPa) dropped 124 dropsondes over wide swaths of Africa and the Atlantic Ocean between end of August and end of September 2006, in order to document the meteorological environment of mesoscale convective systems (MCS) and TCs in the Atlantic [6]. This deployment of the so-called driftsonde system was performed in the frame of the African Monsoon Multidisciplinary Analysis (AMMA) program, initiated in 2002 with an intensive field campaign in 2006, and focusing on the physical changes in the environment of the West African monsoon and their impacts on society [20]. MCSs are the main precursors of TCs in the Atlantic (e.g., [2]), and may even contribute to tropical cyclogenesis in the Pacific (e.g., [10]). It is believed that scale interaction processes drive the tropical cyclogenesis that occurs over the Atlantic off the West African coast during late summer. This interaction involves:

- The African Easterly Jet (AEJ) develops at about 600-hPa pressure level and 4°N-5°N latitude because heating of the West African land mass during summer creates a surface temperature and moisture gradient between the Gulf of Guinea and the Sahara, and the atmosphere responds by generating vertical wind shear to maintain thermal wind balance.
- The African easterly waves (AEWs) which are synoptic scale, westward propagating disturbances produced by barotropic and baroclinic instabilities embedded in the AEJ.
- The Saharan air layer (SAL).
- The westward propagating MCSs.

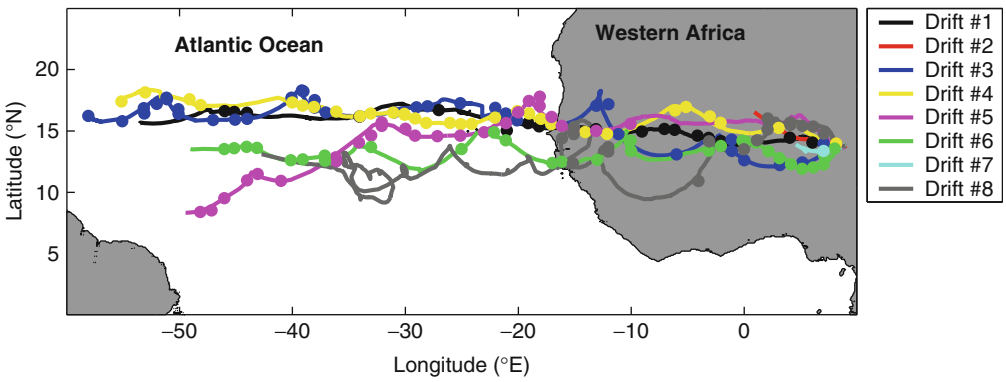

Hurricane and Monsoon Tracking with Driftsondes. Figure 1
Trajectories of the eight driftsondes launched from Zinder (Niger) between August 28 and September 22, 2006. The *dots* indicate the location of a dropsonde

It is already known that some Atlantic tropical cyclones have their origin in MCSs propagating over the African continent [23]. For example, Hill and Lin [13] related the genesis of Hurricane Alberto (2000) to a MCS initiated over the Ethiopian highlands. Lin et al. [17] documented this case study and identified three successive convective genesis and lysis periods before the final cyclogenesis event off the Guinea coast. Berry and Thorncroft [3] also showed that the MCSs associated with the pre-Alberto disturbance were embedded in an AEW. The SAL may significantly impede the development of incipient tropical waves or disturbances and can even weaken preexisting tropical cyclones.

During the AMMA, the driftsondes sampled squall lines in the troughs of AEW and the southeastern edge of the tropical storm Florence, hurricanes Gordon and Helene. In addition to tracking potential hurricanes, the driftsondes gathered bird's-eye data on surges of hot, dry air that cascade into the Atlantic from the Sahel region of Africa. These surges carry huge amounts of dust as far west as Florida, influencing air chemistry, upper-ocean biology, and Atlantic weather systems. Although driftsondes have been tested over the last few years, this was the first time they were used in weather research and prediction. Based on this new type of dataset, this entry aims at illustrating and analyzing the potential of such observation system for tracking high-impact weather system such as cyclone and hurricanes in area generally void of in situ data, and provides additional observation for real-time forecast improvement.

Section"The Driftsonde Observations" presents the driftsonde system which was first used in the frame of a large scientific research program. Section"Analysis of the Driftsonde Trajectories and the Respective Synoptic Environment" describes the synoptic environment (including AEW activity) of the meteorological processes (MCS and tropical storm initiation) investigated with the series of vertical profiles provided by the dropsondes. Section "Analyses of AEW with the Driftsondes" describes the AEW activity and spatial pattern in relation with the dropsonde location. Section"Conclusion" concludes the description of the driftsonde system, lists the ongoing research activity using the driftsonde data collected during AMMA, and proposes perspectives for the use of such observation system.

The Driftsonde Observations

The concept of using driftsondes to take measurements over remote but scientifically important locations around the globe comes from THORPEX, a global program of the World Meteorological Organization (WMO) to accelerate improvements in the prediction of high-impact weather. A driftsonde is composed of a drifting stratospheric balloon and a gondola carrying dropsondes.

For the AMMA project, the drifting stratospheric balloons were developed by the Centre National d'Études Spatiales (CNES) whereas the dropsondes were designed at the National Center for Atmospheric Research (NCAR) and their development was funded by the National Science Foundation (NSF) and the National Oceanic and Atmospheric Administration (NOAA). To build the driftsonde system, scientists and engineers at NCAR and CNES had to overcome many hurdles. Each driftsonde had to be robust enough to endure days of extreme stratospheric cold (averaging −60°C) as well as the intense sunlight of the high, thin atmosphere. For the balloon deployment to be affordable and practical, the system also required low-cost, lightweight, off-the-shelf instruments capable of operating reliably in low pressure and in temperature extremes with very low power. Each gondola held about 35 dropsondes designed by NCAR (the number of dropsondes could differ between the driftsondes) carried on the ballooning systems designed by CNES. In order to make the driftsonde concept practical, NCAR developed a highly compact instrument package, roughly the size of a small bottle of water but weighing only about 140 g. Called MIST (Miniature In situ Sounding Technology), it weighs less than half as much as older dropsondes, which were designed at NCAR in the 1990s. Although driftsondes have been tested over the last few years, this was the first time they were used in weather research and prediction.

The Zinder site, located 740 km east of Niamey, was selected in order to study the AEW, that serve as seedlings for hurricanes during the late African monsoon period (August–September). Dozens of these waves moved across Africa into the Atlantic between about 10°N and 20°N. A small number developed into tropical storms. During July–September 2006 period, a total of 27 AEWs were objectively analyzed (compared with 31 in 2004 and 28 in 2005). July was very different from the

later months with six out of seven of the first waves forming close to the longitude of Niamey or west of it. In August, the AEWs were initiated further east, between 10°E and 20°E, but AEWs over Niamey were still weak. Starting at the end of August and going into September, the AEWs became more coherent with stronger amplitudes over most of tropical North Africa. Interestingly, several AEWs also appeared to start further east, between 20°E and 30°E at this time. It should also be noted that all seven of the AEWs that became named tropical cyclones (Chris – AEW number 6; Ernesto – AEW number 13; Debby – AEW number 14; Florence – AEW number 18; Gordon – AEW number 19; Helene – AEW number 20; Isaac – AEW number 23; see [14]) were initiated east of Niamey and six of these occurred after the middle of August. After being launched from Zinder, each balloon drifted from Africa toward the Caribbean at heights of around 20 km height, where light easterly winds prevail. The trajectories exhibited cycloid-like patterns due to the presence of near-inertial waves [12] (Fig. 1). At least twice per day (0000 and 1200 UTC), each gondola released a dropsonde that fell by parachute, sensing the weather conditions during its 20-min descent and radioing data back to the gondola and then, by satellite, to the operation center in Paris. Whenever promising weather system developed, the operation center signaled the gondola to release additional dropsondes as often as in 3-h intervals. Eight driftsondes were released from Zinder during the late African monsoon period coinciding with the peak period for hurricane formation over the tropical Atlantic (August–September) and 124 sondes were successfully dropped from the eight driftsondes with 15 vertical profiles from the last dropsondes of driftsonde 8 sent to the GTS for assimilation. However, the number of successfully dropped sondes differed between driftsondes. Table 1 summarizes the operation during the driftsonde deployment. Table 1 shows that the most successful flights corresponded to driftsondes 1, 3, 4, 5, 6, and 8. However, the synoptic environment documented with driftsonde 1 was not of high scientific interest. Driftsonde 8 trajectory was particularly complex and difficult to manage since the flight period corresponded to the weakening of the 50 hPa easterly winds due to a change of the Madden Julian oscillation (MJO) phase. So driftsonde 8 did not allow the tracking of any interesting meteorological event. In the following, we thus analyze in detail the data collected with driftsondes 3–6. They documented in an unprecedented way AEW initiating continental mesoscale convective systems (MCS) evolving over the ocean into tropical storm like Florence and hurricanes like Gordon and Helene, some of them skirting with the US Atlantic and Gulf coasts and all experiencing extra-tropical transition.

Analysis of the Driftsonde Trajectories and the Respective Synoptic Environment

Figure 2 shows the space-time "distances" of the dropsondes from the center of tropical storms

Hurricane and Monsoon Tracking with Driftsondes. Table 1 Summary of driftsonde operations

Driftsonde number	First dropsonde coordinates and date	Last dropsonde coordinates and date	Number of successful dropsondes
1	(6.04°E,14.05°N) – August 28 1406 UTC	(−44.03°E,16.47°N) – September 2 1217 UTC	8
2	(8.13°E,13.93°N) – August 29 2118 UTC	(8.13°E,13.93°N) – Augember 29 2118 UTC	1
3	(7.04°E,13.99°N) – September 1 2351 UTC	(−58.07°E,16.22°N) – September 9 1312 UTC	33
4	(8.14°E,13.97°N) – September 4 1942 UTC	(−55.14°E,17.40°N) – September 11 1110 UTC	14
5	(−10.07°E,15.58°N) – September 9 0807 UTC	(−50.09°E, 8.39°N) – September 13 1808 UTC	25
6	(8.00°E,13.57°N) – September 9 2055 UTC	(−46.03°E,13.52°N) – September 18 0005 UTC	26
7	(7.03°E,13.37°N) – September 12 2358 UTC	(7.03°E,13.37°N) – September 12 2358 UTC	1
8	(6.10°E,15.36°N) – September 16 0603 UTC	(−15.07°E,15.33°N) – September 22 1742 UTC	16

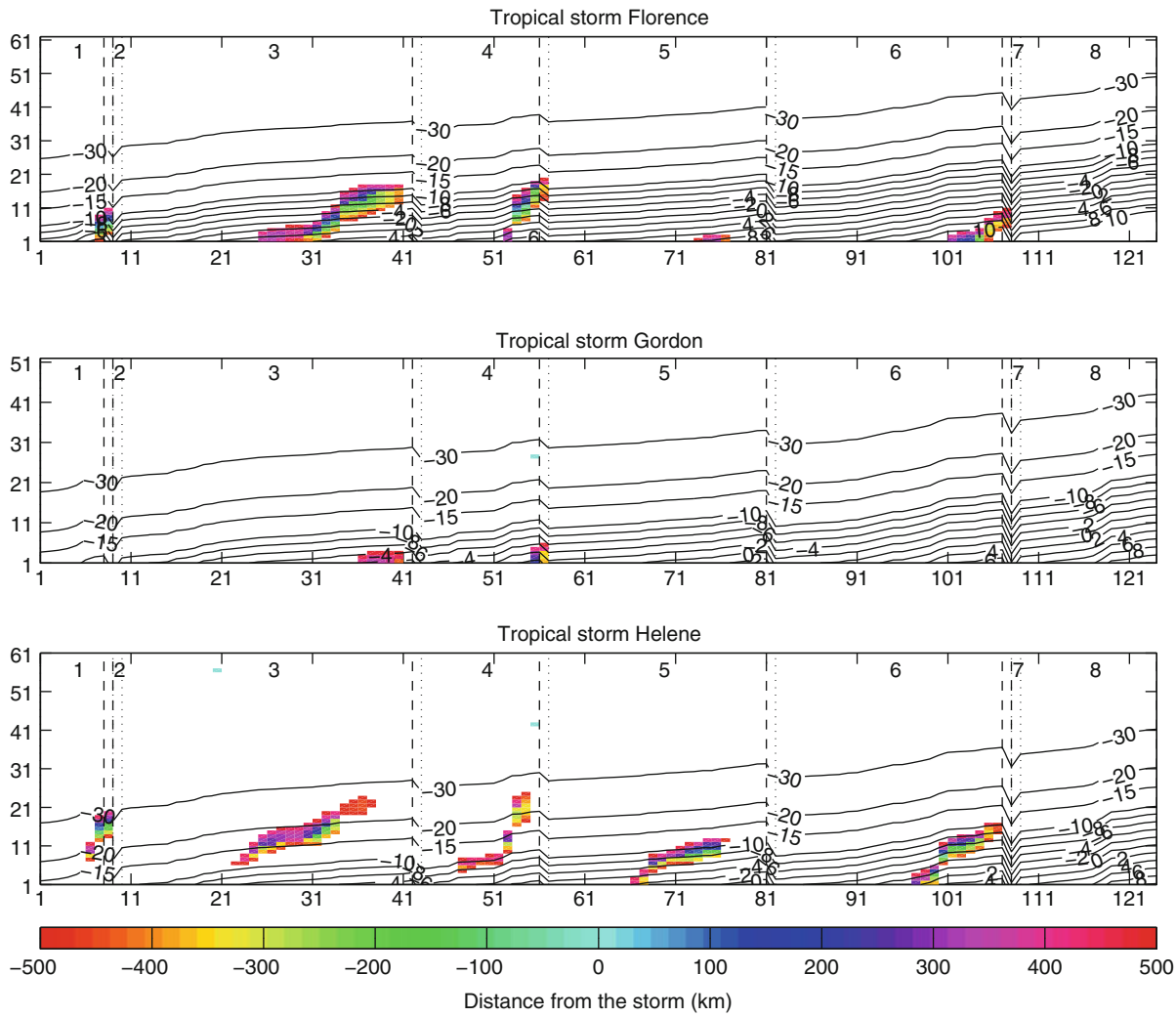

Hurricane and Monsoon Tracking with Driftsondes. Figure 2
Space (color code) and time (iso-contours) "distances" of the dropsondes from the center of tropical storms (TS) Florence (**a**), Gordon (**b**), and Helene (**c**) (color code). The abscissa corresponds to the number of space-time coordinate information available for the TS trajectory. The ordinate corresponds to the number of successful dropsondes available for the whole field campaign. The numbers at the top of the figure indicate the identification number of the driftsonde. Only distances smaller than 500 km are shown, the positive (negative) sign indicates that the sonde is dropped ahead (behind) of the center of the storm. The iso-contours are shown for −30, −20, −15, −10, −8, −6, −4, −2, 0, 2, 4, 6, 8, and 10 days, the positive (negative) sign indicate that the sonde is dropped before (after) the storm

Florence, Gordon, and Helene. The closest in space and time from the storm center is the best. Figure 2a shows that driftsonde 1 approaches Helene track at less than 500 km about a week in advance, whereas driftsondes 3 and 4 followed tropical storm Florence dropping several sondes less than 500 km from the storm track. Gordon track was sampled by driftsonde 4 1 day after its passage (Fig. 2b) whereas Helene track was sampled by driftsonde 6 less than 1 day after its passage (Fig. 2c).

Figure 3 displays the Meteosat Second Generation (MSG) 10.8 μm channel brightness temperature which indicates that convective activity as well as the filtered 700 hPa wind field is shown with arrows (the absence of arrows indicate winds weaker than 1 m s^{-1}). It shows

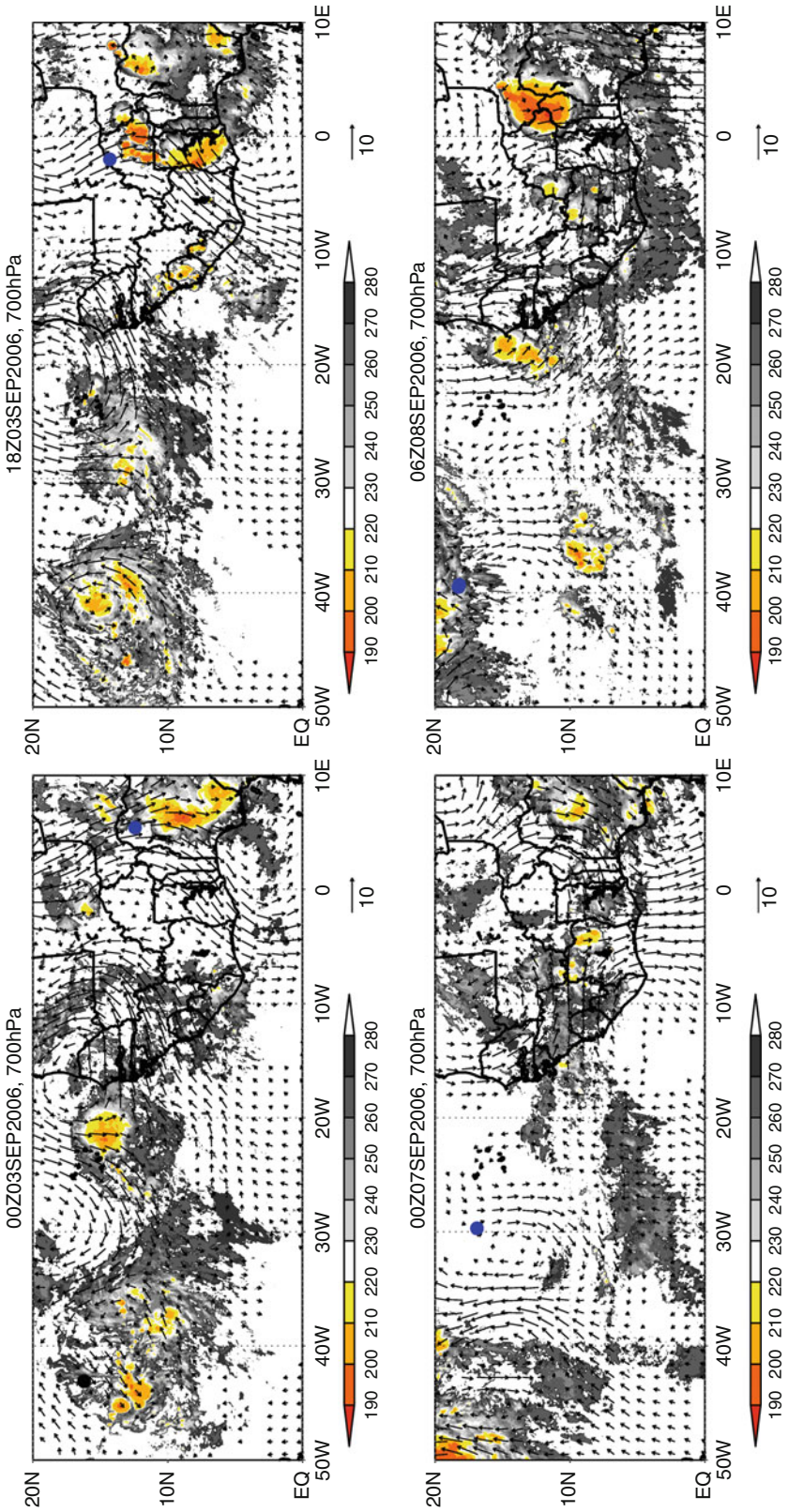

Hurricane and Monsoon Tracking with Driftsondes. Figure 3
Meteosat Second Generation (MSG) 10.8 μm channel brightness temperature which indicates convective activity with superimposed filtered 700 hPa wind field shown with *arrows* (the absence of arrows indicate winds weaker than 1 m s^{-1}) on September 3, 2006, (Julian day 246) at 0000 UTC (**a**), on September 3, 2006, (Julian day 246) at 1800 UTC (**b**), on September 7, 2006, (Julian day 250) at 0000 UTC (**c**) and on September 8, 2006, (Julian day 251) at 0600 UTC (**d**). The black and blue filled dots indicate the locations of dropsondes from driftsondes 1 and 3, respectively

that driftsonde 3 drifts in the vicinity of an MCS propagating westward over the continent at about 15 m s^{-1}. At about 40°W, tropical depression Florence is forming. Figure 4 (first column) shows a time versus height cross section of wind speed, temperature, and humidity constructed with the vertical profiles obtained by the sondes dropped from driftsonde 3. Figure 4a shows evidence of a strong wind tongue between 4 and 5 km height corresponding to the AEJ. Figure 4i shows the moist African planetary boundary layer between Julian days 245 and 248 (September 2–5, 2006) (75% relative humidity) extending up to about 1 km height. Above the planetary boundary layer, layers of saturated air between 5 and 8 km height reveal the proximity of the convective activity. On Julian day 250 (September 7, 2006), dropsondes are released from driftsonde 3 few hundreds of kilometers downstream of Florence, located at about 50°W, which in the meantime has been classified as a tropical storm (it becomes a hurricane on September 10, 2006). The near-surface wind decreases in the disturbed environment near tropical storm Florence as shown in Fig. 4a while the planetary boundary layer humidity and depth increase (up to about 90% relative humidity and up to 3 km

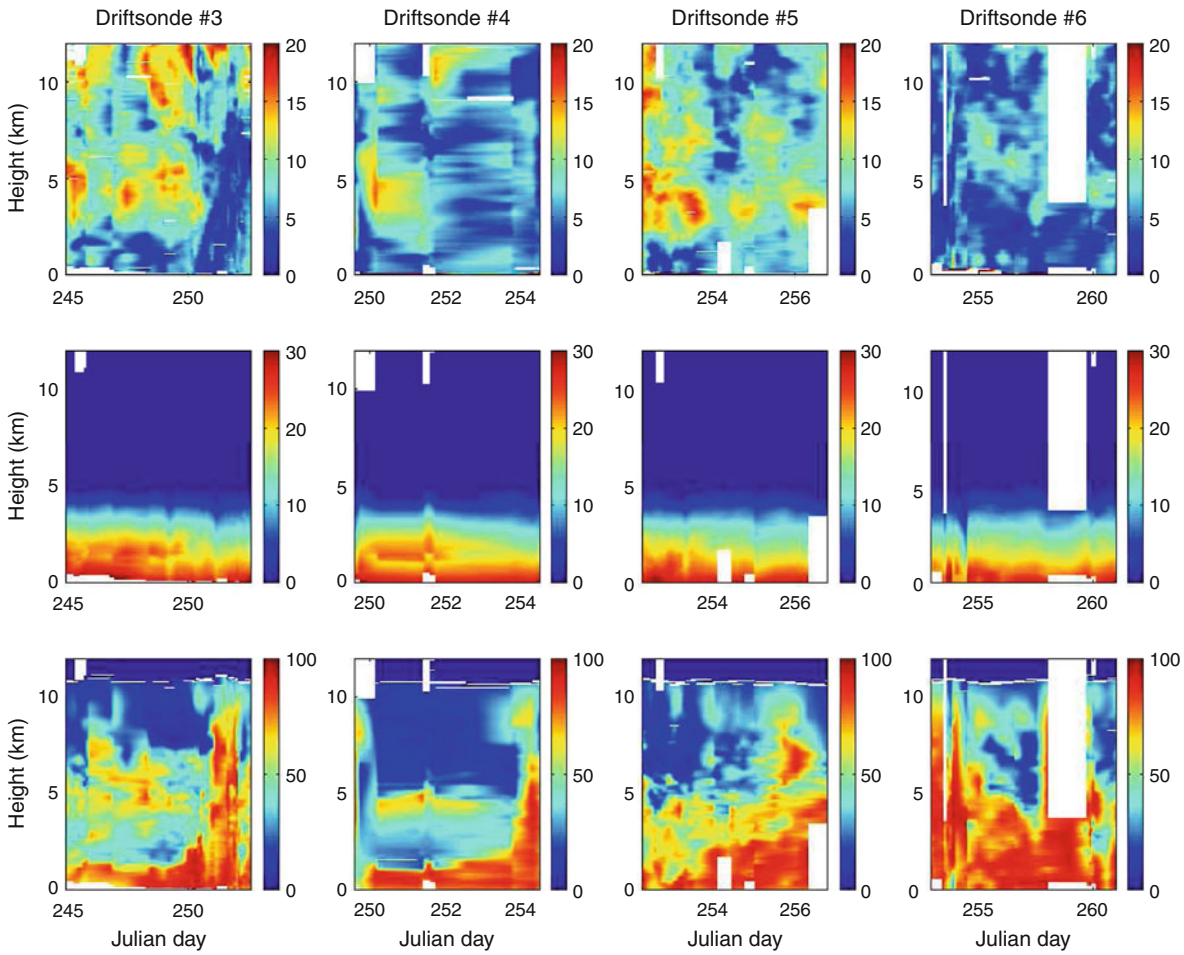

Hurricane and Monsoon Tracking with Driftsondes. Figure 4
Time versus height cross section of wind speed (*first row*, panels **a**, **b**, **c**, and **d**), temperature (*second row*, panels **e**, **f**, **g**, and **h**) and humidity (*third row*, panels **i**, **j**, **k**, and **l**) constructed with the vertical profiles obtained by the sondes dropped from driftsonde 3 (first column; blue trajectory in Fig. 1), 4 (second column; yellow trajectory in Fig. 1), 5 (third column; purple trajectory in Fig. 1), and 6 (fourth column; green trajectory in Fig. 1)

during day 250) before reaching the disturbed environment near Florence where very intense convection occurs (Fig. 4i). Figure 4b is similar to Fig. 4a for driftsonde 4. However, the much lower number of successful dropsondes does not allow the documentation of fine-scale structures over the Atlantic Ocean. It however shows a disturbed environment similar to driftsonde 3 less than 200 km south of the developing tropical storm Gordon at about 55°W (not shown) and Julian day 254 with large humidity extending up to the tropopause and weak near-surface winds. The existence of weak-surface winds is surprising since one may associate naturally developing tropical storms with large evaporation and thus strong winds. The vertical profiles of relative humidity documented by the dropsondes of driftsonde 4 around Julian day 250 also show evidence of very low humidity values just above the planetary boundary layer (around 20% relative humidity) and at about 5–6 km height (below 10% relative humidity) corresponding the AEJ (Fig. 4). The low level dry layer was identified as a strong dry air outflow from the Sahara by the Meteosat-8/Goes-10 combined Saharan air layer product. The very dry air conveyed by the AEJ originated in the upper levels (200–250 hPa) on the anticyclonic side of the polar jet stream at 50°N as diagnosed by the method proposed by Roca et al. [21].

Figure 5 is similar to Fig. 3 between September 11, 2006, and September 17, 2006. Driftsondes 5 and 6 represented by purple and green filled dots, respectively, sensing the atmosphere ahead and downstream the tropical storm Helene which initiates on September 11, 2006, at 1800 UTC over the coast of Senegal and moves westward at a propagation speed of about 8 m s^{-1}. Figure 4 shows that after the formation of three successive storms in about 2 weeks, all evolving into hurricane category, driftsondes 5 and 6 probe a much more disturbed environment than for Florence, with higher convective activity both over the continent and the ocean with nearly saturated air observed up to 5 km along the driftsonde tracks. The AEJ tends to weaken during driftsonde 6 flight.

Analyses of AEW with the Driftsondes

As AEWs are the dominant synoptic weather systems in West Africa and the tropical Atlantic during boreal summer and are an important component of the regional climate by modulating West African rainfall including mesoscale convective systems (MCSs) which can be precursors of tropical cyclones in the Atlantic, the respective locations of the dropsonde and AEW are now investigated.

A method based on the wavelet analysis with a Morlet mother wavelet [24] of the meridional wind field at 700 hPa is used to detect AEW activity. The sum of the spectral density between 3 and 5 days period allows to perform an index which estimates the wave activity over each grid points. The spatial average of this index is then computed to observe the large-scale AEWs activity. This method has been proposed by Lavaysse et al. [16]. Figure 6 shows the longitude/latitude field of the mean AEW index averaged between August 15 and September 30, 2006, as well as the Hovmöller space-time diagram of the 2–6 day bandpass filtered meridional wind at 700 hPa averaged between 5°N and 20°N. Using this method, we detect in 2006 three periods of large AEW activity over West Africa and the tropical Atlantic (i.e., 50°W, 10°E and 5°N, 20°N): middle of July, middle of August, and middle of September. This is in accordance with other methods of AEW as the variance of the 700 hPa meridional wind filtered in the 3–5 days band period, and the 700 hPa curvature vorticity method by Berry et al. [4] and illustrated by Janicot et al. [14]. These results are also in accordance following different analyses as ECMWF and national centers for environmental predictions (NCEP) (not shown) and different geopotential levels (700 or 850 hPa). During the period of driftsonde operations (i.e., August 29 to September 23, 2006), the AEW activity shows two distinct periods. Driftsonde 1 (black trajectory, Fig. 1) flies during a period of low AEW activity preceding the initiation of Helene tropical storm on September 3, 2006, at 40°W also during the period of low AEW activity. The AEW activity increases on September 1, 2006, over West Africa. The area of large waves activity propagates westward in association with the westward propagation of the filtered meridional wind. Driftsonde 3 (blue trajectory) follows the ridge sector of the strengthening wave train (Fig. 3) but the AEW activity abruptly decreases when the waves reach the ocean (around 20°W). A similar scenario occurs for driftsonde 4 (yellow trajectory). Around September 7, 2006, AEW

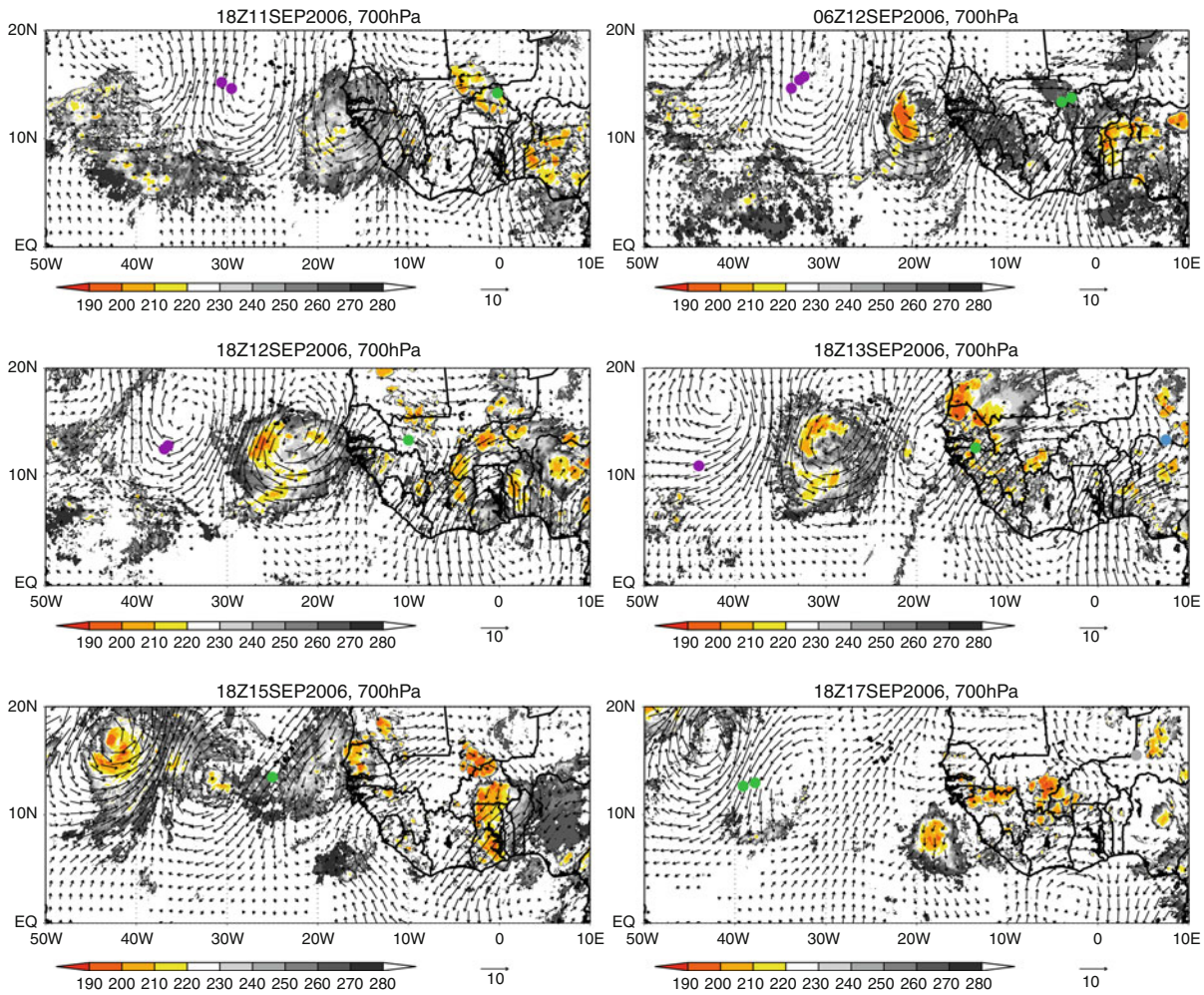

Hurricane and Monsoon Tracking with Driftsondes. Figure 5
Meteosat Second Generation (MSG) 10.8 μm channel brightness temperature which indicates convective activity with superimposed filtered 700 hPa wind field shown with *arrows* (the absence of *arrows* indicate winds weaker than 1 m s^{-1}) on September, 11, 2006, (Julian day 254) at 1800 UTC (**a**), on September 12, 2006, (Julian day 255) at 0600 UTC (**b**), on September 12, 2006, (Julian day 255) at 1800 UTC (**c**), on September 13, 2006, (Julian day 256) at 1800 UTC (**d**), on September 15, 2006, (Julian day 258) at 1800 UTC, (**e**) and on September 17, 2006, (Julian day 260) at 1800 UTC (**f**). The *purple*, *green*, and *cyan filled dots* indicate the locations of dropsondes from driftsondes 5, 6, and 7, respectively

activity is maximum over West Africa. In the same time, driftsonde 5 (purple trajectory) is launched (Table 1). Ten sondes are dropped in the ridge sector of the AEW over West Africa (Fig. 5). Above the coast, the westward propagation speeds of the driftsonde and the AEW are different thus on September 11, driftsonde 5 drops sondes in the trough sector of the AEW ahead of the ridge sector. Driftsonde 5 is particularly interesting when flying over the continent because of its proximity to the trough of the AEW associated with large convective activity. This AEW-MCS system is the precursor of tropical storm Florence initiating around September 12, at 20°W. This storm propagates along a maximum of the mean AEW activity index with the largest value over the tropical Atlantic (September 15 at 42°W; Fig. 6). Driftsonde 6 (green trajectory) covers the largest longitudinal cross section with a first drop at 7°E and the last drop at 47°W. Driftsonde 6 remains

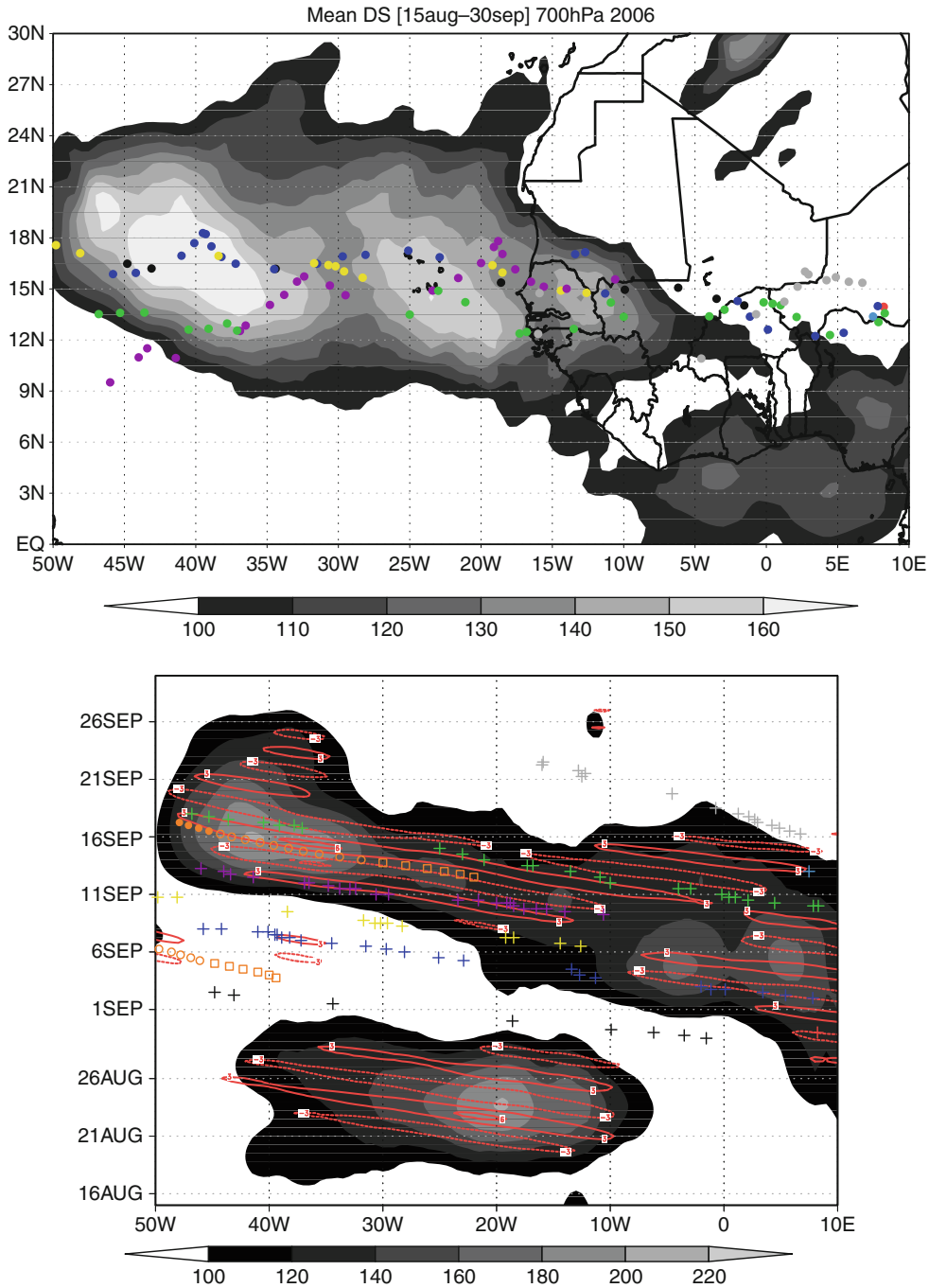

Hurricane and Monsoon Tracking with Driftsondes. Figure 6

Left panel: Mean AEW index with the location of the dropsondes superimposed. *Right panel*: Hovmöller space-time diagram of the 2–6 day bandpass filtered NCEP-2 meridional wind at 700 hPa (*red contour* for +1 m s^{-1}) and AEW index (*gray shading*) averaged between 5°N and 20°N. Superimposed are the locations of the dropsondes of the eight driftsondes ("+" marker with same color code as in Fig. 1) and the 1-day averaged location of the tropical storms Florence and Gordon (*squares*, *circles*, and *filled circles* when classified as tropical depression, tropical storm, and hurricane, respectively). Gordon is not visible since forming at about 55°W, that is, out of the abscissa scale

over the same ridge sector along the whole operation period and provides temporal-longitudinal evolution of the activity and characterization of the ridge.

Conclusion

It is worth emphasizing that all the driftsondes deployed during AMMA were still on probation. This status explains the late dissemination of the data on the GTS (driftsonde 8, only) and the technically mitigated success. The driftsonde system has gradually reached the stage of maturity. During T-PARC, 16 driftsondes were launched from Hawaii during August 2008 [9]. About 250 dropsondes were targeted eventually that correspond to a 64% success rate. The launch site of the pre-Concordiasi test-campaign was in the Seychelles in February 2010 and 3 driftsondes with limited dropsondes were deployed. Finally, Concordiasi test-campaign took place from September to December 2010 [19] over Antarctica. More than 620 dropsondes were deployed from a fleet of 13 driftsondes launched at McMurdo station. The mission success rate was close to 95%, most of the data were disseminated on the GTS.

Whenever the dropsonde data are disseminated or not, the evaluation of the NWP-wise benefit of deploying these observing platforms requires some specific impact studies. These imply to compare the quality of forecasts when the NWP system processes the dropsondes' data or not. The data collected over West Africa and the Atlantic Ocean during AMMA have been used to evaluate numerical weather prediction of the late 2006 African monsoon [8]. They will also be used for a posteriori analysis of their added value for numerical weather forecast. The evaluation of NWP impact of T-PARC driftsondes has not been carried out yet, though many phenomenological studies have been carried out. The evaluation of Concordiasi is currently being done. As the NWP benefit is gained as soon as the data are assimilated in operational NWP systems, the exact assessment of this benefit triggers a limited motivation. Indeed, this evaluation is crucial to correctly assess the NWP efficiency of data targeting with such platforms.

Future Directions

The idea of a network of high atmosphere balloons distributed in the stratosphere and dropping sondes on demand has existed for more than a decade. Some projects have emerged with the advent of THORPEX. Many of them were intractable. The driftsonde system, which appeared to be one of the less ambitious projects, eventually emerged in AMMA 2006. The system has been improved in T-PARC 2008 and for Concordiasi in 2010. The system will be upgraded in 2011–2013, but this last technical step will prevent the system to be deployed in the joint T-NAWDEX/HyMeX framework in 2012–2014 (T-NAWDEX stands for THORPEX-North Atlantic Waveguide and Downstream impact Experiment and HyMeX means Hydrological Cycle in the Mediterranean Experiment). In this last field campaign, the challenge would have been to deploy driftsondes above the Atlantic Ocean, from the USA. The objective was to sample the whole Atlantic, upstream from Europe and the Mediterranean region. Hopefully, the new generation system will probably be deployed in further future specific observation campaigns.

In near future and NWP-wise, the main interest of the driftsonde system is its ability to sample a whole atmospheric environment in which a weather threat is likely to emerge. This mode is especially effective if driftsondes are deployed in a network of several units. This is typically the level of targeting that should be achieved for adaptive observation. Indeed, several factors contribute to the suboptimality of single-use (single weather event) driftsondes' deployment.

- The release of driftsonde is a delicate art, highly dependent on environmental conditions. The system has a limited capacity to respond to a very specific request (short time and very localized area).
- After having drift above the area of interest as defined for the targeted event, the balloon is lost to its initial targeting mission.
- Controlling the trajectory is currently not possible. In the cases and T-PARC and AMMA (summer) the trajectories showed rather zonal despite a few fluctuations. But during the probe campaign for Concordiasi in the Seychelles (February 2010), the trajectories were poorly predictable and let the balloons drift out of the Tropics.

However, regular sampling of regions void of any observations can be very profitable for weather forecasting. Furthermore, deployment in areas (space-time)

where the flow is periodic preserves driftsondes' fleet on the region of interest: around the globe inter-tropical circulation in summer or polar vortex in winter. The specific impact remains to be shown clearly with the existing datasets. This should be a prerequisite to any further deployment and the time left by the upgrade of the driftsonde system should be used to demonstrate the usefulness of these data in some global prediction systems.

Finally, there are other aerostats that may be more suitable for adaptive deployment in response to the possible occurrence of some weather event in particular. Boundary layer pressurized balloon (BLPB) is one example. The BLPB is a balloon drifting in the atmospheric boundary layer and carrying an instrumented gondola which collects measurements of the typical meteorological variables. The proof of concept will be given during the HyMeX special observing periods. In the HyMeX field campaigns, the BLPBs will be deployed above the marine surroundings of some intense convective systems that occur at the periphery of the Mediterranean basin [7].

Acknowledgments

We are thankful to J. Fox, K. Romberg, J. VanAndel, H. Cole, C. Martin, G. Granger, D. Flanigan, and D. Lauritsen (NCAR) for assistance in operation of the driftsonde system. Based on French initiative, AMMA was built by an international scientific group and is currently funded by a large number of agencies, especially from France, UK, Germany, USA, and Africa. It has been the beneficiary of a major financial contribution from the European Community's Sixth Framework Research Program. Detailed information on scientific coordination and funding is available on the AMMA International website http://www.amma-international.org.

Bibliography

1. Aberson SD (2003) Targeted observations to improve operational tropical cyclone track forecast guidance. Mon Wea Rev 131:1613–1628
2. Avila LA, Pasch RJ (1992) Atlantic tropical systems of 1991. Mon Wea Rev 120:2688–2696
3. Berry GJ, Thorncroft C (2005) Case study of an intense African easterly wave. Mon Wea Rev 133:752–766
4. Berry GJ, Thorncroft C, Hewson T (2007) African easterly waves during 2004 – analysis using objective techniques. Mon Wea Rev 135:1251–1267
5. Burpee RW, Franklin JL, Lord SJ, Tuleya RE, Aberson SD (1996) The impact of omega dropwindsondes on operational hurricane track forecast models. Bull Am Meteorol Soc 77:925–933
6. Drobinski P, Parsons D, Cocquerez P, Cardonne A, Cole H, Fox J, Lefevre JP, Redelsperger JL, Romberg K, VanAndel J, Vénel S (2006) Des ballons stratosphriques traquent la mousson africaine. La Météorologie 55:2–3
7. Drobinski P, Basdevant C, Doerenbecher A, Pannekoucke O, Fesquet C, Verdier N, Vargas A (2010) Balloon deployment during the HyMeX (Hydrological in the Mediterranan EXperiment) project. 38th COSPAR Scientific Assembly, Bremen
8. Drobinski P, Karbou F, Bauer P, Cocquerez P, Lavaysse C, Hock T, Parsons D, Rabier F, Redelsperger JL, Vénel S (2011) Driftsonde observations to evaluate numerical weather prediction of the late 2006 African monsoon. J Appl Meteorol Climatol (submitted)
9. Elsberry RL, Harr PA (2008) Tropical cyclone structure (TCS-08) field experiment science basis, observational platforms, and strategy. Asia-Pacific J Atmos Sci 44:209–231
10. Frank NL (1970) Atlantic tropical systems of 1969. Mon Wea Rev 98:307–314
11. Harnisch F, Weissmann M (2010) Sensitivity of typhoon forecasts to different subsets of targeted dropsonde observations. Mon Wea Rev 138:2664–2680
12. Hertzog A, Vial F, Mechoso CR, Basdevant C, Cocquerez P (2002) Quasi-Lagrangian measurements in the lower stratosphere reveal an energy peak associated with near-inertial waves. Geophys Res Lett 29:1229. doi:10.1029/2001GL014083
13. Hill CM, Lin YL (2003) Initiation of a mesoscale convective complex over the Ethiopian Highlands preceding the genesis of Hurricane Alberto (2000). Geophys Res Lett 30:1232. doi:10.1029/2002GL016655
14. Janicot S, Thorncroft CD, Ali A, Asencio N, Berry G, Bock O, Bourles B, Caniaux G, Chauvin F, Deme A, Kergoat L, Lafore JP, Lavaysse C, Lebel T, Marticorena B, Mounier F, Nedelec P, Redelsperger JL, Ravegnani F, Reeves CE, Roca R, de Rosnay P, Schlager H, Sultan B, Tomasini M, Ulanovsky A (2008) ACMAD forecasters team: large-scale overview of the summer monsoon over West Africa during the AMMA field experiment in 2006. Ann Geophys 26:2569–2595
15. Joly A, Browning KA, Bessemoulin P, Cammas J-P, Caniaux G, Chalon J-P, Clough SA, Dirks R, Emanuel KA, Eymard L, Gall R, Hewson TD, Hildebrand PH, Jorgensen D, Lalaurette F, Langland RH, Lematre Y, Mascart P, Moore JA, Persson PO, Roux F, Shapiro MA, Snyder C, Toth Z, Wakimoto RM (1999) Overview of the field phase of the Fronts and Atlantic Storm-Track Experiment (FASTEX) project. Bull Am Meteorol Soc 125:3131–3163
16. Lavaysse C, Diedhiou A, Laurent H, Lebel T (2006) African easterly waves and convective activity in wet and dry sequences of the West African Monsoon. Clim Dyn 27: 319–332
17. Lin YL, Robertson KE, Hill CM (2005) Origin and propagation of a disturbance associated with an African easterly wave as

a precursor of Hurricane Alberto (2000). Mon Wea Rev 133:3276–3298
18. McNally T (2002) A note on the occurrence of cloud in meteorologically sensitive areas and the implications for advanced infrared sounders. Q J Roy Meteorol Soc 128:2551–2556
19. Rabier F, Bouchard A, Brun E, Doerenbecher A, Guedj S, Guidard V, Karbou F, Peuch V-H, El Amraoui L, Puech D, Genthon C, Picard G, Town M, Hertzog A, Vial F, Cocquerez P, Cohn SA, Hock T, Fox J, Cole H, Parsons D, Powers J, Romberg K, VanAndel J, Deshler T, Mercer J, Haase JS, Avallone L, Kalnajs L, Mechoso CR, Tangborn A, Pellegrini A, Frenot Y, Thpaut J-N, McNally A, Balsamo G, Steinle P (2010) The Concordiasi project in Antarctic. Bull Am Meteorol Soc 91:69–86
20. Redelsperger JL, Thorncroft CD, Diedhiou A, Lebel T, Parker DJ, Polcher J (2006) African monsoon multidisciplinary analysis: an international research project and field campaign. Bull Am Meteorol Soc 87:1739–1746
21. Roca R, Lafore JP, Piriou C, Redlesperger JL (2005) Extratropical dry-air intrusions into the West African monsoon midtroposphere: an important factor for the convective activity over the Sahel. J Atmos Sci 62:390–407
22. Szunyogh I, Toth Z, Zimin A, Majumdar SJ, Persson A (2002) On the propagation of the effect of targeted observations: the 2000 Winter Storm Reconnaissance Program. Mon Wea Rev 130:1144–1165
23. Thorncroft C, Hodges K (2001) African easterly wave variability and its relationship to Atantic tropical cyclone activity. J Clim 14:116–1179
24. Torrence C, Compo GP (1998) A practical guide to wavelet analysis. Bull Am Meteorol Soc 79:61–78
25. Wu C-C, Chen J-H, Lin P-H, Chou K-H (2007) Targeted observations of tropical cyclone movement based on the adjoint-derived sensitivity steering vector. J Atmos Sci 64:2611–2626

Hybrid Electric and Hydraulic Technology Applications in Off-Road Vehicles

M. Abul Masrur[1], Vijay K. Garg[2]
[1]College of Engineering & Science, University of Detroit Mercy, Detroit, MI, USA
[2]Dublin, OH, USA

Article Outline

Glossary
Definition of the Subject and Its Importance
Introduction
Off-Road Vehicles
Diesel Electric Locomotives
Hybrid Hydraulic Vehicles
Future Directions
Appendix
Bibliography

Glossary

Plug-in hybrid A plug-in hybrid is a regular hybrid vehicle that has a large high-capacity battery bank that can be charged by plugging in to normal household outlet. While standard hybrids require a combination of regenerative braking and energy from the engine to recharge the batteries, plug-ins can essentially operate as electric vehicles with an internal combustion engine backup. This is also known as PHEVs (Plug-in Hybrid Electric Vehicles)

Alternator An electromechanical device used to translate mechanical power into AC electrical power.

Battery state of charge SOC or state of charge is the equivalent of a fuel gauge for a battery, that is, a measure of how much energy is left in the battery with respect to its full rated capacity. Although many times SOC is related directly by measuring the terminal voltage, SOC cannot be accurately determined in general by voltage measurement, because the terminal voltage of a battery may stay substantially constant until it is completely discharged. SOC is also highly dependent on temperature.

Complex hybrid vehicles In this system, in addition to the ICE and the motor, there is an additional motor/generator set (along with a power electronic converter) which can be used to charge the battery as needed. This can continue charging the battery while the main motor is driving the wheels.

Converter A generic term for a system which translates one form of power (DC or AC) into another.

Diesel IC engine An IC engine that uses the heat of highly compressed mixture of air and spray of fuel (diesel) near the end of the compression stroke to create the combustion.

Drive cycle It is a relationship of either speed versus time or power versus time, for a particular vehicle which is driven in a given road profile. The road profile can be city streets, highways, steep grade,

or some chosen mixed combination of these or other profiles, which will be predefined.

Fuel cell It is a stationary device used to directly translate chemical energy into electrical energy.

Generator It is the generic name used to imply something that translates mechanical energy into electrical energy.

Hybrid electric vehicle (HEV) A vehicle which uses more than one source (two being most common) of propulsion, one being the internal combustion engine, and the other uses an electric motor driven by either a generator run by the IC engine or a combination of generator and a battery which can be charged by the generator to provide the electricity, or it can be a fuel cell instead of a battery or generator, which can directly run the motor.

Internal combustion engine (ICE) ICE is the one in which combustion of the fuel (e.g., gasoline) takes place internally inside a cylinder or other enclosed space using spark ignition or compression ignition to some combustible gas, which will expand and produce high pressure that will produce mechanical power. ICE is thus a converter of chemical energy in mechanical energy.

Inverter A system which converts DC into AC.

Microgrid If an HEV is provided with an additional converter, which can translate the battery power into a utility level AC power, then it can be interfaced with either the main utility grid directly or with other HEVs or other smaller subsystems using utility level AC voltage. An interfaced set of vehicles, other utility level AC voltages, and utility grid, all or part of these entities taken together can be termed a microgrid.

Off-road vehicle An off-road vehicle is a vehicle, which is capable of driving on and off paved or gravel surface. Vehicles that do not travel public streets or highways are generally termed off-highway vehicles, for example, tractors, forklifts, cranes, backhoes, bulldozers, and golf carts.

Parallel hybrid vehicles In parallel hybrid, the IC engine and the electric motor, both are mechanically connected to the wheel. The ICE is also used to charge the batteries.

Power electronics It is a system using solid state high-power and high-voltage electronic switches to turn on/off a voltage or current, which together with other elements like inductance, capacitance to convert DC, AC, etc., into another form of controlled power.

Rectifier A system which converts AC into DC.

Series hybrid vehicles It is a hybrid vehicle, in which the electric motor (or motors) is the only unit which is used to run the wheels. The IC engine charges the batteries by means of a generator.

Ultracapacitor A capacitor that has much greater energy density and power per pound than regular capacitors. It uses chemicals, but the energy is stored in the electrostatic form and, unlike a battery, the energy is not stored through the chemical reaction and no change in chemicals take place while storing energy. It is also sometimes referred to as "supercapacitor."

Definition of the Subject and Its Importance

Hybrid electric vehicle (HEV), as discussed elsewhere in this entry, basically involves hybridization or mixing of power and propulsion sources and/or loads, leading to the achievement of better overall system efficiency and accompanying pollution control. In short, it hinges on the principle that not every "type of" power source (which, e.g., could be IC engine, battery, generator, etc.) is always the best to provide power to every type of load demand, which can vary over time. So, the idea is to use the best source as the load changes. Here, the word "best" is defined in terms of efficiency, performance, and similar attributes. The technology evolved in different forms over the years. The main motivation behind the technology in the recent past has been due to cost of fossil fuel, that is, gasoline and diesel in particular, which showed an ever-increasing trend. But additional benefit like less pollution has also accompanied the technology. HEV technology has already been in existence for use in diesel electric locomotives for quite a while. There the intent was to get very high torque to move the vehicle from rest, by using electric motor instead of a mechanical system (with engine and transmission directly propelling the wheels), thus avoiding the use of bulky mechanical transmission system. At this time, the technology, which is highly interdisciplinary in nature, requires further improvement in the areas of battery, power

electronics, and motor. To this end better materials are being investigated to develop lightweight and high temperature withstanding systems. The importance of the technology is obviously evaluated mainly by how much it can help with fuel economy, followed by pollution control, and then the performance, weight, and size. Depending on the application, one or more of these criteria can be of importance to one user (e.g., small-size automobiles), whereas as another set of criteria can be of importance to another user (e.g., heavy construction and off-road vehicles). Obviously, there is much to gain from the development of this important technology and the future seems very promising at this time with significant technical and social ramifications.

Introduction

There are many HEV (hybrid electric vehicle) applications which include both vehicular and electrically operated nonpropulsion-type military usages. Vehicle applications are directly related to vehicular propulsion. However, interfacing of the vehicular electrical system to create a microgrid to supply/receive power to/from utility grid is gaining popularity. Multiple HEVs, with proper interfacing mechanisms, can create utility-level voltages to run various stationary equipments. This can be done by running the HEV battery (and if necessary, the IC engines [ICE] in the HEV). In another application, several HEVs, along with an industrial/utility power system, can form a microgrid environment and help enhance the overall power system robustness and availability. Hybrid vehicles can be interfaced with a utility grid or a microgrid, where a number of vehicles could be supplying power through some common bus. It is, in principle, possible to have an IC engine–based generator, and fuel cell, vehicles, all properly synchronized and then exchanging power. A system-level diagram of such a situation is shown in Fig. 1. However, in this entry only off-road vehicles/machines applications will be discussed.

One of the most important reasons for considering HEV for vehicular applications is the cost of the fuel, reduced emissions, and acoustic noise. Several different architectures have been implemented in HEV, depending on the application. For example, a series HEV (SHEV) architecture can be implemented by using several hub motors, with one motor on each wheel, or alternatively, there could be one motor per axle for propulsion. This can take advantage of redundancy in case one of the motors fails. In this case, the vehicle can run in a gracefully degradable mode, with somewhat lesser performance and drive to safety as needed. A brief introduction of architectures used in vehicular applications is given in the following section.

Series, Parallel, and Complex Architectures for Ground Vehicle Applications

For the sake of continuity, various types of automotive HEV architectures are discussed in this section briefly. HEV architectures used in off-road vehicles are similar to automotive HEV architectures, except the engine technology. Automotive HEVs use gasoline IC engines in general, while off-road vehicles in general use diesel-based engines. (In this chapter, IC engine implies regular automotive gasoline engine unless explicitly indicated otherwise.) A very informative research paper [1] has made a comparison between the series and parallel HEV architectures (Fig. 2a, b) with a regular IC engine vehicle. From the reference cited above [1], it has been found that IC engine vehicles are slightly lighter than

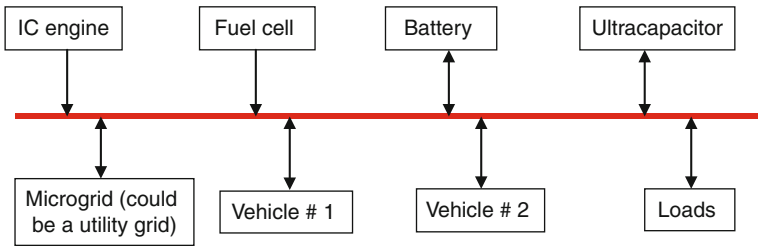

Hybrid Electric and Hydraulic Technology Applications in Off-Road Vehicles. Figure 1
A generic hybrid power system

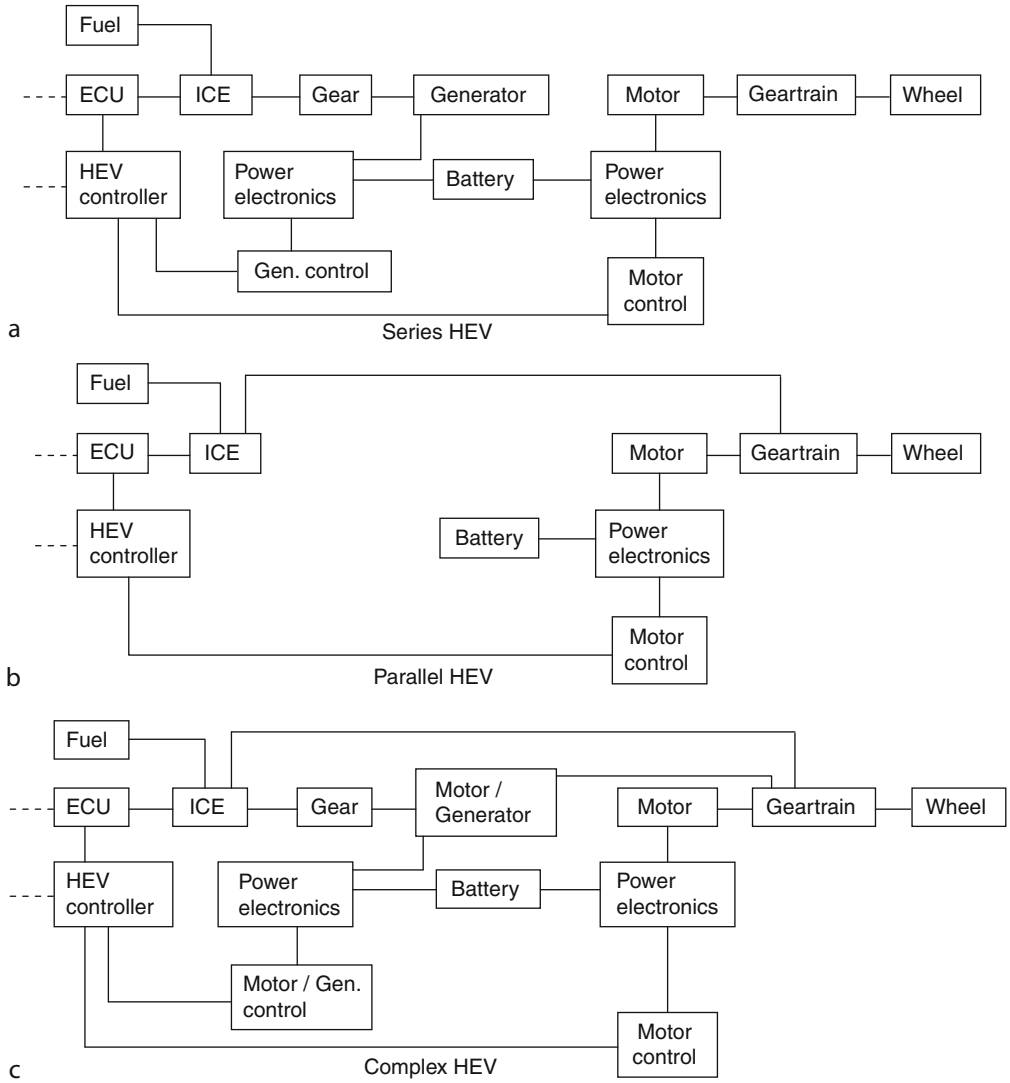

Hybrid Electric and Hydraulic Technology Applications in Off-Road Vehicles. Figure 2
(**a**) Series HEV configuration, (**b**) parallel HEV configuration, (**c**) complex HEV configuration (Courtesy: Pubs-Permissions @ieee.org)

parallel HEVs. However, the series hybrid vehicle was found to be relatively heavier. If a nonhybrid IC engine vehicle is considered a baseline, then one can compare the other architectures as follows. To match the performance of the baseline vehicle, obviously it is necessary to make the electric motor in a Series HEV (SHEV) to have the same size as the IC engine. The authors believe that comparison of vehicle weight and volume of an IC engine vehicle and "series HEV" should be based on drive cycle, and the average energy efficiency of the propulsion system, that is, the comparison should be done under similar circumstances in terms of its operation and type of engine used.

The peak power can be handled by the battery, which should be charged within its bounds. The authors recommend simulation and experimental studies of different drive cycles and then coming up with a worst case scenario to help decision making. The battery and other storage devices play an important role in decision making, depending upon whether

they can provide the maximum power needed or not. Only if the battery is kept under completely floating condition all the time, and the power from the ICE and generator is fed to the motor in parallel with the battery, will require the generator to be sized equal to the maximum power demand. The intent of the battery or any peak power source is to address the maximum power demand in SHEV, and hence ICE and generator size in SHEV could be reduced. However, the size of ICE and the generator in SHEV will definitely depend on the average power demand by the vehicle based over the expected drive cycle in which it will operate. In a parallel HEV, the size of the electric motor could be less than half the size of SHEV motor.

The reference [1] assigns the balance of power to the ICE in the Parallel HEV (PHEV). The mechanism to split the power assignment to the motor and the ICE in the parallel HEV assumes that the original ICE in the baseline vehicle was chosen based on the maximum power needed under the worst possible drive cycle scenario. There is also no separate generator in the PHEV in the reference cited above. However, in some architectures, like Toyota Prius and some others as well, there is a motor/generator that is separate from the main propulsion motor, which can be used as generator and starter as well.

The reason for having this generator is highly dependent on the strategy for control. Under certain conditions of the battery state of charge (SOC) and power demand in the propulsion, it may be necessary to provide additional charge to the battery, through this generator.

The battery, or any other storage elements like the ultracapacitor, is an important part of the SHEV or PHEV. In specifying batteries, normally voltage and amp-hrs are used as metric. But in PHEV and SHEV applications, it is also necessary to know the current (or equivalent power) rating to satisfy the maximum current (or equivalent power) demand by the propulsion motor. The current (and power) demand from the propulsion motor can be met by the generator and the battery working together. As noted earlier, quite often the battery is used to meet some high transient (or peak) current demand from the motor. Hence, it is very important to know the battery current rating, both continuous and instantaneous, in addition to its voltage and amp-hrs. All these issues require a vital decision-making process in developing the design specifications for an HEV. The discussion above applies to both gasoline- and diesel-based HEV for better fuel economy and other benefits, such as reduced emissions.

Another question that requires a serious discussion is the choice of HEV architecture, that is, whether it should be series, parallel, or complex (Fig. 2a–c). The question can be best answered depending on what is the priority – is it fuel economy, performance, size or weight, reliability, or emissions, which are briefly answered below.

- If fuel economy is of utmost priority, then it should be a PHEV.
- On the other hand, if the performance of the vehicle is important (i.e., power output), then SHEV is a better choice. This might help reduce transmission package as well as it makes the system capable of providing high power on demand quickly. This is due to the fact that motor reacts to control the commands faster than the ICE.
- If size and lightweight are of concern due to the vehicle requirements, then PHEV will be a better choice than SHEV. In general, SHEV is to some extent heavier than PHEV, hence this fact might also affect fuel economy slightly.
- Reliability is not to be underestimated in both PHEV and SHEV. However, reliability considerations might be better addressed in general by using PHEV, because of redundancy in propulsion due to ICE and the motor. However, PHEV control system is more complex, in addition to complexity in its mechanical coupling. A thorough study of failure modes of these devices is needed before one can conclusively make a decision on reliability matters.
- Another issue accompanying reliability in vehicular systems is maintenance. It appears that maintenance of an SHEV is somewhat simpler due to several reasons. Its control and mechanical linkage, unlike PHEV, are simple. If there are hub motors in its propulsion, they can be rather quickly replaced in case of failure.
- Off-road and military applications of these vehicles require device ruggedness. This implies that both mechanical and electrical as well as other design

aspects like high temperature extremes (both hot and cold) must be considered. In general, high temperature and mechanical vibrations can negatively impact items like power electronics and batteries. This means the devices can get physically larger and bulky to provide for appropriate cooling needs, if performance is to be achieved at these extreme conditions.

- The above discussion indicates that there are pros and cons of PHEV and SHEV. Having said that, it should be noted that the decision regarding the choice between PHEV and SHEV could be very much application and drive cycle dependent. Final decision on the above requirements is quite complex, and systematic trade-off studies are required for all requirements like performance, fuel economy, reliability, etc., to reach most optimum decision.

Off-Road Vehicles

Success in hybrid electric vehicles in automotive applications has led certain other vehicular areas to consider this technology as well. These include ships and aircrafts, which are nonground vehicles. Diesel electric locomotives have already been using the technology in a slightly different form and these will be discussed as well. Off-road vehicles are ground vehicles for heavy-duty applications. These vehicles, in general, do not use normal roads for their operation. This entry specifically focuses on heavy-duty applications of off-road vehicles. Examples of such vehicles are construction vehicles and equipments (e.g., mining vehicles/trucks, refuse trucks, agricultural vehicles like tractors, etc.) and some military vehicles. Off-road vehicles, in general, operate at low speeds compared to regular passenger vehicles and use diesel engines, instead of gasoline IC engines. Use of diesel engines has certain advantages compared to gasoline IC engines as discussed in the following.

- The compression ratio of diesel engine can be much higher than the gasoline, for example, it can be around 15–20% compared to 9–12% for the gasoline engine. The higher compression ratio necessitates the engine to be heavier, which helps in construction to sustain the cylinder pressure.
- At low speeds diesel engines are more efficient than gasoline IC engines and are better in terms of fuel economy due to the absence of throttle vales, and avoid parasitic losses. This leads to smaller-sized (HP ratings) engines, specifically at lower speeds.
- Other benefits of diesel engines include lower greenhouse gas emissions such as CO_2.
- Low speed characteristics of diesel engines are better compared to gasoline engine, in terms of starting torque generation.
- Diesel engine has less components due to the absence of ignition system, and hence leads to higher overall system reliability.

A comparison of gasoline and diesel engine speed–power characteristics is shown in Fig. 3. It is apparent that at lower speed range diesel engine can provide higher power compared to a gasoline engine of comparable size. This makes it suitable for high-power low-speed type of operation, which is more consistent with off-road vehicles.

The drive cycles and speed-torque demands of these off-road vehicles can be quite different as compared to regular automobiles. Off-road mining/trucks and construction vehicles operate in rough terrain and at low speeds or under stationary conditions. Therefore, high power and torque are required due to the nature of these vehicle operations. In order to supply high torque and power requirements from a diesel engine, it is necessary to have a large gear box and transmission system, etc. In addition, the overall efficiency of diesel engine is still low (of the order of 40%, but still may be

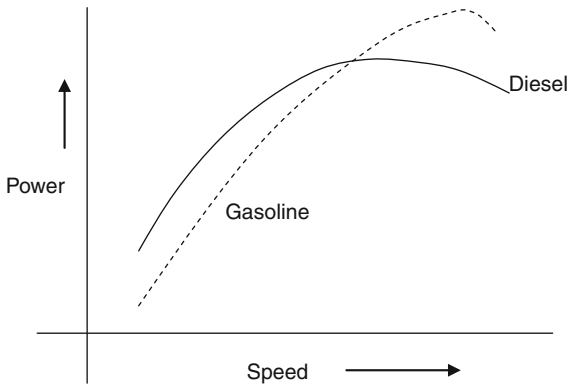

Hybrid Electric and Hydraulic Technology Applications in Off-Road Vehicles. Figure 3
Comparison of gasoline and diesel engine curves

higher than gasoline engine) over the complete drive cycles (or torque speed demand of the load).

To alleviate these issues, hydraulic or electric hybrid propulsion systems are being developed and have been used lately. Hydraulic systems operate by continuously running the engine, which is a low-torque high-speed system relative to load. The engine is used to drive a hydraulic pump which can drive a hydraulic motor. Through the use of an incompressible fluid one can achieve very high pressure, which can be applied at the load drive end. However, the hydraulic systems, in general, can cause problems. Examples of such problems are complex plumbing system with pipes, which, under rough terrain conditions, can cause plumbing system failures. This may be due to fluid leaks, leading to degraded performance and eventually hydraulic system failure. Other disadvantage of hydraulic systems is the parasitic losses.

Based on the above discussion of diesel engines and their use in off-road vehicles, it can be concluded that the merits of diesel engine combined with electric propulsion (diesel HEV) can lead to most fuel-efficient vehicles, subject to the specific application needs. Hence, for the same performance, and particularly during acceleration, it is beneficial to use diesel hybrid, within the same package size. This is especially beneficial in a parallel configuration, when both the engine and the electric propulsion are required to play an important role to achieve optimum performance in terms of power and acceleration. The issue of performance is inherently better addressed in series hybrids, since propulsion is done only by electric motor.

In HEV, energy storage and electric propulsion motor systems offer very high efficiency of the order of 75% and above. In present HEV, engine is used to charge battery and the propulsion torque/power can be shared between the electric propulsion and the engine. Hence, lately various heavy off-road vehicle manufacturers of mining and construction equipments are paying serious attention to transform their system to electric hybrid type of propulsion. These systems offer clean environmental advantages in addition to the fuel economy. It must be noted that hybrid electric off-road vehicles (HEV) are different than the regular automotive HEV, and do not use normal roads for their operation. Mining vehicles, agricultural vehicles like tractors, and some military vehicles also fall in this category. Off-road vehicles will be discussed further in the following section, which have quite different drive cycles and speed-torque demands, as opposed to a regular automobile.

Off-Road HEV

In the preceding sections off-road heavy vehicular applications like mining and construction were mentioned. These vehicles require large transmission system when equipped with only a diesel engine drive, which has relatively low overall efficiency. These issues can be circumvented through HEV system having overall efficiencies of the order of 75%. In an off-road HEV a diesel engine is used to drive a generator or alternator, which in general will generate a variable speed (hence variable frequency) variable voltage (amplitude) system. This variable frequency and variable voltage is then converted to a DC voltage of constant value using an AC to DC converter/rectifier. The constant DC voltage is then converted to a three-phase AC system (inverter) to drive a three-phase AC motor. The inverter can be electronically controlled to deliver desired three-phase voltage (amplitude, frequency, and phase) to drive an electric motor to handle the vehicle load. It should be noted that in the system just described, one can avoid the use of a battery. Although battery is a vital storage element in a regular HEV, in very large off-road vehicles, the battery system can be avoided to reduce cost and package size. In addition, in certain types of vehicles sufficient energy is not available for storage during the vehicle operation. Such a system is very similar to a diesel electric locomotive system.

Various architectures of the off-road and other construction vehicle systems are possible. Two possible systems are shown below. In this architecture the IC diesel engine, in general, is operated at its optimal speed to achieve maximum efficiency. IC engine drives an alternator/generator, which generates a variable three-phase AC voltage (amplitude and frequency). This is rectified and a DC is produced. The DC power is then fed to the inverter to produce desired voltage (amplitude and frequency) to drive a propulsion motor. In general, for very heavy mining applications, induction motors are found to be more robust and suitable in rough terrain/environment. The motor is

then used to drive the vehicle wheels. Generally, large off-road vehicles have two axles and two motors (one on each axle) for propulsion.

In the architecture shown in Fig. 4, the use of battery is avoided. In principle, a battery could be used for energy storage in vehicles, but the size of the battery in that case would be large. In some applications an ultracapacitor bank can also be used. The mechanical energy, during slowing down of the vehicle or some of its movable parts, can be stored in the ultracapacitor as electrical energy. The ultracaps normally have high specific power and low specific energy, that is, it can provide very high burst of power input to a device for a short duration. During the slow down, the controller commands the ultracapacitor, inverter, and the alternator/rectifier to coordinate properly, so that energy flows through the motor and inverter (with the motor operating as a generator) into the ultracapacitor. The stored energy can be utilized to accelerate the vehicle, if so needed at a later time, to save energy and thus leading to better system efficiency and fuel economy. An architecture for such a system noted above is shown in Fig. 5. In this architecture to drive the motor, the DC power could be provided by the ultracapacitor or the IC engine/rectifier. The system will have the necessary switches to select either the ultracapacitor or the alternator/rectifier or both.

It will be interesting to visit some typical sizes involved in such off-road vehicles discussed above. For example [2–4]:

- A Caterpillar engine model Cat 3524B EUI has gross power 2,648 kW (3,550 HP), machine gross operating weight 623,690 kg (1,375,000 lb).
- A particular Komatsu has gross horsepower 2,611 kW (3,500 HP), and weight of 505,755 kg (1,115,000 lb).
- A particular Liebherr has gross horsepower @ 1,800 rpm of 722 kW (3,650 HP), 592 t (British)/652.5 t (US).

The sizes of the tires of these vehicles are in general of the order of 4 m, as is evident from the specifications. This indicates the huge size of these vehicles, some pictures of which are given in Fig. 6.

All the above vehicles, that is, Caterpillar, Komatsu, and Liebherr, are transitioning to hybrid (HEV) power train. Appendix 1 provides additional specifications from the Komatsu information sheet [3] for vehicle shown in Fig. 6b.

The traction motors in both Komatsu and Liebherr are induction motors. The alternators are normally brushless. The gear ratio, reduction from motor to wheel, is of the order of 32–37. The gross engine horsepower of the vehicles is about 2.6–2.7 MW. The inverter

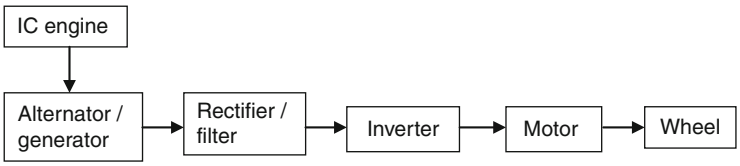

Hybrid Electric and Hydraulic Technology Applications in Off-Road Vehicles. Figure 4
System-level architecture of a diesel electric HEV

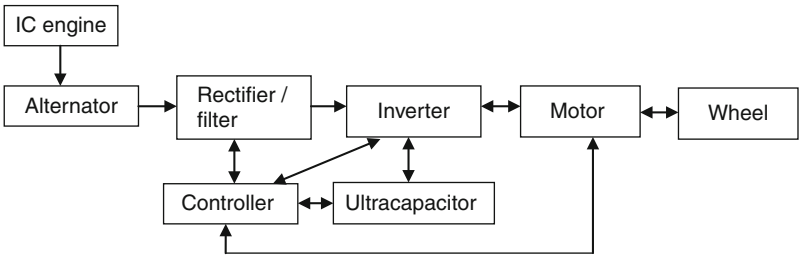

Hybrid Electric and Hydraulic Technology Applications in Off-Road Vehicles. Figure 5
System-level architecture of a diesel electric HEV with ultracapacitor

Hybrid Electric and Hydraulic Technology Applications in Off-Road Vehicles. Figure 6
Typical mining vehicles: (**a**) Caterpillar, (**b**) Komatsu, (**c**) Liebherr (Courtesy: Caterpillar http://catsays.blogspot.com/2005/01/caterpillar-797b-mining-truck.html, http://www.cat.com/contact. Komatsu http://www.komatsuamerica.com/default.aspx?p=equipment&f1=view&prdt_id=947, http://www.komatsuamerica.com/contact. Wikimedia http://commons.wikimedia.org/wiki/File:Liebherr_T282.jpg [2–4])

used to drive the motor generally uses IGBT for switches. Assuming alternator and inverter efficiencies of the order of 0.95 each, the inverter power output (or motor power input) is about 2.35–2.44 MW. So it is reasonable to assume that each induction motor size has to be of the order of 1.2–1.25 MW (assuming two motors for the system, with one at each axle). The vehicle at maximum speed amounts to a wheel revolution of about 84 rpm (assuming a tire diameter of about 4 m). With a gear ratio of about 32.62 the motor speed should be about 2,700 rpm. Nominally, this leads to about 3,000 rpm, which, at 50 Hz, leads to a four-pole induction motor. Four-pole induction motor is normally a common standard for such applications.

Another application of HEV in current off-road vehicles involves construction vehicles such as excavators and scrapers (also known as "track"-type tractor). It is expected that an array of other off-road vehicles may transition to HEV technology, once the customers start accepting the advantages offered by this technology.

Presently in excavators the usage of HEV concept is used in its arm movement, and is not used in vehicle propulsion. The excavator arms need brief burst of high power followed by low power return and then slow down its speed to stop the arm. Such an application is very well catered by using a diesel engine driving a generator to produce electricity to drive the excavator arm motor, which is an electric drive. The possible architecture is shown in Fig. 7.

This architecture is basically the same as the HEV architecture shown previously for the mining truck

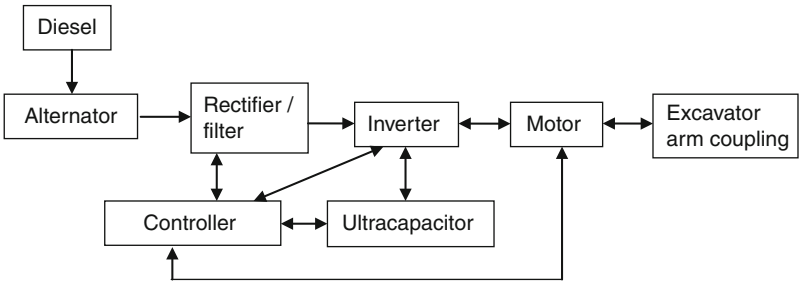

Hybrid Electric and Hydraulic Technology Applications in Off-Road Vehicles. Figure 7
System-level architecture of an excavator with hybrid electric technology and using ultracapacitor

(or hauler) propulsion. Only difference in this case is that the propulsion size is much smaller. It has been claimed that the Komatsu hybrid excavator leads to an additional fuel economy of order of 25% and that some users have achieved fuel economy enhancement as high as 41% for specific applications. A picture of the Komatsu PC 200–8 hybrid excavator is shown in Fig. 8 [5].

Presently, excavators are considered to be good candidates for the installation of energy storage devices such as battery or ultracapacitors. This is perhaps due to size of the machines which require smaller and lower cost storage devices as compared to mining trucks. Some manufacturers prefer to use battery instead of ultracapacitor for the purpose of storage. An example is the New Holland's excavator, which uses a 36 HP diesel engine, 20 kW generator, and a 288 V lithium battery. The choice of storage is highly dependent on exact usage and duty cycle. If it is just a high-power excavator, then ultracapacitor seems to be a suitable candidate. However, if in addition to excavator application, there are other auxiliary equipments, which call for energy that may not be immediately available from an ultracapacitor, a battery may be used. The duty cycle in terms of torque requirement, duration of the torque, auxiliary equipments, cost, size, and similar factors all together leads to the decision process in terms of what will be best, that is, ultracapacitor or battery.

Track-Type Tractor Scraper/Bulldozer Another application of off-road construction and agricultural equipment is a bulldozer or scraper. This was first introduced by Caterpillar in late 2009 [11] and should be available in 2010. The structure of the vehicle, the D7E model is shown in Figs. 9 and 10 [11, 12].

The propulsion is achieved by a diesel electric system with a net power of 175 kW. Here a diesel engine drives a generator. The AC generator and propulsion module voltage is 480 V. The electrical power from the generator is processed by an inverter, which drives a motor. D7E has three-phase induction motors for its drive [13]. It has been indicated [11] that the cost of this model is 20% more than its previous D6 and D8 models. This 20%, which is about $100,000, is claimed to be recoverable in 2 years due to fuel savings of about 10–30%. Performance of this is also claimed to be better than its previous versions. While gas mileage is of importance, in this type of machines the efficiency is measured through how much material can be moved per gallon of fuel, because these machines are not predominantly vehicles in the sense of traveling distances. In terms of materials moved, it is apparently 10–30% more efficient than its nonhybrid equivalent. This machine does not have battery for energy storage, and the power from the generator is directly processed by the inverter and transferred to the motor. The machine can apparently save about 6 gal of fuel over an 8-h period, which can be significant if it is used continuously throughout the year.

Off-Road Military Vehicles

In addition to commercial off-road vehicles, military application also includes similar vehicles. These vehicles, in principle, have similar requirements.

Several pictures of off-road military vehicles are shown in Fig. 11 as illustration and to help readers get visual perspectives of these machines [14–20].

Figures above show vehicles which are regular propulsion type, and could be enhanced by HEV technology.

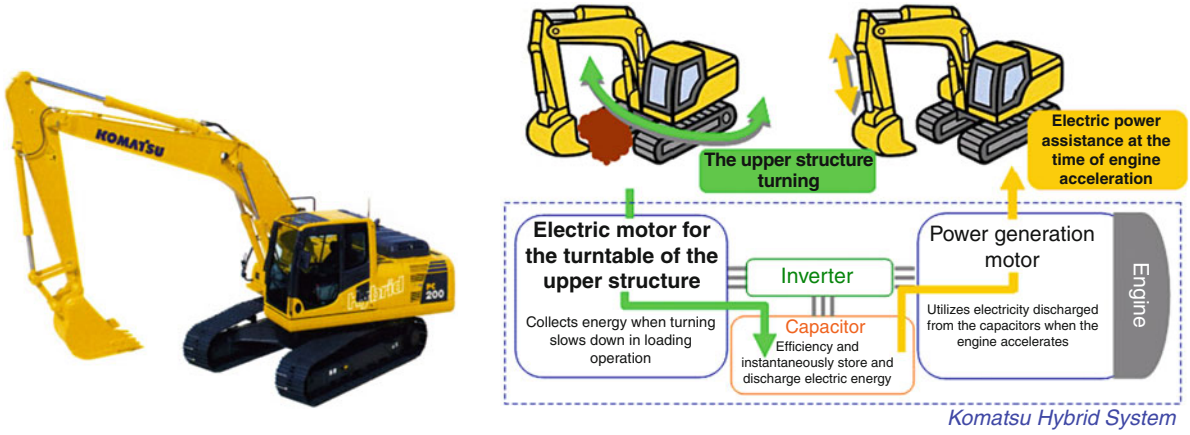

Hybrid Electric and Hydraulic Technology Applications in Off-Road Vehicles. Figure 8
Komatsu excavator system (Courtesy: Komatsu news item http://www.komatsu.com/CompanyInfo/press/200805131511360458 8.html [5])

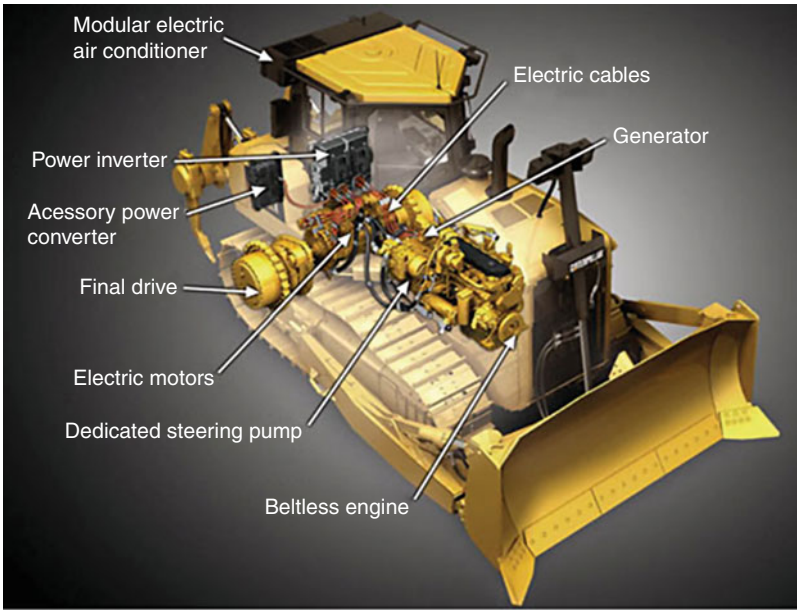

Hybrid Electric and Hydraulic Technology Applications in Off-Road Vehicles. Figure 9
Caterpillar D7E propulsion system (Courtesy: Caterpillar Information Brochure Web article, http://gas2.org/2009/09/18/caterpillar-builds-worlds-first-hybrid-bulldozer/, Web article, http://www.cleanmpg.com/forums/showthread.php?t=33855, http://www.cat.com/contact [11, 12])

From the various types of vehicles shown in the pictures above, it must be noted that these vehicles have different operating requirements in terms of their drive cycles and power when compared to regular automotive applications.

Some vehicles run long distances, and some have extreme power demand and performance needs, such as survivability and fuel economy. Introduction of hybrid propulsion can lead to fuel economy, which has direct and indirect benefits. Direct benefits come

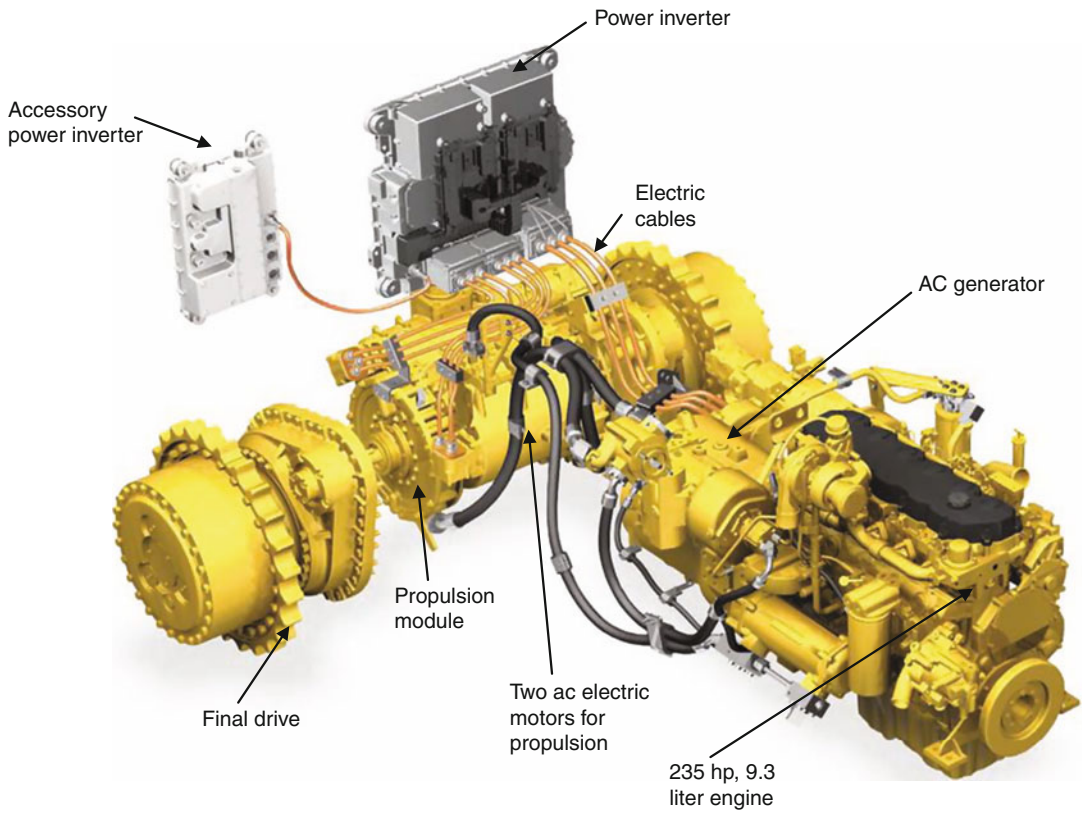

Hybrid Electric and Hydraulic Technology Applications in Off-Road Vehicles. Figure 10
Details of the diesel electric power train organization in Caterpillar D7E (Courtesy: Caterpillar Information Brochure Web article, http://gas2.org/2009/09/18/caterpillar-builds-worlds-first-hybrid-bulldozer/, Web article, http://www.cleanmpg.com/forums/showthread.php?t=33855, http://www.cat.com/contact [11, 12])

in the form of fuel economy, which leads to cost savings. However, for military applications, carrying of fuel to the field involves additional cost and need for logistic vehicles; hence the impact of fuel economy is even higher, compared to commercial vehicles. Hybridization can also lead to redundancy (particularly for parallel architecture with both IC engine and electric propulsion), which can have positive impact on vehicle survivability in case of partial failure. It is also important to note that military environment can involve a wide temperature range and high NVH (noise, vibration, harshness). Power electronics and electric motors have to withstand such situations. These are important enabling technologies which have to undergo further transformation to make HEV technology to gain wide acceptance in military applications.

Summary of Off-Road HEV

Regarding the rating of the motor for the mining truck – nominal DC link rating of these motors can be around 2,600 V, leading to about 1,600 V line-to-line rms input to the three-phase motor. A 1.2 MW motor corresponds to about 541 A AC rms, assuming a power factor of about 0.8. In this case the DC link current for just one motor will be 1.2 MW/2,600 = 461 A DC per motor. All these are assuming no additional loss in the system and the numbers are merely giving an idea of the voltage and current values. Some systems [6] use 3.3 kV IGBT technology to drive these motors, which is consistent with the above ratings indicated for the motor. For the excavator example above the numbers are much lower. As per preceeding paragraph, at 288 V DC, the DC link current will be about 70 A,

Hybrid Electric and Hydraulic Technology Applications in Off-Road Vehicles. Figure 11
(**a**) Stryker (http://commons.wikimedia.org/wiki/File:14_stryker.jpg) (**b**) HEMTT (http://commons.wikimedia.org/wiki/File:HEMTT.jpg) (**c**) Bradley (http://commons.wikimedia.org/wiki/File:Two_M-3_Bradleys.jpg) (**d**) Abrams (http://commons.wikimedia.org/wiki/File:M1A1_Abrams_Tank_in_Camp_Fallujah.JPEG) (**e**) Fennek (European) (http://commons.wikimedia.org/wiki/File:BundeswehrFennek.jpg) (**f**) MRAP (http://commons.wikimedia.org/wiki/File:FBI_Mine_Resistant_Ambush_vehicle.jpg) (**g**) Gladiator (http://commons.wikimedia.org/wiki/File:Gladiator_RSTA.jpg) Courtesy of the websites indicated in the above references [14–20]

the three-phase line-to-line rms for the motor will be about 0.612 × 288 = 176 V, motor current will be about 82 A.

Diesel Electric Locomotives

Diesel engine–based locomotives are commonly used nowadays. In diesel electric locomotives the propulsion system is electric as explained through the block diagram in Fig. 12. There are advantages why diesel electric system is used, as explained in sections "Introduction" and "Series, Parallel, and Complex Architectures for Ground Vehicle Applications" (i.e., if the propulsion was purely mechanical, then a big-sized transmission system with gearbox etc. will be needed to create the needed torque). A second advantage in using electric propulsion system in locomotives is that the electric propulsion system provides continuously variable speed system. This is particularly advantageous in improving the transmission efficiency of short haul trains where speed fluctuations are encountered frequently. Otherwise, a diesel engine with a finite number of gears is required to be operated at different speeds other than the most optimum speed at which the efficiency is highest. In this system (HEV), the diesel engine in general runs

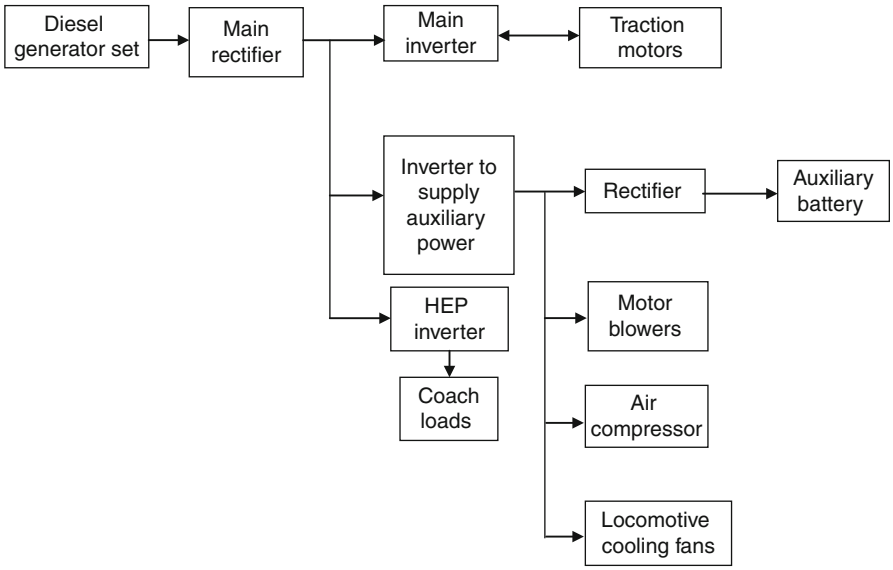

Hybrid Electric and Hydraulic Technology Applications in Off-Road Vehicles. Figure 12
System-level architecture of a diesel electric locomotive

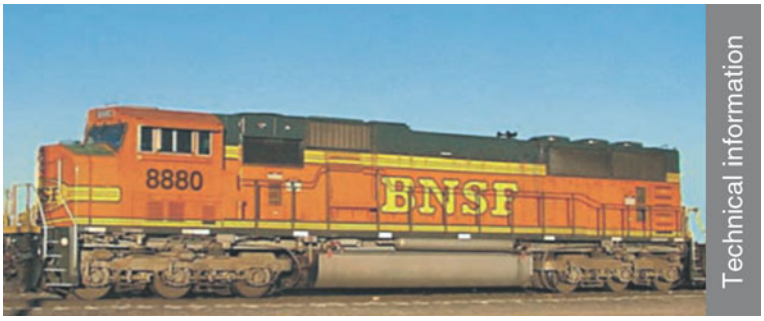

Hybrid Electric and Hydraulic Technology Applications in Off-Road Vehicles. Figure 13
A large diesel electric locomotive (Courtesy: Siemens Technical Information Brochure http://www.siemens.cz/extra/msv/cd/TS/Vozidla/Diesel-Electric_Loco_SD70MAC_EN.pdf, contact.mobility@siemens.com [7])

at the most optimal speed and drives the generator to produce electricity, which is used to run a traction motor mechanically connected to run the wheels as shown in Fig. 9. With the advent of power electronics, this system is rather easy to realize, using reliable and efficient traction motors, which can be induction or synchronous motor – either permanent magnet or field-excited types. With this background, let us look at the architecture of the diesel electric system shown in Fig. 12.

In general, the traction motors are placed on each axle of the locomotive to drive the wheel pairs. These traction motors used in heavy locomotives are AC induction motors. The squirrel cage induction motors are a very reliable device for such applications, due to their robust designs and structures and resilient to temperature conditions, unlike permanent motors.

A picture of a diesel electric locomotive is shown in Fig. 13 [7].

Its diesel engine is rated at 4,000 HP and power at wheels is 3,350 HP. Six motors are used in this engine, with one per axle. The motors are four-pole squirrel cage three-phase induction motors, with a maximum voltage of 2,030 V and 433 kW continuous power rating. The net motor power rating is 2,598 kW, or about 3,500 HP. The maximum speed of the motor is 3,220 rpm, and there is a gear ratio of 85:16 between the motor and the wheel. Although specific power density of induction motors can be somewhat lower than permanent magnet motors, in locomotive applications, where the system package size may not be an important consideration (as in small passenger cars), this may be an ideal choice. As shown in block diagrams, in general, no traction system batteries are presently used in locomotive applications. To start the diesel engine, either electric, hydraulic, or pneumatic starting mechanism can be used. In case of electrical start, a small starter battery is needed.

Recent advances in technology, for capturing regenerative energy, involve some storage battery, ultracapacitor, or a combination of both. Even a flywheel storage unit, can be considered for regeneration. Regeneration can help improve fuel economy and is of more importance for short haul trains and may not be as important for a long haul train.

The architecture of a locomotive system capable of regeneration is shown in Fig. 14. The system is essentially the same in principle as the one in Fig. 12, except that it has a propulsion battery and/or ultracapacitor, which can provide energy to the propulsion motor.

Hybrid Hydraulic Vehicles

Nonelectric hybrid vehicles, specifically *hybrid hydraulic vehicles* (HHV), are being considered by the technical community as viable and can sometimes be more beneficial than an electric hybrid vehicle.

Energy Storage

As compared to electric energy storage system, for example, battery in HEV, in a hydraulic system the

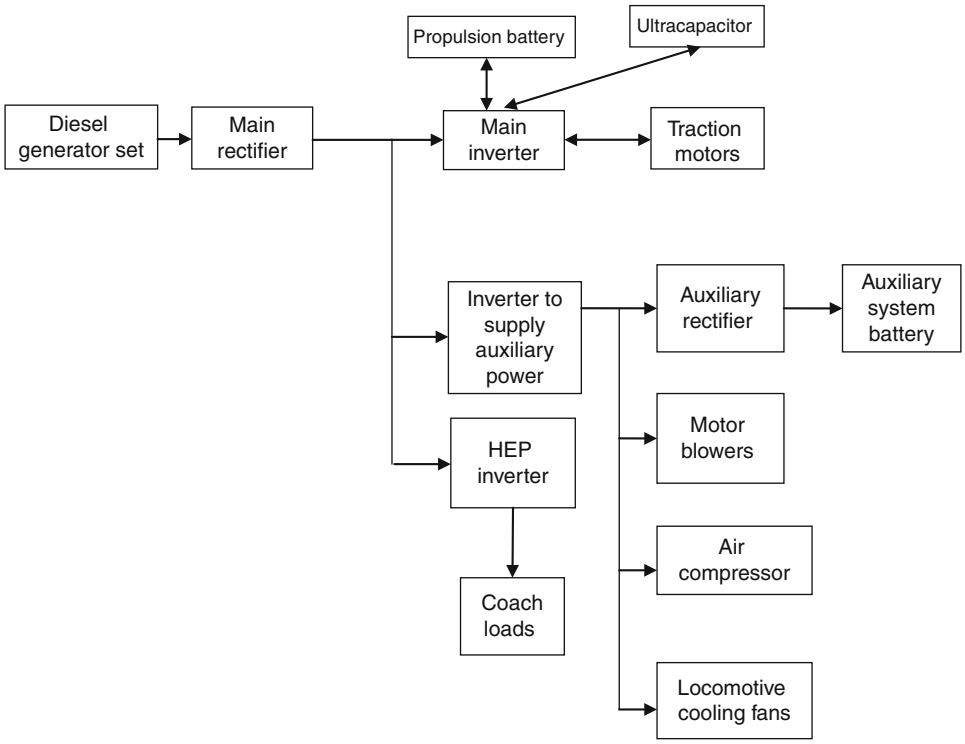

Hybrid Electric and Hydraulic Technology Applications in Off-Road Vehicles. Figure 14
System-level architecture of a diesel electric locomotive including the usage of ultracapacitor

energy is stored in the form of compressed gas in a cylinder. To pressurize a gas, one needs power and energy, which comes from the IC engine to activate the hydraulic pump. While extracting the energy one can use a hydraulic motor. In other words, the hydraulic pump is analogous to an electrical generator, since the latter converts mechanical power into electrical, whereas hydraulic pump converts mechanical power into fluid power. Similarly, hydraulic motor is analogous to an electric motor, and the pressurized gas in the cylinder is analogous to a battery. The efficiency of the hydraulic pump, motor, and storage is around 90%.

To illustrate the hydraulic hybrid system, one can compare Figs. 15 and 16.

For the hybrid hydraulic vehicle architecture shown above, the correspondence with its electrical system counterpart is shown in Table 1.

Figure 17 shows a full series hybrid hydraulic power train configuration [8], which corresponds with the system-level diagram shown in Fig. 16. This includes a high-pressure (HP) accumulator (Appendix 2) containing benign gas such as nitrogen, which can be compressed or expanded by means of incompressible hydraulic fluid acting through some piston type of

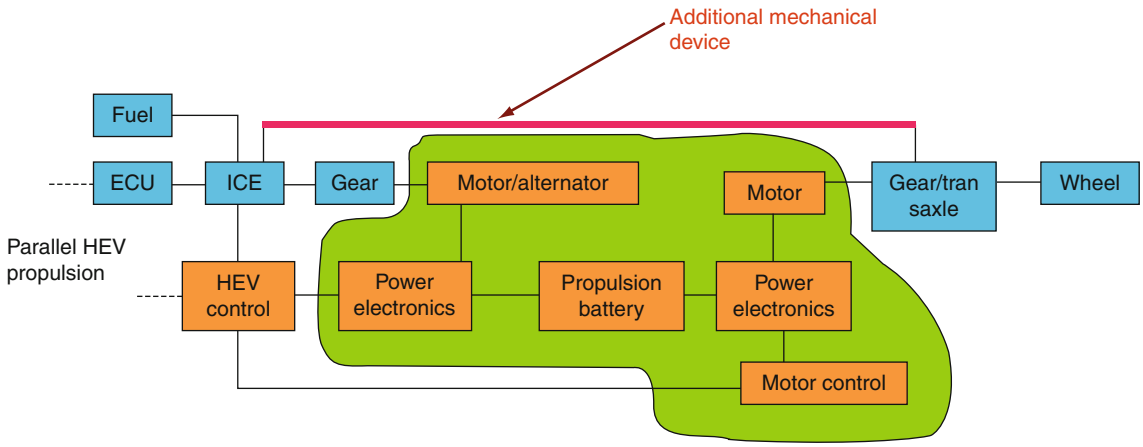

Hybrid Electric and Hydraulic Technology Applications in Off-Road Vehicles. Figure 15
System-level diagram of HEV

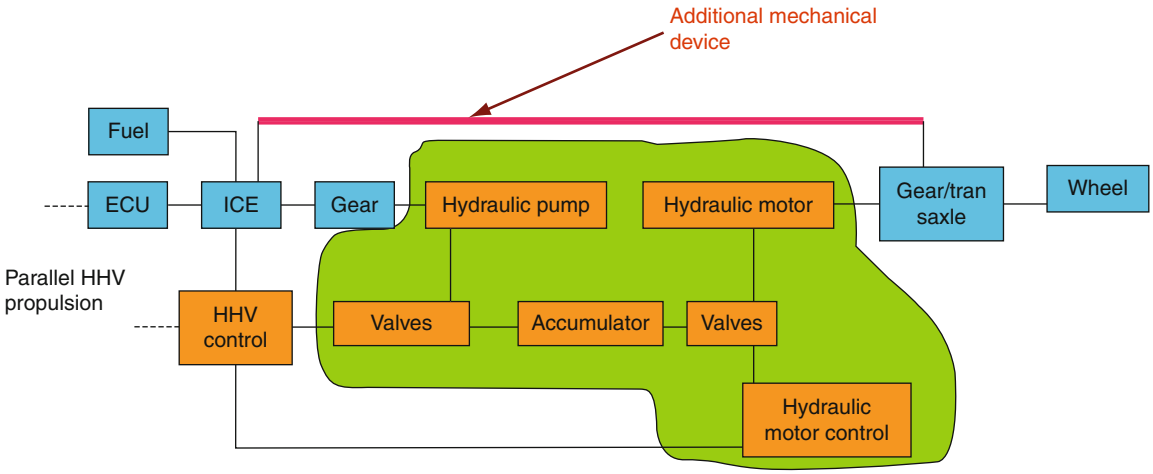

Hybrid Electric and Hydraulic Technology Applications in Off-Road Vehicles. Figure 16
System-level diagram of HHV

mechanism. The pressure in HP cylinder and the pipeline can be as high as 3,000–5,000 psi, whereas the low-pressure cylinder and the corresponding pipeline containing incompressible fluid can be of the order of a few hundred psi. The IC engine drives a pump, which converts the pressure from low to high as the fluid is moved from LP to HP cylinder. To drive the vehicle wheels, the high-pressure gas from the HP cylinder may be allowed to expand and the hydraulic fluid is moved through the motor drive assembly. The hydraulic motor takes the high-pressure fluid in its input port, and converts it to mechanical power at the wheels. When the fluid has passed through the hydraulic motor, its pressure drops and the low-pressure fluid is transferred to the LP cylinder.

The amount of energy stored in the hydraulic accumulator system is quite low in terms of kW-h/kg. As a comparison, the specific energy density in hydraulic accumulator can be of the order of 1.9 w-h/kg [Ref EPA], whereas a battery can have specific energy density of 30 w-h/kg. However, the specific power density of hydraulic system can be of the order of 2,500 W/kg, whereas the electrical system–specific power density (e.g., a battery) can be about 650 W/kg. Therefore, the hydraulic hybrid system can be more suitable for high-power and relatively low-energy applications, particularly where short bursts of high-power acceleration and deceleration are involved.

It is evident from the earlier discussions that an IC engine can run at optimum efficiency to drive the hybrid hydraulic system to deliver the energy to the wheels. A few scenarios can take place here. If the energy needed by the vehicle propulsion matches the energy from the IC engine, the power generated will be used effectively in propulsion. However, if the energy coming from the IC engine is greater than the propulsion load, the excess energy will go to the accumulator for storage. The energy stored in the hydraulic accumulator is rather low, hence this option cannot continue too long, since excessive gas pressure in the accumulator will then be needed, which can be difficult

Hybrid Electric and Hydraulic Technology Applications in Off-Road Vehicles. Table 1 Equivalence of major components between hybrid electric and hybrid hydraulic vehicular systems

Electrical system component	Hydraulic system component
Alternator	Hydraulic pump
Electric motor	Hydraulic motor
Battery	Hydraulic accumulator
HEV controller	Hybrid hydraulic vehicle (HHV) controller
Power electronic system	Hydraulic valve system

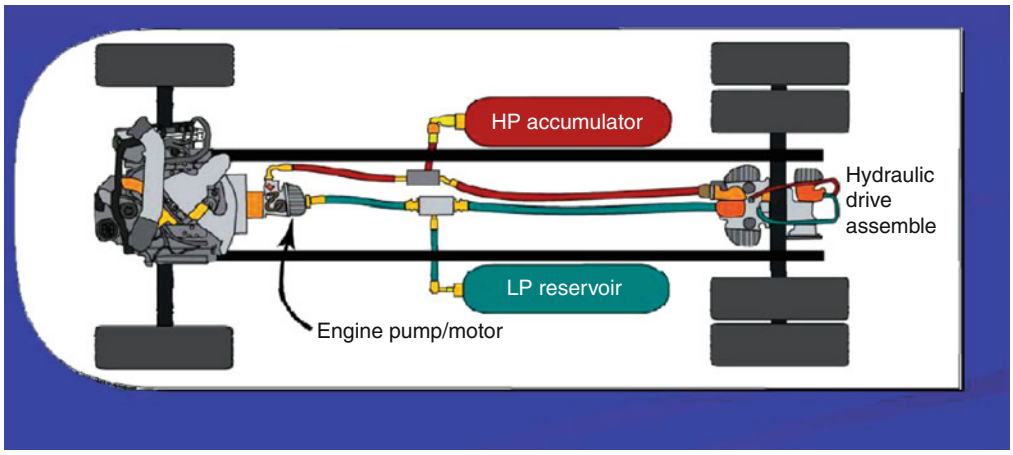

Hybrid Electric and Hydraulic Technology Applications in Off-Road Vehicles. Figure 17 Series HHV system architecture (Courtesy: EPA Kargul, J.J. "Hydraulic hybrids – demonstration for port yard hostlers," in EPA presentation, www.epa.gov/otaq/technology, July 11, 2007 [8])

to sustain. If the HP accumulator cannot store any additional energy, then it will be necessary to change the engine operating point, so as to match the propulsion needs. Alternatively, it may be possible to stop the engine for a short while and use the energy from the hydraulic accumulator, and then start the engine again. As long as the average energy consumption by the motor is same as the average energy delivered by the engine, the process is sustainable, with transients absorbed by the accumulator. If there is no energy storage accumulator in the system, then in principle it is possible to keep the engine running at an optimal speed-torque point. In that case it will be necessary to switch the hydraulic valves on and off in a way such that the average fluid flow corresponds to the average power and energy used by the hydraulic motor. By following this process, it may not be necessary to perform any stop-and-go operation by the engine. But this will lead to a pulsating torque at the motor shaft output, whose average value will correspond to the average load demand.

One of the major advantages of using hydraulic system for propulsion is the fact that it can eliminate the need for a massive conventional transmission system. Also, hydraulic fluid can be more easily moved from one point to another without the need for an elaborate transmission gearbox etc. However, this concept of transmission can be used in a regular nonhybrid vehicle as well, where only the transmission system could be hydraulic. But as described in the previous paragraph, to be able to drive an IC engine at its most optimum point and at the same time eliminate torque-speed pulsations at the load will need some sort of storage, which can be an accumulator. Without a storage, it is, in principle, possible to realize the optimum operating point of the engine by switching the valves on and off to match the average load demand, but the output torque-speed at the load will then be pulsating, which can be smoothed by using a flywheel etc.

Regenerative Braking in Hybrid Hydraulic Vehicles

Hybrid hydraulic vehicles offer the benefit of regeneration and the ability to capture the regenerative energy (which would have been otherwise wasted) during slowing down due to braking and later use it to accelerate again. The hydraulic system–specific energy density or W-h/kg is relatively low compared to a battery. However, hydraulic system can be quite adequate for storing the regenerated energy during braking, since power is high but energy involved is typically low in this situation. Figure 18 shows the regeneration process [8].

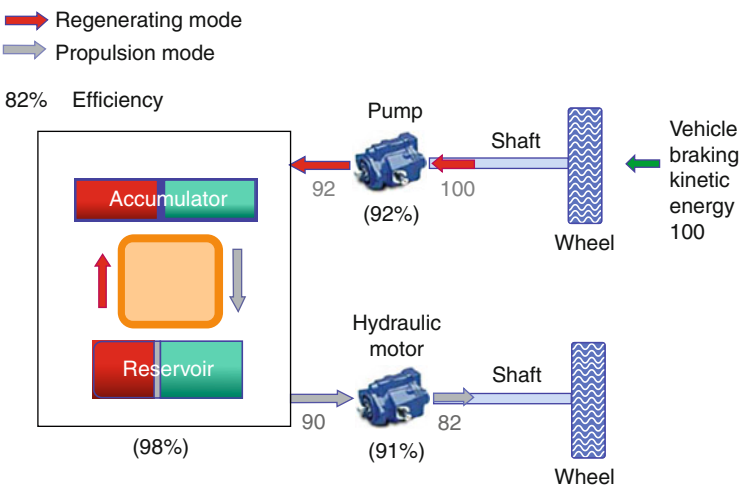

Hybrid Electric and Hydraulic Technology Applications in Off-Road Vehicles. Figure 18
Regenerative braking efficiency in HHV (Courtesy: EPA US EPA, "Clean Automotive Technology. . . Innovation that Works," in www.epa.gov/otaq/technology World's First Full Hydraulic Hybrid SUV, Presented at 2004 SAE World Congress [8])

In Fig. 18, the given efficiency of both the hydraulic pump and the motor are little over 90%. The efficiency of the accumulator (HP and LP together) is about 98%. Hence, the efficiency of the whole regeneration process is 82%.

One advantage of the hybrid hydraulic system is the maturity of the hydraulic system technology. Components used in a hydraulic system, shown in the figure above, have very high efficiency. Figure 19 shows a typical hydraulic motor/pumps (hydraulic pump and hydraulic motor are similar in appearance and their speed-torque characteristics) used in hybrid hydraulic vehicles. This figure shows a bent-axis hydraulic motor, which is from a Bosch-Rexroth specification sheet [9]. For this motor the nominal gas pressure at the entrance can be over 5,000 psi, maximum speed can be 4,500 rpm, and torque @ 5,100 psi can be 371 lb-ft. The length of the unit excluding the geared shaft is about 5.15 in.

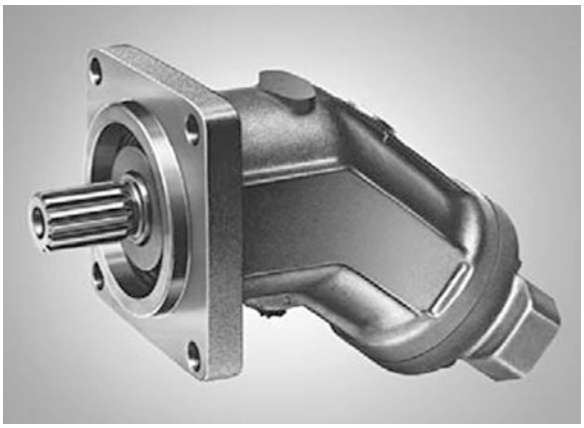

Hybrid Electric and Hydraulic Technology Applications in Off-Road Vehicles. Figure 19
Bent-axis hydraulic pump/motor (Bosch-Rexroth) (Courtesy: Bosch-Rexroth Rexroth – Bosch Group, "Axial Piston Fixed Displacment Motor AA2FM (A2FM)," in Product brochure from Bosch. https://www.boschrexroth.com/various/utilities/contact/index.jsp?cont_country=5&oid=3901 [9])

Future Directions

All people (technical, management, and nontechnical alike) involved with Advanced Heavy Hybrid Propulsion Systems need to work on developing and validating cost-effective, advanced next-generation heavy hybrid components and systems, which at the vehicle level could enable a power train efficiency increase as high as 100% relative to today's conventional power train technology. It is important to focus on the development and improvement of various interdisciplinary technologies, systems, and tools, such as:

- *Improved diesel engine concepts:* Advanced and novel concepts in the areas of hybrid diesel engines, fuel-injection systems, combustion- and emission-

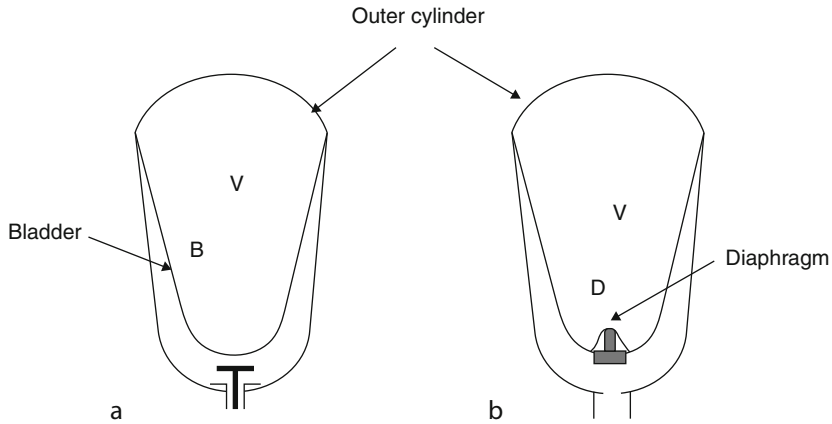

Hybrid Electric and Hydraulic Technology Applications in Off-Road Vehicles. Figure 20
(**a**) Bladder accumulator (**b**) Diaphragm accumulator

control technologies, lightweight materials, particularly for diesel engine structure, to withstand high pressure, and other novel hybrid diesel engine concepts with the potential of increased fuel efficiency and reduced emissions.

- *Low-cost, lightweight, high temperature withstandable power electronics:* Heavy hybrid vehicles will require low-cost, lightweight, simpler power electronic systems that can be easily integrated into off-road vehicular system architectures. It will also call for power electronics that can withstand very high temperature environment.
- *Energy conversion for auxiliary power and energy storage technologies and systems*: Although auxiliary systems are not used for propulsion, newer vehicles have significant amount of nonpropulsion power demand. Hence, new technologies and concepts in areas like integrated thermoelectric systems, photovoltaic, and even wind energy type of technologies are important.
- *Energy storage technology*: Battery, ultracapacitor, and flywheels need significant development to support heavy vehicle hybridization.
- *Advanced transmission and power train components and systems*: Better continuously variable transmissions (CVTs) technology and their integration into heavy hybrid applications are of importance, which can help the hybridization process.
- *Advanced materials for hybrid power trains and vehicle systems*: High-temperature materials, composites, and various polymer materials that lead to enhanced energy use and management, and reduced component and system weight and volume.
- *Rare-earth free materials*: One important area that needs to be attended to is the development of electric motor and machines technology, particularly those involving permanent magnet machines, without using rare-earth materials. This can help reduce the use of strategic elements, and also can help achieving high temperature withstanding ability by these electromechanical devices. In fact, rare-earth free materials are important for some advanced battery systems, hence this area will help with battery technology.

Appendix

Appendix 1: Specifications of Komatsu Mining Truck

Information given below is taken from the Komatsu data sheet [3]. Although exact details on the systems are normally proprietary information of the manufacturers, some commonality can be noticed between these systems and some reasonable idea about the sizes of the components can be obtained, based on the information in these publicly available specification sheets.

AC current	
Alternator	GTA-39
Dual impeller in-line blower	453 m^3/min 16,000 cfm
Control	AC Torque Control System
Motorized wheels	GDY106 AC Induction Traction Motors
Ratio	32.62:1
Speed (maximum)	64.5 km/h 40 mph

Appendix 2: Accumulators

Accumulators basically consist of cylinders which have valves to let the gas in or out with appropriate safety mechanisms. Other types of accumulators are the bladder or diaphragm types as shown in Fig. 20a, b. Bladder-type accumulator consists of a flexible bladder submerged in an incompressible fluid. Inside the bladder there is a gas, which can be pressurized to compress or depressurized to expand. There are several working mechanisms for the accumulators, for example, in the hydropneumatic scheme the liquid pushes a piston, which then pushes a gas stored in the cylinder and compresses it, whereby energy is stored. Piston separates the liquid from the gas.

In the diaphragm accumulator a diaphragm B is pushed by some liquid from the bottom, which then changes the volume of the gas in the upper part of B, that is, between the diaphragm and the cylinder itself. In a bladder accumulator, the bladder B contains the gas which can be compressed. When the liquid enters the cylinder from the bottom, the bladder can expand

or contract, thus energy can be stored in the gas when compressed and taken out from the gas when expanded. The energy is transferred through the fluid itself.

Bibliography

1. Ucarol H, Kaypmaz A, Tuncay RN, Tur O (2005) A performance comparison study among conventional, series hybrid and parallel hybrid vehicles. web article. http://www.emo.org.tr/ekler/c792a8279211dec_ek.pdf
2. Caterpillar. http://catsays.blogspot.com/2005/01/caterpillar-797b-mining-truck.html
3. Komatsu product brochure. http://www.komatsuamerica.com/default.aspx?p=equipment&f1=view&prdt_id=947
4. Wikimedia http://commons.wikimedia.org/wiki/File:Liebherr_T282.jpg (also see Liebherr product brochure, http://www.liebherr.com/ME/en-GB/products_me.wfw/id-14270-0
5. Komatsu product brochure. http://www.komatsu.com/CompanyInfo/press/2008051315113604588.html
6. Brown GN, Ebacher BJ, Koellner WG, Increased productivity with AC drives for mining excavators und haul trucks. http://info.industry.siemens.com/data/presse/docs/2050e.pdf
7. http://www.siemens.cz/extra/msv/cd/TS/Vozidla/Diesel-Electric_Loco_SD70MAC_EN.pdf
8. Kargul JJ (2007) Hydraulic hybrids – demonstration for port yard hostlers, in EPA presentation. www.epa.gov/otaq/technology, Accessed 11 July 2007
9. Bosch Rexroth product brochure, Bent axis hydraulic motor, Rexroth – Bosch Group, Axial Piston Fixed Displacement Motor AA2FM (A2FM), Bosch. https://www.boschrexroth.com/various/utilities/contact/index.jsp?cont_country=5&oid=3901
10. Olaer product brochure, Diaphragm and bladder accumulators, Olaer Inc., "Bladder and diaphragm accumulator product brochure, including High-pressure diaphragm accumulator conforming to EC regulations", ELM Series. http://www.olaer.fr/en/recherche.php?idr=13, http://www.olaer.fr/en/recherche.php?idr=11
11. http://gas2.org/2009/09/18/caterpillar-builds-worlds-first-hybrid-bulldozer/
12. http://www.cleanmpg.com/forums/showthread.php?t=33855
13. Kwak S, Kim T, Park G (2010) Phase-redundant-based reliable direct AC/AC converter drive for series hybrid off-highway heavy electric vehicles. IEEE Trans Veh Technol 59(6):2674–2688
14. http://commons.wikimedia.org/wiki/File:14_stryker.jpg (Stryker)
15. http://commons.wikimedia.org/wiki/File:HEMTT.jpg (HEMTT)
16. http://commons.wikimedia.org/wiki/File:Two_M-3_Bradleys.jpg (Bradley)
17. http://commons.wikimedia.org/wiki/File:M1A1_Abrams_Tank_in_Camp_Fallujah.JPEG (Abrams)
18. http://commons.wikimedia.org/wiki/File:BundeswehrFennek.jpg (Fennek - European)
19. http://commons.wikimedia.org/wiki/File:FBI_Mine_Resistant_Ambush_vehicle.jpg (MRAP)
20. http://commons.wikimedia.org/wiki/File:Gladiator_RSTA.jpg (Gladiator)

Hybrid Energy Storage Systems for Vehicle Applications

Mehrdad Ehsani
Department of Electrical & Computer Engineering, Texas A&M University, College Station, TX, USA

H

Article Outline

Glossary
Definition of the Subject
Introduction
Electric Load Characteristics
Candidates of Vehicle Energy Storage
Hybrid Energy Storage
Battery/Ultracapacitor System
Flywheel/Ultracapacitor System
Future Directions
Bibliography

Glossary

Electric load A device or system connected to the electrical power circuit for the purpose of demanding power.

Energy storage A device or system capable of storing energy in one of many physical forms.

Hybrid A combination of two or more items sharing a common function.

Hybrid energy storage A combination of two or more energy storage devices with complimentary capabilities.

Non-traction load Power demand for all purposes other than traction.

Traction load Power demand for the purpose of propelling the vehicle.

Definition of the Subject

The electric load of a vehicle can be decomposed into two components – static and dynamic load. The static component is slowly varying power with limited

magnitude, whereas the dynamic load is fast varying power with large magnitude. The energy storage system, accordingly, comprises of two basic elements. One is energy source to support the static load and other is a power source to support the dynamic load. A smart combination of the available energy storages, which have different characteristics, may result in a high-performance energy storage system.

Introduction

It is widely agreed that vehicle electrification will lead to revolutionary improvements on vehicle performance, energy resource conservation, and pollution emissions. High-quality energy storage system is one of the most crucial components. Unfortunately, the currently available chemical, electrical, and mechanical energy storage systems, including various kinds of chemical batteries, ultracapacitors, and flywheels, cannot meet these requirements alone. In this entry, the possibility of composing a high-energy, high-power hybrid energy storage system is presented based on the analysis of inherent characteristics of different energy storage methods. The basic components in this system are chemical batteries, ultracapacitors, and flywheels (mechanical batteries). The objective is to fully utilize the advantages and suppress the disadvantages of each component to compose a compact energy storage system with high energy capacity and high power capability [3, 4, 6, 10].

Electric Load Characteristics

The electric load in a hybrid vehicle comprises of traction load and non-traction load. Regarding traction load, the energy storage is only responsible to supply a intermittent peak power which may be from a few seconds, such as in hard acceleration, steep hill climbing, obstacle negotiation, etc., to several minutes, such as in cross-country operation, medium hill climbing, etc. The vehicle in the former operation needs the energy storage to supply peak power in a few seconds with high magnitude, whereas in the latter situation, the vehicle needs the energy storage device to supply power in several minutes with medium magnitude. In normal road operation, the primary power source (engine or fuel cell) should be able to produce sufficient power to support the vehicle operation and, at the same time, produce additional power to charge the energy storage device to recoup its past discharge [7].

Similar to the traction motor load, the non-traction electric load can also be characterized by continuous power demand and intermittent peak power demand. Non-traction electric load is the total of electric loads that are used to serve the vehicle operation and auxiliaries. For a conventional vehicle, the non-traction electric loads consist of continuous loads, prolonged loads, and intermittent loads. The continuous loads, includes engine ignition, fuel injection, instrument panel, fuel pump, etc. These may need around 200 W. The prolonged loads, mainly including all the lights, may need about 260 W. Intermittent loads, mainly including, heater, front and rear wipers, brake light, electric windows, radiator cooling fan, heater blower motor, rear fog light, electric seat movement, electric mirror, etc., may need a total power of 1,700 W. The total of the non-traction electric peak power could reach about 2,140 W. However, the average is about 610 W. It is certain that more non-traction electric loads will be added in near future vehicles. They may include direct electrically driven power steering, direct electrically driven air conditioning, direct electrically engine cooling pump, electrically actuated braking, electrically driven active suspension, electrically driven engine valve actuator, etc. The total peaking power for the future electric loads may reach 20–25 kW while the average power may be only about 5 kW, one fourth or one fifth of the peak power [10].

The average of the electric loads needs the energy storage device to possess sufficient energy to support the vehicle's long-time operation, and the peak of the electric loads needs the energy storage device to be capable of delivering sufficient power in a short time period (usually less than 1 min).

Candidates of Vehicle Energy Storage

As mentioned above, the basic requirement for vehicle energy storage device is to have sufficient energy and also be able to deliver high power for a short time period. With the present technology, chemical

batteries, ultracapacitors, and flywheel system (mechanical battery) are the main candidates for the vehicle energy storage device.

Chemical Batteries

The chemical battery is an energy storage device that stores energy in the chemical form and exchanges its energy with outside devices in electric form. Basically, a cell of battery has one positive electrode, which accepted electrons, one negative electrode, which gives out electrons and an electrolyte, which conducts ions and isolates electrons between the electrodes. The battery operation (discharging and charging) follows principles of electrochemistry and thermodynamics [2, 6, 9, 13].

Theoretical Specific Energy of Chemical Batteries

The amount of energy stored in a battery is completely determined by the amount of active reactants inside the battery, or more precisely, the free energy, ΔG, of the chemical reaction. The commonly used terms to measure the energy capacity of a battery are Watt-hours per kilogram (Wh/kg) called specific energy capacity and Watt-hours per liter (Wh/L) called energy density. The theoretical specific energy (maximum available) can be expressed as

$$E_{\text{specific}} = \frac{-\Delta G}{3.6 \sum M_i} \quad (\text{Wh/kg}), \tag{1}$$

where ΔG is the free energy of the reaction in a battery cell and ΣM_i is the sum of the molecular weight of the individual species involved in the battery reaction. The free energy, ΔG of a reaction is closely associated with the number of electrons transferred in the reaction and the electric potential (voltage), V_r, by

$$\Delta G = -n\ F\ V_r, \tag{2}$$

where n is the number of electrons transferred in the reaction and F is the Faraday constant, 96,495 ampere-seconds per gram-equivalent. Thus, the specific energy can be written as

$$E_{\text{specific}} = \frac{V_r\ F\ n}{3.6 \sum M_i} \quad (\text{Wh/kg}). \tag{3}$$

From theoretical electrochemistry and thermodynamics, the reaction potential of a battery cell can be described by

$$V_r = V_r^0 - \frac{RT}{nF} \ln \left[\frac{\Pi(\text{activities of products}}{\Pi(\text{activities of reactants}} \right], \tag{4}$$

where V_r^0 is a standard voltage at standard conditions when the battery is fully charged, R is gas constant, 8314 $J/^\circ K.\ mole$ and T is absolute temperature. The value in square brackets is nearly unity when the battery is charged, increasing with the process of battery discharging. When the reaction reaches equilibrium, V_r becomes zero, and the battery is fully discharged.

Practical Specific Energy of Chemical Batteries

Generally, practical batteries have much lower specific energies than their theoretical values. Figure 1 shows an example of the weight distribution of the components

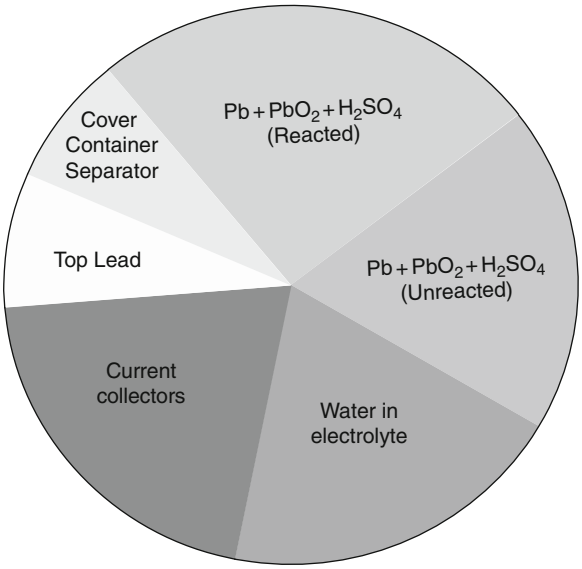

Hybrid Energy Storage Systems for Vehicle Applications. Figure 1
Weight distribution of the components of a lead-acid EV battery with a specific energy of 45 Wh/kg at the C_5/5 rate [13]

of a lead-acid EV battery with a specific energy of 45 Wh/kg at the $C_5/5$ rate. In this example, only about 25% of the total weight of the battery is useful, that is, the practical specific energy is only about 25% of the theoretical one. Table 1 shows the data for some existing batteries.

Specific Power of Chemical Batteries

Specific power is the maximum power, per unit battery weight, that the battery can produce in a short period. The specific power of a chemical battery depends mostly on the battery internal resistance. With the battery model as shown in Fig. 2, the maximum power that the battery can supply to the load is

$$P_{\text{peak}} = \frac{V_0^2}{4(R_c + R_{\text{int}})}, \tag{5}$$

where R_c is the conductor resistance (Ohmic resistance) and R_{int} is the internal resistance caused by chemical reaction.

Internal resistance R_{int} represents the voltage drop, ΔV, which is associated with the battery current. The voltage drop ΔV, termed overpotential in battery terminology, includes two components: one is caused by reaction activity ΔV_A and the other caused by electrolyte concentration ΔV_C. General expressions of ΔV_A and ΔV_C are

$$\Delta V_A = a + b \log I \tag{6}$$

Hybrid Energy Storage Systems for Vehicle Applications. Table 1 Status of battery systems for EV

	Specific energy (Wh/kg)	Peak power (W/kg)	Energy effi.(%)	Cycle life	Cost ($/kW.h)
Acidic aqueous solution					
Lead-acid	35–50	150–400	>80	500–1,000	120–150
Alkaline aqueous solution			75	800	250–350
Nickel/cadmium	40–60	80–150	65	1,500–2,000	200–400
Nickel/iron	50–60	80–150	70	300	100–300
Nickel/zinc	55–75	170–260	70	750–1,200+	200–350
Ni-metal-hydride	70–90	200–300	<50	?	?
Aluminum/air	200–300	90	60	500+	50
Iron/air	80–120	90	60	600+	90–120
Zinc/air	100–200	30–80			
Flow					
Zinc/bromine	70–85	90–110	65–75	500–2,000	200–250
Vanadium redox	20–30	110	75–85	-	400–450
Molten salt					
Sodium/Sulfur	150–240	230	85	800+	250–450
Sodium/Ni/Cl	90–120	130–160	80	1,200+	230–345
Li-ion-sulfur (FeS)	100–130	150–250	80	1,000+	110
Organic/lithium					
Lithium-ion	80–130	200–300	>95	1,000+	200
Li-ion high power[a]	85–95	~4,000	–	–	–
Li-ion high energy[a]	135–150	~600	–	–	–

[a]Reported by SAFT [14]

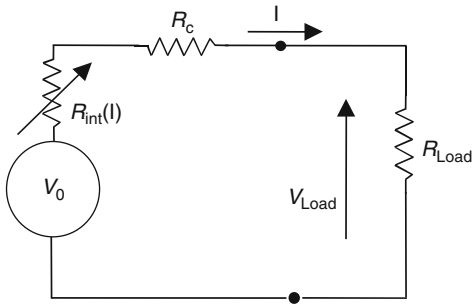

Hybrid Energy Storage Systems for Vehicle Applications. Figure 2
Battery circuit model

and

$$\Delta V_C = -\frac{RT}{nF}\ln\left(1 - \frac{I}{I_L}\right), \tag{7}$$

where a and b are constants, R is gas constant, 8314 $J/°K.\ mole$, T is the absolute temperature, n is the number of electrons transferred in the reaction, F is the Faraday constant, 96,495 ampere-seconds per gram-equivalent, and I_L is the limit current. Accurate determination of battery resistance by analysis is difficult. Specific powers are usually obtained by measurement.

Table 1 shows the status of battery systems potentially available for EV [13]. It can be seen that although specific energies are high in advanced batteries, the specific powers show no significant improvement. About 300 W/kg might be the optimistic estimate. Recent Li-ion high-power and high-energy batteries have been reported with as high as 4,000 and 150 Wh/kg, respectively. However, their practicality and cost need much improvement.

Energy Loss and Thermal Management

The presence of internal resistance in batteries causes energy loss in the battery discharging and charging process. This dissipated energy causes the battery temperature to rise, shortening the battery life. The energy loss can be expressed as

$$E_{loss} = R_{batt} I^2, \tag{8}$$

where $R_{batt} = R_c + R_{int}$ is the battery internal resistance and I is the battery current. The battery resistance is usually related to the battery temperature and battery state-of-charge. Low temperature usually leads to high battery resistance because of less reaction activities of the reactants. Thermal management is usually needed to maintain the battery in an appropriate temperature range. Discharging at low state-of-charge and charging at high state-of-charge can also lead to high battery resistance because of the nonuniformity in the concentration of the reactants. Thus, the battery should be managed to operate in a middle range of state-of-charge, such as 40–60%. Furthermore, high charging and discharging current should be avoided so that the energy loss in battery can be reduced (refer to Eq. 8), and consequently, the thermal management can be simplified.

Ultracapacitors

The ultracapacitor is another candidate for energy storage in the hybrid vehicle. The ultracapacitor is characterized by high specific power, high efficiency, excellent temperature adaptability, and long service life. However, it suffers from very limited specific energy. The characteristics of a 42-V ultracapacitor pack specifically designed for HEV are listed in Table 2 [11]. Reference [8] has reportedly developed 2700-F ultracapacitors with 2.5 V of cell voltage, 2.55 kW/kg of specific power, and 3.23 Wh/kg of specific energy. It is believed that the unit power cost of the ultracapacitor is lower than that of batteries. However, due to its low specific energy and its high dependence of the state-of-charge on voltage, it is difficult to use ultracapacitors alone as the energy storage on hybrid vehicles. The most promising approach is to hybridize the ultracapacitors with other energy storage devices, such as batteries or flywheels as will be discussed in following sections.

Flywheel

Flywheel is an energy storage device which directly stores mechanical energy in an extra high-speed rotating wheel. Because of the difficulty of using the mechanical energy of the flywheel directly for traction, a high-speed electric machine is usually connected to the flywheel to constitute a system, called "mechanical battery," as shown in Fig. 3. The flywheel can be charged and discharged through the electric machine. The major advantages of flywheel system are their

Hybrid Energy Storage Systems for Vehicle Applications. Table 2 Characteristic data of an ultracapacitor

Rated capacitance (DCC[a], 25°C)	[F]	145
Capacitance tolerance	[%]	±20
Rated voltage	[V]	42
Surge voltage	[V]	50
Max. series resistance, ESR (DCC, 25°C)	[mΩ]	10
Specific power density (42 V)	[W/kg]	2,900
Max. current	[A]	600
Max. stored energy	[J]	128,000
Specific energy density (42 V)	[Wh/kg]	2.3
Max. leakage current (12 h, 25°C)	[mA]	30
Weight	[kg]	15
Volume	[L]	22
Operating temperature	[°C]	−35 to +65
Storage temperature	[°C]	−35 to +65
Life time (25°C)	[y]	10 ΔC <20% of initial value, ESR <200% of initial value
Cyclability (25°C, I = 20 A)		500,000, ΔC <20% of initial value, ESR <200% of initial value

[a]*DCC* discharging at constant current
Source: Ref. [11]

relative high energy capacity and low environmental dependence, especially temperature. However, high speeds require high-strength materials, special design bearings (mostly magnetic bearings), and high vacuum housing to reduce the aerodynamic drag. These requirements may cause technical difficulties in their application to vehicles.

Energy Capacity of Flywheel System

The energy stored in a high-speed flywheel is expressed as

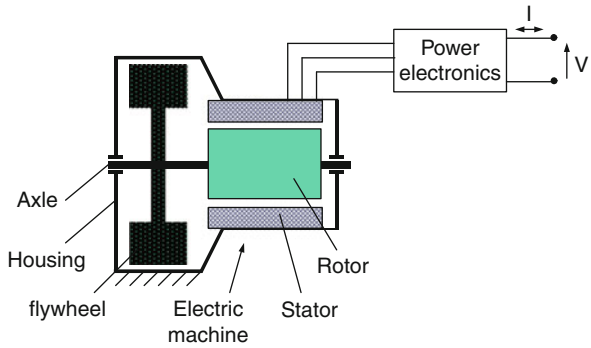

Hybrid Energy Storage Systems for Vehicle Applications. Figure 3
Configuration of a flywheel system (mechanical battery)

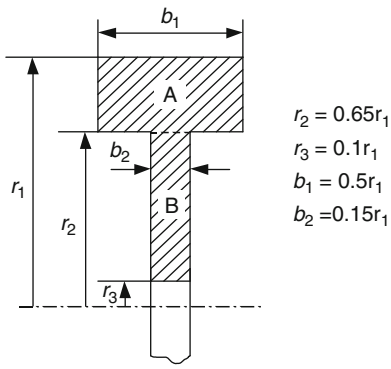

Hybrid Energy Storage Systems for Vehicle Applications. Figure 4
Geometry of a flywheel

$$E_f = \frac{1}{2} J_f \omega_f^2, \tag{9}$$

where J_f is the moment of inertia of the flywheel in kgm^2 and ω_f is the angular velocity of the flywheel in *rad/s*. High energy capacity demands high speed (usually 50,000–60,000 rpm) and high moment of inertia from the flywheel.

The moment of inertia of a flywheel per unit flywheel mass (weight) depends exclusively on its geometric design (refer to Fig. 4), as expressed by

$$\frac{J_f}{M_f} = \frac{1}{2}\left[\frac{b_1(r_1^4 - r_2^4) + b_2(r_2^4 - r_3^4)}{b_1(r_1^2 - r_2^2) + b_2(r_2^2 - r_3^2)}\right]. \tag{10}$$

The effective approach to increase the J_f/M_f is to increase b_1 and r_1. That is, to put as much mass as far

away from its rotating center as possible. This is usually limited by the rotor material strength. So high-strength materials are usually employed in high-speed flywheels. Figure 5 shows the spatial size of a flywheel, which is represented by r_1, versus the moment of inertia of the flywheel per unit mass, using the geometric numbers in Fig. 4.

The theoretical specific energy of a flywheel can be calculated by Eqs. 9 and 10 for the geometrically specified flywheel in Fig. 4. Figure 6 shows the theoret-

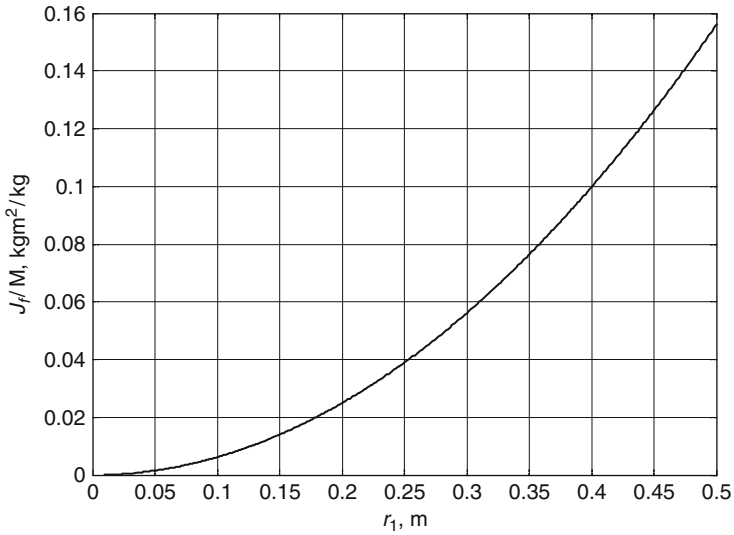

Hybrid Energy Storage Systems for Vehicle Applications. Figure 5
Outer radius of the flywheel versus the moment inertia of the flywheel per unit mass

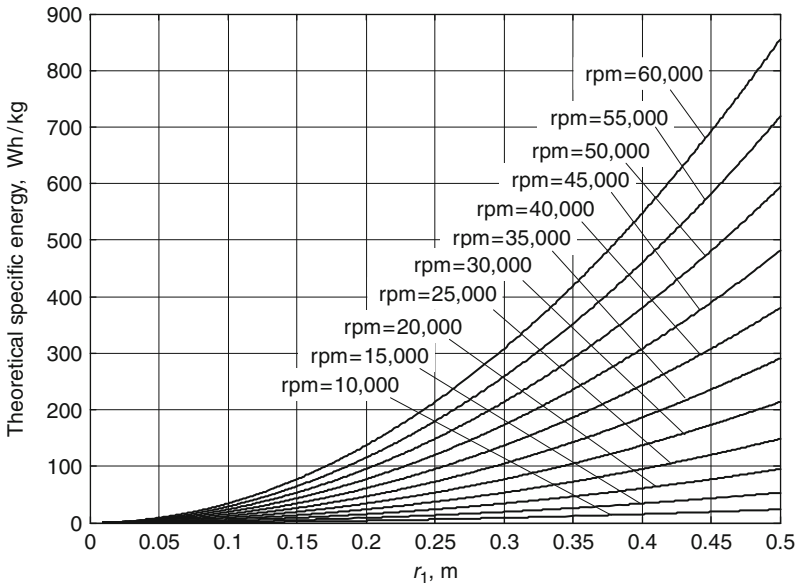

Hybrid Energy Storage Systems for Vehicle Applications. Figure 6
Theoretical specific energy of flywheel versus flywheel geometry size, r_1

ical specific energy of the flywheel versus the flywheel geometric size r_1 and flywheel angular speed. This figure indicates that with increasing flywheel size, r_1, and angular speed, the specific energy can be increased significantly. For a midsize vehicle, r_1 = 035 m and rpm = 50000 may be good estimates. In this case, the theoretical specific energy of flywheel will reach about 300 W/kg.

In practice, the effective mass used to store energy in a flywheel system only takes part of the total system mass. The ineffective masses, such as the housing, the stator of the electric machine, the bearings, etc., and the less effective mass, such as the rotor of the electric machine, may make up to over half of the total system mass. Thus, the practical specific energy of a flywheel system is much lower than its theoretical value and may be in the range of 100–150 Wh/kg, which is in the same range as that of advanced chemical batteries, such as NiMH and lithium batteries, but much high than that of the traditional batteries, such as lead-acid and nickel/cadmium batteries.

Power Capability of Flywheel System

The power of a flywheel system can be expressed as

$$P_f = \frac{dE_f}{dt} = J_f \omega_f \frac{d\omega_f}{dt}, \tag{11}$$

where $T_m = J_f \frac{d\omega_f}{dt}$ is the torque of the electric machine to accelerate (charging) or decelerate the flywheel (discharging). Thus, the power capability of the flywheel system is completely determined by the power capability of its electric machine.

The electric machine used in the flywheel system should be have high speed, high efficiency, light weight, and small volume. Further, in order to simplify the control of the vehicle electric loads, such as traction motors, actuators, etc., the terminal voltage of the flywheel system should be maintained approximately constant in the intended operating speed range of the flywheel. Electric machine theory indicates that varying the machine speed while keeping a constant terminal voltage can be accomplished by controlling its magnetic field. Thus, wide speed operating range with constant voltage requires the machine to have wide "field weakening" capability and a long constant power speed range.

Referring to the motors that are appropriate for electric and hybrid electric vehicles, the induction motor (IM), permanent magnet (PM), brushless dc motor (BLDC), and switched reluctance motor (SRM) seem to be possible candidates for application to the flywheel system. The induction motor is the most mature technology among these motors. Its maximum speed can be extended up 3–4 times of its base speed by using field oriented control technology [1]. The BLDC is well known for its lightweight, small volume, and high efficiency due to its permanent magnet field. However, the extent of its speed range beyond its base speed is very limited due to its limited capability of the field weakening, resulting in a limited constant voltage speed range. The SRM is well known for its simple structure, straightforward control, excellent reliability, high speed, and long maximum speed beyond its base speed. These inherent properties make the SRM an attractive candidate for application to the flywheels system, notwithstanding its relative low torque density, relative to the BLDC. Based on our analysis and development of traction motors for EV and HEV [12], at Texas A&M University, it is believed that the specific power of the overall flywheel system will not be much more than 500 W/kg. This is similar to that of advanced lead-acid batteries and less than that of advanced high-power batteries, such as lithium batteries and ultracapacitors.

Efficiency of Flywheel System

Energy losses in the flywheel system are not mainly mechanical, such as friction and aerodynamic drag, but also electrical losses in its electric machine. With high vacuum inside the housing of the flywheel system and with magnetic bearings, it is believed that mechanical efficiency may reach 98–99%. The electric efficiency mostly depends on the electric motor/generator, whose efficiency may be around 85–90%. Thus, the total efficiency of the flywheel system may be around about 83–87%, which is similar to that of advanced high-efficiency batteries and higher than that of conventional batteries, but much less than that of ultracapacitors.

Hybrid Energy Storage

As discussed above, chemical batteries, ultracapacitors, and flywheels each have their specific operating

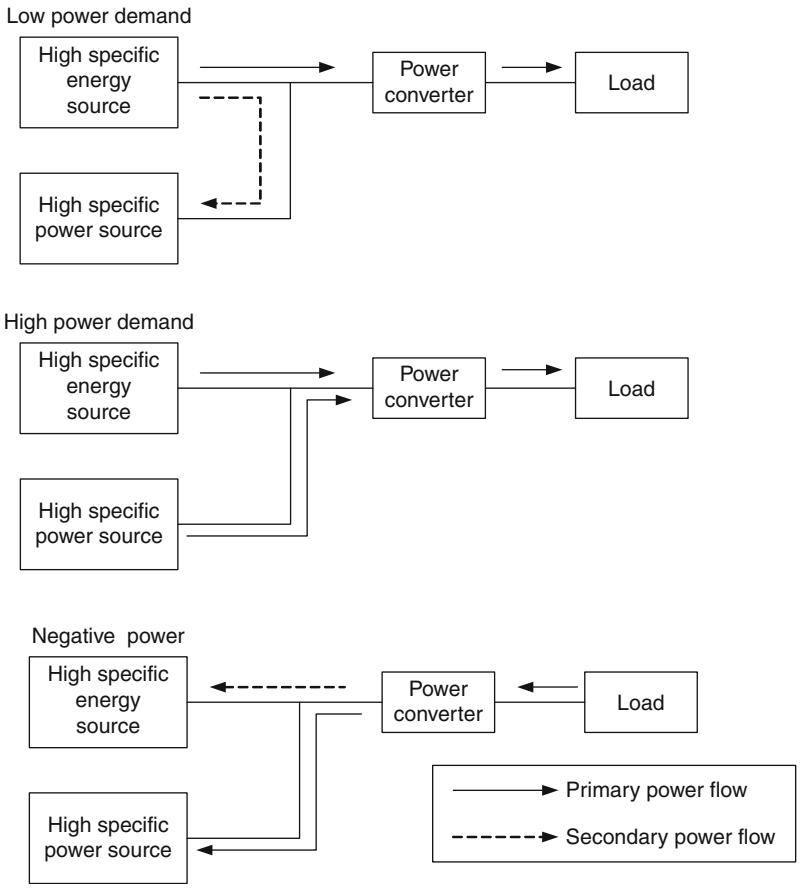

Hybrid Energy Storage Systems for Vehicle Applications. Figure 7
Conceptual operation of the hybrid energy storage

characteristics. The chemical battery and flywheel are more for high energy storage and deliver their energy with medium power for a relatively long period of time. Whereas, the ultracapacitor is more for high-power source and delivers its high power in a relatively short period of time. It is possible, by combining two of these basic energy storage technologies together to constitute a high-energy and high-power storage system. This is the hybrid energy storage system as is conceptually shown in Fig. 7.

Battery/Ultracapacitor System

Passive Interconnection

The most straightforward approach is to directly connect ultracapacitors to batteries as shown in Fig. 8. This configuration has the simplest structure and no control unit. The behavior of the ultracapacitors is more like a current filter. Thus, the high-peak battery currents are leveled, as illustrated in Figs. 9 and 10. In Fig. 9, a step load current is applied to the storage system. First, this step current is in the ultracapacitors and then the load current gradually transfers from the ultracapacitors to the batteries due to the voltage drop in the ultracapacitors. When the load current disappears, the ultracapacitors are charged back up by the batteries automatically. Figure 10 shows the simulation results of the battery current and the ultracapacitor current while a random load current applied.

The leveled battery current, due to the ultracapacitors, can have many benefits for the batteries. These include smaller battery pack, higher battery

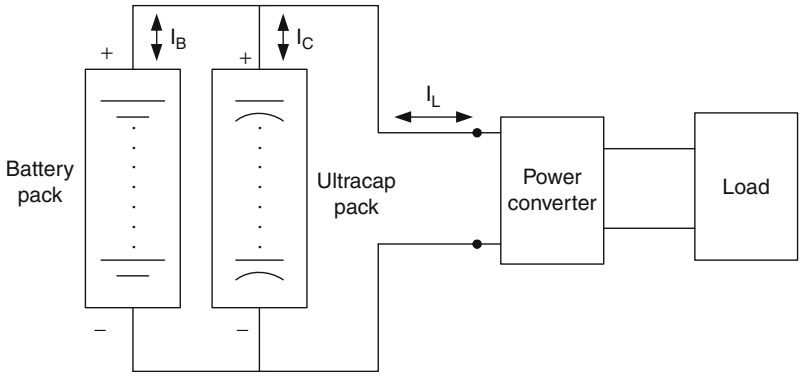

Hybrid Energy Storage Systems for Vehicle Applications. Figure 8
Passively connected batteries/ultracapacitors system

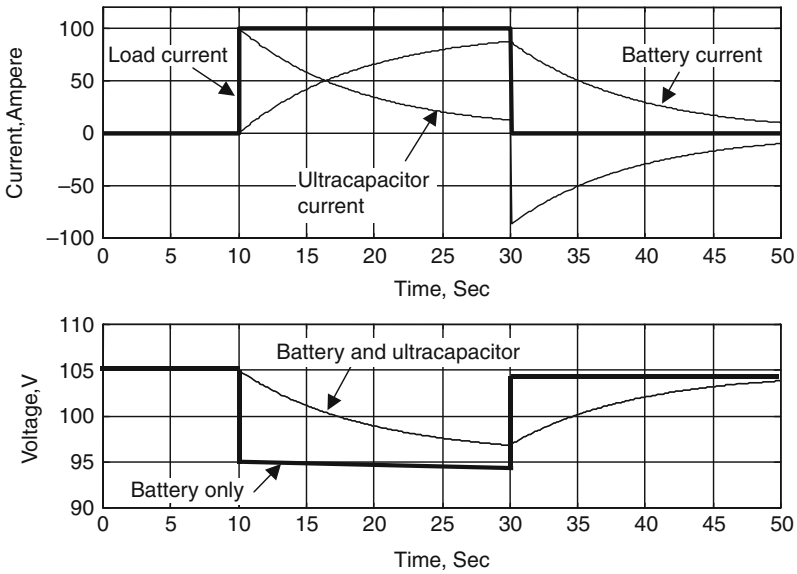

Hybrid Energy Storage Systems for Vehicle Applications. Figure 9
Battery current and ultracapacitor current with a step load current input

operating efficiency, easier battery thermal management, and longer battery life. The limited variation of hybridized battery terminal voltage can also ease the control of the connected load power converter. With proper design of all the components, this simple hybrid structure may yield a high-power, high-energy, and high-efficiency energy storage system.

Active Interconnection

Clearly, in the passively connected battery/ultracapacitor system, the power flow between the battery pack, the ultracapacitor pack, and the load cannot be managed. Consequently, the high power benefits of the ultracapacitors may not be best utilized. Figure 11 shows the concept of an actively controlled battery/ultracapacitor system. In this system, a power electronic regulator is used to manage the power flow between the battery pack, the ultracapacitor pack, and the load.

Basically, the power conditioning operation can be divided into three different modes: (1) ultracapacitor peaking operation for high power demand, (2) ultracapacitor charging from batteries, and (3) battery alone operation. These operation modes are

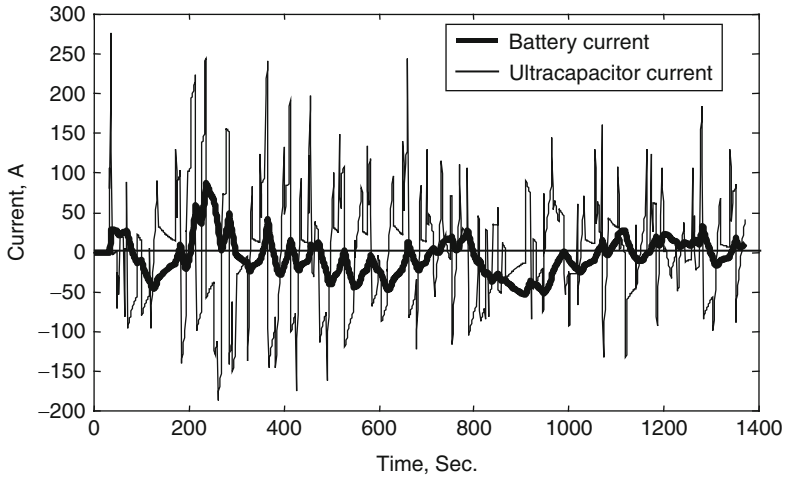

Hybrid Energy Storage Systems for Vehicle Applications. Figure 10
Battery current leveled by passively connected ultracapacitors

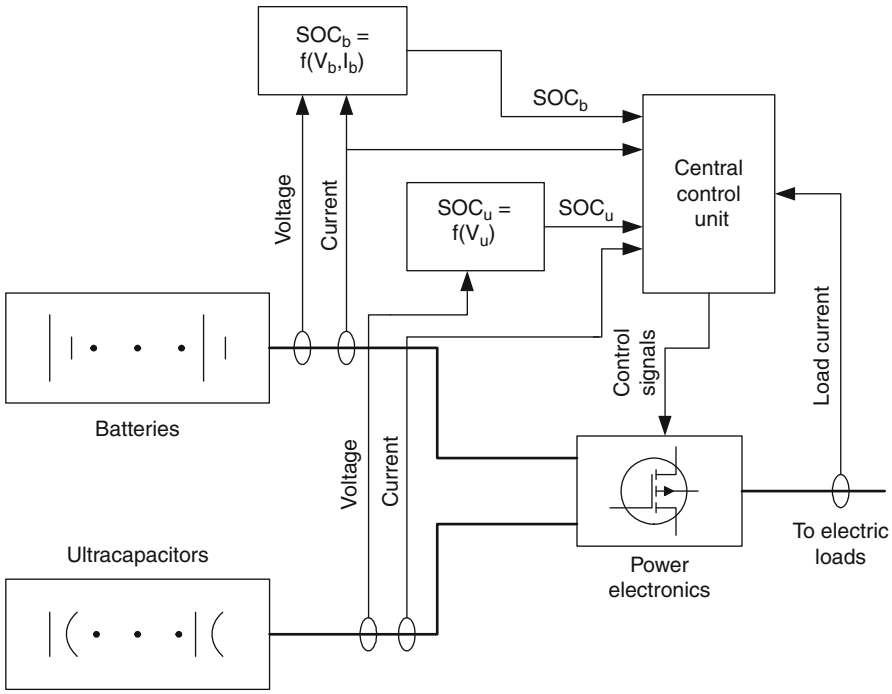

Hybrid Energy Storage Systems for Vehicle Applications. Figure 11
Conceptual illustration of the actively controlled battery/ultracapacitor system

implemented by a central control unit. The central control unit commands the power electronics, according to the control strategy and the received signals from the current and voltages sensors, as shown in Fig. 11. The control objectives are (1) to meet the load power requirement, (2) to keep the battery current in a preset band, and (3) to keep the battery state-of-charge, SOC, in its safe region (e.g., 0.4–0.6), where the battery efficiency are usually optimized.

This system can fully use the high power property of the ultracapacitors, resulting in a smaller battery pack. Further, the actively controlled battery current can lead to more efficient battery operation and easier thermal management.

Flywheel/Ultracapacitor System

As discussed in the flywheel section, the flywheel system, similar to batteries, can be categorized as an energy intensive storage device. This is mainly due to its power capability being constrained by its electric machine. Integration of the high-power ultracapacitors with the high-energy flywheel system may result in a high-power, high-energy and high-efficiency storage system.

As before, the ultracapacitors can be either passively connected to the flywheel system, as shown in Fig. 12, or through an electronic power management unit, as shown in Fig. 13. The passively connected flywheel/ultracapacitor system may be expected to have a performance similar to that of the passively connected battery/ultracapacitor system, as shown in Figs. 9 and 10. The actively controlled flywheel/ultracapacitor system can be expected to have the advantage of a smaller flywheel electric machine, stable operation, and high efficiency.

Compared with battery/ultracapacitor hybrid system, flywheel/ultracapacitor system would have the additional advantage of extended service life, wide temperature tolerance, and lower maintenance. These advantages are very important in vehicle applications.

Future Directions

The vehicle energy storage should be able to supply sufficient energy and power to meet both the steady and dynamic load requirements. Thus, high specific energy and high specific power are necessary to achieve compact vehicle energy storage. Chemical batteries and mechanical flywheels can be categorized as energy sources and ultracapacitors as power sources. By hybridizing these storage devices, a high-energy and high-power-energy storage system may be developed. In the passively connected battery/ultracapacitor hybrid system, the battery peak currents can be significantly moderated. Consequently, the battery efficiency, service life, and thermal management can be significantly improved. In the actively controlled battery/ultracapacitor hybrid system, the power flow between the batteries, ultracapacitor and loads can be actively controlled. Therefore, the operation of the whole system can be better optimized. Flywheel/ultracapacitor hybrid systems, either passively connected or actively controlled, can have the advantages of compact design, high efficiency, extended service life, wide temperature tolerance, and low maintenance requirements. These advantages are very important for advanced vehicles.

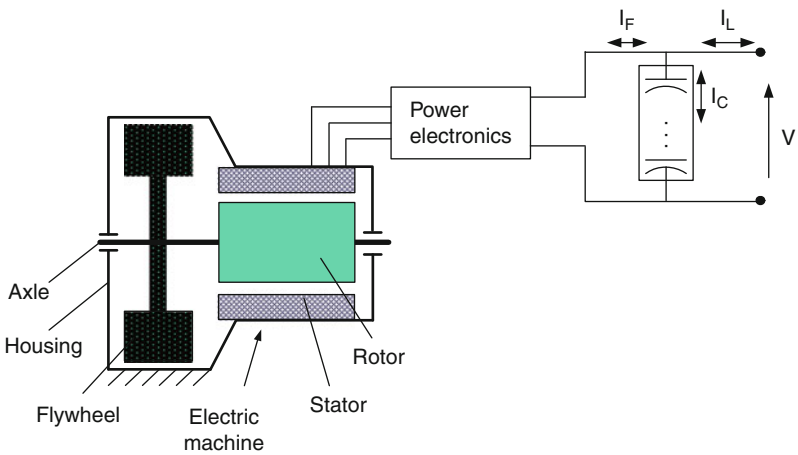

Hybrid Energy Storage Systems for Vehicle Applications. Figure 12
Passively connected flywheel/ultracapacitor system

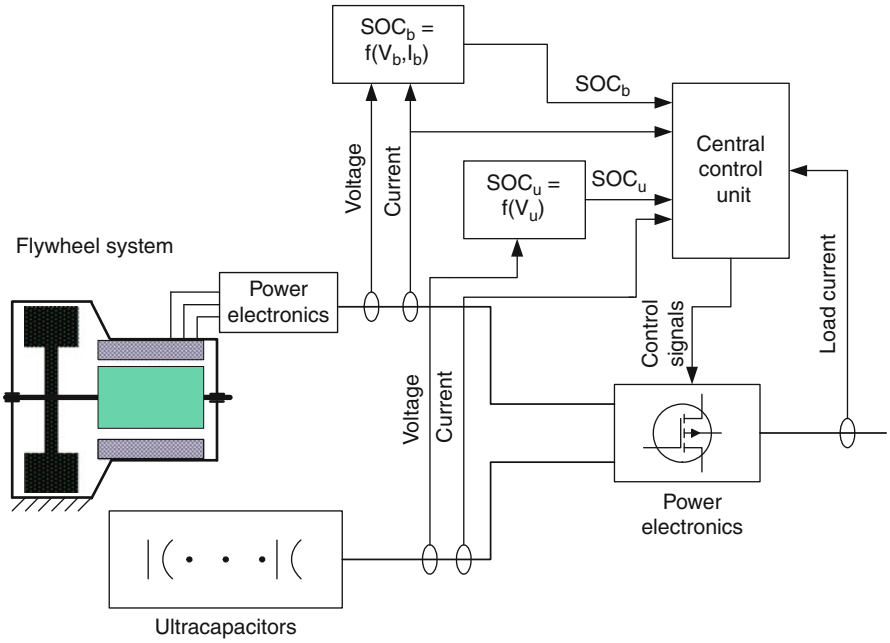

Hybrid Energy Storage Systems for Vehicle Applications. Figure 13
Actively controlled flywheel/ultracapacitor system

Although all of the above systems have been used individually in EV and HEV designs, the hybridized concepts, described here remain to be applied to the commercial EV and HEV products of the future. As the ultracapacitor technology and applications become more mature, their use in vehicle-hybrid-energy storage applications is likely to spread. However, as the power capability of chemical batteries continues to improve, the use of hybrid energy storage becomes less imperative. The eventual outcome of the above competing developments is not clear at this time. However, hybrid energy storage may find uses in advanced vehicles in one form or another for traction and other loads.

Bibliography

1. Chan CC, Chau KT (2001) Modern electric vehicle technology. Oxford University Press, New York
2. Crompton TR (1996) Battery reference book, 2nd edn. Society of Automotive Engineering
3. Delphi Automotive Company, http://www.delphi.com/news/pressReleases/pr11607-04112002
4. Ehsani M, Gao Y, Butler KL (1999) Application of electrically peaking hybrid (ELPH) propulsion system to a full size passenger car with simulated design verification. IEEE Trans Veh Technol 40:6
5. Ehsani M et al (2003) Investigation of high-energy and high-power storage systems for military vehicle applications. SAE-FTT 2003
6. Gao Y, Ehsani M (2002) An investigation of battery technologies for the army's hybrid vehicle application. In: Vehicular technology conference, 2002. Proceedings VTC 2002-Fall. 2002 IEEE 56th, vol 3, pp 1505–1509
7. Kajs J (2001) Combat vehicle mobility requirements. Seminar at Texas A&M University
8. Maxwell Technologies, http://www.maxwell.com
9. Messerle HK (1969) Energy conversion statics. Academic, New York
10. Miller JM, Emadi A, Rajarathnam AV, Ehsani M (1999) Current status and future trends in more electric car power systems. In: Proceedings of the IEEE vehicular technology conference Houston
11. Montena, Montena components. http://www.montena.com
12. Rahman Z, Butler KL, Ehsani M (2000) Effect of extended-speed, constant-power operation of electric drives on the design and performance of EV-HEV propulsion system. SAE future car congress, Apr 2000, Crystal City, Paper No. 2000-01-01557
13. Rand DAJ, Woods R, Dell RM (1998) Batteries for electric vehicles. Society of Automotive Engineering
14. SAFT Batteries, http://www.saftbatteries.com/automotive/uk/f/f.htm
15. ThermoAnalytics, http://www.thermoanalytics.com/support/publications/batterytypesdoc.html

Hydrogen from Biomass

Ralf Schmersahl[1,2], Marco Klemm[3], Ruth Brunstermann[4], Renatus Widmann[4]
[1]Deutsches BiomasseForschungsZentrum GmbH, German Biomass Research Centre (DBFZ), Leipzig, Germany
[2]Institute of Agricultural Engineering Bornim e.V. (ATB), Potsdam, Germany
[3]German Biomass Research Centre (DBFZ), Leipzig, Germany
[4]Department of Urban Water and Waste Management, University of Duisburg-Essen, Essen, Germany

Article Outline

Glossary
Definition of the Subject and Its Importance
Introduction
Biological Hydrogen Production
Hydrogen Production by Solid Biomass Gasification
Future Directions
Bibliography

Glossary

Biohydrogen Hydrogen derived from biomass.

Biological biohydrogen generation Production of hydrogen based on a biological resp. biochemical conversion of biomass.

Biomass From a scientific and technical point of view, biomass is defined as material of biological origin excluding material embedded in geological formations and/or transformed to fossil.

Thermochemical biohydrogen generation Production of hydrogen based on a heat-induced resp. thermochemical conversion of biomass.

Definition of the Subject and Its Importance

Today, there is no disputing that the use of renewable energy has to be increased in order to reduce anthropogenic CO_2 emission as well as the dependence on the fossil fuels. Approximately 95% of the hydrogen produced today comes from carbonaceous raw material, but primarily with a fossil resource as original energy source. Only a fraction of this hydrogen is currently used for energy purposes; the bulk serves as feedstock for manifold purposes, e.g., in the petrochemical industry as well as for food, electronics, and metallurgical processing. However, the share of hydrogen in the energy market is increasing, and hydrogen production will need to keep pace with this growing market [1]. In this sense, this paper summarizes the state of the art of the most important processes, techniques, and research activities in the field of hydrogen production using biomass resources.

Introduction

Hydrogen (H_2) is a secondary energy carrier that has to be produced from other energy carriers. A more and more discussed option for H_2 production is the use of biomass. It may be carried out either by biological or thermochemical processes. The characteristics of thermochemical H_2 production differ significantly from those of biological processes. The differences cover the feedstock basis as well as the reaction chemistry, the plant design, and the plant scales.

In the case of biological H_2 production, H_2 may be produced as a photosynthesis product (e.g., by microalgae). A second option is the use of fermentative microbiological degradation pathways, where H_2 occurs as metabolism product. Both pathways are still in the research scale.

Thermochemical biomass processes, such as combustion, pyrolysis, and gasification, are applied to produce different forms of energy carriers and chemicals. From those basic processes, gasification complies best with the requirements for the production of H_2. However, none of the present biomass gasifier designs is a genuine H_2 supplier: the product gas needs sophisticated posttreatment techniques to achieve both high H_2 yield and a sufficient H_2 purity.

Within the following explanations, these two hydrogen provision routes are discussed in detail.

Biological Hydrogen Production

Biological hydrogen production can be carried out by a wide variety of different organisms [2]. The biological processes differ according to the essential boundary conditions. Below, the process principles as well as some examples are discussed.

Hydrogen from Biomass. Table 1 Possible biochemical reactions of biological hydrogen production processes [3]

Process	Biochemical reaction	Boundary conditions
Direct photolysis	$2H_2O + light \rightarrow 2H_2 + O_2$	E.g., green algae in pure cultures, sterile conditions, lack of sulfur inhibition of the enzyme Fe-hydrogenase by oxygen
Indirect photolysis	$12H_2O + 6CO_2 + light \rightarrow C_6H_{12}O_6 + 6O_2$	Photoautotrophic bacteria, e. g., Cyanobacteria in pure culture, sterile conditions, enzymes: hydrogenase
	$C_6H_{12}O_6 + 2H_2O \rightarrow 4H_2 + 2CH_3COOH + 2CO_2$	
	$2CH_3COOH + 4H_2O + light \rightarrow 8H_2 + 4CO_2$	
Dark fermentation	$Biomass + H_2O \rightarrow H_2 + CO_2 + VFA$ (e.g., acetic acid)	Exclusion of methane-producing bacteria, mixed culture generated from different origin
Photofermentation	$CH_3COOH + 2H_2O + light \rightarrow 4H_2 + 2CO_2$	Photoheterotrophic bacteria (e.g., purple bacteria), enzyme nitrogenase, lack of nitrogen

Process Principles

An overview about different biohydrogen production methods is given in Table 1. Biohydrogen production by photolysis and dark fermentation and photofermentation are described and discussed below.

Photolysis Hydrogen production by the microalgae (i.e., *Chlamydomonas reinhardtii*) has been studied intensively in the recent years. This algae use the direct photolysis pathway to produce hydrogen out of water, if the microorganisms are stressed by lack of sulfur. Under these conditions, the algae produce hydrogen and oxygen but cannot grow. By this reason, a second stage with optimal conditions for the growth of the algae is necessary. Therefore, carbon dioxide is needed to build organic compounds like carbohydrates by photosynthesis. Additionally, by this pathway, hydrogen and oxygen are produced simultaneously, and the produced oxygen inhibits the enzyme hydrogenase, which is involved in the process. The color of the photosystems of the algae and phototrophic bacteria limits the dimension of the reactor because the penetration of light is reduced by the microorganisms itself [12]. For this reason, different reactor types are designed, for example, tubular or flat panels with a diameter or depth respectively of 10 cm at maximum [5]. Most of the experiments are done in lab scale by using artificial light. An advantage of this process is the clean energy production, because only hydrogen and oxygen are produced by this process.

However, the development of photobiological algae systems for biohydrogen production is still fundamental research. Due to the fact that the produced hydrogen yield per lightened area is very low – 1.5% based on a full solar spectrum [4] – further investigations are necessary to develop economic, viable, large-scale applications. Via genetic modification and cloning of the microorganisms, higher yields may be achieved [5]. Apart from that, H_2 and O_2 are produced simultaneously, which requires careful handling.

In contrast to the direct photolysis, it is possible during indirect photolysis to separate the oxygen formation by photosynthesis from hydrogen production in either time or space; this process is divided in three steps (Table 1). First, the photosynthesis takes place. In this step, CO_2 is needed, and oxygen is produced. Biochemical reaction of dark fermentation and photofermentation takes place in the second and third steps. This avoids the inhibition of the enzyme by oxygen. Still, the overall efficiency of the process is low like direct photolysis [4].

Dark Fermentation Dark fermentation is based on anaerobic degradation pathway, which is currently used for methane production with different biomass as feedstock. The biological process is divided in four steps. Depending on the composition of the biomass, different degradation pathways are used, and different microorganisms are involved. In steps 2 and 3, hydrogen is produced as an intermediate in several degradation pathways by a variety of microbes. In a conventional anaerobic digestion, this hydrogen is transformed into methane by methanogenic bacteria

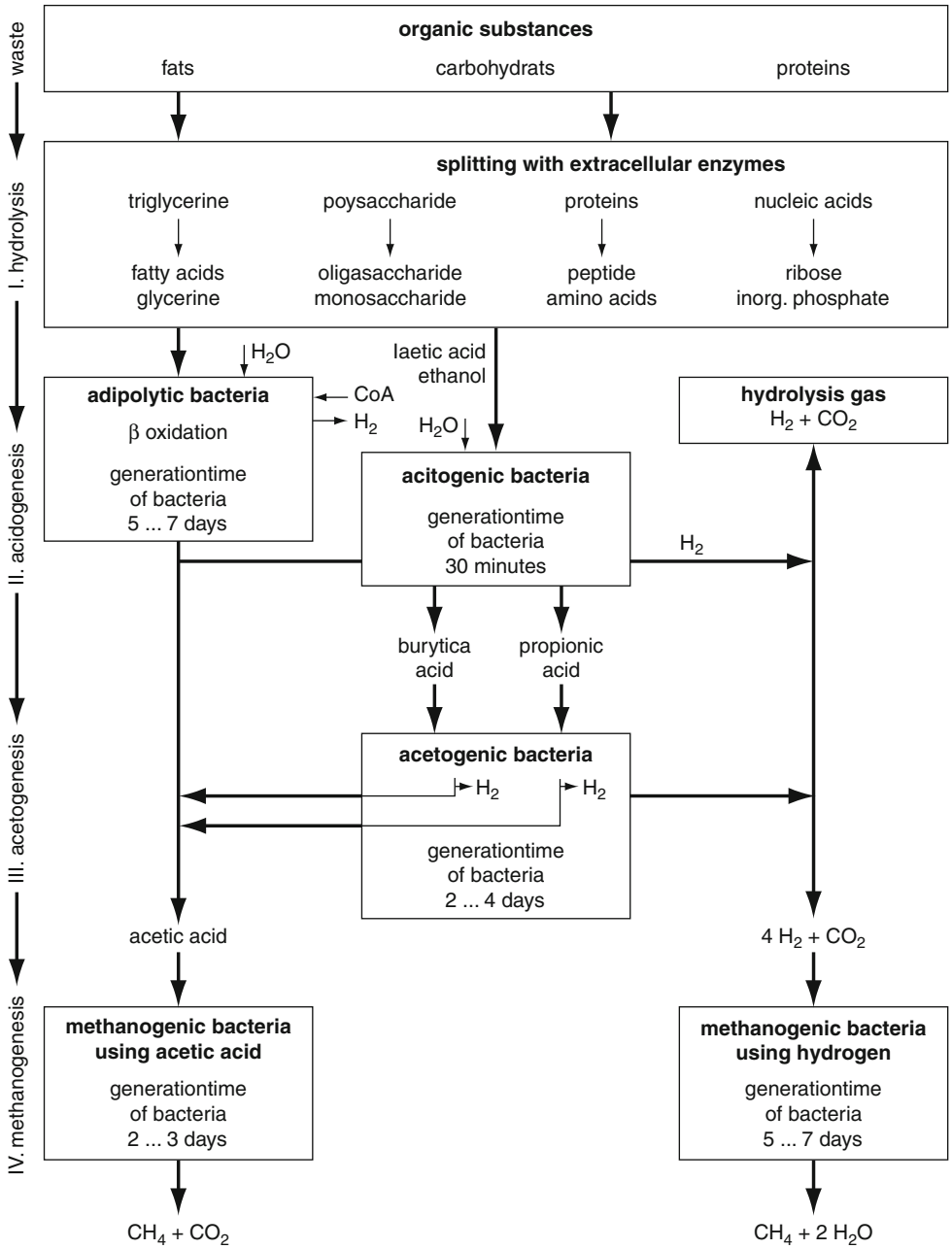

Hydrogen from Biomass. Figure 1
Degradation pathway during anaerobic digestion

in the fourth step. The degradation pathways during anaerobic digestion depending on the composition of feedstock are shown schematically in Fig. 1. There, the biomass is divided in fats, carbohydrates, and proteins because the anaerobic degradation pathway depends on the structure of molecules.

If the hydrogen consumption is stopped by elimination of the hydrogen-consuming microorganisms (i.e., the methanogenic bacteria), hydrolysis gas accrue, which consist mainly of hydrogen and carbon dioxide. The methanogenic microorganisms might be eliminated by heat treatment of the start culture, for

example, digested sludge [6, 7], or by using a seed material without strict anaerobic hydrogen-consuming bacterial-like compost or soil [3, 8] or pure stains of hydrogen-producing bacteria [4].

An opportunity to prohibit the hydrogen consumption by using a mixed culture out of digested sludge is to optimize the applied condition for hydrogen production and suppress hydrogen consumption. This is possible because methane is generated at a pH value between 6.0 and 8.0, whereas the hydrolytic and acidogenic bacteria prefer pH value between 4.5 and 6.0 for the degradation of carbohydrates. Nevertheless, the generation time of the methane-producing bacteria is within 2–7 days, much higher than the generation time of hydrogen-producing bacteria. Due to the fact that the generation time of carbohydrate-degrading acidogenic bacteria is only 30 min at optimal conditions, the hydraulic retention time (HRT) might be shorter. In contrast to the hydrogen-producing bacteria, the methane bacteria cannot accumulate in the reactor at a hydraulic retention time less than 48 h. These facts indicate as well that carbohydrates are most suitable for the dark fermentation process by using mixed cultures, which are generated out of digested sludge.

The process might be driven in the mesophilic [3, 7], thermophilic [6], or hyperthermophilic temperature range. Every temperature has its own advantages and disadvantages.

The extreme thermophilic anaerobic bacteria provide the highest hydrogen yields, reaching almost a maximum of 4.0 mol H_2/mol of glucose by using pure stains. Using pure cultures implicates that the feedstock has to be sterilized to avoid an accumulation of other microorganisms in the reactor. Additionally, the energy demand of the process is higher than at lower temperatures. The above-mentioned hydrogen yield of 4.0 mol H_2/mol glucose (this corresponds with 498.38 Nl H_2/kg glucose) is only reached if the combination of feed (different kinds of sugar) and microorganisms is optimal [4, 10, 11]. That implicates that a small change of feedstock (e.g., hexose instead of glucose) results in less efficiency of the plant. For this reason, a pretreatment step for the conversion of more complex biomass to simple sugars is necessary, which reduce the efficiency of the plant as well.

Hence, with the diversity in a mixed culture of strict anaerobic bacteria like Clostridia and facultative anaerobic hydrogen-producing bacteria, a variety of biomass can be converted to hydrogen. This process may be realized in the mesophilic or thermophilic temperature range. Due to the less energy demand, better stability of the process and approximately the same hydrogen yields [3], the mesophilic temperature range seems to be most promising for a technical application with a mixed bacteria culture as seed material and biowaste as feedstock in short term.

Beside the hydrogen yield (given in Nl hydrogen per kg of substrate), the gas and especially the hydrogen production rate is important for a technical application. Due to the fact that the bacteria density has to be low as well as the organic concentration in the influent, only the reduction of hydraulic retention times (HRT) provides an increase of hydrogen production rate. Hence, different reactor types were used. Continuous stirred-tank reactor (CSTR) is the easiest technique, which is similar to the used technique in wet anaerobic digestion. But the hydraulic retention has to be higher than the generation time of the microorganisms to provide an accumulation of these bacteria. Therefore, the hydraulic retention time has to be higher than 12 h.

A disadvantage of dark fermentation is the inhibition by its end product hydrogen. This is caused by biochemical equilibrium and thermodynamics of reactions. Figure 2 shows the energy yield of different reactions based on the hydrogen partial pressure, which affects the solubility of hydrogen in the liquids. Only if the hydrogen partial pressure is less than 0.1 bar will the conversion of organic acids to hydrogen become exothermic.

To provide these conditions, the produced hydrogen has to be removed from the system continuously. This can be done by:

- Purging with nitrogen or another inert gas
- Stirring with a high frequency

The purging with inert gas results in an increase of gas production. In parallel, the hydrogen concentration within the produced gas is decreasing, and therefore, an upgrading before the use (e.g., in a fuel cell) is necessary.

In general, hydrogen production by dark fermentation is restricted by the incomplete degradation of organic matter into volatile fatty acids, hydrogen, and carbon dioxide. Consequently, a further conversion of the liquid residues into an energy carrier is necessary.

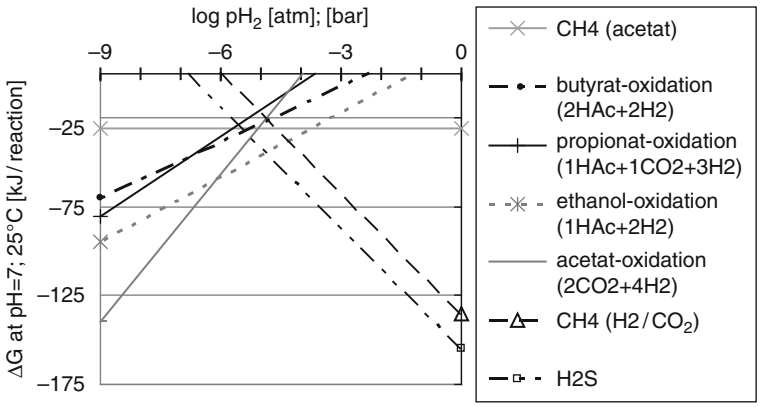

Hydrogen from Biomass. Figure 2
Energy yield of reactions dependent on hydrogen partial pressure

Photofermentation Photofermentation is driven by photoheterotrophic microorganisms, like purple bacteria (i.e., different strains of *Rhodobacter*). These bacteria are unable to split water. However, under anaerobic condition, these bacteria are able to degrade simple organic components like volatile fatty acids and alcohols into hydrogen and carbon dioxide under nitrogen-limited circumstances. The catalyst of the process is nitrogenase, which is sensitive to oxygen like hydrogenase. There are certainly no problems because no oxygen is produced. Normally, this enzyme catalyzed the fixation of molecular nitrogen (N_2) to ammonia NH_3, which is needed by the bacteria to grow. In absence of nitrogen, the enzyme is able to catalyze the evolution of hydrogen. The produced gas consists of hydrogen (80–90% (v/v)) and carbon dioxide (10–20% (v/v)) [4, 5].

The process depends on light. So, the reactor needs a high surface-to-volume ratio like the direct and indirect photolysis. By using sunlight, the increase of temperature has to be taken into account to prevent the system from damage by high temperature.

The above-mentioned limitation to convert only organic acids and alcohols by using of light as an energy source makes it a possible second treatment step after dark fermentation.

Comparison So far, all biohydrogen production technologies have been tested in lab scale. The feasibility of a technical implementation for hydrogen-producing photosystems is currently restricted by space requirements [12]. Additionally, the surface-to-volume ratio is restricted by the penetration of light into the reactor. Table 2 shows a comparison of required dimensions of bioreactors to produce enough gas to power a PEM fuel cell.

Up to now, very few technical and economic studies for biological hydrogen production systems have been carried out [4, 5, 13].

Regarding space requirements, no algae photosystem provides a sufficient amount of hydrogen in relation to the necessary reactor size. Without intensive further research and development of the methods, a technical realization in the large scale seems to be impossible within the next decade. Additionally, most of the photosystems work with pure strains of microorganisms and lack of nutrients (sulfur or nitrogen). Therefore, antiseptic techniques are needed to avoid an accumulation of other bacteria or yeast. Furthermore, circumstances in respect to nutrient limitations have to be taken into account.

Although the process of biohydrogen production by dark fermentation has been investigated very intensively during the last decade, there are still a lot of open questions. Most of the research has been carried out in batch test systems, just small continuous systems have been operated yet. The reactor dimensions usually do not exceed a working volume of a few liters. Additionally, the dark fermentation is an incomplete degradation of organic matter with volatile fatty acids in the liquid phase. Consequently, the dark and photofermentation are promising processes. In case of dark fermentation, a second treatment step is necessary. In case of photofermentation, a pretreatment step is required.

Hydrogen from Biomass. Table 2 Size of bioreactor required to power PEM fuel cells 0

System	Size of bioreactor (m^3) required to power a PEM fuel cell of			
	1.0 kW	1.5 kW	2.5 kW	5.0 kW
Direct photolysis	341	512	856	1,710
Indirect photolysis	67.3	101	169	337
Photofermentation	149	224	374	758
Dark fermentation min.	0.198	0.297	0.495	0.989
Dark fermentation max.	2.91	4.38	7.31	14.62

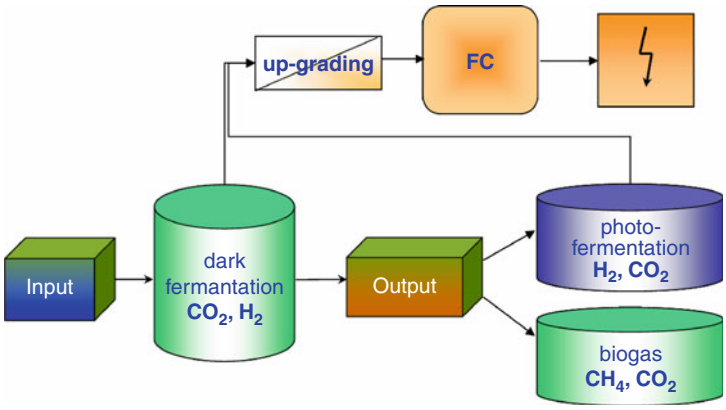

Hydrogen from Biomass. Figure 3
Biological-based biomass to hydrogen concepts

Biomass to Hydrogen Systems

A complete biological conversion into hydrogen and carbon can only be realized by a combined multistage treatment (e.g., dark fermentation as the first stage and conversion of the produced volatile fatty acids into hydrogen by photofermentative microorganisms as the second stage [4]). For implementation, even combined dark fermentation/methane fermentation plants or a material utilization of the reactor effluent is conceivable.

With conventional anaerobic digestion, an energy carrier in form of biomethane is already established. Therefore, methane fermentation combined with steam reforming will lead to energy losses by the hydrogen production step. Hence, it should be carefully considered whether methane could be used directly for energy generation, e.g., in a suitable fuel cell (MCFC, SOFC) or in the mobility sector (gas upgrading to natural gas quality).

Below, some examples of combined systems are discussed in detail (Fig. 3).

Combination of Dark Fermentation and Photofermentation The combined dark fermentation and photofermentation process connects two new technologies with high research requirements because they have only been realized in lab scale and not in pilot or technical scale yet. This will cause additional problems for technical implementation [9]. Figure 4 shows a scheme of the combined dark and photofermentation system.

Caused by the specific microorganisms and to increase the conversion of biomass to hydrogen during dark fermentation with pure bacteria strains, a pretreatment step is used. Here, hydrolytic bacteria and/or addition of chemicals should degrade a variety of biomass (especially carbohydrates) to simple molecules. The thermophilic temperature range is supplied

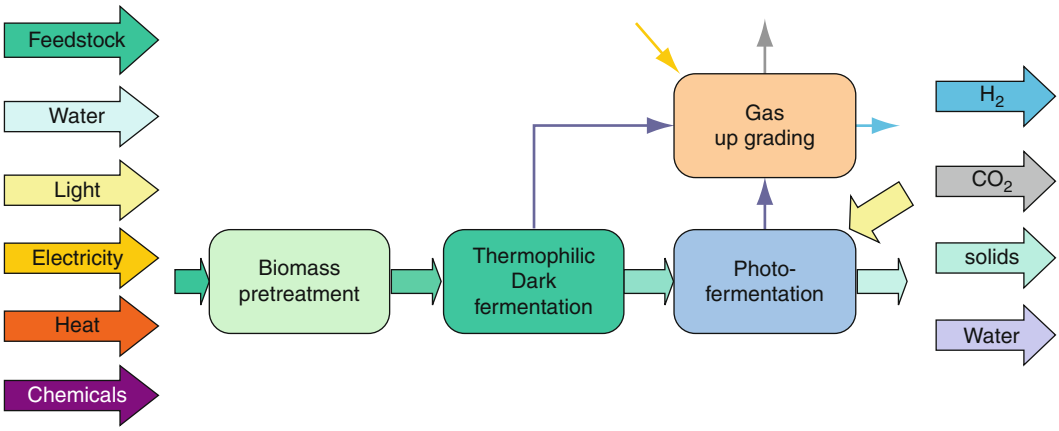

Hydrogen from Biomass. Figure 4
Scheme of combined dark and photofermentation [9] (simplified)

Hydrogen from Biomass. Table 3 Biochemical reactions for the combination of dark and photofermentation with glucose as substrate

Substrate	First reactor (dark fermentation)	Second reactor (photofermentation)
$C_6H_{12}O_6$ + 2 H_2O→	2CH_3COOH + **2CO_2 + 4H_2** [3, 4]	**8 H_2 + 4 CO_2** [14]
	2CH_3COOH + 4H_2O + Light→	

by heating the system. This process operates with specific anaerobic bacteria specialized to degrade only different kinds of sugar or starch to H_2, CO_2, and organic acids. The thermophilic temperature in this stage provides sanitation and decreases the competition with other microorganisms. Additionally, chemicals are used in this stage for nutrient supply and pH stabilization. The effluent contains mainly volatile fatty acids and alcohols dissolved in water. This effluent is pumped in photobioreactor. Here, the light-dependent photofermentation takes place. The biochemical reactions in this combined system, except the biomass pretreatment, are shown in Table 3.

Combined Dark and Methane Fermentation Hydrogen yields of 4 mol/mol glucose (Eq. 1) at maximum are possible by dark fermentation with only 2 mol acetates as by-product [2, 15]. If only butyric acid occurs as by-product, the hydrogen yield decreases to 2 mol/mol glucose (Eq. 2) [15]. Typically, the end product of dark fermentation by using mixed microflora is a mix of different volatile fatty acids like acetic and butyric acid [7, 16]. Accordingly, the biochemical possible hydrogen yield is 2.5 mol/mol glucose (Eq. 3).

If the liquid effluent of the H_2 reactor is used as carbon source in a methane reactor, the organic acids become degraded to CO_2 and CH_4. The theoretical methane yield that can be generated depends on the liquid products of the hydrogen stage. If the acidogenesis takes place in the first reactor, only acetic acids would be transferred into the methane reactor, and only these acids would be converted into CH_4 and CO_2. This case is signed by line 2 in Fig. 5. Line 1 indicates that only the hydrolysis and acetogenesis take place in the first reactor. If so, the hydrogen yield decreases, and the methane yield increases according to Eq. 2 and Eq. 3. The stoichiometries of some possible biochemical reactions for the combined hydrogen and methane production with glucose as carbon source are given in Table 4. The chemical equation for the optimal degradation of glucose by a conventional fermentation (Eq. 4) is also given in this table.

An engineered approach towards a technical system has not been made yet. However, up to now, the combined hydrogen/methane fermentation system

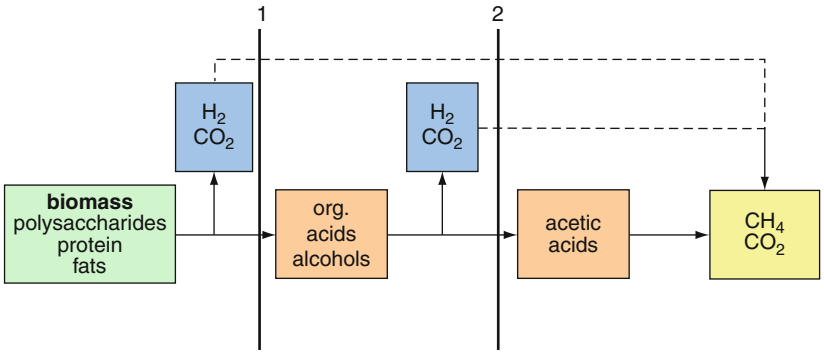

Hydrogen from Biomass. Figure 5
Combined biological hydrogen and methane production out of biomass

Hydrogen from Biomass. Table 4 Biochemical equation for the combined biological hydrogen and methane production with glucose as energy source

	Substrate	First reactor (H_2)	Second reactor (CH_4)
Eq. 1	$C_6H_{12}O_6 + 2\ H_2O \rightarrow$	$2CH_3COOH$ **+ $2CO_2$ + $4H_2$** [2, 15]	
		$2CH_3COOH \rightarrow$	**$2CH_4 + 2CO_2$**
Eq. 2	$2\ C_6H_{12}O_6 \rightarrow$	$2C_3H_7COOH$ **+ $4CO_2$ + $4H_2$** [17]	
		$2C_3H_7COOH + 2H_2O \rightarrow$	**$5CH_4 + 3CO_2$**
Eq. 3	$8\ C_6H_{12}O_6 + 4\ H_2O \rightarrow$	$4CH_3COOH + 6C_3H_7COOH$ + **$16CO_2$+ $20H_2$** [7, 16]	
		$4CH_3COOH + 6C_3H_7COOH + 6H_2O \rightarrow$	**$19CH_4 + 13CO_2$**
Eq. 4	$C_6H_{12}O_6 \rightarrow$		**$3CH_4 + 3CO_2$**

offers the highest realization potential regarding the biological hydrogen production methods. This is due to the fact that only one pretreatment module has to be implemented in a proved technology.

Hydrogen Production by Solid Biomass Gasification

Thermochemical hydrogen production can be carried out by a wide variety of different processes. Below, the basic principles as well as some examples are discussed.

Process Principles

Generally, gasification is a thermochemical process that converts a carbon-containing substance, here lignocellulosic biomass, by partial oxidation into a fuel gas. A gasification agent (i.e., air, oxygen, or steam) provides the required oxygen. While air gasification generates a low-calorific-value gas suitable for power generation, oxygen and steam gasification lead to a medium-calorific-value gas, referred to as syngas. Syngas is suitable for the production of energy carrier such as H_2, methane, and liquid hydrocarbons.

The overall gasification reaction for biomass may be expressed after Eq. 5.

$$\text{Biomass} + H_2O + O_2 \rightarrow H_2 + CO + CO_2 + CH_4 + \text{hydrocarbons} + \text{char} \quad (5)$$

The heat of reaction (ΔH_R) is positive for steam gasification (endothermic reaction) and negative for oxygen gasification (exothermic reaction). Reaction stoichiometry favors steam as gasification agent for a maximum H_2 output, but pure steam gasification requires an external heat supply adding up to a concept called allothermal steam gasification. At first glance, oxygen gasification is comparatively less

attractive for H_2 production since less H (in form of steam) enters the gasifier. But other aspects have to be considered that prohibit such a simple conclusion:

- Oxygen gasification achieves higher temperatures enabling higher carbon-to-gas ratios.
- Autothermal operation is advantageous for overall process efficiency since heat transfer losses are smaller.
- Steam addition in downstream processing may balance the initial lower H content.

Biomass gasification typically operates under thermodynamic conditions that imply an almost complete carbon conversion into gaseous species (i.e., CO, CO_2, and CH_4). Assuming carbon conversion is complete, the equilibrium gas composition is given by two homogenous gas reactions, methane steam reforming (Eq. 6) and water–gas shift (Eq. 7).

$$CH_4 + H_2O \leftrightarrow CO + 3H_2 \quad \Delta H_R = +206\ \mathrm{KJ/mol} \tag{6}$$

$$CO + H_2O \leftrightarrow CO_2 + H_2 \quad \Delta H_R = -41\ \mathrm{KJ/mol} \tag{7}$$

In practice, carbon conversion is restricted due to mass transfer limitations and reaction kinetics. The raw syngas often contains light and heavy hydrocarbons being intermediates in terms of volatilization of the biomass organics. Especially aromatic compounds, known as tars, require a sophisticated conversion process or in depth removal before downstream gas processing.

Biomass gasification for fuel production relies on different gasification concepts, namely entrained flow, fluidized bed, and dual fluidized bed steam gasification:

- Fluidized bed gasification is realized by a bed of fine, inert or catalytic active, material that is fluidized by blowing oxygen upwards through the bed. In contrast to power and heat applications, air is an improper gasification agent as nitrogen dilutes the syngas, boosting the downstream gas treatment effort. Depending on the gas velocity, the bed material is agitated (bubbling fluidized bed, BFB) or suspended throughout the gasifier (circulating fluidized bed, CFB). The syngas leaves the reactor at the top. In case of CFB, it has to be separated from the bed material with a cyclone. Fluidized bed gasifiers allow for pressurized operation. Typical gasification temperatures are in the range of 850–950 C. Compared to other gasification options, the main advantages of CFB gasifiers are high cold gas efficiencies, low investment costs, and a wide applicable power range of some tens to some hundreds of megawatts. Major drawbacks are related to comparatively low H_2 content in syngas and limited operating pressure because of feeding and fluidization issues.
- Entrained flow gasification takes on a special position in biomass gasification. In contrast to fluidized bed gasifier designs, it refers to established fossil fuel technologies for large-scale implementation. The key measure to enable entrained flow gasification for biomass is to manipulate the biomass properties by pyrolysis processes, such as torrefaction and carbonization, in a way that they become more similar to coal. The resulting bio-oil, char, or slurry are pressurized and then atomized with pure oxygen in a burner at the top of the gasifier. Gasification temperatures are in a range of 1,300–1,600°C, high enough to convert ash into slag. Entrained flow biomass gasification has some advantages compared to other gasification processes: (1) the high syngas pressure is favorable for H_2 purification and distribution, (2) the raw gas is tar-free and therefore requires only modest gas cleaning efforts, and (3) the possibility to combine decentralized, small-scale biomass pretreatment with centralized, large-scale gasification avoids the long-distance transport of raw biomass with a low energy density while still profiting from economy of scales. On the other hand, there are some major drawbacks: (1) the overall concept implies an efficiency penalty due to losses during thermochemical pretreatment, (2) formation and discharge of slag is difficult to handle since biomass feedstock provides a wide range of ash properties, and (3) the H_2 content in syngas is low, providing a heavy duty for downstream gas conditioning.
- Dual fluidized bed steam gasification provides a major advantage for H_2 production by increasing the amount of H entering the process. But because the gasification process is endothermic, an external

heat source and a heat transfer medium are required. Therefore, steam gasification concepts usually work with two fluidized beds, one for the gasification process and a second one for combustion. As an example, the process principle of the Fast Internally Circulating Fluidized Bed (FICFB) technology is shown in Fig. 6 0. Here, biomass is fed into the gasification chamber where it is converted into nitrogen-free syngas and char using steam as gasification agent. Char, recycled syngas, and recycled tars are burnt with air in the combustion chamber, heating the accompanying catalytic bed particles. The hot bed material is then fed back into the gasification chamber, providing the required reaction heat. Dual fluidized bed gasifiers operate at ambient pressure with a gasification temperature of 800–870°C [18].

In case of H_2 production, all presented biomass gasifiers require further downstream gas processing to achieve better H_2 yield und purity. Gas conditioning by steam reforming (Eq. 6) and water–gas shift (Eq. 7) utilize steam to generate additional H_2:

- Steam reforming is the process where methane and other hydrocarbons are converted into carbon dioxide, carbon monoxide, and H_2 in the presence of steam. In technical applications, reforming is performed utilizing a catalyst, which is usually nickel-based. Steam reforming should be performed at high temperatures to shift the equilibrium to the right side of Eq. 6. There should be an excess of steam to prevent coking. At temperatures below 900°C, most of the nickel catalysts are sensitive to sulfur poisoning. Methane steam reforming is strongly endothermic. As for the gasification process itself, the question arises, whether the heat is provided autothermal by oxygen supply or allothermal from an external source. Low pressure is favorable since it shifts the reaction equilibrium towards H_2.
- In contrast, the water–gas shift reaction is exothermic. Unfortunately, the excess heat is not suitable to support steam reforming because the temperature level is too low. Water–gas shift is often performed in two steps: a high temperature shift and a low temperature shift. The high temperature shift usually is performed at 300–400°C using iron–chrome catalysts, and the low temperature shift operates below 250°C utilizing copper and zinc oxide catalysts. The amount of carbon monoxide can be lowered to less than 1%. The equilibrium is not sensitive to pressure.

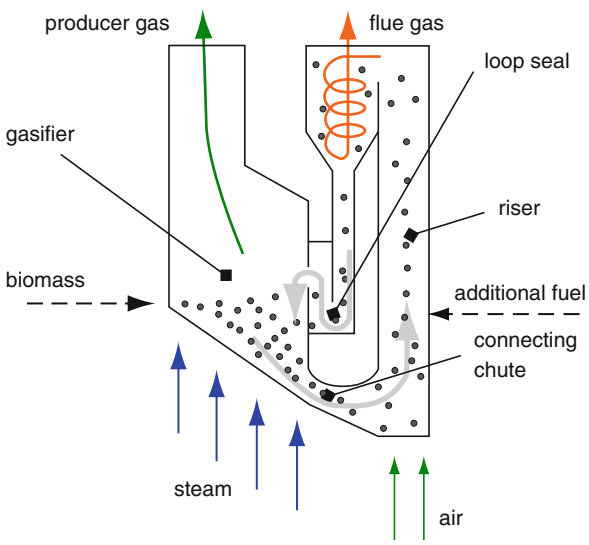

Hydrogen from Biomass. Figure 6
Fast Internally circulating fluidized bed (FICFB) gasification 0

Biomass gasification with downstream gas conditioning results in an H_2-rich gas that typically contains a significant amount of accompanying gas species (e.g., carbon dioxide, carbon monoxide, nitrogen, and a variety of trace components). Physical or chemical scrubbers for acid gas removal (AGR) permit a comparatively cheap and efficient bulk CO_2 removal, but high purity H_2 output requires (additional) pressure swing adsorption, membrane separation, or preferential CO oxidation upstream of the acid gas removal.

Pressure swing adsorption works on the principle of molecular sieving. Molecular sieves are zeolites or activated carbon with a defined pore structure allowing for the separation of molecules according to size and polarity. The gas is fed to a system of packed beds. Frequent pressurization of the beds leads to, alternately, adsorption and release of the unwanted gas species. After desorption, the bed is purged. In the time, the first bed is regenerated; the second bed is pressurized, after which the gas feed is switched back to the first bed.

Biomass to Hydrogen Systems

The basic concept of biomass gasification plants for H_2 production is presented in Fig. 7. It involves several main process steps: (1) biomass pretreatment, mainly drying and sizing, but in case of entrained flow gasification also thermochemical treatment such as fast pyrolysis or torrefaction; (2) the gasification process itself, performed either allothermal with a dual fluidized bed design or autothermal with fluidized bed or entrained flow gasifiers; and (3) downstream gas processing that covers gas cleaning for the removal of impurities, gas conditioning by reforming and water–gas shift reaction, and H_2 purification.

A biomass gasification plant is not energy autonomous. Most of the processes require a significant amount of electrical energy. Steam generation is also an issue. Depending on infrastructural and business conditions, it could be a favorable option to integrate power and heat generation. If so, some of the syngas is used to fire an engine or a gas turbine for the simultaneous generation of electricity, heat, and fuel. Another option is the conversion of surplus heat with a steam turbine. In the future, the operation of a fuel cell feed with H_2 is another possibility. If power and heat generation exceeds the demand of the plant, surpluses can be sold in addition to the H_2 product. This approach is referred to as polygeneration concept [19].

Present biomass gasification plants are originally designed for the production of biofuels other than H_2. But a proper downstream process design allows for H_2 production as well. If designed for H_2 output, the fuel synthesis island has to be replaced by H_2 purification processes.

In case of entrained flow gasification concepts, biomass pretreatment and the gasification process itself will be the same for all biofuel output option. Gasification parameters do not allow for further optimization of the H_2 yield because there is a trade-off between efficiency and H_2 yield: a higher steam input requires more oxygen to achieve the necessary operating temperatures. Carbon conversion in entrained flow gasifiers is almost complete. The hot raw gas consists of H_2, CO, and CO_2. It is cooled by a water quench using the sensible heat of the gas stream for water vaporization. The amount of water fed into the gas stream lowers the demand for additional steam during the water–gas shift.

H_2 production asks for an as high as possible CO conversion since the energy content of unconverted CO is lost for H_2 output. Therefore, a staged water–gas shift layout is essential. Available catalysts are sensitive to sulfur poisoning so that sulfur components have to be removed upstream. Depending on the requested H_2 quality, different H_2 purification processes have to be applied. Figure 8 provides at the left side a basic scheme of a process chain for H_2 production based on entrained flow gasification.

Recently, several large-scale biofuel production concepts based on entrained flow gasification were developed:

- The production of FT-Diesel from wood on a 45-MW scale with a staged gasification process has been demonstrated. The Carbo-V® process operates at 5 bar pressure. First, biomass is converted into tar-containing gas and charcoal by autothermal pyrolysis at 400–500°C. Second, the

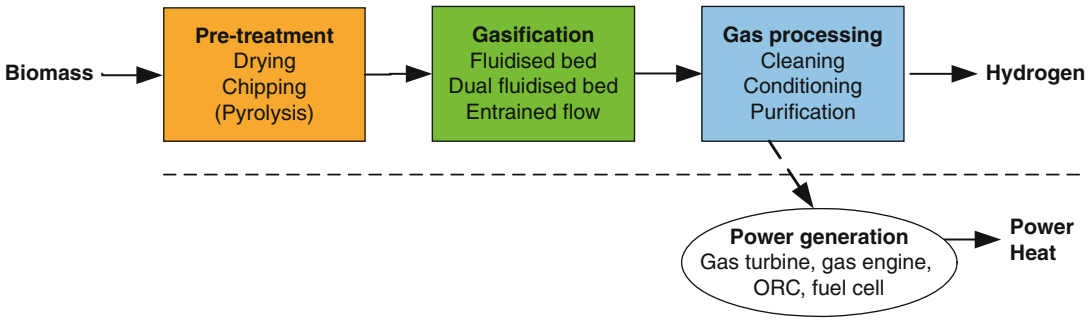

Hydrogen from Biomass. Figure 7
Concept of biomass gasification plants for H_2 production

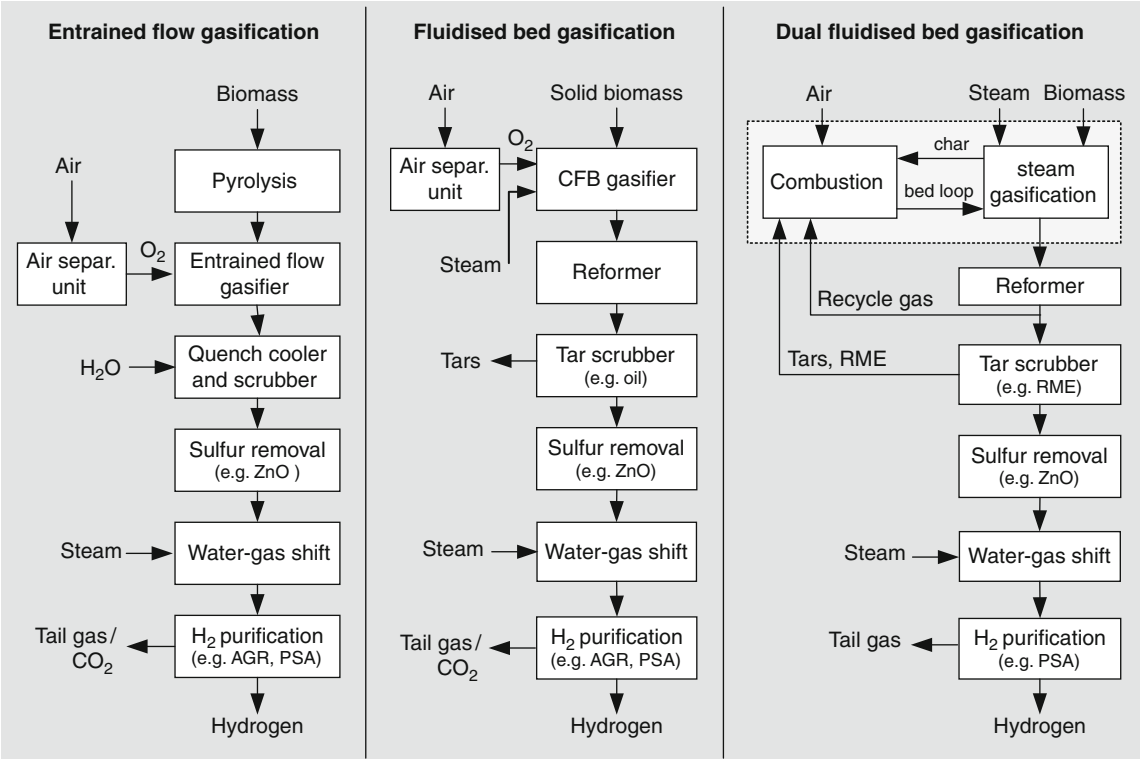

Hydrogen from Biomass. Figure 8
Biomass gasification process chains for H_2 production

pyrolysis gas is fed to an entrained flow gasifier operating at about 1,500°C. Third, charcoal is used for cooling the hot gas down to 900°C by a chemical quench process. The tar-free raw gas contains 30–40% of both H_2 and CO, balanced by CO_2 and H_2O 0.

- The bioliq® concept couples decentralized fast pyrolysis of straw with centralized entrained flow gasification of the resulting bioslurry. The fast pyrolysis is performed at ambient pressure and 500°C. The resulting char and pyrolysis oil are mixed to form slurry, which is transported to the gasification plant. There, it is fed to an entrained low gasifier operating at 30 bar and 1,200°C. The raw gas contains 30–40% CO and 20–30% H_2, balanced by N_2, CO_2, and H_2O. Favored product outputs are FT-Diesel and dimethyl ether, but H_2 production is considered as an option [20].

Fluidized bed gasification concepts, as shown in the middle part of Fig. 8, avoid the need for thermochemical biomass pretreatment. They have milder requirements regarding feedstock drying and sizing. Wood chips are a common fuel. Circulating fluidized bed (CFB) gasifiers are in some major aspects similar to entrained flow gasifiers. They use the same gasification agent – oxygen – and may operate pressurized.

An important difference compared to entrained flow gasifiers is related to ash. Because sintering and slag formation would create problems in terms of bed fluidization, the operating temperature is limited to roughly 1,000°C. At this operating condition, carbon conversion is around 95%. The limited carbon conversion is linked to a major problem of fluidized bed gasifiers: syngas quality suffers from tars. Since tars are not only impurities but also carry a significant amount of the chemical bound energy, tar treatment is crucial for the overall efficiency. A preliminary reforming of tars – and other hydrocarbons including methane, which is a major component in CFB raw gas – recovers the chemical energy to a large extent in form of CO and H_2 before a secondary tar removal process

purifies the syngas. Further downstream processes are similar to those of entrained flow gasification based H_2 concepts. Differences in syngas composition and pressure level decide over the choice of the most suitable H_2 purification steps.

At present, CFB biomass gasification for H_2 is still under development. In Scandinavia, different demonstration projects deal with a slipstream H_2 train:

- In Värnamo (Sweden), the VVBGC demonstration project rebuilds a biomass-fueled IGCC plant into a synthesis gas producing unit with research and development [21].
- In Varkaus (Finland), a consortium is demonstrating a 12-MW syngas atmospheric oxygen/steam–blown CFB gasifier. The ultra clean gas (UCG) project focuses on syngas treatment to provide a reliable interface for different production targets, including H_2 [22, 23].

Dual fluidized bed gasification concepts, as shown in the right part of Fig. 8, cover process steps similar to those of CFB-based process chains. The major differences are: (1) the carbon conversion in the gasification chamber of roughly 75% leads to a smaller amount of syngas containing a higher percentage of H_2, (2) the duty of the water–gas shift is lower because the raw syngas composition provides a higher H_2/CO ratio due to the utilization of steam as gasification agent, and (3) tars are recycled to the combustion chamber because the segregation of gasification and combustion permits an easy handling of additional fuel.

Dual fluidized bed gasification concepts for the production of fuels and chemicals are mainly designed for methane output, often as a part of a polygeneration concept. But some concepts are as well optimized for H_2 production:

- A biomass gasification concept for the production of gaseous and liquid fuels has been introduced. A dual fluidized bed gasifier integrates a tar reformer utilizing the heat of the flue gases to boost the syngas H_2 content from 20% up to more than 45% [24, 25].
- The so-called Güssing model follows the strategy of decentralized, local energy production from all available renewable resources in a region. Here, an 8-MW_{th} FICFB gasifier (Fig. 6) is operated in CHP mode [26]. Additionally, the gasifier provides opportunities for testing different bed materials and for the use of a syngas side stream for process development purposes, for example, the development of methane and BtL fuel production downstream equipment.

Table 5 summarizes the characteristics of the presented biomass gasification process chains regarding H_2 production. Those process chains provide a basis for additional or pure H_2 output but rely on an initial design for other output options. H_2 production is specified as a potential output stream but has not been demonstrated on an industrial scale. From the view of process economics, a major drawback of current gasifier designs is the initial low H_2 content of the syngas. Recently, new processes with higher H_2 concentrations have gained interest. Particularly, a process called adsorption enhanced reforming (AER) provides good opportunities for commercial H_2 production from wood and herbaceous biomass [27] 0.

Case Study: The AER Process

The AER process is a new approach to improve dual fluidized bed gasification. Figure 9 describes the process principle. By using a bed material such as mineral calcite ($CaCO_3$) in a dual fluidized bed gasifier, a chemical loop is established where the bed material not only acts as a heat carrier but also adsorbs CO_2 and transports it from the gasification reactor to the combustion chamber where it is released.

CO_2 absorption in the gasifier part shifts the equilibrium of the water–gas shift reaction towards H_2 (Eq. 7). Hence, an H_2-rich product gas results with reduced CO_2 and CO concentration. The idealized sum reaction of the AER gasification – without considering the formation of methane and other secondary products – is given by Eq. 8 [28].

$$CH_xO_y + (2-y)H_2O + CaO \rightarrow CaCO_3 + (0.5x + 2 - y)H_2 \quad (8)$$

$$CaO + CO_2 \leftrightarrow CaCO_3 \quad \Delta H_R = -181.4\ \mathrm{kJ/mol} \quad (9)$$

The operating temperature of the gasification reactor is 600–700°C. According to Eq. 9, CO_2 adsorption (carbonation) is highly exothermal so that the heat

Hydrogen from Biomass. Table 5 Main characteristics of biomass gasification process chains for fuels and chemicals

	Dual fluidized bed	Circulating fluidized bed	Entrained flow
Gasification characteristics			
Reactor type	Dual fluidized bed	Fluidized bed	Entrained flow
Gasification agent	Steam	Oxygen (+steam)	Oxygen (+steam)
Heat supply	Bed loop	Autothermal	Autothermal
Temperature level (°C)	800–870	900–1,000	1,300–1,600
Pressure level (bar)	1	1–20	5–80
Residues	Ash	Ash	Slag
H_2 at outlet (vol%)	30–40	20–30	25–35
CH_4 at outlet (vol%)	9–12	10–15	<1
Required downstream processes for H_2 production			
Tar removal/conversion	Yes	Yes	No
Steam reforming	Yes	Yes	No
CO shift	Yes	Yes	Yes
H_2 purification	Yes	Yes	Yes
Plant characteristics			
Conversion efficiency[a]	50–60	50–60	45–55
Target scale (MW_{th})	10–100	30–200	250–1,000
Drawbacks	Tar load	Feeding system (pressurization), tar load	Biomass pretreatment, process control
Announced products	CH_4, BtL, polygeneration	BtL, CH_4, H_2, IGCC	BtL, CH_4, H_2

[a]Biomass to H_2 on LHV basis, estimation

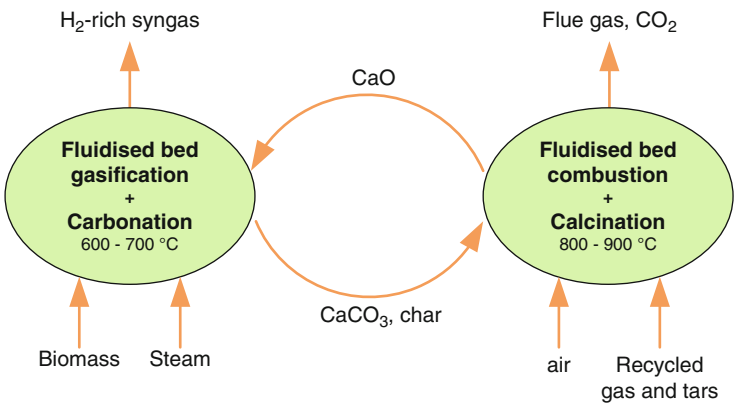

Hydrogen from Biomass. Figure 9
Principle of AER gasification process

demand of the gasifier part is lower as compared to FICFB steam gasification. The fluidized bed material – calcite ($CaCO_3$) and char at this moment – is directed to the combustion chamber where char and additional fuel are burned to provide the calcination temperature well above 800°C. The heated bed material – now quicklime (CaO) – is recycled to the gasification chamber. Because the temperature difference of more than 200°C between gasifier and combustor is much higher than those 50°C of the FICFB process, it is necessary to reduce the bed material circulation rate. In order to do so, the particle size of the bed material is increased, and the primary fluidization in the combustor is decreased [29].

The desired properties on the bed material for AER gasification are:

- High mechanical stability to avoid dust problems in downstream equipment
- High CO_2 capacity and sufficient reaction rate of carbonation and calcination
- High catalytic activity towards tar conversion and CO shift reaction

Different limestones as a bed material have been tested with two biomass fuels, wood pellets, and straw pellets in a 100-kW_{th} process development unit [29]. The tested bed material consisted mainly of calcite coming from different mining companies. Clear variations in overall performance of wood gasification regarding gas composition and dust load have been observed:

- The H_2 concentration varies in a range from 59% to 70%.
- The tar content in raw syngas varies from 0.4 to 2.8 g/Nm^3 with most of the values lower than 1 g/Nm^3.
- The dust content is between 12 and 42 g/Nm^3.

In contrast to conventional dual fluidized bed steam gasification, the AER process provides favorable conditions for straw gasification. Straw is a difficult fuel for biomass gasification because of its low sintering point at 700–750°C, causing bed agglomeration in reactors operating at the temperatures above. The lower gasification temperature and the positive influence of CaO on the melting behavior of straw enable this widely available biomass resource for H_2 production. Compared to wood pellets, drawbacks are a higher dust load (~80 g/Nm^3) due to the high ash content, a higher tar content of 2–3 g/Nm^3, and a lower H_2 concentration of 52% [29].

The same 100-kW_{th} apparatus have been used to perform a comparison between FICFB and AER

Hydrogen from Biomass. Table 6 Comparison of wood gasification with conventional FICFB and AER process [30]

	FICFB	AER
Operating parameter		
Bed material	100 kg olivine	100 kg calcite
Steam/fuel ratio (kg/kg)	0.63	0.79
Gasification temperature (°C)	841	645
Combustion temperature (°C)	920	894
Syngas properties		
H_2 (vol%, dry)	39.1	73.9
CO (vol%, dry)	29.1	6.1
CO_2 (vol%, dry)	17.5	6.0
CH_4 (vol%, dry)	11.4	11.7
Hydrocarbons C2–C6 (vol%, dry)	2.9	2.3
Dust (g/Nm^3)	5.9	22.8
Char (g/Nm^3)	35.2	28.8
Tar (g/Nm^3)	3.5	1.4
H_2O (vol%)	33.2	51.4
Energy balance		
Fuel, wood pellets (kW)	123.5	123.5
Additional fuel, oil (kW)	26.6	9.6
Auxiliaries and steam (kW)	11.4	12.0
Syngas chemical power (kW)	105.6	66.5
Conversion efficiency[a] (%)	70.4	50.0
H_2 yield (l_{H2}/kg_{wood})	280	580

[a]Fuels to syngas, LHV

gasification regarding mass and energy balances [30]. The bed materials were olivine in case of FICFB gasification and calcite for the AER process. Oil was used as additional fuel. Table 6 provides an overview of the main results of those test runs. In contrast to conventional steam gasification, syngas properties of the AER process are more advantageous for H_2 production since the effort for downstream processing is much lower, but the conversion efficiency is comparatively low.

Future Directions

The market implementation of hydrogen from biomass is strongly influenced by the aimed utilization. The fields of use are significant:

- Chemical industry, replacing hydrogen from fossil fuel
- Transportation fuel
- Energy carrier for the storage and dissemination to decentralized applicants

The barrier for market access will be the lowest one in the first case because the market is established, the infrastructure is still available, and there is hardly any alternative to hydrogen as a raw material for processes realized within the chemical industry. The replacement of fossil fuel in the hydrogen production can generate an important environmental benefit. This can be done step by step if the production plants based on fossil fuels reached their end of the lifetime.

In the other market mentioned above (use as a transportation fuel and/or storage medium), a new infrastructure has to be installed before a hydrogen use in the large scale is possible. The creation of such a new infrastructure may be much more expensive than exclusive erection of the production plants. In addition, for these fields of application, renewable alternatives such as biomethane and liquid fuels still exist. It cannot be foreseen which position hydrogen will achieve within this competition field with the given fuel alternatives in years to come.

Some H_2 production methods from biomass are well developed, and several processes are demonstrated. Nevertheless, a commercial status could not be reached until now, neither based on the thermochemical nor on the biochemical or biological route:

- The process steps for the thermochemical hydrogen production based on biomass are well known and scientifically analyzed. Demonstration of the whole provision pathway in a near commercial size has to be the next implementation step. Basically, these processes have to show their economic performance.
- Biochemical pathways for the generation of hydrogen are still in the status of basic research. Therefore, these pathways might have the potential for an important contribution to bioenergy supply only if basic questions are solved based on increased research activities.

The viability of a future biomass to H_2 technology critically depends on the development of efficient, large-scale, cost-effective, and sustainable H_2 production systems. There are lots of activities ongoing, but so far, an economic breakthrough on the market cannot be seen. The years to come will show if this option has a realistic chance to contribute with a considerable share within the overall energy system [1, 31].

Bibliography

Primary Literature

1. Milne TA, Elam CC, Evans RJ (2001) H_2 from biomass – state of the art and research challenges. A report for the international energy agency agreement on the production and utilization of H_2; Task 16, H2 from carbon-containing materials. National Renewable Energy Laboratory, Golden. http://ieahia.org/pdfs/H2_biomass.pdf. Accessed July 2010
2. Hallenbeck PC, Benemann JR (2002) Biological hydrogen production; fundamentals and limiting processes. Int J Hydrogen Energy 27(11):1185–1193
3. Brunstermann R (2010) Entwicklung eines zweistufigen anaeroben Verfahrens zur kontinuierlichen Wasserstoff- und Methanerzeugung aus organischen Abfällen und Abwässer. Forum Siedlungswasserwirtschaft und Abfallwirtschaft, Universität Duisburg-Essen. Shaker, Aachen
4. Reith JH, Wijffels RH, Barten H (2003) Bio-methane and bio-hydrogen status and perspectives of biological methane and hydrogen production. Dutch Biological Hydrogen Foundation, The Hague. ISBN 9090171657
5. Petrovic T, Wagner HJ, Lente A, Widmann R (2005) Photobiologische Wasserstofferzeugung durch Mikroalgen – Beschreibung konkurierender Systeme zur H_2-Erzeugung. Stärkung der technologischen Position an den Ruhruniversitäten Teilprojekt 8 ef. Ruhr Förderkennzeichen 856569-T-170
6. Rechtenbach D (2009) Fermentative Erzeugung von Biowasserstoff aus biogenen Roh- und Reststoffen.

Dissertation am Institut für Abfallressourcenwirtschaft, Technische Universität Hamburg-Harburg. In: Stegmann R (ed) Hamburger Berichte 34. Verlag Abfall aktuell, Stuttgart
7. Krupp M (2007) Bio hydrogen production from organic waste and waste water by dark fermentation – a promising module for renewable energy production. Forum Siedlungswasserwirtschaft und Abfallwirtschaft, Universität Duisburg-Essen. Shaker, Aachen
8. Van Ginkel SW, Logan B (2005) Increased hydrogen production with reduced organic loading. Water Res 39:3819–3826
9. Hyvolution. http://www.fch-ju.eu/sites/default/files/documents/ga2010/pieternel_claassen.pdf
10. Modigell M, Schumacher M, Claassen PAM, Friedl A, Wukovits W (2006) Entwicklung eines zweistufigen Bioprozesses zur Produktion von Wasserstoff aus Biomasse. GVC IT, Wiesbaden
11. Zeidan AA, van Niel EWJ (2007) Developing a thermopilic hydrogen-producing co-culture for efficient utilization of mixed sugars. WHTC, Montecationi Terme
12. Levin DB, Pitt L, Love M (2004) Biohydrogen production: prospects and limitations to practical applications. Int J Hydrogen Energy 29(2):173–185
13. Hemmes K, de Groot A, den Uil H (2003) Bio-H2 Application potential of biomass related hydrogen production technologies to the Dutch energy infrastructure of 2020–2050. ECN-C-03-028. Energy Research Center, Petten
14. Schlegel HG (1997) Allgemeine Mikrobiologie, 1st edn. Thieme, Stuttgart. ISBN 3-13-444607-3
15. Hawkes FR, Dinsdale RM, Hawkes DL, Huss I (2002) Sustainable fermentative H_2 production: challenges for process optimization. Int J Hydrogen Energy 27:1339–1347
16. Benemann JR (2004) Biological production of hydrogen-methane mixtures for clean electricity production. In: 15th hydrogen energy conference, Japan
17. IHS (2005) CEN/TS 14961 Solid biofuels – fuel specification and classes. IHS, Englewood Cliffs
18. Hofbauer H, Veronik G, Fleck T, Rauch R (1997) The FICFB gasification process. In: Bridgwater AV, Boocock D (eds) Developments in thermochemical biomass conversion, vol 2. Blackie Academic & Professional, Glasgow, pp 1016–1025
19. Thrän D, Seidenberger T, Zeddies J, Offermann R (2010) Global biomass potentials – resources, drivers and scenarios. Energy Sustain Dev 14(3):200–205
20. Dinjus E, Kolb T, Dahmen N (2009) State of the art of the bioliq BTL process. In: European biomass conference and exhibition 2009, Hamburg
21. Albertazzi S, Basile F, Brandin J, Einvall J, Hulteberg C, Fornasari G et al (2005) The technical feasibility of biomass gasification for H_2 production. Catal Today 106:297–300. doi:10.1016/j.catted.2005.07.160
22. McKeough P, Kurkela E (2008) Process evaluations and design studies in the UCG project 2004–2007. VTT Research Notes 2434. http://www.vtt.fi/publications/index.jsp
23. Harju-Jeanty T, Nuortimo K, Hotta A, Coda-Zabetta E, Palonen J, Kokki S et al (2009) Innovative utilization of renewable energy sources to combat climate change. In: Fourth international bioenergy conference 2009, Jyväskylä
24. Paisley MA, Overend RP (2002) Verification of the performance of future energy resources' SilvaGas® biomass gasifier – operating experience in the Vermont gasifier. Paper presented at the Pittsburgh coal conference, 24–26 September 2002, Pittsburgh
25. Paisley M (2007) Advanced biomass gasification for the production of biopower, fuels, and chemicals. AIChE, Salt Lake City
26. Hofbauer H, Rauch R, Loeffler G, Kaiser S, Fercher E, Tremmel H, et al (1998) Six years experience with the FICFB-gasification process. In: Twelfth European conference and technology exhibition on biomass for energy, industry and climate protection, Amsterdam
27. Koppatz S, Pfeifer C, Rauch R, Hofbauer H, Marquard-Moellenstedt T, Specht M et al (2009) H_2 rich product gas by steam gasification of biomass with in situ CO_2 absorption in a dual fluidized bed system of 8 MW fuel input. Fuel Process Technol 90(7–8):914–921. doi:10.1016/j.fuproc.2009.03.016
28. Marquard-Möllenstedt T, Sichler P, Specht M, Michel M, Berger R, Hein K et al (2004) New approach for biomass gasification to H_2. In: Proceedings of the second world conference and technology exhibition on biomass for energy, industry and climate protection, Rome, pp 10–14
29. Soukup G, Pfeifer C, Kreuzeder A, Hofbauer H (2009) In situ CO_2 capture in a dual fluidized bed biomass steam gasifier – bed material and fuel variation. Chem Eng Technol 32 (3):348–354. doi:10.1002/ceat.200800559
30. Pfeifer C, Puchner B, Hofbauer H (2009) Comparison of dual fluidized bed steam gasification of biomass with and without selective transport of CO_2. Chem Eng Sci 64(23):5073–5083. doi:10.1016/j.ces.2009.08.014
31. IEA Hydrogen Implementing Agreement (2006) Prospects for hydrogen from biomass, Annex 16 Subtask B, Final report

Books and Reviews

Bienert K (2009) Commercial scale BTL production on the verge of becoming reality. Biomass gasification seminar, Stockholm, 22–23 Oct 2009

Crotogino F, Hamelmann R (2007) Wasserstoff-speicherung in Salzkavernen. In: Tagungsband "14. symposium zur nutzung regenerativer energiequellen und wasserstofftechnik", Stralsund

Droste-Franke B, Bert H, Kötter A et al (2009) Brennstoffzellen und virtuelle kraftwerke. In: Gethmann CF (ed) Ethics of science and technology assessment, vol 36. Springer, Berlin, pp 43–131. http://www.springerlink.com/content/vu43p4/

DWV (2005) Deutscher Wasserstoff- und Brennstoffzellen-Verband e.V.; Press Release No. 5/05: Wasserstoff Spiegel 5/2005

DWV (2007) Deutschland schließt wieder zur Weltspitze auf–aber die Konkurrenz schläft nicht. Deutscher Wasserstoff- und Brennstoffzellen-Verband e.V.; Press Release No. 1/07 (22 Feb 2007)

Erdle EK (2001) Grundlagen, stand und perspektiven der brennstoffzellen-technik. In: VDI-Gesellschaft Energietechnik (ed) Stationäre brennstoffzellenanlagen: markteinführung Tagungsband. VDI, Düsseldorf, pp 3–14

FNR (ed) (2006) Wasserstoff aus biomasse, vol 25. Gülzower Fachgespräche, Gülzow

Gao M, Krishnamurthy R (2009) Hydrogen transmission in pipelines and storage in pressurized and cryogenic tanks. In: Gupta RB (ed) Hydrogen fuel – production, transport and storage. CRC-Press, Boca Raton, pp 341–379

Hoogwijk M, Faaji A, van Den Broek R, Berndes G, Gielen D, Turkenburg W et al (2003) Exploration of the ranges of the global potential of biomass for energy. Biomass Bioenerg 25:119–133. doi:10.1016/S0961-9534(02)00191-5

Jorde F (2006) Laboruntersuchungen zur fermentativen erzeugung von Biowasserstoff in den testsystemen sensomat und ATS unter Einsatz von Rein- und Mischkulturen. Diploma Thesis at the Institute of WasteRessourceManagement, TUHH, unpublished

Jurschik E-M (2007) Optimierung diskontinuierlicher versuche zur fermentativen bio-wasserstoffproduktion, sowie aufbau und inbetriebnahme eines bio-methanreaktors. Diploma Thesis at the Institute of WasteRessourceManagement TUHH, unpublished

Maddy J, Cherryman S, Hawkes FR, Hawkes DL, Dinsdale RM, Guwy AJ, Premier GC, Cole S (2003) Hydrogen 2003. Report Number 1, ERDF part-funded project entitled "A sustainable energy supply for Wales: towards the hydrogen economy." University of Glamorgan, Pontypridd, Mid Glamorgan, Wales, ISBN 1-840540-90-7

Meyer M, Rechtenbach D, Stegmann R (2007) Biological production of H2 from organic raw and waste materials by fermentation with pure and mixed cultures. In: 15th European biomass conference, Berlin, 05 July–05 Nov 2007 (Proceedings CD)

Nandi R, Sengupta S (1998) Microbial production of hydrogen: an overview. Crit Rev Microbiol 24(1):61–84

Noike T, Takabatake H, Mizuno O, Ohba M (2002) Inhibition of hydrogen fermentation of organic wastes by lactic acid bacteria. Int J Hydrogen Energy 27:1367–1371

Pehnt M, Höpfner U (2009) Wasserstoff- und stoffspeicher in einem energiesystem mit hohen anteilen erneuerbarer energien: analyse der kurz- und mittelfristigen perspektiven. Kurzgutachten. IFEU -Institut für Energie und Umweltforschung, Heidelberg. http://www.bmu.de/files/pdfs/allgemein/application/pdf/ifeu_kurzstudie_elektromobilitaet_wasserstoff.pdf. Accessed 22 Feb 2010

Plath M (2006) Untersuchung und Optimierung der diskontinuierlichen erzeugung von biowasserstoff in dem testsystem ATS unter einsatz von klärschlamm und glukose. Project work at the Institute of WasteRessourceManagement, TUHH, unpublished

Rechtenbach D (2009) Fermentative erzeugung von biowasserstoff aus biogenen roh-und reststoffen. Hamburger Berichte 34, Abfallwirtschaft, T.U.Hamburg- Harburg, Germany, Verlag Abfall aktuell

Rechtenbach D, Meyer M, Stegmann R (2006) Fermentative production of bioH2 from organic raw and waste materials. In: Proceedings of the international conference ORBIT 2006 – biological waste management from local to global, 13–15 Sept 2006, Weimar; Kraft E, Bidlingmaier W, de Bertoldi M, Diaz LF, Barth J (Hrsg) Lombego systems & goldwiege. Visualle Projekte, Weimar, pp 869–877, ISBN 3-935974-09-4

Reiß T, Hüsing B (1993) Biologische wasserstoffgewinnung – forschungsperspektiven und technikfolgen. Verlag TÜV Rheinland, Köln. ISBN 3-8249-0150-1

Tanksale A, Beltramini JN, Lu GM (2010) A review of catalytic H_2 production processes from biomass. Renew Sustain Energy Rev 14(1):166–182. doi:10.1016/j.rser.2009.08.010

van Ginkel S, Sung S, Lay J-J (2001) $BioH_2$ as a function of pH and substrate concentration. Eviron Sci Technol 35:4726–4730

Zurawski D, Susanto AL, Stegmann R (2004a) Fermentative erzeugung von bio-wasserstoff aus biogenen roh- und reststoffen. In: Proceedings (CD-ROM) des 10. Internationalen kongresses für nachwachsende rohstoffe und pflanzenbiotechnologie NAROSSA, Magdeburg, 07–08 June 2004

Zurawski D, Susanto AL, Stegmann R (2004b) Sind bioabfälle und energiepflanzen zur biologischen wasserstofferzeugung geeignet? In: Fricke K, Kosak G, Wallmann R, Fischer J, Vogtmann H (eds) Schriftenreihe des ANS, 65. Informationsgesprächs des ANS e.V. "EEG und Emissionshandel – Neue Chancen für Biomassenutzung und Abfallwirtschaft", 06–07 Dec 2004, Braunschweig, pp 189–200. ISBN 3-935974-06-X

Zurawski D, Meyer M, Stegmann R (2005) Fermentative production of $bioH_2$ from biowaste using digested sewage sludge as inoculum. In: Cossu R, Stegmann R (eds) Proceedings of Sardinia 2005 – tenth international waste management and landfill symposium. CISA Environmental Sanitary Engineering Centre, Santa Margerita di Pula, Cagliari, 03–07 Oct 2005

Hydrogen Production from High-Temperature Fuel Cells

Jacob Brouwer, Pere Margalef
National Fuel Cell Research Center, University of California, Irvine, CA, USA

Article Outline

Glossary
Definition of the Subject
Introduction
Background
Key Principles of Poly-Generation of H_2 with HTFC

Cycle Configurations for Poly-Generating HTFC
Comparative Efficiency Analyses
Hydrogen Transport Impacts on Comparative Analyses
Discussion of Scientific Basis for Observed Performance
World's First Poly-Generating HTFC System
Future Directions
Bibliography

Glossary

Distributed energy resources (DER) Small-scale power generation, energy conversion, storage, and/or control technologies (typically in the range of 3–10,000 kW) that are installed and operated close to the energy demand (e.g., a home or business). These resources can provide an alternative to or an enhancement of the existing electric power and thermal energy systems. Among the main advantages of the DER are the energy saving associated with the transport of energy from the centralized plants to the points of use and the potential to poly-generate power, heating, cooling, and/or fuels close to the point of use.

Distributed generation (DG) According to the California Energy Commission [7], distributed generation (DG) comprises small-scale power generation technologies (typically in the range of 3–10,000 kW) located close to where electricity is used (e.g., a home or business) to provide an alternative to or an enhancement of the existing electric power system. Among the main advantages of the distributed generation are the energy saving associated with the transport of energy from the centralized plants to the points of use and the potential for cogeneration of heat and power.

High-temperature fuel cells (HTFC) HTFC are electrochemical conversion devices that produce electricity directly from the chemical potential difference between a fuel and oxidant. There are two common types of high-temperature fuel cells: (1) molten carbonate fuel cells (MCFC) and (2) solid oxide fuel cells (SOFC).

The *molten carbonate fuel cell* uses a carbonate electrolyte, which is generally a mixture of lithium and potassium carbonates (salts). At the high operating temperature (typically 550–650°C) the alkali carbonates become a highly conductive molten salt, with CO_3^{2-} ions providing ionic conduction. Anode materials are typically Ni–Cr/Ni–Al alloys and cathode materials are comprised of lithiated NiO [2]. The fuel cell operation is the result of a complex conjunction of physical, chemical, and electrochemical processes that together oxidize fuel and reduce oxidant in separate compartments to produce electricity, heat, and redox reaction products. The anode and cathode half reactions and overall electrochemical reaction are [3]

$$\text{Cathode}: 0.5O_2 + CO_2 + 2e^- \rightarrow CO_3^{2-} \quad (1)$$

$$\text{Anode}: H_2 + CO_3^{2-} \rightarrow H_2O + CO_2 + 2e^- \quad (2)$$

$$\text{Overall}: H_2 + 0.5O_2 + CO_{2,\text{cat}} \rightarrow H_2O + CO_{2,\text{an}} + \text{electricity} + \text{heat} \quad (3)$$

Note that carbon dioxide must be supplied to the cathode as well as oxygen. The CO_2 is converted to carbonate ions which provide the means of ion transfer between the cathode and the anode. Therefore, there is a net transfer of CO_2 from cathode to anode. There are different ways of CO_2 recycling. The most common method feeds the anode exhaust gas to an anodic gas oxidizer (AGO), which converts any unused hydrogen or carbon monoxide into water and CO_2. A portion of the exhaust gas from the anodic gas oxidizer is then mixed with fresh air and fed into the cathode inlet. This process also serves to preheat the reactant air, burn the unused fuel, and bring the waste heat into one stream for use in a bottoming cycle [4].

The *solid oxide fuel cell* uses an oxide ion-conducting ceramic material as the electrolyte. Since only two phases (solid and gas) are required and CO_2 recirculation is not required, these systems are conceptually simpler than other fuel cells [5]. As in the molten carbonate case, no precious metal catalysts are needed due to the high operating temperatures (700°C–1,000°C). SOFC have typically used materials sets based upon a yttria-stabilized zirconia (YSZ) electrolyte comprised of 8–10% Y_2O_3 in ZrO_2 [2]. Above 700°C, YSZ becomes a conductor of oxygen ions (O^{2-}). The negatively charged ion (O^{2-}) is transferred

from the cathode to the anode [6]. The half-reactions produce water in the anode as follows:

$$\text{Anode}: H_2 + O^{2-} \rightarrow H_2O + 2e^- \quad (4)$$

$$\text{Cathode}: 0.5O_2 + 2e^- \rightarrow O^{2-} \quad (5)$$

$$\text{Overall}: H_2 + 0.5O_2 \rightarrow H_2O + \text{electricity} + \text{heat} \quad (6)$$

The remaining SOFC fuel from the anode reactions is typically oxidized by the remaining oxygen from the cathode in a combustor to produce heat. This heat is used in the fuel cell plant to preheat the inlet streams and/or overcome the endothermicity of steam reforming reactions elsewhere in the system.

Hydrogen separation When hydrogen is produced by thermochemical processes such as steam methane reformation (SMR), the output gas is a hydrogen-rich gas (i.e., reformate) that contains water vapor, carbon monoxide, carbon dioxide, and other trace gases. Therefore, hydrogen must be separated from the reformate gas and purified to reach the specific requirements for hydrogen use.

Hydrogen separation in refineries has been traditionally done by established technologies such as pressure swing adsorption (PSA), selective permeation processes using polymer membranes, or cryogenic separation processes. Each process is based upon different separation principles. Economic aspects and other project considerations such as process flexibility, reliability, and scalability have to be taken into account to decide the hydrogen separation method [10].

Besides the traditional methods, alternative techniques for hydrogen separation are being developed. These include the Electrochemical Hydrogen Separation method (EHS) and Hydrogen Separation Membrane Reactor (HSMR) [11].

Parasitic loads In power generation devices, parasitic loads are those loads associated with the normal operation of the system that are required to sustain the normal operation of the system in a safe and reliable manner. Typical parasitic loads are associated with the preparation of the reactants, handling of products, exchanging of heat and flows, and thermal management. The power required for these parasitic loads must be produced by the same generator and subtracted from the generator power to produce the net system power output. Ideally, parasitic loads should be minimized in order to achieve higher system efficiencies.

Poly-generation Poly-generating systems include energy conversion systems that convert fuel chemical energy into multiple useful forms of energy or power. For instance, a specific poly-generation system instance that produces only two products is a combined heat and power (CHP) system that generates electrical and thermal power from fuel in a single, integrated system. Poly-generating systems are typically comprised of a number of individual components, including for example a heat engine, generator, heat recovery equipment, and electrical interconnection hardware that are configured into an integrated whole system. The primary energy conversion device (i.e., the prime mover) is typically used to identify the type of poly-generating system. Prime movers include reciprocating engines, gas or steam turbines, and fuel cells that can produce electrical and thermal power from a variety of fuels, including natural gas, coal, and biofuels. Thermal energy from the system can be used in direct process applications or indirectly to produce steam, hot water, hot air for drying, or chilled water for process cooling [8]. High-temperature fuel cells, in particular, can be designed and operated to poly-generate electricity, heat, and useful chemicals (such as hydrogen) in a variety of configurations [9].

Steam methane reformation (SMR) Steam methane reforming is a mature industrial technology that is typically used for hydrogen production. The basic reforming reaction for methane is

$$CH_4 + H_2O \rightarrow 3H_2 + CO \quad (7)$$

SMR is an endothermic reaction so that heat must be provided to drive the reaction forward to produce hydrogen. The overall process for hydrogen production typically also includes the water–gas-shift reaction defined below.

Synergy Synergy describes the complementary interaction of processes to create an outcome that is in some way of more value than the sum of the individual values that would otherwise have been

produced by the individual processes operating independently.

Water–gas shift (WGS) The reaction of carbon monoxide with water to produce hydrogen and carbon dioxide as follows:

$$CO + H_2O \rightarrow CO_2 + H_2 \quad (8)$$

The WGS reaction is reversible and exothermic.

Well-to-tank (WTT) efficiency Well-to-tank efficiency is defined as the total energy of a ready-to-be-used fuel (i.e., in the tank of the vehicle), divided by the total energy required for the extraction, preparation, transport, and dispensing of the same fuel. This efficiency calculation is widely used in the automotive sector to compare the energy intensity of different fuels. On the other hand, well-to-wheel (WTW) efficiency accounts for the inefficiencies of the vehicle propulsion system. WTT are higher than WTW efficiencies.

Definition of the Subject

Hydrogen is a likely energy carrier of the future due to the absence of carbon, low emissions when converted in various end-use technologies, and ability to be cleanly and efficiently produced from various domestic primary energy sources. In 2003 the Federal government launched the Hydrogen Fuel Initiative with a total budget of $1.2 billion over 5 years in order to accelerate research and development of fuel cell technologies [12]. Importantly, major automobile manufacturers are operating fuel cell vehicles that run on pure hydrogen gas, and several fuel cell buses are in operation in major cities around the world. Companies such as Shell, Air Products and Chemicals, Chevron, and Air Liquide are developing hydrogen production, distribution, and dispensing technologies for hydrogen vehicles along with strategies to deploy them. Moreover, the state of California intends to reduce the carbon content of transportation fuels through the Low Carbon Fuel Standard. Additional legislation in the areas of energy and climate, such as that contained in California laws entitled AB32, AB1493, SB76, and SB1368, highlight California's commitment to ensuring low greenhouse gas emissions for both electricity and transportation fuels [12]. Many other places around the world, including Germany and fellow European Union countries, Japan, China, and Korea, are advancing hydrogen fueling and vehicle technology. Therefore, developing a highly efficient, low-emission, and economically viable hydrogen production and delivery methodology is of great importance from environmental, social, economic, and political perspectives.

The production of hydrogen from high-temperature fuel cells is accomplished by a synergistic integration of fuel processing, electrochemical conversion in a fuel cell, and hydrogen separation that leads to an ability to locally produce and deliver hydrogen with ultralow criteria pollutant and greenhouse gas emissions. The resulting system comprised of a high-temperature fuel cell that produces electricity, heat, and hydrogen fuel uses a hydrogen separation unit (HSU) that separates and purifies the hydrogen from the anode off-gas, and is typically referred to as a poly-generating or tri-generating fuel cell. Figure 1 shows a basic schematic of a poly-generating HTFC.

Introduction

Since it is not naturally occurring, hydrogen must be produced from water via electrolysis, photolysis, or thermal splitting, or from hydrocarbon fuels (e.g., natural gas, coal, biogas, biomass) via reformation or gasification. Currently, hydrogen is typically produced at large centralized steam methane reformation (SMR) plants from natural gas. SMR is a convenient and

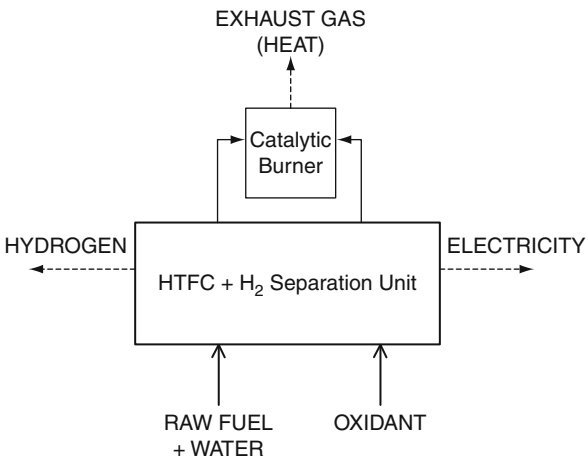

Hydrogen Production from High-Temperature Fuel Cells. Figure 1
Basic schematic of a poly-generating HTFC

cost-effective method that has been implemented to produce a substantial commercial supply for petroleum refining, metals processing, and other industrial uses. Not only hydrogen production (e.g., SMR plants and a host of other cost-effective and environmentally sensitive production technologies) but also energy-efficient and environmentally sensitive technologies for transport, distribution, and dispensing of hydrogen will be needed in the future [13].

Distributed generation of hydrogen, while typically less efficient than centralized generation, is foreseen by many as a viable strategy to produce hydrogen due to the savings associated with transport and distribution of the hydrogen, which can be energy and emissions intensive. Significant efforts to develop small-scale hydrogen production plants have led to commercialization of relatively affordable systems. Ogden [14] reviewed the development and commercialization status of various types of small-scale reformers.

Conventional steam methane reformers consisting of long catalyst-filled tubes that operate at high pressures (15–25 atm) and high temperatures (850°C) have been successfully scaled down to units that produce as little as 10–100 kg/h. However, at such small sizes, relative capital costs are too high to compete with large-scale hydrogen production. In addition, the footprint of these systems may be too large to be placed at conventional fueling stations. For this reason, more compact and inexpensive designs have been, and are being, developed by many manufacturers. The average hydrogen production efficiency reported for good systems ranges between 60% and 77% (on a LHV basis) [14]. The main technical challenges of distributed reformers include relatively larger system heat losses at small scale and inability to produce hydrogen on demand that may require large hydrogen storage capabilities, especially during the early stages of hydrogen vehicle deployment.

Background

As indicated above, most hydrogen is produced today from fossil fuels in large SMR plants and is used at or near the production site [13]. As fuel cells and hydrogen vehicles become more widely used, an entire infrastructure for the distribution and dispensing of hydrogen will be needed with the additional goal of producing and delivering hydrogen to consumers in an environmentally sensitive manner [15].

An integrated energy future that meets transportation fuel and stationary power and thermal energy demands could be made from the same primary energy sources. For example, the primary feedstock currently used for the production of hydrogen (i.e., natural gas) is also a significant primary energy source for electricity production. As both energy sectors (transportation and electricity generation) come to rely on the same primary energy sources, there are significant opportunities to integrate them, which can introduce profound changes in how our energy is converted and distributed. The integration of these two energy sectors at the level of a production plant via poly-generation of hydrogen, heat, and electricity could lead to lower prices for both transportation and stationary applications and ultimately enhance overall efficiency and flexible use of diverse resources [9].

Electricity and hydrogen poly-generation can be accomplished at large or at small scale. For the large-scale approach, hydrocarbon feedstocks such as coal, natural gas, or biomass can be converted via thermochemical processes to a syngas. Syngas is comprised of hydrogen, water, carbon monoxide, and carbon dioxide and can be used to generate electricity in a fuel cell, steam cycle, gas turbine, or combination of these technologies (i.e., combined cycle). Since the syngas produced has a high concentration of hydrogen, part of the gas stream can be diverted and the hydrogen can be separated from the rest of the gas to produce high-purity hydrogen for fuel cell vehicle use.

For the small-scale approach, poly-generating fuel cells represent a viable technology to produce hydrogen, electricity, and heat on demand in a distributed fashion. Excess heat released during the electrochemical fuel cell reactions can be used to produce hydrogen through steam reformation of hydrocarbon fuels. The highly synergistic nature of the poly-generating concept at high temperatures leads to higher production efficiencies compared to conventional hydrogen and electricity generation [16]. If successfully developed, poly-generating HTFC that produce electricity, heat, and hydrogen from a variety of hydrocarbon fuels will provide high efficiency and low emissions distributed hydrogen production and delivery. In addition, such a concept

could aid fuel cell market viability, stakeholder confidence, and energy security and sustainability together with emissions reduction [17].

Key Principles of Poly-Generation of H_2 with HTFC

The key principles that apply to high-temperature fuel cell systems that poly-generate electricity, heat, and hydrogen are as follows:

1. Fuel flexibility of high-temperature fuel cells
2. High-temperature fuel cell–fuel processing relationship
3. Low entropy associated with exchanging heat at similar temperature
4. Fuel utilization concept requires excess fuel processing
5. Lower fuel utilizations lead to higher electrochemical efficiencies
6. Endothermicity of hydrocarbon reformation provides needed cell cooling
7. Production of excess hydrogen produces higher fuel cell efficiency
8. Chemical synergy associated with reactant/product interactions
9. All synergies lead to lower fuel cell system parasitic losses
10. Electrochemical and catalytic processes are inherently low emissions
11. Processes are efficient even at small size enabling distributed production
12. Hydrogen transport involves emissions and energy penalties

A brief description of each of these key principles is presented in this section.

Fuel Flexibility of High-Temperature Fuel Cells

High-temperature fuel cells, such as the molten carbonate fuel cell (MCFC) and solid oxide fuel cell (SOFC), can be operated on a variety of hydrocarbon fuels including natural gas, digester gas, landfill gas, coal and biomass synthesis gases. MCFC and SOFC technologies comprise specific characteristics that make them especially amenable to operation on such hydrocarbon fuels. These characteristics include the use of an oxidizing ion in the electrochemical reactions (CO_3^{2-} for MCFC and O^{2-} for SOFC) and high-temperature operation (550–650°C for MCFC and 700–1,000°C for SOFC) which promotes sufficiently rapid chemical and electrochemical reactions.

High-Temperature Fuel Cell: Fuel Processing Relationship

Solid oxide fuel cells (SOFC) and molten carbonate fuel cells (MCFC) generate electricity and heat through exothermic electrochemical reactions. Oxidation of hydrogen takes place in the anode compartment, which overall thermodynamics are described by the global reaction:

$$H_2 + 0.5O_2 \rightarrow H_2O \quad \Delta\bar{h}_f = -241.83\,\mathrm{KJ\,mol^{-1}} \tag{9}$$

The electrochemical oxidation reactions that convert hydrogen to water in the SOFC and MCFC anode compartments are, respectively:

$$H_2 + O^{2-} \rightarrow H_2O + 2e^- \tag{10}$$

$$H_2 + CO_3^{2-} \rightarrow H_2O + CO_2 + 2e^- \tag{11}$$

These reactions are complemented by corresponding oxidant reduction reactions in the cathode compartment, ion transport, and electron flow to perpetuate the electrochemical reactions. Since electricity is produced by these electrochemical reactions at less than 100% efficiency, the remaining portion of the enthalpy of reaction produces heat as reactants are converted to products.

HTFC system designs typically incorporate fuel processing with electrochemical conversion. The global fuel processing reaction includes steam methane reforming and water–gas-shift reactions and is described by:

$$CH_4 + 2H_2O \rightarrow 4H_2 + CO_2 \quad \Delta\bar{h}_f = -165\,\mathrm{KJ\,mol^{-1}} \tag{12}$$

The heat generated by the electrochemical reactions of Eq. 9 tends to be greater than the heat required by the endothermic fuel processing reactions of Eq. 12 for the amount of electricity produced [6]. Surplus heat is typically used to preheat the fuel and oxidant streams before they enter the fuel cell and to produce the steam required for system operations. Therefore, more hydrocarbon fuel than that required for the electric power

generation could be processed in a HTFC, creating a hydrogen-rich stream that could be subsequently purified and delivered to the point of use without the need of an additional reformer.

Low Entropy Associated with Exchanging Heat at Similar Temperature

To proceed at a sufficiently fast rate and to completion (i.e., consume all the hydrocarbon fuel to produce hydrogen-rich syngas), the fuel processing reactions (e.g., steam reformation reaction of Eq. 12) must occur at a reasonably high temperature. Irreversible heat transfer processes between the exothermic fuel cell reactions (i.e., heat source) and the endothermic reforming reactions (i.e., heat sink) increase the entropy generation of the system. This irreversible heat transfer must be provided to a typical reformer reactor in a fuel cell system, using either fuel combustion or fuel cell exhaust heat at temperatures above those at which the reformation reactions proceed. However, the operating temperatures of HTFC (550–650°C for MCFC and 700–1,000°C for SOFC) are similar to the temperatures at which hydrogen production rate and reaction completion are acceptable for steam methane reformation processes (i.e., ~700°C). Therefore, heat can be transferred from the exothermic to the endothermic process with minimal (or zero) temperature difference leading to low entropy generation for heat exchange, resulting in overall high efficiency.

Fuel Utilization Concept Requires Excess Fuel Processing

Fuel and oxidant utilization factors refer to the fractions of the total fuel and oxidant flowing through the anode and cathode compartments that are consumed to generate electricity. If fuel and/or oxidant species concentrations become too low, the chemical potential difference becomes unable to sustain a voltage difference. The Nernst potential (V_{Nernst}) describes the relationship between voltage and reactant and product concentrations that applies to a fuel cell

$$V_{\text{Nernst}} = E_0 + \frac{RT}{2F} \ln \frac{x_{H_2} x_{O_2}^{\frac{1}{2}}}{x_{H_2O}} \tag{13}$$

where E_0 is the ideal reversible potential, F is Faraday's constant [96,487 kC/kmol], R is the gas constant, T is the operating temperature, and x_k is the concentration of the species k [6].

Since fuel cell electrodes are good electronic conductors (they act as equipotential surfaces), low reactant concentrations anywhere in the anode or cathode compartments leads to voltage that cannot be sustained. Therefore, fuel utilization (U_f) and oxygen utilization (U_{O_2}) must be always lower than 100%. In other words, the amount of fuel and oxidant fed into the fuel cell must always and continuously be greater than the amount consumed within the stack to produce electricity even when hydrogen is not produced.

Lower Fuel Utilizations Lead to Higher Electrochemical Efficiencies

In operational fuel cell systems, cell voltage increases as fuel utilization decreases, which results in higher electrochemical efficiencies. The electrochemical efficiency is defined as the actual cell voltage (V_{cell}) divided by the thermodynamically possible cell voltage ($V_{\max}$), or

$$\eta_{\text{cell}} = \frac{V_{\text{cell}}}{V_{\max}} \tag{14}$$

where $V_{\max}$ is defined as the maximum theoretical voltage that would be achieved if all the energy from the hydrogen fuel were transformed into electrical energy [16], or

$$V_{\max} = \frac{-\Delta \bar{g}_f}{n_i F} \tag{15}$$

where $\Delta \bar{g}_f$ is the Gibbs free energy, n_i is the number of electrons transferred during the electrochemical oxidization of fuel species i ($n_i = 2$ for H_2 and CO, $n_i = 8$ for CH_4), and F is Faraday's constant.

From the Nernst voltage equation Eq. 13, it can be observed that higher species concentrations lead to higher cell voltages. At lower fuel utilizations, reactant species concentrations are higher along the electrode channels. Thus, it can be stated that lower fuel utilization results in higher cell voltages that raise the electrochemical efficiency of the fuel cell as described by Eq. 14.

An alternative concept that provided insight into the effects of the fuel utilization on the electrochemical

efficiency relates to the mixing of products with reactants to dilute the electrochemically active species concentrations. Water product mixes with the anode gas as it is formed by the electrochemical reactions in an MCFC or SOFC. The concentration of water product in the anode increases as the fuel utilization factor increases. Mixing processes are irreversible so they produce entropy. As a result, a completely reversible fuel cell operation would be only approached as $\mathbf{U_f} \rightarrow 0$. In other words, irreversibilities increase as the utilization factor increases [18].

Consequently, one desires to operate a fuel cell at the lowest possible utilization factor to maximize the cell voltage and reduce mixing irreversibilities. However, unless one recycles or otherwise uses the anode off-gas then one alternatively desires high utilization to achieve high overall stack electrical efficiency. Typically, fuel utilization is selected in the 70–90% range to balance these considerations.

One of the key principles of poly-generating fuel cells is related to the capability of operating the fuel cell at lower fuel utilizations without compromising the overall system electrical efficiency. As already stated, hydrogen that is not electrochemically oxidized will be separated and considered as a valuable system output. Therefore, inasmuch as additional hydrogen is separated and used, there is the opportunity to take advantage of the higher electrochemical efficiency that is a natural by-product of the lower fuel utilizations required for hydrogen production.

Endothermicity of Hydrocarbon Reformation Provides Needed Cell Cooling

The fact that fuel cells must be cooled to maintain steady state operating temperature allows for synergistic coupling of endothermic steam reforming with exothermic fuel cell electrochemical reactions to yield unprecedented efficiency. Adding more endothermic reforming reactions for the same amount of electrochemical reactions results in a reduced requirement for air cooling of the cell. The synergistic performance benefits related to these lower cooling requirements are caused by: (1) the additional endothermic reformation at lower fuel utilization that provides additional cooling to the fuel cell stack; and (2) less electrochemical heat generated per mol of input fuel due to the higher voltages achieved at lower fuel utilizations. Both phenomena reduce the auxiliary power associated with forcing air through the cathode compartment, which is the primary means of otherwise removing heat from the fuel cell.

Chemical Synergy Associated with Reactant/Product Interactions

High-temperature fuel cells operate at high enough temperatures to convert methane into fuels that are more amenable to electrochemical oxidation such as hydrogen and carbon monoxide within the anode compartment. This concept is known as internal reformation (IR) and represents one of the key features of high-temperature fuel cells that can yield exceptionally high electrical efficiencies when compared with low-temperature fuel cells that process fuel in a separate reactor (i.e., external reformation). The main synergy associated with IR is related to the direct consumption of the hydrogen product of the reforming reaction by the electrochemical fuel cell reactions that produce water, a reformation reactant, which all occurs at the same time and physical location [17]. The immediate consumption of products and provision of reactants by the fuel cell reactions drives the reformation reaction forward and assures reaction completeness. Continual production of hydrogen and consumption of water by reformation also directly facilitates electrochemical reaction progress. This chemical synergy is introduced in addition to the heat exchange synergy between exothermic fuel cell reactions and endothermic fuel processing reactions with minimum losses since both reactions occur at the same time and place. Figure 2 shows the main

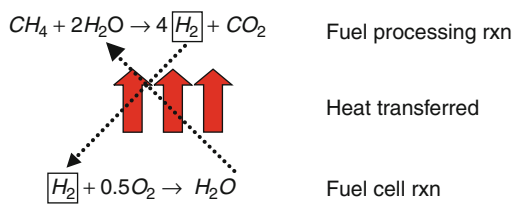

Hydrogen Production from High-Temperature Fuel Cells. Figure 2
Internal reformation chemical and thermal synergy mechanisms

reactions, chemical exchange synergy, and heat transfer processes occurring during internal reformation in high-temperature fuel cells.

All Synergies Together Work in the Same Direction to Increase Fuel Cell System Efficiency

At low fuel utilizations, the ratio between endothermic heat from the fuel processing reactions and exothermic heat from the electrochemical reactions increases, leading to a reduction of the auxiliary power required to circulate cooling air through the cathode. In addition, thermodynamic analyses demonstrate that cooling required per mol of fuel input drops at lower fuel utilizations due to the higher operational voltages at low fuel utilizations [16]. The design and operating changes that produce these synergies require changes in the same direction. Therefore, all of the described synergies of poly-generating high-temperature fuel cells can work together to result in higher fuel cell efficiencies compared to conventional fuel cell system designs that do not poly-generate. There remain design challenges, such as managing the fuel cell temperature gradient in poly-generating systems, but, the overall design and operating changes required for poly-generation work together to improve efficiency.

Integration with Hydrogen Separation Produces Higher System Efficiency

Fuel cells are by nature required to produce somewhat more hydrogen than is electrochemically converted in the anode compartment. However, operating at lower fuel utilization leads to higher electrochemical efficiency and the chemical synergies of internal reforming, and the endothermicity of fuel processing reactions leads to lower parasitic losses due to reduced air blower power. These features by themselves would not be beneficial to overall system efficiency until and unless they are integrated into a system design that produces a significant amount of product hydrogen leading to remarkably higher overall efficiency. This is accomplished by using the above principles in combination with hydrogen separation technology that is integrated with the system design requirements in a manner that exchanges more heat for useful electrochemical and hydrogen production purposes.

Electrochemical and Catalytic Processes Are Inherently Low Emissions

The inherent electrochemical and catalytic nature of high-temperature fuel cells and poly-generating fuel cells yields ultralow criteria pollution emissions.

- Thermal NO_x requires high-temperature combustion in air whereas in HTFC, all of the fuel is processed and converted either electrochemically or by catalytic processes at low temperature.
- SO_x cannot be produced since sulfur is removed from the fuel before entering the system.
- Particulate matter (PM) is not produced due to high water content, catalyst presence, and low-temperature conditions extant in the anode compartment, followed by catalytic and/or low-temperature oxidation of the anode off-gas.
- CO is amenable to the electrochemical oxidation to release electrons in the anode compartment and the remainder is consumed by catalytic and/or low-temperature oxidation of the anode off-gas.
- Hydrocarbons are usually converted into methane in a pre-converter reactor before entering the fuel cell stack and the remainder is consumed by catalytic and/or low-temperature oxidation of the anode off-gas.
- Air toxics, such as higher hydrocarbons, aldehydes, and alcohols, are not present or are removed from the incoming fuel and typically no air toxic compounds are produced by any of the processes involved in a fuel cell system. If any air toxics would be produced then they would likely be destroyed at the high-temperature catalytic conditions of the anode compartment or anode off-gas oxidizer.

Processes Are Efficient Even at Small Size Enabling Distributed Production

Heat engine energy conversion is driven by a temperature difference while fuel cell energy conversion is driven by a chemical potential difference. The efficiency of any heat engine is limited by the efficiency that could be achieved by the reversible cycle operating upon a temperature difference, known as the Carnot efficiency [19]. On the other hand, fuel cells are limited by the Nernst equation and chemical potential difference that can be established in the

cell, since they convert the chemical potential difference directly into electrical energy [6]. Heat engines for electricity production also have additional losses associated with the conversion of mechanical energy (e.g., piston movement, spinning turbine) to electricity through cranks, gears, and a generator.

Heat engines have reduced efficiency at reduced size because surface-to-volume ratios increase leading to higher percentage heat losses and inability to sustain the high cycle temperature for smaller engines. This leads to an inherent inability to establish a high temperature difference leading to a lower efficiency limit (i.e., lower Carnot efficiency). In addition, small-scale heat engines have proportionally larger friction, non-isentropic compressions and expansion, and other losses in comparison to larger heat engines. As a result, we currently tend to produce most of our power in very large central power plants based upon the heat engine – smaller plants are inherently less efficient.

On the other hand, fuel cell power production and efficiency depends upon the establishment of a chemical potential difference which can be established in equal difference regardless of the size of the cell.

Hydrogen Transport Involves Emissions and Energy Penalties

Today, most hydrogen is produced from natural gas in large steam methane reformation (SMR) plants in a centralized fashion. To produce hydrogen at large scale in centralized reformation plants is more efficient than producing hydrogen at small-scale reformation plants.

The main steps of a well-to-tank hydrogen supply chain may be defined as production, treatment, distribution, storage, and dispensing. Each step can be accomplished with a variety of different technologies which may be more or less energy intensive and environmentally friendly [20]. For long distances, transportation of liquefied hydrogen by diesel truck is the most common strategy. However, liquefaction of hydrogen is the most energy intensive process and it makes sense only for very long delivery distances. Shorter distance hydrogen transport may be resolved by the transportation of compressed hydrogen which takes less energy than liquefaction, but delivers less hydrogen per unit truck volume. Hydrogen can also be transported via high-pressure pipeline, which is one of the least energy intensive methods. But, in comparison to other gaseous or liquid fuels, hydrogen pipeline delivery is more energy intensive [26]. In all of these cases, the relatively low volumetric energy density of hydrogen leads to relatively large energy and emissions penalties associated with hydrogen transport and delivery. These penalties can result in mediocre well-to-tank efficiencies compared to other fuels. These penalties can be averted by the production of hydrogen in a distributed fashion with a technology that scales down with high efficiency, such as poly-generating HTFC [16]. Nonetheless, energy and emissions penalties associated with hydrogen transport must be accounted for in all analyses.

Cycle Configurations for Poly-Generating HTFC

Brouwer and Leal [21] investigated the production of hydrogen with high-temperature fuel cells by analyzing and comparing eight different cycle configurations using solid oxide fuel cells (SOFC) and molten carbonate fuel cells (MCFC). Six of the eight configurations use fuel cell heat to drive hydrogen production in an external reformer placed in different positions in the cycle. The other two configurations use the internal reformation capabilities of high-temperature fuel cells to produce hydrogen.

Based upon the cycle configurations developed by Brouwer and Leal [21], Margalef et al. [9] investigated in detail how placing the external reformer in different positions affects the fuel cell performance and the hydrogen production efficiency. In addition, Margalef et al. investigated the performance of the poly-generating plant at different fuel utilizations together with the integration of commercially available hydrogen separation and purification technologies (i.e., pressure swing adsorption) with the fuel cell balance of plant (BOP).

High-Temperature Fuel Cell Subsystem

High-temperature fuel cells (HTFC) generate electricity and heat through exothermic electrochemical reactions. Generated heat by the fuel cell reactions is typically utilized internally or externally by the endothermic fuel processing reactions, which in turn

provide cooling to the system [22]. Surplus heat is used to preheat the fuel and oxidant streams before they enter the fuel cell and to produce the steam required for system operations. In addition, the remaining thermal energy contained in the exhaust gases can be used downstream of the fuel cell for poly-generation applications that require or value heat [22].

One possible configuration is to use the fuel cell heat to produce hydrogen via steam methane reforming in an external reformer (i.e., external reformation). Another possibility relies on the internal reforming capabilities of HTFCs and on the fact that the amount of high-quality heat produced by the exothermic reactions within the stack is typically greater than the heat required for fuel processing [6]. Therefore, more hydrocarbon fuel than that required for the electricity generation can be processed in an HTFC, creating a hydrogen-rich stream that could be subsequently purified and delivered at the point of production without the need of an external reformer [17] (i.e., internal reformation). This mode of operation implies lower stack fuel utilization factors and has been associated with synergies such as lower cell polarization losses and lower parasitic losses correlated with lower cooling air [16].

Separation/Purification Subsystem (Hydrogen Separation Unit (HSU))

Hydrogen separation and purification in refineries has been traditionally accomplished by using established technologies such as pressure swing adsorption (PSA), selective permeation processes using polymer membranes, or cryogenic separation process. Each process is based on a different separation principle, so each method differs significantly from each other. Economic aspects and other project considerations such as process flexibility, reliability, and scalability have to be taken into account to decide the hydrogen separation method [23].

Other hydrogen separation technologies include electrochemical hydrogen separation (EHS), which is foreseen as a promising technology to separate hydrogen fuel from a fuel cell anode exhaust stream. However, EHS technology is not currently mature and has not been used in poly-generating applications to date. In any case, the hydrogen-rich stream is treated and prepared in the hydrogen separation unit (HSU) according to the selected separation/purification technology. For this work, PSA technology has been selected due to its commercial readiness and recent use in poly-generating systems [24].

The HSU configuration depends upon the specific requirements of the hydrogen separation technology and the anode off-gas conditions. PSA technology requires relatively low inlet temperatures and high inlet pressures. Additionally, hydrogen separation with PSA becomes more efficient at high hydrogen partial pressures [23]. Therefore, to extract the hydrogen from the anode off-gas of a HTFC using a PSA, the HSU is required to:

- Decrease the hydrogen-rich stream temperature
- Increase the hydrogen-rich stream pressure
- Increase the hydrogen partial pressure of the hydrogen-rich stream

Table 1 shows representative PSA feed gas requirements and the current configuration design points.

A simplified HSU block consisting of a series of heat exchangers and compressors designed to meet the PSA temperature and pressure requirements is shown in Fig. 3.

As shown in Fig. 3, an electric chiller has been placed upstream of the PSA reactor to meet the temperature requirements when ambient air temperature (used as a cold media in the upstream heat exchangers) is too high. The electric chiller represents a small fraction of the total parasitic loads. Interestingly, required PSA inlet temperature is low enough to condense out sufficient water vapor from the gas stream. As shown in Fig. 3, condensed water may be removed upstream of the PSA reactor resulting

Hydrogen Production from High-Temperature Fuel Cells. Table 1 State-of-the-art PSA feed gas requirements

Parameter	State-of-the-art value range	Notes
Absolute pressure (kPa)	303–2,026	Based on the state of the art [25]
Temperature (°C)	4–50	Based on the state of the art [25]

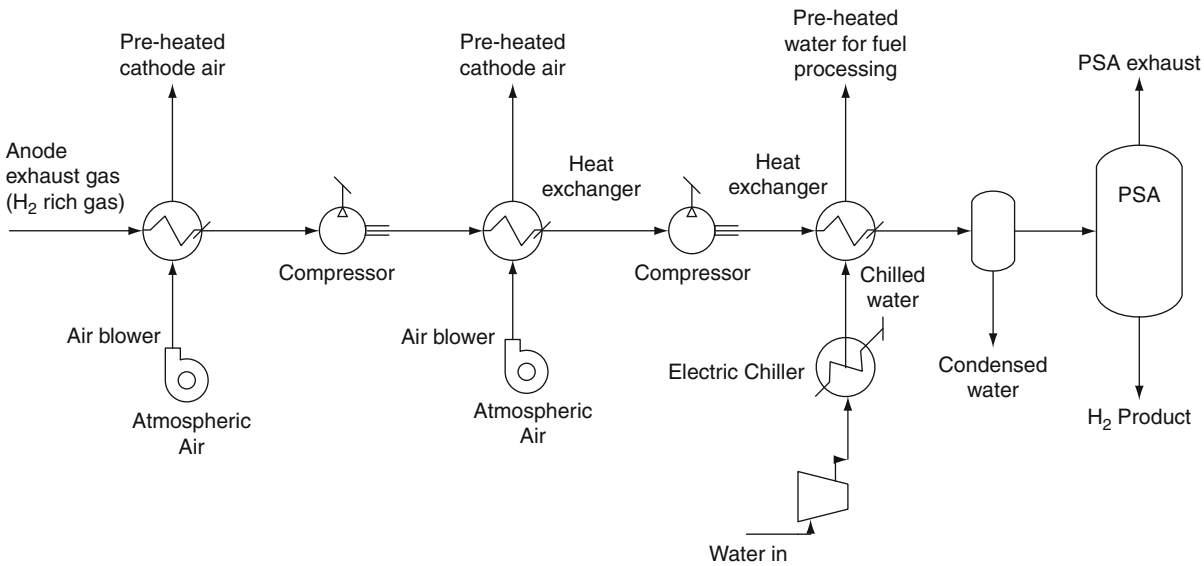

Hydrogen Production from High-Temperature Fuel Cells. Figure 3
Hydrogen separation unit configuration

in higher hydrogen partial pressures and facilitating the PSA separation process.

In the internal reformation cases, the air and water that is heated in the HSU represents an opportunity to thermally integrate the HSU with fuel cell balance of plant. This thermal integration strategy is crucial in order to ensure overall thermal balance within the plant, which may be jeopardized at certain operating conditions if hydrogen is separated from the anode off-gas [16].

Integrated Poly-Generating HTFC Cycles According to Fuel Processing

Steam methane reformation (SMR) and water–gas shift (WGS) are the main fuel processing reactions that convert raw fuel (i.e., natural gas) into fuels more amenable to electrochemical oxidation (i.e., hydrogen and carbon monoxide) occurring on the nickel-based anode of HTFC.

Steam methane reforming is an endothermic reaction that consists of the reaction of methane and steam over a supported nickel catalyst to produce a mixture of hydrogen, carbon monoxide, carbon dioxide, and methane. The basic reforming reaction for methane is

$$CH_4 + H_2O \rightarrow 3H_2 + CO \quad \Delta H = 206\,\text{kJ mol}^{-1} \tag{16}$$

Heat has to be provided to drive the reaction forward to the hydrogen production direction. As shown in Fig. 4, hydrogen concentration under equilibrium conditions is highest between 900 and 1,100 K [17].

The water–gas-shift (WGS) reaction (starting from steam) is slightly exothermic and occurs at the same time as steam reforming [6]. During the shift reaction, additional hydrogen is produced. The basic water–gas-shift reaction for carbon monoxide is

$$CO + H_2O(g) \rightarrow H_2 + CO_2 \quad \Delta H = -41\,\text{kJ mol}^{-1} \tag{17}$$

In poly-generating HTFC, if external reformer is used to produce hydrogen, special attention has to be given to the temperature at which heat from the fuel cell stack is transferred to the external reformer. Therefore, it is important to analyze different cycle configurations consisting on different positions of the external reformer within the system.

In the internal reformation cases where additional hydrogen production occurs at the same physical location than fuel cell reactions (i.e., direct internal reformation) or in a location that is thermally connected with the anode (i.e., indirect internal reformation), the temperature at which heat is

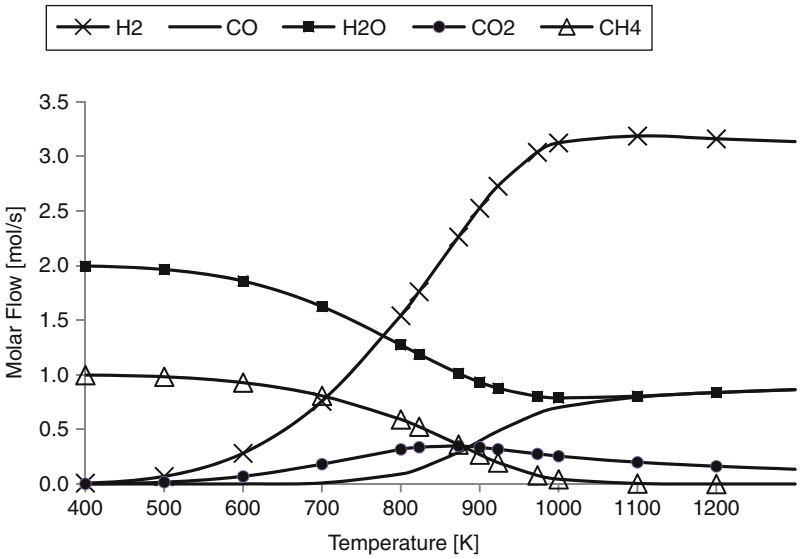

Hydrogen Production from High-Temperature Fuel Cells. Figure 4
Equilibrium composition as a function of temperature (steam-to-carbon ratio S/C = 2) [17]

transferred to the fuel processing reactions corresponds to the operating stack temperature which is equal to the temperature at which hydrogen production is maximized. This feature constitutes one of the key principles that lead to unprecedented high efficiencies achieved by poly-generating HTFC [8].

External Reformation Configurations High-temperature fuel cells (HTFC) can be integrated with an external reformer in multiple ways. Based on preliminary designs by Brouwer and Leal [17], Margalef et al. [9] analyzed in detail the external reforming configurations of poly-generating HTFC shown in Fig. 5.

In all cases, steam reformation is driven by the fuel cell exhaust heat in an external reformer, which takes as much heat as possible without compromising the fuel cell operating temperatures. Inlet temperatures of the fuel, steam, and air streams are kept constant at 1,173 K in order to sustain the electrochemical reactions within the stack. Therefore, depending upon the external reformer location, more or less heat is available to produce hydrogen with the external reformer. Note that in all the configurations, a hydrogen separation unit (HSU) block, based on PSA technology, is placed downstream of the reformer to separate and purify the hydrogen stream from the reformate gas.

Internal Reformation Configurations Internal reforming promotes hydrogen production within the fuel cell stack and provides cooling to the fuel cell stack due to its endothermic nature. Generally, fuel cell systems do not electrochemically consume all the fuel that is supplied (a fundamental limitation for all fuel cells) and they produce enough heat to reform much more fuel than the amount they consume. Remaining fuel exiting the anode presents a unique opportunity for low-cost hydrogen [17].

Margalef et al. [16] analyzed in detailed one internal reformation SOFC configuration at 80% and 60% fuel utilization (U_F). Figure 6 shows the schematic of this configuration. As shown, the HSU block is placed at the anode gas exit upstream the catalytic oxidizer.

Representative Performance Characteristics Modeling capabilities developed at the National Fuel Cell Research Center (NFCRC) of the University of California, Irvine have been used to evaluate the fuel cell performance and the hydrogen production capabilities of the presented poly-generating HTFC configurations. The complete model consists of an SOFC stack; heat exchangers to preheat the fuel, water, and air; an external SMR reactor placed in different locations for each of the different configurations; an adiabatic catalytic combustor that captures

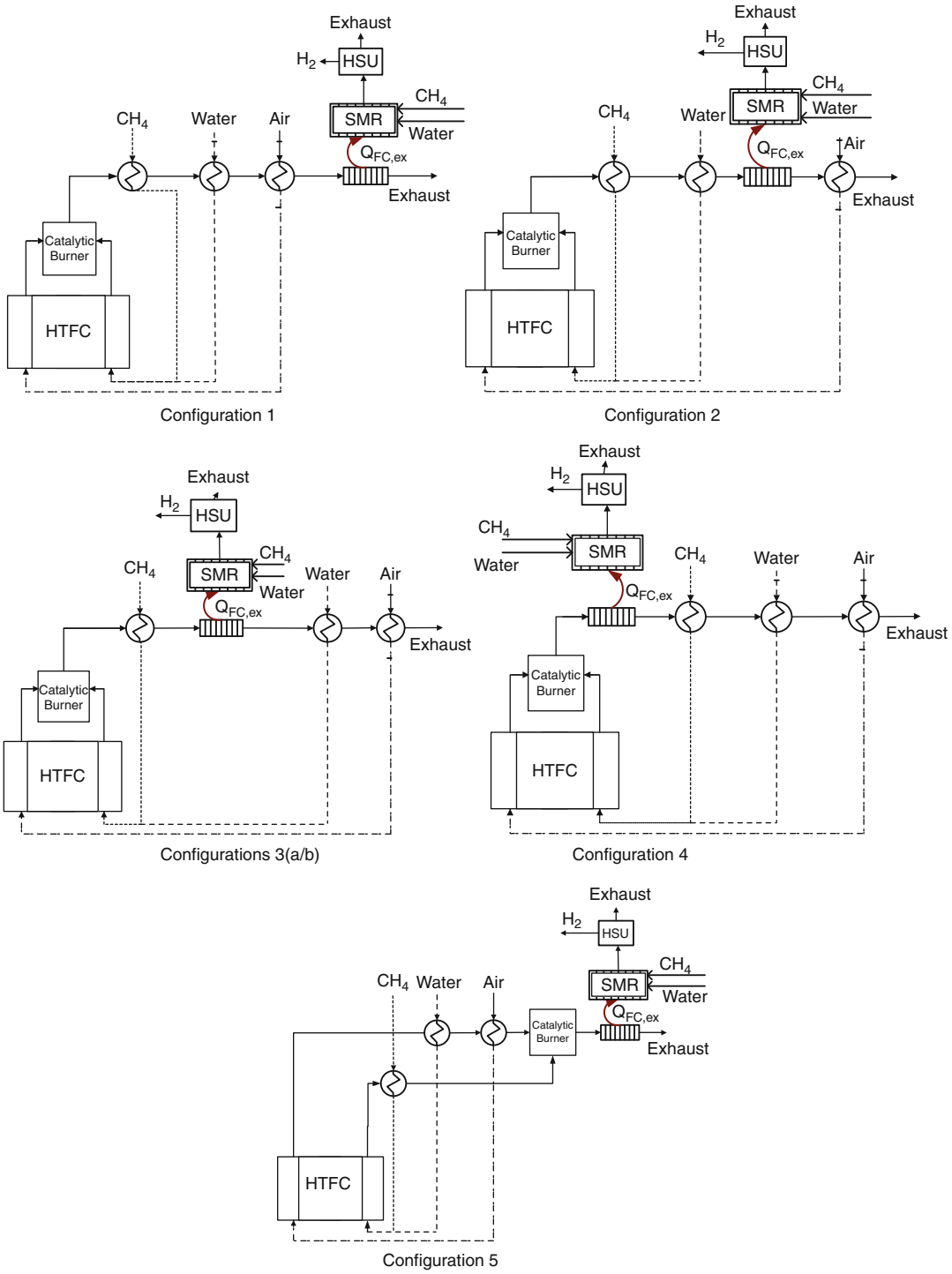

Hydrogen Production from High-Temperature Fuel Cells. Figure 5
Poly-generating HTFC configurations based upon external reformation

the thermal energy of the unused fuel downstream of the stack; and an HSU block based on PSA technology.

Each configuration has been analyzed following the same approach. For the external reformation cases (Conf. 1–5), stack input temperatures of the fuel, air, and steam have been fixed at 1,173 K whereas the amount of reformed methane varies depending upon how much heat is available after preheating all the input streams. Pinch analyses for each heat exchanger have been performed in order to avoid temperature crossovers within the heat exchangers. Similarly, for the internal reformation cases (Conf. 6a/6b), the amount of hydrogen extracted in the HSU block depends upon how much thermal energy has to be extracted from the anode off-gas in order to preheat the input streams to the specified temperatures [9].

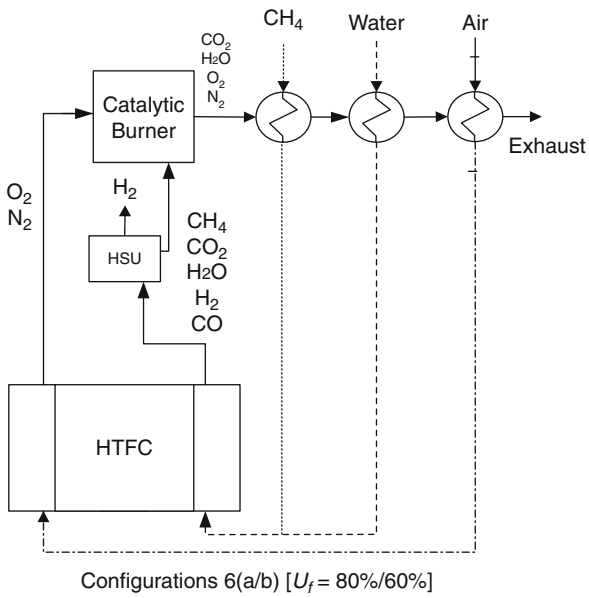

Hydrogen Production from High-Temperature Fuel Cells. Figure 6
Poly-generating HTFC based upon internal reformation

Bulk Stack and External Reformer Temperatures

For the external reformation cases, the heat available to produce hydrogen without compromising the thermal balance of the fuel cell determines how much methane will be taken by the external reformer. However, the hydrogen yield will be a function of the temperature at which the reformation takes places. As shown in Fig. 4, hydrogen yield peaks between 900 and 1,000 K and it flattens out after this point. Therefore, the external reformer should operate in this temperature range in order to maximize the hydrogen production.

Figure 7 shows both fuel cell stack and external reforming temperatures for all the configurations.

As expected, stack temperatures are the same for all cases since inlet stream temperatures have been fixed to a certain value. Importantly, in configurations 6a and 6b, stack and reformation temperatures are equal due to the fact that hydrogen is produced by internal reforming.

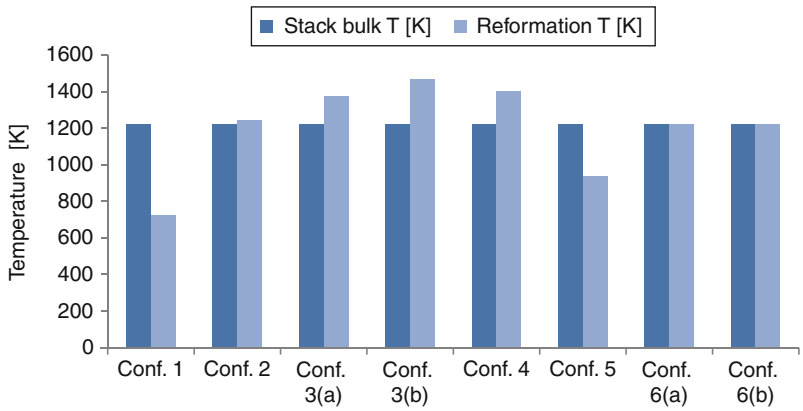

Hydrogen Production from High-Temperature Fuel Cells. Figure 7
Stack and reformer temperatures

Configuration 1 presents the lowest reformation temperature. This makes sense since the external reformer is placed downstream of all the heat exchangers where exhaust gas temperatures are lowest. Configuration 3b achieves the highest reformation temperature among the configurations. This configuration is the only external reforming configuration where the fuel utilization factor has been lowered to 60%. Therefore, more hydrogen will be oxidized in the catalytic combustor raising the exhaust gas temperature considerably. The rest of the configurations present similar reformation temperature values, all of them in range where hydrogen yield is high.

Hydrogen Production Rate Figure 8 shows the amount of hydrogen produced with each configuration. As observed, there is a significant difference between the hydrogen produced with the external reforming configurations and the amount of hydrogen produced with the internal reformation configurations.

The amount of hydrogen produced with configuration 1 is low. As shown in Fig. 7, the temperature at which reformation occurs in configuration 1 is 724 K, at which temperature hydrogen yield under equilibrium conditions is very small.

Figure 7 shows that in configurations 2, 3a, 3b, and 4, external reforming occurs at temperatures at which hydrogen yield is high. However, the amount of hydrogen produced is not comparable to the internal reformation cases or configuration 5. As mentioned previously, hydrogen production is a function of the temperature at which the reformation occurs but is also a function of the amount of transferred heat from the exhaust gas stream to the external reformer. Although in configurations 2, 3, and 4, steam reforming occurs at relatively elevated temperatures, the heat that can be transferred from the fuel cell exhaust to the reformer without compromising the fuel cell thermal balance is not enough to reform large amounts of methane. As a result, the amount of hydrogen that can be produced with these configurations is not large.

Configuration 5 presents higher hydrogen production than the other external reforming configurations. In this case, since the external reformer is placed after the catalytic combustor, the temperature at which the reformation occurs is high enough to achieve significant hydrogen yields. Importantly, since there is no preheater downstream of the reformer, more heat can be extracted from the fuel cell exhaust stream without affecting any fuel cell stream input temperatures.

Finally, configurations 6a and 6b achieve the highest hydrogen production. This is due to the fact that the reformation takes place within the SOFC stack, which operates within the range of temperatures

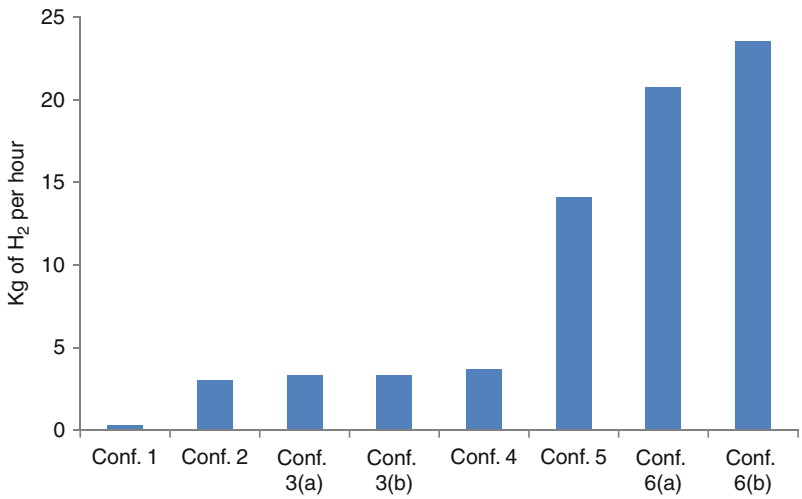

Hydrogen Production from High-Temperature Fuel Cells. Figure 8
Hydrogen production after PSA

at which hydrogen yield is high. Additionally, the reformation reactions and the fuel cell reactions occur in the same physical space. Therefore, heat from the source (i.e., exothermic fuel cell reactions) to the sink (i.e., endothermic reformation reactions) is directly transferred without the need of a heat exchanger. Thus, more heat can be captured resulting in higher hydrogen yields. The total hydrogen production for each configuration is shown in Fig. 8.

Parasitic Loads Associated with the Hydrogen Separation Unit Energy required to separate the hydrogen from the reformate stream varies in each configuration. The HSU is required to increase the pressure and drop the temperature of the reformate gas in order to meet the PSA requirements. This process requires energy and as a result, decreases the overall efficiency of the poly-generating plant. Margalef et al. [9] estimated the amount of energy required to separate 1 kg of hydrogen with the HSU design presented in Fig. 3. The HSU model consists of a series of heat exchangers and compressors that decrease the temperature and increase the pressure of the reformate gas to the design point levels, accordingly, for each configuration. Figure 9 shows the energy per kilogram of hydrogen required for the preparation of the reformate gas to meet the PSA requirements, as a function of the molar concentration of hydrogen.

As seen, the energy required to separate 1 kg of hydrogen from the reformate stream does not decrease linearly with the hydrogen molar concentration and depends upon the hydrogen concentration in the anode off-gas. This is due to the fact that for lower hydrogen concentrations, relatively more gas has to be cooled and compressed to produce the same amount of hydrogen. Therefore, the amount of energy required to separate 1 kg of hydrogen with PSA technology is lower when the hydrogen concentration of the feed gas is high [9]. Figure 10 shows the molar hydrogen concentrations of the PSA feed gas for each configuration.

For all of the external reformation configurations except for configuration 1, hydrogen concentrations remain around 60%. Although the heat available to produce hydrogen in configuration 1 is comparable to the rest of the configurations, the temperature at which the reformation occurs is not high enough to achieve significant methane conversion. Similarly, configurations 6a and 6b present low hydrogen concentrations compared to the rest of the configurations. This makes sense since the produced hydrogen is mixed with the anode off-gas products which include all the carbon dioxide and steam products from the stack reactions, including internal reforming and electrochemical reactions. As a result, the hydrogen concentration of the reformate gas for the internal reformation cases is relative low when compared with the external reformation configurations.

Figure 11 shows the energy required to separate 1 kg of hydrogen with each configuration. As shown, higher

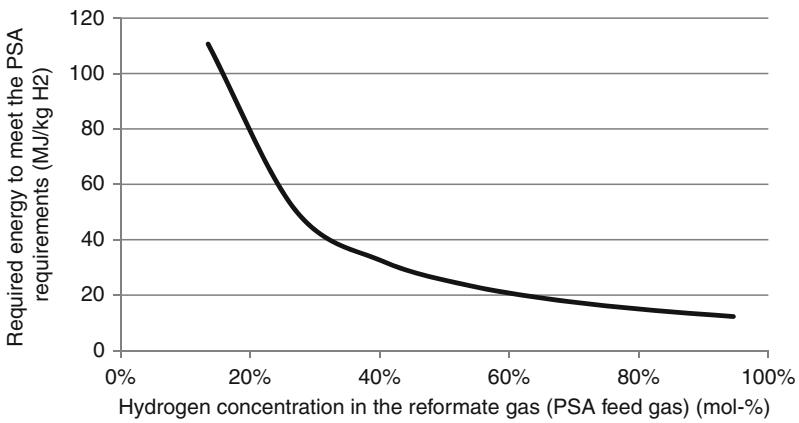

Hydrogen Production from High-Temperature Fuel Cells. Figure 9
Specific energy required for the PSA process

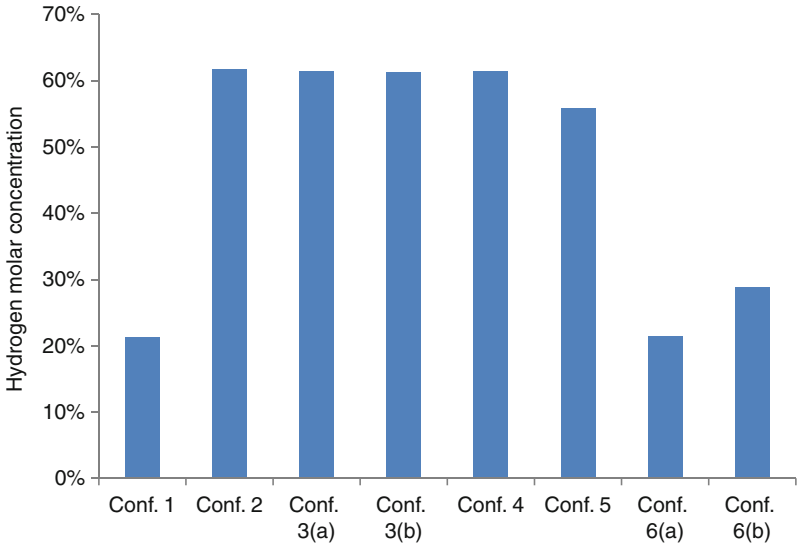

Hydrogen Production from High-Temperature Fuel Cells. Figure 10
Hydrogen concentration in the PSA feed gas

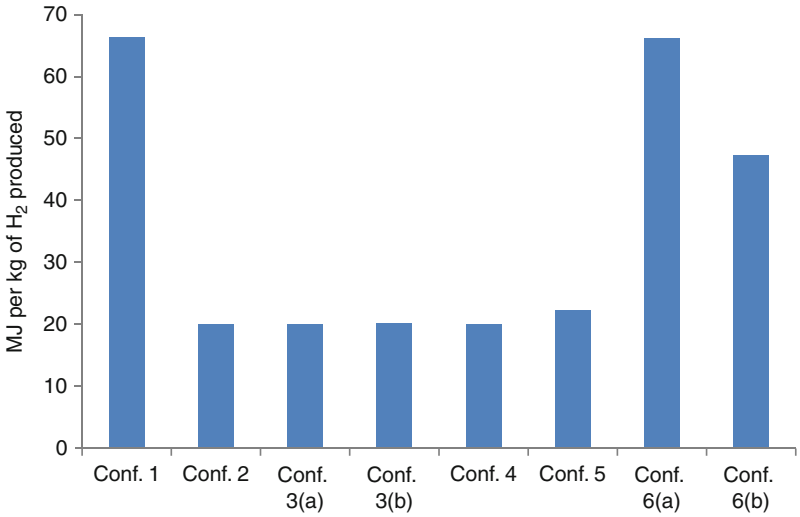

Hydrogen Production from High-Temperature Fuel Cells. Figure 11
Parasitic load required to separate 1 kg of H_2 at the HSU

hydrogen concentration streams require less energy to separate the hydrogen from the reformate gas.

Comparative Efficiency Analyses

Because a poly-generating HTFC simultaneously produces electricity, hydrogen, and useful thermal energy, efficiencies can be measured and expressed in a number of different ways. Margalef et al. developed three different methods to appropriately calculate the overall and coproduct production efficiencies [8]. Table 2 shows the developed equations for each method. The methods have been labeled as: (1) *State-of-the-art Method*; (2) *Ideal Poly-generation Method*, and (3) *Supplemental Input Method*.

Hydrogen Production from High-Temperature Fuel Cells. Table 2 Efficiency equations for (1) state-of-the-art method, (2) ideal poly-generation method, and (3) supplemental input method [8]

		Electrical efficiency	Thermal efficiency	Hydrogen efficiency	Total mixed efficiency
1		$\frac{P_{net}}{E_{tot} - \frac{Q_{net}}{\eta_{boiler}} - \frac{H_2}{\eta_{SMR}}}$	$\frac{Q_{net}}{E_{tot} - \frac{P_{net}}{\eta_{CC}} - \frac{H_2}{\eta_{SMR}}}$	$\frac{H_2}{E_{tot} - \frac{P_{net}}{\eta_{CC}} - \frac{Q_{net}}{\eta_{boiler}}}$	$\frac{P_{net} + Q_{net} + H_2}{E_{tot}}$
2		$\frac{P_{net}}{E_{tot} + Q_{net} + H_2}$	$\frac{Q_{net}}{E_{tot} + P_{net} - H_2}$	$\frac{P_{PSA}}{E_{tot} - P_{net} - Q_{net}}$	$\frac{P_{net} + Q_{net} + H_2}{E_{tot}}$
3	External reforming	$\frac{P_{net}}{E_{tot} - \frac{Q_{e^-}}{\eta_{boiler}} - \left(F_{H_2} + \frac{P_{PSA}}{\eta_{CC}}\right)}$	$\frac{Q_{net}}{\frac{Q_{net}}{\eta_{boiler}}} = \eta_{boiler}$	$\frac{H_2}{F_{H_2} + \frac{P_{PSA}}{\eta_{CC}}}$	$\frac{P_{net} + Q_{net} + H_2}{E_{tot}}$
	Internal Reforming.	$\frac{P_{net}}{E_{tot} - \frac{Q_{e^-}}{\eta_{boiler}} - \left((U_f - U_{f,H2ES})E_{tot} + \frac{P_{PSA}}{\eta_{CC}}\right)}$		$\frac{H_2}{(U_F - U_{f,H2ES})E_{tot} + \frac{P_{PSA}}{\eta_{CC}}}$	

Hydrogen Production from High-Temperature Fuel Cells. Table 3 Efficiency results obtained with the Supplemental Input Method (LHV)

Configuration	1	2	3a	3b	4	5	6a	6b
Electrical efficiency	53.4%	53.3%	53.3%	46.9%	53.3%	52.8%	50.0%	58.4%
Hydrogen efficiency	18.0%	73.5%	73.2%	68.2%	73.2%	62.1%	90.7%	83.5%
Overall efficiency	52.3%	54.7%	54.8%	48.5%	55.0%	55.7%	70.0%	69.5%

These methods are based upon different and reasonable assumptions for the allocation of input energy to each of the coproducts. It should be clear that there is not a unique or superior method for calculating poly-generation efficiencies so that each of the methodologies proposed can be used in comparative analyses if based upon accurate assumptions. For the current specific analyses, the *Supplemental Input Method* is used to estimate the overall electrical and hydrogen production efficiencies for each configuration. Thermal efficiency has not been calculated since it depends upon the thermal requirements of each specific application and there may be cases when thermal energy is not required. Results are presented in Table 3.

The efficiency results shown in Table 3 correspond to the Supplemental Input Method [8] and do not include the heat products shown in the equations presented in Table 2. With this method, electrical efficiency is the net power output P_{net} divided by the energy flow allocated exclusively for the electricity production, which corresponds to the total energy flow in E_{tot} minus the energy flow that has been specifically used to produce hydrogen product. The energy flow used to produce hydrogen product includes feedstock energy (i.e., additional fuel) as well as the necessary fuel to generate the electricity required for the hydrogen separation as if it was produced with a state-of-the-art combined cycle plant. The lowest electrical efficiency value corresponds to configuration 3b. In this case, hydrogen is produced externally and the fuel cell is operating at 60% utilization factor. As expected, the electrical efficiency is low since more fuel is used without obtaining any additional energy flow output (i.e., hydrogen fuel). On the other hand, the highest electrical efficiency value corresponds to configuration 6b, in which hydrogen is produced internally and the fuel cell is operated at 60% utilization factor.

Due to the synergies associated with higher voltages at lower fuel utilizations, electrical efficiency is significantly higher than the rest of the configurations. Nevertheless, one must recall the discussion associated with the key principles above that this analysis confirms that these synergies are only captured if hydrogen is separated from the anode off-gas. Otherwise, more fuel is being used to obtain the same mix of energy outputs. The rest of configurations present similar electrical efficiencies.

With the Supplemental Input Method, hydrogen efficiency is calculated in a similar way as specified in Table 2. The chemical power output of the hydrogen produced, H, is divided by the energy flow input specifically allocated to produce hydrogen. Once again, it corresponds to the feedstock energy (i.e., additional fuel) as well as the necessary fuel to generate the electricity required for the hydrogen separation as if it was produced with a state-of-the-art combined cycle plant. As seen in Table 3, the highest values correspond to the internal reformation cases. Interestingly, although the parasitic load per kilogram of hydrogen produced is higher in configuration 6a than in configuration 6b (see Fig. 11), hydrogen production efficiency is greater in the former case due to the fact that when hydrogen is produced at 80% utilization factor, the additional fuel feedstock allocated to produce hydrogen is equal to zero.

Finally, overall efficiency values are similar in all the external reformation cases, even for configuration 1 where the hydrogen output is almost negligible. This indicates that the hydrogen production does not affect the overall performance when the amount of hydrogen is relatively small (i.e., external reformation cases). As expected, both internal reformation cases achieve the highest overall fuel-to-product efficiency values.

Hydrogen Transport Impacts on Comparative Analyses

Today, most hydrogen is produced from natural gas in large steam-methane reformation (SMR) plants in a centralized fashion. To produce hydrogen at large scale in a centralized plant is more efficient than producing hydrogen at small scale [26]. Stephens-Romero et al. [20] define production, treatment, distribution, storage, and dispensing as the main steps of a well-to-tank hydrogen supply chain. Each step can be accomplished with a variety of different technologies. Figure 12 shows the main steps of a generic hydrogen supply chain from well to tank with the most widely used technologies.

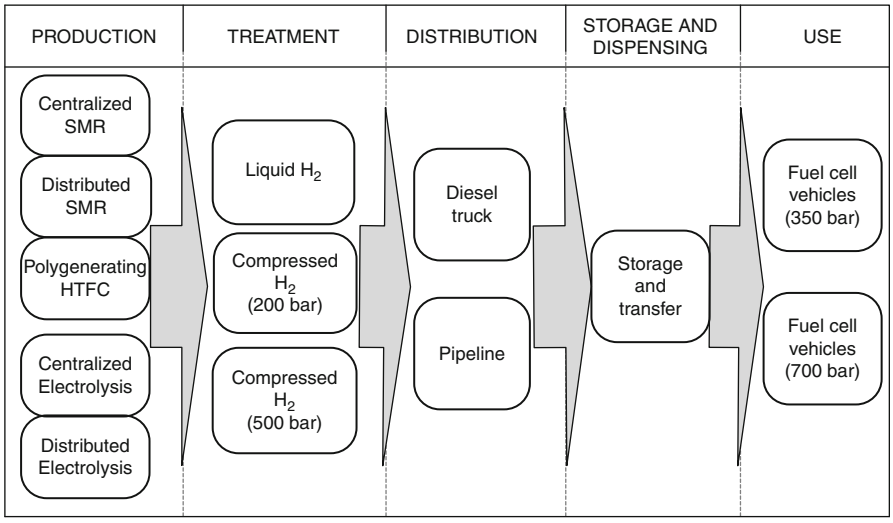

Hydrogen Production from High-Temperature Fuel Cells. Figure 12
Steps in well-to-tank efficiency analysis of H_2

One of the main benefits of producing hydrogen in a distributed manner versus centralized manner is the elimination of the fuel transport and delivery steps (fuel distribution) which can be energy intensive. Furthermore, if hydrogen is produced on demand as in poly-generating HTFC, hydrogen storage may be considerably reduced compared with the distributed reformer case.

Comparative Analysis of Ten Different Hydrogen Supply Chains

To evaluate the benefits of producing hydrogen in a distributed fashion versus centralized production, different hydrogen supply chains with different technologies for each step are analyzed from an energy perspective, resulting in ten different cases. Details of each supply chain are provided in Table 4. As shown, two different final uses corresponding to the two available fuel cell vehicle tank pressures (i.e., 350 bar and 700 bar) [27] are evaluated. In addition, when hydrogen is produced in a centralized SMR plant, the three available treatment methodologies are investigated. As a result, ten different supply chains have been evaluated.

After evaluating the energy required for each step from *production* to *dispensing* of hydrogen, well-to-tank (WTT) efficiencies of the ten different hydrogen supply-chain scenarios were calculated. Figure 13 shows the main results obtained from the analyses.

As shown, the lowest WTT efficiency values are observed for the distributed steam- methane reformation (SMR) cases whereas the highest values correspond to poly-generating HTFC. As expected, due to the significant energy penalties associated with liquefaction processes, WTT efficiencies of centralized SMR with liquid hydrogen transportation are almost as low as the distributed SMR cases. Importantly, the production step includes the energy content of the fuel feedstock. The WTT efficiency values have

Hydrogen Production from High-Temperature Fuel Cells. Table 4 Definition of the ten unique hydrogen supply chain cases

Case	Production	Treatment	Distribution	Storage	Dispensing
1	Centralized SMR	Liquid H_2	Diesel truck (100 km)	Liquid H_2	Use = 350 bar (Transfer = 7 bar to 400 bar)
2	Centralized SMR	Liquid H_2	Diesel truck (100 km)	Liquid H_2	Use = 700 bar (Transfer = 7 bar to 800 bar)
3	Centralized SMR	Compressed H_2 (200 bar)	Diesel truck (100 km)	Compressed H_2 (200 bar)	Use = 350 bar (Transfer = 200 bar to 400 bar)
4	Centralized SMR	Compressed H_2 (200 bar)	Diesel truck (100 km)	Compressed H_2 (200 bar)	Use = 700 bar (Transfer = 200 bar to 800 bar)
5	Centralized SMR	Compressed H_2 (500 bar)	Diesel truck (100 km)	Compressed H_2 (500 bar)	Use = 350 bar (Transfer = 500 bar to 400 bar)
6	Centralized SMR	Compressed H_2 (500 bar)	Diesel truck (100 km)	Compressed H_2 (500 bar)	Use = 700 bar (Transfer = 500 bar to 800 bar)
7	Distributed SMR	Compressed H_2 (500 bar)	n/a (0 km)	Compressed H_2 (500 bar)	Use = 350 bar (Transfer = 500 bar to 500 bar)
8	Distributed SMR	Compressed H_2 (500 bar)	n/a (0 km)	Compressed H_2 (500 bar)	Use = 700 bar (Transfer = 500 bar to 800 bar)
9	Poly-generating HTFC	Compressed H_2 (500 bar)	n/a (0 km)	Compressed H_2 (500 bar)	Use = 350 bar (Transfer = 500 bar to 500 bar)
10	Poly-generating HTFC	Compressed H_2 (500 bar)	(0 km)	Compressed H_2 (500 bar)	Use = 700 bar (Transfer = 500 bar to 800 bar)

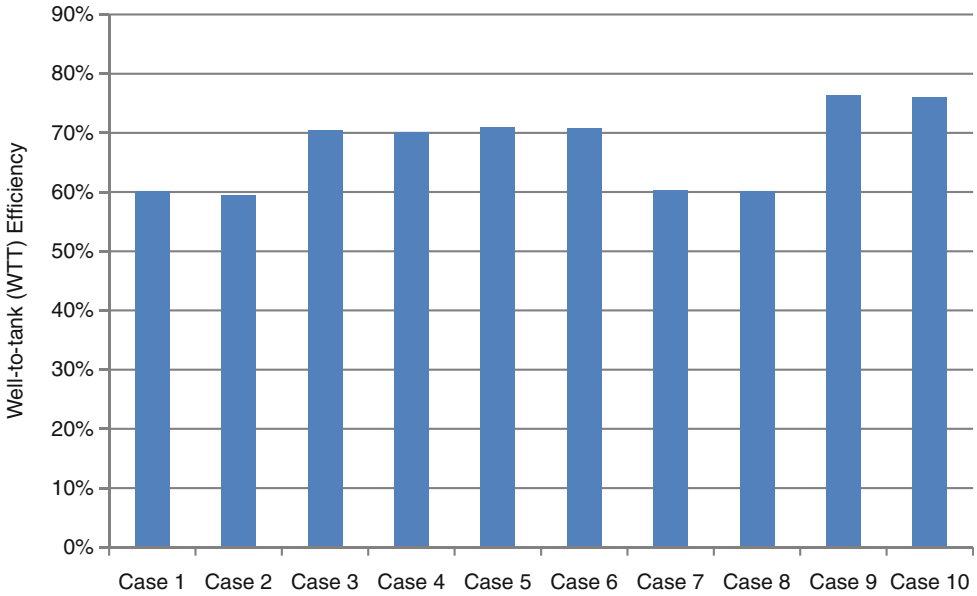

Hydrogen Production from High-Temperature Fuel Cells. Figure 13
Well-to-tank efficiencies of the evaluated supply-chains

been obtained by dividing the energy content of 1 kg of hydrogen (on a LHV basis) by the total energy required from WTT corresponding to each case.

From these energy-based comparative analyses, it is concluded that, of all the analyzed cases, poly-generating HTFC provide the most efficient way to produce and deliver hydrogen.

Discussion of Scientific Basis for Observed Performance

High-temperature fuel cells (HTFC) operate at high enough temperature and produce enough heat and water from the electrochemical reactions to provide heat to the internal fuel processing reactions (i.e., internal reformation). Importantly, the overall heat generated by the fuel cell reactions is typically greater than the heat consumed by the endothermic fuel processing reactions occurring within the fuel cell stack [6]. Surplus heat is partially used to preheat the fuel and oxidant streams before they enter the fuel cell and to produce the steam required for system operations. Therefore, more hydrocarbon fuel than that required for the electricity generation could be processed in an HTFC, creating a hydrogen-rich stream that could be subsequently purified and delivered to the point of use without the need of an external reformer. This represents the main concept that defines and allows the production of hydrogen in addition to electricity and heat with an HTFC. Such systems have been identified as poly-generating HTFC or tri-generation systems (Fig. 14).

Poly-generation systems can produce and deliver hydrogen fuel with lower marginal costs, fuel use, and emissions than conventional hydrogen production and delivery methods [28]. Since hydrogen is produced in a distributed generation fashion there is no energy or emissions penalty associated with the transport and delivery of the hydrogen to its point of use. Recent studies performed at the National Fuel Cell Research Center (NFCRC) of the University of California Irvine demonstrate that less energy is needed to transport and deliver hydrogen to vehicles compared with distributed and centralized steam methane reforming (SMR) resulting in higher well-to-tank (WTT) efficiencies [16].

Definition and Quantification of the Synergies Associated with Poly-Generating HTFC

Among the main benefits associated with the production of hydrogen with HTFC, there are synergistic

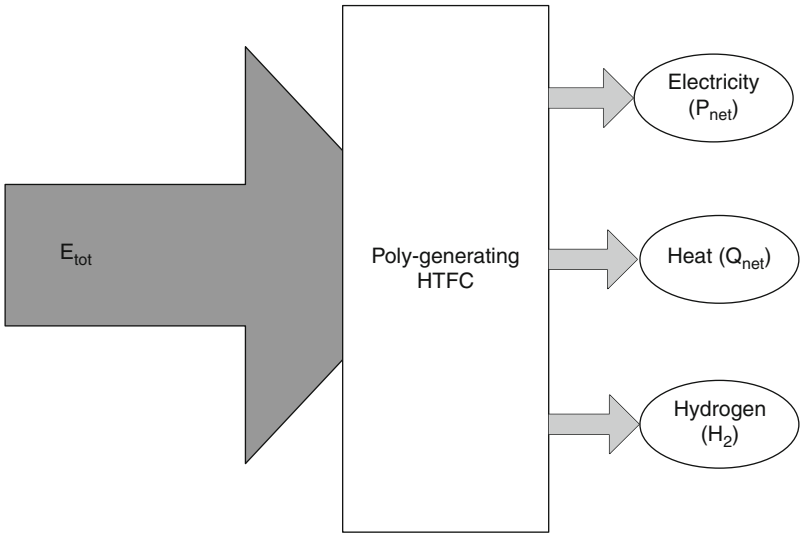

Hydrogen Production from High-Temperature Fuel Cells. Figure 14
Inputs and outputs of a poly-generating HTFC

effects intimately related with operating the fuel cell at low fuel utilization factors:

1. Synergistic impact of lower fuel utilization leads to higher cell voltages which result in:
   (a) Higher electrochemical efficiencies
   (b) Less electrochemical heat generated per mol of input fuel
2. Synergistic impact of lower fuel utilization increases the heat sink associated with the endothermic SMR reaction (i.e., internal fuel processing), reducing excess air requirements for cooling.

Synergies 1(b) and 2 reduce the excess air requirements for the stack cooling. Consequently, lower cooling requirements will lower the parasitic loads from the cathodic air blowers, increasing the net power of the system and the overall system efficiency. In this section, more details about each of the identified synergies are provided.

Synergistic Impact of Lower Fuel Utilization Leads to Higher Electrochemical Efficiencies Ideal reversible voltage (E_0) drops as soon as current is being produced due to the changes in product and reactant concentrations. Importantly, reactants and products concentrations along the electrode channels vary at different utilization factors. Therefore, operating the fuel cell at different fuel utilizations may affect the cell voltage. The voltage reduction caused by the change of species concentrations is known as *Nernstian losses* (η_{Nernst}), which added to the reversible voltage E_0, results on the Nernst Voltage (V_{Nernst}).

$$V_{\text{Nernst}} = E_0 + \eta_{\text{Nernst}} = E_0 + \frac{RT}{2F} In\left(x_{H_2} x_{o_2}^{\frac{1}{2}}\right) \quad (18)$$

$$x\text{H}_2\text{O}$$

Figure 15 shows the Nernstian losses (η_{Nernst}) as a function of the utilization factor obtained with the poly-generating SOFC modeling efforts by Li and Margalef [16, 30].

As shown in Fig. 15, voltage drop related with the Nernstian losses decreases at lower fuel utilizations. This effect represents in fact one of the synergies associated with poly-generating fuel cells, which typically operate at lower fuel utilizations than stand-alone fuel cells (i.e., electricity and heat production only).

To quantify this synergy, the system can be analyzed at two different fuel utilizations. The first value corresponds to the typical utilization factor of a stand-alone SOFC (e.g., $U_f = 0.9$) whereas the second value corresponds to the typical utilization factor of a poly-generating SOFC (e.g., $U_f = 0.6$). The difference in Nernst losses (V_{Nernst}) between both operating points represents the voltage gain of operating the fuel cell at lower fuel utilizations and quantifies this synergistic effect. Approximately, a gain of 0.06 V in the

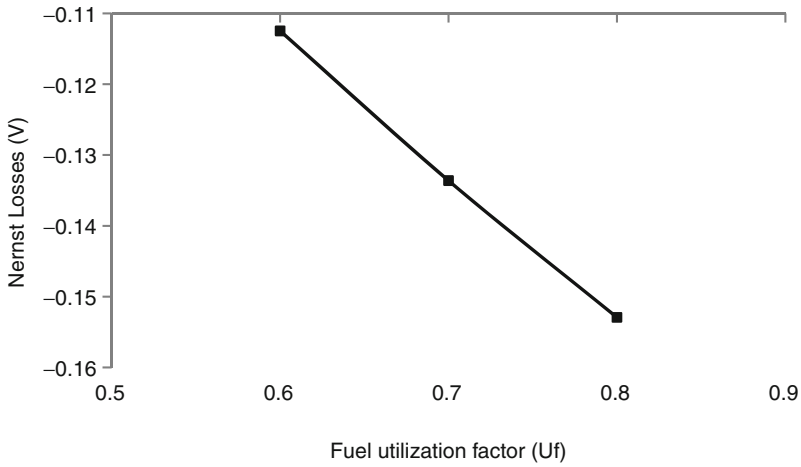

Hydrogen Production from High-Temperature Fuel Cells. Figure 15
Nernst losses (η_{Nernst}) versus the fuel utilization factor

Nernst voltage has been observed by operating the fuel cell at typical utilization factor used in poly-generating fuel cells ($U_f = 0.6$ compared to $U_f = 0.9$).

Additionally, the utilization factor affects the fuel cell performance through reaction kinetics since they also depend upon the reactant and product concentrations at the reaction sites [22]. The voltage drop associated with the reaction kinetics at different fuel utilizations is known as *reaction loss* ($\eta_{rxn\ \text{rate}}$). However, previous analyses performed by Margalef et al. [16] show that reaction losses represent a small fraction of the total voltage drop related with the concentration changes associated with different fuel utilizations. Therefore, the overall effects of operating the fuel cell at lower fuel utilizations on the cell voltage can be defined as

$$\Delta V_{\text{cell,conc}} = \Delta V_{\text{cell,Nernstian}} + \Delta V_{\text{cell},rxn\ \text{rate}} \sim \Delta V_{\text{cell,Nernstian}} \tag{19}$$

If all the energy from the hydrogen fuel were transformed into electrical energy, the cell voltage would correspond to the maximum voltage $v_{\max}$. The maximum voltage would be given by

$$V_{\max} = \frac{-\Delta \overline{g}_f}{n_i F} = 0.97\ V \text{ if using the LHV} \tag{20}$$

where $\Delta \overline{g}_f$ is the Gibbs free energy at 900°C, n_i is the number of electrons transferred during the electrochemical oxidization of fuel species i ($n_i = 2$ for H_2 and CO, $n_i = 8$ for CH_4), and F is the Faraday's constant. This voltage would be obtained from a 100% efficient system [6]. Therefore, the actual efficiency of the cell (or electrochemical efficiency) is the actual voltage divided by the maximum voltage, or

$$\eta_{\text{cell}} = \frac{V_{\text{cell}}}{V_{\max}} = \frac{V_{\text{cell}}}{0.97} \text{ if using the LHV} \tag{21}$$

Therefore, the electrochemical efficiency gain associated with lower utilization factors can be written as

$$\Delta\eta_{\text{cell}} = \frac{\Delta V_{\text{cell,conc}}}{V_{\max}} = \frac{0.06}{0.97} \times 100 = 6.2\% \text{ if using the LHV} \tag{22}$$

This result demonstrates and quantifies the first synergy associated with generating hydrogen with HTFC. As seen, by lowering the utilization factor at typical values of poly-generating SOFC, the electrochemical efficiency increases by 6.2%.

A more philosophical approach to explain the cell voltage drop as the fuel utilization factor increases is related to the mixing of products with reactants to dilute electrochemically active species concentrations. Water product mixes with the anode gas as it is formed throughout the electrochemical reactions. Note that mixing of products with reactants can occur in either the anode (e.g., MCFC, SOFC) or cathode (e.g., PEMFC, PAFC) compartments. The concentration of water product in the anode increases

as the fuel utilization factor increases. Mixing processes are irreversible so they produce entropy. As a result, a completely reversible SOFC operation would be only approached as $U_f \rightarrow 0$. In other words, irreversibilities increase as the utilization factor increases. Consequently, one wants to operate a fuel cell at the lowest possible utilization factor in order to reduce the mixing irreversibilities. However, there is a compromise between the cell efficiency and the fuel utilization efficiency that counterbalances this consideration with a desire for high utilization to achieve high overall system electrical efficiency.

Synergistic Impact of Lower Fuel Utilization Increases the Heat Sink Associated with the Endothermic SMR Reaction, Reducing Excess Air Requirements for Cooling A high-temperature fuel cell (HTFC) is an electrochemical device that converts chemical energy of a fuel and oxidant directly to electricity. Fuel cell electrochemical reactions are exothermic, thus electrochemical heat is produced. In addition, during the operation of an HTFC, ohmic resistance across the electrodes and bipolar plates generates heat. The specific electrochemical heat released qFC can be calculated applying the first law of thermodynamics, according to Eq. 23. Sign convention for this analysis is specified in Fig. 16:

$$\Delta\overline{h}_f = qFC - wFC \tag{23}$$

where $\Delta\overline{h}_f$ is the enthalpy of combustion of hydrogen corresponding to the reaction

$$H_2 + \frac{1}{2}O_2 \rightarrow H_2O(\text{liquid}) \quad \Delta\overline{h}_f = -285.84\,\text{kJ}\,\text{mol}^{-1} \tag{24}$$

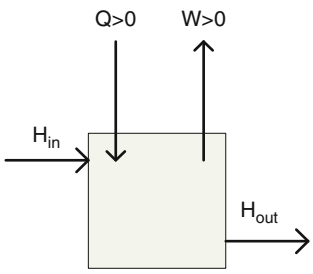

Hydrogen Production from High-Temperature Fuel Cells. Figure 16
Sign convention

and w_{FC} is the electric work produced by the fuel cell, given by the Eq. 23

$$w_{FC} = n_e F V_{\text{cell}} \tag{25}$$

where V_{cell} is the operational cell voltage, n_e is the number of electrons transferred during the electrochemical reactions (i.e., $n_e = 2$ for hydrogen), and F is the Faraday's constant. Combining Eq. 23 and Eq. 25, the specific heat generated during a real fuel cell operation can be calculated as follows:

$$qFC = \Delta\overline{h}_f + w_{FC} = \Delta\overline{h}_f + n_e F V_{\text{cell}} \left[\frac{\text{kJ}}{\text{mol}\,H_2}\right] \tag{26}$$

In a real fuel cell, although part of the heat is exchanged and used in several ways, including fuel processing and air preheating, excess air is usually required to prevent overheating [29]. Assuming that the fuel processing consists of steam reformation (SMR) and water–gas shift (WGS), the total specific heat absorbed by the fuel processing reactions qFC including the steam production is

$$\begin{aligned} qFP &= \Delta\overline{h}_{SMR} + \Delta\overline{h}_{WGS} + 2 \times \Delta\overline{h}_{vap} \\ &= 206.1 - 41.2 + 2 \times 44.1 = 253.1 \left[\frac{\text{kJ}}{\text{mol}\,CH_4}\right] \end{aligned} \tag{27}$$

where $\Delta\overline{h}_{SMR}$ is the enthalpy of steam reforming reaction, $\Delta\overline{h}_{WGS}$ is the enthalpy of water–gas-shift reaction, and $\Delta\overline{h}_{vap}$ is the enthalpy of vaporization of water. Therefore, remaining heat that has to be transferred to the excess air for cooling purposes q_{cool} is the difference between the heat liberated during the fuel cell reactions qFC and the heat absorbed by the fuel processing reactions qFP:

$$q_{\text{cool}} = m \cdot qFC + qFP \left[\frac{\text{kJ}}{\text{mol}\,CH_4}\right] \tag{28}$$

where m is the number of moles of hydrogen produced during the fuel processing reactions. For this specific case, the overall fuel processing reaction includes SMR and WGS, and is given by Eq. 29.

$$CH_4 + 2H_2O \rightarrow 4H_2 + CO_2 \tag{29}$$

Therefore, m is equal to 4. Combining Eqs. 27–29, the specific cooling required can be written as

$$q_{\text{cool}} = 4\left(\Delta\overline{h}_f + n_e F V_{\text{cell}}\right) + qFP\left[\frac{\text{kJ}}{\text{mol of CH}_4}\right] \quad (30)$$

As expected, more electrochemical heat is liberated per mole of hydrogen qFC at higher fuel utilizations. Consequently, by operating the fuel cell at lower utilization factors reduces the fuel cell cooling requirements per mole of input fuel, due to the higher cell voltages that result in less electrochemical heat generated. Lower cooling requirements mean lower parasitic loads from the air blowers, increasing the net power of the system and the overall system efficiency.

World's First Poly-Generating HTFC System

The world's first installation to poly-generate electricity and hydrogen with high-temperature fuel cells (i.e., a molten carbonate fuel cell) has been installed at the Orange County Sanitation District (OCSD) in Fountain Valley, California [24]. The system that has been installed at OCSD is the world's first hydrogen coproduction system installed at a customer site. In addition, it has begun to produce electricity, heat, and hydrogen from renewable digester gas fuel. The prime contractor in the effort is Air Products and Chemicals, Inc., who is working with FuelCell Energy and the National Fuel Cell Research Center and OCSD on the project. The main funding agencies are the US Department of Energy, California Air Resources Board, and the South Coast Air Quality Management District.

This important installation of a prototype poly-generating HTFC operating on digester gas at OCSD will provide important data and experience that will benefit the advancement of the poly-generation concept. The installation itself and measured performance characteristics may also identify important areas for research, development, improvement, and application of the concept.

Future Directions

Recommendations for future research work on poly-generating HTFC development include the development of a detailed dimensional and dynamic SOFC model that is required to solve the complicated internal temperature and species concentration profiles that are not resolved by nondimensional models. Thermodynamic and nondimensional SOFC insights are nonetheless useful for system design and comparative analyses. In addition, the overall system performance obtained by these models generally sets the ideal system performance target. However, since the outlet flow temperatures do not necessarily represent the maximum temperatures in the SOFC, and peak temperatures often occur internal to the stack, a dimensional SOFC model and/or internal temperature measurements could be used to determine if the SOFC working voltage is achievable and practical.

All the analyses performed in previous literature have been performed at a fixed current density value. Therefore, the same analyses described in this chapter should be performed at lower current densities. At such operating conditions, it is likely that the operational cell voltage will rise, increasing the electrochemical efficiency. However, less electrochemical heat will be generated, which is likely to reduce the hydrogen production potential. Therefore, it is possible to adjust the system performance for each specific market depending upon which product is more valuable by varying the operational current density in addition to the fuel utilization.

It has been found that pressure swing adsorption (PSA) might not be the best technology for extraction and purification of the hydrogen from the anode off-gas due to the PSA feed gas requirements. A complex HSU configuration is required in order to meet pressure, temperature, and hydrogen concentration requirements. Therefore, different purification strategies such as electrochemical hydrogen separation and selective permeation membranes might be more suitable for the poly-generation application.

An economic analysis of poly-generating high-temperature fuel cells should be performed in detail. From an efficiency perspective and considering only the configurations presented herein, poly-generating HTFC are the best solution. However, the economics of such novel systems should be analyzed and compared with conventional production methods. Additionally, due to the poly-generating nature of these systems, different strategies to fit each of the specific market requirements should be designed. These strategies might be resolved by dynamic modeling efforts to investigate the ability of system configurations to dynamically dispatch each of the respective products depending upon demand profiles for each product.

Bibliography

1. Samuelsen GS (2005) Energy station concept. In: California hydrogen blueprint plan, vol 2. California Environmental Protection Agency, Sacramento. http://www.hydrogenhighway.ca.gov/plan/reports/volume2_050505.pdf
2. EG & G Technical Services, Inc. (2004) Fuel cell handbook, 7th edn. U. S. Department of Energy Office of Fossil Energy, Morgantown
3. Brouwer J, Jabbari F, Leal EM, Orr T (2006) Analysis of a molten carbonate fuel cell: numerical modeling and experimental validation. J Power Sour 158(1):213–224
4. Sundmacher K et al (2007) Molten carbonate fuel cells modeling, analysis, simulation, and control. Wiley, Weinheim
5. Aguiar P, Chadwick D, Kershenbaum L (2002) Modelling of an indirect internal reforming solid oxide fuel cell. Chem Eng Sci 57:1665–1677
6. Larminie J, Dicks A (2003) Fuel cell systems explained. Wiley, West Sussex
7. Online resource available at: http://www.energy.ca.gov/distgen/
8. Margalef P, Brown T, Brouwer J, Samuelsen GS (2010) Efficiency of polygenerating high temperature fuel cells. J Power Sour POWER_POWER-D-10-02363
9. Margalef P, Brown T, Brouwer J, Samuelsen GS (2010) Conceptual design and configuration performance analyses of polygenerating high temperature fuel cells. Intl J Hydrog Energy. Accepted 11 May 2011
10. Dufour J et al (2009) Life cycle assessment of processes for hydrogen production. Environmental feasibility and reduction of greenhouse gases emissions. Intl J Hydrog Energy 34:1370–1376
11. Holladay JD, Hu J, King DL, Wang Y (2009) An overview of hydrogen production technologies. Catal Today 139(2009):244–260
12. California Fuel Cell Partnership Action Plan (2009) Hydrogen fuel cell vehicle and station deployment plan: a strategy for meeting the challenge ahead. California Fuel Cell Partnership Action Plan, West Sacramento
13. Spath P, Mann M (2001) Life cycle assessment of hydrogen production via natural gas steam reforming. NREL/TP-570-27637. NREL National Renewable Energy Laboratories, Golden
14. Ogden JM (2002) Review of small stationary reformers for hydrogen production. Technical Report to the International Energy Agency
15. Sverdrup GM et al (2006) Status of hydrogen production pathways – comparison of energy efficiencies, fossil fuel use, greenhouse gas emissions, and costs. In: WHEC 16, 13–16 June 2006, Lyon
16. Margalef P (2010) On the polygeneration of electricity, heat and hydrogen with high temperature fuel cells. PhD dissertation, University of California, Irvine
17. Brouwer J, Leal E (2006) A thermodynamic analysis of electricity and hydrogen polygeneration using a solid oxide fuel cell. J Fuel Cell Sci Technol 3:137–143
18. Singhal SC, Kendall K (2003) High temperature solid oxide fuel cells: fundamentals, design and applications. Elsevier, Oxford
19. Cengel YA, Boles MA (2006) Thermodynamics: an engineering approach, 6th edn. McGraw Hill, Boston
20. Stephens-Romero S (2010) Systematic planning to optimize investments in hydrogen infrastructure deployment. Intl J Hydrog Energy 35:4652–4667
21. Brouwer J, Leal E (2005) Production of hydrogen using high-temperature fuel cell: energy and exergy analysis. In: 18th international congress of mechanical engineering. ABCM, Ouro Preto
22. O'Hayre R, Cha S, Colella W, Prinz FB (2006) Fuel cell fundamentals. Wiley, New York
23. Miller QM, Stocker J (1989) Selection of a hydrogen separation process. In: NPRA Annual Meeting held 19–21 March 1989, San Francisco
24. Heydorn EC, Patel P (2010) Development of a renewable hydrogen station. ICEPAG, Costa Mesa
25. QuestAir H-3200 Commercial Brochure. http://www.xebecinc.com/hydrogen-purification-h3200.php
26. Bossel U (2003) Energy and the hydrogen economy
27. Air Products & Chemicals Inc. Recovery process using pressure swing adsorption technology. http://texasiof.ces.utexas.edu/texasshowcase/pdfs/presentations/c6/pcook.pdf
28. Vollmar HE et al (2000) Innovative concepts for the coproduction of electricity and syngas with solid oxide fuel cells. J Power Sour 86:90–97
29. Van Herle J et al (2003) Energy balance model of a SOFC cogenerator operated with biogas. J Power Sour 118:375–383
30. Li M (2010) Detailed fuel cell modeling for coal-based integrated gasification fuel cell system design and analysis. Mechanical and aerospace doctoral studies dissertation, University of California, Irvine

Hydrogen Production Science and Technology

Timothy E. Lipman
Institute of Transportation Studies, University of California – Berkeley, Berkeley, CA, USA

Article Outline

Introduction
Review of Hydrogen Production Methods
Reformation of Fossil Hydrocarbons and Bioderived Liquids
Hydrogen Production Costs
Conclusion
Bibliography

Introduction

Hydrogen is an abundant element that is currently produced for a wide range of industrial uses. In recent years, it is also starting to be used for stationary power production in fuel cell systems and to power fuel cell electric vehicles including buses, forklifts, and passenger cars. One highly compelling attribute of hydrogen is that it can be produced in many different ways and using a variety of feedstocks; however, it does have to be *produced* through one of a variety of processes rather than simply "discovered" and delivered to market as is, for example, natural gas.

Approximately 10–11 million metric tonnes of hydrogen is produced in the USA each year [1]. For reference, this is enough to power 20–30 million cars (using 700–1,000 gal energy equivalents per car per year) or about 5–8 million homes. Globally, the production figure is around 40.5 million tonnes (equal to about 44.4 million short tons or about 475 billion cubic feet) and is expected to grow 3.5% annually through 2013 [2]. Major current uses of the commercially produced hydrogen are for oil refining, where hydrogen is used for hydrotreating of crude oil as part of the refining process to improve the hydrogen-to-carbon ratio of the fuel; food production (e.g., hydrogenation); treating metals; and producing ammonia for fertilizer and other industrial uses.

A range of potential hydrogen production methods and pathways is presented below in Fig. 1. These include reformation, gasification, electrolysis, and other advanced processes. In addition to these more well-established pathways, there are various emerging production pathways also possible. These are mostly at the laboratory scale and present and include such concepts as direct "photoelectrochemical" water splitting; a wide array of biological processes involving biogas conversion, algae, and microbial electrolysis cells; and other novel methods such as high-temperature thermochemical systems.

This chapter reviews a variety of established and emerging hydrogen production methods and their current status. Key remaining issues and research and development (R&D) challenges are highlighted for many of the pathways.

Review of Hydrogen Production Methods

Hydrogen in molecular form can be produced from many different sources and in many different ways. Hydrogen is most typically produced today for industrial uses through the steam reformation of natural gas

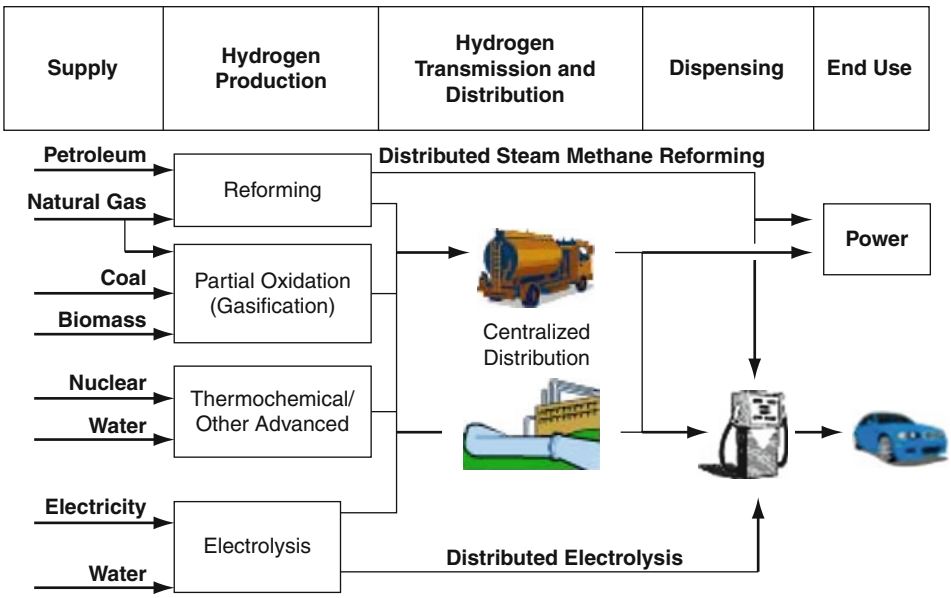

Hydrogen Production Science and Technology. Figure 1
Example hydrogen production pathways (Source: [1])

(known as "steam methane reforming") and from other hydrocarbons in oil refinery locations, but also is produced through electrolysis of water and as a by-product of some industrial processes such as chlor-alkali production. While hydrogen production methods often have several aspects and can be grouped in various ways, they can be organized as follows for purposes of this entry:

- Reformation of fossil hydrocarbons and bioderived liquids
- Gasification of coal and other hydrocarbons
- Electrolysis of water
- Biomass gasification and pyrolysis
- Biological production
- Nuclear-related pathways
- Photoelectrochemical methods
- High-temperature thermochemical methods
- Fuel-cell-based coproduction

These production pathways are briefly reviewed below, along with identification of key remaining challenges associated with the ones that are not yet commercially viable. A section that compares production cost estimates of hydrogen by several of the methods is then presented followed by the overall conclusions of the chapter.

Reformation of Fossil Hydrocarbons and Bioderived Liquids

The most widely used hydrocarbon reformation process is steam methane reforming (SMR). SMR is the process by which natural gas, other hydrocarbon, or other methane-rich stream such as biogas or landfill gas is reacted with steam in the presence of a catalyst to produce hydrogen and carbon dioxide. In the SMR process, carbon monoxide is first produced with hydrogen (this blend is known as "syngas"), and then, a series of water–gas shift reactions converts the carbon monoxide to carbon dioxide and additional hydrogen through the injection of additional steam. The water–gas shift occurs first in a high-temperature step at about 350°C and then in a lower-temperature step at about 190–210°C. Four hydrogen molecules are produced for every one carbon dioxide molecule, making SMR a relatively low-carbon process when, for example, the use of SMR-based hydrogen is used in a fuel cell vehicle compared with the use of gasoline in a combustion-engine vehicle on a "full fuel cycle" basis [3, 4].

The overall SMR reactions are as follows:

$$CH_4 + H_2O\ (\text{steam}) \rightarrow CO + 3H_2\ (\text{syngas production})$$

$$CO + H_2O\ (\text{steam}) \rightarrow CO_2 + H_2\ (\text{water gas shift})$$

$$\text{Overall}: CH_4 + 2H_2O \rightarrow CO_2 + 4H_2$$

SMR produces a hydrogen-rich gas that is typically on the order of 70–75% hydrogen on a dry basis, along with smaller amounts of methane (2–6%), carbon monoxide (7–10%), and carbon dioxide (6–14%) [5]. The efficiency of the SMR process using natural gas as a feedstock is typically about 74% on an LHV basis (CK) [6].

Bioliquids such as ethanol, sugars, and bio-oils can also produce hydrogen through reformation processes as well as via gasification and pyrolysis. Anderson and Carole [7] provide a useful review of the key advantages and disadvantages of various feedstocks as well as potential feedstock prices, hydrogen yield rates, and commercial production time frames. They examine ethanol, glucose, glycerol, sorbitol, ethylene and propylene glycol, cellulose/hemicellulose, methanol, and bio-oils as potential hydrogen feedstocks that are viable for use in reformation processes. They find that ethanol, glucose, glycerol, and bio-oils are potentially viable in the 2012–2017 time frame, while sorbitol, ethylene and propylene glycol, cellulose/hemicellulose, and methanol are possible in the 2017+ longer-term time frame. For the medium-term feedstocks, they find that the highest yield rates are possible for ethanol (0.26 kg hydrogen/kg ethanol) and crude glycerol (0.24 kg hydrogen/kg crude glycerol), with lower rates possible for pure glycerol (0.15 kg hydrogen/kg pure glycerol), glucose (0.13 kg hydrogen/kg glucose), and bio-oils (0.13 kg hydrogen/kg bio-oil). The longer-term options all have similar yield rates, ranging from 0.22 kg/ hydrogen/kg of feedstock (for methanol and propylene glycol) to 0.13/kg hydrogen/kg for sorbitol and cellulose/hemicellulose, while ethylene glycol has a more intermediate estimated hydrogen yield of 0.15 kg per kg of feedstock [7]. They do not present overall levelized costs of hydrogen from each of the feedstocks, but based on the feedstock prices and yield rates presented, it appears that glucose, crude glycerol, and cellulose/hemicellulose could be particularly attractive from a rough feedstock cost

and yield rate perspective (ignoring differences in capital equipment and process energy required, etc.).

US DOE production (not delivered) target costs are for $3.80/gal equivalent for hydrogen from bioderived liquids in 2012 and under $3.00/gal by 2017. Key technical challenges for achieving these goals include advances in catalyst systems, purification technologies, and system integration. A key issue is catalyst deactivation due to coking, when products from side reactions become deposited on the catalyst. An additional important area of research is low-temperature (<500°C) reforming, including aqueous-phase reforming that can be applied to glucose, ethylene glycol, sorbitol, glycerol, and methanol. Advantages include reduced energy intensity, better characteristics for the water–gas shift reactions, minimization of decomposition reactions (that can lead to the coking issue described above), and compatibility with membrane separation/purification techniques [7].

Gasification and Pyrolysis of Coal and Other Hydrocarbons

In the partial oxidation (POX) process, also known more generally as "gasification," hydrogen can be produced from a range of hydrocarbon fuels, including coal, heavy residual oils, and other low-value refinery products. The hydrocarbon fuel is reacted with oxygen in a less than stoichiometric ratio, yielding a mixture of carbon monoxide and hydrogen at 1200–1350°C. Hydrogen can also be produced through pyrolysis-based hydrocarbon gasification processes in the absence of oxygen.

The chemistry of hydrogen production from gasification of coal and other heavy hydrocarbons is complex, involving molecular cracking, POX, steam gasification, water–gas shift, and methanation reactions. The first stages involve progressive devolitization of the feedstock with increasing temperature, yielding a mix of oils, phenols, tars, and light hydrocarbon gases. This is followed by water–gas shift reactions, where additional hydrogen along with carbon dioxide are produced from carbon monoxide and water, and methanation reactions where methane (which can be later reformed into additional hydrogen) instead of hydrogen is formed with any remaining carbon monoxide. Depending on temperature and pressure conditions, the "syngas" produced from hydrocarbon gasification can have varying amounts of carbon dioxide, methane, and water, along with other trace components [8]. Several metals and metal oxides have been found to catalyze the gasification reactions and can alter the kinetic constants. Iron oxides such as Fe_2O_3 and Fe_3O_4 affect the rates of steam gasification of coal and other hydrocarbons, and some gasification reactions are also catalyzed by nickel and calcium-based substances [8].

One recent study [9] examines the potential life cycle impacts of hydrogen produced through gasification and pyrolysis of coal, along with two other pathways – the thermochemical sulfur–iodine cycle and the thermochemical "Westinghouse" cycle that both make use of solar thermal energy (or other source of waste heat such as from nuclear power) and sulfuric acid to produce hydrogen. These other chemical cycles are discussed in more detail in the thermochemical and nuclear-power-assisted hydrogen production sections later in this entry. The study uses SimaPro™ life cycle analysis software for the analysis, which includes major indices for human health impacts, ecosystem impacts (including air, water, and soil impacts), and resource use.

The study finds that, of these four methods of hydrogen production, from a life cycle (system construction and operation) perspective, gasification of coal has the lowest human health impacts and almost as low ecosystem quality impacts as the Westinghouse cycle, while the Westinghouse cycle has the lowest resource impacts. The sulfur–iodine cycle has somewhat higher ecosystem impacts, comparable human health impacts to the Westinghouse cycle, and comparable resource impacts to coal gasification (i.e., somewhat higher than for the Westinghouse cycle). Pyrolysis of coal, meanwhile, has by far the highest impacts across all three categories, primarily because the amount of hydrogen produced through coal pyrolysis is about 3.5 times lower than for gasification per unit of coal used as feedstock [9].

An interesting aspect of gasification is that it could lend itself to carbon dioxide capture, owing to the large scale of many gasification systems and the production of carbon dioxide through the water–gas shift reactions. Particular attention has focused on calcium oxide (CaO) as an inexpensive carbon dioxide acceptor, yielding calcium carbonate that could then be

sequestered [9]. This could prevent the product carbon dioxide from entering the atmosphere, if appropriate geological or oceanic reservoirs are available in the area for long-term storage.

Electrolysis of Water

Electrolysis is the process through which water molecules are split into hydrogen and oxygen molecules using electricity and an electrolyzer device. Electrolyzers are, effectively, fuel cell devices that operate in reverse. The overall electrolysis reaction is:

$$e^- + H_2O \rightarrow \tfrac{1}{2}O_2 + H_2 \text{ (“water splitting”)}$$

The two most common types of electrolyzers are alkaline (using a potassium hydroxide electrolyte) and PEM (using a solid polymer membrane electrolyte). A schematic of an alkaline electrolysis system is provided in Fig. 2. The electrolysis reaction produces pure oxygen as a by-product along with pure hydrogen. The oxygen can then be used for productive purposes such as enriching the oxygen content of greenhouses for food production.

Hydrogen can be produced via electrolysis of water from any electrical source, including utility grid power, solar photovoltaic (PV) power, wind power, hydropower, or nuclear power. The “Electrochemical Hydrogen Production” section of this encyclopedia reviews the basic science and materials issues with electrochemical hydrogen production in detail.

Electrolysis is currently done at a wide range of scales, from a few kilowatts to up to 2,000 kW per electrolyzer device. Additional research involves high-temperature electrolysis, where heat that is coproduced from another process, such as nuclear power as discussed below, is used to generate steam that can then be electrolyzed into hydrogen and oxygen with less electrical energy input than with lower-temperature electrolysis.

Biomass Gasification and Pyrolysis

Biomass conversion technologies can be divided into thermochemical and biochemical processes. Thermochemical processes tend to be less expensive because

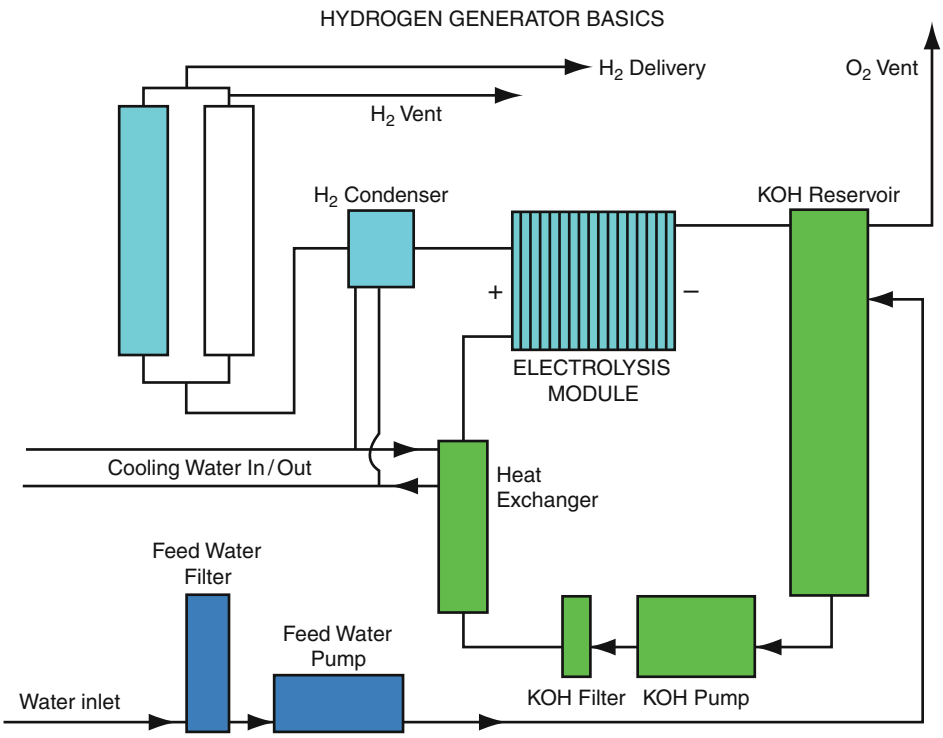

Hydrogen Production Science and Technology. Figure 2
Hydrogen production by alkaline electrolysis (Courtesy of teledyne energy systems)

they can be operated at higher temperatures and therefore obtain higher reaction rates. They involve either gasification or pyrolysis (heating biomass in the absence of oxygen) to produce a hydrogen-rich stream of gas known as "syngas" (a blend of hydrogen and carbon monoxide). They can utilize a broad range of biomass types. In contrast, enzyme-based fermentative-type processes (discussed below) are at present mainly limited to wet, sugar-based feedstocks but could include cellulosic feedstocks in the future with continued improvements in process techniques and systems.

Biomass feedstocks can be gasified in a similar manner as fossil hydrocarbons as discussed above and can also be converted through pyrolysis. Gasification involves POX and/or steam reforming to produce a combination of gas and char products, where the char can then be reduced to ultimately produce a mix of hydrogen, carbon monoxide, carbon dioxide, and methane. Water–gas shift can then be used to produce additional hydrogen from carbon monoxide and water, and the methane can also be further reformed into additional hydrogen using SMR. Example chemical reactions include these, using glucose as an example hydrocarbon [10]:

$$C_6H_{12}O_6 + O_2 + H_2O \rightarrow CO + CO_2 + H_2 + \text{other species}$$

$$CO + H_2O \rightarrow CO_2 + H_2 + \text{small amount of heat("water gas shift")}$$

A key issue with biomass gasification is the formation of tar that occurs during the process, which is an unwanted product because it cannot be readily reformed into hydrogen. In order to minimize tar formation, careful design of the gasifier, incorporation of additives or catalysts, and careful control of operation variables can be effective strategies [8].

Biomass can also produce oxygenated oils through pyrolysis (without oxygen input), which can then be cracked and steam reformed to produce hydrogen and carbon dioxide syngas. An advantage of this method is that bio-oils are easier to transport than either biomass or hydrogen, and hydrogen can thus be produced in a two-step process at different locations with optimization of feedstock supply and hydrogen distribution [11].

Depending on application, there are potential additional cleanup steps (with associated costs) that may need to be added for hydrogen produced from biomass for the provision of high-purity hydrogen (e.g., for low-temperature fuel cell applications for transportation and stationary markets). These may be similar to those required for hydrogen production from other "fossil" hydrocarbons, but with considerable variability in both cases depending on the nature of the feedstock (i.e., natural gas or refinery coke), the amount of sulfur present, and other factors related to details of the production process.

Biological Production Methods

There are a wide range of additional biological production methods, beyond gasification or pyrolysis and reformation of biomass and reformation of biogases. These include:

- Photolytic hydrogen production from water
- Photosynthetic bacterial hydrogen production including dark fermentative methods
- Hydrogen production from algae
- Microbial electrolysis cells
- Other concepts such as combined biological systems

The primary of these additional biological production methods (the first four from the above list) are briefly discussed below.

Photolytic Hydrogen Production from Water

The photolytic hydrogen process produces hydrogen from water directly, without the use of a more conventional electrolyzer device. This is accomplished through the use of a photoelectrochemical (PEC) cell that employs a semiconductor material and involves movement of electrons through the material. This is similar to the operation of solar photovoltaic systems but where instead of the current being collected, it is immediately used at the site of the PEC to split water molecules in either an aqueous or flat-plate type of system.

In the photoelectrochemical water-splitting process, discussed in detail in the "► Photo-catalytic Hydrogen Production" entry in this encyclopedia [12], a photoanode is subjected to solar radiation, generating an electronic charge and an electron–hole

pair (as in photovoltaics). Second, however, oxidation of water occurs at the holes of the anode, yielding molecular oxygen. Then, hydrogen ions and electrons are transported from the photoanode by way of an electrolyte (for the hydrogen ions) and an electrical connection (for the electrons), forming molecular hydrogen as the hydrogen ions are reduced with the electrons at the cathode. PEC cells can thus use sunlight as the only energy input to produce hydrogen [13].

Since only some of the solar spectrum involves photons with sufficient energy to generate these voltage levels, multilayer photovoltaic junction materials can be used to allow multiple low-energy photons to be grouped together to exceed the electrolysis threshold. For example, early research investigated $GaInP_2$/GaAs "p/n, p/n tandem cells" at the National Renewable Energy Agency, that incorporated a top $GaInP_2$ junction with a band gap of 1.83 eV, to absorb the visible part of the light spectrum, with a bottom GaAs junction with a band gap of 1.42 eV to absorb the near-infrared portion that gets transmitted through the top junction. This type of system was shown to have a hydrogen production efficiency of 12.4%, based on the estimated hydrogen yield and the incident light intensity of 1190 mW/cm^2, consistent with theoretical calculations showing a 24% maximum efficiency but more like 10–16% practical efficiencies for two-layer devices of this types [13].

The selection of semiconductor materials for the photoanode is critical for PEC cells, as discussed extensively in the ► Hydrogen via Direct Solar Production contribution to this encyclopedia [14]. Key issues identified in the chapter are for the semiconductor to have the proper band gap (the level of energy in electron volts needed, between about 1.6 and 2.0 eV for the primary cell) and the ability to avoid immediate recombination of the charge carriers.

Challenges to PEC-cell-based hydrogen production include materials issues including corrosion problems and uncertain performance over time, as the lifetimes of current cells being tested in laboratories are on the order of hundreds of hours where tens of thousands of hours of operation are needed for practical systems [15, 16]. Furthermore, there are challenges with the physical assembly of the supramolecular complexes needed for PEC cells, in order to make sure that the various sequential reactions needed are not restricted at any step by poor collection and distribution to the water substrate of the reducing equivalents. It is also important to note that understanding the factors that control multi-electron photochemistry is still at an early stage, meaning both that there are knowledge deficiencies as well as opportunities for future system improvements [14].

Practical PEC systems of several different designs can be contemplated, and four of these have undergone recent economic analysis for the US Department of Energy for an example 10 t/day hydrogen production plant. Of the four types studied – single-bed aqueous suspension, dual-bed aqueous suspension, fixed flat panel, and tracking concentrator – the first type was estimated to have the lowest costs of hydrogen produced ($1.63/kg) compared with $3.19/kg for the dual-bed suspension system, $4.05/kg for the tracking concentrator system, and $10.36/kg for the fixed flat panel system [17]. Given the early stage of development of PEC cells and systems for hydrogen production, however, these economic estimates should be treated as preliminary.

Photosynthetic Bacterial Hydrogen Production

A number of fermentative processes for producing hydrogen using bacteria are being investigated. These can generally be categorized into "photobiological" methods where solar energy is captured to help drive the fermentation process, or those that use organic materials that were previously produced from photosynthetic process contain hydrogen that is associated with the fixation of carbon. Key issues with the direct photobiological methods are the relatively low conversion efficiencies of solar systems and the fact that oxygen is produced along with hydrogen, creating safety risks as well as difficulties in regulating the oxygen level in the fermentative environment (an important factor to the efficacy of these systems) [18].

Another option that involves conversion of existing organic materials to hydrogen is known as anaerobic or "dark" fermentation. This process uses some type of hydrogenase as an enzyme (the two main types being [NiFe] and [FeFe] hydrogenases), uses pyruvate as a key intermediate in the fermentation pathway, and works best with carbohydrate-rich feedstocks. Fermentation of proteins does not yield much hydrogen

because protein amino acids are mostly fermented in pairs through "Strickland" reactions where one amino acid is an electron receptor for oxidation of the second amino acid, without hydrogen production [18]. Fermentation of carbohydrate-rich materials such as glucose can yield a series of products following the pyruvate intermediary, including formate that yields hydrogen and Acetyl-CoA that yields acetate and acetaldehyde that can be further processed into ethanol with the addition of NADH. This is known as "enteric-type mixed-acid fermentation" as shown in Fig. 3 below.

As with other biological hydrogen production methods that tend to be relatively slow in terms of yields, low yield rates for practical systems are a constraint for photosynthetic/bacterial methods as well. Based on known metabolic pathways, thermodynamic and metabolic limitations restrict hydrogen production to a maximum of 4 moles of hydrogen per mole of glucose [18]. This is because acetate is necessarily produced as well as hydrogen and carbon dioxide, effectively "locking up" half of the available hydrogen. Strategies to increase yields include optimizing parameters for the fermentation bioprocesses, attempting to limit competing reactions in order to channel more reductant for hydrogen production, decreasing hydrogen partial pressures in the reactor vessels (but then leading to more dilute streams of product gas), using thermophilic strains of bacteria that increase output at higher temperatures (but then requiring additional reactor vessel heating), and identifying and employing more active hydrogenases as enzymes [18].

Hallenbeck [18] reviews these strategies in some detail and concludes that it will be difficult to exceed the "Thauer limit" of 4 moles of hydrogen produced per mole of glucose, even though it is theoretically possible to produce 12 moles of hydrogen per mole of glucose by the reaction:

$$C_6H_{12}O_6 + 6H_2O \rightarrow 12H_2 + 6CO_2$$

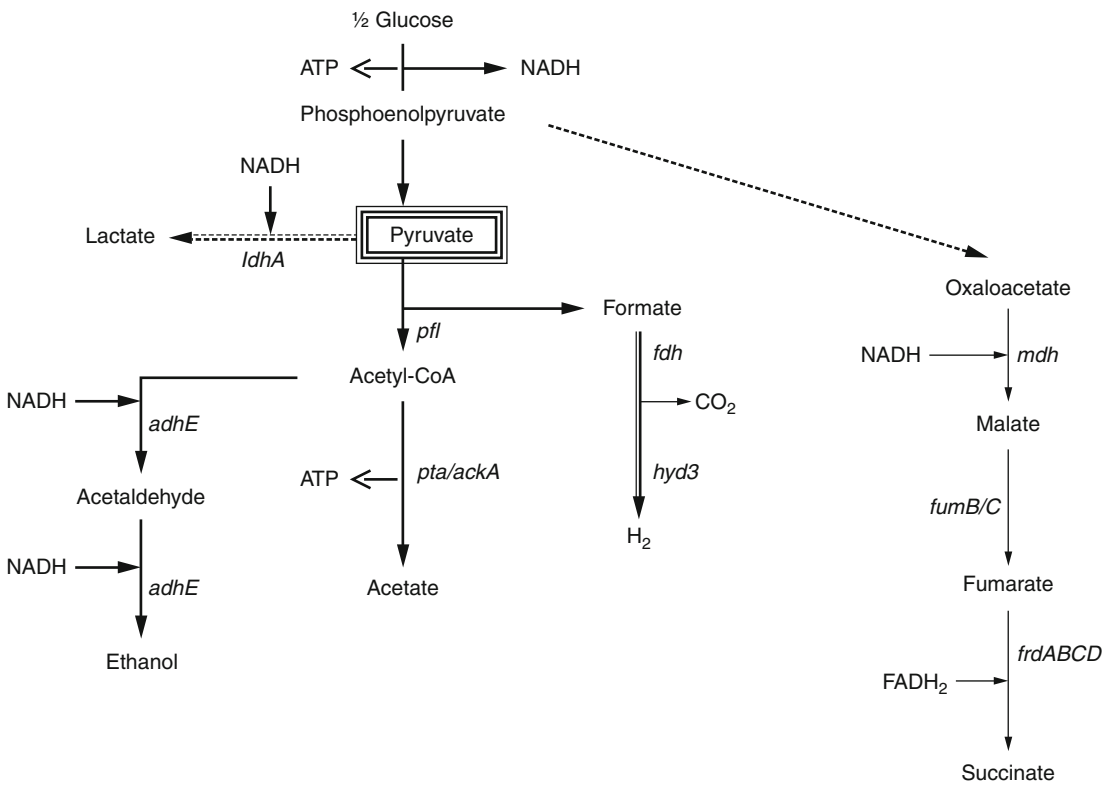

Hydrogen Production Science and Technology. Figure 3
Enteric-type mixed-acid fermentation for hydrogen production (Source: [18])

The existing conversion efficiency of only 33% (maximum) of this theoretical limit is too low for practical systems unless additional steps can be employed to convert more of the organic feedstock into useful products. These have been proposed in the forms of a second stage fermentation for methane production, a second stage photofermentation for additional hydrogen production, and (more radically) metabolic engineering to develop novel hydrogen-producing pathways. Active research continues to address the current limitations, with the goal of developing more efficient and complete conversion levels in practical systems.

Hydrogen Production from Algae

The ability of various strains of algae to produce hydrogen has been studied for some time, with particular attention on unicellular green algae and potential combination of hydrogen production from green algae with additional hydrogen production from bacteria in a coproduction concept. Melis and Menecki [19] have proposed this type of system, where photosynthesis is employed in the first step to produce algae biomass and hydrogen gas using the [Fe]-hydrogenase enzyme. In the second stage, the green algal process is coupled with production of an anoxygenic bacteria (such as *Rhodospirillum rubrum*) to produce adenosine triphosphate (ATP), which is required for the evolution of hydrogen using the nitrogenase enzyme. Finally, during a third stage, fermentative bacteria such as *Clostridium pasteurianum* catabolize the algae/bacteria biomass and further enhance the hydrogen yield [19].

This type of three-organism system thus couples algal hydrogen production with a similar dark fermentative reaction step similar to the bacterial production process described above. Key areas of continuing research with algal-based hydrogen production systems include limiting oxygen evolution during the algal growth phase, exploring the role of sulfate availability to the chloroplasts to regulate the rate of photosynthesis, and examining various means for further increasing hydrogen yields to enable more practical hydrogen production systems [19].

Microbial Electrolysis Cells

In a related concept to photosynthetic biological production, microbial electrolysis cells (MECs) can be used to produce hydrogen by providing some of the voltage potential needed for electrolysis, thus reducing energy requirements. Experiments have determined that the bacteria can produce an anode working potential of around 0.3 V and that only an additional 0.11 V are needed to produce hydrogen in theory – but that in practice, more like an additional 0.25 V are needed due to overpotential at the cathode [20]. This means that it appears that approximately halving the energy needed for electrolysis is possible with MECs, but with still unexplored overall system efficiency. The complete system includes maintaining MEC operating conditions, delivering feedstocks to the production facility, replacing other expendable materials, and performing any gas separation and cleanup needed.

The MEC-based production concept requires two key steps. First, one group of bacteria turns unused sugar and unwanted vinegar from improper fermentation into electricity. Only a small amount of electricity is produced, however, and not enough to reach the 1.2 V necessary to split water in a typical electrolysis reaction. Therefore, some additional electricity from the power grid is also used. Second, another group of bacteria uses the electricity to split water molecules into oxygen and hydrogen in what is known as "microbial electrolysis" [20].

One of the biggest problems that practical systems have to overcome is the bacteria variability of the runoff water, making production rates difficult to predict because the bacteria have to build to a certain level of concentration to be effective. Another issue is that much of the hydrogen can be consumed by "methanogenic" microbes before leaving the solution, leading to much greater production of methane than hydrogen. While this methane could then be "reformed" into hydrogen by SMR, direct production would be far preferable from an overall energy-use standpoint. Research is underway in the laboratory to improve this hydrogen-to-methane production ratio [20].

Nuclear-Related Pathways

Many nuclear-energy-based hydrogen production schemes are possible. These include nuclear thermal conversion of water using various chemical processes such as the sodium-iodine cycle, electrolysis of water using nuclear power, and high-temperature

electrolysis that additionally would use nuclear system waste heat to lower the electricity required for electrolysis. The basic concept is that heat from nuclear plants can be used to assist the production of hydrogen in various ways, with over 100 identified cycles that could benefit from association with nuclear power [21].

A recent US national laboratory study examined hydrogen production costs from nuclear cycles based on the sulfur–iodine (S–I) thermochemical water-splitting cycle, a hybrid sulfur (HyS) thermochemical water-splitting cycle (a modified Westinghouse-type cycle), and a high-temperature steam electrolysis (HTSE) cycle. The study focused on various sensitivities associated with cost estimates for these systems and generally found somewhat higher expected costs than have been reported previously (see Table 1 for details).

The S–I cycle has been studied since the 1970s and involves a three-step chemical reaction process. The first produces HI and sulfuric acid (H_2SO_4) from I_2, SO_2, and water at about 120°C; the second produces SO_2, water, and O_2 from the H_2SO_4 at about 830°C (assisted with heat from nuclear power); and the third produces I_2 and H_2 from the initial HI at about 450°C [22]. The sulfur and iodine compounds are recovered and reused. Based on a reactive distillation design, hydrogen production costs of about $7.27/kg are believed possible with this design with a system producing 380 t/day of hydrogen, assuming some future system cost reductions [23].

The HyS design differs from S to I in that it uses thermal input energy for oxygen generation and a separate low-temperature electrolysis step for hydrogen generation, but also involves sulfuric acid decomposition. The HyS cycle was first explored by Westinghouse in the 1980s and is sometimes called the "Westinghouse hybrid cycle." The key steps in the Westinghouse HyS cycle are [24]

Hydrogen Production Science and Technology. Table 1 Estimated hydrogen production costs

Technology and fuel	Production capacity (1,000 kg/day)	Hydrogen production cost ($/kg)				Source
		Capital ($)	Feedstock ($)	O&M ($)	Total ($)	
Central SMR of natural gas	380	0.16	1.15	0.14	1.47	[1]
Distributed SMR of natural gas	1.5	0.40	1.72	0.51	2.63	[1]
Central coal gasification with CCS	308	0.83	0.56	0.43	1.82	[1]
Central coal gasification without CCS	284	0.57	0.56	0.09	1.21	[1]
Biomass gasification	155	0.37	0.52	0.55	1.44	[1]
Distributed electrolysis	1.5	0.96	5.06	0.73	6.75	[1]
Central wind electrolysis	124.5	1.46	1.69	0.65	3.82	[1]
Distributed wind electrolysis	0.5	3.00	3.51	0.74	7.26	[1]
Central nuclear thermochemical	1,200	0.76	0.20	0.43	1.39	[1]
Nuclear S–I	343.5	2.61	0.35	5.31	7.27	[23]
Nuclear HyS	343.5	1.48	0.22	2.25	4.95	[23]
Nuclear HTSE	343.5	1.05	0.03	3.15	4.23	[23]
Single-bed aqueous PEC	1	–	–	–	1.63	[17]
Dual-bed aqueous PEC	1	–	–	–	3.19	[17]
Fixed panel PEC	1	–	–	–	4.05	[17]
Tracking concentrator PEC	1	–	–	–	10.36	[17]

Notes: *CCS* carbon capture and sequestration, *HTSE* high-temperature steam electrolysis, *HyS* hybrid sulfur cycle, *O&M* operations and maintenance, *PEC* photoelectrochemical cell, *S–I* sulfur–iodine, *SMR* steam methane reforming

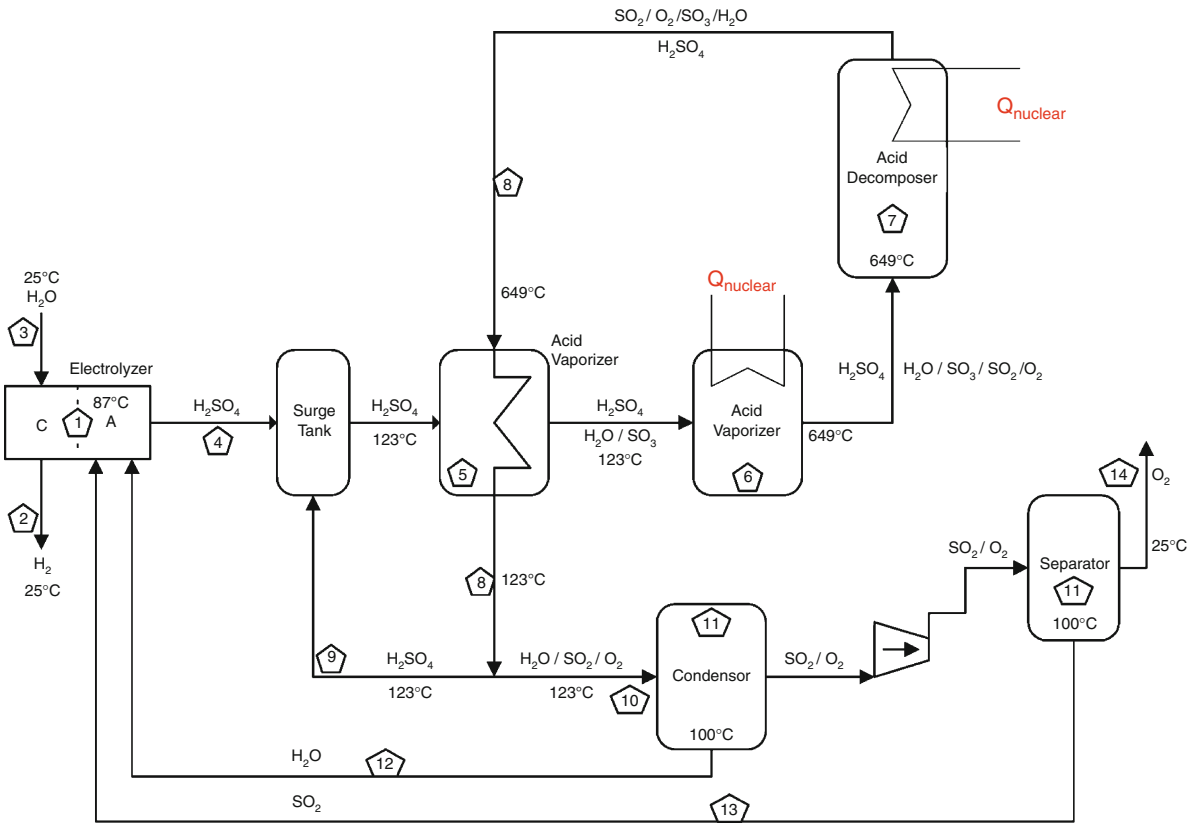

Hydrogen Production Science and Technology. Figure 4
Westinghouse hybrid sulfur cycle schematic (Source: [24])

$$H_2SO_4 \rightarrow H_2O + SO_3 \rightarrow SO_2 + 1/2O_2 + H_2O \text{ (thermal decomposition, } 871^\circ C)$$

$$2H_2O + SO_2 \rightarrow H_2SO_4 + H_2 \text{ (electrolysis, } 87^\circ C)$$

Hydrogen production costs of about \$4.95/kg are believed possible with this type of hybrid system design with a system producing 345 t/day of hydrogen [23]. A schematic of the HyS cycle is presented in Fig. 4:

The third design explored in the recent study, HTSE, involves electrolysis of water at about 800°C, assisted with heat from nuclear power systems. Key elements of the system include sweep gas coupling heat exchangers, process coupling heat exchangers, solid oxide electrolyzer systems, and feed and product purification systems. Hydrogen production costs of about \$4.23/kg are believed possible with HTSE with a system producing 345 t/day of hydrogen [23].

Thermochemical Production Methods

In this set of pathways, high-temperature (500–2,000°C) heat is used to drive chemical reactions to produce hydrogen, including via direct thermolysis of water. This can be done in conjunction with solar thermal power, nuclear power, or other heat sources. Of the over 200 pathways that have been identified, several are being pursued by US DOE for further research [25].

Thermochemical production typically involves the use of metal oxides in a two-step process where a metal oxide is first decomposed into the metal and oxygen in an endothermic step, and then, the metal is then combined with water to re-form the metal oxide and hydrogen in a second exothermic step [26]. In one example known as the zinc oxide cycle, zinc oxide powder passes through a reactor heated by a solar concentrator operating at about 2,300 K. At this temperature, the zinc oxide dissociates to zinc and oxygen gases. The zinc

cools, separates, and reacts with water to form hydrogen gas and solid zinc oxide:

$$2ZnO + heat \rightarrow 2Zn + O_2$$

$$2Zn + 2H_2O \rightarrow 2ZnO + 2H_2$$

The net result is hydrogen and oxygen, produced from water, where the hydrogen can be separated and purified for subsequent use. The zinc oxide can be recycled and reused to create more hydrogen through subsequent phases of the process. Key limitations at present include the rapid reoxidation of the zinc vapor and challenges with keeping the receiver windows clean when the system is coupled with solar thermal systems for delivery of the heat required [26].

An additional type of thermochemical system has been proposed that would also involve a photon component, essentially coupling thermochemical and photoelectrochemical hydrogen production pathways. One concept would use a carbon dioxide/carbon monoxide cycle, where carbon dioxide molecules would absorb near-ultraviolet photons and high temperatures and dissociate into carbon monoxide, helping to enable the production of hydrogen. Research has showed that this can be done at temperatures of around 2,000–2,500 K, which would be compatible with solar thermal concentrator systems [26].

Other concepts involve modifications to the Westinghouse cycle discussed above, including a proposed sulfur–ammonia cycle that makes use of solar power in two ways –to drive both a solar photocatalytic reactor and a sulfuric acid decomposition reactor. The process would use ammonia, sulfuric acid, and aqueous ammonium sulfate – (NH4)2SO4 – at various stages, with the principal advantages using solar photons to directly produce the chemical energy of hydrogen along with using solar heat in the thermochemical step, thus eliminating the need for electrical energy input [26].

Fuel Cell Coproduction

High-temperature fuel cells based on molten carbonate (MCFC) or solid oxide (SOFC) technology operate at sufficiently high temperatures to run directly on methane. This is sometimes called "internal reforming." Thus, MCFC and SOFC systems do not need a pure or relatively pure hydrogen stream as do proton exchange membrane (PEM) and phosphoric acid (PAFC) systems, but can run directly on natural gas or biogas or landfill gas. Furthermore, such systems can be designed to produce additional purified hydrogen as a by-product (e.g., for use as a vehicle fuel), by feeding additional fuel and then purifying the hydrogen-rich "anode tail gas" from the fuel cell into purified hydrogen. This concept is discussed in some detail in the case studies section below. A detailed review of this concept for hydrogen production can be found in the "► Hydrogen Production from High-Temperature Fuel Cells" entry in this encyclopedia [27].

FuelCell Energy (FCE) of Danbury, Connecticut, has teamed up with Air Products and Chemicals, Inc., (APCI) to demonstrate renewable hydrogen production based on the FCE molten-carbonate fuel cell technology and a novel hydrogen gas cleanup system. This system, called the "DFC-H2®" system, has undergone initial testing at FCE's research laboratories and is now being readied for deployment at a landfill site at the Orange County Sanitation District in southern California [28]. Figure 5 below shows the system pictured during initial testing.

The basic concept behind the energy station is that hydrogen and electricity are coproduced, where the electricity is produced using methane (natural gas or biogas) as a feedstock in the high-temperature fuel cell, but additional hydrogen is produced within the fuel cell stack leading to a hydrogen-rich stream of gas leaving the fuel cell unit. This hydrogen-rich "anode tail gas" can then be purified for other uses, such as fuel cell vehicles or other types of fuel cells (e.g., PEM and PAFC) that require pure hydrogen. The following schematic presents the concept and how there are also opportunities for waste heat recovery to help boost overall efficiency.

FCE and APCI have recently released a technical paper about the system that suggests that 125 kg/day of hydrogen can be produced along with an electrical output of 250 kW, based on over 8,500 h of system testing and a "pressure swing adsorption" (PSA) process for hydrogen separation. The purity of the product hydrogen was measured at 99.99%, while also meeting a target of 0.2 ppm of carbon monoxide.

The company believes that a novel electrochemical hydrogen separation unit, which they are also testing, could offer up to a 50% reduction in operating cost compared to the more conventional PSA unit while

Hydrogen Production Science and Technology. Figure 5
"DFC-H2®" system being tested prior to field deployment (Source: [28])

offering an overall electrical power plus hydrogen production efficiency increase to 68% from 66% (with no waste heat recovery) on a lower-heating-value basis [28].

Hydrogen Production Costs

Table 1 presents a set of hydrogen-production-only costs (i.e., not including delivery if centralized production) by some of the production methods discussed in this entry that are either used at present or that are possible in the future. These estimates are all as reported by the US Energy Information Administration or based on analysis for the National Academy of Science or the US Department of Energy. These and other estimates were used to report the production cost ranges by production methods that were discussed in the preceding sections of this entry. Note that some of the cleanest methods of producing hydrogen are currently the most expensive (e.g., based on electrolysis from wind or other clean electricity sources), but biomass gasification offers a renewable hydrogen pathway with costs that can potentially be competitive with fossil sources.

In comparison with these projections, in the current hydrogen market, deliveries of industrial-grade high-purity (99.95%+) hydrogen at medium to large volumes of hundreds to a few thousands of kilograms are typically priced at around $4–5 per 100 standard cubic feet (SCF) (or $17–21/kg), plus freight, rental, and hazmat charges. For smaller volumes of between 4 and 15 kg, or about 1,600–6,100 SCF, gas costs are estimated to vary widely from $5 to $20 per 100 SCF ($21–83/kg) depending on service model, delivery frequency, and distance from the gas supplier fill plant [29].

Conclusion

In conclusion, hydrogen is a promising energy carrier and fuel for stationary and transportation uses, but the potential expanded use of hydrogen involves many technical and infrastructure-related challenges. Approximately 10–11 million metric tonnes of hydrogen are used each year in the USA and about 40 million tonnes globally, but mostly in internal industrial settings. Dispensing hydrogen to wider consumer and fleet-use markets, such as for private and fleet vehicles and for stationary power uses, involves considerable challenges due to hydrogen's low energy density (by volume) and other unusual characteristics (i.e., small molecule size, relative ease of ignition in mixes with air, and need for high gas purity when used in certain applications such as in PEM fuel cells).

There are many available and emerging hydrogen production pathways based on a myriad of thermochemical, photochemical, and electrochemical mechanisms and reactions. Perhaps the most compelling aspect of hydrogen as a potential fuel is the incredible diversity in the means and methods by which it can be produced – literally by everything from basic algae to high-temperature fuel cells using ceramic materials and

customized catalysts. Because hydrogen can be produced from such a wide range of feedstocks – from fossil sources such as natural gas or coal to a variety of renewable sources including those based on solar power and wind, geothermal, and biomass energy.

Options for hydrogen production include various pathways using fossil hydrocarbons or biogas using gasification or pyrolysis processes; steam methane reforming; electrolysis of water; nuclear-power-assisted cycles including the sulfur–iodine cycle; fermentative, algae-based, and other biological pathways; and more recently developed electrochemical and thermochemical processes including the use of PEC cells, microbial electrolysis cells, and tailored molecules that can facilitate the splitting of water molecules into hydrogen and oxygen with lower energy requirements than conventional electrolysis.

Of these, several pathways have been studied with regard to potential production costs at commercial-scale operations. While cost estimates are somewhat preliminary for some of the more novel production methods, particularly attractive hydrogen production costs appear possible for centralized SMR of natural gas, gasification of coal and biomass, nuclear thermochemical systems, and single-bed aqueous photoelectrochemical methods. Also potentially attractive are smaller-scale decentralized production systems based on SMR or electrolysis, as these can avoid the expense and difficulty of transporting bulky hydrogen gas or cryogenic liquid by generating the hydrogen close to the point of end use.

Bibliography

1. US Energy Information Administration (EIA) (2008) The Impact of Increased Use of Hydrogen on Petroleum Consumption and Carbon Dioxide Emissions, Report #: SR-OIAF-CNEAF/2008-04. www.eia.doe.gov/oiaf/servicerpt/hydro/appendixc.html, August
2. Freedonia Group (2010) World hydrogen demand and 2013 forecast. February
3. Lipman TE, Delucchi MA (2010) Expected greenhouse gas emission reductions by battery, fuel cell, and plug-in hybrid electric vehicles. In: Pistoia G (ed) Battery, hybrid, and fuel cell vehicles. Elsevier, Amsterdam. ISBN: 978-0-444-53565-8
4. Wang M, Wu Y, Elgowainy A (2007) GREET1.7 fuel-cycle model for transportation fuels and vehicle technologies. Argonne National Laboratory, Argonne
5. Hirschenhofer JH, Stauffer BD, Engleman RR, Klett MG (2000) *Fuel Cell Handbook*, Fourth Edition. Department of Energy, Federal Energy Technology Center, B/T Books, Orinda
6. US Department of Energy (2010) The Department of energy hydrogen and fuel cells program plan an integrated strategic plan for the research, development, and demonstration of hydrogen and fuel cell technologies – DRAFT
7. Anderson A, Carole T (2006) Bio-derived liquids to hydrogen distributed reforming working group background paper. U.S. Department of Energy, HFCIT Program, September
8. Navarro RM, Pena MA, Fierro JLG (2007) Hydrogen production reactions from carbon feedstocks: fossil fuels and biomass. Chem Rev 107:3952–3991
9. Smitkova M, Janicek R, Riccardi J (2009) Life cycle analysis of processes for hydrogen production. Int J Hydrog Energy 34(3):1370–1376
10. U.S. Department of Energy (2011) Hydrogen production: biomass gasification. Web document, http://www1.eere.energy.gov/hydrogenandfuelcells/production/biomass_gasification.html?m=1&
11. Czernik S, French R, Penev M (2010) Distributed bio-oil refining. DOE hydrogen program FY 2010 annual progress report, pp 38–41
12. Zhu J (2011) Photocatalytic hydrogen production, (this volume)
13. Khaselev O, Turner JA (1998) A monolithic photovoltaic-photoelectrochemical device for hydrogen production via water splitting. Science 280:425–427
14. Arachchige SM, Brewer KJ (2011) Hydrogen via direct solar production. (this volume)
15. Joshi AS, Dincer I, Reddy BV (2010) Exergetic assessment of solar hydrogen production methods. Int J Hydrog Energy 35:4901–4908
16. Brewer KJ, White T, Quinn K, Wang J, Arachchige S, Knoll J (2011) Photoinitiated electron collection in mixed-metal supramolecular complexes: development of photocatalysts for hydrogen production. DOE hydrogen and fuel cells program 2011 annual merit review meeting
17. James BD, Baum GN, Perez J, Baum KN (2009) Technoeconomic analysis of photoelectrochemical (PEC) hydrogen production. Prepared by Directed Technologies Inc. for the U.S. Department of Energy under DOE Contract Number: GS-10 F-009J, December
18. Hallenbeck PC (2009) Fermentative hydrogen production: principles, progress, and prognosis. Int J Hydrog Energy 34:7379–7389
19. Melis A, Melnecki MR (2006) Integrated biological hydrogen production. Int J Hydrog Energy 31:1563–1573
20. Logan BE, Regan JM (2006) Microbial fuel cells – challenges and applications. Environ Sci Technol 1:5173–5180
21. Brown LC, Besenbruch GE, Funk JE, Marshall AC, Pickard PS, Showalter SK (2002) High Efficiency Generation Of Hydrogen Fuels Using Nuclear Energy. Presentation at U.S., Department of Energy Hydrogen Fuel Cells and Hydrogen Review, Nuclear Energy Research Initiative (NERI)
22. Mathias PM, Brown LC (2003) Thermodynamics of the sulfur-iodine cycle for thermochemical hydrogen production. Presented at the 68th annual meeting of the society of chemical engineers. Japan, 23 March 2003

23. Allen D (2009) FY09 projected hydrogen cost estimates for nuclear hydrogen initiative baseline processes. SAND2009-6630P Sandia National Laboratory, Albuquerque
24. Jeong YH, Kazimi MS, Hohnholt KJ, Yildiz B (2005) Optimization of the hybrid sulfur cycle for hydrogen generation. MIT–NES–TR–004, May
25. US Department of Energy (2011) High-temperature water splitting. http://www1.eere.energy.gov/hydrogenandfuelcells/production/water_splitting.html
26. T-Raissi A, Muradov N, Huang C, Adebiyi O (2007) Hydrogen from solar via light-assisted high-temperature water splitting cycles. Trans ASME 129:184–189
27. Brouwer J, Margalef P (2011) Hydrogen production from high temperature fuel cells (this volume)
28. Patel P, Lipp L, Jahnke F, Heydorn E, Abdallah T, Holcomb F (2010) Co-production of renewable hydrogen and electricity: technology development and demonstration. ECS Trans 26(1):493–504
29. Cohen M, Snow GC (2008) Hydrogen delivery and storage options for backup power and off-grid primary power fuel cell systems. Published in IEEE Intelec 2008 proceedings

Hydrogen via Direct Solar Production

Shamindri M. Arachchige, Karen J. Brewer
Department of Chemistry, Virginia Polytechnic Institute and State University, Blacksburg, VA, USA

Article Outline

Glossary
Definition of the Subject
Introduction
Solar Hydrogen Photocatalysis
Conclusions and Future Directions
Acknowledgments
Bibliography

Glossary

bpy A bidentate terminal ligand, 2,2′-bipyridine.

dpp A bidentate bridging ligand, 2,3-bis(2-pyridyl) pyrazine.

dpq A bidentate bridging ligand, 2,3-bis(2-pyridyl) quinoxaline.

dpb A bidentate bridging ligand, 2,3-bis(2-pyridyl) benzoquinoxaline.

EA A subunit that functions to accept an electron in a redox reaction, electron acceptor.

ED A subunit that functions to donate an electron in a redox reaction, electron donor.

TL A ligand that is located at the end of a supramolecule and bound to only one metal center, terminal ligand.

BL A ligand that is located between two metals in a supramolecule, bridging ligand.

CAT The site of a reaction that occurs via catalysis, facilitated by the catalyst without the destruction of this subunit occurring multiple times in a cycle.

I_a Intensity of incident light.

et Excited state electron transfer, oxidation or reduction reaction involving the loss or gain of an electron that occurs in an electronic excited state.

GS Electronic ground state of a molecule.

HOMO Highest occupied molecular orbital for a molecule.

ic Internal conversion, a non-radiative process that allows conversion between two electronic states of the same spin multiplicity.

isc Intersystem crossing, a non-radiative process that allows conversion between two electronic states of different spin multiplicity.

k_x Rate constant of process "x."

LA Ground electronic state of a light absorber.

*LA Excited electronic state of a light absorber.

LUMO Lowest unoccupied molecular orbital for a molecule.

Me_2bpy A bidentate terminal ligand, 4,4′-dimethy-2,2′-bipyridine.

Me_2phen A bidentate terminal ligand, 4,7-dimethylphenanthroline.

L-pyr A monodentate terminal ligand, [(4-pyridine) oxazolo(4,5-f)phenanthroline].

dmgH Dimethylglyoximate.

dmgBF_2 (Difluoroboryl) dimethylglyoximate.

dpgBF_2 (Difluoroboryl)diphenylglyoximate.

ppy A monodentate terminal ligand, 2-phenylpyridine.

py A N containing aromatic ring, pyridyl.

MLCT Metal-to-ligand charge-transfer, an electronic excited state.

MMCT Metal-to-metal charge-transfer, an electronic excited state.

nr Non-radiative decay or movement between electronic states via processes that do not involve the absorption or emission of light.

phen A bidentate terminal ligand, 1,10-phenanthroline.

q Bimolecular deactivation, a reaction of an electronic excited state of a molecule which results in relaxation to the ground state via interaction with another molecule without transfer of electrons or generation of an excited state.

Q Quencher, a molecule that is engaged in a reaction with an electronic excited state of another molecule leading to generation of the ground state of the excited molecule.

rxn Photochemical reaction from the electronic excited state of a molecule.

tpy A tridentate terminal ligand, 2,2′:6′,2″-terpyridine.

Φ^{em} Quantum yield of emission providing the number of photons emitted by an electronic excited state of a molecule divided by the number of photons absorbed.

Φ Quantum yield or a process provides the number of events of interest that occur from an electronic excited state as related to the number of excited molecules.

λ_{max}^{abs} Absorption maximum.

λ_{max}^{em} Emission maximum.

Definition of the Subject

Developing renewable sources of energy to replace reliance on fossil fuels remains a major challenge. Sunlight is recognized as the largest of all carbon-neutral energy sources with 4.3×10^{20} J reaching the earth's surface in 1 h, larger than the current energy consumption by humans in a year [1, 2]. Plants harness solar energy through photosynthesis, which is used to power the biological world and ultimately stored in carboniferous fossil fuels. The rate of production of fossil fuels is exceeded by current consumption leading to interest in artificial means to harvest solar energy. Growing energy demands due to rising living standards and increased population have stimulated a global initiative to exploring alternative means to harness solar energy and alternative energy sources. Current methods to harness solar energy for practical purposes do not compete with fossil fuel use. Artificial photosynthesis, use of synthetic systems that mimic photosynthetic energy conversion, provides an attractive avenue for solar fuel production [1–4]. The "hydrogen economy," transformation from an oil-based economy to a hydrogen-based one, has been proposed as an attractive energy solution for the future [1–6]. Hydrogen provides a high energy content per gram (120 kJ/g), can be used in fuel cells, and has low environmental impact. Hydrogen is found in various feedstocks on earth, combined with oxygen in water and carbon in fossil fuels. Steam-methane reforming currently provides about 95% of the hydrogen used in the United States [7]. Visible light-induced solar hydrogen production from water would be the ultimate clean, renewable energy solution. Molecule-based systems for artificial photosynthesis offers unique insight into electron transfer processes amenable to study by conventional experimental techniques. A molecular-based artificial photosynthetic fuel production system requires an antenna to capture light, generation of a potential, and a catalyst for reduction of the substrate, water. Water reduction to produce hydrogen fuel is complex involving charge separation, multielectron reactions, and chemical bond reorganization. Functioning molecular photocatalysts for water reduction have emerged recently, but practical systems do not yet exist. Engineering systems that can efficiently produce hydrogen from water is a topic of extensive research and developmental efforts with significant progress made in identifying the molecular components necessary for this complicated chemistry.

Introduction

This contribution highlights recent progress in the use of complex molecular systems that reduce water or protons for solar hydrogen production. Supramolecular complexes in this forum are large molecular assemblies composed of multiple components whose individual properties provide a unique function to the supramolecule [8]. The focus will be on supramolecular complexes that couple a light-absorbing unit (LA) to a reactive metal center that is the catalyst (CAT). Systems are designed so that the orbital energetics of the molecular components allow efficient intramolecular charge-transfer to the CAT upon light

activation. Although the properties of the components are typically perturbed in the supramolecular assemblies, the individual components bring to the molecular device a unique function retained by each subunit in the assembly. A sacrificial electron donor (ED) is typically used to reductively quench the oxidized LA. The foundation for supramolecular photochemistry was established by the pioneering work using separate LAs and hydrogen-generating CATs in solar energy conversion schemes [9–11]. Recent progress using homogeneous multicomponent systems in solar hydrogen production will also be presented. The multicomponent systems consist of a LA, electron relay (ER), and a CAT that are not covalently linked. Illustrative examples of different molecular architectures are provided and the photochemistry discussed. Factors impacting system efficiency, including light-absorbing ability at desired wavelengths, the quantum yield of product formation (Φ), and the turnover number (TON) for system components, will be highlighted.

Photochemical Water Splitting

Solar water splitting uses energy from the sun to split water into hydrogen and oxygen. The splitting of water is an energetically uphill process requiring 1.23 eV. The overall reactions for water splitting are multielectron processes (Eqs. 1, 2, and 3):

$$2\,H_2O(l) \rightarrow 2\,H_2(g) + O_2(g) \quad E = -1.23\ \text{V vs NHE} \tag{1}$$

$$4\,H_2O(l) + 4e^- \rightarrow 2\,H_2(g) + 4OH^-(aq) \quad E = -0.83\ \text{V vs NHE} \tag{2}$$

$$4\,OH^-(aq) \rightarrow 2\,H_2O(l) + O_2(g) + 4e^- \quad E = -0.40\ \text{V vs NHE} \tag{3}$$

The redox potentials are pH dependent with proton reduction at pH = 1 occurring at 0.00 V vs. NHE. Multielectron chemistry is key as multielectron water is energetically much more favorable (1.23 V vs. NHE) [1] than water splitting using single electron pathways (5 V vs. NHE) [11]. Most of the solar spectrum has energies >1.23 eV and can be used for the multielectron splitting of water. Many systems are reported to split water using ultraviolet radiation but the fraction of available solar power in this region is smaller, and focus has been to use more abundant, lower energy light to power water photolysis [3, 4]. Due to the complicated nature of designing complete water splitting systems, researchers typically focus on understanding either water oxidation or water reduction, by replacing the other half with a sacrificial electron acceptor or a sacrificial ED.

Components for Supramolecular Solar Hydrogen Photocatalysis

The individual components within the supramolecule provide the overall photocatalytic activity to the supramolecule, thus careful consideration must be given to selecting structural components. The perturbation of each component upon assembly in a supramolecule must be predictable and controllable, with the overall function being maintained.

Light Absorption LA is used in this forum to absorb light and transfer that energy or an electron to other parts of the supramolecule. Incorporation of a LA within the molecular architecture that absorbs in the visible region allows for the use of more of the solar spectrum in solar hydrogen production schemes. A LA absorbs a photon of light to form an electronically excited state, *LA, which has distinctive properties compared to the ground state system, Eq. 4:

$$LA + h\nu \xrightarrow{I_a} {}^*LA \tag{4}$$

Once excited, relaxation of the *LA to the ground state can occur in a non-radiative fashion, through heat loss or in a radiative fashion by emitting light, Eqs. 5 and 6:

$${}^*LA \xrightarrow{k_{nr}} LA + \text{heat} \tag{5}$$

$${}^*LA \xrightarrow{k_r} LA + h\nu' \tag{6}$$

Excited states can be quenched by energy or electron transfer, see Eqs. 7, 8, and 9:

$${}^*LA + Q \xrightarrow{k_{en}} LA + {}^*Q \tag{7}$$

$${}^*LA + EA \xrightarrow{k_{et}} LA^+ + EA^- \tag{8}$$

$${}^*LA + ED \xrightarrow{k'_{et}} LA^- + ED^+ \tag{9}$$

The thermodynamic driving force (E_{redox}) of excited state electron transfer depends on the excited state reduction potential of the LA ($E(^*LA^{n+}/LA^{(n-1)+})$) and the ground state oxidation potential of the ED ($E(ED^{0/+})$) for excited state reduction, Eq. 10, or the excited state oxidation potential of the LA ($E(^*LA^{n+}/LA^{(n+1)+})$) and the ground state reduction potential of the EA ($E(EA^{0/-})$) for excited state oxidation, Eq. 11. The excited state redox potentials, $E(^*LA^{n+}/LA^{(n-1)+})$ and $E(^*LA^{n+}/LA^{(n+1)+})$, differ significantly from the ground state potentials as electronic excited states are both better oxidizing and reducing agents relative to their ground states. The excited state redox potentials can be calculated based on the ground state reduction or oxidation potential of the LA and the energy gap between the ground vibronic state of the electronic ground and excited states (E^{0-0}), Eqs. 12 and 13:

$$E_{redox}(red) = E\left(^*LA^{n+}\Big/LA^{(n-1)+}\right) - E\left(ED^{0/+}\right) \tag{10}$$

$$E_{redox}(oxd) = E\left(^*LA^{n+}\Big/LA^{(n+1)+}\right) - E\left(EA^{0/-}\right) \tag{11}$$

$$E\left(^*LA^{n+}\Big/LA^{(n-1)+}\right) = E\left(LA^{n+}\Big/LA^{(n-1)+}\right) + E^{0-0} \tag{12}$$

$$E\left(^*LA^{n+}\Big/LA^{(n+1)+}\right) = E\left(LA^{n+}\Big/LA^{(n+1)+}\right) - E^{0-0} \tag{13}$$

Common Light Absorbers Ruthenium and late transition metal complexes are widely applicable LAs with strong absorptivity and good spectral coverage as well as long-lived emissive metal-to-ligand charge-transfer (MLCT) excited states [9, 10, 12–15]. Some commonly used LAs used in solar energy conversion schemes are shown in Fig. 1. The excited state of $[Ru(bpy)_3]^{2+}$ is capable of excited state electron- [16–18] and energy-transfer reactions. $[Ru(bpy)_3]^{2+}$ absorbs light with high extinction coefficients in the ultraviolet and visible regions of the spectrum. The UV-region is dominated by intense absorptions that are intraligand (IL) $\pi \rightarrow \pi^*$ in nature, while the visible region is dominated by $Ru(d\pi) \rightarrow bpy(\pi^*)$ MLCT transitions with λ_{max}^{abs} = 450 nm [12–14]. Following the absorption of a photon of light to generate the ^{1}MLCT excited state, rapid intersystem crossing occurs with unit efficiency to populate a relatively long-lived ^{3}MLCT excited state (excited state lifetime, τ = 850 ns in room temperature (RT) acetonitrile solution, quantum yield, Φ = 0.07 emitting at λ_{max}^{em} = 620 nm in RT) [13]. The excited state lifetime, τ, is the inverse of the sum of all the rate constants for deactivation of an electronic excited state in the absence of a quencher, Eq. 14:

$$\tau = \frac{1}{k_r + k_{nr}} \tag{14}$$

The quantum yield for emission, Φ^{em}, for an excited state can be calculated by considering the ratio between the rate constants for the process of interest and the sum of all the rate constants for the deactivation of a state, multiplied by the fraction of light that populates this state, Eq. 15:

$$\Phi^{em} = \Phi_{^3MLCT}\frac{k_r}{k_r + k_{nr}} \tag{15}$$

$\Phi_{^3MLCT}$ is the quantum efficiency for generation of the ^{3}MLCT state, which is one for $[Ru(bpy)_3]^{2+}$ and most Ru(II) polyazine LAs. The relationship between Φ of photochemical processes with concentration of a Q is described using Stern-Volmer kinetics, Eq. 16:

$$\Phi^o/\Phi = 1 + K_{sv}[Q] \tag{16}$$

Φ^o and Φ are quantum yields in the absence and presence of Q, respectively, and K_{sv} is the Stern-Volmer quenching constant. The excited state properties of Ru polyazine–type LAs can be modulated by modification of the ligands bound to the metal center. Complexes use similar properties with higher energy Os(dπ) orbitals and lower energy-excited MLCT states. Table 1 provides spectroscopic properties of Ru and Os LAs. Although the excited state of $[Ru(bpy)_3]^{2+}$ is thermodynamically capable of reducing water to produce hydrogen, this reaction does not occur. Recent studies have also used Ir- or Pt-based LA in photochemical hydrogen production schemes [19–21]. The use of metalloporphyrin types of complexes as LAs have been investigated as they mimic dyes found in nature in photosynthesis [22].

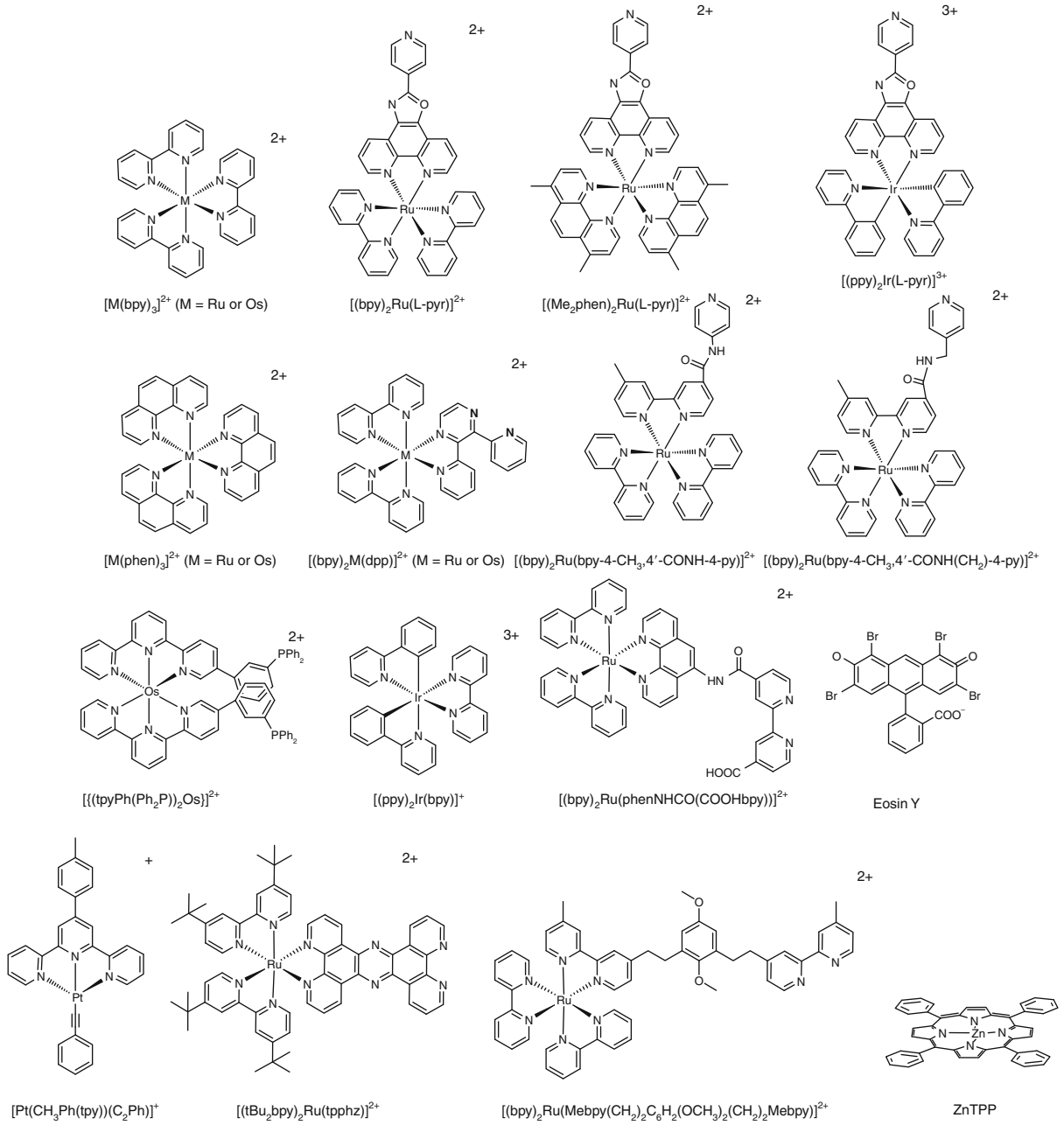

Hydrogen via Direct Solar Production. Figure 1
Representative light absorbers used in solar hydrogen production schemes

Electron Relay Multicomponent systems rely on a suitable relay to transport electrons from an excited LA to the CAT. This electron relay must be able to accept electrons from the *LA. In supramolecular complexes, bridging ligands (BL) are used as electron relays and serve to covalently couple the individual components. A wide range of BLs has been used for this purpose, providing varied degrees of coupling between the LA and CAT and with varied acceptor orbital energetics [12]. Polyazine BLs are commonly

Hydrogen via Direct Solar Production. Table 1 Spectroscopic and redox properties of Ru^{II} and Os^{II} polyazine complexes

Complex	λ_{max}^{abs} (nm)	λ_{max}^{em} (nm)	τ (ns)	Ref.
$[Ru(bpy)_3]^{2+}$ [a]	449	605	850	[13]
$[Ru(phen)_3]^{2+}$ [a]	443	604	400	[13]
$[Ru(Ph_2phen)_3]^{2+}$ [b]	460	613	4,680	[23]
$[Os(bpy)_3]^{2+}$ [a]	640	723	20[b]	[24]
$[(bpy)_2Ru(dpp)]^{2+}$ [a]	470	675	240	[25, 26]
$[(phen)_2Ru(dpp)]^{2+}$ [a]	465	652	252	[27]
$[(bpy)_2Os(dpp)]^{2+}$ [a]	485	798	37	[28, 29]
$[Ru(tpy)_2]^{2+}$	476[c]	629[a]	0.25[b]	[30, 31]
$[Os(tpy)_2]^{2+}$	477[c]	718[c]	269[a]	[31]

[a]In acetonitrile solution at room temperature
[b]In aqueous solutions
[c]In ethanol–methanol (4/1)

used to couple molecular components within supramolecular assemblies. Polyazine BLs separated by short rigid spacers allow for significant electronic communication between components and directional electron or energy transfer [32–35]. $[(bpy)_2Ru(dpp)]^{2+}$ is a well-studied LA derived from $[Ru(bpy)_3]^{2+}$ with one of the bpy replaced by the polyazine BL, dpp (dpp = 2,3-bis(2-pyridyl)pyrazine) [25, 26, 33, 34]. The lowest lying excited state of $[Ru(bpy)_2(dpp)]^{2+}$ is a $Ru(d\pi) \rightarrow dpp(\pi^*)$ CT state, transferring charge from the ruthenium to the dpp ligand. This ^{1}MLCT absorption occurs at 470 nm with the ^{3}MLCT emission at 675 nm (τ = 210 ns). The two remote nitrogen donor atoms on the dpp ligands provide points of attachment for a second metal center, allowing the construction of polymetallic complexes. The $dpp(\pi^*)$ acceptor orbital is stabilized when it is bridging two metals. In the homobimetallic system $[\{(bpy)_2Ru\}_2(dpp)]^{4+}$, a red shifted $Ru(d\pi) \rightarrow dpp(\pi^*)$ CT transition at 525 nm is observed with a shortened ^{3}MLCT lifetime of 80 ns [10, 25].

Catalysts Photochemical water reduction to produce hydrogen is an energetically uphill process involving bond dissociation and formation. Catalysts are used to promote this reaction. Most multicomponent systems are heterogeneous with considerable progress being made recently in homogeneous photocatalysis [19–21]. These systems typically use Pt, Pd, Rh, Co, or bioinspired diiron dithiolate (contains an Fe_2 core) catalysts. The non-precious metal-based Co and Fe systems are proposed as being economically viable. Homogeneous catalysis allows catalyst engineering to promote electron transfer from the LA and allows understanding of the mechanism of action through conventional solution-based analysis methods. Care must be taken in the selection of CATs to ensure that that they do not compete for light with the LA.

Turnover Number (TON) and Quantum Yield (Φ) The observed TON and Φ of a reaction are key parameters describing catalytic system efficiency and stability. The TON relative to the CAT is defined as the ratio of amount of hydrogen produced (n H_2) to the initial amount of CAT present (n_o CAT), Eq. 16:

$$\mathrm{TON} = \frac{n\ \mathrm{H_2}}{n_o\ \mathrm{CAT}} \tag{17}$$

Photoinitiated Charge Separation Solar energy conversion schemes that proceed via photoreduction of substrates are initiated with photoinduced charge separation that generates a potential at the molecular level. A simplified supramolecular device for photoinitiated charge separation is represented in Fig. 2. Optical excitation, followed by intramolecular electron transfer affords a charge separated state consisting of a positively charged electron donor, ED^+, and negatively charged electron acceptor, EA^-. The photogenerated charge separated (CS) state should persist for enough time to drive useful chemistry during the excited state lifetime. In supramolecular systems, the duration of charge separation can be modulated by fine tuning the orbital overlap between the ED and LA through modification of distance between these two subunits. The efficiency of charge separation is also key to functioning and often factors enhancing lifetime reduce quantum efficiency.

Photoinitiated Electron Collection Photoinitiated electron collection (PEC) is a process by which at least two electrons are collected on a central site

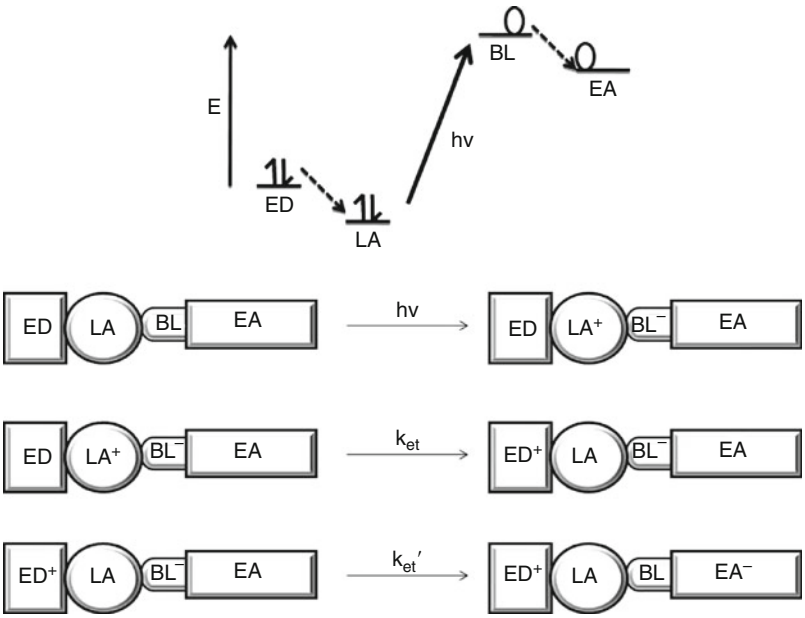

Hydrogen via Direct Solar Production. Figure 2
Photoinduced charge separation in a ED-LA-BL-EA molecular device (*ED* electron donor, *LA* light absorber, *EA* electron acceptor)

following optical excitation. For PEC, supramolecular complexes can be designed so that two ED-LA units are connected to a single EA that can accept at least two electrons (an electron collector, EC) to give a ED-LA-BL-EC-BL-LA-ED structural motif. Following multiple optical excitations, this system collects two electrons at the EC creating two ED^+, Fig. 3. PEC is of considerable importance in solar fuel production as multielectron reduction of the substrate is required in many fuel producing reactions. In the important monograph by Balzani in 1987, the design considerations for functioning photoinitiated electron collectors were discussed [8]. Since then many supramolecular systems that couple multiple LAs have been constructed, but only a few functioning PEC systems exist.

Photoinitiated Electron Collectors that Collect Electrons on Ligand Orbitals Photoinitiated electron collectors are devices that allow the use of light energy to collect the reducing equivalents needed to produce fuels. Molecular-based PEC systems are engineered so that the subunits are connected in an order with orbital energetics that allow multiple electrons to be collected on a single site following light activation. Current systems that undergo PEC have LA units connected to EC through BLs that function as electron relays. The first functioning photoinitiated electron collector is $[\{(bpy)_2Ru(dpb)\}_2IrCl_2](PF_6)_5$ (dpb = 2,3-bis(2-pyridyl)benzoquinoxaline) which collects two electrons on the dpb(π^*) orbitals upon two sequential excitations and electron transfer events, Fig. 4 [36]. Electron transfer from the dpb(π^*) orbitals to the Ir-based orbitals is energetically uphill. Homobimetallic ruthenium systems, $[(phen)_2Ru(tatpq)Ru(phen)_2]^{4+}$ (phen = 1,10-Phenanthroline, tatpq = 9,11,20,22-tetraazatetrapyrido[3,2-a:2′3′-c:3″,2″-1:2‴,3‴-n]pentacene-10,21-quinone) and $[(phen)_2Ru(tatpp)Ru(phen)_2]^{4+}$ (tatpp = 9,11,20,22- tetraazatetrapyrido[3,2-a:2′3′-c:3″,2″-1:2‴,3‴-n]pentacene) are the next PECs studied with multiple electrons also being collected on the BL(π^*) orbitals, Fig. 4 [37, 38]. Although these initial systems undergo PEC, they are not known to reduce substrates. The monometallic system, $[Ru(bpy)_2(pbn)]^{2+}$ (pbn = 2-(2-pyridyl) benzo[b]-1,5-naphthyridine), couples a Ru-based LA to an NAD^+ (NAD^+ = nicotinamide adenine dinucleotide) model ligand, Fig. 4. The NAD^+ model ligand acts as a reservoir for two electrons and uses

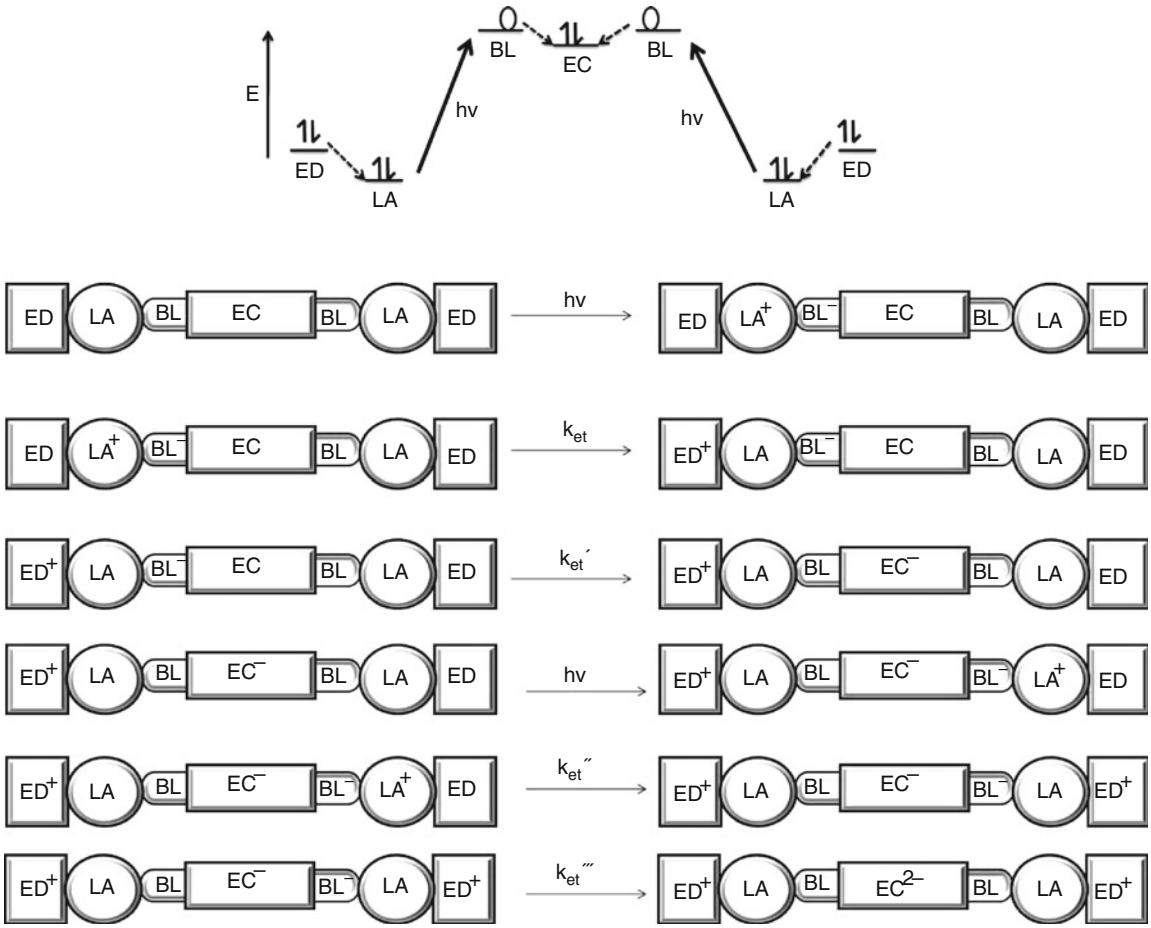

Hydrogen via Direct Solar Production. Figure 3
Photoinduced electron collection in a ED-LA-EA-LA-ED molecular device (*ED* electron donor, *LA* light absorber, *EA* electron acceptor)

proton coupled electron transfer. Photolysis of a solution containing $[Ru(bpy)_2(pbn)]^{2+}$ and triethylamine (Et_3N) leads to the formation of NADH like $[Ru(bpy)_2(pbnHH)]^{2+}$, a potential hydride donor for reduction of organic substrates [39, 40].

Solar Hydrogen Photocatalysis

This entry will focus on the recent developments in molecular-based solar hydrogen photocatalysis using Fe, Co, Rh, Pt, and Pd-based CATs and Ru, Os, Pt, Re, and Ir-based LAs. Illustrative examples will be provided with discussions on system function, TON, and efficiency. The hydrogen TON, quantum yield, and system properties are summarized in Table 2.

Iron-Based System

Metabolism of protons in certain bacteria and algae are catalyzed by a certain class of metalloenzymes coined hydrogenases. Iron hydrogenases are important in proton reduction producing hydrogen gas. Recent research efforts focus on biomimetic diiron systems containing an Fe_2S_2 core, structurally similar to the iron hydrogenase active sites, for solar hydrogen photocatalysis [19–21, 41]. Interest in these systems has been inspired by the superior catalytic activity of hydrogenases which can reach 6,000–9,000 molecules of hydrogen s^{-1} [42]. Most Fe_2S_2 systems have been used in electrocatalytic proton reduction, requiring strongly acidic conditions and large overpotentials [43].

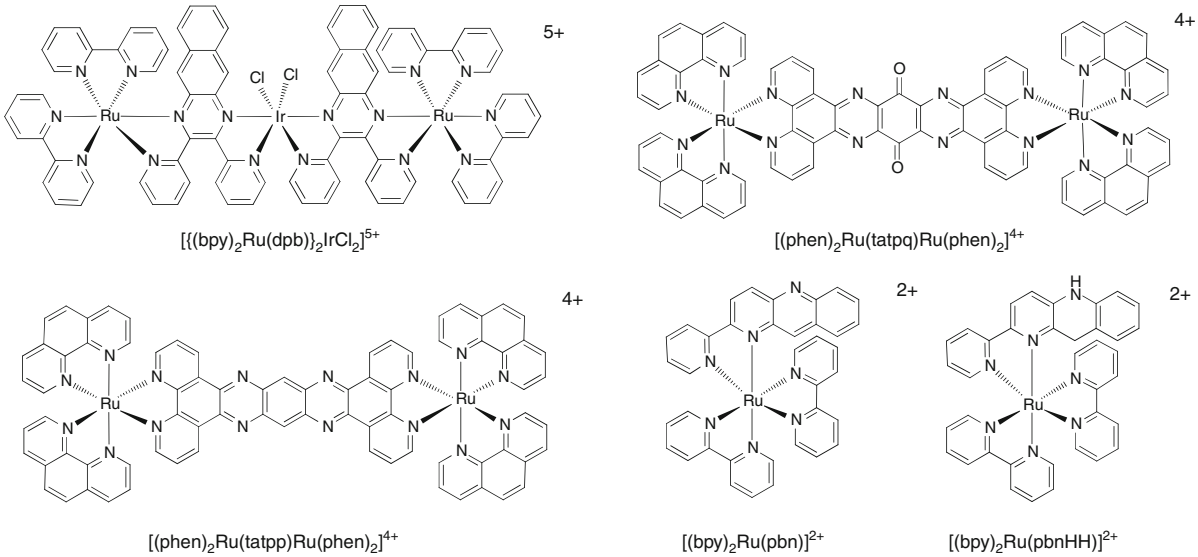

Hydrogen via Direct Solar Production. Figure 4
Photoinitiated electron collectors that collect electrons on ligand orbitals

Supramolecular Iron-Based System The Ru-Fe_2S_2 dyads, $[(bpy)_2Ru(MebpyCONHPhCOO(Fe_2\{\mu\text{-}S_2(CH_2)_2CH\}(CO)_6))]^{2+}$, $[(tpy)Ru(tpyC_2Ph(Fe_2\{\mu\text{-}S_2(CH_2)_2\ N\}(CO)_6))]^{2+}$, $[(bpy)_2Ru(MebpyCONHPh(Fe_2\{\mu\text{-}S_2(CH_2)_2\ N\}(CO)_6))]^{2+}$, and $[(bpy)_2Ru(bpy\ C_2Ph(Ph_2)P(Fe_2\{\mu\text{-}S_2(CH_2)_3\}(CO)_5))]^{2+}$, in which a model iron hydrogenase active site is attached to a $[Ru(bpy)_3]^{2+}$ type chromophore, are supramolecular architectures constructed for possible application in solar hydrogen production, Fig. 5 [44–47]. These systems couple the favorable optical properties of the Ru-based chromophore to the catalytic properties of the diiron active site. It was anticipated that the optically populated ^{3}MLCT excited state would reduce the diiron species by two electrons and catalyze water reduction to produce hydrogen. It was found that electron transfer to the diiron dyads is thermodynamically unfavorable in this structural motif as the reduction potentials of the diiron units are more negative than the excited state oxidation potential of the ruthenium LAs. These Ru-Fe_2S_2 dyads are not solar hydrogen photocatalysts, but provide important design considerations for catalyst engineering. Component modification at the diiron center to facilitate electron transfer from the ^{3}MLCT excited state of the photosensitizer and/or photogeneration of a ^{3}MLCT excited state with a higher energy acceptor orbital have been suggested as a means to promote excited state electron transfer from the ruthenium LA to the diiron core [45–47].

A pyridine (py)-functionalized hydrogenase active site model complex bound to a zinc tetraphenylporphyrin [ZnTPP] LA, $[ZnTPP(pyCOO(CH_2)_2(Fe_2\{\mu\text{-}S_2(CH_2)_2N\}(CO)_6))]$, has been used in solar hydrogen production, Fig. 6 [48]. The photoinduced intramolecular electron transfer from the ^{1}MLCT state of the LA to the diiron unit has been established by fluorescence spectroscopy and laser flash photolysis technique. The weak interaction between the diiron center and the LA allows the two units to separate following intramolecular electron transfer, minimizing charge recombination through back electron transfer. The system can also reassemble to mediate intramolecular electron transfer.

Photolysis of ZnTPP, $[pyCOO(CH_2)_2(Fe_2\{\mu\text{-}S_2(CH_2)_2\ N\}(CO)_6)]$, and the electron donor 2-mercaptobenzoic acid in presence of CF_3COOH acid as the proton source in methylene chloride at $\lambda > 400$ nm resulted in photochemical hydrogen production with 0.16 TON based on $[pyCOO(CH_2)_2(Fe_2\{\mu\text{-}S_2(CH_2)_2N\}(CO)_6)]$ and 16 TON based on [ZnTPP]. The amount of hydrogen increases almost linearly in the first 40 min and reaches a plateau in 2 h. This decrease in rate of hydrogen production is attributed to CAT decomplexation through CO loss.

Hydrogen via Direct Solar Production. Table 2 Summary of hydrogen photocatalysis data

Solvent (electron donor)	λ (nm)	LA	LA-CAT	CAT	TON (time, h)	QY	Ref
CH_2Cl_2/CF_3COOH (2-mercaptobenzoic)	≥400		$[ZnTPP(pyCOO(CH_2)_2(Fe_2\{\mu\text{-}S_2(CH_2)_2N\}(CO)_6))]$		0.16 (Fe_2) (2) 16 (LA) (2)		[48]
CH_3CN/H_2O (ascorbic acid)	>400	$[Ru(bpy)_3]^{2+}$		$[Ph(CH_2)(Fe_2\{\mu\text{-}S_2(CH_2)_2N\}(CO)_5(P(N\text{-}pyr)_3))]$	4.3 (Fe_2) (3) 86 (LA) (3)		[51]
CH_3CN/H_2O (ascorbic acid)	>400	$[(bpy)_2Ru(Me_2bpy)]^{2+}$		$[Ph(CH_2)(Fe_2\{\mu\text{-}S_2(CH_2)_2N\}(CO)_5(P(N\text{-}pyr)_3))]$	3.9 (Fe_2) (3) 76 (LA) (3)		[51]
CH_3CN/H_2O (ascorbic acid)	>400	$[Ru(Me_2bpy)_3]^{2+}$		$[Ph(CH_2)(Fe_2\{\mu\text{-}S_2(CH_2)_2N\}(CO)_5(P(N\text{-}pyr)_3))]$	1.9 (Fe_2) (3) 38 (LA) (3)		[51]
CH_3CN/H_2O (ascorbic acid)	>400	$[Ru(bpy)_3]^{2+}$		$[Ph(CH_2)(Fe_2\{\mu\text{-}S_2(CH_2)_2N\}(CO)_6)]$	0.78 (Fe_2) (3)		[51]
CH_3CN/H_2O (ascorbic acid)	>400	$[Ru(bpy)_3]^{2+}$		$[Ph(CH_2)(Fe_2\{\mu\text{-}S_2(CH_2)_2N\}(CO)_4(P(N\text{-}pyr)_3)_2)]$	1.7 (Fe_2) (3) 34 (LA) (3)		[51]
DMF/H_2O (ascorbic acid)	455–850	$[Ru(bpy)_3]^{2+}$		$[Fe_2(\mu\text{-}Cl_2bdt)(CO)_6]$	200 (Fe_2) (2.5)	0.01	[52]
CH_3COCH_3/H_2O (Et_3N)	>400	$[(ppy)_2Ir(bpy)]^+$		$[Ph(CH_2)(Fe_2\{\mu\text{-}S_2(CH_2)_2N\}(CO)_5(P(N\text{-}pyr)_3))]$	466 (Fe_2) (8) 660 (LA) (8)		[53]
CH_3CN/H_2O (N,N′-Dimethylaniline)	470		$[\{(bpy)_2Ru(dpp)\}_2RhCl_2]^{5+}$		28 (CAT) (4) 20 (CAT) (2)		[54]
CH_3CN/H_2O (N,N′-Dimethylaniline)	470		$[\{(bpy)_2Ru(dpp)\}_2RhBr_2]^{5+}$		38 (CAT) (4) 26 (CAT) (2) 3 (CAT) (4)[a]		[55–57]
CH_3CN/H_2O (N,N′-Dimethylaniline)	470		$[\{(phen)_2Ru(dpp)\}_2RhCl_2]^{5+}$		18 (CAT) (2)		[56]

CH_3CN/H_2O (triethylamine)	470		$[\{(bpy)_2Ru(dpp)\}_2RhCl_2]^{5+}$		4 (CAT) (2)		[56]
CH_3CN/H_2O (triethylamine)	470		$[\{(bpy)_2Ru(dpp)\}_2RhBr_2]^{5+}$		6 (CAT) (2)		[56]
CH_3CN/H_2O (triethylamine)	470		$[\{(phen)_2Ru(dpp)\}_2RhCl_2]^{5+}$		3 (CAT) (2)		[56]
CH_3CN/H_2O (triethanolamine)	470		$[\{(bpy)_2Ru(dpp)\}_2RhBr_2]^{5+}$		1 (CAT) (2)		[56]
CF_3SOOH/H_2O (sodium ascorbate)	>380		$[\{(tpyPh(Ph_2P))_2Os\}RhCl(CO)]^{2+}$		36 (CAT) (18)		[58]
CF_3SOOH/H_2O (sodium ascorbate)	>380		$[\{(tpyPh(Ph_2P))_2Os\}RhCl_2]^{3+}$		87 (CAT) (18) 594 (CAT) (240)	0.007	[58]
CF_3SOOH/H_2O (sodium ascorbate)	>380	$[Os(tpy)_2]^{2+}$		$RhCl_3 \bullet 3H_2O$/dppe	24 (CAT) (18)		[58]
HCl/THF	300–400		$[Rh_2^{0,II}(dfpma)_3X_2(L)]$		27/h (CAT) (3)	0.01	[59]
H_2O (triethanolamine)	450	$[Ru(bpy)_3]^{2+}$, $[Rh(bpy)_3]^{3+}$		Pt	500 (LA) (240)	0.11[b]	[11, 60]
THF/H_2O (triethanolamine)		$[Ir(f\text{-}mppy)_2(dtbbpy)]^+$		$[Rh(dtbbpy)_3]^{3+}$	5,000 (LA or CAT) (20–24)	0.34	[61]
CH_3COCH_3/Et_3NH^+ (triethylamine)[c]	UV-VIS		$[(bpy)_2Ru(L\text{-}pyr)Co(dmgBF_2)_2(OH_2)]^{2+}$		56 (Co) (4)		[62]
CH_3COCH_3/H_2O (triethylamine)[c]	UV-VIS		$[(bpy)_2Ru(L\text{-}pyr)Co(dmgBF_2)_2(OH_2)]^{2+}$		22 (Co) (4)		[62]
CH_3COCH_3/Et_3NH^+ (triethylamine)[c]	>350		$[(bpy)_2Ru(L\text{-}pyr)Co(dmgBF_2)_2(OH_2)]^{2+}$		103 (Co) (15)		[62]
CH_3COCH_3/Et_3NH^+ (triethylamine)[c]	UV-VIS		$[(bpy)_2Ru(L\text{-}pyr)Co(dmgH)_2Cl]^{2+}$		17 (Co) (4)		[62]
CH_3COCH_3/Et_3NH^+ (triethylamine)[c]	UV-VIS		$[(bpy)_2Ru(L\text{-}pyr)Co(dpgBF_2)_2(OH_2)]^{2+}$		12 (Co) (4)		[62]

Hydrogen via Direct Solar Production. Table 2 (Continued)

Solvent (electron donor)	λ (nm)	LA	LA-CAT	CAT	TON (time, h)	QY	Ref
CH_3COCH_3/Et_3NH^+ (triethylamine)[c]	>380		$[(Me_2phen)_2Ru(L\text{-}pyr)Co(dmgBF_2)_2(OH_2)]^{2+}$		9 (Co) (4)		[63]
CH_3COCH_3/Et_3NH^+ (triethylamine)			$[(ppy)_2Ir(L\text{-}pyr)Co(dmgBF_2)_2(OH_2)]^+$		90 (Co) (4) 210 (Co) (15)[e]		[63]
CH_3COCH_3/Et_3NH^+ (triethylamine)[e]	>380	$[Ir(ppy)_2(phen)]^+$		$[Co(dmgBF_2)_2(OH_2)_2]$	165 (Co) (15)	0.11[d]	[63]
CH_3COCH_3/Et_3NH^+ (triethylamine)[e]	>380	$[Re(CO)_3Br(phen)]$		$[Co(dmgBF_2)_2(OH_2)_2]$	273 (Co) (15)	0.16[f]	[63]
CH_3COCH_3/Et_3NH^+ (triethylamine)[d]	>400		$[(bpy)_2Ru(bpy\text{-}4\text{-}CH_3,4'\text{-}CONH\text{-}4\text{-}py)Co(dmgBF_2)_2(OH_2)]^{2+}$		38 (Co) (8)		[64]
CH_3COCH_3/Et_3NH^+ (triethylamine)[d]	>400		$[(bpy)_2Ru(bpy\text{-}4\text{-}CH_3,4'\text{-}CONH(CH_2)\text{-}4\text{-}py)Co(dmgBF_2)_2(OH_2)]^{2+}$		47 (Co) (8)		[64]
CH_3CN/H_2O (Eu^{2+})	450	$[Ru(bpy)_3]^{2+}$		$[Co^{II}L]$	10 (LA) 1 (Co)		[65]
CH_3CN/H_2O (triethanolamine)	465	$[Ir(F\text{-}mppy)_2(bpy)]^+$		$[Co(bpy)_3]^{2+}$	920 (LA) 18 (Co)		[66]
CH_3CN/H_2O (triethanolamine)	>410	$[Pt(ttpy)(C \equiv CPh)]ClO_4$		$[Co(dmgH)_2pyCl]$	2,100 (10)		[67]

CH_3CN/H_2O (triethanolamine)	>450	Eosin Y		$[Co(dmgH)_2pyCl]^{2+}$	900 (LA) (14)[g]	0.04[h]	[68]
$DMF/H_2O/AcOH$ (triethanolamine)	>400	$[ReBr(CO)_3bpy)]$		$[Co(dmgH)_2]$	150 (LA) (9)	0.26	[69]
H_2O/acetate buffer (EDTA)	>350		$[(bpy)_2Ru(phenNHCO(COOHbpy))PtCl_2]^{2+}$		5 (CAT) (10)	0.01	[70]
CH_3CN/H_2O (N,N′-Dimethylaniline)	470		$[\{(phen)_2Ru(dpp)\}_2Ru(dpq)PtCl_2]^{6+}$		115 (CAT) (5)		[71]
CH_3CN/H_2O (N,N′-Dimethylaniline)	530		$[\{(bpy)_2Ru(dpp)\}_2Ru(dpq)PtCl_2]^{6+}$		40 (CAT) (3)	0.01	[72]
H_2O/MES (EDTA)	350–550		[PtCl(tpy)]Cl		3 (LA or CAT) (7)	0.02	[73]
CH_3CN/triethylamine (triethylamine)	470		$[(^tBu_2bpy)_2Ru(tpphz)PdCl_2]^{2+}$		56 (CAT) (30)		[74]

[a]In water/phosphate buffer using TEOA ED (Ref. [57])
[b]Ref. [11]
[c]100-fold excess of both Et_3NH^+ and Et_3N were used
[d]300-fold excess of both Et_3NH^+ and Et_3N were used
[e]600-fold excess of both Et_3NH^+ and Et_3N were used
[f]λ = 412 nm, irradiation time 2 h
[g]dmgH was added to the system
[h]λ = 520 nm, irradiation time 2 h

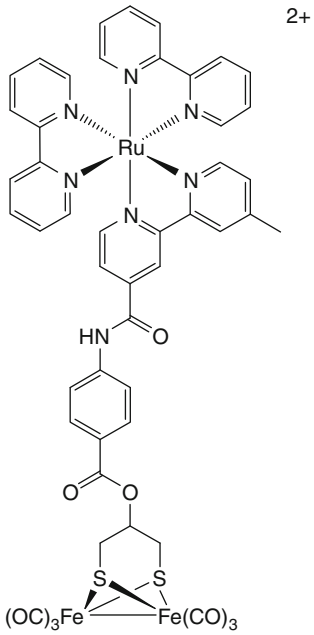

$[(bpy)_2Ru(MebpyCONHPhCOO(Fe_2\{\mu\text{-}S_2(CH_2)_2CH\}(CO)_6))]^{2+}$

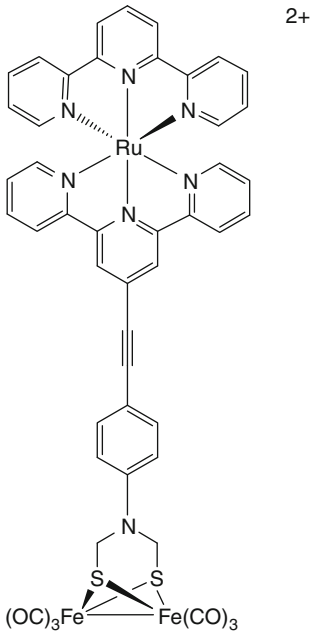

$[(tpy)Ru(tpyC_2Ph(Fe_2\{\mu\text{-}S_2(CH_2)_2N\}(CO)_6))]^{2+}$

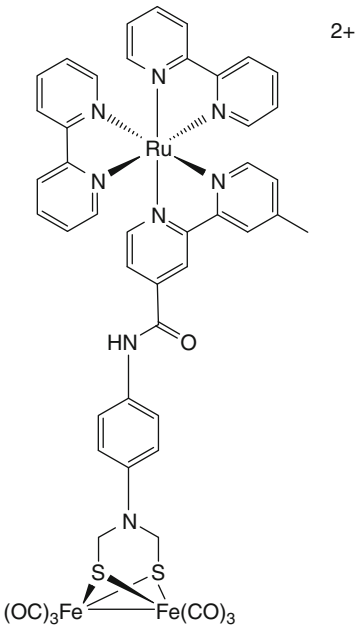

$[(bpy)_2Ru(MebpyCONHPh(Fe_2\{\mu\text{-}S_2(CH_2)_2N\}(CO)_6))]^{2+}$

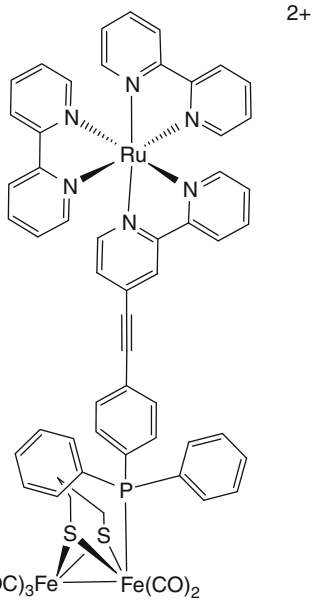

$[(bpy)_2Ru(bpyC_2Ph(Ph_2)P(Fe_2\{\mu\text{-}S_2(CH_2)_3\}(CO)_5))]^{2+}$

Hydrogen via Direct Solar Production. Figure 5
Systems that couple a ruthenium chromophore to an iron-based catalyst

Hydrogen production does not occur when $[pyCOO(CH_2)_2(Fe_2\{\mu\text{-}S_2(CH_2)_2N\}(CO)_6)]$ is replaced by $[OH(CH_2)_2(Fe_2\{\mu\text{-}S_2(CH_2)_2N\}(CO)_6)]$. This suggests that assembly of the system and the intramolecular electron transfer events are crucial for solar hydrogen catalysis as $[OH(CH_2)_2(Fe_2\{\mu\text{-}S_2(CH_2)_2N\}(CO)_6)]$ does not

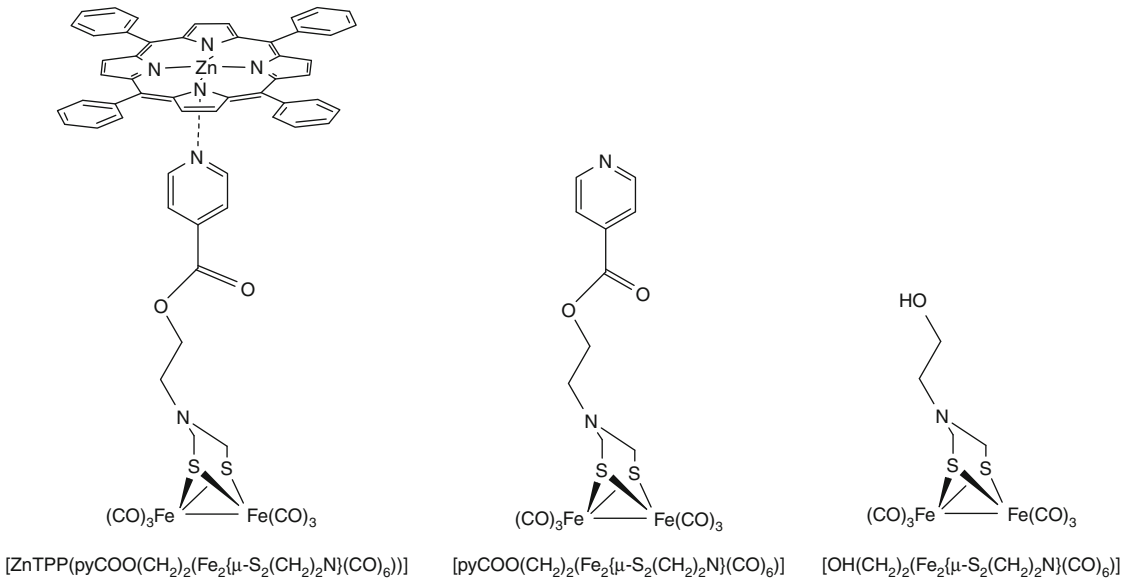

Hydrogen via Direct Solar Production. Figure 6
Representations of ZnFe self-assembling system and the FeFe subunits

coordinate with ZnTPP and hydrogen production does not occur. It is proposed that the singlet excited state intramolecular electron transfer forms the charge separated state [$ZnTPP^{\cdot+}pyCOO(CH_2)_2(Fe_2\{\mu\text{-}S_2(CH_2)_2N\}(CO)_6)^{\cdot-}$], which undergoes dissociation to form [$ZnTPP^{\cdot+}$] and [$pyCOO(CH_2)_2(Fe_2\{\mu\text{-}S_2(CH_2)_2N\}(CO)_6)]^{\cdot-}$. [$ZnTPP^{\cdot+}$] is reductively quenched by the ED, while [$pyCOO(CH_2)_2(Fe_2\{\mu\text{-}S_2(CH_2)_2N\}(CO)_6)]^{\cdot-}$ is protonated. The protonated radical anion facilitates the second electron transfer event, which is followed by further protonation and hydrogen release. Further protonation of the protonated radical anion prior to the second electron transfer has been observed in electrochemical hydrogen production catalyzed by Fe_2S_2 hydrogenases [49]. This is the first photoactive hydrogenase model system that incorporates the self-assembling principle for photochemical hydrogen production. This system is interesting as both CAT and LA are based on bioinspired materials.

In photosynthesis, the light-dependent reactions are carried out by two photosystems, photosystem I (PS I) and photosystem II (PS II). PS I catalyzes the optically induced electron transfer from reduced cytochrome c to oxidized ferredoxin that are directly used to reduce nutrients or used to produce NADH. Systems that couple PS I to active hydrogen producing CATs are known. A recent review describes this technology employing molecular wires to connect PS I directly to CAT including Pt nanoparticles or the distal [4Fe-4S] of a Fe_2 or NiFe hydrogenase [50].

Multicomponent Iron-Based Systems A few multicomponent systems have been reported that use biomimetic iron hydrogenase model complexes as CATs in solar hydrogen production schemes. Multicomponent systems are solution systems with multiple molecules interacting through diffusion to allow individual molecules to perform the acts associated with solar hydrogen production. The photocatalytic system typically consists of three main components: LAs, CATs, and EDs functioning through intermolecular interactions in solution. A photoactive multicomponent system for solar hydrogen production using biomimetic iron hydrogenase model complexes was first reported in 2008 [51]. This system uses [$Ru(bpy)_3]^{2+}$ type LAs, Fe_2S_2 CATs, and ascorbic acid as the ED irradiating at $\lambda > 400$ nm, Fig. 7. The system consisting of [$Ru(bpy)_3]^{2+}$ LA, [$Ph(CH_2)(Fe_2\{\mu\text{-}S_2(CH_2)_2\ N\}(CO)_6)$] CAT containing all CO ligands, and ascorbic acid in CH_3CN/H_2O has the lowest activity attributed to decomplexation of the CO from the CAT. One or two of the CO ligands on the Fe_2S_2

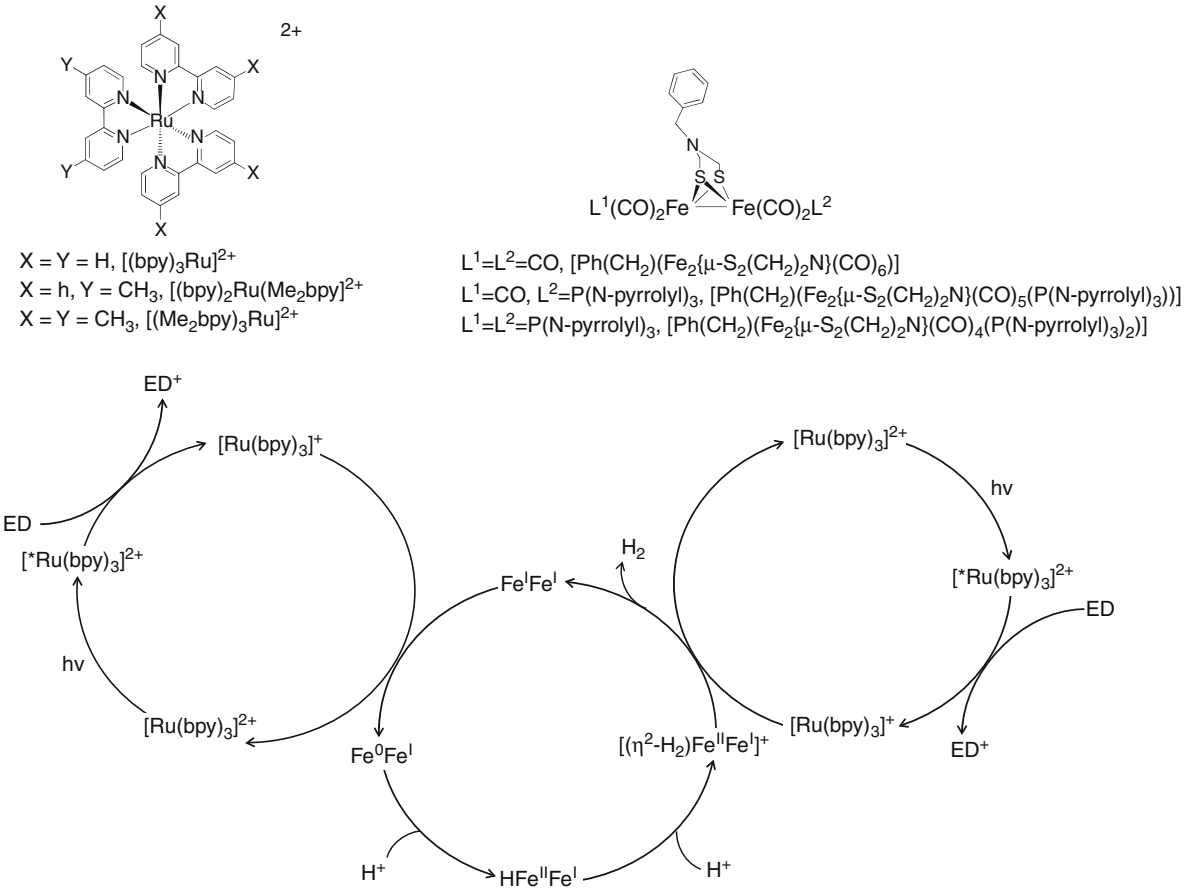

Hydrogen via Direct Solar Production. Figure 7
Homogeneous three-component system for solar hydrogen production catalyzed by biomimetic diiron hydrogenase catalyst

unit were replaced by a phosphine-based ligand to improve the photostability and catalytic activity of the system. The photosystem consisting of the $P(pyr)_3$-monosubstituted CAT (Ph = phenyl, $P(pyr)_3$ = tris (N-pyrrolyl)phosphine), $[Ph(CH_2)(Fe_2\{\mu\text{-}S_2(CH_2)_2N\}(CO)_5(P(N\text{-}pyr)_3))]$, showed greater photostability and catalytic activity albeit low turnovers, 4.3 TON relative to CAT and 86 TON relative to the LA. The photosystem consisting of $[Ru(bpy)_3]^{2+}$ showed the greatest hydrogen production relative to $[(bpy)_2Ru(Me_2bpy)]^{2+}$ or $[(Me_2bpy)_3Ru]^{2+}$ LAs. The decline in the hydrogen production when $[(bpy)_2Ru(Me_2bpy)]^{2+}$ or $[(Me_2bpy)_3Ru]^{2+}$ is used is attributed to inefficient reductive quenching of the excited LA by the ascorbate anion. Methyl substitution renders the excited state reduction potential of the LA more negative making reductive quenching by ascorbate anion less thermodynamically favorable.

It is proposed that the excited $[^*Ru(bpy)_3]^{2+}$ LA is reductively quenched by the electron donor to form $[Ru(bpy)_3]^+$. Intermolecular electron transfer to the diiron unit is thermodynamically feasible and a Fe^0Fe^I species is formed. Based on the redox potentials it is established that further reduction of the CAT is thermodynamically unfavorable. Protonation of the Fe^0Fe^I species to form $HFe^{II}Fe^I$ followed by further reduction HFe^IFe^I is likely. One proposal is that hydrogen production occurs through protonation of HFeIFeI with regeneration of the CAT. An alternative mechanism is the second protonation of HFeIIFeI to generate $[(\eta^2\text{-}H_2)Fe^{II}Fe^I]^+$ that is capable of being reduced to generate hydrogen and regenerate the CAT, Fig. 7.

Higher TON for photochemical hydrogen production has been achieved using $[Fe_2(\mu\text{-}Cl_2bdt)(CO)_6]$ (Cl_2bdt = 3,6-dichlorobenzene-1,2-dithiolate) as the CAT [52]. $[Fe_2(\mu\text{-}Cl_2bdt)(CO)_6]$ is a known electrocatalyst for hydrogen production, allowing electrochemical reduction of protons at low potentials [75]. This complex is unusual displaying electrochemical reversibility. Electrochemical reversibility in these systems could be particularly relevant for hydrogen photocatalysis as proton reduction occurs by consecutive one electron reduction steps. Photolysis of a system consisting of $[Ru(bpy)_3]^{2+}$, $[Fe_2(\mu\text{-}Cl_2bdt)(CO)_6]$, ($[Ru(bpy)_3]^{2+}/[Fe_2(\mu\text{-}Cl_2bdt)(CO)_6]$ 10:1), and ascorbic acid (pH = 5.5) in DMF/H_2O at λ = 455–850 nm provides over 200 TON relative to the CAT in 2.5 h at which time photocatalysis discontinues attributed to CAT deactivation. The maximum TON frequency is 2.7 H_2 CAT^{-1} min^{-1}. The Φ of hydrogen production is 0.01 per absorbed photon. A Φ = 0.014 with a frequency of 3.7 H_2 CAT^{-1} min^{-1} has also been obtained at pH = 6.4, but with lower TON and system stability. The proposed mechanism of action is represented in Fig. 8. Transient absorption and emission spectral data have established the elementary steps of the catalytic cycle to involve the reductive quenching of the excited LA by ascorbic acid to form $[Ru(bpy)_3]^+$ and reoxidation of $[Ru(bpy)_3]^+$ by the diiron unit.

Photochemical hydrogen production in a more basic medium has been investigated using the three-component system using $[(ppy)_2Ir(bpy)]^+$ LA (ppy = phenylpyridine), $[Ph(CH_2)(Fe_2\{\mu\text{-}S_2(CH_2)_2N\}(CO)_5(P(N\text{-}pyr)_3))]$ CAT, and Et_3N electron donor in CH_3COCH_3/H_2O irradiating at $\lambda > 400$ nm [53]. Turnover numbers of 466 relative to the CAT and 660 relative to the LA in 8 h has been achieved in this system. The impact of solvent, ED, LA, and CAT concentrations on solar hydrogen production has been investigated to determine the optimized concentrations to achieve the high TON reported. Unlike in the previous diiron systems, system deactivation occurs through decomposition of the LA, as re-addition of the LA showed total system recovery. The mechanism of catalyst function under basic conditions is unclear but it is proposed to occur through a Fe^0Fe^I species which is formed through reductive quenching of the LA by Et_3N followed by reduction of the Fe^IFe^I form of the CAT.

Rh-Based Supramolecular and Multicomponent Systems

Tris-(2,2′-bipyridine)Rh^{III}, $[Rh(bpy)_3]^{3+}$, is known to undergo excited state electron transfer of $[^*Ru(bpy)_3]^{2+}$ [76]. The one electron reduction product, $[Rh(bpy)_3]^{2+}$,

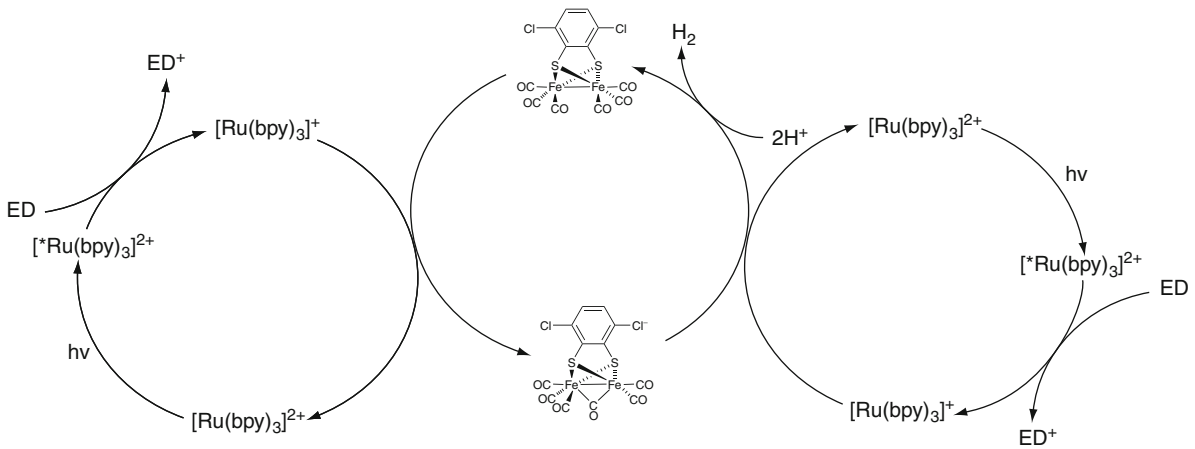

Hydrogen via Direct Solar Production. Figure 8
Proposed mechanism for photochemical hydrogen generation using $[Ru(bpy)_3]^{2+}$ LA, $[Fe_2(\mu\text{-}Cl_2bdt)(CO)_6]$ CAT, and ascorbic acid in DMF/H_2O

is kinetically unstable and rapidly disproportionate to form $[Rh(bpy)_3]^+$ and $[Rh(bpy)_3]^{3+}$. Rh-based systems are used as the electron relays in solar hydrogen production schemes.

Systematic Studies Using Rh-Based Supramolecular Photocatalysts for Solar Hydrogen Production The coupling of Rh centers to Ru light absorbers in supramolecular frameworks is reported [77–81]. The majority of this work focuses on the study of chelated complexes of Rh^{III} coupled to Ru polyazine charge-transfer complexes. In these studies the Rh acts as an intramolecular electron acceptor for the MLCT excited state of the Ru LA. In many of the systems, the Rh centers are bound to only chelating ligands, which can limit the chemistry that can follow intramolecular electron transfer. Brewer et al. reported the supramolecular complex $[\{(bpy)_2Ru(dpp)\}_2RhCl_2]^{5+}$, the first photoinitiated electron collector that collects multiple electrons on a metal capable of photocatalyzing hydrogen production from water [54–57, 82, 83]. This supramolecular system incorporates two $[(bpy)_2Ru(dpp)]^{2+}$ LAs and a single Rh EC allowing for multiple electron reduction. This system is unique from the previously reported systems as the Rh center is bound to monodentate Cl^- ligands that can be lost following photoreduction. This allows the metal to become coordinatively unsaturated, allowing complexation and/or reaction with substrates. The redox properties of $[\{(bpy)_2Ru(dpp)\}_2RhCl_2]^{5+}$ demonstrate that the Ru LAs are electronically isolated, important to PEC and multielectron photochemistry.

Brewer et al. subsequently reported other systems incorporating a similar architecture that are photoinitiated electron collectors catalyzing solar hydrogen production. These systems also couple two Ru^{II} or Os^{II} LAs to a single Rh^{III} acceptor. The supramolecular assemblies provide a LA-BL-RhX_2-BL-LA structural motif (LA = Ru^{II} or Os^{II} polyazine LA, X = Cl^- or Br^-, BL = dpp). Visible light irradiation affords PEC resulting in Rh reduction and loss of the labile ligands, Fig. 9. Studies have established $[\{(bpy)_2Ru(dpp)\}_2RhX_2]^{5+}$ (X = Cl^- or Br^-) and $[\{(phen)_2Ru(dpp)\}_2RhCl_2]^{5+}$ as photochemical molecular devices for electron collection at a metal center and are photocatalysts for solar hydrogen production from water with a hydrogen yield of $\Phi \approx 0.01$ [54, 56, 82]. Modification of the LA to Os and/or the TL to tpy and a Cl destabilizes the LA metal-dπ orbitals providing systems that absorb light at lower energy. The complexes $[\{(bpy)_2Os(dpp)\}_2RhCl_2]^{5+}$, $[\{(tpy)OsCl(dpp)\}_2RhCl_2]^{3+}$, and $[\{(tpy)RuCl(dpp)\}_2RhCl_2]^{3+}$ have been studied and their photocatalytic activity evaluated [56]. Studies show that $[\{(bpy)_2Os(dpp)\}_2RhCl_2]^{5+}$ and $[\{(tpy)RuCl(dpp)\}_2RhCl_2]^{3+}$ are solar hydrogen photocatalysts but provide lower activity consistent with significantly lower driving forces for excited state reductive quenching by the ED. Factors that impact photocatalytic efficiency have been evaluated by studying the redox and photophysical properties of these systems.

Rhodium-Based Supramolecular Photocatalysts: Redox Properties The electrochemical analysis of the supramolecular systems provides meaningful

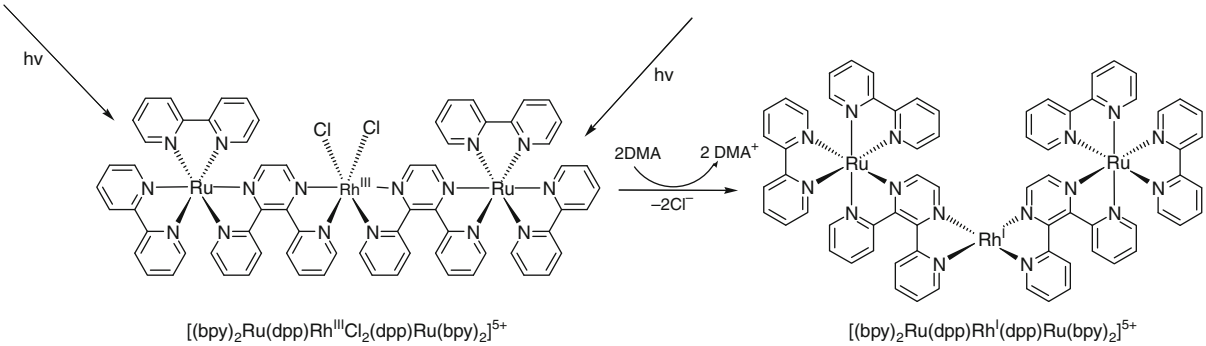

Hydrogen via Direct Solar Production. Figure 9
Photoinitiated electron collection on a metal center

information to understand excited state electron transfer and photocatalyst function. Electrochemical analysis provides a good estimation of the energy of the highest occupied molecular orbital (HOMO) and the lowest unoccupied molecular orbital (LUMO), allowing the study of the orbital energetics. Electrochemically the trimetallic complexes of the general formula $[\{(TL)_2\ M(dpp)\}_2RhX_2]^{5+}$ (TL = bpy or phen, M = Ru or Os, X = Cl or Br) and $[\{(tpy)MCl(dpp)\}_2RhCl_2]^{3+}$ (M = Ru or Os) demonstrate reversible metal-based oxidations and irreversible Rh- and reversible ligand-based reductions [56]. All the trimetallics show overlapping $Ru^{II/III}$ or $Os^{II/III}$ based oxidations for the two terminal ligands, indicating minimal electronic interaction between the two terminal metal LA subunits. The Ru centers of the RuRu bimetallic systems $[\{(bpy)_2Ru\}_2(dpp)]^{4+}$ or $[\{(phen)_2Ru\}_2(dpp)]^{4+}$ are electronically coupled showing two $Ru^{II/III}$ oxidations at *ca.* +1.47 and +1.66 V vs. SCE [84]. These bimetallic systems do not display photoinitiated electron collection and/or reduction of substrates. $[\{(bpy)_2Ru(dpp)\}_2RhX_2]^{5+}$ systems (X = Cl or Br) or $[\{(phen)_2Ru(dpp)\}_2RhCl_2]^{5+}$ show overlapping oxidative couples at *ca.* 1.60 V vs. SCE. Rh^{III} centers coordinated to polyazine ligands typically display irreversible reductions corresponding to $Rh^{III/II/I}$ processes [85]. The $Rh^{III/II/I}$ reductions are followed by the loss of halides as observed for $[Rh(bpy)_2Cl_2]^+$. In the trimetallic systems, the $Rh^{III/II/I}$ reduction is followed by two reversible $dpp^{0/-}$ reductions. The halides on the Rh^{III} center impact the redox properties as evidenced by a slightly more positive $Rh^{III/II/I}$ reduction, −0.36 V vs. SCE for $[\{(bpy)_2Ru(dpp)\}_2RhBr_2]^{5+}$ relative to $[\{(bpy)_2Ru(dpp)\}_2RhCl_2]^{5+}$, −0.40 V vs. SCE [54–56]. This positive shift in the $Rh^{III/II/I}$ couple is consistent Br^- being a weaker σ donor than Cl^-. The $Os^{II/III}$ couple occurs at 1.17 V vs. SCE in $[\{(bpy)_2Os(dpp)\}_2RhCl_2]^{5+}$. The more positive oxidation potential is a result of more destabilized Os(dπ) orbitals relative to the Ru (dπ) orbitals in the Ru-based systems. The $Ru^{II/III}$ oxidation of $[\{(tpy)RuCl(dpp)\}_2RhCl_2]^{3+}$ occurs at 1.09 V vs. SCE, more positive than the $Ru^{II/III}$ oxidations of the analogous bpy-based systems, and consistent with a more electron rich ruthenium center due to Cl^- coordination in place of a pyridine ring. The $Os^{II/III}$ couple in $[\{(tpy)OsCl(dpp)\}_2RhCl_2]^{3+}$ occurs at 0.81 V vs. SCE, consistent with even more destabilized Os(dπ) orbitals. The reductive electrochemistry of $[\{(tpy)MCl(dpp)\}_2RhCl_2]^{3+}$ shows irreversible $Rh^{III/II/I}$ reductions at −0.51 and −0.55 V vs. SCE (M = Ru or Os), respectively, followed by two reversible $dpp^{0/-}$ couples. The electrochemistry of the trimetallic supramolecular complexes predict Ru(dπ)- or Os(dπ)-HOMOs with energy tuned by the TL or LA metal and Rh(dσ*)-based LUMOs with energy tuned by the halides bound to Rh. The electrochemistry predicts a lowest lying metal-to-metal charge-transfer state (MMCT) with an oxidized Ru and a reduced Rh, Fig. 10.

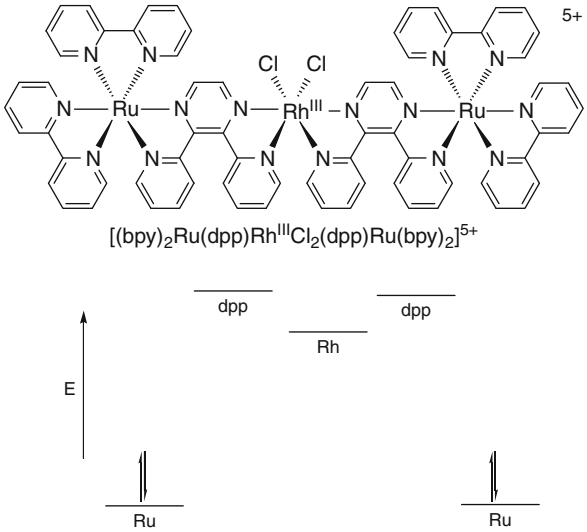

Hydrogen via Direct Solar Production. Figure 10 Orbital energy diagram of Rh-centered photoinitiated electron collection of the form LA-BL-RhX_2-BL-LA (LA = bpy or phen, BL = dpp, X = Cl or Br)

Rhodium-Based Supramolecular Photocatalysts: Spectroscopic Properties The optical properties of the trimetallic supramolecular complexes are evaluated by electronic absorption spectroscopy [54–56]. The trimetallic supramolecular assemblies are efficient light absorbers throughout the UV and visible regions of the spectrum with transitions characteristic of each subunit of the LA-BL unit. The electronic absorption spectra of $[\{(bpy)_2Ru(dpp)\}_2RhX_2]^{5+}$ (X = Cl or Br) and $[\{(phen)_2Ru(dpp)\}_2RhCl_2]^{5+}$ exhibit intense π → π* TL and dpp transitions in the UV, Ru(dπ) → TL (π*) (TL = bpy or phen) CT transitions between 410 and 420 nm, and Ru(dπ) → dpp(π*) CT transitions at

λ_{max}^{abs} = 520 nm ($\varepsilon = 2.6 \times 10^4\ M^{-1}\ cm^{-1}$) [56]. The lowest energy Ru(dπ) → dpp(π*) CT transition for $[\{(bpy)2Ru\}_2(dpp)]^{4+}$ or $[\{(phen)_2Ru\}_2(dpp)]^{4+}$ occurs at λ_{max}^{abs} = 526 nm demonstrating that the Ru (dp) → dpp(π*) CT are dominating in this region. This is verified by the nearly identical electronic absorption spectra of $[\{(bpy)_2Ru(dpp)\}_2RhCl_2]^{5+}$ and $[\{(bpy)_2Ru(dpp)\}_2RhBr_2]^{5+}$ demonstrating that the halide on the Rh does not significantly impact the optical properties. The electronic absorption spectra for the tpy-based systems are similar to the bpy analogs showing changes consistent with the destabilized metal orbitals showing Ru(dπ) → dpp(π*) CT transitions at λ_{max}^{abs} = 540 nm. For the Os analogs, $[\{(bpy)_2Os(dpp)\}_2RhCl_2]^{5+}$ and $[\{(tpy)OsCl(dpp)\}_2RhCl_2]^{3+}$, the Os(dπ) → dpp(π*) CT transitions occur at slightly lower energies relative to the ruthenium-based systems, consistent with the destabilized Os(dπ) orbitals. The Os systems show pronounced intensity of the ^{3}MLCT absorption in the low energy region due to a high degree of spin-orbit coupling.

Rhodium-Based Supramolecular Photocatalysts: Photophysics Emission spectroscopy is used to probe intramolecular electron transfer within a supramolecular assembly possessing emissive MLCT light absorbers. The Ru-based $[\{(TL)_2Ru(dpp)\}_2RhX_2]^{5+}$ (TL = bpy or phen, X = Cl or Br) systems possess ^{3}MLCT emissive excited states [54–56]. Model systems are used for comparison of the excited state properties to better understand the nature of energy and/or electron transfer within the supramolecular architecture. The bimetallic complex $[\{(bpy)2Ru\}_2(dpp)]^{4+}$ that lacks the Rh^{III} typically serves as the model for the interpretation of the emissive properties of these supramolecules due to the similar excited state energies and nature of the emissive ^{3}MLCT excited states. Determination of the rate of electron transfer requires that the energy and nature of the emissive state of the model must closely match that of the supramolecular assembly. In the $[\{(TL)_2Ru(dpp)\}_2RhX_2]^{5+}$ (TL = bpy, X = Cl or Br) and $[\{(phen)_2Ru(dpp)\}_2RhCl_2]^{5+}$ systems, the optically excited ^{1}MLCT state populates a ^{3}MLCT state that is quenched by intramolecular electron transfer to populate a low-lying ^{3}MMCT state (see Fig. 11) [54–56]. The complexes $[\{(bpy)_2Ru(dpp)\}_2RhCl_2]^{5+}$, $[\{(bpy)_2Ru(dpp)\}_2RhBr_2]^{5+}$, and $[\{(phen)_2Ru(dpp)\}_2RhCl_2]^{5+}$ display weak emissions from the Ru(dπ) → dpp(π*) ^{3}MLCT state at λ_{max}^{em} = 760 nm for $[\{(bpy)_2Ru(dpp)\}_2RhCl_2]^{5+}$ and $[\{(bpy)_2Ru(dpp)\}_2RhBr_2]^{5+}$ and λ_{max}^{em} = 746 nm for $[\{(phen)_2Ru$

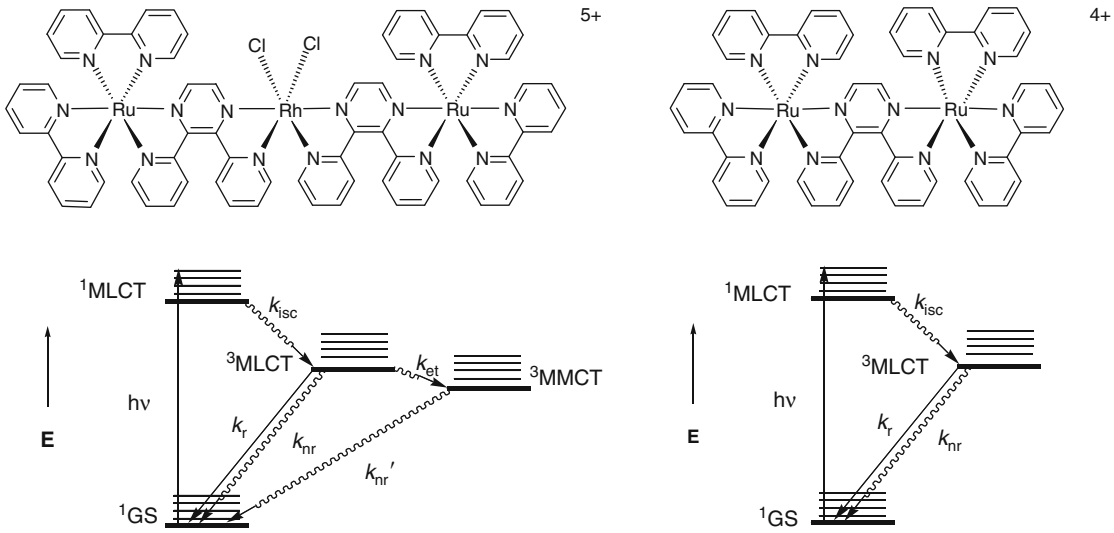

Hydrogen via Direct Solar Production. Figure 11
State diagrams for $[\{(bpy)_2Ru(dpp)\}_2RhX_2]^{5+}$ (X = Cl^- or Br^-) and $[\{(phen)_2Ru(dpp)\}_2RhCl_2]^{5+}$ (*left*) and $[\{(bpy)_2Ru\}_2(dpp)]^{4+}$ (*right*)

$(dpp)\}_2RhCl_2]^{5+}$ with $\Phi^{em} = 7.3 \times 10^{-5}$, 1.5×10^{-4}, and 1.8×10^{-4}, respectively, at RT in deoxygenated acetonitrile solutions following excitation at 520 nm. The emission from the ^{3}MLCT state is quenched by *ca.* 85–90% relative to $[\{(bpy)_2Ru\}_2(dpp)]^{4+}$ (λ_{max}^{em} = 744 nm, $\Phi^{em} = 1.38 \times 10^{-3}$) indicating intramolecular electron transfer to populate a lower lying state. Electrochemical analysis predicts this state to be a ^{3}MMCT excited state with oxidized Ru LAs and a reduced Rh. The τ of the ^{3}MLCT states in deoxygenated acetonitrile solutions at RT for $[\{(bpy)_2Ru(dpp)\}_2RhCl_2]^{5+}$, $[\{(bpy)_2Ru(dpp)\}_2RhBr_2]^{5+}$, and $[\{(phen)_2Ru(dpp)\}_2RhCl_2]^{5+}$ are 32, 26, and 27 ns, respectively, reduced relative to the τ of $[\{(bpy)_2Ru\}_2(dpp)]^{4+}$, τ = 140 ns [56, 84]. The k_{et} to populate the ^{3}MMCT states, estimated by assuming k_r and k_{nr} of the trimetallic systems are the same as $[\{(bpy)_2Ru\}_2(dpp)]^{4+}$, are comparable with $k_{et} = 1.2 \times 10^8\ s^{-1}$, $5.2 \times 10^7\ s^{-1}$, and $4.4 \times 10^7\ s^{-1}$, respectively, for $[\{(bpy)_2Ru(dpp)\}_2RhCl_2]^{5+}$, $[\{(bpy)_2Ru(dpp)\}_2RhBr_2]^{5+}$, and $[\{(phen)_2Ru(dpp)\}_2RhCl_2]^{5+}$. Efficient intramolecular electron transfer is seen in this trimetallic motif.

Rhodium-Based Supramolecular Photocatalysts: Solar Hydrogen Production Solar hydrogen production from water using a series of supramolecular photoinitiated electron collectors of the general form LA-BL-RhX_2-BL-LA has been evaluated [54–56]. These systems photoreduce by two electrons, following visible light excitation in the presence of DMA. This mechanism proposes that $[\{(bpy)_2Ru(dpp)\}_2Rh^I]^{5+}$ species is formed by the excited trimetallic molecule using a sacrificial electron donor and passes through an intermediate Rh^{II} species, Fig. 12. These complexes are unusually oxidizing in their excited states, allowing for excited state oxidation of a variety of electron donors. Reductive quenching of both the ^{3}MLCT and ^{3}MMCT states are feasible. Kinetic investigation by Stern-Volmer emission quenching as well as product

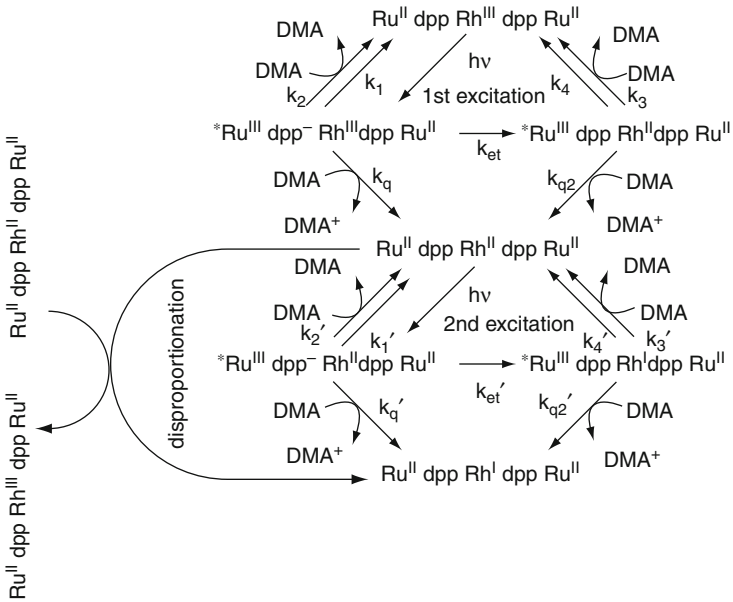

Hydrogen via Direct Solar Production. Figure 12
Proposed mechanism for photoinitiated electron transfer. bpy, Cl, and charges are omitted for clarity. $Ru^{II}dppRh^{III}dppRu^{II}$ is $[\{(bpy)_2Ru(dpp)\}_2RhCl_2]^{5+}$, where bpy = 2,2.-bipyridine and dpp = 2,3-bis-2-pyridylpyrazine. DMA is dimethylaniline. k_1 and k_4 are the unimolecular decay pathways from the ^{3}MLCT and ^{3}MMCT states, respectively, whereas k_2 and k_3 are the bimolecular deactivation rates from the same states. k_{et} is the rate of electron transfer to generate the ^{3}MMCT state. k_q and k_{q2} are the rates of reductive quenching by DMA to generate the Rh^{II} complex from the ^{3}MLCT and ^{3}MMCT states, respectively

formation was performed focusing on the formation of the single electron reduced Rh^{II} species. The rate of reductive quenching to generate the Rh^{II} species from the ^{3}MLCT excited state would be 1.9×10^9 M^{-1} s^{-1} if reduction only occurs via this pathway [82]. A Stern-Volmer emission quenching analysis showed that the ^{3}MLCT excited state is efficiently quenched by DMA close to diffusion limit, $k_q = 2 \times 10^{10}$ M^{-1} s^{-1}. The estimated excited state reduction potentials of the ^{3}MLCT and ^{3}MMCT states for $[\{(bpy)_2Ru(dpp)\}_2RhCl_2]^{5+}$are 1.23 and 0.84 V vs. SCE, respectively. Positive driving forces for reductive quenching of both excited states are predicted, using Eq. 10, the oxidation potential of DMA, $E_{1/2}$ = 0.81 V vs. SCE. Very similar driving forces for reductive quenching of the excited states by DMA are also predicted for $[\{(bpy)_2Ru(dpp)\}_2RhBr_2]^{5+}$ and $[\{(phen)_2Ru(dpp)\}_2RhCl_2]^{5+}$ based on their excited state reduction potentials and the oxidation potential of DMA.

The trimetallic complexes $[\{(bpy)_2Ru(dpp)\}_2RhCl_2]^{5+}$, $[\{(bpy)_2Ru(dpp)\}_2RhBr_2]^{5+}$, $[\{(phen)_2Ru(dpp)\}_2RhCl_2]^{5+}$, $[\{(bpy)_2Os(dpp)\}_2RhCl_2]^{5+}$, $[\{(tpy)RuCl(dpp)\}_2RhCl_2]^{3+}$, $[\{(tpy)OsCl(dpp)\}_2RhCl_2]^{3+}$, and the first photoinitiated electron collector $[\{(bpy)_2Ru(dpb)\}_2IrCl_2]^{5+}$ were evaluated with respect to their functioning as hydrogen photocatalysts in the presence of water and DMA, Et_3N, or TEOA [56]. All complexes demonstrate photocatalytic activity with the exceptions of $[\{(bpy)_2Ru(dpb)\}_2IrCl_2]^{5+}$ and $[\{(tpy)OsCl(dpp)\}_2RhCl_2]^{3+}$. The lack of photocatalysis by $[\{(bpy)_2Ru(dpb)\}_2IrCl_2]^{5+}$ demonstrate that the functioning systems require a Rh center and a ^{3}MLCT and/or ^{3}MMCT states with sufficient driving forces for excited state reduction by the ED. It is predicted that the coordinatively unsaturated species generated by Rh reduction, $[\{(TL)_2Ru(dpp)\}_2Rh^I]^{5+}$ (TL = bpy or phen), is reactive and susceptible to interaction with substrates such as water.

Photolysis of acetonitrile solutions of $[\{(bpy)_2Ru(dpp)\}_2RhX_2]^{5+}$ (X = Cl^- or Br^-) or $[\{(phen)_2Ru(dpp)\}_2RhCl_2]^{5+}$ in the presence of DMA and water at λ = 470 nm leads to water reduction to produce hydrogen with Φ = 0.01 with 18–26 TON in 2 h (36–54 TON relative to the LA as 2 TON of the LA are needed per catalytic cycle). $[\{(bpy)_2Ru(dpp)\}_2RhBr_2]^{5+}$ shows higher photocatalytic activity relative to the chloride analog implying that the rate of halide loss is kinetically important. The complexes $[\{(bpy)_2Os(dpp)\}_2RhCl_2]^{5+}$ and $[\{(tpy)RuCl(dpp)\}_2RhCl_2]^{3+}$ yield similar amounts of hydrogen when irradiated at 470 nm in the presence of DMA and water, but with much lower efficiency than $[\{(bpy)_2Ru(dpp)\}_2RhCl_2]^{5+}$. The excited state reduction potentials of the ^{3}MLCT and ^{3}MMCT were predicted as 0.91 and 0.54 V vs. SCE, respectively, for $[\{(bpy)_2Os(dpp)\}_2RhCl_2]^{5+}$ and 1.01 and 0.61 V, respectively, for $[\{(tpy)RuCl(dpp)\}_2RhCl_2]^{3+}$ making quenching of the ^{3}MMCT excited state by DMA unlikely.

The production of hydrogen despite the negative driving force for reductive quenching of the ^{3}MMCT excited state suggests that hydrogen production can occur through quenching of only the ^{3}MLCT excited state. The lower driving force for reductive quenching of the ^{3}MLCT and the lower τ may account for the lower photocatalytic efficiency of these complexes. $[\{(tpy)OsCl(dpp)\}_2RhCl_2]^{3+}$ does not function as a photocatalyst under the conditions investigated. Based on the excited state reduction potentials of the ^{3}MLCT and ^{3}MMCT states, 0.71 and 0.37 V vs. SCE, respectively, the reductive quenching of both excited states by DMA are thermodynamically unfavorable, explaining the lack of photocatalytic activity of this system. Addition of Hg(l) to the photocatalytic systems does not impair hydrogen production suggesting that hydrogen production catalyzed by Rh colloid formation is not an active pathway and that the supramolecular architecture remains intact during photocatalysis [54, 86, 87]. Interestingly, $[\{(bpy)_2Ru(dpb)\}_2IrCl_2]^{5+}$ is not a solar hydrogen photocatalyst although PEC occurs on the dpb(π^*) orbitals and a thermodynamically favorable driving force for reductive quenching of the ^{3}MLCT state by DMA exists. This implies that other factors in addition to PEC and favorable thermodynamics for reductive quenching are important for solar hydrogen production. The lack of hydrogen production by the Ir-system implies that the Rh center is essential for photocatalysis.

The impact of the ED on the most efficient photocatalysts $[\{(bpy)_2Ru(dpp)\}_2RhCl_2]^{5+}$, $[\{(bpy)_2Ru(dpp)\}_2RhBr_2]^{5+}$, and $[\{(phen)_2Ru(dpp)\}_2RhCl_2]^{5+}$ shows that the efficiency of hydrogen production varies in the order DMA (18–26 TON in 2 h) > Et_3N (3–6 TON in 2 h) > TEOA (1 TON in 2 h) [56]. TEOA has a slightly higher driving force for reductive quenching

of the photocatalysts than Et_3N, but results in lower hydrogen yields. An important factor to be considered in water reduction is the solution pH. The effective pH of the photolysis solutions using DMA, Et_3N, or TEOA were estimated as *ca.* 9.1, 14.7, and 11.8, respectively, on the assumption that the pK_a values of their conjugated acids remain unchanged in the photocatalytic solutions relative to aqueous conditions (pK_a = 5.07 ($DMAH^+$), 10.75 (Et_3NH^+), and 7.76 ($TEOAH^+$)). The lower catalyst function when TEOA is the ED may be attributed to the higher effective pH of the solution. The reduction potential of water is pH dependent occurring at lower potentials at lower pH. In addition the protonation of the Rh center may be critical to photocatalysis and this equilibrium would be very sensitive to pH. In addition, the ability of DMA to form donor-LA π-stacking interactions may be advantageous for more efficient reductive quenching of the excited states affording the highest hydrogen yields compared to the aliphatic electron donors. Recent studies have focused on the scale up of photochemical hydrogen production using the lead photocatalyst $[\{(bpy)_2Ru(dpp)\}_2RhBr_2]^{5+}$. Studies show that increased [DMA], increased headspace, volume, and a DMF solvent provide enhanced catalyst function [88].

Photochemical properties of $[\{(bpy)_2Ru(dpp)\}_2RhBr_2]Br_5$ in aqueous medium have been investigated [57]. Studies have established this complex to function as a photoinitiated electron collector in water, the first system shown to display this function in aqueous medium. $[\{(bpy)_2Ru(dpp)\}_2RhBr_2]Br_5$ functions as a photocatalyst for the production of hydrogen in the presence of TEOA with added triflic acid, hydrobromic acid, or phosphoric acid. The photocatalytic efficiency is lower in the aqueous medium, typical of these systems.

The Rh-centered supramolecular complexes are efficient photocatalysts for water reduction to produce hydrogen fuel. The variation of component identity within this molecular architecture allows for optimization of functioning of these systems and the understanding of the mechanism of action. The functioning of these systems is also modulated by system parameters such as solvent, temperature, reagent concentrations, hydrogen partial pressure, etc. This provides a unique forum to explore the multidimensional space needed to optimize solar hydrogen production via direct water reduction. Often preliminary studies appear without the long-term study needed to explore the full potential of these new supramolecular catalysts for hydrogen production.

Supramolecular solar hydrogen photocatalysts that couple a $[Os(tpy)_2]^{2+}$ LA to a Rh CAT are reported, Fig. 13 [58]. The OsRh dyads have been synthesized and analyzed in situ by treatment with $[RhCl(CO)_2]_2$ or $RhCl_3$. The dyads are potent LAs absorbing in the visible at 480 and 655 nm, attributed to Os(dπ) → tpy (dπ*) ^{1}MLCT and ^{3}MLCT absorptions, respectively. An Os(dπ) → tpy(dπ*) ^{3}CT emission is observed at 728 nm (Φ^{em} = 0.52 in an acetonitrile/water mixture) with reduced intensity relative to the parent LA (Φ^{em} = 0.73 in an acetonitrile/water mixture) suggestive of intramolecular electron transfer to the Rh. The emission is decreased when sodium ascorbate is added to the dyad efficient quenching of the excited state by sodium ascorbate.

Irradiation of catalytic amounts of the dyad generated in situ at λ > 380 nm in a trifluoromethanesulfonic

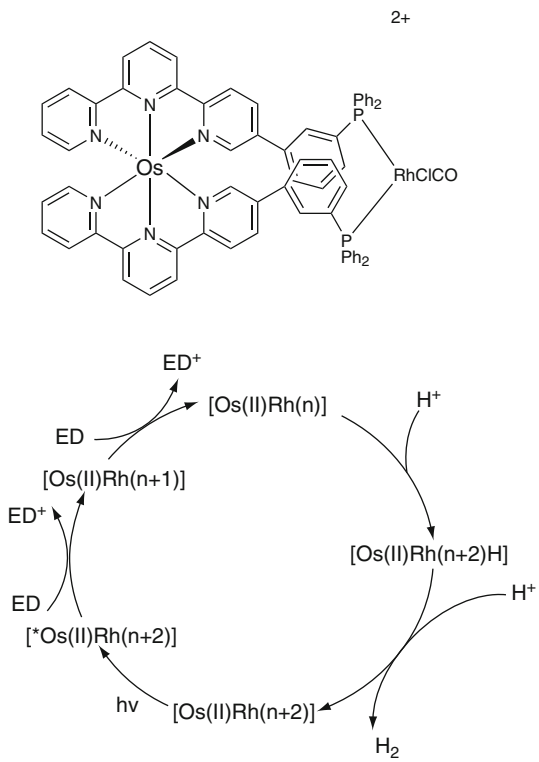

Hydrogen via Direct Solar Production. Figure 13 OsRh dyad systems for solar hydrogen production

acid/sodium ascorbate mixture at pH = 5.2 for 18 h affords hydrogen with 36 TON [58]. Use of $RhCl_3$ in place of $[RhCl(CO)_2]_2$ yields 87 TON with $\Phi = 0.007$. Electron donors including TEOA or L-cysteine are not effective for hydrogen photocatalysis. Lower catalytic function is observed when $RhCl_3 \bullet 3H_2O$/dppe (dppe = 1,2-bis(diphenylphosphino)ethane) with $[Os(tpy)_2]^{2+}$ is used as the photosystem (24 TON) with no detectable hydrogen if only $RhCl_3 \bullet 3H_2O$/dppe, RhCl(CO)(dppe), or only the LA is used. This suggests that the supramolecular architecture is important for photocatalysis and intramolecular electron transfer from Os to Rh is a key step. A schematic for the proposed mechanism is shown in Fig. 13. It is proposed that upon optical excitation, intramolecular electron transfer to Rh by two electrons leads to a reduced Rh which can react with a proton to form a Rh-H, which generates hydrogen.

Photochemical hydrogen production from hydrohalic acid solutions by a Rh-based dinuclear mixed-valence complex capable of multielectron photochemistry has been reported, Fig. 14 [59, 89]. Hydrogen production occurs with $\Phi = 0.01$ with 27 TON/h during the initial 3 h, in the presence of a halogen trap. The mixed-valence compounds have been constructed to drive multielectron chemistry and are of the form $M^{n+} \cdots M^{n+2}$. Rhodium bimetallics, $[Rh_2(dfpma)_3X_4]$, when ligated by three dfpma ligands transform to a two-electron mixed-valence state, $[Rh_2^{0,II}(dfpma)_3X_2(L)]$ (dfpma = $MeN(PF_2)_2$, X = Cl or Br, L = CO,

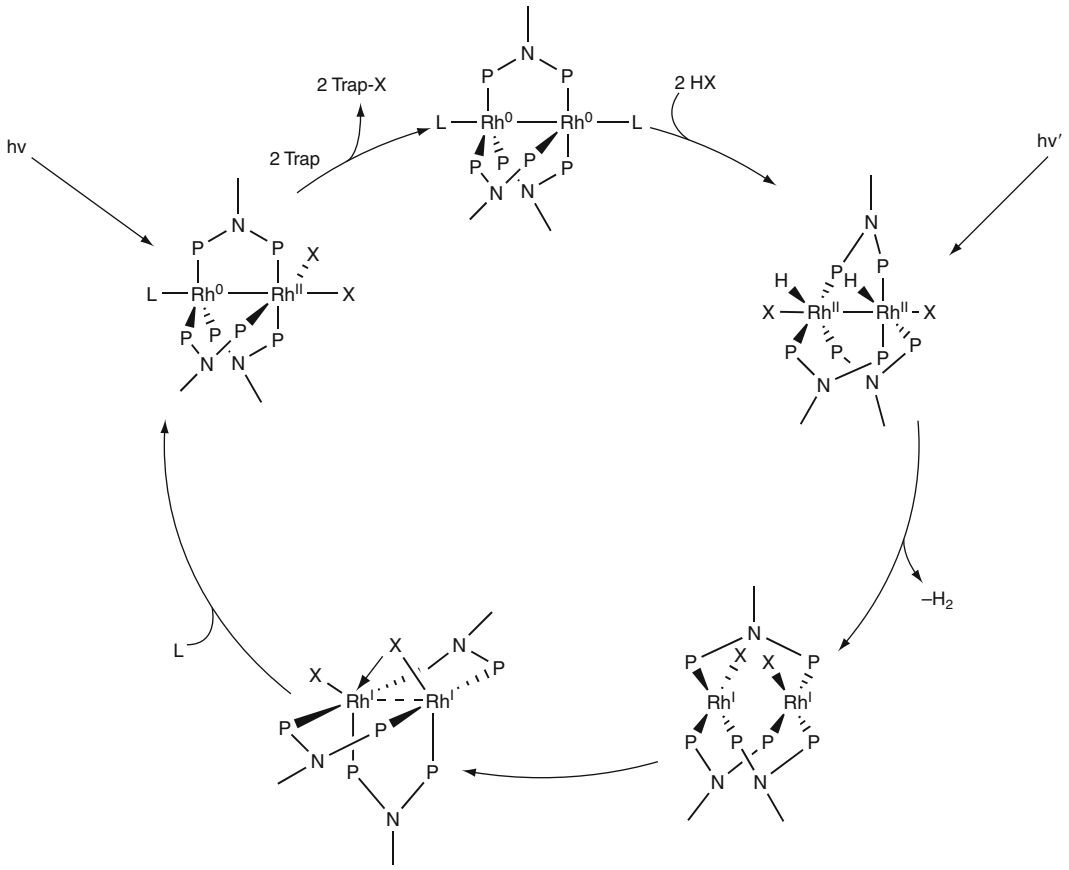

Hydrogen via Direct Solar Production. Figure 14
Mechanism for the photocatalytic generation of hydrogen from hydrohalic acids using a dirhodium mixed-valence photocatalyst (Figure adapted from Ref. [59])

PR_3, or CNR) when irradiated at excitation wavelengths between 300 and 400 nm in the presence of excess L and a halogen-atom trap. The dfpma ligand provides stability to the mixed-valence state by acting as both a π-acceptor and a π-donor. Further irradiation activates a Rh^{II}-X, which is the rate limiting step, to generate a doubly reduced form, $[Rh_2^{0,0}(dfpma)_3\ L_2]$. Photolysis of $[Rh_2^{0,0}(dfpma)_3\ L_2]$ in the presence of HCl results in an intermediate Rh^{II},Rh^{II} dihydride, dihalide, $[Rh_2^{II,II}(dfpma)_3Cl_2H_2]$, which upon photolysis produces hydrogen with the generation of the $[Rh_2^{I,I}(dfpma)_3Cl_2]$ which undergoes internal disproportionation affording $[Rh_2^{0,II}(dfpma)_3X_2(L)]$. New systems $[Rh^IAu^I(tfepma)_2(CN^tBu)_2]^{2+}$ and $[Pt^{II}Au^I(dppm)_2PhCl]^+$ (tfepma = $MeN(P(OCH_2CF_3)_2)_2$ and dppm = $CH_2(PPh_2)_2$) have been constructed with the aim of promoting more efficient M-X bond activation [90, 91]. The Pt^{III}-Au^{II} species, $[Pt^{III}Au^{II}(dppm)_2PhCl_3]^+$, formed by photooxidation displays enhanced efficiency of metal-halide bond activation with respect to the dirhodium complexes.

Rhodium-Based Multicomponent Photocatalysis The pioneering work in photochemical hydrogen production using molecular systems used $[Rh(bpy)_3]^{3+}$ as an electron relay in solar hydrogen production schemes using $[Ru(bpy)_3]^{2+}$ and TEOA [11, 60]. In the presence of a heterogeneous platinum catalyst, photocatalytic hydrogen production from water occurs with Φ = 0.11 irradiated at λ = 450 nm with *ca.* 80 TON relative to $[Rh(bpy)_3]^{2+}$ reported under similar conditions [11, 60]. The MLCT excited state of $[Ru(bpy)_3]^{2+}$ undergoes intermolecular electron transfer to $[Rh(bpy)_3]^{3+}$ to produce the oxidized LA and $[Rh(bpy)_3]^{2+}$. The photogenerated Rh^{II} system is kinetically unstable and can rapidly disproportionate to $[Rh^I(bpy)_2]^+$ and $[Rh^{III}(bpy)_3]^{3+}$ deactivating the system. The catalytic species in this system is colloidal Pt, which facilitates hydrogen photocatalysis by accepting electrons from the reduced Rh. In-depth studies of $[Rh^I(bpy)_2]^+$ have established that at low concentrations in alkaline solutions $[Rh^I(bpy)_2]^+$ predominates, while a dimer, $[Rh^I(bpy)_2]_2^{2+}$, is dominant at higher $[Rh^I(bpy)_2]^+$ [92, 93]. $[Rh^{III}(bpy)_2(H)(H_2O)]^{2+}$ and $[Rh^I(bpy)_2]_2(H)^{3+}$ are formed by protonation of $[Rh^I(bpy)_2]^+$ or $[Rh^I(bpy)_2]_2^{2+}$ at low pH. Thermodynamic and kinetic parameters for the oxidative addition of hydrogen to $[Rh^I(bpy)_2]^+$ and photoinduced reductive elimination of hydrogen have been studied, $K_H = 1.45 \times 10^3\ M^{-1}$ [94]. Studies show that *cis*-$[Rh^{III}(H)_2(bpy)_2]^+$ dissociates to hydrogen and $[Rh^I(bpy)_2]^+$ when irradiated (λ > 300 nm).

Cyclometalated Ir^{III} complexes have been used as LAs in photochemical schemes for production of hydrogen from water using tris-2,2′-bipyridyl Rh^{III} complexes as CATs, Fig. 15 [61]. The study of the system function with varied $[Ir(C\wedge N)_2(N\wedge N)]^+$ LAs and $[Rh(N\wedge N)]^{3+}$ CATs has allowed the development of an optimized photosystem for solar hydrogen production. An optimal catalyst combination of $[Ir(f\text{-}mppy)_2(dtbbpy)]^+$ and $[Rh(dtbbpy)_3]^{3+}$ has been identified through catalyst screening, studies of the impact of hydrogen production by LA, CAT, solvent environment, and electron donor (f-mpy = 5-methyl-2-(4-fluoro)phenylpyridine). Irradiation of 80% THF-H_2O system at 460 nm shows 5,000 TON relative to either the LA or the CAT when one component is limiting in excess of the other. The use of 1:1 of LA and CAT balances the performance of both components resulting in 3,400 TON and a maximum catalytic rate of turnovers of 520 h^{-1} with Φ = 0.32 in *ca.* 20–24 h. The rate constants for reductive quenching of the excited state of the LA by Et_3N and oxidative quenching by $[Rh(dtbbpy)_3]^{3+}$ are similar, $k_{ox} = 6.7 \times 10^7\ M^{-1}\ s^{-1}$ and $k_{red} = 6.4 \times 10^7\ M^{-1}\ s^{-1}$, but the presence of excess of Et_3N suggests that a reductive quenching mechanism is dominant. Addition of Hg does not impede system function providing evidence that the system is a true homogeneous system for photocatalytic hydrogen production.

Co-Based Supramolecular and Multicomponent Systems

Cobalt complexes with diglyoxime ligands are electrocatalysts for hydrogen production at low overpotentials. The electrochemical and photochemical hydrogen evolution catalyzed by cobaloximes with thermodynamic analysis of hydrogen evolution pathways has been reviewed recently [95]. Supramolecular systems as well as multicomponent systems which incorporate cobaloximes sensitized by Ru or Ir base LAs are known. These systems provide a means to utilize first-row transition metal complexes as CATs.

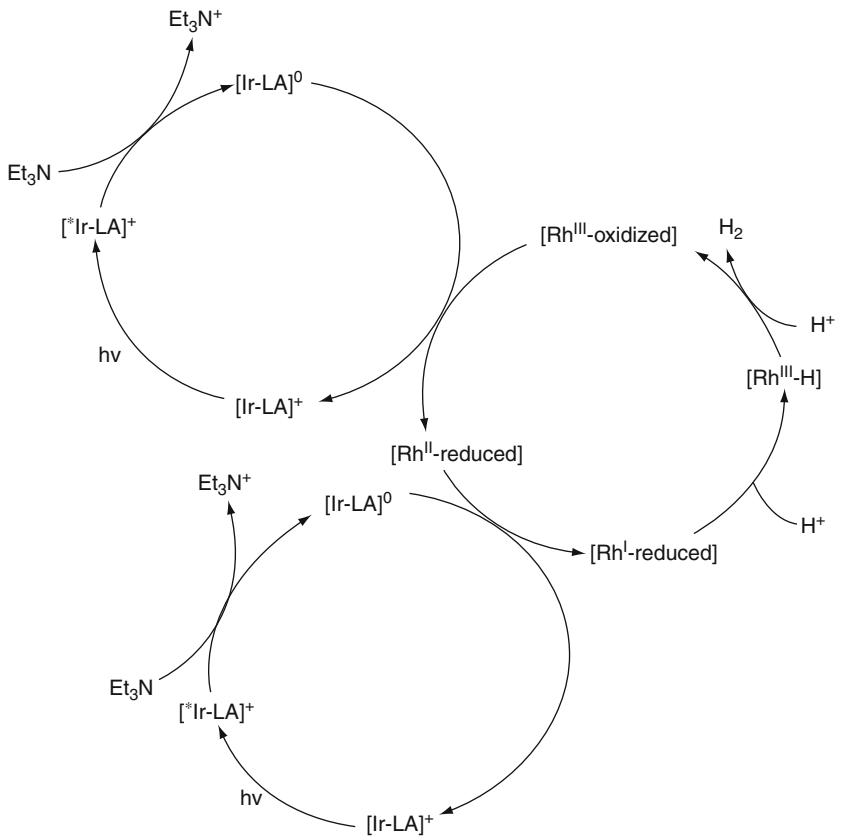

Hydrogen via Direct Solar Production. Figure 15
Mechanism for the photocatalytic generation of hydrogen from water in a Ir-Rh multicomponent system with Et_3N electron donor

Co-Based Supramolecular Systems Supramolecular systems have been engineered taking advantage of the light-absorbing properties of Ru^{II} or Ir^{III} chromophores and the catalytic properties of cobaloximes in single molecules [62, 63]. Supramolecular dyads $[(bpy)_2Ru(L\text{-}pyr)Co(dmgBF_2)_2(OH_2)]^{2+}$, $[(bpy)_2Ru(L\text{-}pyr)Co(dmgH)_2Cl]^{2+}$, $[(bpy)_2Ru(L\text{-}pyr)Co(dpgBF_2)_2(OH_2)]^{2+}$ [62], $[(Me_2phen)_2Ru(L\text{-}pyr)Co(dmgBF_2)_2(OH_2)]^{2+}$, and $[(ppy)_2Ir(L\text{-}pyr)Co(dmgBF_2)_2(OH_2)]^{+}$ (L-pyr = [(4-pyridine)oxazolo(4,5-f) phenanthroline], dmgH = dimethylglyoximate, $dmgBF_2$ = (difluoroboryl)dimethylglyoximate, $dpgBF_2$ = (difluoroboryl)diphenylglyoximate, Me_2phen = 4,7-dimethylphenanthroline, ppy = 2-phenylpyridine) [63] are photocatalysts for solar hydrogen production, Fig. 16. The BF_2-bridged systems are more resistant toward acid hydrolysis and undesired hydrogenation reactions. The Co^{II} state is easier to reduce in the BF_2-bridged systems vs. the H-bridged cobaloximes. The L-pyr BL facilitates intramolecular excited state electron transfer.

Photochemical hydrogen production from Et_3NH^+ occurs when acetone solutions of $[(bpy)_2Ru(L\text{-}pyr)Co(dmgBF_2)_2(OH_2)]^{2+}$, $[(bpy)_2Ru(L\text{-}pyr)Co(dmgH)_2Cl]^{2+}$, or $[(bpy)_2Ru(L\text{-}pyr)Co(dpgBF_2)_2(OH_2)]^{2+}$ are photolyzed using a CdI-doped Hg light source in the presence of 100-fold excesses of Et_3N and Et_3NH^+ [62]. Turnover numbers of 56, 17, and 12 over 4 h are seen for $[(bpy)_2Ru(L\text{-}pyr)Co(dmgBF_2)_2(OH_2)]^{2+}$, $[(bpy)_2Ru(L\text{-}pyr)Co(dmgH)_2Cl]^{2+}$, or $[(bpy)_2Ru(L\text{-}pyr)Co(dpgBF_2)_2(OH_2)]^{2+}$, respectively. Increasing Et_3N and Et_3NH^+ to 300-fold excess had slight effect with 60 TON observed for $[(bpy)_2Ru(L\text{-}pyr)Co(dmgBF_2)_2(OH_2)]^{2+}$ in 4 h. The impact of solvent on photocatalytic efficiency of $[(bpy)_2Ru(L\text{-}pyr)Co(dmgBF_2)_2(OH_2)]^{2+}$ showed lower TON in acetonitrile

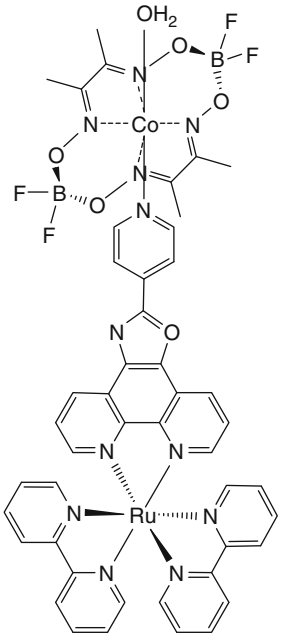

$[(bpy)_2Ru(L\text{-}pyr)Co(dmgBF_2)_2(OH_2)]^{2+}$

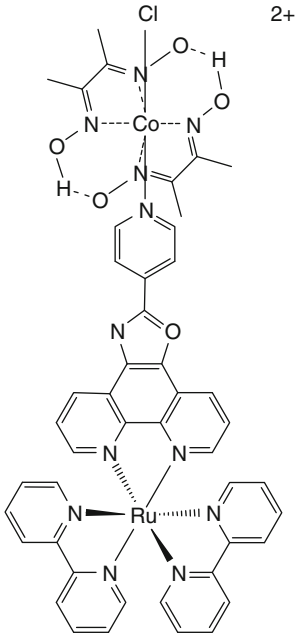

$[(bpy)_2Ru(L\text{-}pyr)Co(dmgH)_2Cl]^{2+}$

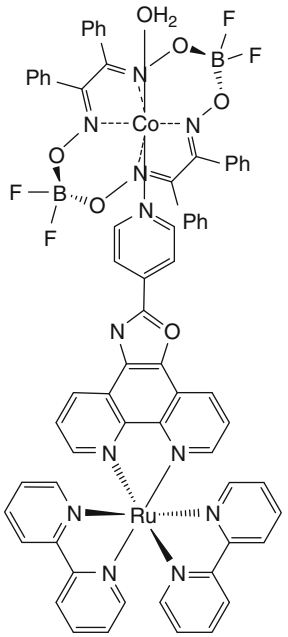

$[(bpy)_2Ru(L\text{-}pyr)Co(dpgBF_2)_2(OH_2)]^{2+}$

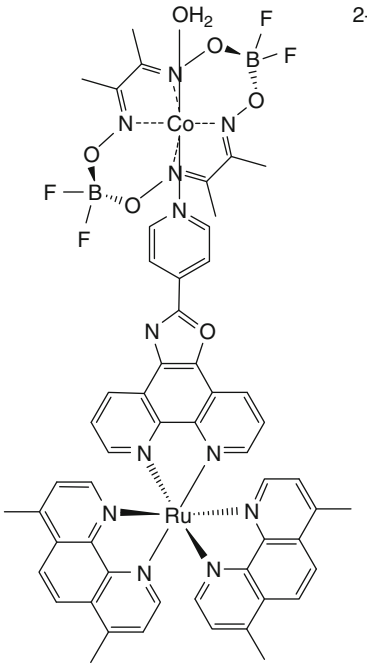

$[(Me_2phen)_2Ru(L\text{-}pyr)Co(dmgBF_2)_2(OH_2)]^{2+}$

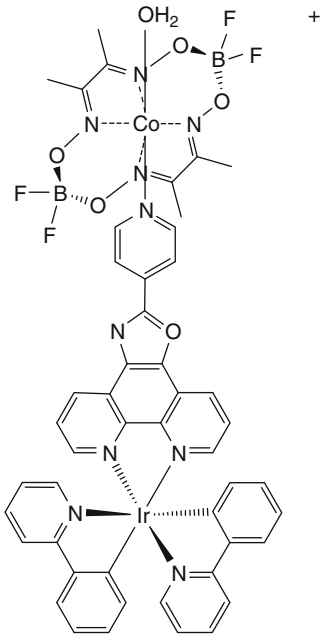

$[(ppy)_2Ir(L\text{-}pyr)Co(dmgBF_2)_2(OH_2)]^{+}$

Hydrogen via Direct Solar Production. Figure 16
Representations of cobalt-based supramolecular dyads

(TON = 10), methanol (TON = 9), DMF (TON = 3), or 1,2-dichloroethane (TON = 0). The lower TON in DMF or 1,2-dichloroethane is attributed to decomplexation of the photocatalyst in these solvents. When the proton source is water (100-fold excess of both water and Et_3N), 22 TON in 4 h is seen for $[(bpy)_2Ru(L\text{-}pyr)Co(dmgBF_2)_2(OH_2)]^{2+}$. It is likely that the lower activity is due to pH changes that are significant when water is used as the proton source. Visible light-induced excitation ($\lambda > 350$ nm) of the $[(bpy)_2Ru(L\text{-}pyr)Co(dmgBF_2)_2(OH_2)]^{2+}$ system afforded 103 TON in 15 h. Lower TON is obtained when a UV cutoff filter is used, implying both UV and visible light promote photocatalysis. It is mentioned that the analogous system of $[(bpy)_2Ru(L\text{-}pyr)Co(dmgBF_2)_2(OH_2)]^{2+}$ with the BL oxazole O replaced by NH shows a twofold increased photocatalytic activity with 104 TON achieved in 4 h using 100-fold excesses of Et_3N and Et_3NH^+. For comparison, photolysis of the multicomponent system consisting of $[Ru(bpy)_3]Cl_2$ and one equivalent of $[Co(dmgBF_2)_2(OH_2)_2]$ in 100-fold excess of both Et_3N and Et_3NH^+ yields only 20 TON using UV-VIS light with only traces of hydrogen observed when a UV cutoff filter is used.

Photochemical hydrogen production occurs when acetone solutions of $[(Me_2phen)_2Ru(L\text{-}pyr)Co(dmgBF_2)_2(OH_2)]^{2+}$ (Me_2phen = 4,7-dimethylphenanthroline), in which bpy has been substituted by Me_2phen, or $[(ppy)_2Ir(L\text{-}pyr)Co(dmgBF_2)_2(OH_2)]^+$, in which an Ir-based LA is used, are irradiated at $\lambda >$ 380 nm in the presence of 300 equivalents of Et_3N and Et_3NH^+ with 9 and 90 TON in 4 h, respectively [63]. The Ir-based system demonstrates enhanced photocatalytic efficiency to the Ru-based system, with 210 turnovers in 15 h in the presence of 600 equivalents of ED and proton source. For comparison the multicomponent system $[Ir(ppy)_2(phen)]^+$ and $[Co(dmgBF_2)_2(OH_2)_2]$ under the same irradiation conditions yields similar initial rates, but the dyad shows greater stability as the hydrogen production rate levels off at 165 TON in 15 h. This implies that intramolecular electron transfer in the dyad may not be the rate limiting step in the hydrogen production scheme, but the reductive quenching of the excited photosensitizer by Et_3N may be important.

This study also uses a multicomponent system based on a $[Re(CO)_3Br(phen)]$ LA and $[Co(dmgBF_2)_2(OH_2)_2]$ CAT with 273 TON in 15 h using 600-fold excess of both Et_3N and Et_3NH^+ [63]. The use of the Re-based LA provides enhanced system functioning with Φ (½ H_2) = 0.16 relative to Φ (½ H_2) = 0.10 in the Ir-based multicomponent system (λ = 412 nm, irradiation for 2 h). This study demonstrates superior system functioning when Ir- or Re-based LAs are employed relative to the Ru-based LAs. The Ru-based dyads demonstrate superior photocatalytic efficiency to the multicomponent $[Ru(bpy)_3]^{2+}$/cobaloxime system. By contrast, the Ir-based dyad shows similar catalytic efficiency to the multicomponent $[Ir(ppy)_2(phen)]^+$/cobaloxime system, but the supramolecular dyad shows greater stability. It is predicted that intramolecular electron transfer affords a Co^I species which is protonated to yield a Co^{III}-H intermediate that can be further protonated to generate hydrogen. Electron transfer to the catalytic Co center can occur either directly from oxidative quenching of the photoexcited LA or from a reduced LA generated from the reductive quenching by an electron donor. A favorable driving force for oxidative quenching of the LA by the attached Co^{II} site is predicted, as the observed electrocatalytic potentials are more positive than the standard excited state reduction potential for $[Ru(bpy)_3]^{2+}$ [96]. Thus, the mechanism for photochemical hydrogen production by the supramolecular Ru-based systems is predicted to proceed through intramolecular electron transfer to the cobalt center from a photoexcited Ru LA. Faster reductive quenching of the excited Re- or Ir-based LA by Et_3N is attributed to the enhanced hydrogen production observed when the photosystem uses these LAs.

The complex $[(bpy)_2Ru(bpy\text{-}4\text{-}CH_3,4'\text{-}CONH\text{-}4\text{-}py)Co(dmgBF_2)_2(OH_2)]^{2+}$ in which the Ru LA and the cobaloxime CAT are connected by a conjugated bridge, and $[(bpy)_2Ru(bpy\text{-}4\text{-}CH_3,4'\text{-}CONH(CH_2)\text{-}4\text{-}py)Co(dmgBF_2)_2(OH_2)]^{2+}$, in which the two components are connected by an unconjugated bridge, have been used in solar hydrogen production schemes, Fig. 17 [64]. Intramolecular electron transfer is evidenced by the emission quenching of the ^{3}MLCT charge-transfer state by 35% and 25% relative to the parent LAs $[(bpy)_2Ru(bpy\text{-}4\text{-}CH_3,4'\text{-}CONH\text{-}4\text{-}py)]^{2+}$ and $[(bpy)_2Ru(bpy\text{-}4\text{-}CH_3,4'\text{-}CONHCH_2\text{-}4\text{-}py)]^{2+}$,

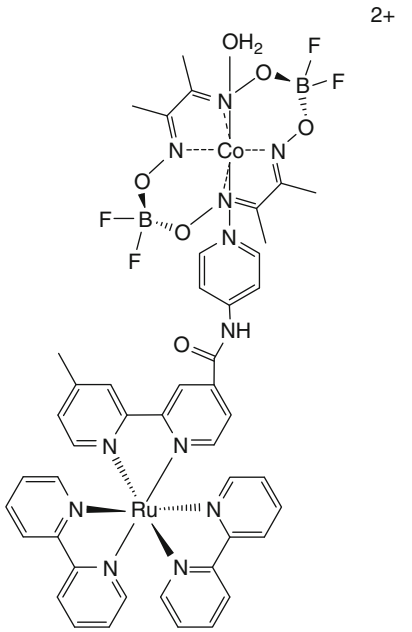

[(bpy)$_2$Ru(bpy-4-CH$_3$,4′-CONH-4-py)Co(dmgBF$_2$)$_2$(OH$_2$)]$^{2+}$

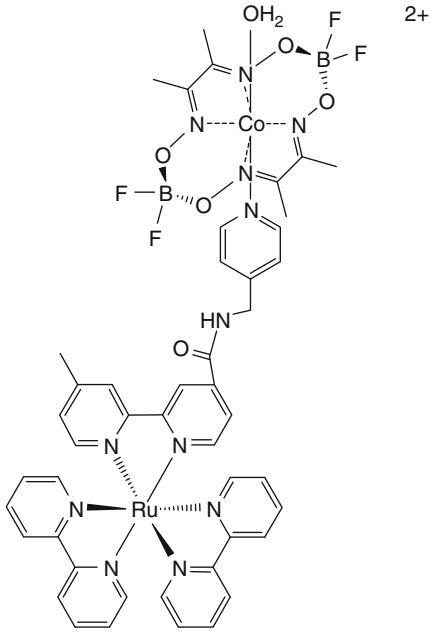

[(bpy$_2$)Ru(bpy-4-CH$_3$,4′-CONH(CH$_2$)-4-py)Co(dmgBF$_2$)$_2$(OH2)]$^{2+}$

Hydrogen via Direct Solar Production. Figure 17
Representations of [(bpy)$_2$Ru(bpy-4-CH$_3$,4′-CONH-4-py)Co(dmgBF$_2$)$_2$(OH$_2$)]$^{2+}$ and [(bpy)$_2$Ru(bpy-4-CH$_3$,4′-CONH(CH$_2$)-4-py)Co(dmgBF$_2$)$_2$(OH$_2$)]$^{2+}$

respectively. The lower emission intensity in the dyad containing the conjugated bridge is attributed to more efficient deactivation through radiative and non-radiative decay, due to the shorter distance between the LA and the cobaloxime. Photolysis of [(bpy)$_2$Ru(bpy-4-CH$_3$,4′-CONH-4-py)Co(dmgBF$_2$)$_2$(OH$_2$)]$^{2+}$ or [(bpy)$_2$Ru(bpy-4-CH$_3$,4′-CONH(CH$_2$)-4-py)Co(dmgBF$_2$)$_2$(OH$_2$)]$^{2+}$ at λ = 400 nm in the presence of 300-fold excess of both Et$_3$N and Et$_3$NH$^+$ in acetone results in hydrogen production with 38 and 48 TON in over 8 h for [(bpy)$_2$Ru(bpy-4-CH$_3$,4′-CONH-4-py)Co(dmgBF$_2$)$_2$(OH$_2$)]$^{2+}$ and [(bpy)$_2$Ru(bpy-4-CH$_3$,4′-CONH(CH$_2$)-4-py)Co(dmgBF$_2$)$_2$(OH$_2$)]$^{2+}$, respectively. Lower TONs are observed when DMF or acetonitrile are the solvent. The complex [(bpy)$_2$Ru(bpy-4-CH$_3$,4′-CONH-4-py)Co(dmgBF$_2$)$_2$(OH$_2$)]$^{2+}$ with a conjugated bridge shows similar photocatalytic efficiency to [(bpy)$_2$Ru(L-pyr)Co(dmgBF$_2$)$_2$(OH$_2$)]$^{2+}$. The unconjugated bridge may impede the possible deactivation routes promoting higher photocatalytic TON. In [(bpy)$_2$Ru(bpy-4-CH$_3$,4′-CONH-4-py)Co(dmgBF$_2$)$_2$(OH$_2$)]$^{2+}$ and [(bpy)$_2$Ru(bpy-4-CH$_3$,4′-CONH(CH$_2$)4-py)Co(dmgBF$_2$)$_2$(OH$_2$)]$^{2+}$, oxidative quenching of the excited Ru LA by the Co^{II} through intramolecular electron transfer has been suggested as the dominant quenching process based on the favorable driving forces and the fact that the excited states of the parent LAs are not quenched efficiently with Et$_3$N.

Other Multicomponent Co-Based Systems The pioneering work using Co-based CAT for solar hydrogen production was in the late 1970s utilizing [Ru(bpy)$_3$]$^{2+}$ LA and a Co(II) macrocycle system as the CAT. Optical excitation of a system containing [Ru(bpy)$_3$]$^{2+}$, [Co^{II}L] ([Co^{II}L] = Co^{II}(Me$_6$ [14]dieneN$_4$)(H$_2$O)$_2$)$^{2+}$, and Eu^{2+} at λ = 450 nm afforded hydrogen providing 10 TON with respect to [Ru(bpy)$_3$]$^{2+}$ and 1 TON with respect to [Co^{II}L], with a Φ = 0.05 [65]. Optical excitation of the LA leads to intermolecular electron transfer generating a Co^{I} species which reduces water to produce hydrogen. Early work using cobaloximes for photochemical hydrogen production entailed a photosystem

consisting of $[Ru(bpy)_3]^{2+}$, $[Co(dmgH)_2(OH_2)_2]$, and triethanolamine (TEOA) in DMF with 16 TON in 1 h relative to the CAT [97].

A series of heteroleptic Ir complexes of the molecular architecture $[Ir(C^\wedge N)_2(N^\wedge N)]^+$ (C^N = ppy or F-mppy and N^N = bpy, phen, Ph_2phen (4,7-diphenyl-1,10-phenanthroline)) have been investigated as LAs in photochemical hydrogen production from water using $[Co(bpy)_3]^{2+}$ as the CAT, Fig. 18 [66]. Irradiation of photosystems consisting of an Ir-based LA, $[Co(bpy)_3]^{2+}$ and TEOA in a CH_3CN/water mixture at λ = 465 nm affords hydrogen with 800–920 TON relative to the LA and 16–18 TON relative to the CAT with the system consisting of $[Ir(F\text{-}mppy)_2(bpy)]^+$ LA providing the highest TON. The fluorinated compounds typically show slightly higher activity. It is proposed that intramolecular electron transfer from the excited LA to the CAT affords a reduced Co species that promotes proton reduction to make hydrogen. The Ir-based systems are about 20 times more efficient than $[Ru(bpy)_3]^{2+}$ and 3–6 times more efficient than $[Ru(Me_2phen)_3]^{2+}$. The multicomponent Ru-based photosystem consisting of $[Ru(bpy)_3]^{2+}$ or $[Ru(Me_2phen)_3]^{2+}$ (Me_2phen = 4,7-dimethyl-1,10-phenanthroline) provides lower TON (100 TON relative to $[Ru(bpy)_3]^{2+}$ and 2 TON relative to the CAT or 290 TON relative to $[Ru(Me_2phen)_3]^{2+}$ and 12 TON relative to the CAT). The excited states of the Ir-based systems are quenched efficiently by both $[Co(bpy)_3]^{2+}$ and TEOA whereas the excited states of the Ru LAs are only quenched by $[Co(bpy)_3]^{2+}$. The rate of quenching of the excited state of the Ir-system by $[Co(bpy)_3]^{2+}$ is about an order of a magnitude faster than TEOA quenching rate and also faster than for the Ru-based systems. The rates of quenching of the Ir-based excited states by $[Co(bpy)_3]^{2+}$ range from 4.8 to 6.9 $\times$ 10^8 M^{-1} s^{-1}. System modification of the LA has provided $[Ir(dF(CF_3)ppy)_2(dtbbpy)](PF_6)$ ($dF(CF_3)ppy$) = 2-(2,4-difluorophenyl)-5-trifluoromethylpyridine and dtbbpy = 4,4′-di-tert-butyl-2,2′-dipyridyl) with enhanced excited state lifetime and significant reducing power that shows dramatically improved system function with a relative Φ that is ca. 14 times larger than $[Ru(Me_2phen)_3]^{2+}$ [98].

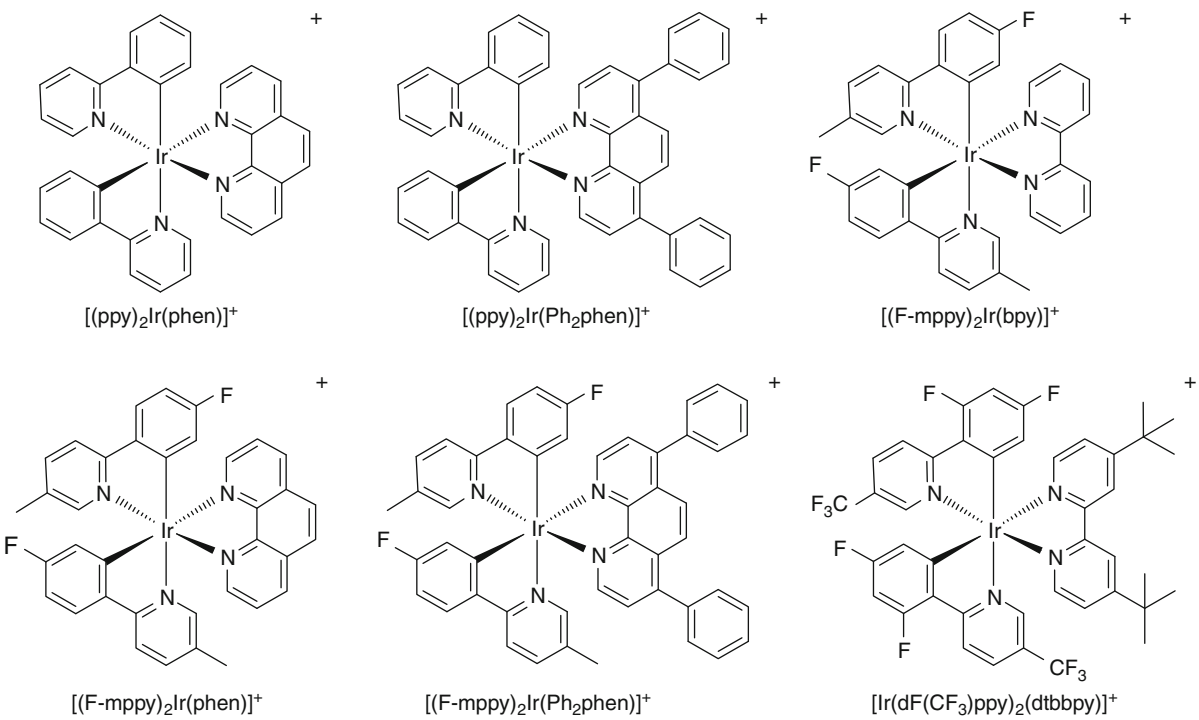

Hydrogen via Direct Solar Production. Figure 18
Ir-based LAs used in photosystems incorporating $[Co(bpy)_3]^{2+}$ CAT for photochemical hydrogen production from water

A series of cobaloxime complexes, [Co(dmgH)$_2$pyCl], [Co(dmgH)$_2$(4-COOMe-py)Cl], [Co(dmgH)$_2$(4-Me$_2$N-py)Cl], [Co(dmgH)(dmgH$_2$)Cl$_2$], [Co(dmgH)$_2$(py)$_2$]$^+$, [Co(dmgH)$_2$(P(n-Bu)$_3$)Cl], and [Co(dmgBF$_2$)$_2$(OH$_2$)$_2$], (dmgH$_2$ = dimethylglyoxime) have been investigated as molecular catalysts photochemical hydrogen generation from water in systems containing a Pt terpyridyl acetylide chromophore and TEOA in acetonitrile, Fig. 19 [67, 99]. Characterization of the cobaloximes, hydrogen photocatalysis, and the investigation of the impact of photosystem functioning with respect to LA, CAT, TEOA, solvent, and CH$_3$CN/water ratio are reported. The cobaloximes oxidatively quench the emission of the excited state LA efficiently, close to the diffusion controlled limit, with the fastest quenching of 1.7×10^9 M^{-1} s^{-1} by [Co(dmgH)$_2$(4-COOMe-py)Cl].

The rate of oxidative quenching by [Co(dmgH)$_2$(py)$_2$]$^+$ is 4.0×10^7 M^{-1}s^{-1}; this lower rate is attributed to the lack of a Cl ligand in this complex that can interact with the Pt LA during the quenching process. It was found that a photosystem consisting of [Pt(ttpy)(C≡CPh)]ClO$_4$ (ttpy = 4′-p-tolyterpyridine), [Co(dmgH)$_2$pyCl], TEOA, and water in CH$_3$CN gives 2,100 TON in 10 h, irradiated at $\lambda > 410$ nm, when the optimized [TEOA] and CH$_3$CN/H$_2$O ratio are used. No hydrogen is observed after 5 h of photolysis in systems consisting of [Pt(ttpy)(C≡CPh)]ClO$_4$, [Co(dmgH)$_2$(P(n-Bu)$_3$)Cl] or [Co(dmgBF$_2$)$_2$(OH$_2$)$_2$], and TEOA. In the system consisting of [Co(dmgH)$_2$(P(n-Bu)$_3$)Cl], it is likely that the stable hydride formed, [CoH(dmgH)$_2$(P(n-Bu)$_3$)] known to yield hydrogen only upon thermolysis at 150°C, prevents hydrogen photocatalysis. The complex [Co(dmgBF$_2$)$_2$(OH$_2$)$_2$] is thermodynamically incapable of proton reduction as evidenced by the Co$^{II/I}$ reduction potential of −0.29 V vs. NHE which is more positive of proton reduction (−0.48 V) at the pH used for photocatalysis (pH = 8.5). Induction periods of 1–2 h are observed for the hydrogen-generating systems. This induction period is impacted by the solvent conditions, LA, and TEOA concentration. The induction period is consistent with the requirement for the formation of Co^{I} for photogeneration of hydrogen to occur. The photochemical cycle can proceed through the oxidative quenching of the photoexcited LA by Co^{III} to form LA$^+$ and Co^{II}, or through reductive quenching by TEOA to form LA$^-$ and TEOA$^+$, Fig. 19. Electron transfer from the LA$^-$ to Co^{III} occurs regenerating the LA. The catalytic cycle proceeds with further reduction of Co^{II} to Co^{I} followed by protonation to give a Co^{III}-H intermediate. One pathway is the protonation of Co^{III}-H to yield hydrogen and Co^{III}. An alternative pathway is utilizing a single Co pathway, which entails reduction of the Co^{III}-H to Co^{II}-H which subsequently gets protonated to generate hydrogen and Co^{II}. This single Co mechanism is supported by the observed linear dependence of the Co concentration on photochemical hydrogen production in a system consisting [Pt(ttpy)(C≡CPh)]ClO$_4$ (ttpy = 4′-p-tolyterpyridine), [Co(dmgH)$_2$pyCl], TEOA, and water in CH$_3$CN irradiating at $\lambda > 410$ nm. An alternative kinetically distinguishable proposal is the homolytic reaction mechanism involving two Co^{III}-H to give hydrogen and Co^{II}. Kinetics of electron transfer reactions of hydrogen evolving cobaloximes have been reported recently [100]. Studies demonstrate that the homolytic pathway (Co^{III}H + CoI^{II}H → 2 Co^{II} + H$_2$) is favored over a pathway involving protonation of Co^{III}-H to yield hydrogen and Co^{III}.

A photocatalytic system using the organic dye, Eosin Y as the LA, [Co(dmgH)$_2$pyCl]$^{2+}$, and TEOA produces hydrogen with an initial rate of 100 TON/h upon irradiation at $\lambda > 450$ nm [68]. Addition of free dmgH$_2$ provides increased stability to the photosystem providing 900 TON relative to the LA (*ca.* 20 mL of hydrogen) in 14 h. A maximum $\Phi = 0.04$ is observed when a bandpass filter at 520 nm is employed, but with a lower TON relative to $\lambda > 450$ nm. The rate of hydrogen evolution shows marked pH dependence with maximum at pH = 7 and decreases sharply at more acidic or basic pH.

Photochemical hydrogen production occurs in a photosystem consisting of [ReBr(CO)$_3$bpy)], [Co(dmgH)$_2$], acetic acid/water, TEOA in DMF at $\lambda > 400$ nm [69]. Turnover numbers are approximately twice compared to when [Ru(bpy)$_3$]$^{2+}$ is the LA under the same conditions (150 TON in 9 h for [ReBr(CO)$_3$bpy)] relative to 65 TON when [Ru(bpy)$_3$]$^{2+}$ is the LA). The quantum yield for hydrogen production is 0.26. The rate of hydrogen production shows a square dependence on the total Co concentration. This square dependence implies a homolytic pathway for hydrogen photocatalysis. The rate of hydrogen production

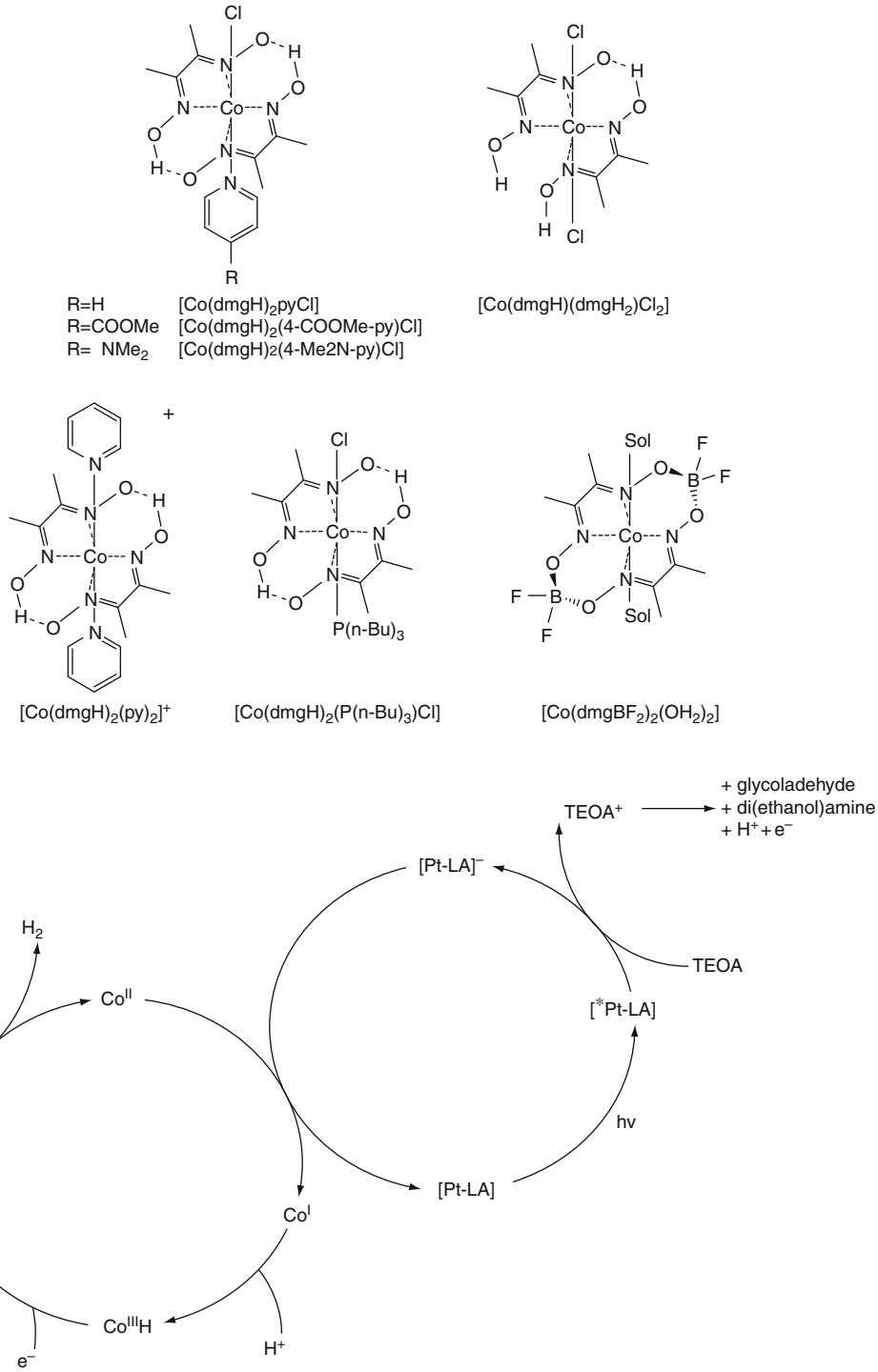

Hydrogen via Direct Solar Production. Figure 19
Representative cobaloximes used for solar hydrogen photocatalysis and the proposed photocycle for hydrogen production by reductive quenching of the LA

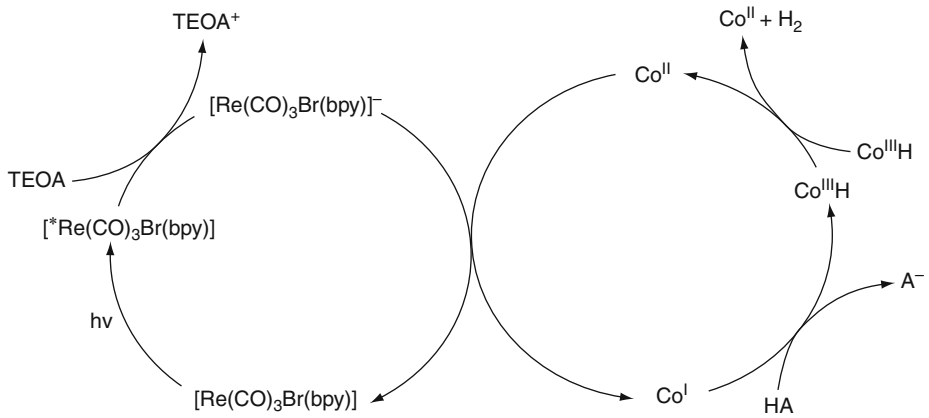

Hydrogen via Direct Solar Production. Figure 20
General representation of a homolytic pathway using a Co-based hydrogen producing photosystem

exhibited a linear dependence on the photon flux. Forward electron transfer between the LA and the CAT occurs at a rate close to diffusion control, with a rate of 2.5×10^8 M^{-1} s^{-1}. An excess of dimethylglyoxime is systematically added to the system to ensure the complete formation of the CAT and reduce the portion of free $[Co]_{solv}{}^{2+}$, which is also an efficient quencher of the excited state of the LA, Fig. 20.

Pt and Pd-Based Homogeneous Systems for Solar Hydrogen Production

Pt- and Pd-based systems have been used in solar hydrogen production schemes. Supramolecular systems that couple polyazine LAs with bridged Pt or Pd CATs for proton reduction are known [70, 73, 74, 101, 102]. The use of the supramolecular design allows for increased electron transfer rates and component modification to enhance device function and light-absorbing properties. The bridged systems use rigid or flexible spacers between the LA and the CAT which controls the level of electronic communication between components. The formation of metallic colloids during photoreduction of the supramolecular assembly has been reported in some studies using similar supramolecular assemblies, implying that heterogeneous catalysis is dominant with the colloidal metal being the active catalytic species [103, 104]. Photoinduced decomposition of $[(bpy)_2Ru(Mebpy(CH_2)_2C_6H_2(OCH_3)_2(CH_2)_2Mebpy)PdCl_2]^{2+}$, Fig. 21, was observed by ESI-MS and the formation of Pd colloid observed by TEM and XPS of evaporated reaction mixtures during photochemical hydrogen production [103]. Mercury tests are employed to deactivate photoproduced metal colloids via formation of inactive alloys with colloidal metals eliminating the impact of the colloid on photochemical activity [86, 87].

These tests can provide meaningful information regarding the mechanism of action for solar hydrogen production, but care must be taken in drawing conclusions as this is a complicated issue. Concentration of the medium to study solids through TEM and XPS can also lead to system decomplexation resulting in formation of metallic solids. Reduced polyazine complexes including those produced electrochemically are known to adsorb to electrodes or metal surfaces such as Hg(l) and this could deactivate a catalytic system. The study of complicated multistep photocatalytic processes is complex, and detailed analyses with carefully selected comparison to determine the catalytically active species are necessary.

A RuPt bimetallic system $[(bpy)_2Ru(phenNHCO(COOHbpy))PtCl_2]^{2+}$, which employs an amide linkage on the phenanthroline as a bridge, produces hydrogen from water when illuminated at $\lambda > 350$ nm in aqueous acetate buffer solutions in the presence of EDTA, with a $\Phi = 0.01$ and 5 turnovers in 10 h [70]. This complex displays an emission from the ^{3}MLCT state at $\lambda_{max}{}^{em} = 610$ nm in an aqueous solution with its intensity quenched by 67% relative to the parent $[(bpy)_2Ru(phenNHCO(COOHbpy))]^{2+}$

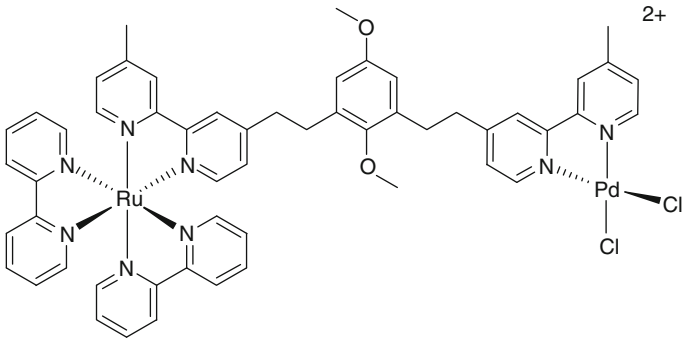

Hydrogen via Direct Solar Production. Figure 21
Representation of $[(bpy)_2Ru(Mebpy(CH_2)_2C_6H_2(OCH_3)_2(CH_2)_2Mebpy)PdCl_2]^{2+}$ (bpy = 2,2′-bipyridine)

suggestive of intramolecular electron transfer process occurring in the bimetallic system. To ascertain that there is no interference from any photodecomposition products, comparisons are made with analogous multicomponent photosystems. The system consisting of $[Ru(bpy)_3](NO_3)_2$, N,N′-dimethyl-4,4′-bipyridinium, and $[PtCl_2(dcbpy)]$ (dcbpy = 4,4′-dicarboxy-2,2′-bipyridine) is effective providing a $\Phi = 0.02$, but completely retarded in the absence of N,N′-dimethyl-4,4′-bipyridinium. Hydrogen production does not occur when $[Ru(bpy)_2(5\text{-amino-phen})]^{2+}$ and $[PtCl_2(dcbpy)]$ or the parent LA, $[(bpy)_2Ru(phenNHCO(COOHbpy))]^{2+}$, and K_2PtCl_4 is the photosystem. The lack of activity by these multicomponent systems suggests the bridge between Ru and Pt is essential for photoreactivity in this system. Hydrogen production shows a linear response to photon flux implying that one-photon excitation of a molecule operates. Rate of hydrogen production shows a linear dependence on supramolecular complex concentration. Lower photocatalytic activity is observed when the COOH on bpy is replaced by a COOEt group demonstrating that a clear relationship exists between the energy of the LUMO and the hydrogen evolving activity which was greatest when the more electron withdrawing COOH is the substituent [105].

The hydrogen evolution rate by $[(bpy)_2Ru(phenNHCO(COOHbpy))PtCl_2]^{2+}$ is shown to obey Michaelis-Menten enzymatic kinetics with regard to the concentration of EDTA, suggesting that an ion-pair formation between $[(bpy)_2Ru(phenNHCO(COOHbpy))PtCl_2]^{2+}$ and $EDTA^{2-}$ is an important step in the photocycle [106]. Bimetallic RuPt systems that incorporate aliphatic linkages to bridge $[(bpy)_2Ru(bpy(CONH(CH_2)_3NH_2)_2)PtCl_2]^{2+}$ and $[(bpy)_2Ru(bpy(CONH(CH_2)py)_2)PtCl_2]^{2+}$, Fig. 22, do not display photocatalytic activity. This implies that aromaticity of the bridge connecting the LA and the CAT is important for intramolecular electron transfer in $[(bpy)_2Ru(phenNHCO(COOHbpy))PtCl_2]^{2+}$. Recently a tetrametallic system that shows higher catalytic activity to the original bimetallic system has been reported, $[(bpy)_2Ru(phenNHCO(CONH(CH_2)bpy))PtCl_2]_2^{4+}$ [106]. This system shows enhanced catalytic activity with a $\Phi = 0.014$.

The tetrametallic $[\{(phen)_2Ru(dpp)\}_2Ru(dpq)PtCl_2]^{6+}$ and $[\{(bpy)_2Ru(dpp)\}_2Ru(dpq)PtCl_2]^{6+}$ systems have been investigated as photoinitiated electron collectors (dpq = 2,3-bis(2-pyridyl)quinoxaline), which photocatalyze the production of hydrogen from water with $\Phi = 0.01$ [71, 72]. These systems couple two terminal $(TL)_2Ru^{II}(dpp)$ LA units to a central ruthenium which is connected to a reactive platinum component through a dpq bridge, Fig. 23. $[\{(phen)_2Ru(dpp)\}_2Ru(dpq)PtCl_2]^{6+}$ displays a Ru $(d\pi) \rightarrow dpp(\pi^*)$ CT absorption observed at 541 nm and an emission from the ^{3}MLCT state (λ_{max}^{em} = 752 nm and $\Phi^{em} = 3.0 \times 10^{-4}$) with reduced intensity relative to $[\{(phen)_2Ru(dpp)\}_2Ru(dpq)]^{6+}$ (λ_{max}^{em} = 752 nm and $\Phi^{em} = 12.3 \times 10^{-4}$) in acetonitrile [71]. The τ of $[\{(phen)_2Ru(dpp)\}_2Ru(dpq)PtCl_2]^{6+}$ is 120 ns, also reduced relative to the $[\{(phen)_2Ru(dpp)\}_2Ru(dpq)PtCl_2]^{6+}$, 170 ns. The reductions in the Φ^{em} and τ are characteristic of intramolecular electron transfer in $[\{(phen)_2Ru(dpp)\}_2Ru(dpq)PtCl_2]^{6+}$

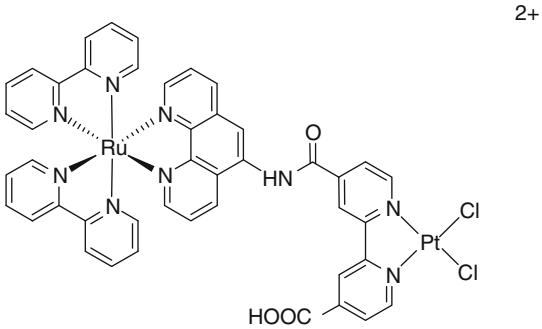

$[(bpy)_2Ru(phenNHCO(COOHbpy))PtCl_2]^{2+}$

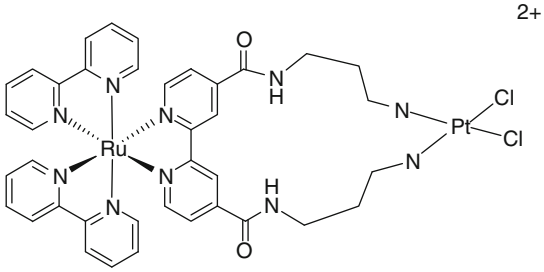

$[(bpy)_2Ru(bpy(CONH(CH_2)_3NH_2)_2)PtCl_2]^{2+}$

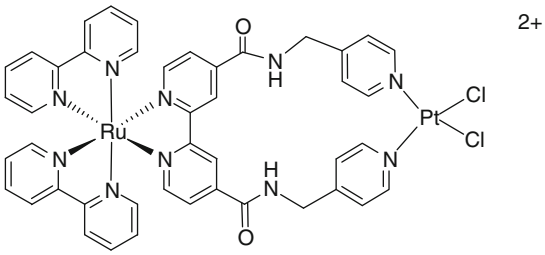

$[(bpy)_2Ru(bpy(CONH(CH_2)py)_2)PtCl2]^{2+}$

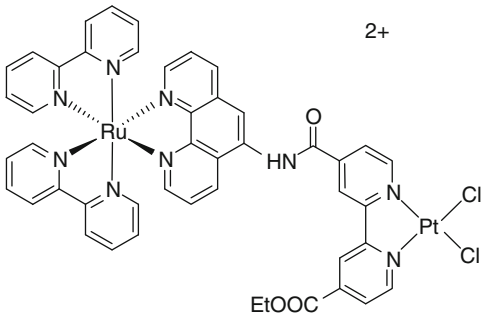

$[(bpy)_2Ru(phenNHCO(COOEtbpy))PtCl_2]^{2+}$

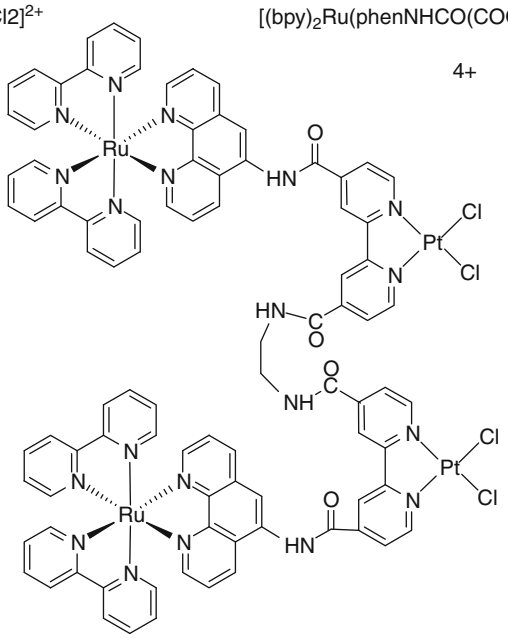

$[(bpy)_2Ru(phenNHCO(CONH(CH_2)bpy))PtCl_2]_2^{4+}$

Hydrogen via Direct Solar Production. Figure 22
RuPt supramolecular systems for solar energy conversion

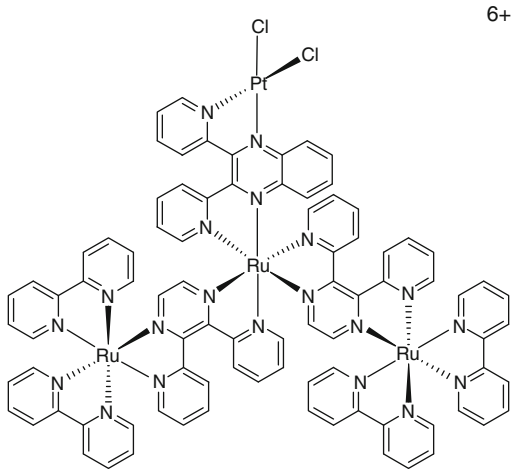

$[\{(bpy)_2Ru(dpp)\}_2Ru(dpq)PtCl_2]^{6+}$

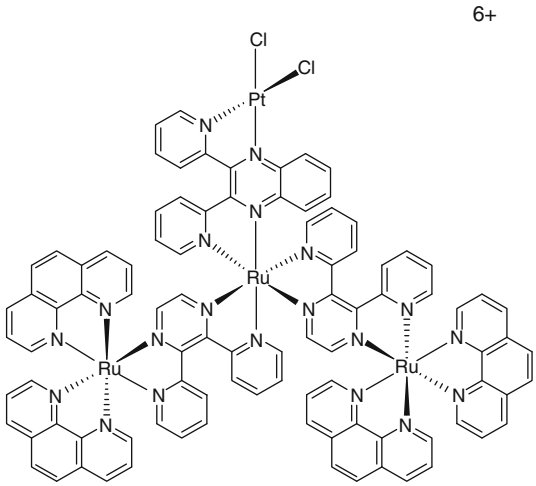

$[\{(phen)_2Ru(dpp)\}_2Ru(dpq)PtCl_2]^{6+}$

Hydrogen via Direct Solar Production. Figure 23
Representations of $[\{(bpy)_2Ru(dpp)\}_2Ru(dpq)PtCl_2]^{6+}$ and $[\{(phen)_2Ru(dpp)\}_2Ru(dpq)PtCl_2]^{6+}$

populating a lowest energy CS state with k_{et} = 2.5×10^6 s^{-1}. The τ = 1.7 μs at 77 K in a solid glass matrix in both tetrametallic and trimetallic systems. The emission of $[\{(phen)_2Ru(dpp)\}_2Ru(dpq)PtCl_2]^{6+}$ is quenched efficiently by DMA with k_q of 4.8×10^9 M^{-1} s^{-1}. The properties of $[\{(bpy)_2Ru(dpp)\}_2Ru(dpq)PtCl_2]^{6+}$ with bpy substituted TL are similar. $[\{(bpy)_2Ru(dpp)\}_2Ru(dpq)PtCl_2]^{6+}$ displays Ru(dπ) → dpp(π*) CT absorption at 540 nm and an emission from the ^{3}MLCT state ($\lambda_{max}{}^{em}$ = 745 nm and Φ^{em} = 2.5×10^{-4}) with reduced intensity relative to $[\{(bpy)_2Ru(dpp)\}_2Ru(dpq)]^{6+}$ ($\lambda_{max}{}^{em}$ = 745 nm and Φ^{em} = 6.0×10^{-4}) in acetonitrile [72]. The τ of $[\{(bpy)_2Ru(dpp)\}_2Ru(dpq)PtCl_2]^{6+}$ is 92 ns, also reduced relative to the $[\{(bpy)_2Ru(dpp)\}_2Ru(dpq)]^{6+}$, 133 ns. The reductions in the Φ^{em} and τ are characteristic of intramolecular electron transfer in $[\{(bpy)_2Ru(dpp)\}_2Ru(dpq)PtCl_2]^{6+}$ populating a lowest energy CS state with k_{et} = 3.4×10^6 s^{-1}. Intramolecular electron transfer is hindered at 77 K in a solid glass matrix with τ = 1.7 μs in both tetrametallic and trimetallic systems. The emission of $[\{(bpy)_2Ru(dpp)\}_2Ru(dpq)PtCl_2]^{6+}$ is quenched efficiently by DMA with k_q of 5.4×10^9 M^{-1} s^{-1}.

A unique feature in these tetrametallic systems is that a greater degree of reduction of the Φ^{em} in the tetrametallic vs. the trimetallic is observed relative to the reduction of the τ of the tetrametallic vs. trimetallic. For $[Ru(bpy)_3]^{2+}$ and similar systems, the $\Phi_{^3MLCT} = 1$. The differences in the degrees of quenching of Φ^{em} and τ of the tetrametallic vs. model trimetallic systems imply that $\Phi_{^3MLCT} \neq 1$, which suggests a reduction in population of the emitting ^{3}MLCT excited state due to an alternative intramolecular electron transfer pathway (k_{et}') in which the higher-lying central Ru(dπ) → dpq(π*) CT state directly populates the ^{3}CS, Fig. 24.

Both $[\{(bpy)_2Ru(dpp)\}_2Ru(dpq)PtCl_2]^{6+}$ and $[\{(phen)_2Ru(dpp)\}_2Ru(dpq)PtCl_2]^{6+}$ are photoinitiated electron collectors with electrons being collected on the molecular orbitals of the central Ru and the surrounding BLs. Spectroscopic changes that occur when the systems are photochemically reduced in the presence of DMA or electrochemically reduced by two electrons are almost identical, implying that the photoproduct and electrochemically reduced product are the same. For $[\{(bpy)_2Ru(dpp)\}_2Ru(dpq)PtCl_2]^{6+}$, photochemical hydrogen production occurs in the presence of DMA and water when photoexcited at λ = 530 nm with Φ = 0.01 representing 40 turnovers in 3 h. The amount of hydrogen produced by $[\{(bpy)_2Ru(dpp)\}_2Ru(dpq)PtCl_2]^{6+}$ is much higher than that

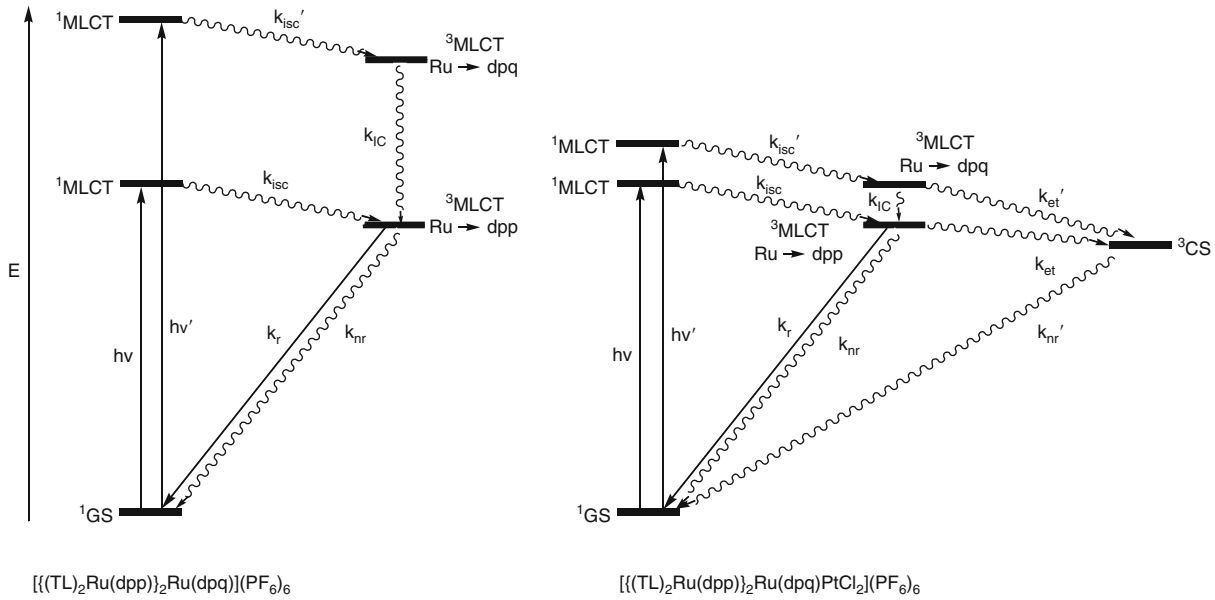

Hydrogen via Direct Solar Production. Figure 24
State diagram showing excited state photophysical properties of $[\{(TL)_2Ru(dpp)\}_2Ru(dpq)PtCl_2]^{6+}$ and $[\{(TL)_2Ru(dpp)\}_2Ru(dpq)PtCl_2]^{6+}$ (TL = bpy or phen)

produced by $[\{(bpy)_2Ru(dpp)\}_2Ru(dpq)]^{6+}$ and Pt colloid. For $[\{(phen)_2Ru(dpp)\}_2Ru(dpq)PtCl_2]^{6+}$, photochemical hydrogen production occurs in the presence of DMA when photoexcited at λ = 470 nm with 115 TON in 5 h. Addition of excess Hg does not impede catalytic activity, which implies that the supramolecular architecture remains intact during the photocycle and colloidal Pt is not operative.

Bifunctional Pt-Based System The complex [PtCl(tpy)]Cl is a single molecule that acts in a bifunctional manner promoting both photosensitization and catalysis [73]. Photolysis of [PtCl(tpy)]Cl in aqueous buffer at λ = 350–550 nm in the presence of EDTA affords 3 TON in 7 h with a Φ = 0.02. 2-Morpholinoethanesulfonic acid is the buffer used to avoid coordination of buffer reagents to the Pt^{II} by replacing Cl, shown to lower hydrogen yield. Contribution from catalytically active Pt colloids seems not operative as the system functions with added Hg(l). It is suggested that photochemical hydrogen production proceeds through a bimolecular mechanism. Photosensitization is suggested to occur through a ^{3}MMLCT state (MMLCT = metal-metal-to-ligand charge-transfer) in dimer formation facilitated by Pt⋯Pt association. The saturation kinetics with regard to the EDTA concentration suggests that the dimer of $[PtCl(tpy)]^+$ and the dianionic form of EDTA form an ion-pair adduct to facilitate reductive quenching by EDTA during the photochemical processes.

Palladium-Based Supramolecular Solar Hydrogen Photocatalysts

The RuPd bimetallic system $[(^tBu_2bpy)_2Ru(tpphz)PdCl_2]^{2+}$ (^{t}Bu = tertiary butyl, tpphz = tetrapyridophenazine, Fig. 25) is a solar hydrogen photocatalyst producing hydrogen, with 56 TON in 30 h, in the presence of the electron donor, Et_3N, in acetonitrile when optically excited at λ = 470 nm [74]. The proton source is Et_3N. A weak emission at λ_{max}^{em} = 650 nm with τ = 27 ns is observed significantly quenched relative to the parent $[(^tBu_2bpy)_2Ru(tpphz)]^{2+}$ (λ_{max}^{em} = 638 nm, τ = 154 ns). It is suggested that the Ru^{II}-phenazine$^-$-Pd^{II} radical photogenerated in the presence of Et_3N is involved in the photochemical hydrogen generation step, initiating chloride loss from palladium. Photoinduced electron transfer

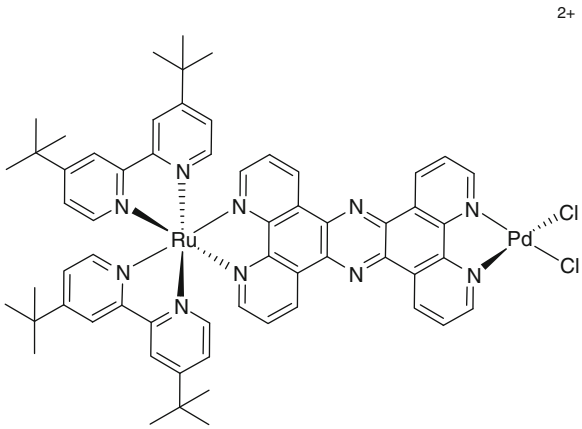

Hydrogen via Direct Solar Production. Figure 25 Representation of $[(^{t}Bu_2bpy)_2Ru(tpphz)PdCl_2]^{2+}$

processes to reduce the Pd site have been studied by resonance Raman and ultrafast time-resolved spectroscopy showing rapid Pd reduction [107].

Conclusions and Future Directions

The conversion of solar energy to a transportable fuel is challenging but important in meeting increasing energy demands. The production of hydrogen fuel via solar water splitting is an attractive approach to alternative energy conversion and storage as the amount of energy reaching the Earth's surface from the sun in 1 h is sufficient to power our planet for more than a year. Photocatalysis to reduce water to produce hydrogen is complicated involving multielectron transfer, bond breaking, and bond formation. Despite these challenges and the lack of consistent substantial long-term funding, a number of photosystems for solar hydrogen production have been developed recently. Pioneering work on multicomponent systems was critical to success. Water splitting to produce hydrogen is complicated and involves energetically demanding chemical reactions with bond breaking and formation and is a multielectron process. Solar energy conversion is promoted via water reduction by multistep processes with multiple photons used sequentially.

Work has focused on the LA and/or CAT design for solar hydrogen production schemes. Structural diversity is starting to be available. Many systems incorporate Ru-based LAs and reactive metal centers in the photocatalytic schemes. Ir, Pt, Re, and Zn-based systems have emerged recently showing promise as LAs. Biomimetic iron-based systems, Rh, Co, Pt, and Pd-based CATs have been typically used is these schemes. The Rh- and Co-based systems take advantage of ability of Rh or Co to cycle through three oxidation states reducing from M^{III} to M^{II} and M^{I} for multielectron chemistry. The application of typical Ru (II) trischelate systems with ligands such as bpy or phen provide for absorption in the visible region to *ca.* 450 nm. The light absorption energy can be modulated by ligand substitution and the use of ligands with stabilized π^* orbitals provide for longer wavelength excitation often to *ca.* 550–650 nm.

Using bridging ligands provides a means to covalently attach the LA to the CAT allowing more efficient intramolecular electron transfer pathways from the LA to the catalytic site. In addition, factors that impact intramolecular electron transfer can be studied and modulated within molecular systems. Coupling of a LA to CAT often dramatically perturbs the properties of these components. The ability to modulate the electrochemical and photochemical properties by component modification in supramolecular systems can be exploited in molecular design. The application of large molecular systems to address hydrogen photocatalysis allows system study using conventional molecular characterization methods allowing for the ability to probe the processes involved in the photocatalytic process.

Many factors are considered during photosystem design for hydrogen photocatalysis. The redox potentials of the LA, CAT, and coordinated ligands dictate the driving force of electron transfer reactions. LA properties including absorptivity and excited state lifetimes are contributing factors which determine wavelength response and overall photosystem efficiency. System parameters including, solvent, electron donor, pH, wavelength of excitation, etc., also determine functioning system efficiency and stability. Often solvent choice can have dramatic impact with systems showing good photoreactivity in organic solvents that are not functional in aqueous media. Catalysts and electron donors selected should not compete for light with the LA. Study and comparison of system parameters that impact hydrogen photocatalysis is crucial as many conditions impact photocatalysis and no set of standard conditions exist. For example, some solvents that show

enhanced system function for photocatalytic systems have been shown to deactivate other systems. Comparison of systems is complicated by these widely varied conditions.

The study of electron transfer between components is key to understanding photosystem properties. The electron transfer events occurring in supramolecular systems are studied with comparison using model systems that should have similar spectroscopic and photophysical properties, but is always not the case. Careful selection of model systems is essential to these studies as the assumption that k_r and k_{nr} are the same in the model systems and supramolecular systems is inherent to this analysis. Sample purity is also important in these studies as the rate of electron transfer could be underestimated in the presence of other emissive impurities or overestimated in the presence of impurities which quench the emissive excited state. The study of these electron transfer events become more complicated as model systems to probe excited state processes are not readily available.

Design and development of functioning photocatalysts for the reduction of water to produce hydrogen fuel has become an international effort as the world recognizes the significance for the need for environmentally friendly, renewable, economically viable alternatives for fuel production. There has been much success in this field given the complexity of the systems and processes.

The iron-based systems exploit the ability of iron-based hydrogenases to catalyze water reduction to produce hydrogen. Interesting biomimetic assemblies have been produced that couple ruthenium to diiron catalytic centers but these complexes have not shown applicability to solar hydrogen photocatalysis. The unfavorable thermodynamic driving force for electron transfer from the ruthenium to the CAT impedes the use of the supramolecules diiron systems as photocatalysts for solar hydrogen production. The coupling of alternative ZnTPP LA units to these diiron cores provides for thermodynamically favorable electron transfer and has provided for photocatalytic systems with low TON. The ZnTPP LA unit possesses a higher energy singlet excited state that allows electron transfer to the diiron unit. These supramolecular assemblies reduce acidic solutions of 2-mercaptobenzoic acid to produce hydrogen following optical excitation with low turnovers. The multicomponent systems using diiron catalytic centers and Ru-based LA have shown promise providing higher TON using high CAT loading. In these systems, the stability of the CAT determines system stability with system malfunction occurring often after few hours due to CAT decomposition. Use of Ir-based LAs have shown better promise with higher TON relative to the LA and CAT, but system deactivation occurs due to decomplexation of the CAT.

Rhodium-centered photoinitiated electron collectors are known to catalyze water reduction to hydrogen. $[\{(bpy)_2Ru(dpp)\}_2RhCl_2]^{5+}$, $[\{(bpy)_2Ru(dpp)\}_2RhBr_2]^{5+}$, and $[\{(phen)_2Ru(dpp)\}_2RhCl_2]^{5+}$ are the lead photocatalysts in this area, demonstrating higher hydrogen yields and turnover capacities. The use of a bridging dpp on the Ru LA provides significant coverage of the solar spectrum to the low energy visible. The Ru LA displays an emissive ^{3}MLCT excited state. The spectroscopic and photophysical properties display population of the emissive ^{3}MLCT excited state followed by intramolecular electron transfer to populate the ^{3}MMCT excited state. Optical excitation in the presence of an electron donor leads to at least two intramolecular electron transfer steps affording a coordinatively unsaturated Rh^I species which can interact with and reduce a substrate such as water. These systems couple two charge-transfer light absorbers to a single electron collector. Studies on the design considerations for a functioning system for optical multielectron reduction of water to produce hydrogen have shown that this general structural motif is applicable in solar hydrogen production schemes. A related photoinitiated electron collector, $[\{(bpy)_2Ru(dpb)\}_2IrCl_2]^{5+}$, does not demonstrate photocatalytic activity implying that the Rh center is necessary and facilitates the chemical steps involved in bond transformations. The coordination environment on the rhodium center impacts the photocatalytic activity as evidenced by the greater hydrogen yields when weaker σ-donors are present on rhodium (Br vs. Cl), further implying that the reactive rhodium center and/or the ^{3}MMCT excited state may be important. $[\{(bpy)_2Ru(dpp)\}_2RhBr_2]^{5+}$ provides a system with a lower lying $Rh(d\sigma^*)$ acceptor orbital with a larger driving force for intramolecular electron transfer to produce the ^{3}MMCT state and/or promotes

halide loss to generate the Rh^I system. Systematic studies on factors impacting hydrogen production, including the driving force for reductive quenching of the excited states by the electron donor, excited state lifetime of the photocatalyst, effective pH of the solution, and electron donor-catalyst interactions, has been studied. Photocatalytic activity of $[\{(tpy)RuCl(dpp)\}_2RhCl_2]^{3+}$ and $[\{(bpy)_2Os(dpp)\}_2RhCl_2]^{5+}$ is observed with lower efficiency, consistent with the lower driving force for reductive quenching of the ^{3}MLCT excited state by DMA. The result is important, showing hydrogen can be evolved employing the ^{3}MLCT excited state as electron transfer quenching of the ^{3}MMCT state is not thermodynamically favorable in these systems. The system pH and the electron donor-catalyst interactions are important factors to be considered as varied photocatalytic activity is observed with variation of electron donors.

Multicomponent systems incorporating cyclometalated Ir complexes have been used as LAs in photochemical schemes for production of hydrogen from water using $[Rh(NN)_3]^{3+}$ CATs. A preliminary study of a library of LA and CAT has enabled the identification of the most efficient system providing high TON and good system stability. Ir LAs provide varied excited state lifetimes and redox potentials relative to the classical Ru LAs.

The use of cobalt CATs have been investigated in solar hydrogen production schemes. The often substitutionally labile cobalt centers are stabilized by the use of cobaloximes often with excess ligand in solution. The supramolecular systems incorporating Ir-based LAs show superior activity to the Ru-based system and enhanced stability relative to the analogous multicomponent system. The use of a Re-based LA with cobaloxime CAT has provided good functioning. Use of Pt- or Ir-based LAs with cobaloxime CATs has shown to be the most promising, providing high TON and good system stability.

Recent studies have focused on the coupling of Pd and Pt reactive metal centers to Ru charge-transfer light absorbers for multielectron solar hydrogen photocatalysis. There have been conflicting reports on these systems with follow-up studies showing that in some RuPt and RuPd systems the reduction of the complex may lead to colloidal Pd or Pt. It was proposed that Pt(s) or Pd(s) are the active catalyst for hydrogen generation. Some systems are proposed to function without colloidal metal formation. Careful analysis of these catalytic systems is needed to provide insight into the function of these photocatalysts and the optimization of the future generation of catalysts.

The area of solar hydrogen production through the use of photocatalysts that collect and deliver reducing equivalents is an active area of current research in inorganic photochemistry. The design and development of systems that catalyze this complicated process can play a significant role in the development of efficient photocatalysts for solar hydrogen production. The fundamental understanding of the properties of the LA, bridging ligand, CAT, and system parameters that determine hydrogen production efficiency is critical to the successful development of efficient and stable photocatalysts for the reduction of water to produce hydrogen fuel. The development of structurally diverse systems which couple a LA to a CAT is needed in this field with systematic variation of device components. Basic chemical studies of the perturbation of properties upon assembly of the supramolecules are also needed. Careful analysis of results and comparisons are needed. It is important that long-term studies of these important systems for light to fuel conversion are undertaken to understand the functioning of these systems and explore the multidimensional parameter space needed to optimize the performance of these systems that are still in their infancy. Detailed mechanistic studies are necessary to uncover factors that limit the functioning of these systems and design of more promising molecular architectures that carry out this complicated photocatalytic reaction. A wide array of system parameters can impact system functioning further complicating this process. The research and development in this very important area requires long-term interest and research funding to assemble the fundamental chemical knowledge needed to establish efficient solar hydrogen production schemes. Sustained and focused research is needed to bring these systems to completion.

Acknowledgments

Acknowledgment is made to all the students and research scientists who have worked in this area in the Brewer Group. Special acknowledgment to Ms. Jessica D. Knoll for help with the manuscript. Acknowledgment is also made to the Chemical Sciences,

Geosciences and Biosciences Division, Office of Basic Energy Sciences, Office of Sciences, US Department of Energy for their generous support of our research and to the financial collaboration of Phoenix Canada Oil Company which holds long-term license rights to commercialize our Rh-based technology.

Bibliography

1. Bard AJ, Fox MA (1995) Artificial photosynthesis: solar splitting of water to hydrogen and oxygen. Acc Chem Res 28:141–145
2. DOE (2005) Report of the basic energy sciences workshop on solar utilization. Department of Energy, Washington, DC
3. Lewis NS (2009) A perspective on forward research and development paths for cost-effective solar energy utilization. ChemSusChem 2:383–386
4. Nocera DG (2009) Living healthy on a dying planet. Chem Soc Rev 38:13–15
5. Bockris JO'M (1999) Hydrogen economy in the future. Int J Hydrogen Energ 24:1–15
6. Lubitz W, Tumas W (2007) Hydrogen: an overview. Chem Rev 107:3900–3903
7. http://www.fsec.ucf.edu/EN/consumer/hydrogen/basics/production.htm
8. Balzani V, Moggi L, Scandola F (1987) Towards a supramolecular photochemistry: assembly of molecular components to obtain photochemical molecular devices. In: Balzani V (ed) Supramolecular photochemistry. Reidel, Dordrecht, pp 1–28
9. Kalyanasundaram K (1982) Photophysics, photochemistry and solar energy conversion with tris(bipyridyl)ruthenium(II) and its analogues. Coord Chem Rev 46:159–244
10. Juris A, Balzani V, Barigelletti F, Campagna S, Belser P, Von Zelewsky A (1988) Ru(II) polypyridine complexes: photophysics, photochemistry, eletrochemistry, and chemiluminescence. Coord Chem Rev 84:85–277
11. Kirch M, Lehn J-M, Sauvage J-P (1979) Hydrogen generation by visible light irradiation of aqueous solutions of metal complexes. An approach to the photochemical conversion and storage of solar energy. Helv Chim Acta 62:1345–1384
12. Balzani V, Juris A, Venturi M, Campagna S, Serroni S (1996) Luminescent and redox-active polynuclear transition metal complexes. Chem Rev 96:759–834
13. Kawanishi Y, Kitamura N, Tazuke S (1989) Dependence of spectroscopic, electrochemical, and excited-state properties of tris chelate ruthenium(II) complexes on ligand structure. Inorg Chem 28:2968–2975
14. Durham B, Caspar JV, Nagle JK, Meyer TJ (1982) Photochemistry of $Ru(bpy)_3^{2+}$. J Am Chem Soc 104:4803–4810
15. Demas JN, Adamson AW (1971) A new photosensitizer. Tris (2,2′-bipyridine)ruthenium(II) chloride. J Am Chem Soc 93:1800–1801
16. Gafney HD, Adamson AW (1972) Excited state $Ru(bipyr)_3^{2+}$ as an electron-transfer reductant. J Am Chem Soc 94:8238–8239
17. Bock CR, Meyer TJ, Whitten DG (1974) Electron transfer quenching of the luminescent excited state of tris(2,2′-bipyridine)ruthenium(II). Flash photolysis relaxation technique for measuring the rates of very rapid electron transfer reactions. J Am Chem Soc 96:4710–4712
18. Bock CR, Connor JA, Gutierrez AR, Meyer TJ, Whitten DG, Sullivan BP, Nagle JK (1979) Estimation of excited-state redox potentials by electron-transfer quenching. Application of electron-transfer theory to excited-state redox processes. J Am Chem Soc 101:4815–4824
19. Tinker LL, McDaniel ND, Bernhard S (2009) Progress towards solar-powered homogeneous water photolysis. J Mater Chem 19:3328–3337
20. Wang M, Na Y, Gorlov M, Sun L (2009) Light-driven hydrogen production catalysed by transition metal complexes in homogeneous systems. Dalton Trans 33:6458–6467
21. Inagaki A, Akita M (2010) Visible-light promoted bimetallic catalysis. Coord Chem Rev 254:1220–1239
22. Balzani V, Credi A, Venturi M (2008) Photochemical conversion of solar energy. ChemSusChem 1:26–58
23. Lin CT, Böttcher W, Chou M, Creutz C, Sutin N (1976) Mechanism of the quenching of the emission of substituted polypyridineruthenium(II) complexes by iron (III), chromium(III), and europium(III) ions. J Am Chem Soc 98:6536–6544
24. Kober EM, Sullivan BP, Dressick WJ, Caspar JV, Meyer TJ (1980) Highly luminescent polypyridyl complexes of osmium (II). J Am Chem Soc 102:7383–7385
25. Braunstein CH, Baker AD, Strekas TC, Gafney HD (1984) Spectroscopic and electrochemical properties of the dimer tetrakis (2,2′-bipyridine)(μ-2,3-bis(2-pyridyl)pyrazine)diruthenium(II) and its monomeric analogue. Inorg Chem 23:857–864
26. Fuchs Y, Lofters S, Dieter T, Shi W, Morgan R, Strekas TC, Gafney HD, Baker AD (1987) Spectroscopic and electrochemical properties of dimeric ruthenium(II) diimine complexes and determination of their excited state redox properties. J Am Chem Soc 109:2691–2697
27. Wallace AW, Murphy WR, Petersen JD (1989) Electrochemical and photophysical properties of mono- and bimetallic ruthenium(II) complexes. Inorg Chim Acta 166:47–54
28. Richter MM, Brewer KJ (1991) Synthesis and characterization of osmium(II) complexes incorporating polypyridyl bridging ligands. Inorg Chim Acta 180:125–131
29. Abdel-Shafi AA, Worrall DR, Ershov AY (2004) Photosensitized generation of singlet oxygen from ruthenium(II) and osmium (II) bipyridyl complexes. Dalton Trans 7:30–36
30. Winkler JR, Netzel TL, Creutz C, Sutin N (1987) Direct observation of metal-to-ligand charge-transfer (MLCT) excited states of pentaammineruthenium(II) complexes. J Am Chem Soc 109:2381–2392
31. Beley M, Collin J-P, Sauvage J-P, Sugihara H, Heisel F, Miehé A (1991) Photophysical and photochemical properties of ruthenium and osmium complexes with substituted terpyridines. J Chem Soc Dalton Trans 23: 3157–3159

32. Rillema DP, Mack KB (1982) The low-lying excited state in ligand π-acceptor complexes of ruthenium(II): mononuclear and binuclear species. Inorg Chem 21:3849–3854
33. Berger RM (1990) Excited-state absorption spectroscopy and spectroelectrochemistry of tetrakis(2,2′-bipyridine)(μ-2,3-bis (2-pyridyl)pyrazine)diruthenium(II) and its Monomeric counterpart: a comparative study. Inorg Chem 29:1920–1924
34. Balzani V, Campagna S, Denti G, Juris A, Serroni S, Venturi M (1998) Designing dendrimers based on transition-metal complexes: light-harvesting properties and predetermined redox patterns. Acc Chem Res 31:26–34
35. Campagna S, Pietro CD, Loiseau F, Maubert B, McClenaghan N, Passalacqua R, Puntoriero F, Ricevuto V, Serroni S (2002) Recent advances in luminescent polymetallic dendrimers containing the 2,3-Bis(2′-pyridyl)pyrazine bridging ligand. Coord Chem Rev 229:67–74
36. Molnar SM, Nallas GNA, Bridgewater JS, Brewer KJ (1994) Photoinitiated electron collection in a mixed-metal trimetallic complex of the form $[\{(bpy)_2Ru(dpb)\}_2IrCl_2](PF_6)_5$ (bpy = 2,2′-bipyridine and dpb = 2,3-bis(2-pyridyl)benzoquinoxaline). J Am Chem Soc 116:5206–5210
37. Konduri R, Ye H, MacDonnell FM, Serroni S, Campagna S, Rajeshwar K (2002) Ruthenium photocatalysts capable of reversibly storing up to four electrons in a single acceptor ligand: a step closer to artificial photosynthesis. Angew Chem Int Edit 41:3185–3187
38. Konduri R, de Tacconi NR, Rajeshwar K, MacDonnell FM (2004) Multielectron photoreduction of a bridged ruthenium dimer, $[(phen)_2Ru(tatpp)Ru(phen)_2](PF_6)_4$: aqueous reactivity and chemical and spectroelectrochemical identification of the photoproducts. J Am Chem Soc 126:11621
39. Polyansky DE, Cabelli D, Muckerman JT, Fukushima T, Tanaka K, Fujita E (2008) Mechanism of hydride donor generation using a Ru(II) complex containing an NAD^+ model ligand: pulse and steady-state radiolysis studies. Inorg Chem 47:3958–3968
40. Fukushima T, Fujita E, Muckerman JT, Polyansky DE, Wada T, Tanaka K (2009) Photochemical stereospecific hydrogenation of a Ru complex with an $NAD^+/NADH^-$Type ligand. Inorg Chem 48:11510–11512
41. Lomoth R, Ott S (2009) Introducing a dark reaction to photochemistry: photocatalytic hydrogen from [FeFe] hydrogenase active site model complexes. Dalton Trans 7:9952–9959
42. Frey M (2002) Hydrogenases: hydrogen-activating enzymes. Chembiochem 3:153–160
43. Capon J-F, Gloaguen F, Pétillon FY, Schollhammer P, Talarmin J (2009) Electron and proton transfers at diiron dithiolate sites relevant to the catalysis of proton reduction by the [FeFe]-hydrogenases. Coord Chem Rev 253:1476–1494
44. Wolpher H, Borgström M, Hammarström L, Bergquist J, Sundström V, Styring S, Sun L, Åkermark B (2003) Synthesis and properties of an iron hydrogenase active site model linked to a ruthenium tris-bipyridine photosensitizer. Inorg Chem Commun 6:989–991
45. Ott S, Kritikos M, Åkermark B, Sun L (2003) Synthesis and structure of a biomimetic model of the iron hydrogenase active site covalently linked to a ruthenium photosensitizer. Angew Chem Int Edit 42:3285–3288
46. Ott S, Borgström M, Kritikos M, Lomoth R, Bergquist J, Åkermark B, Hammarström L, Sun L (2004) Model of the iron hydrogenase active site covalently linked to a ruthenium photosensitizer: synthesis and photophysical properties. Inorg Chem 43:4683–4692
47. Ekström J, Abrahamsson M, Olson C, Bergquist J, Kaynak FB, Eriksson L, Sun L, Becker H-C, Åkermark B, Hammarström L, Ott S (2006) Bio-inspired, side-on attachment of a ruthenium photosensitizer to an iron hydrogenase active site model. Dalton Trans 4599–4606
48. Li X, Wang M, Zhang S, Pan J, Na Y, Liu J, Åkermark B, Sun L (2008) Noncovalent assembly of a metalloporphyrin and an iron hydrogenase active-site model: photo-induced electron transfer and hydrogen generation. J Phys Chem B 112:8198–8202
49. Chong D, Georgakaki IP, Mejia-Rodriguez R, Sanabria-Chinchilla J, Soriaga MP, Darensbourg MY (2003) Electrocatalysis of hydrogen production by active site analogues of the iron hydrogenase enzyme: structure/function relationships. Dalton Trans 4158–4163
50. Lubner CE, Grimme R, Bryant DA, Goldbeck JH (2010) Wiring photosystem I for direct solar hydrogen production. Biochemistry 49:404–414
51. Na Y, Wang M, Pan J, Zhang P, Åkermark B, Sun L (2008) Visible light-driven electron transfer and hydrogen generation catalyzed by bioinspired [2Fe2S] complexes. Inorg Chem 47:2805–2810
52. Streich D, Astuti Y, Orlandi M, Schwartz L, Lomoth R, Hammarström L, Ott S (2010) High-turnover photochemical hydrogen production catalyzed by a model complex of the [FeFe]-hydrogenase active site. Chem Eur J 16:60–63
53. Zhang P, Wang M, Na Y, Li X, Jiang Y, Sun L (2010) Homogeneous photocatalytic production of hydrogen from water by a bioinspired $[Fe_2S_2]$ catalyst with high turnover numbers. Dalton Trans 39:1204–1206
54. Elvington M, Brown J, Arachchige SM, Brewer KJ (2007) Photocatalytic hydrogen production from water employing a Ru, Rh, Ru molecular device for photoinitiated electron collection. J Am Chem Soc 129:10644–10645
55. Arachchige SM, Brown J, Brewer KJ (2008) Photochemical hydrogen production from water using the new photocatalyst $[\{(bpy)_2Ru(dpp)\}_2RhBr_2](PF_6)_5$. J Photochem Photobiol A 197:13–17
56. Arachchige SM, Brown JR, Chang E, Jain A, Zigler DF, Rangan K, Brewer KJ (2009) Design considerations for a system for photocatalytic hydrogen production from water employing mixed-metal photochemical molecular devices for photoinitiated electron collection. Inorg Chem 48:1989–2000
57. Rangan K, Arachchige SM, Brown JR, Brewer KJ (2009) Solar energy conversion using photochemical molecular devices: photocatalytic hydrogen production from water using mixed-metal supramolecular complexes. J Energ Environ Sci 2:410–419

58. Miyake Y, Nakajima K, Sasaki K, Saito R, Nakanishi H, Nishibayashi Y (2009) Design and synthesis of diphosphine ligands bearing an osmium(II) bis(terpyridyl) moiety as a light-harvesting unit: application to photocatalytic production of dihydrogen. Organometallics 28:5240–5243
59. Heyday AF, Nocera DG (2001) Hydrogen produced from hydrohalic acid solutions by a two-electron mixed-valence photocatalyst. Science 293:1639–1641
60. Brown GM, Chan SF, Creutz C, Schwarz HA, Sutin N (1979) Mechanism of the formation of dihydrogen from the photo-induced reactions of tris(bipyridine)ruthenium(II) with tris (bipyridine)rhodium(III). J Am Chem Soc 101:7638–7640
61. Cline ED, Adamson SE, Bernhard S (2008) Homogeneous catalytic system for photoinduced hydrogen production utilizing iridium and rhodium complexes. Inorg Chem 47:10378–10388
62. Fihri A, Artero V, Razavet M, Baffert C, Leibl W, Fontecave M (2008) Cobaloxime-based photocatalytic devices for hydrogen production. Angew Chem Int Edit 47:564–567
63. Fihri A, Artero V, Pereira A, Fontecave M (2008) Efficient H_2-producing photocatalytic systems based on cyclometalated iridium- and tricarbonylrhenium-diimine photosensitizers and cobaloxime catalysts. Dalton Trans 5567–5569
64. Li C, Wang M, Pan J, Zhang P, Zhang R, Sun L (2009) Photochemical hydrogen production catalyzed by polypyridyl ruthenium-cobaloxime heterobinuclear complexes with different bridges. J Organomet Chem 694:2814–2819
65. Brown GM, Brunschwig BS, Creutz C, Endicott JF, Sutin N (1979) Homogeneous catalysis of the photoreduction of water by visible light. Mediation by a tris(2,2′-bipyridine)ruthenium(II)-cobalt(II) macrocycle system. J Am Chem Soc 101:1298–1300
66. Goldsmith JI, Hudson WR, Lowry MS, Anderson TH, Bernhard S (2005) Discovery and high-throughput screening of heteroleptic iridium complexes for photoinduced hydrogen production. J Am Chem Soc 127:7502–7510
67. Du P, Schneider J, Luo G, Brennessel WW, Eisenberg R (2009) Visible light-driven hydrogen production from aqueous protons catalyzed by molecular cobaloxime catalysts. Inorg Chem 48:4952–4962
68. Lazarides T, McCormick T, Du P, Luo G, Lindley B, Eisenberg R (2009) Making hydrogen from water using a homogeneous system without noble metals. J Am Chem Soc 131:9192–9194
69. Probst B, Kolano C, Hamm P, Alberto R (2009) An efficient homogeneous intermolecular rhenium-based photocatalytic system for the production of H_2. Inorg Chem 48:1836–1843
70. Ozawa H, Haga M-A, Sakai K (2006) A photo-hydrogen-evolving molecular device driving visible-light-induced EDTA-reduction of water into molecular hydrogen. J Am Chem Soc 128:4926–4927
71. Knoll JD, Arachchige SM, Brewer KJ (2011) A structurally diverse Ru(II), Pt(II) tetrametallic motif for photoinitiated electron collection and photocatalytic hydrogen production. ChemSusChem 4:252–261
72. Miao R, Zigler DF, Brewer KJ Manuscript to be submitted to Inorg Chem
73. Okazaki R, Masaoka S, Sakai K (2009) Photo-hydrogen-evolving activity of chloro(terpyridine)platinum(II): a single-component molecular photocatalyst. Dalton Trans 6127–6133
74. Rau S, Schäfer B, Gleich D, Anders E, Rudolph M, Friedrich M, Görls H, Henry W, Vos JG (2006) A supramolecular photocatalyst for the production of hydrogen and the selective hydrogenation of tolane. Angew Chem Int Edit 45:6215–6218
75. Schwartz L, Singh PS, Eriksson L, Lomoth R, Ott S (2008) Tuning the electronic properties of Fe_2(μ-arenedithiolate) $(CO)_{6-n}(PMe_3)_n$ (n = 0, 2) complexes related to the [Fe–Fe]-hydrogenase active site. CR Chim 11:875–889
76. Sutin N, Creutz C, Fujita E (1997) Photo-induced generation of dihydrogen and reduction of carbon dioxide using transition metal complexes. Comment Inorg Chem 19:67–92
77. Balzani V, Credi A, Venturi M (1998) Photochemistry and photophysics of coordination compounds: an extended view. Coord Chem Rev 171:3–16
78. Venturi M, Credi A, Balzani V (1999) Electrochemistry of coordination compounds: an extended view. Coord Chem Rev 185:233–256
79. Scandola F, Argazzi R, Bignozzi CA, Indelli MT (1994) Photoinduced energy and electron transfer in inorganic covalently linked systems. J Photochem Photobiol A 82:191–202
80. Serroni S, Juris A, Campagna S, Venturi M, Denti G, Balzani V (1994) Tetranuclear bimetallic complexes of ruthenium, osmium, rhodium and iridium. Synthesis, absorption spectra, luminescence and electrochemical properties. J Am Chem Soc 116:9086–9091
81. Indelli MT, Scandola F, Collin J-P, Sauvage J-P, Sour A (1996) Photoinduced electron and energy transfer in rigidly bridged Ru(II)-Rh(III) binuclear complexes. Inorg Chem 35:303–312
82. Elvington M, Brewer K (2006) Photoinitiated electron collection at a metal in a rhodium-centered mixed-metal supramolecular complex. Inorg Chem 45:5242–5244
83. White TA, Rangan K, Brewer KJ (2010) Synthesis, characterization, and study of the photophysics and photocatalytic properties of the photoinitiated electron collector $[\{(phen)_2Ru(dpp)\}_2RhBr_2](PF_6)_5$. J Photochem Photobiol A 209: 203–209
84. Kalyanasundaram K, Nazeeruddin MK (1990) Photophysics and photoredox reactions of ligand-bridged binuclear polypyridyl complexes of ruthenium(II) and of their monomeric analogs. Inorg Chem 29:1888–1897
85. Kew G, DeArmond K, Hanck K (1974) Electrochemistry of rhodium-dipyridyl complexes. J Phys Chem 78:727–734
86. Anton DR, Crabtree RH (1983) Dibenzo[a, e]cyclooctatetraene in a proposed test for heterogeneity in catalysts formed from soluble platinum-group metal complexes. Organometallics 2:855–859
87. Baba R, Nakabayashi S, Fujishima A, Honda K (1985) Investigation of the mechanism of hydrogen evolution during photocatalytic water decomposition on metal-loaded semiconductor powders. J Phys Chem 89:1902–1905

88. Arachchige SM, Shaw R, White TA, Shenoy V, Tsui H-M, Brewer KJ (2011) Modification of system parameters for high turnover in a photocatalytic system for water reduction to produce hydrogen using a Ru, Rh, Ru photoinitiated electron collector. ChemSusChem 4:514–518
89. Esswein AJ, Veige AS, Nocera DG (2005) A photocycle for hydrogen production from two-electron mixed-valence complexes. J Am Chem Soc 127:16641–16651
90. Esswein AJ, Dempsey JL, Nocera DG (2007) A $Rh^{II} - Au^{II}$ bimetallic core with a direct metal-metal bond. Inorg Chem 46:2362–2364
91. Cook TR, Esswein AJ, Nocera DG (2007) Metal – halide bond photoactivation from a $Pt^{III}Au^{II}$ complex. J Am Chem Soc 129:10094–10095
92. Chou M, Creutz C, Mahajan D, Sutin N, Zipp AP (1982) Nature of bis(2,2′-bipyridine)rhodium(I) in aqueous solutions. Inorg Chem 21:3989–3997
93. Schwarz HA, Creutz C (1983) Reactions of tris- and bis(2,2′-bipyridine)rhodium(II) complexes in aqueous solution. Inorg Chem 22:707–713
94. Fujita E, Brunschwig BS, Creutz C, Muckerman JT, Sutin N, Szalda D, van Eldik R (2006) Transition state characterization for the reversible binding of dihydrogen to Bis(2,2′-bipyridine) rhodium(I) from temperature- and pressure-dependent experimental and theoretical studies. Inorg Chem 45:1595–1603
95. Dempsey JL, Brunschwig BS, Winkler JR, Gray HB (2009) Hydrogen evolution catalyzed by cobaloximes. Acc Chem Res 42:1995–2004
96. Kölle U (1992) Transition metal-catalyzed proton reduction. New J Chem 16:157–169
97. Hawecker J, Lehn JM, Ziessel R (1983) Efficient homogeneous photochemical hydrogen generation and water reduction mediated by cobaloxime or macrocyclic cobalt complexes. Nouv J Chim 7:271–7
98. Lowry MS, Goldsmith JI, Slinker JD, Rohl R, Pascal RA, Malliaras GG, Bernhard S (2005) Single-layer electroluminescent devices and photoinduced hydrogen production from an ionic iridium(III) complex. Chem Mater 17:5712–5719
99. Du P, Knowles K, Eisenberg R (2008) A homogeneous system for the photogeneration of hydrogen from water based on a platinum(II) terpyridyl acetylide chromophore and a molecular cobalt catalyst. J Am Chem Soc 130:12576–12577
100. Dempsey JL, Winkler JR, Gray HB (2010) Kinetics of electron transfer reactions of H_2-evolving cobalt diglyoxime catalysts. J Am Chem Soc 132:1060–1065
101. Sakai K, Ozawa H (2007) Homogeneous catalysis of platinum (II) complexes in photochemical hydrogen production from water. Coord Chem Rev 251:2753–2766
102. Ozawa H, Yokoyama Y, Haga M-A, Sakai K (2007) Syntheses, characterization, and photo-hydrogen-evolving properties of tris(2,2′-bipyridine)ruthenium(II) derivatives tethered to a cis-Pt(II)Cl_2 unit: insights into the structure–activity relationship. Dalton Trans 1197–1206
103. Lei P, Hedlund M, Lomoth R, Rensmo H, Johansson O, Hammarström L (2008) The role of colloid formation in the photoinduced H_2 production with a Ru^{II}-Pd^{II} supramolecular complex: a study by GC, XPS, and TEM. J Am Chem Soc 130:26–27
104. Du P, Schneider J, Li F, Zhao W, Patel U, Castellano FN, Eisenberg R (2008) Bi- and terpyridyl platinum(II) chloro complexes: molecular catalysts for the photogeneration of hydrogen from water or simply precursors for colloidal platinum? J Am Chem Soc 130:5056–5058
105. Masaoka S, Mukawa Y, Sakai K (2010) Frontier orbital engineering of photo-hydrogen-evolving molecular devices: a clear relationship between the H2-evolving activity and the energy level of the LUMO. Dalton Trans 39:5868–5876
106. Ozawa H, Kobayashi M, Balan B, Masaoka S, Sakai K (2010) Photo-hydrogen-evolving molecular catalysts consisting of polypyridyl ruthenium(II) photosensitizers and platinum(II) catalysts: insights into the reaction mechanism. Chem Asian J 5:1860–1869
107. Tschierlei S, Presselt M, Kuhnt C, Yartsev A, Pascher T, Sundström V, Karnahl M, Schwalbe M, Schäfer B, Rau S, Schmitt M, Dietzek B, Popp J (2009) Photophysics of an intramolecular hydrogen-evolving Ru-Pd photocatalyst. Chem Eur J 15:7678–7688

Hydrothermal Systems, Geochemistry of

David Nieva, Rosa María Barragán, Víctor Arellano
Instituto de Investigaciones Eléctricas, Cuernavac, Morelos, Mexico

Article Outline

Glossary
Definition of the Subject
Introduction
Geothermometry
Geochemical Modeling of Hydrothermal Fluids
Future Directions
Bibliography

Glossary

Adiabatic process A process undergone by a system during which there is no heat exchange between the system and its surroundings.

Enthalpy Thermodynamic potential (akin to the internal energy) of a system that remains constant when the system undergoes an adiabatic process at constant pressure and composition.

Geothermal reservoir engineering Branch of engineering that applies scientific principles to the problems arising during the extraction of mass and heat from a geothermal resource.

Geothermal resource, Unless otherwise specified, in this article the meaning is restricted to a hydrothermal system selected for exploitation with the purpose of extracting usable heat.

Magma chamber Large accumulation of molten rock found beneath the surface of the Earth.

Definition of the Subject

In its most ample definition, geochemistry involves the study of the abundance, distribution, transformation, and transport of the elements, and their isotopes and compounds in the Earth and other planets. In this entry, this extremely ample subject is drastically reduced by two constraints. In the first instance, it is restricted to the discussion of hydrothermal systems, the only type of high-temperature geothermal resource that is exploitable with current conventional technology for the production of electricity and process heat. The second constraint consists of the pragmatic approach to the subject. Indeed, the entry refers to the interplay between science and technology, which has led to the development of techniques based on geochemical considerations that have proven useful for the characterization and exploitation of hydrothermal systems.

Early studies of hydrothermal systems were concerned with the underground flow of heat and water [1–4]. Soon afterward, the systematic study of geochemical features of these systems started [5–7]. Since then, geochemistry has accompanied the development of technology for the exploration and exploitation of geothermal resources. Geochemical techniques provide information on the structure and the distribution of temperature and other physicochemical parameters in a hydrothermal system. When combined with reservoir engineering considerations, geochemistry provides information on processes induced in the geothermal reservoir by the continuous extraction of mass and heat.

Introduction

A hydrothermal system is a volume of rock which is permeated by water or steam and heated to a temperature higher than normal for the particular depth. The source of heat is usually a magma chamber lying a few kilometers underneath; less frequently, the source of heat is a crustal site with an abnormally high concentration of radioisotopes, mainly potassium (^{40}K), thorium (^{232}Th), and uranium (^{235}U and ^{238}U). The origin of the fluid is meteoric, that is, rain water that infiltrates the ground to depths of up to a few kilometers, frequently mixed with fluids and solutes of magmatic origin. The essential features of a hydrothermal system are shown in Fig. 1, which is similar to an early sketch by White [8]. A third feature is the so-called cap rock, which is a layer of less permeable rock overlying the volume of permeated rock (i.e., the "reservoir"). The permeability and degree of fracturing of this cap rock varies from site to site and so do the intensity and the abundance of the surface manifestations of hydrothermal systems (boiling springs, steam vents, hot ponds, geysers).

A more detailed model from a geochemical perspective is that shown in Fig. 2 [9]. Degassing of magma produces a fluid that, on the basis of the analysis of high-temperature gases released from basaltic [10] and andesitic magmas [11] is estimated to consist of water vapor with 20–40% by weight of CO_2, 5% of sulfur (SO_2/H_2S), and 1–2% HCl. As this fluid ascends, mixes with deeply circulating ground water and experiences a reduction in temperature, it forms a highly acidic fluid which interacts with the wall rock in a process called "primary neutralization." The result of this process is postulated to be a virtually complete cation leaching of the rock, forming close to neutral solutions with cation contents similar to the composition of the original rock, and with chloride and sulfate as the main anions. It is postulated further that magnesium and calcium are rapidly redeposited in the form of Mg- and Ca- rich minerals and sulfate is also deposited in the form of pyrite, alunite, or anhydrite. The result of this "primary neutralization" process is the production of the typical brine encountered in geothermal reservoirs, that is, a neutral or close to neutral aqueous solution with chloride as the main anion and sodium and potassium as the main cations. This brine, which contains much of the magmatic CO_2 and some of the sulfur as H_2S [9], may reach the surface mixed with varying proportions of meteoric water in natural hot springs or could be brought to the surface by man-

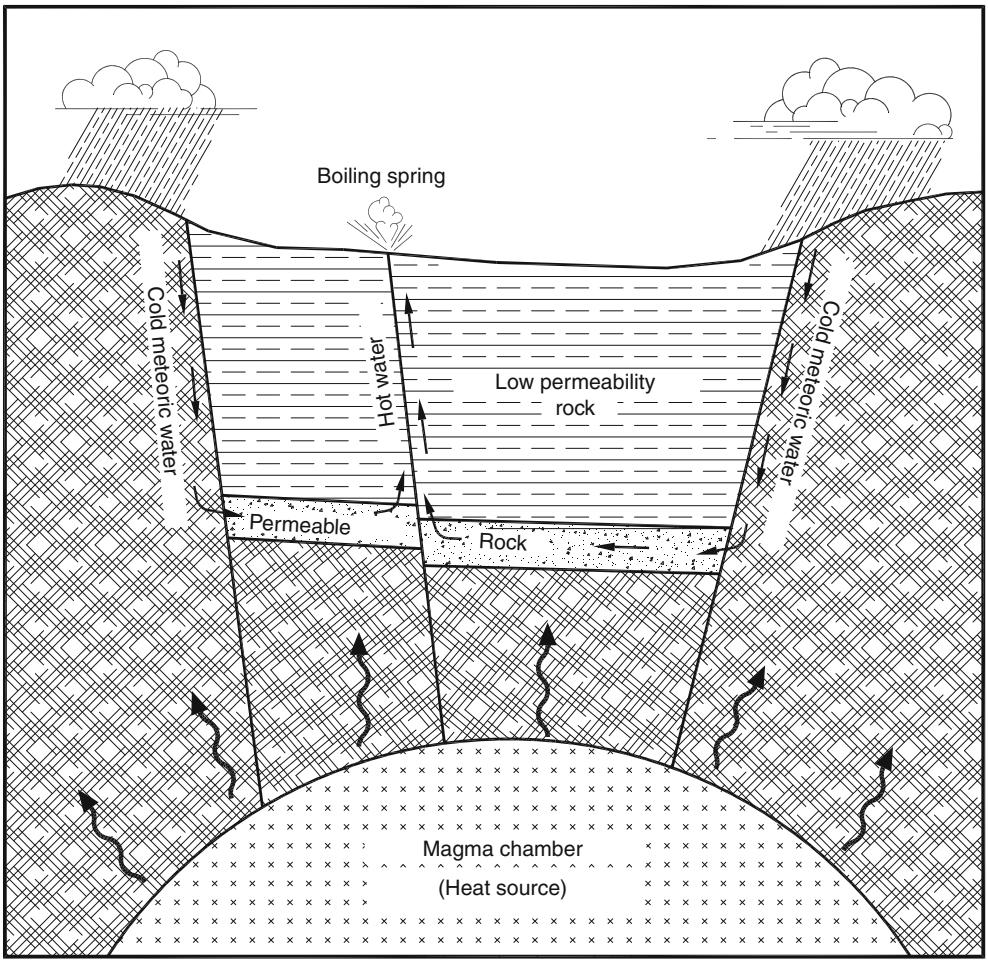

Hydrothermal Systems, Geochemistry of. Figure 1
Schematic model of a hydrothermal system

made wells. The natural upward migration of this NaCl/KCl brine through the main upflow zone (i.e., the "geothermal reservoir") causes some characteristic alteration of the rock which leads to its enrichment in potassium (K-metasomatism).

In some hydrothermal systems, the deep, pre-neutralized liquid phase, finds its way to the surface, mixed with meteoric waters. The oxidation by atmospheric oxygen of the H_2S to produce H_2SO_4 gives rise to surface discharges with very low pH and high concentrations of chloride and sulfate ions; the cation composition of these waters may approach the composition of the original (dissolved) rock [12].

A third type of surface discharge originates from CO_2-rich steam separation from the rising brine, its interaction with the rock at shallower levels to produce calcite, and its mixture with oxygen-rich meteoric waters, which produce surface discharges with bicarbonate as the dominant ion, close to neutral pH, and varying concentrations of sulfate and chloride ions. The mineralogical consequences of this acid-induced alteration (H-metasomatism) of the rock are observable in the periphery of the main upflow zone.

A hydrothermal system is clearly not in equilibrium; there are thermal, mechanical, chemical, and nuclear processes that lead to conductive, convective, and radiative transport of energy, and to mass transport in and out of the system as well as between parts of the system (fluid flow, dissolution and precipitation of material, chemical reactions in liquid, gaseous, and solid phases).

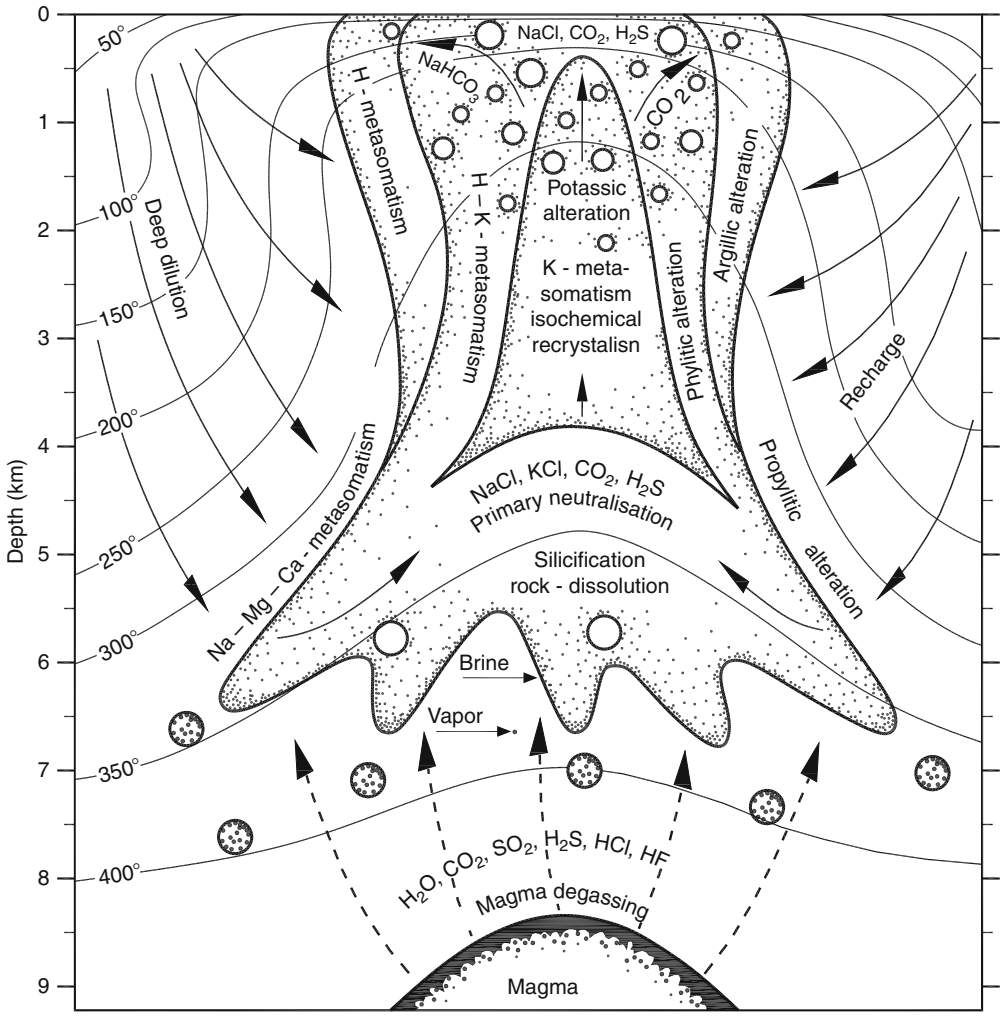

Hydrothermal Systems, Geochemistry of. Figure 2
Schematic cross section of a hydrothermal system with details of fluid genesis and fluid-rock interaction, as drawn by Giggenbach [9]

However, in certain stages of development, and certain parts of the system, where temperature and pressure vary only very slowly, fast chemical reactions adjust to the conditions prevailing at any given time and may be said to be at equilibrium. Many of the useful geochemical inferences that may be made on the prevailing physicochemical conditions in a hydrothermal system depend on these partial equilibrium states, which may be best referred to as *steady states*.

In the early stages of exploration of a hydrothermal system, when only evidence available from the surface is at hand, the aim of a geochemical survey is the generation of a model that would assess the temperature and chemical conditions of the fluid at depth. Naturally, the confidence that may be placed on this assessment increases with the ability of the model to accommodate as much of the available evidence as possible, and to explain the composition of all surface discharges [13–16].

Geothermometry

Perhaps the single most important hydrothermal reservoir parameter that could be estimated with

geochemical techniques is the temperature. Indeed, there are algorithms, called geothermometers, which relate the geothermal reservoir temperature to mathematical expressions involving the concentrations of ionic and neutral species in the hydrothermal fluid. In this section, a general discussion of the bases and application of geothermometers is provided.

Cation Geothermometry

Geothermometers based on the ionic composition of hydrothermal fluids explicitly or implicitly refer to mineral–solution reactions of the following type:

$$\begin{aligned}&\text{Mineral assemblage } 1 + \mathrm{aA}^{w+} + \mathrm{bB}^{x+}\\&\quad = \text{Mineral assemblage } 2 + \mathrm{cC}^{y+} + \mathrm{dD}^{z+}\end{aligned} \tag{1}$$

where A, B, C, and D stand for cations in solution; a, b, c, and d are stoichiometric coefficients, and the charge conservation condition: $aw + bx = cy + dz$ is obeyed.

To a first approximation, the activities of minerals in contact with hydrothermal solutions may be taken as constant and equal to unity. Also, many hydrothermal aqueous solutions are only moderately concentrated, so the activity coefficients of ionic species in solution approach unity. With these simplifications, the equilibrium constant for reaction 1 is given by

$$Keq = \frac{[C^{y+}]^c[D^{z+}]^d}{[A^{w+}]^a[B^{x+}]^b} \tag{2}$$

where the quantities in brackets refer to molal concentrations.

The natural logarithm of the equilibrium constant is related to the reaction changes in standard enthalpy and entropy by the following expression:

$$\ln Keq = -\frac{\Delta \mathrm{H}^0}{\mathrm{RT}} + \frac{\Delta \mathrm{S}^0}{\mathrm{R}} \tag{3}$$

where ΔH^0 and ΔS^0 are the reaction change in standard molal enthalpy and entropy, respectively, T stands for the absolute temperature and R is the gas constant. For many reactions, ΔH^0 and ΔS^0 vary only slightly with temperature and pressure in the range of interest (25–300°C; 1–200 bar), so one would expect to find an approximately linear relationship between the logarithm of the equilibrium constant and the reciprocal of the absolute temperature.

The first indicator of this sort that was identified is the ratio of the concentrations of sodium and potassium ions in the hydrothermal fluid, as it was observed that the ratio K/Na increases with temperature [5, 6]. Mercado [17] generated a model of natural flow in the Cerro Prieto geothermal field (Mexico) based on this indicator.

Several relations of the type:

$$\ln \frac{[\mathrm{K}^+]}{[\mathrm{Na}^+]} = -\mathrm{A}\left(\frac{1}{\mathrm{T}}\right) + \mathrm{B} \tag{4}$$

where A and B are constants, have been fitted to data on fluid chemical composition and measured underground temperature from geothermal wells, oil field brines, and natural hot springs [5, 18–24]. Those relations which were fitted to sufficiently ample data bases from geothermal wells and oil field brines [22–24] approach the expression that would be obtained for Eq. 3 from modern thermodynamic data [25] for the reaction:

$$\text{albite} + \mathrm{K}^+ = \mathrm{K} - \text{feldspar} + \mathrm{Na}^+ \tag{5}$$

Fournier and Truesdell [19] developed a geothermometer based on two hypothetical mineral–solution reactions represented by the single expression:

$$\begin{aligned}&\text{Mineral assemblage } 1 + \mathrm{K}^+\\&\quad = \text{Mineral assemblage } 2 + (\beta/2)\mathrm{Ca}^{2+} + (1-\beta)\mathrm{Na}^+\end{aligned} \tag{6}$$

where β could take one of two possible values, namely, 1/3 and 4/3. Those authors proposed a graphical method to estimate reservoir temperatures in a plot of the type of Eq. 3 for the above reactions. An analytical expression for this geothermometer, provided by Fournier [26], is as follows:

$$\log_{10} \frac{(\mathrm{Na}^+)^{1-\beta}(\mathrm{Ca}^{2+})^{\frac{\beta}{2}}}{\mathrm{K}^+} = 1647\left(\frac{1}{T}\right) - 2.47 - 2.06\beta \tag{7}$$

where the parentheses on the left-hand term refer to concentrations in mg/kg. The procedure proposed by the authors is to apply Eq. 7, on a first trial, utilizing a value of 1/3 for the parameter β. In case the result obtained is a temperature greater than 100°C, one is to

consider it the final value; otherwise, one should utilize the value of 4/3 for β. As pointed out by Giggenbach [9], the fact that a single value for the coefficient of (1/T) is utilized implies that β is to be considered a statistical weighing factor rather than a stoichiometric coefficient in reaction 6.

This Na–K–Ca geothermometer has been applied extensively in the exploration of hydrothermal resources. Several authors have identified systematic errors in its application which seem to be associated with high contents of CO_2 in the hydrothermal fluid [9, 27, 28], and a modified expression has been proposed [27]. In addition, Fournier and Potter [29] have proposed a correction term to be used when this geothermometer is applied to Mg-rich thermal waters.

Geothermometers based on the concentration of the four main cations (Na^+, K^+, Ca^{2+}, Mg^{2+}) have been developed. Nieva and Nieva [24] developed a procedure that leads to the utilization of one of four possible equations with a given sample, depending on its chemical characteristics. This geothermometer, called the Cationic Composition Geothermometer (CCG), is designed to ensure that the equation:

$$\log_{10}\frac{[K^+]}{[Na^+]} = -1178\left(\frac{1}{T}\right) + 1.239 \tag{8}$$

similar to the expression developed by Fournier [22], is applied only to waters showing preliminary signs of having a high-temperature origin, thus adopting a conservative approach which avoids overestimation of temperatures at depth. Application of this geothermometer to a hot-spring NaCl/KCl brine with close to neutral pH is safe and the resulting estimated temperature should be considered a lower bound for the reservoir temperature. In Eq. 8 brackets indicate molal concentrations.

Giggenbach [9] also developed a procedure to estimate temperatures at depth based on the consideration of chemical equilibria involving the four main cations. This author concluded that the mineral assembly muscovite, clinochlore, silica, albite, and K-feldspar is at chemical equilibrium in the deep parts of the main upflow zone of the hydrothermal system according to the following reactions:

$$\begin{aligned} &0.8\ \text{muscovite} + 0.2\ \text{clinochlore} + 5.4\ \text{silica} + 2\ Na^+ \\ &\quad = 2\ \text{albite} + 0.8\ \text{K} - \text{feldspar} + 1.6\ \text{water} + Mg^{2+} \end{aligned} \tag{9}$$

and

$$\begin{aligned} &0.8\ \text{muscovite} + 0.2\ \text{clinochlore} + 5.4\ \text{silica} + 2\ K^+ \\ &\quad = 2.8\ \text{K} - \text{feldspar} + 1.6\ \text{water} + Mg^{2+} \end{aligned} \tag{10}$$

The above reaction system includes, of course, reaction 5. From these considerations, and taking as a reference modern thermodynamic data, Giggenbach [9] proposed the use of a K-Na geothermometer and a K-Mg geothermometer, as given respectively by the following expressions:

$$\log_{10}\frac{[K^+]}{[Na^+]} = -1390\left(\frac{1}{T}\right) + 1.75 \tag{11}$$

and

$$\log_{10}\frac{[K^+]^2}{[Mg^{2+}]} = -4410\left(\frac{1}{T}\right) + 14 \tag{12}$$

In Eqs. 11 and 12 concentrations are in mg/kg. Reaction 5 seems to re-equilibrate very slowly as the fluid ascends and encounters strata with lower temperatures. Thus, as mentioned above, K-Na geothermometers applied to waters from hot springs provide a reasonable lower bound for reservoir temperature at depth. On the other hand, the proportion of magnesium and potassium ions readjusts more rapidly and the application of Eq. 12 yields estimates of temperature in shallower parts of the hydrothermal system [9].

Just as in the case of the development of the CCG geothermometer [24], Giggenbach [9] faced the need to develop an indication, based on the concentration of Mg^{2+}, to determine if thermal water had been at equilibrium at depth. This author proposed the use of the triangular diagram shown in Fig. 3, based on the parameters $Na^+/1{,}000$, $K^+/100$, $(Mg^{2+})^{1/2}$. In this diagram, data points of waters such as those produced by geothermal wells, which have a cationic composition compatible with chemical equilibrium of reactions 9 and 10, fall on the "fully equilibrated waters" curve. In contrast, data points of water with composition compatible with full dissolution of crustal rocks fall in the lower right-hand corner. The region in the

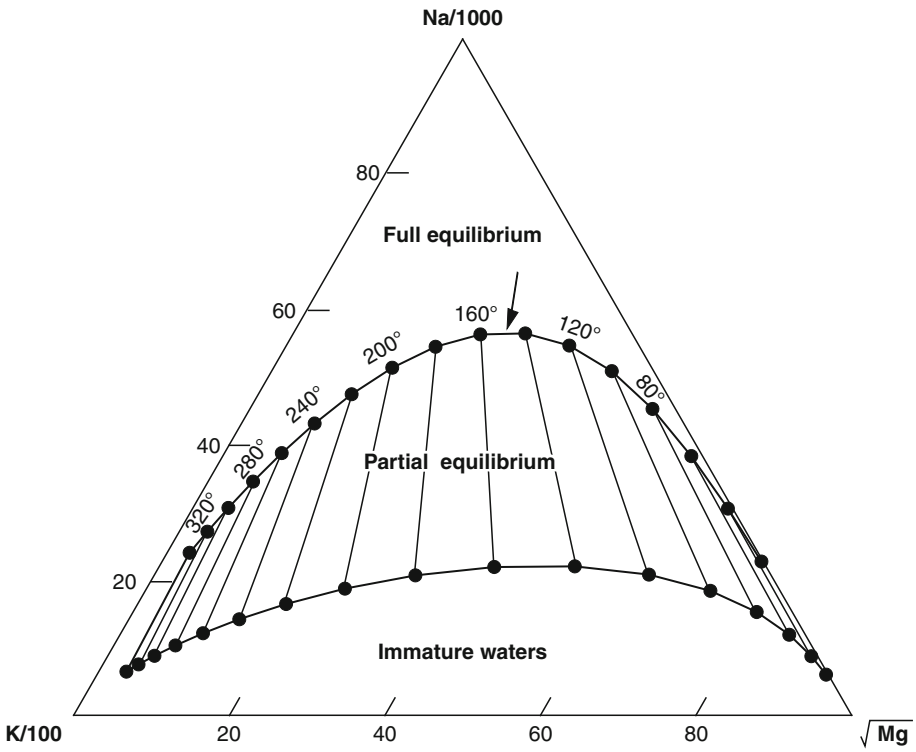

Hydrothermal Systems, Geochemistry of. Figure 3
Triangular diagram for estimation of equilibrium reservoir temperatures by simultaneous application of geothermometric expressions from Eqs. 11 and 12. The "full equilibrium" curve represents the loci of intersections of isotherms drawn by use of Eqs. 11 and 12. Dot-joining lines are isotherms drawn by use of Eq. 12. Figure constructed with information provided by Giggenbach [9]

diagram belonging to "partially-equilibrated waters" is bounded on the top by the "fully equilibrated waters" curve and on the bottom by a rather arbitrary curve. This lower curve is drawn by plotting data as for the "fully equilibrated waters" but first dividing the concentration of sodium by 4.57. Giggenbach [9] recommends the use of the K-Mg geothermometer for samples that fall in the partially-equilibrated waters area of the diagram, but to exercise caution when they fall near the lower curve.

Table 1 illustrates the application of the CCG [24] and the Na-K-Mg [9] geothermometers, as applied to samples from geothermal wells and hot springs from a number of hydrothermal systems. For most wells, the CCG yields temperatures quite close to the measured values. When applied to hot springs, the CCG yields temperatures that, in the context of a survey of a geothermal area, could be safely taken as a lower bound for the reservoir temperature. The Na-K-Mg geothermometer yields temperatures close to the measured value but in some cases, it overestimates the temperature of the reservoir. For this reason, some authors [30, 31] prefer to construct the triangular diagram of Giggenbach [9] using Eq. 8 of the CCG instead of Eq. 11 of the Na-K-Mg geothermometer. Cationic geothermometers fail when applied to ocean water, yielding high-temperature values possibly reflecting the interaction of ocean water with basaltic rock in mid-ocean ridges [9]. In cases of hydrothermal systems with an important intrusion of ocean water, care must be taken in the application of cationic geothermometers; their application should be limited to brines produced by deep wells which presumably have been subject to interaction with reservoir rocks at high temperatures for long periods of time.

Hydrothermal Systems, Geochemistry of. Table 1 Application of the CCG [24] and the Na-K-Mg [9] geothermometers to geothermal wells and associated hot springs. Concentrations are in mg/kg and temperatures are in Celsius. Data is from [9]

Origin	Reservoir Temperature	pH	Na	K	Mg	Ca	t CCG	t K-Na	t K-Mg
Geoth. well NG-9, Ngawha, New Zealand	230	7.7	893	79	0.110	3	194	223	204
Jubilee pool, New Zealand	230	7.2	842	72	1.600	9	191	220	147
Geoth. well WK66, Wairakei, New Zealand	240	8.5	995	142	0.040	17	236	262	258
Champagne Pool, New Zealand	240	8.0	1,070	102	0.400	26	200	229	187
Geoth. well BR-11, Broadlands, New Zealand	260	7.4	675	130	0.011	1	266	291	291
Ohaki Pool, New Zealand	260	7.1	860	82	0.100	3	200	229	208
Geoth. well 10, Miravalles, Costa Rica	250	7.8	1,750	216	0.110	59	222	250	254
Sal. Bagaces, Costa Rica	250	8.6	2,063	85	6.600	33	140	170	129
Geoth. well ZQ-3, Zunil, Guatemala	295	8.1	933	231	0.012	15	294	317	327
Zunil Spring	295	7.0	384	32	39	17	189	218	77
Geoth. well from Cerro Prieto, Mexico	280	7.3	5,600	1,260	0.270	333	283	307	337
Spring N29, Cerro Prieto, Mexico	280	7.6	5,120	664	4.600	357	227	254	216
Geoth. well from Tongonan, Philippines	330	7.0	3,580	1,090	0.200	128	320	340	337
Banati Spring, Philippines	330	8.3	1,990	210	0.400	86	208	237	219
Salton Sea well, USA	330	5.2	38,400	13,400	10	22,010	338	357	381
Seawater	4	7.8	10,760	390	1,290	410	132	162	97

Most cation geothermometers involve only the major cations (Na^+, K^+, Mg^{2+}, Ca^{2+}) but some are based on lithium equilibrium between the aqueous solution and some mineral assembly [32, 33]. Lithium–magnesium geothermometers yield values close to the measure reservoir temperature when applied to water produced by geothermal and oil wells; however, when applied to hot spring water, the calculated temperatures are frequently too low, presumably due to the re-equilibration at lower temperatures of reactions involving magnesium [26].

Silica Geothermometry

The concentration of silica in hydrothermal fluids is determined by the solubility of quartz [34]. The fact that the solubility of quartz shows strong temperature dependence [34–36] provides the basis for the silica geothermometer [37, 38], which has been applied extensively for the exploration of geothermal resources.

Two basic assumptions underlie the application of the silica geothermometer. The first assumption is that the solubility of quartz in moderately saline hydrothermal fluids is similar enough to its solubility in pure water, so that the latter could be taken as reference. This assumption is quite plausible as long as the salinity is below 2% by weight and temperatures are below 300°C, which is the case for many hydrothermal systems; a correction must be made when salinity or temperature are higher [26].

The second assumption is that the hydrothermal fluid does not gain or lose silica after it has reached equilibrium with quartz in the reservoir. This assumption does not hold in cases when the hydrothermal fluid undergoes a relatively slow rise to the surface. This is the reason why the silica geothermometer

applied to hot spring waters does not yield temperatures higher than about 230°C; the reactions of quartz dissolution or precipitation are very fast above this temperature [39, 40]. However, when applied to hydrothermal fluids produced by lined wells that deliver the fluid to the surface much more rapidly and without interaction with the rock, the silica geothermometer is quite useful to estimate the reservoir temperature.

In addition to the above assumptions, when applying the silica geothermometer to hot spring waters, one must make some conjecture as to the processes affecting the sample on its way to the surface. When reaching the point of discharge, the hydrothermal liquid must have reduced its temperature to some value at or below the boiling point. There are basically three mechanisms by which this may be accomplished: mixing with colder waters, loss of heat to the rock by conduction, and adiabatic separation of steam; in most cases, at least two of these mechanisms intervene. When modeling these processes, it is much more convenient to deal with enthalpy (i.e., heat content) rather than temperature because the former is a conservative quantity. Thus, when the hydrothermal liquid loses heat to the rock by conduction, the heat transferred is subtracted from the enthalpy of the liquid. When the hydrothermal liquid mixes with a colder water, the enthalpy (and silica) content of the mixture is simply the sum of the quantities contributed by each of the mixing components. Likewise, when a hydrothermal fluid undergoes adiabatic steam separation at a given temperature, the enthalpy distributes itself between the resulting liquid and steam phases according to the specific enthalpy (i.e., the heat content per unit mass) of each phase:

$$H_{hf} = (1 - f)\bar{H}_{t,l} + f\bar{H}_{t,s} \tag{13}$$

where f is the mass fraction of steam, H_{hf} stands for the specific enthalpy of the hydrothermal liquid before undergoing steam separation, and $\bar{H}_{t,l}$ and $\bar{H}_{t,s}$ refer to the specific enthalpies at temperature t of saturated liquid and steam, respectively. Specific enthalpies of saturated steam and liquid are usually taken as those for pure H_2O and could be obtained from steam tables. The silica content of the hydrothermal liquid also distributes itself between the separated phases:

$$[SiO_2]_{hf} = (1 - f)[SiO_2]_l + f[SiO_2]_s \tag{14}$$

When the steam separation occurs at temperatures of 260°C or less, the silica concentration in the separated steam could be approximated safely as zero.

These processes could be modeled graphically in a Cartesian plot of silica concentration vs. enthalpy. Fournier and Potter [37] provide a plot of the equilibrium silica concentration in H_2O at the vapor pressure of the solution, as a function of enthalpy, covering the range of liquid water at 20°C to temperatures close to the critical point; Fig. 4, which reproduces a portion of that plot, was constructed with information provided in the cited reference. In such a plot, a point representing the hydrothermal liquid would fall on the quartz solubility curve. A point representing the mixture of the hydrothermal liquid with a cold water component would fall on the tie line joining the points which represent the two mixing components. In order to represent a process of adiabatic steam separation, one would locate the point representing the separated steam, with zero silica concentration and the specific enthalpy of the steam; then one would draw a line joining this point with the point representing the original hydrothermal liquid; by extending this line to the value of the specific enthalpy of the separated (saturated) liquid, one would find the resulting silica concentration and thus the position of the point representing this liquid. As an example, the following process is depicted graphically in Fig. 4: A hydrothermal liquid at 240°C undergoes adiabatic cooling by expansion with single-stage steam separation at 120°C. The separated liquid then mixes (w/w) with 60% meteoric water at 15°C, containing 5 mg/kg of silica, giving rise to a thermal water at about 57°C and a silica concentration of about 224 mg/kg.

As mentioned above, in spite of the potential complexity of the processes affecting the silica content of hot spring fluids the silica geothermometer has been applied extensively for the exploration of geothermal resources. When applied to hydrothermal liquid produced by geothermal wells, the situation is particularly simple. The liquid is brought to the surface rapidly, with negligible loss of heat to the walls and without mixing with other fluids; the only mechanism that intervenes is the adiabatic separation of steam. For these reasons, the silica geothermometer applied to well fluids is a powerful tool for the estimation of the reservoir temperature.

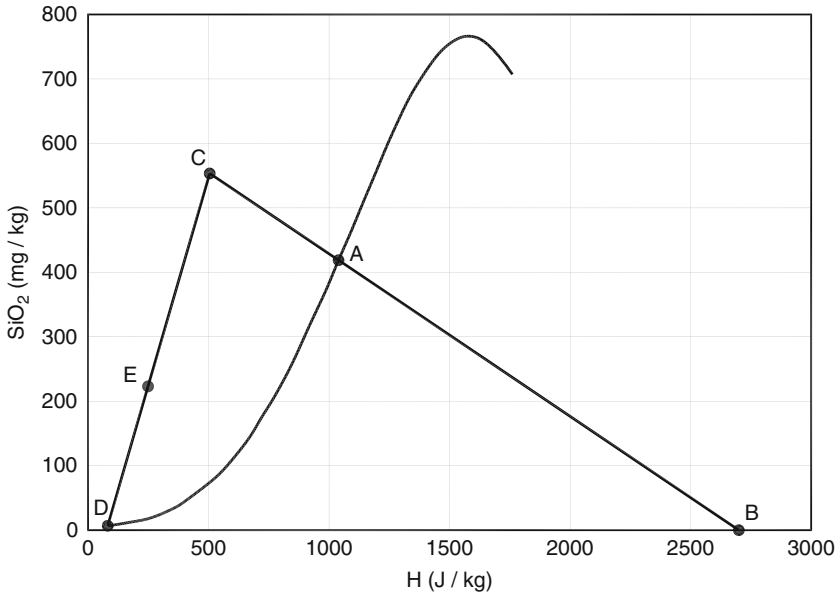

Hydrothermal Systems, Geochemistry of. Figure 4
Graph of equilibrium silica concentration in H2O at the vapor pressure of the solution vs. specific enthalpy. A process of adiabatic cooling of a hydrothermal liquid (point A), followed by mixing with a local meteoric water component (point D), is depicted graphically (see main text). Points (A, B, C, D, E) and compositions (specific enthalpy in J/kg, dissolved silica in mg/kg) are as follows: Original hydrothermal liquid: A (1,037, 418); steam separated adiabatically at 120°C: B (2,706, 0); liquid separated adiabatically at 120°C: C (503.7, 552); cold meteoric water: D (62.99, 5); resulting thermal water: E (239.3, 224)

Gas Geothermometry

Reactions that involve gaseous substances that are present and measurable in the hydrothermal fluid may provide the basis for gas geothermometers. These reactions may or may not involve solid (mineral) phases. Examples of reactions which take place in the hydrothermal fluid and do not involve a mineral phase are the so-called Fischer–Tropsch reaction:

$$CH_4 + 2H_2O = CO_2 + 4H_2 \quad (15)$$

and the conversion of nitrogen to ammonia:

$$2NH_3 = N_2 + 3H_2 \quad (16)$$

An example of a gas reaction which involves mineral phases is the oxidation of pyrite to produce magnetite:

$$3FeS_2 + 2H_2 + 4H_2O = Fe_3O_4 + 6H_2S \quad (17)$$

The collection and handling of samples for the analysis of gaseous species in hydrothermal fluids is, in general, more complicated than is the case for species completely dissolved in the liquid phase [41]. Furthermore, the relative proportions of the gaseous species sampled in the hydrothermal fluid may have been altered by a number of untraceable processes that affect the fluid on its transit from the reservoir to the surface. All these circumstances introduce uncertainty in the interpretation of these analyses, as will be discussed below.

The equilibrium proportions of chemical species that participate in a reaction at a given temperature in, say, the steam phase, are known from thermochemical data. It is safe usually to assume that there exists phase equilibrium between liquid and steam phases, so from the knowledge of liquid–steam partition coefficients, one may know also the equilibrium proportions of species in the liquid phase.

The most favorable situation for the interpretation of the gaseous composition of the hydrothermal fluid is one in which the undisturbed liquid phase is sampled

directly from the reservoir. This situation is approximated closely when one knows that a geothermal well is fed only by liquid phase. In such situation, one may determine the temperature of equilibration of the chemical reaction (i.e., the reservoir temperature) from the analyses of the fluid and the temperature dependence of the equilibrium constant (Eq. 3).

In most cases, however, a geothermal well receives a mixture of liquid and steam phases from the reservoir. This leads to a situation that is considerably more complex [42] because the mobilities of liquid and steam phases in the porous medium are different; thus, the proportions of liquid and steam phases reaching the well will be somewhat different than the proportions in the undisturbed reservoir. In spite of these drawbacks, in these situations the gas composition of the produced fluid is utilized to estimate the fractions of reservoir steam and liquid that make up the mixture feeding the well [43–45]. The fraction of reservoir steam that results from these calculations, which is referred to as the *reservoir steam fraction* and frequently represented by the letter y, approximate as it may be, is a useful reservoir parameter, particularly when employed to detect variations in the conditions of the reservoir resulting from exploitation.

The reservoir temperature, which is a necessary piece of information for the calculations described in the last paragraph, is measured directly, or estimated by the use of other geothermometers. D'Amore and Truesdell [46] developed a graphical method to calculate *both* the reservoir temperature and the reservoir steam fraction by considering simultaneous equilibrium in two reactions in the gas phase.

Some of the reactions that serve as a basis for the calculation of the reservoir steam fraction, namely, the Fischer–Tropsch reaction (Eq. 15) and the conversion of nitrogen to ammonia (Eq. 16), have been reported NOT to be at equilibrium in hydrothermal systems with reservoir temperatures below 250°C [47, 48], so these calculations must be interpreted with caution for such systems.

If the interpretation of the gas composition of fluids produced by geothermal wells is complicated, the case of natural steam vents is even more so. Indeed, there are several processes that may occur during the rise of the hydrothermal fluid to the surface that may affect its composition. For example, the hydrothermal fluid may lose steam at different stages (and different pressures and temperatures) during its rise; the rising steam–liquid mixture may suffer partial condensation at different stages; also, partial re-equilibration of chemical reactions may occur in transit to the surface. Nevertheless, Arnorsson and Gunnlaugsson [47] developed a number of geothermometers based on the concentration of gaseous species, and applied them to steam vents in Icelandic geothermal fields. For some of these sites, the calculated temperatures compare surprisingly well with temperatures measured in nearby wells, but this may be due to particularly favorable hydrological conditions.

Giggenbach [49] proposes a geothermometer based on the ratio of molar concentrations of argon and hydrogen in the hydrothermal fluid, which is designed to be relatively insensitive to processes of steam separation or partial condensation occurring as the hydrothermal fluid ascends toward the natural steam vents. Since both argon and hydrogen are very insoluble in water, and would separate almost quantitatively from the liquid phase upon separation of even a small mass fraction of steam, they are likely to keep their relative proportions unchanged during the rise of the hydrothermal steam to the surface. This geothermometer is based on the following main assumptions. (a) In liquid-dominated systems, the chemical equilibration of species, including volatile components, occurs in the liquid phase. (b) The redox conditions in a fully equilibrated hydrothermal system are quite invariant and keep the ratio of the fugacities of hydrogen to water at a value of approximately $10^{-2.8}$ at temperatures up to 1,200°C. (c) The argon concentration in the reservoir liquid corresponds to that of air-saturated groundwater. With these assumptions, Giggenbach [49] arrives to the expression:

$$t(^{o}C) = 71\left(\log_{10}\frac{X_{H2}}{X_{Ar}} + 2.5\right) \tag{18}$$

where X_i stands for the molar fraction of species i in the sampled fluid. This geothermometer was tested with appreciable success in samples from New Zealand and elsewhere. One serious drawback with this geothermometer is the fact that even the smallest contamination of the sample with air may lead to very erroneous results. Another problem is the possibility that, during its rise to the surface, the fluid may

have lost argon and hydrogen by steam separation, followed by recuperation of hydrogen via chemical re-equilibration, thus leading to an erroneous high ratio of hydrogen to argon, and thus to an overestimation of the reservoir temperature.

It is fair to say that for the exploration of a geothermal site, gas geothermometers should be interpreted with extreme care, and only in conjunction with other techniques such as the cationic or silica geothermometers. This may not be possible in sites where most or all the surface manifestations consist of steam vents and steam-heated waters, in which case the gas geothermometer results should be taken as a rough reference.

Solid Solution Geothermometry

Some minerals tend to form solid solutions through substitution of ions at specific sites in the crystal structure, or by inclusion of ions at interstitial spaces. These ion substitutions or inclusions do not change the crystal structure except for rather minor dimensional distortions. The extent of ion replacement depends on various physical and chemical factors, such as the composition of the surrounding medium, the temperature, and the pressure. In principle, this property of minerals offers the opportunity to identify solid-solution geothermometers when the dominating factor that controls the composition of the solid solution is the temperature.

When drilling a geothermal well in a new area, where there are no nearby wells that provide an indication of the temperature vs. depth profile, a relatively accurate temperature estimation that one could obtain, say from the study of drill cuttings, would be extremely useful. This is so because the information would help decide when to stop drilling and complete construction of the well. At present, engineers need to run costly and time-consuming temperature logs in order to obtain this information. This is an important motivation to develop solid-solution geothermometers.

A geothermometer based on the composition of chlorites has been developed [50–52]. Indeed, linear correlations have been observed of increasing crystallization temperature with increasing aluminum substitution for silicon in the tetrahedral site and with decreasing octahedral site vacancy. In spite of the successful substitution of the original automatic electron microprobe technique with the use of X-Ray Diffractometry [53], the process of sample isolation, analysis, and interpretation is much too complex and time consuming for this geothermometer to be useful in the context described in the preceding paragraph. Nevertheless the geothermometer has been quite useful for the determination of paleotemperatures in a variety of studies.

Geochemical Modeling of Hydrothermal Fluids

In the exploratory stage of development of a hydrothermal resource, the main purpose of geochemical modeling is to determine the temperature and composition of the reservoir fluid, based on the available evidence from surface discharges. This is done by tracing back the processes occurring during the rise to the surface of the hydrothermal fluid. As mentioned above, the reliability of the resulting model will depend on its ability to account for all available evidence, that is, its ability to explain through simple but reasonable processes the origin of all surface discharges, as originating from deep reservoir fluids.

Our ability to model the rise of the hydrothermal fluid depends on our knowledge of the behavior of certain elements and compounds, generally called tracers, upon occurrence of processes of steam–liquid separation and mixing of different fluids.

Stable Isotopes of Hydrogen and Oxygen

Two of those tracers are the stable isotopes of hydrogen and oxygen, deuterium (^2H) and oxygen-18, present in natural waters. Indeed, the species $H_2{}^{18}O$ is present in ocean water in concentrations of the order of 2,000 parts per million. Also, the species HDO, where D stands for deuterium, is present in concentrations of the order of 300 parts per million.

The hydrogen and oxygen isotopic composition of water is measured with a mass spectrometer that determines the ratio of the rare to the common isotopic species (i.e., the ratios HDO/H_2O and $H_2{}^{18}O/H_2O$). Rather than expressing these ratios in absolute terms, they are conveniently expressed in the delta notation (δ) as a per thousand (‰) difference with respect to a water standard.

Thus, the sample's deuterium composition, δD, is calculated as follows:

$$\delta D = \frac{R_{\text{sample}} - R_{\text{standard}}}{R_{\text{standard}}} \times 1000 \quad (19)$$

where R stands for the ratio HDO/H_2O. The oxygen-18 composition, $\delta^{18}O$, is calculated in a similar manner.

The standard that has been adopted almost universally is Standard Mean Ocean Water (SMOW), a water sample with oxygen and hydrogen isotope ratios close to the mean isotope ratios of ocean water [54].

When water separates in two phases (by condensation of steam or evaporation of liquid water), its isotopic composition undergoes *fractionation*, that is, the isotopic composition of the resulting phases is different than the isotopic composition of the original phase. At atmospheric temperatures, the resulting liquid phase will be enriched in the heavy isotopes, deuterium and ^{18}O, and the resulting steam phase will be depleted of them.

As part of the hydrological cycle, water from the ocean continuously evaporates. As the resulting mass of water vapor moves into the continental area, it condensates and looses part of its mass as precipitation (rain). In every precipitation event, the remaining atmospheric steam is depleted further of the heavy isotopes. The process continues as the mass of atmospheric steam moves further into the continental area, giving rise to a distribution of isotopic composition of surface waters, also referred to as "meteoric" waters. This isotopic composition of meteoric water may be seen as a natural label. It was first pointed out by Craig [55] that the isotopic compositions of meteoric waters, which had not undergone appreciable evaporation, were such that the deuterium and oxygen-18 concentrations were linearly related by the following expression:

$$\delta D = 8\delta^{18}O + 10 \quad (20)$$

After Craig's original observation and with more data, Taylor [56] observed a better fit to the expression:

$$\delta D = 8\delta^{18}O + 5 \quad (21)$$

This linear expression is known as the Global Meteoric Water Line (GMWL), and serves as a frame of reference not only for the composition of "fresh" meteoric waters, but also for the isotopic composition of surface waters that have undergone other processes, such as evaporation or isotope exchange with rocks.

There are some natural processes that may alter the isotopic composition of meteoric waters accumulated in the surface or infiltrated in the ground. One of these processes is evaporation. The isotopic composition of a series of surface waters that have originated from the same meteoric water, but which have undergone evaporation to different degrees, would deviate from the GMWL usually along a line of the form

$$\delta D = y\delta^{18}O + x \quad (22)$$

where the slope y would have a value between 4 and 6. The residual waters after evaporation would have higher concentrations of the heavy isotopes and therefore would deviate "to the right" of the GMWL in a δD vs. $\delta^{18}O$ Cartesian plot (see Fig. 5).

Craig [57] observed that thermal waters had a deuterium concentration similar to that of local meteoric waters, but had larger concentrations of oxygen-18, a phenomenon that has been termed the "^{18}O shift." This was ascribed to isotope exchange between water and rock, in such a manner that the comparatively small degree of hydrogen exchange leaves the deuterium content of the water virtually unchanged, but its oxygen-18 content is substantially increased. These observations led to the concept that the main component of thermal waters is, by far, meteoric water that has infiltrated the ground to great depth.

Craig made his observations on what was at the time a comprehensive set of data from known thermal sites. However, as data from more thermal areas has accumulated, it has provided grounds to postulate the existence of a deep water component from partial magmatic origin, called "andesitic water," which in hydrothermal systems found in convective plate boundaries mixes with local meteoric water to form the reservoir fluid tapped by geothermal wells [58, 59] (See Fig. 5). According to this alternative proposition, most of the isotopic exchange with the rock occurs at depths greater than those which are normally reached by drilling, presumably in the site where the "primary neutralization" of magma fluids occurs (see "Introduction"), and the result of this neutralization

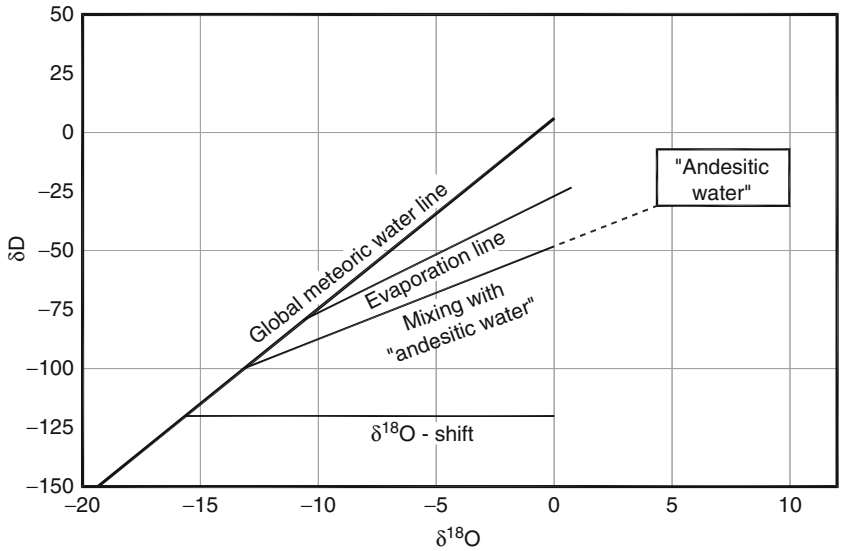

Hydrothermal Systems, Geochemistry of. Figure 5
δD vs. $\delta^{18}O$ diagram showing the position of meteoric waters (Global Meteoric Water Line) and the positions of meteoric waters subjected to evaporation, oxygen-exchange with the rock, and mixing with a deep magmatic component (andesitic water)

is the formation of andesitic water. At the very high temperatures at which this process occurs (close to magma temperatures), it is expected that the proportion of deuterium (and of oxygen-18) in the andesitic water be completely determined by the isotopic composition of the rock or magma phases. It has been suggested that this composition should fall in the ranges of +5‰ to +10‰ for $\delta^{18}O$ and −30‰ to −10‰ for δD [59–61]. It is further postulated that part of this andesitic water would ascend and mix with more meteoric water to form the hydrothermal or reservoir fluid which is reached by drilling in geothermal fields.

As explained in section on "Introduction," in the natural state of a hydrothermal system, the reservoir fluid ascends to the surface through a variety of processes and gives rise to thermal springs, steam vents, and other features typical of thermal areas. In the absence of drilled wells, these are the only sources of information on the chemical and isotopic characteristics of the reservoir fluid. It is the task of geochemistry to infer the temperature and composition of the reservoir fluid from the available evidence.

As explained in relation to the application of the silica geothermometer (Section on "Silica Geothermometer"), with the consideration of parameters that are conserved in the fluid (silica, enthalpy, chloride ion), it is possible to model the processes affecting the rising fluid on its transit to the surface. Under the reasonable hypothesis that no further isotopic exchange occurs between the fluid and the rock during this transit, the deuterium and oxygen-18 contents of the fluid constitute two more conservative parameters.

When liquid water boils, the resulting liquid and steam phases will in general not have identical isotopic compositions. The parameter that describes the equilibrium distribution of isotopes between the two resulting phases (i.e., the isotopic *fractionation*) is the fractionation factor, α. For a given isotope, the fractionation factor is given by:

$$\alpha = \frac{R_{\text{liquid}}}{R_{\text{steam}}} \tag{23}$$

where R stands for the ratio HDO/H_2O in the case of deuterium, and for the ratio $H_2{}^{18}O/H_2O$ in the case of

oxygen-18. For these two isotopes, Truesdell et al. [14] have given a compendium of values of α at temperatures from 0°C to 374°C. The fractionation factor is related to the isotopic compositions of the resulting liquid and steam phases by the following expression:

$$\alpha = \frac{1000 + \delta_{\text{liquid}}}{1000 + \delta_{\text{steam}}} \tag{24}$$

On its rise to the surface, the reservoir liquid may cool by adiabatic boiling, with the steam and liquid remaining in physical contact (and isotopic equilibrium) until the two phases are physically separated at a given temperature. This process shall be called *single-step adiabatic steam separation*. The term adiabatic means that no heat is transferred from or to any surrounding solid (rock) phases. The conservation of enthalpy demands that the mass fraction, y, of generated steam be given by:

$$y = \frac{H_{\text{ol}} - H_{\text{sl}}}{H_{\text{ss}} - H_{\text{sl}}} \tag{25}$$

where H_{ol} represents the specific enthalpy of the original liquid, and H_{sl} and H_{ss} represent the specific enthalpy of liquid water and steam at the separation temperature, respectively.

The conservation of mass for deuterium (or oxygen-18) leads to the following expressions relating the isotopic compositions of the original liquid and the resulting liquid and steam phases:

$$\delta_{\text{ol}} + 1000 = (\alpha + y(1 - \alpha))(\delta_{\text{ss}} + 1000) \tag{26}$$

and

$$\delta_{\text{sl}} + 1000 = \alpha(\delta_{\text{ss}} + 1000) \tag{27}$$

where α represents the value of the fractionation factor at the temperature of separation.

In a real situation, the ascending fluid may suffer more than one event of steam–liquid separation at decreasing temperatures. In fact, one could conceive of a process in which the generated steam separates immediately and continuously from the remaining liquid as soon as it is formed. This process shall be termed *continuous adiabatic steam separation* and, together with the *single-step adiabatic steam separation* described above, constitute the two extreme possible mechanisms of adiabatic boiling of the reservoir fluid on its way to the surface. Both mechanisms lead to an increase in deuterium and oxygen-18 contents of the boiling liquid, but the extent of enrichment is different from one case to the other. An intermediate mechanism that may be called *multiple-stage steam separation* leads, correspondingly, to intermediate enrichments.

The rising reservoir fluid may cool by adiabatic boiling or by mixing with cooler meteoric waters. It may also boil and then mix with meteoric waters, or mix first and then boil, depending on the particular hydrological situation. Truesdell et al. [14] were able to explain the variety of isotopic and chemical compositions of thermal spring waters in Yellowstone National Park, United States, as resulting from a single reservoir liquid at 360°C and particular deuterium and chloride ion contents.

Other Useful Tracers

Other useful tracers are atomic, molecular, or ionic species that exhibit very low chemical reactivity under the conditions prevailing in geothermal reservoirs and upper strata of hydrothermal systems. Some of these tracers partition very favorably (almost exclusively) in the liquid phase, such as chloride ion; some partition very favorably in the steam phase, such as the noble gases, and some distribute themselves in the two phases, but in a manner that can be calculated quantitatively from known partition coefficients (such as the cases of deuterium and oxygen-18). The particular case of silica was discussed in section on "Silica Geothermometer."

When a relatively high flow of the hydrothermal fluid has passed through some natural conduit to the surface, or through a geothermal well, for a sufficiently long time, the radial distribution of temperature around that conduit or well has reached a steady state. Under these conditions, the transfer of heat between the fluid and the rock could be considered negligible, and the enthalpy of the fluid remains constant (see the appendix of reference [14], for a quantitative discussion on this subject). Under these circumstances the enthalpy is another useful "tracer," or conserved parameter, that could be quite useful in modeling the processes affecting the fluid on its rise to the surface [62]. In preceding paragraphs, when referring to adiabatic processes, we have implicitly assumed conditions that support the conservation of the enthalpy of the fluid.

The combined use of tracers and conserved parameters has made possible the determination of conditions at depth in hydrothermal systems [13–16, 63].

Future Directions

There are, of course, many scientific questions remaining to be answered regarding the geochemistry of hydrothermal systems, among them the details of the contribution of magmatic fluids to the formation of the hydrothermal brine. From a technological perspective, however, one would expect more future activity in the interplay between geochemistry and reservoir engineering in studies regarding the sustainability of hydrothermal systems under exploitation.

The next type of geothermal resources to be exploited for electric power generation on a large scale will probably be the so-called Enhanced (or Engineered) Geothermal Systems (EGS). These consist of volumes of hot, impermeable rock, located at reachable depths, which contain substantial amounts of heat. Their development as an exploitable reservoir consists of creating a network of fractures, so as to allow the injection of a working fluid (water) at some point and its extraction through wells located at other points, in such a way that the working fluid extracts the heat from the rock. Important practical issues will arise as a result of the interaction of the working fluid with the rock, which will lead to the dissolution of some minerals and the formation of others, with concomitant changes in porosity and permeability. Geochemistry is expected to play an important role in dealing with these issues.

Bibliography

Primary Literature

1. von Knebel W (1906) Studien in den Thermengebieten Islands. Naturwissenschaftliche Rundschau
2. Thorkelsson T (1910) The hot springs of Iceland. Det kongelige danske Videnskabernes Seleskabs Skrifter
3. Ingersoll LR, Zobel OJ (1913) Mathematical theory of heat conduction. Ginn, Waltham
4. Einarsson T (1942) Ueber das Wesen der heissen Quellen Islands. Soc Sci Islandica 42:91
5. White DE (1957) Magmatic, connate and metamorphic waters. Geol Soc Am Bull 69:1659–1682
6. Ellis AJ, Wilson SH (1960) The geochemistry of alkali metal ions in the Wairakei hydrothermal system. N Z J Geol Geophys 3:593–617
7. Ellis AJ, Mahon WAJ (1977) Chemistry and geothermal systems. Academic, New York, p 392
8. White DE (1967) Some principles of geyser activity, mainly from Steamboat Springs, Nevada. Am J Sci 265:641–684
9. Giggenbach WF (1988) Geothermal solute equilibria. Derivation of Na-K-Mg- Ca geoindicators. Geochim Cosmochim Acta 52:2749–2765
10. Giggenbach WF, Le Guern F (1976) The chemistry of magmatic gases from Erta'Ale Ethiopia. Geochim Cosmochim Acta 40:25–30
11. Giggenbach WF (1987) Redox processes governing the chemistry of fumarolic gas discharges from White Island, New Zealand. Appl Geochem 2:143–161
12. Giggenbach WF (1990) Water and gas chemistry of Lake Nyos and its bearing on the eruptive process. J Volcanol Geoth Res 42:337–362
13. Truesdell AH, Fournier RO (1977) Conditions in the deeper parts of the hot spring systems of Yellowstone National Park, Wyoming, US Geological Survey Open-file report No. 76-428. US Geological Survey, Reston
14. Truesdell AH, Nathenson M, Rye RO (1977) The effects of subsurface boiling and dilution on the isotopic compositions of Yellowstone thermal waters. J Geophys Res 82:3694–3704
15. Giggenbach WF (1978) The isotopic composition of waters from the El Tatio geothermal field. Northern Chile. Geochim Cosmochim Acta 42:979–988
16. Nieva D, Verma MP, Santoyo E, Portugal E, Campos A (1997) Geochemical exploration of the Chipilapa geothermal field, El Salvador. Geothermics 26:589–612
17. Mercado (1975) Movement of geothermal fluids and temperature distribution in the Cerro Prieto geothermal field, Baja California, Mexico. In: United Nations Symposium on the Development and Use of Geothermal Resources, San Francisco, 1975, vol 1. U. S. Government Printing Office, Washington, pp 487–494
18. Ellis AJ, Mahon WAJ (1967) Natural hydrothermal systems and experimental hot water/rock interactions (Part II). Geochim Cosmochim Acta 31:519–538
19. Fournier RO, Truesdell AH (1973) An empirical Na-K-Ca geothermometer for natural waters. Geochim Cosmochim Acta 37:1255–1275
20. Truesdell AH (1975) Geochemical techniques in exploration. In: National Energy Authority (ed) Proc. 2nd. UN Symp. on the development and use of geothermal resources, San Francisco, 1975, vol 1. National Energy Authority, Reykjavik, pp 53–86
21. Arnorsson S, Gunnlaugsson E, Svavarsson H (1983) The chemistry of geothermal waters in Iceland III. Chemical geothermometry in geothermal investigations. Geochim Cosmochim Acta 42:567–577
22. Fournier RO (1979) A revised equation for the Na/K geothermometer. Geoth Res Counc Trans 3:221–224
23. Giggenbach WF, Gonfiantini R, Jangi BL, Truesdell AH (1983) Isotopic and chemical composition of Parbati Valley geothermal discharges, NW-Himalaya, India. Geothermics 12:199–222

24. Nieva D, Nieva R (1987) Developments in geothermal energy in Mexico – Part Twelve. A cationic composition geothermometer for prospecting of geothermal resources. Heat Recovery Syst CHP 7:243–258
25. Bowers TS, Jackson KI, Helgeson HC (1984) Equilibrium activity diagrams. Springer, Berlin
26. Fournier RO (1991) Water geothermometers applied to geothermal energy. In: D'Amore F (ed) Application of geochemistry in geothermal reservoir development, Series of technical guides on the use of geothermal energy. UNITAR/UNDP, New York, p 37
27. Paces T (1975) A systematic deviation from Na-K-Ca geothermometer below 75°C and above 10^{-4} atm P_{CO2}. Geochim Cosmochim Acta 39:541–544
28. Fouillac C, Michard G (1977) Sodium, potassium, calcium relationships in hot springs of Massif Central. In: Pacquet H, Tardy Y (eds) Proc. 2nd. Intl. Symp. on Water-Rock Interaction, Strasbourg, 17–25 August 1977, vol 3. Université Louis Pasteur, Strasbourg, pp 109–116
29. Fournier RO, Potter RW (1979) Magnesium correction to the Na-K-Ca chemical geothermometer. Geochim Cosmochim Acta 43:1543–1550
30. Truesdell AH, Nakanishi S (2005) Chemistry of neutral and acid production fluids from the Onikobe geothermal field, Miyagi prefecture, Honshu, Japan. In: IAEA (ed) Use of isotope techniques to trace the origin of acidic fluids in geothermal systems, Technical document 1448. IAEA, Vienna, p 197
31. Baca Gómez A, Segovia N, Martínez Miranda V, Armienta MA, Barragán Reyes RM, Iturbe García JL, López Muñoz BE, Seidel JL (2006) Physical, chemical, bacteriological and radioisotopic parameters from springs and wells around Jocotitlán volcano, Mexico. Int J Environ Pollut 26:266–283
32. Kharaka YK, Mariner RH (1989) Chemical geothermometers and their application to formation waters from sedimentary basins. In: Naeser ND, McCollon TH (eds) Thermal history of sedimentary basins. Springer, New York, pp 99–117
33. Fouillac C, Michard G (1981) Sodium/lithium ratios in water applied to geothermometry of geothermal reservoirs. Geothermics 10:55–70
34. Fournier RO, Rowe JJ (1966) Estimation of underground temperatures from the silica content of water from hot springs and wet-steam wells. Am J Sci 264:685–697
35. Kennedy GC (1950) A portion of the system silica-water. Econ Geol 45:629–653
36. Morey GW, Fournier RO, Rowe JJ (1962) The solubility of quartz in water in the temperature interval 25 °C to 30 °C. Geochim Cosmochim Acta 26:1029–1043
37. Fournier RO, Potter RW (1982) A revised and expanded silica (quartz) geothermometer. Geoth Res Counc Bull 11:3–12
38. Truesdell AH, Fournier RO (1977) Procedure for estimating the temperature of a hot-water component in a mixed water by using a plot of dissolved silica versus enthalpy. USGS J Res 5:49–52
39. Fournier RO (1973) Silica in thermal waters: laboratory and field investigations. In: Ingerson E (ed) Proceedings: International Symposium on Hydrogeochemistry and Biogeochemistry, Tokyo, 7–9 September 1970, vol 1. Clarke, Washington, DC, pp 122–139
40. Rimstidt JD, Barnes HL (1980) The kinetics of silica-water reaction. Geochim Cosmochim Acta 44:1683–1699
41. Giggenbach WF, Goguel RL (1989) Collection and analysis of geothermal and volcanic water and gas samples, Report No. CD 2387. DSIR, Petone, p 53
42. Nieva D, Quijano León JL (1991) Applications of geochemistry to the study of geothermal resources in Mexico: case study of Los Azufres field. In: D'Amore F (ed) Application of geochemistry in geothermal reservoir development, Series of technical guides on the use of geothermal energy. UNITAR/UNDP, New York, pp 299–316
43. Giggenbach WF (1980) Geothermal gas equilibria. Geochim Cosmochim Acta 44:2021–2032
44. D'Amore F, Celati R (1983) Methodology for calculating steam quality in geothermal reservoirs. Geothermics 12:129–140
45. Nieva D, Fausto J, González J, Garibaldi F (1982) Afluencia de vapor a la zona de alimentación de pozos de Cerro Prieto I. In: Fourth Symp. on the Cerro Prieto Field, Baja California, Mexico, vol 1, p 145
46. D'Amore F, Truesdell AH (1985) Calculation of geothermal reservoir temperatures and steam fraction from gas compositions. Geoth Res Counc Trans 9(1):305–310
47. Arnorsson S, Gunnlaugsson E (1985) New gas geothermometers for geothermal exploration – calibration and application. Geochim Cosmochim Acta 49:1307–1325
48. Taran Y (1986) Gas geothermometers for hydrothermal systems. Geochem Int 20:111–126
49. Giggenbach WF (1991) Chemical techniques in geothermal exploration. In: D'Amore F (ed) Application of geochemistry in geothermal reservoir development, Series of technical guides on the use of geothermal energy. UNITAR/UNDP, New York, p 119
50. Cathelineau M, Nieva D (1985) A chlorite solid solution geothermometer. The Los Azufres (Mexico) geothermal system. Contrib Mineral Petrol 91:235–244
51. Cathelineau M (1988) Cation site occupancy in chlorites and illites as a function of temperature. Clay Miner 23:471–485
52. Kranidiotis P, MacLean WH (1987) Systematics of chlorite alteration at the Phelps Dodge massive sulfide deposits, Matagami, Quebec. Econ Geol 82:1898–1911
53. Battaglia S (1999) Applying X-ray geothermometer diffraction to a chlorite. Clays Clay Miner 47:54–63
54. Craig H (1961) Standard for reporting concentrations of deuterium and oxygen-18 in natural waters. Science 133:1833
55. Craig H (1961) Isotopic variations in meteoric waters. Science 133:1702–1703
56. Taylor HP (1974) The application of oxygen and hydrogen isotope studies to problems of hydrothermal alteration and ore deposition. Econ Geol 69:843–883
57. Craig H (1963) The isotopic geochemistry of water and carbon in geothermal areas. In: Tongiorgi E (ed) Nuclear geology on geothermal areas: Spoleto 1963. Consiglio Nazionale della Richerche, Pisa, pp 17–53

58. Giggenbach WF (1989) The chemical and isotopic position of Ohaaki field within the Taupo Volcanic Zone. In: Proc. 11th New Zealand Geothermal Workshop, Aukland, 1989, pp 81–88
59. Giggenbach WF (1991) Isotopic composition of geothermal water and steam discharges. In: D'Amore F (ed) Application of geochemistry in geothermal reservoir development, Series of technical guides on the use of geothermal energy. UNITAR/UNDP, New York, pp 253–273
60. Sakai H, Matsubaya O (1977) Stable isotope studies of Japanese geothermal systems. Geothermics 5:97–124
61. Taran YA, Pokrovsky BG, Esikov AD (1988) Deuterium and oxygen-18 in fumarolic steam and amphiboles from some Kamchatka volcanoes: "Andesitic" waters. IAVCEI, Commission on the Chemistry of Volcanic Gases Newsletter No. 1, pp 15–18
62. Fournier RO (1979) Geochemical and hydrologic considerations and the use of enthalpy-chloride diagrams in the prediction of underground conditions in hot- spring systems. J Volcanol Geoth Res 5:1–16
63. Giggenbach WF, Stewart MK (1982) Processes controlling the isotopic composition of steam and water discharges from steam vents and steam- heated pools in geothermal areas. Geothermics 11:71–80

Books and Reviews

D'Amore F (ed) (1991) Application of geochemistry in geothermal reservoir development. Series of technical guides on the use of geothermal energy. UNITAR/UNDP, New York

Henley RW, Truesdell AH, Barton PB Jr (eds) (1984) Fluid-mineral equilibria in hydrothermal systems. Reviews in Economic Geology, vol I

IAEA (1983) Guidebook on nuclear techniques in hydrology. International Atomic Energy Agency, Technical Report Series No. 91, Vienna

Valley JW, Taylor HP Jr, O'Neil JR (1986) Stable isotopes in high temperature geological processes. Reviews in Mineralogy, vol 16

Incineration Technologies

Alfons Buekens
Vrije Universiteit Brussel, VUB, Brussels, Belgium
Zhejiang University, Hangzhou, China

Article Outline

Glossary
Definition of the Subject
Introduction
Evaluation of Waste Incineration
Waste Incineration
Incinerator Furnaces and Boilers
Conclusions
Selection of Incinerator Furnaces
Refuse-Derived Fuel
Public Image of Incineration
Future Directions
Bibliography

Glossary

Air equivalence ratio Also, air ratio or air factor, (λ or k), is ratio of actual air supply to the theoretical (stoichiometric) requirements for complete combustion.

Combustion residues Ash remaining after combustion and consisting of bottom-ash or clinker, and of fly ash, entrained by flue gas and eventually separated. Chemical neutralization of flue gas also yields salts, by reaction of acid gas components with basic additives.

Emissions Output of pollutants through the stack (= guided emissions), to a minor extent also as diffuse emission, e.g., from waste pit, evaporation of spills, spreading of fly ash, and outgoing leaks.

Gasification Partial combustion generating flammable gas and conducted with deficiency of air in various reactor types.

Higher heating value (HHV) Amount of heat produced by complete combustion of a specific unit amount of fuel in oxygen.

Immission Added atmospheric concentrations attributed to specific sources, e.g., an incinerator plant, and markedly varying with atmospheric conditions. Immissions are modeled on a basis of (a) emissions, (b) their dispersion, and (c) according to variable atmospheric conditions (wind direction and speed, atmospheric stability).

Municipal solid waste (MSW) Waste produced in a city and collected by the municipality.

Pyrolysis Thermochemical decomposition of organic material in the absence of oxygen, yielding gaseous (pyrolysis gas), condensable (tar), and solid products (char).

Refuse-derived fuel (RDF) Fuel from waste, produced by mechanical processing, (possibly biological), drying, and possibly densification.

Waste-to-energy (WtE) Incineration process in which solid waste is converted into thermal energy to generate steam that drives turbines for electricity generators (http://www.businessdictionary.com/definition/waste-to-energy.html).

Definition of the Subject

Waste incineration is the art of completely combusting waste, while maintaining or reducing emission levels below current emission standards and, when possible, recovering energy, as well as eventual combustion residues. Essential features are as follows: achieving a deep reduction in waste volume; obtaining a compact and sterile residue, yet treating a voluminous flow of flue gas while deeply eliminating a wide array of pollutants.

Robert A. Meyers (ed.), *Encyclopedia of Sustainability Science and Technology*, DOI 10.1007/978-1-4419-0851-3,
© Springer Science+Business Media, LLC 2012

Destruction by fire is almost as old as humanity. Incineration was systematically applied at some locations, both in England and the USA, from the second half of the nineteenth century [1–4]. Furnaces widely differed in conception, yet were still poked and deashed manually. A successful furnace design was the cell furnace, composed of a series of juxtaposed combustion cells with a fixed grate, or also with two superposed retractable grates [4–6]. In 1895, the first large continental incinerator was mounted in Hamburg [7] after traditional export to the countryside of *municipal solid waste* (MSW) was jeopardized by an outbreak of cholera.

The technology was strongly inspired by that of coal firing: *mechanical grate* stokers developed from the 1920s and 1930s were continuously improved to suit the special requirements of firing waste and distributing primary air, while cooling the grate bars [4, 8]. After World War II, *fluidized bed* techniques were introduced mainly in the Nordic countries, where MSW was co-fired together with forest products and residues from pulp and paper industry, and also in Japan, where the suitability of fluidized bed combustors for one- or two-shift operation was valued [9–11]. *Slagging operation*, with tapping of molten residue, remained unusual until the end of the twentieth century; then it became mandatory in Japan to melt fly ash and destroy its organic contents, while either volatilizing or immobilizing its heavy metal content by conversion into a glassy state (vitrification) [12]. A search on "melting" yields more than 130 different processes, as proposed by numerous Japanese corporations [13].

Gasification of waste, a partial combustion conducted with deficiency of air, yields flammable gas, suitable as cleaned gaseous fuel or even for driving engines or turbines [9, 13–16]. This thermal conversion method is mainly apt for high-calorific waste, the complete combustion of which is difficult to control otherwise. Wood waste has been proposed as a decentralized source of heat and power [17, 18].

Pyrolysis, or thermal decomposition of waste [9, 13], may be suitable for specific waste, such as plastics [19], rubber, sewage sludge [20], or wood. These different thermal processes are not to be recommended for general waste, since their process complexity is higher and their availability, hence, lower, whereas most of the advantages claimed often failed to realize [21, 22]. Selecting unproven technology is probably about the worst possible decision in waste management.

Waste varies erratically in *composition* and *properties* and these greatly influence the selection of incinerator furnaces, heat recovery, and flue gas cleaning. Important *waste characteristics* are those determined by *proximate analysis* (moisture, ash, combustibles, subdivided further into fixed carbon and volatile matter) and *elementary analysis* (C, H, N, S, Cl. . . + O, by difference from 100%) of the combustible fraction. Moist refuse is difficult to ignite. Ash content confines the reduction in weight achievable and determines the burden of residue extraction; important is the composition of ash and its softening and melting behavior at high temperature. *Volatile matter* will lead to flaming combustion and *fixed carbon* to glowing combustion, each of these two modes showing their specific demands. Data from these analyses also allow establishing the necessary material balances, as well as estimating the *higher heating value* (HHV).

Combustion of solid waste proceeds in successive steps as schematically represented in Table 1.

In an incinerator furnace, these successive steps may well proceed in parallel and overlap partly. A combination of chemical reactor engineering and of computer fluid dynamics (CFD) may be used in modeling both physical (flow, mass, and heat transfer) and chemical phenomena (combustion, a complex chemical process, proceeding over numerous reactions involving a large number of intermediates, such as free radicals and ions). Cfr. Furnaces, Their Duties, Peripherals, Operation, Design and Control.

Combustion is never *entirely* complete, even though – thermodynamically – equilibrium approach

Incineration Technologies. Table 1 Successive steps in the combustion of waste

Step	Drying	Pyrolysis	Gasification	Combustion
Evolving to the gas phase	Water vapor	Volatile matter	Carbon monoxide, hydrogen, methane	Carbon dioxide, water vapor
Residue	Dry waste	Char and ash	Ash	Ash

could come close to unity. In practice, when most combustibles are burned, the rate of heat generation drops, temperature falls and combustion slows down and eventually stops. The reason for further completing combustion is strictly environmental: *Products of incomplete combustion* (PICs) are major atmospheric pollutants and responsible for reduced visibility, photochemical smog, as well as *soot* or *black carbon* formation. PIC's scientific and health aspects are at the heart of dedicated biannual PIC conferences [23]. Cfr. Post-combustion, Dioxins.

Coarse *combustion residues* (USA: *bottom ash* or slag; UK: *clinker*) are the principal residues of MSW incineration. After removal of unburned material and metals, these may be weathered, graded, and recycled as an aggregate material in sub-road construction and embankments [24–26] Cfr. Residues.

Fly ash is separated by flue gas dust filtration. It is considered *hazardous*, because it accumulates volatilized heavy metals (e.g., Hg, Cd, Pb, and Zn), as well as PICs, some of which are semi-volatile, such as *polycyclic aromatic hydrocarbons* (PAHs) and *dioxins* i.e., polychlorinated dibenzo-p-dioxins (PCDD) and dibenzofurans (PCDF), listed and targeted for removal and destruction by the *Stockholm Convention* on *principal organic pollutants* (POPs). Thermal processes have been applied to detoxify such residues [27–29], yet this treatment is expensive.

Incinerator furnaces. The selection of *furnace types* mainly depends on the characteristics of the waste and the strategies followed to feed the waste to be fired, to contact it with combustion air and to extract the combustion residues from the furnace. Construction of furnaces has evolved mainly empirically, with trial and error as the main method. Tremendous progress made in combustion sciences has started to see some more applications in incinerator design and operation.

Incineration requires sufficient *combustion air*, as well as suitable levels of the three T's, i.e., *T*emperature, residence *T*ime, and *T*urbulence. Turbulence is required to sustain the required macro- and micro-scale mixing to bring together combustibles and air oxygen. Conditions during incineration vary according to the technology employed and the characteristics of the waste fired. Some combustors feature active heat and mass transfer so that combustion takes place much faster, e.g., in vortex or fluidized bed burning. These require, however, size-reduced waste, i.e., preliminary shredding and grading, so that the residence time provided allows either complete burnout even of the largest particles or their recycling after separation.

Temperature ranges from as low as about 750°C (bed temperature of fluidized bed combustion) to more than 1,200°C (destruction of hazardous waste, such as PCBs, slagging operation). High temperatures are only moderately beneficial, for de-mixing of fuel, and oxygen controls combustion rates. *Pressure* is often slightly below atmospheric, to restrict the emanation of combustion products, smoke, and grit. *Residence time* at high temperature is only few seconds (generally 2–3 s) for flue gas. Solid waste and its combustion residue have a much longer residence time, from about a minute in fluidized bed combustion (time required to dry, heat and burnout the ash) to typically half an hour on a mechanical grate; yet, much depends on the time required for drying and heating. After ignition, combustion of volatile matter proceeds rapidly, but burnout of fixed carbon may take time in case of diffusion-controlled combustion, e.g., of ash-occluded carbon.

Some codes prescribe minimum values for temperature and time (e.g., 850°C for 2 s), or they limit the amount of products of incomplete combustion in flue gas (*carbon monoxide*, CO; *total organic carbon*, TOC) and carbon in residues.

Combustion air is supplied to the furnace with several purposes: *primary air* activates the fire bringing oxygen to the reaction surroundings, whereas *secondary air* (also termed over-fire air) is injected at high speed (typically 100 m/s) to induce mixing, as far as its momentum reaches. Increasing primary airflow accelerates combustion until a point at which higher cooling supersedes this stimulating effect. Air may also be used for cooling furnace walls and mechanical grates. Since several decades, water-cooled grates are also in use.

Incinerators are thermal units: liberating more combustion heat also requires supplemental combustion air. A simple rule of thumb states that this amount is directly proportional to the higher heating value, whatever the fuel fired (gas, oil, coal, or garbage of any kind).

In order to obtain complete combustion, it is essential that an adequate amount of air oxygen is supplied. The *air equivalence ratio* indicates the actual air supply, compared to the theoretical, stoichiometric

requirements for complete combustion. The difference, the excess air, merely cools the flame and inflates the volume of gas to be cleaned. Better mixing of fuel and air allow operating at lower air equivalence ratios.

One Mg (metric tonne) of MSW typically generates some 5,000–6,000 m^3 of flue gas! Flue gas flow varies proportionally with both the higher heating value and with the amount of excess air. In numerous plants, the uncontrolled entrance of air leaking into furnace and flues seriously inflates the volume of gas to be cleaned.

During waste combustion, the spatial distribution of flames (formed by combustion of volatile matter) is unpredictable and hence results in erratically active combustion zones, showing oxygen deficiency and less active zones, where oxygen requirements are much less and oxygen plentiful. This results in a complex pattern of oxygen-rich and oxygen-deficient strands that should be mixed intimately in order to reach complete combustion.

Combustion air may also be replaced by oxygen-enriched air, or even by pure oxygen, in order to improve and accelerate combustion. Such practice markedly reduces the volume of flue gas, yet it considerably adds to operating expense and is limited to exceptional cases, such as gasification by means of oxygen/steam mixtures to convert waste into *synthesis gas*.

Municipal solid waste incineration evolved into a complex plant, as represented in Table 2.

MSW storage generally takes place in a deep pit, made of impervious concrete. Storage bridges the gaps between the schedules of collection rounds and continuous firing. A traveling crane allows mixing waste of different origins, stacking waste against the bunker wall, and feeding it into the hopper on top of the load shaft. In the USA, storage floors are in widespread use.

Boiler plant. The heat from flue gas is transferred to the water, boiling in vertical pipe panels, constituting the boiler and organized around the combustion chamber (for an integrated boiler) and in successive vertical passes of the flue gas. An alternative is to suspend boiler tube panels in a horizontal flue gas channel. The resulting medium pressure steam (at 2–4.5 MPa) is superheated in case the steam is used for power generation. At lower temperature, the flue gas preheats the boiler feedwater in an economizer, and possibly the combustion air in a flue gas/air heat exchanger.

Flue Gas Cleaning

Incineration was once a source of smoke and grit. These have been mastered by improved combustion conditions and deep removal of fine dust: once reduced to below 100 mg/Nm^3 by an electrostatic precipitator, the flue gas becomes invisible, a feature that still satisfied the public in the 1950s and 1960s.

Incineration Technologies. Table 2 Composition of current municipal solid waste incinerator plant

Unit	Function	Potential problems
Storage	Bridging the gaps between delivery and firing of MSW	Dust, smells, fires
Crane	Traveling crane to mix and load MSW into a hopper	Mechanical
Hopper	Receiving mixed MSW from the storage bunker	Bridging
Valve	Sliding valve to close the furnace	Mechanical
Shaft	Junction with the combustion chamber	Air infiltration
Furnace	Combustion chamber	Refractory spalling or slagging
Grate	Mechanical grate, supporting, conveying, and poking MSW	Wear, clogging
Burner	Start up combustion, maintain temperature if required	
Boiler	Recovers the heat of combustion from flue gas	Fouling, corrosion, erosion
Dust collection	Separate the bulk of the dust from flue gas	
Scrubber	Acid gas neutralization	Corrosion, erosion, deposits

The German emission code *TA-Luft* (Technische Anleitung zur Reinhaltung der Luft), already in its first version (1974) specified emission levels requiring acid gas levels to be reduced. Since, cleaning the flue gas from waste incineration has steadily become more complex and comprehensive, throughout the 1980s and 1990s. Tables 3 and 4 show both the extent of this gas cleaning duty and the frenetic evolution of these codes in time. The European Union also promulgated successive directives on waste incineration (last directive – Directive 2000/76/EC of the European Parliament and of the Council of 4 December 2000 on the incineration of waste) and prepared codes of good practice (BREF reports: BREF stands for *BAT Ref*erence Document; BAT = *B*est *A*vailable *T*echnology). Other countries (the USA, Japan, and China) use distinct sets of emission Codes and reporting procedures.

For a good understanding of emission limit values, it is of interest to look at the ratio:

$$\text{Reduction ratio} = (\text{Input value})/(\text{Output value})$$

The reduction efficiencies required (in Table 3) of 95% and 99.9% respectively convert into a reduction ratio of 20 and 1,000, respectively. The first two numbers seem deceptively nearby, separated only by 4.9%; the second, the reduction ratios, come closer to the efforts really required in flue gas cleaning, which differ by a factor of 50!

Incineration Technologies. Table 3 Raw gas concentration, emissions, and required separation rate of flue gas cleaning devices (Adapted from [30])

	Raw gas concentration (mg/Nm^3, dry)	Emission limit value (mg/Nm^3, dry)	Required reduction rate(%)
Dust	2,000–10,000[a]	10	99.9
HCl	400–1,500	10	>99
HF	2–20	1	95
SO_2	200–800	50	94
NO_x (as NO_2)	200–400	200	50
Hg	0.3–0.8	0.05	88
Cd, Tl	3–12	0.05	>99.5
Dioxins and furans	1–10 (in ng I-TEQ/Nm^3)	0.1 (in ng I-TEQ/Nm^3)	99

[a]For fluid bed plant these figures are typically 10,000–50,000 mg/Nm^3, dry

The present emission values are monitored and registered continuously. Some parameters (O_2, CO_2, H_2O) remain rather constant; others are more variable (HCl) or are marked by a continuous value, spiked by peaks (CO, TOC). Dioxins cannot be monitored continuously, yet may be sampled continuously and checked on a weekly or biweekly basis.

Dust Collection

Traditionally, cyclones or *electrostatic precipitators* (ESPs) featuring 2, 3, or 4 consecutive fields were arresting the evolving grit and dust, with an efficiency approaching unity according to an exponential curve. As a consequence, it is increasingly difficult to collect the last particles. Important parameters are the size and electric resistivity of the particles to be collected, as well as their behavior (cake severance or re-entrainment) at the moment of rapping the collection electrodes. Moreover, ESPs operating at temperatures substantially above 200°C were found to generate considerable amounts of dioxins.

Current codes require retention also of the small particles around a micrometer in diameter: even though they correspond to only minor amounts when expressed in mass units (mg/Nm^3), they represent relatively large numbers of particles, strongly enriched in pollutants. *Baghouse filters* (BHFs) are capable of efficiently collecting these particles; moreover, they accumulate a layer of basic substances (injected lime, fly ash) that react with acid gases, such as HCl, SO_2, and HF, from the flue gas and adsorb some semi-volatiles.

Neutralization of Acid Gases

Historically, several solutions have been developed to the acid gas problem: wet scrubbing, dry scrubbing, semi-wet scrubbing, and semi-dry scrubbing. Generally, to neutralize these acid gases, hydrated lime is injected into the flue gas (*dry*, *semi-dry*, i.e., after further moistening the flue gas, and *semi-wet scrubbing*, using water slurries of lime). Wet scrubbing is even more efficient, since the principal acid gas, HCl, is eminently water soluble; yet it is also more complex and capital intensive because of the necessity of

Incineration Technologies. Table 4 Some milestones in the evolution of emission limit values (Germany and the European Union)

Compound	TA-Luft Germany, 1974	EU directive 89/369	17. BImSchV[b,c] Germany, 1990	Unit
Dust	100	30	10 (30)	mg/Nm^3
HCl	100	50	10 (60)	mg/Nm^3
HF	5	2	1 (4)	mg/Nm^3
SO_2	–	300	50 (200)	mg/Nm^3
NO_x	–	–	200 (400)	mg/Nm^3
TOC			10 (20)	mg/Nm^3
CO			50 (100)	mg/Nm^3
Heavy metals,[a]				
• Class I	20	0.2	0.5	mg/Nm^3
• Class I + II	50	0.2	0.05	mg/Nm^3
• Class I + II + III	75			mg/Nm^3
Dioxins and furans	–	0.1	0.1	ng TE/Nm^3

[a]The comparison is distorted by changes in the definition of various classes
[b]17. BImSchV Ausfertigungsdatum: 23.11.1990. Complete citation: "Verordnung über die Verbrennung und die Mitverbrennung von Abfällen in der Fassung der Bekanntmachung vom 14. August 2003 (BGBl. I S. 1633), die durch Artikel 2 der Verordnung vom 27. Januar 2009 (BGBl. I S. 129) geändert worden ist" Cfr.: http://www.gesetze-im-internet.de/bundesrecht/bimschv_17/gesamt.pdf
[c]The 17th BundesImmissionsSchutzVerordnung gives values for a daily average, as well as for a 30-min average, the latter in parentheses

maintaining a water circuit and treating the resulting wastewater, removing organic compounds as well as sludge and heavy metals. Moreover, wet scrubbing generally is conducted in two steps: in the first, acid scrubbing (pH 0–2) the bulk of HCl is removed and SO_2 follows in the second step, conducted under mild acid or basic conditions (pH 6–8). However, unless the scrubbed flue gas is reheated, wet scrubbing generates a visible plume of condensing water droplets, with its concomitant negative psychological impact. Still, deeper cooling of scrubber liquors also deepens the removal of virtually all pollutants, including mercury and the various PICs (Table 5).

Incineration Technologies. Table 5 Typical stoichiometric factors applied in flue gas cleaning (acid gas neutralization) [30]

Flue gas cleaning	Semi-dry	Semi-wet	Wet
Range (as cited)	2.4 to >3	2.2–3.0	1.1–1.4

Products of Incomplete Combustion – Organic Semi-volatile Micropollutants

In principle, ensuring steady, high-quality combustion and avoiding all combustion upsets should control *products of incomplete combustion* or *PICs*. The latter relate to large masses burning together rapidly and to poor mixing of the intrinsically heterogeneous input.

Much attention has been given to organic *semi-volatile micropollutants* (PAHs, dioxins) that occur in only minute amounts ($\mu g/Nm^3$and even ng/Nm^3), yet are persistent and bio-accumulating. These compounds are largely removed (>99%) by baghouse filters, after their adsorption onto fine activated carbon particles (typically injected at a dosage of 50–200 mg/Nm^3) or else provided as a fixed adsorption bed.

As an alternative, they are oxidized by means of suitable DeNOx-catalysts, active already at a very low temperature (200°C). A number of preventive measures also allow reducing the formation of PAHs and dioxins (cfr. Dioxins).

Nitrogen Oxides

Nitrogen oxides are formed during combustion, by means of complex free radical and even ionic mechanisms. NO is formed at high temperature and eventually emitted into the atmosphere. In air, slow oxidation of NO takes place, forming strongly oxidizing NO_2. Together with NO, this NO_2 forms an atmospheric oxidizing-reducing system, responsible for the formation of photochemical smog (smog = smoke + fog) and haze. Nitrogen oxides are hence termed "NOx" (NO + NO_2) and generally expressed as their NO_2 equivalent.

NOx in flue gas derives from mainly two sources: the incineration of organic N-compounds (fuel NOx) and incineration at high temperature, e.g., in cement kilns or during slagging operation (thermal NOx and also prompt NOx).

When desirable or required by codes, such NOx can be thermally (*selective non-catalytic reduction*, SNCR) or catalytically reduced (*selective catalytic reduction*, SCR) by means of suitable reducing agents, such as ammonia, urea, amines (N-compounds), hydrocarbons (reburning), and others. Thermal reduction is only possible in a high temperature window, of 760–1,000°C. Catalytic reduction is active already at much lower temperatures, typically 250–450°C.

Another nitrogen oxide is known as nitrous oxide (N_2O), or laughing gas. It forms preferentially at medium-low combustion temperature, such as the fluidized bed combustion of sewage sludge, and during reduction of the conventional NOx. It is a naturally occurring regulator of stratospheric ozone and a major greenhouse gas and air pollutant.

Heat Recovery

Heat recovery has always been central in incineration, and at times waste was regarded as free fuel, yet heat recovery is generally uneconomic in small plants. Some plants incorporate captive uses for the heat produced, e.g., by being linked to district heating systems (Denmark, Sweden) or integrated with civic centers, featuring swimming pools, sauna, and hot baths (Japan), yet generally it is difficult to market the heat produced, so that power generation emerges as a last resort, albeit at limited efficiency. Moreover, the presence of boiler and turbo-generator inflates plant downtime.

Sensible heat is difficult to recover from flue gas, since it is both fouling and corrosive. These limit the possible operating pressure of a *waste heat boiler* (consecutive to the incinerator furnace) or of an integrated boiler, with the furnace fully integrated into its boiler structure (used for highly calorific waste only). Low boiler pressure limits the possible conversion efficiency of steam energy into power. Typically, such conversion efficiency into power is only 16–24%, based on the HHV of waste compared to better than 40% for large fossil fuel–fired thermal power plants (cfr. Heat Recovery).

Co-firing. Waste can also be co-fired in non-dedicated thermal units, such as thermal power plants, cement or limekilns, and in large industrial boilers. Not all waste is suitable, though, because of both combustion and gas cleaning considerations. Table 6 lists the

Incineration Technologies. Table 6 Some specifications for RDF to be fired in cement kilns [31]

Element	Typical value (ppm)	Limit value (ppm)	Hazardous waste* (ppm)
As	9	20	300
Be	0.4	2	50
Cd	3	5	(+ Tl) 90
Co	8	15	300
Cr	40	120	3,000
Cu	100	150	3,000
Hg	0.6	1	5
Mn	50	150	2,500
Ni	50	100	2,000
Pb	50	100	2,000
Sb	25	60	150
Se	5	10	80
Sn	10	40	1,500
Te	5	20	80
Tl	1	2	
V	10	20	1,500
Zn	n.a.	n.a.	15,000

Source: Reference [31]

typical requirements for co-firing in cement kilns (cfr. Co-firing of Waste or of RDF, Thermal Power Plants, Cement and Lime Kilns).

Cost and Plant Availability

Incineration is a technically complex and expensive operation. In the European Union, an all-in cost factor for MSW incineration is ca. 100 €/Mg (1 Mg = 1 metric tonne). In Japan, this cost is about three times higher. Internal comparison is difficult, because of highly variable cost factors corresponding to buildings, other infrastructure and, in Japan, land.

Plant availability typically ranges from 84% to 92%, the latter catering for an annual shutdown, the former accounting for repeated and unscheduled stops. Availability heavily depends on the quality of plant management and maintenance.

Public Acceptance

For a variety of reasons, environmentalists have fought incineration as a waste management option: it is not natural (like composting), destroys recyclables, and generates toxic compounds. This opposition is often termed the *not in my backyard* (NIMBY) syndrome and is sometimes counterproductive to the development of adequate solutions on a sound technical and economic basis. (cfr. Public image of Incineration).

Whatever the quality or foundation of the arguments against incineration, the design and operating standards have been much further improved over recent years and today's incinerator emission standards are probably the toughest in industry.

Introduction

This introduction situates the position of waste incineration in a wider scope of waste management. Traditional waste management was limited to the three options: landfill, composting, and incineration. Landfill was suitable for reclaiming low-value lowlands or restoring the landscape affected by mines and quarries (sand, gravel, clay). Some large cities (e.g., London!) used MSW to fill lowlands, as well as empty quarries of sand, gravel, or clay, to build artificial islands (Tokyo), or even dumped MSW into the sea (New York, Istanbul). Lack of preliminary hydrogeological study and of adequate barriers to contain the leachate has led at times to serious contamination of groundwater. Moreover, landfills are responsible for important high greenhouse gas emissions (methane, carbon dioxide). Composting is still applied nowadays on selectively collected organic fractions; raw MSW yields an unacceptable quality of compost, due to the presence of heavy metals. Incineration has been widely practiced in densely populated regions, where land is at a premium (large municipalities, Japan, Switzerland) and volume reduction primordial.

The 1970s introduced numerous new concepts into waste management, such as the concept of special (Germany), poisonous (England), toxic (Belgium), chemical (the Netherlands) or otherwise hazardous waste (USA, OECD), producer responsibility, the Polluter Pays principle, and mandatory recycling. In the early 1970s, the European Union declared itself competent in environmental matters and the first Framework Directive on Waste (1975) specified the necessity of appointing authorities responsible for waste management, granting licenses, and inspecting waste processing premises. A number of waste streams received particular attention, e.g., hazardous waste, PCBs, waste oil, and packaging. Industrialized countries were repeatedly confronted with waste scandals; industrial and hazardous waste infrastructure was set up step by step and became a booming business. The lowest possible cost disposal was gradually replaced by high-tech, high-cost options. This transition was smoothened through subsidies supporting the options preferred by government and through levies penalizing low-cost landfill. Waste management was borne by the public sector, the private sector, or by public-private initiatives.

According to the Ladder of Lansink (after Dr. Ad Lansink who is a Dutch politician famous for proposing this waste management hierarchy in the Tweede Kamer [Dutch Parliament] in 1979), the generation of waste should in the first place be either prevented or reduced. Next options are reuse and recycle. Lower-ranking options are incineration (preferably with heat recovery), and landfill. Waste management is a legislation-driven business. In several EU countries and in Switzerland, the landfill option is increasingly restricted, so that combustible waste can no longer be landfilled.

Developing countries are often confronted with fast urbanization, so that public services cannot follow demand. Moreover, waste is rich in organics and barely combustible. Large Chinese cities at present are entirely surrounded by a girdle of landfills, polluting groundwater and generating hazardous fermentation gas. Incineration makes rapid progresses, using imported as well as adapted self-developed technology. The severe acute respiratory syndrome (SARS) was material in promoting incineration, in particular for hospital waste. As in numerous developing countries, Chinese MSW is still barely combustible, without resorting to auxiliary fuel!

Evaluation of Waste Incineration

In brief, waste incineration can be summarized as follows.

Advantages

- It eliminates objectionable and hazardous properties, such as being flammable, infectious, explosive, toxic, or persistent.
- Putrescible matter is sterilized and destroyed. Pathogen count becomes low and generally negligible, except in cases of deficient operation.
- It thermally treats solids while realizing a large reduction in volume, for MSW often by a factor of 10 or more.
- It destroys gaseous and liquid waste streams leaving little or no residues, except for those linked to flue gas neutralization and treatment.
- The heat of combustion generated may be put to good use.

Disadvantages

- Incineration is technically a complex process, requiring huge investment and operating cost as well as good technical skill in maintenance and plant operation, in order to conform to modern standards.
- Heat recovery takes place under adverse conditions (boiler fouling, erosion, corrosion) and is often costly and inefficient.
- Incineration generates an amount of pollutants which are not easy to control.
- Complete burnout of flue gas and residues needs to be ensured.
- As emission codes become more stringent, operating costs rise and the volume of secondary waste streams requiring further disposal increases (in decreasing order with dry, semi-wet, or wet gas scrubbers).

Some types of waste are banned from incinerator plants, unless they are specifically equipped to cope with such waste, e.g.:

- Volatile metal (i.e., principally mercury, thallium, and cadmium) bearing waste.
- PCB-containing waste, which requires special incinerators with unusually high destruction efficiency.
- Radioactive waste. The absence of such waste is now routinely checked in MSW, due to widespread use of medical radioactive preparations for either diagnostic or treatment purposes. Radioactive waste can be incinerated like other waste, with (a) volume reduction and (b) immobilization of radionuclides in ash as major aims; yet, containment is essential. Incineration may hence be conducted under slagging conditions. Dust filters should substantially retain all dust.

Waste Incineration

Waste Incineration can be described as "the controlled burning of solid, liquid or gaseous combustible wastes so as to produce gases and residues containing little or no combustible material" (Ph. Patrick, 1980. Past president of the Waste Management Institute (UK)). The technique is now considered from various viewpoints:

- Waste streams of interest
- Phenomena in waste incineration
- Stoichiometry
- Mass balances
- Incineration products
- Residues
- Thermal aspects
- Furnace capacity
- Safety aspects
- Incinerator furnaces – principles – operations – fields of application
- Post-combustion

- Heat recovery
- Corrosion problems
- Flue gas composition and cleaning
- Dioxins

Next, the major types of incinerator furnaces and the conversion of waste into refuse-derived fuel are discussed.

Waste Streams of Interest

Incineration generally addresses combustible waste, whether it is gaseous, liquid, sludge, paste like, melting or solid. Particular streams are municipal solid waste (MSW); commercial, industrial, and hazardous waste; sewage sludge; and hospital waste. Waste that fails being auto-combustible can still be incinerated by means of auxiliary fuel.

Municipal solid waste (MSW) has been routinely analyzed by manual sorting (and sieving of fines) in the Netherlands even on an annual basis and for different types of residential areas (TNO). Argus, Berlin, produced a very much detailed analysis in the early 1980s [32, 33]. Each major sorting fraction (fines, vegetal matter, paper and board, plastics, etc.) was analyzed for its pollutant contents (elementary composition, heavy metals, and dioxins).

Industrial process streams can be very diverse, e.g., gaseous, aqueous, and organic effluents from the most diverse industrial processes, sludge and dust from treating such effluents, waste oil and solvents, and, finally, solid waste. Process waste with stable characteristics is often disposed in-plant, in boilers, or furnaces. Occasional waste and small arising is stored in empty drums, bags, or barrels, grouped and sent to waste disposal centers. Some large factories, such as *BASF* (Ludwigshafen) or *Ford* (Cologne), have operated their own centers since the 1960s. The community operates some comprehensive centers (Denmark, Bavaria); private or public/private entrepreneurs manage others.

Green waste (branches, brush, and logs) may be collected separately for shredding and/or composting or for use in waste-to-energy (WtE) schemes.

Sewage sludge is also a generally occurring municipal waste, mainly consisting of water, so that mechanical dewatering and drying yield tremendous reduction in volume. Co-firing has been practiced many different ways, in mass burning, power plant, etc. Dedicated furnaces are mainly fluidized bed, multiple hearth, and rotary kiln.

Bulky waste or bulky refuse relates to waste types too large to be accepted by the regular waste collection, such as discarded furniture, large household appliances, and plumbing fixtures. The tendency to incinerate such items directly has declined: bulky waste is diverted increasingly for reuse and recycling; what remains is shredded before incineration. Some plants for bulky loads were operated on a full-day burning, nighttime cooling cycle. For fuel economy and especially for environmental reasons, such practices are no longer recommended. Dismantling for recycling and shredding of nonrecyclables is a better option.

Automotive shredder residue (ASR) often contains hazardous substances such as lead, cadmium, and PCBs. Some countries have classified ASR as hazardous waste and have established legislative controls.

Hospital waste is another stream often earmarked for incineration. Its composition varies with local systems for segregated collection. Specific compounds are sharps and disposables and infectious waste. Hospital waste is often incinerated in a two-step process, first partial oxidation then high-temperature post-combustion of fumes, derived from the pyrolyzer. There is a tendency to concentrate incineration in centralized units rather than in scattered and ill-managed small local plants.

Hazardous waste as a rule loses its hazardous properties during incineration. The hazards are more relevant during collection, storage, and pretreatment than during incineration proper. One category of waste stands out: *chlorinated waste* can best be fired to eliminate its persistent, lypophilic, and bioaccumulating properties. Alternatives, such as dehalogenation exist, yet are an order of magnitude more expensive. Particular aspects of chlorinated waste incineration are:

- Very high combustion efficiency ($\eta_{Comb} > 0.9999\ldots$) is required.
- Hence, a minimum combustion temperature of 1,200°C is stipulated.
- The Deacon reaction (forming chlorine gas) is avoided by operating with minimal excess of air, possibly addition of steam (both to steer the

equilibrium), and fast cooling or even water quenching (to freeze the high temperature composition).
- The formation of phosgene ($COCl_2$) is also avoided, by reducing Cl_2 formation and striving for complete conversion of CO into CO_2.

Dedicated thermal units are developed for *recovery* and cleaning of metal or metal parts, contaminated with paint, lacquers, or polymers.

Important Properties of Waste

Important properties of waste are related to:

- Storage behavior and potential hazards during storage (cfr. Safety Aspects)
- Form and size of individual particles and their distribution, physical and bulk density, specific surface, angle of repose
- Flammability and putrescence of *solid wastes*
- Bulk and physical density, viscosity, heat conductivity, reactivity, explosion limits, flash point, ignition temperature, vapor pressure, boiling point, gas evolution or decomposition during preheating, corrosiveness, toxicity, possibility of auto-oxidation, spontaneous polymerization or other incontrollable, exothermic or dangerous reactions of *liquid wastes*
- Density, explosion limits, toxicity, and corrosiveness of *gaseous wastes*.

Waste Gases – Liquids - Solids

The *heat of combustion* of pure chemical compounds is simply derived as the difference between the heat of formation of products and reactants.

The *higher heating value* (HHV) of fuel is derived by burning a known amount with oxygen in a bomb calorimeter and monitoring the amount of heat liberated that is largely transferred to the water mass surrounding the combustion chamber. The resulting temperature rise is proportional to the heat liberated; heat losses to the surroundings are corrected for by calibration. Several empirical formulas were developed to estimate the heat of combustion of a fuel, from its elementary composition, e.g., the Dulong equation (originally developed for coal and later modified to accommodate a variety of fuels, including municipal solid waste).

The heat of combustion of the combustible fraction of refuse is given by:

$$327.81(\mathrm{C}) + 1504.1(\mathrm{H} - \mathrm{O}/8) + 92.59\mathrm{S} + 49.69\mathrm{O} + 24.36\,\mathrm{N} \quad \mathrm{kJkg}^{-1} \tag{1}$$

In this formula C, H, O, S, and N stand for the mass percent of each of these elements. These are expressed on a moisture and ash-free (maf) basis. More formulas are cited in Niessen [35].

The *lower heating value* (LHV), also termed *calorific value*, is lower, because from the HHV value one must subtract the *latent heat of condensation* of water vapor present in the flue gas, but which generally is lost with the flue gas in the plume.

The *proximate analysis* establishes the moisture and ash content (wt.%) and – by difference – the combustible part of the waste (wt.%). Thus the proximate analysis defines the amount of moisture to be evaporated prior to combustion and the required dimension of the ash handling equipment. Moist wastes, such as garbage, sewage sludge, and aqueous solutions, burn only after evaporation of most of the moisture contained. Hence, adequate measures should be taken to ensure fast and complete drying.

The *elementary* or *chemical analysis of the combustibles* should be known in order to estimate the composition of the flue gas at a given excess of air and to determine whether wet or other scrubbing of the flue gas is required.

The other properties are helpful to select and specify the waste storage, handling and feeding facilities and the required safety provisions. Information is also required on the frequency and timing of the deliveries, the kind of containers and packaging, etc.

Individual gaseous combustible compounds are characterized by means of their chemical formula and structure and molecular mass (often termed molecular weight). Density is proportional to molecular mass, which is easily derived as the sum of all atomic masses. Denser gas requires proportionally more combustion air and hence a larger supply of air to the burner. The HHV is roughly proportional to the mass of fired gas. Gases are also often characterized by their Wobbe-index, a factor combining HHV and density.

Important properties for *liquid fuels* or waste are viscosity, density, flash point, surface tension, sooting

tendency, etc. These affect oil atomization and combustion, as well as burner construction, operation, and maintenance (Table 7).

Solid fuels or waste vary in chemical composition and thermal behavior. Coal consists of highly condensed aromatic structures capable of thermal softening, melting, and decomposing. Depending on its rank, coal generates combustible gas and volatiles during combustion, giving rise to flaming combustion and leaving a carbonizing residue. Biomass predominantly consists of cellulose structures, bounded by lignin. Worldwide, it is still an important fuel; yet, it loses much of its importance in terms of industrial use and trade.

Phenomena in Waste Incineration

Combustion science has evolved enormously, with respect to both theoretical concepts and experimental study. Some relevant references as well as past and ongoing conferences are cited in the general bibliography. Incineration is much more an empirical engineering science [35–38]. The last reference provides a state-of-the art review, composed on the basis of European experience.

Combustion of *flammable gas* follows two distinct modes: fast combustion in premixed flames (*mixing is burning*) and diffusion-controlled flames, those relevant in this context. Since waste flammable gases are difficult to store in oil refineries or petrochemical plants, they are commonly disposed of by either elevated or ground *flares*. Severe sooting may occur during an emergency, when large flows need to be flared. Sooting is reduced by addition of steam through ejectors located in nozzles that draws in ambient air. Smaller, better controllable gas streams are often burned in available boilers or furnaces. Where necessary, they are combusted either thermally in a dedicated yet simple combustion chamber, or catalytically on a fixed catalytic bed.

Combustible liquid wastes are generally fired, dispersed into fine droplets, each of which burns as a small entity, composed of evaporating liquid and diffusion flames around the periphery.

Solid fuels first dry, and then thermally decompose while heating, with evolving volatiles sustaining flaming combustion and the charring residue much slower glowing combustion. Converting fuel or waste into volatiles and fixed carbon is an essential step (pyrolysis) in their combustion. Mimicking this process is an essential test; for coal this test was standardized differently in each industrial country, yet 950°C is a typical temperature for defining the split between volatiles and fixed carbon. Heating rate applied and test duration also influence this split (Fig. 1).

In practice, these steps proceed partly in parallel, rather than in a strict sequence.

Drying is a gradual process: moisture can be absorbed quite loosely, e.g., by plastics, or firmly, physicochemically bound to its substrate.

Incineration Technologies. Table 7 Some models for combustion of liquid and solid particles

Model	Hypotheses				
	Number of compounds	Surface temperature compared to gas temperature	Heat exchange	Oil thermal conductivity	Diffusion in droplet
The d^2 law	One	Lower	Radiation	High	–
Scale model	One	Comparable		Nil	–
Homogeneous temperature	One	Comparable	Radiation + losses	High	–
Diffusion control in droplets	Several	From enthalpy balances	Rate laws	Rate laws	Species balances
Direct simulation	Several	From enthalpy balances	Rate laws	Rate laws	Species balances

Source: After Görner K [34]

Incineration Technologies. Figure 1
Flaming combustion of solids [39] (By courtesy of Wikipedia)

All organic materials decompose upon heating, generating generally smaller and simpler molecules. The emerging volatiles contain inorganic (CO, CO_2, H_2O, H_2, etc.) as well as aliphatic and aromatic organic compounds; their product distribution depends on numerous factors, such as raw materials, temperature, residence time of volatiles and solid fraction and – not in the least – catalytic effects exerted by ash, bed material, or furnace walls.

Primary pyrolysis products show structures close to those of the molecules pyrolyzed. The longer the residence times, the more these structures evolve toward thermally more stable molecules. Ultimately, mainly carbon, hydrogen, and water vapor remain when pyrolysis is concluded in the absence of air.

Cellulosic compounds, such as paper or wood, decompose already at ca. 250°C according to quite complex mechanisms that thermally soon become self-sustaining. Some plastics, conversely, follow simple-looking *unzipping* mechanisms, yielding monomer or oligomer (low polymers, such as di-mer, tri-mer, etc.) as a product. This is the case for, e.g., polymethylmetacrylate (PMMA) and polystyrene (PS).

Vinyl compounds (polyvinylchloride, polyvinyl alcohol, polyvinyl acetate) decompose at unusually low temperatures, releasing hydrochloric acid HCl, water, and acetic acid (CH_3COOH), respectively.

PVC also decomposes in two steps. HCl evolves almost quantitatively from PVC between 225°C and 275°C. This step also produces some benzene. The second step yields further, mainly aromatic compounds, by internal cyclization [40].

Polyolefins, such as polyethylene and polypropylene pyrolysis attains a maximum rate of decomposition at ca. 450°C [41]. Primary products are polyolefinic and paraffinic chain fragments, following a Gaussian molecular weight distribution: higher temperature generates in average shorter product molecules. Secondary products from polyethylene, as well as primary products from polypropylene, show more branched chain products.

Solid waste incinerators generally feature a *mechanical grate* that supports, conveys, and pokes the waste, while primary combustion air activates the fire and cools the grate. Traveling grates, roller grates, and reciprocating grates show *plug flow* characteristics, i.e., an almost even residence time for the different refuse parcels that move through the furnace. This leads to successive zones of drying, heating, ignition, and flaming combustion of waste, and residue burnout. *Reverse-reciprocating grates* create back-mixing, by pushing the burning waste upstream, underneath the incoming fresh refuse.

Incinerators burn highly flammable plastics, side by side with wet vegetal waste. Once heated high enough (>400°C) for fast pyrolysis to occur, plastics decompose swiftly and hence burn rapidly, creating oxygen-deficient flames and leaving craters in the original refuse layer. On the other hand, wet waste is slow to ignite, for first it must be superficially dried before it can start rising in temperature, generating flammable vapors, and eventually catching fire. Even then, large lumps of moist vegetal matter may remain wet internally and survive incineration. Also, massive wood, or a thick book, takes time to burn, the carbonized material thermally insulating the flammable core.

Thus, burning refuse is heterogeneous and produces strands of oxygen-deficient hot gas as well as

other gases, still prior to ignition and composed of moist air, charged with smelly products, arising in drying and heating. Unless hot oxygen-deficient and cold oxygen-rich flue gas strands are thoroughly mixed by blowing in secondary air at high speed, products of incomplete combustion will likely leave the furnace unconverted (Fig. 2).

Draft is the most important physical factor determining incinerator capacity. Only the smallest units operate on natural draft, as generated by the chimney. Fans (forced draft) blow in primary and secondary air; a much larger fan in front of the stack provides induced draft. The stepwise extension of flue gas cleaning, necessitated by past progression of the cleaning levels, has inflated the head losses and increased the required capacity and the power consumption of induced draft fans.

The *residence time* of gaseous and liquid wastes in an incinerator amounts to only few seconds. The residence time required for complete combustion of solids is generally about half an hour.

Hence, incinerator feed should always be made as *homogeneous* and *constant* as possible, e.g., by mixing, blending, and for municipal solid waste (MSW) ageing, to provoke moisture transfer and to account for a wide difference of flammability between easily igniting plastics on the one hand and moist vegetal waste on the other.

Stoichiometry

Gaseous and liquid waste can be completely combusted using *low excess of air* (5–15%) as far as their composition is sufficiently predictable and constant and mixing of air and fuel well organized. In principle, much more excess is required when firing solid waste, except in incinerator types featuring first-rate air/solids contact, e.g., fluidized bed or vortex units. Lower airflow

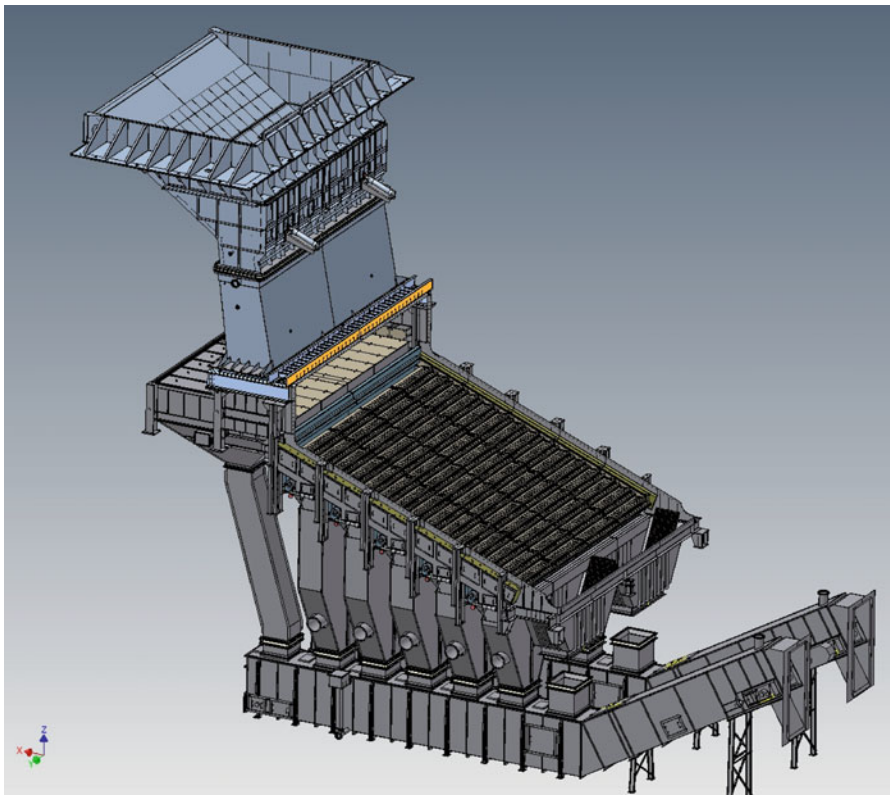

Incineration Technologies. Figure 2
Representation of a mechanical grate incinerator (By courtesy of Keppel-Seghers)

also has other advantages: it elevates the combustion temperature, extends the residence time in a given furnace volume, and reduces entrainment of fly ash with flue gases, as well as thermal losses with flue gas in the stack.

The amount of *combustion air* provided markedly exceeds stoichiometric requirements, following from formal reaction formulas, such as:

$$C + O_2 \Rightarrow CO_2(12g + 32g = 44g) \quad (2)$$

$$2H + \frac{1}{2}O_2 \Rightarrow H_2O(2g + 16g = 18g) \quad (3)$$

$$S + O_2 \Rightarrow SO_2(32g + 32g = 64g) \quad (4)$$

Combustion equations are normally marked in atomic or mol units; the corresponding weight amounts are marked in grams. Under standard conditions 1 mol of gas has a volume of 22.4 l or dm^3.

Mass Balances

The *Law of Mass Conservation* also applies to incineration. Hence, the sum of all *input streams* equals the sum of all *output streams*, whether

- In *total* mass flows (kg/h)
- *Any individual element* entering and leaving the plant, and expressed either in mass units (kg/h) or in number of moles (mol/h). In combustible waste, the main elements (symbol, atomic mass) are carbon (C, 12), hydrogen (H, 1), oxygen (O, 16), sulfur (S, 32), nitrogen (N, 14), and chlorine (Cl, 35.5).

Input streams are typically (1) waste, (2) auxiliary fuel (when needed), and (3) primary and secondary combustion air and also uncontrolled air entering through leaks. The latter can be estimated along the flue gas path, simply by measuring the rising oxygen or the declining carbon dioxide content of the flue gas.

During *flue gas cleaning*, additional compounds may be added, such as basic additives (hydrated lime $Ca(OH)_2$, lime CaO, or even – at high temperature – ground limestone $CaCO_3$, and also sodium bicarbonate $NaHCO_3$ or hydroxide NaOH), ammonia or urea (DeNOx), and activated carbon, as an adsorbent for principal organic pollutants (cfr. Flue Gas Treatment).

Typical *output streams* are grate siftings, bottom ash, boiler slag, fly ash, flue gas neutralization residues, and cleaned flue gas. In some plants, the different flue gas treatment residues are extracted as a mixture, in others separately.

Mass balances directly relate input streams to output streams.

One Mg (tonne) of MSW requires 6.5–7.8 Mg (5,000–6,000 Nm^3) of combustion air. Typically, mechanical grate incineration generates (EU conditions):

- 250–350 kg of bottom ash
- 5–15 kg of boiler slag
- 20–40 kg of fly ash
- 5–15 kg of neutralization salts
- 7–8.6 Mg of flue gas

Incineration Products

On the basis of aforementioned balances, the amount and identity of the incineration products can now be derived.

The *proximate analysis* splits the waste to be fired up into three parts: (1) moisture W, (2) ash A, and (3) combustibles C. The first reports to the flue gas, the second forms the residues, whereas the third is converted into combustion products also reporting to the flue gas. Starting from W% + A% + C% = 100, Tanner represented waste composition in a triangular diagram, in which a zone of auto-combustible MSW is identified (Fig. 3).

Slight disparity occurs between ashes, as originally present in waste, the "real" ash resulting during the proximate analysis test and that formed during incineration proper. Depending on the ash minerals on the one hand and the combustion conditions on the other, the original ash may differ from actual incinerator ash, because of occurrence of various thermal reactions, such as,

$$Ca(OH)_2 \Rightarrow CaO + H_2O \quad (5)$$

$$CaCO_3 \Rightarrow CaO + CO_2 \quad (6)$$

$$CaSO_4 + C \Rightarrow CaO + SO_2 + \frac{1}{2}CO \quad (7)$$

as well as many others that can only be identified by a detailed study of the ash minerals through methods such as X-ray fluorescence (XRF) or scanning electron microscopy (SEM), their thermodynamic stability, potential reactions, and state of conversion.

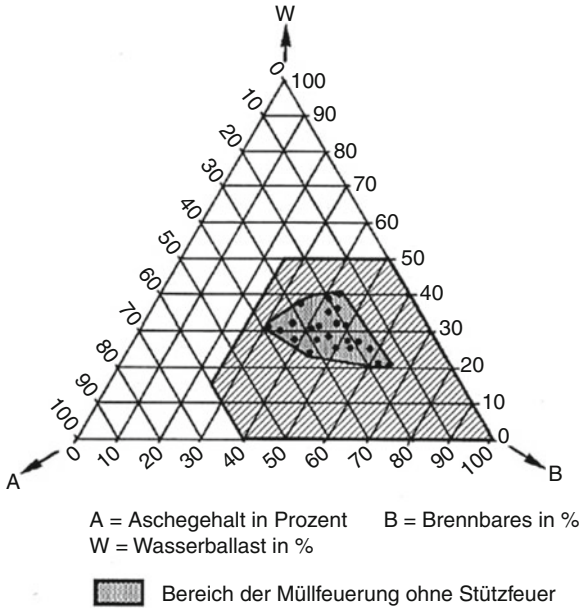

Incineration Technologies. Figure 3
The Tanner diagram [37]

Generic classes of such reactions are: dehydration, decarbonatation, sulfate decomposition, and decomposition of higher oxides into lower oxides. Another reason for disparity is the occurrence of volatilization at flame temperature; such volatilization depends on temperature, presence of oxidizing or reducing conditions and speciation [124]. Halogenides (chloride, bromide) are much more volatile than oxides or sulfides, carbonates, and sulfates.

Coarse or sintered ash materials report to the bottom ash, fines are at risk to be entrained. Bottom ash consists of coarse objects, such as stones, glass, or cans, and of ash proper. Low burnout temperatures preserve the original ash structures; high temperatures first cause sintering, generating larger and more solid sintered structures, and eventually more and more fusion.

The major gaseous incineration products are carbon dioxide and, to a variable extent, water vapor and, of course, a large amount of air nitrogen. *Carbon dioxide* generation is directly proportional to the amount of carbon burned, since the background carbon dioxide content in combustion air is insignificant (0.03 vol.%), compared to carbon dioxide in flue gas. This carbon dioxide concentration varies widely, from few vol.% to about 12 vol.%, depending on waste composition and on the excess air used.

Incomplete combustion leads to the formation of *carbon monoxide (CO)*, *total organic carbon (TOC)*, and *black carbon (BC)* or *soot*. The amount of carbon monoxide formed is highly variable, with generally a stable background value, spiked by rare or more frequent peaks (from less than 1 ppm to peaks of some 10,000 ppm, or 1 vol.%, occurring only during combustion upsets), yet only rarely influences the carbon dioxide content (Fig. 4).

The *moisture content* of flue gas is composed of:

- The original *moisture content* of the fuel fired, which upon drying reports to the flue gas. This is normally negligible for oil and gas fuels, but it reaches several percentages for powdered coal, and is quite substantial for peat, lignite, most forms of biomass, such as sewage sludge or green wood, and for municipal solid waste (MSW).
- *Moisture* contained in *combustion air*, varying markedly with both temperature and relative humidity.
- *Chemically formed water*, derived from the hydrogen content of fuel. The amount can easily be derived by simple stoichiometric computations, based on reaction equations such as:

$$[C_6H_{10}O_5]_n + 6nO_2 \Rightarrow 6nCO_2 + 5nH_2O \qquad (8)$$

with, e.g., five volumes of water vapor formed per anhydro-cellulose unit $C_6H_{10}O_5$ (the cellulose monomer) fired, or in mass units 90 g of water vapor formed per 162 g of solid fuel.

- Water added and evaporated during *quenching* of flue gas by water injection, a usual practice in small incinerators and in the incineration of chlorinated waste.
- *Pre-conditioning* of flue gas, prior to scrubbing, to enhance the elimination of fine dust, HCl, and SO_2. The first become denser, the acid gases are absorbed more easily by hydrated lime in the presence of water vapor.
- Water evaporated in wet scrubbers, used for scrubbing out acidic gases. This treatment saturates the flue gas with water vapor; the resulting temperature is typically 65°C. Sometimes, the scrubbing water is

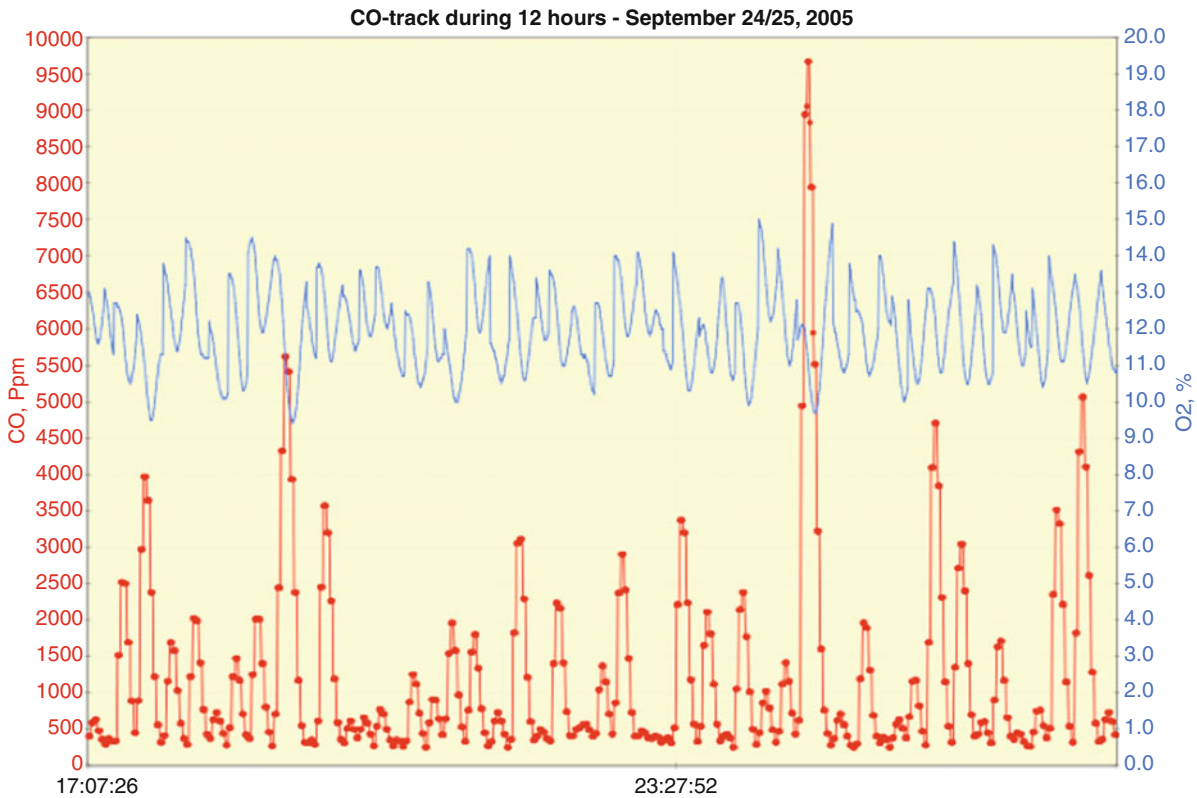

Incineration Technologies. Figure 4
Time evolution of carbon monoxide as a function of time [42]

cooled by heat exchangers to obtain a deeper separation of various pollutants (e.g., mercury, soluble gases, and organic vapors).

Oxygen, present in the fuel, reduces the amount of combustion air required, but does not contribute to the heating value. Heteroatoms, such as sulfur, nitrogen, chlorine, and other halogens may contribute to air pollution, since they are converted largely (sulfur, chlorine) or partly (nitrogen) into pollutants. Still, flue gas cleaning will eliminate the resulting pollutants, down to the limit values specified (cfr. Tables 3 and 4).

Formation of Pollutants

Combustion converts the S-, Cl-, and N-content into SO_2, HCl, and NO, at least as a first approximation. When the resulting flue gas is cooled down slowly and in the presence of catalytic fly ash (transition metal oxides, including iron, manganese, or vanadium oxides are catalysts), a fraction of SO_2 can oxidize further to SO_3, and HCl to Cl_2.

At high temperature (1,000°C), SO_2 and HCl are the most stable compounds; yet, below 500°C SO_3 and Cl_2 become the more stable. On the other hand, a fraction of SO_2/SO_3 and HCl/Cl_2 is removed by adsorption and neutralization by basic fly ash components, e.g., CaO.

Thus *elementary analysis* of fuel allows predicting the major combustion products:

$$\begin{aligned} &C_aH_bO_cS_xN_yCl_z + [a + 0.5(b - c) + x]O_2 \\ &\quad \Rightarrow aCO_2 + (b - 0.5z)H_2O + xSO_2 \\ &\quad + y[\alpha NO + 0.5(1 - \alpha)N_2] + zHCl \end{aligned} \tag{9}$$

Nitrogen oxide (NO) forms from *fuel*-N (i.e., the organic nitrogen, e.g., from proteins, in sewage sludge, hair or leather, or from polyamides) and also from combustion air, yet mainly at elevated temperatures, as *thermal* NO. Such NO formation is lower when the

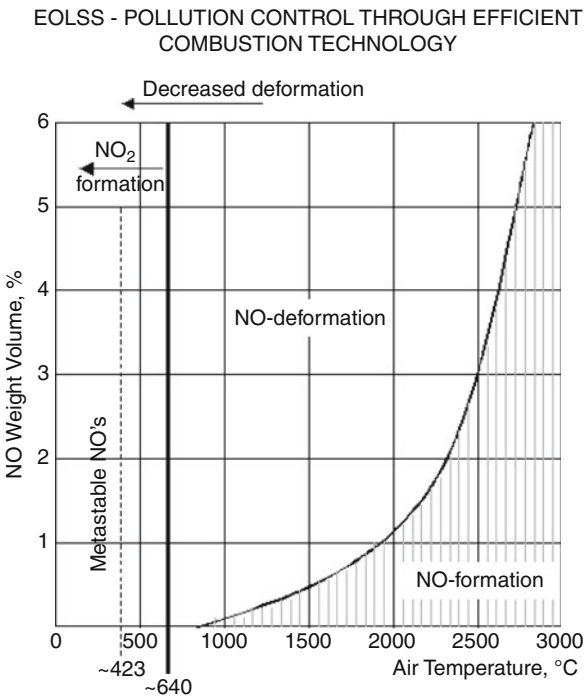

Incineration Technologies. Figure 5
NO as a function of combustion temperature [37]

flame is cooled, e.g., by radiant heat losses or by the presence of water vapor, and also when combustion is conducted in two steps: the first under reducing conditions, the second oxidizing, yet at low temperature.

To cater for this uncertainty, fuel NO formation is given a proportion α ($0 < \alpha < 1$), the balance being reduced or decomposed to molecular nitrogen ($1 - \alpha$). The formation of thermal NO is neglected in Eq. 9 (Fig. 5).

Chlorinated Compounds

Most waste contains chlorides and also chlorinated organic compounds.

The Bundesweite Hausmüllanalyse (comprehensive analysis of refuse and its sorting fractions in the German Federal Republic) established the amount of, e.g., heavy metals, PAH, and dioxins in MSW for fractions such as fines, vegetal, synthetic, paper, and board. All these sorting fractions are contaminated with all kinds of pollutants [32, 33].

During incineration, organic compounds are destroyed and their chlorine content is converted to HCl. Typically 50% of the Cl-content comes from PVC [38]. During combustion, PVC, as well as a vast majority of organic and inorganic chlorinated compounds, is partly or completely converted into HCl. PVC liberates HCl very easily. Such release is also likely to be complete, unless some other compounds, e.g., $CaCO_3$, capture it; the latter is plausible in numerous applications featuring fillers of precipitated calcium carbonate or ground dolomite/calcite.

The presence of NaCl is ubiquitous, especially in marine surroundings. At high temperatures, NaCl reacts with steam, yet its conversion into NaOH and HCl is limited by thermodynamic equilibrium. It shifts largely to the right, however, in case NaOH is itself converted into silicates, aluminates, or other composite compounds [43, 44], e.g.:

$$\mathrm{NaCl} + \mathrm{H_2O} \Rightarrow \mathrm{NaOH} + \mathrm{HCl} \tag{10}$$

$$2\mathrm{xNaOH} + \mathrm{y\,SiO_2} \Rightarrow \mathrm{xNa_2O\,y\,SiO_2} + \mathrm{H_2O} \tag{11}$$

$$2\mathrm{xNaOH} + \mathrm{z\,Al_2O_3} \Rightarrow \mathrm{xNa_2O\,z\,Al_2O_3} + \mathrm{H_2O} \tag{12}$$

Thermodynamically, the formation of chlorine gas from hydrogen chloride is described by the industrially important Deacon equilibrium:

$$4\mathrm{HCl} + \mathrm{O_2} = 2\mathrm{Cl_2} + 2\mathrm{H_2O} + \mathrm{Heat} \tag{13}$$

At combustion temperatures, HCl is by far the main Cl-compound yet – below 500°C – equilibrium conditions reverse and elemental chlorine gains ground. Chlorine is much more reactive and corrosive; moreover, it is slower to dissolve in water and thus difficult to remove. Fortunately, this reaction also becomes slower and slower, so that there is little progress towards equilibrium during the few seconds while flue gas moves from furnace to stack. The Deacon reaction also shows an effect of oxygen partial pressure, an even stronger effect of water vapor, as well as an effect of total pressure.

Other halogens follow similar equilibriums, with the elementary amount rising in a sequence: $F_2 < Cl_2 < Br_2 < I_2$. The Deacon reaction is a potential source of both corrosion and dioxin. No doubt, chlorine is only rarely produced in significant quantities and only in the presence of oxidants, such as iron ore (Fe_2O_3) or manganese ore (MnO_2).

In industry, the Deacon process is of paramount importance: chlorine is a potent reactant required in

organic chemistry and synthesis. Its use leaves HCl as a useless by-product. However, reaction (Eq. 13) allows recovering chlorine from HCl. Typical reaction conditions are: fixed or fluid bed, 450°C, $CuCl_2$ catalyst, and in dry air or pure oxygen.

Residues

In principle, incinerator residues are inert and sterile. Often, the major components in ash are silica (SiO_2), alumina (Al_2O_3), and lime (CaO), which are also the main components of the earth crust; yet virtually all elements are represented and ash composition may differ greatly from that of the earth, especially in industrial waste. Numerous studies have been devoted to the physical nature and the minerals of bottom ash and fly ash [24–26, 45, 46]. The International Ash Working Group merged worldwide experience in characterization, treatment, and leaching tests for evaluation of eventual environmental impacts of incinerator residues. Fly ash, a by-product of fossil fuel firing (coal, lignite, peat) is the subject of a site of Kentucky University and of periodic conferences published there.

Chemical analysis of the mineral ash gives information on the softening and melting behavior of the ash and hence about its tackiness and possible attack on refractory. As a rule, Na- and K-compounds decrease the melting point, in particular when present as persulfates, vanadates, borates, etc. The same holds for fluxing elements, such as boron, vanadium, or fluor. The presence of volatile compounds, such as mercury, thallium, cadmium, arsenic, antimony, and other volatile heavy metals makes the related wastes improper for incineration in conventional units. In numerous cases, stable mineral forms are different at the conditions of high-temperature combustion and at room temperature, e.g., volatile chlorides, stable at combustion temperature, tend to convert into sulfates once they condense on boiler tubes.

Thermal Aspects

During incineration, the heat content of waste, in particular its higher heating value (HHV), is liberated almost entirely. The only exceptions are the unburned materials in bottom ash, fly ash, and flue gas. Combustion efficiency η_{Comb} addresses these chemical losses by:

$$\eta_{Comb} = 1 - \text{Ash}\,C_{ash}\text{HHV}_C - (\text{Fly Ash})C_{fly\ ash}\text{HHV}_C - (\text{TOC})\text{HHV}_{TOC} \tag{14}$$

An incinerator plant is a thermal plant and should be operated as evenly and constantly as possible, close to the setpoint in its operating diagram (Fig. 6). Capacity is expressed either as (nominal) thermal load (GJ/h), or as weight throughput (Mg/h).

The *operating temperature* of an incinerator combustion chamber can be estimated from a heat balance and depends on:

- The higher heating value of waste
- The *excess air* applied
- The cooling of furnace walls (e.g., by tubes of an integrated boiler or by heat losses to the environment)
- The initial temperature of air and waste streams

A theoretical *flame temperature* (°C) can be derived simply by plotting the heat content of flue gas ($MJ/Nm^3 \times Nm^3$/kg waste) as a function of temperature: the flue gas reaches the theoretical flame temperature when its sensible heat equals the liberated heat of combustion (MJ/kg waste). A more complete *heat balance* over the furnace, the boiler, and all downstream equipment gives:

$$Q_{fuel} + H_{fuel} + H_{air} = (H.H.V.)F_{fuel} = Q_{heat\ duties} + Q_{wall\ losses} + Q_{sensible\ heat} \tag{15}$$

The first three terms contain the chemical energy (Q_{fuel}) liberated by combustion, augmented by the enthalpies of fuel (H_{fuel}) and air (H_{air}) when entering the furnace. After combustion, the energy entering the furnace is eventually redistributed as:

- *Useful energy* ($Q_{heat\ duties}$), taken up by the various heat duties, generally the boiler, the economizer, and the air preheater
- *Wall losses* ($Q_{wall\ losses}$) by convection and radiation
- *Sensible heat* ($Q_{sensible\ heat}$) and *latent heat* (water vapor) contained in the flue gas at the stack, i.e., the stack losses

I

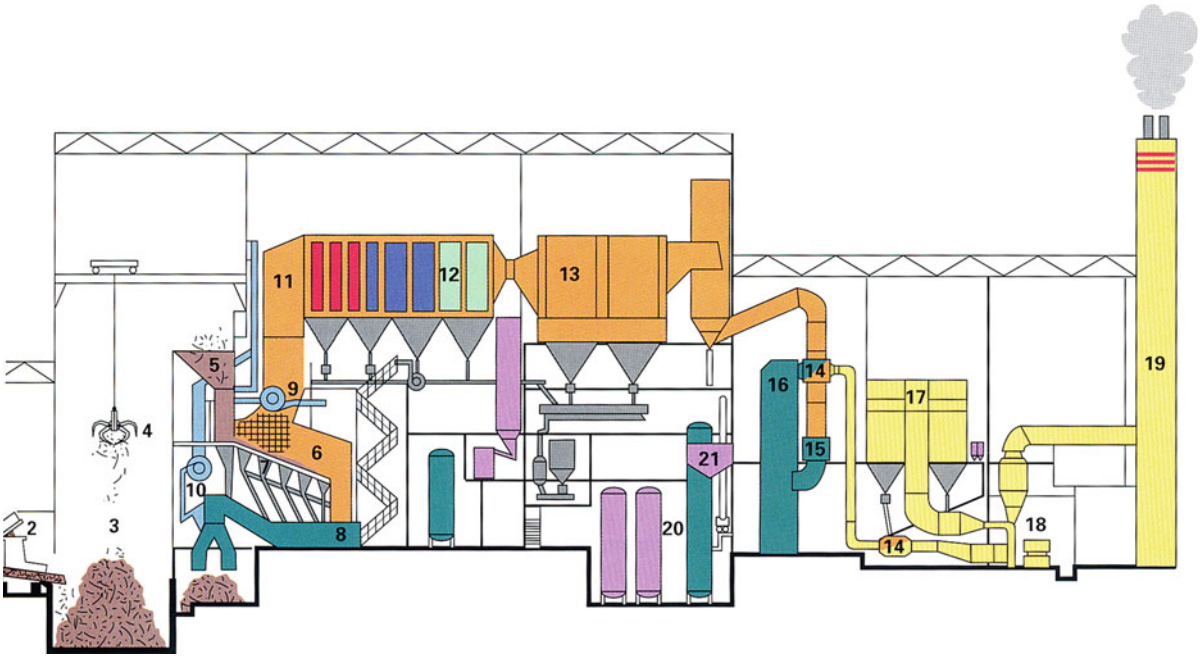

1 Hall de déchargement
2 Cisaille pour déchets encombrants
3 Fosse à ordures
4 Grappin du pont roulant
5 Trémie d'alimentation du four
6 Chambre de combustion
7 Trémies sous grille
8 Canal à mâchefers
9 Brûleur d'allumage
10 Ventilateur d'air comburant
11 Chambre de post-combustion
12 Chaudière de récupération
13 Filtre dépoussiéreur
14 Echangeurs de chaleur
15 Injection d'eau (Quench)
16 Tour de lavage des fumées
17 Filtre à manches
18 Ventilateur de tirage
19 Cheminée
20 Bacs de réactifs chimiques
21 Systèmes d'épuration d'eau

Incineration Technologies. Figure 6
Operating diagram of a mechanical grate incinerator (After [37])

Thermal efficiency η_{Therm} addresses these wall losses and stack losses by:

$$\eta_{\text{Therm}} = 1 - Q_{\text{wall losses}} + Q_{\text{sensible heat}} \tag{16}$$

It indicates the fraction of the energy entering that is recovered for useful purposes. Typical values are 0.6–0.85, or 60–85%. It can be used for district heating, water desalination, or industrial purposes. Since all these applications are site dependent and not generally available, the heat recovered as steam can be converted into electric power, by means of a turbo-alternator.

Finally, there is one more important ratio, indicating the yield of electric power derived from the initial energy in MSW or other waste incinerated. Typical values are 0.16–0.24, or 16–24%.

Air Preheating

Primary air preheating facilitates ignition, increases the flame and combustion temperature, and improves the thermal balance of the process by recovering more heat from flue gas. Combustion air is often preheated, either by flue gas/air or by steam/air heat exchangers, to assist in drying and ignition. Such heat exchangers are relatively voluminous (gas/gas heat transfer is slow) and hence capital intensive. Combustion air may also be replaced by oxygen-enriched air, or even by pure oxygen, in order to improve and accelerate combustion. This is an unusual option, since combustion air is free of charge and pure oxygen is expensive.

Low operating temperatures lead to slower and less complete combustion; excessive temperatures may

render combustion control more difficult and cause severe slagging of ash and fly ash. Tacky ash gradually builds up onto the furnace walls, the deposits eventually limiting the throughput of the furnace. Similarly, clogging problems may occur in the convection sections of the boiler, when excessive approach velocities are practiced or insufficient tube clearance is provided.

Some plants operate under *slagging conditions*, at temperatures at which the ash is molten and tapped in that state. It is important to ensure steady slag flow by:

- Carefully controlling the composition of the ash, at or close to a suitable eutectic composition; iron silicates and glass are two examples of compositions with accessible melting point
- Providing auxiliary burners and, when required, adding fluxes such as fluorspar, to enhance slag fluidity

Furnace Capacity

Nominal capacity is often expressed as the *throughput* or weight capacity (Mg/h) at which the incinerator was designed. The *load factor* of the incinerator is the ratio of the actual operating rate (Mg/h) to the nominal one (Mg/h).

Incinerator furnaces are characterized best by a minimum and a maximum *thermal capacity* (MW). Below its minimum value, the heat generation rate is so low that the furnace no longer reaches adequate temperatures to ensure smooth drying, heating, and ignition, and eventually complete combustion. When the flue gas temperatures descend below 850°C, European Union Codes stipulate that auxiliary burners must ignite and heat the combusting gases, to ensure their sufficient burnout. Excessive combustion temperatures are also undesirable, because fly ash becomes too tacky, creating deposits on furnace walls and boiler tubes. Ash similarly starts slagging; the resulting deposits on the furnace walls become ampler and ampler, eventually even restricting the movement of waste on a grate.

Furnaces feature also a minimum weight capacity (Mg/h), dictated by the necessity to maintain some minimum coverage of the grate for protecting it against furnace radiation and atmosphere. Maximum related to bed density. Finally, the relation between thermal and weight capacity is also bounded, by the necessity of producing sufficient heat for heating furnace and waste; the ratio represents the heat of combustion (MJ/kg). These different boundary conditions are represented in thermal capacity vs. weight capacity diagrams, indicating the area of smooth operation of the plant. The latter is possibly extended toward low heating values by preheating combustion air or toward high-calorific waste by cooling the combustion chamber. Thus, there are links between furnace requirements and waste characteristics.

The *volumetric heat release rate* (MJ/Nm^3, s) of a given furnace is mainly determined by the quality of contact with combustion air and by fuel reactivity, which generally decreases with larger size, higher moisture content, and lower HHV. Since combustion intensity is often unevenly distributed over the furnace, the method to consider furnace volume should be carefully defined, when citing values for volumetric heat release rates. In some cases this volume has been defined as the furnace volume at temperatures exceeding 850°C, rather than as a physical geometric volume of the combustion chamber. Dead zones at lower temperature indeed may consume a sizeable fraction of furnace volume, thus reducing real residence times and combustion efficiency η_{Comb}. Conversely, the first flue of a waste heat boiler may operate above 850°C and thus become eligible as supplemental furnace volume.

The operating domain and the limits of furnace operation may be dictated by various considerations, e.g.:

- *Heat balances*, and the concomitant higher and lower *temperature* limit (°C)
- Excessive, adequate, or insufficient *thermal load* (GJ/h)
- Adequate coverage of a mechanical grates, and hence maximum and minimum *feeding rate* (Mg/h)
- Provision of sufficient combustion air

During reception tests, the operators were supposed to deliver the proof of capacity of a given incinerator furnace over a time period of 24 h. Realizing their presumable failure, they started overcharging the furnace, bringing in more and more MSW. Due to the excessive thermal load, the furnace interior evolved from orange-red to orange, then to yellow, then turning whiter and whiter as the furnace temperature rose. Still, at that moment, more and more unburned materials

appeared among the residue: remarkably, a telephone book had crossed this furnace without even starting to convert into char!

Hazardous Waste

Hazardous waste can be identified either on the basis of inclusive lists, as proposed by the European Union [47], or on the basis of hazardous properties, an approach followed by the US EPA. In the USA, hazardous waste is waste that poses substantial or potential threats to public health or the environment. There are four factors that determine whether or not a substance is hazardous [48]:

- Ignitability (i.e., flammable)
- Reactivity
- Corrosivity
- Toxicity

The US Resource Conservation and Recovery Act (RCRA) additionally describes "hazardous waste" as waste that has the potential to [48]:

- Cause, or significantly contribute to, an increase in mortality (death) or an increase in serious
- Irreversible, or incapacitating reversible, illness
- Pose a substantial (present or potential) hazard to human health or the environment when improperly treated, stored, transported, or disposed of, or otherwise managed

Most of these hazards are entirely eliminated by incineration. Hence, HW may be incinerated at high temperature. Many cement kilns burn hazardous wastes like used oils or solvents. A more detailed discussion is to be found in various books listed at the end of this entry and in [49]. Hazardous waste poses much more problems at the levels of collection, bulking up (i.e., grouping similar waste in the same container or vessel), transportation, and intermediate or final storage than at that of incineration. Obviously, flue gas cleaning must take into account the chemical composition of the hazardous waste concerned.

Safety Aspects

Swiss Re provided a systematic discussion of some safety problems and accidents in incinerator plants. At the times of construction and annual maintenance of incinerators, lots of unusual activities take place onsite, bringing various hazards with them. During normal operation, these hazards reduce to more normal proportions, yet, numerous safety problems may occur around incinerator plants; just to name a few [50]:

- Waste bunker fires
- Explosions during the shredding of waste
- Flame flashback into the system of feeding locks
- Explosive combustion by simultaneous ignition of a large mass of waste, bringing the furnace under overpressure, with flames sorting out
- Hydrogen explosions following decomposition of water in contact with hot metal in a wet ash extractor
- Pressure vessels (boiler)
- Low levels of boiler feed water
- Boiler corrosion and tube failure
- Accidents connected to chemicals on-site, e.g., boiler feedwater treatment acids and bases and ammonia for DeNOx operation
- Rotary and moving equipment
- Transformer fires
- Fires in the wet scrubber, during shutdown

An even larger array of accidents may take place in plants treating hazardous waste, as a consequence of chemical reactivity, flammability, and corrosivity. During collection and storage it is usual practice bulking up liquid waste of similar composition and origin. Mixing distinct waste streams often leads to undesirable events; to avoid such happenings it is desirable to consult compatibility charts and data, such as [51–56], and also to mix small amounts in a test tube and then observe carefully any heating, gas evolution, precipitate formation, or other processes taking place.

Pool burning, *boiling liquid expanding vapor explosions* (BLEVEs) and *vapor cloud explosions* (VCE) are relevant concepts in industrial safety techniques [57]. Even comprehensive waste treatment centers do not necessarily reach the scale of operations or storage required to resort under COMAH eligibility conditions, although specific risk derives from the multitude and variability of waste streams potentially handled. Fires at chemical storage sites are generally impressive

and the storage, blending, and feed preparation facilities upfront a chemical waste incinerator are exposed to such occurrences.

Incinerator Furnaces and Boilers

Furnaces, Their Duties, Peripherals, Operation, Design, and Control

Most problems with incinerator plant proper are basically mechanical and arise mainly at two levels: (a) the introduction of waste into the furnace and (b) the extraction of the various combustion residues. Both should proceed without undesirable and uncontrolled entrance of ambient air.

Duties

Basically, a furnace is a heat-resistant enclosed space that should fulfill several duties simultaneously:

- Limiting the heat losses to the surroundings (heat losses ⇒ flame cooling ⇒ incomplete combustion).
- Ensuring controlled entries to primary and secondary combustion air, and exclude any notable uncontrolled entries, e.g., through the feeding or the ash removal system.
- Ensuring sufficient combustion + post-combustion time to both flue gas and solid phase (fuel, ash) to allow for their thorough and controlled burnout. This implies avoidance of short-circuiting, as well as creation of dead corners.
- Providing peripheral facilities for feeding the various waste streams to be incinerated and (when required) ash removal facilities.

Feeding Equipment

Fuel feeding peripherals strongly depend on fuel characteristics, such as the state of aggregation of the waste to be fired in a primary combustion chamber. Examples are a conventional or more specialized burner for firing gas, liquid, or pulverized, coal, in case of flammable waste gases, pumpable waste liquids, molten solids, and finely divided, free flowing solids. Burners for liquid waste may be based on centrifugal dispersion (rotary cup burners) or on pressure or auxiliary medium (steam, high pressure air) dispersion.

Chlorinated waste has been fired using the dispersion provided by a patented small auxiliary burner situated inside the main burner: the liquid chlorinated waste is supplied through apertures in a duct, leading the combustion productions from the auxiliary burner into the main combustion chamber (Vicarb technology). Some burners are even built to receive several types of wastes simultaneously, such as waste oil, emulsions, suspensions, as well as auxiliary fuel, to sustain combustion.

Solid waste can be fired by means of:

- Gravity feeding from a fuel hopper, separated from the furnace by means of a lock, composed of two sliding doors, a rotary valve, or even a pile of waste locking out the ambient air.
- Spreader stokers [59]
- Screw or piston feeders
- Mechanical or traveling grate stokers
- Pneumatic feeding of free-flowing fuel, e.g., to cyclonic or fluidized bed combustors

Cooling and extinguishing provisions may be required for preventing backfire in feeding systems, or excessive thermal decomposition in feed lines. Another frequent issue is the presence of oversized materials, metal pieces, etc., that create problems during feeding and/or residue extraction: waste containers seem to exert a fatal attraction to all kinds of extraneous matter that can block or even destroy the most sophisticated mechanical feeding or residue extraction equipment. Operators should scrutinize incinerator feed for items such as pressurized gas bottles, ammunition, or oversized concrete or metal parts.

Ash Extraction

Dry or wet ash extraction equipment is generally installed at the bottom of an ash pit or of a sequence of these ash pits, located below successive sections of a grate. It may be based on drag conveyors with suspended flights, screw conveyors, inclined vibrating conveyors, or even pneumatic conveying. These systems must be designed as a function of flow rate and the handling characteristics of fuel and ash. Failing feeding or extraction mechanisms can cause undesirable, expensive downtime (1 day of a commercial incinerator line typically costs US $20,000–$50,000).

Dry extraction plant is somewhat simpler to maintain, yet tends to be a source of persistent dust in and around the basement, where it is located. Dry extractors create considerable chimney effects and – as a consequence – they may turn into an unwelcome source of uncontrolled air in the furnace.

Wet extraction has the merit of quenching the residue and at the same time it brings in some water vapor at the level of the discharge point. Discharging hot metal may decompose water, forming potentially explosive hydrogen.

Air Supply

The combustion chamber provides suitable plenum chambers for *primary* and entrance ports for *secondary air*, supplied at possibly substantial overpressure. Primary air activates the fire, burns out combustion residues, and cools the mechanical grate, if existing. Secondary air is injected at a high speed (typically 80–150 m/s), providing the required momentum for thorough mixing of flue gas and completing their burnout. As capacity is scaled up, the available momentum declines relative to the dimensions of the furnace. Some furnace suppliers also bring in secondary air through hollow beams, situated at the level of the furnace outlet: the secondary air is split into four parts, some supplied though nozzles situated in the side walls, the remaining from the hollow beam in the middle of the furnace exit (Fig. 7).

Flow Patterns

The flow patterns in a combustion chamber are rather complex, determined by the momentum of all inputs (burners, primary and secondary air) and outputs (extraction of combusting gas), as well as by buoyancy effects caused by flames and the hot combusting gas generated.

Whatever the geometry, there is strong tendency toward short-circuiting between, on the one hand, the point(s) of entry and, on the other hand, the point(s) of

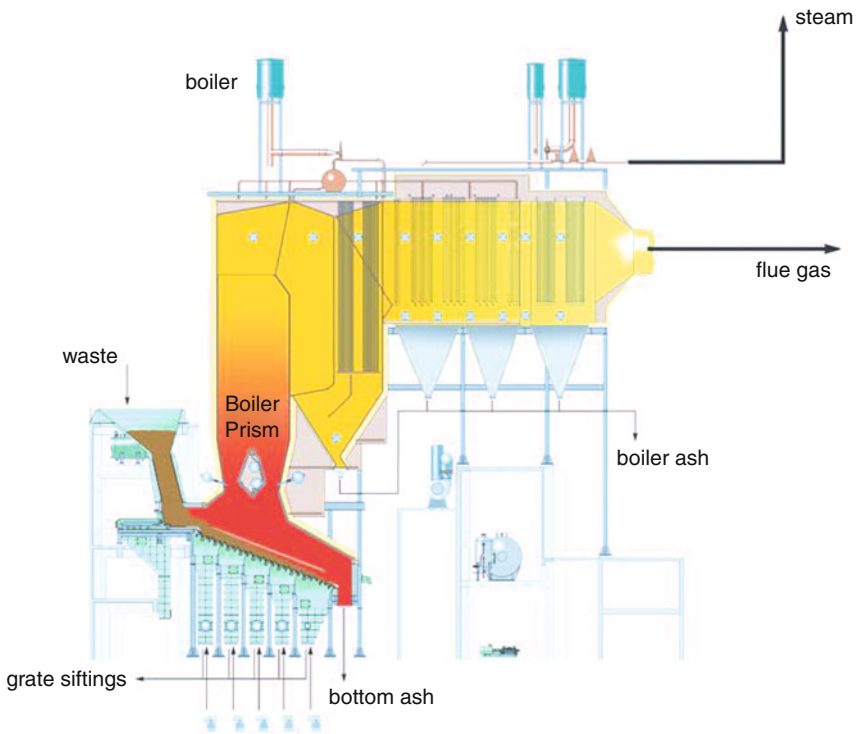

Incineration Technologies. Figure 7
Secondary air distribution beam in the middle of the exit from a combustion chamber (Courtesy of Keppel-Seghers, Willebroek [Belgium])

exit. Short-circuiting is minimal in a perfect plug flow furnace. It becomes important in the case of a voluminous combustion chamber with single entry and single exit, strong short-circuiting between entry and exit, and inactive zones in between furnace walls and short-circuit flows (Fig. 8).

A short-circuiting combustion chamber is inefficient: the short-circuiting threads show a very low, reduced residence time, the short-circuited volumes unduly long residence times, albeit at low combustion rates and temperatures. Hence, both are inefficient.

Flow patterns can be influenced by combustion chamber geometry, positioning of input and exit locations, selection of input momentum, and influencing the combusting gas pathways, e.g., by provision of baffles and changes in direction.

Design Aspects

Thirty years ago, only an empirical approach was practicable when designing incinerators. Tanner devised a triangle diagram to represent MSW as a ternary mixture, indicating zones with auto-combustible waste and others where auxiliary fuel was needed; Hämmerli proposed different nomograms for comparing and assessing grate loadings for mechanical stokers and rotary kilns. Today, *computer fluid dynamics* (CFD) easily derives the flow and mixing characteristics, the rates of heat generation, and the temperature and flow fields [58, 60].

Moreover, the trajectories of particles of various sizes can be predicted stochastically. Swithenbank et al. modeled the various zones (drying, pyrolysis, gasification, incineration) of a mechanical grate incinerator, using CFD, as well as the results of experimental testing at different scales [61–63]. A representative list of recent SUWIC work is given in [64]. Other important sources of solid waste incineration test work are due to ForschungsZentrum Karlsruhe, with experimental research on units such as TAMARA (small mechanical grate incinerator unit) and THERESA (rotary kiln incinerator unit).

Computer Fluid Dynamics (CFD)

Computer fluid dynamics are based on subdividing the volume of interest, i.e., the combustion chamber (or other parts of the plant) into a grid of elementary volumes. The relevant equations of conservation (mass, momentum, energy) are then applied to each of those elements, after defining all inputs, outputs, and boundary conditions. The resulting system is integrated from start to finish, after introducing momentum, mass, and heat transfer (adapted from the Laws of

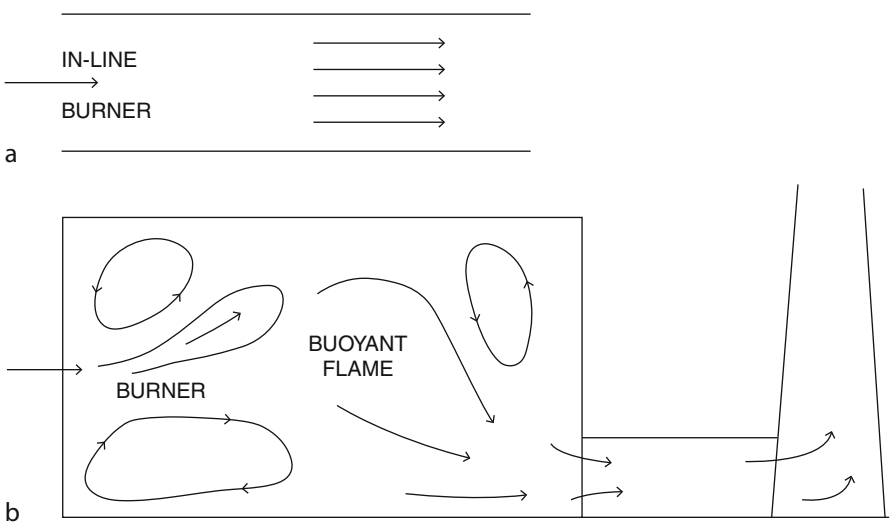

Incineration Technologies. Figure 8
Plug flow versus plug flow with dead zones

Newton, Fick, Fourier, and Stefan-Boltzmann), taking into account dimensional analysis, turbulent flow, and the state functions of relevant compounds, as well as chemical kinetic reaction systems of variable complexity [60].

CFD thus allows visualizing some cardinal aspects of the combustion chamber, i.e., the fluid flow field (flow vectors, indicating flow direction, and rate in each point), temperature and pressure field, and combustion rate field and – depending on nature and composition of the reaction models – fields for any other chemical compounds of interest (PICs, specific pollutants). Modeling thermal behavior of specific compounds or waste can be conducted at a milligram or even a lower scale [65, 66] (Fig. 9).

Draft Considerations

An incinerator plant usually operates under balanced draft: a balance is struck between forced draft (blowing in combustion air) and induced draft (ID, drawing out flue gas through the stack). ID arises by means of chimney draft, supplemented by the ID-fan, so that the furnace operates steadily with a combustion chamber at a slight subatmospheric pressure, of the order of say 10 or 15 cm water column (1 atm equals more than 10 m w.c.).

Chimney draft follows from the *Law of Archimedes*: the stack is filled with light hot gas, taking the place of an equivalent physical volume of much denser ambient air. Hence, the hot stack gas aspires being replaced by the latter, which enters the furnace by all controlled inlet ports, as well as by those uncontrolled, such as a dry ash extractor or non-tight junctions between distinct parts of the plant and non-tight plant parts, e.g., a fly ash discharge valve.

Very small plants (such as a big stove) may rely on *natural draft*, controlled by means of variable obstructions regulating at the supply side or at the chimney. Medium and large plants use both *forced* and *induced draft fans*. These are major consumers of electric power. Due to the gradual extension of heat recovery and pollution control, these draft requirements have steadily risen over time. For example, power consumption in mechanical grate plant was typically 40–80 kWh/Mg of MSW around 1970. Today, it is more like 160–240 kWh/Mg of MSW.

Mechanical Drives

Until the 1920s, loading the furnace, poking the fire, and extracting ashes was largely manual, somewhat aided by gravity and appropriate tools. Mechanical grates, fans and blowers, and the use of mechanical and later hydraulic drives were first introduced to alleviate the hard labor of the stokers. Today, these tasks are largely automated and sensors monitor every operating detail.

Regulation and Controls

Almost all operating parameters (action of drives, position of valves, temperatures, pressures, flows, levels) are registered continuously, for every part of the plant, as well as all relevant emission parameters (O_2, CO_2, CO, H_2O, SO_2, HCl, NOx, TOC, dust, etc.) so that all incidents can be carefully analyzed, even months post factum. Computer screens synoptically present information on storage and feeding, and on the operation of furnace, boiler, boiler feedwater treatment, steam turbo-alternator and condensers, residues extraction, air pollution control techniques, and forced and induced draft fans. Control systems are quite sophisticated and directly influence draft, furnace temperatures, and the position of the fire.

Combustion control follows complex algorithms, developed to ensure the right operating conditions, regarding temperature, pressure, airflows, etc.

Conclusions

A furnace is to achieve adequate control of air supply and draft, and thus of all major combustion conditions (temperature, time, turbulence) and emissions. Typically, combustion is conducted at more than 850°C, a residence time of combustion products in the gas phase of at least 2–3 s at these 850 C (or higher), and adequate turbulence to render these reasonably homogeneous. A minimum level of oxygen (e.g., 6 vol.% in MSW incineration) may also be specified, either by legal codes or by good practice. Ideally, combustion proceeds at a pressure slightly below atmospheric, so that combustion products do not spread to the surroundings, through the inevitable leaks that occur in between the main parts of the incinerator plant, as well as at its appendages.

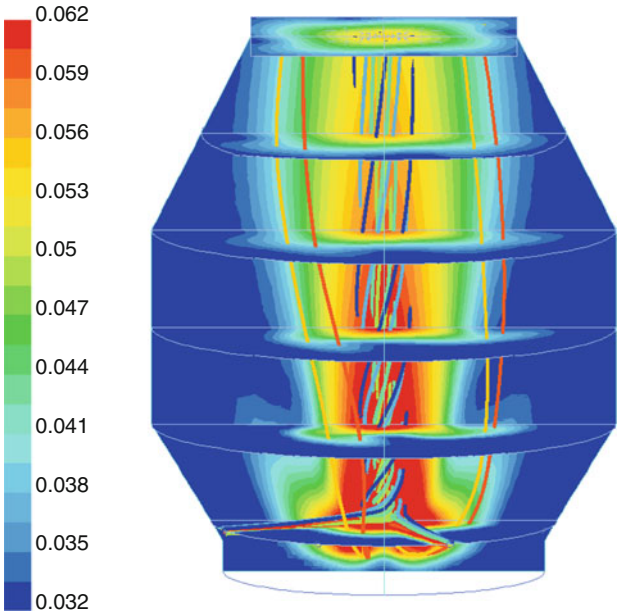

a Contours of Mole fraction of 02 May 15, 2000 FLUENT 5.3 (3d, segregated, spe5, rngke)

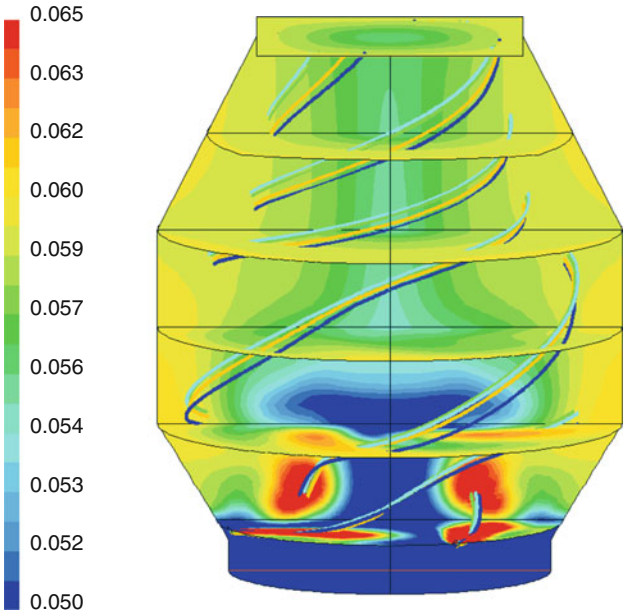

b Contours of Mole fraction of 02 May 15, 2000 FLUENT 5.3 (3d, segregated, spe5, rngke)

Incineration Technologies. Figure 9
Computer fluid dynamics (CFD) representation of a combustion chamber (By courtesy of Prof. J. Swithenbank [SUWIC])

I

Post-combustion

The average *residence time* (s) in the combustion chamber is given by the ratio of the physical volume of this combustion chamber (m^3) to the volumetric flow (m^3/s) at the furnace conditions (temperature, pressure) prevailing, and determined, e.g., at the combustion chamber exit. The real *residence time* follows a distribution determined by internal flow conditions, including short-circuiting and dead zones. Such distributions are rarely established, whether by computer fluid dynamics, or by tracer experiments, as described in [67].

Combusting gas leaving the primary combustion chamber is still at about the average temperature of this chamber, i.e., typically >850°C, yet its burnout must still be completed. There are several physical and chemical reasons for this, e.g.:

- *Residence times* in the (primary) combustion chamber are rather short, to make the best use of intense combustion and the concomitant high temperatures. Too large combustion chambers operate at too low combustion temperatures, causing incomplete combustion. Conversely, too small combustion chambers operate at too high combustion temperatures, causing severe slagging of refractory walls, unless these are adequately cooled, as well as thermal NOx. Cooling of such furnace walls is technically possible by integrating the combustion chamber into the boiler, or by blowing part of the secondary air through channels prepared in the refractory walls.
- Part of the combusting gas *short-circuits* parts of the (primary) combustion chamber, so that its *real* residence time is only a fraction of the *average* residence time. Hence, it is advantageous to promote plug flow by judicious selection of furnace dimensions, make use of any constructive features promoting plug flow and avoiding dead zones, and testing the resulting furnace designs by CFD.
- In zones of intense combustion, local or even general *deficiencies of oxygen* are likely to occur, either permanently, or only in case of fast, flaming combustion of unusually large lumps of waste. As a consequence, incinerator furnaces should be fed steadily, yet in small unit doses.
- Very high combustion temperatures lead to the partial dissociation of major combustion products, such as

$$CO_2 \Rightarrow CO + \frac{1}{2}O_2 \tag{17}$$

$$H_2O \Rightarrow H_2 + \frac{1}{2}O_2 \tag{18}$$

From chemical reaction theory it follows that the best results are obtained under *plug flow* conditions. Theoretically, these can be approached by a sufficiently large number of combustion chambers. In practice, such an ideal situation can be strived for by:

- Separating the combustion chamber into a main, primary chamber, followed by a secondary and possibly third chamber. This secondary chamber is in general use when incinerating, e.g., hospital waste in the sequence (1) primary partial oxidation chamber, yielding incomplete combusted fumes, and (2) secondary post-combustion chamber fitted with an auxiliary burner for raising the temperature and provisions for generating swirl and thus promoting complete combustion.
- Conventional combustion chamber (e.g., featuring a mechanical grate stoker), followed by a zone of highly turbulent mixing, produced by the injection of high-speed secondary air.

Total organic carbon is a lump parameter of flue gas organics, measured off-line by means of flame ionization detectors and expressed as mg CH_4-equivalent per Nm^3. Detailed identification is both seldom conducted and tedious, yet of possible interest in a larger environmental debate, or for dedicated monitoring of POHC (principal organic hazardous constituent) during test burns of hazardous waste [68, 69], e.g., at the Incineration Research Facility (IRF). US EPA monitored the environmental performance of hazardous waste incinerators by ordering test burns to be conducted. The legal framework is described in [70].

Under controlled laboratory conditions Dellinger et al. applied the gas-phase thermal stability method to rank the incinerability of 20 hazardous organic compounds, selected on the basis of frequency of occurrence in hazardous waste samples, apparent prevalence in stack effluents, and representativeness among

hazardous organic waste materials. Their major findings were [71]:

- Gas-phase thermal stability is effective in ranking the incinerability of hazardous compounds in waste.
- Numerous PICs were formed during thermal decomposition of most of the compounds tested.
- A destruction efficiency of 99.99% is achieved after 2 s mean residence time in flowing air at 600–950°C (Table 8).

Conclusions

Post-combustion is essential because primary combustion chambers are too limited in residence time and in mixing and homogenization capabilities to ensure steady burnout reliably and permanently. Post-combustion is preceded by a zone of intense mixing, to homogenize oxygen-rich with oxygen-lean strands; it proceeds as long as temperature remains above, say, 500°C. As temperature decreases, all reaction rates tend to fall.

Below 500°C, oxidation may proceed further in case the remaining PICs can be adsorbed and converted catalytically.

The advent of selective catalytic reduction (SCR) paved the way for organized oxidation of PICs, the semiconductor catalysts used being capable of (first) NO reduction and (second) semi-volatile PICs (PAHs, dioxins) oxidation, even at temperatures of only 200°C.

Incineration Technologies. Table 8 Processes influencing upon the formation of products of incomplete combustion in mechanical grate municipal solid waste incinerators, factors of influence, possible remedial action, and influence of the 850°C, 2 s Rule

Nr	Process	Factors of influence	Possible positive action	Influence of the 850°C, 2 s Rule
1	Drying	Heat radiation	Mix dry and wet waste	May be mildly positive, without exerting much direct influence
		Early ignition of high-calorific materials	Preheat air	
			Use a reverse reciprocating grate (mixing)	
2	Heating and Ignition	Radiating Heat	Noncritical process	Almost none
		Ignition of adjacent materials		
3	Thermal decomposition	Material Type	Premixing refuse	None
		Temperature	Poking and mixing action of the grate	
		Heat supply rate		
4	Flaming combustion	Rate of thermal decomposition	Adapt air distribution along the grate	May be mildly negative, by requiring a hot furnace operation
		Supply of air	Enrich with oxygen	
5	Mixing the gases	Furnace geometry position and diameter of air injection nozzles	Improve the design to increase turbulence	None
			Injection of more high velocity secondary air	
6	Post-combustion	Contact time	Apply the 850°C, 2 s Rule	Important
		Temperature		
7	Avoidance of soot formation	Correlated with (3), (4), and (5)	As for (3), (4), and (5)	None

Heat Recovery

The sensible heat contained in flue gas can largely (thermal efficiency η_{Therm} typically 75–85%) be recovered in waste heat boilers. Normally, medium-pressure (1.5–4.5 MPa) boiler operation is favored, to avoid high-temperature super-heater corrosion problems. Fly ash is often tacky above 600°C; hence the contact surfaces are preceded by radiant cooling surfaces. These are specially designed for:

- Limiting adherence and deposition of hot, tacky particles
- Convenient cleaning (rapping of boiler tube panels, soot blowing, shot cleaning of tube banks)
- Easy inspection

During a furnace standstill, it is advisable to keep the boiler tubes hot, by means of imported steam, in order to avoid corrosion by hygroscopic acidic deposits, such as chlorides. The same holds for flue gas cleaning plants.

Plants Without Heat Recovery

In small or batch-operated plants, flue gas is cooled by injecting quench water in a cooling tower surmounting or following the furnace, or by admixing cooling air [9]. These methods increase the gas flow at standard temperature and pressure typically by 30–50% for water injection and by 300–400% for admixing air, which quite considerably inflate investment and operating costs of the gas cleaning plant.

In large-scale incinerators, *heat recovery* using either waste heat or integrated boilers is the most appropriate for cooling the flue gas prior to its cleaning, provided that the steam generated can be used for in-plant or other useful purposes, such as power generation, district heating (winter) and cooling (summer), water desalination, sludge drying, vacuum generation, etc. Still, such heat recovery proceeds under adverse conditions (corrosive and fouling flue gas), requiring considerable investment and diminishing plant availability.

Generated revenues and avoiding the extra cost of requiring much larger gas cleaning plant may offset these disadvantages. Moreover, since heat recovery is a more sustainable option, recovery may be mandatory, even regardless of economic factors.

Boiler Design

The design of a boiler mainly depends on steam quality (boiler pressure + superheat temperatures), water circulation requirements (MSWI boilers feature natural convection), and flue-gas characteristics (corrosion, erosion, and fouling potential). When selecting steam parameters for waste fired boilers, a compromise is searched between yield of power generation and superheater lifetime: an operating pressure of ca. 40 bar (4 MPa) and 400°C are common choices when power is generated [9].

Corrosion becomes more severe, as steam temperature increases. Steam superheaters are especially vulnerable: since they operate at the highest temperatures of the steam circuit they are located at the high temperature side of flue gas and boiler. Moreover, their internal cooling is of low grade (medium pressure steam, stead of boiling water). Corrosion-resistant materials and coatings are key in increased conversion efficiency and reduced maintenance in waste-to-energy (WTE) plants. Another possibility is to heat the steam superheater in a separate natural gas or oil-fired furnace, an option first tested at Moerdijk, the Netherlands.

During the 1960s, boilers were designed according to conventional rules: compact construction and a high rate of heat transfer, sustained by relatively high linear gas velocities. This design was at the source of failures: some superheaters, designed for 20,000 operating hours, barely reached 3–4,000 h. Linear gas velocities selected for high heat transfer rates also create conditions leading to rapid fouling or even complete clogging of entire tube banks and to rapid corrosion [72–74]!

From the 1970s, some simple rule-of-thumbs emerged that led to the design of large-volume, less efficient boilers, however, without the operating problems cited afore:

- Convection surfaces in the boiler passes are placed only after 1, 2, or even 3 empty boiler passes, so that the flue gas temperature is lower than 600°C or at most 650°C. In this temperature range, fly ash is no longer too tacky thus less fouling.
- The clearance between superheater tubes is wide and the approach velocity is low (only few ms^{-1}) limiting inertial fly ash deposition.

- Deposited fly ash is periodically removed using steam jets or dropping shot onto tube banks.

Chlorides, chlorine, and hydrogen chloride play an important role in some forms of corrosion. Yet, also other factors play a synergetic and decisive role, often related to the creation of electrochemical cells with on one side tube metal, on the other the tube deposits. Rate controlling is the electric conductivity of the deposition layer, not the amount of chlorine in the system. Basically, the presence of molten phases on the tubes must be avoided. Rasch studied the thermodynamics of the formation of these phases in some detail [75].

Corrosion Problems

Most gases attack plain steel. Combustion of MSW generates a highly corrosive environment composed of combustion gases and ash and laden with HCl, SO_2, chlorides, and (subsequently) sulfates. Corrosion rates rise with temperature and – depending on metal structure and composition – diminish by formation of protective layers. Coherent consideration of corrosion processes is difficult, as physical, chemical, operational, metallurgical, and crystallographic parameters interact and the precise origins of corrosion vary from case to case, are multiple, and generally difficult to identify. Thermodynamically speaking, some extent of corrosion is unavoidable. Countermeasures may help to reduce corrosion damage to acceptable levels. These require both constructive and operational countermeasures. Low steam parameters in the boiler system, long residence and reaction times (for preliminary sulfatation of chlorides) before entering in contact with convective heat surfaces, lowering the flue-gas speed, and leveling of the speed profile may all be successful. Protective shells, tooling, stamping, and deflectors can also be used to protect and safeguard heated surfaces. A compromise must be found in determining the boiler cleaning intensity between best possible heat transfer (metallic pipe surface) and optimal corrosion protection [76–79].

Currently, corrosion phenomena are observed on superheater tubes particularly. The key role of formation of a molten phase is obviously associated with ash composition and flue gas temperature. The deposit morphology is related to the flue gas flow pattern, to the mechanisms of corrosion and corrosion rates. A theoretical analysis and enumeration of corrosion's numerous forms and appearances are given in the EU Reference Document on the Best Available Techniques for Waste Incineration [38].

In the 1950s and 1960s, Germany built numerous large MSWI plants. Refuse was assimilated to fuel free of charge and the first generation of plants was designed to squeeze maximum power from this resource. Soon, severe corrosions were encountered and their sources were analyzed; several major areas of concern were identified [38, 72–79]:

- Severe corrosion occurred in integrated boilers, affecting mainly the lower half of the boiler tubes surrounding the combustion chamber. This form of corrosion derives from alternating oxidizing and reducing conditions, which prevent protective and coherent oxide films to form. It proceeds through formation of $FeCl_2$ in an oxygen-deficient flue-gas atmosphere, e.g., below oxide films, tube contaminations, or fireproof material especially in the furnace area. $FeCl_2$ is sufficiently volatile at these temperatures to be mobilized. An indicator for such conditions is the periodic appearance of CO. Corrosion products appear in flakey layers. Today, this part of the boiler is clad with protective refractory, often thermally conductive silicon carbide.
- High-temperature superheater corrosion. Corrosion occurs in synergy with other factors, such as inapt boiler design and the accumulation of tacky deposits on the superheater tube banks. Hydrogen chloride and chlorine play a major role in an electrochemical system constituted by boiler and especially superheater tube deposits: hydrogen chloride is released by conversion of alkaline chlorides into sulfates, and attacks iron. Corrosion is observed in MSW incinerators with flue-gas temperatures $>700°C$ and at pipe wall temperatures above 400°C. The corrosion products are black, firmly bonded, and include red hygroscopic $FeCl_3$.
- Molten salt corrosion. Flue-gas contains alkali salts, which form low-melting persulfates (Na- and $K_2S_2O_7$) and various eutectics. Such molten systems are highly reactive and cause severe corrosion or even react with the refractory lining and destroy it mechanically.

I

- Standstill corrosion creates problems mainly after a shutdown, whether scheduled or accidental. $CaCl_2$ deposits are hygroscopic and show deliquescence, whereas some heavy metal chlorides may even hydrolyze, liberating free HCl. Electric tracing is required to keep such deposits dry during standstill periods.
- Dewpoint corrosion is associated with acid gases that condense at the cold, rear end of the boiler. Temperatures below 110°C may suffer from HCl condensation; sulfuric acid may even condense below 160°C.
- Superheaters may suffer damage from erosion due to excessive flue gas approach velocities and/or excessively strong soot blowing. Such soot blowers are difficult to adjust: if the jets blow too hard they cause erosion, if too soft, soot blowing is useless. Specialized services now blast deposits by appropriate use of explosive charges.

Sulfatation

Salts and metal chlorides sublimate at furnace temperature, leaving bottom ash as a cleaner residue [75]. In the first boiler passes the temperature remains still above 650°C and fly ash is still tacky. Below 600°C, flue gas may come into contact with tube banks, without excessive risk of fouling these rapidly. Nevertheless, tube deposits still form by separation of nonsticky particles, by inertia and interception. These deposits also collect chloride salts that de-sublimate and condense. Thermodynamically, most chloride salts are no longer stable, as they were at furnace temperature. Upon contact with SO_2 they gradually convert into sulfates by generic reactions such as:

$$\begin{aligned} &MeCl_2 + SO_2 + \frac{1}{2}O_2 = MeSO_4 + 2HCl \\ &(Me = \text{bivalent metal}) \end{aligned} \tag{19}$$

Such reactions also consolidate and harden deposits. Moreover, while liberating HCl they contribute to corrosion processes: HCl slowly oxidizes to Cl_2 that diffuses to the tube metal and attacks it; after it is reduced to HCl the same corrosive cycle starts over. From this viewpoint, it is favorable that the flue gas is rich in SO_2 and that sulfatation proceeds before the salt-laden fly ash deposits on the tubes.

Flue Gas Composition

Flue gas composition is determined by several factors of influence. The most important one is waste composition: all entering elements will also leave the plant, whether as flue gas or as solid residue. Mass balances, together with waste composition data, allow estimating the flue gas and the residue composition, even though some assumptions are needed regarding the distribution of the relevant elements over the various output streams. A second factor is the technology used: mass burning of MSW yields much more bottom-ash (typically 20–30 wt.% of MSW) than fly ash (2–3 wt.% of MSW). Fluid bed incineration of the same MSW will turn this relation in favor of fly ash, which may reach, e.g., 10–12 wt.% of MSW. As a consequence, the coarse fraction of fly ash will be less contaminated, following an effect of dilution by bed material and other fines. A third factor is related to the operating conditions used: lower flow and velocity of primary air reduces the entrainment of fly ash and also leads to higher bed temperatures and hence to more sintering of ash and to more volatilization of various heavy metals, e.g., Cd, Cu, Pb, and Zn, that eventually de-sublimate onto the fly ash.

Flue gas composition is also influenced by the excess air amounts practiced: primary air activates the fire in the combustion zone, yet cools the furnace in the drying and burnout zones; excess secondary air merely dilutes the flue gas. To avoid willful dilution with ambient air (to make concentration figures look lower), analytical data are generally expressed at some standard concentration of either oxygen (e.g., 11 vol.% O_2) or carbon dioxide (e.g., 6 or 8 vol.% O_2). Similarly, the concentration of obnoxious compounds is generally expressed on a dry gas basis.

In modern plants, numerous parameters are monitored continuously, e.g.:

Oxygen, on the basis of its paramagnetic properties, or using semiconductors reacting to the oxygen concentration.

Carbon dioxide, water vapor, sulfur dioxide by Fourier-transformed infrared (FTIR) absorption

Hydrogen chloride and fluoride

Nitrogen oxides

The residue composition also depends on the partition between bottom ash, boiler slag (only

a small amount), fly ash, neutralization residues, and fine dust and aerosols that escape uncollected. Numerous studies have considered such issues.

Dioxins

More than a century ago dioxins first drew the attention, while their synthesis afflicted laboratory workers with chloracne. The same happened after isolated incidents in chemical industry, e.g., Monsanto at Nitro, BASF at Ludwigshafen, or Philips-Duphar at Amsterdam. A much more spectacular accident occurred at Seveso (N. of Milan): after a run-away in a herbicide synthesis reactor, its contents were vented all over Seveso, causing trees to lose their leaves, death to various animals, as well as the evacuation of 10,000 inhabitants (1976). People exposed to dioxins are still being monitored today, to detect any eventual symptoms or mortality. Epidemiological investigations show the appearance of rare, soft tissue cancers and neurological afflictions, yet no net increase in mortality (cfr. Public Image).

Dioxins were discovered on MSW incinerator fly ash in 1977 [80]; it took some 15 years more to recognize as major sources several processes in iron and steel industry, as well as in the melting of metal scrap. Dioxins have been at the center of enormous efforts, first to develop, standardize, apply, and ameliorate analytical methods and determine potential dioxin sources as well as possible pathways to formation, then to try and meet the extremely low emission limit values during everyday operation [81–86].

Details of the mechanisms forming dioxins still today remain controversial [87–89]. Theories started with the trace chemistries of flame (Dow Chemicals Co.), continuing with various precursor theories (many researchers) and culminating with the de novo theories, worked out in most detail at Forschungs-Zentrum Karlsruhe. In the first theory, dioxins are inseparable from any combustion process [90]. Precursor theories focus on chemical, often catalytic conversion of dioxin-related structures [91–93], such as phenoxy radicals, chlorophenols, chlorobenzenes, polychlorinated biphenyls (PCBs), and also polycyclic aromatic hydrocarbons and related structures, converting into dioxins. Finally, de novo theory is based on a low-temperature catalytic conversion of almost any carbonaceous structure, such as soot or its various precursors, into dioxins and furans, or PCDD/F [94–98].

Several pathways lead to dioxins [109], yet their relative importance, as well as the precise nature of the catalysis at work will always remain elusive in each particular reactive system. Moreover, there is no mutual exclusion between pathways. Much attention was also given to metal catalysis in dioxins formation [99–102]. Other work related to the prevention of dioxins formation [103–105] or its destruction in fly ash [106–108]. Early and current abatement of dioxins from flue gas is covered in [109–111].

Dioxins in Incineration

During several decades, incinerators have formed the major source of dioxins emissions.

Strangely enough, they were also destroying dioxins, namely, those entering the furnace together with the MSW [112]. Dioxin balances have been established several times in the 1980s, showing that the input and output of dioxins in the plant was similar, yet not necessarily the dioxins fingerprint, i.e., the distribution of various isomer groups and congeners.

Although dioxins are considered to be extremely environmentally stable, they do not survive the combustion process. So, more than 99% of the dioxins entering are destroyed. At the entrance of the furnace and even after the practical end of active post-combustion, no dioxins can be found; at most their basic structures are present [112–115].

Rapid dioxin formation occurs once the flue gas attains a window between 400 and 250°C. A rate maximum of formation occurs at 300–350°C [96].

Explanations differ, yet it seems accepted that the formation is a catalytic process, so that particles play a role, whether suspended in flue gas or deposited from it. Oxygen is required, probably to reactivate the catalyst, after it is reduced while chlorinating aromatic and aliphatic structures.

Salient Factors in Dioxins Formation

Dioxins formation is affected by quite a large number of significant factors, subdivided into two groups: first, operational factors, second, related to chemical,

composition, and catalytic factors, such as catalysis, carbon, oxygen, water vapor, and chlorine [116]. Each of these has several impacts, often with various mutual interactions and it is unlikely that their ranking and relative importance under varied conditions in diverse systems will ever be established once and for all. An intrinsic difficulty in studying dioxins formation is a matter of timescale: the occurrence of a combustion setup, start-up, or shutdown has a certain timescale [117], yet that of dioxins may follow hours, days, or even weeks later (memory effects) [85, 118]. Several factors explain such memory effects: dioxins form from fly ash deposits slowly, and even slower in lower deposit temperatures. In some cases, there may be chromatographic effects, semi-volatiles such as dioxins getting adsorbed and desorbing again later. Wet scrubbers made of plastic dissolve dioxins during upsets and start-ups that desorb again into clean gas later [119].

Incinerator operating factors are of paramount importance. Poor combustion conditions may result from "bad" waste, i.e., either too poor (low temperature) or too rich (excess evolution of volatile matter). These "bad" operating conditions not only lead to more PICs and PAHs (a small fraction of which converts into dioxins), but also to a prolonged increase in dioxins (memory effects: PICs adsorb on boiler deposits and continue generating dioxins afterward). Poor combustion conditions result often from feeding too much at a time, without adequate premixing wastes of different origins and quality. Combustion upsets are notable by a development of peaks of carbon monoxide accompanied by total organic carbon (TOC), a measure for the amount of PICs present. Combustion conditions may be improved by both technology (grates, furnace geometry) and operating skills (mixing and feeding waste, providing primary and secondary air). Nevertheless, firing fuels such as MSW always bring in a factor of chance. With respect to dioxins, the following factors may help:

- Firing well-mixed, homogenized waste only. Humidity transfer from moist vegetal waste to paper and board and dispersion and mixing of high-calorific waste (plastics and rubber) in the bulk of MSW are positive factors, i.e., prolonged storage and periodic mixing of the bunker's content, or mixing moist garden waste with high-calorific commercial waste.
- Using low rates of primary air. This reduces the amount of excess oxygen in the flue gas, as well as the entrainment of dust particles, which is a source of dust deposits and of boiler fouling and corrosion.
- Steady combustion conditions. No large packs of high-calorific waste taking fire together.
- High-quality mixing of gases at the furnace exit.
- Ample post-combustion chamber volumes, at adequately high temperatures and mixing levels.
- Designing post-combustion volumes by means of computer fluid dynamics, for good mixing and avoiding short-circuiting as well as dead zones.
- Limiting residence times in a temperature window ranging from 500°C down to 200°C.
- Operating electrostatic precipitators, at low temperature, not more than 200°C, by extending waste heat boiler surfaces and limiting boiler fouling.
- Avoiding building up and extending deposits on boiler tubes, collection plates in electrostatic precipitators, in flues, etc., by limiting the approach velocity.

The quality of operation can be judged by the permanent absence of CO- and TOC-peaks.

Ideally, their frequency should be nil on a daily basis. Should such peaks still occur, they can be termed "very serious" (CO = 10^3–10^4 mg/Nm^3), "serious" (10^2–10^3 mg/Nm^3), or "benign" (10–10^2 mg/Nm^3). TOC-peaks concur with CO-peaks, yet their height and width differ. The reason for such short-lived peaks is either overfeeding (too much at a time) of fluid beds, or inadequate mixing of MSW fed to mechanical grate units [42].

Complete combustion, mixing of flue gas by blowing in secondary air at high speed, and absence of setups are all primordial operating factors; definitely less dioxin is formed in case excess oxygen is limited.

Another important operational domain is related to the cooling of flue gas: fast and deep cooling limits dioxins formation. Slow cooling of flue gas, in contact with deposited dust, has an opposite effect. For small plants, e.g., metal foundries, quenching off-gas is a suitable prevention measure.

Dust removal takes dioxins away, since these semi-volatiles report to fly ash, especially at low temperatures. Baghouse filters are designed to clean gas down to the very low dust levels required to reach the level of 0.1 ng TE/Nm^3. Any imperfections should be observed by means of tribo-electric sensors, opacity measurement, providing immediate warning in case of dust breaking through.

Chemical and Catalytic Factors

A cardinal chemical factor is related to the presence of transition metals providing the catalytic effects required to fix chlorine on carbon structures and also to oxidize the latter so that dioxins are liberated, together with scores of other surrogate and precursor compounds [47]. Catalytic metals are likely to be associated with particulate, in particular its finest fraction. The latter absorbs the de-sublimating metal salts (Zn, Pb, Cu, Cd, etc.) condensing after having been volatilized at flame temperature [67]. Copper is obviously a premium catalyst; it is often better represented in fly ash from fluidized bed units than in that from mechanical grate units [42]. This could be due to erosion effects, affecting copper wire. In China, fly ash is much leaner in heavy metals than in the EU. Another catalytic substance is iron oxide.

Mixing fly ash with inert materials and carbon creates de novo, dioxin-generating activity. Matrix effects and its particulate carrier are important [120], so is the supply of oxygen to the system: after chlorinating carbon or oxidizing carbon structures, the catalyst is in its reduced form. Oxygen restores a higher valence, required for reactivity. The relations between carbon structure and dioxin formation are still all but elucidated. The presence of the element chlorine is essential in dioxin formation, yet chlorine is ubiquitous in incineration. Factors of influence are numerous and their effects are manifestly complex, interdependent and difficult to pinpoint! Dioxins formation has been studied at full plant level [112], at pilot scale [113–115], and at laboratory level [121, 122]; it was simulated by CFD [123]. Thus, the discovery of dioxins eventually has prompted enormous research efforts, with the fortunate result that incineration became a much more controlled technical process and that the cleaning of flue gas became much deeper (cfr. Tables 3 and 4).

Flue Gas Cleaning

In MSWI flue gas a deep cleaning is essential. Public and political pressures have been so powerful that MSW incineration is at present the most regulated and best controlled form of combustion. Flue gas cleaning addresses successively [30, 37]:

- Particulates and dust, including the associated heavy metals
- Acid gases, such as HCl, HF, and SO_2
- Nitrogen oxides such as NO, NO_2, and N_2O
- Semi-volatile organic compounds, such as PAHs, PCDD/Fs (dioxins), and PCBs

Yet, the precise composition of the flue gas cleaning train depends on numerous options that can be combined in a large variety of flue gas cleaning schemes. Most existing plant during the 1980s and 1990s were forced to revamp this train at least once or even several times, leading to redundancy in the ways these various duties are addressed, e.g.,

- Baghouse filters were often added at the tail of the plant, to complete the preliminary separation by a preexisting electrostatic precipitator; in other plants the ESP was scrapped, because of redundancy and the formation of dioxins at high ESP operating temperatures.
- Dry acid gas scrubbing was supplemented at times by semi-wet or wet units.
- Activated carbon adsorption retains semi-volatile organics that eventually would be destroyed during selective catalytic reduction of NOx.

A survey of best practicable options is given in [37].

HCl is an acid, irritating gas, yet it is eminently soluble in water and thus easily scrubbed out from flue gas (together with HF and HBr, both present at about 100 times lower concentration levels). The resulting diluted solution can be distilled to yield a commercial concentration. Yet, HCl is not in high demand and sales may require removal of trace organics as well as iron. An alternative is using it as a leaching agent, to remove heavy metals from fly ash. In case such recovery options are not followed, yet, the acid needs to be neutralized, e.g., by means of lime.

Selection of Incinerator Furnaces

Selection Criteria

The *selection* of a particular type of *furnace* mainly depends not only on the type(s) of waste to be incinerated (which also determines the possible feeding methods), but also on numerous other factors, such as plant capacity, the operating schedule required, heat recovery, the amount of ash to be handled, and also its physicochemical nature and softening point, etc.

Off-gases and *liquids* are relatively easy to handle using an adapted burner in a simple, tailored combustion chamber, but the incineration of solids, sludge, and paste... may take place under a wide range of combustion conditions and in different types of furnaces.

Furnace types can be classified, according to:

- The contact of waste with combustion air (i.e., in co-current, counter-current, or cross-current relative flow; mechanical and pneumatic agitation, etc.)
- The degree of filling the combustion chamber with solid material
- The choice made between *dry* ash and slag melting conditions (so-called wet-bottom furnaces (not to be mistaken for dry or wet (in water) extraction of combustion residues).

Possible *plant capacity* may be limited by either construction methods, or experience factors; e.g., for mechanical grate at typical capacity 2–20 Mg of MSW/h or rotary kiln furnaces (typically 0.5–5 Mg of waste/h there is only limited experience available once a given size is exceeded. Higher capacity is achieved by providing parallel lines of generally identical capacity and make. Spreading capacity over two or more lines also allows more flexibility, in case of shutdown of one train or of variable supply of waste. Extrapolating existing units to an untested scale may lead to unexpected problems in thermal units. Such was the case in the 1970s for Monsanto's Landgard partial oxidation plant at Baltimore, the Andco-Torrax gasification plant at Leudelange, and the Occidental Petroleum Garrett Pyrolysis plant at El Cajon, Ca. [9, 21, 22].

Heat recovery often features a separate *waste heat boiler*, consecutive to the combustion chamber. Waste with high HHV may also be fired in a furnace, integrated into the boiler structure (*integrated boiler*). The ceiling and sidewalls of the combustion chamber are structurally formed from vertical and inclined boiler tube panels constituted from parallel finned tubes welded together. The tubes are covered by studs sustaining refractory mass, rammed onto the tubes so as to protect them from fouling and corrosion [9].

Pollutant control at times may decide upon the type of furnace to be used or on its operating conditions. Sulfur dioxide (SO_2) is easily captured in a fluidized bed combustor, operating at 850°C, which is the optimal temperature for reacting SO_2 with lime or limestone. Similarly, thermal NOx can largely be avoided at that temperature. Nevertheless, there is always a negative correlation between two types of pollutants: NOx on the one hand and CO + TOC (or PICs) on the other. In case fuel-NOx problems are expected the technique of *staged combustion* is used, which is composed of two steps:

1. Combustion conducted with a deficiency of air (first step, at high temperature), thermally reducing fuel-NOx
2. Post-combustion with ample air and at low temperature

In most cases, this technique will alleviate the problem. Combustion conditions also fix two important factors: (1) ash tends to sinter, soften, and eventually melt, as temperature rises, and (2) the distribution between fly ash and bottom ash also evolves with temperature. Other cardinal factors are the presence of oxidizing or reducing conditions and of halogens, sulfur, etc. [124].

Small-scale incinerators (capacity <2 Mg waste/h) were often operated in a one- or two-shift schedule, but today continuous operation is always to be preferred, since it enhances useful capacity and reduces auxiliary fuel requirements during start-up, thermal wear on refractory, and plant emissions.

Start-up and *shutdown periods* are much more polluting [85], and there is a strong tendency to allow only pure auxiliary fuel to be burnt during these periods. Waste firing can only start once the operating temperature is reached.

Simple, Small-Scale Forms of Incineration

Burning in the open, e.g., in a dedicated open pit, a barrel, or the foot of an old stack, is both highly

polluting and difficult to master technically. An open pit burner was developed by DuPont to incinerate waste [35]. Wigwam or tepee conical burners were used for burning trash, mostly in remote communities [35], in a more controlled manner than is feasible in the open. American apartment buildings used at times to be equipped with chute fed incinerators [125, 126].

These practices should be banned from any densely populated area. Still, in remote areas, e.g., in parts of the USA and Canada, it is often considered the only option practicable and these units are still largely advertized in the USA, even though their use would probably be forbidden in the EU and Japan. Open burning is obviously a major source of pollutants [127–129].

Stationary Furnaces

Summary. Simple, stationary furnaces are in general use for firing gaseous and liquid fuels or even solid waste, on fixed or rotary grates.

Principles. A furnace combines several essential functions, namely:

- Limiting the cooling of the flames and sustaining an adequate furnace temperature
- Providing adequate retention time in the combustion chamber
- Preventing the uncontrolled entrance of air
- Organizing the flows of incoming primary and secondary air and outgoing flue gas, without undesirable dead corners, entries of false (uncontrolled) air, or diffuse spreading of fumes in case of a temporary rise in furnace pressure

Avoiding *smoke* spreading around requires operating at slightly subatmospheric pressure, since incinerators are always somewhat leaky, a consequence of the heating and cooling cycles inflicted upon refractory and casing. For this reason, furnaces formed from welded membrane steel or boiler tube panels are very popular, ever since their first introduction ca. 1970. The selection of waste burners, their position and capacity, flame orifice, air supplies, mixing, and thermal buoyancy characteristics are prime factors determining performance. The mixing characteristics of the furnace are enhanced by appropriate injection of secondary air, enhanced back-mixing of flue gas, created by reducing the cross section of the outlet and by providing periodic changes in the direction of flue gas flow.

Heat release rates are high when burning high-calorific gases or atomized hydrocarbon liquids; they are much lower when burning sludge or wastewater. Where required, a separate post-combustion chamber is used to control PICs, soot, or smells, with its temperature controlled by an auxiliary burner. An alternative is to provide a catalytic post-combustor [130].

Construction and operation. Stationary furnaces refer to a plain combustion chamber, either horizontal or vertical, of a cylindrical shape or box-type, and fitted with the required start-up and auxiliary burners. Horizontal tubular furnaces are most common, possibly aligned with equally tubular waste heat firetube boilers. Box furnaces exhibit dead corners and were used less than half a century ago.

Vertical furnaces occupy less floor space, gradually narrowing to form the stack and deriving draft from this geometrical design. Nowadays, this arrangement becomes less common, since incinerator flue gas generally requires stepwise and multistage cleaning.

Applications. The stationary furnace is used for burning gaseous and liquid waste flows, including off-gases, solvents, oils, wastewater, pumpable sludge, and meltable and paste-like waste streams. Plastics proper are difficult to fire through a burner, for liquid burners will spin threads of molten plastics. Special burner designs fire several streams simultaneously, e.g., auxiliary fuel, waste oil, wastewater, and pumpable sludge. Alternatively, various wastes may be injected either into a stable flame or tangentially to it. Wastewater may be largely evaporated in a forced circulation evaporator and then radially blown into the flame of an auxiliary oil burner.

Advantages and disadvantages. The main technical limitation of an empty combustion chamber is the lack of provisions for eliminating ash or other residues. Ideally, the ash is fine and high melting and blown out of the furnace, and then separated by the air pollution control devices. Residual ash can be eliminated according to different schedules, such as:

- Operating on a daily shutdown schedule for manual or mechanical cleaning
- Periodic or continuous elimination of ash using suitable mechanical means, such as drag conveyers, augers, retractable grates, rotary grates, etc.

Larger units may incorporate rugged, resilient, yet flexible mechanical provisions to convey ash outward. Since it is undesirable that air leaks in through the ash removal system, a wet or dry sealing system is necessary.

Mechanical Grate Incinerators

Summary. Mechanical grate stokers were originally developed for coal [8, 59], yet since the 1930s they have increasingly been used for MSW.

Principles. Traveling grates support the fuel, while conveying it through the furnace, from the front feeding to the ash-discharging side. Staircase grates provide some tumbling action, when fuel drops from one section to the next. *Reciprocating grates* feature individual grate bars, mounted on alternating moving and fixed frames or sledges; moving the sledge conveys the overlaying fuel and – upon its retreat – turns it over that resting on bars from fixed frames. Several arrangements are possible, e.g., with alternating fixed and mobile steps, or with alternating fixed and mobile staircases juxtaposed. A survey of patent literature reveals a richness of ideas to move waste and separate ash [8].

Construction and operation. Most mechanical grates are subdivided conceptually or physically into successive and distinct drying, combustion, and burnout sections, sometimes separated by small walls, where waste tumbles from one level to the next. The position of the fire is somewhat controlled by the mechanical action of the grate, which supports, conveys, and stirs the refuse during drying, combustion, and burnout. The most common types of grate are reciprocating, reverse reciprocating, roller, rocking, and traveling grates. Proprietary, patented devices provide controlled motion, poking, mixing, and sifting ash between individual grate bars.

Primary combustion air is supplied under the various grate sections to cool the grate and accelerate the burnout of the residue. Today less primary air is used, reducing dust entrainment and the flow of flue gas per unit, and improving thermal efficiency.

Air requirements for drying refuse or for burning out clinker residue are quite low, but supply is ill-adapted to real requirements when active combustion takes place. The vapor and gases, resulting from drying and heating the refuse, are rich in oxygen; combustion products evolve as hot, oxygen-deficient strands. Both should be thoroughly mixed by means of powerful jets of secondary air, blown in through high-velocity nozzles, located at the exit of the combustion chamber. After completing further combustion the flue gas is cooled by a waste heat boiler or – in small plant – by injection of water into a cooling tower. Finally the flue gas is cleaned.

Typical combustion conditions are 850–1,050°C, excess air of 80–200%, but there is a strong tendency to limit it to 6–9 vol.% of oxygen in the flue gas. Some operating conditions are specified by codes, e.g., the EU Directive 2000/76/EC:

- Minimum operating temperatures of 850°C and minimum residence time of 2 s at this temperature
- Minimum level of 6 vol.% of oxygen

Applications. The basic application of mechanical grate stokers used to be for firing calibrated coal. Calibration ensures that all lumps or particles burn out after the same residence time, i.e., by the time the coal arrives at the end of the grate. MSW, however, is all but homogeneous. Deviations from uniformity are catered for by providing a feed that has been homogenized and aged (moisture transfer) in the MSW pit and by specific grate action. A number of options are available for co-firing sewage sludge, waste oil, plastic-rich fractions, etc.

Advantages and disadvantages. Mechanical grate operation has been evaluated a number of times, and in the Western society it can boast decisive advantages with respect to the numerous alternatives tested over more than a century.

Its major limitations are:

- Limited to waste that is supported by a grate. Powders, sludge, and liquid or melting waste are excluded, except for marginal amounts. Reporting to grate siftings impairs their quality.
- Less suitable for waste with extremely low or very high HHV, unless both are well mixed. Fluid bed units are much more flexible in this respect.

In southern climates and developing countries, MSW largely consists of putrescible organics and may be too moist to sustain combustion without auxiliary fuel.

Shaft Furnaces

Summary. Shaft furnaces were rather extensively used a century ago, yet they are currently unusual in waste management [9]. Their fields of potential application are briefly discussed.

Principles. The charge is always fed on top, and slowly descends to the hearth by gravity. The air rises generally from the bottom of the unit, activating the fire in the hearth (countercurrent operation). Unless the feed is carefully calibrated, the gas preferentially rises along bigger channels, reducing the quality of contact with air, as well as volumetric capacity. For this reason, shaft furnaces were unsuccessful in tackling raw municipal solid waste; preliminary shredding markedly improved their performance.

Vertical shaft furnaces have been operated in co-current, crosscurrent, or countercurrent (Fig. 10). Usually the last option is selected, since it easily materializes and ensures heat economy, the incoming charge being dried and preheated by the outgoing gas. As a consequence, any moisture and volatile matter evolving from the charge reports to the gas stream, charging it with organics, tars, and odors. Co-current operation hence has been applied in some gasifiers, with the purpose of cracking tars. Crosscurrent operation was applied by WSL/Foster Wheeler in an unsuccessful rubber tire pyrolysis process.

Construction and operation. The shaft furnace consists of a vertical, cylindrical shell protected by inner refractory and thermally insulating lining. Top feeding features a suitable lock for exclusion of air and possibly a distributor for equal distribution of the feed over the entire cross section. Ash extraction proceeds mostly either by means of a rotary grate for ash extraction, or by periodic molten slag tapping.

Applications. Already in Roman times shaft furnaces were used, for calcining limestone. Traditionally, they have been used in the iron and steel industry (blast furnaces), foundries (cupola furnaces for melting metals), and for wood and coal gasifiers.

Shaft furnaces appeared in some ancient incinerator systems (1880–1930), either as combustor or as ash burnout element, the inherent heat exchange assisting in burning low calorific waste with combustion air preheated by hot ash. The rising gas is heavily charged with thermal decomposition products from waste and hence it requires post-combustion. Early Dörr, Didier, Stockholm furnaces are discussed in some detail by Reimann [4].

Advantages and disadvantages. Major advantages are countercurrent heat exchange and a relatively low load of dust. Major areas of potential operating problems with shaft furnaces are [9, 22]:

- Volatiles and moisture emanating from the charge report to the gas, requiring either post-combustion or adequate treatment of these compounds.
- Unless special care is taken to homogenize size and shape of the feed, the rising gas will be channeling through preferential pathways in the charge and along the wall, due to both irregular bed porosity and chimney effects.
- Peripheral fires occur, due to the larger voidage of the charge close to the walls.
- Failing possibilities for controlling temperature, gas flow, and oxygen distribution throughout the charge.
- Controlling ash extraction, whether as cinders or as molten slag.

Rotary Kiln Incinerators

Summary. Rotary kiln incinerators since the 1960s are state of the art in the incineration of industrial waste, including commercial and hazardous waste. These kilns operate either in countercurrent (cfr. long cement kilns), or in co-current (in short kilns, usual in industrial waste incineration). Cross-flow is possible only when using special constructions, e.g., involving telescopic kilns, or in mid-kiln feeding over a complex fixed feeding/rotary kiln device.

Principles. More or less as the shaft furnace, it can operate in countercurrent, co-current, or – with some more difficulty – in crosscurrent mode. Incinerator operation is generally in co-current, with either solid or liquid ash discharge. Tumbling the waste renews the furnace. Since there are no provisions for mixing gas phase strands, a post-combustion chamber is always required.

Construction and operation. A rotary kiln incinerator is typically composed of a stationary feeding system, a rotary kiln with slightly inclined cylindrical shell, a stationary ash discharge system, and

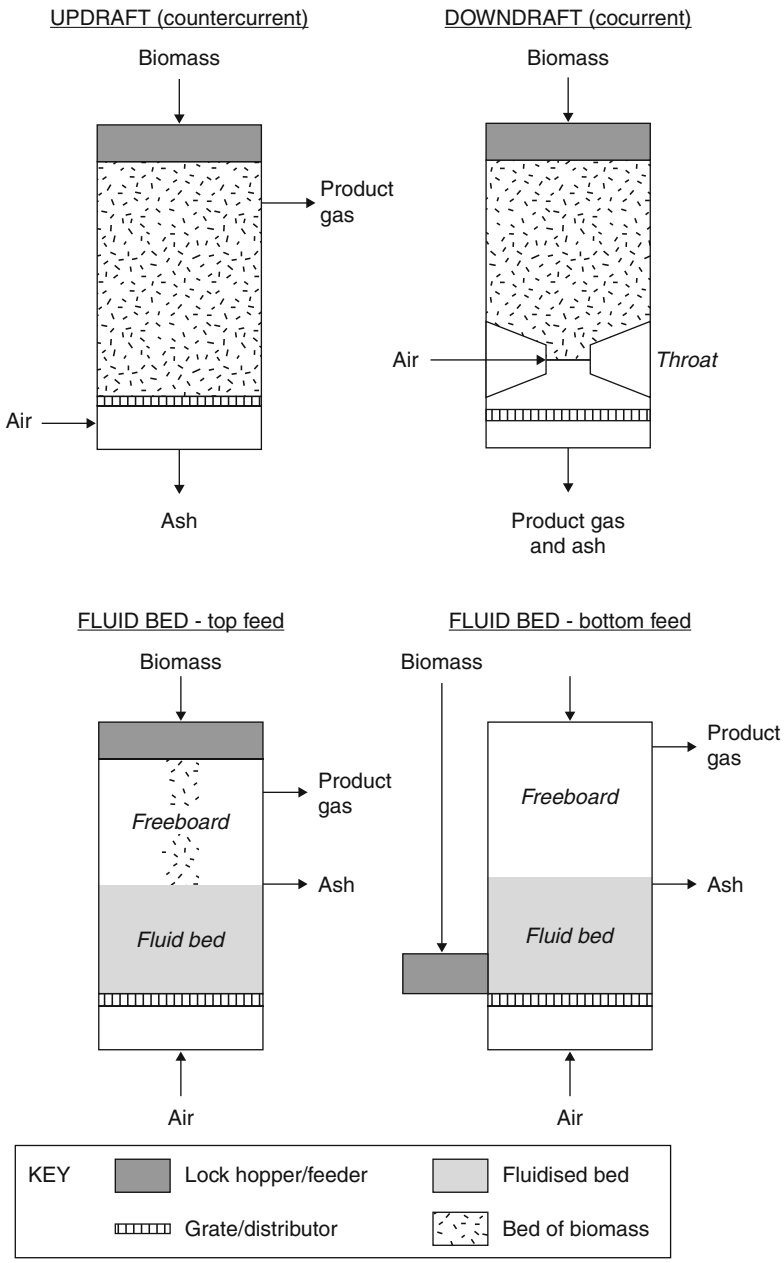

Incineration Technologies. Figure 10
Co-current, crosscurrent, and countercurrent operation of vertical shaft furnaces

a post-combustion chamber, followed by a waste heat boiler (or quench cooler), and air pollution control units [42].

The stationary feeding system consists of a feed hopper, a lock, and a steeply inclined chute. The whole fixed front panel can be mounted on rails. In a patented system, a knife rides on the sides of the feed hopper, cutting off ribbons, plastic film, and textiles, preventing a flashback of the flame into lock and hopper. The lock is formed by two mechanically, hydraulically, or pneumatically operated slides, which are interlocked so that a slide only opens when the other

is closed. The lower slide and the chute are both water cooled. The feeding system can be provided with an explosion relief system, diverting a shock wave into an innocuous direction.

Several systems were tested for homogenizing feed materials and supplying them at a constant rate. Some rotary kilns were fed by a screw conveyor or hydraulically operated ram feeders. Early BASF plants used simple, strong centrifugal pumps with large clearance between rotor and housing, capable of macerating material and pumping the resulting slurry. The rotary kiln was fed from a rotating mixing and storage drum, blanketed with nitrogen.

Kiln lining. The cylindrical shell is internally lined with refractory, selected with regard to the expected operating temperature and slag melting point and reactivity. When using high-quality, dense brick, a continuous operation is necessary to avoid thermal stresses. Gradual heating up may take as much as 60 h and cooling down 24 h. A lifetime of 2 years is considered to be good in normal operation.

No general rules can be formulated regarding the best or more economic furnace lining. In some plants, inexpensive ramming compound or hard chamotte bricks were successfully used. In others, chemical attack was so extensive that lifetimes remained too short, even with expensive high-alumina or magnesia bricks. Chemical attack depends on chemical composition of both lining and ash, and on temperature. Refractory is also subject to abrasion and spalling [35].

Protecting the walls with a layer of solidified molten slag and outward cooling by water sprays have been successfully applied for lengthening lifetimes. Slag accretions can be melted away periodically by slightly elevating the temperature. Iron oxide, when burning barrels, forms low melting silicates enhancing slag fluidity. Slag reactivity and melting point has sometimes been decreased successfully by addition of suitable charges, e.g., sand.

Kiln movement. The peripheral speed of the kiln can be varied continuously using a single drive, with driving pinion and bull gear. The shell is provided with riding rings, rolling on support rollers to obtain a uniform distribution of bearing forces over the shell. In case of power failure, an auxiliary motor should drive the shell to prevent thermal deformation.

Air sealing between rotary shell and stationary loading and discharging equipment at the ends is critical. Excessive air leakage should be prevented by provision of suitable angle or segment seal rings.

In the most usual *co-current operation* both wastes and combustion air are introduced at the front end of the furnace. An auxiliary burner is installed in the fixed front panel of the kiln to enhance drying and accelerate preheating and ignition of the wastes. In the absence of such a burner, drying and preheating completely depends on radiant heat transfer from the rear part; the rate of radiant heat transfer is proportional to the fourth power of temperature (in °K), attained in the hottest part of the kiln. Operation is at 1,200–1,500°C in a slagging operating mode or below 1,000°C in the dry extraction mode.

The rotary kiln is sometimes operated in *counter-current* when relatively wet wastes with a low heating value are to be incinerated (e.g., sewage sludge). Counter-current operation is unsuitable for other waste, because of the risk of flame flashback into the charging lock.

A *partial countercurrent* operation is sometimes used in very short kilns. A good mixing pattern is obtained by using an auxiliary burner in the fixed rear panel. The burner creates a backward gas flow along the kiln axis Fig. 8.

Kiln Internals

The residence time and flow pattern in principle can be modified by installing conveying spirals to guide the materiel flow, ring-dams to retain melted or chains for granular material, or by providing an enlarged cross section near the discharge end to reduce the gas velocity and provide a soaking period at high temperature. A spiraling dentition can be provided in the refractory to retard the forward movement of wastes and enhance the contact between burning wastes and combustion air. The higher cost of the lining limits the practical use of these various patented devices, also prone to erosion and clogging.

Air Supply

Primary air is blown in through a set of nozzles, located on the fixed, front side of the furnace. No secondary air can be distributed along the kiln, unless it is composed of several sections of a different diameter in a telescopic arrangement. The excess of air is large, to make up for

sudden variations in calorific value, and often amounts to 200–300%. Typically 8.000–12.000 m^3 of flue gas is generated per ton of waste.

Combustion air is blown in tangentially at the front end and creates a whirling movement along the wall. Superposition of the two different flow patterns results in a reasonable amount of gas phase mixing, a more uniform temperature and increased kiln capacity.

Residence time and turbulence in the gas phase are both limited. Hence, combustion is to be completed in post combustion chambers providing a supplemental residence time of 2–3 s. The temperature in these chambers is often maintained above 800°C with auxiliary burners firing fuel or liquid waste (solvents, oil).

Facts and Figures

The volumetric rate of heat generation varies, depending on the combustion temperature, between ca. 400,000 and 1,000,000 MJ h^{-1} m^{-3}. Thermal efficiency of the rotary kiln plant is low, limited typically to 55–60%, due to the large excess of air and the various heat losses.

Rotary kilns are built industrially with diameters from 1 to 4.5 m and a length typically from 3 to 15 m. The largest kilns have a capacity of 60 GJ h^{-1}. Scaling-up problems arise, because kiln volume is proportional to the square of the inner diameter, the available exposed surface of waste only to the inner diameter D_i. Hence, multiple kilns are preferred over a single, large diameter one.

Applications

The concept of rotary kiln incinerators was developed at BASF-Ludwigshafen, probably inspired by the much longer units used for producing cement clinker, for calcining limestone or for roasting pyrite and sulfide ores. Yet, the short rotary kilns used in incineration retain the tumbling action rather than countercurrent operation and intrinsic heat exchange.

Dedicated rotary kiln incinerators are capable of eliminating almost any type of industrial wastes, e.g., plastics, oil contaminated sludge, waste paint, solvents, pesticides, spent chemicals, and even explosives (in small amounts). Explosive combustion is relatively harmless, the combustion chamber being spacious and followed by a post-combustion chamber. The rotary kiln is not highly regarded as an incinerator of municipal refuse because of excessive wear of the lining and the absence of possibilities for longitudinal air distribution.

Solid and paste-like wastes, sometimes even complete barrels filled with waste are introduced into a hopper, with a lock system and a chute, located at the stationary upper end of a slowly rotating, slightly inclined cylindrical furnace. The wastes slowly slide and tumble by the rotary movement of the kiln; this provides for mixing and a periodic surface renewal of the burning charge. On their way from the higher feeding side to the lower discharge end, the wastes are rapidly dried, heated, and ignited under the action of radiant heat from the furnace walls. The kiln is generally filled up to 10–20% of its volume. The *residence time* of solid and paste-like waste depends on the length of the kiln, its speed of rotation, the possible presence of a profile in the refractory lining, and gas velocity. Generally residence times of less than 1 h are selected. The ash is discharged into a water bath, located under the lower end of the kiln. In some plants larger pieces of residue are retained on grizzly screen bars, to protect the ash-discharging conveyor [131].

The rotary kiln is used as a drying furnace for, e.g., sewage sludge, in the roasting of pyrites and sulfide ores, the calcination of limestone and the production of cement clinker. In Great Britain, Belgium, and Germany, pulverized refuse was used as a supplemental fuel in coal-fired kilns. Later, rubber tires and hazardous waste in numerous plants became a standard supplement in cement clinker manufacturing.

Westinghouse proposed a unique combination of a rotary combustor with an integrated boiler (O'conner) [35]. In only few cases wastes have been treated or incinerated in a metal-walled rotary kiln having no refractory lining at all (the red factory, of Prayon, Engis, Belgium).

Advantages and Disadvantages

The following problem areas have been identified:

- The charging chute is exposed to heavy wear because of feed sliding and tumbling and condensation of corrosive vapors. Sometimes cracks occur along the welding.

- The kiln lining is exposed to heavy wear and chemical attack. The action of corrosive melted slag is important at the kiln end mainly.
- Air sealings are exposed to dirt, wear, and high temperatures.
- The lower part of the combustion chamber is exposed to attack by entrained droplets of melted ash.

Tilting Furnaces

There are various kinds on rotary kilns, distinguished by their shape (cylindrical, conical), their aspect ratio L/D, or even their rotary movement.

Laurent-Bouillet proposed a particular type of furnace, with a typical conical-cylindrical shape, in which MSW is subjected to an oscillating movement [132].

Multiple Hearth Furnaces (MHF)

Summary MHF have been developed in the nineteenth century for ore roasting and treatment and metallurgical applications are still leading in Europe. Especially in the USA, they have been applied for sewage sludge incineration.

Principles The MHF is a cylindrical construction, composed of a number of circular hearths mounted one above the other. Each hearth contains an air-cooled rabble arm, driven from a common central shaft. Blades, fitted to the slowly rotating rabble arm move the material forward – depending on the angle at which they suspend from the arms – either toward the center or toward the periphery, until it passes over a discharge aperture and falls onto the lower hearth.

The retention time of the charge is varied by changing the speed of rotation of the rabble arms or, rarely, by adapting their relative position to the floor.

Construction and Operation Multiple hearth furnaces (MHFs) consist of a series of superimposed hearths, solids being fed on top and descending stepwise by gravity, after describing a spiraling movement on each hearth, starting at the discharge point of the higher hearth and ending at that to the lower hearth. Gases generally mount, in countercurrent to the movement of solids, aided by buoyancy. The feed material is charged onto the upper hearth and slowly makes its way down, falling from one hearth to the next, while it is progressively dried, heated, ignited, combusted, and finally cooled by the combustion air. The latter is introduced in part or all at the bottom of the furnace, preheated by the ash on the lower hearth(s), and partly consumed on successive combustion hearths. The resulting flue gas is cooled by the incoming feed and leaves the unit toward possible post-combustion and cleaning. Auxiliary burners are used for preheating and adapting and controlling the temperature profile. The atmosphere is controlled by balanced introduction of air, recirculation, or other means [131].

Applications MHFs were originally developed for roasting sulfide ores (Nichols-Herreshoff). Later they were adapted for sewage sludge incineration and for competing with fluidized beds. They provide a controllable temperature record to the feed, generally involving sequential drying, heating, reacting, and cooling hearths. There is much contact surface with air and this surface is periodically renewed by the passing rabble arms with attached plates, plowing through the material.

The main application in waste is incinerating sewage sludge and regeneration of spent carbon or lime. The heat required for drying sludge can – when desirable – be supplied by firing pulverized refuse on lower hearths as an auxiliary fuel.

Lucas Furnace Developments, Ltd., once designed a rotary, single hearth furnace, sloping down from the periphery toward the center. It was proposed for incinerating sewage sludge, old tires (without any prior size reduction), and plastics. After preheating the furnace, waste was fed at regular intervals by means of a ram feeder. As the solid hearth slowly rotates the waste first moves along the outer periphery and gradually spirals to the central discharge point. Finally, the ash falls into a quench tank and is removed by a scraper conveyor.

In this Lucas furnace, the gas flow is organized for cyclonic combustion. High-velocity nozzles direct the combustion airflow tangentially into the furnace, cooling the walls to 850–900°C. The central temperature attains 1,450°C. The plant operates at 80–100% excess of air. Operation at reduced capacity suffers from loss of turbulence in the gas phase, a problem that can be tackled using auxiliary steam jets.

Advantages and Disadvantages

MHFs are a proven and traditional technology that allows a flexible adaptation of operating conditions on each hearth. This versatility is less available in rotary kilns or shaft furnaces.

Because of its complex construction this furnace is limited in its maximum capacity. Moreover, it takes long times to preheat and shutdown MHFs, since it is important to avoid thermal shocks.

Fluidized Bed Incinerators

Summary Fluidized (bubbling) bed combustors are exceptionally adaptable, allowing to burn (or gasify, if air supply is sub-stoichiometric) solid, pasty, melting, liquid, sludge, slurried, and gaseous waste, simultaneously and at unusually low temperatures. Moreover, they admirably accomplish in-bed solids mixing and heat transfer and leave a neatly polished solid residue, sinking in the bed. Fine ash is entrained, including particulate formed by attrition or erosion. Desulfurization with limestone or dolomite is possible in bed at combustion temperature and thermal NO_x-formation remains negligible. The principle limitations are the relatively important pressure drop, as well as bed agglomeration, in the presence of tacky ash or salts. Draining decanted residues requires a dedicated circulation circuit of bed materials, adding to mechanical complication: the extracted bed material is sieved and the underflow returns to the bed.

Circulating bed incinerators have been developed and used since the late 1990s by Zhejiang University and also by Tsinghua University. In China, circulating fluid bed units are unusually popular, since combustion stability can be maintained simply by adding cheap coal, instead of using expensive oil [133].

Principles of Fluidization Consider a fixed bed of granular media, such as sand, ash, or limestone, supported on a porous plate, the distributor plate. An upward current of fluid traversing this layer incurs a pressure drop Δp, which rises as the fluid flow rate increases. Meanwhile, the bed porosity (i.e., the void volume) gradually expands. At a given flow rate the pressure drop Δp even equals the pressure, exerted by bed weight. Then, the minimum velocity of fluidization u_{mf} is reached and the head loss corresponds to the weight of the entire bed per unit of cross section (+ the friction loss, omitted here):

$$\Delta p(u_{mf}) = \rho A H g \tag{20}$$

with Δp = pressure drop, m^2
u_{mf} = minimum fluidization velocity, m s^{-1}
A = bed cross-section, m^2
H = bed height, m
g = acceleration of gravity, m s^{-2}

In principle, the bed thus reaches kind of a state of levitation. However, the fluid (further termed "primary air") will not carry the bed upward, given its granular structure. Rather, excess air trickling through the bed starts forming bubbles at the orifices of the distributor. Such bubbles, after a while, leave the distributor and rise through the bed, more or less like bubbles do in boiling water. The bubbling bed thus resembles a boiling liquid, with series of bubbles rising from the bottom and bursting at the surface. This upward movement of air bubbles creates excellent mixing patterns in the bed leading to temperature homogeneity. Light materials tend to float; dense materials sink to the bottom of the bed. Fluidized beds may be used both as separator of stones or metals present in waste, at low gas velocities, and as a mixer, at velocities a multiple of u_{mf}.

The value of u_{mf} can be estimated using empirical correlations. The gas flows both as bubbles and as a "dense phase" trickling flow. Smooth fluidization is obtained only at a gas velocity of three to four times u_{mf}, together with suitable particle mixing and heat transfer characteristics.

With rising gas velocity, entrainment of fines becomes more important, depending on their terminal falling velocity. The entrainment of bed particles specifies an upper limit of gas velocity. Depending on particle size (often 0.3–0.8 mm), gas velocities typically range between 0.3 and 5 m s^{-1}. There is gradual transition from a bubbling bed to a circulating fluid bed, the latter characterized by a cycle of entrainment, particle separation, and recirculation (Figs. 9 and 11).

Principles Fluidized bed incinerators burn waste, suspended and moved around erratically in a vigorously bubbling bed of hot granular material. High heat generation rates can be obtained despite the low operating temperatures, typically 750–900°C.

EOLSS-WASTE INCINERATION TECHNOLOGY

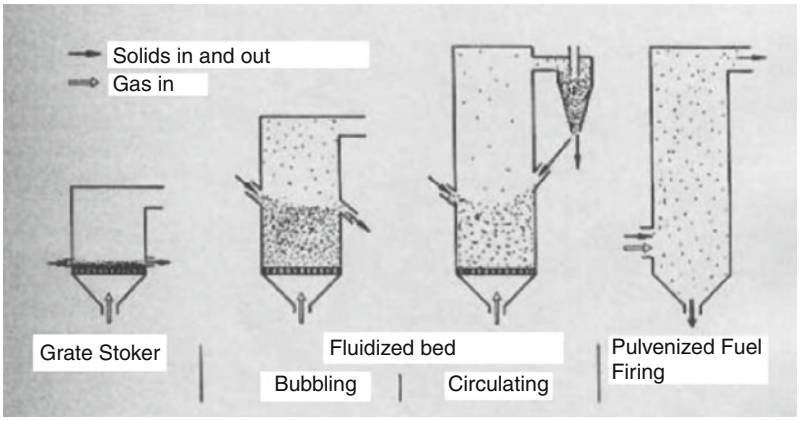

Incineration Technologies. Figure 11
Evolution from a fixed bed, over a bubbling bed and a circulating fluid bed to an entrained flow combustor, with rising gas flow (Görner [34])

In bubbling fluidized beds, combustion of volatile matter mainly takes place in the freeboard zone, i.e., above the bed. This freeboard zone should be ample and well mixed, so that reducing and oxidizing strands can mix and burn out completely. Secondary air provides the swirl required for mixing. The bed material provides a thermal flywheel that effectively copes with short-term fluctuations in feed rates and quality.

Construction and Operation A fluidized bed incinerator consists (starting below and moving upward) of an empty plenum chamber; a distributor supporting the bed; the bed of granular material to be fluidized; a freeboard zone ensuring disengagement of entrained particles and post-combustion, and adapted feeding; start-up and auxiliary heating burners; waste heat boiler; and pollution abatement equipment. The *distributor* supports the bed material and evenly distributes the primary combustion air over the entire cross section. Even distribution requires the pressure drop over the distributor to be at least 0.1–0.2 times the pressure drop over the bed. The distributor should also prevent weeping of bed material into the plenum chamber, or its cycling between both zones, with erosion as a consequence. The distributor is made of heat-resistant alloy or forms an arch of refractory material. In principle, there is a wide range of possible designs; a bubble cap distributor is selected most often.

The *bed material* consists of a graded fraction of clean heat-resistant material, such as sand, more seldom alumina, limestone, dolomite, or ash. Pollutants, such as SO_2, can be removed in situ by simply feeding limestone or dolomite into the bed. The bed is preheated to operating temperature by generating hot air in a separate furnace or using a start-up burner directed toward the surface of the bed and then fluidizing gently.

Combustible waste and *auxiliary fuel* are generally fed into the bed to ensure that the heat of combustion is largely generated inside, rather than above the bed, in the freeboard zone. Yet, much of the combustion of the volatile matter will burn above the bed. Gas is fed through independent bubble caps, liquid fuel, slurries and pumpable sludge, and lances, and solids by means of a screw or a pneumatic feeder.

Low-calorific wastes can be dropped onto the top of the bed by a chute fed by a conveyor belt, or sprayed over the bed by means of suitable nozzles. Mechanical spreaders may assist in obtaining a more uniform distribution of the feed. The falling droplets or particles are partly dried while dropping onto the bed. Once in the bed, drying, heating, ignition, and burnout proceed very rapidly. Feeding large pieces lead to the local evolution of excessive amounts of volatiles, causing total depletion of oxygen, evolution of clouds of pyrolysis and gasification products, and, eventually, of

sequences of CO and TOC peaks. For this reason the feeding rate should be bit by bit and steady, and feed materials should not be larger than 5 or 10 cm.

Bubbling beds project particles into the freeboard. Most settle in the *freeboard zone*, but the finer ones are partly entrained. Finer particles are separated in internal or subsequent cyclones and flow back into the bed, to complete their combustion. Secondary air is injected into the freeboard zone to complete the combustion.

Applications Fluidized bed technology was first applied in the 1920s, in coal gasification (Winkler) [134]. Fluid catalytic cracking of gas-oil to gasoline followed during World War II (Massachusetts Institute of Technology, Esso) [134]. Other important industrial applications are the roasting of sulfide ores and the drying of polymer powders. The most significant applications are the incineration of wastewater sludge and black liquors from wood pulp manufacturing [135].

Fluidized bed incineration, gasification, and pyrolysis of shredded or classified refuse have been widely developed in Japan, Finland, and Scandinavia.

Advantages and Disadvantages Fluidized bed incinerators are relatively simple to build, operate, automate, and maintain. They have no moving parts at high temperatures. Yet, high heat generation rates and bed-to-wall heat transfer rates are obtained due to the high-quality gas-solids contact. Complete combustion is possible already at a low temperature (750–850°C) and a low excess of air (15–35%); hence the volume of flue gas to be cleaned and the NO_x generation rate are relatively small. Bed material can easily be added or removed (draining at the bottom or overflow), which allows adding also lime or dolomite.

Thanks to the large thermal capacity it is also possible to absorb important step changes in feeding rate and even to operate intermittently: cooling of the bed after shutting down is very slow, so that proper operating conditions can rapidly be reached after a standstill of 1 or 2 days.

On the other hand, both the power requirements for fluidization and the dust content of flue gas are quite high. Dense material may segregate and accumulate on the distributor plate, which can be avoided by using an appropriate distributor design, such as sloping distributor plates or arrays of spaced perforated tubes sparging air into the bed. A waste heat boiler and/or preheated air are required to reduce the stack heat losses.

The most serious operating problem occurs when the combustion temperature increases beyond the softening point of the ash. Rapid particle agglomeration then occurs, followed by solidification of part or all of the bed material. When this happens, the solidified material has to be excavated by pneumatic hammers after cooling of the bed.

Vortex Combustors

Summary Vortex incinerators can be used for high-rate combustion of gaseous, liquid, and finely divided solid fuels or wastes. Larger particles require longer residence times and may not burn out completely; in this case, supplemental mechanical means, such as a specific burnout grate, have to be provided for retaining the burning residue [9].

Principles Vortex firing involves a highly turbulent mode of combustion, featuring fast transfer of heat and mass and resulting in high volumetric rates of heat release.

Construction and Operation Fuel (or waste) is blown in tangentially into a conical or cylindrical furnace. The rotary movement of combustibles suspended in combustion air as a carrier creates excellent mixing conditions and hence high combustion intensities and temperature homogeneity.

Two vortices are formed: an outer one consisting of combustion air and waste and an inner one of burning gases. The cooler outer flow shields the refractory walls from overheating and it is rapidly preheated by the hot inner core, considerably stabilizing a steady combustion. A wide range of operating temperatures and a low excess of air can be used. This may lead to a slagging operation.

Applications Tangential firing involving vortex combustion has been used extensively in coal-fired utility boilers. In one design, pulverized coal is fired in a separate cylindrical vessel, somewhat inclined to the horizontal. In a second design, pulverized coal, together with combustion air, is injected from the

four corners of a vertical chamber with a square cross section. Jets are directed tangentially to an imaginary circle contained in this section.

Heat rates in such cyclonic furnaces allow liquid tapping of slag, also with medium HHV waste, such as dry straw or wood chips. Wet bottom cyclonic furnaces for firing coal with an unusually low ash melting point have been developed.

Advantages and Disadvantages Cyclonic furnaces are compact and highly productive. These advantages weigh more, in case the unit capacity is important. The principle is applied less often for small plants. A high-temperature operation may lead to considerable NOx formation, unless excess oxygen is really minimized.

Slagging Incineration

Summary *Slagging incineration* also termed "wet bottom operation", is an option whenever combustion is conducted at quite high temperatures, or when the resulting ash has an unusually low melting range. This occurs when the waste contains certain groups of chemicals in its ash, such as borates and numerous alkali salts.

Principles *Wet bottom* combustors fire fuel (coal, or waste) at temperatures exceeding the melting point of ash. Incinerators may operate in this slagging mode in case:

- Waste is sufficiently high calorific and combustion temperatures are adequately high
- The resulting slag either has adequate fluidity, or fluxes are added
- Provisions for tapping molten slag are available

Preheating combustion air, enriching it with oxygen, providing auxiliary fuel, and dissipating electric power in the charge (Ohm effect, electric arc, hot plasma) all allow to raise combustion temperature to higher levels and addition of fluxing agents (fluorspar, iron oxides, lime) may be used to lower the melting range and enhance slag fluidity. Molten slag can be tapped discontinuously and discharged to solidify to large crystalline blocks. Generally, however, it is quenched by pouring the melt into a water bath, converting it into small glassy grains. Continuous tapping is uncommon, given the small capacity. When treating metal rich waste, two phases might be formed: a light slag floating on top of molten metal.

Construction and Operation There are numerous different methods to conduct incineration or even gasification under slagging conditions. Such methods encompass, e.g.:

- Shaft furnaces, operating like a blast furnace. Examples: Lurgi pressurized moving bed oxygen/steam gasifiers. Union Carbide, Andco-Torrax and Nippon Steel gasifiers.
- Rotary kiln incinerators operating on high-calorific waste and in a slagging mode.
- Mechanical grate incinerators, fitted with a dedicated furnace to melt the residue.
- Electric arc furnaces (cfr. metallurgical Industry).
- Suspension firing. Cfr. The Vortex Furnace and Koppers-Totzek Coal Gasifiers.

Applications Already in 1934 Rummel [134] pioneered the concept of using molten material (these could be slag, metals, or salts) as heat carrier and oxygen transfer agent. Ever since these 1930s, slagging incinerators have been experimented with, in association with cokes addition, electric arc furnaces, plasma torches, with special waste with unusually low ash melting traject, or with waste streams, warranting high disposal cost, e.g., radioactive waste, or PCBs.

Recently, slagging operation in Japan became a standard, following the necessity of converting incinerator residues into glassy slag.

Nippon Steel has developed blast furnace technology, applied to MSW.

Ebara Co. has pioneered a fluidized bed gasification plant, featuring post-combustion under slagging conditions of the gas.

Advantages and Disadvantages Slagging incineration has several potential advantages, such as

- Simpler furnaces, ash flowing along an inclined floor
- Generating dense glassy slag, with low leaching rates and almost free from combustible inclusions
- Operating at low excess of air, reducing flue gas flows to be cleaned as well as stack losses.

The major problem is ensuring steady fluidity of slag, while still limiting its attacks on refractory. A thin layer of solidified slag may be maintained on the refractory lining to cover and protect the refractory (Fig. 12).

It is recommendable to separate combustion from ash melting, by providing a controlled supply of heat and possibly flux in the slag tapping area. Slagging operation exists in many variants. Heat supply is secured by the following means, alone or in combination:

- Plasma torch
- Addition of coke
- Auxiliary burners
- Combustion of gasification products

Example: Incineration in a Molten Salt Bath Incineration in a molten salt bath has also been applied when dealing with hazardous wastes, such as pesticides, explosives, etc. Combustion in a bath of molten salts (e.g., sodium carbonate, potassium carbonate,) could present the following advantages:

- Molten salt acts as a heat carrier and combustion catalyst, ensuring complete oxidation at temperatures lower than normally required.
- Carbonized residues and dust and ash particles are entrapped in the bath.
- Acidic pollutants in the off-gas react with the salt and are also retained in the bath.

A potential disadvantage is the required disposal or regeneration of spent salt. Moreover, managing volatilizing salts is problematic, since deposits of desublimated salt fumes will need to be removed periodically.

Submerged Combustion

Summary Submerged combustion combines a vertical conventional combustion chamber with immediate

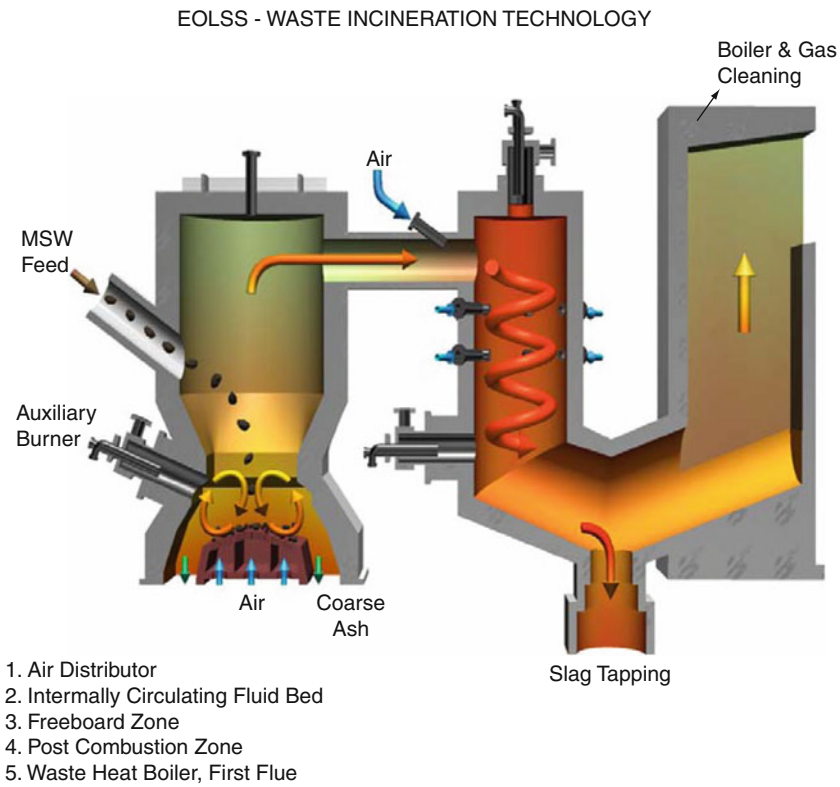

Incineration Technologies. Figure 12
Fluid bed gasifier with slagging post-combustor (By Courtesy of Ebara Co., Japan)

direct-contact quenching of flue gas by its immersion in aqueous liquor, brine, lye or acid, ensuring fast heat and mass transfer in a bubbling liquid mass.

Principles Submerged combustors feature a vertical, refractory lined steel shell furnace equipped at the top with a down-firing burner, the flue gas of which bubbles through a reservoir filled with quenching and scrubbing water or other aqueous liquids (Fig. 13).

Construction and Operation The plant consists of a slender, elongated, vertical furnace, plunging as a downcomer tube into a bath retained in a wider container. Frequently, a concentric tube surrounds the downcomer, forming an annular space, acting as an airlift and promoting internal mixing of the liquor contained in a quenching bath. As a result the gas is suddenly quenched, freezing undesirable reactions, such as forming chlorine according to the Deacon equilibrium of reaction (13).

Waste sulfuric acid, brine, or other corrosive solutions can thus be concentrated by direct contact between hot flue gas and the liquor to be treated. Heat and mass transfer between flue gas and liquid quench are almost instantaneous: the quenched flue gas is almost completely saturated with water vapor and leaves substantially at the temperature of the quenching bath.

Applications Submerged combustors have a long tradition, with first patents in the nineteenth century. Chemico used it as a means to concentrate dilute sulfuric acid, Nittetu Chemical Engineering to treat chlorinated waste [137]. It is mentioned in the IPPC report [136]. Submerged combustors are used to:

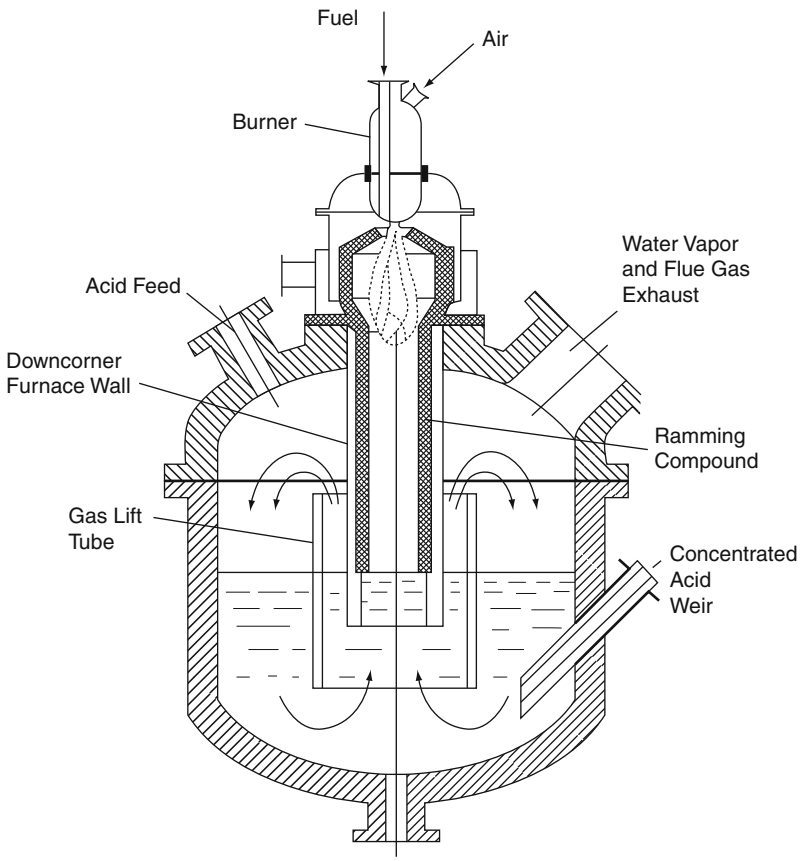

Incineration Technologies. Figure 13
Submerged combustor (Günther [34])

- Quench and clean flue gas, arising from the combustion of chlorinated organics [137] or CFCs [138, 139]
- Concentrate wastewaters or corrosive acids, maintained as quenching bath
- Recover a solution of inorganic salts, when firing aqueous solutions of organic or inorganic salts
- Recover dilute hydrochloric acid of acceptable concentration when firing chlorinated wastes

The liquid wastes are atomized and injected into the flame, so that they are rapidly dried, thermally decomposed, and completely combusted. Inorganic compounds are converted to tiny molten salt particles and are recovered as a salt solution or slurry in the quench vessel.

Another design (Nittetu) features a fractionating column mounted on top of the water vessel. Wastewater contaminated with volatile hydrocarbons is fed on top of the column and hydrocarbons are stripped off in contact with a rising mixture of flue gas and water vapor. After condensation of the vapors, the condensed heavier hydrocarbons are recycled to the quench vessel. The noncondensable is combusted.

Advantages and Disadvantages Submerged combustors are relatively simple, efficient equipment. Quenching and scrubbing are fast and direct-contact. Chlorine formation is suppressed when firing halogenated solvents and vapors. Also dioxins formation is suppressed.

A dedicated website is [140]; various hardware are presented in [141] (Table 9).

Refuse-Derived Fuel

Rather than firing waste as it comes, one can convert it into storable fuel, following a suitable sequence of operations, composed of primary and secondary shredding, grading, wind sifting and screening, magnetic and eddy-current separation, etc. Suitable combinations of such operations may convert municipal solid waste, packaging, wood, paper and plastics, etc., into better manageable and storable refuse-derived fuel (RDF) with more predictable characteristics and specifications, such as HHV, and proximate and ultimate analysis. RDF assumes different forms, such as fluff, powdered (after adding embrittling agents), or densified, i.e., in bales, pellets. Already in the 1970s, the National Centre for Resource Recovery (Washington) tried to standardize RDF, to improve its acceptance and access to the energy markets [9, 142].

The preparation of RDF may proceed according to very simple as well as more complex schemes, promising higher quality as well as more investment and operating cost. EcoFuel® was a powdered product, obtained by raising the temperature and adding an embrittling agent, e.g., sulfuric acid. In one case, processing started by wet pulping (Black Clawson at Franklin, Ohio); the resulting RDF was wet during processing, which is counterproductive for thermal utilization. Moreover, the only large plant in Florida suffered from odor problems and was eventually dismantled. Yet the processing generates clean fractions of metals and glass.

Today, mechanical biological treatment [143, 144] is proposed as a generic group of processes to produce a fuel fraction and sorting fractions.

The complete combustion of solids generally requires residence times of typically half an hour, except for some high-intensity incinerators, such as those firing a *refuse-derived fuel* (RDF). In principle, the residence time available for combustion is comparable now to that of flue gas, i.e., a matter of seconds only for suspension firing up to about a minute in bubbling fluidized bed plants. Circulating fluidized bed units feature cyclonic separators that collect coarse matter for recycling. In practice, the denser RDF will thus be retained by suitable aerodynamic and geometrical means (gravity or centrifugal force) that extend its residence time until the residue is so fine that it is entrained.

RDF preparation is expensive, typically in the range of 20–80 US$/Mg. These costs derive both from investment and operations and include power consumption and heavy wear on equipment. Fire and explosion hazards are notoriously present during shredding, drying, and even longer-term storage.

Co-firing of Waste or of RDF

In most cases waste is incinerated in dedicated furnaces. In some instances, it may be more attractive to

Incineration Technologies. Table 9 Typical combustion conditions

Combustion conditions	Combustion temperature (°C)	Furnace temperature (°C)	Gas velocity (m s^{-1})	Residence time (s)	Air number (–)	Thermal volumetric load (MW m^{-3})	Thermal cross-sectional load (MW m^{-2})
Power plant:							
Natural Gas	1,100–1,400	1,000–1,100	5–10	1–3	1.05–1.1	0.25–0.35	5–8
Oil	1,100–1,400	1,000–1,100	5–10	1–3	1.05–1.2	0.25–0.35	5–8
Grate stoker	1,100–1,300	1,000–1,100	4–9	1–3	1.3–2.5	0.15–0.35	0.5–2.5
Fluidized bubbling bed combustor	750–1,050	750–1,050	0.5–5	1–3	1.2–1.4	2–5	1–2
Circulating fluid bed combustor	750–950	750–950	5–8	0.5–6	1.12–1.3	8–20	2–8
Pulverized coal firing	1,100–1,500	1,050–1,250	5–10	1–3	1.13–1.3	0.06–0.3	0.6–3
Pulverized lignite firing	1,100–1,300	950–1,150	4–8	1–3	1.2–1.5	0.06–0.15	2.5–5
Pulverized coal firing (wet bottom)	1,300–1,600	1,000–1,150	5–10	1–3	1.15–1.3	0.1–0.4	4–6
Mechanical grate MSW-incinerator	1,000–1,250	1,000–1,100	3–8	3–6	1.5–2.0	0.15–0.35	1.4–1.6
Fluid bed sludge combustor	750–900				1.05–1.8	1–3	0.5–1
Stationary combustion chamber					1.2–3	0.1–0.3	0.1–1
Rotary kiln incinerator					1.6–3.5	0.15–0.2	1.5–2.5
Postcombustion chamber	1,050–1,300	1,050–1,250			>1.4	0.08–0.35	1–1.5

Source: Compiled from Görner

incinerate waste in preexisting plants, such as industrial furnaces, power plant, cement kilns, etc. The advantages are obvious:

- Investment cost is limited to the additional plant, required to prepare, store, feed, and fire the waste.
- The energy content of waste is put to good use, often at much higher efficiency than is possible in a dedicated plant. A thermal power plant typically operates at an efficiency of HHV to power of ca. 44%, against typically 16–24% for dedicated incinerators.

Theoretically, it would thus be attractive to replace dedicated incineration by usage of waste as a fuel. Yet there also disadvantages, such as below:

- Integrating distinct activities (waste elimination and heat and power generation) also means declining the operating flexibility of each individual activity.
- Incineration is subject to much more stringent emission codes, compared to those for thermal power plants, industrial furnaces, or cement kilns.

Co-firing has been denigratingly termed "solution by dilution." The EU directive on incineration has considered this problem and offered a solution featuring flexible emission limits.

- The waste composition should be confronted with that of the conventional, generally solid, fuel with respect to the pollutants S, N, Cl, and heavy metals.
- The ash arising from waste may affect and often lower product quality, e.g., in cement and especially limekilns.
- Some elements contribute not only to pollution, but also to the creation of operating problems, such as superheater fouling and corrosion (biomass or RDF co-firing) or cycling of heavy metals (cfr. Cement Kilns).

Thermal Power Plants

Co-firing RDF in thermal power plants offers solutions that hold the promise of limited investment, related to the production (possibly off-site), storage, and firing of RDF. Conversely, RDF co-firing may create serious problems at the level of boiler fouling and emissions.

Thermal power plants in general are large-capacity units (40–400 MW_{el}), typically one order of magnitude larger than the usual waste-to-energy (WtE) projects. As they stand, they are fully equipped with provisions for fuel supply, firing, and ash storage, boiler feedwater production, steam generation at high pressure, turbo-alternator, transmission lines, steam cooling, and condensation provisions. Sharing these provisions with incineration plant allows sharing all provisions related to the steam circuit and power generation.

Co-firing of RDF has been proposed consistently since the early 1970s. Ideally, the hosting power plant fires solid fuels such as coal or lignite. The RDF must be reduced in size, so that the individual particles burn out in suspension. Dense parts falling out can be collected on a dump grate for completing their combustion.

Co-firing of biomass has also been considered, at first in Denmark, to eliminate the polluting practice of field burning. Biomass is often lean in pollutants (sulfur, nitrogen, heavy metals). Unfortunately, the ash is also rich in low-melting potassium salts and hence tacky, causing extensive superheater fouling and corrosion. Pure wood is low in ash (0.5–2 wt.%), yet real biomass, such as straw, is much higher, up to 8 wt.%.

Cement and Lime Kilns

Cement (and lime) kilns are increasingly used for incinerating hazardous and also high-calorific waste. The kilns always operate in countercurrent (Fig. 12) and feature combustion temperatures of almost 2,000°C, with kiln lengths ranging from some 50 m (dry process) to about 150 m (wet process). This ensures longer residence times at temperatures above 850°C than any other furnace. Even hazardous pollutants, such as PCBs, requiring a destruction efficiency of at least six 9s (99.9999%), are completely combusted in such kilns. The waste is fired at the lower end of the kiln so that all flue gas starts at flame temperature and then remains in contact with the high temperature reaction zone in which the clinker is formed. Most ash drops out at high temperature and is incorporated into the clinker.

Wet kilns are even longer, since the raw materials mix is to be dried, dehydrated, decarbonated (conversion of $CaCO_3$ into lime), and eventually reacted to clinker at around 1,500°C.

Wet kilns allow separating dust from flue gas and sluicing it out, since the feed enters as a paste. Much shorter dry kilns do not have this feature, the incoming dry meal being heated in direct contact in batteries of cyclonic heat exchangers and enter the much shorter kiln already at high temperature, after preliminary decarbonatation at ca. 800°C. Because of energetic considerations, dry kilns are always preferred for cement manufacturing.

Waste serves primarily as substitute fuel. Yet, waste with appropriate mineral composition (silica, alumina, lime, and iron) may also replace natural feed materials (clay, shale, limestone), alleviating the needs for quarrying (Fig. 14).

Cement kilns are thus prime substitutes for hazardous waste incinerators, as long as the wastes are introduced as solid or liquid fuels at the lower, kiln discharge side. There is sufficient oxygen, temperature, and time to complete combustion of even the most refractory hazardous compounds, such as PCBs, even though the mixing in the gas phase tends to be weak. The solids are in better contact, due to the tumbling action of the kiln. Typical feed requirements are presented in Table 6.

When waste is introduced mid-kiln, however, or – worse – at the higher end of the kiln (in a dry plant, yet after the battery of heat exchangers),

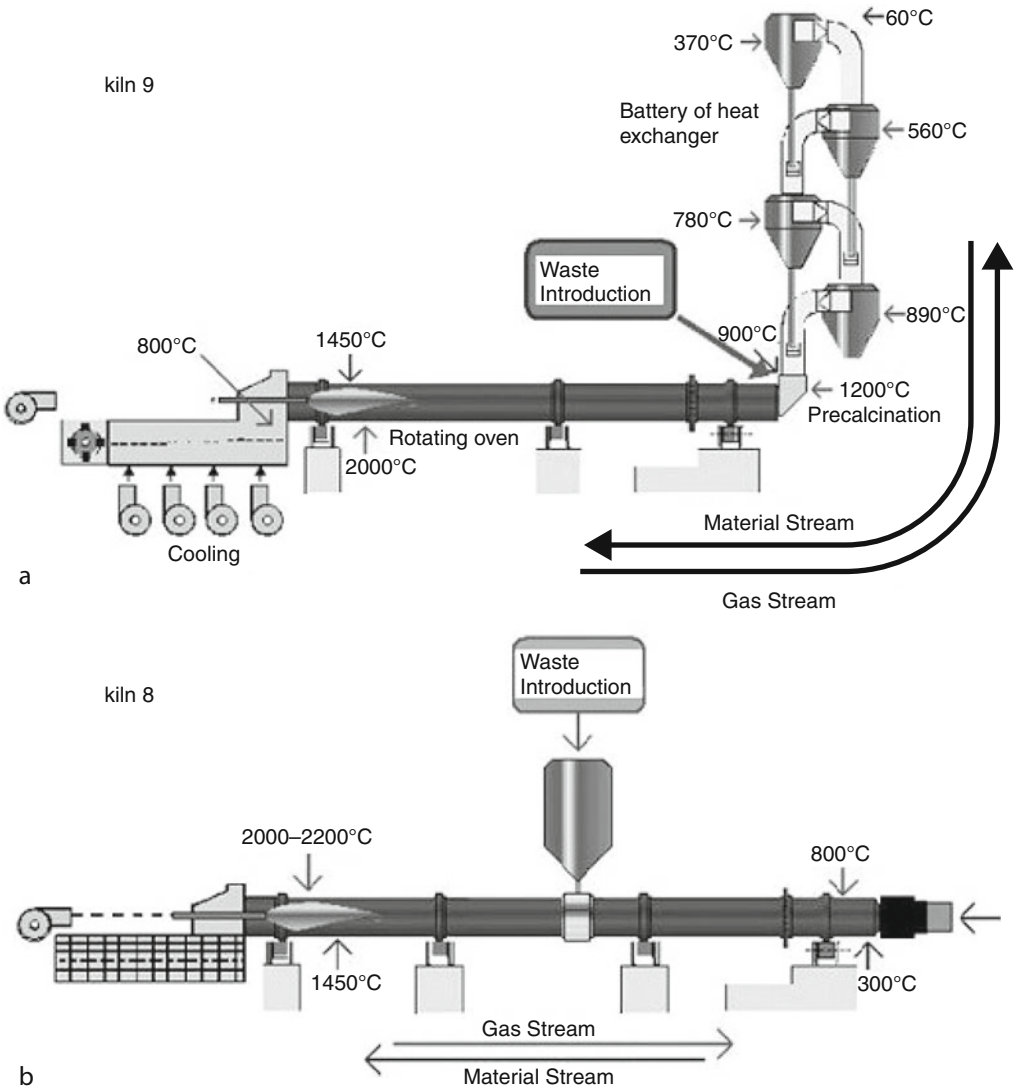

Incineration Technologies. Figure 14
Cement kilns treating contaminated soil with feed point (**a**) after the cyclonic heat exchangers and (**b**) mid-kiln. (14**a**) Shows a battery of four cyclonic heat exchangers, featuring direct contact with hot rising flue gas. The feed entering the plant is dried and heated from 60°C to 900°C, completely calcining the limestone in the feed. In the rotary kiln, it converts into clinker. In this unit, contaminated soil is added at the kiln entrance and it is not certain how far emerging volatiles are still combusted completely. (14**b**) Shows an alternative with mid-kiln feeding, and still converts the contaminated soil into clinker, yet leaves more room for post-combustion than in the first case

a sizeable part of this high-temperature residence time is sacrificed. Feeding organics along with the raw materials, however, must be considered carefully from an environmental viewpoint, since any volatiles evolving from the feed report to the off-gas without post-combustion or cleaning.

The ash from waste is largely incorporated into the clinker. This has raised questions regarding the

eventual leaching of any heavy metals from clinker, as well as regarding the state of oxidation of chromium, i.e., Cr^{III} or Cr^{VI}. Halogens and volatile heavy metals create cycling and emission problems. Several heavy metals (Pb, Zn, and Cu) volatilize in the presence of chlorides, yet de-sublimate and deposit during cooling.

Cement kilns are important emitters of carbon dioxide, dust, and nitrogen oxides. Emission limit values are much more lenient than for dedicated incinerator plants. The cement route has hence been denigrated as "solution by dilution." Nevertheless it is clear that there is scope, worldwide, for the cement route especially in countries devoid of dedicated plant.

There is very extensive literature regarding the cement route [145–148]. Individual cement plants are well documented, relative to inputs and emissions. The lime route has been much less publicized. Obviously, any ash reporting to the product deteriorates product quality.

Public Image of Incineration

Incineration has been branded as a substantial source of environmental pollution (dioxins, heavy metals), as well as an easy way around voluntary or even mandatory recycling. Greenpeace has been quite vocal in these criticisms, attacking incineration, and also PVC as a source of dioxins [149–152]. In the meantime it became clear that dioxins in MSW incineration are formed at comparable rates whether or not PVC is present: the element chlorine is so ubiquitous that its concentration in MSW as a rule is not rate controlling [153]. Much more important factors are the steady quality of combustion, the catalytic effects of transition metals, and dioxins forming increasingly in electrostatic precipitators as their operating temperatures rise (Fig. 15).

Plume dispersion computations show that immission values of state-of-the-art incinerators are negligible, compared to background values. Such

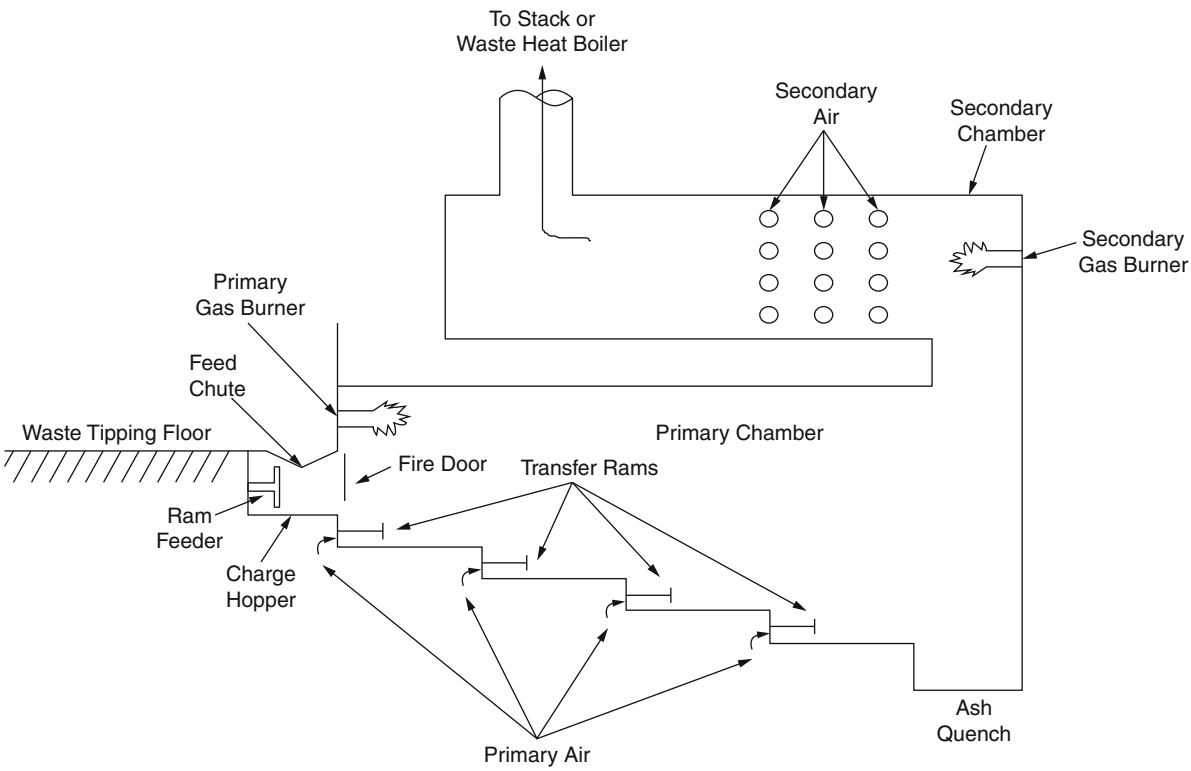

Incineration Technologies. Figure 15
Starved air incinerator (By courtesy of)

deposition values also have been measured many times [154]. Epidemiological studies relating incinerator emissions to public health never clearly condemned the old generations of incinerators, let alone current units with much lower emission values [155, 156]. One reason for these results is that the body burden of most toxic organics relates to food uptake, rather than to inhalation [157]. Today, the main medical interest is related to minute submicron particles that readily migrate through the lung membranes. Also prenatal exposure to dioxins and POPs has been studied.

Other important aspects are related to absorption, digestion, and eventual health effects of dioxins and dioxin-like compounds, in particular polychlorinated diphenyls (PCBs). PCBs are man-made chemicals, yet they also form (with a different congener profile) in thermal processes, typically representing less than 5% of dioxins and furans, when expressed in toxicity equivalents (TEQs). Dioxin diets were established in numerous countries, since food is the major route to take up TEQs. One pathway between the incinerator stack and the food chain is as follows: emission – particle deposition – absorption by grazing cattle – secretion with the milk. In the past, cow milk has been declared unfit for consumption around both incinerator and metallurgical plants. Halting the emissions at Zaandam (the Netherlands) rapidly restored milk quality. Far higher dioxin emission levels at Gien (France) produced no undesirable effects: dioxins were emitted in the gas phase and apparently degraded in the atmosphere, rather than impairing the quality of dairy products.

Incinerators are no longer major polluters, given the extremely stringent emission codes applied today. There is a tendency at present to compare incineration to its traditional alternatives, landfill and composting, incorporating additional criteria, concepts and methods, such as the impact upon climate change and global warming. Landfill is responsible for important greenhouse gas emissions; evolving fermentation gas contains carbon dioxide and also methane, a much more potent greenhouse gas. Composting also emits greenhouse gases, yet does not get the bonus of producing green energy. Markets for compost are as precarious as those for incinerator heat.

Waste incineration is also held responsible for destroying values, available for recycling. Yet, the main bottlenecks of recycling are markets for secondary raw materials showing low-grade specifications or containing *pernicious contraries*: any imbalance between supply and demand exerts strong leverage on market prices.

Future Directions

At present, *waste incineration* has evolved to mature technology, with mechanical grate incinerators as standard in MSW incineration, rotary kiln plant for firing industrial and hazardous waste, and fluidized bed units for sewage sludge, as well as for co-firing wastes with extremely dissimilar properties. Yet, each of these units still has some technical limitations. Mechanical grate stokers must support the waste during combustion, yet have difficulty in coping with both very wet and high-calorific waste. For rotary kiln units, gas phase mixing and wear are major problem areas. Fluid bed units require steady, size-reduced feed and may experience loss of fluidization in the presence of low-melting ash and at too high temperatures.

Flue gas cleaning has evolved considerably since the early 1970s, under pressure of ever tightening limit values (Tables 3 and 4). Given the thorough cleaning generally practiced, it seems unlikely that these limit values would evolve even further. In particular cases, e.g., dioxins, emission values were promulgated on the basis of rather thin evidence and in the absence of proven technology to reach the new limit values. Yet, it cannot be excluded that still new parameters would be brought forward, such as nanoparticles and nitrous oxide (N_2O). However, it is obvious that more can be gained by cracking down on open burning of waste and other primitive and polluting forms of combustion.

The concept of *refuse-derived fuel* (RDF) production holds the promise of conducting incineration in non-dedicated units, such as thermal power plant, and cement and lime kilns. Although RDF is still produced and fired in such plants, initial promise has been mitigated by the added cost and complexity of fuel preparation, by both environmental and product quality (lime, cement) concerns, and by logistic and operational requirements.

Gasification and *pyrolysis* processes have frequently been proposed and tested at laboratory, pilot, and full-scale level. Their theoretical advantages, such as simpler

operation and lower volumetric rates of gas production, have materialized in practice in only few cases. A decisive disadvantage is poor reliability and availability. A large majority of actually constructed plants have actually been scrapped after realizing precarious operating records (e.g., Siemens at Fürth, Thermoselect at Karlsruhe). Some communities were forced to pay for an entire generation for such plants (Andco-Torrax plant in Grasse). By far the most experience has been gathered in Japan, with slagging shaft furnace operation (Nippon Steel) and fluidized bed gasification, followed by post-combustion and fly ash melting and granulating (Ebara Co.) as most successful representatives.

Slagging operation produces glassy aggregate, rather than clinker and fly ash. The question rises whether the more attractive residue can justify considerable supplemental cost, higher energy consumption, and lower availability.

Some organizations important in matters of incineration:

- Air & Waste Management Association (A&WMA)
- American Academy of Environmental Engineers (AAEE)
- American Institute of Aeronautics & Astronautics (AIAA)
- American Institute of Chemical Engineers (AIChE)
- American Society of Mechanical Engineers (ASME)
- Chartered Institution of Wastes Management, London
- Coalition for Responsible Waste Incineration (CRWI)
- Electric Power Research Institute
- Institute for Professional Environmental Practice (IPEP)
- Institute of Chemical Engineers – United Kingdom (IChemE)
- Institution of Mechanical Engineers – United Kingdom (IMechE)
- Integrated Waste Services Association
- International Solid Waste Association (ISWA)
- Japan Waste Management Association ()
- Korea Associate Council of Incineration Technology (KACIT)
- Korea Society of Waste Management (KSWM)
- National Institute for Environmental Studies ()
- National Institute of Environmental Health Sciences (NIEHS)
- Society of Chemical Engineers – Japan
- Solid Waste Association of North America
- Swedish Chemical Society – Sweden
- UK Environmental Agency – United Kingdom
- United States Department of Energy (US DOE)
- United States Environmental Protection Agency (US EPA)
- Waste-to-Energy Research and Technology Council (WtERT)

Bibliography

Primary Literature

1. Lewis H (2007) Centenary history of waste and waste managers in London and South East England, Chartered Institution of Wastes Management, London. http://www.iwm.co.uk/web/FILES/LondonandSouthernCentre/London_and_Southern_Centenary_Histroy.pdf. Accessed July 2011
2. Kleis H, Dalager S (2007) 100 years of waste incineration in Denmark – from refuse destruction plants to high-technology energy works. DTU, Copenhagen. http://www.ramboll.com/services/energy%20and%20climate//media/Files/RGR/Documents/waste%20to%20energy/100YearsLowRes.ashx. Accessed July 2011
3. Reimann DO (1991) Abfallentsorgung mit integrierter Abfallverbrennung – Verfahren von gestern und heute. In: Reimann DO (ed) Rostfeuerungen zur Abfallverbrennung. EF-Verlag für Energie und Umwelt, Berlin, pp 1–20
4. Reimann DO (1991) Die Entwicklung der Rostfeuerungstechnik für die Abfallverbrennung – Vom Zellenofen zur vollautomatischen, emissions- und leistungsgeregelten Rostfeuerung. In: Reimann DO (ed) Rostfeuerungen zur Abfallverbrennung. EF-Verlag für Energie und Umwelt, Berlin, pp 21–60
5. Reimann DO (1991) Rostfeuerungen zur Abfallverbrennung. EF-Verlag für Energie und Umwelt, Berlin
6. Tanner R (1965) Die Entwicklung der Von Roll-Müllverbrennungsanlagen. Schweizer Bauzeitung 83(16)
7. Picture of the first Hamburg incinerator (1985) http://fr.wikipedia.org/wiki/Fichier:Erste_M%C3%BCllverbrennungsanlage_Hamburg.jpeg. Accessed 29 Dec 2011
8. Schoeters J (1975) Patent study on mechanical grate development. VUB, Brussels
9. Buekens A, Schoeters J (1984) Final Report Thermal methods in waste disposal – pyrolysis, gasification – incineration – RDF-firing, Contract Number ECI 1011/B 7210/83B
10. Ebara Co. (1993) Fluidised-bed combustion of municipal solid waste in Japan. Company document
11. Buekens A (1978) Resource recovery and waste treatment in Japan. Resour Recov Conserv 3(3):275–306

12. Buekens A (2008) Schmelzverfahren – erfahrungen in Japan. In: Bilitewski B, Urban AI, Faulstich M (eds) Schriftenreihe des Fachgebietes. Abfalltechnik Universität, Kassel
13. Global Environment Centre Foundation, Japanese Advanced Environment Equipment, http://www.gec.jp/JSIM_DATA/company_index.html
14. E.U. (2009) E.U. Guideline for safe and eco-friendly biomass gasification (gasification – guide). http://www.gasification-guide.eu/. Accessed 11 July 2011
15. Buekens A, Bridgwater AV, Ferrero GL, Maniatis K (eds) (1990) Commercial and marketing aspects of gasifiers. Commission of the European Communities, Elsevier Applied Sciences, Luxembourg, pp 1–239
16. Malkow T (2004) Novel and innovative pyrolysis and gasification technologies for energy efficient and environmentally sound MSW disposal. Waste Manag 24(1):53–79
17. Buekens A, Masson H (1980) Wood waste gasification as a source of energy. Conserv Recycl 3(3–4):275–284
18. Siemons RV (2002) A development perspective for biomass-fuelled electricity generating technologies. PhD thesis, University of Amsterdam. http://www.cleanfuels.nl/Projects%20&%20publications/Siemons_PhD%20Thesis_Internet.pdf. Accessed 11 July 2011
19. Scheirs J, Kaminsky W (2006) Feedstock recycling and pyrolysis of waste plastics. Wiley, Chichester
20. Inguanzoa M, Dominguez A, Menéndez JA, Blancoa CG, Pisa JJ (2002) On the pyrolysis of sewage sludge: the influence of pyrolysis conditions on solid, liquid and gas fractions. J Analy Appl Pyrol 63(1):209–222
21. Buekens A, Schoeters J (1980) Basic principles of waste pyrolysis and review of European processes. ACS Symposium Series 130:397–421
22. Buekens A (1978) Schlussfolgerungen hinsichtlich der praktischen Anwendung der Hausmüllpyrolyse aufgrund weltweiter Erfahrungen. Müll und Abfall 12(6):184–191
23. 12th international congress on combustion by-products and their health effects: combustion engineering and global health in the 21st century – issues and Challenges, Zhejiang University in Hangzhou, China, 5–8 June 2011
24. Chandler AJ, Eighmy TT, Hartlén J, Hjelmar O, Kosson DS, Sawell SE, van der Sloot HA, Vehlow J (1997) Municipal solid waste incinerator residues. Elsevier, Amsterdam\Lausanne\New York\Oxford\Shannon\Tokyo
25. Izquierdo M, López-Soler A, Ramonich EV, Barra M, Querol X 2002) Characterisation of bottom ash from municipal solid waste incineration in Catalonia. J Chem Technol Biotechnol 77(5):576–583
26. Vehlow J (2002) Bottom ash and APC residue management. Expert meeting on power production from waste and biomass – IV, Hanasaari Cultural Center, Espoo, 8–10 Apr 2002. VTT Information Service, Espoo, pp 151–176
27. Sakai S, Hiraoka M (2000) Municipal solid waste incinerator residue recycling by thermal processes. Waste Manag 20:249–258
28. Bergfeldt B, Jay K, Seifert H, Vehlow J, Christensen TH, Baun DL, Mogensen EPB (2004) Thermal treatment of stabilized air pollution control residues in a waste incinerator pilot plant. Part 1: fate of elements and dioxins. Waste Manag Res 22:49–57
29. Baun DL, Christensen TH, Bergfeldt B, Vehlow J, Mogensen EPB (2004) Thermal treatment of stabilized air pollution control residues in a waste incinerator pilot plant. Part 2: leaching characteristics of bottom ashes. Waste Manag Res 22:58–68
30. Achternbosch M, Richers U (2002) Materials flows and investment costs of flue gas cleaning systems of municipal solid waste incinerators. Forschungszentrum Karlsruhe Wissenschaftliche Berichte (FZKA), Karlsruhe, 6726
31. CBR (2011) Personal communication
32. ARGUS – ARBEITSGRUPPE UMWELTSTATISTIK (1981) Bundesweite Hausmüllanalyse 1979/80. Umweltbundesamt, Berlin. Forschungsbericht 103 03 503.
33. ARGUS –ARBEITSGRUPPE UMWELTSTATISTIK (1986) Bundesweite Hausmüllanalyse 1983-1985;Laufende Aktualisierung des Datenmaterials. Umweltbundesamt, Berlin. Forschungsbericht 103 03 508
34. Görner K (1991) Technische verbrennungssysteme, grundlagen, modellbildung, simulation. Springer, Berlin\Heidelberg\New York, p 27
35. Niessen WR (2010) Combustion and incineration processes: applications in environmental engineering. Taylor and Francis, Baco Raton
36. Brunner CR (1996) Incineration systems handbook. Incinerator Consultants, Reston
37. Hämmerli H (1991) Grundlagen zur Berechnung von Rostfeuerungen. In: Reimann D (ed) Rostfeuerungen zur Abfallverbrennung. EF-Verlag, Hrsg
38. European Commission (2006) Integrated pollution prevention and control – reference document on the best available techniques for waste incineration
39. http://en.wikipedia.org/wiki/File:Et_baal.jpg
40. Wilkes JW, Summers CE, Daniels CA, Berard MT (2005) PVC handbook. Hanser Verlag, MŘnchen
41. Buekens A (2006) Introduction to feedstock recycling of plastics. In: Scheirs J, Kaminsky W (eds) Feedstock recycling and pyrolysis of waste plastics: Converting waste plastics into diesel and other fuels. John Wiley & Sons
42. Buekens A (2008) Solving emission problems in a fluid bed MSWI. In: 5th i-CIPEC: international conference on combustion, incineration/pyrolysis and emission control – eco-conversion of biomass and waste, Chiang Mai
43. Briner E, Roth P (1948) Recherches sur l'hydrolyse par la vapeur d'eau de chlorures alcalins seuls ou additionnés de divers adjuvants, Helv Chim Acta 31(2):1352–1360
44. Buekens A, Schoeters J (1986) PVC and waste incineration. APME, Brussels
45. Chimenos JM, Segarra M, Fernández MA, Espiell F (1999) Characterization of the bottom ash in municipal solid waste incinerator. J Hazard Mater 64(3):211–222
46. Meima JA, Comans RNJ (1997) Geochemical modeling of weathering reactions in municipal solid waste incinerator bottom ash. Environ Sci Technol 31(5):1269–1276

47. Commission Decision of 3 May 2000 replacing Decision 94/3/EC establishing a list of wastes pursuant to Article 1(a) of Council Directive 75/442/EEC on waste and Council Decision 94/904/EC establishing a list of hazardous waste pursuant to Article 1(4) of Council Directive 91/689/EEC on hazardous waste (notified under document number C (2000) 1147)
48. Wikipedia, Hazardous Waste
49. Buekens A (2011) Hazardous waste and pollution prevention, course organized by VMAC, Premier Provider of Business Intelligence, Abu Dhabi (U.A.E.)
50. Suisse de Réassurance (1995) Les usines de traitement des déchets urbains, Zurich
51. EPA's Chemical Compatibility Chart (1980) http://www.uos.harvard.edu/ehs/environmental/EPAChemicalCompatibilityChart.pdf. Accessed 11 July 2011
52. Mallinckrodt Specialty Chemicals Co–Chemical compatibility list, 5/1989 http://www.uos.harvard.edu/ehs/environmental/MallinckrodtChemicalCompatibilityList.pdf. Accessed 29 Dec 2011
53. Cole-Palmer Instrument Company-Chemical compatibility (2011) http://www.coleparmer.com/techinfo/ChemComp.asp. Accessed 29 Dec 2011
54. University of Georgia-Chemical storage plans for laboratories (2003) http://www.esd.uga.edu/chem/chemstorage.htm, http://www.esd.uga.edu/chem/pub/lsmanual.pdf, http://www.esd.uga.edu/chem/pub/hmrelocating.pdf. Accessed 29 Dec 2011
55. The University of Vermont, http://www.uvm.edu/~esf/chemicalsafety/chemicalstorage.html. Accessed 29 Dec 2011
56. Magazine Lab Manager, Chemical storage plan fundamentals. http://www.labmanager.com/?articles.view/articleNo/1161/article/8-Chemical-Storage-Plan-Fundamentals. Accessed 29 Dec 2011
57. COMAH (Control of Major Accident Hazards), http://www.hse.gov.uk/comah/
58. Ferziger JH, Peric M (2001) Computational methods for fluid dynamics, 2nd edn. Springer, Berlin, http://elib.tu-darmstadt.de/tocs/100561322.pdf
59. Reményi K (1987) Industrial firing. Akadémiai Kiado, Budapest, 496 p
60. Ferziger JH, Peric M (2001) Computational methods for fluid dynamics, 2nd edn. Springer, New York, http://elib.tu-darmstadt.de/tocs/100561322.pdf
61. Yang YB, Nasserzadeh V, Swithenbank J (2002) Mathematical modelling of MSW incineration in a travelling bed. J Waste Manag 22(4):369–380
62. Yang YB, Goodfellow J, Nasserzadeh V, Swithenbank J (2002) Parameter study on the incineration of MSW in packed beds. J Inst Energy 75(504):66–80
63. Lim CN, Nasserzadeh V, Swithenbank J (2001) The modelling of solid mixing in waste incinerator plants. J Powder Technol 114(1):89–95
64. SUWIC papers (2011) http://www.suwic.group.shef.ac.uk/Journal%20Papers.html. Accessed 29 Dec 2011
65. Buekens A, Mertens J, Schoeters J, Steen P (1979) Experimental techniques and mathematical models in the study of waste pyrolysis and gasification. Conserv Recycl 3(1):1–23
66. Moilanen A (2006) Thermogravimetric characterisations of biomass and waste for gasification processes, VTT Publications 607. 103 pp. + app. 97 pp. Espoo, Finland
67. Nasserzadeh V, Swithenbank J, Lawrence D, Garrod N, Jones B (1995) Measuring gas-residence times in large municipal incinerators, by means of a pseudo-random binary signal tracer technique. J Inst Energy 68(476):106–120
68. Gorman P, Bergman F, Oberacker D (1984) Field experience in sampling hazardous waste incinerators. US Environmental Protection Agency, Washington, DC, EPA/600/D-84/134 (NTIS PB84201573)
69. Carroll GJ (1994) Pilot scale research on the fate of trace metals in incineration. In: Hester RE (ed) Waste incineration and the environment. Royal Society of Chemistry (Great Britain), Cambridge, pp 95–121
70. http://cfr.vlex.com/vid/270-62-hazardous-waste-incinerator-permits-19820277, (2010). Accessed 29 Dec 2011
71. Dellinger B, Torres JL, Rubey WA, Hall DL, Graham JL (1984) Determination of the thermal decomposition properties of 20 selected hazardous organic compounds. Prepared for the U.S. EPA Industrial Environmental Research Laboratory. Prepared by the University of Dayton Research Institute. EPA-600/2-84-138. NTIS PB-84-232487
72. von Paczkowski K (1979) Der Kessel als Bestandteil einer Müllverbrennungsanlage. Seine Entwicklung, sein Entwurf, WÄRME 85:121–125
73. von Paczkowski K (1984) Tendenzen bei Kesseln in Müllverbrennungsanlagen. In: Thome-Kozmiensky KI (ed) Recycling international. EF-Verlag, Berlin
74. Jachimowski A (1978) Kessel für Abfallverbrennungsanlagen. Chemie-Technik 7:403–5
75. Rasch R (1976) Korrosionsvorgänge im Feuerraum. In Kumpf, Maas, Straub, Müll und Abfallbeseitigung, E. Schmidt Verlag, 39 Lfg/III, 7300
76. Vaughan DA, Krause HH, Boyd WK (1974) Study of corrosion in municipal incinerators versus refuse composition. EPA-R-800055
77. Schroer C, Konys J (2002) Rauchgasseitige hochtemperaturkorrosion in müllverbrennungsanlagen – ergebnisse und bewertung einer literaturrecherche. Forschungszentrum Karlsruhe (FZKA), Karlsruhe, 6695
78. Brossard JM, Lebel F, Rapin C, Mareche JF, Chaucherie X, Nicol F, Vilasi M (2009) Lab-scale study on fireside superheaters corrosion in MSWI Plants. In: Proceedings of the 17th annual north american waste-to-energy conference, NAWTEC17, 18–20 May 2009, Chantilly
79. Deuerling C, Maguhn J, Nordsieck H, Benker B, Zimmermann R, Warnecke R (2009) Investigation of the mechanisms of heat exchanger corrosion in a municipal waste incineration plant by analysis of the raw gas and variation of operating parameters. Heat Trans Engin 30(10–11):822–831

80. Olie K, Vermeulen PL, Hutzinger O (1977) Chlorodibenzopdioxins and chlorodibenzofurans are trace components of fly ash of some municipal incinerators in the Netherlands. Chemosphere 6:455–459
81. Rappe C, Andersson R, Bergqvist PA, Brohede C, Hansson M, Kjeller LO, Lindström G, Marklund S, Nygren M, Swanson SE, Tysklind M, Wiberg K (1987) Overview on environmental fate of chlorinated dioxins and dibenzofurans-sources, levels and isomeric pattern in various matrices. Chemosphere 16:1603
82. Rappe C, Andersson R, Bergqvist PA, Brohede C, Hansson M, Kjeller LO, Lindström G, Marklund S, Nygren M, Swanson SE, Tysklind M, Wiberg K (1987) Sources and relative importance of PCDD and PCDF emissions. Waste Manag Res 5(3):225–237
83. Huang H, Buekens A (1995) On the mechanisms of dioxin formation in combustion processes. Chemosphere 31:4099–4117
84. Weber R, Iino F, Imagawa T, Takeuchi M, Sakurai T, Sadakata M (2001) Formation of PCDF, PCDD, PCB, and PCN in de novo synthesis from PAH: mechanistic aspects and correlation to fluidized bed incinerators. Chemosphere 44:1429–38
85. Weber R, Sakurai T, Ueno S, Nishino J (2002) Correlation of PCDD/PCDF and CO values in a MSW incinerator–indication of memory effects in the high temperature/cooling section. Chemosphere 49:127–34
86. Sakai SI, Hayakawa K, Takatsuki H, Kawakami I (2001) Dioxin-like PCBs released from waste incineration and their deposition flux. Environ Sci Technol 35:3601–7
87. McKay G (2002) Dioxin characterisation, formation and minimisation during municipal solid waste (MSW) incineration: review. Chem Engin J 86:343–368
88. Everaert K, Baeyens J (2002) The formation and emission of dioxins in large scale thermal processes. Chemosphere 46:439–448
89. Stanmore BR (2004) The formation of dioxins in combustion systems. Combust Flame 136:398–427
90. Bumb RR, Crummett WB, Cutie SS, Gledhill JR, Hummel RH, Kagel RO, Lamparski LL, Luoma EV, Miller DL, Nestrick TJ, Shadoff LA, Stehl RH, Woods JS (1980) Trace chemistries of fire: a source of chlorinated dioxins. Science 210(4468):385–90
91. Karasek FW, Dickson LC (1987) Model studies of polychlorinated dibenzo-p-dioxin formation during municipal refuse incineration. Science 237(4816):754–756
92. Gullett BK, Bruce KR, Beach LO (1990) Formation of chlorinated organics during solid waste combustion. Waste Manag Res 8:203
93. Sidhu S, Edwards P (2002) Role of phenoxy radicals in PCDD/F formation. Int J Chem Kinet 34:531
94. Vogg H, Metzger M, Stieglitz L (1987) Recent findings on the formation and decomposition of PCDD/PCDF in municipal solid waste incineration. Waste Manag Res 5(3):285–294
95. Hagenmaier H, Kraft M, Brunner H, Haag R (1987) Catalytic effects of fly ash from waste incineration facilities on the formation and decomposition of polychlorinated dibenzo-p-dioxins and polychlorinated dibenzofurans. Environ Sci Technol 21(11):1080–1084
96. Stieglitz L, Zwick G, Beck J, Roth W, Vogg H (1989) On the de-novo synthesis of PCDD/PCDF on fly ash of municipal waste incinerators. Chemosphere 18:1219–1226
97. Schwarz G, Stieglitz L (1992) Formation of organohalogen compounds in fly ash by metal-catalyzed oxidation of residual carbon. Chemosphere 25(3):277–282
98. Stieglitz L, Jay K, Hell K, Wilhelm J, Polzer J, Buekens A (2003) Investigation of the formation of polychlorodibenzodioxins /-Furans and of other organochlorine compounds in thermal industrial processes, Forschungszentrum Karlsruhe, Wissenschaftliche Berichte – FZKA 6867
99. Gullett B, Bruce K, Beach L (1990) The effect of metal catalysts on the formation of polychlorinated diobenzo-p-dioxin and polychlorinated diobenzofuran precursors. Chemosphere 20:1945–1952
100. Olie K, Addink R, Schoonenboom M (1998) Metals as catalysts during the formation and decomposition of chlorinated dioxins and furans in incineration processes. J Air Waste Manag Assoc 48:101–105
101. Kuzuhara S, Sato H, Kasai E, Nakamura T (2003) Influence of metallic chlorides on the formation of PCDD/Fs during low-temperature oxidation of carbon. Environ Sci Technol 37(11):2431–5
102. Hinton WS, Lane AM (1991) Characteristics of municipal solid waste incinerator fly ash promoting the formation of polychlorinated dioxins. Chemosphere 22:473–483
103. Tuppurainen K, Halonen I, Ruokojärvi P, Tarhanen J, Ruuskanen J (1998) Formation of PCDDs and PCDFs in municipal waste incineration and its inhibition mechanisms: a review. Chemosphere 36(7):1493–1511
104. Addink R, Paulus RHWL, Olie K (1996) Prevention of polychlorinated dibenzo-p-dioxins/dibenzofurans formation on municipal waste incinerator fly ash. Environ Sci Technol 30(7):2350–2354
105. Pandelova M, Lenoir D, Schramm K-W (2007) Inhibition of PCDD/F and PCB formation in co-combustion. J Hazard Mater 149(3):615–8
106. Vehlow J, Braun H, Horch K, Merz A, Schneider J, Stieglitz L, Vogg H (1990) Semi-technical demonstration of the 3R process. Waste Manag Res 8(6):461–472
107. Weber R, Nagai K, Nishino J, Shiraishi H, Ishida M, Takasuga T, Kondo K, Hiraoka M (2002) Effects of selected metal oxides on the dechlorination and destruction of PCDD and PCDF. Chemosphere 46:1247–1253
108. Stach J, Pekarek V, Grabic R, Lojkasek M, Pacakova V (2000) Dechlorination of polychlorinated biphenyls, dibenzo-p-dioxins and dibenzofurans on fly ash. Chemosphere 41:1881–1887
109. Alderman SL (2005) Infrared and X-ray spectroscopic studies of the copper (II) oxide mediated reactions of chlorinated aromatic precursors to PCDD/F, Ph.D. Dissertation Louisiana State University, Chapter 1. http://etd.lsu.edu/docs/available/etd-01112005-150557/unrestricted/Alderman_dis.pdf. Accessed 11 July 2011

110. Buekens A, Huang H (1998) Comparative evaluation of techniques for controlling the formation and emission of chlorinated dioxins/furans in municipal waste incineration. J Hazard Mater 62:1–33
111. Wielgosiński G (2010) The possibilities of reduction of polychlorinated dibenzo-p-dioxins and polychlorinated dibenzofurans emission. Int J Chem Eng. Review article 392175:11
112. Düwel U, Nottrodt A, Ballschmiter K (1990) Simultaneous sampling of PCDD/PCDF inside the combustion chamber and on four boiler levels of a waste incineration plant. Chemosphere 20(1):839–846, More papers are to be found at: http://www.nottrodt-ing.de/de/publi.htm
113. Wikström E, Ryan S, Touati A, Tabor D, Gullett BK (2004) Origin of carbon in polychlorinated dioxins and furans formed during sooting combustion. Environ Sci Technol 38(13):3778–84
114. Wikström E, Ryan S, Touati A, Gullett BK (2004) In situ formed soot deposit as a carbon source for polychlorinated dibenzo-p-dioxins and dibenzofurans. Environ Sci Technol 38(7):2097–101
115. Wikström E, Ryan S, Touati A, Tabor D, Gullett BK (2003) Key parameters for de novo formation of polychlorinated dibenzo-p-dioxins and dibenzofurans. Environ Sci Technol 37(9):1962–70
116. Addink R, Olie K (1995) Mechanisms of formation and destruction of polychlorinated dibenzo-p-dioxins and dibenzofurans in heterogeneous systems. Environ Sci Technol 29:1425–1435
117. Konduri R, Altwicker ER (1994) Analysis of time scales pertinent to dioxin/furan formation on fly ash surfaces in municipal solid waste incinerators. Chemosphere 28(1):23–45
118. Zimmermann R, Blumenstock M, Heger HJ, Schramm K-W, Kettrup A (2001) Emission of nonchlorinated and chlorinated aromatics in the flue gas of incineration plants during and after transient disturbances of combustion conditions: delayed emission effects. Environ Sci Technol 35:1019–1030
119. Kreisz S, Hunsinger H, Vogg H (1997) Technical plastics as PCDD/F absorbers. Chemosphere 34(5–7):1045–1052
120. Pekarek V, Weber R, Grabic R, Solcova O, Fiserova E, Syc M, Karban J (2007) Matrix effect on the de novo synthesis of polychlorinated dibenzo-p-dioxins, dibenzofurans, biphenyls and benzenes. Chemosphere (Eng) 68(1):51–61
121. Altwicker ER (1994) Formation of PCDD/F in municipal solid waste incinerators: laboratory and modeling studies. J Hazard Mater 47(1–3):137–161
122. Buekens A, Tsytsik P, Carleer R (2007) Methods for studying the de novo formation of dioxins at a laboratory scale. In: International conference on power engineering-2007, Hangzhou, 23–27 Oct 2007
123. Buekens A, Swithenbank J (2007) CFD modelling of industrial plant from a viewpoint of dioxins formation. In: International conference on power engineering (ICOPE-2007), Hangzhou
124. Verhulst V, Buekens AG, Spencer P, Eriksson G (1996) The thermodynamic behaviour of metal chlorides and sulfates under the conditions of incineration furnaces. Environ Sci Technol 30:50–56
125. http://www.termwiki.com/EN:chute-fed_incinerator_(Class_IIA). Accessed 29 Dec 2011
126. http://www.seas.columbia.edu/earth/wtert/sofos/nawtec/1964-National-Incinerator-Conference/1964-National-Incinerator-Conference-25.pdf. Accessed 29 Dec 2011
127. http://www.dioxinfacts.org/sources_trends/trash_burning.html. Accessed 29 Dec 2011
128. http://www.epa.gov/oaqps001/community/details/barrelburn.html. Accessed 29 Dec 2011
129. Gullett BK, Lemieux PM, Lutes CC, Winterrowd CK, Winters DL (1999) PCDD/F emissions from uncontrolled, domestic waste burning. Presented at Dioxin '99, the 19th international symposium on halogenated environmental organic pollutants and POPs, Organohalogen compounds, vol 41, Venice, 12–17 Sept 1999, pp 27–30
130. Lemieux PM, Lutes CC, Abbott JA, Aldous KM (2000) Emissions of polychlorinated dibenzo-p-dioxins and polychlorinated dibenzofurans from the open burning of household waste in Barrels. Environ Sci Technol 34:377–884
131. iran
132. http://www.sittommi.fr/fonctionnement-usine-incineration-ordures-menageres-pontivy.html. Accessed 29 Dec 2011
133. Buekens A, Yan M, Jiang XG, Li XD, Lu SY, Chi Y, Yan JH, Cen K (2010) Operation of a municipal solid waste incinerator – Pontivy. i-CIPEC
134. Winnacker
135. Saxena SC, Jotshi CK (1994) Fluidized-bed incineration of waste materials. Prog Energy Combust Sci 20(4):281–324
136. Integrated pollution prevention and control reference document on best available techniques for the waste treatments industries, August 2006
137. Santoleri JJ (1972) Chlorinated hydrocarbon waste recovery and pollution Abatement. In: Proceedings of the 1972-National-incinerator-conference, New York
138. Mizuno K (2002) Destruction Technologies for ozone depleting substances in Japan. National Institute for Resources and Environment, in UNEP: http://www.unep.fr/ozonaction/information/mmcfiles/3521-e-file2.pdf. UNON Nairobi
139. http://www.uneptie.org/ozonaction/information/mmcfiles/3521-e-file2.pdf. Accessed 29 Dec 2011
140. http://submergedcombustion.org.uk/Default.aspx. Accessed 29 Dec 2011
141. Tsukishima Kankyo Engineering (2010) http://www.tske.co.jp/english/index.html. Accessed Dec 2011
142. Buekens AG, Schoeters JG, Jackson DV, Whalley LW (1986) Status of RDF-production and utilization in Europe. Conserv Recycl 9:309–309
143. Friends of the Earth (2008) Briefing – mechanical and biological treatment (MBT)
144. Wikipedia, Mechanical and biological treatment (MBT)

145. IPPC (1999) Integrated pollution prevention and control (IPPC): reference document on best available techniques in the cement and lime manufacturing industrie. Formation and release of POPs in the cement industry, 2nd edn. European Commission, Directorate General JRC, Institute for Prospective Technological Studies, Seville
146. Ökopol (1999) Economic evaluation of dust abatement techniques in the European cement industry, Report for EC DG11, contract B4-3040/98/000725/MAR/E1; and "Economic evaluation of NOx abatement techniques in the European cement industry", Report for EC DG11, contract B4-3040/98/000232/MAR/E1. Ökopol GmbH, Hamburg
147. Rabl A (2000) Criteria for limits on the emission of dust from cement kilns that burn waste as fuel. ARMINES/Ecole des Mines de Paris, Paris
148. SINTEF (2006) Formation and release of POPs in the cement industry, second edition. Report of the World Business Council for Sustainable Industry, Cement sustainability initiative, Geneva
149. Greenpeace International (1991) http://archive.greenpeace.org/toxics/reports/gopher-reports/inciner.txt. Amsterdam. Accessed 29 Dec 2011
150. Greenpeace International (1994) http://archive.greenpeace.org/toxics/reports/azd/azd.html. Greenpeace Communications, London
151. Costner P (2001) Chlorine, Combustion and Dioxins: Does Reducing Chlorine in Wastes Decrease Dioxin Formation in Waste Incinerators? http://archive.greenpeace.org/toxics/reports/chlorineindioxinout.pdf
152. PVC WASTE AND RECYCLING. Solving a Problem or Selling a Poison? (1999) http://archive.greenpeace.org/toxics/html/content/pvc3.html#top. Accessed 29 Dec 2011
153. Buekens A, Cen KF (2011) Waste incineration, PVC, and dioxins. J Mater Cycles Waste Manag 13:190–197
154. Xu MX
155. Travis CC (1991) Municipal waste incineration risk assessment: deposition, food chain impacts, uncertainty, and research needs. Plenum Press, New York
156. Hattemer-Frey HA, Travis CC (1991) Health effects of municipal waste incineration. CRC Press, Baco Raton
157. Roberts SM, Teaf CM, Bean JA (1999) Hazardous waste incineration: evaluating the human health and environmental risks. Lewis, Boca Raton

Books and Reviews

Air Pollution Control Association, American Society of Mechanical Engineers. Research Committee on Industrial and Municipal Wastes (1988) Hazardous waste incineration: a re-source document sponsored by the ASME Research Committee on Industrial and Municipal Wastes; co-sponsored by the Air Pollution Control Association, the American Institute of Chemical Engineers, the United States Environmental Protection Agency

Alter H, Horowitz E (1975) STP 592, Resource recovery and utilization. In: Proceedings of the national materials conservation symposium. http://www.astm.org/BOOKSTORE/PUBS/STP592.htm. Accessed July 2011

Bilitewski B, Härdtle G, Marek K (2000) Abfallwirtschaft. Handbuch für Praxis und Lehre. Springer, Berlin

Bonner T, Dillon AP (1981) Hazardous waste incineration engineering, pollution technolo-gy review 88. Noyes Data Corporation, Park Ridge

Gershman, Brickner & Bratton, Inc. (1986) Small-scale municipal solid waste energy recovery systems. Van Nostrand Reinhold, New York

de Souza-Santos ML (2004) Solid Fuels combustion and gasification: modeling, simulation, and equipment operations. Marcel Dekker, New York

Freeman HM (1988) Incinerating hazardous wastes. Technomic, Lancaster

Görner K (1991) Technische Verbrennungssysteme. Springer, Berlin\Heidelberg\New York

Grover VI (2002) Recovering energy from waste: various aspects. Science, Enfield

Günther R (1974) Verbrennung und Feuerungen. Springer, Berlin \Heidelberg\New York

Hester RE (1994) Waste incineration and the environment. Royal Society of Chemistry (Great Britain), Cambridge

Institute of Electrical and Electronics Engineers (1975) Incineration and treatment of hazardous waste. In: Proceedings of the eighth annual research symposium CRE: conversion of refuse to energy, vol 1. World Environment and Resources Council, Institute of Electrical and Electronics Engineers

International conference on combustion, incineration/pyrolysis (i-CIPEC). In: Proceedings of the 1st (Seoul, Korea in 2000), 2nd (Jeju, Korea in 2002), 3rd (Hangzhou, China in 2004), 4th (Kyoto, Japan in 2006), 5th (Chiangmai, Thailand in 2008), and 6th International Conference on Combustion, Incineration/Pyrolysis (Kuala Lumpur, Malaysia, 2010)

International conference on thermal treatment technologies

National Research Council (US). Committee on Health Effects of Waste Incineration (2000) Waste incineration and public health. National Academies, Washington

National-Incinerator-Conference 1964, 1966, 1968, 1970, 1972, 1974 (visit the proceedings at the WTERT-site of Columbia University, e.g. at http://www.seas.columbia.edu/earth/wtert/sofos/nawtec/1966-National-Incinerator-Conference/). Accessed July 2011

National-Waste-Processing-Conference 1976, 1978, 1980, 1982, 1984 1986, 1988, 1990, 1992, 1994 (visit the proceedings at the WTERT-site of Columbia University, e.g., http://www.seas.columbia.edu/earth/wtert/sofos/nawtec/1980-National-Waste-Processing-Conference/). Accessed July 2011

North American Waste to Energy Conferences (NAWTEC) http://nawtec.swana.org/. Accessed July 2011

EPA (1989) Environment Canada. Proceedings of the international conference on municipal waste combustion. Hollywood, Florida

Robinson WD (1986) The solid waste handbook: a practical guide. Wiley, Chichester

I

Rogoff MJ, Screve F (2011) Waste-to-energy: technologies and project implementation. Elsevier Science, Amsterdam
Santoleri JJ, Theodore L, Reynolds J (2000) Introduction to hazardous waste incineration. Wiley-IEEE, New York
Solid Waste Association of North America (1998) Asian-North American solid waste management conference. Paper presented at the 17th biennial waste processing conference, Atlantic City (Proceedings available at the WTERT-site of Columbia University)
Theodore L, Reynolds J (1987) Introduction to hazardous waste incineration. Wiley, New York
Warnatz J, Maas U, Dibble RW (2001) Combustion – physical and chemical fundamentals, modeling and simulation, experiments, pollutant formation, 3rd edn. Springer, Berlin\Heidelberg\New York
World Health Organization. Regional Office for Europe (1985) Solid waste management: selected topics. World Health Organization, Copenhagen
Young GC (2010) Municipal solid waste to energy conversion processes: economic, technical, and renewable comparisons. Wiley, Hoboken

Incinerator Grate Combustion Phenomena

J. Swithenbank[1], Vida N. Sharifi[1,2]
[1]Energy and Environment Engineering (EEE), Sheffield University, Sheffield, UK
[2]EEE Group, Chemical and Biological Engineering, Sheffield University, Sheffield, UK

Article Outline

Glossary
Definition of the Subject
Introduction
Brief Overview of Materials and Energy Recovery from Solid Wastes
Energy Recovery by Thermal Treatment of Wastes
Energy Recovery from MSW by Incineration
Incineration with Combined Heat and Power (CHP)
The Waste Combustion Process
Mathematical Modeling of Combustion in an Energy-from-Waste Plant
Mass and Energy Balance in the Incineration Process
Incineration Modeling Equations
Steady-State Model for Packed Bed Combustion
General Transport Equations
Evaporation of Moisture
Devolatilization
Char Burnout
Combustion of Volatiles in the Porous Bed
NO Formation and Destruction
Nomenclature
Solution Technique
Modeling Validation
Future Directions
Acknowledgments
Bibliography

Glossary

AD Anaerobic digestion
CFD Computational fluid dynamics
CHP Combined heat and power
CHP/DHC Combined heat and power/District heating and cooling
CV Calorific value
DEFRA Department of Environment Food and Rural Affairs
DHC District heating and cooling
DVC Depolymerization-vaporization-cross-linking model
EfW Energy-from-Waste
E.U. European Union
FG Functional group
FG-DVC Functional group model and a depolymerization-vaporization-cross-linking model.
GJ Gigajoule
kWh Kilowatt hours
kW_h Kilowatt heat
MBT Mechanical biological treatment
MSW Municipal solid waste
MRF Material recovery facility
MW Megawatt
NO Nitric oxide
NO_x Nitrogen oxides
PCDD/Fs Polychlorinated dibenzo-dioxins and furans
RDF Refuse-derived fuel
ROC Renewable Obligation Certificate
SRF Solid-recovered fuel
TEQ Toxic equivalent
TGA Thermogravimetric analysis
WID Waste incineration directive
WTE Waste-to-energy

Definition of the Subject

Historically, waste materials from cities were simply dumped in huge piles of polluting material. The liquid runoff usually polluted water courses, and the rotting material continued to emit greenhouse gases, methane, and carbon dioxide for 50 years. The area of land required also became a problem and most societies now accept that such waste dumps are unacceptable. However, an important fact is recognition that dumping of wastes without recovering reusable materials is unsustainable and waste should be: (a) minimized at source, (b) the recovery of reusable or recyclable materials should be optimized, and (c) the recovery of energy-from-waste (EfW) must be maximized.

Minimization of waste at source poses many problems. For example, most cultures have celebrations, such as weddings, which result in waste from gift packaging. Yet these events contribute to the quality of life, and it would be unpopular to ban them. However, packaging consists of paper or cardboard which are biofuels similar to wood, and their combustion in an energy-from-waste plant simply returns captured carbon dioxide to the atmosphere and displaces fossil fuel that would otherwise be used. The important point is that waste material that it is not viable to reuse or recycle should be used in an energy-from-waste plant.

Waste consists of a wide variety of materials such as cans and paper that are initially separate but become mixed in a crude waste-collection system. The subsequent separation or de-mixing requires considerable cost and energy, and usually results in cross-contaminated products. Thus, in accordance with the principle of entropy (or disorder), wastes should be separated at source wherever it is viable. Nevertheless, material handling machines can recover some recyclable material such as metal, paper, and some plastics. The residue, which amounts to about 50% of the raw waste, is flock or pellets known as Solid-Recovered Fuel (SRF), which can be burned or possibly gasified to generate power.

Composting raw municipal waste converts much of the material to carbon dioxide without recovering energy and leaves a semi-toxic residue, whereas methane generation by anaerobic digestion is generally more suitable for wet food wastes.

This presentation focuses on thermal energy-from-waste technology using incineration since this is now a mature and bankable technology that is delivering electricity from hundreds of plants worldwide. Nevertheless, attention is drawn to the fact that the efficiency of the electrical power generation is only about 23% due to boiler corrosion problems. Fortunately, there is an engineering solution to this situation since the remaining energy is available as hot water that can be used for district heating (or building cooling), thus raising the energy conversion efficiency to about 90%. Not only does this save fossil fuels, but because most of the waste residue is biomass, the net carbon dioxide emission is quite low, whilst the heat is generated close to the consumer and transport of waste is minimized.

A key feature of this environmentally friendly "trash-into-resource" strategy is that it helps to reduce global warming by reducing the **net** emissions of carbon dioxide to the atmosphere.

In the light of these observations, it is clear that EfW is a key technology for modern society. The aim of this article is to present; the rationale, the underpinning scientific principles, and key engineering aspects of this topical subject.

Introduction

The impending Fossil Fuel Poverty that is developing in the world largely explains why countries such as Denmark, which have no national fossil fuels, have developed efficient energy-from-waste (EfW) systems incorporating district heating that exploit low-grade heat from waste and integrate it with low-grade heat from their electricity power generation. The result is that two thirds of their buildings are already connected to district heating, and these two systems should be generally considered together for an energy-efficient city. Furthermore, the common perception that old cities cannot have district heating is false since many old cities like Vienna and Paris have successfully installed very extensive heat distribution networks.

The relation between process plant-scale and plant-capital cost generally follows the 0.6 power law, leading to the relative economy of large-scale process plants. Waste plants such as incinerators follow this rule; however, smaller plants can be operated, provided the waste

is suitably shredded. However, in many cases, the problem of large-scale waste supply is solved by the use of waste transfer stations to integrate the wastes sources from several towns.

An important point that is not usually emphasized sufficiently is the relative efficiency of different energy-from-waste technologies. Firstly, many studies assume that the low-grade heat from power generation can be ignored. However, as pointed out above, the efficiency of power generation is usually less that 25%, and this results in ignoring about 60% of the energy that is available to displace fossil fuels currently used to heat buildings. Surely, society will not be able to ignore this issue for long.

The recent development of materials recovery facility (MRF) plants that separate recyclables from residual waste are already starting to produce millions of tons per year of solid-recovered fuel (SRF or RDF). However, the SRF from a particular process will be much more consistent in quality than raw MSW. Complex process plants such as gasifiers generally require the feed to be tightly specified and, hence, will be better suited to use such wastes. It is also noteworthy that SRF can be shipped and stored more easily than raw MSW. An important factor is the need to apply the Waste Incineration Directive (WID) to emissions from all waste combustion systems. The importance of defining the status of new fuels derived from wastes therefore requires considerable attention, especially with regard to the emission of organic material and inorganics, such as heavy metals.

The importance of the moisture content of wastes must be also recognized. In the case of thermal processes, this simply represents 2 MJ/kg heat gain for every 10% reduction in moisture content. The calorific value (CV) of raw MSW is about 10 MJ/kg, hence drying results in a very significant gain in CV. The significance of reducing this moisture in order to recover energy from materials such as AD and sewage sludge requires appropriate recognition. The UK sewage industry often uses centrifuges and thermal systems to dry sewage sludge before burning it in an autothermal fluidized bed; however, the additional use of a belt press can result in a waste cake that delivers enough heat to generate power.

A similar question arises when the power-generation capability of different technologies is compared. In the case of incineration, a typical EfW plant generates electrical energy at 600 kWh/t plus 2,500 kWh/t of heat for buildings. By comparison, an anaerobic digestion plant generates electrical energy at 75–160 kWh/t of the organic fraction of the waste. In the future, new thermal gasification plants could double the electrical energy that can be generated from each ton of waste.

Brief Overview of Materials and Energy Recovery from Solid Wastes

Municipal solid wastes (MSW) can be treated by various methods, as illustrated in Fig. 1. However, direct combustion, also called incineration, of post-recycling-mixed MSW is currently the main route for energy and metals recovery practiced by the global energy-from-waste industry (EfW; also called waste-to-energy or WTE).

The predominant MSW incinerators burn wastes of a wide range of calorific values on a moving grate, without any waste preprocessing. However, in some countries, these incineration systems suffer from unfavorable public perception. The main treatment alternatives to incineration are:

(a) Production of solid-recovered fuel (SRF) from mechanical/biological treatment,
(b) Pretreatment of MSW to "refuse-derived fuel" (SRF) as discussed in another section of this document.
(c) Gasification of preprocessed or as-received waste followed by either combustion or use of the gas as a fuel.

Such processes have *potentially* higher energy efficiency when compared to incineration and perhaps more flexibility in the use of primary products. However, further technology developments with appropriate regulatory drivers are still required for them to compete effectively with incineration.

Another thermal route available for treating the high calorific components of MSW is pyrolysis, in order to produce cheap and storable fuel products. Pyrolysis is normally only suitable for specific types of waste material such as plastics or waste wood, where it is used to produce charcoal, a storable fuel product.

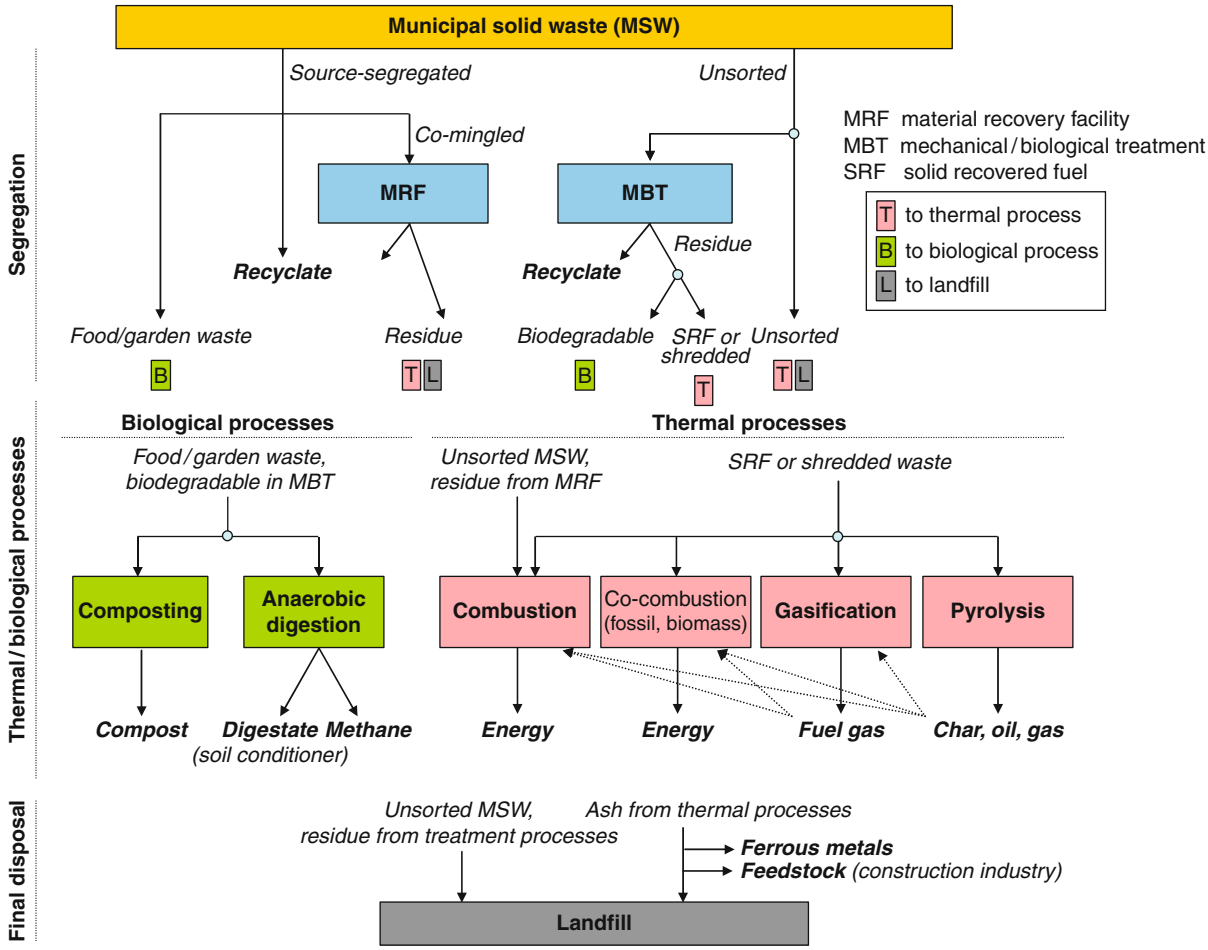

Incinerator Grate Combustion Phenomena. Figure 1
Various methods for recovering materials and energy from municipal solid wastes

Energy Recovery by Thermal Treatment of Wastes

The energy output available from a material is conveniently specified by its calorific value in MJ/kg. Thus, if the fuel feed is 1 kg/s (i.e., 3.6 t/h or ~31,500 t of waste per year), a typical municipal waste fuel containing 10 MJ/kg can produce a maximum of 10 MJ/s, that is, 10 MW of combined heat and power. In practice, the efficiency of the appropriate electrical power generating system is only 23%, so a more realistic figure for the electrical output would be 2.3 MW_e of electricity. However, the rest of the thermal energy is available as low-grade heat that is suitable for district heating and can provide about 6.2 MW_h of district heating.

Putting these figures into perspective, the average person in the E.U. produces approximately half a ton of nonrecyclable waste per year, so the example above would correspond to a fairly large city with a population of 60,000 and 20,000 homes. Heating each home requires up to 5 kW_h, hence the number of homes that could be heated from their own MSW is 6,200/5 = 1,240, or a proportion of 20%. The electricity generated from the waste also provides power for a similar proportion of households in a community served by EfW.

Therefore, the energy available from the waste generated by a local population can make a significant contribution to fulfilling the local demand for heat and electricity, while also replacing the use of an

important amount of nonrenewable fossil fuel. Furthermore, by doing so, the local urban population assumes the responsibility for managing their waste instead of sending it to pollute a rural area. The fact that the waste volume is reduced by a factor of 10 in an energy-from-waste plant is also an important consideration in minimizing the transportation involved in waste management.

To access the energy available in the waste, it must be converted from chemical energy to heat and/or power. The direct method of recovering EfW is thus incineration, which actually involves all the complex reaction processes of pyrolysis, gasification, and oxidation. The other two processes (Gasification and Pyrolysis) produce intermediate products of combustion that can be burned for energy generation or used as a feedstock, depending on process conditions. Furthermore, a gasification or pyrolysis system used to produce heat and power energy also involves combustion of the gas or char and thus conversion of the initial feed to carbon dioxide, water, and ash. Each alternative process should therefore be considered holistically, where one starts from the raw waste and then follows the process to completion of the reaction of the fuel with air, the production of heat and power, and the disposal of the ash residue. Also, any gas cleaning operation that is required to meet the air and water environmental control regulations must be included in such a comparison of alternatives.

An important consideration is the internal use of power within the plant; systems should be compared on the basis of net power production rather than the output of the electricity generator. The internal power-consuming devices include waste preprocessing shredders, fans, material conveyers, pumps, etc.

Incineration is a mature technology that can meet all regulations and that is bankable. Why then are other technologies being considered? The reason lies in the potential efficiency of electrical power production. In the case of the mass-burn system, the combustion gases are used to raise steam for use in the turbine/generator with a Rankine power-generation cycle. Thermodynamic considerations show that the efficiency of the power generation depends on the top temperature of steam generation. This temperature is limited by the acceptable material life of the superheater steam tubes. In a conventional coal-fired power station, steam temperatures are typically about 565°C and result in a power-generation efficiency of about 35%. In the case of a conventional energy-from-waste plant, the composition of the flue gas is more corrosive and a steam temperature yielding an acceptable superheater tube life is about 400°C, resulting in power-generation efficiency of about 23–25%. Although most of the balance of the energy is available as heat for a district heating system, electricity is a more valuable form of energy than heat; hence, research workers are striving to develop a more efficient system.

In principle, if one could generate gas from waste with an efficiency of about 70% and use the gas in an internal combustion engine or a combined gas turbine/steam turbine generator with an efficiency of 45–55%, then an overall power-generation efficiency of 31.5–38.5% should be attainable. However, this target has been elusive and remains a "gleam-in-the-eye" at the present time. For this reason, the following discussion will largely focus on conventional incinerator combustion as the route to produce energy from waste. Furthermore, since the waste combustion process is particularly complex and its study is a specialty of the authors, this entry will focus on this aspect of energy-from-waste.

Energy Recovery from MSW by Incineration

Typical incineration systems are mass-burn combustion chambers that operate at high temperatures (i.e., 850°C at the furnace exit) and with excess air (typically 50–80% of stoichiometric air) in order to ensure efficient combustion of waste material and complete destruction of toxic organic pollutants. As mentioned above, mass-burn incinerators can handle wastes with a wide range of calorific value without any specific waste pretreatment, which is a key advantage of this technology.

The major public issues concerning the "incineration option" are pollution, health risks, and low energy efficiency. All combustion systems inevitably generate certain amounts of pollutants. In the case of incineration, the main flue gases are; nitrogen, oxygen, water vapor, carbon dioxide, acidic gases, NO_x, particulates, heavy metals, and dioxins. The pollutants are efficiently removed by a combination of gas cleaning technologies to a level below the emission limits set by the Waste Incineration Directive of the E.U. (Table 1). Modern

incinerators operate well below these emission limits. Dioxins and fly ash are of particular public interest. However, the dioxin level from modern incineration systems is far below the European emission limits, for example, the total UK dioxin emissions from incineration account for only about 1% of the UK national total [1]. A similar result was also reported for Germany and other nations.

Incinerator Grate Combustion Phenomena. Table 1
Daily average values of air emission limits for incineration in WID

Pollutants	Values
Total dust	10 mg/m^3
Total organic carbon	10 mg/m^3
HCl	10 mg/m^3
HF	1 mg/m^3
SO_2	50 mg/m^3
NO_x	200 mg/m^3
CO	50 mg/m^3
Hg	0.05 mg/m^3
Cd/Tl	Total 0.05 mg/m^3
Sb, As, Pb, Cr, Co, Cu, Mn, Ni, V	Total 0.05 mg/m^3
PCDD/Fs	0.1 ng I-TEQ/m^3

Incineration with Combined Heat and Power (CHP)

As noted above, due to corrosion problems the efficiency of electricity generation by incinerators using a steam turbine is about 25%, which is rather low compared to about 35% for coal-fired power plant. However, the use of combined heat and power systems (CHP) can dramatically increase the overall energy efficiency by exploiting the low-grade heat from the steam turbine for heating (or cooling) domestic, commercial, and industrial buildings. The overall energy efficiency of a CHP system using conventional or waste-derived fuels is as high as 85%. The best example in the UK is the Sheffield incinerator operated by Veolia Sheffield Ltd (Fig. 2). It produces up to 60 MW thermal plus 19 MW electrical energy from a waste throughput of 225 kt/year and supplies heat to commercial properties and over 5,000 residential buildings through a network of 42 km of piping.

An important factor concerning EfW plants in the UK is their eligibility for the Renewable Obligation Certificates (ROCs), which provides an incentive to promote electricity generation from renewable sources, such as the biomass content of wastes.

Incineration is capital intensive (Fig. 3). The major cost factors are equipment and building costs, land acquisition, planning, labor, maintenance, and ash

Incinerator Grate Combustion Phenomena. Figure 2
Sheffield incinerator

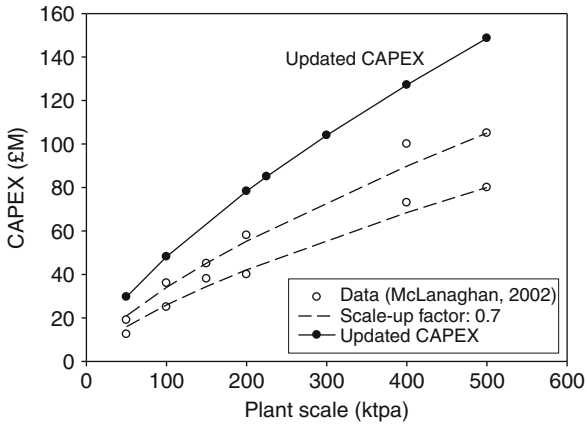

Incinerator Grate Combustion Phenomena. Figure 3 Curve-fitted and updated (2009) for various plant scales

disposal. The costs are very much site-dependent and are affected by a number of parameters such as:

- Scale of the plant (typically ranging from 50 to 400 kt/year)
- Requirement for flue gas treatment
- Treatment and disposal process for the bottom and fly ash, including recovery of metals from the bottom ash and their sale
- Efficiency of energy recovery

The Waste Combustion Process

Two alternative technologies are available to burn waste. These are the mass-burn grate and the fluidized bed. The former consists of a moving grate that burns waste travelling on a grate from a feed shaft to the ash pit. The latter consists of a fluidized bed of near mono-size sand particles enveloping the burning waste material. Air passing up through the bed is almost universally used as the source of oxidant.

The two systems differ in the peak temperature achieved during combustion. In the case of a mass-burn grate, the maximum temperature is about 1,300°C, whereas the fluidized bed operates at about 850°C. Because the ash melting temperature lies between these two temperatures, the ash from a mass-burn grate can contain large pieces of slag. These two processes also differ in the amount of power that is used within the process. In the case of a fluidized bed, the waste must be preprocessed by shredding, which incurs a significant cost and efficiency penalty; also the air pressure needed to suspend the fluidized bed is much greater than that used with a mass-burn grate. The overall effect is that the net electrical power output of a fluidized bed system tends to be less than with a mass-burn grate. These and other considerations have led to a preference for installation of the mass-burn system in Europe, where there is more emphasis on power production, whereas in Japan the balance between the uses of each system is more nearly even.

Mathematical Modeling of Combustion in an Energy-from-Waste Plant

Travelling grate combustion systems such as that illustrated in Fig. 4 are commonly used in industry for incineration of MSW waste. In this type of reactor, waste burns on top of the moving grate with primary air supplied from below. The fresh waste fed onto the grate at one end ignites by radiation from the hot environment and the ignition front propagates into the bed, as it is slowly transported to the discharge end of the moving grate. The combustion products are released to a gas plenum above the bed, where further oxidation of combustible gases takes place. Secondary air is injected through jets into the gas in the shaft above the bed to enhance the gaseous mixing and combust the volatile gases and carbon monoxide that emanate from the burning bed of solids.

Mathematical modeling of the burning bed of waste particles ("FLIC" code) was developed at Sheffield University for thermal processes in a packed bed such as moving grate combustion, fixed bed air-steam gasification, and slow pyrolysis. After establishing the governing equations for the two-phase reacting bed, the heat transfer and reaction parameters are optimized using test results carried out in parallel in a so-called pot burner. This code is usually coupled with a gas flow modeling ("FLUENT" code) to provide comprehensive information on the thermal processes in a furnace. This novel simulation technique has been applied widely to provide a detailed understanding of the combustion process and to help optimize the design and operation of energy-from-waste plants worldwide.

To segregate recyclables, the unsorted MSW can be mechanically treated before being fed into the furnace, as shown in Fig. 5. This can be an attractive waste

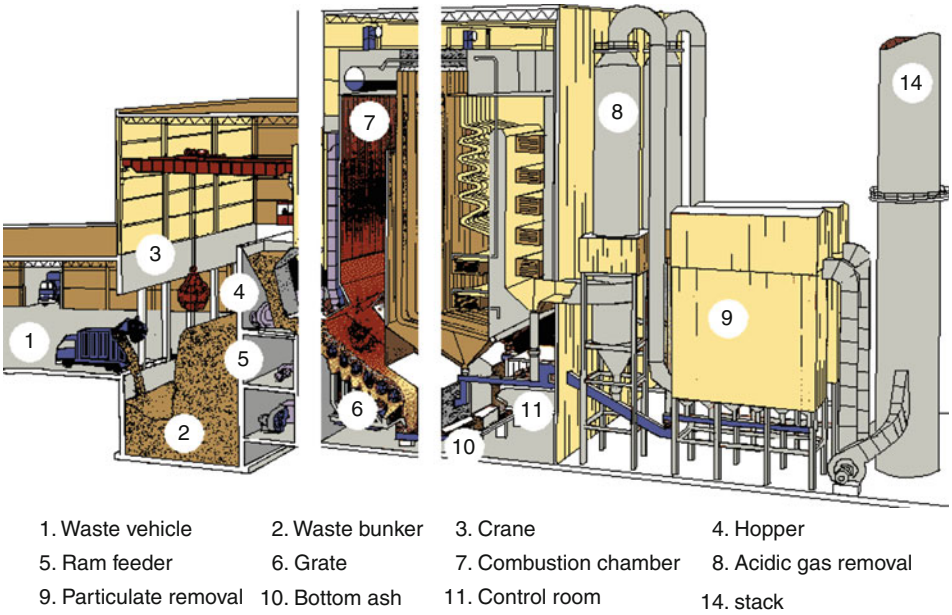

Incinerator Grate Combustion Phenomena. Figure 4
Typical EfW plant [2]

disposal route for local authorities in order to meet the recycling targets by post-collection segregation and reduce landfilling. Based on a least-cost optimization of the waste management options, incineration with mechanical treatment of waste is most likely to be adopted in the near future. However, the recent trend is for more recyclables to be source-separated and collected [3] rather than for post-collection segregation of unsorted wastes, principally due to the poor quality of recyclables sorted out from mixed MSW.

Mass and Energy Balance in the Incineration Process

Incineration generally operates at temperatures between 850°C and 1,100°C with a large excess of oxygen and converts waste materials into ash and exhaust gas while producing thermal/electrical energy from the chemical energy of waste. The overall reaction for incineration can be written as:

$$\begin{aligned} &\textit{waste} + \textit{air}\,(\textit{products}) \\ &\quad w(H_2O) \bullet CxHyOz \bullet Ash \\ &\quad + (1+\lambda)a(O_2 + 3.76\,N_2) \rightarrow x\,CO_2 \\ &\quad + (w + 2/y)H_2O + a\lambda\,O_2 + 3.76(1+\lambda)a\,N_2 + Ash \end{aligned}$$

where λ: excess air ratio and $a = x + y/4 - z/2$.

The chemical composition of waste varies significantly between locations and seasons. For an indicative mass and energy balance calculation, typical ultimate and proximate analyses for MSW, such as that shown in Table 2, must be obtained. In this case, the combustible component of MSW becomes $C_{20}H_{37.3}O_{11.6}$ with 31.2% by weight of moisture and 24.2% by weight of noncombustible ash.

A simple mass and energy balance for incineration based on the above properties of waste is shown in Fig. 6. For 1,000 kg of waste, the amount of air required at 70% excess air ($\lambda = 0.7$) is 5,377 kg. The amount of solid residues is 242 kg. Most of these are bottom ash, and the balance is collected in bag filters as fly ash. The amount of exhaust gas is 6,120 kg in which the fraction of oxygen is 8.8% on a dry basis. The typical temperatures of exhaust gas in the gas cleaning process, and at the chimney are 200°C and 130°C, respectively. The electricity output is 2.15 GJ from 8.6 GJ of chemical energy stored in 1,000 kg of waste. This is based on 25% electrical energy efficiency which is typical in a large-scale incineration plant with a steam turbine. As mentioned above, for incineration with combined heat and power (CHP), the energy efficiency can be as high as 85%.

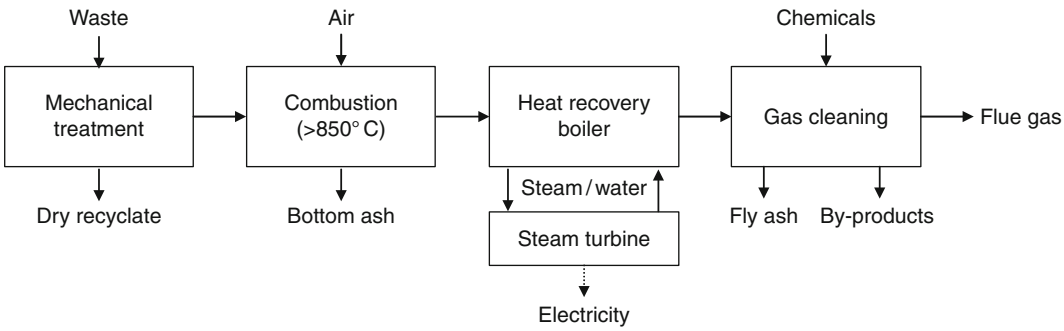

Incinerator Grate Combustion Phenomena. Figure 5
Schematic of mass flow for mechanical treatment followed by incineration

Incineration Modeling Equations

A mathematical model [4], also known as the FLIC code, is used to predict the fixed bed combustion of the waste materials. This model assumes the fuel bed to be a unidimensional bed of uniform spherical particles and gas voids and tracks the combustion in the bed as a function of time. The combustion processes of moisture evaporation, devolatilization, and char burnout for the solid phase, and also the reactions in the gas phase are simulated by various sub-models and modes of heat transfer. The details of the model assumptions, governing equations, various sub-models for reaction and heat transfer, and the numerical scheme are presented below. Application of the FLIC code to the mathematical modeling of the characteristics of a burning bed has provided very valuable results for various solid fuels in fixed or moving bed furnaces.

Early development of solid waste reaction models was largely based in previous work on coal combustion and was linked to biomass combustion due to the fact that a large proportion of municipal solid wastes is biomass or originates from it [4–6]. The devolatilization rate depends not only on fuel type but also on particle size, heating rate, and final temperature. For experimental studies, thermogravimetric analysis (TGA) has been used at low heating rates. However, the pyrolysis processes in an actual incineration furnace or packed-bed pyrolyser differ from the conditions of TGA tests in terms of sample weight and particle sizes. Furthermore, evidence [7] indicated that a bed filled with charcoal at elevated temperatures could reduce tar concentration in the exit gases by 95%; therefore, mathematical models for an actual solid-fuel pyrolysis

Incinerator Grate Combustion Phenomena. Table 2
Ultimate analysis of MSW

Material	% by weight
Water	31.2
Carbon	24.0
Hydrogen	3.2
Oxygen	15.9
Nitrogen	0.7
Sulphur	0.1
Chlorine	0.7
Ash	24.2

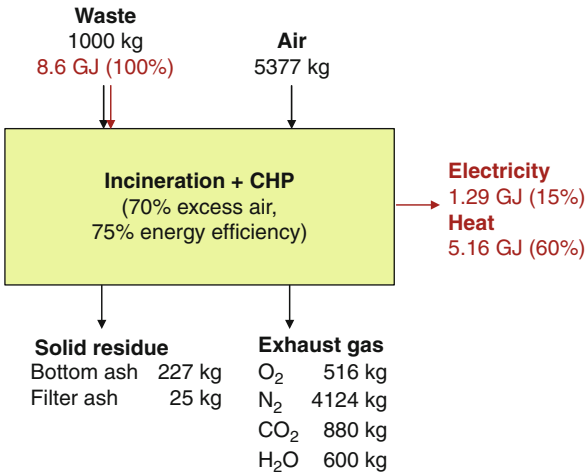

Incinerator Grate Combustion Phenomena. Figure 6
Typical mass and energy balance for incineration with combined heat and power

system should include the tar cracking and re-polymerization processes. In the following discussion, solid waste pyrolysis is modeled by two different methods and the effect of devolatilization rate on the combustion of MSW is investigated by numerical simulations. A specific tar cracking feature is also mathematically simulated to optimize the process operation.

Char from solid wastes constitutes an important part of the waste-to-energy conversion process as the burnout time of char can be more than 10 times the devolatilization time. In addition, chars from different parent fuels are expected to have different kinetic rates since minerals in the ash can act as catalysts and, also, the burnout rate of char also depends heavily on mass transport between the gas and solid phases through the outer ash layer. Thus, collapse of this outer ash layer or particles breaking down into smaller fragments during the char burnout processes can significantly affect the results. This effect is taken into account in the mathematical model by introducing a particle mixing coefficient in a packed-bed agitated by a moving grate; numerical predictions indicate that the overall burning rate of the solid fuel can be doubled. To investigate the effect of grate movement on the combustion processes, a transient mathematical model has also been developed which can reflect the random nature observed for the dynamic processes. However, to analyze the effect of fuel properties and most of the other operating parameters such as airflow rate, the transient mathematical model is unnecessary. Therefore, the average or "steady-state" mathematical model has been generally used.

One of the earliest models for packed-bed solid combustion was proposed by [6]. Early models were generally based on the assumption of thermally thin particles; however, in the case of MSW combustion, particle sizes may be very large in some cases. To correctly model the combustion processes of thermally thick particles, an advanced double-mesh numerical model was developed that takes into account the three-dimensional nature of the boundary conditions for an individual particle in a packed bed. The advantage of such a model is its ability to take into account the temperature gradient inside thermally thick particles, making the modeling more realistic.

Radiation penetration is important in packed-bed waste combustion as it is the major mode of heat transfer inside packed beds of burning solid fuels and one of the major factors influencing the combustion characteristics. The absorption and scattering coefficients of the packed-particle assembly are therefore important parameters required for advanced modeling of heat transfer inside packed-beds. Detailed 3D calculations of radiation penetration in packed beds of various bed configurations were carried out by employing the Discrete Ordinates method and treating the particle surface as wall boundaries. The radiation absorption and scattering coefficients for the particle assembly were thus deduced and correlated to particle size, shape, surface emissivity, and bed porosity.

Most of the model developments have been validated against small-scale bench-top experiments for obvious economic and practical reasons. Scale-up rules allow for the developed models to be applied to large-scale industrial plants, which is the ultimate goal of all the modeling work.

Steady-State Model for Packed Bed Combustion

A schematic description of a solid-to-energy conversion bed is shown in Fig. 7. Layers of solid particles are packed on a grate and under-fire air flows upward through the bed. Solid material is supplied continuously at one end of the grate and the force of gravity and motion of the grate slowly propel the solids to the discharge end of the grate. Most of the combustible material in the solid is burned within the bed and the freeboard zone above the bed, producing CO_2, H_2O, and minor traces of CO and unburned hydrocarbons. The combustible gases are later burned in the over-bed region by adding secondary air. The solid products are bottom ash and fly ash carried in the combustion gases.

It is assumed that the major bed properties, i.e., temperatures of gas and solid phases inside the bed, gas compositions (O_2, H_2, CO, CO_2, etc.), and solid compositions (moisture, volatiles, fixed carbon and ash), can be described as continuous functions of space. It is also assumed that the bed can be treated as a porous medium, where mass and heat transfer take place between the solid and gas phases and that the shape of the particles is spherical (the surface-volume averaged diameter is used). Under such assumptions, the individual bed processes (moisture evaporation, devolatilization, and char burning) can be viewed as

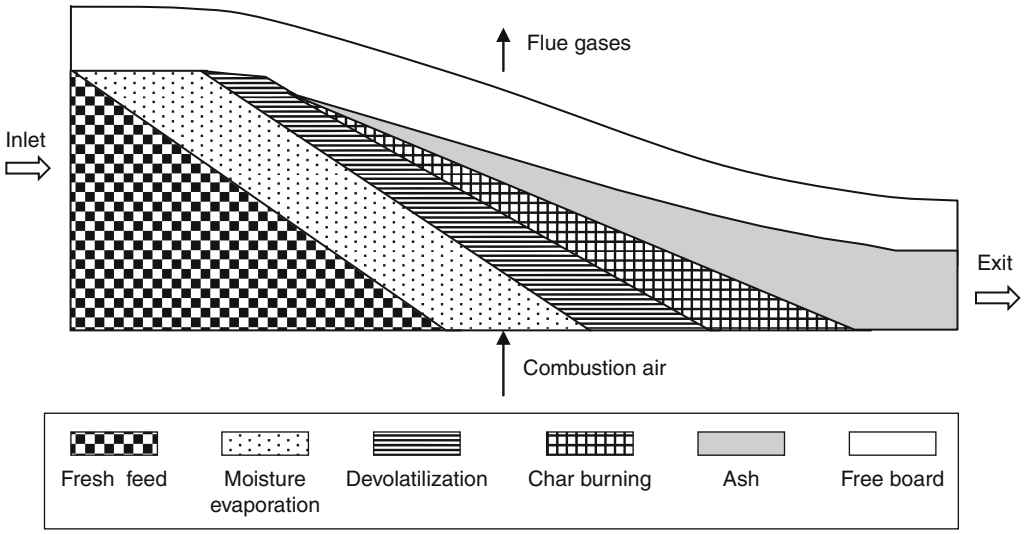

Incinerator Grate Combustion Phenomena. Figure 7
Schematic of the solid combustion processes in a moving packed bed

taking place layer by layer from the bed top to the bottom. This model is suitable for thermally thin particles. However, for much larger particles, the combustion processes may not occur layer by layer from the bed top to the bottom. Instead, the burning process may be more on an individual particle basis, and the numerical model for thermally thick particles must be used.

General Transport Equations

The general governing equations for both the gas and solid phases in a moving bed include mass and momentum conservation, heat transfer, and species transport. For the gas phase, the following equations apply,

$$\text{Continuity:}\quad \partial\left(\phi\rho_g\right)/\partial t + \nabla\bullet\left(\phi\rho_g\left(V_g - V_B\right)\right) = S_{sg} \tag{1}$$

$$\text{Momentum:}\quad \partial\left(\phi\rho_g V_g\right)/\partial t + \nabla\bullet\left(\phi\rho_g\left(V_g - V_B\right)V_g\right) = -\nabla\rho_g + F(\mathbf{v}) \tag{2}$$

$$\text{Species transport:}\quad \partial\left(\phi\rho_g Y_{ig}\right)/\partial t + \nabla\bullet\left(\phi\rho_g\left(V_g - V_B\right)Y_{ig}\right) = \nabla\bullet\left(D_{ig}\nabla\left(\rho_g Y_{ig}\right)\right) + S_{y_{ig}} \tag{3}$$

$$\text{Energy:}\quad \partial\left(\phi\rho_g H_g\right)/\partial t + \nabla\bullet\left(\phi\rho_g\left(V_g - V_B\right)H_g\right) = \nabla\bullet\left(\lambda_g\nabla T_g\right) + S_a\, h_s'\left(T_s - T_g\right) + Q_h \tag{4}$$

In the above equations, $F(\mathbf{v})$ represents resistance of solids to fluid flow in a porous medium and is calculated by Ergun's equations. The fluid dispersion coefficients, D_{ig} for mass and λ_g for thermal, consist of diffusion and turbulent contributions. For Re $>$ 5, the corresponding cross-flow and in-flow dispersion coefficients are given by the following equations [8]:

$$D_r = E^0 + 0.1\, d_p|V_g| \text{ and } D_{ax} = E^0 + 0.5\, d_p|\mathbf{V}_g| \tag{5}$$

$$\lambda_r = \lambda_g{}^0 + 0.1\, d_p|\mathbf{V}_g|\rho_g C_{pg} \text{ and } \lambda_{ax} = \lambda_g{}^0 + 0.5\, d_p|\mathbf{V}_g|\rho_g C_{pg} \tag{6}$$

For the solid-phase processes, the equations of particle movement, species transport, and heat transfer are described below,

$$\text{Continuity:}\quad \partial\rho_{sb}/\partial t + \nabla\bullet\left(\rho_{sb}\left(\mathbf{V}_s - \mathbf{V}_B\right)\right) = S_s \tag{7}$$

$$\text{Momentum:}\quad \partial\rho_{sb}\mathbf{V}_s/\partial t + \nabla\bullet\left(\rho_{sb}\left(\mathbf{V}_s - \mathbf{V}_B\right)\mathbf{V}_s\right) = -\nabla\bullet\sigma - \nabla\bullet\tau + \rho_{sb}\mathbf{g} + A \tag{8}$$

$$\text{Species: } \partial\rho_{sb}Y_{is}/\partial t + \nabla\bullet(\rho_{sb}(\mathbf{V}s - \mathbf{V}_B)Y_{is}) = \nabla\bullet(D_s\nabla(\rho_{sb}Y_{is})) + Sy_{is} \quad (9)$$

$$\text{Energy: } \partial\rho_{sb}H_s/\partial t + \nabla\bullet(\rho_{sb}(\mathbf{V}_s - \mathbf{V}_B)H_s) = \nabla\bullet(\lambda_s\nabla T_S) + \nabla\bullet q_r + Q_{sh} \quad (10)$$

The fourth term on the right-hand side of (8) is included to account for particle random movements (mixing) caused by the mechanical disturbance of the moving grate and other random sources. However, for simplicity, the particle velocities are not actually calculated from (8). Instead, predetermined values are given to the horizontal average particle velocity, and the vertical velocity is then calculated by means of (7).

The solid bed effective thermal conductivity λ_s in (10) consists of two parts: the solid material conductivity, λ_{s0}, and the thermal transport caused by random movement of the particle, λ_{sm}.

$$\lambda_g = \lambda_{s0} + \lambda_{sm} \quad (11)$$

The transport coefficients of the solid-phase, i.e., μ_s, D_s, and λ_{sm} in a packed bed have to be estimated. "Particle Prandtl Number" can be defined as Pr_s, and "Particle Schmidt Number," Sc_s, by analogy to the fluid phase; by assuming that $Pr_s/Sc_s = 1$,

$$\mu_s = \rho_{sh}D_s \quad \text{and} \quad \lambda_{sm} = \mu_s C_{ps} = \rho_{sh}C_{ps}D_s \quad (12)$$

In the above transport equations, steady-state is achieved by setting the time-differentiation term to zero.

As discussed previously, thermal radiation is the major heat transfer mode in the packed bed under combustion conditions. The radiation heat transfer in the bed is represented by a four-flux radiation model [9]:

$$dI_r^{\pm}/dr = -(k_a + k_s)I_r^{\pm} + 1/4\,k_a E_b + 1/4\,k_s\left(I_x^{+} + I_x^{-} + I_z^{+} + I_z^{-}\right) \quad (13)$$

where $r = x$ or $r = z$. The scattering coefficient, k_s, is assumed zero as the first approximation, and the absorption coefficient, k_a, is taken as [10],

$$k_a = -1/d_p\,\ln(\phi) \quad (14)$$

Evaporation of Moisture

It is assumed that the progress of drying is limited by the transport of heat inside the particle and the moisture evaporation rate is approximated by (6)

$$\dot{r}_M = \begin{cases} f_M\dfrac{(T_s - T_{evop})\rho_M c_{pM}}{\Delta H_M \delta t} & \text{if } T_s \geq T_{evap} \\ 0 & \text{if } T_s < T_{evap} \end{cases} \quad (15)$$

where $f_M = 1$.

To overcome potential numerical instability during the computation, the above equation is modified with $f_M = X_M/M$, where M is the initial moisture content in the fuel.

Devolatilization

There are two types of models that are generally used to simulate solid-fuel pyrolysis:

(a) Parallel reaction models
(b) The function-group, depolymerization, vaporization, cross-linking (FG-DVC) model

The FG-DVC model is advocated by Advanced Fuel Research, Inc. in USA [11] and was originally developed for coal pyrolysis. The model combines two previously developed models, a functional group (FG) model, and a depolymerization-vaporization-cross-linking (DVC) model. The DVC subroutine is employed to determine the amount and molecular weight of macromolecular fragments, the lightest of which evolves as tar. The FG subroutine is used to describe the gas evolution and the elemental and functional group compositions of the tar and char. The reaction rates are assumed to follow first-order kinetics with distributed activation energy of width σ. In particular, the rate constant k_i for release of the i-th functional group (also called: pool) is expressed by an Arrhenius expression of the form

$$k_i = A_i\,\exp\left(-\frac{E_i \pm \sigma}{RT}\right) \quad (16)$$

where A_i is the pre-exponential factor, E_i is the activation energy, and σ_i the width of distribution in activation energies.

Direct application of the FG-DVC model data to large particles and fuel batches may encounter difficulty due to secondary cracking of tar and re-polymerization, both inside a pyrolyzing particle and on the activated surfaces of other particles; this can significantly increase the char yield and reduce tar production. It has been found that char yield can increase as much as 30–100% in the packed-bed pyrolyser as

I

compared to standard TGA tests on which the FG-DVC model data are based. Parallel reaction models, on the other hand, provide a much simpler tool to predict the distribution of char, tar, and gases under more realistic conditions, but the elemental composition of each of the products are not predicted. Parallel reaction models are also known as two-stage, semi-global models [12]. In these models, the virgin material is considered as a homogeneous single species and reaction products are grouped into gas, tar, and char. The virgin fuel undergoes thermal degradation according to primary reactions giving as products gas, tar, and char. Tar may undergo secondary reactions in the gas/vapor phase within the pores of the solid matrix, related either to cracking, to give light hydrocarbons, or to depolymerization to give char, as illustrated in the following:

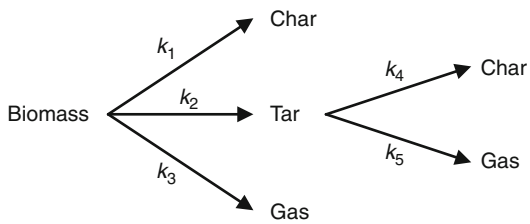

The Function-Group model can be reduced to the more traditional one-step global reaction model if a representative single species is employed

$$dv/dt = k_v(v_\infty - v) \quad s^{-1} \tag{17a}$$

$$\text{where} \quad k_v = A_v \exp(-E_v/RT_s) \tag{17b}$$

In the above equations, v_∞ denotes the ultimate yield of volatile, and v the remaining volatile amount at time t. A_v and E_v are parameters determining the kinetic rate.

Char Burnout

The primary products of char combustion are CO and CO_2,

$$C(s) + \alpha O_2 \rightarrow 2(1-\alpha)CO + (2\alpha - 1)CO_2$$

where the ratio of CO and CO_2 can be expressed as [14]:

$$CO/CO_2 = 2500 \exp(-6420/T) \tag{18}$$

for temperatures between 730 and 1170 K. Ratios outside of this temperature range are calculated using one of the limiting temperatures.

The char consumption rate is expressed as [9]:

$$R_C = P_{O_2}/(1/k_r + 1/k_d) \tag{19}$$

where k_r and k_d are rate constants due to chemical kinetics and diffusion, respectively.

Combustion of Volatiles in the Porous Bed

Gaseous fuels released from the devolatilization process have first to mix with the surrounding air before they can be combusted. Therefore, burning of the volatile hydrocarbon gases is limited not only by the reaction kinetics (temperature dependent), but also by the mixing-rate of the gaseous fuel with the under-fire air. The mixing rate inside the bed is assumed to be proportional to energy loss (pressure drop) through the bed and by recalling the Ergun equations can be expressed as:

$$R_{mix} = C_{mix}\,\rho_g \left\{ 150 \frac{D_g(1-\phi)^{2/3}}{{d_p}^2 \phi} + 1.75 \frac{V_g(1-\phi)^{1/3}}{d_p \phi} \right\} \min\left\{ \frac{C_{fuel}}{S_{fuel}}, \frac{C_{O_2}}{S_{O_2}} \right\} \tag{20a}$$

where C_{mix} is an empirical constant, D_g the molecular diffusivity of the combustion air, V_g the air velocity, d_p the particle diameter, ϕ the local void fraction of the bed, C the molar fractions of the gaseous reactants, and S their stoichiometric coefficients in the reaction.

In the freeboard area immediately above the bed surface, "flame tongues" form and the mixing rate of the volatile gases with surrounding air decreases with increasing distance from the bed surface. Detailed CFD calculations with simulated particle beds were conducted and have produced the following correlation between mixing rate and the distance from the bed top:

$$R_{mix} = R'_{mixo}\left(2.8e^{-0.2y^{++}} - 1.8e^{-2y^{++}}\right) \min\left\{ \frac{C_{fuel}}{S_{fuel}}, \frac{C_{O_2}}{S_{O_2}} \right\} \tag{20b}$$

$$y^{++} = y^{+}/l_p \tag{20c}$$

where R'_{mixo} is calculated from (20a) without the species concentration terms at the bed surface. y^+ denotes the physical distance from the bed top.

A representative hydrocarbon species, $C_mH_nO_l$, can be assumed in the devolatilization products. It is oxidized to produce CO and H_2:

$$C_mH_nO_l + (m/2 - l/2)O_2 \rightarrow mCO + n/2\ H_2$$

CO is then burned by further oxidization to form CO_2

$$CO + {}^1\!/_2O_2 \rightarrow CO_2$$

and H_2 is combusted to H_2O:

$$H_2 + {}^1\!/_2O_2 = H_2O$$

The kinetic rate for $C_mH_nO_l$ oxidation, $R_{C_mH_nO_l}$, is assumed to be the same as that for C_mH_n:

$$R_{C_mH_nO_l} = 59.8\ T_g\ P^{0.3}\ \exp(-12200/T_g)\ C_{C_mH_nO_l}{}^{0.5}\ C_{O_2} \tag{21}$$

and the kinetic rate for CO, R_{co} was shown by [15] to be

$$R_{co} = 1.3 \times 10^{11} \exp(-62700/T_g)\ C_{CO}\ C_{H_2O}{}^{0.5}\ C_{O_2}{}^{0.5} \tag{22}$$

The kinetic rate for H_2, R_{H2} is adopted from [17] as

$$R_{H_2} = 3.9 \times 10^{17} \exp(-20500/T_g) \times R_{H_2}{}^{0.85}\ C_{O_2}{}^{1.42}\ C_{C_mH_nO_l}{}^{-0.56} \tag{23}$$

where the original $C_{C_2H_4}$ has been replaced with $C_{C_mH_nO_l}$ as an approximation.

For tar combustion, a similar reaction rate as $C_mH_nO_l$ is adopted.

In the above equations, C_{CO}, C_{H_2O}, C_{O_2}, and $C_{C_mH_nO_l}$ represent species concentrations, and P the pressure (taken as atmospheric for the packed-bed combustion). The actual reaction rates of volatile species are taken as the minimum of the temperature-dependent kinetic rates and their mixing-rates with oxygen:

$$R = \mathrm{Min}[R_{\mathrm{kinetic}}, R_{\mathrm{mix}}] \tag{24}$$

NO Formation and Destruction

Fuel-nitrogen is assumed to be the dominant source of NO formation in the incinerator furnace. Fuel-nitrogen is released from the solids during pyrolysis either as HCN or NH_3, depending on fuel type and heating rate. In the presence of oxygen, NH_3 or HCN is further oxidized to produce NO and, at the same time, it can also act as a de-NO_x agent to reduce the already-formed NO to nitrogen molecules. In this study, NH_3 is assumed to be the only intermediate product and the well-known De-Soete model is used to calculate the rates:

$$R_{NO} = 4.0 \times 10^6\ X_{NH3}\ X_{O_2}^h \exp\left(\frac{134,400}{RT}\right) \quad s^{-1} \tag{25}$$

and

$$R_{N_2} = 1.8 \times 10^6 X_{NH_3}\ X_{NO} \exp\left(\frac{134,400}{RT}\right) \quad s^{-1} \tag{26}$$

where R_{NO} and R_{N_2} are the NO formation and destruction rates, respectively.

It is assumed that the nitrogen remaining in the char after devolatilization can be heterogeneously oxidized to NO at a rate proportional to the rate of char burnout by a factor related to the relative distribution of carbon and nitrogen in the char [16]. At the same time, the surface oxidation of the char carbon by NO to from N_2 can be calculated from:

$$(dNO/dt) = 4.18 \times 10^4 \exp(-34.70\ \mathrm{Kcal}/RT)\ A_E P_{NO} \quad \mathrm{moles/sec} \tag{27}$$

where A_E is the external surface area of the char in m^2/g, and P_{NO} is in atmospheres.

Nomenclature

A	Particle surface area, m^2m^{-3}
A_r	Pre-exponent factor in char burning rate, $kgm^{-2}s^{-1}$
A_v	Pre-exponent factor in devolatilization rate, s^{-1}
C	Constant; molar fractions of species
C_{fuel}	Fuel concentration, kgm^{-3}
C_{pg}	Specific heat capacity of the gas mixture, $Jkg^{-1}K^{-1}$
C_{mix}	Mixing-rate constant, 0.5
$C_{w,g}$	Moisture mass fraction in the gas phase
$C_{w,s}$	Moisture mass fraction at the solid surface
D_{ig}	Dispersion coefficients of the species Y_i, m^2s^{-1}
d_p	Particle diameter, m

I

E_b	Black body emission, Wm^{-2}
E_r	Activation energy in char burning rate, $Jkmol^{-1}$
E_v	Activation energy in devolatilization rate, $Jkmol^{-1}$
E^0	Effective diffusion coefficient.
H_{evp}	Evaporation heat of the solid material, Jkg^{-1}
H_g	Gas enthalpy, Jkg^{-1}
H_s	Solid-phase enthalpy, Jkg^{-1}
h_s	Convective mass transfer coefficient between solid and gas, $kgm^{-2}s^{-1}$
h_s'	Convective heat transfer coefficient between solid and gas, $Wm^{-2}K^{-1}$
I_x^+	Radiation flux in positive x direction, Wm^{-2}
I_x^-	Radiation flux in negative x direction, Wm^{-2}
k_a	Radiation absorption coefficient, m^{-1}
k_d	Rate constants of char burning due to diffusion, $kgm^{-2}s^{-1}$
k_r	Rate constants of char burning due to chemical kinetics, $kgm^{-2}s^{-1}$
k_v	Rate constant of devolatilization, s^{-1}
k_s	Radiation scattering coefficient, m^{-1}
p_g	Gas pressure, Pa
Q_h	Heat loss/gain of the gases, Wm^{-3}
Q_{sh}	Thermal source term for solid phase, Wm^{-3}
q_r	Radiative heat flux, Wm^{-2}
R	Universal gas constant; process rate, $kgm^{-3}s^{-1}$
R_{mix}	Mixing-rate of gaseous phase in the bed, $kgm^{-3}s^{-1}$
S	Stoichiometric coefficients in reactions
S_{sg}	Conversion rate from solid to gases due to evaporation, devolatilization, and char burning, $kgm^{-3}s^{-1}$
Sy_{ig}	Mass sources due to evaporation, devolatilization, and combustion, $kgm^{-3}s^{-1}$
Sy_{is}	Source term, $kgm^{-3}s^{-1}$
t	Time instant, s
T	Temperature, K
U	x velocity, ms^{-1}
V	y velocity, ms^{-1}
VM	Volatile matter in fuel, wt%
x	Coordinate in bed forward-moving direction, m
y	Coordinate in bed height direction, m
Y_{ig}	Mass fractions of individual species (e.g., H_2, H_2O, CO, CO_2, C_mH_n, . . .).
Y_{is}	Mass fractions of particle compositions (moisture, volatile, fixed carbon, and ash)
ε_s	System emissivity
σ_b	Stefan–Boltzmann constant, 5.86×10^{-8} $Wm^{-2}K^{-4}$
υ	Remaining volatile in solid at time, t
υ_∞	Ultimate yield of volatile
Φ	Void fraction in the bed
λ_g	Thermal dispersion coefficient, $Wm^{-1}K^{-1}$
λ_g^0	Effective thermal diffusion coefficient, $Wm^{-1}K^{-1}$
λ_s	Effective thermal conductivity of the solid bed, $Wm^{-1}K^{-1}$
Subscripts	
env	Environmental
g	Gas phase
i	Identifier for a component in the solid
p	Particle
s	Solid phase

Solution Technique

Except for radiation, the governing equations described above (summarized in Table 3) are generalized into a standard form:

$$\frac{\partial \rho \Phi}{\partial t} + \nabla \bullet (\rho V \Phi) = \nabla \bullet (\lambda \nabla \Phi) + S_\Phi \tag{28}$$

where ρ represents density, V velocities, Φ the parameter to be solved, λ transport coefficient, and S_Φ the source term. The whole geometrical domain of the bed is divided into a number of small cells and (28) is discretized over each cell and solved numerically using the SIMPLE algorithm [13]. For each cell, the equation becomes:

$$a_{i,j}\Phi_{i,j} + a_{i-1,j}\Phi_{i-1,j} + a_{i+1,j}\Phi_{i+1,j} + a_{i,j-1}\Phi_{i,j-1} + a_{i,j+1}\Phi_{i,j+1} = S_{i,j} \qquad (i = 1, M;\ j = 1, N) \tag{29}$$

The radiation equations are solved by the fourth-order Runge–Kutta method.

Incinerator Grate Combustion Phenomena. Table 3 Transport equations and reaction rates used in the mathematical models

Process rate equations	Moisture evaporation	$R_m = A_p h_s \left(C_{w,s} - C_{w,g}\right)$ when $T_s < 100°C$
		$R_m = \frac{A_p\left[h'_s\left(T_g - T_s\right) + \varepsilon_s \sigma_b \left(T_{env}^4 - T_s^4\right)\right]}{H_{evp}}$ when $T_s = 100°C$
	Devolatilization	$R_v = (1-\phi)\rho_s k_v (v_\infty - v)$ $\quad k_v = A_v \exp\left(-\frac{E_v}{RT_s}\right)$
		$C_mH_n + \frac{m}{2}O_2 \rightarrow mCO + \frac{n}{2}H_2$ $\quad R_{C_mH_n} = 59.8\ T_g P^{0.3} \exp\left(\frac{-12200}{T_g}\right) C_{C_mH_n}^{0.5} C_{O_2}$
	Combustion of volatiles	$CO + \frac{1}{2}O_2 \rightarrow CO_2$ $\quad R_{CO} = 1.3 \times 10^{11} \exp\left(\frac{-62700}{T_g}\right) C_{CO} C_{H_2O}^{0.5} C_{O_2}^{0.5}$
		$H_2 + \frac{1}{2}O_2 \rightarrow H_2O$ $\quad R_{H_2} = 3.9 \times 10^{17} \exp\left(\frac{-20500}{T_g}\right) C_{H_2}^{0.85} C_{O_2}^{1.42}$
		$R_{mix} = C_{mix}\rho_g \left[150 \frac{D_g(1-\phi)^{2/3}}{d_p^2 \phi} + 1.75 \frac{V_g(1-\phi)^{1/3}}{d_p \phi}\right] \min\left[\frac{C_{fuel}}{S_{fuel}}, \frac{C_{O_2}}{S_{O_2}}\right]$ $\quad R = \min[R_{kinetic},\ R_{mix}]$
	Char gasification	$C(s) + \alpha O_2 \rightarrow 2(1-\alpha)CO + (2\alpha - 1)CO_2$ $\quad \frac{CO}{CO_2} = 2500 \exp\left(-\frac{6420}{T}\right)$
		$R_4 = A_P C_{O_2} \Big/ \left(\frac{1}{k_r} + \frac{1}{k_d}\right)$ $\quad k_r = A_r \exp\left(-\frac{E_r}{RT_s}\right)$
Gas-phase conservation equations	Continuity	$\frac{\partial\left(\rho_g \phi\right)}{\partial t} + \frac{\partial\left(\rho_g U_g \phi\right)}{\partial x} + \frac{\partial\left(\rho_g V_g \phi\right)}{\partial y} = S_{sg}$
	x – Momentum	$\frac{\partial\left(\rho_g U_g \phi\right)}{\partial t} + \frac{\partial\left(\rho_g U_g U_g \phi\right)}{\partial x} + \frac{\partial\left(\rho_g U_g V_g \phi\right)}{\partial y} = -\frac{\partial p_g}{\partial x} + F\left(U_g\right)$
	y – Momentum	$\frac{\partial\left(\rho_g V_g \phi\right)}{\partial t} + \frac{\partial\left(\rho_g V_g U_g \phi\right)}{\partial x} + \frac{\partial\left(\rho_g V_g V_g \phi\right)}{\partial y} = -\frac{\partial p_g}{\partial y} + F\left(V_g\right)$
	Species	$\frac{\partial\left(\rho_g Y_{i,g} \phi\right)}{\partial t} + \frac{\partial\left(\rho_g U_g Y_{i,g} \phi\right)}{\partial x} + \frac{\partial\left(\rho_g V_g Y_{i,g} \phi\right)}{\partial y} = \frac{\partial}{\partial x}\left(D_{ig} \frac{\partial\left(\rho_g Y_{i,g} \phi\right)}{\partial x}\right) + \frac{\partial}{\partial y}\left(D_{ig} \frac{\partial\left(\rho_g Y_{i,g} \phi\right)}{\partial y}\right) + S_{Y_{i,g}}$
		$D_{ig} = E^0 + 0.5 d_p \left\lvert V_g \right\rvert$
	Energy	$\frac{\partial\left(\rho_g H_g \phi\right)}{\partial t} + \frac{\partial\left(\rho_g U_g H_g \phi\right)}{\partial x} + \frac{\partial\left(\rho_g V_g H_g \phi\right)}{\partial y} = \frac{\partial}{\partial x}\left(\lambda_g \frac{\partial T_g}{\partial x}\right) + \frac{\partial}{\partial y}\left(\lambda_g \frac{\partial T_g}{\partial y}\right) + Q_h$
		$\lambda_g = \lambda^0 + 0.5 d_p \left\lvert V_g \right\rvert \rho_g C_{pg}$
Solid-phase conservation equations	Continuity	$\frac{\partial((1-\phi)\rho_s)}{\partial t} + \frac{\partial((1-\phi)\rho_s U_s)}{\partial x} + \frac{\partial((1-\phi)\rho_s V_s)}{\partial y} = -S_{s_g}$
		$U_s = f(x)$, predefined
	Species	$\frac{\partial\left((1-\phi)\rho_s Y_{i,s}\right)}{\partial t} + \frac{\partial\left((1-\phi)\rho_s U_s Y_{i,s}\right)}{\partial x} + \frac{\partial\left((1-\phi)\rho_s V_s Y_{i,s}\right)}{\partial y} = -S_{Y_{i,s}}$
	Energy	$\frac{\partial((1-\phi)\rho_s H_s)}{\partial t} + \frac{\partial((1-\phi)\rho_s U_s H_s)}{\partial x} + \frac{\partial((1-\phi)\rho_s V_s H_s)}{\partial y} = \frac{\partial}{\partial x}\left(\lambda_s \frac{\partial T_s}{\partial x}\right) + \frac{\partial}{\partial y}\left(\lambda_s \frac{\partial T_s}{\partial y}\right) + \frac{\partial q_{rx}}{\partial x} + \frac{\partial q_{ry}}{\partial y} + Q_{sh}$
Radiation heat transfer	$\frac{dI_{sj}^*}{dx_i} = -(k_a + k_s) I_{xi}^{\pm} + \frac{1}{2N} k_a E_b + \frac{1}{2N} k_s$ $\quad \left(I_{xi}^{+} + I_{xi}^{-}\right), i = 1, N$	
	$k_s = 0$ $\quad k_a = -\frac{1}{d_p} \ln(\phi)$	

Modeling Validation

The modeling predictions have been investigated experimentally for a number of sample materials, where the model parameters were not changed other than the fuel properties. In the simulation, the fuel bed was generally divided into 200 cells, and the time step was fixed at 2 s.

Figures 8a and 8b show the measured temperature history, gas composition, and mass left on the grate for cardboard samples at a low airflow rate (468 kg/m^{2}h).

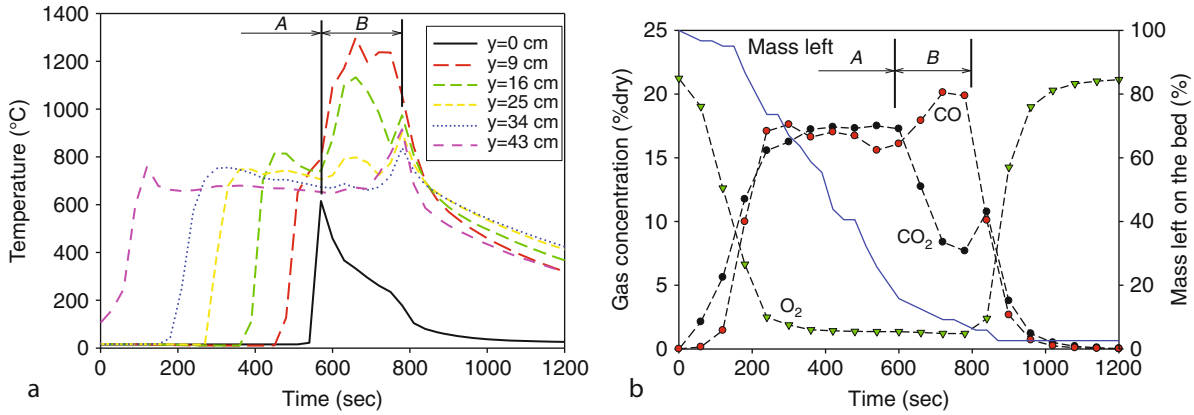

Incinerator Grate Combustion Phenomena. Figure 8

(**a**) Bed temperatures for cardboard combustion at an airflow rate of 468 kg/m^{2}h. (**b**) Gas composition and mass left on the bed for cardboard combustion at an airflow rate of 468 kg/m^{2}h

This type of temperature history is typical for fixed bed combustion as reported in the literature. The temperature plot in Fig. 8a shows two distinct stages with different combustion characteristics. In the ignition propagation stage designated as "A" in Figs. 8a and 8b, the ignition front initiated by the start-up burner propagated into the bed. As the ignition front passed one of the thermocouples in the bed, the volatiles from the burning particles ignited and formed local flames around them and above. This resulted in the temperature increases to around 800°C within a few minutes. The heat released from the reaction of volatiles and char with air transfers downward toward the fresh particles (below the ignition front). This heat is then consumed for further evaporation and heating of fresh fuel. Since oxygen is consumed first by the volatile gases, a layer of char normally accumulates above the ignition front as it propagates downward.

When the ignition front reaches the grate ($y = 0$ cm), the devolatilization of the particles terminated and only the gasification of the remaining char takes place. This stage is designated as "B" in Figs. 8a and 8b. Glowing char particles without flames and high bed temperatures characterize this stage of the combustion process. The temperature at $y = 0$ cm dropped immediately due to the convective cooling. At the same time, the temperatures at $y = 9$ and 16 cm increased rapidly due to active char gasification in this region. As a result, the level of CO immediately began to rise and reached a peak within 150 s as shown in Fig 8b. Note that there were about 60 s delays in the indicated gas composition due to the retention time needed for the sample gas to reach the gas analyzer. The char gasification stages for the cases at an airflow rate of 587 and 702 kg/m^{2}h did not have a CO peak and were shorter than for the above case.

Figures 9a to 9c show the results predicted by the FLIC code for cardboard and waste wood both at an airflow rate of 468 kg/m^{2}h. The thin burning layer and hot spot at 800 s (Fig. 9a) illustrates the key features of bed combustion. As shown, the predicted temperature, weight loss, and gas composition results were in good agreement with the measured data. There was some minor discrepancy between the predicted and measured results for CO and CO_2 during the char gasification stage, although the overall trend was similar. The possible reasons are underprediction of char by the CO_2 to CO reaction or the unaccounted effect of the water gas shift reaction ($CO + H_2O \leftrightarrow CO_2 + H_2$) in this model. In a later model, the char was assumed to be pure carbon, although the char contains a small amount of H element, which is released to the gas phase in the char gasification stage. There was also discrepancy in the bed height in the char gasification stage. Therefore, more information is required on the properties of char particles.

Figure 10 compares the predicted and measured mass loss, ignition rate, and burning rate as a function of airflow for samples of cardboard and waste wood. The predicted ignition rate for cardboard

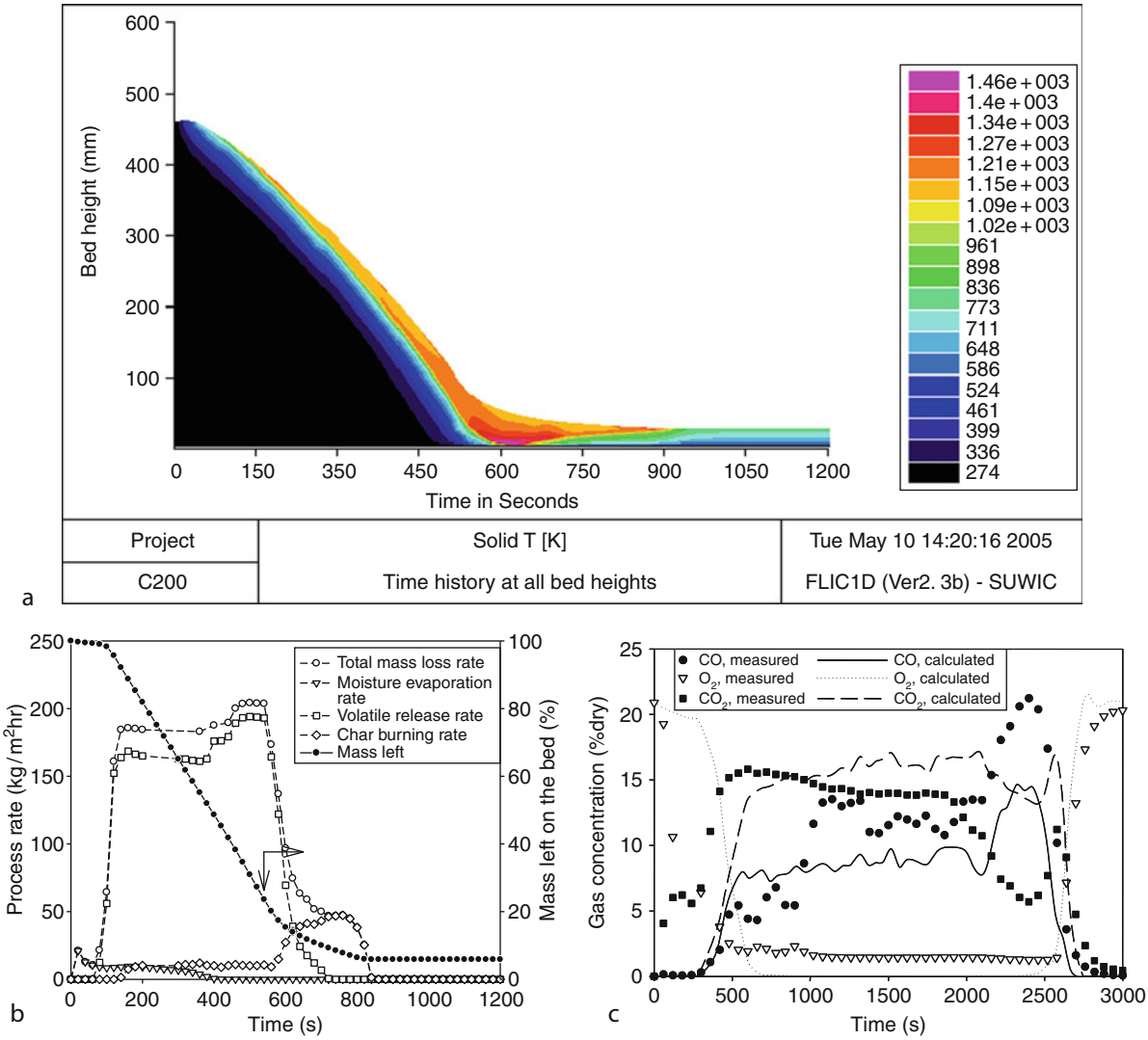

Incinerator Grate Combustion Phenomena. Figure 9

(**a**) Predicted solid temperature for cardboard combustion at an airflow rate of 468 kg/m^{2}h. (**b**) Predicted process rates for cardboard combustion at an airflow rate of 468 kg/m^{2}h. (**c**) Predicted and experimental gas composition for waste wood at an airflow rate of 468 kg/m^{2}h

shown in Fig. 10a was reasonably close to the measured values, but the burning rate was underpredicted. This point will now be discussed to illustrate some of the issues to be taken into account when modeling the combustion of municipal wastes:

Particle size determines the surface to volume ratio of a particle, which directly affects the heat transfer (i.e., radiation penetration through the bed and convection) and the reaction rates of char. Since the model herein assumes the fuel particles to be spherical, the particle diameter was determined to be 10 mm in order to maintain the specific surface area (surface area to volume ratio of a particle). However, the cardboard particle has internal corrugated layers, which significantly increase the area available for mass transfer and heterogeneous reactions. The ignition rate is not significantly affected by the particle size since the bulk density of the bed and the calorific value are unchanged. However, it directly increases the predicted burnout time for char, which gives slower burning rates

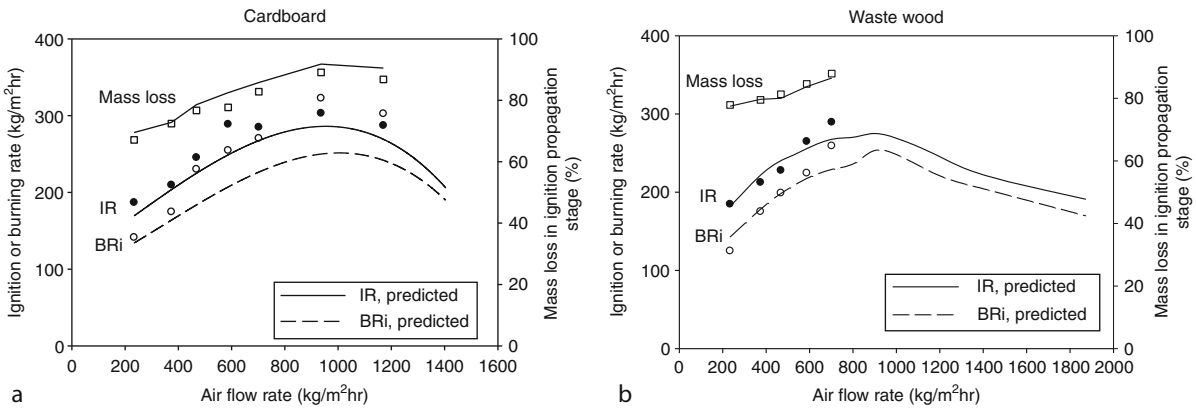

Incinerator Grate Combustion Phenomena. Figure 10
Comparison of measured and predicted ignition and burning rates for cardboard and waste wood (*IR*: ignition rate, *BRi*: burning rate) for the ignition propagation stage. (**a**) Cardboard. (**b**) Waste wood

than the measured values. The char gasification stage also appears at high airflow rates in the prediction. Therefore, more parametric studies for different particle sizes and corresponding model improvement would be required for cardboard. The introduction of a shape factor would be essential in the model in order to consider the actual surface area of a complex particle shape.

However, as expected, the FLIC model prediction for the waste wood shown in Fig. 10b matched well with the measurements. The predicted ignition rate and burning rate had maximum values at an airflow rate of 936 kg/m^{2}h and gradually decreased at higher airflow rates.

Future Directions

- The incineration of a bed of waste by combustion on a moving grate is a widely used and mature technology. Numerical modeling has helped engineers and scientists to understand the key features of the process and optimize plant design and operation.
- The Sheffield CHP/DHC system represents a successful demonstration of this technology. This waste management strategy is already used widely in several European cities but could be applied in many other towns and cities worldwide to reduce fossil fuel consumption and achieve socioeconomic and environmental objectives.
- As indicated above, the potential electricity output of energy-from-waste plants could be almost doubled by the development of an efficient waste gasification system operating with a gasification efficiency of about 70%. The use of this fuel gas in a modern combined cycle gas turbine power plant that has an efficiency of 55% would give and overall efficiency of electricity generation of 38.5%. Since electricity is a more valuable form of energy than low-grade heat, this is an attractive opportunity for further research and development

Acknowledgments

The contribution of the EEE team to this article is gratefully acknowledged: Q Chen, X Zhang, H Li, K M Finney, C Ryu, N Phan, A Khor and Y B Yang.

Bibliography

1. DEFRA (2004) Review of environmental and health effects of waste management: municipal solid waste and similar wastes. London. Available from http://www.defra.gov.uk/ENVIRONMENT/waste/research/health/
2. http://www.ref-fuel.com.technology.htm
3. Department of Environment, Food and Rural Affairs (DEFRA) (2007) Municipal waste management statistics. London. Available from http://www.defra.gov.uk/environment/statistics/wastets/index.htm
4. Yang YB, Goh YR, Zakaria R, Nasserzadeh V, Swithenbank J (2001) Mathematical modelling of MSW incineration, IT3-2001, Philadelphia

5. Goh YR, Siddall RG, Nasserzadeh V, Zakaria R, Swithenbank J, Lawrence D, Garrod N, Jones B (1998) Mathematical modelling of the waste incinerator burning bed. J I Energy 71:110–118
6. Peters B (2003) Thermal conversion of solid fuels. WIT Press, Southampton
7. San SH, Lu A, Stewart DF, Connor MA, Fung PYH, Ng HS (2004) Tar levels in a stratified downdraft gasifier. Science in thermal and chemical biomass conversion. Victoria, pp 1–6, 30 Aug–2 Sept 2004
8. Wakao N, Kaguei S (1982) Heat and mass transfer in packed beds. Gorden & Breach, New York
9. Smoot LD, Pratt DT (1979) Pulverized-coal combustion and gasification. Plenum Press, New York
10. Shin D, Choi S (2000) The combustion of simulated waste particles in a fixed bed. Combust Flame 121:167–180
11. http://www.afrinc.com/products/fgdvc/default.htm
12. Di Blasi C (1996) Heat, momentum and mass transport through a shrinking biomass particle exposed to thermal radiation. Chem Eng Sci 51(7):1121–1132
13. Patankar SV (1980) Numerical heat transfer and fluid flow. Hemisphere, Washington/London
14. Arther JA (1951) Reactions between carbon and oxygen. Trans Faraday Soc 47:164–178
15. Howard JB, William GC, Fine DH (1973) Kinetics of carbon monoxide oxidation in postflame gases. In: Proceedings of the 14th symposium (international) on combustion, the Combustion Institute, Pittsburgh, pp 975–986
16. Jones J, Williams A, Bridgeman T, Darvell L (2005) Modelling pyrolysis and modelling potassium release. EPSRC (UK) Supergen bio-energy consortium, Annual Researchers' Meeting. Stafford, UK, 23–25 Nov 2005
17. Hautman AN, Dryer FL, Schlug KP, Glassman I (1981) A multiple-step overall kinetic mechanism for the oxidation of hydrocarbons. Combust Sci Technol 25:219

Increasing Salinity Tolerance of Crops

Stuart J. Roy, Mark Tester
Australian Centre for Plant Functional Genomics, University of Adelaide, Adelaide, SA, Australia

Article Outline

Glossary
Definition of the Subject
Introduction
Effects of Salt Stress on Plant Growth
Variation in Plant Salinity Tolerance
Mechanisms of Salt Tolerance
Generation of Salt Tolerant Crops
Future Directions
Acknowledgments
Bibliography

Glossary

Exclusion The ability to maintain low concentrations of toxic ions in the plant shoot.

Ionic stress The stress imposed on a plant by the accumulation of salts to toxic concentrations in cells, particularly those of the shoot, leading to premature death.

Genetically modified plant A plant which has been transformed by artificial means with single or multiple genes from another variety or species.

Osmotic stress The stress imposed on a plant by the accumulation of high concentrations of salt around the root, which reduces plant growth.

Osmotic tolerance The ability of a plant to maintain growth under osmotic stress.

Saline soil Soils affected by excess accumulation of salts. Accumulation of sodium chloride (NaCl) on agricultural land has a severe impact on crop yield.

Salt tolerant plant A plant with the ability to grow and set seed in saline environments without significant reductions in plant biomass or yield.

Selective breeding Where two plant species with desirable phenotypes are bred together in an attempt to produce an offspring with both traits.

Tissue tolerance The ability to withstand high concentrations of toxic ions in the shoot.

Definition of the Subject

Plant growth and yield are severely affected by saline soils. High concentrations of salt in the soil make it difficult for plants to take up water, while the accumulated salts in cells, particularly the sodium (Na^+) and chloride (Cl^-) ions, are toxic to plant metabolism. These two factors result in a reduction in plant growth, an increase in the rate of leaf senescence, and a loss in crop yield. The fact that significant areas of farmland worldwide are affected by salt brings with it potentially serious implications for crop yield.

Introduction

Saline soils have been defined as areas where the electrical conductance (ECe; a means of measuring the amount of ions in the soil) is greater than 4 dS/m. It is at around 4 dS/m (approximately 40 mM NaCl) that most plants start to exhibit significant reductions in yield [1]. Over 800 million hectares of land worldwide are affected by saline soils; this accounts for more than 6% of the total land area of the world [2]. Most of this salt-affected land has arisen from natural causes, such as the weathering of rocks, which releases a variety of soluble salts including Cl^-, Na^+, calcium, magnesium, sulfates, and carbonates [3]. Other sources of salt accumulation include the deposition of salts from seawater that is transported by wind and rain, as well as from salts carried in rainwater. It has been estimated that rainwater contains 6–50 mg/kg of sodium chloride (NaCl) which, over time, results in large-scale salt depositions [1].

In addition to the natural processes of salinization, farmland areas are affected by secondary types of salinity which are a consequence of human activities such as land clearing and/or irrigation. This secondary form of salinity results in the raising of water tables and an increase in the concentration of salts around plant roots. Approximately 32 million hectares of the 1,500 million hectares farmed by dryland agriculture are affected by secondary salinity, while 45 million hectares of the 230 million hectares of irrigated land are salt affected [2]. Although it accounts for only 15% of the total cultivated area, irrigated land is twice as productive as dryland agriculture. Consequently, losses of yield which result from an increase in soil salinization in irrigated areas have a disproportionally large effect. Unfortunately, the areas of farmland affected by salinization are increasing and irrigated land is particularly at risk [1].

The deleterious effect of soil salinity on agricultural yields is enormous. To solve this problem will require a variety of approaches including altering farming practices to prevent soil salinization; the implementation of remediation schemes to remove salt from soils; and programs aimed at increasing the salt tolerance of crop plants, either through traditional breeding or by genetic manipulation technologies. By increasing crop salinity tolerance, plant varieties can be generated which will grow on marginal saline soils while longer term land management practices are being introduced. However, before crop salinity tolerance can be improved, an understanding is required of the two separate stresses imposed on a plant when it is grown on a saline soil: osmotic stress and ionic stress.

Effects of Salt Stress on Plant Growth

Osmotic Stress

Osmotic stress affects a plant as the salt concentration around the root reaches 4 dS/m and results in an immediate reduction in shoot growth [1, 4, 5] (Fig. 1). Osmotic stress reduces the rate at which growing leaves expand, the rate of emergence of new leaves, and the development of lateral buds. As this stage of salt stress concerns the inability of a plant to maintain water relations, the cellular and metabolic processes

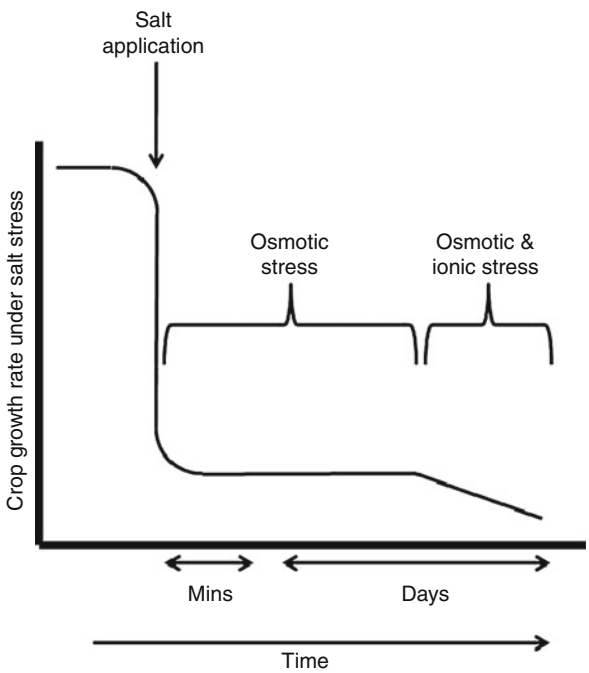

Increasing Salinity Tolerance of Crops. Figure 1
The effect of salt stress on the growth rate of a crop plant. Plants experience an immediate reduction in growth rate after exposure to salt as a result of osmotic stress. Overtime, the effect of ionic stress increases as shoot Na^+ concentrations build to toxic levels (Adapted from [1])

involved are similar to those observed in drought-stressed plants [6]. In dicotyledonous crop species, such as soybean, this osmotic stress results in reductions in the size of leaves and the number of branches [1]; in the monocotyledonous cereals, such as wheat, barley, and rice, the major effect is a reduction in total leaf area and number of tillers [6, 7].

Although it is the roots that are initially exposed to the saline soil, it is actually the growth of the shoot which displays a greater sensitivity to salt; root growth recovers quickly even after exposure to high levels of NaCl [4, 8]. The reduction in leaf development has been attributed to the high salt concentration outside the roots and not to toxic levels of Na^+ or Cl^- within the tissues of the plant [9–11]. This is supported by experiments where plants demonstrate reduced shoot growth when grown in a mixture of salts which individually are at concentrations below those necessary for ionic toxicity but together cause osmotic stress [7, 12]. The mechanisms underlying this down regulation of leaf growth and shoot development remain unclear, but a decrease in shoot area is likely to reduce water use by the plant, thereby conserving soil moisture and preventing an increase in the soil salt concentration. It has been suggested that this reduction in growth rate is regulated by long distance signals in the form of plant hormones and, as the reduction in growth rate is independent of carbohydrate or water supply, is not due to nutrient deficiency [13, 14]. However, it is not just vegetative growth that can be affected by osmotic stress but also the reproductive development of a crop plant – osmotically stressed plants have been found to exhibit either early flowering and/or a reduced number of flowers [1].

Osmotic stress has other detrimental effects on crop plants. On the surfaces of their leaves, plants have stomatal pores, tiny holes through which carbon dioxide (CO_2) enters the leaf for use in photosynthesis and carbohydrate production, and water and oxygen leave the plant. Due to reduced water uptake, osmotically stressed plants close these stomatal pores [1, 15]. The consequent reduction in CO_2 assimilation results in a reduction of carbohydrate production which is detrimental to crop yield. Many plants are able to compensate partially for the reduction in the amount of CO_2 entering the leaf by producing smaller, thicker leaves with more densely packed chloroplasts although this is expensive in terms of expenditure of energy [1]. The decrease in photosynthesis caused by the closure of stomatal pores has the secondary effect of a build up of reactive oxygen species (ROS) [16, 17]. Reactive oxygen species are high energy forms of oxygen, such as superoxide and hydrogen peroxide, which can damage plant DNA and proteins. These ROS accumulate in plant leaves when the energy absorbed from sunlight by chloroplasts cannot be used to synthesize carbohydrates as there is insufficient CO_2 in the leaf to provide the carbon source. If left unchecked these ROS can cause significant damage to plants so cells must produce a range of enzymes, such as superoxide dismutase, ascorbate peroxidase, and catalase, to detoxify and convert the ROS into harmless forms [16, 17]. These detoxifying enzymes are naturally present in plants to protect leaves from sudden burst of sunlight, such as that which occurs when the sun emerges from behind a cloud, but more must be manufactured in response to salt stress, this again being an energy expensive process.

Ionic Stress

Ionic stress has a slower speed of onset than osmotic stress (Fig. 1). It occurs only when the Na^+ or Cl^- accumulation in older leaves reaches a high concentration which results in premature leaf senescence [1, 4, 6, 18]. All salts at high concentrations can affect plant growth but in saline soils it is the Na^+ and Cl^- ions which cause the most detrimental effects on growth. For some plant species, especially citrus, soybean, and grapevines, it is the accumulation of Cl^- ion in the shoot which leads to toxicity, as Na^+ is retained within the roots and the stem [18–22]. However, for most crop plants including the cereals, Na^+ reaches toxic concentrations before Cl^- and is the ion responsible for most of the damage caused to plants [1].

Na^+ and Cl^- are delivered to the shoot in the transpiration stream, that is, in the water which is being transported from the root to the shoot in the xylem of the plant. For most plants, the movement of Na^+ and Cl^- back from the shoot to the roots via the phloem is relatively small, most of the salt delivered to the shoot remaining there [1, 18]. High concentrations of Na^+ in the shoot can cause a range of metabolic and osmotic problems for plants [1, 23]. The metabolic toxicity of Na^+ is largely as a result of its ability to

I

compete with K^+, which is required for many essential cellular functions. Over 50 essential enzymes have been shown to be activated by K^+. Consequently, high levels of cellular Na^+, which will increase the cellular Na^+:K^+ ratio and decrease the availability of K^+, can disrupt a variety of enzymatic processes [24]. In addition, protein synthesis requires high concentrations of K^+ so that tRNA can bind to ribosomes [25]. A reduction in the amount of available cellular K^+ due to high concentrations of Na^+ will disrupt protein synthesis [26]. As older leaves have ceased expanding they cannot use additional water to dilute the salt being transported into, and this leads to an increase in the senescence of older leaves. Consequently, a failure to exclude Na^+ from the shoot over time will result in the accumulation of toxic levels of ions leading to premature senescence and leaf death [4, 27]. If the rate of leaf death is greater than leaf production, the photosynthetic capacity of the plant will be reduced, the plant will be unable to supply carbohydrates to any new leaves, and the growth rate of the plant will decrease.

There is also an osmotic component to ionic stress. During ionic stress, Na^+ and/or Cl^- remain when water from the transpiration stream evaporates and can, therefore, accumulate to high concentrations in the leaf apoplast [5, 28]. These high extracellular concentrations of ions will result in water leaving cells with a consequent severe impact on cellular function. High concentrations of Na^+ and Cl^- in the leaf also present another osmotic problem, that of maintaining cellular water potential below that of the soil, thereby facilitating water uptake for growth. Under conditions of elevated salt concentrations in the soil, plants need to accumulate solutes in order to maintain water uptake. Under such circumstances, the most readily available and energy efficient solutes are the Na^+ and Cl^- ions; however, high cellular concentrations of these ions are toxic. Although Na^+ and Cl^- can be stored within the vacuole of a cell or in the apoplastic space, plant cells have difficulty in maintaining low cytosolic Na^+ and Cl^- [29–31]. Therefore, in order to reduce the water potential within the cell, plants need to synthesize solutes which can be accumulated at high concentrations in the cytoplasm of cells without interfering with metabolism [32, 33]. The synthesis of such compatible solutes, however, is energetically expensive and can make significant demands on the energy resources of a plant.

Overall, in comparison with non-stressed plants, salt stressed plants grow more slowly and die more rapidly. It has been estimated that, due to its immediate effect on plant growth, the osmotic stress has a greater impact than ionic stress on the growth rate of a crop [1]. Ionic stress affects plants only at a later stage and has a lesser effect than osmotic stress, particularly at moderate salinity levels. Only when salt levels are high or if a plant is extremely salt sensitive will the ionic effect be greater than the osmotic.

Variation in Plant Salinity Tolerance

Plants vary widely in their response to saline soils. Many show reduced rates of growth and yield while others, such as the salt tolerant saltbush (*Atriplex amnicola*), only reach an optimal growth rate when a moderate level of salt is present [1, 34]. Depending on their sensitivity to saline soils, plants can be divided into two groups: the salt sensitive glycophytes, which are relatively easily damaged by salt; and the salt tolerant halophytes which can tolerate, and may even require, high concentrations of salt in the soil. Indeed, the halophytic saltbush has been shown to survive at concentrations of salt similar or higher than that of seawater [34]. It has been estimated that only 2% of plant species are true halophytes, while the majority of species, including most crops, are glycophytes [35]. Within the monocotyledonous cereals, rice (*Oryza sativa*) is one of the most salt sensitive [36–39], and shows a significant decrease in growth and yield when exposed to moderate levels of NaCl. By contrast, barley (*Hordeum vulgare*) is significantly more salt tolerant [1, 40]. While not as tolerant as barley, the hexaploid bread wheat (*Triticum aestivum*), which contains the genomes of three different wheat species (AABBDD), is moderately salt tolerant and is able to exclude 97–99% of Na^+ entering the shoot. The tetraploid durum wheat (*T. Turgidum* ssp *durum*), which has the genomes of two species (AABB), is more salt sensitive than bread wheat as it lacks genes for salinity tolerance found on the bread wheat D genome and can exclude only 94–95% of the Na^+ entering the root [6, 30]. In durum wheat, there is a clear deleterious relationship between the amount of Na^+ that accumulates in its shoot and the yield of the plant: the higher the Na^+ concentration, the lower the yield [41].

The variation in salinity tolerance of dicotyledonous crop species is even greater than that observed in the cereals. On a scale of salt sensitivity, sugar beet has been reported as salt tolerant, cotton and tomatoes intermediate in tolerance, and chickpea, beans, and soybean as sensitive to salt [42, 43]. Many fruit trees, such as citrus, are classified as very salt sensitive [43]. A number of legumes have been shown to be extremely salt sensitive, even more so than rice; others, such as alfalfa (*Medicago sativa*) are more salt tolerant than barley [1]. In addition to this variation in salinity tolerance between different crop species, variation also exists within species, some varieties and lines having significantly greater salinity tolerance than others [40–44].

Mechanisms of Salt Tolerance

Osmotic Tolerance

Osmotic stress immediately reduces the expansion rate of shoots and roots. It also results in the closure of stomatal pores. Plants that are more tolerant to osmotic stress will exhibit greater leaf growth and stomatal conductance. This would be desirable in irrigated farmland where water is not limiting, but may be problematic in dryland agricultural systems if the soil water content is depleted before the end of the growing season.

Although it is believed that considerable variation for osmotic tolerance may exist within crop species, until recently this was not easily measured. The estimation of growth rates requires daily measurements of leaf growth or measurements of stomatal conductance [7, 41, 45–47]. These methods are usually either time consuming or have required destructive measurements of plant material to ensure accuracy. Nondestructive imaging technologies have been developed which use digital photographs to calculate plant area and mass [48], or infrared thermography to measure leaf temperature and, thereby, stomatal conductance [49]. These technologies have been used to measure the growth rates of plants in saline environments and, hence, measurement of osmotic tolerance. Variation for osmotic tolerance has now been observed in durum wheat [45, 49] and in wild relatives of wheat, such as *T. monococcum* which is a modern day variety of the plant which donated the A genome to both durum and bread wheat [48].

Ionic Tolerance

Na^+ can accumulate in the shoots of plants to reach toxic levels at concentrations which are below those required of Cl^- for toxicity. Consequently, most studies have focused on revealing any variation in shoot Na^+ accumulation and on the transport of Na^+ within the plant. Ion concentrations in specific tissues can easily be measured at a specific developmental age, and either image analysis [48] or a meter that measures chlorophyll content can be used to measure leaf senescence.

Ionic Tolerance: Exclusion A long established mechanism for salinity tolerance in crop plants is the exclusion of ions, particularly Na^+, from the shoot. Due to the ease of experimentation, this is the mechanism perhaps most studied. A strong correlation between salt exclusion and salt tolerance has been shown for many crops, such as in durum wheat [41, 50], rice [51, 52], barley [40, 53, 54], lotus [55], and *Medicago* [56]. Na^+ enters a plant initially from the soil through the root and is then rapidly transported to the shoot in the water of the transpiration stream. Roots are able to maintain relatively constant levels of NaCl by exporting excess salt either back to the soil or to the shoot. As a result, there is a higher accumulation of Na^+ in the shoot compared with the root. If the net delivery of Na^+ to the shoot could be reduced, this may enable a plant to become more salt tolerant. There are four distinct components that can be modified in order to reduce shoot Na^+ and Cl^- concentrations, all of which occur in the root: reduction in the initial influx of ions from the soil into the root; maximization of the efflux of ions from the roots back to the soil; reduction of the efflux of ions from the inner root cells into the xylem cells which are carrying water and ions to the shoot in the transpiration stream; and maximization of ion retrieval from the transpiration stream into root cells thereby retaining Na^+ and Cl^- in the root.

Ionic Tolerance: Tissue Tolerance Tissue tolerance is the ability to accumulate Na^+ or Cl^- ions in the absence of any detrimental effects on plant health. Tolerance requires the toxic ions to be compartmentalized into areas where they can do no damage. At the cellular level, this usually involves avoiding the accumulation of Na^+ and Cl^- in the cytoplasm of the plant cell where

most of important metabolic processes occur. One strategy of tissue tolerance involves compartmentalization of ions within the vacuole, a large plant cell organelle which can be used as a storage structure. Employing such a mechanism will allow a plant to accumulate high concentrations of Na^+ and Cl^- within the shoot, while avoiding all of the toxicity effects. There already exists a large body of evidence for variation between different varieties of crops in terms of the rates of accumulation of shoot Na^+ and Cl^-, as well as for the concentrations of these ions which the different varieties can tolerate.

Generation of Salt Tolerant Crops

Salt tolerant crop plants may be generated only once there is a clear understanding of the mechanisms underlying salinity tolerance, and of the variation between plant species in effecting such mechanisms. Once identified, the benefit of introducing these salinity tolerance mechanisms into crops must be considered. For example, there would be little point in introducing into a cereal the salinity tolerance mechanisms from a slow growing highly tolerant halophyte if that mechanism involved a slow growth phenotype which would result in the cereal taking years to reach maturity for flowering. In addition, a salt tolerant crop plant must do as well as a sensitive plant when grown in the absence of salt. A high yielding salt sensitive crop which shows a 50% yield reduction under salt stress will still be of greater value to a farmer than a salt tolerant variety which displays little reduction in yield but which produces only 40% as much grain as the salt stressed sensitive variety in the first place.

Crop plants developed to have increased tolerance to both ionic and osmotic stresses would be able to grow at productive rates throughout the life cycle, and the severe losses of yield experienced for most crops growing on saline soils would be reduced. It should also be noted that it may be necessary to develop crop plants with different salinity tolerance mechanisms depending on the environment in which the plants will grow. Crops grown by dryland agriculture may benefit particularly from possessing tissue tolerance mechanisms, as the accumulation of high concentrations of ions within the vacuoles of the plant cells may assist the plant in retrieving more water from the soil. By contrast, an osmotic tolerance strategy, combined with Na^+ exclusion, may be more beneficial to crops grown under irrigation so that water availability is not an issue but the Na^+ content in that water may be high.

Two approaches may be taken to improve the salt stress tolerance of current crops: the exploitation of natural variation in salinity tolerance between different varieties and species of crops; or, the generation of transgenic plants with altered gene expression to increase salinity tolerance. Both approaches have advantages and disadvantages as discussed below.

Exploitation of Natural Variation

For many crop species there exists large natural variation in salinity tolerance mechanisms, with some lines and varieties producing significant yields under salt stressed environments. The screening of 5,000 accessions of bread wheat led to the identification of 29 accessions which produced seed when grown in 50% seawater [57], while screening of 400 Iranian wheats identified several accession with high grain yield under both salt stressed and control environments [58]. Varietal differences in yield in saline conditions have been observed in many crops such as durum wheat [41, 45, 59], barley [60, 61], soybean [62], citrus [19, 63], chickpea [42, 64], and rice [65, 66]. The selection and breeding of these salt tolerant varieties with the current elite varieties grown by farmers would be a step forward in the generation of salt tolerant plants.

The selective breeding of lines with desirable salt tolerance traits with those lines possessing desirable traits for yield is an approach for generating salinity tolerant crops that has been practiced for thousands of years. One limitation with this approach is the time and space necessary to grow offspring from these crosses, test their salinity tolerance, obtain viable seed, and then repeat the crossing with a parent to produce the next generation. Recently, new molecular technologies have been developed which have aided this approach considerably. Different varieties and species have different DNA sequence. The difference between the DNA may be subtle, such as between varieties of the same species where there may be a single nucleotide change in the coding sequence of a gene, or the differences can be extreme, such as the gene duplications or deletions observed between species. Modern molecular techniques

enable the detection of these differences between individuals, varieties, and species and allow the design of molecular markers which recognize specific differences in the DNA between two individuals. Using these molecular markers as DNA landmarks it is possible to produce a map of plant chromosomes which can be divided into regions. By finding differences in regions of DNA between two varieties of plants and then observing the phenotype of the offspring produced by breeding the two original varieties, it is possible to identify regions in DNA linked to that phenotype. These regions are often called quantitative trait loci (QTL). By identifying two different plant varieties with differences in salinity tolerance and by observing molecular markers that are different between the two parents, it is possible to identify QTL linked to salinity tolerance by screening their offspring. As salt tolerance is a complex trait, both genetically and physiologically, it is not uncommon to observe several QTL associated with tolerance.

QTL have now been identified for salinity tolerance in a number of plant species including barley [67, 68], tomato [69], rice [70], citrus [63], bread wheat [71], and durum wheat [41]. When QTL have been discovered, one approach is to then identify the gene in that region of DNA which is responsible for the salt tolerance phenotype. The *SKC1* QTL identified on chromosome 1 in rice and the *Nax1* and *Nax2* loci observed in durum wheat on chromosomes 2A and 5A, respectively, have been narrowed down to genes belonging to a family of Na^+ transporters [70, 72, 73], which have been shown previously to be important for exclusion of Na^+ from the shoot [74–79]. Once a QTL has been discovered, the plant which contains that important piece of DNA for salt tolerance can be bred with salt sensitive varieties to introduce into them the salt tolerant phenotype. As a molecular marker will be linked to the QTL, it is not necessary to screen every offspring produced from this cross with a salt sensitivity assay, rather, it is possible to identify which of the offspring have the piece of DNA important for salt tolerance by screening for the molecular marker linked to the salt tolerance QTL. While this does not necessarily speed up the length of time it takes an individual plant to reach maturity, it does reduce the necessity to screen hundreds of plants in saline conditions looking for those that are salt tolerant, so that more focus can be placed on breeding tolerance traits into crops.

While one approach is to identify a variety of a crop with good salt tolerance and then cross it to other members of that species, a second approach is to introduce salt tolerance traits from related species or near-wild relatives.

Bread wheat and durum wheat are two separate plant species, but because of their genetic background there is the possibility of breeding these two species together to exchange valuable traits. Durum wheat is a tetraploid (AABB) containing two genomes from an ancient ancestral cross, the A genome and the B genome. Bread wheat is a hexaploid (AABBDD), with the same A and B genomes as durum wheat and also a third genome, the D genome [80]. It is possible to breed a bread wheat and durum wheat together to produce a pentaploid hybrid offspring, which has an AABBD genome. During sexual reproduction, there is the possibility of the chromosomes from the different wheat backgrounds to swap DNA, a process called recombination, thereby transferring genes from bread wheat to durum wheat and vice versa. Importantly, however, only chromosomes from the same genome can recombine, i.e., durum genome A with bread genome A and not durum genome A with bread genome B. By crossing this offspring with either bread wheat or durum wheat it is possible to re-obtain tetraploid durum wheat and hexaploid bread wheat, only now containing genes from the other species. This has been done successfully to transfer disease resistance genes [80] and could be used for transferring salt resistance traits between the two species. Although difficult, because durum wheat contains no D genome, it is possible to introduce genes from the bread wheat D genome into durum wheat; however, a special wheat plant, with a mutation that affects the way in which chromosomes align in recombination, is required [81]. This technique was used to transfer the K^+/Na^+ discrimination locus *Kna1* from chromosome 4D of bread wheat to chromosome 4B of durum wheat [82]. This new durum wheat line was able to maintain a high K^+/Na^+ ratio in the leaves [82, 83], thereby increasing its salinity tolerance. However, there was no significant difference in grain yield between durum plants with the bread wheat *Kna1* and those without, perhaps due to a yield penalty imposed by having a large section of the bread wheat D genome in durum wheat. Unfortunately, no agronomically

acceptable durum variety containing the bread wheat *Kna1* locus has been released [80].

In addition to looking for variation in plant salt tolerance in current cultivars, there is the possibility of introducing salinity tolerance traits to crop from their near-wild relatives. These species may have been evolving in areas of high salinity, away from the selective pressures inflicted on domesticated crops. It is, therefore, likely these relatives have developed novel salt tolerance mechanisms which might be introduced into current crops. This approach is not new and there have been many attempts to introduce genes from salt tolerant wild relatives to current salt sensitive crops. Traits for salt tolerance have been discovered in wild relatives of tomato, [84], potato [85], rice [44], wheat [80, 86–88], and barley [40, 86] and several attempts have been made to introduce them to cultivated crops. Screening of eight wild *Hordeum* species, wild relatives of domesticated barley, revealed that seven of the eight had better Na^+ and Cl^- exclusion than domesticated barley under a variety of salt stressed environments. A number of these relatives, such as *H. spontaneum*, *H. marinum*, and *H. intercedens*, had significantly higher relative growth rates than domesticated barley when grown under high salinity stress [40, 89].

T. urartu (AA) is the modern day ancestor of the species that gave rise to the A genomes of durum and bread wheat. Both *T. urartu* and other closely related A genome species, such as *T. monococcum* spp. *monococcum* and *T. monococcum* spp. *aegilopoides*, show greater Na^+ exclusion than durum wheat [80, 90]. Lines of *T. monococcum* also show great variation in both osmotic and Na^+ tissue tolerance [48] and are, therefore, a potential source of novel genes for salinity tolerance. It is possible to cross these species with durum wheat and transfer salinity tolerance traits. One success story of breeding a salinity tolerant crop has been the introduction of a Na^+ exclusion trait into durum wheat from a near-wild relative *T. monococcum*. Screening of multiple durum wheat lines for Na^+ exclusion from the shoot identified a durum landrace, line 149, with significantly lower shoot Na^+ than cultivated durum [59]. It was discovered that Na^+ exclusion in these lines was controlled by two major genes, *Nax1* and *Nax2*, which had been introduced into durum from a cross with *T. monococcum* [91]. These two genes have now been introduced separately into the Australian durum wheat Tamaroi and have undergone field trials.

Another wild relative source for wheat is from *Aegilops tauschii*, which is the modern day version of the species that donated the D genome to bread wheat – there appears to be no modern day equivalent of the B genome [80]. Several screens of *Ae. tauschii* have identified lines with lower shoot Na^+ accumulation and enhanced K^+/Na^+ discrimination than durum wheat, although the phenotype was comparable to bread wheat [29, 71, 92]. As the natural environment of *Ae. tauschii* is dry and moderately saline [80], there exists the possibility of introducing novel salinity tolerant genes into wheat. One possibility is the re-creation of the original cross that generated bread wheat by breeding durum wheat (AABB) with *Ae. tauschii* (DD), thereby creating a synthetic wheat (AABBDD) with a genome similar in style to bread wheat. While the technique is tricky, it has been successful in the past [92]. The advantage of this technique is that the Na^+ exclusion locus found on the D is introduced which is not on the A or B genomes of wheat. Synthetic hexaploid lines with enhanced Na^+ exclusion have been created successfully to have Na^+ exclusion similar to that of the parent *Ae. tauschii* and significantly greater exclusion than that of the durum parent [29] at both high and moderate levels of salt. Indeed, some of the synthetic hybrids produced have significantly lower shoot Na^+ accumulation than bread wheat and often greater yield under salt stress conditions [80, 93]. These results indicate that the approach clearly has validity.

The use of wild relatives in breeding programs remains controversial as few salt tolerant crops are released through this approach [39]. Wheat was one of the earliest crops to be crossed with halophytic wild relatives but over 25 years have elapsed since that initial cross, and no new tolerant varieties has yet been released to farmers [39]. However, a recent report of significant yield advantage in a saline field site of durum wheat plants incorporating a Na^+-excluding locus, *Nax2*, from *T monococcum* appears to be particularly promising [94].

A considerable disadvantage with introducing salinity tolerance traits into crops which are already well adapted for cultivation is the introduction of

undesirable traits encoded by genes which may be physically close to the desirable gene for salinity tolerance in the plant genome [80]. This is a particular problem when breeding current crop varieties with wild relatives, as cultivated crops have been designed by breeders for thousands of years to have desirable traits such as high grain yield, appropriate height and disease resistance. When new traits are introduced into crops by breeding it is not possible to introduce only the gene responsible for that trait. The piece of DNA introduced from the wild relative can be quite large and will contain many genes, for most of which the functions are unknown. If these genes have an undesirable effect which impacts on the agricultural value of the crop leading, for example, to low yield or incorrect flowering time, the crop will be of no value to a farmer. This phenomenon is known as linkage drag [39, 80]. It is possible to reduce the size of the DNA insertion from the wild species by breeding the line with a cultivated crop as, over time, fragments of the wild species DNA will be replaced by that of the cultivated crop. This process, however, can take many generations and requires the breeder to have a molecular marker specific to the Na^+ tolerance gene that has been inserted into the genome; otherwise this gene also would be lost [80].

Transgenic Approaches to Generating a Salt Tolerant Crop

Transgenic approaches are attractive in the generation of salinity tolerant plants, as the sequences of genes known to encode proteins involved in salinity tolerance can be artificially introduced directly into the target variety, without the compounding effects of bringing in multiple, and often undesirable, genes through traditional breeding approaches. In theory, the transformation of commercially relevant crop plants directly with genes for salinity tolerance would help to reduce the time required before farmers can use these crops in the field.

There are numerous possibilities for generating transgenic crops with increased salinity tolerance, either by introducing novel genes for salinity tolerance into crops from other plant species, or by altering the expression of existing genes within the crop (see Fig. 2 for examples).

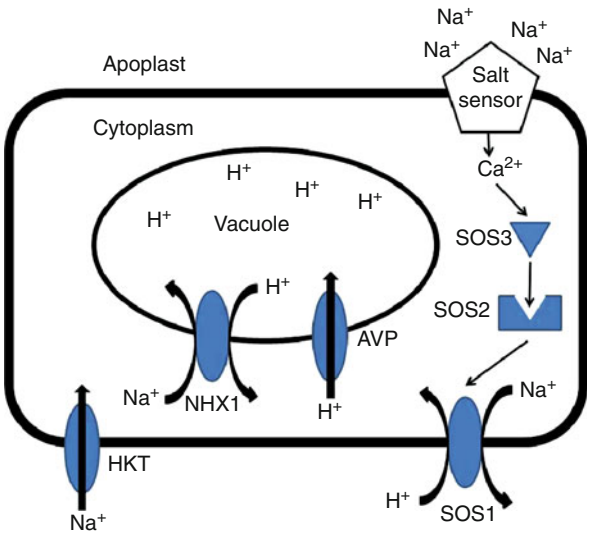

Increasing Salinity Tolerance of Crops. Figure 2 Intracellular location of proteins in a plant cell which are encoded by candidate genes for transformation into transgenic crop plants. NHX1 is a transporter which is involved in the compartmentation of Na^+ into the vacuole by swapping a cytoplasmic Na^+ ion with a vacuolar proton (H^+). AVP is a proton pump that uses the energy released from the breakdown of PPi to move protons into the vacuole. These protons can then be used by transporters such as NHX to transport Na^+ into the vacuole. HKT proteins are involved in the transport of Na^+ from the extracellular space (apoplast) into the cytoplasm. In the salt overly sensitive (SOS) pathway, high concentrations of Na^+ are detected by a membrane bound salt sensor, which results in the release of Ca^{2+} to the cytoplasm. This cytoplasmic Ca^{2+} binds to the calcium binding protein SOS3, which activates the protein kinase SOS2. Together SOS3 and SOS2 activate the Na^+ transporting ability of the SOS1, which moves Na^+ out of the cell

To date, the greatest success with the development of transgenic salinity tolerant crops has been the generation of plants which are better able to compartmentalize Na^+ in the vacuole, where Na^+ can accumulate to high levels without detrimental effects on the plant cells. Central to this process of vacuolar compartmentation is a gene encoding a vacuolar Na^+/H^+ antiporter (NHX), which transports Na^+ into the vacuole in exchange for a proton (H^+) [1, 95, 96] (Fig. 2). The activity of this transporter has been shown to increase

I

under salinity and it is expressed in a variety of different plant species including barley [97], maize [98], sunflower [99], tomato [100], cotton [101], and Arabidopsis [102]. Constitutive expression in yeast of the *NHX* gene from Arabidopsis, *AtNHX1*, had the effect of significantly increasing the salinity tolerance of the yeast [103, 104]. Transgenic plants which have been created to constitutively overexpress the same Arabidopsis *AtNHX* gene, such as Arabidopsis [105], tomato [106], *Brassica napus* [107], and cotton [108], also show increased Na^+ accumulation in the shoot and greater salinity tolerance. These plants are, therefore, Na^+ tissue tolerators. Importantly from a farmer and a consumer point of view, Na^+ accumulation only occurred in the green tissue and not in the fruit, as in the case for tomato [106]. Of particular interest is that both increasing or decreasing the expression of the Arabidopsis *AtNHX* gene has been shown to significantly affect the expression patterns of other genes involved in salinity tolerance mechanisms [96, 109, 110]. This finding has significant implications for the generation of transgenic crops as it indicates that it may not be necessary to transform a plant with multiple salinity tolerant genes but rather with one gene which can regulate others.

Several homologues of the *AtNHX1* gene have now been identified in a number of crops including wheat [111, 112], barley [113], cotton [101], *Medicago* [114], Maize [98], and rice [115, 116], and the constitutive overexpression of these gene in Arabidopsis [111], rice [115–117], wheat [118], tobacco [101], and barley [113] has also been reported to improve salinity tolerance.

Another candidate gene family for the generation of salinity tolerant transgenic crops are the vacuolar H^+ pyrophosphatase genes [1, 96, 119]. Similar to the *NHX* genes, H^+ pyrophosphatase genes, such as Arabidopsis *AVP1*, are involved in Na^+ sequestration to the vacuole. These genes do not encode proteins that are directly responsible for the transport of Na^+ into the vacuole, but rather ones that use the energy released from the breakdown of the high energy molecule inorganic pyrophosphate (PPi) to pump protons (H^+) into the vacuole (Fig. 2). PPi is produced as a by-product of a wide range of biosynthetic pathways. Use of PPi as an energy donor for the activity of the vacuolar H^+-PPase allows ATP to be conserved and improves plant cell performance under more demanding environmental conditions. Once the vacuolar H^+ pyrophosphatase proteins have transported protons into the vacuole, these protons can then be used by Na^+ transporters such as NHXs to move Na^+ into the vacuole. Analysis of plants that are growing under salt stress, such as barley and Arabidopsis, reveals that these genes are significantly upregulated [102, 113]. Arabidopsis, alfalfa (*Medicago sativa*), tobacco (*Nicotiana tabacum*), bentgrass (*Agrostis stolonifera* L.), and rice plants genetically engineered to either express *AVP1* alone, or in combination with *NHX*, have been shown to have increased salinity tolerance [111, 117, 119–122]. Transgenic alfalfa which was constitutively overexpressing *AtAVP1* maintained a greater shoot biomass than wild type alfalfa when grown on 200 mM NaCl [122]. Similarly, transgenic bentgrass expressing the *AtAVP1* gene was not greatly affected when grown on 100 mM NaCl, and was able to survive salt stress of 200 and 300 mM NaCl, levels which severely reduced the growth of wild type bentgrass [123].

In addition to the success in generating salt tolerant plants using genes involved in the mechanisms for sequestering Na^+ in the vacuole, transformation of plants with genes controlling other processes, such as exclusion of Na^+ from the plant, have also been successful. Other candidate genes for increasing the salinity tolerance of crop plants include members of the Salt Overly Sensitive (SOS) pathway.

Many aspects of plant growth, development, and responses to environmental stresses are mediated by the calcium ion (Ca^{2+}) as a secondary messenger signaling molecule. The external cue is first perceived by receptors on the plant cell membrane and this then activates a signaling cascade, using calcium, which regulates the activities of proteins and gene expression [124–127]. The SOS pathway mediates the response of a plant cell to salinity stress. The SOS pathway was so named due to the extreme salt sensitivity of plants which had mutations in key genes of this pathway [128]. Initially, three genes from these mutants, *AtSOS1*, *AtSOS2*, and *AtSOS3*, were identified in Arabidopsis as being important in salinity tolerance [129]. It should be noted, however, that the SOS name refers to a specific salt sensitive phenotype and that the genes sharing the same SOS identifier are unrelated to each other. Indeed, the proteins encoded

by these genes are quite different: AtSOS1 is a plasma membrane Na^+ transporter [130]; AtSOS2 is a protein kinase belonging to a large family of Calcineurin B-like Interacting Protein Kinases (CIPKs) [125, 127]; and AtSOS3 is a plasma membrane bound Ca^{2+} binding protein which belongs to the Calcineurin B-Like proteins (CBL) [125, 127]. However, although they have completely different functions, it is the interactions of these proteins that help a plant cell survive salt stress.

It has been shown in Arabidopsis that under salt stress Ca^{2+} is released into the plant cell cytoplasm from either internal or external cellular stores and it binds to the plasma membrane bound AtSOS3 (AtCBL4). CBL proteins have specific regions which allow them to bind to specific CIPKs, such as SOS2. When Ca^{2+} becomes bound to AtSOS3, it recruits AtSOS2 to the plasma membrane where the kinase phosphorylates the Na^+/H^+ antiporter AtSOS1, thereby activating the transporter and allowing the movement of Na^+ out of the cell [1, 124, 125, 127] (Fig. 2). Although these genes were identified initially in Arabidopsis, homologues for all three genes have now been discovered in a variety of plant species, including crops, such as *Thellungiella halophila* [131], poplar [132], and rice [133]. In all of these species, the genes involved in the SOS pathway have been shown to be significantly upregulated under salt stress, particularly in the plant roots. This would make them ideal as candidate genes for transformation into transgenic crops to increase salinity tolerance.

Arabidopsis plants that were engineered to constitutively express the *AtSOS1* gene had significantly increased salinity tolerance, showing greater biomass, increased chlorophyll retention, and reduced concentrations of Na^+ in the shoot when compared to wild type plants when grown under high saline conditions [134]. Importantly, these plants did not suffer any yield penalty when grown under non-stressed conditions. The increase in the salinity tolerance of the transgenic plants was attributed to them having a great efflux of Na^+ at the cellular level, when compared to control plants.

It is not always necessary to generate a salt tolerant plant by altering the expression level of a gene that encodes a transporter of ions. The salinity tolerance of a plant can also be increased by overexpressing genes encoding molecules that are involved in signaling or activating genes. Overexpression of the transcription factor *Alfin1* in alfalfa resulted in plants with increased root and shoot growth under both control and salt stressed conditions [135]. Enhanced expression of genes involved in signaling pathways, such as those encoding calcium binding CBL proteins and the protein kinase CIPKs, increases the salt tolerance of Arabidopsis, rice, and tobacco [136–139], presumably through enhancing the signaling response of the cell when it is under salt stress. However, the way in which some genes contribute to overall salt tolerance remains unclear. Transgenic tomato that had been transformed with the yeast gene *HAL1* showed increased salt tolerance under stressed conditions but had reduced shoot weight when grown in control conditions, significantly lower than non-transformed plants [140]. This demonstrates that there remains significantly more to understand about the timing and regulation of genes *in planta* before a transgenic salt tolerant plant can successfully be produced.

Certain genes that have been identified as important for plant salinity tolerance have nevertheless not been shown to increase the salinity tolerance of genetically modified plants when constitutively overexpressed. For example, although the *HKT* gene family has been shown to be important in salinity tolerance, the constitutive overexpression of an *HKT* gene was found to have a detrimental effect. The *HKT* gene family can be divided into those genes encoding a Na^+ transporting protein (subfamily 1) or a K^+/Na^+ transporting protein (subfamily 2) [23, 74]. Members of subfamily 2 are considered to be involved in nutrition and the uptake from the soil of ions essential to plant growth (small quantities of Na^+ can be beneficial to plant growth) [141–144], whereas members of subfamily 1 are believed to be important for plant salt tolerance [1, 23, 96]. Members of the subfamily 1 *HKT* gene family have been shown to encode proteins important for the retrieval of Na^+ from the xylem in both the root and the shoot, thereby reducing the accumulation of Na^+ in the shoot [23, 74, 75, 79, 96, 145]. The protein moves Na^+ from the transpiration stream into the cells surrounding the xylem (Fig. 2). Evidence for this function has now been found in a number of plant species in addition to Arabidopsis, such as rice [70] and wheat [72, 73]. Both naturally occurring ecotypes and mutant lines of Arabidopsis

which have reduced expression of this gene show increased shoot Na^+ accumulation [75, 102, 146, 147]. However, constitutive overexpression of this subfamily 1 *HKT* gene also results in higher concentrations of Na^+ and salt sensitive plants [77]. As HKT proteins move Na^+ into cells, the increased salt sensitiveness of constitutive overexpressing plants may be due to the fact that, when the gene is expressed throughout the plant, the protein encoded by the gene transports more Na^+ from the soil into the root, resulting in more Na^+ being transported to the shoot in the transpiration stream. Expression of this gene only in the cells surrounding the xylem would result in a plant being more efficient in retrieving Na^+ from the transpiration stream.

Plants consist of multiple tissues and multiple cells. Each tissue is adapted for a specific purpose – roots for nutrient uptake, leaves for photosynthesis, stems for support – and, therefore, will not necessarily express the same genes. Genes responsible for the maintenance of photosynthesis in the leaves will not be expressed in the roots, and genes for nutrient uptake from the soil will not be expressed in floral tissue. Similarly, not all genes in a plant are expressed all the time; many genes are activated only when required. When growing in non-stressed environments there is little point in a plant using critical energy supplies to generate and maintain proteins important for salinity tolerance. It is unsurprising, therefore, that the continuous expression throughout a plant of a gene important for salinity tolerance, such as *AtHKT1;1*, often results in detrimental effects [77]. A critical feature in the generation of crops engineered to have increased salinity tolerance is the spatial and temporal control of the transgene which has been introduced.

Recently, transgenic Arabidopsis plants have been produced with cell-specific expression of the *AtHKT1;1* gene in the root cells surrounding the xylem [148]. Unlike plants with constitutive overexpression of *AtHKT1;1*, these cell-specific plant lines showed a significant reduction in shoot Na^+ and increased salt tolerance [148].

In a different approach, rice plants designed to overexpress a gene involved in the synthesis of trehalose only when the plants experienced stress exhibited reduced shoot Na^+ concentrations and better growth in saline conditions than non-transformed plants [149]. Trehalose is a sugar involved in protecting cells from long periods of desiccation and possibly aids salinity tolerance through an ability to scavenge reactive oxygen species, thereby protecting cellular proteins [39]; however, plants with constitutive overexpression of genes for trehalose synthesis display severe stunting [150]. The use of a stress-inducible promoter is, therefore, an important control to minimize growth inhibition of transgenic plants when grown in non-stressed environments. The focus now is the identification of gene promoters (sequences of DNA which are used to activate genes) which allow the cell- and temporal-specific expressions of genes in crops.

In addition to the fine control of genes transformed into transgenic crops, there is also the need to identify gene combinations which may have the potential to increase crop salt tolerance. As has been observed, plants employ multiple salinity tolerance mechanisms to survive saline soils, all of which rely on a variety of different genes and proteins. It seems unlikely, therefore, that the generation of a successful commercial salt tolerant crop will be achieved by the constitutive overexpression of one single gene. Recent research promoting salt tolerance in plants focuses on either boosting the intracellular salt-sequestering processes, or on the Na^+ exclusion mechanisms by transferring into selected crop species genes for salinity tolerance from model organisms (such as *Arabidopsis*) or from salt tolerant plants. A complementary approach focuses on the challenging task of reducing net input of salt into plants by perturbing the function of channels and transporters involved in sodium uptake but without disturbing potassium uptake. An ideal scenario contemplates the generation of transgenic plants with an enhanced capability for vacuolar salt sequestration combined with a reduced uptake of salt. While a number of genes involved in these processes have now been identified, the challenge is to switch these genes on at the appropriate time and in the appropriate tissues where they can be most effective. In order to achieve this aim, improved knowledge is required of gene promoters that are stress-inducible and cell specific.

While it is clear that there are potentially many avenues for the generation of a genetically modified salt tolerant plant, there remain significant challenges.

Although it is now possible to generate salt tolerant plants in a laboratory, it has yet to be shown whether this relates to actual yield improvements in the field. There are cases where using genetic modification to generate a salt tolerant plant has a negative effect on yield when no stress is present. It is clear, therefore, that more information on gene promoters is required to enable the activation of salt tolerant genes in specific tissues/cell types only when plants are grown in salt. Furthermore, there are areas of the world, such as Europe, where there remains considerable resistance to the acceptance of genetically modified plants. This may well be due to the lack of availability to consumers of clear, accurate information as well as the prevalence of extremist views. A more open, transparent approach by scientists is required explaining the potential advantages and disadvantages of this technology. Only then will consumers be able to make their own informed choices about genetically modified organisms.

Future Directions

Crops growing on saline soils suffer severe reductions in yield due to both ionic and osmotic stresses. As considerable areas of farmland are currently affected by saline soils much research has been undertaken to enhance crop salinity tolerance by exploitation of natural variation in salinity tolerance or through the generation of transgenic plants expressing genes shown to be important for salt tolerance. While salinity tolerant plants have been generated by both approaches, the focus should now be on the production of viable crop plants for farmers to grow in affected areas. For this to occur, the new cultivars of tolerant plants need to be tested under rigorous field conditions and those with enhanced salt tolerance and, as equally important, no yield penalties when grown in nonsaline conditions pass to breeders for incorporation into future crops.

Approaches are still required to help speed up the generation of salinity tolerance crops through the exploitation of natural variation. Sequencing of cereal genomes will greatly speed up the identification of candidate genes underlying salt tolerance QTL, thereby enabling highly specific molecular markers that are tightly aligned to the trait. Using these markers will help reduce the effects of linkage drag bringing undesirable traits into the population.

For transgenic plants, it is clear that refined control over when and where a gene is expressed is essential. As there are now multiple candidate genes, with potential for enhancing salinity tolerance, research should now focus more on identifying the controlling elements in a plant's genome, which dictate when and where a gene is expressed, and less on the identification of candidate genes. In addition, combinations of genes which have additive effects on salinity tolerance need to be identified, thereby allowing the production of the most optimal salt tolerant plants. When these factors are known, crops can be produced which have the ability to activate multiple genes for salinity tolerance in different areas of the plant but only when saline soils are experienced.

Although further research is clearly still required, considerable progress has been made in generating salt tolerant *plants* through the exploitation of natural variations and the generation of genetically modified organisms. The next step is to deliver salt tolerant *crops* to farmers.

Acknowledgments

We thank Christina Morris for her comments on the manuscript, and the Australian Research Council and Grains Research Development Corporation for financial support.

Bibliography

Primary Literature

1. Munns R, Tester M (2008) Mechanisms of salinity tolerance. Annu Rev Plant Biol 59:651–681
2. FAO. FAO Land and Plant Nutrition Management Service (2008) Available from http://www.fao.org/ag/agl/agll/spush
3. Szabolcs I (1989) Salt-affected soils. CRC Press, Boca Raton
4. Munns R (2002) Comparative physiology of salt and water stress. Plant Cell Environ 25:239–250
5. Flowers TJ, Hajibagherp MA, Yeo AR (1991) Ion accumulation in the cell walls of rice plants growing under saline conditions: evidence for the Oertli hypothesis. Plant Cell Environ 14: 319–325
6. Munns R, James RA, Lauchli A (2006) Approaches to increasing the salt tolerance of wheat and other cereals. J Exp Bot 57:1025–1043

I

7. Yeo AR et al (1991) Short- and long-term effects of salinity on leaf growth in rice (*Oryza sativa L.*). J Exp Bot 42:881–889
8. Frensch J, Hsiao TC (1994) Transient responses of cell turgor and growth of maize roots as affected by changes in water potential. Plant Physiol 104:247–254
9. Hu Y et al (2007) Short-term effects of drought and salinity on mineral nutrient distribution along growing leaves of maize seedlings. Environ Exp Bot 60:268–275
10. Hu Y, Fricke W, Schmidhalter U (2005) Salinity and the growth of non-halophytic grass leaves: the role of mineral nutrient distribution. Funct Plant Biol 32:973–985
11. Fricke W (2004) Rapid and tissue-specific accumulation of solutes in the growth zone of barley leaves in response to salinity. Planta 219:515–525
12. Termaat A, Munns R (1986) Use of concentrated macronutrient solutions to separate osmotic from NaCl specific effects on plant growth. Aust J Plant Physiol 13:509–522
13. Munns R et al (2000) Leaf water status controls day-time but not daily rates of leaf expansion in salt-treated barley. Aust J Plant Physiol 27:949–957
14. Fricke W, Peters WS (2002) The biophysics of leaf growth in salt-stressed barley. A study at the cell level. Plant Physiol 129:374–388
15. Fricke W et al (2004) Rapid and tissue-specific changes in ABA and in growth rate in response to salinity in barley leaves. J Exp Bot 55:1115–1123
16. Apel K, Hirt H (2004) Reactive oxygen species: metabolism, oxidative stress and signal transduction. Annu Rev Plant Biol 55:373–399
17. Logan BA (2005) Reactive oxygen species and photosynthesis. In: Smirnoff N (ed) Antioxidants and reactive oxygen species in plants. Blackwell, Oxford, pp 250–267
18. Tester M, Davenport R (2003) Na^+ tolerance and Na^+ transport in higher plants. Ann Bot 91:503–527
19. Storey R, Walker RR (1999) Citrus and salinity. Sci Hortic 78:39–81
20. Flowers TJ, Yeo AR (1988) Ion relations of salt tolerance. In: Baker D, Halls J (eds) Solute transport in plant cells and tissues. Longman, Harlow, pp 392–416
21. Läuchli A (1984) Salt exclusion: an adaptation of legumes for crops and pastures under saline conditions. In: Staples RC (ed) Salinity tolerance in plants: strategies for crop improvement. Wiley, New York, pp 171–187
22. Teakle NL, Tyerman SD (2010) Mechanisms of Cl^- transport contributing to salt tolerance. Plant Cell Environ 33:566–589
23. Horie T, Hauser F, Schroeder JI (2009) HKT transporter-mediated salinity resistance mechanisms in Arabidopsis and monocot crop plants. Trends Plant Sci 14:660–668
24. Bhandal IS et al (1988) Potassium estimation, uptake, and its role in the physiology and metabolism of flowering plants. Int Rev Cytol 110:205–254
25. Wyn Jones RG, Brady CJ, Spears J (1979) Ionic and osmotic relations in plant cells. In: Laidman DL, Wyn Jones RG (eds) Recent advances in the biochemistry of cereals. Academic, London, pp 63–103
26. Blaha G et al (2000) Preparation of functional ribosomal complexes and effect of buffer conditions on tRNA positions observed by cryoelectron microscopy. Methods Enzymol 317:292–306
27. Munns R (1993) Physiological processes limiting plant growth in saline soils: some dogmas and hypotheses. Plant Cell Environ 16:15–24
28. Öertli JJ (1968) Extracellular salt accumulation, a possible mechanism of salt injury in plants. Agrochimica 12: 461–469
29. Gorham J (1990) Salt tolerance in the *Triticeae*: K/Na discrimination in synthetic hexaploid wheats. J Exp Bot 41:623–627
30. Dubcovsky J et al (1996) Mapping of the K^+/Na^+ discrimination locus *Kna1* in wheat. Theor Appl Genet 92:448–454
31. Maathuis FJM, Amtmann A (1999) K^+ nutrition and Na^+ toxicity: the basis of cellular K^+/Na^+ ratios. Ann Bot 84:123–133
32. Hu YC, Schnyder H, Schmidhalter U (2000) Carbohydrate deposition and partitioning in elongating leaves of wheat under saline soil conditions. Aust J Plant Physiol 27:363–370
33. Chen THH, Murata N (2002) Enhancement of tolerance of abiotic stress by metabolic engineering of betaines and other compatible solutes. Curr Opin Plant Biol 5:250–257
34. Aslam Z et al (1986) Effects of external NaCl on the growth of *Atriplex amnicola* and the ion relations and carbohydrate status of the leaves. Plant Cell Environ 9:571–580
35. Glenn EP, Brown JJ, Blumwald E (1999) Salt tolerance and crop potential of halophytes. Crit Rev Plant Sci 18:227–255
36. Aslam M, Qureshi RH, Ahmed N (1993) A rapid screening technique for salt tolerance in rice (*Oryza sativa* L.). Plant Soil 150:99–107
37. Walia H et al (2005) Comparative transcriptional profiling of two contrasting rice genotypes under salinity stress during the vegetative growth stage. Plant Physiol 139:822–835
38. Flowers TJ, Yeo AR (1981) Variability in the resistance of sodium chloride salinity within rice (*Oryza sativa* L.) varieties. New Phytol 88:363–373
39. Flowers TJ (2004) Improving crop salt tolerance. J Exp Bot 55:307–319
40. Garthwaite AJ, von Bothmer R, Colmer TD (2005) Salt tolerance in wild *Hordeum* species is associated with restricted entry of Na^+ and Cl^- into the shoots. J Exp Bot 56:2365–2378
41. Munns R, James RA (2003) Screening methods for salinity tolerance: a case study with tetraploid wheat. Plant Soil 253:201–218
42. Flowers TJ et al (2010) Salt sensitivity in chickpea. Plant Cell Environ 33:490–509
43. Greenway H, Munns R (1980) Mechanisms of salt tolerance in nonhalophytes. Ann Rev Plant Phys 31:149–190
44. Sengupta S, Majumder AL (2010) *Porteresia coarctata* (Roxb.) Tateoka, a wild rice: a potential model for studying salt-stress biology in rice. Plant Cell Environ 33:526–542
45. James RA et al (2008) Genetic variation in tolerance to the osmotic stress component of salinity stress in durum wheat. Funct Plant Biol 35:111–123

46. James RA et al (2002) Factors affecting CO_2 assimilation, leaf injury and growth in salt-stressed durum wheat. Funct Plant Biol 29:1393–1403
47. Silva C, Martínez V, Carvajal M (2008) Osmotic versus toxic effects of NaCl on pepper plants. Biol Plantarum 52:72–79
48. Rajendran K, Tester M, Roy SJ (2009) Quantifying the three main components of salinity tolerance in cereals. Plant Cell Environ 32:237–249
49. Sirault XRR, James RA, Furbank RT (2009) A new screening method for osmotic component of salinity tolerance in cereals using infrared thermography. Funct Plant Biol 36:970–977
50. Poustini K, Siosemardeh A (2004) Ion distribution in wheat cultivars in response to salinity stress. Field Crop Res 85: 125–133
51. Lee K-S et al (2003) Salinity tolerance of japonica and indica rice (*Oryza sativa* L.) at the seedling stage. Planta 216: 1043–1046
52. Zhu GY, Kinet JM, Lutts S (2001) Characterization of rice (*Oryza sativa* L.) F3 populations selected for salt resistance. I. Physiological behaviour during vegetative growth. Euphytica 121:251–263
53. Forster B (2001) Mutation genetics of salt tolerance in barley: an assessment of Golden Promise and other semi-dwarf mutants. Euphytica 120:317–328
54. Wei W et al (2003) Salinity induced differences in growth, ion distribution and partitioning in barley between the cultivar Maythorpe and its derived mutant Golden Promise. Plant Soil 250:183–191
55. Teakle N et al (2007) *Lotus tenuis* tolerates the interactive effects of salinity and waterlogging by 'excluding' Na^+ and Cl^- from the xylem. J Exp Bot 58:2169–2180
56. Sibole JV et al (2003) Ion allocation in two different salt-tolerant Mediterranean Medicago species. J Plant Physiol 160:1361–1365
57. Kingsbury RW, Epstein E (1984) Selection for salt-resistant spring wheat. Crop Sci 24:310–315
58. Jafari-Shabestari J, Corke H, Qualset C (1995) Field evaluation of tolerance to salinity stress in Iranian hexaploid wheat landrace accessions. Genet Resour Crop Evol 42:147–156
59. Munns R et al (2000) Genetic variation for improving the salt tolerance of durum wheat. Aust J Agric Res 51:69–74
60. Richards RA et al (1987) Variation in yield of grain and biomass in wheat, barley, and triticale in a salt-affected field. Field Crop Res 15:277–287
61. Slavich P, Read B, Cullis B (1990) Yield response of barley germplasm to field variation in salinity quantified using the EM-38. Aust J Exp Agr 30:551–556
62. Lee J-D et al (2009) Inheritance of Salt Tolerance in Wild Soybean (*Glycine soja* Sieb. and Zucc.) Accession PI483463. J Hered 100:798–801
63. Tozlu I, Guy CL, Moore G (1999) QTL analysis of Na^+ and Cl^- accumulation related traits in an intergeneric BC_1 progeny of *Citrus* and *Poncirus* under saline and nonsaline environments. Genome Biol 42:692–705
64. Vadez V et al (2007) Large variation in salinity tolerance in chickpea is explained by differences in sensitivity at the reproductive stage. Field Crop Res 104:123–129
65. Gregorio GB et al (2002) Progress in breeding for salinity tolerance and associated abiotic stresses in rice. Field Crop Res 76:91–101
66. Sahi C et al (2006) Salt stress response in rice: genetics, molecular biology, and comparative genomics. Funct Integr Genomics 6:263–284
67. Mano Y, Takeda K (1997) Mapping quantitative trait loci for salt tolerance at germination and the seedling stage in barley (*Hordeum vulgare* L.). Euphytica 94:263–272
68. Shavrukov Y et al (2010) *HvNax3* – a locus controlling shoot sodium exclusion derived from wild barley (*Hordeum vulgare* ssp. *spontaneum*). Funct Integr Genomics 10:277–291
69. Bretó MP, Aśins MJ, Carbonell EA (1994) Salt tolerance in *Lycopersicon* species. III. Detection of quantitative trait loci by means of molecular markers. Theor Appl Genet 88:395–401
70. Ren Z-H et al (2005) A rice quantitative trait locus for salt tolerance encodes a sodium transporter. Nat Genet 37: 1141–1146
71. Gorham J et al (1987) Chromosomal location of a K/Na discrimination character in the D genome of wheat. Theor Appl Genet 74:584–588
72. Huang S et al (2006) A Sodium Transporter (HKT7) Is a Candidate for Nax1, a Gene for Salt Tolerance in Durum Wheat. Plant Physiol 142:1718–1727
73. Byrt CS et al (2007) HKT1;5-like cation transporters linked to Na^+ exclusion loci in wheat, *Nax2* and *Kna1*. Plant Physiol 143:1918–1928
74. Platten JD et al (2006) Nomenclature for HKT transporters, key determinants of plant salinity tolerance. Trends Plant Sci 11:372–374
75. Davenport RJ et al (2007) The Na^+ transporter AtHKT1; 1 controls retrieval of Na^+ from the xylem in Arabidopsis. Plant Cell Environ 30:497–507
76. Huang S et al (2008) Comparative mapping of HKT genes in wheat, barley, and rice, key determinants of Na^+ transport, and salt tolerance. J Exp Bot 59:927–937
77. Rus A et al (2004) AtHKT1 facilitates Na^+ homeostasis and K^+ nutrition in Planta. Plant Physiol 136:2500–2511
78. Rus A et al (2001) AtHKT1 is a salt tolerance determinant that controls Na^+ entry into plant roots. Proc Natl Acad Sci USA 98:14150–14155
79. Sunarpi H et al (2005) Enhanced salt tolerance mediated by AtHKT1 transporter-induced Na^+ unloading from xylem vessels to xylem parenchyma cells. Plant J 44:928–938
80. Colmer TD, Flowers TJ, Munns R (2006) Use of wild relatives to improve salt tolerance in wheat. J Exp Bot 57:1059–1078
81. Dvořák J, Gorham J (1992) Methodology of gene transfer by homoeologous recombination into *Triticum turgidum*: transfer of K^+/Na^+ discrimination from *Triticum aestivum*. Genome Biol 35:639–646
82. Dvořak J et al (1994) Enhancement of the salt tolerance of *Triticum turgidum* L. by the Kna1 locus transferred from the

I

Triticum aestivum L. chromosome 4D by homoeologous recombination. Theor Appl Genet 87:872–877
83. Gorham J et al (1997) Genetic analysis and physiology of a trait for enhanced K^+/Na^+ discrimination in wheat. New Phytol 137:109–116
84. Perez-Alfocea F et al (1994) Comparative salt responses at cell and whole-plant levels of cultivated and wild tomato species and their hybrid. J Hortic Sci Biotech 69:639–644
85. Sherraf I et al (1994) Production and characterization of intergeneric somatic hybrids through protoplast electrofusion between potato (*Solanum tuberosum*) and *Lycopersicon pennellii*. Plant Cell Tissue Organ Cult 37:137–144
86. Nevo E, Chen G (2010) Drought and salt tolerances in wild relatives for wheat and barley improvement. Plant Cell Environ 33:670–685
87. Gorham J et al (1986) Salt Tolerance in the Triticeae: Solute Accumulation and Distribution in an Amphidiploid derived from *Triticum aestivum* cv. Chinese Spring and Thinopyrum bessarabicum. J Exp Bot 37:1435–1449
88. King IP et al (1997) Introgression of salt-tolerance genes from *Thinopyrum bessarabicum* into wheat. New Phytol 137:75–81
89. Yan J et al (2008) Phenotypic variation in caryopsis dormancy and seedling salt tolerance in wild barley, Hordeum spontaneum, from different habitats in Israel. Genet Resour Crop Evol 55:995–1005
90. Gorham J et al (1991) The presence of the enhanced K/Na discrimination trait in diploid Triticum species. Theor Appl Genet 82:729–736
91. James RA, Davenport RJ, Munns R (2006) Physiological characterization of two genes for Na^+ exclusion in durum wheat, *Nax1* and *Nax2*. Plant Physiol 142:1537–1547
92. Shah SH et al (1987) Salt tolerance in the Triticeae: the contribution of the D genome to cation selectivity in hexaploid wheat. J Exp Bot 38:254–269
93. Schachtman DP, Lagudah ES, Munns R (1992) The expression of salt tolerance from *Triticum tauschii* in hexaploid wheat. Theor Appl Genet 84:714–719
94. CSIRO. CSIRO develops highest yielding salt tolerant wheat (2010) Available from http://www.csiro.au/news/CSIRO-develops-highest-yielding-salt-tolerant-wheat.html
95. Blumwald E, Aharon GS, Apse MP (2000) Sodium transport in plant cells. Biochim Biophys Acta 1465:140–151
96. Plett DC, Skrumsager Møller I (2010) Na^+ transport in glycophytic plants: what we know and would like to know. Plant Cell Environ 33:612–626
97. Garbarino J, DuPont FM (1989) Rapid induction of Na^+/H^+ exchange activity in barley root tonoplast. Plant Physiol Biochem 89:1–4
98. Zörb C et al (2005) Molecular characterization of Na^+/H^+ antiporters (*ZmNHX*) of maize (*Zea mays* L.) and their expression under salt stress. J Plant Physiol 162:55–66
99. Ballesteros E et al (1997) $Na^+//H^+$ antiport activity in tonoplast vesicles isolated from sunflower roots induced by NaCl stress. Physiol Plant 99:328–334
100. Wilson C, Shannon MC (1995) Salt-induced Na^+/H^+ antiport in root plasma membrane of a glycophytic and halophytic species of tomato. Plant Sci 107:147–157
101. Wu C-A et al (2004) The cotton *GhNHX1* gene encoding a novel putative tonoplast Na^+/H^+ antiporter plays an important role in salt stress. Plant Cell Physiol 45:600–607
102. Jha D et al (2010) Variation in salinity tolerance and shoot sodium accumulation in *Arabidopsis* ecotypes linked to differences in the natural expression levels of transporters involved in sodium transport. Plant Cell Environ 33:793–804
103. Aharon GS et al (2003) Characterization of a family of vacuolar Na^+/H^+ antiporters in *Arabidopsis thaliana*. Plant Soil 253:245–256
104. Gaxiola RA et al (1999) The *Arabidopsis thaliana* proton transporters, AtNHX1 and AVP1, can function in cation detoxification in yeast. Proc Natl Acad Sci USA 96:1480–1485
105. Apse MP et al (1999) Salt tolerance conferred by overexpression of a vacuolar Na^+/H^+ antiport in Arabidopsis. Science 285:1256–1258
106. Zhang H-X, Blumwald E (2001) Transgenic salt-tolerant tomato plants accumulate salt in foliage but not in fruit. Nat Biotechnol 19:765–768
107. Zhang H-X et al (2001) Engineering salt-tolerant *Brassica* plants: characterization of yield and seed oil quality in transgenic plants with increased vacuolar sodium accumulation. Proc Natl Acad Sci USA 98:12832–12836
108. He C et al (2005) Expression of an Arabidopsis vacuolar sodium/proton antiporter gene in cotton improves photosynthetic performance under salt conditions and increases fiber yield in the field. Plant Cell Physiol 46:1848–1854
109. Sottosanto J, Gelli A, Blumwald E (2004) DNA array analyses of Arabidopsis thaliana lacking a vacuolar Na+/H+ antiporter: impact of AtNHX1 on gene expression. Plant J 40:752–771
110. Sottosanto J, Saranga Y, Blumwald E (2007) Impact of *AtNHX1*, a vacuolar Na^+/H^+ antiporter, upon gene expression during short- and long-term salt stress in *Arabidopsis thaliana*. BMC Plant Biol 7:18
111. Brini F et al (2007) Overexpression of wheat Na^+/H^+ antiporter *TNHX1* and H^+-pyrophosphatase *TVP1* improve salt- and drought-stress tolerance in *Arabidopsis thaliana* plants. J Exp Bot 58:301–308
112. Yu J et al (2007) An Na+/H+ antiporter gene from wheat plays an important role in stress tolerance. J Biosci 32:1153–1161
113. Fukuda A et al (2004) Effect of salt and osmotic stresses on the expression of genes for the vacuolar H^+-pyrophosphatase, H^+-ATPase subunit A, and Na^+/H^+ antiporter from barley. J Exp Bot 55:585–594
114. Zahran HH et al (2007) Effect of salt stress on the expression of NHX-type ion transporters in Medicago intertexta and Melilotus indicus plants. Physiol Plant 131:122–130
115. Fukuda A et al (2004) Function, intracellular localization and the importance in salt tolerance of a vacuolar Na^+/H^+ antiporter from rice. Plant Cell Physiol 45:146–159

116. Chen H et al (2007) Over-expression of a vacuolar Na^+/H^+ antiporter gene improves salt tolerance in an upland rice. Mol Breed 19:215–225
117. Zhao F-Y et al (2006) Co-expression of the *Suaeda salsa SsNHX1* and Arabidopsis *AVP1* confer greater salt tolerance to transgenic rice than the single *SsNHX1*. Mol Breed 17: 341–353
118. Xue Z-Y et al (2004) Enhanced salt tolerance of transgenic wheat (*Tritivum aestivum L.*) expressing a vacuolar Na^+/H^+ antiporter gene with improved grain yields in saline soils in the field and a reduced level of leaf Na^+. Plant Sci 167: 849–859
119. Gaxiola RA et al (2001) Drought- and salt-tolerant plants result from overexpression of the *AVP1* H^+ -pump. Proc Natl Acad Sci USA 98:11444–11449
120. Duan X-G et al (2007) Heterologous expression of vacuolar H^+-PPase enhances the electrochemical gradient across the vacuolar membrane and improves tobacco cell salt tolerance. Protoplasma 232:87–95
121. Gao F et al (2006) Cloning of an H^+-PPase gene from *Thellungiella halophila* and its heterologous expression to improve tobacco salt tolerance. J Exp Bot 57:3259–3270
122. Bao A-K et al (2009) Overexpression of the Arabidopsis H+-PPase enhanced resistance to salt and drought stress in transgenic alfalfa (*Medicago sativa* L.). Plant Sci 176:232–240
123. Li ZG et al (2010) Heterologous expression of Arabidopsis H^+-pyrophosphatase enhances salt tolerance in transgenic creeping bentgrass (*Agrostis stolonifera L.*). Plant Cell Environ 33:272–289
124. Zhu J-K (2003) Regulation of ion homeostasis under salt stress. Curr Opin Plant Biol 6:441–445
125. Luan S (2009) The CBL-CIPK network in plant calcium signaling. Trends Plant Sci 14:37–42
126. Batistic O, Kudla J (2004) Integration and channeling of calcium signaling through the CBL calcium sensor/CIPK protein kinase network. Planta 219:915–924
127. Weinl S, Kudla J (2009) The CBL-CIPK Ca^{2+}-decoding signaling network: function and perspectives. New Phytol 184:517–528
128. Wu SJ, Ding L, Zhu JK (1996) SOS1, a genetic locus essential for salt tolerance and potassium acquisition. Plant Cell 8: 617–627
129. Qiu Q-S et al (2002) Regulation of SOS1, a plasma membrane Na^+/H^+ exchanger in *Arabidopsis thaliana*, by SOS2 and SOS3. Proc Natl Acad Sci USA 99:8436–8441
130. Qiu Q-S et al (2003) Na^+/H^+ exchange activity in the plasma membrane of Arabidopsis. Plant Physiol 132:1041–1052
131. Vera-Estrella R et al (2005) Salt stress in *Thellungiella halophila* activates Na^+ transport mechanisms required for salinity tolerance. Plant Physiol 139:1507–1517
132. Wu Y et al (2007) Molecular characterization of PeSOS1: the putative Na+/H+ antiporter of *Populus euphratica*. Plant Mol Biol 65:1–11
133. Kolukisaoglu U et al (2004) Calcium sensors and their interacting protein kinases: genomics of the arabidopsis and rice CBL-CIPK signaling networks. Plant Physiol 134: 43–58
134. Shi H et al (2003) Overexpression of a plasma membrane Na^+/H^+ antiporter gene improves salt tolerance in *Arabidopsis thaliana*. Nat Biotechnol 21:81–85
135. Winicov I (2000) Alfin1 transcription factor overexpression enhances plant root growth under normal and saline conditions and improves salt tolerance in alfalfa. Planta 210: 416–422
136. Cheong YH et al (2003) CBL1, a calcium sensor that differentially regulates salt, drought, and cold responses in Arabidopsis. Plant Cell 15:1833–1845
137. Tripathi V et al (2009) CIPK6, a CBL-interacting protein kinase is required for development and salt tolerance in plants. Plant J 58:778–790
138. Xiang Y, Huang YM, Xiong LZ (2007) Characterization of stress-responsive CIPK genes in rice for stress tolerance improvement. Plant Physiol 144:1416–1428
139. Zhao J et al (2009) Cloning and characterization of a novel CBL-interacting protein kinase from maize. Plant Mol Biol 69:661–674
140. Gisbert C et al (2000) The yeast *HAL1* gene improves salt tolerance of transgenic tomato. Plant Physiol 123:393–402
141. Garciadeblás B et al (2003) Sodium transport and HKT transporters: the rice model. Plant J 34:788–801
142. Golldack D et al (2002) Characterization of a HKT-type transporter in rice as a general alkali cation transporter. Plant J 31:529–542
143. Horie T et al (2001) Two types of HKT transporters with different properties of Na^+ and K^+ transport in *Oryza sativa*. Plant J 27:129–138
144. Wang T-B et al (1998) Rapid up-regulation of *HKT1*, a high-affinity potassium transporter gene, in roots of barley and wheat following withdrawal of potassium. Plant Physiol 118:651–659
145. Horie T et al (2006) Calcium regulation of sodium hypersensitivities of sos3 and athkt1 mutants. Plant Cell Physiol 47:622–633
146. Maser P et al (2002) Altered shoot/root Na^+ distribution and bifurcating salt sensitivity in Arabidopsis by genetic disruption of the Na^+ transporter *AtHKT1*. FEBS Lett 531:157–161
147. Rus A et al (2006) Natural variants of AtHKT1 enhance Na^+ accumulation in two wild populations of Arabidopsis. PLoS Genet 2:1964–1973
148. Møller I et al (2009) Salinity tolerance engineered by cell type-specific over-expression of a Na^+ transporter in the Arabidopsis root. Plant Cell 21:2163–2178
149. Garg AK et al (2002) Trehalose accumulation in rice plants confers high tolerance levels to different abiotic stresses. Proc Natl Acad Sci USA 99:15898–15903
150. Romero C et al (1997) Expression of the yeast *trehalose-6-phosphate synthase* gene in transgenic tobacco plants: pleiotropic phenotypes include drought tolerance. Planta 201: 293–297

I

Indoor Environmental Quality and Health Improvement, Evidence-Based Design for

Charlene W. Bayer
Georgia Tech Research Institute, Georgia Institute of Technology, Atlanta, GA, USA

Article Outline

Glossary
Definition of Evidence-Based Design
Introduction
Application to Healthcare Facilities
Application to Other Types of Facilities
Future Directions
Summary/Conclusions
Bibliography

Glossary

AIA (The American Institute of Architects) The AIA has been the leading professional membership association for licensed architects, emerging professionals, and allied partners since 1857.

Cfm (cubic feet per minute) A non-SI (non-International System) unit of measurement of the flow of a gas or liquid that indicates how much volume in cubic feet passes by a stationary point in one minute. The ASHRAE standards and guidelines give ventilation rates for the IEQ in a specified number of cfm/person. 1 cfm = 0.472 L/s.

EBD (evidence-based design) The process of basing decisions about the built environment on credible research to achieve the best possible outcomes.

Health A state of complete physical, mental, and social well-being and not merely the absence of disease or infirmity.

HVAC (heating, ventilation, and air-conditioning system) The systems used to provide heating, cooling, and ventilation in buildings.

IAQ (indoor air quality) The air quality within buildings, related to conditions around buildings and structures, and its relationship to the health and comfort of building occupants.

IEQ (indoor environmental quality) Beyond IAQ to encompass all aspects of the indoor setting including air quality, thermal, visual, and acoustic quality. Focuses on the strategies and systems that result in a healthy indoor environment for building occupants.

WHO (World Health Organization) A United Nations agency that coordinates international health activities and aids governments in improving health services.

Definition of Evidence-Based Design

Evidence-based design (EBD), as defined by the Center for Health Design [1], is "the process of basing decisions about the built environment on credible research to achieve the best possible outcomes." EBD is an approach to facilities design that treats the building and its occupants as a system and gives importance to design features that impact health, well-being, mood and stress, safety, operational efficiency, and economics. To date, EBD has been applied primarily to healthcare facility design, where it has been shown to frequently reduce costs, improve staff productivity, and decrease the length of patient hospital stays. The evidence-based designer, in collaboration with the informed client, develops appropriate solutions to the individual design project based on the needs and expectations of the client, research on similar projects, and experience [2]. EBD provides data on successful strategies for the design process for healthy, high quality buildings.

Introduction

Concepts

Healthy, high-performance buildings should have positive outcomes in terms of energy, sustainability, health, and productivity. A healthy building should meet the World Health Organization (WHO) [3] definition of health, "a state of complete physical, mental and social well-being and not merely the absence of disease or infirmity". The use of this definition of health is particularly applicable to green buildings, intent on not only reducing exposures to chemicals, but also promoting exercise, lowering stress, increasing social interactions, and otherwise fostering physical, social, and mental

health for the occupants. EBD not only meets the WHO health definition, but also encompasses productivity, operational efficiency, economic performance, and occupant/customer satisfaction. Effective EBD needs to be combined with sustainable design, incorporating all practices that reduce the negative impact of development on ecological health and indoor environmental quality [4].

Sustainable, creative design features for application of EBD fall into four major categories, which impact health, economic performance, and operational efficiency of the building system:

- Innovative building enclosures that incorporate load balancing, natural ventilation, and daylighting
- Advanced HVAC systems that incorporate natural conditioning, increased environmental contact, and local control
- Innovative data/voice/power "connectivity" and individual control
- New interior system designs in workstations and workgroup designs for improvements in spatial, thermal, acoustic, visual, and IAQ parameters [5]

Innovative enclosures and advanced HVAC systems particularly impact IAQ, health, productivity and learning, stress reduction, and operational economics. Innovative connectivity and new interior system designs chiefly impact health both as physical well-being and social well-being via connectivity to the organization as a whole, stress reduction, and health.

Indoor Environmental Quality

Healthy buildings encompass all aspects of indoor environmental quality (IEQ) including optimum thermal comfort, lighting with effective daylighting and access to views, IAQ, acoustical performance, ventilation effectiveness integrated with natural ventilation when applicable, and human comfort and health. Healthy buildings are designed for ease of operation and maintenance, because buildings with inadequate IEQ adversely impact occupants' overall health and productivity.

Rashid and Zimring [6] suggest that poor indoor environments may initiate a process leading to stress whenever the individual or workplace IEQ does not meet an occupant's needs, as is shown in Fig. 1. Their framework groups physical environmental variables into two primary groups: (1) IEQ variables including noise, lighting, ambient temperature, and IAQ, and (2) interior design variables including use of space, furniture, fixtures and equipment, finishing materials, color, artwork, natural views, and environmental graphics. These variables are interlinked in the design of the indoor environment and its conditioning systems. Factors leading to stress, similar to individual responses to odors, vary among individuals, further complicating the issues [7]. The collaboration between the designer and the user in the EBD design process is critical in reducing stressors in the indoor environment.

Examples of potential environmentally induced stressors that need to be assessed in the EBD process are:

1. Open office plans creating feelings of lack of privacy [8]
2. Open office plans, selection of hard-surfaced flooring and furnishing materials, office equipment location, HVAC system vibration, and/or or outdoor traffic that may increase noise levels resulting in difficulties in concentration, speech intelligibility, headaches, and other physical and emotional stress responses that impact learning and productivity [9–11]
3. Cafeteria, cleaning, furnishings, or systems odors permeating throughout the work areas of a building due to improper ventilation system design or poor materials selection [12, 13]
4. Daylight glare on work surfaces due to lack of effective window glazing or absence of blinds, and unshielded electric lighting that may result in headaches or eyestrain and poor productivity [14–16]

The Academy of Neuroscience for Architecture (www.anfarch.org) is using evidence-based design as a means to assess the linkage between neuroscience research and human responses to the built environment; thus seeking to relate behavioral changes to brain function changes based on the built environment. The Academy, in its studies, defines the dimensions of functional comfort as: (1) air quality, (2) thermal comfort, (3) spatial comfort, (4) collaborative or teamspace, (5) visual comfort, (6) workstation comfort, (7) lighting quality, (8) noise control, and (9) security. These nine parameters are used to direct the

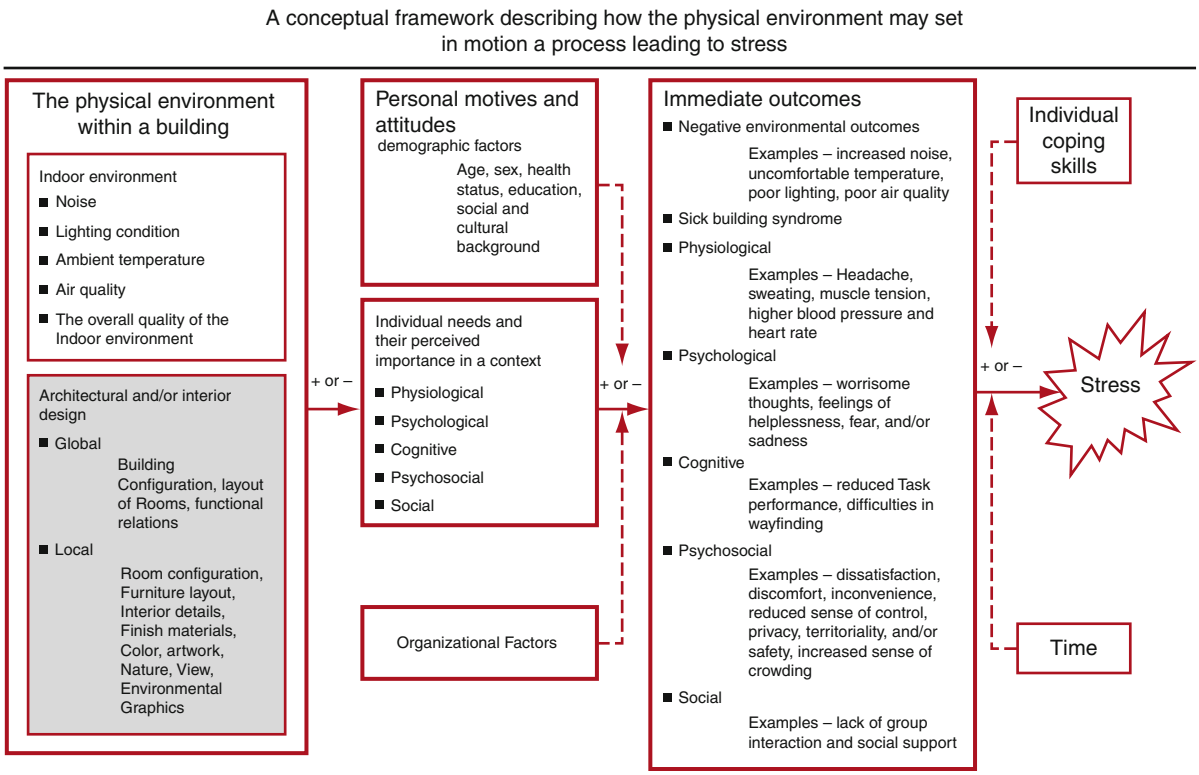

Indoor Environmental Quality and Health Improvement, Evidence-Based Design for. Figure 1
Rashid and Zimring [6] conceptual framework describing how the physical environment may initiate a process leading to stress

evidence-based design practices to reduce human stress, poor behaviors and attitudes, and overall human health, as defined by WHO.

Indoor Air Quality The primary design strategies that are used to improve IAQ in green buildings are the use of low-emitting furnishings and building materials, designed to meet an iteratively tightening set of standards [17–20]. This strategy addresses one of the most important IAQ determinants that is clearly in the realm of the designer – source control. However, the construction process, including installation sequence and protection of materials prior to installation, is also an important factor to be addressed by the EBD team. Installation of carpet prior to painting of walls can result in long-term low level emissions of paint fumes due to adsorption by the carpet and slow reemission into the indoor environment. Key furnishing and material sources that must be specified as low-emitting and eco-friendly include office furniture, flooring, paints and coatings, adhesives and sealants, wall coverings, wood products, textiles, insulation, and cleaning products. The potential adverse health impacts of pollutants that may emit from these products has been determined though many emissions investigations [21].

Another strategy available for reducing exposures to airborne contaminants is source control of indoor equipment and activities. Office machines, stoves, and other appliances that are known to be active pollutant generators benefit from the use of local source control via the installation of dedicated exhaust fans. The use of local source control systems needs to be part of the design process and the location of the areas needing dedicated ventilation and exhausts need to be defined early in the design process. The use of well-maintained air cleaners is another strategy that may be appropriate to selected areas and types of facilities, such as in hospitals.

Ventilation systems are the primary method to dilute and transport airborne contaminants out of

the building. Natural and mixed-mode systems, if employed, must be designed to provide sufficient pollutant dilution and transport out of the building.

Ventilation System Design/Environmental Control The ventilation system is the primary means of transporting contaminants into, throughout, and out of the indoor environment. The placement and design of the system is critical to the quality of the indoor environment. Superior ventilation has been shown to improve learning, productivity, satisfaction, and health. At the same time the ventilation system can transport unwanted outdoor pollutants indoors, transfer indoor pollutants from one space to another, or transport infections [22].

In most buildings, the ventilation system is linked to the thermal conditioning (temperature control) system. Combined thermal comfort and ventilation systems may inadvertently compromise ventilation potentially adversely impacting IEQ, health, and occupant satisfaction. If a decision has to be made between thermal comfort and ventilation response, EBD reveals that the lack of temperature control is a primary stressor in the indoor environment, impacting productivity, learning, mood, and overall health [23].

On the other hand, lower temperatures, especially when combined with increased ventilation rates, tend to increase productivity and student performance. Wargocki and Wyon found that lowering the classroom temperature approximately 5°C improved elementary school students' performance on two numerical tasks and two language-based tasks [24, 25]. The children also reported lower incidence of headaches. When the classroom effective outdoor air supply rate was raised from 11 cfm/person (5 L/s) to 20 cfm/person (10 L/s), the students' performance was improved on four numerical tasks by improving the task performance speed. The children also reported feeling that the air felt fresher with the lower ambient temperatures. Similar results on the relationship of temperature and ventilation on productivity have been reported in adult work situations [26–29]. As a result, EBD reveals the importance in the design of the environmental control/ventilation system of separating the ventilation system from the thermal conditioning system and providing the ability for occupants to individually control the ambient temperature.

Numerous studies show health, productivity, and learning improvements with higher ventilation rates; however, this must also be balanced with sustainable design for greater energy efficiency through the use of innovative ventilation systems and maximizing ventilation efficiency. Haverinen-Shaughnessy et al. [30] found a linear association between classroom ventilation rates within the range of 0.9–7.1 L/s/person and students' academic achievement. In this study of fifth graders, it was determined that for every unit (1 L/s/person) increase in the ventilation rate, the proportion of students passing standardized tests increased by 2.9% for math and 2.7% for reading. Studies have shown that occupants in buildings or spaces with higher ventilation rates on average have fewer communicable respiratory illnesses, and lower asthma rates, and fewer absences from work or school [30–32]. The European Multidisciplinary Scientific Consensus Meeting (EUROVEN) [32] found that ventilation is strongly associated with perceived air quality and health (sick building syndrome symptoms, inflammation, infections, asthma, allergy, short-term sick leave) and that there is an association between ventilation and productivity in offices. The EUROVEN group also concluded that outdoor air supply rates below 25 L/s/person increased the risk of sick building syndrome symptoms, increases in short-term sick leave, and decreased productivity among occupants of an office building. Additionally improper maintenance, design, and functioning air-conditioning systems contribute to increased prevalence of sick building syndrome symptoms.

The research clearly demonstrates significant associations between ventilation system design that allows increased levels of ventilation, at least 10 L/s per person of outdoor air supply in buildings for optimized health, productivity/learning, and reduced stress. In order to meet sustainable design practices meeting the goal of energy efficiency and reduced operating costs, innovative ventilation strategies and systems must be used. Natural ventilation and hybrid systems are important innovative approaches, to be combined with next generation active systems.

Lighting/Daylighting/Access to Views Studies have shown that daylighting has a positive impact on humans, improving accuracy of work performance,

reducing stress and fatigue, and improving patient outcomes [32]. Loftness et al. [14] found that improved lighting quality design decisions are linked with 0.7–23% gains in individual productivity. The lighting quality design ranged from indirect–direct lighting systems, higher quality fixtures, and daylighting simulation. When daylight responsive dimming was employed energy savings of 27–87% were realized.

Access to the natural environment is associated with individual health and productivity. Design decisions for exposure to views include access to windows and view, daylighting through windows and skylights, natural and mixed-mode ventilation systems, and direct accessibility to landscaped indoor and outdoor spaces. Access to the natural environment has been shown to result in 3–18% increases in individual productivity [14] including access to operable windows.

Evidence from school lighting research indicates that improved school lighting can enhance both visual (healthy vision) and non-visual (achievement outcomes). Lighting conditions in classrooms have important non-visual effects on students including potentially raising test scores and faster responding on tests [33].

Acoustics/Noise Control Acoustics is an area of continued dissatisfaction in many green buildings [9]. In a number of projects, the open plan design, large areas of glass, hard-surface materials and furnishings, and natural ventilation strategies used in many green buildings have led to ongoing concerns with acoustic conditions. Building acoustical problems are generally classified in three categories: excessive noise, lack of speech privacy, and lack of speech clarity. Excessive noise is usually the result of high background noise emanating from outdoor noise sources that are transmitted through to the indoor environment, as well as noise from other rooms, building equipment, and/or noise from other occupants. Acoustical design strategies need to control noise levels at the source, reduce sound transmission pathways, and employ sound isolation techniques. Speech privacy is the extent to which speech is unintelligible to an *unintended* listener. The worst speech privacy situations are those where the background noise is very low. In open office plan environments, the lack of speech privacy may be a significant stressor. Design strategies to help improve speech privacy include possibly reconsideration of the open office plan, designing private areas adjacent to the open office area for use in private situations as needed, or increasing background noise. A lack of speech clarity occurs when the acoustics or a room design deteriorate the acoustical communication channel, rendering speech to the *intended* listener unintelligible, creating communication problems. This is particularly an issue in school classrooms and conference rooms. The problem may be caused by excessive background noise or excessive reverberation. EBD solutions to improve acoustics while maintaining sustainable design strategies include the use of acoustically absorbing materials, such as ceiling absorbers, acoustical ceiling tiles or wall-mounted panels.

Operation and Maintenance

A critical area that EBD needs to address for long-term building sustainability and occupant health is designing for maintainability. The life-cycle costing must include the maintenance and operating costs over the facilities lifetime, and EBD feedback on the long-term integrity and maintainability of the materials, components or systems. Metrics should be defined during the design process for the ability to maintain the facility in order to meet health and client economic performance needs. These metrics, at a minimum, should include:

- Labor hours per year that will be required to maintain each integral part of the facility, such as the HVAC system(s), the electrical system, lighting, windows, skylights, floors, and furnishings
- Frequency, extensiveness, and difficulty to perform required cleaning (including avoided toxicity)
- Cost of cleaning and replacement materials
- Equipment and furnishings life expectancies
- Training costs in labor hours and dollars for maintenance staff and occupants/building users

Magee [33] defined the specific maintenance objectives of the majority of facilities as follows:

- Perform necessary daily housekeeping and cleaning to maintain
- Promptly respond and repair minor discrepancies
- Develop and execute a system of regularly scheduled maintenance actions to prevent premature failure of the facility, its systems, and/or components

- Complete major repairs based on lowest life-cycle costs
- Identify and complete improvement projects to reduce and minimize total operating and maintenance costs without increasing indoor toxicity
- Operate the facility utilities in the most economical manner that achieves reliability and optimum functioning, while minimizing or eliminating indoor toxicity
- Provide for easy and complete reporting and identification of necessary repair and maintenance work
- Perform accurate cost estimating to ensure lowest cost and most effective solutions
- Maintain a proper level of materials and spare parts to minimize downtime
- Actively track all costs of maintenance work
- Schedule all planned work in advance allocating and anticipating staff requirements to meet planned and unplanned events
- Monitor progress of all maintenance work
- Maintain complete historical data concerning the facility in general and equipment and components in particular
- Continually seek workable engineering solutions to maintenance problems

Maintenance has a considerable impact on a building's performance and upon occupants' health and satisfaction. Maintenance-related problems over a building's lifetime can be minimized by making appropriate design decisions early in the process.

For example, maintainability is a critical measure for the performance for all ventilation systems including innovative high-performance ventilation systems and may have a significant impact on the health of the building occupants. In a study conducted by Bayer et al. [34] on the benefits of active humidity control and continuous ventilation at a minimum level of at least 15 cfm/person in schools using high-efficiency total energy heat recovery desiccant cooling ventilation system, the importance of system particulate filter maintenance was clearly demonstrated. As can be seen in Fig. 2, the carbon dioxide (CO_2) concentrations in the classroom exceeded 2,000 ppm during occupied times in the classrooms prior to replacement of the particulate filter in the system. Once the filter was changed, reducing the impedance to outside air delivery, the CO_2 levels dropped to approximately 800–1,000 ppm during occupied periods of the classroom. This result clearly demonstrates the necessity of system maintenance for effective ventilation even when a high-efficiency ventilation system is employed. In this school, filter replacement was inadequate due to difficulty in accessing the filter for replacement, a design and maintenance flaw.

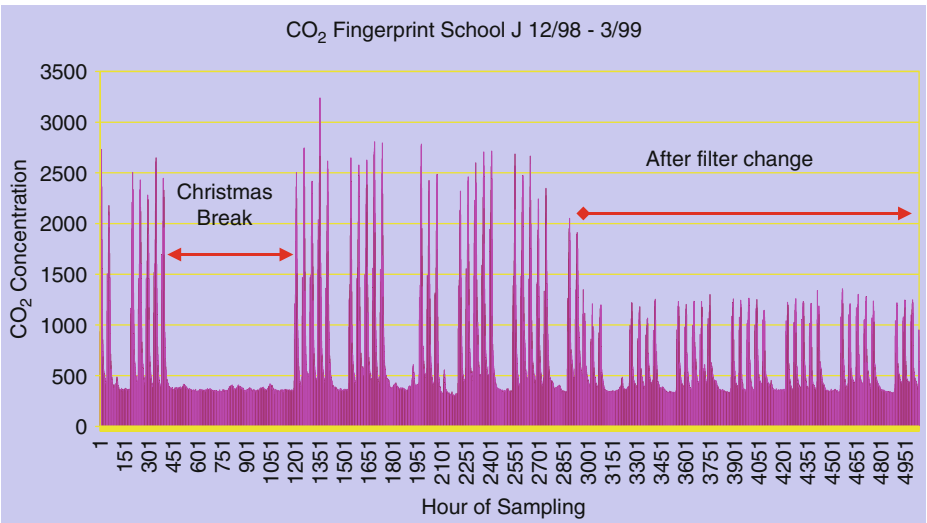

Indoor Environmental Quality and Health Improvement, Evidence-Based Design for. Figure 2
CO_2 levels demonstrate the importance of particulate filter maintenance for effective ventilation in an occupied classroom

Maintaining the cleanliness of the ventilation filters has been found to impact productivity and learning in office buildings and schools. Wargocki et al. [35], in a study on the performance and subjective responses of call-center operators, found that replacing a used filter with a clean filter reduced operator talktime by about 10% at a outdoor air supply rate of approximately 34.4 L/s, but no effect was noted when the filter was replaced and the outdoor air supply rate was only 34.4 L/s. Additionally the operators reported a decrease in sick building syndrome symptoms with clean filters and the increased ventilation rates.

These investigations clearly demonstrate the importance of filter changeouts and ventilation system maintenance for IEQ, health, and productivity. The building systems need to be designed for easy performance of ventilation system maintenance tasks.

Arditi and Nawakorawit [36] surveyed 211 of the largest US building design firms to investigate the relationship between design practices and maintenance considerations. The study examined the extent to which maintenance issues are considered when designers specify building materials and service equipment; the level of designers' knowledge in maintenance-related issues; the degree to which design personnel are exposed to training in maintenance-related matters; the extent to which designers consult property managers and maintenance consultants; the relative importance of maintenance issues to other design factors; the level of difficulty in cleaning, inspecting, repairing, and replacing various building components; and the magnitude and frequency of maintenance-related complaints that designers receive from clients and tenants. Their findings indicate that maintenance consideration follow cost and aesthetics issues when designers specify building materials, but maintenance considerations constitute the number one issue when specifying service equipment. For most firms, the mechanical system was considered to be the most important consideration with regard to difficulty of cleaning, inspection, repair, and replacement with both the designers and the property managers. However ease of repair and replacement, access to cleaning area, and ease of cleaning were ranked by designers to be among the least important design factors for building systems and the facility. This in spite of the fact that the primary complaint that designers reported receiving from clients and tenants concerned issues of ease of repair, access to cleaning area, and ease of cleaning. Property managers also reported frequently receiving similar complaints. The design firms considered themselves to be knowledgeable in maintenance issues and design, and stated that they consulted property managers and maintenance consultants during the designing of selected projects, primarily in the schematic and preliminary design phases.

This is an area where EBD demands increased collaboration among all of the interested parties throughout the entire design process. EBD maintenance planning and design will enhance the life-long performance of the building.

Human Factor Impacts/Occupant/Customer Satisfaction on Sustainable Designs

Many sustainable design strategies reduce the use of walls and partitions – with more open space planning – to reduce material use, enhance views and daylight, and increase ventilation airflow, particularly when natural and hybrid ventilation strategies are used. Although this may increase satisfaction with daylight and access to views, it may also increase dissatisfaction with noise, privacy, and the ability to concentrate [37]. This situation was encountered in the LEED Platinum certified Philip Merrill Environmental Center in Annapolis, MD [38]. This facility placed the entire workforce into an open plan setting, regardless of status in the company, including the president and the key executives, without doors and low partitions for almost all employees (Fig. 3). This allows access to views and daylighting for all employees and the occupants' satisfaction ratings are very high. However, the primary complaints that remain are lack of privacy, noise, distractions, and interference with work concentration. At the same time, the occupants rated the views, daylighting, and interactive behaviors and communication highly.

Evidence-based design is an effective strategy for determining the potential effectiveness of open space planning in different types of buildings and task situations [39, 40]. For example, an elementary school in Atlanta, GA, organized in pods, uses four-foot high partitions among lower grade classrooms in each pod rather than floor-to-ceiling walls to increase interaction between grade classes. The partition heights

Indoor Environmental Quality and Health Improvement, Evidence-Based Design for. Figure 3
Open floor plan at Philip Merrill Environmental Center. Picture available at http://www.cbf.org/Page.aspx?pid=445

Indoor Environmental Quality and Health Improvement, Evidence-Based Design for. Figure 4
Open classroom style at Atlanta, GA, elementary school

increase as the grade level increases until in fifth grade (Fig. 4), the traditional classroom style is used. Staff interviews expressed mixed attitudes about this open design style. Noise between classrooms is a problem; however, as with the Philip Merrill Environmental Center, there was satisfaction with the feeling of community between the grade levels [41]. What has not been sufficiently studied at the school is the potential interference with student concentration in a school with an open floor plan such as is used in this school. The use of the lower partitions in the lower grade levels is actually the converse of what is needed for optimum acoustical performance for learning. Younger children in K-2 grades require a higher signal-to-noise ratio (clearer voices in a quieter environment) since they need to be able to carefully listen to develop the ability to discriminate among minor differences in words, which is extremely difficult in noisy environments [42].

Application to Healthcare Facilities

Hospitals are embracing evidence-based health care design for the promotion of therapeutic, supportive, and efficient environments. EBD is undertaken to develop appropriate solutions to design problems and unique situations in order to improve the organization's clinical outcomes, economic performance, efficiency, and customer satisfaction. EBD helps to provide solutions to the healthcare challenges of cost control, financial stability, avoidance of harm, quality improvements, sustainability, staff retention, and improved patient experience.

Ulrich et al. [43] reviewed the research literature on EBD healthcare design. Their overall findings indicated the importance of improving patient outcomes through a range of design characteristics including single-bed rooms, effective ventilation systems, good acoustical environments, increased views of nature, improved daylighting and interior lighting, better ergonomic design, acuity-adaptable rooms, and improved floor layouts and work settings. A number of significant results were found by optimization of environmental measures through the design process.

EBD can help eliminate hospital-acquired infections through better control of the three most significant vehicles for transmission: air, contact, and water. The most important design measures for infections controls are: (1) effective air quality control measures during construction and renovation using high-efficiency particulate air filters (HEPA) filtration and installation of barriers isolating construction areas (minimize airborne transmission); (2) installation and use of alcohol-based handrub dispensers at the bedside and other accessible locations (minimize contact transmission); (3) easy to clean floor, wall, and furniture coverings (minimize contact transmission);

(4) water system maintained at proper temperatures with adequate pressure to minimize stagnation and backflow (minimize waterborne transmission); and (5) single-bed rooms with private toilets for better patient isolation (minimize airborne and contact transmission).

Medical errors may be reduced through control of several environmental factors including noise, light, and acuity-adaptable single-patient rooms. Noise, both as unacceptable background and episodic interruptions, is responsible for loss of concentration, slower learning, and poor memorization. Additionally excessive noise adversely impacts patient recovery by increasing stress and interrupting sleep. Lighting levels impact task performance, which in a hospital may result in transcription errors [44]. Conversely, better lighting and daylighting design results in improved patient care and outcomes, staff satisfaction, safety, and decreased operational costs [45]. The acuity-adaptable rooms have adequate square footage in the room to accommodate several clinical activities without moving the patient, well-defined zones for patient care activities, strategic placement of handwashing sink and handrub dispensers, convenient access to medical supplies, headwalls designed with adequate critical care services, maximum patient visibility, and patient lifts to ease strain on staff. Another desirable feature is a family zone so that a visitor is able to stay with the patient comfortably [46] (Fig. 5).

Indoor Environmental Quality and Health Improvement, Evidence-Based Design for. Figure 5
Acuity-adaptable, well-lit hospital rooms improve patient care and staff satisfaction

Studies are showing that patient pain levels and length of hospital stays can be reduced by exposure to nature and exposure to higher levels of daylight [47]. Walch et al. [48] found that spinal surgery patients in bright daylight lit rooms required 22% less opioid-equivalent analgesic medications than those in rooms without the bright daylight. Beauchemin and Hays [49] found that myocardial infarction patients in bright daylight lit rooms had shorter hospital stays of at least a day shorter. Ulrich [50] showed that surgery patients with views of nature had reduced hospital stays and used lower levels of pain medicine. EBD reveals that providing patients with high levels of daylight and views of nature (even if only pictures of nature if access to actual outdoor views are not possible) offers an opportunity to reduce patient pain medicine use and length of hospital stays, improving overall patient outcomes.

Reduction in ambient noise levels has been shown through EBD studies to improve patient sleep and reduce patient stress [51, 52]. For example, studies have shown reduced wound healing with exposure to noise, primarily attributed to increased levels of stress [53, 54]. EBD strategies that are applicable to noise control in hospitals include single-patient rooms, use of high-performance sound absorbing materials (although these must be easily cleanable), reduced noise from carts in the hallways, and noiseless paging systems.

EBD has led to improvements in staff workspace design as well as in patient care. EBD reveals that staff workspace needs to be designed with closer alignment to work patterns to improve staff satisfaction, productivity, and reduce stress reduction, which in turn will improve patient outcomes [38]. Potential design features may include decentralized nursing stations, more efficient layouts that allow staff interaction with patients and family members, and decentralized supply locations. Early EBD studies also reveal that the location of family members near the patients may also improve patient outcomes and reduce hospital stay lengths [55].

Economic Performance

Salaries and worker benefits generally exceed energy costs by approximately a factor of 100 [56]. Healthy,

high-performance sustainable buildings that are based on EBD principles have a strong potential to have positive economic performance, as long as the EBD design principles meet the organizational and health needs of the users as well as sustainable design principles. Therefore, a significant potential exists for businesses and building owners to employ EBD principles that improve worker performance, improve health, reduce health insurance costs, and reduce absenteeism.

Heerwagen [57] examined the range of benefits of green building features and attributes in buildings. She found that

- Green buildings are relevant to business interests across the full spectrum of concerns, from portfolio issues to enhanced quality of individual workspaces.
- Outcomes of interest that research should address include workforce attraction and retention, quality of work life, work output, and customer relationships.
- Green buildings can provide both cost reduction benefits and value added benefits.
- The benefits are most likely to occur when the building and organization are treated as an integrated system from the initiation of the design process, as in Evidence-Based Design approaches.

The Carnegie Mellon Center for Building Performance and Diagnostics (CBPD) and the Advanced Building Systems Integration Consortium have developed a decision support tool (The Building Investment Decision Support Tool – BIDS) to enable building decision makers to calculate returns on investments in high-performance building systems and to advance the understanding of the relationship between land use and buildings and health [56]. BIDS is based on a collection of building case studies as well as laboratory and simulation study results to statistically link the quality of buildings. BIDS uses "soft" and hard life-cycle costs to calculate the return on investment. The diverse building-related costs in the USA, including salaries and health benefits, technological and spatial turnover, rent, energy, and maintenance costs, normalized in dollars per person per year, are shown in Fig. 6.

Using statistics from the Bureau of Labor Statistics, the CBPD [56] calculated that the average employer health insurance cost was approximately $5,000 per employee per year in 2003. The CBPD went on and linked the cost of several specific health conditions and illnesses to IEQ (colds, headaches, respiratory illnesses, musculoskeletal disorders, and back pain), which account for approximately $750 of the $5,000 annual costs per employee – 14% of all annual health insurance expenditures. These direct costs would be additionally multiplied by the indirect costs of lost productivity. The results from employing BIDS provide the impetus to demonstrate the financial benefits of using EBD to design better building environments.

Fisk and Seppanen [58] demonstrated a benefit-cost ratio as high as 80 and an annual economic benefit as high as $700 per person when measures are made to improve indoor temperature control and increased ventilation rates based on a review of the existing literature of the health linkages between temperature control and increased ventilation rates. Table 1 shows the estimated productivity gains as a result of four categories of sources.

Application to Other Types of Facilities

The in-depth studies to support EBD in healthcare settings are readily adaptable to other types of facilities, particularly K-12 schools, including methods for infection control, better lighting, access to views and daylighting, improved acoustical performance, interior workspace layouts, and community design. The application of EBD in conjunction with sustainable design should result in optimal facilities for learning, healthcare, and work with maximum emphasis on human and ecological health as well as economic performance.

Schools

The impact of environmental design on the educational performance of students in the UK was investigated by Edwards [59]. In this study, Edwards investigated if "green" schools provide teaching and learning benefits beyond those in conventional schools, and what aspects of classroom design appear to be most critical in improving enhanced educational performance. Green schools were defined as being resource efficient particularly in terms of energy use; healthy both physically and psychologically; comfortable, responsive, and flexible; and based on ecological principles. In the study of

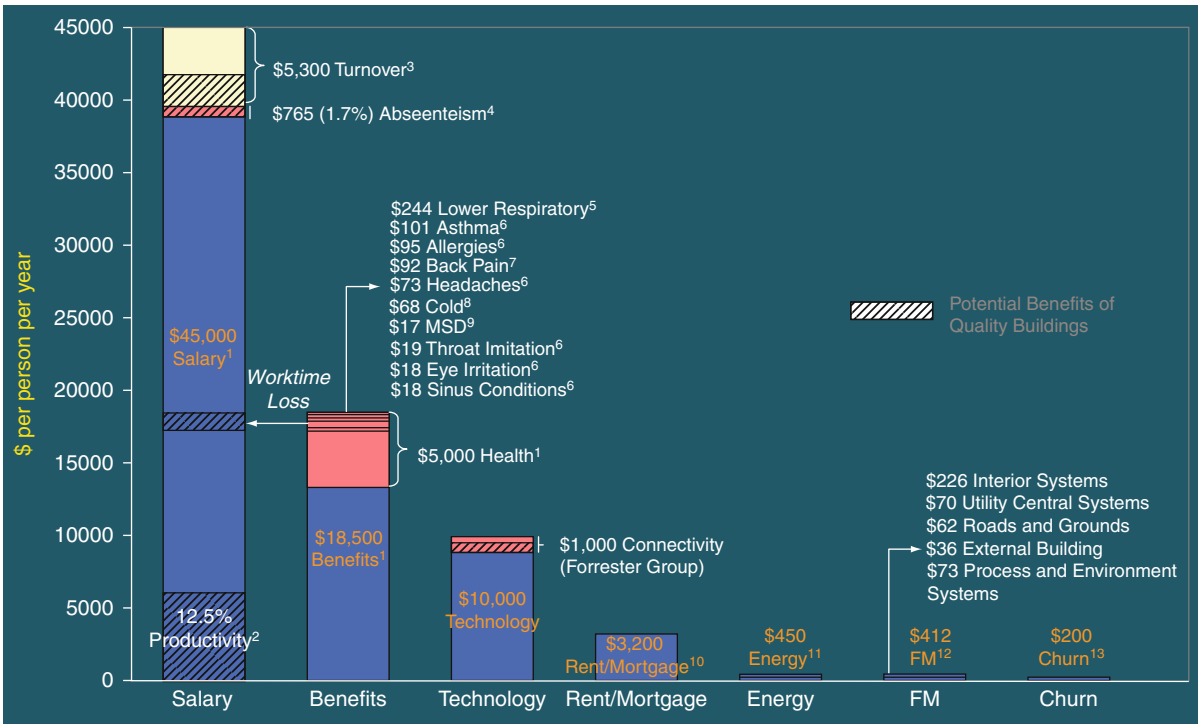

Indoor Environmental Quality and Health Improvement, Evidence-Based Design for. Figure 6
The true cost of least-cost buildings in the USA (US baselines from CMU BIDS) [50]

Indoor Environmental Quality and Health Improvement, Evidence-Based Design for. Table 1 Estimated potential productivity gains [58]

Source of productivity gain	Potential annual health benefits	Potential US annual savings or productivity gain (1996 US $$)
Reduced respiratory illness	16–37 million avoided cases of common cold or influenza	$6–14 billion
Reduced allergies and asthma	8–25% decrease in symptoms within 53 million allergy sufferers and 16 million asthmatics	$1–4 billion
Reduced sick building syndrome symptoms	Health symptoms experienced frequently at work by ~15 million workers	$10–30 billion
Improved worker performance from changes in thermal environment and lighting	Not applicable	$20–160 billion

54 schools built between 1975 and 1995, it was demonstrated that there is relationship between design, energy conservation, and educational performance. Overall the study demonstrated that green schools resulted in enhanced student performance and greater teacher satisfaction with the greatest impact on elementary schools. Benefits were greater in the newer schools with higher levels of ventilation. Absenteeism was reduced in the green schools. The student performance improvement appeared to be particularly related to the

level of daylight in the classroom, but also the level of ventilation, the temperature control, and noise level controls.

Elzeyadi [60] conducted a study to develop the Green Classroom Toolbox with green design guidelines for retrofitting existing educational spaces. The guidelines are based on carbon neutrality metrics and student achievement metrics, developed from a meta-analysis of reported studies and energy modeling simulations. The guidelines center on best practices that increase productivity, comfort, and health of students in retrofitted classrooms; facilitate integrated design and cooperation between designers; reduce environmental impacts and move toward carbon neutrality environments in schools; and are a model for future replication and dissemination. The strategic categories relevant to building professionals are based on the USGBC LEED criteria (1) energy and atmosphere (envelope, lighting, HVAC, and ventilation); (2) materials and resources (site construction, structural, and nonstructural); (3) environmental quality (IAQ, comfort, and acoustics); (4) sustainable sites (density, light pollution, and transportation); and (5) water and waste (building fixtures, landscaping, and recycling). Elzeyadi's method examined the facility as a whole system. He used a framework that treated the students and the school environment as interdependent elements of a system. The system is comprised of "people" and "buildings" on the macro-scale and "buildings" and "environment" on the megascale. This study resulted in three primary decision support tools of evidence-based guidelines to help architects, school designers, and school/school system staff to make informed decisions for implementing green retrofit measures in classrooms. The first tool is a check list of best practices compiled from focus groups and interviews of affected and interested parties. The second tool is a prioritization guide that provides a comparative analysis and ranking of the best practices list (in Tool 1) based on their impacts on building energy consumption and carbon emissions. The third tool is a meta-analysis guide that links the Tool 1 best practices to their impact on student and staff health and performance in schools. All of the tools were based on the specific climates and school typologies of the Pacific Northwest in the USA. The primary reason found for adoption of the best practices in schools was energy conservation followed by providing improved IEQ and connections to nature, reflected in energy and atmosphere, IEQ, and materials and resources gains. Better IAQ, based on the meta-analysis, was found to positively impact occupants' performance in a range of 5–20% improvement. This included reduced illnesses, both chronic and acute, and improved performance on testing. Improved temperature control was found to improve student performance in the range of 3–10%. Access to views and daylighting improved student performance in the range of 5–20%. This study emphasizes the need for evidence-based design guidelines for schools, especially to focus on improving IAQ, improved temperature control, and access to views and daylighting. The manner in which the study was conducted simulates the evidence-design process – interaction between the designers and the users, studying best practices and strategies in other successful facilities, and implementing the practices expected to have the most positive impact based on all of the stakeholders needs.

Office Buildings and Other Types of Facilities

The Academy of Neuroscience for Architecture has applied evidence-based design practices to office building design – focusing on the previously enumerated parameters (1) air quality, (2) thermal comfort, (3) spatial comfort, (4) collaborative or teamspace, (5) visual comfort, (6) workstation comfort, (7) lighting quality, (8) noise control, and (9) security. In their office building study [61], conducted via post-occupancy questionnaires, it was found that the office design features that support security, wayfinding, and feeling part of a cohesive organization created increased satisfaction and "workability" (considered to be neuro-environmental factors) among the employees over their previous office space. This was hypothesized to result in reducing stress, improving attention, focus, and mood. The office space design features included a centralized three-story open stairway connecting the three office floors, providing a naturally mapped sense of place, a "public square" housing centralized communications and meeting areas, a main entry area, centralized lunchroom, well-labeled directional signage, and use of porcelain tile paving across primary transit areas.

The Academy of Neuroscience for Architecture [62] also conducted a limited intervention study exploring the potential applications of neuroscience concepts and evidence-design based methods to correctional facilities. The specific focus topics were (1) daylight and views, (2) exposure to nature, (3) space size, (4) ambient noise levels, (5) color, and (6) environmental design features and their impact on inmate–staff relationships – reducing stress and aggressive behaviors. The overall goal of the study was to develop evidence-based design decisions for correctional settings and operations. The results of this study seemed to indicate that views of nature was the most effective measure of stress reduction, even if they were only projected nature views on a wall.

Future Directions

It is critical that EBD be applied much more widely across the spectrum of buildings. EBD has a tremendous potential to set a new paradigm for designing healthy, sustainable buildings, by including the building managers and occupants as a central player in the entire system's resolution of ecological and human health.

Even in the limited time that evidence-based design has been embraced, the data demonstrate important shifts for the building design and management community. For example, the need for increased ventilation rates significantly above those currently being used in the majority of buildings demands the development and implementation of innovative solutions that simultaneously meet reduced energy usage and cost. These include systems that separate ventilation and thermal conditioning, and new HVAC system types, such as underfloor air distribution and chilled beams. These also include improvements in system maintenance, such as the application of the ASHRAE Indoor Air Quality Procedure (IAQP) employing gaseous phase filtration to aid in air cleaning so that the ventilation level can be reduced. Ongoing research in more effective technologies and systems management is critical.

Future research must also include the development of protocols and metrics to accurately and realistically measure human impact improvements in health and productivity/learning, operational efficiencies, and sustainability. These metrics must consider the entire system in the occupied setting and not a just a single unit of the system. Metrics in specific will greatly aid in providing the necessary parameters for effective EBD studies in a wide range of buildings.

In the future, disparities between sustainable design practices and EBD will need to be resolved. Many practices are fully concurrent, but there are still areas where there is conflict, such as lack of acoustical satisfaction in open office planning and the potential energy costs of higher rates of ventilation for improved health and productivity/learning.

EBD takes the first step in rigorous research of "real" buildings by actively engaging in feedback through occupant questionnaires, and pursuing multi-configuration studies (in the form of layout or building system variations) or multi-building studies for comparative evaluation by end users. The lack of consistent feedback from building occupants and managers in the building design community has led for far too long to anecdotal design decision making, either in the form of untested shifts (such as open classrooms) or a dogged commitment to the status quo. EBD is an invaluable step forward, employing a range of post-occupancy tools – both qualitative and quantitative – to develop design innovations for human and environmental and economic benefit. EBD does not eliminate the need for controlled experimentation, both in the lab and in the field, to advance innovations in building materials, components, and systems design and operation.

Summary/Conclusions

The use of Evidence-Based Design to improve the IEQ in buildings has the potential to significantly impact the total health, productivity, learning, operational efficiency, and economic performance of a facility and its occupants. To begin with, a wide variety of studies have shown the importance of a connection to nature through access to views and daylighting to reduce stress, improve patient outcomes, improve health, and increase productivity. In the available literature, this connection to nature may be the most important design feature for overall impact studied to date. Secondly, an improved, innovative ventilation system has been shown to be critical to improving health and

productivity in buildings, of at least 25 L/s per person. Thirdly, the separation of temperature control from the ventilation system is another important component for improving thermal comfort without compromising ventilation air delivery. Finally, acoustical control is one of the most challenging parameters for EBD innovation, yet critically needed to achieve occupant satisfaction, stress reduction, and optimum learning in schools. EBD combined with sustainable design principles is an important tool for retrofitting and designing healthy, high-performance buildings.

Bibliography

1. The Center for Health Care Design (2008) Defined on their website http://clinicdesign.healthdesign.org/about#cfhd. Accessed 26 Jan 2011
2. Vischer JC (2009) Applying knowledge on building performance: from evidence to intelligence. Intell Build Int 2009: 239–248
3. WHO (1948) Preamble to the Constitution of the World Health Organization as adopted by the International Health Conference, New York, 19–22 June, 1946; signed on 22 July 1946 by the representatives of 61 States (Official Records of the World Health Organization, no. 2, p. 100) and entered into force on 7 April 1948
4. Lawson B (2010) Healing architecture. Arts Health Int J Res Policy Pract 2(2):95–108
5. Hartkofp V, Loftness V, Mahdavi A, Lee S, Shankavaram J (1997) An integrated approach to design and engineering of intelligent buildings – The intelligent workplace at Carnegie Mellon University. Autom Constr 6:401–415
6. Rashid M, Zimring C (2008) A review of the empirical literature on the relationships between indoor environment and stress in health care and office settings. Environ Behav 40(2):151–190
7. McEwen BS, Stellar E (1993) Stress and the individual. Mechanisms leading to disease. Arch Intern Med 157:2093–2101
8. Kaarlela-Tuomaala AA, Helenius RR, Keskinen EE, Hongisto VV (2009) Effects of acoustic environment on work in private office rooms and open-plan offices - longitudinal study during relocation. Ergonomics 52(11):1423–1444
9. Muehleisen RT (2010) Acoustics of green buildings, implications. A newsleter by InformeDesign vol 8(1). www.informedesign.umn.edu. Accessed 3 Oct 2010
10. Nabelek AK, Robinson PK (1982) Monaural and binaural speech-perception in reverberation for listeners of various ages. J Acoust Soc Am 71(5):1242–1248
11. Ryherd EE, Wang LM (2008) Implications of human performance and perception under noise conditions on indoor noise criteria. J Acoust Soc America 124(1):218–226
12. Ryherd EE, Wang LM (2007) Effects of exposure duration and type of task on subjective performance and perception in noise. Noise Control Eng J 55(1):334–347
13. Wilkins KK, Wolkoff PP, Knudsen HN, Clausen PA (2007) The impact of information on perceived air quality –"organic" vs. "synthetic" building materials. Indoor Air 17(2):130–134
14. Wolkoff PP, Wilkins CK, Clausen PA, Nielsen GD (2006) Organic compounds in office environments – sensory irritation, odor, measurements and the role of reactive chemistry. Indoor Air 16(1):7–19
15. Loftness V, Hartkopf V, Gurtekin B, Hansen D, Hitchcock R (2003) Linking energy to health and productivity in the built environment. Presented at the 2003 Greenbuild Conference, Chicago, IL, Nov 2003
16. Okcu S, Ryherd E, Bayer C (2011) The role of the physical environment on student health and education in green schools. Rev Environ Health (submitted)
17. Azuma K, Uchiyama IIK (2008) The regulations for indoor air pollution in Japan: a public health perspective. J Risk Res 11:301–314
18. Koistinen K, Kotzias D, Kephalopoulos S, Schlitt C, Carrer P, Jantunen M, Kirchner S, McLaughlin J, Mølhave L, Fernandes EO, Seifert B (2008) The INDEX project: executive summary of a European Union project on indoor air pollutants. Allergy 63:810–819
19. Olesen BW (2004) International standards for the indoor environment. Indoor Air 14:18–26
20. Kristen K (2005) California looks at tackling indoor air quality. Environ Sci Technol 39:256A
21. Spengler JD, Chen Q (2000) Indoor air quality factors in designing a healthy building. Ann Rev Energy Environ 25:567–601
22. Liddament MW (2000) A review of ventilation and the quality of ventilation air. Indoor Air 10:193–199
23. Wargocki P, Wyon DP (2007) The effects of moderately raised classroom temperatures and classroom ventilation rate on the performance of schoolwork by children (RP-1257). HVAC&R Res 13(2):193–220
24. Wargocki P, Wyon DP (2006) Effects of HAVC on student performance. ASHRAE J 48:22–28
25. Wyon DP, Wargocki P (2005) Room temperature effects on office work. In: Clements-Croome D (ed) Creating the productive workplace, 2nd edn. Taylor and Francis, London, pp 181–192
26. Tanabe Shin-ichi, Kobayashi K, Kiyota O, Nishihara N, Haneda M (2009) The effect of indoor thermal environment on productivity by a year-long survey of a call centre. Intell Buildings Int 1:184–194
27. Milton DK, Glencross PM, Walters MD (2000) Risk of sick leave associated with outdoor air supply rate, humidification, and occupant complaints. Indoor Air 10(4):212–221
28. Shendell DG, Prill R, Fisk WJ, Apte MG, Blake D, Faulkner D (2004) Associations between classroom CO_2 concentrations and student attendance in Washington and Idaho. Indoor Air 14(5):333–341
29. Sundell J, Levin H, Nazaroff WW, Cain WS, Fisk WJ, Grimsrud DT, Gyntelberg F, Li Y, Persily AK, Pickering AC, Samet JM, Spengler JD, Taylor ST, Weschler CJ (2010) Ventilation rates and health: multidisciplinary review of the

scientific literature. *Indoor Air*, an accepted article, Available online at http://onlinelibrary.wiley.com/doi/10.1111/j.1600-0668.2010.00703.x/pdf. Accessed 27 Jan 2011

30. Haverinen-Shaughnessy U, Moschandreas DJ, Shaughnessy RJ (2010) Association between substandard classroom ventilation rates and students' academic achievement. Indoor Air, Article first published online: 28 Oct 2010. http://onlinelibrary.wiley.com/doi/10.1111/j.1600-0668.2010.00686.x/pdf
31. Wargocki P, Sundell J, Bischof W, Brundrett G, Fanger PO, Gyntelberg F, Hanssen SO, Harrison P, Pickering A, Seppanen O, Wouters P (2002) Ventilation and health in non-industrial indoor environments: report from a European Multidisciplinary Scientific Consensus Meeting (EUROVEN). Indoor Air 12:113–128
32. Baron RA, Rea MS, Daniels SG (1992) Effects of indoor lighting (illuminance and spectral distribution) on the performance of cognitive tasks and interpersonal behaviors: the potential mediating role of positive affect. Motiv Emotion 16:1–33
33. Magee GH (1988) Facilities maintenance management. R.S. Means, Kingston
34. Bayer C, Hendry RJ, Cook A, Downing C, Crow SC, Hagen S, Fischer JC (2002) Active humidity control and continuous ventilation for improved air quality in schools. Presented at the DOE integrated energy systems peer review meeting, Nashville, TN, April 30–May 2 2002
35. Wargocki P, Wyon DP, Fanger PO (2004) The performance and subjective responses of call-center operators with new and used supply air filters at two outdoor air supply rates. Indoor Air 14(Suppl 8):7–16
36. Arditi D, Nawakorawit M (1999) Designing building for maintenance: Designer's perspective. J Architect Eng 5(4):107–116
37. Molhave L, Bach B, Pederson OF (1986) Human reactions to low concentrations of volatile organic compounds. Environ Int 12:167–175
38. Smith SW, Rea MS (1982) Performance of a reading test under different levels of illumination. J Illum Eng Soc 1:29–33
39. Veitch JA (1990) Office noise and illumination effects on reading comprehension. J Environ Psychol 10:209–217
40. Heerwagen J, Zagreus L (2005) The human factors of sustainable building design: post occupancy evaluation of the Philip Merrill Environmental Center, Annapolis, MD. Report for Drury Crawley, US Department of Energy, Building Technology Program. http://www.cbe.berkeley.edu/research/publications.htm
41. Bayer CW (2009) Unpublished work on IAQ investigations in Atlanta elementary schools
42. Anderson K (2004) The problem of classroom acoustics: the typical classroom soundscape is a barrier to learning. Semi Hear 25:117–129
43. Ulrich RS, Zimring C, Zhu X, DuBose J, Seo HB, Choi YS, Quan X, Joseph A (2008) A review of the research literature on evidence-based healthcare design. Health Environ Res Des J 1(3):101–532
44. Buchanan TL, Barker KN, Gibson JT, Jiang BC, Pearson RE (1991) Illumination and errors in dispensing. Am J Hosp Pharm 48(10):2137–2145
45. Zigmond J (2006) Built-in benefits. Mod Healthc 36(11):30–38
46. Lipschutz LN (2008) Acuity-adaptable rooms: design considerations can improve patient care. Healthcare Construction and Operations, Jan/Feb 10–11
47. Malenbaum S, Keefe FJ, Williams AC, Ulrich R, Somers TJ (2008) Pain in it environmental context: implications for designing environments to enhance pain control. Pain 134:241–244
48. Walch JM, Rabin BS, Day R, Williams JN, Choi K, Kang JD (2005) The effect of sunlight on postoperative analgesic medication use: a prospective study of patients undergoing spinal surgery. Psychosom Med 67:156–163
49. Beauchemin KM, Hays P (1998) Dying in the dark: sunshine, gender, and outcomes in myocardial infarction. J R Soc Med 91:352–354
50. Ulrich RS (1984) View through a window may influence recovery from surgery. Science 224:420–421
51. Topf M, Bookman M, Arand D (1996) Effects of critical care unit noise on the subjective quality of sleep. J Adv Nurs 24:545–551
52. Freedman N, Gazendam J, Levan L, Pack A, Schwab R (2001) Abnormal sleep/wake cycles and the effect of environmental noise on sleep disruption in the intensive care unit. Am J Respir Crit Care Med 163(2):451–457
53. Wysocki A (1996) The effect of intermittent noise exposure on wound healing. Adv Wound Care 9(1):35–39
54. Toivanen S, Hulkko S, Naatanen E (1960) Effect of psychic stress and certain hormone factors on the healing of wounds in rats. Ann Med Exp Bio Fenn 38:343–349
55. France D, Throop P, Joers B, Allen L, Parekh A, Rickard D, Deshpande JK (2009) Adapting to family-centered hospital design: changes in providers' attitudes over a two-year period. Health Environ Res Des J 3:79–96
56. Loftness V, Hartkopf V, Poh LK, Snyder M, Hua Y, Gu Y, Choi J, Yang X (2006) Sustainability and health are integral goals for the built environment. Presented at the 2006 Healthy Buildings Conference, Lisbon, Portugal, 4–8 June 2006
57. Heerwagen J (2000) Green buildings, organizational success and occupant productivity. Build Res Inf 28(5/6): 353–367
58. Fisk W, Seppanen O (2007) Providing better indoor environmental quality brings economic benefits. In: Proceedings of Clima 2007: well-being indoors. FINVAC, Helsinki, Finland, 10–14 June 2007
59. Edwards BW (2006) Environmental design and educational performance. Res Educ 76:14–32
60. Elzeyadi, Ihab MK (2008) Green classroom retrofit toolbox (GCRT): Evidence-based design guidelines to adapt K-12 school facilities for climate change. http://www.aia.org/aiaucmp/groups/aia/documents/pdf/aiab079900.pdf. Accessed 26 Jan 2011

61. Zeise J, Vischer J (2006) Executive summary: environment/behavior/neuroscience pre and post-occupancy evaluation of new offices for society of neuroscience. http://www.anfarch.org/pdf/SfNExecutiveSummary.pdf. Accessed 26 Jan 2011
62. Farbstein J, Farling M, Wener R (2009) The evidence for evidence-based design: nature views reduce stress in a jail intake area. Presented at The American Institute of Architects Annual Meeting, Orlando, FL, June 2009. http://www.aia.org/akr/Resources/Documents/AIAB086133?dvid=&recspec=AIAB086133. Accessed 26 Jan 2011

Infectious Disease Modeling

Angela R. McLean
Zoology Department, Institute of Emerging Infections, University of Oxford, Oxford, UK

Article Outline

Glossary
Definition of the Subject
Introduction
The SIR Model
Host Heterogeneity
Within-Host Dynamics
Multi level Models
Future Directions
Bibliography

Glossary

Basic reproductive number A summary parameter that encapsulates the infectiousness of an infectious agent circulating in a population of hosts.

Host An organism that acts as the environment within which an infectious agent replicates.

Infectious agent A microorganism that replicates inside another organism.

Pathogen An infectious agent that damages its host.

Variant One of several types of an infectious agent, often closely related to and sometimes evolved from other variants under consideration.

Definition of the Subject

Infectious disease models are mathematical descriptions of the spread of infection. The majority of infectious disease models consider the spread of infection from one host to another and are sometimes grouped together as "mathematical epidemiology." A growing body of work considers the spread of infection within an individual, often with a particular focus on interactions between the infectious agent and the host's immune responses. Such models are sometimes grouped together as "within-host models." Most recently, new models have been developed that consider host–pathogen interactions at two levels simultaneously: both within-host dynamics and between-host transmissions. Infectious disease models vary widely in their complexity, in their attempts to refer to data from real-life infections and in their focus on problems of an applied or more fundamental nature. This entry will focus on simpler models tightly tied to data and aimed at addressing well-defined practical problems.

Introduction

Why is it that smallpox was eradicated in 1979 [1] but measles, once scheduled for eradication by the year 2000, still kills over a hundred thousand children each year [2]? Both diseases can be prevented with cheap, safe, and effective vaccines which probably induce lifelong immunity, and neither virus has an environmental or animal reservoir.

One way to address this question is to consider the comparative ease of spread of the two infections. A useful parameter that summarizes this ease of spread is the "basic reproductive number" always denoted as R_0. The definition of the basic reproductive number is the number of secondary infections caused during the entire duration of one infection if all contacts are susceptible (i.e., can be infected). The concept has widespread currency in the literature on infectious disease models with varying degrees of affection [3]. There is no question that it has been a useful, simple rule of thumb for characterizing how easily an infection can spread [4]. Furthermore, the simplest of calculations relate R_0 to the degree of intervention needed to bring an infection under control and, eventually, eradicate it. The relationship between the basic reproductive number and disease control arises from the simple fact that if each infectious person causes less than one secondary case, then the number of infections must fall. If it is always true, even when there is no infection circulating,

that each new case causes less than one secondary case, then the infection will die out. This simple observation leads to a straightforward calculation for the proportion of a population that must be vaccinated in order to achieve eradication, p_c:

$$p_c = 1 - \frac{1}{R_0} \tag{1}$$

This relationship arises from the fact that if $(R_0 - 1)$ out of the R_0 people a case might have infected have been vaccinated, then each case, in a population vaccinated to that degree, will cause less than one secondary case. For example, say $R_0 = 10$, if 9/10 of the population are successfully immune following vaccination, then infection cannot spread. Thus, in general, $p_c = (R_0 - 1)/R_0$, as stated in Eq. 1. If the fraction of the population that are successfully vaccinated is greater than p_c, then each case will cause, on average, less than one case, and infection cannot spread.

Comparing estimated values for R_0 for measles and smallpox and inferred values for the proportion that need to be vaccinated to ensure eradication (Table 1) leads to a simple answer to the question why has smallpox been eradicated, but not measles? Smallpox, with a basic reproductive number around three, was eradicated with vaccination coverage of around 67%. The higher R_0 for measles, nearer to 15, requires vaccination coverage close to 95% to ensure eradication. Many parts of the world remain unable to achieve such high coverage; measles remains suppressed by tremendous efforts at vaccination but is not yet eradicated.

These calculations are so straightforward that they can be made without recourse to any formal modeling. However, embedding these ideas inside a formal modeling framework has proven very useful. The next section describes the simplest applicable model.

Infectious Disease Modeling. Table 1 The basic reproductive number, R_0, and the critical vaccination proportion for eradication, p_c, for measles and smallpox

Infection	Place	Time	R_0	p_c (%)
Smallpox	India	1970s	3	67
Measles	India	1970s	15	93
Measles	UK	1960s	15	93

The SIR Model

The "plain vanilla" model of mathematical epidemiology is called the SIR model because it splits the host population into three groups:

- The susceptible (S) can be infected if exposed
- The infectious (I) are both infected and infectious to others
- The recovered (R) are no longer infectious and are immune to further infection

The SIR model's structure then consists of a set of assumptions about how people flow into, out of, and between these three groups. Those assumptions can be represented graphically as in Fig. 1.

The assumptions of the SIR model with vaccination are the following: People are born at a constant rate B, and a proportion p of them are vaccinated at birth. Vaccinated newborns are immune for life and so they join the recovered class. Unvaccinated newborns enter the susceptible class. Susceptibles are infected at a per capita rate proportional to I, the number of infectious people in the population. This gives rise to a transfer from the susceptible to the infectious class at rate βIS. Susceptibles are also subject to a per capita background death rate μ. Infectious people recover into the recovered class I at per capita rate γ or die at the per capita background death rate μ. Recovered individuals are immune for the rest of their lives, so the only exit from the recovered class is at the per capita background death rate μ.

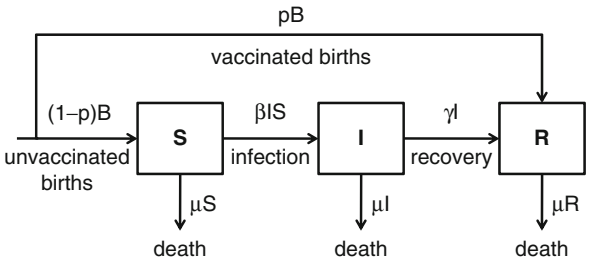

Infectious Disease Modeling. Figure 1
The SIR model in graphical form. The host population is divided into three groups, and transitions of people between those groups are described. Those transitions represent the five processes: birth, vaccination, death, infection, and recovery

These assumptions can be written in several different forms of equations, for example, difference equations, ordinary differential equations, or stochastic differential equations. The difference equation form is as follows:

$$S(t+1) = S(t) + (1-p)B - \beta I(t)S(t) - \mu S(t) \quad (2)$$

$$I(t+1) = I(t) + \beta I(t)S(t) - \gamma I(t) - \mu I(t) \quad (3)$$

$$R(t+1) = R(t) + pB + \gamma I(t) - \mu R(t) \quad (4)$$

This difference equation form is particularly easy to handle numerically and can be straightforwardly solved in a spreadsheet. Figure 2a shows the solutions to Eqs. 2–4 over 50 years with a 1-week timestep. Parameters are set so that an infection with a basic reproductive number of 5 and a 1-week duration of infection is spreading in a population of 100,000 individuals. The figure illustrates how this model shows damped oscillations towards a stable state. The same is true for the ODE version of this model.

This model is useful for understanding the impact of vaccination. In Fig. 2b, the solutions to Eqs. 2–4 are shown when vaccination at birth is introduced 10 years into the model run. With a basic reproductive number of 5, Eq. 1 tells us that vaccination of over 80% of newborns will lead to eradication. This is exemplified in the pink line where 90% vaccination leads to no further cases. Vaccination coverage below this threshold value reduces the numbers of cases and increases the inter-epidemic period but does not lead to eradication. Notice the very long inter-epidemic period at 70% vaccination. This phenomen occurs when vaccine coverage levels are close to but do not achieve the critical coverage level. Under these circumstances, it takes a very long time to accumulate enough susceptibles to trigger the first epidemic after vaccination is introduced. It may therefore appear as though eradication has been achieved even though vaccination coverage is below the critical level. This phenomenon, named "the honeymoon period," [5] was first described in modeling studies and later identified in field data [6].

The ability to identify target vaccination levels predicted to lead to disease eradication has been widely influential in policy circles [7]. Models with the same fundamental structure as the SIR model are used to set targets for vaccination coverage in many settings [8]. Similar models are also used to understand the likely impact of different interventions of other sorts, for example, drug treatment [9] or measures for social distancing [10]. However, models for informing policy need to explore more of the wrinkles and complexities of the real world than are acknowledged in the simple equations of the SIR model. The next section describes some of the types of host heterogeneity that have been explored in making versions of the SIR model that aim to be better representations of the real world.

Host Heterogeneity

There are many aspects of host heterogeneity that have bearing on the transmission and impact of infections. Two of the most important are host age and spatial distribution. In this section, the modeling of these two types of host heterogeneity is introduced with reference to two specific infections: rubella and foot-and-mouth disease.

Rubella is a directly transmitted viral infection that usually causes mild disease when contracted during childhood. However, infection of a woman during early pregnancy can lead to serious birth defects for her unborn child. The set of consequent conditions is labeled "congenital rubella syndrome" or CRS. Because vaccination acts to extend the time between epidemics (Fig. 1b), it also acts to increase the average age at infection. This sets up a complex trade-off when introducing rubella vaccination to a community. On the one hand, vaccinated girls are protected from catching rubella at any age, but on the other hand, the girls who remain unvaccinated are likely to catch rubella when they are older, more likely to be in their childbearing years and so at greater risk of CRS. This means that vaccination with low coverage can actually lead to more CRS, and only when coverage levels get above a certain level do the benefits of vaccinating the community outweigh the costs. Calculating where that level lies then becomes an important public health question.

Because age is such an important component of the risks associated with rubella infection, models of this system need to take account of host age. The relevant versions of Eqs. 2–4 are difference equations with two independent variables, age (a) and time (t):

$$S(a+1, t+1) = S(a,t) - S(a,t)[\Sigma_{a'}\beta(a,a')I(a,t)] - \mu(a)S(a,t) \quad (5)$$

I

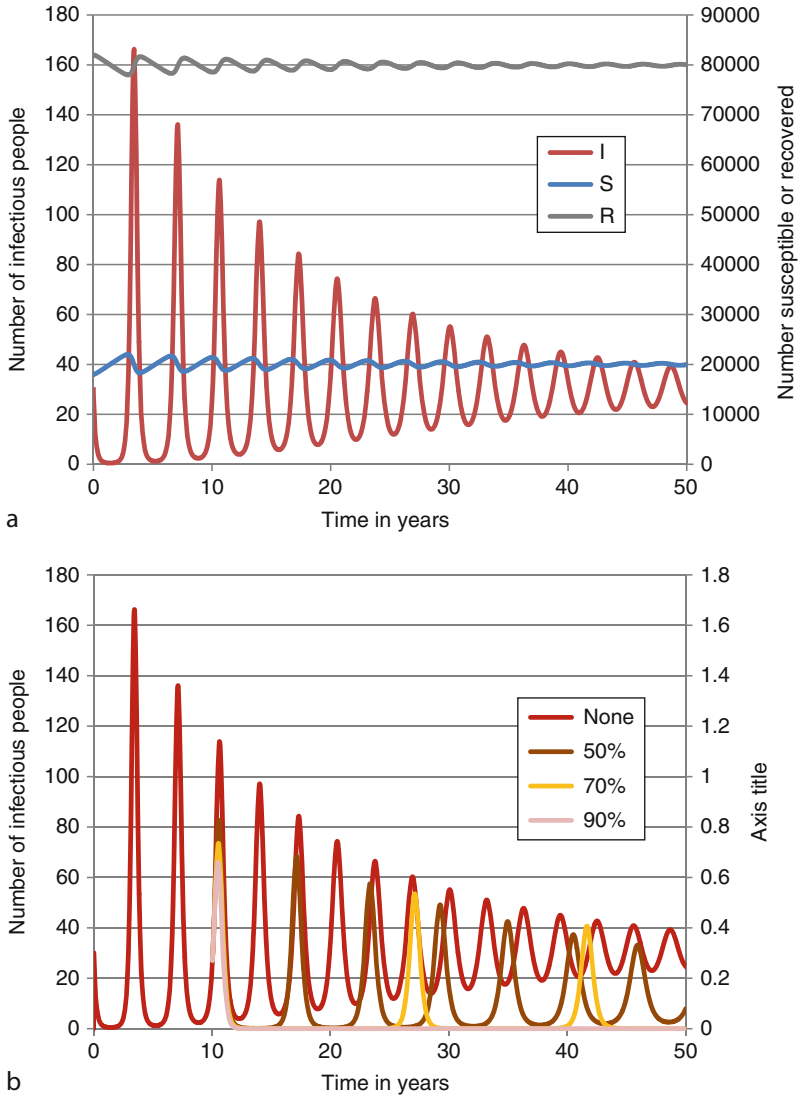

Infectious Disease Modeling. Figure 2

Numerical solutions to the SIR difference equation model. Infection circulates in a population of 100,000 individuals, with an expectation of life at birth of 50 years. The infectious period is 1 week, and the basic reproductive number is 5. This gives the following model parameters: B = 38 per week, μ = 0.00385 per person per week, γ = 1 per person per week, and β = 0.00005 per infected per susceptible per week. (**a**) shows damped oscillations in all three classes after an initial perturbation of 20% of the susceptible class into the recovered class. In (**b**), vaccination of 50%, 70%, or 90% of newborns is introduced at time 10 years. With $R_0 = 5$, the critical vaccination proportion $p_c = 0.8$. Vaccination coverage above this level (at 90%) leads to eradication

$$I(a+1,t+1) = I(a,t) + S(a,t)[\Sigma_{a'}\beta(a,a')I(a,t)] - \gamma(a)I(a,t) - \mu(a)I(a,t) \quad (6)$$

$$R(a+1,t+1) = R(a,t) + \gamma(a)I(a,t) - \mu(a)R(a,t) \quad (7)$$

Notice how these equations, by taking account of age as well as time, allow consideration of several different kinds of age dependence. Firstly, Eq. 6 calculates the number of cases of infection *of a given age* over time. Since the main consideration in balancing up the

pros and cons of rubella vaccination is the number of cases in women of childbearing age, this is an essential model output. Secondly, the per capita rate at which susceptibles become infected depends on their age and on the age of all the infected people. This model is thus able to take account of the complexities of family, school, and working life which drive people of different ages to age-dependent patterns of mixing. Thirdly, the recovery rate $\gamma(a)$ and, more importantly, the background death rate $\mu(a)$ can both be made to depend on age. Since a fixed per capita death rate is a particularly bad approximation of human survival, this is another important advance on models without age structure.

Models with age structure akin to that presented in Eqs. 5–7 have been essential components of the planning of rubella vaccination strategies around the world [11, 12]. A model as simple as these equations would never be used for formulating policy; furthermore, most age-structured models use the continuous time and age versions and so have the structure of partial differential equations. Nevertheless, Eqs. 5–7 illustrate the fundamentals of how to include age in an epidemiological model.

The spatial distribution of hosts is another important aspect of their heterogeneity. If the units of infection are sessile (e.g., plants), the assumption that all hosts are equally likely to contact each other becomes particularly egregious and models that acknowledge the spatial location of hosts more important. One example of units of infection that do not move is farms. If trade between farms has been halted because of a disease outbreak, then disease transmission between farms is likely to be strongly dependent upon their location. This was the case during the 2001 foot-and-mouth disease epidemic in the UK, and spatial models of that epidemic are nice examples of how to explicitly include the distance between hosts in a model epidemic.

On February 19, 2001, a vet in Essex reported suspected cases of foot-and-mouth disease (FMD) in pigs he had inspected at an abattoir. FMD is a highly infectious viral disease of cloven-hoofed animals. Because of its economic and welfare implications for livestock, FMD had been eradicated from Western Europe. The FMD outbreak that unfolded in the UK over the ensuing months had a huge impact with millions of farm animals killed and major economic impact in the countryside as tourism was virtually shut down.

There was heated debate about the best way to control the spread of infection from farm to farm. FMD virus is so very infectious that no attempt was made to control its spread within a farm. Once infection of livestock on a farm was detected, all susceptible animals were slaughtered. Mathematical models of the spread of this epidemic thus treat each farm as a unit of infection, and, as before, farms can be categorized as susceptible, infectious, etc. The best of these models [13] keeps track of every single farm in the United Kingdom, characterizing farms by their location and the number of sheep and cattle they hold. The model classifies farms into four groups: susceptible, incubating, infectious, or slaughtered. As in all epidemic models, the heart of the model is the per capita rate at which susceptible farms become infected – the so-called force of infection. Because this FMD model is an individual-based, stochastic simulation, it is not possible to write out its equations in a simple form as before, but the probability of infection for a single farm can easily be written.

Suppose all farms in the UK are listed and indexed with i. Then p_i, the probability that an individual farm i becomes infected during one unit of time, is:

$$p_i = \beta_i \Sigma_{\text{all infectious farms} j} \tau_j K(d_{ij}) \tag{8}$$

where β_i is the susceptibility of farm i, determined by the number of sheep and cows it holds; τ_j is the infectiousness of farm j, also determined by the number of sheep and cows it holds; and $K(d_{ij})$ is a function of the distance between the pair of farms i and j which determines how quickly infectiousness falls off with increasing distance. K is known as the "infection kernel." In the FMD example, the infection kernel was estimated from contact tracing data on farms that were sources of infection and their secondary cases. This observed relationship shows a very sharp falling off of infectiousness, with a farm just 2 km distant being less than tenfold as infectious to a susceptible farm than one that is adjacent.

This section describes just two of the possible heterogeneities that are often included when making models of the spread of epidemics. There is almost no end to how complex an epidemiological model can become. However, it is very easy for complex models

I

to outstrip the data available to calculate their parameters. In some cases, this can mean that models become black boxes concealing ill-informed guesswork, rather than prisms unveiling the implications of well-sourced and well-understood data.

Within-Host Dynamics

Mathematical models can also be used to investigate the dynamics of events that unfold within infected hosts. In these models, the units of study are often infected cells and immune cells responding to infection. As with epidemiological models, there is a wide range of modeling styles: Some models detail many different interacting components; others make a virtue of parsimony in their description of within-host interactions. In this section, a simple model of the within-host evolution of HIV is used to illustrate how pared-down, within-host models of infection can address important practical questions.

Several trials of prophylactic HIV vaccines have shown little or no effect [14–16], and understanding why these vaccines failed is a major research priority [17]. A quantitative description of the interaction between HIV and host immune cells would be an asset to such understanding. For one component of host immunity – the cytotoxic T cell (CTL) response – such a description can be derived. The question is how effective are host CTL responses at killing HIV-infected cells? Not how many CTLs are present, nor which cytokines they secrete, but how fast do they kill HIV-infected cells?

During the course of a single infection, HIV evolves to escape from the selection pressure imposed by host CTLs [18]. In this process, new HIV variants emerge that are not recognized by the host CTLs. These variants are called "CTL escape mutants." These CTL escape mutants can be seen to grow out in hosts who mount relevant CTL responses (Fig. 3) and to revert in hosts who do not. The rate of reversion in hosts without relevant CTL responses reflects the underlying fitness cost of the mutation. The rate of outgrowth in hosts who do mount relevant CTL responses is a balance between the efficacy of those responses and the fitness cost of the mutations. These costs and benefits need to be examined in the context of the underlying rate of turnover of HIV-infected cells. All this can be represented in a two-line mathematical model [19].

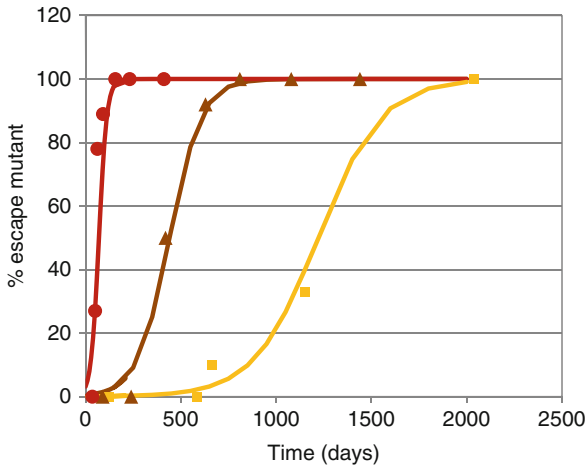

Infectious Disease Modeling. Figure 3
The outgrowth of HIV CTL escape mutants through time. Data sets from three different patients (reviewed in [19]) are shown as *red*, *brown*, and *yellow* symbols. Equation 12 is fitted to these data, yielding rates of outgrowth, $c-(a-\hat{a})$, of 0.048 (*red*), 0.012 (*brown*), and 0.006 (*yellow*)

Let x be the number of host cells infected with "wild-type" virus – that is, virus that can be recognized by the relevant host CTL responses. Let y be the number of host cells infected with escape mutant virus. The model then consists of a pair of ordinary differential equations describing the growth rate of each population of infected cells. The wild-type population grows at rate a, is killed by the CTL response in question at rate c, and is killed by all other processes at rate b. The escape mutant population grows at rate $\hat{a}$ ($\hat{a} < a$, reflecting the underlying fitness cost of the mutation) and is killed by all other processes at rate b. Escape-mutant-infected cells are not killed by the CTL response in question because of the presence of the escape mutation in the viral genome. These assumptions give rise to the following pair of linear ordinary differential equations:

$$x' = ax - bx - cx \tag{9}$$

$$y' = \hat{a}y - by \tag{10}$$

The observed quantity, call it p, is the fraction of virus that is of the escape mutant type; $p = y/(x + y)$. Simple application of the quotient rule for differentiation yields the single differential equation

$$p' = (c - (a - \hat{a}))p(1 - p) \tag{11}$$

with solution:

$$p = (k \exp(-(c - (a - \hat{a}))t) + 1)^{-1} \tag{12}$$

where for p_0, the fraction escaped at time 0:

$$k = \frac{(1 - p_0)}{p_0} \tag{13}$$

It is straightforward to fit the analytic expression (12) to data on the outgrowth of escape mutants to obtain estimates of the quantity $c - (a - \hat{a})$. Figure 3 shows fitted curves with estimates of $c - (a - \hat{a})$ of 0.048, 0.012, and 0.006. The quantity of interest is the parameter c – the rate at which CTL kills cells infected with wild-type virus. Fortunately, independent estimates of the fitness cost of the escape mutation $(a - \hat{a})$ are available. The median of several such observations yields $(a - \hat{a}) = 0.005$ [19]. Taken together and combined with further data, the inference is that on average, a single CTL response kills infected cells at rate 0.02 per day.

The half-life of an HIV-infected cell is about 1 day. This figure was itself derived from the application of elegantly simple models to data on the post-treatment dynamics of HIV [20, 21]. If a single CTL response kills infected cells at rate 0.02 per day and their overall death rate is one, then just 2% of the death of infected cells can be attributed to killing by one CTL response. Patients will typically mount many responses – but probably not more than a dozen. This analysis shows that even though CTL responses are effective enough to drive viral evolution, they are, in quantitative terms, very weak. A vaccine to protect against HIV infection would have to elicit immune responses that are manyfold stronger than the natural responses detected in ongoing infection. This simple, model-based observation greatly helps understand why the vaccines trialed so far have failed.

Multilevel Models

The models discussed so far deal either with events inside individuals or with transmission amongst individuals (people or farms) in a population. Some questions require simultaneous consideration of events at both levels of organization. This is particularly true for questions about the evolution of infectious agents as their evolution proceeds within individual hosts, but they are also transmitted between hosts. Models that capture events at both the within-host and between-host levels are fairly recent additions to the literature on infectious disease modeling. Here, they are illustrated with two examples, a set of models that consider the emergence of a zoonotic infection in humans and a model of the within-host evolution and between-host transmission of HIV.

Emerging infections are a continuing threat to human well-being. The pandemics of SARS in 2003 and H1N1 swine flu in 2009 illustrated how quickly a new infectious agent spreads around the world. Neither of these was as devastating as some predicted, but the continuing pandemic of HIV is ample proof that emerging infectious diseases can have devastating consequences for human communities. Many novel emerging infections arise as zoonoses – that is, infections that cross from animals into humans [22]. To become a successful emerging infection of humans – that is, one that spreads widely amongst people – is a multi-step process [23]. First, the pathogen must cross the species barrier into people, then it must transmit between people, and finally, it must transmit *efficiently enough* that epidemics arise. This latter step amounts to having a basic reproductive number, R_0, that is greater than 1. The emerging infections mentioned already, SARS, swine flu, and HIV, have transited all these steps. But there are other zoonoses that transmit to humans without emerging as epidemics or pandemics. For example, simian foamy virus, a retrovirus that is endemic in most old-world primates [24], can be detected in people who work with primates [25] or hunt them [26]. There is no record of any human-to-human transmission, implying that this zoonosis only completes the first step in becoming an emerging infection. Other infections, whilst spreading from person to person, still do not cause epidemics because that spread is insufficiently efficient. An example of such an infection is the newly discovered arenavirus from Southern Africa called "Lujo virus" [27]. This virus caused a small outbreak in the autumn of 2008. Very dramatically, four out of the five known cases died, but with five cases and just four transmission events, the basic reproductive number stayed below one, and there was no epidemic.

Acquiring $R_0 > 1$ is thus an important threshold that zoonoses must breach before they can become emerging infections. Antia and colleagues [28] developed an elegant model of the within-host evolution and between-host transmission of a zoonotic infection that initially has $R_0 < 1$, but through within-host adaptation in humans can evolve to become efficient enough at transmitting from one human to another that R_0 increases above 1 and epidemics become possible. They developed a multi-type branching process model of the transmission and evolution of a zoonosis. They found that the probability of emergence depends very strongly on the basic reproductive number of the pathogen as it crosses into humans. This is because, even when $R_0 < 1$, short chains of transmission are still possible (as exemplified with Lujo virus described above). During ongoing infections in humans, the zoonosis has opportunities to evolve towards higher transmissibility. The higher its initial R_0, the more opportunities there are for such ongoing evolution and hence for emergence.

This model of the emergence of a novel infection has been extended by other authors to address questions about the interpretation of surveillance data [29] and the role of host heterogeneity in the process of emergence [30]. These extensions confirm the original finding that the transmission efficiency (R_0) of the introduced variant (and any intermediate variants) is a very important driver of the probability of emergence. Kubiak and colleagues explored the emergence of a novel infection in populations split into several communities, with commuters acting to join those communities together. They found that most communities are sufficiently interconnected to show no effect of spatial distribution on the emergence process, even a small number of commuters being sufficient to successfully transmit any novel pathogen between settlements. Thus, although many zoonotic events happen in isolated parts of the world, unless they are really cut off from urban centers, that isolation offers little barrier to the transmission of newly emerged infections.

HIV emerged as a human infection sometime during the end of the 1800s and the early 1900s [31]. It was only recognized as a new human infection in the 1980s when cases of immunodeficiency in young Americans were unusual enough to warrant investigation [32]. As discussed above, during the course of a single infection, HIV is able to adapt to escape from the selection pressures imposed by its host's immune response. HIV variants that cannot be recognized by current host CTLs are termed "CTL escape mutants." These mutants yield important information about the strength of the immune responses that they evade. However, since they were shown to transmit from one host to another, their status has been raised to potential drivers of evolutionary change across the global HIV pandemic [33, 34].

Different hosts respond to different parts of HIV's proteins (known as epitopes). For CTL responses, it is the host class 1 human leukocyte antigen (HLA) type that determines which epitopes are recognized. When CTL escape mutants are transmitted into a host who does not make immune response to that epitope, the mutations are no longer advantageous, and the virus can revert to the wild type [35]. Global change in the prevalence of CTL escape mutants is therefore driven by three parallel processes: the selection of escape mutants in some hosts, transmission between hosts, and reversion of escape mutants in other hosts. Once again, this is a process that takes place across multiple levels of organization, evolution and reversion of escape mutations within infected hosts, and transmission between hosts.

Fryer and colleagues [36] developed a multilevel model of the three processes of within-host evolution, within-host reversion, and between-host transmission. The model is a version of the so-called SI model which is a simplified version of the SIR model presented above which does not allow recovery. The model allows heterogeneity in hosts and in the infecting virus so that there are hosts who do and do not mount immune responses to a given epitope and there are viruses that do and do not have escape mutations in that epitope. This model is represented in Fig. 4. As in the SIR model described in section "The SIR Model," the rate at which susceptibles become infected is determined by the number of infectious people present. However, in this model, because it represents the spread of a sexually transmitted disease, it is the proportion of hosts who are infectious that drives new infections. Furthermore, there are now two virus types circulating – wild type and escape mutant. Within-host adaptation allows hosts who do mount immune responses to the epitope to drive the evolution of escape mutants, and conversely, hosts who do not mount such responses can

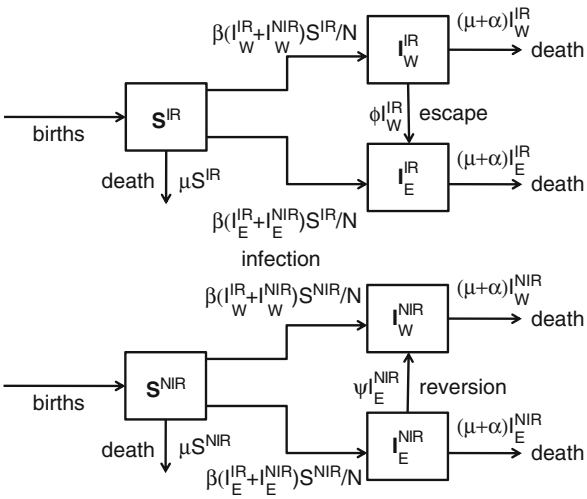

Infectious Disease Modeling. Figure 4
A model of the within-host evolution and between-host transmission of HIV escape mutants [36]. Hosts are divided into two types: immune responders (superscript IR) and nonimmune responders (superscript NIR). There are also two variants of virus, wild type (subscript WT) and escape mutant (subscript E). Hosts are either susceptible, S, or infectious, I, and the type of virus with which they are infected is denoted by the subscript. Rates of infection are determined by the number of people infectious with each virus type. Immune responding hosts infected with the wild-type virus drive immune escape at per capita rate ϕ, whilst nonimmune responding hosts infected with escape mutant virus drive reversion at per capita rate ψ. All hosts are prone to per capita death rate μ, and infected hosts have an additional death rate α

drive the reversion of escape mutant viruses back to the wild type.

This model's behavior is easy to understand. The total numbers of susceptible and infectious people simply follow the well-characterized SI model. Figure 5a shows total cases through time. The total epidemic goes through three phases: an initial exponential growth, a saturation phase, and then settling to a long-term equilibrium. Figure 5b shows the proportion of all cases that are escape mutants through time. Not surprisingly, faster escape rates and slower reversion rates lead to higher prevalence of escape mutants. Less intuitive are the following characteristics of Fig. 5b. Whilst the epidemic is in its exponential growth phase, so long as reversion rates are reasonably fast (say once in 10 years or faster), the prevalence of escape is expected to stabilize quite quickly. However, this is not a long-term equilibrium, and as the total epidemic turns over, the escape prevalence shifts again. For an epitope that escapes fast but reverts at an intermediate rate, this leads to a substantial drop in the prevalence of escape. Secondly, fixation of escape variants only occurs if they never revert, and even then fixation takes a very long time – much longer than it takes for the underlying epidemic to equilibrate. Thirdly, the predicted dynamics and equilibrium are very sensitive to the reversion rate when that is slow. Notice the big difference, in the long term, between no reversion (brown line) and average time to reversion of 50 years (yellow line).

As well as predicting the future spread of escape mutations for different rates of escape and reversion, this model can be used to infer escape and reversion rates from data on their current prevalence. This exercise reveals a surprisingly slow average rate of escape. Across 26 different epitopes, the median time to escape was over 8 years. There is close agreement between rates of escape inferred using this model and those estimated from a longitudinal cohort study. These slow rates are in marked contrast to the general impression given by a large number of case reports in which escape is described as occurring during the first year of infection. However, a collection of case reports is a poor basis upon which to estimate an average rate of escape.

These are just two examples from the new family of infectious disease models that encapsulate processes at multiple levels of organization. As data on pathogen evolution continues to accrue, this approach will doubtlessly continue to yield new insights.

Future Directions

It seems likely that infectious diseases will continue to trouble both individuals and communities. Whilst technological advances in new drugs, new vaccines, and better methods for surveillance will undoubtedly assist with the control of infection, several trends in society pull in the opposite direction. Chief amongst these is a growing population, and second is increasing population density as more and more people live in towns and cities. What can infectious disease modeling do to help?

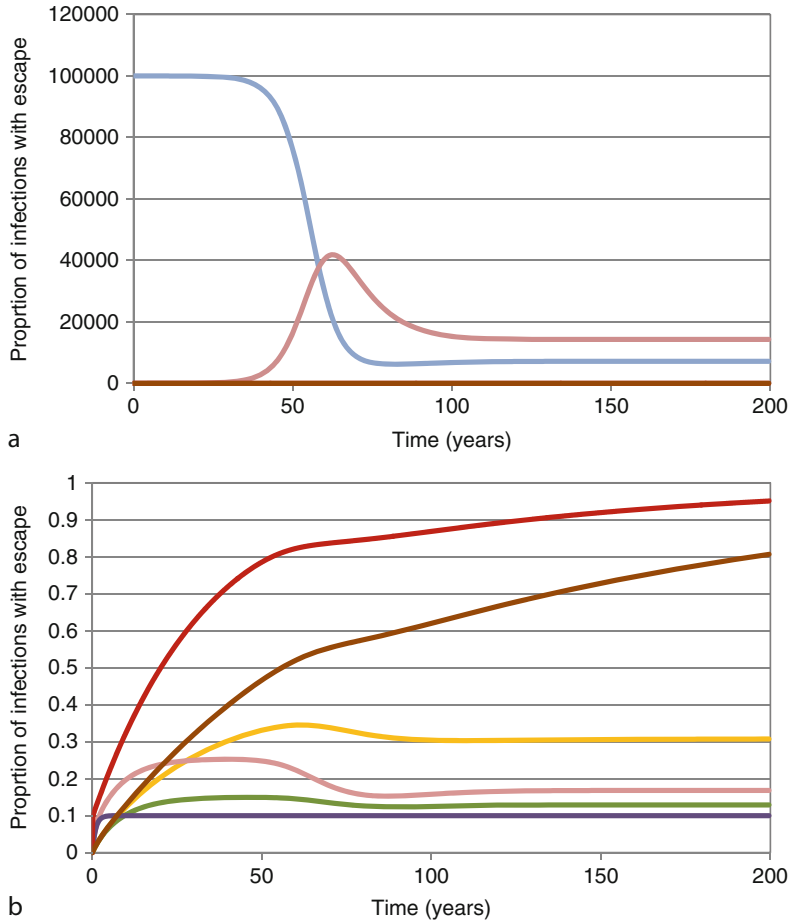

Infectious Disease Modeling. Figure 5
Predictions of a model of within-host evolution and between-host transmission of HIV. (**a**) shows total numbers of susceptible (*blue*) and infectious (*red*) people through time. (**b**) shows the proportion of infections that are with escape mutant virus for a range of escape and reversion rates. The mean times to escape and reversion for each curve are as follows: *red* – escape 1 month, reversion never; *brown* – escape 5 years, reversion never; *yellow* – escape 5 years, reversion 50 years; *pink* – escape 1 year, reversion 10 years; *green* – escape 5 years, reversion 10 years; *mauve* – escape 1 year, reversion 1 year

Models can help in two different ways. The first is to assist the understanding of systems that are intrinsically complicated. Many different interacting populations, events that occur on multiple timescales, and systems with multiple levels of organization can all be better understood when appropriate models are used as an organizing principle and a tool for formal analysis. Sometimes, the problem is that there is not enough data. A systematic description can be very revealing in searching for which new data are most needed. There are also situations where the problem is a deluge of data. In these circumstances, well-constructed models provide a useful organizing scheme with which to interrogate those data.

The second use of models is as representations of well-understood systems used as tools for comparing different intervention strategies. The model of the farm-to-farm spread of FMD described at section "Host Heterogeneity" is a fine example of this use of modeling. It includes enough detail to be a useful tool

for comparing different interventions, but is still firmly rooted in available data so does not rest on large numbers of untested assumptions.

Bibliography

Primary Literature

1. Fenner F (1982) A successful eradication campaign. Global eradication of smallpox. Rev Infect Dis 4(5):916–930
2. Moss WJ, Griffin DE (2006) Global measles elimination. Nat Rev Microbiol 4:900–908
3. Farrington CP, Kanaan MN, Gay NJ (2001) Estimation of the basic reproduction number for infectious diseases from age-stratified serological survey data. J R Stat Soc Ser C Appl Stat 50:251–292
4. Anderson RM, May RM (1991) Infectious diseases of humans. Oxford University Press, Oxford
5. McLean AR, Anderson RM (1988) Measles in developing countries. Part II: the predicted impact of mass vaccination. Epidemiol Infect 100:419–442
6. McLean AR (1995) After the honeymoon in measles control. Lancet 345(8945):272
7. Babad HE et al (1995) Predicting the impact of measles vaccination in England and Wales: model validation and analysis of policy options. Epidemiol Infect 114:319–344
8. McLean AR (1992) Mathematical modelling of the immunisation of populations. Rev Med Virol 2:141–152
9. Arinaminpathy N, McLean AR (2009) Logistics for control for an influenza pandemic. Epidemics 1(2):83–88
10. Longini IM et al (2005) Containing pandemic influenza at the source. Science 309(5737):1083–1087
11. Anderson RM, Grenfell BT (1986) Quantitative investigations of different vaccination policies for the control of congenital rubella syndrome (CRS) in the United Kingdom. J Hyg 96:305–333, Cambridge University Press
12. Metcalf CJE et al (2010) Rubella metapopulation dynamics and importance of spatial coupling to the risk of congenital rubella syndrome in Peru. J R Soc Interface 8(56):369–376
13. Keeling MJ et al (2001) Dynamics of the 2001 UK foot and mouth epidemic: stochastic dispersal in a heterogeneous landscape. Science 294(5543):813–817
14. Flynn NM et al (2005) Placebo-controlled phase 3 trial of a recombinant glycoprotein 120 vaccine to prevent HIV-1 infection. J Infect Dis 191(5):654–665
15. Buchbinder SP et al (2008) Efficacy assessment of a cell-mediated immunity HIV-1 vaccine (the Step Study): a double-blind, randomised, placebo-controlled, test-of-concept trial. Lancet 372(9653):1881–1893
16. Rerks-Ngarm S et al (2009) Vaccination with ALVAC and AIDSVAX to prevent HIV-1 infection in Thailand. N Engl J Med 361(23):2209–2220, Epub 2009 Oct 20
17. Council of the Global HIV Vaccine Enterprise (2010) The 2010 scientific strategic plan of the global HIV vaccine enterprise. Nat Med 16(9):981–989
18. Phillips RE et al (1991) Human immunodeficiency virus genetic variation that can escape cytotoxic T cell recognition. Nature 354:453–459
19. Asquith B et al (2006) Inefficient cytotoxic T lymphocyte-mediated killing of HIV-1-infected cells in vivo. PLoS Biol 4:e90
20. Wei X et al (1995) Viral dynamics in human immunodeficiency virus type 1 infection. Nature 373(6510):117–122
21. Ho DD et al (1995) Rapid turnover of plasma virions and CD4 lymphocytes in HIV-1 infection. Nature 373(6510):123–126
22. Woolhouse MEJ (2002) Population biology of emerging and re-emerging pathogens. Trends Microbiol 10(10):s3–s7
23. Wolfe ND et al (2007) Origins of major human infectious diseases. Nature 447:279–283
24. Meiering CD, Linial ML (2001) Historical perspective of foamy virus epidemiology and infection. Clin Microbiol Rev 14:165–176
25. Switzer WM et al (2004) Frequent simian foamy virus infection in persons occupationally exposed to nonhuman primates. J Virol 78(6):2780–2789
26. Wolfe ND et al (2004) Naturally acquired simian retrovirus infections in central African hunters. Lancet 363:932–937
27. Briese T et al (2009) Genetic detection and characterization of Lujo virus, a new hemorrhagic fever–associated arenavirus from Southern Africa. PLoS Pathog 5(5):e1000455. doi:10.1371/journal.ppat.1000455
28. Antia R et al (2004) The role of evolution in the emergence of infectious diseases. Nature 426:658–661
29. Arinaminpathy N, McLean AR (2009) Evolution and emergence of novel human infections. Proc R Soc B 273:3075–3083
30. Kubiak R et al (2010) Insights into the evolution and emergence of a novel infectious disease. PLoS Comput Biol 6(9): e10000947
31. Worobey M et al (2008) Direct evidence of extensive diversity of HIV-1 in Kinshasa by 1960. Nature 455(7213):661–664
32. CDC (1981) Kaposi's sarcoma and *Pneumocystis pneumonia* among homosexual men – New York City and California. MMWR 30:305–308
33. Kawashima Y et al (2009) Adaptation of HIV-1 to human leukocyte antigen class I. Nature 458:641–645
34. Goulder PJ et al (2001) Evolution and transmission of stable CTL escape mutations in HIV infection. Nature 412:334–338
35. Leslie AJ et al (2004) HIV evolution: CTL escape mutation and reversion after transmission. Nat Med 10:282–289
36. Fryer HR et al (2010) Modelling the evolution and spread of HIV immune escape mutants. PLoS Pathog 6(11):e1001196

Books and Reviews

Anderson RM, May RM (1991) Infectious diseases of humans. Oxford University Press, Oxford

Keeling MJ, Rohani R (2008) Modeling infectious diseases in humans and animals. Princeton University Press, Princeton

Nowak MA, May RM (2000) Virus dynamics. Oxford University Press, Oxford

Infectious Diseases, Climate Change Effects on

Matthew Baylis, Claire Risley
LUCINDA Group, Institute of Infection and Global Health, University of Liverpool, Neston, Cheshire, UK

Article Outline

Glossary
Definition of the Subject and Its Importance
Introduction
Weather, Climate, and Disease
Climate Change and Disease
Other Drivers of Disease
Climate Change and Disease in Wildlife
Evidence of Climate Change's Impact on Disease
Future Directions
Bibliography

Glossary

Climate The weather averaged over a long time or, succinctly, climate is what you expect, weather is what you get!

El Niño Southern Oscillation (ENSO) A climate phenomenon whereby, following reversal of trade winds approximately every 4–7 years, a vast body of warm water moves slowly west to east across the Pacific, resulting in "an El Niño" event in the Americas and leading to a detectable change to climate (mostly disruption of normal rainfall patterns) across 70% of the earth's surface.

Emerging disease An infection or disease that has recently increased in incidence (the number of cases), severity (how bad the disease is), or distribution (where it occurs).

Endemic stability The counter-intuitive situation where the amount of disease rises as the amount of infection falls, such that controlling infection can exacerbate the problem.

Infection The body of a host having been invaded by microorganisms (mostly viruses, bacteria, fungi, protozoa, and parasites).

Infectious disease A pathology or disease that results from infection. Note that many diseases are not infectious and not all infections result in disease.

Intermediate host A host in which a parasite undergoes an essential part of its lifecycle before passing to a second host, and where this passing is passive, that is, not by direct introduction into the next host (see *vector*).

Vector Usually, an arthropod that spreads an infectious pathogen by directly introducing it into a host. For diseases of humans and animals, the most important vectors are flies (like mosquitoes, midges, sandflies, tsetse flies), fleas, lice, and ticks. Aphids are important vectors of diseases in plants. In some instances, other means of carriage of pathogens, such as human hands, car wheels, etc., are referred to as vectors.

Vector competence The proportion of an arthropod vector population that can be infected with a pathogen.

Zoonosis An infection of animals that can spread to, and cause disease in, humans (plural, zoonoses).

Definition of the Subject and Its Importance

Infectious diseases of humans continue to present a significant burden to our health, disproportionately so in the developing world. Infectious diseases of livestock affect their health and welfare, are themselves important causes of human disease and, exceptionally, can threaten our food security. Wildlife infections again present a zoonotic risk to humans, but additionally, such diseases may threaten vulnerable populations and be a cause of extinction and biodiversity loss. Wild populations are inherently more susceptible to environmental change, largely lacking any human protective influence that domesticated species and human populations may benefit from.

Many infectious diseases of humans and farmed or wild animals are influenced by weather or climate, affecting where or when disease occurs, or how severe outbreaks are, and it is therefore likely that future climate change, whether human caused or natural, will have an impact on future disease burdens. Understanding the processes involved may enable prediction of how disease burdens will change in the future and, therefore, allow mitigative or adaptive measures to be put in place.

While climate change will likely be an important cause of change in some infectious diseases in the

future, there are other disease drivers which will also change over similar time scales and which may exacerbate or counteract any effects of climate change. Assessment of the future importance of climate change as an influence over future disease burdens must therefore be considered alongside other causes of change.

Introduction

The impact of infectious diseases of humans and animals seems as great now as it was a century ago. While many disease threats have disappeared or dwindled, at least in the developed world, others have arisen to take their place. Important infectious diseases of humans that have emerged in the last 30 years, for a range of reasons, include Acquired immune deficiency syndrome (AIDS), variant Creutzfeldt-Jakob disease (vCJD), multidrug resistant tuberculosis, severe acute respiratory syndrome (SARS), *E. coli* O157, avian influenza, swine flu, West Nile fever, and Chikungunya [1, 2]. The same applies to diseases of animals: Indeed, all but one of the aforementioned human diseases have animal origins – they are zoonoses – and hence the two subjects of human and animal disease, usually studied separately by medical or veterinary scientists, are intimately entwined.

What will be the global impact of infectious diseases at the end of the twenty-first century? Any single disease is likely to be affected by many factors that cannot be predicted with confidence, including changes to human demography and behavior, new scientific or technological advances including cures and vaccines, pathogen evolution, livestock management practices and developments in animal genetics, and changes to the physical environment. A further, arguably more predictable, influence is climate change.

Owing to anthropogenic activities, there is widespread scientific agreement that the world's climate is warming at a faster rate than ever before [3], with concomitant changes in precipitation, flooding, winds, and the frequency of extreme events such as El Niño. Innumerable studies have demonstrated links between infectious diseases and climate, and it is unthinkable that a significant change in climate during this century will not impact on at least some of them.

How should one react to predicted changes in diseases ascribed to climate change? The answer depends on the animal populations and human communities affected, whether the disease changes in severity, incidence, or spatiotemporal distribution and, of course, on the direction of change: Some diseases may spread but others may retreat in distribution. It also depends on the relative importance of the disease. If climate change is predicted to affect mostly diseases of relatively minor impact on human society or global biodiversity/ecosystem function, while the more important diseases are refractory to climate change's influence, then our concerns should be tempered.

To understand climate change's effects on infectious diseases in the future it is necessary to first understand how climate affects diseases today. This entry begins by first presenting examples of climate's effects on diseases of humans and livestock today and, from the understanding gained, then describes the processes by which climate change might affect such diseases in the future. Diseases of wildlife are important, to some extent, for different reasons to those of humans and livestock, and are therefore considered separately. The relative importance of climate change as a disease driver, compared to other forces, is considered, with examples provided of where climate change both is, and is not, the major force. Finally, the future prospects and the uncertainties surrounding them are considered.

Weather, Climate, and Disease

Many diseases are affected directly or indirectly by weather and climate. Remarkably, no systematic surveys of links between diseases and weather/climate seem to exist and, therefore, it is not possible to indicate whether these diseases represent a minority or majority.

The associations between diseases and weather/climate fall broadly into three categories. The associations may be *spatial*, with climate affecting the distribution of a disease; *temporal* with weather or climate affecting the timing of outbreaks; or they may relate to the *intensity* of an outbreak. Temporal associations can be further broken into at least two subcategories: *seasonal*, with weather or climate affecting the seasonal occurrence of a disease, and *interannual*, with weather or climate affecting the timing, or frequency of years in which outbreaks occur. Here a selection of these associations is presented, which is by no means exhaustive

but is, rather, intended to demonstrate the diversity of effects. Furthermore, the assignment of diseases into the different categories should not be considered hard-and-fast as many diseases could come under more than one heading.

Spatial

- Schistosomosis is an important cause of human mortality and morbidity in Africa and, to a lesser extent, in Asia. The disease is caused by species of *Schistosoma* trematode parasite, for which water-living snails are intermediate hosts. The distribution of suitable water bodies is therefore important for its distribution. However, there must also be suitable temperature: In China, *Oncomelania hupensis* snail intermediate hosts cannot live north of the January 0°C isotherm (the "freezing line") while *Schistosoma japonicum* only develops within the snail at temperatures above 15.4°C. Shistosomosis risk in China is therefore restricted to the warmer southeastern part of the country [4].
- Diseases transmitted by tsetse flies (sleeping sickness, animal trypanosomosis) and ticks (such as anaplasmosis, babesiosis, East Coast fever, heartwater) impose a tremendous burden on African people and their livestock. Many aspects of the vectors' life cycles are sensitive to climate, to the extent that their spatial distributions can be predicted accurately using satellite-derived proxies for climate variables [5].
- Mosquitoes (principally *Culex* and *Aedes*) transmit several viruses of birds that can also cause mortality in humans and horses. Examples are West Nile fever (WNF) and the viral encephalitides such as Venezuelan, western, and eastern equine encephalitis (VEE, WEE, and EEE, respectively) [6]. The spatial distributions of the mosquito vectors are highly sensitive to climate variables.

Temporal-Seasonal

All of the previous examples of spatial associations between diseases and climate can also be classified as temporal-seasonal, as the effects of climate on the seasonal cycle of the intermediate hosts (snails, tsetse flies, and mosquitoes, respectively) also determines in part the seasonal cycle of disease. There are other diseases where the associations can be described as seasonal-temporal.

- Salmonellosis is a serious food-borne disease caused by *Salmonella* bacteria, most often obtained from eggs, poultry, and pork. Salmonellosis notification rates in several European countries have been shown to increase by about 5–10% for each 1°C increase in ambient temperature [7]. Salmonellosis notification is particularly associated with high temperatures during the week prior to consumption of infected produce, implicating a mechanistic effect via poor food handling.
- Foot-and-mouth disease (FMD) is a highly contagious, viral infection of cloven-footed animals, including cattle, sheep, and pigs. Most transmission is by contact between infected and susceptible animals, or by contact with contaminated animal products. However, FMD can also spread on the wind. The survival of the virus is low at relative humidity (RH) below 60% [8], and wind-borne spread is favored by the humid, cold weather common to temperate regions. In warmer drier regions, such as Africa, wind-borne spread of FMD is considered unimportant [9].
- Peste des petits ruminants (PPR) is an acute, contagious, viral disease of small ruminants, especially goats, which is of great economic importance in parts of Africa and the Near East. It is transmitted mostly by aerosol droplets between animals in close contact. However, the appearance of clinical PPR is often associated with the onset of the rainy season or dry cold periods [10], a pattern that may be related to viral survival. The closely related rinderpest virus survives best at low or high relative humidity, and least at 50–60% [11].
- Several directly transmitted human respiratory infections, including those caused by rhinoviruses (common colds) and seasonal influenza viruses (flu) have, in temperate countries, seasonal patterns linked to the annual temperature cycle. There may be direct influences of climate, such as the effect of humidity on survival of the virus in aerosol [12], or indirect influences via, for example, seasonal changes in the strength of the human immune system or more indoor crowding during cold weather [13].

Temporal-Interannual

The previous examples of spatial associations between diseases and climate, which were further categorized as temporal-seasonal, can also be classified as temporal-interannual, as the effects of climate on the intermediate hosts (snails, tsetse flies, and mosquitoes, respectively) will determine in part the risk or scale of a disease outbreak in a given year. There are other diseases where the associations can be described as seasonal-interannual.

- Anthrax is an acute infectious disease of most warm-blooded animals, including humans, with worldwide distribution. The causative bacterium, *Bacillus anthracis* forms spores able to remain infective for 10–20 years in pasture. Temperature, relative humidity, and soil moisture all affect the successful germination of anthrax spores, while heavy rainfall may stir up dormant spores. Outbreaks are often associated with alternating heavy rainfall and drought, and high temperatures [14].
- Cholera, a diarrheal disease which has killed tens of millions of people worldwide, is caused by the bacterium *Vibrio cholerae*, which lives amongst sea plankton [15]. High temperatures causing an increase in algal populations often precede cholera outbreaks. Disruption to normal rainfall helps cholera to spread further, either by flooding, leading to the contamination of water sources, such as wells, or drought which can make the use of such water sources unavoidable. Contaminated water sources then become an important source of infection in people.
- Plague is a flea-borne disease caused by the bacterium *Yersinia pestis*; the fleas' rodent hosts bring them into proximity with humans. In Central Asia, large scale fluctuations in climate synchronize the rodent population dynamics over large areas [16], allowing population density to rise over the critical threshold required for plague outbreaks to commence [17].
- African horse sickness (AHS), a lethal infectious disease of horses, is caused by a virus transmitted by *Culicoides* biting midges. Large outbreaks of AHS in the Republic of South Africa over the last 200 years are associated with the combination of drought and heavy rainfall brought by the warm phase of the El Niño Southern Oscillation (ENSO) [18].
- Rift Valley Fever (RVF), an important zoonotic viral disease of sheep and cattle, is transmitted by *Aedes* and *Culex* mosquitoes. Epizootics of RVF are associated with periods of heavy rainfall and flooding [19–21] or, in East Africa, with the combination of heavy rainfall following drought associated with ENSO [20, 22]. ENSO-related floods in 1998, following drought in 1997, led to an epidemic of RVF (and some other diseases) in the Kenya/Somalia border area and the deaths of more than 2000 people and two-thirds of all small ruminant livestock [23]. Outbreaks of several other human infections, including malaria and dengue fever have, in some parts of the world, been linked to ENSO events.

Intensity

In addition to associations between climate and the spatial and temporal distributions of disease outbreaks, there are some examples of associations between climate and the intensity or severity of the disease that results from infection. It is theoretically possible, for example, that climate-induced immunosuppression of hosts may favor the multiplication of some microparasites (viruses, bacteria, rickettsia, fungi, protozoa), thereby increasing disease severity or, alternatively, reduce the disease-associated immune response to infection, thereby reducing disease severity.

However, the clearest examples pertain to macroparasites (helminth worms) which, with the notable exception of *Strongyloides* spp., do not multiply within the host. Disease severity is therefore directly correlated with the number of parasites acquired at the point of infection or subsequently, and in turn this is frequently associated with climate, which affects both parasite survival and seasonal occurrence.

- Fasciolosis, caused by the *Fasciola* trematode fluke, is of economic importance to livestock producers in many parts of the world and also causes disease in humans. In sheep, severe pathology, including sudden death, results from acute fasciolosis which occurs after ingestion of more than 2,000 metacercariae (larval flukes) of *Fasciola hepatica* at pasture, while milder pathology associated with

subacute and chronic fasciolosis occurs after ingestion of 200–1,000 metacercariae [24]. Acute fasciolosis is therefore most common in places or in years when rainfall and temperature favor the survival of large numbers of metacercariae.

- *Nematodirus battus* is a nematode parasite of the intestine of lambs. Eggs deposited in the feces of one season's lambs do not hatch straightaway; instead, they build up on the pasture during summer and remain as eggs over winter, not hatching until temperatures the following spring exceed 10°C [25]. Once the mean daily temperature exceeds this threshold the eggs hatch rapidly, leading to a sharp peak in the number of infective larvae on the pasture. If this coincides with the new season's lambs grazing on the pasture, there is likely to be a large uptake of larvae and severe disease, called nematodiriasis. If, however, there is a warm spell early in the year, the peak in larvae on pasture may occur while lambs are still suckling rather than grazing, such that fewer larvae are ingested and the severity of nematodiriasis is reduced.

Climate Change and Disease

There is a substantial scientific literature on the effects of climate change on health and disease, but with strong focus on human health and vector-borne disease [5, 26–42]. By contrast, the effects of climate change on diseases spread by other means, or animal diseases in general, have received comparatively little attention [43–48]. Given the global burden of diseases that are not vector-borne, and the contribution made by animal diseases to poverty in the developing world [49], attention to these areas is overdue.

The previous section demonstrates the range of climate influences upon infectious disease. Such influences are not the sole preserve of vector-borne diseases: Food-borne, water-borne, and aerosol-transmitted diseases are also affected. A common feature of non-vector-borne diseases affected by climate is that the pathogen or parasite spends a period of time outside of the host, subject to environmental influence. Examples include the infective spores of anthrax; FMD viruses in temperate regions; the *Salmonella* bacteria that contaminate food products; the cholera-causing *vibrio* bacteria in water; and the moisture- and temperature-dependent survival of the parasites causing schistosomosis and fasciolosis.

By contrast, most diseases transmitted directly between humans (for example, human childhood viruses, sexually transmitted diseases (STDs), tuberculosis) have few or no reported associations with climate. This is also the case for animal infections such as avian influenza, bovine tuberculosis, brucellosis, Newcastle's disease of poultry, and rabies. Clear exceptions are the viruses that cause colds and seasonal flu in humans, and PPR in small ruminants; these viruses are spread by aerosol between individuals in close contact but are nevertheless sensitive to the effects of ambient humidity and possibly temperature.

The influence of climate on diseases that are not vector-borne appears to be most frequently associated with the timing (intra- or interannual) of their occurrence rather than their spatial distribution. There are examples of such diseases that occur only in certain parts of the world (for example, PPR) but most occur worldwide. By contrast, the associations of vector-borne diseases with climate are equally apparent in time and space, with very few vector-borne diseases being considered a risk worldwide. This is a reflection of the strong influence of climate on both the spatial and temporal distributions of intermediate vectors. If there are exceptions to this rule, the vectors are likely to be lice or fleas, with lives so intimately associated with humans or animals that they are relatively protected from climate's influences.

In the scientific literature, many processes have been proposed by which climate change might affect infectious diseases. These processes range from the clear and quantifiable to the imprecise and hypothetical. They may affect pathogens directly or indirectly, the hosts, the vectors (if there is an intermediate host), epidemiological dynamics, or the natural environment. A framework for how climate change can affect the transmission of pathogens between hosts is shown in Fig. 1. Only some of the processes can be expected to apply to any single infectious disease.

Effects on Pathogens

Higher temperatures resulting from climate change may increase the rate of development of certain pathogens or parasites that have one or more lifecycle stages

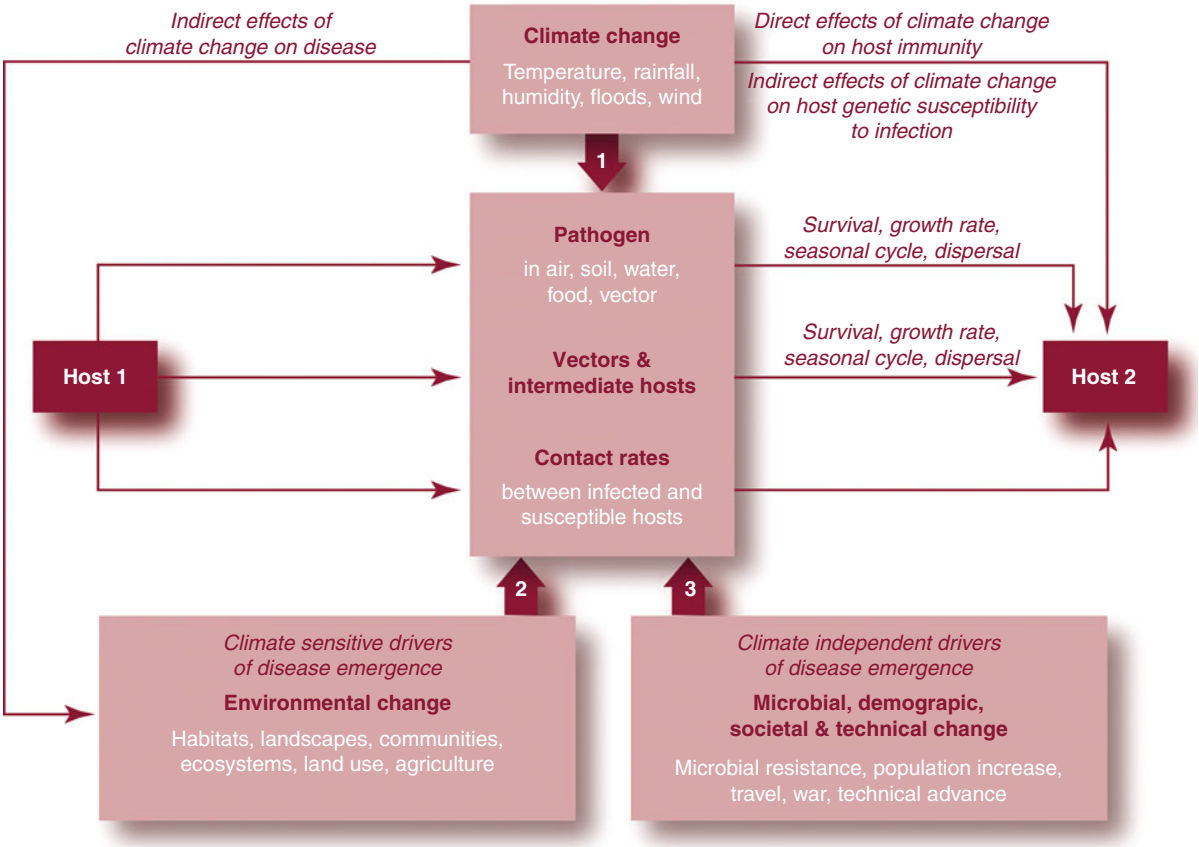

Infectious Diseases, Climate Change Effects on. Figure 1
A schematic framework of the effects of climate change on the transmission of diseases of humans and animals. Climate change can act directly on pathogens in a range of external substrates, or their vectors and intermediate hosts, thereby affecting the processes of survival, growth, seasonality, and dispersal. It can also directly affect hosts themselves or the contact rates between infected and susceptible individuals. Climate change can have indirect effects on disease transmission via its effects on the natural or anthropogenic environment, and via the genetics of exposed populations. Environmental, demographic, social, and technical change will also happen independently of climate change and have as great, or much greater, influence on disease transmission than climate change itself. The significance of climate change as a driver of disease will depend on the scale of *arrow 1*, and on the relative scales of *arrows 2* and *3*

outside their human or animal host. This may shorten generation times and, possibly, increase the total number of generations per year, leading to higher pathogen population sizes [48]. Conversely, some pathogens are sensitive to high temperature and their survival may decrease with climate warming.

Phenological evidence indicates that spring is arriving earlier in temperate regions [50]. Lengthening of the warm season may increase or decrease the number of cycles of infection possible within 1 year for warm or cold-associated diseases respectively. Arthropod vectors tend to require warm weather so the infection season of arthropod-borne diseases may extend. Some pathogens and many vectors experience significant mortality during cold winter conditions; warmer winters may increase the likelihood of successful overwintering [41, 48].

Pathogens that are sensitive to moist or dry conditions may be affected by changes to precipitation, soil moisture, and the frequency of floods. Changes to winds could affect the spread of certain pathogens and vectors.

Effects on Hosts

A proposed explanation for the tendency for human influenza to occur in winter is that the human immune system is less competent during that time; attributable to the effects of reduced exposure to light on melatonin [51] or vitamin D production [52]. The seasonal light/dark cycle will not change with climate change, but one might hypothesize that changing levels of cloud cover could affect exposure in future. A second explanation, the tendency for people to congregate indoors during wintertime, leads to a more credible role for a future influence of climate change.

Mammalian cellular immunity can be suppressed following heightened exposure to ultraviolet B (UV-B) radiation – an expected outcome of stratospheric ozone depletion [53, 54]. In particular, there is depression of the number of T helper 1 lymphocytes, cells which stimulate macrophages to attack pathogen-infected cells and, therefore, the immune response to intracellular pathogens may be particularly affected. Examples of such intracellular pathogens include many viruses, rickettsia (such as *Cowdria* and *Anaplasma*, the causative agents of heartwater and anaplasmosis), *Brucella, Listeria monocytogenes* and *Mycobacterium tuberculosis*, the bacterial agents of brucellosis, listeriosis, and tuberculosis, respectively, and the protozoan parasites *Toxoplasma gondii* and *Leishmania* which cause toxoplasmosis and visceral leishmanosis (kala-azar), respectively, in humans [55].

A third host-related effect worthy of consideration is genetic resistance to disease. Some human populations and many animal species have evolved a level of genetic resistance to some of the diseases to which they are commonly exposed. Malaria presents a classic example for humans, with a degree of resistance to infection in African populations obtained from heterozygosity for the sickle-cell genetic trait. Considering animals, wild mammals in Africa may be infected with trypanosomes, but rarely show signs of disease; local Zebu cattle breeds, which have been in the continent for millennia, show some degree of trypanotolerance (resistance to disease caused by trypanosome infection); by contrast, recently introduced European cattle breeds are highly susceptible to trypanosomosis. In stark contrast, African mammals proved highly susceptible to rinderpest which swept through the continent in the late nineteenth century, and which they had not previously encountered. It seems unlikely that climate change will directly affect genetic or immunologic resistance to disease in humans or animals. However, significant shifts in disease distributions driven by climate change pose a greater threat than simply the exposure of new populations. Naïve populations may, in some cases, be particularly susceptible to the new diseases facing them.

Certain diseases show a phenomenon called *endemic stability*. This occurs when the severity of disease is less in younger than older individuals, when the infection is common or endemic and when there is life-long immunity after infection. Under these conditions most infected individuals are young, and experience relatively mild disease. Counter-intuitively, as endemically stable infections become rarer, a higher proportion of cases are in older individuals (it takes longer, on average, to acquire infection) and the number of cases of severe disease rises. Certain tick-borne diseases of livestock in Africa, such as anaplasmosis, babesiosis, and cowdriosis, show a degree of endemic stability [56], and it has been proposed to occur for some human diseases like malaria [57]. If climate change drives such diseases to new areas, nonimmune individuals of all ages in these regions will be newly exposed, and outbreaks of severe disease could follow.

Effects on Vectors

Much has already been written about the effects of climate change on invertebrate disease vectors. Indeed, this issue, especially the effects on mosquito vectors, has dominated the debate so far. It is interesting to bear in mind, however, that mosquitoes are less significant as vectors of animal disease than they are of human disease (Table 1). Mosquitoes primarily, and secondarily lice, fleas, and ticks, transmit between them a significant proportion of important human infections. By contrast, biting midges, brachyceran flies (e.g., tabanids, muscids, myiasis flies, hippoboscids), ticks, and mosquitoes (and, in Africa, tsetse) all dominate as vectors of livestock disease. Therefore, a balanced debate on the effects of climate change on human and animal disease must consider a broad range of vectors.

There are several processes by which climate change might affect disease vectors. First, temperature and moisture frequently impose limits on their distribution. Often, low temperatures are limiting because of high winter mortality, or high temperatures because they involve excessive moisture loss. Therefore, cooler regions which were previously too cold for certain vectors may begin to allow them to flourish with

Infectious Diseases, Climate Change Effects on. Table 1 The major diseases transmitted by arthropod vectors to humans and livestock (Adapted from [58])

Vector	Diseases of humans	Diseases of livestock
Phthiraptera (Lice)	Epidemic typhus Trench fever Louse-borne relapsing fever	
Reduvidae (Assassin bugs)	Chagas' disease	
Siphonaptera (Fleas)	Plague Murine typhus Q fever Tularaemia	Myxomatosis
Psychodidae (Sand flies)	Leishmanosis Sand fly fever	Canine leishmanosis Vesicular stomatitis
Culicidae (Mosquitoes)	Malaria Dengue Yellow fever West Nile Filiariasis Encephalitides (WEE, EEE, VEE, Japanese encephalitis, Saint Louis encephalitis) Rift Valley fever	West Nile fever Encephalitides Rift Valley fever Equine infectious anemia
Simulidae (Black flies)	Onchocercosis	Leucocytozoon (birds) Vesicular stomatitis
Ceratopogonidae (Biting midges)		Bluetongue African horse sickness Akabane Bovine ephemeral fever
Glossinidae (Tsetse flies)	Trypanosomosis	Trypanosomosis
Tabanidae (Horse flies)	Loiasis	Surra Equine infectious anemia *Trypanosoma vivax*
Muscidae (Muscid flies)	Shigella *E. coli*	Mastitis Summer mastitis Pink-eye (IBK)
Muscoidae, Oestroidae (Myiasis-causing flies)	Bot flies	Screwworm Blow fly strike Fleece rot
Hippoboscoidae (Louse flies, keds)		Numerous protozoa
Acari (Mites)	Chiggers Scrub typhus (tsutsugamushi) Scabies	Mange Scab Scrapie?

Infectious Diseases, Climate Change Effects on. Table 1 (Continued)

Vector	Diseases of humans	Diseases of livestock
Ixodidae (Hard ticks) Argasidae (Soft ticks)	Human babesiosis Tick-borne encephalitis Tick fevers Ehrlichiosis Q fever Lyme disease Tick-borne relapsing fever Tularaemia	Babesiosis East coast fever (Theileriosis) Louping ill African Swine Fever Ehrlichiosis Q fever Heartwater Anaplasmosis Borreliosis Tularaemia

climate change. Warmer regions could become even warmer and yet remain permissive for vectors if there is also increased precipitation or humidity. Conversely, these regions may become less conducive to vectors if moisture levels remain unchanged or decrease, with concomitant increase in moisture stress.

For any specific vector, however, the true outcome of climate change will be significantly more complex than that outlined above. Even with a decrease in future moisture levels, some vectors, such as certain species of mosquito, could become more abundant, at least in the vicinity of people and livestock, if the response to warming is more water storage and, thereby, the creation of new breeding sites. One of the most important vectors of the emerging Chikungunya virus (and to a lesser extent dengue virus) is the Asian tiger mosquito (*Aedes albopictus*) which is a container breeder and therefore thrives where humans store water. Equally, some vectors may be relatively insensitive to direct effects of climate change, such as muscids which breed in organic matter or debris, and myiasis flies which breed in hosts' skin.

Changes to temperature and moisture will also lead to increases or decreases in the abundance of many disease vectors. This may also result from a change in the frequency of extreme weather events such as ENSO. Outbreaks of several biting midge and mosquito-borne diseases, for example, have been linked to the occurrence of ENSO [18, 22, 59–62] and mediated, at least in part, by increase in the vector population size in response to heavy rainfall, or rainfall succeeding drought, that ENSO sometimes brings [18, 22]. Greater intra- or interannual variation in rainfall, linked or unlinked to ENSO, may lead to an increase in the frequency or scale of outbreaks of such diseases.

The ability of some insect vectors to become or remain infected with pathogens (their vector competence) varies with temperature [63, 64]. In addition to this effect on vector competence, an increase in temperature may alter the balance between the lifespan of an infected vector, its frequency of feeding, and the time necessary for the maturation of the pathogen within it. This balance is critical, as a key component of the risk of transmission of a vector-borne disease is the number of blood meals taken by a vector between the time it becomes infectious and its death [65]. Accordingly, rising ambient temperature can increase the risk of pathogen transmission by shortening the time until infectiousness in the vector and increasing its feeding frequency at a faster rate than it shortens the vector's lifespan, such that the number of feeds taken by an infectious vector increases. However, at even higher temperatures this can reverse [66] such that the number of infectious feeds then decreases relative to that possible at lower temperatures. This point is extremely important, as it means that the risk of transmission of vector-borne pathogens does not uniformly increase with rising temperature, but that it can become too hot and transmission rates decrease. This effect will be most important for short-lived vectors such as biting midges and mosquitoes [30].

Lastly, there may be important effects of climate change on vector dispersal, particularly if there is a change in wind patterns. Wind movements have been associated with the spread of epidemics of many *Culicoides*- and mosquito-borne diseases [67–72].

Effects on Epidemiological Dynamics

Climate change may alter transmission rates between hosts by affecting the survival of the pathogen or the intermediate vector, but also by other, indirect, forces that may be hard to predict with accuracy. Climate change may influence human demography, housing, or movement or be one of the forces that leads to changes in future patterns of international trade, local animal transportation, and farm size. All of these can alter the chances of an infected human or animal coming into contact with a susceptible one. For example, a series of droughts in East Africa between 1993 and 1997 resulted in pastoral communities moving their cattle to graze in areas normally reserved for wildlife. This resulted in cattle infected with a mild lineage of rinderpest transmitting disease both to other cattle and to susceptible wildlife, causing severe disease, for example, in buffalo, lesser kudu, and impala, and devastating certain populations [73].

Indirect Effects

No disease or vector distribution can be fully understood in terms of climate only. The supply of suitable hosts, the effects of co-infection or immunological cross-protection, the presence of other insects competing for the same food sources or breeding sites as vectors [74], and parasites and predators of vectors themselves, could have important effects [48]. Climate change may affect the abundance or distribution of hosts or the competitors/predators/parasites of vectors and influence patterns of disease in ways that cannot be predicted from the direct effects of climate change alone.

Equally, it has been argued that climate change-related disturbances of ecological relationships, driven perhaps by agricultural changes, deforestation, the construction of dams, and losses of biodiversity, could give rise to new mixtures of different species, thereby exposing hosts to novel pathogens and vectors and causing the emergence of new diseases [40]. A possible "example in progress" is the reemergence in the UK of bovine tuberculosis, for which the badger (*Meles meles*) is believed to be a carrier of the causative agent, *Mycobacterium bovis*. Farm landscape, such as the density of linear features like hedgerows, is a risk factor for the disease, affecting the rate of contact between cattle and badger [75]. Climate change will be a force for modifying future landscapes and habitats, with indirect and largely unpredictable effects on diseases.

Other Drivers of Disease

The future disease burden of humans and animals will depend not only on climate change and its direct and indirect effects on disease, but also on how other drivers of disease change over time. Even for diseases with established climate links, it may be the case that in most instances these other drivers will prove to be more important than climate. A survey of 335 events of human disease emergence between 1940 and 2004 classified the underlying causes into 12 categories [2]. One of these, "climate and weather," was only listed as the cause of ten emergence events. Six of these were non-cholera *Vibrio* bacteria which cause poisoning via shellfish or exposure to contaminated seawater; the remaining four were a fungal infection and three mosquito-borne viruses. The other 11 categories included, however, "land use changes" and "agricultural industry changes," with 36 and 31 disease emergence events, respectively, and both may be affected by climate change. The causes of the remaining 77% of disease emergence events – "antimicrobial agent use," "international travel and commerce," "human demography and behavior," "human susceptibility to infection," "medical industry change," "war and famine," "food industry changes," "breakdown of public health," and "bushmeat" – would be expected to be either less or not influenced by climate change. Hence, climate change's indirect effects on human or animal disease may exceed its direct effects, while drivers unsusceptible to climate change may be more important still at determining our disease future.

Climate Change and Disease in Wildlife

Wildlife disease is important for different reasons to those which make disease in humans and domestic

animals important. It has the potential for endangerment of wildlife and can be a source of zoonoses and livestock disease.

Wildlife Disease as a Cause of Endangerment

Disease in wild populations may limit or cause extreme fluctuations in population size [76] and reduce the chances of survival of endangered or threatened species [77]. Indeed, disease can be the primary cause of extinction in animals or be a significant contributory factor toward it. For example:

- The Christmas Island rat, *Rattus macleari*, is believed to have been extinct by 1904. There is molecular evidence that this was caused by introduction of murine trypanosomes apparently brought to the island by black rats introduced shortly before 1904 [78].
- Similarly, the last known Po'o-uli bird (*Melamprosops phaeosoma*) in Hawaii died from avian malaria brought by introduced mosquitoes [79].
- Canine Distemper in the Ethiopian Wolf (*Canis simensis*) has brought about its decline [80].
- Devil facial tumor disease, an aggressive nonviral transmissible parasitic cancer, continues to threaten Tasmanian Devil (*Sarcophilus harrisii*) populations [81].
- The white nose fungus G*eomyces destructans* is decimating bat populations in Northeastern US states and is currently spreading in Europe [82]. This is perhaps the most recent emergence of a disease of concern to wildlife endangerment.

Although disease can cause endangerment and extinction, its importance relative to other causes is uncertain. A review of the causes of endangerment and extinction in the International Union for Conservation of Nature (IUCN) red list of plant and animal species found that disease was implicated in a total of 254 cases, some 7% of the total examined [83]. Although the other factors may be more important overall, disease remains an important cause of endangerment and extinction for certain animal groups. A contender for the single issue of greatest current conservation concern is the epidemic of the chytrid fungus *Batrachochytrium dendrobatidis* in amphibians. With a broad host range and high mortality, this pathogen is likely to be wholly or partly responsible for all recent amphibian extinction events, which, remarkably, comprise 29% of all extinctions attributable to disease since the year 1500 [77].

Wildlife Disease as a Source of Infections for Humans and Livestock

Many diseases of wildlife frequently cross the species barrier to infect humans or domestic animals [84, 85]. Closely related organisms often share diseases. A particular risk to humans is presented by diseases of primates: The human immunodeficiency viruses (HIV) that cause AIDS originated as simian immunodeficiency viruses in African monkeys and apes. Humans acquire or have acquired many other pathogens from mammals other than primates, especially those that humans choose to live close to (livestock, dogs, cats), or that choose to live close to us (rodents, bats) [86]. In addition, there are examples of human infections shared with birds (e.g., avian influenza), and reptiles and fishes (e.g., *Salmonella* spp.). Insects are frequent carriers of pathogens between vertebrate hosts, and there may even be a pathogen transmissible from plants to humans [87].

Wildlife populations are the primary source of emerging infectious diseases in humans. A search of the scientific literature published between 1940 and 2004 attempted to quantify the causes of disease introductions into human populations and found that about 72% were introduced from wildlife [2].

How Climate Change Can Influence Wildlife Disease

The effects of climate change on wildlife disease are important when the changes produced lead to increased risk of endangerment or extinction of the wildlife, or increased transmission risk to humans or domestic animals.

Climate change can increase the threat of endangerment or extinction, via reduction in population size of the wildlife host (by altering habitats, for example), or increase in pathogen range or virulence, such that the persistence of a host population is at risk, and climate change can increase the risk of disease emergence and spread to humans or livestock via change to

the distribution of wildlife hosts, such that encroachment on human or livestock populations is favored.

Changes in species' distribution may arise directly under climate change as a result of an organism's requirement for particular climatic conditions or indirectly via ecological interactions with other species which are themselves affected. Climate change can cause the appearance of new assemblages of species and the disappearance of old communities [88], which can create new disease transmission opportunities or end existing ones.

Climatic factors potentially affecting wildlife disease transmission more directly include the growth rate of the pathogen in the environment or in a cold-blooded (ectothermic) wildlife host (e.g., fish, amphibian, reptile). Therefore, effects which are more marked in wildlife disease in comparison to human or livestock disease include the occurrence of ectothermic hosts, and also the vast range of potential vectors that may transmit disease. It is therefore more difficult to generalize about the effects of climate change on wildlife.

In colder climates, the parasite that causes the most severe form of human malaria, *Plasmodium falciparum* does not develop rapidly enough in its mosquito vectors for there to be sufficient transmission to maintain the parasite. Avian malaria (*Plasmodium relictum*) exhibits an elevational gradient due mainly to temperature and is subject to similar constraints [89].

An example of a wildlife pathogen constrained due to its dependence on environmental transmission is anthrax. Infective spores of anthrax bacilli can lie dormant in soils for decades, becoming dangerous when climatic conditions, particularly precipitation, favor it. It is well established that when a host population size is reduced, the pool of susceptible individuals may be too small for pathogen survival. This effect is particularly acute for host-specific diseases, such as the transmissible cancer of Tasmanian devils, *Sarcophilus harrisii*, DFTD or Devil facial tumor disease (discussed in [81]); at low host population sizes, DFTD may become extinct. By contrast, diseases with a broad host range may threaten individual species down to the last individual. As anthrax has both a broad host range and can lie dormant in the environment, it is a particular threat for species with very low numbers, and is currently a conservation consideration for many species. For example the Javan rhinoceros population is down to fewer than 60 individuals and identified as a priority for conservation (an "EDGE" species) because of its uniqueness and scarcity [90].

Climate change may have particular impact on marine animals, because of the preponderance of ectothermic animals in the sea, the multiple ways in which climate change is predicted to affect the marine environment, and the multiple stresses that marine organisms and ecosystems are already experiencing due to anthropogenic influence. Disease is an important part of this impact. For example, warming of the Pacific in the range of the oyster *Crassostrea virginica* caused range expansion of the protozoan parasite *Perkinsus marinus* probably due to a combination of increased overwinter survival, greater summer proliferation, and increased host density [91]. Coral reefs are also sensitive to at least 12 potential factors associated with climate change: [92] CO_2 concentration, sea surface temperature, sea level, storm intensity, storm frequency, storm track, wave climate, run off, seasonality, overland rainfall, and ocean and air circulation [92]. Although these factors might not all increase levels of disease, the synergism between disease, climate, and other stressors might lead to accelerating degradation of the coral reef habitat.

From a geographic perspective, there is evidence that the greatest change in ecosystems attributable to climate change is likely to be in the tropics; the second being the arctic [88]. The impacts of this change on wildlife disease and its consequences may be particularly great in these two regions, and there is evidence that it is already occurring. The tropics have the most species in imminent danger of extinction [93] while tropical coral reefs comprise much of the biodiversity of the oceans. In addition to extinction risks, tropical forests may also pose a zoonosis risk. An increase in animal-human interaction is likely in tropical forests, which have a diverse fauna subject to increasing human encroachment.

With regard to the Arctic, a model of the effect of global warming on a protostrongylid lung-dwelling nematode *Umingmakstrongylus pallikuukensis*, in Canadian Arctic muskoxen *Ovibos moschatus*, found that warming was likely to significantly influence infection, making the muskoxen more susceptible to predation [94]. Muskoxen were also subject to climate-influenced outbreaks of fatal pneumonia [95]. Indeed,

the combination of climate change's effects on pathogen survival and transmission, and the stress to host species from changing environmental conditions, may have serious impact on arctic populations of fish, muskoxen, sheep, and others [96].

Dependency of Disease on Climate: The Example of Chytridiomycosis in Amphibians

In wildlife epidemiology, the host may be of equal importance to the pathogen and vector when considering the impact of climate, as wildlife may be impacted by climate in more diverse ways than humans or domestic animals, and are subject to much reduced human mitigation of those impacts. The importance of climate in *Batrachochytrium dendrobatidis* epidemiology, the cause of chytridiomycosis, and numerous amphibian extinctions is fiercely debated. Although the pathogen *B. dendrobatidis* is neither vector-borne nor has a prolonged environmental phase, it is affected by temperature because the environment of its ectothermic hosts is not kept constant when external temperature varies. It belongs to a basal group within the fungi and has a brief motile zoospore stage for dispersal, followed by the penetration of the outer layers of amphibian skin and asexual intracellular multiplication [97]. Its growth is limited by warmer temperatures, perhaps because amphibians shed their outer layers of skin more frequently in warmer temperatures [97]. Pounds et al. [98] were the first to make a connection between climate and *B. dendrobatidis*-mediated amphibian extinctions, reporting spatiotemporal associations between warming and last year of detection of frog species. The development rate of the *B. dendrobatidis* fungus depends on summer temperature [99], and its survival is dependent on winter freezing [100]. The fungus appears to cause more mortality in mountainous regions [101], yet may be limited at the upper extremes of altitude. Climate may also affect the impact of the disease due to host factors. The habitat of the golden toad *Bufo periglenes* in 1987, the last year of its existence, was much reduced due to an especially dry summer. This may have caused crowded conditions in the remaining ponds, facilitating the spread of chytridiomycosis [102].

In addition, climate may affect mortality associated with the disease. The mortality of frogs exposed to *B. dendrobatidis* spores as adults has been shown to be dependent on the condition of the frogs [103]. In a changing climate where amphibians are shifting their ranges into suboptimal areas, hosts are likely to be more susceptible to the damaging effects of *B. dendrobatidis* infection.

On the other hand, it has been argued that climate is not important in *B. dendrobatidis* outbreaks [104]. The authors contrast the climate-linked epidemic hypothesis with the hypothesis that disease outbreaks occur largely due to introduction into unexposed, naive populations, and describe spatiotemporal "waves" of declines across Central America as evidence that it is disease introduction (and not climatic variables) causing declines.

Evidence of Climate Change's Impact on Disease

Climate warming has already occurred in recent decades. If diseases are sensitive to such warming, then one might expect a number of diseases to have responded by changing their distribution, frequency, or intensity. A major difficulty, however, is the attribution of any observed changes in disease occurrence to climate change because, as shown above, other disease drivers also change over time. It has been argued that the minimum standard for attribution to climate change is that there must be known biological sensitivity of a disease or vector to climate, and that the change in disease or vector (change in seasonal cycle, latitudinal or altitudinal shifts) should be statistically associated with observed change in climate [28]. This has been rephrased as the need for there to be change in both disease/vector and climate at the same time, in the same place, and in the "right" direction [105]. Given these criteria, few diseases make the standard: Indeed, only a decade ago one group concluded that the literature lacks strong evidence for an impact of climate change on even a single vector-borne disease, let alone other diseases.

This situation has changed. One disease in particular, bluetongue, has emerged dramatically in Europe over the last decade and this emergence can be attributed to recent climate change in the region. It satisfies the right time, right place, right direction criterion [64], but in fact reaches a far higher standard: A model for the disease, with variability in time driven

only by variation in climate, produces quantitative estimates of risk which fit closely with the disease's recent emergence in both space and time.

Bluetongue

Bluetongue is a viral disease of sheep and cattle. It originated in Africa, where wild ruminants act as natural hosts for the virus, and where a species of biting midge, *Culicoides imicola*, is the major vector [106]. During the twentieth century bluetongue spread out of Africa into other, warm parts of the world, becoming endemic in the Americas, southern Asia, and Australasia; in most of these places, indigenous *Culicoides* became the vectors. Bluetongue also occurred very infrequently in the far extremes of southern Europe: once in the southwest (southern Spain and Portugal, 1955–1960), and every 20–30 years in the southeast (Cyprus, 1924, 1943–46); Cyprus and Greek islands close to Turkey (1977–1978); the presence of *C. imicola* was confirmed in both areas and this species was believed to be the responsible vector. Twenty years after this last 1977–1978 outbreak, in 1998 bluetongue once again reappeared in southeastern Europe [107]. Subsequent events, however, are unprecedented.

Between 1998 and 2008 bluetongue accounted for the deaths of more than one million sheep in Europe – by far the longest and largest outbreak on record. Bluetongue has occurred in many countries or regions that have never previously reported this disease or its close relatives. There have been at least two key developments. First, *C. imicola* has spread dramatically, now occurring over much of southern Europe and even mainland France. Second, indigenous European *Culicoides* species have transmitted the virus. This was first detected in the Balkans where bluetongue occurred but no *C. imicola* could be found [108]. In 2006, however, bluetongue was detected in northern Europe (The Netherlands) from where it spread to neighboring countries, the UK and even Scandinavia. The scale of this outbreak has been huge, yet the affected countries are far to the north of any known *C. imicola* territory [109].

Recently, the outputs of new, observation based, high spatial resolution (25 km) European climate data, from 1960 to 2006 have been integrated within a model for the risk of bluetongue transmission, defined by the basic reproduction ratio R_0 [110]. In this model, temporal variation in transmission risk is derived from the influence of climate (mainly temperature and rainfall) on the abundance of the vector species, and from the influence of temperature alone on the ability of the vectors to transmit the causative virus. As described earlier, this arises from the balance between vector longevity, vector feeding frequency, and the time required for the vector to become infectious. Spatial variation in transmission risk is derived from these same climate-driven influences and, additionally, differing densities of sheep and cattle. This integrated model successfully reproduces many aspects of bluetongue's distribution and occurrence, both past and present, in Western Europe, including its emergence in northwest Europe in 2006. The model gives this specific year the highest positive anomaly (relative to the long-term average) for the risk of bluetongue transmission since at least 1960, but suggests that other years were also at much higher-than-average risk. The model suggests that the risk of bluetongue transmission increased rapidly in southern Europe in the 1980s and in northern Europe in the 1990s and 2000s.

These results indicate that climate variability in space and time are sufficient to explain many aspects of bluetongue's recent past in Europe and provide the strongest evidence to date that this disease's emergence is, indeed, attributable to changes in climate. What then of the future? The same model was driven forward to 2050 using simulated climate data from regional climate models. The risk of bluetongue transmission in northwestern Europe is projected to continue increasing up to at least 2050 (Fig. 2). Given the continued presence of susceptible ruminant host populations, the models suggest that by 2050, transmission risk will have increased by 30% in northwest Europe relative to the 1961–1999 mean. The risk is also projected to increase in southwest Europe, but in this case only by 10% relative to the 1961–1999 mean.

The matching of observed change in bluetongue with quantitative predictions of a climate-driven disease model provides evidence for the influence of climate change far stronger than the "same place, same time, right direction" criterion described earlier. Indeed, it probably makes bluetongue the most convincing example of a disease that is responding to climate change. In this respect, bluetongue differs remarkably from another vector-borne disease, malaria.

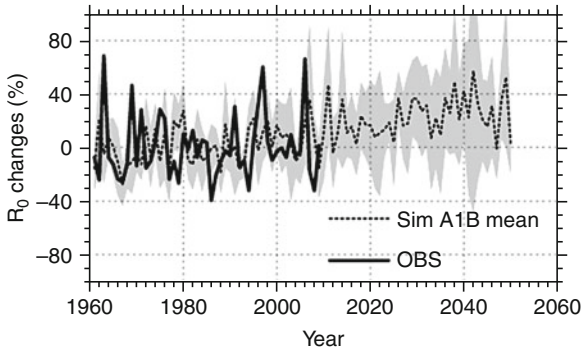

Infectious Diseases, Climate Change Effects on. Figure 2 Projections of the effect of climate change on the future risk of transmission of bluetongue in northern Europe. The *y-axis* shows relative anomalies (%) with respect to the 1961–1999 time period for the risk of bluetongue transmission, during August-October in northwest Europe, as defined by the basic reproductive ratio, R_0. R_0 was estimated from climate observations (*OBS – thick black line*), and an ensemble of 11 future climate projections (*SimA1B*), for which the *dashed line* presents the mean and the *grey* envelope the spread (Adapted from [110])

Malaria

Some 3.2 billion people live with the risk of malaria transmission, between 350 and 500 million clinical episodes of malaria occur each year and the disease kills at least one million people annually [111]. Of these, each year about 12 million cases and 155,000–310,000 deaths are in epidemic areas [112]. Interannual climate variability primarily drives the timing of these epidemics.

Malaria is caused by *Plasmodium* spp. parasites. Part of the parasite's life cycle takes place within anopheline mosquitoes while the remainder of the life cycle occurs within the human host. The parasite and mosquito life cycles are affected by weather and climate (mainly rain, temperature, and humidity), allowing models of the risk of malaria transmission to be driven by seasonal forecasts from ensemble prediction systems [113], thereby permitting forecasts of potential malaria outbreaks with lead times of up to 4–6 months [114, 115].

Among scientists there are contrasting views about the overall importance of climate on the transmission of malaria, and therefore on the importance of future climate change. Some argue that climate variability or change is the primary actor in any changing transmission pattern of malaria, while others suggest that any changing patterns today or in the foreseeable future are due to non-climate factors [35, 116, 117].

A key insight is that while global temperatures have risen, there has been a net reduction in malaria in the tropics over the last 100 years and temperature or rainfall change observed so far cannot explain this reduction [118]. Malaria has moved from being climate sensitive (an increasing relationship between ambient temperature and the extent of malaria transmission) in the days before disease interventions were widely available to a situation today where regions with malaria transmission are warmer than those without, but within the malaria-affected region, warmer temperatures no longer mean more disease transmission. Instead, other variables affecting malaria, such as good housing, the running of malaria control schemes, or ready access to affordable prophylaxis, now play a greater role than temperature in determining whether there are higher or lower amounts of transmission. This would suggest that the importance of climate change in discussions of future patterns of malaria transmission is likely to have been significantly overplayed.

What is clearly recognized, by all sides in the malaria and climate debate, is that mosquitoes need water to lay their eggs in, and for larval development, and that adult mosquitoes need to live long enough in an environment with high humidity and with sufficiently high temperature for transmission to be possible to the human host. Hence, while the spatial distribution of higher versus lower degrees of malaria transmission appears to have become, in a sense, divorced from ambient temperature, it seems likely that the weather plays as important a role as ever in determining when seasonal transmission will start and end. Climate change may therefore still have a role to play in malaria: not so much affecting where it occurs but, via changing rainfall patterns and mosquito numbers, when or for how long people are most at risk.

Malaria has only recently become confined to the developing world and tropics. It is less than 40 years since malaria was eradicated in Europe and the United States; and the 15°C July isotherm was the northern limit until the mid nineteenth century [119]. Changes in land use and increased living standards, in particular,

acted to reduce exposure to the mosquito vector in these temperate zones, leading ultimately to the final removal of the disease. In the UK, a proportion of the reduction has been attributed to increasing cattle numbers and the removal of marshland [120]. In Finland, changes in family size, improvements in housing, changes in farming practices, and the movement of farmsteads out of villages lead to the disappearance of malaria [121], where it had formerly been transmitted indoors in winter. While future increases in temperature may, theoretically, lead to an increased risk of malaria transmission in colder climes than at present [120, 122], the much-altered physical and natural environment may preclude this risk increasing to a level that merits concern. Once again, a more important future driver of malaria risk, in the UK at least, may be the pressure to return some of our landscape to its former state, such as the reflooding of previously drained marshland.

Future Directions

Climate change is widely considered to be a major threat to human and animal health, and the viability of certain endangered species, via its effects on infectious diseases. How realistic is this threat? Will most diseases respond to climate change, or just a few? Will there be a net increase in disease burden or might as many diseases decline in impact as increase?

The answers to these questions are important, as they could provide opportunities to mitigate against new disease threats, or may provide the knowledge-base required for policy makers to take necessary action to combat climate change itself. However, both the methodology to accurately predict climate change's effects on diseases and, in most cases, the data to apply the methodology to a sufficiently wide-range of pathogens is currently lacking.

The majority of pathogens, particularly those not reliant on intermediate hosts or arthropod vectors for transmission, either do occur, or have the potential to occur, in most parts of the world already. Climate change has the capacity to affect the frequency or scale of outbreaks of these diseases: Good examples would be the frequency of food poisoning events from the consumption of meat (such as salmonellosis) or shellfish (caused by *Vibrio* bacteria).

Vector-borne diseases are usually constrained in space by the climatic needs of their vectors, and such diseases are therefore the prime examples of where climate change might be expected to cause distributional shifts. Warmer temperatures usually favor the spread of vectors to previously colder environments, thereby exposing possibly naïve populations to new diseases.

However, altered rainfall distributions have an important role to play. Many pathogens or parasites, such as those of anthrax, haemonchosis, and numerous vector-borne diseases, may in some regions be subject to opposing forces of higher temperatures promoting pathogen or vector development, and increased summer dryness leading to more pathogen or vector mortality. Theoretically, increased dryness could lead to a declining risk of certain diseases. A good example is fasciolosis, where the lymnaeid snail hosts of the *Fasciola* trematode are particularly dependent on moisture. Less summer rainfall and reduced soil moisture may reduce the permissiveness of some parts of the UK for this disease. The snail and the free-living fluke stages are, nevertheless, also favored by warmer temperatures and, in practice, current evidence is that fasciolosis is spreading in the UK [123].

One way to predict the future for disease in a specific country is to learn from countries that, today, are projected to have that country's future climate [37, 39]. At least some of the complexity behind the multivariate nature of disease distributions should have precipitated out into the panel of diseases that these countries currently face.

For example, in broad terms, the UK's climate is predicted to get warmer, with drier summers and wetter winters, becoming therefore increasingly "mediterranean." It would seem reasonable, therefore, to predict that the UK of the future might experience diseases currently present in, or that occur periodically in, southern Europe. For humans, the best example would be leishmanosis (cutaneous and visceral) [124], while for animals, examples include West Nile fever [125], *Culicoides imicola*–transmitted bluetongue and African horse sickness [41], and canine leishmanosis [126]. The phlebotomid sandfly vectors of the latter do not currently occur in the UK, but they are found widely in southern continental Europe, including France, with recent reports of their detection in

Belgium [127]. The spread of the Asian tiger mosquito into Europe and the recent transmission in Europe of both dengue fever [128] and Chikungunya [129] by this vector are further cause for alarm.

However, the contrasting examples of bluetongue and malaria – one spreading because of climate change and one retreating despite it – show that considerations which focus entirely on climate may well turn out to be false. Why are these two diseases, both vector-borne and subject to the similar epidemiological processes and temperature dependencies, so different with respect to climate change? The answer lies in the relative importance of other disease drivers. For bluetongue, it is difficult to envisage epidemiologically relevant drivers of disease transmission, other than climate, that have changed significantly over the time period of the disease's emergence [64]. Life on the farm for the midges that spread bluetongue is probably not dramatically different today from the life they enjoyed 30 years ago. Admittedly, changes in the trade of animals or other goods may have been important drivers of the increased risk of introduction of the causative viruses into Europe, but after introduction, climate change may be the most important driver of increased risk of spread.

For malaria, change in drivers other than climate, such as land use and housing, the availability of prophylaxis, insecticides and, nowadays, insecticide-treated bed nets, have played far more dominant roles in reducing malaria occurrence than climate change may have played in increasing it. Two key reasons, then, for the difference between the two diseases are, first, that life for the human hosts of malaria has changed more rapidly than that of the ruminant hosts of bluetongue, and second, the human cost of malaria was so great that interventions were developed; while the (previously small) economic burden of bluetongue did not warrant such effort and our ability to combat the disease 5 years ago was not very different from that of 50 years before. The very recent advent of novel inactivated vaccines for bluetongue may now be changing this situation.

This entry began by asking whether climate change will affect most diseases or just a few. The examples of malaria and bluetongue demonstrate that a better question may be as follows: Of those diseases that are sensitive to climate change, how many are relatively free from the effects of other disease drivers such that the pressures brought by a changing climate can be turned into outcomes?

Bibliography

Primary Literature

1. Morens DM, Folkers GK, Fauci AS (2004) The challenge of emerging and re-emerging infectious diseases. Nature 430:242–249
2. Jones KE, Patel NG, Levy MA, Storeygard A, Balk D, Gittleman JL, Daszak P (2008) Global trends in emerging infectious diseases. Nature 451:990–993
3. IPCC (2001) Climate change 2001: the scientific basis. Intergovernmental Panel on Climate Change, Cambridge
4. Zhou XN, Yang GJ, Yang K, Wang XH, Hong QB, Sun LP, Malone JB, Kristensen TK, Bergquist NR, Utzinger J (2008) Potential impact of climate change on schistosomiasis transmission in China. Am J Trop Med 78:188–194
5. Rogers DJ, Packer MJ (1993) Vector-borne diseases, models, and global change. Lancet 342:1282–1284
6. Weaver SC, Barrett ADT (2004) Transmission cycles, host range, evolution and emergence of arboviral disease. Nat Rev Microbiol 2:789–801
7. Kovats RS, Edwards SJ, Hajat S, Armstrong BG, Ebi KL, Menne B (2004) The effect of temperature on food poisoning: a time-series analysis of salmonellosis in ten European countries. Epidemiol Infect 132:443–453
8. Donaldson AI (1972) The influence of relative humidity on the aerosol stability of different strains of foot-and-mouth disease virus suspended in saliva. J Gen Virol 15:25–33
9. Sutmoller P, Barteling SS, Olascoaga RC, Sumption KJ (2003) Control and eradication of foot-and-mouth disease. Virus Res 91:101–144
10. Wosu LO, Okiri JE, Enwezor PA (1992) Optimal time for vaccination against peste des petits ruminants (PPR) disease in goats in the humid tropical zone in southern Nigeria. In: Rey B, Lebbie SHB, Reynolds L (eds) Small ruminant research and development in Africa: proceedings of the first biennial conference of the African small ruminant research network. International Laboratory for Research in Animal Diseases (ILRAD), Nairobi
11. Anderson J, Barrett T, Scott GR (1996) Manual of the diagnosis of Rinderpest. Food and Agriculture Organization of the United Nations, Rome
12. Soebiyanto RP, Adimi F, Kiang RK (2010) Modeling and predicting seasonal influenza transmission in warm regions using climatological parameters. PLoS ONE 5:e9450
13. Lowen AC, Mubareka S, Steel J, Palese P (2007) Influenza virus transmission is dependent on relative humidity and temperature. PLoS Pathog 3:e151
14. Parker R, Mathis C, Looper M, Sawyer J (2002) Guide B-120: anthrax and livestock. Cooperative Extension Service, College of Agriculture and Home Economics, University of New Mexico, Las Cruces

15. Eiler A, Johansson M, Bertilsson S (2006) Environmental influences on *Vibrio* populations in northern temperate and boreal coastal waters (Baltic and Skagerrak Seas). Appl Environ Microbiol 72:6004–6011
16. Kausrud KL, Viljugrein H, Frigessi A, Begon M, Davis S, Leirs H, Dubyanskiy V, Stenseth NC (2007) Climatically driven synchrony of gerbil populations allows large-scale plague outbreaks. Proc R Soc B Biol Sci 274:1963–1969
17. Davis S, Begon M, De Bruyn L, Ageyev VS, Klassovskiy NL, Pole SB, Viljugrein H, Stenseth NC, Leirs H (2004) Predictive thresholds for plague in Kazakhstan. Science 304: 736–738
18. Baylis M, Mellor PS, Meiswinkel R (1999) Horse sickness and ENSO in South Africa. Nature 397:574
19. Davies F, Linthicum K, James A (1985) Rainfall and epizootic Rift Valley fever. Bull World Health Org 63:941–943
20. Linthicum KJ, Anyamba A, Tucker CJ, Kelley PW, Myers MF, Peters CJ (1999) Climate and satellite indicators to forecast Rift Valley fever epidemics in Kenya. Science 285:397–400
21. Linthicum KJ, Bailey CL, Davies FG, Tucker CJ (1987) Detection of Rift Valley fever viral activity in Kenya by satellite remote sensing imagery. Science 235:1656–1659
22. Anyamba A, Linthicum KJ, Mahoney R, Tucker CJ, Kelley PW (2002) Mapping potential risk of Rift Valley fever outbreaks in African savannas using vegetation index time series data. Photogramm Eng Remote Sens 68:137–145
23. Little PD, Mahmoud H, Coppock DL (2001) When deserts flood: risk management and climatic processes among East African pastoralists. Clim Res 19:149–159
24. Behm CA, Sangster NC (1999) Pathology, pathyophysiology and clinical aspects. In: Dalton JP (ed) Fasciolosis. CAB International, Wallingford, pp 185–224
25. Christie MG (1962) On hatching of *Nematodirus battus*, with some remarks on *N. filicollis*. Parasitology 52:297
26. Githeko AK, Lindsay SW, Confalonieri UE, Patz JA (2000) Climate change and vector-borne diseases: a regional analysis. Bull World Health Org 78:1136–1147
27. Hay SI, Cox J, Rogers DJ, Randolph SE, Stern DI, Shanks GD, Myers MF, Snow RW (2002) Climate change and the resurgence of malaria in the East African highlands. Nature 415:905–909
28. Kovats RS, Campbell-Lendrum DH, McMichael AJ, Woodward A, Cox JS (2001) Early effects of climate change: do they include changes in vector-borne disease? Philos Trans R Soc Lond B 356:1057–1068
29. Kovats RS, Haines A, Stanwell-Smith R, Martens P, Menne B, Bertollini R (1999) Climate change and human health in Europe. Br Med J 318:1682–1685
30. Lines J (1995) The effects of climatic and land-use changes on insect vectors of human disease. In: Harrington R, Stork NE (eds) Insects in a changing environment. Academic Press, London, pp 157–175
31. McMichael AJ, Githeko AK (2001) Human health (Chapter 9). In: McCarthy OFCJJ, Leary NA, Dokken DJ, White KS (eds) Climate change 2001: impacts, adaptation, and vulnerability: contribution of working group II to the third assessment report of the Intergovernmental Panel on Climate Change. Cambridge University Press, Cambridge, pp 453–485
32. Patz JA, Kovats RS (2002) Hotspots in climate change and human health. Br Med J 325:1094–1098
33. Randolph SE (2004) Evidence that climate change has caused 'emergence' of tick- borne diseases in Europe? Int J Med Microbiol 293:5–15
34. Reeves WC, Hardy JL, Reisen WK, Milby MM (1994) Potential effect of global warming on mosquito-borne arboviruses. J Med Entomol 31:323–332
35. Reiter P, Thomas CJ, Atkinson PM, Hay SI, Randolph SE, Rogers DJ, Shanks GD, Snow RW, Spielman A (2004) Global warming and malaria: a call for accuracy. Lancet Infect Dis 4:323–324
36. Rogers DJ, Randolph SE (2000) The global spread of malaria in a future, warmer world. Science 289:1763–1766
37. Rogers DJ, Randolph SE, Lindsay SW, Thomas CJ (2001) Vector-borne diseases and climate change. Department of Health, London
38. Semenza JC, Menne B (2009) Climate change and infectious diseases in Europe. Lancet Infect Dis 9:365–375
39. Sutherst RW (1998) Implications of global change and climate variability for vector-borne diseases: generic approaches to impact assessments. Int J Parasitol 28:935–945
40. WHO (1996) Climate change and human health. World Health Organisation, Geneva
41. Wittmann EJ, Baylis M (2000) Climate change: effects on *Culicoides*-transmitted viruses and implications for the UK. Vet J 160:107–117
42. Zell R (2004) Global climate change and the emergence/re-emergence of infectious diseases. Int J Med Microbiol 293:16–26
43. Baylis M, Githeko AK (2006) State of science review: the effects of climate change on infectious diseases of animals. Office of Science and Innovation, London
44. Cook G (1992) Effect of global warming on the distribution of parasitic and other infectious diseases: a review. J R Soc Med 85:688–691
45. Gale P, Adkin A, Drew T, Wooldridge M (2008) Predicting the impact of climate change on livestock disease in Great Britain. Vet Rec 162:214–215
46. Gale P, Drew T, Phipps LP, David G, Wooldridge M (2009) The effect of climate change on the occurrence and prevalence of livestock diseases in Great Britain: a review. J Appl Microbiol 106:1409–1423
47. Harvell CD, Kim K, Burkholder JM, Colwell RR, Epstein PR, Grimes DJ, Hofmann EE, Lipp EK, Osterhaus A, Overstreet RM, Porter JW, Smith GW, Vasta GR (1999) Review: marine ecology – emerging marine diseases – climate links and anthropogenic factors. Science 285:1505–1510
48. Harvell CD, Mitchell CE, Ward JR, Altizer S, Dobson AP, Ostfeld RS, Samuel MD (2002) Ecology – climate warming and disease risks for terrestrial and marine biota. Science 296:2158–2162

49. Perry BD, Randolph TF, McDermott JJ, Sones KR, Thornton PK (2002) Investing in animal health research to alleviate poverty. International Livestock Research Institute, Nairobi
50. Walther GR, Post E, Convey P, Menzel A, Parmesan C, Beebee TJC, Fromentin JM, Hoegh-Guldberg O, Bairlein F (2002) Ecological responses to recent climate change. Nature 416:389–395
51. Dowell SF (2001) Seasonal variation in host susceptibility and cycles of certain infectious diseases. Emerg Infect Dis 7:369–374
52. Cannell JJ, Vieth R, Umhau JC, Holick MF, Grant WB, Madronich S, Garland CF, Giovannucci E (2006) Epidemic influenza and vitamin D. Epidemiol Infect 134:1129–1140
53. Aucamp PJ (2003) Eighteen questions and answers about the effects of the depletion of the ozone layer on humans and the environment. Photochem Photobiol Sci 2:9–24
54. de Gruijl FR, Longstreth J, Norval M, Cullen AP, Slaper H, Kripke ML, Takizawa Y, van der Leun JC (2003) Health effects from stratospheric ozone depletion and interactions with climate change. Photochem Photobiol Sci 2:16–28
55. Jankovic D, Liu ZG, Gause WC (2001) Th1- and Th2-cell commitment during infectious disease: asymmetry in divergent pathways. Trends Immunol 22:450–457
56. Eisler MC, Torr SJ, Coleman PG, Machila N, Morton JF (2003) Integrated control of vector-borne diseases of livestock – pyrethroids: panacea or poison? Trends Parasitol 19:341–345
57. Coleman PG, Perry BD, Woolhouse MEJ (2001) Endemic stability – a veterinary idea applied to human public health. Lancet 357:1284–1286
58. Mullen G, Durden L (2002) Medical and veterinary entomology. Academic, Orlando
59. Gagnon AS, Bush ABG, Smoyer-Tomic KE (2001) Dengue epidemics and the El Nino Southern Oscillation. Clim Res 19:35–43
60. Gagnon AS, Smoyer-Tomic KE, Bush ABG (2002) The El Nino Southern Oscillation and malaria epidemics in South America. Int J Biometeorol 46:81–89
61. Hales S, Weinstein P, Souares Y, Woodward A (1999) El Niño and the dynamics of vector borne disease transmission. Environ Health Perspect 107:99–102
62. Kovats RS (2000) El Nino and human health. Bull World Health Org 78:1127–1135
63. Kramer LD, Hardy JL, Presser SB (1983) Effect of temperatures of extrinsic incubation on the vector competence of *Culex tarsalis* for western equine encephalomyelitis virus. Am J Trop Med 32:1130–1139
64. Purse BV, Mellor PS, Rogers DJ, Samuel AR, Mertens PPC, Baylis M (2005) Climate change and the recent emergence of bluetongue in Europe. Nat Rev Microbiol 3:171–181
65. Macdonald G (1955) The measurement of Malaria transmission. Proc R Soc Med Lond 48:295–302
66. De Koeijer AA, Elbers ARW (2007) Modelling of vector-borne disease and transmission of bluetongue virus in North-West Europe. In: Takken W, Knols BGJ (eds) Emerging pests and vector-borne diseases in Europe. Wageningen Academic, Wageningen, pp 99–112
67. Sellers RF (1992) Weather, *Culicoides*, and the distribution and spread of bluetongue and African horse sickness viruses. In: Walton TE, Osburn BI (eds) Bluetongue, African horse sickness and related Orbiviruses. CRC Press, Boca Raton, pp 284–290
68. Sellers RF, Maarouf AR (1991) Possible introduction of epizootic hemorrhagic disease of deer virus (serotype 20) and bluetongue virus (serotype 11) into British Columbia in 1987 and 1988 by infected *Culicoides* carried on the wind. Can J Vet Res 55:367–370
69. Sellers RF, Pedgley DE (1985) Possible windborne spread to Western Turkey of bluetongue virus in 1977 and of Akabane virus in 1979. J Hyg Camb 95:149–158
70. Sellers RF, Pedgley DE, Tucker MR (1977) Possible spread of African horse sickness on the wind. J Hyg Camb 79:279–298
71. Sellers RF, Pedgley DE, Tucker MR (1978) Possible windborne spread of bluetongue to Portugal, June-July 1956. J Hyg Camb 81:189–196
72. Sellers RF, Pedgley DE, Tucker MR (1982) Rift Valley fever, Egypt 1977: disease spread by windborne insect vectors? Vet Rec 110:73–77
73. Kock RA, Wambua JM, Mwanzia J, Wamwayi H, Ndungu EK, Barrett T, Kock ND, Rossiter PB (1999) Rinderpest epidemic in wild ruminants in Kenya 1993–97. Vet Rec 145:275–283
74. Davis AJ, Jenkinson LS, Lawton JH, Shorrocks B, Wood S (1998) Making mistakes when predicting shifts in species range in response to global warming. Nature 391:783–786
75. White PCL, Brown JA, Harris S (1993) Badgers (*Meles meles*), cattle and bovine tuberculosis (*Mycobacterium bovis*) – a hypothesis to explain the influence of habitat on the risk of disease transmission in southwest England. Proc R Soc Lond B 253:277–284
76. Tompkins DM, Dobson AP, Arneberg P, Begon ME, Cattadori IM, Greenman JV, Heesterbeek JAP, Hudson PJ, Newborn D, Pugliese A, Rizzoli AP, Rosa R, Rosso F, Wilson K (2001) Parasites and host population dynamics. In: Hudson PJ, Dobson AP (eds) Ecology of wildlife diseases. Oxford University Press, Oxford, pp 45–62
77. Smith KF, Sax DF, Lafferty KD (2006) Evidence for the role of infectious disease in species extinction and endangerment. Conserv Biol 20:1349–1357
78. Wyatt KB, Campos PF, Gilbert MTP, Kolokotronis SO, Hynes WH, DeSalle R, Daszak P, MacPhee RDE, Greenwood AD (2008) Historical mammal extinction on christmas island (Indian ocean) correlates with introduced infectious disease. PLoS ONE 3(11):e3602
79. Freed LA, Cann RL, Goff ML, Kuntz WA, Bodner GR (2005) Increase in avian malaria at upper elevation in Hawai'i. Condor 107:753–764
80. Haydon DT, Laurenson MK, Sillero-Zubiri C (2002) Integrating epidemiology into population viability analysis: managing the risk posed by rabies and canine distemper to the Ethiopian wolf. Conserv Biol 16:1372–1385

81. McCallum H, Jones M (2006) To lose both would look like carelessness: Tasmanian devil facial tumour disease. PLoS Biol 4:1671–1674
82. Frick WF, Pollock JF, Hicks AC, Langwig KE, Reynolds DS, Turner GG, Butchkoski CM, Kunz TH (2010) An emerging disease causes regional population collapse of a common North American bat species. Science 329:679–682
83. Smith KF, Acevedo-Whitehouse K, Pedersen AB (2009) The role of infectious diseases in biological conservation. Anim Conserv 12:1–12
84. Daszak P, Cunningham AA, Hyatt AD (2000) Wildlife ecology – emerging infectious diseases of wildlife – threats to biodiversity and human health. Science 287:443–449
85. Gortazar C, Ferroglio E, Hofle U, Frolich K, Vicente J (2007) Diseases shared between wildlife and livestock: a European perspective. Eur J Wildl Res 53:241–256
86. Wolfe ND, Dunavan CP, Diamond J (2007) Origins of major human infectious diseases. Nature 447:279–283
87. van der Riet FD (1997) Diseases of plants transmissible between plants and man (phytonoses) exist. Med Hypotheses 49:359–361
88. Williams JW, Jackson ST, Kutzbacht JE (2007) Projected distributions of novel and disappearing climates by 2100 AD. Proc Natl Acad Sci USA 104:5738–5742
89. Benning TL, LaPointe D, Atkinson CT, Vitousek PM (2002) Interactions of climate change with biological invasions and land use in the Hawaiian islands: modeling the fate of endemic birds using a geographic information system. Proc Natl Acad Sci USA 99:14246–14249
90. Isaac NJB, Turvey ST, Collen B, Waterman C, Baillie JEM (2007) Mammals on the EDGE: conservation priorities based on threat and phylogeny. PLoS ONE 2(3):e296
91. Ford SE, Smolowitz R (2007) Infection dynamics of an oyster parasite in its newly expanded range. Mar Biol 151:119–133
92. Sokolow S (2009) Effects of a changing climate on the dynamics of coral infectious disease: a review of the evidence. Dis Aquat Organ 87:5–18
93. Ricketts TH, Dinerstein E, Boucher T, Brooks TM, Butchart SHM, Hoffmann M, Lamoreux JF, Morrison J, Parr M, Pilgrim JD, Rodrigues ASL, Sechrest W, Wallace GE, Berlin K, Bielby J, Burgess ND, Church DR, Cox N, Knox D, Loucks C, Luck GW, Master LL, Moore R, Naidoo R, Ridgely R, Schatz GE, Shire G, Strand H, Wettengel W, Wikramanayake E (2005) Pinpointing and preventing imminent extinctions. Proc Natl Acad Sci USA 102:18497–18501
94. Kutz SJ, Hoberg EP, Polley L, Jenkins EJ (2005) Global warming is changing the dynamics of Arctic host-parasite systems. Proc R Soc Lond B 272:2571–2576
95. Ytrehus B, Bretten T, Bergsjo B, Isaksen K (2008) Fatal pneumonia epizootic in musk ox (*Ovibos moschatus*) in a period of extraordinary weather conditions. EcoHealth 5:213–223
96. Bradley M, Kutz SJ, Jenkins E, O'Hara TM (2005) The potential impact of climate change on infectious diseases of Arctic fauna. Int J Circumpolar Health 64:468–477
97. Berger L, Hyatt AD, Speare R, Longcore JE (2005) Life cycle stages of the amphibian chytrid *Batrachochytrium dendrobatidis*. Dis Aquat Organ 68:51–63
98. Pounds JA, Bustamante MR, Coloma LA, Consuegra JA, Fogden MPL, Foster PN, La Marca E, Masters KL, Merino-Viteri A, Puschendorf R, Ron SR, Sanchez-Azofeifa GA, Still CJ, Young BE (2006) Widespread amphibian extinctions from epidemic disease driven by global warming. Nature 439:161–167
99. Ribas L, Li MS, Doddington BJ, Robert J, Seidel JA, Kroll JS, Zimmerman LB, Grassly NC, Garner TWJ, Fisher MC (2009) Expression profiling the temperature-dependent amphibian response to infection by *Batrachochytrium dendrobatidis*. PLoS ONE 4(12):e8408
100. Gleason FH, Letcher PM, McGee PA (2008) Freeze tolerance of soil chytrids from temperate climates in Australia. Mycol Res 112:976–982
101. Fisher MC, Garner TWJ, Walker SF (2009) Global emergence of *Batrachochytrium dendrobatidis* and amphibian chytridiomycosis in space, time, and host. Annu Rev Microbiol 63:291–310
102. Pounds JA, Crump ML (1994) Amphibian declines and climate disturbance – the case of the golden toad and the harlequin frog. Conserv Biol 8:72–85
103. Garner TWJ, Walker S, Bosch J, Leech S, Rowcliffe JM, Cunningham AA, Fisher MC (2009) Life history tradeoffs influence mortality associated with the amphibian pathogen *Batrachochytrium dendrobatidis*. Oikos 118: 783–791
104. Lips KR, Diffendorfer J, Mendelson JR, Sears MW (2008) Riding the wave: reconciling the roles of disease and climate change in amphibian declines. PLoS Biol 6:441–454
105. Rogers DJ, Randolph SE (2003) Studying the global distribution of infectious diseases using GIS and RS. Nat Rev Microbiol 1:231–237
106. Mellor PS, Boorman J, Baylis M (2000) Culicoides biting midges: their role as arbovirus vectors. Annu Rev Entomol 45:307–340
107. Mellor PS, Wittmann EJ (2002) Bluetongue virus in the Mediterranean basin 1998–2001. Vet J 164:20–37
108. Purse BV, Nedelchev N, Georgiev G, Veleva E, Boorman J, Denison E, Veronesi E, Carpenter S, Baylis M, Mellor PS (2006) Spatial and temporal distribution of bluetongue and its Culicoides vectors in Bulgaria. Med Vet Entomol 20:335–344
109. Mellor PS, Carpenter S, Harrup L, Baylis M, Mertens PPC (2008) Bluetongue in Europe and the Mediterranean basin: history of occurrence prior to 2006. Prev Vet Med 87:4–20
110. Guis H, Caminade C, Calvete C, Morse AP, Tran A, Baylis M (2011) Modelling the effects of past and future climate on the risk of bluetongue emergence in Europe. J Roy Soc Interface (in press)
111. WHO (2005) World Malaria report, rollback Malaria programme. World Health Organisation, Geneva

112. Worrall E, Rietveld A, Delacollette C (2004) The burden of malaria epidemics and cost-effectiveness of interventions in epidemic situations in Africa. Am J Trop Med 71:136–140
113. Palmer TN, Alessandri A, Andersen U, Cantelaube P, Davey M, Delecluse P, Deque M, Diez E, Doblas-Reyes FJ, Feddersen H, Graham R, Gualdi S, Gueremy JF, Hagedorn R, Hoshen M, Keenlyside N, Latif M, Lazar A, Maisonnave E, Marletto V, Morse AP, Orfila B, Rogel P, Terres JM, Thomson MC (2004) Development of a European multimodel ensemble system for seasonal-to-interannual prediction (DEMETER). Bull Am Meteorol Soc 85:853–872
114. Morse AP, Doblas-Reyes FJ, Hoshen MB, Hagedorn R, Palmer TN (2005) A forecast quality assessment of an end-to-end probabilistic multi-model seasonal forecast system using a malaria model. Tellus Ser A 57:464–475
115. Jones AE, Morse AP (2010) Application and validation of a seasonal ensemble prediction system using a dynamic malaria model. J Clim 23:4202–4215
116. Lafferty KD (2009) The ecology of climate change and infectious diseases. Ecology 90:888–900
117. Epstein P (2010) The ecology of climate change and infectious diseases: comment. Ecology 91:925–928
118. Gething PW, Smith DL, Patil AP, Tatem AJ, Snow RW, Hay SI (2010) Climate change and the global malaria recession. Nature 465:342–344
119. Reiter P (2008) Global warming and malaria: knowing the horse before hitching the cart. Malar J 7:S3
120. Kuhn KG, Campbell-Lendrum DH, Armstrong B, Davies CR (2003) Malaria in Britain: past, present, and future. Proc Natl Acad Sci USA 100:9997–10001
121. Hulden L (2009) The decline of malaria in Finland – the impact of the vector and social variables. Malar J 8:94
122. Lindsay SW, Hole DG, Hutchinson RA, Richards SA, Willis SG (2010) Assessing the future threat from vivax malaria in the United Kingdom using two markedly different modelling approaches. Malar J 9:70
123. Pritchard GC, Forbes AB, Williams DJL, Salimi-Bejestani MR, Daniel RG (2005) Emergence of fasciolosis in cattle in East Anglia. Vet Rec 157:578–582
124. Dujardin JC, Campino L, Canavate C, Dedet JP, Gradoni L, Soteriadou K, Mazeris A, Ozbel Y, Boelaert M (2008) Spread of vector-borne diseases and neglect of leishmaniasis, Europe. Emerg Infect Dis 14:1013–1018
125. Gould EA, Higgs S, Buckley A, Gritsun TS (2006) Potential arbovirus emergence and implications for the United Kingdom. Emerg Infect Dis 12:549–555
126. Shaw SE, Langton DA, Hillman TJ (2008) Canine leishmaniosis in the UK. Vet Rec 163:253–254
127. Depaquit J, Naucke TJ, Schmitt C, Ferté H, Léger N (2005) A molecular analysis of the subgenus *Transphlebotomus* Artemiev, 1984 (Phlebotomus, Diptera, Psychodidae) inferred from ND4 mtDNA with new northern records of *Phlebotomus mascittii* Grassi, 1908. Parasitol Res 95:113–116
128. La Ruche G, Souares Y, Armengaud A, Peloux-Petiot F, Delaunay P, Despres P, Lenglet A, Jourdain F, Leparc-Goffart I, Charlet F, Ollier L, Mantey K, Mollet T, Fournier JP, Torrents R, Leitmeyer K, Hilairet P, Zeller H, Van Bortel W, Dejour-Salamanca D, Grandadam M, Gastellu-Etchegorry M (2010) First two autochthonous dengue virus infections in metropolitan France, September 2010. Euro Surveill 15:2–6
129. Eitrem R, Vene S (2008) Chikungunya fever-a threat for Europeans. A review of the recent literature. Parasitol Res 103: S147–S148

Books and Reviews

International Panel on Climate Change (2007) Climate change 2007: impacts, adaptation and vulnerability. Cambridge University Press, Cambridge

Infectious Diseases, Introduction

Phyllis J. Kanki
Department of Immunology and Infectious Diseases, Harvard School of Public Health, Boston, MA, USA

Infectious diseases of humans and animals are illnesses resulting from an infection caused by the presence or growth of a biological organism, often termed a pathogen, for its disease-causing behavior. The term derives from the transmissibility of the pathogen to others and when this results in large numbers of infections in a region can be responsible for epidemics. Pathogens responsible for infectious diseases can be viruses, bacteria, protozoa, fungi, multicellular parasites, and prions. While antibiotics and vaccines have made major progress in the treatment and prevention of major infectious diseases, largely in the developed world, the developing world still bears a significant burden of disease due to infectious disease pathogens such as malaria, tuberculosis, and the Human Immunodeficiency Virus (HIV). Changes in the environment, zoonotic pathogens and their interaction with human populations, and medical practice including treatment and vaccines are just some examples of determinants that can modulate the impact of infectious diseases, in terms of spread, ability to cause disease, or even response to prevention or treatment measures. The ever-changing dynamic nature of infectious diseases is not only due to some pathogen's intrinsic propensity for diversity and fitness but also complex

lifecycles involving intermediate nonhuman hosts. Therefore, our ability to control or eradicate various infectious diseases must entail new technologies and analytic methods.

There is significant disparity in the burden of infectious diseases globally. According to the 2008 Global Health Observatory report, infectious diseases only account for one of the top ten causes of death in high-income countries of the world, whereas in low- and middle-income countries, four of the ten leading causes of death are infectious diseases [1]. However, the mobility of populations globally has resulted in infectious disease outbreaks such as the H1N1 influenza outbreak in Mexico in March 2009 that led to 28,000 confirmed cases in the United States just 3 months later. The WHO raised the pandemic alert level to phase 6, the highest level indicating a global pandemic, because of widespread infection beyond North America to Australia, the United Kingdom, Argentina, Chile, Spain, and Japan. Six months after the initial outbreak in Mexico, H1N1 infection had been confirmed in over 200,000 people from more than 100 countries and several thousand deaths [2]. While influenza virus infections are found in both high- and low- and middle-income countries, the virus responsible for this pandemic appeared to be a novel virus with characteristics of North American and Asian swine influenza viruses, as well as human and avian influenza viruses. Thus, the viruses' propensity for variation through genetic reassortment, various animal reservoirs and their contact with human populations, and the mobility of populations led to an epidemic of global proportions in a short time period.

In the past decade, international donor agencies have supported large-scale programs to address the gap in prevention and treatment of HIV/AIDS, malaria and tuberculosis. The burden of these three infectious diseases is disproportionately high in Africa, where health systems are weak and heavily dependent on foreign aid. The President's Emergency Plan For AIDS Relief initiated in 2005 is the single largest funded program for a disease in the history of US government support, active in 30 countries primarily in Africa and responsible for the initiation of antiretroviral therapy to 3.2 million adults and children with AIDS. A summary of the "► HIV/AIDS Global Epidemic" describes the many challenges posed by the HIV virus, first described in the early 1980s. The HIV/AIDS epidemic most severe in Africa has also led to a concurrent increase in tuberculosis, where the presence of either infection increases the risk of coinfection, and as a result in the past decade, TB incidence has tripled. HIV and TB coinfected patients are more difficult to treat and are responsible for the highest mortality rates in both untreated and treated populations. The complex "► Tuberculosis, Epidemiology of" described by Mario Raviglione and colleagues illustrates both the severity of the public health problem and the efforts by the WHO Stop TB alliance in its control. Development of improved, cost-effective, and point-of-care diagnostics is an emphasis for all three of these pathogens.

The development of drug resistance is another feature common to many infectious disease pathogens. The widespread use of chloraquine to treat malaria in the 1940s and 1950s, led to the detection of chloraquine resistant malaria first in South America and Asia and later in Africa by the late 1970s. It became widespread across Africa within a decade. Continued surveillance for drug resistance is critical to adjust treatment policies and the need for more effective drugs is ever present. In 2006 in Tugela Ferry, South Africa, the interaction between tuberculosis and HIV resulted in the recognition of an "extensively drug resistant" tuberculosis strain (XDR), where the bacteria was not only resistance to the common first line drugs, rifampicin and isoniazid but also to drugs in the quinolone family and at least one of the second line drugs [3]. The XDR tuberculosis epidemic in Tugela Ferry was unusually severe with rapid (~2 weeks) mortality, demonstrating the grave consequences of pathogens that readily evolve under drug pressure. As a result of these biologic propensities, the need for new drugs that target resistant strains is an ongoing process. The cost of second and third line drug therapy is prohibitive in most low-income countries and the need for more efficacious and cost-effective drugs is an important priority. Unfortunately, despite the importance of these pathogens like malaria and TB primarily in low-income countries, major biotechnology firms do not prioritize these diseases agents for diagnostic, vaccine, or drug development. The example of malaria and the structural barriers to solutions for low-income (tropical) settings is well described by J. Kevin Baird in "► Tropical Health and Sustainability."

It is widely believed that prevention measures including vaccines are the most effective means of combating infectious diseases whenever possible and this becomes of paramount importance in infectious diseases with high burden and mortality. In the case of malaria, the ubiquity of the mosquito vector, difficulty in its control, and prevalent drug resistance all lend support for the search for an effective malaria vaccine. As described by Christopher Plowe in "► Malaria Vaccines," a study conducted in a single African village, documented more than 200 variants of blood stage malaria antigens. Thus evidence of the difficulty in developing vaccines that must elicit cross-protective immunity to an ever-expanding set of antigens, such as the multiple parasitic stages of malaria. Despite these many challenges, Christopher Plowe describes progress toward a malaria vaccine that would reduce parasite burden, rather than sterilizing protection, such a vaccine would be an important milestone to be reached in the short-term future of malaria control.

While effective vaccines against poliomyelitis have been available since the 1950s, the global eradication campaign is still in effect, with >99% reduction in the number of cases since 1988 and the inception of the Global Poliomyelitis Eradication Initiative by the World Health Assembly. Indigenous poliovirus remains in only four countries of the world, including Afghanistan, Pakistan, Nigeria, and India. "► Polio and its Epidemiology" by Lester Shulman describes the complexity of a disease system with both natural and vaccine strains of the poliovirus, and the many challenges to its future eradication. The use of the live oral polio vaccine has generated vaccine-derived poliovirus, which contributes to the complex molecular epidemiology of polioviruses in countries with residual infection. The cost and implementation considerations for polio's ultimate eradication are therefore far from simple. It is possible that alternative inactivated vaccines may need to be developed if the ultimate phase out of the current oral polio vaccine is to be considered.

Worldwide, one billion people are infected with pathogens termed neglected tropical diseases, largely in low-income countries. Many infectious diseases in this category are considered waterborne. A comprehensive review of major waterborne diseases is covered in "► Waterborne Infectious Diseases, Approaches to Control" by Fenwick and colleagues. Where the water serves as the habitat for the intermediate animal host or vector and the proximity of human populations facilitates the lifecycle. These include diseases such as schistosomiasis, a protozoa transmitted by snails and guinea worm, transmitted by contaminated water, onchocerciasis or river blindness transmitted by flies, as examples. Protozoal and parasitic infections often have complex lifecycles involving multiple hosts, creating challenges to prevention and treatment. Since 1986, the Carter Foundation has devoted its efforts to neglected tropical diseases such as guinea worm in Africa. More than 3.5 million people were affected by this parasitic roundworm untreatable infection caused by *Dracunculus medenisis* in the 1980s and today, the eradication of this disease through prevention is imminent, despite its neglect in the global health agenda.

Zoonotic diseases are infectious diseases transmitted from animals to humans, and constitute more than half of infectious diseases to humans [4]. There are examples of viruses, bacteria, protozoa, parasites, and prions (transmissible proteins) that are considered zoonotic diseases, where their biology and epidemiology are influenced by the animal host, its behavior, and ecology. Examples such as anthrax (*Bacillus anthrasis*), bovine tuberculosis (*Mycobacterium bovis*), brucellosis (*Brucella* sp), cysticercosis (*Taenia solium*, the pork tapeworm), echinococcosis (*Echinococcus* sp), and rabies virus are endemic in many developing countries of Africa, Asia, and South and Central America. Many of which have poor human and veterinary infrastructure to control these important pathogens. Interdisciplinary research is needed to develop novel and more effective control measures. The divided responsibilities between veterinary and medical governing bodies and resources needs to be further integrated as envisioned by the "One Health" initiatives that study the risks of biological pollution on wildlife and humans.

Climate change has long been considered an important determinant of many infectious diseases but the field has been recently expanding in its scope. Pathogens requiring an intermediate host or insect vector may be particularly sensitive to climate change. Warmer temperatures will be predicted to provide an expanded environment for vectors such as mosquitoes, potentially changing the distribution of vector borne human disease. Climate change has also been associated with the frequency or magnitude of outbreaks of food poisoning

due to salmonellosis in meat or Vibrio infection in shellfish. This field is expanding to consider infectious diseases that are nonvector borne with consideration of climate's impact on seasonality, pathogen replication, dispersal, and survival. However, as described in "► Infectious Diseases, Climate Change Effects on" by Matthew Baylis and Claire Risley, the methodology for predicting climate change's impact on disease is yet to be fully developed and more research is needed to collect data on pathogens that might be influenced.

Disease control in humanitarian emergencies should rely on joint situation analysis and technical support involving experts from related specialties and include the development of standards, guidelines, and tools adapted for field use. Communicable disease epidemiological profiles and risk assessments specific to countries or crisis situations prioritize interventions and provide policy guidance to national authorities and humanitarian partner agencies for the control of communicable diseases in specific settings [5]. As an example, in an 8-week period in 2011, a cholera outbreak was reported in the Democratic Republic of Congo (DRC) and Republic of Congo, a poliomyelitis outbreak in Pakistan, and cases of avian influenza in humans in Egypt. Thus highlighting the ever-changing threat of infectious disease infections on a global and temporal scale.

The dynamic nature of various infectious disease agents is thus evident from a variety of examples, and the harnessing of new technologies for the rapid diagnosis and response to infectious disease agents is described in "► Infectious Diseases, Vibrational Spectroscopic Approaches to Rapid Diagnostics" by Jeremy Driskell and Ralph Tripp. These new high-resolution approaches are being developed and evaluated for both bacterial and viral pathogens. Their further instrumentation and commercialization envisions point-of-care, mobile, and cost-effective spectroscopic based diagnostic methods, which has great potential for the sustainability of infectious disease agent control in our ever-changing environment.

The development of new treatments for current, emerging, and drug resistant infectious disease pathogens is also a priority. In "► Antibiotics for Emerging Pathogens," Vinayak Agarwal and Satish Nair describe improvements and innovations to the approach of identification of antibiotics through metabolic connections between the host and microbe, as well as synthesis and mining of new potential antibiotic candidates. Added to these more conventional approaches is the use of genomics and bioinformatics to identify antibiotic gene clusters and microbial ecological evaluations to better understand the interactions of natural antibiotic with their microbial targets. Future emphasis on narrow spectrum antibiotics coupled with more discriminating diagnostic methods may reduce the emergence of drug resistance already associated with use of broad-spectrum agents.

"► Infectious Disease Modeling," as described by Angela McLean, has become an important methodology to characterize disease spread, both in populations and within a single host. While within-host modeling, often considers the spread of infection within an individual and its interface with the host's immune responses, newer models employ multiple levels simultaneously; such as within-host dynamics and between host transmissions. Modeling has become an even more important tool in characterizing infectious diseases particularly with the challenges of growing population and densities. These methods can organize available data and identify critical missing data. Perhaps most important is the use of modeling techniques to compare or project the impact of various intervention strategies.

Globally, infectious diseases account for more than 17 million deaths each year. While modern medicine and technology have diminished the threat of many of these pathogens in high-income countries, the ever present threats of reemerging infections, population mobility, and pathogen genetic variability are but some of the reasons for the dynamic threat of this broad category of risks to human health. The majority of infectious disease burden remains in the tropics, in low- and middle-income countries with scare resources, infrastructure, and health systems to mount or sustain control efforts in the absence of outside support. It is therefore critical that efforts from the scientific research community and international donor agencies continue to increase their efforts with integrated goals of vigilant surveillance, improved and cost-effective diagnostics, and treatment with a goal of sustainable control.

Cross-References

► Airborne Toxic Chemicals
► Biomarkers and Metabolomics, Evidence of Stress

I

▶ Bioremediation and Mitigation
▶ Biosensors and Bioassays for Ecological Risk Monitoring and Assessment
▶ CERCLA, Sustainability and Public and Environmental Health
▶ Ecological and Health Risks at Low Doses
▶ Ecological Risk Assessment and Animal Models
▶ Environmental Toxicology: Carcinogenesis
▶ Environmental Toxicology: Children at Risk
▶ Microbial Risk Assessment of Pathogens in Water
▶ Recreational Water Risk: Pathogens and Fecal Indicators
▶ Science, Policy, and Risk Management: Case of Seafood Safety
▶ Xenobiotic Protection/Resistance Mechanisms in Organisms

Bibliography

1. WHO. http://www.who.int/gho/mortality_burden_disease/causes_death_2008/en/index.html
2. WHO. Influenza A (H1N1): special insights. http://www.who.int/en/
3. Gandhi NR, Moll A, Sturm AW, Pawinski R, Govender T, Lalloo U, Zeller K, Andrews J et al (2006) Extensively drug-resistant tuberculosis as a cause of death in patients co-infected with tuberculosis and HIV in a rural area of South Africa. Lancet 368: 1575–1580
4. Taylor LH, Latham SM, Woolhouse MEJ (2001) Risk factors for human disease emergence. Philos Trans R Soc Lond B 356:983–989
5. WHO. Global alert and response. http://www.who.int/csr/en/

Infectious Diseases, Vibrational Spectroscopic Approaches to Rapid Diagnostics

Jeremy D. Driskell, Ralph A. Tripp
Department of Infectious Diseases, College of Veterinary Medicine, Animal Health Research Center, University of Georgia, Athens, GA, USA

Article Outline

Glossary
Definition of the Subject and Its Importance
Introduction
Spectroscopy-Based Diagnostics
Future Directions
Bibliography

Glossary

Chemometrics A term to describe the use of multivariate statistics used to extract chemical information.

Fourier-transform infrared spectroscopy (FTIR) A specific technique for acquiring IR absorption spectra in which all wavelengths are simultaneously measured.

Infrared spectroscopy An absorption-based vibrational spectroscopic technique which primarily probes non-polar bonds.

Polymerase chain reaction (PCR) An enzymatic method for amplifying a specific nucleic acid sequence.

Raman spectroscopy A scattering vibrational spectroscopic technique which primarily probes polar bonds.

Surface-enhanced Raman spectroscopy (SERS) A technique used to amplify Raman scattered signal via adsorption to a nanometer-scale metallic surface.

Vibrational (molecular) spectroscopy A general term for the use of light to probe vibrations in a sample as a means of determining chemical composition and structure.

Definition of the Subject and Its Importance

Importance of Rapid Diagnosis of Infectious Diseases

Infectious diseases are a major burden on human health with the World Health Organization (WHO) reporting that infectious diseases are responsible for one in ten deaths in the world's richest nations. The impact of infectious diseases is even greater in poorer regions of the world where six of every ten deaths are caused by a spectrum of infectious diseases that include bacteria, viruses, parasites and fungi. These infectious agents can further be described as classical pathogens, e.g., tuberculosis and malaria, seasonal epidemics, e.g., influenza and rhinoviruses, emerging infectious

disease, e.g., highly pathogenic avian influenza and hemorrhagic fevers, or global pandemics such as the most recent outbreak of novel H1N1 influenza virus. Central to the management of each of these diseases are diagnostics. Early and rapid detection of an infectious agent is not only imperative to prevent the spread of disease, but it is also an essential first step to identify appropriate therapeutics that target the disease, as well as to overcome inappropriate administration of ineffective drugs that may drastically lead to drug-resistant pathogens such as methicillin-resistant *Staphylococcus aureus* (MRSA). This is just a succinct example which highlights the importance of diagnostic testing; however, the sections that follow discuss the current status of diagnostics and introduce an emerging approach to diagnostics based on vibrational spectroscopy which has tremendous potential to significantly advance the field.

Introduction

Classical Culture-Based Diagnostics

Despite the importance of diagnostic tests for infectious diseases, relatively few technological advances have supplanted classical microbiological approaches, e.g., in vitro culture, as a diagnostic standard. Clinical laboratories routinely rely on selective and chromogenic growth media to identify bacterial agents. For example, an αβ−chromogenic medium, which includes two substrates, has been developed to selectively isolate *Salmonella* spp. with 100% sensitivity and 90.5% specificity [1]. More recently chromogenic media have been developed to identify *Staphylococcus aureus* and distinguish methicillin-resistant strains (MRSA) [2, 3]. Culture-based diagnostics provide a method for definitive identification of many bacteria, and the tests are relatively inexpensive; however, the identification process has generally low throughput and substantial time is required for diagnostics. Typically, culture requires 24–72 h to allow the bacteria to grow while slow-growing organisms such as mycobacteria require substantially longer (6–12 week) incubation times. Obviously, this is not ideal as the time frame can delay patient treatment. It should also be noted that not all pathogens can be cultured in a laboratory environment, thus the technique cannot be universally applied. There are several additional drawbacks of culture-based diagnostic methods including the requirement for species specific reagents, appropriate culture and storage environments, and labor intensive procedures.

Antibody-Based Diagnostics

Antigen detection and serology are common approaches used in clinical laboratories as alternative or complementary tools to culture-based detection. Common to both of these methods is the use of antibodies either to directly label and detect the antigen or to capture the host response, e.g., antibody responses to infection. Typically, an enzyme-linked immunosorbent assay (ELISA) is employed for antigen detection in diagnostic laboratories. As a first step, ELISA requires an unknown amount of antigen in a sample to be specifically, via a capture antibody in a sandwich assay format, or nonspecifically, via adsorption, immobilized to a solid phase such as a microtiter plate. After removing excess antigen, a known amount of detection antibody specific to the pathogen is then introduced to bind any immobilized antigen. The detection antibody is either directly labeled with an enzyme, or in an additional step, detected with an enzyme-labeled secondary antibody. After removal of excess reagent, a substrate is introduced to react with the enzyme producing a quantifiable color change. A slight modification of this approach replaces the enzyme with a fluorophor for fluorescence-based readout, eliminating the final substrate incubation step. A similar approach is taken for ELISA-based serological assays in which a known amount of purified antigen is immobilized onto the solid phase and incubated with serum to detect the presence of antibodies. While the procedure requires multitudinous steps, reagents, and substantial labor, ELISA is considered rapid relative to culture-based diagnostics as in many cases the assay can be completed within several hours. ELISA-based assays continue to be an integral part of laboratory diagnostics, but in their original form they are limited to the laboratory.

Lateral flow immunoassays, also called dipstick assays, immunochromatography, sol particle immunoassays, or rapid diagnostic tests, have been developed to overcome many limitations of ELISAs by eliminating the complex multi-step procedure, reducing labor, and allowing field or point-of-care testing. Lateral

flow assays, like ELISAs, utilize pathogen-specific antibodies for the direct detection of antigen or detection of antibody response. However, for the case of lateral-flow assays the labeled detection antibody, capture antibody, and control reagents are dried on a prefabricated carrier strip. By design, these assays overcome diffusion-limited kinetics to exploit the rapid kinetics of antibody-antigen recognition [4, 5] to yield results in 10–20 min. Thus, because of the "reagentless" nature and rapid results, these assays are well suited for field use and resource-poor regions where reagent storage and test sites are severely limited. It should be noted, however, that these benefits are at the loss of quantitative information and often a lower threshold of detection.

Numerous lateral flow immunoassays have been developed commercially for clinical diagnostics. Several competing manufacturers offer rapid diagnostic tests for influenza virus in which a conserved antigen is detected in a lateral flow assay format. Some detect influenza A and influenza B without distinction of the subtypes, e.g., QuickVue Influenza Test (Quidel), others detect and differentiate A and B strains, e.g., QuickVue Influenza A + B Test (Quidel) and 3 M™ Rapid Detection Flu A + B Test, and some only identify A or B strains, e.g., SAS Influenza A Test, (SA Scientific). Similarly, commercial rapid diagnostic tests are available for detection of a conserved protein for rotavirus A, e.g., IVD Rotavirus A Testing Kit. Not all lateral flow assays are designed for antigen detection; a rapid diagnostic test developed for leptospirosis diagnosis target anti-*Leptospira* IgM antibodies [6].

Despite continued advancements in antibody-based diagnostics these platforms will always be limited by the need for species-specific reagents, i.e., antibodies where the assays can only perform with the sensitivity and specificity inherent to the antibody. For example, commercial lateral flow assays for influenza only provide 50–70% sensitivity and 90–95% specificity with respect to culture-based diagnosis [7]. While the lateral flow assays may be performed rapidly, their low sensitivity may preclude early diagnosis due to low levels or unsustained levels of antigen through disease available for detection. Moreover, serological-based assays developed to detect agent-specific antibodies require that the infection elicit a detectable sustained immune response before the assay can be performed, a feature which substantially delays diagnosis.

Molecular Diagnostics

Nucleic acid and sequence-based methods for diagnostics offer significant advantages over conventional culture- and antibody-based diagnostics with regard to sensitivity, specificity, speed, cost, and portability. Central to molecular diagnostics is the use of a complementary nucleic acid probe that hybridizes to a unique species-specific region of the infectious agents RNA or DNA. While several molecular platforms have been developed for infectious diseases diagnostics, e.g., fluorescence in situ hybridization (FISH), polymerase chain reaction (PCR) is the most commonly employed molecular method for diagnostics. PCR is a method of amplifying targeted segments of nucleic acid by several orders of magnitude to facilitate detection. In principal, complementary primer sequences are used to hybridize to a target nucleic acid sequence. A thermostable DNA polymerase, e.g., Taq polymerase, is then employed to extend the primer sequence. Thermal control facilitates extension, melting, and annealing, and via temperature-controlled cycling, the number of target sequences increases exponentially with each cycle. Amplification of the target sequence can be read out in an ethidium bromide-stained agarose gel or in real-time via cleavage of a fluorescent tag from the primer during the extension step. Appropriate selection of the primers provides extremely specific detection, while the amplification of the target nucleic acid provides excellent sensitivity.

PCR has been demonstrated to be sensitive to single-copy numbers of DNA/RNA targets. In these most sensitive PCR assays, primers are chosen to fully complement a region of the target sequence. Perfect complement probes are also ideal for maximizing the assay specificity to a particular infectious agent. However, in practice, genetic mutations, particularly prevalent in RNA viruses such as influenza, can render a primer/probe set ineffective for diagnosis. Thus, degenerate probes are sometimes chosen to encompass some genetic diversity at the expense of sensitivity.

Multiplexed PCR utilizes multiple primer/probe sets that target different pathogens. Multiplexed assays are implemented when the sample size is limited, preventing multiple individual singleplex PCR analyses, and the clinician is unable to determine the most likely causative agent based on early clinical

presentation. Multiplexed PCR assays are not quantitative due to target competition for reagents, are typically less sensitive than singleplex assays, and because of increased reagents, are more expensive to perform than singleplex assays. Moreover, multiple PCR products cannot be simultaneously read out by fluorescence, thus microarray analysis or electrophoresis to identify PCR products of different lengths is required to detect multiple PCR products. However, breakthroughs in multiplexed detection and quantitation are forthcoming [8–10].

Thus, for detection and diagnosis of many diseases such as viruses, PCR offers many advantages over classical methods of diagnostics, and its role will continue to expand in clinical diagnostic laboratories. However, there are challenges associated with PCR. For pathogens in which culture and microscopy can be used, molecular diagnostics are not the most cost effective. For example, the cost of a commercial PCR assay for tuberculosis ranges from $40 to $80, whereas microscopy and culture can be implemented for $1 and $5, respectively. Another consideration is how to interpret PCR results. Due to the sensitivity afforded by PCR, extremely low levels of infectious agent can be detected which may be below clinically relevant thresholds for disease presentation. Thus, quantitative PCR rather than qualitative PCR is typically more informative when correlating to clinical diagnosis. PCR assays developed in the laboratory are not always translational to analysis of clinical samples. In general, PCR cannot be performed directly on biological fluids such as blood because compounds such as hemoglobin, lactoferrin, heme, and IgG inhibit amplification [11–13]. Therefore, DNA and RNA are extracted as a first step, prior to PCR, but inefficiency of extraction kits often lead to a decrease in analytical performance compared to laboratory cultures [14, 15]. Moreover, isolation of nucleic acids is time consuming and technically challenging unless automated, which requires expensive equipment and reagents. A final consideration is the need for temperature-sensitive reagents, thermocyclers, skilled workers, and a clean laboratory environment to prevent contamination leading to false-negative results. While tremendous efforts are focused on PCR automation, incorporation of microfluidics [16, 17], and isothermal amplification [18–21], e.g., loop-mediated isothermal amplification (LAMP), to overcome these challenges, the current status of PCR precludes widespread use of PCR diagnostics in point-of-care settings and developing nations.

Limitations of Classical and Conventional Diagnostics

As discussed above, diagnostics are essential to healthcare and disease management. While there is merit in further advancing current diagnostic methods, there are shortcomings for each approach. As noted above, culture is sensitive, but the length of time prevents rapid and early diagnosis. Antibody-based techniques are often limited in sensitivity, and like molecular diagnostics, are expensive, and require species-specific detection reagents. It is likely that any improvements in these methods to address these challenges will be incremental; however there are several next generation diagnostics that offer potential paradigm shifting approaches to detection and diagnoses that are currently being investigated. One important area is the use of molecular or vibrational spectroscopy for "whole-organism" fingerprinting. This innovative approach to diagnostics promises to be rapid, specific, and truly reagentless.

Spectroscopy-Based Diagnostics

Vibrational spectroscopy includes a number of nondestructive analytical techniques which provide molecular information about the chemical makeup, e.g., functional groups, of a sample. Subtle changes in the frequency of a particular functional group vibration, e.g., group frequency, provides additional details of chemical structure, local environment surrounding the bond, bond angle, length, geometry, and conformation. These attributes of vibrational spectroscopy have led to the development of vibrational spectroscopic approaches to generate whole-organisms fingerprints to serve as unique biochemical signatures for pathogen identification. Unique to this approach of infectious agent identification is rapid readout, and perhaps most importantly, there is no need for species-specific reagents or other reagents of any kind. Three of the most developed vibrational spectroscopic techniques include infrared absorption spectroscopy, Raman scattering spectroscopy, and surface-enhanced Raman spectroscopy (SERS). These three methods, as

well as their development for diagnosing infectious diseases are described in detail below.

Infrared Spectroscopy

Infrared spectroscopy is an absorption technique in which the sample is irradiated most commonly with mid-infrared light with wavelengths in the range of 2.5–50 μm. Photons of appropriate energy to bring about a transition from one vibrational state to an excited vibrational state are absorbed by the analyte. Selection rules govern which vibrations are allowed to absorb IR photons, providing chemical and structural information. These rules require a net change in the dipole moment of the molecule as a result of the vibration. Thus, IR absorption spectra are dominated by asymmetrical vibrations. With consideration to these selection rules, proteins and nucleic acids (building blocks of bacteria, viruses, etc.) are excellent absorbers of IR radiation making IR spectroscopy an ideal tool for characterization of infectious agents.

The chemical complexity and sheer size of bacteria and viruses tend to produce complex spectra with broad and overlapping bands. Yet subtle changes in band shape, slight shifts in band peak positions, and variation in relative band intensities provide significant insight into chemical structure. Thus, careful evaluation of the full spectral fingerprint of whole-organisms, rather than analysis of single peaks common to small molecule studies, can lead to identification and classification of microorganisms.

IR spectroscopy as a technique for whole-organism fingerprinting dates back to 1952 [22]. In this early study, Stevenson and Boulduan showed that the IR spectra for *Escherichia coli*, *Pseudomonas aeruginosa*, *Bacillus subtilis*, and six other species of cultured bacteria are unique to each species. In addition to species identification, six strains of *Bacterium tularense* were spectroscopically differentiated. This initial work did not immediately translate to the diagnostic applications of IR spectroscopy. Two major breakthroughs that did not occur for several decades after the original findings were essential to further increase the utility of IR for whole-organism fingerprinting. First, prior to the 1980s when Fourier transform infrared spectroscopy (FTIR) was introduced, dispersive instruments were typically used. Dispersive instruments do not provide the speed or analytical performance required for IR-based diagnostics. FTIR instruments provide much better signal-to-noise spectra with improved spectral resolution, and are acquired in less time. These advantages provided by FTIR were essential to accurately analyze these complex biological spectra by distinguishing subtle changes in spectral band shape and to rapidly collect data. Additional developments in the methods of data analysis were also essential to move IR whole-organism fingerprinting forward. The large number of variables, i.e., wavelengths, each containing relevant information, inherent to IR spectra and rather subtle changes in intensity prevented traditional single-peak analysis for bacterial identification. Moreover, visual inspection of the spectra by the analyst is too labor intensive, prone to operator error, and unrealistic for large numbers of spectra and/or organisms from which to identify. The introduction of chemometrics, i.e., multivariate statistics applied to spectroscopy, led to the continued interest and advancement of IR-based diagnostics. These methods, including principal component analysis [23, 24], discriminant analysis, multiple regression analysis [25], and artificial neural networks [26, 27], function to simplify the high dimensional dataset by identifying the most significant variables with the ultimate goal of sample identification or quantification.

FTIR has received the greatest attention with respect to vibrational spectroscopic techniques over the last 2 decades and has been developed to the point that it can be considered an established method for the identification of both bacterial species and strains [28–33]. Researchers continue to investigate laboratory cultures of bacteria in an effort to standardize sampling protocols so that spectral databases can be shared among laboratories and to standardize the methods of analysis including spectral preprocessing, feature selection, and classification algorithms. As the method has matured, and while it continues to be tweaked and standardized, FTIR is now being applied to the analysis of clinical specimens. For example, FTIR has been successfully used to analyze clinical sputum samples collected from cystic fibrosis patients [26]. This FTIR capability is important as historically, lung infection caused by *Pseudomonas aeruginosa*, *Staphylococcus aureus*, and *Haemophilus influenzae* were the major causes of morbidity and mortality in cystic

fibrosis patients; however, the number of emerging nonfermenting species is on the rise [34], and many of these species are closely related and not appropriately identified using typical clinical diagnostics and microbiological approaches [35]. Using a FTIR spectral library and an artificial neural network built for pathogen identification, the results from the FTIR method were compared to conventional microbiology detection methods. A two-tiered ANN classification scheme was built in which the top-level network identified *P. aeruginosa*, *S. maltophilia*, *Achromobacter xylosoxidans*, *Acinetobacter* spp., *R. pickettii*, and *Burkholderia cepacia* complex (BCC) bacteria. The second-level network differentiated among four species of BCC, *B. cepacia*, *B. multivorans*, *B. cenocepacia*, and *B. stabilis*. Ultimately, this method resulted in identification success rates of 98.1% and 93.8% for the two ANN levels, respectively. However, before this optimized method was established, the research highlighted three important considerations. First, not all bacterial isolates produce poly-β-hydroxybutyric acid (PHB) which contributes to the IR spectra and confounds classification. To overcome this, each isolate was cultured on TSA medium and harvested after 5 h of growth, prior to the expression of PHB. This step enriches the bacteria for analysis and eliminates interference from PHB. Second, flagella or pilus fibers were determined to contribute to spectral heterogeneity. Vigorous vortexing and subsequent centrifugation removes the fibers to significantly improve spectral reproducibility and classification results (Fig. 1). Third, the classification algorithm significantly affects the classification results. The authors show that hierarchical clustering algorithms (HCA) discriminate between reference and clinical strains rather than based on bacterial identity. Advanced methods, such as ANN, that determine spectral variables that vary only as a result of the bacteria was necessary to correctly classify according to strain. This example work demonstrates the power of IR-based diagnostics, but suggests that these methods may require problem-specific standardization of experimental protocols and data analysis.

These groundbreaking efforts to develop IR for bacterial analysis have led to the realization that spectroscopic methods have advantages for exploring detection of other pathogens. For example, FTIR has been employed for the distinction of yeast and fungi with success [36, 37]. More recently IR has been investigated as a method to detect viral infections, although current experiments are limited to viral infection of cells in culture [38–41]. While mock-infected and herpes simplex virus type 1-infected Vero cells are readily distinguished via IR, infection-induced spectral changes are inconsistent [39, 40]. Thus, substantially more research effort is necessary to standardize protocols and correlate the spectral response to the biochemical response upon infection.

Reports continue to support the utility of FTIR-based diagnostics in the clinical laboratory, but there are certain limitations to consider. First, water is a particularly strong absorber of IR light. Thus, care must be taken to completely dehydrate the sample prior to data acquisition. This obviously does not prevent IR-based diagnostics, it is merely an inconvenience. Second, IR absorption spectroscopy is not an inherently sensitive method and trace levels of a pathogen are not readily apparent. Hence, clinical samples will likely require a culture step to generate sufficient biomass for IR analysis. As noted above, this sample enrichment can be as short as 5 h, and with IR data acquisition on the order of minutes, the total analysis time is still more rapid, less labor intensive, and more informative in many cases than conventional diagnostic methods and does not require species-specific reagents.

Raman Spectroscopy

Raman spectroscopy is a scattering technique, in which the sample is irradiated with a monochromatic light source, almost always a laser. The majority of the scattered photons are elastically scattered and maintain the same frequency as the excitation source; however, a small fraction of the photons are shifted in frequency relative to the excitation source. The difference in the energy between the excitation and inelastically, i.e., Raman, scattered photons correspond to the energy necessary to bring about a transition from one vibrational state to an excited vibrational state. Thus, much like IR spectroscopy, Raman spectra provide insight into the chemical structure, local environment, geometry, and conformation of the sample and can serve as a whole-organism fingerprinting method. Selection rules also govern which vibrations are Raman active.

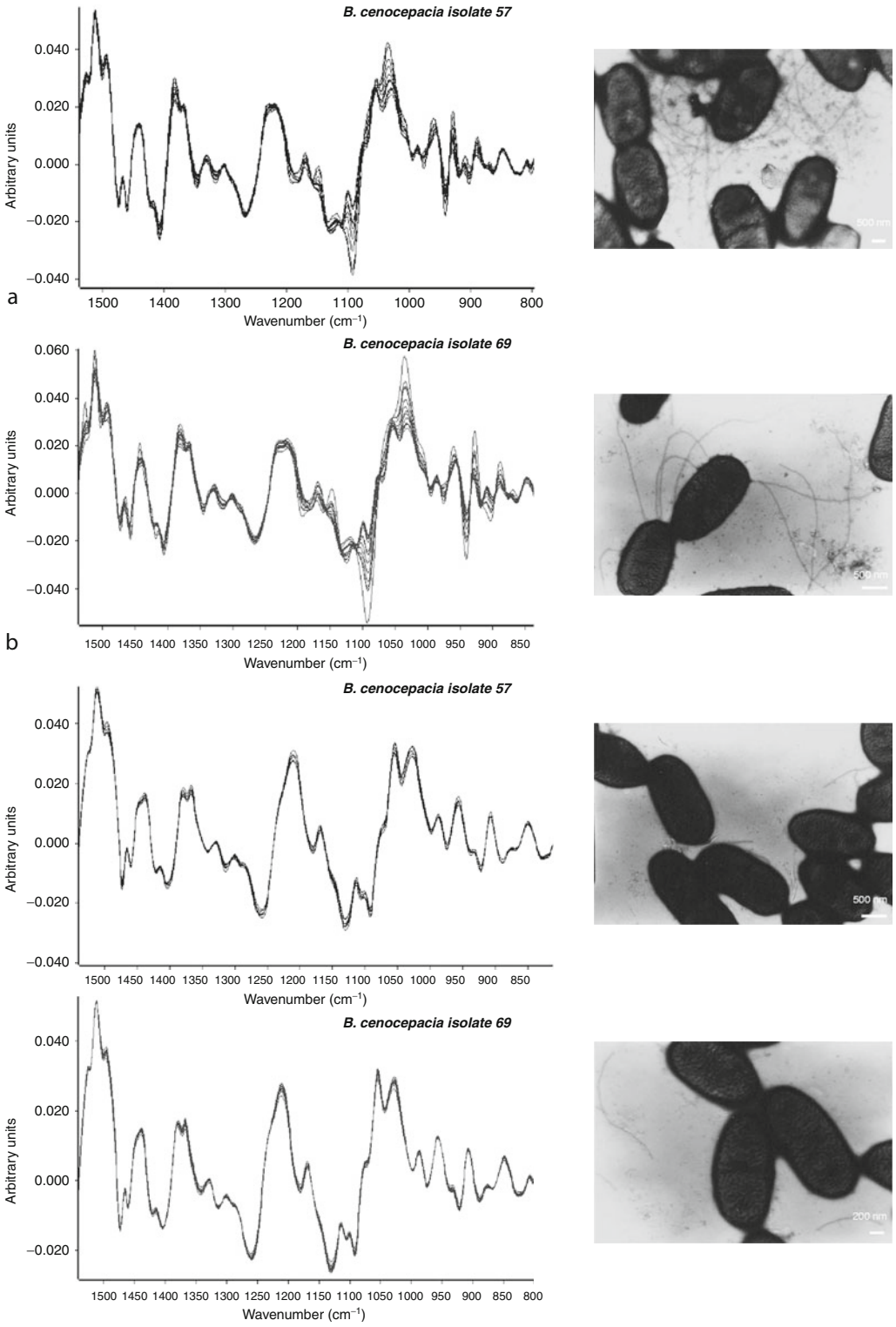

Infectious Diseases, Vibrational Spectroscopic Approaches to Rapid Diagnostics. Figure 1 (Continued)

These rules require a change in the polarizability during the vibration to be Raman active. Thus, Raman spectra are dominated by symmetrical vibrations and the technique is often seen as a complementary rather than competing technique with IR spectroscopy. However, for application to the analysis of biological materials and whole-organism fingerprinting methods, Raman offers many inherent advantages over IR spectroscopy.

Because of the selection rules, the main chain and aromatic side chains of peptides rather than aliphatic side chains are probed via Raman scattering in contrast to IR. Raman bands of nucleic acids are limited to heterocyclic bases or phosphodiester groups making up the backbone. Raman bands are narrower and less likely to overlap, thus the spectra are much less complicated compared to IR spectra because of the many more nonsymmetric vibrations that are possible. Another major advantage of Raman is that water does not interfere since its vibrations do not fit the selection rules criteria. This is an extremely important consideration when analyzing biological samples which are endemic to aqueous environments. Other advantages of Raman include the flexibility to analyze samples in any state, e.g., gas, liquid, or solid, and the ability to analyze small sample volumes and masses because of the tight focus of incident laser light (square microns) compared to the incident IR beams (square centimeters).

Viruses were the first infectious agent analyzed by Raman spectroscopy, although not in a diagnostic capacity [42]. In this first work, Raman spectroscopy was used to probe the RNA and protein structure upon viral packaging. In the 1970s, Raman spectroscopy suffered from poor sensitivity due to instrument limitations. The first evaluation of Raman spectroscopy for pathogen detection was not until 1987 when spectra were collected for five species of bacteria including *E. coli*, *P. fluorescens*, *S. epidermidis*, *B. subtilis*, and *E. cloacae* [43]. To overcome the limited sensitivity of the instruments at the time, an ultraviolet laser was used for excitation to enhance spectral features of RNA, DNA, tyrosine, and tryptophan via resonance Raman. Unique spectra were observed for each bacterium, although analysis relied on visual interpretation since chemometrics had not been implemented for spectral analysis yet. UV Raman instruments, while producing the requisite sensitivity for pathogen analysis, is quite expensive and non-resonant vibrations are not observed which results in a significant loss in information that is valuable for differentiation.

Despite the recognized benefits of Raman-based diagnostics, particularly when compared to conventional and IR-based diagnostics, instrumentation has limited the maturation of Raman-based diagnostics. After development of UV Raman for pathogen detection [43–46], Fourier transform Raman (FT-Raman) instruments were introduced for microbiological studies which increased instrument sensitivity [47, 48]. Raman instruments have now evolved to include NIR lasers to reduce fluorescence from biological and NIR-sensitive CCD detectors. These modern instruments have only been developed in this decade to fully explore the potential of Raman as a diagnostic technique [49–55]. Thus Raman-based whole-organism fingerprinting is less developed than IR-based methods and examples are generally limited to the analysis of laboratory cultures.

In an early study, Maquelin et al. [54] utilized Raman spectroscopy to directly analyze five bacterial strains, including three strains of *Staphylococcus* spp., *E. coli*, and *E. faecium*, on solid culture medium. The flexibility in sample type afforded by Raman spectroscopy allowed direct measurement on the culture plate that would not be possible using IR spectroscopy.

Infectious Diseases, Vibrational Spectroscopic Approaches to Rapid Diagnostics. Figure 1
Vector-normalized first-derivative spectra of two *B. cenocepacia* clinical isolates (isolates 57 and 69) in the 1,500–800 cm^{-1} range. (**a**) The heterogeneity of 15 replicate measurements for each strain in the spectral ranges of 1,200–900 cm^{-1} and 1,500–1,300 cm^{-1} and the corresponding micrographs obtained by TEM are shown. (**b**) Vector-normalized first-derivative spectra measured after vortexing of similar cells at the maximum intensity for 15 min and subsequent centrifugation at 8,000 × g for 5 min to separate the cells from free pilus appendages in the supernatants. Micrographs of the cells obtained by TEM after they were vortexed without centrifugation show the small fragments of pili or fibers suspended in the supernatants (From [26])

The background Raman spectrum resulting from the culture medium was subtracted from those spectra collected from the bacterial microcolonies. Hierarchical cluster analysis yielded two major groupings, one consisting of the three *Staphylococcus* strains and one consisting of the *E. coli* and *E. faecium*. The *E. coli* and *E. faecium* spectra clearly grouped according to species within the latter subcluster while spectra in the *Staphylococcus* subcluster grouped according to strain. While chemometric analysis of these spectra collected from same-day cultures yielded a successful classification rate of 100% for external validation samples, combined data collected from 3 days dropped the accuracy to 83% for classification of two *S. aureus* strains (ATCC 29213 and UHR 28624). However, these two strains are extremely similar and in general the results demonstrate the utility of Raman-based diagnostics.

The most rigorous evaluation of Raman spectroscopy for reagentless detection and identification of pathogens was performed in collaboration with a US government laboratory. In this work, a comprehensive library of Raman spectra has been established for over 1,000 species, including 281 CDC category A and B biothreats, 146 chemical threats, 310 environmental interferents, and numerous others [52]. Spectral signatures were collected using Raman chemical imaging spectroscopy (RCIS) [56]. RCIS technology combines digital imaging and Raman spectroscopy. Digital imaging automatically discriminates against background particulates and identifies regions of interest on a sample platform that are then targeted for Raman analysis. Sample analysis is faster and completely automated using this approach. Two commercially available instruments were tested, one in the laboratory (ChemImage Corp., Falcon) and the other in the field (ChemImage Corp., Eagle). To test the robustness of the Raman spectral library and classification scheme, blinded samples containing one of four *Bacillus* strains were analyzed and identified. The predictive performance ranged from 89.4% to 93.1% for these closely related bacteria. It was concluded that key to the success of this diagnostic approach is the extensiveness of the spectral library. There are many more bacterial phenotypes than genotypes, and it has been found that Raman fingerprints correlate with cell phenotype, thus an all-inclusive library must contain spectra for each bacterial strain grown under different conditions and at different stages of development. In a subsequent study untrained personnel at the Armed Forces Institute of Pathology evaluated 14 bacteria to generate a spectral library and sent 20 blinded samples to ChemImage for external validation in which all 20 samples were correctly identified. This comprehensive study is the first to establish the true utility of automated Raman-based diagnostics carried out off-site by untrained personnel. However, these samples were prepared in water, cell culture media, or spiked nasal swabs, none of which are truly clinical samples.

An early study to evaluate clinical samples for *Acinetobacter* by Raman spectroscopy and compare the results with an established diagnostic method were among the first showing the power and speed of Raman-based detection [55]. In this study, 25 *Acinetobacter* isolates from five hospitals in three countries were analyzed using selective amplification of restriction fragments (AFLP), an established molecular technique for typing bacteria strains. Dendograms resulting from the hierarchical cluster analysis of Raman and AFLP fingerprints for the isolates were generated and compared (Fig. 2). Both dendograms resulted in five clusters that separate the strains according to the five outbreaks, with the exception of one Basildon isolate RUH 3242 which clustered with isolates from Venlo in the Raman-based dendogram. Overall results from Raman fingerprinting of these clinical isolates were very similar to those obtained for established methods, but with the advantage of faster analysis and less complicated procedures.

Despite the advancement of Raman spectroscopy instrumentation and methods for pathogen fingerprinting, Raman is still often limited by poor sensitivity. Only $\sim$1 in 10^6–10^8 photons are inelastically scattered as the vast majority are elastically scattered. This means that high quality spectra with the requisite signal-to-noise can take minutes to acquire. While this may not be a limitation in laboratory experiments, or developmental stages in research, it prohibits its usefulness in clinical diagnostic laboratories which analyze hundreds to thousands of samples per day. Thus, there is great interest in enhancing the Raman signal. One such method is to excite the sample with a frequency that resonates with an electronic transition, so called resonance Raman spectroscopy. For biological samples, this requires UV lasers for excitation, and as noted

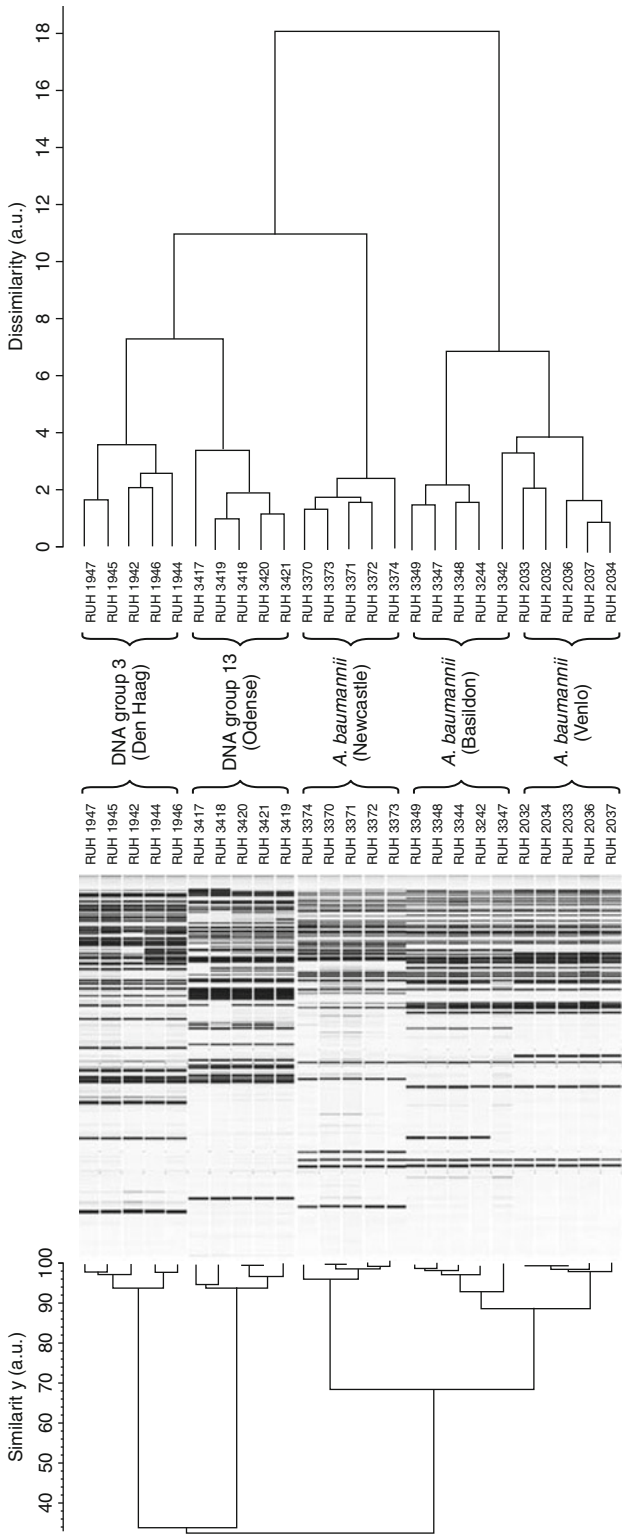

Infectious Diseases, Vibrational Spectroscopic Approaches to Rapid Diagnostics. Figure 2
Dendrograms resulting from the hierarchical cluster analysis of (*left*) AFLP analysis and (*right*) Raman analysis of the isolates. The asterisk marks the strain RUH 3242 misclassified via Raman fingerprinting (From [55])

I

above, is cost prohibitive to widespread adoption of this method. Moreover, chemical information is lost when performing resonance Raman which would likely reduce classification accuracy of closely related pathogens. An alternative method to amplify Raman scattering is surface-enhanced Raman spectroscopy (SERS). SERS has received a great deal of attention, particularly with respect to whole-organism fingerprinting and is the subject of the next section.

SERS

Surface-enhanced Raman spectroscopy is a technique in which the Raman signal of a sample is significantly amplified via adsorption onto a metallic nanostructured surface. A laser excitation frequency is selected such that it is in resonance with the collective oscillation of the conduction electrons in the nanostructures, i.e., surface plasmon resonance. When resonance conditions are met, the local electromagnetic field experienced by molecules in close proximity to the surface is significantly increased to yield rather large enhancements in the Raman scattering. While the signal enhancement is substrate and sample dependent, typical enhancements are on the order of 10^4–10^{14} with respect to normal Raman intensities, with several studies reporting the detection of single molecules using this technique [57, 58]. SERS offers the benefits of normal Raman compared to IR spectroscopy while providing a markedly improved sensitivity. Recent advances in nanofabrication methods and SERS theory has led to significant improvements in SERS substrates in the last several years and has driven increased efforts to develop SERS for whole-organism fingerprinting [59–78].

The major focus of whole-organism fingerprinting via SERS has been on bacteria identification [51, 64–74, 77, 78]. Most of these studies report differentiation among bacteria species, with many demonstrating discrimination of different strains of the same species. However, there are several inconsistencies that have been noted by researchers, particularly in the earlier studies. For example, Grow et al. found SERS spectra for strains that belong to the same species were sometimes less similar than spectra collected from different species [65], and Jarvis and Goodacre observed similar spectra for the same bacteria using different preparations of silver nanoparticles, but noted subtle changes in signal intensities among nanoparticle batches [68]. These discrepancies evident in these early studies highlight the primary challenge of SERS-based diagnostics, i.e., the enhancing substrate. The SERS signal is highly dependent on the enhancing substrate, thus a reliable means of fabricating nanostructured materials is vital to the success of SERS-based diagnostics.

Several research laboratories have analyzed and published SERS spectra for both *Bacillus subtilis* and *E. coli*; however, each reported incongruent spectral fingerprints [67, 68, 71, 72]. The experimental protocols, however, varied among each study. For example, in two different reports Jarvis et al. used two different chemical synthesis preparations to generate colloidal silver, citrate reduction [67] and borohydride reduction [51], to serve as the SERS substrate. The SERS spectra were drastically different in each study. It is well known that spectra are dependent on the enhancing nanostructure, e.g., material, size, shape, interparticle spacing, etc., but given the same final nanostructure similar spectra were expected. The authors attributed the differences to the effect of diverse chemistries used to prepare each silver colloid [79]. However, it should be noted that different excitation sources, 532 nm and 785 nm, were employed in the two studies. For normal Raman, the Raman shifts should be independent of the excitation source, thus spectral fingerprinting should not be affected by the choice of the laser. SERS spectra, however, can be influenced by the excitation source because of the requisite pairing of the excitation frequency and plasmon resonance of the substrate. Therefore, it is perhaps more probable that spectral differences observed by Jarvis et al. are due to greater signal enhancement for the 532 nm excitation source rather than due to differences in chemical preparation of the colloidal silver. This interpretation is supported by a study in which a third variation in experimental parameters was implemented utilizing citrate-reduced silver colloid but acquired spectra with a 647 nm laser [71]. Results from this study closely resembled the results for *B. subtilis* obtained by Jarvis et al. employing borohydride reduced silver nanoparticles and 532 nm excitation. Collectively, these studies also demonstrate the need for procedural consistency.

In a pivotal study, scientists at a US Army research laboratory evaluated the SERS signatures for many bacteria using a standardized sampling protocol and instrumentation. To date, three SERS substrates were directly compared using the standardized protocol: silver nanoparticles, silver film over nanospheres (FONS), and commercially available Klarite. Interaction between substrate and bacteria vary significantly as visualized with electron microscopy which likely results in different spectral fingerprints. Moreover the signal intensities varied significantly among the substrates reflecting differences in enhancing quality. Details of these experiments are approved for public release as a technical report (ARL-TR-4957).

In another key study, SERS and Raman fingerprints were directly compared to assess the advantages of SERS analysis [72]. Raman and SERS spectra were collected for several bacteria, including four strains of *Bacillus*, *S. typhimurium*, and *E. coli*. As noted above, the substrate is a critical factor in SERS analysis, and in this study aggregated gold nanoparticle films were grown in-house and established as a reliable means of substrate preparation for acquisition of repeatable spectra. As anticipated, SERS yielded much greater signal-to-noise spectra compared to normal Raman. The study also identified two unexpected benefits of SERS. Normal Raman signal for *Bacillus* species was overwhelmed by native fluorescence of the sample; however, in the SERS analysis, the metal substrate functioned to quench the fluorescence component in addition to enhancing the Raman signal. It was also observed that normal Raman spectra are more complex than SERS spectra. This is explained by the fact that bulk Raman interrogates all components throughout the entire bacterium equally, while the distance-dependence of SERS enhancement preferentially probes the region of the bacterium closest to the metal substrate and bands for the internal components are not detected. Fortunately, most chemical variation among bacterial strains and species are expressed on the cell surface, thus greater spectral differences are observed among SERS spectra of different samples than compared to bulk Raman spectra. This added advantage is exemplified by greater discrimination of bacteria when utilizing SERS spectra as compared to Raman spectra [72].

A number of novel nanofabrication methods have recently emerged for producing SERS substrates with the potential for addressing the issues noted above due to substrate heterogeneity. These include electron beam lithography [80, 81], nanosphere lithography [82–84], a template method [85–88], oblique angle vapor deposition (OAD) [89–91], and a proprietary wet-etching technology used to produce commercially available Klarite (D3 technologies). It should be noted, however, that with the exception of OAD and Klarite, these fabrication methods are not adaptable to large-scale production due to the complexity of the fabrication procedure. Not only is it likely that these substrates will lead to significant advances in SERS-diagnostics of bacteria, the use of OAD and Klarite substrates has already lead to successful application to virus identification [59, 60, 62, 63, 75, 76].

In the most recent investigation of SERS-based viral fingerprinting, eight strains of rotavirus were analyzed [63]. These isolates were recovered from clinical fecal samples and propagated in MA104 cells and represent the 5 G and 3 P genotypes responsible for the most severe infections. Unique SERS fingerprints were acquired for each strain when adsorbed onto OAD-fabricated silver nanorods. Representative spectra for each strain and negative control, as well as the difference spectra which subtract out the background cell lysate signal are displayed in Fig. 3. Classification algorithms based on partial least squares discriminant analysis were constructed to identify the samples according to (1) rotavirus positive or negative, (2) P4, P6, or P8 genotype, (3) G1, G2, G3, G4, or G9 genotype, or (4) strain. Respectively, these four classification models resulted in 100%, 98–100%, 96–100%, and 100% sensitivity and 100%, 100%, 99–100%, and 99–100% specificity.

Compilation and critical analysis of reports to date demonstrate the potential of Raman-based diagnostics and its advantages over IR, normal Raman spectroscopy, and convention diagnostic methods, but also highlight the need for standardization. The challenge in the future is standardization of substrates and sampling protocols since background can "quench" signal from the analyte. For example, blood analysis requires sample processing to remove some competing elements [92], yet SERS spectra highly dependent on the sample pretreatment procedure as remaining chemical species will also contribute signal and degrade the performance of matching in spectral library databases. The outlook

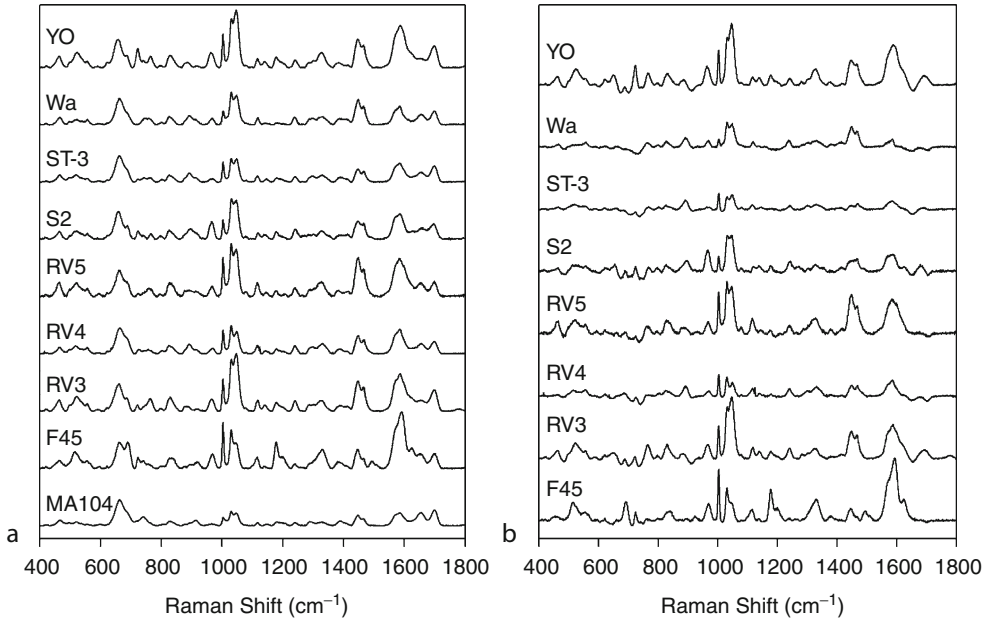

Infectious Diseases, Vibrational Spectroscopic Approaches to Rapid Diagnostics. Figure 3
(**a**) Average SERS spectra for eight strains of rotavirus and the negative control (MA104 cell lysate). Spectra were baseline corrected, normalized to the band at 633 cm^{-1}, and offset for visualization. (**b**) Difference SERS spectra for eight strains after subtraction of MA104 spectrum (From [63])

of SERS is not a question of spectral quality and reproducibility in a controlled environment, the question is how to control the environment across laboratories.

Future Directions

The future of spectroscopic-based diagnostics is bright as demonstrated by the many studies cited and discussed above. In addition to the success found in these studies, areas of improvement have also been identified. An important area of potential development is the methods used for statistical analysis. Well-established algorithms such as PCA, HCA, and discriminant analysis continue to provide high predictive accuracy, but recent examples have shown that more creative and novel approaches such as artificial neural networks, "bar-coding" [70], or innovative uses of PLS [59] can further improve the predictive value. A revolution in instrumentation is also occurring. Vibrational spectroscopy has recently filled niches in quality control of pharmaceuticals and raw materials as well as identification of chemical threats. The nature of these applications and explosion in interest have driven the instrumentation industry to invest in the development and production of high-quality yet affordable handheld instruments for mobile, on-site analysis. This market-driven commercialization, in effect, is paving the way for point-of-care, mobile, and cost-effective spectroscopy-based diagnostics. The most important factor for widespread realization of spectroscopic diagnosis will be the emergence of a universal protocol for sampling, and for the case of SERS, a standard substrate. The accepted protocol must then be used to build a spectral database covering a variety of phenotypes and developmental stages as illustrated above. Implementing a standard practice is crucial for the success of the technique, but once developed this technology has the potential to become the first and immediate response to clinical cases in which infection is suspected.

Bibliography

Primary Literature

1. Perry JD, Ford M, Taylor J, Jones AL, Freeman R et al (1999) ABC medium, a new chromogenic agar for selective isolation of *Salmonella* spp. J Clin Microbiol 37:766–768

2. Hedin G, Fang H (2005) Evaluation of two new chromogenic media, CHROMagar MRSA and S. aureus ID, for identifying Staphylococcus aureus and screening methicillin-resistant S-aureus. J Clin Microbiol 43:4242–4244
3. Perry JD, Davies A, Butterworth LA, Hopley ALJ, Nicholson A et al (2004) Development and evaluation of a chromogenic agar medium for methicillin-resistant *Staphylococcus aureus*. J Clin Microbiol 42:4519–4523
4. Nygren H, Stenberg M (1985) Kinetics of antibody-binding to surface-immobilized antigen – influence of mass-transport on the enzyme-linked immunosorbent-assay (ELISA). J Colloid Interface Sci 107:560–566
5. Nygren H, Werthen M, Stenberg M (1987) Kinetics of antibody-binding to solid-phase-immobilized antigen – effect of diffusion rate limitation and steric interaction. J Immunol Methods 101:63–71
6. Gussenhoven GC, vanderHoorn M, Goris MGA, Terpstra WJ, Hartskeerl RA et al (1997) LEPTO dipstick, a dipstick assay for detection of Leptospira-specific immunoglobulin M antibodies in human sera. J Clin Microbiol 35:92–97
7. Gordon A, Videa E, Saborio S, Lopez R, Kuan G et al (2010) Diagnostic accuracy of a rapid influenza test for pandemic influenza A H1N1. Plos One 5:e10364
8. Erdman DD, Weinberg GA, Edwards KM, Walker FJ, Anderson BC et al (2003) GeneScan reverse transcription-PCR assay for detection of six common respiratory viruses in young children hospitalized with acute respiratory illness. J Clin Microbiol 41:4298–4303
9. Lassauniere R, Kresfelder T, Venter M (2010) A novel multiplex real-time RT-PCR assay with FRET hybridization probes for the detection and quantitation of 13 respiratory viruses. J Virol Methods 165:254–260
10. Li H, McCormac MA, Estes RW, Sefers SE, Dare RK et al (2007) Simultaneous detection and high-throughput identification of a panel of RNA viruses causing respiratory tract infections. J Clin Microbiol 45:2105–2109
11. Abu al-Soud W, Radstrom P (2001) Purification and characterization of PCR-inhibitory components in blood cells. J Clin Microbiol 39:485–493
12. Abu Al-Soud W, Radstrom P (2001) Effects of amplification facilitators on diagnostic PCR in the presence of blood, feces, and meat. J Clin Microbiol 38:4463–4470
13. Widjojoatmodjo MN, Fluit AC, Torensma R, Verdonk G, Verhoef J (1992) The magnetic immunopolymerase chain-reaction assay for direct detection of salmonellae in fecal samples. J Clin Microbiol 30:3195–3199
14. Chui LW, King R, Lu P, Manninen K, Sim J (2004) Evaluation of four DNA extraction methods for the detection of *Mycobacterium avium* subsp *paratuberculosis* by polymerase chain reaction. Diagn Microbiol Infect Dis 48:39–45
15. McOrist AL, Jackson M, Bird AR (2002) A comparison of five methods for extraction of bacterial DNA from human faecal samples. J Microbiol Methods 50:131–139
16. Kaigala GV, Hoang VN, Stickel A, Lauzon J, Manage D et al (2008) An inexpensive and portable microchip-based platform for integrated RT-PCR and capillary electrophoresis. Analyst 133:331–338
17. Zhang NY, Tan HD, Yeung ES (1999) Automated and integrated system for high-throughput DNA genotyping directly from blood. Anal Chem 71:1138–1145
18. Aryan E, Makvandi M, Farajzadeh A, Huygen K, Bifani P et al (2010) A novel and more sensitive loop-mediated isothermal amplification assay targeting IS6110 for detection of *Mycobacterium tuberculosis* complex. Microbiol Res 165:211–220
19. Fang XE, Liu YY, Kong JL, Jiang XY (2010) Loop-mediated isothermal amplification integrated on microfluidic chips for point-of-care quantitative detection of pathogens. Anal Chem 82:3002–3006
20. Notomi T, Okayama H, Masubuchi H, Yonekawa T, Watanabe K et al (2000) Loop-mediated isothermal amplification of DNA. Nucl Acids Res 28:e63
21. Shivakoti S, Ito H, Murase T, Ono E, Takakuwa H et al (2010) Development of reverse transcription-loop-mediated isothermal amplification (RT-LAMP) assay for detection of avian influenza viruses in field specimens. J Vet Med Sci 72:519–523
22. Stevenson HJR, Bolduan OEA (1952) Infrared spectrophotometry as a means for identification of bacteria. Science 116:111–113
23. Lin MS, Al-Holy M, Al-Qadiri H, Kang DH, Cavinato AG et al (2004) Discrimination of intact and injured *Listeria monocytogenes* by Fourier transform infrared spectroscopy and principal component analysis. J Agric Food Chem 52:5769–5772
24. Ngo-Thi NA, Kirschner C, Naumann D (2003) Characterization and identification of microorganisms by FIF-IR microspectrometry. J Mole Struct 661:371–380
25. Janbu AO, Moretro T, Bertrand D, Kohler A (2008) FT-IR microspectroscopy: a promising method for the rapid identification of *Listeria* species. FEMS Microbiol Lett 278:164–170
26. Bosch A, Minan A, Vescina C, Degrossi J, Gatti B et al (2008) Fourier transform infrared spectroscopy for rapid identification of nonfermenting gram-negative bacteria isolated from sputum samples from cystic fibrosis patients. J Clin Microbiol 46:2535–2546
27. Rebuffo-Scheer CA, Schmitt J, Scherer S (2007) Differentiation of Listeria monocytogenes serovars by using artificial neural network analysis of Fourier-transformed infrared spectra. Appl Environ Microbiol 73:1036–1040
28. Bouhedja W, Sockalingum GD, Pina P, Allouch P, Bloy C et al (1997) ATR-FTIR spectroscopic investigation of *E coli* transconjugants beta-lactams-resistance phenotype. FEBS Lett 412:39–42
29. Goodacre R, Timmins EM, Rooney PJ, Rowland JJ, Kell DB (1996) Rapid identification of *Streptococcus* and *Enterococcus* species using diffuse reflectance-absorbance Fourier transform infrared spectroscopy and artificial neural networks. FEMS Microbiol Lett 140:233–239
30. Helm D, Labischinski H, Naumann D (1991) Elaboration of a procedure for identification of bacteria using

I

Fourier-transform IR spectral libraries – a stepwise correlation approach. J Microbiol Methods 14:127–142
31. Helm D, Labischinski H, Schallehn G, Naumann D (1991) Classification of bacteria by Fourier-transform infrared-spectroscopy. J Gen Microbiol 137:69–79
32. Naumann D, Fijala V, Labischinski H, Giesbrecht P (1988) The rapid differentiation and identification of pathogenic bacteria using Fourier-transform infrared spectroscopic and multivariate statistical-analysis. J Mole Struct 174:165–170
33. Naumann D, Helm D, Labischinski H (1991) Microbiological characterizations by FT-IR spectroscopy. Nature 351:81–82
34. Ferroni A, Sermet-Gaudelus I, Abachin E, Quesne G, Lenoir G et al (2002) Use of 16 S rRNA gene sequencing for identification of nonfermenting gram-negative bacilli recovered from patients attending a single cystic fibrosis center. J Clin Microbiol 40:3793–3797
35. Miller MB, Gilligan PH (2003) Laboratory aspects of management of chronic pulmonary infections in patients with cystic fibrosis. J Clin Microbiol 41:4009–4015
36. Fischer G, Braun S, Thissen R, Dott W (2006) FT-IR spectroscopy as a tool for rapid identification and intra-species characterization of airborne filamentous fungi. J Microbiol Methods 64:63–77
37. Sandt C, Sockalingum GD, Aubert D, Lepan H, Lepouse C et al (2003) Use of Fourier-transform infrared spectroscopy for typing of *Candida albicans* strains isolated in intensive care units. J Clin Microbiol 41:954–959
38. Erukhimovitch V, Karpasasa M, Huleihel M (2009) Spectroscopic detection and identification of infected cells with Herpes viruses. Biopolymers 91:61–67
39. Erukhimovitch V, Mukmanov I, Talyshinsky M, Souprun Y, Huleihel M (2004) The use of FTIR microscopy for evaluation of herpes viruses infection development kinetics. Spectrochimica Acta Part A-Mole Biomol Spectrosc 60:2355–2361
40. Hastings G, Krug P, Wang RL, Guo J, Lamichhane HP et al (2009) Viral infection of cells in culture detected using infrared microscopy. Analyst 134:1462–1471
41. Salman A, Erukhimovitch V, Talyshinsky M, Huleihil M, Huleihel M (2002) FTIR spectroscopic method for detection of cells infected with herpes viruses. Biopolymers 67:406–412
42. Hartman KA, Clayton N, Thomas GJ (1973) Studies of virus structure by Raman spectroscopy 1. R17 virus and R17 RNA. Biochem Biophys Res Commun 50:942–949
43. Dalterio RA, Baek M, Nelson WH, Britt D, Sperry JF et al (1987) The resonance Raman microprobe detection of single bacterial-cells from a chromobacterial mixture. Appl Spectrosc 41:241–244
44. Chadha S, Manoharan R, Moenneloccoz P, Nelson WH, Peticolas WL et al (1993) Comparison of the UV resonance Raman-spectra of bacteria, bacteria-cell walls, and ribosomes excited in the deep UV. Appl Spectrosc 47:38–43
45. Ghiamati E, Manoharan R, Nelson WH, Sperry JF (1992) UV resonance Raman-spectra of bacillus spores. Appl Spectrosc 46:357–364
46. Manoharan R, Ghiamati E, Dalterio RA, Britton KA, Nelson WH et al (1990) UV resonance Raman-spectra of bacteria, bacterial-spores, protoplasts and calcium dipicolinate. J Microbiol Methods 11:1–15
47. Edwards HGM, Russell NC, Weinstein R, Wynnwilliams DD (1995) Fourier-transform Raman-spectroscopic study of fungi. J Raman Spectrosc 26:911–916
48. Williams AC, Edwards HGM (1994) Fourier-transform Raman-spectroscopy of bacterial-cell walls. J Raman Spectrosc 25:673–677
49. Choo-Smith LP, Maquelin K, van Vreeswijk T, Bruining HA, Puppels GJ et al (2001) Investigating microbial (micro) colony heterogeneity by vibrational spectroscopy. Appl Environ Microbiol 67:1461–1469
50. Huang WE, Griffiths RI, Thompson IP, Bailey MJ, Whiteley AS (2004) Raman microscopic analysis of single microbial cells. Anal Chem 76:4452–4458
51. Jarvis RM, Brooker A, Goodacre R (2004) Surface-enhanced Raman spectroscopy for bacterial discrimination utilizing a scanning electron microscope with a Raman spectroscopy interface. Anal Chem 76:5198–5202
52. Kalasinsky KS, Hadfield T, Shea AA, Kalasinsky VF, Nelson MP et al (2007) Raman chemical imaging spectroscopy reagentless detection and identification of pathogens: signature development and evaluation. Anal Chem 79:2658–2673
53. Maquelin K, Choo-Smith LP, Endtz HP, Bruining HA, Puppels GJ (2002) Rapid identification of *Candida* species by confocal Raman micro spectroscopy. J Clin Microbiol 40:594–600
54. Maquelin K, Choo-Smith LP, van Vreeswijk T, Endtz HP, Smith B et al (2000) Raman spectroscopic method for identification of clinically relevant microorganisms growing on solid culture medium. Anal Chem 72:12–19
55. Maquelin K, Dijkshoorn L, van der Reijden TJK, Puppels GJ (2006) Rapid epidemiological analysis of *Acinetobacter* strains by Raman spectroscopy. J Microbiol Methods 64:126–131
56. Schaeberle MD, Morris HR, Turner JF, Treado PJ (1999) Raman chemical imaging spectroscopy. Anal Chem 71:175A–181A
57. Kneipp K, Wang Y, Kneipp H, Perelman LT, Itzkan I et al (1997) Single molecule detection using surface-enhanced Raman scattering (SERS). Phys Rev Lett 78:1667–1670
58. Nie SM, Emory SR (1997) Probing single molecules and single nanoparticles by surface-enhanced Raman scattering. Science 275:1102–1106
59. Alexander TA (2008) Development of methodology based on commercialized SERS-active substrates for rapid discrimination of Poxviridae virions. Anal Chem 80:2817–2825
60. Alexander TA (2008) Surface-enhanced Raman spectroscopy: a new approach to rapid identification of intact viruses. Spectroscopy 23:36–42
61. Bao PD, Huang TQ, Liu XM, Wu TQ (2001) Surface-enhanced Raman spectroscopy of insect nuclear polyhedrosis virus. J Raman Spectrosc 32:227–230
62. Driskell JD, Shanmukh S, Liu YJ, Hennigan S, Jones L et al (2008) Infectious agent detection with SERS-active silver

nanorod arrays prepared by oblique angle deposition. IEEE Sens J 8:863–870
63. Driskell JD, Zhu Y, Kirkwood CD, Zhao YP, Dluhy RA et al (2010) Rapid and sensitive detection of rotavirus molecular signatures using surface enhanced Raman spectroscopy. Plos One 5(4):e10222
64. Goeller LJ, Riley MR (2007) Discrimination of bacteria and bacteriophages by Raman spectroscopy and surface-enhanced Raman spectroscopy. Appl Spectrosc 61:679–685
65. Grow AE, Wood LL, Claycomb JL, Thompson PA (2003) New biochip technology for label-free detection of pathogens and their toxins. J Microbiol Methods 53:221–233
66. Guicheteau J, Christesen SD (2006) Principal component analysis of bacteria using surface-enhanced Raman spectroscopy. Proc SPIE 6218:62180G
67. Jarvis RM, Brooker A, Goodacre R (2006) Surface-enhanced Raman scattering for the rapid discrimination of bacteria. Faraday Discuss 132:281–292
68. Jarvis RM, Goodacre R (2004) Discrimination of bacteria using surface-enhanced Raman spectroscopy. Anal Chem 76:40–47
69. Laucks ML, Sengupta A, Junge K, Davis EJ, Swanson BD (2005) Comparison of Psychro-active arctic marine Bacteria and common Mesophillic bacteria using surface-enhanced Raman spectroscopy. Appl Spectrosc 59:1222–1228
70. Patel IS, Premasiri WR, Moir DT, Ziegler LD (2008) Barcoding bacterial cells: a SERS-based methodology for pathogen identification. J Raman Spectrosc 39:1660–1672
71. Pearman WF, Fountain AW (2006) Classification of chemical and biological warfare agent simulants by surface-enhanced Raman spectroscopy and multivariate statistical techniques. Appl Spectrosc 60:356–365
72. Premasiri WR, Moir DT, Klempner MS, Krieger N, Jones G et al (2005) Characterization of the surface enhanced Raman scattering (SERS) of bacteria. J Phys Chem B 109:312–320
73. Premasiri WR, Moir DT, Lawrence DZ (2005) Vibrational fingerprinting of bacterial pathogens by surface enhanced Raman scattering (SERS). Proc SPIE 5795:19–29
74. Sengupta A, Laucks ML, Davis EJ (2005) Surface-enhanced Raman spectroscopy of bacteria and pollen. Appl Spectrosc 59:1016–1023
75. Shanmukh S, Jones L, Driskell J, Zhao Y, Dluhy R et al (2006) Rapid and sensitive detection of respiratory virus molecular signatures using a silver nanorod array SERS substrate. Nano Lett 6:2630–2636
76. Shanmukh S, Jones L, Zhao Y-P, Driskell JD, Tripp RA et al (2008) Identification and classification of respiratory syncytial virus (RSV) strains by surface-enhanced Raman spectroscopy and multivariate statistical techniques. Anal Bioanal Chem 390:1551–1555
77. Yan F, Vo-Dinh T (2007) Surface-enhanced Raman scattering detection of chemical and biological agents using a portable Raman integrated tunable sensor. Sens Actuat B-Chem 121:61–66
78. Zeiri L, Bronk BV, Shabtai Y, Czege J, Efrima S (2002) Silver metal induced surface enhanced Raman of bacteria. Colloids Surf A-Physicochem Eng Aspects 208:357–362
79. Jarvis RM, Goodacre R (2008) Characterisation and identification of bacteria using SERS. Chem Soc Rev 37:931–936
80. DeJesus MA, Giesfeldt KS, Oran JM, Abu-Hatab NA, Lavrik NV et al (2005) Nanofabrication of densely packed metal-polymer arrays for surface-enhanced Raman spectrometry. Appl Spectrosc 59:1501–1508
81. Kahl M, Voges E, Kostrewa S, Viets C, Hill W (1998) Periodically structured metallic substrates for SERS. Sens Actuat B-Chem 51:285–291
82. Haynes CL, Van Duyne RP (2001) Nanosphere lithography: a versatile nanofabrication tool for studies of size-dependent nanoparticle optics. J Phys Chem B 105:5599–5611
83. Hulteen JC, Treichel DA, Smith MT, Duval ML, Jensen TR et al (1999) Nanosphere lithography: size-tunable silver nanoparticle and surface cluster arrays. J Phys Chem B 103: 3854–3863
84. Jensen TR, Malinsky MD, Haynes CL, Van Duyne RP (2000) Nanosphere lithography: tunable localized surface plasmon resonance spectra of silver nanoparticles. J Phys Chem B 104:10549–10556
85. Broglin BL, Andreu A, Dhussa N, Heath JA, Gerst J et al (2007) Investigation of the effects of the local environment on the surface-enhanced Raman spectra of striped gold/silver nanorod arrays. Langmuir 23:4563–4568
86. Lombardi I, Cavallotti PL, Carraro C, Maboudian R (2007) Template assisted deposition of Ag nanoparticle arrays for surface-enhanced Raman scattering applications. Sensor Actuat B-Chem 125:353–356
87. Ruan CM, Eres G, Wang W, Zhang ZY, Gu BH (2007) Controlled fabrication of nanopillar arrays as active substrates for surface-enhanced Raman spectroscopy. Langmuir 23:5757–5760
88. Yao JL, Pan GP, Xue KH, Wu DY, Ren B et al (2000) A complementary study of surface-enhanced Raman scattering and metal nanorod arrays. Pure Appl Chem 72:221–228
89. Chaney SB, Shanmukh S, Zhao Y-P, Dluhy RA (2005) Randomly aligned silver nanorod arrays produce high sensitivity SERS substrates. Appl Phys Lett 87:31908–31910
90. Driskell JD, Shanmukh S, Liu Y, Chaney SB, Tang XJ et al (2008) The use of aligned silver nanorod arrays prepared by oblique angle deposition as surface enhanced Raman scattering substrates. J Phys Chem C 112:895–901
91. Liu YJ, Fan JG, Zhao YP, Shanmukh S, Dluhy RA (2006) Angle dependent surface enhanced Raman scattering obtained from a Ag nanorod array substrate. Appl Phys Lett 89:173134
92. Premasiri WR, Moir DT, Klempner MS, Ziegler LD (2007) Surface-enhanced Raman scattering of microorganisms. New Approaches Biomed Spectrosc 963:164–185

Books and Reviews

Carter EA, Marshall CP, Ali MHM, Ganendren R, Sorrell TC, Wright L, Lee Y-C, Chen C-I, Lay PA (2007) Infrared spectroscopy of microorganisms: characterization, identification, and differentiation. In: Kneipp K, Aroca R, Kneipp H, Wentrup-Byrne E (eds)

I

New approaches in biomedical spectroscopy. American Chemical Society, Washington, DC, pp 64–84
Huang WE, Li M, Jarvis RM, Goodacre R, Banwart SA (2010) Shining light on the microbial world: the application of Raman microspectroscopy. In: Laskin A, Sariaslani S, Gadd GM (eds) Advances in applied microbiology, vol 70. Elsevier, San Diego, pp 153–186
Ince J, McNally A (2009) Development of rapid, automated diagnostics for infectious disease: advances and challenges. Expert Rev Med Devices 6(6):641–651
Posthuma-Trumpie G, Korf J, van Amerongen A (2009) Lateral flow (immune)assay: its strengths, weakness, opportunities and threats. A literature survey. Anal Bioanaly Chem 393: 569–582
Premasiri WR, Moir DT, Klempner MS, Ziegler LD (2007) Surface-enhanced Raman scattering of microorganisms. In: Kneipp K, Aroca R, Kneipp H, Wentrup-Byrne E (eds) New approaches in biomedical spectroscopy. American Chemical Society, Washington, DC, pp 164–199
Quan P-L, Briese T, Palacios G, Lipkin WI (2008) Rapid sequence-based diagnosis of viral infection. Antiviral Res 79:1–5
Sharaf MA, Illman DL, Kowalski BR (1986) Chemometrics. Wiley, New York
Tuma R, Thomas GJ Jr (2002) Raman spectroscopy of viruses. In: Chalmers JM, Griffiths PR (eds) Handbook of vibrational spectroscopy applications in life, pharmaceutical and natural sciences, vol 5. Wiley, West Sussex, pp 3519–3535

Integrated Assessment Modeling

James A. Edmonds, Katherine V. Calvin, Leon E. Clarke, Anthony C. Janetos, Son H. Kim, Marshall A. Wise, Haewon C. McJeon
Joint Global Change Research Institute (JGCRI), Pacific Northwest National Laboratory (PNNL), College Park, MD, USA

Article Outline

Glossary
Definition of the Subject
Introduction
The Variety of Integrated Assessment Models
GCAM as an Example of a Higher Resolution IAM
Using Higher Resolution IAMs to Analyze the Impact of Policies to Mitigate Greenhouse Gas Emissions
Future Directions: Integrating Human Earth Systems with Natural Earth Systems
Bibliography

Glossary

Climate policy (greenhouse gas mitigation policy) A climate policy refers to a policy scheme designed to deliberately limit the magnitude of climate change, often involving mitigation of greenhouse gases. Integrated assessment models (IAMs) represent climate policies in abstract forms. The most commonly modeled climate policy is attaching a universal price on emissions of carbon dioxide (or carbon dioxide equivalent of other greenhouse gases). Such policy represents a universal carbon tax or an economy-wide cap-and-trade policy. Other forms of climate policies, such as differential carbon price by sector or renewable portfolio standards, have also been used in IAMs.

Cost of greenhouse gas mitigation (economic cost) Integrated assessment models (IAMs) employ varies metrics for estimating the economic cost of mitigation policy. One common approach estimates reduction in GDP, a proxy for slowdown in economic activity due to increased price of energy and agricultural products. Another approach estimates the (gross) loss in social welfare due to a policy by measuring the area under the marginal abatement cost curve. Other metrics include foregone consumption, compensated variation, and equivalent variation.

Integrated assessment model (IAM) Integrated assessment model (IAM) in climate change research is a model which simulates the interactions of human decision-making about energy systems and land use with biogeochemistry and the natural Earth system. IAMs can be divided into two categories.

Higher resolution IAMs focus on explicitly representing processes and process interactions among human and natural Earth systems.

Highly aggregated IAMs use highly reduced-form representations of the link between human activities, impacts from climate change, and the cost of emissions mitigation.

Integrated earth system model (iESM) Integrated Earth System Models (iESMs) are a class of models under development by collaboration between integrated assessment modeling community and

climate modeling community. By fully integrating the human dimension from an IAM and the natural dimension from a climate model, iESM allows simultaneously estimating human system impacts on climate change and climate change impacts on human systems, as well as examining the effects of feedbacks between the components.

Land use (land-use emissions) Land use is one of the largest anthropogenic sources of emissions of greenhouse gases, aerosols, and short-lived species. Emissions, as well as sequestration of emissions, may occur from land-use practices, changes in land cover, or changes in forested area or the density. On the other hand, land-use patterns are affected by the changes in the climate. As such, modeling land use has been an important component of the integrated assessment modeling of climate change.

Representative concentration pathways (RCPs) The Representative Concentration Pathways (RCPs) are the most recent set of emission scenarios generated by integrated assessment models. Four scenarios explicitly considering emission mitigation efforts that were sufficiently differentiated in terms of radiative forcing at the end of the century were selected from published literature. RCPs are designed to facilitate the interactions with climate models by including geospatially resolved emissions and land-use data.

Definition of the Subject

This entry discusses the role of integrated assessment models (IAMs) in climate change research. IAMs are an interdisciplinary research platform, which constitutes a consistent scientific framework in which the large-scale interactions between human and natural Earth systems can be examined. In so doing, IAMs provide insights that would otherwise be unavailable from traditional single-discipline research. By providing a broader view of the issue, IAMs constitute an important tool for decision support. IAMs are also a home of human Earth system research and provide natural Earth system scientists information about the nature of human intervention in global biogeophysical and geochemical processes.

Introduction

Integrated assessment models (IAMs) are a class of models which simulate the interactions of human decision-making about energy systems and land use with biogeochemistry and the natural Earth system (see Fig. 1). In so doing, IAMs provide insights that would otherwise be unavailable from investigating either natural systems or human systems, or their various components, alone. By their nature, IAMs capture interactions between complex and highly nonlinear systems. IAMs serve multiple purposes. One purpose is to provide natural science researchers with information about human systems such as greenhouse gas emissions, land use, and land cover. Another purpose of IAMs is to help human system researchers – such as social scientists – better understand the nature of the human impacts on the natural Earth systems.

Traditionally, researchers have relied on models that are each built on the foundations of a single discipline – such as economics, geography, meteorology, etc. By integrating research methods from various disciplines that characterize both the human and natural Earth systems, IAMs produce insights that would not otherwise be available from disciplinary research. The work of Wigley, Richels, and Edmonds [1] provides a classic example of the nature of insights that are available from the explicit linking of human and Earth systems. Wigley et al. showed that the consideration of economic efficiency in the context of the physical carbon cycle carried important implications for the timing of emissions and emissions mitigation in a world seeking to stabilize the concentration of atmospheric CO_2. In other words, the imposition of human system considerations – in this case economic efficiency considerations – led to a different and smaller set of emissions pathways for consideration than were indicated by Earth system considerations alone.

This entry discusses a range of selected topics associated with the development and use of IAMs. This is not an extensive survey of the literature and the available models. Instead, it focuses on a selected set of topics required to understand the various types and uses of IAMs as well as those required to understand the direction of cutting-edge IAM research. In addition, the entry focuses more heavily on the strain

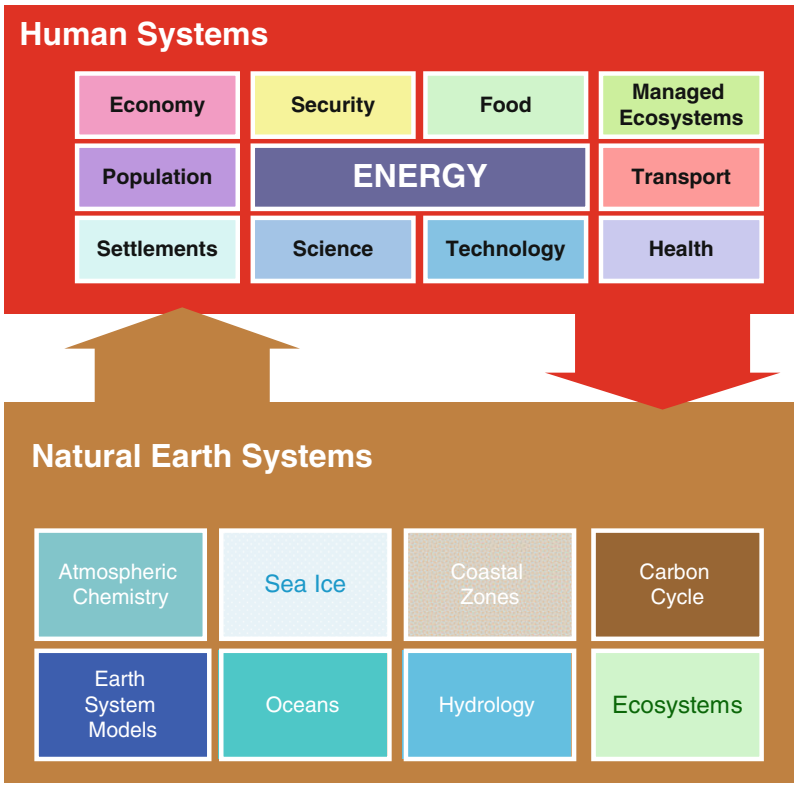

Integrated Assessment Modeling. Figure 1
Integrated assessment models integrate human and physical Earth system climate science (Source: Janetos et al. [72])

of IAMs and integrated assessment modeling (IA modeling) research focused on more effectively modeling human and Earth system processes (higher resolution IAMs) than on the strain of IAMs and IA modeling research that focuses on more aggregate representations of these systems to allow for cost-benefit analysis. The remainder of this entry proceeds as follows. Section "The Variety of Integrated Assessment Models" focuses on the emerging distinction between highly aggregated and higher resolution IAMs. Section "GCAM as an Example of a Higher Resolution IAM" then follows with a discussion of the Global Change Assessment Model (GCAM) as an example of a higher resolution IAM. Section "Using Higher Resolution IAMs to Analyze the Impact of Policies to Mitigate Greenhouse Gas Emissions" discusses the long history of using IAMs to explore the costs of greenhouse gas policies as well as several of the most important conceptual issues that the IAMs have had to wrestle with in this regard. Section "Future Directions: Integrating Climate Impacts with IAM" then explores an important cutting-edge research direction for higher resolution IAMs: the inclusion of structural or process models of climate impacts.

The Variety of Integrated Assessment Models

There are many approaches that have been used to develop and use IAMs. Indeed, every IAM is different. One of the most important ways that IAMs are distinguished from one another is the level of resolution at which they model the underlying human and natural Earth system process. At one end of the spectrum are *highly aggregated* IAMs. Highly aggregated IAMs use highly reduced-form representations of the link between human activities, impacts from climate change, and the cost of emissions mitigation. At the other end of the spectrum are *higher resolution* IAMs. Higher resolution IAMs focus on explicitly representing processes and process interactions among human and natural Earth systems. The following two subsections provide background on each of these two classes of IAMs.

Highly Aggregated IAMs

The highly aggregated class of IAMs was developed to be able to explore the general shape of optimal climate policy, taking into account both the economic costs of mitigation and the economic damages from a changing climate. Highly aggregated IAMs typically frame the climate change mitigation problem in a cost-benefit framework, choosing emission pathways by explicitly weighing the economic costs of mitigation with the economic benefits of reduced impacts. For this reason, highly aggregated IAMs often focus on issues such as the social cost of carbon or optimal tradeoffs over time between mitigation and impacts. Simplicity and parsimony are main virtues of highly aggregated IAMs.

The oldest of the highly aggregated IAMs is the DICE (Dynamic Integrated model of Climate and the Economy) model, whose antecedents have roots in the work of Nordhaus and Yohe [2]. The original DICE model [3] was utilized to explore the integration of human and natural Earth systems as part of a cost-benefit calculation. Originally developed as a one-region global model, DICE was soon followed by a multiregional version, RICE (Regional dynamic Integrated model of Climate and the Economy) [4]. Other such models also emerged building on the Nordhaus-Yohe and DICE paradigm of combining economic costs and benefits in a single framework. These models include, among others, ICAM (the Integrated Climate Assessment Model) [5], PAGE (Policy Analysis of the Greenhouse Effect) [6], and FUND (Climate Framework for Uncertainty, Negotiation and Distribution) [7] (Weyant et al. [8] and Parson and Fisher-Vanden [9] provide good sources of information on pioneering IAMs).

Highly aggregated IAMs are generally composed of three parts: emissions and mitigation, atmosphere and climate, and climate impacts. Mitigation cost and climate change damages are typically monetized (i.e., expressed in dollars or another currency) to allow comparison between mitigation and impacts on a common basis. Highly aggregated IAMs do not attempt to describe in detail either the energy system or the land-use systems that generate emissions. Similarly, detailed descriptions of the physical process links between climate change and emissions are generally beyond their scope. Instead these models use emissions mitigation supply schedules and climate damage functions. The former maps the relationship between the degree of emissions mitigation and associated cost, while the latter represents the relationship between a measure of climate change and the economic value of damages including both damages from market and nonmarket activities. The strength of these reduced-form representations is that they allow highly aggregated IAMs to weigh costs and benefits explicitly. The drawback is that they cannot provide insight into the actual processes that lead to these costs and benefits.

The technical structure of highly aggregated models is simple, but the equations and associated parameterizations are carefully estimated to capture the behavior of more complex systems. These functions are parameterized by either approximating the behavior of more complex process models, or by fitting simple equations to highly aggregated variables. Analyses using FUND, for example, often produce simple equations that capture the behavior of systems that are represented in more complex models and data. Some models use a simpler approach, in which the economic damages from a prescribed level of climate change are first estimated – for example, a 2°C global mean surface temperature change (GMST) relative to preindustrial level – and a simple function that passes through the estimate – for example, a power function – is assigned to represent the relationship between GMST and total economic damages.

A principle role of highly aggregated IAMs is to integrate and to compare in a common metric, both mitigation effort and climate change impact – each estimated from different disciplines – in order to determine the optimal pathway of emissions reductions or the social cost of carbon. Valuation of damages provides substantial conceptual challenges for highly aggregated IAMs. For example, they must put a value on the loss of human lives as well as nonmarket damages. Another difficult challenge faced by highly aggregated IAMs concerns the relative valuation of impacts that occur at different points in time. See Box 1 for details.

Other issues that arise within the highly aggregated IAM paradigm include the problem of interactive effects, that is, the state of one system directly affects the state of another. For example, emissions mitigation may have large-scale effects on land use, which in turn

affect the climate, or the climate system may change as a consequence of land-use policy. A challenge for highly aggregated IAMs is to represent such complex interactions in a simple model structure.

Box 1. Valuation over Time and Across Generations

Climate change is an issue that is inherently long term as well as global. The nature of carbon cycle processes and their associated time scales create a cumulative relationship between CO_2 emissions and concentrations in the atmosphere (and ocean). Thus, unlike traditional atmospheric pollution problems, control of emissions to a level is insufficient to control the concentration of greenhouses in the atmosphere. In other words, CO_2 and other greenhouse gases are stock pollutants.

One of the most important determinants of the social cost of carbon is the rate at which future events are discounted back to the present. Nordhaus [10] argues that the order of magnitude difference between his estimate of the social value of carbon, derived using DICE, and the value estimated in the Stern Report [11], derived using PAGE, is predominantly a result of the differences in valuing the present relative to the future.

The problem is that there is no consensus on precisely how to approach discounting over periods of time long enough to connect multiple generations. The issues are laid out in Portney and Weyant [12], where the editors note in their overview chapter that "those looking for guidance on the choice of a discount rate could find justification for a rate at or near zero, as high as 20% and any and all values in between" ([12], p. 4). The range of estimates for the appropriate discount rate is generally nonnegative, though even that generalization has its exceptions, for example [13].

Methods for determining the appropriate method for discounting the future can be grouped into two general categories – those which are *prescriptive* and those which are *descriptive*. The prescriptive approach appeals to ethical and moral grounds for choosing a discount rate, while the descriptive approach appeals to observed rates of return on assets in economic markets. It is frequently observed that prescriptive approaches tend to generate lower discount rates than descriptive approaches.

Another challenge for highly aggregated IAMs is to determine how to treat impacts occurring outside of the country undertaking the valuation. Early work with highly aggregated IAMs looked at the problem of climate change from the perspective of a single, global, infinitely lived decision maker. But, more recent work has shifted from the perspective of the globe (e.g., [3, 11]) to the perspective of a single country, for example, the United States [14].

The Higher Resolution IAMs

The higher resolution IAMs have roots in the same era as the highly aggregated IAMs. However, they were developed along different lines to serve different purposes. The higher resolution IAMs were developed to provide detailed information about human and natural Earth system processes and the interactions between these processes. The initial focus of these models was the determinants of anthropogenic carbon emissions. To address this problem, IAMs developed detailed representations of the key features determining long-term energy production, transformation, and end use. The higher resolution models distinguished different forms of energy, their supplies, demands, and their transformation from primary energy to fuels and electricity for use in end-use sectors such as buildings, transportation, and industry. Examples of higher resolution IAMs are provided in Table 1.

Over time these models have grown in complexity. The models have added increasing detail to their representations of both the energy system and the economy. They also broadened their scope, adding natural Earth system processes such as carbon cycle. The current generations of higher resolution IAMs also typically contain representations of agriculture, land use, land cover, and terrestrial carbon cycle processes in addition to representations of atmosphere and climate processes. While all of the higher resolution IAMs model both human and natural Earth system processes, each model was developed independently and each IAM development path emphasized different features of the climate change problem. Some emphasized the development of detailed atmosphere and climate system models. Some focused on detailed representations of technology. Others focused on regional differences in emission patterns and energy systems data.

Integrated Assessment Modeling. Table 1 Some higher resolution integrated assessment models

Some higher resolution integrated assessment models with interdisciplinary research teams		
Model	**Home institution**	**Web link**
AIM Asia-Pacific integrated model	National Institutes for Environmental Studies, Tsukuba, Japan	http://www-iam.nies.go.jp/aim/
GCAM Global change assessment model	Joint Global Change Research Institute, PNNL, College Park, MD	http://www.globalchange.umd.edu/models/gcam/
IGSM Integrated global system model	Joint Program on the Science and Policy of Global Change, MIT, Cambridge, MA	http://globalchange.mit.edu/igsm/
IMAGE The integrated model to assess the global environment	PBL Netherlands Environmental Assessment Agency, Bildhoven, The Netherlands	http://themasites.pbl.nl/en/themasites/image/
MERGE Model for evaluating the regional and global effects of GHG reduction policies	Electric Power Research Institute, Palo Alto, CA	http://www.stanford.edu/group/MERGE/
MESSAGE Model for energy supply strategy alternatives and their general environmental impact	International Institute for Applied Systems Analysis; Laxenburg, Austria	http://www.iiasa.ac.at/Research/ENE/model/message.html
ReMIND Refined model of investments and technological development	Potsdam Institute for Climate Impact Research; Potsdam, Germany	http://www.pik-potsdam.de/research/sustainable-solutions/models/remind/

The complex nature of the models requires interdisciplinary research and modeling teams, some of which are listed in Table 1.

Because the higher resolution IAMs have grown in their complexity over time, describing the structure of each model in detail is beyond the scope of this entry. For a reference, comparison of three IAMs – IGCM, MERGE, and MiniCAM (the direct ancestor of GCAM) – can be found in [14]. Here, we present the summary comparison table from the report in Table 2. All three of these modeling systems have evolved considerably in the subsequent years.

GCAM as an Example of a Higher Resolution IAM

Introduction to GCAM

Rather than try to describe and compare the set of higher resolution IAMs, we have chosen to describe here the Global Change Assessment Model (GCAM) as an example of the higher resolution IAM genre. GCAM is the oldest of the higher resolution IAMs. It traces its roots to work initiated in the late 1970s. The model's first applications were completed in the early 1980s by Edmonds and Reilly [15–18]. Over time the model has developed and evolved through a series of advances documented in a variety of papers including [19–22]. Documentation for GCAM under its previous name, MiniCAM, can be found at http://www.globalchange.umd.edu/models/MiniCAM.pdf/. Other higher resolution IAMs, such as IMAGE and MESSAGE, also use MAGICC to represent atmosphere and climate processes.

At the top level the GCAM model is broken into two interacting system, human Earth system and natural Earth systems. Each of these systems in turn is made up of subsystems. This is the basic structure of all IAMs. GCAM and the other higher resolution IAMs are distinguished from the highly aggregated IAMs in the degree of detail that is incorporated in describing human and natural Earth systems.

All higher resolution IAMs emphasize the representation of human activities and their connection to the sources of greenhouse gas emissions. However, each modeling team has taken a different approach.

Integrated Assessment Modeling. Table 2 Characteristics of the three integrated assessment models

Feature	IGSM (with EPPA economics component)	MERGE	MiniCAM
Regions	16	9	14
Time horizon, time steps	2100, 5-year steps	2200, 10-year steps	2095, 15-year steps
Model structure	General equilibrium	General equilibrium	Partial equilibrium
Solution	Recursive dynamic	Inter-temporal optimization	Recursive dynamic
Final energy demand sectors in each region	Households, private transportation, commercial transportation, service sector, agriculture, energy-intensive industries, and other industry	A single, nonenergy production sector	Buildings, transportation, and industry (including agriculture)
Capital turnover	Five vintages of capital with a depreciation rate	A putty clay approach wherein the input-output coefficients for each cohort are optimally adjusted to the future trajectory of prices at the time of investment	Vintages with constant depreciation rate for all electricity-sector capital; capital structure not explicitly modeled in other sectors
Goods in international trade	All energy and nonenergy goods as well as emissions permits	Energy, energy-intensive industry goods, emissions permits, and representative tradable goods	Oil, coal, natural gas, biomass, agricultural goods, and emissions permits
Emissions	CO_2, CH_4, N_2O, HFCs, PFCs, SF_6, CO, NOx, SOx, NMVOCs, BC, OC, NH_3	CO_2, CH_4, N_2O, long-lived F-gases, short-lived F-gases, and SOx	CO_2, CH_4, N_2O, CO, NOx, SO_2, NMVOCs, BC, OC, HFC245fa, HFC134a, HFC125, HFC143a, SF_6, C_2F_6, and CF_4
Land use	Agriculture (crops, livestock, and forests), biomass land use, and land use for wind and/or solar energy	Reduced-form emissions from land use; no explicit land-use sector; assume no net terrestrial emissions of CO_2	Agriculture (crops, pasture, and forests) as well as biomass land use and unmanaged land; the agriculture-land-use module directly determines land-use change emissions and terrestrial carbon stocks
Population	Exogenous	Exogenous	Exogenous
GDP growth	Exogenous productivity growth assumptions for labor, energy, and land; exogenous labor force growth determined from population growth; endogenous capital growth through savings and investment	Exogenous productivity growth assumptions for labor and energy; exogenous labor force growth determined from population growth; endogenous capital growth through savings and investment	Exogenous productivity growth assumptions for labor; exogenous labor force growth based on population demographics
Energy efficiency change	Exogenous	Proportional to the rate of GDP growth in each region	Exogenous

Integrated Assessment Modeling. Table 2 (Continued)

Feature	IGSM (with EPPA economics component)	MERGE	MiniCAM
Energy resources	Oil (including tar sands), shale oil, gas, coal, wind and/or solar, land (biomass), hydro, and nuclear fuel	Conventional oil, unconventional oil (coal-based synthetics, tar sands, and shale oil), gas, coal, wind, solar, biomass, hydro, and nuclear fuel	Conventional oil, unconventional oil (including tar sands and shale oil), gas, coal, wind, solar, biomass (waste and/or residues and crops), hydro, and nuclear fuel (uranium and thorium); includes a full representation of the nuclear fuel cycle
Electricity technologies	Conventional fossil (coal, gas, and oil), nuclear, hydro, natural gas combined cycle (NGCC) with and without capture, integrated coal gasification with capture, and wind and/or solar, biomass	Conventional fossil (coal, gas, and oil), nuclear, hydro, new coal and gas with and without CCS, other renewables	Conventional fossil (coal, gas, and oil) with and without capture; IGCCs with and without capture; NGCC with and without capture; Gen II, III, and IV reactors and associated fuel cycles; hydro, wind, solar, and biomass (traditional and modern commercial)
Conversion technologies	Oil refining, coal gasification, and bio-liquids	Oil refining, coal gasification and liquefaction, bio-liquids, and electrolysis	Oil refining, natural gas processing, natural gas to liquids conversion, coal, and biomass conversion to synthetic liquids and gases; hydrogen production using liquids, natural gas, coal, biomass; and electrolysis, including direct production from wind and solar, and nuclear thermal conversion
Atmosphere – ocean	2-dimensional atmosphere with a 3-dimensional ocean general circulation model, resolved at 20 minute time steps, 4° latitude, 4 surface types, and 12 vertical layers in the atmosphere	Parameterized ocean thermal lag	Global multi-box energy balance model with upwelling-diffusion ocean heat transport
Carbon cycle	Biogeochemical models of terrestrial and ocean processes; depends on climate and/or atmospheric conditions with 35 terrestrial ecosystem types	Convolution ocean carbon cycle model assuming a neutral biosphere	Globally balanced carbon cycle with separate ocean and terrestrial components, with terrestrial response to land-use changes
Natural emissions	CH_4, N_2O, and weather and/or climate dependent as part of biogeochemical process models	Fixed natural emissions over time	Fixed natural emissions over time
Atmospheric fate of GHGs, pollutants	Process models of atmospheric chemistry resolved for urban and background conditions	Single box models with fixed decay rates. No consideration of reactive gases	Reduced-form models for reactive gases and their interactions
Radiation code	Radiation code accounting for all significant GHGs and aerosols	Reduced form, top-of-the-atmosphere forcing	Reduced form and top-of-the-atmosphere forcing; including indirect forcing effects

Source: Clarke et al. [14]

For example, the IGSM employs a computable general equilibrium (CGE) model of the economy [23]. CGE models emphasize the structure of the economy and the interaction of economic sectors with each other and with labor and capital markets. The MERGE model also employs a highly aggregated CGE model in combination with more highly disaggregated energy sector models all embedded in an intertemporal optimization framework [24, 25]. The Asia-Pacific Integrated Model (AIM) employs a set of models that are used in combination [26]. The GCAM model uses a partial equilibrium framework, rather than a CGE framework. Partial equilibrium models delve into more detail in sectors that are directly related to the analysis in question (e.g., energy supply and demand, agricultural production, land use, and land-use change), and treat other sectors of the economy in aggregate.

The GCAM model drives the scale of human activities for each of its 14 geopolitical regions utilizing assumptions about future labor force – determined by working-age population, labor participation, and unemployment rate assumptions – along with the assumptions about labor productivity growth. The highly disaggregated energy, agriculture, and land-use components of GCAM are driven by the scale of human activity. The GCAM geopolitical regions are explicitly linked through international trade in energy commodities, agricultural and forest products, and other goods such as emissions permits.

The human dimension of the Earth system as shown in Fig. 2 integrates the energy system and the agriculture and land-use system, as well as the economic system that drives the activity in both systems. An important feature of the GCAM architecture is that the GCAM terrestrial carbon cycle model is embedded within the agriculture-land-use system model; that is, the agriculture-land-use system model explicitly calculates net land-use-change emissions from changes in land-use patterns over time. The energy system model produces and transforms energy for use in three end-use sectors: buildings, industry, and transport. The global human Earth systems are modeled for 14 geopolitical regions.

GCAM is a dynamic-recursive market equilibrium model. In each period of time the model's solution algorithm reconciles the supplies and demands for goods and services in all markets by finding a set of market-clearing prices. That market solution establishes the foundation from which the model steps forward to the next time period. Other IAMs, such as MERGE and MESSAGE, are built on an intertemporal optimization framework. These models solve all periods simultaneously so that expectations about the future are consistent with the model's future realizations in each time period. In contrast, GCAM, and other dynamic-recursive models, do not assume such intertemporal optimization takes place. Decisions taken in one period contain only expectations about future market conditions. These expectations will not necessarily be realized in the future. In other words, the economic agents in GCAM make decisions based on a less-than-perfect foresight, and the agents' only recourse in the subsequent period is to make another set of decisions, which can also be suboptimal.

The GCAM's time step is variable, but in general is set to 5 years, which is relatively common among integrated assessment models. GCAM tracks 16 different greenhouse gases, aerosols, and short-lived species. The GCAM physical atmosphere and climate are represented by the Model for the Assessment of Greenhouse-Gas Induced Climate Change (MAGICC) [27–29].

In the remainder of this section, we discuss in more detail two of the most important model components in GCAM: the representation of the energy system and the representation of agriculture and land use more generally.

The Energy System in GCAM

In GCAM, the energy system represents processes of energy resource extraction, transformation, and delivery, ultimately producing services demanded by end users (Fig. 3). In each time period, the market prices of all goods and services, including primary energy resources, land, agricultural goods, and other products, are determined by the market equilibrium.

Primary energy production is limited by regional resource availability. Fossil fuel and uranium resources are finite, graded, and depletable. Wind, solar, hydro, and geothermal resources are also finite and graded, but renewable. Bioenergy is also renewable, but is treated as an explicit product of the agriculture-land-use portion of the model. Extraction costs for

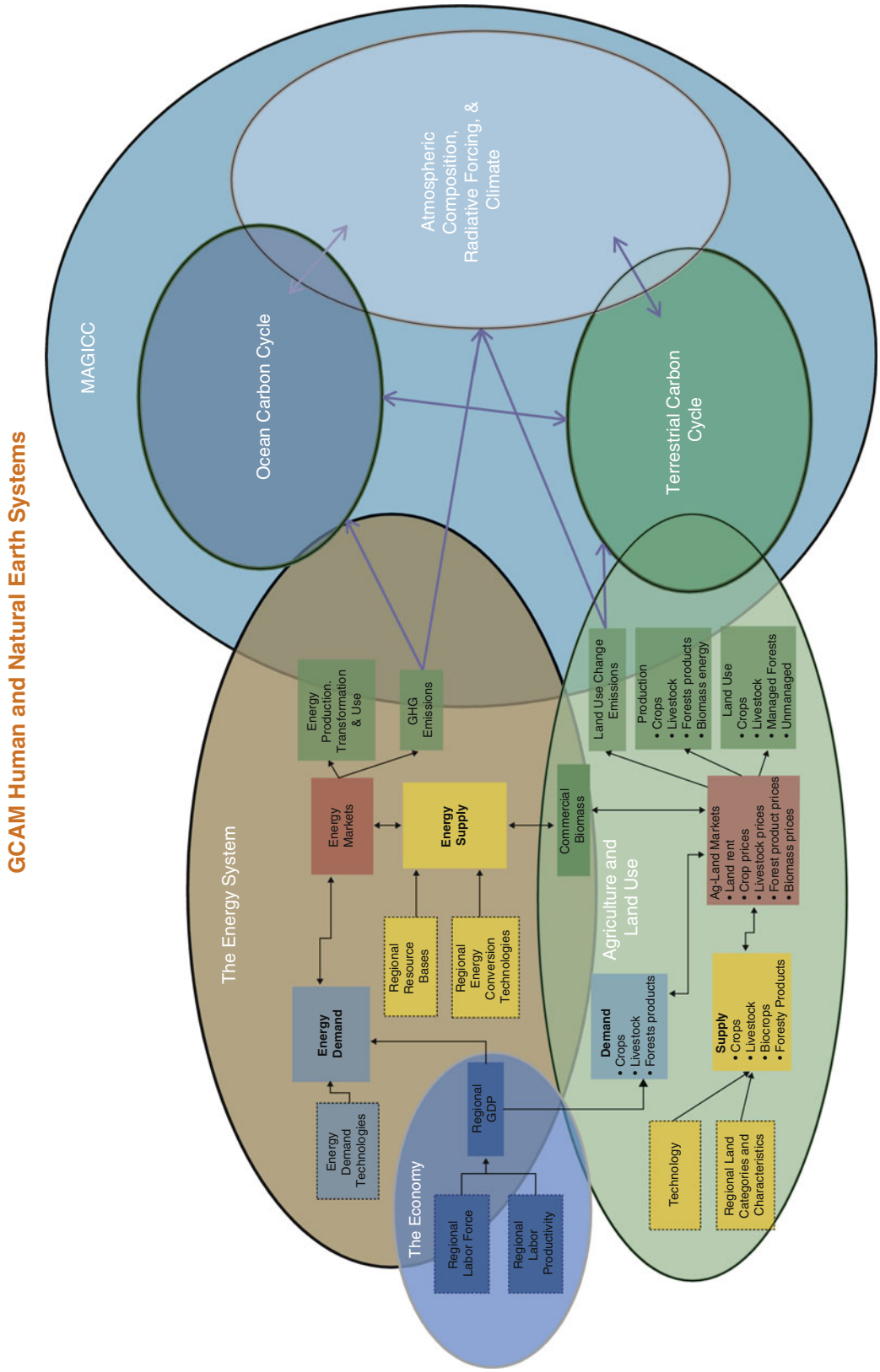

Integrated Assessment Modeling. Figure 2
Human and natural Earth systems of the global change assessment model

I

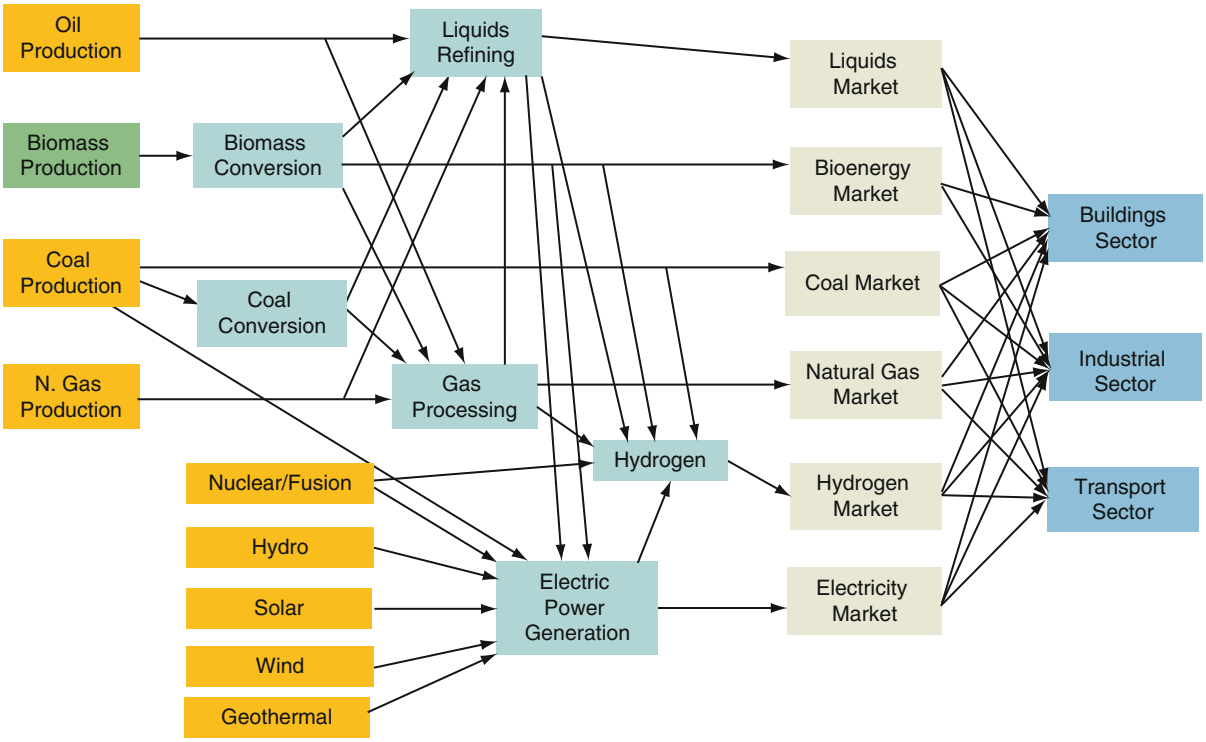

Integrated Assessment Modeling. Figure 3
The energy system in GCAM

graded resources rise as the resource consumption increases, but can fall with improvement in extraction technologies, and can rise or fall depending on other environmental costs.

Primary energy forms can be transformed into six final energy products:

- Refined liquid energy products (oil and oil substitutes)
- Processed gas products (natural gas and other artificially gasified fuels)
- Coal
- Bioenergy solids (various forms of biomass)
- Electricity
- Hydrogen

Energy transformation sectors convert resources initially into fuels, which may be consumed by either other energy transformation sectors or ultimately into goods and services consumed by end users. In each energy sector, multiple technologies compete for market share; shares are allocated among competing technologies using a logit choice formulation [30–32]. The cost of a technology in any period is determined by two key exogenous input parameters – the nonenergy cost and the efficiency of energy transformation – as well as the prices of the fuels it consumes. The nonenergy cost represents all fixed and variable costs incurred over the lifetime of the equipment (except for fuel costs), amortized into a unit cost of output. For example, a coal-fired electricity plant incurs a range of costs associated with construction (a capital cost) and annual operations and maintenance. The efficiency of a technology determines the amount of fuel required to produce each unit of output (e.g., the fuel efficiency of a vehicle in passenger-km per GJ, or the electricity generation efficiency of a coal-fired power plant). The prices of different fuels are calculated endogenously in each time period based on supplies, demands, and resource depletion.

The representation of energy technologies in GCAM is highly disaggregated. Table 3 shows, for example, the set of technologies with accompanying assumptions of

Integrated Assessment Modeling. Table 3 Residential sector efficiencies by service and technology (Source: Kyle et al. [79])

Residential				Reference		Advanced	
Service	Technology	unit	2005	2050	2095	2050	2095
	Building shell	W/m^2	0.232	0.182	0.150	0.163	0.125
Heating	Gas furnace	Out/in	0.82	0.90	0.97	Same as Ref	
	Gas heat pump	Out/in	n/a	n/a	n/a	1.75	2.45
	Electric furnace	Out/in	0.98	0.99	0.99	Same as Ref	
	Electric heat pump	Out/in	2.14	2.49	2.79	2.94	4.12
	Oil furnace	Out/in	0.82	0.86	0.93	Same as Ref	
	Wood furnace	Out/in	0.40	0.42	0.44	Same as Ref	
Cooling	Air conditioning	Out/in	2.81	3.90	4.88	4.59	7.19
Water heating	Gas water heater	Out/in	0.56	0.61	0.64	0.79	0.88
	Gas HP water heater	Out/in	0.89	1.09	1.22	1.75	2.45
	Electric water heater	Out/in	0.88	0.93	0.97	Same as Ref	
	Electric HP water heater	Out/in	n/a	2.46	2.75	2.75	3.45
	Oil water heater	Out/in	0.55	0.56	0.59	Same as Ref	
Lighting	Incandescent lighting	Lumens/W	14	15	16	Same as Ref	
	Fluorescent lighting	Lumens/W	60	75	94	Same as Ref	
	Solid-state lighting	Lumens/W	100	112	125	156	245
Appliances	Gas appliances	Indexed	1.00	1.12	1.25	Same as Ref	
	Electric appliances	Indexed	1.00	1.23	1.38	1.44	2.01
Other	Other gas	Indexed	1.00	1.12	1.25	Same as Ref	
	Other electric	Indexed	1.00	1.08	1.21	1.40	1.96
	Other oil	Indexed	1.00	1.12	1.25	Same as Ref	

technology change over time, for the detailed US representation of residential buildings in GCAM.

Other energy sectors in GCAM have similar, high degrees of technology disaggregation. There are, for example, multiple technology options for generating electric power which include a variety of technologies utilizing solar energy as well as technology options to capture, transport, and store CO_2 in geologic repositories (CCS). The deployment of CCS technology in conjunction with bioenergy is of special interest in the consideration of very low long-term limits on CO_2 concentrations in that this combination potentially allows the production of energy with negative net CO_2 emissions. We discuss this particular technology combination in greater detail in a subsequent section of this entry.

Agriculture and Land Use in GCAM

Overview of the Agriculture and Land-Use Model in GCAM Land use is one of the largest anthropogenic sources of emissions of greenhouse gases, aerosols, and short-lived species. The conversion of grasslands and forests to agricultural land results in a net emission of CO_2 to the atmosphere. In the nineteenth century, the conversion of forests to agricultural land was the largest source of anthropogenic carbon emissions. In the future, biomass energy crops could compete for

agricultural land with traditional agricultural crops, providing a crucial linkage between land use and the energy system. Efforts to sequester carbon in terrestrial reservoirs, such as forests, may limit deforestation activities, and potentially lead to afforestation or reforestation activities. Interactions with crop prices may also prove important. Since land is limited, increasing the demand for land either to protect forests or to plant bioenergy crops could put upward pressure on crop prices that would not otherwise occur [33].

Many higher resolution IAMs include representations of agriculture, land use, and land cover. For some models, such as IGSM or IMAGE, a separate ecosystem model is used to represent terrestrial systems, which is then loosely coupled to the other elements of the IAM. These models represent land use, land cover, and the terrestrial carbon cycle. The IGSM model employs the Terrestrial Ecosystems Model [23], while IMAGE employs their terrestrial environment system submodel [34]. Since these models represent terrestrial processes at fine geographic scales – ½ degree by ½ degree gridded maps, for example – land use is determined by coupling an aggregated model of agriculture with a downscaling algorithm.

GCAM uses a model of land use and land cover, which allocates land area within each of its 14 global geopolitical regions among different land uses and tracks production from these uses and corresponding carbon flows into and out of terrestrial reservoirs. The GCAM agriculture, land use, land cover, terrestrial carbon cycle module determines the demands for and production of agricultural products, the prices of these products, the allocation of land to competing ends, and the carbon stocks and flows associated with land use.

Land is allocated between alternative uses based on expected profitability, which in turn depends on the productivity of the land-based product (e.g., mass of harvestable product per hectare), product price, and non-land costs of production (labor, fertilizer, etc.). The allocation of land types takes place in the model through global and regional markets for agricultural products. These markets include those for raw agricultural products as well as those for intermediate products such as poultry and beef. Demands for most agricultural products, with the exception of biomass products, are driven primarily by income and population. Land allocations evolve over time through the operation of these markets, in response to changes in income, population, technology, and prices.

The boundary between managed and unmanaged ecosystems is assumed to be elastic in GCAM. The area of land under cultivation expands and contracts as crops become more or less profitable. Thus, increased demands for land result in higher cropland profitability and expansion into unmanaged ecosystems and vice versa. Competition between alternative land uses in the GCAM is modeled using a nested logit architecture [30–32] as depicted in Fig. 4.

The costs of supplying agricultural products are based on regional characteristics, such as the productivity of land and the variable costs of producing the crop. The productivity of land-based products is subject to change over time based on future estimates of crop productivity change. It has been shown that the rate of crop yield improvement is a critical determinant of land-use change emissions [33, 35–37].

Bioenergy in GCAM's Agriculture and Land-Use Model Bioenergy supply is determined by the agriculture-land-use component (AgLU) of GCAM, while bioenergy demand is determined in the energy component of the model. For example, the larger the value of carbon, the more valuable biomass is as an energy source and hence the greater the price the energy markets will be willing to pay for biomass. Conversely, as populations grow and incomes increase, competing demands for land may drive down the amount of land that would be available for biomass production at a given price.

There are three types of bioenergy produced in GCAM: traditional bioenergy production and use, bioenergy from waste products, and purpose-grown bioenergy. Traditional bioenergy consists of straw, dung, fuel wood, and other energy forms that are utilized in an unrefined state in the traditional sector of an economy. Traditional bioenergy use, although significant in developing nations, is a relatively small component of global energy. Traditional bioenergy is modeled as a function of regional income levels with its use diminishing as per capita incomes rise.

Other two types of bioenergy products are fuels that are consumed in the modernized sectors of the economy. Bioenergy from waste products are

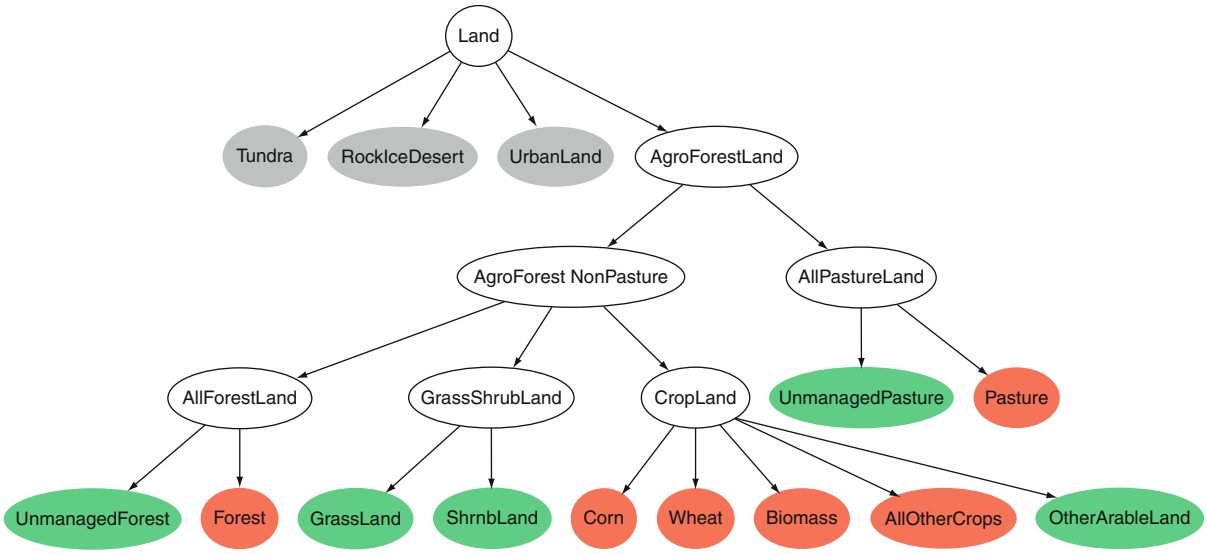

Integrated Assessment Modeling. Figure 4
Competition for land in GCAM. Gray exogenous in future periods, *Green* unmanaged land use, *Red* managed land use. AgLU tracks carbon content in different land uses. Changes in land use result in carbon flux to the atmosphere. Land owners compare economic returns across crops, biomass, pasture, and (future) forest, based on underlying probability distribution of yields per hectare

by-products of another activity. Examples in the model include forestry and milling by-products, crop residues in agriculture, and municipal solid waste. The availability of byproduct energy feedstocks is determined by the underlying production of primary products and the cost of collection. The total potential agricultural waste available is calculated as the total mass of the crop less the portion that is harvested for food, grains, and fibers, and the amount of bioenergy needed to prevent soil erosion and nutrient loss and sustain the land productivity. The amount of potential waste that is converted to bioenergy is based on the price of bioenergy.

The third category of bioenergy is purpose-grown energy crops. Purpose-grown bioenergy refers to crops whose primary purpose is the provision of energy. These would include, for example, switchgrass and woody poplar. The profitability of purpose-grown bioenergy depends on the expected profitability of growing and selling that crop relative to other land-use options in GCAM. This in turn depends on numerous other model factors: in the agricultural sector, bioenergy crop productivity (which in turn depends on the character of available land as well as crop type and technology) and nonenergy costs of crop production, and in the fuel processing sector, cost and efficiency of transformation of purpose-grown bioenergy crops to final energy forms (including liquids, gases, solids, electricity, and hydrogen), cost of transportation to the refinery, and the price of final energy forms. Furthermore, the price of final energy forms is determined endogenously as a consequence of competition between alternative energy resources, transformation technologies, and end-use energy service delivery technologies. In other words, prices are determined so as to simultaneously match demand and supplies in all energy markets as well as all land-use markets.

A variety of crops could potentially be grown as bioenergy feedstocks. The productivity of those crops will depend on where they are grown – which soils they are grown in, climate characteristics and their variability, whether or not they are fertilized or irrigated, the availability of nitrogen and other minerals, ambient CO_2 concentrations, and their latitude. GCAM typically include a generic bioenergy crop, with its characteristics similar to switchgrass that is assumed to be grown in all regions. Productivity is based on

region-specific climate and soil characterizes and varies by a factor of three across the GCAM regions. GCAM allows for the possibility that bioenergy could be used in the production of electric power and in combination with technologies to provide CO_2 emissions captured and stored in geological reservoirs (CCS). This particular technology combination is of interest because bioenergy obtains its carbon from the atmosphere and if that carbon were to be captured and isolated permanently from the atmosphere the net effect of the two technologies would be to produce energy with negative CO_2 emissions. See, for example, [33, 38].

Pricing Carbon in Terrestrial Systems Efficient climate policies are those that apply an identical price to greenhouse gas emissions wherever they occur. Hence, an efficient policy is one that applies identical prices to land-use change emissions and fossil and industrial emissions. This efficient approach is used as the default for emissions mitigation scenarios, though other policy options have also been modeled (A change in atmospheric CO_2 concentration has the same impact on climate change no matter what the source. Thus, to a first approximation land-use emissions have the same impact as fossil emissions. But, there are important differences. Land-use emissions do not have the same impact on atmospheric concentrations as fossil emissions because land-use emissions also imply changes in the future behavior of the carbon cycle. A tonne of carbon emitted due to deforestation, for example, is associated with a decrease in forest that would otherwise act as a carbon sink in the future. This effect, however, is not currently captured in GCAM).

Carbon in terrestrial systems can be priced using either a flow approach or a stock approach. The flow approach is analogous to the pricing generally discussed for emissions in the energy sector: landowners would receive either a tax or a subsidy based on the net flow of carbon in or out of their land. If they cut down a forest to grow bioenergy crops, then they would pay a tax on the CO_2 emissions from the deforestation. In contrast, the stock approach applies a tax or a subsidy to landowners based on the carbon content of their land. If the carbon content of the land changes, for example, by cutting forests to grow bioenergy crops, then the tax or subsidy that the landowner receives is adjusted to represent the new carbon stock in the land. The stock approach can be viewed as applying a "carbon rental rate" on the carbon in land. Both approaches have strengths and weaknesses. Real-world approaches may not be explicitly one or the other. By default, GCAM uses the stock approach.

Using Higher Resolution IAMs to Analyze the Impact of Policies to Mitigate Greenhouse Gas Emissions

A Brief Overview of IAMs in Mitigation Policy Analysis

Higher resolution IAMs have been used extensively to estimate the effects of measures to reduce greenhouse gas emissions. Until recently, the great bulk of the literature focused on the analysis of idealized policy instruments, particularly carbon taxes and cap-and-trade policies. For example, an important vein of early analysis focused on the question of emissions trading. In general, this literature showed that emissions mitigation undertaken with tradable permits resulted in lower costs to all parties without any reduction in overall emissions mitigation (see, for example, [39, 78]. The basic architecture of the Kyoto Protocol [40] reflected this line of thought. The application of these idealized pollution pricing mechanisms was inherently straightforward in higher resolution IAMs because these IAMs' representations of the energy and terrestrial systems are all built on economic principles. Furthermore, these mechanisms were of interest because they were theoretically attractive for the efficiency with which they reduced emissions.

In all the stabilization scenarios, the carbon price rises, by design, over time until stabilization is achieved (or the end-year 2100 is reached), and the prices are higher the more stringent is the stabilization level. There are substantial differences in carbon prices between MERGE and MiniCAM stabilization scenarios, on the one hand, and the IGSM stabilization scenarios on the other. Differences between the models reflect differences in the emissions reductions necessary for stabilization and differences in the technologies that might facilitate carbon emissions reductions, particularly in the second half of the century.

Whether for CO_2 or for multiple gases, a major focus of analysis has been to compute minimum-cost emissions trajectories for meeting long-term

stabilization goals. The minimum cost is generally calculated on the assumption that all regions of the world undertake emissions mitigation in a coordinated, intertemporal program that reduces emissions in an economically efficient manner. One key characteristic of this pathway is that the marginal cost of emissions mitigation is equal in all sectors and in all regions at any point in time. It also means that the price of CO_2 rises at the rate of interest plus the rate of removal of CO_2 from the atmosphere until stabilization is reached [41]. After stabilization is reached, the CO_2 price no longer rises at this roughly constant rate, but instead is determined so as to ensure that at any point in time emissions match uptake so concentrations remain constant. Examples of classic stabilization CO_2 price pathways are shown in Fig. 5.

While mitigation cost may be one of the core questions addressed by the higher resolution IAMs, it is not the only question. A second and complementary set of questions focuses on implications for energy and agricultural systems, the next level of detail upon which higher resolution IAMs focus. How fast must the energy system change? Which technologies need to be deployed and when (see, e.g., [42, 43])? Stabilization of the concentration of CO_2 at any level requires that net anthropogenic carbon emissions must peak and decline indefinitely toward zero [1], but an almost infinite set of combinations of technology could in

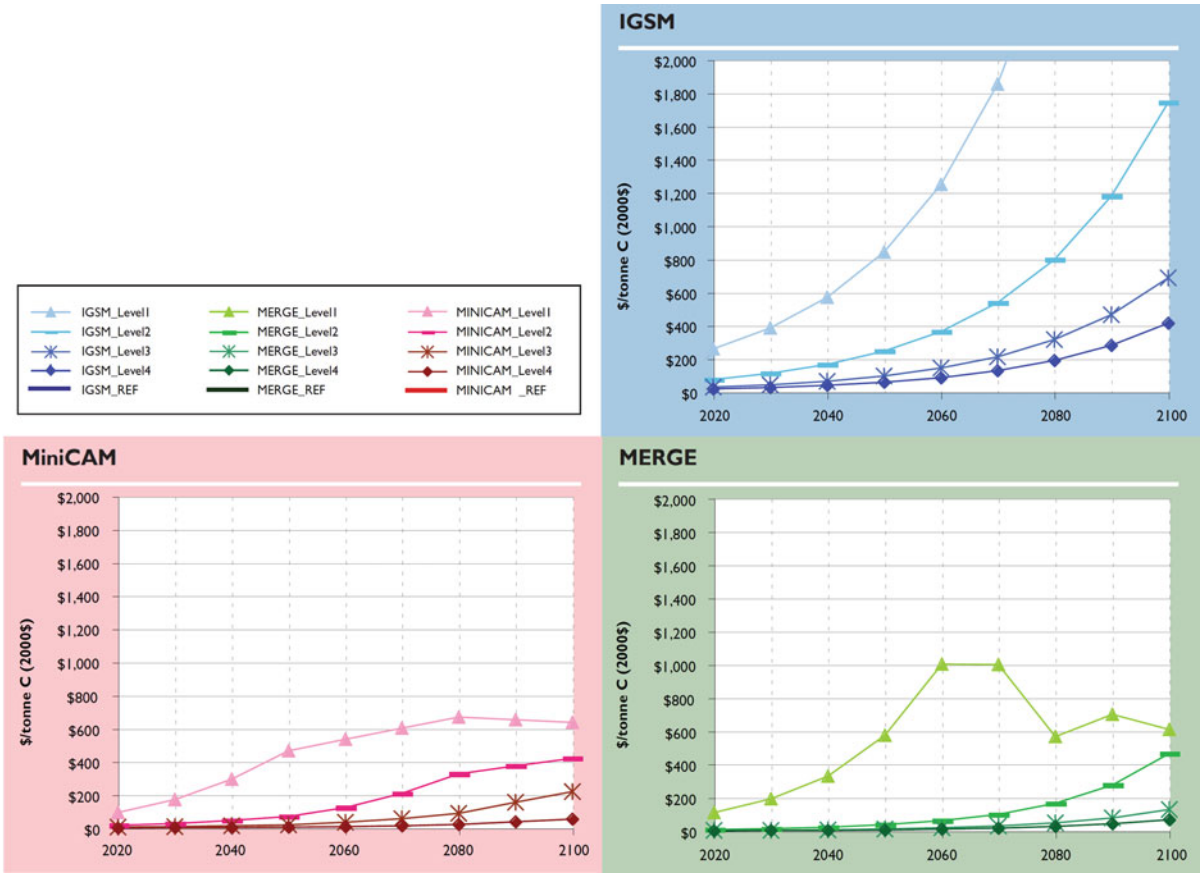

Integrated Assessment Modeling. Figure 5
Carbon prices across stabilization scenarios ($/ton C, 2000$) from three higher resolution IAMs leading to stabilization at approximately 750 ppmv CO_2 (Level 4), 650 ppmv CO_2 (Level 3), 550 ppmv CO_2 (Level 2), and 450 ppmv CO_2 (Level 1) (Source: Clarke et al. [14])

principle deliver that outcome. For example, fossil fuel use could be replaced with renewable energy forms in combination with energy efficiency improvements. Alternatively, fossil fuels could continue to be deployed in the global energy system in combination with CO_2 capture and storage (CCS), nuclear power, renewable energy, and energy efficiency. The combinations that emerge from different models depend on assumptions about technology performance and availability, scale of the economic system, and climate policy. A wide range of studies has made evolution of the energy system to meet long-term goals a focus of analysis (see, e.g., Fig. 6 from [14]).

Stabilization in IAMs with Multiple Greenhouse Gases

The United Nations Framework Convention on Climate Change (UNFCCC) has as its goal the stabilization of the concentration of greenhouse gases in the atmosphere. As discussed above, examination of the cost of stabilization of CO_2 and other gases has been the focus of a great number of papers utilizing higher resolution IAMs. Early studies focused exclusively on stabilization. However, more recent efforts have explored stabilization considering multiple greenhouse gases [14, 44].

When multiple greenhouse gases are considered simultaneously the problem emerges as to how to compare the greenhouse effects across the various constituents. In terms of climate change, the natural aggregate measure is radiative forcing (see Box 2). It is relatively straightforward to compute the radiative forcing for a group of gases, aerosols, and short-lived species and then to estimate what concentration of CO_2 would yield that radiative forcing level if all other species were set at their preindustrial levels. The answer to that question is the CO_2-equivalent concentration for that bundle of gases.

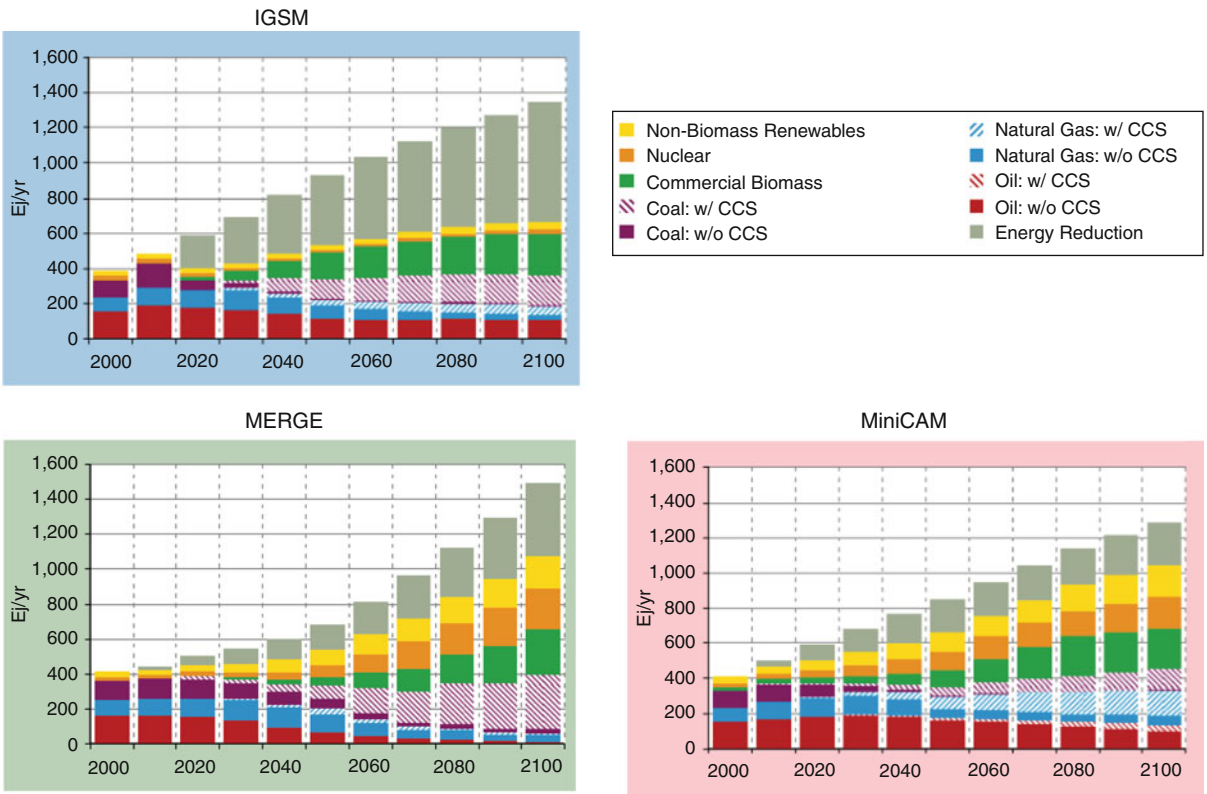

Integrated Assessment Modeling. Figure 6
Global primary energy production across scenarios from three higher resolution IAMs leading to approximately 450 ppmv CO_2 (Source: Clarke et al. [14])

Box 2. Radiative Forcing

Most of the Sun's energy that reaches the Earth is absorbed by the oceans and land masses and radiated back into the atmosphere in the form of heat or infrared radiation. Some of this infrared energy is absorbed and reradiated back to the Earth by atmospheric gases, including water vapor, CO_2, and other substances. As concentrations of GHGs increase, there are direct and indirect effects on the Earth's energy balance. The direct effect is often referred to as a radiative forcing, a subset of a more general set of phenomena referred to as climate forcings. The National Research Council [45] offers the following set of definitions:

- Factors that affect climate change are usefully separated into forcings and feedbacks. . . . A climate forcing is an energy imbalance imposed on the climate system either externally or by human activities. Examples include changes in solar energy output, volcanic emissions, deliberate land modification, or anthropogenic emissions of greenhouse gases, aerosols, and their precursors. A climate feedback is an internal climate process that amplifies or dampens the climate response to an initial forcing. An example is the increase in atmospheric water vapor that is triggered by an initial warming due to rising carbon dioxide (CO_2) concentrations, which then acts to amplify the warming through the greenhouse properties of water vapor.. . .

  Climate forcing: An energy imbalance imposed on the climate system either externally or by human activities.

- *Direct radiative forcing*: A climate forcing that directly affects the radiative budget of the Earth's climate system; for example, added carbon dioxide (CO_2) absorbs and emits infrared radiation. Direct radiative forcing may be due to a change in concentration of radiatively active gases, a change in solar radiation reaching the Earth, or changes in surface albedo. Radiative forcing is reported in the climate change scientific literature as a change in energy flux at the tropopause, calculated in units of watts per square meter (W/m^2); model calculations typically report values in which the stratosphere was allowed to adjust thermally to the forcing under an assumption of fixed stratospheric dynamics.
- *Indirect radiative forcing*: A climate forcing that creates a radiative imbalance by first altering climate system components (e.g., precipitation efficiency of clouds), which then almost immediately lead to changes in radiative fluxes. Examples include the effect of solar variability on stratospheric ozone and the modification of cloud properties by aerosols.
- *Nonradiative forcing*: A climate forcing that creates an energy imbalance that does not immediately involve radiation. An example is the increasing evapotranspiration flux resulting from agricultural irrigation.

Source: Clarke et al. [14], Box 1.1; NRC [45]

I

Two approaches have been used to determine the optimal mix of abatement across gases in stabilization. One approach is to minimize the total costs of meeting a long-term radiative forcing target, based on the combined mitigation costs for all greenhouse gases using intertemporal optimization. This is the approach employed by intertemporal optimization models such as MERGE. In this structure, all of the prices of the different greenhouse gases rise at relatively constant rates until stabilization is reached, consistent with the general result for minimum-cost CO_2 pathways discussed in the previous section [41], but the rates vary among gases. This leads to different timing of mitigation across gases. Indeed, one of the outcomes of this sort of approach to multi-gas stabilization is that the rate of increase in greenhouse gas prices is higher for gases with shorter lifetimes, with the implication that mitigation for these gases is delayed relative to CO_2. For example, this approach leads to scenarios in which mitigation of CH_4 is relatively modest in the early term and then increases dramatically as the total radiative forcing target gets close.

An alternative, though less rigorous methodology that is used to compare greenhouse gases in multi-gas emissions mitigation programs is the application of Global Warming Potential (GWP) coefficients. This is the approach generally used by dynamic-recursive models such as GCAM. The GWP was developed as an analogue to the Ozone Depletion Potential (ODP) coefficients employed to compare the various

stratospheric ozone depleting substances [46]. GWPs are defined as the effect on radiative forcing of the release of an additional kilogram of a gas, relative to the simultaneous release of a kilogram of CO_2, integrated over one of three time horizons: 20 years, 100 years, and 500 years. Values for the GWPs calculated by IPCC Working Group I in the Fourth Assessment Report [47] are given in Table 4. GWPs are something of a mixture between the relative contribution of a gas to radiative forcing, which would be better calculated directly if possible, and an incomplete estimate of climate damage associated with the release of an additional kilogram of a greenhouse gas.

The primary virtue in the GWP is its application as an estimate of the relative importance of various greenhouse gases by national, local, and regional parties. Multi-gas policy instruments often employ GWPs as a means of comparing emissions of different greenhouse gases. The ratio of any pair of GWPs serves as the inverse of the relative price of any pair of greenhouse gases.

In application to stabilization studies in IAMs, GWPs yield constant estimates of the relative contributions of various greenhouse gases to climate change. In other words, since the GWPs are assumed to be constant over time, the relative prices of CO_2 and other gases are also constant over time. Hence, in studies that use GWPs to achieve multi-gas stabilization, mitigation for gases with shorter lifetimes generally takes place more quickly that would be the case in models that employ an intertemporal optimization approach. In this sense, although GWPs are a reality in policy design, they are an imperfect tool for comparing greenhouse gases over time. Manne and Richels [52] showed that if the total cost is the only criteria by which emissions pathways are judged then GWPs were not constant, but would rather change systematically with time. Peck and Wan [41] showed that if minimizing the total cost of limiting radiative forcing were the sole criterion by which greenhouse gas concentrations were controlled then the shadow price of each greenhouse gas rises at the interest rate plus the rate of removal from the atmosphere. Hence the corresponding GWP ratio of any two gases changes over time at a rate equal to the removal rate difference between the two gases. This notion is profoundly different than the concept of the GWP as a constant.

Manne and Richels [52] did show that the inclusion of secondary criteria, in addition to limiting radiative forcing, such as limiting the rate of change of radiative forcing, could produce very different GWPs and rates of change in GWPs over time. Some combinations of objective criteria could generate relatively stable GWPs.

Integrated Assessment Modeling. Table 4 Direct global warming potential coefficients

Industrial designation or common name (years)	Chemical formula	Lifetime (years)	Radiative efficiency (Wm^{-2} ppb^{-1})	IPCC [48] (100^{-year})	20^{-year}	100^{-year}	500^{-year}
Carbon dioxide	CO_2	See notes[a]	[b]1.4×10^{-5}	1	1	1	1
Methane[c]	CH_4	12[c]	3.7×10^{-4}	21	72	25	7.6
Nitrous oxide	N_2O	114	3.03×10^{-3}	310	289	298	153

[a]The CO_2 response function used in this report is based on the revised version of the Bern carbon cycle model (Bern2.5CC) [49] used in IPCC [47] Chap. 10 Global Climate Projections using a background CO_2 concentration value of 378 ppm. The decay of a pulse of CO_2 with time t is given by $a_0 + \sum_{l=1}^{3} a_i \cdot e^{-t/\tau_l}$

where $a_0 = 0.217$, $a_1 = 0.259$, $a_2 = 0.338$, $a_3 = 0.186$, $\tau_1 = 172.9$ years, $\tau_2 = 18.51$ years, and $\tau_3 = 1.186$ years

[b]The radiative efficiency of CO_2 is calculated using the IPCC [50] simplified expression as revised in the TAR, with an updated background concentration value of 378 ppm and a perturbation of +1 ppm (see IPCC [47], Sect. 2.10.2)

[c]The perturbation lifetime for methane is 12 years as in the IPCC [48] (see also [47], Sect. 7.4). The GWP for methane includes indirect effects from enhancements of ozone and stratospheric water vapor (see [47], Sect. 2.10.3.1)

Source: IPCC [43], Table 2.14, pp. 212–213

The Economic Costs of Implementing the Framework Convention on Climate Change

As mentioned above, estimating the costs of meeting long-term targets is a primary function of IAMs. Typical estimates for global costs of limiting CO_2 equivalent concentrations to alternative levels from the IPCC [43] are shown below for two representative years, 2030 (Table 5) and 2050 (Table 6).

While the question of the measurement of the economic cost of emissions mitigation has not generated as much debate as questions about discounting, there are important differences in methodology that different modeling teams employ. Perhaps the most commonly used metric comparable across models is the price of carbon. This metric is useful for comparing across models when simple policy instruments to mitigate emissions are employed – specifically either an economy-wide carbon tax or the carbon price emerging from an economy-wide cap-and-trade. As policy assumptions become more complex the usefulness of this metric fades. In fact, in mixed emissions mitigation systems, where only part of the economy is controlled

Integrated Assessment Modeling. Table 5 Estimated global macroeconomic costs in 2030[a] for least-cost trajectories toward different long-term stabilization levels[b, c]

Stabilization levels (ppm CO_2-eq)	Median GDP reduction[d] (%)	Range of GDP reduction[d, e] (%)	Reduction of average annual GDP growth rates[d, f] (percentage points)
590–710	0.2	−0.6 to 1.2	<0.06
535–590	0.6	0.2 to 2.5	<0.1
445–535[g]	Not available	<3	<0.12

[a]For a given stabilization level, GDP reduction would increase over time in most models after 2030. Long-term costs also become more uncertain
[b]Results based on studies using various baselines
[c]Studies vary in terms of the point in time stabilization is achieved; generally this is in 2100 or later
[d]These are global GDP-based market exchange rates
[e]The median and the 10th and 90th percentile range of the analyzed data are given
[f]The calculation of the reduction of the annual growth rate is based on the average reduction during the period till 2030 that would result in the indicated GDP decrease in 2030
[g]The number of studies that report GDP results is relatively small and they generally use low baselines
Source: IPCC [43], SPM, p. 12

Integrated Assessment Modeling. Table 6 Estimated global macroeconomic costs in 2050 for least-cost trajectories toward different long-term stabilization levels[a]

Stabilization levels (ppm CO_2-eq)	Median GDP reduction[b] (%)	Range of GDP reduction[b, c] (%)	Reduction of average annual GDP growth rates[b, d] (percentage points)
590–710	0.5	−1 to 2	<0.05
535–590	1.3	Slightly negative-4	<0.1
445–535[e]	Not available	<5.5	<0.12

[a]This corresponds to the full literature across all baselines and mitigation scenarios that provide GDP numbers
[b]These are global GDP-based market exchange rates
[c]The median and the 10th and 90th percentile range of the analyzed data are given
[d]The calculation of the reduction of the annual growth rate is based on the average reduction during the period until 2050 that would result in the indicated GDP decrease in 2050
[e]The number of studies is relatively small and they generally use low baselines. High emissions baselines generally lead to higher costs
Source: IPCC [43], SPM, p. 18

by a tax or cap-and-trade program, the carbon price and real economic cost can move in opposite directions. That is, as more of the high-cost sectors of the economy are controlled with less-efficient nonmarket-based policies, the price of carbon may fall while the total economic cost rises.

A variety of approaches have been applied to obtain the total economic cost. These include integration under the marginal abatement cost schedule, measurement of foregone consumption, and compensated/equivalent variation. Each of these approaches traces its method back to welfare economics. While measures that directly link to welfare functions are in principle best, welfare cannot be directly observed and unless highly unlikely circumstances prevail, Arrow [53] has shown that a welfare function with the properties needed to get a measure on real economic cost cannot exist – a distinct disadvantage for numerical simulations.

While the choice of methodological approach to measuring real economic cost will doubtless affect valuation, two larger sources of variation in cost estimates are the policy instruments applied and the assumed rate of technological improvement. It is well known that different policy instruments can attain the same mitigation level with different costs [54]. Differences in technology assumptions can also produce substantial differences in cost (see, e.g., [42, 55]). Exploring the implication of different policy instruments and technology availability are two important directions of future work by the higher resolution IAM research community.

The principal research question which the higher resolution IAMs addressed has been different from that of the highly aggregated IAMs. Whereas the highly aggregated IAMs focused on the problem of determining the optimal balance between emissions mitigation and adaptation to climate change, the higher resolution IAMs focused more on the cost of implementing a policy to limit emissions, concentrations, or combined radiative forcing of greenhouse gases. The higher resolution IAM community has generally taken an agnostic position on the question of whether the policy instrument or the policy goal in question was desirable or not and simply went about the task of calculating the cost of achieving the given goal of implementing the prescribed policy.

As time has passed, the political conversation has moved away from the question of the use of cap-and-trade to control emissions to consider hybrid policy architectures in which emissions mitigation is pursued through a combination of policy measures some of which differ substantially from the conventional market mechanisms, such as carbon taxes or cap-and-trade. For example, many current emissions mitigation proposals contain renewable portfolio standards (RPS). These policy instruments require a minimum fraction of total power generation to be provided by renewable energy forms such as wind and solar.

There are many reasons for the shift. The prospects for a comprehensive international agreement based on the principles of cap-and-trade have diminished. Many parties in the international negotiations were less concerned with economic efficiency and cost-minimization than they were with a sense of moral obligation to achieve domestic emissions mitigation targets without resorting to emission trading. Within the United States similar forces are at work. Efforts to develop a comprehensive countrywide emissions cap-and-trade system show little prospect for entering into effect. Also, the European Union and Japan have either chosen alternatives to cap-and-trade or employ cap-and-trade within limited sectors of the economy. Such policies have pushed IAMs to develop more sophisticated representations of policies in order to estimate the policy effects [56]. In the same context, the IAMs have begun to explore the implications of international regimes in which nations begin emissions mitigation at different times [57, 58].

Future Directions: Integrating Human Earth Systems with Natural Earth Systems

Integrated Assessment modeling research is a continuously evolving field. As the models have matured and diversified, researchers have pushed the development frontiers in multiple directions simultaneously in order to answer a wide range of research questions. For example, researchers have broadened the scope of the models to include more sectors of the human Earth system such as land use and agriculture. They have expanded coverage of various types of the greenhouse gases by including an increasingly diverse set of their sources and activities. They have also lengthened the

time horizon of analysis, pressing past the year 2100 and multiple centuries beyond. At the same time, the researchers have elaborated the key model components by slicing each of them in smaller pieces, for example, by adding finer spatial and temporal resolution and disaggregated representation of technologies.

An increasingly prominent research frontier has been the formal integration with other fields of climate change research, namely climate modeling (CM) and impacts, adaptation, and vulnerability (IAV) research. Although many research questions do not require the use of IPCC-class models of human and natural Earth systems, others cannot be addressed adequately without the development of integrated Earth systems models. The development of integrated Earth systems models opens the door to formally modeling the simultaneous interactions between human activities, climate change, and climate change impacts on human systems.

The Representative Concentration Pathways: An Example of Interactions with Climate Models

The assessment of climate change has traditionally been a linear research process. IA researchers produce emissions scenarios which in turn are transferred to the climate modeling community for use as inputs. The climate modeling community employs these scenarios to force future climate calculations. These climate calculations are then used by IAV researchers to produce estimates of the consequences of climate change. In the past, there has been little communication or feedback between research communities. Each community conducted its research independently and left it for others to figure out how or whether to use it. Beginning in 1990, the integrated assessment modeling community began to interact with the climate modeling community, though interactions with the carbon cycle and other natural Earth system researchers go back even further (see, e.g., [59], and more generally, [60]). Moss et al. [61] provide a succinct history of scenario development, which is summarized in Fig. 7.

There have been numerous long-term scenarios of global greenhouse gas emissions. Three important benchmarks were the publication of scenarios referred to as SA90 [51], IS92 [62], and SRES [63]. These scenarios are notable in that the climate modeling community used them to simulate potential effect of future emissions paths on the climate system. The earliest scenarios considered only fossil fuel CO_2 emissions. Over time scenarios became richer, including land-use change emissions, non-CO_2 greenhouse gases, and short-lived species. While these scenarios span a wide range of potential future emissions, none considered limitations on emissions, that is, until Moss et al. [61] and the publication of the Representative Concentration Pathways (RCPs).

The RCPs are the most recent set of scenarios developed for use in the climate models. They were chosen to initiate an assessment cycle by providing the climate modeling community with a set of scenarios that were sufficiently differentiated by the end of the century to be scientifically relevant and to provide detailed information on the sources of emissions of greenhouse gases and short-lived species from all anthropogenic sources. RCPs differ from earlier scenario development activities in that they were selected from existing scenarios that were available in the peer-reviewed literature rather than being developed de novo. Selected scenarios from the open literature were named corresponding to their century's end radiative forcing levels: 8.5, 6.0, 4.5, and 2. 6 Wm^{-2} (see Table 7).

Subsequent to selection, the four scenarios were updated and harmonized to include the most recent observational data and downscaled to produce harmonized gridded outputs for emissions, land use, and land cover. The resulting time-paths for radiative forcing are given in Fig. 8 (The detailed scenario data are available at www.iiasa.ac.at/web-apps/tnt/RcpDb/).

The RCPs differ from previous scenarios employed by the climate modeling community in that they

1. Include scenarios with explicit emissions mitigation
2. Provide geospatially resolved emissions at ½ degree by ½ degree
3. Provide geospatially resolved land use and land cover at ½ degree by ½ degree

The most recent set of scenarios, while highly useful to the climate modeling community, are less useful from the perspective of the impacts, adaptation, and vulnerability community. While the scenarios contain detailed information that would be of interest to climate modelers, they do not carry associated socioeconomic information, or energy or commodity prices.

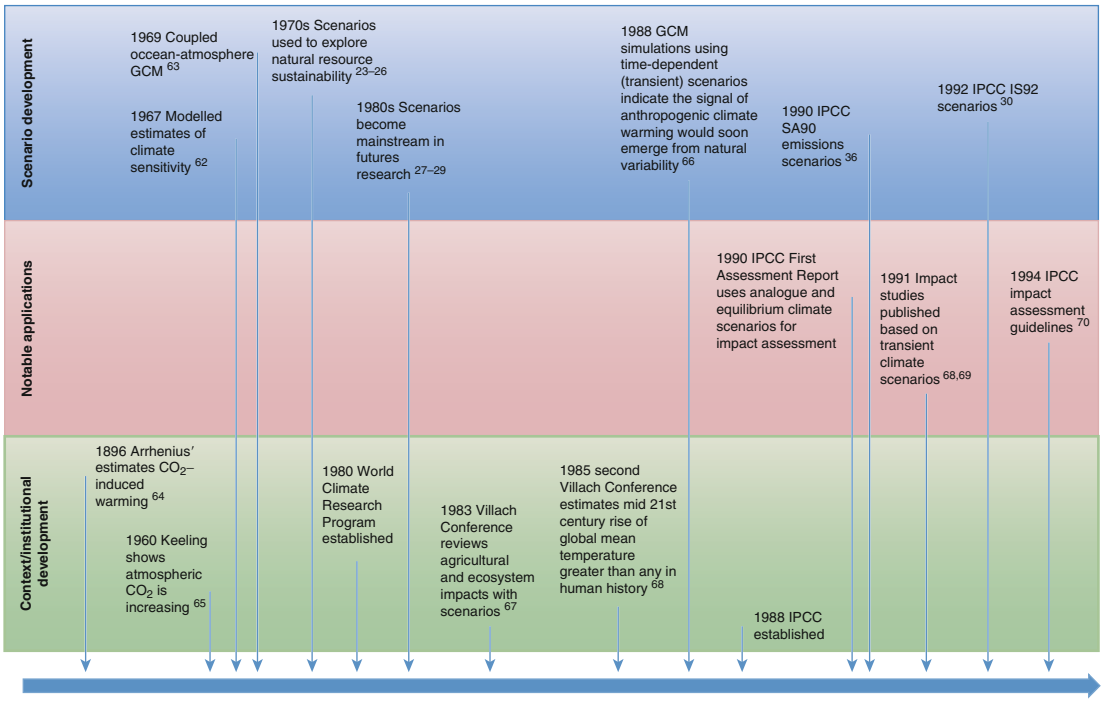

Figure 1 | Timeline highlighting some notable developments in the creation and use of emissions and climate scenarios. The entries are illustrative of the Overall course of model-based scenario development (blue) and application (beige) described in this Perspective, and also give some context (green); they do

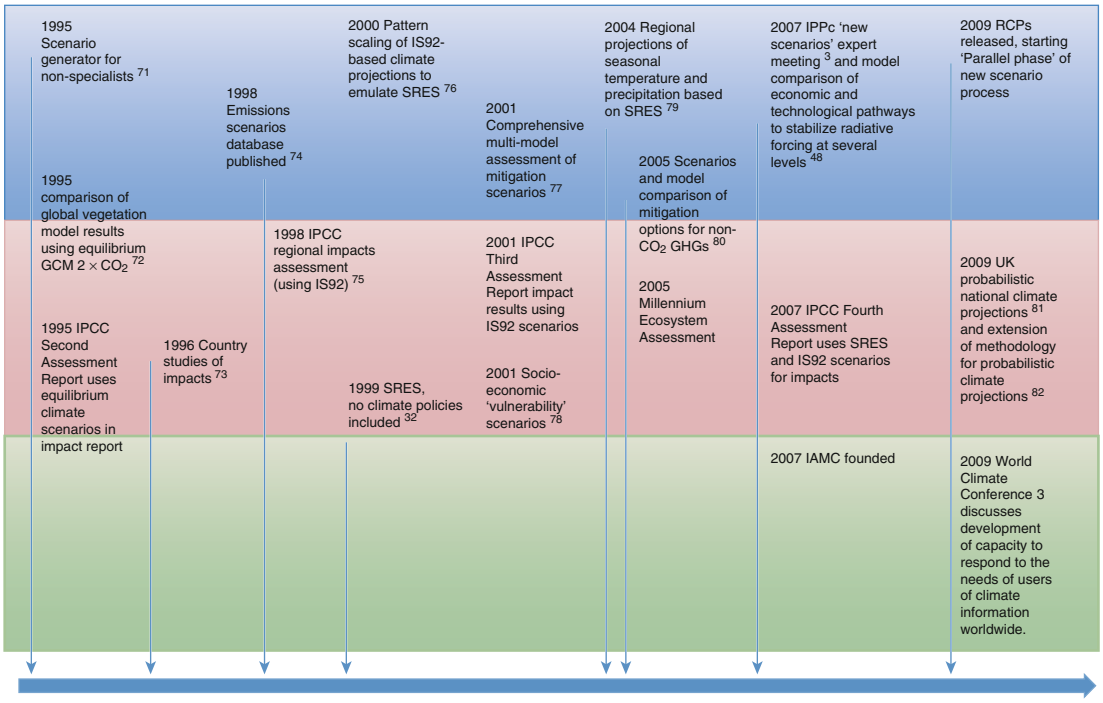

not provide a comprehensive account of all major scenarios and significant studies or assessments that have used them. See Supplementary Information for details. GCM, general circulation model; GHG, greenhouse gas; IAMC, Integrated Assessment Modelling Consortium.

Integrated Assessment Modeling. Figure 7

Timeline highlighting some notable developments in the creation and use of emissions and climate scenarios (Source: Moss et al. [61], pp 748–749)

Integrated Assessment Modeling. Table 7 The four representative concentration pathways

Name	Radiative forcing	Concentration	Pathway	Model providing RCP	References
RCP8.5	>8.5 W/m^2 in 2100	>1,370 CO_2-eq in 2100	Rising	MESSAGE	Riahi et al. [64]
RCP6.0	~6 W/m^2 at stabilization after 2100	~850 CO_2-eq (at stabilization after 2100)	Stabilization without overshoot	AIM	Fujino et al. [65], Hijioka et al. [66]
RCP4.5	~4.5 W/m^2 at stabilization after 2100	~650 CO_2-eq (at stabilization after 2100)	Stabilization without overshoot	MiniCAM (GCAM)	Clarke et al. [14], Smith and Wigley [67]
RCP2.6	Peak at ~3 W/m^2 before 2100 and then decline	Peak at ~490 CO_2-eq before 2100 and then decline	Peak and decline	IMAGE	Van Vuuren et al. [68, 69]

Source: Moss et al. [61], p. 753

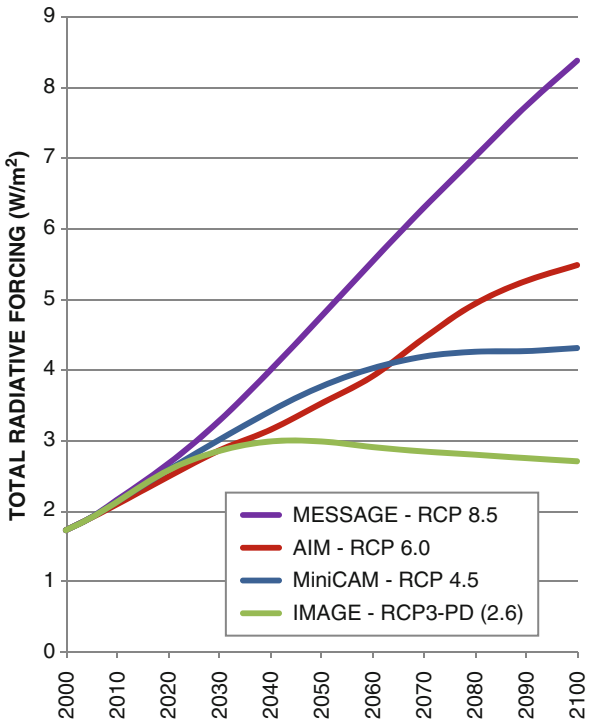

Integrated Assessment Modeling. Figure 8
The radiative forcing trajectories of the four RCP scenarios (Source: Moss et al. [61], P. 748–749)

Furthermore, even if the socioeconomic data were included for these scenarios, each of the scenarios was crafted by a different modeling team, using different assumptions about key socioeconomic and other variables. For instance, it would be difficult, if not impossible to determine if the difference in estimated impacts of climate change associated with RCP4.5 and RCP2.6 was the result of differences in the magnitude

of climate change or that of differences in the underlying human Earth systems that characterize the GCAM and IMAGE scenarios, respectively.

In order to establish a framework, in which the human system impact of climate change could be coupled with emissions scenario and climate model, a new scenario matrix architecture is under development. This architecture would create a suite of scenarios that are defined in terms of two bundles of descriptors: shared socio-ecosystem pathways (SSPs) and shared climate policy assumptions (SPAs).

SSPs have three components: a set of quantitative assumptions that are used by IAMs, such as population and economic growth; a set of quantified assumptions about variables that are not part of IAMs, for example, governance index; and a narrative which describes the general state of the world and its evolution over the course of the twenty-first century.

SPAs define the state of climate policy and its evolution around the world. They are defined with quantitative descriptors, where appropriate, and a qualitative narrative. The quantitative descriptors could be, for example, a limit on radiative forcing, such as was used to define the RCPs. In addition, information regarding the nature of policies that are to be employed to affect the prescribed outcome could be included.

The virtue of harmonizing SPAs with RCPs is that the new scenarios could be coupled smoothly with climate model output from ensemble calculations. This in turn would facilitate analysis that could potentially be fully integrated across three broad research communities: climate modeling, integrated assessment modeling and impacts, and adaptation and vulnerability. Two examples of such scenario matrix architectures can be found in [70, 71].

Climate Impacts in Higher Resolution IAMs

Higher resolution IAMs are increasingly focusing on explicitly modeling the physical impacts of climate change [72]. This work builds on a long tradition of modeling climate impacts in the higher resolution IAM community (see, e.g., [26, 73–75]). However, to date higher resolution IAMs have examined climate impacts using a sequential methodology, that is, they start with emissions, which are assumed to be given by climate models, and then analyzed the consequences of the ensuing climate change.

New model development is increasingly focused on methods and tools that will allow higher resolution IAMs to examine impacts simultaneously with mitigation and therefore to allow the two to interact. For example, there are on-going research efforts that utilize the higher resolution IAMs to study scenarios in which interactions between policies to mitigate emissions through changes in land-use and land cover – e.g., afforestation policies – and adaptive responses to climate change in agricultural sectors are simultaneously examined. Two complementary model development directions are also worthy of note. First, the higher resolution models are beginning to couple with state-of-the-art natural Earth system models (discussed later in this section) and second, they are beginning to move to finer spatial and temporal resolutions.

The increasing attention to climate impacts implies that the higher resolution IAMs will produce new results that will also contribute to the impacts, adaptation, and vulnerability (IAV) research. For nonmarket impacts of climate change, higher resolution IAMs will compute physical consequences, but not necessarily economic damage estimates, as it has generally been the case with climate impacts that the higher resolution IAMs have examined to date. For climate impacts associated with marketable goods and services, economic costs can also be estimated. But, the nonlinear nature of the human and natural Earth system means that separating out the impact of emissions mitigation from the impact of climate change will be nontrivial.

A good example of new work on the interactions between mitigation and impacts within higher resolution IAMs is land use and land cover. Land use will be affected both by a changing climate and by emissions mitigation effort. Mitigation effects will take the form of forest expansion to reduce land-use change emissions along with the use of bioenergy crops for energy production. A changing climate will bring about many changes in the nature of terrestrial systems, including changes in crop yields. All of these dynamics will interact.

To illustrate these interactions, the effects of climate change on crops were modeled as a response function derived from data reported in IPCC [76]. Figure 9 shows the distribution of estimates of crop yields for maize and wheat for low and other latitudes.

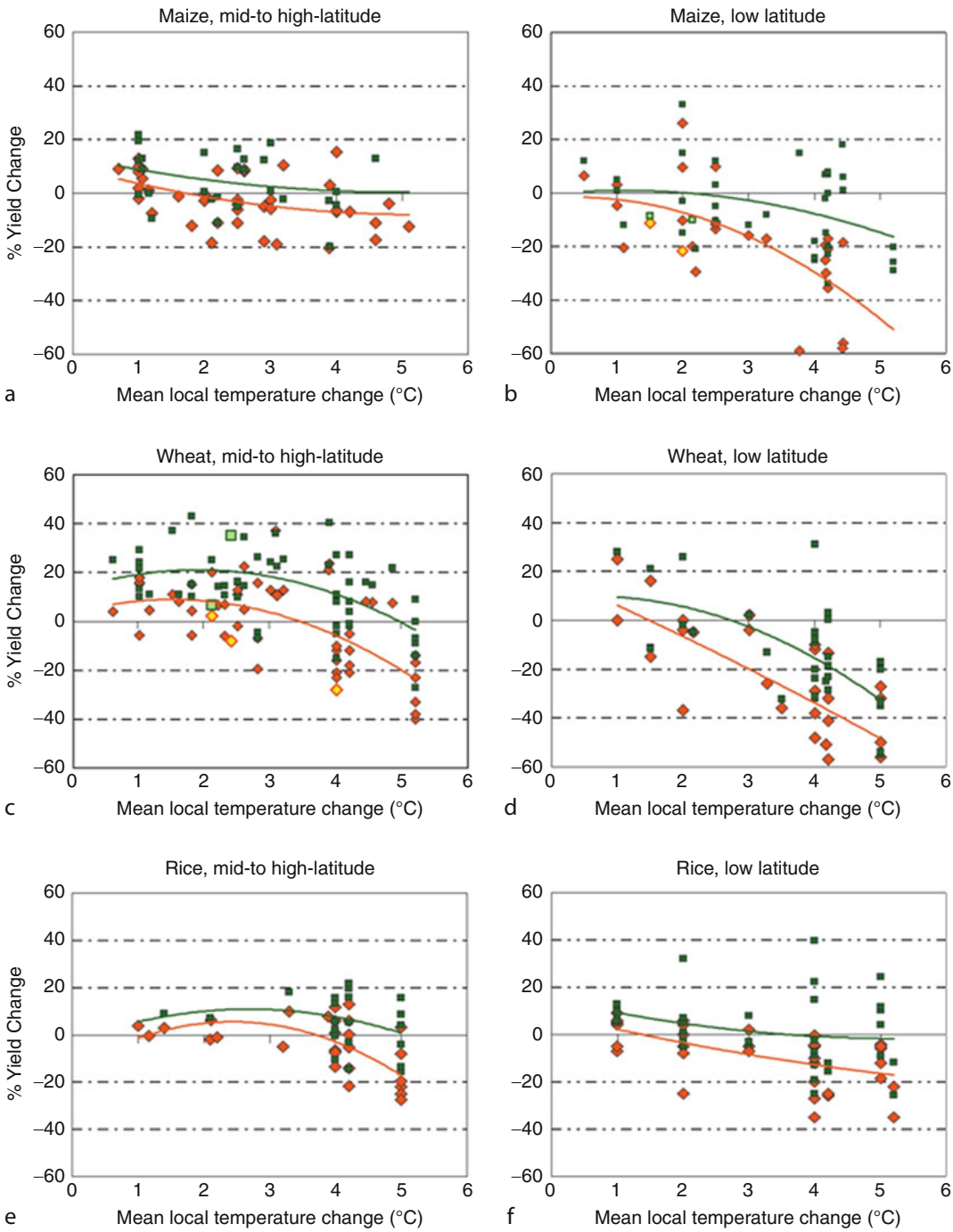

Integrated Assessment Modeling. Figure 9
(Continued)

Both a reference scenario and a policy scenario in which CO_2 concentrations were limited to stay below 500 ppm were presented. Land-use change emissions of CO_2 were recorded for the two scenarios, with and without consideration of climate feedbacks through agricultural crops. These results are displayed in Fig. 10.

Note that cumulative land-use change emissions vary significantly when climate change effects are considered in the reference scenario, with land-use change emissions significantly higher as a consequence of crop yield reductions in the face of climate change.

Results for the scenario in which CO_2 concentrations were not allowed to exceed 500 ppm exhibit lower emissions than either of the reference scenarios. This is because the mitigation scenario valued terrestrial carbon emissions equally with fossil fuel emissions (results would have been very different had terrestrial carbon not been valued; see also [33, 77]). Equally as interesting, land-use change emissions with and without consideration of climate change effects on crop yields are not significantly different between the two scenarios. This result follows directly from the fact that limiting CO_2 concentrations to 500 ppm would also limit the magnitude of climate change, which in turn moderates the effects on crop yields. The purpose of this example is not so much to showcase results, but rather to motivate the joint consideration of impacts, adaptation, and vulnerability with integrated assessment of emissions mitigation.

Linking Higher Resolution IAMs into integrated Earth System Models (iESMs)

Several research teams have undertaken joint work with the climate modeling community. The IGSM team has developed a relationship with climate researchers at the US National Center for Atmospheric Research (NCAR). The IMAGE team has developed several collaborative relationships including those with the Oak Ridge National Laboratory (ORNL), the Centre National de Recherches Météorologiques Coupled global climate Model (CNRM-CM3) team of France, and other European climate modeling teams to develop coupled scenarios. The MESSAGE integrated assessment modeling team has developed a collaboration with the NASA Goddard Institute for Space Studies climate modeling team. The GCAM team has developed a collaboration with ORNL and the Lawrence Berkeley National Laboratory (LBNL) in the development of a modeling system that joins the Community Earth System Model (CESM) representation of natural Earth systems with the GCAM representation of human Earth systems. To date, the collaborations have produced one-way coupling models, where emission scenarios from IAMs affect the climate, while the resulting climate change does not feedback to emissions. However, current effort is focused around developing a two-way coupled system.

The goal of the joint collaborations is to create a first-generation integrated Earth System Model (iESM) by fully integrating the human dimension from an IAM and a natural dimension from a climate model, that is, to create the capability of simultaneously estimating human system impacts on climate change and climate change impacts on human systems. After creating the capacity to examine the coupled natural and human Earth systems, the project could apply the model to the examination of feedbacks between human systems, the climate systems, and land-use systems. For instance, the policy response

Integrated Assessment Modeling. Figure 9

The modeled effects of climate change on crops. Sensitivity of cereal yield to climate change for maize, wheat and rice, as derived from the results of 69 published studies at multiple simulation sites, against mean local temperature change used as a proxy to indicate magnitude of climate change in each study. Responses include cases without adaptation (red dots) and with adaptation (dark green dots). Adaptations represented in these studies include changes in planting, changes in cultivar, and shifts from rain-fed to irrigated conditions. Lines are best-fit polynomials and are used here as a way to summarise results across studies rather than as a predictive tool. The studies span a range of precipitation changes and CO_2 concentrations, and vary in how they represent future changes in climate variability. For instance, lighter-coloured dots in (**b**) and (**c**) represent responses of rain-fed crops under climate scenarios with decreased precipitation. (Source: Parry et al. [76], P. 286)

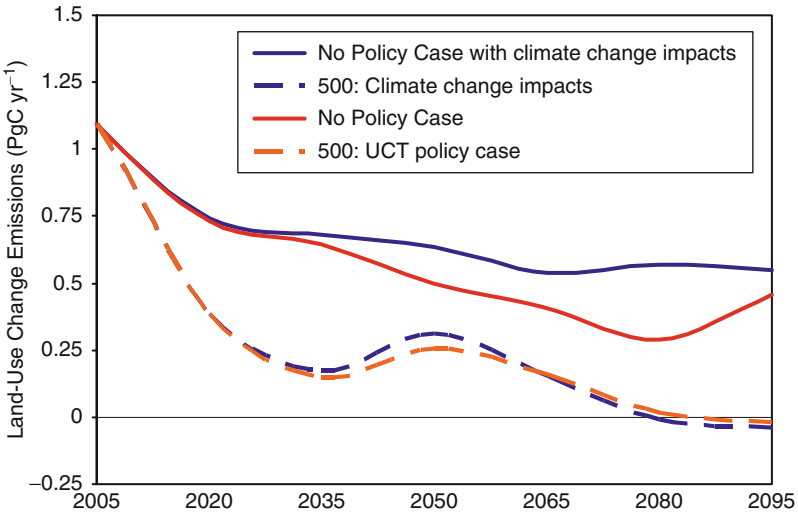

Integrated Assessment Modeling. Figure 10
Land-use change emissions of CO_2 under the scenarios with and without consideration of climate feedbacks through agricultural crops

of land-use change presented in [33] could be revisited to estimate the magnitude of feedbacks in the system.

Significant effort is required before such research becomes routine. Nonetheless, as the research potential this collaboration opens up is virtually limitless, the importance of integrating human Earth systems with natural Earth systems is sufficiently compelling to drive future collaborations between ESMs and IAMs.

Bibliography

1. Wigley TML, Richels R, Edmonds JA (1996) Economic and environmental choices in the stabilization of atmospheric CO_2 concentrations. Nature 379:240–243
2. Nordhaus WD, Yohe GW (1983) Future carbon dioxide emissions from fossil fuels. Changing climate: report of the carbon dioxide assessment committee. National Academy Press, Washington DC, pp 87–153
3. Nordhaus WD (1993) Optimal greenhouse-gas reductions and tax policy in the "DICE" model. Am Econ Rev 83:313–317
4. Nordhaus WD, Yang Z (1996) A regional dynamic general-equilibrium model of alternative climate-change strategies. Am Econ Rev 86:741–765
5. Dowlatabadi H, Morgan MG (1993) A model framework for integrated studies of the climate problem. Energy Policy 21:209–221
6. Hope C, Anderson J, Wenman P (1993) Policy analysis of the greenhouse effect: an application of the PAGE model. Energy Policy 21:327–338
7. Tol RSJ (1997) On the optimal control of carbon dioxide emissions: an application of FUND. Environ Model Assess 2:151–163
8. Weyant J, Davidson O, Dowlatabadi H, Edmonds J, Grubb M, Parson EA, Richels R, Rotmans J, Shukla PR, Tol RSJ (1996) Integrated assessment of climate change: an overview and comparison of approaches and results. In: Bruce JP, H-sŏng Yi, Haites EF (eds) Climate change 1995: economic and social dimensions of climate change. The contribution of working group III to the second assessment report of the intergovernmental panel on climate change. Cambridge University Press, UK/New York, pp 367–396
9. Parson EA, Fisher-Vanden K (1997) Integrated assessment models of global climate change. Annu Rev Energy Env 22:589–628
10. Nordhaus W (2007) Critical assumptions in the Stern Review on climate change. Science 317:201–202
11. Stern NH (2007) The economics of climate change: the Stern Review. Cambridge University Press, Cambridge, UK/New York
12. Portney PR, Weyant JP (eds) (1999) Discounting and intergenerational equity. Resources for the Future, Washington, DC
13. Dasgupta P, Mäler KG, Barrett S (1999) Intergenerational equity, social discount rates and global warming. In: Portney PR, Weyant JP (eds) Discounting and intergenerational equity. Resources for the Future, Washington, DC
14. Clarke L, Edmonds J, Jacoby H, Pitcher H, Reilly J, Richels R (2007) Scenarios of greenhouse gas emissions and atmospheric concentrations. Synthesis and assessment product 2.1a, report by the U.S. Climate Change Science Program and the Subcommittee on Global Change Research. U.S. Government Printing Office, Washington, DC

I

15. Edmonds J, Reilly J (1983) A long-term global energy-economic model of carbon dioxide release from fossil fuel use. Energy Econ 5:74–88
16. Edmonds J, Reilly J (1983) Global energy and CO_2 to the year 2050. Energy J 4:21–48
17. Edmonds J, Reilly J (1983) Global energy production and use to the year 2050. Energy 8:419–432
18. Edmonds J, Reilly JM (1985) Global energy: assessing the future. Oxford University Press, New York
19. Brenkert A, Smith S, Kim S, Pitcher H (2003) Model documentation for the MiniCAM. Pacific Northwest National Laboratory. Technical report PNNL-14337
20. Kim SH, Edmonds JA, Smith SJ, Wise M, Lurz J (2006) The object-oriented energy climate technology systems (ObjECTS) framework and hybrid modeling of transportation in the MiniCAM long-term, global integrated assessment model. Energy J 27:63–91
21. Clarke L, Wise M, Kim S, Smith S, Lurz J, Edmonds J, Pitcher H (2007) Model documentation for the minicam climate change science program stabilization scenarios: CCSP product 2.1 a. Pacific Northwest National Laboratory, PNNL-16735
22. Wise MA, Calvin KV, Thomson AM, Clarke LE, Bond-Lamberty B, Sands RD, Smith SJ, Janetos AC, Edmonds JA (2009) The implications of limiting CO_2 concentrations for agriculture, land use, land-use change emissions and bioenergy. Pacific Northwest National Laboratory
23. Sokolov AP, Schlosser CA, Dutkiewicz S, Paltsev S, Kicklighter DW, Jacoby HD, Prinn RG, Forest CE, Reilly JM, Wang C, et al (2005) MIT integrated global system model (IGSM) version 2: model description and baseline evaluation, MIT Joint Program for the Science and Policy of Global Change. Report 124, Cambridge, MA
24. Manne A, Mendelsohn R, Richels R (1995) MERGE: a model for evaluating regional and global effects of GHG reduction policies. Energy Policy 23:17–34
25. Blanford GJ, Richels RG, Rutherford TF (2009) Feasible climate targets: the roles of economic growth, coalition development and expectations. Energy Econ 31:S82–S93
26. Kainuma M, Matsuoka Y, Morita T (eds) (2003) Climate policy assessment: Asia-Pacific integrated modeling. Springer-Verlag, Tokyo
27. Wigley TML, Raper SCB (1992) Implications for climate and sea level of revised IPCC emissions scenarios. Nature 357:293–300
28. Wigley TML, Raper SCB (2002) Reasons for larger warming projections in the IPCC third assessment report. J Climate 15:2945–2952
29. Raper SCB, Wigley TML, Warrick RA (1996) Global sea-level rise: past and future. In: Milliman JD Haq BU (eds) Sea-level rise and coastal subsidence: causes, consequences, and strategies. Kluwer Academic Publishers, Dordrecht, Netherlands
30. Clarke JF, Edmonds JA (1993) Modeling energy technologies in a competitive market. Energy Econ 15:123–129
31. McFadden D (1974) Conditional logit analysis of qualitative choice behavior. In: Zarambka P (ed) Frontiers of econometrics. Academic, New York, pp 105–142
32. McFadden D (1981) Econometric models for probabilistic choice among products. In: Manski C, McFadden D (eds) Structural analysis of discrete data with econometric applications. MIT Press, Cambridge, MA, pp 198–272
33. Wise M, Calvin K, Thomson A, Clarke L, Bond-Lamberty B, Sands R, Smith SJ, Janetos A, Edmonds J (2009) Implications of limiting CO_2 concentrations for land use and energy. Science 324:1183–1186
34. Bouwman AF, Kram T, Goldewijk KK (2006) Integrated modeling of global environmental change: an overview of Image 2.4. Netherlands Environmental Assessment Agency
35. Searchinger T, Heimlich R, Houghton RA, Dong F, Elobeid A, Fabiosa J, Tokgoz S, Hayes D, Yu T-H (2008) Use of U.S. Croplands for biofuels increases greenhouse gases through emissions from land-use change. Science 319:1238–1240
36. Lal R (2004) Soil carbon sequestration impacts on global climate change and food security. Science 304:1623–1627
37. Fargione J, Hill J, Tilman D, Polasky S, Hawthorne P (2008) Land clearing and the biofuel carbon debt. Science 319:1235–1238
38. Luckow P, Wise MA, Dooley JJ, Kim SH (2010) Large-scale utilization of biomass energy and carbon dioxide capture and storage in the transport and electricity sectors under stringent CO_2 concentration limit scenarios. Int J Greenh Gas Control 4:865–877
39. Edmonds JA, Scott MJ, Roop JM, MacCracken CN (1999) International emission trading and the cost of greenhouse gas emissions mitigation. The Pew Center on Global Climate Change, Arlington
40. Kyoto Protocol: the kyoto protocol to the united nations framework convention on climate change. UNEP/WMO, Kyoto
41. Peck SC, Wan YS (1996) Analytic solutions of simple optimal greenhouse gas emission models. In: van Ierland E, Górka K (eds) Economics of atmospheric pollution. Springer, Berlin, pp 113–121
42. Edmonds JA, Wise MA, Dooley JJ, Kim SH, Smith SJ, Runci PJ, Clarke LE, Malone EL, Stokes GM (2007) Global energy technology strategy: addressing climate change phase 2 findings from an international public-private sponsored research program. Pacific Northwest National Laboratory (PNNL), Richland
43. Metz B, Davidson O, Bosch P, Dave R, Meyer L (eds) (2007) Climate change 2007: mitigation of climate change; contribution of working group III to the 4th assessment report of the intergovenmental panel on climate change. Cambridge University Press, Cambridge, UK/New York
44. Weyant JP, Francisco C, Blanford GJ (2006) Overview of EMF-21: multigas mitigation and climate policy. Energy J 27:1–32
45. National Research Council (U.S.) (2005) Climate research committee: radiative forcing of climate change: expanding the concept and addressing uncertainties. Academic, Washington, DC
46. Wuebbles DJ, Edmonds J (1991) Primer on greenhouse gases. Lewis Publishers, Chelsea, Michigan
47. Solomon S, Qin D, Manning M, Marquis M, Averyt K, Tignor M, LeRoy Miller H, Chen Z (eds) (2007) Climate change 2007. The physical science basis: contribution of working group I to the

fourth assessment report of the intergovernmental panel on climate change. Cambridge University Press, Cambridge, UK/New York
48. Houghton JT, Meiro Filho LG, Callander BA, Harris N, Kattenburg A, Maskell K (eds) (1996) Climate change 1995: the science of climate change. Cambridge University Press, Cambridge, UK
49. Joos F, Prentice IC, Sitch S, Meyer R, Hooss G, Plattner G-K, Gerber S, Hasselmann K (2001) Global warming feedbacks on terrestrial carbon uptake under the Intergovernmental Panel on Climate Change (IPCC) emission scenarios. Global Biogeochem Cy 15:891–908
50. Houghton JT, Jenkins GJ, Ephraums JJ (eds) (1990) Climate change: the IPCC scientific assessment. Cambridge University Press, Cambridge, UK
51. Houghton JT, Jenkins GJ, Ephraums JJ (eds) (1990) Climate change: the IPCC response strategies. Cambridge University Press, Cambridge, UK
52. Manne AS, Richels RG (2001) An alternative approach to establishing trade-offs among greenhouse gases. Nature 410:675–677
53. Arrow KJ (1950) A difficulty in the concept of social welfare. J Polit Econ 58:328–346
54. Milliman SR, Prince R (1989) Firm incentives to promote technological change in pollution control. J Environ Econ Manag 17:247–265
55. McJeon HC, Clarke L, Kyle P, Wise M, Hackbarth A, Bryant BP, Lempert RJ (2011) Technology interactions among low-carbon energy technologies: what can we learn from a large number of scenarios? Energy Econ 33:619–631
56. Böhringer C, Rutherford TF, Tol RSJ (2009) THE EU 20/20/2020 targets: an overview of the EMF22 assessment. Energy Econ 31:S268–S273
57. Edmonds J, Clarke L, Lurz J, Wise M (2008) Stabilizing CO_2 concentrations with incomplete international cooperation. Clim Policy 8:355–376
58. Clarke L, Edmonds J, Krey V, Richels R, Rose S, Tavoni M (2009) International climate policy architectures: overview of the EMF 22 international scenarios. Energy Econ 31: S64–S81
59. Edmonds JA, Reilly J, Trabalka JR, Reichle DE (1984) An analysis of possible future atmospheric retention of fossil fuel CO_2, TR013, US Department of Energy Carbon Dioxide Research Division, Washington DC
60. Trabalka JR, Reichle DE (eds) (1986) The changing carbon cycle: a global analysis. Springer, New York
61. Moss RH, Edmonds JA, Hibbard KA, Manning MR, Rose SK, van Vuuren DP, Carter TR, Emori S, Kainuma M, Kram T, Meehl GA, Mitchell JFB, Nakicenovic N, Riahi K, Smith SJ, Stouffer RJ, Thomson AM, Weyant JP, Wilbanks TJ (2010) The next generation of scenarios for climate change research and assessment. Nature 463:747–756
62. Leggett J, Pepper WJ, Swart RJ, Edmonds J, Meira Filho LG, Mintzer I, Wang MX, Wasson J (1992) Emissions scenarios for the IPCC: an update. Climate change 1992: The supplementary report to the IPCC scientific assessment. Cambridge University Press, Cambridge, UK/New York
63. Nakicenovic N, Alcamo J, Davis G, de Vries B, Fenhann J, Gaffin S, Gregory K, Grubler A, Jung TY, Kram T (2000) Special report on emissions scenarios: a special report of working group III of the Intergovernmental Panel on Climate Change. Cambridge University Press, Cambridge, UK/New York
64. Riahi K, Grübler A, Nakicenovic N (2007) Scenarios of long-term socio-economic and environmental development under climate stabilization. Technol Forecast Soc 74:887–935
65. Fujino J, Nair R, Kainuma M, Masui T, Matsuoka Y (2006) Multi-gas mitigation analysis on stabilization scenarios using AIM global model. Energy J SI3:343–354
66. Hijioka Y, Matsuoka Y, Nishimoto H, Masui M, Kainuma M (2008) Global GHG emissions scenarios under GHG concentration stabilization targets. J Global Environ Eng 13:97–108
67. Smith SJ, Wigley TML (2006) Multi-gas forcing stabilization with MiniCAM. Energy J SI3:373–392
68. van Vuuren DP, Eickhout B, Lucas PL, den Elzen MGJ (2006) Long-term multi-gas scenarios to stabilize radiative forcing-exploring costs and benefits within an integrated assessment framework. Energy J SI3:201–234
69. van Vuuren DP, Elzen MGJ, Lucas PL, Eickhout B, Strengers BJ, Ruijven B, Wonink S, Houdt R (2007) Stabilizing greenhouse gas concentrations at low levels: an assessment of reduction strategies and costs. Clim Change 81:119–159
70. van Vuuren DP, Riahi K, Moss R, Edmonds J, Thomson A, Nakicenovic N, Kram T, Berkhout F, Swart R, Janetos A, Rose SK, Arnell N (2011) A proposal for a new scenario framework to support research and assessment in different climate research communities. Global Environ Chang (In Press)
71. Kriegler E, O'Neill BC, Hallegatte S, Kram T, Lempert R, Moss RH, Wilbanks TJ (2010) Socio-economic scenario development for climate change analysis. CIRED working paper. Centre International de Recherche sur l'Environnement et le Développement, Paris, France
72. Janetos AC, Clarke L, Collins W, Ebi K, Edmonds J, Foster I, Jacoby HJ, Judd K, Leung L, Newell R, Ojima D, Pugh G, Sanstad A, Schultz P, Stevens R, Weyant J, Wilbanks T (2008) Science challenges and future directions: climate change integrated assessment research. U.S. Department of Energy, Office of Science. http://science.energy.gov/~/media/ber/pdf/Ia_workshop_low_res_06_25_09.pdf. Accessed 5 Dec 2011
73. Leemans R, Eickhout B (2004) Another reason for concern: regional and global impacts on ecosystems for different levels of climate change. Global Environ Change Part A 14:219–228
74. Reilly J, Paltsev S, Felzer B, Wang X, Kicklighter D, Melillo J, Prinn R, Sarofim M, Sokolov A, Wang C (2007) Global economic effects of changes in crops, pasture, and forests due to changing climate, carbon dioxide, and ozone. Energy Policy 35:5370–5383
75. Edmonds JA, Rosenberg NJ (2005) Climate change impacts for the conterminous USA: an integrated assessment summary. Clim Change 69:151–162
76. Parry M, Canzaiani O, Palutikof J, Van der Linden P, Hanson C (eds) (2007) Climate change 2007: impacts, adaptation and

I

vulnerability; Contribution of working group II to the fourth assessment report of the intergovernmental panel on climate change. Cambridge University Press, Cambridge, UK/New York
77. Melillo JM, Reilly JM, Kicklighter DW, Gurgel AC, Cronin TW, Paltsev S, Felzer BS, Wang X, Sokolov AP, Schlosser CA (2009) Indirect emissions from biofuels: how important? Science 326:1397–1399
78. Weyant JP, Hill J (1999) The costs of the Kyoto protocol: a multi-model evaluation; introduction and overview. Energy J 20(Special Issue):vii–xliv
79. Kyle P, Clarke L, Rong F, Smith SJ (2010) Climate policy and the long-term evolution of the US buildings sector. Energy J 31:145–172

Integrated Pest Management

Ramon Albajes
Department of Plant Production and Forest Sciences, Universitat de Lleida, Centre UdL-IRTA, Lleida, Spain

Article outline

Glossary
Definition of the Subject
Introduction: Agriculture and Insect Pests
Injuries and Losses Caused by Pests
Strategy for Integrated Pest Management
Tools for IPM
Taxonomic Adscription of Major Pests
Pesticides
Crop Resistance
Biological Control
Microbial Control
Behavioral Control
Genetic Control
Cultural Control
Biotechnology and IPM
Implementation of IPM: Incentives and Constraints
Future Directions
Acknowledgments
Bibliography

Glossary

Agroecosystem, agrosystem – agricultural ecosystem An ecosystem that is managed to optimize the production of a crop plant or part of it.

Biological control Use or manipulation of natural enemies (predators, parasitoids, or diseases of pests) to suppress pest populations.

Crop resistance to pests One or more qualities that some crop plant varieties have resulting in less damage by a number of pest individuals in comparison with a variety without those qualities when it is exposed to the same pest numbers.

Damage caused by a pest Damage is the monetary value lost to the commodity as a result of injury by the pest, for instance by yield reduction.

Economic injury level of a pest The pest population density at which the cost to control the pest equals the amount of damage it inflicts.

Economic threshold of a pest The pest population density at which a control measure has to be taken to prevent population from reaching the economic injury level.

Genetically modified (GM) crop, transgenic crop A crop whose genetic material has been modified by genetic engineering techniques, through which novel genes have been introduced into the crop.

Integrated pest management (IPM) A system for controlling pests in an economically, ecologically, and sociologically sound manner by the use of multiple tactics in a compatible manner. The term has many (if not all) common elements with integrated control.

Metapopulation A set of populations occupying different patches among which individuals can occasionally move.

Pest Any herbivore that feeds and causes damages on crop plants in an agroecosystem resulting in crop damages if control measures are not taken. In this entry the term "pest" includes only insects and mites but for other authors the same term would additionally include plant diseases and weeds.

Pheromones Chemicals that are released in the environment by one individual and trigger a behavioral response in other individuals of the same species.

Precision agriculture Precision agriculture aims to apply inputs only when and where they are needed and at optimal amounts according to variable field or environment characteristics.

Definition of the Subject

In addition to producing food and fiber to satisfy an increasing world population, agriculture is being asked to supply energy at reasonable prices thus contributing to the acceleration of the demand for agricultural commodities. Increase of crop yields may be achieved by maximizing the proportion of sunlight energy that is fixed by the crop plant or by reducing the amount of energy that is lost by insect pests, diseases, and weeds. More than 50% of the potential yield of agricultural crops is lost by the three causes. To diminish losses caused by insect pests in agriculture in an economically, ecologically, and sociologically acceptable manner is the goal of integrated pest management (IPM). Given the complexity of agricultural ecosystems, IPM has to consider and manage all the elements and relationships involved in agriculture, including those related to nonagricultural ecosystems. Providing a scientific approach to better understand processes in agroecosystems in order to implement more rapidly sustainable IPM systems is a major challenge for ecology.

Introduction: Agriculture and Insect Pests

Agriculture and Productivity

Providing stable food for human subsistence has been the main goal of agriculture throughout the centuries. Probably because more than 50% of world population lives in urban areas and because developed countries do not feel threatened by hunger, society is not aware that agriculture needs to secure the world's food supplies. Increase of both world population and its income lead to increasing rates of food demand and to remarkable changes in the commodity composition of food consumption, particularly a bigger demand for livestock products.

In addition to producing food and fiber to satisfy an increasing world population, agriculture has been asked to supply energy at reasonable prices, mostly for replacing gasoline and petrol for motor vehicles. Although nowadays, as in 2007 and 2008, biofuel demand is linked to rising petrol prices, production of agricultural commodities for bioethanol and biodiesel conversion is expected to increase in the coming years, particularly if their price is competitive with petroleum. Biofuel production has accelerated the demand growth rate for agricultural commodities, which may largely exceed an annual rate of 2% in the coming years (Fig. 1). Reduction of basic food stocks, higher food prices, and increased land use may follow the stronger demand for agricultural commodities. Complementarily, agriculture in developed countries faces increasing environmental, human health, traceability, and competition challenges. Only a significant increase of agricultural productivity and sustainable improvement of protection techniques may respond to these challenges.

Agricultural Ecosystems: Ecological Basis for an Integrated Approach to Pest Control

It cannot be forgotten that agricultural ecosystems (also called agroecosystems) have their origin in natural ecosystems which human activity has transformed along millennia to better achieve the goal of agriculture: to provide us with sufficient food. Therefore, objectives of agroecosystems are substantially different to those of natural ecosystems; whereas, in the first case, growers manipulate the ecosystem to obtain an optimal amount of one species or part of one species (grain and not plant biomass, e.g., in cereal systems), natural ecosystems tend to perpetuate the system by themselves and do not favor one particular species or group of species. Agroecosystems differ from natural ecosystems in several ways among which two are particularly relevant in this chapter: (a) agroecosystems introduce a certain amount of energy previously processed (e.g., fuel) in comparison with the second which uses almost exclusively the energy provided by the sun; (b) agroecosystems are generally manipulated to deal with a unique plant species (the crop) and this leads to a drastic simplification of biodiversity in producer and ulterior consumer food web levels.

Composition and relationships in an agroecosystem are of crucial importance to the dynamics of its components. Figure 2 represents a simplified scheme of the main components and relationships concerning crop loss agents.

This chapter only deals with the control of those herbivores that cause damage to crops, the so-called pests. In the literature the term "pest" sometimes refers to pathogens and weeds but here the term will be restricted to herbivore species, mainly insects and

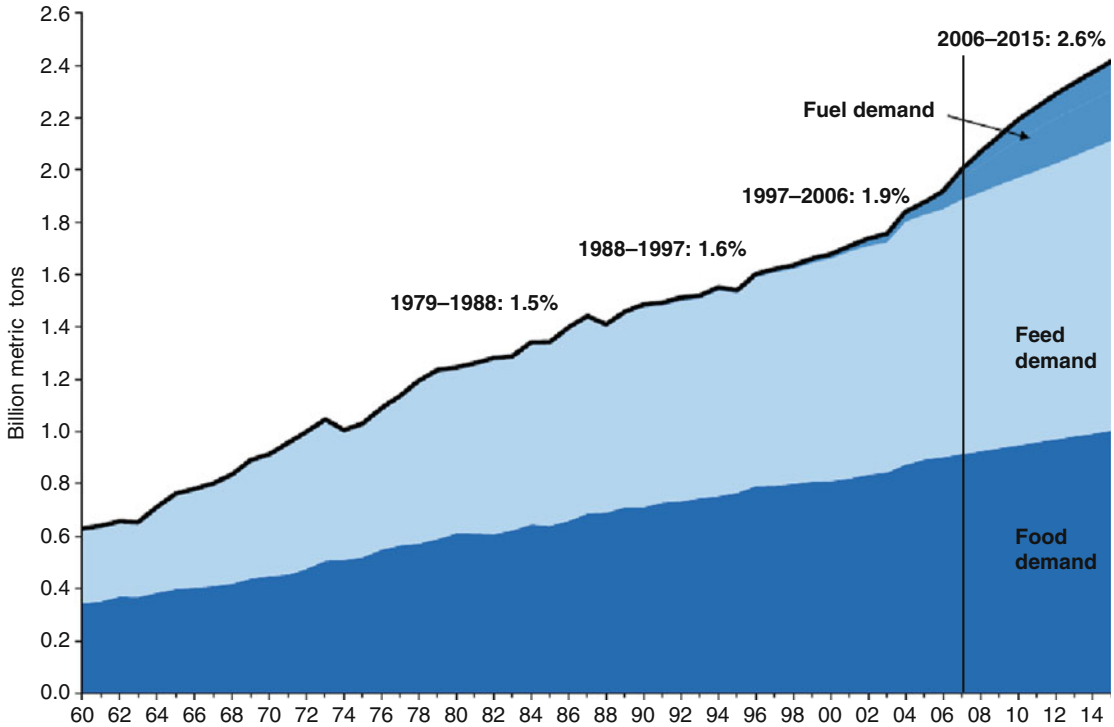

Integrated Pest Management. Figure 1
Evolution of demand of agricultural commodities for food, feed, and fuel use in the last 50 years (http://www.gceholdings.com/pdf/GoldmanReportFoodFeedFuel.pdf. Accessed 17 October 2009)

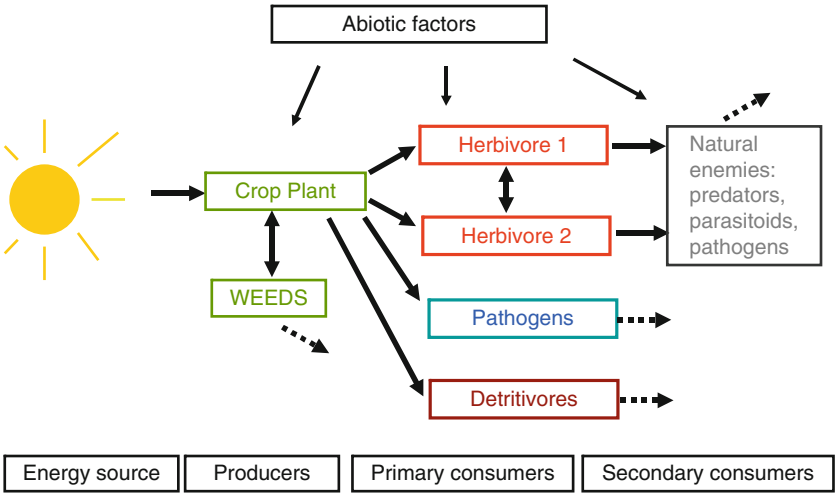

Integrated Pest Management. Figure 2
Main components and relationships related to insect pests and their control in an agroecosystem food web. *Arrows* show the direction of energy flow between components of adjacent trophic levels. *Double arrows* show competition between components within a trophic level. *Broken arrows* show that energy flow continues but the further components involved are not represented

mites, causing damages to crop yield if preventive measures are not adopted. In order to avoid constant repetition of words such as insects and arthropods the term "pest" will be preferred along all the text.

Maximization of crop yield in Fig. 2 may be achieved by increasing the proportion of sunlight energy that is fixed as biomass by the crop plant or by reducing the amount of energy that is lost by competition of weeds, by damages caused by pests, or by diseases caused by plant pathogens. The process of accumulating biomass in a crop plant to reach a yield may be compared to the process of filling a water deposit that loses water through three holes (pests, diseases, and weeds). More water may be stocked in the deposit by opening the tap (more photosynthetic production) or by repairing holes. The complex nature of the agroecosystem demands an integrated approach to manage all the components and relationships taking into account that any change in a part of them may lead to undesirable consequences in the whole system. Considering the entire complexity of the agroecosystem is crucial to develop sound integrated pest management programs.

Continuously Increasing New Insect Pests: Pest Invasion

Elements and links in the picture of Fig. 2 may change in space and time. Introduction and establishment of invasive alien species and climatic change are among the most decisive factors influencing the composition and relationships in an agroecosystem. Many of the insect pests in agriculture originated as exotic herbivores introduced in the past; this process continues to accelerate, mainly as a consequence of globalization of agricultural trading. The introduction, establishment, and spread in Europe of the Colorado potato beetle may exemplify the impact of insect pest invasions on agriculture. It originally restricted its distribution to the Rocky Mountains (USA) where it fed on wild plants. In the second half of the nineteenth century, the cultivation of potatoes close to that area allowed the beetle to multiply its populations, spread out of its original area, and distribute around the world where it has become the most harmful insect pest of potatoes in general terms. Hundreds of exotic arthropods have been documented as invading agricultural areas, establishing themselves and becoming important pests. The objective of eliminating or limiting the spread of pests has led several national and international institutions to develop legislation and tools to restrict the movement of insect species with a high potential to become agricultural pests. Regional sections of the International Plant Protection Convention have been particularly active in this direction and its Web site (www.ippc.int) is an important source of information. To categorize the risk of potential invasive alien species is a first step to adopt correct and ad hoc measures. Then, measures of exclusion, early detection, containment, or control of the most risky species may be adopted at the national or international level. Prevention of the introduction and spread of crop pests is an important first step of integrated pest management although it is sometimes difficult to implement due to the ease of international travel of both people and plants, and the increasing trade of agricultural commodities.

Injuries and Losses Caused by Pests

Pest control, and particularly integrated pest management, is therefore necessary to safeguard crop productivity against losses caused by herbivore insects and assure human nutrition. Losses caused by insect and mite pests derive mostly from their feeding activity on plants. Insects consume plant materials with their chewing or sucking mouthparts; in addition to lowering plant vigor, some insects are also able to transmit plant pathogens, with additional losses due to disease development, or injection of toxic substances that interfere with plant physiology. Consequently, potential crop yield is not attained and a variable level of losses results according to the amount of insects feeding on plants, the type of injury caused, and the susceptibility of the plant to the amount of injury infringed.

Potential and actual losses due to animal (mostly insect and mite) pests have been estimated by Oerke and Dehne in major crops [1]. Those were estimated as quite variable according to the crop and geographical area but on average they were 17.6% and 10.1% of the attainable yield in the world that give a control efficacy (percentage of losses prevented) of 42.4%. Efficacy to prevent losses from animal pests was higher than from

bacterial and fungal diseases (33.8%) but considerably lower than from weeds (70.1%). These moderate values of efficacy in crop protection, which averaged 52.5% in the world, were reached in spite of particularly high pesticide consumption in Western Europe and North America.

Strategy for Integrated Pest Management

What IPM Is

The necessity to change the strategy of controlling insect pests derived from both theoretical considerations and practical collapse of control systems. Although humans were soon aware of weaknesses in relying on control systems based solely on single tactics, control failure of pesticides due to pesticide resistance in important insect pest species and the consciousness of pesticide transfer to environment might have been the detonators of strong criticism about the mass use of pesticides in the 1950s. Soon after that, scientists, especially applied entomologists, defined new concepts and terms among which were integrated control and integrated pest management (IPM) [2]. These two terms share basically the same underlying concepts although some authors have justified the different use of these two expressions [3]. A broad definition of integrated pest management is this: a pest control system in an economically, ecologically, and sociologically sound manner by the use of multiple tactics in a compatible manner.

Sustainability should be an inherent qualification of IPM systems. However, development of novel insect pest control methods has often focused more on replacing chemical pesticides than implementing low input tactics, two objectives that do not necessarily progress in parallel ways. Classical biological control provides us with some examples of reduced sustainability when mass-reared natural enemies are repeatedly released to control insect pests in short-lived annual crops as practiced in some Mediterranean greenhouses. Paradoxically, many of pest natural enemies that are mass produced with energetically costly procedures and released into isolated Mediterranean greenhouses are native to the same area and could be managed to enhance their entrance into greenhouses by conservation biological control practices. Early IPM aimed to decrease the use of pesticides and, fortunately, it succeeded in many cases. The novel era of IPM should put emphasis on the agroecosystem management and various entries in the encyclopedia will give some indications on how to proceed in such direction. Nonetheless, some fundamental concepts of IPM as enounced decades ago have kept most of their validity in theory and practice. This is the case of economic threshold which is still a key concept that, under several formulations and criticisms, occupies a central point in IPM development.

Concept of Economic Threshold

A first question that an IPM practitioner has to face when he/she detects a certain number of pests on the crop is whether intervention is justified. Some criteria to make decisions based on economic, social, ecological, and toxicological needs are necessary. Economic injury level (EIL) and economic threshold (ET) are concepts that primarily were developed to make decisions founded on economic cost-benefit analysis to include later a richer set of the so-called bioeconomic elements that relate pest numbers, crop plants responses to pest injury, and resulting crop losses. With minor modifications these two concepts of EIL and ET still form the basis of the current IPM programs providing the potential to improve economic profits but also reduce environmental impact [4].

Relationships between pest numbers and resulting crop losses are the result of two other subrelationships succeeding each other very closely in time. Pest numbers are grossly related to total injury in a linear manner, whereas the latter relates to crop loss (i.e., lowered yield) by nonlinear figures (Fig. 3) so that the result of combining both curves gives a nonlinear relationship between pest numbers and crop loss (or yield reduction), as that represented in Fig. 4, if crop loss is converted into yield reduction.

As seen in Fig. 4, yield is reduced at low pest numbers very slightly, if at all, but as pest numbers become higher yield is increasingly reduced in a near linear manner until the declining yield per pest number increase decelerates and finally becomes insensitive to pest population growth. Of course the shape and values of this relationship is a function of several factors linked with the plant and pest species. The following are the most significant: yield based on fruit is more

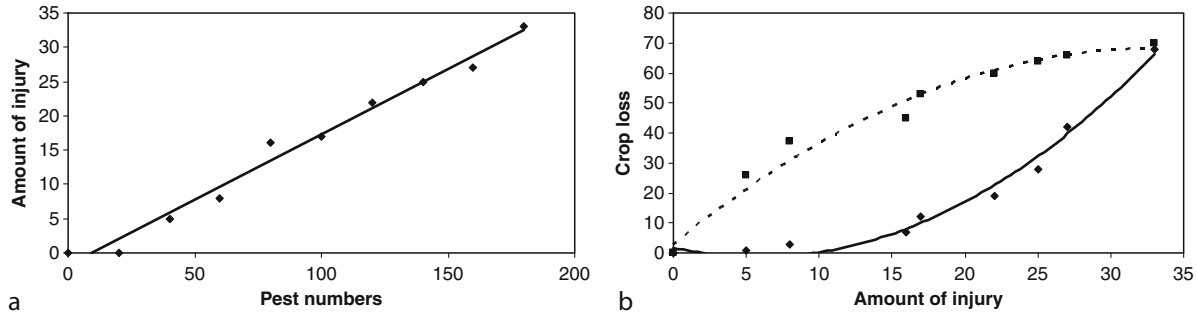

Integrated Pest Management. Figure 3
Relationship between pest numbers and amount of injury (*left*) and two common relationships between the amount of injury and losses caused on the crop (*right*)

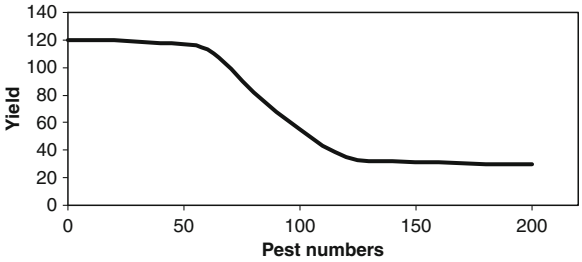

Integrated Pest Management. Figure 4
The relationship between pest numbers and yield as a result of combining the relationships of Fig. 3 and converting crop loss to yield reduction

sensitive than is biomass, injury on plant tissues contributing directly to yield are more yield reducing, dissimilar host-plant growth stages are differentially sensitive to injury in terms of yield loss in a manner that young plants have a higher capacity to recover or compensate injuries, and finally biotic and abiotic stressors other than the pest may magnify the consequences of injuries.

Knowledge of the curve relating pest numbers and yield is the basis for the calculation of EIL and ET. Simply defined, EIL is the lowest pest population numbers that will cause economic damage this being the amount of damage that equals control cost. EIL shows the amount of pests (and therefore the amount of injury) that can be tolerated by a crop. Operational consequences of the EIL are summarized by the ET, which determines if management action against a pest is needed. As the time needed to make a decision and to take the action may cause pest population to surpass the EIL, decisions have to be made before the population reaches the EIL and thereby prevent economic damage; this value is called economic threshold, ET. When decision making is delayed, pest population continues to grow, control methods are less efficient, and ET is lower in relation to EIL. On the contrary, if pest population is expected to decrease after reaching the EIL, ET may be higher than EIL. There are still many gaps in the knowledge of the mechanisms of herbivorous insect and host–plant relationships and this may be the cause of the insufficient development of ETs in practice; in addition, a rather confusing literature and proliferation of nomenclatures, often with no novel concepts provided, do not help in the implementation of tools for economically, ecologically, and toxicologically sound pest control.

Limitations of Economic Thresholds

In addition to the complexity of determining ET values already stressed, a number of other limitations may constrain the application of criteria for decision making in IPM. One of the limitations derives from the fact that many factors affect the amount of injury (or pest numbers) and yield (crop losses) relationship, and therefore it is quite unrealistic to use deterministic models – as those based on ET – in insect pest control. If different levels of crop loss may be associated to probabilities of occurrence, IPM practitioners may decide on a risk assumption basis. Risk is common in economic activities and growers have to compare the

risk of crop losses with control costs. Furthermore, growers may have to choose among a number of control methods, each with a different cost and a different expected efficacy. To further complicate the grower's decision, the benefits of different control options – including no action – may be considered in the short or long term, which are often different. For example, application of an insecticide may be more effective at short time if the chemical has a good knockdown but less effective later in the season if the insecticide kills most of the pest natural enemies and pest population outbreaks occur soon after chemical application. Finally, decisions concerning pest control may be altered if derived actions are adopted at farm or regional levels; in the first case, market price is unlikely to change as a consequence of actions undertaken; but when pest control actions are adopted at a regional level, resulting yields may affect the price.

Tools for IPM

Precision Agriculture and IPM

The so-called precision agriculture applied to pest control aims to apply control inputs only when and where they are needed and at optimal amounts according to variable field characteristics. Whereas it is understood that decisions must account for temporal changes in population densities, much less attention has been given to spatial heterogeneity probably because pest control actions are mostly decided and implemented at the farm level. For very mobile pests, when control implementation needs to operate over areas larger than just the farm, or simply because pest dynamics is decisively influenced by the spatial structure of the habitat, area wide pest management strategies have to be developed [5]. This has been practiced in the past, such as with human insect-borne diseases or in a few agricultural problems (i.e., locust plagues). Larger and systematic use of area wide control applied to agricultural pests has been implemented only in the last decades.

One of the most common causes for control failures is pest migration into managed areas from unmanaged areas or from areas managed at different times, particularly when the pest is able to move through several kilometers in a short time. Disposal of fields with different crops or different crop phenologies, or those submitted to different abiotic conditions in a patchwork landscape facilitates the movement of flying pests searching for the best environments to develop and reproduce. An area wide IPM approach differs from local pest management in some important characteristics. Whereas local IPM implementation focuses the control in specific parts of the habitat, the area wide approach considers the control in all potential niches. On the other hand, as area wide strategies need to consider and implement the control on a multiyear basis, this is an incentive for building a more permanent organization for such a purpose and thus leading to more professional management tools. These include geographical information systems (GIS), satellite imagery and remote sensing, online processing of climate data and weather forecasting, and kits to detect potential insecticide-resistant populations that can be useful for prevention of spreading resistance genes across the regional population. Finally, area wide implementation of IPM programs may allow the use of methods – sterile insect techniques, mating disruption, and inundative biological control – that are effective only when applied on big surfaces. Even if these and other methods may be used at individual farm level, economies of scale may derive from acquiring large amounts of materials. On the negative side of area wide IPM, there is the increased complexity of decision making if the area covered by the program is not uniform and many inputs are needed to respond with control measures adapted to each condition.

Area wide IPM application is based on a large amount of data referenced to each geographical position which needs to be stored and organized in a systematic and recoverable way. Once data are stored and organized they can be used to monitor some variables, manage resources, and develop forecasting models. GIS technology serves such a purpose. In recent years, GIS techniques have monitored the influence of crop plant, crop phenology, topographical variables, or climatic variability on insect distribution; movement of herbivore insects or predators at landscape scale; impact of crop rotations or cropping system on pest damage; agricultural production

techniques, insect community structure and impact of damages caused by insect pests; and invasion and establishment processes by alien invasive insects.

Acquisition of data to feed GIS technology may be a long-lasting and tedious process and it is a major limitation for GIS application in IPM. Remote sensing – acquisition of information on an object without being in contact with it – may reduce the efforts for data acquisition. For instance, remote sensing techniques have been developed to map several types of vegetation or plants that are stressed by damage caused by different amounts of herbivore insects and which display changes in absorption and reflectance in the visible and near infrared light due to chlorophyll content decrease, alteration of other pigments, or some other changes in the internal plant anatomy. Plants stressed by insects or diseases also may alter their temperature and thermal imagery may be used to detect these plants. Images may be field-based or taken from planes or satellites and thus cover big surfaces. Before using remote sensing to make maps of insects or insect-damaged plant distribution, accuracy of sensing images should be verified by means of ground surveys. Signals from damaged plants may not be very specific and insect populations or damage caused by one species may be overestimated.

As more data are needed and available for decision making, more sophisticated are the algorithms used to process the information. Processes relating input data with conclusions leading to actions may be performed by expert personnel or by more automatic procedures as computer software; the latter are called expert systems. To consider the role that expert systems may play in IPM, let us recall the steps of any decision in pest control [6]: pest identification, assessment of injury level (density), estimation of likely crop losses, identification of control options, cost/benefit analysis, identification of constraints, integration in the larger framework of crop production [6]. Ideally, expert systems are linked with data bases that allow input and review of historical series of data to analyze past decisions in the light of real posterior events.

Expert systems not only serve for decision making in IPM but may be used as a common base for discussion among scientists or IPM practitioners in order to identify incorrect algorithms or gaps in the current knowledge or incorrect recommendations made in the past. Expert systems can also be used as training tools. Via simulation, students can examine and check situation rules to sample, make calculations, and convert the conclusions into recommendations. When expert systems are used for training or when they have to be presented for demonstration purposes, input variables, algorithms, and logical rules for decision making should be shown in a more explicit format than just computer software, for example, a set of matrices or as a decision chart such as in Fig. 5.

The decision chart in Fig. 5 was designed for field technicians to decide if insecticide treatments are needed in tomato crops. Decision algorithms take into consideration not only the amount of pest (greenhouse whitefly) but also the amount of predators (two mirid bugs) that can keep pest populations under control when the predator–prey ratio is high enough. As mirid bugs are omnivorous predators that may feed on and damage tomato fruit when lacking prey, the strategy adopted was to manage insecticide sprays. This maintained a sufficient number of whiteflies to provide predators with food and prevent tomato damage but was not too high to avoid having honeydew and sooty mold on plants and fruits. Technicians have to sample the field by choosing a number of plants at random and taking seven terminal well-developed leaves to count the number of whitefly adults and predators (adults + nymphs). According to the position in the graph of the values recorded in the field for whiteflies or predators, the decision made is: (a) doing nothing, (b) or spraying against whiteflies, (c) or predators; (d) a four region in the chart does not lead to specific recommendations. Chart is accompanied by keys to identify the targeted whitefly and the predators, some rules to take samples (including a table of random numbers), and an updated list of eligible insecticides with recommendations about their application.

Estimating Insect Population Densities

To make decisions in pest control, pest density needs to be known. As it is normally impossible to count all the insects in a habitat, it is necessary to estimate

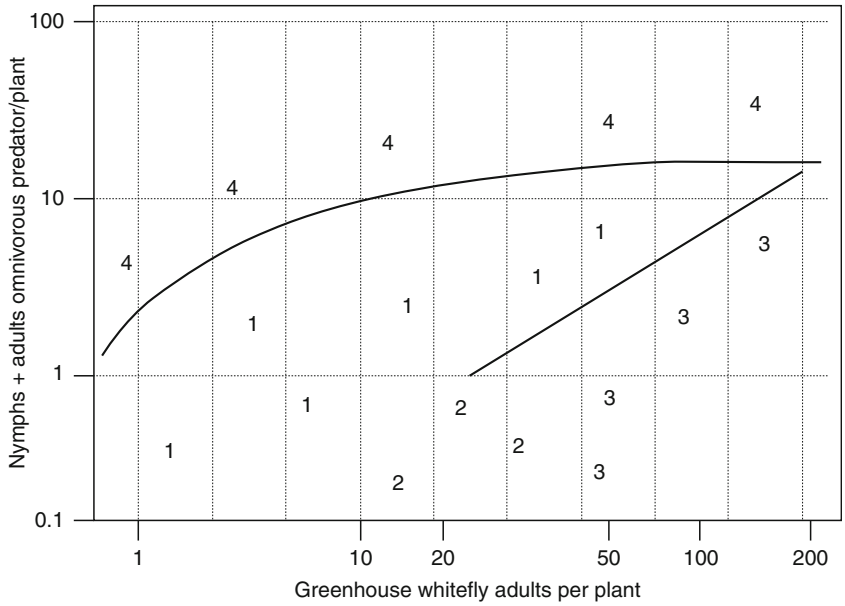

Integrated Pest Management. Figure 5

Decision chart to make recommendations for insecticide spraying in tomato crops against the greenhouse whitefly and the omnivorous predators according to the number of whiteflies and predators recorded on tomato plants. Figure has been simplified to show the most significant elements. Numbers indicate the action to be undertaken after recording densities of the omnivorous predator and the greenhouse whitefly on tomatoes in the field: (1) no action, (2) sample again in one week, (3) spray against whitefly if the recorded numbers remain in zone 2 for two consecutive weeks, and (4) spray against mirids

the population density by sampling. An estimation of absolute or relative population may be needed. In absolute estimations, the estimated number of individuals in a certain surface or volume may be known, whereas in relative estimation a certain and unknown proportion of the population changes in the time or space is determined. The first type of estimate is useful when we want to know if a population has reached the economic threshold or not. The second type serves to compare population numbers in time and space for monitoring purposes. If population numbers may be related to their products – for example, total amount of honeydew excreted by an aphid population – a population index may be more useful than determining the real number of individuals.

An accurate estimate of the density of pests or natural enemies is therefore a major necessity for IPM. To estimate population densities it is necessary to sample the habitat where the population may occur and this may require knowing various aspects. Sampling universe, sampling unit, number of samples to be taken for a certain precision, and data analysis are some of the aspects to be considered in a sampling plan. Readers interested in this concept should consult the Southwood and Henderson book for wider development [7].

How individuals of an insect population are disposed in space – dispersion or distribution of the population – greatly affects the sampling program. Theoretically, three different types of population distributions may be found (Fig. 6). In *uniform distributions* individuals are evenly distributed in space whereas in *random distributions* any point in space has the same probability for occupation by an individual. Finally, most commonly, individuals are clumped on relatively few foci in *aggregated distributions*.

Population dispersion has been described by means of aggregation indices or by fitting mathematical distributions to experimental data. Use of aggregation indices is based on the relationship between variance

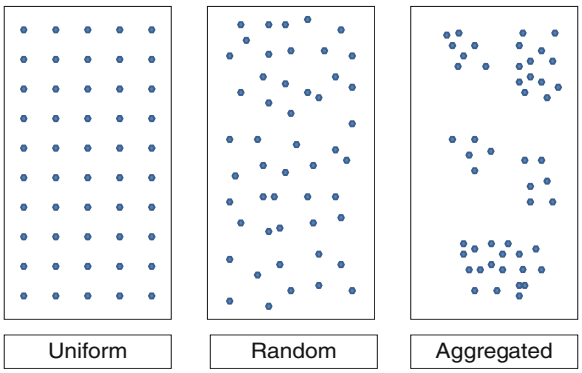

Integrated Pest Management. Figure 6
Three kinds of insect population distributions

and mean in the three types of distribution models. In uniform distributions variance is null independently of the mean; in random models mean equals variance; in aggregated distributions variance is higher than mean. The simplest aggregation index uses the variance/mean ratio so that when the ratio is 1 it means that distribution is at random, it is more uniform as the ratio decreases below 1 and, inversely, aggregated models show variance/mean ratios increasing higher than 1 as individuals are more clumped. Other aggregation indices relating variance and mean in different ways have been used – for example Lloyd', Morisita' indices – but most of them have shown a high dependency from sampling unit size and population density, a disturbing inconvenience to characterize a population distribution pattern. Relationship between estimated variance (s^2) and mean (m) has been empirically fitted to a power law: $s^2 = am^b$, where a and b are constants; a is largely a sampling factor while b appears to depend on the degree of aggregation of individuals and thus may be used as an aggregation index. Taylor's power law has shown to overcome some of the limitations mentioned for aggregation indices but usually needs many experimental data to fit a sound power function.

Several mathematical models have been proposed to describe population distributions; for insects many populations have been adequately fitted to the negative binomial distribution which is basically described by the parameter k, which is a measure of the degree of clumping. Although the approach of mathematical models to study population distribution patterns has given more accurate descriptions than aggregation indexes, it often depends on population density and sampling technique. In summary, none of these methods describing population distributions is free from limitations and this can explain why insect ecologists have used so large a variety of approaches to characterize patterns of insect disposition in space.

When populations are very clumped and most individuals occupy a few dense patches among empty patches a question arises: are individuals in one patch moving to another patch? If yes, how often and to which extent does this movement occur? Such a perspective deals with metapopulation ecology. Ecology has classically considered that individuals of a population are capable of unrestricted interaction with each other within a habitat. However, habitats usually occur in a patchwork within a landscape – as islands in the ocean – and populations inhabiting those habitats are consequently patchy. Populations occupying each patch may become extinct but individuals coming from other patches may recolonize that patch and rebuild a new population. Between-patch movement also may be caused by factors other than just extinction and recolonization. In any case, individuals initially belonging to a population in a certain patch occasionally may interact with individuals of other patches. The set of all populations initially occupying different patches is called a metapopulation. There has been a lot of interest in metapopulation ecology in the last decades because of its practical application. In the field of IPM, metapopulation ecology may bring new tools for analyzing the dynamics of insect populations that occur in partially isolated patches (fields or group of fields). Understanding how populations work in a metapopulation may help to increase environmental resistance to pest population development or to favor populations of pest natural enemies. Management of metapopulations and not just local populations may be a valuable approach not only for unstable annual crop systems but also for more permanent crops that are periodically disturbed (i.e., cut, pruned, sprayed with insecticides) so insects are regularly obliged to leave and recolonize fields. In the context of area wide IPM programs, metapopulation ecology may be more predictive than just considering individual populations.

Taxonomic Adscription of Major Pests

Main Animal Taxa with Damaging Species

Most agents causing injuries to crop plants are species belonging to the Phylum Arthropoda and among these the class Insecta includes the majority of arthropods that are crop pests. That is why the discipline dealing with pests and their control very often is called agricultural entomology, the science about insects in relation to agriculture. The class Arachnida, particularly the order Acari (mites), also contains some important pest species. Notice that some herbivorous insects and mites cause injuries to crop plants whereas pathogens are responsible for crop plant diseases.

The class Insecta comprises more than one million identified species and probably even more that have not been identified yet. Insects are grouped in 28 orders – this varies according to the authority– a common taxonomical level to refer to insects. Among those, seven major orders include most of the important insect pests: Orthoptera (grasshoppers and others), Hemiptera (true bugs), Homoptera (hoppers, psyllids, whiteflies, aphids, scale insects), Coleoptera (beetles), Lepidoptera (moths and butterflies), Diptera (mosquitoes, flies), Hymenoptera (ants, wasps, insect parasitoids, and others). Table 1 shows the main families of mites and insects including economically important pests and their most significant pest characteristics.

Other taxa of the animal kingdom include species that can potentially become serious pests. Mollusks (snails and slugs), fishes, reptiles, birds, and mammals may include species that in some circumstances are very damaging.

Identification of Insects and Mites

When a technician observes insects or mites on a crop, the first question that arises is "what are they?" To precisely answer this question is a key starting point for finding an efficient solution if the population grows to become a pest. A wrong answer may lead us to make incorrect decisions as many solutions are specific for each insect pest and crop. Sometimes, even specific identification is needed to adopt correct measures.

Identification of insects and mites is usually done by means of taxonomic keys. Keys are arrangements of related taxa put in clusters. Morphological characters – complemented sometimes with anatomy, appearance, or behavioral features – are mainly used to segregate individuals into clusters. The process goes from more general characteristics (i.e., with wings or wingless) and taxa to more particular characteristics until reaching species-level determination. Even for easy identifications, a certain expertise is needed. For routine identifications field technicians may perform quite well in recognizing common species; when dealing with a new species, correct identification may require sending a sample to a family-level specialist usually working in universities or musea. Availability of good insect taxonomists is therefore critical for developing sound IPM programs, not only to identify insect pests but also their natural enemies (predators and parasitoids).

Molecular techniques are still insufficiently developed to identify insects but rapid progress has been made in recent years. Molecular tools are usually developed to distinguish between two or more taxonomically close species. Molecular identification keys based on a targeted DNA sequence or marker may be useful for such purposes and have some advantages in relation to classical morphological keys. These advantages include: applicability to all developmental stages; less variation than for morphological characters; they may be applied to fragments of the individual to be identified; the technique may be applied for a variety of insects if appropriate specific material and personnel trained in molecular tools are available, in contrast with morphological-based keys that usually require family-level specialists.

Pesticides

Use of Pesticides

In the coming sections, major *control methods* are reviewed in the light of how they can contribute to the sustainability of agriculture. Ecological bases, common applications, and how they can be integrated into IPM systems are presented in each method.

Use of pesticides (mainly herbicides, insecticides, fungicides, and nematocides) in western world agriculture has decreased or been maintained in general.

Integrated Pest Management. Table 1 Main orders and families of arthropods including economically important pest species

Class	Order	Family	Main characteristics and features as pests
Arachnida	Acari	Tetranychidae	Plant-feeding spider mites. They feed on several aerial plant parts but mainly on leaf undersides with loss of photosynthetic products and water
		Eriophyidae	Microscopic mites with only two legs; they feed on plant parts often causing galls
Insecta	Orthoptera	Acrididae	Insects that at high density may aggregate in groups and migrate long distances and become very destructive on many crop and forest plants
	Hemiptera	Pentatomidae	They suck plant sap from several tissues resulting plant wilt, abortion of fruits, or tissue malformations
		Miridae	Numerous, but not only, herbivore species that feed on plant sap causing foliar chlorosis, cankers, abnormal growth, and many kinds of lesions
	Homoptera	Cicadellidae	Usually they feed on leaves where they suck juices and reduce chlorophyll contents and produce small white spots. Plant vigor decrease and disease transmission are common injuries
		Psyllidae	They feed on the phloem causing plant stunting or poor plant growth and sometimes gall forming
		Aleyrodidae	They feed on the phloem and reduce plant vigor, exude honeydew where sooty mold may develop causing fruit depreciation and some species are active plant disease vectors
		Aphididae	As mentioned for Aleyrodidae with special importance for plant virus transmission
		Coccoidea	In addition to the injuries mentioned for the other Homoptera, scale insects may inject saliva into the host causing discoloration, malformations, galls, and also esthetic damages in ornamental plants
		Diaspididae	
		Asterolecaniidae	
		Coccidae	
		Margarodidae	
		Pseudococcidae	
	Coleoptera	Scarabaeidae	As pests they mainly feed on plant roots in larval stages causing plant vigor decrease and even plant death
		Elateridae	Larvae feed below ground on roots and tiller base and kill the plant when it is young. Crops harvested for roots or tubers are more easily injured
		Curculionidae	Many species whose larvae and adults feed on several plant tissues including roots, tillers, leaves, flowers, and fruits. A very damaging family
		Chrysomelidae	Adults and larvae feed on foliage and fruit; in some other species larvae feed on roots
		Scolytidae	Larvae feed internally in tree tissues, below the bark; particularly harmful in forest trees but also in orchard and ornamental trees
	Lepidoptera	Tortricidae	Larvae feed on leaves, fruit, buds, and stems
		Pyralidae	Larvae are leaf-rollers, borers, and detritivorous attacking a large number of crops including stored products
		Crambidae	Larvae are mostly grass stem borers

Integrated Pest Management. Table 1 (Continued)

Class	Order	Family	Main characteristics and features as pests
		Noctuidae	Larvae feed on leaves, stem, and fruits devastating many crops. This is one of the most important families with many economically important species
	Diptera	Cecidomyiidae	Main injury comes from their capacity to cause galls in several plant tissues
		Tephritidae	Larvae feed internally in fruits. They have a high destructive potential
		Agromyzidae	Larvae mine leaves by feeding parenchyma cells between up and down epidermis
	Hymenoptera	Tenthredinidae	Most damage is caused by larvae feeding on leaves that reduce photosynthesis activity and thus plant vigor. They commonly defoliate forest trees but also some agricultural crop plants
		Cephidae	Larvae bore into stems of grass plants and cause their breakage

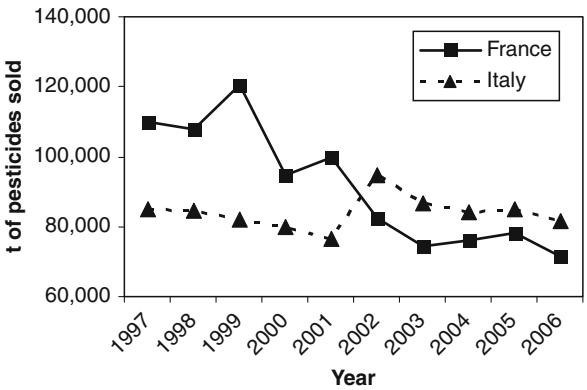

Integrated Pest Management. Figure 7
Evolution of sales of active ingredients with pesticide activity in two significant consumers in Western Europe (From http://epp.eurostat.ec.europa.eu/tgm.Accessed 6 February 2010)

In Fig. 7, the amount of pesticides sold in two main consumer European countries is shown. Whereas in France, the highest consumer of pesticides in Europe, the amount of pesticides sold (mostly applied in France) has decreased significantly, in Italy the amount of pesticides is more or less stable or shows a slight increase taking into account that modern pesticides are used at considerably lower doses than classical active ingredients. Beyond differences due to variable economic and climatic conditions, an important part of the decrease in many countries has been achieved by the progress of application of IPM systems to control insect pests, diseases, and weeds.

Pesticides are chemicals aimed to kill any kind of plant pest or otherwise lower their populations to prevent their reaching economic thresholds. Pesticides include four main groups of substances according to their target: herbicides against weeds, insecticides against insects or other pests, fungicides against in general disease-causing agents, and nematocides against plant pathogenic nematodes. A number of characteristics of pesticide use may explain the success of pesticides for pest control in the last decades although probably the amount applied has started to decrease in the developed world in recent years due to the restrictions posed by the legislation and also by the progress experimented by the R&D in implementing IPM systems.

Pesticides are easy to use; growers may fill the tank and spray many hectares while sitting in the tractor and listening to the radio. When used correctly they are effective to lower pest populations and frequently cheaper than other control alternatives. In spite of the better selectivity and lower permanence of modern pesticide active ingredients, at least one pesticide is usually available in the market for each pest. Until the discovery of insecticide properties of DDT in the 1940s, most pesticides were inorganic or extracted from plants. Since the 1940s until the end of the century, the amount of pesticides applied in the world multiplied dramatically per 20 or 30 times according to the country and several chemical families were available to

control insect pests. Since the 1950s, however, scientists were aware of the problems derived from the excessive confidence in the efficacy of pesticides. Fewer than 20 years of mass application of pesticides in western agriculture were sufficient to display some of their negative effects. In ulterior years, problems became harder and many field data confirmed first concerns. Development of alternatives to chemical pesticides therefore became the goal of R&D programs in most of those countries.

Problems Associated to Pesticide Use

Problems derived from inadequate and excess pesticide use include (a) risks to public health and environment (e.g., wildlife and groundwater), (b) disturbance within agrosystems due to the common toxicity to natural enemies and secondary pest resurgence, (c) development of pesticide resistance in the targeted pests (more than 600 pest species related to agriculture and human and livestock health are nowadays confirmed to be resistant to one of more pesticides) (www.pesticideresistance.org accessed on February 10, 2010), and (d) shorter and shorter shelf life and increasing costs to innovate by producing more selective and environmentally friendly new active ingredients. Industry has tried to develop new more compatible chemicals in order to integrate selective chemicals in IPM strategies but innovation is increasingly slow and expensive. Legislation is becoming very strict for registration of new pesticides and obliges repeated registration of old active ingredients for health and environmental safety. As a consequence the number of active ingredients available for chemical pest control is decreasing constantly. It is expected that the number of active ingredients registered as insecticides in the coming years in the EU will be less than a third of those allowed at the end of the twentieth century. Lack of effective insecticides is pressing research in and the development of new and efficient IPM systems.

Controversy on pesticide use in modern agriculture cannot lead us to forget that pesticides, at the moment, have still an important role in IPM systems. Some important pests lack sufficiently effective control methods so that no-chemical methods have to be combined with chemical ones. In other, although few, cases, pests have only chemical insecticides to control them. Invasive exotic insect pests, due to short experience in their control and novelty, may be contained only by the regional application of chemical pesticides. A rigorous analysis of how sustainable is the use of each insecticide for each pest should permit detection of those pest problems in which insecticides are irreplaceable at least at short time and those other pests in which one insecticide is superfluous – therefore that pesticide can be banned – because at least one efficient nonchemical method is available. Unfortunately the control of unnecessary use of chemicals is frequently difficult but should be implemented to speed up the adoption of IPM technology.

Crop Resistance

Ecological Bases of Crop Resistance

Most pests cause plant damage when feeding. However, it is well known by interested observers of nature that not all herbivore insects may feed on any plant. Usually some insects may feed on a few close plant species (monophagous insects), or on plant species belonging to one family or only a few families (oligophagous insects), and finally some others may feed on a broad range of plants (polyphagous insects). Even polyphagous species feeding is usually restricted to a relatively small number of plants available in the habitat. These associations between herbivore insects and host plants are the result of the coevolution of the two components; in such coevolution, plants develop mechanisms to defend themselves from herbivore insects and insects try to develop mechanisms to overcome plant defenses. That a plant possesses some characteristics that diminish its access for one insect pest and that such a trait may be introduced into a host plant for pest control is an old idea. Still, until well into the twentieth century crop resistance to insects was not systematically considered as a universal tool for pest control in spite of early successes in the use of plant resistance. Probably, the most famous early case of using crop plant resistance for pest control was the control of grape phylloxera in European grapevines. Practically all the European wine industry was ruined by the entrance into Europe of the North American phylloxera aphid in the 1860s. Successful control of the pest was achieved at the very end of that century by grafting European vineyards on resistant American rootstocks.

Insect–Plant Relationships and Plant Characteristics for Crop Resistance

Many physical and chemical factors are involved in insect–plant interactions. Plant stimuli and elicited insect responses are usually studied in a sequence of five behavioral steps: (a) host habitat searching, (b) host searching within the habitat, (c) recognition of a host as suitable for feeding and ovipositing, (d) host acceptance, and (e) host suitability. Step (a) is important for species that migrate or disperse over long distances and it is only occasional for pests staying in the crop habitat. Preferred abiotic conditions of the habitat are usually the most involved signals in habitat selection whereas in host selection (step b) visual and olfactory stimuli have a major relevance to bring the herbivore close to the host plant and not only olfactory but also tactile inputs stimulate the herbivore to remain on the plant. The host is recognized through gustatory receptors that identify particular host substances when bitten by the herbivore or when the female starts ovipositing. Similar mechanisms but different substances in the host plant cause the herbivore to continue or stop feeding or ovipositing after the recognition phase. Host adequacy for the herbivore and descendants is determined by the nutritional value of the plant and the absence of toxic compounds.

Physical and chemical plant characteristics that confer resistance to the host plant against the exploitation by the herbivore may be found in each of the behavioral steps and mechanisms and those traits may be incorporated into the crop plant genotype for pest control. Mechanisms involved in host-plant resistance to herbivores may be grouped into two main categories:

- *Antixenotic* mechanisms prevent herbivores from approaching or establishing on a plant to feed or oviposit on it. There is a varied array of chemical and physical deterrents in plants to prevent or modulate preference of herbivores for feeding/ovipositing. Chemicals may be plant volatiles that act at long distances or nonvolatiles that intervene once the herbivore has landed on the plant or after it has probed the host. Physical characteristics in plants with antixenotic properties include morphological and structural features that interfere with normal feeding or oviposition. For example, plant epidermis hairs and trichomes are common morphological features that impede normal feeding in many herbivore insects and confer resistance to hairy cultivars.
- *Antibiotic* mechanisms cause deleterious effects, including mortality, for the herbivore once it has ingested a certain amount of the host plant. Antibiotic effects on herbivores that have fed on resistant plants may be expressed in a variety of consequences, and not only mortality: lowered development rates, failure of development features like pupation or adult emergence, reduced fecundity or fertility, and irregular behavior. Antibiosis is caused by toxic plant compounds or by other nontoxic plant characteristics like low nutritional quality, unbalanced composition in nutrients, or presence of enzymes interfering with normal insect digestive physiology.

There are mechanisms of plant resistance that are not related to host-plant constitution. These are "ecological resistance," "induced resistance," and "tolerance." Although they have been often neglected in plant breeding programs, their consideration when crop cycling and crop management practices are planned may contribute greatly to reduce crop losses by pests. *Ecological resistance* derives from the phenological asynchrony of crop and pest populations that prevents or diminishes the coincidence of the most susceptible crop growth stages with the most pest stages that are able to attack the host; sowing date may thus be planned for enhancing ecological resistance. *Induced resistance* is the response of a host plant to an environmental stress that reduces herbivore insect fitness or the plant availability for the insect. Once again, many agricultural techniques, like fertilization or irrigation, may alter plant physiology to enhance or decrease induced resistance. *Tolerance* is the capacity of some crop plants or crop cultivars to recover from injuries caused by the pest so that tolerant plants may attain yields that a similar amount of pest on a nontolerant plant would reduce. Several physiological processes have been identified in plants that may compensate for the injury caused by a herbivore insect and those processes may be facilitated by good agricultural practices.

Crop Resistance and IPM

Host crop resistance has been used profusely for disease control but it is increasingly considered and applied for integrated pest management. It is largely *compatible* with other IPM tactics, particularly biological control, although interferences of the host plant in predator–prey relationships have been reported recently. Its effectiveness is cumulative as its effects on pest population is exerted on several pest generations and usually persists after a pest's long exposure to the resistance traits; however, some cases of pests that have overcome resistance barriers at midterm have been described. One of the major advantages of crop resistance as a pest control method in the framework of IPM programs is that growers may easily adopt it as no particular expertise is needed. From a point of view of environment, crop resistance is in general safe, a required trait of any IPM method.

There are also some important limitations for a wider adoption of crop resistance in IPM. Frequently a long time is needed to develop a resistant cultivar, particularly in tree crops, and reaction to new and urgent problems is very slow. Modern biotechnology techniques, particularly genetic engineering (see below), are contributing to mitigate this handicap. Additionally, resistance traits are not always identified and available or they are very difficult to introduce into crop plants (also genetic engineering may favor the transfer of resistance genes between nonsexually compatible organisms). Another difficulty to implement crop resistance for pest control is the incompatibility of the resistance trait and commercial requirements; bad taste for consumers, for example, has been found in some resistant cultivars. In spite of the persistence of crop resistance mentioned as an advantage of the method, and as also mentioned earlier, local biotypes of the pest that are able to overcome or avoid resistance characters in the plant may develop and rapidly multiply as a consequence of their supremacy to exploit the resistant cultivar.

Biological Control

Ecological Basis of Biological Control

Biological control may be defined in general terms as the use or manipulation of natural enemies to suppress pest populations. Some authors include in the term any kind of nonchemical method that is biology-based. However, this is generally considered as incorrect and the narrower meaning given above is preferable. Although biological control may be practiced under several modalities, its principle is unique and responds to the scientific background of predator–prey ecology.

Natural enemies have been signaled as major components of natural control keeping populations within cyclic oscillations between maximal and minimal bounds in the framework of a "spontaneous balance of nature." Therefore the idea that exotic pests greatly increase their densities mainly due to lack of natural enemies in the new habitat led to attempts of reconstituting that balance by importation and release of exotic natural enemies. The ecological basis of biological control may be represented as shown in Fig. 8. A pest population that oscillated around a mean density very often above economic threshold is reduced to oscillations below that threshold after a release of an effective natural enemy. An important part of recent population ecology developments has dealt with prey-predator models that should provide the theoretical basis of biological control allowing it to progress from a rather empirical practice to a scientifically based technology. Unfortunately, the contribution of theoretical developments on predator–prey relationships has not been as fruitful as expected for biological control applications although they have clearly helped to progress beyond the "trial and error" stage of the first half of the twentieth century.

Understanding relationships between predators and prey and between parasitoids and hosts is important to optimize biological control practices. Prey consumption or host parasitization is the successful result of several behavioral steps of predator/parasitoid including:

- Selection of a *suitable habitat* where prey/host is more likely to occur. Predators and parasitoids may respond to biotic and abiotic characteristics of habitats where prey may be found. Several long-distance visual and olfactive stimuli from habitat components, including the proper prey/host, may be involved in habitat suitability recognition by searching predators and parasitoids.
- Once in the suitable habitat the predator/parasitoid has to *find a prey/host*. Within the habitat vision and

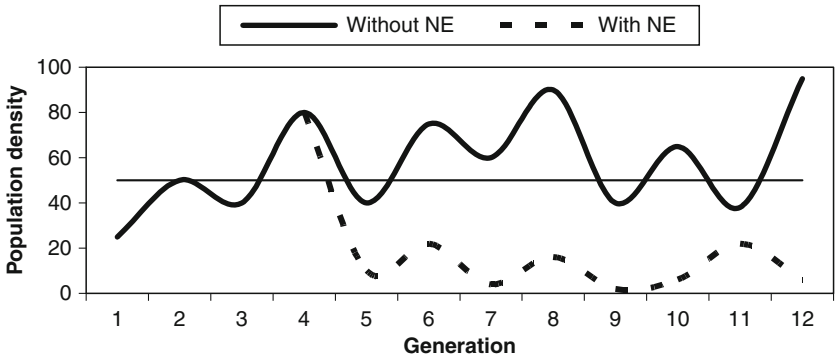

Integrated Pest Management. Figure 8
Fluctuations of a pest population before and after releasing an effective natural enemy. *Broken line* shows the fluctuation under the action of the natural enemy whereas *solid line* shows the dynamics of the pest without the natural enemy. *Horizontal line* represents the value of economic threshold

olfaction also play a major role, but short distance stimuli may be decisive as adults sometimes look first for a prey in a random way until they come in contact with a potential prey.

- *Acceptance of a prey/host* when it is attacked by the predator/parasitoid is influenced by physical and chemical characteristics of the prey/host but also by hunger of the predator. Abundance may also determine if a prey is attacked or not.
- Prior to the final decision to consume/parasitize requires checking that a *prey/host is suitable* for the predator/parasitoid. Internal composition of prey largely determines if the predator rejects or continues to feed on it.

A relatively low amount of predatory arthropods are quite specific (they feed only on a particular family of prey) whereas generalist predators (they may feed on a wide range of prey taxa) are more common among both insects and spiders. In some groups both juvenile and adult stages are predatory but in some others only juveniles or adults prey. Parasitoids are usually more specific than predators and in general they can parasitize species belonging to one family or to a narrow range of families.

Taxonomic Adscription of Insect Natural Enemies

Natural enemies include three kinds of organisms: predators, parasitoids, and entomopathogens. Biological control only deals with the former two types whereas the third is the subject of microbial control. Predators are organisms that kill and consume a number of other organisms, called prey, along their lifespan from which they obtain the energy needed to grow, develop, and reproduce. Parasites are organisms that usually need to consume only one organism, the host, to develop and reproduce. When the host dies as a result of the action of one parasite this is called parasitoid.

Predaceous habits are relatively common in classes Insecta and Arachnida. Among insects, five orders include particularly important predators in agrosystems: Hemiptera (true bugs), Neuroptera (nerve-winged insects), Coleoptera (beetles), Diptera (flies), and Hymenoptera (wasps and ants). Among Arachnida, the order Acari includes some predatory families, particularly Phytoseiidae, and many predatory species grouped in several families belong to Araneae (spiders). Whereas predators are located in many insect and mite families, parasitoids mainly belong to certain families of Hymenoptera and a few to Diptera. Early on biological control almost exclusively used entomophagous insects but currently a wide range of organisms are being applied or manipulated to control pests. Table 2 shows those predators and parasitoids that are or have been commercially used in Europe and Mediterranean countries (http://archives.eppo.org/EPPOStandards/biocontrol_web) (accessed in December 2009).

Integrated Pest Management. Table 2 Main predators and parasitoids that are or have been commercially provided for biological control in Europe and non-European Mediterranean countries

Phylum/order	Family	Species	Main target pests
Predators			
Insecta/Hemiptera	Pentatomidae	*Podisus maculiventris*	Lepidoptera larvae, Colorado potato beetle
		Picromerus bidens	Lepidoptera larvae
	Anthocoridae	*Orius albidipennis*	Thrips
		O. laevigatus	Thrips
		O. majusculus	Thrips
		Anthocoris nemoralis	Psyllidae in orchards
		A. nemorum	Pear psylla
	Miridae	*Macrolophus caliginosus*	Whiteflies
Thysanoptera	Aeolothripidae	*Franklinothrips megalops*	Thrips
		Franklinothrips vespiformis	Thrips
		Karniothrips melaleucus	Scales
Neuroptera	Chrysopidae	*Chrysoperla carnea*	Aphids
Coleoptera	Staphylinidae	*Aleochara bilineata*	Larvae of *Delia* sp. flies in soil
	Coccinellidae	*Adalia 2-punctata*	Aphids
		Chilocorus baileyii	Armored scale insects
		C. bipustulatus	Armored scale insects, olive black scale
		C. circumdatus	Armored scale insects
		C. nigrita	Armored scale insects, pit scales
		Coccinella septempunctata	Aphids
		Cryptolaemus montrouzieri	Mealybugs
		Delphastus catalinae	Whiteflies
		Rhyzobius lophanthae	Armored scale insects
		Rodolia cardinalis	Cottony cushion scale
		Scymnus rubromaculatus	Aphids
		Stethorus punctillum	Red spider mite
Diptera	Cecidomyiidae	*Aphidoletes aphidimyza*	Aphids
		Feltiella acarisuga	Red spider mite
	Syrphidae	*Episyrphus balteatus*	Aphids
Arachnida/Acari	Phytoseiidae	*Amblyseius barkeri*	Thrips, tarsonemid mites
		A. degenerans	Thrips
		Hypoaspis aculeifer	Sciarid flies in soil substrates
		Metaseiulus occidentalis	Spider mites
		Neoseiulus californicus	Spider mites

Integrated Pest Management. Table 2 (Continued)

Phylum/order	Family	Species	Main target pests
		N. cucumeris	Thrips
		Phytoseiulus persimilis	Red spider mite
		Typhlodromus pyri	Some spider and eriophyoid mites
	Laelapidae	*Stratiolaelaps miles*	Sciarid flies in soil substrates
	Cheyletidae	*Cheyletus eruditus*	Storage mites
Parasitoids			
Insecta/Hymenoptera	Mymaridae	*Anagrus atomus*	Leafhoppers
	Encyrtidae	*Anagyrus fusciventris*	Mealybugs
		A. pseudococci	Mealybugs
		Comperiella bifasciata	Armored scale insects
		Encyrtus aurantii	Scales
		E. infelix	Scales
		Gyranusoidea litura	*Pseudococcus longispinus* (mealybug)
		Leptomastidea abnormis	Mealybugs
		Leptomastix dactylopii	*Pseudococcus citri* (mealybug)
		L. epona	Mealybugs
		Metaphycus flavus	Soft scales
		M. helvolus	Soft scales
		M. lounsburyi	Soft scales
		M. swirskii	Soft scales
		Microterys nietneri	Soft scales
		Pseudaphycus maculipennis	Mealybugs
		Tetracnemoidea peregrina	Mealybugs
	Aphelinidae	*Aphelinus abdominalis*	Some aphids
		Aphytis diaspidis	Some armored scales
		A. holoxanthus	Armored scales
		A. lingnanensis	Some armored scales
		A. melinus	*Aonidiella aurantii* (armored scale)
		Coccophagus lycimnia	Soft scales
		C. rusti	Soft scales
		C. scutellaris	Soft scales
		Encarsia citrina	Armored scales
		E. formosa	Greenhosue whitefly
		Eretmocerus eremicus	*Bemisia tabaci* (whitefly)
		E. mundus	*Bemisia tabaci* (whitefly)
		Cales noacki	*Aleurothrixus floccosus* (whitefly)

Integrated Pest Management. Table 2 (Continued)

Phylum/order	Family	Species	Main target pests
	Aphidiidae	*Aphidius ervi*	Aphids
		A. colemani	Aphids
		A. matricariae	Aphids
	Braconidae	*Bracon hebetor*	Lepidoptera
		Cotesia marginiventris	Lepidoptera
		Dacnusa sybirica	*Liriomyza* spp. (leafminers)
		Opius pallipes	*Liriomyza* spp. (leafminers)
		Praon volucre	Aphids
	Eulophidae	*Aprostocetus hagenowii*	Cockroaches
		Diglyphus isaea	*Liriomyza* spp. (leafminers)
		Thripobius javae	Thrips
	Trichogrammatidae	*Trichogramma brassicae*	Lepidoptera
		Trichogramma cacoeciae	Lepidoptera
		Trichogramma dendrolimi	Lepidoptera
		Trichogramma evanescens	Lepidoptera
	Pteromalidae	*Scutellista caerulea*	Soft scales

The dozens of natural enemies included in Table 2 are only a part of those used in biological control in Europe. At least the same amount can be added when established agents managed for biological control by conservation (conservation and enhancement of natural enemies by crop and habitat management, see biological control by conservation below) are considered. Many other arthropod (e.g., dermapterans, carabids, staphylinids, coccinellids, syrphids, mirids, nabids, lygaeids, spiders, phytoseiids, and stigmaeids) and non-arthropod groups include predatory species that are or have been directly or indirectly managed to suppress pest populations in agriculture in Europe. Similarly, the same or close families to those cited in Table 2 include other species of parasitoids that have been used in biological control by conservation.

Strategies of Biological Control

To achieve pest suppression biological control may follow three main strategies: release of new natural enemies in a habitat (classical biological control); augmentation of natural enemies in the habitat (augmentative biological control); and conservation of those natural enemies already established in the habitat (conservation biological control) [8].

Classical biological control. Modern biological pest control began at the end of the nineteenth century when an exotic pest, the cottony cushion scale, invaded Californian citrus orchards and caused severe damages. Among other species, a predatory coccinellid beetle, *Rodolia cardinalis*, was imported from its Australian origin and released in some orchards of California. In a few years the predators spread throughout the citrus growing area and greatly reduced scale densities. Success of the strategy created much enthusiasm and many other cases of introduction of exotic natural enemies to control exotic pests followed the release of the Rodolia beetle. Some of them resulted in successful pest suppression but some other failed due to several causes. In spite of this, several benefits derived from successful and failed attempts. First, biological control was shown as a feasible technique to suppress pests. Second, a network of entomology laboratories – mainly

American – spread around the world to support expeditions to look for natural enemies and some of them were the embryo of future biological control institutes. Third, successes and failures have pushed entomology science to develop the taxonomy of many families of predators and parasitoids, to furnish an ecological basis of predator–prey relationships for a more theoretically founded biological control and convince governments and policy makers that nonchemical methods may be as efficient as pesticides in controlling insect pests (if not more so). Although there are no reliable records of all introductions of new natural enemies for biological control, more than 1,000 cases have been reported in the last 100 years and about 60% provided a complete control or a substantial reduction of pest damage. A classical reference on the history of biological control in the twentieth century is DeBach [9].

A major concern and limitation of classical biological control is the potential impact that introduced exotic natural enemies may cause on native fauna. Criticism of biological control by introduction of exotic natural enemies was soon theoretically enounced and several authors have advocated for limiting the trade of commercial biological control agents. In spite of little field data supporting the idea of strong impacts on native fauna, several countries have prepared regulations to forbid the importation of the most risky species of natural enemies. Although some principles have been established to assess risks of classical biological control agents much more knowledge on natural enemy interactions is needed. Two references may be useful for readers interested in environmental impact of biological control agents [10, 11].

Conservation biological control. As shown in Fig. 2, pest population development is the result of interactions among many biotic and abiotic components among which are herbivores and their natural enemies. In fact, pest population outbreaks are often due to agricultural practices which interfere with natural enemies that exert a certain control on herbivore populations in agrosystems. The goal of conservation biological control is to restore or enhance conditions for natural enemy survival, reproduction, and activity.

Conservation biological control may be implemented by manipulating the crop or the habitat. Main concerns of this kind of biological control are the identification of the natural enemies that can play a major role in keeping pest population at tolerable levels and what practices interfere with their functioning. Of course, pesticides are one of the principal interferences with natural enemies either by directly causing mortality or by indirectly influencing their biology, behavior, and movement at sublethal concentrations. Nowadays, data on the effects of pesticides on common natural enemies are needed before a pesticide is authorized; today, selectivity and low persistence in the environment, contrarily to that of years ago, are positive characteristics of pesticides used in pest control. Innovation in pesticide application techniques also tries to reduce the amount of pesticide and concentrates the application on certain sites, two goals that may increase selectivity in relation to natural enemies.

Certain practices to manage soil, water, and crop residues may contribute to natural enemy enhancement. Many insect pests live in the soil or have a part of their life cycle in the soil where they may be attacked by natural enemies; soil tillage has to be practiced in a safe and timely manner for such natural enemies. This includes crop residue management. After harvesting, crop plants may host a high variety of pest natural enemies; destroying crop residues also destroys pest individuals but may inflict a higher damage on natural enemy populations. Water management must provide relative humidity values that are optimal for natural enemies while damaging for pests.

Generally, the more stable is the agrosystem, the more chance natural enemies have to play their role as biological control agents. Whereas permanent crops allow population establishment and increase year after year, annual crops have to be colonized each year by natural enemies. However, cropping patterns may be designed to promote earlier and more abundant field colonization by natural enemies or enhance their survival and reproduction once the crop is established. Manipulation of sowing and harvesting dates may facilitate earlier colonization in the season and maintenance of natural enemies after season. Some other practices may also contribute to stabilize agrosystems. Some examples of crop manipulation to benefit

natural enemy survival and activity include strip harvesting, variable crop phenology, and inclusion of banker plants to keep prey and predators in the field between seasons.

Crop diversification seeks to delay crop colonization by insects, both pests and natural enemies, or reduce their retention in the crop. Intercropping – growing two or more crops in the same field at the same time – can cause a more abundant colonization by natural enemies although there are records of the contrary phenomenon. In non-crop-diversified agrosystems, herbivore colonizers arrive earlier and in higher numbers and consequently higher populations of natural enemies may be built up. Crop diversification may be performed by different spatial and temporal patterns of crops in the landscape where one field is the source for colonization of neighboring fields. Diversification of landscape with nonagricultural vegetation is another way to enhance natural enemy presence and activity. Non-crop plants in inter-rows, margins, roads, "fallow" plots, etc., may provide shelter and even food for natural enemies when conditions on crop plants are not suitable for natural enemies and may facilitate the movement of predators and parasitoids among fields in a patchwork landscape.

Biological control by conservation has shown to be very efficient when practiced after a sound knowledge of the agrosystem. Furthermore it is safe as managed natural enemies are already established in the habitat and no negative effects on the environment may be expected. Unfortunately, biological control by conservation is not always possible due to a lack of effective natural enemies in the habitat or a lack of knowledge about how crop or habitat may be managed to effectively enhance predator or parasitoid action. Research needed to implement a program of conservation biological control has to be closely linked with local conditions, and solutions are not universal but related to each particular location.

Augmentative biological control. Although natural enemies exist, sometimes conservation and enhancement practices are not sufficient to increase their populations until reaching levels which are capable to suppress pest populations at desirable levels. In these cases the release of reared natural enemies is needed. Augmentative releases may be necessary when the natural enemy is not present at the place and time needed. There are two types of augmentative releases:

- A relatively low number of individuals of the natural enemy is released and the suppression is expected to be achieved by the first or ulterior descendants: *inoculative augmentation.*
- A high number of individuals are released and control is expected to be exerted by them: *inundative augmentation.*

As in the previously described biological control strategies, augmentative releases use natural enemies that are able to search, locate, recognize as suitable, and attack the prey, but supplementary characteristics in the natural enemy are required in augmentative releases. Biocontrol agents have to be reared, and in inundative releases, they have to be mass reared. Rearing techniques have to meet several economical and quality requirements. The high costs of rearing are mainly due to a lack of true artificial diets but also by the necessity of labor to manipulate materials and individuals and the necessity of producing natural enemies for a rather narrow interval of time in the year. Predators and parasitoids need to be reared on their natural herbivore prey/host or, in some cases, an easily reared alternative prey/host, as in the case of flour moth eggs that can be produced daily for millions at relatively low cost and supplied as food to rear many generalist predators. In addition, herbivores have to be reared on their natural host plant, or similar alternatives, that usually need specific temperature, humidity, and light conditions, sufficient space, and a lot of manpower. Automatic processes to produce plants and natural enemies in biofactories have been designed but much more still has to be done to lower production costs. The extra cost of producing for a few demand peaks in the year may be mitigated if an effective storage method is available. For instance, the egg parasitoids *Trichogramma* spp. may be produced throughout the year and stored for months as diapaused larvae that are reactivated in their development some weeks before they have to be applied in the field.

Continuous rearing of natural enemies in nonnatural conditions and ulterior transport to the field may alter their quality to perform as biological control agent. Genetic uniformity and inbreeding,

negative selection for desirable characteristics to perform in the field, high impact of diseases in mass rearing colonies, and lack of learning opportunities of natural features may be some of the problems derived from natural enemy mass rearing. Procedures for quality control are being developed for the most common natural enemies [12]. Dispersal and search capacities, fecundity, health, correct species, and biotype are some of the characteristics checked in natural enemies for quality control.

Biological Control and IPM

Biological control is an important component of many successful IPM programs. The success of biological control has pushed pesticide companies to design new active ingredients with less impact on natural enemies. Whereas a few decades ago long persistence and broad action spectrum were two positive characteristics of new pesticides, current innovation of chemicals for integrated pest management looks for high selectivity and short persistence thus helping pesticides to become more compatible with biological control. The introduction of a new natural enemy in agrosystems to control a certain pest may allow reduced pesticide application and express the full potential of native natural enemies to control other pests.

Predator–prey interactions may be mediated by the host plant so that a natural enemy that is able to successfully control a pest on a certain crop may fail to do so on another crop. Hairy cucumber cultivars, which are more resistant to greenhouse whitefly than glabrous ones, were preferred to control the whitefly before *Encarsia formosa* was profusely used for biological control of this pest. Once the biological control was generally adopted in Dutch greenhouses, objectives of plant breeding shifted 180º and less hairy cultivars were again cultivated because these facilitated the inspection of leaves by the parasitoid to select and parasitize a host, thus improving the efficacy of greenhouse whitefly biological control. Tritrophic relationships – host plant, herbivore, and natural enemy – have to be considered before planning a biological control program. For IPM programs based on biological control, crop plant management and general cultural practices also have to be adapted to enhance natural enemy activity. Detection of those cultural practices that injure natural enemies may allow cultural modification in order to make predators or parasitoids more compatible with agricultural environments. For instance, tomato deleafing to produce more colored fruits has been found to interfere with the establishment of whitefly parasitoids that are inside the host in lower leaves. Tomatoes may be equally deleafed but leaves should be left on the soil between rows for some days until adult parasitoids emerge and fly to upper leaves to parasitize the host there.

Microbial Control

Entomopathogenic Organisms as a Natural Mortality Factor on Insect Populations

Insects are naturally affected in nature and also in agroecosystems by a varied array of pathogenic organisms, called entomopathogens, that cause diseases on insect pests. When naturally occurring epizootics are not efficient enough to lower pest populations under economic thresholds or they occur too late (natural epizootics are very dependent on natural abiotic conditions), the entomopathogen can be released into the environment at the time needed or manipulate the habitat to enhance the impact of the disease on the pest population. Entomopathogens may be mass produced and formulated for applying as a chemical pesticide. Many aspects described and discussed in biological control may be applied to microbial control. For instance, microbial control can be employed with classical, conservation, and augmentation techniques. In classical microbial control, a pathogen is isolated in a foreign insect and inoculated into a population that previously has never been exposed to that pathogen, whereas in conservation microbial control the impact of an already established pathogen is enhanced by manipulating crop or habitat conditions. Finally, augmentative microbial control inoculates a nonexotic pathogen at the time needed, or the crop field is inundated by microbial pesticides whose efficacy relies on the primary infection and not the secondary one as in the other techniques.

Main Insect Pathogens Used for Microbial Control

There are several kinds of microbes that cause diseases in insects and are used to control insect pests. Groups

with more species and microbial control uses are: bacteria, viruses, fungi, and nematodes.

- Bacteria. The most known and used bacterium is *Bacillus thuringiensis* (Bt). This bacterium has some interesting properties that make its use very compatible with other IPM methods. Entomopathogenic action of Bt originates in some insecticidal toxins – the so-called delta endotoxins – that are produced by the bacterium during its sporulation and once ingested by the insect is activated in the digestive system and causes gut paralysis, feeding cessation, and later larvae show general paralysis. One of the most valuable characteristics of Bt toxins is their selectivity according to the Bt strain. Historically Bt has been used to control specific Lepidoptera pests and, to less extent, some Diptera and Coleoptera. Nowadays, the range of pests targeted by Bt toxins include species of some other insect groups. Also importantly, Bt can be produced in large scale and at a reasonable price by fermentation and then formulated like an insecticide to easily spray or powder the crop. Genes encoding the production of Bt toxins may be transferred by genetic engineering to crop plants which become resistant to insects that are susceptible to the Bt toxins introduced into the plant (see section "Crop Resistance"). Biopesticides based on Bt are widely used in world agriculture, particularly in IPM programs and organic farming. Their relatively high prices and low permanence on the crop plant, mainly reduced by UV radiation when the crop is grown in the open air, are major limitations. Bt biopesticides are less than 1% of the pesticide world market in economic terms.
- Viruses. There are many types of insect pathogenic viruses but only baculoviruses are commercially available for insect pest control, mainly for Lepidoptera and Hymenoptera pests. Baculoviruses have a characteristic that gives them some advantages in comparison with other entomopathogens: they are able to create secondary inoculums and ulterior epizootics so that permanence of control efficacy may be longer than for other microbial control agents, although, like Bt, they are very sensible to deactivation by UV radiation. Furthermore, viruses are very selective and thus especially good for integrating their use in IPM programs. Genetic engineering techniques have shown a high potential to overcome some of the limitations of baculoviruses; higher knockdown effects and host range are two of the traits introduced in genetically modified baculoviruses. Probably their high price is the principal constraint for repeated field applications.
- Fungi. They comprise microorganisms that cause diseases on a variety of insect groups. In comparison with the two above, fungi are able to act in topical applications and do not need to be ingested to be active. This is why they are preferably used against sucking insects like whiteflies, scales, or aphids. Several fungal entomopathogens occur naturally and reduce insect pest incidence in agroecosystems but they are also mass produced and applied as biopesticides. Efficacy of fungal biopesticides is largely limited by low relative humidity although suitable formulations may attenuate this constraint; also UV-radiation protectors in fungal biopesticides are being tried to prolong their persistence on crop plants.
- Nematodes. Nematodes are a quite large group including many species that have several kinds of associations with insects. Facultative and obligate parasitism is among these. Some insect parasitic species have established a symbiotic relationship with entomopathogenic bacteria that confer to these kinds of nematodes a more virulent action against insect pests. In this case the bacterium is responsible for killing the host and, once dead, to preserve the host insect from being invaded by other microorganisms and therefore available for the nematode. These entomopathogenic nematodes are the most valuable for pest control, especially when part of their life cycle is in the soil, where nematodes are more effective. For pests that do not inhabit the soil, nematode desiccation at low humidity conditions is a major limitation of these agents for use in microbial control.

Use of Entomopathogens for Insect Control in IPM: Advantages, Disadvantages, and Techniques

Microbial control is one of the most promising methods to control insect pests within IPM programs. It is highly specific and selective for nontarget

arthropods like natural enemies, it is harmless for vertebrates including man, it has very little risk of environmental pollution, it is easy to apply as most of them are formulated to be sprayed with conventional machinery, and there are techniques for engineered modified entomopathogens with improved performance. Disadvantages include short permanence in the environment for pest control, slow efficacy, moderate probability of generating resistance to the active ingredient in targeted pests, host production cost, and poor acceptance of biotechnology products by consumers in certain countries. In summary, microbial control is an easy method to integrate in IPM and should substantially replace chemical treatments if efficacy and cost problems are solved and biopesticides are perceived by public opinion as a safe replacement for chemicals.

Behavioral Control

Pheromones and Other Semiochemicals

It is well known that insects, and other animals, communicate within the same species and with individuals of other species by chemical signals; chemicals involved in communication are called semiochemicals. Intra-population semiochemicals are called pheromones and those devoted to communicating among species are allelochemicals. These are divided into two categories depending if they benefit the chemical releaser (allomones) or to the receiver (kairomones). As more is known about insect behavior, more relevance is given to the role of semiochemicals in the communication governing crucial insect functions and more applications of semiochemicals are envisaged for insect control. Several kinds of semiochemicals have been investigated for both scientific and practical purposes but most attention has focused on pheromones.

Although chemical signals in insect communication had been observed some centuries ago, the chemical identification, synthesis, and demonstration of the sex attraction capacity of a pheromone was performed in the 1950s. A general enthusiasm on potentialities to govern insect behavior and suppress insect pests followed that pioneering work with considerable practical achievements but also with some limitations. The number of insect functions governed or mediated by pheromones is large; in addition to courtship behavior – the most studied for practical applications – social, physiology, trail, defense, finding, discriminating, and aggregating on the host plant are among insect biology features with pheromone involvement. The chemical nature of pheromones is quite diverse according to insect taxon and function. Pheromone composition usually has to meet two main requirements: be highly specific and be easily transportable by air currents. This double requirement is in part contradictory as volatile compounds need to be short molecules, with low molecular weights, but long enough to make possible several combinations of atoms for specificity. As pheromones are typically blends of several organic components synthesized by the insect or less commonly sequestered from the plant, specificity is achieved not only by chemical structure of components but also by the exact composition of the mixture.

Main Application of Pheromones for IPM

The main applications of pheromones for insect pest control may be included in one of the three following groups:

- Pheromones for *detection and monitoring* pest populations. One first application of pheromones is to know when and where a pest population is present. The pheromone is put in a trapping device and number of trapped individuals recorded. There are many kinds of traps that have been used; optimal trap design depends on pheromone composition and insect species. Generally, trap catch numbers will give relative estimates from which absolute numbers of pest population cannot be derived. Early warning, determination of timing for control intervention according to the pest population phenology, early detection for quarantine actions, and dispersal studies are some of the purposes that may be reached with pheromone trapping. However, decisions that need to know population numbers or densities rarely may be based solely on trap catch records unless a sound relationship between relative and absolute estimates had been previously established.
- Pheromones may be used to directly control insect pests by *mass trapping*, that is, by trapping

a sufficient number of individuals from a pest population. Usually a huge amount of traps is needed to remove a significant number of individuals to lower pest damage. The rice stem borer – as other Lepidoptera – is controlled nowadays by mass trapping in the Mediterranean area. A first interesting variant of mass trapping with pheromone traps is practiced with *trap trees* in bark beetles. When a pioneer bark beetle recognizes a tree as a suitable host, it starts releasing an aggregation pheromone. This is soon followed by another attractant emitted by the tree that complements aggregation of many bark beetles on the same tree that may be destroyed, burnt, or sprayed with insecticides to kill many beetles. A second variant of mass trapping is when the attracted insect is not glued on the trap but killed or sterilized and in any case eliminated. Some of the most harmful fruit flies are caught in traps, sterilized, and released again to the environment for control as in the sterile technique programs (see below in the section "Genetic Control"). Principles of mass trapping are very simple but many limitations have prevented successful application. One major constraint of the method is its low efficacy when pest population densities are high; in these circumstances a reducing treatment is needed before applying mass trapping.

- Species in which orientation of one sex to the other for mating is performed by sex pheromones are sensitive to the application of *mating disruption* techniques. The principle, as in the other cases where pheromones are involved, is rather simple. The permeation of the air with synthetic pheromone components – or the whole pheromone blend – interferes with the orientation of the searching sex that usually is unable to meet the other sex; oviposition is thus prevented and population rapidly declines. Despite many studies conducted on the mechanisms underlying mating disruption techniques, much remains still unknown. A number of factors influence feasibility and efficacy of these techniques. Systems for pheromone delivery have to assure air permeation for all the period during which males and females may meet and mate, a requirement difficult to satisfy for very volatile molecules. Synthetic components to be delivered have to be produced and released at reasonable prices; otherwise, the technique is not competitive with insecticides that are cheaper and relatively easy to apply. Efficacy of mating disruption has repeatedly shown to be drastically limited by high pest population densities and this means that mating disruption has to be applied in early generations when populations are still low and forecasting whether they will reach economic thresholds is difficult. In many countries authorization to sell pheromones for mating disruption purposes has to follow hard administrative processes too close to chemical insecticide registration; this sometimes deters companies from investing money in research and development. Dozens of pests are controlled nowadays by mating disruption techniques with acceptable efficacies, especially to manage Lepidoptera in vineyards and fruit orchards.

Compatibility of Pheromones in IPM Systems

Pheromones are easy to integrate into IPM systems because they are very compatible with other control systems such as biological control. Selectivity of the method is a major advantage. As environmentally friendly substances they do not cause pollution problems, generally have no toxic effects on nontarget species, and permanence in the environment is low. When used for monitoring pheromones are easy to work with and field technicians do not need particular skills.

Pheromones are an elegant tool for IPM and used more and more profusely sometimes without sufficient rigor. On the other side, scientific research is not sensible enough for solving real problems that would lead to a faster adoption of pheromones in the field. As stated by Millar [13] more pragmatism is necessary in research on pheromones [13]. The deeper knowledge of how pheromones work acquired in the last decades should allow focusing our efforts on those systems that can be most effective. Furthermore, globalization of insect pests should push local and national efforts to more international cooperation because "my pest today may be your pest tomorrow" and vice versa.

Genetic Control

Genetic pest control comprises those techniques that use the insect pest for its own destruction. Genetic

control consists of the release of sterilized, sterile, or incompatible individuals of one species into its wild population to cause a high proportion of sterile matings and hence reduce or eliminate the wild population. Three main methods causing sterility by different mechanisms are available for agricultural pests: sterile insects, incompatible insects, and hybrid sterility. Some other mechanisms have been exploited to control pests by genetic methods. Note that use of resistant/tolerant host crops is not considered within this section of genetic control.

In the sterile insect technique, insects are mass reared in controlled conditions, sterilized, and then released into the field. Insects can be sterilized by irradiation or by chemosterilization. Gamma irradiation, in which dominant lethal mutations arise as a result of chromosome break in treated cells, has been the most used technique in field programs. One of the key aspects to be determined before applying the technique in the field is the optimal irradiation dose to produce enough degree of sterility without causing somatic damages in the sterilized individual. The optimal dose is a function of several factors including insect species, its sex and physiological age, and the level of sterility required. Males are usually sterilized and released. Efficacy of the method relies on the capacity of released males to compete with wild males to mate with wild females. Progeny of females mated with sterile males will die soon after egg oviposition. Ideally insect mass rearing procedures should target males for sterilizing and releasing because females may need a higher dose for sterilization and once released they may be harmful for the crop as a consequence of ovipositing.

With no doubt the successful eradication of the parasitic screwworm fly – the larvae of which eats the living tissue of warm-blooded animals including humans in some circumstances – in wide areas of North and Central America contributed decisively to an increase in the amount of funds devoted to the research and applications of the sterile insect technique. In agricultural pests there have also been a number of successful male sterile programs, particularly in fruit flies. The Mediterranean fruit fly, *Ceratitis capitata*, has been eradicated in some countries of Latin America and they have been declared medfly-free regions; those countries can export fruits to countries which have fruit flies as quarantine pests. In contrast, attempts to use sterile male techniques in several moth pests have failed mainly due to the difficulty or mass rearing the moth at reasonable prices.

Insect incompatibility has been also used in field conditions but less extensively than the sterile insect technique. One of the methods of insect incompatibility used is based on the effect of crossing sexes in two conspecific populations resulting in only partial embryonation and thus population decrease. Incompatibility may be caused by microorganisms that are present in one population and not in the other. For practical pest control purposes, the release of one sex of one geographic population into another location may result in nonviable progeny and therefore population suppression.

Finally, sterility also may be achieved by crossing individuals of two species that produce apparently normal but completely or partially sterile hybrids. If the hybrid mates with at least one of the parent species, it can be mass reared and released in the field for genetic control. An advantage of this system comes from the fact that it does not need a sterilization method and the quality of released individuals is better than in the case of irradiation.

Genetic control has been shown as successfully practicable in commercial conditions in several cases. However, some failures have taught us about the constraints of the method. Reinvasion of treated areas by gravid females is one of the common causes of failure. Real knowledge of the dispersal capacity of the targeted species should prevent applying the sterile male technique in too small areas. Area wide programs are particularly needed for sterile insect technique application to prevent early recolonization of the treated area from neighboring zones.

One of the key factors for successful pest control with the sterile male technique is the ability of treated individuals to compete with wild males for wild females. Lack of adequate information on how to assure competitive treated males and about mating behavior could have been the main failure cause of many genetic control programs. More attention was then devoted to developing quality control of

mass-reared insects that are now routinely applied in many programs. A major conclusion after several years of applying genetic control programs is that the method by itself may be insufficiently effective to be uniquely applied and in many situations it may be useful when integrated in IPM systems to control the target and other interacting species.

Another perspective about the future of genetic control relates to potential contributions of insect molecular biology, more developed in model insects like the fly Drosophila but increasingly interesting for insect pests and pest natural enemies. As genetic control was soon seen as very limited by the lack of appropriate genetic material or by too reduced fitness in irradiated individuals, transgenesis may contribute to renewing the interest for genetic pest control. Introduction of desired transgenes into target insect species or the release of insects infected with engineered microorganisms – mainly rickettsia-like, Wolbachia – which mate with no infected individuals cause reduced fitness progeny. The reader curious about potential contributions of molecular biology to genetic control should consult the review by [14].

Cultural Control

As for any organism, insect populations – and thus pests – have a variable rate of increase depending on, among other factors, biotic and abiotic factors (see Fig. 2). An insect population becomes a pest in the agroecosystems when the insect environment is favorable enough to enhance population increase until economic threshold is reached and control measures have to be adopted. To manipulate that environment to make it less favorable for pests is called cultural control. Many kinds of crop or habitat manipulations devoted to constrain pest population development or enhance natural enemy numbers and activity may be included within the term.

It is quite difficult to list the practices that may be applied to reduce pest populations or enhance natural enemies. Some of the practices routinely applied are apparently unrelated to pests and natural enemies and only when they are eliminated or modified their implication in pest control is discovered. In other cases growers abandoned cultural practices that had been used to control pests due to the efficacy and reliability of cheap pesticides and they had to rediscover their usefulness. (a) Crop rotation, for example, prevented populations of non-generalist herbivorous insects from building up high populations without moving from the same field; crop monoculture provoked a high resource concentration on the same place for a long time and facilitated insect development and reproduction.

In addition to crop rotation, some general cultural practices are used to lower pest populations: (b) removal of crop residues between two successive seasons may reduce insect survival in unfavorable seasons (e.g., cold winters or dry summers); (c) management of planting or harvesting can avoid pest populations peaking at particularly susceptible crop growth stages; (d) unbalanced fertilization use to favor some herbivore insects like aphids that can multiply per several units their rate of increase when fed on plants with an excess of nitrogen; (e) the same as in the previous point could be said for other agricultural inputs like water, mulching, or plant hormones that alter physical environment and crop plant physiology in favor of or detriment to pests.

Many cultural practices have an important impact on pest populations by enhancement of *natural enemies*. Weed management, beyond preventing damages to the crop should take into account their role in insect biology. Nonagricultural vegetation in margins and hedgerows may offer shelter, refuge, or food sources for predators and parasitoids, but also for herbivorous insects that colonize crops early in the season. This double role of margins has to be carefully studied before margin management practices are recommended. The behavioral manipulation of the insect pest and their natural enemies may allow making the protected resource (e.g., the crop) unattractive for the pest and attract it to an unprotected resource (e.g., nonagricultural plants). The opposite done for natural enemies in this kind of strategy is called "push and pull" [15]. *Intercropping* – the cultivation of two or more crops simultaneously on the same field – is another potential way to manipulate the environment for making it unfavorable to the pest. It is frequently observed that there are fewer pests in fields with intercropping than in monoculture; more

attractiveness for natural enemies and less for herbivorous insects are two hypotheses to explain such a phenomenon.

Biotechnology and IPM

Emerging Biotechnological Techniques for IPM

Developments in plant biotechnology have contributed decisively to progress in agriculture in general and IPM in particular in the last decades of the twentieth century [16]. Biotechnology has been defined by the United Nations Convention on Biological Diversity as any technological application that uses biological systems, living organisms, or derivatives thereof, to make or modify products or processes for specific use (http://www.cbd.int/convention/ accessed on January 27, 2010). Probably, genetically engineered crops are the most socially known products of biotechnology applied to plant breeding. However, there are many other achievements and tools issued from plant biotechnology that have allowed progress in the scientific basis of IPM and multiple applications in the last decades and may allow even faster progress in the future. Following are some achievements of plant biotechnology that are relevant for IPM: (a) incorporation of insect resistance genes into commercial crop varieties; (b) the design of chemical and biological novel insecticides; (c) genetic modification of insect pests with lethal characters for genetic control or with beneficial traits to improve activity and efficacy of biological control agents; (d) rapid and reliable detection of insecticide resistance before genes responsible of resistance are widespread in the pest population and control fails in the field; and (e) identification of arthropod species and biotypes for pest diagnostics or trophic studies.

Host-Plant Resistance: Integrating GM Crops into IPM Systems

Host-plant resistance has been used in IPM to a rather limited degree (see above). Host resistance to herbivore insects is generally a quantitative trait that is difficult to manage and long to be incorporated into crop plants in conventional plant breeding programs. Techniques of genetic engineering have allowed some of those problems to be overcome by faster identification of insect resistance sources by means of molecular markers associated to resistance traits and by speeding up gene transfer from those sources to crop varieties to produce the genetically modified (GM) crops. The capacity to produce entomopathogenic toxins and digestive enzymes inhibitors have been the most used characters to confer insect resistance to crop plants by means of genetic engineering techniques. However, a varied array of other characters has also been successfully introduced into crop plants for insect pest control purposes. Insecticidal capacity of an entomopathogenic bacterium, *B. thuringiensis* (Bt) is caused by some of the toxins that the microorganism produces when it sporulates. Truncated genes expressing Bt toxins (dozens of Bt toxins and corresponding genes have been identified) have been transferred to several crop and forest plants to give the so-called Bt crops and plants. More than 35 million ha of maize and 15 million ha of cotton with Bt-expressing genes (alone or stacked with other transgenes) were grown in the world in 2009 [17] to control mainly Lepidopteran pests [17]. In Spain – the European country with the largest surface of Bt maize, the only GM crop allowed for cultivation in Europe – a survey conducted among more than 400 growers on the economic, social, and environmental impact of Bt maize found this: a mean increase of 12% in the gross margin in Bt growers, more than a 50% decrease in the number of insecticides applied due to the cultivation of Bt maize; this reduction was not very high because only a minority of growers used to spray against the pest targeted by the GM crop due to low efficacy [18].

In spite of the potential contribution of Bt crops to the sustainability of IPM through the selective control of key pests and the important savings of insecticide sprays, the deployment of GM crops has been very controversial in some areas like the European Union. Major risks concern potential development of resistance to Bt toxins in targeted pests and negative effects that Bt crops could have on nontarget organisms (NTO). The development of resistance to Bt toxins in targeted pests would cause a significant loss of an important tool for selective control of certain pests in the framework of IPM programs and organic agriculture and could drastically reduce the lifetime of Bt crops. Most countries that grow Bt crops have specific programs to monitor targeted pest populations for the

evolution of resistance and have implemented strategies to prevent resistance development. Until now, no Bt-resistance has been reported even in areas with almost 15 years of cultivation of Bt crops. More public attention has been paid to potential negative effects of GM crops on nontarget organisms. Most of the work conducted in this area has been devoted to Bt maize and practically no negative effects on biological control functions have been reported [19]. Consequently, Bt crops may prevent a substantial part of current insecticide usage and they can be integrated with biological control into more sustainable IPM programs.

Introduction of Traits into Insects

The introduction of deleterious or beneficial traits into insects has been achieved in several cases for varied purposes. Lethal gene inoculation into wild pest populations for genetic control may overcome some of the problems of conventional sterile insect techniques in which insects may be harmed when they are sterilized with irradiation or chemosterilization techniques and their competitive ability decreased. However, introduction of desirable traits for enhanced efficacy of biological control agents is a remarkable contribution of biotechnology to IPM. Unfortunately, most programs in that last respect have focused on insecticide-resistant genes that increase the possibility of using chemical insecticides and biological control in a compatible way. Despite this innovative approach, which may contribute to increasing the effective application of biological control, it also may lead to increased use of chemical insecticides.

Detection and Monitoring of Insecticide Resistance

Insects, like any other organism, may become resistant to insecticide active ingredients if they are submitted to frequent pressure of that ingredient. More than 600 insect species are nowadays resistant to one or more insecticides (http://www.pesticideresistance.org/search/1/). As fewer insecticide active ingredients are available in world agriculture, more is needed to increase the lifetime of registered substances and to implement strategies for resistance development prevention.

Several tactics to prevent resistance development in the pest population may be implemented and may succeed at least to delay the wide spread of resistance genes in the targeted population. Commonly, insecticide resistance in a pest is first detected when typical doses fail to control it and usually it is too late. Even at low frequency, earlier detection of the presence of resistance genes in the targeted population before they become common is crucial for the successful implementation of any antiresistance strategy application. As resistance is caused by a varied set of mechanisms, there are also several methods to detect resistance genes. Biochemical, immunological, and molecular methods are available now for the most common insecticides that allow screening a large amount of individuals for resistance gene presence. Improved comprehension of resistance mechanisms should lead to developing more specific, faster, and cheaper methods in order to monitor more populations at reasonable prices.

Identification of Arthropods

IPM needs the correct identification of insect species (or even biotype) in multiple situations: to apply a specific and selective method to control a certain species, to release a biological control agent that needs particular characteristics only available at biotype level, to detect quarantine pests in border inspections, and to study predator diet in trophic ecological studies. Morphological features that classically have been used for insect identification are frequently unknown or they are difficult to observe for nonspecialists. Biotechnological tools also may be valuable for various ecological studies that need markers for distinguishing target individuals from nontarget ones. Some of the current applications of biotechnology for identifying insects and their functions include: markers for dispersal measurements or to estimate insect densities by capture, release, and recapture of marked individuals, silencing genes for investigation of the function of certain proteins, invasion and spreading processes, and phylogenetic relationships between taxonomical groups.

Novel Bioinsecticides and Tension Actives

As described in microbial control, entomopathogenic microorganisms are used to control pests although

some factors linked with their costly production and narrow host range are limiting applicability. Entomopathogens may be genetically engineered to incorporate genes expressing foreign proteins with new insecticidal capacities, including larger host range, or proteins that negatively interfere with insect metabolism and physiology like insect hormones or juvenile hormone esterase that are involved in insect metamorphosis. A major concern about the bioengineered entomopathogens deals with the fate and permanence of foreign genes in the environment. Another promising line of biotechnological research in relation to IPM includes biosurfactants. A considerable amount of pest control agents is applied as sprays that need surfactants for correct application and spreading on target surfaces. Classical chemical surfactants are increasingly rejected by consumers and legislation due to their environmental impact and this stimulates the research on alternative biosurfactants. These are a group of heterogeneous secondary metabolites produced by a variety of microorganisms during their growth with significantly improved characteristics in comparison with homologous chemicals: those are biodegradable, have a lower per se toxicity, have more environment-friendly characteristics, require cheaper fermentative processes to produce them, are efficient at more variable conditions and at lower quantities, and have the potential of tailoring to suit specific applications. In addition to their activity as surface tension reducers and other chemical functions, biosurfactants have shown considerable biological antifungal and antiviral activity although in many cases their mode of action is poorly understood.

Implementation of IPM: Incentives and Constraints

More than 20 years ago, Wearing [20] wrote an article reporting results of a survey conducted among researchers and extensionists of three regions of world agriculture (Australia–New Zealand, Europe, and USA) on the IPM implementation process [20]. Still in 2010, many of the conclusions remain valid and following is a summary of those aspects of IPM implementation that enhance or constrain the adoption of IPM systems in western agriculture. There is general agreement among scientists about the accelerated progress of research on pest knowledge and control as well as the slow adoption of the new methods in practice. Knowing the key elements in the technology transfer and implementation of IPM may accelerate its application.

Among incentives to adopt IPM systems in Wearing's work, most surveys first perceived the cost advantage, followed by the development of pesticide resistance in local pest populations, the hazard to the grower from using pesticides, and environmental issues. The surveys also examined the major constraints for IPM implementation. The importance of obstacles for faster and wider application of IPM varied from one region to another. Whereas in USA over the 50% of respondents ranked social/market obstacles first, in Australia–New Zealand organizational obstacles were the first ranked, and technical obstacles were signaled in Europe as the least important to implement IPM.

In Europe much has been done in labeling agricultural products issued from IPM technology, particularly from regional administrations: IPM labels and integrated production (IP) labels have proliferated in the second half of the twentieth century in northern and southern Europe as well. The International Organization for Biological and Integrated Control (IOBC/WPRS) soon established the bases of IP and later developed guidelines in specific crop groups (see the organization Web site www.iobc-wprs.org). Food retailers and marketing food chains more recently have developed auditing procedures, in part inspirited in IPM principles which have pressed growers to progress more rapidly to more integrated production techniques. The impact of labeling and certification initiatives on IPM adoption has been quite variable in each country and commodity but the initiatives probably have contributed to publicize IP and IPM techniques among consumers.

A common question among policy makers is how to measure IPM adoption. Most likely, data on acquisition and use of tools for implementing IPM in the field (for instance, monitoring devices, meteorological receptors, users of warning systems and significant Web sites, and varied software for decision making among others) in combination with data related to pesticide usage (amount and economic value of pesticides sold,

commodity rejection because of high residue levels, inspection of pesticide residues in food trading, and significant habitat and ecosystem elements) may give an approximate idea of the progress made by the implementation of IPM. The number and size of companies (including small local firms) devoted to selling IPM products (e.g., natural enemies for biological control) may be another realistic way to monitor IPM adoption in world agriculture. Data on all these indicators are very disperse but perhaps they allow moderate optimism for faster IPM adoption in developed and emerging countries. Additionally, more strict legislation on pesticide use and the "disappearance" of most insecticides in the coming years may accelerate this process.

Future Directions

Most elements of IPM are among the factors that contribute greatly to the sustainability of agriculture. Beyond IPM, integrated control of insect pests, diseases, and weeds should progress toward the integration of all elements of agroecosystems to produce a balanced and harmonized growth of plants through true integrated production techniques. Exploitation of local natural resources and energy saving are common benefits of implementing novel integrated management systems. Additionally, most insecticides are being prohibited by western legislations. This should be the main focus of IPM progress to accelerate the transition of classical pest control based on chemicals to more integrated approaches.

Review of the vast literature on IPM confirms that success has come from a fundamental understanding of the processes acting in agroecosystems, rarely from a revolutionarily new control tactic. However, faster adoption of IPM strategies and tactics should also come from a more intense linkage among research, development, education, extension, and production. It is well documented that much of the scientific progress issued from R&D is not applied in practice or it takes too long to do it. Analysis of surveys conducted to identify the major incentives for the adoption of IPM systems by growers shows that an innovation is not adopted unless it contributes to producers' economic goals and meets the requisites for acceptance by the whole society.

Acknowledgments

Mr. Thomas Holland, MA from Stanford University in California, and now working at the Centro de Linguas at the Universidade da Coruña, proofread the English for this entry. His patience and professionalism has, I hope, helped ensure a comprehensible reading.

Bibliography

1. Oerke EC, Dehne HW (2004) Safeguarding production-losses in major crops and the role of crop protection. Crop Prot 23:275–285
2. Stern VM, Smith RF, van den Bosch R, Hagen KS (1959) The integrated control concept. Hilgardia 29:81–101
3. Kogan M (1998) Integrated pest management: historical perspectives and contemporary developments. Annu Rev Entomol 43:243–270
4. Higley LG, Pedigo LP (1996) Economic thresholds for integrated pest management. University of Nebraska Press, Lincoln
5. Klassen W (2008) Area-wide insect pest management. In: Capinera JL (ed) Encyclopaedia of entomology, vol 2. Springer, Dordrecht, pp 266–282
6. Mumford JD, Norton GA (1993) Expert systems. In: Norton GA, Mumford JD (eds) Decision tools for pest management. CAB International, Wallingford, pp 167–179
7. Southwood TRE, Henderson PA (2000) Ecological methods, 3rd edn. Blackwell Science, Oxford
8. Van Driesche RG, Bellows TS (1996) Biological control. Chapman & Hall, New York
9. DeBach P (1974) Biological control by natural enemies. Cambridge University Press, London
10. Bigler F, Babendreier D, Kuhlmann U (eds) (2006) Environmental impact of invertebrates for biological control of arthropods: methods and risk assessment. CAB International, Wallingford
11. Follett PA, Duan JJ (eds) (2000) Nontarget effects of biological control. Kluwer, Boston
12. Van Lenteren JC (ed) (2003) Quality control and production of biological control agents. CAB International, Wallingford
13. Millar JG (2007) Insect pheromones for integrated pest management: promise *versus* reality. Redia 90:51–55
14. Gould F, Schliekelman P (2004) Population genetics of autocidal control and strain replacement. Annu Rev Entomol 49:193–217
15. Cook SM, Khan ZR, Pickett JA (2007) Push and pull strategies for insect pest management. Annu Rev Entomol 52:375–400
16. Shelton AM, Bellinder RR (2007) Role of biotechnological advances in shaping the future of integrated pest management. In: Koul O, Cuperus GW (eds) Ecologically based integrated pest management. CAB International, Wallingford, pp 269–288

17. James C (2009) Global status of commercialized biotech/GM crops: 2009. ISAAA brief n. 41. Ithaca, NY
18. Gomez-Barbero M, Berbel J, Rodríguez-Cerezo E (2008) Bt corn in Spain – the performance of the EU's first GM crop. Nat Biotechnol 26:384–386
19. Romeis J et al (2008) Assessment of risk of insect-resistant transgenic crops to non target arthropods. Nat Biotechnol 26:203–208
20. Wearing CH (1988) Evaluating the IPM implementation process. Annu Rev Entomol 33:17–38

Intelligent Vehicles Technology, Introduction

Fei-Yue Wang
Institute of Automation, Chinese Academy of Sciences, Beijing, China

The basic goal of intelligent vehicle research is to provide a safe and comfortable ride for drivers and passengers. To reach this goal, an intelligent vehicle needs to dynamically sense the surrounding environment, receive the correct command from drivers, and make appropriate movements in real time.

In the 15 chapters in this book, 11 address how to sense the environment via vision sensors, 3 study how to monitor drivers' status and understand their commands, and 1 discusses vehicle motion control. The basis and content of these chapters are described below.

To obtain richer and more accurate visual information, researchers are trying to design more powerful vision sensors. One important direction combines different vision sensors to achieve better image quality. For example, how to obtain true color night vision video was studied in the chapter "► True Color Night Vision Video Systems in Intelligent Vehicles." The proposed night vision cameras sense the near-infrared radiation of the car's own headlights to extend the range of forward vision. The near-infrared and visible spectrum can then be combined into natural-looking color images for the driver to read.

Adjusting the focus of high-resolution video cameras and directing them to the regions of interest can provide better image data of certain objects. "► Active Multifocal Vision System, Adaptive Control of" presents methods for obtaining active pointing and gaze stabilization camera systems via an adaptive multi-focal vision system. Sliding mode control has been shown to be an effective control strategy to reach this goal.

Stereo vision sensors have become more popular because they can recover more three-dimensional information about nearby objects via stereo video data. In "► 3D Pose Estimation of Vehicles Using Stereo Camera," neighboring vehicles pose a detection problem and are discussed as a special application of the 3D stereo vision technique. The common characteristic points clustering problem is discussed and a model-based scene flow method is applied to determine the positions and instantaneous motion states of the vehicles.

"► Dynamic Environment Sensing Using an Intelligent Vehicle" studies the 3D environment reconstruction problem. Not only moving vehicles but also stationary objects (e.g., trees, walls, etc.) are recognized and modeled in such applications. Similarly, "► Driver Assistance Systems, Automatic Detection and Site Mapping" discusses how to reconstruct objects in the environment, particularly when driving in constructing sites.

LIDAR (Light Detection And Ranging) sensor is another frequently used vision sensor and often serves as a supplement to ordinary vision sensors. It can measure the distance between objects and the vehicle and provides depth information that cannot be directly collected via ordinary vision sensors. In "► Vehicle Detection, Tightly Coupled LIDAR and Computer Vision Integration for," a calibration algorithm was developed to map the geometry transformation collected via a multi-plane LIDAR system into camera vision data. Both simulations and real-world experiments have been carried out to show its reliability. "► Active Pedestrian Protection System, Scenario-Driven Search Method for" studies pedestrian detection problem via the fusion of LIDAR and camera systems.

Another type of approach combines camera vision systems and radar systems. Some related discussion is presented in "► Night Vision Pedestrian Warning in Intelligent Vehicles." The pedestrian detection problem is studied as an example to prove the merit of radar/camera fusion systems.

Since occlusion is generally unavoidable, the vision capability of a single vehicle is always limited. One straightforward way to solve this difficulty is to employ vision information that is collected from different vehicles in a small area. Clearly, this objective requires us to share the understandings of surrounding environments in an efficient way. As an early attempt, "► Cooperative Group of Vehicles and Dangerous Situations, Recognition of" discusses how to define the objects around several vehicles and share their position information.

The final chapter in vision sensory field, "► Driving under Reduced Visibility Conditions for Older Adults," discusses how to enhance the gathered vision information in reduced visible conditions and transform it sufficiently for older adults. This chapter can be viewed as an interdisciplinary study that crosses the boundaries of vision sensor system design and driver assistance systems.

The first chapter on driver assistance, "► Driver Assistance System, Biologically inspired," is hard to categorize. It discusses how drivers pay attention to certain changes in vision and how we can learn from drivers' response. It points out that advanced driver assistance systems may be designed to alert drivers in way that fit their biological characteristics. However, a detailed notification method is yet to be developed.

"► Driver Behavior at Intersections" provides a relatively mature approach that identifies drivers' turning features at intersections based on the sampled vehicle motion records. Following a stylized procedure, it first introduces how to gather the required driving data. Then a decision model of drivers' side turn behavior is proposed and the gathered driving data are used to calibrate the model. This chapter can be viewed as a representative of related reports.

The final chapter on driver assistance is "► Driver Characteristics Based on Driver Behavior." It presents a classical method to model driver characteristics, the driver behavior questionnaire. If well designed, a driver behavior questionnaire can tell us how drivers make their decisions under certain conditions. This method is not novel but may still useful to driver modeling.

The only chapter on vehicle motion control is "► Unscented Kalman filter in Intelligent Vehicles." It covers vehicle tire friction monitoring. Because a vehicle's motion is primarily determined by the friction forces transferred from the road via the tires, tire friction features receive attention. This chapter illustrates how researchers consider the connection between vehicle motion dynamics and tire friction features. It also presents application of the Unscented Kalman Filter (UKF) to realize tire feature monitoring.

There is an additional chapter related to intelligent vehicles. As mentioned above, sharing information between vehicles and infrastructures is a hot topic in recent studies. In "► Vehicular ad hoc networks, enhanced GPSR and Beacon-assist Geographic Forwarding in," utilization of real-time vehicle location information to accelerate vehicle ad hoc communication is discussed.

Internal Combustion Engines, Alternative Fuels for

Thomas Wallner[1], Scott A. Miers[2]
[1]Energy Systems Division, Argonne National Laboratory, Argonne, IL, USA
[2]Mechanical Engineering, Michigan Technological University, Houghton, MI, USA

Article Outline

Glossary
Definition of the Subject and Its Importance
Introduction
Limitations
Legislation
Overview of Alternative Fuels
Fuel Properties
Alternative Fuels for Spark-Ignition (SI) Engines
Alternative Fuels for Compression-Ignition (CI) Engines
Future Directions
Bibliography

Glossary

Advanced biofuel Renewable fuel not produced from food crops such as cellulosic biofuel and biomass-based diesel.

Alternative fuel A fuel that can serve or be used in place of another or an unconventional fuel choice.

Diesel gallon equivalent (DGE) The amount of alternative fuel required to match the energy content of 1 gal of diesel fuel.

Gasoline gallon equivalent (GGE) The amount of alternative fuel required to match the energy content of 1 gal of gasoline.

Mixture calorific value The amount of energy contained per volume of fresh charge typically at stoichiometric conditions that can be introduced into the cylinders of an internal combustion engine.

Renewable fuel A fuel created from resources that are never used up or can be replaced by new growth.

Definition of the Subject and Its Importance

Alternative fuels for internal combustion engines include a wide range of liquid and gaseous chemicals for both spark-ignition (SI) and compression-ignition (CI) applications. *Alternative* in this context describes a fuel that can be used in place of a conventional fuel such as gasoline or diesel. Alternative fuels are not equivalent but to a wide extent include renewable fuels since *renewable* only suggests a fuel can be created from resources that are never used up or can be replaced by new growth. The most common alternative fuels for SI engines are ethanol in blends with gasoline as well as compressed natural gas (CNG), liquefied natural gas (LNG), and liquefied petroleum gas (LPG). Biodiesel, synthetic diesel, green diesel, and DME are the most common alternative fuels for CI engines. In light of increasing energy demand worldwide, limited fossil fuel reserves partially located in politically unstable regions, growing environmental awareness and concern related to air pollutants as well as greenhouse gas emissions, alternative fuels have transitioned into social and political focus. Legislation and mandates were put in place specifying required amounts of alternative fuels in the fuel mix in Europe, Asia, and the United States. This article highlights some of the dominant alternative fuels, their market share, properties as well as their implication on engine and vehicle design, engine efficiency, and emissions.

Introduction

Although gasoline and diesel are nowadays considered conventional fuels, early engine concepts were designed to use other fuels. Combustion engines date back as early as 1807 with François Isaac de Rivaz of Switzerland and his combustion engine that used a mixture of hydrogen and oxygen for fuel [1]. The idea of alternative fuels is as old as engines themselves with Rudolf Diesel including considerations for use of gaseous, liquid and solid fuels in "Theory and Construction of a Rational Heat Motor" in 1894 [2]. The first mass produced vehicle, Ford Model T, was designed to run on ethanol.

Economic growth and prosperity are closely linked with availability and cost of energy. A large portion of worldwide energy demand and the majority of energy used for transportation are covered through fossil resources. The two most dominant fuels for transportation applications are gasoline in spark-ignition engines and diesel in compression-ignition engines. Announcements of newly discovered crude oil reserves and uncertainty on size of known reserves result in a large error band in prediction of the time span in which fossil fuels will be depleted. However, the fact that fossil fuels are finite is indisputable and with increasing worldwide energy demand the need for viable and sustainable alternative fuels becomes ever more pressing.

Today more than ever, society is concerned with the availability of energy which has become a matter of national security. The transportation sector alone accounted for 70% of the total US oil consumption in 2007. Foreign sources continue to outpace domestically produced fuel in the United States as well as Europe and Asia, leading to increased dependence on oil from politically unstable regions. Alternatives, either from domestic reserves or locally produced have been identified as a critical factor in ensuring national security and also as a means to stabilizing fuel prices in times of fluctuating crude oil prices.

As third-world countries develop and further growth of other countries continues, the amount of transportation-borne pollution increases. This development poses a threat due to local pollution resulting from emissions of regulated constituents and air toxics as well as the global impact of increased greenhouse gas emissions. Alternative fuels can play a major role in reducing regulated emissions through cleaner combustion, and renewable fuels in particular can help reduce greenhouse gas emissions.

There are several potential solutions to these issues from reduced consumption, increased production, and/or alternative sources of energy. It is this last

option that is the focus of this article and how alternative fuels and their properties impact engine as well as vehicle operation.

Limitations

This article is focused on technical implications of alternative fuels on engines and vehicles, their performance and emissions characteristics with particular focus on automotive applications. The characteristics of the most dominant alternative fuels are defined and compared to conventional gasoline and diesel fuel. The discussion on engine and fuel efficiency is strictly limited to the effects of alternative fuels on engine performance. Differences of alternative fuels in production pathways, production efficiency and challenges for their distribution are not included in this article. The interested reader is referred to [3] for detailed well-to-wheel analysis of alternative fuel pathways.

Before an attempt is made to classify alternative fuels it is important to define alternative fuels. The word alternative in the context of fuels suggests that a fuel can serve or be used in place of another and might also suggest an unconventional choice. However, alternative fuels are not to be confused with renewable fuels since renewable suggests that the resources used to create the fuel are never used up or can be replaced by new growth. Alternative fuels and renewable fuels are neither mutually exclusive nor mutually inclusive; although the vast majority of renewable fuels are also considered alternative fuels, by far not all alternative fuels are renewable. Methanol is just one example for a fuel that is renewable if produced, e.g., from biomass, and since not widely used also an alternative fuel. Ethanol is a renewable fuel if produced from corn or sugarcane, but since it is commonly used it may or may not be considered an alternative fuel in the sense of an unconventional choice. For our discussion ethanol is still considered an alternative since it is used in place of other fuels. Natural gas is just one example for an alternative fuel that, if fossil reserves are used, is not a renewable fuel.

Legislation

Recently introduced legislation worldwide mandates the increased use of alternative fuels. Directive 2009/28/EC of the European Parliament and of the Council of 23 April 2009 on the promotion of the use of energy from renewable sources and amending and subsequently repealing Directives 2001/77/EC and 2003/30/EC states the need to increase energy efficiency as part of the triple goal of the "20-20-20" initiative for 2020, which means a saving of 20% of the European Union's primary energy consumption and greenhouse gas emissions, as well as the inclusion of 20% of renewable energies in energy consumption.

Japan issued a New National Energy Strategy in 2007 targeting to expand the domestic biofuel production to cover approximately 10% of the fuel consumption by 2030 mainly through increased bioethanol and biodiesel utilization [4].

US legislation through the Renewable Fuel Standard (RFS) mandates a fourfold increase in renewable fuel production from approximately 9 billion gallons in 2008 to 36 billion gallons in 2022. The RFS also limits the amount of conventional biofuels to 15 billion gallons [5]. Figure 1 shows the mandated biofuels production in the United States which regulates contribution by conventional biofuels, advanced cellulosic and non-cellulosic and biomass-based diesel. Despite the rapid growth, US biofuels consumption remains a small contributor to US motor fuels, comprising about 4.3% of total transportation fuel consumption (on an energy-equivalent basis) in 2009 which is expected to grow to about 7% with the mandated 36 billion gallons by 2022 [6].

Overview of Alternative Fuels

Alternative fuels for internal combustion engines include fuels used in blends with conventional fuels such as ethanol which is used in low level gasoline/ethanol blends (e.g., E10) or biodiesel in low level blends with diesel (e.g., B5) as well as fuels requiring a dedicated fuel system design such as compressed natural gas (CNG) or liquefied petroleum gas (LPG). The following chapters focus on these mainstream alternative fuels, including their market share, properties, and impact on engine efficiency and emissions as well as other renewable fuel options with considerable market share either globally or in local markets.

Classification of Alternative Fuels

As mentioned earlier, different alternative fuels require more or less significant changes to vehicle fuel system

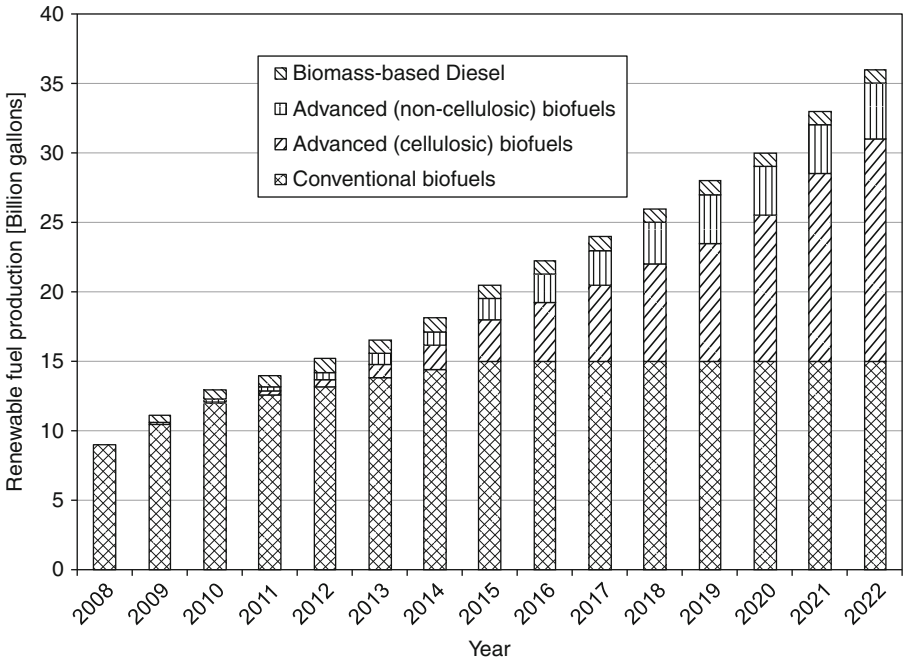

Internal Combustion Engines, Alternative Fuels for. Figure 1
Mandated biofuel production in the United States

design, engine calibration, and safety equipment. Some of these changes will be addressed in detail when discussing individual alternative fuels. In general, a classification can include dedicated vehicles, flexible fuel vehicles, and multi-fuel vehicles. Dedicated vehicles only operate on a single (alternative) fuel and are therefore typically purpose-built and optimized for this specific fuel. Dedicated vehicles are typically built for applications with fuels that cannot be stored in conventional fuel tanks, such as compressed gaseous fuels or liquefied fuels. On the other hand, blended operation describes usage of two or more fuels of the same type (liquid or gaseous) at varying mixture ratios. Vehicles capable of operating on varying blends of gasoline and ethanol are commonly referred to as FlexFuel vehicles. Finally, multi-fuel vehicles are defined here as vehicles that can operate on two or more fuels and feature multiple fuel storage and delivery systems.

According to their most common use, alternative fuels can also be classified as alternatives for spark-ignition engines or compression-ignition engines. This very generic classification is used for the following discussion although there are examples of alternative fuels that can be used in both applications. Gasoline is used as the baseline fuel for spark-ignition engine applications. For compression-ignition engine applications diesel is used as the reference.

Market Share of Alternative Fuels

Worldwide approximately 5% of the automobile fleet are alternative fuel or advanced technology vehicles [7]. These vehicles can be grouped into dedicated vehicles that are designed and built for a certain type of fuel on the one hand and vehicles that are capable of operating on alternative or conventional fuels on the other hand. Total vehicle population is an estimated 884 million vehicles which includes all types of vehicles such as light-duty, medium-duty, and heavy-duty vehicles as well as busses.

Considering all vehicle types CNG is the dominant alternative fuel for dedicated vehicles with a share of 1.27% which amounts to a total of more than 11 million NG vehicles worldwide. However, distribution and share of CNG vehicles is not uniform and strongly

depends on local fuel supplies. Figure 2 shows the absolute number of vehicles for all countries with a total CNG vehicle population in excess of 10,000 units. In addition the fraction of natural gas vehicles compared to the countries' total vehicle population is presented. The leading nations in terms of total CNG population are Pakistan (2.25 million units), Argentina (1.8 million units), Iran (1.7 million units), and Brazil (1.6 million units). Following India with approximately 700,000 units is Italy with 677,000 units as the largest European CNG vehicle fleet. The CNG vehicle fleet in the United States is approximately 100,000 vehicles, which accounts for only 0.04% of the entire vehicle population. The number of CNG vehicles available in the United States dropped from eight models in MY2004, to five in MY2005, and one in MY2006 [8].

In terms of market share of alternative fuel technology, CNG is only exceeded by ethanol and gasoline/ethanol flexible fuel (FlexFuel) vehicles. FlexFuel vehicles are vehicles that can run on gasoline and any gasoline/ethanol blend up to 85 vol % (E85). Since their introduction in 1979, more than 12.5 million ethanol and FlexFuel vehicles have been sold in Brazil [9]. In the United States, the FlexFuel fleet in 2009 accounted for approximately 8.35 million vehicles [10]. Although the number of FlexFuel vehicles exceeds that of natural gas–fueled vehicles, the total number of vehicles likely operated on ethanol is lower than that of CNG. In the United States, the number of vehicles actually operated on E85 is only 450,000 [11]. Figure 3 shows the development of alternative fuel vehicles in use in the United States since 1995. While LPG was the dominant alternative fuel in 1995 with more than 170,000 units, this number dropped to approximately 150,000 units in 2008. In the same time frame, the number of CNG vehicles increased from approximately 50,000 units in 1995 to more than 110,000 units in 2008. As mentioned earlier, the number of E85 vehicles that are actually fueled with gasoline/ethanol blends was around 450,000 units in 2008, still making it the dominant alternative fuel in the United States. Methanol as an alternative fuel was fairly popular in the 1990s with a peak of more than 21,000 units in 1997. Although the number of hydrogen powered vehicles has been steadily increasing since 2003, their market share with slightly over 300 vehicles in 2008 was less than 0.05% of all alternative fuel vehicles.

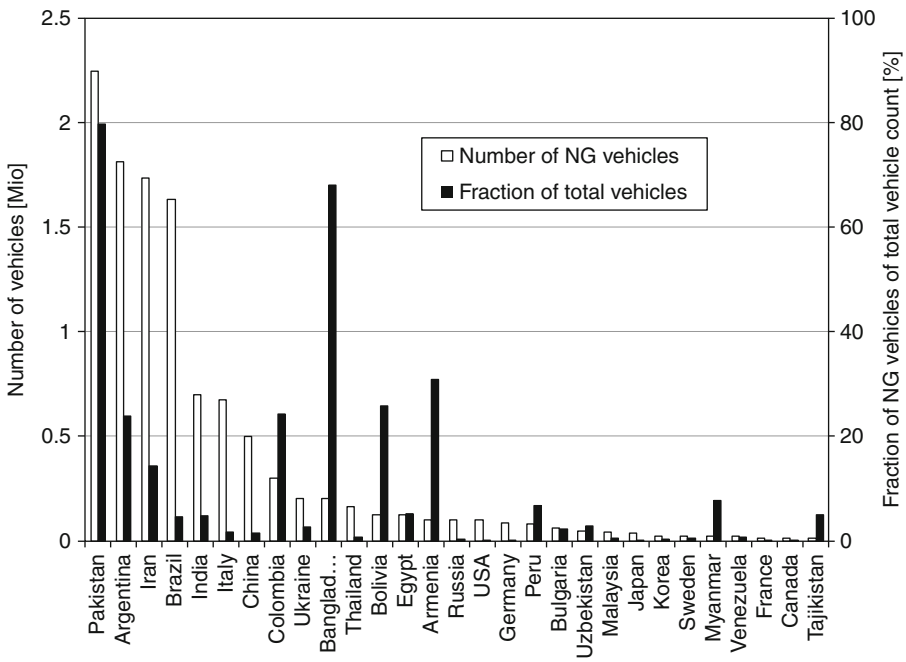

Internal Combustion Engines, Alternative Fuels for. Figure 2
NG vehicles worldwide (Based on data supplied via NGVA Europe and the GVR)

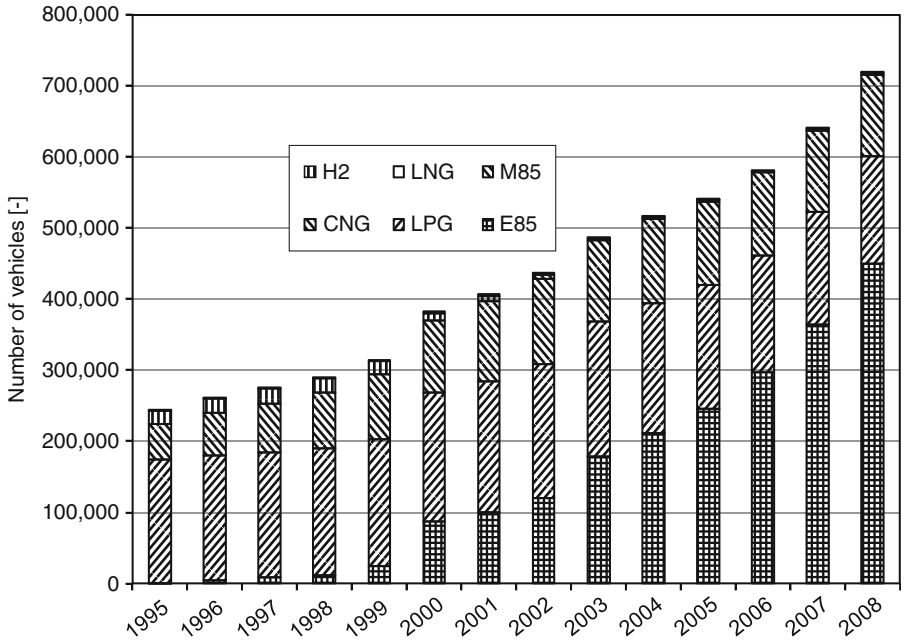

Internal Combustion Engines, Alternative Fuels for. Figure 3
Alternative fuel vehicles in use in the USA [11]

The United States consumed approximately 43 billion gallons of petroleum diesel fuel in 2005. Europe consumed 59.4 billion gallons, and Asia (excluding the middle east) consumed 48.5 billion gallons in 2005. In 2009, Europe produced the largest percentage of worldwide biodiesel followed by the United States and Asia Pacific. Figure 4 shows the distribution of biodiesel production for EU member states from 1998 to 2010 [12]. Overall biodiesel production has been declining in Europe since 2001, while it is increasing in the United States and Asia Pacific.

Since 2000, US production of biodiesel has increased by a factor of 350, as shown in Fig. 5. Government-imposed incentives combined with the requirements of the Renewable Fuel Standard have been the primary reasons behind the expansion of biodiesel production and associated utilization in the United States.

In 2009, the United States produced 17.7% of the world's biodiesel, making it the second largest producer behind Europe. The biodiesel market is expected to grow in the United States over the next several years and is predicted to reach ~6,500 million liters (1,717 million gallons) by 2020. Biodiesel is considered a biomass-based diesel source, and a minimum of 3.79 billion liters (1 billion gallons) must be produced by 2012. This is a 50% increase over 2010 production. The biodiesel market in Germany is not anticipating growth but rather a decline in production. Taxes have made the biodiesel too expensive for consumers combined with export subsidies for US producers. The European Union has imposed import tariffs on US biodiesel to promote and protect European production.

Fuel Properties

An understanding of alternative fuels and their impact on vehicle design as well as engine performance and emissions characteristics requires knowledge of fuel properties. For this purpose the fuel properties of the most common liquid as well as gaseous fuels are discussed in detail and compared to conventional fuels as a baseline. The alternative fuels are grouped into alcohol fuels including methanol, ethanol as well as *iso*-butanol as the most promising butanol isomer;

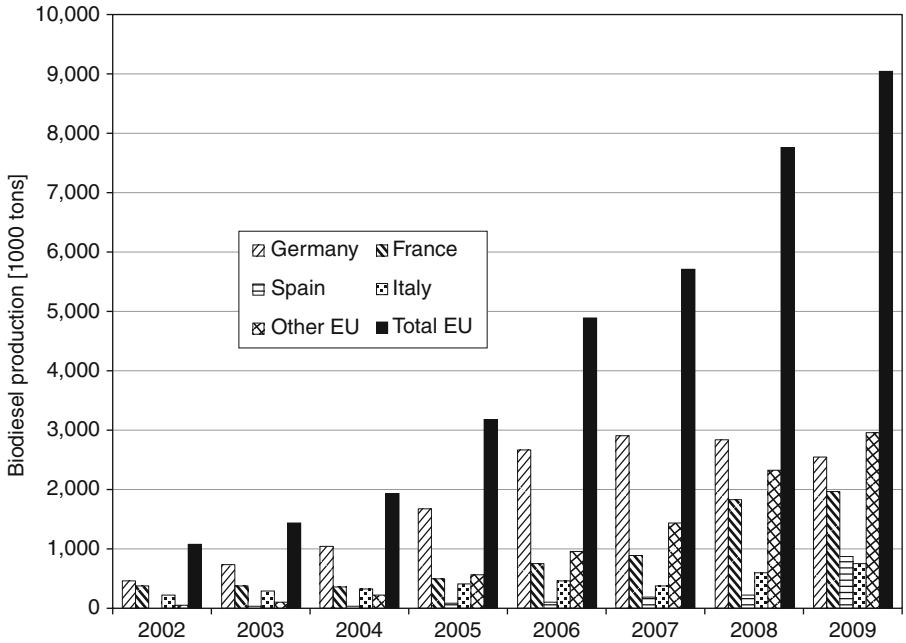

Internal Combustion Engines, Alternative Fuels for. Figure 4
EU biodiesel production [12, 13]

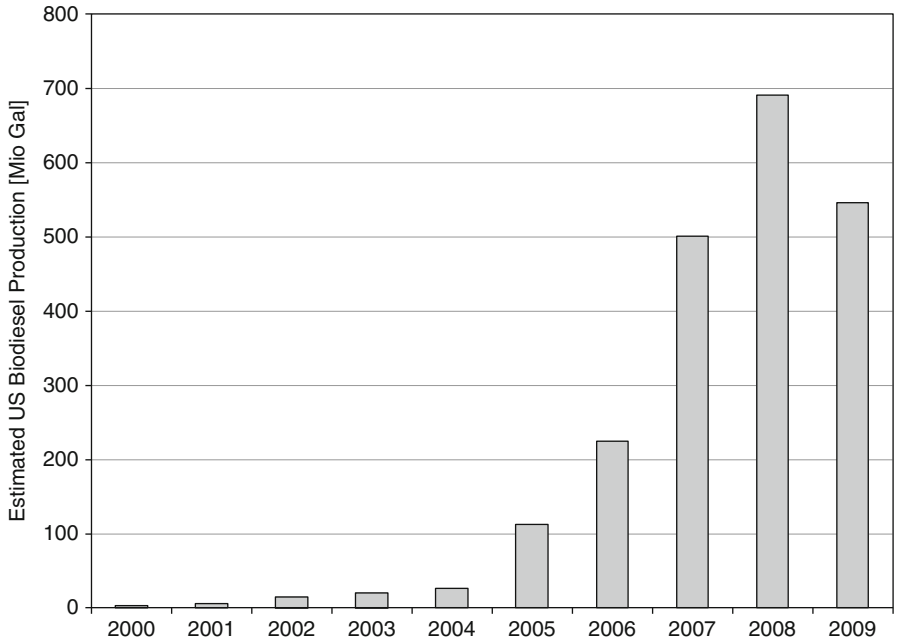

Internal Combustion Engines, Alternative Fuels for. Figure 5
Estimated US Biodiesel Production by year [14]

liquefied fuels including liquefied natural gas (LNG) and liquefied petroleum gas (LPG), and gaseous fuels including methane/CNG and hydrogen. Since these fuels are mainly used in spark-ignition (SI) engines, gasoline as the most common SI engine fuel is used as the baseline for comparison. Biodiesel and synthetic diesel fuel produced through the Fischer–Tropsch process, green diesel as well as dimethyl ether (DME) are compared to diesel fuel for CI engine applications.

In order to compare the energy content of alternative fuels to a conventional fuel, gasoline gallon equivalent (GGE) is introduced. GGE refers to the amount of alternative fuel required to match the energy content of 1 gal of gasoline. Although this measure is somewhat controversial due to the variability in the energy content of gasoline as well as alternative fuels [15], it is used here to simplify the discussion regarding energy content of alternative fuels. In a similar way, diesel gallon equivalent (DGE) is defined as the amount of alternative fuel required to match the energy content of 1 gal of diesel fuel. GGE is used for alternative fuels that are mainly used in spark-ignition engines and therefore displace gasoline whereas DGE is used for alternative fuels used in compression-ignition engines with the potential to substitute diesel fuel. The conversion factor between GGE and DGE is approximately 0.88.

Alcohol Fuels

Table 1 summarizes the fuel properties of the most common alcohol fuels and compares them to gasoline as a baseline. Characterized by a hydroxyl functional group (-OH) bound to a carbon atom the most common alcohols are methanol, with only a single carbon atom, ethanol (C2) as well as butanol, a four carbon alcohol. The negative impact of the oxygen in the hydroxyl group on the energy content decreases with increasing carbon count. While the lower heating value of methanol is less than 47% of gasoline, it increases with carbon count to approximately 63% for ethanol and 78% for butanol. Since the density of these fuels is in a similar range, the ratio of volumetric energy

Internal Combustion Engines, Alternative Fuels for. Table 1 Comparison of fuel properties – gasoline versus common alcohol fuels [16, 18, 19]

Parameter	Unit	Gasoline	Methanol	Ethanol	*iso*-Butanol
Chemical formula		$C_4 - C_{12}$	CH_3OH	C_2H_5OH	C_4H_9OH
Composition (C, H, O)	wt.%	86, 14, 0	37.5, 12.6, 49.9	52, 13, 35	65, 13.5, 21.5
Lower heating value	MJ/kg	42.7	20	26.9	33.1
Density	kg/m^3	720–780	792	789	805
Volumetric energy content	MJ/l	31.6	15.8	21.2	26.5
Vol. energy content relative to gasoline	%	100	50	67	84
GGE	gal	1	2.01	1.5	1.19
Research octane number (RON)	–	92–98	106–114	107–111	105
Motor octane number (MON)	–	80–90	91–95	89–94	91
AKI		90	100	100	98
Stoichiometric air/fuel ratio	–	14.7	6.45	9.0	11.2
Solubility in water @ 20°C	ml/100 ml H_2O	<0.1	Miscible	Miscible	7.6
Boiling temperature	°C	25–215	64.7	78.4	107–108
Flashpoint	°C	–43	12	17	28
Ignition limits	vol % λ	1.0–7.6 0.4–1.4	4–75	3.5–15	1.2–10.9
Latent heat of vaporization	MJ/kg	0.305	1.103	0.84	0.69

content is similar to the lower heating value with a significant advantage of gasoline compared to the alcohols in general and the short chain alcohols in particular. The lower volumetric energy content is also reflected in the GGE values for alcohol fuels. Approximately 2 gal of methanol contain the same energy as 1.5 gal of ethanol, 1.2 gal of butanol, or 1 gal of gasoline. A major advantage of these most common alcohol fuels compared to gasoline is their higher knock resistance expressed as octane number, which is around 100 for methanol as well as ethanol and 98 for *iso*-butanol compared to approximately 90 for gasoline. Although concerns have been voiced that laboratory engine Research and Motor octane rating procedures are not suitable for use with neat oxygenates [16], the presented values are still indicators to evaluate knock resistance. The difference in oxygen content is once again apparent when comparing the stoichiometric air demand. It increases from 6.45 for methanol to 9 for ethanol and 11.2 for butanol compared to 14.7 for gasoline. Finally, the solubility of ethanol in water is known to present a challenge for transporting gasoline/ethanol blends in pipelines [17].

A critical factor for liquid fuels is their evaporation characteristics. These characteristics affect engine behavior, in particular at cold start, as well as evaporative vehicle emissions. Vapor pressure curves for alcohol fuels as a function of blend level are shown in Fig. 6 based on data from Anderson et al. [20]. The vapor pressure of alcohols is lower than that of gasoline. When alcohols are mixed with gasoline, they form an azeotropic mixture with some components of the gasoline which results in an asymmetric relation between vapor pressure of the blended fuel and the volumetric blend ratio [21]. Evaporation of ethanol produces 4.6 times as much cooling of the charge as *iso*-octane, a major component of gasoline, while methanol produces 8.4 times as much cooling. Charge cooling reduces the tendency of the end gas to autoignite and therefore, further decreases the tendency for combustion knock [22].

Liquefied Fuels

Table 2 compares the properties of liquefied natural gas (LNG) and liquefied petroleum gas (LPG) to those of

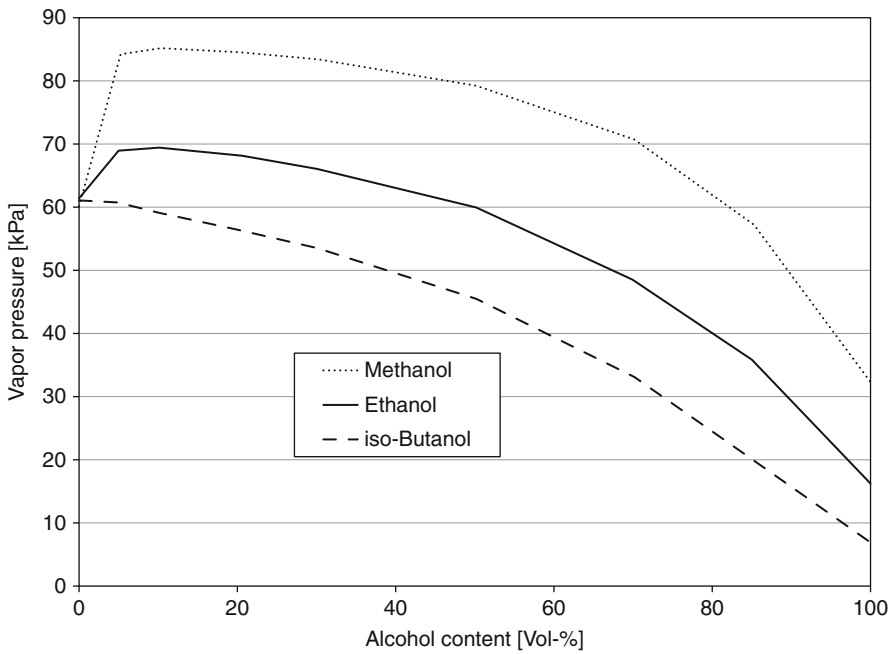

Internal Combustion Engines, Alternative Fuels for. Figure 6
Vapor pressure of alcohol fuels blends based on data from [20]

Internal Combustion Engines, Alternative Fuels for. Table 2 Comparison of fuel properties of gasoline with LNG and LPG [18]

Parameter	Unit	Gasoline	LNG	LPG (USA)
Chemical formula		$C_4 - C_{12}$	CH_4 (typ. > 95%)	C_3H_8 (maj) C_4H_{10} (min.)
Lower heating value	MJ/kg	42.7	46.7	46
Density	kg/m^3	715 – 765	430–470	508
Volumetric energy content	MJ/l	31.6	21	23.4
Vol. energy content relative to gasoline	%	100	66	74
GGE	gal	1	1.5	1.35
Octane number ((R + M)/2)	–	90	120	105
Stoichiometric air/fuel ratio	–	14.7	17.2	15.8
Boiling temperature	°C	25–215	–162	–42
Physical state for storage	–	Liquid	Cryogenic liquid	Pressurized liquid
Ignition limits	vol % λ	1.0–7.6 0.4–1.4	5.3–15 0.7–2.1	2.1–9.5 0.4–2

gasoline. Natural gas, after it has been cooled down to its liquid state at a temperature of –161°C, is referred to as liquefied natural gas (LNG). Since the liquefaction requires the removal of certain components that could form solids during the process, LNG typically contains approximately 95% methane [23]. Liquefied petroleum gas (LPG), also called autogas, is a mixture of propane (C_3H_8) and butane (C_4H_{10}) with changing composition depending on the region as well as seasonal differences. In the United States, Canada, and Japan, LPG consists mainly of propane, whereas the butane content in other areas of the world can be significant and typically increases for countries with warmer climate (butane content in Greece is 80%). The actual composition of LPG significantly affects its properties. Figure 7 shows the vapor pressure of propane and butane, the two main constituents of LPG as a function of temperature. Although the lower heating value of both LNG and LPG is higher than that of gasoline, the volumetric energy content of both fuels is significantly lower. This is due to the lower density of the two alternative fuels compared to gasoline and results in a volumetric energy content of LNG of only 66% and 74% for LPG compared to gasoline. The resulting GGE values of LNG and LPG are 1.5 and 1.35, respectively. The octane rating of LNG is approximately 120 and significantly higher than gasoline (90) and LPG with an octane rating of 105.

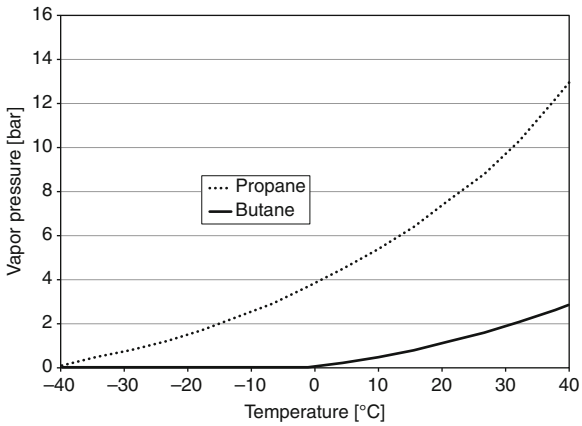

Internal Combustion Engines, Alternative Fuels for. Figure 7
Vapor pressure as a function of temperature for propane and butane

Gaseous Fuels

As mentioned earlier, LNG typically contains more than 95% methane (CH_4) since other impurities are removed for the liquefaction process. Although compressed natural gas (CNG) also mainly contains methane, its range of composition is wider than that of LNG and varies geographically. In addition to methane it

typically includes significant amounts of ethane, propane, and butane as well as other constituents in smaller amounts, as shown in Table 3.

Given that methane is by far the dominating constituent of CNG, the comparison of fuel properties of gaseous fuels shown in Table 4 uses the properties of methane as representative for CNG. Although not widely used for transportation applications at this point, the fuel properties of hydrogen as another promising alternative fuel are included in this comparison. The mass-specific lower heating value increases from gasoline to methane to hydrogen starting at 43.5–50 MJ/kg and 120 MJ/kg respectively. It is interesting to note that the lower heating value increases with increasing hydrogen content in the mass-specific fuel composition. However, since both methane and hydrogen are gaseous at ambient conditions with a density that is several orders of magnitude lower than that of gasoline, it takes 912 gal of methane or 3,075 gal of hydrogen to achieve the energy equivalent of 1 gal of gasoline. The comparison is more favorable on a weight basis, suggesting that 1 kg of hydrogen contains the same energy as 2.5 kg of methane and 2.86 kg of gasoline.

Internal Combustion Engines, Alternative Fuels for.
Table 3 Typical composition of natural gas [24]

Methane	CH_4	70–90%
Ethane	C_2H_6	0–20%
Propane	C_3H_8	
Butane	C_4H_{10}	
Carbon dioxide	CO_2	0–8%
Oxygen	O_2	0–0.2%
Nitrogen	N_2	0–5%
Hydrogen sulfide	H_2S	0–5%
Rare gases	A, He, Ne, Xe	Trace

Biodiesel and Synthetic Diesel

The average properties of petroleum diesel fuel and biodiesel are shown in Table 5. In addition, to accentuate the differences in properties between biodiesel

Internal Combustion Engines, Alternative Fuels for. Table 4 Comparison of fuel properties of gasoline and gaseous fuels (methane and hydrogen) [18, 19]

Parameter	Unit	Gasoline	Methane	Hydrogen
Chemical formula		$C_4 - C_{12}$	CH_4	H_2
Composition (C, H, O)	wt.%	86, 14, 0	75, 25, 0	0, 100, 0
Lower heating value	MJ/kg	43.5	50	120
Density gaseous liquid	kg/m^3	– 730–780	0.72 430–470	0.089 71
GGE (by volume)	gal	1	912	3075
GGE (by weight)	kg	2.86	2.5	1
Stoichiometric air demand	–	14.7	17.2	34.3
Boiling temperature	°C	25–215	–162	–253
Ignition limits	vol % λ	1.0–7.6 0.4–1.4	5–15 0.7–2.1	4–75 0.2–10
Minimum ignition energy	mJ	0.24	0.29	0.02
Self-ignition temperature	°C	approximately 350	595	585
Diffusion coefficient	mm/s	–	1.9×10^{-6}	8.5×10^{-6}
Quenching distance	Mm	2	2.03	0.64
Laminar flame speed	cm/s	40–80	40	200

Internal Combustion Engines, Alternative Fuels for. Table 5 Fuel properties for diesel, biodiesel, and synthetic diesel [25, 27]

Parameter	Unit	Diesel	Biodiesel	Synthetic diesel
Chemical formula		C_8–C_{25}	C_{12} – C_{22}	
Composition (C, H, O)	wt%	87, 13, 0	77, 12, 11	85–87, 13–15, 0
Lower heating value	MJ/kg	42–44	36–38	43.9
Density	kg/m^3	810–860	870–895	770–780
Volumetric energy content	MJ/l	34–37.8	31–34	33.8–34.2
Vol. energy content relative to diesel	%	100	93	94.4–95.5
DGE	gal	1	1.074	1.05–1.06
Cetane number	–	40–55	45–65	73–80
Viscosity @ 40°C	mm^2/s	2.8–5.0	2–6	2.0–3.5
Flash point	°C	60–78	100–170	59–109
Cloud point	°C	−24 – −10	−5–5	−19–0
Stoichiometric air/fuel ratio	–	14.7	13.8	
Boiling range/temperature	°C	180–340	315–350	160–350
Ignition limits	vol %	0.6–6.5	0.3–10	
Lubricity		Baseline	Higher	Lower

and other alternative diesel fuels, the properties of a typical synthetic diesel fuel produced through the Fischer–Tropsch process are included in Table 5 as well.

Diesel fuel properties are controlled by ASTM D975. Hundred percent biodiesel has been specified as an alternative fuel to diesel and has its own standard, ASTM 6751. For blends between 6% and 20% biodiesel, a third standard is used, ASTM D7467. Before neat biodiesel can be blended with petroleum diesel, both fuels must meet their respective ASTM standards and then be analyzed as a blend using D7467 if the biodiesel content is between 6 and 20 vol %.

For example, if the cetane number falls too low, it can lead to increased ignition delay, combustion pressure, and noise, along with increased smoke during cold start.

Increased viscosity has been shown to increase fuel spray penetration resulting in cylinder wall wetting and impingement. Biodiesel has a slightly higher viscosity than petroleum diesel, while synthetic diesel is similar to petroleum diesel. In addition, the atomization of the fuel is reduced as fuel viscosity is increased. Too low of viscosity will increase pump wear due to reduced lubricity. Biodiesel has been utilized as a lubrication additive recently.

Sulfur content has previously been utilized for lubrication in fuel injection systems but increased emissions controls have forced the reduction of sulfur in diesel fuel. The sulfur can be converted into sulfur dioxide and sulfur trioxide, poisoning the catalyst and sensors in the exhaust stream. In addition, small droplets of sulfuric acid and other sulfates can become nucleation sites for particulate matter emissions. In the United States, the sulfur content of on-road diesel fuel was mandated to not exceed 15 ppm sulfur as of 2006. Biodiesel and synthetic diesel do not contain sulfur.

The cloud point is the temperature at which crystals begin to form in the fuel and prevent the flow of fuel through filters and pumps. A significant challenge for biodiesel fuels is overcoming the significant increase in cloud point temperature compared to petroleum diesel fuel. Additives, tank heaters, and various blends of petroleum and biodiesel have all been experimented with to improve the cold-weather operation of biodiesel.

Synthetic diesel fuel whether produced from biomass (BTL), coal (CTL), or natural gas (GTL) does not vary widely in properties based on the feedstock due to the consistent processing techniques employed. If the Fischer–Tropsch process is employed, the feedstock is first converted to a synthesis gas (syngas) consisting of hydrogen and carbon monoxide. This process involves combustion of the feedstock in a reduced oxygen environment. Once the hydrogen and carbon monoxide are produced, the effect of the feedstock composition is removed from the final fuel properties. The remaining process to produce liquid fuel (Fischer–Tropsch) basically receives the same input regardless of feedstock. The other method of producing synthetic diesel fuel is to first convert the biomass to bio-oil through pyrolysis (zero oxygen environment) and then convert the bio-oil to fuel. Again, the pyrolysis step removes the effect of feedstock composition, thus producing a consistent fuel. Both processes produce a high quality alternative diesel fuel with high cetane, good cold-flow and oxidative stability properties, and ultra low sulfur content. The Fischer–Tropsch process was first commercialized by Sasol in South Africa. They produce over 165,000 barrels/day of transportation fuel from coal. However, the process is on the order of three times more expensive to produce fuel than conventional petroleum production processes [28].

Green Diesel and DME

Hydrogenated-derived renewable diesel fuel or "green" diesel is an alternative compression-ignition engine fuel that is produced by utilizing the conventional processing method for petroleum diesel fuel, fractional distillation. The process is feedstock tolerant and unlike transesterification, the properties of the fuel do not change significantly when the feedstock varies from vegetable oil to waste grease. However, there are significant differences in properties compared to biodiesel and even petroleum diesel. Green diesel has a higher cetane number, typically 75–90 compared to 40–50 for petroleum diesel. The pour point and energy content can be nearly the same as petroleum diesel, alleviating the negative aspects of biodiesel. Green diesel is not oxygenated so the oxidative stability is very good. The process of producing green diesel is more energy intensive and requires higher temperatures and pressures compared to transesterification. The majority of research is currently focused on increasing the output of fuel and scaling up production facilities.

Dimethyl ether (DME) is a two-carbon, oxygenated molecule that has unique properties in the liquid state as an alternative diesel fuel. DME is primarily produced by converting hydrocarbons such as natural gas to synthesis gas (syngas). The syngas is then converted to methanol in the presence of a copper-based catalyst. An additional dehydration process of methanol using a silica-alumina catalyst results in the production of DME. This two-step process is the most widely utilized currently, but a one-step production process is currently being researched. Because DME is in the vapor state at standard temperature and pressure, it must be compressed, like liquid propane, and stored in tanks for transportation and consumption. Table 6 shows some of the primary differences between green diesel and DME compared to petroleum diesel fuel.

Effect of Feedstock Composition on Biodiesel Properties Unlike ethanol whose properties are relatively unaffected by the feedstock due to the processing technique employed (distillation), biodiesel properties have been shown to vary widely depending on the feedstock properties (fatty acid profile) and catalyst employed (typically methanol or ethanol) during the fuel production process.

The fatty acid profile of the feedstock directly influences the properties of the biodiesel. The primary features of interest for the fatty acid include chain length, degree of unsaturation, and branching of the chain. The properties of the biodiesel that are most directly impacted by changes in the fatty acid profile include cetane number, heat of combustion, cold-flow, oxidative stability, viscosity, and lubricity. Table 7 shows the fatty acid profiles for the primary feedstock options in biodiesel and the wt% of each fatty acid contained in the feedstock. Note that C18:1 refers to an 18 carbon chain molecule with one double bond. Increasing numbers of double bonds reduce the saturation of the molecule. If no double bonds exist, the molecule is said to be fully saturated.

It is well known that cetane number decreases with decreasing chain length and increasing branching. As well, oxidative stability increases with degree of saturation. Table 8 shows the range of cetane number,

Internal Combustion Engines, Alternative Fuels for. Table 6 Green diesel and DME fuel properties compared to petroleum diesel [26–29]

	Unit	Petroleum diesel	Green diesel	DME
Chemical formula		C_8–C_{25}		C_2H_6O
Lower heating value	MJ/kg	42–44	44	28
Density (+20°C)	kg/m^3	810–860	780	675
Volumetric energy content	MJ/l	34–37.8	34.3	18.9
Vol. energy content relative to diesel	%	100	94	52
DGE	–	1	1.06	1.92
Cetane number	–	40–55	98–99	>65
Viscosity @ 40°C	mm^2/s	2.8–5.0	3.0–3.5	0.21
Flash point	°C	52		–41
Auto ignition temperature	°C	250		350
Cloud point	°C	–24 – –10	–15	n/a
Lubricity		Baseline	Similar to baseline	Poor
Stoichiometric air/fuel ratio	–	14.7		8.99
Ignition limits	vol %	0.6–6.5		3.4–28

Internal Combustion Engines, Alternative Fuels for. Table 7 Fatty acid profile for the most common biodiesel feedstocks [30, 31]

Vegetable oil	C16:0	C18:0	C18:1	C18:2	C18:3
Castor	1	1	3	4	
Coconut	7.5–10.5	1–3.5	5–8	1–2.6	
Cottonseed	22–26	2–3	15–22	47–58	
Palm	40–47	3–6	36–44	6–12	
Peanut	6–14	2–6	36.4–67.1	13–43	
Rapeseed (Canola)	2–6	4–6	52–65	18–25	10–11
Soybean	10–12	3–5	18–26	49–57	6–9
Sunflower	5–7	3–6	14–40	48–74	

heat of combustion, cloud point or cold filter plugging point (CFPP), and kinematic viscosity for several biodiesel fuels.

Figure 8 shows the effect of 33 different feedstocks on fuel oxidative stability, measured in hours. This data shows that as the number of double bonds increases (increased degree of unsaturation), the oxidative stability decreases significantly. A test of iodine number of the biodiesel provides a measure of the degree of unsaturation of the fuel.

One of the significant advantages of biodiesel is the ability to improve the lubricity of the fuel with only a small quantity of ester. As shown in Fig. 9, the lubricity improves significantly for the first 1% of methyl ester added to the baseline diesel fuel. Lubricity is measured using the ASTM D6078 Scuffing Load

Internal Combustion Engines, Alternative Fuels for. Table 8 Fuel properties of biodiesel fuels from various feedstocks [31]

Vegetable oil	Cetane number	Heat of combustion [KJ/kg]	Cloud point or CFPP [°C]	Kinematic viscosity [40°C, mm^2/s]
Coconut ethyl	67.4	38,158	5	3.08
Cottonseed	51.2		−5 (pour point)	6.8 (21°C)
Palm ethyl	56.2	39,070	8	4.5 (37.8°C)
Rapeseed (Canola)	48–56	37,300–39,870	−3; CFPP −6	4.53
Soybean	48–56	39,720–40,080	from −2 to 3	4.0– 4.3
Sunflower	54–58	38,100–38,472	0–1.5	4.39

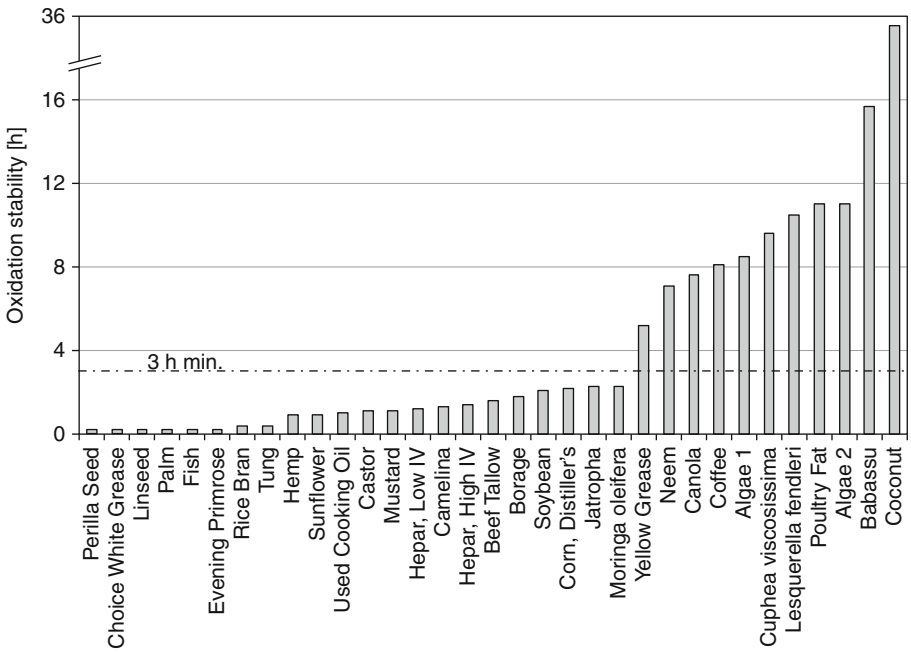

Internal Combustion Engines, Alternative Fuels for. Figure 8 Dependence of biodiesel oxidative stability on feedstock [32]

Ball-on-Cylinder Lubricity Evaluator (SLBOCLE) test rig. The higher the value, the higher the load before scuffing occurs which translates to a fuel with improved lubricity.

The impact of biodiesel on cetane number can be clearly identified in Fig. 10. As a general rule regardless of feedstock, increasing quantity of biodiesel volume increases the cetane number and improves the overall combustion quality. The data shown in Fig. 10 utilized a baseline petroleum diesel fuel meeting ASTM D975 specifications.

Comparison of Fuels Based on Mixture Calorific Value

In addition to the fuel properties highlighted in Tables 1–9, the mixture calorific value for different fuels and mixture formation strategies can be calculated

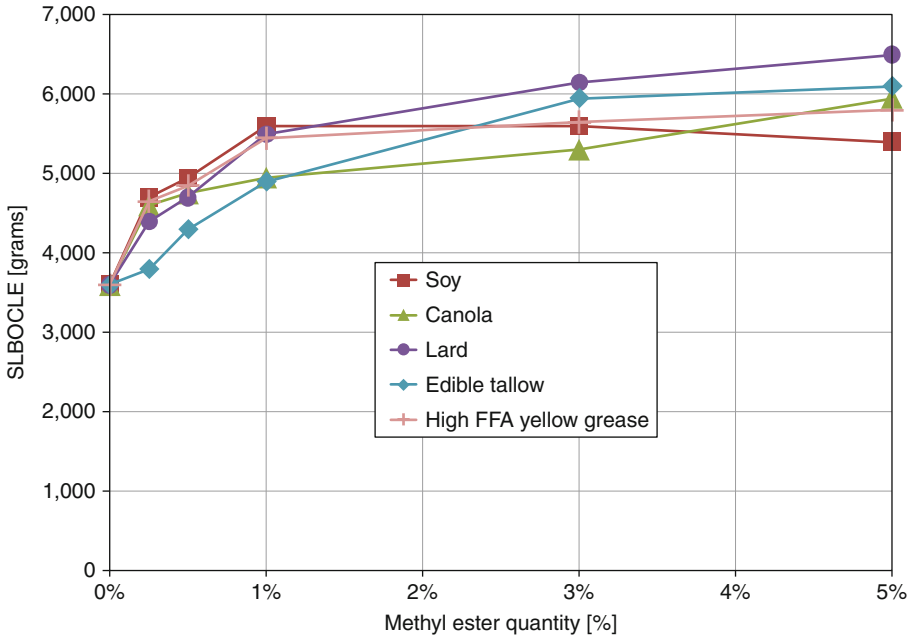

Internal Combustion Engines, Alternative Fuels for. Figure 9
Lubricity improvement with methyl ester quantity [33]

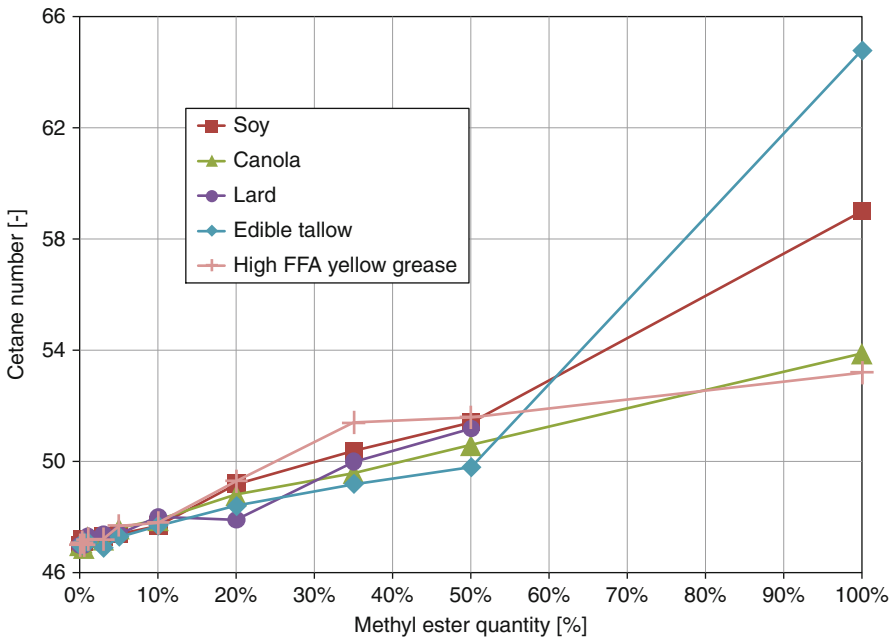

Internal Combustion Engines, Alternative Fuels for. Figure 10
Effect of methyl ester on cetane number [33]

Internal Combustion Engines, Alternative Fuels for. Table 9 Comparison of methyl ester and ethyl ester properties with a soybean feedstock

Ester	Acid No.	Iodine No.	Peroxide No.	Glycerol- free/ Glycerol-bound	Water/ Sediment	Cetane No.	Density g/cm^3	Oxygen wt%	Kinematic viscosity	
									40°C	100°C
Methyl soy	0.15	121	340	0.007/0.223	0	52.3	0.8836	11.44	4.03	1.64
Ethyl soy	3.02	122	123	0.003/0.031	0	47.3	0.8817	11.55	4.33	1.74

and presents a measure for the volume-specific energy content of fuel/air mixtures. It specifies the amount of energy contained per volume of fresh charge typically at stoichiometric conditions that can be introduced into the cylinders of an internal combustion engine. The mixture calorific value is not only used to describe the fuel properties of a specific fuel and mixture formation strategy, but also allows estimation of the theoretical power density of a specific alternative fuel. The brake mean effective pressure (BMEP) or engine torque can be calculated based on the volumetric efficiency (VE) of a specific engine, the brake thermal efficiency (BTE), and the mixture calorific value (H_G). Under the (theoretical) assumption that volumetric efficiency and brake thermal efficiency remain unchanged when switching from one fuel to another, any change in mixture calorific value is directly reflected in corresponding change in (maximum) brake mean effective pressure, in other words, maximum torque.

$$\mathrm{BMEP} = \mathrm{VE} \times \mathrm{BTE} \times \mathrm{H_G} \tag{1}$$

For mixture-aspirating engines (carbureted or port injected/external mixture formation) the mixture calorific value is defined relative to 1 m^3 of mixture and for air-aspirating engines (direct injection/internal mixture formation) to 1 m^3 of air. The mixture calorific value for mixture-aspirating operation is calculated based on lower heating value (LHV), density of the fuel/air mixture (ρ_{Mixture}), relative air/fuel ratio (λ), and stoichiometric air demand (L_{St}) and is defined as:

$$\mathrm{H_G} = \frac{\mathrm{LHV}\rho_{\mathrm{Mixture}}}{\lambda \mathrm{L_{St}} + 1} \tag{2}$$

For air-aspirating operation the density of air (ρ_{Air}) is used instead of the fuel/air mixture density and the value is defined as:

$$\bar{H}_{\mathrm{G}} = \frac{\mathrm{LHV}\rho_{\mathrm{Air}}}{\lambda \mathrm{L_{St}}} \tag{3}$$

Figure 11 shows the mixture calorific value for various alternative fuels both for air-aspirating and mixture-aspirating operation as a function of stoichiometric air/fuel ratio. To achieve high power density, the mixture calorific value should be as high as possible. With liquid fuels the difference in the mixture calorific value between air- and mixture-aspirating operation is minimal since the liquid fuel due to its high density takes up only a small volume. However, for gaseous fuels the difference between the mixture calorific value in air-aspirating and mixture-aspirating operation increases significantly with decreasing gas density ($\rho_{\mathrm{Propane}} = 1.83$ kg/m^3, $\rho_{\mathrm{Methane}} = 0.72$ kg/m^3, $\rho_{\mathrm{Hydrogen}} = 0.089$ kg/m^3). The impact is most pronounced for hydrogen as a fuel, because it displaces approximately 30% of the aspirated air at stoichiometric conditions with external mixture formation. Even for liquid fuels there is noticeable difference in mixture calorific values that should be considered when comparing alternatives.

Alternative Fuels for Spark-Ignition (SI) Engines

Alcohol Fuels (Ethanol, Butanol, Methanol)

Methanol As per the Energy Policy Act of 1992, Methanol (CH_3OH), also known as wood alcohol, is considered an alternative fuel. The main production routes for methanol all use natural gas as a feedstock. Methanol can be used to make methyl tertiary-butyl ether (MTBE), an oxygenate that was used in blends with gasoline as an octane booster. MTBE production and use has declined in recent years because it has been found to contaminate ground water. As an engine

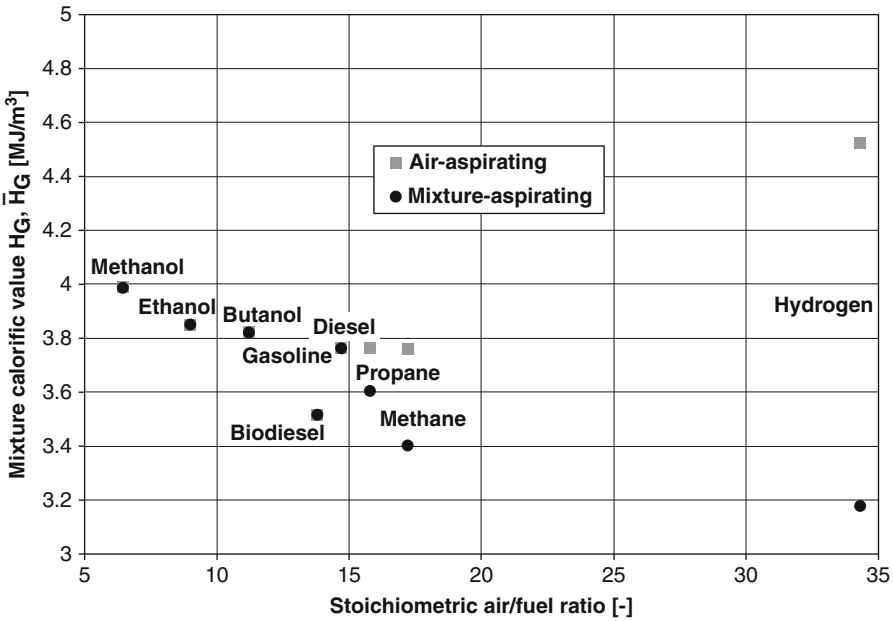

Internal Combustion Engines, Alternative Fuels for. Figure 11
Mixture calorific value for conventional and alternative fuel options

fuel, methanol has similar chemical and physical characteristics to ethanol.

A limited study of low level methanol gasoline blends up to 15 vol % on a four-stroke, single-cylinder, variable compression ratio engine with a displacement volume of 582 cm^3 suggests an approximately 10% increase in torque at the highest blend level which is attributed to the improved volumetric efficiency due to the higher heat of vaporization [34]. An experimental evaluation of engine cold start behavior with gasoline as well as 10 vol % and 30 vol % blends of methanol in gasoline on a small three-cylinder engine came to the conclusion that the addition of methanol improves combustion stability, indicated mean effective pressure (torque), and reduces misfires. In addition a 70% reduction in CO emissions as well as a 40% reduction in HC emissions were also observed. These positive effects of methanol addition were attributed to higher vapor pressure, lower boiling temperature as well as the high oxygen content of methanol [35]. A detailed thermodynamic evaluation of alcohol fuels including their effect on engine efficiency and NO_x emissions concluded that the use of methanol could result in increase in engine brake thermal efficiency of up to 1% regardless of engine load and speed. This increase was attributed to slightly reduced pumping losses because of the increased amount of fuel vapor at constant load compared to the *iso*-octane baseline. The study further found that a 25% NO_x emissions reduction can be expected with methanol compared to the baseline fuel which is mainly caused by reduced process temperatures [36]. The high octane rating of methanol also makes it well suited for knock-free operation at high compression ratios. A study that was performed on single-cylinder, four-stroke, naturally aspirated, high-compression direct-injection stratified charge spark-ignition engine revealed the potential of methanol for high engine efficiencies. Performing optimization of injection timing and spark timing at the research engine with a compression ratio of 16:1 at full load conditions at 1,600 RPM resulted in a maximum indicated efficiency of approximately 51% [37].

Due to challenges with methanol such as toxicity as well as safety related issues due to invisible methanol flames widespread use of methanol as a transportation fuel is rather unlikely.

Ethanol Ethanol is probably the most widely used liquid alternative fuel and is typically used in blends

with gasoline. The two main variables when using gasoline/ethanol blends are the blend level and whether hydrous or anhydrous ethanol is used. Typically gasoline is blended with anhydrous ethanol whereas neat ethanol when used in vehicles is hydrous (E100). Although attempts are made to get higher blends approved, the most commonly used blend throughout the world is E10, a blend of 90 vol % gasoline with 10 vol % anhydrous ethanol. US legislation limits the amount of oxygen content in blends of gasoline with alcohol fuels. In 1991, the maximum oxygen content was increased from 2 wt.% to 2.7 wt.% for blends of aliphatic alcohols and/or ethers excluding methanol [38]. To ensure sufficient gasoline base was available for ethanol blending, the EPA also ruled that gasoline containing up to 2 vol % of MTBE could subsequently be blended with 10 vol % of ethanol [39]. Only recently EPA granted a partial waiver to allow gasoline that contains greater than 10 vol % ethanol and up to 15 vol % ethanol (E15) for use in model year 2007 and newer light-duty motor vehicles, which includes passenger cars, light-duty trucks, and sport utility vehicles (SUV) [40].

Several markets also promote higher ethanol blends, with E85 being the most prominent one with existing distribution networks in several countries including the United States and Sweden.

Due to its large domestic production capabilities of ethanol from sugarcane Brazil has a special role in the worldwide ethanol market with a distribution network for both, Type C gasoline as well as neat hydrous ethanol (~5 vol % water content). Type C Gasoline describes a 25 ± 1 vol % anhydrous ethanol blend with gasoline [41] and is referred to as gasohol in Brazil.

A critical aspect potentially limiting the maximum blend level of any alcohol fuel with gasoline is the vapor pressure of the fuel blend since it is critical for cold startability. Figure 6 shows the vapor pressure for several alcohol fuels as a function of volumetric blend level. Vapor pressures below 45 kPa [42] are known to potentially cause cold start problems which effectively limits the maximum ethanol blend level without taking additional measures to approximately 75% during winter months. Other limitations when increasing the amount of ethanol in the fuel might be inferred due to incompatibility of the blend with metals, plastics, and elastomers in the fuel system. Despite these direct effects, higher ethanol blends potentially also limit the use of existing fuel infrastructure, in particular pipelines [17]; however, these limitations are beyond the focus of this article.

A more detailed overview of vehicle components that are affected by ethanol addition as a function of blend level are shown in Fig. 12 [43]. Blend levels below

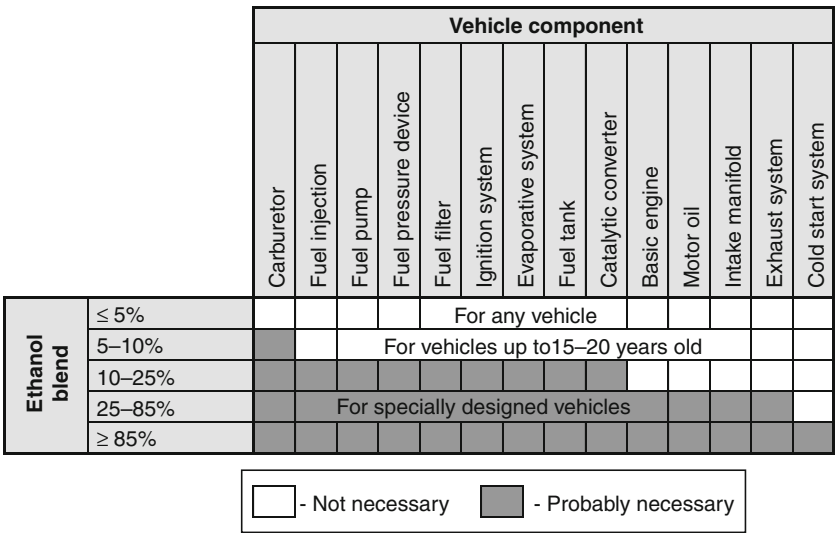

Internal Combustion Engines, Alternative Fuels for. Figure 12
Required vehicle modifications with ethanol blend level (Based on [43])

5 vol % do not require any changes to the vehicle regardless of vehicle age. Typically, modifications are also not required at blend levels up to 10 vol % for most vehicles less than 15–20 years of age. Only older vehicles might require changes to the engine carburetors. Although studies suggest that most fuel system components are not negatively affected at a blend level of 20 vol % [44–46], modifications to the fuel system including injectors, pumps, regulators and filters, the ignition system as well as the catalytic converters are common for blend levels up to 25 vol %. At higher blend levels up to 85 vol % additional modifications include the base engine, engine oil as well as intake and exhaust system. Only for blend ratios beyond 85 vol % and neat ethanol, a separate cold start system might be required.

As mentioned earlier, specific engine designs are typically only found for engines that are intended to run on higher ethanol blends in excess of 25 vol %. Experimental results with port fuel injection on a 1.8 L four-cylinder engine converted to single cylinder operation revealed the efficiency and emissions potential of high ethanol blends. In particular at moderate engine speed of 1,500 RPM torque could be improved significantly due to the increased knock resistance resulting in a 20% increase with E100 compared to gasoline, while improving indicated thermal efficiency from 32% to 40%. At the same time a reduction in oxides of nitrogen emissions by approximately 125 ppm together with a 2°C reduction in exhaust temperature per 10% increase in liquid volume fraction of ethanol in the fuel could be observed which was attributed to lower adiabatic flame temperatures [47]. A theoretical as well as experimental study comparing performance, efficiency, and emissions of gasoline and E85 with direct fuel injection concluded that at full load at 2,000 RPM a 9% improvement in efficiency as well as maximum torque could be achieved while reducing exhaust gas temperatures by 60°C [48]. The Saab Biopower, a turbocharged sedan built to operate on gasoline as well as E85 utilizes the advantageous fuel properties of the ethanol blend. Rated at a maximum power of 110 kW at 5,500 RPM and a peak torque of 240 Nm at 1,800 RPM with gasoline, the same engine achieves a maximum power of 132 kW at 5,500 RPM and a peak torque of 280 Nm at 2,400 RPM with E85 [49]. With a compression ratio of 9.3:1 the 2.0 L engine takes advantage of the higher octane rating of the ethanol blend by operating the turbo engine at higher combustion pressures, producing more power without risk of engine knock. Independent vehicle dynamometer testing of the Saab Biopower showed that the vehicle acceleration time with E85 was 1 s faster than with gasoline, and that the car also met US Tier 2, Bin 5 emissions levels on both gasoline and E85, which is significant since Europe, where the car is certified, does not require emissions certification on E85 and applicable Euro 4 emissions standards are less stringent. In addition, a detailed exhaust speciation revealed that ethanol and aldehyde emissions were higher on E85 while hydrocarbon-based hazardous air pollutants were higher on gasoline [50]. A detailed study of the impact of alcohol blends on regulated emissions and air toxics with direct injection and ethanol blend levels of up to 50 vol % also concluded that ethanol addition resulted in an increase in aldehyde emissions, in particular acetaldehyde, whereas formaldehyde emissions remained almost constant with ethanol addition. The same study also concluded that with E50 oxide of nitrogen emissions were reduced by approximately 15% compared to gasoline operation, which was attributed to a temperature reduction as a result of direct injection and the increased in-cylinder cooling effect of ethanol compared to gasoline. Specific emissions trends for oxides of nitrogen as well as relevant air toxics at a typical part load engine operating point are summarized in Fig. 13 [51]. These trends hold true independent of engine load, the magnitude changes slightly depending on engine speed and load conditions.

A study targeted at designing an engine specifically for neat ethanol application suggested that a combination of direct injection and turbocharging at increased compression ratios is ideally suited for operation on E100. The proposed direct injection, turbo charged engine differs in the direct injector operating pressure, piston shape and compression ratio to efficiently run with E100 and gasoline. The E100 version operates at an increased injection pressure (300 bar vs 200 bar) and an increased compression ratio (13:1 vs 9:1). Improvements in power and torque vary from 20% to 28% over the range of engine speed, while the fuel conversion efficiency increases 17% to 23% with a peak efficiency of approximately 40% [52]. The report acknowledges

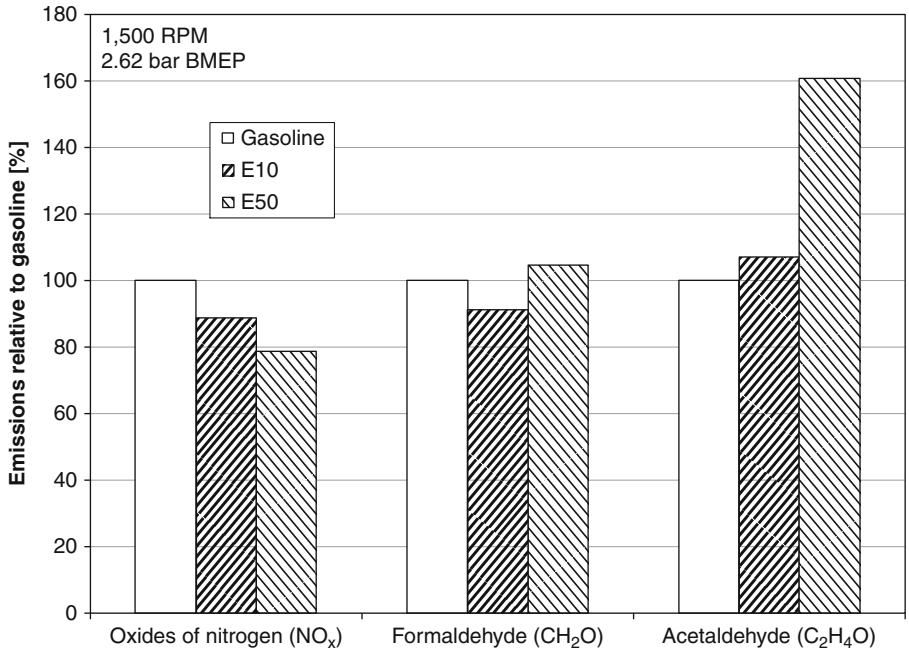

Internal Combustion Engines, Alternative Fuels for. Figure 13
Influence of ethanol content on oxides of nitrogen and air toxics [51]

that cold start issues exist for E100 engines and indicates that fuel is injected after intake valve closing which helps to insure complete vaporization of the ethanol and prevents or minimizes wall wetting, however, no specific measures to ensure proper cold start behavior are discussed.

Measures to mitigate the cold start issue with E100 include fuel choice, e.g., E85 where the 15 vol % of highly volatile gasoline are typically sufficient to improve cold startability, sometimes combined with intentional overfueling to further improve the cold start behavior. However, it would be preferable to use neat ethanol to fully utilize its fuel properties and also avoid overfueling in order to reduce cold start emissions. Technical solutions that have been developed to mitigate the cold start problem include heated fuel injectors [53], heated fuel-rails as well as installation of a second tank, filled with highly volatile gasoline to run the engine for a few seconds before switching to ethanol [54].

Ethanol currently is one of the most dominant alternative fuels which is mainly due to its favorable properties and production pathways. The properties and challenges of ethanol as a fuel are well understood and most technical hurdles for use of ethanol in internal combustion engines have been overcome. It is likely that ethanol will remain a dominant alternative fuel for both, low and mid-level blends with gasoline for the majority of applications as well as high level blends and neat ethanol for local markets. Further development is expected in dedicated engines for high level blends and neat ethanol, however, the main area for advancement will have to be in renewable production pathways which create ethanol from biomass rather than food crops.

Butanol Butanol, a four carbon alcohol that exists in several isomers, is currently under investigation as a potential alternative fuel. Butanol is particularly attractive compared to ethanol due to its higher volumetric energy content and its lower affinity to water (see Table 1). In a joint venture BP and DuPont founded Butamax™ Advanced Biofuels LLC to market and promote biobutanol, which consists mainly of *iso*-butanol. In addition to 135 cars, including 1995 – 2009 model years, that have been tested to date with 1.5 million miles driven, a retail demonstration was completed in 2009 in the UK. A total of 10 million liters of

biobutanol were blended and supplied to ten retail sites as EN228 compliant gasoline. Over the course of the demonstration approximately 250,000 vehicle fills were performed and 80 million miles driven suggesting biobutanol can be treated as a normal fuel component and used without special procedures [55]. Since butanol has a lower oxygen content than ethanol, a 16 vol % blend of butanol with gasoline contains the same amount of oxygen, approximately 3.7 wt.%, than a 10 vol % blend of ethanol with gasoline (E10).

In addition to vehicle tests performed and publicized by BP and DuPont, few engine performance and efficiency tests have been performed on *iso*-butanol as well as other butanol isomers. A comparative study performed with gasoline as well as 10 vol % ethanol in gasoline (E10) and 10 vol % *n*-butanol in gasoline on a 2.2 L Direct-injection engine suggests that engine efficiency and emissions characteristics are almost identical throughout a majority of the engine operating regime. Apparent differences were only found at the highest speed and load conditions which could be attributed to differences in the knock resistance of the different fuels [56]. Consequently the study was extended to include *iso*-butanol in addition to *n*-butanol and blend levels were increased up to 85 vol % with similar findings as for the low level blends. Even at the highest blend levels for ethanol, *n*-butanol, and *iso*-butanol, the engine efficiency and emissions characteristics are almost identical to the gasoline baseline. However, at high load conditions the engine could be run with significantly earlier spark timing with ethanol and *iso*-butanol compared to *n*-butanol and gasoline. The earlier combustion phasing due to the increased knock resistance of ethanol and *iso*-butanol compared to gasoline resulted in an increase in brake thermal efficiency in excess of 1% [57]. Due to its lower octane rating *n*-butanol does not exhibit the advantages in terms of knock resistance that ethanol and *iso*-butanol show compared to gasoline. In fact, *n*-butanol was found to behave very similar to regular gasoline in terms of combustion knock [58]. A study of gasoline-butanol blends with up to 80 vol % alcohol content on a port injected spark-ignition engine suggests that the emissions characteristics remain similar with increasing blend ratio, however, improved combustion stability with increasing butanol was observed which could be attributed to shorter ignition delays [59]. An issue that was raised specifically with the use of alcohol fuels is the amount of aldehydes and other air toxics as a result of the combustion. A study of regulated and non-regulated emissions as a result of combustion of various blends of gasoline with ethanol, *n*-butanol, and *iso*-butanol suggests that aside from a consistent reduction in engine-out emissions of oxides of nitrogen regardless of blending agent, both formaldehyde and acetaldehyde emissions increased with addition of butanol to the fuel blend, whereas formaldehyde did not increase significantly with addition of ethanol. Figure 14 shows oxides of nitrogen as well as formaldehyde and acetaldehyde emissions for *n*-butanol as well as *iso*-Butanol gasoline blends at blend levels of 16 and 83 vol % [51]. Since the load point is identical and the butanol blends with 16, and 83 vol % contain the same amount of oxygen as ethanol gasoline blends at 10 and 50 vol %, these results are directly comparable to those for ethanol blends shown in Fig. 13. Although the increase in air toxics in engine-out emissions is noticeable, further studies will have to clarify the effect on tailpipe emissions.

Butanol appears to be a promising alternative fuel with certain fuel properties superior to ethanol such as volumetric energy content and affinity to water. Several studies suggest that butanol is well suited as a fuel for spark-ignition internal combustion engines. However, butanol nowadays is produced mainly as an industrial chemical rather than a transportation fuel. Since feedstock and production pathways for butanol are similar to ethanol, the higher alcohol also faces the same challenges in terms of economy of production from celluloses.

Liquefied Fuels (LPG, LNG)

Liquefied Petroleum Gas At normal ambient pressure the boiling point of methane is –162°C, propane is at –42°C, isobutane –10°C, and *n*-butane 1°C. Special measures have to be taken to keep liquefied fuels from evaporating at ambient conditions. As mentioned earlier, LPG composition differs depending on regional supplies which affect vapor pressure and storage conditions (see Fig. 7). Typically LPG is stored in a steel or composite tank at moderate pressure around 10 bar. The two most common mixture formation strategies for LPG are vapor fumigation and LPG injection into the intake. More recently work has also been

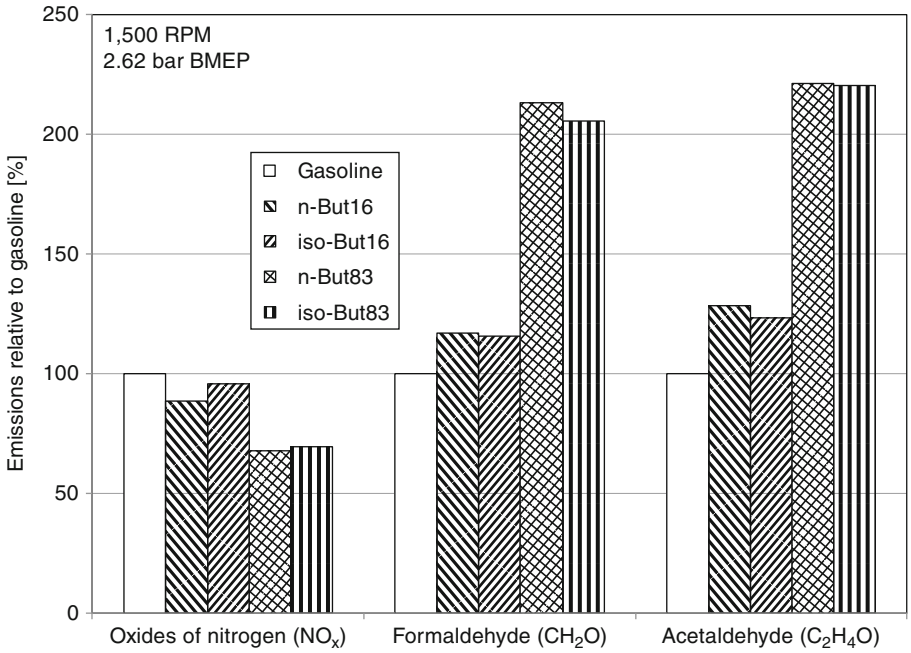

Internal Combustion Engines, Alternative Fuels for. Figure 14
Influence of butanol content on oxides of nitrogen and air toxics [51]

reported on LPG direct injection. For vapor fumigation the LPG supply to the engine is typically controlled by a regulator or vaporizer, followed by a mixer in the intake manifold. For a typical vaporizer system a power density that is up to 15% lower than a comparable gasoline engine can be expected [60, 61]. LPG injection systems supply the liquid phase to the intake manifold, where a phase change occurs once the fuel is injected. Since this phase change results in increased charge density due to the cooling effect of the evaporation, LPG injection systems are superior compared to fumigation systems in terms of power density and also reduce the tendency for backfiring [62]. An increase in power density of LPG injection systems of approximately 5–10% compared to the gasoline baseline has been reported [60, 61]. Most recently LPG engines have also been operated with direct injection, and a performance advantage in excess of 10% compared to a gasoline baseline has been reported [61]. Figure 15 shows the maximum engine torque as a function of engine speed for gaseous LPG port injection, liquid LPG port injection, and LPG direct injection relative to gasoline.

A comparative emissions study of a bi-fuel vehicle capable of operating on gasoline or LPG using a vaporizer system showed significant emissions advantages for LPG. Depending on the drive cycle a reduction in CO emissions of 10–30%, 30–50% in HC, and 40–77% in NO_x was reported [63]. The same study also concluded that CO_2 emissions were reduced by approximately 10% when operated on LPG compared to gasoline regardless of drive cycle. Given that the CO_2 emissions factor per unit energy for LPG is approximately 12% lower than that of gasoline [64], the previously mentioned reduction in CO_2 emissions suggests that the two fuels are equivalent in fuel economy. Due to the rapid vaporization of LPG a significant advantage also in terms of particulate emissions can be realized. A study of combustion and emissions characteristics with direct injection of LPG and gasoline concluded that the particulate emissions in LPG operation were lower by a factor of 100 compared to gasoline [65]. Finally, the higher octane rating of LPG compared to gasoline indicates that a dedicated LPG engine could possibly run at a higher, more efficient compression ratio. A computational study that focused on developing an engine design for direct injection of CNG and LPG proposed 14.2:1 as a suitable compression ratio for LPG operation [66]. Since the fuel properties of

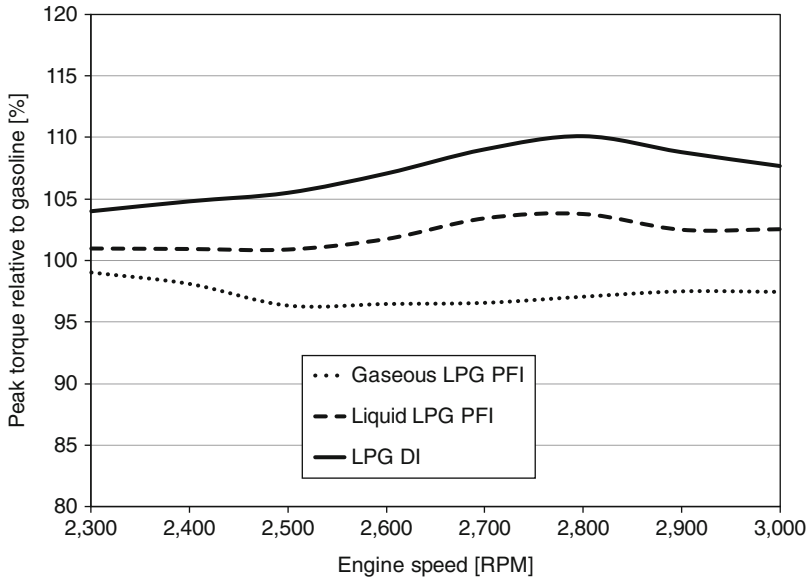

Internal Combustion Engines, Alternative Fuels for. Figure 15
Relative peak torque of LPG mixture formation concepts compared to gasoline (Based on [61])

propane were used for the study, the actual compression ratio for real world LPG with a higher butane content might be lower. Nonetheless the proposed compression ratio is still significantly higher than that of typical gasoline engines with compression ratios below 10.5:1 for port injection and less than 12:1 for gasoline direct injection [67].

Liquefied petrol gas (LPG) is well established as an alternative fuel in certain markets and the combustion properties of LPG are well understood. However, the market share compared to mainstream fuels is small in most markets limiting dedicated vehicle development. Besides the challenges due to the liquefied state of the fuel, additional issues with infrastructure limitations and safety concerns appear to further limit the interest in large scale deployment.

Liquefied Natural Gas LNG is stored on-board of vehicles as a cryogenic liquid in super-insulated storage tanks. The typical operating pressure of these tanks is in the range of approximately 5 bar but can reach up to 15 bar. Although LNG is stored in its liquid form, it is typically evaporated before use. The quality of the evaporated gas differs depending on whether natural boil-off gas or forced boil-off gas is used. The gaseous phase in the top portion of LNG tanks is called natural boil-off gas, consists mainly of methane and some nitrogen, and has a high knock resistance. If LNG is extracted from the liquid phase and evaporated separately, it is considered forced boil-off gas which could have a different knock resistance than the natural boil-off gas. In addition to the potential difference in knock resistance the lower heating value of natural boil-off gas is approximately 33–35 MJ/m^3 and significantly lower than that of forced boil-off gas with an LHV of 38–39 MJ/m^3 [68].

Regardless of which type of gas from an LNG tank is used, the fuel is delivered to the engine in its gaseous state. Therefore, an engine combustion system designed and marketed for operation on LNG is in fact designed to run on natural gas or methane and does not necessarily differ from CNG engines [69, 70]. There are, as outlined above, significant differences in the fuel storage, supply, and conditioning systems. For engine design, efficiency, performance, and emissions the same considerations as for compressed natural gas apply.

Gaseous Fuels (Natural Gas, Hydrogen)

Compressed Natural Gas Compressed natural gas is typically stored on-board a vehicle in pressure cylinders, with single steel cylinders mainly used in the past

which are more and more replaced by several smaller composite cylinders. The gas is typically stored at pressures around 200–270 bar with the additional cylinders adding around 60 kg of extra weight to the average vehicle [71].

The first CNG model of the Honda Civic released in 1998 had a natural gas storage capacity of approximately 8 GGE at a fuel economy of 24 MPG City and 34 MPG Highway [72]. The 2011 model still has the same storage capacity (7.8 GGE) at reported fuel economy numbers of 24/36 MPG allowing for a vehicle range of up to 450 km (280 miles) [73].

Vehicle range and weight of the fuel storage system are challenges for natural gas vehicles. At constant range a gaseous storage system operating at 200 bar requires approximately four times the storage volume and outweighs the gasoline system by a factor of 3. Lightweight materials, increased storage pressures, and improved engine efficiencies are expected to improve the volumetric ratio to 1:2.9 and the gravimetric ratio to 1:1.4 with a vehicle range of up to 600 km [74].

The dominant mixture formation strategy for natural gas in automotive applications is intake manifold injection. The higher knock resistance of natural gas compared to gasoline allows for dedicated NG engines to operate at higher compression ratios resulting in higher thermal efficiencies on the one hand and higher NO_x emissions on the other. The lower mixture calorific value of natural gas with external mixture formation (see Fig. 11) compared to gasoline causes reduced power density with the gaseous fuel which can be further compromised when a lean burn strategy is employed. The increased NO_x levels with NG also warrant the use of exhaust gas recirculation (EGR), however, EGR is limited due to combustion instabilities and misfires which occur at increased rates. The reduced power density with injection into the intake manifold can be compensated with supercharging or turbocharging with intercooling. More recently, attempts have also been made to employ direct injection (DI) of natural gas but efforts are hampered since high pressure gaseous injection hardware is not available on the open market [75].

A comparative study of gasoline and CNG on a four-cylinder spark-ignition engine showed significant differences between the two fuels at identical operating conditions. At wide open throttle operation at speeds between 1,500 and 5,000 RPM the engine produced between 8% and 16% less torque with sequential CNG injection relative to gasoline port fuel injection which was mainly attributed to the reduced mixture calorific value. The increased reduction in engine torque at higher speeds was further attributed to the lower flame speeds of CNG compared to gasoline. Similar results in terms of reduction in maximum torque had been reported on the same engine when operated with a mixer type CNG system instead of the sequential fuel injection. However, the fuel conversion efficiency with intake manifold injection was reported to be an average of 13% higher compared to gasoline whereas the carburetor system only showed an average 3% improvement over the gasoline baseline. Both the carburetor and the sequential injection system showed emissions reductions of up to 80% for CO, 8–20% for CO_2, and an average reduction in hydrocarbons of approximately 50%, while NO_x emissions were increased by around 33% with the carburetor system compared to gasoline and no NO_x emissions were reported for the sequential injection system [76, 77].

The previously mentioned results are representative of stoichiometric engine operation just like conventional gasoline engines. However, the relatively wide ignition limits of natural gas suggest that a lean burn strategy which is beneficial for engine efficiency be applied.

Experiments on a 1.3 L four-cylinder engine with one cylinder operated with port fuel injection of natural gas showed that lean operation with relative air/fuel ratios up to 1.3 is feasible without a dramatic decrease in combustion stability. The lean burn strategy also resulted in an up to 75% reduction in NO_x emissions compared to the stoichiometric case with only a moderate increase in HC and CO emissions [78]. Modern stationary natural gas engines operate at relative air/fuel ratios around 1.7 which is close to the misfire region which results in a further increase in engine efficiency while minimizing NO_x emissions [79].

Further extension of the lean combustion limits can be achieved with stratification of the fuel/air mixture which is frequently accomplished by employing direct injection. Research on a single-cylinder 0.9 L engine with direct injection during the compression stroke

suggests that the lean limit could be expanded to approximately 1.8 also identifying the injection timing as a critical parameter to influence combustion and emissions characteristics [80]. A comparison of early injection, late injection, and split injection on a 1 L single-cylinder research engine further showed that stratified mixtures resulting from late and split injection can extend the lean limit up to relative air/fuel ratios in excess of 2.5, eliminating NO_x emissions. However, decreased combustion stabilities and exponential increase in hydrocarbon emissions were reported for these conditions [81]. Finally, hydrogen addition has also been examined as a tool to extend the lean limit of natural gas engines. Results on a 1.6 L single cylinder engine with hydrogen addition rates of up to 19% showed an extension of the lean limit from a relative air/fuel ratio around 1.8 without hydrogen addition to almost 2 with 19% hydrogen. A simultaneous increase in indicated efficiency which can be attributed to the increased burn rate with hydrogen addition was also reported [82].

Energy security and domestic production in addition to natural gas being considered a clean-burning fuel are the main drivers for renewed interest in natural gas in the United States [83]. Natural gas has been widely used for stationary power supply at outstanding engine efficiencies and emissions levels. However, most natural gas vehicle applications rely on conversion from conventional gasoline engines for light-duty applications or diesel natural gas dual fuel applications for heavy duty applications. Future development for natural gas applications is expected to result in dedicated engines optimized to cater to the specific properties of the gaseous fuels. In terms of storage technology both compressed natural gas as well as liquefied natural gas storage will have their market share since either one is well suited for certain applications.

Hydrogen Although the situation for hydrogen in terms of fuel storage is similar to that of natural gas with compressed and cryogenic storage as the two dominant techniques, hydrogen vehicles are not typically classified based on their storage system. Since, as for natural gas, the fuel supply to the engine is almost exclusively in gaseous form, engine technology does not depend on the storage system. Attempts have been made to utilize the low temperature of gaseous hydrogen from liquid storage to increase the power density of hydrogen port injection engines [84].

Hydrogen storage is a significant challenge for the development and viability of hydrogen-powered vehicles. On-board hydrogen storage in the range of approximately 5–13 kg is required to enable a driving range of greater than 300 miles for the full platform of light-duty automotive vehicles using fuel cell power plants or hydrogen internal combustion engines. Current on-board hydrogen storage approaches involve compressed hydrogen gas tanks, liquid hydrogen tanks, cryogenic compressed hydrogen, metal hydrides, high-surface-area adsorbents, and chemical hydrogen storage materials. Storage as a gas or liquid or storage in metal hydrides or high-surface-area adsorbents constitutes "reversible" on-board hydrogen storage systems because hydrogen regeneration or refill can take place on-board the vehicle. For chemical hydrogen storage approaches (such as a chemical reaction on-board the vehicle to produce hydrogen), hydrogen regeneration is not possible on-board the vehicle and thus, these spent materials must be removed from the vehicle and regenerated off-board. On-board hydrogen storage system performance targets were developed through the FreedomCAR and Fuel Partnership, a collaboration among DOE and the US Council for Automotive Research, and the major energy and utility companies. The targets developed are system-level targets and are customer-driven based on achieving similar performance and cost levels as competitive vehicles. The storage system includes the tank, storage media, safety system, valves, regulators, piping, mounting brackets, insulation, added cooling capacity, and any other balance-of-plant components. In order to achieve system-level capacities of 1.8 kWh/kg system (5.5 wt.% hydrogen) and 1.3 kWh/L (0.040 kg hydrogen/L) in 2015 and the ultimate targets of 2.5 kWh/kg system (7.5 wt.% hydrogen) and 2.3 kWh/L (0.070 kg hydrogen/L), the gravimetric and volumetric capacities of the material alone must clearly be higher than the system-level targets [85, 86].

A primary classification of mixture formation strategies of hydrogen engines can be done based on the location of mixture formation or the location of the hydrogen dosing devices. External mixture formation refers to concepts in which hydrogen and air are mixed

outside the combustion chamber, whereas internal mixture formation refers to concepts with hydrogen being introduced directly into the combustion chamber. Some researchers have also proposed combined concepts with a combination of external and internal mixture formation [87]. As indicated in Fig. 11, the mixture formation strategy, especially in hydrogen operation, has significant impact on the theoretical power output of the engine. The dramatic difference in theoretical power output is mainly caused by the low density of hydrogen, resulting in a significant decrease in mixture density when external mixture formation is employed [88].

A study of hydrogen mixture formation concepts in comparison to gasoline performed on an automotive single-cylinder engine confirmed the superior power density with hydrogen direct injection. A 15% improvement in torque at 2,800 RPM with hydrogen direct injection compared to gasoline port injection could be achieved; the relative torque improvement of direct injection compared to hydrogen port injection exceeded 75% [89].

In terms of engine efficiency hydrogen internal combustion engines have been shown to be superior to other, more conventional fuels. Peak efficiency numbers reported by several research groups around the globe suggest that brake thermal efficiencies in the range of 45% can be achieved with hydrogen direct injection [90–93].

Since hydrogen is the only fuel that does not contain any carbon, its combustion does not create any carbon-based emissions constituents except for traces that are expected to result from lube oil combustion. The major challenge for hydrogen combustion engines is their NO_x emissions which are a result of high temperatures during the combustion process (Fig. 16). A trade-off between relative air/fuel ratio and NO_x emissions for homogeneous hydrogen combustion resulting from port injection or early direct injection has been reported by several researchers [89, 94]. Combustion of lean hydrogen–air mixtures with fuel-to-air equivalence ratios of less than 0.5 ($\lambda > 2$) results in extremely low NO_x emissions. Due to the excess air available in the combustion chamber, the combustion temperatures do not exceed the NO_x critical value of approximately 1,800 K [94]. Exceeding the NO_x critical equivalence ratio results in an exponential increase in

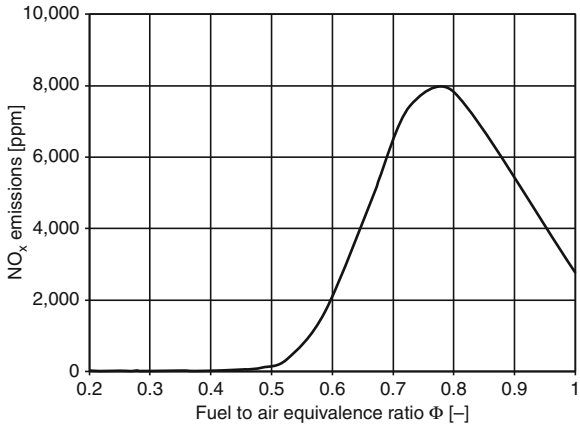

Internal Combustion Engines, Alternative Fuels for. Figure 16
NO_x emissions trends for hydrogen fuelled engines

oxides of nitrogen emissions, which peaks around a fuel-to-air equivalence ratio of 0.75 ($\lambda \sim 1.3$). At stoichiometric conditions, the NO_x emissions are at around 1/3 of the peak value. The highest burned gas temperatures in hydrogen operation occur around a fuel-to-air equivalence ratio near 1.1, but at this equivalence ratio oxygen concentration is low so the NO_x concentration does not peak there [95]. As the mixture gets leaner, increasing oxygen concentrations initially offset the falling gas temperatures, and NO_x emissions peak around a fuel-to-air equivalence ratio of 0.75 (λ 1.3). Since hydrogen engines, due to the efficiency advantages, are generally operated with fuel lean conditions, the above mentioned NO_x emissions trade-off with air/fuel ratio also limits the power output.

If NO_x emissions have to be avoided, hydrogen engine operation with port injection is frequently limited to air/fuel ratios below 0.5 and supercharging is employed to increase power density [96, 97]. With hydrogen direct injection the mixture homogeneity can be influenced through tailored design of injection strategy including injector location and nozzle design as well as injection strategy. Parameter studies with hydrogen direct injection revealed that the NO_x emissions characteristics significantly depend on the injection strategy. A consequent optimization of injection timing with conventional hydrogen direct injection allowed a NO_x tailpipe emissions reduction below the

level of a comparable gasoline engine; with a multiple injection approach NO_x emissions could be further reduced to a level of less than 25% compared to single-injection strategies [98].

A recently released hydrogen internal combustion engine vehicle has been pushing the envelope in terms of emissions levels achievable with combustion engines. A BMW Hydrogen 7 Mono-Fuel demonstration vehicle that was tested for fuel economy as well as emissions on the Federal Test Procedure FTP-75 cold-start test as well as the highway test achieved emissions levels that were only 3.9% of the Super Ultra Low Emissions Vehicle (SULEV) standard for nitric oxide (NO_x) and 0.3% for carbon monoxide (CO) emissions. For non-methane hydrocarbon (NMHC) emissions the cycle-averaged emissions are actually 0 g/mile, which require the car to actively reduce emissions compared to the ambient concentration [99].

The properties of hydrogen make it well suited for internal combustion applications with excellent engine efficiency potential and inherently low emissions signatures for carbon based emissions. Further development of injection equipment will be required for production applications of advanced mixture formation concepts. The main challenges for a widespread utilization of hydrogen in transportation remain the lack of a fuel infrastructure as well as sufficient on-board storage density.

Alternative Fuels for Compression-Ignition (CI) Engines

Operation of compression-ignition engines on non-petroleum fuel is not a new concept. In fact, Rudolf Diesel, one of the pioneers of the diesel engine, originally designed the compression-ignition engine to run on a variety of fuels, including straight vegetable oil. In 1900, at the World Exhibition in Paris, he demonstrated his engine running on pure peanut oil.

Operation of today's modern, highly sophisticated compression-ignition engines on straight vegetable oil is not recommended due to the higher viscosity and increased contaminants in the oil. While short-term operation may be possible, long-term effects include build-up of engine deposits, ring sticking, lube oil gelling, and other significant maintenance problems that can reduce engine life.

The primary alternative fuels for compression-ignition engines include biodiesel and synthetic diesel. Emerging fuel technologies include hydrogenated-derived diesel fuel ("green" diesel) and dimethyl ether (DME).

Biodiesel

Biodiesel is the most widely used alternative diesel fuel in the world. Biodiesel is defined as, "a fuel comprised of mono-alkyl esters of long chain fatty acids derived from vegetable oils or animal fats, designated B100, and meeting the requirements of ASTM D 6751" [100]. The properties of biodiesel can vary widely, depending on the feedstock and processing technique employed.

Biodiesel is produced from a fat or oil by reacting it with an alcohol like methanol or ethanol in the presence of a catalyst such as sodium or potassium hydroxide. The transesterification process produces esters (biodiesel) and glycerin. Typically, the alcohol is supplied in excess to ensure a quick reaction and it can be reused. The processing temperatures are around 65°C and the pressures rarely exceed 140 kPa. The conversion efficiency, from oil to methyl ester exceeds 98%. If the alcohol is methanol, then the biodiesel is called a fatty acid methyl ester (FAME). If the alcohol is ethanol, then the biodiesel is called a fatty acid ethyl ester (FAEE). The two "biodiesels" have significantly different properties, as shown in Table 9 for a biodiesel derived from a soybean feedstock. As the properties of biodiesel change, there is a direct impact on fuel economy, emissions, performance, and engine efficiency.

Experimental testing has shown that particulate matter, CO, and HC emissions can be significantly reduced with relatively low levels of biodiesel blend, while NO_x emissions have been shown to increase. Figure 17 shows a typical trend in emissions as the quantity of biodiesel is increased.

One theory as to why NO_x increases with increasing biodiesel content relates to the reduction in PM. As the combustion event occurs, the formation of soot and particulate matter is reduced due to the presence of oxygen in the fuel. Typically, this mass in the cylinder would increase the specific heat of the burned-gas mixture and lower the overall temperature. With the reduction in particulate matter mass, the temperature rises and the production of NO_x increases [102].

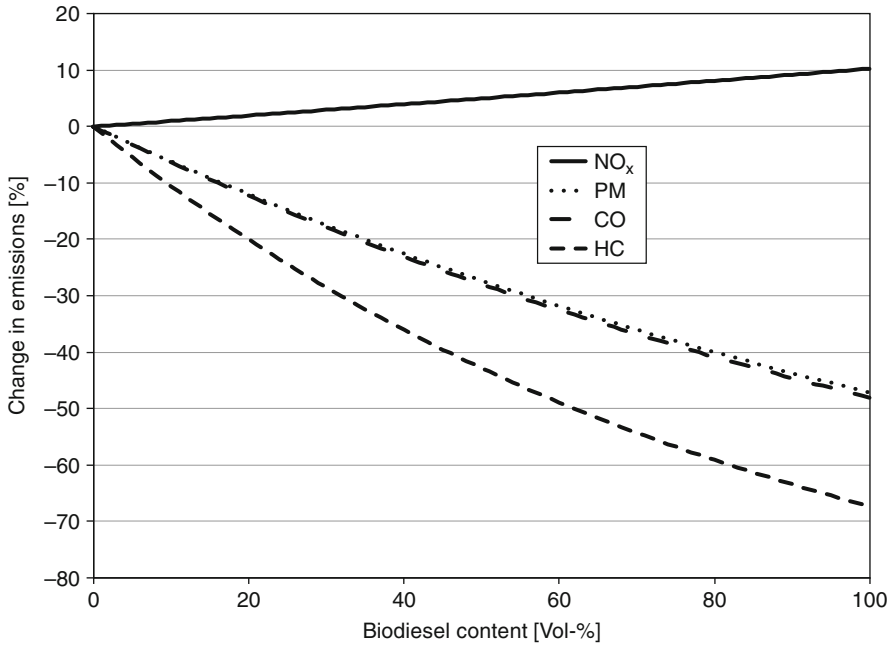

Internal Combustion Engines, Alternative Fuels for. Figure 17
Impact of emissions on biodiesel percentage [101]

A comparison of unregulated, gaseous toxic emissions for two biodiesel blend ratios is shown in Fig. 18. Except for Styrene and Toluene, all toxic emissions levels reduced as the biodiesel blend quantity increased from 20% to 100%. Even for the 20% blend compared to a base petroleum diesel fuel, all but three toxic emissions constituents decreased measurably.

Because of the lower energy density compared to petroleum diesel fuel, biodiesel is associated with a decrease in fuel economy. As the blend volume increases, the impact on fuel economy becomes greater. One would expect up to a 15% reduction in fuel economy due to the reduction in lower heating value. To maintain equivalent power, additional fuel must be injected when operating on biodiesel. This is achieved through an increase in injection pressure or injection duration. It is advantageous to increase injection pressure to not only increase the fuel delivery rate but also improve atomization of the liquid fuel. However, field data has not shown the significant reduction in fuel economy as expected. The oxygenated fuel is also associated with an increase in combustion efficiency up to 5% at blend levels below 25% [104]. The positive impact on combustion efficiency reduces as the blend level increases beyond 30%. The higher cetane number of biodiesel reduces the ignition delay, resulting in reduced noise and vibration from the engine [104]. This also reduces the premixed combustion event of diesel operation, known to have a significant influence on the production of NO_x emissions.

Hydrogenated-Derived Renewable Fuel, Hydrogenated Vegetable Oil (HVO), or Green Diesel

Green diesel refers to the diesel-like fuel product produced from renewable feedstocks utilizing the conventional distillation process for petroleum fuel. Because conventional distillation methods are used to produce this fuel, the properties are very similar to petroleum diesel and it blends well with conventional fuel. The fuels are straight chain paraffinic hydrocarbons that do not contain aromatics, oxygen, or sulfur. Neste claims that their green diesel, named NExBTL results in an 18% reduction in NO_x and almost a 30% reduction in PM, compared to petroleum diesel fuel [105]. This data was the result of a delayed injection event from a lower bulk modulus compared to petroleum diesel. It has been found that the bulk modulus on

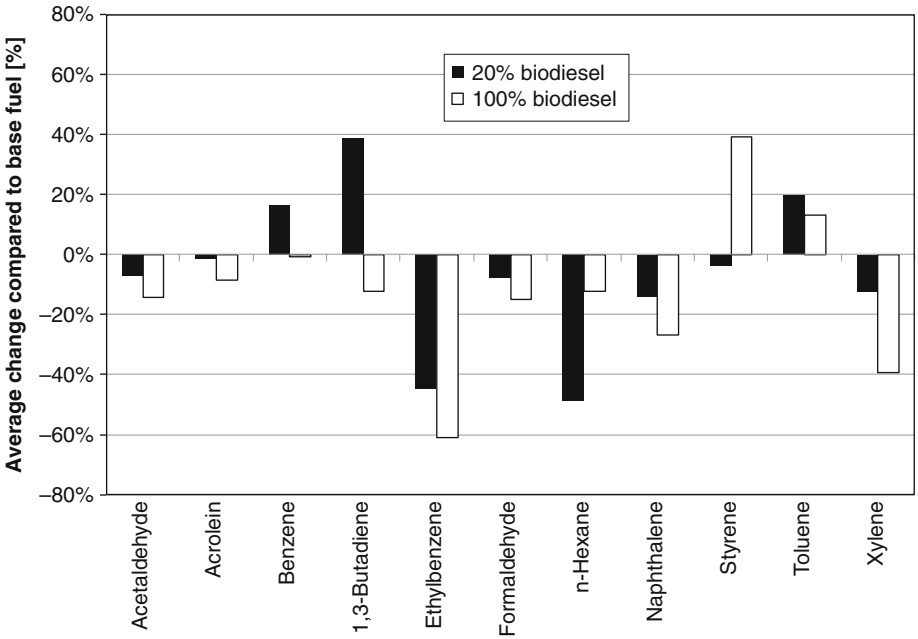

Internal Combustion Engines, Alternative Fuels for. Figure 18
Comparison of gaseous, toxic emissions at two biodiesel blend ratios [103]

pump-line-nozzle injection systems is a sensitive parameter in affecting the start of injection. Therefore, each fuel system needs to be custom tuned for different alternative fuels to ensure optimum performance and minimal emissions. This requires advanced sensors and significantly more involved calibration to enable flex-fuel operation in the field.

In another study using a common-rail injection system, the impact of 30% and 100% HVO on emissions and fuel consumption was studied. Figure 19 shows the significant reduction in emissions and even gravimetric fuel consumption when no changes were made to the injection system. Additional benefits were realized by modifying the injection timing depending on the parameter of interest. For example, when specific fuel consumption (SFC) was held constant for all three fuels, the 100% HVO reduced NO_x by 16% and smoke by 23% compared to petroleum diesel fuel [106].

Synthetic Diesel

Synthetic diesel fuel is characterized by high cetane number, low pour point, low sulfur content, and high energy density. These characteristics provide a high quality alternative diesel fuel that is capable of blending with petroleum diesel at any ratio. In one study utilizing a synthetic diesel fuel derived from biomass feedstock (BTL), emissions and fuel consumption were positively impacted when operating the engine on the BTL fuel. The engine was a 1.7 L, four-cylinder, direct injected diesel (Euro II) with intercooled turbocharging. A single speed/load point was utilized for all the testing, which simulated a typical cruise point for this engine. The fuel was produced by Choren Industries under the brand name SunDiesel. The impact on NO_x and BSEC is shown in Fig. 20. Brake specific energy consumption (BSEC) was utilized instead of brake specific fuel consumption (BSFC) due to the varying energy densities between the baseline D2 diesel fuel and SunDiesel. Depending on the parameter of concern, a significant reduction in NO_x emissions at the same BSEC level was achievable with the synthetic diesel fuel [107].

A significant reduction in the number of soot particles in the exhaust stream was measured when the engine was operated on SunDiesel, as shown in Fig. 21. There is also a slight shift toward smaller particles for

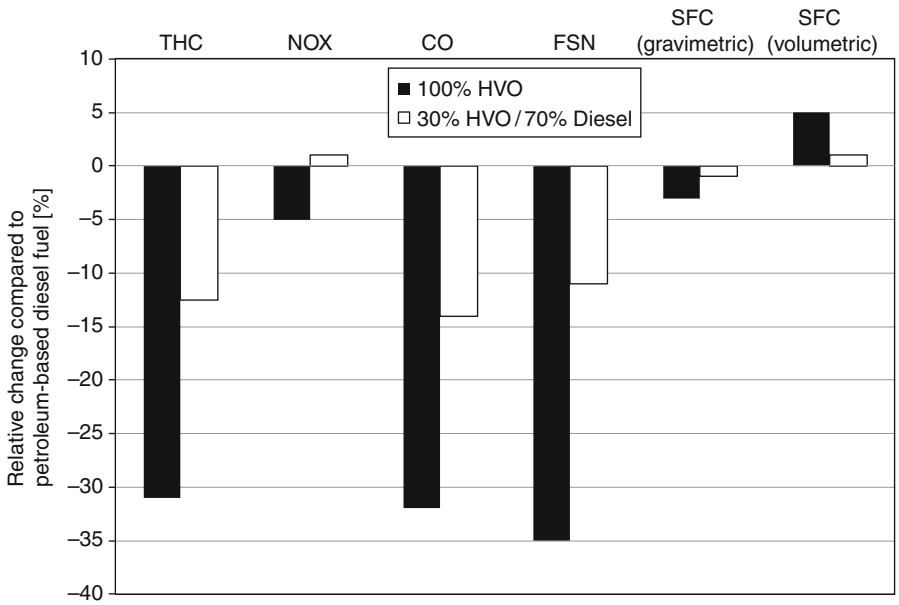

Internal Combustion Engines, Alternative Fuels for. Figure 19
Impact of green diesel (HVO) on emissions and fuel consumption [106]

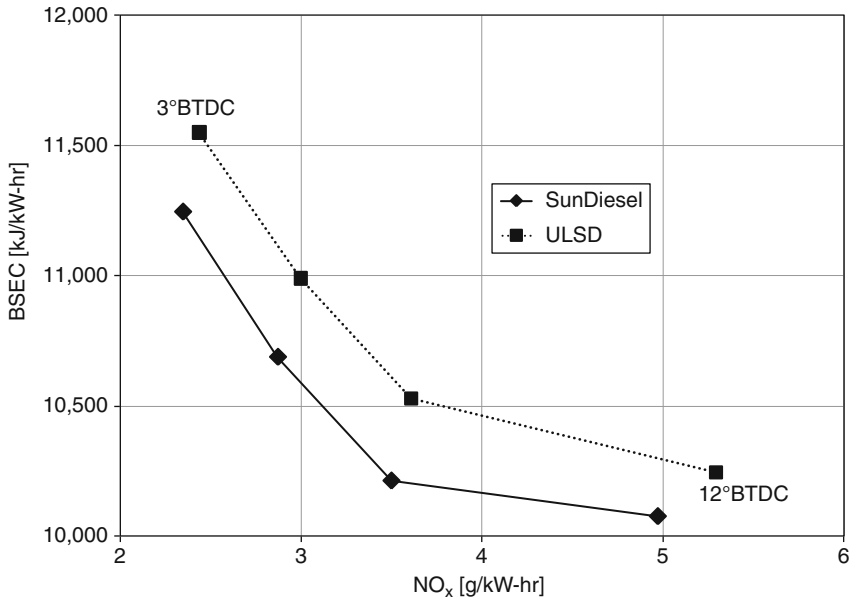

Internal Combustion Engines, Alternative Fuels for. Figure 20
Brake-specific energy consumption versus specific NO_x emissions for D2 and SunDiesel [107]

the synthetic diesel fuel compared to the petroleum based fuel. This modification of the particulate matter size and quantity can have implications on the particulate filter efficiency and regeneration.

In a comprehensive look at GTL, BTL, and CTL fuels produced using the Fischer–Tropsch process, Gill et al. [108] concluded that the higher cetane number and lower aromatic content were the primary fuel

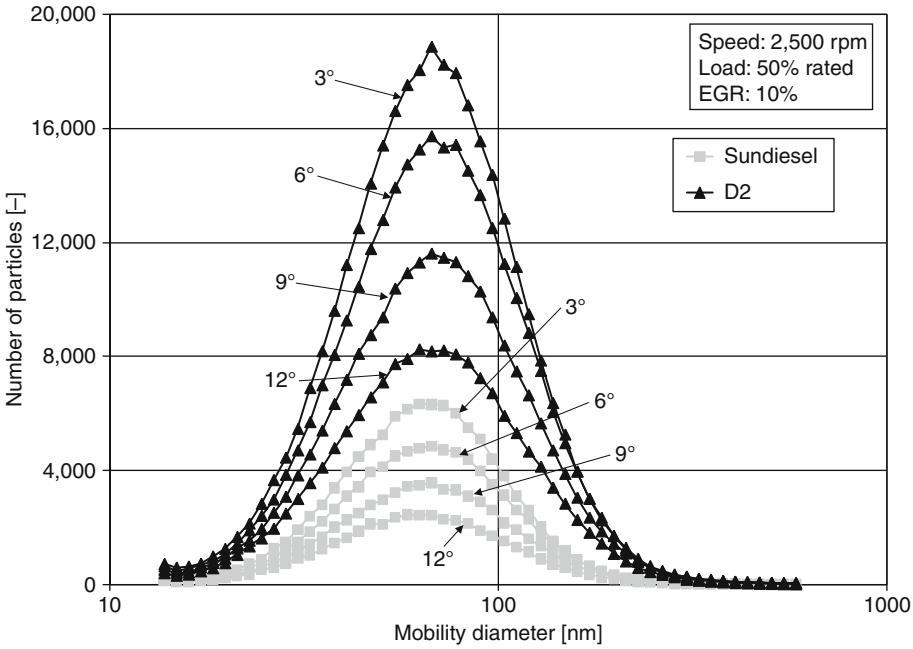

Internal Combustion Engines, Alternative Fuels for. Figure 21
Soot particle size and distribution for D2 and SunDiesel [107]

properties that directly affected the emissions. The higher cetane number reduced the ignition delay, leading to a reduction in NO_x emissions. Typically, injection timing is retarded to reduce NO_x emissions but at the expense of fuel consumption (higher BSFC). With a higher cetane number and thus lower ignition delay, the injection timing can be delayed with almost no impact on the BSFC. The shorter ignition delay also provides additional time for the oxidation of soot particles and subsequently reduced the engine-out particulate matter. The reduced aromatic content of the XTL fuels reduced the formation of soot by removing soot nucleation sites [108]. EGR is another effective method of reducing NO_x emissions but typically increases the PM production. XTL fuels with their lower aromatic content have a higher tolerance to EGR, producing less PM emission for the same EGR rate as petroleum diesel fuel.

Dimethyl Ether (DME)

DME is characterized by high cetane (>55) and low emissions characteristics. The oxygenated fuel has been shown to reduce PM, NO_x, and THC emissions compared to petroleum diesel fuel and engine noise is typically reduced as well. The absence of carbon–carbon bonds combined with high oxygen content (~35 wt.%) and rapid evaporation are the primary reasons for the emissions reduction with DME. This makes it an attractive alternative fuel for compression-ignition engines and provides additional means to reduce NO_x emissions through injection timing without a significant increase in PM emissions. However, DME has poor lubricity and high compressibility compared to diesel fuel and thus requires modification to the fuel delivery and storage system. To achieve comparable mileage to a petroleum diesel vehicle, the fuel storage capacity for a DME-powered vehicle would have to be doubled [110].

As shown in Fig. 22, DME has shown significant reductions in HC, CO, and NO_x emissions compared to petroleum diesel. Smoke emissions for DME were too low to be measured. Of interest is the associated reduction in BSFC, though perhaps a BSEC comparison would be more meaningful due to differences in energy density.

DME can be produced from the conversion of natural gas, coal, oil residues, and bio-mass [109]. DME is

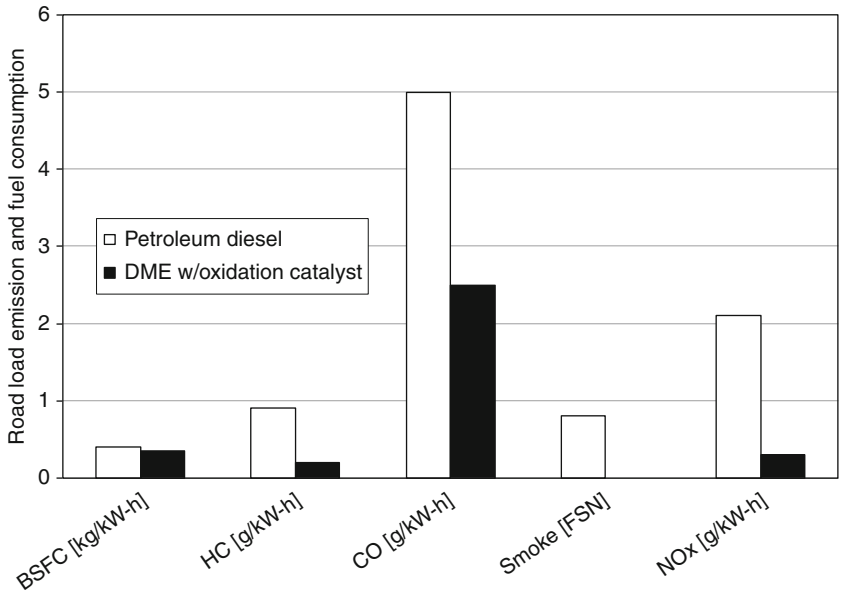

Internal Combustion Engines, Alternative Fuels for. Figure 22
Road load emissions and fuel consumption for DME and conventional petroleum diesel [110]

an effective energy carrier and reforming of DME to produce hydrogen-rich fuel-cell streams is currently being researched. In fact, hydrogen yields have been found to be equivalent to methanol at comparable operating temperatures [110].

When comparing alternative fuels on a well-to-wheels analysis for efficiency and GHG production, DME combined with existing engine technology is quite favorable. For example, compression-ignition engines operating on DME has the highest well-to-wheel efficiency of all non-petroleum–based fuel utilizing conventional, hybrid-electric, and fuel processor fuel cell technologies (excluding natural gas) [110]. When compared against existing engine technology, DME produces the lowest amount of well-to-wheel GHG emissions compared to FT diesel, biodiesel, methanol, and ethanol [110].

Alcohol/Diesel Blends

Various drivers including energy security and potential for emissions reduction of diesel engines have triggered attempts to blend diesel with alcohol fuels. A variety of factors including blend stability, viscosity and lubricity, materials compatibility, energy content, cetane number, safety and biodegradability have to be considered if alcohol is to be added to conventional diesel fuel for engine applications. Although all factors require attention, the safety aspect is particularly emphasized at this point. Diesel fuel has a flashpoint of 64°C and is therefore classified as a Class II or combustible liquid according to NFPA guidelines. Alcohol fuels as well as gasoline with flashpoints below 37.8°C (see Table 1) are classified as Class I or flammable liquids requiring more stringent storage requirements such as greater distance in location of storage tanks from property lines, buildings, and other tanks. Studies have shown that blends of 10, 15, and 20 vol % of ethanol in diesel exhibit combustion safety characteristics essentially identical to those for pure ethanol. Essentially any blend of alcohol with diesel fuel has to be stored and handled like gasoline rather than diesel [111, 112].

Blends of diesel and ethanol, also referred to as E-Diesel, generally show increased specific fuel consumption due to the lower energy content of ethanol compared to diesel. However, engine efficiencies remain constant or improve slightly with addition of ethanol. It is also accepted that the addition of ethanol to diesel fuel has a beneficial effect in reducing the PM emissions at least. The amount of improvement varies

from engine to engine and also within the working range of the engine itself [113]. A heat release and emissions study of 5, 10, and 15 vol % ethanol/diesel blends also concluded that soot, NO_x, and CO emissions decreased with increasing blend levels while hydrocarbon emissions showed an opposite trend [114].

A comparative study of methanol diesel and ethanol diesel blends at blend levels of 5 and 10 vol % on a single-cylinder engine concluded that trends for both alcohols were similar. The results suggest a consistent reduction in soot and CO emissions as well as increased specific fuel consumption with alcohol addition. However, the reported trends of decreasing HC emissions and increasing NO_x emissions with addition of ethanol and methanol are inconsistent with earlier studies. All reported trends did not show any significant difference between addition of ethanol and methanol [115].

A study was performed using a four-cylinder Mercedes Benz C220 turbo-diesel vehicle and comparing the emissions for conventional diesel fuel, 20 vol % and 40 vol % *n*-butanol. Tests were performed for the cold-start UDDS, hot-start UDDS, and HWFET drive cycles as well as several steady-state points. The results showed that for the urban drive cycle, both total hydrocarbon (THC) and carbon monoxide (CO) emissions increased as larger quantities of butanol were added to the diesel fuel. Oxides of nitrogen (NO_x) were not significantly affected by the 20% butanol blend and decreased with the 40% butanol blend. Drivability of the vehicle decreased noticeably for the 40% butanol blend, especially for the cold-start urban drive cycle. Fuel consumption increased and thus fuel economy decreased (mpg) as the blend ratio of butanol increased, as shown in Fig. 23 due primarily to the lower energy density of butanol compared to diesel.

For the steady state tests, a significant reduction in filter smoke number (FSN) with increasing butanol quantity was observed, as shown in Fig. 24 [116].

A performance and emissions study performed on a 6.0 L bus engine at several steady state operating points reached similar conclusions. At the tested blend levels of 8 and 16 vol % of *n*-butanol with diesel, smoke, NO_x, and CO emissions were consistently reduced with increasing butanol content. At the same time increasing butanol content also resulted in increased HC emissions as well as increased specific

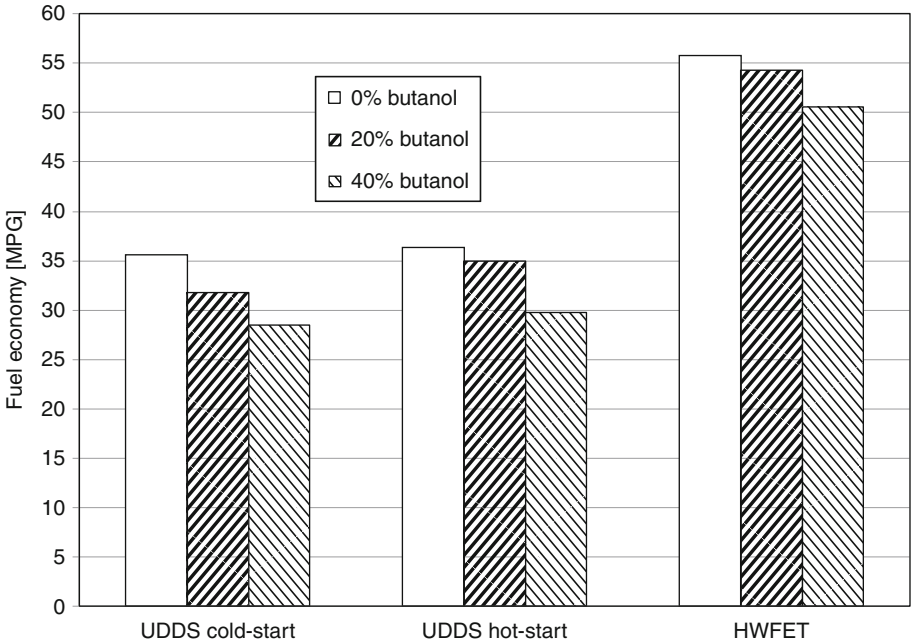

Internal Combustion Engines, Alternative Fuels for. Figure 23
Impact on fuel economy for butanol/diesel blends over three drive cycles [116]

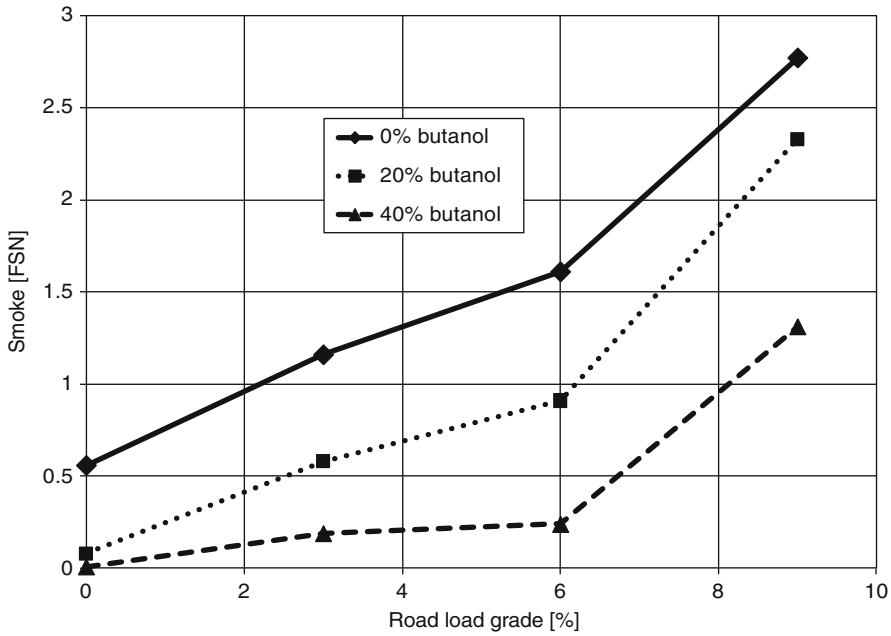

Internal Combustion Engines, Alternative Fuels for. Figure 24
Effect of *n*-butanol in diesel fuel on smoke emissions [116]

fuel consumption despite a simultaneous increase in engine efficiency [117].

Although the technical advantages of alcohol addition to diesel have been demonstrated other limiting factors such as blend stability, materials compatibility and, especially, safety have to be critically evaluated. Given that even addition of small amounts of alcohol changes the flammability dramatically raises the question on whether a transition to alcohol diesel blends is economically viable.

Future Directions

Although alternative fuels can be grouped according to their fuel properties or suitability for certain engine types, their diversity requires dedicated engines to fully utilize their unique characteristics. Due to the wide range of engine applications with their specific requirements such as emissions limits or efficiency targets and the variety of alternative fuel options with specific advantages and limitations it is likely that a future transportation scenario will rely on an increased range of fuels. Meeting current and future engine and vehicle efficiency as well as emissions targets will likely also require advanced combustion concepts to be implemented which in turn might benefit from introduction of alternative fuels. To this extent a stronger link between engine development and fuel development is desirable which should result in optimized utilization of certain fuel properties in dedicated engines. This would put an end to the currently applied approach of developing fuels that best mimic the properties of gasoline or diesel which themselves are far from optimal for certain engine concepts.

Further, an isolated evaluation of fuels based on their efficiency potential or emissions characteristics will likely yield a suboptimal solution. Assessment of alternative fuel options must include technical merits and downsides as well as economical aspects. While technical considerations have been discussed here, an economical assessment including the entire vehicle and fuel life cycle known as "well-to-wheel" analysis has to be performed. These assessments have to include factors such as fuel production, storage and distribution options as well as secondary factors such as water use, recycling, or land usage. Furthermore, findings and recommendations of such studies might vary dramatically depending on regional factors such as climate as

well as typical driver behavior. To this extent a link between engine and fuel related aspects and vehicle related aspects will have to be established which will clarify the impact of engine and fuel choices for different powertrain configurations such as hybrid vehicles.

Overall improving energy security while reducing harmful pollutants as well as greenhouse gas emissions will require a combination of improved transportation efficiency and increased use of alternative fuels. Any efficiency benefit a new engine technology can provide is also desirable when burning alternative fuels along the lines of "Using alternative fuels is desirable, having to use less even more so."

Bibliography

Primary Literature

1. Dutton K (2006) A brief history of the car. New Ideas 1
2. Diesel R (1894) Theory and construction of a rotational heat motor. Spon & Chamberlain, London
3. MacLean H, Lave LB (2003) Evaluating automobile fuel/propulsion system technologies. Prog Energy Combust Sci 29:1–69
4. Tanaka R (2007) Biofuels in Japan. Report by the British Embassy in Tokyo
5. Section 201-202 Renewable Fuel Standard (RFS) Energy Independence and Security Act of 2007 (Pub.L. 110-140, originally named the CLEAN Energy Act of 2007)
6. Schnepf R, Yacobucci B (2010) Renewable Fuel Standard (RFS): Overview and issues. CRS Report for Congress, Order Code R40155
7. Sperling D, Gordon D (2009) Two billion cars: driving toward sustainability. Oxford University Press, New York, pp 42–43. ISBN 978-0-19-537664-7
8. Yacobucci BD (2008) Natural gas passenger vehicles: availability, cost, and performance. CRS Report for Congress. Order Code RS22971
9. Brazilian Automotive Industry Association – ANFAVEA, Brazilian Automotive Industry Yearbook 2010. Available online at http://anfavea2010.virapagina.com.br/anfavea2010/
10. Energy Information Administration (2008) Annual survey of alternative fuel vehicle suppliers and users, "as reported in" Alternatives to traditional Transportation fuels 1998–2008 reports (Tables 14 or S1 depending on year of report). www.eia.doe.gov/cneaf/alternate/page/atftables/afv-atf2008.pdf
11. US Energy Information Administration (EIA) (Apr 2010) EIA's Alternatives to traditional transportation fuels, Table V1. www.eia.doe.gov/cneaf/alternate/page/atftables/afv-atf2008.pdf
12. European Biodiesel Board (2009) http://www.ebb-eu.org/stats.php
13. International Energy Agency (IEA) Statistics division (2007) Energy balances of OECD countries (2008 edition)–Extended balances and energy balances of Non-OECD countries (2007 edition)–Extended balances. IEA, Paris. http://data.iea.org/ieastore/default.asp
14. http://www.biodiesel.org/buyingbiodiesel/plants/
15. Boyd RA (2009) Proposed method of sale and quality specification for hydrogen vehicle fuel. Summary of current information. Standards Fuel Specifications Subcommittee (FSS). U.S. National Work Group for the Development of Commercial Hydrogen Measurement
16. American Petroleum Institute (API) (2001) Alcohols and ethers, Publication No. 4261, 3rd edn. API, Washington, DC
17. Whims J (2002) Pipelines considerations for ethanol, Agricultural marketing resource center. Kansas State University
18. Perry RH, Green DW (1999) Perry's chemical engineers' handbook. McGraw Hill, Malaysia
19. Heywood JB (1988) Internal combustion engine fundamentals. McGraw-Hill, New York
20. Andersen V, Anderson JE, Wallington TJ, Mueller SA, Nielsen OJ (2010) Vapor pressures of alcohol-gasoline blends. Energy Fuels 24:3647–3654
21. The Royal Society (2008) Sustainable biofuels: prospects and challenges. The Royal Society, London. ISBN 978 0 85403 662 2
22. Bradley D (2009) Combustion and the design of future engine fuels. Proc. IMechE Part C: J. Mech Eng Sci 223:JMES1519. doi: 10.1243/09544062JMES1519
23. Foss M (2007) Introduction to LNG. An overview on liquefied natural gas (LNG), its properties, organization of the LNG industry and safety considerations
24. http://www.naturalgas.org/overview/background.asp
25. Lapuerta M, Armas O, Rodrıguez-Fernandez J (2008) Effect of biodiesel fuels on diesel engine emissions. Prog Energy Combust Sci 34:198–223
26. Teng H, McCandless JC, Schneyer JB (2004) Thermodynamic properties of dimethyl ether – an alternative fuel for compression-ignition engines. SAE Technical Paper 2004-01-0093
27. Tilli A, Kaario O, Imperato M, Larmi M (2009) Fuel injection system simulation with renewable diesel fuels. SAE Technical paper 2009-24-0105
28. Teng H, McCandless JC, Schneyer JB (2001) Thermochemical characteristics of dimethyl ether — an alternative fuel for compression-ignition engines. SAE Technical Paper 2001-01-0154
29. Teng H, McCandless JC, Schneyer JB (2002) Viscosity and lubricity of (Liquid) dimethyl ether – an alternative fuel for compression-ignition engines. SAE Technical Paper 2002-01-0862
30. Knothe G (2008) "Designer" biodiesel: optimizing fatty ester composition to improve fuel properties. Energy Fuels 22:1358–1364
31. Knothe G (2005) Dependence of biodiesel fuel properties on the structure of fatty acid alkyl esters. Fuel Process Technol 86:1059–1070
32. Sanford SD et al (2009) Feedstock and biodiesel characteristics report, Renewable Energy Group, Inc. www.regfuel.com

33. Kinast JA (2003) Production of biodiesel from multiple feedstocks and properties of biodiesel and biodiesel/diesel blends, NREL/SR-510-31460, March 2003
34. Abu-Zaid M, Badran O, Yamin J (2004) Effect of methanol addition on the performance of spark ignition engines. Energy Fuels 18:312–315
35. Song R, Hu T, Liu S, Liang X (2008) Combustion characteristics of SI engine fueled with methanol gasoline blends during cold start. Front Energy Power Eng China 2(4):395–400
36. Caton JA (2009) A thermodynamic evaluation of the use of alcohol fuels in a spark-ignition engine. SAE Paper No. 2009-01-2621
37. Li J, Gong C, Su Y, Dou H, Liu X (2010) Effect of injection and ignition timings on performance and emissions from a spark-ignition engine fueled with methanol. Fuel 89:3919–3925
38. Environmental Protection Agency. Regulation of fuels and fuel additives; definition of substantially similar. [FRL-3856-9]
39. http://www.faqs.org/faqs/autos/gasoline-faq/part1/section-4.html
40. http://www.epa.gov/otaq/regs/fuels/additive/e15/420f10054.htm
41. Ré-Poppi N, Almeida FFP, Cardoso CAL, Raposo JL Jr, Viana LH, Silva TQ, Souza JLC, Ferreira VS (2009) Screening analysis of type C Brazilian gasoline by gas chromatography – Flame ionization detector. Fuel 88:418–423
42. Bennett J (2007) Bioethanol in road transport fuels. Presentation at the Royal Society 'International Biofuels Opportunities' conference and workshop, London
43. Joseph Jr H (2007) The vehicle adaptation to ethanol fuel. Presentation at the Royal Society 'International Biofuels Opportunities' conference and workshop, London
44. Jones B, Mead G, Steevens P, Timanus M (2008) The Effects of E20 on metals used in automotive fuel system components. Report by the Minnesota Center for automotive research at Minnesota State University, Mankato
45. Jones B, Mead G, Steevens P (2008) The Effects of E20 on plastic automotive fuel system components. Report by the Minnesota center for automotive research at Minnesota State University, Mankato
46. Jones B, Mead G, Steevens P, Connors C (2008) The Effects of E20 on elastomers used in automotive fuel system components. Report by the Minnesota center for automotive research at Minnesota State University, Mankat
47. Kar K, Cheng W, Ishii K (2009) Effects of ethanol content on gasohol PFI engine wide-open-throttle operation. SAE Paper No. 2009-01-1907
48. Grabner P, Eichlseder H, Eckhard G (2010) Potential of E85 direct injection for passenger car application. SAE Paper No. 2010-01-2086
49. Saab engine specifications (2008) http://dyc.saab-web.com/main/GLOBAL/en/model/95/techspecs.shtml. Accessed 31 May 2011
50. West B, López A, Theiss T, Graves R, Storey J, Lewis S (2007) Fuel economy and emissions of the ethanol-optimized Saab 9-5 biopower. SAE Paper No. 2007-01-3994
51. Wallner T, Frazee R (2010) Study of regulated and non-regulated emissions from combustion of gasoline, alcohol fuels and their blends in a DI-SI engine. SAE Paper No. 2010-01-1571
52. Boretti A (2010) Analysis of design of pure ethanol engines. SAE Paper No. 2010-01-1453
53. Kabasin D, Hoyer K, Kazour J, Lamers R, Hurter T (2009) Heated injectors for ethanol cold starts. SAE Paper No. 2009-01-0615
54. Jeuland N, Montagne X, Gautrot X (2004) Potentiality of ethanol as a fuel for dedicated engine. Oil & Gas Sci Technol Rev IFP 59(6):559–570
55. Schubert A (2010) Expanding the role of biofuels through development of advanced BioButanol. Biofuels Workshop. SAE International Fuels & Lubricants Meeting. Rio de Janeiro
56. Wallner T, Miers S, McConnell S (2009) A comparison of ethanol and butanol as an oxygenate and their effect on efficiency, combustion performance and emissions of a direct-injected 4-cylinder engine. J Engin Gas Turbines Power 131(3):032802–032809
57. Cooney C, Wallner T, McConnell S, Gillen J, Abell C, Miers S (2009) Effects of blending gasoline with ethanol and butanol on engine efficiency and emissions. In: ASME Spring technical conference. Milwaukee/WI. ASME Paper No. ICES2009-76155
58. Szwaja S, Naber JD (2010) Combustion of *n*-butanol in a spark-ignition IC engine. Fuel 89:1573–1582
59. Dernotte J, Mounaim-Rousselle C, Halter F, Seers P (2010) Evaluation of Butanol–gasoline blends in a port fuel-injection, Spark-ignition engine. Oil & Gas Science and Technology – Rev IFP 65(2):345–351
60. http://www.lpgli.com/features.html
61. Li X, Yang L, Pang M, Liang X (2010) Effect of LPG injection methods on engine performance. Adv Mater Res 97–101:2279–2282
62. LPG Autogas (2005) Expansion Issue 1
63. Saraf RR, Thipse SS, Saxena PK (2009) Comparative emission analysis of gasoline/LPG automotive bifuel engine. Int J Environ Sci Eng 1:4
64. Energy Information Administration, Documentation for Emissions of Greenhouse Gases in the U.S. 2005, DOE/EIA-0638 (2005), Oct 2007
65. Oh S, Lee S, Choi Y, Kang K, Cho J, Cha K (2010) Combustion and emission characteristics in a direct injection LPG/Gasoline spark ignition engine. SAE Paper No. 2010-01-1461
66. Boretti AA, Watson HC (2009) Development of a direct injection high flexibility CNG/LPG spark ignition engine. SAE Paper No. 2009-01-1969
67. Heywood JB, Welling OZ (2009) Trends in performance characteristics of modern automobile SI and diesel engines. SAE Paper No. 2009-01-1892
68. CIMAC Working Group "Gas Engines" (2008) Information about the use of LNG as engine fuel. CIMAC position paper
69. Westport Innovations Inc (2010) Direct injection natural gas demonstration project. Westport GX Geavy-Duty LNG engine, Canada

70. Mattas G, Thijssen B (2004) Dual-fuel diesel engines for LNG carriers. Marine News 1
71. ETSAP (2010) Energy Technology Systems Analysis Programme. Automotive LPG and Natural gas engines. http://www.etsap.org
72. NREL (1999) Honda civic dedicated CNG Sedan. Fact Sheet
73. Honda website. http://automobiles.honda.com
74. Thien U (2008) Widening the driving range of NGV 's. Presentation 6th European Forum Gas, Bratislava
75. Korakianitis T, Namasivayam AM, Crookes RJ (2011) Natural-gas fueled spark-ignition (SI) and compression-ignition (CI) engine performance and emissions. Prog Energy Combust Sci 37(1):89–112
76. Aslam MU, Masjuki HH, Kalam MA, Abdesselam H, Mahlia TMI, Amalina MA (2006) An experimental investigation of CNG as an alternative fuel for a retrofitted gasoline vehicle. Fuel 85:717–724
77. Geok HH, Mohamad TI, Abdullah S, Ali Y, Shamsudeen A, Adril E (2009) Experimental investigation of performance and emission of a sequential port injection natural gas engine. Eur J Sci Res 30(2):204–214, ISSN: 1450-216X
78. Cho HM, He B-Q (2008) Combustion and emissions characteristics of a lean burn natural gas engine. Int J Automot Technol 9(4):415–422
79. Packham K (2007) Lean-burn engine technology increases efficiency, reduces NO_x emissions. Power topic #7009. Technical information from cummins power generation
80. Zeng K, Huang Z, Liu B, Liu L, Jiang D, Ren Y, Wang J (2006) Combustion characteristics of a direct-injection natural gas engine under various fuel injection timings. Appl Therm Eng 26:806–813
81. Goto Y, Sato Y, Narusawa K (1998) Combustion and emissions characteristics in a direct injection natural gas engine using multiple stage injection. Proceedings of the International Symposium on Diagnostics and Modeling of Combustion in Internal Combustion Engines (COMODIA), 1998. Japan Society of Mechanical Engineers, pp 543–548
82. Tunestål P, Christensen M, Einewall P, Andersson T, Johansson B (2002) Hydrogen addition for improved lean burn capability of slow and fast burning natural gas combustion chambers. SAE Paper No 2002-01-2686
83. ASTM Standardization News (2010) The renewed promise of natural gas. ASTM Committee D03 and natural gas standards by Adele Bassett. May/June 2010
84. Hallmannsegger M, Fickel H-C (2004) The mixture formation process of an internal combustion engine for zero CO_2-emission vehicles fueled with cryogenic hydrogen. In: IFP International Conference, Rueil-Malmaison, France
85. DOE EERE website. http://www1.eere.energy.gov/hydrogenandfuelcells/storage/current_technology.html?m=1&
86. Wallner T (2009) Opportunities and risks for hydrogen internal combustion engines in the United States. In: Conference proceedings "Der Arbeitsprozess der Verbrennungskraftmaschine." Verlag d. Technischen Universität Graz. ISBN 978-3-85125-068-8
87. Rottengruber H, Berckmueller M, Elsaesser G, Brehm N, Schwarz C (2004) Operation strategies for hydrogen engines with high power density and high efficiency. In: 15th annual U.S. hydrogen conference, Los Angeles, CA
88. Verhelst S, Wallner T (2009) Hydrogen-fueled internal combustion engines (H2ICEs). Prog Energy Combust Sci 35:490–527
89. Eichlseder H, Wallner T, Freymann R, Ringler J (2003) The potential of hydrogen internal combustion engines in a future mobility scenario. SAE Paper No. 2003-01-2267
90. Welch A, Mumford D, Munshi S, Holbery J, Boyer B, Younkins M, Jung H (2008) Challenges in developing hydrogen direct injection technology for internal combustion engines. SAE Paper No. 2008-01-2379
91. Heindl R, Eichlseder H, Spuller C, Gerbig F, Heller K (2009) New and innovative combustion systems for the H2-ICE: compression ignition and combined processes. SAE Paper No. 2009-01-1421
92. Obermair H, Scarcelli R, Waller T (2010) Efficiency improved combustion system for hydrogen direct injection operation. SAE Paper No. 2010-01-2170
93. Tanno S, Ito Y, Michikawauchi R, Nakamura M, Tomita H (2010) High-efficiency and Low-NO_x hydrogen combustion by high pressure direct injection. SAE Paper No. 2010-01-2173
94. Tang X, Stockhausen WF, Kabat DM, Natkin RJ, Heffel JW (2002) FordP hydrogen engine dynamometer development. SAE Paper No. 2002-01-0242
95. Salimi F, Shamekhi AH, Pourkhesalian AM (2009) Role of mixture richness, spark and valve timing in hydrogen-fuelled engine performance and emission. Int J Hydrogen Energy 34:3922–3929
96. ETEC hydrogen internal combustion engine full-size pickup truck conversion. Hydrogen ICE truck brochure
97. Wallner T, Lohse-Busch H, Shidore N (2008) Operating strategy for a hydrogen engine for improved drive-cycle efficiency and emissions behavior. Int J Hydrogen Energy 34:4617–4625
98. Wimmer A, Wallner T, Ringler J, Gerbig F (2005) H2-direct injection – a highly promising combustion concept. SAE Paper No. 2005-01-0108
99. Wallner T, Lohse-Busch H, Gurski S, Duoba M, Thiel W, Martin D, Korn T (2008) Fuel economy and emissions evaluation of a BMW hydrogen 7 mono-fuel demonstration vehicle. Int J Hydrogen Energy 33:7607–7618
100. http://www.biodiesel.org/resources/biodiesel_basics/
101. United States Environmental Agency (2002) A comprehensive analysis of biodiesel impacts on exhaust emissions. EPA420-P-02-001, Oct 2002
102. Mueller CJ, Boehman AL, Martin GC (2009) An experimental investigation of the origin of increased NO_x emissions when fueling a heavy-duty compression-ignition engine with soy biodiesel. SAE Int J Fuels Lubr 2:789–816
103. Graboski et al (2003) The effect of biodiesel composition on engine emissions from a DDC series 60 engine. NREL/SR-510-31461

104. Agarwal AK (2006) Biofuels (alcohols and biodiesel) applications as fuels for internal combustion engines. Prog Energy Combust Sci 33:233–271
105. Kuronen M, Mikkonen S, Aakko P, Murtonen T (2007) Hydrotreated vegetable oil as fuel for heavy duty diesel engines. SAE Technical Paper 2007-01-4031
106. Aatola H, Larmi M, Sarjovaara T, Mikkonen S (2008) Hydrotreated Vegetable Oil (HVO) as a renewable diesel fuel: trade-off between NO_x, particulate emission, and fuel consumption of a heavy duty engine. SAE Technical Paper 2008-01-2500
107. Miers SA, Ng H, Ciatti SA, Stork K (2005) Emissions, performance, and In-cylinder combustion analysis in a light-duty diesel engine operating on a Fischer-Tropsch, Biomass-to-Liquid Fuel. SAE Technical Paper 2005-01-367
108. Gill SS et al (2010) Combustion characteristics and emissions of Fischer Tropsch diesel fuels in IC engines. Progr Energy Combust Sci 31:466–487. doi:10.1016/j.pecs.2010.09.001
109. Arcoumanis C, Bae C, Crookes R, Kinoshita E (2008) The potential of di-methyl ether (DME) as an alternative fuel for compression-ignition engines: a review. Fuel 87:1014–1030
110. Semelsberger TA, Borup RL, Greene HL (2006) Dimethyl ether (DME) as an alternative fuel. J Power Sour 156:497–511
111. McCormick RL, Parish R (2001) Advanced petroleum based fuels Program and renewable diesel program milestone report: technical barriers to the use of ethanol in diesel fuel. NREL/MP-540-32674
112. Waterland LR, Venkatesh S, Unnasch S (2003) Safety and performance assessment of ethanol/diesel blends (E-diesel). Subcontractor Report NREL/SR-540-34817
113. Hansen AC, Zhang Q, Lyne PWL (2005) Ethanol - diesel fuel blends – a review. Bioresour Technol 96:277–285
114. Rakopoulos CD, Antonopoulos KA, Rakopoulos DC (2007) Experimental heat release analysis and emissions of a HSDI diesel engine fueled with ethanol–diesel fuel blends. Energy 32:1791–1808
115. Sayin C (2010) Engine performance and exhaust gas emissions of methanol and ethanol–diesel blends. Fuel 89:3410–3415
116. Miers S, Carlson R, Ng H, McConnell S, Wallner T, LeFeber J (2008) Drive cycle analysis of butanol/diesel blends in a light-duty vehicle. SAE Paper No. 2008-01-2381
117. Rakopoulos DC, Rakopoulos CD, Hountalas DT, Kakaras EC, Giakoumis EG, Papagiannakis RG (2010) Investigation of the performance and emissions of bus engine operating on butanol/diesel fuel blends. Fuel 89:2781–2790

Books and Reviews

Agarwal AK (2007) Biofuels (alcohols and biodiesel) applications as fuels for internal combustion engines. Prog Energy Combust Sci 33:233–271

Eichlseder H, Klell M (2008) Hydrogen in automotive engineering (in German, Wasserstoff in der Fahrzeugtechnik). Vieweg + Teubner, Wiesbaden. ISBN 978-9-8348-0478-5

Huo H, Wu Y, Wang M (2009) Total versus urban: well-to-wheels assessment of criteria pollutant emissions from various vehicle/fuel systems. Atmos Environ 43:1796–1804

MacLeana HL, Lave LB (2003) Evaluating automobile fuel/propulsion system technologies. Prog Energy Combust Sci 29:1–69

Pischinger R, Klell M, Sams T (2002) Thermodynamics of internal combustion engines (in German: Thermodynamik der Verbrennungskraftmaschine). Springer, Wien. ISBN 3-211-83679-9

Internal Combustion Engines, Developments in

Timothy J. Jacobs
Department of Mechanical Engineering,
Texas A&M University, College Station, TX, USA

I

Article Outline

Greek Symbols
Symbols
Glossary
Definition of the Subject
Introduction
The Basics of Internal Combustion Engines
A Case Study: Diesel Engines Versus Gasoline Engines
Future Directions of Internal Combustion Engines
Acknowledgments
Abbreviations
Bibliography

Greek Symbols

η_c Combustion efficiency
η_f Fuel conversion efficiency
$\eta_{f,b}$ Brake fuel conversion efficiency
$\eta_{f,i}$, Indicated fuel conversion efficiency
η_m Mechanical efficiency
η_{th} Thermal efficiency
$\eta_{th,Carnot}$ Thermal efficiency of the ideal Carnot cycle
$\eta_{th,Otto}$ Thermal efficiency of the ideal heat engine Otto cycle
η_v Volumetric efficiency
γ Ratio of specific heats
γ_b Ratio of specific heats of the burned mixture

φ Fuel–air equivalence ratio. For $\varphi < 1$ mixture is lean. For $\varphi = 1$, mixture is stoichiometric. For $\varphi > 1$, mixture is rich. Note that φ is the inverse of the often-used air–fuel equivalence ratio, or λ.
$\rho_{a,i}$ Inlet air density
τ Engine torque

Symbols

BMEP Brake mean effective pressure
$C_{p,b}$ Constant pressure specific heat of the burned mixture
$C_{v,b}$ Constant volume specific heat of the burned mixture
f Residual fraction
f_{final} Final calculated residual fraction
$f_{final-1}$ Previous iteration residual fraction to final calculated residual fraction
(F/A) Fuel–air ratio
FMEP Friction mean effective pressure
h_1 Specific enthalpy at state 1
h_2 Specific enthalpy at state 2
h_3 Specific enthalpy at state 3
h_{3a} Specific enthalpy at state 3a
h_5 Specific enthalpy at state 5
h_6 Specific enthalpy at state 6
h_e Specific enthalpy of exhaust mixture
h_i Specific enthalpy of inlet mixture
$\mathbf{IMEP_g}$ Gross indicated mean effective pressure
$\mathbf{IMEP_n}$ Net indicated mean effective pressure
m Mass
m_1 Mass at state 1
m_2 Mass at state 2
m_3 Mass at state 3
m_4 Mass at state 4
m_6 Mass at state 6
m_a Mass of air
m_f Mass of fuel
m_r Residual mass
m_{total} Total mass
$\dot{m}_a$ Mass flow rate of air
$\dot{m}_f$ Mass flow rate of fuel
MEP Mean effective pressure
M_b Molecular weight of the burned mixture
n_R Number of revolutions per engine cycle
N Engine speed
$\overline{R}$ Universal gas constant
R Gas constant
R_5 Gas constant of mixture at state 5
R_6 Gas constant of mixture at state 6
R_e Gas constant of exhaust mixture
P Cylinder pressure or power
P_1 Pressure at state 1
P_2 Pressure at state 2
P_3 Pressure at state 3
P_{3a} Pressure at state 3a
P_4 Pressure at state 4
P_5 Pressure at state 5
P_6 Pressure at state 6
P_7 Pressure at state 7
P_b Brake power
P_e Exhaust pressure
P_i Inlet (initial) pressure
P_{in} Net indicated power
P_{limit} Limit pressure
PMEP Pumping mean effective pressure
${}_1Q_2$ Heat transfer of process 1–2
${}_6Q_1$ Heat transfer for process 6–1
Q_{HV} Heating value of fuel
$Q_{HV,f}$ Heating value of fuel
$Q_{HV,i}$ Heating value of specie i
r_c Compression ratio
s_1 Entropy at state 1
s_2 Entropy at state 2
s_3 Entropy at state 3
s_4 Entropy at state 4
s_5 Entropy at state 5
T_1 Temperature at state 1
T_4 Temperature at state 4
T_5 Temperature at state 5
T_6 Temperature at state 6
$T_{cv,adiabatic}$ Constant volume adiabatic flame temperature
T_e Exhaust temperature
T_H Temperature of a source reservoir
T_i Inlet temperature
T_L Temperature of a sink reservoir
T_r Residual fraction temperature
u_1 Specific internal energy at state 1
u_2 Specific internal energy at state 2
u_3 Specific internal energy at state 3
u_{3a} Specific internal energy at state 3a
u_4 Specific internal energy at state 4
U_1 Internal energy at state 1

U_2 Internal energy at state 2
U_3 Internal energy at state 3
U_4 Internal energy at state 4
v_1 Specific volume at state 1
v_2 Specific volume at state 2
v_3 Specific volume at state 3
v_{3a} Specific volume at state 3a
v_4 Specific volume at state 4
V Cylinder volume
V_1 Volume at state 1
V_2 Volume at state 2
V_3 Volume at state 3
V_5 Volume at state 5
V_6 Volume at state 6
V_d Displaced volume
V_{max} Maximum cylinder volume
V_{min} Minimum cylinder volume
W Thermodynamic work
${}_1W_2$ Work for process 1–2
${}_2W_3$ Work for process 2–3
${}_3W_4$ Work for process 3–4
${}_4W_5$ Work for process 4–5
${}_5W_6$ Work for process 5–6
${}_6W_1$ Work for process 6–1
W_b Brake work
W_f Friction work
W_{gross} Gross work
W_{ig} Gross indicated work
W_{in} Net indicated work
W_{ip} Pump work
W_{net} Net work
x_i Mole fraction of specie i
y_i Mass fraction of specie i

Glossary

Combustion Rapid oxidation of a fuel–air mixture (reactants) converting reactants to products and in the process releasing thermal energy.

Lean Air–fuel mixture is such that there is more air than is chemically necessary to oxidize the available fuel.

Products Species formed as the result of a chemical reaction (in the context of this article species formed as the result of a combustion reaction).

Reactants Species that are to be involved in a chemical reaction (in the context of this article species that are to be involved in a combustion reaction).

Rich Air–fuel mixture is such that there is less air than is chemically necessary to oxidize the available fuel.

Stoichiometric Air–fuel mixture is chemically balanced such that there is the correct amount of air to fully oxidize the available fuel.

Definition of the Subject

An internal combustion (IC) engine is a thermodynamic work conversion device that converts chemical energy (typically delivered to the engine in the form of a liquid or gaseous fuel) to work energy (typically in the form of shaft work issuing from a rotating crankshaft). The internal combustion engine markedly distinguishes itself from other types of power-producing equipment – most notably, the heat engine (e.g., steam engine or steam-cycle plant). In the former, chemical energy is released, via combustion (i.e., rapid oxidation) mechanism, internal the same device that converts the released energy to work energy. In the latter, thermal energy is passed into the device via heat transfer; the device thereby converts the thermal energy to work energy. Because of this subtle difference, the thermodynamic limits of maximum efficiency of the internal combustion engine are constrained differently than the thermodynamic limit of maximum efficiency of the heat engine.

There are several types of internal combustion engines; the two most common being the piston/cylinder reciprocating engine and the gas turbine engine. This article constrains its discussion to just piston/cylinder reciprocating engines. As this article is meant to be brief, readers seeking additional and thorough information are referred to the associated cited articles and the authorities listed in "Books and Reviews".

Introduction

Internal combustion engines are pervasive to our daily activities. They are the primary powerhouse of the transportation industry. They serve as neighborhood and small municipality backup power generators or primary power stations. They provide convenience by powering lawnmowers, leaf blowers, and weed trimmers. They deliver excitement and entertainment in pleasure boats, race cars, and motor bikes. Their scale of usability nearly spans the scales of classical physics,

from as small as "micro engines" that fit in the palm of your hand to as large as marine engines that scale three stories and use human-sized doorways for entry into the cylinder block.

The story of the internal combustion engine dates back around 150 years ago, when J.J.E. Lenoir built an engine that combusted coal–air mixtures in a cylinder outfitted with a piston with a two-stroke type fashion (without compression). Soon thereafter, Nicolaus A. Otto and his colleague Eugen Langen expanded on the Lenoir concept, creating an engine that had 11% efficiency compared to Lenoir's 5%. Determined to improve efficiencies of internal combustion engines (which at 11%, were not much better than the steam engine), Otto built the first engine operating on the four-stroke principle which today serves as the primary operating cycle of engines [1]. It is here noted that, although Otto built the first working four-stroke engine, Alphonse Beau de Rochas described in theory the principles of the four-stroke cycle. Further, Beau de Rochas outlined several conditions to achieve maximum efficiency of the internal combustion engine [1].

From this point, and with the aid of several important developers including Rudolf Diesel, Sir Harry Ricardo, Robert Bosch, and Charles Kettering, the internal combustion engine has become one of the most highly efficient, power dense, cost-effective, easily maintained, and versatile power machinery available to consumers. This article will provide some of the important basic information about internal combustion engines, and indicate some of the more recent developments that continue to make internal combustion engines competitive as the preferred power-producing technology.

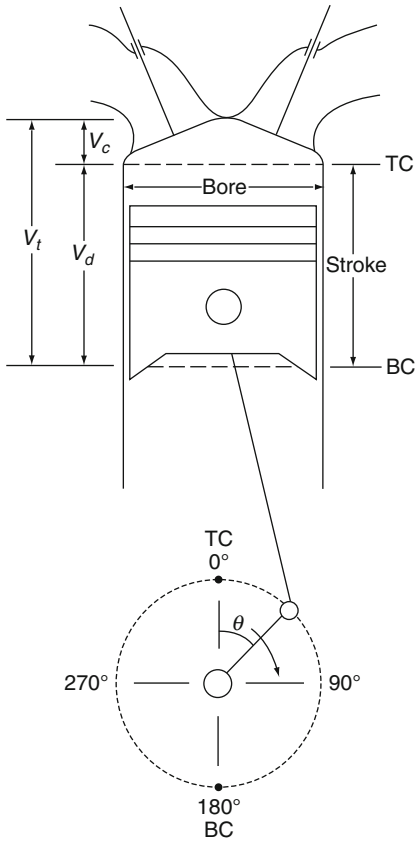

Internal Combustion Engines, Developments in.
Figure 1
Illustration of a piston/cylinder arrangement, as often employed in a reciprocating-piston internal combustion engine (Used with permission from [2])

The Basics of Internal Combustion Engines

Basic Operating Cycle

As this article concentrates its discussions of IC engines on those of the piston/cylinder reciprocating type, Fig. 1 [2] shows the basic geometrical considerations of the piston/cylinder/crankshaft arrangement, which kinematically is described as a crank-slider mechanism. The chemical energy to work energy conversion occurs inside the cylinder, usually bound on the sides by the cylinder walls, on the top by the cylinder head (which typically houses the gas exchange valves, such as the intake and exhaust valves, and other important hardware such as spark plugs and/or fuel injectors), and on the bottom by the piston which reciprocates within the cylinder. A rigid connecting rod fastens the piston to an eccentric location on the rotating crankshaft. The eccentric placement of the connecting rod converts the reciprocating motion of the piston (i.e., boundary motion work) to the rotating motion of the crankshaft (i.e., shaft work). The eccentric placement of the connecting rod to the crankshaft also dictates the important geometrical parameter of the piston engine called the "stroke." The stroke and "bore," or diameter of the cylinder, create the displaced volume, V_d, of the piston engine. The maximum volume of the cylinder, V_{max}, is attained when the piston is at its bottom-most

position; a position referred to as "bottom dead center," or BDC. The minimum volume, or clearance volume, V_c, is attained when the piston is at its top-most position; a position referred to as "top dead center," or TDC. The ratio between V_{max} and V_{min} is called the compression ratio, r_c, and is given as Eq. 1:

$$r_c = \frac{V_{max}}{V_{min}} \tag{1}$$

The compression ratio, as will be described in section on "Thermodynamic Analysis of Internal Combustion Engines", is a fundamentally critical parameter for controlling the efficiency (i.e., the ratio of work energy out to chemical energy in) of an internal combustion piston engine.

There are two major cycles used to exploit the piston engine's conversion of chemical energy to work energy: a "two-stoke" cycle and a "four-stroke" cycle. The earliest prototype engines were of the two-stroke variety (e.g., Lenoir and Otto/Langen engines) [1]. In pursuit of achieving higher efficiency, Otto (for whom the thermodynamic ideal "Otto Cycle" is named) built the four-stroke version of his engine [1]. Today, four-stroke cycle engines are the dominant form; thus, most of the article will center on the details of the four-stroke cycle.

Four-stroke cycle engines require four strokes of the piston to complete one power-producing cycle, as shown in Fig. 2 [3]; the reader is also referred to Fig. 4a to aid the discussion. Consider first the cycle starting with the piston at TDC and the intake valve open. The piston moves from TDC to BDC, inducting fresh mixture (conventionally, fuel and air in a gasoline engine and only air in a diesel engine) through the open intake valve in what is called the "intake stroke." At some location near BDC, the intake valve closes, and the piston reverses its motion at BDC. Once the valve closes, the piston/cylinder arrangement creates a closed system. As the piston moves from BDC to TDC, the trapped mixture is compressed in what is called the "compression stroke," increasing the mixture's temperature, pressure, and decreasing its specific volume (i.e., increasing its density). At a point near TDC combustion is expected to commence. In the case of a spark ignition engine (e.g., a conventional gasoline engine), combustion is initiated by the release of spark at a point near (usually advanced of) TDC. In the case of a compression ignition engine (e.g., a conventional diesel engine), combustion is initiated by injecting liquid fuel directly into the cylinder; the compressed air at elevated temperature and pressure atomizes, vaporizes, and mixes with the injected fuel. After a period of time,

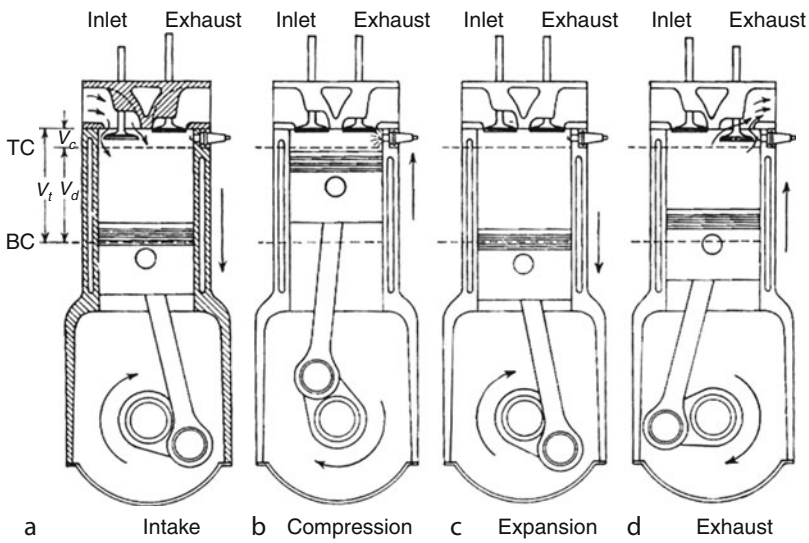

Internal Combustion Engines, Developments in. Figure 2
Illustration of the four-stroke operating principle (Used with permission from [3])

the high temperature environment causes chemical reaction and start of combustion. Around start of combustion, the piston reaches TDC, reverses direction, and expands the cylinder volume as combustion converts chemical energy into work energy. This stroke takes on many names, including "power stroke," "combustion stroke," and "expansion stroke." As the piston approaches BDC, the exhaust valve opens, allowing the products of combustion to escape the cylinder. At BDC, the piston reverses direction and motions toward TDC with the exhaust valve open, in what is called the "exhaust stroke." Depending on the engine's crankshaft rotational speed – which can vary from as low as 100 rev/min for large marine-application engines to as high as 15,000 rev/min for race car engines – the four-stroke cycle requires as much as about 1.2 s to as little as 8 ms to complete.

Up to this point, the discussion has centered on the processes occurring in a single cylinder. Most engines, however, are composed of many cylinders and take on various forms (e.g., in-line four-cylinder, "V6", "V8", and "W" engine). In such cases, each cylinder undergoes the same processes but usually out of phase. For example, in an in-line four-cylinder engine (i.e., an engine that has four cylinders oriented sequentially in a single-line bank, an example of which is shown in Fig. 3), the cylinder processes are typically out of phase by 180° (720°/4). The firing order is usually not linear, however, in order to ensure smooth and continuous operation. For example, a four-cylinder firing order may go 1-3-2-4; that is, as the engine crankshaft rotates cylinder 1 produces a power stroke first, followed by cylinder 3, then cylinder 2, and finally by cylinder 4 (which is then followed again by cylinder 1). Finally, when describing an engine's displacement, it refers to a summation of each cylinder's displacement; thus, each cylinder displacement is on average the total engine displacement divided by the number of cylinders.

Internal Combustion Engines, Developments in.
Figure 3
Illustration of the Audi 2.0-L TSI, an example of an in-line four-cylinder engine (Used with permission from [4])

How an Engine Makes Power

The reciprocating motion of the piston in a cylinder is the means by which the chemical energy released during combustion is converted into useful work. Work is transferred when a force acts through a displacement; in the case of the piston/cylinder engine, the in-cylinder pressure, P, is interpreted as the force and the changing cylinder volume, dV, during piston strokes is interpreted as the displacement. Thus, the thermodynamic work of an engine cycle is given by Eq. 2:

$$W = \oint P\,dV \qquad [\text{kJ/cycle}] \tag{2}$$

The work of the cycle given by (Eq. 2) is considered *boundary work*, since it results from the changing boundary of the control system (in this context, the control system is that enclosed by the piston/cylinder arrangement, and the moving boundary is manifested by the moving piston). Conventional engines convert this boundary work of the piston to *shaft work* through the piston connecting rod's eccentrically located connection to the crankshaft. The shaft work issuing from the crankshaft is often best interpreted as *torque*, τ; the work given by Eq. 2 is related to the torque of the crankshaft via Eq. 3:

$$W = 2\pi n_R \tau \qquad [\text{kJ/cycle}] \tag{3}$$

where n_R is the number of crankshaft revolutions per power cycle (i.e., $n_R = 2$ for a four-stroke cycle and $n_R = 1$ for a two-stroke cycle). The units for τ in Eq. 3 are kN-m.

The torque of an engine is routinely measured with a dynamometer; in this way, the torque is considered "brake torque," or the amount of resistance torque the dynamometer must apply to "brake" the engine to a certain speed condition. Via application of Eq. 3, the "brake work," W_b, is determined. Only determining brake work, however, reveals no insight into the in-cylinder work processes. The in-cylinder work processes can be calculated using in-cylinder pressure measurement that is precisely coupled to the in-cylinder volume via a crankshaft encoder and detailed knowledge of the cylinder's and crank-slider's geometries. An example "pressure–crankangle" diagram is shown Fig. 4a, where crankangle is reported in degrees after top dead center (° ATDC) relative to "combustion TDC." Also shown in Fig. 4a are the four strokes of the four-stroke cycle as described in section "Basic Operating Cycle". In-cylinder pressure is typically measured with a piezo-electric pressure transducer which is able to provide a fast-response indication during the engine cycle [5]. It should be noted that measuring in-cylinder pressure is not a trivial task and great care must be taken to do it properly [6–9]. When using digital equipment (i.e., an analog–digital converter) to electronically record in-cylinder pressure, it becomes necessary to determine the sample rate, which is usually determined by the crankshaft encoder. Varying crankangle resolutions can be used, depending on the level of precision needed of the analysis. For calculating in-cylinder work (described next), a crankangle resolution of up to 10° [6] can be used; for detailed combustion analysis much finer resolution must be used (e.g., about 1° for gasoline engine combustion and 0.25° for diesel engine combustion). The data shown in Fig. 4 is recorded every 0.2°. In addition to the crankangle resolution, the engine speed also determines the needed sample rate of the data acquisition system. Finally, it is equally important to know the cylinder volume at each record of pressure when calculating in-cylinder work. This requires precise phasing between the piston's location and the crankshaft encoder; it also requires knowing the precise geometries of the cylinder and crank-slide mechanism. Specifically, the minimum volume (i.e., clearance volume), the piston stroke, and the cylinder bore must be precisely known. It is often best to determine these using precise measuring instruments, rather than rely on manufacturer specifications (which, although have

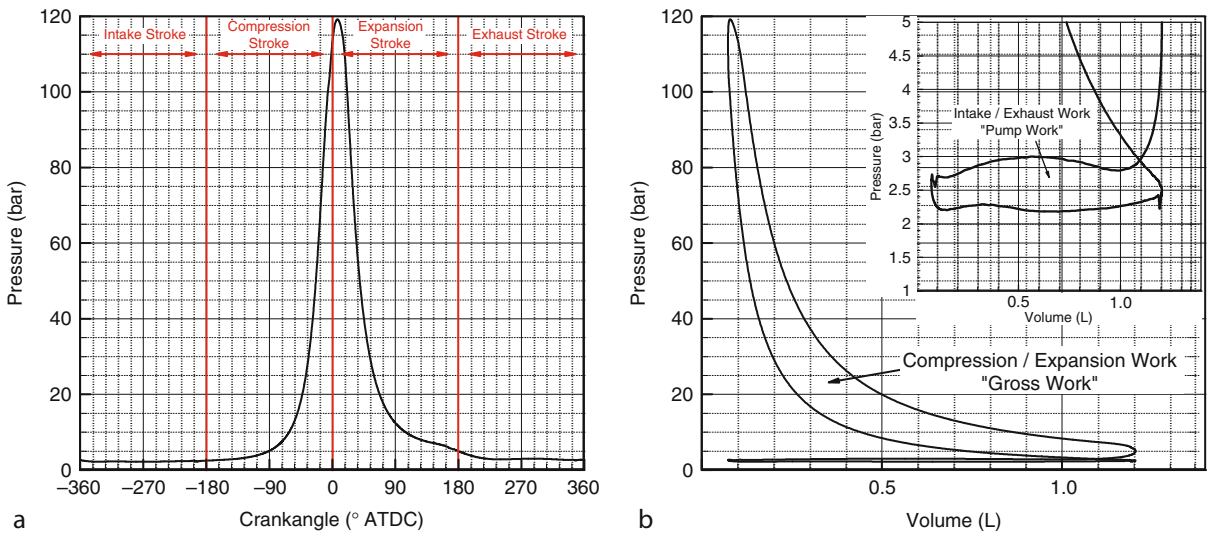

Internal Combustion Engines, Developments in. Figure 4
(**a**) Pressure as a function of crankshaft rotation, or crankangle, in degrees after top dead center (° ATDC), and (**b**) pressure as a function of cylinder volume, also illustrating the areas of the *P–v* plane that render gross work and pump work (Data from author's laboratory, Texas A&M University)

tight tolerances, are nominal values). An example "pressure–volume," or "P–V," diagram is shown in Fig. 4b.

Once a precise P–V diagram is determined, the in-cylinder work associated with each process can be determined. The area between the P–V curves, as suggested by Eq. 2, represents the in-cylinder work, or "indicated" work (named for the antiquated use of a mechanical stylus-indicator device to record pressure [10]). There are two portions of the typical four-stroke engine cycle, as shown in Fig. 4: (1) compression and expansion strokes which in combination result in the "gross work," W_{ig}, and (2) intake and exhaust strokes which in combination result in the "pump work," W_{ip}. It is important to note that gross work and pump work correspond to the respective strokes of the piston, not necessarily the valve events (i.e., not necessarily the closed portion of the cycle versus open portion of the cycle). In combination, i.e., the sum of gross work and pump work result in the "net work," as given by Eq. 4:

$$W_{in} = W_{ig} + W_{ip} \tag{4}$$

Note that the subscript "*i*" on the terms in Eq. 4 represents "indicated"; since terms "gross," "pump," and "net" only have relevance from indicated data (i.e., in-cylinder pressure data), it is often dropped as a designator on the work terms.

Pump work, which will be nonzero when intake pressure is different from exhaust pressure (nearly all situations), often decreases net work relative to gross work (i.e., the gas exchange process requires the piston to do work on the gas, or, pump work is negative). There are a few situations, with the use of a turbocharger or supercharger for example, when intake pressure is greater than exhaust pressure and pump work is positive. In such situations, net work will be greater than gross work.

The difference between net work and brake work, as shown in Eq. 5, is the friction work, W_f, of the engine. Friction, of course, always requires work from the system; thus, brake work will always be less than net work. In Eq. 5, W_f captures all forms of mechanical friction of the engine, including friction among crank-slider components, in bearings, in valve springs, and in various accessories (e.g., water and oil pumps):

$$W_f = W_{in} - W_b \tag{5}$$

Engine researchers typically quantify all of the above-described work parameters on volume-normalized parameters, which in general represent a "mean effective pressure." The general definition for mean effective pressure, MEP, is given as Eq. 6:

$$\text{MEP} = \frac{W}{V_d} \tag{6}$$

The various mean effective pressures and their definitions are summarized in Table 1.

One of the major benefits of describing the work of an engine in terms of mean effective pressure is that the "size" of the cylinder is removed from consideration. In other words, it is possible to produce more work from an engine that has a larger displaced volume; however, the mean effective pressure may be lower (relative to a lower displaced volume engine) due to a number of other possible influencing parameters that affect and engine's ability to make power (i.e., fuel conversion and volumetric efficiencies, fuel–air ratio, inlet air density, and fuel heating value). To make these types of assessments, refer to Eq. 7, which is developed from the basic definition of power, P (i.e., work per unit time), and respective definitions of other involved parameters as shown by Heywood [11]. An example of the use of Eq. 7 to assess factors affecting power in a technology comparison is provided in [12].

$$P = \frac{\eta_f \eta_v \rho_{a,i} (F/A) Q_{HV} V_d N}{n_R} \tag{7}$$

where

Internal Combustion Engines, Developments in.

Table 1 Summary of various mean effective pressures describing the various work transfers defined for a reciprocating-piston internal combustion engine

Name	Definition
Gross indicated mean effective pressure (gross IMEP)	$\text{IMEP}_g = W_{ig}/V_d$
Net indicated mean effective pressure (net IMEP)	$\text{IMEP}_n = W_{in}/V_d$
Pump mean effective pressure (PMEP)	$\text{PMEP} = W_{ip}/V_d$
Friction mean effective pressure (FMEP)	$\text{FMEP} = W_f/V_d$
Brake mean effective pressure (BMEP)	$\text{BMEP} = W_b/V_d$

η_f Fuel conversion efficiency (described in section on "Thermodynamic Analysis of Internal Combustion Engines").

η_v Volumetric efficiency, or the engine's effectiveness at "breathing" air. It is defined as $\eta_v = \frac{m_a}{\rho_{a,i} V_d}$, where m_a is the actual mass of air inducted per cycle (kg) and $\rho_{a,i}$ is the density of the intake air at some reference point (kg/m^3) (usually the intake manifold, but also may be atmospheric air upstream of the engine air filter). Note that V_d has units of (m^3) in Eq. 7. It is important to note that volumetric efficiency only quantifies the engine's ability to breath air, i.e., not a fuel–air mixture. Thus, for example, premixing fuel with air prior to induction tends to lower the engine's volumetric efficiency. It is also important to note that volumetric efficiency of the engine depends on the chosen reference point. Thus, if the volumetric efficiency of the whole breathing stream is desired, the reference point is taken as upstream of the intake air filter (for example). If, however, volumetric efficiency of just the intake ports and through the valves is desired, then the reference point is taken as the intake manifold.

$\rho_{a,i}$ As defined above, the density of the intake air at some reference point (kg/m^3).

F/A The mass-based fuel–air ratio of the mixture.

Q_{HV} Heating value of the fuel (typically, lower heating value is used since the products leaving the piston/cylinder system with water as a vapor) (kJ/kg).

N Engine speed (rev/s)

To reveal the form of mean effective pressure, Eq. 8 is given as a modified form of Eq. 7.

$$\mathrm{MEP} = \eta_f \eta_v \rho_{a,i} (F/A) Q_{HV} \tag{8}$$

Thus, it is apparent from Eq. 8 how an engine with a relatively small displacement might have a higher mean effective pressure than an engine with a large displacement, even though the larger-displaced engine may produce more power. It is also clear from Eqs. 7 and 8 how the performance (i.e., power) of an engine may be improved beyond the "easy" action of increasing displaced volume. One parameter, for example that benefits the power and mean effective pressure of the engine is the fuel conversion efficiency. This very important parameter is discussed in the next section.

Finally, this section concludes by illustrating a typical power/torque/speed curve. Apparent from Eq. 3 and the definition of power, there is a relationship among power, torque, and speed of an engine. This relationship for a typical internal combustion engine is shown in Fig. 5. There are a few interesting features to point out in this figure. The first, a practical feature, is the identification of "rated torque" and "rated power". Engines are usually "sized" based on the speed at which they develop maximum torque (also known as rated torque) and the speed at which they develop maximum power (also known as rated power). The second feature, which is apparent from the knowledge that rated torque exists, is the seemingly dependent relationship of torque on engine speed. It is clear from the definition of power that it should have a functional relationship on the speed of the engine, which dictates the amount of work per unit time the engine can deliver. But, based on assessment of Eq. 3, there is not a direct relationship between in-cylinder work per cycle and the speed of the engine. In fact, in an ideal sense, the torque of the engine should be constant with engine speed (and, if constraining to an ideal engine, higher than the maximum attained torque of the real engine), similar to how torque of an electric motor is nearly constant with motor speed. Thus, the behavior seen in Fig. 5 suggests that there exist factors in a real engine that depend on engine speed and also affect the work produced per cycle (thereby affecting the torque of the engine). These factors predominantly consist of heat transfer and friction; both of which have dependencies on the speed at which the engine operates. Heat transfer of course is a time-dependent phenomenon. At low engine speeds there is more time per cycle for thermal energy to be transferred from the cylinder; thus, torque droops at low engine speeds as heat transfer diminishes the energy available for in-cylinder work production. Friction, too, is a speed dependent function due to the mechanical behavior of the engine's interacting components. At high engine speeds, there is increased friction to be overcome on a per cycle basis; thus torque droops at high engine speeds as increased work energy is required to overcome increased friction.

Relating this discussion to Eq. 7, both heat transfer and friction effects tend to decrease η_f. There is, however, another factor of Eq. 7 being influenced by heat transfer and friction and thus serving as a major

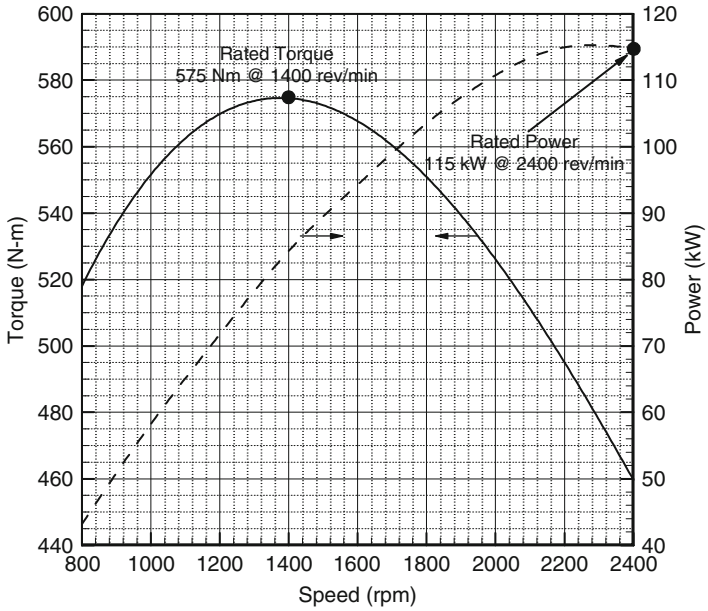

Internal Combustion Engines, Developments in. Figure 5
Torque and power as functions of engine speed for a typical internal combustion engine. Data is collected from 4.5 L medium-duty diesel engine with advanced technology such as turbocharging and exhaust gas recirculation (Data from author's laboratory, Texas A&M University)

contributor to the behavior of the torque curve shown in Fig. 5; this factor is the volumetric efficiency. The maximum amount of work that can be developed per cycle is firstly dependent on the amount of air (or oxidizer) the engine can breathe; the amount of air the engine can breathe ultimately dictates the amount of fuel that can be delivered, which of course serves as the energy carrier to be converted in the cylinder.

A representative volumetric efficiency curve as a function of mean piston speed (which is correlated to engine speed) is shown in Fig. 6. There is much important detail in this figure, and the following will describe this in detail; after this discussion, a return to the effect of volumetric efficiency on the torque curve of Fig. 5 will be made. First, notice that under ideal situations the volumetric efficiency curve would be 100% and independent of engine speed (like work, trapped mass per cycle ideally has no functional dependency on the number of cycles per unit time, or, speed of the engine). It is noted that, depending on the reference point chosen for quantifying it, volumetric efficiency could be greater than 100% if the engine is, for example, boosted. In such a situation, the chosen reference point is upstream of the boosting device

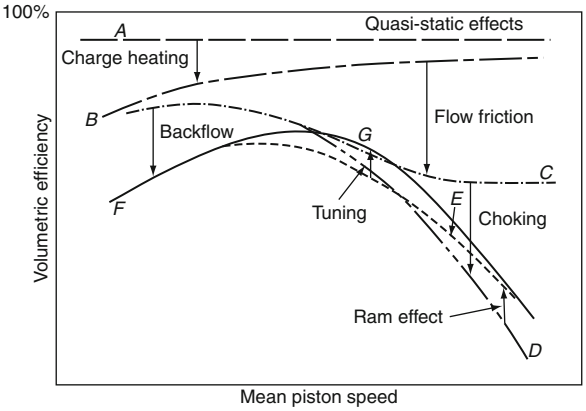

Internal Combustion Engines, Developments in. Figure 6
Example of volumetric efficiency, illustrating the many factors that impact the engine's ability to effectively breathe air (Used with permission from [13]). Improvements to the engine's volumetric efficiency can yield substantial improvements to its ability to make power, evident from Eq. 7

(e.g., turbocharger compressor inlet). Although such a chosen reference point is useful to indicating the quantity of trapped mass in the cylinder, it prevents the quantification of the engine's breathing system outside of the boosting device, and masks opportunities for further improvement to the engine's design.

Returning to the volumetric efficiency curve of Fig. 6, and for the specific case of premixed charge engines such as conventional gasoline spark-ignited engines, the premixing of fuel with air prior to induction diminishes the amount of trapped mass of air in the cycle. Such a factor is considered a "quasi-static" effect since it will be present regardless of the speed of the engine. Other quasi-static effects include factors such as, for example, residual fraction due to manifold pressure differences (between exhaust manifold and intake manifold) and exhaust gas recirculation. Thus, notice secondly that the diminishing effect of quasi-static factors is represented as curve "A" in Fig. 6. The next phenomenon to be captured in the volumetric efficiency curve is called "charge heating" and is a heat transfer effect. During normal engine operation, the breathing system of the engine reaches a steady state temperature that is higher than the ambient temperature. Thus, the elevated temperature of the intake port results in heat transfer to the intake air, increasing the air temperature, decreasing its density, and decreasing the amount of mass per unit volume. As described above, heat transfer is a time-dependent phenomenon, therefore its presence is most notable at low engine speeds (low mean piston speeds); notice thirdly in Fig. 6 the effect of charge heating on the volumetric efficiency curve, which in combination with quasi-static effects lowers it to the curve labeled "B." Similar to how friction affects work per cycle, friction also affects air flow and has a dependency on mass flow rate (i.e., has a dependency on engine speed). The fourth factor to notice in Fig. 6 is the effect of flow friction; its effect in concert with quasi-static and charge heating factors result in the curve labeled "C." Notice at very high speeds, the flow friction effect seems to level off and play a speed-independent role as engine speed increases; this results from the flow attaining choke conditions where, regardless of the pressure drop across the intake system, the mass flow rate remains constant as its velocity reaches the speed of sound. Thus, the fifth factor to notice in Fig. 6 is the effect of choking on the volumetric efficiency curve. The net result of all combined effects including choke is the curved labeled "D." Interestingly, some phenomena help to increase the engine's volumetric efficiency; ram effect is one such example. Ram effect occurs at high flow rates where fluid momentum results in continued charging of the cylinder even as the in-cylinder motion of the piston no longer provides the pumping action (i.e., volume increase during intake stroke). The sixth factor to note in Fig. 6 is the increase in volumetric efficiency due to ram effect. The combined effects, including ram effect, result in the curve labeled "E." A similar but diminishing gas exchange phenomenon occurs at low engine speeds, known as backflow. Backflow occurs during the valve overlap period (the period during which both exhaust and intake valves are open as exhaust valves close and intake valves open) where in-cylinder motion becomes quiescent as the piston reaches top dead center and exhaust products of combustion backflow into the intake port. The seventh factor to notice in Fig. 6 is the effect of backflow on the engine, which tends to pervade at low engine speeds where exhaust momentum is low. The combined effects, including backflow, on volumetric efficiency result in the curve labeled "F." Finally, to end on a positive note, the eighth and last factor to observe in Fig. 6 is that of tuning. Tuning is the effort to make use of established resonating sound waves in the intake and exhaust systems to either aid in charging the cylinder (intake tuning) or discharging the cylinder (exhaust tuning). Because this charging or discharging benefits relies upon the timing of compression and rarefaction waves being positioned at precise locations in the intake or exhaust systems, fixed geometry intake and exhaust systems can only be tuned at a narrow speed range. The benefit of tuning is shown in Fig. 6, where for this particular application tuning is designed for the mid-speed range of the engine. Variable tuning systems are becoming available in production, which through the use of creative flow channeling and blocking, can change the "effective" runner length of the flow passage and allow for tuning across broader speed ranges than allowed by fixed geometry runners. With all factors considered, the final volumetric efficiency curve is the solid curve labeled "G."

Now that the details of the volumetric efficiency curve as a function of engine speed, identified as

curve "G" in Fig. 6, have been discussed, a return to its effect on engine torque will be made. In fact, it is interesting to note the similarities between the final volumetric efficiency curve (curve "G") of Fig. 6 and the torque curve of Fig. 5. Such a similarity is not a coincidence, as the maximum amount of work attainable per cycle is a strong function of how well the engine breathes air per cycle. Correspondingly, based on the assessment of Eq. 7, significant improvements to an engine's ability to make power can be realized through creative improvements to the engine's volumetric efficiency.

Thermodynamic Analysis of Internal Combustion Engines

At its core, an internal combustion engine is a thermodynamic device. That is, it takes one form of energy (i.e., chemical energy) and converts it into another form of energy (i.e., mechanical "shaft work" energy). There are several considerations that should be given to the thermodynamics of the internal combustion engine, in pursuit of improving its ability to make power and, more importantly, to make power *efficiently*. Efficiency is an important thermodynamic concept which quantifies the ability of a work conversion device to convert one form of energy (e.g., chemical energy) into work energy (i.e., mechanical shaft work). In the context of internal combustion engines, *fuel conversion efficiency* is used, as given by Eq. 9:

$$\eta_{\mathrm{f}} = \frac{W}{m_{\mathrm{f}} Q_{\mathrm{HV}}} \tag{9}$$

where m_{f} is the mass of fuel per cycle. Typical maximum fuel conversion efficiencies for internal combustion engines vary from ca. 20% to 45%, depending on engine design and type of combustion system. Fuel conversion efficiency, like power, can be designated as brake or indicated fuel conversion efficiency. The relationship between brake and indicated fuel conversion efficiency is given as Eq. 10:

$$\eta_{\mathrm{f,b}} = \eta_{\mathrm{f,i}} \eta_{\mathrm{m}} \tag{10}$$

where $\eta_{\mathrm{f,b}}$ is brake fuel conversion efficiency, $\eta_{\mathrm{f,i}}$ is net indicated fuel conversion efficiency, and η_{m} is mechanical efficiency and given by $\eta_{\mathrm{m}} = \frac{W_{\mathrm{b}}}{W_{\mathrm{in}}} = \frac{P_{\mathrm{b}}}{P_{\mathrm{in}}} = \frac{\mathrm{BMEP}}{\mathrm{IMEP_n}}$. In words, fuel conversion efficiency is the ratio of work output to fuel energy delivered. There is another efficiency definition that can be considered, called *thermal efficiency*, which is the ratio of work output to fuel energy released. In other words, since the combustion process converts the fuel's chemical energy to thermal energy, the thermal efficiency indicates the conversion of thermal energy to work energy. It is not possible to precisely measure the energy released by the fuel during the combustion process; it is, however, possible to precisely determine the extent of incomplete combustion, or combustion inefficiency. Thus, *combustion efficiency* is introduced to allow for the determination of the engine's thermal efficiency. Combustion inefficiency is defined as the energy of unreacted fuel in the exhaust to fuel energy delivered to the engine. Combustion efficiency, η_{c}, is thusly given as Eq. 11 [14]:

$$\eta_{\mathrm{c}} = 1 - \frac{\sum y_{\mathrm{i}} Q_{\mathrm{HV,i}}}{\left[\dot{m}_f \Big/ \dot{m}_f + \dot{m}_a\right] Q_{\mathrm{HV,f}}} \tag{11}$$

where y_{i} is an unreacted fuel specie in the exhaust (e.g., carbon monoxide), $Q_{\mathrm{HV,i}}$ is the heating value of specie i, $\dot{m}_f$ and $\dot{m}_a$ are the fuel and air mass flow rates, respectively, and $Q_{\mathrm{HV,f}}$ is the fuel's heating value. Fuel conversion efficiency, combustion efficiency, and thermal efficiency, η_{th}, are all related by Eq. 12:

$$\eta_{\mathrm{f}} = \eta_{\mathrm{c}} \eta_{\mathrm{th}} \tag{12}$$

Note that η_{f} of Eq. 12 could be either brake or indicated, in which case the corresponding η_{th} will have the same basis.

At this point, it is instructive to question what the maximum possible fuel conversion or thermal efficiency of an internal combustion engine could be. To begin to answer this question, it should be established that, contrary to what is sometimes simply conveyed, an internal combustion engine is not, by rigid definition, a *heat engine* [15–17]. A heat engine is a device that collects thermal energy, via heat transfer mechanism, from a high temperature reservoir and converts the *available portion* of this thermal energy to useful work. The portion of thermal energy that is not available for conversion to useful work (i.e., the entropy of the thermal energy) is rejected to a low temperature sink via heat transfer mechanism. A practical example of a heat engine is the steam engine. It is the steam

engine that caused N.L. Sadi Carnot to establish his two postulates on the maximal conditions of the heat engine [18], thus laying the foundation for what would become the second law of thermodynamics and the mathematical axioms for the property entropy. The fully reversible heat engine cycle, i.e., the Carnot cycle, is the most efficient cycle for converting thermal energy into useful work (which, because of its reversible nature, is the most efficient cycle for converting work energy into thermal energy). These details are provided because a common misconception is that the maximum efficiency of an internal combustion engine is limited by a so-called Carnot efficiency; this really has no technical basis because the internal combustion engine does not operate on the same principle (i.e., the heat engine principle) around which the Carnot cycle is created.

Perhaps much of the misdiagnosis of considering an internal combustion engine a heat engine comes from the use of ideal heat engine cycles to "model" an internal combustion engine; namely the Otto and Diesel cycles. These cycles do serve an important purpose in that certain fundamental parameters affecting the efficiency of the ideal heat engine cycles (i.e., Otto and Diesel cycles) transcend to also affecting the efficiency of the internal combustion engine. An example of such is compression ratio. Thermodynamic analysis of the Otto Cycle, the four processes of which are shown in Fig. 7, on (a) pressure–volume and (b) temperature–entropy diagrams reveal that efficiency of the cycle, $\eta_{\text{th,Otto}}$, is given by Eq. 13:

$$\eta_{\text{th,Otto}} = 1 - \frac{1}{r_c^{\gamma-1}} \tag{13}$$

where γ is the ratio of specific heats for the working fluid (e.g., $\gamma_{\text{air}} = 1.4$ at 300 K). This result reveals the asymptotic relationship of increasing thermal efficiency with compression ratio, as shown in Fig. 8. Similar behavior is observed in internal combustion engines (i.e., increasing efficiency with increasing compression ratio) as the capability to expand the working fluid (i.e., combustion products), and thus the ability to convert thermal energy to work energy, increases with increasing compression ratio. Another fundamental behavior is apparent Fig. 8 related to the changing value of γ. Notice that thermal efficiency tends to increase with an increase in γ; similar to the increase in compression ratio, a mixture with a higher γ suggests it requires more energy to increase its temperature during a work-transfer (i.e., constant pressure) process compared to a nonwork (i.e., constant volume) process. The corollary to this is more work energy is transferred out of a mixture with higher γ as the mixture is expanded. In internal combustion engines,

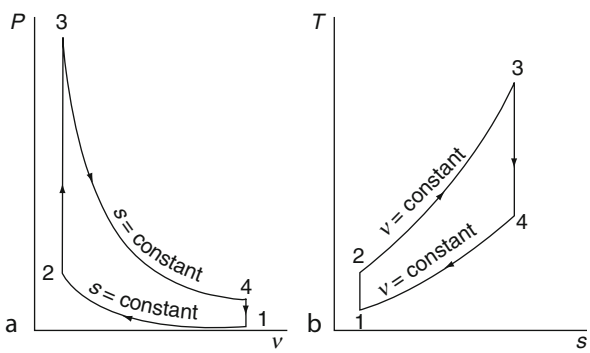

Internal Combustion Engines, Developments in.
Figure 7
(**a**) Pressure–volume and (**b**) temperature–entropy diagrams of the air-standard Otto cycle (Used with permission from [19])

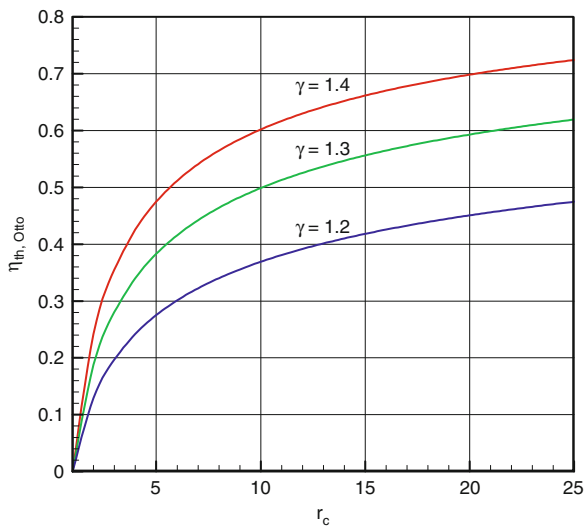

Internal Combustion Engines, Developments in.
Figure 8
Otto cycle thermal efficiency as a function of compression ratio for several γ values

I

leaner fuel/air mixtures (i.e., those with less than stoichiometric, or chemically complete, concentrations of fuel in the mixture) have higher γ values, and thus realize an efficiency improvement.

Although the examples of using the Otto cycle to assess the effects of compression ratio and γ value on thermal efficiency are helpful, the Otto cycle efficiency cannot be used to predict maximum attainable efficiency limits of an internal combustion engine. There are several inaccuracies in applying the Otto cycle (or any ideal heat engine cycle) to predict internal combustion engine performance and efficiency. Specifically, the assumptions that go into the development of Eq. 13 are as follows (refer to Fig. 7):

1. Processes 1–2 and 3–4 are *reversible and adiabatic* (i.e., *isentropic*, or constant entropy) processes.
2. Process 2–3 is a constant volume *heat addition* process, where thermal energy of the system increases due to heat transfer with the surroundings at a temperature of no less than T_3.
3. Process 4–1 is a constant volume *heat rejection* process, where thermal energy of the system decreases due to heat transfer with the surroundings at a temperature no greater than T_1.
4. Properties of the working fluid are constant throughout the cycle.

Of the above four assumptions, all four are impractical (meaning, an actual engine's efficiency will be less than the ideal limit because of real effects, which will be discussed in more detail below). Further, assumptions 2–4 are theoretically improper to impose on an internal combustion engine. Assumptions 2–4 imply a heat engine cycle, which has already been established that an internal combustion engine is not. Instead, an internal combustion engine operates as a collection of processes, all which have ideal limits dictating, in aggregate, the ideal maximum efficiency of the engine. Energy is transferred to the control system (i.e., the cylinder of the engine) through mass flow rate, as opposed to heat transfer mechanism (as in the heat engine apparatus). This energy, initially in the form of chemical energy, is converted to thermal energy during the combustion process and the expansion of the piston thereby converts the thermal energy to work energy. Additionally, because of the change from reactants to products during the combustion process and the dependence of species' properties on temperature and pressure, it is not appropriate to assume properties of the working substance remain constant during the engine's operation (i.e., assumption no. 4 is not valid).

Instead, maximum ideal efficiency limits of internal combustion engines could be assessed by improving upon the inappropriate assumptions of the Otto heat engine cycle, i.e., allow energy to be transferred into the system via mass flow (i.e., via the intake process) and allow properties of the mixture to change with species, temperature, and pressure. The resulting analysis, referred to as *Fuel–Air Cycle Analysis* [20], employs the following processes (refer to Fig. 9) and assumptions in modeling an internal combustion engine cylinder (i.e., the control volume):

Process 6–7–1: Ideal intake process of fuel and air and adiabatic mixing with residual gas from the preceding cycle. Residual gas, or often referred to as "residual fraction," is left-over products of combustion not fully exhausted from the cylinder during the previous cycle's exhaust displacement process.

Process 1–2: Reversible and adiabatic compression of the fuel/air/residual mixture (i.e., the reactants). Chemical species are frozen.

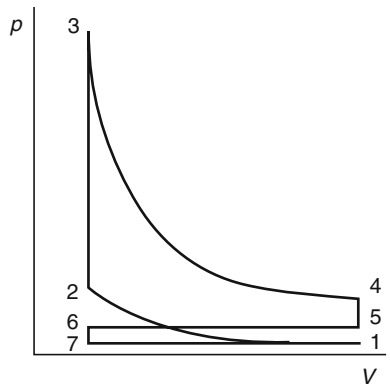

Internal Combustion Engines, Developments in.
Figure 9
Pressure–volume diagram illustrating the processes assumed in *Fuel–Air Cycle Analysis* of an internal combustion engine. Note that shown cycle is representative of an engine under "throttled" conditions, where intake pressure is less than atmospheric (Used with permission from [21])

Process 2–3: Complete, adiabatic combustion of reactants to products (the latter of which are assumed to exist in equilibrium concentrations). Combustion, in ideal sense, is modeled as constant volume, constant pressure, or limited pressure. Limited pressure is a combination of constant volume and constant pressure processes. Constant volume combustion occurs until a "limit pressure" is reached, when remainder of combustion occurs at constant pressure.

Process 3–4: Reversible and adiabatic expansion of products, which remain in chemical equilibrium throughout the process.

Process 4 – 5: Reversible and adiabatic "blowdown" of products to exhaust pressure of products remaining in the cylinder. Products remain in fixed composition based on concentrations at State 4.

Process 5–6: Ideal, constant pressure, and adiabatic exhaust displacement of products, remaining in fixed composition.

Ideal gas behavior of the mixture and conserved mass are assumed throughout the analysis. Further, mass transfers only occur during intake and exhaust processes (i.e., no leakage, blow-by, or crevice flow during the cycle). By employing first and second laws and various assumptions to each of the processes, respective states can be thermodynamically fixed, thus allowing determination of work transfers. An item to note about *Fuel–Air Cycle Analysis*, because it accommodates changing species, is that *three* independent properties must be known to fix the states (i.e., two thermodynamic properties, such as temperature and pressure, and species composition). Process 6–7–1 is assumed adiabatic. Further, it is assumed that during the stroke from TDC to BDC, the cylinder pressure is constant and equal to the intake pressure, P_i:

$$P_7 = P_1 = P_i$$

$${}_6Q_1 = 0$$

With these two statements, and use of first law, the enthalpy at State 1, h_1, is given as:

$$h_1 = f\left[h_e + R_e T_e\left(\frac{P_i}{P_e} - 1\right) - h_i\right] + h_i$$

where f is residual gas fraction, h_e is enthalpy of the exhaust (and equal to $h_6 = h_5$), R_e is the gas constant of the exhaust (and equal to $R_6 = R_5$), T_e is temperature of the exhaust (and equal to $T_6 = T_5$), P_e is pressure of exhaust (and equal to $P_6 = P_5$), and h_i is the enthalpy of the fresh intake mixture. Residual fraction, as explained above, is the residual mass, m_r (which is equal to m_6, the mass at State 6), divided by the total cylinder mass, m_{total} (which is equal to $m_1 = m_2 = m_3 = m_4$, the mass of the system at States 1, 2, 3, and 4, respectively), and is related to r_c, P_e, T_e, and the pressure and temperature at State 4, P_4 and T_4, respectively, by the following:

$$f = \frac{m_r}{m_{total}} = \frac{m_6}{m_1} = \frac{m_6}{m_4} = \frac{1}{r_c}\frac{P_e T_4}{P_4 T_e}$$

It is clear from the equations for h_1 and f that a priori knowledge of the cycle is needed in order to fix State 1 (note that r_c, P_i, P_e, h_i are chosen based on desired cycle compression ratio, manifold conditions, inlet composition, and inlet temperature, T_i, respectively). Thus, initial values for State 1 are typically assumed for the first iteration; State 4 temperature, pressure, and composition from the initial iteration are then used to estimate f and h_1 for the next iteration. This iterative process continues until some convergence criterion is met (e.g., close match between f_{final} and $f_{final\ -\ 1}$). Rather than assume values of f and h_1, it is perhaps more intuitive to assume initial values of f and temperature at State 1, T_1; the following expressions [22] are approximations for establishing initial iteration State 1 properties:

$$f = \left\{1 + \frac{T_e}{T_i}\left[r_c\left(\frac{P_i}{P_e}\right) - \left(\frac{P_i}{P_e}\right)^{(\gamma-1)/\gamma}\right]\right\}^{-1}$$

$$T_1 = T_e r_c f\left(\frac{P_i}{P_e}\right)$$

It is also noted that composition of the residual gas must be assumed to fully fix State 1; it is suggested that ideal products of stoichiometric combustion of the fuel–air mixture be used as the residual gas species.

Work analysis of Process 6–7–1 gives the intake work quantity:

$${}_6W_1 = P_i(V_1 - V_6)$$

Process 1–2 is assumed reversible and adiabatic (i.e., ${}_1Q_2 = 0$); from second law, this gives:

$$s_1 = s_2$$

Geometric relationship gives: $v_1 = r_c v_2$

The assumption that chemical composition remains fixed during compression (i.e., Process 1–2) gives chemical composition at State 2; thus, State 2 is fixed. First law analysis of Process 1–2 gives:

$$_1W_2 = U_2 - -U_1 = m(u_2 - u_1)$$

Process 2–3 is the adiabatic combustion process, where reactants become products (products assumed to be in chemical equilibrium) modeled typically in three simple fashions: (1) constant volume combustion, (2) constant pressure combustion, and (3) limited pressure combustion. First law analysis for each of the three cases results in the following, respectively:

1. Adiabatic constant volume combustion
   $u_3 = u_2$
   $v_3 = v_2$
   $_2W_3 = 0$
2. Adiabatic constant pressure combustion
   $h_3 = h_2$
   $P_3 = P_2$
   $_2W_3 = P_2(V_3 - V_2) = P_3(V_3 - V_2)$
3. Adiabatic limited pressure combustion
   Constant volume portion
   $u_{3a} = u_2$
   $P_{3a} = P_{\text{limit}}$
   $v_{3a} = v_2$
   Constant pressure portion
   $h_3 = h_{3a}$
   $P_{3a} = P_3 = P_{\text{limit}}$
   $_2W_3 = P_3(V_3 - V_2)$

At this point, it becomes necessary to describe a way in which product species of combustion can be modeled. It is clear from the above discussion that combustion is modeled as adiabatic and (a) constant volume, (b) constant pressure, or (c) limited pressure. In order to capture a representative combustion reaction, it is necessary to assume that several product species may exist and will exist in equilibrium. Also, it is important to clarify that this approach assumes initial and final equilibrium states in predicting combustion; i.e., the thermodynamic process goes from one equilibrium state (reactants) to a different equilibrium state (products). This is in contrast to using a more detailed approach that models the progression of combustion and relies upon reaction kinetics to predict intermediate species and their nonequilibrium concentrations. See, for example, Foster and Myers [16] for overview of detailed engine modeling and, for example, Westbrook and Dryer [23] for overview of kinetic modeling of combustion. While perhaps hundreds of species could be included as products, Olikara and Borman [24] propose a combustion reaction, given as Reaction (R1), that might nearly be general for internal combustion engine purposes:

$$\begin{aligned} x_{13}\Big[\mathrm{C}_n\mathrm{H}_m\mathrm{O}_l\mathrm{N}_k + \frac{n+m/4-l/2}{\varphi}(\mathrm{O}_2 + 3.7274\,\mathrm{N}_2 \\ + 0.0444\,\mathrm{Ar})\Big] \rightarrow x_1\mathrm{H} + x_2\mathrm{O} + x_3\mathrm{N} + x_4\mathrm{H}_2 \\ + x_5\mathrm{OH} + x_6\mathrm{CO} + x_7\mathrm{NO} + x_8\mathrm{O}_2 + x_9\mathrm{H}_2\mathrm{O} \\ + x_{10}\mathrm{CO}_2 + x_{11}\mathrm{N}_2 + x_{12}\mathrm{Ar} \end{aligned} \quad \text{(R1)}$$

where x_1 through x_{12} are the mole fractions of the respective product species. x_{13} represents the moles of fuel per mole of products. Solution of the 13 unknowns of course requires 13 independent equations; five of these equations come from the species balance (i.e., balance of C, H, O, N, and Ar species). The remaining eight equations come from the assumption of equilibrium among various product species [24]. As a final note, it is recognized that NO appears as a product species; this represents the equilibrium concentration of NO at the reaction temperature and pressure. Because both the formation and decomposition of NO in the post-flame gas regions are rate limited [25], it is necessary to take a chemical kinetic approach to modeling IC engine exhaust NO concentrations (see, e.g., [26–29]).

Process 3–4 is reversible and adiabatic expansion with the mixture in chemical equilibrium (resulting in different species at State 4 relative to State 3), resulting in the following thermodynamic state (along with geometrical constraint imposed):

$$s_4 = s_3$$

$$v_4 = v_1$$

First law analysis gives the following expression, which is the expansion work of the cycle:

$$_3W_4 = U_4 - U_3 = m(u_4 - u_3)$$

Process 4–5 is the ideal blowdown process (i.e., mixture that remains in the cylinder expands isentropically, filling the cylinder volume voided by the products irreversibly escaping past the open exhaust valve).

Species are fixed based on State 4 concentrations. Thus, State 5 is fixed with the following relationships:

$$s_5 = s_4$$

$$P_5 = P_e$$

Although specific volumes change during the blowdown process (due to mass transfer), total volume is constant; thus, work transfer is 0:

$${}_4W_5 = 0$$

Finally, Process 5–6 is the ideal exhaust displacement process, i.e., cylinder contents are transferred out of the adiabatic control volume via piston displacement at constant pressure.

At this point, it is useful to describe the attainment of various property values indicated above (e.g., s_1). Because *Fuel–Air Cycle Analysis* seeks to capture the effects of changing properties on the cycle analysis, the approximations for constant-specific heat ideal gas property equations cannot be used. Instead, it becomes necessary to employ techniques that accommodate changes to mixture properties based on the mixture's temperature, pressure, and species composition. One such technique is to use NASA's Chemical Equilibrium with Applications program [30–34] coupled with the JANAF Thermochemical Tables. By doing so, species at any given temperature and pressure can be predicted (using NASA's Chemical Equilibrium with Applications program) and the corresponding mixture's properties (using JANAF Thermochemical Tables) can be determined. This type of technique, for example, can be programmed into a computer routine.

Based on first law analysis and constant pressure assumption, State 6 is fixed as follows:

$$T_6 = T_5 = T_r$$

$$P_6 = P_5 = P_e$$

The exhaust work is given by the following:

$${}_5W_6 = P_e(V_6 - V_5)$$

Based on the above analysis, the net work and gross work of the cycle are given by:

$$W_{net} = {}_6W_1 + {}_1W_2 + {}_2W_3 + {}_3W_4 + {}_5W_6$$

$$W_{gross} = {}_1W_2 + {}_2W_3 + {}_3W_4$$

Pump work is as defined by Eq. 4.

Further, various efficiencies can be calculated using Eqs. 9, 11, and 12. Note that although *Fuel–Air Cycle Analysis* is ideal, there may still be incomplete combustion due to the assumption of species existing in chemical equilibrium. Thus, combustion inefficiency will occur at fuel–air mixtures approaching stoichiometric and rich conditions, as dissociation creates concentrations of CO, H_2, and other partially oxidized species. Upon execution of the above analysis in a computer routine, for example, the theoretical limits of maximum efficiency of an internal combustion engine can be determined. Examples of such ideal efficiencies for constant volume combustion of isooctane/air mixtures at two different EGR levels are given in Fig. 10.

Figure 10 reveals interesting behavior of two important internal combustion engine parameters on the various efficiencies, i.e., fuel–air equivalence ratio (often designated as φ) and EGR level. First, notice that as φ approaches stoichiometric (i.e., $\varphi = 1$), η_{th} decreases, and then begins to increase as φ goes rich (i.e., $\varphi > 1$). Further, η_{th} increases as EGR level increases. To understand this behavior, it is necessary to understand how mixture properties are affected by (a) effect of varying φ on species, (b) effect of varying EGR level on species, and (c) effects of φ and EGR level on temperatures and pressures of the cycle. Ultimately, as fundamentally revealed by Eq. 13, a change to mixture properties that results in an increase in γ will cause an increase in efficiency. Figure 11 [35] summarizes how burned gas mixture properties of an isooctane/fuel mixture are affected by various parameters such as φ and temperature. The behaviors of the parameters shown in Fig. 11 can be related to γ by recognizing that γ can be written as given by Eq. 14:

$$\gamma_b = \frac{1}{1 - \frac{\bar{R}}{M_b C_{p,b}}} \tag{14}$$

where γ_b is γ for the burned gas mixture, $\bar{R}$ is the universal gas constant (i.e., $\bar{R} \approx 8.314$ kJ/kg-K), M_b is the molecular weight of the burned gas mixture, and $C_{p,b}$ is the constant pressure specific heat of the burned gas mixture. As an example of the type of analysis that might be done on Fig. 11, notice that M_b, (Fig. 11a) decreases as φ increases (for any given temperature of the burned mixture); although concentrations of CO_2 ($M_{CO_2} \approx 44$ g/mol) increase as φ increases, so too do concentrations of H_2O ($M_{H_2O} \approx 18$ g/mol). Since

I

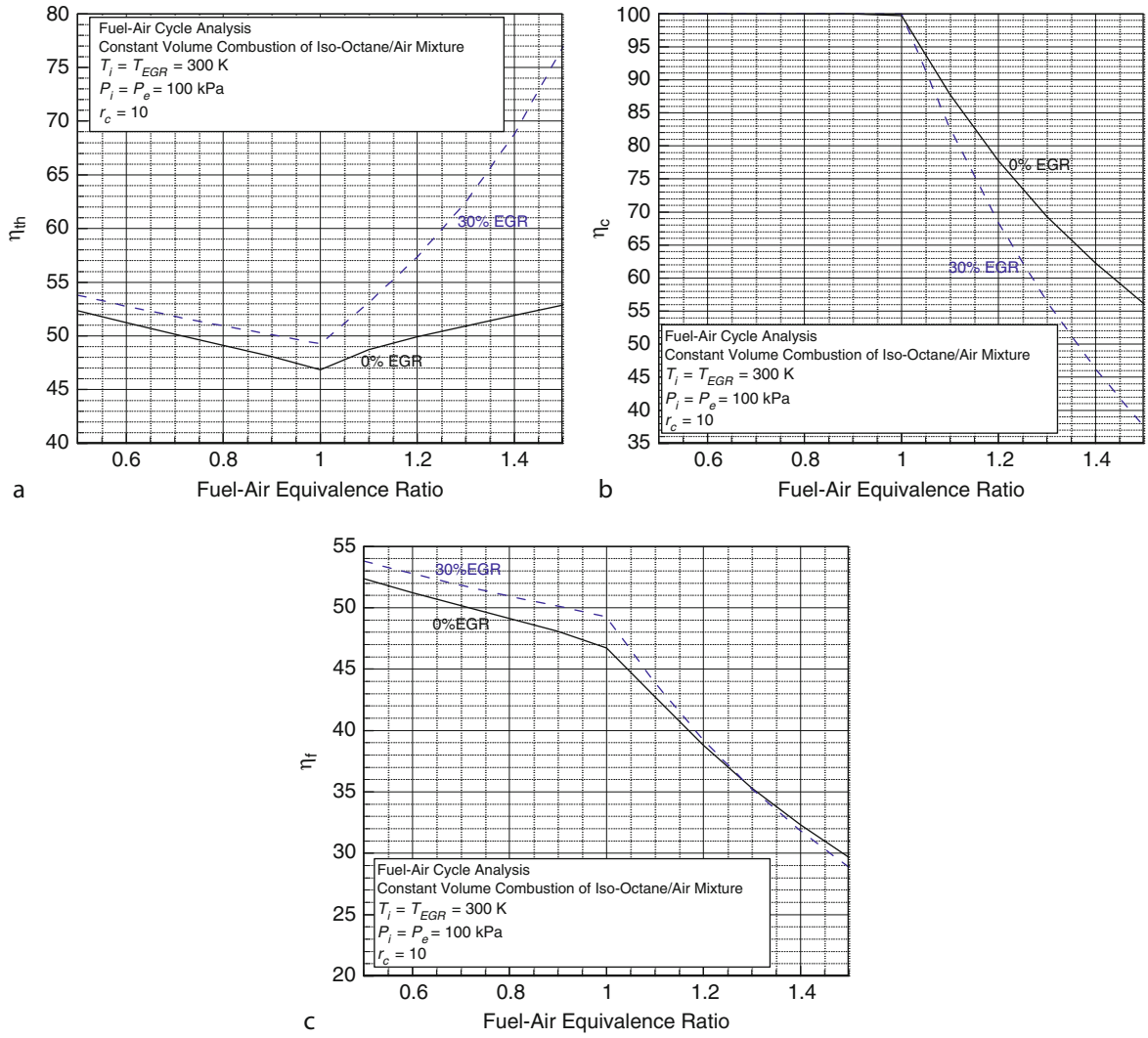

Internal Combustion Engines, Developments in. Figure 10
(**a**) Thermal efficiency, (**b**) combustion efficiency, and (**c**) fuel conversion efficiency of an ideal fuel–air cycle analysis of an internal combustion engine assuming constant volume combustion of isooctane (C_8H_{18}) with T_i = 300 K, $P_i = P_e$ = 100 kPa, T_{EGR} = 300 K, and r_c = 10

isooctane, being a paraffin, produces more H_2O than CO_2 in the products, the lighter, higher concentration of H_2O dominates the net effect of decreasing M_b with increasing φ. As the mixture approaches $\varphi = 1$ and becomes rich ($\varphi > 1$), M_b decreases substantially as concentrations of partially oxidized species (e.g., CO and H_2) with relatively lighter molecular weights increase. Based on analysis of Eq. 14, a decrease in M_b will tend to increase γ_b, which tends to increase η_{th}. Also contributing to γ_b behavior, however, is $C_{p,b}$, which is shown in Fig. 11b. Notice that, up to about $\varphi = 1$, $C_{p,b}$ increases with φ. A portion of this increase is due to the increasing concentration of species with higher constant pressure specific heats as φ increases (e.g., At 1,750 K, $(C_p/R)_{H_2O} \approx 5.94$ and $(C_p/R)_{CO_2} \approx 7.15$ whereas $(C_p/R)_{N_2} \approx 4.28$ and $(C_p/R)_{O_2} \approx 4.46$, as shown in Fig. 12b); another portion, however, comes from the increase in burned gas temperature which causes an increase in constant pressure specific heat for most species. Specifically, as φ increases, adiabatic

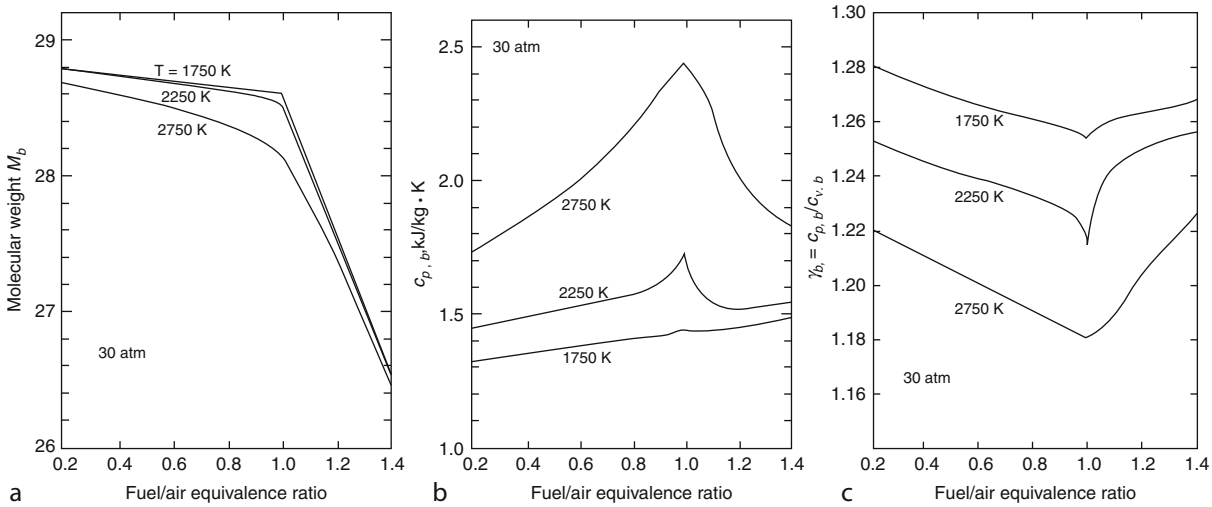

Internal Combustion Engines, Developments in. Figure 11
Burned mass (**a**) molecular weight, (**b**) constant pressure specific heat, and (**c**) ratio of specific heats as functions of equivalence ratio of isooctane/air mixtures at various burned mass temperatures and pressure of 30 atm (Used with permission from [35])

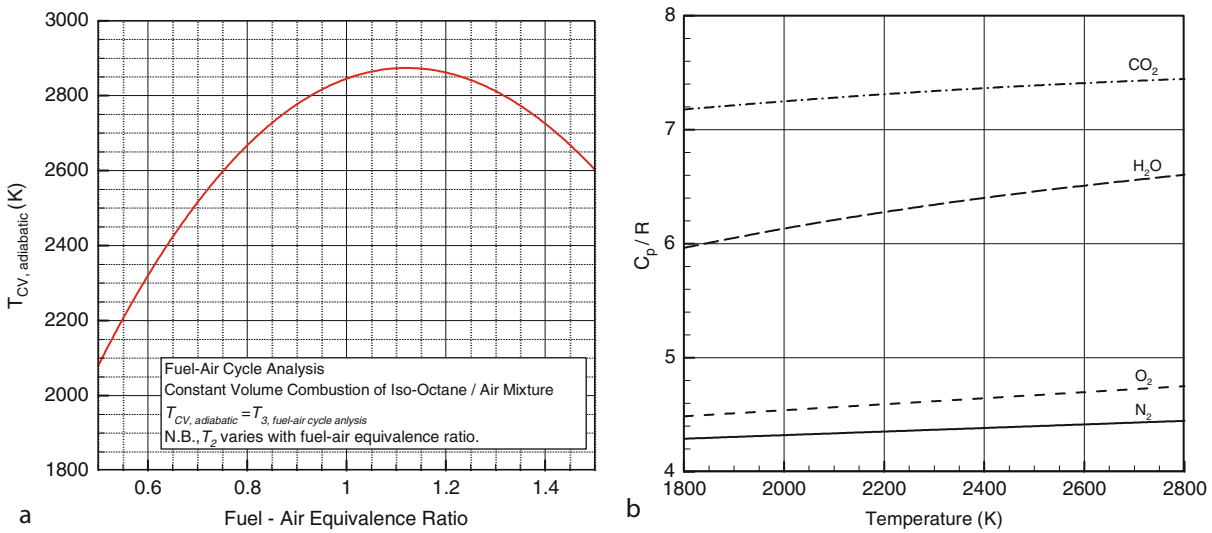

Internal Combustion Engines, Developments in. Figure 12
(**a**) Constant volume adiabatic flame temperature as function of fuel–air equivalence ratio of isooctane with initial temperature and pressure as predicted by *Fuel–Air Cycle Analysis* of isooctane/air mixture and 0% EGR, and (**b**) C_P/R for various species typically found in burned mixtures as function of temperature (Data adapted from JANAF *Thermodynamic Tables* [36])

flame temperature and thus burned mixture temperature increases up to a peak that occurs slightly rich of stoichiometric (for isooctane; location of peak adiabatic flame temperature will vary depending on the type of fuel), as shown in Fig. 12a for isooctane/air–fuel cycle analysis with 0% EGR (note that adiabatic flame temperature, or $T_{CV,adiabatic}$ is equal to State 3 temperature, or T_3 of *Fuel–Air Cycle Analysis* and that

T_3 is partially influenced by the changing State 2 temperature, or T_2, as φ varies). The effects of increasing burned gas temperature on the various species' constant pressure specific heats are shown in Fig. 12b. Thus as φ increases $C_{p,b}$ increases as species concentrations change (i.e., increased concentrations of CO_2 and H_2O) and burned gas temperature increases. An increase in $C_{p,b}$, like M_b, will cause γ_b to decrease. Thus, for φ less than stoichiometric, there are two competing effects on γ_b; a decreasing M_b and an increasing $C_{p,b}$ as φ increases. The net result, as shown in Fig. 11c, is a decrease in γ_b which correspondingly explains the decrease in η_{th} as φ increases up to stoichiometric (see Fig. 10a).

The behaviors of M_b and $C_{p,b}$ change as φ increases beyond $\varphi = 1$ (i.e., the mixture becomes rich), causing a corresponding change in γ_b and ultimately in η_{th}. As explained above, M_b decreases more dramatically rich of stoichiometric due to the abundantly increasing concentrations of CO, H_2, and other dissociated species which have lower molecular weights than the fully associated (i.e., CO_2 and H_2O) species. The dramatic decrease in M_b generally dominates any potential increase in $C_{p,b}$, resulting in a net increase in γ_b. Thus, as φ becomes larger than 1, η_{th} increases. Further, at certain temperatures (e.g., 2,750 K) $C_{p,b}$ decreases as φ becomes greater than 1; the higher temperature of the burned mixture causes higher dissociation, which causes increased concentrations of dissociated species (e.g., CO and H_2), which have lower constant pressure specific heats than the fully associated species (e.g., at 2,750 K, $(C_p/R)_{H_2O} \approx 6.6$ whereas $(C_p/R)_{H_2} \approx 4.4$). For such temperatures where $C_{p,b}$ simultaneously decreases along with M_b as φ becomes larger than 1, there is a dramatic increase in γ_b and a corresponding dramatic increase in η_{th}.

Although η_{th} may tend to increase as φ becomes larger than 1, η_c tends to decrease (again, as concentrations of dissociated species such as CO and H_2 increase as φ becomes larger than 1). The result is a general decrease in η_f. Similar analysis can be conducted to understand the effect of EGR on the various efficiencies. It becomes necessary at this point, however, to assess the extent of the utility of such "first law analysis" – i.e., an analysis centered only on energy transfer – in pursuing future developments of internal combustion engines. For example, an engineer may "dream" of a situation where an engine operates rich at a fuel–air equivalence ratio of 1.4 and 30% EGR, yielding a η_{th} of nearly 70%; this certainly outperforms an engine operating lean at a fuel–air equivalence ratio of 0.5 and 30% EGR (see Fig. 10a). If only an energy-analysis is conducted to assess this "dream," the idea will immediately be discounted because the corresponding η_f for the engine running at 1.4 fuel–air equivalence ratio and 30% EGR is only ca. 32% (compared to the lean operation which is close to 54%). But, the products of the rich combustion still have useful energy, that is, energy that can be converted to useful work. While it is true the cycle cannot convert such *available* energy to useful work, it is more than a "dream" that some other device could convert it (e.g., a fuel cell or a thermoelectric generator). Thus, it might be conceivable to design an engine that allows it to operate at maximal η_{th} and couple it to another device that, while not having as high of a η_{th}, has a high enough η_{th} to suitably convert the available chemical energy to useful work, so that the net efficiency of both devices is greater than the η_f of the internal combustion engine operating at the lean condition (for example).

Analysis of such "dreams" can only be completed by (a) introducing the concept of *available energy*, or modernly called *exergy*, by employing second law considerations on the analysis and (b) introducing real effects on the engine analysis that include such factors as heat transfer, friction, and other energy "losses" – but not necessarily exergy losses (friction is, of course, an exergy loss). Thus, a brief discussion will follow describing the major benefit of conducting an exergy analysis of an engine system. The idea of available energy – or, that portion of energy which is available to do useful work – is introduced by Gibbs [37] and, in its basic form, suggests that a system with a given amount of energy can transfer that energy out of the system as useful work until the point of equilibrium between the system and its environment (i.e., its surroundings). Using a simplified example, a piston/cylinder arrangement that contains a gas at 2 atm. will, if allowed to interact with its surroundings at 1 atm., expand and transfer work energy until the system pressure is in equilibrium with the surrounding's pressure (i.e., 1 atm.). In a more theoretical sense, it captures the notion that only an orderly flow of energy (e.g., like that established because of a temperature gradient

between a system and its surroundings) can be converted into useful work; disorderly energy cannot be converted to useful work. Entropy is the idea of disorder within a system; thus, exergy analysis combines the effect of a system's entropy on its ability to convert its energy into useful work. Because real processes in net increase entropy (i.e., real processes are irreversible and result in entropy generation), systems undergoing real processes destroy exergy; that is, the opportunity to convert energy into useful work is destroyed via some disordering of what had been an orderly flow of energy.

Examples of real effects, or irreversibilities, either in a general thermodynamic system or between a general thermodynamic system and its environment (all of which happen to be present, also, in internal combustion engines) are heat transfer through a finite temperature difference, mixing, unrestrained expansion, combustion, and friction. The general premise of an irreversibility is one which renders a system/environment combination changed as the system undergoes a cycle and returns to its initial state. For example, if a warm body exchanges thermal energy with a cold body (i.e., heat transfer through a finite temperature difference), there is heat transfer, but not work transfer, until the two bodies are in thermal equilibrium. To return the two bodies to their initial states (i.e., transfer thermal energy from the cold body to the warm body), work energy must be transferred into the system to effect the heat transfer. In the forward process (i.e., the bodies attaining thermal equilibrium), heat transfer occurs without work transfer; in the reverse process (i.e., the bodies returning to their initial states), heat transfer is manifested by a necessary work transfer. A net effect has been made to the surroundings (transfer of work energy) as the system is returned to its initial state; thus, the process is irreversible. If, on the other hand, a device had been positioned between the two bodies of dissimilar temperature that was able to extract the orderly sense of energy motion into useful work (i.e., a heat engine), the irreversibility of the heat transfer through finite temperature difference is diminished. Further, if the heat engine is conceived to be ideal itself, then all the orderly sense of energy motion is converted into useful work; hence, the concept of the Carnot heat engine, or, fully reversible heat engine.

On the one hand, the heat transfer is viewed as a loss; on the other hand, it becomes apparent that there may still be an opportunity to extract useful work from the heat transfer. It is the latter supposition that exergy analysis centers on. To begin a discussion of energy and exergy analysis of an internal combustion engine, a revisit to the assumptions made in the *Fuel–Air Cycle Analysis* is necessary. First, the assumption that the engine is adiabatic is not realistic; all real engines have heat transfer. Thus, it becomes necessary to capture an understanding of the effects of heat transfer on the engine cycle. Second, the assumption of how combustion is modeled is inaccurate. Of course, constant volume combustion in an operating engine is not physically possible due to the finite time required by chemical kinetics to decompose the fuel molecule. Even constant pressure combustion is not realistic because it supposes a constant burn rate with instantaneous starts and ends of combustion. Thus, it becomes necessary to include the effects of "real" combustion on the engine cycle. Third, if it is desired to know the actual torque from the engine (as opposed to what is indicated by the pressure–volume relationship), then a sense of friction must be included in the analysis.

The inclusion of "real effects" in engine cycle analysis is well established. For example, comparisons between actual engine cycles and *Fuel–Air Analysis Cycles* are made by Edson and Taylor [38]. Inclusion of heat transfer, finite combustion rates, and mechanical losses is demonstrated by Strange [39]. The beginnings of detailed combustion modeling, including spatial location of start of combustion and flame propagation, are demonstrated by Patterson and Van Wylen [40]. Such early demonstrations, and the corresponding advancement in digital computers, result in advanced models of heat transfer (e.g., [41–43]), friction [44, 45], and combustion; the latter of which are described in the context of doing a complete engine cycle simulation (e.g., [44, 46–51]). The influences of "real effects" on both energy and exergy perspectives of internal combustion engines are also well established (see, e.g., the reviews by Caton [52] and Rakopoulos and Giakoumis [53]). For example, Fig. 13 illustrates both the energy (Fig. 13a) and exergy (Fig. 13b) distributions of using 0% and 20% adiabatic EGR in a spark ignition engine, as computed by a thermodynamic simulation [54]. Note that when real factors, such as heat transfer and

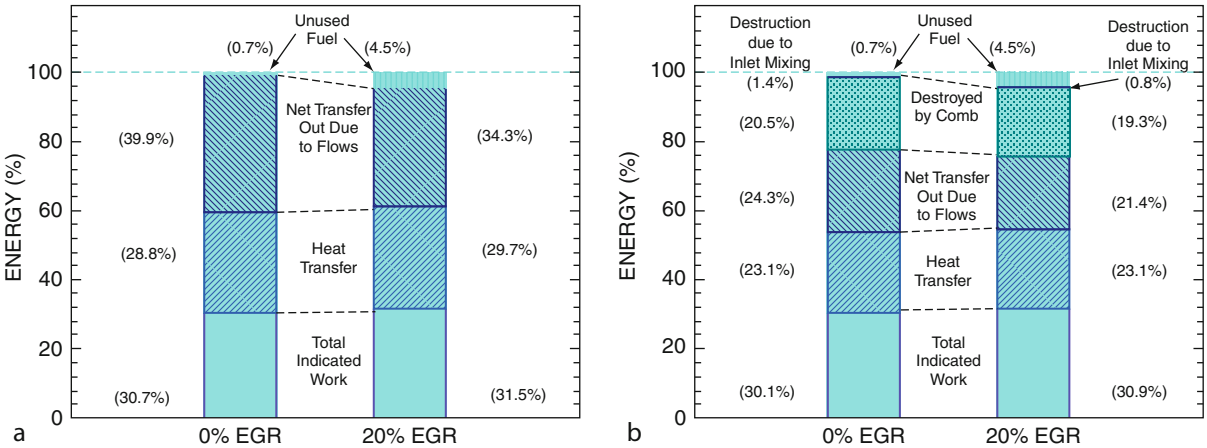

Internal Combustion Engines, Developments in. Figure 13
(**a**) Energy distribution and (**b**) exergy (availability) distribution of various transfer and destruction (in the case of exergy) mechanisms for 0% EGR and 20% EGR in a spark ignition engine modeled using a thermodynamic simulation [54] (Used with permission from Professor J. Caton, Texas A&M University)

real combustion, are considered, the maximum indicated fuel conversion efficiency is about 30.7% for non-EGR case (0% EGR) and 31.5% for 20% EGR case. Most of the balance of energy is transferred to the coolant (ca. 29% for non-EGR case) due to nonadiabatic control system and out the exhaust (ca. 40% for non-EGR case) due to underutilized conversion of thermal to work energy. Thus, the importance of considering real effects is clear. It is noted that the data shown in Fig. 13 do not include the effect of friction; the brake fuel conversion efficiency for the studied conditions of Fig. 13 are available in [54]. It is further noted that friction offers no opportunity for conversion to useful work (i.e., energy lost to friction is all destroyed exergy). Finally, it is noted that EGR seems to have a small to negligible effect on the calculated friction of the simulation [54].

Also clear from Fig. 13 is the importance of considering the internal combustion engine from an exergy perspective. If considering only the energy transfers of Fig. 13a, it may appear that ca. 70% of the energy is "lost," or unavailable for conversion to useful work. While it is correct to say that a fraction of the fuel's energy is underutilized in the engine control system's (i.e., piston/cylinder chamber) conversion to useful work, it is not correct to say that all this energy is lost. As explained above, exergy provides insight into the fraction of energy that is available to do useful work. For example, Fig. 13 illustrates that (for non-EGR cases) 28.8% of the fuel's *energy* is transferred out of the control system via heat transfer, whereas only 23.1% of the fuel's *exergy* is transferred out of the control system via heat transfer. That is, for one unit of fuel, 0.288 unit of energy is transferred via heat transfer, but only ca. 80% (0.231/0.288) of that energy is available to do useful work; thus, 0.231 unit of fuel exergy are a missed opportunity for conversion to useful work. This 0.231 unit of missed opportunity could be exploited by configuring an ideal heat engine between, for example, the cylinder walls and the environment (i.e., representative T_H and T_L). Such a conceptualization seems impractical, but exergy is not just passed into the coolant. Exergy is also transferred to the exhaust; ca. 24.3% of the fuel's exergy for the non-EGR case under study in Fig. 13b. The high temperature exhaust, with ease of accessibility, offers an opportunity to exploit the fuel's exergy transferred through the exhaust system. There are several practical technologies that offer an opportunity to extract the fuel's exergy transferred out of the engine control system; these are discussed in more detail in the section "Waste Heat Recovery".

One of the important features of Fig. 13b is the exergy destroyed due to combustion. Combustion, in any application, is an irreversible phenomenon and thus will render entropy generation (i.e., exergy

destruction). Like friction, the ca. 20% of fuel exergy destroyed due to combustion cannot be recovered for conversion to useful work. The major causes for exergy destruction of a typical hydrocarbon-based combustion process include (1) thermal energy exchange among particles within the system, (2) diffusion among fuel/oxidizer particles, and (3) mixing among product species [55]; of these three, the dominant exergy destruction source is the thermal energy exchange among particles. At the onset of combustion, with the system containing reactants, a metastable equilibrium exists as gradients exist between fuel and oxidizer molecules. As combustion proceeds during the process, natural phenomena cause the system to eliminate such gradients and maximize entropy in the pursuit of attaining a more stable equilibrium (i.e., the products state). The maximization of entropy in reducing the gradients is manifested entirely through entropy generation. Using the dominant source of exergy destruction (i.e., entropy generation) during combustion as an example: internal thermal gradients among particles [56] established during the combustion process create microscopic opportunities to do useful work (i.e., thermal gradients can be converted to useful work via a heat engine). Of course, practical implementations of microscopic heat engines do not exist, thus, the thermal gradients are reduced to zero during the combustion process without any conversion to useful work; heat transfer through a finite temperature difference, as described above, generates entropy (destroys exergy).

The general behavior of exergy destruction due to combustion in internal combustion engines is generally well characterized, as summarized by [57]; generally, an increase in combustion temperature decreases exergy destroyed due to combustion. This statement should not be confused with the situation of internal thermal gradients which, as mentioned above, are a major source of combustion-based exergy destruction. While it is tempting to seek ways to minimize (or even eliminate) combustion irreversibilities (and thus minimize or eliminate combustion-based exergy destruction), it should be recognized that such efforts may decrease the conversion of exergy in other ways. Consider, for example, the use of a lean mixture versus the use of a stoichiometric mixture; the former has higher exergy destruction than the later. While a stoichiometric mixture reduces exergy destruction, its mixture composition also causes lower conversion of thermal to work energy during the expansion process (and, coincidentally, increases exergy transfer via heat transfer). Thus, overall efficiency is lower with a stoichiometric mixture. Again, energy- and exergy-based analyses, such as that presented in Fig. 13, are necessary to quantitatively make such assessments. In the case of eliminating combustion irreversibilities, a reversible combustion process [58] can be conceptualized [59, 60] where initially separated reactant species are isentropically compressed to their respective partial pressures and a certain temperature; concentrations of individual species, when allowed to interact with each other, will be in equilibrium. After compression, individual species will be collected forming a mixture that is a priori in equilibrium (thus, there are no irreversibilities due to mixing) and allowed to expand isentropically. Because of the increase in moles of the mixture as it expands isentropically maintaining equilibrium along the path, net work is extracted from the collection of processes. Quantitative analysis [60] of such a concept reveals 0% exergy destruction; because of exergy retention in the exhaust products, however, thermal efficiency of the "reversible combustion engine" is around 28% (for a fuel–air equivalence ratio of 1.0, compression pressure and temperature of 10 MPa and 6,000 K, respectively, and an expansion ratio of 18:1). Of course, such concepts are presently impractical; but the notion of reversible combustion is theoretically possible.

In fact, it is briefly noted that, although not explicitly calling his concept one of "reversible combustion," a close inspection of Diesel's original engine design [61] describes a method of nearly attaining reversible combustion (at least, one which eliminates internal thermal gradients). This is described in more detail in section "A Case Study: Diesel Engines Versus Gasoline Engines".

In closing this section on "Thermodynamic Analysis of Internal Combustion Engine", it is noted that assigning a "maximum possible efficiency" of an internal combustion engine is anything but straightforward. *Fuel–Air Cycle Analysis* reveals that the efficiency of an engine cycle depends on several different characteristics of the control system. A more advanced and appropriate analysis of an engine – that which includes real

I

effects of heat transfer, real combustion, friction, and other irreversibilities – gives realistic senses of tangible factors that engineers can strive to improve. Further, exergetic-based analysis offers the important insight of what future opportunities might be exploited in improving the overall system efficiency associated with an internal combustion engine. In returning to the engineer's "dream" engine concept described above, such computed numbers as shown in Fig. 13 are more realistic than the ideal *Fuel/Air Cycle Analysis* numbers shown in Fig. 10. Further, the exergy-based analysis of Fig. 13 could be used to make the necessary assessment of the engineer's dream, to quantify if there are real opportunities of "downstream" exergy conversion when the engine is operated close to maximum theoretical thermal efficiency levels.

Spark Ignition Combustion

As discussed in section on "Thermodynamic Analysis of Internal Combustion Engines", real combustion in an internal combustion engine is not ideal in the sense that it can be modeled as precisely constant volume, constant pressure, or even the combination of the two (limited pressure). Real combustion, instead, involves several complex and interacting features that, on the one hand, make it difficult to predict and model, but on the other hand create opportunities for further development. Conventional engines are either spark ignited or compression ignited. Since the type of ignition results in substantially different combustion features, the two are separated into respective sections. This section describes spark ignition combustion.

Spark ignition combustion is the typical form of combustion found in the commonly called "gasoline" engine (also commonly called either "petrol" engine or "otto" engine); it is more descriptive to refer to such engines as spark ignition engines. The "spark" aspect of the term implies that combustion is initiated by introducing a high voltage electrical arc, typically through the use of a spark plug, into the reactant mixture at a point during the cycle where sustained combustion reaction will proceed. Most spark ignition engines (exceptions are described in section on "Future Directions of Internal Combustion Engines") induct a premixed and homogeneous mixture of fuel and air during the intake process. At a point near the end of compression, the spark plug discharges an arc into the mixture. This arc, in the near-by region of the spark plug, forms a high temperature plasma that evolves into a flame kernel. The flame kernel transitions from the plug region in a laminar sense establishing a flame front with initial velocity close to the laminar flame speed. This initial flame development is referred to as the flame-development period. Because of turbulent motion among particles composing the mixture, the flame then rapidly spreads throughout the mixture in a turbulent fashion, enveloping microscale eddies with flame. This rapid flame propagation is referred to as the turbulent entrainment period. Upon flame envelopment of the turbulent eddies within the mixture, the flame then laminarly burns the microscale eddies in the final stage of the process referred to as rapid burnup. Turbulent entrainment and rapid burn practically occur simultaneously, and together compose what is referred to as rapid-burning period. This described sequence of spark ignition combustion for a typical operating point (i.e., 1,400 rev/min, part-load condition) is shown in Fig. 14 [62], and, for the same typical operating point, requires about 10 ms from spark to finish.

One of the important features of Fig. 14, along with the shown in-cylinder pressure, is the corresponding mass fraction burned. Using the first law of thermodynamics, it possible to develop an expression that determines the chemical-to-thermal energy conversion rate (commonly called the "heat release rate") of the combustion process. Since the mass of fuel present in the cylinder, along with the fuel's heating value, are known, the mass fraction burned rate of fuel can be calculated from the heat release rate. Figure 15 illustrates a typical mass fraction burned curve, as a percent of the total fuel, and defines the above-described periods referred to as flame-development period (shown in Fig. 15 as the flame-development angle, $\Delta\theta_d$) and the rapid-burning period (shown in Fig. 15 as the rapid-burning angle, $\Delta\theta_b$). These periods are conventionally defined as the angle swept from spark release to 10% mass fraction burned and the angle swept from 10% mass fraction burned to 90% mass fraction burned, respectively.

The mass fraction burned profile of spark ignition combustion can be modified, and the parameters that

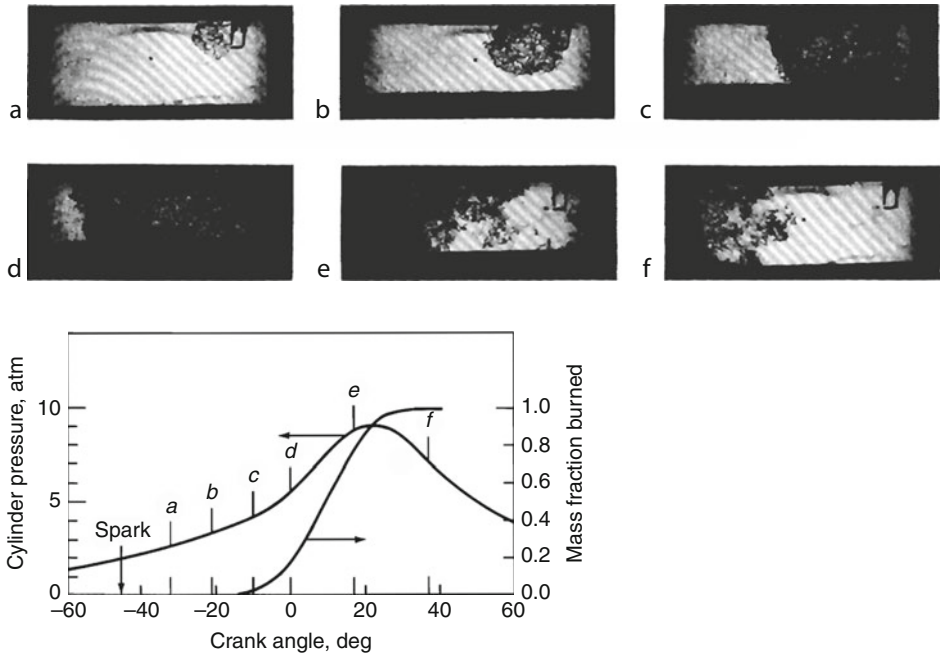

Internal Combustion Engines, Developments in. Figure 14
In-cylinder images capture the sequence of spark ignition combustion with the corresponding result on in-cylinder pressure and mass fraction burned. The various steps of spark ignition combustion shown include the spark release (indicated by "Spark"), flame kernel development (**a**–**c**), turbulent entrainment and burn up (**d**–**e**), and flame termination (**f**) (Used with permission from [62])

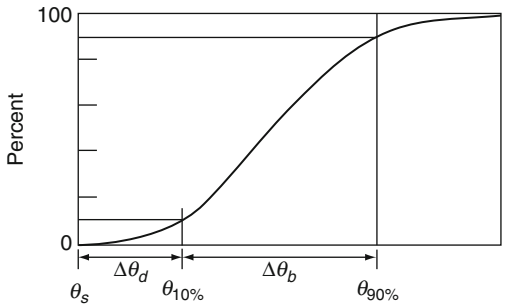

Internal Combustion Engines, Developments in. Figure 15
Mass fraction burn rate (as a percent of total fuel) of spark ignition combustion in an internal combustion engine, illustrating the definitions of the flame-development angle, $\Delta\theta_d$, and the rapid-burning angle, $\Delta\theta_b$ (Used with permission from [63])

cause alterations to the mass fraction burned profile are often coupled. Perhaps the most obvious parameter that can affect the mass fraction burned profile is the spark timing, or sometimes called the spark advance. By adjusting the time in the cycle when combustion is initiated (i.e., the spark advance), the times required for flame development and rapid-burning periods are altered. An advance in spark timing (i.e., spark timing is moved earlier into compression stroke) generally results in combustion occurring earlier in the cycle and in-cylinder pressures becoming higher in magnitude. Correspondingly, a retard in spark timing (i.e., spark timing is moved later into the compression stroke, or possibly even into the expansion stroke) generally results in combustion occurring later in the cycle and in-cylinder pressures becoming lower in magnitude. There are several other parameters, however, that can affect the burn profile of spark ignition combustion. Examples of such parameters include the mixture's fuel–air ratio (i.e., stoichiometry), the level of EGR, the level of turbulence in the mixture, the level of heat transfer, initial mixture pressure (i.e., load variation), initial mixture temperature, and engine speed. Analysis of each of these parameters is

outside the scope of this article; readers are referred to the "Books and Reviews" for additional reference text on the subject.

One item that is important to mention, however, is the effect of burn profile on engine-scale parameters such as performance, efficiency, and emissions. The rate of combustion, and its corresponding effect on in-cylinder pressure, flame temperature, and mixture gas temperature, alters the performance, efficiency, and emissions of the spark ignition engine. For example, Fig. 16 illustrates the effect of spark timing (spark advance) on in-cylinder pressure and relative torque to maximum brake torque (MBT). MBT is the maximum torque attained over a given parametric sweep, most commonly over a spark-timing sweep. Note that there is nearly a single spark timing that yields the maximum torque delivered by the engine. Too early of a timing (advanced) or too late of a timing (retarded) renders a lower torque than MBT. Three spark timings are shown in Fig. 16: 50°, 30°, and 10° before TDC (BTDC). The most advanced timing (50° BTDC) renders the earliest burn profile (of the studied timings), the highest magnitude of in-cylinder pressure, and the earliest location of peak pressure (occurring around 0° BTDC). Although it may appear from Fig. 16 that the spark advance of 50° BTDC yields the maximum area under the pressure-volume curve (and thus, the maximum work for the cycle), it should be noted that its pressure is lower through most of the expansion stroke than the other two shown spark timings (i.e., 30° and 10° BTDC). This lower pressure through the expansion stroke results from the increased level of heat transfer manifested by the higher gas mixture temperature caused by the faster burn rate-induced higher cylinder pressures. Thus, spark timings advanced of MBT timing result in lower torque due to higher levels of compression work, heat transfer, and friction. Conversely, the most retarded timing (10° BTDC) renders the latest burn profile (of the studied timings), the lowest magnitude of peak pressure, and the latest location of peak pressure (occurring around −40° BTDC). Because of the later-phased combustion, the location of the rise in pressure misses the full opportunity of the expansion stroke. Thus, spark timings retarded of MBT result in lower torque due to expansion losses. It is clear that MBT occurs in the balance of minimized compression work and maximized expansion work, both of which are affected by combustion phasing, heat transfer, and friction. In the example of Fig. 16, this balance occurs around 30° BTDC. Notice that peak pressure for this timing is around −20° BTDC; a general "rule of thumb" is that MBT occurs when peak pressure is positioned between −15° and −20° BTDC. As revealed in Fig. 16, this rule of thumb extends to the mass fraction burned profile, where maximum brake torque is timed when 50% of

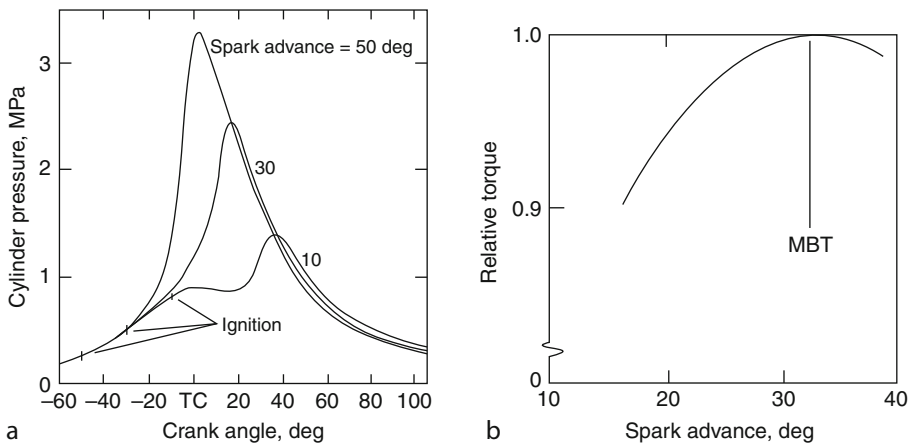

Internal Combustion Engines, Developments in. Figure 16
(**a**) In-cylinder pressure as a function of engine crankangle and (**b**) relative torque to maximum brake torque (MBT) as a function of spark advance of a typical spark ignition engine (Used with permission from [64])

the fuel burns by −10° BTDC. In some cases, MBT timing may be "knock limited," meaning that a higher torque could be attained at an earlier timing if fuel knock were not present. Fuel knock is a combustion abnormality of spark ignition engines that, due to the combustion-generated compression of the reactive mixture in the end regions of the cylinder, results from autoignition of the mixture prior to its controlled burn by the propagating flame. Fuel knock can be very damaging because the uncontrolled combustion tends to cause dramatic rises in pressure near critical mechanical components (such as piston rings). The octane rating of a fuel indicates the fuel's resistance to knock in a spark ignition engine; a fuel with a higher octane has a higher resistance to autoignition. Additional discussion about this is provided in the sections. on "A Case Study: Diesel Engines Versus Gasoline Engines" and "Direct Injection, Spark Ignition Engines".

At MBT timing, since fuel flow rate is generally held constant during spark-timing sweeps, efficiency will also be correspondingly maximized. In the case of emissions, however, the trends are not straightforward and a brief discussion of emissions is reserved for the section on "Emissions Formation and Exhaust Pollution".

Finally, it is noted that several parameters affect the spark ignition burn profile. Thus, for each change to a given parameter (e.g., initial pressure, initial temperature, fuel–air equivalence ratio, engine speed, and level of mixture turbulence), a potentially different spark timing will correspond to maximum brake torque. Again, the general trend of spark timing will be such that 50% mass fraction burned occurs at −10° BTDC for maximum brake torque.

Compression Ignition Combustion

In contrast to spark ignition combustion – which uses an electrical arc, or spark, to initiate combustion of a reactive mixture – compression ignition combustion relies on compressive heating – or, the increase in temperature of a gas due to the increase in pressure resulting from the decrease in volume – where combustion initiation is kinetically driven by exceeding the ignition temperature of the fuel–air mixture. Compression ignition combustion is the typical mode of combustion used in the commonly called diesel engine, an engine which more descriptively is called a compression ignition engine.

It is immediately recognized that one challenge of compression ignition engines is the lack of a direct trigger of ignition; the spark acts as the direct trigger of combustion initiation in a spark ignition engine. Conventional applications of compression ignition engines (e.g., the conventional diesel engine) overcome this challenge by using the fuel injection event as the direct trigger. Thus, conventional compression ignition engines typically induct an air and residual mixture (i.e., no premixing of fuel) during the intake stroke. This same unreactive mixture is compressed during the compression stroke until near the point when combustion is desired to begin. At this point fuel is introduced into the mixture, which, due to compression, is a high temperature, high pressure environment. After several complex and coupled processes occur (described below), combustion initiates and chemical to thermal energy conversion takes place.

At this point, it is instructive to briefly describe the role of "glow plugs" often used in compression ignition engines. Glow plugs should not be confused with spark plugs. A glow plug is a resistive heating element inserted into the cylinder of a compression ignition engine to aid in the initial starting of the engine. It acts as a warming device during "cold start"; after engine warm up and stable operation, the glow plugs deactivate. They are not necessary on a cyclic-basis. Spark plugs, on the other hand, are integral components of spark ignition engines; they provide the source of ignition for every combustion cycle of a spark ignition engine.

The method by which fuel is injected into the compressed mixture typically falls into one of two categories: (1) direct injection, or (2) indirect injection. Indirect injection involves injecting fuel into a "prechamber" which is connected to the main chamber. Fuel injected into the prechamber ignites and causes the mixture to issue into the main chamber where main heat release and work extraction occurs. Indirect injection engines are used primarily in applications where motion of the nonreactive mixture in the main chamber is too quiescent for ignition; this typically occurred in the early implementations of small, high speed automotive compression ignition engines. Use of a prechamber, where nonreactive mixture forced

through orifices or nozzles connecting the main chamber to the prechamber suitably increased mixture swirl and turbulence, generated sufficient fluid motion to allow ignition to occur. Technological developments in intake port design, combustion chamber design, and fuel injection systems have rendered indirect injection systems nearly obsolete and technically inferior to direct injection techniques.

Direct injection, as the name implies, indicates that the fuel is injected directly into the cylinder at the point near when combustion is desired to begin. Because of the compressed nature of the nonreactive mixture into which fuel is injected, fuel injection pressures must be very high; i.e., modern fuel injection systems inject fuel at pressures on the order of 100–2,000 bar (ca. 3,000–30,000 psi). The processes of fuel injection, combustion initiation, and subsequent combustion propagation (or burning) are very complex in compression ignition engines. The following discussion will briefly highlight these complexities.

Figure 17 illustrates the sequence of events that occur in a typical direct injection compression ignition engine. Two load conditions at 1,400 rev/min are shown, with a high-load condition (ca. 75% peak load which is about 11.3 bar BMEP) shown as Fig. 17a and a low-load condition (ca. 25% peak load which is about 1.9 bar BMEP) shown as Fig. 17b. Both plots illustrate the fuel injector needle lift profile (which roughly correlates to the fuel delivery rate), the rate of heat release profile, and the mass fraction burned profile. Focusing first on the high-load condition (Fig. 17a), notice that fuel injection occurs near 2° BTDC. Fuel in typical compression ignition engines is injected as a liquid. Thus, the fuel must undergo a series of physical processes (e.g., penetration, breakup, atomization, and vaporization) before it undergoes its chemical process of bond fragmentation and eventual ignition. This period of time – i.e., the time between start of fuel injection and ignition (commonly called start of combustion) – is often called the ignition delay period. As will be described below, the ignition delay period of a compression ignition engine is an important parameter that affects the remainder of the burn profile and is affected by several other parameters. The end of the ignition delay period after start of injection will witness start of combustion and noticeable heat release, as indicated in Fig. 17a as the positive rate of heat release. During heat release, the mass fraction burned profile steadily increases until end of combustion when all the fuel is most nearly completely burned.

An interesting and important feature of Fig. 17 is the rate of heat release profile between start of

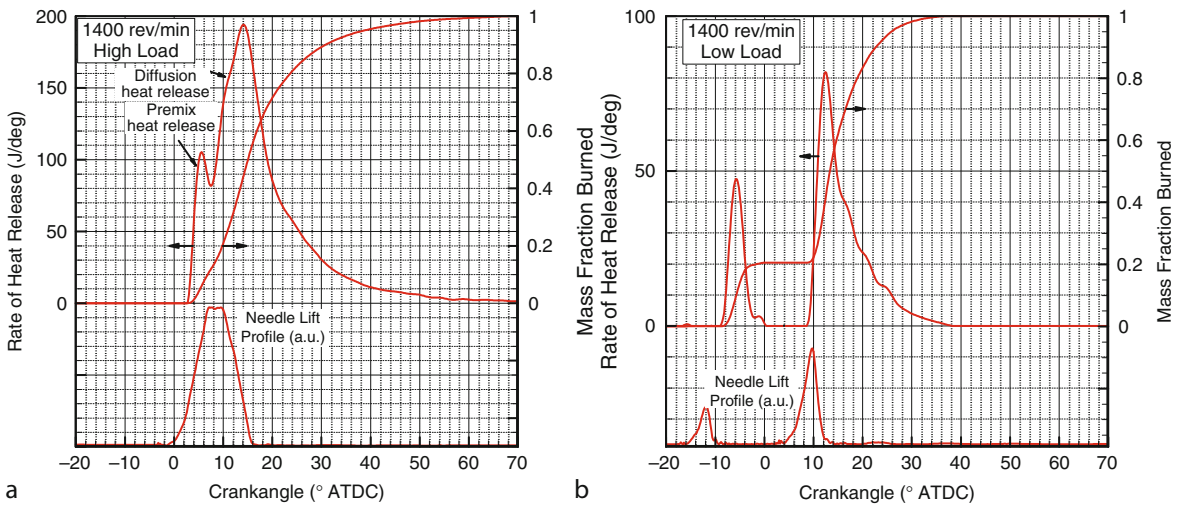

Internal Combustion Engines, Developments in. Figure 17
Fuel injector needle lift profile, rate of heat release, and mass fraction burned for a typical diesel engine operating at 1,400 rev/min (**a**) high-load condition (ca. 75% peak load = 11.3 bar BMEP) and (**b**) low-load condition (ca. 25% peak load = 1.9 bar BMEP) with the use of pilot injection (Data from author's laboratory, Texas A&M University)

combustion and end of combustion. Notice in Fig. 17a there are two distinct components of the rate of heat release: a premixed component and a diffusion component. These two respective components are nearly an exclusive feature of compression ignition combustion that relies on fuel injection as the ignition trigger. The premixed heat release component results from the complex processes involved in physically preparing the initial "packets" of fuel for chemical decomposition [65]; as described above, the injected liquid fuel must be prepared and sufficiently mixed with the cylinder gases before chemical decomposition can begin. Once ignition occurs, the parcels of fuel that prepared for burning during the ignition delay period react under kinetic control, with relatively high rates of burning for the given mixture temperature. Fuel continues to inject during the premixed portion, and the increase in temperature due to premixed combustion accelerates the physical preparation of the newly introduced parcels of fuel. In spite of this acceleration of fuel preparation, the burn rate becomes limited by the fuel's mixing rate with the air. Since the time scales for mixing are larger than the time scales for chemical kinetic decomposition [66], the burn rate becomes mixing-controlled, rather than kinetically controlled. The mixing-controlled, or diffusion-controlled, component of heat release is observed in Fig. 17a as the longer heat release following premixed heat release and is identified as "diffusion heat release." The burn rate of diffusion heat release is generally slower than premixed heat release at any given reaction temperature. Figure 17a shows diffusion heat release having a much higher burn rate than premixed heat release; this is manifested, however, by the associated higher mixture temperature effected by the combustion process.

The situation is slightly different for the low-load case, shown as Fig. 17b. Conventional compression ignition engines that use fuel injection as the ignition trigger typically also use the amount of fuel delivery as the means to control engine load. Thus, the need to produce less power at a given engine speed is effected by decreasing the amount of fuel delivered during the injection process. This is evident in Fig. 17b where the area under the fuel injector needle lift profile is less than that of the high-load case (for the moment, disregard the bimodal fuel injection profile, which will be explained below). Consequently, the distribution of premix versus diffusion heat release is not apparent on the low-load heat release profile. This does not imply that mixing-controlled combustion does not occur during low-load operation; it does imply, however, that combustion is predominantly kinetically controlled at low-load conditions whereas it is predominantly diffusion-controlled at high-load conditions.

The bimodal feature of the fuel injection profile in Fig. 17b is the result of the use of a double-injection strategy on this particular engine at this particular condition. Modern advanced engine fuel systems are capable of introducing fuel in sequences, or pulses, in what is commonly called "multi-injection strategies." In the case of the engine highlighted in Fig. 17b, the first injection is considered a "pilot" injection, while the second injection is considered a "main" injection. The pilot injection introduces only a small portion (e.g., ca. 10%) of the total fuel to be delivered in the cycle, creating an opportunity to prepare a smaller portion of fuel for burning during the ignition delay period. This small pilot increases cylinder temperature, so that the ignition delay period of the main injection is much shorter, and there correspondingly is a lower fraction of premixed heat release during the main combustion event. Such a strategy is used, for example, to reduce combustion-generated noise of a diesel engine. Interestingly, diesel engine noise is an "age-old" problem, serving as a primary focus of development for Sir Harry Ricardo (a pioneer in the development of high speed diesel engines) [67].

The above-described use of multiple injections hints at an ever-present relationship within compression ignition combustion systems using fuel injection as the direct trigger; i.e., a relationship among ignition delay, fraction of premix heat release, and fraction of diffusion heat release exists. This relationship is shown in Fig. 18a, which illustrates the rates of heat release at two different injection timings of a typical compression ignition engine operating at 1,400 rev/min, high-load condition (11.3 bar BMEP, nominal). Notice for the advanced injection timing there is a substantial level of premix heat release and a correspondingly lower fraction of diffusion heat release relative to the retarded injection timing. The advanced injection timing, due to the injection of fuel into a relatively cool environment when rates of physical and chemical processes are low, results in a relatively longer ignition delay. Because of

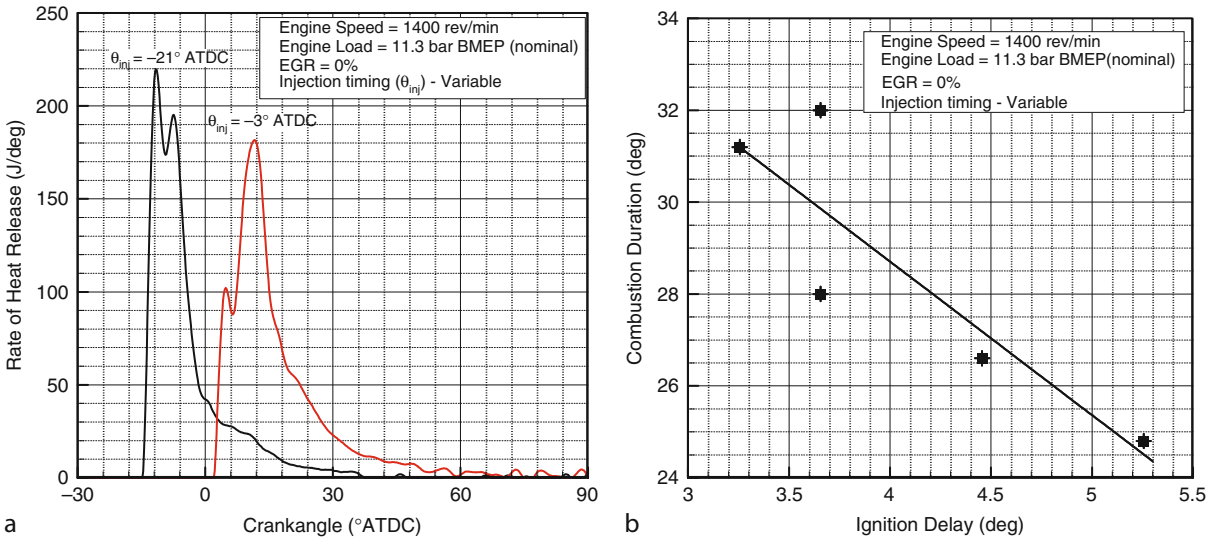

Internal Combustion Engines, Developments in. Figure 18
(**a**) Rate of heat release at an advanced injection timing (21° BTDC) and a retarded injection timing (3° BTDC) and (**b**) the relationship between ignition delay and combustion duration via an injection timing sweep for a typical compression ignition engine operating at 1,400 rev/min, high-load condition (11.3 bar BMEP, nominal) (Data from author's laboratory, Texas A&M University)

the longer ignition delay, there is more time for fuel preparation prior to ignition; once ignition occurs, there is a relatively higher concentration of fuel that is prepared for burning and correspondingly combusts in a premix and kinetically controlled fashion. As more fuel is prepared during the ignition delay period for premix burn, there consequently is less fuel available for diffusion heat release; thus, as premix burn fraction increases, diffusion burn fraction decreases. Likewise, at the retarded injection timing, fuel is injected in a relatively hotter environment which enables fuel preparation for burning at a faster rate and combustion commences relatively sooner (i.e., shorter ignition delay). Because of the shorter ignition delay, there is less fuel prepared for burning, thus there is lower fraction of premix heat release and correspondingly larger fraction of diffusion heat release.

Because premix heat release rate is relatively faster (at a given temperature) than diffusion heat release, the "combustion duration" – or, the time taken between start of combustion and end of combustion – for a mostly premix heat release combustion event will be shorter than that of a mostly diffusion heat release combustion event. Thus, there tends to be an inverse relationship between ignition delay and combustion duration, as shown in Fig. 18b, where changes to ignition delay are manifested by alterations to injection timing. The shorter ignition delay results in less premix heat release, more diffusion heat release, and correspondingly a longer combustion duration.

Injection timing is just one parameter that can affect ignition delay, and thus the burn profile of a compression ignition combustion event when fuel injection is used as the ignition trigger. Other engine parameters such as EGR level [68], initial temperature and initial pressure [69], injection pressure [70–72], and swirl and turbulence [69, 73] all have certain effects on ignition delay and the resulting relative fractions of premix and diffusion heat release. Like the effect of various parameters of spark ignition engine performance, efficiency, and emissions, the various effects of compression ignition engine parameters on ignition delay and burn profile also have an effect on engine efficiency, performance, and emissions. For example, overly advanced or retarded injection timings will cause decreases in engine torque for a given fuel delivery rate. Additionally, fuel quality is particularly important for conventional diesel combustion operation, where low

volatility fuels with high ignitability are generally used to ensure ignition occurs during the cycle. An important fuel parameter – i.e., its cetane number – is used to identify the quality of fuels appropriate for use in a diesel combustion system. A higher cetane corresponds to a fuel with a shorter ignition delay.

Finally, in closing, it is important to recognize the above-described phenomena are largely phenomenological observations that can be made using conventional diagnostics with relatively straightforward analysis. Considerable development (e.g., [49, 74, 75]) has been made to provide substantial insight into the complex fluid, heat transfer, and chemical processes that occur during compression ignition combustion where fuel injection is used as the direct ignition trigger. Description of these details is outside the scope of this work.

Emissions Formation and Exhaust Pollution

A discussion on the basics of internal combustion engines, actually any combustion-based device, is incomplete without a description of the associated harmful species that may exist in the products of combustion. Such harmful species are generally called "exhaust pollution" and many governing agencies around the world place restrictions on the emission of certain pollutants from combustion-based devices. Because the application of the internal combustion engine is so varied, emission regulations tend to be application-oriented. For example, in the USA, emission regulations are placed on passenger vehicles differently than emission regulations placed on heavy trucks or hand-held engine devices (such as lawn mowers). Because of such variability in regulation, the time-oriented nature of the regulations (i.e., regulations have, to this point, been in a state of flux), and variation in regulation among various governing agencies around the world, further description of specific emissions will not be provided. The basic issues at hand, however, can be briefly described.

As shown in Reaction (R1), there are several species formed during the combustion reaction of a typical hydrocarbon–air mixture. Some of these species are generally stable and nonreactive in the atmosphere, thus pose little to no harm to the five kingdoms of nature. Other species, however, are either harmful or reactive in ways that lead to harmful consequences. Specifically, there is little scientific debate about the harmful nature of certain combustion products such as CO, NO/NO_2, unburned hydrocarbons (HC), and particulate matter (PM, or the solid/liquid components of exhaust that can be collected on a filter. It is noted that historically sulfur oxides and sulfates have been considered either separately from [76] or in combination with [77, 78] particulate matter). There is, perhaps, continued debate about the potential consequences of other products of combustion; in particular, there is current debate on the consequence of CO_2 and the role it may play in the presently observed warming of the planet (i.e., so-called global warming or global climate change). Because of the certainty of the effects of the former species, attention will be given to them and basic information on their formation during combustion. Because of the uncertainty of the effects of the latter species, readers are referred to other literature to uncover the current state-of-debate of CO_2 and its potential impact on global trends currently believed to occur (see, e.g. [79, 80]).

The first such species to describe is CO, which due to its fatal effects on human/animal life is one of the first combustion products to be considered a pollutant [76]. It is well established [76] that all precursor hydrocarbon decomposition reactions firstly form CO. Thus, increased concentrations of CO in engine exhaust result from incomplete reaction of the principal CO oxidation step [26], given as Reaction (R2):

$$CO + OH \leftrightarrow CO_2 + H \qquad \text{(R2)}$$

In internal combustion engines, the incomplete oxidation of CO most typically occurs during rich engine operation [76], where available oxidants for final CO oxidation are lacking [81]. Fuel–air mixtures close to stoichiometric or even slightly lean, however, result in nonnegligible concentrations of CO.

The next species to consider is NO. NO emerged as combustion-generated pollutant due to its observed effect of reacting with hydrocarbons in the presence of sunlight to produce tropospheric ozone [82]. Its formation in a combustion system is rather complex, as there are several major pathways through which it can form. These major pathways include thermal (or commonly called Zeldovich), prompt, and fuel-based nitrogen [26]. For reciprocating-type internal

combustion engines, the primary NO formation mechanism is the thermal mechanism where atmospheric air serves as the principal source of nitrogen in the mechanism [27]. There are three reactions that compose the mechanism, given as Reactions (R3)–(R5):

$$O + N_2 \leftrightarrow NO + N \tag{R3}$$

$$N + O_2 \leftrightarrow NO + O \tag{R4}$$

$$N + OH \leftrightarrow NO + H \tag{R5}$$

The forward and reverse reaction rate constants of Reactions (R3) and (R4) are generally exponentially dependent on temperature. To demonstrate the substantial role temperature plays on NO formation, several simplifying assumptions (see below) are applied to Reactions (R3) and (R4) to yield Eq. 15 [26]:

$$\frac{d[NO]}{dt} = \frac{6 \times 10^{16}}{T^{\frac{1}{2}}} \exp\left(\frac{-69090}{T}\right) [O_{2,eq}]^{\frac{1}{2}} [N_{2,eq}] \cdot \left(\text{mol/cm}^3\text{-s}\right) \tag{15}$$

where [NO] is the concentration (mol/cm^3) of NO at time, t (s), and $[O_{2,eq}]$ and $[N_{2,eq}]$ represent the equilibrium concentrations (mol/cm^3) at temperature T (K) of oxygen and nitrogen, respectively. The several simplifying assumptions that go into Eq. 15 include the following. The first assumption is that the nitrogen chemistry is de-coupled from the combustion reactions. Although combustion reactions generally occur much faster than nitrogen chemistry [25], the presence of O and OH radicals in the thermal mechanism (which are also important species in combustion reactions) may require the chemistries to be coupled for accurate NO prediction [27]. By assuming the chemistries are de-coupled, O, O_2, OH, H, and N_2 can be approximated by their equilibrium concentrations at equilibrium temperature; assuming equilibrium temperature is the second assumption applied to Eq. 15. The third and last assumption applied to Eq. 15 is that nitrogen radical (N) is in steady-state concentration (i.e., $\frac{d[N]}{dt} = 0$). Finally, it is reinforced that the forward reaction rate constant of Reaction (R3) is used from [26] in Eq. 15; updated reaction rates are available in Dean and Bozzelli [29]. It is clear from Eq. 15 the strong dependency NO formation rate has on temperature.

Because of the dominance of the thermal mechanism on NO formation in internal combustion engines, combustion-based efforts to reduce NO center on reducing the reaction temperature and O_2 concentration. Such techniques include altering spark advance [83, 84] or injection timing [85–87] for spark ignition or compression ignition engines, respectively, and introducing EGR into the mixture [87–90].

As described above with NO, unburned hydrocarbons (HC) play a role in the formation of tropospheric ozone. Further, they represent unreacted fuel; if left to discharge into the atmosphere, there is lost opportunity to convert that chemical energy into useful work. Formation of HC species during combustion reaction are complex and varied depending on the type of fuel used [91]. A general cause for HC emissions, however, is insufficient mixing between fuel and air [76], where most of the HC emission species are formed during low temperature ($T < 1{,}000$ K) reactions [26]. Typically, in conventional reciprocating internal combustion engines, most of these species are oxidized as combustion enters high temperature mechanisms [26]. Reciprocating engines, however, contain "sources" for hydrocarbon storage that, if not oxidized upon release in the gas mixture in the later portion of the cycle, emit as HC emissions in the exhaust [92]. Although there are special considerations given to engines operating under cold-start conditions [93], the general storage locations of HC species (and thus, the major source of HC emissions [94]) include cylinder head gasket crevice, spark plug crevices, piston ring pack crevices, and valve seat crevices. In addition to crevice HC storage, other sources of HC emissions [94] include single-wall flame quenching, oil film layers, combustion-chamber deposits, exhaust valve leakage, and liquid fuel (i.e., HC species not vaporized during the process). Because of the relative importance of crevice storage on HC emissions, much of the combustion-based effort to decrease HC emissions has centered on reducing the volume and flow pattern of crevices in the piston/cylinder arrangement.

The final major pollutant to briefly describe is particulate matter, or PM. PM is essentially any exhaust specie that can be collected on a filter; it typically is structured on a solid organic component (which is mostly pyrolized carbon particles, or "soot") upon which organic (e.g., unburned HC) and nonorganic (sulfates) components build. Since soot serves as the building block for PM, much of the research efforts are

dedicated to understanding soot formation processes [95–99]. The general path for soot formation begins with the high temperature pyrolysis, or fragmentation to hydrocarbon radical, of the hydrocarbon fuel. Such pyrolysis typically leads to a certain group of hydrocarbon radicals called polyaromatic hydrocarbons. Such polyaromatic hydrocarbons that do not oxidize during the reaction serve as the nucleation site for soot growth. Nuclei then begin to coalesce and substantially increase surface area. Now particles, the high surface area soot particles agglomerate and allow other species (i.e., liquid HC, condensed gaseous HC, and sulfates) to absorb onto the surfaces [99]. Soot formation is strongly dependent on mixture fuel–air ratio and also temperature (both tend to govern the rate of pyrolysis). Formed soot can, however, undergo oxidation as well. Soot oxidation is likewise a function of temperature, but has a stronger dependency on temperature than soot formation [99]. The difference between soot that is formed and soot that oxidizes is ultimately released in the engine exhaust, and is commonly called "net soot release." Compression ignition engines (e.g., diesel engines) are often plagued with high PM emissions, largely due to the heterogeneity induced into the fuel/air mixture by use of fuel injection as a direct trigger for ignition. Spark ignition engines, however, are recently being considered as sources of nanoscale soot particles [100, 101].

It is clear from the above discussion that soot and PM emission processes are complex. From phenomenological considerations, however, Khan et al. [86, 102] and Ahmad [103] provide insight into the general behavior of PM with, in particular, diesel engine combustion. Specifically, it is observed that increases in diffusion heat release generally increase the emissions of PM. A portion of this may be due to the overall lower reaction temperatures, manifested by relatively lower premix heat release, decreasing the rate of soot oxidation through the diffusion flame. This observation is also supported, however, by Dec's [74] observation that precursor soot formation occurs in the standing premix reaction zone within a diffusion flame sheet that exists in diesel combustion. Thus, increased diffusion burn correspondingly results in increased soot emission. Either way, it becomes apparent when relating this discussion to the known effects of injection timing, for example, on diffusion combustion and NO emissions that an attempt to decrease soot by creating higher temperatures with, perhaps, more premix heat release will correspondingly increase NO emissions; hence, the establishment of the conventional "soot-NO_x" tradeoff of diesel engines.

As described briefly above with each species, there are in-cylinder and combustion-based methods to reduce the formation of various exhaust pollutants. Advanced development of combustion systems continues to focus on these in-cylinder methods, as described in section on "Future Directions of Internal Combustion Engines". Also in use to eliminate exhaust pollution are exhaust after treatment systems, which conventionally are catalyzed devices (hence, their common name of "catalyst" or "catalytic converter") [104–106]. The basic idea of a catalyst is to promote a reaction that otherwise would not proceed. In aftertreatment of engine exhaust, there are several catalysts in use depending on the species composition of the exhaust. For example, the conventionally named "three-way catalyst" is often used with conventional gasoline spark ignition engines. Such a catalyst is typically an exhaust flow-through device composed of a ceramic monolith (the substrate) with thru-hole passages to allow exhaust gases to flow and a metal-oxide "washcoat" that suspends catalytic particles on the surfaces of the monolithic passages. The monoliths are usually constructed of coerderite and the metal-oxide washcoat is often an alumina washcoat. Catalyzed particles are often from the precious metals group (e.g., platinum, palladium, and rhodium), with platinum being the most commonly used metal. The general operation of the three-way catalyst is to promote the reduction–oxidation reactions among CO and HC (the reductants) and NO/NO_2 (the oxidants). In other words, the catalyst promotes the reduction of NO or NO_2 to yield stabilized N_2 and the oxidation of CO and HC to yield stabilized CO_2 and H_2O. The efficiency of the three-way catalyst – or, the conversion effectiveness of converting a given species to its more stable species, e.g., CO to CO_2 – is strongly dependent on the constituent composition on the inlet mixtures, as shown in Fig. 19 [104]. Notice that maximum conversion efficiencies of NO_x, CO, and HC occur very near stoichiometric air–fuel ratios; a small departure from stoichiometric conditions – e.g., about 0.5% increase or decrease in A/F ratio – results in a nearly

I

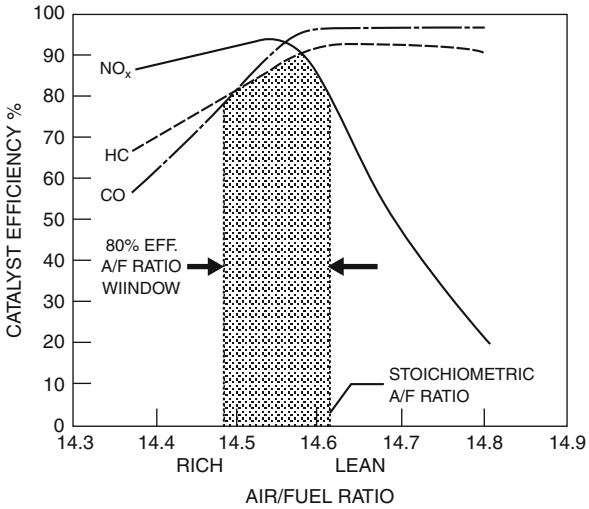

Internal Combustion Engines, Developments in. Figure 19
Catalyst efficiency of a typical three-way catalyst interacting with exhaust from a typical gasoline spark ignition engine as a function of mixture air–fuel ratio (A/F ratio) (Used with permission from [104])

20% decrease in conversion efficiency. Because of such an intolerable response of the catalyst, effective control of gasoline spark ignition engines requires precise control of the mixture stoichiometry during operation.

Also clear from Fig. 19 is the challenge of outfitting a typical platinum-based catalyst with non-gasoline spark ignition engine technology. Diesel engines which typically operate fuel lean (i.e., oxygen rich), for example, create constituent exhaust species that are difficult to catalyze using conventional techniques. Advanced aftertreatment technologies for diesel engines, or other advanced combustion/engine systems, are under development and beginning to appear in production applications [105, 106].

A Case Study: Diesel Engines Versus Gasoline Engines

At this point, with the basics of internal combustion engines having been described, it is useful to do a "state-of-the-art" technology comparison between the two dominant conventional internal combustion engines – i.e., the gasoline spark ignition engine and the diesel compression ignition engine – to set the stage for discussions on future directions in internal combustion engines. The elementary comparison is provided in Table 2; note that this comparison is neither comprehensive nor general. It is intended to highlight the common state-of-the-art of the two technologies, and create a sense for the trends of future directions in internal combustion engine development.

It is clear from Table 2 that the two engine types differ in virtually every way, save for their common use of the kinematic elements of the crank-slider and piston/cylinder components. Consider first the spark ignition engine; its use of spark requires a relatively tight control on the fuel–air mixture equivalence ratio. The flame travel time is minimized when fuel–air equivalence ratio is near stoichiometric, and greater than about 20–40% departure from stoichiometric will typically cause misfire [107]. It is noted that this requirement [107] is only for ignition and flame propagation. The integration of a three-way catalyst with a conventional spark ignition engine requires even more precise control over fuel equivalence ratio, as described in section on "Emissions Formation and Exhaust Pollution" [104]. Thus, conventional spark ignition engines are not able to tolerate substantial departures from stoichiometric conditions. Further, because of this requirement, it is necessary to avoid mixture striations between fuel and air. Thus, conventional spark ignition engines make use of premixing devices (e.g., carburetors or throttle body and port fuel injectors) to prepare the fuel–air mixture prior to induction. The result is a homogeneous mixture of fuel, air, and other residuals such as residual fraction and purposefully introduced constituents such as EGR. In order to assist with the homogenization of the fuel–air mixture, light distillates and aromatics with high volatility are typically used as the fuel for conventional spark ignition engines. The most common, of course, is the mixture of light distillates and aromatics commonly called "gasoline" or "petrol." Interestingly, largely due to the reactive nature of the homogeneous and near-stoichiometric mixture [108], compression ratios of spark ignition engines are limited to around 11. Compression ratios higher than this promote the undesirable autoignition of certain regions of the fuel–air mixture during the combustion process; a phenomenon known as "fuel knock." Fuel knock can be very damaging to an engine, mostly due to its occurrence in the end regions of cylinder, where

Internal Combustion Engines, Developments in. Table 2 Elementary comparison between conventional spark ignition engines and conventional compression ignition engines. The comparison is not comprehensive nor general, rather it is intended to highlight the common state-of-the-art and create a sense for the trends of future directions in internal combustion engine development

Feature	Conventional spark ignition engine (homogeneous charge spark ignition)	Conventional compression ignition engine (heterogeneous charge compression ignition)
Also known as	Gasoline, petrol, Otto engine	Diesel engine
Method of ignition	Spark	Compression
Fuel equivalence ratio	Precisely controlled to stoichiometric	Varies depending on engine load; typically remains lean
Fuel/air mixture preparation	Carburetion, throttle-body injection, port injection	Direct injection or indirect injection
Degree of fuel/air mixing	Homogeneous	Heterogeneous
Fuels used	Gasoline, alcohols, ethanol, hydrogen, high volatility hydrocarbons	Diesel, oils (transesterified), hydrogen, low volatility hydrocarbons
Compression ratios	Ca. 8–11	Ca. 14–21
Method of load control	Throttle restriction of air or fuel/air mixture (depending on mixture preparation)	Fuel injection duration (i.e., fuel quantity)

uncontrolled autoignition of the mixture results in excessively high rises in pressure near susceptible components of the piston/cylinder arrangement (e.g., piston rings). As an aside, initially tetra-ethyl lead and eventually other lead alkyls were used in gasoline as anti-knock agents, allowing for compression ratios to increase in spark ignition engines [109]. Concerns over the effect of lead on human and animal life, as well as the implications of lead on catalytic devices, have mostly eliminated lead-based additives from fuels [110]. Finally, and similarly related to the spark's need to ignite a near-stoichiometric and homogeneous mixture, conventional spark ignition engines control their load, or power output, via the use of a throttle. In other words, the power of the engine at any given speed is minimized by decreasing the efficiency by which the engine can induct fresh mixture.

Consider now the conventional compression ignition engine, or commonly called diesel engine. It seems that from its first inception, the diesel engine was to be a compressively ignited machine, as Diesel intended to create an isothermal reaction where air and fuel were (separately) compressed to the combustion temperature and expansion occurred isothermally as chemical energy converted directly into mechanical energy [61]. Of course, Diesel never succeeded in attaining this isothermal process (nor has anyone since); but, the foundation had been laid for a compression ignition engine. By using compression ignition combustion, many of the constraints placed on the spark ignition engine (i.e., near-stoichiometric fuel equivalence ratio, homogeneous mixture, and throttle of intake mixture) no longer need apply to the diesel engine. It also seems that from its initial inception, Diesel intended the fuel to be directly delivered to the compressed air [61]; of course, it is also clear that direct (or indirect) injection of the fuel to compressed air is necessary so as to control start of combustion. Further, to aid in the gradual and isothermal conversion from chemical to mechanical energy, Diesel stipulated that there be a chemical abundance of air (i.e., fuel lean) in the mixture [61]; practical implementations of diesel engines make use of varying fuel-equivalence ratios to control the load of the engine. The direct (or indirect) injection of fuel into the compressed air, contrary to Diesel's conception, establishes a heterogeneous mixture that within itself has widely varying fuel–air ratios and reaction temperatures. Further, since ignition is

manifested through compression, fuels with high ignitability (e.g., heavy distillates and aromatics) are required (correspondingly, the fuels also have relatively lower volatility, further establishing the heterogeneous nature of diesel combustion). Also related to the use of compression to ignite the mixture is the need to have high compression ratios (i.e., typically varying between 14 and 21). Finally, as already described, engine load is controlled by the direct and exclusive control of fuel; thus, engine load varies as mixture fuel–air equivalence ratio varies. Due to the heterogeneous nature of diesel combustion, and the dependency of soot formation on mixture stoichiometry under conventional conditions, fuel equivalence ratios rarely exceed 90% of stoichiometric to avoid "smoke limitation."

In the context of the three common attributes of internal combustion engines (i.e., performance, efficiency, and emissions), and the comparison given in Table 2, brief comments will be made about the pros and cons of each conventional technology.

In terms of power, consider Eq. 7 and the qualitative relation of each parameter for a given technology at their "wide-open throttle" or full-load operation, as given in Table 3. Described in more detail below, diesel engines tend to have higher fuel conversion efficiencies. Because of not premixing the fuel with air and generally lower engine speeds (which allows the avoidance of flow choke), diesel engines tend to have higher volumetric efficiencies (refer to the discussion surrounding Fig. 6 and [111] for more detail on factors affecting volumetric efficiency of engines). Typical applications of diesel engines use turbocharging, which increase the inlet mixture density to above atmospheric conditions (typical spark ignition engines operate naturally aspirated). As described above, spark ignition engines generally operate stoichiometric, whereas compression ignition engines generally operate lean even at full power. The heating value of diesel fuel is marginally higher than that of gasoline. Displaced volumes of typical compression ignition engines tend to be larger than those of typical spark ignition engines. Correspondingly, peak power speeds for typical spark ignition engines tend to be higher than compression ignition engines. Mostly due to the larger displaced volumes, but also assisted by higher fuel conversion and volumetric efficiencies, higher inlet density, and higher heating value of the fuel, typical compression ignition engines tend to exhibit higher peak powers than typical spark ignition engines. If the power is normalized by displaced volume to render the specific power, however, spark ignition engines tend to have higher specific power than compression ignition engines (in spite of compression ignition engines having high efficiencies, density, and heating value, the stoichiometric and high speed operation of the spark ignition engine tends to yield higher specific power).

Internal Combustion Engines, Developments in.

Table 3 Comparison of the various parameters that control an engine's ability to make power (Eq. 7) between typical applications of conventional spark ignition and conventional compression ignition engines at wide-open throttle or full load condition. It should be noted that these are qualitative assessments of typical technology, and should not be viewed as absolute truths of the respective technologies. Since typical applications of internal combustion engines operate on the four-stroke principle, its effect on the comparison is neutral

Parameter	Parameter's effect on power[a]	Conventional spark ignition engine	Conventional compression ignition engine
η_f	↑		↑
η_v	↑		↑
$\rho_{a,i}$	↑		↑
(F/A)	↑	↑	
Q_{HV}	↑		↑
V_d	↑		↑
N	↑	↑	
n_R	↓	↔	

[a]In other words, an increase in the parameter will have the listed effect on power

As described in section on "Thermodynamic Analysis of Internal Combustion Engines", engines operating with high compression ratios and lean fuel equivalence ratios will tend to have higher efficiencies than engines operating with relatively lower compression ratios and near-stoichiometric equivalence ratios. As a result, typical compression ignition engines tend to have higher efficiencies than typical spark ignition engines. In some instances, turbocharging that is

typically found on compression ignition engines could increase efficiency if intake manifold pressure is boosted to higher than exhaust manifold pressure; the primary function of a turbocharger, however, is to increase inlet mixture density to increase the power capabilities of the engine (as shown in Eq. 7). The efficiency improvement of compression ignition engines at part-load conditions becomes amplified as (a) the mixture becomes leaner for the compression ignition engine and (b) the use of throttle to manifest part load in the spark ignition engine introduces a thermodynamic loss parameter in the cycle.

Finally, a brief comparison of emissions between the two engines at wide-open throttle or full load condition is made. Because of their near-stoichiometric operation, engine-out emissions of HC and CO for spark ignition engines tend to be relatively higher for those of compression ignition engines (where the latter uses fuel-lean mixtures, creating an oxygen rich exhaust and high level of oxidation of partially oxidized species such as CO and HC). Engine-out emissions of NO tend to be nearly the same between engine technologies. Engine-out emissions of PM are much higher for compression ignition engines, where mixture heterogeneity creates numerous opportunities for soot formation. Of course, it is important to note that conventional spark ignition engines are typically coupled with an effective catalyst, substantially lowering the catalyst-out emissions of the various species to levels well below the engine-out emissions of compression ignition engines. While the use of aftertreatment systems with conventional compression ignition engines are less straightforward, technology is becoming available to also allow substantial reduction of their engine-out emissions [106].

At this point, it becomes clear both engine technologies have features which are more favorable than the other for power, efficiency, and emissions considerations. For example, the high compression ratio and lean mixture required by compression ignition are attractive from efficiency perspectives. The homogeneous mixture of spark ignition is attractive from uniform combustion and emissions perspectives. The lack of a throttle to control load of a compression ignition engine is attractive, but the direct ignition trigger of a spark ignition engine is also attractive. Thus, it is clear that future engine developments could exploit the favorable features of engine technologies to create the next generation internal combustion engine. The next section will describe such efforts and offer insight into the likely future direction of internal combustion engines.

Future Directions of Internal Combustion Engines

There are several types of advanced technology that exist for internal combustion engines. Some of this technology is very prevalent on engines (e.g., turbocharging on diesel engines). Some technology is beginning to appear on production models (e.g., variable valve timing). Other technology is still in its development stages, awaiting its potential entry into full-scale production (e.g., homogeneous charge compression ignition combustion). This section will briefly describe such technology.

Engine Downsizing

A general idea that permeates much of the technology under development of internal combustion engines is that of engine downsizing – or, the effort to use advanced technology to enable the use of smaller-sized engines to produce the same power (i.e., increase power density) [112]. The application-oriented benefit is that a smaller engine likely weighs less, thus could improve application efficiency (e.g., better vehicle fuel economy with a lighter engine). The engine itself, however, will likely realize improved efficiency. For example, a smaller engine that uses turbocharging to maintain same power (as a larger-sized engine) will generally operate more often near the location of peak efficiency. Some benefit of such is realized in diesel engines, which typically have best efficiencies near mid-speed, and 75% peak load conditions. More benefit, however, is realized in gasoline engines where throttles are used; a smaller engine with higher power density will require less throttle and thus realize larger gains in efficiency improvement. Overall, the major purpose of engine downsizing is to improve parameters other than V_d in Eq. 7. This idea will become more apparent as specific technology is discussed below.

Turbocharging/Supercharging/Boosting

Boosting an engine – i.e., increasing the inlet mixture density to increase the trapped mass per cycle – is a very

common means to increase the power density of an engine. As evident from Eq. 7, an increase in the inlet air density will directly increase the power of the engine. There are two major types of boosting technology: turbocharging and supercharging. The major difference between the two technologies is the former uses a centrifugal device (i.e., a turbine) to exploit available exhaust energy for conversion to shaft work whereas the latter absorbs shaft work via a direct mechanical connection to the engine. In both cases, the shaft work of the device is coupled to a boosting component – typically, either a centrifugal-based compressor or a positive-displacement compressor – which acts as an "air pump" to increase density of the inlet air. In most applications, a turbocharger uses a centrifugal turbine/compressor configuration while a supercharger uses a positive-displacement compressor.

Diesel engines are typically favorable engines to outfit with boosting devices (further, usually with turbochargers as they assist over the entire engine operating map). Boosting compensates for the diesel engine's typical use of fuel-lean mixtures to improve its power density. Further, since diesel engines do not employ throttles for load control, boosting of a diesel engine provides benefit over the entire operating map. For this latter reason, and due to the general higher efficiency of a turbocharger over a supercharger, turbochargers are the most common boosting device on a diesel engine. Gasoline engines also can be outfitted with boosting devices, with additional complexity to consider. First, boosting devices on gasoline engines usually offer benefit only at wide-open throttle conditions; a point of operation for most applications of engines that is rarely used. Also, for this reason, directly coupled superchargers are often used where improved response to boost is provided. Second, increasing density of the inlet mixture tends to increase the propensity to knock. Thus, while boosting provides additional trapped mass to deliver increased power, a potential retard in timing to avoid fuel knock likely decreases fuel conversion efficiency and introduces a tradeoff in how much additional power can be expected from the boost. Third, because of the typical use of superchargers when boosting is applied to gasoline engines, the system efficiency tends to decrease as shaft work is transferred to provide the boosting action (whereas turbocharging uses available energy of the exhaust).

Often times, boosting devices – in particular, turbochargers – are viewed as devices to increase the overall system efficiency of the engine. In other words, it is thought that because a turbocharger uses exhaust energy that would otherwise be wasted, its conversion to useful work (i.e., boosting) should increase efficiency. This work transfer, however, usually does not leave the control system (i.e., the shaft work of the turbine is directly coupled to the pumping action of the compressor). In some instances, efficiency improvements can be realized if a "negative pumping loop" is created by boosting the intake manifold to a higher pressure than the exhaust manifold. It is also possible to improve the overall engine efficiency if boosting an engine enables the use of a smaller-sized engine for a given application; an effort, as described above, known as downsizing. In most instances, however, overall system efficiency may decrease even with the use of a turbocharger, as the major objective of increasing inlet density to increase power density requires additional energy transfer through the exhaust than out as shaft work. This latter aspect is often realized as an increase in exhaust manifold pressure to "drive" the turbocharger.

An area of technology development for turbocharging is the use of waste-gated and variable geometry turbochargers. In non-waste-gated or non-variable geometry turbochargers, the turbine has fixed geometry and thus fixed flow characteristics. As such, a fixed geometry turbocharger is restrictively designed to provide maximum benefit to the engine at a narrow operating range which usually centers on the peak power condition of the engine. As such, at low speed or low-load conditions, the turbocharger's boosting benefits are diminished. While decreasing the turbocharger's maximum benefit over a broader regime of the engine's operating map, such a constraint also typically creates a dynamic issue during engine accelerations known as "turbo lag." The large turbine designed for maximum engine flow rates requires substantial inertia to rotationally accelerate to maximum boosting benefit. Waste-gated and variable geometry turbochargers offer opportunities to overcome such issues. In the case of a waste-gated turbocharger, usually a smaller turbine with less inertia is used with an exhaust "waste-gate." The smaller turbine provides faster response and better boosting at low-loads and

speeds; upon approach of the engine's peak power condition (where either boosting becomes excessive for the intake system or turbocharger speeds exceed maximum limits) a waste-gate opens that allows exhaust energy to bypass the turbine. Thus, the turbocharger is supplied by a fraction of the available exhaust energy providing suitable boost at allowable rotational speeds of the turbocharger at the engine's peak power condition. A variable geometry turbocharger uses a similar concept, except that it is designed to change the flow momentum of the exhaust gases and create multiple pressure ratios for a given exhaust flow rate [113, 114].

Finally, it is noted that outfitting a boosting device to an engine is not a trivial task [115]. There is not an exclusive match between an engine and a given boosting device; instead, the match of a boosting device to its engine application is dictated by the objectives of adding the device, whether it is to exclusively increase power density, efficiency, and/or emissions of the engine system [116–118].

Advanced Engine Controls

Much of the advanced technology that appears on modern engines, or will appear on future engines, is enabled by advanced engine controls. Engine control has always been an integral component of the engine's success at delivering cost-effective and efficient power. Early engine control systems were purely mechanical and only concerned with controlling the level of power (e.g., throttle or rack position) or holding a constant speed with variable load (such as a generator system, using a speed governor). Modern-day engine control systems, however, are virtually all electrical-based, and at the very least sense several aspects of the engine's operation (e.g., cam position, throttle position, manifold temperatures and pressures, and air flow) and typically control most aspects of the engine (e.g., spark timing, injection timing, injection pressure, EGR level, and boost pressure) [119].

Like the engine itself, engine controls are becoming more sophisticated and advanced. Specifically, a general trend to use in-cylinder information as a feedback signal is an example of the type of complexity future engine control systems intend to resolve. Knowledge of in-cylinder pressure, for example, can provide immediate information to the engine controller about load produced by the engine. Additionally, in-cylinder pressure is the major property necessary for assessing the rate of energy release during the combustion process; having such information could allow engine control systems to change parameters based on a desired burn profile in the cylinder [120–122]. Further, along with the continuing advancements in engine model development (e.g., [46–50]), a trend toward model-based engine control [123, 124] intends to decrease engine development time and improve control over the several parameters now present on internal combustion engines.

Variable Geometry Engine Designs

Along with efforts to effect engine downsizing, and made possible with advancements in engine control systems, is the notion of variable geometry engine designs. In other words, conventional reciprocating internal combustion engines have mechanically fixed geometries, i.e., constant compression ratios and constant displaced volumes. A variable compression ratio is attractive, for example, since it might enable high compression ratio operation for a spark ignition engine at part-load conditions where there is decreased propensity for knock. Similarly, it could be used in diesel engines to avoid excessively high peak pressures at full load conditions. Variable displacement engines are attractive since they enable high peak powers, but use less throttle at part-load conditions (thus diminishing pumping losses).

An early concept of variable compression ratio was proposed by J. Atkinson, for whom the Atkinson Cycle is named. As described by [125], Atkinson's original conception involved mechanical linkages to displace the piston such that the engine's compression ratio is lower than its expansion ratio; the main idea being that more expansion work will yield higher efficiency. Similar in idea, but different in implementation, is the Miller concept [125] which uses either late intake valve closing or late exhaust valve opening to shorten or extend the compression or expansion strokes, respectively. Both concepts are attempted in modern-day applications, using both variable compression ratio techniques [112, 126, 127] and altered valve timing techniques [112, 127, 128]. The latter approach, of

using altered valve timing techniques, is fluidly made possible through the use of variable valve timing [112, 127], a concept discussed in more detail in the next section.

While variable compression ratio concepts attempt to increase engine efficiency by way of increasing expansion, variable displacement engines attempt to increase engine efficiency by decreasing the use of throttle (thereby, decreasing the pumping work associated with the gas exchange process of a conventional spark ignition engine). With variable displacement, an engine is able to deliver high power using full displacement; at part-load conditions, rather than use throttle, cylinders can be "deactivated" so that they produce no power and allow the engine to deliver part-load power [129]. The deactivated cylinders typically continue to stroke and exchange gases; the closed portion of the cycle (i.e., compression and expansion) realize some loss due to heat transfer and friction but this is intended to be less than the gain realized through decreased pumping work.

Variable Valve Timing

Briefly discussed in the above sections is the idea of variable valve timing, or, the ability to change the valve events (i.e., intake and exhaust valve opening and closing) at any given point during the engine's operation [130]. In conventional engine design, the valve events are "fixed" by mechanical positions of the lobes on the cam shaft. The effectiveness of an engine to induct and exhaust mixture depends on many things including, for example, engine speed, engine load, the use of EGR, spark timing, and injection timing. Thus, there are not valve events that will universally yield peak power, efficiency, and/or emission for any given engine design.

The idea of variable valve timing allows the engineer to decouple the valve events from the in-cylinder processes. In other words, flexibility of intake and exhaust is afforded with the use of variable valve timing. This not only allows the valve events to be uniquely tuned for each operating point of the engine for improved performance [131] and efficiency [132], but it also can enable other advanced technology. For example, having variable valve timing allows the implementation of the Miller approach to effecting variable compression ratio at part-load conditions, but enabling conventional operation at peak power conditions [127]. Another example is the use of variable valve timing to control the amount of residual fraction in the cylinder, which can affect emission of certain pollutants [133]; controlling residual fraction is a way to enable advanced modes of combustion, described in more detail below. Finally, variable valve timing can be used to replace a throttle, for example, for load control [134]; in doing so, trapped mass can be controlled without inducing pumping work in the engine. Although not widespread technology, variable valve timing is becoming more prevalent on modern-day engines.

Waste Heat Recovery

Waste heat recovery is the effort to take advantage of temperature gradients created between the engine and its environment. As described in section on "Thermodynamic Analysis of Internal Combustion Engines", thermal energy is transferred out of the system through heat transfer (e.g., through engine coolant) and exhaust flow. Because of the temperature gradient that exists between, for example, the high temperature exhaust and the low temperature surroundings, an orderly flow of thermal energy tends to cause the exhaust system to attain thermal equilibrium with the environment. Conventionally, this orderly flow of thermal energy is wasted (i.e., the heat transfer completely dissipates as generated entropy). It is practically possible to instead intercept the orderly flow of thermal energy and convert it to useful work. In the theoretical limit, this conversion of thermal energy to work energy is given by the completely reversible cycle, often called the Carnot cycle. The corresponding efficiency of useful work converted from thermal energy is thusly the Carnot efficiency, as is given by Eq. 16:

$$\eta_{\mathrm{th,Carnot}} = 1 - \frac{T_{\mathrm{L}}}{T_{\mathrm{H}}} \tag{16}$$

where $\eta_{\mathrm{th,Carnot}}$ is the Carnot efficiency (maximum possible conversion of thermal energy to work energy), T_{L} is the sink's temperature (e.g., the environment temperature), and T_{H} is the source's temperature (e.g., the exhaust temperature). Considering that a typical automotive exhaust temperature may be 900 K operating in a 300 K environment, ideal

efficiencies could be on the order of 67%. Of course, real process irreversibilities diminish actual device efficiencies from the ideal Carnot efficiency. In spite of the diminished efficiency from ideal, though, waste heat recovery in an automotive application, for example, is reported to decrease vehicle fuel consumption by as much as 7.4% [135].

There are several technologies available to make use of internal combustion engine exhaust waste heat energy; because of its spatial accessibility and concentrated high temperature, exhaust energy has been the focus of much of the waste heat recovery. Example major technologies include: (1) mechanical or electrical turbo-compounding/generating devices, (2) Rankine cycle-type devices, and (3) thermoelectric-type devices. Turbo-compounding or turbo-generating [136] converts exhaust thermal energy to mechanical energy (in the form of pressure and kinetic energy) and couples the mechanical energy either directly to the engine driveshaft (to deliver additional brake power) or to an electric generator. One disadvantage of turbo-compounding (like its turbocharging companion) is the method of converting thermal energy to mechanical energy; the centrifugal device increases an engine's exhaust pressure based on its operation. The increased exhaust pressure affects the engine's operation by altering the pumping work and initial mixture composition (increased exhaust species in the initial mixture); such factors can deteriorate the engine's cycle efficiency.

Rankine cycle-type devices make use of the thermodynamic Rankine cycle – typically with an organic fluid designed to undergo phase change within the temperature ranges of a typical engine exhaust system – to output shaft work for either direct-coupling to the engine driveshaft or electrical generation. In such a device, the engine exhaust stream provides the thermal energy to boil or vaporize the organic working fluid of the cycle. After becoming saturated vapor, the fluid expands through a turbine converting the thermal energy to mechanical energy; the cycle completes with the usual condenser and pump processes. Such a device is reported to increase the combined engine + waste heat recovery efficiency by up to 10% [137]; a potential downside is the added complexity of adding four processes (as opposed to one, for example, in the case of a turbomachine) to waste heat recovery system.

Another example major waste heat recovery device is the thermoelectric device. The thermoelectric effect, first observed by Seebeck in 1821, is the generation of a voltage due to a temperature difference between two junctions of two dissimilar materials [138]; principally, the Seebeck effect describes the operation of a thermocouple measurement of temperature. The practical use of the Seebeck effect to produce electricity as a thermoelectric device has recently emerged with semiconductor materials having favorable properties to transmit electricity with little resistance heating (Joule heating) and thermal conductivity (which would tend to "short-circuit" the thermoelectric device). In fact, the advent of semiconductor materials first made possible practical thermoelectric devices as refrigerators exploiting the Peltier Effect (i.e., the opposite of the Seebeck effect, where an applied voltage creates a temperature difference between two junctions of two dissimilar metals) [138]. Now, however, thermoelectric devices create promise to exploit the available thermal energy in an internal combustion engine's exhaust for conversion to electricity [135, 139].

Direct Injection, Spark Ignition Engines

At the end of the section on "A Case Study: Diesel Engines Versus Gasoline Engines", it is suggested that spark ignition and compression ignition engines each have favorable features for power, efficiency, and emissions, but that each has conventionally designed limitations. Thus, it becomes attractive to design each ignition system's limitations out of the engine, and potentially realize gains in the engine's attributes (i.e., power, efficiency, and emissions). Two now-common technologies exist to do so: (1) direct injection spark ignition combustion and (2) homogeneous charge compression ignition combustion. This and the next section will describe these two technologies.

Direct injection spark ignition combustion attempts to create a stratified fuel–air mixture "charge" around the spark plug so that, at the point of spark release, the spark ignites a near-stoichiometric mixture. It is intended that outside of the stratification zone there is little to no fuel, thus creating an overall lean fuel–air mixture. The use of the word "stratified" to describe the fuel–air mixture is used here, as opposed to heterogeneous, to reinforce the notion that under

ideal conditions the fuel–air mixture would be homogeneous (i.e., homogeneously stoichiometric) throughout the fuel–air mixture, but pure air outside the stratification zone (i.e., outside the fuel–air mixture). This is in contrast to the use of "heterogeneous" to describe a mixture (e.g., diesel engine mixture), where it is expected that substantial fuel–air ratio gradients exist throughout the fuel sprays.

In order to manifest the stratified mixture concept (see, e.g., [140–148]), fuel is injected directly into the cylinder. Typically, the combustion chamber of a direct injection spark ignition engine is specially designed to assist the stratification of the fuel–air mixture, and center it on the spark plug. The intake stroke draws air and residual mixture into the cylinder – notably, fuel is not inducted during intake as is done in conventional spark ignition operation. After intake, direct fuel injection into the cylinder usually occurs at some point during the piston's travel from BDC to TDC during the compression stroke. Spark advance is typically timed at around the same point as that in a conventional spark ignition engine (i.e., at a point near the piston reaching TDC-compression). The remaining processes of the direct injection spark ignition engine are basically the same as the conventional spark ignition engine.

There are several potential benefits of direct injection spark ignition combustion. Perhaps the clear benefit is the ability to use lean mixtures in a spark ignition engine. Because the combustion chamber is designed to stratify the mixture and create a stoichiometric mixture near the spark plug, the overall equivalence ratio of the mixture filling the entire chamber can be lean. As described in section on "Thermodynamic Analysis of Internal Combustion Engines", overall lean mixtures possess higher ratios of specific heats (γ), which translate to higher fuel conversion efficiencies. Another, less obvious, benefit of a stratified mixture is the decreased propensity to fuel knock (or, at least decreased propensity of fuel knock in the regions of the cylinder able to cause harm such as near cylinder walls and piston rings). The lack of a reactive mixture – manifested by charge stratification – in the regions furthest from the spark plug – which are the last to be controllably burned by the propagating flame – decreases the propensity that the mixture will autoignite and burn uncontrollably. Such a feature enables the direct injection spark ignition engine to have increased compression ratios relative to conventional spark ignition engines; again, this is an attribute that promotes an increase in efficiency of the novel engine concept. Finally, the use of direct fuel injection into the cylinder enables the elimination of a throttle to control engine load. In other words, engine load is controlled by the quantity of fuel injected into the cycle, similar to the load control of a diesel engine. Elimination of the throttle, as repeatedly described, will improve part-load efficiency by eliminating pumping losses effected by throttle.

Although the benefits are plentiful, the challenges are also present. From practical perspectives, perfect attainment of a stratified charge is difficult to accomplish. As such, heterogeneities within the stratified mixture emerge and can lead to products of incomplete combustion such as CO, HC, and PM. This, of course, is amplified at full load conditions; thus, peak power attainment through direct injection means alone would likely be limited by smoke limitations (similar to full load limitations of a diesel engine). Further, and like the challenges faced by diesel engines, outfitting direct injection spark ignition engines with after treatment devices is complicated by the use of overall lean mixtures (as described in section on "Emissions Formation and Exhaust Pollution"). In spite of such challenges, direct injection spark ignition engines are in production; continued development of in-cylinder flow modeling tools and engine controls contribute toward the concept's potential success.

Homogeneous Charge Compression Ignition Engines

An attractive feature of the conventional spark ignition engine is its use of a homogeneous mixture. Although this tends to promote knock (as described in section "Direct Injection Spark Ignition Engines"), it provides the benefit of being kinetically rate-limiting as opposed to mixing rate-limiting (as in the case of diesel engines). One issue with using a spark, or single point, to ignite a homogeneous mixture is the establishment of a flame that must propagate the mixture to convert the chemical energy. In order to more quickly react the mixture, in a volumetric sense, multi-point ignition is required; i.e., ignition that occurs in several locations throughout the mixture will result in a faster

burn rate. Such a voluminous ignition can be effected through compression of a homogenous mixture.

This is the basic idea of homogeneous charge compression ignition (HCCI); use compression to ignite a homogeneous mixture (similar to a diesel engine, except that diesel engines use compression to ignite an inherently heterogeneous mixture). The homogeneous mixture could, for example, be formed through premixing of fuel and air prior to mixture induction during the intake stroke. A faster burn rate effected by homogeneous charge compression ignition allows heat release to occur at near constant volume conditions; thus establishing the possibility to approach theoretical limits of maximum efficiencies of internal combustion engines. Further, because compression is used to ignite the mixture rather than spark, lean mixtures can be used at part-load conditions which further promotes higher efficiencies of the HCCI concept. Similar to the direct injection spark ignition concept, HCCI engines could eliminate throttles as load is controlled directly by the quantity of fuel mixed with the intake mixture. Finally, the common issue of particulate matter emissions faced by diesel engines (which also use compression ignition) are substantially decreased through the avoidance of locally rich fuel–air mixture zones (due to the use of a homogeneous mixture in an HCCI concept).

Of course, immediately the obvious problem becomes the method of ignition control. HCCI concepts do not have a direct ignition trigger, as do conventional gasoline (i.e., a spark) or diesel (i.e., direct fuel injection) engines. Controlling ignition in the HCCI concept depends on very precise control of the mixture's initial state at start of compression and the compression path followed up to the point of ignition. Several factors which are present – even in tightly controlled research environments – such as heat transfer, turbulence, and the history of preceding combustion events make the practical application of HCCI very challenging. The payoffs, of course, are correspondingly very high.

Practical implementation of HCCI is first reported by Onishi et al. [149] with theoretical developments experimentally provided by Najt and Foster [150]. Several control parameters could be adjusted such as compression ratio (e.g., with the use of variable valve timing), initial temperature, and quantity of residual fraction (e.g., effected either through exhaust gas recirculation or variable valve timing). Identifying the key control parameters, and the optimal way to adjust them during real-time operation of the engine, continue to be on-going research activities [151–156].

Advanced Compression Ignition Engines

A technique to control combustion of an HCCI engine is to use precisely metered amounts of residual fraction, which not only act to alter the kinetics of combustion but also result in substantially lower combustion temperatures. As such, much of HCCI combustion is characterized by low temperature mechanisms commonly referred to as *low temperature combustion* (LTC). LTC offers a few benefits. First, efficiency improvements in the engine can be realized (in spite of increased exergy destruction due to low reaction temperatures) due to more favorable thermodynamic properties (i.e., higher ratio of specific heats, see Fig. 11) of the burned mixture and lower rates of heat transfer. Second, and typically the driver for LTC technology development, lower nitric oxide formation per the discussion in section on "Emissions Formation and Exhaust Pollution".

With this in mind, and reconsidering the prevailing issue of HCCI implementation – i.e., control of start of combustion – it becomes plausible to consider developing an "HCCI-type" mode of combustion in a diesel engine. That is, rather than induct a homogeneous mixture of fuel and air and rely upon indirectly controlled parameters to control ignition, perhaps fuel can be injected directly into the cylinder allowing for better control of ignition. In order to manifest LTC and harvest its benefits (e.g., possibly higher efficiency and substantially emission), high levels of EGR and strategic injection timings are used to extend ignition delay and create a nearly all-premixed combustion event. The long ignition delay, coupled with low temperature mechanisms, establishes the phenomenological observation of two-stage ignition characterized by the presence of cool-flame reactions [150, 157]. Interestingly, because of attainment of LTC, soot precursor formation is substantially abated, and the engine is made to operate with very low emissions of nitric oxide and particulate matter [158–168]. The combustion concept has become known as premixed compression ignition or premixed charge compression ignition combustion.

The ability to attain LTC in compression ignition engines is attributed to the advancement of technology now in place on such machines, such as common-rail and electronic fuel pressure systems, variable geometry turbochargers, and exhaust gas recirculation systems.

Alternative Fuels

The term "alternative fuels" for an internal combustion engine is somewhat baseless, as an internal combustion engine has considerable flexibility in the type of fuel it uses. Of course, conventional fuels are the commonly called "gasoline" and "diesel" fuels, but generally engines have been shown to operate on virtually any gaseous, liquid, and solid dust particle specie that has heating value (i.e., will release thermal energy in a chemical oxidation process). Because of the wide variability of fuels available to internal combustion engines, this topic will not be expanded in this article. There are, however, certain considerations that should be given to the use of a fuel in an engine which was not intently designed for use with such fuel (e.g., use of ethanol in a gasoline engine or use of biodiesel in a diesel engine). First, ignition characteristics of the fuel may not be favorable for the particular engine design. For example, short-chain volatile hydrocarbons do not generally ignite well in conventional unmodified compression ignition engines of typical compression ratios. Likewise, long-chain nonvolatile hydrocarbons do not generally vaporize well in conventional unmodified spark ignition engines. Second, flame temperatures of the combustion of the fuel may exceed material limits of any given engine construction. Third, fuels may react with other support components of the engine system (e.g., solvency of fuels with rubber hoses). Finally, combustion process will likely be altered when using an unconventional fuel in a conventional unmodified engine yielding different emissions, efficiency, and peak power capabilities. Thus, although internal combustion engines have inherent fuel-flexibility, their use with unconventional fuels is not straightforward and requires careful design and engineering considerations.

Acknowledgments

The author wishes to thank several people who have helped to make this work possible. First, the State of Texas is acknowledged for their financial support of some of the research highlighted here; specifically, their support through the Texas Commission on Environmental Quality and the Houston Advanced Research Center is acknowledged. Second, Professor Jerald A. Caton of Texas A&M University is acknowledged for his contributions to this article and for providing a thorough proof of its contents. Third, Margaret Fisher is acknowledged for her assistance in preparing the copyrighted materials from other sources and securing permissions to use them. Fourth, Wiley is acknowledged for providing permission of copyrighted material *au gratis*. Fifth and lastly, but certainly not least, I acknowledge the contributions and assistance of my graduate and undergraduate students, some of whom have research highlighted in this work. Specifically, these individuals include: Mr. Josh Bittle, Mr. Jason Esquivel, Ms. Sarabeth Fronenberger, Mr. Blake Gettig, Mr. Mark Hammond, Mr. Bryan Knight, Mr. Jeffrey Kurthy, Mr. Jimmy McClean, Ms. Claire Mero, Mr. Yehia Omar, Ms. Gurlovleen Rathore, Mr. Kyle Richter, Mr. Sidharth Sambashivan, Mr. Chris Schneider, Ms. Amy Smith, Mr. Hoseok Song, Mr. Jiafeng Sun, Mr. Brandon Tompkins, Mr. Brad Williams, Mr. R. Kevin Wilson, Mr. Whit Wilson, and Mr. Jesse Younger.

Abbreviations

BDC	Bottom dead center
EGR	Exhaust gas recirculation
HCCI	Homogeneous charge compression ignition
IC	Internal combustion
LTC	Low temperature combustion
TDC	Top dead center

Bibliography

Primary Literature

1. Cummins C Jr (1976) Early IC and automotive engines. SAE Trans 85(SAE Paper No. 760604):1960–1971
2. Heywood J (1988) Internal combustion engine fundamentals. McGraw-Hill, New York, p 9
3. Heywood J (1988) Internal combustion engine fundamentals. McGraw-Hill, New York, p 10
4. Automot Eng Int (January 2010), 118(1):47. http://www.sae.org/automag/
5. Brown W (1967) Methods for evaluating requirements and errors in cylinder pressure measurement. SAE Trans 76(SAE Paper No. 670008):50–71

6. Lancaster D, Krieger R, Lienesch J (1975) Measurement and analysis of engine pressure data. SAE Trans 84(SAE Paper No. 750026):155–172
7. Randolph A (1990) Methods of processing cylinder-pressure transducer signals to maximize data accuracy. SAE Trans J Passenger Cars 99(SAE Paper No. 900170):191–200
8. Kuratle R, Marki B (1992) Influencing parameters and error sources during indication on internal combustion engines. SAE Trans – J Engines 101(SAE Paper No. 920233):295–303
9. Davis R, Patterson G (2006) Cylinder pressure data quality checks and procedures to maximize data accuracy. SAE Paper No. 2006-01-1346
10. Amann C (1983) A perspective of reciprocating-engine diagnostics without lasers. Prog Energy Combust Sci 9:239–267
11. Heywood J (1988) Internal combustion engine fundamentals. McGraw-Hill, New York, pp 56–57
12. Tompkins B, Esquivel J, Jacobs T (2009) Performance parameter analysis of a biodiesel-fuelled medium duty diesel engine. SAE Paper No. 2009-01-0481
13. Heywood J (1988) Internal combustion engine fundamentals. McGraw-Hill, New York, p 217
14. Heywood J (1988) Internal combustion engine fundamentals. McGraw-Hill, New York, p 154
15. Lauck F, Uyehara O, Myers P (1963) An engineering evaluation of energy conversion devices. SAE Trans 71(SAE Paper No. 630446):41–50
16. Foster D, Myers P (1984) Can paper engines stand the heat? SAE Trans 93(SAE Paper No. 840911):4.491–4.502
17. The K, Miller S, Edwards C (2008) Thermodynamic requirements for maximum internal combustion engine cycle efficiency, Part 1: optimal combustion strategy. Int J Engine Res 9:449–465
18. Carnot NLS (1824) Reflections on the motive power of heat (Trans and ed: Thurston RH), 2nd edn (1897). Wiley, New York
19. Borgnakke C, Sonntag R (2009) Fundamentals of thermodynamics. Wiley, New York, p 497
20. Heywood J (1988) Internal combustion engine fundamentals. McGraw-Hill, New York, p 177
21. Heywood J (1988) Internal combustion engine fundamentals. McGraw-Hill, New York, p 163
22. Edson M (1964) The influence of compression ratio and dissociation on ideal otto cycle engine thermal efficiency, Digital calculations of engine cycles. SAE, Warrendale, pp 49–64
23. Westbrook C, Dryer F (1984) Chemical kinetic modeling of hydrocarbon combustion. Prog Energy Combust Sci 10:1–57
24. Olikara C, Borman G (1975) A computer program for calculating properties of equilibrium combustion products with some applications IC engines. SAE Paper No. 750468
25. Lavoie G, Heywood J, Keck J (1970) Experimental and theoretical study of nitric oxide formation in internal combustion engines. Combust Sci Technol 1:313–326
26. Bowman C (1975) Kinetics of pollutant formation and destruction in combustion. Prog Energy Combust Sci 1:33–45
27. Miller J, Bowman C (1989) Mechanism and modeling of nitrogen chemistry in combustion. Prog Energy Combust Sci 15:287–338
28. Turns S (1995) Understanding NO_x formation in nonpremixed flames: experiments and modeling. Prog Energy Combust Sci 21:361–385
29. Dean A, Bozzelli J (2000) In: Gardiner WC Jr (ed) Combustion chemistry of nitrogen in gas-phase combustion chemistry. Springer, New York, pp 125–341
30. McBride B, Gordon S (1992) Computer program for calculating and fitting thermodynamic functions. NASA Report No. RP-1271
31. Svehla R (1995) Transport coefficients for the NASA Lewis chemical equilibrium program. NASA Report No. TM-4647
32. Gordon S, McBride B (1999) Thermodynamic data to 20000K for monatomic gases. NASA Report No. TP-1999-208523
33. McBride B, Gordon S, Reno M (2001) Thermodynamic data for fifty reference elements. NASA Report No. TP-3287/Rev 1
34. McBride B, Zehe M, Gordon S (2002) CAP: a computer code for generating tabular thermodynamic functions from NASA Lewis Coefficients. NASA Report No. TP-2001-210959-Rev1
35. Heywood J (1988) Internal combustion engine fundamentals. McGraw-Hill, New York, pp 136–137
36. Stull D, Prophet H (1971) JANAF thermochemical tables, NSRDS-NBS 37. http://www.nist.gov/data/nsrds/NSRDS-NBS37.pdf. Accessed July 5, 2010
37. Keenan J (1951) Availability and irreversibility in thermodynamics. Br J Appl Phys 2:183–192
38. Edson M, Taylor C (1964) The limits of engine performance – comparison of actual and theoretical cycles. In: SAE digital calculations of engine cycles, pp 65–81
39. Strange F (1964) An analysis of the ideal Otto cycle, including the effects of heat transfer, finite combustion rates, chemical dissociation, and mechanical losses. In: SAE digital calculations of engine cycles, pp 92–105
40. Patterson D, Van Wylen G (1964) A digital computer simulation for spark-ignited engine cycles. In: SAE digital calculations of engine cycles, pp 82–91
41. Woschni G (1967) Universally applicable equation for the instantaneous heat transfer coefficient in the internal combustion engine. SAE Trans 76(SAE Paper No. 670931): 3065–3083
42. Hohenberg G (1979) Advanced approaches for heat transfer calculations. SAE Trans 88(SAE Paper No. 790825): 2788–2806
43. Borman G, Nishiwaki K (1987) Internal-combustion engine heat transfer. Prog Energy Combust Sci 13:1–46
44. Heywood J, Higgins J, Watts P, Tabaczynski R (1979) Development and use of a cycle simulation to predict SI engine efficiency and NO_x emissions. SAE Paper No. 790291
45. Sandoval D, Heywood J (2003) An improved friction model for spark-ignition engines. SAE Trans J Engines 112(SAE Paper No. 2003-01-0725):1041–1052
46. Blumberg P, Lavoie G, Tabaczynski R (1979) Phenomenological models for reciprocating internal combustion engines. Prog Energy Combust Sci 5:123–167
47. Assanis D, Heywood J (1986) Development and use of a computer simulation of the turbocompounded diesel system for

engine performance and component heat transfer studies. SAE Trans 95(SAE Paper No. 860329):2.451–2.476
48. Filipi Z, Assanis D (1991) Quasi-dimensional computer simulation of the turbocharged spark ignition engine and its use for 2 and 4-valve engine matching studies. SAE Trans J Engines 100(SAE Paper No. 910075):52–68
49. Kamimoto T, Kobayashi H (1991) Combustion processes in diesel engines. Prog Energy Combust Sci 17:163–189
50. Reitz R, Rutland C (1995) Development and testing of diesel engine CFD models. Prog Energy Combust Sci 21: 173–196
51. Caton J (2003) Effects of burn rate parameters on nitric oxide emissions for a spark ignition engine: results from a three-zone, thermodynamic simulation. SAE Paper No. 2003-01-0720
52. Caton J (2000) A review of investigations using the second law of thermodynamics to study internal-combustion engines. SAE Trans J Engines 109(SAE Paper No. 2000-01-1081): 1252–1266
53. Rakopoulos C, Giakoumis E (2006) Second-law analyses applied to internal combustion engines operation. Prog Energy Combust Sci 32:2–47
54. Shyani R, Caton J (2009) A thermodynamic analysis of the use of exhaust gas recirculation in spark ignition engines including the second law of thermodynamics. Proc Inst Mech Eng Part D: J Automobile Eng 223:131–149
55. Dunbar W, Lior N (1994) Sources of combustion irreversibility. Combust Sci Technol 103:41–61
56. Som S, Datta A (2008) Thermodynamic irreversibilities and exergy balance in combustion processes. Prog Energy Combust Sci 34:351–376
57. Caton J (2000) On the destruction of availability (exergy) due to combustion processes – with specific application to internal-combustion engines. Energy 25:1097–1117
58. Keenan J (1941) Thermodynamics. Wiley, New York, p 269
59. Obert E (1970) Internal combustion engines, 3rd edn. International Textbook Company, Scranton, p 459
60. Patrawala K, Caton J (2008). Potential processes for "reversible" combustion with application to reciprocating internal combustion engines. In: Proceedings of the 2008 technical meeting of the central states section of the combustion institute, Tuscaloosa
61. Diesel R (1897) Diesel's rational heat motor. A lecture delivered at the general meeting of the society at Cassell, June 16, 1897. Original published in Zeitschrift des Vereines Deutscher Ingenieure (Trans: Leupold R). Progressive Age, New York (Reprinted)
62. Heywood J (1988) Internal combustion engine fundamentals. McGraw-Hill, New York, p 391
63. Heywood J (1988) Internal combustion engine fundamentals. McGraw-Hill, New York, p 390
64. Heywood J (1988) Internal combustion engine fundamentals. McGraw-Hill, New York, p 374
65. Lyn W (1963) Study of burning rate and nature of combustion in diesel engines. Proc Combust Inst 9:1069–1082
66. Plee S, Ahmad T (1983) Relative roles of premixed and diffusion burning in diesel combustion. SAE Trans 92(SAE Paper No. 831733):4.892–4.909
67. Ricardo H (1941) The high-speed internal combustion engine (Rev: Glyde HS), 3rd edn. Interscience Publishers, New York
68. Ladommatos N, Abdelhalim S, Zhao H, Hu Z (1998) Effects of EGR on heat release in diesel combustion. SAE Paper No. 980184
69. Meguerdichian M, Watson N (1978) Prediction of mixture formation and heat release in diesel engines. SAE Paper No. 780225
70. Lyn W, Valdmanis E (1968) Effects of physical factors on ignition delay. SAE Paper No. 680102
71. Kamimoto T, Aoyagi Y, Matsui Y, Matsuoka S (1981) The effects of some engine variables on measured rates of air entrainment and heat release in a DI diesel engine. SAE Trans 89(SAE Paper No. 800253):1163–1174
72. Dent J, Mehta P, Swan J (1982) A predictive model for automotive DI diesel engine performance and smoke emissions. Paper presented at the international conference on diesel engines for passenger cars and light duty vehicles. Institution of Mechanical Engineers, London. IMECE Paper No. C126/82
73. Binder K, Hilburger W (1981) Influence of the relative motions of air and fuel vapor on the mixture formation processes of the direct injection diesel engine. SAE Trans 90(SAE Paper No. 810831):2540–2555
74. Dec J (1997) A conceptual model of DI diesel combustion based on laser-sheet imaging. SAE Trans J Engines 106(SAE Paper No. 970873):1319–1348
75. Flynn P, Durrett R, Hunter G, zur Loye A, Akinyemi O, Dec J, Westbrook C (1999) Diesel combustion: an integrated view combining laser diagnostics, chemical kinetics, and empirical validation. SAE Trans J Engines 108(SAE Paper No. 1999-01-0509):587–600
76. Chigier N (1975) Pollution formation and destruction in flames – Introduction. Prog Energy Combust Sci 1:3–15
77. Beltzer M (1976) Non-sulfate particulate emissions from catalyst cars. SAE Trans 85(SAE Paper No. 760038):198–208
78. Khatri N, Johnson J, Leddy D (1978) The characterization of the hydrocarbon and sulfate fractions of diesel particulate matter. SAE Trans 87(SAE Paper No. 780111):469–492
79. Hoffert M, Caldeira K, Benford G, Criswell D, Green C, Herzog H, Jain A, Kheshgi H, Lackner K, Lewis J, Lightfoot H, Manheimer W, Mankins J, Mauel M, Perkins L, Schlesinger M, Volk T, Wigley T (2002) Advanced technology paths to global climate stability: energy for a greenhouse planet. Science 298:981–987
80. Ghoniem A (2011) Needs, resources and climate change: clean and efficient conversion technologies. Prog Energy Combustion Sci 37:15–51
81. Henein N (1976) Analysis of pollutant formation and control and fuel economy in diesel engines. Prog Energy Combust Sci 1:165–207
82. Haagen-Smit A, Fox M (1955) Automobile exhaust and ozone formation. SAE Trans 63(SAE Paper No. 550277):575–580

83. Huls T, Nickol H (1967) Influence of engine variables on exhaust oxides of nitrogen concentrations from a multicylinder engine. SAE Paper No. 670482
84. Starkman E, Stewart H, Zvonow V (1969) Investigation into formation and modification of exhaust emission precursors. SAE Paper No. 690020
85. Hames R, Merrion D, Ford H (1971) Some effects of fuel injection system parameters on diesel exhaust emissions. SAE Paper No. 710671
86. Khan I, Greeves G, Wang C (1973) Factors affecting smoke and gaseous emissions from direct injection engines and a method of calculation. SAE Trans 82(SAE Paper No. 730169):687–709
87. Yu R, Shahed S (1981) Effects of injection timing and exhaust gas recirculation on emissions from a D.I. diesel engine. SAE Trans 90(SAE Paper No. 811234):3873–3883
88. Newhall H (1967) Control of nitrogen oxides by exhaust recirculation, a preliminary theoretical study. SAE Trans 76(SAE Paper No. 670495):1820–1836
89. Benson J, Stebar R (1971) Effects of charge dilution on nitric oxide emission from a single-cylinder engine. SAE Trans 80(SAE Paper No. 710008):7–19
90. Komiyama K, Heywood J (1973) Predicting NO_x emissions and effects of exhaust gas recirculation in spark-ignition engines. SAE Trans 82(SAE Paper No. 730475):1458–1476
91. McEnally C, Pfefferle L, Atakan B, Kohse-Hoinghaus K (2006) Studies of aromatic hydrocarbon formation mechanisms in flames: progress toward closing the fuel gap. Prog Energy Combust Sci 32:247–294
92. Cheng W, Hamrin D, Heywood J, Hochgreb S, Min K, Norris M (1993) An overview of hydrocarbon emissions mechanisms in spark-ignition engines. SAE Trans J Fuels Lubricants 102(SAE Paper No. 932708):1207–1220
93. Henein N, Tagomori M (1999) Cold-start hydrocarbon emissions in port-injected gasoline engines. Prog Energy Combust Sci 25:563–593
94. Alkidas A (1999) Combustion-chamber crevices: the major source of engine-out hydrocarbon emissions under fully warmed conditions. Prog Energy Combust Sci 25:253–273
95. Haynes B, Wagner H (1981) Soot formation. Prog Energy Combust Sci 7:229–273
96. Smith O (1981) Fundamentals of soot formation in flames with application to diesel engine particulate emissions. Prog Energy Combust Sci 7:275–291
97. Kennedy I (1997) Models of soot formation and oxidation. Prog Energy Combust Sci 23:95–132
98. Richter H, Howard J (2000) Formation of polycyclic aromatic hydrocarbons and their growth to soot – a review of chemical reaction pathways. Prog Energy Combust Sci 26:565–608
99. Tree D, Svensson K (2007) Soot processes in compression ignition engines. Prog Energy Combust Sci 33:272–309
100. Hassaneen A, Samuel S, Morrey D, Gonzalez-Oropeza R (2009) Influence of physical and chemical parameters on characteristics of nanoscale particulate in spark ignition engine. SAE Paper No. 2009-01-2651
101. Ericsson P, Samson A (2009) Characterization of particulate emissions propagating in the exhaust line for spark-ignited engines. SAE Paper No. 2009-01-2654
102. Khan I (1969–1970) Formation and combustion of carbon in a diesel engine. Proc Inst Mech Eng 184(3J):36–43
103. Ahmad T, Plee S, Myers J (1982) Diffusion flame temperature – its influence on diesel particulate and hydrocarbon emissions. Paper presented at the international conference on diesel engines for passenger cars and light duty vehicles. Institution of Mechanical Engineers, London. IMECE Paper No. C101/82
104. Kummer J (1980) Catalysts for automobile emission control. Prog Energy Combust Sci 6:177–199
105. Koltsakis G, Stamatelos A (1997) Catalytic automotive exhaust aftertreatment. Prog Energy Combust Sci 23:1–39
106. Johnson T (2010) Diesel emission control in review. SAE Int J Fuels Lubricants 2(SAE Paper No. 2009-01-0121):1–12
107. Taylor C (1985) The internal combustion engine in theory and practice, Vol 2: Combustion, fuels, materials, design (rev. edition). The MIT Press, Cambridge, MA, pp 21–23
108. Taylor C (1985) The internal combustion engine in theory and practice, Vol 2: Combustion, fuels, materials, design (rev. edition). The MIT Press, Cambridge, MA, p 50
109. Heywood J (1988) Internal combustion engine fundamentals. McGraw-Hill, New York, pp 4–5
110. Heywood J (1988) Internal combustion engine fundamentals. McGraw-Hill, New York, p 475
111. Heywood J (1988) Internal combustion engine fundamentals. McGraw-Hill, New York, pp 217–220
112. Clenci A, Descombes G, Podevin P, Hara V (2007) Some aspects concerning the combination of downsizing with turbocharging, variable compression ratio, and variable intake valve lift. Proc Inst Mech Eng D J Automobile Eng 221:1287–1294
113. Van Nieuwstadt M, Kolmanovsky I, Morael P (2000) Coordinated EGR-VGT control for diesel engines: an experimental comparison. SAE Trans – J Engines 109(SAE Paper No. 2000-01-0266):238–249
114. Arnold S, Slupski K, Groskreutz M, Vrbas G, Cadle R, Shahed S (2011) Advanced turbocharging technologies for heavy-duty diesel engines. SAE Trans J Engines 110(SAE Paper No. 2001-01-3260):2048–2055
115. Kessel J, Schaffnit J, Schmidt M (1998) Modeling an real-time simulation of a turbocharger with variable turbine geometry (VGT). SAE Paper No. 980770
116. Hawley J, Wallace F, Pease A, Cox A, Horrocks R, Bird G (1997) Comparison of variable geometry turbocharging (VGT) over conventional wastegated machines to achieve lower emissions. In: IMechE autotech conference, Birmingham, UK, pp 245–259 (IMechE Seminar Publication: Automotive Engines and Powertrains, Paper No. C524/070/97)
117. Hawley J, Wallace F, Cox A, Horrocks R, Bird G (1999) Reduction of steady state NO_x levels from an automotive diesel engine using optimized VGT/EGR schedules. SAE Trans J Engines 108(SAE Paper No. 1999-01-0835):1172–1184

118. Tanin K, Wickman D, Montgomery D, Das S, Reitz R (1999) The influence of boost pressure on emissions and fuel consumption of a heavy-duty single-cylinder DI diesel engine. SAE Trans J Engines 108(SAE Paper No. 1999-01-0840):1198–1219
119. Cook J, Sun J, Buckland J, Kolmanovsky I, Peng H, Grizzle J (2006) Automotive powertrain control – A survey. Asian J Control 8(3):237–260
120. Leithgoeb R, Henzinger F, Fuerhapter A, Gschweitl K, Zrim A (2003) Optimization of new advanced combustion systems using real-time combustion control. SAE Paper No. 2003-01-1053
121. Corti E, Moro D, Solieri L (2007) Real-time evaluation of IMEP and ROHR-related parameters. SAE Paper No. 2007-24-0068
122. Leonhardt S, Muller N, Isermann R (1999) Methods for engine supervision and control based on cylinder pressure information. IEEE/ASME Trans Mechatron 4(3):235–245
123. Yoon M, Chung N, Lee M, Sunwoo M (2009) An engine-control-unit-in-the-loop simulator of a common-rail diesel engine for cylinder-pressure-based control. Proc Inst Mech Eng D J Automobile Eng 223:355–373
124. Turin R, Zhang R, Chang M (2008) Systematic model-based engine control design. SAE Int J Passenger Cars Electron Electr Syst 1(SAE Paper No. 2008-01-0994):413–424
125. Caton J (2008) Results from an engine cycle simulation of compression ratio and expansion ratio effects on engine performance. J Eng Gas Turbines Power 130(5):052809-1–052809-7
126. Wirbeleit F, Binder K, Gwinner D (1990) Development of pistons with variable compression height for increasing efficiency and specific power output of combustion engines. SAE Trans J Engines 99(SAE Paper No. 900229):543–557
127. Sugiyama T, Hiyoshi R, Takemura S, Aoyama S (2007) Technology for improving engine performance using variable mechanisms. SAE Trans J Engines 116(SAE Paper No. 2007-01-1290):803–812
128. Boggs D, Hilbert H, Schechter M (1995) The Otto-Atkinson cycle engine: fuel economy and emissions results and hardware design. SAE Trans J Engines 104(SAE Paper No. 950089):220–232
129. Leone T, Pozar M (2001) Fuel economy benefit of cylinder deactivation – Sensitivity to vehicle application and operating constraints. SAE Trans J Fuels Lubricants 110(SAE Paper No. 2001-01-3591):2039–2044
130. Gray C (1988) A review of variable engine valve timing. SAE Trans J Engines 97(SAE Paper No. 880386):6.631–6.641
131. Payri F, Desantes J, Corberaan J (1988) A study of the performance of an SI engine incorporating a hydraulically controlled variable valve timing system. SAE Trans J Engines 97(SAE Paper No. 880604):6.1133–6.1145
132. Ma T (1988) Effect of variable engine valve timing on fuel economy. SAE Trans J Engines 97(SAE Paper No. 880390):6.665–6.672
133. Meacham G (1970) Variable cam timing as an emission control tool. SAE Trans 79(SAE Paper No. 700673):2127–2144
134. Tuttle J (1980) Controlling engine load by means of late intake-valve closing. SAE Trans 89(SAE Paper No. 800794):2429–2441
135. Stobart R, Wijewardane A, Allen C (2010) The potential for thermo-electric devices in passenger vehicle applications. SAE Paper No. 2010-01-0833
136. Patterson A, Tett R, McGuire J (2009) Exhaust heat recovery using electro-turbogenerators. SAE Paper No. 2009-01-1604
137. Srinivasan K, Mago P, Zdaniuk G, Chamra L, Midkiff K (2008) Improving the efficiciency of the advanced injection low pilot ignited natural gas engine using organic Rankine cycles. ASME J Energy Resour Technol 130:022201-1–022201-7
138. Goldsmid H (1960) Principles of thermoelectric devices. Br J Appl Phys 11:209–217
139. Hussain Q, Brigham D, Maranville C (2010) Thermoelectric exhaust heat recovery for hybrid vehicles. SAE Int J Engines 2:1(SAE Paper No. 2009-01-1327):1132–1142
140. Barber E, Reynolds B, Tierney W (1951) Elimination of combustion knock ~ Texaco combustion process. SAE Trans 59(SAE Paper No. 510173):26–38
141. Davis C, Barber E, Mitchell E (1961) Fuel injection and positive ignition ~ A basis for improved efficiency and economy. SAE Trans 69(SAE Paper No. 610012):120–131
142. Mitchell E, Cobb J, Frost R (1968) Design and evaluation of a stratified charge multifuel military engine. SAE Trans 77(SAE Paper No. 680042):118–131
143. Alperstein M, Schafer G, Villforth F III (1974) Texaco's stratified charge engine – multifuel, efficient, clean, and practical. SAE Paper No. 740563
144. Pischinger F, Schmidt G (1978) Experimental and theoretical investigations of a stratified-charge engine with direct fuel injection. SAE Paper No. 785038
145. Hiraki H, Rife J (1980) Performance and NO_x model of a direct injection stratified charge engine. SAE Trans 89(SAE Paper No. 800050):336–356
146. Ullman T, Hare C, Baines T (1982) Emissions from direct-injected heavy-duty methanol-fueled engines (one dual injection and one spark-ignited) and a comparable diesel engine. SAE Trans 91(SAE Paper No. 820966):3154–3170
147. Giovanetti A, Ekchian J, Heywood J, Fort E (1983) Analysis of hydrocarbon emissions mechanisms in a direct injection spark-ignition engine. SAE Trans 92(SAE Paper No. 830587):2.925–2.947
148. Kato S, Onishi S (1988) New mixture formation technology of direct fuel injection stratified charge SI engine (OSKA) ~ Test result with gasoline fuel. SAE Trans J Engines 97(SAE Paper No. 881241):6.1497–6.1504
149. Onishi S, Jo S, Shoda K, Jo P, Kato S (1979) Active thermo-atmosphere combustion (ATAC) ~ A new combustion process for internal combustion engines. SAE Trans 88(SAE Paper No. 790501):1851–1860
150. Najt P, Foster D (1983) Compression-ignited homogeneous charge combustion. SAE Trans 92(SAE Paper No. 830264):1.964–1.979

151. Martinez-Frias J, Aceves S, Flowers D, Smith J, Dibble R (2000) HCCI engine control by thermal management. SAE Trans J Fuels Lubricants 109(SAE Paper No. 2000-01-2869):2646–2655
152. Law D, Kemp D, Allen J, Kirkpatrick G, Copland T (2001) Controlled combustion in an IC engine with a fully variable valve train. SAE Trans J Engines 110(SAE Paper No. 2001-01-0251):192–198
153. Rausen D, Stefanopoulou A, Kang J, Eng J, Kuo T (2005) A mean-value model for control of homogeneous charge compression ignition (HCCI) engines. J Dyn Syst Meas Contr 127:355–362
154. Shaver G, Gerdes J, Roelle M, Caton P, Edwards C (2005) Dynamic modeling of residual-affected homogeneous charge compression ignition engines with variable valve actuation. J Dyn Syst Meas Contr 127:374–381
155. Bengtsson J, Strandh P, Johansson R, Tunestal P, Johansson B (2006) Multi-output control of a heavy-duty HCCI engine using variable valve actuation and model predictive control. SAE Paper No. 2006-01-0873
156. Chiang C, Stefanopoulou A (2009) Sensitivity analysis of combustion timing of homogeneous charge compression ignition gasoline engines. J Dyn Syst Meas Contr 131:014506-1–014506-5
157. Fish A, Read I, Affleck W, Haskell W (1969) The controlling role of cool flames in two-stage ignition. Combust Flame 13:39–49
158. Takeda Y, Keiichi N, Keiichi N (1996) Emission characteristics of premixed lean diesel combustion with extremely early staged fuel injection. SAE Trans J Fuels Lubricants 105(SAE Paper No. 961163):938–947
159. Akagawa H, Miyamoto T, Harada A, Sasaki S, Shimazaki N, Hashizume T, Tsujimura K (1999) Approaches to solve problems of the premixed lean diesel combustion. SAE Trans J Engines 108(SAE Paper No. 1999-01-0183):120–132
160. Iwabuchi Y, Kawai K, Shoji T, Takeda Y (1999) Trial of new concept diesel combustion system – premixed compression-ignited combustion. SAE Trans J Engines 108(SAE Paper No. 1999-01-0185):142–151
161. Kimura S, Aoki O, Kitahara Y, Airoshizawa E (2001) Ultra-clean combustion technology combining a low-temperature and premixed combustion concept for meeting future emission standards. SAE Trans J Fuels Lubricants 110(SAE Paper No. 2001-01-0200):239–246
162. Kaneko N, Ando H, Ogawa H, Miyamoto N (2002) Expansion of the operating range with in-cylinder water injection in a premixed charge compression ignition engine. SAE Trans J Engines 111(SAE Paper No. 2002-01-1743):2309–2315
163. Shimazaki N, Tsurushima T, Nishimura T (2003) Dual mode combustion concept with premixed diesel combustion by direct injection near top dead center. SAE Trans J Engines 112(SAE Paper No. 2003-01-0742):1060–1069
164. Hasegawa R, Yanagihara H (2003) HCCI combustion in DI diesel engine. SAE Trans J Engines 112(SAE Paper 2003-01-0745):1070–1077
165. Okude K, Mori K, Shiino S, Moriya T (2004) Premixed compression ignition (PCI) combustion for simultaneous reduction of NOx and soot in diesel engines. SAE Trans J Fuels Lubricants 113(SAE Paper No. 2004-01-1907):1002–1013
166. Jacobs T, Bohac S, Assanis D, Szymkowicz P (2005) Lean and rich premixed compression ignition combustion in a light-duty diesel engine. SAE Trans J Engines 114(SAE Paper No. 2005-01-0166):382–393
167. Lechner G, Jacobs T, Chryssakis C, Assanis D, Siewert R (2005) Evaluation of a narrow spray cone angle, advanced injection timing strategy to achieve partially premixed compression ignition combustion in a diesel engine. SAE Trans J Engines 114(SAE Paper No. 2005-01-0167):394–404
168. Jacobs T, Assanis D (2007) The attainment of premixed compression ignition low-temperature combustion in a compression ignition direct injection engine. Proc Combust Inst 31:2913–2920

I

Books and Reviews

Ferguson CR, Kirkpatrick AT (2001) Internal combustion engines: applied thermosciences, 2nd edn. Wiley, New York

Heywood J (1988) Internal combustion engine fundamentals. McGraw-Hill, New York

Jennings BH, Obert EF (1944) Internal combustion engines: analysis and practice. International Textbook Company, Scranton

Pulkrabek WW (2004) Engineering fundamentals of the internal combustion engine, 2nd edn. Pearson Prentice-Hall, Upper Saddle River

Taylor CF (1985) The internal combustion engine in theory and practice – Vol 1: Thermodynamics, fluid flow, performance (rev), 2nd edn. The MIT Press, Cambridge, MA

Taylor CF (1985) The internal combustion engine in theory and practice – Vol 2: Combustion, fuels, materials, design (rev). The MIT Press, Cambridge, MA

Invasive Species

Anthony Ricciardi
Redpath Museum & McGill School of Environment, McGill University, Montreal, QC, Canada

Article Outline

Glossary
Definition of Subject
Introduction
Pattern and Process in Biological Invasion
Ecological Impacts

Socioeconomic Impacts
Management of Invasions
Future Directions
Bibliography

Glossary

Biological invasion The process by which an organism is introduced to, and establishes a sustainable population in, a region beyond its native range.

Eradication The managed extirpation of an entire nonnative population.

Impact The effect of a nonnative species on its environment.

Invasibility The vulnerability of a habitat, community, or ecosystem to invasion.

Invasion ecology A multidisciplinary field that examines the causes and consequences of biological invasions.

Invasional meltdown The phenomenon in which multiple nonnative species facilitate one another's invasion success and impact.

Invasive species Nonnative species with conspicuously high colonization rates. Such species have the potential to spread over long distances. The term *invasive* is also used (often by policy makers) to describe colonizing species that cause undesirable ecological or economic impacts.

Nonnative species (synonyms: alien, exotic, foreign, nonindigenous) Species present in a region beyond their historic range.

Propagule pressure The quantity or rate of nonnative organisms released into an area.

Definition of the Subject

Biological invasion is the process by which a species is introduced, deliberately or inadvertently, into a new geographic region where it proliferates and persists. Outside their historic range (in which they evolved) such species are described as *nonnative* (or nonindigenous, exotic, alien). For a variety of reasons, the vast majority of introduced nonnative organisms fail to persist. Many of those that do establish self-sustaining populations do not spread very far or very fast beyond their point of introduction, and they often do not have conspicuous impacts on their environment. However, a small proportion (but a large and growing number) of nonnative species becomes *invasive* – that is, they may spread aggressively and/or have strong environmental effects. Invasive species are a global problem that threatens native biodiversity, the normal functioning of ecosystems, natural resources, regional economies, and human health. As such, they pose a major concern for conservation and management, and are the focus of a highly productive multidisciplinary field called *invasion ecology*.

Introduction

The potential impact of nonnative species has long been recognized by naturalists. In *The Origin of Species*, Darwin (1859) warned "Let it be remembered how powerful the influence of a single introduced tree or mammal has been shown to be [on native communities]." A century later, Charles Elton's groundbreaking monograph *The Ecology of Invasions by Animals and Plants* [1] helped inspire two generations of scientists to study what has become one of the world's most challenging environmental problems.

The major findings of this burgeoning research are summarized in recent texts by Lockwood et al. [2], Davis [3], Blackburn et al. [4], and Richardson [5].

This entry describes the causes and consequences of biological invasions, by synthesizing concepts from population biology, community ecology, evolution, biogeography, and conservation biology. First, the patterns and process of invasion are explored; then, some of its potential ecological and socioeconomic impacts are examined. Some major hypotheses and theoretical concepts explaining patterns of colonization and impact are presented. Next, management approaches to assessing, preventing, and mitigating this problem are considered. The entry ends with a brief glimpse at some of the emerging issues that will likely be the foci of future research.

Pattern and Process in Biological Invasion

The process of invasion comprises a sequence of events involving the transport, introduction, establishment, and spread of organisms into a new region. Organisms in various life stages may be moved by natural dispersal (e.g., passive transport by wind, water currents, or animals; active transport by the organism's own movements) or, far more frequently, by human activities

(e.g., transportation systems carrying people or material) across a geographic barrier that previously defined the limits of the historic range of the species. Most organisms will die soon after arrival, or reproduce for only a couple of generations; thus, the vast majority of introduction events fail to produce a sustainable population. If a sufficient number of healthy individuals arrive in a suitable habitat when conditions are favorable, then a self-sustaining population will develop and the species is said to be established. Although populations can sometimes establish from very small numbers, higher numbers of introduced individuals and more frequent introduction events (collectively termed *propagule pressure*) contribute to a higher probability of establishment [6].

In general, the more species introduced to an area, the more that become established in that area [7]. Lonsdale [8] presented an instructive model to describe the number of nonnative species in a region, E:

$$E = I \times S$$

where I is the number of species introduced (*colonization pressure* [7]) and S is the product of the survival rate of each species. S is a function of both the biological traits of the nonnative species and the environmental conditions of the target habitat; for example, all other things being equal, a higher survival rate would result from a closer match between the species' physiological requirements and the prevailing habitat conditions.

There is a variable time lag between initial introduction and establishment, followed by an exponential increase in abundance until the population reaches limits imposed by local abiotic and biotic conditions, at which point population growth diminishes. The range expansion of the species (increase in area occupied per unit time) is correlated with its population growth. The lag phase may range from being negligible (e.g., for a rapidly reproducing species) to extensive – during which the species may remain inconspicuous for years or decades prior to becoming abundant and widespread [9, 10]. For example, the first outbreak of the European gypsy moth (*Lymantria dispar*) in North America occurred two decades after it was initially released. A mussel introduced from the Red Sea remained rare for about 120 years prior to developing dense colonies on the Israeli Mediterranean coast [9]. Recognition of the lag phase phenomenon is critical to management; otherwise, it may lead to inaccurate assessments of benign invasion risk and low impact, as well as missed opportunities to control a nonnative species population while it was still small [10]. Non-mutually exclusive factors contributing to lag phases include: (1) density-dependent (Allee) effects, in which the organism's birth rate is correlated with its population density [11]; (2) adaptation and selection of new genotypes; (3) a change in the composition of the recipient community (e.g., the introduction of a pollinator or seed disperser [12], or the extinction of a dominant resident predator) that triggers the explosive growth of a previously subdued nonnative species; and (4) changing abiotic conditions (e.g., climate change [13]) that release the nonnative species from physiological constraints. Furthermore, the inability to detect an inconspicuous population in its early growth stages is often responsible for a substantial delay in the discovery of a nonnative species. Substantial lags in detection, caused by inadequacies in monitoring and taxonomic expertise, are a major hindrance to effective management [14].

The range expansion of an introduced species tends to fall into a few general patterns, each of which is characterized by an establishment lag phase, an expansion phase, and, when a geographic limit to suitable habitat is realized, a saturation phase [15]. In the simplest pattern, the species expands its range linearly through time; this pattern is the result of random short-distance dispersal outward in all directions through a homogeneous environment, and is often exhibited by rodents such as muskrats. The expanding range is modeled as a circle whose radius increases at a constant rate [16]. The probability of invasion at a given site is inversely proportional to the distance from the edge of the expanding colony and directly proportional to time.

A second pattern is defined by a slow initial rate of linear spread followed by an abrupt shift to a higher linear rate. This biphasic pattern, which has been observed in invasive birds such as the European starling (*Sturnus vulgaris*), occurs when long-distance migrants generate new satellite colonies not far from the primary colony; the coalescence of satellites into the expanding primary colony generates a higher linear rate of expansion. A third pattern occurs when long-distance

dispersers create numerous remote satellite colonies that begin to expand their range independent of each other; their continuous coalescence generates an exponential expansion phase, as exhibited by European cheatgrass (*Bromus tectorum*) in North America and tiger pear cactus (*Opuntia aurantiaca*) in South Africa [15, 17]. In this pattern, a prolonged lag phase often occurs prior to conspicuous exponential growth. Genetic adaptation is another mechanism that can produce the enhanced rate of expansion that characterizes the second and third patterns, but the occurrence of long-distance migrants is probably the more common cause. Via long-distance "jumps," migrants may establish satellite colonies that are remote from the expanding edge of the primary colony; the overall rate of range expansion is driven more by the number of these satellite colonies than by their individual size [16]. The pattern is more pronounced where human vectors dominate dispersal, such that there would be multiple introductions of satellite colonies within a region (e.g., the transport of zebra mussels and aquatic weeds between river basins by recreational boats, or introductions of a marine invertebrate along a coastline via ballast water release at various ports). In this case, the probability of dispersal to a given site is nearly independent of time and distance from the primary colony but instead is driven largely by human-mediated dispersal opportunity [18].

Factors Affecting Establishment Success

In addition to propagule pressure, other biotic and abiotic factors have been hypothesized to explain why some species are better invaders, and why some systems are more invaded, than others. Attributes associated with highly invasive species include an ability to rapidly reproduce from small numbers (a high intrinsic rate of population growth), broad environmental tolerance, and mechanisms of exploiting human transportation vectors and human-modified landscapes. A popular view is that generalist species are better invaders than specialists, because the former can thrive in a broader range of habitat conditions (*niche breadth-invasion success hypothesis* [19]). As such, traits that enable species to cope with new environments (e.g., diet breadth, physiological tolerance [20, 21]), or proxy variables that suggest broad tolerance (e.g., latitudinal range [22]), are generally good predictors of invasion success. Among vertebrates, brain size also generally predicts invasion success [23–25], perhaps because it facilitates behavioral flexibility in new environments (but see [26]). Similarly, invasive plants tend to be more phenotypically plastic than noninvasive plants [27]. Traits associated with reproduction are often correlated with the post-establishment success (abundance and range size) of plants [20, 28]. However, the most important factor limiting the large-scale distribution of a species is whether it is valued by humans for domestication [29–32] or, for a species that is not introduced deliberately, whether its life history allows it to be easily transported by human vectors operating on a global scale [33, 34].

Much research on the question of why some communities or systems are more invasible has addressed the concept of *biotic resistance*, which posits that biotic interactions between nonnative species and resident enemies can limit establishment and post-establishment success. The logical extension of this concept is that resident species diversity may act as a barrier to invasion – an idea promoted by Elton [1] to explain the seemingly disproportionate invasibility of species-poor systems such as oceanic islands and highly disturbed areas such as agricultural fields. Most support for Elton's hypothesis is derived from terrestrial plant communities and is equivocal. Over a range of scales, from small garden plots to regional landscapes, positive correlations between native and nonnative species richness have been observed, reflecting shared responses to external variables [35]. Where negative correlations exist, they are found only at local (m^2) scales in experimental manipulations [36]. Numerous studies suggest that competition, herbivory, and native species richness can strongly inhibit the performance (and impact) of nonnative plants following establishment [37, 38], but little evidence suggests that these interactions can prevent establishment when abiotic conditions are favorable and propagule pressure is high. The lesson for managers from these studies is that even highly diverse native communities are often readily invaded by nonnative species, but the reduction of local species richness may accelerate invasion [35].

Most recent studies of invasion mechanisms focus on two popular hypotheses: *fluctuating resource availability* and *enemy release*. The former hypothesis

proposes that a system's susceptibility to plant invasions varies with fluctuations in unused resources (e.g., light, water, space, nutrients). Where propagule pressure exists, invasion will be promoted by a sudden increase in resource supply (such as through nutrient pollution) or reduced uptake by resident species (following a disturbance such as clearcutting or fire) [39, 40]. Nutrient-rich habitats do experience more plant invasions, but native plants may not always outperform nonnatives in low-resource conditions [41]. Highly disturbed environments are also believed to be more invasible [1]. Nonnative species may dominate a habitat following a disturbance event that is outside the evolutionary experience of the natives; otherwise, natural disturbance may contribute to a system's resistance to invasion [42].

The enemy release hypothesis attributes the success of nonnative species to their escape from specialized natural enemies upon arrival to a new region, and their inherent advantage over resident competitors that are burdened by their own enemies [43]. One reason why plants that are subject to strong herbivory in their native range can thrive in novel regions is that, in the absence of specialized enemies, they may reallocate the energetic costs of defense toward reproduction and growth, and thus become more competitive [44]. It follows that fast-growing species adapted to resource-rich environments may benefit most from the absence of specialized enemies; thus, multiple mechanisms (enemy release, disturbance, resource addition) may act synergistically to drive such invasions [45].

Modern Invasions as Unprecedented Global Change

The spread of species into regions beyond their native range has accelerated exponentially during the past millennium because of human activities such as agriculture, international travel, and global trade. There is a strong link between trade activity and the global distribution of nonnative species [46, 47]. International trade often involves cargo moved by transoceanic ships, which can carry an enormous number of organisms on their hulls and especially in their ballast tanks. Tens of thousands of ships are estimated to be collectively transporting several thousand species around the planet on any given day [48].

Most countries have recorded the establishment of several hundred nonnative species, including invertebrates, vertebrates, plants, bacteria, and fungi (Fig. 1). Human influence is reflected in the improbable composition of modern species assemblages worldwide: African grasses dominate large tracts of the Neotropical region [30], European mammals and birds are abundant in Australia and New Zealand [29, 32], Eurasian invertebrates and fishes dominate food webs in the North American Great Lakes [34], and over 25% of the nonnative species in the Baltic Sea originate from the Pacific and Indian Oceans [50]. Over a decade ago, it was estimated that nonnative plants covered at least 3% of the Earth's ice-free land mass, excluding the already immense area under agricultural cultivation [51]. Nonnative species comprise substantial fractions of flora and fauna on continental areas and, especially, on islands (Table 1). The majority of these invasions have occurred over the past few centuries, coinciding with steep increases in global trade, human travel, and land use. Invaders are presently colonizing new regions at rates that are several orders of magnitude faster than prior to human arrival (Fig. 2). Even the seemingly remote Antarctic continent and its surrounding islands have been colonized by nearly 200 nonnative species of terrestrial plants, invertebrates, and vertebrates within the past two centuries, owing to the effects of scientific exploration, increased accessibility by air and by sea, a burgeoning tourist industry (tens of thousands of visitors annually), and a changing climate [59]. The modern rate and geographic extent of invasion is without historical precedent [58].

Ecological Impacts

Most nonnative species appear to have only minor effects on their invaded systems, but this observation is tempered by two caveats: The impacts of the vast majority of invasions have not been studied [60], and even species that are generally benign can become disruptive at different times or different locations [61]. In many cases, nonnative species can profoundly affect ecosystems by altering community composition, resident species interactions, physical habitat structure, hydrology, nutrient cycling, contaminant cycling, primary production, and natural disturbance (fire, flood, erosion) regimes [17, 62–64]. They can disrupt food

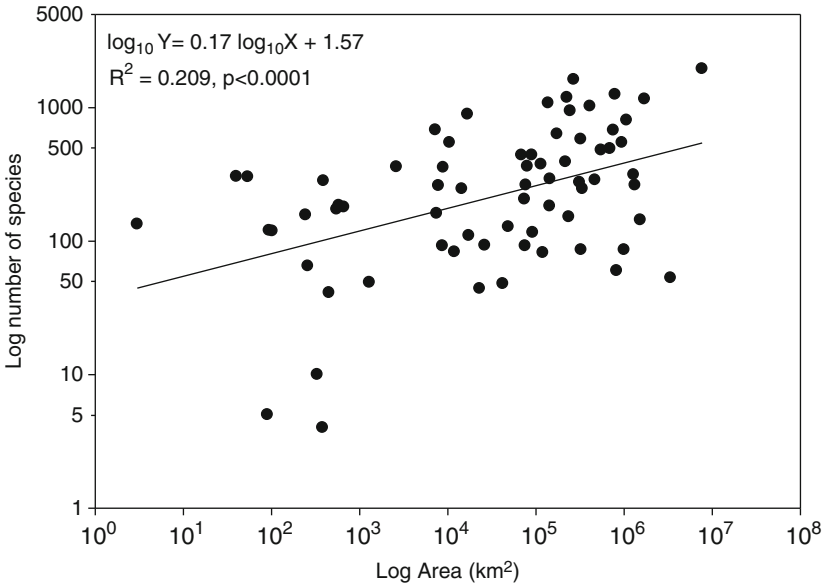

Invasive Species. Figure 1
Number of nonnative vascular plant species versus area for regions worldwide (Data from [49]. Line is fitted by least-squares regression)

Invasive Species. Table 1 Proportion (%) of extant species comprised by established nonnative freshwater fishes, breeding birds, land mammals, and vascular plants in selected regions (Data from [32, 49, 52–57])

Region	Fishes	Birds	Mammals	Plants
Continental areas				
Europe	10	3	19	6
Russia	7	n/a	17	n/a
Southern Africa	11	1	12	4
North America (north of Mexico)	8	4	19	11
South America	<1	<1	4	n/a
Australia	13	6	14	1
Islands				
Puerto Rico	71	35	40	12
Bahamas	14	9	n/a	18
Bermuda	n/a	30	50	65
Hawaii	88	33	89	44
Madagascar	17	2	5	3
Japan	15	2	14	n/a
New Zealand	38	18	40	40

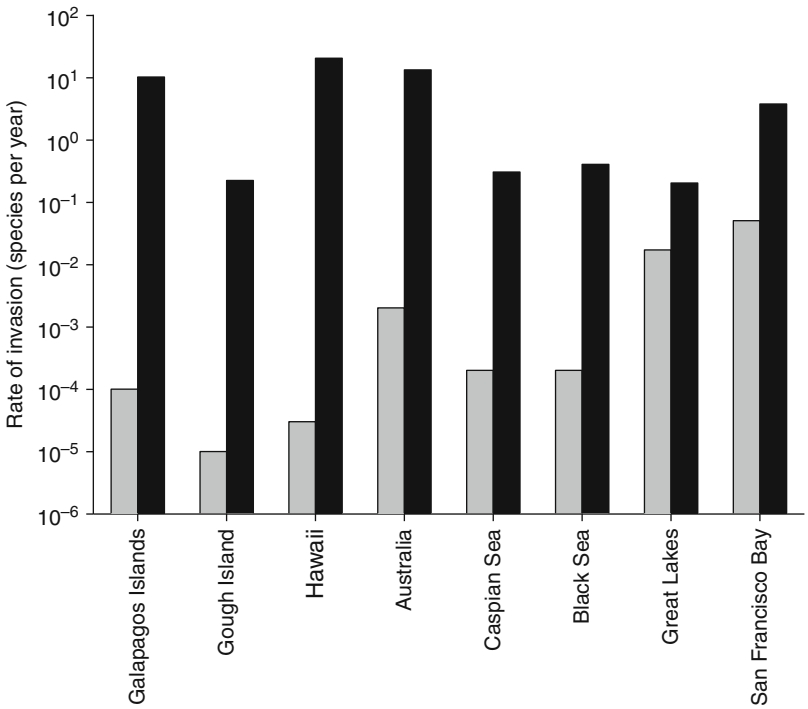

Invasive Species. Figure 2

Prehistoric versus modern rates of invasion (number of nonnative species established per year) for various regions. Prehistoric rates (grey bars) are before human settlement and were estimated from the fossil record or by calculating numbers of "native" species (excluding endemics) that have become established in the region over time. Modern rates (black bars) are inferred from discovery rates averaged over the past 40–100 years (Modified from [58])

webs [65, 66] and plant-animal mutualisms that are crucial for pollination and seed dispersal [67, 68]. Even where environmental stressors such as habitat degradation have already caused population declines of native species, invasions can accelerate these declines [69]. They are a major cause of animal extinctions [70, 71], particularly in insular habitats, such as lakes, river basins, and islands [72, 73]. The invasion-mediated loss of genetically distinct native populations in continental regions has likely been grossly underestimated. There are examples of once widely distributed species being reduced to near extinction as a result of introduced pathogens [17]. Some of the greatest impacts on biodiversity are caused by nonnative predators, and the most conspicuous examples involve introductions to oceanic islands [74, 75] and freshwater ecosystems [76]. Large mammalian herbivores have also had devastating effects on island biodiversity [77, 78]. Other factors contributing to species loss at local to global scales include hybridization [79, 80], competition [69], disease transfer [81], food web alteration [65, 66, 68], and physical habitat alteration [17].

Entire ecosystems may be transformed by invaders that alter resource availability, disturbance regimes, or habitat structure. Some invaders alter the disturbance regime of habitats through fire suppression (e.g., the shrub *Mimosa pigra* in Australian flood plains), fire enhancement (e.g., Eurasian cheatgrass *Bromus tectorum* in the Western United States), increased erosion (e.g., the Australian shrub *Acacia mearnsii* in South Africa), reduced erosion (e.g., exotic plants with extensive root systems that stabilize hills, stream banks, or sand dunes), and increased soil disturbance (e.g., the rooting activities of feral European pigs *Sus scrofa* can destroy the herbaceous understory of a forest, causing soil mineral depletion, rapid organic decomposition, and loss of habitat). Through its

filter-feeding activities, the zebra mussel (*Dreissena polymorpha*) has dramatically increased water transparency in North American and European lakes, thus stimulating the growth of benthic algae and macrophytes and altering physical habitat for invertebrates and fishes [82]. In Hawaii, a nitrogen-fixing tree, *Myrica faya*, significantly enriched nutrient-poor volcanic soils at a rate 90-times greater than native plants and thus has a dominant influence on ecosystem properties including soil chemistry and productivity [83]; *Myrica* has also added habitat structure, shading, and high-quality leaf litter that has promoted enhanced populations of nonnative earthworms [84].

Socioeconomic Impacts

The economic value of cultivated nonnative species (such as crop plants) is widely appreciated, but the same cannot be said for the enormous costs incurred by invasions in general. In several countries, nonnative species comprise more than 40% of all harmful weeds, 30% of arthropod pests, and 70% of plant pathogens, and cause substantial losses in total crop production each year [85]. A single invasive forest insect, the emerald ash borer beetle, is projected to cost the United States $10 billion over the next decade [86]. The 2001 outbreak of foot-and-mouth disease in the United Kingdom, linked to illegal meat imports, cost $25 million USD and required the slaughter of ~11 million animals [87]. The annual costs of 16 nonnative species to fisheries, agriculture, and forestry in Canada are projected to be as high as $34 billion CDN [88]. The combined annual costs of biological invasions in the United States, United Kingdom, Australia, India, South Africa, and Brazil are estimated to be $314 billion USD. Assuming similar costs worldwide, the global economic damage attributable to invasions amounts to US $1.4 trillion per year, which constitutes 5% of the global economy [85].

Whereas some nonnative species perform valuable roles, other nonnatives can degrade ecosystem services – including water purification, soil stabilization, agricultural yield, disease regulation, and climate regulation [89]. The conservation of water resources in African countries is threatened by introduced plants [90], whereas pollination services provided by European honeybees are threatened by Asian *Varroa* mites, whose parasitism has destroyed entire hives [91]. Animal (including human) health, in general, is threatened by invasions that spread parasites, diseases, and their vectors (e.g., mosquitoes [92]). Invasions can also alter the transmission of parasites to humans by introducing hosts to novel regions [93]. About 100 species (~6%) of nonnative invertebrates (e.g., spiders, mosquitoes, nematodes) in Europe adversely affect human or animal health, and these are a subset of ~1,300 nonnative species in the region that have documented socioeconomic impacts [94]. Climate change is expected to drive a new wave of such invasions, as suggested by the recent occurrence in Northern Europe of the tropical virus that causes "bluetongue disease" that resulted from the introduction of infected livestock from a Mediterranean country [95].

Management of Invasions

Risk Assessment

Managers have few tools for prioritizing invasion threats because reliable predictive methods are scarce (but see [96, 97]). Progress in developing a predictive understanding of impact has been hampered by the lack of standardized metrics. Parker et al. [60] proposed a metric for impact (I) that can be compared across species and invaded sites:

$$I = R \times A \times E$$

where R is the total area occupied by the nonnative species in its invaded range, A is its abundance (in numbers or biomass per square meters) in the invaded range, and E is its per-capita effect based on the functional ecology and behavior of individuals (e.g., filtration rate of mussels, functional response of predators, rate of habitat conversion for ecosystem engineers). Data on per-capita effects are often scarce, but inferences regarding the magnitude of impact may be drawn from abundance, which has been shown to be a useful predictor of impact [61]. Range size, in contrast, may not necessarily be a good predictor. Beyond the trivial expectation that the impacts of an invading species accumulate as it occupies more territory, there is no statistical correlation between the invasion success of a species (i.e., its rate of establishment success or spread) and the magnitude of its impact [98]. Even relatively poor invaders can have strong local

impacts on native populations (e.g., the Asian clam *Potamocorbula amurensis*; Atlantic salmon *Salmo salar*), whereas highly successful colonizers do not necessarily displace native species (e.g., freshwater jellyfish *Craspedacusta sowerbyi*). One generalization that has emerged from numerous case studies is that high-impact invaders often represent novel life forms in the invaded system. They acquire and use resources differently than resident species, possess defense mechanisms and "weapons" that are foreign to the invaded community [99], and may have predatory capabilities to which residents are poorly adapted. Such species tend to belong to taxonomic or functional groups that were not present in the ecosystem prior to invasion [100–102]. As such, the phylogenetic distinctiveness of the invader in its novel environment might be an indicator of its impact potential [101, 102].

A major challenge to prediction is context-dependent variation generated by site-specific environmental factors [60, 61]. The best predictor of the colonization success and impact of an introduced plant or animal is its invasion history [20, 61]. Although impacts vary across a heterogeneous environment, models may be developed to predict the impact (or abundance) of a species with a well-documented impact history [61], but the predictive power of such models is diminished at sites that have been highly invaded. Nonnative species can interact in multiple ways to produce unpredictable effects [12, 75], sometimes by facilitating each other's spread and impact (i.e., *invasional meltdown* [103]).

Prevention

Given the growing frequency of invasions, their profound impacts, and the substantive resources required to control rapidly spreading species after they become established, the most cost-effective management strategy is prevention [14]. Arguably, invasions warrant similar investments in preparedness and response planning as natural disasters; despite being slower in their onset, invasions have more persistent impacts and a greater scope of ecological and economic damage than natural disasters [104].

Prevention involves controlling either species entry or establishment. Preventing entry of nonnative species begins with the identification and control of dominant transportation vectors and pathways [14]. The effectiveness of vector-control policies requires rigorous inspection, enforcement, evaluation, and – where necessary – refinement, as has been demonstrated by the evolution of a management program to control ballast water–mediated invasions in the Great Lakes [105]. An additional preventative approach is to manage ecosystems so as to reduce their vulnerability to invasions – e.g., via restoration of intact native communities in degraded areas, managed disturbance (e.g., fire, river flow) regimes, and manipulation of resource supply (nutrients, water supply) [14, 106]. Cultivated systems can be designed with resistance in mind; for example, the use of polycultures (e.g., diversified crops, mixed forest stands) has been demonstrated to reduce harmful outbreaks of invasive pests [107]. The spatial modification of habitats (such as the use of small-scale dispersal barriers) may also be employed to limit colonization [11].

Eradication

The Convention on Biological Diversity [article 8(h)] directs signatory nations to "prevent the introduction of, control or eradicate those alien species which threaten ecosystems." Eradication, the removal of a nonnative population, can lead to the recovery of previously threatened native species [108, 109]. Several conditions must be met for an eradication program to be successful [110]: (1) The target species must be detected at low densities. (2) Its biology must make it susceptible to control measures. (3) Resources must be sufficient to complete the project. (4) Managers must have the authority and public support to take all necessary steps. (5) Re-invasion must be prevented. Also influencing the success of eradication are the reproductive and dispersal capabilities of the invader, both of which determine how fast it will spread. The probability of success is highest in the initial stages of invasion when spatial spread is still limited; hence, early detection and rapid response are crucial, particularly for species that can reproduce and disperse rapidly [14].

Owing to the indirect effects of nonnative species, eradication can have unanticipated negative consequences. Where multiple invaders exist, particularly in simple food webs (e.g., on islands), the removal of a nonnative predator or herbivore can cause the

proliferation of a second invader that was previously controlled by the target species through top-down regulation [111, 112]. For example, the eradication of feral cats from Macquarie Island led to a population explosion of an invasive herbivore – European rabbit [112]. The explosion of rabbits was accompanied by large-scale habitat alteration characterized by a shift in vegetation that favored fast-growing plants, some of which themselves were nonnative. Similarly, the removal of cats from Little Barrier Island, New Zealand, released the introduced Pacific rat (*Rattus exulans*) from top-down control and led to a reduction in the breeding success of an endangered endemic seabird (Cook's petrel, *Pterodroma cookii*), apparently due to nest predation by the rat; subsequent eradication of the rat was followed by a rapid rise in the seabird's breeding success [111]. Additional effects of eradication on multiply invaded systems might be to increase predation pressure on natives as a result of nonnative predators shifting their diets following the removal of nonnative prey, or to release one or more nonnative species from competition by removing a superior competitor.

Maintenance Control

When dealing with nonnative species with strong Allee effects, eradication may involve culling individuals to bring a population below sustainable levels [11]. If eradication fails, or is impossible, the next option is maintenance control of the invader at acceptable population levels, using mechanical, chemical, or biological control methods. Mechanical control, such as hunting, may be particularly effective on islands and other geographically restricted areas. Chemical control involves the application of pesticides to reduce the abundance of a target species, but high economic costs and human health risks constrain the application of chemicals over large areas. Moreover, pesticides often impact nontarget species (including native competitors), sometimes to the benefit of the target itself [113].

Biological control involves the introduction of a nonnative species (usually a predator, herbivore, or parasite) to reduce an established nonnative pest to less harmful densities. This technology is considered to be a more desirable alternative to pesticide use, despite its potential for unanticipated consequences. Because the introduced agents can disperse beyond the target area and evolve to exploit new hosts, nontarget species may be attacked and even driven to extinction [17, 114]. The assumption underlying biological control is that nonnative species proliferate to harmful levels because they have escaped their natural enemies. However, indirect (e.g., competitive) effects may sometimes be more important than top-down consumer regulation. Under these situations, the introduction of a biological control species may have a counterproductive effect [115]. Difficulties in predicting such complex community interactions can obviously compromise ecological risk assessments.

Future Directions

The questions underlying invasion ecology – that is, why some species are more successful and have greater impact than others, why some systems are more vulnerable to invasion, and how ecosystem functions and services are affected by invasion – are clearly of societal importance and will remain relevant in the future, as invasive species are increasingly viewed as a biosecurity issue [87]. The extent and impact of invasions will be further exacerbated by climate change, and synergies between nonnative species and other human-mediated stressors will become more frequent. Future research foci will include the consequences associated with cultivation of novel biofuels and bioenergy crops [116] and the expanded use of genetically modified organisms [117]. Moreover, there may be increasing interest among conservation biologists to relocate native species deemed to be threatened by climate change or other stressors, and some plants and animals could be moved well beyond their historical ranges [73]. Each of these practices will have potentially high ecological risks whose assessment will require more powerful forecasting methods than are currently available. Thus, we can anticipate a growing need for invasion ecology to develop a more predictive understanding of the impact of nonnative organisms.

Bibliography

Primary Literature

1. Elton CS (1958) The ecology of invasions by animals and plants. Methuen, London
2. Lockwood JL, Hoopes MF, Marchetti MP (2007) Invasion ecology. Blackwell, Oxford

3. Davis MA (2009) Invasion biology. Oxford University Press, Oxford
4. Blackburn TM, Lockwood JL, Cassey P (2009) Avian invasions. Oxford University Press, Oxford
5. Richardson DM (ed) (2011) Fifty years of invasion ecology – the legacy of Charles Elton. Wiley-Blackwell, Chichester
6. Simberloff D (2009) The role of propagule pressure in biological invasions. Annu Rev Ecol Evol System 40:81–102
7. Lockwood JL, Cassey P, Blackburn TM (2009) The more you introduce the more you get: the role of propagule and colonization pressure in invasion success. Divers Distrib 15: 904–910
8. Lonsdale WM (1999) Global patterns of plant invasions and the concept of invasibility. Ecology 80:1522–1536
9. Rilov G, Benayahu Y, Gasith A (2004) Prolonged lag in population outbreak of an invasive mussel: a shifting habitat model. Biol Invasions 6:347–364
10. Crooks JA (2005) Lag times and exotic species: the ecology and management of biological invasions in slow-motion. Ecoscience 12:316–329
11. Tobin PC, Berec L, Liebhold AM (2011) Exploiting allee effects for managing biological invasions. Ecol Lett 14:615–624
12. Richardson DM, Allsopp N, D'Antonio CM, Milton SJ, Rejmànek M (2000) Plant invasions – the role of mutualisms. Biol Rev 75:65–93
13. Witte S, Buschbaum C, van Beusekom EE, Reise K (2010) Does climatic warming explain why an introduced barnacle finally takes over after a lag of more than 50 years? Biol Invasions 12:3579–3589
14. Hulme PE (2006) Beyond control: wider implications for the management of biological invasions. J Appl Ecol 43:835–847
15. Shigesada N, Kawasaki K (1997) Biological invasions: theory and practice. Oxford University Press, Oxford
16. Hengeveld R (1989) Dynamics of biological invasions. Chapman and Hall, New York
17. Mack RN, Simberloff D, Lonsdale WM, Evans H, Clout M, Bazzazz FA (2000) Biotic invasions: causes, epidemiology, global consequences, and control. Ecol Appl 10:689–710
18. MacIsaac HJ, Grigorovich IA, Ricciardi A (2001) Reassessment of species invasions concepts: the Great Lakes basin as an example. Biol Invasions 3:405–416
19. Vasquez DP (2006) Exploring the relationship between niche breadth and invasion success. In: Cadotte M, McMahon SM, Fukami T (eds) Conceptual ecology and invasion ecology. Springer, Dordrecht, pp 307–322
20. Hayes KR, Barry SC (2008) Are there any consistent predictors of invasion success? Biol Invasions 10:483–506
21. Blackburn TM, Cassey P, Lockwood JL (2009) The role of species traits in the establishment success of exotic birds. Glob Chang Biol 15:2852–2860
22. Goodwin BJ, McAllister AJ, Fahrig L (1999) Predicting invasiveness of plant species based on biological information. Conserv Biol 13:422–426
23. Sol D, Timmermans S, Lefebvre L (2002) Behavioural flexibility and invasion success in birds. Anim Behav 63:495–502
24. Sol D, Bacher S, Reader SM, Lefebvre L (2008) Brain size predicts the success of mammal species introduced to novel environments. Am Nat 172:S63–S71
25. Amiel JJ, Ringley R, Shine R (2011) Smart moves: effects of relative brain size on establishment success of invasive amphibians and reptiles. PLoS One 6(4):e18277
26. Drake JM (2007) Parental investment and fecundity, but not brain size, are associated with establishment success in introduced fishes. Funct Ecol 21:963–968
27. Davidson AM, Jennions M, Nicotra AB (2011) Do invasive species show higher phenotypic plasticity than native species and, if so, is it adaptive? A meta-analysis. Ecol Lett 14:419–431
28. Ordonez A, Wright IJ, Olff H (2010) Functional differences between native and alien species: a global-scale comparison. Funct Ecol 24:1353–1361
29. Long JL (1981) Introduced birds of the world. Universe Books, New York
30. Mack RN, Lonsdale WM (2001) Humans as global plant dispersers: getting more than we bargained for. BioScience 51:95–102
31. Reichard SH, White P (2001) Horticulture as a pathway of invasive plant introductions in the United States. BioScience 51:103–113
32. Long JL (2003) Introduced mammals of the world. CSIRO Publishers, Collingwood
33. Suarez AV, Holway DA, Case TJ (2001) Patterns of spread in biological invasions dominated by long-distance jump dispersal: insights from Argentine ants. Proc Natl Acad Sci USA 98:1095–1100
34. Ricciardi A (2006) Patterns of invasion in the Laurentian Great Lakes in relation to changes in vector activity. Divers Distrib 12:425–433
35. Fridley JD, Stachowicz JJ, Naeem S, Sax DF, Seabloom EW, Smith MD, Stohlgren TJ, Tilman D, Von Holle B (2007) The invasion paradox: reconciling pattern and process in species invasions. Ecology 88:3–17
36. Herben T, Mandák B, Bímova K, Münzbergova Z (2004) Invasibility and species richness of a community: a neutral model and a survey of published data. Ecology 85:3223–3233
37. Levine JM, Adler PB, Yelenik SG (2004) A meta-analysis of biotic resistance to exotic plant invasions. Ecol Lett 7:975–989
38. Olofsson J, Oksanen L, Callaghan T, Hulme PE, Oksanen T, Suominen O (2009) Herbivores inhibit climate-driven shrub expansion on the tundra. Glob Chang Biol 15:2681–2693
39. Davis MA, Grime JP, Thompson K (2000) Fluctuating resources in plant communities: a general theory of invasibility. J Ecol 88:528–534
40. Davis MA, Pelsor M (2001) Experimental support for a resource-based mechanistic model of invasibility. Ecol Lett 4:421–428
41. Funk JL, Vitousek PM (2007) Resource-use efficiency and plant invasion in low-resource systems. Nature 446:1079–1081
42. Leprieur F, Hickey MA, Arbuckle CJ, Closs GP, Brosse A, Townsend CR (2006) Hydrological disturbance benefits a native fish at the expense of an exotic fish. J Appl Ecol 43:930–939

43. Keane RM, Crawley MJ (2002) Exotic plant invasions and the enemy release hypothesis. Trends Ecol Evol 17:164–170
44. Blossey B, Nötzold R (1995) Evolution of increased competitive ability in invasive nonindigenous plants: a hypothesis. J Ecol 83:887–889
45. Blumenthal D, Mitchell CE, Pyšek P, Jarošik V (2009) Synergy between pathogen release and resource availability in plant invasion. Proc Natl Acad Sci USA 106:7899–7904
46. Westphal MI, Browne M, MacKinnon K, Noble I (2008) The link between international trade and the global distribution of invasive alien species. Biol Invasions 10:391–398
47. Lin W, Cheng X, Xu R (2011) Impact of different economic factors on biological invasions on the global scale. PLoS One 6(4):e18797
48. Carlton JT (1999) The scale and ecological consequences of biological invasion in the World's oceans. In: Sandlund OT, Schei PJ, Viken Å (eds) Invasive species and biodiversity management. Kluwer, Dordrecht, pp 195–212
49. Vitousek PM, D'Antonio CM, Loope LL, Rejmanek M, Westbrooks R (1997) Introduced species: a significant component of human-caused global change. N Z J Ecol 21:1–16
50. Leppäkoski E, Olenin S (2000) Non-native species and rates of spread: lessons from the brackish Baltic Sea. Biol Invasions 2:151–163
51. Mack RN (1997) Plant invasions: early and continuing expressions of global change. In: Huntley B, Cramer W, Morgan AV, Prentice HC, Allen JRM (eds) Past and future rapid environmental changes: the spatial and evolutionary responses of terrestrial biota. Springer, Berlin, pp 205–216
52. Bogustkaya NG, Naseka AM (2002) Freshwater fishes of Russia database. http://www.zin.ru/animalia/pisces/. Accessed 22 July 2011
53. Callmander MW, Phillipson PB, Schatz GE, Andriambololonera S, Rabarimanarivo M, Rakotonirina N, Raharimampionona J, Chatelain C, Gautier L, Lowry PP (2011) The endemic and non-endemic vascular flora of Madagascar updated. Plant Ecol Evol 144:121–125
54. Froese R, Pauly D (2011) FishBase. www.fishbase.org, version (06/2011). Accessed 11 July 2011
55. Hockey PAR, Dean WRJ, Ryan PG (2005) Roberts – birds of southern Africa, 7th edn. The Trustees of the John Voelcker Bird book Fund, Cape Town
56. Koehn JD, MacKenzie RF (2004) Priority management actions for alien freshwater fish species in Australia. N Z J Mar Freshw Res 38:457–472
57. Lehtonen H (2002) Alien freshwater fishes of Europe. In: Leppakoski E, Gollasch S, Olenin S (eds) Invasive aquatic species of Europe: distribution, impacts and management. Kluwer, Dordrecht
58. Ricciardi A (2007) Are modern biological invasions an unprecedented form of global change? Conserv Biol 21:329–336
59. Frenot Y, Chown SL, Whinam J, Selkirk PM, Convey P, Skotnicki M, Bergstrom DM (2005) Biological invasions in the Antarctic: extent, impacts and implications. Biol Rev 80:45–72
60. Parker IM, Simberloff D, Lonsdale WM, Goodell K, Wonham M, Kareiva PM, Williamson MH, Von Holle B, Moyle PB, Byers JE, Goldwasser L (1999) Impact: toward a framework for understanding the ecological effects of invaders. Biol Invasions 1:3–19
61. Ricciardi A (2003) Predicting the impacts of an introduced species from its invasion history: an empirical approach applied to zebra mussel invasions. Freshw Biol 48:972–981
62. Brooks ML, D'Antonio CM, Richardson DM, Grace JB, Keeley JE, DiTomaso JM, Hobbs RJ, Pellant M, Pyke D (2004) Effects of invasive alien plants on fire regimes. BioScience 54:677–688
63. Croll DA, Maron JL, Estes JA, Danner EM, Byrd GV (2005) Introduced predators transform subarctic islands from grassland to tundra. Science 307:1959–1961
64. Simberloff D (2011) How common are invasion-induced ecosystem impacts? Biol Invasions 13:1255–1268
65. Spencer CN, McClelland BR, Stanford JA (1991) Shrimp stocking, salmon collapse, and eagle displacement. BioScience 41:14–21
66. Burghardt KT, Tallamy DW, Philips C, Shropshire KJ (2010) Non-native plants reduce abundance, richness, and host specialization in lepidopteran communities. Ecosphere 1(5):1–22
67. Traveset A, Richardson DM (2006) Biological invasions as disruptors of plant reproductive mutualisms. Trends Ecol Evol 21:208–216
68. Sekercioglu CH (2011) Functional extinctions of bird pollinators cause plant declines. Science 331:1019–1020
69. Ricciardi A (2004) Assessing species invasions as a cause of extinction. Trends Ecol Evol 19:619
70. Clavero M, García-Berthou E (2005) Invasive species are a leading cause of animal extinctions. Trends Ecol Evol 20:110
71. Clavero M, Brotons L, Pons P, Sol D (2009) Prominent role of invasive species in avian biodiversity loss. Biol Conserv 142:2043–2049
72. Ebenhard T (1988) Introduced birds and mammals. Swed Wildl Res (Viltrevy) 13(4):1–107
73. Ricciardi A, Simberloff D (2009) Assisted colonization is not a viable conservation strategy. Trends Ecol Evol 24:248–253
74. Fritts TH, Rodda GH (1998) The role of introduced species in the degradation of island ecosystems: a case history of Guam. Annu Rev Ecol Syst 29:113–140
75. Blackburn TM, Petchey OL, Cassey P, Gaston KJ (2005) Functional diversity of mammalian predators and extinction in island birds. Ecology 86:2916–2923
76. Witte F, Goldschmidt T, Wanink J, Vanoijen M, Goudswaard K, Wittemaas E, Bouton N (1992) The destruction of an endemic species flock – quantitative data on the decline of the haplochromine cichlids of Lake Victoria. Environ Biol Fish 34:1–28
77. Spear D, Chown SL (2009) Non-indigenous ungulates as a threat to biodiversity. J Zool 279:1–17
78. Carrete M, Serrano D, Illera JC, López G, Vögeli M, Delgado A, Tella JL (2009) Goats, birds, and emergent diseases: apparent and hidden effects of exotic species in an island environment. Ecol Appl 19:840–853

79. Simberloff D (2006) Hybridization between native and introduced wildlife species: importance for conservation. Wildl Biol 2:143–150
80. Ayres DR, Zaremba K, Strong DR (2004) Extinction of a common native species by hybridization with an invasive congener. Weed Technol 18S:1288–1291
81. Wyatt KB, Campos PF, Gilbert MTP, Kolokotronis S-O, Hynes WH, DeSalle R, Ball SJ, Daszak P, MacPhee RDE, Greenwood AD (2008) Historical mammal extinction on Christmas Island (Indian Ocean) correlates with introduced infectious disease. PLoS One 3(11):e3602
82. Higgins SN, Vander Zanden MJ (2010) What a difference a species makes: a meta–analysis of dreissenid mussel impacts on freshwater ecosystems. Ecol Monogr 80:179–196
83. Vitousek PM, Whiteaker LR, Mueller-Dombois D, Matson PA (1987) Biological invasion by *Myrica faya* alters ecosystem development in Hawai'i. Science 238:802–804
84. Aplet GH (1990) Alteration of earthworm community biomass by the alien *Myrica faya* in Hawaii. Oecologia 82:414–416
85. Pimentel D, McNair S, Janecka J, Wightman J, Simmonds C, O'Connell C, Wong E, Russel L, Zern J, Aquino T, Tsomondo T (2001) Economic and environmental threats of alien plant, animal, and microbe invasions. Agric Ecosyst Environ 84:1–20
86. Kovacs KF, Haight RG, McCullough DG, Mercader RJ, Siegert NW, Liebhold AM (2010) Cost of potential emerald ash borer damage in U.S. communities, 2009–2019. Ecol Econ 69:569–578
87. Chomel BB, Sun B (2010) Bioterrorism and invasive species. Rev Sci Tech 29:193–199
88. Colautti RI, Bailey SA, van Overdijk CDA, Amundsen K, MacIsaac HJ (2006) Characterised and projected costs of nonindigenous species in Canada. Biol Invasions 8:45–59
89. Pejchar L, Mooney HA (2009) Invasive species, ecosystem services and human well-being. Trends Ecol Evol 24:497–504
90. Le Maitre DC, Versfeld DB, Chapman RA (2000) The impact of invading alien plants on surface water resources in South Africa: a preliminary assessment. Water SA 26:397–408
91. Cook DC, Thomas MB, Cunningham SA, Anderson DL, De Barro PJ (2007) Predicting the economic impact of an invasive species on an ecosystem service. Ecol Appl 17:1832–1840
92. Lounibos LP (2002) Invasions by insect vectors of human disease. Annu Rev Entomol 47:233–266
93. Lv S, Zhang Y, Steinmann P, Yang G-J, Yang K, Zhou X-N, Utzinger J (2011) The emergence of angiostrongyliasis in the People's Republic of China: the interplay between invasive snails, climate change and transmission dynamics. Freshw Biol 56:717–734
94. Vilà M, Basnou C, Pyšek P, Josefsson M, Genovesi P, Gollasch S, Nentwig W, Olenin S, Roques A, Roy D, Hulme PE (2010) How well do we understand the impacts of alien species on ecosystem services? A pan-European, cross-taxa assessment. Front Ecol Environ 8:135–144
95. Purse BV, Mellor PS, Rogers DJ, Samuel AR, Mertens PPC, Baylis M (2005) Climate change and the recent emergence of bluetongue in Europe. Nat Rev Microbiol 3:171–181
96. Reichard S, Hamilton CW (1997) Predicting invasions of woody plants introduced into North America. Conserv Biol 11:193–203
97. Kolar CS, Lodge DM (2002) Ecological predictions and risk assessments for alien species. Science 298:1233–1236
98. Ricciardi A, Cohen J (2007) The invasiveness of an introduced species does not predict its impact. Biol Invasions 9:309–315
99. Callaway RM, Ridenour WM (2004) Novel weapons: invasive success and the evolution of increased competitive ability. Front Ecol Environ 2:436–443
100. Short J, Kinnear JE, Robley A (2002) Surplus killing by introduced predators in Australia – evidence for ineffective anti-predator adaptations in native prey species? Biol Conserv 103:283–301
101. Ricciardi A, Atkinson SK (2004) Distinctiveness magnifies the impact of biological invaders in aquatic ecosystems. Ecol Lett 7:781–784
102. Strauss SY, Webb CO, Salamin N (2007) Exotic taxa less related to native species are more invasive. Proc Natl Acad Sci U S A 103:5841–5845
103. Simberloff D, Von Holle B (1999) Positive interactions of nonindigenous species: invasional meltdown? Biol Invasions 1:21–32
104. Ricciardi A, Palmer ME, Yan ND (2011) Should biological invasions be managed as natural disasters? BioScience 61:312–317
105. Bailey SA, Deneau MG, Jean L, Wiley CJ, Leung B, MacIsaac HJ (2001) Evaluating efficacy of an environmental policy to prevent biological invasions. Environ Sci Technol 45: 2554–2561
106. Huston MA (2004) Management strategies for plant invasions: manipulating productivity, disturbance, and competition. Divers Distrib 10:167–178
107. Risch SJ, Andow D, Altieri MA (1983) Agroecosystem diversity and pest control: data, tentative conclusions, and new directions. Environ Entomol 12:625–629
108. Pascal M, Siorat F, Lorvelec O, Yésou P, Simberloff D (2005) A pleasing consequence of Norway rat eradication: two shrew species recover. Divers Distrib 11:193–198
109. Donlan CJ, Campbell K, Cabrera W, Lavoie C, Carrion V, Cruz F (2007) Recovery of the Galapagos rail (*Laterallus spilonotus*) following the removal of invasive mammals. Biol Conserv 138:520–524
110. Myers JH, Simberloff D, Kuris AM, Carey JR (2000) Eradication revisited: dealing with exotic species. Trends Ecol Evol 15:316–320
111. Rayner MJ, Hauber ME, Imber MJ, Stamp RK, Clout MN (2007) Spatial heterogeneity of mesopredator release within an oceanic island system. Proc Natl Acad Sci U S A 104:20862–20865
112. Bergstrom DM, Lucieer A, Kiefer K, Wasley J, Belbin L, Pedersen TK, Chown SL (2009) Indirect effects of invasive species removal devastate World Heritage Island. J Appl Ecol 46:73–81

113. Rinella MJ, Maxwell BD, Fay PK, Weaver T, Sheley RL (2009) Control effort exacerbates invasive-species problem. Ecol Appl 19:155–162
114. Louda SM, Arnett AE, Rand TA, Russell FL (2003) Invasiveness of some biological control insects and adequacy of their ecological risk assessment and regulation. Conserv Biol 17:73–82
115. Callaway RM, DeLuca TH, Belliveau WM (1999) Biological-control herbivores may increase competitive ability if the noxious weed *Centaura maculosa*. Ecology 80:1196–1201
116. Lonsdale WM, FitzGibbon F (2011) The known unknowns – managing the invasion risk from biofuels. Curr Opin Environ Sustain 3:31–35
117. Andow DA, Zwahlen C (2006) Assessing environmental risks of transgenic plants. Ecol Lett 9:196–214

Books and Reviews

Catford JA, Jansson R, Nilsson C (2009) Reducing redundancy in invasion ecology by integrating hypotheses into a single theoretical framework. Divers Distrib 15:22–40

Ionizing Radiation Detectors

Wm. David Kulp, III
Mechanical Engineering, Georgia Institute of Technology, Atlanta, GA, USA

Article Outline

Glossary
Definition of the Subject
Introduction
Gas-Filled Detectors
Scintillation Detectors
Semiconductor Detectors
Neutron Detectors
Future Directions
Bibliography

Glossary

Alpha particle A particle emitted during radioactive decay that is comprised of two protons and two neutrons, equivalent to the nucleus of a ^{4}He atom.

Beta particle An electron or a positron (the positively charged antimatter twin of an electron) emitted during radioactive decay.

Electron volt (eV) A unit of energy measurement defined by the kinetic energy gained by a free electron when accelerated through a potential difference of 1 V; approximately equivalent to 1.602×10^{-19} joule.

Gamma radiation Highly energetic electromagnetic radiation (energy greater than approximately 100 keV) emitted from the nucleus during radioactive decay.

Ionizing radiation Particles or light with sufficient energy to remove an electron from an atom or molecule.

Nuclide A species of atomic nuclei, defined by the number of protons and neutrons present in the nucleus; nuclides are represented by the chemical symbol and atomic mass number. Two examples are ^{14}C (carbon-14, six protons and eight neutrons) and ^{235}U (uranium-235, 92 protons and 143 neutrons).

Radioactive Describes an unstable atomic nucleus that releases energy through ionizing radiation.

Scintillator A type of detector that uses fluorescence to detect radiation.

Spectroscopy The measurement of radiation intensity as a function of radiation energy; a device or system of detectors capable of spectroscopy is referred to as a spectrometer.

Definition of the Subject

Equipment to detect, identify, and measure radioactivity is a key component in the safe and responsible development of nuclear science and technology. Whether designed to monitor radioactive processes, provide an alert, or characterize the radiation measured, these systems "see" what is undetectable to human senses. Used in nuclear power, industry, medical imaging, nuclear medicine, scientific exploration, and nuclear security, radiation detectors provide information about the radiation present and can be used to interpret what the source of the radioactivity is.

Experimental data exist for about 2,900 nuclides, or species of atomic nuclei, characterized in the laboratory. Yet less than 300 nuclides are found in measurable abundance in the environment. Most of these naturally occurring nuclides are stable nuclei, meaning that they do not decay to other nuclei over time. However,

some unstable, or radioactive, nuclei are found in everyday objects. Examples of naturally occurring radioactive material (NORM) are ^{40}K in bananas and the nuclides in the uranium and thorium decay series that are found in cat litter. The identification of radioactive nuclides is accomplished through detection and measurement of the radiation emitted during the decay of the unstable nucleus.

The decay of a radioactive atomic nucleus results in energy being released in the form of particles or electromagnetic radiation. Particles emitted during radioactive decay include alpha particles, beta particles, neutrons, and photons. Alpha and beta radiation are electrically charged particles ejected from the decaying nucleus. Alpha particles are positively charged helium nuclei. Beta particles are electrons or positrons (the antiparticle of an electron), which carry negative and positive charges, respectively. Neutrons have no electric charge. Photons, X and gamma rays, are electromagnetic radiation; treated as particles, they have zero charge, zero rest mass, and travel at the speed of light.

Introduction

The detection and characterization of radiation originated with Wilhelm Conrad Röntgen, who was awarded the first Nobel Prize in Physics in 1901 [1]. This work was continued and led to the discovery of spontaneous radioactivity, for which Antoine Henri Becquerel, Pierre Curie, and Marie Curie shared the 1903 Nobel Prize in Physics [1]. The mature nature of the field is demonstrated by the many textbooks available on nuclear physics and radiation detection. Suggested reading for in-depth study with focused discussion on radiation detection are Glasstone [2], Kantele [3], Knoll [4], Krane [5], Leo [6], and Tsoulfinidis [7].

Nuclear radiation ranges in energy from a few thousand electron volts (kilo-electron volts, or keV) to millions of electron volts (mega-electron volts, or MeV). Particles in the keV or MeV energy range are energetic enough that as they pass through matter they can cause the ejection of one or more electrons from a neutral atom in the material, ionizing the atom. Because of this interaction, nuclear radiation is also referred to as ionizing radiation. The physical processes that lead to ionization as radiation passes through matter depend upon the kind of radiation. Charged particles, photons, and neutral particles all interact with matter in different ways.

Alpha particles and other heavy, charged particles interact with matter through a variety of mechanisms, but the primary reaction is simply Coulomb scattering, an interaction between charged particles that is kinematic in nature. When energy is imparted to a target atom in the material, an inelastic collision has occurred with atomic electrons. Where no energy is transferred to the target material, the incident particle has elastically scattered from a target nucleus. These interactions have two basic results for the incident particle: (1) the particle loses energy, and (2) the particle is deflected from its initial trajectory.

Electrons and positrons also lose energy through Coulomb scattering in matter. However, they are more easily deflected in the electric field near an atomic nucleus due to the small mass of these particles or in collisions with atomic electrons (same mass). When electrons collide, energy is directly transferred to the atomic electrons. When electrons are accelerated or decelerated, electromagnetic energy is emitted in a process known as bremsstrahlung. Above a few MeV in energy, this mechanism is the predominant interaction for high-energy electrons and positrons.

Gamma rays and X rays are very different from the charged particles discussed above. They are electromagnetic radiation, called photons; a photon has zero electric charge and zero rest mass. Photons have three main interactions with matter:

1. The photoelectric effect, where an atomic electron is ejected from an atom after the absorption of the photon
2. Compton scattering, the scattering of photons by free electrons
3. Pair production, where a photon is transformed into an electron-positron pair

Neutrons are similar to photons in that they lack electric charge and will not interact with matter through Coulomb scattering. Instead, a neutron interacts with nuclei through the strong force. This is a relatively rare occurrence due to the short range of the strong force (effective only within 10^{-15} m). The result of interaction may be:

1. Elastic scattering from nuclei, so that no nuclear reaction takes place.
2. Inelastic scattering, where the target nucleus is left in an excited state.
3. Neutron capture, where the target nucleus is transformed through absorption of the neutron; most of the time the new nucleus is radioactive and decays by emitting beta particles and/or gamma rays (and neutrons, too, in a few cases).
4. Nuclear reactions with the emission of a charged particle.
5. Fission, the splitting of a heavy atomic nucleus.

Radiation detectors make use of these interactions with matter to produce a measurable effect that signals the presence of radioactivity. In general, a radiation detector can be characterized through three traits: (1) the radiation absorber (the materials of which the detector is made), (2) an observable that signals the interaction with radiation, and (3) a way to measure the signal.

The radiation absorber may be gas, liquid, or solid and can be made from a range of materials. The choice of detection medium phase depends on the type of radiation to be measured. Heavy charged particles have a range of less than about 100 μm (0.01 cm or 0.004 in.) in a solid absorber, but the resulting signals may be hard to distinguish from electronic noise. Neutrons and gamma rays, on the other hand, may penetrate centimeters of solid matter without producing any observable response. For detecting neutrons, the use of enriched isotopes may be used in order to take advantage of specific nuclear reactions that have higher probabilities of occurring.

The choice of observable effect produced by the detector is usually more dependent upon the application and the material used as the radiation absorber, rather than the type of radiation. Early researchers Henri Becquerel and Marie and Pierre Curie recorded data on photographic plates. While this method of observation provided long-lasting visible evidence of radiation, other detection methods such as electronic signals, scintillation light emissions, and changes in temperature are more advantageous for modern radiation detection. For example, light emissions produce the fastest detector response, thus a scintillation detector is the best choice for a measurement that requires precision timing. On the other hand, semiconductor detectors provide excellent energy resolution with good timing resolution, and are used for detailed nuclear spectroscopy.

If the radiation detection application requires only a qualitative measure of the presence of radiation, then an effective method of measurement would be an audible alarm that sounds when a threshold radiation level is reached, measured as a current generated within the detector volume. Nuclear science, however, requires quantitative analysis of the number and energy of individual particles emitted by atomic and nuclear transitions. For nuclear spectroscopy, it is therefore necessary to measure each electronic pulse registered in the detector, amplify the pulses and perhaps shape the signals as necessary, and record these signals for later analysis.

Given the different types of radiation and the range of energies, no single detector will be sensitive to all nuclear radiations at all applicable energies. Further, the diverse applications for radiation detection preclude a general list of radiation detectors that could be considered comprehensive. In the sections that follow, the most common detector types will be discussed and some recent advancements in the field will be introduced.

Gas-Filled Detectors

Ionizing radiation produces pairs of positively charged ions and negatively charged electrons as it passes through matter. It follows that a simple way to measure radioactivity is to apply an electric field across the radiation-absorbing material and count the ion-electron pairs produced in the detector. Such a detector can be envisioned as a parallel-plate capacitor filled with a gas. An electric potential applied across the capacitor creates an electric field that separates the electrons and ions. The electrons drift toward the positively charged anode plate, while the ions drift in the opposite direction toward the negatively charged cathode. This separation prevents the electrons and ions from recombining and enables measurement of the electronic signal produced by the ionizing radiation.

Ionization Chambers

The applied voltage across the capacitor influences how quickly charged particles move in the ionization

chamber. Electrons and ions tend to recombine to form neutral atoms at low voltages, with the result that only a weak signal is collected. This recombination region is indicated in the range where $V < V_1$ as in Fig. 1. Above some threshold potential, the electric field prevents recombination. This is indicated in the region where $V_1 < V < V_2$, where the total charge detected is insensitive to the applied voltage, as all of the electron-ion pairs that are created by the initial ionizing event are collected. A detector operating in this region collects only the charge produced directly by the incident radiation and is thus called an ionization chamber.

How big is the output electronic signal from an ionization chamber? The average energy required to produce an ion in dry air is about 30 electron volts (eV). An ionization chamber consisting of two square plates, each 10 cm long on a side, separated by a 1-cm air gap has a capacitance of 9×10^{-12} farads. Based on the energy to produce one ion in air, a 1-MeV gamma ray that deposits all of its energy in this detector would produce a maximum of about 3×10^4 electron-ion pairs, and a 2-MeV gamma ray would produce twice as many pairs. The voltage pulse resulting from these events would be about 0.5 or 1 mV, respectively.

To analyze individual pulses, the small signals produced by the direct radiation interaction require amplification. The two curves illustrated in Fig. 1 correspond to radiations that deposit different energies in the detector, e.g., an alpha particle and a beta particle or two gamma rays of different energies. The more energetic radiation produces more electron-ion pairs, resulting in a larger output signal.

Proportional Counters

A larger output signal can also be generated by increasing the applied voltage across the capacitor. The increased electric field accelerates the ions and electrons in the chamber to higher kinetic energy. Above a second threshold voltage, indicated as V_2 in

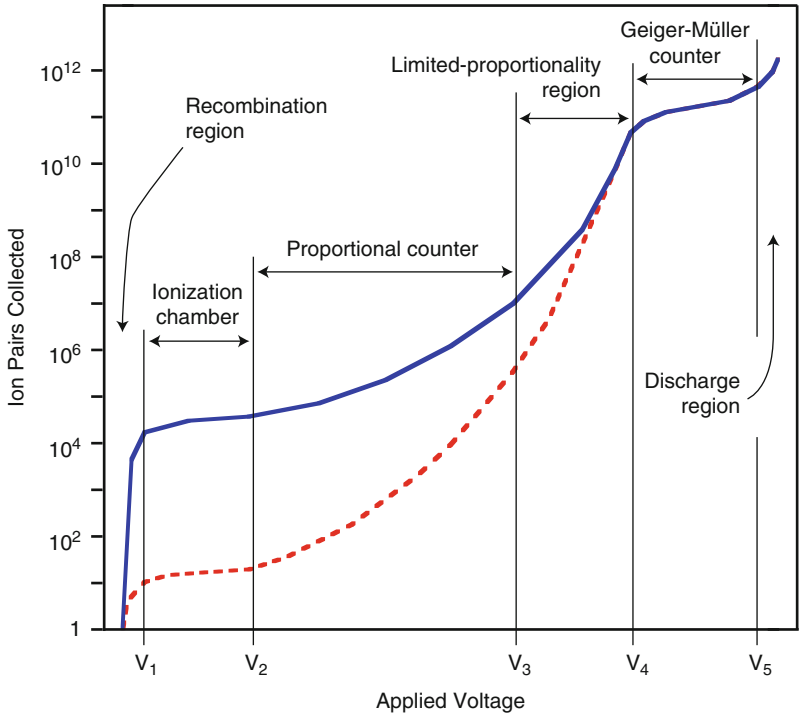

Ionizing Radiation Detectors. Figure 1
The number of ion-electron pairs collected in a gas-filled detector depends on the applied voltage and on the energy deposited in the active volume of the detector

Fig. 1, free electrons, produced by the incident radiation, are accelerated to sufficient energy such that they ionize additional gas atoms during collisions and produce more free electrons. This process is known as *gas multiplication* and results in a larger output signal.

The electrons produced in the knock-on reactions are called *secondary electrons*. The secondary electrons accelerate and produce additional ionization, resulting in a *Townsend avalanche*, where 10^3–10^5 secondary events occur for each original ion produced. As shown in region $V_2 < V < V_3$, the number of electron-ion pairs is proportional to the number of pairs produced in the primary event. Detectors operating in this range are called *proportional counters*. Using such a detector, the measurement of the incident particle energy is possible because the final signal is proportional to the energy deposited in the detector.

Proportional counters are typically cylindrical in shape, as shown in Fig. 2. This geometry results in an electric field that has an inversely proportional 1/r dependence, where r is the distance from the distance from the center of the detector. The site of the original interaction is not critical in such a detector. However, as an electron accelerates closer to the central anode wire, the field becomes very intense, resulting in a Townsend avalanche, indicated as a shower of electrons in Fig. 2. Because this occurs near the anode, the secondary electrons created are highly localized and no additional cascades form.

Increasing the applied voltage beyond $V = V_3$, the total ionization produced through gas multiplication continues to increase, but with reduced proportionality. This is the result of the creation of clouds of ions near the anode wire that have significantly lower drift speeds than the electrons. As a result, as the voltage increased in the region $V_3 < V < V_4$, the ions build up a space charge that shields the anode and changes the effective electric field.

Further increasing the voltage beyond V_4 results in a discharge occurring in the gas. Instead of a single, localized avalanche for each original electron-ion pair, *secondary avalanches* occur all along the anode wire. The secondary avalanches are the result of photons emitted by de-exciting gas molecules in the detector causing further ionization and avalanches elsewhere in the detector. A saturation effect thus takes place in the region indicated by $V_3 < V < V_4$: the discharge always has the same output, independent of the energy of the initial event.

Geiger-Müller Counters

Detectors operating in the $V_4 < V < V_5$ region are called *Geiger-Müller counters*. As shown in Fig. 1, there is no difference in count rate due to the energy initially

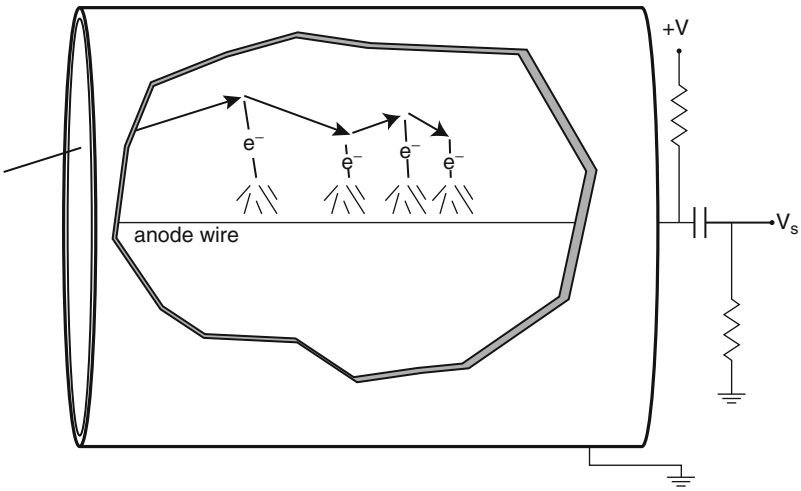

Ionizing Radiation Detectors. Figure 2
Radiation enters a proportional counter through a thin window and interacts with the gas within the cylinder, creating electron-ion pairs. The electrons accelerate toward the anode wire and produce avalanches of secondary electrons

deposited in the detector. Moreover, while the measured pulse size changes because the charge collected increases with increasing voltage, the pulse count rate does not change significantly, as shown in Fig. 3.

What is happening here is that the potential difference is so large in the active region of the detector that secondary avalanches cause a chain reaction of avalanches and total breakdown occurs. The discharge ends only when a large number of slow-moving secondary ions are formed near the anode wire. This localized concentration of ions represents a *space charge* that reduces the magnitude of the electric field, diminishing the attractive force accelerating the secondary electrons, and quenching the breakdown so that all radiation interacting with the detector produces the same current, regardless of particle type or initial energy.

Increasing the voltage to $V > V_5$ results in continuous breakdown in the gas, producing a steady current, whether radiation is present or not. This discharge region should be avoided in order to prevent damage to the detector. For this reason, Geiger-Müller tubes are typically operated at a voltage in the middle of the Geiger plateau.

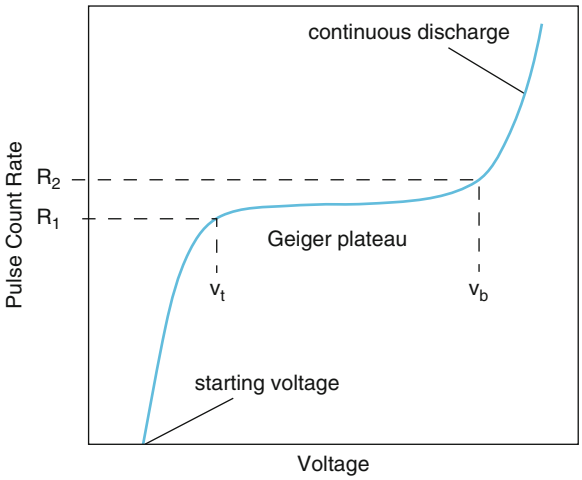

Ionizing Radiation Detectors. Figure 3
The operating point of a Geiger-Müller tube is the middle of a region between a threshold voltage, V_t, and a breakdown voltage, V_b. In this region, called the *Geiger plateau*, the count rate changes very little as a function of the applied voltage. Beyond the breakdown voltage, the tube discharges continuously

In general, gas-filled detectors are the simplest detectors to operate, but have relatively low radiation detection efficiency. For electrons, ions, and low-energy X rays and gamma rays, the low density of matter in the active volume of the detector is sufficient. However, for high-energy photons, gas-filled detectors lack sufficiently high density to stop the radiation effectively. Practically, this is demonstrated using a rule of thumb: the thickness of material required to attenuate by half the intensity of a beam of 1 MeV photons is ~10 g/cm^2. To halve the intensity of a 1 MeV source of gamma rays using air (density = 0.00129 g/cm^3 at standard temperature and pressure) would require a detector 78 m thick. In comparison, only 2.7 cm thickness of sodium iodide (density = 3.667 g/cm^3) is needed to reduce the beam intensity by half.

Scintillation Detectors

The principle of operation for a scintillation detector is very different from that of a gas-filled detector. Rather than collecting the electrons produced directly in the ionizing event in the radiation absorber, scintillation detectors use light as the observable that signals radiation detection.

The basic principle of operation of a scintillation detector, illustrated in Fig. 4, is as follows:

1. Incident radiation ionizes an atom in the scintillator material.
2. The excited atom *fluoresces*, i.e., produces light, as it relaxes to its initial state.
3. The light strikes the front surface of a *photomultiplier tube* (*PMT*) called a *photocathode* that yields a *photoelectron* through the photoelectric effect.
4. The photoelectrons are accelerated and multiplied through a series of electrodes (called *dynodes*) to produce a shower of secondary electrons.
5. The secondary electrons are collected at the anode as an output signal pulse.

The scintillator medium may be a solid, liquid, or gas. Scintillator material may be selected from organic crystals, organic liquids, plastics, glasses, inorganic

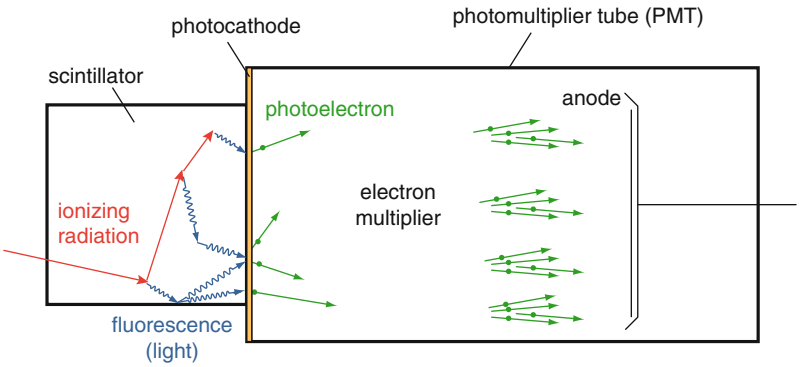

Ionizing Radiation Detectors. Figure 4
Ionizing radiation produces flashes of light in a scintillation detector. This light is focused to produce photoelectrons, which are multiplied to produce a measurable signal

crystals, glasses, and gases. With the exception of the crystalline detectors, organic scintillators are referred to using manufacturer designations. For example, a common liquid scintillator used in fast neutron detection is known as NE-213 (Nuclear Enterprises), BC-501A (Bicron/St. Gobain), and EJ-301 (Eljen). Plastic scintillation detectors, such as NE-102A (alternatively marketed as BC-400 or EJ-212), are manufactured by dissolving organic scintillators in a solvent such as styrene or polyvinyltoluene (PVT) that can be polymerized. These detectors have a notable advantage in that they may be cut or shaped as needed and are fairly durable, but the choice of material ultimately depends on the detection application.

The characteristics of a good scintillator are:

1. Efficient *luminescence*, i.e., it converts most of the energy deposited in the material into light.
2. Transparent to its own light output to enable light transmission through the absorbing material.
3. Has an index of refraction approximately that of glass ($n = 1.5$) to allow coupling to a light sensor.
4. Emits light within a wavelength range that matches existing light sensors.
5. Emits light pulses with a short decay time constant (τ).

Organic detectors are characterized by the shortest decay time constants; however, these lighter compounds lack the efficiency of detectors made using materials of higher atomic number. Inorganic crystals can be made from materials as heavy as bismuth (atomic number, Z = 83), and typically have better energy resolution than organic detectors. Scintillators in common use are:

- Anthracene ($C_{14}H_{10}$), an organic crystal with a short decay constant (τ = 30 ns) used in general radiation detection
- Stilbene ($C_{14}H_{12}$), a very fast (τ <5 ns) organic crystal used in neutron detection
- NE-102A, a general-purpose plastic scintillator (τ = 2.4 ns)
- NE-213, an organic liquid used in neutron detection (τ = 3.7 ns)
- NaI(Tl) (sodium iodide activated with a thallium dopant), an inorganic crystal in wide use in radiation detection (τ = 230 ns)
- LiI(Eu) (lithium iodide doped with europium), an inorganic crystal used in neutron detection (τ = 1,200 ns)
- $Bi_4Ge_3O_{12}$ (bismuth germanate, or BGO), used in PET scanners and in nuclear spectroscopy (τ = 300 ns)
- BaF_2 (barium fluoride), used for fast timing in nuclear spectroscopy (two components to the pulse τ = 0.6 and 630 ns, respectively)

Semiconductor Detectors

Semiconductor detectors are essentially solid-state ionization chambers. With higher mass density, and requiring less energy per charge generated (on the

order of 3 eV, compared with about 30 eV in gaseous detectors), however, semiconductor detectors provide both increased detection efficiency and superior energy resolution compared with gaseous detectors. Ionizing radiation excites electrons into the conduction band of the semiconductor crystal. These electrons and the positively charged *holes* left behind in the valence band of the semiconductor migrate under the influence of the applied electric field, which is on the order of a few thousand volts.

The band gap in a semiconductor is on the order of about 1 eV. Such a small energy difference results in a measurable output signal from semiconductor detectors at room temperature. To reduce this thermal noise, some semiconductor detectors are operated at cryogenic temperatures.

The two operational constraints on semiconductor detectors, high voltage and cryogenic temperatures, limit widespread use of these devices. However, semiconductor detectors typically have significantly better energy resolution than scintillator detectors. This is illustrated in the gamma-ray spectrum measured during the decay of ^{152}Eu, shown in Fig. 5.

The upper pulse-height spectrum in Fig. 5 shows the response of an array of barium fluoride (BaF_2) scintillation detectors, while the lower spectrum is that collected using an array of high-purity germanium (HPGe) semiconductor detectors. Individual lines resolved by the HPGe detector appear as a continuum with mound-like features in the BaF_2 spectrum. This difference makes semiconductor detectors the tool of choice in nuclear spectroscopy. With a higher atomic number (Z = 32), germanium detectors are typically used for gamma-ray spectroscopy, while silicon detectors (Z = 14) are used in X-ray spectroscopy and in charged particle spectroscopy.

Neutron Detectors

The absence of an electric charge complicates neutron detection. Neutrons do not directly produce ionization in matter. However, neutrons interact with atomic nuclei through absorption or scattering, and are thus detected through reaction products that do produce ionization.

Absorption through neutron-induced nuclear reactions is most probable at very low energies (eV); the probability of a reaction occurring increases with decreasing neutron energy with a 1/v relationship, i.e., inversely proportional to the neutron velocity. Most nuclear power reactors are designed to work at thermal energies (on the order of 0.025 eV), where a neutron has a speed of 2,200 m/s, and the probability is high for neutron-induced fission in uranium. The 1/v

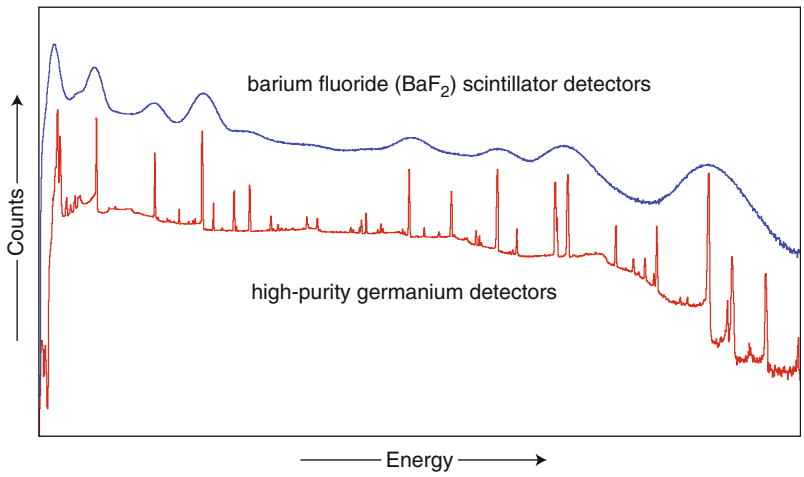

Ionizing Radiation Detectors. Figure 5
Gamma-ray spectra from the radioactive decay of ^{152}Eu demonstrate the difference in energy resolution between that of a barium fluoride (BaF_2) scintillator detector array (*top*) and that of a high-purity germanium semiconductor detector array (Spectra courtesy of D. Cross)

relationship implies that nuclear reactions will be most useful for detecting *slow* neutrons, categorized by a neutron energy < 0.5 eV. Neutrons with an energy above this threshold are more effectively detected through scattering in the detector material.

Slow Neutron Detectors

Nuclear reactions used to detect slow neutrons (neutron energy <0.5 eV) typically produce heavy charged particles such as protons and alpha particles. These reactions are referred to as activation reactions, because they usually leave the product nucleus in an excited state, which subsequently decays through gamma-ray emission. Two common reactions used in detectors are the (*n,p*) and (*n,α*) activation reactions. In the (*n,p*) reaction a neutron, *n*, is absorbed and a proton, *p*, is emitted. Similarly, in the (*n,α*) reaction an alpha particle, α, is emitted. These reactions release considerable energy (approximately 1 MeV or more), so that the incident neutron energy (< 0.5 eV) cannot be determined from the reaction. Subsequently, detectors designed for slow neutrons are used only for indicating the presence of neutrons, and not for neutron spectroscopy.

The primary reactions used to detect slow neutrons are:

- $^{10}B(n,\alpha)^{7}Li$, where the detector requires enriched boron that is >90% ^{10}B (boron is naturally found in ratios of 19.8% ^{10}B and 80.2% ^{11}B)
- $^{6}Li(n,\alpha)^{3}H$, which uses ^{6}Li enriched to over 90% (the natural abundance of lithium is 7.59% ^{6}Li and 92.41% ^{7}Li)
- $^{3}He(n,p)^{3}H$, where the detector relies on rare ^{3}He gas that has a natural abundance of 0.00137% and is very expensive to produce
- $^{157}Gd\ (n,\gamma)^{158}Gd$, used in liquid scintillator detectors

Because the nuclear reactions require the use of specific isotopes, the availability of enriched isotopes contributes to the cost of fabrication for these detectors. In the case of ^{3}He, this cost is significant, if sufficient quantities of the material can be acquired at all. Helium-3 is not only for neutron detection, but also for cryogenics and is in high demand in many fields of research. Manufactured through the decay of tritium produced in a nuclear reactor, ^{3}He was available in greater quantities during the Cold War, because tritium is a critical component in thermonuclear weapons.

Fast Neutron Detectors

Neutron-induced nuclear transformations such as the $^{6}Li(n,\alpha)$ and $^{3}He(n,p)$ reactions may be used to detect fast neutrons. Unlike the case for slow neutrons, where the incident neutron energy is negligible compared with the reaction energy, it is possible to measure the neutron energy. However, the efficiency of these detectors is limited because the reaction probability decreases rapidly with increasing neutron energy. More commonly, scattering reactions are used to detect and measure the energy of fast neutrons.

Kinematics limit the energy that may be transferred in the neutron-nucleus collision. Because the mass of the neutron and the mass of the proton are nearly the same, it is only possible to transfer all of the neutron energy in a single collision in the (n,p) reaction. As the mass of the recoil nucleus increases, the fraction of energy transferred decreases. For the case of a deuterium recoil nucleus (atomic mass A = 2), a maximum of 88.9% of the energy can be transferred. In the case of ^{3}He, this maximum value falls to 75%. It is evident that a radiation absorber made from light nuclei is preferred, as it is possible to transfer more energy to the detector nuclei in fewer collisions. To provide higher efficiency, a solid-state detector is preferable, and materials with relatively high concentrations of hydrogen are desired.

The *proton recoil scintillation detector* takes advantage of kinematics and the high availability of scintillators that contain hydrogen. The kinematic advantage of these detectors is that the energy distribution of the recoil protons does not depend on the collision angle, resulting in a rectangular-shaped distribution in an ideal case. The shape of the detector output pulse may be used to separate gamma rays from neutrons, and the energy of the incident neutrons may be determined by comparing the response of the detector with calibration spectra obtained using a monoenergetic neutron source.

The availability of organic scintillators in many forms, including plastic and liquid detectors, provides a broad range of available materials for detector

construction. The hydrogen in the aromatic compounds provides an efficient mechanism for energy transfer in the absorbing medium, but the response of the detector is complicated by the presence of other elements such as carbon and oxygen. If the source of neutrons is pulsed, such as at an accelerator facility, then the energy may be extracted using a *time-of-flight* method. This method relates the detection time to the pulse structure of the beam used to create the neutrons and extracts the neutron energy from the amount of time it takes for the neutron to travel to the detector.

Moderating Detectors

A third type of neutron detector uses a layer of hydrogen-containing material to slow down, or *moderate*, neutrons in order to use neutron-induced nuclear reactions as the detection method. Called *moderating detectors*, these systems are useful if there is a broad range of neutron energies to be detected or if the neutron energy distribution is unknown. This type of detector has a relatively slow response time due to the moderating process. This is unsuitable for situations where the neutron energy distribution changes with time or when it is desirable to relate the neutron with another event, such as the detection of a gamma ray.

Examples of moderating detectors include *Bonner sphere spectrometers* and *spherical neutron dosimeters*. Used to detect fast neutrons, the Bonner sphere spectrometer consists of a set of different-diameter solid polyethylene moderating spheres that slow incident neutrons and a thermal neutron detector such as a lithium iodide scintillator. The spheres are placed over the detector in turn, and the count rate is recorded for each sphere. The neutron energy spectrum is then interpreted from this data using calibration data.

A spherical neutron dosimeter is essentially the same construction as a Bonner sphere spectrometer, but only uses a single sphere. The sphere is modified to provide a response that coincidentally resembles the neutron dose equivalent delivered curve as a function of energy. This detector is often used for neutron monitoring to provide neutron dose estimates.

Future Directions

Advances in radiation detection may result from the development of new radiation absorber materials, the refinement of methods to signal radiation interactions, and innovations in signal measurement. Some recent advances are discussed in the following section. The impact of these new developments and future directions may have an effect on the ability to detect small quantities of nuclear materials for safety and security, provide better tools for medicine and medical imagining, characterize the rarest nuclei in the cosmos, provide key data for understanding astronomical interests such as supernovas and neutron stars, and investigate dark matter and the nature of neutrinos.

Advancements in Detector Materials (Radiation Absorbers)

It is the interaction of radiation with matter which provides a signal to be measured. Perhaps because of this, and because of the limitations of current radiation detectors, it may be presumed that the primary need in radiation detection is in the characterization of new materials that are sensitive to radiation. Indeed, the physical characteristics of some of these materials in use are not optimal. Some examples are found in gamma-ray detectors: HPGe crystals require cryogenics temperatures for operation and the hygroscopic nature of NaI(Tl) leads to performance degradation as water is absorbed in the crystal. In other cases, the optimal materials are simply difficult to acquire: the scarcity of ^{3}He for cryogenics and for neutron detectors since the reduction of tritium production is a case in point [8].

There are many open areas of research, including applications in nanotechnology and crystal growth. Suspension of nanoparticles in liquid scintillators may lead to improved scintillation detectors or detectors based on novel new materials. Development of crystal growth techniques for newer CdZnTe-based detectors [9] may reduce the defects found in these detectors and enable the growth of larger crystals. It is important to note, however, that the common materials already in use have been selected through years of research, and that a breakthrough in detector materials may take decades to come to fruition.

Near-term improvements may come from refining methods to make detectors, as in the case of the high-purity germanium crystal. Originally, germanium semiconductors required a lithium dopant in the

crystal matrix. This dopant would degrade as the lithium migrated out of the crystal, unless the detector was constantly kept at liquid nitrogen temperature. By refining the technique for growing germanium crystals, the lithium dopant is no longer used in these detectors.

Simply modifying compounds already in use can advance the field as well. A case in point is in the use of deuterated benzene scintillators for neutron detection. Benzene (C_6H_6) is commonly used in neutron scintillation detectors. In neutron spectroscopy, neutron energy is generally extracted using the time-of-flight method. This is because the detector response is essentially featureless, as shown in Fig. 6a, b taken with NE-213 scintillators. On the other hand, Fig. 6c, d are from deuterated benzene scintillators measured at the same energies. The peaks in these spectra appear due to the kinematics of scattering from deuterium. By combining these detectors with advanced pulse-shape analysis electronics, the energy information may be extracted in addition to the time-of-flight method, allowing for fast neutron spectroscopy in laboratory experiments.

Advancements in Detection Methods (Observables)

The types of detectors discussed here, gas-filled ionization detectors, scintillation detectors, semiconductor detectors, and neutron detectors, represent the majority of radiation detectors currently in use.

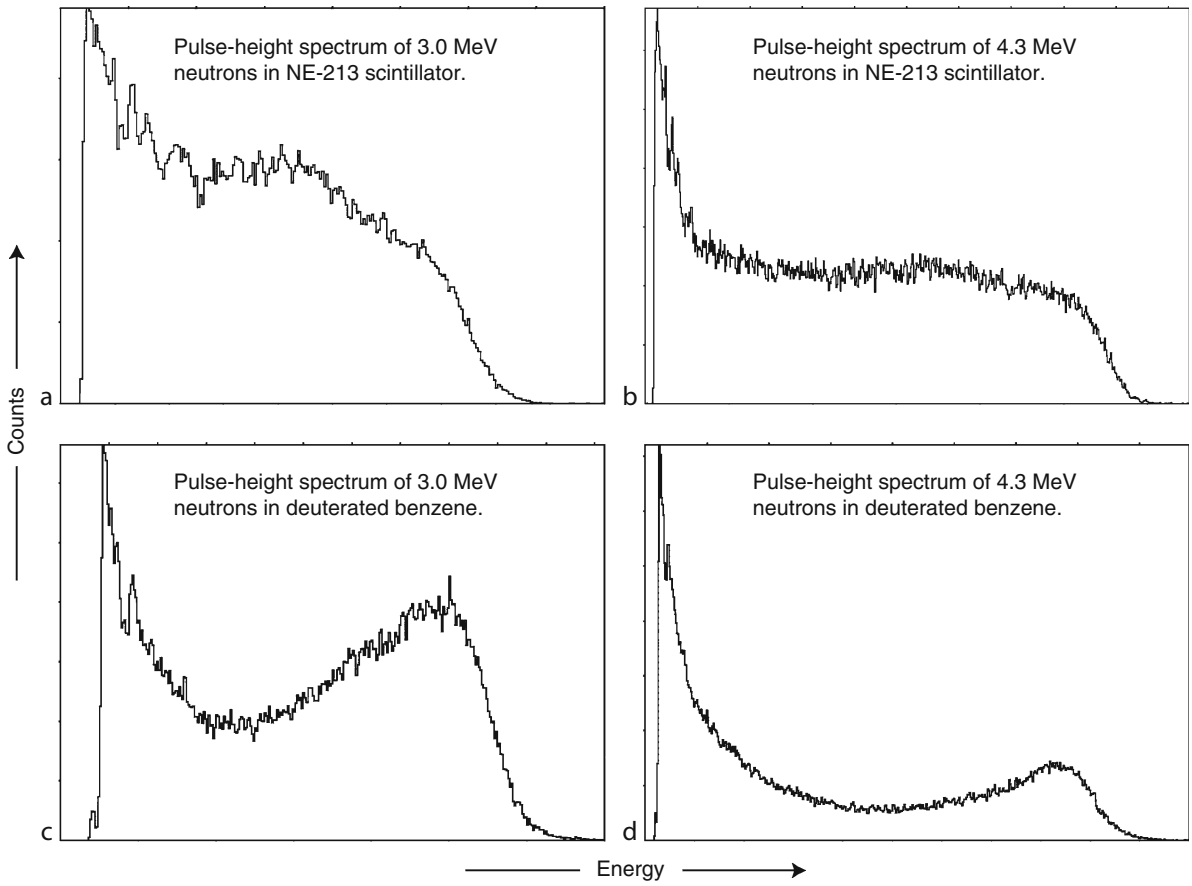

Ionizing Radiation Detectors. Figure 6
Pulse-height spectra of monoenergetic neutrons collected using NE-213 scintillators and deuterated benzene scintillators. Neutron energy may be extracted from the deuterated benzene detectors using pulse-shape discrimination electronics (Spectra courtesy of P. E. Garrett)

The primary observables have been the electronic signals or light output based on direct or indirect ionization to signal the interaction of radiation in the detector. These represent the basic interactions which can be measured in common detectors.

Another possible observable is to measure temperature changes in a material to indicate radiation detection. Such a detector is called a *bolometer*, and the radiation absorber in this kind of detector is a material that has electric resistance that is highly dependent upon the material temperature. These detectors are at the forefront of dark matter and neutrinoless double-beta decay experiments [10] and are typically small metal, semiconductor, or even superconductor devices. The size is limited in order to maximize the temperature rise and the measured change in resistance. A drawback to this kind of detector is the need to maintain a consistent temperature.

One simple advancement in this area is to combine multiple types of detectors to filter the signal that is recorded for later use. An example of this is found in the *Compton-suppressed* germanium detector [11]. A germanium semiconductor detector is surrounded by high-efficiency scintillation detectors that act as an anticoincidence shield. If a gamma ray is detected only in the HPGe detector, but not in the surrounding detectors, it is presumed to have deposited the full energy in the germanium crystal. However, when signals are detected in coincidence with the surrounding scintillators, this indicates that the gamma ray has

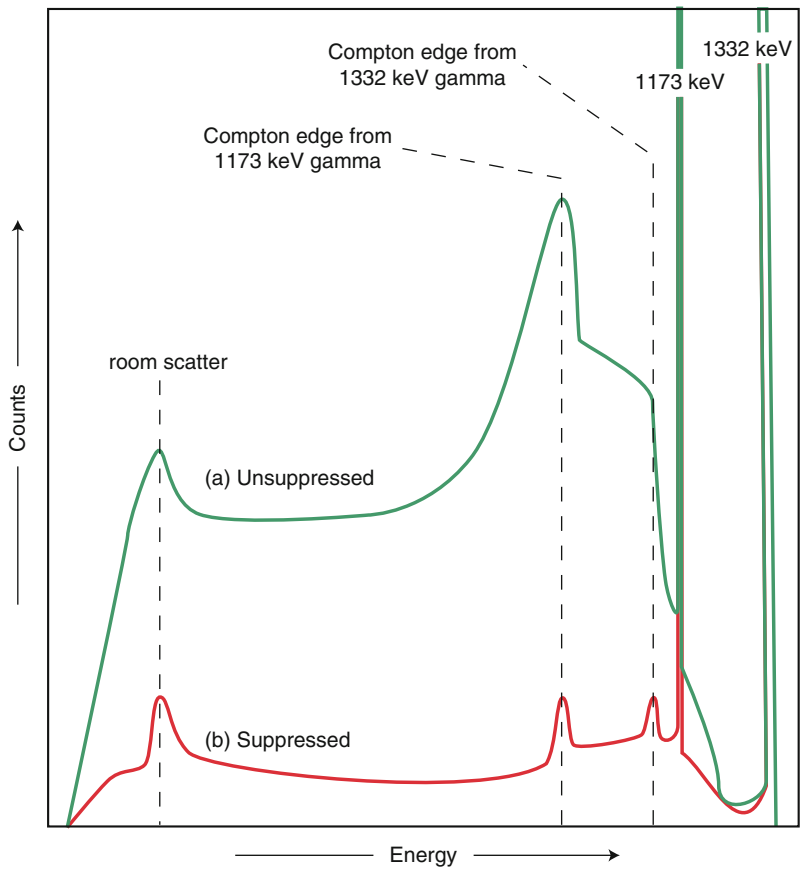

Ionizing Radiation Detectors. Figure 7
The spectrum of a ^{60}Co source with characteristic gamma-ray lines at 1,173 and 1,332 keV collected using (**a**) a high-purity Ge semiconductor (HPGe) detector, and (**b**) the same HPGe detector operated in anticoincidence with a Compton-suppression shield of scintillators

scattered out of the HPGe detector, and a full-energy pulse will not be detected. By suppressing these Compton scattering events using nanosecond coincidence timing circuits, the background spectrum of the detector can be greatly reduced, as shown in Fig. 7. This enables the detection of much lower intensity peaks than would normally be visible with an unsuppressed detector.

Advancements in Signal Measurement

The basic method for radiation spectroscopy is to measure signal outputs and record the data to build up statistics for interpretation. Typically, each signal is passed through electronic circuits comprised of amplifiers, discriminators, and analog-to-digital convertors in order to electronically record each event as it is detected. Computer analysis is later used to scan the recorded data, sort out events that fit requisite criteria, and fit the data for interpretation.

In some cases, such as in neutron detection, pulse-shape discrimination is used to distinguish between the types of radiation detected. This is typically done off-line during the computer analysis in order to separate the neutrons from gamma rays. An advancement to this technique is to use a computer in the data acquisition system in order to fit and digitize pulses during the data collection, and record only the signals of interest.

Very advanced gamma-ray spectrometers GRETA (Gamma-Ray Energy Tracking Array) [12] and AGATA (Advanced GAmma Tracking Array) [13] are being constructed in the United States and in Europe, respectively, to follow gamma-ray interactions as they scatter in germanium detectors. These *gamma-ray tracking spectrometers* use segmented germanium crystals connected by electronic contacts to determine where gamma rays interact in the detector. Off-line computer analysis is used to reconstruct the history of interaction. The full energy of the gamma ray is determined by summing up the energy of the individual interactions, and the first point of interaction in the detector may be determined for use in analysis based on angular distributions.

The GRETA and AGATA spectrometers are the most advanced research-class systems in gamma-ray spectroscopy and come with multimillion dollar (euro) price tags. Such systems are in development to support large groups of scientists at national laboratories, and as such are of specialized interest, rather than directly applicable to the general field of radiation detection. However, the future in this area will be closely tied to computational power and to the development of specialized electronics and programs for signal processing and data analysis. Adoption of better in-line and off-line computational power may overcome some of the inherent barriers in radiation detection and open opportunities for the development of new materials and new observables for detectors.

Bibliography

1. Nobel Lectures, Physics 1901–1921. Elsevier, Amsterdam, 1967
2. Glasstone S (1958) Sourcebook on atomic energy. D. Van Nostrand, Princeton
3. Kantele J (1995) Handbook of nuclear spectroscopy. Academic, San Diego
4. Knoll GF (2010) Radiation detection and measurement. Wiley, New York
5. Krane KS (1988) Introductory nuclear physics. Wiley, New York
6. Leo WR (1994) Techniques for nuclear and particle physics experiments. Springer, New York
7. Tsoulfanidis N (1995) Measurement and detection of radiation. Taylor & Francis, Washington, DC
8. Kouzes RT et al (2010) Nucl Instr Meth A 623:1035
9. Erickson JC, Yao HW, James RB, Hermon H, Greaves M (2000) J Electron Mater 29:699
10. Arnaboldi C et al (2008) Phys Rev C 78:035502
11. Nolan PJ, Gifford DW, Twin PJ (1985) Nucl Instr Meth A 236:95
12. Deleplanque MA et al (1999) Nucl Instr Meth Phys Res A 430:292
13. Eberth J, Simpson J (2008) Prog Part Nucl Phys 60:283

Ionizing Radiation on Nonhuman Biota, Effects of Low Levels of

Glen A. Bird
EcoMetrix Incorporated, Mississauga, ON, Canada

Article Outline

Glossary
Definition of the Subject
Introduction
Characteristics of Radiation
Protection of the Environment

Effects of Radiation on Animals
Effects of Radiation on Plants
Radiation Effects Synthesis
Future Directions
Bibliography

Glossary

Acute dose A single dose generally greater than 500 mGy of ionizing radiation to most or all of the body in a short time, usually a matter of minutes.

Adaptive response Adaptation to the presence of a low concentration of a contaminant, rendering subsequent treatment with high doses of the same agent less effective.

Alpha radiation The emission of alpha particle (the nucleus of a helium atom consisting of two protons and two neutron) from the nucleus of an unstable atom (radionuclide). Since alpha particles transfer their energy in a very short distance and cannot penetrate the outer layer of skin, alpha radiation is only an internal radiation hazard if it is inhaled or absorbed following ingestion. Most members of the U and Th decay chains are alpha emitters, e.g., ^{210}Po, ^{226}Ra, ^{232}Th, ^{238}U, ^{239}Pu.

Becquerel (Bq) The SI unit of radioactivity for measuring the rate of decay of a radioactive substance. It is equivalent to the disintegration of one radioactive nucleus per second.

Beta radiation The emission of electrons or positrons from the nucleus of an unstable atom (radionuclide). Beta particles can penetrate biological tissue to a depth of 1–2 cm. They may pose both an internal and an external hazard, e.g., ^{3}H, ^{14}C, ^{90}Sr.

Cancer An abnormal growth of cells which tend to proliferate in an uncontrolled way and in some cases to metastasize or spread. Cancer can involve any tissue of the body and have many different forms in each body area.

Chronic dose A dose of ionizing radiation received either continuously or intermittently over a prolonged period of time comprising a major portion of an organisms life cycle.

Deoxyribonucleic acid (DNA) Nucleic acid that contains the genetic instructions used in the development and functioning of all known living organisms with the exception of some viruses.

Deterministic effect Both the incidence and severity increase as a function of dose after a threshold dose is reached and usually involves cell killing.

Gamma radiation The emission of photons (gamma rays), which carry energy but no charge, by nuclear transition or interaction (radionuclide). Gamma radiation is the most penetrating radiation.

Gray (Gy) The SI unit of absorbed dose for ionizing radiation, equal to 1 J of radiation energy absorbed in 1 kg of the material of interest.

LD_{50} The dose of a substance that causes mortality in 50% of the organisms exposed.

Linear energy transfer (LET) The rate of energy loss per unit path length.

Radiation dose The energy absorbed per unit mass of any material exposed to ionizing radiation, measured in grays (Gy).

Relative biological effectiveness (RBE) The ratio of the absorbed doses of reference to the test radiation types that produce the same biological effect.

Stochastic effect The severity of the effect is independent of the absorbed dose, there is no threshold, and the probability of the effect occurring is proportional to the dose absorbed.

Track The path of a particle of ionizing radiation.

Definition of the Subject

Radiation is present in the environment from both natural and anthropogenic sources. Civilian use of nuclear materials results in chronic releases of low levels of radiation to the environment, particularly from the nuclear fuel cycle, i.e., the mining and milling of uranium ore to the operation of nuclear power plants, the reprocessing of spent nuclear fuel and nuclear waste disposal. Genetic effects such as chromosomal aberrations are observed in biota living in areas of elevated natural background levels of radiation. High exposure levels affect rates of morbidity, reproduction, and mortality. In introducing the topic of radiation effects on biota, a brief discussion of biological response is presented covering stochastic and deterministic effects, tissue sensitivity, dose fractionation, relative biological effectiveness, adaptive response, and radiation as just another environmental contaminant.

The focus of the chapter is on the effects of radiation on biota at low dose levels similar to those

associated with chronic releases from normal operations of nuclear facilities. However, a scarcity of information is available on the effects of exposure to low doses possibly because the effects are small, are difficult to quantify, and are only temporary, i.e., are reversible. Acute doses of radiation, like those of most other contaminants, produce more severe effects. Acute exposures of radiation are never observed under natural conditions and are seldom observed in the environment except for severe accident situations, i.e., Kyshtym and Chernobyl accidents or in tailing ponds. Information from laboratory studies, field irradiator studies, industrial contaminated sites, and accidents is reviewed to ascertain the effects of radiation on the environment. Information provided on the effects of low levels of radiation on biota may be useful to practitioners in establishing ecotoxicological benchmarks to meet their regulatory requirements to protect the environment.

Introduction

A growing global human population has fuelled increased energy demand, which together with concern over climate change and dependence on foreign supplies of fossil fuels have created renewed interest in nuclear power [1]. Most of this interest is in countries that already use nuclear power. There were 438 reactors in operation globally at the end of 2008 with a total nuclear capacity of 372 GW(e) [2]. The IAEA [2] projected that nuclear capacity would increase to between 473 and 748 GW(e) by 2030. The World Nuclear Association [1] projection is for at least 1,100 GW(e) of nuclear capacity by 2060, and possibly up to 3,500 GW(e). In association with this expansion, there will also be increased activity in the remainder of the nuclear fuel cycle: mining and milling of uranium (and thorium) ore, refining, conversion, enrichment, fabrication of fuels, and reprocessing and disposal of spent fuel. All components of the nuclear fuel cycle release some contaminants to the environment. Radionuclide releases from the fuel cycle are greatest from the mining and milling of ore and from reprocessing of spent fuel. In recent years, strict environmental regulations, advances in pollution prevention technology, and more modern designs have greatly curtailed releases to the environment compared with earlier operations. Future releases will result in large areas being influenced by low levels of radiation. The present chapter focuses on the potential effects that low levels of radiation may have on the environment.

Characteristics of Radiation

Radiation is energy that is transmitted in the form of rays, waves, or particles as either ionizing or nonionizing radiation. Ionizing radiation has energy of at least 12.4 eV, and the ability to remove an orbital electron from an atom, thereby forming an ion–electron pair from a neutral atom. Nonionizing radiation is also electromagnetic radiation but does not have enough energy to ionize atoms or molecules. Nonionizing radiation interacts with biological tissue primarily by generating heat. Examples of nonionizing radiation include radio waves, microwaves, and visible light. This chapter focuses on ionizing radiation.

Radiation is measured using a gamma-, beta-, or alpha spectroscopy, and other mass spectroscopy techniques. Advances in the level of detection of radiation have improved with the development of low-level and ultralow-level gamma ray spectrometry, and the ability to directly count atoms using mass spectrometry (i.e., accelerator mass spectrometry (AMS), inductive coupled plasma mass spectrometry (ICPMS), thermal ionization mass spectrometry (TIMS), and resonance ionization mass spectrometry (RIMS) (see "► Radionuclides as Tracers of Ocean Currents"). Improvements in detection limits have increased our ability to measure the movement of radionuclides in the environment but do not affect dose calculations in any significant manner or the interpretation of older literature with respect to radiation dose measurements and effects, i.e., the older literature is still valid today.

Major types of ionizing radiation are: X-rays, gamma (e.g., ^{60}Co, ^{134}Cs, ^{65}Zn), beta (e.g., ^{3}H, ^{12}C, ^{90}Sr) and alpha (e.g., ^{210}Po, ^{226}Ra, ^{232}Th, ^{238}U, ^{239}Pu), and neutrons. X-rays and gamma rays are ionizing electromagnetic radiations produced from atomic and nuclear transitions respectively. When absorbed in matter, energy is deposited unevenly in discrete packets with enough energy to break chemical bonds, hence, the termed ionizing.

Gamma radiation is the emission of photons from the nucleus. Gamma radiation is much more

penetrating than alpha and beta radiation, and has no precise range. Gamma radiation is both an external and internal hazard. The intensity of gamma radiation attenuates exponentially with distance in dense media. Beta and alpha are particulate ionizing radiation. Beta particles are highly energetic electrons that originate in the nucleus and may carry either a −1 or +1 charge. Alpha particles are highly energetic helium nuclei lacking orbital electrons with 2^+ charges when ejected from the nucleus during decay. Alpha and beta particles are less penetrating, so their energy is more likely to be transferred within the organism and cause more damage locally. Beta particles may be both an external and an internal hazard, whereas alpha particles are only an internal hazard.

Alpha radiation has high linear energy transfer (LET) and is more biologically damaging for the same absorbed dose than gamma and beta radiation with low LET [3]. Radiation damage can be divided into two general types: direct effects due to molecular damage occurring, where the energy has been absorbed in the molecule (target has been hit); and indirect effects where the molecular damage is brought about by the chemical reactions of free radicals produced by the radiation (e.g., in cell water) [4]. The free radicals can then diffuse and damage the critical target, an indirect action verses a direct effect. Direct and indirect ionization result in essentially the same effect, an ionized atom. DNA is the most important target, although a large diversity of molecules may be affected.

In the following, radiation doses presented in rads in referenced material have been converted to grays (Gy), whereas doses given in roentgens (R or r) have been converted to rads then grays using the following conversion factors, 1 R = 0.9 rad [5] = 10 mGy. Most dose rates are presented in milliGray per day to allow easier comparison of chronic exposures. Where possible, the period of exposure is given along with the radiation exposure rate. Where exposure rates to biota are given for field studies or nuclear accidents, it is assumed that the exposure period is over most of the organism's life cycle or for perhaps several generations. Likewise, implicit for international guidance on radiation dose rates protective of nonhuman biota is that exposure is over a large portion of the organism's life cycle.

Biological Response to Radiation

Radiation effects may be either stochastic or deterministic. A stochastic effect is "a radiation-induced health effect, the probability of occurrence of which is greater for a higher radiation dose and the severity of which (if it occurs) is independent of dose." A deterministic effect is "a radiation effect for which generally a threshold level of dose exists above which the severity of the effect is greater for a higher dose" [6]. Cancer is a stochastic effect. Cell death, reddening of the skin, opacity of the eye lens, and permanent sterility are examples of deterministic effects.

For short-lived animal species, cancer is unlikely to be important at the population level. At the population level, cancer may be more important in more long-lived species such as marine mammals, and terrestrial animals with long reproductive life spans, slow recruitment, and low numbers of individuals, although this needs to be demonstrated.

Much of the information on the effects of radiation on humans comes from laboratory studies primarily with small mammals such as mice and rats. The findings of these studies are equally applicable to other animals.

For all endpoints from cell death to tumor induction, cancer induction and life shortening, reduction in dose rate in general results in reduced biological effects. The risk per unit dose of low-LET radiation has been observed in experimental systems to depend upon both the magnitude of the dose and its temporal distribution. Dose–response curves for low-LET radiation for late effects and genetic effects generally increase in slope with increasing dose and dose rate. The response for tumorigenesis may pass through a maximum and turn downward after a single high-dose-rate exposure at doses above 2.4–4 Gy; the dose often attributed to cell killing. Although dose–response relationships differ from one biological effect to another, qualitatively, the relationships are similar. Linear interpolation of effects from high doses and dose rates to effects of either low doses or dose rates overestimate effects by a factor of 2–10. Hence, the assumption of a linear, no-threshold dose–response relationship is a conservative approach to estimate risk for low dose and dose rate exposure. This is the dose rate effectiveness factor [7].

Radiation doses are defined as:

- Low – between 0 and 200 mGy;
- Intermediate – between 200 and 1,500 mGy;
- High – between 1.5 and 3.5 Gy; and
- Ultrahigh – greater than 3.5 Gy [8].

The biological effect of a given dose of low-LET radiation is dependent on the duration of exposure, time frame for biological repair, and biological target, which may change with age [8]. Lesions at low doses are formed almost entirely by single-hit kinetics, i.e., radiation events singly capable of inducing the complete lesion. The resultant effect is expected to be proportional to dose over the low-dose range. However, it is extremely difficult to detect radiation-induced effects in animals in the low-dose range at any dose rate, and thus the shape of the dose–response curve is better defined for high doses and dose rates [8].

Linear-Quadratic Model The linear-quadratic model adequately describes the dose response for solid cancers and describes chromosome aberrations, incidence of myeloid leukemia, and breast and lung cancer in mice [9] and plants such as the spiderwort (*Tradescantia*) [8]. Radiation effects on the spider plant can be used to illustrate the model. The spiderwort has flower buds that contain stamen hairs consisting of 25 blue colored cells. Mutation events cause the cells to turn pink. Pink mutations can be quantified down to less than 3 mGy of X-ray radiation and lower doses for high-LET radiation. The region below a radiation dose of 100 or 150 mGy shows an almost linear response, whereas the region of the curve beyond about 1 Gy shows a flattening and then declines, consistent with the effect of cell killing. The mortality of mice exposed to gamma radiation (Fig. 1) shows a similar respond [7]. The intermediate portion of the curve between 100 and 1,000 mGy is essentially linear on a log plot with a slope of 2, a value which indicates a quadratic relationship [8]. The dose–response relationship can be defined by the equation

$$I_\gamma = aD + bD^2$$

where I_γ is the induced incidence, D is absorbed dose in mGy, and the a and b terms are coefficients for the specific radiobiological conditions.

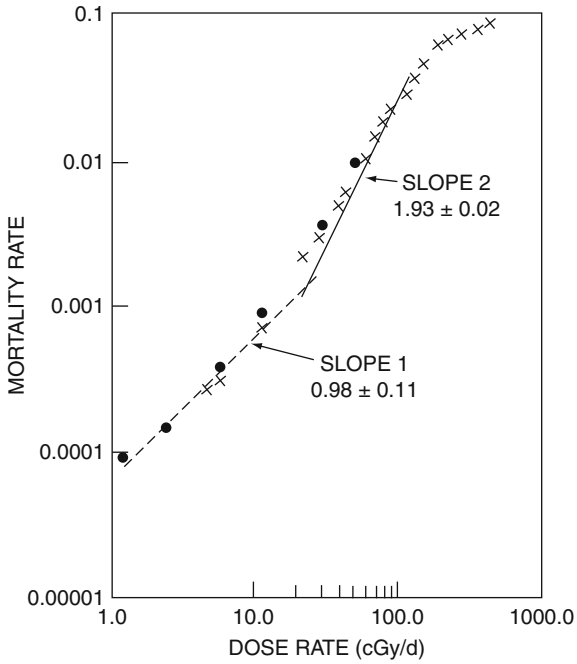

Ionizing Radiation on Nonhuman Biota, Effects of Low Levels of. Figure 1
Log-log plot of mortality rate of mice exposed to ^{60}Co at various dose rates for about 10 h per day (From Fry [7])

Radiation acts as if it is made of two separate components, an aD component and a bD^2 component. The aD component is considered the single hit response, which is all or none. The bD^2 component is a two-hit response, i.e., two hits are necessary at a sensitive site to produce the effect. The second hit can only produce the effect if it occurs soon enough after the first. The probability of an effective second hit increases with dose and dose rate, and is negligible at low doses and dose rates, leaving only the aD component to describe the effect. Most of the effect below about 1 Gy is considered to be the sum of the linear (aD) and squared (bD^2) components. The liner component contributes the same degree of effect per unit of absorbed dose at all doses, while the quadratic term dominates at higher doses. Therefore, the linear term coefficient for low-LET radiation is important only at low absorbed doses.

Radiation induced chromosome damage is detectable in cultured human lymphocytes for an

adsorbed dose of 100–250 mGy. The relation between chromosomal aberrations and dose is

$$I = C + aD + bD^2$$

where C is the spontaneous aberration frequency. Of the two-event lesions induced in irradiated cells, the dicentric chromosome is considered a reliable indicator of radiation exposure in lymphocytes. Most studies of dicentric chromosomes use a dose of 0.5–4 Gy since few dicentrics occur at lower doses. Most dicentric lesions (94%) are attributed to the linear component at 50 mGy and follow the two component theory at doses above 300 mGy [8].

Tissue Sensitivity to Radiation Rapidly dividing cells are generally the most sensitive to acute radiation, suggesting that chromosomal structure is most vulnerable during division. Thus, cell absorption of ionizing radiation leads to abnormal mitosis, growth, and metabolism. Undifferentiated cells are also usually more sensitive to radiation than differentiated cells. In male fish, sensitive germ cells are type B spermatogonia and spermatocytes [10]. In female fish, the most sensitive germ cells are the oogonia in the process of mitosis and oocytes at the start of the prophase changes of meiosis. Oocytes and lymphocytes are very sensitive despite being differentiated (resting) cells. In the small intestinal crypts, stem cells are more sensitive to ionizing radiation than their differentiated progeny and are more sensitive than the stem cells of the large intestinal crypts. Although rapidly dividing cells are sensitive to radiation and the small intestine is characterized by high cell proliferation, the small intestine is more resistant to cancer formation than the large intestine [11].

Effects of prenatal irradiation on growth and development depend on the gestational age when irradiated, the total dose, the dose rate, the linear energy transfer (LET) of the radiation, and on the particular endpoint or type of response expected. The period of organogenesis is a susceptible period for the induction of growth retardation, microcephaly, and mental retardation. The sensitivity of the stage of development and total dose delivered during a sensitive period are critical factors in determining the radiation effect.

The primitive germ cell (gonocyte) is the most radiosensitive cell type, and the level of response depends upon the prenatal time period during which the gonocyte persists. The rate of gonocyte killing in mammals with long gestation periods (>50 days) and, therefore, with long gonocyte life spans, appears to depend only upon the total dose and not upon dose rate down to rates of 10 $\mu Gy \cdot min^{-1}$ or less. Biological injury to the fetus occurs following exposure to either low single doses (~10 mGy) at a sensitive stage or low-dose-rate exposures (~14.4 mGy day^{-1}) over most of the prenatal period. Effects include germ cell depletion, growth retardation, central nervous system damage, or depressed central nervous system growth and cytogenetic abnormalities [8]. Immature mouse oocytes are very sensitive to radiation with a LD_{50} of 81 mGy. At 450 mGy, 99% of the cells are killed. Nevertheless, sufficient oocytes survive that mice are able to produce litters and maintain their population in both the laboratory and the environment. This may be because germ cells in the adult mouse remain in an arrested, nondividing oocyte stage, which in the late follicles is not easily killed by radiation [8].

Mutations are proportional to the amount of radiation absorbed and depend upon the amount of DNA in the cell, the functional state of the cell, and the effectiveness of the repair mechanisms. Generally, a higher dose rate will cause a greater impact than a lower dose rate, given the same total dose. This is assumed to be because repair mechanisms are better able to keep pace with damage caused by a lower dose rate. Note that cells that are irradiated during dormancy can store the damage without being able to repair it. When conditions permit cell division, accumulated damage may be manifested to a greater degree than in cells that are continuously active. Most examples of this occur in plants or in animals that greatly reduce their metabolic rates during cold or dry weather conditions. For example, fish, amphibians, reptiles, and certain mammals avoid cold weather by going into diapauses or hibernation. Likewise, certain insect species go into diapause to avoid periods of drought or warm weather.

The biological effect on cells is dependent on the number of cells struck by ionizing radiation, and the radiation energy and type – alpha, beta, or gamma. The lowest possible dose to a cell is the dose deposited by a single photon. For ^{60}Co gamma radiation, 1 mGy corresponds to an average of one track (path of a particle of ionizing radiation) per cell. This is

the lowest possible dose to a cell [12]. Below 1 mGy, not all cells receive a track of damage, but those that do still receive 1 mGy. Exposures at low doses are not uniform and, at 1 mGy, some cells receive two tracks, whereas about a third of the cells receive no track. However, at 1 mGy, all cells respond as if they received a track because of communication or the bystander effect [13]. There are about 100 tracks per nucleus at a dose of 100 mGy of low LET [14]. At moderate to high doses (>100 mGy) of sparsely ionizing radiation, all cells and tissues receive a nearly uniform exposure.

Dose Fractionation Dose fractionation is the repeated exposure to fractions of the total dose, rather than the same total dose being delivered at an essentially constant average dose rate. The effect of dose fractionation is highly dependent on the size of the fractions, the dose rate within each fraction, and age-dependent changes that may occur over the exposure period, which affect the radiosensitivity of the target. The magnitude of dose, dose rate, and protraction of dose interact to influence the dose effect [8]. Protraction allows for more repair and more effective repair because of the time between depositions of energy [7].

When the fractions of dose are administered at a time longer than the time required to rejoin the breaks (4 h), the yields of translocations are generally equal to the sum of those resulting from the individual fractionations. For example, 2.7 Gy delivered as 30 equal exposures reduces the yield of translocations to about 25% of that after an acute dose, whereas five exposures of 540 mGy reduced the yield to about 40%. Repair of chromosomal damage in oocytes takes between 1½ to 3 h. In general, closely spaced, large fractions are about as effective as a single dose. As the interval between fractions is prolonged and/or the dose per fraction is reduced, the effect on life shortening lessens [8]. Once-weekly exposure was less than half as effective in shortening the life of mice as the single exposure, and continuous exposure was only 20% as effective as the single exposure [15]. UNSCEAR [16] estimated that a radiation dose of 7 Gy to the mouse over its lifetime is equivalent to 5% life shortening due to cancer induction.

For immobile organisms such as barnacles and tube-dwelling benthic invertebrates and organisms with small home ranges, such as mice and muskrats, it is continuous (chronic) exposure over the life cycle of the organism that is of interest. For more mobile organisms with a large home range such as deer, moose, and wolves, exposure may be intermittent or fractured.

Adaptive Response The response by organisms to preexposure to a stressor is termed an adaptive response and is attributed to the stimulation of repair mechanisms by low dose exposure [17]. An adaptive response is a general response to stress induced by many different contaminants. For example, exposure of lymphocytes and other cells to low doses of ionizing radiation and subsequently to a high dose lessens the genetic damage. Fewer chromosomal aberrations are found in cells that had been preexposed before exposure. Various stress conditions induce an adaptive response to subsequent radiation-induced chromosome damage, including exposure to low-dose radiation, low concentrations of chemical mutagens, anticancer drugs (bleomycin, mitomycin C, and actinomycin D), free radical–generating chemicals such as hydrogen peroxide (H_2O_2), mild hypothermia, heavy metals (zinc), and low levels of double-strand DNA breaks [17, 18]. For example, pretreatment of rabbit peripheral lymphocytes with Zn results in resistance to gamma radiation (2 Gy) induced chromosome aberrations such as dicentrics, centric rings, and cells with chromosome aberrations. An increase in apoptosis is a cytogenetic adaptive response because cell death occurs at a lower dose than more serious effects [18]. For example, exposures of mouse spermatogonial cells to about 4.5–5.4 Gy results in cell killing, selectively eliminating germ cells with chromosomal damage.

Stimulated effects at low doses are often considered a positive effect but should be considered a negative effect as they can entail disorder of homeostasis, change of dominating species, and reduction of biological diversity [19]. Stimulation is an early response to stress and is a warning of potential harm should stress levels increase.

Relative Biological Effectiveness The extent and type of damage from radiation exposure depends on the type of radiation and the amount and rate of energy absorbed at the site of impact. Gamma rays and X-rays penetrate through biological tissue, deposit less energy (i.e., low-LET) and, at low dose rates, tend to produce

single-strand breaks in chromosomes. At low dose rates, alpha radiation is of much greater concern than gamma or beta. Alpha particles penetrate only about 70 μm into tissues (i.e., does not penetrate the outer layer of dead skin and hence is an internal hazard), deposit much more energy at the site of impact (i.e., high LET), and are more likely to cause double-strand breaks and more rapid cell death. The repair of single-strand breaks is typically efficient and rapid, whereas double-strand breaks are more difficult to repair and may be fatal to the cell but not the organism. The vast majority of genetic effects are removed by selection at the tissue, organism, or population level. At the population level, genetic damage to individuals may be offset by immigration of unaffected individuals from surrounding areas that contribute to the local gene pool as observed following the Chernobyl accident [20].

The higher energy deposition associated with high-LET radiation has been shown to produce unique types of damage that are not observed with low-LET radiations [21–24]. The greater clustering of ionization damage in high-LET tracks is apparently more favorable to induce mutation than cell death. The increased damage to cells from high-LET radiation is caused by the cluster of ionizations in the region of an alpha track. The biological effect of low-LET radiations are predominantly due to track-end clustered ionizations rather than from the large number of sparse ionizations, i.e., sparse ionizations are biologically unimportant, and clusters of different sizes are likely the cause of biological damage of different repairability.

The clustering of ionizations on the scale of nanometers is a prime determinant of radiation effectiveness. High-LET lethal damage is predominantly from clusters of about 10 or more ionizations in a 3.4 nm target thickness, the diameter of a DNA molecule, whereas low-LET is predominantly from clusters of $\geq$3 ionizations in a similar target thickness. For mutagenic damage, the increase in RBE with high-LET is due to clusters of about 15–20 ionizations or more in 3–5 nm. High-LET radiation is also qualitatively different than low-LET due to the greater complexity of damage in larger volumes, comparable to nucleosomes, which include numerous breaks, base damages, and cross-links that are much less repairable [23]. Despite the greater damage caused by alpha radiation, cells have a high probability of surviving the passage of a high-LET particle through the nucleus of the cell. Studies also indicate that cells of irradiated tissue that have not been hit by an alpha particle contribute significantly to the response because of the "bystander effect," which is mediated through gap junction cell–cell communication [25].

As discussed, radiations differ in their relative biological effectiveness (RBE) per unit of absorbed dose. The RBE is the ratio of the absorbed doses of two different radiation types (e.g., alpha radiation to a reference radiation usually either X-rays or gamma) that produce the same biological effect. At low dose rates (e.g., <100 mGy), high-LET radiations such as alpha particles and neutrons have a higher effectiveness for producing biological effects than low LET at the same absorbed dose. Use of a weighting factor (w_R) to account for RBE allows the summation of the absorbed dose for each type of ionizing radiation to give the total dose for biological effects such as cancer induction and genetic defects at low doses [3].

In human radiological protection, it is the absorbed dose averaged over a tissue or organ and weighted for the radiation quality that is of interest for setting dose limits [26]. The w_R is used for this purpose. The w_R is selected for the type and energy of the radiation incident on the body or within the body. The values of w_R are based on review of the biological information for a variety of exposure circumstances that include inducing stochastic effects (e.g., cancer) at low doses as well as the quality factor (Q), which is related to LET, a measure of the density of ionization along the track of an ionizing particle [26, 27]. W_Rs of 20 for alpha emitters and 1 for beta particles and gamma are recommended by the ICRP [26] for radiation protection of workers and the public. These w_Rs are set against X-rays as the reference radiation. More recently, a RBE of 2 has been recommended for beta radiation for tritium ([28] and see "► Tritium, Health Effects and Dosimetry"). The RBE values for high-LET radiation are greatest at low dose rates and for stochastic effects such as carcinogenesis and lowest for high dose rates and deterministic effects such as impairment of fertility. At high radiation doses, all cells are exposed to radiation and, at very high doses, there is in essence no difference between the effect of alpha and gamma radiation (damage is extreme) and RBE is about one.

The increase in the RBE at low dose rates is not due to the effect of the alpha radiation increasing. The effect of alpha remains the same, it is the effect of the gamma radiation that becomes smaller and harder to measure in comparison to the effect of alpha which causes the RBE to increase at low doses. RBE does not increase to infinity. Double-strand breaks induced by alpha particles are repaired more slowly and a higher fraction remains unrepaired, whereas repair is more effective at low gamma doses, so their effect is harder to quantify. This accounts for higher RBE values at low doses [29, 30].

There is currently no consensus on the value of a radiation w_R that should be used in calculating doses to nonhuman biota from exposures to alpha particles. Weighting factors of 1–40 have been used to estimate the radiation dose from alpha radiation to nonhuman biota. Some investigators have not modified the calculated absorbed dose (in Gy) due to alpha particles (e.g., Amiro [31]), whereas others have used a value of 20 [32, 33]. UNSCEAR [34] suggested a lower w_R of 5 for alpha radiation and a w_R of unity for beta and gamma radiation. Kocher and Trabalka [35] expressed the view that an appropriate w_R for alpha particles for use in protection of biota probably lies in the range of about 5–10 as the endpoints of concern in protection of biota are deterministic effects (e.g., cell killing). A value of 20 is used for stochastic effects for humans and 5–10 for deterministic effects [36] such as impairment of fertility [3]. Pentreath and Woodhead [37, 38] recommended a value of about 40 for provisional application until sufficient data become available, whereas EC and HC [39] used a value of 40 to represent the low dose rates and endpoints relevant to their assessment of releases from Canadian nuclear facilities.

The subject of RBE is reviewed by NCRP [40], EC, and HC [39] and, subsequently, by Chambers et al. [41]. Chambers et al. [41], in establishing an RBE of 5 for alpha, rejected studies giving high RBE values as being of poor quality, whereas EC and HC [39] considered these studies of acceptable quality and their RBE included these studies in deriving a RBE value of 40.

Studies conducted using plant systems have also shown that low doses of radiation yield large RBE values, while high doses yield lower values. For example, exposure of plant systems to high doses and high dose rates resulted in an average RBE value of 12±3 (average of 16 studies), while exposure to a low dose administered at any dose rate resulted in an average RBE value of 65±5 (average of 23 studies) [40]. NCRP [40] also concluded that for many plant systems with either greater DNA content per cell or larger nuclear volumes than mammalian cells, the RBE values tend to be larger than those observed in mammalian test systems by a factor of 2 or more.

The choice of a radiation w_R to account for the difference in the RBE per unit of absorbed dose is currently not defined but is dependent on the endpoint and the radiation dose rate of interest. A lower value for w_R seems appropriate when protection is at the population level for deterministic effects at higher doses. Where protection is at the individual level from low chronic doses typical of modern nuclear facilities, a larger value for w_R seems more appropriate, e.g., EC and HC [39].

Radiation: Just Another Environmental Contaminant

Radiation differs from most other contaminants in that it can be quantified precisely at very low concentrations at the atom level and that external exposure may lead to health effects. Otherwise, exposure to low levels of radiation is much like that for many other contaminants. For certain radionuclides, it is possible to measure their presence down to a small fraction of a Becquerel (Bq), where a Becquerel is one disintegration per second. For example, 1 $Bq \cdot L^{-1}$ of tritium is one tritium molecule in 100,000 million molecules (“► Tritium, Health Effects and Dosimetry”). In the case of tritium, the drinking water quality guideline in Canada is 7,000 $Bq \cdot L^{-1}$, which sounds like a huge number, but this represents only a tenth of the public dose limit of 1 $mSv \cdot year^{-1}$ [42], which in itself has a large safety factor associated with it and is much less than the 2.4 billion Becquerels of ^{99m}Tc routinely injected into human patients for nuclear medicine diagnostic purposes.

As with other contaminants, radiation effects increase with dose and there is a minimum dose-rate below which further reductions in the dose rate do not result in further diminution of response per unit of

dose [13]. High-radiation doses and high concentrations of other contaminants are harmful to the environment; however, their effects are much less than natural ecological events that regulate animal abundance [43].

Expression of radiation-induced biological effects and responses may be at either the cell, organ, or organism level. Induction of cancer and genetic effects can have their origin in the interaction of a single charged particle within the cell nucleus. Changes in the cell can initiate organ effects and responses and, because the cell nucleus contains essentially all of the genetic material, it is the target where this change occurs [12].

Deoxyribonucleic acid (DNA) strands in our cells are continuously being exposed to and broken by ionizing radiation such as ultraviolet light, X-rays, and gamma rays, and by other natural and man-made mutagenic chemicals. The latter include heavy metals, polycyclic aromatic hydrocarbons, polychlorinated biphenyls, pesticides, oxyradicals generated by ionizing radiation or processes such as redox cycling by heavy metal ions, radio-mimetic drugs which create oxyradicals, asbestos fibers, certain plant toxins, hydrolysis, thermal disruption, and viruses [44–47]. Therefore, many contaminants produce single- and double-strand breaks (DSBs) and chromatid aberrations. DSB can also be caused by mechanical stress on chromosomes, or when a replicative DNA polymerase encounters a DNA single-strand break or other type of DNA lesion [44]. DSBs occur when DNA polymerase runs into an unrepaired nick in the DNA. Topoisomerase inhibitors also cause breaks: topoisomerase breaks and rejoins DNA in the course of its function, and inhibitors can block the rejoining step. Cells may break their DNA on purpose for special functions, most notably during the gene shuffling that occurs as lymphocytes mature, which generates diversity in antibodies, T-cell receptors, and other highly variable immune system proteins [45].

Cancer is not caused by just one unique cause, e.g., radiation, therefore one must be very cautious in attributing any excess cancers to a sole cause, be it radiation or any other singe contaminant [11]. The ability of ionizing radiation to induce a unique fingerprint in DNA, which leads to a molecular marker mutation in a tumor suppressor gene of tumors in experimental animals, has not been demonstrated. The non-specificity of final effects of ionizing irradiation and chemical toxicants on the environment makes it difficult to recognize their independent contribution to harmful effects to organisms [48]. It has been suggested that the analysis of the distribution of chromosome aberrations in cells and of the frequency of the different types of aberrations may be a means of differentiating between the effects of radiation and that of other chemicals [49], although this needs to be confirmed.

Repair of DNA

Two major methods to repair double-stranded DNA breaks are (1) homologous recombination – the break is repaired using the duplicate set as a template which is very precise since the cell can use the undamaged DNA strand to ensure that the repair is correct; and (2) nonhomologous end joining – repairs the break directly without any outside information. The latter is less accurate and may result in the addition or removal of a few nucleotides at the repair site [45]. DSBs are the most dangerous form of DNA damage and are formed when the two complementary strands of the DNA double helix are broken simultaneously at sites that are sufficiently close to one another that base-pairing and chromatin structure are insufficient to keep the two DNA ends juxtaposed. As a consequence, the two DNA ends generated by a DSB are liable to become physically dissociated from one another, making repair difficult. This may lead to inappropriate recombination with other sites in the genome. Error also occurs because DNA termini have sustained base damage, which means DSB ligation cannot occur until processing by DNA polymerases and/or nucleases has taken place. DSBs are potent inducers of mutations and of cell death [44].

Inaccurate repair or lack of repair of a DSB can lead to mutations or to larger-scale genomic instability through the generation of dicentric or acentric chromosomal fragments. Such genome changes may have tumorogenic potential [44]. Breaks can cause serious problems as a single break in a key gene can kill a cell or cause it to kill itself by apoptosis. For this reason, cells have powerful methods to repair damage as soon as it happens. In the human lifetime, each of the body's cells

will have repaired more or less successfully several thousand double-stranded DNA breaks. In cancer treatment, radiation therapy is used to overwhelm the natural repair mechanism using high doses of radiation to fragment the DNA in cancer cells [45].

Protection of the Environment

Biota residing downstream of nuclear facilities will be exposed over their entire life cycle, and perhaps for several generations, to low levels of radionuclides released in effluents. Therefore, protection of the environment is concerned with chronic exposures from routine releases. The exposures also are mainly internal from alpha, beta, and gamma emitters incorporated into the tissues of organisms. In the case of biota exposed to releases from uranium mines and mills, over 90% of the dose is from alpha emitters deposited internally from ingestion of food and water. For organisms exposed to routine discharges from nuclear power plants and some waste management facilities, tritium, "a beta emitter," may comprise a major component of the radiation dose. Other radionuclides such as ^{14}C, ^{60}Co, ^{90}Sr, and ^{137}Cs may also be important.

The goal of environmental protection is to prevent or minimize the effects of ionizing radiation on organisms, including the induction of cytogenetic effects, morbidity, decreased reproduction, and early mortality [39, 50, 51]. Cytogenetic effects such as mutations include genetic changes in a somatic cell that may alter its function or in a germ cell that may be inherited. Morbidity includes effects on growth, immune system, and behavioral modifications which may lead to a loss of individual fitness. Decreased reproduction results from reduction in fertility and fecundity rates, whereas early mortality occurs due to damage to tissues and organs [50, 51].

The effects of exposure to radiation have been reviewed by several international agencies for the purpose of identifying a radiation dose below which effects on populations of organisms would not likely occur (Table 1) [34, 52–54]. These reports have suggested that doses of approximately 10 mGy day^{-1} to maximally exposed individuals for aquatic organisms and 10 mGy day^{-1} for terrestrial plants, and 1 mGy day^{-1} to maximally exposed individuals of terrestrial animals would not put populations at risk. This approach assumes that in a heterogeneously contaminated environment, only a few individuals in a population would be exposed to elevated doses of radiation, and that if doses to only a limited number of individuals of a large population are greater than 1 or 10 mGy day^{-1}, then the population should not be adversely affected. In contrast, the United States Department of Energy adopted a radiation dose standard of 10 mGy day^{-1} for the protection of aquatic animals and

Ionizing Radiation on Nonhuman Biota, Effects of Low Levels of. Table 1 Radiation levels defined as protective of the population by international agencies and lower effect levels to individuals recorded in the present paper

	Terrestrial animals	Terrestrial plants	Aquatic organisms	References
Population	1 mGy day^{-1}	10 mGy day^{-1}	10 mGy day^{-1}	IAEA [52, 53], NCRP [54], UNSCEAR [34]
Individual	0.13 mGy day^{-1}[a] to a mouse	0.5 – 2.4 mGy day^{-1} [c,d,e]	0.4 mGy day^{-1} to fish[f]	Present paper
	0.84 mGy day^{-1}[b] to the earthworm		0.12 mGy day^{-1} to invertebrate[g]	

[a]Fluctuating asymmetry in yellow-necked mouse [55]
[b]Integument epithelium and midgut epithelium changes [56]
[c]Delayed growth of wheat, barley, and beans [57]
[d]Reduced growth and morphoses in pine trees [58]
[e]Reduced growth of Scotch pine seedlings [59]
[f]Reduced spermatogenesis and survival in *Tilapia mossambica* [60]
[g]Abnormalities and mortality of embryo-larvae of *Mytilus edulis* [61]

proposed dose standards of 10 mGy day^{-1} for terrestrial plants and 1 mGy day^{-1} for terrestrial animals [62] for the population as opposed to the maximally exposed individual.

The above radiological protection guidelines based on the maximally exposed individuals assumes that populations of organisms possess compensatory capabilities such that impacts on a few individuals should not affect the integrity of a population or community [63]. These radiological protection guidelines have shortcomings for the protection of populations composed of a small number of organisms or organisms with a small home range. Another shortcoming of guidance based on the maximally exposed individual is demonstrating that the radiation dose is to the maximum exposed individual as opposed to the larger population. This is because large sample sizes are required to demonstrate the maximally exposed individual, i.e., sampling such large numbers may have a greater impact on the local population than the contaminant. In support of this guidance, the FASSET Radiation Effects Database [64] contained few indications of readily observable effects on biota at dose rates less than 2.4 mGy day^{-1} and the LC_{50} for radiation exposures over a period of 30 days is more than 150 mGy day^{-1} for even the most radiosensitive organisms [65].

Protection of the environment from radiation has been governed by the anthropocentric approach that "radiological control of the environment to the standard necessary to protect humans will ensure that other species are not put at risk" [26, 53, 54]. In the past, this has been considered reasonable except when human access is restricted without restricting access by biota; unique exposure pathways exist; rare or endangered species are present; or other stresses are significant [66]. However, this approach is not defensible for several reasons: the importance of exposure pathways to biota may differ from that of humans; many organisms are just as sensitive to radiation as humans; and in most environments, humans are likely to be the least exposed to radiation. For example, from 1949 to 1952, large quantities of liquid radioactive waste were discharged into the Techa River, Russia, from the Mayak processing facility [67]. Evaluation of radiation doses from 1950 to 1951 data and again in 1991–1994 showed doses to aquatic biota were much higher than those to humans. Doses to humans decreased from maximum individual rates of 2–4 Sv and average of 0.1 Sv to an average of 0.2 mSv·year^{-1} (0.1–2 mSv·year^{-1}) from consumption of local foods. In comparison, doses to fish decreased from 10 Gy·year^{-1} to 4 mGy·year^{-1}, mollusks from 20 Gy·year^{-1} to 20 mGy·year^{-1}, and algae from 30 Gy·year^{-1} to 3 mGy·year^{-1}; values 100–300 times higher than for humans. In the upper reach of the river, radiation doses were estimated to be as high as 200 Gy·year^{-1} to fish, 500 Gy·year^{-1} to mollusks, and 700 Gy·year^{-1} to algae [67]. Unfortunately, radiation effects were not reported. Likewise, following the Chernobyl accident, terrestrial biota were exposed to higher levels of radiation than humans [58]. The same may also apply to the uranium mining and milling industry, where human access to the receiving water is usually restricted.

The anthropocentric approach for radiation also differs from that taken for the protection of the environment from other contaminants and does not demonstrate that the environment is adequately protected [68]. There is no reason to treat ionizing radiation differently to other environmental stressors [68–71]. Nonhuman species should be protected in their own right [71, 72]. The level of protection depends on the component of the environment to be protected: individual, population, community, or ecosystem. Most jurisdictions focus on protection of populations rather than individuals. As noted by Oughton [72], individuals can suffer, individual humans matter, but individual animals tend not to.

Protection of individuals (within reason) will ensure that the population is protected. When population changes are observed in response to a stressor, it may already be too late to protect the population as the effect has occurred. The philosophy that the loss of the local population (maximally exposed individuals) is acceptable as migration of healthy individuals from surrounding populations will repopulate the area once radiation levels decline is not acceptable for other contaminants and is in conflict with the philosophy of sustainable development. With conventional contaminants, emphasis is placed on protection of exposed individuals, whereas with radiation protection, emphasis is on protection of populations. Individuals may be harmed as long as the larger population is protected.

Once the radiation contamination has decayed or been diluted to a low enough level that the quality of the environment has improved enough, organisms from the surrounding areas can recolonize the area.

When assessing the effects of radiation on biota, the life history of the organism should be taken into consideration along with the dose rate and total radiation dose. For example, chromosomal aberrations were seen in the benthic invertebrate *Chironomus tentans* exposed to 6 mGy day^{-1} in White Oak Lake, Tennessee, USA [73]. In the warm waters of White Oak Lake, presumably about 22°C, *C. tentans* would complete its life cycle in about 30 days and be exposed to a radiation dose of about 180 mGy. However, at low temperatures found in northern climates, over-wintering *C. tentans* may take 8–10 months to complete its life cycle. This would be an exposure of about 1.8 Gy at a dose rate of 6 mGy day^{-1}. Would this same exposure rate over a longer time frame produce a more severe effect than chromosomal aberrations? Longevity should be considered in assessing dose effects. For example, in a breeding facility, the American alligator (*Alligator mississippiensis*) had complete reproductive failure by 21 years of age due to the accumulation of high levels of lead from their diet [74]. The accumulation of contaminants over time in long-lived, late-reproducing species such as the alligator should be of environmental concern.

Populations generally exhibit compensatory mechanisms to increase reproduction in response to population decline. For example, following control of rodents and insects, their populations are often seen to bounce back to original levels or increase to greater numbers. Pollutants that disturb the reproductive function of animals have the greatest potential for consequences [43]. Inhibition of reproduction in response to population decline may lead to the destruction of the population. In assessing potential effects, the presence of high abundance of a species in certain habitats is not always a reliable indicator of population well-being. This is because high abundance may be supported by the inflow of migrants after reproduction has ceased. For example, elevated water temperature in industrial reservoirs in the Dnieper region, Russia, created favorable conditions for marsh frogs (*Rana arvalis*) which became abundant. However, discharge of wastewater to the reservoirs resulted in marsh frogs ceasing reproduction and their high abundance was maintained only due to in-migration [43]. Similar observations have been observed with tundra voles at contaminated sites (section "Technically Enhanced Naturally Occurring Radioactive Material (TENORM)").

Effects of Radiation on Animals

Information on the effects of radiation on biota comes from laboratory studies, field irradiation studies, and observations at sites of industrial releases, nuclear tests, and accidents. Radiosensitivity generally increases with increasing organism complexity [34, 53, 75]. Polikarpov [48] provides a conceptual model for the response of organisms, populations, and ecosystems to radiation dose rates (Table 2).

The following sections briefly review the relevant radiation effects data with emphasis on more sensitive studies for both aquatic and terrestrial organisms. Other information on the effects of radiation exposure can be found in EC and HC [39], Harrison [76], Anderson and Harrison [77], Real et al. [78], and the reviews cited above.

In the following sections, dose rates reported are for gamma radiation, unless otherwise noted.

Ionizing Radiation on Nonhuman Biota, Effects of Low Levels of. Table 2 Response of biota to ionizing radiation as described by Polikarpov [48]

Zone	Radiation dose (Gy·year^{-1})	
Obvious action	4–>3,000	Above lower boundary of evident effects
Ecological masking	0.05–4	Above natural background where see effects, but effects are not significant
Physiological masking	0.005–0.05	Area of overlap between minor radiation effects and natural variability
Radiation well-being	0.00004–0.005	Natural background
Uncertainty	<0.00001–0.00004	Below natural background

In comparison to the effects of acute radiation on organisms, relatively few studies have investigated the effect of chronic exposure on biota. Within the literature, it is common to find studies presenting information on radiological effects but without providing information on absorbed doses, although concentrations may be provided. Information on absorbed dose is essential to interpret radiation effects [79]. For example, in the case of the Chernobyl literature, Polikarpov and Trytsugina [79] noted that 10 out of 16 studies reporting radiation effects did not provide radiometric or dosimetric data, but only the location of the study, i.e., zone of radiation contamination.

Interpretation of the literature on radiation effects is difficult because of the variety of dose rates, total dose exposure, time frame, and endpoints studied, and uncertainty in the relevance of certain endpoints with respect to protection of species. It is also sometimes difficult to estimate the radiation dose that organisms have been exposed to. The presence of other contaminants or stressors in field studies also complicates matters, i.e., it is difficult to determine whether the effect is due to radiation or other contaminants. The response of organisms to contaminants is essentially the same, whether it is exposure to radiation or another contaminant. Most studies have employed high doses of gamma radiation over short-time periods from an external source [3, 39]. Few studies have looked at the effects of internal exposure to alpha radiation or effects on more long-lived, slow-reproducing organisms.

Acute Doses

At high doses, effects are expressed by the death of cells, which may ultimately result in loss of tissue and organ function and, if the dose is high enough, the death of the organism. The mechanisms of radiation-induced mortality in invertebrates and lower vertebrates are similar to those observed in mammals. Major systems affected by high acute exposures are the hematopoietic, gastrointestinal, and immune systems. Lower doses and dose rates affect reproduction and can cause chromosomal aberrations and mutations. Genetic effects, such as point mutations, single-strand breaks, double-strand breaks, and sister chromatid exchanges occur at lower doses in both somatic and germinal cells and may be expressed at the population level.

Most research has been done using acute exposures with high doses generally given as a single dose but, in some cases, continuously for a specific period or until fatal. In the case of earlier studies, this is because the focus was on the potential effects of a nuclear war and accidental acute exposures to humans. Although information has been gained on potential effects of radiation to the environment from acute exposure studies, it should be recognized that most of the exposures used in these studies would be lethal to larger mammals, including humans, and are not representative of levels of radiation seen in the environment as a result of releases from nuclear facilities under normal operations. For our purposes, a radiation dose of greater than 100 mGy in less than a day may be considered an acute exposure, although mortality is not expected following such an exposure.

Chronic Doses

The data on the effects of chronic radiation exposure on mammals are extremely variable. The IAEA [53] concluded that a dose rate of 10 mGy day^{-1} is a threshold at which reproductive capacity may be affected in some mammals. Acute doses of 100 mGy are very unlikely to produce persistent, measurable deleterious changes in populations or communities of terrestrial plants or animals; and irradiation at a rate of 1 mGy day^{-1} is unlikely to cause observable changes in terrestrial animal populations. UNSCEAR [34] concluded that dose rates below 10 mGy day^{-1} to the most exposed members of the population would not seriously increase the death rate of mammal populations, and reproductive effects are unlikely at 10% of this dose rate, or 1 mGy day^{-1}. UNSCEAR [34] also cited a study in which the developing oocytes of the squirrel monkey (*Saimiri sciureus*) had an LD_{50} of 1 mGy day^{-1}, giving total doses in the range of 40–200 mGy over the study. As a general rule, chronic effects begin at 10% of the LD_{50} value, and effects on oocytes occur at 1% of the LD_{50}. Harrison and Knezovich [80] concluded that in mammals, adverse effects on fertility are first observed at a critical range of 0.48–4.8 mGy day^{-1}. Rose [81] concluded that the lowest dose rate producing a spectrum of effects is around 2.7 mGy day^{-1}, although effects have been observed at lower dose rates. For example, a dose rate of 0.2 mGy day^{-1}

(42 mGy) increased the mortality of offspring of laboratory mice provided with tritiated water [82], and a dose rate of 1 mGy day^{-1} (210 mGy) reduced testicular mass and epididymal sperm counts of mice after 30 weeks exposure to alpha radiation from plutonium [83].

Genetic effects in nonhuman species are the major consequence from radiation exposure at low and moderate dose rates. Radiation causes many types of damage to genetic material. Small errors in DNA repair and changes in the gene expression regulatory mechanisms can lead to cancer. Cancer is the primary concern in human radiation protection strategies. Nonhuman vertebrate species also develop cancers in response to radiation [84]. The development of cancer and mortality later in life, after the reproductive life cycle is complete, is considered to have little effect on the population. However, this may not be the case for long-lived, slowly reproducing species, such as elephants and whales or perhaps slow-growing fish in northern lakes. Can cancer be a limiting factor for local populations of animals like the bear that frequently live for more than 20 years in the wild and reproduce every 2 or 3 years, or for local populations like the alligator, which does not start to breed until 10–12 years of age in the wild [74], in areas where their population numbers are low? Certainly the loss of older members of the community in long-lived animals like the elephant that depend on the experience and leadership of elders for guidance under adverse conditions such as drought can be detrimental to the local population.

Survival, reproduction, and growth are the endpoints most relevant to protection of the population. With respect to reproduction, the processes from gametogenesis to embryonic development are limiting endpoints in terms of survival of the population [76]. Endpoints that measure changes in the ability to reproduce are the factors that affect fertility and sterility, such as reduction in number of gametes produced, gamete death, and increased abnormalities and mortality of early-life-stages [76]. Changes in fertility (an indicator of reproductive success) have been attributed to damage to cytogenetic material [54, 78, 85–87]. Although there is much interest in genetic effects because they may be transmitted to subsequent generations, genetic damage per se is generally not considered a limiting endpoint because of the difficulty in interpreting the significance at the population level (i.e., population fitness and survival). However, genetic damage provides an early warning that damage is occurring and may be important at the individual level.

Minor effects may be seen at low dose rates in more sensitive species and systems, the threshold for statistically significant effects in most studies is about 2.4 mGy day^{-1}. The significance of effects on the individual or population of minor responses at dose rates <2.4 mGy day^{-1} has not been determined, especially for morbidity and cytogenetic effects. The response increases progressively with increasing dose rate and is usually very clear at >24 mGy day^{-1} sustained for a large fraction of the lifespan [78]. In the present chapter, exposure to chronic radiation doses of <10 mGy day^{-1} to biota are considered most relevant to exposures biota may receive from continuous routine releases from modern nuclear facilities.

Effects at Elevated Background Concentrations

When assessing the effect of radiation on biota, it is the incremental radiation dose above background that is of concern. Normal background radiation is about 2.4 mGy·year^{-1}. Background radiation is generally in the range of 0.6–7 mGy·year^{-1} for leaves and needles of terrestrial plants, 1–5 mGy·year^{-1} for terrestrial mammals, and 0.7–1.7 mGy·year^{-1} for freshwater organisms [34]. However, some species of wildlife may receive much higher doses of background radiation. For example, the accumulation of ^{210}Pb and ^{210}Po in the liver and kidney of some herds of Canadian caribou (*Rangifer tarandus*) [88] may result in doses 10–100 times higher than background (see "► Radiation Effects on Caribou and Reindeer"). Similarly, burrowing animals living in radon-rich soils may receive exposures resulting from short-term peaks in radon concentrations, equivalent to over 100 mGy·year^{-1} [89].

Naturally occurring alpha-emitting radionuclides appear to be the most significant sources of background radiation exposure to organisms. In the terrestrial environment, background radiation is mainly from ^{222}Rn and its short-lived decay products, whereas in aquatic environments, ^{210}Po is the major contributor [34], although it is important in the terrestrial environment as seen in the example for caribou above. Po-210 is

about 8,000–50,000 times less abundant than ^{40}K, but the dose rate from ^{210}Po is sometimes 10–100 times higher than for ^{40}K [90]. K-40 is a major source of internal and external gamma radiation, and together with members of the ^{238}U and ^{232}Th decay chain, are part of the natural background dose (see "► Radiation in the Environment, Sources of").

In certain areas, normal background radiation may be greatly elevated with radiation levels of up to about 100 mGy·year^{-1} (see "► Radiation in the Environment, Sources of"). In the state of Kerala in South India, natural radiation levels are as high as 1 mGy day^{-1}, or about 250 times the normal background (4.3 μGy·day^{-1}), due to ^{232}Th and its daughters in the monazite soil. At these elevated radiation levels, a higher incidence of chromosomal aberrations is reported. For example, higher frequency of meiotic abnormalities and pollen sterility is reported in plants in the presence of monazite soil in comparison with plants from control areas [91]. Bats (*Chiroptera*) living in an abandoned monazite mine showed a dose-dependent increase in DNA damage at 0.5 mSv·day^{-1} and 2.4 mSv·day^{-1} compared to bats from a control area [92]. Rabbits exposed to naturally high radioactivity in areas in southwest France of about 1.9 mGy·day^{-1} and up to 700 mGy·day^{-1} gamma rays and >6 Gy of alpha radiation to the bronchial region from inhalation of radon showed a small but significant increase of chromosomal aberrations (dicentrics) in their lymphocytes. Chromosomal aberrations are also reported in spermatocytes of scorpions (*Tityus bahiensis*), inhabiting areas with radiation levels of 0.7 mGy·day^{-1} and 252 mGy·year^{-1} in the state of Minas, Brazil [93]. Increased levels of chromosomal aberrations in peripheral blood lymphocytes are also observed in humans living in areas with elevated natural background radiation levels in India, China, and Iran [94]. Thus, naturally elevated background levels of radiation may be having subtle effects on biota.

Effects on Mammals

There is an apparent inverse relationship between the $LD_{50/30}$ and the weight of the animal [34]. Lethal radiation doses for small mammals are in the range of 6–10 Gy for several species of rodents (Table 3) with the lowest doses to cause death in the range of 3–6 Gy·year^{-1} [96]. Lethal radiation doses (LD_{50}s) for large domestic animals such as cattle, sheep, goats, pigs, burros, and horses are in the range of 1.2–3.9 Gy [34] and that for large wild animals is in the same range [96]. Dose rates < 4 Gy·year^{-1} do not seriously affect the population of small mammals. However, individual specimens are affected at these doses.

Effects of radiation on larger agricultural animals were observed following the Kyshtym (Mayak) and

Ionizing Radiation on Nonhuman Biota, Effects of Low Levels of. Table 3 The LD_{50} (Gy) of several types of rodents and larger mammals exposed to acute doses based primarily on Dunaway et al. [95]

Species/strain	LD_{50} (Gy)
Larger mammals, including humans	1.5–6 Gy
Four strains of mice and two reciprocal crosses	4.9–6 Gy
Marsh rice rat (*Oryzomys palustris*)	5.3 Gy $LD_{50/30}$
Feral house mouse (*Mus musculus*)	5.5 Gy
Wild house mouse (*M. musculus*)	6.3 Gy
Thirteen strains of laboratory mice	5.1–7.2 Gy
Short-tailed shrew (*Biarina brevicauda*)	7.8 Gy
Wild house mouse (*M. musculus*)	8.2 Gy
Least shrew (*Cryptotis parva*)	8.4 Gy
Norway rat (*Rattus norvegicusl)*	8.7 Gy
RF strain (*M. musculus*)	8.8 Gy
Pine vole (*Microtus pinetorum*)	9.4 Gy $LD_{50/30}$
Eastern harvest mouse (*Reithrodontomys humulis*)	9.5 Gy $LD_{50/30}$
Hisoid cotton rat (*Sigmodon hispidus*)	9.6 Gy $LD_{50/30}$
Golden mouse (*Peromyscus nuttalli*)	10 Gy $LD_{50/30}$
Old-field mice (*Peromyscus polionotus*)	10.1 Gy
Cotton mice (*Peromyscus gossypinus*)	10.1 Gy
Cotton rat (*Sigmodon hispidus*)	10.4 Gy
White-footed mouse (*Peromyscus leucopus*)	10.7 Gy $LD_{50/30}$
Eastern harvest mouse (*Reithrodontomys humulis*)	10.8 Gy
Little pocket mouse (*Perognathus longimembris*)	13.7 Gy

I

Chernobyl accidents [55]. Following the Kyshtym accident in the Urals, cows feeding in pastures received a radiation dose of 1.4–3 Gy from external gamma exposure within 12 days following the accident, whereas their large intestine received a radiation dose of about 4–23 Gy. Cows began dying on days 9–12 from acute radiation exposure. Similarly, sheep received about 1.4–3 Gy from external gamma exposure and from 8 to 15 Gy up to 30–54 Gy to the large intestine through ingestion of forage. The sheep died within 9–12 day due to acute radiation sickness. Where fallout was less (170 $MBq{\cdot}m^{-2}$), cows and sheep received 0.13 Gy from external radiation and 1–4 Gy to the large intestine during the first 12 days after the accident. These animals showed radiation induced changes to their blood but, when evacuated from the area, they recovered. Based on a decline in the population of elk and roe deer in areas with 3.7–37 $MBq{\cdot}m^{-2}$ of ^{90}Sr, a die off of elk and roe deer occurred. The estimated radiation dose to the intestines was 0.1–1 Gy for elk and ~10–30 Gy for roe deer [55]. Similar findings were reported for the Chernobyl accident [20, 97].

The lowest acute dose in the literature that caused sublethal effects is 10 mGy to pregnant rats, which impaired the reflexes of their offspring (Semagin 1975 cited in [81]). Mice are among the most sensitive species to the reproductive effects of radiation with impairment of reproduction being observed at an acute dose as low as 0.2 Gy for females, while males are less sensitive (3.2 Gy) [53]. An increase in the number of mice embryos resorbed and, in the frequency of abnormalities, is seen in specimens exposed to a radiation dose of 5 mGy or more [98]. However, increases in fertility are also observed at low dose rates, and normal breeding mice are reported at high doses. For example, no effect was observed on fertility for 10 generations of rats exposed to 7 $Gy{\cdot}year^{-1}$ or for six successive litters produced by female rats exposed to 36 $Gy{\cdot}year^{-1}$ [99]. Exposure of male mice to high doses (9 Gy for each of eight generations, 3 Gy for 15 generations, or 2 Gy for 35 generations) resulted in no change in health or fitness of offspring. Slight changes in bull semen occur at an acute dose of 0.5 Gy, but recovery is complete in about 30 weeks post-irradiation.

The dog (beagle) is another sensitive species with a dose rate of 4.3 $mGy{\cdot}day^{-1}$, producing cellular regression and sterility in a few months. However, no effects are observed at a dose rate of 0.9 $mGy{\cdot}day^{-1}$ throughout the dog's lifespan of 12 years [96].

Natality is generally a more radiosensitive parameter than mortality. In general, within the same species, the ovary is more sensitive to radiation than the testis. The most sensitive endpoint for mammals appears to be the killing of 50% of immature oocytes as a result of exposure to 1 $mGy{\cdot}day^{-1}$ (total of 210 mGy) of tritium (^{3}H) during the last trimester of fetal development in monkeys [82]. A dose of 3.1 $mGy{\cdot}day^{-1}$ to neonatal mice from ^{3}H produced a 50% reduction in number of immature oocytes. However, more immature oocytes are produced than can be utilized for reproduction, so oocyte killing does not necessarily affect reproduction and population size. For example, chronic exposure to gamma radiation at a rate of 13–26 $mGy{\cdot}day^{-1}$ over 10 generations did not produce changes in the litter size of mice or sex ratios of progeny. Likewise, survival of mammals in an irradiated hardwood forest was not affected at a dose rate of 20 $mGy{\cdot}day^{-1}$ [100]. Wild rodents living on the dry bed of White Oak Lake exposed to lifetime doses of 2–3 Gy showed no effects that could be ascribed to radiation [101].

In their review on the effects of chronic irradiation on animals, Real et al. [78] found no effects on morbidity and mortality at a radiation dose rate of <2.4 $mGy{\cdot}day^{-1}$, but evidence of life shortening at dose rates of 2.4–24 $mGy{\cdot}day^{-1}$ to the dog and mouse, and reproduction effects to the pig, rat, and mouse.

Chromosomal damage may occur at low doses. An increase in micronuclei in the bank vole (*Clethrionomys glareolus*) was observed at dose rates up to 14.4 $mGy{\cdot}year^{-1}$ [102]. Similar chromosomal effects were observed in caribou in Norway after Chernobyl (see "► Radiation in the Environment, Sources of," "► Radionuclide Fate and Transport in Terrestrial Environments") at doses of 50–60 mGy [103]. However, no difference was seen in the frequency of micronuclei in bank voles exposed to a maximum dose rate of 86 $mGy{\cdot}day^{-1}$ within the Chernobyl exclusion zone and unexposed voles [104]. This observation is in conflict with reports of increased micronuclei in rodents exposed at low dose rates. Evidence is also accumulating that damage occurs to genetic material that is not expressed in the irradiated generation but may be expressed several generations later [105].

Effects on Life Span: Life Shortening Life-shortening studies have been mainly focused on rodents using gamma radiation. Mortality at daily doses above 216 mGy·day^{-1} primarily reflects radiation effects to the blood system such as depression of platelets, red cell count, white cell count, etc. Radiation induced life-span shortening of mammals at low and moderate doses (<216 mGy·day^{-1}) are essentially due to carcinogenesis, i.e., premature death due to the induction of tumors and to specific diseases such as neoplasias, amyloidosis, kidney degeneration, etc., which have opportunity to more fully develop with radiation survival times beyond 200 days. There is about a 6 month mean latent time for neoplastic and degenerative diseases in the mouse [5].

Carnes et al. [106] reported that the lowest doses in studies performed at Argonne National Laboratory at which radiation induced mortality caused by primary tumors could be detected was about 1–2 Gy for gamma rays and 100–150 mGy for neutrons. Increased pathological burdens were detected in irradiated mice at doses lower than those that increased mortality, i.e., at 220 mGy for gamma rays and 20 mGy for neutrons. Adverse health effects at low doses, other than cancer, involve multiple organ systems (cardiovascular, kidney, lungs and pleura, and reproductive organs). These pathologies were speculated to have as great an effect on the animal's health as those reported for tumors [106].

Life shortening of mice averaged 35 days·Gy^{-1} at high doses of >0.5 Gy·d^{-1} but only about 4 days·Gy^{-1} at daily doses of 3–560 mGy over their life span (Table 4) [8]. At lower daily doses of a few mGy·day^{-1}, a consistent life shortening affect is not seen. Sensitivity decreases with age and is strongly dependent on age at exposure during the first 2 months of life [5]. Because the response to radiation exposure decreases with age, the lifetime accumulated dose is not truly representative of the biological response [5].

At dose rates <2.4 mGy·day^{-1} of gamma or beta, no detriment effects on morbidity or reproductive capacity are seen. However, neutrons (1 or 5 MeV) at dose rates lower than 2.4 mGy·day^{-1} for 475 days result in increased mortality (50%) of mice. Dose rates of 2.4–24 mGy·day^{-1} of gamma shorten the life of mice and dogs, and reduces the number of primitive stem germ cells by 41% and the weight of ovary and testes by 44% in prenatal pigs compared to controls. The mortality rate of dogs exposed to dose rates ranging from 3–540 mGy·day^{-1} is dependent on the accumulated total dose rather than the dose rate with a slope of 1 for tumor deaths and slope of 2 for non-tumor deaths [7]. Thompson and Grahn [15] concluded that at dose rates lower than 2.0 mGy·day^{-1}, life shortening depends only on total dose and is independent of dose rate. These findings are in contrast to the statement that for life shortening, daily or monthly exposure rate throughout life is more important than the total dose [8].

Ionizing Radiation on Nonhuman Biota, Effects of Low Levels of. Table 4 Estimated life shortening for the mouse at low radiation dose rates and total dose measured in the laboratory at 400–450 mGy·min^{-1} of gamma

Dose rate (mGy day^{-1})	Total dose (mGy)	Life shortening (days)
1	650	3
2	1,290	5
3	1,930	8
5	3,190	13
8	5,030	21

Source: Modified from NCRP [8]

Searle [107] irradiated C3H mice with ^{60}Co for many generations at a rate of 9 mGy over a 11–17 h night starting at the age of 4–8 weeks through an average generation time of 80 days to first reproduction. Three sublines persisted successfully for 25–30 generations. However, after the second litter, the successive litter sizes became smaller than those of controls. Most mice became sterile before producing a fifth litter. For specimens receiving 18 mGy per night, only one mouse out of 66 produced more than three litters. The effect on litter size was attributed to the killing of oocytes in the ovary, which reduced the number of oocytes ovulated resulting in the early onset of sterility. Early oocyte stages in 10-days old mice were particularly sensitive to irradiation with a LD_{50} of 75.6 mGy for stage I oocytes after gamma irradiation of 26 mGy·min^{-1}. Searle [107] concluded that significant depletion of oocyte stocks occurred at low dose rates of 9 mGy per night and 720 mGy per generation. Vivarium studies have also demonstrated life shortening of mice at a few mGy·day^{-1} [55].

Continuous exposure to gamma radiation at 8 mGy·day^{-1} and 10 mGy·day^{-1} in two studies resulted in about a 50% reduction in oocytes on day 14 of life in mice irradiated from conception [108]. Effects on female fertility occurred over 33 days at a total dose of only 0.26 Gy. Chronic irradiation of sibling matings of four strains of mice at 12–24 mGy·day^{-1} for ten generations did not alter reproductive success, and average litter sizes remained the same because there is a huge over production of oocytes in mice [107]. This is why population effects are usually not seen in small mammals exposed to low levels of radiation in the field.

Hibernation In poikilotherms and hibernating animals at low temperatures radiation damage may be latent, so radiation effects may not be apparent in winter, but at warmer temperatures the lesions may manifest themselves [109].

The pocket mouse (*Perognathus* subfamily Perognathinae Heteromyidae) exhibits a high degree of radiation resistance compared to the other rodents. This is attributed to the capability of heteromyids to become hypothermic under certain adverse environmental conditions [110]. Hibernation after exposure to X-rays prevents damage leading to death in the ground squirrel (*Citellus tridecemlineatus*) and door mouse [111]. However, this was not the case for the brown bat (*Myotis lucifugus*). Therefore, there are species differences with respect to the development of cellular damage in hibernation [111].

Field Irradiator Studies Several field irradiation studies were carried out to assess the effect of radiation on various natural ecosytems (section "Field Irradiator Studies" – Table 10). These studies in general were not very successful in assessing effects to small mammals because of their mobility, the small areas irradiated, the nonuniform delivery of exposure and the short duration of some studies. The results of several of these irradiation studies have been reviewed by Turner [112]. Only a brief synopsis is presented here.

French et al. [113] irradiated Mojave Desert shrub type habitat in the Nevada test site to assess the effect of radiation on plant and animal life, particularly on heteromyid rodents. Nine hectare enclosures were continuously exposed to radiation for 5 years on average 310 days·year^{-1} with about 3.1 Gy in 1965, 3.2 Gy in 1966, and 1.9 Gy in 1967. A sixfold variation in dose rate was observed along the 550-m radius of the plot with most (77%) of the area receiving between 2.7 and 54 mGy day^{-1}. Radiation dose to individual animals was measured using a thermoluminescent dosimeter attached to the skin of their back.

Desert rodents are relatively long lived (e.g., 2–5 years) and maintain reproduction throughout life. Food supply is an important limiting factor for rodents. In good years, the population increased about fivefold, but in poor years there was no reproduction. Sampling to assess the population was nondestructive using live traps. Trapping was successful during summer months when the rodents were active, but less successful during the winter, when they largely remain underground and inactive. This seasonal behavior resulted in animals receiving a radiation dose of about 13.5 mGy day^{-1} in summer and <0.9 mGy day^{-1} in mid-winter [113].

The pocket mouse *Perognathus formosus* was exposed to 5–9 mGy day^{-1} (1.9–3.2 Gy·year^{-1}), which reduced survival particularly before the age of 6 months. The instantaneous rate of death for the irradiated population was 0.219 during this period and 0.075 and 0.104 for the two control populations. Life expectancy at age 1 month for the irradiated population was 9.2 months, and 11.4 and 14.4 months for the control populations. Laboratory studies confirmed that these levels of chronic radiation were sufficient to double mortality in preweaning age animals [113]. Thus, the pocket mouse suffered increased early mortality due to irradiation. The intrinsic rate of increase for the irradiated population was 0.314 compared to 0.493 and 0.498 per year for controls. This is a rate that would result in a 40% reduction in the multiplication rate per generation for the irradiated animals. However, Turner [112] considered this an over interpretation of the data for survival since plot-specific estimates of fertility were not available. Two long-lived specimens of *P. formosus*, a female 4 years 9 months old and a male 4 years 10 months of age (sacrificed about 8 months after radiation ceased) received an average dose of about 4.5 mGy day^{-1} for a lifetime exposure of about 16.9 Gy.

French et al. [113] speculated that a population of 3-year-old *P. formosus* subjected to such radiation likely would not be able to reproduce. Hence, when reproduction is curtained by unfavorable conditions,

radiation effects would be detrimental to the population. The rapid turnover of generations prevents the population from accumulating damaging effects at low levels of exposure.

Large kangaroo rats *Dipodomys merriami* and *Dipodomys microps* did not perform well in the enclosures and became extinct in the irradiated plot in <1 year and in one of two control plots after 5 years. The enclosures were too small for kangaroo rats and, with immigration curtailed, these rats became extinct. French et al. [113] concluded that chronic exposure to 8.1 mGy day^{-1} of gamma radiation was clearly detrimental to both the large kangaroo rat and pocket mouse.

Mihok [114] reported that exposure of meadow voles (*Microtus pennsylvanicus*) to radiation from a ^{137}Cs irradiator on six 1-ha meadows in Manitoba over 1–1.5 years resulted in no effects to the population or individuals at measured dose rates as high as 81 mGy day^{-1}. Third generation voles received up to about 5.7 Gy at a dose rate of 44 mGy day^{-1}. Mihok [114] concluded that voles that received a chronic dose of 5–6 Gy survived as well as controls and small numbers of overwintering animals survived and reproduced at doses up to 10 Gy.

Technically Enhanced Naturally Occurring Radioactive Material (TENORM) Tundra voles (*Microtus oeconomus*) inhabit an area of technically enhanced natural radiation near old plants where radium was processed from radium rich groundwater. Dose rates were 800 times reference values at Radium Site No 1 and Uranium-Radium Site No 1 and 400 times at Radium Site No 2 [55, 57, 115]. Tundra voles spend considerable time in their holes in the top 20 cm of soil, which results in radiation doses of 0.84–2.5 mGy day^{-1} in contaminated areas [57] and 2–7 mGy day^{-1} exposures from radon in burrows. Of 3,590 tundra voles evaluated from the exposed sites, 61% showed a decreased fat level compared to 21% for 2,135 control animals. All exposed voles were parasitized compared to 41% of those for control sites. Other effects included: changes in blood composition indicating chronic radiation sickness; low liver weight in young mice and degenerative changes in the liver, spleen, kidneys, testicles and ovaries; cytogenic changes in chromosomal aberrations in bone marrow; individuals with changed karyotype; significant alterations in the lipid peroxidation regulation in tissues; and serious reproductive problems.

Sexual maturity of male voles was inhibited up to 9 months of age compared to controls, which matured at 1–3 months of age. A lower number of females were involved in reproduction and these had half the number of embryos per female than the control population. The reproduction period and survival of young voles under 3 months of age were lower than reference levels (Table 5). Young males voles showed decreased fertility, reduction of testicular weight, and vacuolization of the seminiferous tubules parenchyma from Radium Site No 2, which suggests inhibition of spermatogenesis to complete termination of spermatogenesis [57]. This was more severe in young 1–2 months old specimens. The results reported for tundra voles are in agreement with other studies [107, 116, 117] that have reported increased mutation rate and reduction in life span, litter size, and reproductive capacity at low doses and dose rates of about 0.8 Gy per generation.

Despite a reduced reproduction period and decreased life span, exposed voles showed compensatory effects in fertility which together with immigration helped maintain the population size. Immigrants formed 30% of the population, or 1.5 to 2 times more of the population at contaminated sites than the

Ionizing Radiation on Nonhuman Biota, Effects of Low Levels of. Table 5 Radiation effects on tundra voles exposed to elevated radium concentrations near Vodnyi, Komi Republic, Russia

Parameter	Reference site	Ra No. 1 Site	U-Ra No. 2 Site
^{226}Ra in voles (mBq·g^{-1} ash)	26±12	201±99	265±198
Life span (months)	16.2±2.3	12.6±2.8	16.4±2.9
Reproductive period (months)	9.6±1.8	7.9±1.8	4.8±2.2
No of litters	6.7±0.8	8.6±1.6	6.3±1.1
Young per female	25.7±3.1	31.2±5.8	28.6±4.0
% loss of young in 3 months	13.9±2.32	31.8±3.75	51.4±4.73

Source: Based on Geras'kin et al. [57]

I

reference site. However, within a month, the immigrants were as contaminated as resident specimens [55].

Effects were observed in otters (*Lutra lutra*) and game birds living in an area of elevated natural thorium in the northern taiga, Komi region. The area has up to 1 mg Th·g^{-1} ashed soil and a gamma radiation background of 0.2–0.25 mGy day^{-1}. Otters living along a river in the elevated thorium area weigh less than controls, and spent less time in the water, i.e., hunt less, possibly due to disruption of thermoregulation. They were also 33% less numerous along a 127-km stretch of river than the reference area. In the same area, populations of great grouse (*Tetrao urogallis*) and black grouse (*Lyrurus tetrix*), two large game birds, had higher radionuclide concentrations than smaller grouse, hazel grouse (*Tetrastes bonsai*) and ptarmigan (*Lagopus lagopus*). They also have smaller populations per km^2 than in a reference area; 13–25% less for great grouse and 14–35% less for black grouse. Large grouse weighed less than reference specimens and were more heavily infested with feather parasites and endoparasites [55].

Nuclear Accidents

Kyshtym Accident In September 1957, the Kyshtym accident at the Mayak nuclear materials production complex (Mayak Production Association) east of the town of Kyshtym in the southern Urals, Russia, resulted in the release of ~7.4 × 10^{17} Bq of fission products from a concrete tank of liquid radioactive waste contaminating a stretch of forest called the East Urals Radioactive Track. Initially, about 90% of the radiation was from short-lived radionuclides (^{89}Sr, ^{144}Ce, ^{95}Zr, and ^{95}Nb) with ^{90}Sr accounting for only about 2.7% of the radioactivity. Initial maximum contamination was up to 1.5 × 10^8 Bq·m^{-2} for ^{90}Sr near the explosion. An area of 23,000 km^2 was contaminated with ^{90}Sr at a density of 3.7 kBq·m^{-2} and an area of 1,000 km^2, about 105 km in length by 8–9 km wide, with 74 kBq·m^{-2} of ^{90}Sr [55].

In the first fifteen years following the Kyshtym accident, during which radiation doses decreased from 100 mGy day^{-1} to 1 mGy day^{-1}, an increase in mortality of mice and a reduction in their fertility and life span was observed (Table 6)[55, 118]. Mortality of mice increased by a factor of two to ten, life span decreased by a factor of 1.5 to 2, and their fertility decreased by a factor of 1.25 at a radiation dose of 10 mGy day^{-1}. These changes had no effect on the population, but population structure and condition changed with bloodsucking ectoparasites increasing by a factor of five on small mammals. More than fifteen years after the accident, deviations were still evident in the morphology of blood and marrow of mice at total doses of 0.18 to 1.8 Gy·year^{-1}.

Chernobyl Accident The Chernobyl reactor accident in April 1986 released about 3–6 × 10^5 TBq of ^{137}Cs and 2–4 × 10^5 TBq of ^{90}Sr to the atmosphere of which about half was deposited within 20 km [119]. This resulted in the death of trees and other biota, and the establishment of a human exclusion zone. In the first 10–20 days, radiation doses in the exclusion zone may have reached up to 880 Gy mainly due to beta radiation [119]. From April 26 to June 1, 1986, external radiation was one to two orders of magnitude higher than that of the internal radiation dose. Initial exposure was mainly due to aerosols precipitated on the trees. Two months after the accident, most radionuclides moved to the leaf-litter layer with 95% or more of the radionuclide inventory residing in the litter layer 1–2 years after the cessation of radioactive fallout [120] and remained in the upper 3–5 cm soil layer for ~7 year. After the initial exposure to aerosols, exposure to vegetation was by root uptake [121].

Maximum absorbed dose following the Chernobyl accident occurred in the first year after deposition. External exposure to beta radiation, because of the path length of beta particles, was more an issue with smaller animals than large animals since their skin and fur absorbed most of the external beta dose [120]. Radiation dose declined monotonic mainly as a result of the decline in external gamma radiation. Exceptions were due to delayed maximum internal exposure [122]. Maximum levels of radiocesium occurred at 1–2 years after deposition, followed by an exponential decrease. Incorporation of ^{90}Sr increased up to the tenth year after deposition. Uptake of transuranic elements (^{238}Pu, ^{239,240}Pu, ^{241}Pu, and ^{241}Am) were much lower. Considerable ^{241}Am was first detected in animals, the bank vole (*C. glareolus*) and yellow-necked mouse (*Apodemus flavicollus*), in areas of high contamination five years after deposition and concentrations continued to increase over the next 5 or more years.

Ionizing Radiation on Nonhuman Biota, Effects of Low Levels of. Table 6 Radiation dose and dose rates to biota and observed effects following the Kyshtym nuclear accident at Mayak Production Association in the Urals, Russia, in 1957

Dose rate and accumulated dose	Effect
0.6–5 mGy day^{-1} and total dose of 0.1–1 Gy	No effect on average number of embryos in female northern red-backed mouse (*Clethrionomys rutilus*)
20 mGy day^{-1} and external dose of 0.13 Gy, 1–2 Gy large intestine	12 days after the accident, cows and sheep had abnormal blood but recovered when moved to an uncontaminated area
0.28 Gy day^{-1} and 10 Gy	Slight life shortening of northern red-backed mouse (*C. rutilus*)
60 mGy day^{-1} and 12–20 Gy	Life shortening of short-tailed vole (*Microtus agrestis*), 16% of contaminated adults had anomalous growth of upper teeth, which interfered with feeding – not seen in controls
11 mGy day^{-1} and total dose of 4 Gy	Shortening of the reproductive period of the European wood mouse (*Apodemus sylvaticus*) because of early death of adults
15 mGy day^{-1} and total dose of 5 Gy per lifetime, 0.57 mGy day^{-1} to bones with total dose of 0.2 Gy	Increased leukocyte concentration in short-tailed vole (*M. agrestis*) and weakened resistance to blood parasites (*Leucocytgrenarinae mieroti*) by a factor of 6 from control specimens; life shortening, i.e., 344±53 days for Kyshtym mice in vivarium versus 433±134 days for controls; poor health of the European wood mouse (*A. sylvaticus*), i.e., heavily infested with mites, eye diseases, loss of hair, and a reduced immune response compared to controls
11 mGy day^{-1} and 4.3 Gy	Altered blood composition with signs of leucopoenia, anemia and inversion in lymphocyte/neutrophile proportion, percent composition relative to controls was: 60%±5 for erythrocytes; 96%±8 for hemoglobin; 127%±20 for thrombocytes; 46%±7 for leucocytes; 295%±60 for neutrophiles; and 37%±4 for lymphocytes. Life shortening decreased the reproductive period of adults with 5–10% of the control females being pregnant verses 0.8–1% in exposed females. In autumn, the proportion of older animals in the population was 5–10% less than in the control population; number of progeny/female was the same as the control
3 mGy day^{-1} and total dose of 1 Gy	*A. sylvaticus* had a higher average rectal temperature and average breathing rate than controls. At a 3.7–370 kBq ^{90}Sr·kg^{-1} mice were more vulnerable to predation by the bird buzzard (*Buteo buteo*) than less contaminated mice, i.e., about 80% mice eaten had ~35 kBq ^{90}Sr·kg^{-1} in their bones, while only 20% trapped had this level, most (60%) had about 3.7 kBq·kg^{-1}

Source: Based on Sazykina and Kryshev [55]

Within 2–3 years after the Chernobyl accident, mice populations practically recovered in the Chernobyl zone. However, radiation effects typical of animals living in contaminated areas were present in subsequent years, e.g., negative changes in blood, infestation with parasites, hypooxygenia, and cytogenetic effects [55]. Ecological differences in mice species affected their response to the accident. Species that either fed on less contaminated food items, root voles (*M. oeconomus*), and/or lived in sheltered places, the house mouse (*M. musculus*), substantially increased in numbers after the Chernobyl accident due to evacuation of people from the area and abandonment of agricultural plants in fields. Fluctuating asymmetry in yellow-necked mouse (*Apodemus flavicollis*) was higher in close proximity to the Chernobyl reactor for both size and shape. Detectable effects of radiation on developmental stability probably start to occur between 3 and 7 μGy day^{-1}. Fluctuating asymmetry was highest (3.6 times reference) in specimens from the 10-km exclusion zone at a dose rate of 100 μGy day^{-1}, intermediate (2.3 times reference) in the 30-km exclusion zone at a dose rate of 7 μGy day^{-1}, and lowest in the reference area with a dose rate of 1.3 μGy day^{-1} [123].

I

Chesser et al. [124] reported that the bank vole (*C. glareolus*) living in the highly contaminated Red Forest area near Chernobyl Reactor 4 experienced an average dose of 18 mGy day^{-1} from ^{137}Cs and 25 mGy day^{-1} from ^{90}Sr, most of which is taken up from the diet. Total accumulated dose (internal and external) for voles was about 1.1 Gy over 30 day and 1.5 Gy for the house mouse (*M. musculus*). No evidence was found for reproductive failure in mammals from the Red Forest, i.e., the rodents were able to maintain their populations. In another study, Baker et al. [125] trapped small mammals within the 10-km exclusion zone of the Chernobyl Reactor 4, within the 30-km exclusion zone that received minimal radioactive pollution, and five sites outside of the 30-km exclusion zone. In total, 355 specimens representing 11 species were collected within the exclusion zone, and 224 specimens representing 12 species outside the exclusion zone. They concluded that diversity and abundance of small mammals were not reduced in the exclusion zone, and there were no aberrant gross morphological features other than enlargement of the spleen within the contaminated zone. Gross chromosomal rearrangements were not recorded, and 8–9 years after the Chernobyl accident, the small mammal community appeared normal [125]. These latter findings differ from those of Oleksyk et al. [123] and Sazykina and Kryshev [55].

Within the 10-km exclusion zone red fox (*Vulpes vulpes)* grey wolf *(Canus lupus*), moose (*Alces alces*), river otter (*L. lutra*), roe deer (*Capreolus capreolus*), Russian wild boar (*Sus scrofa*), and brown hare (*Lepus europaeus*) were observed, while only a single brown hare was observed beyond the 30-km exclusion zone. Exodus of the human population from the exclusion zone allowed wildlife to flourish [125], although the data for small mammals indicates that they are heavily contaminated. Actual radiation exposure to large animals and birds immigrating to the exclusion zone is less than that for small mammals because of their mobility, large feeding areas, and the nonuniform distribution of the contamination.

Animal populations were able to maintain themselves in the Chernobyl exclusion zone several years following the accident and even flourished in the absence of humans. However, effects typical of radiation exposure were observed in small mammal populations, and these populations should not be considered normal. In a review of the effects of the Chernobyl accident on biota, Polikarpov and Trytsugina [78] noted that 10 out of 18 studies reported deleterious effects over a wide range of dose rates (3 μGy day^{-1} up to 100–200 mGy day^{-1}), whereas the other 8 studies reported no damage below dose rates of 4–0.8 mGy day^{-1}. In three studies where the exposed dose was controlled, individual effects were observed at dose rates below 0.07–0.7 mGy day^{-1}.

Turner [112] concluded that chronic radiation of $>$ 1 mGy day^{-1} reduced fertility in rodents. Real et al. [78] concluded that dose rates lower than 24 mGy day^{-1} do not produce clear irreversible effects on morbidity, mortality, or reproductive capacity in nonhuman mammals. Impairment of reproductive capacity occurs at a threshold of ~2.4 mGy day^{-1}, although detrimental effects are reversible. The data support the finding that 1 mGy day^{-1} for mammals is protected at the population level, although there are effects on individuals [78]. However, it must be recognized that there is a lack of information on alpha emitters on mammals and for the effect of radiation on other species than rodents. Based on Chernobyl data, Fesenko et al. [58] derived a threshold dose for radiation effects of 1.6 mGy day^{-1} for cattle and 1 mGy day^{-1} for small mammals. Bird et al. [126] and EC and HC [39] also concluded 1 mGy day^{-1} is protective for small mammals.

Birds

Wild birds appear to exhibit LD_{50} values (5–12 Gy) in the same general range as small mammals [34]. The effect of radiation on birds has been reviewed by Brisbin [127] and Mellinger and Schultz [128]. Effects are seen at dose rates that may be considered acute exposures. Three eggs in a swallow's nest exposed to 1.5 Gy day^{-1} did not hatch despite prolonged incubation by the adults [129]. In four nests exposed to dose rates of 1 Gy day^{-1} (total dose of about 16–20 Gy), hatching was suppressed (56.3±14.7% compared with 82% and 91% for controls), but fledging success was not affected. Increased embryonic mortality was observed in birds irradiated at about 300 mGy day^{-1} in a Wisconsin forest [130], and impaired gametogenesis of irradiated chicken embryos was observed at 240 mGy day^{-1} in the laboratory [131].

Breeding tree swallows (*Tachycineta bicolor*) were exposed to a radiation dose of up to 45 times background levels (up to 0.14 mGy day^{-1}) [129, 132] without affecting breeding success [132]. In a field irradiation study, breeding tree swallows and house wrens (*Troglodytes aedon*) were exposed to radiation dose rates up to 5 mGy day^{-1} without any apparent effects on hatching, fledging, or breeding.

In the East Urals Radioactive Track, a reduction in hatching and a growth delay of chicks by 20% in nest volume was observed after the accident at radiation doses of 10 mGy day^{-1} [133]. Reproductive failure of flycatchers in man-made nests was reported in the Kyshtym area [56], but reproductive failure was not associated with specific radiation doses or dose rates. A loss of fitness was observed in the barn swallow *Hirundo rustic* breeding close to Chernobyl with an increase in partial albinism observed in the population. The number of breeding pairs also decreased 74% from 292 pairs in 1991 to 76 pairs in 1996 in nine villages near Chernobyl compared to a reduction of 19.8% from 202 pairs in 1991 to 162 pairs in 1996 in six villages in control areas. Unfortunately, radiation dose estimates were not available [134]. UNSCEAR [34] reported that swallows and sparrows produced young that appeared normal 4 months after the Chernobyl accident. From the above, it appears that birds do not seem to be particularly sensitive to radiation.

Amphibians and Reptiles

Data on the effects of radiation on survival of amphibians and reptiles are generally available only from studies with acute exposures where the post-irradiation observation period is often 30 days (30-d LD_{50}). Extending the observation period usually lowers the dose causing 50% mortality. In the case of poikilothermic (cold-blooded) animals, temperature can control the time of expression of radiation effects. Therefore, for fish, amphibians and reptiles, which are poikilotherms, a 60- or 90-day study period is more appropriate than the 30-day period normally employed for mammals.

LD_{50} values for frogs, salamanders, turtles, snakes, and lizards tend to be in the range of 2–22 Gy [34]. Although both reptiles and amphibians appear to be less sensitive to radiation than mammals [34, 135], work by Sparrow et al. [136] indicates that the LD_{50} for the mud puppy (*Necturus maculosus*) is less than 1 Gy when a longer study period is used, putting it in the same range of sensitivity as mammals. For the mud puppy, the 30-d LD_{50} of 35.5 Gy drops to 0.8 Gy at 200 days following a single exposure (i.e., 200-d LD_{50}). Other examples can be found in Woodhead and Pond [137]. It is hypothesized that *Necturus* is more sensitive than other amphibians because of a very large interchromosomal volume [138] and lack of a suitable system to repair the radiation damage [136]. LD_{50} values for adult anurans (frogs and toads) range from about 6 to 20 Gy [135]. Panter [139] showed that the most sensitive stage for acute exposure for the spotted grass frog (*Limnodynastes tasmaniensis*) is the fertilized egg, with a 40-d LD_{50} of 0.6 Gy. Urodeles (e.g., newts, mud puppy) are also sensitive, with LD_{50} values between 1 and 5 Gy, assuming up to 300-days postexposure for the time of lethality [136]. Juvenile life stages have lower LD_{50} values, ranging as low as 0.9 Gy (4.5 mGy day^{-1}) for Fowler's toad (*Bufo woodhousei fowleri*). The LD_{50} for acute radiation changes markedly through the developmental stages of a frog, increasing from <1 Gy in the early stages of development to over 25 Gy in the adult [140]. LD_{50} values for reptiles are in the same range as those for adult amphibians (>8 Gy).

In the Kyshtym area, the brown frog (*R. arvalis*) had smaller eggs, lower reproductive success, and 17% more morphological deformities than control specimens. Young brown frogs grew faster, but adults were smaller than control specimens [55]. Also in the Kyshtym area, the viviparous lizard *Lacerta viviparous* had 26.6% morphological deformities verses 2.1% in the nonexposed population [55]. Similarly, at the highly contaminated Izumrudnoye site 3 km from the Chernobyl NPP, in the first year after the accident, over 33% of the frog eggs were infertile, 17% in 1988, and 3% in 1989 compared to 0.01% in the control area [55]. Unfortunately, in the above studies, effects were not associated with specific radiation doses or dose rates.

For the moor frog (*R. arvalis*), the dose rate was highest when the frog was buried in sediment and lowest in the egg stage when suspended in water. This is because of the low ^{137}Cs concentration in water. A 1-cm layer of water between the egg mass and the sediment reduces the dose by 45% [141]. No effects were specified at external doses of 21–160 mGy·y^{-1} and

an internal dose rate between 1 and 14 mGy·y^{-1} measured in their study [141].

Continuous irradiation of lizards at about 20 mGy day^{-1} for 4 years from a ^{137}Cs source resulted in sterility at a cumulative dose of 15 Gy [112]. The annual radiation dose to the iguanid lizard (*Uta stansburianna*) was about 3.6–18 Gy, depending on location in the enclosure with most individuals receiving about 7.5 Gy. Dose rates to leopard lizard (*Crotaphytus wislizenii*) are estimated at 6.8–13.5 mGy day^{-1}, to the horned lizard (*Cnemidophorus tigris*) at about 3.5–7 mGy day^{-1}, and as high as 20–50 mGy day^{-1} to the iguanid lizard (*U. stansburianna*). Population survival depended on the individual species' life span, time to sexual maturity, and population age structure. *U. stansburiana* was protected by its rapid turnover (early sexual maturation and high fecundity), whereas longer-lived lizards, the horned lizard (*C. tigris*) and the leopard lizard (*C. wislizenii*), that matured later in life and produced fewer offspring suffered population losses, becoming nearly extinct [112]. All mature females became sterile, and there was no reproduction. Some of the irradiated *U. stansburianna* also became sterile by the age of 19–20 months. In the fourth year of the study, no female leopard lizards went into breeding colors, and three specimens sacrificed in the fifth year all lacked ovaries.

In summary, there is a lack of information on the effects of prolonged exposure to low levels of ionizing radiation for sensitive species such as frogs and the mud puppy, and most amphibian and lizard species in general. Based on the available information, amphibians and reptiles are as sensitive of chronic radiation exposure as mammals and a protective dose would be $\leq$1 mGy day^{-1}. However, no information is available on long-term exposures to more long-lived, slower-reproducing species such as alligators, crocodiles, and turtles. In the wild, the American alligator does not reach sexual maturity until about 10–12 years of age [74] and hence could accrue a considerable radiation dose even at low chronic dose rates before their first reproduction.

Fish

Several reviews on the effects of radiation on aquatic organisms have been published [39, 142–144]. Fish are considered the most radiosensitive of the nonmammalian aquatic organisms, with reproductive capacity being the most sensitive endpoint. Behavior and feeding habits affect the exposure of fishes to contaminants. Predatory fish tend to accumulate greater concentrations of contaminants than nonpredatory fish. For example, Koulikov [145] reported that the average ^{137}Cs levels were about 6.3 times higher in perch (*Perca fluviatilis*) and 4.4 higher in pike (*Esox lucius*) than nonpredatory species bream (*Abramis brama*), silver bream (*Blicca bjoerkna*), and rudd (*Scardinius erythrothalmus*). For tench (*Tinca tinca*) and goldfish (*Carassius* sp.), the factor was ~2. Differences were due to ecological and physiological factors. Bream fed mainly on *Chironomus* larvae while trench show a preference for mollusks and insect larvae. Other examples are given in "► Nuclear Accidents, Chernobyl Fallout in Scandinavian Watersheds."

Fish is the only non-mammal vertebrate studied in relatively more detail for dose rate or total dose effects. Most studies have involved acute exposures. Only 34 chronic studies were found at low-dose exposure to fish in the FASSET Radiation Effects Database [78]. The IAEA [87] concluded that reduced reproductive success would likely occur at dose rates in the range of 24–240 mGy day^{-1}, well above chronic exposures normally seen at modern nuclear facilities. Real et al. [78] reported a reduction in testis mass and sperm production, lower fertility and delayed spawning at a radiation dose of 2.4–24 mGy day^{-1} in plaice, medaka and roach. Anderson and Harrison's [146] synthesis of the data on effect levels for a number of endpoints indicated that a dose rate of 5–100 mGy day^{-1} would encompass the level at which a variety of low-level effects on reproduction, development, and genetic integrity are detectable in sensitive tissues and organisms. Increased mortality is also expected at a sustained dose rate of 240 mGy day^{-1} [146]. Dose rates (5–100 mGy day^{-1}) at which detrimental effects on fertility are first observed in fish are similar to those observed in mammals [146, 137].

The 30-d LD_{50} values, which are generally between 8.8 and 44 Gy, suggest that fish are less sensitive to radiation than mammals. These conclusions are based primarily on short-term acute toxicity studies. As noted above (section "Amphibians and Reptiles"), the

30-day period to assess radiation effects is too short for poikilotherm vertebrates. However, extending the study period reduces the LD_{50} considerably and into the lethal range for mammals [137]. For example, for mummichog (*Fundulus heteroclitus*), the 30-day LD_{50} is 12 Gy, whereas at 60 days, the LD_{50} is 3–3.5 Gy [147].

The LD_{50} for adult fishes ranges from 3.8 to 30 Gy, whereas the LD_{50} for fish embryos ranges from 0.16 to 25 Gy [39]. The lowest LD_{50} reported for fish was 0.16 Gy in coho salmon (*Oncorhynchus kisutch*) exposed at the one-cell stage and observed for 150 days [148]. The next lowest LD_{50} was 0.58 Gy for the one-cell stage of rainbow trout (*Oncorhynchus mykiss*) [149], then 0.9 Gy from exposure to X-rays for plaice (*Pleuronectes platessa*) larvae irradiated at the blastula stage [150]. The lowest acute exposure causing effects on reproductive tissue of fish appears to be 0.25 Gy [146]. A significant reduction in growth rate was observed when rainbow trout embryos were acutely exposed to 0.38 Gy [149]. In the same study, an increased frequency of abnormalities was observed in embryos irradiated at 2 Gy. Major malformations were observed when developing eggs of the mummichog were exposed to 3–4 Gy [151]. An acute dose of 5 Gy caused a 50% reduction in hatching of carp (*Cyprinus carpio*) eggs [152].

Few studies have been conducted to determine radiation doses that would cause mortality in fish as a result of chronic exposures. Significant reductions in fecundity have been observed at chronic doses ranging from $<$14.4 to 312 mGy day^{-1}. Chinook (*Oncorhynchus tshawytscha*) and coho salmon embryos exposed for 16–20 days and for periods up to 80 days to an external ^{60}Co source at a dose rate of 5 mGy day^{-1} (total dose of 330–400 mGy) showed a significant increase in deformities [153, 154] but no difference in survival at time of release, or in the number of adult salmon returning. The latter is possibly because at best only 1.2% of the salmon released returned to spawn. Opercular defects and fusion of vertebrae were observed in first-generation (F1) irradiated coho alevins [153]. Deformities were also more severe in F1-generation chinook salmon. When controls from the 1960 brood that returned in 1963 were mated with control and experimental (irradiated brood) fish, the resultant F1 generation, which had not been irradiated but were the offspring of irradiated parents, showed an increase in deformities. Twinning of the head was the most common deformity observed in chinook alevins, then curvature of the body and shortening of the body (fusion of vertebrae, omissions and incomplete tails) and opercular defects [153, 154]. Deformities were not observed in adults that returned to spawn, which may suggest that deformed fish were removed from the population. Exposure to 100 mGy day^{-1} or more was required to produce a significant change in the number of adult salmon returns [155]. These high radiation doses resulted in decreased growth and increased mortality of young fish in freshwater, decreased return of adult salmon, increased age at return and sterility in adult males [155].

In mosquitofish (*Gambusia affinis*) living in White Oak Lake (Oak Ridge National Laboratory, Tennessee, USA), a pond contaminated with radionuclides, exposure to 0.6 mGy day^{-1} and other contaminants over a lifetime produced a small but significant increase in embryo mortality over controls [156]. This small increase in mortality, although statistically significant, is not considered biologically significant, as the rapidly reproducing (spawning one or more times a year) mosquitofish population was thriving. Chronic exposure of the guppy (*Poecilia reticulata*) to 41 mGy day^{-1} caused reduced fecundity [157]. However, the guppy is a radio-resistant fish species with a 30-day LD_{50} of 23.5 Gy when irradiated with an acute dose of X-rays and no significant increase in mortality is seen in young guppies exposed to a total dose of 3.4–47 Gy from ^{3}H [158]. In a short-lived, rapidly reproducing fish species, the zebra fish (*Danio rerio*), exposure to a chronic radiation dose of 178 mGy day^{-1} from ^{137}Cs, caused complete sterility, with an EC_{25} for reproduction of approximately 24 mGy day^{-1} from ^{137}Cs [159]. In the same study, the highest dose rate from the alpha emitter ^{210}Po that caused no effects was reported to be 5 mGy day^{-1}.

Tilapia mossambica raised in ^{90}Sr contaminated aquaria for 800 days showed essentially normal reproduction at 4–5 μGy day^{-1}. At 0.4–0.5 mGy day^{-1}, male gonads were smaller in mass than those of control specimens and spermatogenesis was reduced, whereas no effects were observed on female gonads. At 30–40 mGy day^{-1}, 100% of males were sterile, 30% of females had underdeveloped ovaries, and 80% of females had anomalies of ovaries. Complete

suppression of reproduction occurred. Impregnation of exposed females with control males resulted in larvae that died by day 160 [60]. Overall survival decreased with radiation dose: 71% for controls, 54% for the 0.4 mGy day^{-1} fish, and 33% for 30 mGy day^{-1}. Weakening of the immune system also occurred with radiation exposure, i.e., experimental infection of fish exposed to 30 mGy day^{-1} with parasites increased mortality by 2–4 times compared to controls [60]. Reduced fecundity of the roach (*Rutilus rutilis*) that lived their entire lives in aquaria exposed to ^{90}Sr was also observed at dose rates > 5 mGy day^{-1} and all males became sterile [60].

Exposure of the carp, *C. carpio*, to concentrations of 1,850 Bq·L^{-1} and 37,000 Bq·L^{-1} of ^{90}Sr in aquaria for 15, 30, 90, 180, and 270 days resulted in radiation doses to the kidney of 0.2 mGy, 1.2 mGy, 42 mGy, 200 mGy, and 340 mGy. This affected the lymph system. Leucocyte concentrations and their phagocytic activity decreased with dose, and the immune response was delayed and weakened. Early signs of effects were detected at dose rates of 1 mGy day^{-1} and accumulated doses above 0.05–0.2 Gy. At lower doses, recovery was seen in 180 days. At a dose rate of 7–12 mGy day^{-1} and an accumulated dose of 2.5–3 Gy, distinct effects on fish immunity were seen. At 90 days and a radiation dose of >0.04 Gy, leucocyte concentrations were lower and were depressed at doses greater than 0.7 Gy by 40–50%. Changes in proportions of leucocytes were also seen along with negative biochemical changes in male gonads. At 0.4 Gy, the glycogen concentration in gonads was not detectable and testicles had up to 95 mg of fat per gram gonad. This increased to 127 mg fat per gram gonad at 0.7 Gy [60]. In nature, inhibition of the immune system results in increased parasite infection, development of morbid effects such as loss of competitive capacity and early mortality. Early signs of effects on the lymph system are detected at chronic dose rates of 1 mGy day^{-1} and accumulated doses above 0.05–0.2 Gy. At dose rates of 7–12 mGy day^{-1} and accumulated doses of 2.5–3 Gy, the effects on fish immunity are clearly distinct [60].

Studies on the effect of chronic exposure to radiation in the contaminated Chernobyl cooling pond demonstrated radiation effects to fish at low dose rates [10, 160–162]. Both caged silver carp (*Hypophthalmochthys molitrix*) and free-swimming specimens from the Chernobyl cooling pond were monitored from 1989 to 1992 to assess the effect radiation exposure had on their reproductive system.

Silver carp are planktivores; therefore, they accumulate lower concentrations of radionuclides than benthic and predatory fishes. Silver carp reaches sexual maturity at three years of age. From 1989 to 1992, first-generation silver carp received a radiation dose of about 0.2 Gy annually (0.55 mGy day^{-1}), i.e., about 0.6 Gy for the 1989 generation, 0.4 Gy for the 1990 generation, and 0.2 Gy for the 1991 generation [160]. Over the study period, the internal dose to silver carp was about 150 mGy·year^{-1}. This was primarily from consumption of plankton in summer and periphyton (filamentous algae) that colonized the cages in winter. In comparison, the parent stock, which was present in the cooling pond in 1986 as 1–2 year olds, received a radiation dose of 7–10 Gy, primarily from external radiation [160]. The external radiation dose was measured using dosimeters suspended at different depths, whereas the internal radiation dose was based on radionuclide concentrations in tissues. Internal radionuclide contamination was from ^{137}Cs and ^{134}Cs in flesh, ^{90}Sr in bone and ^{144}Ce, ^{141}Ce, ^{106}Ru, ^{95}Zr, and ^{95}Nb absorbed to the gut wall.

An increase in the number of silver carp (*H. molitrix*) with anomalies of their reproductive system occurred following the Chernobyl accident. From 47% to 90% of the fish exhibited anomalies in their sex cells. Anomalies included sterile individuals, morphological changes in the gonads such as gonad asymmetry, and degeneration of sexual cells. Fish with gonad asymmetry had one normal ovary or testis, and the other either degenerated or completely absent. Other anomalies such as those associated with the eye, e.g., absence of eye pupil and lens, and blindness in one eye may have been due to radiation or parasites.

The number and severity of reproductive anomalies in caged silver carp increased with time (Table 7). Despite abnormalities in their reproductive system, the high fecundity of silver carp allowed them to maintain their population in the cooling pond [60, 160].

Radiation effects were also investigated in the bighead carp (*Aristichthys nobilis*) [161]. Bighead carp was not as radiosensitive as silver carp. Only one female specimen exhibited gonadal abnormalities, large vacuoles in the oocyte cytoplasm. Male specimens showed

Ionizing Radiation on Nonhuman Biota, Effects of Low Levels of. Table 7 Effect of radiation on caged silver carp in the Chernobyl cooling pond following the Chernobyl accident

Year	Sterility (%)	Male gonadal malfunction (%)	Anomalies of male sex cells (%)	Anomalies of female oocytes (%)	Gonad asymmetry (%)
1989	5.7	25	25		8.6
1990	12.5	33	47.1	55	16.7
1991	0	57	68.8	78	23.1
1992	0 15.4[a]	100	100 89.5[a]	33 89[a]	9.1[a]
Reference[b]	0.25				4.6

[a]Free – swimming silver carp in Chernobyl cooling pond
[b]Experimental fish farm near Uzbekistan, which had water temperatures close to that in the cooling pond; 10–14°C in winter and 25–30°C in summer
Source: Based on Makeyeva et al. [160]

I

some effects, i.e., enhanced growth of connective tissue in gonads, lower sperm concentrations, and anomalous spermatozoa, but not to the same extent as for silver carp [161]. Catfish (*Ictalurus punctatus*) in the Chernobyl cooling pond were also found to exhibit greater genetic damage in relation to the radiocesium concentration in individual fish [163]. Similar finding were reported for the frequency of micronucleated erythrocytes in northern pike and the concentration of ^{137}Cs in pike in the Tom River downstream of the Siberian Chemical Complex [164].

In the Mayak Southern Urals field studies, the effect of radiation on several species of fish was investigated. The Siberian roach (*R. rutilus*) exposed to an external radiation dose of 4.8 mGy day^{-1}, 7 mGy day^{-1} to gonad, and 15 mGy day^{-1} to bone had lower fertility by a factor of ~2 and more morphological deformities (6–9% vs 0.5–1) than reference fish. A small percent (0.5–2%) had underdeveloped gonads and signs of hermaphroditism. In the roach (*R. rutilus*), asymmetry in the number of soft rays in pectoral fins was observed in fish living in the canal for liquid wastes from the Leningrad nuclear power plant. These fish were exposed to a dose rate of about 2 mGy day^{-1} [162].

A sample of 358 goldfish (*Carassius auratus gibelio*) was collected over a 3-year period from a triploid population of female fish from 1972 to 1975 in two lakes in the Mayak Southern Urals area. In Berdenish, the goldfish were exposed to a radiation dose of 30–40 mGy day^{-1} in 1957, which had decreased to 0.5 mGy day^{-1} in 1972–1975. Absorbed doses were 350–600 mGy for 2-year-old specimens, 730–1,300 mGy for 3-year-old specimens and 1.1–2 Gy for 5-year-old specimens. Morphological deformities, mainly deformities of gonads, were observed in about 24% of the specimens. The frequency of sterility was 17% for fish in the age group 3+ fish, and up to 25% for 4+ and older fish; 13.4% of the fish had only one ovary, 18.2% were without gonads, and 18% had curvature of the fins and tail, and irregular scale structure. Chlorine was also noted as present, but no information was given on concentrations. For the Lake Uruskul population, the radiation dose was about 30–40 mGy day^{-1} in 1957 and 3–5 mGy day^{-1} in 1972–1975. Two-year-old fish received 2.2–3.3 Gy, 3-year-old fish 3.3–4.45 Gy, and 5-year-old fish 5.5–7.75 Gy. About 15% of the goldfish in Lake Uruskul had morphological deformities and gonad anomalies (unpaired gonads and sterility). Despite increased numbers of deformities in gonads, growth and nutritional status of fish were normal in the contaminated lakes. In the two Ural Lakes, Uruskal and Berdenish, no goldfish specimens older than 8 years were present; 4–6-year-old specimens dominated spawning shoals. This suggests that radiation had a life shortening effect since older specimens are usually present [60, 90].

In the Southern Urals, anomalies are seen in the development of northern pike (*Esox lucius*) living in

Reservoir No. 10, which receives radioactive wastes (^{90}Sr, ^{137}Cs) and chemicals from radiochemical plants at the Mayak complex, i.e., the water was sulfuric with a pH of 4.5–5 [162]. The pike were tested for their ability to reproduce by mixing roe from 100 fish and examining the development of 1,000 fore larvae in comparison to control specimens from Lake Alabuga. An order of magnitude increase in anomalies above the reference population was observed at dose rates of 5–10 mGy day^{-1} (about 6.5 mGy day^{-1} from beta radiation and 1 mGy day^{-1} of gamma). About 8.3% of the exposed pike had serious deformities – no eyes, no yolk sac compared to 1.1% for controls. About 19–27% of the fish had curvature of the spinal cord in both exposed and control specimens. The latter was attributed to transportation from the distant lake to the fish farm. Nine types of deformities were present in exposed fish verses two types in controls. Immature fish exhibiting anomalies were removed from the population in the first few months of their life by natural selection. Despite the anomalies and loss in recruitment, the pike population in the reservoir remained viable over a period of 30 years [162].

Based on the observation of radiation effects on fish in the Chernobyl cooling pond and on fish at other contaminated sites in the former Soviet Union, Kryshev and Sazykina [162] concluded that dose rates below 10 mGy day^{-1}, in combination with other anthropogenic factors, affect reproduction and cause anomalies in fish species. Sazykina and Kryshev [60] concluded that obvious morphological and functional effects occur in the reproduction system of fish at chronic exposures above 2–5 mGy day^{-1}, and minor chemical changes occur around 0.5 mGy day^{-1}. Nevertheless, fish are able to maintain their population in highly contaminated water bodies.

For fish, the lowest acute LD_{50} is 0.16 Gy in coho salmon exposed in the one-cell stage [148]. At 5 mGy day^{-1}, anomalies are seen in the development of northern pike [162] and deformities are seen in coho salmon (total dose of 0.4 Gy) [153, 154]. The lowest reported chronic exposures to produce reproductive effects were observed in carp subjected to chronic exposures of 0.6 mGy day^{-1} in the Chernobyl cooling pond. The value of 0.6 mGy day^{-1} for reproductive effects in carp was used as an estimated-no-effect-value by EC and HC [39]. The carp, a more long-lived species that is slower to mature and reproduce, is affected by 0.6 mGy day^{-1}, whereas the mosquito fish, a short-lived, early to mature, fast reproducing fish, is not affected at this dose rate.

Considering the large number of eggs produced and natural losses, radiation may not be a controlling factor for most fish populations. For fish with long development times, such as the fish eggs of Arctic fish or viviparous fish with a relatively small number of eggs, radiation effects on embryos may limit the population [60]. This needs more detailed investigation. Effects on fish are in general similar to the effects reported for warm-blooded vertebrate animals. At the organism level, the following radiation effects are important for the survival of populations: weakening of the immune system, decreased reproduction, increased number of abnormalities, and life shortening [60].

At low doses, an increase in mortality is not observed directly, but mortality usually occurs in the form of a reduction in age-dependent survival. The effect of life shortening may be a cumulative result of effects on morbidity as well as abnormalities in reproduction and cytogenetic damages [60]. Slight life shortening may occur at relatively low dose rates of chronic exposure and may have a greater effect on long-lived species than on short-lived organisms.

Sazykina and Kryshev [60] concluded approximate threshold levels of chronic exposure above which specific types of effects can be detected are:

- 0.5–1 mGy day^{-1} with total doses above 0.05–0.2 Gy for the first appearance of negative changes in fish blood composition and early signs of a decrease in immune system function.
- 2–5 mGy day^{-1} with accumulated doses above 1.5 Gy for the appearance of negative effects on the reproductive system.
- 5–10 mGy day^{-1} of chronic lifetime exposure leads to life shortening of adult fish.

These effect levels are lower than the 10 mGy day^{-1} recommended or adapted for protection of aquatic populations. Sazykina and Kryshev [165] provided a threshold dose level of 0.3 mGy day^{-1} for fish, which is similar to the 0.6 mGy day^{-1} of Bird et al. [126] and EC and HC [39], whereas Fesenko et al. [58] used a value of 1.6 mGy day^{-1}.

Radiation is a pollutant that is frequently found in combination with other stressors. In the field, it is difficult to separate out the effect of radiation from that of other contaminants. In cooling ponds, water temperature is elevated. Elevated temperatures accelerate sexual maturation resulting in an increase in duration of gonad maturation of stages II-III in females, shorter duration of vitellogenesis, and reduced size and weight of mature eggs. In species that deposit eggs in batches, the number of eggs per batch decreases, and the spawning period is longer. Individual fecundity decreases in most species. For example, in the roach, fecundity increases as a result of higher temperature, but the percentage of oocyte resorption is high, and fecundity is actually lower than without elevated temperatures. In bream inhabiting cooling ponds, mass asynchronism of oocyte maturation is observed. Oocytes in the second generation usually undergo resorption with mass resorption occurring at all development stages in cooling reservoirs [43].

In water bodies heavily polluted with mixtures of contaminants (heavy metals, pesticides, organics), the reproductive system of fishes may be affected. Disturbances include asymmetrical development of ovaries and testicles, constriction of gonads, the absence of gonads in some individuals, testicular tissue degeneration, substitution of generative tissues by connective and adipose tissue in testicles, hermaphroditism in various forms (one gonad is an ovary and another is a testicle, or both types of generative tissue are found in the same gonad), mass reabsorption of oocytes, spermatocytes at different developmental stages, and mass abortive ovulation long before spawning. Many of these responses are associated with radiation effects. When mixtures of contaminants are present, it is difficult to assess what is causing the effect, i.e., a particular contaminant acting alone or in combination to produce the effect.

Invertebrates

Terrestrial Invertebrates Adult insects are relatively hardy when it comes to radiation exposure because very little cell division and differentiation occur in adults. Juvenile stages of insects are much more sensitive to radiation because of higher rates of cell turnover and differentiation. About 0.1 Gy kills the eggs of the braconid wasp (*Bracon hebetor*) [166], and <1.3 Gy kills the eggs of the housefly (*Musca domestica*) [167].

An impact on soil invertebrates as a result of elevated radium concentrations in soil was reported in an area where radium was commercially extracted from groundwater at Vodnyi in the Komi Republic in northern Russia (see section "Technically Enhanced Naturally Occurring Radioactive Material (TENORM)"). In these areas, soil invertebrates populations, particularly earthworms, are reduced [56, 57, 133, 168]. Immature earthworms were absent in plots with elevated radium concentrations but common in the reference plot. Earthworm numbers were reduced by a factor of 7 at 0.021 mGy day^{-1} recorded at the soil surface and changes in the earthworm integument epithelium, and midgut epithelium were observed at a radiation dose of 0.84 mGy day^{-1} [56]. In contrast to these findings, Hertel-Aas et al. [169] reported that the lowest dose rate to produce an effect on the earthworm *Eisenia fetida* was 96 mGy day^{-1}. Adult earthworms are radioresistant, but their juvenile stages are much more sensitive [170]. Slow-developing organisms and tardigrade species were also identified as being sensitive to elevated levels of radiation at the Vodnyi site [57].

Following the Kyshtym accident, earthworms and myriapods populations in the East Urals Radioactive Track were reduced by more than a factor of 10–100, where the radiation dose exceeded 6 Gy [119]. An estimated radiation dose of 30 Gy 2 months after the Chernobyl accident did not impact the number of adult invertebrates, but juvenile numbers were reduced due to mortality of eggs and early-life stages and the reproductive failure of adults [170]. Invertebrate numbers, including those for earthworms, were reduced only in the first two years or so after the accident. Earthworm numbers were more abundant than at the reference site in 1988 with only one species *Dendrobaena octaedra* present at contaminated sites and two species (*D. octaedra* and *Apporectodea caliginosa*) at the reference site [171]. Sampling of four sites within the Chernobyl exclusion area in 2002 revealed only one earthworm from the Parshev area (low contamination), three earthworms from the Forestry area (medium contamination), and no earthworms from the Pine Trees (medium contamination) and the Red Forest (high contamination) areas [119]. It was suggested

that the low pH 4.5–5.5 of the soils may not have been ideal habitat for the earthworms [119]; however, worms tend to be pH tolerant.

Jackson et al. [119] noted a general loss of invertebrate diversity in the Chernobyl exclusion zone with increasing radiation levels, but no change in biomass [119]. A noticeable reduction in number of soil invertebrates (mites, earthworms, myriapods, etc.) was observed at a radiation dose of 5–10 Gy [58, 120]. Asynchronous development was also reported between the hatching of leafworm eggs and their food source, the blossoming of leaves, following the Chernobyl accident [120, 172].

In field irradiation studies, invertebrates are more affected by indirect effects of chronic exposure from an external radiation source, such as loss of litter, than by the irradiation itself [112, 173]. Some examples are as follows:

- Increased diversity of microarthropods with increased diversity of lower vegetation
- Increase density in leaf miners due to scarcity of leaves
- Increase in ant populations as a result of removal of standing dead plant material which increased the area's attractiveness to foraging
- An outbreak of aphids on white oak leaves as irradiated leaves contained a higher sugar concentration [112]

A decrease in numbers only occurred at high doses. The effects of field irradiation studies on animals, including invertebrates, have been reviewed by Turner [112].

Fesenko et al. [58] suggested a radiation dose of 2.5 mGy day^{-1} as a threshold effects level based on Chernobyl data and because inhibition of reproduction usually occurs at doses an order of magnitude lower than lethal doses. Effects on earthworms are reported at a dose of <1 mGy day^{-1}.

Aquatic Invertebrates Most invertebrates are relatively tolerant of radiation. For example, Marshall [174, 175] showed that *Daphnia* are very resistant to radiation with sterilization occurring at about 105 Gy. Populations tolerated 13.3 Gy day^{-1} [174]. A significant decrease in percent hatch occurs in the calanoid copepod *Diaptomus clavipes* at a dose of 10 Gy [176]. The data on marine invertebrates suggest that acute LD_{50} values range from 2.1 Gy (*Palaemonetes pugio*) to 560 Gy (*Callinectes sapidus*, adults) [146]. Significant reductions in fecundity occur at doses ranging from 1.7 to 13,200 mGy day^{-1}. More recent studies exposing *Daphnia magna* to alpha radiation revealed that low doses of $\geq$ 2.6 mGy day^{-1} produced a significant (15%) reduction in body mass, smaller egg masses, and smaller neonates [177]. At a radiation dose of $\geq$7.2 mGy day^{-1}, the proportion of breeding females in the second generation was reduced, body mass was smaller, and oxygen consumption was increased [178].

A radiation dose of only 0.24 mGy day^{-1} is reported to accelerate cell division in the protozoa *Colpoa* sp [81, 90]. Embryos of the goose barnacle (*Pollicipes polymerus*) were most sensitive to radiation, showing a reduction in molting relative to controls when exposed to tritiated water for 32 days at a dose rate of 1.7 mGy day^{-1} [179] or dose rate of 3.4 mGy day^{-1} when the RBE of 2 for tritium is accounted for. However, the cultures were under considerable stress. Only about 55% of the control larvae molted from naupluis stage I to stage II, and antibiotics were required for successful culture. In a subsequent study with the marine mollusc *Mytilus edulis* exposed to tritium, significant effects on abnormalities and mortality of embryo-larvae accrued at a dose of about 0.12 mGy (corrected for a RBE of 2 and a 72 h exposure period) [61]. Tritium was genotoxic to *M. edulis* as measured by micronucleated hemocytes and induction of DNA strand breaks (Comet test) in a dose dependent manner at dose rates of 0.3, 2.2 and 11.6 mGy day^{-1} [180].

Chronic exposure of polychaete worms, *Neanthes arenaceodentata*, to a dose rate of 4.6 mGy day^{-1} for a total radiation dose of 0.55 Gy from a ^{60}Co source over their life cycle resulted in a significant reduction in live embryos per brood and hatchlings per brood and a significant increase in abnormal embryos per brood [77]. In contrast to the findings with *N. arenaceodentata* [77], the lowest dose rate to produce a significant effect on the polychaete worm *Ophryotrocha diadema* was 77 mGy day^{-1} [181]. Sensitivity of *N. arenaceodentata* is attributed in part to its gametogenic and spawning strategy; the gametes develop synchronously, and the female spawns only once [80]. In addition, little or no repair appears to

occur during egg development. In comparison, *O. diadema* lays eggs over several weeks [181]. A large variety of life-history strategies are observed in invertebrates, from synchronous development of gametes following a single spawning to laying several egg sacs to parental care of offspring. Considerable variation in radiosensitivity is observed and should be expected in invertebrates, much like that seen in other taxonomic groups.

In aquatic ecosystems, benthic organisms are likely to be the most highly exposed organisms due to the partitioning of radionuclides to sediment. Chronic irradiation of *C. tentans* larvae in White Oak Lake, Oak Ridge, Tennessee, at about 6 mGy day^{-1} increased the frequency of chromosomal aberrations but had no apparent additional effects on the population [73]. Reduction of the dose rate to about 0.3 mGy day^{-1} due to radiological decay resulted in the frequency of chromosomal aberrations decreasing to that found in reference populations. In the warm waters of White Oak Lake, *C. tentans* would complete its life cycle in about 30 days for a total dose exposure of about 180 mGy at a dose rate of 6 mGy day^{-1}. In a colder climate, it would take *C. tentans* much longer to complete its life cycle, especially for the over-wintering generation exposing the larvae to a much larger total dose and possibly greater effects.

In White Oak Lake, the snail *Physa heterostropha* experienced a reduction in egg capsule production at a radiation dose of about 6 mGy day^{-1}, but there was no difference in reproduction compared with the nonirradiated population because the number of eggs per capsule increased in the irradiated population [182–184]. In the laboratory, a dose rate of 240 mGy day^{-1} from ^{60}Co had no significant effect on reproduction, mortality, or size of the snail [183]. The pond snail (*Physa acuta*) exposed as a four-celled embryo had an acute LD_{50} of 10.8 Gy [185]. In contrast to the findings for the pond snail, the freshwater gastropod *Pila luzonica* appears to be more sensitive to irradiation [186]. Five velagis stages (embryos) were exposed to ^{3}H at concentrations of 3.7×10^3, 3.7×10^5, and 3.7×10^7 Bq·L^{-1}. Concentrations of 3.7×10^5 Bq·L^{-1} and greater resulted in histological abnormalities in the digestive tract. Abnormalities included infolding of the stomach wall, smaller stomach, variation in the thickness of the stomach wall, and hypertrophied cells. This was a dose-dependent response. At an estimated dose of about 0.06 mGy day^{-1}, 10–20% of the embryos exhibited abnormalities, whereas 45–65% of the exposed embryos were deformed at a dose rate of 6 mGy day^{-1} corrected for a RBE of 2. These abnormalities of the digestive tract occurred in nonfeeding embryo stages and were interpreted by the authors as effects on growth. It is not known whether the nature of these abnormalities could adversely influence growth and survival of affected individuals in later stages of life.

Tsytsugina and Polikarpov [187] studied the genotoxic effect of radiation on three species of oligochaetes *Dero obtuse, Nais pseudobtusa*, and *Nais pardalis* in a Chernobyl contaminated lake located in the 5-km zone of the Red Forest near Yanov. The lake was contaminated with metals, chloro-organic compounds, and high concentrations of ^{90}Sr, 5,872 Bq·kg^{-1} dw sediment with a dose rate of 0.2 mGy day^{-1}. The reference lake was located 20-km south of the Chernobyl NPP and had a ^{90}Sr sediment concentration of 105 Bq·kg^{-1} dw and a dose rate of 16 μGy day^{-1}. In the exposure lake, asexual reproduction and paratomous division was stimulated in *D. obtuse*, whereas activation of sexual reproduction occurred in the other two species. Asexual reproduction is the norm in these worms, with sexual reproduction occurring under stressed conditions. The change from asexual to a sexual mode of reproduction occurred at about ~0.3 mGy day^{-1}.

Increased cytogenetic damage in somatic cells of the three worms (6–8.3% in the contaminated lake verses 1.7–4.9% in the reference lake) was possibly due to low levels of radiation (0.2 mGy day^{-1}), although the other contaminants may also be responsible [187]. Where radiation effects could be excluded and the damage attributed to chemicals, chromosomal aberrations more closely followed a geometric distribution and the aberration spectrum included mostly bridges. With beta and gamma exposure, the distribution of chromosome aberrations between cells is described by the Poisson distribution. In the presence of both chemicals and radiation, the distribution is closer to a Poisson distribution if the effect is mainly from radiation and to a geometric distribution if the effect is mainly from the chemicals [49, 188]. Tsytsugina and Polikarpov [187] concluded more work is required on irradiation effects in the ~0.005 to ~4 Gy·year^{-1} range

since these doses affect a larger area and greater population than higher doses. Further information is required on the toxicity of mixtures that include radiation at low doses and whether there is indeed a difference in the type and distribution of chromosomal aberrations in the presence of different contaminants.

Circumstantial information suggests that tardigrade may be sensitive to radiation. Tardigrada were reported to be abundant in a control pond but were absent from an adjacent pond contaminated with ^{137}Cs [189]. In the experimental pond, the radiation dose to benthic invertebrates was estimated to vary from about 0.2 mGy day^{-1} in the centre to 9 mGy day^{-1} at the perimeter in the pond [39]. The effect of radiation on Tardigrada needs further study.

Fesenko et al. [58] derived threshold effect values of 7 mGy day^{-1} for zooplankton and 2.5 mGy day^{-1} for benthic invertebrates. Bird et al. [126] and EC and HC [39] in their assessment of radiation effects on nonhuman biota used the value of 4.6 mGy day^{-1} as a no effect level based on the response of the polychaete worm to radiation [77] because the endpoint (reproductive success) is most relevant to population health. Chronic exposure of *C. tentans* larvae to about 6 mGy day^{-1} resulted in measurable effects on individuals but did not result in population-level effects [73]. It can be concluded that radiation doses of <10 mGy day^{-1} may not affect populations but may affect individuals.

Effects of Radiation on Plants

Terrestrial Plants

Larger plants are generally more radiosensitive than small ones [96] and young plants are much more sensitive than mature plants [190]. Plant parts vary in their radiosensitivity. The apical meristem, the growing tip of the main root or stem is most sensitive, whereas the dry seed is considered most resistant. In general, plants that have many small chromosomes are more resistant to ionizing radiation than plants with a few large chromosomes. Woody species tend to be about twice as sensitive as herbaceous species, for a given interchromosomal volume [75]. Low-stature plants and dormant seeds are more resistant to radiation effects [75]. The order of radiosensitivity is as follows: coniferous trees > deciduous trees > shrubs > herbaceous species > lichen and fungi. In general, strong growth inhibition occurs at 40–50% of the lethal dose and inhibition of seed production occurs at 25 - 35% of the lethal dose [96].

The LD_{50} values for 60 woody plants range from 4.1 Gy for sugar pine (*Pinus lambertiana*) to 77 Gy for bitternut hickory (*Carya cordiformis*) and mockernut hickory (*C. tomentosa*) [39]. Gymnosperms (conifers trees) are more sensitive, by almost an order of magnitude, than angiosperms (deciduous trees) and are among the most sensitive of all plants. Plant morphology affects the radiation dose, the size, shape, and density of plant stands alters exposure and consequently radiation dose, e.g., shades sensitive parts [78].

There are relatively few studies involving chronic exposure of plants to radiation because of the logistic difficulties in having plants grow for an extended time in elevated radiation fields. Studies are primarily from field irradiator studies and from areas contaminated by nuclear releases and older contaminated waste disposal sites. Long-term irradiation experiments with plants showed that the most sensitive endpoint is the loss of viability or mortality. A few data indicate that the production of viable seed is at least as sensitive an indicator of radiation damage as mortality [191].

Some more sensitive studies in which effects were observed for plants exposed to low acute doses include: a 50% reduction in seed yield at 0.51 Gy to a flowering plant; a small portion of young Douglas fir trees (*Pseudotsuga douglasii*) were killed by a dose of 0.8 Gy [192]; a radiation effect at 0.1 Gy on an enzyme related to auxin, a growth regulator hormone in plants [193]; and an increase in root growth of seeds at 0.2 Gy. Lethal radiations are usually between 10 and 1,000 Gy for plants [96]. Some plant species predicted to be more sensitive to radiation at acute doses of <10 Gy are given in Table 8. UNSCEAR [194] noted that spruce trees are more radiosensitive than pine trees with absorbed doses of 0.7–1 Gy, resulting in malformed needles, buds, and shoot growth.

For chronic exposures, a more sensitive finding was reduced growth (13%) of Scotch pine seedlings grown in small pots above a waste management facility at a dose rate of 2.4 mGy day^{-1} [195]. Amiro [196] and Amiro and Sheppard [197] reported a no-observed effect level for sensitive species of 2.4 mGy day^{-1} in

Ionizing Radiation on Nonhuman Biota, Effects of Low Levels of. Table 8 Predicted sensitivity to gamma radiation of major woody ecosystems and the dominant plant species that are affected by an acute radiation dose of less than 10 Gy

Major ecosystem and vegetation type	Dominant species	Common name	Predicted H 16-h acute gamma LD_{50} (Gy)
Coniferous forests			
Boreal	*Abies balsamea*	Balsam fir	8.9 I
	Picea glauca	White spruce	8.5 I
	Picea abies	Black spruce	5 I[a]
Subalpine and montane	*Abies lasiocarpa*	Alpine fir	6.2
	Picea engelmanni	Englemann spruce	7.3
	Pinus ponderosa	Ponderosa pine	5.8
	Pseudotsuga douglasii	Douglas fir	9.9
	Pseudotsuga douglasii	Douglas fir	4 I[a]
Sierra-Cascades	*Abies concolor*	White fir	8.1
	Pinus jeffreyi	Jeffrey pine	6.7
	Pinus lambertiana	Sugar pine	4.1
	Pinus ponderosa	Ponderosa pine	5.8
	Pseudotsuga douglasii	Douglas fir	4.6
Pacific conifer	*Abies grandis*	Grand fir	6.2
	Tsuga heterophylla	Western hemlock	8.0
Deciduous forests			
Beech-maple-basswood	*Tsuga canadensis*	Canada hemlock	7.2
Hemlock-hardwood	*Pinus resinosa*	Red pine	7.8 I
	Pinus strobus	Eastern white pine	4.7 I
	Tsuga canadensis	Canada hemlock	7.0 I
Oak-hickory	*Pinus taeda*	Loblolly pine	6.3

H – Based on calculations of interphase chromosome volumes from active meristems
I – Observed mortality in actual experiments
I[a] – from UNSCEAR [34]
Source: Modified from Sparrow et al. [192]

a field irradiation study. These studies and those of Gunckel and Sparrow [193], Sparrow et al. [198] and Whicker and Fraley [199] all reported effects at dose rates between 2.4 and 20 mGy day^{-1}.

Pine Trees

Kyshtym Accident The Kyshtym accident at the Mayak nuclear materials production complex in the southern Urals Russia contaminated an area of 23,000 km^2 with ^{90}Sr at a density of 3.7 $kBq{\cdot}m^{-2}$, and a smaller area of 1,000 km^2, about 105 km in length by 8–9 km wide, with 74 $kBq{\cdot}m^{-2}$ of ^{90}Sr [55]. About half the contaminated area was covered with birch trees and to a lesser extent birch-pine forests. An average radiation dose of 40 Gy to the crown of pine trees resulted in their death. The LD_{100} was 30 Gy to up to 50 Gy and represented an area of 20 km^2. At doses of 15–20 Gy, a wide spectrum of radiation effects were observed such as a 50% and greater reduction in sprout growth, under development of needles, up to 70%

die-off of needles in the crown and inhibition of radial growth of wood tissue [118]. More sensitive herbaceous plants showed a 10–25% reduction in growth at an absorbed dose of 5 Gy. Stimulation of plant growth such as an increase in length of sprouts and needles by up to 20% occurred at doses below 1 Gy.

Chernobyl Accident The Chernobyl accident had a marked effect on the surrounding pine forest. Pine trees close to the reactor in an area of 500–600 ha were estimated to be exposed to doses greater than 80–100 Gy, doses above the acute LD_{50} level which killed the trees. In a second zone, with an area of approximately 3,000 ha, pine trees received doses above 8–10 Gy. Die back of new vegetative shoots of pine trees and damaged needles and buds were observed. In a third zone of about 12,000 ha, pine trees received doses of about 3.5–4 Gy. In this zone, moderate effects to pine trees were observed, including suppression of growth and needle loss, reduced capacity, and genetic damage [34].

Pine Trees as a Sentinel Species As already noted, pine trees are highly sensitive to radiation (and other contaminants). This, together with their widespread distribution, makes pine trees an ideal organism to biomonitor for ecological and genetic effects of radiation. The reproductive organs of conifers have a complex organization with a long generative cycle, so sensitive tissues are exposed to contaminants for prolonged periods and contaminants are highly retained. Most angiosperms species have a reproductive cycle lasting several months, but Scotch pine (*P. sylvestris*) seeds require at least 18–20 months to mature from micro- and megaspore formation. This allows for significant DNA damage to accumulate in undifferentiated stem cells at low dose rates and low contaminant concentrations. The cytogenetic anomalies in the intercalary meristem of young pine needles are sensitive biomarkers of contaminant effects. Damage to the DNA mainly appears as chromosome aberrations at the first mitosis [200].

The Chernobyl accident occurred in spring when the reproductive organs of plants were highly radiosensitive. Short-lived radionuclides made up most the dose in the first 10–20 days. By late summer–early autumn, the dose rate on the soil had dropped to 20–25% of the initial value. Thus, the initial acute radiation dose was replaced by low-dose chronic exposure. Variation in the distribution of radionuclides resulted in greater than an order of magnitude variation in the radiation dose even in small localized areas. For example, at four sites within the exclusion zone, the air kerma levels were: 2.4–12 μGy day^{-1} at Paryshev, 74–142 μGy day^{-1} at Pine Trees, 86–398 μGy day^{-1} at Forestry, and 1.2–3.3 mGy day^{-1} at the Red Forest [119].

In the first acute period of the Chernobyl accident, the absorbed dose was primarily due to external β and γ-irradiation, which resulted in cytogenic damage similar to acute gamma irradiation at comparable doses [201]. Mass mortality of pine trees occurred at a radiation dose of more than 60 Gy, the dying of the trees being accelerated by an evasion of pathogenic insects. Injury to pine stands was high at 10–60 Gy, medium at 1–10 Gy, and low at 0.1–1 Gy [172]. By May 1986, the pine forest had became known as the "red forest" because of the orange colored needles on the dead trees. These trees were cut down and buried. Since 1988, the forest has been replaced with grasses, shrubs, and young trees of deciduous species. By autumn 2000, young pine trees had started to reappear at the periphery of the red forest [121].

Geras'kin et al. [200] studied the frequency and spectrum of cytogenetic anomalies for reproductive (seeds) and vegetative (needles) tissues to assess the effect of different levels of radiation on Scotch pine (*P. sylvestris*) in the Chernobyl NPP 30-km zone and areas used for the processing and storage of radioactive wastes, the Leningrad regional waste processing enterprise radon site at Sosnovy Bor, Leningrad Region, Russia. In the Chernobyl, 30-km exclusion zone ionizing radiation predominated, whereas chemical toxins were the main contributors to contamination in the Sosnovy Bor area. Pine seeds in the Chernobyl area were collected from two areas in the exclusion zone, the asphalt–concrete plant at Chernobyl which received 10–20 Gy in 1986 and the village of Cherevach a relatively clean area within the 30-km zone, and the town of Obninsk in Kaluga Region, a remote control area [200]. Pine seeds in the Sosnovy Bor area were obtained from cones collected in 1995 from three areas: the Radon Leningrad regional waste processing enterprise site, the town of Sosnovy Bor, and a control area.

Cell aberrations in the root apical meristem are the result of aberrations induced during the period from gametogenesis to the maturation and harvesting of the seeds. Cytogenetic damage found in seed (roots from seedlings) and needle samples from the Chernobyl NPP 30-km zone increased with radiation exposure. Likewise, cytogenetic damage at Radon Leningrad regional waste processing enterprise site was higher than controls but cannot be solely attributed to radiation. Tripolar mitoses, which are rare anomalies possibly linked to spindle damage, were found in preparations from seeds sampled at both the Leningrad regional waste processing enterprise radon site and Sosnovy Bor, but not in samples from the Chernobyl NPP 30-km zone [200].

Cytogenetic effects of radiation on chromosome aberrations in anaphase cells in seedlings in the first mitosis of embryonic wood were higher in seeds of the first two reproductions than seeds produced subsequently [121]. The effect of radiation on *P. sylvestris* in the 30-km exclusion zone following the Chernobyl accident is given in Table 9.

Exposure to 0.5 mGy day^{-1} over long time periods increased radiosensitivity of pine trees indicating the accumulation of unrepaired damage. A decrease in pine shoot growth rate was observed at 0.43 Gy and cessation in growth occurred at 3.45 Gy in the Chernobyl area. Morphological alterations in pine needles occurred at a dose rate of 24 mGy day^{-1} and an accumulated dose of 13 Gy [78]. In the Chernobyl 0.2–20.4 TBq·km^{-2} area, a linear dose-dependent relationship was observed for cytogenic and genetic effects induced in *P. sylvestris* [121]. Acute radiation induced cytogenic and genetic effects that were significantly higher at 0.5 Gy than controls. Acute radiation at doses >1 Gy induced formation of morphoses and depressed growth and, at doses >2 Gy, the reproductive ability of the trees declined. The minimum dose at which

Ionizing Radiation on Nonhuman Biota, Effects of Low Levels of. Table 9 Effect of radiation dose rate on the Scotch pine (*Pinus sylvestris*) in the 30-km exclusion zone following the Chernobyl accident in 1986

Radiation dose (Gy)	Effect
0.5–1.0	Stimulation – an increase in secondary shoot growth
1–5	Slight damage, decrease in annual growth, morphological alteration of vegetative organs (variable needle length, intense budding at tips of annual shoots, secondary growth) in the first two years, then disappeared, frequency of chromosomal aberrations approached control levels by 7 years
5–15	Frequency of chromosomal aberrations was seven times control over the first two years then decreased to 2–3 times control by the eleventh year; moderate damage, depression of shoot, needle and wood growth, partly damaged crown and mortality of low tree classes, disturbed morphogenesis of vegetative organs and needle ultrastructure, shortened shoots with intense needle growth (broomlike shoots), distorted spatial orientation of needles and shoots (crushed needles and shoots), gigantic and dwarfed needles and shoots, significantly altered reproductive organs (small or absent male flowers, low number of seeds in cones), seeds had low germinating capacity and power, normal growth and development restored in 3 years, maintained its initial structure and function, i.e., the population did not decline in number, and more radioresistant offspring were produced
5–10	Threefold decrease in seed number per cone, a 12-fold increase in yield of unfilled seeds and 23% decrease in weight of 1,000 seeds. Effects were far less pronounced after 11 years
10–20	Most pine trees perished, surviving trees showed delayed reproduction in the sublethal zone for 5–7 years
0.36–0.96 mGy day^{-1}	After 14 years, restoration of trees was in progress, with mortality absent, increase in shoot growth, amount of needles, number of male strobiles, and pines reappearing

Source: Based on Kal'chenko and Fedotov [121]

morphologic effects occurred to pine trees following the Chernobyl accident was 1.2 mGy day^{-1} and involved reduction of shoot growth and morphoses [58].

Gene expression was assessed in *P. sylvestris* needles in the year 2000 at about 10 km from the Chernobyl NPP, where the absorbed dose in the first year was about 3–5 Gy but had subsequently decreased to 0.24–0.48 mGy day^{-1}. Changes in gene expression were small and in agreement with other studies of the flora and fauna in that considerable recovery had occurred in the Chernobyl area over the 10 years or more after the accident [202].

Other Plants Morphological effects were observed in plants at doses of 4.8–7.2 mGy day^{-1} with enhanced vegetative reproduction observed in heather and gigantism in other plants at 18–36 mGy day^{-1} following the Chernobyl accident [194]. The effect of chronic radiation up to 17.3 mGy day^{-1} on herbaceous plants was assessed at fifteen sites within the Chernobyl 30-km exclusion zone based on mass of 1,000 seeds, germination of seeds, and frequency of aberrant cells in roots of germinated seeds. No significant radiation effect was observed possibly because herbaceous plants are less sensitive to radiation than conifer trees [203]. Fesenko et al. [58] identified 8 mGy day^{-1} as a threshold effect dose for herbaceous plants at Chernobyl as cytogenic disturbances and point mutations were observed at this dose rate. Sterility, decrease in germination of seeds and morphological anomalies occurred at radiation doses greater than 27 mGy day^{-1}.

Radiation-induced effects were evident in agricultural plants. Increased cytogenetic damage was seen in the root apical meristem of seedlings in rye and wheat in the10-km zone of the Chernobyl NPP in 1987–1989. At an absorbed dose of 3.1 Gy, plants showed a significant increase in the yield of aberrant cells. Microsatellite mutations increased from 1.03×10^{-3} to 6.63×10^{-3} per locus over one generation at a total dose of about 300 mGy in wheat grown on contaminated soil (27 MBq·m^{-2}) near Chernobyl. Percent germination decreased by about 50% at 12 Gy [201].

Mutation induction in cornflower *Arabidopis* and barley plants near Chernobyl indicated that doses of >2.5 mGy day^{-1} are less effective than low doses of 0.1–1.1 mGy day^{-1} in inducing mutations when exposure was mainly from internal irradiation [78]. At the East Ural RadiationTrack, an elevated frequency of chlorophyll mutations in cornflower *Arabidopis* was still observed 38 years after the Kyshtym accident. Thus, decline in cytogenic damage induced by radiation lags the decrease in radiation dose as a result of radioactive decay. Mutation rates significantly greater than the spontaneous rate occurred at 0.3 mGy day^{-1} at a total dose of between 1 and 10 mGy.

External gamma radiation at 0.52 mGy day^{-1} delayed the growth and development and yield of wheat, barley, and beans in uncontaminated soil at Uranium-Radium Site No. 2 [57]. A dose rate of 0.3 mGy day^{-1} and total dose between 1 and 10 mGy gave mutation rates significantly higher than the spontaneous rate in barley plants exposed to internal irradiation from ^{90}Sr [78]. Apparently, exposure to both internal and external gamma radiation results in increased frequencies of both fragments and vagrant chromosomes, in suppressed DNA synthesis, and in homologous recombination, whereas exposure to only external gamma radiation resulted in an increased frequency of bridges [57].

Seeds of wild vetch collected at Uranium–Radium Site 2 had low weight per 1,000 seeds and when germinated in the control field, more than half the plants did not survive. Those that survived had lower productivity than reference plants [57]. In wild vetch seedlings, a significant increase in cytogenetic disturbances was observed in meristem root tip cells, sterile buds (4–6%), and partial sterility (11–23%), including polyploidy in exposed plants compared to <2 and 3–12% in control plants. However, interpretation of these findings is complicated by the fact that the Uranium–Radium site had nutrient deficiency (sand-gravel soil), high concentrations of natural radionuclides, toxic metals, chlorides, and sulfates [57].

Field Irradiator Studies Studies on the effects of external radiation from a radiation source on the surrounding environment are not directly analogous to the potential effects that may be caused by chronic releases to the environment. This is because radionuclides are not incorporated into the organisms and alpha radiation may be more harmful in an organism than gamma radiation. Also, for larger plants, such as mature trees, radiation exposure may be much greater on one side of the tree than the other, which is largely shielded. Field irradiation

studies allow one to relate absorbed doses in vegetation to observed effects. However, it is hard to draw conclusions from these studies because of differences in the quality, intensity, and duration of radiation in each of the field irradiator studies (Table 10).

Irradiation of a slash pine (*Pinus ellottii*) and longleaf pine (*Pinus palustris*) forest sharply decreased the growth of long-leaf pine at 3.6 Gy for small trees, 4.5 Gy for medium sized trees, and 5.4 Gy for the largest individuals. Species diversity increased in the portion of the forest, where all trees were killed (>27 Gy) and numerous old field species (weeds) such as *Heterotheca subaxillaris* colonized the area. At high doses (>27 Gy), there was a complete change in species composition. Only minor changes in species composition occurred at 7.7 Gy [215]. Irradiation of a white oak and evergreen oak forest in southern France for 18 years resulted in little change at radiation doses of 360 mGy day^{-1} or less. The original woody plants remained in place, though visibly deformed [216].

Irradiation of the Canadian Boreal forest for 14 years from a point source resulted in the die-back of sensitive coniferous trees such as *Abies balsamea* and *Picea mariana* at dose rates greater than 48 mGy day^{-1} [69]. These conifers were replaced by more resistant species, such as *Populus tremuloides* and *Salix bebbiana*, in some locations. Effects on canopy cover could not be detected at dose rates of <2.4 mGy day^{-1}. Dose rates greater than 24 mGy day^{-1} suppressed growth of needles and branches and decreased the number of lateral and terminal buds. Buds were often killed at dose rates greater than 48 mGy day^{-1}. Germination of jack pine seeds was sensitive to radiation with deleterious effects observed at 26 mGy day^{-1} [217]. Dugle and Mayoh [218] reported on the response of 56 species of shrubs to radiation. LC_{50}s at the end of the sixth year ranged from 48 to >1488 mGy day^{-1}. The estimated no effect value of 2.4 mGy day^{-1} for mortality in this study was used by EC and HC [39] in their assessment of the potential effects of radiation released by Canadian nuclear facilities on plants.

Aquatic Plants

There are few studies on the effects of radiation on aquatic plants (macrophytes and algae), particularly macrophytes. The lowest dose causing sublethal effects on aquatic plants is 0.07–0.12 mGy day^{-1}, which caused a loss of synchrony in growth of *Chlorella pyrenoidosa* cultures [195]. Circumstantial evidence that low radiation doses may impede algal development also comes from analysis of algae species invading

Ionizing Radiation on Nonhuman Biota, Effects of Low Levels of. Table 10 Field irradiator studies

Project	Location	References
Enterprise radiation forest	Enterprise, Wisconsin, USA	Rudoph [204], Zavikoewski [205]
Mediterranean forest	Cadarache, France	Fabries et al. [206]
Brookhaven oak-pine forest	Upton, New York, USA	Woodwell [207]
Puerto Rico radiation forest (Montane tropical rain forest)	El Verde, Puerto Rico	Odum and Pigeon [208]
Mojave desert	Rock Valley, Nevada, USA	French et al. [113]
Short-grass Prairie	Nunn, Colorado, USA	Fraley and Whicker [209]
Savannah river irradiations (old field)	Aiken, South Carolina, USA	Miller [210], McCormick and Golley [211]
Field Irradiator Gamma (FIG) (boreal forest)	Pinawa, Manitoba, Canada	Amiro [69], Guthrie and Dugle [212]
Zoological Environment Under Stress (ZEUS) (meadows surround by boreal forest)	Pinawa, Manitoba, Canada	Turner and Iverson [213], Mihok [114]
USSR pine and birch forest	South Urals	Alexakhin et al. [214]

a ^{137}Cs-contaminated pond and a control pond [189]. The control pond developed a thick bloom of algae, but surface algal growth was sparse in the contaminated pond. Green algae were dominant in the contaminated pond, whereas blue-green algae were dominant in the control pond. Whether this was a radiation effect or a chance event is not clear. However, radiation appeared to have affected the succession of algal species in the artificial pond. Properly designed studies employing replication should be performed to confirm these observations.

Algae tend to be more resistant to radiation than higher plants when exposed to acute doses. This may be because of the minute size of their chromosomes and polyploid condition in many algal species. *Prorocentrum* and *Oedogonium* have relatively large chromosomes of about the same size as common in higher plants and are more sensitive algal genera; a lethal dose for *Prorocentrum* is 20 Gy [219] and, for *Oedogonium*, about 6.7 Gy [4].

In general, chronic exposure to radiation from routine releases from nuclear facilities is unlikely to have an effect on algae because of the low dose rates involved and the rapid turnover time for algae. A radiation dose rate of 20.9 mGy·y^{-1} increased the growth rate of *Synechococcuslividus* in the laboratory [220]. Whether low levels of radiation exposure stimulate algal production leading to more eutrophic conditions in the environment has not been documented. A threshold effect value of 8 mGy day^{-1} was suggested by Fesenko et al. [58].

Radiation Effects Synthesis

International guidance on radiation levels protective of the population of 1 mGy day^{-1} for the maximally exposed individuals of terrestrial animals, and 10 mGy day^{-1} for the maximally exposed individuals of aquatic organism is inadequate. The concept that it is okay to impact the local population as long as a nearby healthy population remains intact to repopulate the area through immigration is not in the spirit of sustainable development and is in noncompliance with national environmental regulations supporting environmental protection and pollution prevention. Although, the guidance is in all likelihood protective of populations over a relatively large area, since most individuals would be exposed to a much lower radiation dose, the guidance is difficult to administer. Large sample sizes are required to demonstrate that the maximally exposed individuals are within the criteria, such that sampling can have a major impact on populations. Further, when impacts are seen at the population level, it is too late, the impact is there. It is preferable to monitor effects at the individual level. If the individual is protected, then the population will also be protected. Radiation effects are observed at levels substantially lower than the guidance levels (section "Effects of Radiation on Animals" and Table 1), especially for aquatic organisms, and there are many taxa for which no radiation effects information is available, particularly long-lived, slow reproducing species that are theoretically more sensitive to radiation. It is difficult to rationalize the use of guidance levels that represent more severely polluted environments, i.e., those found following a major nuclear accident or in/near uranium mine/mill waste management areas and effluent discharge areas.

Under normal operating conditions and effluent releases, radionuclide members of the uranium and thorium decay chains potentially represent the most risk to the environment. This is because most members are alpha emitters and give the greatest radiation dose to organisms when ingested, several radionuclides are generally present (the decay chain) and the sum of these individual radionuclide doses gives the total dose (the total dose is additive). Finally, the effect of an internal radiation source appears to be greater than the effect from an external source. These radionuclides are most closely associated with the first stage of the nuclear fuel cycle; the mining and milling of uranium ore. Other radionuclides such as ^{131}I, ^{90}Sr, and ^{137}Cs are of most concern following a nuclear reactor accident.

Research is required into the chronic effects of internally ingested radionuclides, particularly alpha emitters, on biota. Several studies showing effects at low exposure levels warrant follow-up. For example, the effects of tritium on the goose barnacle [179] and on the gastropod *Pila luzonica* [186], the radiosensitivity of Tardigrada [58, 189], and the effect of radiation on the growth of the green alga *Chlorella pyrenoidosa* [195]. Further study on the effect of radiation on long-lived, slow-growing organisms is essential as is the influence of radiation in contaminant mixtures. The results of radiation exposure studies should always

report the exposure levels (radiation dose), duration of exposure, effect level, and dose–response relationship so that data may be standardized to provide estimated-no-effect-levels or low-effect levels.

Future Directions

Radiation like most contaminants shows a spectrum of effects from being harmless at very low doses to lethal at high doses. Radiation differs from other contaminants in that external exposure to elevated concentrations of radioactivity can be harmful in the case of gamma radiation. Most studies have focused on the effect of radiation at high doses where major effects are documented and expected. Relatively few studies have investigated the effects of low doses of radiation representative of chronic releases. Of these studies, most used gamma radiation as an external source. Studies are required on the effects of low doses of internal radiation, particularly alpha, on a variety of organisms. Most studies have investigated the effects of radiation on small, rapidly reproducing organisms such as mice and rats, or in the aquatic environment, small-bodied fish and zooplankton. This is because these organisms are easy to study in the laboratory. However, they are also much more resistant to radiation at the population level than long-lived, slow-reproducing species.

Since radiation is seldom the only contaminant present in the environment, it is important to assess the role of radiation in inducing effects when present in contaminant mixtures.

Finally, the issue of voluntary and regulatory levels protective of the environment needs to be addressed, although it is recognized that it is up to individual governments to set criteria. Presently, protection is at the population level, but there are suggestions that protection should be at the individual level similar to the trend for other contaminants, although even here some jurisdictions protect the individual and others the population. Environmental thresholds are usually based on "no effect" to populations typically defined as the EC_{10} or less, or low effects (EC_{15-25}). It is difficult to justify an international guidance level of 10 mGy day^{-1} for protection of the aquatic environment when a radiation dose level of this magnitude is essentially restricted to major accidents (Kyshtym and Chernobyl) and waste management areas, e.g., uranium tailing ponds. Plants are clearly more tolerant than many animals to radiation. Therefore, international guidance on radiation dose rates protective of plants (10 mGy day^{-1}) is not protective of many inhabitants of plant communities. Garnier-Laplace et al. [221] have suggested a generic screening value of 0.24 mGy day^{-1}, and others [39, 58, 126, 222] have suggested various values for different taxonomic groups. Clearly, better direction is required as to what radiation dose rate is truly protective of the environment.

Bibliography

Primary Literature

1. World Nuclear Association (2009) The nuclear renaissance. http://www.world-nuclear.org/info/inf104.html. Accessed 10 Nov 2010
2. IAEA (International Atomic Energy Agency) (2009) Nuclear technology review 2009. http://WWW.iaea-org/cgl-bin/db.page.pllpris.opris.oprconst.htm. Accessed 10 Nov 2010
3. Jones S, Copplestone D, Zinger-Gize I (2003) A method of impact assessment for ionising radiation on wildlife. In: Third international symposium on protection of the environment from ionizing radiation (SPIER 3). International Atomic Energy Agency (IAEA), Vienna, Australia, pp 248–256
4. Godward MBE (1962) Invisible radiations. In: Lewin AR (ed) Physiology and biochemistry of algae. Academic, New York, pp 551–566
5. Sacher GA, Grha D (1964) Survival of mice under duration-of-life exposure to gamma rays. 1. The dosage-survival relation and the lethality function. J Nat Cancer Inst 32:277–321
6. UNSCEAR (United Nations Scientific Committee on the Effects of Atomic Radiation) (1977) Sources and effects of ionizing radiation. Report to the general assembly with annexes UN sales publication NOE.77.IX.I New York
7. Fry RJM (1996) Effects of low doses of radiation. Health Phys 70:823–827
8. NRCP (National Council on Radiation Protection and Measurements) (1980) Influence of dose and its distribution in time on dose-response relationships for low-LET radiations. Recommendations of the National Council on Radiation Protection and Measurements, Washington, DC, RA121.R2/U58/No.64/1980
9. Gong JK, Glomski CA, Bruce AK (1983) The effects of low dose (less than 1 rad) X-rays on the eythropoietic marrow. Cell Biophysics 5:143–162
10. Belova NV, Verigin BV, Yemel'yanova NG, Makeyeva AP, Ryabov IN (1994) Radiobiological analysis of silver carp (*Hypophthalmichthys molitrix*) from the cooling pond of the Chernobyl Nuclear Power Station in the post-disaster period. Reproductive system of fish exposed to radioactive contamination J Ichthyol 34:16–38

I

11. Trosko JE (1996) Role of low-level ionizing radiation in multi-step carcinogenic process. Health Phys 70:812–822
12. Bond VP, Feinendegen LE, Booz J (1988) What is a 'low dose' of radiation? Int J Radiat Bio 53:1–12
13. Ulsh BA, Miller SM, Mallory FF, Mitchel REJ, Morrison DP, Boreham DR (2004) Cytogenetic dose-response and adaptive response in cells of ungulate species exposed to ionizing radiation. J Environ Radioact 74:73–81
14. Goodhead DT (1988) Spatial and temporal distribution of energy. Health Phy 55:231–240
15. Thompson JF, Grahn D (1989) Life shortening in mice exposed to fission neutrons and γ rays VIII. Exposures to continuous γ radiation. Rad Res 118:151–160
16. UNSCEAR (United Nations Scientific Committee on the Effects of Atomic Radiation) (1982) Ionizing radiation: sources and biological effects. Report to the General Assembly with annexes. United Nations, New York
17. Wolff S (1996) Aspects of the adoptive response to very low doses of radiation and other agents. Mutat Res 358:135–142
18. Cai L, Cherian MG (1996) Adaptive response to ionizing radiation-induced chromosome aberrations in rabbit lymphocytes: effect of pre-exposure to zinc, and copper salts. Mutation Res 369:233–241
19. Polikarpov GG (1998) Biological aspect of radioecology: objective and perspective. In: Imaba J, Nakamura Y (eds) International workshop on comparative evaluation of health effects of environmental toxicants derived from advanced technologies, Chiba, Japan, 28–31 Jan 1998. Kodansha Scientific, Tokyo
20. Kryshev II (1992) Radioecological consequences of the Chernobyl accident. Nuclear Society International, Moscow, p 142
21. Blöcher D (1988) DNA double strand break repair determines the RBE of α-particles. Int J Radiat Biol 54:761–771
22. Goodhead DT, Nikjoo H (1989) Track structure analysis of ultrasoft X-rays compared to high- and low-LET radiations. Int J Radiat Biol 55:513–529
23. Goodhead DT, Thacker J, Cox R (1993) Effects of radiation of different qualities on cells: molecular mechanisms of damage and repair. Int J Radiat Biol 63:543–556
24. Prise KM (1994) Use of radiation quality as a probe for DNA lesion complexity. Int J Radiat Biol 65:43–48
25. Zhou H, Suzuki M, Randers-Pehrson G, Vannais D, Chen G, Trosko JE, Waldren CA, Hei TK (2001) Radiation risk to low fluences of α particles may be greater than we thought. Pro Natl Acad Sci USA 98:14410–14415
26. ICRP (International Commission on Radiological Protection) (1991) 1990 recommendations of the International Commission on Radiological Protection. Ann ICRP 21(1–3):1–201 (ICRP Publication 60)
27. Simmons JA, Watt DE (1999) Radiation protection dosimetry: a radical reappraisal. Medical Physics Publishing, Madison
28. Health Protection Agency (2007) Review of risks from tritium. Report of the independent Advisory Group on ionizing radiation. Chilton, Doc HPA, RCE-4, pp 1–90
29. Barendsen GW (1993) Sublethal damage and DNA double strand breaks have similar RBE–LET relationships: evidence and implications. Int J Radiat Biol 63:325–330
30. Barendsen GW (1994) RBE–LET relationships for different types of lethal radiation damage in mammalian cells: comparison with DNA double strand breaks and an interpretation of differences in radiosensitivity. Int J Radiat Biol 66: 433–436
31. Amiro BD (1997) Radiological dose conversion factors for generic non-human biota used for screening potential ecological impacts. J Environ Radioact 35:37–51
32. Blaylock BG, Frank ML, O'Neal BR (1993) Methodology for estimating radiation dose rates to freshwater biota exposed to radionuclides in the environment. Oak Ridge National Laboratory, Oak Ridge, (ES/ER/TM-78)
33. Copplestone D, Bielby S, Jones SR, Patton D, Daniel P, Gize I (2001) Impact assessment of ionizing radiation on wildlife. Environment Agency, UK, p 222 (R&D Publication 128)
34. UNSCEAR (United Nations Scientific Committee on the Effects of Atomic Radiation) (1996) Effects of radiation on the environment, vol V92–53957. United Nations, New York
35. Kocher DC, Trabalka JR (2000) On the application of a radiation weighting factor for alpha particles in protection of non-human biota. Health Phys 79:407–411
36. ICRP (International Commission on Radiological Protection) (1989) RBE for deterministic effects. ICRP Publication 58. Ann ICRP 20:1–57
37. Pentreath RJ, Woodhead DS (2000) A system for environmental protection: reference dose models for fauna and flora. 10th international congress of the international radiation protection association (IRPA-10), Hiroshima, Japan, 14–19 May 2000, p 6. (P-4b-228). http://www.irpa.net/irpa10/cdrom/00662.pdf. Accessed 10 July 2010
38. Pentreath RJ, Woodhead DS (2001) A system for protecting the environment from ionizing radiation: selecting reference fauna and flora, and the possible dose models and environmental geometries that could be applied to them. Sci Total Environ 277:33–43
39. Environmental Canada, Health Canada (EC and HC 2003) Canadian Environmental Protection Act 1999. Priority substances list assessment report releases of radionuclides from nuclear facilities (Impact on non-human biota). Final Report May 2003
40. NCRP (National Council on Radiation Protection and Measurement) (1990) The relative biological effectiveness of radiations of different quality. Recommendations of the National Council on Radiation Protection and Measurement. Washington, DC, p 218. (NCRP Report No. 104)
41. Chambers DB, Osborne RV, Garva AL (2006) Choosing an alpha radiation weighting factor for doses to non-human biota. J Environ Radioact 87:1–14
42. IAEA (Intenational Atomic Energy Agency) (1996) International basic safety standards for protection against ionizing radiation and for the safety of radiation sources. Safety Series No. 115, Schedule II, Public Exposure, Dose Limits pp 92–93

43. Shilova SA, Shatunovskii MI (2005) Ecophysiological indicators of the state of animal populations exposed to damaging factors. Russian J Ecology 36:27–32
44. Jackson SP (2002) Sensing and repairing DNA double strand breaks. Carcinogenesis 23:687–696
45. Goodsell DS (2005) The molecular perspective: double-stranded DNA breaks. Oncologist 10:361–362
46. Ulsh B, Hinton TG, Congdon JD, Dugan LC, Whicker FW, Bedford JS (2003) Environmental biodosimetry: a biologically relevant tool for ecological risk assessment and biomonitoring. J Environ Radioact 66:121–139
47. Xu A, Smilenov LB, He P, Masumura K-I, Nohmi T, Yu Z, Hei TK (2007) New insights into intrachromosomal deletions induced by chrysotile in the gpt delta transgenic mutation assay. Environ Health Perspect 115:87–92
48. Polikarpov GG (1998) Conceptual model of responses of organisms, populations and ecosystems to all possible dose rates of ionizing radiation in the environment. Rad Prot Dosimetry 75:181–185
49. Tsytsugina VG (1998) An indicator of radiation effects in natural populations of aquatic organisms. Rad Prot Dosim 75:171–173
50. Strand P, Larsson C-M (2001) Delivering a framework for the protection of the environment from ionizing radiation. In: Bréchignac F, Howard BJ (eds) Radioactive pollutants, impact on the environment. EDP Sciences, les Veix France
51. Copplestone DC, Howard BJ, Bréchignac F (2004) The ecological relevance of current approaches for environmental protection from exposure to ionizing radiation. J Environ Radioact 74:31–41
52. IAEA (International Atomic Energy Agency) (1976) Effects of ionizing radiation on aquatic organisms and ecosystems, Vienna, p 131 (Technical Reports Series No. 172)
53. IAEA (International Atomic Energy Agency) (1992) Effects of ionizing radiation on plants and animals at levels implied by current radiation protection standards, Vienna (Technical Reports Series No. 332)
54. NCRP (National Council on Radiation Protection and Measurement) (1991) Effects of ionizing radiation on aquatic organisms. Washington, DC (NCRP Report No. 109)
55. Sazykina T, Kryshev II (2006) Radiation effects in wild terrestrial vertebrates – the EPIC collection. J Environ Radioact 88:11–48
56. Krivolutsky D, Turcaninova V, Mikhaltsova Z (1982) Earthworms as bioindicators of radioactive soil pollution. Pedobiologia 23:263–265
57. Geras'kin SA, Evseena TI, Belykh ES, Majstrenko TA, Michalik B, Taskaev AI (2007) Effects on non-human species inhabiting areas with enhanced level of natural radioactivity in the north of Russia: a review. J Environ Radioact 94:151–182
58. Fesenko SV, Alexakhin RM, Geras'kin SA, Sanzharova NI, Spirin YV, Spiridonov SI, Gontarenko IA, Strand P (2005) Comparative radiation impact on biota and man in the area affected by the accident at the Chernobyl nuclear power plant. J Environ Radioact 80:1–25
59. Chandorkar KR, Dengler NG (1987) Effect of low level continuous gamma irradiation on vascular cambium activity in Scotch pine *Pinus sylvestris* L. Environ Exp Bot 27:165–175
60. Sazykina TG, Kryshev AI (2003) EPIC database on the effects of chronic radiation in fish: Russian/FSU data. J Environ Radioact 68:65–87
61. Hagger JA, Atienzar FA, Jha AN (2005) Genotoxic, cytotoxic, developmental and survival effects of tritiated water in the early stages of the marine mollusc, *Mytilus edulis*. Aquat Toxicol 74:205–217
62. Higley KA, Domotor SL, Antonio EJ (2003) A probabilistic approach to obtaining limiting estimates of radionuclide concentration in biota. J Environ Radioact 66:75–87
63. Barnthouse LW (1997) Extrapolating ecological risks of ionizing radiation from individuals to populations to ecosystems. In: Symposium on radiological impacts from nuclear facilities on non-human species, Ottawa, 1–2 Dec 1996. Canadian Nuclear Society, Toronto, pp 53–60
64. Copplestone D, Zinger-Gize I, Woodhead DS (2002) The FASSET Radiation Effects Database: a demonstration SPIER: 3rd international symposium on the protection of the environment from ionising radiation, Darwin, 2002
65. IAEA (International Atomic Energy Agency) (1991) The international Chernobyl project technical report. International Atomic Energy Agency, Vienna, p 640
66. Barnthouse LW (1995) Effects of ionizing radiation on terrestrial palants and animals: a workshop report, ORNL/TM-1341. Oak Ridge National Laboratory, Oak Ridge
67. Kryshev II, Romanov GN, Chumichevs VB, Sazykina TG, Isaeva LN, Ivanitskaya V (1998) Radioecological consequences of radioactive discharges into the Techa River on the southern Urals. J Environ Radioact 38:195–209
68. Smith J (2005) Effects of ionizing radiation on biota: do we need more regulation? J Environ Radioact 82:105–122
69. Amiro BD (1995) Effects of ionizing radiation on the boreal forest. Prepared for the Atomic Energy Control Board, Ottawa, Ontario by AECL Research, Whiteshell Laboratories, Manitoba, AECB INFO-0581
70. Delistraty D (2008) Radioprotection of non-human biota. J Environ Radioact 99:1863–1869
71. Stone R (2002) Radioecology's coming of age – or its last gasp? Science 297:1800–1801
72. Oughton D (2003) Protection of the environment form ionizing radiation: ethical issues. J Environ Radioact 66:3–18
73. Blaylock BG (1965) Chromosomal aberrations in a natural population of *Chironomus tentans* exposed to chronic low-level radiation. Evolution 19:421–429
74. Lance VA, Horn TR, Elsey RM, de Peyster A (2006) Chronic incidental lead ingestion in a group of captive-reared alligators (*A. mississippiensis*): possible contribution to reproductive failure. Comparative Biochem Phys Part C 142:30–35
75. Whicker FW, Schultz V (1982) Radioecology: Nuclear energy and the environment, vols I and II. CRC Press, Boca Raton
76. Harrison F (1997) Radiobiological endpoints relevant to ecological risk assessment. In: Symposium on radiological

I

impacts from nuclear facilities on non-human species, Ottawa, 1–2 Dec 1996. Canadian Nuclear Society, Toronto, pp 39–52
77. Harrison FL, Anderson SL (1994) Effects of acute irradiation on reproductive success of the polychaete worm, *Neanthes arenaceodentata*. Radiat Res 137:59–66
78. Real A, Sundell-Bergman S, Knowles JF, Woodhead DS, Zinger I (2004) Effects of ionizing radiation exposure on plants, fish and mammals: relevant data for environmental radiation protection. J Radiol Prot 24:A123–A137
79. Polikarpov GG, Trytsugina VG (1996) Radiation effects in the Chernobyl and Kyshtym aquatic ecosystems. In: Luykx FF, Frissel MJ (eds) Radioecology and the restoration of radioactive-contaminated sites. Kluwer Academic Publishers, Netherlands, pp 269–277
80. Harrison FL, Knezovich JP (2001) Effects of radiation on aquatic and terrestrial organisms. In: Van der Stricht E, Kirchmann R (eds) Radioecology: radioactivity and ecosystems. International Union of Radioecology, Liege, pp 317–375
81. Rose KSB (1992) Lower limits of radiosensitivity in organisms, excluding man. J Environ Radioact 15:113–133
82. Dobson RL (1982) Low-exposure tritium radiotoxicity in mammals. In: Matsudaira H, Yamaguchi T, Nakazawa T, Saito C (eds) Proceedings of a workshop on tritium radiobiology and health physics, Chiba City, 27–28 Oct 1981. Biomedical Sciences Division, Lawrence Livermore National Laboratory, Livermore, pp 120–134, NIRS-M-41
83. Searle AG, Beechey CV, Green D, Humphreys ER (1976) Cytogenetic effects of protracted exposures to alpha-particles from plutonium-239 and to gamma rays from cobalt-60 compared in male mice. Mutat Res 41:297–310
84. Gilbert ES, Cross FT, Dagle GE (1996) Analysis of lung tumor risks in rats exposed to radon. Radiat Res 145:350–360
85. IAEA (International Atomic Energy Agency) (1979) Methodology for assessing impacts of radioactivity on aquatic ecosystems, Vienna, p 416. (Technical Reports Series No. 190)
86. Kligerman AD (1979) Cytogenetic methods for the detection of radiation-induced chromosome damage in aquatic organisms. In: Methodology for assessing impacts on radioactivity on aquatic ecosystems. International Atomic Energy Agency, Vienna. pp. 39–367 (Technical Reports Series No. 190)
87. IAEA (International Atomic Energy Agency) (1988) Assessing the impact of deep sea disposal of low level radioactive waste on living marine resources, Vienna, p 127. (Technical Reports Series No. 288)
88. Thomas P, Sheard JW, Swanson S (1992) Transfer of ^{210}Po and ^{210}Pb through the lichen–caribou–wolf food chain of northern Canada. Health Phys 66:666–677
89. Macdonald CR, Laverock MJ (1998) Radiation exposure and dose to small mammals in radon-rich soils. Arch Environ Contam Toxicol 35:109–120
90. Polikarpov GG (1979) Effects of ionizing radiation upon aquatic organisms. In: Methodology for assessing impacts of radioactivity on aquatic ecosystems. Report of an advisory group meeting IAEA, Vienna, 21–22 Nov 1979, STI/DOC/190.1, pp 173–194
91. Gopal-Ayengar AR, Nayar GG, George KP, Mistry KB (1970) Biological effects of high background radioactivity: studies on plants growing in the monazite-bearing areas of Kerala Coast and adjoining regions. Indian J Exp Biol 8:313–318
92. Meehan KA, Truter EJ, Slannert JP, Parker MI (2004) Evaluation of DNA damage in a population of bats (*Chiroptera*) residing in an abandoned maonazite mine. Mutat Res 557:183–190
93. Léonard A, Delpoux M, Decat G, Léonard ED (1979) Natural radioactivity in southwest France and its possible genetic consequences for mammals. Rad Res 77:170–181
94. Ghiassi-Nejad M, Zakeri F, Assaei RGh, Kariminia A (2004) Long-term immune and cytogenetic effects of high level natural radiation on Ramsar inhabitants in Iran. J Environ Radioact 73:107–116
95. Dunaway PB, Lewis LL, Story JD, Payne JA, Inglis JM (1969) Radiation effects in the Soricidae, Cricetidae, and Muridae. In: Nelson DJ, Evans FC (eds) Symposium on radioecology proceedings the second national symposium, United States Atomic Energy Commission Report CONF-670503. Michigan, Ann Arbor, pp 173–184
96. Bréchignac F (2001) Impact of radioactivity on the environment: problems, states of current knowledge and approaches for identification of radioprotection criteria. Radioprotection 36:51–535
97. IAEA (International Atomic Energy Agency (2001) Present and future environmental impact on the Chernobyl accident. IAEA-TECDOC-1240
98. Ohzu E (1965) Effects of low-dose X-irradiation on early mouse embryos. Rad Res 26:107–113
99. Brown SO, Krise GM, Pace HB, de Boer J (1964) Effects of continuous radiation on the reproductive capacity and fertility of albino rat and mouse. In: Carlson W (ed) Effects of ionizing radiation on the reproductive system. Pergamon Press, New York, pp 103–110 [cited in Rose, 1992]
100. Buech RR (1977) Small mammals in a gamma-irradiated northern forest community. In: Zavitkovski J (ed) The enterprise, Wisconsin, radiation forest: radioecological studies. US Energy Research and Development Administration, Washington, DC, pp 167–180, (ERDA Report TID-26113-P2
101. Dunaway PB, Kaye SV (1963) Effects of ionizing radiation on mammal populations on the White Oak Lake bed. In: Schultz V, Klement AW Jr (eds) Radioecology. Division of Technical Information Extension, U.S. Atomic Energy Commission, Oak Ridge, p 333
102. Cristaldi M, Ieradi LA, Mascanzoni D, Mattei T (1991) Environmental impact of the Chernobyl accident: mutagenesis in bank voles from Sweden. Int J Radiat Biol 59:31–40
103. Røed KH, Eikelmann IMH, Jacobsen M, Pedersen Ø (1991) Chromosome aberrations in Norwegian reindeer calves exposed to fallout from the Chernobyl accident. Hereditas 115:201–206
104. Rodgers BE, Baker RJ (2000) Frequencies of micronuclei in bank voles from zones of high radiation at Chernobyl, Ukraine. Environ Toxicol Chem 19:1644–1648

105. Mothersill C, Seymour C (1997) Lethal mutations and genomic instability. Int J Radiat Biol 71:751–758
106. Carnes BA, Gavrilova N, Grahn D (2002) Pathology effects of radiation doses below those causing increased mortality. Radiation Res 158:187–194
107. Searle AG (1964) Effects of low-level irradiation on fitness and skeletal variation in an inbred mouse strain. Genetics 50:1159–1178
108. Dobson RL, Kwan TC (1976) The relative biological effectiveness of tritium radiation measured in mouse oocytes increases at low exposure levels. Radiat Res 66:615–625
109. Sazykina TG (2005) A system of dose-effects relationships for the northern wildlife: radiation protection criteria. Radioprotection 40(Suppl 1):S889–S892
110. Gambino JJ, Lindberg RG (1964) Response of the pocket mouse to ionizing radiation. Rad Res 22:586–597
111. Smith DE (1960) The effects of ionizing radiation in hibernation. Bull Museum of Comp Zool 124:493–506
112. Turner FB (1975) Effects of continuous irradiation on animal populations. Adv Radiat Biol 5:83–144
113. French NR, Maza BG, Hill HO, Aschwanden AP, Kaaz HW (1974) A population study of irradiated desert rodents. Ecol Monogr 44:45–72
114. Mihok S (2004) Chronic exposure to gamma radiation of wild populations of meadow voles (*Microtus pennsylvanicus*). J Environ Radioact 7:233–266
115. Kudyasheva AG, Shishkina LN, Shevchenko OG, Bashlykova LA, Zagorskaya NG (2007) Biological consequences of increased natural radiation background for *Microtus oeconomus* Pall. populations. J Environ Radioact 97:30–41
116. Muramatsu S, Sugahara T, Okazawa Y (1963) Genetic effects of chronic low-dose irradiation on mice. Int J Radiat Biol 6:49–59
117. Russell WL (1963) The effect of radiation dose rate and fractionation on mutation in mice. In: Sobels FH (ed) Repair for genetic radiation damage and differential radiosensitivity in germ cells. Pergamon Press, London, pp 205–217
118. Spirin DA (1996) Effects of ionizing radiation on organisms of terrestrial ecosystems in the East Urals radioactive track territory. In: Luykx FF, Frissel MJ (eds) Radioecology and the restoration of radioactive-contaminated sites. Kluwer, Dordrecht, pp 235–244
119. Jackson D, Copplestone D, Stone DM, Smith GM (2005) Terrestrial invertebrate population studies in the Chernobyl exclusion zone Ukraine. Radioprotection 40(Suppl 1):S857–S863
120. Tikhomirov FA, Shcheglov AI (1994) Main investigation results on the forest radioecology in the Kyshtym and Chernobyl accident zones. Sci Tot Environ 157:45–57
121. Kal'chenko VA, Fedotov IS (2001) Genetic effects of acute and chronic ionizing irradiation on *Pinus sylvestris* L. inhabiting the Chernobyl meltdown area. Russian J Genetics 37:341–350
122. Ryabokon NI, Smolich II, Kudryashov VP, Goncharova RI (2005) Long-term development of the radionuclide exposure of murine rodent populations in Belarus after the Chernobyl accident. Radiat Environ Biophys 44:169–181
123. Oleksyk TK, Novak JM, Purdue JR, Gashchak SP, Smith MH (2004) High levels of fluctuating asymmetry in populations of *Apodemus flavicollis* from the most contaminated areas in Chornobyl. J Environ Radioact 73:1–20
124. Chesser RK, Rodgers BE, Wickliffe JK, Gaschak S, Chizhevsky I, Carleton JP, Baker RJ (2001) Accumulation of ^{137}Cesium and ^{90}Strontoium from abiotic and biotic sources in rodents at Chornobyl, Ukraine. Environ Toxicol Chem 20:1927–1935
125. Baker RJ, Hamilton MJ, Van Den Bussche RA, Wiggins LE, Sugg DW, Smith MH, Lomakin MD, Gaschak SP, Bundova EG, Rudenskaya GA, Chesser RK (1996) Small mammals from the most radioactive sites near the Chornobyl Nuclear Power Plant. J Mammalogy 77:155–170
126. Bird GA, Thompson PA, Macdonald CR, Sheppard SC (2002) Ecological risk assessment approach for the regulatory assessment on the effects of radionuclides released from nuclear facilities. In: Third international symposium on the protection of the environment from ionising radiation. Darwin, Australia, 22–26 July, 2002
127. Brisbin IL Jr (1991) Avian radioecology. Curr Ornithol 8:60–140
128. Mellinger PJ, Schultz V (1975) Ionizing radiation and wild birds: a review. Crit Rev Environ Contam 5:397–421
129. Zach R, Mayoh KR (1982) Breeding biology of tree swallows and house wrens in a gradient of gamma radiation. Ecology 63:1720–1728
130. Buech RR (1977) Observations of nesting avifauna under gamma radiation exposure. In: Zavitkovski J (ed) The enterprise, Wisconsin, radiation forest: radioecological studies. U.S. Energy Research and Development Administration, Washington, DC, pp 181–184 (ERDA Report TID-26113-P2)
131. Mraz FR, Woody MC (1972) Effect of continuous gamma irradiation of chick embryos upon their gonadal development. Radiat Res 50:418–425
132. Zach R, Hawkins JL, Sheppard SC (1993) Effects of ionizing radiation on breeding swallows at current radiation protection standards. Environ Toxicol Chem 12:779–786
133. Krivolutsky DA (1987) Radiation ecology of soil animals. Biol Fertil Soils 3:51–55
134. Ellegren H, Lindgren G, Primmer CR, Møller AP (1997) Fitness loss and germline mutations in barn swallows breeding in Chernobyl. Nature 389:593–596
135. Ewing LL, Macdonald CR, Amiro BD (1996) Radionuclide transfer and radiosensitivity in amphibians and reptiles. Atomic Energy of Canada Limited, Pinawa, Manitoba, p 34. (AECL Technical Report TR-731, COG-96-06)
136. Sparrow AH, Nauman CH, Donnelly GM, Willis DL, Baker DG (1970) Radiosensitivities of selected amphibians in relation to their nuclear volume and chromosome volumes. Radiat Res 42:353–371
137. Woodhead AD, Pond V (1987) Effects of radiation exposure on fishes. In: Capuzzo JM, Kester DR (eds) Oceanic processes in marine pollution, vol 1, Biological processes and wastes in the ocean. Robert E Krieger Publishing, Malabar, pp 157–180

138. Conger AD, Clinton JH (1973) Nuclear volumes, DNA contents, and radiosensitivity in whole-body irradiated amphibians. Radiat Res 54:69–101
139. Panter HC (1986) Variations in radiosensitivity during the development of the frog *Limnodynastes tasmaniensis*. J Exp Zool 238:193–199
140. Panter HC, Chapman JE, Williams AR (1987) Effect of radiation and trophic state on oxygen consumption of tadpoles of the frog *Limnodynastes tasmaniensis*. Comp Biochem Physiol 88A:373–375
141. Stark K, Avila R, Wallberg P (2004) Estimation of radiation dose from ^{137}Cs to frogs in a wetland ecosystem. J Environ Radioact 75:1–14
142. Blaylock BG, Trabalka JR (1978) Evaluating the effects of ionizing radiation on aquatic organisms. Adv Radiat Biol 7:103–152
143. Egami N, Ijiri K-I (1979) Effects of irradiation on germ cells and embryonic development in teleosts. Int Rev Cytol 59:195–248
144. Woodhead DS (1984) Contamination due to radioactive materials. In: Kinne O (ed) Marine ecology: a comprehensive, integrated treatise on life in oceans and coastal waters, vol 5, Ocean management. Pt. 3. Pollution and protection of the seas — radioactive materials, heavy metals and oil. John Wiley, Chichester, pp 1111–1287
145. Koulikov AO (1996) Physiological and ecological factors influencing the radiocaesium of fish species from Kiev reservoir. Sci Tot Environ 177:125–135
146. Anderson SL, Harrison FL (1986) Effects of radiation on aquatic organisms and radiobiological methodologies for effects assessment. U.S. Environmental Protection Agency, Washington, DC (Report No. 520/1-85-016)
147. Angelovic JW, White JC Jr, Davis EM (1969) Interactions of ionizing radiation and temperature on the estuarine fish, *Fundulus heteroclitus*. In: Nelson DJ, Evans FC (eds) Proceedings of the 2nd national symposium on radioecology. U.S. Atomic Energy Commission, Washington, DC, pp 131–141, CONF-670503
148. Bonham K, Welander AD (1963) Increase in radioresistance of fish to lethal doses with advancing embryonic development. In: Schultz V, Klement AW (eds) Proceedings of the 1st National Symposium on Radioecology. Reinhold Publishing Corp, New York, pp 353–358
149. Welander AD (1954) Some effects of X-irradiation of different embryonic stages of the trout (*Salmo gairdnerii*). Growth 18:227–255
150. Ward E, Beach SA, Dyson ED (1971) The effect of acute X-irradiation on the development of the plaice *Pleuronectes platessa* L. J Fish Biol 3:252–259
151. Rugh R, Clugston H (1955) Effects of various levels of X-irradiation on the gametes and early embryos of *Fundulus heteroclitus*. Biol Bull 108:318
152. Blaylock BG, Griffith NA (1971) Effect of acute beta and gamma radiation on developing embryos of carp (*Cyprinus carpio*). Radiat Res 46:99–104
153. Donaldson LR, Bonham K (1964) Effects of low-level chronic irradiation of chinook and coho salmon eggs and alevins. Trans Am Fish Soc 93:333–341
154. Bonham K, Donaldson LR (1966) Low-level chronic irradiation of salmon eggs and alevins. In: Proceedings of the symposium on disposal of radioactive wastes into sea, oceans, and surface waters. International Atomic Energy Agency, Vienna, pp 869–883
155. Hershberger WK, Bonham K, Donaldson LR (1978) Chronic exposure of chinook salmon eggs and alevins to gamma irradiation: effects on their return to freshwater as adults. Trans Am Fish Soc 107:622–631
156. Trabalka JR, Allen CP (1977) Aspects of fitness of a mosquitofish *Gambusia affinis* population exposed to chronic low-level environmental radiation. Radiat Res 70:198–211
157. Woodhead DS (1977) The effects of chronic irradiation on the breeding performance of the guppy, *Poecilia reticulata* (Osteichthyes: Teleostei). Int J Radiat Biol 32:1–22
158. Erickson RC (1973) Effects of chronic irradiation by tritiated water on *Poecilia reticulata*, the guppy. In: Nelson DJ (ed) Proceedings of the 3rd national symposium on radioecology. U.S. Atomic Energy Commission, Washington, DC, pp 1091–1099 (CONF-710501)
159. SNIFFER (Scotland & Northern Ireland Forum for Environmental Research) (2002) An investigation into the effects of chronic radiation in fish. Environment Agency, Bristol, UK. (SNIFFER R&D Technical Report P3-053/TR)
160. Makeyeva AP, Yemel'yanova NG, Velova NB, Ryabou IN (1995) Radiobiological analysis of silver carp, *Hypophthalmichthys molitrix*, from the cooling pond of the Chernobyl Nuclear Power Plant since the time of the accident. 2. Development of the reproductive system in the first generation of offspring. J Ichthyol 35:40–64
161. Makeyeva AP, Belova NV, Emer'yanova NG, Verigin BV, Ryabou IN (1996) Materials on the state of reproductive system of bighead *Aristichthys nobilis* from the cooling pond of Chernobyl Nuclear Power Station in the post-disaster period. J Ichthyol 36:181–189
162. Kryshev II, Sazykina TG (1998) Radioecological effects on aquatic organisms in the areas with high levels of radioactive contamination: environmental protection criteria. Radiat Prot Dosim 75:187–191
163. Sugg DW, Bickman JW, Brooks JA, Lomakin MD, Jagoe CH, Dallas CE, Smith MH, Baker RJ, Chesser RK (1996) DNA damage and radiocesium in channel catfish from Chernobyl. Environ Toxicol Chem 15:1057–1063
164. Ilyinskikh NN, Ilyinskikh EN, Ilyinskikh IN (1998) Micronucleated erythrocytes frequency and radiocesium bioconcentration in pikes (*Esox lucius*) caught in the Tom River near the nuclear facilities of the Siberian Chemical Complex (Tomsk-7). Mutat Res 421:197–203
165. Sazykina TG, Kryshev II (1999) Radiation protection of natural ecosystems: primary and secondary dose limits to biota. In: Proceedings of the international symposium on radioactive

waste disposal –health and the environment criteria and standards. Stockholm Environment Institute, Stockholm, pp 115–118
166. O'Brien RE, Wolfe LS (1964) Non genetic effects of radiation. In: Radiation, radioactivity and insects. Academic, New York, pp 23–54
167. Cole MM, LaBrecque GC, Burden GS (1959) Effect of gamma radiation on some insects affecting man. J Econ Entomol 52:448–450 [cited in Rose, 1992]
168. Krivolutsky DA (1980) The effect of an increased Ra content in the soil of soil animals. In: Proceedings of the VII international college of soil zoologists, Syracuse, pp 391–396
169. Hertel-Aas T, Oughton DH, Jaworska A, Bjerke H, Salbu B, Brunborg G (2007) Effects of chronic gamma irradiation on reproduction in the earthworm *Eisenia feida* (Oligochaeta). Radiat Res 168:515–526
170. Krivolutzskii DA, Pokarzhevskii AD (1992) Effects of radioactive fallout on soil animal populations in the 30 km zone of the Chernobyl atomic power-station. Sci Tot Eviron 112:69–77
171. Krivolutzskii DA, Pokarzhevskii AD, Viktorov AG (1992) Earthworm populations in soils contaminated by the Chernobyl atomic power-station accident. Soil Biol Biochem 24:1729–1731
172. Arkhipov NP, Kuchma ND, Askbrant S, Pasternak PS, Musica V V (1994) Acute and long-term effects of irradiation on pine (*Pinus sylvestris*) stands post-chernobyl. Sci Tot Environ 157:383–386
173. Tabone E, Poinsot-Balaguer N (1987) Dynamique de la matière organique dans un sol de forêt miste méditerranéenne (chênes verts-chênes blancs) soumise à une irradiation gamma chronique. Pedobiologia 30:112 [cited in IAEA, 1992]
174. Marshall JS (1962) The effects of continuous gamma radiation on the intrinsic rate of natural increase of *Daphnia pulex*. Ecology 43:598–607
175. Marshall JS (1966) Population dynamics of *Daphnia pulex* as modified by chronic radiation stress. Ecology 47:561–571
176. Gehrs CW, Trabalka JR, Bardill EA (1975) Sensitivity of adult and embryonic calanoid copepods to acute ionizing radiation. Radiat Res 63:382–385
177. Alonzo F, Gilbin R, Bourrachot S, Floriani M, Morello M, Garnier-Laplace J (2006) Effects of chronic alpha radiation on physiology, growth and reproductive success of *Daphnia magna*. Aquat Toxicol 80:228–236
178. Alonzo F, Gilbin R, Zeman FA, Garnier-Laplace J (2008) Increased effects of internal alpha radiation in *Daphnia magna* after chronic exposure over three successive generations. Aquat Toxicol 80:228–236
179. Abbott DT, Mix M (1979) Radiation effects of tritiated seawater on development of the goose barnacle, *Pollicipes polymerus*. Health Phys 36:238–287
180. Jha AN, Dogra Y, Turner A, Millward GE (2005) Impact of low doses of tritium on the marine mussel, *Mytilus edulis*: Genotoxic effects and tissue-specific bioconcentration. Mutation Res 586:47–57
181. Knowles JF, Greenwood LN (1994) The effects of chronic irradiation on the reproductive performance of *Ophryitrocha diadema* (Polychaeta, Dorvilleidae). Mar Environ Res 38:207–224
182. Cooley JL, Nelson DJ (1970) Effects of temperature and chronic irradiation on populations of the aquatic snail *Physa heterostropha*. Oak Ridge National Laboratory, Oak Ridge (ORNL-4612)
183. Cooley JL, Jr Miller FL (1971) Effects of chronic irradiation on laboratory populations of the aquatic snail *Physa heterostropha*. Radiat Res 47:716–724
184. Cooley JL (1973) Effects of chronic environmental radiation on a natural population of the aquatic snail *Physa heterostropha*. Radiat Res 54:130–139
185. Ravera O (1968) Molluscs. In: Proceedings of the symposium on mollusca, part II. Euratom Biology Division, European Atomic Energy Community, Brussels, p 295 (Contribution No. 295)
186. Cruz-Ramos B, Carino VS (1989) Effects of tritiated water on the digestive tract of *Pila luzonica* embryos. Nucleus 27:63–70
187. Tsytsugina VG, Polikarpov GG (2003) Radiological effects on populations of Oligochaeta in the Chernobyl contaminated zone. J Environ Radioact 66:141–154
188. Florou H, Tsytsugina V, Polikarpov GG, Trabidou G, Gorbenko V, Chaloulou CH (2004) Field observations of the effects of protracted low levels of ionizing radiation on natural aquatic population by using a cytogenetic tool. J Environ Radioact 75:267–283
189. Dugle JR, Guthrie JE (1970) Some observations on algae invading a ^{137}Cs contaminated pond. Atomic Energy of Canada Limited, Pinawa (AECL-3463)
190. Mericle LW, Phelps VR, Wheeler AC (1955) Dose-effect relationships in X-irradiated barley embryos. Genetics 40:585 [cited in Luckey, 1980]
191. Woodhead DS (1997) The report on "Effects of Radiation on the Environment" from UNSCEAR (United Nations Scientific Committee on the Effects of Atomic Energy). In: Symposium on radiological impacts from nuclear facilities on non-human species, Ottawa, 1–2 Dec 1996. Canadian Nuclear Society, Toronto, pp 109–119
192. Sparrow AH, Rodgers AF, Schwemmer SS (1968) Radiosensitivity studies with wood plants. I Acute gamma irradiation survival data for 28 species and predictions for 190 species. Radiat Bot 8:149–186
193. Gunckel JE, Sparrow AH (1961) Ionizing radiations: biochemical, physiological and morphological aspects of their effects on plants. In: Ruhland W (ed) External factors affecting growth and development, encyclopedia of plant physiology. Springer, Berlin, pp 555–583
194. UNSCEAR (United Nations Scientific Committee on the Effects of Atomic Radiation) (2008) Sources and effects of ionizing radiation. Report to the general assembly, with

scientific annexes. Annex E. Effects of ionizing radiation on non-human biota
195. Chandorkar KR, Szachrajuk RB, Clark GM (1978) Effect of extremely low radiation dosages on synchronized cultures of *Chlorella pyrenoidosa*. Health Phys 34:494–498
196. Amiro BD (1994) Response of boreal forest tree canopy cover to chronic gamma irradiation. J Environ Radioactivity 24:181–197
197. Amiro BD, Sheppard SC (1994) Effects of ionizing radiation on the boreal forest: Canada's FIG experiment, with implications for radionuclides. Sci Tot Environ 157:371–382
198. Sparrow AH, Schairer LA, Woodwell GM (1965) Tolerance of *Pinus rigida* trees to a ten-year exposure to chronic gamma irradiation from cobalt-60. Radiat Bot 5:7–22
199. Whicker FW, Fraley L Jr (1974) Effects of ionizing radiation on terrestrial plant communities. Adv Radiat Biol 4:1–317 [cited in IAEA, 1992]
200. Geras'kin SA, Zimina LM, Dikarev VG, Dikareva NS, Zimin VL, Vasiliyev DV, Oudalova AA, Blinova LD, Alexakhin RM (2003) Bioindication of the anthropogenic effects on micropopulations of *Pinus sylvestris* L. in the vicinity of a plant for the storage and processing of radioactive waste and in the Chernobyl NPP zone. J Environ Radioact 66:171–180
201. Geraskin SA, Dikarev VG, Ya Zyablitskaya Ye, Oudalova AA, YeV S, Alexakhin RM (2003) Genetic consequences of radioactive contamination by the Chernobyl fallout to agricultural crops. J Environ Radioact 66:155–169
202. Zelena L, Sorochinsky B, von Arnold S, van Syl L, Clapham DH (2005) Indications of limited altered gene expression in *Pinus sylvestris* trees from the Chernobyl region. J Environ Radioact 84:368–373
203. Taskaev AI, Frolova NP, Popova ON, Shevchenko VA (1992) The monitoring of herbaceous seeds in the 30-km zone of the Chernobyl nuclear accident. Sci Tot Environ 112:57–67
204. Rudolph TD (1974) The enterprise, Wisconsin, radiation forest. Pre-irradiation ecological studies. USAEC Report, TID-26116-P1
205. Zavitkovski J (1977) The enterprise, Wisconsin, radiation forest Radioecological studies. TID-26113-P2. National technical Information Service. US Department of Commerce, Springfield
206. Fabries M, Grauby A, trochain JL (1972) Study of a Mediterranean type phytocenose subjected to chronic gamma radiation. Rad Bot 12:125–135
207. Woodwell GM (1963) Design of the Brookhaven experiment on the effects of ionizing radiation on a terrestrial ecosystem. Rad Bot 3:125–133
208. Odum HT, Pigeon RF (1970) A tropical rain forest. A study of irradiation and ecology at El Verde, Puerto Rico. T1D-24270, USAEC Division of Technical Information Extension, Oak Ridge
209. Fraley L Jr, Whicker FW (1973) Response of short-grass plains vegetation to gamma radiation. Rad Bot 13:331–353
210. Miller GL (1968) Influence of season on the radiation sensitivity of an old field community. Thesis, University of North Carolina, Chapel Hill, North Carolina, p 262
211. McCormick JF, Golley FB (1966) Irradiation of natural vegetation. An experimental facility, procedures and dosimetry. Health Phy 12:1467–1474
212. Guthrie JE, Dugle JR (1983) Gamma-ray irradiation of a boreal forest ecosystem: the Field Irradiator-Gamma (FIG) facility and research programs. Can Field Nat 97: 120–128
213. Turner BN, Iverson SL (1976) Project ZEUS: a field irradiator for small-mammal population studies. Atomic Energy of Canada Limited Report, AECL-5524
214. Alexakhin RM, Karaban RT, Prister BS, Spirin DA, Romanov GN, Mishenkov NN, Spiridonov SI, Fesenko SV, Fyodorov YA, Tikhomirov FA (1994) The effects of acute irradiation on a forest biogeocenosis; experimental data, model and practical applications for accidental cases. Sci Tot Environ 157:357–369
215. McCormick JF (1969) Effects of ionizing radiation on a pine forest. In: Neson DJ, Evans FC (eds) Symposium on radioeclogy. United States Atomic Energy Commission, CONF-670503, Washington, DC
216. Poinsot-Balaguer N, Castet R, Tabone E (1992) Impact of chronic gamma irradiation on a Mediterrainean forest ecosystem in Cadarache (France). J Environ Radioact 14:23–36
217. Sheppard SC, Guthrie JE, Thibault DH (1992) Germination of seeds from an irradiated forest: implications for waste disposal. Ecotoxicology Environ Safety 23:320–327
218. Dugle JR, Mayoh KR (1984) Responses of 56 naturally-growing shrub taxa under chronic gamma radiation. Environ Exp Bot 63:1458–1468
219. Godward MBE (1960) Resistance of algae to radiation. Nature 185:706
220. Conter A, Dupouy D, Planel H (1983) Demonstration of a biological effect of natural ionizing radiations. Int J Radiat Biol 43:431–432
221. Garnier-Laplace J, Della-Vedova C, Andersson P, Copplestone D, Cailes C, Beresford NA, Howard BJ, Howe P, Whitehouse P (2010) A multi-criteria weight of evidence approach for deriving ecological benchmarks for radioactive substances. J Rad Prot 30:215–233
222. Woodhead DS, Zinger I (2003) Radiation effects on plants and animals *Deliverable 4* FASSET project. http://www.fasset.org

Books and Reviews

Chipman WA (1972) Ionizing radiation. In: Kinne O (ed) Marine ecology, vol I, part 3. Wiley/Interscience, New York, pp 1579–1657 [cited in Anderson and Harrison, 1986]

Hinton TG, Coughlin DP, Yi Y, Marsh LC (2004) Low dose rate irradiation facility: initial study on chronic exposures to medaka. J Environ Radioact 74:43–55

IAEA (2001) Present and future environmental impact of Chernobyl accident. IAEA-TECDOC-1240

Ophel IL (1976) Effects of ionizing radiation on aquatic organisms. In: Effects of ionizing radiation on aquatic organisms and ecosystems. International Atomic Energy Agency, Vienna, pp 57–88 (Technical Reports Series No. 172)
Polikarpov GG (1966) Radioecology of aquatic organisms. Reinhold Book Division, New York
Smith JT, Beresford NA (2005) Chernobyl – catastrophe and consequences. Springer, Published in association with Praxis Publishing, Chichester
Templeton WL, Nakatani RE, Held EE (1971) Radiation effects. In: Radioactivity in the marine environment. National Academy of Sciences, Washington, DC, pp 223–239

Irrigation Management for Efficient Crop Production

Elías Fereres, Margarita García-Vila
Institute for Sustainable Agriculture, IAS-CSIC and University of Cordoba, Cordoba, Spain

Article Outline

Glossary
Definition of the Subject
Introduction: Background on the Sustainability of Irrigation
The Process of Irrigation at Different Scales: From the Field to the Basin
Irrigation Management Goals for the Improvement of Sustainability
Management Options: Strategic, Tactical, and Operational
Management Under Water Scarcity
Future Directions
Bibliography

Glossary

Application efficiency Relationship between the target irrigation depth (depth of water stored in the root zone to be used by the crop) and the depth of water applied to meet this target during a single irrigation event.

Conservation agriculture (CA) An agricultural production system aimed at achieving a sustainable and profitable agriculture through the application of three principles: minimal soil disturbance, permanent organic soil cover, and diversification of crop species in rotations or associations.

Decision support systems (DSS) Interactive information systems (not limited to computerized systems) that aid decision makers to identify and solve problems, and make decisions, which may be rapidly changing and are not easily specified in advance.

Deficit irrigation (DI) An irrigation strategy based on applying irrigation depths that are less than the full crop water requirements (ET), either throughout the crop life cycle (continuous or sustained deficit irrigation) or during specific stages that are insensitive to water stress (regulated deficit irrigation).

Distribution uniformity A measure of the spatial evenness with which irrigation water is distributed across a field.

Evapotranspiration (ET) The combination of two separate evaporation processes whereby water is lost to the atmosphere, on the one hand from the soil surface and crop surfaces (canopy interception) and on the other hand, from inside the leaves and other organs through pores called stomata, a process termed "transpiration."

Irrigation return flows The combination of surface and subsurface water flows resulting from the runoff and drainage following the application of irrigation water which may be available for subsequent appropriation from either a stream or an aquifer downstream of the original use.

Leaching requirements The depth of water needed to displace the excess salt accumulation in the soil profile resulting from irrigation, and aimed to maintain the salt balance in the crop root zone.

Soil water balance The state of soil water in the crop root zone resulting from the balance between water inputs from precipitation and irrigation and the water losses to evapotranspiration, runoff, and drainage below the root zone.

Water use efficiency (WUE) The ratio between the water volume used for a specific purpose and the water volume derived from a source to accomplish that purpose.

Definition of the Subject

The anticipated population growth in the coming decades will place large worldwide demands to increase

I

the global production of food, animal/fish protein, livestock feed, fiber, and biofuels. Such an increase must come primarily from enhancing productivity, given the constraints in further land expansion for agriculture. Irrigated agriculture currently produces more than 40% of total production on 17% of the land. It is therefore imperative that irrigated agriculture not only sustains its current rates of productivity but that they be increased in the future. Irrigation expansion has taken place over the last 60 years, and is currently under pressure from other sectors to reduce its share of the freshwater resources. Efficient crop production under irrigation in the future would be essential to produce more food with less water than is used today. This goal is a challenge that will not be easy to achieve without new and innovative approaches in irrigation management and in crop productivity. These innovations would also have to address the problems created by the return flows from irrigation which will threaten its sustainability, unless solutions are found to resolve permanently the environmental impacts of irrigation.

Introduction: Background on the Sustainability of Irrigation

The practice of irrigation started soon after agriculture was discovered thousands of years ago. Near the main rivers in the arid zones, water was diverted to the fields where crops were grown in areas and times of lack of rainfall, in an attempt to obtain a stable food supply. The Sumerian civilization that inhabited the Mesopotamia plains is believed to be among the first that used irrigation for crop production. Other locations where major irrigation developments took place early in the history of modern agriculture include the Yellow River basin of China, the Indus River Valley in Pakistan, and the Nile River Valley of Egypt. Many civilizations developed successfully in the past centuries, their food security heavily dependent on irrigation. History is filled with cases, however, where irrigated agriculture failed after some time, leading to the decline and even the disappearance of civilizations (e.g., Mesopotamian civilizations). The causes for failure included technical as well as economical, social, and political factors, but all combined suggest that irrigated agriculture may not be sustainable indefinitely. On the contrary, cases where irrigation has been practiced successfully for millennia, such as the Nile River basin in Africa and many areas of Southeast Asia, prove that it is possible to sustain irrigated agriculture in the long run [1].

Nowadays, irrigation is by far the largest consumer of developed freshwater on a global basis. It is estimated that irrigated agriculture currently uses about two thirds of water diversions, while industry and urban diversions amount to around 20 and less than 10%, respectively [2]. Such a high level of consumption in agriculture is due to the fact that crop plants require a continuous supply of water to replace the water transpired from their leaves and other aerial organs. The water demand arises because the crop is exposed to strong evaporative demand (due to the fluxes of solar and thermal radiation and warm, dry air). For carbon dioxide to enter the leaves, the microscopic leaf pores (stomata) must be open. But when the pores are open, water vapor freely escapes from the interior of the leaves which are nearly saturated with water. Because of the differences in concentration of carbon dioxide and water vapor between the interior of the leaf and the air, 50–100 molecules of water are lost for every molecule of carbon dioxide taken up. Crop water consumptive use is thus an unavoidable consequence of wet crop surfaces being exposed to dry air. Nevertheless, despite the large amounts of water that are transported through the plants, if they are not capable of taking up soil water to replace the losses, water deficits develop which can be detrimental to yield [3]. Therefore, if irrigated agriculture is to be sustainable, it needs sufficient water to meet its requirements at present and in the future.

Presently, more than 260 million ha of irrigated lands exist, representing 17% of the cultivated area but more than 40% of food production worldwide [2]. Future increases in population combined with changes in dietary habits toward the consumption of more animal protein will require sustained increases in crop production in the next decades well above present levels. Additionally, there may be demands on agricultural products for uses other than food production, such as energy from biomass. The increase in production cannot come from a significant expansion of the area devoted to agriculture for at least two reasons. On one hand, the area best suited for agricultural use is already under production, and only in a number of

regions in the American and African continents there is additional land that has not been put under cultivation. Furthermore, that expansion would alter further the balance between agricultural and natural ecosystems, which much of the world population would oppose, arguing for the environmental preservation of the remaining areas that are not in cultivation.

If land expansion will not be possible, the goal would then be to increase productivity, the production per unit of cultivated land. Crop productivity of the main cereals has been increasing steadily since the 1960s, albeit at rates that are apparently declining in recent years [4]. Given that the average productivity of irrigated lands is more than twice that of rainfed areas, it appears that preserving irrigated agriculture would be essential for future food security. The issue is whether it would be possible to expand irrigated agriculture beyond its present level by transforming rainfed into irrigated areas. While some expansion may be possible in the foreseeable future, it is difficult to see how a major world expansion of irrigation would occur, given the present commitments of freshwater (supplies already overcommitted in many arid and semiarid areas), the perceived strong opposition from urban societies, and the uncertainties that climate change brings to future water supplies. It is therefore essential that the productivity of irrigated lands be increased to cope with future demands, and this will have to be done at efficiency levels higher than those achieved at present. The reduction in water used in irrigation per unit production emerges then as a critical issue in the area of crop production in the future.

Irrigated agriculture has to manage large amounts of water that must be utilized with a high level of efficiency. This is not the only requisite of good management, however. All irrigation waters contain salts, and crops transpire pure water; thus, the irrigation process concentrates the salts in the soil profile at a rate which mostly depends on the salt content of the irrigation water. In this respect, the salinity that develops under irrigation would make cropping unsustainable unless the salts are evacuated to prevent the salinization of the crop root zone. In many areas, natural rainfall is sufficient to leach out the salts from the potential root zone. However, when waters of high salinity are used for irrigation in arid areas of limited rainfall, salt leaching must be performed by applying irrigation in excess of the crop needs. The control of salinity is one important requisite of a sustainable irrigated agriculture. However, the water applied in excess of the consumptive use must be disposed of, and this creates a whole host of potential environmental problems associated with water pollution [5]. Many of the problems caused by the return flows from irrigation occur outside the farms, at the level of the irrigation district or at the basin level, and are discussed below.

The Process of Irrigation at Different Scales: From the Field to the Basin

When a field is irrigated, the water applied may be lost via surface runoff or by deep percolation, or may be stored in the crop root zone for subsequent uptake by the crop and lost as ET. However, the focus of irrigation management for efficient crop production extends well beyond a field, up to the farm, the irrigation district, and the watershed. The water balance is the unifying concept that connects the water disposition in the different scales. In any field, farm, or watershed, it is possible to quantify a water balance in which the incoming water in the form of rain or irrigation must be balanced by the water lost as evapotranspiration (ET), runoff, deep percolation, and that stored in the soil profile.

When scaling up from an irrigated field, one needs to consider the situation upstream and downstream of that field. Irrigation water originates from storage reservoirs, flowing streams, or from the groundwater. In all cases it must be conveyed and distributed among the different areas, their farms, and individual fields. The process of distribution entails a number of losses due to direct evaporation from reservoirs and open conduits, leakages from canals, and management losses in the handling of distribution networks that deliver the water to individual farms [6]. Farmers on collective networks do not always have access to water when they need it, and that may cause imbalances between the supply of irrigation water and the crop demand. Those that pump directly from the groundwater have greater flexibility at the expense of additional energy usage. At any rate, by the time the water is delivered to a particular field, there have been distribution and management losses upstream that are often substantial.

The classical work of Bos and Nugteren [7] quantified the efficiency of irrigation along the path from the source of water to the field and found very low values, of the order of 40–50%. Hsiao et al. [8] have also analyzed the efficiency losses in the network, from the dam to the crop, and have highlighted the dramatic differences between good and bad situations, given the multiplicative effects of the chain of efficiencies from the source of water until it is transpired to the atmosphere [8].

At the field scale, water may be used beneficially for ET and for salinity control or may not have a beneficial use when it is lost through runoff or drainage. However, at higher scales, water that evaporates from a watershed is considered a loss or consumption, while water running off a field can be recovered downstream and may not be lost to the system. Equally, water that percolates below the root zone may reach the groundwater from which it can be pumped and recovered. Thus, there are consumptive and nonconsumptive uses of irrigation water. Water applied as irrigation may be used consumptively in the ET process, while the network and runoff losses may be recovered downstream and used by others within the basin. Water used in one farm within a basin is not always consumed in that basin and can be used severa1 times before it leaves the basin.

The difference between water use and consumption is important to understand whether water conservation efforts will result in net water savings [9]. If *all* the water lost outside the ET can be recovered, then efficiency improvements via reducing runoff or percolation losses would not lead to net water savings. On the contrary, if the losses are partially or not recoverable at all, because either the water quality is deteriorated or the losses end in a saline sink, then the water saved at the field scale also represents (partial) savings at the basin scale. Thus, knowing the fate of water all along its path, it is critical to determine whether the water saved on the farm may be part of the recoverable or of the unrecoverable losses.

The basin perspective of water conservation could change the emphasis on where to act when irrigation improvements are sought, and whether such improvements are really needed. Nevertheless, the picture would not be complete if two other issues are not included in the overall assessment of basin irrigation management. One is the fact that field and farm losses, while they could be recovered downstream, often have negative environmental consequences. Surface runoff may carry sediments and chemicals that act as pollutants in streams, lakes, and dams. Drainage waters pick up salts, fertilizers, and other chemicals in the soil profile and may contaminate the groundwater. The other issue is the energy requirements for recovering the losses. Whether is surface runoff recovered at the end of a field or groundwater pumped from the aquifers, additional energy is always needed to recover the losses. Needless to say, the water quality of these return flows would always be worse than that of the original irrigation water.

Irrigation Management Goals for the Improvement of Sustainability

An agriculture that aims toward sustainability should be economically viable, efficient in the use of the natural resource base, socially equitable, and must have a minimal environmental impact. These requisites are essential when defining the goals of irrigation management for efficient crop production. Economic viability in irrigated agriculture is usually associated with *high production levels,* because the investments needed for irrigation development would not be justified under low levels of production. Thus, irrigation must be managed in such a way as to avoid water deficits that reduce economic yield. Not only high production should be sought but also, *high productivity* in relation to the use of production inputs, including water, should be an important goal. Contrary to the common belief, de Wit [10] demonstrated that production inputs are used at their highest efficiency when yields approach the maximum potential. Therefore, it is possible to combine both goals with judicious management.

Equity is an important goal in irrigated agriculture because, first of all, irrigation development represents a quantum leap in terms of increased income relative to rainfed agriculture. Also, sometimes water supplies are managed rigidly by water authorities or are insufficient relative to the potential demand; thus, *equitable distribution* of the available water supply is definitely an important goal of sustainable irrigation management. How this goal is pursued would depend on a number of socioeconomic, political, and cultural factors discussed

below. Finally, irrigation can have a number of detrimental effects on the environment that must be minimized. Firstly, without *control of salinity* agriculture cannot be sustainable [11]. However, the leaching of salts and other chemicals from the soil profile end up as part of the return flows and contribute to the non-point pollution generated by irrigated agriculture. To minimize these negative effects on the environment, irrigation must be managed in such a way as to *avoid runoff* and *minimize deep percolation.* To achieve this goal, the engineering of irrigation systems (to distribute water uniformly) and the scheduling of irrigations (correct timing and application amounts) are the main instruments to be optimized when walking the fine line of achieving high production and productivity while reducing the environmental impact of irrigation.

Management Options: Strategic, Tactical, and Operational

In this entry, we are assuming that farmers have already made a choice among the different irrigation methods, basing their decision on their access to capital, the availability of water and its distribution mode, their management skills, and the labor and energy costs. There are frequent interactions between engineering and management in irrigation that are frequently ignored but are covered here, even though the focus is on management.

The temporal scale determines the nature of irrigation management decisions. Operational decisions are those that must be made in the short term, within days; for instance, the advancing or delaying of one irrigation application. Tactical decisions are those that are taken within the irrigation season once it has started, and have a time scale of days to weeks. One example would be the adjustment of the number of irrigation applications within the season, if the water supply has been reduced after planting. Strategic decisions have a time scale of months to years, and are normally taken before the season starts. The preseason decisions pertaining to the allocation of water to the different fields and crops are examples of strategic decisions.

Crop and Cultivar Selection

Farmers' choice of crops in commercial agriculture is a complex decision that is, above all, based on factors related to production economics and marketing, while other socioeconomic and biophysical factors are considered afterward. The water-related factors such as crop water usage are most important when the supply available is less than the anticipated demand. Crop consumptive use depends primarily on the evaporative demand, the length of season, and the fraction of incoming radiation intercepted by the crop canopy. There are ample differences among the crop ET of different species. These differences are also modulated by the type of climate in which crops are grown. In that respect, there are major differences between tropical and temperate climates. In tropical climates, reference ET (the ET from a standard grass surface: ETo) is relatively constant throughout the year and irrigation is used during the dry season; here, the critical issue is the duration of the growing season, with the goal of producing multiple crops in 1 year. Production per day is the best indicator of efficiency in tropical climates, where crops must follow a sequence that uses best the land and water available.

In temperate climates, evaporative demand during winter is a small fraction than that in the summer. For instance, in Mediterranean-type climates, ETo oscillates between 1–2 mm/day in winter and 6–8 mm/day in summer. Thus, winter crops require much less water than summer crops per unit time. Additionally, seasonal rainfall occurs primarily from fall to spring in those climates, thus reducing the irrigation needs of winter and spring crops. One environmental factor that indirectly affects the crop water requirements in temperate climates is air temperature. Temperatures in winter are low in such climates and that slows down the rate of crop growth and development, thus lengthening crop duration. For instance, the season of winter cereals may last 6–7 months while maize, a summer crop, may be grown in 4 months. These differences in season length balance out some of differences in ETo between winter and summer, but still winter crops generally use less water than summer crops. As an example in some interior valleys of Mediterranean climate, wheat ET is between 350 and 400 mm while maize ET ranges between 600 and 650 mm. Perennial crops have higher ET rates, alfalfa ranging between 800 and 1,200 mm, and deciduous trees between 700 and 1,000 mm. Evergreen tree crops should have the highest ET, however, both citrus and olive have strong stomatal

control of transpiration and their seasonal ET does not exceed values that range between 700 and 1,000 mm, depending on the specific climate.

Crop choice is therefore the most important factor in determining irrigation water requirements. Cultivar differences in water use are considerably smaller than the differences among crops, and are directly related to season length. Early cultivars of maize in temperate climates may use 10–20% less water than late-maturing cultivars. Similar differences have been observed in other crops. Even though such differences are relatively small, they can be important when the crop sequence is such that only short-season cultivars fit in the rotation or when the water supply available is limited. Genetic improvement of the intrinsic transpiration efficiency (TE, g CO_2/g H_2O) [12] has not been successful until now. The limited variability encountered within crop species has not led to cultivars that have higher productivity in irrigated agriculture, although some yield advantage (of the order of 10% at around 1 t/ha yield levels) has been achieved when selecting wheat cultivars for high TE in rainfed environments [13]. The use of genetic engineering in the future [14] may offer new opportunities for enhancing other basic responses that can indirectly improve crop WUE (e.g., maintenance of harvest index under water stress).

Planting dates also have some effects on crop ET in temperate climates. Early plantings of spring or summer crops have lower ET by avoiding the times of peak ETo. One example is that of winter plantings of sunflower in Mediterrranean climates. By planting early, the growing season is displaced away from the summer and the seasonal ET is less, even though the season may be longer due to the slow growth and development in the early crop stages. The irrigation requirements may even be lower because of the higher rainfall probabilities in early spring. In general, plantings of summer crops have been moved as early as feasible to reduce irrigation requirements; this is the case of maize in many areas where the optimal planting dates have moved more than 40 days over the last 30 years. To displace the growing season any further the temperature limitation to growth and development must be overcome. Progress has already been made in crop improvement; for example, maize has expanded significantly into colder areas in the last decades, but more breeding efforts are needed to achieve higher growth rates under low temperatures in the principal irrigated crops.

Contrary to the measurable effects of varying planting dates on crop ET, the variation in planting density within commercial practices has little influence on the ET of annual crops. This is because the differences in radiation interception among different planting densities are small and restricted to the short period of early canopy development. It is important, however, in the case of perennials, as tree or vine densities have a strong influence in the intercepted radiation for several years after the initial planting, and may be carried over the entire life of the orchard or vineyard. Biomass production and thus yield of most crops is directly related to the seasonal intercepted radiation. Any agronomic practice that favors quick canopy development and complete radiation interception should increase production and will have a smaller effect on crop ET, thus increasing the efficiency of water use.

Optimal Use of Rainfall and of Stored Soil Water

The goal of irrigated crop production is to use all sources of water supply as effectively as possible. Soil water storage from rainfall or from preplanting irrigation is an effective way of using the water resource. To maximize stored soil water, infiltration should be enhanced so that surface runoff is minimized. Low infiltration rates decrease the effectiveness of rainfall to the point that only a small fraction of it may be stored in the potential crop root zone for subsequent use by the crop. Many irrigated soils have problems of slow infiltration, either inherent to their physical makeup or caused by the application of irrigation water for a long time that alters negatively the surface infiltration properties of the soil [15].

Excessive tillage of some irrigated soils and, more importantly, the traffic required in crop intensification under irrigation has exacerbated the problems related to low infiltration, which not only reduces the effectiveness of rainfall but also affects the distribution of irrigation water. The use of minimum tillage, no-tillage, surface residues, permanent beds, and of controlled traffic is all being incorporated into what is now known as conservation agriculture [16]. These soil management systems have been used successfully in many world areas for sometime now, primarily under

rainfed agriculture, but they are now increasingly being adopted for irrigated agriculture as well. The benefits of conservation agriculture (CA) include soil surface protection by the crop residues, the maintenance of soil organic matter, increased infiltration, and better distribution uniformity. The limitation of CA is that it needs to be tailored to the specific situation thus requiring field experimentation before it is introduced in a new area or system. The widespread expansion of CA in the main agricultural areas of the world [17] suggests that it will be adapted to many irrigated systems in the near future.

The critical role of rainfall, while being obvious in rainfed agriculture, is nearly as important in irrigated agriculture because it leads to a reduction in irrigation demand. The best strategy for optimal use of stored soil water is the conjunctive use of both, the applied irrigation water and the soil reserve. It is desirable that the soil is partially depleted to allow the storage of anticipated rainfall in the root zone, although such depletion has to be managed to avoid yield-reducing water deficits (See below). As the crop approaches maturity, it is recommended to rely more on the stored reserve and use as much of it as possible, thus reducing irrigation water use. Ideally, the soil reserve should be almost totally depleted when the crop is harvested, assuming it will be replenished by rainfall. Obviously, to manage the soil reserve, it must be quantified from planting to harvest. Growers need to know the level of soil water at planting and the rate of water use (ET) relative to the depths of irrigation and rainfall. Therefore, making best use of the rainfall and of the water reserve requires carrying out a seasonal water budget for each crop. It is also important to evaluate the risk of basing a limited irrigation strategy on using a large fraction of the stored rainfall, because in the event of a drought, irrigation would be insufficient to meet the crop demand and this strategy may not be sustainable.

Technical Irrigation Scheduling

Decisions on when to irrigate and how much water to apply – the irrigation scheduling process – are commonly made by irrigators around the world solely based on experience. There are, however, a collection of technical procedures and tools developed to forecast the timing and amount of irrigation applications. Some sort of irrigation on demand is a prerequisite for the application of these technical procedures, because when the delivery method of the network is on rotation, the farmers have no flexibility to vary the irrigation interval and they tend to use all the water they receive as insurance for uncertain conditions.

Among water-sensing devices, soil water sensors were perhaps the first instruments that were introduced for irrigation scheduling in the 1950s, and it is remarkable that they have enjoyed a certain degree of success until recently. There is now a new generation of soil water sensors that track soil water status continuously, rather than providing point measurements as the traditional instruments such as the tensiometer offer. Unfortunately, the new developments have not resolved the quantification of volumetric soil water content with depth, a parameter that is still most reliably measured with the neutron probe since the early 1970s. The regulatory constraints on this nuclear instrument have limited its use even for research in many countries, with the result that reliable data on soil water balance and crop ET are difficult to obtain with soil water measurement methods. The information from current sensors is treated as trends and these tendencies, often observed at more than one depth, are the basis for making decisions, rather than using a threshold value of soil water at a given depth as the indicator of irrigation timing. Protocols have been developed to automate irrigation scheduling on the basis of soil water status [18].

The use of plant water sensors for irrigation management lagged behind that of soil water sensors by about 2 decades. The pressure chamber was the first portable instrument that was rugged enough to be used under field conditions, although it is manually operated and its readings cannot be automated. It is now used commercially in some areas for irrigation scheduling of tree crops and vines. Other plant sensors have not been as successful for their use in practical scheduling, although they have been around for sometime. The most notable example is that of dendrometers, sensors that detect the variations in stem diameter, which were used since the 1950s and have today the same degree of precision they have had since the 1970s, but they became popular for research 20 years later. Protocols to be used with trunk diameter sensors have

also been proposed [19] although its use, while attractive, has been mostly limited for research purposes. One of the most promising plant-based indicators is the canopy temperature as measured by infrared thermometry. Jackson and coworkers (summarized in [20]) developed several indicators based on canopy temperature, the Crop Water Stress Index (CWSI) being the most popular. Threshold values of CWSI have been found for several crops and its use as a water stress indicator is gaining acceptance. Plant-based parameters are best used as pre-visual indicators of water stress, rather than being indicative of irrigation timing and amount. Their strength resides in providing a specific, crop-based calibration for other methods that use either soil water sensors or the water balance procedure. One important limitation of all soil- and plant-based sensors is the variability in the measurements, as discussed in Coping with Spatial Variability: Precision Irrigation.

The most robust technique for wide use in irrigation scheduling is the one using the soil water budget. Here, irrigation timing is computed by adding the crop ET losses minus effective rainfall until a soil water level termed "the allowable depletion" is reached. The basic information in this method is that of crop ET, computed as the product of a crop coefficient times ETo. After a method for computing ETo has been standarized and widely accepted [21], agrometeorological weather stations provide the information needed for calculating ETo from meteorological variables. In some developed countries, networks of weather stations now provide the ETo information routinely. The pan evaporation is a viable alternative for estimating ETo to the more sophisticated automated weather stations. Computer programs have been developed for calculating the water balance of fields, and irrigation scheduling services have been developed, mostly by public agencies and by consultants as well. These services have been around for several decades now but most farmers have been reluctant to pay for them. Nevertheless, irrigation advisory services are becoming more popular in areas of scarce or expensive water. One pattern that has been observed is that farmers subscribe to these technical procedures or services for a few years and then, they no longer use them. Perhaps they perceive that they have acquired sufficient knowledge during that time period, a reason that may also explain why the use of sensors is discontinued after some time by many growers.

Interactions Between Irrigation Methods and Their Management

Irrigation has been practiced for thousands of years by flooding the soil surface and keeping the water standing until it infiltrates. This method is named surface irrigation and it is still the most popular method worldwide. In surface irrigation, the soil intake rate determines the depth of water that infiltrates and if its properties are spatially variable, the farmer will not have good control of the amount of water applied. Pressurized irrigation methods (sprinkler and microirrigation) were invented much more recently, about 70 years ago. Since then, they have enjoyed increasing popularity in areas where farmers have access to sufficient capital to shift from surface to pressurized systems. In other, newly developed areas where topography and/or water infiltration properties made the use of surface methods impractical, pressurized methods have been preferred over surface irrigation. One advantage of pressurized systems is that the depth of applied water does not depend on soil properties but is determined directly by the run time. Farmers' preferences for pressurized systems are based on the need for better control and the greater skills needed for effective surface irrigation management. The higher capital and energy requirements are two limitations of pressurized systems relative to surface irrigation.

The key feature of irrigation systems in relation to their management is the degree of uniformity of water distribution. Regardless of the method, high distribution uniformity prevents excessive percolation losses in some areas of the field and the development of water deficits in others. To emphasize the importance of high distribution uniformity suffices here to summarize an example in which the performance of two systems with low (70%) and high (90%) distribution uniformity (DU) were compared for maize irrigation [22]. The additional depth of water needed under low uniformity to achieve maximum yields amounted to 400 mm, or 70% of the net irrigation requirements. The requisites for high DU include an appropriate design, good

maintenance, and correct operations. Nowadays, efficient irrigation cannot be practiced unless high to very high DU values are achieved.

All irrigation methods have potentially high performance that can eliminate or minimize runoff and percolation losses, but they seldom achieve their potential due primarily to lack of maintenance or to mismanagement. To optimize the operation of existing surface irrigation systems the water delivery procedures often need to be changed. There are needs relating to adjusting the flow rates delivered to fields, altering the operation of delivery networks, and sometimes land consolidation is also needed. Such changes not only require capital investments but agreements among various users as well. The introduction of pressurized systems (sprinkler and drip) in collective irrigation networks also requires changes in the physical infrastructure (e.g., reservoirs). Thus, there must be economic incentives for the farmers and access to capital to introduce the improvements needed to increase the potential application efficiency and distribution uniformity at the system level.

Control of Salinity and of Return Flows

Irrigated agriculture cannot be sustainable unless salinity is properly managed. Salts that accumulate in the root zone must be leached but the amount of leaching must be kept to the minimum if the environmental impacts of drainage waters and the return flows are to be controlled. Determining the leaching fraction (proportion of the ET that must be added for salt leaching) should be based not only on the quality of irrigation and drainage waters but on the need to avoid excessive percolation. Here again, high DU is essential when the target leaching fraction is of the order of 5–10%, which is only achievable under very high DU values.

The use of salt-tolerant crops is often proposed as a means of controlling salinity. It is true that there is an ample range of salinity tolerance among crop plants and that it is possible to exploit waters of low quality for irrigation of salt-tolerant crops. However, because the process of salt concentration in the profile in the absence of leaching is inexorable, the use of salt-tolerant crops should be considered as a temporary measure until excess salts can be leached out of the potential root zone. Sometimes, tolerant crops have been used for some years in the event of a drought that limits the irrigation supply available for leaching. Their long-term use in dry areas should not be considered sustainable, given the progressive salinization of irrigated soils. After some environmental problems related to toxicity caused by the selenium content of the return flows, the drainage from a large area in California, San Joaquin Valley, was interrupted in 1989 [23]. The rainfall in the area is negligible, thus salt leaching depends on artificial drainage. As of 2010, the area is still under irrigation; irrigation systems installed have high DU values and there is an extensive monitoring program of soil salinity. Perhaps long-term control of salinity would be feasible with systems that have very high DU, and where irrigations are scheduled with precision, keeping most of the salts near the bottom of the root zone, as it was first proposed by Hoffman et al. [24].

At scales beyond that of a field or farm, the concerns shift toward the quality of return flows, its reuse, and the environmental impacts of irrigation. The decline in water quality after the water has gone through the irrigation process has an associated cost that needs to be quantified. The concept that water lost to a farm is recovered downstream needs to have associated an economic analysis of the energy costs and the quality deterioration costs of recovering the return flows. If minimum leaching is practiced at the field scale, the amount of return flows is also reduced but that increases the concentration of salts and other contaminants in the drainage waters. Eventually, it may be possible to reduce the quantity of return flows so much so that they can be disposed of in evaporation ponds that become salt sinks. It would then be possible to either accumulate or export the salts and make the agriculture of that region fully sustainable.

Coping with Spatial Variability: Precision Irrigation

The major challenge that technical farm irrigation management has faced and continues to face is how to cope with variability. Under field conditions, both spatial and temporal variabilities are the norm rather than the exception. The strong spatial heterogeneity of soil water properties even in what are considered uniform soils, combined with the variations in the distribution of irrigation water applications, and the

uncertainties of rooting depth and densities, all contribute to create a heterogeneous environment that farmers have to manage as accurately as feasible. The problem has increased in magnitude over the last decades due to the increase in size of the management units, in an attempt to reduce production costs by managing uniformly larger and larger field units. The complexities involved in dealing with the variability problem are such that, until very recently, the common solution chosen by irrigators was to apply water in excess so that the risk of inducing water deficits in some parts of the field is minimized. Because of the difficulties that farmers and technicians have had in characterizing the variability, significant uncertainty is introduced and often the irrigation management decisions may be in error.

To advance solutions for coping with the variability problem in irrigation management what is needed is to be able to characterize the variation across a field, and also to have the option of applying variable amounts of water within that field. The objective would then be to apply variable water depths under non-uniform crop growing conditions to match the requirements of every area of the field, while minimizing the environmental consequences that uniform irrigation over a variable field would have. The technologies for variable water application are already available in self-propelled sprinkler systems and can lead to significant water conservation [25]. Significant efforts in the engineering of irrigation systems have been undertaken recently to offer the flexibility of applying spatially variable amounts of water (and agrochemicals) for the different pressurized methods, including microirrigation [26]. These new capabilities should enable growers to increase productivity and minimize environmental impacts of irrigation.

While the engineering solutions for precision irrigation are underway, there is still the need, not only to characterize and monitor the variability but to interpret the causes of the variations in crop growth and development. The characterization of irrigation performance through remote sensing [27] is a promising area, as it enables performance evaluation in a fast and an inexpensive way, and can also identify the areas in need of improvement. Interpreting the underlying causes of variations among and within fields is much more difficult, however. The use of remote sensing techniques has progressed substantially in recent years by developing capabilities for detecting a number of vegetation properties with very high resolution (e.g., [28]). High-resolution imagery cannot be acquired from current satellites, and a number of initiatives to obtain them from aerial vehicles flying closer to the ground have been launched recently. As an example that is relevant for irrigation management, Berni et al. [29] applied models based on canopy temperature estimated from high-resolution airborne imagery, obtained with an unmanned aerial vehicle, to calculate tree canopy conductance and the CWSI of heterogeneous canopies, such as those of tree crops.

Use of Simulation Models and of Decision Support Systems

Decision-making in crop production has been the focus of numerous studies, mainly on the description of the decision-making process and decision outcomes [30]. The numerous decisions dealing with irrigation management include, not only the scheduling and application of the available water to different crops over the irrigation season, but also strategic decisions related to crop choices and seasonal water allocation. Irrigation is a complex operation, based on technical and agronomic knowledge, and on sociological factors which may include a negotiating process among irrigators [31]. Recent advances in information and telecommunication technologies allow farmers to acquire vast amounts of site-specific data for their farms, with the ultimate goal of *reducing uncertainty* in decision-making. However, farmers face many difficulties in efficiently managing, analyzing, and interpreting the vast amount of data collected, while considering both the costs and value of the information [30].

The tactical decisions related to irrigation scheduling have been discussed above; however, strategic decisions that must take into account the complex nature of agricultural systems and changes in environmental conditions are difficult to make without tools that assist the farmer in the decision-making process. Among the tools available in the area of water management are the Decision Support Systems (DSS), which were first used in the early 1970s as a radical alternative to large-scale management information systems [32]. There are different types of DSS; many of them are expert systems [33], which have the problem of

handling multiple experts to evolve decisions and uncertainty. Linear programming, dynamic programming, and non-linear programming are the most popular modeling techniques; while recently, genetic algorithms [34] have been used to generate optimal solutions more efficiently [35] than dynamic programming (e.g., [36]). Also, DSS have been shown to help decision-making at different scales: at the field level, considering only one crop (e.g., [37]); and at the farm scale, with multiple crops (e.g., [38]).

Because irrigation decisions include many factors, the DSS combine crop simulation models with econometric models to assist farmers in optimizing irrigation management, according to environmental, socioeconomic, and political prospects [39]. The yield response to different irrigation levels is one of the inputs of DSS that traditionally has been quantified as empirical crop-water production functions [40–42]. Even though these functions have been used profusely, they are site-specific and difficult to extrapolate without costly, empirical calibration. An alternative to crop-water production functions is the use of dynamic crop simulation models [43]. Among the simulation models usable for irrigation decision-making are CropSyst [44], EPIC [45], CROPWAT [46], APSIM [47], and CERES [48]. However, most of these models require detailed information (difficult to obtain) about parameters that describe plant behavior (APSIM, CERES), or make use of simple empirical functions (CROPWAT). The models must be calibrated, validated, and be sufficiently robust to provide reliable predictions. For this reason, detailed models may be less practical than simpler but robust models [49] such as the recently published FAO water productivity model, AquaCrop [50]. AquaCrop is a model focused on simulating attainable yield in response to the water available, and it is thought to have an optimum balance between accuracy, simplicity, and robustness [50]. In water-limited situations, these models can be helpful in determining the optimal level of irrigation water that leads to maximizing income (e.g., [51]).

To make informed decisions that will enhance the efficiency of irrigation, farmers need to be able to assess how agricultural systems respond to internal (e.g., new technology) and external changes (such as those in the economic and political context, water constraints, or climate change). Therefore, DSS may be used for scenario analyses, showing the effects of alternative scenarios on irrigation management for efficient crop production [39]. The possibility of DSS implementation to assist farmers on irrigation management creates opportunities to establish a relationship that leads to the solution of problems and research feedback, redirecting the paths of research to better solve problems. Until now DSS are not commonly used directly by farmers as they are considered complex tools, which usually lack a user-friendly interface that permits easy access by the users. Irrigation advisory services of the irrigator's communities may be the right platform for the introduction of DSS, being potentially a major breakthrough in improving the use and management of irrigation water.

Management Under Water Scarcity

At present and more so in the future, irrigated agriculture will take place under water scarcity. Insufficient water supply for irrigation will be the norm rather than the exception, and irrigation management will shift from emphasizing production per unit area toward maximizing the production per unit of water consumed, the water productivity (WP).

Water Allocation Constraints and Their Impact on Management

While irrigation is an ancient technique, its expansion is very recent. The world area under irrigation has more than doubled in the last 60 years [4], in response to the increase in food demand. This expansion has required the development of additional water supply through the construction of dams for storing surface waters and exploitation of the groundwater resource. The sustainability of supply depends on the long-term rainfall and on the rate of groundwater recharge. As the irrigated areas expanded, the pressures on the finite water resources in some areas increased and the balance between supply and demand was altered (e.g., [52]). Two issues cause the imbalances; first, periodic drought cycles reduce the availability of water supply, some times during several years. Then, the increases in the demands from other sectors of society, notably the environment that has been neglected in the past, compete with irrigation demands, which are often considered the lowest in priority. The expansion of

groundwater use is also a cause of concern; it is possible that the abstraction exceeds the rate of recharge, causing a decline in the water table depth with time. In fact, groundwater may be considered a reservoir of supply that may be overexploited during drought years, when surface supplies are scarce. However, when the aquifers are depleted in the long run and do not recover after years of high rainfall, the groundwater overdraft is unsustainable and the abstraction must be reduced to sustainable levels.

Regardless of the causes for water scarcity, knowing the degree of supply reduction is essential for farmers to make rational decisions regarding how to manage the limited supplies. Preseason decisions are centered on crop choice and/or to land abandonment. Matching demand to supply is achieved by selecting low-water-use crops or by leaving some land in fallow, if the supplies are insufficient to irrigate all the developed land. Once the season starts it is much more difficult to make adjustments, if the reduction in supply is significant. Changes in the irrigation system to reduce percolation and other operational losses, changes in scheduling to reduce the number of applications thus reducing E losses, and the use of deficit irrigation (see below) are the only options left to growers once the season has started and the crops have been planted.

Water scarcity does not occur overnight, and water authorities and farmers have conservative attitudes to avoid risks. Predictions of big cuts in supply that do not materialize reduce economic opportunities, but the reverse may be even more catastrophic. Thus, planning in advance by water authorities and by irrigation districts, and knowing precisely the expected level of reduction are the two key elements to manage successfully the anticipated scarcity. Seasonal predictions of rainfall would be very useful to anticipate droughts and consequently, irrigation supply reductions. One paradox is the enormous investment in climate change research relative to that devoted to medium range weather predictions, and the apparent lack of connections between two areas that should be closely related.

Deficit Irrigation

Deficit irrigation (DI) is defined as the application of water below the crop ET requirements. Therefore, water demand for irrigation can be decreased relative to full irrigation and the water saved can be diverted for alternative uses. Even though DI is simply a technique aimed at the optimization of economic output when water is limited [53], the reduction of irrigation supply to an area imposes many adjustments in the agricultural system. Thus, DI practices are multifaceted, inducing changes at the technical, socioeconomical, and institutional levels.

In the humid and subhumid zones, irrigation supplements the rainfall as a tactical measure during drought spells to stabilize production. This practice has been called supplemental irrigation [54] and, although it uses limited amounts of water due to the relatively high rainfall levels, the goal is to achieve maximum yields and to eliminate yield fluctuations caused by water deficits. Supplementing rainfall in arid areas with one or more irrigation applications is a form of DI as maximum yields are not sought. When irrigation is applied at rates below the ET under DI, the crop extracts water from the soil reservoir to compensate for the deficit. Two situations may then develop. In one case, if sufficient water is stored in the soil and transpiration is not limited by soil water, even though the volume of irrigation water is reduced, the consumptive use (ET) is unaffected. However, if the soil water supply is insufficient to meet the crop demand, growth and transpiration are reduced and DI induces an ET reduction below its maximum potential. The difference between the two situations has important implications at the basin scale [55]. In the first case, DI does not induce net water savings and yields should not be affected. If the stored soil water that was extracted is replenished by seasonal rainfall, the DI practice is sustainable and has the advantage of reducing irrigation water use. In the second case, both water use and consumption (ET) are reduced by DI but yields may be negatively affected in cases where yields are directly related to ET [56].

There are several strategies to impose the water deficits under DI, but basically there are two alternatives [56]. One is to impose the same level of deficit over the entire irrigation season (continuous or sustained DI), while the other concentrates the deficits in certain crop growth stages believed to be the least sensitive to water stress (Regulated DI, RDI). Deficit irrigation, by reducing irrigation water use, can aid in coping with situations where supply is constrained. In field crops, a well-designed DI regime can optimize WP

over an area when full irrigation is not possible. It will reduce yield to a certain extent because of the linear relations between ET and the yield of the major field crops [40]. In many horticultural crops, such as fruit trees and vines, RDI has been shown to improve not only WP but farmers net income as well. Because of the differential responses among the different crops to water deficits it would be important to investigate the basis for the positive responses to water deficits in the cases where water deficits are not detrimental to yield. While DI can be used as a tactical measure to reduce irrigation water use when supplies are limited by droughts or other factors, it is not known whether it can be used over long time periods, given that the reduction in applied water could lead to greater accumulation of salts in the profile. It is imperative to investigate the sustainability of DI via long-term experiments and modeling efforts to determine to what extent it can contribute to the permanent reduction of irrigation water use.

Future Directions

Farmers in irrigated agriculture are confronted, at the start of every season with a critical question: How much water would be available this season, and how should I distribute it among the different crops and fields? There are many procedures and tools to answer those questions in such a way that the water allocation will be used efficiently. In fact efficiency of water use in irrigated agriculture has been steadily increasing with the improvements in science and technology, and as pressures from other sectors of society mount. Irrigation management encompasses several scales, from the network down to the individual field. One of the primary management targets at the field level is, once the amount of water needed is precisely determined, to distribute it over the field as uniformly as possible. Elimination of surface runoff and minimal percolation losses are prerequisites for optimizing irrigation water use and for limiting the environmental impacts of irrigation.

Monitoring, evaluation, and real-time feedbacks for benchmarking and to assess irrigation performance is essential for efficient water use. In the future, performance evaluation will be done routinely and at low cost with the use of remote sensing techniques. These surveys will allow the identification of areas within irrigation networks in need of improvement, and farmers will have the information to modify practices or to change methods, thus achieving greater productivities. Incentives are needed, however, for farmers to adopt new technologies for more efficient water use when water supplies are abundant and/or inexpensive.

The recent expansion of irrigation combined with increased water supply limitations will lead to water scarcity in many areas. In those situations, efficient use of water will be critical for the sustainability of irrigated agriculture. Deficit irrigation will be used more, and other socioeconomic measures, such as water markets, will play a more important role in water scarce situations [57]. Planning ahead in water-limited situations would be critical to achieve optimal use of water, and it is envisaged that robust DSS that include economic models will be used to allocate the limited irrigation water available among different users in networks and among crops in farms.

Finally, bridging the yield gap between potential and actual yields offers another avenue for improving the efficiency of water use in irrigated agriculture. Crops that are limited only by solar radiation and temperatures have potential yields that are several times the current world average yields. For instance, wheat world averages are reaching 3 t/ha, while the potential yield approaches 14 t/ha. In the case of maize, average world yield is about 5 t/ha while the potential yield exceeds 18 t/ha. The yield gap is not only important in rainfed conditions [58], but under irrigated conditions as well. Differences that exist between actual and potential yields are caused by many factors, water being just one of them. Therefore, it is most important to optimize crop agronomy in all of its facets, from soil to crop management, and from pest and disease management to weed control. Most of the time, yield improvement by better agronomy does not increase crop ET significantly, and it has proven over and over again to be a very effective path for enhancing the efficiency of water use now and in the near future.

Bibliography

Primary Literature

1. Fahlbusch H, Schultz B, Thatte CD (2004) The Indus basin: history of irrigation, drainage and flood management. ICID, New Delhi

2. Molden D (2007) Water for food, water for life: a comprehensive assessment of water management in agriculture. Earthscan/IWMI, London
3. Hsiao TC, Acevedo E, Fereres E, Henderson DW (1976) Water stress, growth, and osmotic adjustment. Philos Trans R Soc Lond B 273:479–500
4. FAOSTAT (2010) http://faostat.fao.org/. Verified on 26 May 2010
5. Tanji KK (1990) Nature and extent of agricultural salinity. In: Tanji KK (ed) Agricultural salinity assessment and management. ASCE, New York, pp 1–17
6. Clemmens AJ (2006) Improving irrigation water performance through an understanding of the water delivery process. Irrig Drain 55:223–234
7. Bos MG, Nugteren J (1990) On irrigation efficiencies, 4th edn. International Institute for Land Reclamation and Improvement (ILRI), Publication 19, Wageningen
8. Hsiao TC, Steduto P, Fereres E (2007) A systematic and quantitative approach to improve water use efficiency in agriculture. Irrig Sci 25:209–231
9. Jensen ME (2007) Beyond irrigation efficiency. Irrig Sci 25: 233–245
10. de Wit CT (1992) Resource use efficiency in agriculture. Agric Syst 40:125–151
11. Van Schilfgaarde J (1984) Drainage design for salinity control. In: Shainberg I, Shalhevet J (eds) Soil salinity under irrigation. Springer, New York, pp 190–197
12. Steduto P, Hsiao TC, Fereres E (2007) On the conservative behavior of biomass water productivity. Irrig Sci 25:189–207
13. Richards RA (2006) Physiological traits used in the breeding of new cultivars for water-scarce environments. Agric Water Manage 80:197–211
14. Salekdeh GH, Reynolds M, Bennett J, Boyer J (2009) Conceptual framework for drought phenotyping during molecular breeding. Trends Plant Sci 14:488–496
15. Shainberg I, Levy GJ (1996) Infiltration and seal formation processes. In: Agassi M (ed) Soil erosion, conservation, and rehabilitation. Marcel Dekker, New York, pp 1–22
16. FAO (2010) http://www.fao.org/ag/ca/. Verified on 26 May 2010
17. Derpsch R, Friedrich T (2009) Global Overview of Conservation Agriculture Adoption. Proceedings: 4th World Congress on Conservation Agriculture, 4–7 February 2009, New Delhi, pp 429–438
18. Thompson RB, Gallardo M, Agüera T, Valdez LC, Fernandez MD (2006) Evaluation of the watermark sensor for use with drip irrigated vegetable crops. Irrig Sci 24:185–202
19. Goldhamer DA, Fereres E (2001) Irrigation scheduling protocols using continuously recorded trunk diameter measurements. Irrig Sci 20:115–125
20. Jackson RD (1982) Canopy temperature and crop water stress. Adv Irrig 1:43–85
21. Allen RG, Pereira LS, Raes D, Smith M (1998) Crop evapotranspiration: guidelines for computing crop water requirements, FAO irrigation and drainage paper 56. FAO (Food and Agriculture Organization), Rome
22. Mantovani EC, Orgaz F, Villalobos FJ, Fereres E (1995) Modelling the effects of sprinkler irrigation uniformity on crop yield. Agric Water Manage 27:243–257
23. Benson SM, White AF, Halfman S, Flexser S, Alavi M (1991) Groundwater contamination at the Kesterson reservoir, California 1. Hydrogeologic setting and conservative solute transport. Water Resour Res 27:1071–1084
24. Hoffman GJ, Dirksen C, Ingvalson RD, Maas EV, Oster JD, Rawlins SL, Rhoades JD, Van Schilfgaarde J (1977) Minimizing salt in drain water by irrigation management: design and initial results of Arizona field studies. Agric Water Manage 1:233–252
25. Sadler EJ, Evans RG, Stone KC, Camp CR (2005) Opportunities for conservation with precision irrigation. J Soil Water Conservat 60:371–379
26. Evans RG, Sadler EJ (2007) New technologies to improve crop water use efficiencies [CD-ROM]. S164. Lawrence Media
27. Santos C, Lorite IJ, Tasumi M, Allen RG, Fereres E (2010) Performance assessment of an irrigation scheme using indicators determined with remote sensing techniques. Irrig Sci. doi:10.1007/s00271-010-0207-7
28. Zarco-Tejada PJ, Berni JAJ, Suárez L, Sepulcre-Cantó G, Morales F, Miller JR (2009) Imaging chlorophyll fluorescence from an airborne narrow-band multispectral camera for vegetation stress detection. Rem Sens Environ 113:1262–1275
29. Berni JAJ, Zarco-Tejada PJ, Sepulcre-Cantó G, Fereres E, Villalobos F (2009) Mapping canopy conductance and CWSI in olive orchards using high resolution thermal remote sensing imagery. Rem Sens Environ 113:2380–2388
30. Fountas S, Wulfsohn D, Blackmore BS, Jacobsen HL, Pedersen SM (2006) A model of decision-making and information flows for information-intensive agriculture. Agric Syst 87:192–210
31. Maton L, Leenhardt D, Goulard M, Bergez JE (2005) Assessing the irrigation strategies over a wide geographical area from structural data about farming systems. Agric Syst 86:293–311
32. Arnott D (2006) Cognitive biases and decision support systems development: a design science approach. Inf Syst J 16:55–78
33. Mohan S, Arumugam N (1997) Expert system applications in irrigation management: an overview. Comput Electron Agric 17:263–280
34. Goldberg DE (1989) Genetic algorithms in search, optimization and machine learning. Addison-Wesley, Madison
35. Azamathulla HMd, Wu FC, Ab Ghani A, Narulkar SM, Zakaria NA, Chang CK (2008) Comparison between genetic algorithm and linear programming approach for real time operation. J Hydro Environ Res 2:172–181
36. Kipkorir EC, Raes D, Labadie J (2001) Optimal allocation of short-term irrigation supply. Irrig Drain Syst 15:247–267
37. Bergez JE, Garcia F, Lapasse L (2004) A hierarchical partitioning method for optimizing irrigation strategies. Agric Syst 80: 235–253

38. Bazzani GM (2005) An integrated decision support system for irrigation and water policy design: DSIRR. Environ Model Softw 20:153–163
39. Stoorvogel JJ, Antle JM, Crissman CC, Bowen W (2004) The tradeoff analysis model: integrated bio-physical and economic modeling of agricultural production systems. Agric Syst 80:43–66
40. Stewart JI, Hagan RM (1973) Functions to predict effects of crop water deficits. J Irrig Drain Div 99:421–439
41. Doorenbos J, Kassam AH (1979) Yield response to water, FAO irrigation and drainage paper No. 33. FAO (Food and Agriculture Organization), Rome
42. Vaux HJ, Pruitt WO (1983) Crop-water production functions. In: Hillel DI (ed) Advances in irrigation, vol II. Academic, New York, pp 61–97
43. Loomis RS, Rabbinge R, Ng E (1979) Explanatory models in crop physiology. Annu Rev Plant Physiol 30:339–367
44. Stöckle CO, Donatelli M, Nelson R (2003) CropSyst, a cropping systems simulation model. Eur J Agron 18:289–307
45. Jones CA, Dyke PT, Williams JR, Kiniry JR, Benson CA, Griggs RH (1991) EPIC: an operational model for evaluation of agricultural sustainability. Agric Syst 37:341–350
46. Smith M (1992) CROPWAT: a computer program for irrigation planning and management, FAO irrigation and drainage paper No. 46. FAO (Food and Agriculture Organization), Rome
47. McCown RL, Hammer GL, Hargreaves JNG, Holzworth DP, Freebairn DM (1996) APSIM: a novel software system for model development, model testing and simulation in agricultural systems research. Agric Syst 50:255–271
48. Ritchie JT, Godwin DC, Otter-Nacke S (1985) CERES – wheat: a simulation model of wheat growth and development. Texas A&M University Press, College Station
49. Sinclair TR, Seligman NG (1996) Crop modeling: from infancy to maturity. Agron J 88:698–704
50. Steduto P, Hsiao TC, Raes D, Fereres E (2009) AquaCrop – the FAO crop model to simulate yield response to water: I. Concepts and underlying principles. Agron J 101:426–437
51. García-Vila M, Fereres E, Mateos L, Orgaz F, Steduto P (2009) Deficit irrigation optimization of cotton with AquaCrop. Agron J 101:477–487
52. Sophocleous M (2005) Groundwater recharge and sustainability in the high plains aquifer in Kansas, USA. Hydrogeol J 13:351–365
53. English MJ (1990) Deficit irrigation. I: analytical framework. J Irrig Drain Eng 116:399–412
54. Debaeke P, Aboudrare A (2004) Adaptation of crop management to water-limited environments. Eur J Agron 21:433–446
55. Fereres E, Goldhamer DA, Parsons LR (2003) Irrigation water management of horticultural crops. Historical review compiled for the American Society of Horticultural Science's 100th Anniversary. HortScience 38:1036–1042
56. Fereres E, Soriano MA (2007) Deficit irrigation for reducing agricultural water use. J Exp Bot 58:147–159
57. Jury AJ, Vaux HJ (2007) The emerging global water crisis: managing scarcity and conflict between water users. Adv Agron 95:1–76
58. Sadras VO, Angus JF (2006) Benchmarking water use efficiency of rainfed wheat in dry environments. Aust J Agric Res 57: 847–856

Books and Reviews

Burt CM, Clemmens AJ, Strelkoff TS, Solomon KH, Bliesner RD, Howell TA, Eisenhauer DE (1997) Irrigation performance measures: efficiency and uniformity, Journal of Irrigation and Drainage Engineering 123, No. 6. ASCE (American Society of Civil Engineers), New York, pp 423–442

Evans RG, Sadler EJ (2008) Methods and technologies to improve efficiency of water use: W00E04, Water Resources Research 44, No. 7. American Geophysical Union, Washington

Fereres E, González-Dugo V (2009) Improving productivity to face water scarcity in irrigated agriculture. In: Sadras VO, Calderini DF (eds) Crop physiology: applications for genetic improvement and agronomy. Academic, New York, pp 123–143

Lamm FR, Ayars JE, Nakayama FS (2007) Microirrigation for crop production, Developments in agricultural engineering 13. Elsevier, Amsterdam

Malano H, Burton M (2001) Guidelines for benchmarking performance in the irrigation and drainage sector. IPTRID/FAO, Rome

Molden D (2007) Water for food, water for life, A comprehensive assessment of water management in agriculture. Earthscan/IWMI, London

National Research Council (1996) A new era for irrigation. National Academy, Washington

Passioura JB, Angus JF (2010) Chapter 2 – improving productivity of crops in water-limited environments, Advances in agronomy 106. Academic, San Diego, pp 37–75

I

Isotope Separation Methods for Nuclear Fuel

Shuichi Hasegawa
Department of Systems Innovation, School of Engineering, The University of Tokyo, Tokyo, Japan

Article Outline

Glossary
Definition of the Subject
Introduction

Principles of the Separation Processes
Cascade Theory
Laser Isotope Separation (LIS)
Future Directions
Bibliography

Glossary

Isotope Nuclei of a chemical element which have the same number of protons but different number of neutrons. Some isotopes are stable; some are radioactive.

Separation factor A ratio of a mole fraction of an isotope of interest to that of non-interest in an enriched flow divided by that in a depleted flow from a separation unit. The factor should be larger than unity for the unit to result in isotopic enrichment.

Separation capability A measure of separative work by a cascade per unit time.

Mean free path An average distance of a moving gas molecule between its collisions.

Molecular flow Low-pressure phenomenon when the mean free path of a gas molecule is about the same as the channel diameter; then a molecule migrates along the channel without interference from other molecules present.

Definition of the Subject

Isotope separation, in general, means enrichment of a chemical element to one of its isotopes (e.g., ^{10}B in B; ^{6}Li in Li, ^{157}Gd, etc). In the case of uranium, isotope separation refers to the enrichment in the isotope ^{235}U, which is only 0.711% of natural uranium; today's nuclear power plants require fuel enriched to 3–5% in ^{235}U. Uranium enrichment is the subject of this article.

Efficiencies of sorting out different isotopes of the element (separation factor) are usually very low. For practical enrichment plants, a gaseous diffusion process has been successfully employed to obtain enriched uranium. A gas centrifugation process is the preferred method of enrichment today due to reduced energy consumption. A new process using lasers, which can have a high efficiency of separation, is under development and has the potential to replace the current enrichment methods.

Introduction

The fuel used today by commercial nuclear power plants is the fissile isotope ^{235}U. Unfortunately, ^{235}U is only 0.711% of natural uranium, the rest of which is, essentially, ^{238}U. Light water reactors (LWR) operating dominantly all over the world require isotope enrichment processes because the isotopic ratio of ^{235}U for their fuels should be 3–5%. The processes used to elevate the ^{235}U content from 0.711% to 3–5% are called isotope separation or enrichment processes. Table 1 shows the current trends of isotope separation capabilities of the world. The main countries performing the process are Russia, France, US, and URENCO (Germany, Netherland, and UK). A number of separation processes have been studied so far, but the principles of the current isotope separation processes mainly use gaseous diffusion or gas centrifugation. The diffusion process was commercialized first but the centrifugation is taking over because of less energy consumption. This article following mainly [2, 3] describes the

Isotope Separation Methods for Nuclear Fuel. Table 1
World Enrichment capacity (thousand SWU/year) [1]

Country	2010	2015	2020
France (Areva)	8,500*	7,000	7,500
Germany, Netherlands, UK (Urenco)	12,800	12,200	12,300
Japan (JNFL)	150	750	1,500
USA (USEC)	11,300*	3,800	3,800
USA (Urenco)	200	5,800	5,900
USA (Areva)	0	>1,000	3,300
USA (Global Laser Enrichment)	0	2,000	3,500
Russia (Tenex)	23,000	33,000	30–35,000
China (CNNC)	1,300	3,000	6,000–8,000
Pakistan, Brazil, Iran	100	300	300
Total approx.	57,350	69,000	74–81,000
Requirements (WNA reference scenario)	48,890	55,400	66,535

Source: WNA Market Report 2009; WNA Fuel Cycle: Enrichment plenary session WNFC April 2011
*Diffusion

principles of the two processes and cascade theory, which explains why it is required to repeat the process many times (using successive stages/cascades) to obtain a certain desired enrichment fraction such as 3–5% because a single step provides only a small incremental enrichment. The new enrichment technology using lasers will be described at the end.

Principles of the Separation Processes

Gaseous Diffusion

Figure 1 shows the schematic diagram of the gaseous diffusion process. Consider a chamber divided into two compartments by a porous membrane. When dilute gases are introduced into the bottom compartment of the chamber, the pores of the membrane (membrane) make dependency of the transmission of the gases on their molecular masses.

If we have a mixture of two molecules in a gas with the same kinetic energy (kinetic energy is determined by kT, k = Boltzmann constant; T = temperature in K; ($1/2\ mv^2 \sim kT$)), the lighter molecule is faster than the heavier one. Therefore, their frequencies of hitting the membrane is higher for the lighter than for the heavier molecule. However, the mass preference phenomena occur only when the mean free path of the gas molecule is longer than the diameter of the pores $2r$ and the thickness of the membrane l. The mean free path, λ of the molecule can be written as [2]

$$\lambda = \frac{kT}{4\sqrt{2}\pi\sigma^2 p} \tag{1}$$

where k is the Boltzmann constant, T is the absolute temperature, σ is the radius of the molecule, and p is the gas pressure in the chamber. In this condition, a molecule cannot collide with others during the transmission through the membrane so that its dynamics can be considered as a single molecule process. This process is called molecular flow. The flux of the molecular flow through the flow path with circular cross section is derived by Knudsen as [3]

$$G_{mol} = \frac{8r\Delta p}{3l\sqrt{2\pi mRT}} \tag{2}$$

where G_{mol} is the molecular flow velocity, m is the molecular mass, R is the gas constant, and $\Delta p = p'' - p'$ is the pressure difference between the bottom and top compartments of the chamber. Equation 2 shows that the flow velocity depends on the mass of the gas molecules so that the ratio of the molecules in the mixture transmitted to the upper compartment of the chamber is changed compared with that of the feeding gas. The opposite condition where flows do not depend on the molecular mass is called viscous flow.

We will derive the ideal separation factor in the case of $^{235}UF_6$ and $^{238}UF_6$ [3], the gas molecules used for uranium enrichment. On the ideal condition where p'' is very small and p′ can be neglected compared with p'', when we have a binary mixture of gases which consist of $^{235}UF_6$ (molecular mass: m_{235} = 349, mole fraction: x) and $^{238}UF_6$ (molecular mass: m_{235} = 352, mole fraction: $1 - x$), the molecular flow velocities of $^{235}UF_6$ and $^{238}UF_6$ are

$$G_{235} = \frac{ap''x}{\sqrt{m_{235}}}, \quad G_{238} = \frac{ap''(1-x)}{\sqrt{m_{238}}} \tag{3}$$

where the constant a includes factors in Eq. 2. The ratio of the molecular flow of $^{235}UF_6$ to the whole can be written as

$$s = \frac{G_{235}}{G_{235} + G_{238}} = \frac{\frac{x}{\sqrt{m_{235}}}}{\frac{x}{\sqrt{m_{235}}} + \frac{1-x}{\sqrt{m_{238}}}} = \frac{\frac{x}{1-x}}{\frac{x}{1-x} + \sqrt{\frac{m_{235}}{m_{238}}}} \tag{4}$$

Therefore, the ideal separation factor α_0 of the gaseous diffusion process can be derived as the separation factor of the molecular flow of the porous media

$$\alpha_0 = \frac{\frac{s}{1-s}}{\frac{x}{1-x}} = \sqrt{\frac{m_{238}}{m_{235}}} = \sqrt{\frac{352}{349}} = 1.00429 \tag{5}$$

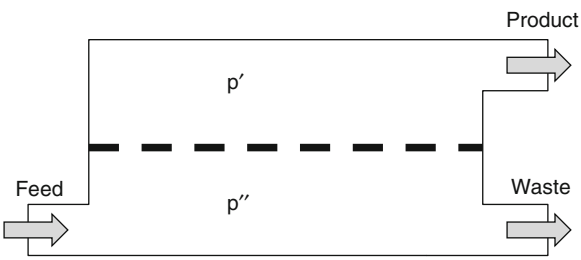

Isotope Separation Methods for Nuclear Fuel. Figure 1 A single gaseous diffusion stage

The separation factor depends on the ratio of the molecular masses so that this method is more effective for the isotope separation of lighter elements. For heavier elements, a larger number of repeated processes is required to obtain sufficiently enriched products.

However, in reality, the real value of the separation factor is smaller than that given by Eq. 5 due to reverse molecular flow from the upper compartment to the bottom one and viscous flow not depending on the molecular mass; these two phenomena work in a direction negating the enrichment process. Furthermore operating conditions (porous media performance, working pressures, etc.) affect the value of the separation factor. The energy consumption to run the process is very high due to pressure controlling of the gases, small separation factors and so on (see discussion about Separative Work Unit). Because of the relatively high energy consumption, uranium enrichment by gaseous diffusion is on the way out and is replaced by the gas centrifugation method.

Gas Centrifugation

The principle of gas centrifugation is based upon centrifugal forces that are created inside a rotating cylinder containing two different gas molecules, forces that depend on the molecular mass. Let's see how it works in detail [2]. When we have a mixture of two gas molecules in a rotating cylinder (centrifuge), pressure gradients develop with respect to the radial direction. The pressures can be written as

$$\frac{dp}{dr} = \omega^2 r\rho \tag{6}$$

where p is the pressure, r is the radial distance, ω is the angular frequency of rotation, and ρ is the density of the gases. By substituting the equation of state $\rho = pm/RT$ into the differential equation, we can derive the following equation,

$$\frac{dp}{p} = \frac{m\omega^2}{RT} r dr \tag{7}$$

When we integrate this differential equation from the radial distance r (pressure p_r) to the inner radius of the cylinder a (pressure p_a), we can obtain this expression,

$$\frac{p_r}{p_a} = \exp\left[-\frac{1}{2}\frac{mv_a^2}{RT}\left\{1-\left(\frac{r}{a}\right)^2\right\}\right] \tag{8}$$

where the speed of the outer circumference of the cylinder $v_a = \omega a$ This equation shows that the ratio of the pressure at radius r to that of radius a depends on the molecular mass of the gases.

If we have the gases which consist of $^{235}UF_6$ (molecular mass: m_{235} = 349, mole fraction: x) and $^{238}UF_6$ (molecular mass: m_{235} = 352, mole fraction: $1 - x$), their ratios of the partial pressures at the radius r to the radius a can be derived as

$$\frac{p_r x_r}{p_a x_a} = \exp\left[-\frac{1}{2}\frac{m_{235}v_a^2}{RT}\left\{1-\left(\frac{r}{a}\right)^2\right\}\right] \tag{9}$$

$$\frac{p_r(1-x_r)}{p_a(1-x_a)} = \exp\left[-\frac{1}{2}\frac{m_{238}v_a^2}{RT}\left\{1-\left(\frac{r}{a}\right)^2\right\}\right] \tag{10}$$

Therefore, the local separation factor at radial distance r of radius a is given by

$$\alpha = \frac{\frac{x_r}{1-x_r}}{\frac{x_a}{1-x_a}} = \exp\left[\frac{(m_{238}-m_{235})v_a^2}{2RT}\left\{1-\left(\frac{r}{a}\right)^2\right\}\right] \tag{11}$$

which depends on the difference of their molecular masses, $\Delta m = m_{238} - m_{235} = 3$. Values of the local separation factor of $^{235}UF_6$ and $^{238}UF_6$ with T = 300 K and v_a = 700 m/s are given in Table 2. This feature is superior to the gaseous diffusion method when the difference of the masses is large, (e.g., for heavier elements). The separation factor increases as the speed of the outer circumference increases. However, the maximum speed v_{max} is limited by stresses created to the cylinder from the force of the centrifugation and can be written as [2]

$$v_{max} = \sqrt{\frac{\sigma}{\rho}} \tag{12}$$

where ρ is the density of the material of the cylinder, and σ is the tensile strength. Although most molecular

Isotope Separation Methods for Nuclear Fuel. Table 2
The local separation factor of $^{235}UF_6$ and $^{238}UF_6$ at r/a with T = 300K, υ_a = 700m/s

r/a	0	0.5	0.8	0.9	0.95	0.98	0.99	1.0
α	1.343	1.247	1.112	1.058	1.029	1.012	1.006	1.0

gases are localized at $\frac{r}{a} \approx 1$ because of the centrifugation, the values of the separation factor could be higher than those obtained from the gaseous diffusion method. These values can be enhanced if we make use of a countercurrent flow in the vertical direction. Figure 2 shows the schematic diagram of countercurrent centrifugation method. Gernot Zippe performed pioneering work on the development of the centrifugation first in the Soviet Union during 1946–1954, and from 1956 to 1960 at the University of Virginia. The countercurrent flow can be induced by heating and cooling centrifuges, or pipes drawing off flows in centrifuges. The temperature control can adjust the flow deliberately but the equipment becomes more complicated than that of the flow control by the pipes (Fig. 2). This countercurrent flow makes enrichment of the lighter isotopes at inner radius as the flow descending along the axis direction, and the heavier isotopes are being enriched at the circumference as the flow ascending. These enriched gases are collected at different radial positions of the both ends (at outer radius for heavier isotope and at inner radius by baffle for lighter isotope). When the centrifuge has a length L, the maximum separative power δU_{max} can be derived as [2, 4]

$$\delta U_{max} = \frac{\pi}{2} L \rho D \left(\frac{\Delta m v_a^2}{2RT} \right)^2 \tag{13}$$

where D is diffusion coefficient. The maximum separative power is proportional to the height of the centrifuge. It is preferable to have a taller centrifuge in the vertical direction, but the length is imposed on the resonant vibration of the centrifuge. The resonant conditions can be written as [3]

$$\left(\frac{L}{a}\right)_i = \sqrt{\lambda_i} \sqrt[4]{\frac{E}{2\sigma'}} \quad \lambda_i = 22.0, 61.7, 121.0, 200.0, 298.2, \cdots \tag{14}$$

where E is coefficient of elasticity. A taller centrifuge can give a larger separative power although excellent mechanical properties are required to overcome the resonant conditions.

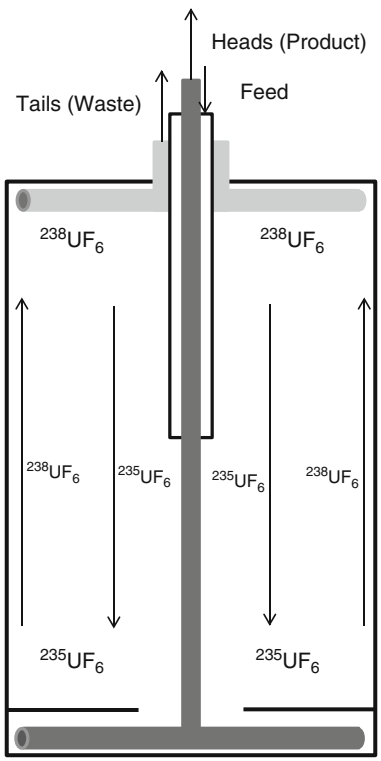

Isotope Separation Methods for Nuclear Fuel. Figure 2 Schematics of gas centrifuge with countercurrent flow

Cascade Theory

The present isotope separation plants make use of these principles of enrichment with small separation factors. In order to obtain high enrichment ratios, cascade theory is necessary [3]. According to the theory, we can enhance the ratios by iterating a single physical stage many times. Figure 3 shows a simple scheme of a cascade. An original material "feed" is provided to the system. The isotope of interest is enriched as going through many separation stages and a final output "product" is obtained. Another output which mainly contains unnecessary isotopes is called "waste." Each flow F, P and W should have the following equation

$$F = P + W \tag{15}$$

and with mole fractions of the isotope of interest in each flow x_F, x_P, x_W, we can obtain

$$Fx_F = Px_P + Wx_W \tag{16}$$

In this system, we have four independent parameters to define. In order to obtain necessary flow of Product "P" and mole fraction "x_P" of the isotope of interest, we need the design methodology to construct stages of separation units. The product of

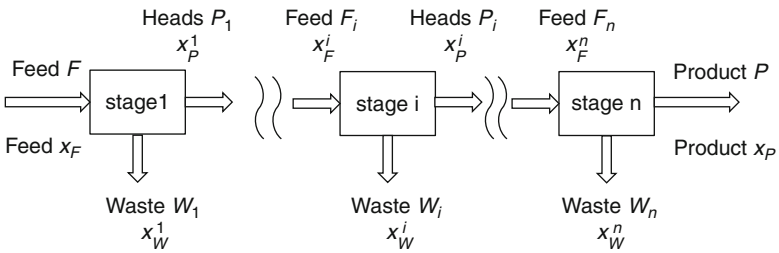

Isotope Separation Methods for Nuclear Fuel. Figure 3
Simple scheme of the cascade

a single stage (unit) is called heads and the waste of that is tails. The ratios of the isotope of interest in the product are usually most important. If, for instance, we have two isotopes "1" and "2," and want to enrich the "1" isotope, we would focus on the variation of the mole fraction ratio of the two isotopes, $\frac{x_1}{x_2}$, which can be rewritten as $\frac{x_1}{1-x_1}$. The capability of each enrichment unit is described as separation factor α. This factor is defined as the ratios of the isotopes of interest to that of not-interest in the heads (product) divided by those in the tails (waste)

$$\alpha = \frac{\dfrac{x_P}{1-x_P}}{\dfrac{x_W}{1-x_W}} \tag{17}$$

In a similar way, we can define the ratio of the heads (product) to the feed as heads separation factor β, and that of the feed to the tails as tails separation factor γ,

$$\beta = \frac{\dfrac{x_P}{1-x_P}}{\dfrac{x_F}{1-x_F}},\ \gamma = \frac{\dfrac{x_F}{1-x_F}}{\dfrac{x_W}{1-x_W}} \text{ and } \alpha = \beta\gamma \tag{18}$$

The ratio of the product to the feed is called "cut" θ and defined as

$$\theta \equiv \frac{P}{F} = \frac{x_F - x_w}{x_P - x_W} \tag{19}$$

The simplest design to accomplish enrichment is to accumulate separation stages in a single line such as Fig. 4. This scheme is called simple cascade.

Simple Cascade

In this scheme, the heads and the mole fraction of the i th stage are equal to the feed flow and the mole fraction of the $i+1$ th stage (Fig. 4).

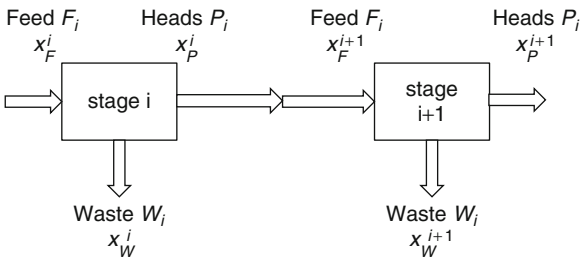

Isotope Separation Methods for Nuclear Fuel. Figure 4
Simple cascade of the i and i + 1 th stages

$$F_{i+1} = P_i, \quad x_F^{i+1} = x_P^i \tag{20}$$

This cascade disposes of the tails of all stages so that the total amount of the isotope of interest in the waste should be given sufficient attention. This can be evaluated by means of the recovery rate of the i th stage r_i

$$r_i = \frac{P_i\, x_P^i}{F_i\, x_F^i} = \theta_i \frac{x_P^i}{x_F^i} = \frac{x_F^i - x_W^i\, x_P^i}{x_P^i - x_W^i\, x_F^i} = \frac{1 - \dfrac{x_W^i}{x_F^i}}{1 - \dfrac{x_W^i}{x_P^i}} = \frac{\alpha_i - \beta_i}{\alpha_i - 1} \tag{21}$$

When we have n stages in the cascade, the total recovery rate r can be expressed as

$$r = \frac{P\, x_P}{F\, x_F} = \frac{P_n\, x_P^n}{F_1\, x_F^1} = \frac{P_1\, x_P^1\, P_2\, x_P^2}{F_1\, x_F^1\, F_2\, x_F^2} = \frac{P_n\, x_P^n}{F_n\, x_F^n} = r_1\, r_2 \cdots r_n \tag{22}$$

The over-all separation factor of the cascade ω can be derived as

$$\omega = \frac{\dfrac{x_P^n}{1-x_P^n}}{\dfrac{x_F^1}{1-x_F^1}} = \beta_1\, \beta_2 \cdots \beta_n \tag{23}$$

Therefore, if α, β do not depend on each stage, the total recovery rate can be rewritten as

$$r = \left(\frac{\alpha - \beta}{\alpha - 1}\right)^n = \left(\frac{\alpha - \omega^{\left\{\frac{1}{n}\right\}}}{\alpha - 1}\right)^n \tag{24}$$

When the feed itself is available without any special cost, the simple cascade is effective. But in case the wastes from each stage should not be disposed because, for instance, it is valuable or the recovery rate has to be increased, the waste flows are recycled as feed flow, which is called countercurrent recycle cascade (Fig. 5).

Countercurrent Recycle Cascade

Since the simple cascade cannot improve the recovery rate, the tail flow is recycled into either stage to use it efficiently, which is called recycle cascade (Fig. 5). If β (heads separation factor) is equal to γ (tails separation factor) in all stages, we can obtain $x_W^{i+2} = x_F^{i+1} (= x_P^i)$. So the tails flow of the $i + 2$ th stage can be merged to the heads flow of the i th stage and fed into the $i + 1$ th stage without any mixing loss. We will consider the case that the tails flow of the second upper stage is refluxed to the i th stage.

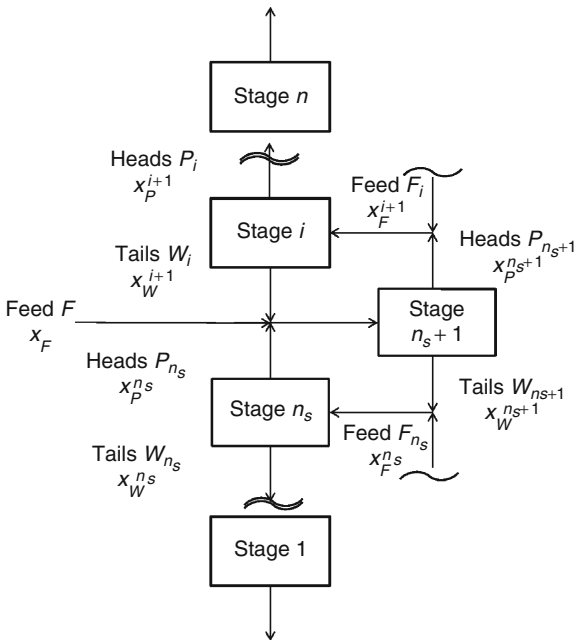

Isotope Separation Methods for Nuclear Fuel. Figure 5 Countercurrent recycle cascade

The flows and the fractions of the isotope of interest in each stage of enriching sections should have the following relationships.

$$P_i = W_{i+1} + P, \quad P_i\, x_P^i = W_{i+1}\, x_w^{i+1} + P x_P \tag{25}$$

In a similar way, those in stripping sections can be expressed as

$$W_{j+1} = P_j + W, \quad W_{j+1}\, x_W^{j+1} = P_j\, x_P^j + W x_W \tag{26}$$

Let's estimate the number of stages. From these equations, we can derive

$$x_P^i - x_W^{i+1} = \frac{x_P - x_P^i}{\frac{W_{i+1}}{P}} \tag{27}$$

At total reflux, where the reflux ratio is infinity,

$$\frac{W_{i+1}}{P} \to \infty \tag{28}$$

the mole fraction of the heads flow at the i th stage x_P^i becomes equal to that of the tails flow at the i + 1 th stage x_W^{i+1} and the number of the stages is minimal.

$$\frac{x_P^{i+1}}{1 - x_P^{i+1}} = \alpha \frac{x_W^{i+1}}{1 - x_W^{i+1}} = \alpha \frac{x_P^i}{1 - x_P^i} = \alpha^2 \frac{x_P^{i-1}}{1 - x_P^{i-1}} = \cdots \tag{29}$$

gives the following equation,

$$\frac{x_P}{1 - x_P} = \alpha^n \frac{x_W}{1 - x_W} \tag{30}$$

and the minimum number of the stages at total reflux can be derived as

$$n = \frac{1}{\ln \alpha} \ln\left(\frac{x_P}{1 - x_P} \frac{1 - x_W}{x_W}\right) \tag{31}$$

On the contrary, the reflux ratio becomes minimum when the mole fraction of the heads at the i + 1 th stage is equal to that of the heads at the i th stage ($x_P^{i+1} = x_P^i$).

Ideal Cascade

Ideal cascade satisfies the condition that the values of β (heads separation factor) at all stages are constant and the mole fraction of the heads flow at the $i + 1$ th stage is equal to those of the tails flow at the $i - 1$ th stage and

of the feed flow at the i th stage ($x_p^{i+1} = x_W^{i-1} = x_F^i$). In this instance, each separation factor satisfies the following relationship.

$$\beta = \sqrt{\alpha} = \gamma \tag{32}$$

In a similar way to the previous section, we can obtain the total number of the stages for an ideal cascade

$$\begin{aligned} n &= \frac{1}{\ln \beta} \ln \left(\frac{x_P}{1 - x_P} \; \frac{1 - x_W}{x_W} \right) - 1 \\ &= \frac{2}{\ln \alpha} \ln \left(\frac{x_P}{1 - x_P} \; \frac{1 - x_W}{x_W} \right) - 1 \end{aligned} \tag{33}$$

The number of stages in stripping n_S and enriching $n_E = n - n_S$ sections can be derived as

$$n_S = \frac{1}{\ln \beta} \ln \left(\frac{x_F}{1 - x_F} \; \frac{1 - x_W}{x_W} \right) - 1 \tag{34}$$

$$n_E = n - n_S = \frac{1}{\ln \beta} \ln \left(\frac{x_P}{1 - x_P} \; \frac{1 - x_F}{x_F} \right) \tag{35}$$

The reflux ratio Eq. 27 can be rewritten using $x_P^i = x_F^{i+1}$ and β as

$$\frac{W_{i+1}}{P} = \frac{x_P - x_P^i}{x_P^i - x_W^{i+1}} = \frac{1}{\beta - 1} \left\{ \frac{x_P}{x_W^{i+1}} - \frac{\beta(1 - x_P)}{1 - x_W^{i+1}} \right\} \tag{36}$$

Mccabe–Thiele Diagram

It is useful to draw McCabe–Thiele diagram to investigate the design of the cascade, the mole fractions of the stages and so on. Figure 6 shows a typical McCabe–Thiele diagram. In this graph, the horizontal and vertical axes correspond to the mole fractions of the heads flow x_P^i and of the tails flow x_W^i, respectively.

First, the following equation is satisfied at the enrichment process of the i th stage because of the definition of the separation factor

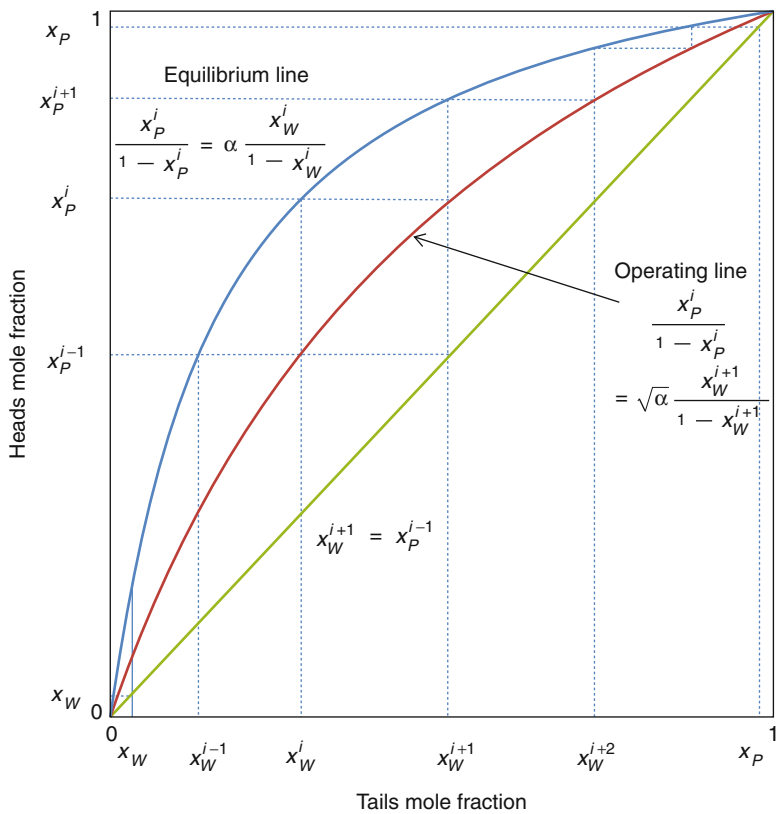

Isotope Separation Methods for Nuclear Fuel. Figure 6
McCabe-Thiele diagram

$$\frac{x_P^i}{1-x_P^i} = \alpha \frac{x_W^i}{1-x_W^i} \text{(Equilibrium line)} \tag{37}$$

Second, the condition that the tail (waste) flow at the i + 1 th stage is the feed of the i th stage ($x_F^i = x_W^{i+1}$) defines the relationship between the mole fractions of the tail (waste) and head (product) flows at different stages as follows

$$\frac{x_P^i}{1-x_P^i} = \beta \frac{x_F^i}{1-x_F^i} = \sqrt{\alpha} \frac{x_W^{i+1}}{1-x_W^{i+1}} \text{(Operating line)} \tag{38}$$

And third, the feed flow at the i th stage consists of the tails flow of the i + 1 th stage and the heads flow of the i − 1 th stage and their mole fractions are the same.

$$x_W^{i+1} = x_P^{i-1} \tag{39}$$

These three formulae can be shown in the McCabe–Thiele diagram as shown in Fig. 6. We can estimate the number of necessary stages, mole fractions of the stages, and overview the total processes through the graphical construction.

Separative Work Unit

The total flow in the cascade can be derived as

$$\sum_i (P_i + W_i) = \frac{\beta+1}{(\beta-1)\ln\beta}\left[W(2x_W-1)\ln\left(\frac{x_W}{1-x_W}\right) + P(2x_P-1)\ln\left(\frac{x_P}{1-x_P}\right) - F(2x_F-1)\ln\left(\frac{x_F}{1-x_F}\right)\right] \tag{40}$$

The first term of Eq. 40 including β indicates the difficulty of the separation and increases as the value of β approaches to unity. The second term corresponds to the amount of work for separation, and it has the same dimension as flow rates and is called separative capacity or separative power. This value is important because it is considered to be proportional to the initial cost of the plant. When we use the unit of the amounts of material (mole, kg, etc.) instead of flow rates, this is called separative work. The sum of the annual investment and operation costs can be expressed by the product of the separative work SW (kg SWU/year) and unit price of separative work c_s (\$/kg SWU). SWU is the abbreviation of Separative Work Unit. The separative work is defined as

$$SW = W\phi(x_W) + P\phi(x_P) - F\phi(x_F) \tag{41}$$

where $\phi(x_i)$ is called separation potential and written as

$$\phi(x_i) = (2x_i - 1)\ln\frac{x_i}{1-x_i} \tag{42}$$

When we use kg SWU/year for the separative work, the unit of W, P, and F should be kg/year.

For operating the plant, we need the raw materials, the amount of which is F (kg/year) and unit price of the raw materials c_F (\$/kg). The total cost per year c (\$) can be written as

$$c = SWc_S + Fc_F \tag{43}$$

When the amount of the product per year is P (kg), the unit cost of the product $c_P = \frac{c}{P}$. could be derived as

$$c_P = \frac{SWc_s}{P} + \frac{Fc_F}{P} = \left\{(\phi(x_P) - \phi(x_F)) - (x_P - x_F)\frac{\phi(x_F) - \phi(x_W)}{x_F - x_W}\right\}c_s + \left(\frac{x_P - x_W}{x_F - x_W}\right)c_F \tag{44}$$

Example

With the ideal cascade of the gaseous diffusion method (α = 1.00429), the mole fraction of the feed flow 0.711% (x_F = 0.00711) would be enriched to 3% (x_P = 0.03) and the mole fraction of the waste is planned to be 0.3% (x_W = 0.003). In this case, the necessary moles of the feed and the waste to obtain the product of 1 [mol] are

$$F = \frac{P(x_P - x_W)}{x_F - x_W} = \frac{1\times(0.03-0.003)}{0.00711-0.003} = 6.569[mol]$$

$$W = \frac{P(x_P - x_F)}{x_F - x_W} = \frac{1\times(0.03-0.00711)}{0.00711-0.003} = 5.569(=6.569-1)[mol]$$

The total number of stages n and the number of stages in stripping section n_S and in enriching section n_E are calculated as

Stripping Section

$$n_S = \frac{2}{\ln\alpha}\ln\left(\frac{x_F}{1-x_F}\,\frac{1-x_W}{x_W}\right) - 1$$
$$= \frac{2}{\ln 1.00429}\ln\left(\frac{0.00711}{1-0.00711}\,\frac{1-0.003}{0.003}\right) - 1 = 404$$

Enriching Section

$$n_E = \frac{2}{\ln\alpha}\ln\left(\frac{x_p}{1-x_p}\,\frac{1-x_F}{x_F}\right)$$
$$= \frac{2}{\ln 1.00429}\ln\left(\frac{0.03}{1-0.03}\,\frac{1-0.00711}{0.00711}\right) = 683.5$$

The total number of stages

$$n = \frac{2}{\ln\alpha}\ln\left(\frac{x_p}{1-x_p}\,\frac{1-x_W}{x_W}\right) - 1$$
$$= \frac{2}{\ln 1.00429}\ln\left(\frac{0.03}{1-0.03}\,\frac{1-0.003}{0.003}\right) - 1 = 1087.5$$

The heads flow rate in the enriching section can be written as

$$P_i = P + W_{i+1}$$
$$= P + \frac{P}{\beta - 1}\{x_p(1-\beta^{i-n}) + (1-x_p)\beta(\beta^{n-i}-1)\}$$

and that in the stripping section

$$P_i = \frac{W}{\beta - 1}\{x_W\beta(\beta^i - 1) + (1-x_W)(1-\beta^{-i})\}$$

These flows as a function of the number of the stages can be shown as Fig. 7 in this example.

When we need higher concentration, such as 5%, $F = 11.436[mol]$, $W = 10.436[mol]$, $n = 1336$ and $n_E = 932$.

Laser Isotope Separation (LIS)

The photon absorbing frequencies of isotopes show small differences caused by shifts of atomic electron energies due to the differences in the number of neutrons among isotopes. This is called isotope shift. The invention and development of lasers enable to resolve the isotope shift sufficiently and make isotope-selective photo-chemical reaction possible. Laser Isotope Separation may lead to almost 100% isotope separation in a single stage. Mainly, two methods such as Atomic Vapor Laser Isotope Separation (AVLIS) and Molecular Laser Isotope Separation (MLIS) were intensively studied. AVLIS uses uranium atomic vapor that is struck by lasers of such wavelength that only ^{235}U atoms are excited and then ionized; once ionized, the

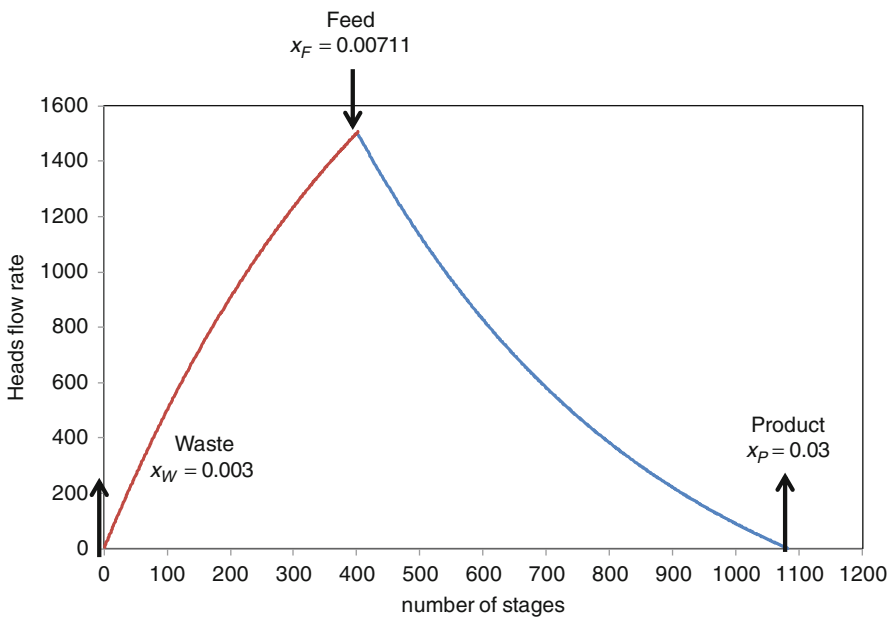

Isotope Separation Methods for Nuclear Fuel. Figure 7
Heads flow rate

^{235}U ions are collected by an electromagnetic field. MLIS uses UF_6, and vibrationally excites and multiphoton-dissociates only $^{235}UF_6$ into $^{235}UF_5$ by infrared lasers. The research to commercialize them has faded on a global scale.

A new process called Separation of Isotopes by Laser Excitation (SILEX) is under development. All details are not out in the open yet; but SILEX is considered to be a kind of molecular LIS using UF_6. The method only isotope-selectively excites but not dissociates $^{235}UF_6$. The separation factor announced by the company has been 2–20 [5]. Silex Systems Ltd was originally established as a subsidiary of Sonic Healthcare Limited of Australia in 1988. In 2007, the SILEX Uranium Enrichment project was transferred to GE's nuclear fuel plant in the United States. Global Laser Enrichment (GLE) was formed as a subsidiary of GE-Hitachi in 2008 [5]. In June 2009, GE-Hitachi submitted a license application to construct a commercial laser enrichment plant in Wilmington, NC. The NRC staff is currently reviewing that application. They announced that they succeeded the initial measurement program at Test Loop in 2010 and proceeded to evaluate the program to decide the commercialization of the process [6].

Future Directions

As of today, the gaseous diffusion and centrifuge processes have been used on a commercial scale. For the future, it seems that laser enrichment (the SILEX process) may be the successor to current enrichment methods. Preliminary results, based on enrichment by lasers, are encouraging. However, considerable improvements are needed before this method achieves commercial competitive status. Every uranium enrichment process is linked to nuclear proliferation issues. It would be very beneficial for the world if a method of enrichment is devised which inherently offers non- proliferation safeguards for nuclear materials.

Bibliography

1. World Nuclear Association, Uranium Enrichment, World Enrichment capacity - operational and planned. http://www.world-nuclear.org/info/inf28.html
2. Villani S (1976) Isotope separation. American Nuclear Society, Hillsdale
3. Benedict M, Pigford TH (1957) Nuclear chemical engineering. Mcgraw-Hill, New York; Benedict M, Pigford TH, Levi HW (1981) Nuclear chemical engineering (second edn.), (trans: by Kiyose R into Japanese)
4. Kemp RS (2009) Gas centrifuge theory and development: a review of U.S. programs. Science and Global Security 17, 1; Wood HG, Glaser A, Kemp RS (2008) The gas centrifuge and nuclear weapons proliferation. Physics Today 40
5. Silex Systems Limited home page. http://www.silex.com.au/
6. World Nuclear News (2010) Initial Success from SILEX test loop, 12 April 2010. http://www.world-nuclear-news.org/NN-Initial_success_from_SILEX_test_loop-1204104.html

K

Karst Terrane and Transportation Issues

Harry Moore[1], Barry Beck[2]
[1]Tennessee Department of Transportation, Retired, Blaine, TN, USA
[2]Karst, P.E. LaMoreoux, Inc., Oak Ridge, TN, USA

Article Outline

Glossary
Definition of the Subject
Introduction
The Character of Karst
Karst Features and Highway Construction
Reactive Approaches and Remedial Measures
Proactive Measures
Future Directions
Bibliography

Glossary

Carbonate rocks Bedrock that is composed of calcium carbonate, such as sedimentary rocks like limestone and dolostone.

Cave A natural cavity or series of galleries that is produced by solution of limestone and is large enough to be entered by man.

Centerline A term that refers to the center of a road or highway and runs the length of the road or highway.

Collapse A term used in conjunction with the formation of sinkholes; the subsidence of land or bedrock due to an underlying cavity.

Ditchline A term used in roadway design and construction that refers to a drainage ditch that is parallel to the roadway and located on either side of the road, and sometimes in the median of the road.

Gabion basket A basket configuration constructed from double-twist wire meshing; typically the basket is backfilled with rock or gravel to form a semirigid retaining wall.

Geomembrane Typically a synthetic man-made material that is usually impervious to water penetration; e.g., is a swimming pool liner; used in roadway construction to reinforce embankments and line ditches.

Groundwater That part of the subsurface water which is in the zone of saturation; also called phreatic water.

Grout A term that refers to thin fluid mortar; commonly used in construction and often used to fill in cavities in limestone to produce a stable foundation for a road, bridge footing, or dam.

Karst A landscape underlain by carbonate rocks, such as limestone and dolostone, that exhibit such features as sinkholes, sinking streams, caves, and subsurface drainage; e.g., central Kentucky Mammoth Cave region.

Lined ditch A term used in highway design and construction that refers to a drainage ditch that has an engineered "bottom" such as concrete, asphalt, or geomembrane.

Ponor A karst feature where a surface stream disappears into the subsurface, usually via a sinkhole or cave entrance.

Recharge A term that usually refers to the replenishing of a substance, usually used in association with the groundwater table; i.e., recharging the groundwater.

Regolith The layer or mantle of loose weathered rock and soil debris that forms the surface of the land and rests upon hard bedrock material; most commonly associated with the soil horizons overlying bedrock.

Reinforced concrete Concrete that is strengthened by using steel bars.

Robert A. Meyers (ed.), *Encyclopedia of Sustainability Science and Technology*, DOI 10.1007/978-1-4419-0851-3,
© Springer Science+Business Media, LLC 2012

Roadway alignment The general configuration and direction of a roadway.

Rock pad A term used in construction that refers to a layer of quarried and/or crushed rock that is used to form a hard stable layer or foundation, and also provides for drainage of water seeps.

Sinkhole A circular or funnel-shaped depression in the landscape of a limestone region usually formed by the solution of limestone and the subsurface erosion of the overlying regolith; can occur rapidly and catastrophically causing great damage to roads and structures.

Solution Typically the change from a solid, such as limestone into the liquid state by its combination with a liquid; usually associated with karst.

Definition of the Subject

As roads, highways, bridges, and railroad corridors are built to better transport our society, the terrane that they are located in may dictate design and construction procedures necessary to produce a stable and safe transportation route. One such terrane is karst, a landscape that is typically underlain by carbonate rocks such as limestone and weathers chemically and physically to produce features such as sinkholes and caves.

Designing, constructing, and maintaining these transportation systems that are located in karst terrane require proactive techniques to better stabilize the road or bridge. Too often a reactive approach to dealing with karst issues is pursued by transportation agencies. Being more proactive toward karst issues can lessen maintenance costs and also protect the environment.

Introduction

Dissolution of bedrock in areas underlain by carbonate rocks (usually limestone or dolomite) results in a terrane characterized by sinkholes, sinking streams, underground (cave) streams, and springs. (The entire landscape formed in soluble rock areas is known as a karst terrane. The term *terrane* is used rather than *terrain* to include subsurface features as well as surface features.) This terrane is usually referred to as karst. Groundwater in these settings is more susceptible to contamination because surface water may pass directly into the subsurface with little or no filtration by soil. Because karst groundwater typically flows through relatively large fractures and conduits within the bedrock, it may transport contaminants rapidly from points of recharge (such as sinkholes) to distant cave streams, water wells, springs, and surface streams.

A karst landscape can be composed of gently rolling hills and valleys textured with sinkholes, cave entrances, sinking streams, and outcroppings of weathered limestone (Fig. 1) as is typically found in Kentucky and Tennessee and the Virginia/West Virginia/Pennsylvania sections of karst. Dramatic topography that exhibits tall "haystack"-type karst terrane as found in the Li River section of southwest China (Fig. 2) can be impressive and a daunting landscape for highway construction.

Existing roads in karst areas usually experience the sudden collapse of a sinkhole or the flooding of a sinkhole basin crossed by a road. In addition, issues of groundwater pollution often go unchecked or not addressed by highway agencies as well as developers and city planners.

To the geologist and geotechnical engineer, caves are more than just curious features because they reveal information about the groundwater movement and solution processes that act on carbonate rocks. The patterns in which the solution cavities and resulting caves develop generally indicate the attitude of the bedrock, fracture density, and groundwater movement. Cave passage patterns, sinkholes, and springs are important features that may contribute to an understanding of the local groundwater flow. The recognition of areas of active karst subsidence and collapse is of considerable importance to those engaged in the design and implementation of highways, especially the construction of infrastructure.

Some of the problems that have resulted from human modification of karst into subdivisions, highways, and commercial properties include the subsidence of building foundations and the collapse of lawns due to leaking swimming pools, and inappropriately located septic tanks (Fig. 3). The collapse of highway surfaces (Fig. 4), ditch lines, and bridge foundations, as well as numerous instances of flooding are also karst-related problems triggered by human construction activity. In most instances, it is the impact of human construction activity and alteration to the surface drainage that induces the collapse of a highway

Karst Terrane and Transportation Issues. Figure 1
Features such as sinkholes and cave entrances such as this Roane County, Tennessee cave entrance, often characterize karst terrane

Karst Terrane and Transportation Issues. Figure 2
A karst region in China is characterized by remarkable landscape relief as shown here along the Li River near Guilin, China

or house foundation or results in the flooding of a commercial strip mall.

Solution cavities developed in karst terrane characteristically have numerous open subsurface flow paths. Accordingly, any contaminating fluids are able to be rapidly dispersed along difficult-to-predict routes. This type of groundwater contamination from highway runoff is becoming a greater a concern as transportation routes are expanded into karst areas.

Karst Terrane and Transportation Issues. Figure 3
Sinkholes can occur most anywhere in karst areas, as evidenced by this sinkhole near Morristown, Tennessee

This is particularly so in karst areas where toxic or hazardous spills along highways can directly flow from the highway into sinkholes and cave systems that recharge groundwater aquifers. Everyday highway runoff including tar, gasoline, diesel fuel, asbestos, and metals from the roadway can also contaminate groundwater supplies where the runoff flows into sinkholes affecting the groundwater quality.

Most of the remedial activity concerning karst problems has been reactive in nature. In most instances it is highway maintenance personnel that tend to remediate these sinkhole collapse and runoff problems. The reactive approach to dealing with karst problems involves responding in an emergency situation.

Remedial action is usually adopted in response to karst problems. Remedial concepts used for correcting karst problems include bridging, drainage, and relocation measures. Bridging a collapse with a rock fill or a concrete structure may be one alternative. Trying to solve flooding problems may require the use of existing sinkholes for drainage outlets (possibly resulting in groundwater contamination) or even constructing special ditches to bypass sinkhole areas to access a nearby stream. Sometimes moving a section of road or relocating a house is the course of action required.

Karst Terrane and Transportation Issues. Figure 4
Karst terrane can impact our highways as shown in this photo of a sinkhole along I-40 near Knoxville, Tennessee

If proper consideration is given to karst problems in advance of a construction project, then proactive measures can be taken that involve the understanding of karst processes. By simply avoiding a karst area when planning a highway or developing a commercial zone or residential subdivision, one can save future agony as well as dollars for the home owner, developer, or government agency. If avoidance is not possible, then there must be certain integrated measures taken that address not only potential subsidence but also flooding and groundwater contamination.

In general, transportation issues in karst terrane deal mostly with sinkhole collapse problems, sinkhole flooding, groundwater pollution, and environmental issues dealing with caves and cave inhabitants. How these issues are dealt with usually falls into reactive measures and proactive measures.

The Character of Karst

As would be expected the character of karst can be varied and unusual, and is often dramatic. Caves and sinkhole collapse are the most common karst characters and are often the features encountered when designing and constructing highways. Sinkhole plains, disappearing streams, resurging streams, subsurface drainage, and delicate ecosystems are also characteristic of karst and presents tenuous issues when locating or constructing transportation infrastructure.

The geologic character of the bedrock also plays an important role in the development of karst features. In addition to lithology, structural characteristics such as fracture density, folding, and faulting also contribute to the development of karst. Long linear belts of karst tend to develop on folded and faulted strata whereas flat-lying strata tend to develop wider, dendritic-type expanses of karst. In addition, highly fractured strata provide more avenues for solution activity of groundwater and therefore develop into a karst landscape quicker than less fractured strata. There are numerous studies that describe the relationship between geologic structure and karst development such as [4, 14, 31, 32, 38, 51, 52].

Cave development in karst areas, like those in the East Tennessee region, central Kentucky, and other karst areas around the USA, follows the more soluble zones or lines of weakness within the host bedrock. These weak areas are generally parallel to zones of fractures (joints and faults) or bedding planes of the rock. Solution enlargement of these weak areas of fractured rock generally coalesce into interconnecting passages that form intricate caverns, some of which are profusely decorated with cave formations (speleothems or dripstone) [26, 29].

Surface expression of the subsurface conditions in karst areas is usually manifested as depressions and sinkholes (Fig. 5). The sinkholes vary in size from several feet to several hundred feet across and up to tens of feet in depth. Some of the sinkholes may have active swallets or openings into the cave environments, while others may be simply silted in and covered with vegetation. Additionally, numerous rock outcrops are present, as well as sinking streams, cave entrances, and springs. Most all of these conditions are present along highways in the karst areas of the USA.

Sinkhole development along highways usually results from the collapse of the residual clay soil into cavities developed in the subsurface soil due to erosion of the residual clay. As these "soil cavities" enlarge and approach the surface, the remaining soil bridge over the cavity loses strength and collapses forming a typical sinkhole collapse. The eroded soil is flushed down into the solution cavities in the bedrock. This type of induced sinkhole failure has been previously described by Donaldson [9], Jennings, et al. [15], Moore [22, 24], and Newton [34, 35].

The majority of sinkhole collapse incidents experienced along most highways in karst areas are usually the soil collapse type (Fig. 6a, b, c, d, and e) as defined by [24] for sections of East Tennessee karst. Extremely rare are occurrences of bedrock collapse into large open caves; however, they do occur.

Karst Features and Highway Construction

There are a number of features that characterize the karst landscape that can, and often do, present problems for highway engineering projects. Features such as subsidence depressions (no visible cave opening) and sinkholes should be considered in any planning study. Likewise, known cave systems, springs, "dry valleys," and areas of numerous limestone outcrops should be closely studied. Ponors, sinkholes that receive surface streams, and flooded or water-filled sinkholes and

Karst Terrane and Transportation Issues. Figure 5
Naturally occurring sinkholes often expose limestone bedrock as shown in this photo from Middle Tennessee

depressions should be avoided if at all possible. Large karst valleys known as uvalas and poljes may be overlooked due to their enormous size relative to other karst features.

Building roadways over existing sinkholes and other karst features is obviously not the preferred engineering choice. However, when building roads across karst areas these features are often unavoidable. The construction practice of dumping soil into a depression or sinkhole without proper investigation and design procedures will usually result in subsidence of the fill.

Collapse

One of the most recognizable features of karst is sinkholes. The result of human activity on the karst landscape often includes subsidence or collapse of a building, roadway, house, or even a yard (Fig. 7). When subsidence develops beneath structures or highways, it may have a catastrophic impact resulting in high repair costs.

The construction and maintenance of highways and appurtenant structures in karst terrane often will trigger sinkhole collapse, subsidence, and flooding. The collapse of highways in karst areas has been well documented in the literature [18, 21, 22, 27, 33].

The relationship between construction activity and the occurrence of sinkholes has also been documented [17, 34, 37]. More specifically, Moore [22, 24] relates the occurrence of sinkhole collapses to highway construction, particularly the grading and ditching operations where surface and subsurface water flow paths have been altered. Studies conducted by Moore [24] cited above show that over 75% of the sinkhole collapses that have been documented along the roadways by the Tennessee Department of Transportation (TDOT) in East Tennessee were found to have occurred in the drainage ditch of the roadway.

Sinkhole collapse and flooding problems along Tennessee highways have been described by Royster [44] and Moore [22, 23]. In addition, Sowers [46], Newton [33], Foose and Humphreville [11], and Amari and Moore [1] have detailed possible geotechnical solutions to subsidence, flooding, and groundwater contamination in the Valley and Ridge Province from Alabama to Pennsylvania.

In 2003 Moore updated the 1987 study by analyzing 163 cases of sinkhole collapse incidents in East Tennessee between 1969 and 2002. Of the 163 sinkhole incidents studied, 86.5% of the sinkhole occurrences were located in highway ditch lines [27]. The 2003

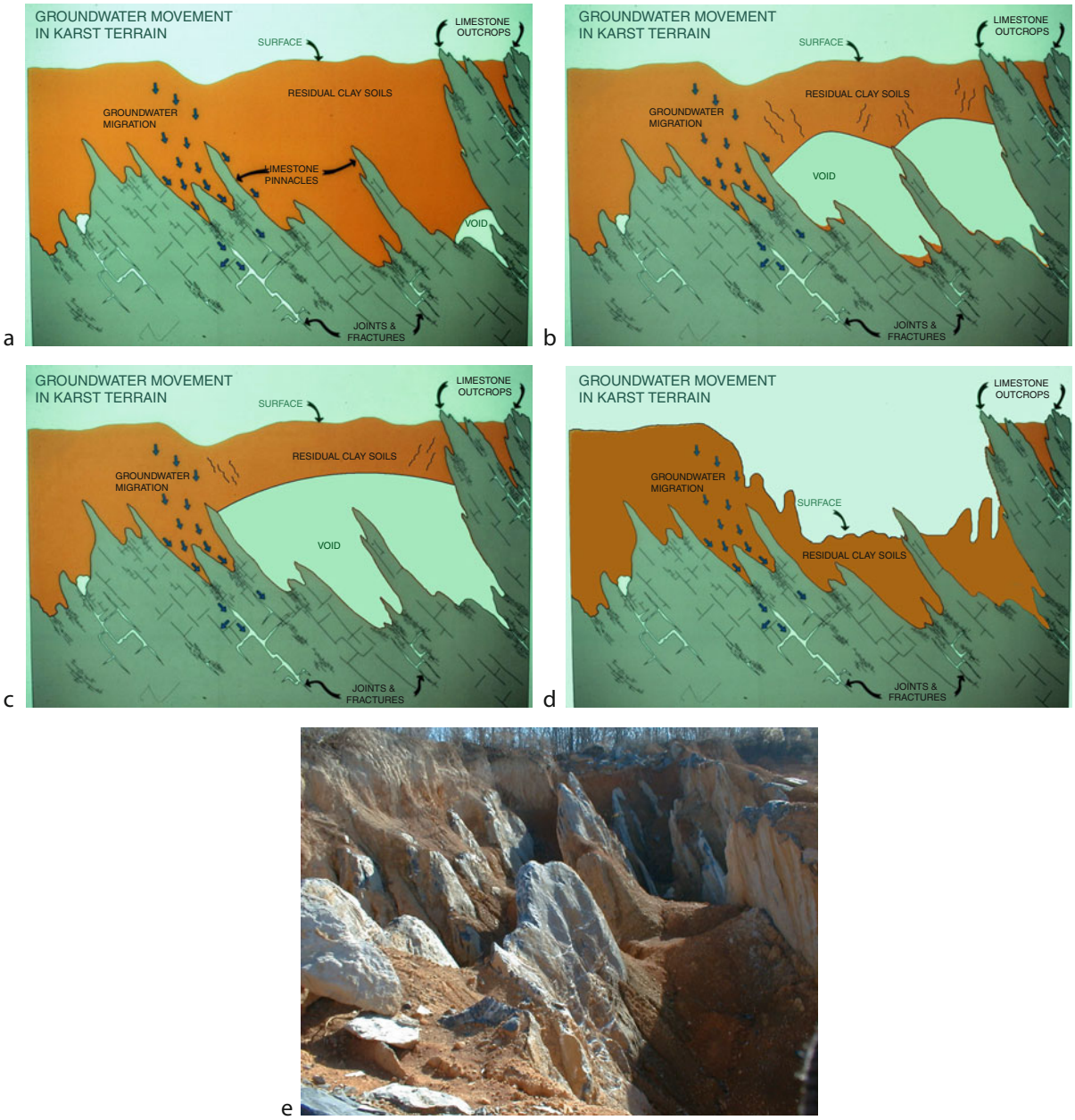

Karst Terrane and Transportation Issues. Figure 6

This sequence of drawings shows a hypothetical development of a cover collapse type sinkhole, common in much of the karst areas of the eastern USA: (**a**) shows void developing in the residual soil covering tilted limestone; (**b**) shows the void becoming larger and spanning between two rock pinnacles; (**c**) shows a larger soil bridge over the void; (**d**) shows the result of the soil bridge collapsing into the void below, causing a cover collapse sinkhole; and (**e**) shows a real example of the collapse as depicted in the above drawings

Karst Terrane and Transportation Issues. Figure 7 Some sinkholes are often filled with trash and other debris which leads to the contamination of the surrounding groundwater

study also supported the findings of the 1987 study by showing that of the ditch line collapse incidents analyzed, 93% also involved unlined ditches (the same percentage disclosed in the 1987 study).

Warning Signs of Collapse

Catastrophic sinkhole collapses can engulf entire houses and sections of roadways. Predicting sinkhole development can be extremely challenging.

However, evidence of subsidence is sometimes evident prior to catastrophic sinkhole formation. One of the initial signs of collapse sinkhole development is the initially minor subsidence of an area. The effects of minor or initial subsidence are often evident. Minor pooling of surface water may occur in normally dry areas. Shallow puddles of water on a highway surface or along a ditch line are also initial signals of possible collapse.

Signs of settlement around houses and other structures may indicate subsidence. Cracks in house foundations, bridge abutments, or piers are signs of subsidence. The tilting of trees or other vegetation also indicates movement of soils. This type of evidence is often associated with landslides, but can develop in association with catastrophic sinkhole collapse.

Under most conditions these early warning signs may develop over a considerable amount of time (months or even several years). In construction areas, induced sinkholes may occur suddenly without any indication of an impending collapse.

The formation of a sinkhole in a natural setting or on a construction site may occur in a sequence of settlement, significant subsidence, and collapse. Settlement of the ground may be noticed at first where minor movement of the soil, on the order of a few centimeters, may occur. Subsidence usually follows with drastic and very noticeable downward warping of the ground surface but with no large-scale cracks or scarps, sometimes many meters in diameter, but with no actual surface collapse of soil or bedrock. Finally, a sinkhole results from the collapse of the overlying soil (or bedrock) into the void below. This sequence may occur over a long period of time (months to years) or may occur quickly in a matter of hours.

Sinkhole Formation in Roadway Ditches

The greatest number of karst problems that develop along highways in East Tennessee involves subsidence and collapse of the drainage ditch (Fig. 8). These karst problems are referred to as being "induced" by some type of construction activity as opposed to being naturally developed [34].

In most highway design situations, roadway ditches with gradients of 3% or less, are designed to be left barren or sodded. Only when the ditch line gradient exceeds 3%, according to most standard roadway design procedures, are the ditches paved or treated with an impervious material (i.e., concrete, polyethylene, geofabrics).

Within karst areas, the problem with untreated ditches often results when run-off accumulates in the ditch line and percolates into the underlying soil and rock. As the surface water migrates downward, clay particles are taken from the soil and carried into existing solution channels in the top of the bedrock and into the underlying bedrock conduits and caves. A cavity develops in the soil mass (above the bedrock) and enlarges from the bedrock toward the surface over a variable period of time (Fig. 9). Where the soil can no longer span the subsurface void, then the soil mass collapses into the underlying cavity and the collapse progressively works upward to form a surface depression or a collapse sinkhole [10].

Karst Terrane and Transportation Issues. Figure 8 Sinkholes often form along highway ditchlines as surface water is concentrated there leading to the subsurface erosion of the soil which forms these sinkholes

Karst Terrane and Transportation Issues. Figure 10 When roadway bridges are constructed in karst terrane, sinkholes can develop beneath the supporting structures as shown here along I-24 in Montgomery County, Tennessee

Karst Terrane and Transportation Issues. Figure 9 Soil voids usually form over the limestone bedrock before the soil collapses forming a cover collapse sinkhole

Construction projects are notorious for disregarding the surface runoff and usually result in serious siltation problems. In addition, the pooling of surface run-off in recently graded or excavated karst areas can result in sinkhole collapse. A significant aspect to consider is the new drainage path along the grade of the roadway (a drainage ditch) that concentrates the runoff and increases infiltration into the subsurface. An example of this process occurred on a highway construction project in Montgomery County, Tennessee, where surface runoff from a rain event was allowed to pond around newly constructed bridge pier footings on I-24. The concentration of water on the freshly excavated ground (which happened to be in an active karst area) triggered a collapse (Fig. 10) of residual clay soils around the pile-supported footings [44].

Drainage

Other types of karst features and hazards are associated with drainage issues. Flooding and groundwater pollution problems are two major concerns associated with drainage in karst.

Flooding of highways constructed across sinkholes is a relatively common occurrence in some karst areas. A number of sinkhole flooding problems of this type have been studied and documented (Tennessee: [16, 20, 22, 23]; and Royster [44]; Kentucky: [5]).

In most instances of highway flooding, the subject road was constructed across (or into) the sinkhole following the natural topography (Fig. 11). Prior to construction, land use may have been agricultural with little runoff and the sinkhole did not flood. Many such sites are now urbanized and the sinkhole can no longer adequately drain the increased runoff.

Groundwater pollution due to the infiltration of highway surface runoff into a sinkhole feature has become a major environmental concern associated with highway routes in karst. While a number of researchers have studied the effects of highway runoff

Karst Terrane and Transportation Issues. Figure 11
Roads built across and in sinkholes may flood if the subsurface drainage becomes blocked as shown in this photo of Prosser Road in Knoxville, Tennessee

on the surface environment, few have dealt with the effects on the subsurface environment. Quinlan and Ewers [40] and Quinlan and Ray [42] discuss the effects of surface runoff on the Mammoth Cave System and their efforts to dye-trace the karst boundary. In their discussions, it was pointed out the necessity to map and dye-trace all sinkholes connected to roadways that traverse through the Mammoth Cave National Park.

Stephenson and Beck [48] made a review of literature regarding the quality of highway runoff and its potential impacts on karst groundwater. They found that little attention was being given by researchers to the issue of groundwater contamination by highway-related surface runoff, and that the highway runoff could contain high concentrations of hydrocarbons and other vehicle-related contaminants.

In 1997, Stephenson and Beck describe the results of a Federal Highway Administration Pooled Fund Study (that involved 15 state DOTs including Tennessee) where a prototype filtration system (Fig. 12) was designed to treat highway runoff in an interchange of I-40 and I-640 in the eastern part of Knoxville, Tennessee. This study described the attention that is required by infrastructure designers to prevent or lessen the pollution of the groundwater system in karst areas.

Reactive Approaches and Remedial Measures

Historically, the remedial approach to karst-related highway subsidence and flooding problems has typically been reactive in nature. Road crews commonly repair the sinkhole collapse after it has happened.

Remedial measures used in correcting karst-related subsidence problems reactively (after they occur) may be divided into three areas: bridging, drainage, and relocation. The techniques used in bridging include graded-rock and shot-rock pads and fills, graded-rock backfill, concrete structures, and grouting [22, 25, 47]. Remedial measures used in drainage include alteration of the existing drainage by the use of paved or geomembrane-lined ditches, special overflow ditches, plastic overlays, pumps, horizontal drains, and the maintenance of obstructed sinkhole entrances. Surface drainage filter systems have been researched and are

Karst Terrane and Transportation Issues. Figure 12
Surface runoff from roadways can be filtered to remove pollutants before the water reenters the groundwater system through sinkholes

beginning to be employed to treat surface runoff from highways in karst areas. Although not widely used, relocation of the highway facility around a karst area may also be a viable corrective measure.

Types of Bridging Remedial Approaches

The treatment of karst-related subsidence and collapse features involving engineered structures can include methods as varied and site specific as the sinkholes themselves. Many remedial treatment techniques involve a method of "bridging" to provide adequate stability and bearing capacity.

There are a number of different approaches to bridging that can be applied. These include, but are not limited to, the following: conventional bridge spans, "muck trestles" (bridge built on grade), drilled shafts, riprap backfill, rock pads, grouting, concrete slabs, geofabrics, and geogrids. In some instances, a combination of these procedures may be needed [29].

Where field conditions warrant, a concrete structure may be used to bridge or span the collapse sinkhole area. This remedial measure may entail the construction of: (1) a free spanning highway concrete or steel bridge; (2) a concrete bridge with the deck constructed on the ground surface (commonly referred to as a "muck trestle"); (3) drilled cast-in-place concrete piers to support a concrete slab or bridge section; or (4) a concrete slab placed over the subsurface opening [29].

Although a very costly approach, a free spanning bridge constructed over the sinkhole area is very effective in eliminating future problems. This approach should be considered when crossing very large and deep sinkholes or in environmentally sensitive areas such as Mammoth Cave National Park.

The "Muck Trestle" bridge has been considered for a severe karst-related flooding and collapse problem in Hamblen County along State Route 34 near Morristown. This concept was applied to a railroad bridge in the same vicinity of Hamblen County where a sinkhole collapse was endangering a rail line [50].

An often recommended measure for structural foundations in karst strata is the use of drilled cast-in-place piers (caissons). Where soluble limestone strata occur beneath a river channel, numerous cavities may exist which are either clay filled or open. In some instances, a series of solution cavities may extend downward to depths of over 30.4 m (100 ft). Karst

strata that extend as much as 8–10 m (25–30 ft) below the surface can make excavation prohibitive and drilled cast-in-place piers more viable.

Another type of bridging concept commonly used in roadway applications is to use concrete grout to seal up cavernous strata. Grouting is often used at the soil/rock interface to close up openings that the soil may filter into – this is referred to as "cap grouting." Royster [44, 45] used this concept to repair a bridge footing along I-24 in Montgomery County, Tennessee where a collapse occurred beneath a pier footing pile cap (Fig. 13). Another instance of using grouting to repair subsidence and sinkhole collapse problems is detailed in Mellett and Maccarillo [19] where the authors warn that grouting can divert underground water flow into other areas, and new sinkholes may occur nearby as a result. As shown in the above example, caution should be used when attempting to use grouting as a method of stabilization of collapse problems.

The Tennessee Department of Transportation applies another effective type of bridging concept which uses rock riprap to backfill the collapse. The interlocking action of the riprap backfill, often referred to as "chunk rock" backfill," and the placement of the backfill on the top of the in-place bedrock effectively bridge the solution cavity (Fig. 14). This concept also provides a free draining structure for groundwater and surface drainage.

These inverse filters using "chunk rock" backfill are designed to prevent overlying materials from filtering down into the interstitial spaces of the clean rock backfill and solution cavity resulting in subsidence or even another collapse.

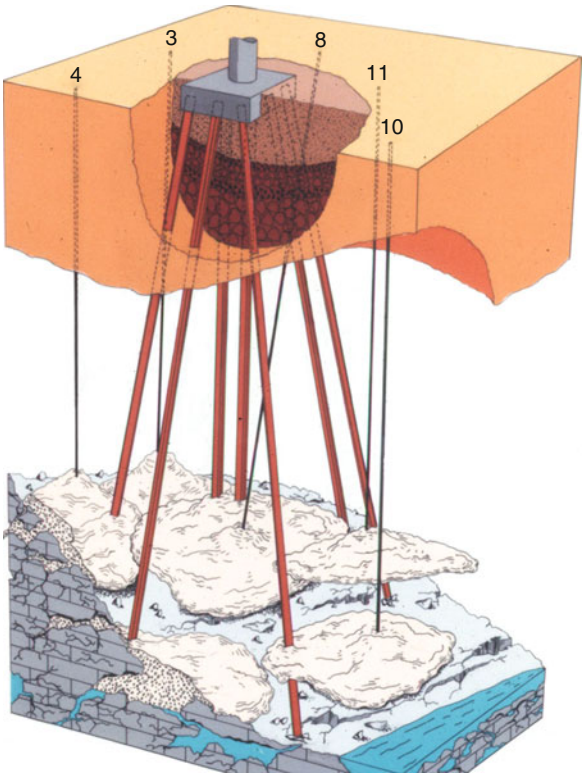

Karst Terrane and Transportation Issues. Figure 13 "Cap grouting," where concrete grout is pumped down to the soil–bedrock interface to seal the rock surface and prevent the migration of soil down into cavities in the bedrock, was used on a bridge footing in Montgomery County, Tennessee along I-24

Karst Terrane and Transportation Issues. Figure 14 Clean graded rock is used to backfill a sinkhole collapse along Interstate 640 in Knoxville, Tennessee by the Tennessee DOT

Karst Terrane and Transportation Issues. Figure 15 A rock pad is constructed over naturally occurring sinkholes on a road project in Tennessee. The rock pad provides not only stability for the road but allows surface drainage to flow into or out of the sinkhole, which had bedrock exposed and not soil

A bridging technique, commonly used in Tennessee, consists of a limestone graded rock pad placed to span an area of intense solution activity (Fig. 15). This technique was used on a section of Tennessee State Route 1 (U.S. 11-W) in Hawkins County where a new four-lane section of State Route 1 was constructed over an area of active sinkholes. This rock pad provided stability for the highway by allowing groundwater to flow freely from the sinkholes to a special channel and box culvert.

The rock pad constructed over this sinkhole area has a minimum thickness of 1.5 m (5 ft) and meets the following rock specifications [29]:

Rock pad material consists of sound, nondegradable limestone with a maximum size of 0.9 m (3 ft) and is free of shale and/or clay; at least 50% (by volume) of the rock is uniformly distributed between 0.3 m and 0.9 m (1 ft and 3 ft) in diameter, and no greater than 10% (by volume) is less than 5 cm (2 in.) in diameter; the rock material is roughly equi-dimensional; thin slabby material is not accepted.

A geotextile filter fabric should be used to separate the rock pad from the overlying fill material (usually soil). The filter fabric specifications should be determined based on the grain size of the overlying fill material.

Drainage-Related Remedial Approaches

The development of proper drainage systems for highways constructed across karst terrane is commonly overlooked, often necessitating reactive approaches to karst drainage problems which involve ditch line collapse and flooding.

A successful technique of drainage control involves the use of lined drainage ditches along roadways in karst areas. This includes using materials such as asphalt, concrete, or geomembrane-lined drainage ditches. Studies [24, 27] have shown that the majority of collapse-type karst problems occur in unlined ditches. Unlined ditches are usually sodded at best and have gradients of less than 3% and more often 1% or less.

Unpaved ditches also provide for increased seepage which may result in subsurface erosion and finally collapse. Bare soil ditches and even sodden ditches are prone to this type of collapse failure (Fig. 16).

Usually, water collecting in an unlined ditch will seep into the underlying soil eventually reaching a conduit developed at the soil/bedrock interface below the ditch. Erosion continues until the soil over the cavity collapses; the result of the erosion being a collapse sinkhole induced by seepage from the drainage ditch. The solution is to line the ditch with an impervious material at the outset, during construction.

Materials that have historically been used to line ditches include sodding, asphalt, riprap, and concrete. Concrete paved ditches have historically been used in these situations and perform moderately well.

In recent years, new emphasis has been put on the use of synthetic geomembranes (Fig. 17). Their use as ditch liners in karst areas is strongly recommended due to the following factors: flexibility, imperious character, strength against puncture, ease of installation.

The geomembrane liners can be installed with a soil or sod cover for aesthetics and UV protection. Riprap can also be placed atop the geomembrane (careful placement is required). In emergency situations, polyethylene sheeting can be used until a more permanent repair can be affected. Finally, if a concrete ditch is desired, the concrete should be applied over a geomembrane liner. Geomembranes that tend to perform well in these applications are 60 mil thickness HDPE and PVC membranes.

Karst Terrane and Transportation Issues. Figure 16 Unlined drainage ditches in karst areas usually bear the brunt of sinkhole formation as shown in this photo of a sinkhole along State Route 72 in Tennessee

Karst Terrane and Transportation Issues. Figure 17 Geomembrane is used for drainage ditches along some highways in karst areas of Tennessee. Most are covered with riprap or concrete paving

Relocation

In some instances relocation of the highway is the best alternative to solving the karst-related problem. This may simply involve shifting the roadway slightly to miss a specific sinkhole or cave entrance. In other cases, the relocation may be several hundred feet from the original alignment and cost thousands of dollars for additional right-of-way.

Proactive Measures

Being proactive in regard to dealing with karst in highway design and construction is to identify the problem and formulate a design that will remediate that problem before construction begins. If a roadway alignment has to be located in sinkhole areas, then design roadway embankments and cut sections so that the impact of the karst on the roadway will be lessened or eliminated. Avoidance measures and some combination of drainage and bridging methods are usually the best direction to take in a proactive approach to designing and constructing highways in karst areas.

Avoidance Measures

The avoidance of karst areas by transportation facilities is recognized as a highly desired approach in highway planning; however, the extensive suburban development necessitating new highway construction commonly limits highway corridors to less desirable land. Identification of the most severe karst areas (with respect to drainage, sinkhole collapse, and other environmental impacts) during location and design phases of highway planning can lessen the impact of karst features on the project and result in a better designed and more stable roadway facility.

Avoidance is only effective where karst is active and recognizable. The construction of new roads with associated increases in runoff along the new landscape can trigger subsidence and flooding problems where previous land uses were in relative equilibrium with the karst.

Locating new roads in areas prone to karst development requires a great dependence upon the geologic information that is available. The geotechnical information gathered during the investigative phase of a proactive approach to highway design is most valuable in determining route location selection relative to karst. Maps and other information that delineate such karst areas (derived from a proactive investigation) can be used to avoid problem areas. The use of geophysical methods such as resistivity, seismic, and radar can be used to aid in the characterization of subsurface conditions in karst areas [3].

Caution should be exercised when using standard 7.5 min U.S.G.S topographic maps to identify sinkhole prone areas. The standard 20 ft (6 m) contour interval used with the 7.5 min quadrangle rarely reveals the true number of sinkholes present. Hubbard [13] researched this issue in the karst regions of the Valley and Ridge of Virginia where he consistently identified more

sinkholes on the ground than were depicted on selected 7.5 min quadrangle maps. In one instance, Hubbard describes a 7.5 min quadrangle with a 20 ft contour interval that revealed 55 sinkhole features, while ground field mapping identified 533 sinkhole features.

In another case that relates this concept to East Tennessee, Moore [28] studied a proposed location of an interchange along I-181 in Sullivan County, Tennessee situated in the Valley and Ridge province and underlain by carbonates. Within an approximately 100 acre site, the standard 7.5 min maps with 20 ft contour intervals revealed some 30 or so sinkhole features. After aerial mapping using a 1 m contour interval, a total of 177 sinkholes and 7 cave entrances were identified at the proposed site (Fig. 18a, b), which was later rejected by the Tennessee Department of Transportation for the interchange location.

Roadway designs may involve the use of broad horizontal curves to miss a sinkhole area or cave complex resulting in a more scenic facility. An example of this process is the Pellissippi Parkway Extension (I-140) in Knox County, Tennessee. The extension of a limited access, four-lane highway facility, "The Pellissippi Parkway" (I-140), involved the possible location of corridors in active karst areas of Knox and Blount counties in East Tennessee. Geotechnical involvement in the location and design phases of this highway development process resulted in the recognition of several unstable areas of karst and led to the adoption of remedial and preventive design measures which were incorporated into the construction plans [23].

Ultimately, the route selected was the most favorable geologic setting of the four proposed routes. Significant consideration by administrative officials was given to the geologic evaluation of the project, a measure of the progress in recognizing and addressing karst processes and teamwork within the geologic and engineering professions.

Mapping karst areas for planning use by government highway organizations (state DOTs) is very proactive and effective in reducing the impact of karst on proposed transportation routes. One such example is the South Knoxville Boulevard Extension (SR 71) in Knox County, Tennessee. The Tennessee Department of Transportation (TDOT) is planning a new roadway alignment (SR 71) that crosses portions of South Knox County in East Tennessee. The proposed corridor

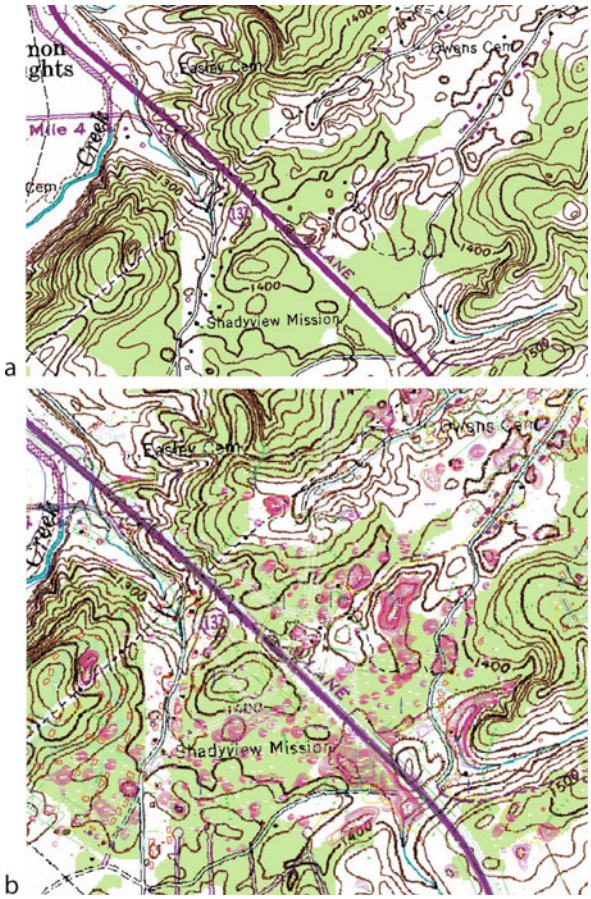

Karst Terrane and Transportation Issues. Figure 18 Using topographic maps is a good source for finding sinkhole terrane. However, the scale of map and the contour interval can be deceiving as shown in the map above. Map (**a**) shows an area on a 20-foot contour scale with some 30 sinkholes developed; map (**b**) shows the same area on a 3-foot contour scale showing over 100 sinkholes

is located in a section of the Valley and Ridge Province of East Tennessee where several ridges and valleys will be crossed, as well as creeks, roads, subdivisions, and rural lands. The proposed corridor connects the current terminus of SR 71 at Moody Ave. in South Knoxville to John Sevier Highway (SR 168) (Fig. 19).

In an attempt to properly evaluate the potential for geologic hazards along the project, an effort was made to locate all sinkholes and caves within the project area,

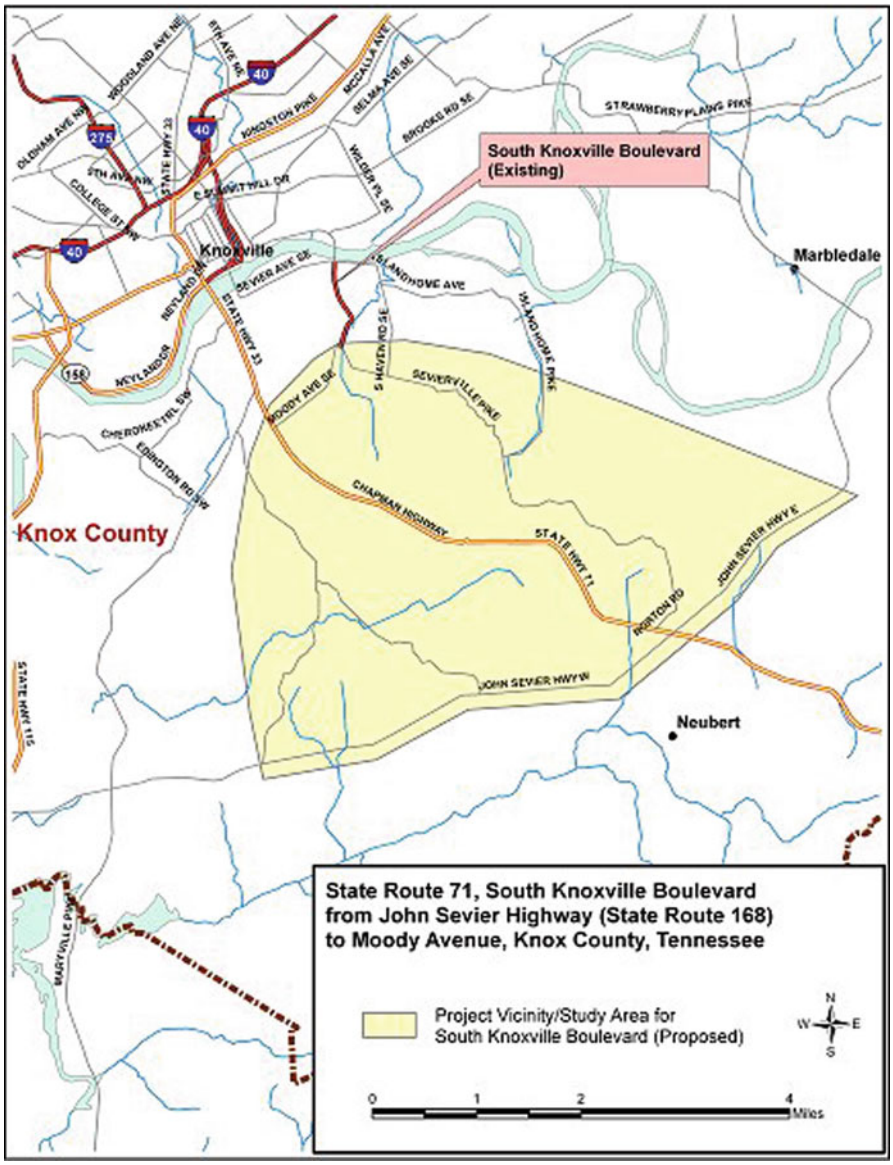

Karst Terrane and Transportation Issues. Figure 19

This map shows the study area for the extension of the SR 71 – South Knoxville Blvd. in Knoxville, Tennessee. The study area contains a large karst sinkhole area shown on Fig. 23

karst being the primary geologic hazard identified. To this effort, a karst map and a map of one cave was completed (Figs. 20 and 21).

The proposed SR 71 corridor is situated in the rolling to hilly topography of the Valley and Ridge Province of East Tennessee and includes a portion of South Knox County. Geologically, the corridor is situated in terrain underlain by folded and faulted middle-Ordovician sedimentary strata composed of several major rock types including limestone, shale, sandstone, and siltstone.

The weathering of the rock strata has produced a knobby terrain that follows the out crop pattern of the specific formations, especially the Holston and Chapman Ridge formations. The weathering has also produced classic karst topography characterized by sinkholes, disappearing streams, and caves, including Meades Quarry Cave (Fig. 22).

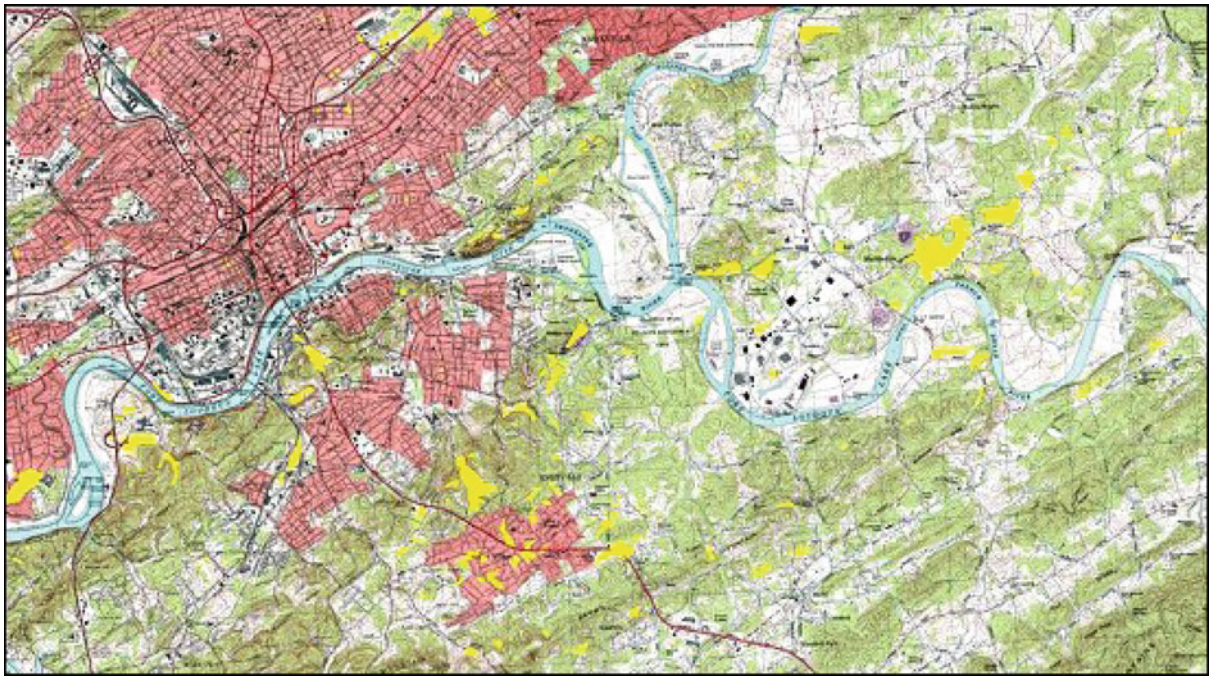

Karst Terrane and Transportation Issues. Figure 20
This map shows sinkholes (*yellow*) that were found in the study area for the proposed SR 71 – South Knoxville Blvd. Extension in Knoxville, Tennessee

A geohazards evaluation was conducted by the Tennessee DOT Geotechnical Engineering Section for the proposed SR 71 route. This study was an effort by the Tennessee DOT to identify the geologic hazards along the corridor and to avoid or reduce the hazard impact on the roadway facility, environment, and the public. The main geohazard found along the proposed SR 71 study area was karst.

The study revealed that the corridor is characterized by features such as sinkholes, caves and cave entrances, sinking streams, and outcroppings of weathered carbonate rock (limestone and dolostone). The recognition of areas of active karst subsidence and collapse is of considerable importance to the design and implementation of the proposed highway infrastructure, SR 71.

TDOT initiated a karst geohazards inventory and assessment to assist in evaluating and selecting a satisfactory alignment within the corridor study area. This study involved the location of caves and sinkholes within and adjacent to the proposed corridor. In addition, the caves were visited and preliminarily evaluated as to their geotechnical and environmental importance. The caves that were found to be of significance to the proposed stability of the roadway or have environmental and archeological significance were surveyed to determine their lateral and vertical extent. Mapping of the caves was performed by both TDOT Geotechnical Engineering staff and local speleologists.

Caves and sinkholes offer special challenges relative to both the physical and environmental issues of highway development. The karst geohazards inventory study, which included mapping karst features, disclosed the presence of both sinkholes and caves, some of which may have detrimental structural, geologic, and environmental issues for alignment and grade design considerations.

Efforts to avoid karst areas with roads and other developments are difficult at best, especially since the "good" land is already mostly developed, leaving only the geologically undesirable land for current development. Geologically undesirable land includes such areas as karst terrane steep terrain, very rocky terrain, landslide-prone areas, soft ground, and areas prone to acid mine drainage, to name a few.

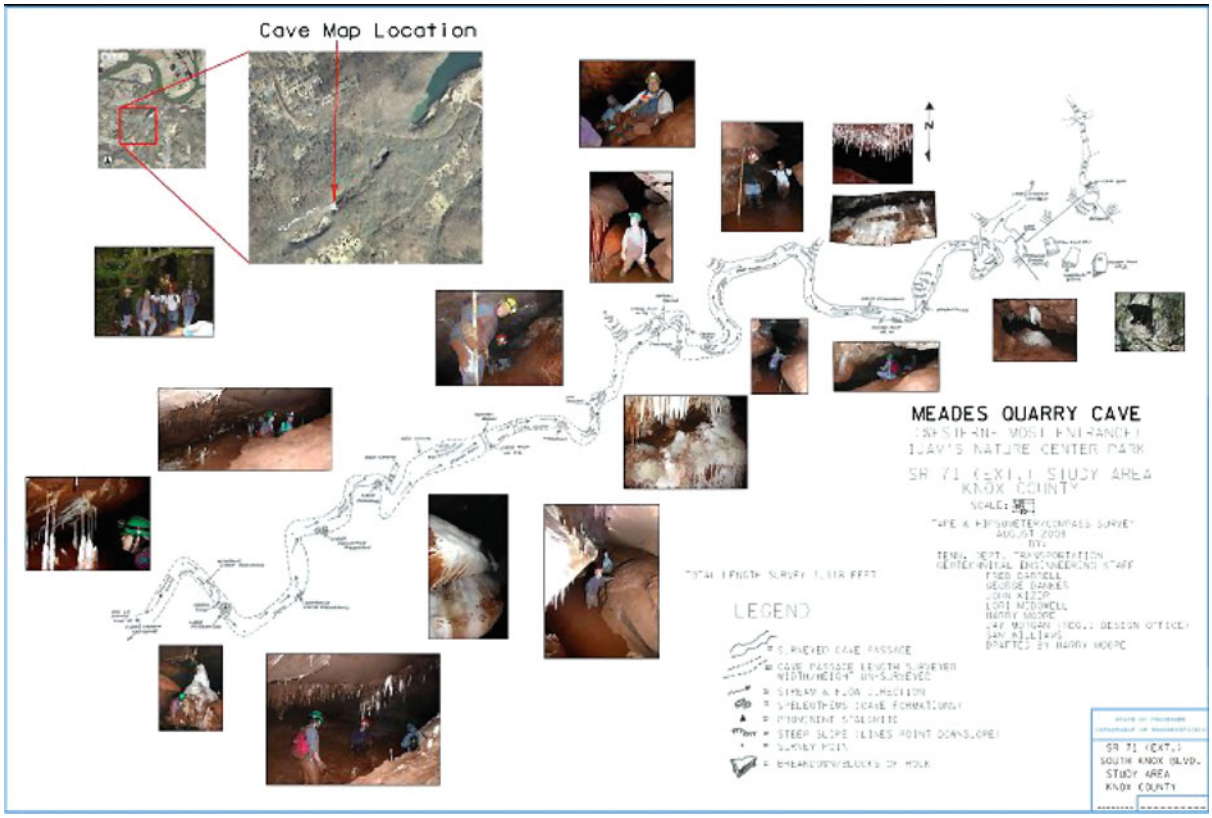

Karst Terrane and Transportation Issues. Figure 21
Cave maps, such as this detailed cave map of Meades Quarry Cave in South Knoxville, Tennessee can be used by highway designers to avoid impacting fragile cave environments when planning and designing future roads

In planning new highway corridors certain constraints must be known and when identified are usually displayed by mapping. The Tennessee Department of Transportation, Geotechnical Engineering Section is involved in studying proposed roadway corridors in East Tennessee in an effort to identify geohazard areas.

The mapping of karst areas generally involves the following procedure as outlined by Moore and McDowell [30]:

- In general, 7.5 min topographic maps (that use a 6 m (20 ft) contour interval) are used to locate karst features such as sinkholes (closed depressions on the contour map), caves, springs, and sinking streams. Once these karst features are identified and located on the topographic maps, then a field reconnaissance is performed to field check the features to make sure that they are there.
- Afterward, the sinkholes and other karst features are enhanced on the topographic maps and subjective boundaries are drawn to encircle these areas. Typically, these encircled areas are identified as "areas of high concentrations of sinkholes" and/or "areas of numerous cave openings." Actual cave entrances are not plotted on the final geohazard map due to access issues and private owner protection.
- The geohazard areas are then expressed as outlined patterns on topographic maps to better illustrate the geohazard relative to the surrounding landscape. In addition, the proposed corridor route is overlain on the geohazard map. This map is then used by the roadway planners to better locate the final roadway centerline.

In addition to the surface mapping of sinkholes, it is becoming more important to map the caves where they may exist in close proximity to the proposed roadway.

Karst Terrane and Transportation Issues. Figure 22 This photo shows the man-made entrance to Meades Quarry Cave which was opened by marble quarrying operations in South Knoxville in the early 1900s

By knowing spatially where the cave passages are located, a more accurate design of proposed roadway cut slopes can be made. This would prevent the unnecessary opening of a cave system to the surface, and benefit the cave biota, such as bat colonies and salamanders to name a few.

The use of experienced cavers (usually cavers who are members of the National Speleological Society, NSS) in combination with engineering survey crews provided the best results for locating the cave passages spatially with respect to the proposed roadway. It is anticipated that mapping of cave passages will become increasingly mandatory as society continues encroaching onto and into the karst environment.

After a review of available geologic data and field investigations, the SR 71 Extension corridor in South Knoxville, Tennessee was found to be located within several strike belts of karst. The belts of karst trend in a northeast to southwest direction, reflecting the strike of the underlying bedrock. In addition, the rock strata are folded into a large structural anticline resulting in the bedrock forming a "U"-shaped pattern in the South Knoxville community (Fig. 23).

Numerous sinkholes and caves were found to be located in these karst areas. A map of the most intensive sinkhole areas was prepared in order to better assess the corridor terrain. A field reconnaissance of the study area was made in an effort to locate as many of the sinkholes as possible. Many were overgrown and difficult to locate. A few of the caves that were identified were found to be located outside of the numerous sinkhole zones (outlined on the attached karst-sinkhole map), but within typical karst terrane.

The possible impacts on the karst environment from constructing the proposed road alignment (or any other structure, building, subdivision, etc.) include sinkhole collapse, sinkhole flooding, groundwater contamination, and environmental effects on the cave and subsurface-dwelling wildlife, such as bats and salamanders.

Mapping Subsurface Karst: Meades Quarry Cave Mapping Initiative

Due to the uncertainty of the existence of Meades Quarry Cave within the proposed study area, it was decided to map the western-most portion of the cave system. The purpose of mapping the cave was to determine if the general trend of the cave and cave stream is toward the sinkhole area around Old Sevierville Pike and Red Bud Drive, which is within the study area of the proposed parkway extension.

The presence of the Berry Cave Salamander (*Gyrinophilus gulolineatus*, a subterranean amphibian listed as a potential threatened species – see Fig. 24) in the Meades Quarry Cave stream has made the cave an important issue of the overall study of the proposed SR 71 extension. The Berry Cave Salamander derives its nutrition from debris and organics that are flushed into the sinkholes by rain events which in turn recharge the cave stream in which the salamander lives. Adversely affecting the sinkholes would directly affect the salamanders.

As a result of the concern over the salamander species found in Meades Quarry Cave, it was decided by Tennessee DOT that a mapping effort of the

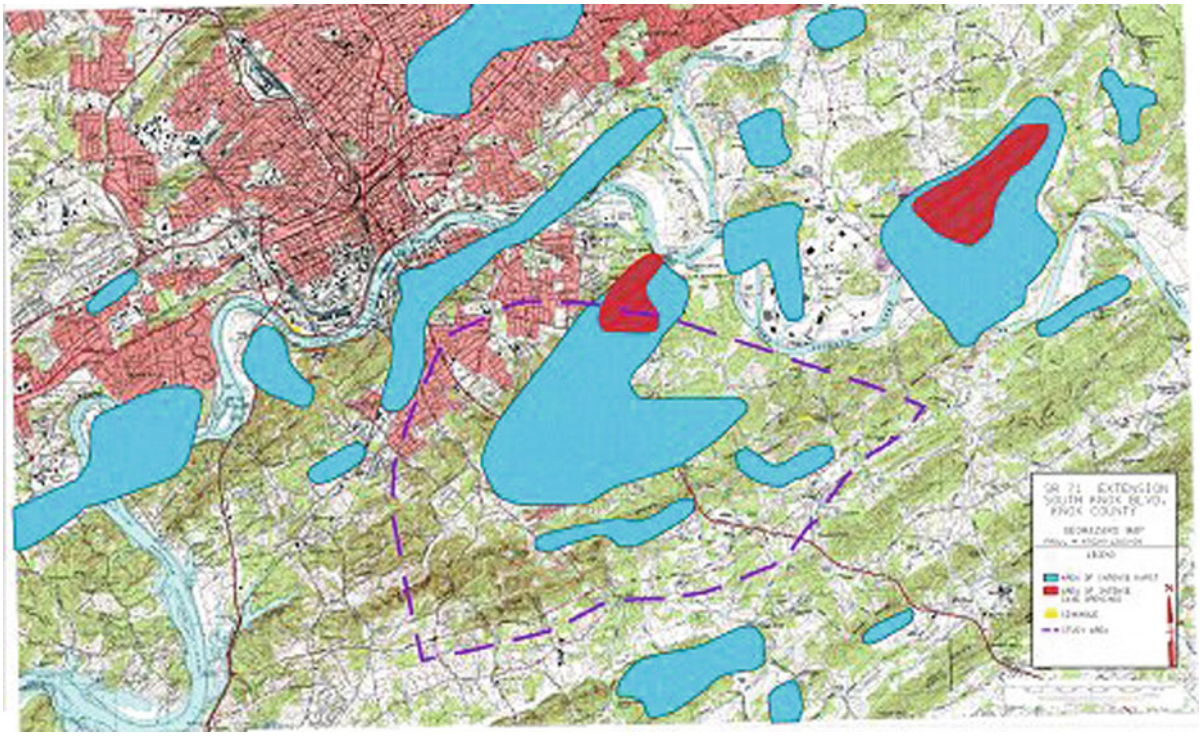

Karst Terrane and Transportation Issues. Figure 23
This map shows the karst and sinkhole area that was mapped by the Tennessee DOT Geotechnical Engineering Section while studying the proposed extension for SR 71 – South Knoxville Blvd. in Knoxville, Tennessee. The dashed area shows the actual study area (base geologic information from Hardeman [12])

cave would be completed. In August of 2008 the Geotechnical Engineering Section initiated an effort to map the western-most portion of the Meades Quarry Cave system (Figs. 25, 26, and 27). This section of the cave system has its entrance in the floor of an old quarry pit which exposed the cave during quarrying operations in the 1930s and 1940s.

As a consequence of our investigation and mapping initiative, it was interpreted that the stream passage of Meades Quarry Cave does indeed lie within the study area of the proposed SR 71 highway extension. In addition, it was decided that a dye trace study was needed to further delineate the groundwater recharge area for Meades Quarry Cave system.

Dye Trace Study

A proven and reliable method of identifying subsurface drainage areas in karst is to use dye tracing. Many studies have disclosed the valuable usefulness of dye tracing (Quinlan and Ray [39–42]). To that end, the South Knoxville SR 71 highway project study has initiated a dye trace study of the proposed highway route in a sinkhole prone section of the corridor.

As noted in the above discussion, the Meades Quarry Cave system of solution channels and stream(s) is located within the study area for the proposed extension of SR 71. Also, it was disclosed by local University of Tennessee biology researchers that the Meades Quarry Cave contains a population of Berry Cave Salamander which is a rare species of animal (Moore and McDowell [30]).

The U.S. Fish and Wildlife Service and the Tennessee Wildlife Resources Agency has noted the presence of the Berry Cave Salamander in the Meades Quarry Cave system and requested that TDOT do an adequate dye trace study of the sinkholes in the area of the proposed project to better understand the geohydrology of the Meades Quarry Cave system. The dye trace study is to better differentiate which sinkholes actually recharge

Karst Terrane and Transportation Issues. Figure 24 This photo of the Berry Cave Salamander made in Meades Quarry Cave in South Knoxville, Tennessee. Cave environments are fragile places and harbor many rare and endangered species of wildlife. (Photo by Matt Niemiller [36] University of Tennessee; from: http://www.herpetology.us/niemiller/)

Karst Terrane and Transportation Issues. Figure 25 Mapping caves is an important process in studying the location of future transportation routes like highways and railroads; shown is Meades Quarry Cave mapping by Tennessee DOT geologists

the cave stream that the Berry Cave Salamander lives in, so that TDOT can avoid any impact on the cave system with the construction of the proposed SR 71 extension. A result of the dye trace study will be an effort to minimize the impact of highway runoff on the local karst system. This will be accomplished with the use of runoff filtration systems.

In summary, the study of the karst of the SR 71 project found that the proposed corridor has numerous karst features that are found within the area topography. Mapping surface and subsurface karst features can greatly aid the evaluation of proposed roadway corridors. A result of this study was the development of a surface karst map which showed areas of numerous sinkholes, which is interpreted as areas of potential future sinkhole development.

The construction of road projects, as well as industrial sites, shopping malls, and subdivisions will be problematic in karst areas and should be avoided when possible. However, if avoidance is not possible, then minimization of the impact of construction on the sinkhole and cave environments should be the objective. Such design measures as minimal cut and fill construction and minimal alterations in the surface drainage of an area (both surface and subsurface) are recommended.

Another result of the karst geohazard study was the development of a karst planning map and the decision that mitigation of the impacts on the karst areas will need to be included with the roadway design and construction plans once the road project is approved. Proactive measures such as surface drainage filtration systems for sinkholes, impermeable lining for ditchlines (to prevent new sinkholes from forming), the use of graded rock embankments (for stability and groundwater impacts), and the use of structural bridges over sensitive sinkholes are recommended to be considered and/or employed during the roadway design phase.

The groundwater contamination issue is an important topic for the SR 71 project due to the potential

Karst Terrane and Transportation Issues. Figure 26 Meades Quarry Cave contains a perennial stream that supports the environment for the Berry Cave Salamander

Karst Terrane and Transportation Issues. Figure 27 Cave speleothems decorate a passage in Meades Quarry Cave in Knoxville, Tennessee. Shown are white soda straws connecting with white stalagmites

impact on the rare Berry Cave Salamander which lives in the Meades Quarry Cave system. Once the groundwater dye trace results are obtained by the Environmental Division (as discussed in the above narrative), then a more appropriate evaluation of the karst groundwater drainage can be made.

Surface water runoff filtration systems, as proposed for the SR 71 project in South Knoxville, have recently been constructed on a Tennessee DOT roadway project in Hamblen County, Tennessee where the runoff empties into a sinkhole (Fig. 28). The filtration system design was based on results of a FHWA Pooled Fund study that involved filtering highway runoff in karst areas. Tennessee DOT was a partner in the FHWA Pooled Fund study [48, 49].

It is important to understand that there will always be an impact on the karst environment (sinkholes, caves, wildlife, and groundwater) when construction occurs in karst areas. In some places, this impact may be significant where caves and sinkholes are exhumed and/or filled in with embankment material, and where surface drainage is directed into sinkholes that empty into the caves and groundwater systems. These impacts can be lessened by appropriate and judicious mitigation during the design and construction phase of the project.

Proactive Drainage and Bridging Concepts

The proactive approach to karst-related drainage problems requires attention to several design-related items. These include lined ditches, rock pads, overflow channels, sinkhole opening improvement/protection, curbs for embankment sections, and drainage wells. The following discussion summarizes the treatment of karst-related drainage problems [28]:

- *Lined ditches* – The single most important item that can be implemented to prevent future sinkhole collapse occurrence is the use of lined drainage ditches. Types of liners that tend to function the best include 60 mil PVC and/or HDPE geomembrane, and concrete and asphalt materials.
- *Rock pads* – Rock pads beneath embankments using clean riprap limestone may be used for bridging depressions and sinkholes (Fig. 29).
- *Overflow channels* – This concept involves the construction of a lined channel or pipe from a negative

Karst Terrane and Transportation Issues. Figure 28
This shows the sinkhole filtration system constructed on a Tennesse DOT road project in Morristown, Tennessee. The filter is in the long rectangular structure near the top center of the photo. The sinkhole receiving the filtered runoff is in the *top left* of the photo

Karst Terrane and Transportation Issues. Figure 29
Shown is a roadway embankment that is underlain by an engineered rock pad across a sinkhole in Knoxville Tennessee

drainage area (sinkhole) to a positive draining system.

- *Sinkhole opening improvement/protection* – This concept involves improving the runoff flowing into subsurface cavities by removing debris and trees from around the throat of a sinkhole and protection of the cavity opening from siltation and debris using such methods as siltation barriers, debris catchment fences, riprap, gabion siltation barriers, and concrete structures (Fig. 30).
- *Drainage wells* – An additional concept that has been implemented in some areas is the use of injection drainage wells [7, 8, 22, 43, 44]. These types of storm water drainage wells are required to be permitted by the State and are known as Class V injection wells.

When implementing any of the above drainage concepts, it is imperative that a maintenance program be established and monitored in order to reduce future problems.

Another proactive method of approaching karst drainage problems is the use of tracer studies (dye, pollen, spores, etc.) in identifying the subsurface drainage regime [6, 39, 41]. As discussed earlier (and in more detail) under proactive remedial measures – investigative measures – the use of tracers placed in the subsurface (via springs, wells, sinkholes, etc.) enables karst hydrologists to define the subsurface drainage basins and recharge areas.

The information gained through tracer studies is extremely useful in both design development and litigation, despite its time-consuming nature.

The use of sinkholes for drainage is often considered in roadway design. In a proactive methodology for environmentally sensitive roadway design in karst, the best approach would be to *avoid placing drainage into a sinkhole*, particularly using the sinkhole as a wastewater disposal feature. The use of sinkholes as drainage features is basically groundwater contamination by design. Eventually, hazardous waste will be spilled and the karst aquifer will become contaminated.

Concerns about groundwater contamination must be addressed by either a filtration system, a retention/sediment basin, or both. A study by Stephenson et al. [49] showed that using a pilot-researched peat-moss filtration system on highway runoff on the I-40/I-640 interchange in Knoxville, Tennessee (Fig. 31) effectively reduced the highway runoff contaminants by

Karst Terrane and Transportation Issues. Figure 30
When roadways are built in sinkhole areas, sinkhole may need to be used for draining the runoff. Shown here is one such sinkhole that was cleaned of debris and protected against erosion and siltation with riprap and straw bales

Karst Terrane and Transportation Issues. Figure 31
This shows the completed and functioning filtration system for a sinkhole that receives runoff from the I-640/I-40 interchange in East Knoxville, Tennessee. This is the prototype for such filtration systems that was the result of a Federal Highway Administration pooled fund study on filtering highway runoff in karst areas

90–99% [2]. This type of treatment of highway runoff is highly recommended for high-volume highways where the roadway runoff recharges karst aquifers via sinkhole features.

As discussed earlier under reactive remedial measures, there are a number of sinkhole improvement techniques that may be employed to ease the impact on the groundwater. These include siltation fences, trash racks, perforated and filter-cloth wrapped stand pipes, gabion revetment, erosion control geotextiles, riprap, and concrete structures such as box culverts and inlet structures.

Regardless of the type of method used to treat the sinkhole that is used for drainage, it is imperative that a maintenance program be established for the drainage facility. Without maintenance of the sinkhole improvement facility, silt and trash will eventually plug the sinkhole resulting in flooding.

Future Directions

The collapse of roadway surfaces, drainage ditches, and bridge foundations, as well as numerous instances of flooding are karst-related issues and problems triggered by human construction activity on the environment. The greatest number of karst problems that develop along highways involves subsidence and collapse. This may involve the road or bridge footing itself or a drainage ditch. In some instances, the construction can trigger sinkhole formation outside of the construction limits of a project.

Remedial measures used in correcting karst-related subsidence problems may be divided into three areas: bridging, drainage, and relocation. Avoidance measures and some combination of drainage and bridging methods are usually the best direction to take in a proactive approach to designing and constructing highways in karst areas.

Innovative and cost-effective remedial concepts for solving karst-related geotechnical problems require modifications and refinement of the standard design to insure proper results to site-specific conditions. Proactive involvement by the geologic and engineering profession will be necessary to insure the success of karst-related remedial design concepts proposed for highways.

Bibliography

1. Amari D, Moore HL (1985) Sinkholes and gabions: a solution to the solution problem. In Proceedings of the 36th annual highway geology symposium, Clarksville, pp 47–68
2. Beck BF, Stephenson JB, Wanfang Z, Smoot JL, Turpin AM (1996) Design and evaluation of a cost effective method to improve the water quality of highway runoff prior to discharge into sinkholes. In Proceedings of the 1996 Florida environmental expo, Tampa, 1–3 Oct 1996, pp 155–164

3. Benson RC, Yuhr L, Kaufmann R (2003) Some considerations for selection and successful application of geophysical methods. 3rd international conference on applied geophysics, geophysics 2003, Orlando, 8–12 Dec 2003
4. Black TJ (1984) Tectonics and geology in karst development of Northern Michigan. In: Barry B (ed) Proceedings of the 1st multidisciplinary conference on sinkholes, 15–17 Oct 1984, Orlando, p 87–91
5. Crawford NC (1981) Karst flooding in urban areas, Bowling Green, Kentucky. Proceedings of the 8th international congress of speleology, Western Kentucky Univ., Bowling Green
6. Crawford NC (2003) Karst hydrogeologic investigation for proposed Kentucky trimodal transpark. In: Barry B (ed) ASCE Special Publ. No. 122, sinkholes and the engineering and environmental impacts of Karst, Huntsville, 6–10 Sept, pp 385–403
7. Crawford NC, Groves CG (1984) Storm water drainage wells in the karst areas of Kentucky and Tennessee. U.S. Environmental Protection Agency and Center for Cave and Karst Studies, Bowling Green, Kentucky, p 52
8. Crawford NC, Groves CG (1995) Sinkhole collapse and groundwater contamination problems resulting from storm water drainage wells on karst terrain. In: Beck B (ed) Karst Geohazards, Proceedings of the 5th multidisc. conf. on sinkholes, Gatlinburg, pp 257–264
9. Donaldson CW (1963) Sinkholes and subsidence caused by subsurface erosion. Proceedings, 3rd regional conference for Africa on soil mechanics and foundation engineering, pp 123–125
10. Drumm EC, Yang MZ (2005) Preliminary screening of residual soil stability in karst terrain. Environ Eng Geosci XI(1):29–42
11. Foose RM, Humphreville JA (1979) Engineering geological approaches to foundations in the karst terrain of the Hershey Valley. Bull of the Association of Eng Geol XVI(3):355–381
12. Hardeman WH (1966) Geologic map of Tennessee. Tennessee Division of Geology, Department of Environment and Conservation, Nashville
13. Hubbard DA (2003) Use of regional sinkhole mapping for sinkhole susceptibility maps. ASCE Geotech. Special Publ. No. 122: sinkholes and the engineering and environmental impacts of Karst. In: Barry B (ed) Proceedings of the 9th multidisciplinary conference on sinkholes, Huntsville, 6–10 Sept, pp 61–71
14. Hubbard DA (1984) Sinkhole distribution in the central and northern valley and ridge province, Virginia. In: Barry B (ed) Proceedings of the 1st multidisciplinary conference on sinkholes, 15–17 Oct, Orlando, pp 75–78
15. Jennings JE, Brink ABA, Louw A, Gowan GD (1965) Sinkholes and subsidences in the transvaal dolomites of South Africa. Proceedings of the 6th international conference of soil mechanics, pp 51–54
16. Kemmerly PR (1981) The need for recognition and implementation of a sinkhole-floodplain hazard designation in urban karst terrains. Environ Geol 3:281–292
17. Ketelle RH, Newton JG (1987) Inventory of karst subsidence in the valley and ridge province of east Tennessee. In Proceedings of 2nd multidisciplinary conference on sinkholes, Orlando, pp 25–29
18. Mathis H, Wright E, Wilson R (1985) Subsidence of a highway embankment on karst terrain. In Proceedings of the 36th annual highway geology symposium, Clarksville, pp 14–27
19. Mellett JS, Maccarillo BJ (1995) A model for sinkhole formation on interstate and limited access highways, with suggestions on remediation. In: Barry B (ed) Karst Geohazards, engineering and environmental problems in Karst Terrane. Proceedings of the 5th multidisciplinary conference on sinklholes, Gatlinburg, 2–5 Apr, pp 335–339
20. Mills HH, Starnes DD, Burden KD (1982) Predicting sinkhole flooding in Cookeville. Tenn Tech J 17:1–20, (Tennessee Technological University), Cookville, Tennessee
21. Moore HL (1976) Drainage problems in carbonate terrain of East Tennessee. In Proceedings of 27th annual highway geology symposium, Orlando, pp 112–131
22. Moore HL (1981) Karst problems along Tennessee highways: an overview. In Proceedings of the 31st annual highway geology symposium, Austin, pp 1–28
23. Moore HL (1984) Geotechnical considerations in the location, design, and construction of highways in karst terrain – 'The pellissippi parkway extension', Knox-Blount Counties, Tennessee. In Sinkholes: their geology, engineering, and environmental impact, Proceedings of the 1st multidisciplinary conference on sinkholes, Orlando, pp 385–389
24. Moore HL (1987) Sinkhole development along 'untreated' highway ditchlines in East Tennessee. In: Beck B, Wilson W (eds) Karst hydrogeology: engineering and environmental applications, Proceedings of the 2nd multidisciplinary conference on sinkholes, Orlando, pp 115–119
25. Moore HL (1988) Treatment of karst along Tennessee highways. In: Sitar N (ed) Geotechnical aspects of karst terrains: exploration, foundation design and performance, and remedial measures, ASCE Geotechnical Special Publication No. 14, pp 133–148
26. Moore HL (1994) A geologictrip across Tennessee by interstate 40. University of Tennessee Press, Knoxville, p 339
27. Moore HL (2003) Recent sinkhole occurrences along highways in East Tennessee, a historical perspective. In: Proceedings of the 54th annual highway geology symposium, Burlington, 24–26 Sept 2003, pp 46–55
28. Moore HL (2004) Preliminary geotechnical investigation of proposed interchange, I-181 with ext of SR 126, Sullivan, Co., unpublished report files, geotechnical engineering section, TDOT Region One, Knoxville Office
29. Moore HL (2006) A proactive approach to planning and designing highways in East Tennessee karst. Environ Eng Geosci XII(2):147–160
30. Moore HL, McDowell L (2008) The development and use of Karst maps in the location of highways in East Tennessee. In: Beck BF (ed) Sinkholes and the engineering and the environmental impacts of karst, Proceedings of the 11th

multidisciplinary conference on sinkholes, 22–26 Sept 2008, Tallahassee, ASCE Geotechnical Special Publication No. 183, pp 680–693
31. Myers PB, Perlow M (1984) Development, occurrence, and triggering mechanisms of sinkholes in the carbonate rocks of the Lehigh Valley, eastern Pennsylvania. In: Barry B (ed) Proceedings of the 1st multidisciplinary conference on sinkholes, 15–17 Oct 1984, Orlando, pp 111–115
32. Mylroie JE (1987) Influence of impermeable beds on the collapse of bedrock voids in the vadose zone. In karst hydrogeology: engineering and environmental applications, Proceedings of the 2nd multidisciplinary conference on sinkholes, Orlando, pp 95–99
33. Newton JG (1976) Early detection and correction of sinkhole problems in Alabama, with a preliminary evaluation of remote sensing applications. Fed. Hwy. Admin. HPR Report No. 76, Project 930–070., p 83
34. Newton JG (1981) Induced sinkholes: an engineering problem. J Irrig Drain Div ASCE 107(IR3):175–185, Proc. Paper 16343
35. Newton JG (1984) Natural and induced sinkhole development_eastern United States: international association of hydrological sciences proceedings, third international symposium on land subsidence, Venice, Italy
36. Niemiller M (2010) Photo of berry cave salamander. Accessed on 2008 from http://www.herpetology.us/niemiller/
37. Newton JG, Tanner JM (1987) Case histories of induced sinkholes in the Eastern United States. In: karst hydrogeology: engineering and environmental applications, Proceedings of 2nd multidisciplinary conference on sinkholes, Orlando, A.A. Balkema, Netherlands, pp 15–23
38. Price DJ (1984) Karst progression. In: Barry B (ed) Proceedings of the 1st multidisciplinary conference on Sinkholes, 15–17 Oct 1984, Orlando, pp 17–22
39. Quinlan JF, Ray JA (1981a) Groundwater basins in the mammoth cave region, Kentucky showing springs, major caves, flow routes, and potentiometric surface. Friends of Karst Occasional Publication, p 2
40. Quinlan JF, Ewers RO (1981) Hydrogeology of the mammoth cave region, Kentucky: Geological Society of America, Cincinnati field trip no. 8. pp 457–82
41. Quinlan JF, Ray JA (1981b) Groundwater basins in the mammoth cave region, Kentucky: plate 1 in central Kentucky cave survey bulletin no. 1, Center for Cave and Karst Studies, Western Kentucky University, 1:138,000 map
42. Quinlan JF, Ray JA (1990) Groundwater remediation may be achievable in some karst aquifers that are contaminated, but it ranges from unlikely to impossible in most: II. Implications for the mammoth cave area of long-term tracer tests and universal, nationwide failure in goal attainment by scientists, consultants, and regulators: In Karst Hydrology_Proceedings of mammoth cave national park's first annual science conference: U.S. National Park Service, Mammoth Cave National Park, Kentucky, 17–18 Dec 1990, pp 113–14
43. Reeder PP, Crawford NC (1989) Potential groundwater contamination of an urban karst aquifer - Bowling Green, Kentucky. In: Beck BF (ed) Engineering and environmental impacts of sinkholes and karst, Proceedings of the 3rd multidisciplinary conference on sinkholes and the engineering and environmental impacts of karst, Orlando, 2–4 Oct 1989, pp 197–206
44. Royster DL (1984a) Use of sinkholes for drainage. In: Construction and difficult geology: karstic limestone, permafrost, wetlands, and peat deposits; Trans. research board record 978, Washington DC., pp 18–25
45. Royster DL (1984b) Unpublished drawing of cap grouting on I-24, Montgomery Co., Tennessee. In: Geotechnical engineering section files, Tennessee Dept. Transp., Nashville
46. Sowers G (1976) Foundations bearing in weathered rock. Proceedings speciality conference on rockeng. for foundations and slopes 2, Univ. of Colorado, 15–18 Aug 1976
47. Sowers GF (1984) Correction and protection in limestone terrain. In: Beck B (ed) Sinkholes: their geology, engineering and environmental impact, Proceedings of the 1st multidisciplinary conference on sinkholes, Orlando, pp 373–378
48. Stephenson JB, Beck B (1995) Management of the discharge quality of highway runoff in karst areas to control impacts to groundwater – A review of relevant literature. In: Beck BF (ed) Karst geohazards – engineering and environmental problems in karst terrane, Proceeding of the fifth multidisciplinary conference on sinkholes and the engineering and environmental impacts of Karst, Gatlinburg, 2–5 Apr 1995, pp 297–321
49. Stephenson JB, Zhou WF, Beck B, Green T (1997) Management of highway storm water runoff in karst areas – baseline monitoring and design of a treatment system for a sinkhole at the I-40/I-640 interchange in eastern Knoxville, Tennessee. In Proceedings of the 48th annual highway geology symposium, Knoxville, 8–10 May 1997, pp 24–34
50. Vance SJ (2003) Perceived risk versus cost in Karst remediation: a case history. In: Beck B (ed) Sinkholes and the engineering and environmental impacts of karst, Proceedings of the 9th multidisciplinary conference on sinkholes, ASCE Geotechnical Special Publication No. 122, pp 652–658
51. Veni G (1987) Fracture permeability: implications on cave and sinkhole development and their environmental assessments. In karst hydrogeology: engineering and environmental applications, Proceedings of the 2nd multidisciplinary conference on sinkholes, Orlando, pp 101–105
52. White WB, White EL (1987) Ordered and stochastic arrangements within regional sinkhole populations. In: karst hydrogeology: engineering and environmental applications, Proceedings of the 2nd multidisciplinary conference on sinkholes, Orlando, pp 85–90

L

Lake and Reservoir Fate and Transport of Chemicals

Heinz G. Stefan[1], Xing Fang[2], John S. Gulliver[3]
[1]St. Anthony Falls Laboratory, Department of Civil Engineering, University of Minnesota, Minneapolis, MN, USA
[2]Department of Civil Engineering, Auburn University, Auburn, AL, USA
[3]Department of Civil Engineering, University of Minnesota, Minneapolis, MN, USA

Article Outline

Glossary
Definition of the Subject
Introduction
Inputs, Outputs, and Transformations of Materials in a Lake or Reservoir
Material Residence Times, Stratification, Mixing, and Currents in a Lake or Reservoir
Simulation of Water Quality in a Lake or Reservoir
Simulation of Sustainable Fish Habitat in Lakes Under Global Warming
Future Directions
Bibliography

Glossary

Dimictic lake A lake that has two complete mixing (circulation) periods per year (one in spring after the ice melts and another in fall before the ice forms).

Hyporheic flow Flow in a region beneath and along a stream bed. It is characterized as mixing of shallow groundwater and surface water which is important to sedimentary oxygen uptake.

Lentic "Stagnant" waterbody as opposed to "flowing".

Limnology Science or the study of inland waters, e.g., lakes and reservoirs.

Oxythermal parameter Variable to define fish habitat in inland waters using dissolved oxygen (DO) and water temperature limits, e.g., TDO3 – temperature at DO = 3 mg/L.

Particulate Tiny subdivisions of solid matter suspended in a gas or liquid, also known as particulate matter (PM) or fine particles.

Residence time The mean amount of time that water or a substance would stay or "reside" in a lake or reservoir. Hydraulic residence time is equal to lake volume divided by outflow rate. The residence time of a substance is equal to the quantity of a substance in volume divided by the change of a substance in volume over time through various lake's removal mechanisms (outflow or flushing, settling, and chemical and biological reactions).

Sedimentation The process or tendency for particles in suspension to settle out of the fluid in which they are entrained and come to rest against a barrier (e.g., lake or river bed).

Solute Material dissolved in water of a lake.

Stratification The formation of horizontal layers (strata) in which water temperature and concentration of substances are different along depth of a lake and reservoir.

Definition of the Subject

"Eutrophication" is originally used to describe aging process whereby a lake is transformed from a lake to a marsh to a meadow (fill the lake with sediments). "Cultural eutrophication" occurs when the lake aging process is quickened or accelerated by excess nutrients from human activities [1]. Understanding of the fate and transport of water quality constituents in lakes and reservoirs is essential to sustaining water quality and fish habitat in these inland waters. Constituent is used generically and does not necessarily mean a polluting substance, e.g., dissolved oxygen (DO) is a relatively benign variable. The fate of a constitute typically

Robert A. Meyers (ed.), *Encyclopedia of Sustainability Science and Technology*, DOI 10.1007/978-1-4419-0851-3,
© Springer Science+Business Media, LLC 2012

depends on its transport (movement) through an inland water system (lake or reservoir) and on sources, sinks, chemical and biological reactions, and other decay mechanisms (e.g., settling). When sediment input is more than sediment outflow or nutrients are more than demands of aquatic plants, a lake or reservoir becomes not sustainable and the aging process of a lake is accelerated. The study of fate and transport of a substance in a lake or reservoir is to qualitatively and quantitatively account for mass balance of the substance through boundaries of and within the waterbody. Using the principle of the conservation of mass to investigate mass balance is not a new topic, but closely examining mass balance of various water quality constituents in inland waters was only started a few decades ago, and sustainability of aquatic systems is a relative new topic to researchers, water resources managers, and the public. Due to waterborne pathogens as one of the prime causes of disease, civil engineers began to plan, design, and construct urban water and wastewater systems in the late nineteenth century, and then the water quality management processes or models from streams to lakes and reservoirs emerged. In the United States (U.S.), Rivers and Harbors Act in 1899 to Federal Water Pollution Control Act in 1972 (subsequently amended and called the Act Clean Water Act) promoted studies on water quality in receiving waters. Sustainability is the capacity to endure. For humans, sustainability is the potential for long-term maintenance of well-being, which has environmental, economic, and social dimensions. Sustainability in lakes and reservoirs involves how biological systems remain diverse and productive over time and how designated uses (e.g., water supply, recreation, fish and wildlife, etc.) endure over time. Lake and reservoir fate and transport involve understanding and maintaining healthy aquatic ecosystems and environments that provide vital goods and services to humans and other organisms.

Inland waterbody provides suitable habitat for survival and reproduction of desirable fish, shellfish, and other aquatic organisms. Sustaining fish habitat in lakes and reservoirs is a major resource management issue. Freshwater fish habitat is constrained by physical, chemical, and biological attributes that relate to water quality, food supply, and human interference [2]. In lakes, water temperature and DO concentration are two of the most significant water quality parameters affecting survival and growth of fishes [2, 3] and sustainability of lake aquatic ecosystem. An increase of atmospheric greenhouse gases is projected to cause climate warming, which would alter water temperature and DO characteristics in lakes. These changes are in turn expected to have an effect on indigenous fish populations. Understanding impacts of future climate changes on water quality and fish habitat in lakes and reservoirs is essential to promoting sustainability of valuable but limited water resources for humanity.

Introduction

"Sustainability" of lakes and reservoirs relates/depends on the transport and transformation of materials into, within, and out of these "lentic" waterbodies. Typically, lakes are formed by natural, i.e., geophysical and hydrogeological processes, whereas reservoirs or impoundments are typically man-made. There is a vast amount of literature on physical, chemical, and biological structure and function of lakes. There is a lot of literature on the engineering of dams and other hydraulic structures, e.g., by Zipparro and Hasen [4], USBR [5], Novak [6], and Press [7], but less on water quality processes in the impoundments they create [8–10]. Decisions on water releases from reservoirs and associated water quality downstream are difficult to make because of overlapping and contradictory objectives such as water storage, flood protection, hydropower generation, sediment transport, recreational water use, and water quality [11].

The study of lakes probably goes back to the scientists of the antiquity with a keen sense of observation such as Plinius. Thieneman in Germany and Birge and Juday in the USA (Wisconsin) were early scientific explorers of the physics, chemistry, and biology of lakes. "Limnology" is the discipline under which early investigators of lakes conducted their research, but geophysicists, biologists, engineers, and people with other diverse backgrounds have contributed significantly. The two volume book by Hutchinson [12] was an early and thorough compilation of the state of scientific knowledge on lakes. An overview of North American Limnology was compiled by Frey [13]. Books, e.g., by Lerman [14], Wetzel [15], Horne and Goldman [16], Lampert and Sommer [17]; conference proceedings of the International Society of Theoretical

and Applied Limnology (SIL); and journal articles, e.g., in Limnology and Oceanography, Hydrobiologia, Water Resources Research, and Aquatic Sciences, have summarized the progressively larger body of knowledge. Physical processes in lakes and their quantitative analysis are described by Henderson-Sellers [18]. Ecosystems in lakes and reservoirs and their modeling are described by Straskraba and Gnauck [19].

Reservoirs were created by man-made dams thousands of years ago in the Middle East and in China to provide water for irrigation of agricultural lands [20]. This practice provided the food source that sustained major cultures. Reservoirs connected by aqueducts to major cities supplied drinking water even in relatively dry regions. Eventually, sediment accumulation in reservoirs as well as natural lakes made it painfully obvious that water-filled depressions in the landscape that receive inflows from a watershed are not sustainable forever. Sedimentary rocks give testimony to this fact on geological timescales.

While sediment transport into reservoirs received some early attention, e.g., in China [21], the limnology of reservoirs has become of interest recently because of fishery issues in the reservoirs (e.g., Columbia River) and water quality and ecological issues in the tailwaters below dams (e.g., Colorado River) [11, 22]. The need to better understand reservoir processes and reservoir operations on the environment became obvious. Information is typically presented at meetings of the major water-resources-oriented societies such as American Geophysical Union AGU, the American Society of Civil Engineers (ASCE), American Water Resources Association (AWRA), International Water Resources Association (IWRA), American Society of Limnology and Oceanography (ASLO), SIL, and International Commission of Large Dams (ICOLD). Symposium proceedings were published by AGU [9] and ASCE [10], and a book on reservoir limnology was written by Thornton et al. [8]. Introductions to the modeling of lakes and reservoirs were given by Imberger in Fischer et al. [23] and Gray [24].

Although often lumped together, lakes and reservoirs differ significantly in several respects: (a) the water levels in a reservoir can be controlled by an outlet structure and, therefore, often varies more widely and at shorter timescales as water demand dictates, whereas the water level of a lake depends on natural outflow, evaporation, and precipitation on the water surface, and groundwater; (b) a reservoirs has typically a shorter hydraulic residence time than a natural lake because a river or stream is flowing through it; (c) horizontal water quality gradients in a reservoir can be far greater than in natural lakes (except the very largest lakes) because of the flow through a reservoir.

Even though entire cultures collapsed because water reservoirs for the irrigation of farm fields could not be sustained, construction of large dams for the purpose of creating new reservoirs has continued to the present (Three Gorges on the Yangtze River in China). Reservoirs have been created now not only for water storage but also to provide hydropower, flood protection, and sufficient water depth in navigable waterways. Small retention and flow retarding structures have been built in large numbers in cities and agricultural areas and in suburban developments for erosion control, to retain stormwater runoff for infiltration and groundwater recharge, and for urban stormwater management, i.e., flow reduction and water quality improvement [25, 26].

Sustainability of lakes and reservoirs is a big issue. Topographic depressions that lead to the formation of lakes in the landscape have been created naturally by a variety of geophysical processes. Large numbers of lakes were created in the northern USA during the last major glacial period only 10,000 year ago. Processes, resulting in over 70 lake types, are reviewed in Hutchinson's 1957 book [12]. However, all lakes and reservoirs are eventually filled by sediments because they are at a low point of a landscape. Prolonging their lifespan while maintaining high water quality and water use potential is the goal of many efforts.

Inputs, Outputs, and Transformations of Materials in a Lake or Reservoir

The fate and transport of a water quality constitute in a lake and reservoir is the study of mass balance of a substance. Mechanistic water quality studies and models are based on the conservation of mass; that is, within a finite volume of water, mass is neither created nor destroyed [1]. A mass balance equation quantitatively accounts for all transfers (fluxes) of matter across the system's boundaries (e.g., water surface and lake

bottom) and all transformations occurring within the system (a lake or reservoir) during a finite period.

$$\text{Accumulation} = \text{loading} \pm \text{transport} \pm \text{reactions}$$

The movement of substances through the volume, along with water flow (surface water and groundwater), is termed transport. Mass of substances is gained or lost by transformations or reactions of the substances within the volume. Chemical and biological reactions either add mass by changing another constituent into the substance being studied or modeled or remove mass by transforming the substance into another constitute [1].

The concept of water and material residence times is intimately linked to the "sustainability" of lakes and reservoirs. As lentic waterbodies, they experience periods of low flow and "flushing." In those times, "deposition" of inorganic or organic particulate matter becomes a crucial and defining process. Material fluxes that can be used to develop material budgets for lakes and reservoirs are crucial for the understanding of how lake chemistry and biology function. Material fluxes and budgets can be for total suspended solids (TSS), total dissolved solids (TDS), specific nutrients such as phosphate (PO_4), ammonia and nitrate (NO_3), silica (SiO_2), sulfate (SO_4), organic matter in terms of total (C) or cell count, dissolved oxygen (DO), or subcategories of nutrients such as total Kjeldahl N (TKN) or dissolved reactive phosphorus or orthophosphorus (P).

If a material budget for a substance is developed, and the control volume is the entire lake or reservoir, the material fluxes can be divided into the following components:

1. External material inputs to a lake or reservoir by runoff from the watershed, i.e., by rivers, small streams, storm sewers, drainage ditches, and "overland" flow from surrounding watersheds
2. External material inputs from the atmosphere through the lake or reservoir surface in form of wet (rain) or dry deposition
3. Material flux to or from the lake or reservoir sediments by organic or inorganic particle deposition or resuspension
4. Material flux of solutes (dissolved substances) into or from the pores of lake or reservoir sediments
5. Material transformations by chemical and biological processes (kinetics) within the various layers of a lake or reservoir

The "overland" flow is storm runoff flowing over the ground surface toward a channel or a waterbody when rainfall has exceeded infiltration capacity and depression storage capacity. Figure 1 gives a schematic of fluxes across the upper and lower boundaries of a lake or reservoir and internal transfer processes with emphasis on fundamental biological processes, and Fig. 2 is an example of biochemical interactions for various phosphorus components within a lake or reservoir.

External Material Inputs to a Lake or Reservoir by Runoff from the Watershed

Besides the water, material inputs to lakes and reservoirs come in particulate or dissolved form as TSS or TDS. Besides suspended particles, there can also be a significant bed load component in rivers and streams. These inputs are often detrimental to water quality. Suspended inorganic sediments cause undesirable turbidity and fill lakes and reservoirs when they settle out, reducing the useful life expectancy of reservoirs. This is one of the main arguments against the construction of dams and impoundments. Since there are no known economical methods to remove sediment from reservoirs, water storage in impoundments becomes unsustainable, until incoming and outgoing sediment loads balance. This is a huge problem for reservoirs on sediment-laden rivers. On the Yellow River in China, the life expectancy of a reservoir can be just a few decades. The Colorado River also has significant sedimentation problems. Bed load carried by inflowing rivers contributes to the loss of storage capacity, mostly by the formation of deltas in reservoirs. Diverting clay-laden turbid inflow from Lake Chico, AK, to the nearby Mississippi River increased light penetration and photosynthesis sufficiently to restore a dysfunctional ecosystem and bass fishery [29].

External materials (substances) that are fully dissolved in water and are not reactive are not likely to accumulate long-term in lakes or reservoirs. An example is road salt which is not only a conservative substance but also highly soluble [30]. Snowmelt water from roads in northern cities of the USA will first flow

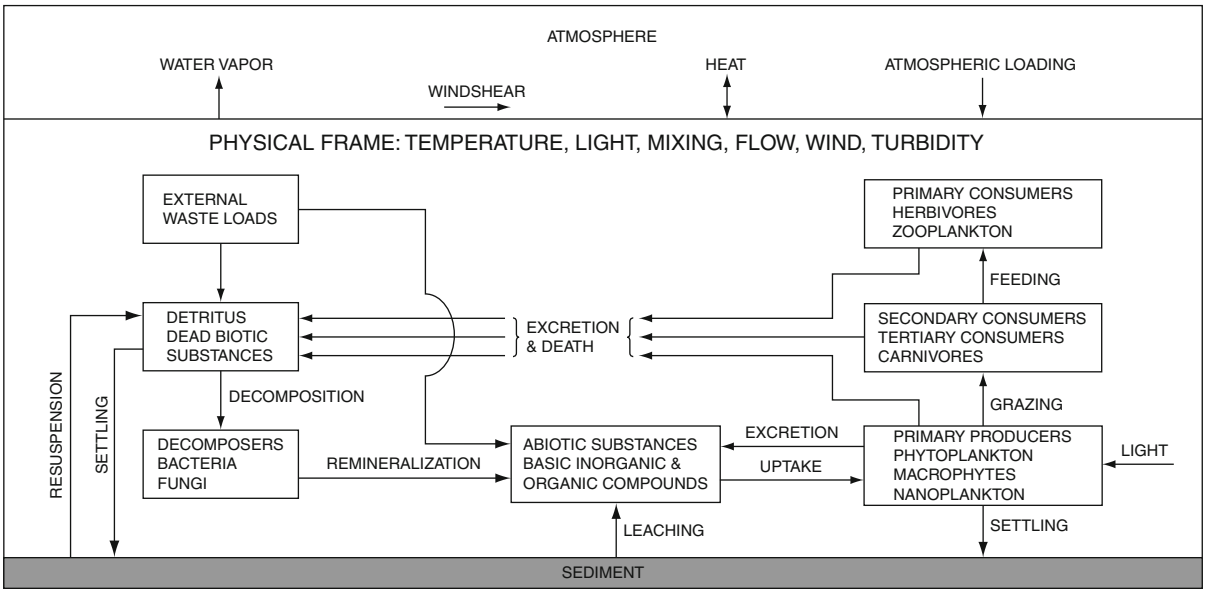

Lake and Reservoir Fate and Transport of Chemicals. Figure 1
Material flow in a lake or reservoir with emphasis on biological processes (From [27])

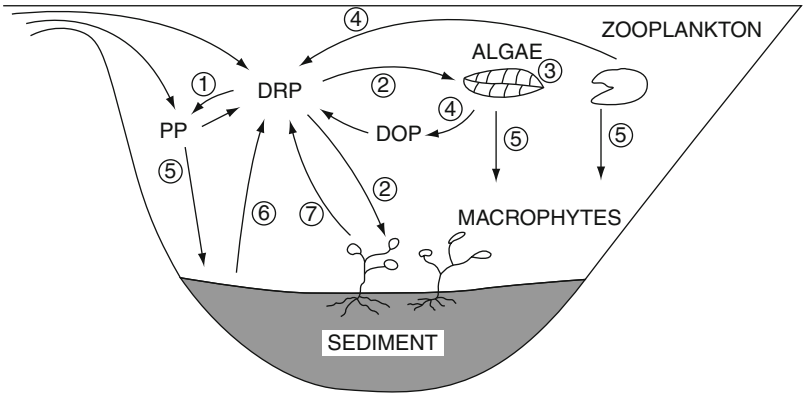

Lake and Reservoir Fate and Transport of Chemicals. Figure 2
Schematic of phosphorus components and interactions in a lake (From [28]). *DRP* dissolved reactive phosphorus, *DOC* dissolved organic phosphorus, *PP* particulate phosphorus. (1) Adsorption/desorption, (2) assimilation, (3) grazing by zooplankton, (4) regeneration, (5) sedimentation, (6) sediment release/recycling, (7) regeneration (From [27])

to and accumulate near the bottom of a lake because the salinity makes the water slightly denser than freshwater, some of it will flow into the pores of the lake sediments and the groundwater table underneath, and some will get mixed into the lake and flushed out if there is an outflow of water from the lake. Depending on the annual salt loading and the hydraulic residence times, each lake receiving road salt runoff will reach an equilibrium concentration, which may be high if the loading rate and the residence times are high. Novotny and Stefan [30] give examples for Twin Cities' lakes (7–104 t of Cl input per year and 3–14 years hydraulic residence time). The associated seasonal maximum Cl concentrations at the end of the winter

for these lakes were projected to be 107 and 387 mg/L, compared to a chronic water quality standard of 230 mg/L. Road salt accumulation is therefore considered to be fully reversible in lakes but not in groundwater because hydraulic residence times can be several order of magnitudes larger.

Nutrients such as phosphate, ammonium, or nitrate also come from watersheds, especially where fertilizers are used for agriculture. They are dissolved in lake or reservoir water in their original form, but they are reactive, and once they are incorporated in plant mass, they are particulates that precipitate to the lake or reservoir bottom. There have been literally thousands of studies of water quality in runoff from watersheds. Studies have progressed from estimates of annual yields of sediment, phosphorus, or nitrate from agricultural and urban watersheds to computer simulations using fairly detailed models such as SWAT [31] and SWMM [32, 33]. Heat transport in urban runoff has been simulated in models such as SNTEMP [34] for natural watersheds and MINUHET [35] in urban watersheds. Stormwater management is being studied to improve the quality of the runoff into lakes and reservoirs. Reducing the inflow of undesirable nutrients or contaminants to lakes or reservoirs is the goal of many TMDL (Total Maximum Daily Load) studies.

External Material Inputs from the Atmosphere and Material Release to the Atmosphere

The term "precipitation" in water quality studies may be used to describe the external material deposited by wet (rainfall) and dry (dustfall) processes on water surface of a lake or reservoir. The dry dustfall is a continuous process, while wet precipitation (rain, snow, sleet, etc.) is an intermittent process. Precipitation contributes chemical substances to surface waters and should be considered (not simply ignored) in analyzing surface water quality [26]. Precipitation impurities or chemical depositions will vary from one location to another and one time period to another, for example, chloride ion concentrations are highest along coastal areas.

Acid rain has harmed lakes in Europe and the USA. Sulfate emissions from the burning of coal were identified as the cause. Another example of atmospheric input is phosphorus loading of Lake Superior, where one third of the total P input was found to be from the atmosphere [36]. On the other hand, Lake Superior cleansed itself of PCB (polychlorinated biphenyl) that had accumulated by transferring it to the atmosphere in gaseous form (volatilization) [37].

Volatilization and gas exchange between atmosphere and water are controlled by mechanisms or processes at either sides of the air–water interface. Several gas transfer theories [1], e.g., Whitman's two-film theory and surface renewal models [38], and many empirical formulas through data synthesis were developed and used to quantify gas transfer process. Air–water equilibrium concentrations of gases dissolved in water are quantified by Henry's law [1]. Resistance to gas transfer for many gases (e.g., O_2, N_2, CH_4, H_2S, and SO_2) is in the liquid phase [1]. Oxygen reaeration is an important process to surface water quality control and modeling and was studied from the early stage of water quality engineering and management research development and applications. Various formulas of oxygen reaeration in rivers, streams, through hydraulic structures, in standing waters, and estuaries were developed, e.g., summarized by Chapra [1] and Gulliver [38].

Particle Settling and Resuspension in a Lake or Reservoir

Organic or inorganic particle deposition is the most significant process that impairs sustainability of lakes and reservoirs. Particles can settle out from the water column when they are no longer kept in suspension; inorganic clay or silica particles settle relatively fast; algae, which are almost neutrally buoyant, settle in dimictic lakes after they have died in fall. The mechanics of particle settling in lakes and reservoirs are very complicated because settling is the net effect of falling and resuspension in an intermittently turbulent or laminar environment. Settling is driven by the density difference between the solid particle and the water. If the two processes are parameterized by a particle fall velocity and a vertical turbulent resuspension coefficient, their interaction can be used to describe profiles of particle distributions in lentic waterbodies [39].

Resuspension of particles in lakes and reservoirs can be an important process that affects water quality,

e.g., turbidity, in lakes and reservoirs. Resuspension of sediment particles on the shoreline of a lake or reservoir can be observed when large enough waves are present. In fact, shorelines may be devoid of fine sediments because their resuspension has carried them to deeper and deeper water by turbidity currents. This process of sediment redistribution in lakes is responsible for the sorting of sediment beds such that shorelines exposed to wind and waves may be devoid of fine sediments, while very fine particulates, particularly organic particles, are settling to the deepest part of a lake [14, 40]. Because resuspension facilitates the redistribution of once deposited materials in a lake, it is an important process. The effect of wind on resuspension in shallow settling basins was investigated by Sheng and Lick [41] and modeled by Rodney and Stefan [42] among others. Erdmann et al. [43] provided data from Duluth harbor.

Because of adsorption and desorption of solutes on particle surfaces, particles also become carriers of substances. These interactions are well known, and descriptions can be found in textbooks, e.g., Thomann and Mueller [44], Clark [45], and Weber and DiGiano [46]. For example, a substantial portion of the TP load to a lake or reservoir can be adsorbed to particles. A seminal article on particle transport in lakes was written by Weilenmann et al. [47].

Flux of Solutes into or from the Pores of a Lake or Reservoir Sediment Bed

The best example of this type of flux is DO transfer from the benthic boundary layer to the surfaces of sediment bed particles, where it is used by microbial biofilms or in chemical reactions. The linkage between DO uptake rates, sometimes referred to sedimentary oxygen demand (SOD), and the flow over, through and below the sediment surface, have been established by field studies (Boynton et al. 1981) and laboratory experiments [48]. Sediment topography and surface waves have been shown to enhance physical transfer rates by "hyporheic flow" between the overlying water and the pore system significantly [49–53]. Connections to the microbial populations have been investigated experimentally, e.g., by Steinberger and Hondzo [54] and O'Connor and Hondzo [55], and modeled, e.g., by Nakamura and Stefan [56] and Higashino et al. [57]. Transfer of solutes other than DO, such as nitrate, iron, and sulfate, at the sediment–water interface have also been studied by Arnon et al. (2007) and Thumdrup et al. [58]. Transfer rates of solutes over a wide range of flow and sediment conditions have been scaled, i.e., linked to dimensionless parameters by O'Connor and Harvey [59]. Transfer of colloids and organic particles into sediment pore systems have been the subject of studies by Packman et al. (2000) and Huettel et al. (1996).

In the long-term, materials incorporated or adsorbed to particles on a lake or reservoir bed may be buried in the sediments, or they may be recycled. The recycling process of phosphate is well understood and depends on chemical reactions with iron [60]. The process has been modeled in detail, e.g., by Nakamura (1994), and as a seasonal bulk process by Lorenzen et al. [61]. The annual recycling of phosphate from the lake or reservoir sediment is referred to as "internal nutrient loading" and can sustain multiple annual algal blooms [62] or blooms over long periods of time because the fertilizer is essentially recycling. The biogeochemical and transport processes associated with the transfer and use of dissolved substances in the sediment pore system are very numerous and complex and have been described, analyzed, and modeled in books, e.g., by Boudreau and Joergensen [63], DiToro [64], Clark [45], and Zheng and Bennett (1995). An experiment on sulfate uptake in lake sediments is described by Manous et al. [65].

Material Transformations by Chemical and Biological Processes (Kinetics) Within the Water Layers of a Lake or Reservoir

Biological processes by which materials in a lake are transformed include plant growth by photosynthesis (primary productivity), grazing by zooplankton, and predation by fish and higher-order animals. Respiration, death, and microbial decomposition affect all organic materials. Chemical processes include oxidation and reduction, and adsorption and desorption round out the menu of possible interactions. Models of lake or reservoir water quality [66, 67] include algorithms that quantify the material fluxes associated by these processes. Chemical and biological kinetics used for this purpose can be simple zero or first order, or can be higher order and/or more complex,

e.g., Michaelis Menten, Monod, Haldane kinetics, or processes in series. Figure 1 gives a very simple flowchart for the principal biological processes in a lake.

Information on the chemical kinetics of lakes can be found in the limnological literature; the literature on chemical kinetics, e.g., by Stumm and Morgan [68, 69], Gobas and McCorquodale [70], Brezonik [71], Weber and DiGiano [46], and Gulliver [38]; and the water quality modeling literature, e.g., by Thomann and Mueller [44], Chapra [1], Zison et al. [72], and Bowie et al. [73].

Studies of lakes and reservoirs have progressed to ever finer detail and are often highly specialized. Earlier studies of the physics of lakes and reservoirs dealt with readily identifiable phenomena such as the seasonal temperature stratification, wind-driven Langmuir circulation, and the thermal bar which are all described in classical textbooks [15, 16]; more recent studies rely on field measurement techniques that record temperature and turbulent velocities at high temporal and spatial resolution, as well as transparency, specific conductance, and other parameters. Similarly, the study of lake chemistry has progressed from dissolved oxygen and nutrients to subspecies of nutrients, toxic substances, and endocrine disruptors [74, 75]. Lake ecology used to concentrate on phytoplankton, zooplankton, and fish, but has evolved to include detailed measurements and analyses of macrophytes, periphyton, and microbial components (see, e.g., Scheffer [76]).

Lake and Reservoir Manipulations to Affect Fluxes of Materials

Manipulation of water quality and lakes and reservoirs has become a subject of considerable interest, and many different tools have been tried. Cooke et al. [77] give an overview of techniques used in lakes. Engineering approaches have been described by Reckhow and Chapra [78]. Examples of simulation model applications to guide lake or reservoir management decisions have been given by Henderson-Sellers [79].

Destratification by air bubble release at the lake bottom was an early tool [80] and has been modeled by Fast [81], Goossens [82], Zic and Stefan [83], and Zic et al. [84]. Instead of air, pure oxygen has been used in deeper lakes. Air bubble plume can cause phosphorus recycling from the lake sediments [85].

The US Army Corps of Engineers in Vicksburg, MS, has developed and applied various techniques to mix stratified reservoir water near dam faces with large propellers before its release through outlet structures, in order to improve the water quality in the tailwater downstream from reservoirs.

Mixing (aeration) of selective layers has been attempted and practiced, particularly for aeration of selective layers in stratified lakes [86, 87]. Hydraulic jet mixing systems are energetically attractive [88–90]. To prevent internal phosphorus loading of eutrophic lakes, various sediment treatment techniques have been developed (alum, RIPLOX). Herbicides have been applied to kill phytoplankton [91] or macrophytes selectively. Biomanipulation by influencing the food chain is an elegant technique that has had some success. Fish stocking and fish management in lakes are very common in some states where recreational fishing is popular.

Lake manipulation techniques (Fig. 3) to control the excessive growth of algae are designed to change one or more of the following:

1. The inflow of water, nutrients (mostly P), or sediments to a lake
2. The loss of algal populations by settling or grazing or outflow from a lake
3. The availability of light to an algal population of a lake
4. The nutrients in the photogenic surface layer of a lake
5. The transfer of nutrients from the hypolimnion to the surface layer of a lake
6. The concentration of nutrients in the hypolimnion
7. The release of nutrients from the sediments

Material Residence Times, Stratification, Mixing, and Currents in a Lake or Reservoir

Residence Times

Hydraulic residence time (years) is a measure of the flushing effect by flow through a lake or reservoir. It can be defined as a lake's or reservoir's volume (m^3) divided by the volumetric outflow rate (m^3/year). Some definitions use inflow instead of outflow rates. Hydraulic residence times range from a few days or

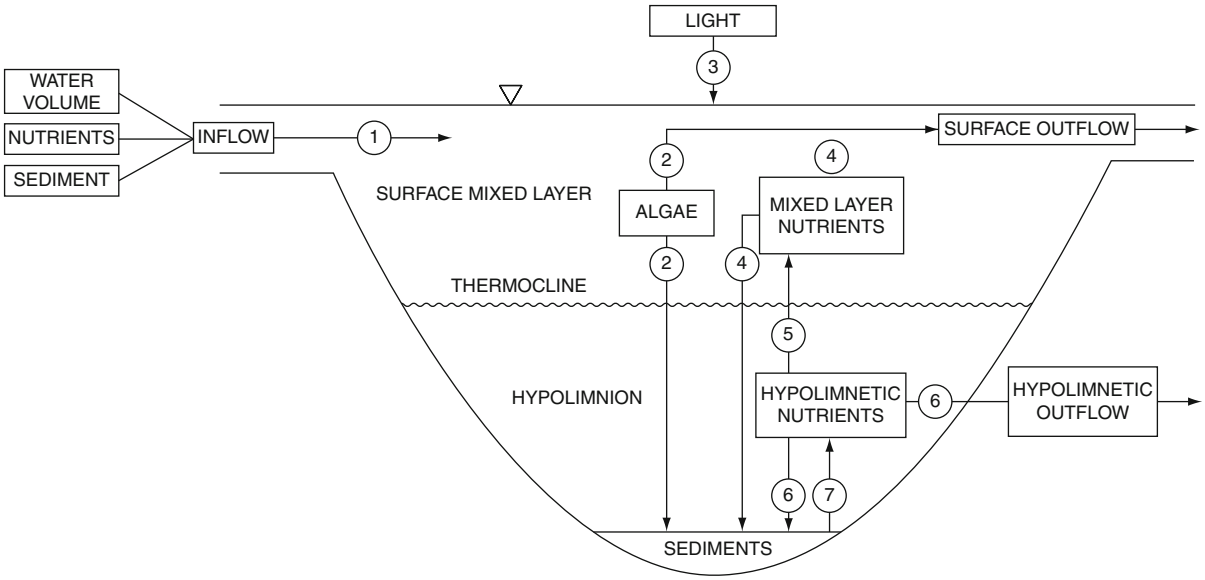

Lake and Reservoir Fate and Transport of Chemicals. Figure 3
Schematic of lake manipulation (processes 1–7) for eutrophication (water quality) control (From Henderson-Sellers [79])

weeks for shallow river impoundments, to several years for quaternary lakes and large reservoirs, to hundreds of years of the world's largest lakes. Hydraulic residence time determines how long different chemical or biological processes can work on the removal or generation of different materials/substances. Lake and reservoir ecosystems depend on hydraulic residence times.

Hydraulic flushing or residence time determines the impact of a nutrient input to a lake. Lake or reservoir eutrophication is in many instances linked to phosphorus supply to a lake. The famous Vollenweider [92] diagram reproduced in Fig. 4 shows annual flushing rate (m/year) = annual outflow per lake surface area on the horizontal axis and annual volumetric P loading rate (g/m^3/year) on the vertical axis. The lines are boundaries between eutrophic, mesotrophic, and oligotrophic lakes, i.e., very high, intermediate, and low primary (plant) productivity. It can be seen that the same trophic state can be achieved with a high P loading rate when the flushing rate is higher.

The rate of removal of a material/substance/organism, e.g., by settling or by volatilization or by uptake, can be used in addition to the flushing rate to define a material residence time. If material is removed, the material residence time will be shorter than the hydraulic residence time. For first-order processes, the following relationship holds:

$$\begin{aligned}(\text{material residence time})^{-1} = {} & (\text{hydraulic residence time})^{-1} \\ & + (\text{settling rate coeff.}) \\ & + (\text{removal rate coeff.}) \\ & + (\text{volatilization rate coeff.})\end{aligned}$$

Stratification or Vertical Mixing of a Lake

For water quality in lakes or reservoirs, it makes a large difference if a lentic waterbody is density (temperature) stratified or not, in addition to the flushing effect by flow through the lake or reservoir. Temperature stratification is driven mostly by solar irradiation of the water surface and seasonal temperature variations. Stratification can occur during the day and be absent during the night, it can be intermittent for several days at a time, it can be seasonal in northern temperate climate regions with one or two full mixing events, or permanent if a saline water layer forms in a lake. Correspondingly, lakes are referred to as well-mixed, polymictic, monomictic, dimictic, or meromictic. Stratification and/or mixing depend on the physical processes that produce them.

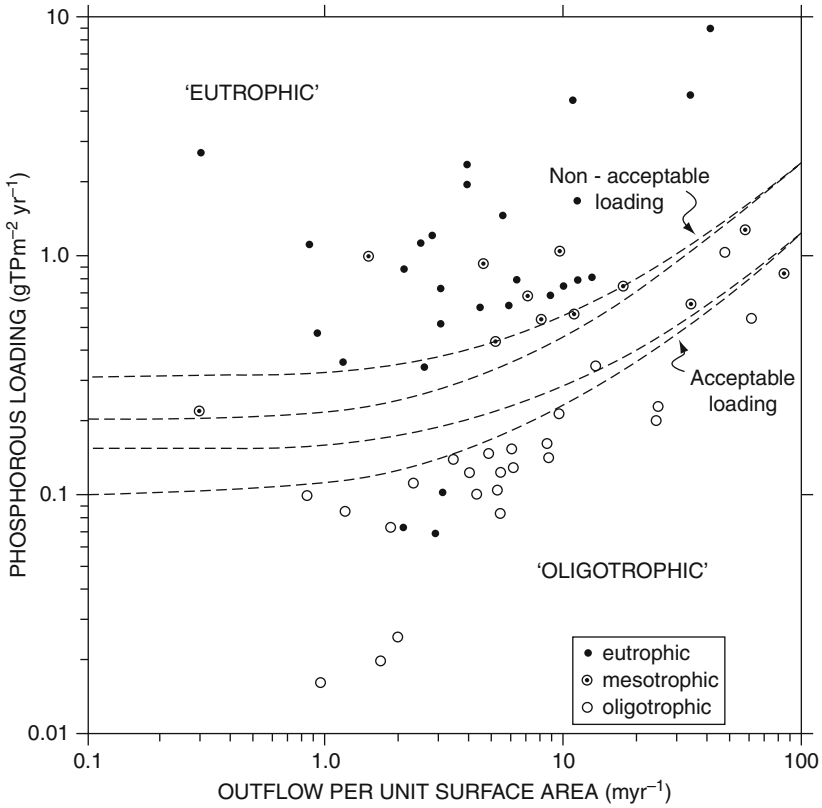

Lake and Reservoir Fate and Transport of Chemicals. Figure 4
Annual phosphorus loading tolerance of a lake as a function of annual hydraulic flushing rate (outflow per unit surface area) (From [92])

The density of freshwater changes ever so slightly with temperature or salinity (concentration of dissolved substances). A lake or reservoir can become density stratified whenever heat or any dissolved substance is added or removed from portions of its water. Because a lake or reservoir is a lentic or standing waterbody, its water will tend to arrange itself in layers of increasing density from top to bottom. The differences are typically very slight, but significant. The stable equilibrium of a density-stratified lake is easily reinforced or upset by many physical mechanisms such as daily heating through the water surface by solar radiation, inflows of warmer or colder water, or wind action on the water surface. These processes and their effects on lake stratification have been studied extensively.

There are two major processes that produce lake mixing: convective mixing induced by density instability, i.e., denser water on top of lighter water; or forced mixing, e.g., by wind or inflows (jet mixing). Density instabilities can be caused by cooling of surface waters (cooler water is denser above 4°C) or by dissolved (e.g., road salt) or suspended (e.g., sediment) materials in inflowing waters. Wind mixing depends on the shear stress exerted by wind on the water surface. That shear causes not only clearly visible "progressive" surface waves with amplitudes dependent on shear stress but also less noticeable and relatively slow "standing" waves on the lake surface. In a stratified lake, internal waves are produced by wind and contribute to mixing at different depths when they break on the sloping beaches, invisible to the eye below the water surface.

Criteria for lake or reservoir mixing have been developed. One of the easiest to use is the "lake geometry ratio" $A_S^{0.25}/H_{max}$ [93]. It is the ratio of the fourth root of the lake surface area A_S (in m^2)

divided by the maximum lake depth H_{max} (in m). In the north-central USA, lakes with a geometry ratio greater than 4 are polymictic; those with a ratio smaller than 1 are dimictic. The lake geometry ratio depends on lake bathymetry only and is climate independent. That makes it easier to use than other criteria, e.g., the Wedderburn number which requires knowledge of the wind shear stress (Imberger in Fischer et al. [23]).

Density- or Wind-Driven Currents in a Lake or Reservoir

When water temperature or dissolved or suspended material content makes a portion of the water in a lake denser than its ambient water, that water will always tend to sink lower in a stratifies lake until it reaches a layer of equal density. This sinking has a huge effect on water quality because it redistributes material at a rate that is much faster than molecular diffusion.

An organized sinking flow is a density current or turbidity current if suspended sediment makes the water heavier than its surroundings. Turbidity currents are sediment-laden underwater rivers that can occur unnoticed because they take place below a quiescent water surface. Only a plunge line visible on the water surface by the accumulation of floating wood or a color contrast between clear lake water and turbid inflow may give away the occurrence of a significant process. Reservoirs in the Yellow River Basin are famous for their turbidity currents, and the routing and the release of these turbidity currents through bottom outlets at a downstream dam site have become management tools to delay the deposition and filling of the Yellow River reservoirs by the fine loess sediments. Plunging flows and density currents in reservoirs have been investigated and modeled among others by Imberger [23], Alavian et al. [94], Akiyama and Stefan [95–98], Johnson et al. [99, 100], Farrell and Stefan [101, 102], and Fang and Stefan [103]. A density current of saline snowmelt water into an ice-covered lake was described by Ellis et al. [104].

When the inflow to a lake or reservoir is warmer than the lake, it will spread out on the surface of the lake [105–109].

Wind induces horizontal exchange flows in multibasin lakes [110–113] that can transport salinity, nutrients, or contaminants from basin to basin. Wind also controls vertical mixing of a lake by progressive waves and standing waves (seiche) both on the lake surface and internally, if a lake is density (temperature) stratified. Wind also has a determining effect on the depth of the surface mixed layer [114, 115]. In nutrient-rich (eutrophic) lakes, wind can become the determinant/controlling factor for algal growth [116]. Wind controls the wind-driven circulation, stratification, and mixing dynamics in lakes, and thereby the fate and transport of organic and inorganic materials as well as the growth of algae [116] and rooted vegetation (macrophytes) in them [117]. Wind sheltering by trees, buildings, or topography can severely hinder wind access and thereby reduce wind shear on the water surface, wave action, and vertical turbulent mixing by waves, turbulent eddies, and Langmuir circulation. The development of the atmospheric boundary layer on a lake surface and its effects on surface mixing and water quality is often ignored and only partially understood and predictable [118].

Simulation of Water Quality in a Lake or Reservoir

Water quality models are often used as tools to guide decisions on lake management and reservoir operation. Without them, decisions have to be made based on experience. Water quality in a lake or reservoir is best simulated by a deterministic model. Physical modeling attempted by the USEPA and the Army Corps of Engineers did not work out because scaling laws for the physics, chemistry, and biology in lakes or reservoirs were incompatible. The simulation models use mathematical descriptions and rely on basic principles, such as conservation of mass, heat, and mass transfer equations, and well-known relationships for chemical and biological kinetics. A review of basic principles of model formulations can be found, e.g., in textbooks by Thomann and Mueller [44], Chapra [1], and Clark [45], and in a monograph by Stefan, Ambrose, and Dortch [119] but also in some user manuals.

A review of major available hydrological and water resources simulation models was given by Wurbs [120]. One- or multidimensional models of lake or reservoir water quality, e.g., WASP (EUTRO04) [66], CE-QUAL-R1 [121], CE-QUAL-W2 [67], DYRESM [122], and MINLAKE [123], are composed of submodels that analyze and project the hydrodynamics

in a lake or reservoir, the heat transfer to obtain temperature distribution and density stratification, sediment particle dynamics, chemical kinetics, biological kinetics and particle–solute interaction. Numerous boundary conditions have to be specified at the water surface or the sediment–water interface. These models require considerable data input and can therefore be tedious to use. Training on the use of some of these models is available from the custodian organizations or from consultants. Information on some of these models can be found on the internet under the name of the model.

Empirical models, e.g., to relate nutrients to lake eutrophication [27, 92, 124], are popular and widely used tools to guide nutrient management in lakes. However, the simplifications necessary in empirical models can lead to outliers and high variance in the results of these models. Empirical models are typically zero-dimensional, i.e., they do not resolve spatial differences and assume well-mixed conditions; they are usually applicable at long (monthly or annual) timescales. Sometimes they apply only to a portion, e.g., the surface mixed layer, of a lake (Fig. 3).

One-dimensional water quality models of stratified lakes describe water quality C(z,t) as a function of depth (z) below the water surface and of time (t). They can be quite sufficient for smaller lakes and work well even at short, e.g., daily, timescales. They do not give water quality changes in the longitudinal direction of reservoirs.

Two-dimensional reservoir water quality models have to resolve the flow through the waterbody and can show longitudinal water quality gradients. Three zones are often found by two-dimensional models [8]: a shallow inflow region where velocities are initially high, sediment settles out, and deltas form; a productive zone where nutrients in the inflow combined with sunlight lead to high primary productivity, i.e., phytoplankton growth; and finally a quiescent region where algae are consumed or settle out and water quality is increased. Two-dimensional (width-integrated) models where water quality parameters C(x, z, t) are functions of distance from the dam or inflow, depth below the water surface, and time are very appropriate for reservoirs. Such models can handle stratified flows such as density and turbidity currents, at least in their developed stages away from the plunge point. A schematic of 0-, 1-, 2-, and 3-dimensional model resolution is shown in Fig. 5.

Three-dimensional models are used to simulate the most demanding and complex waterbodies. A 3-dimensional model developed by HYDROQUAL has been applied to the tidal Chesapeake Bay, San Francisco Bay, and the Upper Mississippi River impoundments and Lake Pepin in the Twin Cities area of Minnesota. Over 30 water quality constituents have been simulated at daily or shorter timescales and for multiyear periods. Another 3-dimensional hydrodynamic and water quality model ELCOM-CAEDYM was developed and applied by Bruce et al. [125] to simulate the role of zooplankton on C, N, and P cycling in Lake Kinneret, Israel. Other applications of this model have been described by Gal et al. [126], Leon et al. [127], and Robson and Hamilton [128]. An introduction and CE-ROM for 3-dimensional hydrodynamic and water quality lake modeling was offered by Edinger [129].

As an example of a water quality model, the structure and use of the MINLAKE model will be described in more detail. The original MINLAKE model [123] simulates the processes shown in Fig. 6. A flowchart is shown in Fig. 7. It was applied, e.g., by West and Stefan [130–132], to several lakes in the Twin Cities, Minnesota, and elsewhere, and modified by Fang et al. [133] to MINLAKE96. This deterministic, process-oriented, dynamic and one-dimensional (vertical) year-round lake water quality model was later modified for water temperature and dissolved oxygen (DO) simulations in deep oligotrophic lakes in Minnesota, and then called MINLAKE2010 [134].

Year-Round Water Temperature and Ice-Cover Model

The MINLAKE numerical simulation model for water temperature profiles in lakes solves the one-dimensional, unsteady heat transfer equation

$$\frac{\partial T}{\partial t} = \frac{1}{A}\frac{\partial}{\partial z}\left[K_z A \frac{\partial T}{\partial z}\right] + \frac{H_w}{\rho c_p} \tag{1}$$

where T (°C) is the water temperature, t (day) is the time, A (m^2) is the horizontal area of a lake as a function of depth z (m), K_Z (m^2 day^{-1}) is the vertical turbulent heat diffusion coefficient, ρc_p (J m^{-3}°C^{-1}) represents heat capacity per unit volume of water and is equal to the density of water (ρ) times heat capacity of water (c_p), and H_w (J m^{-3} day^{-1}) is the heat source or

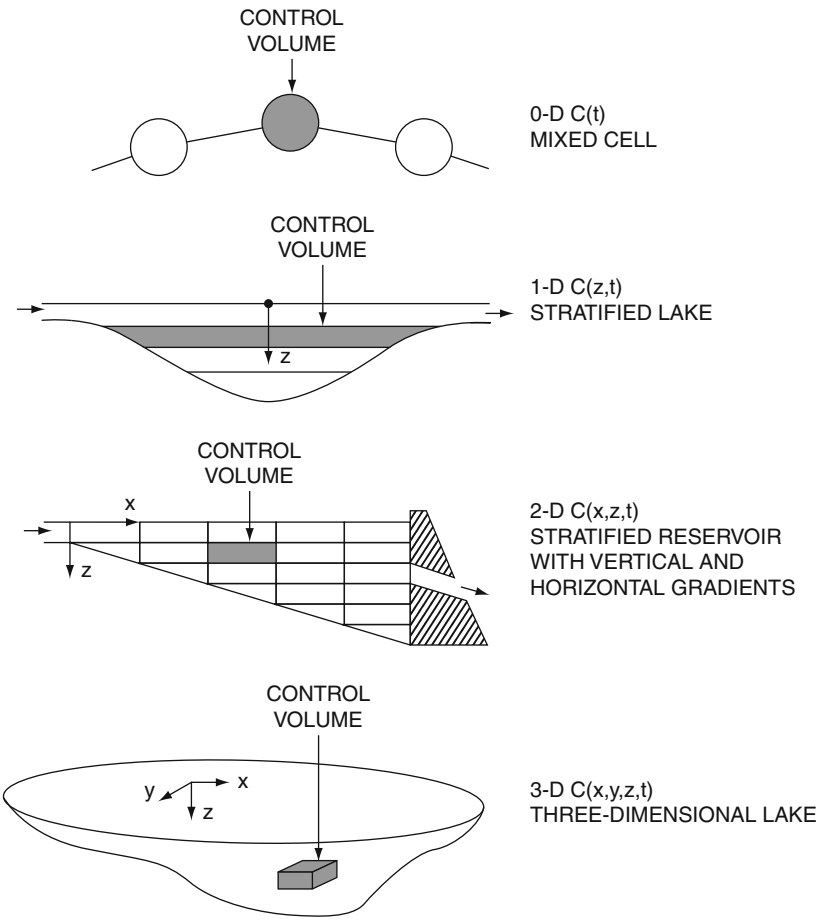

Lake and Reservoir Fate and Transport of Chemicals. Figure 5
Schematic of the spatial resolution of lake or reservoir water quality models. Control volumes are shown as shaded elements. Concentration of a water quality constituent is designated by (C) (From Stefan, Ambrose, and Dortch [119])

sink strength per unit volume of water. Solar radiation absorption in the water column contributes to the heat source term. Heat exchange between the atmosphere and the water during the open-water season (7) is treated as a source/sink term for the topmost water layer in a lake. For the open-water season, the computational scheme and the determination of source and sink terms have been discussed, e.g., by Edinger et al. [135], Ford and Stefan [136], Harleman [137], Hondzo and Stefan [138, 139], among others. Equation 1 is solved numerically using an implicit finite difference scheme and a Gaussian elimination method, e.g., for time steps of 1 day and water layer thicknesses of 1 m. The model uses a stacked layer system to represent a lake and its environment in the open-water and winter ice-cover periods. Besides the water layers, the lake sediments, the ice cover, and the snow cover are included in the model by separate submodels (Fig. 8).

Climate conditions and variations over seasons are driving forces of seasonal variations of water temperature in a lake. Weather parameters needed are: daily average air temperature, dew point temperature, wind speed, sunshine percentage, total daily solar radiation, and precipitation (rainfall and snowfall). They are used as model input parameters to calculate heat fluxes across the water surface or ice and snow cover in winter. If solar radiation has not been measured, it is calculated [141].

Compared to the regional water temperature model for the open-water season [139], the year-round water

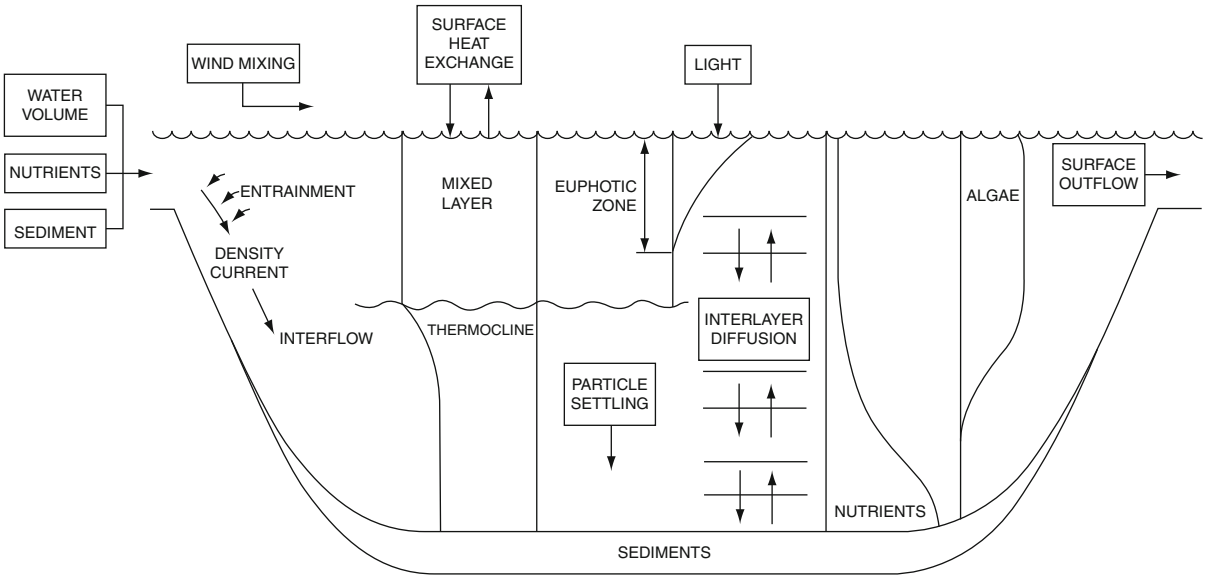

Lake and Reservoir Fate and Transport of Chemicals. Figure 6
Schematic of the variables and processes simulated by the 1-D MINLAKE model [123]

temperature simulation model has been expanded significantly by simulating ice and snow covers above the water and including the heat exchange between each water layer and its adjoining sediments.

The heat flux across the sediment–water interface is treated as a contribution to the source/sink term for each water layer from the water surface to the lake bottom [142]. The direction of the heat flux between the sediment and the water reverses frequently on shorter, e.g., daily, timescales [143]. Heat can transfer into or out of the lake sediment during both the open-water season and the winter ice-cover period. The lake sediments not only provide seasonal heat storage but also add significant thermal inertia to the water column. Sediment heat fluxes are most important in shallow lakes and during winter ice-cover period.

The snow and ice thickness submodels developed by Gu and Stefan [144] have been used with some modifications. The complete set of equations for the ice- and snow-cover simulation has been summarized by Fang and Stefan [142]. During the ice-cover period, the model simulates ice thickness and sediment temperature profiles (heat conduction equation) first, then determines the heat source/sink term H_W in (Eq. 1), and finally solves the heat transfer (Eq. 1) to obtain water temperature profiles below the ice. At the air/snow interface (or air–ice interface if snow is absent), the net heat flux from the atmosphere into or out of the snow/ice cover is calculated. Contributions of heat flux are made by solar radiation (H_{SN}), evaporation (H_E), and convection (H_C). Snow thickness is determined from snow accumulation (precipitation), followed by compaction and snow melting. The model simulates melting of snow by surface heat input (convection, rainfall, solar radiation), melting within the snow layer due to internal absorption of short wave radiation, and transformation of wetted snow to ice when cracks in the ice cover allow the water to migrate on the ice surface [133]. In the model, ice growth occurs at the ice/water interface and at the ice surface [133]; ice decay occurs and is simulated at the snow/ice interface, the ice/water interface, and within the ice layer.

Ice formation on small freshwater lakes generally occurs on a calm, cold night. Rising winds and daytime heating may subsequently break up this cover until calm and cold conditions occur again and the ice cover forms a second time [145]. A process-descriptive algorithm which replaced previous empirical and lake-size-dependent criteria to predict the date of ice

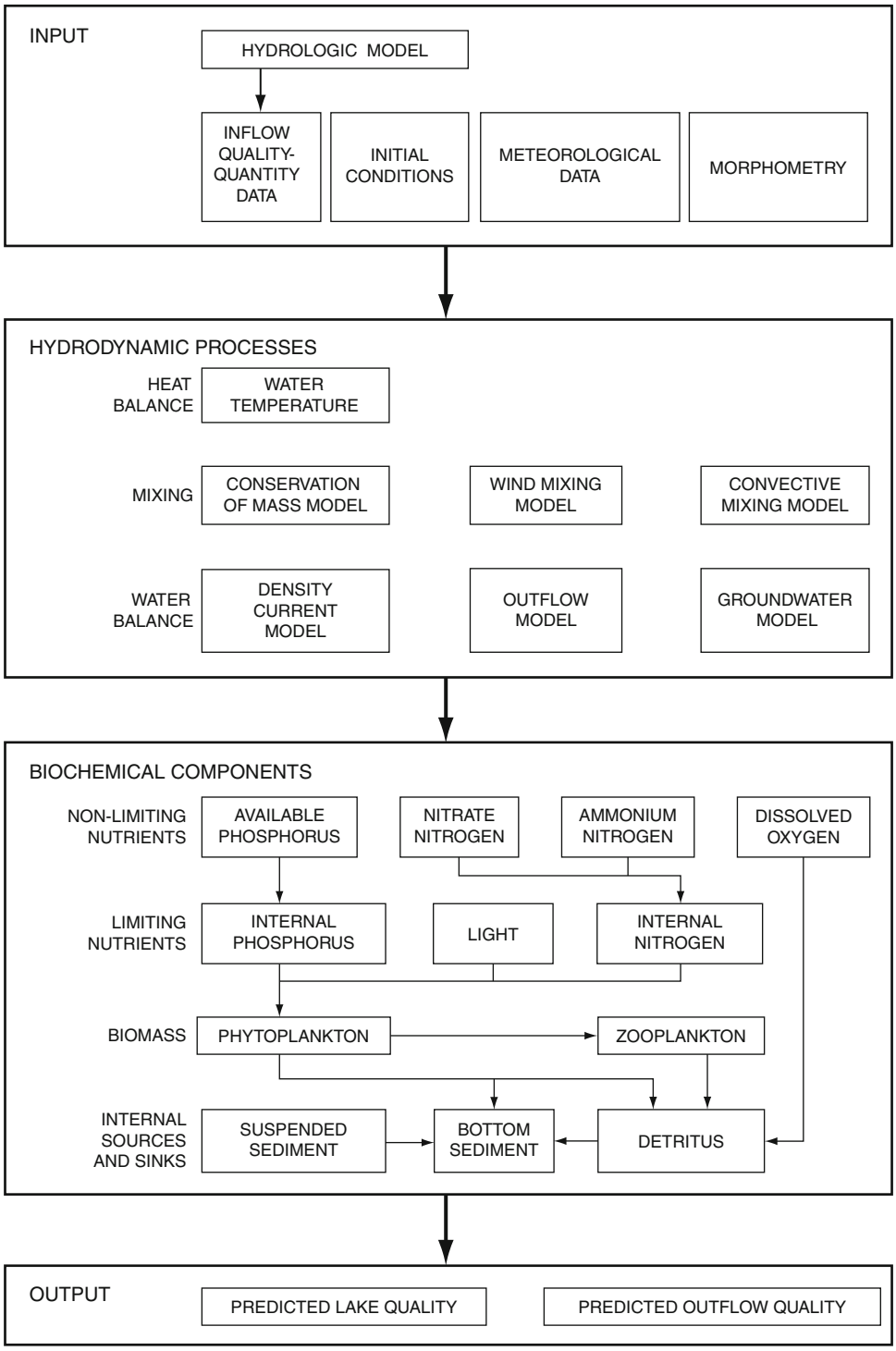

Lake and Reservoir Fate and Transport of Chemicals. Figure 7
Flowchart and major model sections and components in the original MINLAKE model [123]

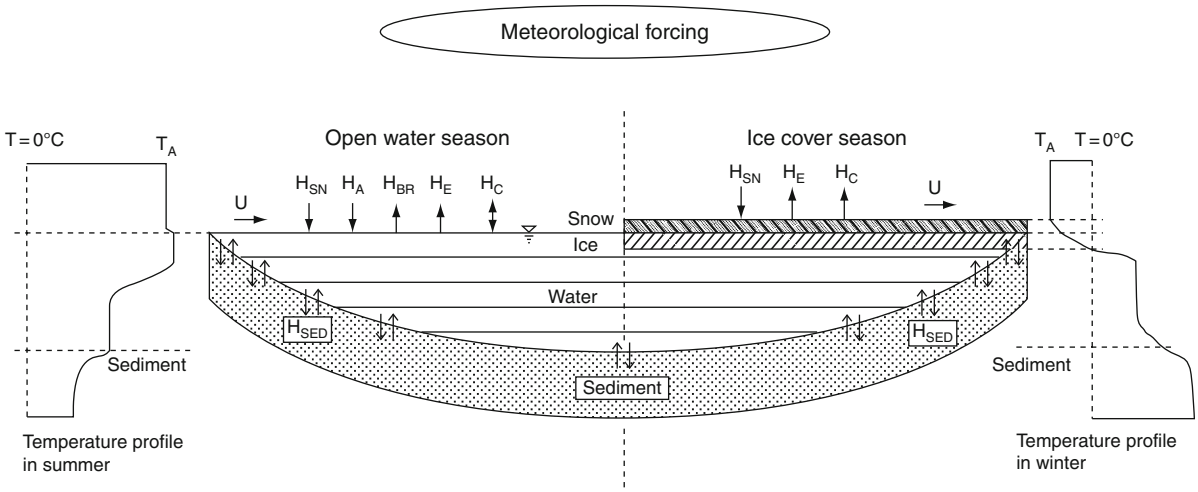

Lake and Reservoir Fate and Transport of Chemicals. Figure 8
Schematic of a stratified lake with a 10-m sediment layer showing heat transfer components and water/sediment temperature profiles in the open-water season and in the ice-cover season [140]

formation is incorporated in the model [146]. The ice-formation algorithm uses a full heat budget equation to estimate surface cooling, quantifies the effect of forced connective (wind) mixing, and includes the latent heat removed by ice formation. The algorithm has a fine spatial resolution near the water surface where temperature gradients before freeze-over are the greatest. Inverse temperature stratification occurs in the near-surface water several hours before ice formation. The ice-formation algorithm is combined with the year-round temperature model and was tested previously against observations in Ryan Lake and eight other Minnesota lakes for multiple (9–36) years. The difference between the simulated and observed (permanent) ice-formation dates was less than 6 days for all lakes studied. Water temperature profiles are typically predicted with an RMSE on the order of 1°C.

The water temperature and ice-cover model can be run in a continuous mode over many simulation years covering sequences of both open-water seasons and ice-cover periods. The model uses a stacked layer system (Fig. 1); lake sediment and water layers during the summer open-water season, and additional ice-cover and snow-cover layers for winter. A lake or reservoir is divided into well-mixed horizontal layers having typical thickness of 1 m.

Year-Round Dissolved Oxygen Model

The one-dimensional, deterministic, unsteady year-round dissolved oxygen transport equation [147], which is the basis of the DO model, is

$$\frac{\partial C}{\partial t} = \frac{1}{A}\frac{\partial}{\partial z}\left(AK_Z\frac{\partial C}{\partial z}\right) - \frac{S_b}{A}\frac{\partial A}{\partial z} + P_{MAX}\,Min[L]Chla - \frac{1}{YCHO2}\,k_r\,\theta_r{}^{T-20}\,Chla - k_b\,\theta_b{}^{T-20}\,BOD \tag{2}$$

where C(z,t) is the dissolved oxygen concentration in mg L^{-1} as a function of depth (z) and time (t), A(z) is the horizontal area at different depths in m^2, K_z is the turbulent diffusion coefficient of DO in m^2 day^{-1}, S_b is the sedimentary oxygen demand (SOD) coefficient in mg O_2 (m^{-2} day^{-1}), P_{max} is the maximum specific oxygen production rate by photosynthesis at saturating light conditions in [mg O_2 (mg Chl-a)$^{-1}$ h^{-1}], Min[L] is the light limitation determined by the Haldane equation, Chl-a is the chlorophyll-a concentration in mg L^{-1}, YCHO2 is the yield coefficient which is the ratio of mg chlorophyll-a to mg oxygen, k_r and k_b are the first-order decay for biochemical oxygen demand (BOD) and respiration rate coefficient (day^{-1}),

respectively, θ_r and θ_b are the temperature adjustment coefficient for plant respiration and BOD, BOD is the biochemical oxygen demand concentration in mg L^{-1}, and T(z, t) is the water temperatures in °C. In the model, the oxygen transfer through the water surface (reaeration) is expressed as

$$k_e(C_s - C)/\Delta z_s \quad (3)$$

It is used as an oxygen source or sink term in the topmost water (surface) layer. Diffusive oxygen flux at the lake bottom is set equal to zero as a boundary condition. (Sedimentary oxygen demand is treated as a source/sink term.)

For the dissolved oxygen simulations in a lake over the winter season (Fig. 9), some modifications had to be made in Eq. 2 to account for the presence of an ice cover and low temperatures. These modifications [142] include: (a) reaeration is zero (k_e is set equal to zero); (b) the respiration rate coefficient k_r is zero; (c) the water column oxygen demand, WOD, by detrital and other organic matter, is set to a constant value (0.010 g O_2 m^{-3} day^{-1}), independent of the trophic status of a lake [148]; and (d) sedimentary oxygen demand (S_b) is dependent on trophic state and set equal to 0.226, 0.152, and 0.075 (g O_2 m^{-2} day^{-1}) for eutrophic, mesotrophic, and oligotrophic lakes, respectively.

Water column oxygen demand in winter (WOD) is constant and very low, whereas the biochemical oxygen demand (BOD) in summer varies as a function of trophic status. Both WOD and BOD describe the same processes, i.e., microbial and chemical decomposition of detrital or nonliving organic material, and can therefore be expected to depend on trophic state. However, the very limited database for WOD and its small value did not justify or require an adjustment of WOD for trophic state.

Trophic state characterizes biological productivity and relates to plant density, especially phytoplankton; nutrient availability; photosynthetic oxygen production; and respiratory consumption. All of these characteristics can be used to measure trophic status. In many, but not all, lakes, trophic states are closely related to phytoplankton concentration and lake clarity. With this in mind, lakes were divided into three trophic states by the mean annual chlorophyll-a concentrations given in Table 1. Secchi depths (SD) of 1.2, 2.5, and 4.5 m were selected for eutrophic, mesotrophic, and oligotrophic lakes using Carlson's trophic state index [159], respectively.

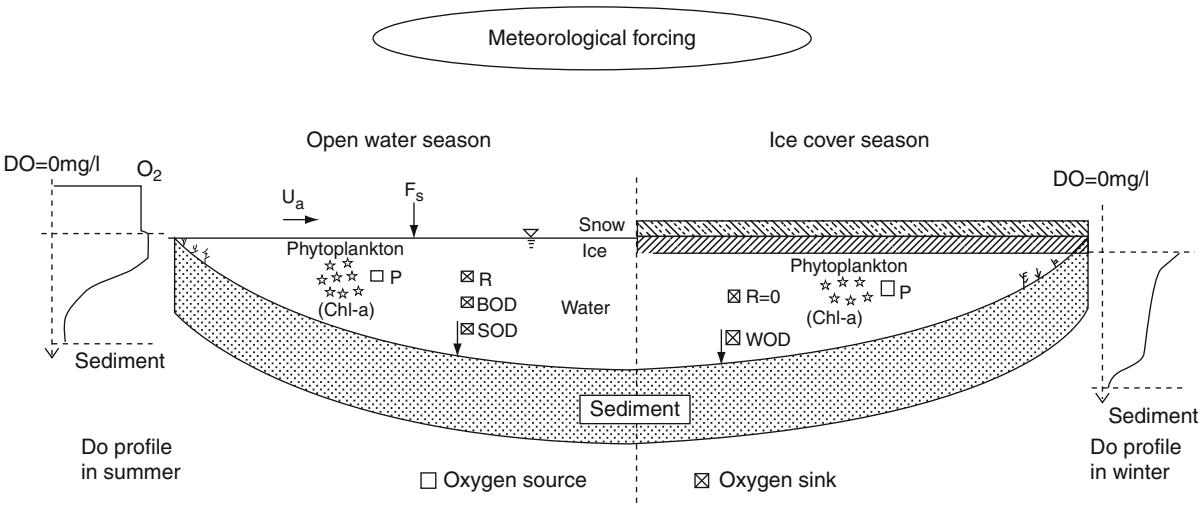

Lake and Reservoir Fate and Transport of Chemicals. Figure 9
Schematic of a stratified lake showing dissolved oxygen source/sink terms and dissolved oxygen profiles in the open-water season and in the ice-cover period [140]

Lake and Reservoir Fate and Transport of Chemicals. Table 1 Parameters and coefficient values in the hydrothermal model [147]

Coefficients and symbols		Units	Range and references	Selected value
Open-water season				
Radiation absorption for water	β_w	–	0.4[a]	0.4
Sediment specific heat	c_{psed}	kcal kg^{-1}°C^{-1}	0.2–0.3[b]	0.28
Sediment thermal conductivity	k_{sed}	kcal day^{-1}°C^{-1} m^{-1}	8.64–51.8[b]	19.25
Radiation attenuation by Chl-a	μ_{chh}	m^2 g^{-1} Chl-a	0.2–31.5[c]	20.0
Radiation attenuation by water	μ_w	m^{-1}	0.33–1.03[d]	0.51
Sediment density	ρ_{sed}	kg m^{-3}	1,650–2,300[b]	1,970
Wind sheltering	W_{str}	–	0.01–1.0[e]	Varies
Winter ice cover				
Surface reflectivity for ice	α_i	–	0.55[f]	0.55
Surface reflectivity for snow	α_{sw}	–	0.4–0.95[g]	0.80
Radiation absorption for ice	β_i	–	0.17–0.32[h]	0.17
Radiation absorption for snow	β_{sw}	–	0.17–0.34[i]	0.34
Snow compaction	c_{sw}	–	0.125–0.5[g]	0.4
Ice thermal conductivity	k_i	kcal day^{-1}°C^{-1} m^{-1}	45.8[b]	53.6
Snow thermal conductivity	k_{sw}	kcal day^{-1}°C^{-1} m^{-1}	2.16[b]	5.57
Ice density	ρ_i	kg m^{-3}	920[b]	920.0
Snow density	ρ_{sw}	kg m^{-3}	100–400[g]	300.0
Radiation attenuation by ice	μ_i	m^{-1}	1.6–7.0[j]	1.6
Radiation attenuation by snow	μ_{sw}	m^{-1}	20–40[k]	40.0
Ice latent heat of fusion	λ_i	kcal kg^{-1}	80[l]	80.0
Snow latent heat of fusion	λ_{sw}	kcal kg^{-1}	80[l]	80.0

[a]Dake and Harleman [149]
[b]Carslaw and Jaeger [150]
[c]Bannister [151]
[d]Megard et al. [152]
[e]Riley and Stefan [123]
[f]Bolsenga [153]
[g]Lock [154]
[h]Wake and Rumer [155]
[i]Scott [156]
[j]Pivovarov [157]
[k]Greene [158]
[l]Ashton [145]

The radiation attenuation in a lake is used to quantify how much of the solar energy reaching the water surface can penetrate through a water column to heat water below the surface and to support photosynthesis of phytoplankton. Total attenuation coefficient, μ (m^{-1}), is given by

$$\mu = \mu_w + \mu_{ch}\,(Chl - a) \tag{4}$$

where μ_w (m^{-1}) is the attenuation coefficient of the lake water excluding chlorophyll-a, μ_{ch} [m^{-1} (g m^{-3} Chl-a)$^{-1}$] is the attenuation coefficient due to chlorophyll-a [152], and *Chl-a* is chlorophyll-a concentration (g m^{-3}). An alternative is to estimate total attenuation coefficient as function of Secchi depth [139] by the Eq. 5. The coefficient 1.84 is empirical, and other similar values have also been proposed.

$$\mu = \frac{1.84}{SD} \tag{5}$$

Model Input and Output

Model parameters and coefficients are shown in Table 1 for the temperature submodel and in Table 2 for the DO submodel of MINLAKE2010.

Lake and Reservoir Fate and Transport of Chemicals. Table 2 Parameters and coefficient values in the dissolved oxygen model [134, 147]

Coefficients and symbols			Units	Range and references	Selected value
Independent of trophic status					
BOD decay coefficient		k_b	day^{-1}	0.02–3.4[a]	0.1
Respiration rate coefficient		k_r	day^{-1}	0.05–0.5[a]	0.1
BOD temperature adjustment		θ_b	–	1.047[a]	1.047
Photosynthesis temperature adjustment		θ_p	–	1.066[b]	1.036
Respiration temperature adjustment		θ_r	–	1.045[c], 1.047[d]	1.047
Sediment temperature adjustment		θ_s	–	1.034–1.13[e]	1.065
Respiration ratio		YCHO2	–	0.0083[f]	0.0083
Water column oxygen demand during winter		WOD	g m^{-3} day^{-1}	0.01	0.01
Dependent on trophic status					
Coefficients and symbols		Units	Eutrophic	Mesotrophic	Oligotrophic
Oxygen equivalent	BOD	mg l^{-1}	1.0[g]	0.5	0.2
Chlorophyll-a	Chl-a	mg m^{-3}	15[h]	6	2
SOD during open-water season	S_{b20}	g m^{-2} day^{-1}	1.5[g]	1.25	1.0
			H_{max} = 24 m	H_{max} = 24 m	H_{max} = 24 m
			1.95	1.75	1.2
			H_{max} = 13 m	H_{max} = 13 m	H_{max} = 13 m
			2.2	1.9	1.25
			H_{max} = 4 m	H_{max} = 4 m	H_{max} = 4 m
SOD during ice-cover period	S_b	g m^{-2} day^{-1}	0.226	0.152	0.075

H_{max} = 4 m = shallow lake, H_{max} = 13 m = medium depth, H_{max} = 24 m = deep lake [147]
[a]From QUAL2E [160]
[b]From [44]
[c]From EUTR04 [66]
[d]From MINLAKE [123]
[e]From [161]
[f]From [68]
[g]From Fang et al. [134]
[h]From Stefan and Fang [147]

MINLAKE2010 model input data are read through ten input files: (1) bathymetry data, (2) weather data (solar radiation optionally from Maxwell et al. 1998), (3) lake-specific model parameter, (4) fixed model parameter, (5) long-term annual and January air temperatures, (6) weather station information (elevations, longitude, and latitude), (7) dimensionless sediment temperature profile [162], (8) seasonal chlorophyll-a pattern file [147, 163], (9) path file directing the program to open model input or output files, and (10) future climate data, e.g., output data of General Circulation Models (GCM) models.

Most of the input data files are common data files for model simulations of many lakes. Only three data files are created for a specific lake: the bathymetry data file, the lake-specific model parameter input file, and the path file. Sediment temperature at 10 m below sediment–water interfaces of a water layer is a model input [162]. These 10-m sediment temperatures have been related to mean annual air temperatures [164]. Long-term air temperature in January is used to specify whether a lake will have an ice cover [162]. The station data files, including long-term air temperatures, were developed for 209 weather stations over the contiguous United States of America. Therefore, in addition to three lake-specific input files mentioned earlier, the station data file and the file with long-term air temperatures were also updated when new weather stations were used.

Because the growth of phytoplankton is not explicitly modeled in the MINLAKE2010 version of the model (it is in the original version by Riley and Stefan [123]), the seasonal pattern of standing algal crops had to be specified, as shown by the solid line in Fig. 10 for mesotrophic lakes. Similar patterns were developed also for eutrophic and oligotrophic lakes [134, 147].

The model output consists of daily vertical profiles of water temperature (example in Fig. 11) and DO in the water column. Three measured temperature profiles on July 5, 1996, in Swan Lake (Fig. 11) indicate that horizontal variations of water temperature at different depths are typically much smaller than vertical temperature difference (stratification) from surface to bottom; therefore, one-dimensional assumption in lake modeling is valid. An example of simulated versus observed water temperatures and DO concentrations in Minnesota lakes is given in Fig. 12.

Simulation of Sustainable Fish Habitat in Lakes Under Global Warming

Sustaining fish habitat in lakes and reservoirs is a major resource management issue. Freshwater fish habitat is

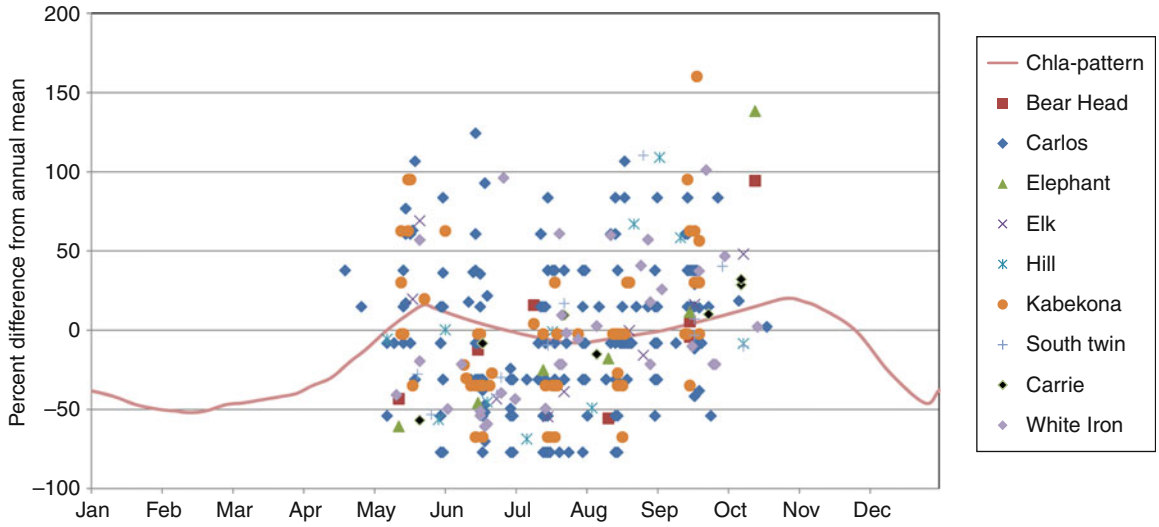

Lake and Reservoir Fate and Transport of Chemicals. Figure 10
Seasonal chlorophyll-*a* distribution specified as MINLAKE2010 model input for mesotrophic lakes. Generic distribution (*solid line*) and field data from nine study lakes

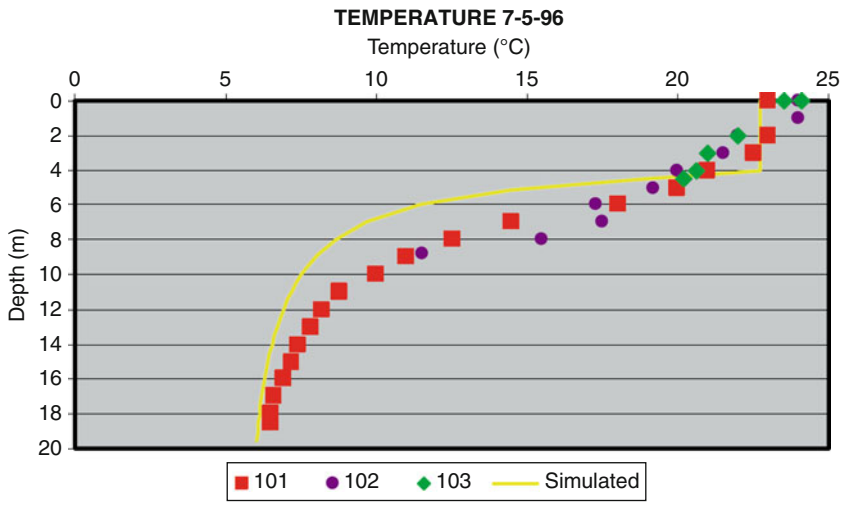

Lake and Reservoir Fate and Transport of Chemicals. Figure 11
Example of simulated (*solid line*) and three measured (sites 101,102,103) temperature profiles in Swan Lake, Minnesota

constrained by physical, chemical, and biological attributes that relate to water quality, food supply, and human interference [2].

In lakes, water temperature and dissolved oxygen (DO) concentrations are two of the most significant water quality parameters affecting survival and growth of fishes [2, 3]. An increase of atmospheric greenhouse gases is projected to cause climate warming, which would alter water temperature and DO characteristics in lakes. These changes are in turn expected to have an effect on indigenous fish populations [165–169]. For example, cold-water species typically have physiological optima at temperatures near 15°C and are generally not found where summer water temperatures are higher than 20–26°C [170]. Can fish habitat, especially of cold-water species, be sustained under global warming? Cold-water fish habitat in lakes can be reduced in several ways: by direct warming of the water, by increased hypolimnetic oxygen depletion during periods of stratification, and by thermocline deepening [165, 171, 172]. Can potential refuge lakes and reservoirs be identified and protected?

Water temperatures and DO concentrations in Minnesota lakes under several projected climate scenarios were previously simulated for the open-water season and the entire year [140, 173], and the results were used to estimate potential future fish habitats [166–169, 174]. Fish habitat estimated from daily temperature and DO profiles under past climate conditions was validated against fish observations [175, 176]. In these studies, fish species were grouped into three thermal guilds – cold-water, coolwater, and warm-water – that differ in the optimal temperature range for physiological function and ecological success.

In a follow-up study, habitat for only one fish species was investigated. Cisco, *Coregonus artedi*, is the most common cold-water stenothermal fish in Minnesota lakes. The combination of a wide geographic distribution and a requirement for cold, oxygenated water make cisco an excellent "canary in a mineshaft" species that is a sensitive indicator of climate change.

After daily water temperature and DO were simulated under past and future climate scenarios, two approaches were explored to determine if cisco habitat existed in a lake. The first approach was based on separate water temperature and DO constraints; this approach had previously been used to examine the potential impact of future climate warming on cold-water, coolwater, and warm-water fish species (guilds) in small lakes in the contiguous United States [166].

The second approach used a single oxythermal habitat variable to define suitable or unsuitable fish habitat. Jacobson et al. [177] developed a generalized oxythermal habitat variable, TDO3, called "temperature at 3.0 mg/L DO." It is determined by interpolating

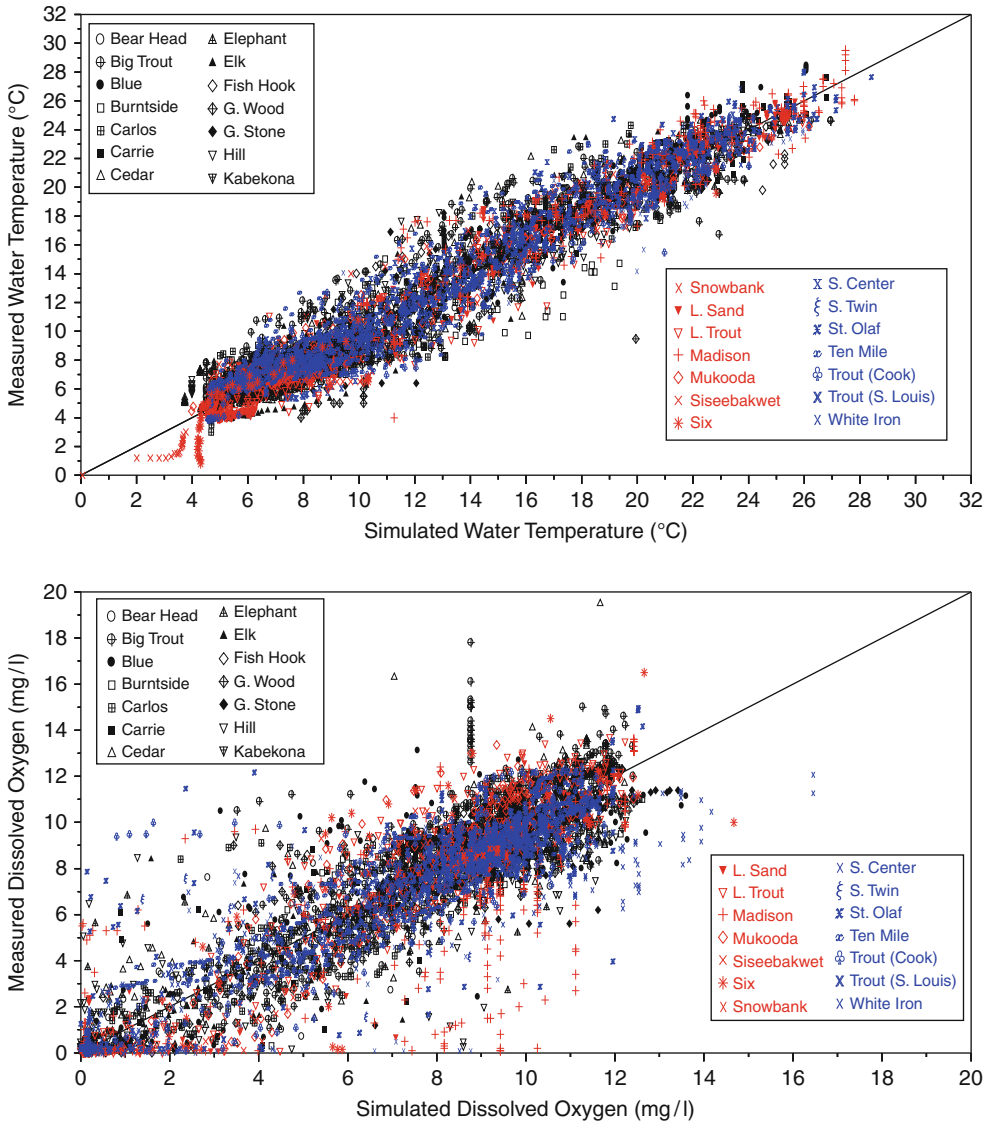

Lake and Reservoir Fate and Transport of Chemicals. Figure 12
Simulated versus measured temperature and dissolved oxygen (DO) in 28 Minnesota lakes. The solid line (1:1) would indicate perfect agreement

the water temperature at a benchmark oxygen concentration (i.e., 3.0 mg/L) from vertical temperature and DO profiles in a lake. DO = 3.0 mg/L is an oxygen concentration limit that is probably lethal or nearly so for many cold-water species [2, 178, 179]. TDO3 has a strong connection with four cold-water taxa (lake trout, cisco, whitefish, and burbot) in Minnesota lakes. Cisco were present in lakes with a broad range of maximum TDO3 values, with central borders of 4.0–16.9°C [177]. TDO3 allows to evaluate or quantify which lake is a better refuge lake for cisco under a future climate scenario.

Simulation of Cisco Habitat by the Constant Values Method (CVM)

Fish habitat for cold-water fish guilds (e.g., cisco) was estimated from simulated daily water temperature (T)

and DO profiles in lakes, similar to the approach by Christie and Regier [3]. Temperature and DO criteria for survival and good growth of a fish species were applied to the simulated year-round daily water temperature and DO profiles, as shown schematically in Fig. 13. This schematic figure is for a lake *where cold-water fish cannot be present* during much of the open-water season. On days when the isotherm of lethal temperature (LT) and the DO limit isopleth for a fish species intersect, the entire depth of a stratified lake is uninhabitable. When the maximum water temperature is lower than the lethal temperature (LT) everywhere in a lake, the isotherm for LT will not show up. In this case, the DO survival limit becomes the only survival criterion; this occurs especially during the winter ice-cover period, as shown in Fig. 14.

In addition to the lethal temperature (LT) isotherm, Fig. 13 also gives the upper good-growth temperature (UGGT) and the lower good-growth temperature (LGGT) isotherms. Between these isotherms/isopleths, three fish habitats are identified:

1. *Uninhabitable space* if temperature is above or DO is below the survival limit
2. *Good-growth habitat* if temperature is between the upper and lower good-growth limits (i.e., LGGT < T < UGGT) and DO is above the survival limit

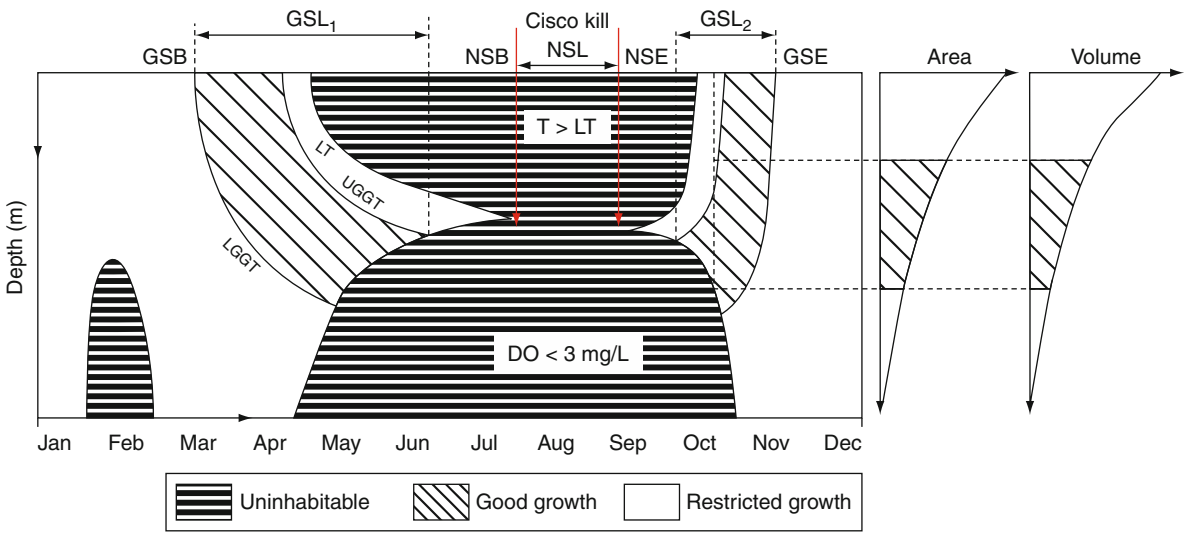

Lake and Reservoir Fate and Transport of Chemicals. Figure 13
Depth versus time plot of the critical isotherm and DO isopleth, showing projected cisco kill in a seasonally stratified lake as dark shaded areas. Habitat parameters (e.g., NSL, GSL) are discussed by Stefan et al. [166]

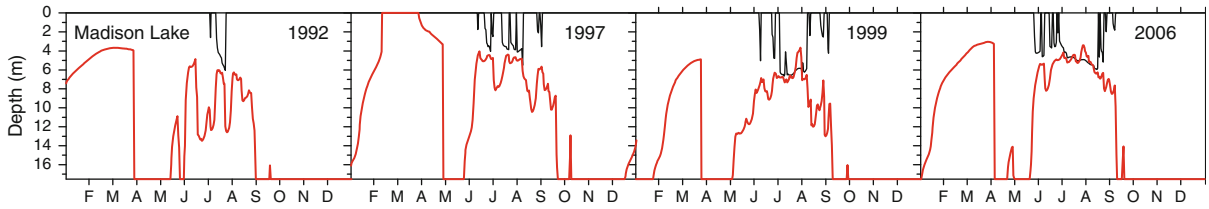

Lake and Reservoir Fate and Transport of Chemicals. Figure 14
Depth versus time contours of cisco fish habitat in Madison Lake for selected years. Thin lines are isotherms and indicate a temperature constraint for fish habitat in the upper part of the stratified lake; bolder lines are DO isopleths that indicate a dissolved oxygen constraint for fish habitat in the lower portion of the lake

3. *Restricted growth habitat* if temperature is above the upper good-growth temperature but below the survival limit (i.e., UGGT < T < LT), or if temperature is below the lower good-growth limit of temperature (i.e., T < LGGT) and DO is above the survival limit

Projections on growth habitat and survival parameters of three fish guilds (cold-water, coolwater, and warm-water) in the U.S. were reported by Stefan et al. [166] and Fang et al. [167–169].

The LT is the water temperature to which fish cannot be acclimated without causing death. The LT = 23.4°C [170] used for the cold-water fish guild in previous studies [166] was the mean value of LT values for ten cold-water fish species (pink salmon, sockeye salmon, chinook salmon, chum salmon, coho salmon, brown trout, rainbow trout, brook trout, lake trout, mountain whitefish).

The DO = 3.0 mg/L requirement for the cold-water fish guild, below which mortality is more likely to occur or growth is impaired [179], was developed from an available US EPA database [180]. The DO = 3.0 mg/L was for the open-water season. In ice-covered shallow, eutrophic or mesotrophic lakes DO can drop below 2.0 mg/L near the end of an extended ice-cover period due to bottom (sediment) and water column oxygen demands. For ice-covered lakes, DO criteria for fish survival could be set at lower values than 3.0 mg/L, but data from previous studies are still inadequate to establish specific tolerance limits of DO for fish winterkill [181]. The use of a single year-round DO criterion had no adverse effect on projections of winterkill under a 2 × CO_2 climate scenario; no winterkill was projected despite using higher DO limits [166, 182].

Figure 14 is an example of contour plots in Madison Lake, Minnesota, which has a maximum depth of 18.0 m, surface area of 4.5 km^2, and mean summer Secchi depth of 0.88 m (eutrophic lake). Isotherms at the lethal temperature of 23.4°C are drawn as thin black lines, and isopleths at the DO limit of 3.0 mg/L are drawn as thicker red lines. The CVM projected fish kill in 42 out of 47 simulation years (1961 to 2008), summer kill in 1999 and 2006, and winterkill in 1997 in Fig. 14 are samples because 2006 was the warmest year and 1997 was the coldest year in the simulation period. No fish kill was projected in 1992, as shown in Fig. 14. The maximum continuous kill days in Madison Lake were projected to last 34 days and occurred in 2006. Madison Lake is classified as a non-cisco lake by Minnesota Department of Natural Resources. The maximum continuous kill days in 15 lakes studied were projected to occur either in 2006 for summer kill (with a few exceptions) or in 1996 or 1997 for winterkill (the coldest 2 years of the simulation period).

Simulation of Cisco Habitat by the Equation Method (EM)

Jacobson et al. [177] developed an equation for the lethal-niche boundary of adult cisco by remapping the measured DO concentrations and temperatures from the profiles in 16 Minnesota lakes that experienced cisco mortality in midsummer of 2006. The equation is given as

$$DO_{lethal} = 0.40 + 0.000006e^{0.59T_{lethal}} \quad (6)$$

where DO_{lethal} and T_{lethal} are the dissolved oxygen concentration and the water temperature that define the lethal-niche boundary. DO_{lethal} is the required or needed minimum DO concentration at a given temperature T_{lethal} for cisco to survive. Equation 6 gives a DO survival limit for cisco that is not constant but instead depends on water temperature. The Equation Method (EM), therefore, uses survival limits for temperature and DO that are variable and related to each other.

The study by Jacobson et al. [177] leading to the EM was done specifically for cisco, whereas the study by Eaton et al. [170] that lead to the CVM was done on the entire cold-water fish guilds and not specifically on cisco (though cisco is a cold-water fish).

Equation 6 was implemented in a fish habitat simulation program to determine potential fish mortality in 15 study lakes. For each simulation day, the required DO concentrations, DO_{lethal}, were computed from simulated water temperatures in all water layers using Eq. 6 and compared with DO concentrations simulated by MINLAKE2010 in the same layers. Fish kill was assumed to occur if the simulated DO was less than the DO_{lethal} value at all water depths on that day. If simulated DO was larger than DO_{lethal} in some of the water layers, fish mortality was not assumed to occur

because cisco could swim to the water layers with suitable DO and temperature conditions.

Sample plots of simulated DO concentrations versus simulated temperatures at the same location in four study lakes on selected summer days when cisco mortality (kill) potential was high were developed. The lethal-niche-boundary curve (Eq. 6) developed by Jacobson et al. [177] was added for reference. Examples of results for South Center Lake are shown in Fig. 15. All simulated data points in Fig. 15 are located to the right of the curve, indicating that adult cisco kill could indeed occur in all water layers (depths) on the days shown [183]. Fish kill of adult cisco was simulated to occur also on some days in four other lakes (Carrie Lake, Hill Lake, White Iron Lake, and Madison Lake) (Fang et al. [183]), and this result agreed with field observations because no cisco had been found in those five lakes. This means that these lakes are not sustainable to cisco or potential other cold-water fish species.

Projection of Sustainable Cold-Water Fish Habitat in Lakes Under Future Climate Scenarios

Fish habitat projections under future climate scenarios were made for cisco in Minnesota lakes using the two methods described above and three future climate scenarios based on the output of three GCMs of the global atmosphere: CCCma GCM 2.0, CCCma CGCM 3.1 (A1B scenario), and MIROC 3.2 (A1B scenario) from the Special Report on Emission Scenarios of the IPCC (2001). Descriptions of the evolving stages of the GCMs and examples of applications were given by Boer et al. [184], McFarlane et al. [185], and Kim et al. [186, 187]. MIROC was described by Hasumi and Emori [188]. One output of the cisco habitat simulations was the projected number of annual cisco kill days; these were summarized and interpreted for the different climate scenarios.

Results obtained by both the CVM and the EM showed a considerable increase in the number of annual cisco kill days under future climate scenarios. Projections of the number of annual kill days under all three future climate scenarios were consistent. The GCM 2.0 scenario projected higher numbers of cisco kill days because the future atmospheric CO_2 concentration was higher for this earlier climate scenario model. Future climate scenarios based on the two more recent CGCMs (CCCma CGCM 3.1 and MIROC 3.2) gave almost the same numbers of projected cisco kill days [183].

As a preliminary conclusion, 19 out of 21 simulated cisco lakes were projected to be viable cisco refuge lakes under a warmer climate. In lakes not supporting cisco habitat, there is a shift in cisco kill days from winter to summer.

Figure 16 shows the distribution of 620 current cisco lakes in Minnesota and 21 selected cisco study lakes in a coordinate system of lake geometry ratio (GR) versus Secchi depth (SD). Under the CCCma CGCM 3.1 future climate scenario, 19 of the 21 simulated cisco lakes were projected to have no cisco kill

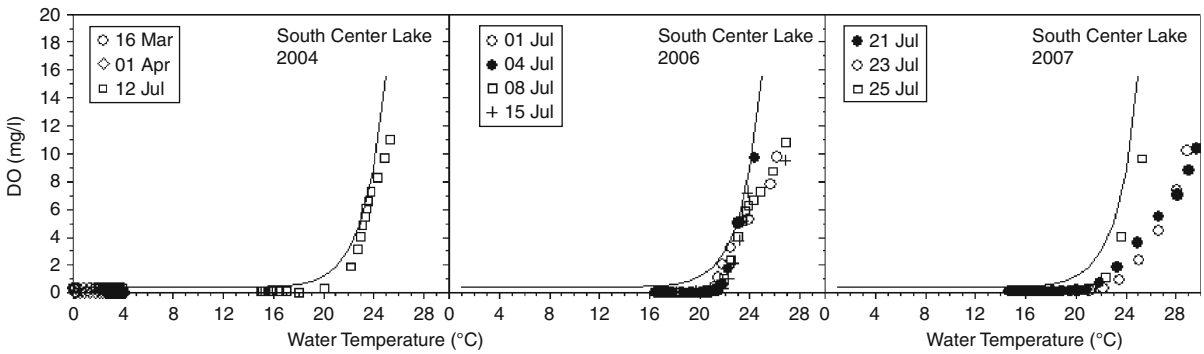

Lake and Reservoir Fate and Transport of Chemicals. Figure 15
Simulated DO concentration versus simulated temperature in South Center Lake on selected summer days in 2006 with potential cisco mortality against the lethal-niche-boundary curve developed by Jacobson et al. [177]

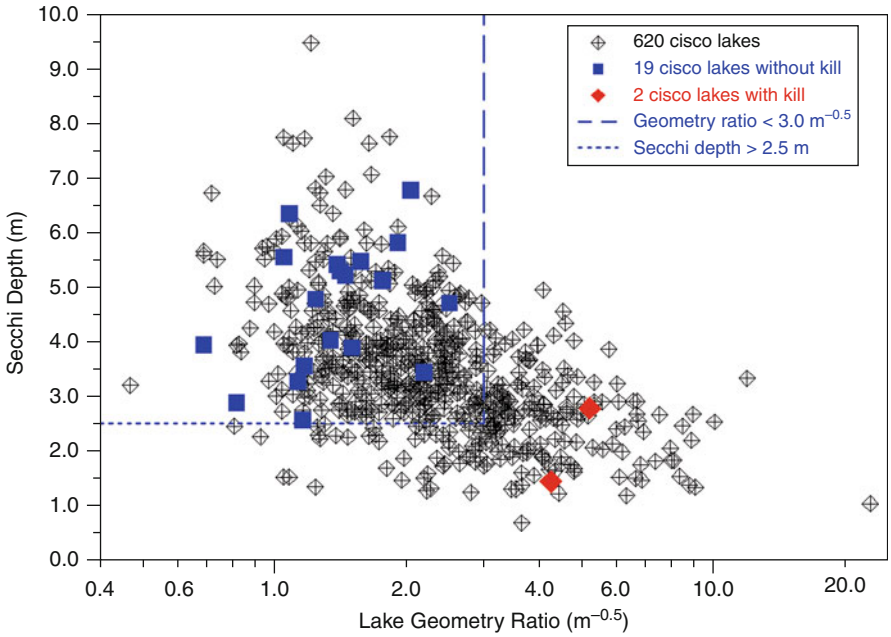

Lake and Reservoir Fate and Transport of Chemicals. Figure 16
Distribution of 21 study lakes among 578 current cisco lakes in Minnesota projecting no future cisco kill in 19 and potential cisco kill in two study lakes under the CCCma CGCM 3.1 future climate scenario

under future climate scenarios. There is a region on the (SD) versus (GR) plot in Fig. 15 with "refuge" lakes that can support cisco habitat under future climate scenarios. Such refuge lakes should have an SD greater than 2.5 m (mesotrophic or oligotrophic lakes) and a GR less than 3.0 m$^{-0.5}$ (typically seasonally stratified, dimictic lakes). Once refuge lakes are identified, watershed protection efforts can be initiated at refuge lakes to prevent deterioration of water quality by anthropogenic activities.

The findings in Fig. 16 were confirmed by projections using the oxythermal habitat parameter TDO3. Jacobson et al. [177] proposed a single variable to quantify oxythermal habitat that allows for comparison across several cold-water fish species (lake trout, cisco, lake whitefish, and burbot) that have different requirements for cold, oxygenated water. The single generalized oxythermal habitat variable is defined as the water temperature at 3 mg/L of DO and is called TDO3. The TDO3 can be determined by interpolating the temperature of water at the DO concentration of 3 mg/L from measured or simulated vertical temperature and DO profiles. When nonmonotonic profiles generate low oxygen concentrations with more than one TDO3 value, the coldest TDO3 is used [177].

The oxythermal parameter TDO3 measures environmental conditions and stress in a lake. Low values of summer TDO3 indicate excellent oxythermal habitat for cold-water fish, i.e., fish have a wide range of temperatures available in the hypolimnion with sufficient oxygen concentrations. High values of TDO3 indicate poor oxythermal habitat for cold-water fish, with little or no cold water with sufficient oxygen. Very high values of TDO3 indicate hypolimnia that are anoxic or are found in unstratified lakes. The conclusion of the fish habitat study [183] was that under fairly stringent selection criteria (DO $>$ 3 mg/L and TDO3 $\leq$ 17°C), at least one fourth to one third of the lakes that currently have cisco populations are projected to maintain cisco habitat under projected future climate scenarios. Many of the "refuge" lakes are located in northeastern and central Minnesota.

Refuge lakes with TDO3 $<$ 17°C under the future climate scenario MIROC 3.2 have Secchi depths greater than $\approx$ 2.5 m, lake geometry ratios less than $\approx$ 2.5 m,

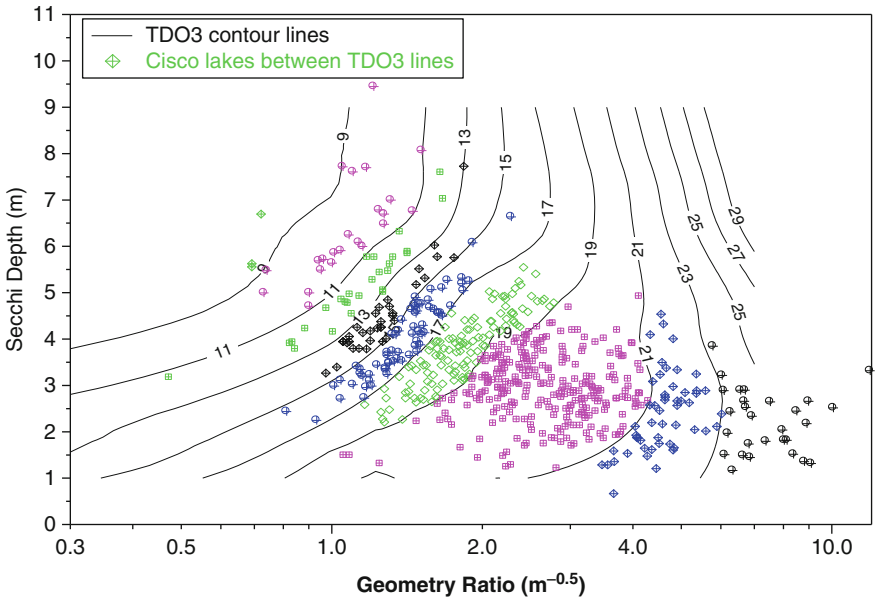

Lake and Reservoir Fate and Transport of Chemicals. Figure 17
Distribution of 620 cisco lakes in Minnesota between *contour lines* of AvgATDO3$_{VB}$ for variable benchmark periods simulated for the MIROC 3.2 future climate scenario using Duluth weather data

maximum depths greater than ≈ 15 m, and surface areas less than ≈ 30 km^2 [183].

Cisco refuge lakes were also ranked in narrow (2°C) bands of TDO3 values (Fig. 17). AvgATDO3$_{VB}$ in Fig. 17 is the average of mean daily TDO3 values over the fixed 31-day benchmark period (Julian day 209–239) in the simulation period (one value for 1962–2008 period). Names and locations of lakes in each band were given to the Minnesota Department of Natural Resources for management decisions. Lakes with the lowest TDO3 values were the best candidates for cisco refuge lakes because a low TDO3 value is presumed to reflect the least stress on adult cisco.

Future Directions

There are many unanswered questions regarding transport and transformation processes that control water quality and habitat in lakes or reservoirs because these processes are numerous and often interacting. This lack of knowledge and information hinders meaningful decision making on lake and reservoir management and can lead to waste of effort and resources. Examples where future research efforts can pay sustained benefits are:

1. Continuous automated data collection in lakes and reservoirs. Existing and future sensors of physical, chemical, and biological lake parameters will enable the collection and recording of time series of information at high temporal and spatial resolution. The installation of measuring stations can be expensive, but the return will be information that can really decipher the timescales and vertical scales of processes.
2. Development of simulation models for critical lakes as a permanent tool for decision making. Existing models can be tailored to specific, valuable lakes and can be used first to simulate the outcome of contemplated actions. In the long-term, model development, modification and validation can benefit greatly when paired with automated data collection advocated above (1).
3. Research on the intermediate-scale coupling between the atmosphere and the hydrosphere of lakes and reservoirs. A missing link in our

understanding of lakes is their coupling to the atmospheric boundary layer. Atmospheric boundary layers over lakes have been all but ignored roughness transitions from the land to water and the transfer of momentum from wind, and the transfer rates of gases at lake and reservoir surfaces have been measured and analyzed as if the atmospheric boundary layer over a lake surface did not have to respond to wakes of canopies, buildings, and hills, and adjust to the roughness transition from land to water.

4. Research on the large-scale coupling between the atmosphere and the hydrosphere of lakes and reservoirs. "Large-scale" here means responses to climate (warming). Climate/weather effects on heat transfer at a water surface and the consequences for stratification and mixing can be estimated. However, the intensification of the hydrologic cycle by global warming has effects on lake and reservoir water budgets, on material import from watersheds, and material budgets of lakes and reservoirs; it also affects internal material transport and transformation processes, and thereby habitat in ecosystems.
5. Interactions and exchange processes at the sediment–water interface are highly diverse and difficult to model in a comprehensive way. Flow of water in the boundary layer can be highly intermittent, possibly density stratified, and possibly affected by sediment settling and/or sediment resuspension. The porous sediment surface allows for some exchange of mass and momentum but also much damping. The pore scale is far shorter than the internal lake modeling scale, and the chemistry of the waters in the sediment pore system can be complex; sediment particle interactions with solutes can be significant, and there are also microbial biofilms. At present, the fluxes of materials across the sediment interface that are needed as boundary conditions in lake water quality models are mostly estimated empirically. Processes in the flowing water boundary layer above the sediment layer and in the sediment pore system need to be better coupled to in lake models.
6. Microbial processes and solute–particle interactions in lakes may have far more impact on water quality and material fluxes than is acknowledged in current lake models. The microstructure of lake and reservoir stratification needs to be better understood because it controls some of these processes.
7. Criteria used to assess fish habitat in lakes are currently fairly crude. What are the proper timescales? Criteria need to be established for different life stages of fish, not only adult fish. More quantitative information on the response of fish to environmental parameters has a bearing on fish survival projections under environmental stress such as global warming.
8. Lake and reservoir management, including goal-setting, data collection and storage, planning, decision making, resource allocation, and implementation, are complicated not only because lakes and reservoirs are complicated but also the multitude of agencies and organizations that are in charge gives an administrative and organizational structure that is not optimal. A single, multidisciplinary entity in charge of a lake or reservoir may do a better job than the compromises developed under current administrative structures. Simplification of the organizational structure and the resulting decision-making process are appropriate.
9. One of the many management issues has to do with internal nutrient loading. Many TMDL studies of external inputs to lakes and reservoirs accomplish little when lake ecosystems function on the basis of internal nutrient recycling.
10. Biomanipulation is practiced in a very empirical way and needs a better basis.
11. Lake and reservoir improvement technologies need to be reviewed and can probably be improved. Guidance manuals need to be developed for these techniques.

Bibliography

Primary Literature

1. Chapra SC (1997) Surface water-quality modeling. McGraw-Hill, New York
2. Fry EFJ (1971) The effect of environmental factors on the physiology of fish. Academic, New York
3. Christie CG, Regier HA (1988) Measurements of optimal habitat and their relationship to yields for four commercial fish species. Can J Fish Aquat Sci 45:301–314

4. Zipparro VJ, Hasen H (eds) (1993) Handbook of applied hydraulics. McGraw-Hill, New York
5. USBR (U. S. Bureau of Reclamation) (1987) Design of small dams. U. S. Govmt. Printing Office, Denver
6. Novák P, Nalluri C (1990) Hydraulic structures. Unwin Hyman, London
7. Press H (1958) Talsperren (in German), 2nd edn. Ernst & Sohn, Berlin
8. Thornton KW, Kimmel BL, Payne FE (1990) Reservoir limnology. Wiley, New York
9. Ackerman WC, White GF, Worthington EB (eds) (1973) Man-made lakes: their problems and environmental effects. American Geophysical Union, Washington, DC
10. Stefan HG (ed) (1980) Surface water impoundments. ASCE, New York
11. NRC (national Research Council) (1987) Glen canyon environmental studies review committee. National Academy, Washington, DC
12. Hutchinson GE (1957) A treatise on limnology. Wiley, New York
13. Frey DG (1966) Limnology in North America. The University of Wisconsin Press, Madison
14. Lerman A, Baccini P (1978) Lakes – chemistry, geology, physics. Springer, New York
15. Wetzel RG (1983) Limnology, 2nd edn. WB Saunders, Philadelphia
16. Horne A, Goldman C (1994) Limnology. McGraw-Hill, New York
17. Lampert W, Sommer U (1997) Limnoecology: the ecology of lakes and streams. Oxford University Press, New York
18. Henderson-Sellers B (1984) Engineering limnology. Pitman Advanced Publication Program, Boston
19. Straskraba M, Gnauck AH (1985) Freshwater ecosystems. Modeling and simulation. Elsevier, Amsterdam
20. Rouse H, Ince S (1957) History of hydraulics. Iowa Institute of Hydraulic Research, Iowa City
21. Chien N, Wang Z (1998) Mechanics of sediment transport. ASCE Press, Reston
22. Dortch MS (1992) Modeling water quality of reservoir tailwaters, Technical Report W-92-1. US Army Corps of Engineers, Waterways Experiment Station, Vicksburg
23. Fischer HB (1979) Mixing in inland and coastal waters. Academic, New York
24. Gray WG (1986) Physics-based modeling of lakes, reservoirs, and impoundments. ASCE Press, Reston
25. Herb WR, Janke B, Mohseni O, Stefan HG (2009) Runoff temperature model for paved surfaces. J Hydrol Eng 14:1146–1155
26. Wanielista MP, Yousef YA (1993) Stormwater management. Wiley, New York
27. Hino M (1994) Water quality and its control. International Association for Hydraulic Research, AA Balkema, Rotterdam
28. Baker LA (1984) A model for phosphorus cycling in lakes. International Memorandum No. 100, St Anthony Falls Laboratory, University of Minnesota, Minneapolis
29. Stefan HG, Dhamotharan S, Schiebe FR, Fu AY, Cardoni JJ (1989) Dynamic simulation of turbidity and its correction in Lake Chico, Arkansas. In: Henderson-Sellers B (ed) Water quality modeling, vol IV. CRC Press, Baco Raton
30. Novotny EV, Stefan HG (2010) Projections of chloride concentrations inurban lakes receiving road de-icing salt. Water Air Soil Pollut 211:261–271
31. Gassman PW (2007) The soil and water assessment tool: historical development, applications, and future research direction. Trans ASABE 50(4):1211–1250
32. James W, Huber W, Rossman L et al (2005) Water systems models: user's guide to SWMM. CHI, Guelph
33. Rossman L (2008) Storm Water Management Model. User's manual Version 5.0. US Environmental Protection Agency, Cincinnati
34. USGS (2008) SNTEMP stream temperature model, http://smig.usgs.gov/cgi-bin/SMIC/model_home_pages/model_home?selection=sntemp
35. Herb WR, Mohseni O, Stefan HG (2009) Simulation of temperature mitigation by a stormwater detention pond. J Am Water Resour Assoc 45:1164–1178
36. PLUARG (1978) Environmental management strategy for the great lakes system. Final Report of the Pollution from Land Use Activities Reference Group (PLUARGE) to the International Joint Commission. Windsor, Ontario
37. Hornbuckle KC, Jeremiason JD, Sweet CW, Eisenreich SJ (1994) Seasonal variations in air-water exchange of polychlorinated biphenyls in Lake Superior. Environ Sci Technol 28:1491–1501
38. Gulliver JS (2007) Introduction to chemical transport in the environment. Cambridge University Press, Cambridge
39. Dhamotharan S, Gulliver JS, Stefan HG (1981) Unsteady one-dimensional settling of suspended sediment. Water Resour Res 17:1125–1132
40. Johnson TC (1980) Sediment redistribution by waves in lakes, reservoirs and embayments. In: Stefan HG (ed) Proceeding of international symposium on surface water impoundements. ASCE, Reston, Minneapolis, pp 1307–1317
41. Sheng YP, Lick W (1979) The transport and resuspension of sediments in a shallow lake. J Geophys Res 84:1809–1826
42. Rodney MW, Stefan HG (1987) Conceptual model for wind-generated sediment resuspension in shallow ponds. In: Proceedings of the national symposium on mining, hydrology, sedimentology and reclamation. University of Kentucky, Lexington, pp 263–269
43. Erdmann JB, Stefan HG, Brezonik PL (1994) Analysis of wind and ship induced sediment resuspension in Duluth-Superior harbor. J Am Water Resour Assoc 30:1043–1053
44. Thomann RV, Mueller JA (1987) Principles of surface water quality modeling and control. Harper & Row, New York
45. Clark MM (1996) Transport modeling for environmental engineers and scientists. Wiley, New York
46. Weber W Jr, DiGiano FA (1995) Process dynamics in environmental systems. Wiley, New York
47. Weilenmann U, O'Melia CR, Stumm W (1989) Particle transport in lakes: models and measurements. Limnol Oceanogr 34:1–18
48. Mackenthun AA, Stefan HG (1998) Effect of flow velocity on sediment oxygen demand: experiments. J Environ Eng 124:222–230

49. Qian Q, Clark JJ, Voller VR, Stefan HG (2009) Modeling of vertical dispersion of a solute in a stream or lake bed enhanced by wave induced interstitial flow. J Am Water Resour Assoc 45:343–354
50. Qian Q, Clark JJ, Voller VR, Stefan HG (2009) Depth-dependent dispersion coefficient for modeling of vertical solute exchange in a lake bed under surface waves. J Hydraul Eng ASCE 135:187–197
51. Elliott AH, Brooks NH (1997) Transfer of non-sorbing solutes to a streambed with bed forms: theory. Water Resour Res 33:123–136
52. Packman AI, Salehin M, Zaramella M (2004) Hyporheic exchange with gravel beds: basic hydrodynamic interactions and bedform-induced advective flows. J Hydraul Eng 130:647–656
53. Roy H, Huttel M, Jorgensen BB (2002) The role of small-scale sediment topography for oxygen flux across the diffusive boundary layer. Limnol Oceangr 47:837–847
54. Steinberger N, Hondzo M (1999) Diffusional mass transfer at sediment-water interface. J Environ Eng 125:192–200
55. O'Connor BL, Hondzo M (2008) Dissolved oxygen transfer to sediments by sweep and eject motions in aquatic environments. Limnol Oceanogr 53:566–578
56. Nakamura Y, Stefan HG (1994) Effect of flow velocity on sediment oxygen demand: theory. J Environ Eng 120:996–1016
57. Higashino M, Clark JJ, Stefan HG (2009) Pore water flow due to near-bed turbulence and associated solute transfer in a stream or lake sediment bed. Water Resour Res 45
58. Thamdrup B, Fossing H, Jorgensen BB (1994) Manganese, iron and sulfur cycling in a coastal marine sediment, Aarhus Bay, Denmark. Geochimica et Cosmochimica Acta 58:5115–5129
59. O'Connor BL, Harvey JW (2008) Scaling hyporheic exchange and its influence on biogeochemical reactions in aquatic ecosystems. Water Resour Res 44:W12423
60. Mortimer CH (1971) Chemical exchanges between sediments and water in the Great Lakes-speculations on probable regulatory mechanisms. Limnol Oceanogr 16:387–404
61. Lorenzen CJ, Welschmeyer NA, Copping AE, Vernet M (1983) Sinking rates of organic particles. Limnol Oceanogr 28: 766–769
62. Stefan HG, Hanson MJ (1981) Phosphorus recycling in five shallow lakes. J Environ Eng Div 107:713–730
63. Boudreau BP, Jørgensen BB (2001) The benthic boundary layer: transport processes and biogeochemistry. Oxford University Press, Oxford
64. DiToro DM (2001) Sediment flux modeling. Wiley, New York
65. Manous JD, Gantzer CJ, Stefan HG (2007) Spatial variation of sediment sulfate reduction rates in a saline lake. J Environ Eng-ASCE 133:1106–1116
66. Ambrose RB, Wool TA, Connolly JP, Schanz RW (1988) WASP (EUTRO4), A hydrodynamic and water quality model – model theory, user's manual, and programmer's guide. US Environmental Protection Agency, Athens, Georgia
67. Cole TM, Wells SA (2004) CE-QUAL-W2: a two-dimensional, laterally averaged, hydrodynamic and water quality model, version 3.2, user's manual. Environmental Laboratory, US Army Engineer Research and Development Center, Vicksburg
68. Stumm W, Morgan JJ (1981) Aquatic chemistry. Wiley-Intersciences, New York
69. Stumm W, Morgan JJ (1996) Aquatic chemistry: chemical equilibria and rates in natural waters, 3rd edn. Wiley, New York
70. Gobas FAPC, McCorquodale JA (1992) Chemical dynamics in fresh water ecosystems. Lewis, Chelsea
71. Brezonik PL (1993) Chemical kinetics and process dynamics in aquatic systems. Lewis, Boca Raton
72. Zison SW, Mills WB, Diemer D, Chen C (1978) Rates, constants, and kinetics formulations in surface water quality modeling. Tetra Tech Incorporation, SEPA, ORD, Athens, Georgia
73. Bowie GL, Mills WB, Porcella DB et al (1985) Rates, constants, and kinetics formulations in surface water quality modeling (2nd edn), EPA/600/3-85/040. Environmental Research Laboratory, Office of Research and Development, US Environmental Protection Agency
74. Novak P, Arnold W, Blazer V et al (2011) On the need for a national (U.S) research program to Elucidate the potential risks to human health and the environment posed by contaminants of emerging concern. Environ Sci Technol 45:3829–3830
75. Calabrese EJ (1985) Age and susceptibility to toxic substances. Wiley, New York
76. Scheffer M (1998) Ecology of shallow lakes. Chapman and Hall, London
77. Cooke GD (1993) Restoration and management of lakes and reservoirs. Lewis, Boca Raton
78. Reckhow KH, Chapra SC (1983) Engineering approaches for lake management, vol 1, Data analysis and empirical modeling. Ann Arbor Science, Boston
79. Henderson-Sellers B (1991) Water quality modeling, vol IV, Decision support techniques for lakes and reservoirs. CRC Press, Boca Raton
80. Burns F, Powling I (1981) Destratification of lakes and reservoirs to improve water quality. Australian Government, Canberra
81. Fast AW (1971) The effects of artificial aeration on lake ecology. US Environmental Protection Agency, Washington, DC
82. Goossens L (1979) Reservoir destratification with bubble columns. Delft University Press, Delft
83. Zic K, Stefan H (1988) Lake Aerator effect on temperature stratification analyzed by "MINLAKE" model. Lake Reserv Manag 4:85–90
84. Zic K, Stefan H, Ellis C (1992) Laboratory study of water destratification by a bubble plume. J Hydraul Res 30:7–27
85. Gulliver JS, Stefan HG (1982) Lake phytoplankton model with destratification. J Environ Eng Div-ASCE 108:864–882
86. Ellis CR, Stefan HG (1990) Hydraulic design of a winter lake aeration system. J Environ Engin-ASCE 116:376–393
87. Stefan HG, Bender MD, Shapiro J, Wright DI (1987) Hydrodynamic-design of a metalimnetic lake aerator. J Environ Eng-ASCE 113:1249–1264

88. Stefan HG, Gu R (1992) Efficiency of jet-mixing of temperature-stratified water. J Environ Eng ASCE 118:363–379
89. Stefan HG, Gu R (1990) Jet mixing in lake or reservoir stratification simulations. Lake Reserv Manag 6:165–174
90. Stefan HG, Gu RC (1991) Conceptual design procedure for hydraulic destratification systems in small ponds, lakes, or reservoirs for water-quality improvement. Water Resour Bull 27:967–978
91. Hanson MJ, Stefan HG (1984) Side effects of 58 years of copper sulfate treatment of the fairmont lakes, Minnesota. Water Resour Bull 20:889–900
92. Vollenweider R (1968) Scientific fundamentals of the eutrophication of lakes and flowing waters, with particular reference to phosphorus and nitrogen as factors in eutrophication. Organisation for Economic Cooperation and Development Technical Report OAS/CSI/68.27, Paris
93. Gorham E, Boyce FM (1989) Influence of lake surface area and depth upon thermal stratification and the depth of the summer thermocline. J Great Lakes Res 15:233–245
94. Alavian V, Jirka GH, Denton RA, Johnson MC, Stefan HG (1992) Density currents entering lakes and reservoirs. J Hydraul Eng 118:1464–1489
95. Akiyama J, Stefan HG (1984) Plunging flow into a reservoir – theory. J Hydraulic Eng ASCE 110:484–499
96. Akiyama J, Stefan H (1985) Turbidity current with erosion and deposition. J Hydraul Eng 111:1473–1496
97. Akiyama J, Stefan HG (1987) Onset of underflow in slightly diverging channels. J Hydraul Eng ASCE 113:825–844
98. Akiyama J, Stefan HG (1988) Turbidity-current simulation in a diverging channel. Water Resour Res 24:579–587
99. Johnson TR, Ellis CR, Farrell GJ, Stefan HG (1987) Negatively buoyant flow in a diverging channel. Part 2: flow field description. J Hydraul Eng ASCE 113:731–742
100. Johnson TR, Farrell GJ, Ellis CR, Stefan HG (1987) Negatively buoyant flow in a diverging channel. Part1: flow Regimes. J Hydraul Eng ASCE 113:716–730
101. Farrell GJ, Stefan HG (1988) Mathematical-modeling of plunging reservoir flows. J Hydraul Res 26:525–537
102. Farrell GJ, Stefan HG (1989) Two-layer analysis of a plunging density-current in a diverging horizontal channel. J Hydraul Res 27:35–47
103. Fang X, Stefan HG (2000) Dependence of dilution of a plunging discharge over a sloping bottom on inflow conditions and bottom friction. J Hydraul Res 38:15–25
104. Ellis CR, Champlin J, Stefan HG (1997) Density current intrusions in an ice-covered urban lake. J Am Water Resour Assoc 33:1363–1374
105. Stefan HG (1970) Modeling spread of heated water over lake. J Power Div 96:469–482
106. Stefan H, Schiebe FR (1970) Heated discharge from flume into tank. J Sanit Eng Div 96:1415–1433
107. Stefan HG (1970) Stratification of flow from channel into deep lake. J Hydraul Div 96:1417–1434
108. Stefan HG, Chu CS, Wing H (1972) Impact of cooling water on lake temperatures. J Power Div 98:253–272
109. Stefan H, Vaidyaraman P (1972) Jet type model for the three-dimensional thermal plume in a crosscurrent and under wind. Water Resour Res 8:998–1014
110. Demetracopoulos AC, Stefan HG (1983) Model of Mississippi river pool: dissolved oxygen. J Environ Eng ASCE 109: 1020–1034
111. Stefan HG, Anderson KJ (1980) Wind-driven flow in Mississippi river impoundment. J Hydraul Div 106:1503–1520
112. Demetracopoulos AC, Stefan HG (1983) Model of Mississippi river pool: mass transport. J Environ Eng 109:1006–1019
113. Manous JD, Stefan HG (2004) Sulfate distribution in a multi-basin, saline lake. Hydrobiologia 529:169–185
114. Stefan H, Ford DE (1975) Temperature dynamics in dimictic lakes. J Hydraul Div ASCE 101:97–114
115. Ford DE, Stefan HG (1980) Stratification variability in three morphometrically different lakes under identical meteorological forcing. J Am Water ResourAssoc 16:243–247
116. Stefan HG, Megard RO, Skoglund T (1976) Wind control of algae growth in eutrophic lakes. J Environ Eng Div 102:1201–1213
117. Herb WR, Stefan HG (2005) Model for wind-driven vertical mixing in a shallow lake with submersed macrophytes. J Hydraul Eng 131:488–496
118. Markfort CD, Perez ALS, Thill JW et al (2010) Wind sheltering of a lake by a tree canopy or bluff topography. Water Resour Res 46:W03530
119. Stefan HG, Ambrose RB, Dortch MS (1990) Surface water quality models:modeler's perspective. In: Proceedings international symposium on water quality modeling of agricultural non-point sources, US Department of Agriculture, American Society of Agricultural Engineers. St. Joseph
120. Wurbs RA (1998) Dissemination of generalized water resources models in the United States. Water Int 23: 190–198
121. Anon (1986) A numerical one-dimensional model of reservoir water qulity. user's manual. Instruction Report E-82-1, US Army Corps of Engineers,Vickburg
122. Imberger J, Patterson JC (1981) A dynamic reservoir simulation model – DYRESM. In: Fischer HB (ed) Transport models for inland and coastal waters. Academic, New York, Chapter 9
123. Riley MJ, Stefan HG (1988) Minlake: a dynamic lake water quality simulation model. Ecol Model 43:155–182
124. Middlebrooks EJ, Falkenbory DH, Maloney TE (1976) Modeling the eutrophication process. Ann Arbor Science, Boston
125. Bruce LC, Hamilton D, Imberger J et al (2006) A numerical simulation of the role of zooplankton in C, N and P cycling in Lake Kinneret, Israel. Ecol Model 193:412–436
126. Gal G, Hipsey M, Parparov A et al (2009) Implementation of ecological modeling as an effective management and investigation tool: Lake Kinneret as a case study. Ecol Model 220:1697–1718
127. Leon LF, Lam D, Schertzer W, Swayne D (2005) Lake and climate models linkage: a 3D hydrodynamic contribution. Adv Geosci 4:57–62

128. Robson B, Hamilton D (2004) Three-dimenstional modelling of a microcystis bloom event in the Swan River estuary, Western Australia. Ecol Model 174:203–222
129. Edinger JE (2001) Waterbody hydrodynamic and water quality modeling, workbook and CD-ROM. ASCE Press, Reston
130. West D, Stefan HG (1998) Simulation of lake water quality using a one-dimensional model with watershed input. Model description and application to lake riley and lake elmo, Project Report No.430. St. Anthony Falls Laboratory, University of Minnesota, Minnesota
131. West D, Stefan HG (1999) Modeling of watershed input and potential climate change effects on water quality in agricultural reservoirs in the little Washita River watershed, Project Report No.437. St. Anthony Falls Laboratory, University of Minnesota, Minnesota
132. West D, Stefan HG (2000) Simulation of water quality and primary productivity control strategies for lake McCarrons, Project Report No.426. St. Anthony Falls Laboratory, University of Minnesota, Minnesota
133. Fang X, Stefan HG (1996) Development and validation of the water quality model MINLAKE96 with winter data. Anthony Falls Laboratory, University of Minnesota, Minneapolis
134. Fang X, Alam SR, Jacobson P, Pereira D, Stefan HG (2010) Simulations of water quality in Cisco Lakes in Minnesota. Anthony Falls laboratory, University of Minnesota, Minneapolis
135. Edinger JE, Duttweiler DW, Geyer JC (1968) The response of water temperatures to meteorological conditions. Water Resour Res 4:1137–1143
136. Ford DE, Stefan HG (1980) Thermal prediction using internal energy model. J Hydraul Div ASCE 106(HY1):39–55
137. Harleman DRF (1982) Hydrothermal analysis of lake and reservoir. J Hydraul Div ASCE 108(HY3):39–49
138. Hondzo M, Stefan HG (1993) Lake water temperature simulation model. J Hydraul Eng 119:1251–1273
139. Hondzo M, Stefan HG (1992) Water temperature characteristics of lakes subjected to climate change. St Anthony Falls Hydraulic Laboratory, University of Minnesota, Minneapolis
140. Fang X, Stefan HG (2009) Simulations of climate effects on water temperature, dissolved oxygen, and ice and snow covers in lakes of the contiguous United States under past and future climate scenarios. Limnol Oceangr 54:2359–2370
141. Maxwell EL (1998) METSTAT – the solar radiation model used in the production of the national solar radiation database (NSRDB). Solar Energy 62:263–279
142. Fang X, Stefan HG (1994) Temperature and dissolved oxygen simulations for a lake with ice cover. Anthony Falls Hydraulic Laboratory, University of Minnesota, Minneapolis
143. Fang X, Stefan HG (1996) Dynamics of heat exchange between sediment and water in a lake. Water Resour Res 32:1719–1727
144. Gu R, Stefan HG (1990) Year-round temperature simulation of cold climate lakes. Cold Reg Sci Technol 18:147–160
145. Ashton GD (1986) River and lake ice engineering. Water Resources, Highlands Ranch
146. Fang X, Ellis CR, Stefan HG (1996) Simulation and observation of ice formation (freeze-over) in a lake. Cold Reg Sci Technol 24:129–145
147. Stefan HG, Fang X (1994) Dissolved oxygen model for regional lake analysis. Ecol Model 71:37–68
148. Mathias JA, Barica J (1980) Factors controlling oxygen depletion in ice-covered lakes. Can J Fish Aquat Sci 37:185–194
149. Dake JMK, Harleman DRF (1969) Thermal stratification in lakes: analytical and laboratory studies. Water Resour Res 5:484–496
150. Carslaw HS, Jaeger JC (1959) Conduction of heat in solids. Oxford University Press, New York
151. Bannister TT (1974) Prediction equations in terms of chlorophyll concentration, quantum yield, and upper limit of production. Limnol Oceangr 19:1–12
152. Megard RO, Combs WS Jr, Smith PD, Knoll AS (1979) Attenuation of light and daily integral rates of photosynthesis attained by planktonic algae. Limnol Oceanogr 24:1038–1050
153. Bolsenga SJ (1977) Preliminary observations of the daily variation of Ice Albedo. J Glaciol 18:517–521
154. Lock GSH (1990) The growth and decay of ice. Cambridge University Press, Cambridge
155. Wake A, Rumer RR Jr (1979) Modeling ice regime of Lake Erie. J Hydraul Div 105:827–844
156. Scott JT (1964) A comparison of the heat balance of lakes in winter. Department of Meteorology, University of Wisconsin, Madison
157. Pivovarov AA (1972) Thermal Condition in Freezing Lakes and Rivers. Wiley, New York
158. Greene GM (1981) Simulation of ice-cover growth and decay in one dimension on the upper St. Lawrence River. NoAA Technical Memorandum Erl GLERL-36
159. Carlson RE (1977) A trophic state index for lakes. Limnol Oceanogr 22:361–369
160. Brown LC, Barnwell TO (1987) The enhanced stream water quality models QUAL2E and QUAL2W-UNCAS: documentation and user manual. U.S. Environmental Protection Agency, Athens
161. Zison SW, Mills WB, Diemer D, Chen CW (1978) Rates, constants and kinetic formulations in surface water quality modeling. Tetra Tech Incorporation, USEPA, ORD, Athens, Georgia
162. Fang X, Stefan HG (1998) Temperature variability in the lake sediments. Water Resour Res 34:717–729
163. Marshall CT, Peters RH (1989) General patterns in the seasonal development of chlorophyll a for temperate lakes. Limnol Oceanogr 34:856–867
164. Todd DK (1980) Groundwater Hydrology, 2nd edn. John Wiley, New York, NY
165. Magnuson JJ, Webster KE, Assel RA et al (1997) Potential effects of climate changes on aquatic systems: Laurentian great lakes and precambrian shield region. Hydrol Process 11:825–871
166. Stefan HG, Fang X, Eaton JG (2001) Simulated potential thermal/DO fish habitat changes in lakes in response to projected climate warming. Trans Am Fish Soc 130:459–477

167. Fang X, Stefan HG, Eaton JG, McCormick JH, Alam SR (2004) Simulation of thermal/dissolved oxygen habitat for fishes in lakes under different climate scenarios: Part 1. Cool-water fish in the contiguous US. Ecol Model 172:13–37
168. Fang X, Stefan HG, Eaton JG, McCormick JH, Alam SR (2004) Simulation of thermal/dissolved oxygen habitat for fishes in lakes under different climate scenarios: Part 2. Cold-water fish in the contiguous US. Ecol Model 172:39–54
169. Fang X, Stefan HG, Eaton JG, McCormick JH, Alam SR (2004) Simulation of thermal/dissolved oxygen habitat for fishes in lakes under different climate scenarios: Part 3. Warm-water fish in the contiguous US. Ecol Model 172:55–68
170. Eaton JG, McCormick JH, Goodno BE et al (1995) A field information based system for estimating fish temperature requirements. Fisheries 20:10–18
171. Schindler DW, Bayley SE, Parker BR et al (1996) The effects of climate warming on the properties of boreal lakes and streams at the experimental lakes area, Northwestern Ontario. Limnol Oceanogr 41:1004–1017
172. Stefan HG, Hondzo M, Fang X, Eaton JG, McCormick JH (1996) Simulated long-term temperature and dissolved oxygen characteristics of lakes in the north-central United States and associated fish habitat limits. Limnol Oceanogr 41:1124–1135
173. Stefan HG, Fang X (1995) A methodology to estimate year-round effects of climate change on water temperature, ice and dissolved oxygen characteristics of temperate zone lakes with application to Minnesota. Anthony Falls Laboratory, University of Minnesota, Minneapolis, MN, St, 55414
174. Stefan HG, Hondzo M, Eaton JG, McCormick JH (1995) Predicted effects of global climate change on fishes in Minnesota lakes. Fish Aquat Sci 121:57–72 (Special Publication)
175. Stefan HG, Hondzo M, Eaton JG, McCormick JH (1995) Validation of a fish habitat model for lakes. Ecol Model 82:211–224
176. Fang X, Stefan HG, Alam SR (1999) Simulation and validation of fish thermal DO habitat in north-central US lakes under different climate scenarios. Ecol Model 118:167–191
177. Jacobson PC, Stefan HG, Pereira DL (2010) Coldwater fish oxythermal habitat in Minnesota lakes: influence of total phosphorus, July air temperature, and relative depth. Can J Fish Aquat Sci 67:2003–2013
178. Evans D (2007) Effects of hypoxia on scope-for-activity and power capacity of lake trout (Salvelinus namaycush). Can J Fish Aquat Sci 64:345–361
179. US EPA (1976) Quality criteria for water. United States Environmental Protection Agency (US EPA), Washington, DC
180. Chapman G (1986) Ambient aquatic life criteria for dissolved oxygen. US Environmental Protection Agency, Washington, DC
181. Barica J, Mathias JA (1979) Oxygen depletion and winterkill risk in small Prairie lakes under extended ice cover. J Fish Res Board Can 36:980–986
182. Fang X, Stefan HG (2000) Projected climate change effects on winterkill in shallow lakes in the northern U.S. Environ Manag 25:291–304
183. Fang X, Alam SR, Jiang LP et al (2010) Simulations of Cisco Fish Habitat in Minnesota Lakes under Future Climate Scenarios. Anthony Falls laboratory, University of Minnesota, Minneapolis, St
184. Boer GJ, McFarlane NA, Lazare M (1992) Greenhouse gas-induced climate change simulated with the CCC second-generation general circulation model. J Clim 5:1045–1077
185. McFarlane G, Boer J, Blanchet JP, Lazare M (1992) The Canadian climate centre second-generation general circulation model and its equilibrium climate. J Clim 5:1013–1044
186. Kim S-J, Flato GM, Boer GJ, McFarlane NA (2002) A coupled climate model simulation of the Last Glacial maximum, Part 1: transient multi-decadal response. Clim Dynam 19:515–537
187. Kim S-J, Flato GM, Boer GJ (2003) A coupled climate model simulation of the Last Glacial maximum, Part 2: approach to equilibrium. Clim Dynam 20:635–661
188. Hasumi H, Emori S (2004) K-1 coupled model (MIROC) description. University of Tokyo, Center for Climate System Research

Books and Reviews

Eaton JG, McCormick JH, Stefan HG, Hondzo M (1995) Extreme-value analysis of a fish temperature-field database. Ecol Eng 4(4):289–305

Ellis CR, Stefan HG (1989) Oxygen demand in ice covered lakes as it pertains to winter aeration. J Am Water Resour Assoc 25(6): 1169–1176

Ellis CR, Stefan HG (1991) Field testing of an ice-preserving winter lake aeration system. J Am Water Resour Assoc 27(6):903–914

Ellis CR, Stefan HG, Gu R (1991) Water temperature dynamics and heat-transfer beneath the ice cover of a lake. Limnol Oceanogr 36(2):324–335

Fang X, Stefan HG (1995) Interaction between oxygen transfer mechanisms in lake models. J Environ Eng 121(6):447–454

Fang X, Stefan HG (1996) Long-term lake water temperature and ice cover simulations/measurements. Cold Reg Sci Technol 24(3):289–304

Fang X, Stefan HG (1997) Simulated climate change effects on dissolved oxygen characteristics in ice-covered lakes. Ecol Model 103(2–3):209–229

Fang X, Stefan HG (1998) Potential climate warming effects on ice covers of small lakes in the contiguous U.S. Cold Reg Sci Technol 27(2):119–140

Fang X, Stefan HG (1999) Projections of climate change effects on water temperature characteristics of small lakes in the contiguous US. Clim Change 42(2):377–412

Gao S, Stefan HG (1999) Multiple linear regression for lake ice and lake temperature characteristics. J Cold Reg Eng 13(2): 59–77

Gao S, Stefan HG (2004) Potential climate change effects on ice covers of five freshwater lakes. J Hydrol Eng 9(3):226–234

Gu R, Stefan HG (1993) Validation of cold climate lake temperature simulation. Cold Reg Sci Technol 22(1):99–104

Gu R, Luck FN, Stefan HG (1996) Water quality stratification in shallow wastewater stabilization ponds. J Am Water Resour Assoc 32(4):831–844

Henneman HE, Stefan HG (1998) Snow and ice albedo measured with two types of pyranometers. J Am Water Resour Assoc 34(6):1487–1494

Henneman HE, Stefan HG (1999) Albedo models for snow and ice on a freshwater lake. Cold Reg Sci Technol 29(1):31–48

Herb WR, Stefan HG (2004) Temperature stratification and mixing dynamics in a shallow lake with submersed macrophytes. Lake Reserv Manag 20(4):296–308

Herb WR, Stefan HG (2005) Dynamics of vertical mixing in a shallow lake with submersed macrophytes. Water Resour Res 41(2): W02023, doi:10.1029/2003wr002613

Herb WR, Stefan HG (2006) Seasonal growth of submersed macrophytes in lakes: the effects of biomass density and light competition. Ecol Model 193(3–4):560–574

Hondzo M, Stefan H (1991) Three case studies of lake temperature and stratification response to warmer climate. Water Resour Res 27(8):1837–1846

Hondzo M, Stefan HG (1993) Regional water temperature characteristics of lakes subjected to climate change. Clim Change 24:187–211

Hondzo M, Stefan HG (1996) Long-term lake water quality predictors. Water Res 30(12):2835–2852

Hondzo M, Stefan HG (1996) Dependence of water quality and fish habitat on lake morphometry and meteorology. J Water Resour Plan Manag 122(5):364–373

Hondzo M, Ellis CR, Stefan HG (1991) Vertical diffusion in small stratified lake: data and error analysis. J Hydraul Eng 117(10):1352–1369

Horsch GM, Stefan HG (1988) Convective circulation in littoral water due to surface cooling. Limnol Oceanogr 33(5): 1068–1083

Johnson SL, Stefan HG (2006) Indicators of climate warming in Minnesota: Lake ICE covers and snowmelt runoff. Clim Change 75(4):421–453. doi:10.1007/s10584-006-0356-0

Manous JJD, Stefan HG (2003) Projected sulfate redistribution as impacted by lake level stabilization scenarios: devils lake, North Dakota. J Water Resour Plan Manag 129(5):399–408

Rasmussen AH, Hondzo M, Stefan HG (1995) A test of several evaporation equations for water temperature simulations in lakes. J Am Water Resour Assoc 31(6):1023–1028

Stefan HG, Fang X (1993) Model simulations of dissolved oxygen characteristics of Minnesota lakes: past and future. Environ Manag 18(1):73–92

Stefan HG, Fang X (1997) Simulated climate change effects on ice and snow covers on lakes in a temperate region. Cold Reg Sci Technol 25(2):137–152

Stefan HG, Fang X, Hondzo M (1998) Simulated climate changes effects on year-round water temperatures in temperate zone lakes. Clim Change 40:547–576

Stefan HG, Fang X, David W, Eaton JG, McCormick JH (1995) Simulation of dissolved oxygen profiles in a transparent, dimictic lake. Limnol Oceanogr 40(1):105–118

Stefan HG, Hondzo M, Fang X (1993) Lake water quality modeling for projected future climate scenarios. J Environ Qual 22(3): 417–431

Stefan HG, Horsch GM, Barko JW (1989) A model for the estimation of convective exchange in the littoral region of a shallow lake during cooling. Hydrobiologia 174(3):225–234

Stefan H, Cardoni J, Schiebe F, Cooper C (1983) Model of light penetration in a turbid lake. Water Resour Res 19(1):109–120. doi:10.1029/WR019i001p00109

Stefanovic DL, Stefan HG (2002) Two-dimensional temperature and dissolved oxygen dynamics in the littoral region of an ice-covered lake. Cold Reg Sci Technol 34(3):159–178

Williams G, Layman KL, Stefan HG (2004) Dependence of lake ice covers on climatic, geographic and bathymetric variables. Cold Reg Sci Technol 40(3):145–164

Williams SG, Stefan HG (2006) Modeling of lake ice characteristics in North America using climate, geography, and lake bathymetry. J Cold Reg Eng 20(4):140–167

Land Disposal

N. C. Vasuki
RGM, Dover, DE, USA

Article Outline

Glossary
Definition of the Subject
Introduction
Finding Sites for Land Disposal (Landfills)
Design of the Landfill
Design of the Landfill Cell

Glossary

Alternate daily cover (ADC) Alternate daily cover (ADC) *consists of chemical foams, tarpaulins; sprayed on sticky cellulosic and clayey materials, and fine residues from recycling of demolition wastes.*

Aquicludes Aquicludes *are impervious geologic strata that prevent movement of water between aquifers.*

Aquifers Aquifers *are pervious water-bearing strata under the surface of the earth. Precipitation (rain and snow) infiltrates the soil layers and finds its way into both shallow and deep geologic layers.*

Closed dumps Closed dumps are areas where accumulated MSW and/or ISW are controlled by reducing the footprint of the dump and capped with

layers of soil or other materials to minimize infiltration of precipitation. Closure involves good engineering practice to minimize leachate formation, safe venting of degradation gases (methane, hydrogen sulfide, etc.), and leachate removal via drilled wells or drains. Once the dump is closed, no further disposal of MSW and/or ISW is permitted.

Commercial solid wastes (CSW) Consist of materials discarded in offices, stores, public and private institutions, and other service provider locations. CSW generally consist of paper products, film and rigid plastics, metal parts, paper, plastic, metal and wooden containers, rags, plastics, carpets, wires, broken electric and electronic devices, yard wastes, etc.

Daily soil cover (DSC) Daily soil cover (DSC) *consists of soil materials spread over the final layer of solid waste at the end of the working day. Environmental regulations of provinces or states dictate the thickness. Generally accepted practice is 15 cm. DSC acts to reduce flying litter (paper and film plastics), infiltration of precipitation, odors, and also as a fire retardant layer.*

Geomembranes Geomembranes are synthetic thin sheets (1- to 1.5-mm thickness) made from polyolefins (polyethylene, polypropylene, polybutylene), polyvinyl chloride, etc. Geomembrane sheets are designed to be impervious to water and are therefore used in leachate containment systems. Using scrims made from nylon to achieve specific engineering requirements strengthens select geomembranes.

Geosynthetic clay liners (GCL) Geosynthetic clay liners (GCL) *are specially manufactured by compressing high quality clays (bentonite) between two layers of nonwoven polyolefin membranes.*

Industrial solid wastes (ISW) Consist of materials discarded in industrial and manufacturing locations. ISW generally consist of materials discarded in the manufacture of a variety of goods such as card board, film and rigid plastics, paper products, rags, broken pipes, residues from manufacturing processes, metal, plastic and paper board containers, broken electrical and electronic goods, yard wastes, etc.

Land disposal Land disposal means placement of MSW and/or ISW in specially engineered cells designed to safely store such wastes without adverse impact on air or surface or groundwater and biological resources. Safe storage involves use of synthetic and natural materials for lining disposal areas, collection of leachate, and degradation products (gases such as hydrogen sulfide, methane, volatile organic compounds, etc.).

Landfill cap Landfill cap *is an engineered system to prevent entry of precipitation into underlying layers of disposed solid wastes. They vary in complexity – from simple compacted clayey soil layers (60–90-cm thickness) to multiple layers of soil, geomembranes, GCL, and drainage materials.*

Landfill gas (LFG) Landfill gas *is the result of biodegradation of solid wastes disposed in open dumps, controlled dumps, and engineered landfills. Bacteria and fungi naturally present in the organic fraction of solid wastes work to breakdown simple and complex chemical compounds. Under anaerobic conditions, one class of select (acid formers) bacterial colonies create organic acids during the breakdown process. Another class of select (methanogens) bacterial colonies use the organic acids to create methane, carbon dioxide, and other gases.*

Leachate Leachate is generated by rainwater percolating through a waste containment unit. In addition, moisture inherent in organic matter disposed in dumps or sanitary landfill cells and water released during the degradation process also mixes with the leachate. Leachate consists of both organic and inorganic compounds, and the strength varies considerably. Leachates are generally light brown in color (presence of iron and manganese salts) and malodorous.

Municipal solid wastes (MSWs) Consist of a mixture of RSW and CSW and vary in composition on a seasonal basis.

Open dumps Open dumps are areas where MSW and/or ISW are disposed without adequate controls thereby causing contamination of air, surface, groundwater, and biological resources. Open dumps harbor rats and other vermin. Open dumps often catch fire (spontaneous or intentional) and release combustion products that could be toxic.

Residential solid wastes (RSW) Consist of solid wastes discarded by residents of single family or multifamily units. Typically discarded materials

consist of paper and paper products, containers made from plastics, metal and paper, rubber, leather, food (unspoiled, spoiled, and uneaten), vegetables, fruits, plant cuttings, meat products (including bones), broken glass, aluminum foil, film plastics, rigid plastics, carpets and carpet backing, wood, gypsum board, yard wastes, etc.

Sanitary landfills Sanitary landfills are specially engineered units (known as cells) to safely store disposed MSW and/or ISW without causing adverse impact on air, surface and groundwater, and biological resources of the community. They have carefully designed leachate containment systems (collection, storage, treatment, and disposal), degradation gas collection systems for beneficial use or for destruction of methane and hydrogen sulfide, full control over access, environmental quality monitoring, planned usage of disposal in cells to maximize density, and dust and runoff controls.

Definition of the Subject

Human beings have always discarded materials they did not need on land and waterways. During the preindustrial revolution period, the discarded solid wastes generally consisted of five packaging materials: wood, leather, metal, ceramics, and glass. Food and vegetative wastes, textiles, ashes, and cinders made up bulk of solid wastes. Most of the materials were discarded in and around the dwellings in open dumps. If the waste became obnoxious, the dump was covered with locally available mud. This method of disposal has assisted archeologists learn much about materials used and discarded over millenniums.

The industrial revolution induced significant changes in the lifestyle of human beings. Food production increased, food preservation methods improved, food distribution systems became more reliable, and communication and transportation systems became vastly reliable. As a result, the discard rate of materials significantly increased – an unanticipated adverse consequence. Industrial revolution also increased use of chemicals in manufacturing, farming, and medical care.

The accepted methods of solid waste disposal on land started showing strains when the population density of human beings increased through urbanization. The usual method of disposal in the backyard became unacceptable.

The two world wars resulted in extraordinary demand for new materials and innovation in chemical industry induced a myriad of new chemicals for improving the general standard of living. The solid waste discard rate increased in tandem with the improvements in the standard of living.

The characteristics of solid waste changed significantly, and the disposal in open dumps resulted in contamination of ground and surface waters threatening public health. Starting in the 1960s, governments of industrialized nations led by the USA and UK initiated regulatory measures to mitigate contamination.

In 1976, the US Congress enacted landmark legislation – The Resource Conservation and Recovery Act – that materially improved standards of disposal of solid wastes on land. The regulatory framework for protecting the environment has resulted in materially reducing the contamination potential.

Introduction

Human needs for survival are clean air, clean water, food, shelter, and companionship. Human beings have always demanded more than their essential needs. The human "wants" induce innovation and adaptation of technology to meet the human "wants" by using available natural resources. Since technology cannot be 100% efficient, inevitably, there will be residues (wastes) that require disposal. Recycling and reuse of discarded materials could reduce the amount of residues requiring disposal.

All human settlements have to contend with the mundane tasks of collection of discarded solid wastes and carting the solid wastes for disposal. The amount of solid waste discarded by humans varies between 0.4 and 1.5 kg per person per day. The amount is also an index of the general standard of living of the settlement and the degree of development.

The characteristic of discarded solid waste also varies considerably and reflects the general wealth of the settlement. In poor neighborhoods, there is a higher level of organic materials in the waste discards and lower amounts of paper, paper products, and metals. In higher income neighborhoods, there are less organic materials and more packaging materials, namely, paper, paper products, metals, and plastics.

In the organization of governance of communities, there are generally three levels of government – national,

state, and local. State governments create local governments and delegate select police powers to protect public health and local environmental quality. Therefore, local governments are held responsible for collection and proper disposal of solid waste discards in their jurisdictions. Local governments select methods of collection of solid waste discards, recyclable materials, shrubbery clippings, grass clippings, etc.

Throughout the world, land disposal of solid waste is the last resort. In North America, nearly 65% of the solid waste discards are landfilled while the remaining 35% is diverted for recycling and for extracting energy from waste. In the European Union and Japan, there is greater emphasis for diverting select fractions of the solid waste discards for energy recovery. Still, they need landfills to dispose noncombustible and nonrecyclable residues in landfills.

Modern landfills are designed to:

1. Safely contain the solid waste for several decades
2. Reduce infiltration of precipitation
3. Extract efficiently all the leachate generated by the landfill
4. Extract continuously a significant portion of the landfill gas
5. Minimize the runoff of precipitation
6. Minimize odor emissions
7. Keep track of the amount of solid waste disposed daily
8. Treat all the leachate generated either in situ or at an external waste water treatment plant
9. Have extensive groundwater, surface water, and air quality measurement systems

Modern landfill design, construction, and operation must meet very exacting standards of environmental protection. Landfill sites could be used as Regional Waste Management Centers where materials recovery facilities (MRF), organic waste composting operations (OWC), and even energy from Wastes (EFW).

Finding Sites for Land Disposal (Landfills)

Selecting a land disposal site is a very controversial process and requires careful planning. Political and civic groups will object to any site considered for land disposal. The discussion is always emotion driven.

Despite the perceived impediments, it is possible to create a rational process for site selection. In general terms, a site selection process could be organized as follows:

1. Defining the problem

   A simple and clear definition of the solid waste disposal problem
   (a) Population to be served
   (b) Geographical area to be served
   (c) Tonnage of solid waste anticipated per year
   (d) Growth rate of the region
   (e) Estimate of nonhazardous industrial and commercial waste anticipated
   (f) Lifetime design for land disposal – minimum of 20 years – preferably 30 years
2. Establishing the criteria for site selection

   Listing specific criteria to be used for evaluating all available sites should be displayed to the public at large and well advertised. The criteria should have as a minimum the following:
   (a) The site should be above the 100-year flood plain.
   (b) Complete evaluation of the flora and fauna of the site.
   (c) Roads and highways near the site.
   (d) Water courses in and near the site.
   (e) Groundwater aquifers underlying the site.
   (f) Airports near the site.
3. Process for site selection

   The following steps allow an open and transparent process allowing full public participation:
   (a) The agency responsible for site selection issues a public notice in newspapers indicating that it is proceeding to identify potential sites for landfills. The notice includes site criteria. It also notifies all local, state, and federal government elected and appointed officials.
   (b) The agency requests land owners and realtors interested in selling land to the agency. A time limit is set for receiving offers.
   (c) After receiving offers, the agency reviews the offered sites and selects those that meet the minimum criteria. It issues another public notice listing the potential sites and informs the elected and appointed officials.

(d) The agency holds a public hearing after due notice and accepts testimony from the public. A verbatim record is maintained for inspection.
(e) The agency performs further review of sites using the testimony offered in the public hearing and selects the sites worth studying in detail and offers reasons for eliminating some sites. The agency negotiates with the site owners an option to purchase the site if it is selected.
(f) The agency performs detailed hydrogeological, environmental, and traffic studies of the sites. The public is kept informed about the progress of the studies.
(g) After completion of the studies, the agency reviews the reports and selects the final number of sites for consideration. Explanation is provided for eliminating additional sites.
(h) The agency issues a complete report on the studies and includes an executive summary. Another public hearing is held about the report, and the public is allowed to provide comments and criticisms. A verbatim record of the public hearing is maintained for inspection.
(i) After reviewing the public hearing comments and criticisms, the agency could decide to perform more studies to answer questions raised. If further studies are deemed not necessary, the agency could list the remaining sites in an order of priority. A public notice is issued to the public and the elected and appointed officials about the priority list.
(j) Any aggrieved party could challenge the priority list in the appropriate courts of law.
(k) Unless a judicial injunction is used, the agency could start negotiating with the owner of the first priority site to take ownership.
(l) On absent permanent judicial injunction, the agency could start planning and design of the landfill. The regulatory agency of the state is appraised of the progress of design.
(m) After the design is completed, a permit application is filed with the regulatory agency.
(n) After receiving the necessary approvals and permits, the agency issues a bid package for interested construction companies to respond. A public notice is issued with a specific date to respond.
(o) The agency awards the construction contract to the company that meets the requirements and offers the lowest price.

Design of the Landfill

1. The first task is to perform a detailed topographic survey of the site and establish boundaries, watercourses, environmentally sensitive areas, neighboring residences, religious and commercial buildings, etc. A good quality aerial photograph of the site is very helpful.
2. The second task is to determine appropriate areas for construction of landfill cells and determining the sequence of cell construction based on entry road to the landfill site. The goal is to set substantial buffer zones around the landfill cells to provide a visual transition between the neighboring land use and the landfill.
3. The third task is to perform a detailed study of the geology of the site including the area where landfill cells are to be located. The number of soil borings should be made to determine the underlying soil structure. In addition, wells should be drilled around the proposed landfill cells to determine depth of groundwater present in one or more aquifers underlying the site. Based on the results of borings and drilled wells, a detailed hydrogeological report should be prepared describing the general geological characteristics of the site, depth of groundwater, and aquifers and aquicludes underlying the site. The report should include a listing of wells used by neighboring properties as well as any surface waters in the immediate vicinity.
4. The fourth task is to gather local meteorological information – precipitation, wind speed, predominant wind directions, solar radiation, storm frequency and intensity, etc.
5. The fifth task is to determine the amount of solid waste to be disposed in the first landfill cell based on population to be served, the growth rate of the area to be served, the design period, the seasonal

variations in solid waste discards, and the general characteristics of the solid waste (paper products, metal containers and devices, glass and ceramics, food fraction, yard or green wastes, leather, textiles, etc.).

6. The sixth task is to determine the optimum traffic flow within the landfill site to determine the placement of weigh scales, landfill office, maintenance buildings, leachate storage tanks, leachate pump stations, landfill gas flare stations, landfill gas to energy plant, etc.
7. The seventh task is to perform a detailed study of the flora and fauna, archeological sites (if any), wetlands, etc.
8. The eighth task is to establish an environmental quality database before start of the project. This would establish a recognized benchmark against which the impact of construction and operation of the landfill could be measured. Measurements must include current conditions of environmental indicators as a minimum for:
   Air quality – sulfur dioxide, nitrogen oxides, hydrogen chloride, particulate matter, mercury, volatile organic compounds, etc.
   Water quality – heavy metals in ground and surface waters, biochemical oxygen demand (BOD%), chemical oxygen demand (COD), specific conductance, pH, dissolved solids, chlorides, volatile organic acids, etc.
   Soil quality – mineral content (heavy metals), pH, pesticide and weedicide levels, salinity, etc.
9. The ninth task is to determine the sequence of construction of the essential infrastructure: roads, utility corridors (for electrical, phone, water sewer, LFG, and information technology), weigh bridges, traffic control gates, temporary and permanent office structures, lay down areas for construction materials, required signage, etc.
10. The tenth task is to prepare a complete report of the project including all the information gathered in the tasks 1 through 9. The report should be tailored for public release and written in a format that the public at large could understand (minimal technical jargon and acronyms).

Design of the Landfill Cell

1. Landfill Cell Capacity
   Based on population to be served, waste discard rate, projected population growth, and the capital available, the tonnage of solid waste discards could be estimated. The size of the cell should serve the community's needs for a minimum of 7 years.
2. Landfill Cell Construction Sequence
   Future landfill cell construction sequence should also be determined to minimize the cost of the general infrastructure necessary for long-term operations. Such planning would be required for obtaining permits from regulatory agencies.
3. Leachate Containment, Recovery, and Treatment
   The objective of leachate containment design is to capture all the leachate generated by the landfill cell and minimizes the head of leachate on the bottom layer of the landfill cell. Generally, regulatory agencies limit the head of leachate to be 31 cm or less. The bottom surface of the landfill cell is graded to create small valleys to allow the leachate to flow by gravity to the lowest point in the valley. Leachate containment is assured by using one or more layers of impermeable materials. The materials used include natural clay layers, bentonite clay mixed with in situ soils, geosynthetic clay liners (GCL – a sandwich created by compressing bentonite clay between nonwoven polypropylene geomembranes), and high-density polyethylene (HDPE) geomembrane (0.75–1.5-mm thickness). Depending on the regulatory framework, many combinations of materials may be used. Perforated HDPE pipes with a minimum diameter of 20 cm are placed in a bed of small-sized gravel placed in the graded valleys. The slopes of the pipes are controlled to allow gravity flow of leachate into sumps. Pumps with level sensors periodically remove the leachate and send it to external storage tanks.
4. Testing Leachate Containment Liners
   When HDPE or other polymeric geomembranes are used for contain leachate, it is a good practice to test for defects (holes in the membrane, cuts made during construction, etc.). The tests are usually based on electrical conductivity and are very reliable. It is important to make sure there is a quality control and quality assurance program for installation of leachate containment systems.

Land Subsidence in Urban Environment

M. Adrián Ortega-Guerrero[1], J. J. Carrillo-Rivera[2]
[1]Centro de Geociencias, UNAM Juriquilla, Querétaro, Mexico
[2]Instituto de Geografía, UNAM, CU México, DF, Mexico

Article Outline

Glossary
Definition of the Subject and Its Importance
Introduction
Causes of Land Subsidence
Related Issues in an Urban Environment
Future Directions
Conclusion
Bibliography

Glossary

Aquifer unit Aquifer unit is a geological formation, part of a formation, or a number of formations that provide water substantially and in an adequate quality for the expected usage.

Aquitard Aquitard is a geological formation that although insufficiently in producing water as an aquifer unit does, the volume of water that it allows to be released from storage may provide an adverse environmental impact as subsidence.

Compressibility Relates the change in volume, or strain, induced in a soil under an applied stress.

Effective stress Represents the stress transmitted to the full-saturated soil skeleton when a force per unit area (total normal stress) is transmitted in a normal direction across the measuring plane.

Hydraulic conductivity Hydraulic conductivity is the rate of water that an unit volume of aquifer material may allow through under a unit hydraulic gradient such value is a function of its degree of saturation attaining it maximum at 100% saturation, and is also function of water density.

Hydraulic head Hydraulic head is the sum of two components: the elevation of the point of measurement and the pressure head (assuming nil flow velocity).

Specific storage Specific storage of a saturated aquifer is the volume of water that a unit volume of aquifer releases from storage under a unit decline in hydraulic head.

Void ratio Void ratio is the ratio of the volume of voids to the volume of solids.

Definition of the Subject and Its Importance

Progressive or sudden decrease in ground surface elevation, defined as land subsidence, has risen due to different issues related to the urban environment. These issues involve primarily the geologic evolution of a region that determines the type of rock formations, presence of natural raw material, morphology, soil, groundwater presence, and ecological complexity where a city might develop. The evolution of the urban environment is closely linked to the extraction of one or more natural raw materials, which under particular situations may expose urban populations to risk from land subsidence and negatively affect integrity of housing, urban infrastructure, public and private property, and also involve costs of damage in the order of several millions of dollars.

Subsidence is a global problem (Fig. 1). More than 200 cases have been reported in the world (USGS International Survey of Land Subsidence Database) and many more may be reported in the near future as the causes and evolution are better understood.

Due to the importance and implications of land subsidence, the United Nations Educational, Scientific and Cultural Organization (UNESCO) included this topic to be studied under the International Hydrological Programme (IHP). Each country has the responsibility of collecting, maintaining, and interpreting the basic related data (fluid extraction, mining, geotechnical properties, etc.) and associated land subsidence rates, usually with the participation of professional organizations in engineering represented by the areas of soil mechanics, groundwater hydraulics, geological and geophysical sciences, as well as consulting companies, and research groups at universities.

Introduction

The scope of land subsidence is wide. Although several of the processes involved are included in this entry, emphasis is given to the slow response of the soil due to the extraction of subsurface fluids, especially groundwater related to the water supply for large urban environments.

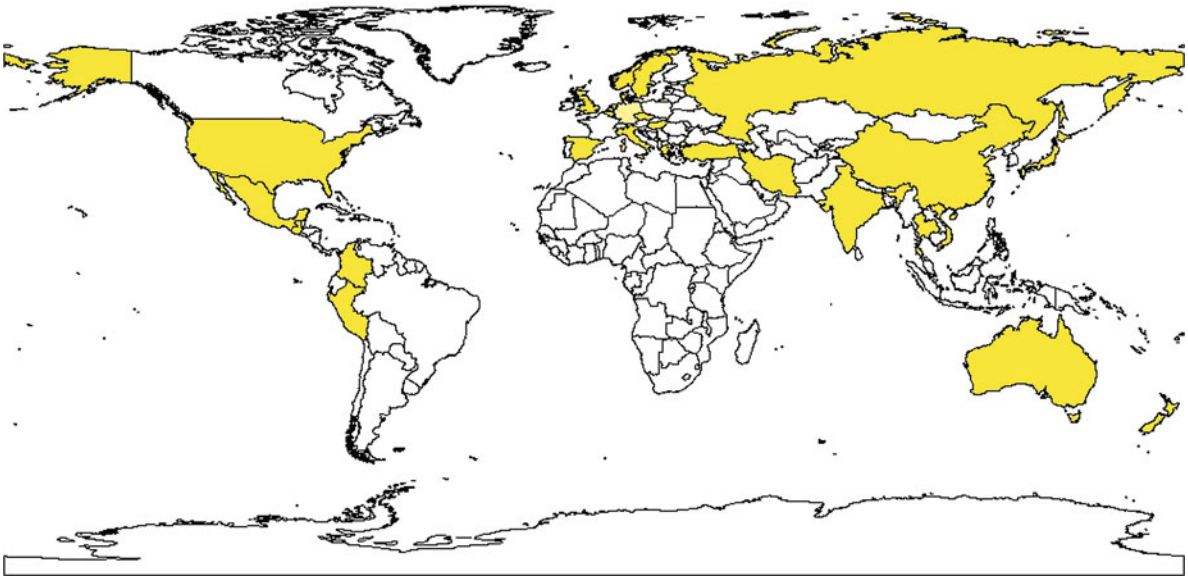

Land Subsidence in Urban Environment. Figure 1
World map showing countries with problems of land subsidence

Causes of Land Subsidence

Land subsidence is caused by different processes on the crust of the Earth resulting from natural or anthropogenic activities such as: (1) direct withdrawal of fluids (water, gas, geothermal, oil, brine); (2) mining (ore deposits, construction earth materials) and tunneling; (3) application of water to unconsolidated moisture deficient soils; (4) dewatering of soils with high organic content usually located in groundwater discharge zones; (5) loading by engineering structures (buildings, bridges); (6) collapse of subsurface cavities in soluble rocks or soft volcanic deposits; (7) geologic loading; and (8) tectonic deformation.

Land subsidence may behave as a gradual soil settling or as a sudden sinking or collapse. Gradual settling of the land is usually due to withdrawal of fluids, application of water to unconsolidated moisture deficient soils, dewatering of organic soils, geologic loading, and tectonic deformation. Whereas, sudden sinking, is usually associated to collapse of the roof of a cavity formed due to underground mining, to the dissolution of soluble rocks (such as limestone) or to water flow under low consolidated volcanic materials, e.g., the well-covered Guatemalan event [9]. Gradual subsidence may affect areas from tens to hundreds of square kilometers, whereas, sudden sinking involves smaller areas in the order of hundreds of square meters. The predictability and the impacts on humans, their property, and urban infrastructure also differ from one case to another.

Different rates of land subsidence or vertical deformation causes development of earth fissures with different urban consequences, and may create risk for humans and damage to housing, buildings, and urban infrastructure, and may also represent more rapid pathways for contaminants to reach groundwater.

Table 1 shows 27 countries where different problems of land subsidence have been reported. From them, groundwater extraction and collapse due to underground mining and karst development represent the highest risk to human population, their properties, and urban infrastructure.

Land subsidence response is particularly critical in the urban environment where population and urban infrastructure are concentrated (housing, buildings, roads, surface and underground transportation system, distribution lines for water, oil, gas, among others).

From the mean causes for land subsidence presented above, the extraction of natural earth fluids (water, oil, gas) that fill pores of underlying sediments and fractures

Land Subsidence in Urban Environment. Table 1 Countries with land subsidence response

Main land subsidence origin	(1)	(2)	(3)	(4)	(5)	(6)	(7)	(8)
Australia		✓			✓	✓		
Belgium		✓						
China	W,G,Gt		✓					✓
Colombia		✓						
Czech Republic								✓
Germany	B					✓		
Greece	W							
Guatemala						✓		
Hungary	W	✓	✓					
India		✓						
Iran	W							
Israel	W					✓		
Italy	W,G,Gt,B	✓					✓	
Japan	W,G	✓		✓	✓			✓
Mexico	W			✓	✓			
Netherlands	W,G	✓		✓	✓			✓
New Zealand	B,Gt							
Norway	W							
Peru								✓
Russia	W	✓						
Spain	W					✓		
Sweden	W			✓				
Thailand	W			✓	✓			
Turkey		✓						
United Kingdom	W,B	✓				✓		
United States	W,B,G,O	✓	✓	✓	✓	✓		✓
Vietnam	W	✓						

Adapted from USGS International Survey on Land Subsidence, land subsidence proceedings 1991, 1995
W Water, *G* Gas, *O* Oil, *B* Brine, *Gt* Geothermal
(1) Direct withdrawal of fluids (water, gas, geothermal, oil, brine)
(2) Mining
(3) Application of water to unconsolidated moisture deficient soils
(4) Dewatering of soils with high organic content
(5) Loading by engineering structures
(6) Collapse of subsurface cavities in soluble rocks or volcanic rocks
(7) Geologic loading
(8) Tectonic deformation

Land Subsidence in Urban Environment. Table 2
Recorded total land subsidence due to groundwater extraction

Locality	Land subsidence (m)	Area affected (km^2)
Central Valley CA, USA	9.0	13,500
Houston TX, USA	2.75	12,170
Eloy ARZ, USA	3.6	8,700
Tokyo, Japan	4.6	2,400
Po Valley, Italy	3.0	780
City of London, Great Britain	0.35	450
Venice, Italy	0.14	400
Mexico City, Mexico	10.0	225
Chalco Plain, near Mexico City	15.0	60

of rocks is paramount. These fluids perform different important services to humans, such as domestic, industrial, and irrigation water; oil and gas for energy generation and combustible formulations; and others. Groundwater extraction represents the more common and critical process of gradual land subsidence (Table 2). Countries like Japan, Mexico, and the United States have reported large-scale land subsidence affecting populated urban environments, such as Mexico City; Tokyo and Osaka; Santa Clara Valley and San Joaquin Valley in California; Houston-Galveston, Texas; Las Vegas, Nevada; and South-Central Arizona. For example, at the beginning of the twenty-first century, observed subsidence response in Mexico City has been recorded to be in the order of 0.01–0.50 m/year. There is local variation in subsidence rates, but at some sites soil consolidation is causing cumulative lowering of the land subsidence of several meters.

A classic example in the technical and scientific literature is the land subsidence response in downtown Mexico City and surrounded areas. The city is built on fine lacustrine sediments, overlying a regional aquifer composed of both granular and fractured volcanic units, in a natural closed basin. More than 50 m^3/s of groundwater are extracted from this aquifer unit causing cumulative land subsidence of more than 10 m by 2010 after more than 150 years of groundwater extraction. In the Chalco Plain, the site of a past lake on the south eastern outskirts of Mexico City, land subsidence reached 15 m in 2010 after 35 years of extraction. Large-scale fractures have also developed associated with land subsidence, increasing the risk to inhabitants. The Chalco Plain suggests the result of one of the most critical land and water use practices carried out to encourage unplanned urban growth; the extracted groundwater is not used locally, but transferred to add to the water supply of the larger Mexico City area. Overpumping is causing severe damage to the local hydraulic infrastructure. In one case, an urban-industrial sewage canal broke due to subsidence which affected the health and property of thousands of people, and had repair and recovery costs of several million dollars.

Related Issues in an Urban Environment

From the international experience, different issues have been identified in an urban environment associated to land subsidence. Better understanding of these issues would permit reduction of risk and associated costs to urban population as well as to private and government property.

Geology

Geology is the science that studies the interior of the Earth and its origin, composition, and evolution. The geological evolution of a particular region determines the type of rock formations and soil characteristics where cities are built. The presence and distribution of fluids (groundwater, oil, gas, geothermal) also depend on the geological evolution. Geological understanding of the urban environment is therefore essential to determine the risk for either gradual soil settling or as a sudden sinking or collapse.

Different disciplines of geology study particular topics associated to geologic evolution and natural raw materials. Among these, hydrogeology, and in particular the flow system theory, proposes a wide system view for the analysis of groundwater in the environment which could assist in the definition of processes involved in land subsidence.

Properties of the Soils

Soils are formed by physical, chemical, or biological destruction (weathering) of rock units assisted by

erosion processes and other factors. Physical weathering takes place in situ by the action of wind, water, or glacier that disintegrate a rock unit (alternate freezing and thawing in cracks in the rock), where the resulting grains or particles retain the same mineralogical composition as that of the parent rock. Chemical weathering, on the other hand, produces changes in the mineral composition of the parent rock, where the presence of water, carbon dioxide, and oxygen play a major role in the chemical reactions. Biological activity plays an important role in the disintegration of a rock unit and in the formation of soils from that of microorganisms to large individuals through, for example, allopathic reactions or through the roots of trees. Clay minerals (< 2 μm) resulting from chemical weathering constitute basic structural units of silicon and oxygen (silica tetrahedron), which may combine with alumina and hydroxyl (alumina octahedron) to form combined sheets. Depending on the packing organization of the silica sheets, alumina sheets, and presence of water molecules or ions such as potassium, magnesium, or iron, different clay minerals are formed with specific physical and chemical properties. Some of these clay minerals have important volumetric changes depending on the water content.

Particle sizes in soils usually vary between less than 0.001 mm to more than 100 mm. Most types of soil consist of a graded mixture of particles between specific limits, this mixture is known as a porous media. The presence of clay minerals usually exerts a major influence on the properties of a soil, an influence out of all proportion to their percentage per weight in the soil [4]. Determination of particle size analysis and physical properties (plasticity, liquid and plastic limits, natural water content, porosity, void ration, compressibility, etc.) of the fine-grained particles (between 0.06 mm and less than 0.001 mm) constitutes an important issue to understand land subsidence.

Among the many different physical properties of a soil, compressibility (α) relates the change in volume, or strain, induced in a soil under an applied stress and may be represented as:

$$\alpha = \frac{-dVt/Vt}{d\sigma e} \tag{1}$$

where

−dVt is the reduction in the total volume of the soil mass

Vt is the total volume of the soil mass

dσe is the change in effective stress

Land Subsidence in Urban Environment. Table 3

Material	Compressibility (α) (m^2/N or Pa^{-1})
Clay	10^{-6}–10^{-8}
Sand	10^{-7}–10^{-9}
Gravel	10^{-8}–10^{-10}
Jointed rock	10^{-8}–10^{-10}
Sound rock	10^{-9}–10^{-11}
Water	4.4×10^{-10}

Modified from Freeze and Cherry [6]

Table 3 shows the range of value of compressibility for different porous materials and rocks large compactions occur in clayey soils due to the larger compressibility (α).

Compressibility controls the magnitude of land subsidence under loading by engineering structures or geologic loading.

Fluid Withdrawal and Properties Variation in Time

Extraction of fluids (water, gas, oil, geothermal) causes a depressurization of the granular materials or fractured rocks that is manifested as compaction. The amount and related importance of parameters of the geologic media and fluid (liquid or gas) vary from one case to another.

To illustrate the hydraulic and geomechanical parameters and to understand the groundwater flow system, the following example for Mexico City is presented. In this case, land subsidence is associated with groundwater extraction, where lacustrine clayey deposits overly a sandy aquifer unit. The transient hydraulic response and consolidation of the lacustrine clayey deposits can be demonstrated by using a coupled, one-dimensional, groundwater flow nonlinear deformation, fine element model [14]. Other aspects of the nonlinearity of parameters for the Mexico City aquitard were presented by Rivera et al. [13]. The 1-D groundwater flow equation that solves for the hydraulic head (h') distribution within an aquitard in terms of the stress-dependent

parameters of hydraulic conductivity (K') and specific storage (Ss') is:

$$\frac{\partial}{\partial z}\left(K'(e)\frac{\partial h'}{\partial z}\right) = Ss'(e,\sigma_e)\frac{\partial h'}{\partial t} \quad (2)$$

This model incorporates empirical expressions that relate K' (L/T) and Ss' to the soil mechanics parameters of void ratio (e) and effective stress (σ_e) (M/LT^2) as:

$$de(\sigma_e) = C_c \log\left(\frac{\sigma_{eo} + d\sigma_e}{d\sigma_{eo}}\right) \quad (3)$$

Equation 3 represents the change in void ratio (e) as a function of a change in effective stress ($d\sigma_e$); C_c is the compression index obtained from the slope of the linear portion of the e-log σ_e plot, and σ_{eo} is the effective stress under current hydraulic head conditions prior to the subsequent pore pressure change:

$$Ss'(e,\sigma_e) = \frac{\rho g C_c \log\left(\frac{\sigma_{eo}+d\sigma_e}{\sigma_{eo}}\right)}{d\sigma_e(1.0 + e_o)} \quad (4)$$

Equation 4 provides an expression for Ss' in terms of void ratio and total stress:

$$dK'(e) = Ko'(e)(10^{de/m} - 1) \quad (5)$$

Equation 5 relates the change in hydraulic conductivity of the aquitard (K') to variations in void ratio (e); where K'_o is the initial hydraulic conductivity and (m) represents the slope of the e-log K' plot [8].

An adequate evaluation of the land subsidence process requires a good understanding of the regional and local groundwater flow system function [15], and a precise quantification of evolution of groundwater flow direction and the hydraulic and geomechanical properties of the porous media in both aquifer units and aquitards in time and space. When the groundwater flow system function is not well understood or ignored, negative consequences have occurred due to arbitrary groundwater extraction. For example, negative changes in groundwater quality could be associated with either the overlying aquitard pore water [10] or the uprising thermal groundwater from deep regional flow systems [5, 7].

Underground Construction (Tunneling) and Solid Extraction

Tunneling is a common practice in the urban environment to conduct fresh or residual water, gasoline, gas, oil, or underground transportation systems. Solid raw material extraction such as from ore deposits, coal, or geologic materials for construction often use tunneling to get access and to extract materials. Surface settlements during tunnel construction depend on a number of factors that include geological conditions, presence of groundwater and geotechnical conditions, design of the tunnel (geometry and depth) and excavation-construction methods. Shallow tunnels will generally have a greater effect on surface structures than deep ones.

Underground construction requires detailed knowledge of the geology, hydrogeologic and geotechnical properties of rocks and soils for a long-term design that reduces the possibilities of sudden settlements. Existing underground constructions can also be analyzed and instrumented to quantify any rate of land subsidence associated to tunneling. Predictive models can be developed to identify zones of potential collapse.

Environmental Effects

Land subsidence is manifested as changes in ground surface elevation that progressively develop topographic depressions where meteoric water may accumulate, affecting native vegetation and fauna, among other. A good example of this environmental effect is a shallow lake that is forming in a topographic depression caused by the land subsidence in the middle of the Chalco plain, in the Basin of Mexico near Mexico City [12]. Land subsidence is causing loss of agricultural land and encroachment of a shallow lake toward the rapidly expanding urban sprawl areas. To control the accumulation of runoff and sewage, drainage canals are being deepened and increased in length. Pumping stations for canal water have been put into operation to control the growth of the surface water body during the rainy season. Land subsidence is also causing damage to sewage canals and their periodic rupture produce consequent flooding in nearby urban areas.

Large-scale fractures in the Chalco Plain have also developed as a consequence of groundwater extraction; these fractures are important due to their hydraulic implications in the groundwater flow and solute transport controls in the lacustrine aquitard to the underlying aquifer [11].

Urban Planning and City Growth

Several issues related to the unplanned growth of Mexico City have accompanied its development since historical times. The Aztecs were the initial dwellers that constructed the city of Tenochtitlan harmoniously with the natural conditions of the prevailing lake system. However, the construction and expansion of the city after the Spanish conquest in 1,521 have included a continuous struggle with water management issues instead of reaching a coexistence with nature. As population increased, flooding due to rainfall made surface water pooling undesirable, so the lakes were desiccated by the turn of the twentieth century through an artificial opening of the basin. Groundwater emerged in mid 1800s as a solution to the water requirements of the city. Population and industrial activities in the City grew rampantly by the second half of the twentieth century. The total population reached 14,987,000 inhabitants [1], so groundwater has been the major component. By 1905, more than 70% of the water supply to the city was from groundwater. Dramatic subsidence incidents reported by the mid 1950s reached 0.44 per year, mainly in the downtown area. By the 1980s, groundwater extraction in Mexico City proper was stopped and shifted to the surrounding areas, such as Chalco Plain, to provide water to Mexico City, as well as for the increasing population of its urban sprawl and increased prominent economic activities.

Monitoring of Land Subsidence

Global Positioning System (GPS) in combination with Total Topographic Stations are traditionally used to develop detailed topographic elevation surveys of the ground surface. Differences in ground surface elevation obtained for different periods of time would permit measurement of the rates and distribution of land subsidence. Yearly topographic surveys are usually recommended. Radar Interferometry is an indirect satellite technique that has also been used to track changes in ground surface elevation.

Economics

Costs and potential costs of damage to private and government property (urban infrastructure) caused by land subsidence are becoming important issues. Insurance against health implications, both physical or psychological, or property damage or loss in some subsidence-prone areas of the world involve millions of dollars to the urban infrastructure and private property.

Economic studies now consider the benefits of fluid, earth materials, or ore deposits extraction against the costs to repair damages caused by land subsidence in the urban centers and surrounding areas.

Future Directions

Prediction of land subsidence and its control represent one of the main scientific challenges in the urban environment. Prediction depends first on understanding the subsidence events occurring on the crust of the Earth resulting from natural processes such as collapse of subsurface cavities in soluble rocks or soft volcanic deposits, geologic loading, and tectonic deformation or from anthropogenic activities, for example, direct withdrawal of fluids, mining and tunneling, application of water to unconsolidated moisture deficient soils, dewatering of soils with high organic matter, and loading by engineering structures. Accurate predictions also depend on the quality and density of long-term instrumentations to measure deformation of the soils and rocks and particularly laboratory and field instrumentation to determine hydraulic and geomechanical parameters involved into the physical processes of land subsidence.

Understanding and quantification of the evolution of the groundwater flow systems represent an important area for research. Long before human intervention, the local environmental system took thousands of years to develop. Location of urban centers usually began in groundwater discharge areas where water was easily available. However, as groundwater and other fluids are extracted from underground, groundwater quality as well as its temperature and flow direction changes with time as extraction progresses. An understanding of these effects and their impact, not only of the obtained physical characteristics of the water, but the imposed constrains on the development of subsidence could became important issues to incorporate into subsidence studies as to understand related processes and possible options for their control. Due to the scale

and time involved in the reaction of these systems, long-term evaluation and monitoring programs are needed.

Conclusion

The particular phenomena of land subsidence is related to geologic evolution, properties and distribution of sediments, rocks fluids and ore deposits, in addition to the urban setting, evolution, and planning. Groundwater extraction represents one of the most important factors causing land subsidence in the urban environment. Therefore, it is important to determine the functioning of the groundwater flow systems at regional and local scales. It is also important to consider that groundwater extraction has different effects on the groundwater flow regime if it is tapped in a recharge, a transit, or a discharge area. The type of flow hierarchy, local, intermediate, or regional [15], to be induced into the particular extraction site could trigger different subsidence responses.

Bibliography

Primary Literature

1. AIC (1995) El Agua y la Ciudad de México. Academia de la Investigación Científica, Academia Nacional de Ingeniería, Academia Nacional de Medicina, National Academy of Sciences (through the National Research Council), pp 364
2. Bouwer H (1978) Groundwater hydrology, Series in water resources and environmental engineering. Mc Graw-Hill, Sydney, p 480
3. Carrillo-Rivera JJ (1998) Monitoring of exploited aquifers resulting in subsidence, example: Mexico City. Studies and reports in hydrology No 57. In: Van Lanen HAJ (ed) Monitoring for groundwater management in (semi-)arid regions. UNESCO, Paris, pp 151–165
4. Craig RF (1987) Soil mechanics. Van Nostrand Reinhold, New York
5. Edmunds WM, Carrillo-Rivera JJ, Cardona A (2002) Geochemical evolution of groundwater beneath Mexico city. J Hydrol 258:1–24
6. Freeze RA, Cherry JA (1979) Groundwater. Prentice-Hall, Englewood Cliffs, p 604
7. Huizar-Alvarez R, Carrillo-Rivera JJ, Angeles–Serrano G, Hergt T, Cardona A (2004) Chemical response to groundwater extraction southeast of México City. Hydrogeol J 12:436–450
8. Lambe TW, Whitman RV (1969) Soil mechanics. Wiley, New York
9. National Geographic (2010) http://news.nationalgeographic.com/news/2010/06/100601-sinkhole-in-guatemala-2010-world-science/
10. Ortega GA, Cherry JA, Rudolph DL (1993) Large-scale aquitard consolidation near Mexico City. Ground Water 31(5):708–718
11. Ortega GA, Rudolph DL, Cherry JA (1999) Analysis of long term land subsidence near Mexico City: field investigations and predictive modeling. Water Resour Res 35(11):3327–3341
12. Ortiz-Zamora DC, Ortega-Guerrero MA (2010) Evolution of long-term land subsidence near Mexico City: review, field investigations, and predictive simulations. Water Resour Res 46:W01513. doi:10.1029/2008WR007398
13. Rivera A, Ledoux E, de Marsily G (1991) Non-linear modelling of groundwater flow and total subsidence in the Mexico City aquifer-aquitard system. In: Land subsidence proceedings of fourth international symposium of land subsidence, vol 200. International Assocation of Hydrological Sciences, Gentbrugge, pp 45–58
14. Rudolph DL, Frind EO (1991) Hydraulic response of highly compressible aquitards during consolidation. Water Resour Res 27(1):17–30
15. Tóth J (1999) Groundwater as a geological agent: an overview of the causes, processes, and manifestations. Hydrogeol J 7:1–14

Books and Reviews

Carrillo N (1947) Influence of artesian wells in the sinking of Mexico City. In: Carrillo VN (ed) Comision Impulsora y Coordinadora de la Investigacion Cientifica, Anuario 47. Secretaria de Hacienda y Credito Publico, Mexico City, pp 7–14, 1969

Dassargues A, Schroeder Ch, Li XL (1993) Applying the Lagamine model to compute land subsidence in Shanghai. Bull Eng Geol (IAEG) 47(1):13–26

Figueroa GE (1987) Structural stability problems of wells and aquifers. en: Workshop on leaky aquifer mechanics, conference proceedings. Universidad Nacional Autónoma de México, Instituto de Geofísica, México, DF, pp 53–61

Figueroa GE (1989) Mecanismos de producción de grietas inducidos por la explotación del agua subterránea. Academia Mexicana de Ingeniería, Alternativas Tecnológicas 29, México, DF, pp 33–48

Juárez-Badillo E (1975) Constitutive relationships for soils. In: Symposium on recent developments in the analysis of soil behaviour and their application to geotechnical structures. University of New South Wales, Kensington, pp 231–257

Juárez-Badillo E, Figueroa GE (1984) Stresses and displacements in an aquifer due to seepage forces (one-dimensional case). J Hidrol 73:259–288

Gambolati G, Freeze RA (1973) Mathematical simulation of the subsidence of venice, 1, theory. Water Resour Res 9(3): 721–733

Helm DC (1976) One-dimensional simulation of aquifer system compaction near Pixley, California, 2, stress-dependent parameters. Water Resour Res 12:375–391
Herrera I, Figueroa GE (1969) Integrodifferential equations for systems of leaky aquifers. Water Resour Res 5(4):900–904
Herrera I, Rodarte L (1973) Integrodifferential equations for systems of leaky aquifers and implications, the nature of approximate theories. Water Resour Res 9(4):994–1005
Herrera IR, Yates R, Henart JP (1982) Estudio de hundimiento y balance de acuíferos subterráneos en la Ciudad de México. In: Proyecto elaborado para el Departamento del Distrito Federal por el Instituto en Investigaciones Aplicadas. Universidad Nacional Autonoma De Mexico, México, DF
Hiriart F, Marsal RJ (1969) The subsidence of Mexico City. In Volumen Nabor Carrillo, Comision impulsora y coordinadora de la investigacion Cientifica, Anuario 47. Secretaria de Hacienda y Credito Publico, Mexico City, pp 109–147
Lambe TW, Whitman RV (1969) Soil mechanics. Wiley, New York
Neuman SP, Witherspoon PA (1969) Applicability of current theories of flow in leaky aquifers. Water Resour Res 5(4):817–829
Neuman SP, Preller C, Narasimhan TN (1982) Adaptive explicit-implicit quasi three-dimensional finete element model of flow and subsidence in multiaquifer systems. Water Resour Res 18(5):1551–1561
Stamatakos JA, Connor CB, Martín RH (1997) Quaternary basin evolution and basaltic volcanism of Crater Flat, Nevada, From detailed ground magnetic surveys of the little cones. J Geol 105:319–330
Telford WM, Geldart LP, Sheriff RE (1990) Applied geophysics, 2nd edn. Cambridge University Press, Cambridge/New York

Landfill Bioreactors

J. Patrick A. Hettiaratchi
Department of Civil Engineering and CEERE,
University of Calgary, Calgary, AB, Canada

Article Outline

Glossary
Definition
Introduction
Historical Evolution of the Landfill Bioreactor Concept
Types of Landfill Bioreactors
Landfill Bioreactor Design, Construction, and Operational Considerations
Cover Systems in Landfill Bioreactors
Waste Degradation and Gas Production in Landfill Bioreactors
Waste Settlement in Landfill Bioreactors
Experience with Field Operations: Gas Production
Future of Landfill Bioreactor
Future Directions
Bibliography

Glossary

Landfill Physical facility used for the disposal of residual solid waste by burial.

Landfill bioreactor Non conventional landfill which performance is based on the manipulation of anaerobic/aerobic conditions and moisture content.

Leachate recirculation Emerging operation associated to the moisture content control in landfills by recirculating the produced leachate into the waste matrix.

Waste management Group of technologies, policies, and procedures associated to the waste generation, collection, transport, storage, reuse, recycle, and disposal.

Definition

Modern waste disposal has evolved from open dumping to the current practice of sanitary landfilling. Although this approach has proved to be a good alternative for preventing a variety of negative human health issues and environmental impacts associated to esthetic conditions and ground/surface water contamination with leachate, conventional sanitary landfills create additional social and environmental concerns, associated mainly to atmospheric emissions and the loss of space and resources. Landfill bioreactors represent a holistic solution to the problems of waste disposal.

Introduction

Until recently, municipal solid waste (MSW) management often represented little more than filling an open hole or marshland with various types of waste. The waste was often not covered properly, sometimes it was burned for volume reduction, and there was little effort to control stormwater runoff and production and escape of landfill leachate into subsurface environment. This type of waste disposal has been the accepted practice until the recognition that uncontrolled open

dumps create a variety of negative human health and environmental impacts.

The modern practice of sanitary landfilling evolved from the past practice of waste disposal in open dumps. The modern sanitary landfills are designed and constructed to eliminate specific problems associated with open dumps. For example, sanitary landfills have features to minimize contamination of groundwater from landfill leachate [1]. Sanitary landfills "entomb" solid waste to minimize landfill leachate production and escape into the surrounding environment, thereby minimizing potential groundwater contamination with landfill leachate. Nevertheless, "dry-tomb" sanitary landfills are known to create further environmental concerns. Although dry-tomb sanitary landfills do not create leachate contamination problems, they are considered environmentally and socially counterproductive because they do not address the landfill gas issues and the loss of space and resources.

Keeping waste as dry as possible within a dry-tomb landfill may decrease leachate production but could be environmentally counterproductive because of the slow production and atmospheric release of methane (CH_4), and perpetual storage of the waste within the landfill boundary. Since a sanitary landfill is designed and constructed as a dry storage facility, new landfill cells should be built upon prime land every few years to accommodate the growing quantities of waste produced by municipalities. Such demand on prime real estate within municipal boundaries could create social and political problems. The dry-tomb landfilling approach also causes financial burden on citizens because of the need to monitor groundwater and air quality in the vicinity of the landfill to ensure that public health is not compromised. The monitoring should be conducted well into the future unnecessarily burdening future generations.

With a view to approach the problem of waste from a different angle, recently some researchers have focused on developing alternatives to dry-tomb sanitary landfilling. Recent advances in landfill research have indicated that the operation of landfills as bioreactors could be viable. Waste entombment in a conventional dry-tomb landfill slows down the process of biodegradation by minimizing moisture entry, whereas landfill bioreactors speed up the biodegradation process by controlled input of moisture (i.e., by leachate recirculation) and increased cycling of nutrients and bacterial populations.

Considering the potential for landfill bioreactors to replace the landfill approach as the "favored alternative," this paper provides a critical review of this approach. The paper includes a brief introduction to landfill bioreactors identifying key advantages, a review of design, construction and operational parameters, design/research questions relevant to landfill bioreactors, and an evaluation of the future of this technique as an integral part of MSW management.

Historical Evolution of the Landfill Bioreactor Concept

Although the landfill bioreactor concept was first introduced to the research community in 1970s [2], waste management regulators and practitioners were not prepared to consider it as an alternative to sanitary landfilling until a few years ago. A number of reasons contributed to the lack of recognition of landfill bioreactors as a credible alternative. One of the primary reasons was the adoption of a piecemeal approach by regulators and practitioners to solve problems with the former practice of open dumping. The dry-tomb sanitary landfilling approach was considered adequate to remedy the biggest threat of open dumps to environment and human health; the release to subsurface of leachate. Dry-tomb landfills were promoted by regulators (especially the US EPA) as a solution to groundwater contamination and esthetic problems. The early view of waste was pessimistic; "waste is a liability and requires high level of resources to manage."

However, with the emergence of NIMBY (Not in My Back Yard) syndrome and the adoption of sustainable development strategies by communities, an optimistic view of waste has emerged: "waste is a resource or material in the wrong place and wrong time." Proliferation of waste to resource (e.g., recycling and composting) and waste to energy (e.g., thermal systems and landfill gas utilization systems) projects throughout the world is the result of this new attitude. Another contributing factor is the adoption of stricter regulations for waste disposal, especially in countries of the European Union. With the implementation of increasingly stringent regulations, sanitary landfills have become highly engineered facilities with

sophisticated containment systems, environmental monitoring, and improved operational practices.

Waste to resources and waste to energy projects are considered sustainable and "green" and receive the blessing of environmentalists. A primary attraction is the potential to decrease the landfill footprint by diverting waste to resource recovery facilities, thereby decreasing the inherent problems associated with sanitary landfills. However, these projects could be costly and may not be economically viable in some situations. Often, these projects require subsidies from governmental sources to be viable. Furthermore, an integrated waste management system still requires a sanitary landfill to accept residual waste either rejected from or not acceptable at resource recovery facilities.

The landfill bioreactor concept was first introduced as a solution to the leachate management problem [2, 3]. In traditional sanitary landfills, the leachate management system includes bottom liners to retard escape of leachate from landfills and a leachate collection and removal system to remove leachate retained above the bottom liner. The removed leachate should be disposed of in an environmentally acceptable manner. In some landfills, on-site leachate treatment plants are used to treat leachate and in others, with relatively low quantities, leachate is removed for off-site treatment at sewage treatment plants. Such disposal methods add to the total cost of operating sanitary landfills. In landfill bioreactors, the waste mass is expected to act as a treatment medium capable of removing both organic and inorganic contaminants from recirculating leachate [4].

A secondary benefit of leachate recirculation in a landfill bioreactor is the accelerated microbial decomposition of waste [3, 5–7], resulting in enhanced landfill gas generation and a faster decrease in the waste volume. Production of landfill gas has received increased attention over the last couple of decades because of the realization that as much as 15% of annual global anthropogenic CH_4 produced and released into the atmosphere could be the result of anaerobic decomposition of waste in landfills [8]. In response, there has been a significant increase in the number of landfill gas extraction and energy recovery projects. However, landfill operators have also realized that economical viability of such landfill gas to energy projects depends on the amount of gas available for extraction at these sites. Two obstacles are encountered with dry-tomb sanitary landfills: first, gas production rates are usually low, and second, the use of low permeable daily/intermediate cover layers restricts the free flow of gases during extraction. Some operators have attempted to retrofit such landfills with leachate recirculation systems, with limited success. In this context, the design, construction, and operation of landfill cells as landfill bioreactors is the perfect remedy.

Recent public outcry against landfills has forced operators to maximize the amount of waste deposited at existing landfills. Another benefit, somewhat less important, that favors the landfill bioreactor utilization is the potential to increase volume available for landfilling because of waste settlement during filling of a cell. Landfill bioreactors, with rapid waste degradation and settlement, could increase capacity of a cell by up to 10% [9].

Types of Landfill Bioreactors

A landfill bioreactor is a landfill cell that utilizes enhanced microbiological processes to transform and stabilize the readily and moderately decomposable organic waste constituents within a few years of bioreactor process implementation. The landfill bioreactor significantly increases the extent of organic waste decomposition, conversion rates, and process effectiveness over what would otherwise occur within a traditional landfill. In a landfill bioreactor, the environmental performance measurement parameters, such as landfill gas (LFG) generation rate and landfill leachate characteristics (generation rate and the concentration of key leachate constituents such as heavy metals and biochemical oxygen demand (BOD)), decrease to low and steady levels within 5–10 years of bioreactor process implementation.

The landfill bioreactor includes specific operational strategies to enhance microbial decomposition processes. The most important strategy is the liquid addition into the waste matrix. Other strategies, including waste conditioning and shredding, pH and nutrient adjustment of leachate, temperature management, and gas outflow and air inflow management, may also serve to optimize the bioreactor process. Therefore, successful implementation requires development and implementation of focused development and

operational plans. Sometimes, leachate alone is not available in sufficient quantity to sustain the bioreactor operational needs. Other non-hazardous liquids and semiliquids are suitable alternatives to leachate. However, such liquid addition requires regulatory approvals depending on the jurisdiction. Furthermore, under certain circumstances, the cell may produce more leachate than needed for bioreactor operation, requiring additional on-site or off-site leachate handling facilities. Such situations arise mostly under humid tropical climatic conditions at bioreactor cells without low permeability (e.g., polyethylene membrane liners) cover systems.

Considering the variety of operational features adopted, landfill bioreactors could be categorized as anaerobic, aerobic, and hybrid (aerobic-anaerobic). Among these anaerobic bioreactors are the most common. The primary objectives of anaerobic bioreactors include leachate management and enhanced LFG production. In anaerobic bioreactors, required conditions are achieved by minimizing oxygen infiltration, whereas in aerobic bioreactors the objective is rapid waste degradation under aerobic conditions by introducing oxygen/atmospheric air into the waste mass. Active aerobic biodegradation processes, such as composting, have been used for centuries to stabilize biodegradable portion of agricultural and household waste in a significantly short time frame. Although oxygen transfer efficiency is lower than that of active composting systems, aerobic bioreactors also utilize the same bacterial decomposition process, albeit at a lower kinetic reaction rate.

The hybrid bioreactors may involve simultaneous or sequential anaerobic-aerobic operation. An example of simultaneous anaerobic-aerobic operational system is the Fukuoka Method [10] which is being widely applied across Japan. This approach utilizes the self-purifying capacity inherent in "nature" to stabilize waste materials with following considerations:

- Quality of leachate improves significantly and more rapidly than in anaerobic conditions, offering considerable cost advantages.
- Generation of the greenhouse gas methane is reduced.
- Stabilization of the waste is enhanced making it possible to return the completed landfill sites to other uses in a short time period.

An example of the sequential anaerobic-aerobic operational system is the concept of *Biocell*. In Biocell approach, a cell is operated in anaerobic and aerobic modes sequentially, with the specific intention of mining in a third stage once the waste is fully stabilized. The Biocell concept involves the operation of a cell as an anaerobic bioreactor first with leachate recirculation to recover the full energy potential of biomass waste. In a second stage, the Biocell is operated in the aerobic mode to produce compost. The input of air and operation of the cell as an aerobic bioreactor enhances waste decomposition to a level where it could be mined in a third stage for resource and space recovery, thus making the landfill operation sustainable. The Biocell is a novel and holistic approach to waste disposal on land; with energy recovery, greenhouse gas (GHG) emission control, groundwater contamination control, and compost and space recovery as direct benefits. The cell is converted from a perpetual waste storage location to a waste processing facility minimizing liability associated with cell monitoring.

With the availability of several modes of operation, landfill bioreactors provide a large number advantages to waste managers, including but not limited to:

- Leachate management: Temporary storage of leachate and the partial in situ treatment of leachate within the waste cell contributing to enhanced leachate quality over time.
- Leachate management: The volume of leachate could be reduced by maximizing evaporative losses during recirculation which can reduce leachate treatment capital and operation costs.
- Landfill Gas management: Improvement of LFG production rate and total yield, thereby increasing the viability of energy recovery.
- Cell volume optimization: Enhanced decomposition increases the rate of MSW settlement with up to 10% during cell filling and up to 25% overall gain in landfill space.
- Post-closure monitoring: Since biological stabilization could be completed in years versus decades in traditional sanitary landfills, there is considerable reduction in time and cost of post-closure monitoring. In the case of Biocells, post-closure monitoring does not arise because the cell is converted to a waste processing facility instead of a waste storage facility.

- Overall environmental impacts: Reduce environmental impacts by containing leachate and controlling greenhouse gas emissions, with minimum impacts on groundwater, surface water, and the neighboring environment.

Landfill Bioreactor Design, Construction, and Operational Considerations

Most design components of a landfill bioreactor cell are similar to that of a traditional sanitary landfill, but differences exist. All landfill bioreactors require additional components such as a leachate recirculation system. Aerobic bioreactors and Biocells require an air delivery system as well. Required primary design components of a cell include the bottom liner and leachate collection system, leachate recirculation system, gas collection and management facilities, and the final cover system.

Cell Configuration

For economic and regulatory reasons, an emerging trend in traditional landfill design is to build deep cells that are filled and completed within 2–5 years. This trend bodes well for landfill bioreactor evolution. Phased cell construction can more easily take advantage of emerging technological developments, rather than committing long term to a design that may prove to be inefficient. Once closed, methanogenic conditions within the cell are optimized and gas generation and extraction are facilitated.

Cell depth is a particularly important consideration in landfill bioreactor operation in cold climates. Shallow cells may exhibit low internal temperatures during winter months. Recent research has shown that a minimum cell thickness of about 15 m is required to maintain acceptable temperatures in a cold climate landfill bioreactor. On the other hand, deep cells could also cause operational problems. Extremely deep landfills may show a high degree of waste compaction in the bottom portions such that low waste permeability could inhibit leachate and gas flow. In these instances, it may be necessary to limit leachate recirculation to the upper levels, or develop adequate internal drainage management capability. Nevertheless, maintaining a maximum cell height of about 25 m could minimize waste settlement, density and permeability gradients, and stability problems.

Leachate Management System

An efficient leachate collection and recirculation system is central to the operation of landfill bioreactors. The bottom liner and leachate collection systems are common to both traditional landfills and landfill bioreactors. However, leachate recirculation and moisture addition within a landfill bioreactor cell will result in greater hydraulic loadings than those of traditional landfills. It is therefore necessary to ensure that the leachate collection system is adequate to accommodate these higher leachate flow rates.

The primary objective of the bottom liner and leachate collection system is to minimize escape of leachate into the subsurface. During the design and construction stages of the cell, the following questions arise:

- What will be the rate of leachate impingement on the collection system?
- What is the best configuration for the leachate drainage and collection system?
- What is the best type and configuration of liner system?
- What are the factors that may contribute to clogging of the leachate collection system, and what is the best way to mitigate them?
- What is the best way to monitor the efficiency of the leachate collection system (required instrumentation)?

Leachate recirculation provides treatment of leachate in addition to increased rate of biodegradation. These positive developments are the result of increased moisture movement within the solid waste matrix that transports enzymes, bacteria, and nutrients to the solid waste. Increased contacts between organic waste and nutrients will increase biodegradation reaction rates. Furthermore, the solid waste matrix may act as a trickling filter medium in removing suspended or soluble organic and inorganic contaminants from leachate.

Since leachate recirculation is a relatively new concept, so far, most researchers have focused their attention on efficient methods of delivering moisture (as leachate) into the waste matrix. The presence of nutrients and seed microorganisms in leachate that may aid the biodegradation process has received less

attention. Most bioreactor operators consider the presence of nutrients and bacteria as a bonus and have not attempted to manipulate these in order to optimize the biodegradation process. In relation to leachate recirculation, the relevant questions are:

- What should be the optimum moisture contents within the refuse to achieve maximum biodegradation, both in anaerobic and aerobic modes of operation?
- What should be the ideal liquid management systems to maintain optimum moisture content?
  - What should be the leachate recirculation rate?
  - What is the best method to monitor moisture content of waste?

Related literature does not reveal a single optimum moisture content (or a universally acceptable empirical model) for waste biodegradation. Several optimum moisture contents are reported in literature: 45–75% for anaerobic, 50–70% for aerobic, and 50% for methanogenesis. The saturated moisture content was reported to be in range of 50–60%. According to the values reported by various researchers the optimum moisture content is very close to saturated moisture content. Reported field capacities are in the range of 40–50%. Leachate appears to reach the collection network when the waste reaches 60–70% of its field capacity due to short-circuiting. The increase in moisture content eliminates mass transfer limitations, the exchange of substrate, nutrients and microorganisms, and the dilution of inhibitors and improved distribution of enzymes and microorganisms within the landfill.

Optimum Leachate Recirculation Rate Volume, rate, and frequency of added water directly impact liquid movement within the waste. Generally liquid addition leads to increased flow through the waste matrix when the field capacity of waste mass is exceeded. Excessive addition of water could significantly reduce flow if the capacity of leachate collection system is exceeded [11]. In addition, high flow rates could potentially flush out nutrients and microbes necessary for high rate biodegradation. The leachate recirculation operation can be continuous or intermittent.

Landfill Bioreactors. Table 1 Leachate production rate and leachate recirculation rates at different sites

Site	Leachate production (m^3/ha/day)	Leachate recirculation (m^3/ha/day)
Alachus county	7.8	4.3
Worcester county	2.6	2.1
Win field county	19.0	13.8
Pecan Row	2.7	1.1
Lower mount valley	14.6	9.5
CRSWMA landfill	16.6	11.7
Lemons	2.2[a]	5.0
Mill Seat		
Test cell 2	2.8[a]	6.8
Test cell 3	2.8[a]	5.2

[a] From HELP model predictions

According to a study by Reinhart et al. [12], the daily recirculation rate generally was in the range of 0.2–5% flow rate per day based on waste mass. Leachate production rate and leachate recirculation rate observed at different sites are tabulated in Table 1 [3]. Although this information cannot be used directly to determine the leachate recirculation rate to be used in a given bioreactor, some interesting observations can be made by analyzing the data provided:

- In locations where leachate production is monitored and observed to be higher than leachate recirculation rate, the ratio of leachate recirculation rate to production rate varied from 0.41 to 0.81, with an average of 0.64.
- In locations where no direct leachate production information is available, researchers have used US EPA supported HELP (Hydrologic Evaluation of landfill Performance) model to determine the leachate production rate. These values are significantly lower than the actual rates reported in other locations.
- Although the values are specific to the particular site under consideration, it is worthwhile to note

that the maximum reported leachate production rate was 19.6 m^3/ha/day (Winfield county landfill). This translates to 2 mm/day or 60 mm/month infiltration rate.

Infiltration Methods and Uneven Moisture Distribution in Landfill Bioreactors

Moisture distribution within the waste matrix depends on several factors, such as characteristics of waste, infiltration method, suspended particles in the leachate to be recirculated, biological activity, degree of compaction of waste, channeling, and effects of cover layers. Homogeneous or even distribution of moisture within the waste matrix can be achieved with proper understanding of the impact of these factors.

Infiltration/leachate recirculation methods play a major role in even distribution of moisture within the waste matrix. The common infiltration methods can be categorized into three main classes according to their water movement patterns (i.e., vertical, horizontal, and water movement in both directions). The first category includes spraying, surface ponding, and horizontal introduction of water using trenches or horizontal pipe network. The second category, horizontal water movement, includes vertical injection of water using vertical wells. The last category includes combinations of first and second.

Horizontal Infiltration Trenches Horizontal infiltration trenches generally consist of perforated PVC pipes surrounded by gravel, tire shreds or automobile fluff, and are usually capped with a flow barrier such as an infiltrator or low permeability clay [10]. The pipe is centered within the trench and is placed at the bottom or center of the trench. The trenches can be located either at surface of the landfill or within each landfill lift. They can be operated either by gravity feed or under pressure. Use of flexible pipes will be helpful to prevent fracturing of the injection line, if a large amount of settlement is anticipated.

Size and spacing of leachate injection holes should be selected to achieve even distribution of moisture. Extra holes should be made to accommodate potential clogging. According to Miller et al. [13], this method requires greater effort in construction than surface ponds. Also, the method requires regular monitoring of pressure and flow rate to minimize the potential for surface seeps and high leachate return to leachate collection system. Moisture distribution resulting from the injection lines has been found to cover a large area, but the distribution was less uniform than that of infiltration ponds.

Horizontal systems can be used during active phases of the landfill or at closure if constructed as a part of the final cover system. Problems associated with this method include freezing (if operated during winter), clogging (of the receiving medium), surface and side slope leachate seeps, limited recharge areas, and system failure due to landfill subsidence. Large quantities of leachate can be successfully introduced through trenches, although long-term use may result in biofouling of trench fill materials and hence a consequent reduction in permeability.

Vertical Infiltration Wells Vertical infiltration wells are generally constructed using a series of perforated manhole sections placed on top of each other and these perforated sections rise to just below the final elevation of landfill. The bottom section is generally not perforated to minimize leachate short-circuiting. A solid section is then added to bring the well above the final grade. Normally these wells are constructed on concrete pads for stability and filled with gravel [10]. Diameter of a well is in the range of 60–120 cm. Well spacing varies from one well per 0.16 ha to one well per 0.8 ha. If wells are spaced too closely, they may interfere with waste placement and compaction operations. Leachate is applied by filling the well from the top. Infiltration rates appear to be enhanced if rest periods are provided between pumping events.

Problems associated with this method include surface and side slope leachate seeps, limited recharge area, system failure due to landfill subsidence, and damages to the liner. Concern has also been expressed over possible tearing of the bottom liner if the well rests on the geomembrane, as well as problems with well integrity during landfill subsidence. On the positive side, this method is compatible with landfill closure.

Infiltration Ponds Leachate recirculation using surface infiltration ponds has been used successfully at several landfills in Florida and with less success in Delaware [3]. Infiltration ponds provide large storage

volume for leachate and a constant source of infiltration of leachate into the solid waste matrix [13]. However, ponds will have limited recharge areas unless moved frequently. Problems with evaporation, flow of surface runoff into the ponds, floating waste, odor, limited influence area, and incompatibility with final cover requirement are reported in literature. This method is not applicable in Northern climates during winter months, because of freezing problems.

Spray Infiltrators Spray application includes standard lawn sprinklers, surface infiltrators, and truck sprayers. Lawn sprinklers and surface infiltrators are generally constructed using a semi rigid PVC framework that can be easily moved to receive waste, to wet a different area, to maximize application rates, and to avoid active landfilling areas. Surface infiltrators have perforations in the PVC framework that distribute the leachate. Although spraying provides the greatest opportunity for volume reduction of all recirculation methods used to date, it cannot be used in periods of rain or freezing conditions, and is not compatible with the application of an impermeable final cover.

Problems associated with this method are clogging of the application device, odor, stormwater contamination, formation of hard-pan deposits that limit infiltration, and incompatibility with final closure. The latter three problems are the most serious.

Pre-wetting of Waste Pre-wetting of waste has been practiced for many years as a method for increasing waste compaction efficiency. More recently, leachate has been used as the wetting agent. Waste wetting is most commonly accomplished using water tankers or by manual spraying using a fire hose. In addition to compaction enhancement, pre-wetting has advantages in terms of simplicity, evaporation opportunity, and a uniform and efficient use of waste moisture holding capacity. However, this technique is rarely used in large-scale operations because of odor problems. Obviously, this technique cannot be used after the landfill closure.

Important Considerations in Installing Infiltration Systems Some issues remain uncertain, including the determination of the area of influence of recirculation devices, the effect of leachate recirculation on leachate collection systems, and appropriate recirculation flow rates. Townsend et al. [14] recommend at least 3 m of waste placed on top of a horizontal injection line, and 6 m distance from side slopes to avoid leachate outbreaks and artesian conditions at the surface of the fill. French drains may be necessary at landfill slopes to control side seeps. Miller et al. [13] selected 6 m spacing for trenches based on results of excavation studies at a recirculating cell operated by Delaware Solid Waste Authority. Intermittent introduction of leachate permits fill and drain operations that prevent development of saturation conditions.

Gas collection systems should not be placed within the area impacted by leachate recirculation devices. If leachate reaches the gas collection wells or trenches, pressure builds up and impedes gas removal. For this reason, leachate recirculation and gas collection systems should not be combined. Gas collection devices also provide a preferential leachate flow path that may result in short-circuiting of leachate and a restricted impact area. Due to the limited impact area and the cone-shaped impact volume of both vertical and horizontal water introduction devices, a combination of vertical and horizontal devices should be considered. Alternative placement of trenches at right angles to each other at each lift may also increase the impact area. Wicks, or capillary layers, are also being used at several landfills to increase impact area [3].

The heterogeneous nature of the waste matrix produces a high degree of preferential flow resulting in pockets of highly saturated areas as well as relatively dry areas. The parameters such as hydraulic conductivity will vary from point to point. This end-result is the formation of voids or channels through which water can flow readily without moving the wetted front downward. The water flows downward unevenly, reaching the leachate collection system long before the waste matrix reaches its field capacity. Research has shown that pretreatment of waste (e.g., reducing particle size of waste by shredding) can reduce heterogeneity of landfill's waste mass, and therefore reduces channeling.

Cover Systems in Landfill Bioreactors

Traditional landfills require three types of covers: daily, intermediate, and final. Since the primary purposes are the reduction of esthetic concerns and moisture infiltration into the waste matrix, usually, the other impacts

of cover systems are ignored. Therefore, operators have been known to use every available material to construct these cover systems. The usual practice is to use low permeable soil material available on site.

However, the use of low permeable material in daily and intermediate cover systems could interfere with performance of landfill bioreactors. For example, daily and intermediate covers may act as barriers to vertical moisture movement, thereby increasing lateral moisture flow. Use of low permeable materials will significantly impede vertical movement of leachate resulting in perched lenses of leachate and potentially side seep problems as leachate moves laterally along the daily cover material. McCreanor and Reinhardt [10] identified several perched lenses of leachate directly above daily cover material at a Delaware landfill. The waste beneath these perched lenses was found to be dry and well preserved.

Considering the above concerns, the selection and application of daily covers is of particular importance for successful leachate recirculation. Options available to landfill operators include the use of highly permeable soils or compost as cover material, the use of alternative daily cover (ADC) material, or the practice of breaking up or removing the daily cover prior to the application of the next layer of waste. However, the use of high permeability materials will not only inhibit vertical flow but sometimes may result in lateral flow to side slopes again resulting in potential seepage problems [10]. The best situation would be to use removable or degradable cover materials within the landfill and to use low permeable materials on the side slope of the cell.

Alternative Daily Cover Materials (ADCs)

Some of the ADCs available for daily and intermediate covers are foundry sand waste, papermill waste, processed infrastructure demolition waste, processed building demolition waste, spill debris, dredged material, and mixtures/blends of waste with soil. Careful assessment of these materials' physical properties is necessary to ensure that the material itself does not have inherent characteristics that could cause operational problems at the landfill bioreactor. Some of these parameters need to have regulatory agency approvals, acceptable material permeability, good material workability, material availability, storage, specialized equipments, etc. Manufactured or processed materials that may be considered as alternative daily cover materials (and typically take up no additional volume in the landfill) are: sprayed foam products, sprayed recycled paper/plastic slurry products and removable/reusable synthetic membrane, or textile products.

Final Cover

Final covers used in landfill bioreactors play two important roles: prevention of uncontrolled infiltration of precipitation, and trapping generated gas within the waste matrix. A final cover generally consists of a vegetative layer, a protective layer, a drainage layer, and a barrier layer. The drainage layer encourages subsurface runoff and reduces the mounding depth of moisture on barrier layer. The barrier layer could be a thick compacted clay layer or a plastic liner. Because of the potential for high differential settlement of the cell, it is more appropriate to use a flexible plastic liner (e.g., low density polyethylene or polyvinyl chloride).

Waste Degradation and Gas Production in Landfill Bioreactors

More recently, increased attention has focused on the role of CH_4 in climate change. Methane from landfills contributes a significant proportion of annual global CH_4 emissions, although the estimation is subject to a great deal of uncertainty. The global CH_4 emissions from landfills range from less than 20–70 Tg/year or about 5–20% of the total estimated emissions of 375 Tg/year from anthropogenic sources globally.

Anaerobic decomposition of organic waste in the landfill environment produces LFG. LFG mainly consists of methane and carbon dioxide, both of which are odorless. Trace constituents of other volatiles, often malodorous or toxic gases, are also found in LFG. LFG can migrate through soil into structures located on or near landfills. Since methane presents a fire or explosive threat, LFG must be controlled to protect property, and public health and safety. Also, many jurisdictions require landfill owners/operators to reduce reactive organic gas emissions to improve regional air quality. Thus, engineered solutions are needed to efficiently and safely monitor, collect, and process LFG. As noted, a positive side to LFG control is energy recovery. Today's technology allows a landfill owner/operator to recover the

energy in LFG while reducing gas emissions. Revenue from the sale of LFG or electricity generated using LFG as a fuel can offset costs for landfill environmental compliance and/or closure.

LFG is the product of microbiological decomposition of land-filled garbage. The microorganisms turn complex organic compounds in garbage into methane, carbon dioxide, and trace amounts of other compounds. The composition of LFG depends on activity of the bacteria involved, the available substrate, and other factors. Methane comprises about 50–55% of LFG, while the rest is mostly carbon dioxide. Methane is the most reduced organic molecule. In other words, no further conversions to simpler organic molecules are possible once methane has been produced. It is produced as an end product of anaerobic metabolism. Methane is a short-lived GHG with an atmospheric lifetime of approximately 12 years compared to over 100 years for carbon dioxide. It is 25 times more potent as a GHG, kilogram for kilogram, than carbon dioxide.

Considering one of the key objectives of an anaerobic landfill bioreactor is to produce the maximum amount of gas in the shortest time period, it is necessary to ensure gas production conditions are maintained at optimum levels. Apart from waste characteristics, various cell operating conditions are the main contributors to gas production. Characteristics of waste as placed in the cell, such as pretreatment of waste and degree of compaction, are critical. The relevant questions are:

- What is the effect of preprocessing the waste (opening plastic bags, etc.) on biodegradation rate of the waste? What would be the effect of reduction of particle size (to provide more homogenous waste) on biodegradation rate of the waste?
- What are the reactions rates for various combinations of feed stocks types (e.g., mixed waste, organic waste alone, organic waste, and sludge etc.)?
- Is it possible to increase the microbial populations within the waste mass to accelerate the biodegradation process? Is it necessary to introduce additional microbial populations into the landfill from sources like digested sewage sludge?

Answers to some, but not all, of these questions are available in literature. Considering the impact initial waste properties may have on other cell parameters such as waste density and permeability, answers to the above questions should not be evaluated by themselves. Questions related to waste compaction are:

- What should be the as filled waste density to ensure even distribution of leachate during recirculation?
- What is the impact of as filled waste density on settlement behavior and eventual creation of a waste density and permeability gradient within the solid waste matrix?

Because of the interrelationship of various processes, it is extremely difficult to answer these questions. Nevertheless, past experience and laboratory/field investigations have shown the following:

- Although a low compaction density aids in leachate delivery to the entire waste mass at the early stages of cell operation, waste density changes over time creating a scenario of high settlement rates, permeability gradients (high permeability in upper parts of the cell and low permeability in lower parts of the cell), and potential lateral migration and channeling of recirculated leachate.
- High rates of gas production during early stages of cell operation, usually exceeding gas production in traditional landfills by an order of magnitude or more.

Waste Settlement in Landfill Bioreactors

Waste settlement could impact landfill bioreactor operations due to the reasons identified above. Within this context, the basic questions raised are as follows:

- How does the waste density profile vary with time and space?
- What is the relationship between initial compaction density and waste settlement?
- Is preprocessing of waste and/or mixing of sewage sludge with high moisture content feasible or desirable in terms of waste settlement?
- Is there any significant effect of swelling (rebound of waste after initial compaction) on compaction/construction?
- What is the impact on stability/settlement of daily/intermediate cover? If so, what should be the most suitable cover material?
- What is the effect of waste density on lift height and total height of a landfill bioreactor?

In a typical landfill, the majority of settlement takes place over a long period of time as a result of the decomposition and mechanical compression. Settlement is often described in three stages: (1) initial compression, (2) primary compression, and (3) secondary compression. The initial compression is seldom discussed because compression happens immediately when a load is applied. However, considerable settlement during the filling phase should be included in landfill bioreactor design because it contributes to the total amount of waste that can be deposited in a cell. This settlement is typically unaccounted for and usually goes unnoticed. It is anticipated that mechanical compression is the dominant mechanism that determines settlement during construction; however, since biodegradation initiates soon after the deposition of waste there may be a contribution from biodegradation as well. The influence of biodegradation on ultimate settlement is of interest to designers but the impact of biodegradation during filling may also be valuable in landfill design since filling typically takes place over a period of several months.

Experience with Field Operations: Gas Production

Although the concept of bioreactor landfilling is relatively new, a number of demonstration anaerobic bioreactors are underway in Northern America and Europe [15]. Crow Wing County Landfill located in north central Minnesota was started in 1998 and accepted 50,000 t of waste annually in an area of 5.7 ha. More than one million liters of treated and untreated leachate were injected via horizontal laterals, working face spray, and spray on yard waste composting over intermediate cover [16]. The Burlington County bioreactor in northwest New Jersey had leachate recirculation from 2002 to 2005 in a 4 ha area accepting about one million tons of MSW. The New River Regional bioreactor was a "research" bioreactor in Union County, north central Florida. It had about one million tons of waste in-place in a 5 ha area. Leachate was recirculated into an existing interim capped landfill with an exposed membrane cover. Volume of leachate recirculated was about 24,600 m^3 [16]. The 2 ha Salem County anaerobic bioreactor in southwest New Jersey received leachate via horizontal injection trenches since 2000. The rate of moisture addition is about 0.167 m^3/t waste [16].

A hybrid bioreactor is in operation in Calgary, Alberta, Canada, since 2006. The Calgary Biocell is a unique facility where the three processes, anaerobic bioreactor, aerobic bioreactor, and mining, are sequentially applied in one cell. The Calgary Biocell is a full-scale facility, which covers an area of 100 m × 100 m with a waste footprint of 85 m × 85 m and a maximum height of 18 m. The schematic diagram of the Biocell is presented in Fig. 1. The base of the Biocell is 50 m × 50 m, and it extends 10 m below the ground surface. The shape of the Biocell is a pyramidal square frustum increasing sectional area with side slope of 3H: 1V up to ground level. The bottom liner/leachate collection systems are used to minimize groundwater contamination and maximize recovery of leachate. The Biocell received 48,000 t of residential (high in organics) and selected commercial wastes, with the resulting feedstock placed in three lifts of 5–6 m each. Collected leachate is recirculated after ensuring the quality is acceptable. A pipe system was added to recirculate the collected leachate. Recirculation of leachate adds the much needed moisture and transfer bacteria from well-inoculated waste to freshly deposited waste, thus accelerating the establishment of microbial community. The Biocell was instrumented to gather time-resolved and real-time moisture, temperature, and settlement data.

The construction of the Biocell began in August 2004 and it accepted approximately 43,000 t of waste from April 2005 until May 2006. The final cover was completed in October 2006 and the Biocell became fully operational as a landfill bioreactor in the same

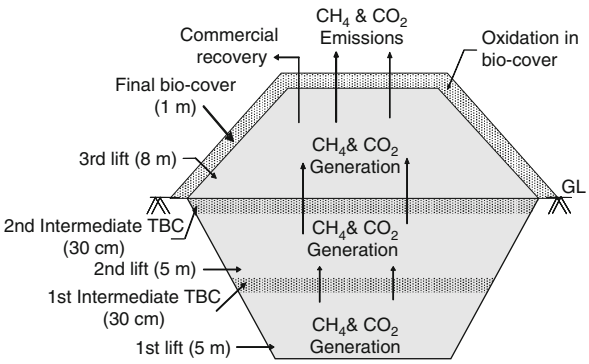

Landfill Bioreactors. Figure 1
Schematic diagram of calgary biocell

month. The intermediate thin-biocovers were made up of a mixture of compost and soil with some mulch used as makeup material in some areas.

The gas production rate from October 2006 to September 2008 is shown on Fig. 2. The initial gas production rate was low. After leachate recirculation was initiated, the gas production rate increased four-fold to 254 m^3/h. Thereafter, the gas production rate decreased gradually and reached a steady state flow rate of 170 m^3/h throughout the winter months. The methane generation potential, calculated from waste composition data, is 120 m^3/t of solid waste. Hence, in October 2006 the theoretical gas generation rate at the Biocell should be approximately 282 m^3/h which is very close to the field measured value of 254 m^3/h reported in Fig. 2.

For comparison purposes, Fig. 2 includes the cumulative methane generation curve for a landfill cell containing 43,000 t of waste and operated as a dry-tomb sanitary landfill. The Scholl Canyon model was used to generate this curve using the parameter values k = 0.023 $year^{-1}$ and Lo = 116.7 m^3/t.

The parameter values are those proposed by Environment Canada for a typical sanitary landfill in the province of Alberta. Evidently, the gas production at the Biocell is more than 400% higher than that of a dry-tomb type sanitary landfill of similar size and configuration located in Calgary, Alberta.

Future of Landfill Bioreactors

Waste disposal practice has evolved over the years from open dumping to the current practice of sanitary landfilling. However, future waste disposal practice lies with landfill bioreactors, anaerobic, aerobic, and/or hybrid. However, being a relatively new technological innovation, full-scale operation of bioreactors could be fraught with uncertainties.

In addition to the unavailability of key design parameters (e.g., optimum moisture content, compaction density), a number of operational difficulties exist. Short-circuiting may occur during leachate recirculation preventing achievement of field capacity for most of the waste matrix. Head build up on liner may require innovative operational practices. Continuous pumping of leachate at two to three times the generation rate may be necessary to avoid head buildup on the liner. The use of permeable daily and intermediate covers may help in attaining field capacity but may give rise to other problems. Accelerated gas production may lead to odor problems if not accommodated by aggressive LFG collection. Leachate infiltration and collection piping are vulnerable to irregular settling and clogging. If the waste is less permeable than anticipated, increased condensate production leads to short-circuiting of moisture into LFG collection pipes. Storage must be provided to manage leachate during

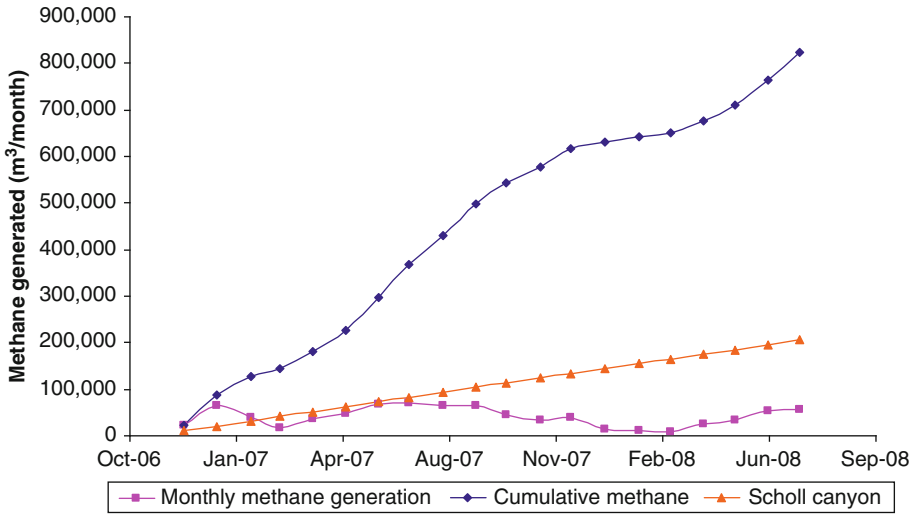

Landfill Bioreactors. Figure 2
Comparison of gas production at the biocell and a conventional landfill

wet weather periods if the final cover is not impermeable. Conversely, leachate may not be sufficient in volume to completely wet the waste, particularly for aerobic bioreactors. Increased internal pore pressure due to high moisture content may lead to reduced factor of safety against slope stability and must be considered during the design process.

In view of the concerns raised here, it is clear that many questions are yet to be answered hence detailed research on different components of bioreactor landfill is required.

Future Directions

Four primary problems are associated with land disposal of solid waste, namely esthetic concerns, ground/surface water contamination with leachate, emission of landfill gas, and extensive space requirements. Over the last three decades, the design and operation of dry-tomb sanitary landfills have managed to solve, to a large extent, the first two problems. However, the last two problems have not been adequately addressed. The landfill bioreactors, especially the Biocell, are proposed to solve all four problems at the same time. The proposed holistic approach is expected to revolutionize waste management throughout both developed and developing countries.

Bibliography

1. Hartz KE, Klink RE, Ham RK (1982) Temperature effects – methane generation from landfill samples. J Environ Eng Division ASCE 108(4):629–638
2. Pohland FG, Gould JP, Ramsey E, Walters DC (1982) The behavior of heavy metals during landfill disposal of hazardous wastes. In: Proceedings of the U.S. EPA 8th annual research symposium on land disposal of hazardous waste, EPA-60019-82-002, pp 360–371
3. Reinhart DR, Townsend TG (1998) Landfill bioreactor design and operation. Lewis, New York
4. Pohland FG (1992) Anaerobic treatment: fundamental concepts, applications and new horizons. In: Design of anaerobic processes for the treatment of industrial and municipal wastes. Technomic, Lancaster, pp 1–40
5. Pohland FG, Kang SJ (1975) Sanitary landfill stabilization with leachate recycle and residual treatment. AIChE Symposium Series No 145, p v 71
6. Warith MA, Smolkin PA, Caldwel JG (2001) Effect of leachate recirculation on enhancement of biological degradation of solid waste: Case study. Pract periodical hazardous toxic radioactive waste management 5(1):40–46
7. McBean EA (2007) Performance results from the Tucumán solid waste bioreactor. Waste Manage 27(12):1783–1791
8. Houghton JT, Callander BA, Varney SK (1992) Climate change 1992: the IPCC supplementary report. Cambridge University Press, Cambridge
9. Hunte C, Hettiaratchi JPA, Meegoda JN, Hettiarachchi CH (2007) Settlement of bioreactor landfills during filling operation. ASCE geotechnical special publication #152-GeoDenver2007, ISBN # 0784408971
10. McCreanor PT, Reinhart DR (1996) Hydrodinamic modeling of leachate recirculating landfills. Water Sci Technol 34(7): 463–470
11. Craig P (2000) Effects of moisture content in solid waste landfills. Master's thesis, AFIT/GEE/ENV/00M-03
12. Reinhart DR, AlYousfi AB (1996) The impact of leachate recirculation on municipal solid waste landfill operating characteristics. Waste Manage Res 14(4):337–346
13. Miller LW, Earle JFK, Townsend TG (1996) Engineering control and augmentation of biological decomposition at solid waste landfills. Report #96-4, Florida Center for Solid and Hazardous Waste Management, Gainesville
14. Townsend TG, Miller WL, Earle JFA (1995) Leachate recycle infiltration ponds. J Environ Eng 121(6):465–471
15. Hettiaratchi JPA, Hsieh H, Meegoda JN, Hunte CA (2010) Sustainable management of household solid waste. Int J Environ Waste Manage (IJEWM) 6(1–2):96–106
16. USEPA (2007). Bioreactor performance. Office of Solid Waste, Municipal and Industrial Solid Waste Management Division, EPA530-R-07-007

Landfill Closure and Reuse of Land

Joseph J. Lifrieri, John T. Bolan, Walter W. Burke
Paulus, Sokolowski and Sartor, LLC, Warren, NJ, USA

Article Outline

Glossary
Definition of Subject
Introduction
Review of Federal Regulations for Landfill Closure
State Adoptions of Subtitle D
Closure and Reuse of Subtitle D Landfills
Viability for Reuse of Landfills
Sustainability Review for Reuse of Landfills
Potential Sustainable Reuses
Conclusion
Future Directions
Bibliography

Glossary

Closure plan The plan for closure of a landfill after it ceases receipt of waste materials.

Hazardous waste A solid waste which due to its quantity, concentration, or physical, chemical, or infectious characteristics may pose a substantial present or potential hazard to human health or the environment when treated, stored or disposed of, or otherwise mismanaged or can cause or contribute to an increase in mortality, or an increase in irreversible or incapacitating illness.

Landfill A disposal site where solid waste is buried between layers of soil and other materials in such a way as to reduce contamination of the surrounding land. The modern version of landfill, also known as a sanitary landfill, is lined and subsequently covered to keep pollutants from leaking into the soil and water.

Leachate A liquid that has passed through or emerged from solid waste and contains soluble, suspended, or miscible materials removed from such waste.

Post-closure plan The plan for the period after a landfill undergoes closure. Post-closure care activities typically include maintenance of the waste containment systems and monitoring of the groundwater to ensure that waste is not escaping and polluting the surrounding environment. In the USA, the required post-closure care period is 30 years from site closure, but this can be shortened or extended by the State Director.

Solid waste Any discarded material that is abandoned by being disposed, burned, or recycled. A solid waste can have the physical form of a solid or semisolid.

State Any of the 50 United States, the District of Columbia, the Commonwealth of Puerto Rico, the Virgin Islands, Guam, American Samoa, and the Commonwealth of the Northern Mariana Islands.

State Director The chief administrative officer of the lead state agency responsible for implementing the state permit program by the United Sates Environmental Protection Agency.

Sustainability It is defined herein as a process that resolves the conflict between various competing goals and involves the simultaneous pursuit of consensus with economic prosperity, environmental quality and social equity.

Sustainable development It is defined herein as a pattern of resource use that aims to meet human needs, at the same time preserving the environment, with the goal that human needs are met in the present and for future generations.

Definition of Subject

This section examines the sustainable reuse of existing landfill sites. Sustainability is examined in the context of the existing regulatory authority of the United States Environmental Protection Agency (USEPA). The viability of reuse is also examined in the context of planning, engineering, and environmental and economic issues. Lastly, sustainability of reuse of existing landfill sites is measured against the goals of sustainability: environmental benefits, economic benefits, and achievement of sociopolitical policies. Based upon these reviews it is concluded that the reuse of existing landfills can meet the goals of sustainability.

Introduction

With the growing scarcity of available land, especially in urban areas, the reuse of existing landfill sites has been frequently accomplished. Landfills have the benefits of filled lands and have been redeveloped for other uses after their life as a waste disposal facility has ended. The sustainability of this practice of reuse is in need of further review.

Review of Federal Regulations for Landfill Closure

As an initial step in the sustainability analysis, a review of the USEPA Regulations for landfills was completed for two types of landfills that are potential candidates for sustainable reuse: landfills that received nonhazardous waste materials and landfills that received hazardous waste materials. There is a far greater number of nonhazardous waste landfills than hazardous waste landfills.

Subtitle C (Hazardous Waste Materials)

Under the Resource Conservation and Recovery Act (RCRA), all hazardous waste disposal, including landfill disposal, is regulated under Subtitle C and its resultant USEPA regulations at 40CFR Part 264. Landfills

authorized to accept hazardous wastes must follow very stringent guidelines for their design and operation. Part 264 requires inspections, personnel training, location standards for disposal facilities, construction quality assurance, detailed facility design and operation, the use of manifests and tracking of received waste materials, preparation of contingency and emergency plans, closure, post-closure care, and extensive financial assurance. Subtitle C reserves the authority for approval of hazardous waste landfills to the USEPA. The most current version of Part 264 is July 2006.

Subtitle D (Nonhazardous Waste Materials)

RCRA Subtitle D and its resultant USEPA regulations at 40CFR Parts 257 and 258 authorize the landfills that serve as disposal sites for all wastes not regulated by Subtitle C, including municipal wastes. Waste materials authorized for disposal at Subtitle D Landfills also include household hazardous waste and hazardous wastes generated by small quantity generators.

RCRA provides a procedure so that States can be become qualified by the USEPA to assume the responsibilities for regulating Subtitle D Landfills in their states (Qualifying States). As detailed in 40CFR Part 239, this procedure entails the submission of a State Solid Waste Management Plan to the USEPA Administrator or designee. This Plan will have the following contents: (1) all sources of solid waste in the State including hazardous wastes, residential, commercial and institutional solid waste, wastewater treatment sludge, pollution control residuals, industrial wastes, mining wastes, agricultural wastes, water treatment sludge, and septic tank cleanout; (2) all aspects of solid waste management: resource conservation, source separation, collection, transportation, storage, transfer, processing (including resource recovery), treatment, and disposal; (3) established and justified priorities for solid waste planning, resources, and management, and schedules and milestones for achieving the objectives of RCRA and meeting the requirements of Part 264; (4) cover a minimum of a 5-year time period from the date submitted to USEPA for approval; and (5) an identification of the State's legal authority for solid waste management including any modifications to regulations necessary to implement Subtitle D.

Comparison of Subtitle C and D

A comparison of the design, closure and post-closure requirements for Subtitle C and Subtitle D Landfills is shown in Table 1.

This comparison indicates that Subtitle D Landfills have generally less stringent requirements. Location criteria prohibit Subtitle C Landfills in certain seismic areas, floodplains, and geologic formations. Bottom liners, leachate controls, and cover systems are more rigorous for Subtitle C Landfills. Extensive contingency, emergency, and release detection plans are also required for Subtitle C Landfills. Lastly, Post-Closure Care requirements, including financial assurance, for Subtitle C Landfills are more rigorous and provide more long-term responsibilities and liabilities for operators/owners of Subtitle C Landfills. Overall, the current USEPA regulatory requirements would serve to preclude the reuse of Subtitle C Landfills and the priority for landfill reuse would be Subtitle D Landfills.

State Adoptions of Subtitle D

To gain a better focus on the available reuse of landfills and their regulatory constraints, a detailed examination of the USEPA Subtitle D regulations was completed. These regulations are intended to provide the minimum standards for the design, operations and closure/post-closure of Subtitle D Landfills. The USEPA regulations at 40CFR Part 239 allow a State to implement the requirements of Subtitle D. Numerous states have adopted the 40CFR Parts 257 and 258 regulations. Most of these States have adopted the USEPA regulations without any change. Some States, such as California, New York, and New Jersey, have adopted additional protective requirements beyond the USEPA regulations which have been approved as part of their submittals under 40CFR Part 239 to address local concerns of their constituencies. Reuse in the States which have gone beyond the USEPA requirements will place additional issues and concerns.

A typical example of a Qualifying State is New Jersey. Through its New Jersey Department of Environmental Protection (NJDEP), the State regulates the permitting, environmental impact, design, operations, maintenance, closure, post-closure, and financial assurance for private, commercial, and municipal

Landfill Closure and Reuse of Land. Table 1 Comparison of subtitle D and subtitle C landfills

Criteria	Subtitle D landfill	Subtitle C landfill	Comparison
Seismic	New sites and lateral expansions cannot be located within 200 ft of a fault that had a displacement within Holocene period	Not located within 200 ft of a fault that had a displacement within Holocene period	No difference for new Sites; Subtitle C more restrictive for old Sites
Flood plains	Site will not restrict the flow of the 100-year flood, reduce the temporary water storage capacity of the floodplain, or result in washout of solid waste	Site located within 100 year flood plain must demonstrate no washout of hazardous waste	No difference
Salt dome	–	Waste disposal prohibited in salt dome	Subtitle C more restrictive
Liner system	Single composite liner system of two components, with the upper component a minimum 30-ml flexible membrane liner (FML), and the lower component a 2-ft layer of compacted soil with a hydraulic conductivity of no more than 1×10^{-7} cm/s	Must prevent release from Site for active life and for entire closure period; composed of top liner and multiple composite 1×10^{-7} cm/s bottom liner including 3 ft minimum thickness soil layer	Subtitle C more restrictive
Leachate collection	Prevent maximum of 1 ft of leachate buildup	Install above top liner to prevent maximum of 1 ft of leachate buildup over liner for life of liner system	Subtitle C more restrictive
Leak detection	Not required	Required between top and bottom liner to verify integrity of top liner	Subtitle C more restrictive
Groundwater protection	Groundwater monitoring required; no potential for migration of hazardous constituents to the uppermost aquifer during the active life of the Site and the post-closure care period	Ensure that the contaminants specified in its permit are not detected in uppermost aquifer beneath the Site during the active life of the Site and the post-closure care period	Subtitle C more restrictive
Run-On Protection	Prevent run-on during a 25 year design storm	Prevent run-on during a 25 year design storm	Equal
Response action plan	Not required	Set forth actions in response to leakage from the Site	Subtitle C more restrictive
Contingency plan	Not required	Minimize hazards due to fire, explosion and release of hazardous waste or constituents	Subtitle C more restrictive
Closure plan	Written plan required; must prove compliance with less restrictive Closure Protection criteria	Written plan required; must prove compliance with rigorous closure protection criteria	Subtitle C more restrictive
Financial assurance for closure	Either Trust Fund, Surety Bond, Letter of Credit or Insurance allowed with closure cost estimate; Disbursement of funds subject to State requirements	Only Trust fund allowed with closure cost estimate; Funds to be disbursed only at the order of the USEPA	Subtitle C more restrictive

Landfill Closure and Reuse of Land. Table 1 (Continued)

Criteria	Subtitle D landfill	Subtitle C landfill	Comparison
Post-closure	30 year period: Maintain final cover and leachate collection system; Monitor groundwater; Maintain and operate gas monitoring system	Minimum 30 year period, can be extended if release is detected; Maintain final cover and leachate collection system; Monitor groundwater; Maintain and operate gas monitoring system; Prevent run-on and run-off from damaging the final cover; Protect and maintain surveyed benchmarks	Subtitle C more restrictive
Post-closure use of site	No specific restriction	Post-closure use of property can never be allowed to disturb the integrity of the final cover, liner(s), or any other components of the containment system, or the function of the facility's monitoring systems which preclude post-closure reuse	Subtitle C reuse is not possible.

landfills located in the state. A landfill in New Jersey has the following closure and post-closure care restrictions:

- No person shall construct or operate a sanitary landfill without an approval from the Department of a Closure and Post-Closure Plan. Such Plan shall consist of both a Closure and Post-Closure Care Plan and a Closure and Post-Closure Financial Plan.
- The owner or operator of every sanitary landfill shall submit to the Department a Closure and Post-Closure Care Plan prepared, signed and sealed by a New Jersey licensed professional engineer to provide for closure and post-closure care of the sanitary landfill upon application for new sanitary landfill.
- The Closure and Post-Closure Care Plan shall provide for the design and implementation of the following: (1) Soil Erosion and Sediment Control Plan certified by the local soil conservation district. (2) Final cover; final cover vegetation, maintenance of final cover, and final cover vegetation. (3) Maintenance of side slopes; run-on and run-off control programs. (4) Maintenance of run-on and run-off control programs. (5) Groundwater monitoring wells. (6) A program for the maintenance of groundwater monitoring wells. (7) A program for the monitoring of groundwater in accordance with NJPDES rules, *N.J.A.C. 7:14A*, and any permit for that sanitary landfill issued pursuant thereto. (8) A methane gas venting or evacuation system. (9) A program for the maintenance of methane gas venting or evacuation system. (10) A leachate collection and/or control system. (11) A program for the operation and maintenance of a leachate collection and/or control system. (12) A program for the installation of a facility access control system. (13) A program for the maintenance of the facility access control system. (14) Measures to conform the site to the surrounding area. (15) A program for the maintenance of measures to conform the site to the surrounding areas.
- The owner or operator of every sanitary landfill shall submit a Closure and Post-Closure Financial Plan to the Department which shall set forth the costs and expenses, and establish the means for meeting those costs and expenses, associated with full implementation of the approved Closure and Post-Closure Plan.
- The Closure and Post-Closure Financial Plan shall include an estimate which details the cost of each provision of the Closure and Post-Closure Care Plan and a projection of funds that will be available from the escrow account. The Plan shall provide that no withdrawals may be made from the escrow account without the approval of the Department. A review of the cost estimate is required every 2 years and, if necessary, the Plan is to be revised.

A revised or updated Financial Plan shall be submitted on the second anniversary of the date of the Plan's last approval. Upon closure of the sanitary landfill, a detailed description of the landfill shall be recorded, along with the deed, with the appropriate county recording office. The description shall include the general types, locations, and depths of wastes on the site, the depth and type of cover material, the dates the landfill was in use and all such other information as may be of interest to potential landowners, and shall remain in the record in perpetuity. The deed shall also provide notice that any future disruption of the closed landfill shall require prior approval from the Department.

- The post-closure care period shall continue for 30 years after the date of completing closure of the sanitary landfill.

The NJDEP regulations provide for disruption of closed landfill and through this process NJDEP addresses the reuse of a landfill. Written approval for disruptions is required prior to any excavation, disruption, relocation, or removal of any deposited material. This action may or may not involve solid waste, from either an active or closed sanitary landfill. Disruptions are defined as "Minor" for the purpose of gathering and evaluating information about the landfill's environmental or physical properties or "Major" for the purpose of the construction of buildings, roadways, parking areas, and other site improvements on top of a landfill. As per the NJDEP Technical Manual on Landfill Permits, judgments regarding the impact of a potential reuse are made on a case-by-case basis dependent on the physical and environmental characteristics. This approach appears to be typical for other Qualifying States.

Closure and Reuse of Subtitle D Landfills

While the USEPA regulations restrict the design and operations of a landfill, these regulations also specify the elements of a Closure Plan. A landfill's closure plan will have a direct impact on the viability of its reuse. The USEPA-required elements of a closure plan include: (1) a description of the final cover and the methods and procedures to be used to install the final cover, (2) an estimate of the largest area of the landfill that requires a final closure during its active life, (3) an estimate of the maximum inventory of wastes disposed on-site over the landfill's active life, (4) a schedule for completing all required final closure activities and improvements, and (5) financial assurance to pay for the cost of the proposed closure improvements. The final cover system must be designed to have a permeability less than or equal to any bottom liner system, but no greater than 1×10^{-5} cm/s; have an infiltration layer of a minimum 18 in. of earthen material; and have a minimum of 6 in. of earthen material that is capable of sustaining native plant growth.

In addition to a Closure Plan, the USEPA regulations also provided for the submission of a written Post-Closure Care Plan. This Plan controls the use of the closed landfill for a minimum period of 30 years after Closure and includes the provision of financial assurance to guarantee post-closure care. Within this Plan, a description of any planned uses of the property must be provided along with their impacts on the provided financial assurance. Post-closure use of the property cannot disturb the integrity of the closure improvements or the function of the monitoring systems. However, a USEPA-approved State may allow any disturbance (reuse) if the owner or operator demonstrates that the disturbance of the closure improvements, including any removal of waste, will not increase the potential threat to human health or the environment. Therefore, the reuse of closed landfill would require a submission which supports no increase in potential threats.

Viability for Reuse of Landfills

Planning and Land Use Issues

Beyond the regulatory requirements imposed by the USEPA and the States, landfill reuse must also meet the tests of viability: planning and land use, permitting requirements, engineering and institutional controls, infrastructure, and economics. State and local jurisdictions control the use of land through master plans and zoning regulations and the reuse of a closed landfill must comply with these requirements.

A key aspect of planning for landfill reuse will be localities' master plan. Ideally, the governing master plan should integrate the overall environment for a community with needed active and passive recreation. The master plan should view landfill reuse as

providing a unique opportunity to restore former aesthetic qualities to the area, while satisfying the open space needs of the community. More intense use also increases site development costs and utility requirements which requires further consideration. The master plan should also have been developed through a visioning process to assist the community and public. It will be important to visualize the former landfill as more than a waste disposal site and to be able to look beyond the current use to the site's potential. A strong understanding of the existing conditions and reasonable accomplishments must be the basis of planning. The master plan should also create a "sustainable and livable" environment, which can meet the community's "standard of maintenance." The plan should balance site development with the protection of surrounding natural and diverse aquatic, terrestrial and wetland habitats, as well as minimize impact on the surrounding neighborhood and community. The plan should foster public–private partnerships for funding project development, sustaining use, and long-term maintenance.

The Master Plan should also have addressed a number of landfill related considerations including: the impact of settlement, impact and operational needs for landfill gas control, storm drainage, long-term post-closure care/maintenance requirements, wetland impacts, slope stability issues, and the need for a risk assessment to support a public reuse of the landfill. The lack of considerations of landfill reuse in the localities' master plan will negatively impact a planned reuse of a landfill site.

As an outgrowth of the localities' master plan, zoning regulations and ordinances will control and limit the type and character of land use that may be implemented within that locality. The zoning will set both bulk and use limits. Bulk limits include lot area, front, rear and side yard setbacks, maximum heights, maximum lot coverage and maximum floor area ratio. Zoning will define uses "as of right" (also known as permitted uses) and prohibited or non-permitted uses. A gray area between permitted and non-permitted uses, known as conditional uses, is also typically included. The reuse of landfills is likely to be controlled as a Conditional Use and would be subject to a detailed review through submission of special documentation and conduct of public hearings.

In addition to bulk and use limits, zoning typically requires compliance with state and federal environmental regulations and permitting. The localities' zoning may also impose its own environmental requirements including wetland buffers, noise/vibration limits, and air quality/permitting.

Permitting

Additional federal, state and local permits will be required for landfill reuse and will include approvals in such areas as wetlands, flood plains, air quality, and coastal zone management. These permits and approvals will have conditions of their approval that will restrict, limit and/or prohibit certain types of landfill reuses and/or designs for reuse. For example, a Section 404 wetlands fill permit issued by the United States Army Corps of Engineers (USACE) may require setbacks or buffers from the landfill due to an adjacent high level ecology. Similarly, a Title V Major Source Air Permit issued by either the USEPA or a qualifying State may require the installation and permanent operation of a flare and/or other control devices to reduce air emissions and the location and operation of these devices will limit the scope of the landfill reuse.

A typical list of required permits and approvals for a landfill reuse is shown in Table 2.

Engineering and Institutional Controls

Closure of a landfill will include both engineering and institutional controls. The engineering and institutional controls provided through the landfill's design and closure will also determine if and how the landfill can be reused. An impact analysis to these two types of controls is a necessary consideration for the sustainable reuse of the selected landfill site.

Engineering controls are structures that have been constructed as per the landfill's construction permit and are required to be maintained during the period of closure and post-closure. These controls typically include the following: leachate collection and treatment; subsurface perimeter barriers; access roads; landfill gas collection, venting, and treatment; stormwater management drains, pipes, swales, and basins, and surface caps; and erosion and sedimentation control systems. Disturbance of the engineering controls triggers regulatory review and will require a written

Landfill Closure and Reuse of Land. Table 2 Typical permits and approvals for landfill site reuse

Permit or approval name	Issuing entity	Regulated aspect
Section 404 permit	US Army Corps of Engineers	Disturbance and/or filling of wetlands or waters of the united states
Section 9 permit	US Coast Guard	Bridge crossings over navigable waters
Landfill closure/post-closure care plan	US Environmental Protection Agency (USEPA)	Approval of plan and /or modifications (if the state has not qualified by USEPA)
NPDES permit	USEPA	Liquid discharges from Landfill including stormwater and leachates (if the State has not qualified by USEPA)
Title V/New source review permit (NSR)	USEPA	Air Emissions from Landfill (if the State has not qualified by USEPA; smaller sites = NSR; larger sites = Title V)
Landfill closure/post-closure care plan	Qualifying state	Approval of plan and/or modifications
Title V/new source review permit	Qualifying state	Air emissions from landfill (smaller sites = NSR; larger sites = Title V)
NPDES permit	Qualifying state	Liquid discharges from landfill including stormwater and leachates
Soil erosion and sediment control certification	Soil Conservation District	Soil erosion
Coastal zone management approval	State	Sites that are located in or will impact coastal areas
Flood plain permits	State	Sites that are located in or will impact regulated flood plains

regulatory consent (i.e., amendment to closure/post-closure care plan, permit modifications or zoning/planning approvals) from the landfill's permitting authority(ies).

Institutional controls are nonstructural, legal documents that control access to the landfill site and/or restrict the future use of the closed landfill site. As per 40CFR 258.60 or similar state requirements, "the owner or operator must record a notation on the deed to the landfill facility property, or some other instrument that is normally examined during title search, and notify the Qualifying State Director that the notation has been recorded and a copy has been placed in the operating record." Typically, the landfill operator will use a form document, provided by the Qualifying State and then submit the completed document to the landfill localities' Registrar of Deeds. A file copy is then submitted back to the Qualifying State.

The deed notation is a perpetual notice to any potential purchaser of the property that the land has been used as a landfill and its use is restricted. The landfill owner or operator also has the option to request permission from the USEPA or Director of the Qualifying State to remove the notation from the deed if all wastes are removed from the Site.

Infrastructure

The lack and/or the need to upgrade available infrastructure such as roads, water, sewer, and electric services will impacts the viability of reuse. Suitable infrastructure will be needed to support the reuse of a landfill site. Roads, sewers, and utilities will be key factors in the reuse planning and design. For example, if an active reuse is proposed, then the condition and viability of local roads will be a critical issue. Is there a connection of these local roads to county, state and federal highways? The location and capacity of storm and sanitary sewers will need to be considered. Will new sewers or extensions to existing sewers be

required? The capacity and availability of treatment facilities for sanitary and other liquid wastes is another key factor and lack of available capacity may otherwise invalidate a potential reuse site.

Economics

Economics will also play a key role in the viability of reuse. The financial assurance provided for both closure and post-closure care will need to be examined in view of the intended reuse. A valuation of the property of an unclosed landfill and for its intended use will need to be completed. A business financial analysis to determine the return on investment and comparison to a reuse on a Greenfield (currently undeveloped) site, where environmental factors are valued higher than economic and sociopolitical factors, will also be needed.

The uniqueness, size and complexity of the landfill reuse will usually cause significant implementation costs. Accurate cost estimates for the purposes of capital budgeting, grant application, and determining project phasing and limits are important. A long-term maintenance program should be established in conjunction with the required post-closure care program. Annual operation and maintenance costs should be developed for consideration of the site use and development.

Full or partial funding of the landfill reuse through state and federal grants should also be factored into the economics analysis. Due to the size, location and regional significance of the site, the landfill may qualify for open space and /or economic development grant funding.

Sustainability Review for Reuse of Landfills

The final step in the process is a review of Sustainability. Sustainability is a process that resolves the conflict between various competing goals and involves the simultaneous pursuit of consensus with economic prosperity, environmental quality and social equity. As coined by the Brundtland Commission, sustainable development is a pattern of resource use that aims to meet human needs, at the same time preserving the environment, with the goal that human needs are met in the present and for future generations.

The Sustainable development review for reuse of landfills is completed in three constituent parts: environmental sustainability, economic sustainability and sociopolitical sustainability. Within the environmental sustainability review, the landfill reuse is viewed against the standard of maintaining a naturally pristine environment and the avoidance of an unsustainable situation where consumption of natural resources exceeds the speed of replenishment. The economic sustainability review measures the landfill's reuse against the added economic value in relation to the landfill's aggregated ecological impacts and resource use. Similar to the environmental sustainability review, the sociopolitical sustainability review examines the relationship between the added value of the landfill reuse and its sociopolitical impacts. Positive and negative sociopolitical impacts of landfill reuse are quantified and measured against the goal of minimizing negative sociopolitical impacts. Based upon the results of this three part review, a determination that the landfill reuse is or is not sustainable development is completed.

For a landfill to be sustainable for reuse it would necessitate that the landfill either be removed or reused in such a way that it would appear that the landfill never existed following its useful life. The most important aspect would be whether or not the landfill is used to dispose of hazardous or nonhazardous wastes. Subtitle C Landfills, where hazardous waste was disposed, would not be sustainable for reuse since current USEPA regulations preclude their use for any other purpose following closure.

Throughout the landfill's useful life, sustainability would require that any resource it produces, like the generation of methane gas or as a source of solid fuel for properly designed energy producing machinery, be utilized to its maximum potential. Following, the depletion of these beneficial byproducts of land filling, any adverse impact upon the environment needs to be eliminated and the site used as it would have been prior to land filling. In this manner the definition of sustainability as "using a resource so that the resource is not depleted or permanently damaged" is preserved.

To preserve the sustainable character of a piece of property used to support a landfill use would require that the landfill's operations, resulting products, and post-closure uses promote favorable environmental, economic, and sociopolitical aspects as it relates to human interaction.

Environmental Aspects Related to Sustainability

Environmental impacts of the proposed use of the site for land filling have the greatest effect upon whether or not it is sustainable. Hazardous materials disposed of throughout the landfill and adverse environmental impacts upon the underlying soil, surrounding air quality and upon the groundwater beneath the site would, by definition, render the use non-sustainable. Therefore, this discussion focuses upon nonhazardous landfills such as municipal solid waste landfills, nonhazardous sludge landfills, and construction and demolition debris landfills.

For landfills constructed prior to the age of environmental awareness and the realization that non engineered landfills have a negative impact upon the environment, their resultant negative environmental impacts may or may not be able to be corrected. These environmental corrections would be required so that the site can be transformed into a sustainable use. Landfills that have severely impacted the various environmental media surrounding the site may require complete excavation, redeposition of waste, and the remediation of underlying soils and groundwater to remove the damage caused by the construction of the landfill that has rendered it non sustainable. Other older types of landfills may be remediated or contained in situ in order to prevent the impacts of future adverse pollution from decomposition and generation of leachate and gases. These measures could include the capping of a closed landfill and other engineering controls to collect and manage produced gases and to minimize and control the introduction of moisture into the landfill thereby minimizing leachate generation. Other measures can include the construction of impermeable barrier walls, with leachate collection systems, to prevent the escape of pollutants already impacting the environment, thereby containing them and collecting them so that they may be treated and rendered inert. Gas collection systems may be constructed to collect gases that are generated by the decomposition of the wastes. The gases can be utilized to run generators to produce energy thereby saving other natural resources for later use. The landfill gases may be cleaned of impurities and placed into natural gas pipelines for use as a heating fuel. The gases can also be destroyed in a controlled manner so that they are not emitted into the atmosphere exacerbating current unacceptable greenhouse warming concerns causing an adverse impact on the environment. These types of landfills require a longer remedial period of time to convert the site back to an environmentally neutral sustainable use.

Landfills that have been developed at present and in recent time are constructed in a controlled manner subject to strict USEPA regulatory mandates outlined in the Code of Federal Regulations under Subtitles C and D discussed elsewhere within this Chapter. Subtitle C regulations apply to hazardous waste landfills and are excluded as a part of this discussion.

These newer landfills have engineered designs that consist of discrete cells with double lined enclosure systems, upper and lower bottom liners, with leachate collection systems, to enable the collection of or recycling of generated leachate. The liner systems contain leak detection measures to alert the operators of a potential breach of the bottom liner enclosure system. The landfills are constructed with intermediate caps during operation to collect generated gases, to minimize external infiltration into the landfill and to control vermin and other vectors. Some bioreactor landfills are equipped such that collected leachate may be recirculated back into the waste mass to enhance the decomposition of the waste allowing decomposition to occur in the least amount of time. This process increases the air space of the landfill and allows more waste volume to be deposited in the landfill over a shorter period of time when compared to bioreactor landfills not subject to recirculation. When waste deposition within a cell is completed capping systems are engineered, designed and constructed to minimize infiltration and collect the gases produced during waste decomposition for beneficial reuse or destruction.

Depending upon the type of landfill that is being closed, the time required for post-closure operation and maintenance will vary. Older landfills will require longer periods of time to utilize and decompose the wastes within its confines due to the restrictions that its original construction design or lack thereof, places upon the use of decomposition enhancing recirculation techniques. Landfills that were designed and engineered using today's more advanced regulation and engineering controls would likely require less post-closure operation and maintenance. Landfills of this type would meet the definition of environmental sustainability.

Economic Aspects Related to Sustainability

The costs related to engineering a landfill so that it can be considered sustainable would ultimately cause the fee to dispose of waste to increase when compared to the tipping fees charged when landfills were unregulated. These initial costs would be necessary to provide funding for closure and post-closure operation and maintenance. Although these costs appear to be significant compared to former costs for disposal, the cost in avoided environmental damages to health, wildlife, and adjoining properties would render this increase insignificant in comparison.

Properly controlled, engineered and constructed landfills will enable a greater volume of waste to be placed within the landfill when compared to older non sustainable landfills. They can also result in the development of sources of renewable resources such as natural gas and solid fuels that can be utilized to produce heat, steam, and electricity. These renewable sources were formerly wasted because they were not collected or utilized for other purposes. The collectable quantity of landfill gas can be enhanced and its production time increased by recycling generated leachate throughout the waste mass. Although the actual amount of gas that the waste can produce is theoretically finite, the length of time required to produce that finite quantity can be reduced significantly in sustainable landfills. The remaining less decomposable solid material within a sustainable landfill may be used to operate resource recovery facilities that can produce electricity and steam. The economic benefits related to these aspects of land filling have increased in recent times due to the rising costs and depletion of our natural resources.

Sustainable landfills can ultimately be transformed into usable land suitable for construction and alternate uses. Recycling of leachate can shorten the time required for complete decomposition of the waste and the ultimate reuse of the site in construction. Once the waste is decomposed its behavior as a structural foundation material can be better determined. A highly decomposed waste reacts to applied stresses in a manner similar to that of natural soils and its behavior under imposed loading can be better predicted. This enables sites to utilize more economical construction means to support required roadways, utilities, sanitary sewer systems, drainage systems, etc., and, in some cases, foundations. The ultimate economic benefit is that the structures cost less to build and result in additional taxable sites.

Sociopolitical Aspects Related to Sustainability

Since sustainable landfills can be reused for many other purposes the affect upon sociopolitical aspects can be enormous. Initially, the control of environmental hazards related to non-sustainable land filling measures, by itself results in a better quality of life for surrounding communities. Air quality and odor concerns would be minimized during operation and would no longer be a concern following closure. Underlying sources of groundwater for potable uses would be preserved. Vermin and unwanted pests would be replaced by desirable forms of wildlife and enhanced wildlife habitats thereby improving the quality of life for nearby residents.

In rural areas and areas in many developing nations where sources of energy are limited or too far away to be utilized, sustainable landfills can provide a renewable source of cheap energy. These areas can benefit by utilizing the gases generated by the decomposition of the wastes to heat their homes, pump their water, improve their sanitation and sanitary waste systems and run their machinery.

Potential Sustainable Reuses

General

This section further examines several post-closure development scenarios that may be considered for possible sustainable reuse. As discussed in the preceding sections, landfill reuse must consider diverse criteria ranging from state and federal landfill regulations, local master plan considerations and zoning ordinances, and state and federal land use permitting issues (e.g., flood plain restrictions, wetlands, threatened and endangered species, and coastal zone management).

The intended reuse must be protective of all engineering controls and not degrade or impact post-closure operations and maintenance requirements. Furthermore, the post-closure redevelopment must satisfy the design, performance, or operational requirements and criteria that are specific to the intended

reuse. The following discussions are intended to highlight some of the major issues that should be considered for several possible sustainable reuses. Detailed studies, constraint evaluations, and engineering analysis are needed to fully quantify whether a candidate sustainable reuse is a viable post-closure redevelopment option.

Energy Generation Considerations

A closed landfill may represent a potential site for sustainable energy generation. In addition to the unique requirements and constraints that are specific to the different technologies, there are factors and considerations which are common to all energy generation technologies. The most common energy generation technologies involve electricity derived using solar, wind, or landfill gas.

Energy generated at a closed landfill may be utilized in several ways. The concept of sustainability is optimized if a long-term power supply is made available to a dedicated end-user. However, several factors must be considered to confirm that this option is technically and economically viable:

- *Infrastructure*: A transmission system is necessary for a customer to utilize energy generated at a landfill. To avoid the cost associated with the design and construction of an extensive power distribution system, the end-user should ideally be located proximate to landfill/energy distribution site. In the event the end-user is located offsite, a more extensive offsite transmission system may be required and at least a portion of the transmission system would be located on-site.
- *Permitting*: In addition to the state and federal permits and approvals associated with the redevelopment of a closed landfill, additional permitting and approvals would be required for the offsite portion of a transmission alignment. These may include the procurement of easements and rights-of-way and environmental permits such as wetlands disturbance.
- *Offsite Distribution*: Consideration should be given to the possibility that the distribution of energy to an offsite end-user may satisfy the definition of a regulated utility which may, in turn, require additional permitting and/or licensing.
- *Operation and Maintenance (O&M)*: Even if the end-user is located on-site, the energy generation and transmission systems will essentially function as localized, dedicated utility. Life cycle O&M of the energy generation and transmission systems will be required.
- *Reliability*: All of the alternate power sources share a common concern regarding reliability. Assuming an end-user requires uninterrupted electricity, back-up measures such as the use of emergency generators or connection to the local utility may be necessary.
- *Economics*: The capital and long-term costs associated with the design, permitting, construction and O&M of the generation and transmission systems must be compared to the costs associated with purchasing power from the local utility.

In the event energy generated at a closed landfill cannot be used by a local, dedicated end-user, the power may be purchased by the local utility. In order to sell power to the local utility, it will be necessary for the alternative energy developer to enter into a power purchase agreement (PPA) with the local utility. The considerations associated with infrastructure, permitting and O&M would also be applicable to this option.

Solar Energy

The generation of energy through the use of photovoltaic (PV) panels is increasingly promoted as a sustainable post-closure landfill redevelopment alternative. Some of the issues to be considered are summarized below:

- *Landfill Orientation*: The functionality of PV panels is optimized when placed in a south-facing orientation. Ideally, the landfill should be oblong with the long axis oriented in the east-west direction.
- *PV Panel Technologies*: The predominant PV panel technology currently in use is crystalline. Crystalline panels are generally considered to be the more efficient with respect to energy generation. Crystalline panels have been in use for several decades. Thin film PV panels have been recently introduced as an alternative to crystalline panels. At present, thin film panels are generally less efficient than

crystalline panels and do not share a demonstrated history of usage and reliability.

- *Panel Support*: Ground-mounted crystalline PV panels are typically supported by a relatively light weight metal frame. Because the foundation should not penetrate through the landfill cover, the metal frame may be supported on concrete ballast pads which are placed on the surface of the landfill cover. The ballast pads must be designed to prevent punching through the cover system while, at the same time, be able to resist uplift forces during periods of high winds. There is less experience regarding the use of thin film panels on landfills. One mounting system uses a backing membrane. The thin film panel is mounted to the backing membrane which, in turn, is bonded to the landfill cover geomembrane. Other mounting systems under consideration involve the use of mats or panels which are, in turn, placed on the landfill surface and secured using anchor trenches.
- *Space Requirement*: Depending on a number of factors, from 3 to 5 acres are required to produce 1 megawatt (MW) of electricity using crystalline panels. The film panels are somewhat less efficient and will therefore require greater available area.
- *Surface Drainage Considerations:* A solar energy system typically covers a significant area; however, the design of landfill mounted PV panels must assure that proper surface water management systems are not adversely impacted. The landfill surface water management components are generally designed for semi-pervious, grassed surfaces. However, because of the surface area required to generate solar energy, the impervious surface area of the landfill can significantly increase. As a result, the surface water management components (e.g., ditches, swales, down chutes, and detention ponds) may need to be redesigned and enlarged to accommodate the higher peak storm flows resulting from the increased impervious surface area. Existing erosion control measures may require modifications to safely accommodate the increased overland run-off velocities.
- *Protection of Existing Features*: Both crystalline and thin film PV panels are area-intensive technologies. The design and construction of solar energy facilities must be protective of existing features and engineering controls including: active and passive landfill gas well, access roads, surface water management systems and groundwater monitoring wells.

Wind Energy

In addition to the use of PV panels, the generation of energy using wind turbines may be a sustainable reuse of closed landfills. Some of the issues to be considered are summarized below:

- *Location*: The wind turbines must be located in an area of reliable wind. Studies are required to confirm that reliable minimum wind velocities and durations can be expected.
- *Space Requirements*: A wind turbine can produce up to 1.5 MW of electricity. However, a wind turbine facility requires a significant land area. The structures are large with rotor diameters up to 250–260 ft and the rotor hub may be located up to 260 ft above the ground. As a planning tool, each wind turbine requires approximately 0.4 acres (wind turbine plus supporting infrastructure) and a spacing of 5–10 turbine diameters is required between adjacent turbines to enable the turbines to operate efficiently.
- *Permitting*: In addition to other required environmental and land use permits and approvals, permitting of a wind turbine facility may require a bird mortality study in the event the landfill is located in a bird migratory path or flyway.
- *Foundations*: The foundation systems needed to support a large wind turbine must resist high shear and moment forces. Landfill materials are relatively loose and weak and cannot be relied upon to provide the necessary support. As a result, it is likely that the foundation loads must be transferred through the landfill mass to underlying competent bearing materials. A pile foundation system is one method of supporting the foundation loads. However, piles would need to penetrate through the bottom of the landfill. This would likely be prohibited if the landfill was constructed with an engineered bottom liner/leachate collection system. If the landfill was not constructed with a bottom liner system, it may be necessary to demonstrate that the use of piles would not result in vertical cross-contamination of the groundwater.

Landfill Gas Energy

Energy generated from the active extraction and combustion of landfill gas (LFG) is a proven technology. The installation and operation of active LFG wells would serve as a major component to control both LFG migration and odors. Factors to consider are discussed below:

- *LFG Generation:* The generation of LFG which can be reasonably extracted for energy production would extend over a finite period of time. As a result of the methanogenic process, peak LFG flows will generally occur after closure and will then decrease exponentially over time. There are several LFG generation models that can be used to estimate the LFG generation curve. Information regarding LFG generation calculation methods can be obtained from the USEPA's Landfill Methane Outreach Program (www.epa.gov/landfill).
- *Energy Utilization:* Two alternatives for the use of the collected LFG would depend on the available local infrastructure. Typically, the collected LFG is used as a fuel for specially designed engines for on-site energy generation. Issues specific to the on-site energy generation have been previously discussed. In the event the appropriate infrastructure is located nearby, it may be possible to remove impurities so that the conditional LFG can be used as low or medium BTU fuel to supplement natural gas.
- *Condensate*: Condensate will form as the relatively warm LFG is cooled in ambient environmental conditions. The condensate resulting from the cooled LFG must be collected, conveyed and managed in a manner compliant with applicable state and federal regulations.
- *Contingencies*: Even properly operated and maintained LFG engines must be taken out of service for repairs and maintenance. As a result, the LFG-to-energy system should incorporate measures to accommodate these contingencies. These measures may include spare LFG engines and/or flares which can be activated when production LFG engines are taken out of service.
- *Other Considerations*: The LFG extraction system would comprise an engineering control measure that would supplement and interact with other engineering controls. The LFG system will require electrical power and control systems; penetrations through the final cover system; monitoring and reporting; and operations and maintenance procedures. The costs associated with these considerations should be considered in the initial planning and design phase.

Post-Closure Development

Reuse of a closed landfill for post-closure vertical development has involved several end-use scenarios. Relatively passive developments have included parks, athletic fields, and golf courses. More aggressive end uses have included entertainment, retail, and residential facilities. Some of the issues to be considered with respect to post-closure development of a landfill are discussed below:

- *Closure Cover*: The post-closure redevelopment can be designed and constructed after the final closure cover is designed, permitted and constructed. Alternatively, the elements of the redevelopment can be incorporated with the final closure system. For example, it may be possible to utilize slabs, pavements, hardscaping and general grading fill as elements of the closure cap. Factors such as the procurement of predevelopment approvals, financing, and other real-estate transaction criteria may dictate that a conventional cover system be designed, permitted, and installed prior to construction of the post-closure redevelopment.
- *Integrity of Engineering Controls*: The post-closure redevelopment must be designed and constructed in a manner that is protective of the necessary engineering controls. Surface water management systems must comply with post-closure design criteria in addition to more restrictive criteria which may be dictated by land use ordinances or state regulations. Control of LFG is critical; the post-closure redevelopment will likely incorporate passive and active LFG systems. In addition, underslab venting systems will likely be required if the redevelopment includes buildings and other occupied (or potentially occupied) spaces. Depending upon applicable regulations, a clean soil cap may be adequate or a more extensive engineered geomembrane system may be required. In the event a geomembrane is necessary,

designs should incorporate appropriate connection and penetration details. In addition, design of the geomembrane system should consider to the stresses that may be imposed by post-closure settlement.

- *Geotechnical Considerations*: Without improvement, landfill materials are relatively loose, weak and unsuitable for support of structures. Landfill materials may contain voids and are subject to decomposition. The placement of grading fill will impose stresses on the landfill mass which will likely result in settlement and the possible presence of voids and/or pockets of very loose materials may result in differential settlements which would adversely impact the final cover system, other engineering controls and the post-closure redevelopment. Dynamic compaction (DC), i.e., impact densification by dropping a large weight on a regular pattern, is one technique used to densify the landfill materials, crush possible voids and loose zones and result in a mass that would have somewhat more predictable settlement characteristics. Even after DC is performed, post-construction settlement should be expected and measures to accommodate settlement should be incorporated in all designs.
- *Foundation Considerations*: Structures may be supported on foundations which transfer building loads through the landfill materials or on shallow foundations bearing on landfill materials which have been improved by DC. Each alternative involves specific risks and considerations. The use of pile foundations has been previously discussed (see Wind Energy). Even if structures are pile-supported, differential settlements relative to the adjacent grades are likely as the landfill materials settle under the weight of new fill. As a result, DC may be required outside of pile-supported building footprints to reduce the potential for sharp differential settlements. In addition, if the landfill is underlain by soft compressible natural soils, it may be necessary to supplement the DC program by implementing a surcharge program to pre-compress the natural soils. Even after the ground improvement program is implemented, designs should incorporate flexible couplings and utilities and other settlement-tolerant measures. It may be possible to support lightly loaded, settlement-tolerant framed structures on conventional spread footings after a comprehensive ground improvement program is implemented. However, designs based on the use of spread footing foundations should not be considered unless it is understood that the risk of settlement can be reduced but not eliminated.

Conclusion

After they have reached their design capacity, landfills often represent an under-utilized resource that can be redeveloped with a sustainable reuse. The selection of the most appropriate post-closure reuse will be controlled by a suite of diverse factors ranging from economics, local market demands, and available infrastructure. All landfill reuse designs should ensure that engineering controls are not adversely impacted while, at the same time, recognizing that landfill materials are not similar to competent natural soils and even if ground improvement measures are properly implemented, the risk of post-closure settlement is not eliminated.

Future Directions

Sustainable development is a unique and evolving concept. Sustainable landfill reuse is a new approach to the old planning technique of adaptive reuse. As sustainable landfill reuse projects are developed, new methods of measuring sustainability will be created. The sustainable development mantra requires current and future generations to use a systems approach to growth and development and to manage the natural, economic, and social aspects of projects. Landfill reuse will be one of the areas where this approach can be successfully implemented.

Bibliography

1. Sustainable development, Wikipedia, the free encyclopedia, http://en.wikipedia.org/wiki/Sustainable_development. Accessed Jan 2010
2. United Nations (1987) Report of the world commission on environment and development (Brundtland Commission), General Assembly Resolution 42/187, 11 Dec 1987
3. 40CFR Part 258, United States Environmental Protection Agency, revised through Nov 1996
4. Solid waste landfill guidance, Section 11: Closure and post-closure, State of Ohio, Ohio Environmental Protection Agency

5. 40CFR Part 264, United States Environmental Protection Agency, revised through July 2006
6. Meegoda JN, Hsieh HN, Borgaonkar A, El Haggar S, Hettiaratchi P, Stressel RI (2007) Towards the development of sustainable landfills. In: 22nd international conference on solid waste technology and management, Philadelphia, 18–21 Mar 2007
7. Hettiaratchi JPA, Perera MDN, Davies D, Hundal J, VanEverdingen D (2006) an innovative technique for ensuring sustainability of landfills: the sustainable biocell technology. In: 21st international conference on solid waste technology and management, Philadelphia, 26–29 Mar 2006
8. Zeiss C, Moore JC (2007) Sustainable landfill operation and care with passive systems and renewable energy. In: Proceedings of 12th SWANA landfill conference, San Diego, June 2007
9. Ezeah C, Roberts CL, Watkin DG, Phillips PS, Odunfa A (2009) Analysis of barriers affecting the adoption of a sustainable municipal solid waste management system in Nigeria. In: 24th international conference on solid waste technology and management, Widener University, Philadelphia, 15–18 Mar 2009
10. Atudorei A, Atudorei LG, Dumitru E, Rusu V (2009) Technical, economical and social solutions for sustainable waste management systems in Rural areas in Romania. In: 24th international conference on solid waste technology and management, Widener University, Philadelphia, 15–18 Mar 2009
11. Bates M, Phillips P, Nwigwe A, Mbeng L, Montasser W, Fairweather R (2009) Driving sustainable waste management: tools for waste management facilities in the midland of England. In: 24th international conference on solid waste technology and management, Widener University, Philadelphia, 15–18 Mar 2009
12. Clarke M (2009) Zero waste and New York's climate footprint. In: 24th annual solid waste technology and management conference, Philadelphia, 16–18 Mar 2009
13. Erses S, Onay TT (2007) The evaluation of the municipal solid waste degradation performance in semi-aerobic landfills. In: Proceedings of the 22nd international conference on solid waste technology and management, Widener University, Philadelphia, 18–21 Mar 2007
14. Morris J, Phillips P (2007) A landfill tax credit scheme funding success: East sussex waste minimisation programme. In: Proceedings of the 22nd international conference on solid waste technology and management, Widener University, Philadelphia, 18–21 Mar 2007
15. Munoz Q, Fischer (2007) A vision of the brand new program on sanitary landfill in Mexico city and its advances. In: Proceedings of 22nd international conference on solid waste technology and management, Philadelphia, 18–21 Mar 2007
16. Kissida JE, Spieler RJ (2009) Case studies in successful landfill reuse
17. N.J.A.C. 7:26-2A, Additional, specific disposal regulations for sanitary landfills, New Jersey Department of Environmental Protection, revised through Feb 2009

Landfill Leachate Control

Haluk Akgün[1], Jaak J. K. Daemen[2]
[1]Department of Geological Engineering, Middle East Technical University (METU), Ankara, Turkey
[2]Department of Mining Engineering, University of Nevada, Reno, NV, USA

Article Outline

Glossary
Definition of the Subject
Introduction
Landfill Liners
Landfill Covers
Landfill Runoff/Infiltration Control
Landfill Leachate Monitoring
Landfill Leachate Treatment
Landfill Leachate Disposal
Landfill Post-closure Control
Future Directions
Acknowledgments
Bibliography

Glossary

Compacted clay liner (CCL) A barrier lining system used in landfills constructed primarily from compacted natural soil materials that are rich in clay, although the liner may contain processed materials such as bentonite.

Cover A multilayer barrier installed on top of the waste emplaced in a landfill, designed, planned, and constructed to control inflow of water, e.g., rain or snowmelt, into the waste to minimize the risk of disturbance by humans, animals, and plant roots, to control erosion, and to improve visual impact, i.e., human perception, of the facility.

Geocomposites A manufactured material used for drainage layers in landfills, which consists of a geonet sandwiched between one or two layers of nonwoven geotextiles.

Geomembranes or flexible membrane liners (FML) An essentially impermeable synthetic membrane used as barrier layers in landfills.

Geonets A net-like polymeric material formed from intersecting ribs joined at the junctions, which is used as drainage layers in landfills.

Geosynthetic clay liners (GCL) Subset of geosynthetics used as barrier layers in landfills consisting of rolls of fabricated thin layers of bentonite clay sandwiched between two geotextiles or bonded to a geomembrane.

Geosynthetics The generic term used for all of the synthetic materials used as barrier and drainage layers in landfills that include geomembranes, geosynthetic clay liners, geonets, geotextiles, and geocomposites.

Geotextiles Woven or nonwoven fabrics made from polymeric fibers generally used as a filter material for drainage layers in landfills.

Hazardous waste A waste with chemical and physical diversity, environmental persistence, and acute and chronic detrimental effects on human, plant, and animal health that is disposed of in landfills utilizing an extension of sanitary landfill technology using very conservative design criteria.

Leachate A potentially foul-smelling liquid, dirty water emanating from landfills, brownish, reddish, sometimes rust-colored acidic or basic water that may be loaded with a wide variety of contaminants, unless carefully and adequately controlled.

Lining A barrier between the void in which landfill waste is emplaced and the underlying soil on which the landfill is constructed. Designed and constructed to reduce any leachate outflow into the underlying soil or rock to an acceptable level.

Municipal solid waste (MSW) Garbage, trash, rubbish; waste collected from private citizens, households, possibly small businesses. Consists of food, food scraps, food leftovers, paper, plastics, textiles, cardboard, etc. Ideally, preferably, should not contain waste classified as hazardous. Ideally, preferably, should not contain recyclables, or not too many of them. Depending on local practices may or may not contain compostable organics, such as grass, plant, and tree cuttings. May contain batteries, paint thinner, nail polish, etc.

Mixed waste (MW) Contains both radioactive and chemically hazardous waste. In the USA, the radioactive waste component is regulated by the US NRC (Nuclear Regulatory Commission), the other hazardous waste by the US EPA (Environmental Protection Agency).

Natural attenuation The decrease in contamination that takes place over time naturally, i.e., without human intervention or interaction, as a result of reactions that take place naturally within landfills. Too slow, and too incomplete, to provide an adequate control method by itself, in most cases.

Nonvolatile dissolved organic carbon (NVDOC) Organic contaminants dissolved in the leachate.

Volatile organic compounds (VOC) Organic compounds that are likely to evaporate under typical landfill conditions, e.g., temperature and pressure. May include, e.g., gasoline, paint thinner, etc. Some are likely to be toxic or carcinogenic.

Definition of the Subject

Leachate refers to the liquid, contaminated water, that results from the interaction between any water in a landfill, e.g., as the result of rainwater infiltration, and the waste emplaced in the landfill. Leachate constitutes one of the major environmental and health risks associated with landfills. Typically, virtually always, leachate is a very complex liquid, with a wide variety of contaminants, many of which may be harmful to people and to the environment. As the waste and the landfill age, i.e., as reactions take place between the waste emplaced and any water within or percolating through a landfill, the composition changes, and hence the leachate composition changes. This further complicates controlling effluents emanating from landfills. Leachate control, i.e., preventing unacceptable damage to people and to the environment is a critical aspect of the design, planning, construction, operation, and closure of landfills. It also is a major challenge for landfill operators, owners, users, and regulators.

Because leachate contamination results from the interaction between waste and water, one line of control is to manage the types of wastes emplaced. A second line of control is to control water inflow and outflow. A third control approach is to operate the landfill in a mode that minimizes the formation of potentially damaging products, and optimizes the probability of enhancing reactions and interactions that reduce the detrimental aspects of leachate composition. Given the complexity of the problem, e.g., the

variety of waste products that may be emplaced, and the variety of operating conditions (e.g., in terms of water content, water flow, temperature), it is not surprising that landfills continue to pose serious challenges, and that leachate control is a difficult target to reach.

Waste input management is accomplished in part by specifying what type of waste can be accepted by landfill operators. In the USA, e.g., a clear distinction is made between landfills that are permitted to accept hazardous waste and landfills that can accept municipal solid waste only. Although conceptually and in principle this might be considered to be a simple and straightforward distinction, in practice it remains fraught with uncertainties. As a most obvious example, it will be understood that it is relatively easy for some types of potentially hazardous materials to become intermixed with municipal waste, whether intentionally or unintentionally, and it is essentially impossible for the operator to check the waste emplaced in a landfill in full detail.

A sea shift of massive proportions with an enormous impact occurred in the 1970s, when the extensive environmental impacts of the up to that time exceedingly casual approach to waste disposal finally became recognized. As a result of the extensive regulations introduced since that time, landfill design, planning, operations, and closure have become an exceedingly sophisticated endeavor, aimed at protecting the public and the environment from the potentially harmful effects of uncontrolled landfill operations, and in particular of uncontrolled leachate formation and releases. In parallel with the regulatory and operational improvement in practices has been the development of major research efforts, aimed at improving the understanding of what actually happens in landfills, and of how the control of leachate in particular can be improved. This ongoing and continuing research has resulted in a vast literature dealing with virtually every conceivable aspect of leachate control.

While it is true that in most advanced societies rigorous rules and regulations have been emplaced in order to control landfill leachate, it is equally true that this frequently is not the case in many less-developed societies, where landfill leachate control frequently is not yet perceived as a high priority. Hence environmental and potential health impacts of landfill operations in many parts of the world can be considered as being more of the open dump–type operations common in most of the world until about 50–70 years ago, i.e., casual dumping in holes in the ground, or even on the surface, with minimal attention paid to any potential health or environmental hazards associated with the waste emplacement.

Introduction

Controlling leachate is an essential yet difficult-to-achieve objective of landfill design, construction, operations, control, and regulations. In relatively wet climates leachate is unavoidably associated with landfills. In arid climates, the amount of leachate may be minor, inconsequential, and of little concern. In semi-arid climates, leachate may develop on an intermittent basis, e.g., seasonably, following periods of intense rainfall or snowmelt.

The composition of the leachate, which largely results from the interactions between water and the waste emplaced in the landfill, will be affected significantly by the waste with which the water comes in contact and with which it interacts. "Leachate may be composed of liquids that originate from a number of sources, including precipitation, groundwater, consolidation, initial moisture storage, and reactions associated with decomposition of waste materials. The chemical quality of leachate varies as a function of a number of factors, including the quantity produced, the original nature of the buried waste materials, and the various chemical and biochemical reactions that may occur as the waste materials decompose [1, 2]." Hence a primary consideration in determining leachate composition will be the determination of the waste inventory and its characteristics. This will notably include the physical, chemical, and biological composition of the waste.

Methods used to maintain an adequate control over the leachate include first and foremost landfill design, construction, and operations. Site selection will be a first major step in providing assurance that leachate discharges can be controlled, and that their impact on the environment, e.g., on groundwater and on surface waters will remain within acceptable limits. Landfill designers will pay particular attention to liners and covers (Fig. 1). These will control the influx into the

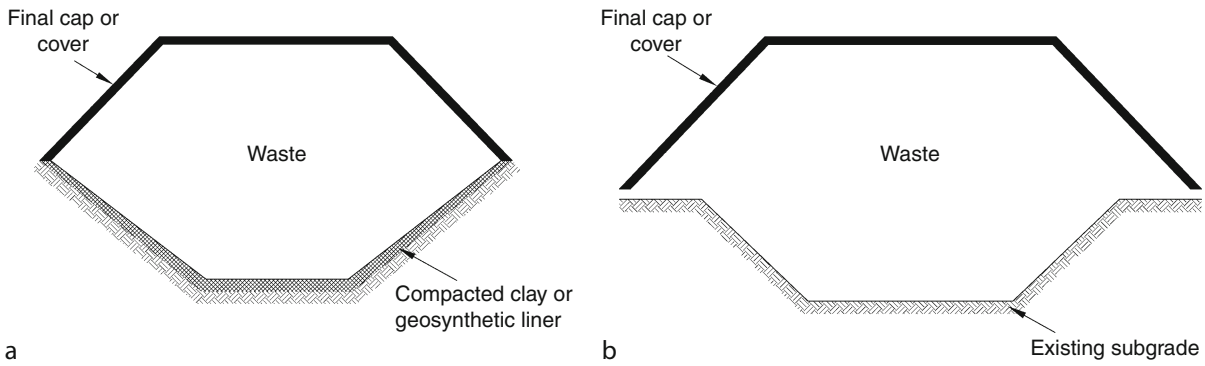

Landfill Leachate Control. Figure 1
(**a**) Waste emplaced in landfill with bottom liner and cover (Modified from Ref. [16], Fig. 6-2, p. 326); (**b**) waste emplaced in landfill installed directly on in situ ground, protected by cover (Modified from Ref. [16], Fig. 6-1, p. 325)

landfill and the outflow from the landfill. Because waste composition is such an important aspect of leachate characteristics, the extent to which waste composition can be controlled will certainly be a significant factor in leachate development, and would be one of the prime modes of control. Waste input control frequently poses difficult challenges.

Liners may be constructed of compacted soil, of soil amended with additives, e.g., clay, to reduce the permeability of the liner, or with geosynthetics such as geomembranes and geosynthetic clay liners. A number of standard, recommended, and widely used designs are available. Design differences are explainable in part based on the performance requirements of a particular liner for a particular application. These performance requirements in turn will depend on a number of variables, notably on the leachate characteristics, on the climate (especially rainfall and temperature ranges), on the topography of the location of the landfill, and on the proximity to the groundwater table and to any surface waters.

Covers control influx into the landfill. Cover design will depend to some extent on the climatic conditions at the site, with somewhat different approaches possible in arid or semi-arid climates as compared to wet ones. The usual classical approach to cover design will emphasize the objective of minimizing water inflow into the landfill. A significant aspect of cover design and construction will be the control of runoff and of infiltration.

Leachate monitoring is a desirable integral part of landfill operations. This includes volumetric control (flow) and quality control (chemical composition, sediment load, etc.). Leachate treatment is extremely helpful in reducing potential harmful impacts of landfill operations.

While it is likely that over time, for many situations, leachate control requirements will decrease as interactions between waste and water slow down, and effluent quality improves, it nevertheless must be assured that post-closure controls, preferably passive only, if at all possible, should be sufficient to assure that no unacceptable detrimental environmental impacts will develop.

The European Council Directive on Landfill classifies landfills into three categories: landfills for hazardous waste, landfills for nonhazardous waste, and landfills for inert waste [3]. Very similarly, roughly parallel, is the US Environmental Protection Agency's classification of landfills into industrial waste landfills, construction and demolition debris landfills, and municipal solid waste landfills (e.g., [4]). The Environmental Protection Authority of New South Wales, Australia, classifies waste in six classes: special waste (clinical and related, asbestos, tires), liquid waste, hazardous waste, restricted solid waste, and putrescible or nonputrescible solid waste [5]. Clearly, whatever classification might be used, broad categories of waste types exist and are recognized. Equally obvious, the leachate resulting from emplacing various waste types in landfills will be very different and will have very different

health and environmental impact implications. As a result, it is clear that correspondingly different regulatory requirements will be imposed on all aspects of landfill planning, design, operation, and closure, and notably on leachate treatment and management.

A critical initial step for leachate control in new landfills is site selection. Geology, hydrology, hydrogeology, geomorphology, and geochemistry are among the topics to be considered when selecting a site for consideration for the location of a future landfill. In principle it would be desirable to consider climate as well, but presumably in general climate variations among potential nearby sites will be fairly minor, unless options are available such as leeside of hills and mountains and consequent significant differences in rainfall, snowfall, wind, and temperature that might provide a basis for preferential location, assuming that the local microclimates are known sufficiently well.

Knowledge of the regional and local geology will be exceedingly helpful in identifying sites that would be attractive for landfill location vs. sites that would be singularly unattractive. It certainly is preferable to consider sites with simple, well-understood geology as compared to sites with complex, especially grossly disturbed geology. Of particular interest will be the hydrology and hydrogeology of the site, in a broad sense: What are surface and underground water flow patterns? Is the surface topography such that any rainfall or snowmelts is likely to result in inflow into a potential landfill? Will extensive, hence expensive, engineering measures be required to minimize such inflows (e.g., diversion ditches, trenches, or berms)? If so, will there be a post closure maintenance requirement for such engineered structures?

Groundwater flow most commonly will be the dominant concern for landfill site selection. At what depth is the water table? What is the flow pattern at the site? What is the flow rate? Head (water pressure)? Will major engineered structures be required to reduce water inflow to an acceptable level (e.g., impermeable barriers installed in trenches upstream of the landfill, grout curtains, formed by injecting grout into the upstream geological formations in order to reduce water inflow into the landfill to an acceptable level)? While such approaches are technologically feasible, they are expensive, and they raise questions with regard to durability, longevity: will they require long-term inspection, monitoring, and maintenance? If so, how extensive, intensive? Who will have the responsibility for these activities?

The first step in a geological/geotechnical site characterization will consist of collecting, collating, and analyzing all available information about the site being considered. This will start from the regional geology, which, in many parts of the world is known sufficiently well to allow an initial assessment as to whether or not a particular location appears promising from a general geological and geotechnical point of view. The next step in what virtually always will be an iterative approach to site characterization may consist of initial onsite geological mapping, and study of aerial photography and remote sensing data that are available. If, on the basis of this initial office and preliminary field work, it is concluded that further investigation is warranted, the site investigation will proceed to a first phase of intense field work.

Detailed geological mapping is likely to be the first step in a comprehensive site characterization, followed by detailed geophysical surveys. A variety of geophysical methods can be used, in order to improve the understanding of the lithological formation configuration at the site and, in particular, to gain an improved understanding of the distribution of geological formations that will facilitate water flows (aquifers) and formations that will impede water flow (aquitards). Geophysical surveys will provide initial information about soil and rock properties important for water flow such as density, porosity, and water table depth. They will provide information about the continuity and uniformity of the host formation, about the depth to bedrock, and bedrock topography, and about major geological disturbances that might affect the containment functionality of the site.

Once a comprehensive understanding of the site geology has been obtained, it is desirable to determine physical characteristics of the host formations. Superficially, this can be accomplished with trenching or the excavation of test sample pits. Sampling to greater depth most likely will require drilling, or, if dealing with relatively weak and soft soils, by driving sampling tubes into the ground. Around this time it also would be desirable to start collecting initial groundwater samples in order to establish a base line of the groundwater composition prior to any landfill construction

disturbance. Similarly, at this time it would be highly desirable to install monitoring wells, as these will allow the determination of a much more precise and reliable understanding of local groundwater flow patterns and rates. It is highly probable that any such wells initially will be used to conduct hydrological site characterization testing including, e.g., pumping and injection tests. Such tests will provide large-scale information about the main parameters that will influence subsurface water flow such as hydraulic conductivity, aquifer transmissivity, piezometric head, and hydraulic gradient. Knowledge of these parameters, combined with the understanding of the geology of the site, will make it possible to numerically model subsurface flow paths, patterns, and intensity, e.g., volumetric flow rates. Such models will assist in estimating what the potential consequences might be of leachate breaching the containment liners.

At sites where the water table is well below the planned bottom of the proposed landfill, it would be highly desirable to also characterize the vadose zone, i.e., the ground in between the landfill bottom and the water table, where the pore space is not fully filled with water. In these situations, it is this unsaturated zone that would be the first recipient of any leaking leachate. Therefore it is highly desirable to understand what the consequences might be of any leakage into this zone. Fluid flow, and even more contaminant flow, and dispersion in soil or rock where pores are filled with water only partially remains a difficult topic, probably at the edge of the current state of the art, and most certainly in need of more research and development.

The geological host formations on which an eventual landfill will be constructed can form a major last line of defense against any contamination by leachate, e.g., in a situation where all engineered components (liners and covers) have failed. Hence, it is highly desirable, if not always possible, to select sites where the host formations can be as effective as possible as natural barriers.

Landfill Liners

A major concern about landfill leachate is that it might affect groundwater and soil, and on some occasions, surface waters. The first line of defense against leachate contamination of groundwater is by installing liners prior to waste emplacement, in order to form a barrier and minimize the risk that leachate might escape the landfill and contaminate nearby soil, ground water, or surface water.

A wide variety of liners, liner systems and liner designs are available. A lining system consists of barrier and drainage layers where compacted clay liners (CCL) or geosynthetics such as geomembranes, geosynthetic clay liners (GCL), and/or a combination of these may be used as barriers for the containment of liquids, sludges, and leachate generating solids. Compacted clay liners are constructed primarily from compacted natural soil materials that are rich in clay, although the liners may contain processed materials such as bentonite. Compacted clay liners are compacted in lifts of 150 mm up to total liner thicknesses generally ranging from 0.6 to 0.9 m up to as much as 3 m. US EPA requires that compacted clay liners have a hydraulic conductivity equal to or less than 1×10^{-9} m/s (e.g., [6–8]). Geomembranes or flexible membrane liners (FML) are essentially impermeable, relatively thin sheets of polymeric materials composed of semi-crystalline thermoplastics such as high-density polyethylene (HDPE), linear low-density polyethylene (LLDPE), very-low-density polyethylene (VLDPE), and flexible polypropylene (FPP); thermoplastics such as polyvinyl chloride (PVC); and thermoplastic elastomers such as chlorosulfonated polyethylene (CSPE). The thickness of geomembranes ranges from 0.75 to 3 mm (30–120 mil) [9]. A geosynthetic clay liner (GCL) is a relatively thin layer of processed clay (typically bentonite) either bonded to a geomembrane or fixed between two sheets of geotextile where a geotextile is a woven or nonwoven polymeric fiber that is less impervious to liquid than a geomembrane, but more resistant to penetration damage. In GCL configurations using a geomembrane, the clay is affixed using an adhesive whereas in GCL configurations consisting of geotextiles, adhesives, stitchbonding, needlepunching, or a combination of the three are used. The main advantages of GCLs are the allocation of more landfill airspace for waste disposal since GCLs are not as thick as a liner system involving the use of compacted clay [10] and the relatively low hydraulic conductivities of most sodium bentonite GCLs that lie in the range of 1×10^{-11} to 5×10^{-11} m/s [9]. Granular material or geosynthetics such as geonets, geotextiles,

and geocomposites may be used for the landfill drainage layers. Granular materials used for drainage layers are sand and gravel where sand is generally used as a filter material and gravel is used as the drainage material. Geonets are net-like polymeric materials formed from intersecting ribs joined at the junctions that meet in-plane flow rate regulations. Geocomposites consist of a geonet sandwiched between one or two layers of nonwoven geotextiles (e.g., [6–9]).

The primary objective of these lining systems is waste containment in the form of low permeability soil ponds, surface impoundments, municipal solid waste, and hazardous waste landfills. Disciplines such as geotechnical engineering and polymer science are utilized in the design of these lining systems. Various types of lining systems with six variations are illustrated by Fig. 2. These six variations fall into two main groups: single liners and double liners. A double lining system is created with the addition of a second liner. It consists of two liners and an intermediate drainage layer. This intermediate drainage layer is depicted as a granular soil but in fact can be comprised of a variety of drainage media, including geosynthetic materials such as geonets or geocomposites in addition to granular soils. The primary feature of the double liner (Fig. 2d–f) is the intermediate leakage detection and removal layer or the secondary leachate collection system, which allows the detection of any leakage through the top liner before that leakage has exited the overall lining system. With a single liner (Fig. 2a–c), leakage detection is only possible outside of the lining system, in which case the containment objective has been violated (e.g., [11, 12]).

Any of the six lining configurations shown in Fig. 2 may also contain leachate collection systems or primary leachate collection systems above the topmost (primary) liners. The leachate collection systems may be either comprised of granular soils, i.e., a sand drainage and protective layer; or geosynthetic materials, i.e., a geotextile filter layer sandwiched between an underlying geonet drainage layer and an overlying sand protective layer. The leachate collection system removes leachate to a sump through some form of collection system in order to reduce the leachate head.

The single liner has all but disappeared as a viable option for the containment of liquids and wastes in the USA, not because of any particular shortcoming on the part of clay-only or geomembrane-only liners, but

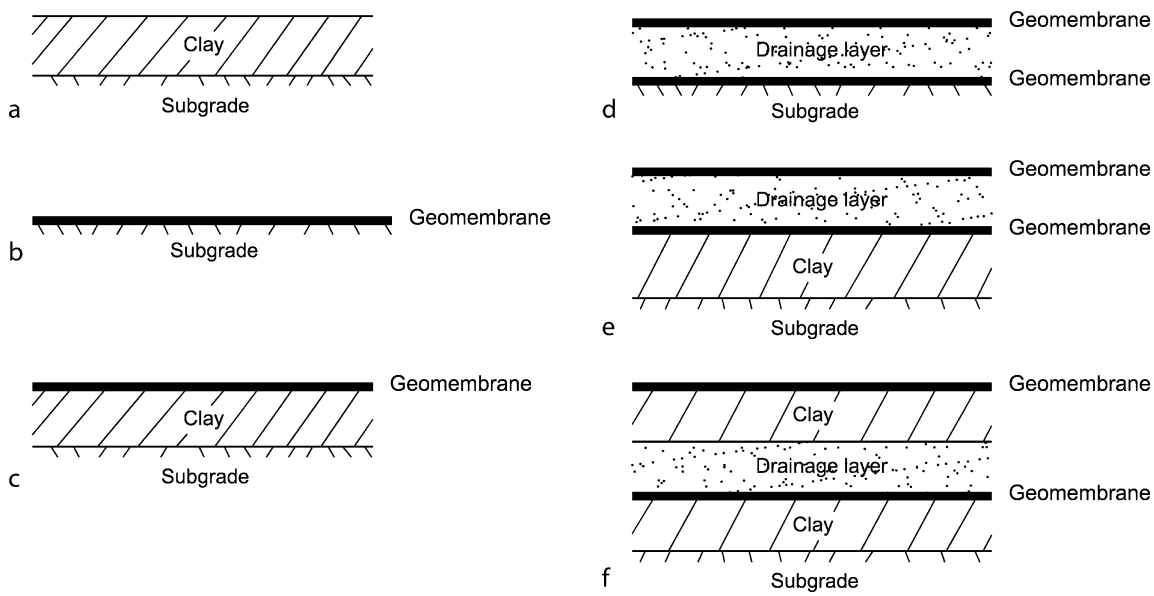

Landfill Leachate Control. Figure 2

Types of lining systems: (**a**) single compacted clay liner; (**b**) single geomembrane liner; (**c**) single composite liner; (**d**) double geomembrane liner; (**e**) double liner with geomembrane top liner and composite bottom liner; and (**f**) double composite liner with composite top and bottom liners (Modified from Ref. [11], Fig. 1, p. 138)

because it has been clearly demonstrated through considerable research, primarily in the USA (e.g., by [13–15]) and as quoted by [9] that a composite liner composed of both geomembrane and compacted clay performs in a superior manner to either alone. Double composite liners with both primary and secondary leachate collection systems have been widely adopted in solid waste landfills in the USA.

Figure 3 presents a section through a typical double-lined landfill composed of a geomembrane top

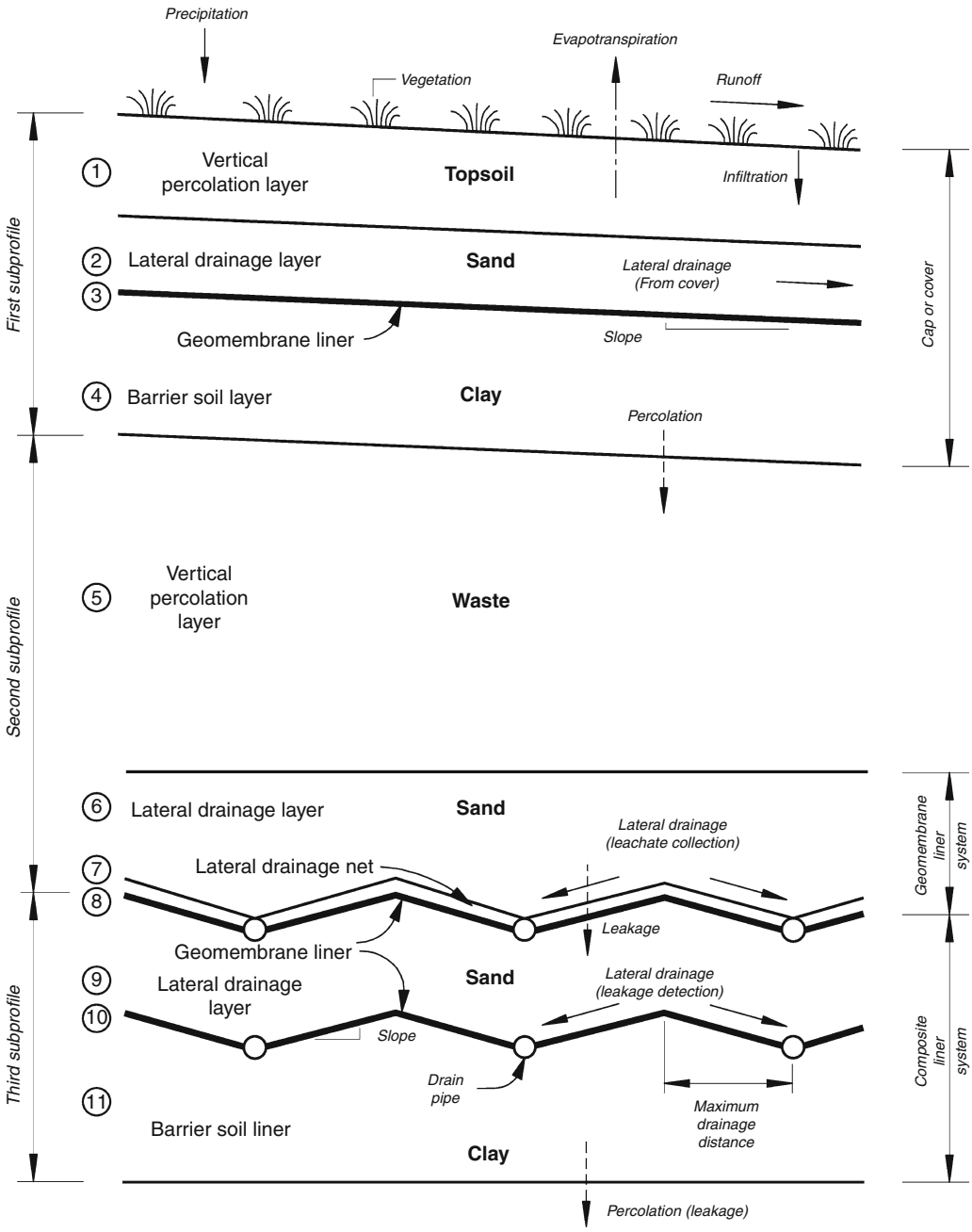

Landfill Leachate Control. Figure 3
Section of a double lined landfill profile (From Ref. [1], Fig. 1, p. 7)

liner and composite bottom liner. The profile is made up of three subprofiles containing a total of 11 layers. Immediately above the bottom (secondary) geomembrane/clay composite liner is the secondary (bottom) leakage detection and drainage layer to collect leakage from the primary geomembrane liner. Above the primary liner is the primary (top) leachate collection layer that is composed of a geosynthetic drainage net (geonet) and a sand layer that serve as drainage layers for leachate collection. The sand drain layers are typically at least 0.305 m (1 ft) thick and have suitably spaced, perforated or open joint drain pipes embedded below the surface of the liner. The leachate collection drainage layer serves to collect any leachate that may percolate through the waste layers in an attempt to avoid significant buildup of the leachate head and to limit the leakage. The liners are sloped to prevent ponding by encouraging leachate to flow toward the drains. The primary goal is to minimize the volume of the leachate that might percolate through the primary (top) liner and to virtually prevent any migration of leachate through the secondary (bottom) composite liner that would eventually be directed to the natural formations below and might lead to violating the containment objective. The first subprofile (topmost part) of the landfill consists of a cap or cover system. At the base of the cap is a drainage layer underneath which a composite liner system is installed similar to the secondary (bottom) lining system used at the base of the landfill. The top of the barrier soil layer is graded so that water percolating into the lateral drainage layer will be diverted toward some kind of removal system (drain or sump). A layer of soil suitable for vegetative growth is placed above the lateral drainage layer to complete the cap system [1, 2].

The US Environmental Protection Agency (US EPA) requires composite lining systems (both clay and geosynthetic) with leachate collection for municipal solid waste landfills (RCRA Subtitle D, 40 CFR §258.40(a) [2]) or equivalent performance (40 CFR §258.40(a) [1]), and double composite liners with leachate collection and detection systems for all hazardous waste landfills (RCRA Subtitle C, 40 CFR § 264.301). Some individual states in the USA require double composite liner systems for municipal solid waste landfills as well (e.g., 6NYCRR Part 360 and Michigan NREPA Part 115 as referenced by [9]). A typical double composite lining system (Fig. 2f) from bottom to top consists of a 0.6 m thick compacted secondary (bottom) clay liner (or an alternative liner that can be equivalent to a 0.6 m thick compacted clay liner), followed by a secondary (bottom) geomembrane liner, secondary (bottom) leachate collection (or leak detection) layer, a minimum 0.6 m thick primary (top) compacted clay liner (or geosynthetic clay liner that can be equivalent to a 0.6 m compacted clay liner), a primary (top) geomembrane liner, and a primary (top) leachate collection system. This succession is overlain by a 0.6 m thick protective sand blanket. The leachate collection system consists of a layer of synthetic geonet and geotextile. The former provides good in-plane drainage conveyance and the latter good cross-plane drainage together with the ability to exclude (filter out) fines. The geomembrane must be at least 1.5 mm (60 mil) thick if made from high-density polyethylene (HDPE), or 0.75 mm (30 mil) thick if made from other resins. The permeability of the subbase and of the compacted clay liner must not exceed 1.0×10^{-9} m/s [9].

Landfill Covers

A major reason for the development of landfill leachate is the interaction between water and emplaced waste. A first line of defense against such interactions is the installation of covers that will minimize the inflow of water into the emplaced waste. A variety of cover methods are available, and a variety of cover design approaches. Cover design will depend significantly on the local climate, and will be different for landfills in wet, dry (arid), or intermediate (semi-arid) environments.

Operational covers, typically emplaced daily, and final closing covers installed at the end of the life of the landfill are distinguished. Daily soil covers are placed in relatively thin lifts and compacted daily to hide the wastes in an attempt to limit the access of nuisance insects and to prevent as much as possible spreading of any potential disease from the landfill.

Figure 4 presents an alternative landfill final cap/cover system composed of seven typical layers, namely, a vegetation/soil top layer, biotic barrier layer, filter layer, drainage layer, barrier layer, gas collection/venting layer, and foundation layer. The vegetation/soil

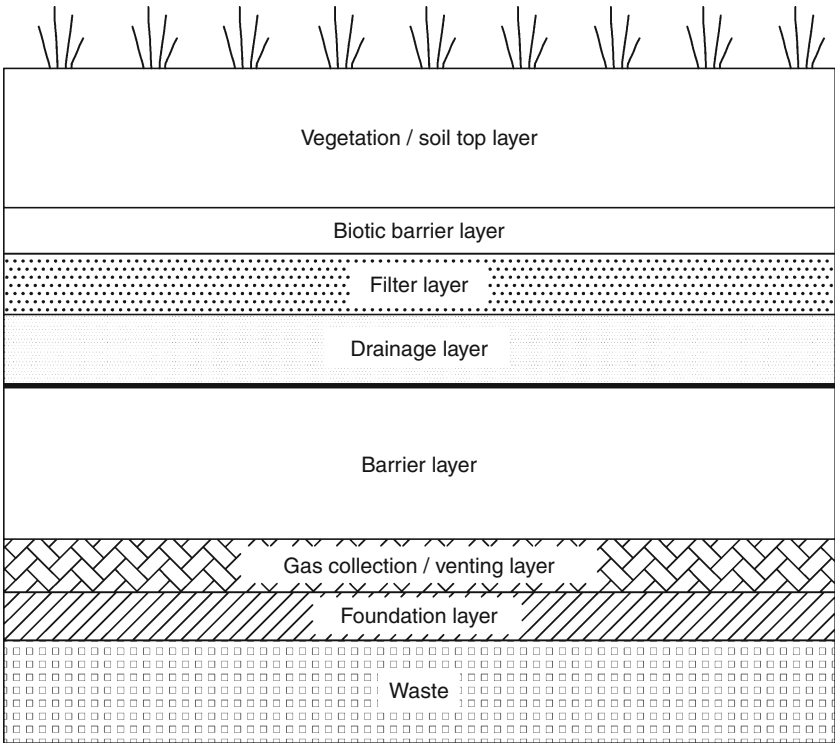

Landfill Leachate Control. Figure 4
Alternative landfill final cover/cap system (Modified from Ref. [16], Fig. 6-6, p. 334)

top or erosion layer consists of fertile topsoil suitable for vegetation growth to minimize erosion and to promote evapotranspiration. The main purpose of the vegetation/soil top layer is to store infiltrated water until it is later removed by evapotranspiration. The biotic barrier layer placed below the vegetation/soil top layer consists of cobbles to form a barrier against plant roots and burrowing animals. A filter layer composed of geotextiles may be placed between the biotic barrier layer and drainage layer to minimize clogging of the drainage layer by soil particles. The drainage layer placed below the protective layer mainly serves to reduce the water head acting on the barrier liner to reduce infiltration and most importantly, to reduce pore pressures in the cover soil to improve slope stability of the final cover. Granular material such as sand or gravel or geosynthetics such as geonets and geocomposites are generally utilized for the drainage layer. It should be noted that a drainage layer may not be needed for a final cover system located in an arid region. The barrier layer, generally consisting of a geomembrane/compacted clay composite liner or a geosynthetic clay liner (GCL), as an alternative to the compacted clay liner, minimizes percolation of water from the overlying cover system and prevents landfill gases from escaping into the atmosphere and causing air pollution. The gas collection/venting layer constructed of granular material (i.e., sand, gravel) or geosynthetics (i.e., geonet, geocomposite, geotextile) serves to collect gasses originating from the decomposition of the waste or volatile organics released from the waste. The foundation layer is generally the interim soil cover that has been placed on the waste and possibly subjected to some additional compaction which supports the final landfill cover. The gas collection layer and the foundation layer may be combined to form a single layer if the gas collection layer is made up of sand [7, 16]. Chapter entitled "► Landfill Closure and Reuse of Land" provides additional information on landfill final covers.

Landfill Runoff/Infiltration Control

A primary method of minimizing the formation of leachate is to minimize water inflow into a landfill. A major method for achieving this objective is to install covers that will minimize infiltration, and that will in part divert some precipitation in the form of runoff. Runoff is promoted but controlled to prevent excessive erosion of the landfill cap. Section "Landfill Covers" above and chapter "► Landfill Closure and Reuse of Land" provide information on infiltration control through landfill final covers.

A good procedure for promoting surface runoff and for controlling erosion is to maintain cap/cover slopes at 2–5% and to increase the slope gradually toward the sides of the cover (e.g., as can be observed in Fig. 1). For long, uniform slopes steeper than 5%, runoff diversion in the form of benches excavated at right angles to the slope which intercept the sheet flow may need to be constructed to control erosion along the cover system. The accumulated flow along the benches may be directed toward down chutes which convey the flow to lower benches or away from the cover. The spacing of the benches and down chutes should be based on climate and local factors and should not be established arbitrarily [7].

Landfill Leachate Monitoring

The formation of leachate depends on numerous complex interactions between the waste in the landfill and the water that penetrates into the landfill. Types of wastes emplaced vary considerably among different types of landfills. As the resulting leachate will depend heavily on the waste types emplaced, and on the waste–water interactions, considerable differences exist among leachates from different landfills. Moreover, the composition of the leachate varies over time, as the reactions change, e.g., in response to the changing composition of the materials in the landfill. In order to obtain a good understanding of leachate development, it is highly desirable to monitor leachate development and flow. This includes monitoring volume, flow rates, and, in particular, composition.

It seems highly likely, virtually certain, that leachate monitoring will become a standard operating practice for most if not all large landfills in the future. Monitoring will give the operator, the regulator, and the public greatly increased confidence that no detrimental consequences are resulting from the landfill operation.

Given that one major concern, usually the ultimate concern, associated with landfill leachate is the risk that it might contaminate groundwater, it is likely that in many situations the highest monitoring priority will be the establishment of a system that provides early warning in the eventuality of a release from the landfill.

The European Communities have established minimum requirements for landfill monitoring ([3], Annex III). These include monitoring of meteorological data, emission data, groundwater monitoring, and monitoring of the landfill topography, i.e., settlement monitoring. Meteorological monitoring is aimed at providing input data for water balance studies, which in turn will help to identify whether or not leakage might be occurring. Weather data to be recorded include precipitation, temperature, wind strength and direction, evaporation, and atmospheric humidity. During the operational phase, these data are to be recorded daily, but the measurement frequency is reduced greatly (mostly to monthly) during the aftercare phase. Leachate and surface water, if any, is to be sampled at representative points. Leachate measuring and sampling is to be performed at all points at which leachate discharges from the site, and will include measurements of volume and of composition. The sampling frequency can be adapted, based on the morphology of the waste, but needs to be specified in the permit. Typically, volumes will be measured monthly, compositions quarterly during the operational phase, every 6 months thereafter. Groundwater protection monitoring is aimed at detecting any early releases that might compromise the integrity of the groundwater. As a minimum, this requires a monitoring point in the inflow region, and two monitoring points in the outflow regions. However, the number of monitoring points can be increased on the basis of local hydrogeology. For landfills to be permitted in the future, base reference-level values must be established prior to commencing waste emplacement. Leachate sample analyses to be performed will be determined based on the expected waste composition and on the quality of the groundwater in the area. Of particular importance is the early recognition of indicator parameters that might provide an early warning of potential problems – indicators such as pH, TOC (Total Organic

Carbon), phenols, heavy metals, oil, and/or hydrocarbons. On the average, for typical situations, groundwater level is to be determined every 6 months, although this frequency is to be increased at sites with significant water level fluctuations. Composition determination of samples is to be performed at a frequency depending on the groundwater flow rate, and in particular on the feasibility of taking responsive remedial action before the next sampling. Trigger levels should be established, based on the local groundwater quality, and taking into account the local hydrogeology. If at all possible the trigger levels should be included in the permit for the site, and should form the basis for reporting to the regulatory authority when reached.

The monitoring program developed by the US Environmental Protection Agency essentially parallels the European community approach [17]. A section through a typical monitoring well installation is shown in Fig. 5. Figure 6 presents an example of an installation to monitor an interbedded aquifer (in this example, a low permeability clay bed in between two much more permeable sand layers): a PVC pipe installed coaxially in a borehole allows withdrawing water samples from the screened section of the hole. Above the screened section the pipe is carefully sealed, in this example with bentonite and cement/bentonite grout, in order to assure that no fluid can flow in the annulus in between the PVC pipe and the well walls. Surface structures protect the installation against vandalism or accidental damage. A critical and very important aspect of monitoring well installation is to minimize, as much as possible, any disturbance and especially contamination of the conditions that one intends to observe with the well.

Major components of monitoring projects include groundwater monitoring, leachate monitoring, monitoring of gas generation, of subsidence, surface erosion, and air quality. This approach stresses that both the quantity and quality of the leachate that develops are good indicators of how successful the operation is controlled.

A serious limitation of many landfill leachate effluent monitoring programs is the heavy reliance on well monitoring. By definition, wells monitor at points. Depending on the local geology and geohydrology, this may or may not be satisfactory. Certain is that in many natural environments fluid flows, and contamination plumes in particular, may pursue highly

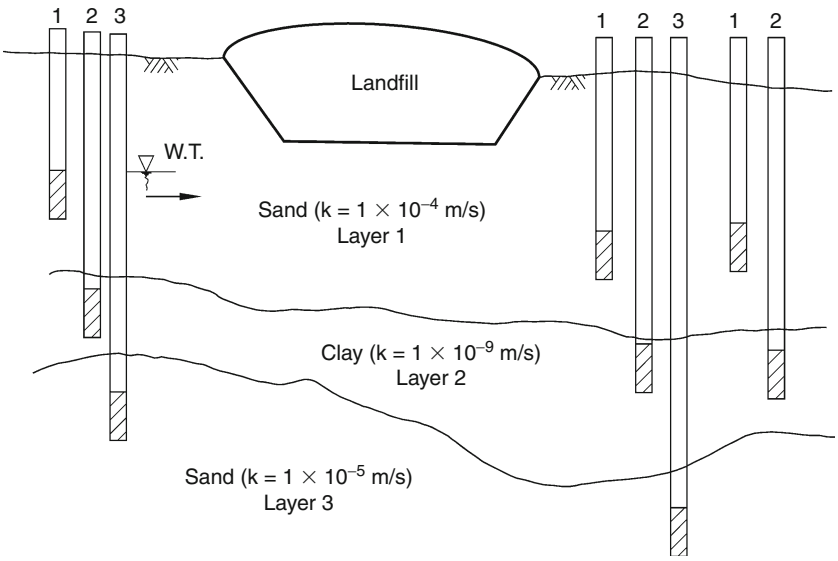

Landfill Leachate Control. Figure 5

Monitoring well arrangement: monitoring wells upstream (*left*) and downstream (*right*) from landfill, with provisions for sampling in aquifers (sand) and aquitard (clay) (From Ref. [17], Fig. 12-1, p. 142). k = hydraulic conductivity; W.T. = water table

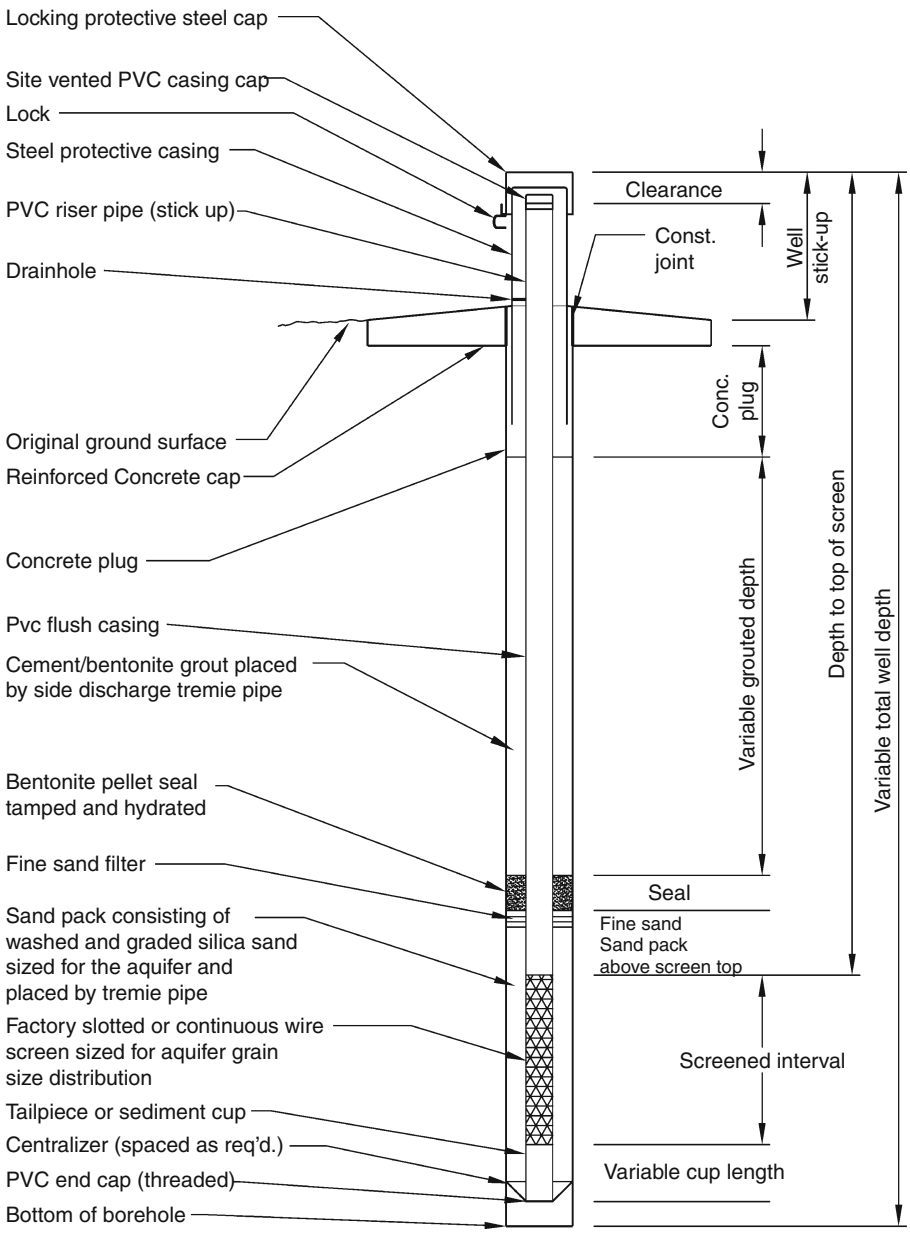

Landfill Leachate Control. Figure 6
Monitoring interbedded aquifer. The monitoring well is installed downstream from the landfill, and allows sampling of groundwater from the screened interval. If excessive concentrations of contaminants are detected in these samples, it indicates that excessive leachate leaking has taken place, and remedial action may be required (From Ref. [17], Fig. 12-2, p. 142)

preferential paths that can readily bypass measurements at a few points only. One possibility to address the uncertainties resulting from monitoring in wells is to complement such measurements with geophysical surveys. Geophysical surveys, by definition, can provide information about large volumes of ground. Geophysical surveys depend on differences in physical properties in the ground surveyed in order to detect

anomalies. If a correlation can be established between some physical property, e.g., electrical resistance, or electrical conductivity, and a contamination plume, it may be possible to gain a much more comprehensive assessment of site conditions, e.g., downstream from a leaking landfill, using geophysical surveys.

Landfill Leachate Treatment

In response to the numerous types of leachate that have developed in landfills, a wide range of leachate treatment methods have been developed, and are being implemented, tried out, and researched, with the objective of identifying methods most appropriate for particular waste types, water inflow and outflow rates, and waste–water interactions. The objective of treatment is to reduce the contaminant load in any effluent to an environmentally acceptable level, at an acceptable cost.

Under unusually successful treatment, it may be possible to discharge the now clean "leachate" directly into surface or underground waters. Under some situations it still may be possible to rely on natural attenuation as the major or exclusive treatment option. However, relying on natural attenuation only is likely to become less and less acceptable, except under the most unusual circumstances where it can be demonstrated convincingly to be adequate. Much more likely today is that leachate will require further treatment. One option is to convey leachate to sewage treatment facilities, and to treat leachate co-jointly with sewage. This certainly will require that the sewage treatment facility has adequate capacity, and allows for treatment that will clean the leachate without interfering with regular sewage treatment operations. This will require careful collaboration with the sewage treatment operations in order to assure mutually beneficial, preferably optimal co-joint treatment.

Major leachate treatment methods include recirculation, physical, chemical, and biological treatments. Recirculation should result in enhancing and accelerating all reactions taking place within the landfill, and hence should promote reaching earlier a waste and leachate composition less likely to result in excessive environmental impacts. Under what would usually be considered the very best practices for municipal waste landfills today, the landfill effectively is operated as a bioreactor, with controls in principle, in concept, very similar to those for chemical reactor vessels in general. Obviously, given the complexity of the system, and the numerous associated uncertainties, e.g., with regard to emplaced waste, and possibly inflow and outflow uncertainties, enhanced by the fact that the "reactor" operates in a natural environment, with far from complete control over the environment, e.g., with respect to temperature, pressure, humidity, designing, planning, and operating such a reactor remains a challenging task. Comprehensive information on landfill bioreactor design and operations is given by [18] and in chapter "► Landfill Bioreactors."

The use of constructed wetlands to treat landfill leachate appears to be gaining favor [19] as one more treatment option that has highly desirable benefits under the appropriate conditions. Considerable experience has been gained about the use of wetlands for the treatment of a variety of wastewaters, notably including acid mine drainage, urban storm water runoff, agricultural wastewaters, and sewage. Obviously one very attractive feature of constructing wetlands is that it assists in rebuilding some of the wetlands that have been lost over the last decades, or centuries. Equally obvious, treatment wetlands must remain environmentally acceptable.

Two major types of constructed wetlands for wastewater treatment are surface flow and subsurface flow systems. As the name implies, surface flow systems rely on water flow in an open system, open to the atmosphere. In a subsurface system, the main flow is below the surface (Fig. 7).

As with all leachate treatment systems the performance will depend on multiple factors with complex interactions, but one basic critical variable will be water flow rate and water replacement. Similarly to landfills themselves, a first step in estimating these variables will be the determination of the water balance:

$$\frac{dV}{dt} = Q_i - Q_o + P - ET$$

where V is the water volume, t is time, Q_i is the leachate inflow rate assuming no other inflows exist (V/t), Q_o is the outflow rate (V/t), P is the precipitation rate (V/t), and ET is the evaporation rate (V/t).

Obvious from this simple equation is that a number of climatological variables will affect the flow rate, possibly the water volume or water level, and hence the treatment effectiveness of a constructed wetland.

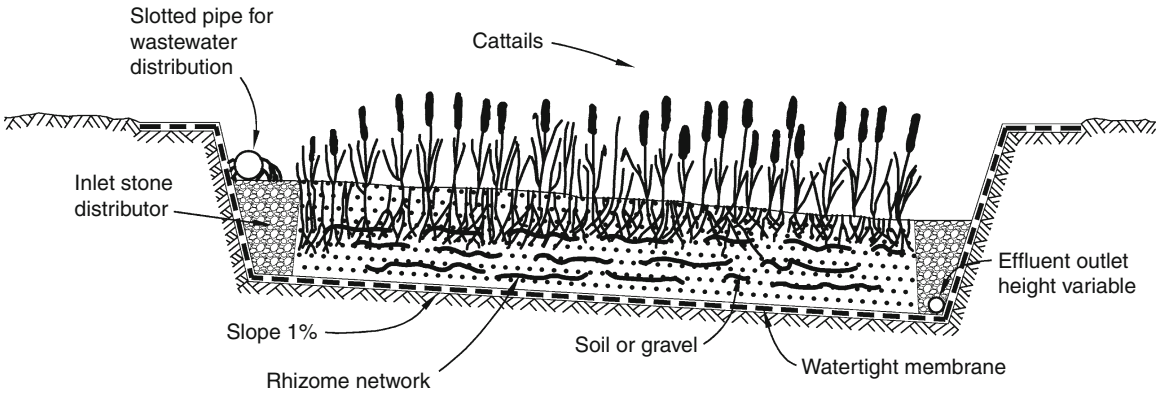

Landfill Leachate Control. Figure 7
Representative section through a subsurface flow system constructed wetlands for the treatment of wastewater (From Ref. [20], Fig. 3-1, p. 16). Leachate flow is guided through a highly permeable layer, e.g., gravel, coarse sand, installed directly above an impermeable base barrier, and covered by a soil that will permit and encourage plant growth

Rainfall intensity and pattern will influence performance, as will evaporation, and hence wind, temperature, and humidity. Strongly preferable is to collect such data on a local and a representative level as possible, although, in particular, for preliminary planning purposes it may be necessary to rely on regional data. As for landfills themselves, site selection, in particular with regard to subsurface hydrology, but also with regard to potential surface water flow, especially flooding, as well as foundation barrier performance, will be given high priority as a first and major line of defense against unacceptable environmental impacts.

The cleansing effects that take place in the wetlands treatment facility are similar to those in other leachate treatments. Physical activities will include the settling out of some solids, precipitation, the filtering out of others, and the adsorption of others on various surfaces within the wetlands. Chemical precipitation and adsorption will remove nitrogen and phosphorous. Chemical decomposition will remove or at least greatly reduce bacterial and viral content. Biological reactions will contribute to the removal of various organics, and may assist in the uptake by plants of heavy metals, at least temporarily. The latter aspect raises a question that needs to be researched more: is there a risk of treatment wetlands becoming cumulatively loaded, over time, with excess contaminants? Could there come a point where further decontamination of treatment wetlands themselves becomes a requirement?

Notwithstanding some remaining uncertainties, it is clear that constructed wetlands for leachate treatment provide multiple benefits that may make them highly attractive. These include typically low operating and maintenance costs, wildlife benefits, and visual attractiveness benefits. An issue that may be of concern, depending on the local climate, and the proximity to human habitat, is the risk of mosquito development.

Landfill Leachate Disposal

Depending upon the treatment that leachate has undergone, a range of options may be available for disposal of the residual wastes left over after leachate treatment. Depending upon the type of treatment to which the leachate has been subjected, the residual waste is likely to be significantly different, and may require different disposal methods, options, and approaches. Disposal requirements are reduced greatly by the ever more common practices of leachate recycling and neutralization.

Landfill Post-closure Control

Landfill post-closure control will be a strong function of potential risks associated with post-closure landfill performance. Of particular concern will be the risk of gas formation, gas collection, gas emissions, and associated health and safety risks. Of prime importance will be any anticipated continued methane gas development. If this is anticipated, gas control measures will be required.

Leachate control will be required to prevent detrimental impacts from leachate escapes. Liners and covers are the primary means of defense against problems caused by leachate formation and outflow. In many situations, it will be desirable to provide active leachate control as well, at least for some time. Active control can be achieved, e.g., by collecting all leachate in low points in the landfills, "sumps," and either allow drainage and collection by gravity flow from such collection points or implement pumping from such points.

To what extent the surface area and the buffer zone surrounding landfills can be redeveloped, put to alternate use, and to what kind of use, will depend on the location as well as on the characteristics of the emplaced waste and of the anticipated future development of leachate, gas, waste, potential releases – what are health, safety, and environmental risks associated with the site post-closure? Whereas in the past, closed landfills, sometimes with minimal, if any, controls, have been used for a variety of purposes, including housing, residential and commercial developments, parks and recreational areas, etc., it is certain that in the future, society will insist on a much more careful approach to such practices, in part at least, because of serious disasters that have resulted from past approaches of this type.

For some hazardous waste landfill sites it seems rather obvious that the operator or some subsequent responsible party will have to maintain and assure physical control over closed landfill sites. On the other hand, for landfills loaded with only relatively innocuous material, it may continue to be possible, given adequate site characterization, possibly complemented by monitoring, that the site might be restored to public use.

Municipal waste landfills, in particular, for obvious reasons, are frequently located relatively close to urban areas. In fact, not uncommonly one of the main challenges for landfill operators is to maintain acceptable relations with an ever closer and more intense encroachment from developments. Conversely, if it were possible to convert the landfill area, upon closure, to an acceptable public use, it obviously would benefit all parties involved.

Landfill leachate monitoring is an integral part of modern landfill operations, including post-closure monitoring. The location of monitoring wells will be determined based on local groundwater flow patterns (Fig. 8). The frequency of sampling and testing will be based on test results (Fig. 9). If test results indicate that unacceptable releases are taking place (Fig. 10), remedial action may be required.

Future Directions

The last few decades have seen major recognition of the potentially serious problems associated with landfill disposal of various wastes. Considerable efforts are being focused on reducing waste generation, on recycling, on composting, on waste incineration, on waste combustion with energy generation, and in general on waste management strategies aimed at reducing and minimizing the need for landfill emplacement. Even so, it appears highly likely that for the foreseeable future landfills will continue to form a major component in waste management and disposal strategies.

Understanding of leachates generated at landfills has improved significantly over the last few decades. This improved understanding in turn has resulted in greatly improved leachate control strategies. Even so, serious doubts and uncertainties remain associated with leachate control, particularly with regard to long-term performance. Hence it is essential that research be continued in this area and, in particular, that an improved understanding about leachate generation and control under actual field conditions over extended periods of time, at least decades, is gained. This unquestionably will assist in the development of further improvements in leachate control strategies and approaches.

Given the vast range of actual implementation options that are being pursued in many parts of the world, under many widely ranging conditions, i.e., waste types and contents, climatological environments, control and operational measures implemented, etc., it is clear that over the next several decades an exceedingly large data base of practical results will be obtained. Most modern landfills are monitored, instrumented, and tested, some extensively. All of this monitoring and testing provides extremely valuable data to calibrate theoretical models that continue being developed. Hence it is certain that models, and input data for the models, will continue to improve. Experience is being gained over decades, eventually many decades. This will provide currently sorely

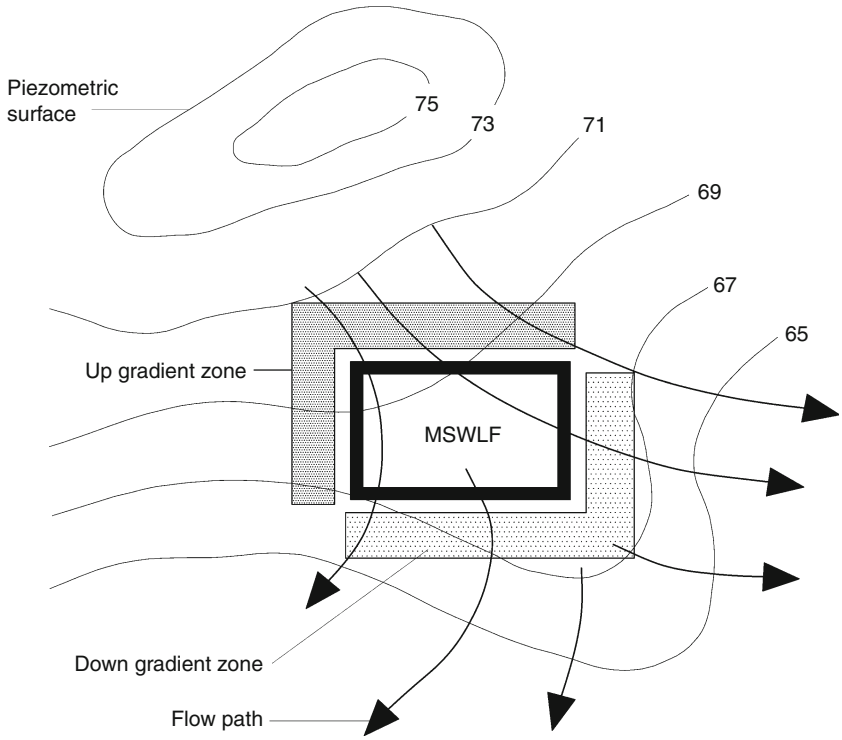

Landfill Leachate Control. Figure 8
Example of possible groundwater flow paths near and through a municipal solid waste landfill (MSWLF). Monitoring wells will be installed downstream, to allow sampling of effluent downstream from the fill, in order to assess whether leachate releases, if any, remain within allowable limits (From Ref. [16], Fig. 5-2, p. 238)

lacking information about long-term in situ leachate development which in turn will provide feedback to improve and optimize future control strategies.

It seems virtually certain that in developed societies landfill operations will continue to shift toward a bioreactor operational mode, i.e., systems in which leachate generation will ever more tightly be controlled through the monitoring and manipulation of operating variables. As a result, it seems highly probable that it will be possible to continue to reduce potential health and environmental impacts of landfills.

Alternatively, especially in dry and in semi-arid regions, the actual implemented approach of minimizing infiltration might result in and promote fossilization, mummification, of the waste. It is not clear that the full implications of the likely extreme longevity of many wastes in many landfills are understood or have been addressed. They probably deserve more attention than they have received to date?

Unfortunately such approaches are expensive. Even though in recent decades considerable efforts have been devoted to study landfills in less-developed countries, it appears that landfill leachate control remains a low priority in many societies. Hence it seems rather likely that they will continue to receive low priority in many parts of the world, and will continue to pose serious risks and hazards.

Leachate quality significantly depends on the characteristics (e.g., chemical composition, physical structure) of emplaced waste. Hence leachate control certainly would be improved by implementing more rigorous controls on landfill input, although this most likely will remain a major challenge for municipal waste in particular. Presumably, as analytical instrumentation and tools continue to improve, it should eventually be possible to provide a better input characterization, and hence improved optimization of operational controls that affect leachate quality. How well

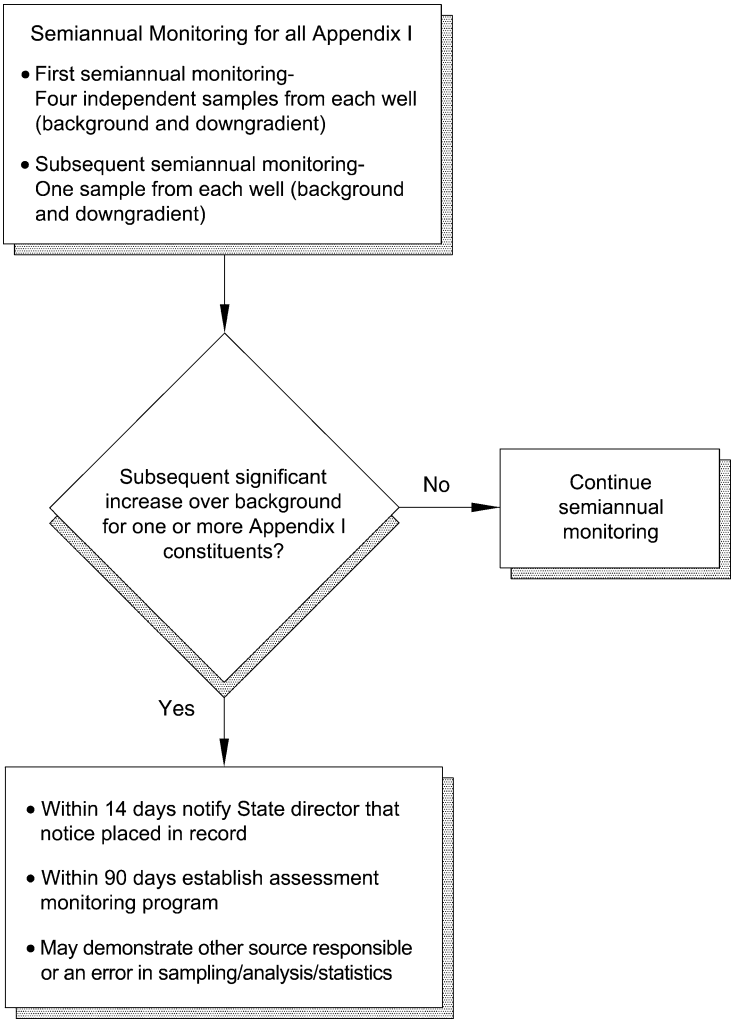

Landfill Leachate Control. Figure 9
Flow chart to determine monitoring requirements for landfill leachate control (Appendix I of ref [16] lists constituents, contaminants, for which testing is required) (From Ref. [16], Fig. 5-5, p. 278)

and reliable and comprehensively waste input can be controlled through regulatory means probably at least to some extent is a function of culture, citizen civic responsibility, and hence may vary across borders.

Liner and cover installations are labor intensive. It is to be hoped that technological improvements will continue, and will result in simpler and more reliable installation methods for these critical components of the leachate control system.

An obvious approach, in principle, to reduce landfill leachate control requirements is to reduce landfill leachate. Among the major methods that are being pursued toward this goal are recycling, composting, and waste incineration. In one way or another, all of these have been practiced and implemented to varying degrees and studied. All have benefits and shortcomings. It can be anticipated that all these methods will continue to be improved and find wider applications. This will reduce landfill requirements, undoubtedly one of the best methods to reduce leachate control requirements. An even more fundamental approach is the ongoing effort to minimize waste production in the first place.

Notwithstanding these efforts, all indications are that waste generation will continue to increase,

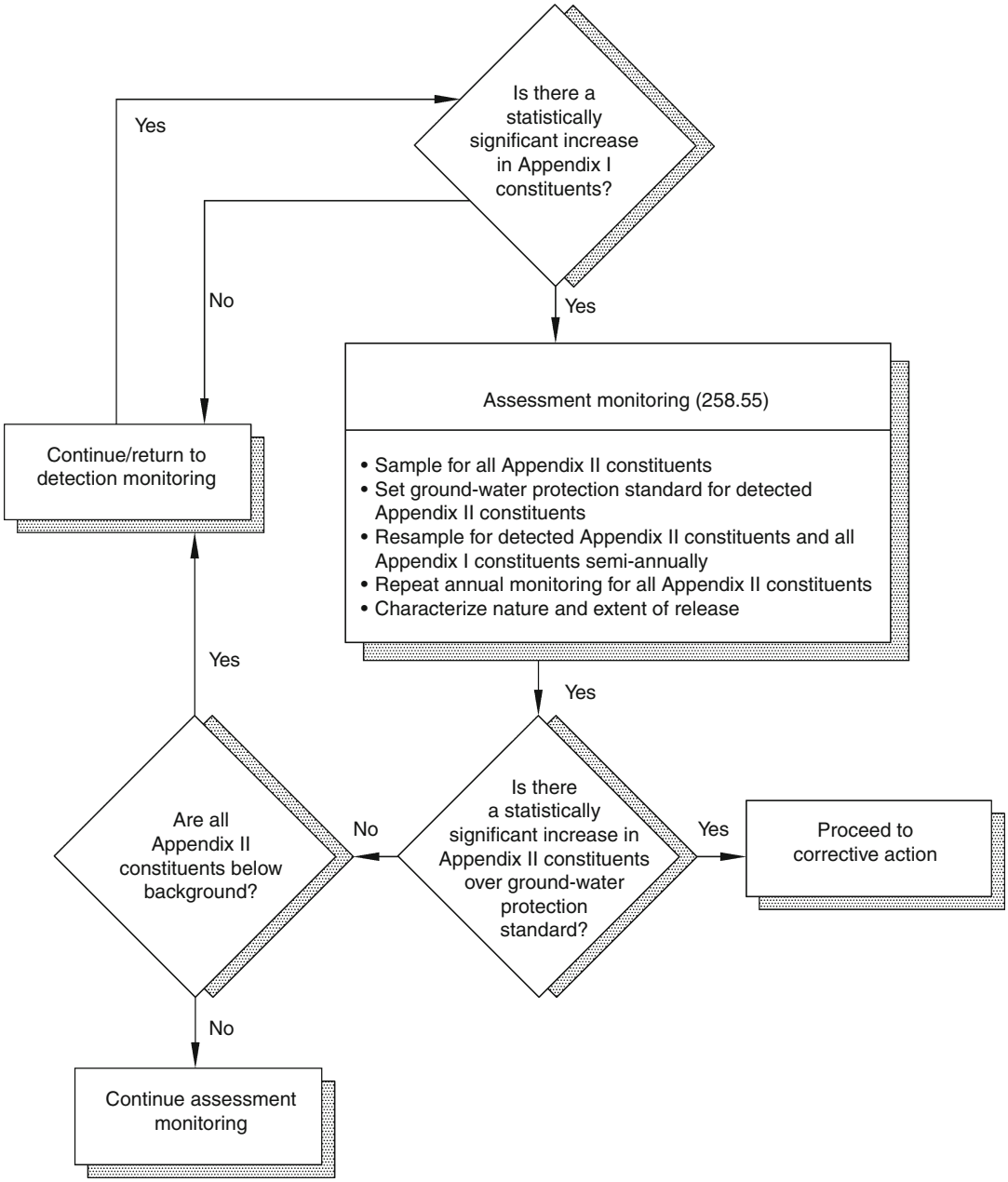

Landfill Leachate Control. Figure 10

Flow chart illustrating the decision making process as to whether remedial action is required as a result of monitored leachate content: excessive concentration of contaminants (Appendix I and/or Appendix II materials of Ref. [16]) in the effluent emanating from the landfill (From Ref. [16], Fig. 5-6, p. 284)

probably increase substantially. According to the Organisation for Economic Co-Operation and Development ([21], p. 235) "The annual generation of municipal waste in OECD countries increased by around 40% between 1980 and 1997," and is expected to increase by about 43% in the years 2000–2020 ([21], p. 236). The same source ([21], p. 237) expects that municipal solid waste generation in non-OECD

countries will increase, over the period 1995–2020, by somewhat over 100%. While recycling and, to a lesser extent incineration, are likely to continue to grow, it is expected that in 2020, landfill will still be used for 50% of municipal waste disposal in OECD countries and for 70% in non-OECD countries. According to OECD's updated 2008 projection ([22], p. 238), municipal solid waste generation in OECD countries is expected to increase by about 250% by 2030 compared to 1980, even though expected population growth over that period in these countries is likely to be only about 40%. Municipal solid waste generation is expected to grow much faster in the BRIICS countries (Brazil, Russia, India, Indonesia, China, and South Africa), and especially in the rest of the world, due to population growth and economic growth. Moreover, in many of the BRIICS countries, inappropriate collection and treatment of municipal waste remains widespread, estimated to range from 20% to, much more commonly, 60% of the waste. Presumably, the situation for the rest of the world most likely is worse. The need for improved and less expensive waste management and leachate collection and treatment are rather obvious. While the research that is going on in advanced societies is impressive in its sophistication, and unquestionably will greatly improve the leachate control with more advanced treatment options, one cannot help but see that most of these result in very expensive and technically challenging treatments. Might there not be a place for relatively inexpensive, even if less completely perfect treatment methods, that provide at least some improved control, at a cost less wealthy societies can afford?

Acknowledgments

The authors would like to thank Mr. Kivanç Okalp, Coordinator of Projects, Beray Engineering Consultancy Ltd., for his kind assistance in drafting the illustrations in this entry.

Bibliography

Primary Literature

1. Schroeder PR, Lloyd CM, Zappi PA, Aziz NM (1994) The hydrologic evaluation of landfill performance (HELP) model: user's guide for version 3. Risk Reduction Engineering Laboratory, Office of Research and Development, US Environmental Protection Agency, Cincinnati. EPA/600/R-94/168a
2. Schroeder PR, Dozier TS, Zappi PA, McEnroe BM, Sjostrom JW, Peyton RL (1994) The hydrologic evaluation of landfill performance (HELP) model: engineering documentation for version 3. Risk Reduction Engineering Laboratory, Office of Research and Development, US Environmental Protection Agency, Cincinnati, EPA/600/R-94/168b
3. Council of the European Union (1999) Council directive 1999/31/EC of 26 April 1999 on the landfill of waste (Official Journal of the European Communities, 16.7.1999, L 182/1-19)
4. US EPA (2010) Landfills (US Environmental Protection Agency, Cincinnati, OH). http://www.epa.gov/waste/nonhaz/municipal/landfill.htm. Accessed 26 Feb 2010
5. EPA NSW (2009) Waste classification guidelines part 1: classifying waste. Environmental Protection Authority, Department of Environment, Climate Change and Water, New South Wales, Sydney, Australia. http://www.environment.nsw.au/waste/envguidlin/index.htm. Accessed 26 Feb 2010
6. Daniel DE, Koerner RM (2007) Waste containment facilities: guidance for construction quality assurance and construction quality control of liner and cover systems, 2nd edn. American Society of Civil Engineers, Reston
7. Koerner RM, Daniel DE (1997) Final covers for solid waste landfills and abandoned dumps, ASCE, American Society of Civil Engineers, Reston, Virginia; Thomas Telford, London
8. US EPA (1989) Requirements for hazardous waste landfill design, construction, and closure. US Environmental Protection Agency, Washington, DC, EPA/625/4-89/022
9. Qian X, Koerner RM, Gray DH (2002) Geotechnical aspects of landfill design and construction. Prentice Hall, Upper Saddle River
10. US EPA (2001) Geosynthetic clay liners used in municipal solid waste landfills. US Environmental Protection Agency, Washington, DC. EPA530-F-97-002
11. Akgün H, Wallace RB (1993) Solid waste containment in double lined systems. J Resour Manage Technol 21:137–141
12. Wallace RB, Akgün H (1994) Leakage in double liner systems: the containment objective. Chapter 2. In: Christensen TH, Cossu R, Stegmann R (eds) Landfilling of waste: barriers. E & FN Spon, London, pp 81–89
13. Bonaparte R, Giroud JP, Gross BA (1989) Rates of leakage through landfill liners. In: Proceedings of Geosynthetics '89 Conference, San Diego, California, Industrial Fabrics Association International (IFAI), St Paul, Minnesota, pp 18–29
14. Giroud JP, Bonaparte R (1989) Leakage through liners constructed with geomembranes – Part I, geomembrane liners. Geotext Geomembr 8:27–67
15. Giroud JP, Bonaparte R (1989) Leakage through liners constructed with geomembranes-Part II, composite liners. Geotext Geomembr 8:71–111
16. US EPA (1993) Solid waste disposal facility criteria technical manual. EPA530-R-93-017, Revised 13 April 1998 (US Environmental Protection Agency, Washington, DC). http://www.epa.gov/wsste/nonhaz/municipal/landfill/techman/index.htm
17. US EPA (1991) Design and construction of RCRA/CERCLA final covers. Seminar publication EPA/625/4-91/025, US

Environmental Protection Agency, Washington, DC (prepared by Eastern Research Group, Inc, Arlington, MA, for Center for Environmental Research Information, US Environmental Protection Agency, Cincinnati, OH)
18. Reinhart DR, Townsend TG (1998) Landfill bioreactor design and operation. Lewis (CRC Press), Boca Raton
19. Mulamoottil G, McBean EA, Rovers F (eds) (1999) Constructed wetlands for the treatment of landfill leachates. Lewis (CRC Press), Boca Raton
20. US EPA (1988) Design manual constructed wetlands and aquatic plant systems for municipal wastewater treatment. US Environmental Protection Agency, Office of Research and Development, Center for Environmental Research Information, Cincinnati, EPA/625/1-88/022
21. OECD (2001) OECD Environmental outlook environment. OECD, Organisation for Economic Co-operation and Development, Paris
22. OECD (2008) OECD environmental outlook to 2030. OECD, Organisation for Economic Co-operation and Development, Paris

Books and Reviews

Abbas AA, Jingsong G, Ping LZ, Ya PY, Al-Rekabi WS (2009) Review on landfill leachate treatments. Am J Appl Sci 6:672–684

Acar YB, Daniel DE (1995) Geoenvironment 2000, characterization, containment, remediation and performance in environmental geotechnics. Geotechnical Special Publication No. 46. American Society of Civil Engineers (ASCE), New York

Alexander JH (1993) Defense of garbage. Praeger, Westport

Alshawabkeh A, Benson CH, Culligan PJ, Evans JC, Gross BA, Narejo D, Reddy KR, Shackelford CD, Zornberg JG (2005) Waste containment and remediation. Geotechnical Special Publication 142, Geo-Frontiers 2005, 24–26 Jan 2005. The Geo-Institute of the American Society of Civil Engineers, American Society of Civil Engineers (ASCE), Reston, VA

Arnould M, Barrès M, Côme B (1993) Geology and confinement of toxic wastes. In: Geoconfine93, Proceedings of the International Symposium, Montpellier, France, AA Balkema, Rotterdam, Brookfield, 8–11 June 1993

Associate Committee of Geotechnical Research (1983) Geotechnical aspects of waste disposal. A Report Prepared by the Task Force on Waste Disposal, Technical Memorandum No. 135. National Research Council of Canada, Ottawa

August H, Holzohner U, Meggyes T (eds) (1997) Advanced landfill liner systems. Thomas Telford, London

Aziz HA, Adlan MN, Hung Y-T (2009) Special issue on landfill leachate management and control. Int J Environ Waste Manag 4:385–398

Bagchi A (1994) Design, construction, and monitoring of landfills, 2nd edn. Wiley, New York

Bagchi A (2004) Design of landfills and integrated solid waste management, 3rd edn. Wiley, New York

Banerji SK (1977) Management of gas and leachate in landfills. In: Proceedings of the Third Annual Municipal Solid Waste Research Symposium, St. Louis, Missouri, 14–16 March 1977, EPA-600/9-77-026, Municipal Environmental Research Laboratory. US Environmental Protection Agency, Cincinnati, Ohio

Barlaz MA, Ham RK, Schaefer DM (1990) Methane production from municipal refuse: a review of enhancement techniques and microbial dynamics. Crit Rev Environ Control 19:557–584

Bentley SP (1996) Engineering geology of waste disposal. Geological Society Engineering Geology Special Publication No. 11. The Geological Society, London

Beranek DA (2001) Engineering and design. Checklist for hazardous waste landfill cover design Ft. Belvoir Defense Technical Information Center, Report ETL-1110-1-162. Corps of Engineers, Washington, DC. http://handle.dtic.mil/100.2/ADA403099. Accessed 11 Feb 2010

Bonaparte R (1990) Waste containment systems: construction, regulation, and performance. In: Proceedings of a symposium sponsored by the Committee on Soil Improvement and Geosynthetics and the Committee on Soil Properties of the Geotechnical Engineering Division, American Society of Civil Engineers in conjunction with the ASCE National Convention San Francisco, California. American Society of Civil Engineers (ASCE), New York, Geotechnical Special Publication No. 26, 6–7 Nov 1990

Bonaparte R, Daniel DE, Koerner RM (2002) Assessment and recommendations for improving the performance of waste containment systems. US Environmental Protection Agency, Washington, DC. EPA/600/R-02/099

Bouazza A, Kodikara J, Parker R (1997) Environmental geotechnics. In: Proceedings of the 1st Australia-New Zealand conference on environmental geotechnics-geoenvironment 97, Melbourne, Victoria, Australia, AA Balkema, Rotterdam, Brookfield, 26–28 November

Bradshaw AD, Southwood SR, Warner SF (eds) (1992) The treatment and handling of wastes. Chapman & Hall, London

Cheremisinoff NP (2003) Handbook of solid waste management and waste minimization technologies. Butterworth Heinemann (Elsevier Science), Amsterdam

Christensen TH, Cossu R, Stegmann R (1992) Landfilling of waste: leachate. E & FN Spon (Chapman & Hall), London

Christensen TH, Cossu R, Stegmann R (1994) Landfilling of waste: barriers. E & FN Spon (Chapman & Hall), London

Christensen TH, Kjeldsen P, Albrechtsen HJ, Heron G, Mielson PH, Bjerg PL, Holm PE (1994) Attenuation of landfill leachate pollutants in aquifers. Crit Rev Environ Sci Technol 24:119–202

Christensen TH, Cossu R, Stegmann R (1996) Landfilling of waste: biogas. E & FN Spon (Chapman & Hall), London

Christensen TH, Cossu R, Stegmann R (1999) Sardinia'99: Seventh international waste management and landfill symposium. CISA, Environmental Sanitary Engineering Centre, Cagliari, Sardinia, Italy

Christenson SC, Cozzarelli IM (2003) The Norman landfill environmental research site: What happens to the waste in landfills? USGS Fact Sheet FS-040-03. US Geological Survey, Washington, DC. http://water.usgs.gov/pubs/fs/fs-040-03.pdf

CLU-IN (2004) NATO/CCMS pilot study: prevention and remediation issues in selected industrial sectors: Rehabilitation of old landfills, Cardiff, Wales, May 23–26. US Environmental Protection Agency Technology Innovation Program. http://www.clu-in.org/wales/. Accessed 5 Feb 2010

Daniel DE (ed) (1993) Geotechnical practice for waste disposal. Chapman & Hall, London

Daniel DE (1993) Landfills and impoundments. In: Daniel DE (ed) Geotechnical practice for waste disposal. Chapman & Hall, London, pp 97–112

Daniel DE, Trautwein SJ (eds) (1994) Hydraulic conductivity and waste contaminant transport in soil. ASTM, Philadelphia, ASTM STP 1142

Defra (2009) Environmental permitting guidance – The landfill directive. Version 2.0, Department for Environment Food and Rural Afffairs, London. Defra Publications, Department for Environment, Food and Rural Affairs, London. www.defra.gov.uk

Defra (2009) Consultation on a strategy for hazardous waste management in England. Department for Environment Food and Rural Afffairs, London. Defra Publications, Department for Environment, Food and Rural Affairs, London. www.defra.gov.uk

Dhamija U (2006) Sustainable solid waste management: issues, policies, and structures. Academic Foundation, New Delhi

Dixon N, Murray EJ, Jones DRV (eds) (1998) Geotechnical engineering of landfills. Thomas Telford, London

Dixon N, Smith DM, Greenwood JR, Jones DRV (2003) Geosynthetics protecting the environment. In: Proceedings of the 1st IGS UK Chapter National Geosynthetics Symposium held at The Nottingham University, Thomas Telford, London, 17 June 2003

Dunn RJ, Singh UP (1995) Landfill closures-environmental protection and land recovery, Geotechnical Special Publication No. 53. American Society of Civil Engineers (ASCE), New York

Dwyer JR (1988) Evaluation of municipal solid waste landfill cover designs. US Environmental Protection Agency, Hazardous Waste Engineering Research Laboratory, Cincinnati

Dwyer SF (1998) Construction costs of six landfill cover designs, Sandia Report SAND98-1988. Sandia National Laboratories, Albuquerque, NM/Livermore, CA

Dwyer SF (2000) Landfill covers: is it time to change current regulations? Sandia Report SAND2000-2302. Sandia National Laboratories, Albuquerque, NM/Livermore, CA

EC (2010) Landfill of waste. http://ec.europa.eu/environment/waste/landfill_index.htm. Accessed 5 Feb 2010

EC (1999) Council directive 1999/31/EC of 26 April 1999, on the landfill of waste. http://eur-lex.europa.eu/pri/en/oj/dat/1999/1_182/1_18219990716en00010019. pdf. Accessed 4 Feb 2010

Enviros Consulting Ltd and University of Birmingham with Risk and Policy Analysts Ltd, Open University and Maggie Thurgood (2004) Review of environmental and health effects of waste management: Municipal solid waste and similar wastes. Defra Publications, Department for Environment, Food and Rural Affairs, London. http://www.defra.gov.uk/environment/documents/health-report.pdf. Accessed 26 Mar 2010

European Commission, DG Environment (2001) A Study on the economic valuation of environmental externalities from landfill disposal and incineration of waste, Final Main Report. http://ec.europa.eu/environment/waste/studies/pdf/econ_landfill_report.pdf. Accessed 4 Feb 2010

European Commission, DG Environment (2007) Follow-up study on the implementation of Directive 1999/31/EC on the landfill of waste in EU-25, Final Report – Findings of the Study. http:ec.europa.eu/environment/waste/pdf/study/cow_report.pdf. Accessed 4 Feb 2010

Evans JC (1997) In situ remediation of the geoenvironment. In: Proceedings of the conference sponsored by the Geo-Institute and the Environmental Engineering Division of the American Society of Civil Engineers, Minneapolis, Minnesota, 5–8 Oct 1997, Geotechnical Special Publication No. 71. American Society of Civil Engineers (ASCE), Reston, VA

FAA (2000) Construction or establishment of landfills near public airports. Federal Aviation Administration, Washington, DC. Advisory Circular AC No: 150/5200-34

Fang H-Y (1997) Introduction to environmental geotechnology. CRC Press, Boca Raton

Fang H-Y, Inyang H (1996) Environmental geotechnology. In: Proceedings of the 3rd International Symposium, San Diego, Technomic Pub Co, Lancaster

Fanjoy J (2003) How to prepare a startup, shutdown, malfunction plan for collection and control systems at municipal solid waste landfills EPA-456/R-03-006. US Environmental Protection Agency, Office of Air Quality Planning and Standards, Information Transfer and Program Integration Division, Research Triangle Park, North Carolina. www.epa/gov/ttn/atw/landfill/lfssm12_03.pdf

Garg VK, Mor S (Guest eds) (2008) Special issue on solid waste management (Part I). Int J Environ Waste Manag 2(1/2):3–199

Garg VK, Mor S (Guest eds) (2008) Special issue on solid waste management (Part II). Int J Environ Waste Manag 2(6): 506–665

Garg VK, Mor S (Guest eds) (2009) Special issue on solid waste management (Part III). Int J Environ Waste Manag 3(1/2):4–192

Gartner L (1987) Site assessment 4B: geology, hydrogeology and geotechnics-potential impacts on ground water from the landfill. Ontario Waste Management Corporation, Toronto

Genetelli EJ, Cirello J (eds) (1976) Gas and leachate from landfills: formation, collection and treatment. US Environmental Protection Agency, Municipal Environmental Research Laboratory, Cincinnati. EPA-600/9–76–004

German Geotechnical Society (1993) Geotechnics of landfill design and remedial works: technical recommendations – "GLR", 2nd edn. Ernst & Sohn, Berlin

Gilbert PA, Murphy WL (1987) Prediction/mitigation of subsidence damage to hazardous waste landfill covers, Project Summary, EPA/600/S2-87/025. US Environmental Protection Agency, Hazardous Waste Engineering Research Laboratory, Cincinnati, Ohio. nepis.epa.gov/Exe/ZyPURL.cgi?Dockey=2000TLFZ.txt. Accessed 12 Feb 2010

Golder Associates (1996) Landsim: landfill performance simulation by Monte Carlo method, Report No. CMW 094/96. Department of the Environment, UK

Golder Europe EEIG (2005) Report on implementation of the landfill directive in the 15 member states of the European Union, Ref ENV.A.2/ETU/2004/0016. The European Commission "Markets" Team DG ENV.F2 (BU-5 00/120), Evere, Belgium. http://ed.europa.eu/environment/waste/pdf/report_a2.pdf. Accessed 4 Feb 2010

Gronow JR, Schofield AN, Jain RK (1988) Land disposal of hazardous waste. Wiley, New York

Hagerty DJ, Pavoni JL, Heer JE Jr (1973) Solid waste management, Van Nostrand Reinhold environmental engineering. Van Nostrand Reinhold Company, New York

Hammer DA (1989) Constructed wetlands for wastewater treatment-municipal, industrial and agricultural. In: Proceedings from the First International Conference on Constructed Wetlands for Wastewater Treatment, Chattanooga, Tennessee. Lewis, Chelsea, MI

Hasan SE (1996) Geology and hazardous waste management. Prentice Hall, Upper Saddle River

International Committee on Environmental Geotechnology (1986) International symposium on environmental geotechnology. Envo, Allentown

International Containment Technology Conference (1997) International Containment Technology Conference: February 9–12 1997, St. Petersburg, Florida, USA: Conference Proceedings. Florida State University Institute for International Cooperative Environmental Research, Tallahassee, Florida

International Water Association (2001) 1st world water congress: operation and management, landfill and sludge management. In: Selected Proceedings of the 1st World Water Congress of the International Water Association, held in Paris, France, International Water Association, London, 3–7 July 2000

ISWA (2010) Landfill operational guidelines, 2nd edn. ISWA Working Group on Landfill, International Solid Waste Association, Vienna, Austria. www.iswa.org. Accessed 19 Feb 2010

ITRC (2003) Technology overview using case studies of alternative landfill technologies and associated regulatory topics. Interstate Technology and Regulatory Council, Washington, DC. www.itrcweb.org/Documents/ALT-1.pdf. Accessed 12 Feb 2010

Johannessen LM (1999) Guidance note on leachate management for municipal solid waste landfills, 5. Working Paper Series. Urban Development Division, Urban Waste Management Thematic Group, The International Bank for Reconstruction and Development, The World Bank, Washington, DC. www.worldbank.org/urban/solid_wm/erm/.../uwp5.pdf. Accessed 5 Feb 2010

Johannessen LM, Boyer G (1999) Observations of solid waste landfills in developing countries: Africa, Asia, and Latin America. Urban Development Division, Waste Management Anchor Team, The International Bank for Reconstruction and Development, THE WORLD BANK, Washington, DC. www.worldbank.org/urban/solid_wm/erm/CWG%20folder/uwp3.pdf. Accessed 23 Mar 2010

Kadlec RH, Knight RL (1996) Treatment wetlands. CRC/Lewis Publishers, Boca Raton

Kadlec RH, Wallace SD (2009) Treatment wetlands, 2nd edn. Taylor & Francis Group, Boca Raton

Khire MV, Alshawabkeh AN, Reddy KR (2008) Geotechnics of waste management and remediation. In: GeoCongress, Proceedings of Selected Sessions of Geocongress 2008. American Society of Civil Engineers (ASCE), Reston, VA

Kjeldsen P, Barlaz MA, Rooker AP, Baun A, Ledin A, Christensen TH (2002) Present and long-term composition of MSW landfill leachate: a review. Crit Rev Environ Sci Technol 32:297–336

Klinck BA, Stuart ME (1999) Human health risk in relation to landfill leachate quality, British Geological Survey Technical Report WC/99/17. British Geological Survey, Keyworth, UK. www-esd.worldbank.org/. . ./Human%20_health_risk_rel_%20lfill_%20leachate_qual.pdf. Accessed 23 Mar 2010

Koerner RM (1990) Geosynthetic testing for waste containment applications, ASTM STP (Special Technical Publication) 1081. ASTM (American Society for Testing and Materials), Philadelphia

Koerner RM (1994) Designing with geosynthetics, 3rd edn. Prentice Hall, Englewood Cliffs

Landreth RE, Rebers PA (1997) Municipal solid wastes: problems and solutions. CRC Lewis, Boca Raton

Landva A, Knowles GD (1990) Geotechnics of waste fills-theory and practice, ASTM STP 1070, ASTM Special technical publication. ASTM (American Society for Testing and Materials), Philadelphia

Lopez A, Dilaconi C, Mascolo G, Pollice A (2010) Innovation and integrated technologies for the treatment of industrial wastewater. IWA, International Water Association, London

Lu JCS, Eichenberger B, Stearns RJ (1985) Leachate from municipal landfills: production and management. Noyes, Park Ridge

MacBean EA, Rovers FA, Farquhar GJ (1995) Solid waste landfill engineering and design. Prentice Hall, Englewood Cliffs

Matrecon Inc (1988) Lining of waste containment and other impoundment facilities, EPA/600/2-88/052. US Environmental Protection Agency, Risk Reduction Engineering Laboratory, Cincinnati, Ohio

Melosi MV (2005) Garbage in the cities (Revised edition). University of Pittsburgh Press, Pittsburgh

Miller DW (ed) (1980) Waste disposal effects on ground water. Premier, Berkeley

Müller WW (2007) HDPE geomembranes in geotechnics. Springer, Berlin

Murphy WL, Gilbert PA (1985) Settlement and cover subsidence of hazardous waste landfills, Project Summary, EPA/600/S2-85/035. US Environmental Protection Agency, Hazardous Waste Engineering Research Laboratory, Cincinnati, Ohio. nepis.epa.gov/Exe/ZyPURL.cgi?Dockey=100019HC.txt. Accessed 12 Feb 2010

Myers GA (2005) Disposable cities: garbage, governance and sustainable development in urban Africa. Ashgate, Aldershot

Nath B, Pelovski Y, Stoyanov SK (2000) Sustainable solid waste management in the southern black sea region. In: Proceedings of the NATO advanced research workshop, Sofia, Bulgaria, Kluwer, Dordrecht/Boston, 27 Sept–1 Oct 1999

Office of Environmental Guidance (1993) Closure of municipal solid waste landfills (MSWLFs), RCRA Information Brief EH-231-036/0793. US Department of Energy. www.osti.gov/bridge/servlets/purl/10133328-qM49KE/.../10133328.pdf

Oweis IS, Khera RP (1998) Geotechnology of waste management, 2nd edn. PWS, Boston

Popov V, Itoh H, Brebbia CA, Kungolos S (2004) Waste management and the environment II, Second International Conference, Landfills, design, construction and monitoring, section 8, WIT Press, Southampton, Boston

Qasim SR, Chiang W (1994) Sanitary landfill leachate: generation, control, and treatment. Technomic, Lancaster

Rathje W, Murphy C (1992) Rubbish! The Archaeology of garbage. HarperCollins, New York

Reddy KR, Kadlec RH (2001) Wetland systems for water pollution control 2000. In: Selected Proceedings of the 7th International Conference on Wetland Systems for Water Pollution Control, held in Lake Buena Vista, Florida, IWA, International Water Association, London, 11–16 Nov 2000

Reddy KR, Smith WH (1987) Aquatic plants for water treatment and resource recovery, selected papers from the International Conference on research and applications of aquatic plants for water treatment and resource recovery held in Orlando, Florida, Magnolia, Orlando, Florida, 20–24 July 1986

Reed SC, Middlebrooks EJ, Crites RW (1995) Natural systems for waste management and treatment, 2nd edn. McGraw-Hill, New York

Richardson GN (2002) Construction quality management for remedial action and remedial design waste containment systems, EPA/540/R-92/073. Office of Solid Waste and Emergency Response, US Environmental Protection Agency, Washington, DC

Richardson GN, Koerner RM (1988) Geosynthetic design guidance for hazardous waste landfill cells and surface impoundments. US Environmental Protection Agency, Hazardous Waste Engineering Research Laboratory, Cincinnati

Rowe RK, Quigley RM, Booker JR (1995) Barrier systems for waste disposal facilities. E & FN Spon (Chapman & Hall), London

Rowe RK, Quigley RM, Brachman RWI, Booker JR (2004) Barrier systems for waste disposal facilities, 2nd edn. Spon, London/New York

Sara MN (1994) Standard handbook for solid and hazardous waste facility assessments. Lewis, Boca Raton

Sarsby RW (1995) Waste disposal by Landfill. In: Proceedings of the Symposium GREEN'93, Geotechnics Related to the Environment, Bolton, United Kingdom, AA Balkema, Rotterdam, Brookfield, 28 June–July 1993

Sarsby RW, Felton AJ (2007) Geotechnical and environmental aspects of waste disposal sites. In: Proceedings of Green4 International Symposium on Geotechnics Related to the Environment, Wolverhampton, Taylor & Francis, London, 28 June–1 July 2004

Sarsby R (2000) Environmental geotechnics. Thomas Telford, London

Serrato MG (2001) Bentonite mat demonstration. Final Report. WSRC-TR-94-0618 Westinghouse Savannah River Company, Aiken, South Carolina. www.osti.gov/bridge/servlets/purl/105732-QPtpgp/.../105732.pdf. Accessed 11 Feb 2010

Sharma HD, Lewis SP (1994) Waste containment systems, waste stabilization, and landfills: design and evaluation. Wiley, New York

Sharma HD, Reddy KR (2004) Geoenvironmental engineering: site remediation, waste containment, and emerging waste management technologies. Wiley, New Jersy

Site Investigation Steering Group (1993) Site investigation in construction Part 4: guidelines for the safe investigation by drilling of landfills and contaminated land. Thomas Telford, London

Spillmann P, Dorrie T, Struve M (2009) Long-term hazard to drinking water resources from landfills. Thomas Telford, London

Stegmann R, Ritzkowski M (eds) (2007) Landfill aeration. CISA, Padova

Stone JJ, Paige G, Hakonson TE, Lane LJ (1994) Design document for landfill capping prototype decision support system, Report Number LA-UR-94-570. USDA-ARS Southwest Watershed Research Center, Tucson, Arizona, Los Alamos National Laboratory, Los Alamos, New Mexico. www.osti.gov/bridge/product.biblio.jsp?osti_id=10132805. Accessed 12 Feb 2010

Stormont JC (1994) Assessment of an active dry barrier for a landfill cover system, Sandia Report SAND94-0301. Sandia National Laboratories for the Department of Energy, Office of Technology Development

Stuart ME, Klinck BA (1998) A catalogue of leachate quality for selected landfills from newly industrialised countries, British Geological Survey Technical Report WC/98/49. British Geological Survey Keyworth. www-esd.worldbank.org/. . ./A_Catalogue_of Leachate_Quality_Selected_.... Accessed 23 Mar 2010

SWANA (2009) 14th Annual Landfill Symposium Proceedings. SWANA: Solid Waste Association of North America, Silver Spring, Maryland. http://swanastore.stores. yahoo.net/lanpub.html. Accessed 19 Feb 2010

Tammemagi HY (1999) The waste crisis: landfills, incinerators, and the search for a sustainable future. Oxford University Press, New York

Tchobanoglous G, Theisen H, Vigil S (1993) Integrated solid waste management: engineering principles and management issues. McGraw-Hill, New York

Testa SM (1994) Landfill disposal, landfill design, siting criteria. In: Testa SM (ed) Geological aspects of hazardous waste management. Lewis, Boca Raton. Chapter 10

Tridata Corporation (2002) Landfill fires: their magnitude, characteristics, and mitigation. Federal Emergency Management Agency, United States Fire Administration, National Fire Data Center. http://www.usfa.dhs.gov/downloads/publivations/fa-225.pdf

Tyagi RD, Surampalli RY, Yan S, Zhang TC, Kao CM, Lohani, BN (2009) Sustainable sludge management production of value-added products. American Society of Civil Engineers (ASCE), Reston

Twardowska I, Allen HE, Kettrup AA, Lacy WJ (2004) Solid waste: assessment, monitoring and remediation. Elsevier, Amsterdam

Usmen MA, Acar YB (1992) Environmental geotechnology. In: Proceedings of the mediterranean conference on environmental geotechnology, Ceşme, Turkey, 25–27 May 1992. AA Balkema, Rotterdam; Brookfield

US Army Corps of Engineers (1997) Quality assurance representative's guide, pamphlet no. EP 415-1-261, Chapter 3: Landfill covers and liners. Vol 5, Department of the Army, Washington, DC

US Army Corps of Engineers (2001) Checklist for hazardous waste landfill cover design, Technical Letter No. 1110-1-162. Department of the Army, Washington, DC

US Army Corps of Engineers (2006) Select fill and topsoil for landfill covers, UFGS-02140. www.wbdg.org/ccb/DOd/UFGS/UFGS%2002%2066%2000.pdf. Accessed 12 Feb 2010. Department of the Army, Washington, DC

US Congress Office of Technology Assessment (1989) Facing America's trash: what next for municipal solid waste? US Government Printing Office, Washington, DC, OTA-O-424

US Congress Office of Technology Assessment (1992) Managing industrial solid wastes from manufacturing, mining, oil and gas production, and utility coal combustion. US Government Printing Office, Washington, DC, Background Paper, OTA-BP-O-82

US Department of the Army (1990) Solid waste management, Navy Manual NAVFAC MO-213, Air Force Regulation No. AFR 91-8, Army Manual No. TM 5-634. Departments of the Army, the Navy and the Air Force, Washington, DC

US DOE (1994) Mixed waste landfill integrated demonstration technology summary, Report Number DOE/EM-0128P. US DOE Office of Environmental Restoration and Waste Management, Office of Technology Development, US Department of Energy, Washington, DC, www.osti.gov/bridge/servlets/purl/143977Ay7G12/NATIVE/143 977.PDF. Accessed 11 Feb 2010

US EPA (1981) Process design manual: land treatment of municipal waste water. US Environmental Protection Agency, Cincinnati, EPA-625/1-81/013

US EPA (1982) RCRA guidance document: landfill design, liner systems and final cover. US Environmental Protection Agency, Washington, DC

US EPA (1989) The solid waste dilemma: An agenda for action. EPA/530-SW-89-019, Solid Waste and Emergency Response. US Environmental Protection Agency, Washington, DC

US EPA (1989) Technical guidance document: final covers on hazardous landfills and surface impoundments. US Environmental Protection Agency, Washington, DC, EPA 530-SW-89-047

US EPA (1990) How to meet requirements for hazardous waste landfill design, construction, and closure, Pollution technology review no. 185. Noyes Data Corp, Park Ridge

US EPA (1993) Criteria for solid waste disposal facilities: a guide for owners/operators. US Environmental Protection Agency, Washington, DC, EPA/530-SW-91-089

US EPA (1993) Engineering bulletin: landfill covers. Office of Emergency and Remedial Response, US Environmental Protection Agency, Washington, DC, EPA/540/S-93/500

US EPA (1993) Constructed wetlands for wastewater treatment and wildlife habitat-17 case studies. US Environmental Protection Agency, Washington, DC, EPA832-R-93-005

US EPA (1994) Seminar publication design, operation, and closure of municipal solid waste landfills. Center for Environmental Research Information, US Environmental Protection Agency, Cincinnati, Ohio. nepis.epa.gov/Exe/ZyPURL.cgi?Dockey=30004O0A.txt. Accessed 30 Mar 2010

US EPA (1997) Landfill reclamation. US Environmental Protection Agency, Washington, DC, EPA530-F-97-001

US EPA (1999) Preparing no-migration demonstrations for municipal solid waste disposal facilities: a screening tool. US Environmental Protection Agency, Washington, DC. EPA530-R-99-008

US EPA (2006) Revegetating landfills and waste containment areas fact sheet. Office of Superfund Remediation and Technology Innovation, US Environmental Protection Agency, Washington, DC

US EPA (2008) Landfills. US Environmental Protection Agency, Washington, DC http://www.epa.gov/waste/nonhaz/municipal/landfill.htm

US EPA (2009) Solid Waste Landfill Publications. US Environmental Protection Agency, Washington, DC. http://www.epa.gov/waste/nonhaz/municipal/landfill/sw_pubs.htm

Venkateswaran SR (1990) How to meet requirements for hazardous waste landfill design, construction and closure. William Andrew/Elsevier, New York

Velinni AA (2007) Landfill research trends. Nova, Hauppauge

Well LW (1997) Testing and acceptance criteria for geosynthetic clay liners, ASTM special technical publication STP 1308. ASTM, West Conshohocken

Westlake K (1995) Landfill waste pollution and control. Albion, Chichester

Wilderer P, Moletta R (2003) Anaerobic digestion of solid wastes III. In: Selected Proceedings of the 3rd IWA International Symposium on anaerobic digestion of solid wastes, held at Garching, Munich, Germany, 11–13 Sept 2002, International Water Association, London

Woods RD (1987) Geotechnical practice for waste disposal'87. In: Proceedings of a specialty conference, University of Michigan, Ann Arbor, Michigan, June 15–17, 1987, sponsored by the Geotechnical Engineering Division of the American Society of Civil Engineers, Geotechnical Special Publication No. 13. American Society of Civil Engineers (ASCE), New York

Yegian MK, Finn WDL (1995) Earthquake design and performance of solid waste landfills. In: Proceedings of the session sponsored by the soil mechanics Committee of the Geotechnical Engineering Division of the American Society of Civil Engineers in conjunction with the ASCE Convention in San Diego, California, October 23–27, 1995, Geotechnical Special Publication No. 54. American Society of Civil Engineers (ASCE), New York

Young M (2007) Garbage and recycling, Opposing Viewpoints Series. Greenhaven Press, an Imprint of Thomson Gale, a part of The Thomson Corporation, Detroit

Zimmie TF (2000) Environmental geotechnics. In: Proceedings of Sessions of Geo-Denver 2000. American Society of Civil Engineers (ASCE), Reston

Zornberg JG, Christopher BR (2000) Advances in transportation and geoenvironmental systems using geosynthetics. In: Proceedings of Sessions of Geo-Denver 2000, Geotechnical Special Publication 103, American Society of Civil Engineers (ASCE), Reston

Landscape Ecology

Jianguo (Jingle) Wu
School of Life Sciences and Global Institute of Sustainability, Arizona State University, Tempe, AZ, USA

Article Outline

Glossary
Definition of the Subject
Introduction
What is Landscape Ecology?
Key Research Topics Landscape Ecology
Future Directions
Bibliography

Glossary

Landscape A geographic area in which variables of interest are spatially heterogeneous. The boundary of a landscape may be delineated based on geographic, ecological, or administrative units (e.g., a watershed, an urban area, or a county) which are relevant to the research questions and objectives.

Landscape connectivity The degree of a landscape to facilitate or impede the exchange of organisms, energy, material, and information among landscape elements. This is sometimes referred to as landscape functional connectivity, which is a function of both landscape structural connectivity and the movement characteristics of the species or process under consideration. Landscape structural connectivity is simply a measure of how spatially connected the elements in a landscape are, without reference to any particular ecological process.

Landscape ecology The science of studying and improving the relationship between spatial pattern and ecological processes in a landscape on multiple scales. Landscape ecology studies the structure, function, and dynamics of landscapes of different kinds, including natural, seminatural, agricultural, and urban landscapes.

Landscape fragmentation The breaking-up of landscape into smaller patches by anthropogenic and natural forces or the introduction of barriers that impede exchange of organisms, energy, material, and information across a landscape. Habitat fragmentation is a similar term to landscape fragmentation, but has a more explicit focus on changes in habitat relevant for organisms of interest.

Landscape pattern The composition (diversity and relative abundances) and configuration (shape, size, and spatial arrangement) of landscape elements, including both spatial patchiness and gradients.

Landscape function The horizontal and vertical exchanges of organisms, energy, material, and information in a landscape.

Landscape structure The composition and spatial arrangement of landscape elements – including patches, corridors, and the matrix.

Landscape dynamics Temporal changes in the structure and function of a landscape, driven by natural and anthropogenic processes.

Landscape sustainability The ability of a landscape to maintain its basic environmental, economic, and social functions under ever-changing conditions driven by human activities and environmental changes. Landscape sustainability emphasizes the optimization of the composition and spatial configuration of the landscape so as to achieve a high level of resilience or persistency.

Metapopulation The total population system that is composed of multiple local populations geographically separated but connected through dispersal.

Patch dynamics A perspective that ecological systems are mosaics of patches, each exhibiting nonequilibrium dynamics and together determining the system-level behavior. Patches can be biotic or abiotic, ranging from a tree gap in a forest or a resource patch in a grassland to a whole ecosystem or a continent.

Pattern analysis The procedures with which landscape pattern is quantified, primarily, using synoptic indices and spatial statistical methods.

Scale The spatial or temporal dimension of a phenomenon. In landscape ecology, scale usually refers to grain and extent. Grain is the finest spatial or temporal unit in a data set, within which homogeneity is assumed, whereas extent is the total spatial area or temporal duration of a study. Grain and resolution are two related but distinct concepts. In general, fine-grained analyses require high-resolution data, but high-resolution data, after rescaling or aggregation, can also be used for coarse-grained analyses.

Scaling The translation of information between or across spatial and temporal scales or organizational levels.

Spatial heterogeneity The combination of discrete and continuous variations of one or more variables in a landscape, which can be characterized as patchiness, gradients, or a mixture of both. Spatial heterogeneity varies with scale in space and time.

Spatially explicit models Models that explicitly take account of the locations of processes in a two- or three-dimensional space so that the spatial arrangement of landscape elements matters.

Definition of the Subject

Landscapes are spatially heterogeneous areas characterized by a mosaic of patches that differ in size, shape, contents, and history. When spatial heterogeneity is considered, the explicit treatment of scale becomes necessary and hierarchies emerge. Landscape ecology is the science of studying and improving the relationship between spatial pattern and ecological processes on a multitude of scales and organizational levels. In a broad sense, landscape ecology represents both a field of study and a scientific paradigm. As a highly interdisciplinary and transdisciplinary enterprise, landscape ecology integrates biophysical and analytical approaches with humanistic and holistic perspectives across natural and social sciences. Landscape ecology was initially developed in Europe. With theoretical developments in spatial ecology and technological advances in remote sensing and geospatial information processing, landscape ecology became an internationally recognized field of study in the 1980s. The most salient characteristics of landscape ecology are its emphasis on the pattern-process relationship and its focus on broad-scale ecological and environmental issues. Key research topics in landscape ecology include ecological flows in landscape mosaics (e.g., movements of water, nutrients, plant propagules, animals, and other materials), land use and land cover change, scaling, understanding the relationship between landscape pattern metrics and ecological processes, and landscape conservation and sustainability.

Introduction

Landscape ecology is an interdisciplinary field that aims to understand and improve the relationship between spatial pattern and ecological processes on a range of scales [1]. Although the term appeared in the 1930s, landscape ecology was not a recognized scientific field of global scope until the 1980s when remote sensing data and computers became widely accessible to ecologists and geographers. The 1980s was also a time period when ecological ideas of spatial heterogeneity and nonequilibrium dynamics flourished, and when landscape ecology took roots in North America. Today, landscape ecology is a well-established field of study, with active participation of ecological, geographical, and social scientists from around the world.

Landscape ecology has been dominated by two schools of thought: the European perspective and the North American perspective. At the risk of oversimplification, the European landscape ecology perspective may be considered as being characterized by a more holistic, humanistic, and society-centered view, with a focus on user-inspired and solution-driven research. The North American landscape ecology perspective, on the other hand, has been dominated by a more analytical and biological ecology–centered view, with a focus on basic science-oriented and question-driven studies. Cautions must be exercised, however, to avoid overinterpretation of such dichotomous characterization [2]. The two perspectives are neither inclusive nor exclusive; they are not contradictory but complementary. There are, and should be, other approaches to landscape ecology. For example, one may argue for an Australian landscape ecology perspective that focuses on pragmatic and functional approaches, typically, tied

with land management, restoration, and conservation issues (e.g., [3]).

Landscape ecology is now a well-established interdisciplinary field of study, which is evidenced by several characteristics. These include an evolving but identifiable system of concepts, theories, principles, methods, and applications, a hierarchy of professional organizations from the international association to local chapters, a flagship journal, Landscape Ecology (http://www.springerlink.com/content/0921-2973), the adoption in educational and training programs by major universities and research institutes around the world, and an increasing number of publications in main-stream scientific journals which indicate its recognized status as well as its expanding impacts on related disciplines.

In this entry, I focus on the key concepts, research topics, and quantitative methods in landscape ecology. A number of textbooks on landscape ecology are available where more details on the contents covered here can be found [4–8].

What is Landscape Ecology?

Diverse Concepts of Landscape

The term, "landscape," is a key concept in a number of fields, from social to geographical and ecological sciences. With the rise of landscape ecology in the past several decades, the concept of landscape has achieved a prominent status in the interdisciplinary literature. However, because of the plurality of its origins and interpretations, landscape has acquired various connotations. For example, the same word may refer to a natural landscape, a cultural landscape, a political landscape, an economic landscape, a mental landscape, an adaptive landscape, a landscape view, landscaping, or landscape painting [9, 10].

Even within the field of landscape ecology, the word, "landscape," has different meanings, and the differences usually hinge on the spatial scale and the contents of a landscape. For example, landscape has been defined as a kilometers-wide geographic area [11, 12], which corresponds to the "human-scale" landscape. This is the scale at which the field of landscape ecology was originally developed in Europe, and at which most landscape studies have been conducted around the world ever since. The human-scale landscape, in general, seems to coincide well with geographic units such as watersheds and urban regions [4], as well as spatial domains of human perception [13]. Thus, it resonates with the public, the decision makers, and researchers who are conscious about the environmental setting in which they live, work, and engage in recreation.

Many other landscape ecologists, however, have treated landscape as a multi-scale or hierarchical concept, meaning that a landscape is a spatially heterogeneous area that may be of various sizes, depending on the subject of study and the research questions at hand [6, 14, 15]. In this case, landscape is an "ecological criterion" [14], and its essence does not lie in its absolute scale but in its internal heterogeneity. Different plant and animal species perceive, experience, and respond to spatial heterogeneity at different scales, and patterns and processes in landscapes tend to have different characteristic scales [16]. Thus, a hierarchical concept of landscape, of course also encompassing the human-scale, is both sensible and necessary. Apparently, one does not need to consider a landscape of tens of square kilometers to study how grassland vegetation pattern affects the movement of beetles [17] or is affected by gophers [18].

The elements that constitute a landscape vary greatly in landscape ecological research. For simplicity, the components of a landscape may be classified as tangible versus intangible and biophysical versus cultural. This is not intended to represent a dichotomous view, but rather a continuum within which a variety of components coexist. Tress and Tress [10] proposed a "transdisciplinary landscape concept" that encompasses five dimensions: (1) landscape as a spatial entity, (2) landscape as a mental entity, (3) landscape as a temporal dimension, (4) landscape as a nexus of nature and culture, and (5) landscape as a complex system. Landscape ecological studies often have focused on some but not all of these dimensions. The concept of landscape provides a meeting ground for a number of disciplines, including archaeology, ecology, geography, geology, history, landscape architecture, and regional economics. To achieve its interdisciplinary and transdisciplinary goals, landscape ecology needs to appreciate and integrate the multifaceted perspectives on the culture-nature/people-place relationships that are offered by these diverse disciplines.

Evolving Concepts of Landscape Ecology

The definitions of landscape ecology are also diverse, although they are not quite as numerous as those of landscape (Table 1). Images can be powerfully inspiring, and this is especially true to someone who has a special interest in landscape patterns. Partly inspired by the conspicuous spatial patterns revealed in aerial photographs, the German geographer and botanist Carl Troll [19] coined the term "landscape ecology" and defined it later as "the study of the main complex causal relationships between the life communities and their environment in a given section of a landscape" [20, 21]. Carl Troll's training and research in multiple disciplines endowed him with the abilities to synthesize across, and innovate at the interface between, different fields. He was trained as a botanist; did his doctoral dissertation in plant physiology; and then spent decades working on the climatic, geologic, geographical, and ecological aspects of various landscapes in Europe, South America, and Africa. It is not difficult to understand why Troll could simultaneously appreciate the then-new idea of "ecosystem" put forward by Arthur Tansley [28], as well as the great potential for geospatial analysis presented by aerophotography. As a result of his attempt to integrate the "vertical" ecological approach with the "horizontal" geographical approach, a new field of study was born.

In the past several decades, landscape ecology has acquired a number of definitions which all are, in some way, related to Carl Troll's original definition. For example, Zonneveld [22] defined landscape ecology as "an aspect of geographical study which considers the landscape as a holistic entity, made up of different elements, all influencing each other." He advocated that the landscape should be studied as the "total character of a region," not "in terms of the separate aspects of its component elements" [22, 29]. This holistic landscape perspective continues and culminates in the work by Naveh [30], who described landscape ecology as the study of "the total spatial and functional entity of natural and cultural living space."

Some key ideas of contemporary landscape ecology, such as patch dynamics [31–33] and the patch-corridor-matrix model [11, 12], began to emerge in North America in the late 1970s, apparently with little connection to the European root. The early ideas of landscape ecology in North America were inspired by the theory of island biogeography [34], with an explicit focus on spatial heterogeneity. The first major communication between North American and European landscape ecologists occurred in 1981 when five American ecologists attended the first International Congress on Landscape Ecology in the Netherlands. Two years later, 25 ecologists (23 Americans, 1 Canadian, and 1 French) gathered at Allerton Park, Illinois of USA, to discuss the nature and future directions of landscape ecology. The report of this historic work, published in the following year [24], became an important guide to the incipient landscape ecologists in North America [35].

Why was such discussion necessary after landscape ecological research had been practiced for more than 40 years in Europe? The answer seems clear from Forman [36]: "What theory explains the spatial heterogeneity of energy, nutrients, water, plants, and animals at the level of a landscape, the setting in which we live? Alas, none." To develop such a landscape theory, broader scales that encompass multiple ecosystems need to be considered, and horizontal interactions have to be a focus of study. Thus, Forman and Godron [11, 12] defined landscape ecology as the study of the structure (spatial relationships among the distinctive landscape elements), function (flows of energy, materials, and species among landscape elements), and dynamics (temporal change in landscape structure and function) of landscapes. The main theme of landscape ecology in North America, with an unmistakable focus on spatial heterogeneity, was set in Risser et al. [24]:

- Landscape ecology focuses explicitly upon spatial pattern. Specifically, landscape ecology considers the development and dynamics of spatial heterogeneity, spatial and temporal interactions and exchanges across heterogeneous landscapes, influences of spatial heterogeneity on biotic and abiotic processes, and management of spatial heterogeneity.

Is landscape ecology a subdiscipline of ecology? The term itself apparently suggests that it is. Many ecologists do consider landscape ecology as a branch of ecology (e.g., [6]), and most ecology programs of

Landscape Ecology. Table 1 A list of definitions of landscape ecology

Definition	Source
The German geographer Carl Troll coined the term "landscape ecology" in 1939, and defined it in 1968 as "the study of the main complex causal relationships between the life communities and their environment in a given section of a landscape. These relationships are expressed regionally in a definite distribution pattern (landscape mosaic, landscape pattern) and in a natural regionalization at various orders of magnitude" (Troll 1968; cited in Troll 1971)	• Troll [19] • Troll [20] • Troll [21]
"Landscape ecology is an aspect of geographical study which considers the landscape as a holistic entity, made up of different elements, all influencing each other. This means that land is studied as the 'total character of a region', and not in terms of the separate aspects of its component elements" (Zonneveld 1972)	• Zonneveld [22]
"Landscape ecology is a young branch of modern ecology that deals with the interrelationship between man and his open and built-up landscapes" based on general systems theory, biocybernetics, and ecosystemology (Naveh and Liberman 1984). "Landscapes can be recognized as tangible and heterogeneous but closely interwoven natural and cultural entities of our total living space," and landscape ecology is "a holistic and transdisciplinary science of landscape study, appraisal, history, planning and management, conservation, and restoration" (Naveh and Liberman 1994)	• Naveh and Lieberman [5] • Naveh and Lieberman [23]
"A landscape is a kilometers-wide area where a cluster of interacting stands or ecosystems is repeated in similar form; landscape ecology, thus, studies the structure, function and development of landscapes" (Forman 1981). Landscape structure refers to "the spatial relationships among the distinctive ecosystems;" landscape function refers to "the flows of energy, materials, and species among the component ecosystems;" and landscape change refers to "the alteration in the structure and function of the ecological mosaic over time" (Forman and Godron 1986).	• Forman [11] • Forman [12]
"Landscape ecology focuses explicitly upon spatial pattern. Specifically, landscape ecology considers the development and dynamics of spatial heterogeneity, spatial and temporal interactions and exchanges across heterogeneous landscapes, influences of spatial heterogeneity on biotic and abiotic processes, and management of spatial heterogeneity" (Risser et al. 1984). "Landscape ecology is not a distinct discipline or simply a branch of ecology, but rather is the synthetic intersection of many related disciplines that focus on the spatial-temporal pattern of the landscape" (Risser et al. 1984).	• Risser et al. [24]
"Landscape ecology emphasizes broad spatial scales and the ecological effects of the spatial patterning of ecosystems" (Turner 1989).	• Turner [25]
"Landscape ecology is the study of the reciprocal effects of the spatial pattern on ecological processes," and "concerns spatial dynamics (including fluxes of organisms, materials, and energy) and the ways in which fluxes are controlled within heterogeneous matrices" (Pickett and Cadenasso 1995).	• Pickett and Cadenasso [14]
"Landscape ecology investigates landscape structure and ecological function at a scale that encompasses the ordinary elements of human landscape experience: yards, forests, fields, streams, and streets" (Nassauer 1997).	• Nassauer [26]
Landscape ecology is "ecology that is spatially explicit or locational; it is the study of the structure and dynamics of spatial mosaics and their ecological causes and consequences" and "may apply to any level of an organizational hierarchy, or at any of a great many scales of resolution" (Wiens 1999).	• Wiens [27]

Landscape Ecology. Table 1 (Continued)

Definition	Source
"Landscape ecology emphasizes the interaction between spatial pattern and ecological process, that is, the causes and consequences of spatial heterogeneity across a range of scales" (Turner et al. 2001). "Two important aspects of landscape ecology . . . distinguish it from other subdisciplines within ecology": "First, landscape ecology explicitly addresses the importance of spatial configuration for ecological processes" and "second, landscape ecology often focuses on spatial extents that are much larger than those traditionally studied in ecology, often, the landscape as seen by a human observer" (Turner et al. 2001).	• Turner [6]
"Landscape ecology is the science and art of studying and influencing the relationship between spatial pattern and ecological processes across hierarchical levels of biological organization and different scales in space and time."	• Wu and Hobbs [1]

major research universities worldwide now offer courses in landscape ecology. On the other hand, Zonneveld [22] indicated that landscape ecology is not part of biological sciences, but a branch of geography. Risser et al. [24] contemplated three ways in which landscape ecology may be viewed: as an intersection of many disciplines, as a separate discipline, or as a branch of ecology. They concluded that only the first option was "intellectually and practically the most persuasive." They further pointed out that "viewing landscape ecology as an interdisciplinary field of research avoids the issue of which discipline 'owns' landscape ecology" (a problem that may have hindered the healthy development of some interdisciplinary fields, such as human ecology, for which geography, sociology, and anthropology all have claimed ownership). The Allerton workshop report clearly recognized the importance of the multidimensionality of landscapes and the interdisciplinarity of landscape ecology:

- A major forcing function of landscapes is the activity of mankind, especially associated cultural, economic, and political phenomena. . . . Landscape ecology is not a distinct discipline or simply a branch of ecology, but rather is the synthetic intersection of many related disciplines that focus on the spatial-temporal pattern of the landscape" [24].

Today, a general consensus seems to have emerged that landscape ecology is not simply an academic discipline, but rather a highly interdisciplinary field of study [2, 37]. Landscape ecology is an interdisciplinary and transdisciplinary science that focuses on the relationship between spatial pattern and ecological processes across scales. The goal of landscape ecology is not only to understand this relationship but also to influence it so as to help achieve landscape sustainability [38–40]. As such, a pluralistic and hierarchical framework has been proposed to facilitate synergistic interactions between biophysical/pattern-process and holistic/humanistic perspectives (Fig. 1) [37, 38]. "Hierarchical" here refers to the varying degrees of interdisciplinary, the hierarchy of organizational levels, and the multiplicity of spatiotemporal scales of landscape ecological studies. "Pluralistic" indicates the necessity and importance of recognizing and valuing the different perspectives and methods in landscape ecology due to its diverse origins and goals.

Key Research Topics Landscape Ecology

Based on the suggestions by a group of leading landscape ecologists (Table 2), Wu and Hobbs [2] identified six key issues that characterize landscape ecology: (1) interdisciplinarity or transdisciplinarity, (2) integration between basic research and applications, (3) Conceptual and theoretical development, (4) education and training, (5) international scholarly communication and collaborations, and (6) outreach and communication with the public and decision makers. Wu and Hobbs [2] also summarized ten key research topics and priorities as follows:

1. Ecological flows in landscape mosaics: A primary goal of landscape ecology is to understand the reciprocal relationship between spatial pattern and ecological processes [14]. Understanding the mechanisms of flows of organisms, energy,

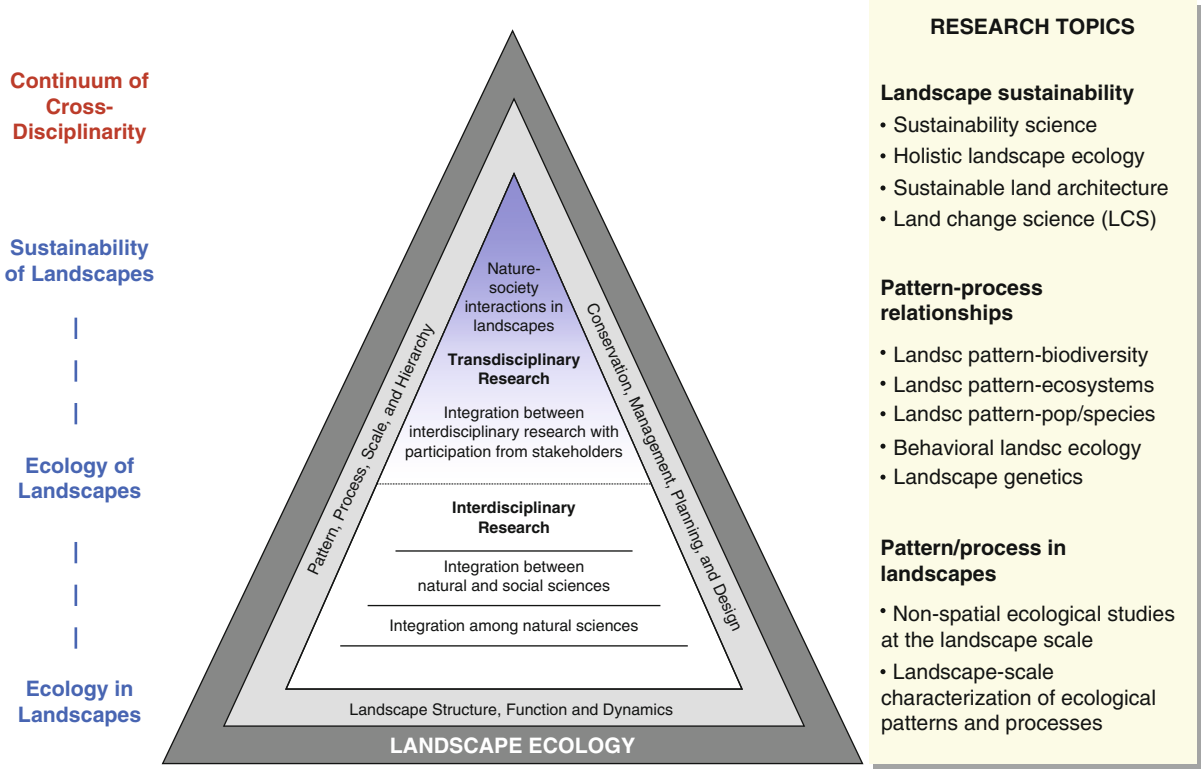

Landscape Ecology. Figure 1
A schematic representation of a hierarchical and pluralistic view of landscape ecology (Modified from [38])

material, and information in landscape mosaics is central to landscape ecology. In particular, the study of the effects of spatial pattern on population and ecosystem processes has made much progress in the past several decades. There is a need to integrate socioeconomic theory of landscape change into metapopulation models to make them more relevant to the issues of biodiversity conservation and landscape sustainability. The spread of invading species has become an increasingly important ecological and economic problem which deserves more research efforts.

2. Causes, processes, and consequences of land use and land cover change: Land use and land cover change is arguably the most important driver for changes in the structure and function of landscapes. Land use and land cover change is driven primarily by socioeconomic forces, and is one of the most important and challenging research areas in landscape ecology. Numerous studies have been carried out to investigate the effects of land use and land cover change on biodiversity and ecological flows in human-dominated landscapes. More research efforts are needed to incorporate the insights of economic geography which studies how economic activity is distributed in space and resource economics which determines how land will be used [41]. Long-term landscape changes induced by economic activities and climate change, as well as "land use legacies" (i.e., the types, extents, and durations of persistent effects of prior land use on ecological patterns and processes) need to be emphasized in future research.
3. Nonlinear dynamics and landscape complexity: Landscapes are spatially extended complex systems which exhibit emergent properties, phase transitions, and threshold behavior. To understand the complexity of landscapes, concepts and methods from the science of complexity and nonlinear dynamics should be helpful.

Landscape Ecology. Table 2 A list of major research topics in landscape ecology suggested by a group of leading landscape ecologists from around the world at the 16th Annual Symposium of the US Regional Association of the International Association for Landscape Ecology, held at Arizona State University, Tempe, in April 2001 [2]

Development of theory and principles	• Landscape mosaics and ecological flows • Land transformations • Landscape sustainability • Landscape complexity
Landscape metrics	• Norms or standards for metric selection, change detection, etc. • Integration of metrics with holistic landscape properties • Relating metrics to ecological processes • Sensitivity to scale change
Ecological flows in landscape mosaics	• Exchanges of organisms, material, energy, and information across the landscape • Effects of connectivity, edges, and boundaries • Spread of invading species • Spatial heterogeneity and ecosystem processes • Disturbances and patch dynamics
Optimization of landscape pattern	• Optimization of land use pattern • Optimal management • Optimal design and planning • New methods spatial optimization
Metapopulation theory	• Integration of the view of landscape mosaics • Incorporation of socioeconomic factors and management decisions
Scaling	• Extrapolating information across heterogeneous landscapes • Development of scaling theory and methods • Derivation of empirical scaling relations for landscape pattern and processes
Complexity and nonlinear dynamics of landscapes	• Landscapes as spatially extended complex systems • Landscapes as complex adaptive systems • Thresholds, criticality, and phase transitions • Self-organization in landscape structure and dynamics
Land use and land cover change	• Biophysical and socioeconomic drivers and mechanisms • Ecological consequences and feedbacks • Long-term landscape changes driven by economies and climate changes
Spatial heterogeneity in aquatic systems	• The relationship between spatial pattern and ecological processes in lakes, rivers, and oceans • Terrestrial and aquatic comparisons
Landscape-scale experiments	• Experimental landscape systems • Field manipulative studies • Scale effects in experimental studies
New methodological developments	• Integration among observation, experimentation, and modeling • New statistical and modeling methods for spatially explicit studies • Interdisciplinary and transdisciplinary approaches
Data collection and accuracy assessment	• Multiple-scale landscape data • More emphasis on collecting data on organisms and processes • Data quality control • Metadata and accuracy assessment
Fast changing and chaotic landscapes	• Rapidly urbanizing landscapes • War zones • Other highly dynamic landscapes

Landscape Ecology. Table 2 (Continued)

Landscape sustainability	• Developing operational definitions and measures that integrate ecological, social, cultural, economic, and aesthetic components • Practical strategies for creating and maintaining landscape sustainability
Human activities in landscapes	• The role of humans in shaping landscape pattern and processes • Effects of socioeconomic and cultural processes on landscape structure and functioning
Holistic landscape ecology	• Landscape ecology as an anticipative and prescriptive environmental science • Development of holistic and systems approaches

For example, self-organization, percolation theory, complex adaptive systems (CAS), fractal geometry, cellular automata, and genetic algorithms have been used in the study of spatiotemporal dynamics of landscapes (e.g., [42–46]). However, the theoretical potential and practical implications of these concepts and methods are yet to be fully explored.

4. Scaling: Scaling refers to the translation of information from one scale to another across space, time, or organizational levels. Spatial scaling, in particular, is essential in both the theory and practice of landscape ecology because spatial heterogeneity does not make any sense without the consideration of scale [47]. While scale effects are widely recognized in landscape ecology, scaling-up or scaling-down across heterogeneous landscapes remains a grand challenge in landscape ecology and beyond [48]. General rules and pragmatic methods for scaling landscape patterns and processes need to be developed and tested.
5. Methodological advances: Landscape variables are often spatially autocorrelated and spatially dependent, which poses serious challenges for using traditional statistical methods based on the assumption of independence of observations. The spatial autocorrelation and dependence that traditional statistical methods try to get rid of are usually what landscape analyses intend to get at. Thus, spatial statistical methods that directly deal with spatial autocorrelation and dependence have increasingly been used in landscape ecology. Also, most landscape ecological problems need to be studied over large and multiple scales in a spatially explicit manner. This need poses problems such as the lack of replicability or "pseudoreplication" [49]. To get to the processes and mechanisms of landscape phenomena, landscape ecology has developed a suite of spatially explicit modeling approaches [50, 51]. In both spatial analysis and modeling of landscapes, remote sensing and GIS (geographic information systems) have become indispensable.
6. Relating spatial pattern measures to ecological processes: To understand the relationship between pattern and process, quantifying landscape pattern is necessary. Indeed, landscape pattern analysis has been a major part of landscape ecological research for the last few decades. A number of landscape metrics (Table 3) and spatial statistical methods have been developed and applied for describing and comparing the spatial patterns of landscapes, monitoring and predicting changes in landscape patterns, and relating spatial pattern to ecological processes at a particular scale or across a range of scales [47, 53, 54]. Nevertheless, a sound ecological understanding of these spatial analysis methods is yet to be fully developed [55].
7. Integrating humans and their activities into landscape ecology: Socioeconomic processes are the primary drivers for land use and land cover change which in turn determines the structure, function, and dynamics of most landscapes. Social and economic processes have increasingly been integrated into landscape ecological studies. The need for incorporating humans, including their perceptions, value systems, cultural traditions, and socioeconomic activities, into landscape ecology has made it a highly interdisciplinary and transdisciplinary enterprise [38, 56]. That said, effectively integrating human-related processes into ecology may remain one of the

Landscape Ecology. Table 3 Some commonly used landscape metrics [4, 52]

Landscape metric	Abbreviation	Description
Patch shape index	PSI	A measure for the complexity of the shape of a given patch: $PSI = \frac{P}{2\sqrt{A\pi}}$ where P is the perimeter of a patch, and A is the area of the patch. $PSI = 1$ for circles; $PSI = 1.1283$ for squares; and $PSI = 1.1968$ for a rectangle (2 L by L). $1/D$ is called "compactness" (see Forman [4]).
Perimeter/area ratio	PAR	A measure of the complexity of the shape of a patch: $PAR = P/A$ where P is the perimeter of a patch, and A is the area of the patch.
Number of patches	NP	The total number of patches in the landscape.
Patch density	PD	The number of patches per square kilometer (i.e., 100 ha).
Total edge	TE	The sum of the lengths of all edge segments (unit: meter).
Edge density	ED	The total length of all edge segments per hectare for the class or landscape of consideration (unit: m/ha).
Patch richness	PR	The number of different patch types in the landscape.
Patch richness density	PRD	The number of patch types per square kilometer (or 100 ha).
Shannon's diversity index	SHDI	A measure of patch diversity in a landscape that is determined by both the number of different patch types and the proportional distribution of area among patch types: $H = -\sum_{i=1}^{m} p_i \ln(p_i)$ where m is the total number of patch types and p_i is the proportion of the landscape area occupied by patch type i.
Dominance index	D	A measure of the degree of dominance by one or a few patch types in a landscape: $D = H_{\max} + \sum_{i=1}^{m} p_i \ln p_i$ where $H_{\max}$ is the maximum diversity when all patch types are present in equal proportions, m is the total number of patch types, and p_i is the proportion of the landscape area occupied by patch type i. Small values of D tend to indicate landscapes with numerous land use types of similar proportions.
Largest patch index	LPI	The ratio of the area of the largest patch to the total area of the landscape (unit: percentage).
Mean patch size	MPS	The average area of all patches in the landscape (unit: ha).
Patch size standard deviation	PSSD	The standard deviation of patch size in the entire landscape (unit: ha).
Patch size coefficient of variation	PSCV	The standard deviation of patch size divided by mean patch size for the entire landscape (unit: percentage).
Landscape shape index	LSI	A modified perimeter/area ratio of the form: $LSI = \frac{0.25E}{\sqrt{A}}$ where E is the total length of patch edges and A is the total area of the landscape (unitless).

Landscape Ecology. Table 3 (Continued)

Landscape metric	Abbreviation	Description
Mean patch shape index	MSI	A patch-level shape index averaged over all patches in the landscape: $MSI = \frac{\sum_{i=1}^{m}\sum_{j=1}^{n}\left[\frac{0.25P_{ij}}{\sqrt{a_{ij}}}\right]}{N}$ where P_{ij} and a_{ij} are the perimeter and area of patch ij, respectively, and N is the total number of patches in the landscape (unitless).
Area-weighted mean patch shape index	AWMSI	Mean patch shape index weighted by relative patch size: $AWMSI = \sum_{i=1}^{m}\sum_{j=1}^{n}\left[\left(\frac{0.25P_{ij}}{\sqrt{a_{ij}}}\right)\left(\frac{a_{ij}}{A}\right)\right]$ where P_{ij} and a_{ij} are the perimeter and area of patch ij, respectively, A is the total area of the landscape, m is the number of patch types, and n is the total number of patches of type i (unitless).
Double-log fractal dimension	DLFD	The fractal dimension for the entire landscape which is equal to 2 divided by the slope of the regression line between the logarithm of patch area and the logarithm of patch perimeter: $DLFD = \frac{2}{\left[\frac{\left[N\sum_{i=1}^{m}\sum_{j=1}^{n}\left(\ln(P_{ij})\ln(a_{ij})\right)\right]-\left[\left(\sum_{i=1}^{m}\sum_{j=1}^{n}\ln(a_{ij})\right)\right]}{\left(N\sum_{i=1}^{m}\sum_{j=1}^{n}\left(\ln(P_{ij}{}^{2})\right)\right)-\left(\sum_{i=1}^{m}\sum_{j=1}^{n}\ln(P_{ij})\right)^{2}}\right]}$ where P_{ij} and a_{ij} are the perimeter and area of patch ij, respectively, m is the number of patch types, n is the total number of patches of type i, and N is the total number of patches in the landscape (unitless).
Mean patch fractal dimension	MPFD	The average fractal dimension of individual patches in the landscape, which is the summation of fractal dimension for all patches divided by the total number of patches in the landscape: $FD = \frac{\sum_{i=1}^{m}\sum_{j=1}^{n}\left(\frac{2\ln(0.25P_{ij})}{\ln(a_{ij})}\right)}{N}$ where P_{ij} and a_{ij} are the perimeter and area of patch ij, respectively, m is the number of patch types, n is the total number of patches of type i, and N is the total number of patches in the landscape (unitless).
Area-weighted mean patch fractal dimension	AWMFD	The patch fractal dimension weighted by relative patch area: $AWMPED = \sum_{i=1}^{m}\sum_{j=1}^{n}\left(\frac{2\ln(0.25P_{ij})}{\ln(a_{ij})}\left(\frac{a_{ij}}{A}\right)\right)$ where P_{ij} and a_{ij} are the perimeter and area of patch ij, respectively, m is the number of patch types, n is the total number of patches of type i, and A is the total area of the landscape (unitless).
Contagion	CONT	An information theory–based index that measures the extent to which patches are spatially aggregated in the landscape [57]: $CONT = \left[1+\sum_{i=1}^{m}\sum_{j=1}^{m}p_{ij}\ln(p_{ij})/2\ln(m)\right](100)$ where p_{ij} is the probability that two randomly chosen adjacent pixels belong to patch type i and j, m is the total number of patch types in the landscape (unitless).

ultimate challenges for landscape ecologists in years to come.

8. Optimization of landscape pattern: If spatial pattern significantly influences ecological processes in the landscape, then there must be certain patterns that are better than others in terms of promoting ecosystem functioning and services. This is a question of landscape pattern optimization (e.g., optimization of land use pattern, optimal landscape management, optimal landscape design, and planning). For example, can landscape patterns be optimized in terms of both the composition and configuration of patches and matrix characteristics to maximize biodiversity and ecosystem services? Are there optimal ways of "spatially meshing nature and culture" to promote landscape sustainability? These are some of the challenging questions that landscape ecologists ought to address now and in the future. Spatial optimization of landscape pattern for environmental purposes presents exciting research opportunities and requires interdisciplinary approaches.
9. Landscape conservation and sustainability: Biodiversity, ecosystem functions, and human activities, all take place in landscapes. Landscape fragmentation profoundly alters ecological and socioeconomic processes. Thus, the importance of applying landscape ecological principles in biodiversity conservation and sustainable development has been increasingly recognized. However, specific landscape ecological guidelines for biodiversity conservation are needed, and a comprehensive and operational definition of landscape sustainability is yet to be developed.
10. Data acquisition and accuracy assessment: Landscape ecological studies use large-scale and multiscale data. A suite of advanced technologies are readily available, including various remote sensing techniques, GIS, GPS (global positioning systems), and spatial analysis and modeling approaches. However, ecological understanding of species and ecosystems is essential in landscape ecology, and this requires the collection of basic biological data of landscapes. Also, to ensure the quality of landscape data, error analysis, uncertainty analysis, and accuracy assessment have become a key issue in landscape ecological research.

Future Directions

Landscape ecology is a highly interdisciplinary field of study which is characterized, most conspicuously, by its spatial explicitness in dealing with ecological problems in theory and practice. Emphasis on spatial heterogeneity begs questions of the pattern-process relationships and scale. Studying spatial pattern without relating it to ecological processes is superficial, and investigating ecological processes without consideration of spatial pattern is incomplete. From this perspective, landscape ecology is a science of heterogeneity and scale, providing a new scientific paradigm for ecology and other related fields.

On the other hand, with increasing human dominance in the biosphere, emphasis on broad spatial scales makes it inevitable to deal with humans and their activities. As a consequence, humanistic and holistic perspectives have been and will continue to be central in landscape ecological research. Thus, landscape ecology has become increasingly relevant to sustainability research and practice [38, 56]. First, landscape ecology provides a hierarchical and integrative ecological basis for dealing with issues of biodiversity and ecosystem functioning from fine to broad scales. Second, landscape ecology has already developed a number of holistic and humanistic approaches to studying nature–society interactions. Third, landscape ecology offers theory and methods for studying the effects of spatial configuration of biophysical and socioeconomic component on the sustainability of a place. Fourth, landscape ecology has developed a suite of pattern metrics and indicators which can be used for quantifying sustainability in a geospatially explicit manner. Finally, landscape ecology provides both theoretical and methodological tools for dealing with scaling and uncertainty issues that are fundamental to most nature–society interactions.

To move forward, future landscape ecological studies need to further address the key research topics as discussed earlier in this entry. In addition, concerted efforts need to be made to focus on sustainability-related research questions. For example, what theories, principles, and methods of landscape ecology are pertinent to sustainability and how can they be operationalized? How does landscape pattern or spatial heterogeneity affect sustainability? How do ecological,

economic, and social patterns and processes in landscapes change with scale and interact to influence sustainability? How is landscape sustainability measured and what roles can landscape metrics play in all this? How can landscape models to project sustainability trajectories in response to environmental, economic, social, and institutional changes be developed? And finally, how can landscape ecology help design sustainable landscapes?

Bibliography

Primary Literature

1. Wu J, Hobbs R (2007) Landscape ecology: the-state-of-the-science. In: Wu J, Hobbs R (eds) Key topics in landscape ecology. Cambridge University Press, Cambridge, pp 271–287
2. Wu J, Hobbs R (2002) Key issues and research priorities in landscape ecology: an idiosyncratic synthesis. Landscape Ecol 17:355–365
3. Ludwig J, Tongway D, Freudenberger D, Noble J, Hodgkinson K (1997) Landscape ecology, function and management: principles from Australia's rangelands. CSIRO, Collingwood
4. Forman RTT (1995) Land mosaics: the ecology of landscapes and regions. Cambridge University Press, Cambridge
5. Naveh Z, Lieberman AS (1984) Landscape ecology: theory and application. Springer, New York
6. Turner MG, Gardner RH, O'Neill RV (2001) Landscape ecology in theory and practice: pattern and process. Springer, New York
7. Burel F, Baudry J (2003) Landscape ecology: concepts, methods and applications. Science, Enfield
8. Farina A (1998) Principles and methods in landscape ecology. Chapman & Hall, London
9. Mitchell D (2000) Cultural geography: a critical introduction. Blackwell, Oxford
10. Tress B, Tress G (2001) Capitalising on multiplicity: a transdisciplinary systems approach to landscape research. Landscape Urban Plan 57:143–157
11. Forman RTT (1981) Interaction among landscape elements: a core of landscape ecology. In: Tjallingii SP, de Veer AA (eds) Perspectives in landscape ecology: contributions to research, planning and management of our environment. Pudoc, Wageningen, pp 35–48
12. Forman RTT, Godron M (1986) Landscape ecology. Wiley, New York
13. Gobster PH, Nassauer JI, Daniel TC, Fry G (2007) The shared landscape: what does aesthetics have to do with ecology? Landscape Ecol 22:959–972
14. Pickett STA, Cadenasso ML (1995) Landscape ecology: spatial heterogeneity in ecological systems. Science 269:331–334
15. Urban DL, O'Neill RV, Shugart HH (1987) Landscape ecology: a hierarchical perspective can help scientists understand spatial patterns. BioScience 37:119–127
16. Wu J, Loucks OL (1995) From balance-of-nature to hierarchical patch dynamics: a paradigm shift in ecology. Quart Rev Biol 70:439–466
17. Wiens JA, Milne BT (1989) Scaling of "landscape" in landscape ecology, or, landscape ecology from a beetle's perspective. Landscape Ecol 3:87–96
18. Wu J, Levin SA (1994) A spatial patch dynamic modeling approach to pattern and process in an annual grassland. Ecol Monogr 64(4):447–464
19. Troll C (1939) Luftbildplan and ökologische Bodenforschung. Zeitschrift der Gesellschaft für Erdkunde zu Berlin 7–8:241–298
20. Troll C (1968) Landschaftsökologie. In: Tuxen B (ed) Pflanzensoziologie und Landschaftsökologie, Berichte das 1963 internalen symposiums der internationalen vereinigung fur vegetationskunde. Junk, The Hague, pp 1–21
21. Troll C (1971) Landscape ecology (geoecology) and biogeocenology–a terminology study. Geoforum 8(71):43–46
22. Zonneveld IS (1972) Land evaluation and land(scape) science. International Institute for Aerial Survey and Earth Sciences, Enschede
23. Naveh Z, Lieberman AS (1994) Landscape ecology: theory and application, 2nd edn. Springer, New York
24. Risser PG, Karr JR, Forman RTT (1984) Landscape ecology: directions and approaches. Illinois Natural History Survey Special Publication 2, Champaign
25. Turner MG (1989) Landscape ecology: the effect of pattern on process. Ann Rev Ecol Syst 20:171–197
26. Nassauer JI (1997) Culture and landscape ecology: insights for action. In: Nassauer JI (ed) Placing nature. Island Press, Washington, DC, pp 1–11
27. Wiens JA (1999) Toward a unified landscape ecology. In: Wiens JA, Moss MR (eds) Issues in landscape ecology. International Association for Landscape Ecology, Snowmass Village, pp 148–151
28. Tansley AG (1935) The use and abuse of vegetational concepts and terms. Ecology 16:284–307
29. Zonneveld IS (1989) The land unit – a fundamental concept in landscape ecology, and its applications. Landscape Ecol 3:67–86
30. Naveh Z (1991) Some remarks on recent developments in landscape ecology as a transdisciplinary ecological and geographical science. Landscape Ecol 5:65–73
31. Burgess RL, Sharpe DM (eds) (1981) Forest Island dynamics in man-dominated landscapes. Springer, New York
32. Levin SA, Paine RT (1974) Disturbance, patch formation and community structure. Proc Nat Acad Sci USA 71:2744–2747
33. Pickett STA, Thompson JN (1978) Patch dynamics and the design of nature reserves. Biol Conser 13:27–37
34. MacArthur RH, Wilson EO (1967) The theory of island biogeography. Princeton University Press, Princeton
35. Wiens JA (2008) Allerton Park 1983: the beginnings of a paradigm for landscape ecology? Landscape Ecol 23:125–128
36. Forman RTT (1983) An ecology of the landscape. BioScience 33:535
37. Wu J, Hobbs RJ (eds) (2007) Key topics in landscape ecology. Cambridge University Press, Cambridge

38. Wu J (2006) Landscape ecology, cross-disciplinarity, and sustainability science. Landscape Ecol 21:1–4
39. Wu J (2008) Making the case for landscape ecology: an effective approach to urban sustainability. Landscape J 27:41–50
40. Wu J (2010) Urban sustainability: an inevitable goal of landscape research. Landscape Ecol 25:1–4
41. O'Neill RV (1999) Theory in landscape ecology. In: Wiens JA, Moss MR (eds) Issues in landscape ecology. International Association for Landscape Ecology, Snowmass Village, pp 1–5
42. With KA, Pavuk DM, Worchuck JL, Oates RK, Fisher JL (2002) Threshold effects of landscape structure on biological control in agroecosystems. Ecol Appl 12:52–65
43. Milne BT (1998) Motivation and benefits of complex systems approaches in ecology. Ecosystems 1:449–456
44. Levin SA (1998) Ecosystems and the biosphere as complex adaptive systems. Ecosystems 1:431–436
45. Levin SA (2005) Self-organization and the emergence of complexity in ecological systems. BioScience 55:1075–1079
46. Gardner RH, Milne BT, Turner MG, O'Neill RV (1987) Neutral models for the analysis of broad-scale landscape pattern. Landscape Ecol 1:19–28
47. Wu J (2004) Effects of changing scale on landscape pattern analysis: scaling relations. Landscape Ecol 19:125–138
48. Wu J, Jones KB, Li H, Loucks OL (eds) (2006) Scaling and uncertainty analysis in ecology: methods and applications. Springer, Dordrecht
49. Hargrove WW, Pickering J (1992) Pseudoreplication: a sine qua non for regional ecology. Landscape Ecol 6:251–258
50. Turner MG, Gardner RH (1991) Quantitative methods in landscape ecology: the analysis and interpretation of landscape heterogeneity. Springer, New York
51. Wu J, Levin SA (1997) A patch-based spatial modeling approach: conceptual framework and simulation scheme. Ecol Model 101:325–346
52. McGarigal K, Marks BJ (1995) FRAGSTATS: spatial pattern analysis program for quantifying landscape structure. Genernal Technnical Report PNW-GTR-351. Pacific Northwest Research Station, USDA-Forest Service, Portland
53. Gustafson EJ (1998) Quantifying landscape spatial pattern: what is the state of the art? Ecosystems 1:143–156
54. Fortin M-J, Dale MRT (2005) Spatial analysis: a guide for ecologists. Cambridge University Press, Cambridge
55. Li HB, Wu JG (2004) Use and misuse of landscape indices. Landscape Ecol 19:389–399
56. Naveh Z (2007) Landscape ecology and sustainability. Landscape Ecol 22:1437–1440
57. Li H, Reynolds JF (1993) A new contagion index to quantify spatial patterns of landscapes. Landscape Ecol 8(3):155–162

Books and Reviews

Barrett GW, Peles JD (eds) (1999) Landscape ecology of small mammals. Springer, New York
Bissonette JA (ed) (1997) Wildlife and landscape ecology: effects of pattern and scale. Springer, New York
Dramstad WE, Olson JD, Forman RTT (1996) Landscape ecology principles in landscape architecture and land-use planning. Harvard University Graduate School of Design/Island Press, Cambridge
Hansson L, Fahrig L, Merriam G (1995) Mosaic landscapes and ecological processes. Chapman & Hall, London
Ingegnoli V (2002) Landscape ecology: a widening foundation. Springer, Berlin
Nassauer JI (ed) (1997) Placing nature: culture and landscape ecology. Island Press, Washington, DC
Naveh Z, Lieberman AS (1994) Landscape ecology: theory and application. Springer, New York
Turner MG (2005) Landscape ecology: what is the state of the science? Ann Rev Ecol Systemat 36:319–344
Wiens J, Moss M (eds) (2005) Issues and perspectives in landscape ecology. Cambridge University Press, Cambridge
Wu J, Hobbs R (eds) (2007) Key topics in landscape ecology. Cambridge University Press, Cambridge
Wu J, Jones B, Li H, Loucks O (eds) (2006) Scaling and uncertainty analysis in ecology. Springer, Dordrecht

Landscape Planning for Minimizing Land Consumption

Henning Nuissl[1], Stefan Siedentop[2]
[1]Geographical Institute, Humboldt-Universität zu Berlin, Berlin, Germany
[2]Institute of Regional Development Planning, University of Stuttgart, Stuttgart, Germany

Article Outline

Glossary
Definition and Relavance of the Subject
Introduction
A Conceptualization of Land Consumption
The Means of Spatial Planning to Minimize Land Consumption
Future Directions
Acknowledgment
Bibliography

Glossary

Development plan A document (often consisting of several written documents and maps) that aims at organizing the spatial development in a particular territory in a comprehensive manner; the term

development plan has different meanings in different legal and administrative contexts, in many countries it is used for indicative rather than compulsory plans that complement land use planning by addressing additional aspects of spatial development (e.g., infrastructure planning).

Density, urban density Urban densities are measured by the number of people (or housing units, floor space, jobs) per unit urban land (e.g., km, hectare, acre); density is an important measure of urban form; the density of a lot, a neighborhood, or city usually indicates the intensity of urban land uses.

Green belt Idea of retaining an area of largely undeveloped, agricultural, or wild or park land surrounding an urban settlement.

Greenfield development Urban development that occurs on previously nonurban (agricultural, forestry, pasture, or other) land (as opposed to brownfield development that occurs on derelict sites); synonym of land consumption.

Growth management A set of policies and interventions used by governments at different tiers to ensure that urban growth occurs in a controlled and sustainable way; the containment of urban growth to counteract urban sprawl, the sufficient supply with urban services, and the protection of valuable land resources are the most important aims of growth management programs.

Land consumption Conversion of land use from nonurban (agricultural, forestry, pasture, or other) to urban uses (mainly residential, industrial, commercial, and transport); the term has a pejorative connotation.

Land cover The observed biophysical cover on the earth's surface, usually expressed in terms of vegetation cover or lack of it; land cover changes can occur as the conversion from one class of land cover to another or as a changing condition within a land cover class.

Land use Human employment of land; land use is characterized by the arrangements, activities, and inputs undertaken by humans in order to use land for productive or reproductive purposes; urban land use change can be attributed to the change of use from a land use class to another or to varying intensities within a land use class.

Land use pattern Spatial configuration of land uses or patches.

Land use plan Product of land use planning that is usually legally binding and prescribes how a piece of land can (and how it must not) be used.

Land use planning Any systematic effort of public authorities to organize (or at least influence) the way people, that is, society, make use of the land.

Spatial planning Any systematic effort of public authorities to organize, that is, influence the pattern of spatial organization of society. (Spatial planning is often used as a synonym of land use planning but can be seen as the broader term that also includes sector-specific planning, e.g., the planning and allocation of infrastructures.)

Suburbanization Suburbanization occurs when the growth of the suburbs (population, employment) dominates that of the central city; suburbanization is driven by relocation decisions of private households and firms leaving the central parts of metropolitan areas in favor of suburban, less dense, and cheaper lands; at the same time, suburbanization can also be caused by in-migration from outside the metropolitan area to the suburban parts.

Urban design plan A specific kind of land use plan, which, according to the planning system of many countries, formulates detailed norms for the land use of smaller areas (e.g., a couple of building blocks); urban design plans are often drawn up for areas that are about to be developed or fundamentally restructured.

Urbanization An increase in the proportion of the population living in urban areas or cities (urban systems).

Urban sprawl A specific, mostly unintended, pattern of land use that exhibits low-density residential and commercial settlements, the spatial segregation of certain land use types in specialized zones, and a spatially discontinuous urban expansion; in metropolitan areas, both in developed and developing countries, urban sprawl is the dominating spatial manifestation of land consumption.

Urban growth boundary (UGB) Line, defined by land use planning, which circumscribes an entire urbanized area and mandates that the area inside the boundary is to be used for higher density urban

development and the area outside for lower density development.

Urban system Human settlements with a minimum population density.

Zoning The practice of designating permitted uses of land to particular areas that are unambiguously separated from each other; zoning is usually enacted via land use plans and primarily aims at segregating uses that are thought to be incompatible.

Definition and Relevance of the Subject

Land use-driven environmental degradation has long been considered a locally scaled phenomenon. Today, the global dimension of land use related environmental change is generally acknowledged by researchers and policy makers [1–4]. The need to provide a still growing world population with housing, food, fiber, and freshwater accompanied with wasteful land use practices has resulted in a cumulative loss of biologically productive land and ecosystem functions. Moreover, land use practices are directly or indirectly responsible for the chemical degradation of environmental resources and high levels of greenhouse gases. Thus, land use has become a more and more important agent of global change that influences fundamental environmental processes. Foley et al. [1, p 572] rightly point out that modern land use processes allow humans to increase the short-term supply of material goods but undermine ecosystem services in the long run on regional and global scales.

Urbanization or – more specifically – land consumption as the conversion of land use from nonurban to urban uses is only a part of land use-driven environmental degradation processes. And it may not be the most important one with respect to the loss of productive land and ecosystem services. Between 0.3% and 4% of the earth's land surface is occupied by impervious or built-up surfaces [2, 4–7]. The pervasive effects of forest clearance, subsistence agriculture, and intensified farmland production are perhaps more important for the ongoing loss of the world's biological resources (Fig. 1). However, when taking the many indirect impact pathways of urban land uses into account (e.g., fragmentation of natural landscapes and habitats, chemical degradation of hydrological systems by polluted urban runoff, roads affecting adjacent habitats by noise), urbanization must be regarded as an important causative factor in models of global and regional environmental change [8].

In addition, there are strong links between urbanization levels and the intensity of rural land use, be it through land-consuming urban lifestyles (tourism and recreational activities, second homes), the relocation of unwanted land uses to the city edge or even peripheral locations (airports, wastewater sites, etc.), or the

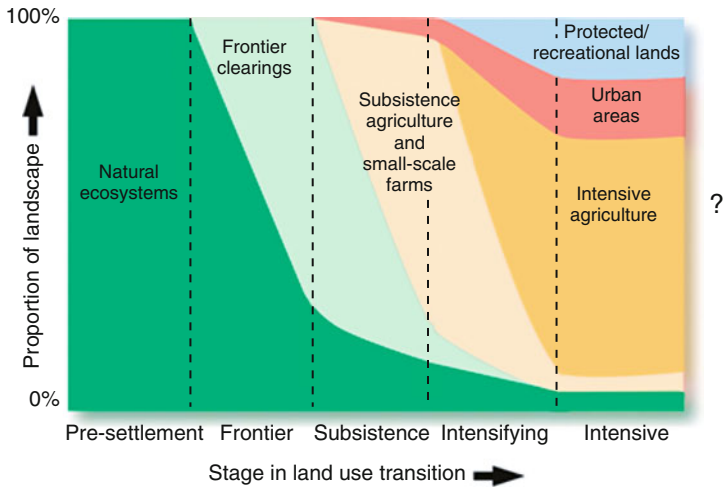

Landscape Planning for Minimizing Land Consumption. Figure 1
Stages of land use transition in human history [1]

demand for facilities that serve the increased intensity of production and energy flows between rural and urban communities (transport infrastructure, warehousing, biofuel production, solar parks, wind parks). Land consumption goes against the objectives of sustainable development in two ways: (1) by increasing the ecological footprint through the addition of land with resource consumptive human activities and (2) by reducing the biocapacity of a region or a country.

At the same time, blaming land consumption for urban purposes as environmentally harmful and generally non-sustainable would be an inappropriate simplification. The phenomenon of urban growth confronts human societies with an intrinsic dilemma. On the one hand, the continuous development of land for residential or commercial purposes is absolutely essential for demographically and economically growing nations [9]. On the other hand, land-consuming human activities degrade ecosystem services upon which demographically growing societies strongly depend. Adding to the dilemma, land-intensive modes of urban growth often represent people's preferences for greener, less dense, and automobile-oriented communities.

While global land use change has become a hot topic over the past few years, urbanization, suburbanization, and urban sprawl at regional and local scales have been the subjects of long-standing academic discussions. Over the years, improving standards of living, the increase in personal mobility, the industrialization of agriculture, the ongoing land demand by households and firms, together with vast changes in societal norms and values have led to widespread conflicts over the use of land [10]. Land consumption changes the physical performance of urban systems in a variety of ways. Among them, the increase in artificial surfaces, the change in densities, and the alteration of land use patterns are the most important ones. Land consumption is being blamed for its contribution to the degradation of natural and seminatural habitats and its stimulating effects on motorized transportation. Consequently, concerns have arisen on the role of changing urban forms for rising greenhouse gas emissions and climate change [11–13]. Moreover, in the recent past other impacts attracted consideration, such as the negative implication of low-density environments on physical activity levels and health outcomes (e.g., [14]).

Recent policy initiatives have further fuelled interest in this subject. In the USA, a number of states have adopted growth management programs that aim at containing urban growth and preserving valuable open space. The English government has set a national target to deliver 60% of all new housing units on previously developed land and through conversions of the existing building stock. The government regards the reuse of urban land a key policy to reduce the development pressure on the open countryside and to improve urban regeneration by upgrading physically and socially deprived cities and neighborhoods with new housing and urban services of higher quality [15]. The Chinese government, concerned about the alarming loss of prime farmland due to urbanization, has introduced regulative policies that aim to protect farmland more effectively [16]. The German federal government introduced a national target to reduce the rate of conversion of nonurban to urban land uses from 130 ha per day in 2000 to 30 ha per day in 2020 [17]. The government argues that land consumption and landscape fragmentation, important aspects of "urban sprawl," are to be acknowledged as key drivers of species loss, landscape deterioration, and the decline of infrastructure efficiency.

While the effectiveness of these legislations and policy initiatives is subject to a highly controversial dispute (e.g., [18–21]), their sheer existence has stimulated further research into the nature of urban expansion patterns, their environmental, social, and economic impacts, and more effective anti-sprawl strategies and policies.

Introduction

Public concern over the undesirable effects of urban growth and land consumption can be traced back to an era when the "exploding metropolis" and its radically changing land use patterns and urban design first became physically visible. The beginning suburbanization process at a metropolitan scale was accompanied by an unprecedented expansion of development at the expense of open space and natural land resources. Not surprisingly, the debate on the unintended effects of urban growth started in the USA where rising affluence, a rapid motorization, public funds for low-density housing, and an antiurban social

climate ("white flight") had formed the precondition for a "mass movement" from the central cities to suburban areas – much earlier than in Europe or other parts of the world. In a 1937 speech to US urban planners, Earl Draper, Director of Tennessee Valley Authority, first used the term "sprawl" to indicate a specific pattern of urban growth that makes the countryside – from his point of view – "ugly, uneconomic [in terms] of services and doubtful social value" (cited from [22]). Since then, the discussion about the impacts of urban sprawl as well as its drivers and remedies has continued (see [23–27] as early contributions) and spread around the globe. Today, urban sprawl and its counterpart, the "compact city," are subject to scientific and political discourses in many developed *and* developing countries (see [28–34] as a few more recent examples).

This debate has clearly broadened its scope and increased in intensity over the decades. The major topics that characterized the debate on urban sprawl before the 1980s had already been established before the Second World War, notably the effects on ecosystem services and landscape beauty, on transportation and the efficiency of network infrastructure [35]. In the last two decades, however, researchers have made substantial progress in empirically addressing spatial manifestations, drivers, and effects of land-consuming human activities as well as the effectiveness of anti-sprawl policies and instruments. As a consequence, the global dimension of land consumption and urban sprawl (as noted above) is now on the agenda of policy makers and researchers worldwide.

Despite the fact that we know much more about the nature of land consumption and its complex societal roots today, many research questions still need to be addressed. On the one hand, it can be said that the quality of information regarding past trends in land use change has significantly improved over the decades, mainly due to the availability of new data sources like remotely sensed data. Likewise, thorough knowledge has been acquired on the many different and complex impacts of land consumption. On the other hand, forecasting future land consumption remains a scientific challenge. Current state-of-the-art prediction models often have to deal with unreliable data, their use is therefore limited to the definition of alternative scenarios within the ranges of uncertainty. In addition, there is still considerable scope for the deepening of scientific knowledge on the driving forces and dynamics of land-consuming developments [36, p 45f].

Apart from these methodological and conceptual challenges, the lack of internationally comparative data on urban land use prevents scientists from analyzing the influence of region-specific political and cultural factors on the spatial formation of urban growth. In this context, research on urban sprawl is largely limited to case studies of selected metropolitan areas in a national context that have limited value for the comparison of regional policies or housing preferences. While economic and population trends are often subject to international cross-sectional research efforts and are therefore well-documented, virtually no information exists on the amounts, rates, and patterns of urban expansion across countries and their metropolitan areas. It has only been in the recent past that empirical studies systematically addressed similarities and dissimilarities in urban land use change across world regions and countries [2, 8, 37–39].

Based on this problem description, this contribution aims to provide a comprehensive overview on the debate on land consumption and its importance for related thematic fields in spatial planning, that is, urban and regional planning as well as environmental and conservation planning. It starts with an elaboration of the meaning of "land consumption" in terms of terminology, causations, and consequences (Section on "A Conceptualization of Land Consumption"). Then, it provides an account of how spatial planning can try to control land consumption, thereby introducing a taxonomy of planning strategies and instruments that appear suited to minimize land consumption (Section on "The Means of Spatial Planning to Minimize Land Consumption"). The contribution concludes with a brief outlook on future challenges regarding both planning practices as well as scientific efforts that endeavor to get a grip on land consumption, either in reality or conceptually (Section on "Future Directions").

A Conceptualization of Land Consumption

What is Land Consumption?

Land consumption, sometimes referred to as land take [38, 40, p 308] can be regarded as a subprocess of land

use change marked by a conversion from nonurban to urban land use types. The visible outcome of land consumption is the spatial expansion of built-up areas accompanied by a significant alteration of land cover features and urban form. The construction of new buildings and infrastructure facilities, the sealing of surfaces and other modifications of the original land surface usually result in a decline of environmental quality. Clearly, it is not land that is consumed. The term "consumption" solely refers to the mostly irreversible loss of ecosystem services (or even entire ecosystems) due to the physical modification of land cover.

In terms of environmental significance, the size of urban areas by itself would be a very poor indicator for the impact of urban land use [6]. In order to adequately address land consumption in terms of its negative (or positive) effects in this context,

- The previous use of land and land cover (agricultural, forestry, or natural)
- The dominant purpose of new urban use (residential, commercial, industrial, recreational, or others) and the corresponding land cover features such as the imperviousness of surfaces
- The location and pattern of new urban land and
- The efficiency of land use

have to be taken into account [8]. To put it bluntly, the development of an acre or hectare of new residential land on former agricultural land has not the same impact as the development of an acre or hectare of industrial land on a drained wetland site. New development in the vicinity of existing settlements has clearly fewer negative impacts on the landscape matrix than the development of many small and disconnected patches throughout the open space (often referred to as "scattered sprawl" or "leapfrogging"). Therefore it is not only the quantity of land converted to urban uses that needs to be considered, but also the spatial patterns and their flow-on effects on environmental qualities that urban planning and management need to take notice of.

Fortunately, improvements in the resolution and quality of digital land use and land cover data have opened up new possibilities for a spatially more refined modeling of urban form, including measures for development patterns. In the recent past, numerous methodological approaches to provide quantitative assessments of urban form and urban sprawl have been introduced [8, 41–45]; see Chin [46] for a brief overview. Table 1 lists prominent measures (indicators) of land consumption and urban sprawl along with their function (description) and sources in the literature.

Looking at recent urbanization trends, land consumption can take very different intensities and forms. In Europe, the annual growth of urban land is expected to range between a maximum of 2% in rapidly growing areas and nearly 0% in remote rural regions [55]. For the period from 1990 to 2000, Angel et al. [2, p 56] estimated that the annual increase in built-up areas in developing countries was around 3.6%, whereas it amounted to only 2.9% on average in industrialized countries. Among the world regions, East Asia, including the Pacific, and Southeast Asia have witnessed the most intensive land consumption with growth rates of 7.2% and 6.4%, respectively.

Other studies provide empirical evidence that the spreading of urban land uses clearly exceeds population growth, resulting in declining overall densities (see, e.g., [2, 50, 53, 55–57]). In Germany, for example, per-capita land use for housing, transport, industrial, and commercial as well as recreational needs increased from 350 m in 1950 to more than 500 m in 1999 [58]. At the same time, in metropolitan areas urban density gradients have significantly flattened over time. It is worth mentioning that urban systems both in developed and developing countries have witnessed this process of decreasing densities, although it was more intense in the developed world [2]. Urban densities decreased between 1990 and 2000 worldwide, in East Asia by as much as 4.9% per annum and in Europe by a relatively moderate 1.9%.

The change of spatial configurations of urbanized areas that results from the shift of private households and firms from central locations to suburban and exurban areas is another highly visible characteristic of land consumption. Over time, metropolitan areas have changed their urban form from a highly concentrated compact structure to a rather dispersed or polycentric pattern [22, 59–63]. The deconcentration of urban systems ("suburbanization") has come along with a change of micro-patterns of urban form, often addressed with terms like "leapfrogging" or "ribbon" development. In this sense, land consumption has contributed to the large-scale transformation of urban

Landscape Planning for Minimizing Land Consumption. Table 1 Frequently proposed land consumption and urban sprawl measures

Indicator	Description	Sources
Size or share of urban land	Size of urban land (km^2 or sqm); percentage of urban land (%)	[2, 8, 42, 45, 47]
New land consumption	Converted urban land (in hectares or acres)	[9, 45]
Urban density	Number of people, jobs, or housing units per hectare of urban land (gross or net)	[2, 41, 45, 46, 48–50]
Change in urban density	Change of urban density between two base years (percentage)	[2, 19, 45, 51]
Density gradient	Regression of density against distance by ordinary least-squares (OLS) means	[41, 44]
Land use mix/land use separation	Degree to which different urban land uses exist in close distance to each other (measured with indices like the Shannon Diversity Index)	[42, 44, 46, 49, 52]
Continuity/dispersion/ fragmentation/complexity	The degree to which developable land is built up continuously; the degree of irregularity of built-up patches (measured with certain indices such as the patch density or more complex statistical measures of spatial regularity)	[8, 37, 42, 45, 46]
Concentration/ decentralization	Degree to which urban development is located near to the CBD (e.g., measured with the percentage of population and employment within concentric rings around the CBD or the median person's/worker's distance in distance units from CBD)	[37, 42, 44, 50, 53, 54]

systems from a compact urban form to an irregular, discontinuous, and dispersed urban land use pattern [31, 41, 42, 52]. Table 2 presents some characteristic "real world" examples for the spatial manifestation of "contiguous," "ribbon," or "leapfrogging" urban growth.

Drivers of Land Consumption

What factors account for the phenomenon of land consumption in general? What explains regional disparities in the rates at which land consumption occurs, and why do the patterns of land use conversions differ significantly between countries and even regions (e.g., [37])? Furthermore, why does land consumption often continue under conditions of stagnation or even decline [64]?

First of all, it has to be said that an explanatory model of land consumption cannot be deduced from a grand theory of urban growth or urban development simply because such a theory does not exist. However, social sciences and economics have offered theories that help to identify important drivers of land-consuming human activities. In particular, neoclassical economic theory provides a closed framework for the explanation of urban growth. It argues that location decisions of private households and firms reflect the aim to get the maximum utility out of matching space needs, location preferences, and financial budget constraints. Given an unregulated land market, land rents near the urban core are highest because transportation costs are lowest and accessibility of urban services is therefore best. It is the sum of all costs within the income elasticities for land and transportation that determines location choice. High-income groups (with more land-demanding aspirations) may prefer to live in a larger distance to the city center where large building lots are available, whereas low-income households will choose a location near the urban core with lower transportation costs. Based on these primary considerations, the monocentric model of urban spatial structure explains the spatial expansion of cities and density gradients with just a few variables, namely, the demand for new housing and commercial land,

Landscape Planning for Minimizing Land Consumption. Table 2 Types of urban sprawl (*grey colors* existing urban area 1990, *red colors* expansion 1990–2006; data sources: CORINE Land Cover 1990, 2000, and 2006, OpenStreetMap)

Types of urban sprawl	Examples
"Contiguous" or "continuous" development • New urban area is located adjacent to existing urban areas, expanding ring-wise around the central city • Structure: compact and "contiguous," possibly interrupted by topographic features • Land use: mono-functional or mixed, with residential and commercial use around subcenters, industrial along radial transport routes • Impact: flattened density gradient from the inner city to the city edge, well suited for mass transit systems, poor open space provision for inner-city dwellers	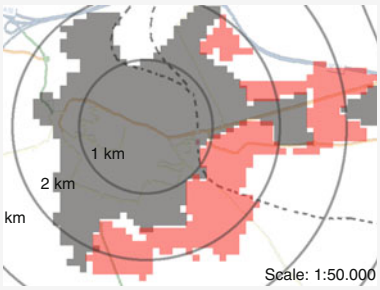
"Ribbon" development • New urban area is located near major transport network facilities (motorway on-ramps, public transport stations) • Structure: the resulting settlement patterns resemble strips or "ribbons" • Land use: often mono-functional residential areas preferred by commuters, extensive industrial (warehousing) or commercial use (shopping malls) • Impact: habitat fragmentation, inefficient in terms of urban service provision	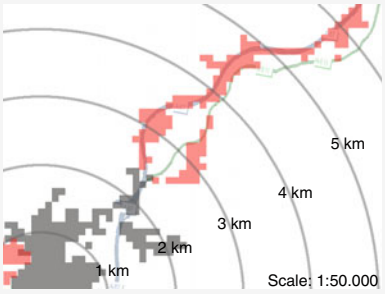
"Leapfrogging" development • New urban area is located in isolated patches far from existing urban areas • Structure: dispersed and disconnected urban structures, surrounded by open space • Land use: mostly mono-functional industrial, commercial, or residential areas • Impact: relies on new infrastructure, inefficient to service with public transport and network infrastructure, fragmentation of open space; availability of nearby open space	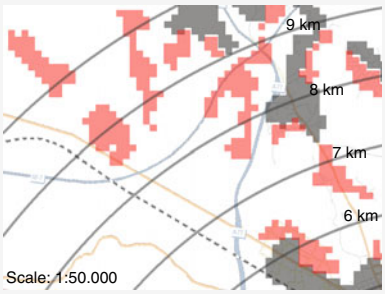

rising incomes, innovations of intra-urban transportation systems, and decreasing transportation costs [65–68]. In this sense, the growing physical footprint of cities and their declining density is the combined effect of a growing population, rising affluence, and enhanced individual mobility due to the increasing affordability of the private motor car.

Critics of the neoclassical monocentric urban model ("Alonso–Muth–Mills model") claim that many other factors than land prices and commuting costs affect location decisions [35]. Examples are the quality of urban services, specific priorities, and demands of different social groups in terms of urban and environmental amenities, or the desire to live in a socially homogeneous neighborhood. The Tiebout Local Public Finance Model [69] suggests that people decide to locate in a particular jurisdiction based on their preferences and taste for local amenities. Tiebout describes factors that "pull" people out of the central areas of metropolitan regions because of attractive characteristics of suburban communities (e.g., good service levels or lower taxes) and others that "push" people out of central areas as a result of central city problems such as crime or poor environmental quality and services.

The disagreement with the Alonso–Muth–Mills model is also fuelled by the empirical emergence of polycentric urban configurations [70–72]. The outward movement of jobs is regarded as a key factor explaining this trend. Suburban and exurban industrialization, beginning in the 1950s and 1960s, have made rural areas attractive to workers as new places to live in. In contrast to the fundamental assumption in the neoclassical city model that employment concentrates in the central business districts (and gradually decreases with increasing distance to the urban core), modern agglomerations in developed countries are characterized by their multinodal settlement system with a complex pattern of primary and secondary centers.

Next to economic theories, technical and social sciences aim to explain urban growth and the change of urban form [73]. Technical viewpoints focus on the role of transport innovations in order to explain the spatial diffusion of urban land uses. They associate the compactness of the preindustrial city with the fact that most trips had to be made on foot or similarly slow modes of transportation. This constraint disappeared with the availability of faster mass transportation technologies and the private automobile [74]. Following this logic, the physical growth of cities became a function of transport technology. Nelson [21] points out that other improvements in technology such as the personal computer, cellular phones, or the Internet may have encouraged the spatial decentralization of people and firms further, setting out the conditions for more land-intensive forms of urbanization.

On the one hand, economic, social, and technical theories help to explain the intensity of urban deconcentration and the associated rate of land consumption. On the other hand, they fall short of explaining the spatial patterns of urban land development. The reasons are manifold: neoclassical theory assumes that an unregulated market exists without any regulating land use policies (e.g., land use zoning) and that biophysical factors unfavorable for urban land use can be ignored. However, it is evident that these factors of urban development need to be taken into account to understand how actual land consumption patterns result from a complex interaction between various social, demographic, economic, and environmental processes. As a consequence, spatially explicit land use models have been developed that not only explain *at what rates* land use change occurs in a given period of time, but also address the question *where* land consumption will take place, that is, the likely location of change [5, 75].

For this purpose, Poelmans and van Rompaey [5] distinguish five groups of explanatory variables that are frequently used in models of land consumption:

- Biophysical factors may have an impact on the suitability of land tracts for the construction of buildings or infrastructure facilities. For example, factors such as slope or environmental hazards strongly influence the cost of development. Therefore, biophysical factors can explain why certain areas are excluded from development.
- Social factors put emphasis on location preferences of households (or household types). Examples are the income level or ethnic composition of nearby neighborhoods and the availability of public green spaces. These factors may encourage or discourage the choice of a development site.
- Economic factors refer to accessibility features as proxy values for market access. Frequently used measures are the distance to urban centers or main roads and the availability of public transport services in a walkable distance. Undeveloped properties with good accessibility are more probable to become urbanized in the future.
- Neighborhood interactions refer to an observed spatial autocorrelation between new developments and existing urbanized areas. In contrast, some potentially conflicting land uses (e.g., residential and industrial development) are unlikely to be located directly next to each other.
- Spatial policies are relevant because of their influence on the location decisions of private households and firms. These policies can be labeled "negative planning" where they aim to protect current land uses (habitat conservation, prime farmland) or "positive planning" where they define the suitability of a piece of land for a specific use (i.e., where they explicitly designate sites for urban development) (see also Legally Binding Land Use Planning).

Clearly, these determinants of land consumption encourage or constrain urban development with a certain spatial logic. Some of them may explain the total pressure on the land within a region or even

a nation state, but are hardly suited to identify the local hot spots of development. Examples are housing policies or mortgage schemes that support private homeownership. Other determinants can explain why certain plots of land were developed – for example, moderate land prices or above-average accessibility – while failing to explain the aggregated regional growth rate of urbanized land. Table 3 presents a set of relevant variables with their estimated explanatory capacity.

Recent studies [76, 77] have found that supply-driven factors of land consumption generally carry higher weights than the demand side. They suggest that land consumption is not only the result of demand driven by demographic and economic growth pressures or social preferences, but is also fuelled and facilitated by policies at national as well as local scales [78, 79]. For instance, the political agenda of local decision-makers in stagnating or economically declining areas often emphasizes the importance of cheap land for residential or commercial uses as a means to attract people and enterprise and thus to generate income tax. This can explain why some regions and municipalities without demographic or economic demand pressure show significant land consumption rates [80, 81]. Government policies like the commuter tax allowance in Germany, the financing of highway infrastructure in the USA, or subsidies for the development of industrial or retail development by the European Union are likely to support this effect [82].

Some scholars present evidence that the institutional fragmentation of local authorities could be another important factor explaining the rate and pattern of land consumption. According to this position, a decentralized land use governance with numerous local governments controlling urban land use is likely to promote urban sprawl as it increases the number of jurisdictions seeking for extra-budgetary revenue through land conversion to urban uses [48, 77, 83]. The size of local government units is also important in other ways – the bigger they are the less likely to be reliant on one particular investor or project, and less vulnerable to the influence of individual land owners with regard to planning policies and decisions. Furthermore, smaller communities are more likely to permit exclusionary zoning policies where local governments intend to exclude low-income groups from their

Landscape Planning for Minimizing Land Consumption. Table 3 Explanatory variables used in land consumption model applications (*dark grey* strong explanation, *pale grey* moderate explanation, *white* not relevant)

Factor	Examples	Explanation of rate of land consumption	Explanation of location of land consumption
Biophysical	Slope		
	Hazardous land		
Economic	Economic growth		
	Land prices		
	Distance to urban centers		
	Distance to the main road		
	Fiscal motives to convert land into urban use		
Demographic/ social	Population growth		
	Income growth and changes in lifestyles		
	Motorization		
	Social preferences for housing types and locations		
Spatial policies	Land use regulation (positive and negative planning)		
	Revitalization and renovation policies		
	Public funds for Greenfield development		

municipalities [79, 84]. These policies are driven by the suburban resident's desire to protect their housing investments and to maintain their social status [83].

Impacts of Land Consumption

Systematization As mentioned above, land consumption is a by-product of demographic and economic change. In a sense, land consumption is an indicator of prosperous development since it seems unrealistic to aim for strong economic growth without any land conversion. Improvements of housing supply, the introduction of modern transport systems, or the rise of economic productivity are mostly land-consuming activities. Downs [83] points out that urban sprawl produces some benefits for metropolitan citizens. Among others, he lists low-density lifestyles and the availability of private green space, an easy access to public open spaces in the countryside, a broad choice of places to work and live, relatively short commuting times for people who both live and work in suburban areas, and the ability of citizens to exercise strong influence on local governments.

At the same time, land consumption is responsible for many undesirable effects. In the scientific literature, numerous approaches to categorize these effects have been introduced (Table 4). They refer to causality, to spatial scales of impact phenomena, specific impact pathways, issues of concern (environmental, economic, or social issues), or the quality of effects as costs or benefits.

A first useful categorization distinguishes between single, that is, direct, and cumulative, that is, indirect, impacts. Conversion of forest to residential land, for example, is a direct effect causing the loss of vegetation or the sealing of natural surfaces. However, significant land use related environmental problems such as the modification of urban climate conditions ("urban heat island") or the increase in urban runoff often result from the cumulative effects of development activities rather than single projects. They build up over a period of time and usually have more than one cause. The individual effects from a single development activity may not be significant in terms of environmental harm (Table 5). However, when considered with other perturbations on the same environmental component (or system), they can become significant either through additive or interactive processes [85]; see also CEQ [86] and Parr [87].

Landscape Planning for Minimizing Land Consumption.
Table 4 Categorization of land consumption impacts

Dimension of categorization	Impact categories
Causality	Direct impacts
	Indirect or cumulative impacts
Spatial scale	Land unit-level impacts
	Context-level impacts
Issue of concern	Environmental impacts
	Economic impacts
	Social impacts
Impact pathway	Land surface related impacts
	Land use pattern related impacts
	Density related impacts
Quality	Impacts as costs
	Impacts as benefits

Closely related to the above-mentioned categorization, Nuissl et al. [92] differentiate a "land unit level" and a "context level" of land use impacts. Unit-level effects are the direct and immediate outcome of a change of land use on a particular plot of land. In contrast, context-level effects depend on the characteristics of the larger territory in which a land use change is taking place. The authors point out that these indirect impacts cannot be comprehended with a narrow spatial focus on the particular piece of land that is subject to a modification of land use or land cover. Examples are fragmentation effects of new roads or the attraction of motorized consumers by large-scale retail facilities.

Siedentop and Fina [45] distinguish three key dimensions of urban land use through which a broad range of land consumption impacts can be explained and modeled. These are land cover features (surface), the pattern of land use as the spatial configuration of urban and nonurban land patches, and the intensity of use (urban density). Table 6 summarizes well-documented impacts of land consumption and attributes them to certain impact pathways.

Landscape Planning for Minimizing Land Consumption. Table 5 A typology of cumulative effects with some examples of land consumption (Adapted from Cooper [85, p 3])

Type	Main characteristics	Examples
Time crowding	Frequent, repetitive, and simultaneous impacts on an environmental resource	Loss of prime farmland [88]
Space crowding	High spatial density of impacts on an environmental system	Emergence of an "urban heat island" caused by the spatial concentration of artificial surfaces and a lack of green space [89]
Cross-boundary movement	Impacts occur some distance away from source	Floods affecting downstream settlements caused – among other reasons – by increases in upstream urban runoff
Compounding/ synergistic effects	Effects resulting from multiple sources or impacts that may be different in nature from the individual impacts	Drawdown of groundwater levels due to increased imperviousness and increases in withdrawal of groundwater
Triggers and thresholds	Fundamental changes in system behavior or structure	Beyond a threshold of 15% imperviousness, urban stream quality becomes poor [90]
Nibbling	Incremental or decreasing effects	Gradual loss of greenbelt land through urban development [91]

Other studies categorize impacts with respect to certain issues of concern [125–127]. Often, a reference to environmental, economic, and social effects is made. Fig. 2 outlines some frequently addressed land consumption impacts and categorizes them with regard to the issue of concern and the spatial scales of their impact in an "urban sprawl" matrix.

Review of Important Impacts First of all, land consumption has sparked environmental concerns. Environmental effects of land consumption can be primarily explained with changes of land cover features that are inevitably related to urban development [99]. Natural or seminatural surfaces are converted to urban uses with a high share of artificial, impervious surfaces and complex effects on ecological systems [90, 100, 128]. Imperviousness is defined as the sum of roads, parking lots, sidewalks, rooftops, and other impermeable surfaces of the urban landscape [90, 129] (see Table 7 for an overview on the mean imperviousness of different land uses). In many studies, imperviousness has been used as an indicator to measure the impacts of land development on terrestrial and aquatic ecosystems. Imperviousness physically limits the infiltration of rainfall into the ground. Rainfall and snowmelt water disabled to infiltrate becomes surface runoff. Studies have shown that the urban runoff can be more than twice as high in urbanized than in rural areas with more natural land cover features [130]. Thus, soil sealing in highly urbanized areas is widely viewed as an important causative factor of flood risks [75]. Due to the fact that urban runoff water carries with it chemical pollutants (e.g., from automobile traffic or industrial land uses) imperviousness also contributes to the biochemical degradation of aquatic ecosystems. Based on many empirical studies, Moglen and Kim [128] estimate that when the rate of paved surfaces exceeds a threshold of 10–15% various indicators of biological stream quality decline markedly.

Moreover, the high percentage of imperviousness is also co-responsible for highly modified meso-climatic conditions in large urbanized areas ("urban heat island"). The spatial concentration of artificial materials with specific thermal characteristics creates local temperature anomalies leading to a higher average temperature in the dense urban fabric as compared to the urban periphery [89, 96, 97].

In addition to the magnitude of land conversion and imperviousness, the characteristics of the land that became urbanized within a specific period of time have to be taken into account (e.g., soil quality, habitat quality, vegetation, etc.). Of particular concern is the

Landscape Planning for Minimizing Land Consumption. Table 6 Land consumption impacts related to distinct impact pathways (Adapted from [45])

Impact pathway	Impacts of land consumption	Sources
Change of land cover (surface)	Continuous urbanization leads to a loss or degradation of valuable open space	[88, 93–95]
	The spatial concentration of pollutants is co-responsible for high air pollution	[51]
	The spatial concentration of artificial surfaces and a lack of green space is one causative factor for the urban heat island	[89, 96–99]
	The spatial concentration of built-up land has negative effects on the provision of green space	[99]
	Urban runoff from sealed surfaces negatively affects aquatic systems (water quality, biodiversity of systems)	[90, 100]
Changes of land use patterns	Dispersed and scattered settlement patterns hold responsible for high development costs (infrastructure)	[36, 101–103]
	Dispersed and scattered settlement patterns lead to higher travel distances and thus higher climate gas emissions	[62, 104–106]
	A discontinuous urban growth brings about higher levels of habitat fragmentation	[107, 108]
	The over-concentration of population and monocentric urban systems have a risk of higher levels of traffic congestion	[109, 110]
Change of urban densities	Low residential densities come along with a high level of automobile dependence	[111, 112]
	Low residential densities are usually associated with higher travel distances	[11, 49, 113–115]
	Low residential densities lead to less cost-efficient and effective public transit	[116–118]
	Low residential densities result in higher per-capita development costs (urban services)	[36, 103, 119]
	Low residential densities lead to higher energy use for housing (heating)	[120, 121]
	Low residential densities are co-responsible for negative health effects (due to physical activity levels)	[14, 122–124]

loss of prime agricultural land due to its importance for the long-term competitiveness and sustainability of agriculture [94]. The European Environment Agency [40, p 176] estimates that the "continent's best soils" are sealed due to the fact that most urban centers were built on fertile valley soils and around estuaries (see also [88, 133]). Hasse and Lathrop [94] present quantitative findings that prime farmland is more vulnerable to urbanization than farmland of lesser quality. Urban development in more and more fragmented agricultural landscapes can also be problematic for the production of food and fiber on the remaining farmland. For instance, conflicts between farmers and their residential neighbors "can arise over noise, chemical applications, and smells that are part of farming" [134, p 2].

In addition, dispersed and fragmented land use patterns are a crucial contributor to landscape fragmentation, which is characterized by a process of perforation, dissection, and isolation of habitat areas and natural or seminatural ecosystems [107]. Many scholars regard fragmentation as a major cause of the alarming loss of species all over the world [108, 135].

The (not purely monetary) costs for providing settlements with public services are commonly addressed in urban sprawl studies that focus on the economic effects of land consumption. In 1974, the "costs of sprawl" study [136] presented empirical evidence for

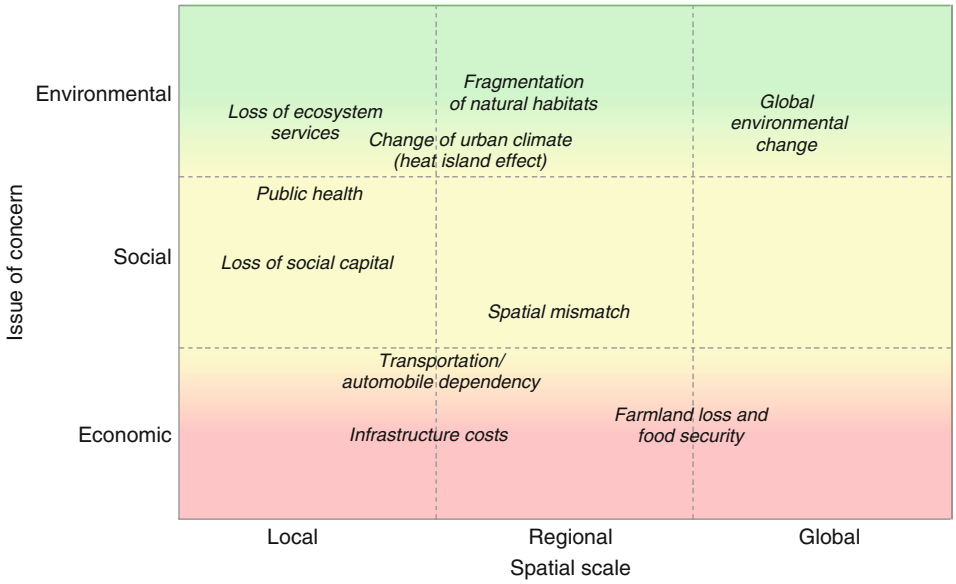

Landscape Planning for Minimizing Land Consumption. Figure 2
The impact matrix of land consumption

Landscape Planning for Minimizing Land Consumption. Table 7 Percentages of imperviousness for different categories of urban land use (Adapted from [92, 128, 131, 132])

Land use category	[131]	[92]	[132]	[128]
	Imperviousness (in percent)			
Residential	35–65	40–80	49	25–65
Mixed use	65	–	44	–
Public open spaces	–	–	15	–
Commercial and business	80	–	–	85
Institutional (public use)	–	–	59	50
Industrial	76–80	80–100	64	72
Transportation	58–63	80–100 (roads) 20–40 (rail)	–	75
Urban recreation (sport fields, public parks, private gardens)	4–8	–	–	–
Agriculture	0	–	2	–
Forest	–	–	2	–

a negative interdependency between the density of residential developments and the fiscal costs for providing basic urban services. The findings of this study triggered an intensive dispute not only with respect to the implications for urban development policies but also in terms of methodological uncertainties. A couple of subsequent studies confirmed the results of the 1974 work (see [36] with many references); others disputed the relevance of urban form variables on infrastructure costs [137, 138]. As a bottom line it can be said that it is

widely acknowledged today that low-density and dispersed urban developments are more cost-intensive than more compact development patterns (see also [101, 139–141]).

The impact of land consumption on motorized transport demand is probably the most frequently discussed issue in this field of research. Many scholars have shown that spatially dispersed urban areas accompanied by low densities contribute to larger travel distances [104, 114, 142, 143]. Based on a meta-analysis of the relevant literature, Ewing and Cervero [113] come to the conclusion that single variables of urban form have a relatively minor effect on motorized transport demand. However, the combined effect of several urban form variables on travel can be significant (see also [144]). Next to urban density, the accessibility of workplaces and other destinations, the mix of different land uses, the availability of public transit and urban design features are regarded as being influential on transport. Some critics dispute the causality between urban form and travel behavior, pointing to the possibility that private households self-select themselves to places that are in accordance with their preferences for particular transportation modes [145]. At the same time, studies that controlled for demographic, socioeconomic, and attitudinal variables (such as household income, family size, or age) presented contrasting results that identify a significant effect of urban form on transport [143, 146, 147]. Everything else being equal, households in peripheral low-density environments have longer travel distances and tend to travel by car more often than their inner-city counterparts.

Lastly, land consumption and urban sprawl have also been criticized for unintended social outcomes (e.g., [148]). The "spatial mismatch" debate, starting in the 1960s (see [149] and [150]), addressed the extent of limitations on residential choice for minority populations (especially Afro-Americans in the USA), combined with the intra-regional decentralization of employment. Proponents of the spatial mismatch hypothesis argue that the exclusion of low-income and nonwhite households from suburban communities together with the continuous spatial dispersal of jobs especially for low-skilled employees is responsible for the high rates of unemployment and low earnings of minority population members living in central cities. More recently, studies found evidence that low job accessibility in public transport catchments negatively affects the employment probability of social groups with a poor availability of cars [151].

The very recent debate concerning the effects of urban sprawl on public health – with a special focus on the relationship between urban form variables and physical activities with their corresponding health implications – demonstrates that the discussion on land consumption impacts is not closed (e.g., [14, 122, 124]). Moreover, the verification of alleged impact hypotheses with credible and disaggregated data and more robust methodological designs will help policy makers in justifying their potentially restrictive policies and measures.

The Means of Spatial Planning to Minimize Land Consumption

The Aim of Spatial Planning

The desire to control the dynamics of land consumption was one of the earliest motivations for spatial planning. However, while this desire used to be of minor importance in comparison to the goal of mitigating land use conflicts and safeguarding the most rational possible form of urban growth, it has become one of the major issues in land use policy only more recently (e.g., [152]). This issue is probably most disputed in the USA where public concern about sprawl grew heavily in the recent past [153], resulting in a strong anti-sprawl movement that meets strong opposition by more liberal academics and planners who emphasize the importance of individual choice and the free market (e.g., [28, 93, 154–156]). However, elsewhere, most notably in Western and Central Europe and Australia, this debate has also gained considerable momentum (e.g., [55, 157]).

As has been shown in the previous part of this contribution, at least in sustainability science and environmental politics it is now widely acknowledged that sprawl causes ecological damage, increases the need to travel, makes service provision more expensive, and has additional social and economic impacts. In 1999 the European Spatial Development Perspective recommended that "member States and regional authorities should pursue the concept of the 'compact city' (the city of short distances) in order to have better control over further expansion of the cities." "For this

purpose," the document continues "co-operation between the city and the surrounding countryside must be intensified and new forms of reconciling interests on a partnership basis must be found" [158 para 84]. This quotation gives a typical example of the risen sensitivity of the land consumption issue. However, while it implies a strong quest for the minimization of land consumption the quotation's latter part hints at the general aim of spatial planning to provide a legal and conceptual framework that facilitates societal progress and economic growth. Insofar, it is a major challenge for spatial planning to balance the minimization of land consumption with other planning goals that are associated with development. To achieve this complex mission, spatial planning has quite some strategies and instruments at hand, many of which are well proven.

A Taxonomy of Planning Instruments

Basically, spatial planning is about the organization and regulation of land uses. Thus, almost all strategic and instrumental approaches developed by spatial planning are potentially apt to contribute to the minimization of land consumption – provided they are used to pursue precisely this goal.

The debate on potential policy responses to land consumption is rather broad and a great variety of policy strategies has actually been put in place across different countries so as to mitigate land consumption. Therefore, first of all a broad categorization of planning instruments seems to be helpful, which groups these instruments according to the general approach they use. A common way to achieve such classification is to divide public policies into those concerned either with (a) regulation, (b) spending, taxation, and subsidy, or (c) advocacy. Considering the phenomenon of urban sprawl in the USA, Bengston et al. [159] employed a similar three-part classification of policy types for the control of urban sprawl. Adopting and slightly modifying their approach, we propose to differentiate the means of spatial planning to minimize land consumption according to where they are located on the continuum that expands between the poles of two basic planning principles:

- *Planning*, reflecting the "traditional" regulatory approach of spatial planning to set legally binding rules for the use of land via regulative plans, and
- *Market*, reflecting the "economic" approach of land use policy that employs "market-based instruments" that modify incentives in a way that leads actors to use the land in the intended manner. For instance, taxation schemes that put an additional cost on the development of land are surely among the most efficient means to minimize the total amount of urbanized land (e.g., [160]).

Between these two poles (somewhere "halfway") one can discern an array of instruments, which are primarily managerial by character and that basically aim at impacting on the decision-making processes that eventually lead to regulative or market-oriented land use policy measures. This group of instruments can be attributed to a third planning principle:

- *Management*, reflecting the "persuasive" approach that tries to change the behavior of land using actors, either by providing them with information on the consequences of their behavior or by involving them in a communicative process together with actors that want to restrict land consumption.

These planning principles are of course ideal types. In reality policy responses and planning instruments that address the problem of land consumption are frequently combinations of several instruments that entail different principles.

Table 8 illustrates the three general approaches land use policy can adopt to pursue its goals, including the goal of minimizing land consumption. However, only the regulative and the persuasive approach fall into the scope of spatial planning in a strict sense, while the modification of incentives is usually to be achieved in other policy fields, for instance taxation or social policy [161]. In the following sections, we shall therefore highlight those spatial planning instruments that can be attributed to either the regulative or the persuasive approach while economic instruments do not fall into the scope of this contribution. (However, this must not be misunderstood as a neglect of the latter's indisputable effectiveness.)

Regulation

Sector-Specific Planning and Comprehensive Land Use Planning In virtually all countries there are different fields of public policy, legislature, and planning

Landscape Planning for Minimizing Land Consumption. Table 8 A taxonomy of land use policy instruments

Governance principle	Planning approach	Examples of strategies and instruments
Planning	Regulation (law)	Land use planning, that is, Zoning, for example, [162, 163]
		Urban design planning (e.g., density controls), for example, [164, 165]
		Transit planning [166, 167] etc.
Management	Persuasion (information and communication)	Forums and roundtables, for example, [168, 169]
		Information campaigns, for example, [170, 171]
		Land use change assessment and forecasting tools, for example, [172, 173] etc.
Market	Modification of incentives	Development taxes, for example, [174, 175]
		Subsides (e.g., urban regeneration), for example, [176, 177]
		Tradable permit schemes, for example, [161, 178] etc.

that define regulations as to the use of land. Frequently we find a differentiation between comprehensive land use planning on the one hand – as a policy field that is focused on resolving land use conflicts and safeguarding the rational use of land – and sector-specific fields of policy making and planning on the other hand. They both produce legal framework conditions on how a piece of land may be used, but the latter formulate only particularistic demands for land (e.g., by defining the location of technical infrastructure, water reserve zones, or nature preservation areas) and leave the task of coordinating these demands and interests to land use planning.

In principle, all kinds of public planning that have an impact on land use can contribute to achieving minimal land consumption. For instance, when planning a new power plant or road infrastructure it is always possible and worthwhile to consider how much land needs to be developed to realize the project. The field of environmental policy is particularly important as to sector-specific plans with the potential to minimize land consumption. The plans that are elaborated within this policy field, frequently labeled landscape planning, are usually restricted to defining nonurban areas that must not be developed in the future and include more or less detailed rules on how these areas ought to be used. However, the kind of planning that is most relevant with regard to land consumption and its minimization is almost always comprehensive land use planning.

Land use planning is an integrative endeavor. Its major task is the coordination and balancing of the different demands for land, which are put forward by industry and commerce, by private households, or, not least, by sector-specific policies, that is, authorities who are in charge for the provision of the public with infrastructure and services. The ability of land use planning to achieve this integrative task, and thus to prevent the formulation of contradictory public demands or rules regarding the use of land, varies between different countries and largely depends on the functionality and powers of the respective system of land use planning (e.g., [179]). However, even in countries with well-established (and more or less sophisticated) systems of comprehensive land use planning it is often the case that sector-specific plans drawn up by different authorities prove inconsistent.

Legally Binding Land Use Planning Virtually everywhere, land use planning builds on the principle of *distinguishing different kinds of land use*. This principle, and the related practice, is usually named "zoning" in the English-speaking world. Zoning basically implies the delineation of particular (non-overlapping) pieces of land for which acceptable and unacceptable kinds of land use are defined more or less precisely. This may

include the definition of the kinds of activities that will be tolerable on a particular lot (such as open space, residential, commercial, etc.), or the regulation of building height, lot coverage, obligatory shares of green space, and similar characteristics, or some combination of these. The primary purpose of zoning is to segregate uses that are deemed incompatible.

The most basic distinction that can be made via zoning is between urban land, including land that is dedicated to future development, and nonurban land. Thus, the principal instrument of regulative land use planning to minimize land consumption consists in the preparation and legal enforcement of land use and development plans, which, by distinguishing between these two land types, confine urban development to a limited area and usually include regulations regarding the character and intensity of urban land use.

Depending on a country's planning legislation, land use planning either formulates rules only for the urban area of a respective administrative unit, including the demarcation of this area that may contain yet undeveloped greenfield land, or it defines land use classes (zones) for an entire administrative territory, which likewise includes the *classification of developable land*. Usually land use planning, like many other forms of public policy, operates at different spatial scales – thus yielding regulatory efforts at the local, regional, national, or even supranational level, which mainly differ as to both the precision and the enforceability of directives (see Fig. 3). This constitutes a *hierarchy of plans*, with the plans on the upper levels specifying the framework conditions the more detailed local plans must meet. At the same time, however, it is a basic principle of regulatory land use planning that the more general "upper-level" plans must not be at odds with existing local (zoning) plans. In the hierarchy of land use planning it is usually only the local plans that enforce the containment of urban development by categorizing the different pieces of land in a way that is legally binding for land owners and investors.

Beyond the fact that most countries in the world have a system of land use planning, which, in one way or other, yields compulsory plans that prescribe how the land may be used, this planning system can be organized rather differently. Accordingly, there is an immense diversity of forms that regulatory land use plans can take in terms of legal foundation, regulatory power, planning symbols, relation between planning tiers, or content – ranging from plans that endeavor

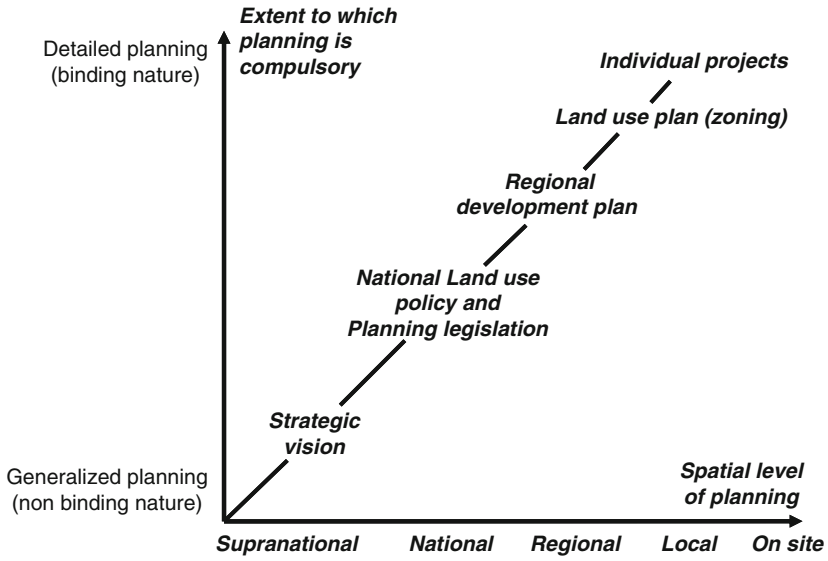

Landscape Planning for Minimizing Land Consumption. Figure 3
Stylized correlation between spatial level of planning and precision as well as enforceability of planning (Source: [180] modified)

to grasp and regulate the full complexity of spatial development on the one hand to elementary zoning plans that include only a few basic predictions as to the permissible developments on the other. In many European countries, for instance, local plans are framed by plans prepared at the regional level, that is, by medium tiers of administration. Where such an intermediate level of spatial planning is lacking there is sometimes a distinctive antagonism between the national state and the communes. In addition to the comprehensive land use plans, in some countries, such as the Netherlands or Germany, detailed urban design plans, specifying the physical form of future development, are prepared, especially for areas where some new development is to be expected. Other countries, such as the UK, rely mainly on the comprehensive land use plans and supplementary policy to control development, without the preparation of detailed urban design plans.

The use of compulsory land use planning can be based on two fundamentally different ideas. On the one hand, land use plans may be drawn up to provide for the legal preparation of future development by defining the location of developments or facilities that are to be realized in future – this can be called "positive planning." On the other hand, land use plans are frequently necessary to steer and curtail urban growth as well as to prevent certain unwelcome developments by excluding particular uses for particular lots – this can be called "negative planning ."

From its beginning in the nineteenth century modern land use planning was basically devised as a response to the rapid outward expansion of urban areas in the course of industrialization. Initially, planning thus adopted the "positive" rather than the "negative" approach in that it was not primarily concerned with the containment of urban development and land consumption but rather with its preparation and coordination. The idea that land is a finite resource emerged only much later, in recent times. It is also important to note that an effective system of land use planning that draws on the principle of zoning did not emerge simultaneously throughout the world. Rather, in contrast to those countries in western, northern, and central Europe where the idea of urban and town planning is well established and accepted, the current planning legislation and planning practice is a fairly recent phenomenon in many countries and, in even more countries, remains a highly contested area of policy and a somewhat toothless tiger.

The "negative" approach toward land use planning is clearly most effective when it comes to curtailing land consumption. At the same time, however, it usually means a considerable limitation of the landowners' discretionary scope regarding the use of their sites. It is therefore also particularly prone to provoke sharp resistance in particular at the local level where it is often in conflict with the interests of land owners, investors, and politicians (e.g., [181]). Hence, it is often recommendable to combine "negative" and "positive" planning regulations as the latter are usually less contested and can help making urban development less land consuming, too. An example for such combination is the permission to develop the land that is dedicated to urban uses at a considerable density (thereby lessening the pressure on greenfield land) while at the same time marking out extensive areas where building activities are strictly prohibited.

Regulatory Planning Instruments Beyond Legally Binding Land Use Planning In addition to its traditional instrument, compulsory land use plans, regulatory land use planning has a wide range of other means at hand that can be used to minimize land consumption either directly or indirectly. Four more recent examples of these additional regulatory means that have earned much attention in contemporary land use policy debates will be sketched out in the following. All of them are inspired by the normative ideas of environmental conservation and sustainability. While one of these instruments aims at influencing land use patterns directly, the other three do so in an indirect fashion.

1. In many countries planning legislation enables authorities to define *minimum lot sizes* or *minimum building density*. Both can be employed in order to prevent land consumption and urban sprawl (e.g., [182]). Minimum lot sizing is usually meant to preserve the rural character of the landscape by prescribing a size of plots that exceeds the usual size of residential sites by far. However, as an attempt to save the rural character of an area minimum lot sizing can easily fail, in particular in the vicinity of urban agglomerations, when affluent households

start acquiring the rural plots in order to build their house there (e.g., [183]). The definition of minimum building density, on the other hand, prescribes an economic use of urbanized plots that does not "waste" land. Involving a rather far-reaching and detailed regulation as to the usability of a certain plot of land, this instrument is most feasible in a spatial context where there already exists a high-density building structure and a political context where the power of spatial planning is generally accepted.

2. The proposal to coordinate the development of land through *tradable permit schemes* combines regulative land use planning with economic principles. In the USA, there are already several examples where this idea has been implemented [178, 184] but its intense discussion has also progressed in other countries such as Germany [185] or Italy [186]. Tradable permit schemes usually involve "a cap-and-trade" approach, which works as follows: State authorities define the maximum amount of developable land and then issue a limited number of permits that allow developing a certain share of this total amount of potentially new urban land. After their assignment to the actors, either authorities or private landowners, who – according to a respective country's legal system – are entitled to use them in order to develop land, these permits can be traded among the actors. Where the demand for building land exceeds the initial assignment of permits, additional allowances can be requested. In turn, actors with a weak demand for building land can put their surplus permits on offer. The basic hypothesis underlying the idea of tradable permit schemes is that the trading of allowances will eventually lead to the most efficient land use pattern (because local planning entities, developers, or property owners are deemed rational actors who compare the expected profitability of new building land to the market price for the required permits). However, the introduction of tradable permit schemes may also entail some difficulties. First of all, it is open to debate how the "cap" should be defined and how the initial allocation of permits should be organized (e.g., via auctioning or via a fair distribution between actors free of charge) without distorting the balance between actors and without jeopardizing institutional rights of local communes or property owners. From an environmental point of view one might also object that the system is only focused on aggregate land consumption figures and neglects the different environmental values and public good functions of different plots of land (e.g., [187, 188]). Yet again, a "cap-and-trade" scheme of tradable permits appears to be a promising instrument for minimizing land consumption as it provides the land-consuming actors with the highest possible decision autonomy, while at the same time assuring the achievement of the cap previously set.
3. In many countries, the rising awareness for environmental issues has led to the introduction of laws and schemes that provide for the *compensation of ecological infringements* by new developments. These are based on the simple principle to ask anyone who is responsible for an investment with negative environmental impact to invest into the improvement of ecological conditions elsewhere. In several countries a system of compensation has developed in recent years, including, among others, pools of plots where compensation measures may be implemented (by improving the ecological value of a respective plot) as well as detailed evaluation schemes that allow quantifying both the environmental impact of a particular development as well as the environmental benefit of compensation measures [189]. Compensation systems of this kind can help minimize land consumption in at least two respects. On the one hand, they simply make the development of new land more expensive, thereby impeding investments that foster land consumption. On the other hand, activities that mitigate previous land consumption can be acknowledged as compensation measures for new developments. Insofar it is for instance possible to oblige land developers to dismantle the water-bound surface of a brownfield plot or tear down empty premises.
4. The *definition of rules concerning the process of land use planning* can be an important control ensuring the efficient use of existing or planned urban areas and infrastructure, avoiding unnecessary land consumption. The obligation to check public plans for their eco-friendliness, including their impact in terms of land consumption, which is required by

a directive of the European Union (SEA Directive 2001/42/EC) since 2004 is a good example. The SEA procedures obligate land use planners and decision-makers to systematically evaluate the likely effects of a plan on the environment and to propose reasonable alternatives of the proposed plan or program. Therefore, the SEA can stimulate planners to look for less land-consuming ways to reach their goals. Another example is the "sequential test" in British land use planning. It requires local authorities to seek suitable brownfield areas first before preparing greenfield land. In the beginning this the "sequential test " only applied to new retail or leisure development [190], but more recently the concept has been extended to planning for residential development, thereby giving priority to reusing previously developed land within urban areas, bringing empty homes back into use and converting existing buildings in preference to the development of greenfield sites. This strategy is particularly relevant with respect to those regions where land consumption occurs in combination with decline (see the contribution by Haase in this volume).

Persuasion – Indicative and Informal Means of Land Use Planning

Besides the "hard" instruments of regulatory land use planning spatial planning has a wide array of "soft" instruments at its disposal. Even though it is the defining characteristic of these instruments that they do not involve the definition of legally binding rules for the use of land, they can nevertheless be very effective when it comes to minimizing land consumption. They include rather different tools such as nonbinding development and actions plans [191] (more or less sophisticated concepts for the organization of), round-table discussions, workshops, and public forums (e.g., [192]); GIS-based decision support systems (e.g., [193]); or initiatives to promote an urban rather than a suburban lifestyle [170]. Generally speaking, these "persuasive" planning instruments attempt to create a commitment to a common goal (i.e., to the goal of minimizing land consumption) and to find cooperative solutions for problems arising from conflicting demands on land use (whereas the regulatory instruments seek to solve these problems by exertion). Reflecting the experience that traditional "blue-print-planning " that mainly draws on regulatory planning tools is often unable to achieve its goals – due to its inability to handle the complexity of societal production of urban space [194, 195] – "persuasive" instruments are broadly accepted today and advocated as an alternative means of progressing in spatial planning.

It hardly comes as a surprise that indicative and informal instruments of spatial planning work fairly well in situations that entail a win-win-structure – for instance, if the national government has decided to allocate a big infrastructure investment in a particular region and the municipalities in the region have to discuss and agree about the details of the project. On the other hand, if a "zero-sum-game" is to be played it is much more difficult to convince the officials in charge to engage in some kind of cooperative action. This becomes manifest, for example, with most attempts to persuade, or push, municipalities to transfer some of their formal competences in spatial planning to the regional level, for example, a new supra-local authority that is installed to organize land development in an urban agglomeration [196].

The provision of information for those actors whose decisions actually determine the pattern of spatial development is a very "soft" but also, at least sometimes, a very promising strategy of spatial planning . With regard to the public actors the monitoring of spatial development and land use change has long been discussed as a means to promote sustainable development (e.g., [197]). The focal point of this discussion is the assumption that an enhanced knowledge on the environmental and social drawbacks of land consumption may lead policy makers to the conclusion that they should call for more efficient forms of spatial development. Moreover, such knowledge can serve as an additional source of legitimacy for the efforts of public authorities (at the supra-local, i.e., regional or national, level) that strive for a containment of land consumption and urban sprawl. Accordingly, various kinds of planning information systems have been designed the main task of which is the continuous provision of information on land use change to decision-makers, and sometimes also the public (e.g., [38, 198]). In addition, there is a further group of instruments that not only aim at monitoring the process of

land use change but also the effectiveness and success of growth management policies altogether (e.g., 75, 199, 200).

Apart from providing decision support to professionals, the publication of data from land use monitoring systems also helps raising public awareness for land consumption and facilitates participation in the planning process. While much of the decision-making surrounding land use changes can be attributed to the calculation of economic costs and benefits by individual firms and households with little concern for wider socio-environmental matters, it is interesting to speculate on the extent to which behavior might be changed through "promoting a non-sprawl culture (...) through education and dissemination" and by "advertising and marketing techniques" [201, p 19], similar to previous campaigns, for example, in support of waste recovery or against smoking in public places.

Models and Paradigms of Urban Development

Whether or not the goal to minimize land consumption can be achieved is not only dependent on the availability of appropriate strategies and instruments to influence or regulate land use changes. Rather, a normative idea on the optimal spatial structure of urban areas that provides orientation in applying these instruments is likewise important. Spatial planning has developed a number of models and paradigms of urban development which, among others, make a strong claim for an economic use of land. As regards the minimization of land consumption, (1) the Green Belt and the Urban Growth Boundary, (2) the various leitmotifs of urban development that promote the compact, polycentric, and mixed-used city, (3) and the prioritization of urban regeneration are among the most important of these normative ideas. Although addressing the complexity of the urban system at rather different levels, these ideas can be seen as specific kinds of planning instruments in that they all entail concrete assertions on how the result of land use change, that is, spatial planning, should look like. They are planning instruments in their own right, but both of a more "substantial" (i.e., material) nature than the instruments discussed above (which are neutral in terms of content and can be used to pursue very different goals). To unfold their instrumental character in the planning process, however, models and paradigms of urban development usually need to be sustained by employing both regulative and persuasive instruments (i.e., the more "instrumental" planning instruments) to implement them.

1. The delineation of *Green Belts* or *Urban Growth Boundaries*, respectively, are among the most famous "tools" designed by spatial planning so as to provide a clear orientation about where to steer new development to and where to prevent urbanization (e.g., [202–204]). While both involve the idea to define a ring of open land that surrounds the urban area, the former notion usually implies a precisely defined line beyond which no building activity must take place whereas the latter is the more generic notion that is often used in nonbinding, regional plans and thus needs to be enforced by specific plans that prohibit development in the Green Belt areas. As long ago as 1944 Abercrombie's Plan for Greater London successfully employed the idea of a green ring that separates the metropolis from the surrounding landscapes – combined with the designation of a series of "new towns" as decentralized growth centers [205, 206]. In particular the concept of the Urban Growth Boundary is difficult to apply in densely populated regions where a sharp distinction between urban and rural areas is often hardly possible. In addition, there is a broad debate in the USA on whether the definition of a rigid boundary around a settlement is indeed the most effective means to curb urban sprawl and its associated negative impacts (e.g., [207]). Several scholars claim to have proven this assumption (e.g., [208]) whereas others doubt it (e.g., [209]). Likewise, Green Belt policies or Urban Growth Boundaries can prove unsuitable in a situation where informal housing is a frequent phenomenon [210]. In such a situation it is hardly possible to limit the outward expansion of the urban area, while, at the same time, it is important to involve the inhabitants of the proliferating informal areas in the planning process, rather than posing threats to their security of tenure by a desk-top zoning of land uses [211]. The implementation of Green Belts and Urban Growth Boundaries requires the decided use of compulsory

land use plans in the way of "negative" planning . It will only be successful if there is broad support for a policy that deprives land owners of the chance to develop their sites if this site is located beyond the imaginary line planners have conceived between the urban and open space [212]. Therefore, whether or not a Green Belt or an Urban Growth Boundary can be implemented in practice largely depends on the distribution of political powers between the main actors of urban development, and in particular on the power of regional planning to pursue its goals.

2. Spatial planning has ever since been strongly influenced by the predominant *leitmotifs and guiding stars* of the time regarding the optimal urban environment – in fact without its foundation in visionary ideas planning would be a somewhat uninspired, bland business. Today the chief guiding stars in urban planning promote, in one way or another, the economic use of land and thus the minimization of land consumption. This is particularly true of the ideal of the mixed use and compact city (e.g., [213]), which is at the heart of, for example, the New Urbanism campaign in the USA [214] as well as the discourse on the European City that has become influential in particular in Central Europe [215]. These guiding stars have developed over the last several decades as a reaction to the neglect of the particular qualities of "urban" environments that was characteristic of the postwar principles and trends of urban development [216]. Decentralized concentration is another leitmotif of spatial development that rather addresses the regional level of planning. It is based on the somewhat dialectic idea that, on the one hand, development (including the development of fresh land) should be promoted in less privileged, peripheral regions but, on the other hand, should be steered to selected locations in order to prevent an inefficient and unwelcome dispersion of development activities [217, 218]. Although the leitmotifs and guiding stars of urban planning are usually not primarily focused on land use issues but rather sketch out a more general idea of "the urban" (which is embedded in an even broader utopian idea of society), their clear intention to concentrate on urban development can mean considerable ideological support for a policy in favor of minimization of land consumption.
3. It is widely acknowledged that policies to minimize land consumption will only be successful if they go hand in hand with efforts to encourage *urban regeneration*, that is, the revalorization or reuse of land that has already been developed [219, 220]. Within the last around 50 years, in many countries a variety of strategies and instruments have emerged to promote urban regeneration. These include specific legislative measures that regulate urban renewal processes (e.g., [176]), urban regeneration schemes aiming to reestablish the attractiveness of inner urban areas (e.g., [221]), congestion charges in inner urban areas [222], or graduated density zoning [223]. These efforts help making the existing urban area as attractive as the newly developed areas as a place in which to invest, develop, produce, live, and work, from the perspectives of economic return, social satisfaction, and environmental quality [224]. If the endeavors to promote urban regeneration are successful they provide a powerful support for the minimization of land consumption; if they fail it will be hardly possible to (re-) direct the focus of investors and households away from suburban Greenfield land and to win them over for more compact development patterns.

Practical Challenges: Spatial Planning as a Governance Endeavor

There is no doubt that spatial planning in most countries in principle disposes of the means to minimize land consumption. Accordingly, we can find countless examples where decided planning efforts have contained land consumption (e.g., [20, 225]) as well as several studies that conducted a comparative evaluation of growth management policies in different regions and found them to have significant impact (e.g., [226–228]). On the other hand, some authors remain somewhat skeptical as to the effectiveness of growth management via spatial planning (e.g., [79, 229]) or even oppose the very idea of intervention in the dynamics of land use change (e.g., [155, 230]). When it comes to discussing whether the actual containment of land consumption has indeed mitigated the negative impacts attributed to urban sprawl,

opinions are even more split as can be seen from countless studies on the urban sprawl issue (see [219, 231, 232], to name but three examples). To give an example from the USA for this divergence of expert views: When comparing federal states with and without growth management programs, Nelson [21] and Kline [233] arrive at completely contrary conclusions as to the success of these programs.

However, the mixed opinions about the overall success of efforts to reduce land consumption by means of spatial planning are only one important aspect. It is likewise essential to account for the fact that the implementation of such efforts is by no means only dependent on whether planners or other experts expect them to be successful. Rather, spatial planning is the result of a political process (and not just a directive endeavor possibly led by public representatives who are highly conscious of environmental issues) [77]. In other words, the mere existence of powerful planning tools that can restrict land consumption does not guarantee their use. Frequently, the problem is not the availability of legal controls but their usage by different public agencies who by no means always regard the minimization of land consumption a top priority (e.g., [234]). Furthermore, minimizing land consumption is a common interest goal that has to be pursued mainly by state authorities (supported by environmental groups) against both other common interest goals (like increasing the number of jobs or the local tax base) as well as the individual interest of land owners and developers to use the land for their purposes (e.g., [235]). Thus, the question arises whether some provision can be made that spatial planning works in favor of a minimization of land consumption at all.

Due to the differences that exist between the planning systems of different countries – and also because of different legal and administrative cultures (e.g., [236]) – it would not be feasible to provide general recommendations as to how spatial planning systems can be instigated to minimize land consumption. Neither is it possible to formulate universally applicable assumptions as to the optimal strategy of land use policy and spatial planning, let alone the use of particular planning instruments. Rather, "anti-sprawl policies must be tailored for the particular patterns extant in the area at hand" [237]. However, it is possible to name a few aspects that should be taken into account wherever spatial planning is expected to help minimizing land consumption.

As we have seen, different state tiers usually have their own means of land use planning that they employ to pursue their specific goals. As a rule, it is at the local level where the opportunity to curtail land-consuming development is usually most, but the willingness to actually inhibit development least pronounced [238] – while we often find the reverse situation at the regional or national level. The task of minimizing land consumption is therefore a characteristic problem of multilevel-governance. This is particularly so where local authorities largely depend on their own tax bases (like in the USA or Germany) because this situation tempts them to use their power to dedicate the land to certain uses to attract tax payers or investments (e.g., [239]). Administrative fragmentation can further aggravate this situation as it increases the number of competitors trying to attract investments by offering fresh land (e.g., [240]; see also Drivers of Land Consumption). Overall, it is important to note that planning law provides local authorities with both the means to minimize or to promote land consumption – and they will often use it to promote growth rather than contain development.

As the containment of urban sprawl and the preservation of the landscape is often an important goal of supra-local land use policies, regional planning can play a key role in controlling land consumption. It can impose a set of aims and provide a framework for the operation of planning on lower government tiers. It can also organize a process in which different actors, including the region's local authorities, develop a joint idea on the future spatial structure and land use patterns of the region [241]. The commitment of local authorities and other actors to such idea will usually be the stronger the tighter they were integrated in the process of designing the common plan, beyond the usual consultations. Generally speaking, it is advisable to enact growth management policies at a spatial scale that is sufficiently large to rein in local parochialism ([31, 226]). With respect to the situation in the USA, Bengston et al. suggest that "with regard to vertical coordination (. . .) growth management is most effective within a statewide context, so that each level of government coordinates their plan with other governmental levels.

Horizontal coordination is needed to help avoid situations in which growth management policies in one jurisdiction undermine policies or create burdens in neighboring communities" [159].

However, it may well be the case that regional or state authorities are hardly inclined to enact a containment of land consumption because they too sometimes emphasize growth as a major aim of public policy. This situation is particularly likely to occur where the responsibility for regional planning lies with an association formed by the region's local authorities (as is the case in many federal states in Germany). Razin [242] has questioned the likelihood of land consumption being successfully controlled by "macro-scale regional plans" and planning regulations and argues in favor of changes to both local tax regimes and local government structures as a more effective approach.

It can be concluded that spatial planning alone will hardly suffice to minimize land consumption. Therefore it should be complemented by other means of public policy (e.g., [19]). In particular three aspects are worthwhile considering in this respect:

1. Firstly it is important to consider the potential land-consuming effects of all types of public policy, for instance, land readjustment policies (e.g., [243]), tax policies (e.g., [244]), subsidies (e.g., [245]), and, in particular, public investments in transportation infrastructures(highways, public transport, parking lots, etc.). There is considerable evidence that the latter stimulate urban sprawl [246, 247]. For instance, radial rapid transit systems in urban agglomerations, together with park and ride facilities, do not only define the potential nodes of compact development but usually also enhance the attractiveness of suburban locations (as compared to the inner city) by improving their accessibility and making the journey from suburbia to the urban core more convenient.
2. Secondly, economic policy instruments can significantly support spatial planning in its attempt to minimize land consumption [187]. These instruments can be used to profoundly alter the framework conditions for individual action and thus to make "land-consuming activities" much less attractive [248]. In this vein, a number of suggestions are available on how fiscal incentives may be introduced that work in favor of the minimization of land consumption [175]. Likewise, the aforementioned tradable permit schemes provide an example of how regulatory land use planning may be combined with economic instruments.
3. Thirdly, it seems obvious that a policy that really aims at minimizing land consumption has to be much more decisive in supporting inner-city (in comparison to suburban) developments than is the case today [249, 250]. In particular, this could mean that subsidies and tax-depreciations for greenfield developments must be abolished, or even allowed only for inner urban projects.

Future Directions

It is widely accepted that extensive land consumption leads to the unwelcome loss of open land and natural resources, causes ecological damage, generates unnecessary traffic, wastes energy, leads to atmospheric pollution, and imposes economic costs on local authorities as inner urban services and amenities lie underused – let alone the potential social effects of urban sprawl such as the exacerbation of spatial social segregation and the exclusion of non-car-owning households from a good deal of work and leisure facilities. The minimization of land consumption is therefore usually an important goal of land use policy. Spatial planning is the major means to pursue and achieve this goal although the heydays of spatial planning and regulation of land use have been in the 1960s and 1970s and are long over. Looking to the future, however, we may expect spatial planning to increase in importance again, mainly because of the risen concern about environmental issues and the introduction in many countries of stronger requirements for considering the environmental impact of development.

Overall, there exists a wide range of strategies and instruments that can be employed by spatial planning to bring land consumption under control. The strategies and instruments that are in use in different countries share many basic features – however different they may be in detail, in particular due to the peculiarities of the respective legal system. Against this background, it will be a crucial task for future applied research on land use and spatial planning to continue with the ongoing

efforts to evaluate the various instruments and strategies that aim at minimizing land consumption (which were mentioned above in particular in Practical Challenges: Spatial Planning as a Governance Endeavor). Apart from this general assertion, regarding the utilization of planning strategies and instruments a series of relevant issues and research questions can be defined that deserve the attention of both academia and practitioners:

1. It appears crucial to embed any attempt to minimize land consumption by spatial planning in a strategy that at the same time eliminates existing incentives for land-consuming development. It is therefore important to identify and then tackle such incentives in, for instance, tax policies or policies for structural development.
2. Given the variety of regulative planning instruments it would be worthwhile to scrutinize the feasibility and effectiveness of possible combinations of different instruments. In this vein, the thorough evaluation of management and containment policies that already exist in different states or regions will be particularly instructive.
3. Since the minimization of land consumption is largely dependent on the political will to achieve this task (which is often lacking), the provision of powerful tools to monitor land use changes and to assess their various impacts is essential. Therefore, current efforts in land use science to develop such tools that are easy to handle and allow establishing the overall effect of land-consuming activities can provide a major contribution to the minimization of land consumption.
4. The ongoing attempts to seek for scientifically sound arguments in favor of compact urban development can supply the efforts to minimize land consumption with weighty arguments.

Finally, it is always important to acknowledge the particular context in which the minimization of land consumption is to be achieved. The existence of a similar set of regulatory means in different countries, for instance, is by no means tantamount to their practical relevance also being similar in these contexts. Likewise, the perception of urban form and density patterns or the reaction of people to anti-sprawl campaigns may vary considerably from place to place. Against this background, it is virtually impossible to transfer planning strategies and instruments by means of which authorities try to minimize land consumption from one legal and cultural context to another without further ado. Therefore, it remains a major research task to keep an eye on practical experiences regarding the applicability of planning strategies and instruments in different contexts as this will provide a basis for their adaption to the context in which they are to be utilized. Without such effort to allow for the particularity of different contexts it seems hardly possible to control, manage, and steer the development of fresh land to the most acceptable locations and to minimize land consumption, and thus to increase the sustainability of land use patterns.

Acknowledgment

We would like to thank Stefan Fina for his valuable guidance and stimulating discussions.

Bibliography

Primary Literature (Cited in the Contribution)

1. Foley JA, DeFries R, Asner GP, Barford C, Bonan G, Carpenter SR, Chapin FS, Coe MT, Daily GC, Gibbs HK, Helkowski JH, Holloway T, Howard EA, Kucharik CJ, Monfreda C, Patz JA, Prentice IC, Ramankutty N, Snyder PK (2005) Global consequences of land use. Science 309:570–574
2. Angel S, Sheppard SC, Civco DL (2005) The dynamics of global urban expansion. Transport and Urban Development Department, The World Bank, Washington, DC
3. Alberti M (2005) The effects of urban patterns on ecosystem functions. Int Reg Sci Rev 28:168–192
4. Lambin EF, Turner BL, Geist HJ, Samuel BA, Angelsen A, Bruce JW, Coomes OT, Dirzo R, Fischer G, Folke C (2001) The causes of land-use and land-cover change: moving beyond the myths. Global Environ Chang 11:261–269
5. Poelmans L, Van Rompaey A (2010) Complexity and performance of urban expansion models. Comput Environ Urban Syst 34:17–27
6. McGranahan G, Marcotullio P (2005) Urban systems. In: Hassan R, Scholes R, Ash N (eds) Ecosystems and human well-being: current state and trends. The Millenium Ecosystem Assessment Project, vol 1. Island, Washington, DC, Covelo, London, pp 797–825
7. World Resources Institute (2003) Domesticating the world: conversion of natural resources. World Resources Institute, Washington, DC
8. Schneider A, Woodcock CE (2008) Compact, dispersed, fragmented, extensive? A comparison of urban growth in

twenty-five global cities using remotely sensed data, pattern metrics and census information. Urban Stud 45:659–692
9. Deng X, Huang J, Rozelle S, Uchida E (2010) Economic growth and the expansion of urban land in China. Urban Stud 47: 813–843
10. EEA (European Environment Agency) (2002) Environmental signals 2002. Benchmarking the millennium. Environmental assessment report 9, EEA, Copenhagen
11. Cervero R, Murakami J (2010) Effects of built environments on vehicle miles traveled: evidence from 370 US urbanized areas. Environ Plann A 42:400–418
12. Ewing R, Bartholomew K, Winkelman S, Walters J, Chen D (2008) Growing cooler, The evidence on urban development and climate change (executive summary). Urban Land Institute, Washington, DC
13. Ewing R, Nelson AC (2008) CO2 reductions attributable to smart growth in California. California Air Resources Board, Sacramento
14. Committee on Physical Activity, Health, Transportation, and Land Use, Transportation Research Board, Institute of Medicine of the National Academies (2005) Does the built environment influence physical activity? Examining the evidence. Transportation Research Board, Washington, DC
15. Ganser R, Williams K (2007) Brownfield development. Are we using the right targets? Evidence from England and Germany. Eur Plan Stud 15:603–622
16. Lichtenberg E, Ding C (2006) Land use efficiency, food security, and farmland preservation in China. Land Lines 18 (online source)
17. Bundesregierung (2002) Perspektiven für Deutschland. Unsere Strategie für eine nachhaltige Entwicklung, Berlin
18. Landis J (2006) Growth management revisited. J Am Plann Assoc 72:411–430
19. Anthony J (2004) Do state growth management regulations reduce sprawl? Urban Aff Rev 39:376–397
20. Carruthers JI (2002) The impacts of state growth management programmes: A comparative Analysis. Urban Stud 39:1959–1982
21. Nelson AC (1999) Comparing states with and without growth management – Analysis based on indicators with policy implications. Land Use Policy 16:121–127
22. Wassmer RW (2002) Defining excessive decentralization in Californial and other Western states, vol 1, An economist's perspective on urban sprawl. California Senate Office of Research, Sacramento
23. Whyte WH (1958) Urban sprawl. In: Whyte WH (ed) The exploding metropolis. Doubleday, Garden City
24. Mumford L (1962) The city in history. Harcourt, Brace & World, New York
25. Mumford L (1963) The highway and the city. Harcourt Brace Jovanovich, New York
26. Clawson M (1962) Urban sprawl and speculation in suburban land. Land Econ 38:99–111
27. Harvey RO, Clark AV (1965) The nature and economics of urban sprawl. Land Econ 41:1–9
28. Benfield KF, Raimi M, Chen DDT (1999) Once there were greenfields: how urban sprawl is undermining America's environment, economy and social fabric. National Resource Defense Council, New York
29. Burgess R (2000) The compact city debate: a global perspective. In: Jenks M, Burgess R (eds) Compact cities: sustainable urban forms for developing countries. Spon, London, pp 9–24
30. Richardson HW, Bae CHC, Baxamusa MH (2000) Compact cities in developing countries: assessment and implications. In: Jenks M, Burgess R (eds) Compact cities: sustainable urban forms for developing countries. Spon, London, New York, pp 25–36
31. Peiser R (2001) Decomposing urban sprawl. Town Plann Rev 72:275–298
32. Gillham O (2002) The limitless city. A primer on the urban sprawl debate. Island, Washington, DC, Covelo, London
33. Burchell RW, Lowenstein G, Dolphin WR, Galley CC, Downs A, Seskin S, Gray Still K, Moore T (2002) Costs of sprawl – 2000. National Academy, Washington, DC
34. Squires GD (ed) (2002) Urban sprawl. Causes, consequences and policy responses. The Urban Institute, Washington, DC
35. Nechyba TJ, Walsh RP (2004) Urban sprawl. J Econ Perspect 18:177–200
36. Burchell RW, Shad NA, Listokin D, Phillips H, Downs A, Seskin S, Davis JS, Moore T, Helton D, Gall M (1998) The costs of sprawl – revisited. National Academy, Washington, DC
37. Huang J, Lu XX, Sellers JM (2007) A global comparative analysis of urban form: Applying spatial metrics and remote sensing. Landscape Urban Plan 82:184–197
38. Kasanko M, Barredo JI, Lavalle C, McCormick N, Demicheli L, Sagris V, Brezger A (2006) Are European cities becoming dispersed? Landscape Urban Plan 77:111–130
39. Fina S, Siedentop S (2008) Urban sprawl in Europe identifying the challenge. Paper presented at the REAL CORP 008, Wien
40. EEA (European Environment Agency) (2005) The European environment. State and outlook 2005. State of the environment report No 1/2005, EEA, Copenhagen
41. Torrens PM, Alberti M (2000) Measuring sprawl. CASA paper 27. University College London
42. Galster G, Hanson R, Ratcliffe MR, Wolman H, Coleman S, Freihage J (2001) Wrestling sprawl to the ground: Defining and measuring an elusive concept. Hous Policy Debate 12:681–717
43. Frenkel A, Ashkenazi M (2008) Measuring urban sprawl: how can we deal with it? Environ Plann B 35:1–24
44. Torrens PM (2008) A toolkit for measuring sprawl. Appl Spatial Anal Policy 1:5–36
45. Siedentop S, Fina S (2010) Monitoring urban sprawl in Germany: towards a GIS-based measurement and assessment approach. J Land Use Sci 5:73–104
46. Chin N (2002) Unearthing the roots of urban sprawl: a critical analysis of form, function and methodology. CASA Working Paper 47, University College London
47. Kolankiewicz L, Beck R (2001) Weighing sprawl factors in large U.S. cities. A report on the nearly equal roles played by

population growth and land use choices in the loss of farmland and natural habitat to urbanization. NumbersUSA, Arlington, VA
48. Razin E, Rosentraub M (2000) Are fragmentation and sprawl interlinked? North American evidence. Urban Aff Rev 35: 821–836
49. Ewing R, Pendall R, Chen DT (2002) Measuring sprawl and its impacts. Smart Growth America, Washington, DC
50. Glaeser EL, Kahn ME (2003) Sprawl and urban growth. Harvard University, Harvard Institute of Economic Research, Cambridge, MA
51. Emison GA (2001) The relationship of sprawl and ozone air quality in United States' metropolitan areas. Reg Environ Change 2:118–127
52. Song Y, Knaap GJ (2004) Measuring urban form. Is Portland winning the war on sprawl? J Am Plann Assoc 70:210–225
53. Lopez R, Hynes HP (2003) Sprawl in the 1990s. Measurement, distribution, and trends. Urban Aff Rev 38:325–355
54. Weber J, Sultana S (2005) The impact of sprawl on commuting in Alabama. University of Alabama, University Transportation Center for Alabama, Birmingham
55. EEA (European Environmental Agency) (2006) Urban sprawl in Europe – the ignored challenge. EEA Report 10/2006, EEA, Copenhagen
56. Theobald DM (2005) Landscape patterns of exurban growth in the USA from 1980 to 2020. Ecol Soc 10:32
57. Fulton W, Pendall R, Nguyen M, Harrison A (2001) Who sprawls most? How growth patterns differ across the U.S. The Brookings Institution, Washington, DC
58. Dosch F, Beckmann G (2003) Stand und Perspektiven der Siedlungsflächenentwicklung. In: Bundesamt für Bauwesen und Raumordnung (BBR) (ed) Bauland- und Immobilienmärkte 16. BBR, Bonn, pp 71–102
59. Lang RE, LeFurgy J (2003) Edgeless cities: examining the noncentered city. Hous Policy Debate 14:427–460
60. Nelson AC (1992) Characterizing exurbia. J Plann Lit 6:350–368
61. Theobald DM (2001) Land-use dynamics beyond the American urban fringe. Geogr Rev 91:544–564
62. Crane R, Chatman DG (2004) Traffic and sprawl: evidence from US commuting, 1985 to 1997. In: Richardson HW, Bae CHC (eds) Urban sprawl in western Europe and the United States. Ashgate, London, pp 311–324
63. Glaeser EL (2001) Job sprawl. Employment location in U.S. metropolitan areas. The Brookings Institution, Washington, DC
64. Siedentop S, Fina S (2010) Urban sprawl beyond growth: from growth to decline perspective on the cost of sprawl. Flux 79(80):90–100
65. Alonso WA (1964) Location and land use. Harvard University Press, Cambridge, MA
66. Mills ES (1972) Studies in the structure of the urban economy. Johns Hopkins University Press, Baltimore
67. Muth R (1969) Cities and housing. Chicago University Press, Chicago
68. Mieszkowski P, Mills ES (1993) The causes of metropolitan suburbanization. J Econ Perspect 7:135–147
69. Tiebout C (1956) A Pure Theory of Local Expenditures. J Polit Econ 64:416–424
70. Davoudi S (2003) Polycentricity in European spatial planning: from an analytical tool to a normative agenda. Eur Plan Stud 11:979–999
71. Champion AG (2001) A changing demographic regime and evolving polycentric urban regions: consequences for the size, composition and distribution of city populations. Urban Stud 38:657–677
72. Garreau J (1991) Edge city. Life on the new frontier. Doubleday, New York
73. Dielemann F, Wegener M (2004) Compact city and urban sprawl. Built Environ 30:308–323
74. Antrop M (2004) Landscape change and the urbanization process in Europe. Landscape Urban Plan 67:9–26
75. Frenkel A (2004) A land-consumption model - Its application to Israel's future spatial development. J Am Plann Assoc 70:453–470
76. Siedentop S, Junesch R, Straßer M, Zakrzewski P, Samaniego L, Weinert J (2009) Einflussfaktoren der Neuinanspruchnahme von Flächen. Bundesamt für Bauwesen und Raumordnung, Bonn
77. Ulfarsson GF, Carruthers JI (2006) The cycle of fragmentation and sprawl: a conceptual framework and empirical model. Environ Plann B 33:767–788
78. Green RK (1999) Nine causes of Sprawl. Illinois Real Estate Letter (Fall 1999):10–13
79. Pendall R (1999) Do land-use controls cause sprawl? Environ Plann B 26:555–571
80. Siedentop S, Fina S (2010) Urban Sprawl beyond Growth: from Growth to Decline Perspective on the Cost of Sprawl. Flux 79(80):90–100
81. Nuissl H, Rink D (2005) The 'production' of urban sprawl in eastern Germany as a phenomenon of post-socialist transformation. Cities 22:123–134
82. Persky J, Kurban H (2001) Do federal funds better support cities or suburbs? A spatial analysis of federal spending in the Chicago metropolis. The Brookings Institution (The Discussion Paper Series), Washington, DC
83. Downs A (1998) How America's cities are growing: the big picture. Brookings Rev 16:8–12
84. Clingermayer JC (2004) Heresthetics and happenstance: intentional and unintentional exclusionary impacts of the zoning decision-making process. Urban Stud 41:377–388
85. Cooper LM (2004) Guidelines for cumulative effects assessment in SEA of plans. Imperial College, London
86. Council on Environmental Quality (1997) Considering cumulative effects under the National Environmental Policy Act. Council on Environmental Quality, Washington, DC
87. Parr S (1999) Study on the assessment of indirect and cumulative impacts as well as impact interactions, Vol 1: Background to the study. Hyder, Cardiff
88. American Farmland Trust (1994) Farming on the edge: a new look at the importance and vulnerability of agriculture near American cities. American Farmland Trust, Washington, DC

89. Voogt JA (2002) Urban heat island. In: Douglas I (ed) Encyclopedia of global environmental change, vol 3, Causes and consequences of global environmental change. Wiley, Chichester, pp 660–666
90. Schueler TR (1994) The importance of imperviousness. Watershed Prot Tech 1:100–111
91. Yang J, Jinxing Z (2007) The failure and success of greenbelt program in Beijing. Urban Forest Urban Greening 6:287–296
92. Nuissl H, Haase D, Lanzendorf M, Wittmer H (2009) Environmental impact assessment of urban land use transitions - a context-sensitive approach. Land Use Policy 26:414–424
93. Ewing R (1997) Is Los-Angeles-style sprawl desirable? J Am Plann Assoc 63:107–126
94. Hasse JE, Lathrop RG (2003) Land resource impact indicators of urban sprawl. Appl Geogr 23:159–175
95. Heimlich RE, Anderson WD (2001) Development at the urban fringe and beyond: impacts on agriculture and rural land. U.S. Department of Agriculture, Washington, DC
96. Park HS (1986) Features of the heat island in Seoul and its surrounding cities. Atmos Environ 20:1859–1866
97. Watkins R, Palmer J, Kolokotroni M (2007) Increased temperature and intensification of the urban heat island: implications for human comfort and urban design. Built Environ 33:85–96
98. Gill SE, Handley JF, Ennos AR, Pauleit S (2007) Adapting cities for climate change: the role of the green infrastructure. Built Environ 33:115–133
99. Pauleit S, Ennos R, Golding Y (2005) Modeling the environmental impacts of urban land use and land cover change – a study in Merseyside, UK. Landscape Urban Plann 71:295–310
100. Arnold CL, Gibbons CJ (1996) Impervious surface coverage. The emergence of a key environmental indicator. J Am Plann Assoc 62:243–258
101. Burchell RW, Mukherji S (2003) Conventional development versus managed growth: the costs of sprawl. Am J Public Health 93:1534–1540
102. Doubek C, Zanetti G (1999) Siedlungsstruktur und öffentliche Haushalte. Österreichisches Institut für Raumplanung, Wien
103. Parsons, Brinckerhoff, Quade & Douglas Inc., ECONorthwest (1998) The full social costs of alternative land use patterns: theory, data, methods and recommendations. U.S. Department of Transportation, Federal Highway Administration, Washington, DC
104. Cervero R (1996) Jobs-housing balance revisited. Trends and impacts in the San Francisco Bay Area. J Am Plann Assoc 62:492–511
105. Naess P (2003) Urban structures and travel behaviour. Experiences from empirical research in Norway and Denmark. European. J Transp Infrastructure Res 3:155–178
106. Sultana S (2000) Some effects of employment centers on commuting times in the Atlanta metropolitan area, 1990. Southeast Geogr 41:225–233
107. Jaeger J (2000) Landscape division, splitting index, and effective mesh size: new measures of landscape fragmentation. Landscape Ecol 15:115–130
108. Theobald DM, Miller JR, Thompson Hobbs N (1997) Estimating the cumulative effects of development on wildlife habitat. Landscape Urban Plann 39:25–36
109. Downs A (1999) Some realities about sprawl and urban decline. Hous Policy Debate 10:955–974
110. Sarzynski A, Wolman HL, Galster G, Hanson R (2006) Testing the conventional wisdom about land use and traffic congestion: the more we sprawl, the less we move? Urban Stud 43:601–626
111. Newman P, Kenworthy JR (2006) Urban design to reduce automobile dependence. Opolis 2:35–52
112. Newman P (1996) Reducing automobile dependence. Environ Urbanization 8:67–92
113. Ewing R, Cervero R (2010) Travel and the built environment. A meta-analysis. J Am Plann Assoc 76:256–294
114. Banister D (1999) Planning more to travel less. Land use and transport. Town Plann Rev 70:313–338
115. Stone JB, Mednick AC, Holloway T, Spak SN (2007) Is compact growth good for air quality? J Am Plann Assoc 73:404–418
116. Bertaud A (2004) The spatial organization of cities: deliberate outcome or unforeseen consequence? University of California, Institute of Urban and Regional Development, Berkeley
117. Campoli J, McLean AS (2004) Visualizing density. Lincoln Institute of Land Policy, Cambridge, MA
118. Cervero R (1998) The transit metropolis. A global inquiry. Island, Washington, DC
119. Ecoplan (2000) Siedlungsentwicklung und Infrastrukturkosten. Gutachten im Auftrag des Bundesamtes für Raumentwicklung, des Staatssekretariats für Wirtschaft und des Amtes für Gemeinden und Raumordnung des Kantons. Bern
120. Ewing R, Rong F (2008) The impact of urban form on U.S. residential energy use. Hous Policy Debate 19:1–30
121. Holden E, Norland IT (2004) Three challenges for the compact city as a sustainable urban form: household consumption of energy and transport in eigth residential areas in the Greater Oslo Region. Urban Stud 42:2145–2166
122. Kelly-Schwartz AC, Stockard J, Doyle S, Schlossberg M (2004) Is sprawl unhealthy? A multilevel analysis of the relationship of metropolitan sprawl to the health of individuals. J Plann Educ Res 24:184–196
123. Ewing R, Schmid T, Killingsworth R, Zlot A, Raudenbush S (2003) Relationship between urban sprawl and physical activity, obesity, and morbidity. Am J Health Promot 18:47–57
124. Mc Cann BA, Ewing R (2003) Measuring the health effects of sprawl, A national analysis of physical activity, obesity and chronic disease. Smart Growth America, Washington, DC
125. Siedentop S (2005) Urban Sprawl - verstehen, messen, steuern. Ansatzpunkte für ein empirisches Mess- und Evaluationskonzept der urbanen Siedlungsentwicklung. DISP 160:23–35
126. Kahn ME (2000) The environmental impact of suburbanization. J Policy Anal Manage 19:569–586
127. Johnson MP (2001) Environmental impacts of urban sprawl: a survey of the literature and proposed research agenda. Environ Plann A 33:717–735

128. Moglen GE, Kim S (2007) Limiting imperviousness. Are threshold-based policies a good idea? J Am Plann Assoc 73:161–171
129. Haase D, Nuissl H (2007) Does urban sprawl drive changes in the water balance and policy? The case of Leipzig (Germany) 1870–2003. Landscape Urban Plann 80:1–13
130. Alberti M (1999) Urban patterns and environmental performance: what do we know? J Plann Educ Res 19:151–163
131. Dahlmann I, Gunreben M, Tharsen J (2001) Flächenverbrauch und Bodenversiegelung in Niedersachsen. Bodenschutz 3:79–84
132. Meinel G, Hernig A (2005) Inwertsetzung von Geobasisdaten für Fachanwendungen am Beispiel der Bodenversiegelungserhebung auf Grundlage des ATKIS Basis-DLM. In: Deutsche Gesellschaft für Photogrammetrie, Fernerkundung u. Geoinformation (ed) 25. Wissenschaftlich-Technische Jahrestagung d. DGPF, Rostock, pp 83–91
133. Bradshaw TK, Muller B (1998) Impacts of rapid urban growth on farmland conversion: application of new regional land use policy models and geographical information systems. Rural Sociol 63:1–25
134. Merenlender AM, Brooks C, Shabazian D, Gao S, Johnston R (2005) Forecasting exurban development to evaluate the influence of landuse policies on wildland and farmland conservation. J Conserv Plann 1:64–88
135. Cieslewicz DJ (2002) The environmental impacts of sprawl. In: Squires GD (ed) Urban sprawl. causes, consequences and policy responses. The Urban Institute, Washington, DC, pp 23–38
136. Real Estate Research Corporation (1974) The costs of sprawl. Detailed cost analysis. Prepared for the Council on Environmental Quality, the Office of Policy Development and Research, Department of Housing and Urban Development, the Office of Planning and Management. Environmental Protection Agency, Washington, DC
137. Ladd H (1991) Population growth, density and the costs of providing public services. Urban Stud 29:273–295
138. Peiser R (1989) Density and urban sprawl. Land Econ 65:193–204
139. Burchell RW, Downs A, McCann B, Mukherji S (2005) Sprawl costs. Economic impacts of unchecked development. Island, Washington, DC, Covelo, London
140. Carruthers JI, Ulfarsson GF (2003) Urban sprawl and the cost of public services. Environ Plann B 30:503–522
141. Speir C, Stephenson K (2002) Does sprawl cost us all? Isolating the effects of housing patterns on public water and sewer costs. J Am Plann Assoc 68:56–70
142. Holtzclaw J, Clear R, Dittmar H, Goldstein D, Haas P (2002) Location efficiency: neighborhood and socioeconomic characteristics determine auto ownership and use – studies in Chicago, Los Angeles and San Francisco. Transp Plann Technol 25:1–27
143. Naess P (2007) The impacts of job and household decentralization on commuting distances and travel modes. Experiences from the Copenhagen region and other Nordic urban areas. Inf Raumentwicklung 2(3):149–168
144. Bento AM, Cropper ML, Mobarak AM, Vinha K (2003) The impact of urban spatial structure on travel demand in the United States. World Bank policy research working paper no. 3007, Washington, DC
145. Handy S (2005) Smart Growth and the transportation-land use connection: what does the research tell us? Int Reg Sci Rev 28:146–167
146. Vance C, Hedel R (2007) The impact of urban form on automobile travel: disentangling causation from correlation. Transportation 34:575–588
147. Cervero R (2003) The built environment and travel. Evidence from the United States. Eur J Transp Infrastructure Res 3: 119–135
148. Power A (2001) Social exclusion and urban sprawl: Is the rescue of cities possible? Reg Stud 35:731–742
149. Kain JF (1992) The spatial mismatch hypothesis: three decades later. Hous Policy Debate 3:371–460
150. Gordon P, Kumar A, Richardson HW (1989) The spatial mismatch hypothesis: some new evidence. Urban Stud 26:315–326
151. Matas A, Ramond J-L, Roig J-L (2010) Job accessibility and female employment probability: The cases of Barcelona and Madrid. Urban Stud 47:769–787
152. Gallent N (2006) The rural-urban fringe: a new priority for planning policy? Plann Pract Res 21:383–393
153. Bengston DN, Potts RS, Fan DP, Goetz EG (2005) An analysis of the public discourse about urban sprawl in the United States: Monitoring concern about a major threat to forests. For Pol Econ 7:745–756
154. Ewing R (1994) Causes, characteristics, and effects of sprawl: a literature review. Environ Plann Urban Issues 21:1–15
155. Gordon P, Richardson HW (2001) The sprawl debate. Let markets plan. J Federalism 31:131–149
156. Bruegman R (2005) Sprawl. A compact history. University of Chicago Press, Chicago
157. Newman P (1992) The compact city. An Australian perspective. Built Environ 18:285–300
158. CEC (Commission of the European Communities) (1999) ESDP – European Spatial Development Perspective: towards balanced and sustainable development of the territory of the European Union. Adopted by the Ministers for Spatial Planning at the Potsdam Council on 10 and 11 May 1999. Office for Official Publications of the European Communities, Luxembourg
159. Bengston DN, Fletcher JO, Nelson KC (2004) Public policies for managing urban growth and protecting open space: policy instruments and lessons learned in the United States. Landscape Urban Plann 69:271–286
160. Song Y, Zenou Y (2006) Property tax and urban sprawl. Theory and implications for US cities. J Urban Econ 60: 519–534
161. Nuissl H, Schröter-Schlaack C (2009) The economic approach towards the containment of land consumption. Environ Sci Policy 12:270–280
162. Hirt S (2007) The devil Is in the definitions. J Am Plann Assoc 7:436–450

163. Köck W, Bovet J, Gawron T, Hofmann E (2007) Activating spatial planning law: options for the reduction of land consumption. J Eur Environ Plann Law 4:2–16
164. Acioly C Jr, Davidson F (1996) Density in urban development. Build Issues 8:3–25
165. Churchman A (1999) Disentangling the concept of density. J Plann Lit 13:389–411
166. Freilich RH (1998) The land-use implications of transit-oriented development: Controlling the demand side of transportation congestion and urban sprawl. Urban Lawyer 30:547–572
167. Handa VK (1996) Construction engineers driving into the 21st century. J Constr Eng Manage – ASCE 122:2–6
168. Healey P (1992) A planner's day: Knowledge and action in communicative practice. J Am Plann Assoc 58:9–20
169. Wates N (2000) The community planning handbook. Earthscan, London
170. Besecke A, Haensch R, Pinetzki M (eds) Das Flächensparbuch. Diskussion zu Flächenverbrauch und lokalem Bodenbewusstsein. ISR-Diskussionsbeiträge 56, Institut of Urban and Regional Planning, Technische Universität Berlin
171. Haughton G (1999) Information and participation within environmental management. Environ Urbanization 11:51–62
172. Criterion Planners/Engineers, Fehr & Peers Associates (2001) INDEX 4D Method. A quick-response method of estimating travel impacts from land-use changes. Technical Memorandum. Portland, OR
173. EPA (U.S. Environmental Protection Agency) (2000) Projecting land-use change: a summary of models for assessing the effects of community growth and change on land-use patterns. Cincinnati, OH
174. Gihring TA (1999) Incentive property taxation - A potential tool for urban growth management. J Am Plann Assoc 65:62–79
175. Korthals Altes WK (2009) Taxing land for urban containment. Reflections on a Dutch debate. Land Use Policy 26:233–241
176. Couch C, Fraser C, Percy S (2003) Urban regeneration in Europe. Blackwell, Oxford
177. Newton PW (2010) Beyond greenfield and bownfield. The challenge of regenerating Australia's greyfield suburbs. Built Environ 36:81–104
178. Pruetz R (2003) Beyond takings and givings: Saving natural areas, farmland and historic landmarks with transfer of development rights and density transfer charges. Arje, Marina Del Ray, CA
179. Newman P, Thornley A (1996) Urban planning in Europe. Routledge, London
180. Sinz M (2000) Gibt es Auswirkungen der europäischen Raumentwicklungspolitik auf nationaler, regionaler oder kommunaler Ebene? (Does European spatial development policy have impacts at the national, regional and municipal levels?). Inf Raumentwicklung 3(4):109–116
181. Brody SD, Carrasco V, Highfield WE (2006) Measuring the adoption of local sprawl - Reduction planning policies in Florida. J Plann Educ Res 25:294–310
182. Miceli TJ, Sirmans CF (2007) The holdout problem, urban sprawl, and eminent domain. J Hous Econ 16:309–319
183. Pasha HA (1996) Suburban minimum lot zoning and spatial equilibrium. J Urban Econ 40:1–12
184. Johnston RA, Madison ME (1997) From landmarks to landscapes: A review of current practices in the transfer of development rights. J Am Plann Assoc 63:365–378
185. Bizer K, Hansjürgens B, Köck W, Siedentop S (2008) Handelbare Flächenausweisungsrechte: Anforderungen aus planerischer ökonomischer und juristischer Sicht. Nomos-Verlag, Baden-Baden
186. Micelli E (2002) Development right markets to manage urban plans in Italy. Urban Stud 39:141–154
187. Brueckner JK (2000) Urban sprawl: Diagnosis and remedies. Int Reg Sci Rev 23:160–171
188. Burkhard B, Kroll F, Müller F, Windhorst W (2009) Landscapes' capacities to provide ecosystem services – a concept for land-cover based assessments. Landscape Online 15:1–22, doi: 10.3097/LO.200915
189. Peters W, Siewert W, Szaramowicz M (2002) Folgenbewältigung von Eingriffen im internationalen Vergleich. BfN-Skripten 82, Bundesamt für Naturschutz, Bonn
190. DCLG (2005) Planning Policy Statement 6: Planning for town centres. The Stationary Office, London
191. Gallent N, Shaw D (2007) Spatial planning, Area Action Plans and the rural-urban fringe. J Environ Plann Manage 50: 617–638
192. Woolston DW (1996) Simply a matter of growing pains? Evaluating the controversy surrounding the growth management hearings boards. Wash Law Rev 71:1219–1253
193. Lee J, Tian L, Erickson LJ, Kulikowski TD (1998) Analyzing growth-management policies with geographical information systems. Environ Plann B 25:865–879
194. Friedman J (1987) Planning in the public domain. From knowledge to action. Princeton University Press, Washington, DC
195. Healey P (1997) Collaborative planning. Shaping places in fragmented societies. Macmillan, London
196. Gillette CP (2001) Regionalization and interlocal bargains. NY Univ Law Rev 76:190–271
197. Koomen E, Rietveld P, de Nijs T (2008) Modelling land-use change for spatial planning support. Ann Reg Sci 42:1–10
198. Schmid WA (2001) The emerging role of visual resource assessment and visualisation in landscape planning in Switzerland. Landscape Urban Plann 54:213–221
199. Conway TM, Lathrop RG (2005) Modelling the ecological consequences of land-use policies in an urbanizing region. Environ Manage 35:278–291
200. Nelson AC, Sanchez TW (2005) The effectiveness of urban containment regimes in reducing exurban sprawl. DISP 160:42–47
201. Kolyvas A (2003) URBS PANDENS. Analysis of Present Policy Structures and Concepts. Draft Version, ICLEI – International Council of Local Environmental Initiatives, European Secretariat, Freiburg (Germany)
202. Abbott C, Margheim J (2008) Imagining Portland's urban growth boundary: Planning regulation as cultural icon. J Am Plann Assoc 74:196–208

203. Al-Hathloul S, Mughal MA (2004) Urban growth management - the Saudi experience. Habitat Int 28:609–623
204. Bengston DN, Youn YC (2006) Urban containment policies and the protection of natural areas: the case of Seoul's greenbelt. Ecol Soc 11(1):3, (URL: http://www.ecologyandsociety.org/vol11/iss1/art3)
205. Osborn FG, Whittick A (1977) New towns: Their origins, achievements, and progress, 3rd edn. L. Hill/Routledge, London, Boston
206. Hall P (2002) Urban and regional planning. Routledge, New York
207. Carlson T, Dierwechter Y (2007) Effects of urban growth boundaries on residential development in Pierce County, Washington. Prof Geogr 59:209–220
208. Weitz J, Moore T (1998) Development inside urban growth boundaries - Oregon's empirical evidence of contiguous urban form. J Am Plann Assoc 64:424–440
209. Bae CHC, Jun MJ (2003) Counterfactual planning – What if there had been no greenbelt in Seoul? J Plann Educ Res 22:374–383
210. Wang YM, Scott S (2008) Illegal farmland conversion in China's urban periphery: Local regime and national transitions. Urban Geogr 29:327–347
211. Field BG (1998) Embracing the informal sector: an inclusive and more sustainable approach to development planning. Int J Sustain Dev World Ecol 5:277–287
212. Pond D (2009) Ontario's greenbelt: Growth management, farmland protection, and regime change in Southern Ontario. Can Pub Policy 35:413–432
213. Williams K, Burton E, Jenks M (eds) (2000) Achieving sustainable urban form. E & FN Spon, London
214. Talen E (2005) New Urbanism and American planning: The conflict of cultures. Routledge, New York and Milton Park, Abingdon
215. Rietdorf W (ed) (2001) Auslaufmodell Europäische Stadt? Neue Herausforderungen und Fragestellungen am Beginn des 21. Jahrhunderts. Verlag für Wissenschaft und Forschung, Berlin
216. Jacobs J (1961) Death and life of great American cities. Random House, New York
217. Gainsborough JF (2002) Slow growth and urban sprawl – support for a new regional agenda. Urban Aff Rev 37: 728–744
218. Yu L (2007) A sustainable development form for metropolises in China - A case study of Beijing. Int Dev Plann Rev 29:451–473
219. Nelson AC, Burby RJ, Feser E, Dawkins CJ, Malizia EE, Quercia R (2004) Urban containment and central-city revitalization. J Am Plann Assoc 70:411–425
220. Lee S, Leigh NG (2005) The role of inner ring suburbs in Metropolitan smart growth strategies. J Plann Lit 19: 330–346
221. Haase A, Kabisch S, Steinführer A (2005) Reurbanisation of inner-city areas in European cities. Scrutinizing a concept of urban development with reference to demographic and household change. In: Sagan I, Smith D (eds) Society, economy, environment – towards the sustainable city. Bogucki Wydawnictwo Naukowe, Gdansk/Poznan, pp 75–91
222. Anas A, Rhee H-J (2006) Curbing excess sprawl with congestion tolls and urban boundaries. Reg Sci Urban Econ 36: 510–541
223. Shoup D (2008) Graduate density zoning. J Plann Educ Res 28:161–179
224. Couch C, Karecha J (2006) Controlling urban sprawl. Some experiences from Liverpool. Cities 23:353–363
225. M'Bala J (2001) Forestalling urban sprawl: The Greber Plan for Montreal, 1950. Urban Hist Rev - Revue d'Histoire Urbaine 29:62–71
226. Yin M, Sun J (2007) The impacts of state growth management programs on urban sprawl in the 1990s. J Urban Aff 29:149–179
227. Howell-Moroney M (2007) Studying the effects of the intensity of US state growth management approaches on land development outcomes. Urban Stud 44:2163–2178
228. Bento AM, Francob SF, Kaffine D (2006) The efficiency and distributional impacts of alternative anti-sprawl policies. J Urban Econ 59:121–141
229. Tomalty R (2002) Growth Management in the Vancouver Region. Local Environ 7:431–445
230. Thornes P, Simons GPW (1999) Letting the market preserve land. The case for a market-driven transfer of development rights program. Contemp Econ Policy 17:256–266
231. Dawkins CJ, Nelson AC (2002) Urban containment policies and housing prices: an international comparison with implications for future research. Land Use Policy 19:1–12
232. Nelson AC, Dawkins CJ, Sanchez TW (2004) Urban containment and residential segregation: a preliminary investigation. Urban Stud 41:423–439
233. Kline JD (2000) Comparing states with and without growth management – analysis based on indicators with policy implications. Comment. Land Use Policy 17:349–355
234. Leo C, Beavis MA, Carver A, Turner R (1998) Is urban sprawl back on the political agenda? Local growth control, regional growth management, and politics. Urban Aff Rev 34: 179–211
235. Chou TL, Chang JY (2008) Urban sprawl and the politics of land use planning in urban Taiwan. Int Dev Plann Rev 30: 67–92
236. Healey P, Williams (1993) European urban planning systems. Diversity and convergence. Urban Stud 30:701–720
237. Cutsinger J, Galster G (2006) There is no sprawl syndrome: A new typology of metropolitan land use patterns. Urban Geogr 27:228–252
238. Sellers JM (2002) Federalism and metropolitan governance in cross-national perspective: the case of urban sprawl. Environ Plann C 20:95–112
239. Wassmer RW (2002) Fiscalisation of Land Use, Urban Growth Boundaries and Non-central Retail Sprawl in the Western United States. Urban Stud 39:1307–1327

240. Carruthers JI (2003) Growth at the fringe: The influence of political fragmentation in United States metropolitan areas. Pap Reg Sci 82:475–499
241. Carruthers JI, Ulfarsson GF (2002) Fragmentation and sprawl. Evidence from interregional analysis. Growth Change 33:312–340
242. Razin E (1998) Policies to control urban sprawl. planning regulations or changes in the ‚rules of the game'? Urban Stud 35:321–340
243. Sorensen A (1999) Land readjustment, urban planning and urban sprawl in the Tokyo Metropolitan Area. Urban Stud 36:2333–2360
244. Brueckner JK, Kim H-A (2003) Urban sprawl and the property tax. Int Tax and Public Finance 10:5–23
245. Su Q, DeSalvo JS (2008) The effect of transportation subsidies on urban sprawl. J Reg Sci 48:567–594
246. Goodwin PB (1996) Empirical evidence on induced traffic – a review and synthesis. Transportation 23:35–54
247. Shoup DC (1997) The high cost of free parking. J Plann Educ Res 17:3–20
248. Atkinson G, Oleson T (1996) Urban Sprawl as a path dependent process. J Econ Issues 30:609–615
249. Couch C (2003) City of change and challenge. Urban planning and regeneration in Liverpool. Ashgate, Aldershot
250. Nuissl H, Couch C (2007) Lines of defence. Policies for the control of urban sprawl. In: Couch C, Leontidou L, Petschel-Held G (eds) Urban sprawl in Europe. Landscapes, land-use change and policy. Blackwell, Oxford, pp 217–241

Books and Reviews

Alberti M (2005) The effects of urban patterns on ecosystem functions. Int Reg Sci Rev 28:168–192
Gillham O (2002) The limitless city. A primer on the urban sprawl debate. Island, Washington, DC, Covelo, London
Burchell RW, Shad NA, Listokin D, Phillips H, Downs A, Seskin S, Davis JS, Moore T, Helton D, Gall M (1998) The costs of sprawl – revisited. National Academy, Washington, DC
EEA (European Environmental Agency) (2006) Urban sprawl in Europe – the ignored challenge. EEA Report 10/2006, Copenhagen
Mieszkowski P, Mills ES (1993) The causes of metropolitan suburbanization. J Econ Perspect 7:135–147
Pendall R (1999) Do land-use controls cause sprawl? Environ Plann B 26:555–571
Ewing R (1997) Is Los-Angeles-style sprawl desirable? J Am Plann Assoc 63:107–126
Gallent N (2006) The rural-urban fringe: a new priority for planning policy? Plann Pract Research 21:383–393
Bengston DN, Fletcher JO, Nelson KC (2004) Public policies for managing urban growth and protecting open space: policy instruments and lessons learned in the United States. Landscape Urban Plann 69:271–286
Atkinson G, Oleson T (1996) Urban Sprawl as a path dependent process. J Econ Issues 30:609–615

Landscape Planning for Sustainable Water Usage

Martin Volk
Department of Computational Landscape Ecology, UFZ Helmholtz Centre for Environmental Research, Leipzig, Germany

Article Outline

Glossary
Definition of the Subject and Its Importance
Introduction
Processes and Planning on Different Scales
Effects of Land Use Pattern on the Hydrological Cycle
Land Use as Controlling Factor for Water and Nutrient Dynamics
Scale Appropriate Application of Models for Integrated Ecological-Economic Assessments and Decision Support
Future Directions
Bibliography

Glossary

Catchment (or river basin) The drainage area of a stream, river, or lake. It has a common outlet for its surface runoff.

Ecosystem An arbitrary ensemble of macroscopic matter that captures, stores, and uses energy to circulate and rearrange matter within the system.

Evaporation (of water) (1) The emission of water vapor by a free surface at a temperature below the boiling point. (2) The amount of water evaporated.

Interception loss Rainfall evaporated from canopy and litter.

Landscape The traits, patterns, and structure of a specific geographic area, including its biological composition, its physical environment, and its anthropogenic or social patterns. An area where interacting ecosystems are grouped and repeated in similar form.

Landscape ecology The science of studying and improving the relationship between spatial pattern and ecological processes on a multitude of landscape scales and organizational levels. Landscape

ecology is highly interdisciplinary and integrates biophysical and analytical approaches with humanistic and holistic perspectives across natural and social sciences.

Landscape structure, function, and pattern structure Is determined by the composition, the configuration, and the proportion of different patches across the landscape, while *function* refers to how each element in the landscape interacts based on its life-cycle events. *Pattern* is the term for the contents and internal order of a heterogeneous area of land.

Landscape planning The aspect of the land use planning process that deals with physical, biological, esthetic, cultural, and historical values and with the relationships and planning between these values, land uses, and the environment.

Landscape water balance Inventory of water based on the principle that during a certain time interval, the total water gain to a given catchment area or body of water must equal the total water loss plus the net change in storage in the catchment or body of water. In hydrology, a water balance equation can be used to describe the flow of water *in* and *out* of a system. A *system* can be one of several hydrological domains, such as a column of soil or a drainage basin.

Scale A definition applied to the time, space, and mass component of any quantity is that scale denotes the resolution within a range of a measured quantity. This definition encompasses two important, interacting facets of scale: resolution and range. Resolution or "grain" refers to the finest distinction that can be made in an observation set, while range or "extent" refers to the span of all entities that can be detected in the data.

Transpiration Process by which water from vegetation is transferred into the atmosphere in the form of vapor.

Definition of the Subject and Its Importance

Extreme events such as floods, droughts, as well as water scarcity and poor water quality have been increasing globally during recent decades. Global change phenomena, increasing population density in some parts of the world, as well as multiple land use of landscapes such as agricultural management, urbanization, and industrialization are some of the main reasons for these problems. Both the mentioned reasons as well as the resulting environmental consequences, represent some of the world's most pressing problems that occur on different scales – from the field to the region or even globally. In recent decades, integrated river basin and environmental management – including landscape planning – have been introduced as a potential but challenging instrument to tackle these complex transdisciplinary problems around the world. However, several problems still exist before an effective integrated planning and management can be realized. This section introduces these problems and presents contributions to the solution for some of these (methodological but also environmental) problems. In the following, the existing problems and needs of the handled topics are briefly argued, and numerous studies on the solutions to these problems are shortly illustrated. In the sense of an integrated methodology, promising developments of decision-support systems are presented as one future direction to support sustainable land use planning and water resources management. Finally, criteria for sustainable water planning are presented.

Introduction

"Water is life. It nourishes our ecosystems, powers our industry, grows our food, and makes life itself possible" [1]. This statement emphasizes the importance of water for humans and nature. The human factor "land use" affects the interactions between the components of a landscape structure in different manners and intensities. Landscape pattern or structures consist of water, soil, geomorphology, vegetation, etc. Water-carried fluxes of matter (nutrients, sediments) and energy play an important role for the landscape balance. All components of the landscape structure are interrelated by these fluxes. Hence, society needs a way to handle a landscape as a whole, so that the human manipulative capabilities do not have too much head start over our knowledge about the impacts of these manipulations [2].

However, extent and rate of effectuate changes in landscapes still exceeds, to a high degree, the scientific capability to reliably predict long-term impacts of technological developments on natural cycles and

processes. Human impact not only on landscape pattern, water balance, material fluxes, habitats for plants and animals, but also on socioeconomic situations has in fact reached a degree that may lead to irreversible changes and put at risk the natural systems essential for life support. Thus, landscape ecology and other environmental sciences have to develop suitable and improved methods to assess the impacts of anthropogenic changes in landscapes and to develop a conceptual base for sustainable land use.

Land use is the parameter by which society controls the landscape water balance [3]. It controls not only parameters such as evaporation, surface runoff, or groundwater recharge in catchments, but also soil erosion and water quality. Figure 1 shows the complex interrelationships within the water cycle. The water cycle links evaporation from the sea, atmospheric water vapor flow, the moistening of continental landscapes, the recharge of aquifers and rivers, and the river discharge back to the sea. The human physical and chemical interventions (including land use in all its forms) influence the atmosphere, the landscape, and the aquifers and rivers [1]. Hence, the investigation of the effect of land use change and land use patterns on the water resources provides information for the development of sustainable land use concepts and integrated environmental and river basin management as demanded by landscape programs or political directives. Examples for such directives are the Clean Water Act [4] in the USA or the European Water Framework Directive (WFD; [5]) in Europe. Due to the oftentimes insufficient water availability or poor water quality of the streams these environmental programs were implemented to achieve good ecological and chemical conditions of water quality of groundwater and surface water bodies.

In addition to these directives, land use plans (for different scales such as communities, counties, states, or even nations) based on ecological principles (landscape ecological plans) are finding increasing application, especially in continental Europe and the USA [6]. This reflects a growing maturity in landscape ecology, enabling it not only to inform theory, but also offer solutions to "real-world" planning problems. In countries with a long history of industrialization, visual distinctiveness and biodiversity have been severely eroded by a combination of habitat removal and fragmentation, intensive farming and forestry, river engineering, transport corridor construction, and industrial pollution and dereliction. More subtle effects, associated with pollution and nutrient transfers by air and water, have also had significant impacts [6].

On the one hand, the spatial distribution of different land use types (settlements, forest, grassland, pasture, arable land) affects the water and nutrient cycle of a landscape, but on the other hand also the different types of land management (crops, tillage, etc.) are important factors that influence these cycles. Table 1

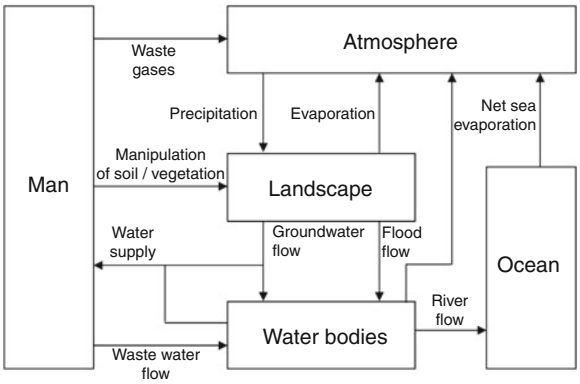

Landscape Planning for Sustainable Water Usage. Figure 1
The continuous water flow through the water cycle, linking sea evaporation, atmospheric vapor flow, moistening of continental landscapes, recharge of aquifers and rivers, and outflow to the ocean ([1], see also [7])

Landscape Planning for Sustainable Water Usage. Table 1 Percentage of soil evaporation, interception loss, and transpiration of different land uses and land cover on total evaporation [8]

	Soil evaporation	Interception loss	Transpiration
Forest	–	40%	60%
Pasture	15%	25%	60%
Arable land	30%	15%	55%
Bare fallow	100%	–	–

gives an impression on the percentage of soil evaporation, interception loss, and transpiration of different land uses and land cover on the total evaporation.

Sustainable land use and management needs a sound knowledge of these influences. Hence, there are numerous examples for studies described in literature where measurements and computer-aided hydrological models are applied successfully for the simulation of the influence of land use and management changes on potential groundwater recharge or streamflow. Mostly variants or scenarios are investigated that are based on assumptions of climatic change or of the influence of political decisions. When simulating water balances for large areas, only considerable land use changes result in noteworthy shifts of the simulated total runoff. Depending on the selected model type, database and regional site conditions of the study site, land use changes can affect the results (and also the further modeling) to varying degrees. The assumptions of land use changes can be made on the basis of plausibility considerations, or models can be applied [9]. Overviews of the prospects and limitations of eco-hydrological models for evaluation of land use options in mesoscale catchments are given by Fohrer et al. [10] and Hörmann et al. [11]. On the one hand, such influences of land use and management have to be reduced that have a negative impact on the water resources. On the other hand, land use and management can be used as instruments to realize sustainable landscape development. The complexity of these interrelationships on different scales makes its study extremely challenging. The examples presented in this chapter are mainly from the "developed" world, such as from Europe, the USA, or Australia. Despite existing problems, the presented examples in these regions are with no doubt "best cases" for landscape planning and sustainable water planning. However, especially in the developing regions with an increasing number of drought and flood events and water quality problems, there is an urgent need for integrated landscape and water management strategies [1]. This becomes even more important with regard to the enormous regional differences of water availability in the world (as presented Fig. 2). Figure 2 shows the global distribution of water availability at country level.

Processes and Planning on Different Scales

Land use affects the interactions between water, soil, geomorphology, vegetation, etc., on several scales in different manners and intensities. That means that both natural processes and environmental problems occur on different spatial and temporal scales, from the field to the region, and even globally [12–15]. Due to the long tradition in scale-specific research in landscape ecology, several methods are available for the investigation of landscape ecological structures and processes on, for instance, fields or farms (the microscale), where the processes have to be measured or mapped, as well as for the whole world, where for instance climate is simulated by using General Circulation Models (GCMs). Only a few studies deal with the optimization of the scale-specific applicability of these methods and models, especially for larger scales [16–18]. But most of the environmental changes and conflicts between land use, conservation, and resource management become obvious at the so-called landscape scale [19]. Special attention should be paid to the investigation of the landscape water balance – at least in temperate and humid zones, because water-carried fluxes of matter and energy play an important role for the landscape balance . All components of the landscape structure are interrelated by these fluxes. Therefore, special indicators and model applications have to be developed for landscape-scale investigations that allow assessments and forecasts about the impacts of land use changes on the landscape balance.

Several papers from different scientific disciplines deal with the hierarchical organization of nature [20]. An overview about hierarchical concepts in landscape ecology is given by Klijn [21]. These concepts are mainly focused to the hypothesis that each of the scale levels (micro-, meso-, and macroscale) is characterized by specific temporal and spatial ranges. As a consequence, each scale level needs data layers with suitable spatiotemporal resolution and specific investigation methods and provides specific knowledge [22]. The main topic here is the definition of a linkage of the different landscape scales. The main hypothesis of the hierarchical approach suggested by Steinhardt and Volk [17, 23] is that the basic components for vertical and horizontal material and energy fluxes – morphology, soil, hydrology, land use and land management, and

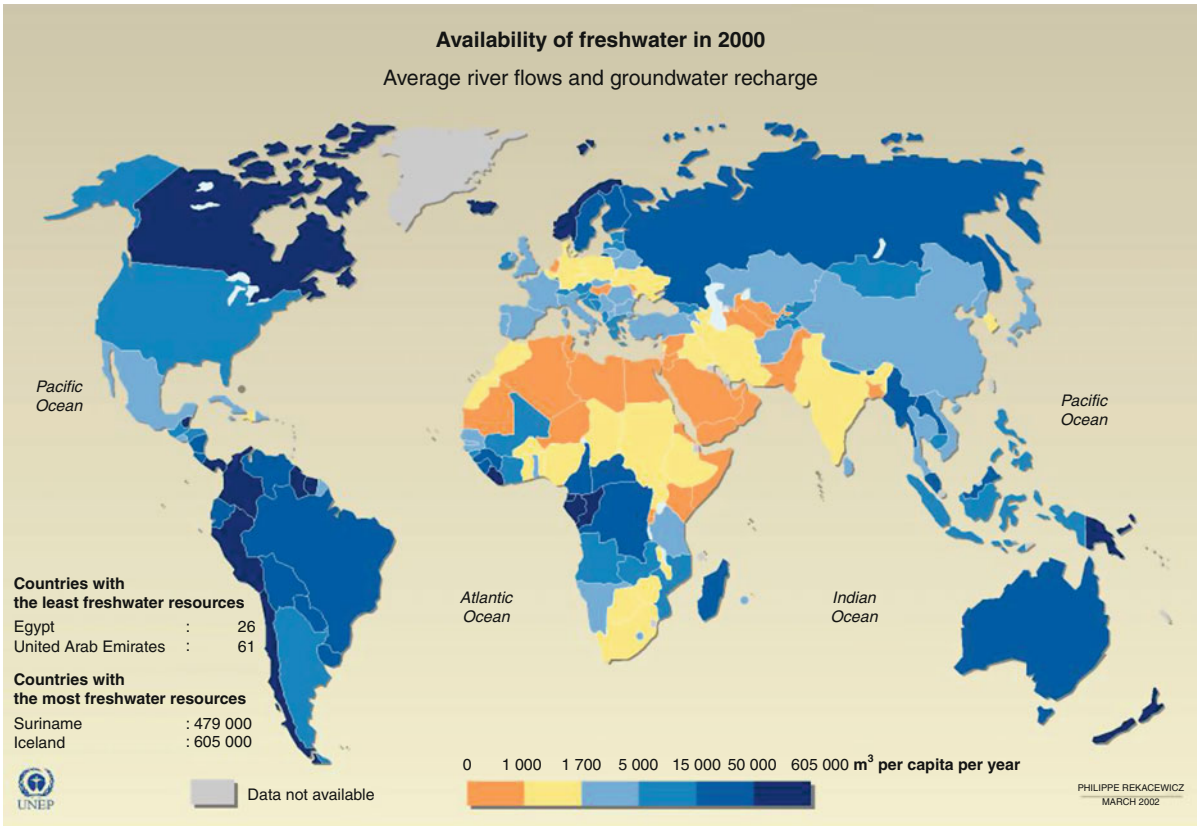

Landscape Planning for Sustainable Water Usage. Figure 2
Availability of freshwater through average river flows and groundwater recharge, in cubic meters per capita per year, at the national level in the year 2000. The graphic highlights the countries with the least freshwater resources (Egypt and the United Arab Emirates) and those with the most (Suriname and Iceland)

climate – are similar over all scale levels. It is only the importance of the factors of these components that changes for each scale [24]. To give an example for morphology and erosion: On the local scale, surface roughness is one of the main factors that will affect erosion disposition, whereas for larger scales (up to river catchments) the factors slope inclination, slope length, slope exposition up to the shapes of streamlet, -net, -order, and direction of flow are responsible for erosion processes.

According to the hierarchical organization of nature spatial planning and forest, biodiversity, agriculture, and water management are also organized hierarchically (Fig. 3, Table 2). In Germany, regional management plans are instruments within the spatial planning system used to set guidelines for landscape development on the regional scale. Priority areas for "landscape functions " are designated at the community level. But there are only few applications of landscape ecological information – especially about the regulation capacity – that are included, and the realization of sustainable development requires the recognition of all landscape functions. Therefore, useful indicators and parameters have to be derived for analyzing and optimizing the regulation and production functions of the existing landscape types for the concerned scales [25, 26].

Effects of Land Use Pattern on the Hydrological Cycle

Measurements

The impact of land use and land cover change on the hydrological cycle can be quantified by using different

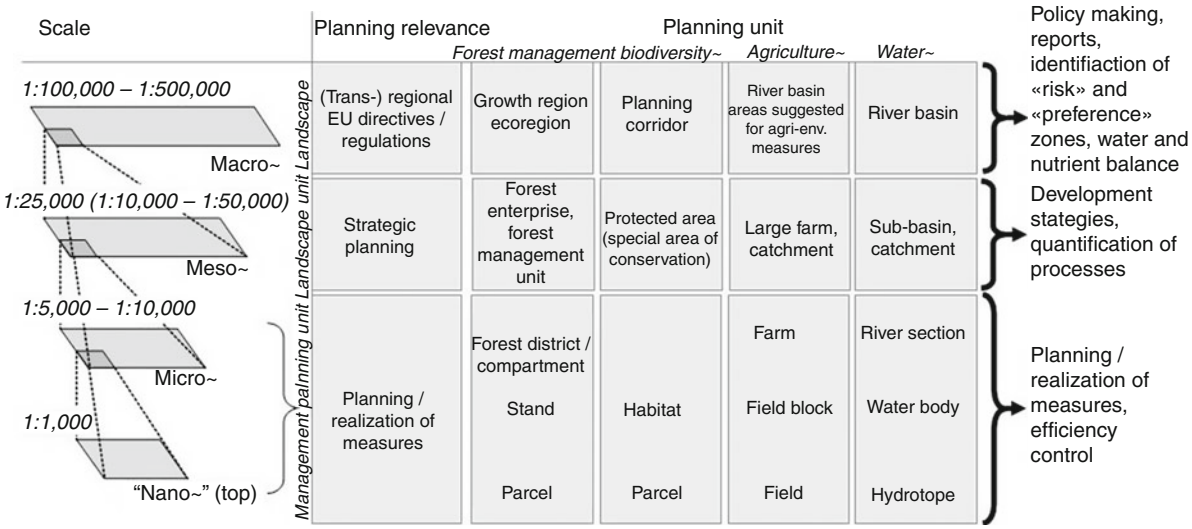

Landscape Planning for Sustainable Water Usage. Figure 3
Scales and planning units in forestry, biodiversity, and agricultural and water management

Landscape Planning for Sustainable Water Usage. Table 2 Hierarchies in landscape and spatial planning in Germany (after [27])

Scale level	Planning level	Spatial planning	Landscape planning
Macroscale	Country	Spatial development policy	–
Mesoscale	Federal scale Region	*Raumordnungsplan* *Regionalplan (= regional planning program)*	*Landschaftprogramm* *Landschaftsrahmenplan (= landscape program, landscape framework plan)*
Microscale	Municipality (town, village) Parts of municipalities	*Flächennutzungsplan* *Bebauungsplan (= land development plan, zoning plan)*	*Landschaftsplan* *Grünordnungsplan (= landscape plan, green structures plan)*

methods – depending on topic and scale one is interested in. One way to quantify the impact of vegetation cover change on the hydrologic cycle is paired watershed experiments [28, 29]. In a paired catchment experiment, land use is held constant on the control catchment and changed on the treatment catchment. Differences in hydrologic response with respect to annual runoff, flood, and low flow response and water quality can then be compared for catchments experiencing the same weather patterns [30]. Hibbert [31] gives a summary of 39 catchment experiments. He concluded that the reduction of forest cover increases water yield and in contrast the establishment of forest cover on sparsely vegetated land decreases water yield. The response to treatment was highly variable and thus for most parts unpredictable. Bosch and Hewlett [32] added another 55 catchment experiments to this review and sorted them by mean annual precipitation, vegetation type, and country. They confirmed the first two statements of Hibbert [31] and concluded that "coniferous forest, deciduous hardwood, bush and grass cover have (in that order) a decreasing influence on water yield of the source areas in which these covers are manipulated." Coniferous forest causes around 40 mm change in annual water yield per 10% change in forest cover. Deciduous hardwoods are associated with

a 25 mm change in yield per 10% cover change, while bush and grassland generate around 10 mm of difference. In their data set, forest cover changes of less than 20% could not be detected by measuring stream flow. Stream flow response to deforestation or afforestation depends both on the region's mean annual precipitation and on the precipitation for the year under treatment. Yield changes are greatest in high-rainfall areas. In low-rainfall areas the effect is less pronounced but more persistent due to slow vegetation regrowth. Decreases in water yield following afforestation seem to be proportional to the growing rate of the stand, while gains in water yields after clearfelling diminish in proportion to the rate of recovery of the vegetation. Smith and Scott [33] found that the dry season flow from forested catchments was lower than from comparable non-forested catchments in South Africa. Burch et al. [34] and Peck and Williamson [35] address the hydrological aspects of forest replacement by annual crops or pasture. The latter focused on the effect of deforestation on groundwater in five Australian paired catchments (0.8–3.5 km). Clearing increased the average recharge rate documented by piezometer hydrographs. Potentiometric heads within the forest and up to 50 m down-gradient from areas that were cleared have responded to clearing after a delay of 2 or 3 years. This delay was consistent with the very low transmissivity of the aquifer under observation. Burch et al. [34] compared two experimental catchments; one vegetated by natural eucalypt forest (5.0 ha) and the other completely clear-cut and maintained in grassland (7.8 ha) for over 80 years. The grassland catchment generated high-peak storm flows and large discharge volumes irrespective of antecedent soil water content, whereas the forested catchment gave little runoff provided the antecedent soil water content was below 60% of the available storage capacity. In the case of woodland establishment a substantial reduction of runoff was reported by Williams et al. [36].

In single-catchment experiments, the effect of land use change is measured by comparing measurements before and after the change occurred. Thus it is more difficult to separate the effect of land use change from the effects of different weather patterns before and after the change. It is a common knowledge that discharge from forest, urban, and agricultural catchments is different, but the experimental quantification is still not easy. A simple, but radical solution is the clear-cut or afforestation of entire catchments [37–39]. An overview of conversion studies from and to forest is given by Whitehead and Robinson [40]. An overview of paired catchment studies, where only a part or a subcatchment is changed, was published by Best et al. [28]. Major influence factors such as soil and relief properties of the catchments are seldom discussed. Paired watershed experiments, however, were limited to a size of 1–2,500 ha.

Modeling

In larger catchments it becomes increasingly costly and difficult to control the experimental boundary conditions and to measure precipitation and stream flow accurately. Thus in recent years the application of simulation models to quantify the effect of land use change on the hydrologic cycle has increased. The first water balance models were produced back in the late 1940s. In a more sophisticated manner, the development of hydrological models started in 1960s with the Stanford watershed model [41]. Until today the number of models and model systems as well as the number of different model concepts grew considerably as indicated in the overview given by Singh [42]. They have evolved in a number of different directions depending on the many purposes for which they are required [43, 44]. Generally speaking, nowadays there are three different approaches to modeling the landscape water balance:

1. *Physical-deterministic models*, which are based on the fundamental laws of physics (chiefly hydrodynamics and thermodynamics), chemistry, biology, etc.
2. *Conceptional models*, which take these laws into account in a simplified manner and also use empirical approaches
3. *Empirical-statistical models*, which are solely based on the empirically measured cause–effect relations of system inputs and outputs without trying to fathom the laws on which they are based

The transitions between the three approaches are in a state of flux. Moreover, hydrological processes always include both deterministic and stochastic characteristics owing to the unavoidable simplifications of

complex reality and the error occurring when capturing input data [45].

Depending on the model type and its purpose, different scales of temporal and spatial resolution are used. Compromises usually have to be made between the accuracy desired and the availability of data. If nonlinear processes are being studied (e.g., precipitation and runoff), hourly or daily steps have to be used, whereas for seasonal or annual properties monthly or even yearly steps suffice. The possible degree of spatial resolution ranges from highly aggregating approaches in which the study area is divided into a few subunits with similar geophysical properties ("lumped models") to models that as far as possible take into account the variability of spatial structures ("distributed models"). The scope for using a higher spatial resolution has improved with the advent of faster, more powerful computers, the development of geographic information systems, and – especially recently – the growing availability of data stored in a Geographical Information System (GIS).

Water balance models are used to depict the impact of land use changes on potential natural groundwater recharge (e.g., [46, 47]). Usually variants or scenarios are investigated, which are for instance based on assumptions concerning climatic change or the impact of political decisions (Table 3). If balancing is performed over the entire study area, only very pronounced land use changes will result in any considerable shifts in the simulated total runoff. What the list in Table 3 fails to show are any local changes, which in certain areas may well considerably exceed the means calculated. The algorithm used to introduce the land use changes forecast into the area also needs to be considered. Depending on local characteristics, the effect on further modeling exerted by a change in land use varies greatly. Assumptions regarding the spatial distribution of land use changes can be made by using plausibility considerations. Alternatively, models can also be used [9].

Hydrologic models can be useful tools to evaluate the effect of landscape patterns or land use change resulting from policy decisions, economic incentives, or changes in the economic framework [9, 50, 51]. One of the earliest works was from Onstad and Jamieson [52], who investigated the effect of land use modifications on runoff. A two-dimensional groundwater model has been applied in several Australian experimental catchments to quantify the response of the underlying aquifer to the removal of deep-rooted native vegetation [53]. The catchment response to clearing was assumed to be a function of the temporal pattern of the clearing, the proportion of the catchment cleared, the location of the clearing within the catchment, and the rainfall amount. Calder et al. [54] carried out a modeling study to determine the effects of land use change from natural forest to agricultural land on a large-scale catchment (124,500 km) in Africa.

Landscape Planning for Sustainable Water Usage. Table 3 Case studies on land use change and water yield [48]

Region	Scenarios in the case studies	Land use change	Simulated change in total water yield (%)	Reference
NE-Germany	EU agricultural reform	Change of 4% AL into forest, change of 32% AL into forest	−1, −10	[49]
Hesse (Germany)	Agricultural policy: grassland premium	Forest: 42 → 13%,	+8	[9]
		AL: 44 → 73%		
Hesse (Germany)	Agricultural policy: cessation of animal husbandry	Forest: 42 → 49%,	+2	[9]
		AL: 44 → 37%		
Saxony-Anhalt (Germany)	Analysis of land use conflicts in priority areas (agriculture vs. groundwater protection)	Change of 10% AL into forest, *Koethener Ackerland, Noerdlicher Mittelflaeming*	−9, −2	[47]

AL arable land

Lørup et al. [55] applied the lumped conceptual hydrologic model NAM in six medium-sized catchments (200–1,000 km) to assess the long-term effect of land use change in Zimbabwe. They stated that despite a significant increase in population density, there have been no major changes in the percentage of each land use type and thus there was no indication of increased surface runoff in the six catchments. The physically based model SHETRAN [56] was applied to characterize the influence of land use on catchment hydrology [57]. Results from those simulations show that the same land use change may have a significant effect on the hydrology of a lowland subcatchment, but an insignificant effect on the hydrology of the upland subcatchment. This underlines the necessity of spatially distributed modeling approaches for land use change studies.

Dunn and Mackay [57] discuss in detail the influence of vegetation type on evapotranspiration and its components' interception and transpiration for the Tyne Basin (>2,000 km) in northeast England. They outline the importance of physical soil properties for the nature of the hydrological response to variations in vegetation cover. Lahmer et al. [58] and Eckhardt et al. [59] addressed the problem of input data uncertainty for land use change studies in large catchments.

Another crucial point is the thorough validation of catchment models for predicting land use change. In large basins there are usually no experimental data for real land use change available. Thus the model calibration and validation is mostly restricted to measured stream flow data. Different validation techniques are discussed critically by Klemes [60] and Ewen and Parkin [61]. Additional information for model testing can be obtained by the application of base-flow separation algorithms, as for example, as proposed by Lyne and Hollick [62] or Arnold et al. [63]. Though one has to be aware that this method is empirically based and thus the applicability to catchments other than those of the original data set is limited, and the results should be interpreted with care.

Land Use as Controlling Factor for Water and Nutrient Dynamics

The investigation of the effect of land use change and land use patterns on hydrologic processes such as groundwater recharge or surface runoff provides information for the development of sustainable land use concepts and integrated environmental and river basin management as demanded by the landscape programs or the European Water Framework Directive (WFD [5]). There are numerous examples for studies described in literature where hydrological models are applied successfully for the simulation of the influence of land use changes on potential groundwater recharge or streamflow. Mostly variants or scenarios are investigated that are based on assumptions of climatic change or of the influence of political decisions. When simulating water balances for large areas, only considerable land use changes result in noteworthy shifts of the simulated total runoff. Depending on the selected model type, database, and regional site conditions of the study site, land use changes can affect the results (and also the further modeling) to varying degrees. The assumptions of land use changes can be made on the basis of plausibility considerations, or models can be applied [9]. Fohrer et al. [10] and Hörmann et al. [11] give an overview of the prospects and limitations of eco-hydrological models for evaluation of land use options in mesoscale catchments. The papers that they analyzed are classified into three categories: analysis of consequences of observed (or historical) land use changes on the water cycle, simulation of hydrologic consequences of land use change based on ecological and mainly economic scenarios, and finally optimization of land use according to economic or ecological criteria, where both components, hydrology and land use change, are simulated.

Lorz et al. [48] emphasize the need of an improved consideration of the spatial distribution and functionality of forests in river basin management. Their review of relevant papers has shown that forests, despite their frequent occurrence in temperate zones, play presently only a minor role in river basin management. In general, most of the studies highlight the positive effect of forests on water and nutrient fluxes in river basins. But hydrologists have also reported consistently flood events in or originating from forested areas. In context of the discussion on forest ecology and water quality it became obvious that forest ecosystems can be sources depending on system properties, time, and atmogenic pollution. The simulation of land use changes on water yield in forested river basins has been carried out in

a great number of research projects, but mostly without considering the spatial distributed function of forests. The objective of Lorz et al. [48] was thus to improve the consideration of spatial distribution of forests in river basins and its effect on water yield and water quality. The most promising approaches in the future are either spatial explicit models or integrated models with both improved forest modules and landscape positioning. The efficiency of these models could be proved by using virtual catchments. As a first conceptual approach towards the base concept of a virtual catchment, they propose a five-unit model (FUM), representing cross-sections with typical land use sequences. The basic idea of their model is to identify major process units and to implement them in the river basin modeling and management.

In much of Europe, the USA, and parts of Australia, increased inputs of especially nitrogen and phosphorus to land in the form of fertilizers, manures, and biosolids means that agricultural runoff now comprises a greater share of these nutrients in groundwater, rivers and lakes, and associated water quality problems [64, 65]. Numerous site-specific field studies have quantified the potential export of nutrients in agricultural runoff. But it is clear that to meet the requirements of end users, the research effort needs to shift towards developing suitable models that are based on expert knowledge to simulate the impact of land use and land management practices on diffuse source pollutant transport. Franko et al. [66] and Neubert et al. [67] give examples for the application of two different model systems: the process-based carbon-and-nitrogen-dynamics models, CANDY, and the (balance-oriented) whole-farm simulation model, REPRO, to determine land usage variants, which, employing the regional regulation potential, lead to a reduction of nutrient outputs into neighboring ecosystems. The hydrological effects were simulated with ABIMO (which is a runoff generation model) that was used to model data for groundwater recharge. This was then taken as a basis in conjunction with area-related nutrient balances to estimate nitrogen discharge by using the model CANDY (***Ca**rbon-and-**N**itrogen-**Dy**namics*; [66, 68]). With regard to the modeling and estimation of the scenario effects, extensive sensitivity analyses were carried out. As a result not only point estimates for the criteria values were generated but also probability distributions reflecting various kinds of data and model uncertainties [69]. The results of the studies presented by Volk et al. [70] and Franko et al. [66] were used as a basis for multi-criteria ecological-socioeconomic assessments described in Horsch et al. [71] and Klauer et al. [69]. The application of an alternative model combination of ABIMO and the model REPRO (Reproduction of Soil Fertility; Hülsbergen [72]) in this study area is presented in Neubert et al. [67]. Models such as REPRO provide efficient tools for evaluating both environmental and economic performance of farming systems. The results indicate an explicit dependency of the nitrate leaching on groundwater discharge and nitrate balance in relation to the variants of cultivation practice like organic, integrated, and conventional farming. The work shows clearly the influence of the quality and availability of data on the simulation results, whereas the model structure seemed to have less influence in this case study.

The experiences of different European and national projects dealing with the model-supported implementation of the WFD revealed that the available *integrated* model systems are still far from being suitable for operational applications with regard to water quality simulations [73–75].

However, complex transdisciplinary problems have to be tackled through implementation of WFD or other environmental directives. Hence, in order to achieve optimal working efficiency of the models in the management processes, it is required that they contribute information over a wide range of abiotic and biotic aspects of hydrology and water quality demanded by the decision makers, which cannot be achieved by individual groundwater, water quality, or erosion models. Consequently, the suitability of the publicly available river basin model Soil and Water Assessment Tool (SWAT) [76], the available database and the existing water quality monitoring network to adequately represent general trends in water quality changes resulting from various measures based on land use and management change in the intensively used Upper Ems Basin was checked by Volk et al. [18, 77, 78] and Ullrich et al. [78].

During the last years, increased cultivation of energy crops influences the landscape water and nutrient balance. Schilling et al. [79] showed that over the

last century, land use and land cover (LULC) in the US Corn Belt region shifted from mixed perennial and annual cropping systems to primarily annual crops. Historical LULC change impacted the annual water balance in many Midwestern basins by decreasing annual evapotranspiration (ET) and increasing streamflow and base flow. Recent expansion of the biofuel industry may lead to future LULC changes from increasing corn acreage and potential conversion of the industry to cellulosic bioenergy crops of warm or cool season grasses. Schilling et al. [79] used SWAT to evaluate potential impacts from future LULC change on the annual and seasonal water balance of the Raccoon River watershed in west-central Iowa. Three primary scenarios for LULC change and three scenario variants were evaluated, including an expansion of corn acreage in the watershed and two scenarios involving expansion of land using warm season and cool season grasses for ethanol biofuel. Modeling results were consistent with historical observations. Increased corn production will decrease annual ET and increase water yield and losses of nitrate, phosphorus, and sediment; whereas increasing perennialization will increase ET and decrease water yield and loss of non-point source pollutants. However, widespread tile drainage that exists today may limit the extent to which a mixed perennial-annual land cover would ever resemble pre-1940s hydrologic conditions. Study results indicate that future LULC change will affect the water balance of the watershed, with consequences largely dependent on the future LULC trajectory.

Scale Appropriate Application of Models for Integrated Ecological-Economic Assessments and Decision-Support

Integrated river basin and environmental management involve all management objectives related to the use, pollution mitigation, pollution rehabilitation, protection and rehabilitation of water bodies, as well as many other impacts on biodiversity, soil protection, water quantity, and quality in river basins or administrative units [80]. An integrated approach implies that relations between the abiotic and the biotic part of the various water systems, between ecological and economic factors, and between various stakeholder interests are considered in decision-making processes. It takes into account three often conflicting main dimensions: ecology, economy, and equity [81]. Directives such as the WFD, the NATURA2000 in Europe, or Clean Water Act (CWA) in the USA call for multidisciplinary approaches of river basin and environmental management. Hence, during recent decades a number of research projects have developed (spatial) decision-making support systems (DSS) for integrated water resources and environmental management (including socioeconomic analyses) with respect to groundwater management and flood prevention problems [80–87]. Most of them offer the possibility of drawing information from geographical information systems and/or supplying interdisciplinary multi-criteria analyses of the hydrological, ecological, and economic consequences of different management strategies, based on either pre-calculated scenarios or model coupling [88]. References [81] and [86–89] give examples and overviews of the development, application, and potential of different types of DSS. Giupponi [86] states that despite the many DSSs developed in the field of environmental management, the risk of Decision Support Systems failing to meet the challenge of real-world problems is reported to be high, and even the criteria for judging whether a DSS has been successful or not are often a matter of discussion (e.g., [90–92]). He emphasizes that there is a widely recognized need to develop new decision-support tools in this field, with greater attention to the needs of potential users and to identification of the application context.

An integrated approach to catchments, that is, administrative units, is essential that would include a necessary basis for balancing and reconciling conflicting interests. Therefore further development of integrated natural resource management is needed to incorporate land use, pollution leads, and vital ecological goods and services [1]. Planners and policy makers have the difficult task to intervene in complex human–natural systems. They cannot focus only on individual processes; rather it is necessary to address the system as a complex integral whole and think about economic values. To fulfill these requirements, tools such as DSS that integrate environmental, social, and economic concerns and that facilitate the involvement of interested parties in the formulation of strategies may be useful. Especially water is considered more and more as an economic good due to competing water use resulting in resource scarcity (e.g., [93–95]). Decision makers

need information about the economic value of water and the economic consequences of water management. The complexity of interactions between water, ecology, and the economy can be captured through formal, mathematical models. These models link relevant hydrological and biogeochemical processes to economic "laws" of supply and demand underlying the provision of scarce water services. Brouwer and Hofkes [95] edited a special issue on "Integrated hydro-economic modeling: Approaches, key issues and future research directions" in the journal of "Ecological Economics." They distinguish between main approaches: modular, holistic, and computable general equilibrium models. The latter top-down models counterbalance the traditional emphasis on bottom-up water engineering approaches. Key issues and future research directions in integrated hydro-economic modeling are discussed and illustrated through a variety of case study applications worldwide. Although the interaction works both ways, feedback effects of water changes on the economy and changes in the economy on the water system are often missing in practice.

The study presented by Rode et al. [96] includes the work on integrated nutrient transport modeling with respect to the implementation of the WFD that was done in the Weisse Elster Case Study, Germany. The implementation of the WFD can only be tackled by comprehensive environmental and economic assessments based on an integrated methodology and decision-support system. The methodology was developed within an interdisciplinary research project on the highly polluted Weisse Elster River basin, a large subcatchment of the Saale basin that is part of the UNESCO-IHP HELP program. The project focuses on nutrient management, river basin management, and decision making to achieve good ecological status of surface waters. From the modeling study using SWAT it can be concluded that the investigated organic farming scenarios do not ensure a considerable reduction in high nitrogen loads from the agricultural land of the studied catchment. Only the scenario on liberalization of the agricultural market leads to a considerable reduction in nitrogen loads due to large reduction of agricultural land use of 42.6%. The scenario analysis shows that sufficient reductions in nitrogen loads with respect to the ambitious goals of the WFD can only be achieved with a considerable change in agricultural land use. With regard to the river water quality modeling study it can be concluded that the impact of the most feasible measures on the concentration of inorganic nitrogen is quite low. Little effect on the yearly mean of inorganic phosphorus is also expected. The reason for this is that the autotrophic assimilation is low and the substance regimes between sediments and the water column are on average balanced, since the seasonal dependence of fixation through sorption or mobilization by desorption or erosion is preponderant. The parameter uncertainties are high and sometimes larger than the effect of the investigated river restoration management scenarios. The case study shows that easily applicable measures for the reduction in diffuse nutrient (especially nitrogen) loads may not be sufficient to reach the goal of good water quality status requested by the WFD.

Volk et al. [18] present the results of the FLUMAGIS project, in which they developed a spatial decision-support system (SDSS) to support the implementation of the WFD. The main objective of the WFD is the achievement of a good ecological and chemical status of the water environment (water bodies). This status corresponds to the limit value of Germany's Working Group of the Federal States on Water Problems Issues (LAWA) for water quality class II (3 mg/l total nitrogen). The rivers in the intensively cropped Upper Ems River basin (Northwestern Germany) show total nitrogen concentrations in excess of 5–10 mg/l. One objective of the project was to find a land use and land management scenario that would reduce the total nitrogen concentration to meet the WFD requirements for good ecological and chemical status [77].

Within the FLUMAGIS project, Volk et al. [77] developed consecutive land use and management scenarios on the basis of policy instruments such as the support of agro-environmental measures by Common Agricultural Policy and regional landscape development programs. The model simulations were done by using SWAT. Table 4 summarizes the agro-environmental measures that they considered in the model. They were developed successively in direction of a target scenario that finally would come close to the water quality objective of the WFD. The areas for the necessary land use changes were mainly chosen by catchment characteristics (permeability of the soils, groundwater table) and the degree of human impairment (river channel regulation, nutrient leaching).

Landscape Planning for Sustainable Water Usage. Table 4 Implementation of agro-environmental measures in the model

Scenario	Measure	Implementation in the model
1	Increase of pasture/decrease of arable land	Modification of the land use file (shape-files). Allocation of the land use type pasture on former arable land.
2	Extensification of pasture	Reduction of livestock density to 1.4 livestock units per hectare by modification of the management scenarios. Reduction of the amount of fertilizers.
3	Afforestation of arable land	Modification of the land use file (shape-files). Allocation of the land use type forest on former arable land.
4/5	Implementation of conservation tillage practices Extensification of arable land Modification of crop rotation schemes	No plowing, only cultivator and harrow (reduction of tillage depth), reduction of mixing efficiency. Reduction of the amount of applied mineral fertilizers accordant to 0.7 livestock units. Implementation of complex management scenarios over several years with short fallow periods.
6	Oxbow reconnection (improvement of river morphology) Riparian buffer strips	Increase of the river length on the HRU level. Modification of Manning's roughness coefficient "n" (CN_N(2)) for main channel flow. Modification of the parameter FILTERW
7	Abandonment of the floodplain use	Conversion of arable land and pasture in riparian zones to areas without management. Change of floodplain pasture into wetland (according soil and groundwater conditions).
8	Additional increase of pasture/decrease of arable land	Conversion of arable land to pasture (randomly chosen).

In order to achieve the good ecological status for nitrogen at the Upper Ems River, the nitrogen concentration has to be reduced by 50% of the mean annual average. This would require substantial, expensive changes of land use and land management intensity as well as of the river morphology. Figure 4a, b shows the current conditions and the target scenario (scenario 8) that comes closest to the requirements of the water quality class II for nitrogen.

In addition to river channel changes, this scenario includes reduction of arable land from 77.2% to 46% (13% organic farming), increase of pasture from 4% to 15%, afforestation from 10% to 21%, increase of protected wetlands from 0% to 9%, etc. However, this is not realistic from an economic point of view, since the drastic cuts for the farmers would be so strong that most of them would have to give up their farms. Agro-economic calculations have shown, for instance, that the mentioned changes in the floodplains alone would cost between 500 and 800 euro per hectare per year (31.6 million euro per year) [18] depending on regional soil qualities and management intensities. This measure is expected to result in intense conflicts with affected farmers [18].

Results of SWAT scenario calculations showed that drastic measures, which are unrealistic from a socioeconomic point of view, would be needed to achieve the water quality target in the basin. The example shows additionally that the achievement of the WFD targets is only possible with a consideration of regional landscape and land use distinctions. A related problem yet to be addressed is the general lack of measured water quality data with which to calibrate and validate water quality models such as SWAT. This adds considerable uncertainty to already complicated and uncertain situations. Thus, improved strategies for water quality monitoring, and data accessibility must be established.

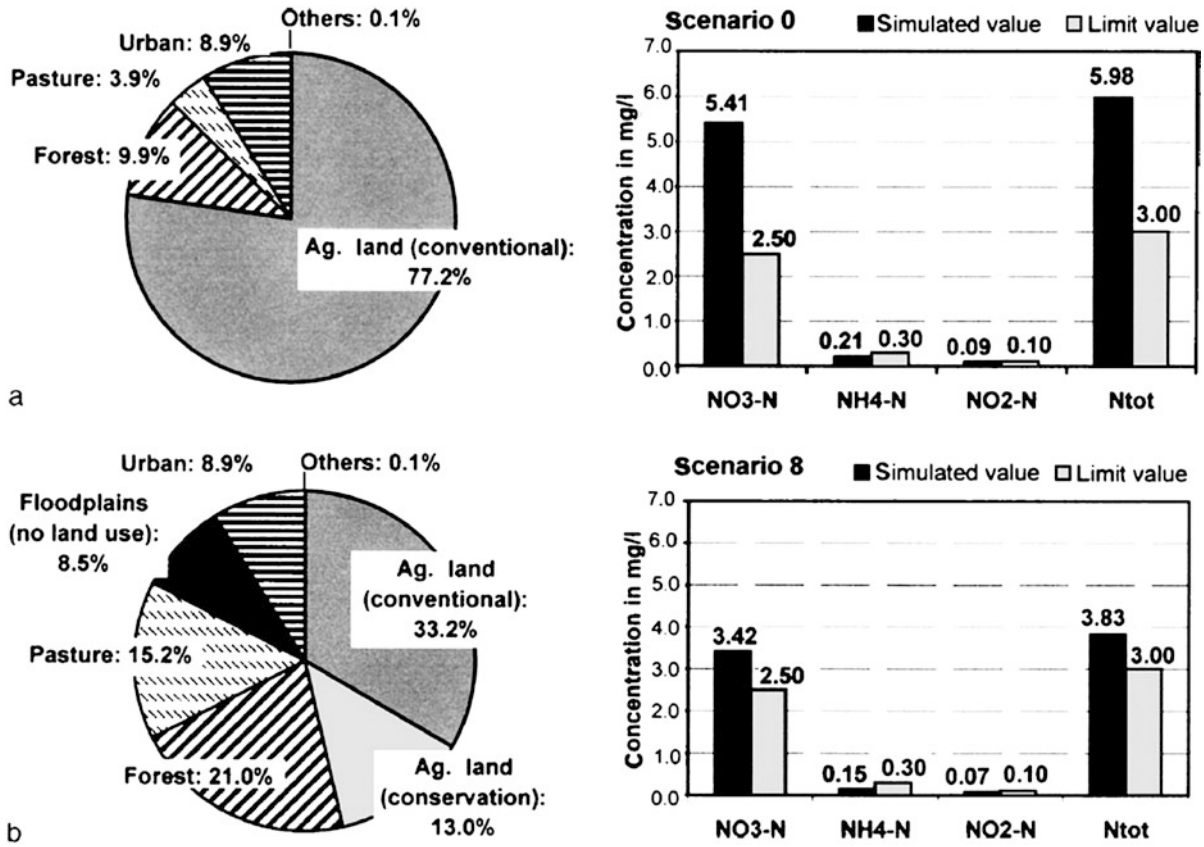

Landscape Planning for Sustainable Water Usage. Figure 4
Current land use distribution and nitrogen concentrations (**a**) and scenario 8 (**b**) with the land use distribution and simulated nitrogen concentrations to achieve the good ecological status for the Upper Ems River. Note values include 0.26 mg organic nitrogen for (**a**) and 0.2 mg/l organic nitrogen for (**b**)

Future Directions

Landscape planning and sustainable water use can only be successful within integrated approaches. In this regard, integrated landscape and river basin management takes into account the three often conflicting dimensions of ecology, economy, and equity [81]. Finding a proper balance between the interests of different stakeholders requires understanding the effects of combined measures on multiple river functions [97]. Uncertain future conditions related to changing political priorities, economic development, and climate change influence the outcome of proposed alternatives. The decisions are inherently a political (and economic) matter, but resulting management plans need scientific underpinning and the support of local stakeholders prior to implementation. There is a need to (a) bridge the gap between the scientific knowledge and demand for information (that requires a combination of a wide range of expertise and data) and (b) make the information available for the analysis and presentation of promising strategies for integrated landscape and river basin management. The benefit of using DSSs in the complex field of integrated landscape and river basin management is that these systems enable comparisons of different land and water management strategies based on the effects on multiple objectives.

With regard to DSS, Volk et al. [98] analyzed benefits and shortcomings of four recently developed decision-support systems. The analysis elaborated on the following aspects: (1) application area/decision problem, (2) stakeholder interaction/users involved,

(3) structure of DSS/model structure, (4) usage of the DSS, and finally (5) most important shortcomings. On the basis of this analysis, they formulated four criteria that are considered essential for the successful use of DSS in landscape and river basin management. The criteria relate to (1) system quality, (2) user support and user training, (3) perceived usefulness, and (4) user satisfaction. Volk et al. [98] could show that the availability of tools and technologies for DSS in landscape and river basin management is good to excellent. However, their investigations indicated that several problems have to be tackled. First of all, data availability and homogenization, uncertainty analysis and uncertainty propagation, and problems with model integration require further attention. Furthermore, the appropriate and methodological stakeholder interaction and the definition of "what end users really need and want" have been documented as general shortcomings of all four examples of DSS. They propose an iterative development process that enables social learning of the different groups involved in the development process, because it is easier to design a DSS for a group of stakeholders who actively participate in an iterative process. Volk et al. [98] also identified two important lines of further development in DSS: the use of interactive visualization tools and the methodology of optimization to inform scenario elaboration and evaluate trade-offs among environmental measures and management alternatives.

In general, new approaches to long-term water planning and management that incorporate principles of sustainability and equity are required and are now being explored by national and international water experts and organizations. Hence, Gleick [99] offered seven sustainability criteria for water planning (Table 5).

These sustainability criteria provide a framework for prioritizing competing interests and for making decisions about future water use and management. The first two criteria require that basic allocations for humans and ecosystems are identified and met, which are to be satisfied before other demands. Thus, the approach suggested by Gleick [99] defines criteria for basic needs as recommended by Agenda 21 of the United Nations. Besides setting out quantity and quality requirements, they also set an upper limit to water use and provided some institutional guidance.

Landscape Planning for Sustainable Water Usage.

Table 5 Sustainability criteria for water planning [99]

A basic water requirement will be guaranteed to all humans to maintain human health.
A basic water requirement will be guaranteed to restore and maintain the health of ecosystems.
Water quality will be maintained to meet certain minimum standards. These standards will vary depending on location and how the water is to be used.
Human actions will not impair the long-term renewability of freshwater stocks and flows.
Data on water resources availability, use, and quality will be collected and made accessible to all parties.
Institutional mechanisms will be set up to prevent and resolve conflicts over water.
Water planning and decision making will be democratic, ensuring representation of all affected parties and fostering direct participation of affected interests.

Bibliography

Primary Literature

1. Falkenmark M, Rockström J (2004) Balancing water for humans and nature. Earthscan Publications Ltd, London
2. Odum E (1969) The strategy of ecosystem development. Science 164:262–270
3. Calder IR, Newson MD (1979) Land use and upland water resources in Britain – a strategic look. Water Resour Bull 15:1628–1639
4. NRC (2001) Assessing the TDML approach to water quality management. Committee to access the scientific basis of the total maximum daily load approach to water pollution reduction, Water Science and Technology Board, Division on Earth and Life Studies. National Research Council, Washington DC
5. EC (European Commission) (2000) Directive of the European Parliament and of the Council 2000/60/EC establishing a framework for community action in the field of water policy. Official Journal 2000L 327/1, European Commission, Brussels
6. Hawkins V, Selman P (2002) Landscape scale planning: exploring alternative land use scenarios. Landscape Urban Plan 60:211–224
7. Flügel W-A (1996) Delineating hydrological response units by geographical information system analyses for regional hydrological modeling using PRMS/MMS in the drainage basin of the river Bröl, Germany. Hydrol Process 9:423–436
8. Wohlrab B, Ernstberger H, Meuser A, Sokollek V (1992) Landschaftswasserhaushalt. Verlag Paul Parey, Hamburg und Berlin, p 352
9. Fohrer N, Eckhardt K, Haverkamp S, Frede H-G (1999) Auswirkungen von Landnutzungsänderungen auf den

Wasserhaushalt eines ländlichen Einzugsgebietes in einer peripheren Region. Z f Kulturtechnik und Landentwicklung 40:202–206
10. Fohrer N, Thielen J, de Roo A (2003) Recent developments in river basin research and development. Phys Chem Earth 28(33–36):1279–1387
11. Hörmann G, Horn A, Fohrer N (2005) The evaluation of land-use options in mesoscale catchments. Prospects and limitations of eco-hydrological models. Ecol Model 187:3–14
12. Steinhardt U, Volk M (eds) (1999) Regionialisierung in der Landschaftsökologie. Teubner, Stuttgart, Leipzig
13. Urban DL (2005) Modeling ecological processes across scales. Ecology 86:1996–2006
14. Bastian O, Krönert R, Lipsky Z (2006) Landscape diagnosis on different space and time scales – a challenge for landscape planning. Landscape Ecol 21:359–374
15. Hein L, van Koppen K, de Groot RS, van Ierland EC (2006) Spatial scales, stakeholders and the valuation of ecosystem services. Ecol Econ 57:209–228
16. Krysanova V, Müller-Wohlfeil D-I, Becker A (1996) Integrated modeling of hydrology and water quality in mesoscale watersheds. PIK-report 18, Potsdam
17. Steinhardt U, Volk M (2003) Meso-scale landscape analysis based on landscape balance investigations: problems and hierarchical approaches for their resolution. Ecol Model 68:251–265
18. Volk M, Hirschfeld J, Dehnhardt A, Schmidt G, Bohn C, Liersch S, Gassman PW (2008) Integrated ecological-economic modeling of water pollution abatement management options in the Upper Ems River Basin. Ecol Econ 66:66–76
19. Riitters KH, Wickham JD (1997) A landscape atlas of the Chesapeak Bay Watershed. Environmental Research Center, Norris
20. O'Neill RV (1986) A hierarchical concept of ecosystems. Princeton University Press, Princeton
21. Klijn JA (1995) Hierarchical concepts in landscape ecology and its underlying disciplines. DLO winand staring centre report 100, Wageningen
22. Steinhardt U, Volk M (2000) Von der Makropore zum Flusseinzugsgebiet – Hierarchische Ansätze zum Verständnis des landschaftlichen Wasser- und Stoffhaushaltes. Petermann's Geogr Mitt 2(2000):80–91
23. Steinhardt U, Volk M (2002) The investigation of water and matter balance on the meso-landscape scale: a hierarchical approach for landscape research. Landscape Ecol 17:1–12
24. Helming K, Frielinghaus M (1999) Skalenaspekte der Bodenerosion. In: Steinhardt U, Volk M (eds) Regionalisierung in der Landschaftsökologie Forschung – Planung – Praxis. Teubner, Stuttgart-Leipzig, pp 79–95
25. Volk M (1999) Interactions between landscape balance and land use in the Dessau region, eastern Germany. A hierarchical approach. In: Hlavinkova P, Munzar J (eds) (1999) Regional prosperity and sustainability. Proceedings of the 3rd moravian geographical conference CONGEO'99, pp 201–209
26. Mitchell B (2005) Integrated water resource management, institutional arrangements, and land-use planning. Environ Plan A 37(8):1335–1352
27. Kiemstedt H, von Haaren C, Mönnecke M, Ott S (1997) Landschaftsplanung – Inhalte und Verfahrensweisen. Der Bundesminister für Umweltschutz und Reaktorsicherheit, Naturschutz und Reaktorsicherheit
28. Best A, Lu Z, McMahon T, Western A, Vertessy R (2003) A critical review of paired catchment studies with reference to seasonal flows and climatic variability. CSIRO land and water technical report 25/03. www.clw.csiro.au/publications/technical2003/tr25–03.pdf. Accessed 17 November 2009
29. Fohrer N, Haverkamp S, Frede H-G (2005) Assessment of the effects of land use pattern on hydrologica landscape functions: development of sustainable land use concepts for low mountain range areas. Hydrol Process 19:659–672
30. Calder IR (1992) Hydrologic effects of land use change. In: Maidment DR (ed) Handbook of hydrology. McGraw-Hill, Inc, New York, pp 13:1–13:5
31. Hibbert AR (1967) Forest treatment effects on water yield. In Sopper WE, Lull HW (eds) International symposium on forest hydrology, Pennsylvania, September 1965, Pergamon, Oxford, pp 99–103
32. Bosch JM, Hewlett JD (1982) A review of catchment experiments to determine the effect of vegetation changes on water yield and evapotranspiration. J Hydrol 55:3–23
33. Smith RE, Scott DF (1992) The effects of afforestation on low flows in various regions of South Africa. Water SA 18:185–194
34. Burch GJ, Bath RK, Moore ID, O'Loughlin EM (1987) Comparative hydrological behaviour of forested and cleared catchments in Southeastern Australia. J Hydrol 90:19–42
35. Peck AJ, Williamson DR (1987) Effects of forest clearing on groundwater. J Hydrol 94:47–65
36. Williams JR, Rose SC, Harris GL (1995) The impact on hydrology and water quality of woodland and set-aside establishment on lowland clay soils. Agric Ecosyst Environ 54:215–222
37. Whitaker A, Alila Y, Beckers J, Toews D (2002) Evaluating peak flow sensitivity to clear-cutting in different elevation bands of a snowmelt-dominated mountainous catchment. Water Resour Res 38:11–17
38. Kiersch B (2000) Land-use impacts on water resources: a literature review. Discussion paper No. 1. Land-water linkage in rural watersheds. Electronic workshop (September 18–October 27, 2000), FAO, Rome www.fao.org/ag/agl/watershed/watershed/en/eworken/idxewken.stm. Accessed 17 November 2009
39. Thomas RB, Megahan WF (1998) Peak flow responses to clearcutting and roads in small and large basins, western Cascades Oregon: a second opinion. Water Resour Res 34:3393–3403
40. Whitehead PG, Robinson M (1993) Experimental basin studies – an international and historical perspective of forest impacts. J Hydrol 145:217–230
41. Crawford NH, Linsey RK (1966) Digital simulations in hydrology – stanford watershed model IV, technical report 39. Department of Civil Engineering, Stanford University, Stanford

42. Singh VP (ed) (1995) Computer models of watershed hydrology. Water Resources Publications, Highland Ranch
43. Dyck S (1983) Overview on the present status of the concepts of water balance models. In: Van der Beken A, Herrmann A (eds) New approaches in water balance computations., pp 3–19, IAHS Publication 148
44. Xu C-Y, Seibert J, Halldin S (1996) Regional water balance modeling in the NOPEX area: developemnt and application of monthly water balance models. J Hydrol 180:211–236
45. Nemec J (1993) Comparison and selection of existing hydrological models for the simulation of the dynamic water balance processes in basins of different sizes and on different scales. Commission Internationale de L'hydrologie du Bassin du Rhin, report II-7, Lelystad, the Netherlands
46. Liebscher H-J, Wilke K, Schultz GA, Schumann A (1996) Mathematisches Modell zur Untersuchung des Einflusses von Klima- und Landnutzungsänderungen auf den Hoch- und Niedrigwasserabfluss im Einzugsgebiet der Model. Umweltbundesamt Texte 33/96, Berlin
47. Volk M, Bannholzer M (1999) Auswirkungen von Landnutzungsänderungen auf den Gebietswasserhaushalt: Anwendungsmöglichkeiten des Modells "ABIMO" für regionale Szenarien. Geoökodynamik 20:193–210
48. Lorz C, Volk M, Schmidt G (2007) Considering spatial distribution and functionality of forests in a modeling framework for river basin management. For Ecol Manage 248:17–25
49. Werner A, Eulenstein F, Schindler U, Müller L, Ryskowski L, Kedziora A (1997) Grundwasserneubildung und Landnutzung. Z f Kulturtechnik und Landentwicklung 38:106–113
50. Fohrer N, Möller D, Steiner N (2002) An interdisciplinary modeling approach to evaluate the effects of land use change. Phys Chem Earth 27:655–662
51. Van Rompaey AJJ, Govers G, Van Hecke E, Jakobs K (2001) The impacts of land use policy on the soil erosion risk: a case study in central Belgium. Agric Ecosyst Environ 83:83–94
52. Onstad CA, Jamieson DG (1970) Modeling the effect of land use modifications on runoff. Water Resour Res 6:1287–1295
53. Hookey GR (1987) Prediction of delays in groundwater response to catchment clearing. J Hydrol 94:181–198
54. Calder IR, Hall RL, Bastable HG, Gunston HM, Shela O, Chirwa A, Kafundu R (1995) The impact of land use change on water resources in sub-Saharan Africa: a modeling study of Lake Malawi. J Hydrol 170:123–135
55. Lørup JK, Refsgaard JC, Mazvimavi D (1998) Assessing the effect of land use change on catchment runoff by combined use of statistical tests and hydrological modeling: case studies from Zimbabwe. J Hydrol 205:147–163
56. Abbot MB, Bathurst JC, Cunge JA, O'Connell PE, Rasmussen J (1986) An introduction to the European hydrological system–syst'eme hydrologique Europ´een, 'SHE'. 1: History and philosophy of a physically based distributed modeling system. J Hydrol 87:45–59
57. Dunn SM, Mackay R (1995) Spatial variation in evapotranspiration and the influence of land use on catchment hydrology. J Hydrol 171:49–73
58. Lahmer W, Pfützner B, Becker A (1999) Großskalige hydrologische Modellierung vor dem Hintergrund unsicherer Eingangsdaten. In: Fohrer N, Döll P (eds) Modellierung des Wasser- und Stofftransports in großen Einzugsgebieten. Kassel University Press, Kassel, pp 153–161
59. Eckhardt K, Breuer L, Frede HG (2003) Parameter uncertainty and the significance of simulated land use change effects. J Hydrol 273:164–176
60. Klemes V (1986) Operational testing of hydrological simulation models. Hydrolog Sci J 31:13–24
61. Ewen J, Parkin G (1996) Validation of catchment models for predicting land-use and climate change impacts. 1. Method. J Hydrol 175:583–594
62. Lyne V, Hollick M (1979) Stochastic time-variable rainfall–runoff modeling. Australian Natl Conf Pub 79:89–93
63. Arnold JG, Muttiah RS, Srinivasan R, Allen PM (2000) Regional estimation of base flow and groundwater recharge in the Upper Mississippi river basin. J Hydrol 227:21–40
64. Heathwaite AL (2003) Making process-based knowledge useable at the operational level: a framework for modeling diffuse pollution from agricultural land. Environ Model Softw 18:753–760
65. Neal C, Heathwaite AL (2005) Nutrient mobility within river basins: a European perspective. J Hydrol 304:477–490
66. Franko U, Schmidt T, Volk M (2001) Modellierung des Einflusses von Landnutzungsänderungen auf die Nitratkonzentration im Sickerwasser. In: Horsch H, Ring I, Herzog F (eds) Nachhaltige Wasserbewirtschaftung und Landnutzung. Methoden und Instrumente der Entscheidungsfindung und - umsetzung. Metropolis, Marburg, pp 165–186
67. Neubert M, Volk M, Herzog F (2003) Modellierung und Bewertung des Einflusses von Landnutzung und Bewirtschaftungsintensität auf den potenziellen Nitrataustrag in einem mesoskaligen Einzugsgebiet. Landnutz Landentwick 44:1–8
68. Volk M, Franko U, Schmidt T, Herzog F, Neubert M (2001) Modeling the impact of land use changes on the groundwater quantity and quality as a base for multicriteria ecological-socioeconomic assessment in a mesoscale watershed. In: Hlavinkova P, Munzar J (eds) The 4th moravian geographical conference CONGEO '01: nature and society in regional context, Tisnov, September 10–14 2001, pp 160–168
69. Klauer B, Drechsler M, Messner F (2006) Multicriteria analysis under uncertainty with IANUS – method and empirical results. Environ Plan C: Govt Policy 24:235–256
70. Volk M, Herzog F, Schmidt T, Geyler S (2001) Der Einfluss von Landnutzungsänderungen auf die Grundwasserneubildung. In: Nachhaltige Wasserbewirtschaftung und Landnutzung. Methoden und Instrumente der Entscheidungsfindung und – umsetzung. Metropolis, Marburg, pp 147–164
71. Horsch H, Ring I, Herzog F (eds) (2001) Nachhaltige Wasserbewirtschaftung und Landnutzung - Methoden und Instrumente der Entscheidungsfindung und - umsetzung. Metropolis, Marburg

72. Hülsbergen K-J (2003) Entwicklung und Anwendung eines Bilanzierungsmodells zur Bewertung der Nachhaltigkeit landwirtschaftlicher Systeme. Shaker Verlag, Aachen
73. Horn AL, Rueda FJ, Hörmann G, Fohrer N (2004) Implementing river water quality modeling issues in mesoscale watershed models for water policy demands – an overview on current concepts, deficits, and future tasks. Phys Chem Earth 29: 725–737
74. Payraudeau S, Cernesson F, Tournoud MG, Beven KJ (2004) Modeling nitrogen loads at the catchment scale under the influence of land use. Phys Chem Earth 29:811–819
75. Euroharp-Project (2007) http://www.euroharp.org/toolbox/scenario.php. Accessed 6 April 2009
76. Arnold JG, Srinivasan R, Muttiah RS, Williams JR (1998) Large area hydrologic modeling and assessment. Part 1: Model development. J Am Water Res Ass 34:73–89
77. Volk M, Liersch S, Schmidt G (2009) Towards the implementation of the European water framework directive? Lessons learned from water quality simulations in an agricultural watershed. Land Use Policy 26:580–588
78. Ullrich A, Volk M (2010) Influence of different nitrate–N monitoring strategies on load estimation as a base for model calibration and evaluation. Environmental monitoring and assessment. (Online First: doi: 10.1007/s10661-009-1296-8)
79. Schilling KE, Jha MK, Zhang Y-K, Gassmann PW, Wolter CF (2008) Impact of land use and land cover change on the water balance of a large agricultural watershed: historical effects and future directions. Water Resour Res 44:W00A09, doi:10.1029/2007WR006644
80. Berlekamp J, Lautenbach S, Graf N, Reimer S, Matthies M (2007) Integration of MONERIS and GREAT-ER in the decision support system for the German Elbe river basin. Environ Model Softw 22:239–247
81. Hirschfeld J, Dehnhardt A, Dietrich J (2005) Socioeconomic analysis within an interdisciplinary spatial decision support system for an integrated management of the Werra River Basin. Limnologica 35:234–244
82. Mödinger J, Kobus H, Schnitzler S, Lehn H (2004) Ansätze fu¨r eine nachhaltige Grundwasserbewirtschaftung und -nutzung im Rhein-Neckar-Raum bei konkurrierenden Interessen. Wasser Wirtschaft 94:40–45
83. Möltgen J, Petry D (eds) (2004) Interdisziplinäre Methoden des Flussgebietsmanagements. Workshopbeiträge, 15./16. März 2004. IfGI prints 21. Münster: Institut für Geoinformatik, Universität Münster, Münster, pp 352
84. Schneck A, Haakh F, Lang U (2004) Multikriterielle Optimierung der Grundwasserbewirtschaftung – dargestellt am Beispiel des Wassergewinnungsgebiets Donauried. Wasserwirtschaft 12:32–39
85. Feld CK, Rödiger S, Sommerhäuser M, Friedrich G (eds) (2005) Typologie, Bewertung, Management von Oberflächengewässern. Limnologie aktuell 11, E. Schweizerbart'sche Verlagsbuchhandlung (Nägele u. Obermiller). Stuttgart, Germany, p 243
86. Giupponi C (2007) Decision support systems for implementing the European water framework directive: the MULINO approach. Environ Model Softw 22:248–258
87. Van Delden H, Luja P, Engelen G (2007) Integration of multi-scale dynamic spatial models of socio-economic and physical processes for river basin management. Environ Model Softw 22:223–238
88. Lautenbach S, Berlekamp J, Graf N, Seppelt R, Matthies M (2009) Scenario analysis and management options for sustainable river basin management: application of the Elbe DSS. Environ Model Softw 24:26–43
89. Burstein F, Holsapple CW (eds) (2008) Handbook on decision support systems, vol 1 (854 pp) and 2 (800 pp). Springer, Heidelberg, Berlin, New York
90. Newman S, Lynch T, Plummer AA (1999) Success and failure of decision support systems: learning aswe go. In: Proceedings of the American society of animal science. http://www.asas.org/jas/symposia/proceedings/0936.pdf. Accessed online 25 February 2009
91. Zapatero EG (1996) A quality assessment instrument for multicriteria decision support software. Benchmarking Qual Manage Technol 3:17–27
92. Uran O, Janssen R (2003) Why are spatial decision support systems not used? Some experiences from the Netherlands. Comput Environ Urban Syst 27:511–526
93. Briscoe J (2005) Water as an economic good. In: Brouwer R, Pearce DW (eds) Cost-benefit analysis and water resources management. Edward Elgar, Cheltenham
94. Young RA (2005) Determining the economic value of water: concepts and methods. Resources for the Future, Washington DC
95. Brouwer R, Hofkes M (2008) Integrated hydro-economic modeling: approaches, key issues and future research directions. Ecol Econ 66:16–22
96. Rode M, Klauer B, Petry D, Volk M, Wenk G, Wagenschein D (2008) Integrated nutrient transport modeling with respect to the implementation of the European WFD: the Weisse Elster case study, Germany. Water SA 34:490–496
97. De Kok J-L, Kofalk S, Berlekamp J, Hahn B, Wind H (2009) From design to application of a decision-support system for integrated river-basin management. Water Resour Manage 23:1781–1811
98. Volk M, Lautenbach S, van Delden H, Newham LTH, Seppelt R (2009): How can we make progress with decision support systems in landscape and river basin management? Lessons learned from a comparative analysis of four different decision support systems. Environ Manage (Online First: doi: 10.1007/s00267-009-9417-2)
99. Gleick PH (1998) Water in crisis: paths to sustainable water use. Ecol Appl 8:571–579

Books and Reviews

Beven KJ (2001) Rainfall-runoff modeling: the primer. Wiley, Chichester

Brutsaert W (2005) Hydrology – an introduction. Cambridge University Press, New York
Davie T (2003) Fundamentals of hydrology. Routledge fundamentals of physical geography. Routledge, London
Dingman SL (2002) Physical hydrology. Prentice Hall, Upper Saddle River
Dunne T, Leopold LB (1978) Water in environmental planning. W.H. Freeman & Company, San Francisco
Evers M (2008) Decision support systems for integrated river basin management: requirements for appropriate tools and structures for a comprehensive planning. Shaker Verlag, Aachen
Federal Interagency Stream Restoration Working Group (FISGRWG, 1998/2001) Stream corridor restoration: principles, processes, and practices. GPO Item No. 0120-A; SuDocs No. A 57.6/2:EN3/PT.653 (http://www.nrcs.usda.gov/technical/stream_restoration/newgra.html). Accessed 11 April 2009
Gassman PW, Reyes MR, Green CH, Arnold JG (2007) The soil and water assessment tool: historical development, applications, and future research directions. Trans ASABE 50:1211–2150
Gooch G, Stlnacke P (2010) Science, policy and stakeholder in water management: an integrated approach to river basin management. Earthscan, London
Heathcote IW (1998) Integrated watershed management principles and practice. Wiley, Chichester
Mysiak J, Henrikson HJ, Sullivan C, Bromley J, Pahl-Wostl C (eds) (2010) The adaptive water resource management handbook. Earthscan, London, Sterling
Shaw E (1994) Hydrology in practice. Stanley Thornes, Cheltenham
Ward RC, Robinson M (1999) Principles of hydrology. McGraw-Hill, London
Wohl EE (2001) Virtual rivers. Lessons learned from the mountain rivers of the Colorado Front Range. Yale University Press, New Haven

Landscape Planning/Design of Shrinking Landscapes

Dagmar Haase
Department of Geography, Humboldt University Berlin, Berlin, Germany
Department of Computational Landscape Ecology, Helmholtz Center for Environmental Research – UFZ, Leipzig, Germany

Article Outline

Glossary
Definition of the Subject
Introduction: Shrinkage and Sustainability – Setting the Scene
Premises of Shrinkage
Consequences of Shrinkage on Sustainability
Response to Shrinkage
Future Directions
Acknowledgments
Bibliography

Glossary

Demographic change Refers to new demographic developments that bring sustained sub-replacement fertility, a multitude of living arrangements other than marriage, the disconnection between marriage and procreation, and no stationary population. Instead, populations would face decline if not complemented by new migrants, and they will also be much older as a result of lower fertility and additional gains in longevity. Migration streams will not be able to neutralize aging, but stabilize population sizes. Demographic change brings new social challenges such as aging, integration of immigrants and other cultures, less stability of households, and high levels of poverty or exclusion among household types like single persons of all ages or single parents. It brings alterations in per capita housing and transport demand.

Ecosystem services Society benefits from a multitude of resources and processes that are supplied by natural ecosystems and landscapes. Collectively, these benefits are known as ecosystem services and include products like clean drinking water or recreation area and processes such as the decomposition of wastes. In 2004, the United Nations 2004 Millennium Ecosystem Assessment (MA) formalized ecosystem services and grouped them into four broad categories: provisioning, such as the production of food and water; regulating, such as the control of climate and disease; supporting, such as nutrient cycles and crop pollination; and cultural, such as spiritual and recreational benefits.

Governance Governance is the activity of governing. It relates to multi-actor and multilevel decision-making that define expectations, grant power, or verify performance. It consists either of a separate process or of a specific part of management or leadership processes. In the case of a nonprofit organization, governance relates to consistent

management, cohesive policies, processes, and decision rights for a given area of responsibility. In case governance refers to land use, it deals with land management.

Landscape planning Landscape planning puts landscape ecology into a spatial planning context. It focuses on landscape function and ecosystem service assessment on different spatial scales. Landscape planning develops strategies for sustainable land use systems including the whole range from natural, cultural landscapes to impacted or devastated areas.

Land use Land use is the human modification of the natural environment, surface, or wilderness into built environment such as fields, pastures, and settlements. Urban land use is characterized by a particular high degree of imperviousness.

Perforation Development of patchwork settlement structures without a compact core and related creation of low-density counter settlements with implications for lower sealing rates, building and population densities. The spatial cohesion of perforated areas is low.

Shrinkage Shrinkage is understood primarily as the quantitative process of population decline in an area which might be the result of very different processes such as deindustrialization, demographic change, or even natural hazards.

Sprawl Urban sprawl is a multifaceted concept, which includes the spreading of impervious surface and built-up area outward of a city and its suburbs to its outskirts to low-density, car-dependent development on rural or virgin land, with associated design features that encourage car dependency.

Sustainability Sustainability is the capacity to endure. In ecology, it describes how biological systems remain diverse and productive over time. For humans, it is the potential for long-term maintenance of well-being, which in turn depends on the well-being of the natural world and the responsible use of natural resources. It includes the maintenance of landscape functions, ecosystem goods and services.

Definition of the Subject

When thinking about sustainability, it is mainly about how to keep intact nature and environmental resources for either future generations and/or, more in terms of environmental justice, for other parts of the world. Land use and spatial planning focus on how to minimize negative effects of urban and industrial growth. Set against this context, urban shrinkage represents a new challenge. This is true due to the fact that one has to deal with the opposite phenomenon of growth – population decline and accompanying processes of de-densification – which, unemotionally, also asks the same questions as even mentioned for growth: How could land use development be steered in order to ensure quality of life of the population under conditions of decline? How high-quality and sustainable urban livelihoods can be developed? Are there visions for sustainable shrinkage?

Resource consumption is a problem particularly in cities due to the concentration of population – that is consumers of environmental goods and ecosystem services. Since some years, more than half of the world population lives in cities. And, what is more, >200 cities worldwide, mostly in Europe, Russia, Japan and the US, are shrinking: they are losing population. Shrinkage and declining population numbers do not mean an automatic decrease of natural resources consumption such as land, energy, or water because the per capita requirements on environmental resources, ecosystem services, and housing space are increasing. Also, in shrinking cities, household numbers increase. In consequence, population losses along with rising per capita housing space lead to further land consumption and enlargement of, for example, transport and infrastructure. Also, in shrinking cities, sprawling settlement development continues because of specific housing preferences such as single family houses and spacious housing with backdoor garden.

Since shrinkage does not follow the logics of growth, there are no receipts for how to sustainably develop or plan a shrinking city. This entry will show that shrinkage appears in many different shapes and argues that there will not be a "one-size-fits-all" or textbook answer to this question. So doing, the entry addresses the relationship between urban decline, socio-demography, infrastructure, land use, and ecosystems, and discusses causes and consequences of shrinkage in the light of sustainability. It ends up with showing how actors in cities react to shrinkage in terms of rethinking their visions, instrumental settings, and strategic planning.

Introduction: Shrinkage and Sustainability – Setting the Scene

Urban Shrinkage

Shrinkage affects many cities across the world, especially old industrial areas (America's Rust Belt, British Midlands, Germany's Ruhr Valley, eastern part of Germany; [1, 2]). The phenomena of urban shrinkage and its concomitant industrial blight, low investment rates, depopulation, and low housing demand can be vividly exemplified in the landscape: dilapidated residential buildings and estates, extensive brownfield and derelict commercial sites, streets with vacant storefronts, underutilized social and technical infrastructure, and neglected parks and squares [3]. Shrinking cities often hold large brownfield sites, particularly in their old built-up inner parts [4].

Urban shrinkage appears in many forms and dynamics. Since their very early history, cities across the world have already seen phases of decline [5]. The same is true if one narrows the focus to look at the recent decades of urban development. Already throughout the entire twentieth century up to the present day, urban shrinkage has become reality for many cities in Europe, Russia, Japan, and the eastern US ([6]; cf. Fig. 1).

Recent studies provided evidence for the fact that about 40% of all European cities >200,000 inhabitants have lost population in a short-, medium- or long-term period for different reasons (for a quantitative analysis, see studies by [6] or [7]). Therefore, urban shrinkage has become the focus of international research and debate, not least because of cross-national projects (e.g., Shrinking Cities, 2002–2008; ShrinkSmart, 2009–2011) or the establishment of scholarly networks (e.g., the Berkeley Cities International Research Network SCIRN; [8]). One of the exceptional cases of urban shrinkage is eastern Germany, which lost between 10 and 20% of its residents in a period of 10 years (mean value for big cities from 1990 to 1999 is about 16%). Thus, in the following, eastern Germany will serve as an example case when analyzing processes and patterns of shrinkage.

How does urban shrinkage relate to sustainability and resource consumption in urban regions? A recent analysis of the relation of population and household development of 195 European cities from 1990 to 2000

Landscape Planning/Design of Shrinking Landscapes. Figure 1
World map of shrinking cities with more than 100,000 inhabitants (adopted from the "Atlas of shrinking cities" by Office Oswalt, [1])

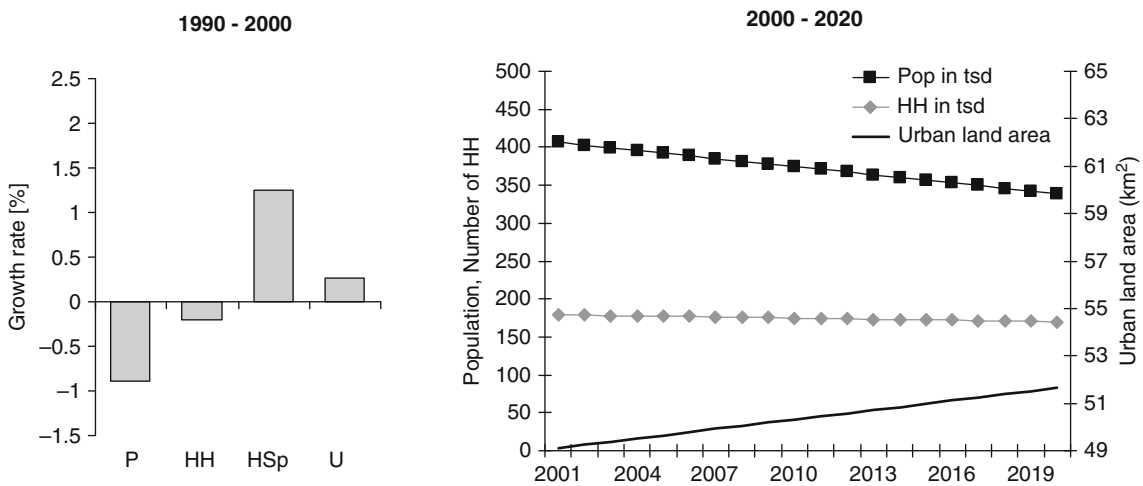

Landscape Planning/Design of Shrinking Landscapes. Figure 2

Left: Annual growth rate of total population (P), number of households (HH), per capita housing space (HSp), and urban land area of shrinking cities across Europe 1990–2000. *Right*: Projection of total population, number of households, and urban land area of shrinking cities in Europe from 2001 to 2020. The annual growth rates were computed for each variable x as Δx from t_0=1990 to t_1=2000, for instance, for the number of households HH: $\Delta HH = HH(t_0) - HH(t_1)$. Assuming that the average aggregate population, the average household size, the average rates of urban and commercial land take in European cities in 2020 remain at the level of 2000 (t_1), the aggregate population at t_2 was estimated as $Pop_{t_2} = Pop_{t_1} + GR_{a_{1990-2000}}$ where $R_{a_{1990-2000}}$ is the average annual growth rate 1990–2000 [9]

to the growth of urban land consumption and housing space [9] found a significant share of cities facing declining population and decreasing household numbers. Nonetheless, the urban (= impervious) areas within the boundaries of these declining cities have continued to spread. No reduction of natural resource consumption in terms of returning sealed surfaces back to their natural states was observed (Fig. 2).

In addition to that, [9] identified an increase in per capita housing space, which also counteracts a reduction of land consumption. A linear projection of population, household numbers, and urban land up to 2020 shows that, exemplified at European cities, urban – that is mostly impervious surface – areas will face further land consumption, regardless of whether population and household numbers increase or decrease. Therefore, the global problem of unsustainable resource consumption seems not to be "simply" solved by population shrinkage.

Urban Sustainability

The concept of "sustainable development" evolved in response to the socio-environmental impacts of economic activities. Already in 1987, the Brundtland report framed it as "meeting the needs of the present without compromising the ability of future generations to meet their own needs" (World Commission on Environment and Development). The application of this concept to urban regions and urban land use development raises many questions. This is, firstly, due to the diverse concept of sustainable development, which combines economic, social, and environmental goals, both locally and globally, and in both the short and longer term [10]. And secondly, because the nature of the urban areas is generally a complex mix of drivers, pressures, and processes in many different sectors, at different spatial scales [11]. In particular, the peri-urban role is as a hinterland and support system for urban core activities [12]: food is produced there, recreational facilities are given, energy is provided, and drinking water delivered [13, 14].

There is also a global dimension to the urban sustainability agenda, which is still dominated by growth: In the next 40 years, current projections show a rapid growth in the urban areas of developing countries of up to 3 billion people [15]. Current trends show that

a majority of urban residents will live in slums or chaotic settlements lacking basic infrastructure [16]. Much of this "urban" development is likely to be in peri-urban areas, or rapidly metropolitanized peri-rural areas [17]. However, next to this spreading growth, demographic aging and low-rate fertility will establish a new urban trajectory also in the developing world. This trend currently has been already reached cities in India or China [18, 19].

When thinking about sustainability, keeping intact nature and environmental resources for either future generations and/or, more in terms of environmental justice, for other parts of the world are talked about. Landscape and regional landscape planning focuses on how to minimize negative effects of urban and industrial growth [12, 20]. In terms of sustainability, urban shrinkage represents a new challenge because one has to deal with the opposite phenomenon of growth – decline and accompanying processes of de-densification and land use perforation – and focus on the following questions: How could land use development be steered in order to ensure quality of life of the population under conditions of shrinkage? Is it possible to direct land preparation toward the inner parts of shrinking cities? Are there visions for sustainable shrinkage?

Premises of Shrinkage

Urban shrinkage has been approached using different ways (see review by [8]): Some scholars interpret shrinkage as a decreasing population development in the urban core (city) as part of wider shifts in the spatial organization of larger urban regions (for example, between the urban core and the peri-urban hinterland) in the course of which existing built environments are devalorized, mainly in economic terms, and made obsolete [21–23].

Others discuss urban shrinkage as an inevitable result of uneven economic development, emerging as something rather natural that is deeply rooted in the nature of capitalist economies [24] and the underlying dynamics of the territorial division of labor [25, 26]. In fact, many shrinking cities exist because of the postindustrial shift from manufacturing (II. Sector) to service industries (III. Sector) and the IT branch (IV. Sector) followed by resulting unemployment and outmigration (such as Pittsburgh and St. Louis in the US, Manchester or Liverpool in UK). In eastern Europe and the former Soviet Union, the collapse of socialist systems led or at least importantly contributed to the decline of urban regions there [2]. Still another explanatory approach discusses urban shrinkage in the light of demographic change and relates it to low-fertility rates, changes in the household formation, and migration impact (see here [27, 28]).

In this entry, shrinkage is defined as the quantitative process of population decline. Population decline is represented by both natural decline (i.e., death surpluses) and losses by out-migration (due to suburbanization, intra-regional migration, emigration). It is frequently used as the main indicator in research on urban shrinkage, which makes the findings presented here in this respect easily comparable with other studies [1, 5, 6, 29]. Overall, shrinkage processes have drained essential resources from the urban regions (mostly the core cities), leaving the cities with a diminishing fiscal base [30].

Urban shrinkage affects the physical space, the society of a city, and the surrounding ecosystems (as well as landscapes) whose mutual fit is diminishing; this leads in turn to phenomena such as mismatches of supply and demand in various respects [31]. Since shrinkage is also a spatial phenomenon, it is important to differentiate between urban shrinkage as a process and its results that are seen as reconfigured or reshaped urban structure or patterns [32]. Urban shrinkage impacts on nearly every sphere of urban life: municipal budgets, land use and urban planning, natural resources, ecosystem services, infrastructure and amenities, housing market and housing mobility, labor market and employment, residential composition, and social inclusion and cohesion. This makes shrinkage a challenge for both landscape planning and sustainability research.

Consequences of Shrinkage on Sustainability

Shrinkage Patterns and Consequences for Urban Land Use

Population decline leads to a decrease in population density and to an oversupply/underuse of urban, residential, and commercial land, infrastructure, and services. Shrinking populations need fewer and modified services and amenities according to the need of the remaining, often aging, population [32]. This leads to

problems for both the public and private sector: Underuse of the building stock leads to housing and commercial vacancies and to a more rapid dilapidation of unused buildings [33]. Whilst in some places, buildings are demolished to "balance" the housing or real estate market, in other places they simply become unusable after a certain time of not being used. [34] introduced the term of "land use perforation " in order to describe the scattered land use development in the inner parts of shrinking cities: Fig. 3 displays a stylized example of land use perforation in comparison of dense (left) and compact (center) urban forms. The simulation results show that despite population decline and decreasing demand for housing space in the inner city, land consumption at the urban periphery continues.

Table 1 provides a detailed overview on the most important processes and impacts of urban shrinkage. It gives a short explanation of the underlying processes. Figure 4, developed based on the Table 1 findings, shows that most of the processes are interrelated and shape the specific appearance or trajectory of shrinkage in a particular city [35]. It shows the fortunes of urban neighborhoods as home or place to work which depend on their attractiveness under the condition of supply surplus, on ownership structures, housing policies, and the local economic situation of enterprises and retail.

Compared to the regular patterns of land use perforation produced by the stylized model given in Fig. 3, often, differences between neighborhoods in a shrinking city vary on a small scale within the urban area [36]. This makes it extremely difficult to identify an overall picture or specified model of urban shrinkage and its impact on the city as a whole or land use patterns in a larger scale as well as in the future [2, 37].

In consequence, the change of land use causes an increasing proportion of derelict land or brownfields within the inner parts of the city. This can foster out-migration decisions of those who do not want to live close to dilapidating building stock or areas of urban wilderness [4, 38]. This cycle will reinforce itself over time and lead to a steady decrease of population density either in specific parts of a city (Fig. 5 "perforated city"), in the central (Fig. 5 "disperse city") or peripheral parts (Fig. 5 "compact city"). In addition to such a patchy way of shrinkage, a widespread and overall decrease of population density across the entire urban area can be found [5].

The project "Leipzig 2030" [39] compared population densities of specific housing forms under conditions of high and low demand (Table 2). Low demand leads to vacancies in the buildings and to a shift of lower population densities in the city. So, for example, partial vacant, old built-up multistory estates almost "reach" population densities that are typical for terraced row houses. This is important for infrastructure development, as, normally, population density determines the network of social and technical infrastructure in cities.

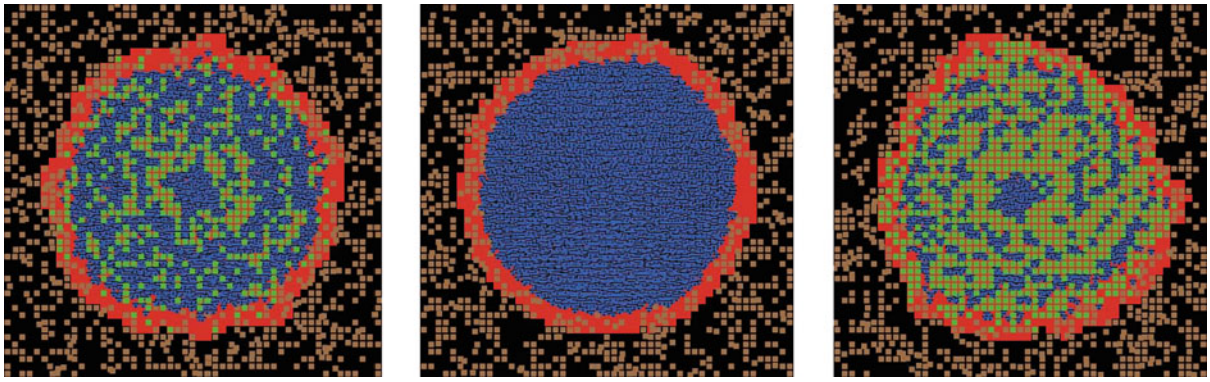

Landscape Planning/Design of Shrinking Landscapes. Figure 3
Stylized representation of urban form: (*left*) a medium density built-up town, (*center*) a very compact city, and (*right*) urban land use perforation. Blue houses represent the built-up area, red patches newly prepared peri-urban land, green patches green area, and brown patches other types of land in the rural surroundings (NetLogo model and draft: D. Haase)

Landscape Planning/Design of Shrinking Landscapes. Table 1 Processes and impacts of urban shrinkage (adopted from [35])

Process/Impact	Explanation
Decrease in density	Population loss and out-migration lead to a decrease in the number of inhabitants of the affected areas and, subsequently, to a decrease in residential, commercial densities.
Increase in housing and commercial vacancies[a]	Decreasing demand leads to supply surplus and an underuse of housing stock, commercial stock, and, subsequently, to vacant stock.
	Vacancies in shrinking cities can affect also renovated or even new build stock due to a mismatch of supply (investment) and real demand (use).
Underuse of urban structures and infrastructures	Population losses and decrease in densities lead to an oversupply of urban structures (see above vacancies) and infrastructures such like schools, kindergartens, public transport, etc.
	Oversized infrastructures have to be either maintained without being used or closed or demolished.
Increase of unused (built) urban land	Due to decreasing densities and increasing underuse or nonuse, the share of unused built urban land increases.
	Demolition activities are necessary and being done.
	Unused built urban land can be vacant buildings, urban brownfields on former industrial, commercial, railways sites, etc.
	Unused built urban land develops to "new urban wildernesses" or even "forests".
Perforation of urban structures	Demolition, abandonment of places and uses within a city lead to the dissolution of the street or block grid of a city or urban area due to vacant lots and brown- resp. greenfields that separate or divide built lands (perforation).
	Perforated areas are characterized by a large percentage of vacant areas within an urban territory or city.
Changing sociodemographic structure of the residential population	Population losses and selective out-migration lead to aging, changing household structures, and a "blurred" age group distribution.
Increase in socio-spatial fragmentation and residential segregation	Selective out-migration and population losses might lead to a "blurred" socioeconomic structure of the remaining inhabitants.
	In shrinking cities, there are often relations between dilapidating areas with high housing vacancies and a concentration of disadvantaged population groups living there.
	Shrinking and resurging areas are situated closely to each other (= rising small-scale fragmentation).
Change in housing mobility within the city and its region	An oversupply of housing might lead to a higher housing mobility and a greater choice for a number of residential groups.
	The level of housing mobility increases due to the greater choice and the good opportunities to get a better flat at many places in the city.
	Vacant housing offers the opportunity for transitory housing, which might become more and more important for residential areas with housing oversupply.

Landscape Planning/Design of Shrinking Landscapes. Table 1 (Continued)

Process/Impact	Explanation
Decrease in municipal budget	Happens due to the decrease in tax revenues as a consequence of population losses. Results in many cases in an increasing dependency on public money.
Need of new planning schemes	Growth-oriented planning schemes have to be replaced by a strategy that aims at the coping with urban shrinkage, either in a long-term perspective or as a phase of urban development that has to be quickly overcome (depending on the causes of shrinkage and the chances of the particular city to reach regrowth).
Shrinkage of the local labor market	Decrease in employment and jobs leads to a decreasing demand on land used for industrial and commercial activities.

[a]Housing and commercial vacancies = housing and commercial stock that is inhabitable and useable but not inhabited or used; perforation = dissolution of the street or block grid of a city or urban area due to vacant lots and brown- resp. greenfields that separate or divide built lands

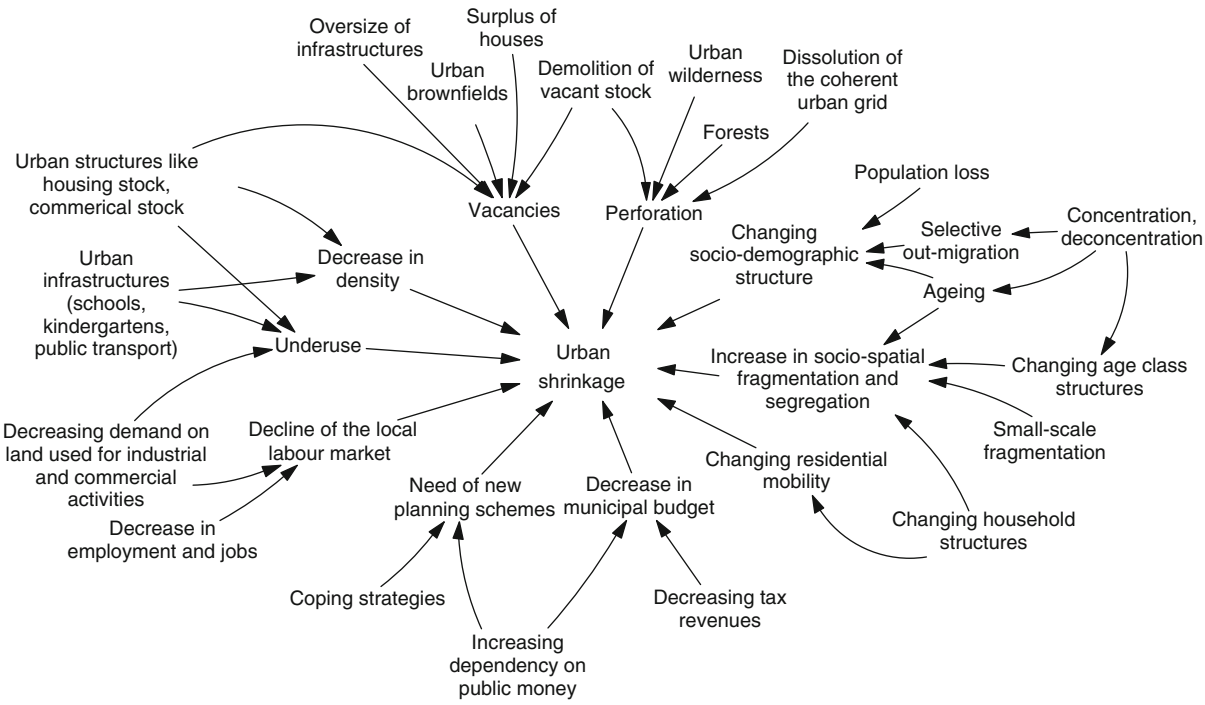

Landscape Planning/Design of Shrinking Landscapes. Figure 4
Compilation of social science indicators about shrinkage, its drivers, processes, and impacts (draft: D. Haase)

Effects on Socio-Demographic Sustainability

Can a city consistently lose population and yet maintain a high quality of life, human well-being, and social equity for all groups of residents? This paper argues it cannot in case planning does not counteract the following trends discussed in the literature or shown by statistical data: Urban shrinkage leads to shifts in the population structure since out-migration is almost always selective and often removes the younger and well-educated parts of the population leading to an

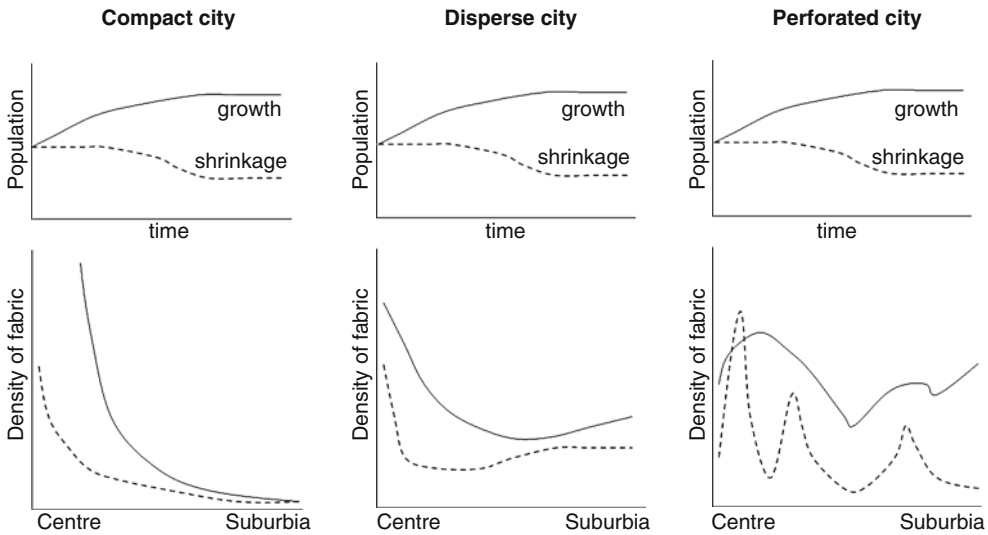

Landscape Planning/Design of Shrinking Landscapes. Figure 5
Stylized urban-to-rural gradient of growing (*black* line) and shrinking (*dotted* line) population development (*upper* diagrams) and respective impacts on urban fabric density (draft: D. Haase). Such fabric densities were already observed in several eastern German but also US cities [1]

Landscape Planning/Design of Shrinking Landscapes. Table 2 Population density of different housing form under conditions of high and low demand [39]

Housing form	Old built-up multistory high demand	Old built-up multistory low demand	Prefabricated multistory high demand	Prefabricated multistory low demand	Row houses	Single houses
Population density (inhabitants/km^2)	149	80	230	75	55	37

enforced aging of the remaining population (cf. again Table 1; Fig. 7b). The same happens when a city loses population due to death surpluses [40]. In shrinking cities, there is often a concentration of neglected population groups such as the unemployed, poor or low-income groups, and foreigners or ethnic minorities ([2]; Fig. 7c). Moreover, the overall household size is declining and accompanied by a temporary increase of the household number (cf. argumentation by [41] and [42]; Fig. 6).

This brings about challenges for social cohesion and may fix and strengthen patterns of socio-spatial and residential segregation and poverty concentration in the respective city [43]. Selective out-migration also has consequences for the labor market since skilled labor becomes scarce [8]. Here, the declining attractiveness of a city can even lead to an accelerated population loss and thus start a vicious circle [33]. In shrinking cities, high unemployment and decreasing investment are closely related to each other, which makes these cities less and less attractive for both in-migrants and developers and forces them, in many cases, into an especially developer-friendly, neoliberal policy to attract investment. This in turn demands low wages and high land consumption at the urban periphery [38, 44].

Figure 7 provides a mapped vision of socio-demographic and land use changes provoked by

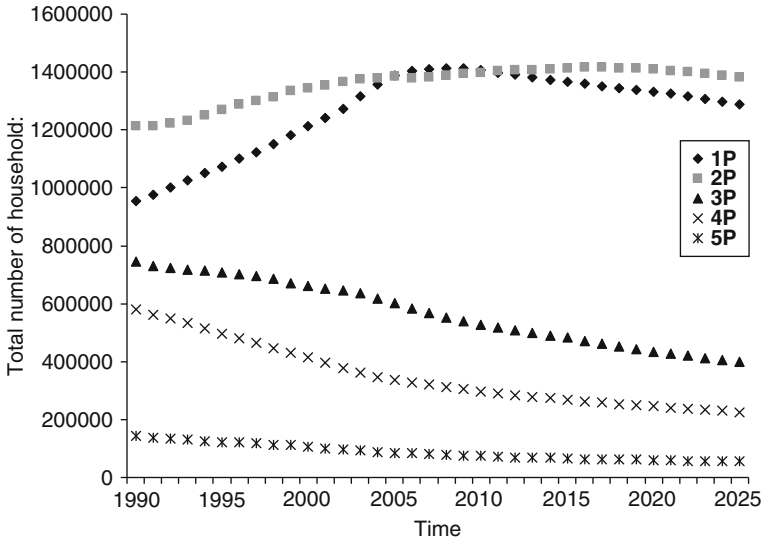

Landscape Planning/Design of Shrinking Landscapes. Figure 6
Development of the total number of households in the shrinking eastern German urban region of Leipzig-Halle measured for 1990–2005 and simulated until 2025 (own analysis based on data by the German Federal Agency for Spatial Planning). The figure shows that particularly the number of large – that is 3 and more person households (3–5P) – will steadily decline whereas one (1P) and two person households (2P) still grow for a while. This is not an effect induced by shrinkage but by demographic transition processes. Both processes overlap in shrinking urban regions

shrinkage in Germany for 2020 [45] when it is defined as population decline: Fig. 7a shows the overall population decline in shrinking regions. Figure 7b then provides evidence that those regions faced with strong population decline – that is northeastern and central eastern Germany – age dramatically. Due to outflow of the young and well-educated people, the unemployment rate increases (Fig. 7c) – this process reinforces the aging. In consequence, settlement and transport development weakens (Figs. 7d and e), which is not by far a problem for the regional sustainability. Thus, reinforced processes of shrinking shape larger regions such as given in Fig. 7f.

Effects on Infrastructure

As far as urban space and its amenities and infrastructure are concerned, population losses bring about a decrease in density and an increasing underuse of infrastructure, urban land, and amenities [46]. Shrinking populations demand fewer services and amenities leading to problems for both the public and private sectors. Underuse of the building stock leads to housing and commercial vacancies and to a more rapid dilapidation of unused buildings [47].

So, for example, shops have to close when there is no longer enough purchasing power, and in most cases public infrastructure sees a thinning-out process – the frequency of services decreases and selected stops and trajectories are close down [48]. Local suppliers of water and electricity face a decreasing demand, which might lead to rising costs for those who still live in areas with a shrinking population, as they still have to cover the maintenance costs of the infrastructure system [49]. Whilst to some extent a decreasing building stock density leads to "relaxation" for a densely built city, at a later stage, it might lead to a fragmentation and even the aforementioned perforation of urban space in terms of dissolution of the street or block structure due to vacant lots [33].

The – at least temporary – result of shrinkage, as discussed in the previous section, is a pattern of (newly) built-up area in rather close vicinity to vacant housing. City intervention programs finally lead to

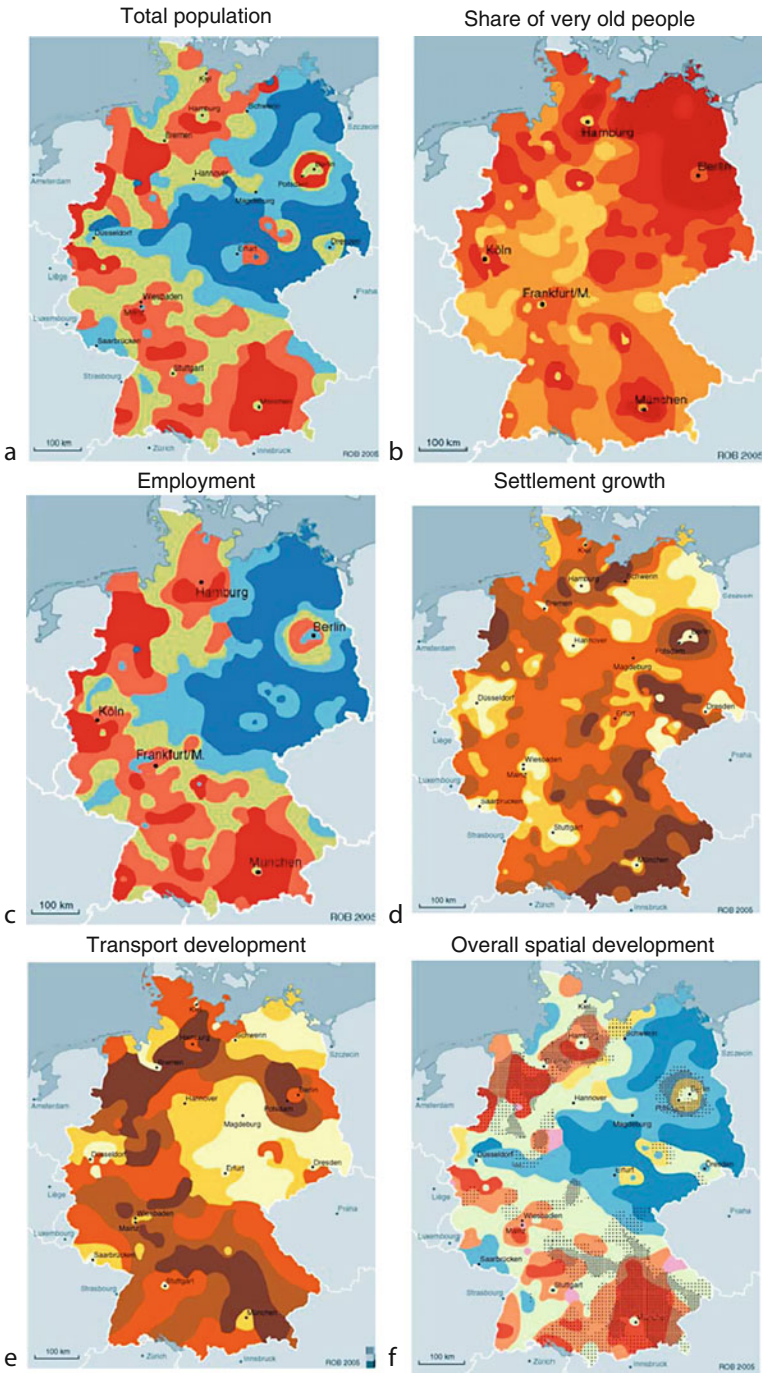

Landscape Planning/Design of Shrinking Landscapes. Figure 7
Changes of the spatial patterns of socio-demographic impacts of population decline exemplified for Germany for the time span of 2000–2020 (BBSR, 2005): Legends in (**a**), (**c**) and (**f**) range from red = very positive to blue = very negative; Legend (**b**) is red = very high to yellow = moderate; Legends of (**d**) and (**e**) is brown = significant to beige = nearly zero. In figure (**f**), the dotted areas mean an overdimensional aging

the partial demolition of the vacant housing stock and to land use perforation [33, 50]. This pattern of vacant, demolished, and new housing poses challenges for urban infrastructure provision. This is obvious for network-dependent infrastructure, like water, sewage, or electricity: Vacant houses no longer need supply of water or electricity or a transport for waste water, so that the pipes and cables leading to this house are no longer used. In an area with a larger proportion of vacant houses, underutilization can pose severe problems for maintenance of the service for the whole area [51, 52].

Social urban infrastructure like schools, kindergartens, as well as roads and public transport also are influenced by vacancy. All of these infrastructures are optimized for a certain demand structure in an area, usually determined by population density and commercial or industrial activity. At least, efficiency decreases in areas with higher rates of vacancy [2, 49]. At the worst, an area might enter a vicious cycle of declining population, underutilized and then dismantled infrastructure, so that the area gets less attractive. Thus, even more residents relocate to another part in the city [52]. Moreover, underutilization causes toxic effects and water resources pollution [46, 49]. In the years to come, housing service and maintenance costs are likely to rise in shrinking or perforating communities. In shrinking cities, lower residential densities may demand a smaller road network. Ironically, the demand for public transit could increase in shrinking cities as populations tend to be increasingly poor and increasingly without access to private transportation [2].

To avoid or at least limit higher ancillary costs and the consequent worsening of local conditions in the municipalities affected, low-cost urban renewal strategies of the spatial adaptation of the technical urban infrastructure need to be set on the agenda (examples are given in Table 3). The pure demographic aspect that a change of household structures and sizes arises, independent from growth or shrinkage, implies further changes in water and energy use [46].

Effects on Ecosystems

Turning to the positive side effects of shrinkage in inner city and peripheral areas – which arguably contribute to urban sustainability – demolition and resulting brownfields should be understood as a chance for ecological restoration and development of green networks in city regions [4]. [53] and [54] found a positive correlation between the amount of urban green and the habitat suitability of urban breeding birds (such as for the Green woodpecker *Picus viridis*). Generally, urban fallow lands (such as shown in Fig. 8) are seen as niches for rare specialist species [55]. The study by [54] reports particular high neighborhood densities of breeding birds in the old built-up housing areas of the inner parts of the city. Thus, demolished sites should be left partially open in order to develop long-term hotspots of urban biodiversity.

In order to measure biodiversity effects of shrinkage, a number of recently demolished sites allocated in a densely built-up and socialist prefabricated housing estates of the eastern German city of Leipzig had been

Landscape Planning/Design of Shrinking Landscapes. Table 3 Adaptation of infrastructure networks to shrinking or perforating contexts ([33]; adapted)

Form of adaptation	Land use and transportation impact
Increasing accessibility	Increase in traffic and road network demand
Reduction	Decrease in traffic and road network demand
Centralization	Decrease in traffic and road network demand
Decentralization (local networks)	Increase in traffic and road network demand
Temporal mobile structures	Optimization of spatial structures
New structures and substitution	No effects for spatial configuration but for total net consumption

Landscape Planning/Design of Shrinking Landscapes. Figure 8
Images of demolished sites within an old built-up residential area: a recently demolished site under spontaneous succession and two planted sites serving for transition and recreation purposes now

analyzed in terms of their spatial shape, configuration, and the resulting habitat quality for an open-land indicating bird species, Whitethroat (*Sylvia communis*). For the comparison of pre- and post-demolition status of about 50 sites, the following indicators have been used: Largest Patch Index (LPI) of open land uses, Edge Density (ED), Habitat Suitability Index (HSI), and Shannon Diversity Index (SHI). In doing so, LPI is defined as

$$LPI = \frac{\max\limits_{j=1}^{n}(a_{ij})}{A} * 100$$

where a is the area of single patches and A the total area. The edge density is

$$ED = \frac{\sum\limits_{k=1}^{m} e_{ik}}{A}(10,000)$$

where ED is edge density, A the total area, and e the edge vector. Finally, the Shannon diversity is formally according to [56]

$$SHDI = -\sum_{i=1}^{m} p_i \ln p_i$$

where p is the single patch. The HSI had been calculated using the approach of the ecological niche which is formalized the $\sum$ of cells with a certain probability of species presence [53, 57]. For calculation and mapping purpose, the *Biomapper* software tool was used [58].

The results of the study are shown in Fig. 9 [59]. Edge density and patch size are the variables that most benefit from selective, single house, or block demolition compared to only slight changes in Shannon diversity due to the uniform grasslands that emerged after demolition at many sites, particularly in the prefabricated peripheral districts. For species like the Whitethroat, demolition seems to offer an increase of its preferred open habitat structures (HSI values in Fig. 9).

However, general positive or negative effects of shrinkage for urban ecosystems and biodiversity are not verified yet through empirical studies. In particular residential vacancy, simple land abandonment (excluding a de-sealing) and perforation are not subsequently followed by positive effects for nature and ecosystems. On the contrary, inefficient solutions could lead to higher environmental impact and more land consumption in shrinking landscapes when, despite an existing urban brownfield, open land at the periphery becomes sealed [4]. Processes and forms of urban perforation are assumed to have the potential to considerably contribute to structural enrichment and an increase in edge densities [60]. They let one further think about a bringing back of nature to former densely populated and built urban centers. At least "wilderness ideas" [38, 61] in urban landscapes for recreational and educational purposes are in discussion among urban planners and landscape architects.

Shrinkage in terms of demolition and land use perforation has also effects for the water regulation flows in the city such as surface runoff and evapotranspiration since they create potentials for de-sealing [62]. [50] found for demolished and regreened sites in Leipzig

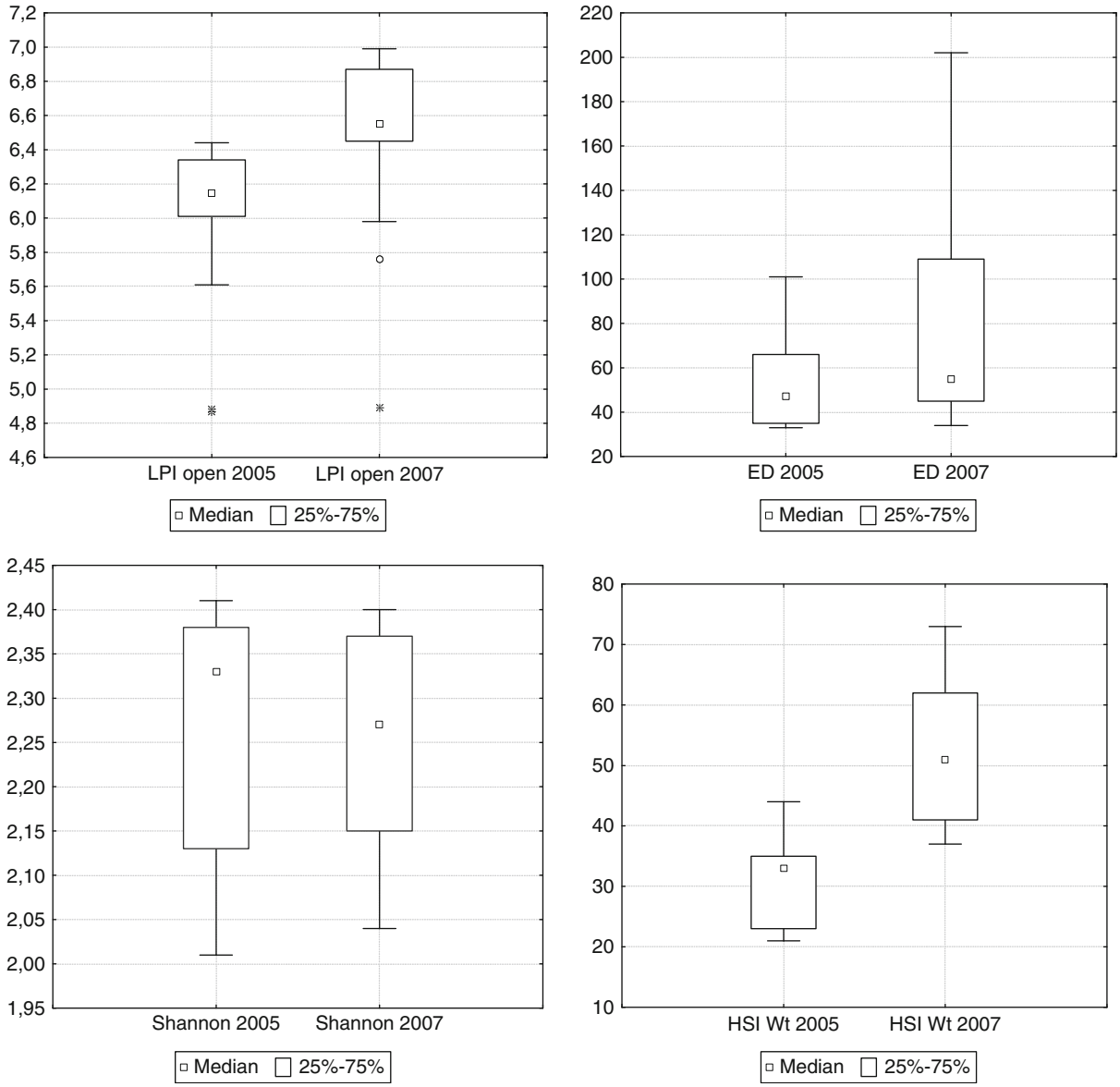

Landscape Planning/Design of Shrinking Landscapes. Figure 9
Largest Patch Index (LPI open) of open land uses such as park, allotment, courtyard, brownfield, wasteland, etc., Edge Density (ED), Shannon Diversity and Habitat Suitability Index (HSI) for a range of recently demolished sites in Leipzig – a comparison of the pre- (2005) and post-demolition (2009) status [59]

a decrease of the share of direct surface runoff and a higher water on-site percolation. The more the urban landscape gets perforated the higher the in situ water sink potential is.

Concerning carbon storage , shrinking cities are of particular interest: they have a high potential for urban reconstruction and new green space (also as brownfields) are abundant and development pressure is low [54]. Newly planted trees unquestionably sequester atmospheric CO_2 as they grow [63–65]. As promising results of a pilot case study by [54] impressively show, tree planting at demolition sites in shrinking cities can be viewed as one contribution to the many efforts that cities have to make in order to decrease their carbon emissions.

Landscape Planning/Design of Shrinking Landscapes. Table 4 Impact of planning policies on climate regulation indicators compared to values of 2000: affected areas [km^2] for the shrinking urban region of Leipzig [66]. Urban renewal policies in bold

Climate impact	Mining redevelopment	Urban renewal	Municipal development plans	Economic land take	Green corridors	Green ring around the city
f-evapotranspiration: no change; emissivity: higher	0.0	**0.0**	8.9	0.0	0.0	0.0
f-evapotranspiration: no change; emissivity: lower	0.0	**0.0**	14.7	1.1	177.0	110.3
f-evapotranspiration: higher; emissivity: no change	0.0	**0.0**	0.0	0.0	0.8	0.0
f-evapotranspiration: lower; emissivity: no change	0.0	**0.0**	0.1	0.0	0.0	0.0
f-evapotranspiration: higher; emissivity: lower	33.0	**6.5**	13.9	0.0	12.5	53.6
f-evapotranspiration: lower; emissivity: higher	0.0	**0.0**	48.5	17.0	15.9	0.9
f-evapotranspiration: higher; emissivity: higher	0.0	**0.0**	0.0	0.0	0.0	0.0
f-evapotranspiration: lower; emissivity: lower	0.0	**0.0**	0.1	0.0	0.4	0.0
No change	999.7	**1026.2**	946.6	1014.6	826.3	868.0

In more general terms, next to the sequestration of CO_2 urban green can also put shade trees on vacant land [2] or cools the air by evapotranspiration fluxes [66]. To measure the climate regulation potential of urban renewal and development policies, an emissivity index value can be used for each land use in order to show differences in thermal emissions between land uses. The f-value is an approximation for the evapotranspiration potential of a land use class and therefore for emitting latent heat rather than sensible heat [66]. Table 4 shows the positive climate regulation contribution of urban renewal policies in consequence of shrinkage: They provide a higher vapor content in the air and release less heat emissions from the urban surface.

Response to Shrinkage

Modes of Collaboration and Governance

To what extent can existing planning tools used in growing communities be adapted to be used in a shrinking environment? And, secondly, how do planners, policy makers, citizens, businesses, and others operate within a shrinking city, how do they conceptualize population decline, how do they manage the physical changes that result from shrinkage, and what can they do to plan more effectively for shrinkage? Shrinking cities might offer a paradigm shift from growth-centered planning to a more careful and place-based approach toward more livable cities [2]. But, does shrinking cities planning mean making them greener, more compact, and thus sustainable?

In a shrinking city, spatial planning strategies to deal with the simultaneousness of urban restructuring and population shrinkage lay a focus on enhancing the quality of life in the city as a way to retain residents. They further control activities consuming land in the urban fringe to prevent urban sprawl and to direct land development to the inner parts. The spatial focus of planning strategies for shrinking cities in Germany, for example, is diverse: Formal strategies are implemented at different administrative levels, that is, municipalities, the city, regions, and the federal state. Informal

strategies are frequently implemented at an intermediate level – larger than municipalities and smaller than regions. The same applies to inter-municipal cooperation, which, by definition, refers to aggregates of municipalities. There is a "gap" regarding formal planning strategies at the level of the urban landscape, which implies that well-rehearsed forms of decision-making by state actors are not prevalent here [67]. In addition to formal planning, governance – equal voice for all participants in decision-making – plays an increasing role for informal spatial planning [68], also and predominantly in urban regions. However, a sustainable future of a shrinking city can only be ensured through shared policies and planning that also involves the land owners and local entrepreneurs. Sustainable development of settlements also demands the expansion of regional cooperation across city boundaries. Wherever there are cities with excess vacant land, local entrepreneurs will attempt to extract value from such vacancy. However, local regulations, liability concerns, and the objections of nearby landowners prevent them from pursuing innovative temporary uses [2].

Shrinking cities have a range of opportunities to adapt their planning, also at very limited financial budgets: Outsourcing of urban green space maintenance, development of a more heterogeneous green network including a new complexity and disorder and the permission of more natural development. It is their chance to bring (less) people closer to nature and to involve private land owners into such programs. Strategies for integrated rural–urban development play an increasingly important role besides classic instruments, such as spatial development plans and zoning [69]. New media and formats such as planning games might facilitate an urban region's process of collectively tackling shrinkage. Models and scenarios make it easier to recognize and estimate land use potential and risks of shrinkage at an early stage [69], but they need to be accepted as communication platform by all participants, particularly local and regional stakeholders [70].

Ways of Implementation – The Pilot Case of Eastern Germany

Creating realistic visions for shrinkage is the main planning approach in eastern Germany, sponsored by the federal funding program "Urban Renewal East" (*in German* "Stadtumbau Ost"), which began in 2001 [2]. As consequence of the population decline, first of all the massive out-migration of the 1990s, eastern German cities are faced with emptying and devastated housing areas, unused infrastructure, and pattern of perforation. Urban policy makers are needed to find solutions to counteract the decline of the urban fabric and, what is more, to create urban livelihoods that "accept" shrinkage and partial vacancies as long-term phenomena. Thus, in the mid-1990s, planners started to talk about urban reconstruction and renewal realizing that prevailing urban structures did not meet the needs of a shrinking development (Fig. 10).

In this context, a set of nationally funded regeneration programs had been developed (Fig. 10): Whereas at the beginning of the 1990s "classical" programs, such as the Federal Program of Urban Renewal or WENG (a program dedicated to enhance the development of prefab housing estates) focusing on an encompassing approach of urban regeneration dominated, the situation changed after having supported the reconstruction of major parts of the eastern German core cities. The problem of a simultaneous emptying of the housing stock remained. Thus, in the late 1990s, reconstructed, old built-up housing estates were as same affected with vacancy as GDR-time prefabricated blocks.

In a second phase, urban planners initiated several new programs to find answers on this urban decline. Accordingly, "integrated programs" as a new approach in urban regeneration focusing not exclusively on the urban fabric but also on social, economic, and ecologic aspects were implemented. A couple of years ago, in 1999, the program "Social City" (*in German* Soziale Stadt) came into action foreseen to counteract the increasing social and spatial segregation as well as results of urban shrinkage and abandonment within eastern German cities. Currently, this program supports 390 initiatives in 260 German cities (www.sozialestadt.de; Fig. 10).

Set against this well-developed planning background for urban areas in the Germany after reunification, it became however clear that urban shrinkage needs specific interventions such as e.g., the opportunity of massive demolition in order to be regulated or steered (www.exwost.de). Consequently, in particular for the eastern part of Germany the intervention program "Urban Renewal East" had been

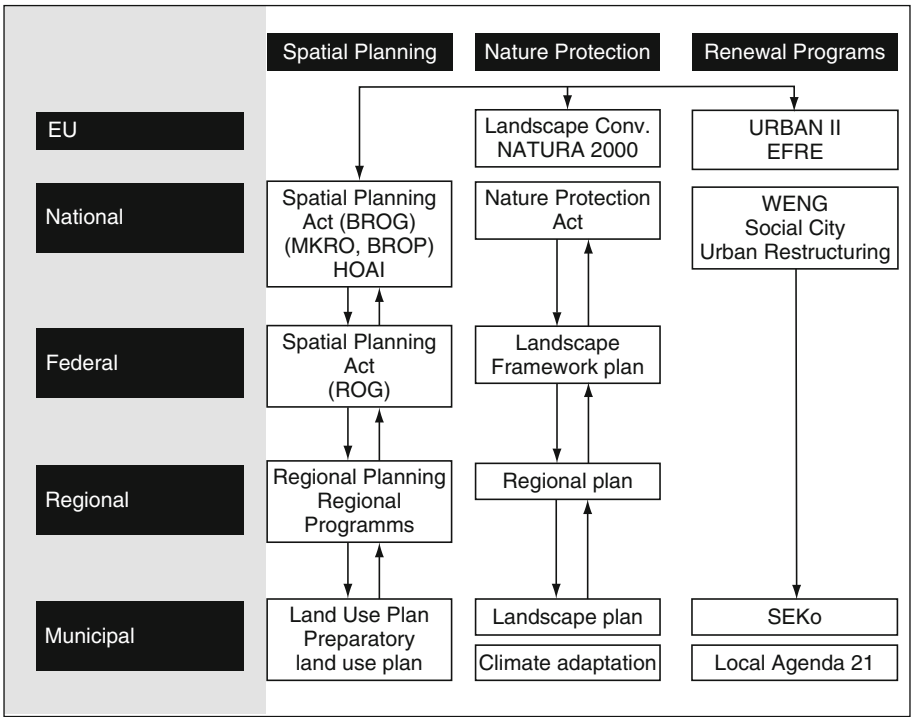

Landscape Planning/Design of Shrinking Landscapes. Figure 10
Spatial and landscape planning repertoire of Germany with respect to urban shrinkage and renewal. SEKo is the new integrated urban development plan for the city of Leipzig that acknowledges simultaneous shrinkage and growth processes

implemented in 2002. To be primarily a reaction on the enormous vacancy rates the urban renewal program predominantly focused on the consolidation of the housing market aiming at a balance between housing demand and supply which is nevertheless until recently not really given: in many districts of cities like Leipzig, Chemnitz, Zwickau, Halle, or Magdeburg, the supply of dwellings outweighs the demand by far. To support the municipal housing cooperatives as well as the private house owners being economically weakened by such high vacancies is a central goal of "Urban Renewal East." In doing so, it focuses on either up-valuation of neighborhoods or on dilapidation of vacant buildings (Fig. 10).

In this vein, three different strategies had been implemented in the city of Leipzig by urban administration: one to foster urban regeneration, the already mentioned initiative "Social City" based on a manifold scenery of subsidies and, the two European programs "URBAN II" and "EFRE" came to action but these are per se spatially up-divided across the urban area of Leipzig. Thus "URBAN II" focuses on the regeneration of the western part of the city being characterized by large housing estates of the Wilhelminian style, devastated factory buildings, and large brownfields. Activities of "EFRE" and the "Social City" support urban regeneration in the eastern part of the city. In terms of urban environment, ecology, and local livelihoods, both programs fund mainly actions to improve the urban quality of life, to assist in cultural and social beliefs, and support medium and small enterprises (Fig. 10). Recently, these strategies found entrance in the new integrated urban development plan SEKo, which had been established in 2009 and covers the entire city area.

Temporary Use of Brownfields – An Innovative City Intervention Strategy

As [2] argue, less regulation and more help for grassroots experimentation may provide large new opportunities for urban regeneration in shrinking cities.

One example is the temporary or interim use of vacant plots. Though temporary or interim use is not completely new (Berlin's Tiergarten after WWII, the 1st community gardens of Los Angeles, etc.), it was first employed as a formal city development strategy in the late 1990s in Germany [71]. Interim land use strategies are extolled as a cost-effective solution to fight urban blight and shrinkage. As examples in Leipzig, Berlin, and Basel have shown, interim uses have the potential to improve esthetics and perceptions of run-down areas, to increase the amount and diversity of green space opportunities and pedestrian routes, and to create new spaces for creative play and performance [71, 72], but they also have the potential to improve the environmental condition of vacant lots.

Perhaps because Leipzig was "the capital of housing vacancies" [73], it was one of the first East German cities to reorient its planning policy to confront shrinkage [3], and it did this with new district development plans, criteria for intervention intensities and priorities, innovative presentation forms, and marketing – "the perforated city" [34] and "more green, less density, greater individuality" [74] – and new planning tools like interim use.

Vacant plots of land growing wild with "weeds" are not pleasant to view for most people and contribute to negative images of neighborhoods. The situation in Leipzig was complicated by the fact that 80% of the vacant buildings and lots belong to private owners, 90% of whom live outside the city; this meant that the city had very few means with which to improve the situation [75].

Improvement of these infill sites necessitated some kind of authorization for property use. Since city acquisition of the plots could only be made in very special circumstances because of the strained municipal budget, and since expropriation is politically unpopular and in any case only possible in exceptional situations, an "authorization agreement" (*in German* Gestattungsvereinbarung) was developed as an informal planning tool to regulate limited term public use of private property while still maintaining the owner's building rights [76]. Advantages for the city include the activation of new green space for public use, connecting green space, and an assurance from the owner to ensure site maintenance, thereby improving quality of life and development attractiveness in the neighborhoods. For the owner, advantages include subsidized land clearance and development, property tax exemption for the duration of the contract, and a reduction of some running costs such as sewage or cleanup from vandalism [71].

So far, 134 public interim use agreements have been concluded for 235 plots totaling 165,905 m^2. When compared to the total area of the city's brownfields (1,942 plots totaling more than 7 million square meters), the scale of interim use agreement interventions seems small, but they are concentrated in three main intervention areas of the city, so in these neighborhoods, the impact is visible. At the program's beginning, contract periods could be for as little as 1 year, though the mean was around 8 years [76]. Now, the Saxon Urban Development Regulation has mandated a 10-year minimum contract period in order to ensure worthwhile use of state funds [71]. Despite this new restriction, interest has remained steady. Current owners under interim use contract often renew contracts because of the lack of city growth. In this sense, interim uses are increasingly becoming more permanent in nature. But what potentials and limitations does this strategy have, and how can these be measured suitably, taking into account both social and environmental factors?

[77] found that, first, interim use sites scored higher overall than their main alternative, recently demolished brownfields, especially on social criteria (i.e., accessibility, recreational interest, and use). Second, interim use sites had a much greater usage rate than other site types, especially by men. The most popular uses of interim use sites are to take shortcuts, to relax, to enjoy nature, and to walk dogs. Third, there was a wide consensus of site condition improvement over the last 6 years. Still, the most desired changes on the six sampled interim use sites are for more benches and better maintenance of the site, especially of dog litter. Fourth, most of the respondents did not know about the city's interim use strategy and do not recognize the sites as being a result of city intervention and development. In so far, it can be hypothesized that public acceptance and support for interim use might be strengthened with increased communication about the strategy and its potential as an urban planning

tool [78]. This could also strengthen use by residents and willingness to participate in site development.

Future Directions

Urban shrinkage is an upcoming phenomenon cities and urban regions face, particularly in the developed world. This entry dealt with the drivers, processes, and patterns behind. Discussing the socio-demographic, land use, and ecological dimension of urban shrinkage, the entry showed the problems and threats related to population decline and economic blight. However, concerning sustainability, urban shrinkage also bears potentials and opportunities.

Urban shrinkage could allow a resurgence of nature into inner cities that are densely populated and have been built up "for ages." In this vein, ideas regarding urban wilderness for recreational and educational purposes are of concern among urban planners and landscape architects who are confronting this shrinkage. The eastern German city of Leipzig, quite a model city, has made the novel suggestion of creating urban greenery in the form of temporary green spaces at core city demolition sites as a kind of planned alternative and spontaneous and ruderal nature on former brownfields as a kind of unplanned alternative. Particularly, green spaces developed from inner-city brownfields represent "flagships" or "experimental fields" that serve as models for future greening endeavors to improve both local biodiversity and human livelihoods. Besides total demolition of houses, shrinkage also leads to a deconstruction of multistory housing stock in the form of a transition toward more spacious housing and living conditions in densely urbanized environments: bigger apartments and integrated patios and terraces, as well as higher shares of urban green and landscape within the neighborhood.

Doubtless, there is considerable potential for social, residential, and ecological improvement in shrinking cities, which, through exploring opportunities as discussed above, might attract new residents for a longer period of time and keep local dwellers in the city, instead of having them choose the detached-house alternative. This opens a new pathway to counteract urban sprawl and thus contributing to urban sustainability.

Acknowledgments

I would like to thank the editor-in-chief of the Encyclopedia for Sustainability Science and Technology, Robert A. Meyers, the Springer Editors, namely, Julia Körting, and my colleague Martin Volk for his useful comments on an earlier version of the manuscript.

Bibliography

Primary Literature

1. Oswalt P, Rieniets T (2006) Atlas of shrinking cities. Hatje Cantz, Ostfildern
2. Blanco H, Alberti M, Olshansky R et al (2009) Shaken, shrinking, hot, impoverished and informal: emerging research agendas in planning. Prog Plan 72:195–250
3. Jessen J (2006) Urban renewal – a look back to the future. The importance of models in renewing urban planning. Ger J Urban Stud 45(1):1–17
4. Haase D (2008) Urban ecology of shrinking cities: an unrecognised opportunity? Nat Culture 3:1–8
5. Rieniets T (2009) Shrinking cities: causes and effects of urban population losses in the twentieth century. Nat Culture 4(3):231–254
6. Kabisch N, Haase D (2010) Diversifying European agglomerations: evidence of urban population trends for the 21st century. Population, space and place (in press)
7. Mykhnenko V, Turok I (2008) East European cities – patterns of growth and decline, 1960–2005. Int Plann Stud 13(4): 311–342
8. Rink D, Haase A, Bernt M (2009) Specification of working model. Shrink smart deliverable (unpublished)
9. Haase D, Kabisch N (2010) The endless city: on the growing mismatch of population development and land consumption. Global environmental change
10. Young OR et al (2006) The globalization of socio-ecological systems: an agenda for scientific research. Global Environ Change 16(3):304–316
11. Nuissl H, Haase D, Wittmer H, Lanzendorf M (2008) Impact assessment of land use transition in urban areas – an integrated approach from an environmental perspective. Land Use Policy 26:414–424
12. Kasanko M, Barredo JI, Lavalle C, McCormick N, Demicheli L, Sagris V, Brezger A (2006) Are European cities becoming dispersed?: a comparative analysis of 15 European urban areas. Landsc Urban Plann 77(1–2):111–130
13. EEA (European Environmental Agency) (2006) Urban sprawl in Europe – the ignored challenge. EEA Report 10/2006. Copenhagen
14. MEA (Millennium Ecosystem Assessment) (2005) Ecosystems and human wellbeing: synthesis. Island Press, Washington, DC

15. UNESA (United Nations Economic & Social Affairs) (2007) World urbanisation prospects: the 2007 revision. United Nations, New York
16. Neuwirth R (2005) Shadow cities: a billion squatters, a new urban world. Routledge, London/New York
17. Scott AJ (1988) Metropolis: from the division of labour to urban form. University of California Press, Berkley, CA
18. Krishnaswamy B, Than S, Davison M, Varghese C, Venkataraman K, Anand L (2008) Ageing in India. Ageing Int (2008) 32:258–268
19. UNFPA China Office (2006) Population ageing in China – facts and figures
20. Cullingworth JB, Caves R (2008) Planning in the USA – policies, issues and processes. Routledge, London
21. Berg L, Drewett R, Klaassen LH, Rossi A, Vijverberg CHT (1982) Urban Europe: a study of growth and decline. Pergamon Press, Oxford
22. Lever WF (1993) Reurbanisation: the policy implications. Urban Stud 30:267–284
23. Garreau J (1991) Edge city: life on the new frontier. Doubleday, New York
24. Harvey D (2006) Spaces of global capitalism: towards a theory of uneven geographical development. Verso, London
25. Amin A, Thrift N (1994) Globalization, institutions and regional development in Europe. Oxford University Press, Oxford
26. Storper M, Manville M (2006) Behaviour, preferences and cities: urban theory and urban resurgence. Urban Stud 43: 1247–1274
27. Müller B, Siedentop S (2004) Growth and shrinkage in Germany – trends, perspectives and challenges for spatial planning and environment. Ger J Urban Stud 43:14–32
28. Kabisch N, Haase D, Haase A (2009) Evolving reurbanisation? Spatio-temporal dynamics exemplified at the eastern German city of Leipzig. Urban Stud 1–24
29. Turok I, Mykhnenko V (2008) Resurgend European cities. Urban Res Practice 1(1):54–77
30. Pallagst KM (2007) Das Ende der Wachstumsmachine. Berliner Debatte Initial 18(1):4–13
31. Bürkner H-J (2003) Schrumpfung, städtische Rekonstruktion und Regenerierung – sozialräumliche Perspektiven. IRS-aktuell 40:1–3
32. Haase D, Seppelt R, Haase A (2007) Land use impacts of demographic change – lessons from eastern German urban regions. In: Petrosillo I, Müller F, Jones KB, Zurlini G, Krauze K, Victorov S, Li B-L, Kepner WG (eds) Use of landscape sciences for the assessment of environmental security. Berlin, Springer, pp 329–344
33. Bernt M (2009) Partnerships for demolition: the governance of urban renewal in East Germany's shrinking cities. Int J Urban Regional Res 33(3):754–769
34. Lütke-Daldrup E (2001) Die perforierte Stadt. Eine Versuchsanordnung. Stadtbauwelt 150:40–45
35. Haase D, Kabisch N, Haase A, Kabisch S, Rink D (revisions) Actors and factors in land use simulation – the challenge of urban shrinkage. Environ Model Software
36. Häußermann H, Glock B (2004) New trends in urban development and public policy in Eastern Germany: dealing with the vacant housing problem on the local level. Int J Urban Regional Res 28:919–930
37. Schwarz N, Haase D, Seppelt R (2009) Omnipresent sprawl? A review of urban simulation models with respect to urban shrinkage. Environ Plann 37:265–283
38. Rink D (2009) Wilderness: the nature of urban shrinkage? The debate on urban restructuring and restoration in Eastern Germany. Nat Culture 3(1):275–292
39. City of Leipzig (2004) Leipzig 2030. Report
40. Kabisch S, Haase A, Haase D (2006) Beyond growth – urban development in shrinking cities as a challenge for modeling approaches. In: Voinov A, Jakeman A, Rizzoli A (eds) Proceedings of the iEMSs third biennial meeting: "Summit on Environmental Modelling and Software". International Environmental Modelling and Software Society, Burlington, USA, July 2006. CD ROM. Internet: http://www.iemss.org/iemss2006/sessions/all.html, ISBN 1-4243-0852-6 978-1-4243-0852-1
41. Liu J, Daily GC, Ehrlich P, Luck GW (2003) Effects of household dynamics on resource consumption and biodiversity. Nature 421:530–532
42. Keilman N (2003) The threat of small households. Nature 421:489–490
43. Dorling D, Rigby J, Wheeler B, Ballas D, Thomas B, Fahmy E, Gordon D, Lupton R (2007) Poverty, wealth and place in Britain, 1968 to 2005. Joseph Rowntree Foundation, York
44. Runge J, Kłoskowski F, Runge A (2003) Conditions and trends of social-economic changes of Katowice region. Bull Geography (Socio-Economic Series) 2:85–101
45. Bundesinstitut für Bau-, Stadt- und Raumforschung (BBSR; Ed.; 2009) Raum-ordnungsprognose 2025/2050. Bevölkerung, private Haushalte, Erwerbspersonen. Bundesamt für Bauwesen und Raumordnung (BBR), Berichte 29, BonnCity of Leipzig (2002). Lücken in der Stadt: Interimslösungen durch Zwischennutzung von Baulücken in Stadterneuerungsgebieten. Amt für Stadterneuerung und Wohnungsbauförderung (ASW): Leipzig. http://www.leipzig.de/imperia/md/content/64_stadterneuerung/Luecken_Flyer.pdf
46. Koziol M (2004) The consequences of demographic change for municipal infrastructure. Ger J Urban Stud 44(1), see: http://www.difu.de/index.shtml?/publikationen/dfk/e-n/04_1/welcome.shtml
47. Endlicher W, Langner M, Hesse M, Mieg HA, Kowarik I, Hostert P, Kulke E, Nützmann G, Schulz M, van der Meer E, Wessolek G, Wiegand C (2007) Urban ecology – definitions and concepts. In: Langner M, Endlicher W (eds) Shrinking cities: effects on urban ecology and challenges for urban development. Peter Lang Verlag Frankfurt/Main, S, New York, pp 1–15
48. Hannemann C (2004) Die Transformation der sozialistischen zur schrumpfenden Stadt. In: Siebel W (ed) Die europäische Stadt. Frankfurt. a. Main, pp 197–207
49. Schiller G, Siedentop S (2005) Infrastrukturfolgekosten der Siedlungsentwicklung unter Schrumpfungsbedingungen

[Follow-up costs of settlement development for infrastructure under conditions of shrinkage]. Disp 160:83–93
50. Schetke S, Haase D (2008) Multi-criteria assessment of socio-environmental aspects in shrinking cities. Experiences from Eastern Germany. Environ Impact Assess Rev 28:483–503
51. Moss T (2008) 'Cold spots' of urban infrastructure: 'Shrinking' processes in eastern Germany and the modern infrastructural ideal. Int J Urban Regional Res 32(2):436–451
52. Schwarz N, Haase D (2010) Urban shrinkage: a vicious circle for residents and infrastructure? – coupling agent-based models on residential location choice and urban infrastructure development. Paper for the iEMSs 2010, Ottawa
53. Mehnert D, Haase D, Lausch A, Auhagen A, Dormann CF, Seppelt R (2005) Bewertung der Habitateignung von Stadtstrukturen unter besonderer Berücksichtigung von Grün- und Brachflächen am Beispiel der Stadt Leipzig. Naturschutz und Landschaftsplanung 2:54–64
54. Strohbach M, Haase D, Kabisch N (2009) Birds and the city – urban biodiversity, land-use and socioeconomics. Ecol Soc 14(2):31
55. Kowarik I, Körner S (eds) (2005) Wild urban woodlands. Springer, Berlin, Heidelberg
56. Forman RT (1995) Land mosaics: the ecology of landscapes and regions. Cambridge University Press, Cambridge
57. Hirzel A, Hausser J, Chessel D, Perrin N (2002) Ecological-niche factor analysis – how to compute habitat-suitability maps without absence data? Ecology 83:2027–2036
58. Hirzel A, Hausser J, Perrin F (2001) Biomapper 2.0. Laboratory for conservation biology, Institute of Ecology, University of Lausanne, http://www.unil.ch/biomapper/enfa.html, 05.08.2003
59. Haase D, Schetke S (2010) Potential of biodiversity and recreation in shrinking cities: contextualisation and operationalisation. In: Müller N, Werner P, Kelcey JG (eds) Urban Biodiversity and Design. Blackwell Academic Publishing "Conservation Science and Practice Series" No.7, pp 518–538
60. Bolund P, Hunhammar S (1999) Ecosystem services in urban areas. Ecol Econ 29(2):293–301
61. Rink D (2005) Surrogate nature or wilderness? Social perceptions and notions of nature in an urban context. In: Kowarik I, Körner S (eds) Wild urban woodlands. Springer, Berlin, Heidelberg, pp 67–79
62. Haase D (2009) Effects of urbanisation on the water balance – a long-term trajectory. Environ Impact Assess Rev 29:211–219
63. Nowak DJ, Crane DE (2002) Carbon storage and sequestration by urban trees in the USA. Environ Pollut 116(3):381–389
64. Rowntree RA, Nowak DJ (1991) Quantifying the role of urban forests in removing atmospheric carbon dioxide. J Arboric 17(10):269–275
65. Zhao M, Kong Z-H, Escobedo FJ, Gao J (2009) Impacts of urban forests on setting carbon emissions from industrial energy use in Hangzhou, China. J Environ Manag (in press)
66. Schwarz N, Bauer A, Haase D (2010) Assessing climate impacts of local and regional planning policies – quantification of impacts for Leipzig (Germany). Environ Impact Assess Rev (in press)
67. Sinn A, Haase D, Walde A (2008) Analysis of regional spatial planning and decision making strategies and their impact on land use in the urban fringe. Deliverable 3.3.6. for the EU project PLUREL (www.plurel.net), internally used document
68. Le Galès P (1998) Regulations and governance in European cities. Int J Urban Regional Res 22(2):482–506
69. Haase D et al (2009) Spatial development in the Leipzig-Halle region, Brochure at www.plurel.net
70. Volk M, Lautenbach S, van Delden H, Newham LTH, Seppelt R (2009) How can we make progress with decision support systems in landscape and river basin management? Lessons learned from a comparative analysis of four different decision support systems. Environ Manage. doi:10.1007/s00267-009-9417-2
71. Heck A, Will H (2007) Interim use: opportunity for new open-space quality in the inner city – the example of Leipzig. Ger J Urban Stud 46(1)
72. Gstach D (2007) Temporary open spaces as incubator for social integration. Presented at the 45th international making cities livable conference, Portland, OR, 10–14 June 2007. Retrieved from http://www.livablecities.org/Gstach_Doris.pdf
73. Wiest K, Zischner R (2006) Upgrading old housing areas in East German inner cities – processes and development paths in Leipzig. Ger J Urban Stud 45(1)
74. Stadt Leipzig (2002) Lücken in der Stadt: Interimslösungen durch Zwischennutzung von Baulücken in Stadterneuerungsgebieten. Amt für Stadterneuerung und Wohnungsbauförderung (ASW): Leipzig. Retrieved from http://www.leipzig.de/imperia/md/content/64_stadterneuerung/Luecken_Flyer.pdf
75. Blumner N (2006) Planning for the unplanned: tools and techniques for interim use in Germany and the United States. German Institute of Urban Affairs occasional papers series. German Institute of Urban Affairs, Berlin. http://www.difu.de/english/occasional/06-blumner_planning.pdf, 26 Oct 2008
76. Heck A (2007) Leipziger Osten-Gestattungsvereinbarungen: Qualitätssicherung bei Zwischennutzungen. Leipzig: City of Leipzig- Amt für Stadterneuerung und Wohnungsbauförderung
77. Lorance ED, Haase D (2010) Creative intervention in a dynamic city: a sustainability assessment of an interim use strategy for brownfields in Leipzig, Germany. Landsc Urban Plann
78. Bontje M (2001) Dealing with deconcentration: population deconcentration and planning response in polynucleated urban regions in north-west Europe. Urban Stud 38(4): 769–785

Books and Reviews

Oswalt P, Rieniets T (2006) Atlas of shrinking cities. Ostfildern, Hatje Cantz
Nature and Culture Special Feature 3(1), 2009

Large-Scale Ocean Circulation: Deep Circulation and Meridional Overturning

Stephen R. Rintoul
Antarctic Climate and Ecosystems Cooperative Research Centre, Wealth from Oceans National Research Flagship, CSIRO Marine and Atmospheric Research, Hobart, TAS, Australia

Article Outline

Glossary
Definition of the Subject
Introduction
Deep Water Masses and Circulation
An Observing System for the Deep Ocean and Overturning Circulation
Future Directions
Acknowledgments
Bibliography

Glossary

Antarctic bottom water A dense water mass formed near the Antarctic continental margin that spreads northward to ventilate the abyssal ocean.

Argo floats Autonomous profiling floats that drift with ocean currents at 1–2 km depth and periodically measure temperature and salinity while rising to the sea surface, where the data is transferred by satellite.

Barotropic The depth-independent component of ocean currents. Direct current measurements are needed to determine the barotropic flow.

Baroclinic The depth-dependent component of ocean currents. The baroclinic flow can be estimated from measurements of ocean density.

Deep western boundary current Strong deep flows intensified along the western boundary of the basins.

Eddy The small-scale, time-variable component of the ocean circulation (also mesoscale eddy).

Ekman transport Wind-driven transport of the surface layer of the ocean to the right (left) of the wind in the northern (southern) hemisphere.

Geostrophic flow The large-scale flow of the oceans is in geostrophic balance, where horizontal pressure gradients are balanced by the Coriolis force.

Glider Like an Argo float with wings, an autonomous instrument that varies its buoyancy allowing it to move both vertically and horizontally, measuring water properties.

Hydrographic sections Ship transects along which measurements are made of seawater properties (e.g., temperature, salinity, carbon, nutrients).

Meridional In the north–south direction.

Meridional overturning circulation A basin-integrated view of the net north–south flow in the ocean basins.

North Atlantic deep water Deep water formed in high latitudes of the North Atlantic that spreads to the south in a deep western boundary current.

Ocean conveyor belt A highly simplified conceptual representation of the large-scale overturning circulation of the oceans.

Overturning circulation A global-scale network of ocean currents consisting of sinking of dense water in a small number of deep water formation regions and a compensating return flow of water in the upper ocean.

Potential vorticity A property of a fluid related to its rotation rate and stratification, which is approximately conserved by the large-scale ocean circulation. Analogous to angular momentum.

Sverdrup A unit of the volume of water carried by ocean currents (1 Sv = 10^6 m^3 s^{-1}).

Thermohaline circulation A term sometimes used as a synonym for the overturning circulation, or more specifically the portion of the overturning circulation driven by exchange of heat and moisture (i.e., thermohaline forcing) at the sea surface.

Ventilation The transfer of surface waters to the interior ocean, resulting in renewal of oxygen levels and other properties of the subsurface ocean.

Water mass A volume of the ocean with similar water mass properties.

Water mass formation The process by which surface water acquires a characteristic set of water mass properties through air–sea interaction, and transfers these properties into the ocean interior when the water mass sinks.

Zonal The east–west direction.

Definition of the Subject

Roughly half the world ocean volume lies below 2,000 m depth. This deep half of the ocean is cold (<3°C), indicating that the abyssal ocean is filled with waters that sink in high latitudes, where cold surface waters are found [1]. The deep ocean circulation transports the cold waters that sink in the polar regions throughout the deep ocean basins. The transfer of surface water to the deep ocean must be balanced by an inflow of water in the upper ocean to the deep water formation regions, to conserve mass. The result is an "overturning circulation ," in which the export of cold deep waters from the source regions is balanced by a return flow of warmer water in the upper ocean. The large temperature contrast between the upper and lower limbs of the overturning circulation makes this flow pattern an efficient means of transporting heat. The large-scale overturning circulation is the primary means by which the ocean stores and transports quantities of relevance to the Earth's climate system and biogeochemical cycles, including heat, freshwater, carbon, and nutrients. The evolution of climate is therefore influenced strongly by the overturning circulation.

The deep ocean, once thought to be largely quiescent, is now recognized to include energetic flows in many locations. The classical description of the deep ocean circulation includes deep boundary currents along the western boundaries of ocean basins, and quieter flows in the ocean interior. Observations from long-term moorings and deep floats have illustrated a more dynamic deep ocean environment, with energetic variability observed at a wide range of space and timescales, including narrow jets, eddies, and recirculating gyres.

The deep and overturning circulations are difficult to observe with existing tools. Most of the knowledge of deep currents has been inferred from the distribution of properties measured along hydrographic transects occupied by ships. The coverage of the deep ocean by full-depth hydrographic sections remains sparse in space and time. In addition, the property distributions reflect the integrated response to a combination of advective and diffusive processes and their interpretation in terms of deep circulation can be ambiguous. Direct measurements of deep currents, for example from current meter moorings, are even less common. The deep ocean circulation, therefore, remains largely unobserved. However, new tools are now making it feasible to obtain sustained measurements of the deep ocean.

Introduction

The conceptual framework developed by Stommel [2] still guides present thinking about the nature of the deep ocean circulation. Deep water that sinks in the polar regions of the ocean must flow away from the source regions. Stommel recognized that on a rotating earth these deep currents will be intensified along the western boundary of the ocean basins, forming "deep western boundary currents" (DWBCs). The sinking in the deep water formation regions was presumed to be balanced by weak upwelling distributed uniformly over the rest of the global ocean. The "stretching" of water columns produced by this upwelling requires that fluid must move poleward in the ocean interior to conserve potential vorticity. Stommel and Arons [3, 4] used these concepts to map the expected circulation pattern in the deep ocean, consisting of concentrated deep flows along the boundary of each basin and weak poleward flow in the interior (Fig. 1).

Both the upwelling and the interior flow are too weak to measure directly. Efforts to test this model of the deep circulation have therefore focused on measurements of the deep western boundary currents [5]. Swallow and Worthington [6, 7] used neutrally buoyant floats to confirm the presence of a deep southward flow along the western boundary of the North Atlantic. Warren and others used measurements of water properties collected by ships and direct velocity measurements from current meter moorings to identify DWBCs in each of the ocean basins [8–10]. In particular, the fact that the DWBCs carry waters that have recently been in contact with the atmosphere, and hence are rich in gases like oxygen and chlorofluorocarbons, means that tracer measurements provide a powerful tool for mapping the deep circulation.

In the modern ocean, deep water is only formed in a few locations in the high-latitude North Atlantic and over the Antarctic continental shelf. The density of seawater depends on both temperature and salinity. To sink from the sea surface to the deep ocean, surface

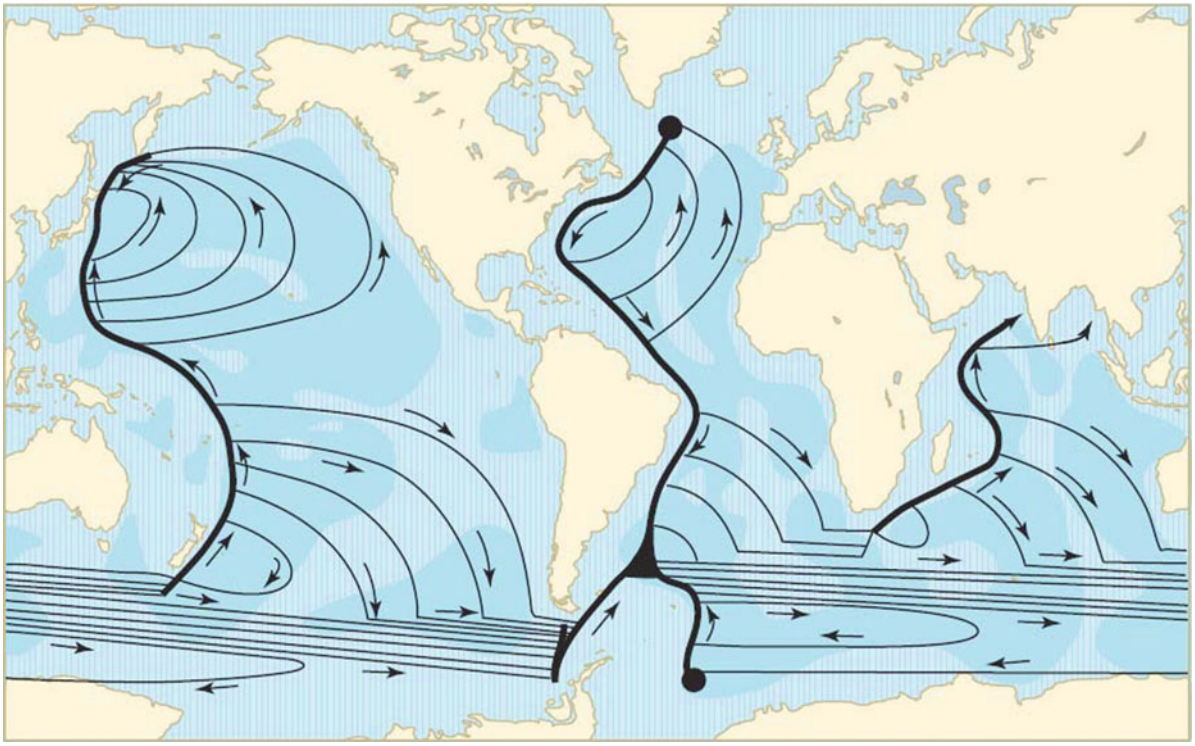

Large-Scale Ocean Circulation: Deep Circulation and Meridional Overturning. Figure 1
The abyssal circulation according to Stomme's model [2]. Sources of deep water in the northern North Atlantic and Antarctica are denoted by *black dots*. These water masses are carried away from the source regions by a network of deep western boundary currents that feed weak poleward flows in the interior of each ocean basin (Reprinted from [4], as modified by [56], with permission)

waters must become sufficiently cold and salty to be denser than the water below. The surface waters in the high-latitude North Pacific are so fresh that even when cooled to the freezing point, they remain too buoyant to sink [11]. Even in the North Atlantic and the Southern Ocean, deep water is only formed in a few particular regions where air-sea heat loss and the release of brine during sea ice formation result in a sufficient increase in density to cause surface waters to sink.

The flow of deep water away from the source regions is balanced by a return flow of warmer, lighter water in the upper ocean. These counter flows, linked by formation of dense water at high latitude, form an overturning cell. The northward transport of warm water in the upper ocean and compensating southward transport of cold water at depth results in a poleward transport of heat in the Atlantic basin. The large temperature contrast between the upper and lower limb of the overturning makes this circulation pattern an efficient means of transporting heat. In fact, at midlatitudes the ocean and atmosphere make roughly equal contributions to the poleward redistribution of heat absorbed in the tropical regions. The overturning circulation is also an important player in the biogeochemical cycles of carbon, nutrients, and other properties.

Various terms have been used to refer to the overturning circulation . Because deep water formation depends on density, and hence on temperature and salinity, the circulation is often referred to as the thermohaline circulation. However, as discussed below, it is not clear that the overturning is driven solely or primarily by the exchange of heat and moisture and so the term "thermohaline" is potentially misleading. In addition, the phrase has been used by many authors to mean different things, adding to the confusion [12].

In the Atlantic, the term "meridional overturning circulation (MOC)" is commonly used. However, the global-scale overturning circulation involves zonal as well as meridional flows, and the zonally averaged perspective inherent in the term MOC is itself potentially misleading. Therefore, the more general term overturning circulation is used here.

Another term, the "great ocean conveyor belt," was introduced by Wally Broecker [13, 14]. He highlighted the link between glacial cycles and variations in the strength of the overturning circulation. In particular, the addition of freshwater from melting continental ice sheets during the transition from glacial to interglacial conditions made surface waters in the North Atlantic too buoyant to sink, slowing the heat transport by the ocean conveyor, and cooling northern hemisphere climate. The switching on and off of the conveyor was linked to temperature changes in Greenland as large as 10°C over periods as short as a decade or two. Broecker's work highlighted the role of the "ocean conveyor" in global climate and renewed interest in the forcing of the circulation and its sensitivity to changes in forcing (in particular, freshwater input).

Broecker's "conveyor belt" picture was intended to serve as a logo or metaphor for the much more complex, three-dimensional, and time-variable circulation now commonly referred to as the overturning circulation, rather than as a realistic depiction of the flow. The actual flow paths involved in the global overturning circulation are much more complex, including narrow boundary currents, recirculation gyres, small-scale eddies, and jets. The deep circulation is steered by the topography of the seafloor and can also be influenced by the deep expression of circulation features in the upper ocean, such as boundary currents and eddies.

The large capacity of the ocean to store heat has a significant influence on climate. For example, more than 93% of the extra heat energy stored by the Earth system over the last 50 years is found in the ocean [15, 16]. The extra heat stored in the ocean has caused a rise in sea level, as a consequence of thermal expansion of the water column. Most of the extra heat stored in the ocean has accumulated in the upper 700 m. However, there is increasing recognition that the deep ocean makes a significant contribution to ocean heat storage and sea-level rise [17]. Accounting for the contribution of the deep ocean is necessary to explain the observed record of past sea-level rise (e.g., [18]) and to close the overall energy budget of the earth [17]. In addition, the warming projected by climate models for a given level of greenhouse gas forcing (called the climate sensitivity) is sensitive to the amount and depth of ocean heat storage [19]. Observations of the deep ocean are therefore needed to improve climate projections and to understand changes in sea level and the planetary energy budget.

Progress in understanding the deep circulation has been slowed by the technical challenge of observing the deep ocean. While new instruments like Argo profiling floats have revolutionized the ability to observe the upper 2 km of the ocean, providing the first year-round, broad-scale measurements of the ocean, no equivalent yet exists for the deep ocean. Deep ocean observing systems still rely heavily on traditional oceanographic platforms like ships and moorings. Because research vessels and long-term deep water moorings are expensive, the spatial and temporal coverage of deep ocean observations remains very limited. The deep ocean is now recognized to be more energetic and to include flows on smaller spatial scales than once believed, characteristics that increase the challenge of observing the deep circulation and its variability.

Deep Water Masses and Circulation

Sources of Deep and Bottom Water

To sink from the sea surface to the deep ocean, surface waters must become sufficiently dense, hence cold and/or salty. These conditions are met in only a handful of places in the present day ocean. Warm, saline waters move north in the upper layers of the Atlantic Ocean, gradually losing heat to the atmosphere, until ultimately sinking in the Norwegian, Greenland, and Iceland seas. These dense waters spill through gaps in the ridge system isolating the northern seas from the North Atlantic. Mixing with ambient waters during the descent into the deep North Atlantic increases the volume and modifies the properties of the dense overflows. Deep convection in the Labrador Sea produces somewhat lighter and warmer water which contributes to the deep waters in the basin. Collectively these dense waters supplied to the basin are known as North Atlantic Deep Water (NADW).

An even denser water mass, known as Antarctic Bottom Water (AABW), is formed in several locations around the margin of Antarctica. Heat lost to the atmosphere cools the ocean and, if the sea temperature reaches the freezing point of about −1.8°C, results in the formation of sea ice. Salty brine released when sea ice forms increases the density of the underlying water and makes an important contribution to the formation of dense shelf waters. As the dense waters flow off the shelf and sink into the deep ocean, they entrain about three times their volume of ambient waters [20]. The mixture of dense shelf waters and entrained fluid forms AABW. The primary sources of AABW are the Weddell Sea in the Atlantic sector, the Ross Sea in the Pacific sector, and the Adélie/Wilkes Land coast south of Australia [20–22].

NADW and AABW are examples of water masses, volumes of water with similar physical and chemical properties, reflecting a common origin. Water masses acquire their characteristic properties (e.g., temperature, salinity, and dissolved gas concentrations) through exchange between the surface ocean and the atmosphere. When water masses sink from the sea surface, they carry these characteristic properties with them into the ocean interior. These properties gradually evolve as the water masses are carried away from the source regions by ocean currents, as a result of mixing with water masses with different characteristics, but mixing is relatively weak in the ocean and water mass properties tend to be retained for long distances. Maps of water properties can thus be used to trace the spreading paths of water masses. In fact, given the difficulty of directly observing deep ocean currents, much of what is known about the deep circulation has been inferred from the distribution of water mass properties.

For example, surface waters in contact with the atmosphere are rich in dissolved gases like oxygen and chlorofluorocarbons (CFCs). The distribution of oxygen and CFC reflects the flow paths of deep water away from the source regions. Figure 2 shows the distribution of CFC-11 in the North Atlantic, illustrating the spreading pathway of the recently ventilated North Atlantic Deep Water [23]. At 24°N in the Atlantic, high CFC concentrations are observed in the deep ocean in the western basin, with the highest values observed adjacent to the boundary. A map of the inventory of CFC-11 in the NADW shows a plume of high CFCs spreading southward along the western boundary from the deep water formation regions in the Greenland –Iceland-Norwegian and Labrador Seas (Fig. 2b). Figure 3 shows a similar plot for the Southern Ocean, illustrating the three main sources of Antarctic Bottom Water in the Weddell and Ross Seas and the Adélie/Wilkes Land coast and the system of boundary currents exporting AABW to lower latitudes [20]. As seen in the North Atlantic, the highest concentrations are observed along the western boundary of each ocean basin. NADW and AABW supply roughly equal amounts ($10 - 15 \times 10^6$ m^3 s^{-1}) of dense water to the deep ocean [24] and AABW occupies roughly twice the volume of NADW [25].

No dense water is formed in the northern Indian and Pacific basins. The north Indian Ocean is limited to relatively low latitudes and so strong cooling of the ocean does not occur there. The Pacific extends to high latitudes and enough heat is lost to freeze the sea surface in winter. However, the surface waters of the Pacific are so fresh that even when cooled to the freezing point they are too buoyant to sink into the deep ocean [11]. These basins are therefore ventilated from the south, by a mixture of NADW exported from the Atlantic and AABW formed in the Southern Ocean, called Circumpolar Deep Water (CDW) [26]. This can be seen clearly in the distribution of oxygen in the deep ocean in these basins. High oxygen values spread northward from the Southern Ocean at 4,000 m depth in the Pacific, with the strongest penetration seen to the east of the large bathymetric obstacle imposed by the Tonga–Kermadec Ridge (Fig. 4). Oxygen values are low in the North Pacific and spatial gradients are small, indicating relatively weak flow there. The oxygen distribution at 33°S in the Indian Ocean shows that the lowest oxygen values are observed at mid-depth, sandwiched between the well-ventilated upper ocean waters that have been in recent contact with the atmosphere and relatively oxygen-rich deep waters spreading northward into the basin along the western sides of the deep basins (Fig. 5).

Deep Ocean Circulation

The distribution of water mass properties in the deep ocean reflects the formation and spreading of dense water formed at high latitudes in the North Atlantic and Southern Oceans. More specifically, the property

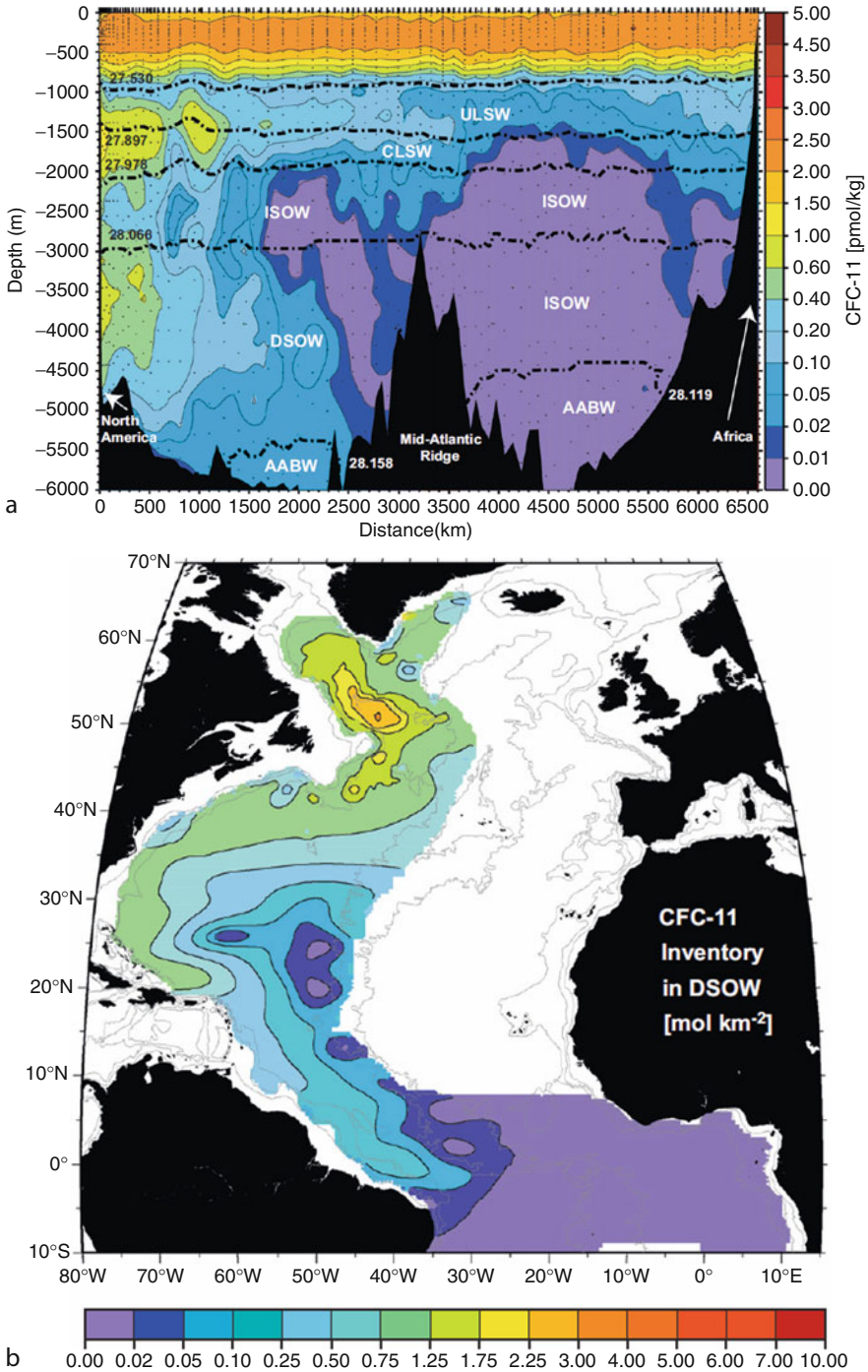

Large-Scale Ocean Circulation: Deep Circulation and Meridional Overturning. Figure 2
(**a**) Vertical section of chlorofluorocarbon – 11 (CFC-11, [pmol kg^{-1}]) in the North Atlantic at 24°N. The initials indicate different water masses; *dashed lines* indicate surfaces of constant density. The neutral density surfaces defining the water mass boundaries are plotted as bold *dashed lines*. (**b**) The inventory of CFC-11 (molkm_2) in the density layer corresponding to dense overflow waters exported from the Greenland–Iceland–Norwegian Seas through the Denmark Straits (DSOW) (From [23], used with permission)

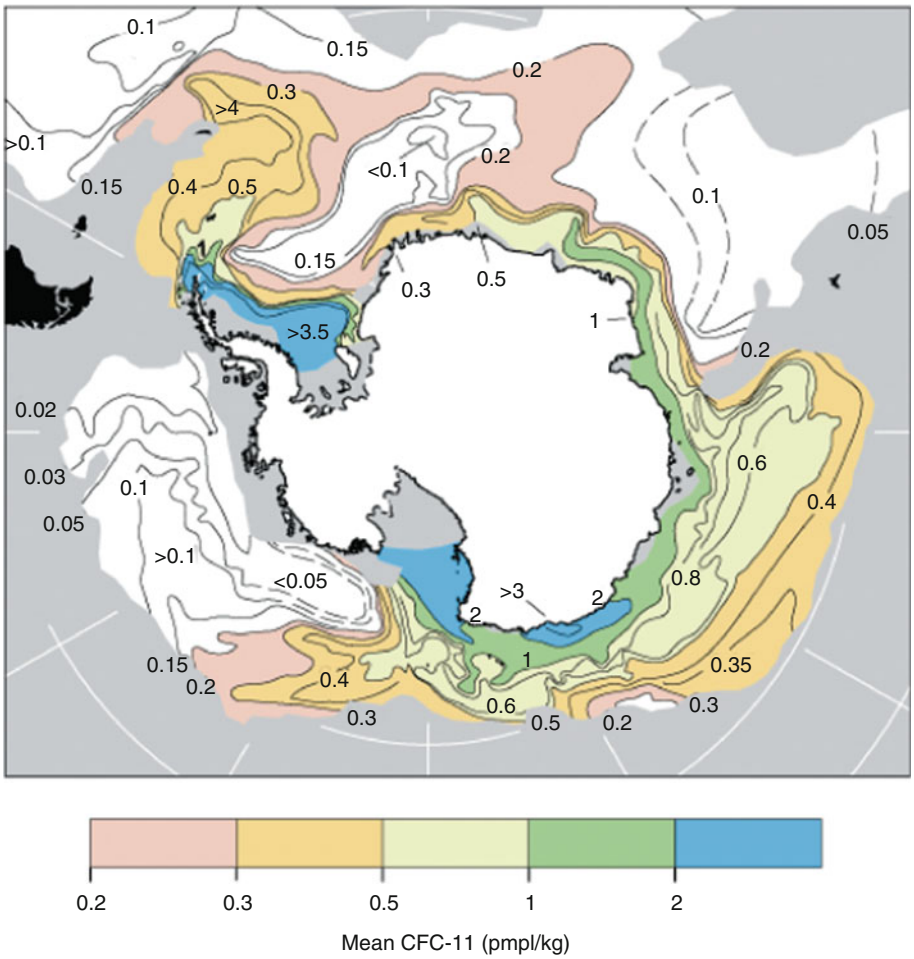

Large-Scale Ocean Circulation: Deep Circulation and Meridional Overturning. Figure 3
Inventory of CFC-11 in the Antarctic bottom water layer. High concentrations (*blue*) near the Weddell Sea, Ross Sea, and Adélie/Wilkes Land Coast indicate the three major sources of Antarctic bottom water (Adapted from [20])

distributions indicate the dominant role played by deep western boundary currents in the deep circulation. Maps of deep ocean properties like Figs. 2, 3, 4 also illustrate several other important aspects of the deep circulation: The flow is strongly steered by bathymetric features like the mid-ocean ridges and fracture zones; water properties gradually evolve along the flow path as a result of mixing; and water mass properties often change more abruptly near sills between basins (e.g., the Samoa Passage near 10 S, 175 W, Fig. 4), suggesting enhanced mixing in these regions.

The transport of the deep western boundary currents have been measured at a number of locations in the Atlantic and at a few locations in the Indian and Pacific basins, from long-term moored experiments or hydrographic sections. Hogg [27] provides a useful summary of measurements that existed at that time. A DWBC carrying NADW southward can be identified throughout the Atlantic (e.g., Fig. 2b). AABW and CDW formed from a mixture of AABW and NADW flows northward along the western boundary of most of the deep basins surrounding Antarctica, as seen in Figs. 3 and 5.

Such measurements confirm the existence of the DWBCs expected from the Stommel's theory. However, as observations of the deep ocean have increased in number and duration, it has become clear that the deep circulation is more complex than illustrated

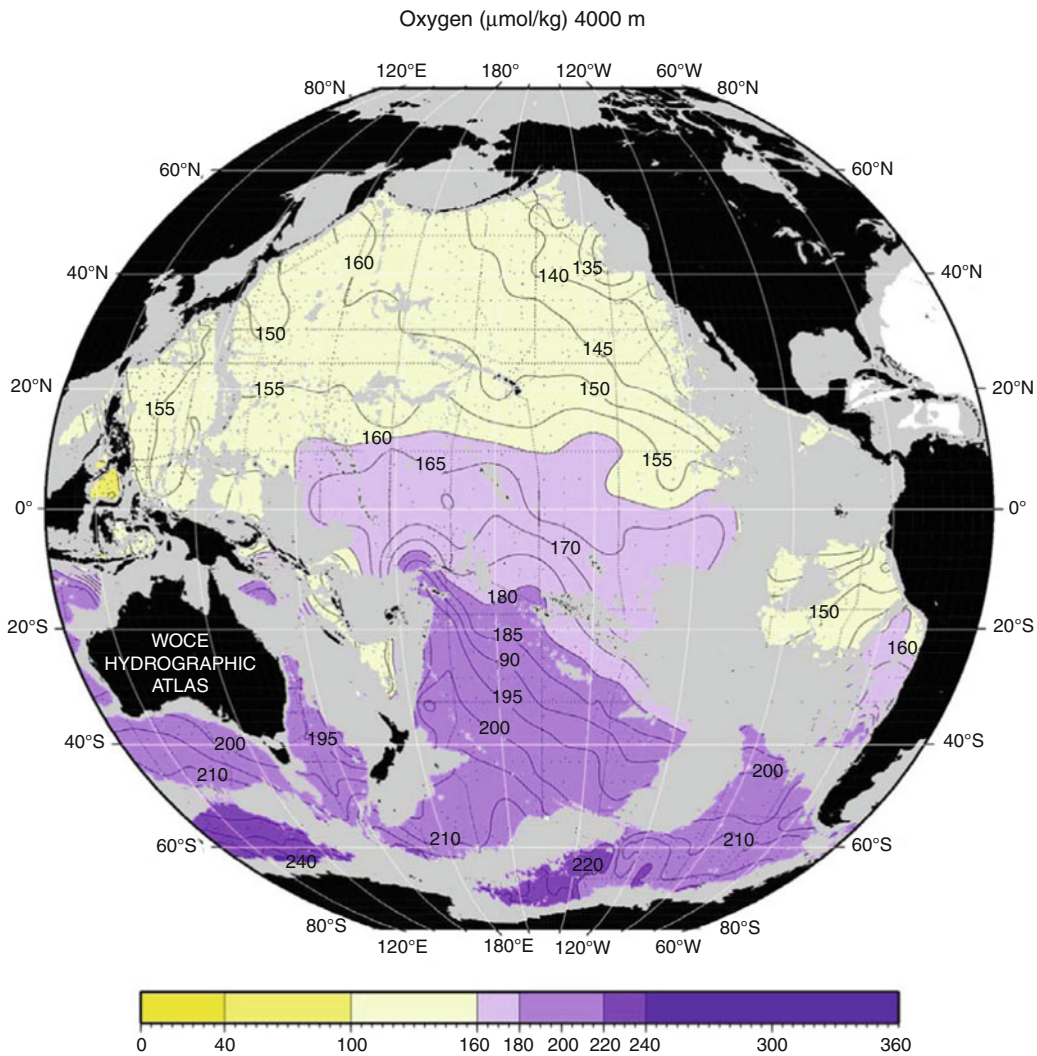

Large-Scale Ocean Circulation: Deep Circulation and Meridional Overturning. Figure 4
Oxygen concentration at 4,000 m depth in the Pacific, illustrating the inflow of relatively oxygen-rich Circumpolar Deep Water in a deep western boundary current to the east of New Zealand. From the WOCE Pacific Atlas; used with permission

in Fig. 1. Energetic eddies are common in the vicinity of the deep boundary currents, produced by dynamical instabilities of the currents. Stable transport estimates therefore require time series of sufficient duration to average over the eddy signal. In addition, momentum fluxes associated with these eddies drive recirculating gyres offshore of many DWBCs (e.g., [28, 29]). The presence of the deep recirculation gyres complicates efforts to measure the net transport of the DWBCs associated with the large-scale overturning circulation: few moored arrays span both the DWBC and the offshore gyres, as required to separate the recirculating and throughflow components of the DWBC.

The weak poleward flow expected from Stommel's deep circulation theory has proven even more elusive to observe. The first attempts to use neutrally bouyant floats to measure the interior flow instead discovered mesoscale eddies [30, 31]. Stommel's theory assumed a flat-bottomed ocean. The presence of seafloor

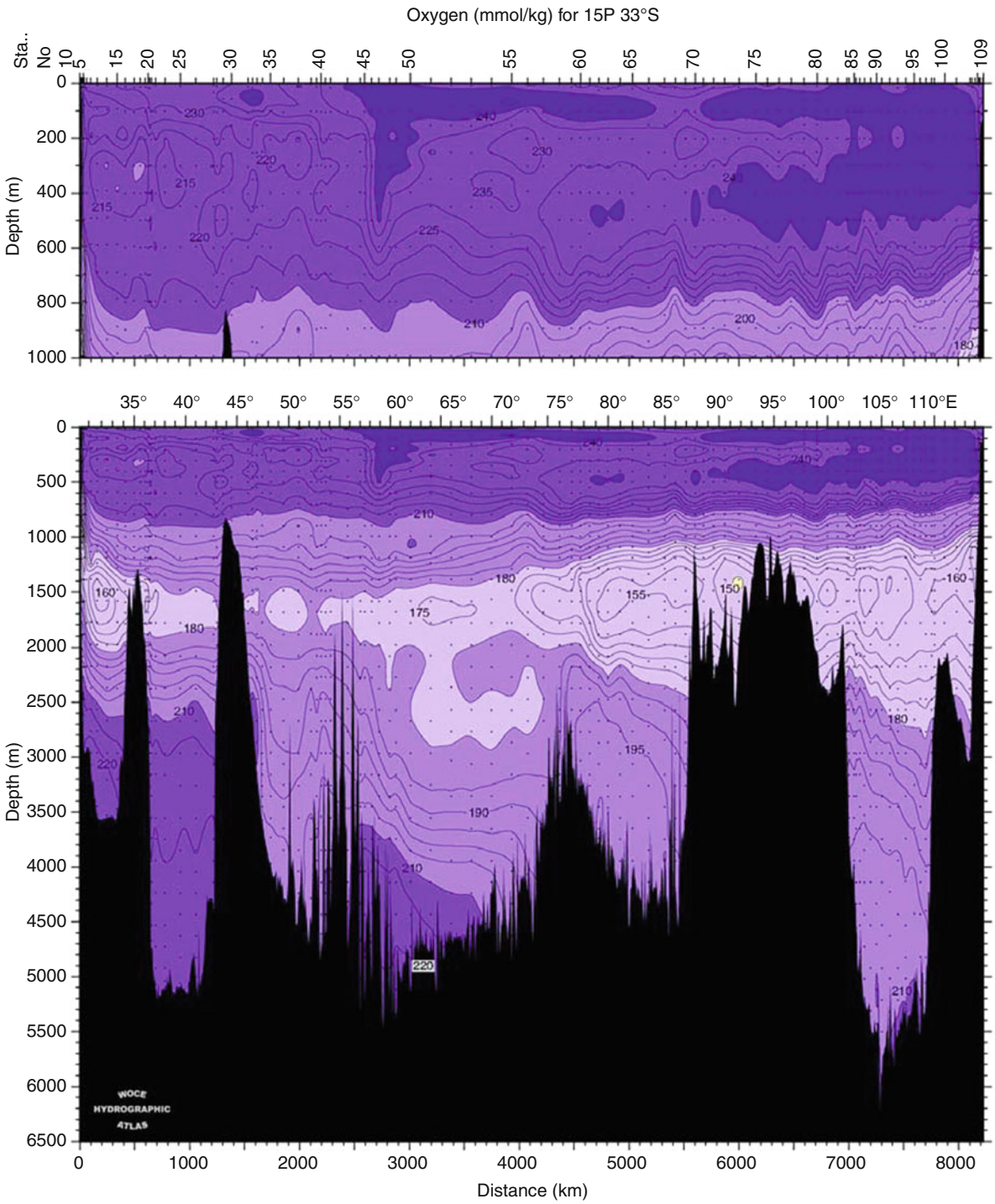

Large-Scale Ocean Circulation: Deep Circulation and Meridional Overturning. Figure 5
Oxygen concentration at 33°S in the Indian Ocean. Abyssal waters are relatively rich in oxygen, with the highest values seen near the seafloor on the western side of each deep basin, reflecting the presence of deep western boundary currents (From WOCE Pacific Atlas; used with permission)

bathymetry both steers the deep flow and can affect the dynamics of the deep circulation by driving vertical motions near the seafloor and hence meridional motion, analogous to the poleward flow caused by upwelling at the top of the deep layer in the Stommel model. In a basin with realistic bathymetry, therefore, one would not necessarily expect to see uniform poleward flow in the interior. Neutrally buoyant floats were used to study the deep flow in the Brazil Basin during the World Ocean Circulation Experiment [32]. Rather than weak poleward flow, the floats revealed alternating east–west (zonal) flows, with short north–south (meridional) scales, in the interior of the basin. The zonal flows in the interior were interpreted to be consistent with the idea that mixing (and therefore upwelling) was limited to the rough topography around the rim of the basin (as directly observed during the experiment, [33]). With no upwelling in the interior, there is no vortex stretching and no requirement for meridional flow in order to conserve potential vorticity. Zonal flows in the ocean interior have since been observed in many parts of the ocean [34].

Global Overturning Circulation

The DWBCs that dominate the circulation of the deep ocean form the lower limb of the global overturning circulation. To balance the sinking of dense water in the North Atlantic and Southern Ocean, an equal volume of water in the upper ocean must flow toward the sinking regions in the upper limb of the overturning circulation. The shallow and deep branches of the OC must be linked by upwelling (and therefore mixing) somewhere in the ocean interior. While the existence of a global-scale circulation pattern linking the high-latitude sources of deep water to lower latitudes, and the upper layers of the ocean to the deep sea, has been recognized for many years, a quantitative understanding of the structure and dynamics of the overturning circulation was lacking.

Role of the Overturning Circulation in Climate and Biogeochemical Cycles The OC is a primary mechanism for the transport and storage of heat and freshwater and carbon by the ocean and therefore has a substantial impact on climate variability and change [35]. For example, in the North Atlantic the ocean carries about 1×10^{15} W of heat to the north, helping to moderate the climate of western Europe. The relative contribution of deep and shallow overturning cells to the net meridional transport of heat and freshwater varies between the ocean basins [36, 37]. Changes in the OC have been linked to past climate variations, including abrupt changes caused by a slowing of the overturning, and climate models suggest the circulation will both respond to and modulate climate change in the future (e.g., [38]). In particular, large inflows of freshwater produced from melting of ice during the transition out of glacial cycles are believed to have made the surface waters of the North Atlantic so buoyant that dense water was no longer formed [14]. The resulting slowdown of the overturning circulation and reduction in heat transport led to rapid cooling. Climate models project a slowdown of the overturning circulation of about 30% over the next century, as a result of warming and freshening of the surface layers of the ocean, although the magnitude and sensitivity to change of the overturning varies widely between models.

The OC also plays an important role in the global cycles of carbon, nutrients, and other properties. Sinking of organic matter transfers nutrients and carbon from the surface to the deep ocean. Upwelling of deep water as part of the OC, particularly in the Southern Ocean, returns nutrients to the surface ocean to support phytoplankton growth [39]. Models suggest that nutrients upwelled and exported by the Southern Ocean support 75% of global primary production north of 30°S [39]. Changes in the overturning circulation would therefore be expected to influence global primary productivity and ecosystem function [40]. Deep water is also rich in carbon and the efficiency with which the ocean sequesters carbon dioxide from the atmosphere depends on a balance between the outgassing from upwelled deep water and the physical and biological processes acting to transport carbon into the ocean interior [41]. Projections of future climate change are sensitive to the rate of carbon uptake by the ocean in climate models and therefore sensitive to the overturning circulation. Atmospheric observations and coarse-resolution ocean model studies have suggested that the carbon sink in the Southern Ocean has "saturated" in recent decades, as a result of an increase in

strength of the overturning circulation (and hence increased outgassing of natural carbon from the deep ocean) in response to stronger winds [41]. This result, however, may significantly change when ocean eddy feedback processes are resolved [42]. The upwelling of carbon-rich deep water will also affect the carbon saturation state and pH of surface waters, with implications for calcifying organisms and marine ecosystems.

Seasonal and interannual climate variability is largely independent of the deep ocean and OC. But as the timescale of climate variability increases, the deep ocean becomes an increasingly important player. For example, a number of recent studies have shown that sea surface temperature variations on multi-decadal timescales are influenced by the overturning circulation (see [43] for a summary). These multi-decadal anomalies in Atlantic sea surface temperature (SST), known as the Atlantic Multi-decadal Oscillation, have in turn been linked to regional climate anomalies, persistent drought, hurricane frequency, and fisheries production (see [44–46] and references therein). On these timescales, the evolution of climate tends to be dominated by the slow dynamics of the ocean rather than the atmosphere [47, 48], suggesting that it may be possible to exploit ocean information to improve the prediction of these phenomena. For example, advection of salinity anomalies by the OC can result in decadal variability of the OC and its heat transport, and therefore in anomalies of sea surface temperature that drive decadal variability in the overlying atmosphere [45].

Conceptual Models of the Overturning Circulation

Observations of the deep circulation (section Deep Ocean Circulation) reveal features both consistent with (e.g., DWBCs) and at odds with (e.g., lack of evidence of poleward flow in the interior) the simple pattern (Fig. 1) expected from Stommel's model for the deep circulation. The limited deep observations available to date also reveal a variety of small-scale, energetic flows that complicate efforts to observe and understand the overturning. The connections between the upper and lower limbs of the overturning and the nature of the interior flows have been particularly difficult to quantify and understand. Nevertheless, a more complete conceptual model of the overturning circulation has gradually evolved over the past 25 years.

In the absence of other information, Stommel assumed the sinking at high latitudes was balanced by uniform upwelling elsewhere. A consequence of uniform upwelling was that much of the return to the upper ocean must take place in the Pacific, the largest ocean basin. There must therefore be exchange pathways in the upper ocean to return fluid upwelled in the Pacific and Indian Oceans to the Atlantic to complete the loop. Broecker and Peng [49] were the first to refer to the resulting global circulation pattern as a "conveyor belt" and to attempt to illustrate the circulation with a two-layer schematic. Gordon's [50] version of this schematic included a more realistic representation of the regional currents and interbasin exchanges involved in the global cell, and was the first to include estimates of the transports carried by the various branches. A visually compelling cartoon of the two-layer schematic published by Broecker [13] with the title "Great Ocean Conveyor Belt" grabbed the imagination of many and was used in Broecker [14] to illustrate the role of the overturning circulation in glacial–interglacial cycles. Figure 6 shows a version of the Broecker conveyor belt, modified to include the Antarctic sources of deep water and the interbasin connection provided by the Antarctic Circumpolar Current.

A series of authors have sought to add to the realism of Broecker's schematic diagram, while retaining the power of a simple representation of the flow. Richardson [51] provides a very useful overview of the history of such diagrams. Here a few of the major contributions are highlighted. Gordon ([52]; figure reproduced in [51]) used a novel three-dimensional representation of the oceans to represent the global nature of the overturning circulation, including the major interbasin exchanges, alternating flows at different depths in each basin, and the upwelling and mixing that link the upper and lower limbs. Schmitz [53, 54] revised and colored Gordon's scheme. Lumpkin and Speer [55] (Fig. 7) further revised this schematic and added estimates of the transport of the major current branches.

Several authors have refined two-dimensional schematics of the overturning. In particular, the reports by Schmitz [53, 54] include a number of multilayer pictures of the global overturning, an example of which is shown in Fig. 8. These schematics were constructed by

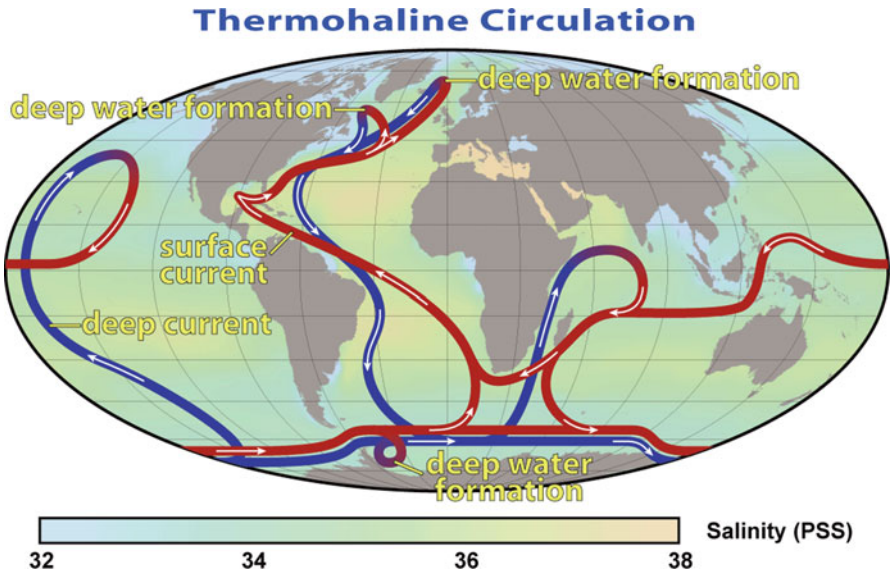

Large-Scale Ocean Circulation: Deep Circulation and Meridional Overturning. Figure 6
An illustration of Broecker's "Great Ocean Conveyor Belt," modified to include sinking of dense water near Antarctica and the interbasin connection provided by the Antarctic Circumpolar Current around Antarctica. *Red arrows* indicate flows of warm water in the upper ocean; *blue arrows* the flow of deep water (Illustration by Robert Simmon, NASA; used with permission)

summarizing the results of a large number of regional and global studies and are particularly notable because they are quantitative, with an internally consistent set of transport estimates provided for each branch of the circulation. Finally, the schematic of Lumpkin (modified by Speich, 2009, personal communication) is a recent attempt to convey the global overturning in a more realistic fashion, including the major pathways, recirculating gyres, interbasin exchanges, water mass transformations, and eddies (Fig. 9).

A number of recent results have called aspects of the "conveyor belt" view of the overturning circulation into question [56]. The fact that an overturning circulation exists in the ocean is clearly supported by ocean observations, model studies and theory. However, it is becoming increasingly clear that it is inappropriate to think of this flow as a continuous, steady "belt" of flow connecting the ocean basins. (This was of course obvious from the start to the authors of early schematics of the overturning circulation, but the conveyor belt metaphor has at times been interpreted more literally than intended, perhaps a victim of its own success.) For example, the DWBC in the Atlantic is apparently not as continuous as once believed [57]. Eddies detrain and re-entrain fluid into the boundary current and into recirculation gyres, diluting waters in the boundary current and spreading the flow over a larger fraction of the interior of the basin. Floats have also revealed the importance of interior pathways [58]. The fact that local, time-varying processes (e.g., wind forcing, eddies, and recirculation gyres) can influence the transport of the DWBC means that variations in the strength of the current with time, or with latitude, do not provide an unambiguous indication of changes in the production of dense water in the source regions, as once assumed [56]. Moreover, evidence is growing that both the upper and lower limbs of the overturning are sensitive to wind and buoyancy forcing and to mixing. For example, it is not clear whether it is more appropriate to think of the overturning circulation as "pushed" by formation of dense water or "pulled" by upwelling driven by winds in the Southern Ocean and by vertical mixing [59]. Attribution of the cause of changes in the overturning is difficult because

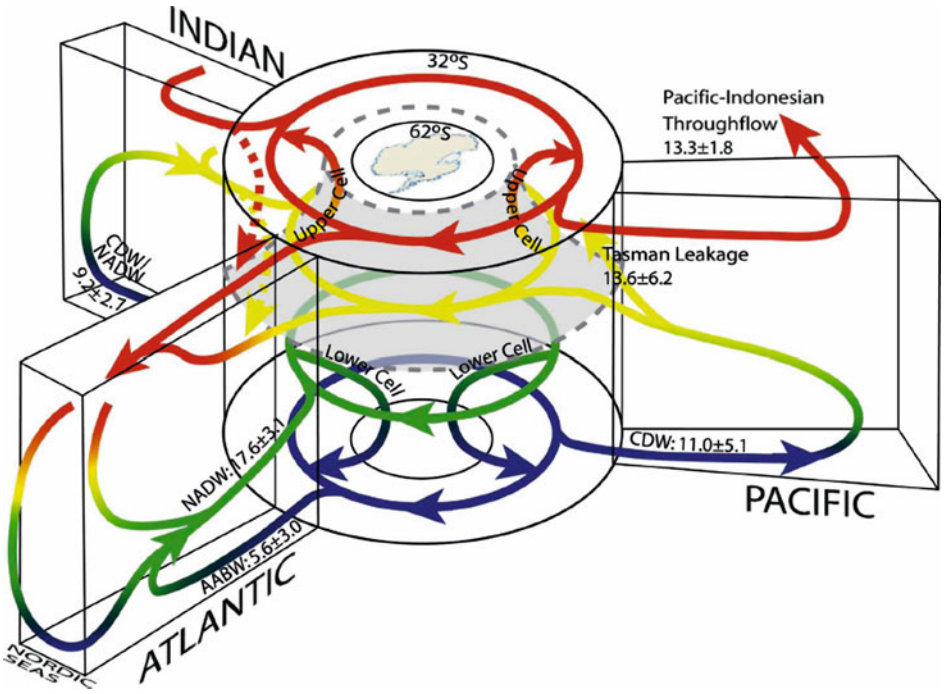

Large-Scale Ocean Circulation: Deep Circulation and Meridional Overturning. Figure 7
A schematic view of the global overturning circulation. Color indicates approximate density ranges. *Red*: upper; *yellow*: intermediate; *green*: deep; *blue*: bottom. *Dashed arrows* indicate Indian-to-Atlantic westward exchange between Africa and the ACC (Format adapted from Gordon [52] and Schmitz [53, 54]; from [55]; used with permission)

variations may reflect the response to a range of physical processes (e.g., eddies and wind) in addition to buoyancy forcing at high latitudes, as believed when the "conveyor belt" concept was developed.

Observations of the Overturning Circulation The transport of properties by the OC depends on the rate of overturning and the difference in property concentration between the upper and lower limbs of the overturning; in many locations, the horizontal gyres also contribute to the meridional transport of heat and other properties. Therefore observations of the property transport by the OC must extend throughout the full depth and breadth of the ocean basins. With present technology, this is generally not feasible because of the expense of deploying a coherent array of current meter moorings across vast regions of the ocean. However, while continuous, direct measurements of the global OC are not yet possible, new approaches have been developed to allow monitoring of the OC at particular locations. An important achievement in the last decade is the first multiyear time series of the meridional mass transport contributing to the overturning circulation in the Atlantic sector.

For example, an array of instruments has been deployed to measure the overturning circulation crossing 26.5°N in the Atlantic [60–62]. Figure 9 shows a 3.5 year time series of the transport of individual components of the OC: the Gulf Stream at Florida Straits, the interior flow in the upper ocean, and the Ekman transport. The mean overturning is 18.5 Sv (1 Sv = 10^6 m^3 s^{-1}), with a standard deviation of 4.9 Sv and a standard error of 1.5 Sv. The fact that the sum of the individual components approximately conserves mass provides additional confidence that the transport estimates are robust [62]. The measurements reveal significant high-frequency variability of the OC on several timescales, underscoring the need for both continuous sampling to avoid aliasing and

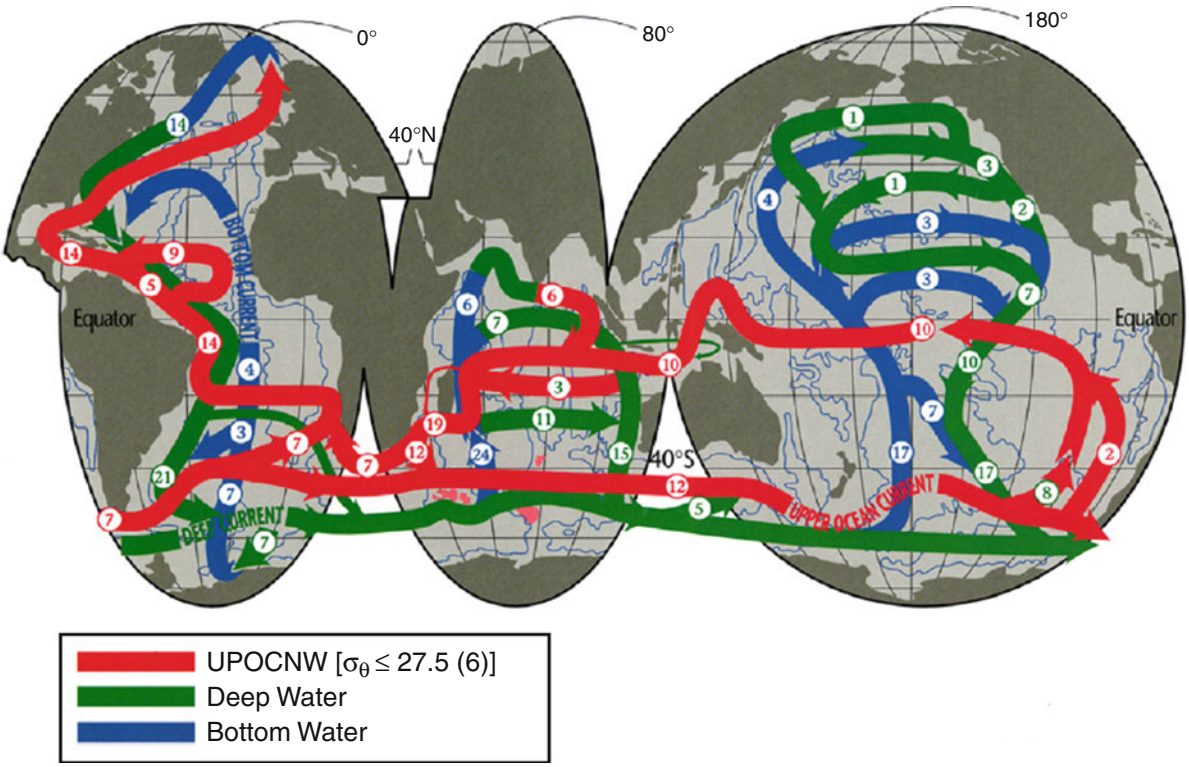

Large-Scale Ocean Circulation: Deep Circulation and Meridional Overturning. Figure 8
A three-layer schematic of the global interbasin circulation by Schmitz [54]. Values in circles represent transport in Sverdrups. UPOCNW designates upper ocean water, a combination of upper layer water and intermediate water (From [54]; used with permission)

for long time series to detect trends. The continuous time series is providing new insights into the dynamics of the OC, including identification of the mechanisms responsible for variability of the OC on different timescales (e.g., [63]).

The 26.5°N array exploits the fact that the net geostrophic transport between two points on a latitude circle can be determined from measurements of the pressure difference between the two points. Therefore the volume transport in the interior can be estimated from measurements on either side of the basin, without the need for a coherent array of instruments spanning the basin. This works well at 26.5 N in the Atlantic because of the particular geometry of the basin there. The strong flows in the boundary currents over the continental slope on the western side of the basin need to be measured directly.

The end-point monitoring approach has also proved effective at 16°N in the Atlantic, where the time series of North Atlantic Deep Water export is now more than 9 years long [64, 65]. Flows in the eastern basin contribute little to the net transport. The near-rectangular geometry of the western Atlantic basin allows the OC to be monitored with a small number of instruments and thus is very cost-effective. As found at 26.5°N, the transport of the lower limb of the OC is highly variable on short timescales (Fig. 10). Despite the large high-frequency variability, the time series is of sufficient duration to detect a weakening trend (significant at 85%), corresponding to a 3 Sv reduction in the NADW export over the duration of the record.

The demonstration that continuous measurements of the basin-scale overturning circulation can be made using a small number of instruments is a remarkable achievement. However, the subtropical North Atlantic represents a special case where the near-rectangular geometry of the ocean basins means that the end-point

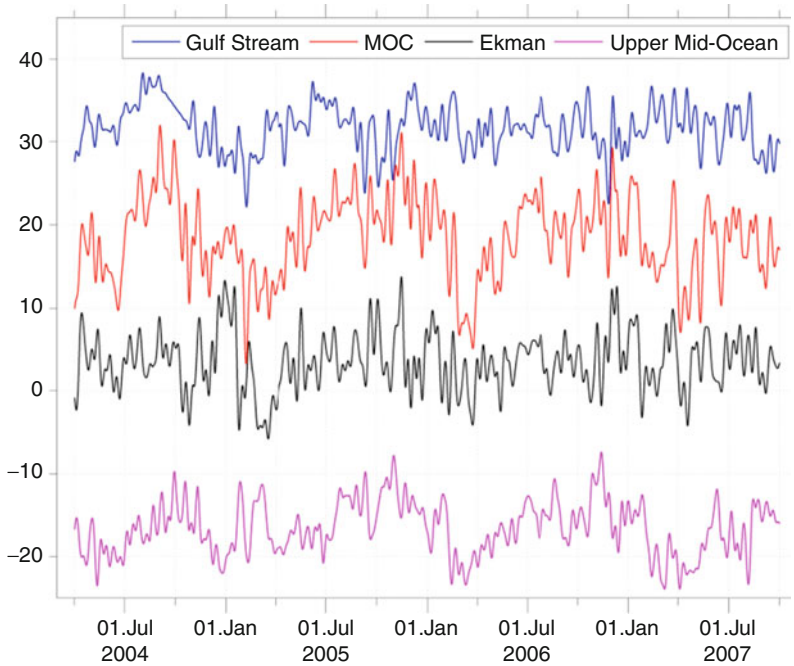

Large-Scale Ocean Circulation: Deep Circulation and Meridional Overturning. Figure 9
Transport of the overturning circulation at 24 N in the Atlantic. Gulf Stream transport through the Florida Straits (*blue*), Ekman transport (*black*), upper mid-ocean transport (*magenta*), and overturning transport (*red*). Transports in Sv, positive northward. Florida Straits transport is based on electromagnetic cable measurements. Ekman transport is based on scatterometer winds. The upper mid-ocean transport is the vertical integral of the transport per unit depth down to 1,100 m. Overturning transport is the sum of Florida Straits, Ekman, and upper mid-ocean transport. The mean $\pm$ standard deviation of Gulf Stream, Ekman, upper-mid ocean, and overturning transports are 31.7 $\pm$ 2.8 Sv, 3.5 $\pm$ 3.4 Sv, -16.6 ± 3.2 Sv, and 18.5 $\pm$ 4.9 Sv, respectively (From [61]; used with permission)

monitoring approach can capture most of the flow. Array design studies using general circulation models [66, 67] have identified some of the requirements for a basin-scale observing system for the overturning circulation. Where barotropic flows make a significant contribution to the mass and heat transport, they need to be measured directly and cannot be inferred from observations at the end points of a section. Where western boundary currents are broad (e.g., over sloping topography), extensive, and expensive, moored arrays may be required to resolve them. Complex bathymetry and barotropic flows in the ocean interior also need to be resolved, for example at subpolar latitudes where the gyre circulation makes a significant contribution to the net heat flux. For accurate estimates of property transports, these measurements need to be horizontally coherent to capture the correlations of velocity and temperature that are responsible for heat transport. In other words, at most latitudes, direct observations of the overturning circulation require massive moored arrays that are not feasible with present technology and resources.

While basin integrals of the OC are not yet feasible at most latitudes, major currents contributing to the overturning circulation have now been measured at several locations, in particular in the dense overflows and along the deep western boundary current carrying NADW southward [60, 68, 69]. These measurements have generally spanned the overflow or deep western boundary current, but not the flows in the interior of the basin. The presence of recirculation gyres offshore of the DWBC, usually not resolved by the moored arrays, often makes it difficult to use these measurements to infer the overall strength (or throughflow) of

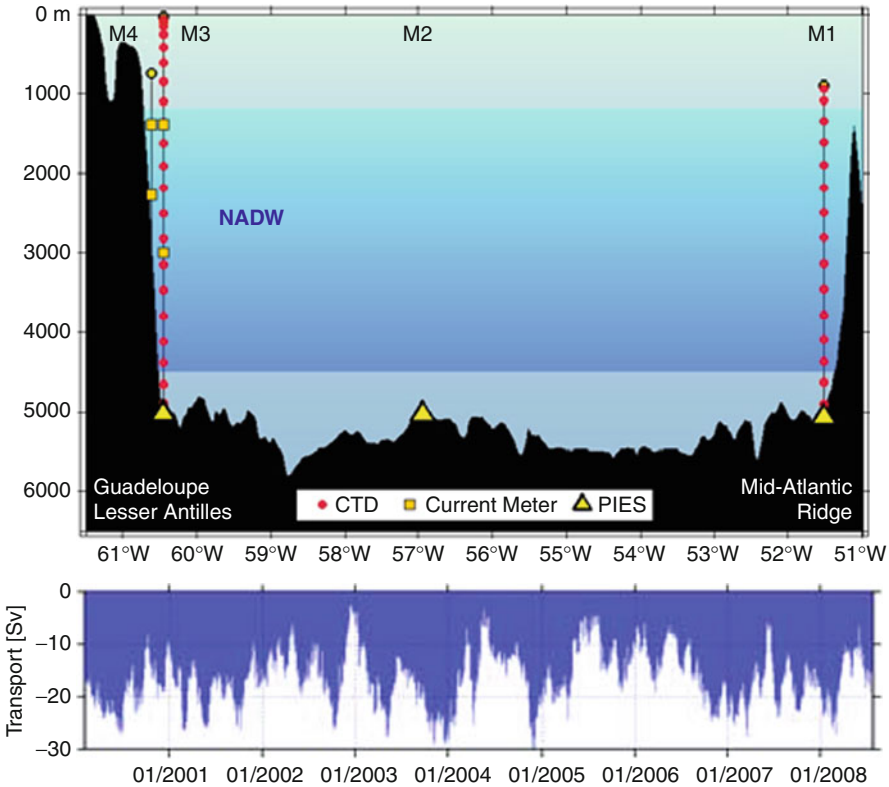

Large-Scale Ocean Circulation: Deep Circulation and Meridional Overturning. Figure 10
Top: the 9°N array in the western basin of the Atlantic. Lines with red dots indicate end-point moorings; *yellow diamonds* indicate inverted echo sounders with pressure sensors (PIES). Bottom – Absolute transport of NADW through the array from end-point moorings with density sensors. The long-term mean is 14.9 Sv (southward) (From [65], used with permission)

the OC [69]. However, they do provide robust estimates of a primary pathway of the deep limb of the overturning. The DWBC estimates can be combined with measurements in the ocean interior (e.g., from hydrographic sections) to estimate the OC and net meridional transport. They also provide valuable constraints for ocean state estimates and for the testing of ocean models.

Some current measurements have been made of the DWBC systems in the Indian and Pacific, but they are typically of less than 2-years duration and often lack the supplementary information needed to estimate the basin-wide overturning. As a consequence, estimates of the strength of the OC in the other ocean basins vary over a wide range (e.g., [70–73]). Examples of DWBC measurements include the flows carrying Antarctic Bottom Water (AABW) northward adjacent to the Kerguelen Plateau [74], into the Argentine Basin [75], through the Vema Channel to the Brazil Basin [76], and crossing the equator to enter the North Atlantic [77]; the flow entering the Indian Ocean through the Madagascar [78] and Perth Basins [79]; and the Pacific DWBC at 30°S [80], the Samoa Passage [81] and at 5°N [82].

Observations of Change in the Deep Ocean In climate models, deep ocean heat uptake has been found to be well correlated with the climate sensitivity of the model, with greater ocean heat uptake implying a larger commitment to future warming and sea-level rise [83, 84]. In fact, the degree to which the deep ocean takes up heat may be the largest uncertainty in determining climate sensitivity [19]. A similar argument applies to the ocean uptake of carbon dioxide.

Hence deep ocean measurements are central to reducing uncertainty in projections of global warming and sea-level rise. Observations suggest that warming of the deep ocean has contributed about 20% of the total increase in ocean heat content over the last decade or so [17].

While time series measurements are sparse in the deep ocean, there is increasing evidence of changes in properties and circulation. For example, the Antarctic Bottom Water (AABW) exported from the Southern Ocean to ventilate the abyss of each ocean basin has warmed in recent decades [17, 85–90] (Fig. 11). The changes in deep ocean temperature are sufficient to account for a significant fraction of the global energy imbalance [16, 18, 72, 87]. Reference [17] has estimated that the warming below 4,000 m depth and below 1,000 m south of the Subantarctic Front contributes about 0.09 W m^{-2} to the global heat budget (compared to 0.5 ± 0.18 W m^{-2} for the 0–700 m layer of the ocean [91]). This contribution to the planetary energy budget will grow in importance as the anthropogenic warming signal propagates to increasing depth with time. The warming below 4,000 m contributes about 0.1 mm $year^{-1}$ to global sea-level rise, while the warming below 1,000 m in the Southern Ocean contributes about 1 mm $year^{-1}$ of sea-level rise there. These new studies complement previous results [16, 92, 93], indicating significant warming between 700 and 3,000 m in the North Atlantic Ocean. The dynamical mechanism responsible for the observed abyssal warming is not yet known, but a recent study has highlighted the importance of wave-like motions that can rapidly transfer anomalies over large distances [94]. In this case, the warming of the deep North Pacific was traced back to changes in air-sea heat exchange at the sea surface off the coast of Antarctica, south of Australia.

The possibility that increased freshwater input to the high latitude ocean could cause a slowing of the thermohaline circulation and changes in climate has focused considerable interest on the high-latitude freshwater budget. Changes in upper ocean salinity have been observed in each of the ocean basins, with an increase in salinity in the subtropical evaporation zones and a decrease at higher latitudes that is consistent with a more vigorous hydrological

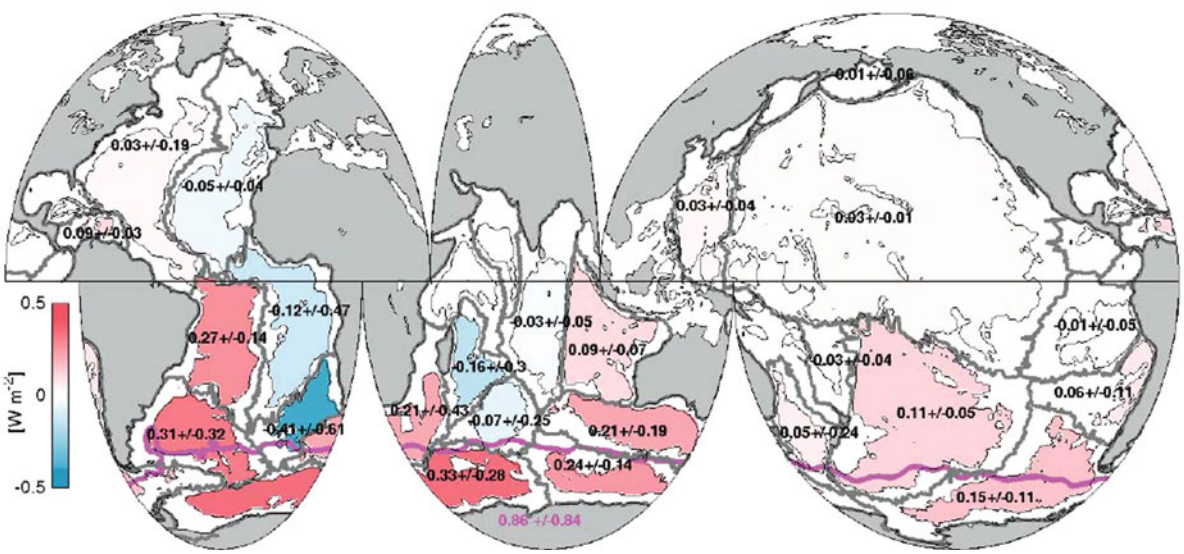

Large-Scale Ocean Circulation: Deep Circulation and Meridional Overturning. Figure 11
Mean local heat fluxes through 4,000 m implied by abyssal warming below 4,000 m from the 1990s to the 2000s, with 95% confidence intervals. Basin boundaries (*thick gray lines*) and 4000 m isobaths (*thin gray lines*) are shown. The local contribution to the heat flux through 1,000 m south of the SAF (*maroon line*) implied by deep Southern Ocean warming from 1,000 to 4,000 m is also given (*maroon number*) with its 95% confidence interval (From [17]; used with permission)

cycle and increased supply of meltwater at high latitudes [91, 95–97]. Numerous studies documented a freshening of North Atlantic Deep Water between the mid-1960s and the mid-1990s, when an atmospheric circulation pattern known as the North Atlantic Oscillation (NAO) evolved to an extreme positive state (e.g., [98]). The freshening reversed in the mid-1990s. Weakening of westerly winds in the mid-1990s to mid-2000s caused a reduction of deep convection in the Labrador Sea, a slowing and contraction of the subpolar gyre, and a northward advance of warm saline subtropical waters [99–104]. The NAO-induced upper ocean changes were rapidly transferred to deeper levels, causing an increase in temperature and salinity of deep waters [105–107].

While measurements are sparse in the Southern Ocean, several recent studies have detected changes in the salinity of Antarctic Bottom Water [86, 108–112]. The Ross Sea and Adélie Land regions supply about 40% of the total input of AABW [21]. Most of the AABW exported from both sources passes through the Australian Antarctic Basin, making it a good place to monitor changes in properties of the AABW formed in the Indian and Pacific sectors. The deep temperature–salinity relationship has changed throughout the basin in recent decades, with a shift toward fresher and lighter bottom water observed in the deepest 1,000 m of the water column [113]. References [110, 114, 115] suggest that the most likely source of the additional freshwater is basal melt of glacial ice in the Pacific sector. Enhanced basal melting there has been linked to warmer ocean temperatures [116]. In contrast, in the Weddell Sea the situation is ambiguous, with freshening of bottom water in the west [117] and a slight increase in the salinity of deep water in the east [89].

The evidence from the North Atlantic and the Southern Ocean suggests that the dense water sinking in both hemispheres responds to changes in the high latitude freshwater balance, and rapidly transmits this climate signal to the deep ocean. However, in only a few places are the observations sufficiently frequent to avoid aliasing of interannual variability. Expanded arrays of continuous measurements of deep ocean properties are needed to better understand the OC and its response to changes in forcing.

An Observing System for the Deep Ocean and Overturning Circulation

Measuring the OC poses a significant challenge. The OC extends throughout the global ocean, reaches from the sea surface to the sea floor, and consists of both intense narrow boundary currents and broad flows in the ocean interior. In essence, measuring the OC and associated heat and freshwater transport requires observations of the global, full-depth, three-dimensional, time-varying flow of the ocean. The tools to do this do not yet exist. Indeed, the deep ocean remains essentially unmeasured by the present ocean observing system, at least in a continuous sense. Nevertheless, substantial progress has been made in recent years, as discussed above. Building on this foundation, the international community recently developed a strategy for sustained observations of the deep ocean and overturning circulation [118], in the context of a decadal review of the status and prospects for global ocean observations known as OceanObs09 [119, 120]. In the following, the strategy for deep ocean observations developed by that community effort is summarized.

Building Blocks for an Observing System for the OC and Deep Ocean

An observing system for the transport of the OC and deep currents needs to rely on a combination of approaches. For some science questions (e.g., quantifying the transport of the OC), focused arrays of instruments are needed in key pathways of the circulation; for others (e.g., quantifying ocean heat content and its contribution to sea-level rise), broad-scale measurements are needed to track the evolving inventory of climate-relevant variables. In this section, the tools available for sampling the transport and inventory of the deep ocean are described; the following section outlines an initial strategy for their deployment.

Much of the transport of the OC is carried in narrow boundary currents and therefore direct velocity measurements are needed there. Both the surface-intensified but deep-reaching western boundary currents of the subtropical and subpolar gyres, and the deep western boundary currents that dominate the abyssal flow need to be measured. Boundary current transports can be observed using current meter arrays

incorporating point measurements and profiling instruments (e.g., acoustic Doppler current profilers (ADCPs)), cables, pressure gauges, and C-PIES (an Inverted Echo Sounder ((IES)) equipped with a pressure sensor (P) and a current meter (C); the combination provides a cost-effective means of monitoring the ocean, especially in the vicinity of strong currents [121]).

The full-depth volume transport in the interior of deep basins can be inferred from deep hydrographic measurements near the end points (from moorings, ships, gliders, or in some cases C-PIES), using the geostrophic relationship, supplemented by additional measurements over the sloping topography at the basin boundaries or mid-ocean ridges. Estimates of the transport of other properties (e.g., heat, freshwater, carbon), on the other hand, require knowledge of the covariance between velocity and concentration and cannot, in general, be made from end-point measurements alone. Given the prohibitive cost of a coherent "picket fence" of tall moorings spanning ocean basins (and the lack of moored sensors for some properties of interest), repeat hydrographic sections are in most cases the only approach available for estimating property fluxes over the full ocean depth. In some locations, where a close relationship exists between an integral property (e.g., acoustic travel time) and a single mode of variability of vertical profiles of temperature and salinity, property fluxes can be measured using a coherent array of C-PIES.

While the main focus of the entry is on the deep ocean, the OC of course includes flows in the upper ocean as well. To measure the OC, measurements of boundary currents and interior flows in the upper ocean are needed, including the wind-driven Ekman transport in the surface layer. Strategies for measuring the upper ocean are summarized in [119, 120].

Measurements of the evolving inventory of heat, freshwater, carbon, and other properties rely heavily on deep repeat hydrography [122]. Hydrographic sections remain the only tool available to sample the deep ocean over broad scales and the only way to collect samples for biological and biogeochemical analyses. The signal of change will appear first and be most prominent near the dense water overflows and along the main pathways of the deep circulation; hence these areas need to be sampled more frequently. Moored instruments provide the only means to obtain continuous time series of ocean currents and water properties and are therefore a key part of the armory, despite their relatively high cost and therefore limited spatial distribution. Repeat glider transects can also contribute to this goal. Remote sensing from satellites (e.g., altimetry and gravity measurements) or by acoustic means (e.g., acoustic tomography and thermometry) can provide integral constraints on ocean heat content [123]. However, each of these tools has limitations and as a result, changes in full-depth ocean heat content and other properties over most of the ocean can still not be measured accurately.

Because the reliance is on a variety of incomplete or indirect measurements to observe the overturning circulation and deep currents, analysis approaches such as inverse methods or state estimation are often required to combine the observations in a dynamically consistent manner and to interpolate between sparse observations.

A Strategy for a Deep Ocean Observing System

An initial strategy for sustained observations of the OC and deep ocean was articulated by Rintoul et al. [118] and is summarized here and in Fig. 12. For further detail, see [118] and references therein.

To understand the response of the OC and associated property transports to changes in forcing, measurements are needed at several latitudes to allow the meridional coherence of the OC to be assessed and understood. The partitioning of the meridional heat transport between the overturning and horizontal gyre circulations, for example, differs strongly with latitude [124]. Model studies suggest that the meridional coherence of the AOC has different timescales at different latitudes, with stronger decadal variability in the subpolar regime and stronger high-frequency variability in the subtropics [125, 126]. Other model studies suggest that measurements at a single latitude in each basin of the Atlantic might be sufficient to detect OC changes on multidecadal scales, but that measurements at additional latitudes are needed to capture interannual to decadal variability and to understand the role that interocean and interbasin exchanges play in the OC and climate [124, 127].

Basin-wide monitoring of the Atlantic OC and meridional heat and freshwater transport is therefore

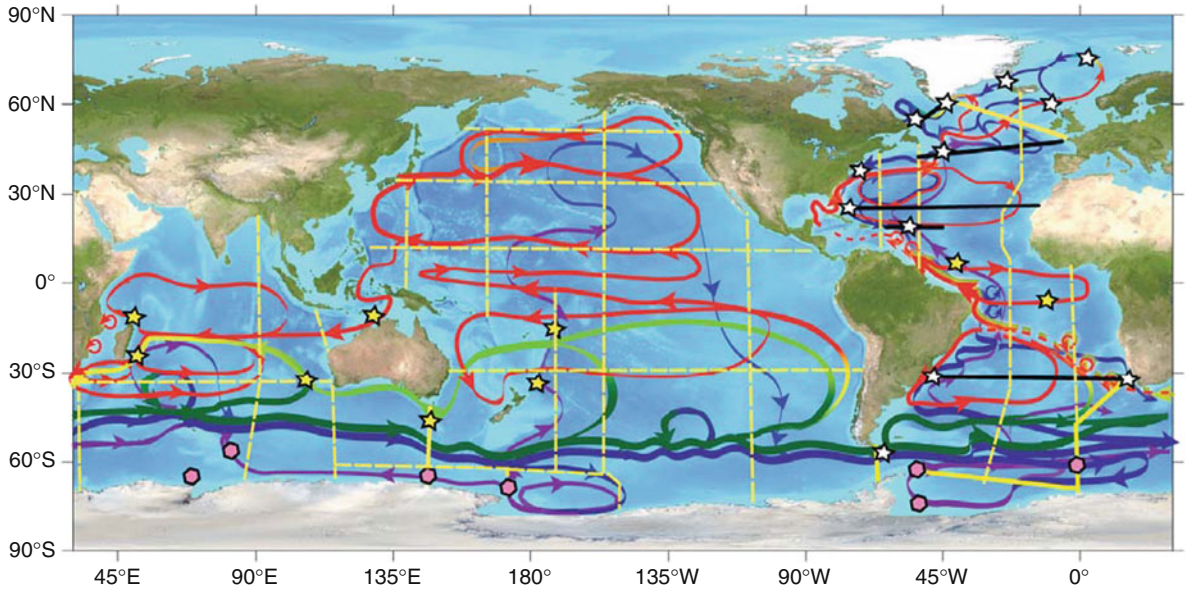

Large-Scale Ocean Circulation: Deep Circulation and Meridional Overturning. Figure 12
Schematic of the global ocean overturning circulation. *Red* indicates upper ocean flow, *blue* and *purple* are deep flows, and *yellows* and *greens* represent transitions between depths. The proposed observing system includes repeat hydrography (*dashed yellow lines*; *solid bold yellow lines* indicate higher frequency repeat lines); basin-scale arrays of moorings and repeat hydrography for main transport lines (*bold black lines*); and moored arrays across deep boundary currents and interbasin exchanges (stars) and in the primary AABW outflows (hexagons). *White stars* indicate locations of existing arrays; *yellow stars* indicate recommended new arrays. For clarity, some components of the proposed observing system are omitted (e.g., floats and broad-scale mooring array, see [129]). Base map from S. Speich, adapted from R. Lumpkin (From [118]; used with permission)

needed in the subpolar and subtropical North Atlantic, at low latitudes, and in the South Atlantic. Based on relevance, feasibility, and the value of continuing existing time series, arrays at 47°N, 26.5°N, 9°N, and 35°S are recommended. The existing monitoring arrays at 26.5°N and 9°N need to be maintained. At 47°N and 35°S, interior measurements of water properties and velocity are needed, as well as boundary arrays and end-point monitoring. Closure of the Labrador Basin with a full-depth transport and flux array is also recommended to monitor the production and export of Labrador Sea Water, an important contributor to the Atlantic OC and a region known to be sensitive to climate variability such as the North Atlantic Oscillation.

Measurements of key components of the OC and deep circulation need to be made in additional locations, where basin-wide monitoring is not possible. Existing long-term measurements of dense overflows and boundary currents in the Atlantic must be continued (see Table 1 of [60] for the location of these measurements). A new array is needed at Cape Farewell to measure the combined flux of the Denmark Strait and Faroe Bank Channel overflows [128]. Monitoring of the boundary currents in the South Atlantic needs to be enhanced [129]. The major pathways for interbasin exchanges (the Southern Ocean and Indonesian Throughflow) need to be monitored [130–132]. The southern hemisphere dense overflows and boundary currents carrying ventilated water northward also need to be measured for a complete understanding of the global OC [133].

Repeat hydrography will remain the backbone of the broad-scale deep ocean observing system [122]. The recommended repeat hydrographic lines are shown in Fig. 12; these lines have been identified as high priority by the Global Ocean Ship-based Hydrographic Investigations Program (GO-SHIP) and

commitments for future occupations exist for most of these sections. On each section, top-to-bottom measurements of temperature, salinity, oxygen, carbon, nutrients, and transient tracers are needed. More frequent sections are recommended near the dense water overflows and boundary currents, where the signal of change is evolving more rapidly (see [122] for the rationale and recommended sampling frequency for specific sections).

The repeat hydrography program , while essential, is still far from adequately sampling the deep ocean, given the infrequent sampling in space and time. The OceanSITES network of long-term time series stations will make an important contribution [134] and needs to be well-integrated with other deep-ocean observing systems, such as observatories established for geophysics or other applications.

In addition to maintaining the existing observing systems for deep ocean velocity, heat, salt, and carbon, there is a critical need to develop new, cost-effective, technologies for observing the deep ocean. Profiling floats capable of deeper profiling would allow broad-scale, sustained sampling of deep ocean properties for the first time. As well as the technological advances necessary to achieve this, design studies are needed urgently to determine the appropriate investment and deployment strategy for deep floats. Deep gliders could also make an important contribution and prototypes are being tested now that are designed to profile to 6,000 m depth. Near-continuous time series are needed to avoid aliasing and to determine the spectrum of deep variability. The OceanSITES network will make a significant contribution to this goal. Development of long-term moorings with the ability to transfer data to the surface (e.g., using expendable data capsules, acoustics, or other means) is needed to allow time series to be measured in remote ocean locations in a cost-effective manner [129]. Development of new sensors and platforms to measure carbon and other biogeochemical parameters is essential to improve the ability to track the evolving ocean inventory of carbon and acidification.

Status and Prospects

The observing system depicted in Fig. 12 is at various stages of readiness and commitment. Most of the hydrography lines have commitments for ongoing repeats, with a repeat time of 5–10 years. Several lines at high latitude are being repeated more frequently (indicated as solid lines in Fig. 12; see [122] for details). The moored arrays identified in Fig. 12 are, from a technology standpoint, ready to go now. More than 20 moored arrays and repeat lines have already been established in the Atlantic basin, as described in more detail in [60]. Many of these have a multiyear commitment. Each of the Southern Ocean sites identified by hexagons in Fig. 12 has been sampled with a moored array of at least 1-year duration in the last decade. The three Weddell Sea sites have been maintained for more than 8 years and are still underway. There are fewer established, long-term moored arrays in the other ocean basins, although pilot experiments are planned or are underway for most of the sites indicated in Fig. 12.

Overall, a large fraction of the recommended observing system for the deep ocean and OC already exists or is being developed – in particular, those components that rely on existing technology. On the other hand, the tools available today leave vast blind spots in the deep observing system: there are no means of making broad-scale, sustained measurements of the properties and circulation of the deep ocean. Three particular elements that are under development would make this possible: Floats capable of profiling throughout the full ocean depth; gliders capable of full-depth, basin-scale missions; and long-endurance moorings with data telemetry capability. For the nonphysical parameters (e.g., carbon, nutrients, biological variables), new sensors suitable for deployment on autonomous vehicles and moorings are urgently needed.

Future Directions

The overturning circulation and deep ocean strongly influence phenomena of direct relevance to sustainability, including climate change and variability, sea level, temperature and precipitation patterns over land, global biogeochemical cycles, and marine productivity. Despite its importance, observations of the deep ocean remain scarce, limiting the ability to understand and predict the overturning and deep circulations, their response to changes in forcing, and the impact of

change. However, substantial progress has been made in recent years, including the first time-series measurements of the strength of the overturning circulation in the Atlantic, the discovery of new current pathways in the deep ocean, evidence for widespread changes in the deep ocean, and a deeper appreciation of the role of the deep ocean and overturning in the climate system. Building on these advances, the community has recently articulated a strategy for sustained observations of the deep ocean and overturning. New tools are needed before a comprehensive observing system for the deep ocean can be established and many of these technologies are under development. An ongoing challenge is the need to complete the transition from a collection of distinct observing elements to an integrated, coherent observing system.

Acknowledgments

Many of the ideas presented here were developed as part of a community-wide effort to develop plans for a sustained deep ocean observing system, as input to the OceanObs09 process.

Bibliography

Primary literature

1. Worthington LV (1981) The water masses of the world ocean: some results of a finescale census. In: Warren BA, Wunsch C (eds) Evolution of physical oceanography. MIT Press, Cambridge, MA, pp 43–69
2. Stommel H (1958) The abyssal circulation. Deep-Sea Res 5:80
3. Stommel H, Arons AB (1960) On the abyssal circulation of the world ocean–I. Stationary planetary flow patterns on a sphere. Deep-Sea Res 6:140–154
4. Stommel H, Arons AB (1960) On the abyssal circulation of the world ocean – II. An idealized model of the circulation pattern and amplitude in oceanic basins. Deep-Sea Res 6:217–218
5. Warren BA (1981) Deep circulation of the world ocean. In: Warren BA, Wunsch C (eds) Evolution of physical oceanography. MIT Press, Cambridge, MA, pp 6–41
6. Swallow JC, Worthington LV (1957) Measurements of deep currents in the western North Atlantic. Nature 179:1183–1184
7. Swallow JC, Worthington LV (1961) An observation of a deep countercurrent in the western North Atlantic. Deep-Sea Res 8:1–19
8. Warren BA (1974) Deep flow in Madagascar and Mascarene basins. Deep-Sea Res 21:1–21
9. Warren BA (1977) Deep western boundary current in eastern Indian Ocean. Science 196:53–54
10. Warren BA (1978) Bottom water transport through Southwest Indian ridge. Deep-Sea Res 25:315–321
11. Warren BA (1983) Why is no deep water formed in the Pacific? J Mar Res 41:327–347
12. Wunsch C (2002) What is the thermohaline circulation? Science 298:1179
13. Broecker WS (1987) The biggest chill. Nat Hist Mag 97:74–82
14. Broecker WS (1991) The great ocean conveyor. Oceanography 4(2):79–89
15. Baringer MO, Arndt DS, Johnson MR (2010) State of the climate in 2009. Bull Am Meteorol Soc 91, S1
16. Levitus S, Antonov J, Boyer T (2005) Warming of the world ocean, 1955–2003. Geophys Res Lett 32:L02604. doi:10.1029/2004GL021592
17. Purkey SG, Johnson GC (2010) Warming of global abyssal and deep Southern Ocean waters between the 1990s and 2000s: Contributions to global heat and sea-level rise budgets. J Climate 23:6336–6351
18. Domingues CM, Church JA, White NJ et al (2008) Improved estimates of upper-ocean warming and multi-decadal sea-level rise. Nature 453:1090
19. Boe J, Hall A, Qu X (2009) Deep ocean heat uptake as a major source of spread in transient climate change simulations. Geophys Res Lett 36:L22701
20. Orsi AH, Johnson GC, Bullister JB (1999) Circulation, mixing and production of Antarctic bottom water. Prog Oceanog 43:55–109
21. Orsi AH, Smethie WM, Bullister JB (2002) On the total input of Antarctic waters to the deep ocean: a preliminary estimate from chlorofluorocarbon measurements. J Geophys Res C8:3122
22. Rintoul SR (1998) On the origin and influence of Adelie land bottom water. In: Jacobs S, Weiss R (eds) Ocean, ice and atmosphere: interactions at the Antarctic continental margin, vol 75, Antarctic Research Series. American Geophysical Union, Washington, pp 151–171
23. LeBel DA, Smethie WM, Rhein M et al (2008) The formation rate of North Atlantic deep water and eighteen degree water calculated from CFC-11 inventories observed during WOCE. Deep-Sea Res Part I-Oceanogr Res Pap 55(8):891–910
24. Orsi AH, Jacobs SS, Gordon AL et al (2001) Cooling and ventilating the abyssal ocean. Geophys Res Lett 28:2923–2926
25. Johnson GC (2008) Quantifying Antarctic bottom water and North Atlantic deep water volumes. J Geophys Res – Oceans 113(C5):C05027
26. Rintoul SR (2006) Circumpolar deep water. In: Encyclopedia of the Antarctic. Routledge, New York, pp 240–242
27. Hogg NG (2001) Quantification of the deep circulation. In: Siedler G, Church J, Gould J (eds) Ocean circulation and climate. Academic, San Diego, pp 259–270
28. McCartney MS (1992) Recirculationg components to the deep boundary current of the northern North Atlantic. Prog Oceanogr 29:283–383
29. Schmitz WJ, McCartney MS (1993) On the North Atlantic circulation. Rev Geophys 31:29–49

30. Crease J (1962) Velocity measurements in deep water of the western North Atlantic – summary. J Geophys Res 67:3173–3176
31. Swallow JC (1971) ARIES current measurements in western North Atlantic. Philos Trans R Soc Lond Ser A-Math Phys Sci 270:451–460
32. Hogg NG, Owens WB (1999) Direct measurement of the deep circulation within the Brazil Basin. Deep-Sea Res Part II-Top Stud Oceanogr 46(1-2):335–353
33. Ledwell JR, Montgomery ET, Polzin KL et al (2000) Evidence for enhanced mixing over rough topography in the abyssal ocean. Nature 403:179–182
34. Maximenko NA, Melnichenko OV, Niiler PP et al (2008) Stationary mesoscale jet-like features in the ocean. Geophys Res Lett 35:L08603
35. Bryden HL, Imawaki S (2001) Ocean heat transport. In: Siedler G, Church J, Gould J (eds) Ocean circulation and climate. Academic, New York, pp 455–474
36. Talley LD (2003) Shallow, intermediate, and deep overturning components of the global heat budget. J Phys Oceanogr 33:530–560
37. Talley LD (2008) Freshwater transport estimates and the global overturning circulation: shallow, deep and throughflow components. Prog Oceanogr 78:257–303
38. Alley RB, Marotzke J, Nordhaus WD, Overpeck JT, Peteet DM, Pielke RA Jr, Pierrehumbert RT, Rhines PB, Stocker TF, Talley LD, Wallace JM (2003) Abrupt climate change. Science 299:2005–2010
39. Sarmiento JL (2004) High-latitude controls of thermocline nutrients and low biological productivity. Nature 427: 56–60
40. Schmittner A (2005) Decline of the marine ecosystem caused by a reduction in the Atlantic overturning circulation. Science 343:628–633
41. Le Quéré C et al (2007) Saturation of the southern ocean CO_2 sink due to recent climate change. Science 316:1735–1738. doi:10.1126/science.1136188
42. Böning CW, Dispert A, Visbeck M, Rintoul SR, Schwarzkopf F (2008) Response of the Antarctic circumpolar current to recent climate change. Nat Geosci. doi:10.1038/ngeo362
43. Latif M et al (2010) Dynamics of decadal climate variability and implications for its prediction. In: Hall J, Harrison DE, Stammer D (eds) Proceedings of OceanObs'09: sustained ocean observations and information for society, vol 2. ESA Publication WPP-306, Venice, 21–25 Sept 2009
44. Hurrell J et al (2010) Decadal climate prediction: opportunities and challenges. In: Hall J, Harrison DE, Stammer D (eds) Proceedings of OceanObs'09: sustained ocean observations and information for society, vol 2. ESA Publication WPP-306, Venice, 21–25 Sept 2009
45. Latif M et al (2006) A review of predictability studies of Atlantic sector climate on decadal time scales. J Clim 19:5971–5987
46. Zhang R, Delworth TL (2006) Impact of Atlantic multidecadal oscillations on India/Sahel rainfall and Atlantic Hurricanes. Geophys Res Lett 33(17). doi:82410.1029/2006GL026267
47. Latif M (1998) Dynamics of interdecadal variability in coupled ocean-atmosphere models. J Clim 11:602–624
48. Bjerknes J (1964) Atlantic air-sea interaction. In: Advances in geophysics, 10th edn. Academic, New York, pp 1–82
49. Broecker WS, Peng T-H (1982) Tracers in the sea. Eldigio Press, Palisades, p 690
50. Gordon AL (1986) Interocean exchange of thermocline water. J Geophys Res 91(C4):5037–5046
51. Richardson PL (2008) On the history of meridional overturning circulation schematic diagrams. Prog Oceanogr 76:466–486
52. Gordon A (1991) The role of thermohaline circulation in global climate change. In: Lamont–Doherty geological observatory 1990 and 1991 report, Lamont–Doherty Geological Observatory of Columbia University, Palisades, pp 44–51
53. Schmitz WJ Jr. (1996a) On the world ocean circulation: volume I, some global features/North Atlantic circulation. Woods Hole Oceanographic Institution technical report WHOI-96-03, 141 pp
54. Schmitz WJ Jr. (1996b) On the world ocean circulation: volume II, the pacific and Indian oceans/a global update. Woods Hole Oceanographic Institution technical report WHOI-96-08, 237 pp
55. Lumpkin R, Speer K (2007) Global ocean meridional overturning. J Phys Oceanogr 37:2550–2562
56. Lozier MS (2010) Deconstructing the conveyor belt. Science 328:1507–1511
57. Dengler M, Schott FA, Eden C, Brandt P, Fischer J, Zantopp RJ (2004) Break-up of the Atlantic deep western boundary current into eddies at 8° S. Nature 432:1018–1020
58. Bower AS, Lozier MS, Gary SF, Böning CW (2009) Interior pathways of the North Atlantic meridional overturning circulation. Nature 459:243–247
59. Visbeck M (2007) Oceanography: power of pull. Nature 447:383
60. Cunningham S et al (2010) The present and future system for measuring the atlantic meridional overturning circulation and heat transport. In: Hall J, Harrison DE, Stammer D (eds) Proceedings of OceanObs'09: sustained ocean observations and information for society, vol 2. ESA Publication WPP-306, Venice, 21–25 Sept 2009
61. Cunningham SA, Kanzow T, Rayner D, Baringer MO, Johns WE, Marotzke J, Longworth HR, Grant EM, Hirschi JJM, Beal LM, Meinen CS, Bryden HL (2007) Temporal variability of the Atlantic meridional overturning circulation at 26.5°N. Science 317(5840):935–938. doi: 10.1126/science.1141304
62. Kanzow T et al (2007) Flow compensation associated with the OC at 26.5°N in the Atlantic. Science 317:938–941
63. Bryden HL, Mujahid A, Cunningham SA, Kanzow T (2009) Adjustment of the basin-scale circulation at 26° N to variations in Gulf stream, deep western boundary current and Ekman transports as observed by the rapid array. Ocean Sci 5:421–433
64. Send U et al (2010) A global boundary current circulation observing network. In: Hall J, Harrison DE, Stammer D (eds)

Proceedings of OceanObs'09: sustained ocean observations and information for society, vol 2. ESA Publication WPP-306, Venice, 21–25 Sept 2009
65. Send U et al (2002) Monitoring the Atlantic meridional overturning circulation at 16 N. CLIVAR Exchanges 25:31–34
66. Hirschi J et al (2003) A monitoring design for the Atlantic meridional overturning circulation. Geophys Res Lett 30(7). doi:10.1029/2002GL016776
67. Baehr J et al (2004) Monitoring the meridional overturning circulation in the North Atlantic: a model-based array design study. J Mar Res 62(3):283–312
68. Schott FA, Fisher J, Dengler M, Zantopp R (2006) Variability of the deep western boundary current east of the grand banks. Geophys Res Lett 33:L21S07. doi:10.1029/2006GL026563
69. Bryden HL, Johns WE, Saunders PM (2005) Deep western boundary current east of Abaco: mean structure and transport. J Mar Res 63:35–57
70. Ganachaud A, Wunsch C (2000) Improved estimates of global ocean circulation, heat transport and mixing *from* hydrographic data. Nature 408(6811):453–457
71. Talley LD, Reid JL, Robbins PE (2003) Data-based meridional overturning streamfunctions for the global ocean. J Clim 16(4). doi:10.1175/2787.1
72. Palmer MD, Bryden HL, Hirschi J, Marotzke J (2004) Observed changes in the south indian ocean gyre circulation, 1987–2002. Geophys Res Lett 31:L15303. doi:10.1029/2004GL020506
73. Sloyan BM, Rintoul SR (2001) The southern ocean limb of the global deep overturning circulation. J Phys Oceanog 31(1):143–173
74. Fukamachi Y, Rintoul SR, Church JA, Aoki S, Sokolov S, Rosenberg M, Wakatsuchi M (2010) Strong export of Antarctic bottom water east of the Kerguelen plateau. Nat Geosci 3:327–331. doi:10.1038/ngeo842
75. Whitworth AB, Whitworth T III, Nowlin WD, Pillsbury RD, Moore MI, Weiss RF (1991) Observations of the Antarctic circumpolar current and deep boundary current in the southwest Atlantic. J Geophys Res 96:15105–15118
76. Hogg NG, Siedler G, Zenk W (1999) Circulation and variability at the southern boundary of the Brazil basin. J Phys Oceanogr 29:145–157
77. Hall MM, McCartney M, Whitehead JA (1997) Antarctic bottom water flux in the equatorial western Atlantic. J Phys Oceanogr 27:1903–1926
78. Warren BA, Whitworth T, LaCasce JH (2002) Forced resonant undulation in the deep Mascarene Basin. Deep-Sea Res II 7–8:1513–1526
79. Sloyan BM (2006) Antarctic bottom and lower circumpolar deep water circulation in the eastern Indian Ocean. J Geophys Res 111:C02006. doi:10.1029/2005JC003011
80. Whitworth T III, Warren BA, Nowlin WD Jr, Rutz SB, Pillsbury RD, Moore MI (1999) On the deep western-boundary current in the Southwest Pacific basin. Prog Oceanogr 43:1–54
81. Rudnick DL (1997) Direct velocity measurements in the Samoan passage. J Geophys Res – Oceans 102:3293–3302
82. Kawabe M, Yanagimoto D, Kitagawa S (2006) Variations of deep western boundary currents in the Melanesian basin in the western North Pacific. Deep-Sea Res I 53:942–959
83. Raper SCB, Gregory JM, Stouffer RJ (2002) The role of climate sensitivity and ocean heat uptake on AOGCM transient temperature response. J Clim 15:124–130
84. Meehl GA, Washington WM, Collins WD et al (2005) How much more global warming and sea level rise? Science 307:1769–1772
85. Johnson GC, Doney SC (2006) Recent western South Atlantic bottom water warming. Geophys Res Lett 33:L14614. doi:10.1029/2006GL026769
86. Johnson GC, Purkey SG, Bullister JL (2008) Warming and freshening in the abyssal southeastern Indian Ocean. J Clim 21:5351–5363. doi:10.1175/2008JCLI2384.1
87. Johnson GC, Mecking S, Sloyan BM, Wijffels SE (2007) Recent bottom water warming in the Pacific Ocean. J Clim 20:5365–5375. doi:10.1175/2007JCLI1879.1
88. Fukasawa M, Freeland H, Perkin R, Watanabe T, Uchida H, Nishina A (2004) Bottom water warming in the North Pacific Ocean. Nature 427:825–827
89. Fahrbach E, Hoppema M, Rohardt G, Schröder M, Wisotzki A (2004) Decadal-scale variations of water mass properties in the deep Weddell Sea. Ocean Dyn 54:77–31
90. Kawano T et al (2006) Bottom water warming along the pathway of lower circumpolar deep water in the Pacific Ocean. Geophys Res Lett 33:L23613. doi:10.1029/2006GL027933
91. Bindoff N, Willebrand J, Artale V, Cazenave A, Gregory J, Gulev S, Hanawa K, Le Quere C, Levitus S, Nojiri Y, Shum CK, Talley L, Unnikrishnan A (2007) Observations: oceanic climate change and sea level. Climate change 2007: the physical science basis. In: Solomon S, Qin D, Manning M, Chen Z, Marquis M, Averyt KB, Tignor M, Miller HL (eds) Contribution of working group i to the fourth assessment report of the intergovernmental panel on climate change. Cambridge University Press, Cambridge, 385–432.79
92. Levitus S, Antonov JI, Wang J, Delworth TL, Dixon KW, Broccoli AJ (2001) Anthropogenic warming of earth's climate system. Science 292:267–270
93. Hansen J, Nazarenko L, Ruedy R, Sato M, Willis J, Del Genio A, Koch D, Lacis A, Lo K, Menon S, Novakov T, Perlwitz J, Russell G, Schmidt GA, Tausnev N (2005) Earth's energy imbalance: confirmation and implications. Science 308:1431–1435
94. Masuda S, Awaji T, Sugiura N et al (2010) Simulated rapid warming of abyssal North Pacific waters. Science 329:319–322
95. Durack PJ, Wijffels SE (2010) Fifty-Year trends in global ocean salinities and their relationship to broad-scale warming. J Clim 23:4342–4362
96. Roemmich D, Gilson J (2009) The 2004–2008 mean and annual cycle of temperature, salinity, and steric height in the global ocean from the Argo Program. Prog Oceanogr 82:81–100. doi:10.1016/j.pocean.2009.03.004
97. Hosoda S, Sugo T, Shikama N, Mizuno K (2009) Global surface layer salinity change detected by argo and its implication for hydrological cycle intensification. J Oceanogr 65:579–586

98. Dickson B, Yashayaev I, Meincke J, Turrell B, Dye S, Holfort J (2002) Rapid freshening of the deep North Atlantic Ocean over the past four decades. Nature 416:832–837
99. Hátún H, Sandø AB, Drange H (2005) Influence of the Atlantic subpolar Gyre on the thermohaline circulation. Science 309:1841–1844
100. Häkkinen S, Rhines PB (2004) Decline of subpolar North Atlantic circulation during the 1990s. Science 304:555–559
101. Bersch M, Yashayaev I, Koltermann KP (2007) Recent changes of the thermohaline circulation in the subpolar North Atlantic. Ocean Dyn 57:223–235
102. Holliday NP, Hughes SL, Bacon S, Beszczynska-Moeller A, Hansen B, Lavın A, Loeng H, Mork KA, Østerhus S, Sherwin T, Walczowski W (2008) Reversal of the 1960s to 1990s freshening trend in the northeast North Atlantic and Nordic Seas. Geophys Res Lett 35:L03614. doi:10.1029/2007GL032675
103. Sarafanov A, Falina A, Sokov A, Demidov A (2008) Intense warming and salinification of intermediate waters of southern origin in the eastern subpolar North Atlantic in the 1990s to mid-2000s. J Geophys Res 113:C12022. doi:10.1029/2008JC004975
104. Hakkinen S, Rhines PB (2009) Shifting surface currents in the northern North Atlantic Ocean. J Geophys Res – Oceans 114: C04005
105. Sarafanov A, Sokov A, Demidov A, Falina A (2007) Warming and salinification of intermediate and deep waters in the Irminger Sea and Iceland Basin in 1997–2006. Geophys Res Lett 34:L23609. doi:10.1029/2007GL031074
106. Yashayaev I (2007) Hydrographic changes in the Labrador Sea, 1960–2005. Prog Oceanogr 73:242–276
107. Sarafanov A (2009) On the effect of the North Atlantic Oscillation on temperature and salinity of the subpolar North Atlantic intermediate and deep waters. ICES J Mar Sci 66:1448–1454
108. Whitworth T III (2002) Two modes of bottom water in the Australian–Antarctic basin. Geophys Res Lett 29(5):1073. doi:10.1029/2001GL014282
109. Jacobs SS (2004) Bottom water production and its links with the thermohaline circulation. Antarct Sci 16(4):427–437
110. Jacobs SS (2006) Observations of change in the Southern Ocean. Philos Trans R Soc A 364:1657–1681. doi:10.1098/rsta.2006.1794
111. Aoki S, Bindoff NF, Church JA (2005) Interdecadal water mass changes in the Southern Ocean between 30E and 160E. Geophys Res Lett 32(L07607):1–5, ISSN 0094-8276
112. Aoki S, Rintoul SR, Ushio S, Watanabe S, Bindoff NL (2005) Freshening of the Adelie land bottom water near 140°E. Geophys Res Lett 32:L23601. doi:10.1029/2005GL024246
113. Rintoul SR (2007) Rapid freshening of Antarctic bottom water formed in the Indian and Pacific Oceans. Geophys Res Lett 34: L06606. doi:10.1029/2006GL028550
114. Jacobs SS, Guilivi CF, Merle P (2002) Freshening of the Ross Sea during the late 20th century. Science 297:386–389
115. Rignot E, Jacobs SS (2002) Rapid bottom melting widespread near Antarctic ice sheet grounding lines. Science 296: 2020–2023
116. Shepherd A, Wingham D, Rignot E (2004) Warm ocean is eroding West Antarctic ice sheet. Geophys Res Lett 31: L23402. doi:10.1029/2004GL021106
117. Heywood KJ, Thompson AE, Fahrbach E, Mackensen A, Aoki S (2009) Cooling and freshening of the Weddell Sea outflow. Geophys Res Abstracts, 11: EGU2009-4336. EGU General Assembly 2009
118. Rintoul SR et al (2010) Deep circulation and meridional overturning. In: Hall J, Harrison DE, Stammer D (eds) Proceedings of OceanObs'09: sustained ocean observations and information for society, vol 1. ESA Publication WPP-306, Venice, 21–25 Sept 2009
119. Hall J, Harrison DE, Stammer D (eds) Proceedings of OceanObs'09: sustained ocean observations and information for society, vol 1. ESA Publication WPP-306, Venice, 21–25 Sept 2009
120. Hall J, Harrison DE, Stammer D (eds) Proceedings of OceanObs'09: sustained ocean observations and information for society, vol 2. ESA Publication WPP-306, Venice, 21–25 Sept 2009
121. Meinen CS, Watts DR, (2000) Vertical structure and transport on a transect across the North Atlantic Current near 428 N. J Geophys Res 105(21869):21891
122. Hood M et al (2010) Ship-based repeat hydrography: a strategy for a sustained global program. In: Hall J, Harrison DE, Stammer D (eds) Proceedings of OceanObs'09: sustained ocean observations and information for society, vol 2. ESA Publication WPP-306, Venice, 21–25 Sept 2009
123. Dushaw B et al (2010) A global ocean acoustic observing network. In: Hall J, Harrison DE, Stammer D (eds) Proceedings of OceanObs'09: sustained ocean observations and information for society, vol 2. ESA Publication WPP-306, Venice, 21–25 Sept 2009
124. Kieke D et al (2007) Changes in the pool of Labrador Sea water in the subpolar North Atlantic. Geophys Res Lett 34: L06605. doi:10.1029/2006GL028959
125. Bingham RJ et al (2007) Meridional coherence of the North Atlantic meridional overturning circulation. Geophys Res Lett 34(L23606). doi:10.1029/2007GL031731
126. Biastoch A et al (2008) Causes of interannual-decadal variability in the meridional overturning circulation of the midlatitude North Atlantic Ocean. J Clim 21(24):6599–6615
127. Baehr J, Stroup A, Marotzke J (2009) Testing concepts for continuous monitoring of the meridional overturning circulation in the South Atlantic. Ocean Model 9:147–153
128. Bacon S, Saunders PM (2009) The deep western boundary current at cape farewell: results from a moored current meter array. J Phys Oceanogr 40:815–829
129. Garzoli S et al (2010) Progressing towards global sustained deep ocean observations. In: Hall J, Harrison DE, Stammer D (eds) Proceedings of OceanObs'09: sustained ocean observations and information for society, vol 2. ESA Publication WPP-306, Venice, 21–25 Sept 2009
130. Gordon A et al (2010) Interocean exchange of thermocline water: indonesian throughflow; "Tassie" leakage; Agulhas

leakage. In: Hall J, Harrison DE, Stammer D (eds) Proceedings of OceanObs'09: sustained ocean observations and information for society, vol 2. ESA Publication WPP-306, Venice, 21–25 Sept 2009
131. Weijer W et al (1999) Impact of interbasin exchange on the Atlantic overturning circulation. J Phys Oceanogr 29:2266–2284
132. Caltabiano A (2007) A monitoring system for heat and mass transports in the South Atlantic as a component of the Meridional Overturning Circulation, Estancia San Ceferino, Buenos Aires, Argentina, May 8, 9, and 10, 2007. In: Workshop report. 2007, International CLIVAR Project Office: Southampton, p 38
133. Rintoul S et al (2010) Southern ocean observing system (SOOS): rationale and strategy for sustained observations of the southern ocean. In: Hall J, Harrison DE, Stammer D eds) Proceedings of OceanObs'09: sustained ocean observations and infomation for society, vol 2. ESA Publication WPP-306, Venice, 21–25 Sept 2009
134. Send U et al (2010) OceanSITES. In: Hall J, Harrison DE, Stammer D (eds) Proceedings of OceanObs'09: sustained ocean observations and information for society, vol 2. ESA Publication WPP-306, Venice, 21–25 Sept 2009

Books and Reviews

Pickard GL, Emery WJ (1990) Descriptive physical oceanography: an introduction, 5th edn. Pergamon, Elsevier Science Ltd., Oxford, U.K. ISBN 008 0379532
Siedler G, Church J, Gould J (eds) (2001) Ocean circulation and climate, vol 77, International Geophysics Series. Academic, San Diego
Tomczak M, Godfrey JS (2003) Regional oceanography: an introduction, 2nd edn. xi+390p., figs., tabls., ind., 25 cm, Pergamon, Elsevier Science Ltd., Oxford, U.K. ISBN: 8170353068
Warren B, Wunsch C (eds) (1981) Evolution of physical oceanography. MIT Press, Cambridge, MA

Lead Acid Battery Systems and Technology for Sustainable Energy

Kathryn R. Bullock
President, Coolohm, Inc., Blue Bell, PA, USA

Article Outline

Glossary
Definition of the Subject
Introduction
Lead-Acid Battery Markets
Sources of Information on Lead-Acid Batteries
Battery Designs
Battery Discharge Reactions
Battery Discharge Rates
Overcharge Reactions
Battery Maintenance and the Effect of Temperature
Future Directions
Bibliography

Glossary

AGM Absorptive glass mat, a battery separator material.
Ah Ampere-hour: dc current multiplied by time of charge or discharge.
Monopolar cell String of cells connected in series (+ − + − + −).
Bipolar plate Conductive, nonporous substrate with negative active material on one side and positive active material on the opposite side.
e^- Electron.
Float V Voltage applied to sustain battery Ah capacity.
Flooded cell Lead-acid cell saturated with aqueous sulfuric acid electrolyte.
Gel cell Lead-acid cell with a gelling agent added to the electrolyte.
HEV Hybrid electric vehicle.
KVA Kilovolt amperes, unit of electrical energy in an ac circuit.
H_2SO_4 Reactant at both electrodes; electrolyte when aqueous.
MSDS Material safety data sheet (for information on a battery product).
Pb Lead metal, the main negative electro-active material.
PbO_2 Lead dioxide, the main positive electro-active material.
$PbSO_4$ Lead sulfate, the discharge product on both electrodes.
SLI Starting, lighting and ignition automotive battery.
UPS Uninterruptible power system.
VRLA cell Lead-acid cell with one-way pressure-relief valve.

Definition of the Subject

Work on optimizing battery designs to fit the needs of each emerging application has been an ongoing process

since Gaston Planté first demonstrated the lead-acid battery in France in 1859 [1]. This article describes many different commercial lead-acid battery designs and electrical requirements in a wide range of applications. Commercial lead-acid batteries are increasingly used for sustainable energy storage and power system regulation. Their global availability and the low cost of their components, their reliability under many operating conditions and their established recycling industry are among the reasons that the technology is finding additional markets in sustainable energy systems.

Adapting battery designs to further optimize their performance in new applications has been a successful international effort for 150 years and continues to generate improved battery designs and power systems for the future.

Introduction

A wide range of designs and sizes of lead-acid batteries are manufactured for traditional markets. Examples of applications are automotive vehicle starting, lighting and ignition; stand-by power back-up for electrical and nuclear energy and safety systems; and vehicle propulsion. Growing use of lead-acid batteries for storing sustainable energy has led to new designs with improved performance and longevity. New lead-acid battery designs for hybrid electric vehicles are under development. A recent 144 V Ultra battery design with negative plates made of carbon and lead in a parallel configuration exceeded 100,000 miles when substituted for nickel metal hydride battery in a Honda Insight [2].

The electro-active ingredients of lead-acid batteries, based on lead, sulfuric acid, water and oxygen, are available around the globe. Small amounts of other common materials such as carbon, barium, and lignin from wood are also added. Plate separators, battery cases and other inert parts are generally made from glass and common plastics, such as polypropylene and polyethylene. Another environmental advantage is that a well-developed commercial battery recycling system has a proven record of recycling more than 97% of spent lead-acid cells and batteries in the United States and Europe. These advantages are major reasons why the lead-acid battery has remained the most widely used energy storage device for large-power sustainable energy systems.

Commercial designs range in size from single cylindrical 2-V "D" cells for portable equipment to large strings of prismatic battery modules for both stationary and motive power. A 6 V battery is achieved with a series connection of three 2-V cells in a string, in contrast to the four cells that are required for 6-V nickel-metal hydride or nickel-cadmium batteries. Higher lead-acid battery voltages in multiples of two are made by adding more cells to the string. Batteries for cars with gasoline engines or micro-hybrid systems typically have 6 cells connected in series to produce 12 V. DC standby-power systems that back-up telecommunication systems are usually 24 or 48 V modules. Medium hybrid electric vehicles (HEVs) with power-assist systems have a battery voltage in the range of 100–150 V. Some large stationary applications, as well as full hybrid electric vehicles, require a battery voltage over 200. The practice of balancing individual cells to maintain optimum electrical performance and long battery life increases in difficulty with the battery string voltage.

Lead-Acid Battery Markets

The largest and most familiar market for lead-acid batteries is vehicle starting, lighting and ignition (SLI). In addition to passenger cars and trucks, the SLI market includes batteries for motorcycles, off-road vehicles, motorboats, airplanes, racing cars, and other mobile devices. Only a small percentage of the total energy in the battery is used to start a car at moderate temperatures but the electrodes must have very high surface areas to yield the larger currents needed for cold engine starts.

SLI batteries must also provide higher amp hour (Ah) capacity at the lower currents needed to power the lighting, entertainment, safety, and other on-board electronic equipment. In addition to electrical drains from on-board equipment, batteries lose charge by internal chemical self-discharge processes. In cold weather these processes are slow, but when the vehicle is parked in hot environments, higher self-discharge rates can reduce the battery voltage and current needed for engine starting. When stored in hot environments, vehicles and boats that are not used regularly can fail to start because of these self-discharge processes.

Lead-acid batteries are also used for emergency power in uninterruptible power systems (UPS),

telecommunications back-up systems, and safety equipment in critical applications such as hospitals and nuclear power plants. Stationary or "standby" battery designs and recharge profiles vary according to the specific system requirements. Large battery strings are connected in series to deliver up to several hundred volts.

In telecommunication back-up power systems, stationary batteries are typically charged continuously at low constant voltage, called the "float voltage" or at low constant current to maintain their energy levels. The batteries contain enough capacity to provide emergency power during long electrical outages of 8 h or longer or until a generator can be brought up to power the system. When power outages are short and infrequent and the battery electrical grid is restored, the float charging will continue. For longer electrical outages, a higher charging rate may be specified to recharge the battery as quickly as possible.

Large digital data centers that support online computers have been increasing rapidly in recent years. The market is driven by the very high cost penalty incurred when computers go offline due to a power outage in one of these centers. The batteries are designed to replace ac power and are therefore rated in KVA.

Deep-cycle batteries store and deliver energy for motive power applications, such as golf carts, forklift trucks, and airport service vehicles. Use of batteries to power robots for duty cycles in highly automated or hazardous applications is also growing. The number of charge–discharge cycles that they can deliver during their lifetime is a function both of the cell design and the battery cycle profile.

In a temperate climate zone, batteries used for solar energy storage generally do not undergo repetitive, deep-discharge cycling. Instead the energy storage system is designed to cycle at a daily partial-state-of-charge cycle in which the battery charges on sunny days and discharges when used at night or on overcast days. During the summer, the photovoltaic system will provide extra energy that can gradually increase the battery state of charge. But during the winter months the battery state of charge will gradually decrease. In temperate climates the use profile may, therefore, be shallow daily cycles within a single deep yearly cycle.

Energy from remote wind turbines can be stored in lead-acid batteries designed to accept high power peaks. These batteries may also be used to filter power peaks and maintain grid stability when wind energy is added to the electrical grid system.

Hybrid electric vehicles (HEVs) are a new and even more demanding partial state-of-charge applications. The battery powers the SLI functions but is also used to assist other functions in the vehicle propulsion system. A high current charges the on-board battery when the vehicle brakes are applied. When the vehicle accelerates, the battery discharges rapidly to provide the required power. If the car is parked for long time in a hot environment, the battery can also self-discharge. Although the battery-operating modes depend on the vehicle design and usage, many of these HEV batteries operate in a narrow range between about 30 and 70% state-of-charge [2].

Nickel metal hydride and lithium batteries are also under development for HEVs. However, safety, low cost and readily available materials give lead-acid batteries some important advantages for a consumer mass market. In addition, an industry is already in place and well capable of recycling nearly 100% of commercial lead-acid batteries.

In early hybrid electric vehicle testing, high currents needed for acceleration and regenerative braking and minimal recharge times limited the cycle life of VRLA batteries. Several modifications to the battery design have greatly improved the battery's high-rate performance in typical HEV driving cycles. For example, conductive particles have been added to the electro-active lead material in the negative plate to increase its electrical conductance and its electrolytic capacitance.

The new lead/carbon acid battery design, called the Ultra battery, shows promise for use in HEV and other partial-state-of-charge applications. Scientists at CSIRO in Australia invented the Ultra battery, and Furukawa in Japan has developed a manufacturing process that has been licensed in the United States and Europe.

The Ultra battery design [2] substitutes a carbon electrode for a portion of each negative lead electrode. The combination of the carbon negative and the lead-dioxide positive electrode provides a pseudo-capacitor in parallel with a normal lead-acid battery in the same cell. The pseudo-capacitor can operate at high currents for short periods of time to reduce the stress on the

battery. Meanwhile, the battery can store chemical energy and supply electrical energy for a longer period of time at a more moderate rate.

Sources of Information on Lead-Acid Batteries

Battery manufacturers often classify lead-acid battery designs in their product specifications and data sheets according to the market application. Common terms are described below so that the reader can understand the type and appropriate use of each battery product.

Battery producers provide technical specifications and material safety data sheets (MSDS) for their products. The data sheets are often available on their websites. Section I of the MSDS shows the battery type and name, and the name and contact information of the manufacturer, including customer service and emergency telephone numbers. Chemicals in the battery are listed in Section 2 and physical and chemical characteristics are shown in Section 3. Section 4 lists fire and explosion hazards based on physical and chemical data. Section 5 provides important safety requirements during shipping and electrical installation and use to avoid shorting and electrical fires. Health hazards and precautions for safe handling, use and disposal are provided in Sections 6 and 7. Control measures, if needed, are provided in Section 8. Information on proper transportation, shipping and handling in Section 9 is essential to ensure good battery performance. Battery manufacturers also give additional information, including disclaimers, in Section 10.

Several large organizations have been instrumental in developing the battery industry in a responsible and innovative approach to meeting the needs of its customers. The Battery Council International [3] publishes manuals, specifications, test methods, and other literature for lead battery users and sponsors symposia on the battery industry. The International Lead Association (ILA) is a consortium of companies in mining, battery design and manufacturing, and recycling, their suppliers, contractors, and other organizations that have a direct interest in lead and its responsible use. ILA also manages an international consortium of companies that are doing cooperative research to develop and improve battery technologies for new applications, as well as environment, health, sustainable development and product-related research programs.

Battery Designs

Monopolar and Bipolar Electrodes

Commercial batteries are typically monopolar designs. Monopolar cells are made in a stack of a single positive electrode, a porous, nonconductive separator, and a single negative electrode. To increase the cell capacity, the series stacking process continues with separator/positive/separator/negative layers to produce a larger stack of plates that will deliver the required cell capacity. In each cell the negative electrodes are all connected in series by a conductive lead strap and terminal called the "top lead." The same method is used to connect the positive plates to the positive top lead.

The negative and positive terminals collect the current in each cell and conduct it to the external negative or positive post, respectively. The battery is sealed to avoid electrolyte leakage and air ingress, but one-way pressure relief valves are required to release small quantities of gas that may be generated during recharge. Most batteries have a pressure valve in each cell, but some designs use a single pressure relief valve for all cells.

Bipolar designs have been tested over many years, but are still under development. They are especially desirable for applications that require high voltage and power but can store only limited capacity per unit cell. One developing application is for hybrid electric vehicles. They require batteries with high current capability for short times to store regenerative braking energy and for vehicle acceleration. Each electrode in a bipolar cell has a positive side and a negative side with a solid partition between them that conducts electrons but not ions. The partition material must also be noncorrosive to prevent shorting through the partition walls.

Bipolar electrodes are stacked to produce a battery of cells connected at the partitions. If the cells in a bipolar battery are not rigorously sealed around the edges, electrolyte leaks can provide a shunt current path between cells, which reduces the battery performance. Researchers continue to look at new materials and designs for commercial bipolar batteries. Recent work to develop bipolar batteries is discussed further in Future Development at the end of this article (Fig. 1).

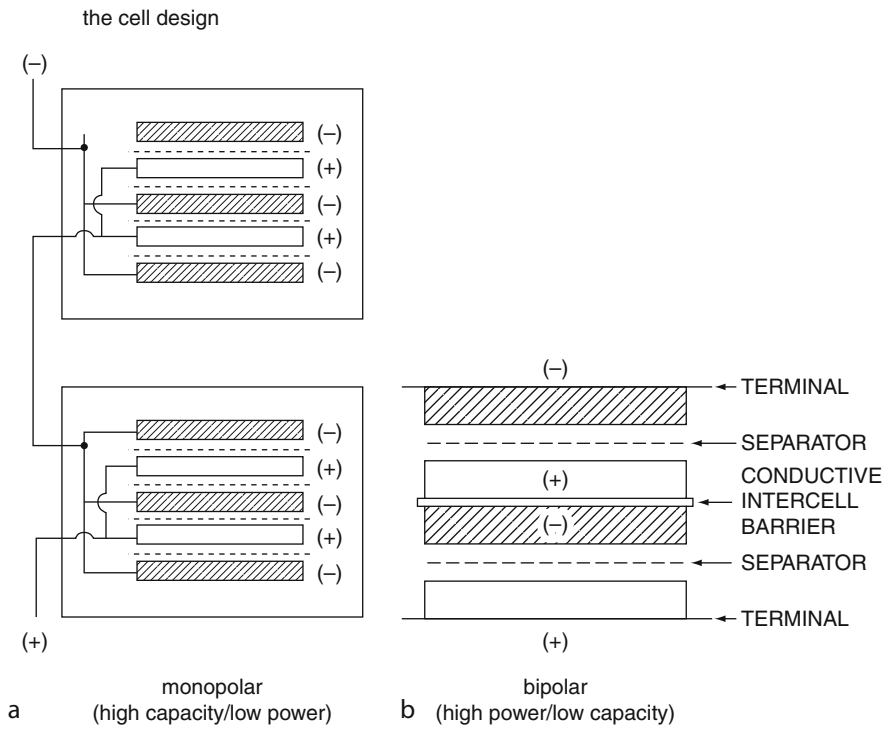

Lead Acid Battery Systems and Technology for Sustainable Energy. Figure 1
Schematic of monopolar and bipolar battery designs [4] (Electrochemical Society approval obtained)

Flat and Tubular Electrodes

Lead-battery electrodes can be made as a flat plate with a lead grid as the current collector or as a tubular plate design with a lead rod current collector in the center of tubes. Monopolar electrode current collectors have a conductive lead grid that connects with the terminal. The current collector physically supports the electrode and also collects and carries the current to the electrical system.

Flat grids are often made by pouring molten lead into a mold and cooling it to form a grid with holes for the active materials. Other approaches to making grids are to punch holes in flat lead sheets or to slit the lead sheets and then expand the slits to make the holes for the active material paste.

Tubular positive plates are sometimes used in batteries for deep-discharge applications to reduce shedding of electro-active materials from the plate during cycling. The positive electrode has interconnected porous tubes that are filled with positive lead paste. Lead rods in the centers of tubes are connected in parallel by a conductive lead bar at the top, and the bar is connected to the positive terminal.

Tubular batteries have flat negative plates opposing the positive tubular plates. Recent approaches to preventing positive plate shedding with improved separator designs have limited the use of tubular positive plate batteries. They are primarily in applications that have deep-discharges or severe vibration.

Lead Alloys in Grids and Gas Venting Systems

Because water electrolysis on pure lead is a very slow process, pure lead grids have good corrosion resistance in aqueous sulfuric acid. However, lead is a soft metal that is easily bent out of shape unless it is alloyed with stronger metals. This problem was solved between 1880 and 1890 by adding up to 12% antimony and a lesser amount of arsenic to the lead. These additives increase the mechanical strength of the grid, but unfortunately they also increase water loss and accelerate hydrogen

evolution when the batteries are charged. Batteries with grids containing antimony are designed to vent the oxygen and hydrogen that water electrolysis produces, but periodic water additions are necessary to maintain life. Higher levels of room ventilation are also required to maintain safety.

Lead-alloys containing calcium were introduced in 1935 by Haring and Thomas of Bell Laboratories [5] to reduce water loss and ventilation requirements. These designs are often called low-maintenance batteries, because water additions are not required and now are often prevented by battery manufacturers to minimize electrolyte contamination. Some of the lead alloys in these designs have lower levels of antimony, typically 1–3%. Others use a combination of calcium and tin in the lead. Specially designed vent valves with a flame arrestor are installed to prevent an external spark from igniting hydrogen gas in the battery.

In about 1970, Sonnenschein in Germany [6] began using finely divided fumed silica to gel the sulfuric acid and reduce acid leakage. The technology was applied to portable or power equipment. At about the same time Don McClelland and John Devitt at Gates Rubber Company [7] invented a valve-regulated lead-acid (VRLA) battery with an absorptive glass mat (AGM). This valve reduces acid leakage while retaining the power capability of a liquid electrolyte system. The spirally wound battery design in Fig. 2, based on the Gates Rubber Company patents, is now manufactured by EnerSys Energy Products, Inc.

VRLA batteries have a one-way pressure relief valve that opens when the internal battery pressure increases to a specified valve design level between 1 and 30 psi. The valve closes when the internal battery pressure decreases. Some VRLA batteries have grids made of pure lead or pure lead with a little tin added. The design intent is to facilitate the recombination of the oxygen and hydrogen within the cell by re-forming the water during charge. This process, often called "the oxygen cycle," can reduce the amount of hydrogen vented over the life of the cell but will not entirely eliminate it. Room ventilation must be adequate to handle a worst-case condition, such as a high battery temperature, when the batteries are on charge. Water electrolysis and hydrogen venting accelerate with increasing battery temperatures during charge. Other options for controlling battery life and safety are monitoring and control of the environment, and smart battery charging using algorithms and electronic control methods.

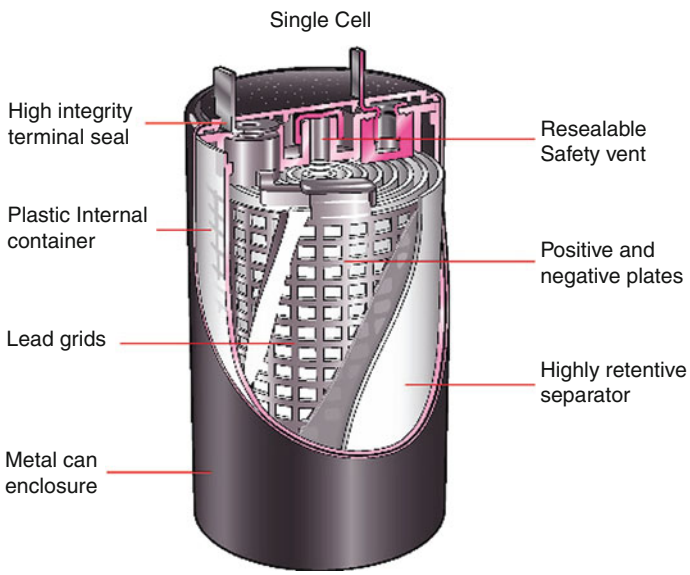

Lead Acid Battery Systems and Technology for Sustainable Energy. Figure 2
Cutaway of valve-regulated lead-acid cell (EnerSys Energy Products, Inc., approval obtained)

Electrode Active Material Preparation

The electrodes in the first lead-acid battery were made by repeatedly charging and discharging lead plates in sulfuric acid mixed with forming agents to facilitate surface corrosion. Because the electrochemical formation process requires a large amount of time and energy to produce high battery capacity, electrochemically formed plates are now typically used mainly for heavy-duty industrial applications where very rugged plate designs are required.

Today, pasted plates are more common. They are made by mixing lead oxide powders with aqueous sulfuric acid and other minor additives to form a lead oxide paste that can be spread onto a lead grid. Since the negative plate surface area tends to shrink during battery cycling, a mixture of fine carbon particles, lignin derived from wood, and barium sulfate is typically added to maintain a high plate surface area. This additive is called an expander mixture. The expander mix is changing as new battery designs and applications emerge.

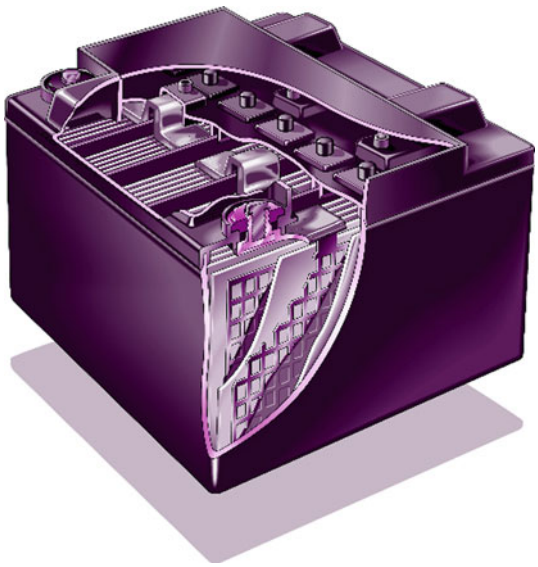

Lead Acid Battery Systems and Technology for Sustainable Energy. Figure 3
Cut-away of VRLA AGM battery with low profile (EnerSys Inc., approval obtained)

Electrolyte Systems: Flooded, Gel, and Absorptive Glass Mat (AGM)

The sulfuric acid used in lead-acid batteries is a combination of sulfuric acid (or dihydrogen sulfate, (H_2SO_4) and water (H_2O)). Acid concentrations in automotive batteries are about 35% H_2SO_4. The cells are "flooded" with excess electrolyte to prevent the battery from drying out during use.

Two types of electrolyte systems use methods to immobilize the liquid battery acid. The first design, which was developed in Germany, is called a "gel" battery because finely divided silica is added to "gel" or thicken the electrolyte. Gelling prevents the aqueous sulfuric acid from leaking or spilling if the battery is tipped. The other method, developed in the USA in about 1970, is absorbing a more highly concentrated acid in a porous glass mat (AGM). The acid concentration in the AGM battery was increased from about 35% in liquid and gel batteries to about 40% acid in AGM batteries. This reduces the water volume in each cell and makes the battery more sensitive to dry-out in hot environments. However, the AGM design has the advantage of higher discharge power compared to a gel battery design (Fig. 3).

A spirally wound, 2 V AGM battery was the first VRLA design used commercially. The valve was designed to open at 30–50 psi. The cell was made by stacking single strips of a positive plate, AGM separator, and a negative plate together, rolling the stack up like a jelly roll, and inserting it in a cylindrical case. The design was called a gas recombinant battery because it reduced the amount of water lost in the battery during charge by recombining the hydrogen and oxygen that are formed on overcharge.

Lower electrolyte volumes and higher acid concentrations of VRLA AGM batteries also allowed designers to lower the height of rectangular cases. Since typical rectangular battery containers cannot withstand high pressures, their valve-opening pressures may be only a few pounds per square inch (psi). Gel batteries became VRLA batteries when they adopted one-way pressure relief valves. Most of the Gel and AGM batteries are now rectangular. All of these designs are called VRLA batteries.

Gel batteries are finding a new market in storing energy from solar cell arrays. The acid concentration in gel batteries is similar to flooded lead-acid batteries. One-way pressure relief valves help to retain the water

in hot environments. Compared to AGM batteries, gel batteries are less susceptible to drying out, because they contain more acid.

Battery Discharge Reactions

The lead-acid battery electrolyte (sulfuric acid) participates in the electrode reaction at both the positive and the negative plate when the battery discharges. Sulfuric acid dissolves in water (H_2O) and dissociates into ions in two steps. First, sulfuric acid forms hydrogen and bisulfate ions [1]

$$H_2SO_4 \Leftrightarrow H^+ + HSO_4^-.$$

These ions transport the electric charge between the electrodes. If the sulfuric acid in the electrolyte is very dilute, the bisulfate ion may dissociate further to hydrogen and sulfate ($SO_4^=$) ions: [2]

$$HSO_4^= \Leftrightarrow H^+ + SO_4^=.$$

The total reaction is [3]

$$H_2SO_4^= \Leftrightarrow 2H^+ + SO_4^=.$$

The standard negative electrode voltage on open circuit is $E_0 = -0.358$ V when measured versus a standard hydrogen electrode. During discharge, lead (Pb) oxidizes by reacting with the bisulfate ion and loses two electrons to form lead sulfate ($PbSO_4$). The reaction is [4]

$$Pb + HSO_4^- \Leftrightarrow PbSO_4 + H^+ + 2e^-.$$

The electrons from reaction [4] are transferred through the external electric circuit to the positive electrode, where lead dioxide (PbO_2) is reduced by reacting with two electrons (e^-), as well as hydrogen and bisulfate ions, forming lead sulfate and water. The reaction is [5]

$$PbO_2 + 3H^+ + HSO_4^- + 2e^- \Leftrightarrow PbSO_4 + 2H_2O.$$

The standard potential of this reaction [5] is +1.690 V versus a standard hydrogen electrode. (May want to use Parsons' book as reference in addition.)

The overall cell reaction is determined by adding reactions [4] and [5] to get the double sulfate reaction [6]

$$PbO_2 + Pb + 2H_2SO_4 \Leftrightarrow 2PbSO_4 + 2H_2O.$$

Reaction [6] is called the double sulfate reaction because sulfuric acid reacts at both electrodes. A resistive layer of lead sulfate crystals forms on both the positive and negative electrode surfaces. The equilibrium cell voltage is the sum of the two electrode reactions:

$$V^0 = +1.690\ \text{V} - (-0.358\ \text{V}) = 2.048\ \text{V}.$$

The voltage decreases as the sulfuric acid concentration decreases. A simple way of determining the relative state of charge of the battery is measuring the battery voltage on open circuit at room temperature. Temperature corrections can be made at higher or lower battery temperatures. Assuming that the battery is at room temperature is usually sufficient unless the batteries have been stored for hours in an uncontrolled hot or cold environment or are operated at high currents.

The theoretical specific energy of the lead-acid battery is calculated below using the molecular weights of the reactants and the chemical formulas. The number of electrons exchanged is an important factor in the energy density of a battery reaction, because it determines the total current that the reactants can deliver. A disadvantage of lead-acid batteries is the high molecular weight of lead. However, the water-based electrolyte is relatively light, and the reaction has the advantage of exchanging two electrons instead of only one.

The number of atoms in these reactions multiplied by the atomic weight of the atom determines the total molecular weight of the reactants:

O weighs 16.0 g/mole($\times$10 moles weighs 160.0 g);
H weighs 1.0 g/mole($\times$4 moles weighs 4.0 g);
Pb weighs 207.2 g/mole($\times$2 moles weighs 414.4 g); and
S weighs 32.1 g/mole($\times$2 moles weighs 64.2 g).

The total equivalent molecular weight of the reactants required to generate 2 moles of electrons in the discharge reaction is 646.6 g.

The calculation of the theoretical specific energy is shown below. The theoretical specific energy at 2.048 V is 170 W h/kg of material weight.

$$170\ \text{Wh/kg of reactants} = \frac{2.048\ \text{V} \times 2\ \text{moles e}^- \times 96{,}500\ \text{As/mole e}^-}{646.6\ \text{g reactants} \times 3600\ \text{s/h} \times 1\ \text{kg/1000 g}}$$

This type of calculation can be useful as a means of comparing the theoretical specific energies of different

batteries. Practical energy densities are design dependent and typically deliver no more than 20–40% of the theoretical specific energy.

Battery Discharge Rates

The reversible voltage of 2.048 V is for the lead-acid battery at a room temperature of 25°C and one atmosphere pressure in a dilute acid concentration. Lead-acid batteries have higher acid concentrations when fully charged, so the reversible voltage is higher. During discharge the reversible voltage drops rapidly at the beginning of the discharge until it reaches an initial voltage plateau. Then the voltage decreases more slowly to the discharge cut-off voltage. The initial drop is in part due to the internal resistance of the battery and in part due to the initial rapid depletion of the sulfuric acid concentration at the surface of both the positive and negative electrodes.

The actual discharge capacity is the current (I) multiplied by the discharge time (t) in ampere hours. The rate of discharge, or current, strongly affects the initial voltage drop and the slope of the plateau voltage. The higher the discharge rate, the shorter the discharge time and the smaller the capacity will be. This is because hydrogen and bisulfate ions must carry the charge between the electrodes through the porous separator and acid film at the electrode surfaces.

The horizontal x axis is the log to the base 3 of the discharge current, and the vertical y axis is the log to the base e in discharge time.

The discharge time is a function of discharge current. $I^n t = C$ where I is current in amperes and t is the discharge time in hours for a specific battery design measured at three or more discharge currents and C is a constant. When these values are plotted on a log–log scale, the constant n is the slope of a straight line. It is typically 1.3–1.4 but approaches 1 at very small currents and 2 at high currents. The example in Table 1 and Fig. 4 is based on three discharges of a VRLA battery.

The discharge reactions are reversed when the cell is recharged. If each of these discharge reactions is reversed and the discharge reactions are added together, the reaction [7]

$$2PbSO_4 + 2H_2O \Leftrightarrow PbO_2 + Pb + 2H_2SO_4$$

is the reverse of the double sulfate reaction [6].

Lead Acid Battery Systems and Technology for Sustainable Energy. Table 1

Discharge amperes (I)	Discharge hours (t)	Ampere hour capacity (AH)[a]
5	9	45
12	3.6	43.2
25	1.4	35
$\ln C = n \ln I + \ln t$		
$4.078 = 1.15 \ln I + \ln t$		

[a]Based on three discharges of one battery

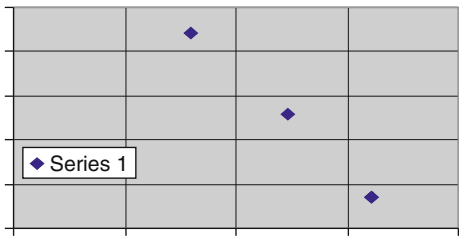

Lead Acid Battery Systems and Technology for Sustainable Energy. Figure 4
Relationship between the discharge time and current in a lead-acid battery

When the battery reaches a voltage level that corresponds to about 90% state of charge, the recharge reaction becomes less efficient as water in the electrolyte begins to form oxygen at the positive plate and hydrogen at the negative plate. This process accelerates as recharge currents and/or internal cell temperatures increase. To control water electrolysis, the charging current is generally decreased as the battery receives its finishing charge. Many lead-acid battery designs are able to recharge up to the gassing level relatively quickly, but the finishing charge will take longer to avoid rapid water loss and high gassing rates. The battery manufacturer's recommendations should be carefully followed, since charge methods and charging times are design-dependent.

Overcharge Reactions

Overcharge is defined as the amp hours of charge put into the battery in excess of the amount of Ah taken out of the battery during the previous

discharge. Because charging is not 100% efficient, all lead-acid batteries must be overcharged to return them to full capacity.

The finishing charge and overcharge reactions that electrolyze water form a mixture of hydrogen (H_2) and oxygen (O_2) gases. At the positive plate, [8]

$$H_2O \Rightarrow 2H^+ + {}^1/_2\, O_2 + 2e^-$$

at the negative plate [9]

$$2H^+ + 2e^- \Rightarrow H_2.$$

The total overcharge reaction is the electrolysis of water to form oxygen and hydrogen [10]

$$H_2O \Rightarrow H_2 + {}^1/_2\, O_2.$$

Thermodynamic measurements of these reactions at platinum electrodes show that it takes less energy to electrolyze water in the electrolyte than to recharge lead sulfate. If this were true in the lead-acid battery, it could not be recharged. Lead-acid batteries recharge efficiently because of the low rate of water electrolysis on lead. The reason is that the hydrogen evolution reaction is impeded on the surface of the lead electrode. As a result, the lead-acid battery can deliver a higher voltage than other aqueous rechargeable batteries.

Impurities in the battery electrolyte lower the cell voltage and may increase water loss. When electrolyte purity is well controlled, the capacity can be returned more rapidly because the end of the recharge is more efficient. The final part of the recharge is controlled either by "floating" the battery at a voltage that is slightly above the open circuit or by applying a small "trickle" current to the battery. Floating or applying a trickle current near the end of charge minimizes the water loss.

The oxygen generated at the positive electrode is not very soluble in the sulfuric acid, so it vents out through the battery valve. However, in a VRLA battery, the oxygen cycle recombines the oxygen and prevents hydrogen from forming at the negative electrode by the following equations.

The positive plate reaction is [8] $H_2O \Rightarrow 2H^+ + {}^1/_2\, O_2 + 2e^-$ shown previously. The negative plate reactions may be a two-step process: [11] $Pb + {}^1/_2\, O_2 + H_2SO_4 \Rightarrow PbSO_4 + H_2O$ and [12] $PbSO_4 + 2H^+ + 2e^- \Leftrightarrow Pb + H_2SO_4$. When these equations are added up, the overall reaction is the double sulfate reaction [1] discussed above

$$2PbSO_4 + 2H_2O \Leftrightarrow PbO_2 + Pb + 2H_2SO_4$$

Since the oxygen generated at the positive electrode is not very soluble in the acid, it will vent out through the valve of a flooded lead-acid battery, and the opportunity to reform the water will be lost. A VRLA battery design allows the oxygen to travel to the negative plate through the AGM separator, because the separator pores are not fully saturated with acid. The acid volume is reduced in the separator by decreasing the percentage of water in the electrolyte. Because of the higher acid concentration, there is free space for oxygen to travel from positive to negative electrode as a gas instead of dissolving in the electrolyte. The oxygen reacts at the negative plate to reform water, because the negative electrode surface has a three-phase gas/liquid/solid interface.

Battery Maintenance and the Effect of Temperature

Lead-acid batteries have a variety of failure modes that depend on the design, the use mode, and the environment. Manufacturers generally provide information about the life of their battery designs in a particular application. Some factors that can shorten the useful battery life are, however, applicable to most designs and applications. One of the most important variables in predicting battery life is the ambient temperature.

Low ambient temperatures reduce the battery voltage and current while high temperatures reduce battery life. For example, automotive batteries often fail to start the engine in the winter for two reasons. First, the power (voltage times current) that is required to start a cold engine increases. And second the battery power is reduced because cold temperatures decrease both the voltage and current that the battery can deliver. High summer temperatures decrease battery life because of increased grid corrosion and other side reactions that lead to battery failure.

Although automotive batteries often fail to start a vehicle in the winter when the ambient temperature is low, battery storage at high temperatures is often the cause of the battery deterioration and failure. If the battery is subjected to high heat for a long time,

reactions that wear out the battery, such as grid corrosion, water loss, and formation of hard lead sulfate on the plate surfaces, will be accelerated.

Application of batteries in other uncontrolled environments, such as outdoor telecommunications cabinets, photovoltaic systems, and marine uses also reduces battery life. When batteries are operated in hot environments, manufacturers often recommend reducing the charging current or float voltage to prevent the battery from overheating.

Battery life can also be reduced by storage on open circuit for a long time. Chemical reactions will self-discharge the battery gradually over its "shelf life." Since heat increases the rates of these chemical reactions, the battery shelf life will be longer if the battery is stored at a moderately cold temperature. The rates of most battery degradation mechanisms are reduced at low temperatures. The electrolyte in a fully charged battery does not freeze until the temperature reaches about minus 40°C. However, the battery freezing temperature will rise to 10–15°C when the battery is discharged.

Future Directions

Increasing use of renewable energy from wind turbines will increase the need for batteries with both higher power and increased energy storage. Wind is variable and tends to be higher at night when electricity is used less by energy consumers. When wind energy is fed into the ac electric grid, this variability frequently causes instability in the grid system. Several new approaches to developing higher-power lead-acid batteries for renewable energy storage are discussed below.

The thixotropic gel that is typically used in VRLA batteries is liquefied by agitation before being poured into the cell. It then solidifies around and within the plate separators. C&D Technologies developed a battery using a colloidal, poly-silica gel that does not have to be liquefied before it is poured into the cell. The gelling solution can be added after the AGM separator between the plates is soaked with acid, so less gel penetrates into plate area. The AGM separator maintains the high power capability of the AGM battery design, while the gel around the edges of the plates provides an additional source of aqueous electrolyte. This extends the cycle life by reducing the rate of water loss. This concept has been tested in a commercial 485 Ah C&D model 12SL 78-13 battery, which is designed for motive power and materials handling equipment [8].

Lead-acid batteries with high power capability may be required to stabilize the future grid system as more wind energy is fed into it. Use of a battery/capacitor combination may be necessary, but the physical space of the system must also be acceptable. The Ultra battery [2], which has both a super capacitor and a storage battery in the same module, is one very interesting way to address this need. In 2010, a 144 V Ultra battery design passed a 100,000-mile test in a Honda Insight at the Millbrook test track in the United Kingdom with no conditioning and in an excellent state of health. After passing that test, the battery was returned to Furukawa in Japan for continued use (Fig. 5) [2, 9].

If the history of lead-acid batteries is an indicator, the performance of a super capacitor and storage battery combination will likely be improved further as additional materials and designs are developed and field experience with the HEV and wind energy applications increases. Other sustainable energy systems that operate over a wide range of currents may also benefit from this work. Many types of carbons as well as other materials are being studied. The challenge is to find materials that are low cost and are also compatible with the lead-acid system.

High battery voltages and power capacities in a small footprint will also be needed to power equipment in off-grid applications. Bipolar lead-acid batteries are most desirable for high voltage applications that do not require large amounts of energy. Researchers continue to look at new materials and designs that will improve the life and performance of bipolar batteries. Atraverda Ltd. in the U.K. uses Ebonex®, a ceramic material based on conductive titanium oxides, for its bipolar battery partitions and case.

Effpower® tested a lead infiltrated ceramic (LIC™) bipolar battery in a Honda Insight for 15,000 km in Gothenburg, Sweden [9]. Their conductive ceramic has pockets containing lead on the negative side and lead dioxide on the positive side of the partition. They have announced plans to start production of 24 V and 150 V lead-acid battery modules in 2011 in partnership with Banner Batterien in Austria. Both batteries are 6 Ah designs. The 24 V lead-acid battery module is rated at 5 KW/8.6 kg in a 90 × 253 × 203 mm

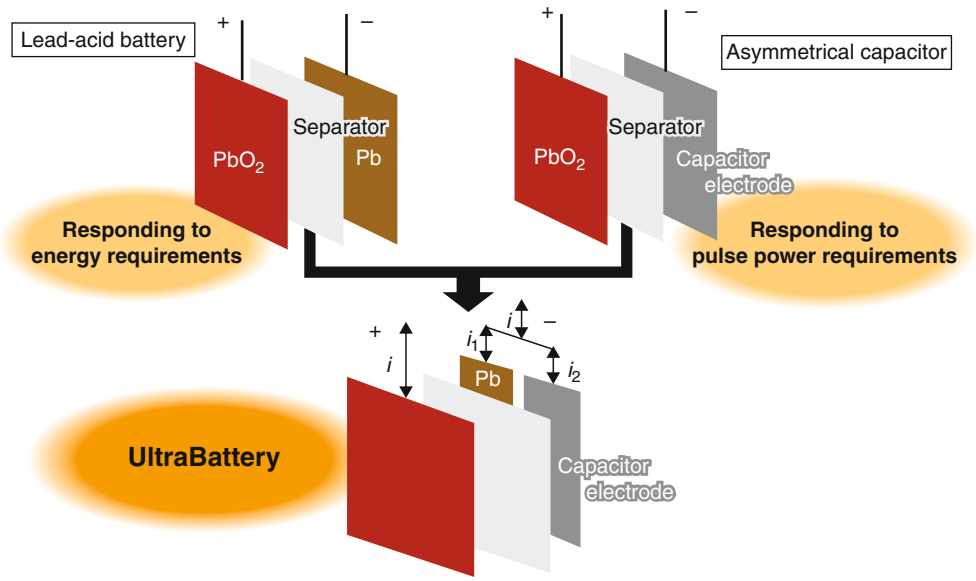

Lead Acid Battery Systems and Technology for Sustainable Energy. Figure 5
Diagram of the construction of the Ultra Battery (Furukawa permission obtained)

module (0.58 KW/kg). The 150 V lead-acid battery module has 0.8 KW/kg. An Effpower® battery has also been installed in a 2007 Honda Civic Hybrid and is undergoing testing at the Millbrook testing grounds in the UK [9].

Bipolar batteries are susceptible to two failure modes that are not found in monopolar designs. (1) When seals around the outside edges of bipolar partitions fail, leakage currents between cells will cause a decline in cell performance. (2) An electrical short through a pinhole in the bipolar partition can cause sudden battery failure. Much progress has been made in bipolar module technologies. Finding the right materials, designs and construction technologies, and improving our understanding of application modes, will be ongoing as new bipolar battery designs are developed and applied.

Bibliography

Primary Literature

1. Planté G (1859) Compt Rend 49:402
2. Cooper A, Furakawa J, Lam L, Kellaway M (2009) The UltraBattery – a new battery design for a new beginning in hybrid electric vehicle energy storage. J Power Sources 188:642–649
3. Battery Council International (BCI), 401 North Michigan Ave, 24th Floor, Chicago, Illinois 60611–4267. www.batterycouncil.org
4. Bullock KR (1995) Progress and challenges in bipolar lead-acid battery development. J Electrochem Soc 142:1726–1731
5. Haring HE, Thomas UB (1935) Trans Electrochem Soc 68:293+
6. Eberts K (1970) In: Collins DH (ed) Power sources 2. Pergamon Press, Oxford, p 69+
7. McClelland DH (1975) US Patents 3,704,173 and 3,862,361
8. Misra SS, Mraz SL, Dillon III JD, Swanson DB (2003) VRLA battery with AGM-gel hybrid for superior performance. DB IEECE/IEEE INTELEC'03, paper 19–2. www.ieee.org/publications_standards/index.html
9. Moseley PT (2010) The work of the advanced lead-acid battery consortium – continuing in the footsteps of Gaston Planté, plenary lecture, Joseph Priestley Society, Chemical Heritage Foundation, Philadelphia

Books and Reviews

Bard AJ, Parsons R, Jordan J (1985) Standard potentials in aqueous solution. CRC Press, Boca Raton

Berndt D (2003) The lead-acid battery system. In: Ecclestone TL, Shepherd PA (eds) Maintenance-free batteries, 3rd edn. Research Press, Baddock

Bode H (1975) Lead acid batteries. Wiley, New York

Bullock KR, Salkind AJ (2011) Valve regulated lead-acid batteries. In: Reddy TB, Linden D (eds) Linden's handbook of batteries, 4th edn. McGraw Hill, New York (Chap 17)

Bullock KR, Vincent CA (1997) Secondary lead-acid cells. In: Vincent CA, Scrosati B (eds) Modern batteries, 2nd edn. University of Chicago Press, Chicago
Rand DAJ, Moseley PT, Garche J, Parker CD (2004) Valve-regulated lead-acid batteries. Elsevier, Amsterdam

Life Cycle Assessments and Their Applications to Aquaculture Production Systems

Patrik J. G. Henriksson[1,2], Nathan L. Pelletier[3], Max Troell[4,5], Peter H. Tyedmers[3]
[1]Institute of Environmental Sciences, Leiden University, Leiden, The Netherlands
[2]Department of System Ecology, Stockholm University, Stockholm, Sweden
[3]Dalhousie University, Halifax, Nova Scotia, Canada
[4]The Royal Swedish Academy of Sciences, The Beijer Institute of Ecological Economics, Stockholm, Sweden
[5]Stockholm Resilience Centre, Stockholm University, Stockholm, Sweden

Article Outline

Glossary
Definition of the Subject
Introduction
LCA – The Method and Its Applicability in Aquaculture
LCA in Food Production
Guiding the Way for More Sustainable Aquaculture and Alternative Farming Methods
Discussion
Future Directions
Bibliography

Glossary

Aquaculture The farming of aquatic organisms, including fish, mollusks, crustaceans, and aquatic plants. Farming implies some form of intervention in the rearing process to enhance production, such as regular stocking, feeding, and protection from predators. Farming also implies individual or corporate ownership of the stock being cultivated.

Co-product allocation Partitioning the input or output flows of a process or a product system between the product system under study and one or more other product systems.

Functional unit The quantified function provided by the product system(s) under study, for use as a reference basis in an LCA, e.g., 1,000 h of light.

Life cycle assessment (LCA) An ISO-standardized analytical tool developed to evaluate environmental performance of products and processes. It constitutes a compilation and evaluation of the inputs, outputs, and potential environmental impacts of a product system throughout its life cycle; the term may refer to either a procedural method or a specific study.

System boundary Defines the inputs and outputs that are included in the study. System boundaries should be set depending on what will be relevant to the aim of the study.

Definition of the Subject

Aquaculture production has grown three times faster than the livestock sector since the 1970s, becoming a major source of edible seafood and other products. This rapid expansion has, however, had a combination of positive and negative environmental, social, and economic effects. A variety of tools are available to evaluate these impacts in an attempt to identify the most sustainable practices. One of the more recent tools that has been applied to the evaluation of aquaculture production is Life Cycle Assessment (LCA), an ISO-standardized biophysical accounting framework that allows for multi-criteria environmental performance assessments. This chapter reviews studies that have applied LCA to studying the environmental dimensions of aquaculture production to date. Methodological differences and alternative approaches are discussed, along with their influence on research outcomes. There is little homogeneity between the studies when it comes to the choice of functional unit, system boundaries, and basis for allocation. However, several clear trends do emerge that point toward imperatives for sustainable practices in aquaculture and considerations for sustainable development of the industry moving forward. Recommendations for further methodological development of LCA for application to seafood sustainability research are advanced.

Introduction

Society is increasingly aware of both the drivers and consequences of natural resource depletion and environmental degradation. Various analytical frameworks have therefore been developed for the purpose of evaluating the environmental performance of products and processes. Finding a suitable tool for assessing sustainability in the rapidly developing aquaculture sector has gained increasing profile over the past 2 decades. What has emerged is the need for a tool that can incorporate multiple environmental performance criteria in the evaluation of diverse aquaculture production technologies. For this reason, there is increasing interest in, and application of, life cycle assessment (LCA) as a research framework to better understand environmental performance in this sector. The interest has, however, not been coming from within the aquaculture industry itself, but rather outside. LCA is a versatile methodology that is well suited to address a broad suite of resource use and emissions-related issues. Over the last decade, it has become an increasingly common tool for characterizing an important subset of environmental impacts in aquaculture and elsewhere.

Aquaculture Development

Even though global capture fisheries landings have declined since the late 1980s, total production of marine fisheries products has increased 67% between 1970 and 2007 (including brackish water fish). This has only been possible through a large increase in aquaculture production over the last 4 decades. Aquaculture currently provides half of all finfish destined for human consumption. Seafood from all sources accounts for about 20% of all animal proteins consumed by humans, and demand continues to grow [1]. The aquaculture industry is the fastest growing animal products' sector, with an average annual growth rate of 6.9%. At present, it provides almost 8 kg of seafood per capita year^{-1} globally [1]. In 2006, aquaculture accounted for more than 70% of global shrimp and prawn production, 47% of total food fish production, and 36% of total fish production. Mariculture of finfish dominates production in developed countries [2]. By mass, however, the majority of global production is accounted for by carp farmed in extensive and semi-intensive farms in Asia.

Aquaculture comprises an enormous diversity of farming technologies, culture settings, and species. From monoculture to polyculture systems operated in ponds, raceways, land-based tanks, along with cages, pens, poles, rafts, and longlines in open water settings, well over 250 species are currently in culture. Production technologies may also reflect traditional farming methodologies or more modern systems [3–5]. In turn, post-production processing yields a diverse range of products, including salted, dried, smoked, and various kinds of preserved fish. About 37% of all fish and fishery products are traded internationally, with the major importers being Japan, the USA, and Spain [1].

Aquaculture and the Environment

It has been proposed that aquaculture represents the most viable option for meeting future demands for fish, as well as providing economic and nutritional benefits to millions [1]. The recent rapid expansion of this sector has, however, been accompanied by a range of environmental and social concerns, including localized nutrient enrichment or depletion, chemical pollution, genetic pollution, introduction of non-indigenous species, habitat destruction, greenhouse gas (GHG) emissions, depletion of wild fish stocks, inefficient energy and biotic resource usage, and spread/amplification of diseases and parasites [2, 3, 6–9]. Of these, local-scale interactions have traditionally attracted the most attention. However, global scale interactions such as greenhouse gas emissions associated with intensive production strategies are of increasing interest. What has become clear is that each production strategy is characterized by a unique suite of environmental interactions at local, regional, and global scales. Informed decision making for improved environmental management in aquaculture, therefore, requires tools, which can provide multi-criteria environmental performance assessments and make clear the environmental trade-offs associated with specific aquaculture technologies and products.

Sustainability Tools in Aquaculture

Increasing aquaculture production to meet future demands is clearly attractive from a policy and development perspective. However, a number of critical questions related to growth in this sector must be

addressed. These questions encompass complex issues associated with sustainability objectives at local, regional, and international scales. For example, a spectrum of negative ecological and social externalities associated with aquaculture and other food production systems bear careful scrutiny and must be weighed against anticipated benefits [10]. Such comparisons need to extend beyond short-term gains and localized impacts and incorporate a long-term social-ecological resilience perspective. This requires tools to identify the most sustainable aquaculture practices, drawing knowledge from both new and traditional culture systems [5].

A wide range of tools/frameworks for assessing various aspects of environmental performance have been advanced [11], some focusing especially on food production. These include techniques such as Risk Assessment, Ecological Footprint, and Energy Analysis. Frameworks more specific to assessing seafood production systems are Fishprint and the Global Aquaculture Performance Index (GAPI) [10, 12, 13]. Most of these, however, encompass a limited range of the environmental concerns associated with aquaculture and some suffer from a lack of methodological standardization [10]. Moreover, the degree of scientific rigor in both the methods and their application is also variable. Data limitations and analytical scope have, therefore, often led to misrepresentation of the environmental consequences of specific management decisions.

LCA – The Method and Its Applicability in Aquaculture

History of LCA

LCA has, since its emergence in the 1970s, evolved from a tool whose primary application was waste management and energy efficiency management to a more general eco-efficiency measurement framework. It has close links to energy analysis, but is unique among biophysical accountancy-type tools in that it has been internationally standardized (ISO 14040-14044) [14, 15]. An LCA typically begins at the "cradle" of a product or service life cycle (i.e., at the point of primary resource extraction), and extends along the supply chain to encompass all life cycle stages of interest to a particular analysis. Single or multiple impact assessment methods may be applied. Estimation of the cumulative environmental impacts along supply chains permits attention to spatially and temporally discrete impacts not typically considered in more traditional environmental impact analyses. Impact categories range from highly quantifiable effects, such as greenhouse gas emissions or energy use, to (less frequently) more diverse social consequences, such as human health effects [16].

The outcome of a LCA is highly influenced by the ambition, skill, and objectives of the practitioner. Modern software with built-in inventory databases and impact assessment methods has simplified the LCA process, to the extent that an aquaculture system may be modeled in hours. However, the rigor of such models is to a large extent dependent on data quality. While use of generic data available in many public and commercial life cycle inventory databases may provide a starting point for scoping analyses, more context-specific data is required for robust modeling of specific production systems and technologies. Unfortunately, the former (simplified analyses) are increasingly common in the peer-reviewed literature, providing what may be misleading signals and eroding the credibility of the research framework, generally.

Software Tools and ISO

The rapid evolution and adoption of LCA have been accompanied by the creation of a variety of guidelines, manuals, and dedicated software [17]. The most commonly used LCA software platforms are GaBi and SimaPro, which are commercial products. Others, such as CMLCA and openLCA, are available free of charge. There are also several life cycle inventory databases, which have been developed, with the most extensive being the EcoInvent database (www.ecoinvent.ch). Such databases provide inventory data for materials and processes common to most product systems – for example, the production of materials such as concrete, steel, and plastic; the provision of energy carriers such as diesel or regionally specific electricity mixes; or transportation modes like air freight, rail freight, or private automobile transport. As these "background" data are often premised on different methods, assumptions, and rigor, sourcing data should be done with care as different databases apply different methodologies. It is therefore recommended to be consistent when

choosing sources of background systems data and also to be aware of the methodology used before making comparisons between studies. ISO compliance does not require that studies are comparable, only that they follow the same requirements. Individual studies also often differ in functional unit (the unit of output against which impacts are quantified), system boundaries, and allocation criteria.

A LCA study is, in accordance to ISO standards, carried out methodically through four phases (Fig. 1). As an initial phase, the goal and scope definition will specify the main characteristics of the study. Goal is specified as the application, audience, and reason for the study, while scope outlines the product system to be studied, functional unit, system boundaries, allocation procedures, impact categories, data requirements, assumptions, limitations, data quality, and format of the report. System boundaries specify the processes that are to be included in the product system and are in turn set by the cutoff criteria. This is followed by a Life Cycle Inventory Analysis (LCI), which involves the collection and calculation of data as well as allocation of burdens, in cases where input or output flows involve more products or processes than the defined unit. The impacts of these results are then, in the third phase (Life cycle impact assessment, LCIA), assessed according to their contribution to the impact categories defined in the goal and scope phase. Finally, the three previous phases are interpreted and communicated to the anticipated audience.

Functional Unit

Seafood commodities are farmed for different purposes, which complicates the choice of functional unit. Most LCA studies to date have used live weight mass at the farmgate or mass of processed product as the functional unit. Variable protein contents and edible portions between aquatic animals therefore may complicate direct comparisons. For example, the edible portion of an oyster is only about 18% of its wet weight, a number that in turn is subject to local variation [18] while the edible yield from an Atlantic salmon (*Salmo salar*) typically exceeds 50%. Local customs may

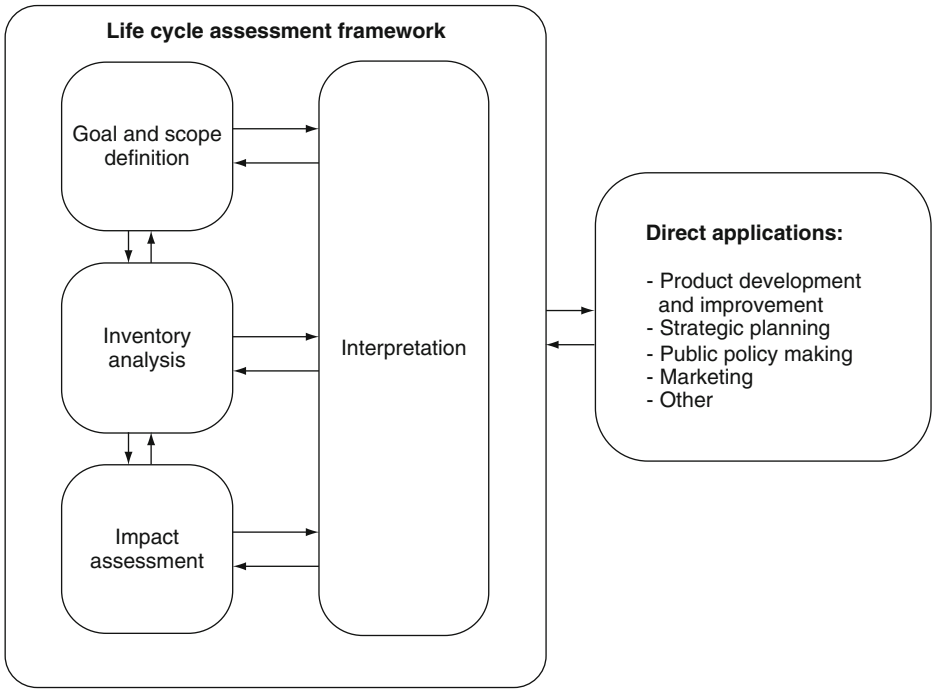

Life Cycle Assessments and Their Applications to Aquaculture Production Systems. Figure 1
The general methodological framework for LCA studies according to ISO 14040 (2006) and its four comprised phases

further confound the decision as certain parts of the fish that may be discarded as inedible in one region are considered good for human consumption in another region. Two such examples are herring roe and catfish stomachs; both of which are considered offal in the western world but are prized in parts of Asia [19, 20]. Ideally, the functional unit should reflect the function of the product system. For aquaculture products intended for consumption as food, such functions might include the provision of caloric energy, protein, or omega fatty acids, etc.

Setting System Boundaries

System boundaries delineate those processes formally included in an analysis from those that are excluded. There are only general requirements on how to set these boundaries, though they should be decided relative to the research objectives and include all elements having a non-trivial influence on research results. Most LCA studies in aquaculture limit their system boundary to the farmgate, whereas some include processing, packaging, marketing, and consumption phases [21–23]. Thrane [24] evaluated the effects of post-harvest stages of the life cycle of seafood products and concluded that they have a significant impact on the overall environmental performance of most seafood products. For example, inclusion of the processing phase contributed an additional 10% to life cycle energy use, while inclusion of the consumption phase resulted in an average 25% increase in cumulative energy demand [24].

Allocation

A common issue faced by many LCA practitioners is how to allocate environmental burdens to products and materials that are co-produced with other products [25]. Examples in aquaculture include the allocation of environmental burdens between targeted catch and bycatch used in fishmeal production, the multiple products derived from corn and other commodity crops used in feeds, and alternative uses of fish by-products or aquaculture wastewater used to fertilize other crops. The ISO standards for LCA do provide guidelines for an allocation decision hierarchy, but leave considerable room for interpretation. According to the standard, environmental burdens are primarily to be allocated according to an underlying physical relationship, if subdivision is unavoidable. The standard further states that where such relationships cannot be established, the allocation should reflect other relationships between the input system and output system. In reality, the final choice of allocation basis will likely reflect the goals of the study, as well as the worldview of the practitioner. Some of the more common bases for allocation in aquaculture and their characteristics are summarized in Table 1. Accessibility of the different allocation factors differs depending on location and situation, where regional differences will play a large role in making generalizations. Time and spatial scales will also have a great influence on the allocation factors that do not represent physical relationships, as these will not remain static.

There are several things to keep in mind when choosing a basis for allocation. The first is that nothing limits a study to only one allocation factor; each allocation scenario may be treated differently depending on the circumstances. Results may also be presented using several of the allocation factors, thus enabling readers to interpret results according to their own perspective or worldview. No matter how the allocation problem is approached, it is very important to be clear in the supporting text about which methods have

Life Cycle Assessments and Their Applications to Aquaculture Production Systems. Table 1 The most commonly used bases for allocation and their characteristics

Allocation factor	Accessibility	Physical relationship	Static	Market oriented
Mass	Good	Yes	Yes	No
Value	Average	No	No	Yes
Nutritional energy content	Average	Yes	Yes	No
System expansion	Poor	Sometimes	Sometimes	Sometimes

been used. It is, however, important to keep in mind that the basis of allocation can influence the allocated burden by as an order of magnitude [26].

Impact Categories and Impact Assessment

Any quantifiable performance measure can be included within the LCA methodology, from emissions to the well-being of workers, as long as: (a) a causal relationship between the variable of interest and the provision of the functional unit can be established and (b) a defensible impact assessment methodology is available [27]. A wide variety of impact assessment methods are available for use in LCA, most of which have been applied to assessments of seafood production systems [27]. These methods may describe environmental interactions that have relevance at local (e.g., eutrophication), regional (e.g., acidification), or global (e.g., greenhouse gas emissions) scales. Generally, impact assessment methods are based on peer-reviewed, internationally accepted environmental accounting protocols. Some of these continue to evolve, and novel methods emerge in response to newly identified issues [27, 28].

Labor

Labor is rarely accounted for in LCA due to the difficulty of establishing defensible system boundaries and quantifying associated environmental impacts. It can also be debatable if the number of employees should be considered as a negative or positive input. It is, however, important to keep labor in mind when comparing traditional and modern production systems. Labor can be presented in a number of different ways, either separately or incorporated into the individual impact categories [28, 29]. Several methods have been suggested on how to quantify the environmental impacts of labor. Suggested reference units include metabolic energy, calorific content of food consumed, national fuel share, or other more complex equations [29].

LCA in Food Production

Working with non-Static Systems

The adaptation of LCA from the characterization of static industrial systems to food production systems typified by significant variability has brought with it new challenges. Annual fluctuations occur both on the farm, as productivity will depend on water temperature, extreme weather events, algae blooms, etc., as well as on indirect variables such as oil prices and public demand. Fisheries providing fishmeal and fish oil for use in aquafeeds offer a good example of such variability, as fuel inputs per tonne of fish landed will fluctuate with season, stock status, gear type, and skipper [30, 31]. The aquaculture sector is particularly dependant on annual production of the anchoveta fishery off South America for both of these commodities, which in turn is strongly influenced by El Niño-Southern Oscillation (ENSO) events [32]. Increased use of compound feeds and higher oil prices have also boosted prices of both fishmeal and oil over the last decade [1]. Such fluctuations not only affect economic allocation but also catch per unit effort. It can therefore be hard to set average fuel consumption for fishing fleets, especially since the species and status of the stocks used for fishmeal production often are unknown [33]. The situation is further complicated in certain parts of the world where low value fish are used directly as fish feed [33].

Agricultural crops – the other major source of aquafeed inputs – may also experience significant annual fluctuations, with larger variability in developed countries, for crops such as maize and wheat [1, 34]. Farmgate prices will further affect the LCA as many feed formulators and aquaculturists quickly adjust to price trends in their choice of feed inputs or cultured species in efforts to maximize profits [20, 35]. One such example is the constant push toward higher stocking densities of shrimp in SE Asian polyculture systems, where the large profits that are to be made often outweigh the risk of white-spot disease [36]. Farming practices, as for feed composition, are also under constant change, which emphasizes the importance of considering the time scales used in LCA studies. Ultimately, a balance must be struck between feasibility and the goals of the study in pursuing representative data and models.

The relevance of such variability will, in part, be determined by the scope of the analysis and specific research questions of interest. Variability might be accommodated when modeling at regional scales by applying average data over specified spatial and temporal horizons. It is increasingly common to account for and report such variability in published outcomes. In other cases, quantifying variability might comprise

research foci – for example, understanding the influence of variable field-level nitrous oxide emissions on the overall greenhouse gas intensity of crop production at local scales.

LCA in Aquaculture

The first LCA studies focusing on aquaculture systems were conducted in the beginning of the new millennium, with an increasing application of the methodology to aquaculture issues toward the end of its first decade [37–39]. As the number of studies increased, so too did the seeming detail of analysis and possibly also the accuracy of the results. Most have focused on production systems in developed countries (see Table 2). The methodological detail used between studies does, however, vary widely and makes broad comparisons between studies difficult. This includes differences in functional unit, system boundaries, data sources and quality, and choice of allocation criteria.

A common theme that has emerged from LCA research of intensive, finfish aquaculture production systems is the importance of feed provision in supply chain environmental impacts [21, 22, 42–44]. For example, Pelletier et al. (2009) found that feed provision accounted for, on average, 92% of quantified impacts in global salmon farming systems. Of particular importance are fisheries and livestock products, which typically have higher impacts per unit mass relative to crop-derived feed inputs (Fig. 2). Also of note is that on-site processes have only made a substantial contribution in highly mechanized systems, where industrial energy inputs are required to maintain water quality [3, 20, 21, 40, 44].

Although animal-derived feed ingredients usually have a higher impact per unit mass compared to crop-derived inputs [22, 43, 45, 46], their inclusion may support more rapid growth of the cultured organisms and, in some cases, result in a higher quality product [47]. By including a larger portion of agriculturally sourced materials in feeds, environmental burdens may be reduced. In this light, it might be anticipated that rearing herbivorous or omnivorous species is environmentally preferable. However, both feed composition and feed conversion efficiency must be considered in determining and comparing impacts between cultured organisms [44].

The choice of impact categories in aquaculture LCAs varies widely (Table 2). These include resource depletion and emissions-related environmental concerns, as well as toxicological potentials. The only categories almost consistently applied are global warming potential, acidification, and eutrophication, while cumulative energy demand is also very commonly evaluated. There is an expected but imperfect correlation of cumulative energy demand and global warming potential (Table 3), since much of the feed-related emissions for agricultural inputs do not arise from fossil fuel combustion. Rather emissions of nitrous oxide and methane are typically as or more important. It is only in systems where ecosystem services have been replaced to a large extent by anthropogenic processes that on-farm energy demand has a significant impact on the total energy consumption.

Guiding the Way for More Sustainable Aquaculture and Alternative Farming Methods

Feed Production

Improvements of feed conversion ratios (FCRs) for piscivorous fish in addition to an increased inclusion of non-fish ingredients has led to great environmental improvements over the last decades [46]. Additional improvements are to be made by identifying and sourcing for the least-environmental-cost feed formulations; especially for sources of fishmeal and oil [22]. In reduction fisheries, effective management will play a major role in reducing fuel consumption along with associated environmental impacts while sustaining output from the industry [30, 50]. In many fisheries, boats today have to travel further to find productive fishing grounds and invest more fishing effort to maintain catches. This has resulted in a sixfold increase in energy consumption for some capture fisheries over the last two decades [51]. A collapse of one of the large reduction fisheries, of the scale that occurred to the anchoveta fishery in the 1970s, would further drive up the energy intensity of aquafeeds and culture products as well as have devastating effects on the aquaculture industry as supply of fishmeal and oil supplies already are outpaced by demand [1, 52].

Decreasing fishmeal inclusion has, to a large extent, been driven by increasing public awareness about "fish-in to fish-out" ratios, as a result of labeling and

Life Cycle Assessments and Their Applications to Aquaculture Production Systems. Table 2 Overview of species, functional unit, system boundary, allocation factor, and impact categories applied for a selection of published LCA studies on aquaculture systems. One ton at farmgate is the most prominent functional unit while global warming potential, acidification, and eutrophication are the only impact categories that are included in all studies

Species	Reference	Functional unit	System boundary	Allocation factor	Cumulative energy demand	Fossil fuel use	Biotic resource use	Abiotic depletion potential	Water dependence	Surface use	Global warming potential	Ozone depletion potential	Acidification	Eutrophication	Phtotochemical oxidant formation	Freshwater aquatic ecotoxicity	Marine aquatic ecotoxicity	Terrestrial ecotoxicity	Human toxicity	Respiratory impacts from inorganics	Carcinogens
Blue mussels	Iribarren et al. [23]	1 kg of dry edible mussel flesh	Post consumption waste	System expansion	✖			✖			✖		✖	✖	✖	✖	✖	✖	✖		
Shrimps	Mungkung [70]	1.8 kg block of frozen shrimp	Post consumption waste	Monetary				✖			✖	✖	✖	✖	✖				✖		
Rainbow trout, sea-bass, and turbot	Aubin et al. [21]	1 t live weight	Farmgate	Monetary	✖		✖		✖		✖		✖	✖							
Salmon, different farming methods	Ayer and Tyedmers [40]	1 t live weight	Farmgate	Gross nutritional energy content	✖			✖			✖	✖	✖	✖			✖		✖		

Arctic char	Ayer and Tyedmers [40]	1 t live weight	Farmgate	Gross nutritional energy content	✖			✖			✖	✖	✖	✖			✖		✖		
Atlantic salmon, different feeds	Pelletier and Tyedmers 2007 [43]	1 t live weight	Farmgate	Gross nutritional energy content	✖		✖				✖		✖	✖			✖				
Trout, flow through/ recirculating system	d'Orbcaster et al. [41]	1 t live weight	Farmgate	Monetary	✖		✖		✖	✖	✖		✖	✖							
Trout	Papatryphon et al. [37]	1 tonne live weight	Farmgate	Monetary	✖		✖				✖		✖	✖							
Atlantic salmon	Ellingsen and Aanondsen [39]	200 g fillet	Processed fillets	Mass/ Monetary		✖					✖	✖	✖	✖			✖			✖	✖
Atlantic salmon	Pelletier et al. [22]	1 tonne live weight	Farmgate	Gross nutritional energy content	✖		✖				✖		✖	✖							

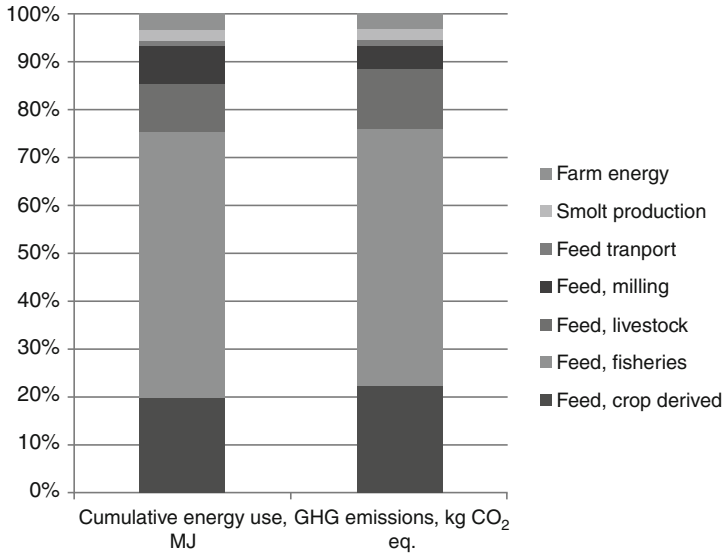

Life Cycle Assessments and Their Applications to Aquaculture Production Systems. Figure 2
Cumulative Energy Use and Greenhouse gas emissions from salmon production. Feed production is by far the largest contributor to environmental concerns, constituting 93% of the energy use and 94% of the GHG emissions. The feed represents an average from farms in Norway, UK, Canada, and Chile with 41.8% of the ingredients derived from crops, 49.4% from fish, and 8.8% from livestock. Data from: Pelletier et al. [22]

certification initiatives [9, 46]. It has also been strongly influenced by rising prices for these commodities, due to increased competition from the aquaculture sector [1]. The overall demand for fishmeal and oil in aquaculture has, despite this, increased due to a larger share of farmers using compound feeds and increasing aquaculture production over time [46, 53]. At present, in most aquaculture LCAs, the amount of fishmeal and oil used is only reported as life cycle inventory data. Beyond the standard impact categories, methods to account for the ecological impacts of producing these products are underdeveloped. To date, only a few researchers have, e.g., applied a measure of biotic resource use in life cycle assessment, following the methods originally advanced by Pauly and Christensen [54]. This method quantifies the net primary productivity, as measured in carbon, required to support the provision of a specified amount of fish-derived material, taking into account trophic level and species-specific meal and oil yield rates. Biotic resources used can differ by as much as an order of magnitude between different sources of fishmeal and oil [22]. Alternative sources of proteins that could in part replace fishmeal include soy meal, wheat gluten, bone, feathers, blood, livestock co-product meal, and seafood processing materials [46, 55]. A variety of vegetables oils may also be partially substitutable for fish oils. The environmental performance of systems using, e.g., agriculture alternatives for fishmeal and oil needs, however, to be carefully analyzed as such substitution does not guarantee improved performance. Switching to the culture of low-trophic species is often described as a solution for more sustainable aquaculture [6]. While this would allow for great reductions in fish inclusion rates, the higher FCRs associated with lower quality feeds may result in only marginal improvements in GHG and related life cycle impacts [44]. In contrast, a switch to more energy and climate-friendly fertilizer production either through efficiency improvements in existing fertilizer plants or the use of biological nitrogen fixation in place of conventional N fertilizers could, however, offset some of the impacts associated with crop production [56, 57].

Improvements of feeding practices on farms can both reduce costs, emissions, and FCR [58]. The amount of feed added is often calculated according to feeding charts or as a percentage of the fish biomass. These generalizations often result in inefficient feed

Life Cycle Assessments and Their Applications to Aquaculture Production Systems. Table 3 Summary of the different results for 1 t of seafood product at farmgate

Species	Country	Source	CED (MJ) t^{-1}	GWP kg CO_2-e t^{-1}
Turbot, recirculating	France	Aubin et al. [21]	290,986	6,017
Sea-bass, cages	Greece	Aubin et al. [21]	54,656	3,601
Rainbow trout, flow through	France	Aubin et al. [21]	78,229	2,753
Atlantic salmon, net-pen	Canada	Ayer and Tyedmers [40]	26,900	2,073
Atlantic salmon, Land base	Canada	Ayer and Tyedmers [40]	97,900	2,770
Atlantic salmon, Bag	Canada	Ayer and Tyedmers [40]	32,800	1,900
Atlantic char, land-based recirculating	Canada	Ayer and Tyedmers [40]	353,000	28,200
Trout, recirculating system	Denmark	d'Orbcastel et al. [41]	63,202	2,043
Trout, flow through	Denmark	d'Orbcastel et al. [41]	34,869	2,015
Atlantic salmon	Norway	Ellingsen and Aanondsen [39]	65,000[a]	N.A.
Blue mussels, fresh	Spain	Iribarren et al. [23]	N.A.	472
White-legged shrimps	Thailand	Zimmo et al. [49] and Mungkung [70]	45,600	N.A.
Trout, portion sized	France	Papatryphon et al. [37]	37,842	1,851
Trout, large sized	France	Papatryphon et al. [37]	62,774	2,499
Atlantic salmon, organic crop/25% soy meal and 100% canola oil substitute	Canada	Pelletier and Tyedmers [43]	9,860	690
Atlantic salmon, organic crop ingredients/ fisheries by-product meals and oils	Canada	Pelletier and Tyedmers [43]	26,900	1,810
Atlantic salmon, organic crop/conventional animal meals and oils	Canada	Pelletier and Tyedmers [43]	17,100	1,250
Atlanti salmon, conventional	Canada	Pelletier and Tyedmers [43]	18,100	1,400
Atlantic salmon	Worldwide	Pelletier et al. [22]	31,100	2,160
Tilapia, Lake	Indonesia	Pelletier and Tyedmers [44]	18,200	1,520
Tilapia, Pond	Indonesia	Pelletier and Tyedmers [44]	26,500	2,100

Energy use in Norwegian salmon farming reported by Ellingsen and Aanondsen [39] was calculated by assuming that 15% of total reported energy use was used in the processing and distribution phases

utilization as it does not take factors such as species, genetic stock, feed composition, water temperature, or growth rate into account [58]. In addition, feeding efficiency is also influenced by the type of farming facility as confined bodies of water, such as raceways or bags, allow for more efficient feeding practices and effluent management [59].

Replacing Ecosystem Services with Anthropogenic Processes at Farm Site

Traditional extensive aquaculture systems depend, to a large extent, on labor and natural energy inputs [3]. Solar energy inputs promote in-situ production utilizable by some farmed animals while tidal energy or other

natural watercourse flows provide means for water exchange. As for energy consumed in highly mechanized production systems, such as most intensive land-based systems, the energy for farm-site activities often originates from fuel as farm-sites typically lack access to alternative sources of energy. It is therefore recommended to consider the location characteristics of the farm-site before implementing artificial services. Farms situated in areas with high water turnover, i.e., in streams, tidal zones, or exposed coasts, may cause little or no impact on the local ecosystem. Farms situated in areas without such hydrodynamic conditions need to treat their wastewater to avoid negative impact on the environment or run as closed systems. It is, however, important to acknowledge that environmental impacts from farm release need to be analyzed from an ecosystem perspective, which implies considering additional pollution sources and more regional scale effects and thresholds.

LCA has limited capacity to predict the actual consequences of many of the estimated impact potentials [60]. It may be justifiable to have such an approach for the impact categories that are operational on a global scale, such as global warming potential or ozone depletion. For more regional consequences, however, it can be highly misleading to make comparisons of the impacts between two localities. To address this in a more justifiable manner, several country-specific factors, such as RECIPE, TRACI, EDIP2003, and LUCAS [61], have been developed and arguments have been raised for similar factors on regional scales [62].

Transmission of disease and parasites between wild and farmed stock and introduction of non-indigenous species are both major concerns associated with aquaculture that have yet have not been addressed by LCA methodology [63, 64]. Nor is the framework necessarily conducive to accommodating such interactions since it is necessary to be able to link the impact to the production of a functional unit following a clear and quantifiable cause-effect pathway. Both of these types of impacts have attracted much public attention and have been major incentives for closed farming facilities. Transmission of sea lice has, apart from having potentially detrimental effects on wild fish stocks, been estimated to account for 6% of the product cost in salmon farming [64]. Floating cages and net cultures allow for free movement of pathogens from farmed to wild stocks [64]. They also run an increased risk of large escape events of domesticated fish due to their vulnerability to extreme weather events, marine mammal interactions, failing infrastructure, and management errors. Such events can lead to the introduction of non-indigenous species as well as undermining the genetic fitness of wild stocks. It has been estimated that aquaculture is responsible for 16% of all introductions of non-indigenous species to European coastal waters, and further introductions are to be expected with changing climate [63].

The use of chemicals and antibiotics on farm sites is still only generally covered by existing impact categories. These practices can result in long-term effects such as antibiotic-resistant bacteria or other public health risks [10]. They may also lead to contaminated water sources and loss of biodiversity [10]. Shrimp farms are implicated most frequently for using large amounts of antibiotics to reduce stock losses. On several occasions, this has resulted in product recalls and import bans by the EU, Canada, and the USA [10]. The social consequences of this might be direct (e.g., lower water quality) or indirect, as import bans can seriously affect the financial viability of many farmers [65]. Even if LCA has the potential to account for such social and economic consequences, there is a lack of metrics to describe how to include socioeconomic indicators [28]. Overcoming the hurdles associated with the development of such impact categories would allow for better estimations of overall sustainability, including environmental, social, and economic variables [28]. However, it should be recognized that LCA is not necessarily conducive to accounting for the full spectrum of sustainability concerns. As such, it should be considered a complement to, rather than a replacement for, other metrics.

Discussion

As the number of LCA studies describing aquaculture systems increases, so too does our understanding of a broader suite of the environmental costs of aquaculture production. In some cases, it would appear that aquaculture may indeed provide an inexpensive and sustainable source of food and other products; however, this will depend on numerous factors including cultured species, production technology, and socioeconomic characteristics. To date, LCA research has helped to identify those aspects of the life cycle that contribute

disproportionately to environmental degradation, allowing for the identification of improvements opportunities. There is, however, always the danger of oversimplification where results get misinterpreted as a result of inaccurate data or where results are not put into their relevant context. LCA should therefore not be seen as an all-encompassing tool, but rather as a screening tool, which allows for the mapping of good practices. Additional environmental and socioeconomic analyses can thereafter be applied to strengthen assessment of sustainability.

As for advancements that can be made within the sector, the major challenge will be to find good sources of low impact feed inputs for fed aquaculture systems, especially for fish oil that currently drives the demand for wild marine resources [46]. This would, of course, ideally be combined with further advances in feed utilization by fish in culture. A shift toward organically produced crop inputs may also reduce the impacts of fed aquaculture, while bringing other benefits such as biodiversity improvements and superior soil quality [57, 66]. However, the choice of some resource intensive "organic" inputs can negate much of the life cycle environmental benefits associated with organic crop production [57]. Another alternative protein source is offal meal from fish processing. Tilapia, for example, has an offal yield of about 67% of live weight [59]. This does, however, increase the risk of disease transmission and/or recycling of environmental contaminants [53]. Moreover, the environmental costs of producing these materials from a life cycle perspective may be high [22]. Recently, there has been increased interest in the use of fish processing co-products for biofuel feedstock [67]. Conversion of high-quality protein into biofuels appears rather wasteful when the environmental burdens associated with producing certain high protein feed inputs are taken into account. It is clearly desirable to identify and implement optimal uses of high-quality protein toward the overarching sustainability objective. This must include, among other things, attention to the environmental dimensions of alternative protein production and use strategies. Since our ability to make informed decisions will be strongly influenced by the robustness of our models and the extent to which they actually reflect the environmental impacts associated with the products and systems of interest, methodological decisions such as choice of allocation criterion should be clearly communicated and defended in the context of each analysis.

Increasing trade flows of aquatic products from developing to developed countries highlights the need for more LCA work beyond production systems in the developed world. It also indicates that there are substantial opportunities for expansion of aquaculture in developed countries. Tyedmers et al. [2] points out that the USA only accounts for 1% of global aquaculture production, half of which is made up by channel catfish. Future developments may also to be expected within mariculture, as much recent effort has focused on the development of marine fin-fish hatcheries and offshore cages.

Impacts involved with on-site activities can more easily be avoided by selecting for better farm locations, use of renewable energy, improved utilization of ecosystem services, and farming of more tolerant species. One example of such a species is Pangasius catfish, which has reached high production levels in Vietnam over the last decade. This fish does not require aeration as it can utilize aerial respiration when the oxygen level drops. The farms also often utilize tidal floods for water exchange [20]. As for tilapia, the tolerance toward hypoxia and changes in pH is much higher than other species normally found in western aquaculture. This would, again, lower the inputs needed for maintaining water quality. Wastewater quality can also be improved by the use of settlement ponds and/or plant production to remove nutrients. Cultivation of plants such as *Azolla* spp. and duckweed within ponds can also enhance carbon fixation and be used as feed inputs [48, 68]. Duckweed may further reduce GHG emissions as it will shade the pond and thereby limit the ammonia volatilization rate [49]. Some of these feed inputs may, however, negatively influence the color and the taste of the final product, which makes them less suitable as feed inputs [48].

Converting to energy conserving practices will not only have environmental benefits, it can also improve the economic profitability of farms and reduce vulnerability to peaks in the price of oil. Lower intensity systems are also less sensitive to mechanical or infrastructure failures, such a black outs, which otherwise can cause mass mortality. This is especially important in developing countries where there is less access to spare parts and power failures are recurring events.

Open systems are, on the other hand, more vulnerable to other events such as algae blooms, pollution, and extreme weather events, which may cause the loss of an entire crop. Areas ravaged by extreme storm events, such as typhoons, may suffer from weeks of poor water quality as large quantities of sediments may lead to high turbidity for long periods of time.

More knowledge on the true carbon emissions associated with aquaculture is needed as there is increasing interest in its potential as a climate-friendly source for food and biofuels [68, 69]. LCA can play an essential part in the screening for sustainable farming practices and also provide information for the implementation of carbon credit schemes. This need is especially critical for developing countries, as this is where the majority of production occurs and exports are increasing. This will, however, pose a challenge as farming methods are highly diverse and data on farm practices are usually limited.

Also, some important environmental impacts from aquaculture are at present not quantifiable using the LCA framework, such as spread of diseases and parasites. These impacts have been attracting widespread public concerns and have influenced development of farming methods in many countries. The associated consequences could, for example, be accounted for as biotic resource use. Concerns associated with deforestation to produce agricultural land should also be further discussed, as it is only partially covered in current LCA practice and literature.

Future Directions

LCA provides a robust tool for dealing with an important subset of sustainability concerns, many of which have historically been overlooked in discussions of environmental management in aquaculture. However, it must be kept firmly in mind that decisions made during the analytical process strongly influence research outcomes.

It is, therefore, important to continue the discussion about such methodological decisions, including the kind of LCA framework applied (i.e., attributional versus consequential LCA), systems boundaries, and choice of allocation methods for LCAs of aquaculture production. In the least, it would be constructive for all practitioners to clearly communicate and defend all methodological choices, as they may ultimately send different signals to the industry and policy makers working with sustainability issues.

A more standardized methodology within the sector would certainly facilitate the advancement of the field. This could be achieved by better communications between major practitioners or by the development of a manual to guide the community toward one common framework. Even still, there will always be deviations from common practice as each study serves a unique purpose, stressing the need for more transparency.

Even though ongoing initiatives for developing the LCA framework exist, it is important to acknowledge that the present framework has limited ability to accommodate the other two pillars of sustainability, namely, social and economic impacts [28]. Thus, even if LCA provides a tool with great potential to guide the aquaculture industry toward more sustainable production, its framework needs to be reinforced by other analytical tools to capture a wider range of sustainability concerns. The need to include other tools alongside LCA has already been recognized and recent projects, such as the SEAT project (www.seatglobal.eu), include complementary tools to give a more holistic measurement of sustainability. Limitations aside, however, the rapid development of this sector, coupled with the diverse range of possible culture species and technologies, demands careful attention to environmental effects at all relevant scales. LCA can and should play an important role in guiding decisions oriented toward sustainability in aquaculture.

Bibliography

Primary Literature

1. FAO (2009) State of world fisheries and aquaculture 2008. FAO, Rome
2. Tyedmers P, Pelletier N, Ayer N (2007) Biophysical sustainability and approaches to marine aquaculture development policy in the United States, A Report to the Marine Aquaculture Task Force
3. Troell M, Tyedmers P, Kautsky N, Rönnbäck P (2004) Aquaculture and energy use. Encyclopedia Energy 1:97–108
4. Troell M, Joyce A, Chopin T, Neori A, Buschmann A, Fang J-G (2009) Ecological engineering in aquaculture – potential for integrated multi-trophic aquaculture (IMTA) in marine offshore systems. Aquaculture 297:1–9
5. Troell M (2009b) Integrated marine and brackish water aquaculture in tropical regions: research, implementation

and prospects. In: Soto D (ed) Integrated mariculture: a global review. FAO Fisheries and Aquaculture Technical Paper, 529. FAO, Rome, pp 47–131
6. Naylor R, Goldburg R, Primavera J, Kautsky N, Beveridge M, Clay J, Folke C, Lubchenco J, Mooney H, Troell M (2000) Effect of aquaculture on world fish supplies. Nature 405:1017–1024
7. Naylor R, Williams S, Strong D (2001) Aquaculture – a gateway for exotic species. Science 294:1655–1656
8. Naylor R (2005) Aquaculture and ocean resources: raising tigers of the seat. Annu Rev Environ Resources 30:185–218
9. Pelletier N, Tyedmers P (2008) Life cycle considerations for improving sustainability assessments in seafood awareness campaigns. Environ Manage 42:918–941
10. Bartley D, Brugére C, Soto D, Gerber P, Harvey B (2007) Comparative assessment of the environmental costs of aquaculture and other food production sectors, Methods for meaningful comparisons, FAO/WFT Expert Workshop, 24–28 April 2006, Vancouver, Canada. FAO Fisheries Proceedings, no. 10, Rome
11. Finnveden G, Moberg Å (2005) Environmental systems analysis tools – an overview. J Cleaner Prod 13:1165–1173
12. Folke C, Kautsky N, Berg H, Jansson Å, Troell M (1998) The ecological footprint concept for sustainable seafood production: a review. Ecol Soc Am 8(1):S63–S71
13. Volpe JP, Beck M, Ethier V, Gee J, Wilson A (2010) Global aquaculture performance index. University of Victoria, Victoria, British Columbia, Canada
14. International Organization for Standardization (2006) Environmental management – life cycle assessment – principles and framework (ISO 14040:2006). International Organization for Standardization, Geneva, Switzerland
15. International Organization for Standardization (2006) Environmental management – life cycle assessment – requirements and guidelines (ISO 14044:2006), Geneva, Switzerland
16. Cordella M, Tugnoli A, Spandoni G, Santarelli F, Zangrando T (2008) LCA of an Italian Beer. Int J LCA 13(2):133–139
17. Baumann H, Tillman A-M (2004) The Hitch Hicker's Guide to LCA. Studentlitteratur, Lund
18. Wright DA, Hetzel EW (1985) Use of RNA: DNA ratios as an indicator of nutritional stress in the American oyster Crassostrea virginica. Mar Ecol Prog Ser 25:199–206
19. Thrane M, Nielsen E, Christensen P (2009) Cleaner production in Danish fish processing – experiences status and possible future strategies. J Cleaner Prod 17:380–390
20. Henriksson P (2009) Energy Intensity in Tropical Aquaculture, MSc thesis, Stockholm University
21. Aubin J, Papatryphon E, van der Werf H, Chatzifotis S (2009) Assessment of the environmental impact of carnivorous finfish production systems using life cycle assessment. J Cleaner Prod 17(3):354–361
22. Pelletier N, Tyedmers P, Sonesson U, Scholz A, Zeigler F, Flysjo A, Kruse S, Cancino B, Silverman H (2009) Not all salmon are create equal: life cycle assessment (LCA) of global salmon farming systems. Environ Sci Technol 43(23):8730–8736
23. Iribarren D, Moreira M, Gumersindo F (2010) Revisiting the life cycle assessment of mussels from a sectorial perspective. J Cleaner Prod 18(2):101–111
24. Thrane M (2004) Environmental impacts from Danish fish products – hot spots and environmental policies, PhD thesis, Ålborg University, Ålborg, Denmark
25. Reap J, Roman F, Duncan S, Bras B (2008) A survey of unresolved problems in life cycle assessment. Int J Life Cycle Assess 13:290–300
26. Thrane M (2006) LCA of Danish fish products. Int J Life Cycle Assess 11(1):66–74
27. Pelletier N, Ayer N, Tyedmers P, Kruse S, Flysjo A, Robillard G, Ziegler F, Scholz A, Sonesson U (2007) Impact categories for life cycle assessment research of seafood production: Review and prospectus. Int J Life Cycle Assess 12(6):414–421
28. Kruse S, Flygsjö A, Kasperczyk N, Scholz A (2009) Socioeconomic indicators as a complement to life cycle assessment – an application to salmon production systems. Int J Life Cycle Assess 14:8–18
29. Zhang T, Dornfeld D (2007) Energy use per worker-hour, evaluating the contribution of labor to manufacturing energy use, part 3:B1, pp 189–193. In: Takata S, Umeda Y (eds) Advances in life cycle engineering for sustainable manufacturing businesses, Proceedings of the 14th CIRP conference on life cycle engineering, Waseda University, Tokyo
30. Tyedmers P, Watson R, Pauly D (2005) Fueling global fishing fleets. Ambio 34(8):635–638
31. Ruttan L, Tyedmers P (2007) Skippers, spotters and seiners: analysis of the "skipper effect" in US menhaden (Brevoortia spp.) purse-seine fisheries. Fish Res 83(1):73–80
32. Sandweiss D, Maasch K, Chai F, Andrus C, Reitz E (2004) Geoarchaeological evidence for multidecadal natural climatic variability and ancient Peruvian fisheries. Quatern Res 61: 330–334
33. Tacon A, Metian M (2009) Fishing for aquaculture: non-food use of small pelagic forage fish – a global perspective. Rev Fish Sci 17(3):305–317
34. Naylor R, Falcon W, Zavaleta E (1997) Variability and growth in grain yields, 1950-94: does the record point to greater instability? Populat Dev Rev 23(1):41–58
35. Tacon A, Silva S (1997) Feed preparation and feed management strategies within semi-intensive fish farming systems in the tropics. Aquaculture 151:379–404
36. Kautsky N, Rönnbäck P, Tedengren M, Troell M (2000) Ecosystem perspectives on management of disease in shrimp pond farming. Aquaculture 191:145–161
37. Papatryphon E, Petit J, Kaushik S, van der Werf H, Kaushik S (6–8 October 2003) Life cycle assessment of trout farming in France: a farm level approach. In: Halberg N (ed) Life Cycle Assessment in the Agri-food sector, Proceedings from the 4th International Conference. Bygholm, Denmark
38. Aubin J, Papatryphon E, van der Werf H, Petit J, Morvan Y (2006) Characterisation of the environmental impact of a turbot (Scophtalmus maximus) re-circulating production systems using Life Cycle Assessment. Aquaculture 261:1259–1268

39. Ellingsen H, Aanondsen S (2006) Environmental impacts of wild caught cod and farmed salmon – a comparison with chicken. Int J Life Cycle Assess 1:60–65
40. Ayer N, Tyedmers P (2009) Assessing alternative aquaculture technologies: life cycle assessment of salmonid culture systems in Canada. J Cleaner Prod 17:362–373
41. d'Orbcaster RE, Blancheton J-E, Belaud A (2009) Water quality and rainbow trout performance in a Danish Model Farm reciculating system: comparison with a flow through system. Aquacult Eng 40:135–143
42. d'Orbcaster RE, Blancheton J-E, Aubin J (2009) Towards environmentally sustainable aquaculture: comparison between two trout farming systems using Life Cycle Assessment. Aquacult Eng 40:113–119
43. Pelletier N, Tyedmers P (2007) Feeding farmed salmon: Is organic better? Aquaculture 272:399–416
44. Pelletier N, Tyedmers P (2010) A life cycle assessment of frozen Indonesian tilapia fillets from lake and pond-based production systems. J Ind Ecol (in press)
45. Alder J, Campbell B, Karpouzi V, Kaschner K, Pauly D (2008) Forage fish: from ecosystems to markets. Annu Rev Environ Res 33:7.1–7.14
46. Naylor R, Hardy R, Bureau D, Chiu A, Elliott M, Farrell A, Forster I, Gatlin D, Goldburg R, Hua K, Nichols P (2009) Feeding aquaculture in an era of finite resources. Proc Natl Acad Sci 106(36):15103–15110
47. de Francescoa M, Parisia G, Médaleb F, Lupia P, Kaushikb S, Poli B (2004) Effect of long-term feeding with a plant protein mixture based diet on growth and body/fillet quality traits of large rainbow trout (*Oncorhynchus mykiss*). Aquaculture 236(1–4):413–429
48. Edwards P, Anh Tuan L, Allan G (2004) A survey of marine trash fish and fishmeal as aquaculture feed ingredients in Vietnam. ACIAR Working Paper No. 57
49. Zimmo O, van der Steer N, Gijzen J (2003) Comparison of ammonia volatilization rates in algae and duckweed-based waste stabilization ponds treating domestic wastewater. Water Res 37:4587–4594
50. Driscoll J, Tyedmers P (2010) Fuel use and greenhouse gas emission implications of fisheries management: the case of the New England Atlantic herring fishery. Marine Policy 34(3):353–359
51. Tlusty M, Lagueux K (2009) Isolines as a new tool to assess the energy costs of the production and distribution of multiple sources of seafood. J Cleaner Prod 17:408–415
52. Pauly D, Christensen V, Guénette S, Pitcher T, Sumaila U, Walters C, Watson R, Zeller D (2002) Towards sustainability in world fisheries. Nature 418:689–695
53. Tacon A, Metian M (2008) Global overview on the use of fishmeal and fish oil in industrially compounded aquafeeds: trends and future prospects. Aquaculture 285:146–158
54. Pauly D, Christensen V (1995) Primary production required to sustain global fisheries. Nature 374:255–257
55. Tacon A, Hasan M, Subasinghe R (2006) Use of fishery resources as feed inputs for aquaculture development: trends and policy, implications. FAO Fisheries Circular. No. 1018. Rome, FAO, 99 p
56. Rafiqul I, Weber C, Lehmann B, Voss A (2005) Energy efficiency improvements in ammonia production-perspectives and uncertainties. Energy 30:2487–2504
57. Pelletier N, Arsenault N, Tyedmers P (2008) Scenario-modeling potential eco-efficiency gains from a transition to organic agriculture: life cycle perspectives on Canadian canola, corn, soy and wheat production. Environ Manage 42:989–1001
58. Cho C, Bureau D (2001) A review of diet formulation strategies and feeding systems to reduce excretory and feed wastes in aquaculture. Aquac Res 32:349–360
59. Boyd C, Tucker C, McNevin A, Bostick K, Clay J (2007) Indicators of resource use efficiency and environmental performance in fish and Crustacean aquaculture. Rev Fish Sci 15:327–360
60. Potting J, Hauschild M (1997) Spatial differentiation in life-cycle assessment via the site-dependent characterisation of environmental impact from emissions. Int J Life Cycle Assess 2(4):209–216
61. ILCD handbook (International Reference Life Cycle Data System) (2010) Analysis of existing environmental impact assessment methodologies for use in life cycle assessment, JRC background document, 1st edn, European Union
62. Gallego A, Rodríguez L, Hospido A, Moreira1 M, Feijoo G (2010) Development of regional characterization factors for aquatic eutrophication. J Life Cycle Assess 15(1):32–43
63. Occhipinti-Ambrogi A (2007) Global change and marine communities: alien species and climate change. Mar Pollut Bull 55:342–352
64. Costello M (2009) How sea lice from salmon farms may cause wild salmonid declines in Europe and North America and be a threat to fishes elsewhere. Proc R Soc 276: 3385–3394
65. Cato J, Lima dos Santos C (1998) European Union 1997 seafood-safety ban: the economic impact on Bangladesh shrimp processing. Mar Resource Econ 13(3):215–227
66. Reijnders L, Soret S (2003) Quantifications of the environmental impacts of different dietary protein choices. Am J Clin Nutr 78:664S–668S
67. Wiggers V, Wisniewski A, Madureira L, Chivanga Barros A, Meier H (2009) Biofuels from waste fish oil pyrolysis: continuous production in a pilot plant. Fuel 88(11):2135–2141
68. Bunting S, Pretty J (2007) Global carbon budgets and aquaculture – emissions, sequestration and management options. Centre for Environment and Society Occasional Paper 2007-1. University of Essex, Essex
69. Hossain S, Salleh A, Boyce A, Chowdhury P, Naqiuddin M (2008) Biodiesel fuel production from algae as renewable energy. Am J Biochem biotechnol 4(3):250–254
70. Mungkung R (2005) Shrimp aquaculture in Thailand: application of life cycle assessment to support sustainable development, PhD thesis, Center for Environmental Strategy, School of Engineering, University of Surrey, Surrey, UK

Books and Reviews

Mungkung R, Gheewala SH (2006) Use of life cycle assessment (LCA) to compare the environmental impacts of aquaculture and agri-food products. In: Barley DM, Brugére C, Soto D, Gerber P, Harvey B (eds) Comparative assessment of the environmental costs of aquaculture and other food production sectors: methods for meaningful comparisons, FAO/WFT Expert Workshop, 24–28 April 2006, Vancouver, Canada. FAO Fisheries Proceedings, no. 10, Rome, FAO, pp 87–96, 207

Ayer N, Tyedmers P, Pelletier N, Sonesson U, Scholz A (2007) Co-product allocation in life cycle assessments of seafood production systems: review of problems and strategies. Int J Life Cycle Assess 12(7):480–487

Baumann H, Tillman A-M (2004) The hitchhiker's guide to LCA: an orientation in life cycle assessment methodology and application. ISBN 91-44-02364-2

Guinée J (ed), Gorrée M, Heijungs R, Huppes G, Kleijn R, de Koning A, van Oers L, Wegener Sleeswijk A, Suh S, Udo de Haes H, de Bruijn J, van Duin R, Huijbregts M (2002) Handbook on life cycle assessment: operational guide to the ISO Standards. Series: Eco-efficiency in industry and science. Springer, Dordrecht

Life Cycle Comparison of Waste-to-Energy to Sanitary Landfill

P. Ozge Kaplan[1], Joseph F. DeCarolis[2]
Morton A. Barlaz[2]
[1]National Risk Management Research Laboratory, Office of Research and Development, U.S. Environmental Protection Agency, Research Triangle Park, NC, USA
[2]Civil, Construction and Environmental Engineering, North Carolina State University, Raleigh, NC, USA

Article Outline

Glossary
Definition of the Subject
Introduction
Background on Life Cycle Assessment
System Boundaries of the WTE LCI
Life Cycle Inventory
Method to Generate Emission Factors per MWh of Electricity Generated
Method to Generate Emission Factors for Landfill Gas to Energy
Results and Discussion
Conclusions and Future Directions
Bibliography

Glossary

APCS Air pollution control systems
ASCC Alaska Systems Coordinating Council
BOD Biological oxygen demand
CAA Clean air act
COD Chemical oxygen demand
EGU Electric generating unit
FRCC Florida Reliability Coordinating Council
HDPE High-density polyethylene
HICC Hawaiian Islands Coordinating Council
ICE Internal combustion engine
LCA Life cycle assessment
LCI Life cycle inventory
LFG Landfill gas
LFGTE Landfill gas to energy
MRO Midwest reliability organization
MSW Municipal solid waste
NERC North American Energy Reliability Council
NPCC Northeast Power Coordinating Council
OCC Old corrugated cardboard
ONP Old newsprint
PET Polyethylene terephthalate
RFC Reliability first corporation
SERC SERC reliability corporation
SPP Southwest power pool
TRE Texas Regional Entity
US EPA United States Environmental Protection Agency
WECC Western Electricity Coordinating Council
WTE Waste-to-energy

Definition of the Subject

This entry provides a detailed life cycle assessment (LCA) of combustion vs. landfilling of post-recycling municipal solid waste (MSW). LCA can be used to evaluate the environmental footprint of products, processes, and services. An LCA allows decision makers to compare products and processes through systematic evaluation of supply chains. LCA takes a "cradle-to-grave" approach, by including each stage of life for a given product or process, which includes the extraction of raw materials, transportation, manufacturing, distribution, use, and final disposal. LCA has been

widely utilized to analyze different solid waste management alternatives [1–9]. In the USA, 220 million Mg (1 Mg = 1 metric ton) of MSW was generated in 2009, of which only 32% was recycled, and 13% was combusted with energy recovery [10]. Despite resource conservation efforts, over 50% of the US MSW is discarded in landfills. This number is significantly higher than other countries such as Denmark, where only 4% of the MSW generated is disposed in landfills. The remaining 96% is recycled or combusted for energy recovery. There is an ongoing debate about the relative environmental merits of landfill gas to energy (LFGTE) vs. waste to energy (WTE). Application of LCA revealed that the relative emissions associated with both options are highly sensitive to the input data in the life cycle inventory (LCI).

Introduction

While per capita generation has been relatively constant for the past decade, the absolute amount of MSW generated is increasing due to population growth. In 2002, the US Environmental Protection Agency (US EPA) established the Resource Conservation Challenge to increase the nationwide recycling rate to 35%. The challenge encourages pollution prevention, resource conservation, efficient use of materials, and a materials management approach to waste management. Current recycling and composting rates in the USA have almost reached the 35% goal [10]. In addition, 13% of MSW is combusted in WTE facilities. The rest of the MSW, totaling 151 million Mg according to the US EPA, is disposed in landfills. Europe's solid waste management (SWM) policies also focus on the minimization of MSW disposal in landfills and maximization of the environmental benefits through material and energy conservation. For example, in Denmark, only 4% of MSW is disposed in landfills. Most of the Danish MSW (55%) is combusted, and the balance (42%) is recycled [11]. The US public generally perceives solid waste combustion as hazardous and toxic, a response to the poor environmental performance of incineration facilities in the 1980s and early 1990s, which lacked air pollution control systems (APCS). This concern was a motivation for the Clean Air Act (CAA) Amendment which required all WTE facilities in the US to have APCS installed [12]. In 2010, there were 86 WTE plants with continuous emission monitoring, operating in 24 states [13]. Each facility is required to submit the result of an annual stack test to measure performance and demonstrate compliance with regulations. These measures have alleviated much of the risk associated with WTE. Now with scientific concern about climate change and GHG emissions, it is a good time to revisit WTE and its role in GHG mitigation. For example: What are the net impacts of WTE, and how do these compare with alternatives such as landfilling without any landfill gas (LFG) collection, landfilling with LFG collection and then flaring, landfilling with LFG collection and then electricity production also called LFGTE? Further, as a source of energy, how do the GHG emissions from WTE compare with those of fossil fuels and nuclear power? LCA provides a means to answer these questions.

This chapter describes the calculation of LCI air emissions from WTE and compares the results with the LCI emissions from landfills with different LFG management options. Background information on LCI is presented in the next section, followed by a description of the system boundaries and design basis for the WTE LCI. The method used to calculate each emission factor and the amount of energy recovered is then described. Emission factors are reported on both a per Mg basis and per unit electricity generated. In addition, sensitivity of emission factors to various parameters such as efficiency of the electricity generation at the power plant, LFG collection efficiency, and waste composition is also investigated and presented along with the results.

Background on Life Cycle Assessment

The design of SWM strategies that are efficient with respect to material and energy conservation requires a site-specific evaluation of multiple SWM alternatives. For example, energy recovery in a WTE facility may represent an efficient way to recover the energy value of the materials while at the same time displacing fossil fuels. However, if the materials are recycled otherwise, this may reduce demand for energy in manufacturing. Thus, a thorough examination of the impacts of WTE facilities must include full life cycle impacts as well as comparison on the benefits of converting recyclables to

new products. Given these many complexities, life cycle models are essential for calculating the energy consumption and environmental emissions. Integrated life cycle models for SWM typically are comprised of modules that represent each unit process of a given solid waste system, including collection, separation, recycling, treatment, and landfill processes.

The goal of LCA is to evaluate the full environmental impacts of a process or product. The LCA is carried out in four phases: goal and scope definition, life cycle inventory, life cycle impact assessment and interpretation. In this chapter, the LCI concept is applied to MSW combustion. The essential feature of LCI methodology is an attempt to thoroughly consider all aspects of a process. In the context of MSW combustion, the LCI methodology requires estimation of both the direct emissions from a combustion facility that recovers energy and the avoided emissions at a power plant (including associated steps for fuel extraction and transportation). General information on LCI methodology as it can be applied to MSW management has been presented previously in [9].

System Boundaries of the WTE LCI

A LCI model for WTE developed by [14] is utilized to calculate the LCI-based emission factors presented in this entry. This model is a part of an integrated SWM life cycle model that has individual unit process models for collection, recycling, transfer, treatment, and disposal of MSW [4, 15]. The LCI-based emission factors for WTE include all the activities associated with the combustion of 1 Mg of MSW as it is received by the WTE facility. A typical mass-burn combustion facility with energy and ferrous metal recovery is assumed for the analysis. The facility is equipped with all necessary APCS to comply with the prevailing air quality regulations. The following APCS are assumed to be present in the facility: spray dryer absorbers for acid gas (i.e., SO_2 and NO_x) control, activated carbon injection for mercury control, injection of ammonia for NO_x control by conventional selective non-catalytic reduction, and a fabric filter for particulate matter (PM) control. The LCI emissions associated with collection, transfer, and separation of MSW and ash disposal are considered in separate unit process LCI models, which can be found in [15].

The LCI model for WTE can track 32 life cycle parameters, including energy consumption, CO_2, CO, NO_x, SO_2, total greenhouse gas equivalents (CO_2e), PM, CH_4, water pollutants and solid wastes associated with combustion of MSW as well as indirect burdens. The CO_2 emissions are represented in two forms: fossil and biogenic. The CO_2 released from anthropogenic activities such as burning fossil fuels or fossil-fuel derived products (e.g., plastics) for electricity generation and transportation are categorized as CO_2-fossil, while the CO_2 from biogenic materials (e.g., paper, food waste) released during combustion, or biodegradation in the case of landfills, is categorized as CO_2-biogenic. The CO_2e represents the summation of CO_2-biogenic, CO_2-fossil and CH_4 emissions, multiplied by their corresponding global warming potentials (GWP). The GWPs for CO_2-biogenic, CO_2-fossil and CH_4 are 0, 1 and 25, respectively [16].

The emission levels depend on waste composition, combustion process details, and the effectiveness of installed APCS. For example, the quantity of CO_2 emissions is composition dependent, whereas the quantity of criteria air pollutants and hazardous air pollutants depends primarily on flue gas treatment procedures. Generally, WTE plants in the USA do not generate wastewater, and the sludge generated from semidry or wet scrubbing is not included in this LCI. The WTE LCI model does not differentiate between bottom ash and fly ash. The quantity of total ash is a function of the materials combusted in the facility, the corresponding ash content, and the assumed uncombusted fractions of each material. The assumptions regarding MSW component characteristics are presented in Table 1. The amount of limestone and ammonia used in the APCS are also added to the total quantity of ash produced. The ash is then taken to an ash landfill for disposal. Another LCI model developed by [17] is used to track emissions associated with the disposal of ash.

The emissions associated with the production of limestone and ammonia for the APCS are included as indirect burdens in the LCI. The emissions associated with the construction of the facility are less than 1% of total LCI emissions occurring during the operation of the facility [18]. As a result, construction emissions were excluded from the results presented here. The steam generated in the WTE facility is converted to

Life Cycle Comparison of Waste-to-Energy to Sanitary Landfill. Table 1 Characteristics of municipal solid waste

Category[a]	Generated total, thousands of Mg[b]	Discarded waste, thousands of Mg[b]	Heating value, BTU/lb[c]	Moisture content, %	WTE residue, Mg/dry Mg of waste item	Ash content (dry basis), %	Carbon type	Additional assumptions
Leaves	6,690	2,547	2,601	60	0.11	6.3	Biogenic	23% of the total yard waste[d]
Grass	17,744	6,756	2,601	60	0.11	6.3	Biogenic	61% of the total yard waste[d]
Branches	4,654	1,772	6,640	60	0.11	6.3	Biogenic	16% of the total yard waste[d]
Old newsprint (ONP)	10,930	1,215	7,541	6	0.06	1.5	Biogenic	
Old corrugated cardboard (OCC)	28,054	8,009	6,895	5	0.10	5.0	Biogenic	
Office paper	5,968	2,231	6,313	6	0.11	6.0	Biogenic	
Phone books	599	490	6,248	6	0.11	6.0	Biogenic	
Books	1,016	780	6,248	6	0.11	6.0	Biogenic	
Old magazines	2,286	1,406	5,386	6	0.27	23.3	Biogenic	
Third class mail	5,288	3,392	6,076	6	0.11	6.0	Biogenic	
Mixed paper	21,995	20,544	6,799	6	0.11	6.4	Biogenic	All other paper categories
High-density polyethylene (HDPE)	4,753	4,281	18,687	2	0.05	0.4	Fossil	
Polyethylene terephthalate (PET)	2,159	1,669	18,687	2	0.05	0.4	Fossil	
Mixed plastic	11,410	11,211	14,101	2	0.15	10.0	Fossil	All other resins
Ferrous cans	2,150	789	301	3	0.97	97.0	Biogenic	Steel packaging

Ferrous metal	10,340	7,229	–	3	0.97	97.0	Biogenic	
Aluminum cans	1,723	1,098	–	2	0.97	97.0	Biogenic	
Aluminum	1,188	1,188	–	2	0.97	97.0	Biogenic	
Glass	9,905	7,401	84	2	0.99	98.9	Biogenic	All glass except durable glass
Food waste	26,512	25,887	1,797	70	0.10	5.0	Biogenic	
Wood	12,635	11,447	6,640	70	0.11	6.0	Biogenic	100% wood
Plastic—non-recyclable	2,649	2,649	10,000 [e]	2	0.15	10.0	Fossil	100% carpets
Miscellaneous organics	11,002	9,460	7,730[f]	20	0.11	6.0	Biogenic	100% clothing, 100% other nondurables
Rubber tires	2,503	1,633	10,890	20	0.11	6.0	50% Biogenic/ 50% Fossil	100% rubber tires
Glass—non-recyclable	1,660	1,660	–	2	0.99	98.9	Biogenic	100% durable glass
Miscellaneous inorganics	16,971	14,431	–	20	1	100.0	Fossil	Other products, other inorganics, other nonferrous metals, durable plastics
Total MSW	222,785	151,175		27			77% biogenic/ 23% fossil	

[a]Unless stated otherwise in the assumptions column, all the categories are consistent with [28]
[b]See Ref [28]
[c]See Ref [32]
[d]The split of yard waste into leaves, grass, and branches is based on [33]
[e]See Ref [34]
[f]Average of heating value of textiles and leather see [32]

electricity, which then contributes to baseload electricity generation within the regional electric grid. Thus, the supply of electricity from the WTE plant avoids emissions from conventional fossil fuel-fired power plants. These avoided emissions are calculated and included in the LCI as an emissions reduction. In addition, most WTE facilities recover ferrous metals from bottom ash. The LCI model takes into account the avoided emission from the manufacturing of iron and steel from raw materials due to ferrous recycling.

Life Cycle Inventory

Method to Generate Emission Factors Per Mg of Waste Item

The WTE LCI model generates emission factors per Mg of each waste item, which is the summation of emissions associated with (1) the combustion of MSW (while accounting for the emission controls), (2) the production and use of limestone and ammonia in the APCS, (3) offsets applied due to avoided regional grid emissions, (4) offsets applied due to ferrous recovery, and (5) emissions associated with ash disposal [14]:

$$\begin{aligned} LCI_WTE_{ij} = (&LCI_Stack_{ij} + LCI_Limestone_{ij} \\ &+ LCI_Ammonia_{ij} - LCI_GridEmissions_{ij} \\ &- LCI_FeOffsets_{ij} + LCI_Ash_{ij}) \quad \text{for all } i, j \end{aligned} \tag{1}$$

where LCI_WTE_{ij} is the LCI emission factor for pollutant i (g/Mg of waste item j); LCI_Stack_{ij} is the controlled stack gas emissions for pollutant i (g/Mg of waste item j); $LCI_Limestone_{ij}$ is the allocated emissions of pollutant i from the production and use of limestone in the scrubbers (g/Mg of waste item j); $LCI_Ammonia_{ij}$ is the allocated emissions of pollutant i from the production and use of ammonia (g/Mg of waste item j); $LCI_GridEmissions_{ij}$ is the allocated emissions of pollutant i associated with the avoided utility emissions (g/Mg of waste item j); $LCI_FeOffsets_{ij}$ is the emission offset for pollutant i per Mg of recycled ferrous material; and LCI_Ash_{ij} is the emissions of pollutant i associated with the disposal of ash from WTE facility (g/Mg of waste item j).

The magnitude of the emission factors thus is a function of heat rate (Btu/kWh) (i.e., the amount of energy input in Btu required to generate 1 kWh of electrical energy), waste composition, and the pollutant removal efficiency of the APCS. The characteristics of MSW assumed for this study are given in Table 1. The composition and amount of MSW determines the total electricity generated, which affects the total avoided emissions from the grid. Avoided grid emissions are allocated based on the energy content of the individual waste item. The emissions remaining after APCS treatment are allocated equally among different waste categories. Facility design assumptions are given in Table 2.

The CO_2 emissions are calculated using a stoichiometric equation for combustion given the quantity, moisture, and ultimate analysis of individual waste items. The emission rates for criteria air pollutants were calculated using field level stack gas concentrations (including the controls) and resultant flue gas volumes [14]. The performance data on WTE plants in the USA reveal that all the facilities' stack gas concentrations are either well below or within the regulatory limits [12]. The WTE LCI model can use either the regulatory concentration limits or average stack gas concentration limits to calculate the emission factors. Table 3 presents these input concentration limits. The results presented here are calculated using the regulatory limits; however, sensitivity analysis is conducted to demonstrate the effects of changes in concentration limits on emission factors.

Life Cycle Comparison of Waste-to-Energy to Sanitary Landfill. Table 2 Summary of major parameters characterizing a combustion facility

Parameter	Units	Assumptions
Lifetime	Years	20
Capacity factor		0.91
Heat rate	Btu/kWh	18,000
Conversion efficiency	%	18%
Limestone usage in the APCS	Mg/Mg of MSW	0.007055
Ammonia usage in the APCS	Mg/Mg of MSW	0.0015
Ferrous ash recovery rate	%	90
Unburned waste	%	5

Life Cycle Comparison of Waste-to-Energy to Sanitary Landfill. Table 3 Regulatory emission concentration limits and average emissions concentrations in the stack gas of WTE facilities

Pollutants	Units	Regulatory emission limits[a]	Average at new facilities[b]
SO_2	(ppmv @ 7% oxygen, dry)	30	10
HCl	(ppmv @ 7% oxygen, dry)	25	11
NO_x	(ppmv @ 7% oxygen, dry)	150	170
CO	(ppmv @ 7% oxygen, dry)	100	100
PM	(mg/dscm @ 7% oxygen, dry)	24	4.7
Dioxins/ Furans	(ng/dscm @ 7% oxygen, dry)	13	4.5

[a]See Ref [12]
[b]See Ref [35]

The WTE LCI accounts for all energy and material recovery activities. The WTE LCI model calculates the total electricity generated per unit mass of waste item based on the assumed heating value, ash content of each waste item, and heat rate of the WTE facility. The electricity generated at the WTE facility is fed into the regional grid to help meet part of the baseload demand. As a result, electricity generation from conventional sources is avoided, leading to a proportional decrease in emissions.

A separate LCI model for the electric sector was developed to calculate emission factors per unit electricity generated in a given region in the USA or the national grid [19]. Each of the electric grid regions in the North American Electric Reliability Council (NERC), an average national grid, or a user-defined grid can be defined in the model through input of fuel mixes. The fuel mixes for NERC regions and the national average are taken from the US EPA's eGRID database [20] and presented in Table 4. The LCI model for the electric sector concurrently calculates emission factors for each of the electric generating units (EGUs) powered by coal, natural gas, oil, biomass, hydroelectric, and nuclear. The factors include both the operating emissions with post-combustion APCS and precombustion emissions including the extraction, processing, and transportation of fuel. The precombustion LCI data for each of the fuels running the EGUs in the grid was obtained from the National Renewable Energy Laboratory (NREL) LCI database [21–24]. The database reports emissions associated with the extraction, processing, and transportation of fuel. These data were reported on a unit mass of fuel bases [21–24]; when converted to emissions per unit of electricity generated, the magnitude of the resultant emissions factor is inversely proportional to the efficiency of the power plant. The efficiency of the EGUs and the corresponding emission factors used in this analysis are presented in Table 5. The results of this analysis include offsets for coal-fired power plants in the SERC regional grid. The SERC grid represents 27% of US electricity generation, and the fuel mix in the SERC region roughly matches the fuel mix of the US national average grid. The emission factors for the SERC regional grid are summarized in Table 6.

Most WTE facilities recover up to 90% of the ferrous materials from the bottom ash. The recycled ferrous material replaces iron ore and other raw materials in the production of steel. As a result, emissions due to steel manufacturing from virgin materials are avoided. In terms of greenhouse gas emissions, 1.05 Mg CO_2e is avoided per Mg of recycled ferrous material as a result of recovery activities. The complete set of LCI emissions is presented in Table 7.

The WTE LCI emission factors per Mg of MSW item are summarized in Tables 8 and 9. Table 8 presents the combustion-related emission factors associated with WTE facilities. These factors exclude offsets associated with electricity generation and ferrous recycling as well as the burdens associated with the use of limestone and ammonia in the facility. Table 9 presents the LCI emissions from WTE facilities that include stack gas emissions, emissions associated with limestone and ammonia production, and offsets associated with the electricity generation in coal-fueled EGUs in the SERC region. Table 10 presents the emissions associated with the disposal of ash from the WTE facility. From these tables, the LCI emission factors for WTE are derived using Eq. 1.

Life Cycle Comparison of Waste-to-Energy to Sanitary Landfill. Table 4 Fuel mix on North American reliability council regions

NERC region	Nameplate capacity	Net generation	Coal	Oil	Gas	Other fossil	Biomass	Hydro	Nuclear	Wind	Solar	Geothermal	Other
	MW	GWh	%										
ASCC	2,010	6,577	9.47	11.56	56.62	0.00	0.08	22.26	0.00	0.01	0.00	0.00	0.00
FRCC	59,453	207,885	26.24	17.87	39.03	0.64	1.54	0.01	13.83	0.00	0.00	0.00	0.84
HICC	2,593	11,523	14.16	78.77	0.00	1.65	2.61	0.83	0.00	0.06	0.00	1.92	0.00
MRO	53,418	209,005	72.72	0.82	5.18	0.21	1.18	4.07	13.98	1.79	0.00	0.00	0.04
NPCC	79,230	282,945	14.42	13.16	29.24	1.06	3.16	11.70	27.22	0.04	0.00	0.00	0.00
RFC	245,899	997,523	64.42	1.43	5.78	0.73	0.70	0.61	26.22	0.07	0.00	0.00	0.05
SERC	288,160	1,109,684	57.14	1.46	11.73	0.42	1.75	3.27	24.17	0.00	0.00	0.00	0.05
SPP	61,500	214,392	62.63	0.74	27.72	0.20	1.05	2.58	4.11	0.85	0.00	0.00	0.12
TRE	89,456	321,072	37.06	0.48	47.52	1.24	0.07	0.31	11.91	1.24	0.00	0.00	0.17
WECC	186,027	695,837	33.45	0.48	26.29	0.44	1.30	24.66	10.09	1.08	0.08	2.08	0.05
USA	1,067,746	4,056,442	49.61	3.03	18.77	0.60	1.30	6.50	19.28	0.44	0.01	0.36	0.10

See Ref [20]

Life Cycle Comparison of Waste-to-Energy to Sanitary Landfill. Table 5 LCI-based emission factors for conventional power plants[a]

		Coal	Natural gas	Oil	Nuclear
System parameters					
Efficiency	%	33	50	33	33
Criteria pollutants					
CO	g/MWh	220	800	340	27
NO_x	g/MWh	3,700	1,500	1,400	280
SO_2	g/MWh	6,900	3,400	6,100	830
PM	g/MWh	1,300	14	120	210
PM-10	g/MWh				
Other pollutants					
HCl	g/MWh	82	0	22	2
Dioxins/ furans	g/MWh				
Ammonia	g/MWh	0.05	9.1	56	0.15
Hg	g/MWh				
Greenhouse gases					
CO_2-biogenic	Mg/MWh	0.00	0.00	0.00	0.00
CO_2-fossil	Mg/MWh	0.97	0.41	0.88	0.03
CH_4	Mg/MWh	0.00	0.00	0.00	0.00
CO_2e	MTCO2E/ MWh	1	0.44	0.89	0.03

[a]See Ref [21–24]; The raw data on precombustion emission factors are collected on a unit mass of fuel; when converted on a per unit electricity generated, the magnitude of resultant emissions depends on the efficiency of the power plant. To provide transparency, the assumed efficiencies are provided along with the factors

Method to Generate Emission Factors per MWh of Electricity Generated

The WTE LCI model also generates emission factors per MWh of electricity generated using the emission factors per Mg of waste item and the energy content of the waste stream received by the facility. The composition and quantity of waste used in this analysis are summarized in Table 1. The analysis assumes that the WTE facility receives the discarded portion of the

Life Cycle Comparison of Waste-to-Energy to Sanitary Landfill. Table 6 LCI-based emission factors for the US grid and South Eastern Reliability Council (SERC) region

		National	SERC
Air emissions			
PM-10	g/kWh	0.00E + 00	0.00E + 00
PM	g/kWh	7.02E−01	7.88E−01
Nitrogen oxides	g/kWh	2.43E + 00	2.46E + 00
Hydrocarbons (non-CH_4)	g/kWh	5.89E−01	3.87E−01
Sulfur dioxide	g/kWh	5.30E + 00	4.85E + 00
Carbon monoxide	g/kWh	4.10E−01	3.46E−01
CO_2 biogenic	g/kWh	6.52E + 00	8.70E + 00
CO_2 fossil	g/kWh	6.57E + 02	6.52E + 02
Ammonia	g/kWh	4.52E−03	2.65E−03
Lead	g/kWh	2.94E−05	2.77E−05
Methane	g/kWh	1.44E + 00	1.44E + 00
Hydrochloric acid	g/kWh	4.23E−02	4.71E−02
Waterborne emissions			
Dissolved solids	g/kWh	2.90E + 00	1.90E + 00
Suspended solids	g/kWh	4.07E−01	4.31E−01
Biological oxygen demand (BOD)	g/kWh	2.94E−03	1.89E−03
Chemical oxygen demand (COD)	g/kWh	4.10E−02	2.67E−02
Oil	g/kWh	5.12E−02	3.34E−02
Sulfuric acid	g/kWh	5.21E−03	5.75E−03
Iron	g/kWh	3.16E−02	3.59E−02
Ammonia	g/kWh	3.97E−04	4.48E−04
Copper	g/kWh	0.00E + 00	0.00E + 00
Cadmium	g/kWh	1.31E−04	8.61E−05
Arsenic	g/kWh	0.00E + 00	0.00E + 00
Mercury	g/kWh	1.03E−08	6.75E−09
Phosphate	g/kWh	2.60E−03	2.87E−03
Selenium	g/kWh	0.00E + 00	0.00E + 00
Chromium	g/kWh	1.31E−04	8.61E−05
Lead	g/kWh	2.17E−08	9.56E−09
Zinc	g/kWh	4.53E−05	2.96E−05
Solid waste	g/kWh	1.09E + 02	1.20E + 02
Energy	BTU/kWh	1.08E + 04	1.08E + 04

Life Cycle Comparison of Waste-to-Energy to Sanitary Landfill. Table 7 LCI emission offsets due to recovery and remanufacturing of ferrous metals from the bottom ash in WTE plants[a]

		Ferrous metals
Air emissions		
PM-10	g/Mg	0.00E + 00
PM	g/Mg	−4.99E + 03
NO_x	g/Mg	−8.35E + 02
Hydrocarbons (non-CH_4)	g/Mg	−4.88E + 03
SO_2	g/Mg	−1.78E + 03
CO	g/Mg	−1.22E + 04
CO_2 biogenic	g/Mg	0.00E + 00
CO_2 fossil	g/Mg	−1.03E + 06
Ammonia	g/Mg	0.00E + 00
Lead	g/Mg	6.90E-01
Methane	g/Mg	−8.56E + 02
Hydrochloric acid	g/Mg	1.80E + 01
Waterborne emissions		
Dissolved solids	g/Mg	−5.84E + 02
Suspended solids	g/Mg	−2.22E + 02
BOD	g/Mg	0.00E + 00
COD	g/Mg	0.00E + 00
Oil	g/Mg	−5.15E + 00
Sulfuric acid	g/Mg	0.00E + 00
Iron	g/Mg	0.00E + 00
Ammonia	g/Mg	−5.07E + 01
Copper	g/Mg	0.00E + 00
Cadmium	g/Mg	0.00E + 00
Arsenic	g/Mg	0.00E + 00
Mercury	g/Mg	0.00E + 00
Phosphate	g/Mg	2.64E + 00
Selenium	g/Mg	0.00E + 00
Chromium	g/Mg	0.00E + 00
Lead	g/Mg	0.00E + 00
Zinc	g/Mg	0.00E + 00
Solid waste	g/Mg	−2.53E + 05
Energy	MBTU/Mg	−1.89E + 02

[a]Negative values indicate the magnitude of emission avoided due to remanufacturing activities

MSW. In addition, the functional unit of LCI is shifted from 1 Mg of waste item to 1 MWh of electricity generated. In order to facilitate a side-by-side comparison of WTE with LFGTE and other electricity generation options, the emission offsets associated with generation of electricity via WTE is excluded from the factors. The emissions per MWh of electricity generated are then calculated using the following equation:

$$WTE_MWh_i = \sum_j \{ (LCI_Stack_{ij} + LCI_Limestone_{ij} + LCI_Ammonia_{ij} + LCI_Ash_{ij}) \times Mass_j \} \div Elec \text{ for all } i \quad (2)$$

where WTE_MWh_i is the LCI emission factor for pollutant i (g/MWh); LCI_Stack_{ij} is the controlled stack gas emissions for pollutant i (g/Mg of waste item j); $LCI_Limestone_{ij}$ is the allocated emissions of pollutant i from the production and use of limestone in the scrubbers (g/Mg of waste item j); $LCI_Ammonia_{ij}$ is the allocated emissions of pollutant i from the production and use of ammonia (g/Mg of waste item j); LCI_Ash_{ij} is the allocated emissions of pollutant i from the disposal of ash (g/Mg of waste item j); $Mass_j$ is the amount of each waste item j processed in the facility (obtained from Table 1); and $Elec$ is the total electricity generated from MSW processed in the facility (MWh) and calculated as follows:

$$Elec = \left(\sum_j HeatingValue_j * Mass_j \right) * \frac{\frac{2000 \frac{\text{lb}}{\text{ton}}}{1000 \frac{\text{kWh}}{\text{MWh}}}}{HeatRate} \quad (3)$$

where $HeatingValue_j$ is the heating value of item j (Btu/lb) and $HeatRate$ is the thermal efficiency of the WTE facility (Btu/kWh). These emission factors exclude the emission offsets associated with generation of electricity.

Method to Generate Emission Factors for Landfill Gas to Energy

The total LCI emissions from landfills are the summation of the emissions resulting from (1) the site preparation, operation, and post-closure operation of a landfill, (2) the decay of the waste under anaerobic

Life Cycle Comparison of Waste-to-Energy to Sanitary Landfill. Table 8 LCI emissions from WTE (controlled emissions only) (g pollutant/Mg of waste component)

	Biogenic CO_2	Fossil CO_2	SO_2	HCl	NO_x	Dioxins/furans	CO	PM	Methane	CO_2e
Leaves	6.44E + 05	0.00E + 00	2.20E + 02	1.04E + 02	5.14E + 02	3.34E−05	3.21E + 02	6.14E + 01	1.50E + 00	3.75E + 01
Grass	5.89E + 05	0.00E + 00	2.04E + 02	9.74E + 01	4.79E + 02	3.10E−05	2.98E + 02	5.74E + 01	1.50E + 00	3.75E + 01
Branches	6.44E + 05	0.00E + 00	2.20E + 02	1.04E + 02	5.14E + 02	3.34E−05	3.21E + 02	6.14E + 01	1.50E + 00	3.75E + 01
ONP	1.58E + 06	0.00E + 00	5.19E + 02	2.48E + 02	1.22E + 03	7.89E−05	7.59E + 02	1.46E + 02	1.50E + 00	3.75E + 01
OCC	1.47E + 06	0.00E + 00	4.82E + 02	2.29E + 02	1.13E + 03	7.34E−05	7.04E + 02	1.35E + 02	1.50E + 00	3.75E + 01
Office paper	1.24E + 06	0.00E + 00	4.20E + 02	1.99E + 02	9.84E + 02	6.34E−05	6.09E + 02	1.17E + 02	1.50E + 00	3.75E + 01
Phone books	1.51E + 06	0.00E + 00	4.99E + 02	2.38E + 02	1.17E + 03	7.59E−05	7.29E + 02	1.40E + 02	1.50E + 00	3.75E + 01
Books	1.44E + 06	0.00E + 00	4.79E + 02	2.28E + 02	1.12E + 03	7.29E−05	6.99E + 02	1.34E + 02	1.50E + 00	3.75E + 01
Old magazines	8.59E + 05	0.00E + 00	2.88E + 02	1.37E + 02	6.74E + 02	4.37E−05	4.20E + 02	8.09E + 01	1.50E + 00	3.75E + 01
Third class mail	1.05E + 06	0.00E + 00	3.65E + 02	1.73E + 02	8.54E + 02	5.54E−05	5.34E + 02	1.02E + 02	1.50E + 00	3.75E + 01
Mixed paper	1.23E + 06	0.00E + 00	4.18E + 02	1.99E + 02	9.79E + 02	6.34E−05	6.09E + 02	1.17E + 02	1.50E + 00	3.75E + 01
HDPE	0.00E + 00	2.91E + 06	1.27E + 03	6.04E + 02	2.98E + 03	1.93E−04	1.86E + 03	3.57E + 02	1.50E + 00	2.91E + 06
PET	0.00E + 00	2.12E + 06	6.64E + 02	3.16E + 02	1.56E + 03	1.01E−04	9.69E + 02	1.86E + 02	1.50E + 00	2.12E + 06
Mixed plastic	0.00E + 00	2.73E + 06	1.11E + 03	5.24E + 02	2.60E + 03	1.68E−04	1.61E + 03	3.10E + 02	1.50E + 00	2.73E + 06
Ferrous cans	4.79E + 04	0.00E + 00	1.56E + 01	7.39E + 00	3.65E + 01	2.36E−06	2.27E + 01	4.36E + 00	1.50E + 00	3.75E + 01
Ferrous metal − other	4.79E + 04	0.00E + 00	1.56E + 01	7.39E + 00	3.65E + 01	2.36E−06	2.27E + 01	4.36E + 00	1.50E + 00	3.75E + 01

Life Cycle Comparison of Waste-to-Energy to Sanitary Landfill. Table 8 (Continued)

	Biogenic CO_2	Fossil CO_2	SO_2	HCl	NO_x	Dioxins/furans	CO	PM	Methane	CO_2e
Aluminum cans	4.84E + 04	0.00E + 00	1.57E + 01	7.49E + 00	3.69E + 01	2.38E−06	2.29E + 01	4.40E + 00	1.50E + 00	3.75E + 01
Aluminum	4.84E + 04	0.00E + 00	1.57E + 01	7.49E + 00	3.69E + 01	2.38E−06	2.29E + 01	4.40E + 00	1.50E + 00	3.75E + 01
Glass	1.70E + 04	0.00E + 00	6.69E + 00	3.19E + 00	1.57E + 01	1.02E−06	9.79E + 00	1.88E + 00	1.50E + 00	3.75E + 01
Paper – non-recyclable	1.24E + 06	0.00E + 00	4.20E + 02	1.99E + 02	9.84E + 02	6.34E−05	6.09E + 02	1.17E + 02	1.50E + 00	3.75E + 01
Food waste	5.04E + 05	0.00E + 00	1.79E + 02	8.49E + 01	4.19E + 02	2.71E−05	2.61E + 02	4.99E + 01	1.50E + 00	3.75E + 01
Wood	4.98E + 05	0.00E + 00	1.77E + 02	8.39E + 01	4.15E + 02	2.69E−05	2.58E + 02	4.95E + 01	1.50E + 00	3.75E + 01
Plastic – non-recyclable	0.00E + 00	2.73E + 06	1.11E + 03	5.24E + 02	2.60E + 03	1.68E−04	1.61E + 03	3.10E + 02	1.50E + 00	2.73E + 06
Miscellaneous organics	1.34E + 06	0.00E + 00	4.67E + 02	2.22E + 02	1.09E + 03	7.09E−05	6.79E + 02	1.31E + 02	1.50E + 00	3.75E + 01
Rubber	1.34E + 06	0.00E + 00	4.67E + 02	2.22E + 02	1.09E + 03	7.09E−05	6.79E + 02	1.31E + 02	1.50E + 00	3.75E + 01
Ferrous – non-recyclable	4.79E + 04	0.00E + 00	1.56E + 01	7.39E + 00	3.65E + 01	2.36E−06	2.27E + 01	4.36E + 00	1.50E + 00	3.75E + 01
Aluminum – non-recyclable	4.84E + 04	0.00E + 00	1.57E + 01	7.49E + 00	3.69E + 01	2.38E−06	2.29E + 01	4.40E + 00	1.50E + 00	3.75E + 01
Glass – non-recyclable	1.70E + 04	0.00E + 00	6.69E + 00	3.19E + 00	1.57E + 01	1.02E−06	9.79E + 00	1.88E + 00	1.50E + 00	3.75E + 01
Miscellaneous inorganics	0.00E + 00	0.00E + 00	0.00E + 00	0.00E + 00	0.00E + 00	0.00E + 00	0.00E + 00	0.00E + 00	1.50E + 00	3.75E + 01

Life Cycle Comparison of Waste-to-Energy to Sanitary Landfill. Table 9 LCI emissions from WTE (controlled emissions + limestone emissions – regional grid offsets) (g pollutant/Mg of waste component)

	Biogenic CO_2	Fossil CO_2	SO_2	HCl	NO_x	Dioxins/ furans	CO	PM	Methane	Ammonia	Hydrocarbons	CO_2e
Leaves	6.44E + 05	−2.97E + 05	−1.92E + 03	7.89E + 01	−6.29E + 02	3.34E−05	2.55E + 02	−3.26E + 02	−6.59E + 02	−1.43E−02	−1.49E + 01	−3.14E + 05
Grass	5.89E + 05	−2.97E + 05	−1.94E + 03	7.14E + 01	−6.64E + 02	3.10E−05	2.33E + 02	−3.31E + 02	−6.59E + 02	−1.43E−02	−1.49E + 01	−3.14E + 05
Branches	6.44E + 05	−7.74E + 05	−5.29E + 03	3.90E + 01	−2.42E + 03	3.34E−05	1.49E + 02	−9.59E + 02	−1.70E + 03	−3.88E−02	−4.14E + 01	−8.17E + 05
ONP	1.58E + 06	−8.79E + 05	−5.74E + 03	1.73E + 02	−2.11E + 03	7.89E−05	5.64E + 02	−1.01E + 03	−1.93E + 03	−4.42E−02	−4.72E + 01	−9.27E + 05
OCC	1.47E + 06	−8.04E + 05	−5.24E + 03	1.61E + 02	−1.91E + 03	7.34E−05	5.24E + 02	−9.24E + 02	−1.76E + 03	−4.03E−02	−4.30E + 01	−8.48E + 05
Office paper	1.24E + 06	−7.34E + 05	−4.82E + 03	1.37E + 02	−1.80E + 03	6.34E−05	4.49E + 02	−8.49E + 02	−1.61E + 03	−3.68E−02	−3.92E + 01	−7.74E + 05
Phone books	1.51E + 06	−7.29E + 05	−4.68E + 03	1.76E + 02	−1.59E + 03	7.59E−05	5.69E + 02	−8.19E + 02	−1.59E + 03	−3.64E−02	−3.88E + 01	−7.69E + 05
Books	1.44E + 06	−7.29E + 05	−4.70E + 03	1.66E + 02	−1.63E + 03	7.29E−05	5.39E + 02	−8.24E + 02	−1.59E + 03	−3.64E−02	−3.88E + 01	−7.69E + 05
Old magazines	8.59E + 05	−6.24E + 05	−4.18E + 03	8.39E + 01	−1.70E + 03	4.37E−05	2.82E + 02	−7.44E + 02	−1.37E + 03	−3.12E−02	−3.32E + 01	−6.59E + 05
Third class mail	1.05E + 06	−7.04E + 05	−4.67E + 03	1.13E + 02	−1.83E + 03	5.54E−05	3.76E + 02	−8.29E + 02	−1.55E + 03	−3.54E−02	−3.77E + 01	−7.43E + 05
Mixed paper	1.23E + 06	−7.89E + 05	−5.24E + 03	1.31E + 02	−2.02E + 03	6.34E−05	4.34E + 02	−9.29E + 02	−1.74E + 03	−3.97E−02	−4.24E + 01	−8.33E + 05
HDPE	−3.05E + 02	7.19E + 05	−1.43E + 04	4.21E + 02	−5.29E + 03	1.93E−04	1.37E + 03	−2.55E + 03	−4.79E + 03	−1.12E−01	−1.20E + 02	5.99E + 05
PET	−3.05E + 02	−6.89E + 04	−1.49E + 04	1.32E + 02	−6.69E + 03	1.01E−04	4.84E + 02	−2.72E + 03	−4.79E + 03	−1.12E−01	−1.20E + 02	−1.89E + 05
Mixed plastic	−2.30E + 02	1.08E + 06	−1.06E + 04	3.87E + 02	−3.64E + 03	1.68E−04	1.25E + 03	−1.88E + 03	−3.61E + 03	−8.39E−02	−8.99E + 01	9.89E + 05

Life Cycle Comparison of Waste-to-Energy to Sanitary Landfill. Table 9 (Continued)

	Biogenic CO_2	Fossil CO_2	SO_2	HCl	NO_x	Dioxins/ furans	CO	PM	Methane	Ammonia	Hydrocarbons	CO_2e
Ferrous cans	4.79E + 04	−2.64E + 04	−2.10E + 02	4.42E + 00	−8.79E + 01	2.36E−06	1.73E + 01	−2.37E + 01	−6.89E + 01	−4.12E−04	1.10E−01	−2.81E + 04
Ferrous metal – other	4.79E + 04	8.99E + 03	4.13E + 01	7.39E + 00	4.56E + 01	2.36E−06	2.52E + 01	2.34E + 01	8.19E + 00	1.41E−03	2.08E + 00	9.19E + 03
Aluminum cans	4.84E + 04	8.99E + 03	4.15E + 01	7.49E + 00	4.60E + 01	2.38E−06	2.54E + 01	2.34E + 01	8.19E + 00	1.41E−03	2.08E + 00	9.19E + 03
Aluminum	4.84E + 04	8.99E + 03	4.15E + 01	7.49E + 00	4.60E + 01	2.38E−06	2.54E + 01	2.34E + 01	8.19E + 00	1.41E−03	2.08E + 00	9.19E + 03
Glass	1.70E + 04	−8.79E + 02	−3.76E + 01	2.36E + 00	−1.23E + 01	1.02E−06	1.00E + 01	7.79E + 00	−1.34E + 01	8.99E−04	1.53E + 00	−1.21E + 03
Paper – non-recyclable	1.24E + 06	−7.54E + 05	−4.94E + 03	1.35E + 02	−1.87E + 03	6.34E−05	4.45E + 02	−8.74E + 02	−1.65E + 03	−3.77E−02	−4.02E + 01	−7.95E + 05
Food waste	5.04E + 05	−2.03E + 05	−1.29E + 03	6.74E + 01	−3.68E + 02	2.71E−05	2.16E + 02	−2.12E + 02	−4.53E + 02	−9.44E−03	−9.69E + 00	−2.14E + 05
Wood	4.98E + 05	−7.74E + 05	−5.34E + 03	1.86E + 01	−2.52E + 03	2.69E−05	8.69E + 01	−9.69E + 02	−1.70E + 03	−3.88E−02	−4.14E + 01	−8.17E + 05
Plastic – non-recyclable	−1.63E + 02	1.56E + 06	−7.19E + 03	4.28E + 02	−1.83E + 03	1.68E−04	1.35E + 03	−1.23E + 03	−2.56E + 03	−5.89E−02	−6.34E + 01	1.50E + 06
Miscellaneous organics	1.34E + 06	−8.99E + 05	−5.94E + 03	1.46E + 02	−2.32E + 03	7.09E−05	4.81E + 02	−1.06E + 03	−1.98E + 03	−4.53E−02	−4.85E + 01	−9.48E + 05
Rubber	1.34E + 06	−1.27E + 06	−8.59E + 03	1.14E + 02	−3.72E + 03	7.09E−05	3.99E + 02	−1.55E + 03	−2.79E + 03	−6.44E−02	−6.89E + 01	−1.34E + 06
Ferrous – non-recyclable	4.79E + 04	8.99E + 03	4.13E + 01	7.39E + 00	4.56E + 01	2.36E−06	2.52E + 01	2.34E + 01	8.19E + 00	1.41E−03	2.08E + 00	9.19E + 03
Aluminum – non-recyclable	4.84E + 04	8.99E + 03	4.15E + 01	7.49E + 00	4.60E + 01	2.38E−06	2.54E + 01	2.34E + 01	8.19E + 00	1.41E−03	2.08E + 00	9.19E + 03
Glass – non-recyclable	1.70E + 04	8.99E + 03	3.24E + 01	3.19E + 00	2.49E + 01	1.02E−06	1.22E + 01	2.09E + 01	8.19E + 00	1.41E−03	2.08E + 00	9.19E + 03
Miscellaneous inorganics	3.35E−01	8.99E + 03	2.57E + 01	8.29E−06	9.14E + 00	0.00E + 00	2.47E + 00	1.90E + 01	8.19E + 00	1.41E−03	2.08E + 00	9.19E + 03

Life Cycle Comparison of Waste-to-Energy to Sanitary Landfill. Table 10 Emission factors for ash landfill (g pollutant/Mg of waste component)

	Biogenic CO_2	Fossil CO_2	SO_2	HCl	NO_x	CO	PM	Methane	Ammonia	Hydrocarbons	CO_2e
Leaves	4.07E−01	1.73E + 03	4.11E + 00	2.06E−03	2.42E + 01	8.19E + 00	2.22E + 00	3.06E−01	2.67E−03	6.18E + 00	1.73E + 03
Grass	4.07E−01	1.73E + 03	4.11E + 00	2.06E−03	2.42E + 01	8.19E + 00	2.22E + 00	3.06E−01	2.67E−03	6.18E + 00	1.73E + 03
Branches	4.07E−01	1.73E + 03	4.11E + 00	2.06E−03	2.42E + 01	8.19E + 00	2.22E + 00	3.06E−01	2.67E−03	6.18E + 00	1.73E + 03
ONP	6.14E−01	2.60E + 03	6.20E + 00	3.11E−03	3.65E + 01	1.24E + 01	3.35E + 00	4.62E−01	4.03E−03	9.32E + 00	2.62E + 03
OCC	6.20E−01	2.63E + 03	6.26E + 00	3.14E−03	3.68E + 01	1.25E + 01	3.38E + 00	4.66E−01	4.07E−03	9.41E + 00	2.64E + 03
Office paper	6.14E−01	2.60E + 03	6.20E + 00	3.11E−03	3.65E + 01	1.24E + 01	3.35E + 00	4.62E−01	4.03E−03	9.32E + 00	2.62E + 03
Phone books	6.14E−01	2.60E + 03	6.20E + 00	3.11E−03	3.65E + 01	1.24E + 01	3.35E + 00	4.62E−01	4.03E−03	9.32E + 00	2.62E + 03
Books	6.14E−01	2.60E + 03	6.20E + 00	3.11E−03	3.65E + 01	1.24E + 01	3.35E + 00	4.62E−01	4.03E−03	9.32E + 00	2.62E + 03
Old magazines	6.14E−01	2.60E + 03	6.20E + 00	3.11E−03	3.65E + 01	1.24E + 01	3.35E + 00	4.62E−01	4.03E−03	9.32E + 00	2.62E + 03
Third class mail	6.14E−01	2.60E + 03	6.20E + 00	3.11E−03	3.65E + 01	1.24E + 01	3.35E + 00	4.62E−01	4.03E−03	9.32E + 00	2.62E + 03
Mixed paper	6.14E−01	2.60E + 03	6.20E + 00	3.11E−03	3.65E + 01	1.24E + 01	3.35E + 00	4.62E−01	4.03E−03	9.32E + 00	2.62E + 03
HDPE	6.38E−01	2.71E + 03	6.44E + 00	3.23E−03	3.79E + 01	1.28E + 01	3.48E + 00	4.80E−01	4.19E−03	9.69E + 00	2.72E + 03
PET	6.38E−01	2.71E + 03	6.44E + 00	3.23E−03	3.79E + 01	1.28E + 01	3.48E + 00	4.80E−01	4.19E−03	9.69E + 00	2.72E + 03
Mixed plastic	6.38E−01	2.71E + 03	6.44E + 00	3.23E−03	3.79E + 01	1.28E + 01	3.48E + 00	4.80E−01	4.19E−03	9.69E + 00	2.72E + 03
Ferrous cans	6.32E−01	2.68E + 03	6.38E + 00	3.20E−03	3.75E + 01	1.27E + 01	3.44E + 00	4.75E−01	4.15E−03	9.60E + 00	2.69E + 03
Ferrous metal − other	6.32E−01	2.68E + 03	6.38E + 00	3.20E−03	3.75E + 01	1.27E + 01	3.44E + 00	4.75E−01	4.15E−03	9.60E + 00	2.69E + 03
Aluminum cans	6.38E−01	2.71E + 03	6.44E + 00	3.23E−03	3.79E + 01	1.28E + 01	3.48E + 00	4.80E−01	4.19E−03	9.69E + 00	2.72E + 03
Aluminum	6.38E−01	2.71E + 03	6.44E + 00	3.23E−03	3.79E + 01	1.28E + 01	3.48E + 00	4.80E−01	4.19E−03	9.69E + 00	2.72E + 03

Life Cycle Comparison of Waste-to-Energy to Sanitary Landfill. Table 10 (Continued)

	Biogenic CO_2	Fossil CO_2	SO_2	HCl	NO_x	CO	PM	Methane	Ammonia	Hydrocarbons	CO_2e
Glass	6.38E−01	2.71E + 03	6.44E + 00	3.23E−03	3.79E + 01	1.28E + 01	3.48E + 00	4.80E−01	4.19E−03	9.69E + 00	2.72E + 03
Paper – non-recyclable	6.14E−01	2.60E + 03	6.20E + 00	3.11E−03	3.65E + 01	1.24E + 01	3.35E + 00	4.62E−01	4.03E−03	9.32E + 00	2.62E + 03
Food waste	3.83E−01	1.62E + 03	3.87E + 00	1.94E−03	2.27E + 01	7.71E + 00	2.09E + 00	2.88E−01	2.51E−03	5.81E + 00	1.63E + 03
Wood	3.83E−01	1.62E + 03	3.87E + 00	1.94E−03	2.27E + 01	7.71E + 00	2.09E + 00	2.88E−01	2.51E−03	5.81E + 00	1.63E + 03
Plastic – non-recyclable	6.38E−01	2.71E + 03	6.44E + 00	3.23E−03	3.79E + 01	1.28E + 01	3.48E + 00	4.80E−01	4.19E−03	9.69E + 00	2.72E + 03
Miscellaneous organics	5.43E−01	2.30E + 03	5.48E + 00	2.75E−03	3.22E + 01	1.09E + 01	2.96E + 00	4.08E−01	3.56E−03	8.24E + 00	2.31E + 03
Rubber	5.43E−01	2.30E + 03	5.48E + 00	2.75E−03	3.22E + 01	1.09E + 01	2.96E + 00	4.08E−01	3.56E−03	8.24E + 00	2.31E + 03
Ferrous – non-recyclable	6.32E−01	2.68E + 03	6.38E + 00	3.20E−03	3.75E + 01	1.27E + 01	3.44E + 00	4.75E−01	4.15E−03	9.60E + 00	2.69E + 03
Aluminum – non-recyclable	6.38E−01	2.71E + 03	6.44E + 00	3.23E−03	3.79E + 01	1.28E + 01	3.48E + 00	4.80E−01	4.19E−03	9.69E + 00	2.72E + 03
Glass – non-recyclable	6−.38E−01	2.71E + 03	6.44E + 00	3.23E−03	3.79E + 01	1.28E + 01	3.48E + 00	4.80E−01	4.19E−03	9.69E + 00	2.72E + 03
Miscellaneous inorganics	5.43E−01	2.30E + 03	5.48E + 00	2.75E−03	3.22E + 01	1.09E + 01	2.96E + 00	4.08E−01	3.56E−03	8.24E + 00	2.31E + 03

Life Cycle Comparison of Waste-to-Energy to Sanitary Landfill. Table 11 Inputs to landfill process model

During	LFG collection system efficiency[a] (%)	Oxidation rate (%)
Venting	0	15
First year of gas collection[b]	50	15
Second year of gas collection	70	15
Third year onward of gas collection	80	15

[a]We assumed efficiency of the collection system based on the year of the operation and the ranges stated in [31]
[b]Gas collection can start anytime during the operation of the landfill. In this analysis, two scenarios were considered. In the first scenario, gas collection starts at the second year of the operation, and in the second one, the gas collection starts at the fourth year of the operation

conditions, (3) the equipment utilized during landfill operations and landfill gas management operations, (4) the production of diesel required to operate the vehicles at the site, and (5) the treatment of leachate [17, 25]. The production of LFG was calculated using a first-order decay equation for a time horizon of 100 years and the measured methane yield from each individual waste component [17, 26]. The LCI model also requires the quantity and composition of the waste disposed, LFG collection efficiency (Table 11), annual LFG management schedule, oxidation rate (15%), emission factors for combustion by-products from LFG control devices, and the emission factors for equipment used on site during the site preparation and operation of a landfill. The LFG collection efficiency can be varied annually. The emission factors are calculated under the following scenario assumptions:

1. A regional landfill subject to CAA is considered.
2. A single cell in the regional landfill is modeled.
3. Waste is initially placed in the new cell in Year 0.
4. The landfill already has a LFG collection network in place.
5. An internal combustion engine (ICE) is utilized to generate electricity.
6. The offline time that is required for the routine maintenance of the ICE is not considered.
7. The LFG control devices are assumed to have a lifetime of 15 years.
8. The LFG will be collected and controlled until Year 65. This assumption is based on a typical landfill with an average operating lifetime of 20 years in which LFG production decreases significantly after about 60 years from initial waste placement. The LFG production is based on the use of a first-order decay equation.

In practice, the timing of LFG-related operations such as the installation of the gas capture system, start of gas capture, and the installation of energy recovery equipment exhibits significant variation that will influence the total emissions from an individual landfill. To capture these variations, several different LFG management schemes were tested. An average or typical LFG management scheme would vary significantly from one location to another. Kaplan et al. [27] enlist a variety of scenarios for comparison. Here, the WTE LCI emission factors were compared in detail against three LFG LCI scenarios, and the sensitivities around various operational assumptions are accounted and presented as lower and upper bounds. The first scenario assumes 100% venting of LFG for the entire life of the landfill. The second assumes venting of the LFG for the first 4 years and then flaring of the LFG until Year 65. The third scenario represents an LFG energy recovery scenario: The LFG is vented for the first 4 years followed by the installation of an LFG collection system in the landfill. The recovered LFG is flared for 2 years, and subsequently combusted in an ICE for electricity generation for 30 year, then flared until Year 65. In practice, this energy recovery period could last anywhere from 10 to 60 years. The extent of this time period depends on the site characteristics such as flow rate and the quality of the captured methane gas, regional climate, and economic feasibility. Table 12 presents the LCI emission factors per Mg of MSW components for the LFGTE case with 30 years of electricity generation through the use of an ICE. These emission factors include offsets associated with the generation of electricity from coal-powered EGUs in the SERC region.

In addition, LCI emission factors per MWh of electricity generated were calculated for LFGTE scenarios. A procedure similar to one detailed for WTE is followed. The reader may refer to [27] for details on

Life Cycle Comparison of Waste-to-Energy to Sanitary Landfill. Table 12 Landfill emission factors (g pollutant/Mg of waste component)

	Biogenic CO_2	Fossil CO_2	SO_2	HCl	NO_x	CO	PM	Methane	Ammonia	Hydrocarbons	CO_2e
Leaves	4.39E + 04	−1.04E + 04	−9.18E + 01	−6.80E−01	2.54E + 01	8.34E + 01	−1.00E + 01	2.59E + 03	1.06E−02	1.43E + 01	5.44E + 04
Grass	1.93E + 05	−6.52E + 04	−4.77E + 02	−3.66E + 00	−1.07E + 02	2.53E + 02	−6.86E + 01	1.39E + 04	2.30E−02	1.33E + 01	2.82E + 05
Branches	8.99E + 04	−2.57E + 04	−1.99E + 02	−1.40E + 00	−1.05E + 01	1.47E + 02	−2.60E + 01	5.30E + 03	1.44E−02	1.41E + 01	1.07E + 05
ONP	2.51E + 05	−7.92E + 04	−5.74E + 02	−3.91E + 00	−1.36E + 02	3.72E + 02	−8.19E + 01	1.48E + 04	2.79E−02	1.33E + 01	2.90E + 05
OCC	5.19E + 05	−1.69E + 05	−1.20E + 03	−8.12E + 00	−3.46E + 02	7.46E + 02	−1.75E + 02	3.06E + 04	5.04E−02	1.19E + 01	5.97E + 05
Office paper	7.33E + 05	−2.40E + 05	−1.70E + 03	−1.15E + 01	−5.13E + 02	1.04E + 03	−2.49E + 02	4.32E + 04	6.83E−02	1.09E + 01	8.41E + 05
Phone books	2.51E + 05	−7.92E + 04	−5.74E + 02	−3.91E + 00	−1.36E + 02	3.72E + 02	−8.19E + 01	1.48E + 04	2.79E−02	1.33E + 01	2.90E + 05
Books	7.33E + 05	−2.40E + 05	−1.70E + 03	−1.15E + 01	−5.13E + 02	1.04E + 03	−2.49E + 02	4.32E + 04	6.83E−02	1.09E + 01	8.41E + 05
Old magazines	2.85E + 05	−9.05E + 04	−6.54E + 02	−4.45E + 00	−1.63E + 02	4.19E + 02	−9.37E + 01	1.68E + 04	3.07E−02	1.31E + 01	3.29E + 05
Third class mail	5.09E + 05	−1.65E + 05	−1.18E + 03	−7.95E + 00	−3.38E + 02	7.32E + 02	−1.72E + 02	3.00E + 04	4.95E−02	1.20E + 01	5.85E + 05
Mixed paper	3.50E + 05	−1.12E + 05	−8.06E + 02	−5.46E + 00	−2.14E + 02	5.10E + 02	−1.16E + 02	2.06E + 04	3.62E−02	1.28E + 01	4.04E + 05
HDPE	1.05E + 00	4.26E + 03	1.07E + 01	7.67E−03	5.98E + 01	2.21E + 01	5.21E + 00	8.42E−01	6.88E−03	1.45E + 01	4.28E + 03
PET	1.05E + 00	4.26E + 03	1.07E + 01	7.67E−03	5.98E + 01	2.21E + 01	5.21E + 00	8.42E−01	6.88E−03	1.45E + 01	4.28E + 03
Mixed plastic	1.05E + 00	4.26E + 03	1.07E + 01	7.67E−03	5.98E + 01	2.21E + 01	5.21E + 00	8.42E−01	6.88E−03	1.45E + 01	4.28E + 03

Ferrous cans	1.05E + 00	4.26E + 03	1.07E + 01	7.67E−03	5.98E + 01	2.21E + 01	5.21E + 00	8.42E−01	6.88E−03	1.45E + 01	4.28E + 03
Ferrous metal − other	1.05E + 00	4.26E + 03	1.07E + 01	7.67E−03	5.98E + 01	2.21E + 01	5.21E + 00	8.42E−01	6.88E−03	1.45E + 01	4.28E + 03
Aluminum cans	1.05E + 00	4.26E + 03	1.07E + 01	7.67E−03	5.98E + 01	2.21E + 01	5.21E + 00	8.42E−01	6.88E−03	1.45E + 01	4.28E + 03
Aluminum	1.05E + 00	4.26E + 03	1.07E + 01	7.67E−03	5.98E + 01	2.21E + 01	5.21E + 00	8.42E−01	6.88E−03	1.45E + 01	4.28E + 03
Glass	1.05E + 00	4.26E + 03	1.07E + 01	7.67E−03	5.98E + 01	2.21E + 01	5.21E + 00	8.42E−01	6.88E−03	1.45E + 01	4.28E + 03
Paper − non-recyclable	3.50E + 05	−1.12E + 05	−8.06E + 02	−5.46E + 00	−2.14E + 02	5.10E + 02	−1.16E + 02	2.06E + 04	3.62E−02	1.28E + 01	4.04E + 05
Food waste	3.20E + 05	−1.11E + 05	−7.98E + 02	−6.07E + 00	−2.17E + 02	4.05E + 02	−1.17E + 02	2.30E + 04	3.36E−02	1.25E + 01	4.65E + 05
Wood	1.05E + 00	4.26E + 03	1.07E + 01	7.67E−03	5.98E + 01	2.21E + 01	5.21E + 00	8.42E−01	−6.88E−03	1.45E + 01	4.28E + 03
Plastic − non-recyclable	1.05E + 00	4.26E + 03	1.07E + 01	7.67E−03	5.98E + 01	2.21E + 01	5.21E + 00	8.42E−01	6.88E−03	1.45E + 01	4.28E + 03
Miscellaneous organics	1.05E + 00	4.26E + 03	1.07E + 01	7.67E−03	5.98E + 01	2.21E + 01	5.21E + 00	8.42E−01	6.88E−03	1.45E + 01	4.28E + 03
Rubber	1.05E + 00	4.26E + 03	1.07E + 01	7.67E−03	5.98E + 01	2.21E + 01	5.21E + 00	8.42E−01	6.88E−03	1.45E + 01	4.28E + 03
Ferrous − non-recyclable	1.05E + 00	4.26E + 03	1.07E + 01	7.67E−03	5.98E + 01	2.21E + 01	5.21E + 00	8.42E−01	6.88E−03	1.45E + 01	4.28E + 03
Aluminum − non-recyclable	1.05E + 00	4.26E + 03	1.07E + 01	7.67E−03	5.98E + 01	2.21E + 01	5.21E + 00	8.42E−01	6.88E−03	1.45E + 01	4.28E + 03
Glass − non-recyclable	1.05E + 00	4.26E + 03	1.07E + 01	7.67E−03	5.98E + 01	2.21E + 01	5.21E + 00	8.42E−01	6.88E−03	1.45E + 01	4.28E + 03
Miscellaneous inorganics	1.05E + 00	4.26E + 03	1.07E + 01	7.67E−03	5.98E + 01	2.21E + 01	5.21E + 00	8.42E−01	6.88E−03	1.45E + 01	4.28E + 03

the calculations of the LCI emission factors. These emission factors, similar to WTE counterparts, exclude the emission offsets associated with the generation of electricity.

Results and Discussion

The LCI emission factors for WTE were generated on a per Mg of MSW item and compared to LCI emission factors for LFGTE scenarios. Table 13 summarizes the CO_2e emission factors for major waste items such as paper, yard waste, and plastics sent to either WTE or LFGTE. The CO_2e emission factors for WTE include all the components presented in Eq. (1). All of the biogenic waste items such as grass, leaves, cardboard, and food waste result in avoided emissions when combusted in a WTE facility. When biogenic items are disposed in landfills—even with energy recovery—the CO_2e emission factors for those items are higher than the factors for fossil-based waste items such as plastics, mainly because organic materials decompose in the landfill under anaerobic conditions, which results in methane emissions. Methane being a more potent greenhouse gas than CO_2 leads to higher CO_2e emission factors. Plastics, on the other hand, do not decompose in landfills. However, their higher carbon content translates to a higher energy content per unit mass, which results in higher CO_2e emissions when combusted in a WTE facility. The average composition of MSW as discarded by weight was calculated to be 77% biogenic- and 23% fossil-based [28]. Based on the average composition of discarded MSW presented in Table 1, average CO_2e factors were calculated. A WTE facility receiving the discarded portion of MSW resulted in avoided or negative emissions of 345 kg CO_2e/Mg of MSW, whereas the emissions from LFGTE were 219 kg of CO_2e/Mg of MSW, which includes the electricity generation offsets.

When waste is buried in a landfill, some of the biogenic material does not degrade, and this material is said to be stored. While carbon storage was not included in this analysis, it could have a significant impact on the results. For example, Staley and Barlaz (2009) report carbon storage factors of about 0.13 kg C/kg dry refuse [29]. At a moisture content of 20%, this translates to 381 kg CO_2e/Mg of wet refuse. This value would be subtracted from the landfill LCI result of 219 kg of CO_2e/Mg of MSW to obtain an LCI emission factor that accounts for the carbon sequestration.

The LCI emissions were calculated per MWh of electricity generated and compared to the LCI-based emission factors for LFGTE. A parametric sensitivity analysis was conducted on the LCI emission factors to establish lower and upper bounds. We hypothesize that the variations in the MSW composition and electricity conversion efficiency of the WTE facility could have significant effects on the LCI emission factors. The sensitivity of emission factors to biogenic- vs. fossil-based waste fraction was also determined. Two compositions (one with 100% biogenic-based waste and another with 100% fossil-based waste) were used to generate the emission factors. In addition, the conversion efficiency of the WTE facility was varied from 15% to 30%. A summary of this analysis is presented in Table 14. For LFG scenarios, the LCI emission factors were varied by changing oxidation rates and analyzing various LFG management scenarios. The LCI emission factors for the conventional EGUs are recalculated while the conversion efficiencies are varied. The lower and upper bounds on the LCI emission factors are established. The results of this analysis are presented in the figures as lower and upper bounds; however, for more details on the assumptions and the full sensitivity

Life Cycle Comparison of Waste-to-Energy to Sanitary Landfill. Table 13 Comparison of LCI emission factors in *kg of CO_2e per Mg* of selected major MSW items and average MSW as received by the WTE facility and landfill with energy recovery

	WTE	LFGTE
Leaves	−312	54
Grass	−312	282
OCC	−846	597
Office paper	−772	841
HDPE	602	4
PET	−186	4
Mixed plastic	991	4
Food	−212	465
MSW	−345	219

Life Cycle Comparison of Waste-to-Energy to Sanitary Landfill. Table 14 Emission factors (g pollutant/MWh) and sensitivity of emission factors for WTE to plant efficiency, waste composition, and remanufacturing benefits of steel recovery

				Sensitivity on				
		Baseline factors		System efficiency	Waste composition		Steel recovery	
Input parameters varied [a]								
Heat rate	BTU/kWh	18,000		*[11,000, 23,000]*	18,000	18,000	18,000	18,000
Conversion efficiency	%	19		*[15, 30]*	19	19	19	19
Composition		Default		Default	*All biogenic*	*All fossil*	Default	Default
Stack gas limits		Reg	Avg	*Reg/Avg*	Reg	Reg	*Reg*	*Avg*
Steel recovery		Excludes		Excludes	Excludes	Excludes	*Includes*	*Includes*
Results: Criteria pollutants								
CO	g/MWh	790	790	[500,1,000]	740	880	−110	−110
NO_x	g/MWh	1,300	1,500	[810, 1,800]	1,200	1,400	1,200	1,400
SO_2	g/MWh	578	221	[140, 730]	550	620	450	90
PM	g/MWh	181	60	[38, 230]	180	190	−190	−310
HCl	g/MWh	260	110	[71, 320]	240	280	260	110
Dioxins/furans	g/MWh	8.1E−05	2.8E−05	[1.8E−05, 1.0E−04]	7.6E−05	9.1E−05	8.1E−05	2.8E−05
Ammonia	g/MWh	3.8E−03	3.8E−03	[2.4E−03, 4.8E−03]	4.4E−03	2.7E−03	3.8E−03	3.8E−03
Hg	g/MWh	5.0E−02	5.0E−02	[3.2E−02, 6.4E−02]	6.5E−02	2.7E−02	5.0E−02	5.0E−02
Results: Greenhouse gases								
CO_2-biogenic	Mg/MWh	0.91	0.91	[0.58, 1.2]	1.5	0.03	0.91	0.91
CO_2-fossil	Mg/MWh	0.56	0.56	[0.36, 0.71]	0.02	1.5	0.49	0.49
CH_4	Mg/MWh	1.3E−05	1.3E−05	[8.1E−06, 1.6E−05]	1.6E−05	7.9E−06	−5.0E−05	−5.0E−05
CO_2e	Mg CO_2E/MWh	0.56	0.56	[0.36, 0.71]	0.02	1.45	0.49	0.49
Results: Electricity generation								
	TWh[b]	98	98	[78, 160]	61	37	98	98
	kWh/Mg	590	590	[470, 930]	470	970	590	590
	GW[c]	12	12	[9.7, 20]	7.6	4.7	12	12

[a]For each sensitivity analysis scenario, the input parameters in *italics* were modified, and resultant emission factors were calculated and reported in the ranges

[b]The values represent the TWh of electricity that could be generated from all MSW disposed into landfills

[c]1 TWh/8,000 h = TW; Capacity factor of approximately 0.91 is utilized

analysis, the reader should refer to Kaplan et al. [27]. In addition, the reader should recognize that the LCI emission factors for WTE and LFGTE per MWh of electricity generated do not include the offsets associated with the avoided electricity generation from the grid.

Figure 1 presents the emission factors for total CO_2e per MWh of electricity generated for landfills,

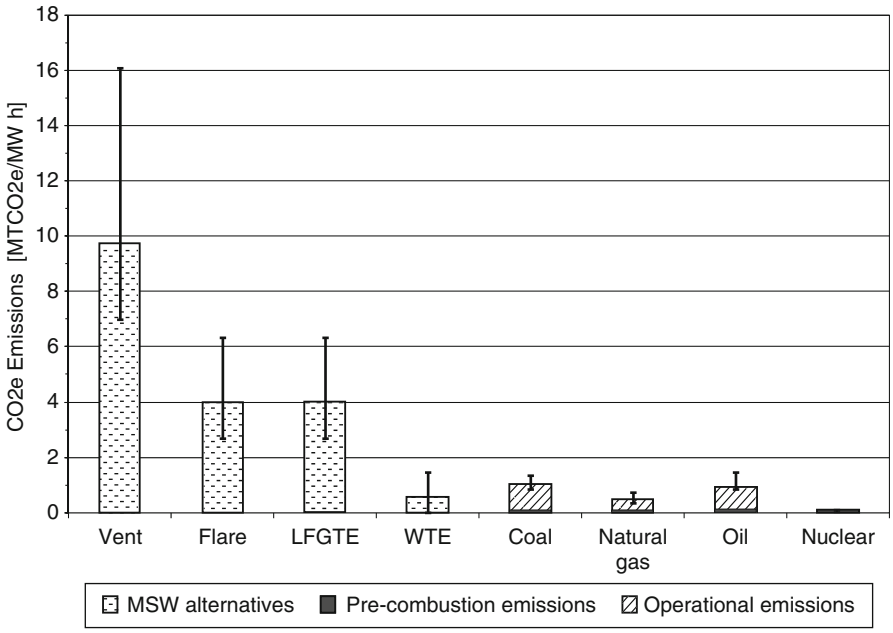

Life Cycle Comparison of Waste-to-Energy to Sanitary Landfill. Figure 1
Comparison of carbon dioxide equivalents for LFGTE, WTE, and conventional EGUs (Note that the Flare and LFGTE options have same CO_2e, this due to the fact that emission factors per MWh do not include offsets associated with the generation of electricity from LFG.)

WTE, coal, natural gas, oil, and nuclear power plants. The WTE scenarios result in less CO_2e emissions than the LFG scenarios. The vented methane in the early years of the landfill operation is the main contributor to the higher CO_2e emissions. The CO_2e emissions from WTE ranged from 0.02 Mg of CO_2e/MWh to 1.5 Mg of CO_2e/MWh, where the low end of the range represents high efficiency and MSW composition with 100% biogenic waste while the high end of the range represents emission factors calculated using MSW composition consisting of 100% fossil-based waste items. However, the CO_2e emissions from WTE—even the ones based on 100% fossil-based waste—are still lower than the most aggressive LFGTE scenario whose CO_2e emissions are 2.3 Mg of CO_2e/MWh. Figure 2 provides a closer look at the CO_2e emission factors for WTE and conventional EGUs and distinguishes between precombustion and combustion-related emissions. The average CO_2e emissions for WTE are 0.56 Mg of CO_2e/MWh, resulting in lower emissions than coal and oil; however, natural gas and nuclear have still lower greenhouse gas emissions than WTE.

SO_2 emissions from WTE facilities occur during the combustion process and are controlled via wet or dry scrubbers. The use of LFG control during operation, closure, and post-closure of the landfill as well as the treatment of leachate contributes to the SO_2 emissions from landfills. Figure 3 presents SO_2 emission factors for WTE, LFG scenarios and conventional EGUs. Overall, the SO_2 emissions resulting from the LFGTE and WTE alternatives are approximately ten times lower than the SO_2 emissions resulting from coal- and oil-fired power plants with flue gas controls. The SO_2 emissions for WTE ranged from 140 to 730 g/MWh, and for LFGTE it ranged from 430 to 900 g/MWh. In a coal-fired power plant, average SO_2 emissions were 6,900 g/MWh. Note that the majority of the SO_2 emissions from natural gas are attributed to the processing of natural gas rather than the combustion of the natural gas for electricity-generating purposes.

During the combustion process, NO_x emissions result from two different oxidation mechanisms. First, a reaction referred to as "thermal NO_x" occurs between nitrogen in the combustion air and excess oxygen at elevated temperatures. A second reaction referred to as

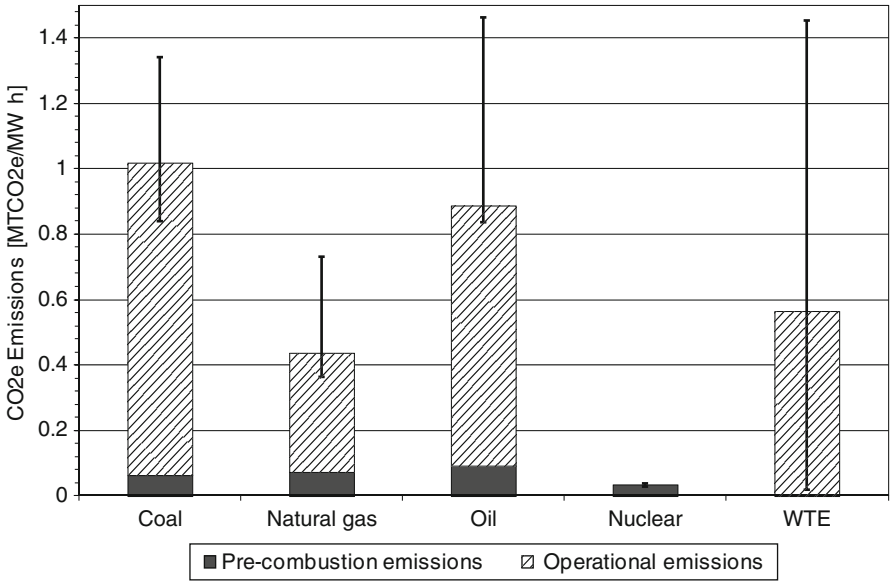

Life Cycle Comparison of Waste-to-Energy to Sanitary Landfill. Figure 2
Comparison of carbon dioxide equivalents for WTE and conventional EGUs

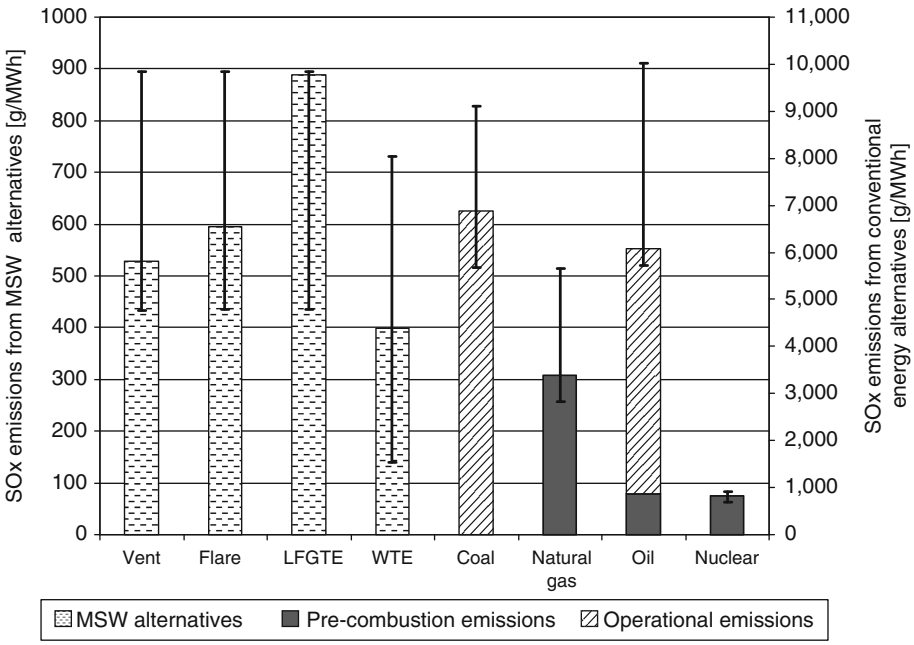

Life Cycle Comparison of Waste-to-Energy to Sanitary Landfill. Figure 3
Comparison of sulfur dioxide emissions for LFGTE, WTE, and conventional EGUs

"fuel NO_x" represents the oxidation of nitrogen that is chemically bound in the fuel. For most coal-fired EGUs, thermal NO_x typically represents about 25%, and fuel NO_x represents about 75% of the total NO_x formed. Figure 4 presents NO_x emission factors for WTE, LFGTE, and conventional EGUs. The NO_x emissions for WTE alternatives ranged from 810 to 1,800 g/MWh, and for LFGTE, NO_x emissions ranged from 2,100 to

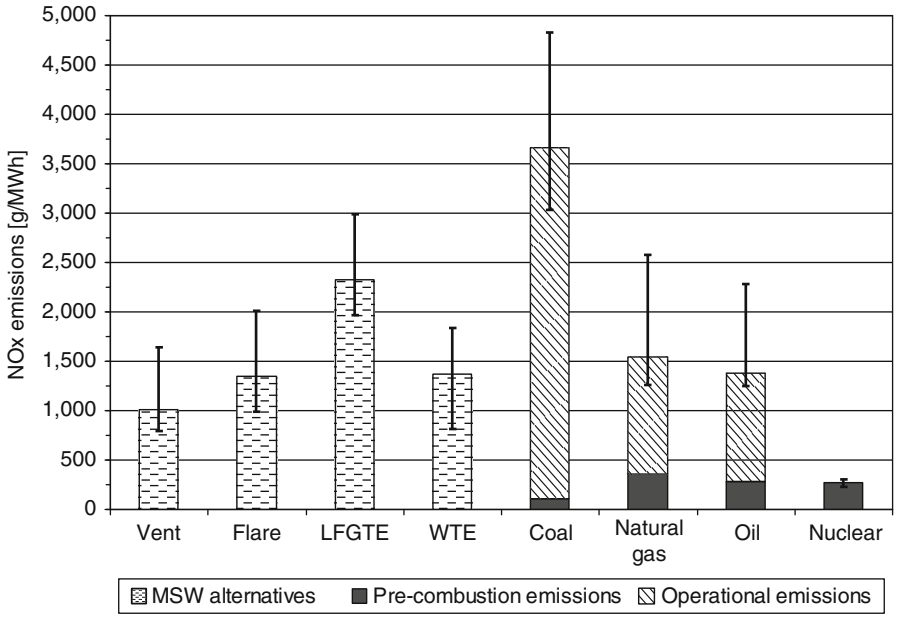

Life Cycle Comparison of Waste-to-Energy to Sanitary Landfill. Figure 4
Comparison of nitrogen oxides emissions for LFGTE, WTE, and conventional EGUs

3,000 g/MWh. In a coal-fired power plant, average NO_x emissions are 3,700 g/MWh. The emission factors for other criteria pollutants are also calculated. Besides CO and HCl emissions, the emission factors for all LFGTE and WTE cases are lower than the ones for the coal-fired generators [27].

In addition, the impact of WTE within the larger energy system is evaluated. Hypothetically, if 166 million Mg of MSW is discarded in regional landfills with energy recovery, on average roughly 10 TWh or 65 kWh/Mg of MSW of electricity can be generated, whereas a WTE facility can generate on average roughly 100 TWh or 600 kWh/Mg of MSW of electricity with the same amount of MSW. WTE can generate an order of magnitude more electricity than LFGTE given the same amount of waste. LFGTE projects would result in significantly lower electricity generation because only the biodegradable portion of the MSW contributes to LFG generation, and there are significant inefficiencies in the gas collection system that affect the quantity and quality of the LFG.

Moreover, if all post-recycling MSW (i.e., excluding recycled and composted portions) is utilized for electricity generation, the WTE alternative could yield a generation capacity of 14,000 MW, which could potentially replace ~4.5% of the 313,000 MW of current coal-fired generation capacity [30]. A significant portion of this capacity could be achieved through centralized facilities where waste is transported from greater distances. The transportation of waste could result in additional environmental burdens, and there are clearly limitations in accessing all discarded MSW in the nation. Wanichpongpan et al. [8] studied the LFGTE option for Thailand and found that large centralized landfills with energy recovery performed much better in terms of cost and GHG emissions than small, localized landfills despite the increased burdens associated with transportation [8].

The landfill emission factors include the decay of MSW over 100 years, whereas emissions from WTE and conventional electricity-generating technologies are instantaneous. The operation and decomposition of waste in landfills continues beyond the monitoring phases for an indefinite period of time. Reliably quantifying the landfill gas collection efficiency is difficult due to the ever-changing nature of landfills, number of decades that emissions are generated, and changes over time in landfill design and operation, including waste quantity and composition. Landfills are an area source, which makes emissions more difficult to monitor.

In a recent release of updated emission factors for landfill gas emissions, data were available for less than 5% of active municipal landfills [31]. Across the USA, there are major differences in how landfills are designed and operated, which further complicates the development of reliable emission factors. This is why a range of alternative scenarios is therefore evaluated with plausible yet somewhat optimistic assumptions for LFG control. For WTE facilities, there is less variability in the design and operation. In addition, the US EPA has data for all the operating WTE facilities as a result of CAA requirements for annual stack testing for pollutants of concern, including dioxin/furan, Cd, Pb, Hg, PM, and HCl. In addition, data are available for SO_2, NO_x, and CO from continuous emissions monitoring. As a result, the higher quality and availability of WTE data make estimation of emission factors less uncertain compared to LFGTE.

Conclusions and Future Directions

Despite increased recycling efforts, US population growth will ensure that the mass of MSW discarded in landfills will remain significant. Discarded MSW is a viable energy source for electricity generation in a carbon-constrained world. One notable difference between LFGTE and WTE is that the latter is capable of producing an order of magnitude more electricity from the same mass of waste. If the goal is greenhouse gas reduction, then WTE should be considered as an option under state and US renewable energy policies. In addition, LFTGE scenarios had on average higher NO_x, SO_2, and PM emissions than WTE. However, HCl emissions from WTE are significantly higher than the LFGTE scenarios.

This analysis does not address location-specific issues such as local air quality concerns. In cases where the remanufacturing and electricity generation offsets occur in locations different from the location of the WTE facility, the direct emissions from WTE could reduce local air quality. For example, if a WTE facility is located in an electric grid with a high penetration of renewable and nuclear, then WTE could result in an increase of CO_2e, NO_x, SO_x, and PM emissions. Future work to account for the geographic and temporal distribution of emissions would yield valuable insight into the life cycle performance and impact of WTE and LFGTE.

Bibliography

1. Christensen TH, Bhander G, Lindvall H, Larsen AW, Fruergaard T, Damgaard A, Manfredi S, Boldrin A, Riber C, Hauschild M (2007) Experience with the use of LCA-modelling (EASEWASTE) in waste management. Waste Manage Res 25(3):257–262
2. Eriksson O, Reich MC, Frostell B, Bjorklund A, Assefa G, Sundqvist JO, Granath J, Baky A, Thyselius L (2005) Municipal solid waste management from a systems perspective. J Cleaner Prod 13(3):241–252
3. Gentil EC, Damgaard A, Hauschild M, Finnveden G, Eriksson O, Thorneloe S, Kaplan PO, Barlaz M, Muller O, Matsui Y, Li R, Christensen TH (2010) Models for waste life cycle assessment: review of technical assumptions. Waste Management 30(12): 2636–2648
4. Harrison KW, Dumas RD, Solano E, Barlaz MA, Brill ED, Ranjithan SR (2001) Decision support tool for life-cycle-based solid waste management. J Comput Civil Eng 15(1):44–58
5. Kaplan PO, Ranjithan SR, Barlaz MA (2009) Use of life-cycle analysis to support solid waste management planning for delaware. Environ Sci Technol 43(5):1264–1270
6. Kirkeby JT, Birgisdottir H, Hansen TL, Christensen TH, Bhander GS, Hauschild M (2006) Environmental assessment of solid waste systems and technologies: EASEWASTE. Waste Manage Res 24(1):3–15
7. Thorneloe SA, Weitz K, Jambeck J (2007) Application of the US decision support tool for materials and waste management. Waste Management 27(8):1006–1020
8. Wanichpongpan W, Gheewala SH (2007) Life cycle assessment as a decision support tool for landfill gas-to energy projects. J Clean Prod 15(18):1819–1826
9. White PR, Franke M, Hindle P (1995) Integrated solid waste management: a lifecycle inventory. Chapman & Hall, New York
10. U.S. Environmental Protection Agency (2010) Municipal solid waste in the United States: 2009 facts and figures. EPA/530/R10/012. Washington, DC
11. European Commission (2005) Waste generated and treated in Europe: data 1995–2003. Luxembourg. http://epp.eurostat.ec.europa.eu/cache/ITY_OFFPUB/KS-69-05-755/EN/KS-69-05-755-EN.PDF. Accessed 14 Nov 2011
12. Standards of performance for new stationary sources and emission guidelines for existing sources: large municipal waste combustors; Final Rule (2006) Federal Register: 71(90)
13. Energy Recovery Council (2010) The 2010 ERC directory of waste-to-energy plants http://www.wte.org/userfiles/file/ERC_2010_Directory.pdf Accessed 12 July 2011
14. Harrison KW, Dumas RD, Barlaz MA, Nishtala SR (2000) A life-cycle inventory model of municipal solid waste combustion. J Air Waste Manage 50(6):993–1003
15. RTI International. Municipal solid waste decision support tool. https://mswdst.rti.org. Accessed 12 July 2011
16. IPCC (2007) Contribution of working group I to the fourth assessment report of the intergovernmental panel on climate

change: The physical science basis. http://www.ipcc.ch/publications_and_data/ar4/wg1/en/contents.html Accessed 18 July 2011
17. Camobreco V, Ham R, Barlaz M, Repa E, Felker M, Rousseau C, Rathle J (1999) Life cycle inventory of a modern municipal solid waste landfill. Waste Manage Res 17(6):394–408
18. Environment Agency (2000) Life cycle inventory development for waste management operations: incineration; R&D project record P1/392/6. Environment Agency, Bristol
19. Dumas RD (1998) Energy consumption and emissions associated with electric energy consumption as part of a solid waste management life cycle inventory model. Dissertation, North Carolina State University, Raleigh
20. U.S. Environmental Protection Agency (2010) The emissions & generation resource integrated database (eGRID). http://www.epa.gov/cleanenergy/energy-resources/egrid/index.html. Accessed 13 July 2011
21. NREL (2011) Bituminous coal, at mine, data years 1999–2002. U.S. LCI database. www.nrel.gov/lci. Accessed 24 June 2011
22. NREL (2011) Natural gas, at extraction site, data years 1997–2001. U.S. LCI database. www.nrel.gov/lci. Accessed 24 June 2011
23. NREL (2011) Fuel grade uranium, at regional storage, data years 1981–2002. U.S. LCI Database. www.nrel.gov/lci. Accessed 24 June 2011
24. NREL (2011) Crude oil, at production site, data years 1997–2001. U.S. LCI database. www.nrel.gov/lci. Accessed 24 June 2011
25. Sich BA, Barlaz MA (2000) Calculation of the cost and life cycle inventory for waste disposal in traditional, bioreactor and ash landfills. https://mswdst.rti.org/docs/Landfill_Model_OCR.pdf. Accessed 15 July 2011
26. Eleazer WE, Odle WS, Wang YS, Barlaz MA (1997) Biodegradability of municipal solid waste components in laboratory-scale landfills. Environ Sci Technol 31(3):911–917
27. Kaplan PO, DeCarolis J, Thorneloe S (2009) Is it better to burn or bury waste for clean electricity generation? Environ Sci Technol 43(6):1711–1717
28. U.S. Environmental Protection Agency (2006) Municipal solid waste in the United States: 2005 facts and figures. EPA/530/R06/011. Washington, DC
29. Staley BF, Barlaz MA (2009) Composition of municipal solid waste in the U.S. and implications for carbon sequestration and methane yield. J Environ Engr 135(10):901–909
30. U.S. Department of Energy (2006) Electric power annual 2005. DOE/EIA-0348(2005). Washington, DC
31. U.S. Environmental Protection Agency background information document for updating AP42 section 2.4 Municipal solid waste landfills. EPA/600/R-08-116 Washington, DC. http://www.epa.gov/ttn/chief/ap42/ch02/draft/db02s04.pdf
32. Tchobanoglous G, Vigil SA, Theisen H (1993) Integrated solid waste management. McGraw-Hill, New York
33. Oshins C, Block D (2000) Feedstock composition at composting sites. Biocycle 41:31–34
34. Realff MJL, P. Lucero, S. Mulholland, J. Smith, P.B. (2005) Characterization of transient puff emissions from the burning of carpet waste charges in a rotary kiln combustor. In: Cement Industry Technical Conference, Kansas City, Missouri, 15–20 May 2005. pp 212–228
35. Nelson B (2002) Performance/test data for large municipal waste combustors (MWCs) at MACT compliance (Year 2000 data). Memo for Walt Stevenson of U.S. EPA, Durham, NC

Light Rail Transit in the US and Abroad, Examination of History and Innovations

José I. Farrán
Adavant Consulting, San Francisco, CA, USA

Article Outline

Glossary
Definition of the Subject
Introduction
Pedestrian Conflicts
Future Directions
Bibliography

Glossary

Bedstead barrier A type of pedestrian-light rail crossing control device whose design prevents a pedestrian from walking straight onto the tracks by forcing them to make one or more turns immediately ahead of the tracks.

Channelization device A physical element that limits pedestrian movements to within the preferred pathway and that guides pedestrians to cross the LRT tracks at the designated crossing location.

Dynamic envelope The clearance on either side of a light rail vehicle required for the overhang resulting from any combination of loading, lateral motion, or suspension failure.

Flashing light signal assembly A warning device consisting of two red signal indications arranged horizontally that are activated to flash alternately when a light rail vehicle is approaching or present at a highway-rail at-grade crossing.

Light rail transit (LRT) A mode of transit service (also called streetcar, tramway, or trolley) operating passenger rail cars singly (or in short, usually two-car or three-car, trains) on fixed rails in right-of-way that is often separated from other traffic for part or much of the way.

Light rail vehicles (LRVs) Vehicles typically driven electrically with power being drawn from an overhead electric line via a trolley or a pantograph driven by an operator on board the vehicle and may have either high platform loading or low-level boarding using steps.

Off-quadrant The location at a light rail crossing, from the perspective of an approaching motorist, on the far side of the tracks and same side of the roadway. Warning devices for pedestrians at highway-rail crossings are typically absent in the off-quadrant.

Pavement markings Markings set into the surface of, applied upon, or attached to the pavement for the purpose of regulating, warning, or guiding traffic.

Pedestrian A person who travels on foot or who uses assistive devices, such as a wheelchair, for mobility.

Pedestrian automatic gate A type automatic gate at a highway-rail at-grade crossing that descends when activated by a light rail vehicle blocking the pedestrian path. The gate is typically delineated with red and white diagonal bars along its length and may include one small red light at the tip, which is illuminated when the gate is activated.

Pedestrian-light rail at-grade crossing The general area where a pedestrian pathway and a light rail vehicle cross at the same level, within which are included the light rail tracks, pathway, design features, and traffic control devices for those traversing the area.

Positive control device An element that provides a temporary or permanent physical barrier between the light rail tracks and locations where pedestrians can safely queue.

Public transportation (also called transit, public transit, or mass transit) Transportation by a conveyance that provides regular and continuing general or special transportation to the public, but not including school buses, charter, or sightseeing service.

Right-of-way (r-o-w) A strip of land devoted to light rail transportation purposes.

Traffic control devices All signs, signals, markings, and other devices used to regulate, warn, or guide motor vehicle, pedestrian, or bicycle traffic.

Swing gate A self-closing, non-locked, fence-type gate designed to swing open away from the track area and return to the closed position upon release.

Z-crossing A type of pedestrian-light rail crossing control device whose design forces a pedestrian to make a 90-degree turn and walk parallel to and facing oncoming light rail vehicles immediately ahead of the tracks.

Definition of the Subject

Descendants of the streetcar, light rail vehicles (LRVs) have their own distinct characteristics, including a broad range of operating environments (both on-street and in semi-exclusive or exclusive rights-of-way) and a wide extent of typical operating speeds (from 15 to 60 mph or 10 to 40 km/h). This flexibility, coupled with passenger attraction and capacity of the vehicles, has made light rail an increasingly viable public transportation option.

Accommodating light rail transit (LRT) in these multiple environments while maintaining or improving safety has led transportation planners and engineers to utilize a variety of innovative traffic control practices. These practices are used to manage conflicting movements with LRVs and to provide motorists, as well as pedestrians and bicyclists with better information upon which to base their decisions and have evolved over time in response to changes in the way that LRVs operate (higher speeds, more silent operation) and pedestrians behave (increased inattentiveness and more distractions). Since increased LRT safety is a worldwide need, traffic engineers and transportation planners in the United States and Europe have implemented and adjusted over the years a number of practices to minimize conflicts between LRVs and pedestrians.

This entry examines and describes the observations resulting from the author's research and firsthand experience in traffic engineering practices in the United States and Europe related to solving LRT conflicts with pedestrians. Those practices and traffic control devices that are most innovative and with the greatest potential for implementation in new or expanding LRT systems are graphically identified.

Introduction

A key strength of LRT is its ability to integrate well into an urban environment sharing the public right-of-way with motorists, bicyclists, and pedestrians. It is this characteristic that makes LRT successful in those urban corridors where a high-capacity mode of transportation is required to operate well in both an exclusive and a shared right-of-way. Although LRT is an inherently safe mode of transportation, accidents sometimes do occur, negatively affecting not only the parties involved in the accident, but also the entire operation of the LRT system and the reputation of the transit property. Furthermore, safety concerns, particularly with pedestrians, are always a subject of great debate between residents and transit planning agencies, in those communities where a new LRT system or an LRT line extension is being proposed.

The interactions between pedestrians and LRVs are substantially different from those between motorists and LRVs. In general, motorists tend to be more aware of their environment, while pedestrians, traveling in the relatively safe venue of protected sidewalk areas, do not routinely share the same continuous attentive edge.

When crossing the travel path of motor vehicles or LRVs, pedestrians are supposed to shift their attention

Light Rail Transit in the US and Abroad, Examination of History and Innovations. Table 1 Aggregate number of LRV collisions by type[a]

LRV collisions with	Resulting in injuries		Resulting in fatalities	
Motor vehicles	184	53%	19	19%
Pedestrians	115	33%	74	76%
Other	50	14%	5	5%
Total	349	100%	98	100%

[a]Provided by LRT agencies in Los Angeles (1990–2006), Portland (1994–2007), San Francisco (2006–2007), and San Jose (1987–2007)

Light Rail Transit in the US and Abroad, Examination of History and Innovations. Table 2 Aggregate number of LRV collisions by type[a] 2002–2007

LRV collisions with	Resulting in injuries		Resulting in fatalities		Property damage only		Total	
Motor vehicles	272	66%	17	24%	278	93%	567	72%
Pedestrians	117	28%	47	67%	4	1%	168	21%
Other	26	6%	6	9%	17	6%	49	6%
Total	415	100%	70	100%	299	100%	784	100%

[a]Reported to the Federal Transit Administration by the LRT agencies in Baltimore, Boston, Buffalo, Cleveland, Dallas, Denver, Houston, Los Angeles, Memphis, Minneapolis, New Jersey, New Orleans, Philadelphia, Pittsburgh, Portland, Sacramento, Salt Lake City, San Diego, San Francisco, San Jose, Seattle, St. Louis, and Tampa

Light Rail Transit in the US and Abroad, Examination of History and Innovations. Table 3 Possible solutions to observed pedestrian conflicts

Situation	Possible solution
Low level of pedestrian awareness	• Install LRV-activated signs and signals • Install LRV-specific passive signage at pedestrian eye level
Poor definition of pedestrian pathways	• Delineate dynamic envelope by contrasting pavement color and/or texture or paint • Construct physical barriers (fence, bollards with chains, landscape)
Cross-street access	• Provide adequate storage/queuing/refuge space • Install positive pedestrian control devices (automatic gates, swing gates, bedstead barriers, or Z-crossings)

Light Rail Transit in the US and Abroad, Examination of History and Innovations. Figure 1
LRV-activated internally illuminated warning sign (urban environment, median operation) Salt Lake City (Utah)

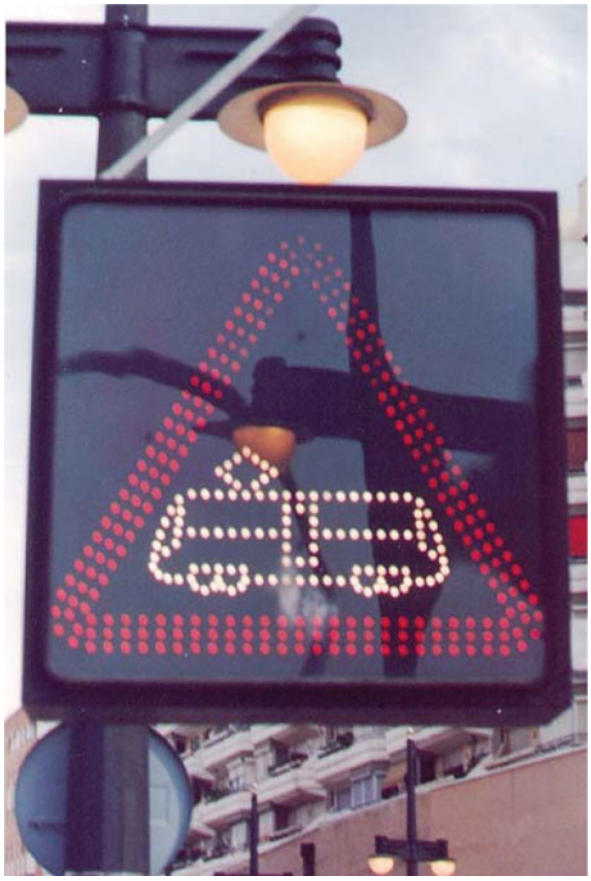

Light Rail Transit in the US and Abroad, Examination of History and Innovations. Figure 2
LRV-activated internally illuminated warning sign (urban environment, median operation) Valencia (Spain)

to a similar state of awareness as that exhibited by motorists or LRV operators. However, this shift does not always occur. Pedestrian inattentiveness is exacerbated when interacting with modern LRVs, which are nearly silent. Moreover, unlike motor vehicles, LRVs cannot swerve or stop quickly enough to compensate for pedestrians who are errant or disobedient of traffic control devices.

According to past research conducted by the author [1], incidents between pedestrians and LRVs are the least prevalent type of LRT-related collisions, representing approximately 10% of the total, but are the most severe and account for at least 50% of all fatalities resulting from such incidents. Additional research conducted for Transit Cooperative Research Board [2] further validated this finding.

Table 1 summarizes the total number of collisions with injuries and fatalities that have occurred at five LRT systems operating in the Western United States (Los Angeles, Portland, San Francisco, and Santa Clara) over the past few years. According to Table 1, more than three fourths of those involved in a pedestrian collision with an LRV are killed, compared to less than one fifth of those involved in a motor vehicle collision.

Similar, more extensive, geographical data provides similar conclusions. Table 2 presents the aggregate number of collisions by type that have occurred at

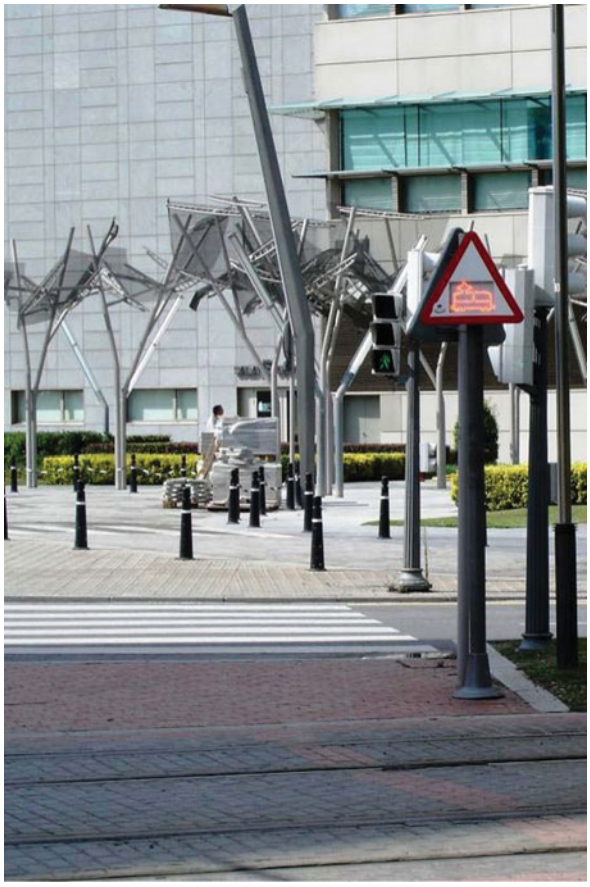

Light Rail Transit in the US and Abroad, Examination of History and Innovations. Figure 3
LRV-activated internally illuminated warning sign (urban environment, median operation) Bilbao (Spain)

Light Rail Transit in the US and Abroad, Examination of History and Innovations. Figure 4
LRV-activated internally illuminated warning sign with directional arrow (urban environment, median operation) Portland (Oregon)

most of the LRT systems in the United States from 2002 to 2007.

According to Table 2, LRV collisions with pedestrians represent approximately one fifth of the total but result in about two thirds of all fatalities resulting from those collisions. Also according to Table 2, an average of three persons are killed for every ten that are involved in a pedestrian collision with an LRV, as opposed to three persons killed for every 100 that are involved in a motor vehicle collision with an LRV. It is clear that finding an effective means of addressing and minimizing pedestrian-LRV collisions is critically important to the operations of LRT systems in the United States and abroad.

The interactions between pedestrians and LRVs are substantially different from those between motorists and LRVs. In general, motorists tend to be more aware of their environment, while pedestrians, traveling in the relatively safe venue of protected sidewalk areas, do not routinely share the same continuous attentive edge. Moreover, unlike motor vehicles, LRVs cannot swerve or stop quickly enough to compensate for pedestrians who are errant or disobedient of traffic control devices.

Possible strategies to minimize LRV/pedestrian conflicts are summarized in Table 3. These solutions address the types of situations identified above, and

Light Rail Transit in the US and Abroad, Examination of History and Innovations. Figure 5
LRV-activated SECOND TRAIN APPROACHING warning sign (suburban environment, separate r-o-w) San Jose (California)

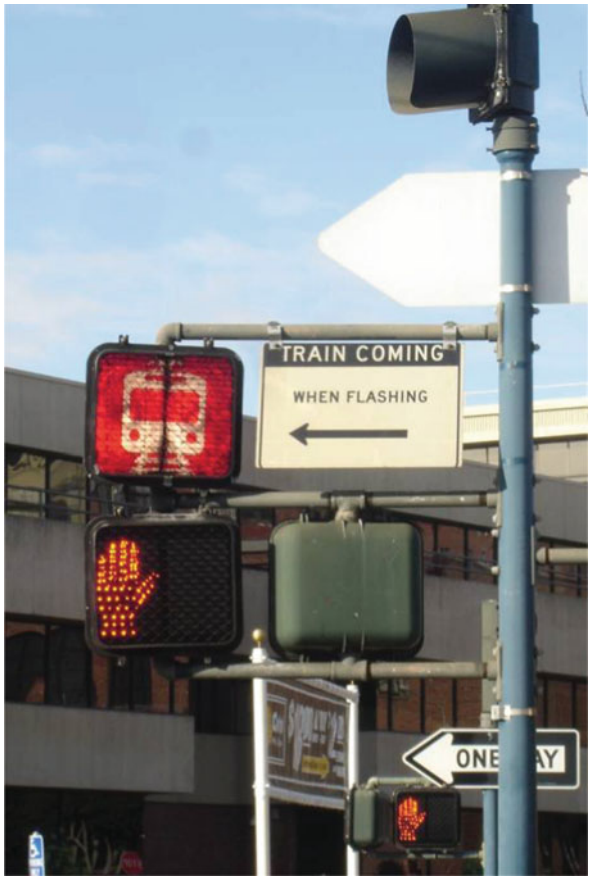

Light Rail Transit in the US and Abroad, Examination of History and Innovations. Figure 6
LRV-activated internally illuminated warning sign with supplemental plaque (urban environment, median operation) San Francisco (California)

underscore the need for establishing a set of principles and guidelines to achieve greater uniformity and consistency in implementing a safer LRT system.

The following sections of this entry provide a summary of innovative pedestrian control designs and practices that have been applied successfully to light rail system in the United States and Europe to address the types of conflicting motor vehicle and pedestrian movements with LRVs described above.

Pedestrian Conflicts

The design of a pedestrian-light rail at-grade crossing is only effective if pedestrians actually cross at the designated point by taking a path that allows them clear observation of the warning devices. Devices to control pedestrian travel across LRT tracks and warn about the presence or approach of an LRV can be grouped under three major categories [3]:

- Regulatory and warning devices (both passive and active)
- Delineation markings
- Positive control devices

This section describes some of the most innovative traffic control devices included under each category and provides graphic examples of their application at several LRT systems in the United States and Europe.

Light Rail Transit in the US and Abroad, Examination of History and Innovations. Figure 7
Two-way LRV warning sign with LRV symbol used with a pedestrian signal (urban environment, median operation) Barcelona (Spain)

Light Rail Transit in the US and Abroad, Examination of History and Innovations. Figure 8
Two-way LRV warning sign with LRV symbol at an unsignalized crossing (urban environment, median operation) Bordeaux (France)

Regulatory and Warning Devices

Pedestrian crossing regulatory and warning devices include signs, pedestrian signals, flashing light signals, and audio devices. Signs used at LRT crossings are typically fixed standard signs, such as the railroad cross buck or the LRV symbol, or LRV-activated internally illuminated depicting words or graphic symbols. LRV-activated internally illuminated signs warn pedestrians of the increased risk associated with violating the crossing in the presence of an LRV. Figure 1 shows an example of an LRV-activated internally illuminated warning sign in Salt Lake City, used in combination with a pedestrian traffic signal. Figures 2 and 3 show similar internally illuminated signs in Valencia and Bilbao, depicting two variations of the international LRT crossing warning sign. These signs are typically installed where substantial pedestrian presence is expected or where additional information is needed due to complicated track or pedestrian crossing geometry.

Figure 4 shows an innovative internally illuminated sign in Portland depicting a side view of an LRV plus an arrow representing its direction of travel. LRV-activated internally illuminated signs are also used to warn

Light Rail Transit in the US and Abroad, Examination of History and Innovations. Figure 9
LRV-activated pedestrian signal (urban environment, pedestrian mall operation) Bordeaux (France)

Light Rail Transit in the US and Abroad, Examination of History and Innovations. Figure 10
Pedestrian flashing red light signals (suburban environment, separate r-o-w) San Jose (California)

pedestrians of additional LRVs approaching the crossing. Figure 5 shows the use of an LRV-activated internally illuminated SECOND TRAIN APPROACHING sign in San Jose, used in combination with a conventional flashing light signal assembly.

Supplemental warning plaques are also used extensively in United States and European cities evaluated in this paper. Figure 6 shows an example of a supplemental plaque used in combination with a pedestrian traffic signal head and an LRV-activated internally illuminated warning sign in San Francisco. Figure 7 shows a similar example used in the Barcelona LRT system, while Fig. 8 shows an installation in Bordeaux where the plaque is combined with an LRV warning sign at a pedestrian-only crossing. The intent of the signs and plaques is to clearly alert pedestrians about the possibility of LRVs approaching the crossings from both sides, and are typically installed at all pedestrian crossings.

Pedestrian crosswalk signals in most cities are similar to those installed at non-LRV crosswalks, with internally illuminated heads depicting the pedestrian WALK and DON'T WALK symbols. The city of Bordeaux, however, has installed LRV-specific

Light Rail Transit in the US and Abroad, Examination of History and Innovations. Figure 11
Pedestrian-LRV crossing delineation (urban environment, separate r-o-w) Dallas (Texas)

Light Rail Transit in the US and Abroad, Examination of History and Innovations. Figure 12
LRV dynamic envelope delineation (urban environment, median operation) Barcelona (Spain)

regulatory signals at key locations with heavy pedestrian usage, such as the pedestrian mall in the old town area (Fig. 9), to emphasize the impending arrival of a train and raise the pedestrian awareness about the prohibition to cross the street. The signal is normally blanked out and becomes activated by the approaching LRV.

Flashing red light signals used at pedestrian-LRV crossings have the same design and type of operation as those used in conventional highway-rail grade crossings, consisting of two red light units mounted on a horizontal line flashing alternately to indicate the approach or presence of an LRV. Figure 10 shows a pedestrian flashing red light signal assembly in San Jose, used in combination with an LRV warning sign and a supplemental plaque.

Delineation Markings

Delineation markings direct pedestrians to cross LRT tracks at a designated location. Pedestrian path delineation can be accomplished with line striping, differential pavement color or texture, contrasting surface materials or landscaping. Delineation is also used to mark the edge of the dynamic envelope of the LRV, that is, the clearance on either side of an LRV required for the overhang resulting from any combination of

Light Rail Transit in the US and Abroad, Examination of History and Innovations. Figure 13
LRV dynamic envelope delineation (urban environment, median operation) Bilbao (Spain)

Light Rail Transit in the US and Abroad, Examination of History and Innovations. Figure 14
LRV directional striping on a one-way track (urban environment, median operation) Barcelona (Spain)

loading, lateral motion, or suspension failure. Figure 11 shows a combination of line striping, contrasting color and differential pavement texture to delineate a pedestrian crossing in Dallas. Figures 12 and 13 depict a similar combination found in Barcelona and Bilbao, respectively, used to delineate the LRV dynamic envelope.

In addition to the dynamic envelope delineations shown in Fig. 12, arrow striping indicating the direction that LRVs typically traverse the crossing is also used extensively in Barcelona at all pedestrian crossings to warn pedestrians and help them look in the most appropriate direction (the opposite from where the arrow is pointing) before they walk onto the track area. The arrow in combination with the LRV symbol is striped between the two rails for a given LRV direction immediately downstream of the pedestrian pathway. A single arrow is used where LRVs typically operate in a single direction (Fig. 14), while two arrows are used when LRVs typically operate two-way in a single track (Fig. 15).

As an alternative to the previous European markings, LRT systems in the United States, such as those in Salt Lake City and San Francisco, have implemented pavement markings at the crosswalk edge with the word LOOK and two arrow heads pointing both ways, either adjacent to the tracks or on the sidewalk, as shown in Figs. 16 and 17.

Light Rail Transit in the US and Abroad, Examination of History and Innovations. Figure 15
LRV directional striping on a two-way track (urban environment, median operation) Barcelona (Spain)

Light Rail Transit in the US and Abroad, Examination of History and Innovations. Figure 16
LOOK pavement marking (urban environment, median operation) Salt Lake City (Utah)

Light Rail Transit in the US and Abroad, Examination of History and Innovations. Figure 17
LOOK pavement marking (urban environment, median operation) San Francisco (California)

Light Rail Transit in the US and Abroad, Examination of History and Innovations. Figure 18
Pedestrian delineation with bollards and chains (urban environment, separate r-o-w) Dallas (Texas)

Positive Control Devices

Positive control devices provide a physical barrier between the outer edge of the LRV dynamic envelope and the area where it is safe for pedestrians to congregate. These devices can be fixed or moveable.

Fixed barriers are used to restrict pedestrian movements as they approach an LRT crossing and lead them toward a designated crossing location. They include fencing, railing, bollards, and chains or wire strung between posts. Fixed barriers, such as those shown in Fig. 18 for the Dallas LRT system, are used to reinforce delineation markings and to increase awareness of the potential presence of an LRV at those locations where a more strict control of pedestrian flows approaching a crossing may be necessary for safety considerations.

Fixed barriers are also used to configure pedestrian-only crossings of the LRT tracks. The most common types of fixed-barrier crossings are Z-crossings and bedstead barrier crossings.

The Z-crossing is designed to turn pedestrians toward the direction of approaching LRVs before they cross each track, forcing them to take note of potential danger. They are typically used at mid-block (away from intersections) pedestrian-only crossings. Bedstead barrier crossings are similar to Z-crossings, but their design is more compact so that they can be used in tight urban spaces.

Light Rail Transit in the US and Abroad, Examination of History and Innovations. Figure 19
Pedestrian Z-Crossing configuration used in combination with a pedestrian signal (urban environment, median operation) San Francisco (California)

Light Rail Transit in the US and Abroad, Examination of History and Innovations. Figure 20
Bedstead barrier at mid-block crossing used in combination with pedestrian signal (urban environment, median operation) Bordeaux (France)

Light Rail Transit in the US and Abroad, Examination of History and Innovations. Figure 21
Pedestrian swing gate installation (suburban environment, separate r-o-w) San Jose (California)

Light Rail Transit in the US and Abroad, Examination of History and Innovations. Figure 22
Pedestrian swing gate installation (urban environment, separate r-o-w) Los Angeles (California)

The barriers are placed in an offset, maze-like manner that requires pedestrians moving across the LRT tracks to turn toward the direction of approaching LRVs before they cross each track. Both Z-crossings and bedstead barrier crossings can also be used in combination with other devices such as signals or automatic gates. Figure 19 depicts a Z-crossing in San Francisco while Fig. 20 shows a bedstead barrier crossing in Bordeaux, both used in combination with pedestrian signals and supplemental warning plaques.

Moveable barriers are used to restrict pedestrian movements as they are about to enter into the dynamic envelope of the LRV. The barriers can be automatically activated and deactivated by an LRV as it approaches and departs the crossing, or they can be operated manually by the pedestrian. The two most common types of moveable barriers at LRV crossings are the swing gate and the pedestrian automatic gate.

A swing gate is a manual device that requires a pedestrian to pull the gate in order to enter the crossing and to push the gate to exit the protected track area. Operating the gate alerts pedestrians to the presence of the LRT crossing, forces them to pause, and prevents them from running freely across the LRT tracks. Swing gates do not lock when closed and are designed to return to the closed position by gravity after passage of the pedestrian.

Light Rail Transit in the US and Abroad, Examination of History and Innovations. Figure 23
Pedestrian automatic gate with secondary arm (suburban environment, separate r-o-w) Dallas (Texas)

Light Rail Transit in the US and Abroad, Examination of History and Innovations. Figure 24
Pedestrian automatic gate with push gate as escape path (urban environment, separate r-o-w) Los Angeles (California)

Swing gates are often used in conjunction with channelization barriers, LRV-activated internally illuminated signs, flashing light signals, and audible warning devices, as shown in Figs. 21 (San Jose) and 22 (Los Angeles), in order to achieve a higher level of positive pedestrian control at the crossing.

Pedestrian automatic gates are configured and operate much the same as vehicular gates, except that the arms are shorter and may include one or three red lights at the center or the tip that flash when the gate is activated. When used at pedestrian-rail at-grade crossings, the gate arm is located approximately 3 feet above the pathway when in the horizontal position.

At those locations where there is a concern about pedestrians ducking under the arm when the gate is closed, a secondary arm may be installed to hang below the primary arm, as shown in Fig. 23 for the Dallas LRT system. Pedestrian automatic gates are used to physically discourage pedestrians from crossing the LRT tracks when an LRV approaches the crossing, particularly at locations with inadequate stopping sight distance.

Because pedestrians may approach the crossing from both ways, the preferred method for pedestrian automatic gate installation is to provide them at both sides of the crossings (in all four quadrants when installed at motor vehicle and pedestrian grade crossings). Establishing clearly marked pedestrian safety zones and escape paths minimizes the possibility of trapping pedestrians in the LRT right-of-way when

pedestrian automatic gates are used at both ends of the crossing. An emergency exit swing gate can be used for this purpose, designated for use only as an escape route for a pedestrian that may remain between the track and a lowered automatic pedestrian gate. Figure 24 presents an example of the placement of emergency exit swing gates at the Los Angeles LRT system.

Future Directions

The previous sections have shown that although accidents between pedestrians and LRVs are the least common type of LRT accident, they are by far the most severe. A means of addressing and minimizing this type of accidents is by installing devices that convey to pedestrians the higher level of risk associated with violating a closed LRV crossing. The types of devices used to control pedestrian travel across the LRT tracks and warn them about the presence of an approaching LRV include regulatory and warning devices (both passive and active), delineation markings, and positive control devices. These pedestrian control devices are typically implemented in combination in order to achieve a higher level of pedestrian control at the LRT crossing.

Bibliography

Primary Literature

1. Korve HW, Farrán JI, Mansel DM, Levinson HS, Chira-Chavala T, Ragland DR (1996) Integration of light rail transit into city streets. In: TCRP 17, Transportation Research Board, Washington, DC
2. Cleghorn D, Clavelle A, Boone J, Masliah M, Levinson HS (2009) Improving pedestrian and motorist safety along light rail alignments. In: TCRP 137, Transportation Research Board, Washington, DC
3. Korve HW, Ogden BD, Siques JT, Mansel DM, Richards HA, Gilbert S, Boni E, Butchko M, Stutts JC, Hughes RG (2001) Light rail service: pedestrian and vehicular safety. In: TCRP 69, Transportation Research Board, Washington, DC

Books and Reviews, Monographs

Farradyne PB (2002) Final report for the second train warning sign demonstration project on the Los Angeles metro blue line. In: FTA-CA-26-7017-01, Los Angeles, CA, US Department of Transportation, Federal Transit Administration, Washington, DC, pp 1–69

Korve Engineering, ATS Consulting, LLC, Fidell Associates, CERS, and Bear Consulting (2007) Audible signals for pedestrian safety in LRT environments. Research Results Digest 84, Transportation Research Board, Washington, DC

State of California Department of Transportation (2006) California manual on uniform traffic control devices for streets and highways, 2006 edn. Part 10: Light rail transit grade crossings. Business, Transportation and Housing Agency Department of Transportation, CA, pp 10A-1–10D-12

State U.S. Department of Transportation – Federal Highway Administration/Rail Grade Crossing Technical Working Group (2002) Guidance on traffic control at highway-rail grade crossings. FHWA, Washington, DC

U.S. Department of Transportation – Federal Highway Administration (2009) Manual on uniform traffic control devices for streets and highways, 2009 edn. Part 8: traffic control for railroad and light rail transit grade crossings. Business, Transportation and Housing Agency Department of Transportation, CA, pp 747–788

U.S. Department of Transportation – Federal Highway Administration – Office of Safety Design (2007) Railroad-highway at-grade crossing handbook, revised 2nd edn. Federal Highway Administration – Office of Safety Design, Washington, DC

Collections

Boorse JW (2003) Delineation of the dynamic envelope of light rail transit cars and trains. In: TRB 2003 Annual Meeting, Transportation Research Board, Washington, DC

Currie G, Smith P (2005) An innovative design for safe and accessible light rail/tram stops suitable for streetcar style conditions In: TRB 2005 Annual Meeting, Transportation Research Board, Washington, DC, pp 1–15

Farrán JI (1998) The light rail transit safety experience in North America. In: Urban transport IV – urban transport and the environment for the 21st century. WIT Press, Computational Mechanics Publications, Ashurst, Southampton, UK, pp 43–52

Farrán JI (2002) The pedestrian paradigm: controlling pedestrians across LRT tracks. In: Commuter rail/transit conference proceedings. Boca Raton, FL, pp 1–9

Farrán JI (2007) Innovative traffic control practices for light rail transit: a European perspective. In: Joint international light rail conference: a World of applications and opportunities, Transportation Research E-C112, TRB, Washington, DC, pp 87–106

Irwin D (2003) Safety criteria for light rail pedestrian crossing. In: Proceedings 9th national light rail transit conference, American Public Transportation Association, TRB, Washington, DC, pp 266–288

Korve HW, Farrán JI, Mansel DM (1995) Pedestrian control systems for light rail transit. In: Seventh national conference on light rail transit: building on success–learning from experience, Compendium of Technical Papers, Baltimore, MD, pp 91–102

Journal Articles

Farrán JI (2006) Pedestrian and motor vehicle traffic control practices for LRT – Innovations in the new Barcelona LRT system, TRB (2006). Trans Res Record 1955:56–61

Siques JT (201) Pedestrian warning and control devices, guidelines, and case studies TRB (2001). Trans Res Record 1762:18–24

Light Rail Transit, Shared Infrastructural Issues

Rongfang Rachel Liu
Department of Civil and Environmental Engineering, New Jersey Institute of Technology, Newark, NJ, USA

Article Outline

Glossary
Definition of the Subject
Introduction
Historical Background
Current Operating Scenarios in the USA
Demand for Commingled Operation
Challenges Faced by the Attempts
Potential Solutions
Future Directions
Acronyms
Bibliography

Glossary

Commingled operation Transit trains and freight trains are separated by headway intervals measured in minutes in an operating schedule.

Light rail transit Also called streetcar, tramway, or trolley, is a system with passenger rail cars operating singly or in short, usually two-car, trains on fixed rails in right-of-way that is not separated from other traffic for much of the way.

Shared corridor Transit and freight operators share a transportation corridor, but tracks are separated by at least 25 ft and no more than 200 ft.

Shared right-of-way The transit vehicles run on separate tracks, but track centers are less than 25 ft, that is, separation between the centerline of the freight track and the centerline of the passenger track is less than 25 ft.

Shared track Heavy or LRT vehicles operate on the same tracks used by freight trains.

Temporal separation Both transit and freight trains utilize the same track but are separated by time windows.

Definition of the Subject

Interest in light rail transit (LRT), as a viable urban transportation system, has been growing worldwide and new LRT systems are appearing in urban areas of many countries. One advantage of LRT is its ability to use existing railroad infrastructure to reduce construction cost and environmental impact. The majority of LRT systems in the USA share right-of-way, or utilize the same tracks but temporally separated from the freight railroads, while commingled or simultaneous operation has been common practice for many countries in Asia and Europe. With the success of LRT applications in recent decades, service providers are looking for more space and infrastructure for expansion. Interest in applying overseas commingled experience in the USA has been growing.

Current Federal Railroad Administration (FRA) policy, dominated by safety concerns, does not allow commingling of LRT and freight rail operations within the same time period. The general practice is that light rail agencies own or control the track system, operate transit service as the host, and lease or permit freight operations in off-peak periods. The majority of the freight rail is local deliveries to businesses involving relatively short, slow-moving trains.

Most of the new light rail services operate through central cities on city streets, but new light rail services tend to be extended into the suburbs on private right-of-way, with longer station spacing. Though the commingled operation between LRT and freight railroad is a practice adopted in Europe, it is currently not permitted in the USA. However, with the technical innovations in rolling stock and control systems, more LRT service providers are looking at the potential applicability of European experience in the USA, and the feasibility of commingled operation between LRT and freight railroad is increasingly being discussed.

According to recent studies [1–3], FRA defined three types of shared-use transit and freight operations, which are shared track, shared right-of-way (ROW), and shared corridor.

Shared Track: Heavy or LRT vehicles operate on the same tracks used by freight trains. FRA regulations govern this type of operation, in which time separation, that is, no simultaneous operation of freight trains and LRVs, is required in most cases.

Commingled Operations (Mixed Operation): Transit trains and freight trains are separated by headway intervals measured in minutes in an operating schedule. Though this approach occurs in Europe and Japan for all sorts of transit operations, it is only approved for commuter services governed by rigid FRA rules in the USA. Joint operation between LRT and freight railroad operation is not allowed [1].

Temporally Separated Operations (Time-Separated Operation): Both transit and freight trains utilize the same track but are separated by time windows. In North America, the common practice is to operate transit during the day and freight at night, generally in the early morning hours [1].

Shared Right-of-Way (ROW): In this case, the transit vehicles run on separate tracks, but track centers are less than 25 ft, that is, separation between the centerline of the freight track and the centerline of the passenger track is less than 25 ft. FRA requires railway maintenance workers to observe specific safety precautions when multiple main tracks are adjacent.

Shared Corridor: Transit and freight operators share a transportation corridor, but tracks are separated by at least 25 ft and no more than 200 ft. FRA believes that intrusion by derailed freight or transit cars onto a parallel railroad track is unlikely beyond 200 ft, so does not consider separations of more than 200 ft to be shared corridor for purposes of safety regulation.

Commingled operation, for the purpose of this entry, is defined as "simultaneous train operation on shared track by railroad trains and by light rail transit vehicles that are not fully FRA compliant." Shared right-of-way, similar to FRA's definition "adjacent tracks," is "the arrangement that the track center spacing between the freight track and adjacent LRT track is less than 25 ft." Shared corridor is "the arrangement that the track center spacing between the freight track and LRT track is more than 25 ft but less than 200 ft."

Seeking a better understanding of the current interaction practices between rail transit and freight railroads, the first three sections of this entry presents the historical background and the general landscape of shared-use practices in the USA and overseas, which are largely based on a survey of transit and freight railroad interaction in North America and extensive research and communication with their counterparts overseas. The fourth and fifth sections of this entry discuss potential demands and challenges faced by transit service providers and freight railroads when and if commingled operation is permitted in the USA. Potential solutions and future directions of research are included in the last two sections.

Introduction

Congestion on highways and urban streets has stimulated renewed interest in rail transit in a large number of US cities. Data compiled by the American Public Transportation Association (APTA) reveal that, over the past three decades, total passenger-miles carried by US public transit almost doubled, from 30 billion in 1997 to 53 billion in 2007 [4]. Among the modes of rail transit, the number of unlinked passenger trips by Light Rail Transit (LRT) quadrupled, from 103 million in 1977 to 419 million in 2007, as shown in Fig. 1. The explosive growth of LRT usage has largely been propelled by the renaissance of LRT in the USA after the long decline of streetcar and interurban systems between 1920 and 1960.

An attractive feature of LRT is that it can use some of the existing real estate of the general railroad system, which significantly reduces the cost of construction and environmental impacts by eliminating the need to build a new rail corridor. However, physical incompatibility, disparate operating practices, and safety regulations have led to separating the two operations temporally. To better understand the interaction between light rail transit and freight railroad, this entry highlights the difference between LRT and freight railroad operations and critical issues in shared use of railroad infrastructure. There are major structural differences between the Federal Railroad Administration

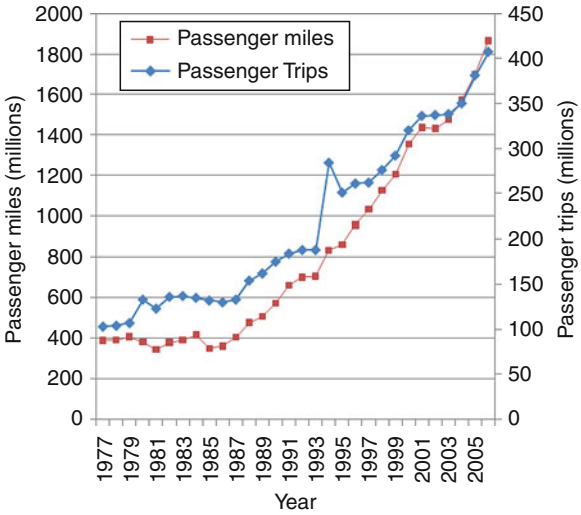

Light Rail Transit, Shared Infrastructural Issues. Figure 1 Historical Growth of LRT Usages Source: Based on Data from APTA, 2009

(FRA)-compliant cars and light rail vehicles (LRV), therefore FRA requires that, to minimize or eliminate the risk of collision between the two types of equipment, complete physical or, at least, temporal separation of their systems must be established.

A few LRT service providers, reaping the benefit of newly developed LRT, and at the same time facing the capacity constraints for more LRT services, are willing to challenge the temporal separation rules. The idea of commingled operation may not be totally irresponsible thinking, given the fact that a number of commingled operations do exist in Europe and Asia [5].

Historical Background

A brief review of historical development of LRT and shared-use issues may help to understand the origins of the conflicts and expedite the pace to derive solutions. Congestion along highways and urban streets in a large number of American cities has stimulated renewed interest in guideway transit, especially light rail transit (LRT). The interest in commingling freight and passenger trains intensifies as potential LRT projects appear on the drawing board or join the existing transit systems in service. The inevitable interaction between railroad and transit stirs up great concern about the safety of these services when they share common track, right-of-way, or corridors. It also raises issues of track capacity, and multiple institutional issues relating to ownership of the right-of-way, control, access, liability, and similar matters.

The modern-day light rail transit (LRT) can easily trace its origin back to horse-drawn wagons or omnibuses in the nineteenth century. Its closest relatives or direct ancestors are "streetcar," "tram," "cable car," or "trolley," some of which are still operating today. The terms are often used interchangeably, even by professional transportation planners and engineers. In the USA, ridership data and operating statistics of streetcars, trams, and trolleys have all been aggregated under the LRT category and can be traced back to 1902 [6]. Figure 2 demonstrates the intensity of streetcar operation in Newark New Jersey during the early twentieth century, and is representative of the USA during that period.

There are a large number of books, papers, and web sites documenting the historical demise of the guideway transit industry in the USA and around the world [7–9]. Some of them have developed theories and hypotheses on the reasons underlying the dramatic mid-century drop in transit usage and others have presented vivid images, such as the one documented in Fig. 3. Limited by the length, this entry has no choice but to leave the colorful stories, sometimes romantic connotations, of streetcars or trams to focus on the modern-day LRT, which is the key stakeholder in the shared use of railroad infrastructure.

Along with increasing gasoline prices and roadway congestion in the 1970s, there came increasing doubt that a single mode or technology, even as flexible and comfortable as the automobile, could effectively serve the broad range of activity patterns and travel demand in large metropolitan areas. Facing the dilemma of extinction or renewal and growth, the lonely survivors of a half-dozen streetcar or tram systems in America, as shown in Fig. 4, became the focus of the transportation professionals. The first national conference on light rail transit, organized by the Transportation Research Board, National Research Council, was held in Philadelphia in 1975, which may serve as a symbol that LRT development in America was at that time opening a new page.

Joining the renaissance of LRT development, San Diego, CA; Buffalo, NY; Portland, OR; San Jose, CA;

Light Rail Transit, Shared Infrastructural Issues. Figure 2
Streetcar Operation in the early twentieth century in Newark, NJ (Source: North Jersey Chapter, National Railway Historical Society)

Light Rail Transit, Shared Infrastructural Issues. Figure 3
Pacific Electric Railway cars piled atop one another at junkyard on Terminal Island, California, 1956 Source: Los Angeles Times Photographic Archive, UCLA Library

and Sacramento, CA established new LRT services in the 1980s. Of these, San Diego LRT initiated shared use of railroad track with freight operations. Their negotiations with freight railroad and navigation of federal regulations will be highlighted in the following section.

According to the 2009 Public Transportation Fact Book published by APTA, the latest data available, by 2007 there were 33 LRT operations, with 1,810 vehicles available for peak service in the USA. The total LRT track miles reached 1,517 miles, including 144.1 miles in

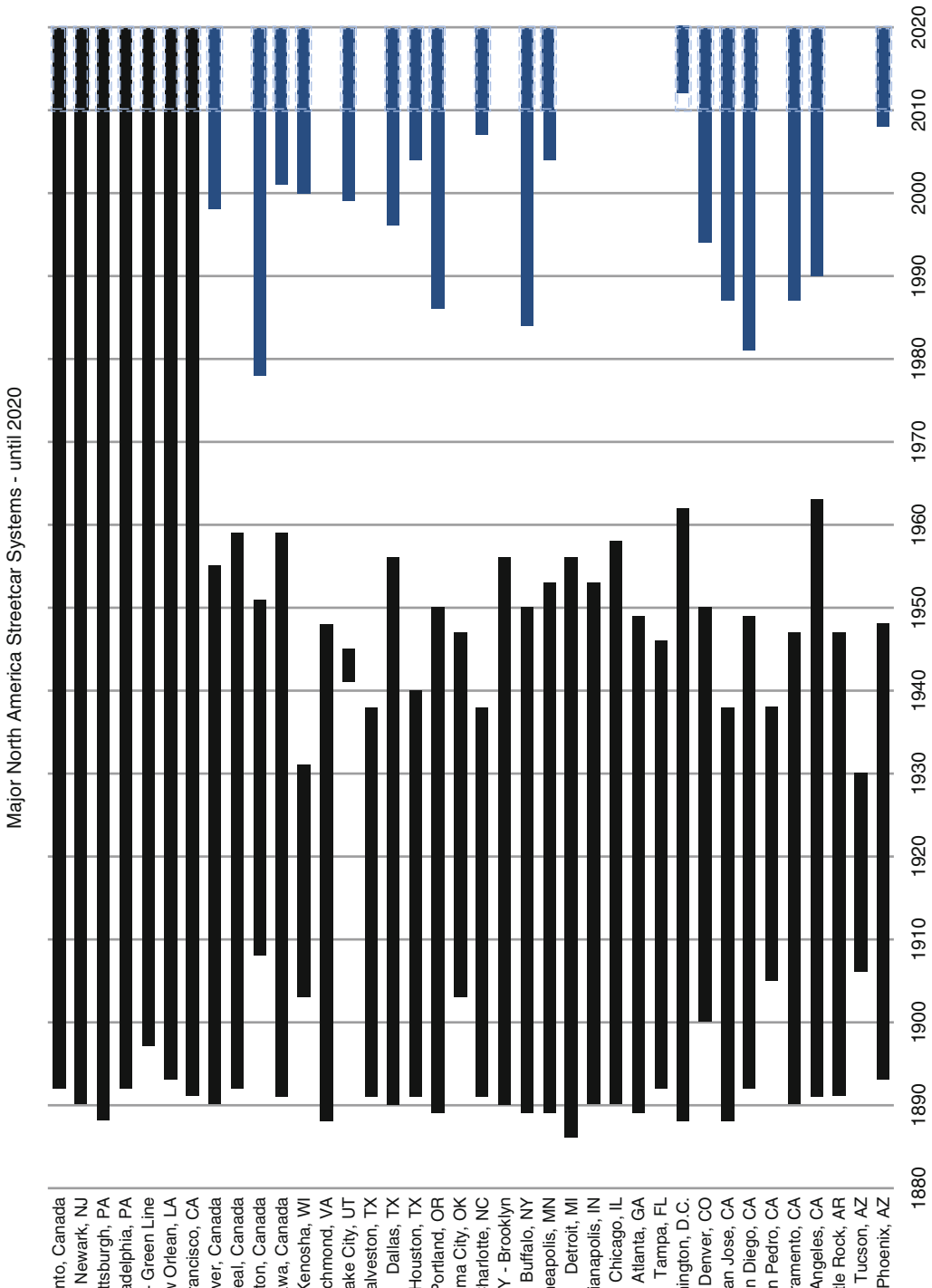

Light Rail Transit, Shared Infrastructural Issues. Figure 4
The Timeline of Major Streetcar Systems in the North America

construction and design and 561.7 mile in future planning as of September 1, 2008. The total number of unlinked passenger trips by LRT had reached 419 million, still a far cry from 13 billion during its heyday in the 1920s, but a fourfold growth from 103 million, the darkest days for LRT in 1977.

As defined by the Transportation Research Board and adapted by the US Department of Transportation [10], modern-day light rail transit is "a metropolitan electric railway system characterized by its ability to operate single cars or short trains along exclusive rights-of-way at ground level, on aerial structures, in subways, or occasionally, in streets and to board and discharge passengers at track or car floor level." Operating along the old tram or streetcar alignment or built along brand new corridors, the modern-day LRT has made great strides in rolling stock technology, which leads to higher efficiency, quick operating responsiveness, and high speed, especially when separate rights-of-way are used.

If the definition by TRB and USDOT has emphasized the operating environment and characteristics of LRT, the definition by America Public Transportation Association (APTA) has focused on the capacity. It states that light rail transit is "an electric railway with a 'light volume' traffic capacity compared to heavy rail. Light rail may use shared or exclusive rights-of-way, high or low platform loading and multi-car trains or single cars."

Joint operation of passenger and freight railroad services is not a revolutionary concept. It has a long tradition in the USA over the last century and is widely practiced in Europe, Asia, and other parts of world [11–13]. However, current Federal Railroad Administration (FRA) policy dictates that freight and LRT trains using the same track must be separated by time of day, primarily because light rail vehicles (LRVs) do not comply with FRA crashworthiness regulations. On the other hand, applications of commingled operations of freight and LRT have been growing overseas, notably in Europe and Asia, where light rail services share track with conventional freight and/or passenger rail services without time-of-day separation.

The commingled operation of freight and LRT, given the growing interest in providing similar services in the USA, has caught the attention of transit operators, government agencies, and the research community. This entry highlights the concerted effort by the FRA, Federal Transit Administration (FTA), and Federal Highway Administration (FHWA), to explore the innovation concept and feasibility of integrated rail operations of short-line or lightly used freight railroads and LRT.

On July 10, 2000, FRA and FTA jointly issued the statement entitled "Joint Statement of Agency Policy Concerning Shared Use of the General Railroad System by Conventional Railroads and Light Rail Transit Systems" (Joint Policy Statement) [14]. The Joint Policy Statement explains how the two agencies will coordinate their safety authority with regard to the sharing of track by rail transit and conventional railroads. On the same date, FRA issued its statement entitled "Statement of Agency Policy Concerning Jurisdiction over the Safety of Railroad Passenger Operations and Waivers Related to Shared Use of the Tracks of the General Railroad System by Light Rail and Conventional Equipment" (Policy Statement). The Policy Statement gives policy guidance and explains the legal basis for safety jurisdiction and agency policy on exercising the same in a shared-use context.

The Joint Policy Statement is general and procedural in nature, while FRA's Policy Statement contains more substantive guidance and practical details. According to FRA, transit operations that will share use of the general railroad system trackage must either comply with the FRA's safety rules or seek a waiver. FRA will be more likely to waive many of its rules where "temporal separation" is in effect and the petitioner demonstrates that its system safety program and state safety oversight program address relevant safety issues. If the transit and conventional railroads operate simultaneously on shared tracks, the petitioners will face a steep burden of demonstrating that extraordinary safety measures are taken to adequately minimize the likelihood of a collision between conventional and light rail equipment. Where a rail transit line shares only a common right-of-way with a general system railroad line, FRA does not consider that situation to involve shared use, and a waiver is not necessary.

The primary reason that collision safety is a major issue is that the structural strength of typical light rail equipment is well below the requirements for rail passenger vehicles, as specified in 49CFR Part 238, reference to the latest edition of FRA safety regulations in

CFR Parts 200–299. A manuscript by a FRA Staff [15] provides an overview of the policy statement with respect to shared track and limited connections. A few tables outlining the likely treatments of various subject rules are given and examples include track, structure, signaling; motive power and equipment; and operating practices. These examples provide helpful guidance for transit operators interested in applying for waivers. A large portion of the entry is devoted to shared rights-of-way and limited connection categories. The author made the following statement on the shared track and commingled operations:

- For joint simultaneous operations on shared track, the petitioner will face a steep burden of demonstrating measures taken to reduce likelihood of collision between light rail and conventional equipment. Fully integrated joint operations, such as the Karlsruhe, Germany system, include advanced train control systems required for all equipment. Accordingly, transit operator will be required to observe the same rules and procedures as the general system, i.e., FRA is less likely to waive rules such as engineer certification for light rail operators.

In another elaboration of the Joint Statement, Sheys and Spear [16] summarized FRA's treatment of shared-use safety issues in petitions filed by Utah Transit Authority (UTA), New Jersey Transit (NJ TRANSIT), and Santa Clara Valley Transportation Authority (VTA). UTA sought a waiver from the injury report requirements, Hours of Service Act record-keeping regulations, and the requirement for flagging a crossing in the event of a grade-crossing activation failure. FRA granted all UTA's requested waivers conditionally, except for part of the Hours of Service Act record-keeping. NJ TRANSIT sought a waiver of several FRA rules related to window glazing and emergency window exits. FRA granted the petitions but required NJ TRANSIT to conduct a public education and awareness campaign to familiarize residents of the area with the new service on the line. VTA's petition related to a 7.6 mile extension, 1.6 miles of which involve temporally separated transit and freight use of a rail corridor, but only extremely infrequently, that is, three or four times per year. This case indicates that FRA is likely to treat shared track/temporal separation cases involving very infrequent usage differently than those involving routine freight usages.

The American Public Transportation Association (APTA) formed a Shared-Use Working Group (SWG) in 1999 when the Federal Railroad Administration and Federal Transit Administration were developing the Joint Policy Statement and Final Rule. The purpose of the SWG was to press for consistent and flexible regulation of transit operations in corridors shared with the general railroad system. The SWG has brought together general managers of transit agencies, federal officials, and technical specialists for a series of energetic, well-attended meetings and forums. The SWG is currently cochaired by John Inglish of the Utah Transit Authority, and Thomas Hickey of Houston Metro.

There were also a few studies addressing the subject of commingled operation of freight and LRT since the late 1990s, among which, three Transit Cooperative Research Program (TCRP) studies, one FRA-sponsored study, and their related publications are most notable and are summarized below.

The Transportation Research Board commissioned a concerted research effort to explore various issues associated with joint operations between light rail transit and freight railroads, driven by the large numbers of urban areas in the USA that were contemplating new or expanded rail transit services, especially where active railroad trackage provides an opportunity for potential cost-effective joint use.

The first TCRP research [13] was conducted and completed before the publication of the FRA/FTA Joint Statement. It reviewed a number of joint operations domestically and overseas and summarized four categories of critical issues related to commingled operations: regulation, operation, infrastructure, and vehicles. The study pointed out that one should be very careful when talking about transferring overseas experiences to the USA. There are a number of different circumstances, such as traffic mix, labor agreements, and safety features that make simple replication of these systems in the USA very difficult. Even the sampling operations in Germany and Japan maybe very different: while in Germany one can find light rail, passenger railroad, and freight railroad sharing track, in Japan these examples are very rare. If it occurs, track sharing is most often by passenger railroads and transit operators. Therefore, all the factors mentioned above vary from case to case and must be studied

independently. The TCRP research also recognized that differences and variations in standards among rail systems in the USA, even in neighboring metropolitan areas, make joint operation even harder to accomplish. The interchange of rolling stock is also very hard to achieve due to all the institutional and technology requirements, even though the use of one another's rolling stock on different commuter lines does occur for various reasons.

In order to recognize the FRA and FTA joint statement of policy concerning shared use, the principal authors of TCRP Report 52 produced another TCRP report [5]. After a brief review and summary of FRA/FTA joint statement and TCRP Report 52, the author proceeded to provide some additional information on Karlsruhe and other track-sharing locations that had occurred since the publication of TCRP Report 52. The detailed descriptions of various locations in Germany are very useful to researchers to identify potential models/aspects for application in North America. The article clearly identified that Karlsruhe may be an ideal model but not for direct application in North America. It also urges others to examine some less intense, simple, and straightforward interactions, such as those at Durren or Zwickau, for more transferable applications in the USA.

The article also emphasized the validity of major issues identified in TCRP Report 52. It included a matrix of interest groups or stakeholders and the intensity of their interest in the shared-use issues. The author provided some key issues and policy suggestions for further research in four large areas: regulation, operation, physical plant and infrastructure, and vehicle. A few key questions raised in this article are directly relevant to the understanding of shared-use issues:

- Is joint use a sound policy worth advancing?
- What risk mitigation measures can be applied to shared track to reduce the risk to tolerable levels?
- Does joint use constitute a hazard to public safety?
- What are the quantifiable risks and liabilities arising from various degrees of joint use?

As an introduction of "shared-use operations" to the general transportation community and a freestanding statement of current conditions, Phraner [17] presented another report at the 8th Joint Conference on LRT in Dallas, which provided a definition and then current applications of joint use. The article also listed motivations and deterrents to shared use.

Another study conducted by the Volpe National Transportation Systems Center [18] for FTA focused on safety and insurance issues. Shared-track operations involve some unique risks, and the liabilities associated with these risks can affect whether such services are offered and, if offered, their operating plans and costs. Insurance is used to mitigate or manage such risks and insurance premiums can be a significant cost item for transit agencies. The authors explored the issues of liability and insurance that arise when operating on track shared between light rail transit and freight railroads. The study included six shared-track operations. The transit agencies that currently operate light rail transit on the same track as freight railroads are: San Diego Trolley, Inc. (SDTI), Utah Transit Authority (UTA), New Jersey Transit (NJ TRANSIT), which has two services, the River Line and Newark City Subway, and the Maryland Transit Administration (MTA).

The most salient risk involved in shared-track operations is that of a collision between a light rail transit vehicle and a freight railroad vehicle. None of the shared-use agreements specifically addresses the possibility of this kind of risk, since it has never occurred. Other risks include one party damaging the other party's property. Track ownership seems to have a significant effect on risk. Part of the reason that freight railroads agree to sell the ownership of track to transit operators is to avoid risk. Some insurance industry officials believe it would be useful to have a study that could quantify the perceived risk of shared operations. However, there has been no published risk assessment performed specifically for the case of shared track between light rail transit and freight railroads until the two recent FRA studies, which will be addressed in the following section.

Freight railroads generally try to minimize their risk for anything related to passenger transit. Based on the six case studies, there are three basic methods for assigning liability: by fault; by financial threshold; and by incident circumstances. By fault is the simplest way to address the issue. However, when the fault for an incident is not clear or if multiple parties are involved, the process of fault determination can be lengthy. Financial thresholds are easier to determine. In many cases cutoff points assign liability. Liability assignment

by circumstance describes various situations and assigns liability based on who is involved and the type of damage is caused. When liability is assigned by financial threshold or incident circumstances, one party is held harmless irrespective of fault. In these cases, there is an implicit lack of incentive for safe behavior.

According to the study, there is no instance where separate liability insurance for the shared-track operations exists because the safety rules and procedures are viewed as effective in mitigating possible risks. A table included in the manuscript gives an overview of the various insurance levels and premiums for each of the case studies. Insurance level varies by agency from $35 million to $250 million and annual premiums ranged from $150,000 to $4.2 million.

The primary objective of another FRA study [19] was to explore the feasibility of concurrent operations of compliant and noncompliant vehicles on the same track, concentrating on identifying and evaluating risk mitigation measures that would meet FRA's requirement of providing "equivalent safety." The study was deliberately constrained to existing noncompliant vehicle types proposed for LRT services in North America, and sharing track with low-density local freight service to best represent the current interest.

The study summarized principal vehicle characteristics and physical plant for five potential shared-track operations, which include: Baltimore LRT in Maryland, SPRINTER DMU from Oceanside to Escondido in California, the River Line in southern New Jersey, San Diego Trolley, and TRAX light rail in Salt Lake City, Utah. The areas of noncompliance, issues related to shared use of LRT and freight railroad, such as railroad operating and maintenance practices, equipment, and operating environment, are discussed.

After furnishing a table summarizing the effects of noncompliance on accident likelihood and severity, the report provided a risk analysis of a representative noncompliant passenger rail operation with concurrent local rail freight service. The primary area of concern with commingled operation is the number and severity of collisions between noncompliant vehicles and conventional freight cars and locomotives. The risk analysis results showed that the incremental risk from shared operation could be mitigated by practical risk mitigation measures, provided that freight operations are confined to a small number of trips during off-peak hours. Mitigation measures include adding a second track to a single-track system, and applying one of several alternative train control systems to reduce the risk of a collision.

A recent draft implementation strategy developed by Tereschuck [20] outlines the core operational requirements for retention of an equivalent level of safety for commingled operation of freight and LRT services. Based on previous TCRP research and Federal fact-finding mission trips to Europe, the author highlighted five essential operating characteristics consistent with the European approach to commingled operations. Corresponding to each characteristic, the manuscript also presented possible actions for pilot application:

- Single authority/ownership of rail corridor/dispatching control
- Uniform/single rule book authority
- Single communication network
- Consistent training/certification process – single authority control
- Application of advanced technology – provide positive train stop or automatic train control capability

A recent study [2], sponsored by FRA, has reviewed the technical feasibility of concurrent shared-track operations in detail focusing on the 1999 FRA/FTA Shared Track Policy Statement, which identifies six factors to be considered in evaluating the operational safety of light rail transit systems that would share track with conventional railroad equipment. The research team pointed out that five of these factors are primarily operational in nature requiring appropriate organization and training but no investment in technology. The final factor, fail-safe train separation and collision prevention, revolves around the deployment of appropriate technology to prevent collisions between trains. Relative to the primary technical consideration of providing fail-safe train separation, the team has identified a number of train control systems that ensure trains sharing track do not collide. All of the systems override the vehicle operator in the event of a signal violation that could result in a collision with another train.

Independent of the federal shared-track policy, the research team identified and evaluated the four most salient risks of concurrent shared-track operations.

The study team found that risk assessment is a valuable tool that can contribute to assuring the safety of commingled shared-track operations. Risk assessment is any structured process of identifying the hazards present in an operation, evaluating the level of risk associated with the hazard, assessing the acceptability of the risk, and determining whether or not risk mitigation will be required. Risk assessment may be applied at all stages in the development and operation of a passenger rail system, but the primary purpose for a shared-track operation is to support the customary safety assurance process for a new shared track operation through planning design and implementation stages.

In addition, the FRA study has also conducted a market assessment to support federal investment in mechanisms and methods that facilitate shared-track operations. The market assessment indicates substantial national applicability and considerable industry interest in concurrent shared-track operations where light transit cars share track with conventional railroad trains. In the context of national applicability, a nationwide review of the 88 urban areas with populations greater than 500,000 inhabitants identified 165 corridors in 65 cities with potential for development as shared track freight/transit rail services. Relative to industry interest, a brief scan identified 15 North American corridors where shared track operations are in current operation, design/construction, or active planning.

The most recent TCRP Report 130 [3], produced under the TCRP A-27 project, has focused on the present and evolving state of the art in the shared-use environment, specifically examining train control technology, operating rules and procedures, communications systems, vehicles, shared-use operations, and governance and business models of existing and planned systems.

The research team took a comprehensive view of "Command and Control" as including the variety of train control and communication systems, operational rules and procedures that are particularly suitable or adaptable to the shared-track environment. The emphasis was on those features that compensate for vehicle structural deficiencies by minimizing the risk of a collision in such an integrated system.

Building on knowledge gained via previous studies, the TCRP project presented the characteristics of freight railroads, suggested business models for future implementation, and included a business case and practical guide for transit agencies or other stake holders to be involved in the shared-use area. To carry the TCRP A-27 to a new height, the study team developed a hypothetical case study and recommended a demonstration program to explore the critical issues and feasibility of sharing track between FRA noncompliant LRT vehicles with lightly used freight railroad operations.

There are various studies, trip reports, and research summaries that document overseas practices in the areas of commingled operations of freight and LRT. The literature presented here may overlap on some cases in Europe but the emphasis and time frame may vary.

Geissenheimer [21] published a manuscript that recognized the opportunities to operate efficient rail service on sparsely used lines using a new generation of self-propelled diesel multiple unit cars (DMUs) or dual-power electric light rail vehicles (LRVs) combined with changes in operation and organization. The focus of this article related to vehicle technologies and their applications, but also provided some pioneer study of shared use cases in Duren and Karlsruhe, Germany; Amsterdam, Holland; and briefly mentioned shared use in Japan and Korea.

Another early introduction to overseas shared-use practices was included in a short article in the Journal of Transportation Engineering [22]. This article highlighted two basic strategies to develop a local LRT or streetcar network into a regional system at relatively low cost. The first strategy is to take over a railroad line, where most or all prior freight service has been or can be abandoned. Examples mentioned in the USA include the Riverside Line in Boston and LRT service between downtown San Diego and the Mexican border. The second strategy is to implement a shared track agreement that provides LRT access to the railroad with freight services. As documented in this manuscript, in contrast to the requirement by the US government regulations, for LRV to meet high buffing strength standards to protect against damage in the event of collision, there is no special buffing strength requirement in Germany. The rationale is that LRV braking rates, being superior to those of main line trains, obviate the need for buffing strength.

The author presented a detailed network and vehicle arrangements of Germany's Karlsruhe system to demonstrate the principles of shared-use applications. A few other applications were also mentioned in the article: Kassel, Saarbrucken, and Zwickau in Germany and other cities in France and Switzerland.

Another detailed study of shared track operations in Karlsruhe is presented in the FTA/FRA fact-finding trip report [23]. In March 2000, a delegation of US transit operators, equipment manufacturers, and consultants led by FTA/FRA went to Karlsruhe to examine shared track operations. After describing the nature and importance of rail transportation in Germany, the trip report documented how shared track operation was achieved in Karlsruhe. Summarizing general observations and specific case studies during the trip, the delegation highlighted the following factors that contributed to the success of shared track operation in Karlsruhe

1. A government-owned national railway system provides accessibility to all rail tracks.
2. Information, communications, and active train control systems and equipment adaptable to mixed usage are employed.
3. Government also requires the labor force to obtain licensing certification to operate the different types of trains running in Karlsruhe, including trains for freight, intercity passengers, regional passengers, and local trams.
4. Institutional factors, such as common operating rules, dual dispatching facilities, and uniform safety regulations, ensure the seamless integration of both light rail and conventional rail operations.

As a member of the delegation of the fact-finding trip organized by FTA/FRA in 2000, Phraner also visited additional cities, such as Saarbrucken, Duren, and Koln. A supplemental report [24] was compiled to provide an independent supplemental study of those systems visited. Recognizing Karlsruhe as an instructive case study but not a readily transferable model to North America, the author defined Karlsruhe as representing the most advanced example of shared track operations. The Karlsruhe case study provided selective lessons and precedents in institutional and regulatory innovations that encourage shared track arrangements. Karlsruhe practice demonstrated operating practice extremes by dispatching tram and mixed LRT train traffic through a peak volume point and confirmed that the German train control technology and control center operated safely.

Another important issue in the Karlsruhe practice is the exemplification of strong political leadership and commitment, necessary to accomplish a shared-use project. Besides abundant field visit photographs of each location, this report also included detailed network maps, schedule, and operating arrangements for Saarbrucken, Duren, and Kohn case studies. One of the important contributions of this report was to identify the potential issues to be encountered in the USA when/if a particular model is to be transferred. In addition, the report also devoted an entire chapter to light-rail-derived DMU rail cars and discussed their importance to shared track in North America.

Similar to previous fact-finding trip reports, the TCRP Research Result Digest Number 47 [23] documented a number of case studies of shared track operations in Germany (Kohn, Durren, Kassel, Karlsruhe, Saarbrucken, Rhine/Ruhr-Dortmund, and Gelsenkirchen), France (Strasbourg), and Luxembourg City. Different from the previous fact-finding trip report is that this digest is organized by functional areas, such as design, technology, and track-sharing relationship to economic and urban development. Each area is demonstrated via specific examples of various cases in Europe. Its Appendix C provided a summary table of German cities with track sharing operations, which may be useful to identify the unique characteristics and similarities of various shared track operations.

Another recent description of shared track operations appeared in the Tramways & Urban Transit Magazine [25]. In this article, the author described a visit to a German city transformed since the end of communist era. Nordhausen, a former part of East Germany, has access to two meter-gauge tramlines. One runs to an informal transfer center with two railway stations and serves a large number of urban, suburban, and interurban bus routes. The Deutsche Bahn Station, a typical busy urban facility, has intercity and regional trains arriving and departing at frequent intervals. The Bahnhof Nord, the terminus of a privately operated but highly subsidized meter-gauge railway system, runs through rural areas and forests and is used

primarily for passenger traffic, with diesel railcars and steam-hauled trains attracting commuters, schoolchildren, and tourists.

Similar to most US cities with growing suburban and rising automobile ownership, Nordhausen wanted to improve transit service and discourage motor traffic from clogging its streets. Following the examples of Karlsruhe, it was thought that a tram-train operation providing through service might substantially reduce the number of cars entering the city. Encouraged by the no-transfer service and low-cost solutions, Nordhausen simply built a track connection between the two systems and a hybrid vehicle to run on busy streets under typical 600 V tramway overhead and self-propelled on traditional railway tracks. Service over the connection began in April 2002 and an extended service of 12 km beyond the privately operated station was inaugurated in May 2004. As observed by the author during his visit in 2005, the shared-use operation in Nordhausen is "very elegant." Using sophisticated layover procedures, the shared track operation provides sufficient service for commuters and makes significant contributions to the local economy.

Current Operating Scenarios in the USA

It is important to have a general understanding of the current LRT operations in order to explore the issues of shared use of infrastructure with freight railroads in the USA. A brief presentation of a national survey of shared use between LRT and freight railroads in North America is included below. The survey results are categorized into four groups: physical characteristics, operating privileges, insurance liability, and regulation.

The difference between propulsion power, capacity, and operating characteristics determined that LRT operations have different issues from commuter rail services, even though they may share certain legal, administrative, and organization issues. According to a recent survey [1], among the 34 LRT operations in North America, about a quarter do not have any interaction with freight railroad and the rest all interact with freight railroad to some extent, as shown in Fig. 5. The majority of the LRTs surveyed, 61%, interact exclusively with local freight; SEPTA light rail interacts exclusively with mainline freight and another light

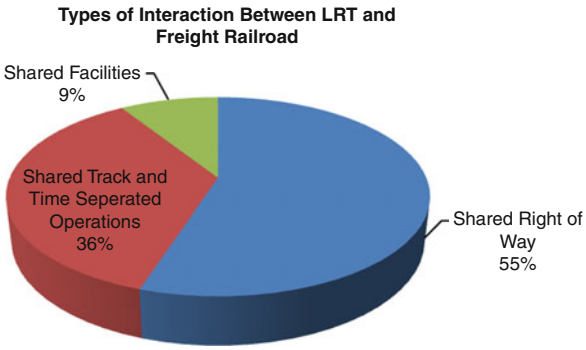

Light Rail Transit, Shared Infrastructural Issues. Figure 5 Types of Interaction between LRT and Freight Railroad

rail transit. It is interesting to note that, in the case of Edmonton LRT, the interaction with the adjacent freight main line has diminished due to changes in freight operations since LRT was built in 1978. At that time, the LRT route was located between main line tracks. Now the alignment is a little used freight spur.

Platform access level is an important element in the interaction between LRT and freight railroad. The Americans with Disabilities Act (ADA, 1990) requires that transit systems provide level access for passengers. Unlike a commuter railroad, whose platform access level can be categorized as low-level platform and high-level platform, LRT platform access level may be better described as "low-floor" versus "high-floor" configuration. In case of low-floor access, the LRT vehicle floor is flush with station platforms that are 8–14 in. above the track, depending on the system, so wheelchairs or strollers can roll on to the vehicle directly. Low-floor cars, which have been used in Europe for more than a decade, were only first introduced to USA in 1997 on Tri-Met MAX in Portland, OR.

Most early low-floor designs were intended for city streetcar or tramway applications and have neither the top speeds nor the ride quality suitable for US and Canadian light rail operations. However, many European LRTs have extensive on-street operation and recent new vehicle procurements have been predominantly for the low-floor type [26]. In the most recent decade, partial low-floor LRVs capable of 55–65 mph top speeds have been delivered to several US cities. These vehicles are capable of providing the speeds and

levels of comfort needed to effectively serve regional LRT lines of 10–20 miles in length.

When high-floor LRT vehicles are used, the floor is higher than the station platform so wheel chairs have to be aided by a lift to roll onto the vehicle. There are often mini platforms situated at the end of the platform so that they can be operated by the train driver when required, which is the case in Sacramento, Dallas, Baltimore, Denver, Salt Lake City. San Diego has elevators mounted on the car itself. High platforms are used exclusively in a number of systems including Los Angeles, St. Louis, Edmonton and Calgary. They are also used in combination with low level loading platforms. Examples include Buffalo, Pittsburgh, and San Francisco. A precise demonstration of both high- and low-floor LRV may be observed in Tri-Met's MAX in Portland, OR. The agency practice coupling one high floor with another low-floor vehicle, this ensures adequate access for wheel chair users at all times and all locations.

As documented in the study [1], the degree of shared operation in light rail transit varies. Five systems, depicted in Fig. 6, share track and are temporally separated from freight operations. They are MTA LRT in Los Angeles, TRAX in Salt Lake City, the LRT system in Baltimore, San Diego Trolley, and Newark Subway in New Jersey. Light rail services usually operate during the day, with freight operations from midnight until the early morning hours. Since that survey was conducted in 2003, a new kid on the block, South Jersey Riverline LRT, has joined the group using the temporally separation arrangement. Six light rail transit systems share right-of-way with freight, with each mode on separate tracks. These include New Orleans Streetcar; SEPTA light rail transit, Denver LRT, Portland MAX, Sacramento LRT and Hudson Bergen LRT. Only the Metro Blue, Green and Red LRT lines, in MTA of Los Angeles, and Edmonton Transit have some shared facilities with freight, but no joint usage.

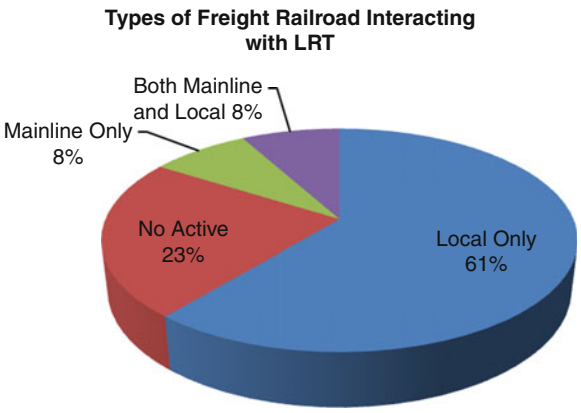

Light Rail Transit, Shared Infrastructural Issues. Figure 6 Types of Freight Railroad Interacting with LRT

In contrast to the mixed ownership of tracks used for commuter rail operations, the ownership for LRT tracks is distinctly defined. According to the same survey [1], about 40% of the shared tracks are owned by freight railroad and 60% by the transit agencies. In general, LRT either uses tracks abandoned by a freight railroad, or the transit agency has acquired the right-of-way, being abandoned, to preserve transit corridors.

Moreover, most of the light rail transits are dispatched by transit agencies themselves, such as Newark Subway, NJ River Line, Edmonton Light Rail Transit, San Diego Trolley, SEPTA LRT, Baltimore light rail transit, and Metro Blue, Green, Red lines in Los Angeles. Two systems are dispatched by third parties, which include TRAX in Salt Lake City and Hudson Bergen LRT in New Jersey.

When compared to the commuter rail systems that have different dispatching protocols during peak and off-peak period, the majority of the LRT systems implement the same dispatching priority timetable during their operating period, which is largely caused by the temporal separation.

None of the light rail transits surveyed has any incentive plan for better coordination between freight and transit operations. The obvious reason is that light rail transit operators are less affected by freight operation, except during the time window that is allocated.

One of the questions included in the survey asked what measures are provided to separate transit and freight operations. The results indicate that the majority of LRT systems do not have any physical barriers to separate LRT and freight operation when they are in the close proximity of each other. Among the ten valid answers, seven do not have any separation measures between transit and freight, two uses fences, and one uses both fencing and intrusion detection. The last example was dictated by the freight railroad due to liability concerns.

The survey results revealed that generally not many changes were made to the transportation system to accommodate passenger operation for LRT. Most changes were just a complete service time separation schedule. For example, Edmonton Light Rail Transit, where the LRT tracks were originally in the center of the right-of-way with mainline tracks on both sides, gave modification details to accommodate LRT operation: "temporary relocation of CN track during construction of a shared LRT/CN bridge. Also CN grade crossing gates were connected to LRT signals system to allow shared use of the gates. They extended the crossing 'gate call-on' provided on CN line and tied it into the LRT crossing 'call on' signal to allow gates called on by LRT to stay down if CN train was approaching. There was also a need for the modification of CN's DC signal system to ensure that there would not be interference caused by LRT DC traction power return. A signalized diamond crossing was installed on CN track to enable LRT line to cross into their yard that was located across the CN westbound track. All of the above were paid for by the City of Edmonton." Since the construction of the LRT the main line freight service has largely been relocated away from the shared right-of-way.

The settlement of insurance and liability issues between the light rail transits and the freight railroads is similar to that of commuter systems. The size of LRT operation and the strict separation of operations defined the insurance premium, liability, and deductible, which are generally smaller than for commuter rail services. For example, the insurance and liability issues for San Diego Trolley were handled through agreement with Metropolitan Transportation Development Board (MTDB) that both own the freight railroad and San Diego Trolley. In the case of the Baltimore LRT, the State MTA holds CSX harmless. The insurance requirement for Edmonton Light Rail Transit is as follows: $5 million liability insurance covering persons using LRT and CN passenger service; $1 million insurance covers liability to cover third parties arising from utilization by the City of the premises and all premiums are paid by City of Edmonton. City waives its rights against CN for damages arising from occupation/use of the leased premises, except if caused by the negligence of CN.

No accidents were recorded as a result of freight and LRT interaction in the survey [1]. This may reflect the safety precaution of the separated operation. But at the same time, we also have to admit that LRT systems have only been in operation for a relatively short period. The oldest among the several "new age" LRT operations in the USA is the San Diego Trolley, which is only 29 years old. Compared with the century old commuter rail operations, the total accident number is low or nonexistent.

Different from the commuter rail operation, most LRT service providers or transit agencies have purchased and now own the railroad lines. Then public transit entities grant trackage rights to the contract freight operators to access the shared-use tracks. For example, Utah Transit Authority (UTA) bought the railroad track from Salt Lake City to Sandy and beyond from Union Pacific and contracted a short line to provide the residual local freight switching service on the LRT line. Similarly, New Jersey Transit purchased the alignment from Conrail for the Riverline LRT in South New Jersey. Conrail has a permanent operating easement, which provides them trackage rights to use the River LINE per the terms of the sale and operating agreements. Many transit entities are in the process of acquiring the shared-use asset; some properties still inherited the historical arrangements. For example, Edmonton Light Rail Transit and Newark Subway get the corridor access through property lease; SEPTA light rail gets their corridor access through a highway crossing agreement between State and railroad, and San Diego Trolley, Inc. via a contract through MTDB, of which SDTI is a wholly owned subsidiary.

Demand for Commingled Operation

While North America pioneered commingled operation in the early twentieth century, the newest and most innovative forms of joint use are found overseas. Transit professionals found that, in terms of commingled operation between LRT and freight railroad, the combination of US engineering and operations best practices is behind international trends. A few LRT service providers argue that commingled operation is feasible, if certain measures are taken to mitigate risks to tolerable levels.

LRT is a relatively inexpensive transit mode to build, compared with urban highway and heavy rail. Yet, LRT is effective in attracting automobile users from congested highways. For example, Baltimore's LRT was

built in 1992, at the cost of $360 million, for the initial 22.5 miles. In year 2000 dollars, that's approximately $422 million, or $19 million per mile. The cost includes right-of-way purchase, line construction, stations, vehicle procurement, maintenance and storage facilities, etc. According to APTA, Baltimore's LRT carries about 25,600 passenger trips per weekday, which is about 2,500 trips in the highest peak hour, or about 2,400 trips in the peak direction, equivalent to almost two freeway lanes. The LRT system has been planned to accommodate future growth with three-car trains, and with a maximum 2-min headways assumed, the system could theoretically accommodate about 23,000 persons per hour, the equivalent of about 20 freeway lanes [27].

LRTs also have the advantages of lower operating cost. For example, the operating cost of LRT services in Boston, which carries the heaviest LRT ridership in the USA, is significantly less than that of bus services. According to FTA's National Transit Database [28], the MBTA's LRT system carried passengers at an average cost of $1.25 per trip, and $0.51 per passenger mile, compared with MBTA average bus costs of $2.04 per trip and 0.71 per passenger mile.

LRT is the USA's big winner in terms of ridership growth among the major transit modes. Despite the economic recession, Americans took more than 10 billion trips on public transportation in 2009, a 35% increase since 1995 [4]. Among which, LRT ridership remain the most stable, contributed by newly inaugurated systems, in Phoenix, AR and Seattle, WA. In addition, a number of existing LRT systems exhibited large ridership increase, such as 12% in Baltimore, MD; 11% in Oceanside, CA; and 9% in Memphis TN.

LRT operations have been developing at an average rate of nearly one new system per year over the past 3 decades. According to APTA [6], there are 27 modern LRT systems (opened after 1981), and another 7 Vintage Trolley systems in USA. The recent openings of LRT include Portland's MAX Yellow Line, streetcar extensions in Memphis and New Orleans, and New Jersey River Line, which is the first to use non-electrified vehicles. Most extensions in San Diego, San Francisco, San Jose, Sacramento, Denver, Dallas, St. Louis, Philadelphia, Pittsburgh, Baltimore, Hudson-Bergen, and Newark subway are now open. New start-ups in Phoenix, Memphis, Minneapolis, and Charlotte are in operation also.

Most new light rail services operate through central cities on streets from which the bulk of automobile travel has been removed. However, outside of the center cities, the new LRT services typically extend into the suburbs on private right-of-way, with longer station spacing. The general practice is that light rail agencies own or control the track, operate transit service as the host and lease or permit freight operations by a contracting railroad in off-peak periods.

Though most LRT agencies own the right-of-way by purchasing the abandoned or branch rail lines, the demand for commingled operation between LRT and freight railroad might increase when rail transit "new starts" exhaust vacant right-of-way. It is possible that the competition for track space will focus on the active railroad lines, not only abandoned or underused lines.

On the other hand, rail freight is booming as well. For the first time since World War II, some railroads have capacity constraints on certain lines. According to the Association of American Railroads [29], railroads are experiencing a surge in traffic volumes for all commodities, including coal, and, for the first time, intermodal freight is the industry's top revenue source. The US railroads originated more than 330,000 carloads per week in 2008. The transformation from once thought to be stodgy and slow carrier to a good-service, high-speed and modern carrier has made freight railroad an indispensable link in providing "just-in-time" supply chain.

The dilemma faced by both freight railroads and rail transit operators is that rail segments, where passenger service providers require additional capacities, are often bottleneck areas within freight operations. This fact can make it even more difficult to share tracks for both freight and passengers.

Though commingled LRT operation with freight railroad is not active in the USA, it is a common practice in Europe and Japan. The European approach to mixed operations is significantly different from the US approach. European operations maximize utilization of the "track resource" through scheduled, on-time freight and passenger operations [30].

Karlsruhe, Germany is acknowledged to provide the most sophisticated and advanced examples of shared-track practice between railroads and light rail. As documented by the supplement of TCRP 52 [5] Karlsruhe integrated its local streetcar and railroad

service on selected lines. LRVs and commuter trains not only run jointly, but also provide joint service on an integrated timetable, with freight and intercity trains interspersed in the operating schedule. Karlsruhe demonstrates operating practice extremes by dispatching tram and mixed LRT and train traffic through peak volume points. The observation made by TRB [5] disclosed the highest level of operating discipline and performance: 16 trains passing in an hour, nine of which were scheduled northbound in the half-hour interval between 12:30 and 13:00. A northbound freight intercity train is followed 1 min later by a high-speed Intercity Express (ICE) train, 10 min later by a Euro International Express, 4 min later by a light rail vehicle making a station stop, 3 min later by an express freight, 4 min later by freight – all sharing the same track [5].

Japan is another leader in commingled operation between rail transit and freight railroad. Japanese National Railways (JNR) split into six passenger carriers which are separate corporations but are marketed as Japanese Railways (JR) and one freight carrier, JR Freight in 1987. JR Freight and the six JRs operate on the same track and catenary system, using the same railway facilities. Unlike freight services in the USA, freight in Japan is subordinate to passenger services on the national railroad system. Freight operation is consistently the tenant on the passenger railroads. Although JR Freight does not pay track usage fees, it is responsible for the incurred incremental costs of operating freight trains on these tracks. An average of 737 freight trains operates each day throughout the country. Of these, 425 are container trains, while the remainders are trains hauling bulky freight in tankers and hoppers. About 90% of JR Freight's rail freight is transported at night [31]. JR Freight is investing heavily to upgrade its fleet with faster and powerful locomotives; developing new freight wagons for high-speed trains; developing new containers for easier loading and more capacity; and upgrading freight station facilities. An advanced freight system may also contribute to more harmonious operations with the rest of the rail transit modes.

It remains to be seen whether FRA is willing to adopt such practices even though Europe and Japan has proven that commingled operation can provide more line capacity. The RiverLine in Southern New Jersey could be an example of efficient use in the USA. NJ Transit's initial plan, developed with Conrail Shared Assets, called for a "limited mixed-use" operation with parallel running on adjacent freight-only tracks, one freight train per day during off-peak hours, and use of automatic trip-stops and derails. The risk assessment indicated that the safety level would meet FRA's requirement. However, FRA rejected this plan, claiming that freight traffic on the Trenton-Camden corridor is expected to grow, making temporal separation impractical. NJ TRANSIT then replaced the original plan with a more rigid time-separated alternative, day and evening for passenger operations and late night freight operations.

Challenges Faced by the Attempts

Though commingled operation could exhibit advantages, such as lower capital investment for infrastructure, reduced operating cost, cheaper and quicker new starts, etc., challenges are yet to be solved, such as incompatible equipment, signals and communications, and inspection and maintenance practices.

The FRA/FTA "Joint Statement" states, "Although compatible in terms of track gage, these two forms of rail service are incompatible in terms of equipment. A collision between a light rail transit vehicle with passengers aboard and heavy-duty freight or passenger equipment would likely result in catastrophe."

The main problem in the USA is the design of different categories of rail vehicles: FRA requires railroad vehicles have certain crashworthiness or buff strength, while these regulations do not apply to rail transit and LRVs. Having different types of vehicles with different weights, crashworthiness, and braking characteristics commingling on the same track imposes safety concerns. As stated in TCRP 52 [30], emphasis in North America is focused on rail safety and collision survival, versus European emphasis on collision avoidance and impact attenuation. For example, railroad buff strength for overseas railroads is in the 300,000–400,000 lb range, while North American railroad requirements are twice that, at 800,000 lb. Typical light rail car buff strength generally is 200,000 lb or less, and rarely, if ever, more than twice the empty weight of the LRV such as CPUC General Order 143-B. Making rail cars stronger to sustain collision

forces creates a heavier car that is unable to stop in shorter distances, thereby increasing costs and power consumption, while sacrificing performance.

Related to the scarcity of North American main line railroad electrification is the potential reintroduction of Diesel Multiple Unit (DMU) rail car to North America. DMUs are similar to LRVs in appearance and performance, except that they can operate independently of wayside traction power infrastructure. New Jersey Transit's River Line is among the first contemporary uses of the light DMU technology as a surrogate for conventional electrified light rail. Analysis indicates that DMU can offer both cost savings and operating advantages.

Operating trains that travel at different speeds reduces capacity on a rail line. The optimum condition can be achieved by operating at about the same speed by all types of trains. All other things being equal, the longer the block length, the lower the capacity. The block length is based on the distance it takes to stop the train. Braking distance varies by the train type. Signal design would have to conform to conventional freight railroad requirements, but also accommodate design elements unique to LRV. For example, freight trains require much greater braking distances than do LRVs, so the design must consider the longer freight braking distance when establishing the signal block layout and establishing speed limits for the various classes of trains to operate over a line. However, longer signal blocks unnecessarily penalize LRVs by causing them to run at reduced speeds under certain signal aspects. This scenario could be compounded under certain topography, such as downhill or grade crossing territories. Special operating rules must therefore be developed to help reduce or eliminate such penalties.

Under the general guideline of the "Joint Statement of Agency Policy Concerning Shared Use of General Railroad System by Conventional Railroads and LRT systems" (Joint Policy Statement) issued in 2000, FRA does not consider the situation, where a rail transit line shares a common right-of-way with a general railroad without sharing track, involves shared use of the general system by the rail transit line, therefore a waiver is not necessary. Where a rail transit line shares track with general railroad, but under strict "temporal separation" as referred in the Policy Statement, the FRA is likely to waive many of its rules. However, the petitioner must demonstrate that its system program and state safety oversight program addresses all relevant safety issues.

For commingled operations on shared track, the petitioner will face a "steep burden" of demonstrating measures taken to reduce likelihood of collision between light rail and conventional equipment, because of concerns over major differences between FRA-compliant cars and light rail vehicles (LRV). It seems that, in this litigious society, chances are slim for winning approval of such waivers from FRA.

In North America, liability is the single biggest institutional obstacle to joint operations between rail transit and freight railroad. In spite of many concerns arising from joint operation, one of the primary fears is a catastrophic event resulting in major loss of life and property damage. Thus, an important condition for a freight railroad to share its track with rail transit is to be held harmless, regardless of fault.

According to General Accounting Office [32], in 1997, Congress limited the aggregate damages that may be awarded to all passengers claims from a particular rail accident to $200 million and permitted providers of rail transportation to enter into indemnification agreements. After reviewing the legislation, the GAO concluded that the liability cap applies to commuter rail operations, which is certainly a good base for commuter service providers to cap their liability insurance to under $200 million per accident. It seems unlikely that such a cap will apply to LRT as well, since LRT is non-FRA compliant.

The level of risk can influence the level of liability. As risk increases, the necessity for liability insurance coverage increases too. Where passengers are involved, risk increases dramatically and liability insurance can become excessively onerous. No freight rail owner is willing to risk the assets of its railroad, but looks for return on investment to find joint operations attractive. Higher risks for passenger operation create a dilemma for transit operators.

Potential Solutions

It is understood that successful experience from overseas cannot be directly transferred to USA because of cultural, regulation, intuition, and physical differences.

However, certain risk mitigation choices can be applied to get USA prepared for future possible commingled operation.

Advanced signal systems, positive train control, or Intelligent Transportation System (ITS) may be applied to improve the efficiency and communication of rail transit. Railway signal systems, in general terms, are made up of block signal system, interlocking systems, and control systems. Block signal systems are designed to inform operators of the need to stop when there is danger of rear end collision. Block lengths are based on the distance it takes the heaviest train to stop. To accommodate disparate operational trains on the same tracks, block signal systems need to be reconstructed to assure the appropriate block length based on the train's speed, braking ability, weight, etc. Automatic cab signaling (ACS), displaying signal aspect information on the operator's control panel, can be used to reduce the possibility of operators missing signals. Further, positive train control systems, including automatic train stop (ATS) and automatic train control (ATC), can take control of the trains if operator does not take appropriate actions upon receiving the signals. The US government requires that for operations above 79 mph, cab signaling or train control systems are installed and used. In addition, all railroad lines carrying passengers must be equipped with an acceptable system of Positive Train Control (PTC) by 2015, as required by the recently enacted Railroad Safety Improvement Act (RSIA, 2008).

Interlocking signals prevent trains from colliding where railroad tracks meet. All interlockings for commingled operations should be designed to ensure that they do not delay trains or cause capacity problems. Centralized traffic control (CTC), commonly used on busy railroads, allows trains to be routed through complex track networks to optimize performance of the overall railroad system. A CTC system allows the dispatcher to safely direct overtaking trains traveling in the same direction and trains meeting in opposite directions. This enables the dispatcher to place a train in a siding or on an additional mainline track, to avoid delay [33].

As described earlier, its punctuality, superb service, and the large crowds of people using it characterize Japanese public transportation. The German rail system is also credited with convenient, on time, superb service. Both systems are the envy of the world. Such success is achieved not only by innovative technologies, but also by good communication, understanding and attitudes among the parties sharing the facilities.

A sophisticated operational plan can be worked out between willing parties. Communication must be established and maintained between the operational managers. Since passenger and freight operations have different operating characteristics, employees from a transit background may not be familiar with freight rail operation and vice versa. Thus, it is important for professionals from both parties to reach a mutual understanding, not only the dispatchers.

Insuring a high standard of employee qualifications and performance is important in commingled operations. Cross training might be helpful to enhance mutual understanding of employees in both operational environments. One of the transit agencies suggested, "Get transit agencies to understand the nature of freight rail business. Get freight railroads to understand the requirements for public funding of transit projects, lengthy time, many steps, public review and comment, etc."

According to a recent TCRP study [3], "Fail-safe" means that any foreseeable failure will result in the system reverting to a safe state. This approach works well for mechanical and electromechanical devices, but has proved very difficult to apply to the programmable processor-based systems that have been coming into use over the past 10–15 years. New safety assurance methods and procedures have been developed for application to safety-critical electronic systems and software and related installation and maintenance activities.

There are a number of train control systems that ensure that trains sharing track do not collide [3]. These systems override the vehicle operator in the event of a signal violation that could result in a collision with another train. A list of various approaches to provide fail-safe train separation in approximate order of their common use is highlighted here but detailed information on each should be referenced in the TCRP Report No. 130 [3] and other engineer publications:

- Automatic Train Stop (ATS)
- Train Protection and Warning System (TPWS)

- Indusi "Punktförmige Zugbeeinflussung" (PZB)
- Automatic Train Control (ATC)
- Communication Based Train Control (CBTC)
- Positive Train Control (PTC)

Three federal agencies, FRA, FTA, and Surface Transportation Board (STB) govern different aspects of railroad operation. FRA focuses on safety; FTA controls funding to transit projects; and STB is responsible for economic regulation of railroads. However, none of these agencies has responsibilities and authority to facilitate transit systems on freight track access issues, leaving transit agencies who desire for a commingled operation in a difficult situation when negotiate with railroad companies. The difficulties create a discouraging effect on the development and expansion of commuter rail and light rail transits. Therefore, an affiliate agency should be established to provide guidance or facilitate the negotiation on track access. The Rail Transit Safety Initiative recently submitted by Secretary LaHood [34] has the potential to empower the safety oversight and facilitate shared-use issues. However, detailed programs and procedures are still under development and their impact on shared use remains to be seen.

FTA and FRA issued Joint Statement to "coordinate the use of respective safety authorities with regard to shared-track operations." However, the waiver program restricts the opportunity to commingled operation since it is a strict and tedious review process. FRA officials are cautious to say "yes" to commingled operation. Though the technologies are sophisticated and plenty experience has been gathered from overseas, no one can guarantee 100% safety and no one can afford the blame of permitting the commingled operation. It is safe to assume that not only concerns over operation safety, but also concerns over public reaction and political impact are important in the FRA decision making.

The objectives of the business model are to establish the core operational requirements essential in order to satisfy oversight agency's concerns for retention of an equivalent level of safety for joint freight/LRT service operations [35]. The business model addresses the spatial, temporal, and institutional changes associated with sharing track by freight and noncompliant passenger vehicles without temporal separation. It will also highlight strategies to deal with incremental risks and liabilities associated with commingled operations.

It is a challenge to develop a business model of commingled operations since there are no domestic cases of "commingled" operations of freight and non-FRA-compliant passenger services, and the number of cases where freight and light transit equipment share tracks on a temporal separation basis is limited. On the other hand, greater opportunities may be created since there are many domestic cases where public passenger transportation and private freight operations share track, and there are many proven international experiences in commingled operations of LRT and freight services [35].

As pointed out by Transportation Research Board [29], the noncompliance, exemption, and buff strength requirement are largely developed based on the American mentality, similar to larger SUVs on the road. That is, if you drive a larger car or heavier train, your damage would be less when an accident happens. On the other hand, the European philosophy relies on accident avoidance, that is, all parties try their best to avoid collision and other accidents altogether. The philosophical difference may serve as a fundamental reason for Karlsruhe, Germany being safely and efficiently operated for years while its American counterpart cannot even pass the pilot stage.

Judging from the current extensive discussion of the shared issues, newly commissioned studies by GAO [32], FRA [2, 19], NJ Transit [1] and TCRP [3], it can be safely predicted that the interest on shared track or commingled operation has been reawakened. Along with the increasingly widespread interest, a pilot program could develop a realistic framework to explore the potential of commingled operations.

Based on the obvious safety concerns, capacity expansion and cost savings are also main factors driving commingled operating practices. Before any commingled operation may be even tested, a thorough cost-benefit analysis coupled with a realistic operation analysis should be conducted. A detailed risk assessment should also be performed and a set of performance measures should be developed to benchmark and mitigate the risks.

Future Directions

Interest in LRT as a viable urban transportation system has been growing worldwide and new LRTs are appearing on urban streets in many countries. Pressed

with a growing demand for extended LRT services, a few LRT agencies seek the possibility of applying overseas experience in USA. After examining existing practices in the USA and overseas, it is hoped that this entry has highlighted that commingled operation has many advantages, including, but not limited to reduced construction costs, increased track usage, and quicker new starts. With strict train scheduling and on-time performance control, the commingled operation proves to be viable overseas. Japan and some European countries, especially Germany pioneered in commingled operation between LRT and freight railroad. However, many issues need to be resolved before the USA can realize similar implementations.

Building on the current knowledge base and momentum on transit demand under the large economic background, it is foreseeable that multiple fronts will be advanced along the lines of technology improvement, regulation changes, and business model development to promote shared use of railroad infrastructure between LRT and freight railroads. A logical next step may be a pilot model to address all these issues in a confined but realistic environment.

Acronyms

ACS	Automatic Cab Signaling
ADA	American with Disabilities Act
APTA	American Public Transportation Association
ATC	Automatic Train Control
ATS	Automatic Train Stop
CBTC	Communication Based Train Control
CFR	Code of Federal Regulation
CN	Canadian National
CTC	Centralized Traffic Control System
DMU	Diesel Multiple Unit
FHWA	Federal Highway Administration
FRA	Federal Railroad Administration
FTA	Federal Transit Administration
GAO	Government Accountability Office or General Accounting Office, prior to 2004
ICE	Intercity Express Train
ITS	Intelligent Transportation System
JNR	Japanese National Railways
JR	Japanese Railways
LRT	Light Rail Transit
LRV	Light Rail Vehicle
MBTA	Massachusetts Bay Transportation Authority
MTA	Maryland Transit Administration
MTDB	Metropolitan Transportation Development Board
NCTD	North County Transit District
NJ TRANSIT	New Jersey Transit
PTC	Positive Train Control System
PZB	Indusi "Punktförmige Zugbeeinflussung" System
ROW	Right-of-Way
RSIA	Railroad Safety Improvement Act
SDTI	San Diego Trolley Inc.
STB	Surface Transportation Board
SWG	Shared-Use Working Group
TCRP	Transit Cooperative Research Program
TPWS	Train Protection and Warning System
TRB	Transportation Research Board
UTA	Utah Transit Authority
VTA	Santa Clara Valley Transportation Authority

Bibliography

Primary Literature

1. Liu RR (2004) Survey of transit/rail freight interaction final report. Submitted to New Jersey Department of Transportation/Federal Highway Administration, submitted by New Jersey Institute of Technology, September 2004
2. Alan B, Nelson D, Stangas P, Liu RR (2006) ITS technologies for integrated rail corridors. Submitted to Federal Railroad Administration (FRA) US Department of Transportation, Washington DC, December 2006
3. Transportation Research Board (2009) Shared use of railroad infrastructure with non-compliant public transit rail vehicles: a practitioner's guide. In Transit cooperative research program report 130, TRB, National Research Council, 2009
4. America Public Transportation Association (APTA) (2010) 10.2 Billion trips taken on US public transportation in 2009, http://www.apta.com/mediacenter/pressreleases/2010/Pages/100308_Ridership_Report.aspx. Accessed in March 2010
5. Transportation Research Record (2001) Supplementing and updating TCRP report 52: joint operation of light rail transit or diesel multiple unit vehicles with railroads. In Research Result Digest, TRB, National Research Council, 2001
6. America Public Transportation Association (APTA) (2009) Public transportation fact book, 60th edn, American Public Transportation Association, April 2009

7. Boorse J, Tennyson E, Schumann J (2000) This is light rail transit. Conference Proceedings of 8th national conferences on light rail transit. Dallas, 2000
8. Grava S (2003) Urban transportation systems. McGraw-Hill, New York
9. Thompson G (2003) Defining an alternative future: birth of the light rail movement in north america, experience, economics, and evaluation from starter lines to growing systems. Proceedings of the 9th national light rail transit conference. Transportation Research Board, Portland, pp 25–36, 2003
10. US Department of Transportation (1996) Transportation expressions, research and special projects administration, Washington DC
11. Schumann J (1977) Historical of railroad and transit joint track use, unpublished paper
12. Vigrass J (1995) Joint use of track by electric railways and railroads: historic view. The proceeding of the 7th joint conference on light rail transit, Vol 1,TRB, National Research Council, Washington DC, pp 154–163, 1995
13. Phraner D, Roberts R, Stangas P, Korach K, Shortreed J, Thompson G (1999) Joint operation of light rail transit or diesel multiple unit vehicles with railroads, TCRP Report 52, TRB, National Research Council, Washington DC, 1999
14. Federal Railroad Administration (2000) Shared use of the tracks of the general railroad system by conventional railroads and light rail transit systems. 2000
15. Schulte CF (2001) General system and rail transit common corridor safety, Rail transit conference, Boston MA, 2001
16. Sheys KM, Spear T (2000) Safety oversight of shared track operations: an update, the Proceeding of the 8th Joint conference on light rail transit, Dallas, Texas, 2000
17. Phraner D (2000a) Light rail sharing track with other rail modes: how far have we come at the millennium? The proceeding of the 8th joint conference on light rail transit, Dallas, Texas, 2000
18. Christner P, Mauri P (2005) Sharing of track by transit and freight railroads access, safety, and insurance issues. Prepared for Walter Kulyk and Venkat Pindiprolu, Federal Transit Administration, US Department of Transportation, John A. Volpe National Transportation Systems Center, United States Department of Transportation, Cambridge MA, 2005
19. Ensco, ICF, KKO, and Mayville (2005) Safety of non-compliant passenger rail equipment, Draft Report, Federal Railroad Administration, Office of Research and Development, 2005
20. Tereschuck P (2005) Draft of implementation strategy. Joint LRT/Freight Operations. Unpublished report
21. Geissenheimer H (1997) New vehicle options for lower-cost rail mobility: using diesel or dual-powered light rail cars as a transfer of technology, Transportation Research Record, No. 1571, Transportation Research Board, Washington DC, pp 125–133
22. Homburger W (1998) Practitioner's forum. J Transp Eng 124(5):402–403
23. Phraner D (2002) German track sharing experience, TCRP Research Result Digest 47. TRB, National Research Council, Washington, DC
24. Phraner D (2000b) German shared track experience independent supplemental technical study tour findings, TCRP Project J06, Task 34. 2000
25. May J (2005) Nordhausen tram trains rule OK, Tramways & Urban transit November 2005
26. Transportation Research Board (2003) Transit capacity and quality of service manual, 2nd edn. In Transit Cooperative Research Program Report 100, TRB, National Research Council, 2003
27. Lightrail Now (2010) Rail transit systems in operation, http://www.lightrailnow.org/. Accessed January 2010
28. Federal Transit Administration (2003) National Transit Database 2003
29. Association of America Railroad (2010) Weekly traffic summary report, http://www.aar.org/NewsAndEvents/WeeklyTrafficReport.aspx. Accessed in January 2010
30. Transportation Research Board (1999) Joint operation of light rail transit or diesel multiple unit vehicles with railroads. In Transit Cooperative Research Program Report 52, TRB, National Research Council, 1999
31. Iwasa K (2001) Rail freight in Japan – the situation today and challenges for tomorrow. Jpn Railway Transport Rev 26:8–17
32. General Accounting Office (2004) Information and guidance could help facilitate commuter and freight rail access negotiations. GAO-04-240, 2004
33. Nash A (2003) Best practices in shared-use high-speed rail systems. Mineta Transportation Institute, College of Business, San Jose State University, 2003
34. Federal Transit Administration (2010) Rail transit safety initiative, http://fta.dot.gov/11039_11052.htm. Access in January 2010
35. Liu RR, Nelson DO, Lu A (2009) Business model for shared operations of freight and passenger services (09-2547). J Transport Res Board (TRB) 2547:86–92, Transportation Research Record (TRR), Washington DC

Books and Reviews

California Public Utilities Commission (1991) General order 143-B, Safety rules and regulations governing light-rail transit, San Francisco, CA, 1991 as amended

Choueiry E, Bullock D (2002) Light rail DMU on shared right of way. Proceedings of commuter rail/rail transit conference, June 9–13, 2002

Liu RR, Yang F, Chen M (2005) Understanding the shared operation of commuter rail transit and freight railroads. J Transport Res Forum 44(1):157–172

Liu RR, Yang F, Bing A (2007) State of the practice on commingled operation of light rail transit and freight rail services. Proceedings of the 86th Annual Conference of Transportation Research Board. January 2007. Peer Reviewed

Liu RR, Yang F (2006) A national survey of shared use of railroad infrastructure and LRT service. Proceedings of the 85th annual

conference of Transportation Research Board. January 2006. Peer Reviewed

Sela E, Randolph R, Hickey T (2003) Shared use corridors: survey of current practice and recommendations for the future. Proceedings of Transportation Research Board 9th national light rail transit conference, November 16–18, 2003

Light Rail Transit, Systemic Viability

Gregory L. Thompson, Jeffrey R. Brown
Department of Urban and Regional Planning, Florida State University, Tallahassee, FL, USA

Article Outline

Glossary
Definition of the Subject
Introduction
Historical Background
Conclusions
Future Directions
Abbreviations
Bibliography

Glossary

Average speed The speed that results by dividing the round trip time of a transit vehicle to traverse a transit route from beginning to end and back to the beginning, including the layover time until the beginning of the next trip, by the roundtrip length of the route. Average speed also may be calculated by dividing annual vehicle miles for a route by annual vehicle hours for the route. Average speed is slower than scheduled speed because average speed includes layover time at each end of the route.

Bus rapid transit An application of buses in a way that emulates rail transit. Bus rapid transit usually provides for a reserved right-of-way for buses that includes wayside stations. Fare collection systems allow passengers to board and alight buses at all doors. Drivers are not involved in fare collection. Buses usually are articulated and contain several wide doors, all of which open when buses stop at online stations. Rights-of-way are usually Type A or B, and scheduled speeds of 20–25 mph are possible.

CBD Central business district. The CBD typically is the largest business center in a metropolitan area and often dates from the streetcar era. At one time, CBDs contained almost all jobs, shops, and recreation in metropolitan areas, but since World War I when autos became the principal form of urban transportation, CBDs have been in relative decline as most job, shopping, and recreation growth has occurred in the suburbs.

Commuter rail A form of rail transit in which transit vehicles use the same tracks (or have the capability of doing so) as do long distance freight and passenger trains. Commuter trains usually are comprised of several large cars containing closely spaced seats and two or three wide doors on each side of the car to allow rapid boarding and alighting of passengers. Commuter trains can be electrically or diesel powered and may be either pulled by locomotives, or have each car equipped with electric motors or diesel engines under the floor. Conductors typically collect fares from passengers while the trains are in motion.

Edge city One of several terms used to describe large urban centers in metropolitan areas that rival central business districts in magnitude and diversity of employment. Edge cities typically cover a much larger area than CBDs, however, with much of the land devoted to parking lots and high-speed, multilane roads. It typically is difficult or impossible to walk from one part of an edge city to another part.

Express bus A form of bus transit in which buses run nonstop over much of their routes. The most typical application is for express buses to run during weekday rush hours between outlying affluent suburbs and the metropolitan CBD. In the morning express, buses typically circulate through neighborhoods in which affluent commuters live, and when they fill up the buses travel nonstop on a reserved freeway lane or sometimes on a specially built busway to the edge of the metropolitan CBD. The express buses may use purpose-built ramps to gain access to or to leave their freeway lanes. Express buses then circulate through the CBD on city streets to distribute their passengers. In the afternoon peak period, express buses retrace their path to the suburbs. Most express bus routes offer a handful of

one-way inbound trips in the morning and one-way outbound trips in the afternoon. Passengers pay their fares to the driver.

Grid route structure A multidestination transit routing method, in which each north–south and east–west arterial road in a metropolitan area has its own bus, streetcar, light rail, or heavy rail route, typically providing frequent service. To travel from one part of a metropolitan area to another, passengers typically walk to a nearby bus or streetcar line, travel to a connecting route, and alight near their final destination. Grid route structures afford passengers the ability to travel from any place to any other place in a metropolitan area without out-of-direction travel, but grid route structures require most passengers to transfer. Grid route structures typically attract much higher passenger volumes than radial transit route structures and are more productive, as well.

Heavy rail The word "heavy" refers to heavy infrastructure that is associated with subway and elevated rapid transit lines. Heavy rail lines are exclusively Type A rights-of-way achieved by directing the paths (or grades) of rail transit lines above or below paths (or grades) of conflicting transportation. Thus, heavy rail is also called, "grade-separated" transit. Typically, heavy rail is operated by trains of up to ten electrically powered cars, each car having two or three wide doors on each side. Stations are designed to be as long as the longest trains, an expensive proposition when, as is typically the case, the entire station is buried far below the surface or erected far above ground. Passengers pay fares at turnstiles or elaborate and expensive fare collection machines before boarding trains.

Interurban A nearly extinct form of US rail transit in which lightly built electric rail lines connected more densely populated rural areas with nearby towns or cities. Lines typically were 15–40 miles long, but both shorter and longer lines were built. The longest through interurban run was from Detroit to Cincinnati, a distance of over 300 miles. Typically, interurbans entered city centers over the tracks of local streetcar companies, but they operated through the countryside either alongside state highways or across county on their own rights-of-way. Interurban cars stopped frequently and offered scheduled speeds typically of about 20 mph. Interurban cars were the size of smaller mainline railroad coaches but typically each car was electrically powered, using streetcar technology. Interurbans usually operated as one-car trains but could operate in multicar trains controlled by a motorman in the lead car, much as rapid transit trains. Interurban lines appeared in the USA during the decade before the automobile appeared and spread rapidly. They declined just as rapidly after World War I and with a few exceptions disappeared before the USA entered World War II.

Light rail "Light" refers to light infrastructure and not to the weight of the rail or of the cars. Light rail evolved from streetcars in northern European cities in the three decades following World War II and is characterized by short trains of high-capacity rail cars operating though metropolitan areas on mostly Type B rights-of-way. Each train has multiple wide doors, and light rail systems employ fare collection systems that obviate the need for employees to be on trains to collect fares. Passengers board and alight at all doors. Light rail lines are intended to function like heavy rail lines but at a much lower capital cost. In the USA, they are most effective where they are configured as long routes up to 30 miles long, along which are situated major destinations. Scheduled speeds typically are in the range of 19–30 mph in contrast to typical local bus speeds of 10–15 mph. Bus routes are reconfigured from CBD-radial service to light rail stations at major destinations in the suburbs, thereby creating multidestination transit systems with improved productivity. Metropolitan transit networks having such characteristics are among the most successful in the USA and Canada.

Mode A type of transportation technology, such as the walk mode, the auto mode, the bus transit mode, or the rail transit mode.

Multidestination transit route networks A transit network so structured that users can reach many destinations in a metropolitan area while avoiding out-of-direction travel. Doing so usually requires a transfer, however. A grid network is one type of multidestination network, but not the only type. Multidestination transit systems stand in

contrast to radial transit systems, where most transit routes radiate outward from the one destination that is deemed the most important to serve, usually the CBD.

PCC Streetcar A streetcar developed by the Presidents' Conference Committee (a committee of the presidents of US and Canadian streetcar companies) between the late 1920s and mid-1930s. The objective of the development was to create a quiet and smoothly riding streetcar that could accelerate and decelerate as rapidly as autos in stop-and-go traffic while not jerking standing passengers off their feet. The PCC car, particularly its control system, is considered one of the marvels of North American industrial engineering, but a streetcar that was like a bus on rails competing with the auto in its own environment was not what was needed to save the transit industry.

Proof-of-payment (POP) Fare Collection System Passengers are required to determine what their fare for a particular trip should be and to then purchase a ticket for that trip before they board the vehicle. They may board any door. Nobody on board monitors fares while passengers board, but roving inspectors may ask for proof of payment at any time. Passengers without valid proof are warned or fined. Managers typically employ a sufficient number of inspectors to inspect 1% or 2% of passengers. The percentage of passengers without valid proof of payment is the fraud rate, which is generally lower than that of driver-administered fare systems. Its chief advantage is allowing passengers to board at all doors, important for high-capacity lines but not important for low patronage bus lines. Most passengers using such systems buy monthly, weekly, or daily passes. Passengers buying 90 min passes may do so at simple vending machines on train platforms.

Radial transit route systems Most transit routes radiate outward from the one destination that is deemed the most important to serve, usually the CBD. Passengers are given a one-seat ride from their homes to the CBD. Underlying a radial route structure is the belief that passengers will not transfer. Radial route systems stand in contrast to multidestination route networks (of which the grid network is an example). Most radial transit systems in the USA are characterized by falling demand and productivity. They typically have higher operating costs per passenger mile than multidestination networks.

Rapid transit The traditional name for what now is known as heavy rail.

Scheduled speed The speed that results by dividing the length of a route by the time that it takes for a transit vehicle to travel from the beginning to the end of the route. Scheduled speed is much slower than the top speed at which transit vehicles operate, because scheduled speed includes time spent at stops, acceleration and deceleration time (which is what transit vehicles are doing much of the time – hence the design objective of the PCC car), and it includes time lost in traffic congestion. Scheduled speed is faster, however, than average speed, because the later includes the layover time at each end of the route.

Streetcar An electrically powered rail transit vehicle, in North America traditionally about 40 ft long and 8 ft wide. Streetcars historically ran on tracks imbedded in the middle of streets, and they competed for street space with vehicular traffic. Thus, they ran on right-of-way type C. Passengers board and alight from streetcars in the centers of streets, sometimes on raised concrete islands. In North America, streetcars typically operated with two-person crews, a motorman to drive the car and a conductor to collect fares while the car was in motion. PCC cars, which appeared in the mid-1930s, were operated with foot pedals that left the driver's hands free to collect fares, enabling one-person operation.

Traction Until the 1920s, streetcar and interurban companies were known as traction companies. One still hears the term, "electric traction."

Transit-oriented development, or TOD A type of development advocated by many planners but not often seen that is comprised of dense, clusters of various types of housing units, retail stores, restaurants, bars, and offices clustered within a quarter of a mile of a transit stop, preferably a rail station. TODs also are characterized by pleasant pedestrian paths linking all of their parts with each other and with the transit station. Studies of the behavior of residents of and visitors

to TODs indicate that most use automobiles but that a significant minority do in fact use transit. TODs built to date usually have large parking structures as well as transit access.

Transit The generic name used today in the United States for fixed-route, scheduled public transportation services, whether they are bus or rail. One may speak of transit agencies, rail transit, bus transit, or just transit.

Trolley bus A bus powered by electricity delivered to the vehicle by overhead wires. Upward-sprung dual trolley poles (one for positive current and the other for negative current) connect with dual parallel overhead wires strung above the street. Trolley buses may travel in the traffic lane under the wires, or they may travel in lanes on either side of the lane under the wire.

Vehicle miles traveled (VMT) An automobile or light truck traveling 1 mile. VMT is the standard unit for measuring the magnitude of auto use in a metropolitan area.

Verkehrsverbund or federation of transit operators A form of transit organization used in several German metropolitan areas. The Verkehrsverbund is characterized by separation of ownership of transit services in the metropolitan region among many different transit operating companies or agencies, and coordination between all of the transit services in the region through a small, centralized public marketing and planning body. Passengers may navigate transit routes throughout the metropolitan area without being aware of boundaries between different transit operating agencies. The idea behind this form of organization is that smaller operators may control their timeliness as well as their operating costs far better than large operating companies, while a central coordinating body insures coordination among all operators through scheduling, fares, and provision of information. The San Diego MTDB created and ran this form of organization from about 1979 to 2003 and experienced better coordination between its various transit services and lower costs per passenger mile than any of the large public transit districts in the USA. It also experienced among the highest rates of passenger growth during this period.

Definition of the Subject

Light Rail Transit

Light rail transit is one of several forms of rail public transportation designed to transport passengers within metropolitan areas, but there is no agreement on its precise definition. The Transportation Research Board of the National Academy of Sciences [1] and the American Public Transportation Association [2] define light rail to include streetcars and tramways. Both organizations also define light rail to include modern metropolitan rail systems characterized by multicar trains operating on tracks that are segregated from motor vehicle traffic except at cross streets. Vuchic [3] defines light rail with respect to the nature of metropolitan rail right-of-way that it uses. He categorizes metropolitan rail rights-of-way according to three types. Type A denotes grade-separated rail rights-of-way that have no conflicts with motor vehicle, other rail, or bicycle and pedestrian traffic. Type A rail rights-of-way characterize subway and elevated rail rapid transit lines in the world's cities. Type B denotes rail rights-of-way where rail vehicles are segregated longitudinally from motor vehicle traffic, bicycles, and pedestrians but have conflicting traffic crossing tracks at cross streets. Type C denotes rights-of-way where the tracks are imbedded in streets shared by motor vehicle and/or pedestrian traffic, and rail vehicles have no preference over other vehicles with which they compete for road space. Traditional streetcars and trams, characterized by the operation of single rail cars in mixed traffic with drivers collecting fares, are associated with right-of-way Type C. Vuchic associates light rail transit primarily with right-of-way type B, upon which short multicar trains operate with fare systems allowing passengers to board at all doors [4]. Vuchic's definition gives light rail much higher level of service, measured in average speeds and passenger-carrying capacity than streetcars and trams (typical scheduled speeds of 10–14 mph), but lower speeds and passenger-carrying capacity compared to subway and elevated rail rapid transit lines (scheduled speeds of 20–45 mph), whose long trains use Type A rights-of-way. According to Vuchic's definition, the cost of constructing light rail often falls between the high cost of constructing subways and elevated lines and the much lower cost of constructing streetcar lines.

Vuchic's definition for light rail is closely aligned with the historical rise of light rail transit in the 1950s, 1960s, and 1970s as a reform mode of metropolitan transportation that addressed shortcomings of traditional streetcars and trams as they succumbed to local bus replacements in city after city throughout the world [5, 6]. Political leaders in many cities wanted a form of urban public transportation that provided faster, higher capacity, and more productive service than traditional streetcars or local buses but that cost less than subways or elevated railways that only the largest cities could afford. Light rail, and more recently bus rapid transit, evolved to fill unmet demand in many medium-sized metropolitan areas for a transit mode offering intermediate capacity.

This entry follows Vuchic's definition for light rail. It defines light rail as the operation of short trains operated with only one person. The trains have many large doors, any of which passengers may board at stops. Drivers are not involved in fare collection. Light rail trains operate primarily on right-of-way Type B, though they have the flexibility to operate over rights-of-way Types A and C. Some segments of a light rail system may exhibit all of the features of a completely grade-separated metro line, while other segments have lower-speed, at-grade operation. Selective investment based on need in specific areas is a key characteristic. What is "light" about light rail is the overall average level of capital investment per unit length of a route; the term does not pertain in any way to physical weight.

Generally, light rail trains operate at faster scheduled speeds (18–30 mph) than either streetcars or local buses and provide higher passenger carrying capacity, as well. Light rail systems also carry more passengers per employee than buses or streetcars.

The intent of light rail construction is to attract more passengers to transit by providing a quality of transit service that approaches what metropolitan subway or elevated rail rapid transit lines could achieve in particular corridors but at a much lower overall capital cost. In some metropolitan areas, the intent of investing in light rail also is to improve the productivity of the transit system by replacing numerous duplicative bus routes running to the central business districts of cities with one or two light rail lines to which passengers transfer at outlying stations. In such cases, transit operators restructure shorter bus routes to suburban light rail transit stations: because buses meet trains at the same time, they also connect with each other, and therefore also make intra-suburban transit usage more feasible. The intent is that fewer bus and train car miles will be more aligned with dispersed travel demands in today's decentralized metropolitan regions, thus attracting more passengers, resulting in more passengers per employee and lower operating cost per passenger. In recent years, some political leaders also have intended light rail investments to attract new urban development to the vicinity of light rail stations.

Viability

To measure viability of light rail transit is to measure how well light rail investments achieve their objectives. Following on Fielding's treatment of transit performance measurement [7], this entry evaluates how light rail investments change overall transit performance in the metropolitan areas where the light rail investments are made compared to similar metropolitan areas where light rail investments are not made. In general, the entry examines trends in metropolitan transit ridership per capita before and after light rail as a measure of light rail's effect on transit ridership in the region. It examines trends in ridership per transit vehicle mile over the entire region as a measure of productivity. It examines regional transit operating expense per passenger or passenger mile as a measure of efficiency. Where results of onboard passenger surveys of passenger characteristics are available, this entry also reports those. The entry also examines how light rail has affected development in the areas that it serves by referencing academic studies on that topic.

Introduction

Light rail transit evolved from streetcars in northern European cities during the 1950s and 1960s. It was what resulted as transit operators incrementally modified their traditional streetcar systems to survive mass motorization and rapidly rising wages. Light rail was characterized by one driver (with the assistance of no other labor) operating a short train comprised of large articulated streetcars with numerous wide doors, fare collection systems allowing passenger to enter and leave all doors, and segregation of trains from

automobile traffic. Light rail was much more productive than buses and proved to be a more successful adaption of streetcars than the earlier American approach to saving streetcars from auto and bus competition. The American approach was based on developing a single unit streetcar about the size of a bus whose performance mimicked that of automobiles, with which streetcars competed for street space. Plagued by congestion from passengers forced to board front doors to pay their fares to the driver, as well as by auto congestion, the American approach resulted in at best marginal productivity superiority over buses. It failed to save streetcars in most US and Canadian cities.

The European light rail idea, carried on the wings of Canadian and US urban advocates and transit reformers, was first adopted in a North American city in 1978 when Edmonton opened a light rail line and restructured buses around its stations, 27 years after it converted its last streetcar line to bus operation. Edmonton's sister city, Calgary, opened its first light rail line in 1981. The US transit industry resisted the light rail idea, but reformers forced transit systems to adopt light rail, first in San Diego in 1981, followed by Portland, San Jose, and Sacramento in 1986–1987. The US Urban Mass Transit Administration (UMTA) sponsored the opening of a demonstration light rail line in Buffalo in 1984 with the full cooperation of the transit system in that city. The next line opened in Los Angeles in 1990, and 12 additional metropolitan areas added light rail lines since then. Many of the metropolitan areas that opened initial light rail lines since have expanded their systems. Some of the North American streetcar lines that survived into the 1970s also have been rebuilt with some light rail characteristics.

Light rail advocates hoped that light rail investments would reverse the fortunes of declining North American transit systems. Some hoped that the investments would do the same for declining downtowns and inner city neighborhoods. Some actually hoped that light rail combined with renewal of urban centers could displace autos as the main form of urban transportation. Actual results have been mixed. Some light rail investments, such as in San Diego, Portland, and St. Louis, have had highly positive impacts on the performance of transit in their metropolitan areas. Others have had little positive impact. Some have been accompanied by greater population densities and more walkable environments. None, however, has reduced significantly the dominance of automobiles as the primary mode of urban transport.

The purpose of this entry is to explain why results are mixed, and in particular to understand what light rail innovations are most effective for better transit system performance. It does this by first explaining how streetcars arose and affected the growth of North American cities before World War I. It then examines reasons for streetcar decline, efforts to stem the decline, and reasons why those efforts failed. It then explains how light rail arose as a fix for streetcar defects, how and why light rail was adopted in various North American cities. The analysis of light rail performance in various US metropolitan regions precedes the entry's conclusions.

Historical Background

Light rail is not synonymous with streetcar (or tramway in English parlance); it is more accurate to see light rail as a mode that evolved as a reaction to shortcomings of streetcar technology and applications. This section makes that evolution understandable. It provides a history of the North American streetcar beginning with a depiction of its technology and how it influenced the form of American cities before World War I. It then considers the streetcar's increasingly apparent shortcomings as auto use intensified, urban form changed, and city bus technology improved. The history considers the American and Canadian transit industry's attempt to modernize the streetcar with new technology in the 1930s (the famous PCC car), and it considers reasons for the failure of that effort, including the American auto industry's involvement in liquidation of American streetcar systems. Finally, it considers the appearance in the postwar period in western Germany of a different, more successful approach to modifying streetcar technology that is known as light rail.

The American Streetcar at the Peak of Its Influence and How It Shaped the City

From 1888 when Frank Sprague implemented the world's first successful streetcar system in Richmond, Virginia through the 1920s, the electric streetcar

symbolized the American transit industry. In cities throughout the country the press followed the expansion and financial scandals of the traction industry, "traction" being the term that the public then used for streetcars. Land owners on the fringes of cities clamored to have traction lines extended to their lots, thereby making the lots much more valuable. In as little as 30 min and for a nickel fare (a fare the middle class could afford), streetcars operating at average speeds of 12 mph could connect lots in the countryside with jobs and opportunity in the center. Such relationships stimulated a huge demand for suburban living, and to meet it, traction lines, sometimes owned by real estate interests, expanded outward in all directions. Population followed. For the first time in their histories, the horribly overcrowded cities of America began to empty outward in the form of new streetcar suburbs, built on previously empty land around the city edges. The center cities from which the middle and working classes fled changed as well, as department stores, specialized shops, corporate offices, financial firms, hotels, theaters, concert halls, and other less reputable types of entertainment rushed in to fill the voids left by the departing middle and working classes [8, 9].

By the 1910s, the streetcar created a new American city characterized by specialized sections. Iconic was the fashionable Central Business District, a vibrant area with specialized subdistricts wherein were located almost all jobs and activities that the middle class wished to reach. Poorer groups remained in cheaper, older housing surrounding the new center cities. Factories and warehouses also remained packed around railroad yards. Further out, extending along the electric car lines, were the new streetcar suburbs. These were middle and working class bedroom districts, each a new homogenous enclave catering to a specialized income and ethnic group. Every day the middle and working class populations surged into the center on electric cars and surged outward in the evenings. Wives and children filled the cars during the middle of the days, and in the evenings and Sundays families used the cars for recreation. For the middle and working classes, the streetcar revolutionized the American city and the way in which they experienced it [8–10].

The streetcar evolved to efficiently fulfill the mass transit role called for it. By the 1910s, the modern streetcar was about 40 ft long and 8 ft wide, riding on two four-wheel trucks. Each axle was driven by its own electric motor that was suspended from the axle. Air pressure controlled the braking power. Cars typically had top speeds of about 30 mph. A cabin (saloon) in which passengers rode constituted about two-thirds of the length of the vehicle. On cars operating in clement climates, cabins often were divided into a weather-protected section and an open-air part. The rest of the length typically was comprised of large platforms projecting from both the front and rear of the car. The platforms, which were lower to the ground than the center sections, contained large doors and vestibules from which passengers could board and alight. The driver, called a motorman, stood at the controls on the front platform, and the conductor, who collected fares, stood on the rear platform. The conductor communicated with the motorman with bells that he (rarely she in 1910) could activate by an overhead cord. Terms like, "platform employees," or, "platform hours," still are used by some transit systems today to denote transit operating personnel (usually bus drivers) and the hours that they work serving the riding public [8]. Figure 1 shows a state-of-the-art streetcar from this period.

In operation, the streetcar was a crowd-eater. Coasting into a stop thronged with waiting passengers, the streetcar's gaping rear door beckoned the crowd to board. As the last passenger cleared the steps, the conductor gave two quick yanks on the bell cord to the motorman, who replied with two loud clangs on the car's traffic-warning brass gong affixed to the front. The car lurched forward, and the conductor then collected fares as the car swayed and trundled along to its next stop, often interrupted by traffic congestion and furious bursts of clangs from the motorman's gong. As passengers paid their fares, they proceeded forward into the cabin to find a seat. Those not finding a seat stood in the aisle holding onto leather straps hung from the ceiling, or they stood on the front platform, from which they ultimately alighted. Cars from this period were not fast, but despite the huge crowds they ingested and disgorged, they did not lose time at passenger stops, because large numbers of passengers could board quickly – and fare collection occurred while the car was under way. They truly were mass transit vehicles [8].

Light Rail Transit, Systemic Viability. Figure 1
Traditional American streetcar. San Francisco Municipal Railway Car No. 1, dating from 1912, in a neighborhood it helped to create. Author's photo, taken in 1981

The Decline of the American Streetcar Beginning During World War I

Several factors began the streetcar's long decline around World War I. Most immediately, the cost of labor and supplies more than doubled during the war, while streetcar companies often found it politically difficult to raise the fare above the accustomed nickel, sometimes written into corporate charters in the 1890s. Profits turned to losses, and investment in tracks and streetcars dwindled commensurately. Companies by and large stopped extending lines to undeveloped areas demanded by developers, and service became less frequent and more overcrowded [11].

Beginning about 1910, automobile registrations also climbed rapidly. Auto ownership initially rose fastest in rural areas, but by World War I automobiles were widely distributed in cities, as well. House builders began shifting their products from clients using streetcars to clients using autos. In cities throughout the country, developers by World War I were offering homes in areas not served by streetcars, though they still were using their political muscle to attempt to force streetcar companies to extend lines into new territory. By 1925, however, housing developers no longer cared whether streetcar companies extended lines into new territory. Streetcars had become irrelevant to them [11].

At the same time, motor trucks cut the tether between retailing and railroad yards and led to the extraordinarily rapid decentralization of retailing. Horse-drawn wagons were slow and expensive, and in the pre-truck era, retailers could not afford to locate their stores beyond a short wagon haul away from the giant merchandise warehouses adjacent to the rail yards. Almost all retailing was in the CBD. With the adoption of trucks, however, retailers of all stripes decentralized. The driving force was demand for free parking from the increasingly large number of customers who came downtown to shop in their autos. Retailers quickly learned that the cheapest solution to the parking problem was building major branch stores, which could be easily supplied by truck from the central city warehouses. By 1925, many established CBD-located firms were opening new stores in the suburbs that were grander and more posh than their original CBD flagship stores. The new stores all were built around auto access and free parking. The highly centralized, streetcar-oriented retailing regime

characteristic of the American city in 1910 had given way by 1925 to a decentralized regime characterized by rampant suburban strip retailing and free parking. Already planners were talking about the decline of the CBD [10, 12].

The combined weight of these forces pushed down streetcar patronage during the 1920s in all but the largest cities, and even there streetcar riders became increasingly dominated by those going to and from work. The smaller the city, the more rapid was the loss of streetcar traffic [11]. Streetcar companies began abandoning lightly used streetcar lines and replacing other lightly used lines with buses.

Revolution in Streetcar Technology: The PCC

Most traction industry leaders thought that streetcars would continue serving the more heavily traveled lines, however, and toward the end of the 1920s, they formed the Presidents' Conference Committee to develop a super streetcar to reequip the "trunk" lines. The committee was comprised of presidents of various streetcar companies and had at its disposal the best electrical engineering talent from the larger operating companies as well as from the streetcar manufacturing companies. The result was the Presidents' Conference Committee car, or PCC car, which was unveiled in 1936, and which is considered today to be one of the marvels of American industrial engineering. Figure 2 shows a train of two PCC cars coupled together in Toronto. More than 5,000 PCC cars were built between then and 1952 for US and Canadian application, and even more were built for foreign use. Despite the car's success as a piece of industrial engineering, however, it failed to save the North American streetcar industry [8, 13].

In the PCC car, the traction industry sought and obtained a streetcar that could keep up with autos in stop and go traffic. The PCC with a full standing load of passengers could accelerate smoothly and silently from a stop as fast as an auto, and it did so without jerking, an important consideration given that many of the

Light Rail Transit, Systemic Viability. Figure 2
Two PCCs coupled together into a train in Toronto in 1974. There is a driver in the second car, as well, to collect fares and transfers from boarding passengers, who are allowed to board only at the front doors of each car. Note passengers queuing at front doors of both cars to pay fares. Also note sign on signal pole prohibiting motorists from turning, so as not to impeded streetcars. Finally, note the illuminated white sign just to right of the streetcar, indicating a subway entrance. This spot was (and remains today) an important transfer point between the north–south Yonge subway and east–west Queen streetcar in Toronto's gridded route network. Author's photo

streetcar passengers were standees. It also could brake to a smooth stop just as rapidly. Although its initial rate of acceleration of about 3.5 mph per second fell off rapidly as it gained speed, the PCC could reach about 45 mph on level ground, if given enough time. The PCC also was quiet. It rode on trucks with rubber inserts to reduce noise. Rubber pads even separated the steel wheel treads from the centers. The car was streamlined, as well, and looked as modern as the latest autos. Finally, the motorman could operate the car entirely with foot pedals, leaving his or her hands free to act as a fare cashier. The industry intended to operate the PCC with a crew of one. Passengers would enter one half of a double width front door, filing past the driver to pay fares. They could exit from the other half of the front door or from a double width center or rear door [8, 13].

Improved Transit Bus Technology and Its Replacement of Streetcars

Contributing to blunting the PCC's promise for saving American streetcars were major improvements to bus technology. At the end of the 1920s, bus manufacturers adopted monocoque construction that integrated body and chassis construction into a high-capacity, strong, and lightweight vehicle. Monocoque buses could carry large passenger loads reliably and in comfort by the end of the 1920s. In 1930, such buses began operating every 3 min through the new road tunnel connecting Detroit and Windsor, demonstrating that buses could accommodate mass passenger movements. By 1940, the Yellow Coach Division of General Motors had married the monocoque bus with a lightweight, two-stroke diesel engine connected to the rear wheels via a hydraulic transmission. The result was a transit vehicle that, according to technological historian Robert Post could perform almost as well as the PCC car at comparable operating cost without the need for tracks or electrical overhead wires [8]. The bus had another major advantage, as well. It did not get trapped behind queues of left-turning autos and trucks at busy intersections, increasingly the bane of streetcar operations.

The transit diesel hydraulic bus did have several major disadvantages. Post cites choking diesel exhaust as one. A second was the roar of accelerating diesel engines [8]. Both exhaust and noise were particularly objectionable on more heavily patronized lines with frequent service, and they were severe nuisances in areas of heavy pedestrian activity and confined spaces, such as found in some downtowns. Although diesel buses are far less polluting and much less noisy today, pollution and noise emanating from them remain issues and have led to the reduction of their use through downtowns in Denver and Minneapolis and perhaps other cities [14]. Hilly terrain also intensifies noise and pollution problems and slows heavily loaded diesel buses to a crawl. Another problem was the fact that bus drivers had to use their hands on the steering wheel and thus could not complete dealing with passengers paying fares as the vehicle accelerated, as they often did on PCC streetcars. Diesel buses also had narrow doors, slowing boarding and alighting of heavy passenger volumes.

By the mid-1930s, there was another bus technology that performed about as well as PCC-equipped streetcar lines but avoided air and noise pollution of diesel buses. This was the electric trolley bus. Like the PCC, trolley buses could accelerate rapidly with full passenger loads, but unlike diesel buses trolley buses could zoom quietly up and down steep hills with full passenger loads. Trolley buses took their power from dual overhead wires and could maneuver into lanes right or left of the traffic lane over which the dual wires were strung. Trolley buses did not require tracks, thus saving a large investment, and while they did require overhead electrical wires, they could use most of the same electrical investment that already was in place for streetcars [8].

With the availability of these two bus technologies, the transit industry in America and Canada began the full-scale replacement of streetcars on the eve of World War II [8]. Most American transit systems still were privately operated and, ignoring pollution issues replaced streetcars mostly with diesel buses. There were exceptions, particularly San Francisco and Seattle. These two cities had hilly terrain and municipally operated transit and electric power systems and replaced most streetcars (all in the case of Seattle) with trolley bus systems. Canadian transit systems, most of which were municipally rather than privately operated, were more likely to turn to trolley buses. Most transit systems that installed trolley buses later replaced trolley buses with diesel buses, however. Today, only two cities

in Canada and the USA continue to operate large trolley bus systems: Vancouver, B.C. and San Francisco. Smaller systems remain in Seattle, Dayton, Philadelphia, and Boston.

By the end of the 1960s, vestigial streetcar services remained in only a handful of US cities, and streetcar patronage all but disappeared (Fig. 3). Most of the remaining street car services were operated with PCCs, and most had elements of right-of-way Types B or A, giving the streetcars a speed advantage over buses. Toronto remained the sole city in Canada and the USA that continued to operate a large and heavily patronized streetcar systems mostly with right-of-way Type C. The director of planning for the Toronto Transit Commission during the early 1970s, Robert Topp at that time told one of the authors of this entry that the TTC retained streetcars on heavily patronized routes because in that environment PCCs cost less to operate and provided faster service than buses. Philadelphia also had several streetcar lines still running almost entirely in mixed traffic, but the transit system there converted those to bus operation during the 1980s and 1990s. San Francisco operated one streetcar line primarily in mixed traffic.

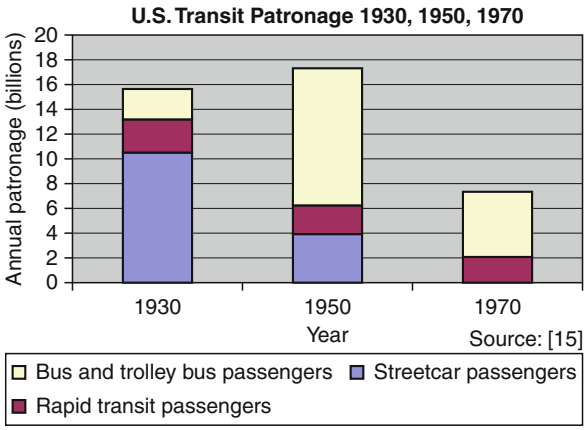

Light Rail Transit, Systemic Viability. Figure 3
Between 1930 and 1970 streetcar passengers almost disappeared. Local bus passengers declined dramatically between 1950 and 1970. Only rapid transit passengers (Type A right-of-way) maintained itself against the onslaught of the automobile [15]

The General Motors Conspiracy Explanation for Streetcar Decline

Whether streetcar loss was inevitable is hotly debated. This history shows that the traction industry ceased influencing the growth pattern of US cities between roughly 1915 and 1925 as the auto became the primary mode of urban transportation. The traction industry became unprofitable during this period, and it began losing passengers at an increasing rate as the 1920s progressed. As a consequence, the industry had difficulty financing track and car renewal. The Great Depression accelerated patronage and financing difficulties. Congress further compounded the financing crisis during the mid-1930s by requiring those private electric utility companies that owned transit systems to divest themselves of the transit systems, thus ending a source of cross-subsidy from utility customers to transit users. This action deprived the transit industry of yet another source of capital for renewing itself. All of these developments, in the context of improved bus designs, are enough to explain the near disappearance of streetcars in Canada and the USA by 1970.

Despite the weight of such evidence, popular American culture views the elimination of streetcars as the result of a conspiracy. The role of General Motors in particular in financing conversions of transit services from streetcars to diesel buses formed the basis of Bradford Snell's widely cited 1974 brief [16] arguing that GM orchestrated the decline of rail transit in America to increase the size of a stagnant auto market. Snell was a staff member of the Senate Judiciary Committee. Research by some academics support the Snell thesis [17, 18], and it has entered the popular culture in outlets such as a popular Spielberg movie *Who Framed Roger Rabbit* (1988) and a widely aired Public Broadcasting System documentary *Taken for a Ride* (1996). Informed rebuttals to the Snell thesis, such as Adler's [19] analysis showing that politics between suburban and downtown real estate interests had a lot to do with transit technology decisions, Bianco's critique [20], Post's [8] and Black's [21] analyses have done little to dispel the GM conspiracy theory of streetcar elimination.

It is a fact that General Motors and other automotive interests financed a holding company in the 1930s, called National City Lines, to purchase transit

operating companies around the country. The purpose was to scrap streetcar systems and replace them with buses built by the General Motors subsidiary, Yellow Coach. From then into the 1950s National City Lines purchased streetcar and bus transit systems, and it continued to operate many of its holdings into the 1960s. NCL eliminated streetcar and electric trolley bus service on most but not all of the systems that it purchased. It also outfitted its systems with new Yellow Coach buses [8, 21]. National City Lines pared management of the companies that it took over to the bone but provided staff management services for its operating properties. It also provided financing for new buses and garages, as well. During this period, independent transit companies, because of their unprofitability, had great difficulty financing new streetcar purchases and track and electrical system renewals. National City Lines supporters point to these facts and state that NCL injected desperately needed capital into the transit industry, improved the efficiency of its management, and kept it going in private hands for another couple of decades [15].

In this debate, the authors' side with Post [8] and Black [21] who view, National City Lines as a symptom rather than a cause of streetcar decline. Many private streetcar companies in the USA were not taken over by National City Lines, but they replaced their streetcars with buses despite that fact. In some US cities, such as Los Angeles and Pittsburgh, public agencies took over private rail transit lines (including some from National City Lines) and scrapped their newly acquired rail systems in favor of new buses. It also is true that most Canadian transit systems were municipally owned, but save for Toronto, all converted from streetcar to bus or electric trolley bus. Most cities in France and England eliminated streetcars just before and after World War II, and most cities in Spain did so in the 1950s and 1960s. None of these conversions were the result of US automobile interests.

In the authors' opinion, the US national interest would have been served by modernizing parts of many US streetcar systems at the end of the 1920s by segregating them from auto traffic, but doing so would have required municipalization and capital infusion from higher levels of government. Neither municipalization nor capital infusion from higher levels of government were even remotely in the cards at that time. Even if they had been, given Canada's experience, and experience with public authorities in Los Angeles and Pittsburgh, it is uncertain whether streetcars would have been modernized in the USA. It is safe to say, however, that in the absence of such government takeover and capital infusion, the American streetcar industry could not have maintained itself in private hands because of its unprofitability and inability to raise capital. If National City Lines had not happened, some other combination of liquidators probably would have.

The American and Canadian PCC streetcar operating in motor vehicle traffic almost disappeared because it offered insufficient advantages over the diesel bus to compensate for the expense of its infrastructure, including track and electrical systems. As Post points out, its strongest suit was quietness and absence of fumes. Operationally, it was marginally faster than buses in heavy patronage conditions, at least on roads where left turns were banned, as in some intersections in Toronto (Fig. 2). According to Toronto officials, PCCs carried passengers at less operating cost than buses under the heavy patronage conditions of that city, but other studies showed that it carried passengers at greater operating expense than diesel buses, perhaps because patronage levels were lower in the cases studied [21]. In any event, if there was a case to be made for the PCC streetcar operating in mixed motor vehicle traffic, it was not a strong enough one, and that primarily is why it almost disappeared in North America.

The Light Rail Revolution

Light rail resulted by tweaking the streetcar concept to reduce its drawbacks while enhancing its advantages. The Canadian and American transit industry itself initiated a few of the tweaks, but the industry initiatives came too late in the decline of the Canadian and American streetcar industry to change the trajectory of decline. The progressive changes that did change trajectory came from Europe and crossed the Atlantic in response to the social protest movement in Canada and the USA that began in the 1960s. Many in the American transit industry, who came directly or indirectly from the National City Lines mold, resisted the European ideas but ultimately some were forced to accept them by outside pressure.

In the USA, most of the few streetcar lines that lasted into the 1970s possessed significant elements of right-of-way Types B and A that gave them speed advantages over buses. The speed advantage is why they remained. Five streetcar lines remained in San Francisco; four of them used long tunnels (one 2.5 miles long, the other 1 mile long) that took the lines from the edge of the central business area to suburbs that were cut off by a steep range of hills. Boston had a central streetcar subway that ran outward from its business center, and several streetcar lines fanned out from it like fingers on a hand. The fingers surfaced on ramps, and then ran through inner suburbs in mixed traffic or on reservations in the center of boulevards. Boston ran its PCC cars in one or two car trains, with drivers in both cars collecting fares. In addition to three or four remaining traditional streetcars that ran almost entirely on narrow streets, Philadelphia still operated remnants of three distinct streetcar systems. It had a similar configuration of subway-surface streetcar lines to that of Boston. Philadelphia also continued to operate three or four traditional long streetcar lines running on narrow streets. Finally, it operated two suburban streetcar lines that fanned out from the end of a rapid transit line into the suburbs largely on rights-of-way Type B. Pittsburgh still had one set of streetcar lines that ran south from its business area, which the lines exited through a long tunnel under a range of hills to get to the southern suburbs. All that remained of streetcars in New Jersey was a short streetcar subway in Newark in which individual PCC cars shuttled back and forth between several stations, crossing but not operating in city streets. In Cleveland two streetcar lines ran on reservations in the centers of boulevards in the community of Shaker Heights. The community's developers in 1920 placed expensive homes so that residents had short, pleasant walks to streetcar stops. The two streetcar lines came together into one and then turned onto a railroad corridor that the streetcar tracks followed with Type A right-of-way to a terminal on the edge of the Cleveland CBD, 6 or 7 miles away. Short trains of PCC cars operated on this commuter line at fast speeds.

Some transit advocates argued that rather than representing the dying gasp of an old technology, the surviving streetcar operations with their rights-of-way Types B and A offered a model of a new mode of transit needed in American cities. Bill Adams, an employee of the Boston redevelopment authority and later the Boston transit system wrote a thoughtful article in 1965 describing how the Boston streetcars could be altered to improve their speed and productivity. He was not aware of the light rail transformation then happening in Germany, but what he advocated was very much like what was happening there [22]. Boston did make a much noticed improvement to its streetcar system in 1959 by punching an additional ramp out of its subway and connecting it to a commuter rail line that just had been abandoned, and which then was converted to streetcar operation. The Boston transit system rebuilt the commuter tracks so they were suitable for streetcars, electrified them, and then it began operating frequent service with two- and three-car PCC trains from the outer terminal at Riverside to central Boston via the streetcar subway [8]. An attendant in each car collected fares. Patronage settled down to about 25,000 per day, much greater than what the commuter trains attracted, and Adams and others felt the Riverside line could be a national model. This model led to no emulation, however, except in 1964 for a short shuttle line in the suburbs of Chicago (on right-of-way Type A, part of an abandoned interurban line) called the Skokie Swift [8].

The impetus for the light rail revolution was the social protest movement of the 1960s and the availability of capital from higher levels of government [5, 6]. Continuously falling demand for transit, particularly for bus service, and rising costs forced the US transit industry into an unprofitable position. Between the late 1960s and early 1970s, almost all public transportation in the USA was municipalized with federal and in some cases, state financial assistance. The passage of federal transit legislation in 1970 also made capital available for building new rail systems [11, 23]. At the same time citizen movements, such as those dedicated to preserving neighborhoods by stopping inner city freeways and others to reducing air pollution, came together in some metropolitan areas with the idea that better public transportation systems could help with urban preservation and revitalization [24]. Rail service was clearly desirable, but there was little in the way of immediate domestic examples that seemed relevant to the needs. It was apparent from transit patronage trends (Fig. 3) that bus and streetcar service was in decline, while rail

rapid transit was holding its own against the automobile. Could surface rail systems be tweaked to perform like rapid transit while costing much less to build? If the answer was "yes," there was hope that introduction of such surface rail lines could reverse the declining fortunes of transit and perhaps contribute to renewal of central cities. Thus was born the light rail movement. Its model was not the American streetcar, even the PCC car, but a new concept coming out of northern European cities.

Public transit in most German cities was centered on streetcar technology before and during World War II. As in the USA and Canada, German streetcars ran on tracks located in the middle of streets. The typical German streetcar was a much shorter vehicle than its North American counterpart, however, and German transit providers typically ran them in two- and three-car trains. The first car was a motor car, staffed with a motorman and a conductor. The motor car pulled one or two small trailers, each with a conductor, so the typical German streetcar train of three diminutive cars had a staff of four. The passenger (based on the capacity of the cars)-to-staff ratio was 45:1 [25].

When faced with rebuilding their war-ravaged cities after World War II, German transit planners contemplated a future urban world dominated by the automobile [26]. Should their streetcar systems be rebuilt? Modern buses promised passenger-to-staff ratios of 60:1 for a regular bus and 75:1 for articulated buses, and German transit systems probably would have made the transition to buses at that time had they been able to obtain buses. They were unable to obtain buses, however, and so they put their streetcar systems back together as best as they could. Rapidly rising wages, however, forced German transit operators to seek ways of improving streetcar productivity. In the mid-1950s, they began obtaining larger vehicles, similar in size to PCCs, and then they experimented with articulating two of the large vehicles together into a long-bendable vehicle. The experiments worked. Transit operators improved productivity further by running large trailers behind the articulated cars. They added third sections to the articulated cars. They introduced proof-of-payment (POP) fare systems. POP fare systems required passengers who did not have weekly or monthly passes to figure out what fares they owed and purchase tickets from simple vending machines or tobacco kiosks before boarding vehicles. No staff would inspect their fare upon boarding, but roving bands of inspectors could ask them to produce proof of payment at any time during their journeys, and if they failed to produce adequate proof, they could be fined. This system added teams of roving inspectors to the payroll, but it eventually eliminated all conductors on all cars. Passenger-to-staff ratios rose to over 200 [25]. The increase in streetcar productivity was so large that many transport undertakings decided to retain streetcars but adapt them to conditions where it was expected that most of the public would use automobiles in the future [26]. A British publication *Modern Tramway* reported regularly on the transition of the streetcar systems in many northern European cities into what later became known in North America as light rail.

Figure 2 offers a vantage point for understanding what the German's were trying to do with their streetcar technology makeover, as evidenced from the pages of *Modern Tramway*. Figure 2 shows a two-car PCC train on the Queen Street line in central Toronto that was given some priority over autos. Both the operation of a second car as well as auto priority were significant improvements over traditional North American streetcar practice and undoubtedly contributed to the higher performance of the Toronto streetcars in handling high passenger volumes compared to buses. Would it not be possible to take such modifications further? Could three-car trains be operated? Could drivers on the second and third cars be eliminated to improve productivity? Could the fare collection system be changed so that passengers could board at all doors on the train, without being impeded by an employee collecting fares and transfer slips? Could motorists be kept off the tracks? Could all left turn conflicts be avoided? Could the service be speeded up by stretching out the distance between stations, and could the stations be designed to be safe from auto traffic and integrated with pedestrian systems, with easy transfers between bus and rail? Could the entire bus route structure in the region be changed to dump the heaviest passenger loads onto streetcar routes experiencing such modification, taking advantage of their speed and high passenger carrying capacity, leaving local diesel buses to handle lighter loads? In short, rather than having the streetcar act

like a slow local bus on rails, could it act more like a quiet fast subway train operating on the surface (perhaps dipping into short subways in the heart of the CBD), becoming the backbone to a regional transit system? The answer to all of these questions was, and is, "Yes," and German transit thinkers (as well as transit thinkers in Switzerland, the Netherlands, Belgium, and Sweden) developed technology and operating procedures for doing it. Getting transit systems in the USA and Canada to adopt and implement such technology and procedures was what the light rail revolution was all about.

In a major study that took place about 1959, Frankfurt am Main in West Germany compared different strategies for region-wide public transport improvements. One was based on building a system of subway lines fed by buses. The other was a system of light rail trains running in short subways in the center of the city and then using Type B rights-of-way everywhere else. Frankfurt decided in 1960 to follow the second path [27, 28]. Figures 4–7 offer several glimpses of the evolution of the Frankfurt streetcar system to a light rail network. Similar modifications were happening to streetcar systems in cities throughout northern Europe at this time [29].

The German concept of light rail entered North America through different channels. *Modern Tramways* was an important conduit, prompting at least two US consultants to visit Germany to see for themselves and then write about their observations in *Traffic Quarterly*. In 1962, Dean Quinby, a consultant working on the BART project in the Bay Area, captured the essence of the idea, which was more than just separating streetcars from autos. It was the idea of creating surface, or *light infrastructure* rapid transit that could be afforded by midsized cities. Door design and efficient fare collection design were important parts of the concept [30]. Eight years later, Stuart Taylor captured the momentum of the idea that was spreading across northern Europe and again argued that the idea had great applicability to the USA [31].

Other readers of *Modern Tramways* included Senator James R. Mills, president pro tempore of the California State Senate, who brought light rail to San Diego in 1981, the first application in the USA. Mills' most vehement opponent in introducing light rail was San Diego Transit's general manager, who also was president of the American Public Transit Association. San Diego's MPO, the Comprehensive Planning Organization, who sought a Washington Metro-like regional

Photos of the transformation from streetcar to light rail in Frankfurt, circa 1966-1972

Light Rail Transit, Systemic Viability. Figure 4
Streetcar tracks being relocated from mixed traffic in center of road to side of road in right-of-way Type B. Frankfurt, 1966. Author's photo

Light Rail Transit, Systemic Viability. Figure 5
The result. Frankfurt right-of-way Type B, 1966. Author's photo

Light Rail Transit, Systemic Viability. Figure 6
Light rail station being built in street right-of-way, Frankfurt 1968. Author's photo

rapid transit system, also opposed light rail, but both San Diego Transit and CPO lost the battle [32].

Readers of *Modern Tramways* also included Tom Parkinson, a British electrical engineer, who introduced the self service, barrier free fare (proof-of-payment or POP) fare system, so critical to the success of light rail, to North America. Parkinson installed POP on Seabus in Vancouver (1978), then on the new light rail line in

Light Rail Transit, Systemic Viability. Figure 7
Delivery in Frankfurt of new light rail cars, four double doors to a side. Manufacturer: DueWag; Type: U2. 1968. A decade to a decade and a half later, this car became the de facto standard light rail car in North America. Author's photo

Edmonton (1978), and then on the San Diego Trolley (1981). With the proof-of-payment fare system, passengers bought passes allowing from 90 min of riding to a month of riding at vending machines on platforms or at retail outlets. Passengers were required while on board trains to have in their possession a valid ticket or pass, inspected at random by roving teams of fare inspectors. This system eliminated the need for drivers to inspect fares and allowed passengers to board through all doors, making it possible for several hundred passengers to board in a matter of seconds [32]. Parkinson, with Walter Quintin of Bechtel, also wrote the car specs for the first San Diego line. Only six pages long, the spec was a stunning contrast to the phonebook sized spec that the Urban Mass Transit Administration issued for the flawed standard light rail vehicle, which ultimately was ordered only by San Francisco and Boston. The Parkinson/Quintin spec led to San Diego selecting the DueWag U2 car (Fig. 7) [32]. The U2 was a rugged, reliable and easily maintained car originally introduced in Frankfurt in 1968 and already selected by Edmonton and Calgary for their light rail lines. In addition to its use in San Diego, updated versions of the U2 car would be used later by Sacramento, Pittsburgh, and other operators, and it became the de facto standard light rail vehicle in North America [8].

The light rail idea also was brought into the USA by academics and high government officials who lived in Europe during this period and then moved to or back to the USA. Such persons included Professors Vukan Vuchic of the University of Pennsylvania, who published a summary of European light rail practice on behalf of the new Urban Mass Transit Administration. Another notable member of this initial group was Professor John Bakker, a civil engineering professor at the University of Alberta who worked closely with Don MacDonald, the Superintendent of the Edmonton Transit System to define a short rail system around which a timed transfer bus system (based on ideas from the Netherlands) could be structured. Edmonton would be the first modern light rail adoption in North America. The group included Bob Burco, who headed the Oregon Department of Transportation when light rail was adopted in Portland, and Ken Orski, who as Deputy Administrator of UMTA wrote a policy directing MPOs to consider light rail among alternatives for transportation improvement in their long-range transportation plans. Vuchic, Stuart Taylor, and Orski worked together to establish what became known

as the Light Rail Subcommittee of the Transportation Research Board's Rail Transit Committee in 1974. Shortly after its formation, the subcommittee branded the German concept of limited tramways as light rail, and held a national conference on light rail in June 1975 to popularize the idea among politicians, regional planning officials, and transit managers in cities in the USA and Canada. Leadership of the American Public Transit Association joined as a cosponsor of the conference at the last minute, though many in leadership positions then were opposed to the idea of light rail [5, 6].

A characteristic of German light rail that differed from American streetcars was the German practice of imbedding light rail lines into regional transit networks. The coordination of light rail and bus routes, as it came to be practiced in North America, was done to accomplish two objectives. One was to take advantage of the high passenger-to-staff ratios of light rail lines to improve overall transit productivity. The idea here was to introduce light rail lines into corridors served by many bus lines, particularly during rush hours. Rather than operating all of the bus routes to the CBD on arterial roads, where there were large amounts of redundant bus service, the transit operator would terminate bus routes at suburban light rail stations. High-capacity light rail trains then could take passengers to the CBD, and perhaps to other important destinations that bus passengers previously could not reach. Staff and operating expense would be saved by discontinuing the duplicative parts of the bus routes running from the suburban stations to the CBD.

The other objective of bus and light rail service coordination was the creation of multidestination transit networks that enabled those passengers without access to autos to reach many metropolitan area destinations in addition to the CBD. Suburban light rail stations where many bus routes converged were excellent places for passengers to transfer not only between buses and trains, but also between trains and buses (so that train passengers could reach nearby destinations), and between one suburban bus line and another.

Ideas of bus/rail coordination to achieve the dual objectives of greater productivity and multidestination travel were new to transit systems in the USA. US transit planners typically viewed the CBD as the only important destination for transit to serve. They believed that to attract as many passengers as possible to the CBD, it was important not to force passengers to transfer from buses to trains [39]. American (but not necessarily Canadian) practice tended to view each transit line as an independent entity that connected suburban neighborhoods with the CBD.

The idea of multidestination transit came into Canada and the USA from several directions. John Bakker and Don MacDonald of Edmonton saw light rail as the core of a restructured city-wide bus network much as they saw happening in Europe. Brian Sullivan of Edmonton, Calgary, and Vancouver also realized the importance of bus rail service integration for both reducing costs and increasing patronage. Sullivan passionately argued for the network approach and attempted to import the German idea of the *Verkehrsverbund*, or traffic federation, to North America. The idea of the *Verkehrsverbund*, pioneered in Hamburg, was that a central planning and marketing agency in an urban region would design a regional transit network to allow easy travel throughout the region by transfers between lines and modes. The traffic union would establish timetables, collect fare revenue, and provide information to the public for all transit services in the urban region. However, it would contract out the construction and operation of different parts of the network to many different entities. From the public's perspective, the entire regional network would seem to be one coordinated entity. There would be only one regional transit map, one source of timetables, and one fare system. The public would be able to transfer freely between all parts of the system, connections would be timed, and transfer stations would be attractive and functional. However, different operators would be able to keep close managerial control over the independent parts of the network, insuring timely operation and low operating costs. Sullivan, Bakker, and MacDonald had considerable success in spreading at least parts of these ideas either directly or through coworkers (such as Tom Matoff and Greg Thompson) to Vancouver, San Diego, Edmonton, Calgary, Portland, Sacramento, and Denver. Under the leadership of Tom Larwin, MTDB's general manager from 1978 to 2003, San Diego was the one region in the USA and Canada that came closest to implementing the *Vehrkehrsverbund*, where the concept was the organizing principle for regional transit in the southern part of San Diego County from 1979 to 2003 [32].

Vancouver also adopted many aspects of the traffic union concept through British Columbia's Bureau of Transit Services. Sullivan, who was deputy director of the province's Bureau of Transit Services from 1973 to 1980, led a team in preparing a transit plan for the region calling for the region's extensive local bus and trolley bus system to be reorganized around a core of regional light rail lines and regional buses, called Fast Buses. The plan largely has been implemented, though the region obtained the funding to build its rail lines as entirely Type A rapid transit lines rather than as light rail. Other regions, such as Denver, also adopted the concept of an integrated regional network but attempt to manage the concept through large public monopolies.

Also important to the transference of the light rail idea from northern Europe to North America was the mass travel of Canadian and US youth to Europe during this period [24]. By and large, these travelers were the offspring of middle class families who grew up in the suburbs using automobiles. In Europe, however, they rode between great urban centers on fast, comfortable, frequent trains on first-class Eurail passes and used the modernizing tram systems in cities throughout northern Europe. Many came back with the realization that there was a viable urban alternative to suburban, auto-based neighborhoods that they experienced as kids. Such individuals, passionate in their beliefs, entered transportation bureaucracies in Edmonton, Vancouver, San Diego, Portland, San Francisco, Sacramento, among other cities in the late 1960s and 1970s, and worked with other such individuals in citizen activist groups to get the light rail idea accepted by top decision makers [24].

Light Rail Adoption in North America

Table 1 summarizes the history of light rail adoption in Canada and the USA as well as the streetcar systems that survived to 1970 and then were modernized. The table shows the year that a previously all-bus urban area opened its first light rail line and the miles of line that it originally opened. The table also indicates growth, if any, from the original length, and the passengers boarding the light rail lines each weekday in a recent year (generally 2006). Some systems cater to passengers who travel only a short distance; others to passengers who travel a long distance. Average distance traveled for each city is shown, as is the speed of service. The next to last column shows the current (usually 2006) traffic density on each mile of line. Density is measured by the average number of passengers passing each mile of line on a typical weekday. The primary purpose of showing the relative traffic intensity of the various systems is to offer a first cut to judging their relative performance.

This section summarizes how the first group of North American bus-only cities to adopt light rail decided how to do so. There are seven such cities. The section shows a great deal of commonalty of objectives among five of the seven pioneer cities, and understanding the commonality assists in evaluating the success of the light rail movement in the section of this entry that follows. This section stops at the first seven because there is a clear gap between the seventh and eighth city in terms of time, after which the rate of adoption increased rapidly.

Edmonton was first. During the 1950s, 1960s, and 1970s, a city department, the Edmonton Transit System operated the area's bus and trolley bus system under the direction of an electrical engineer, Don MacDonald. MacDonald began his career with Edmonton Transit by replacing the system's streetcars with trolley buses just after World War II, when he was made Superintendant. During the 1960s MacDonald collaborated with a Dutch university transit engineering professor, John Bakker, in forming strategy for system change. MacDonald and Bakker developed a plan for a short Type A rail transit line using railroad rights-of-way modeled roughly after a similar line that opened in Cleveland in1955. In contrast to Cleveland where the rail investment resulted in no significant changes to the city's bus system, MacDonald and Bakker intended to restructure the Edmonton bus and trolley bus network around the rail line, eliminating duplication of trunk bus routes running to the CBD, and making suburban destinations more reachable. They could not obtain funding or council approval for the project, however. This changed about 1970 when two university-affiliated activist groups organized to fight city hall's effort to bulldoze inner city neighborhoods, nature corridors, and parks to make way for an inner city freeway ring. Their 1971 book addressed to Edmonton's city council, "Immorality of the Motor

Light Rail Transit, Systemic Viability. Table 1 Light rail adoption in Canada and the USA, 1978–2010

New light rail systems								
Urban area	Opening year	Opening one way miles	Recent one way miles, 2006 unless otherwise noted	Recent light rail average weekday boardings, 2006 unless otherwise noted	Distance traveled by average passenger miles	Average daily density of passengers carried along each mile of route	Scheduled speed, mph	Notes
Edmonton	1978	4.3	15.3	74,000	4.0*	19,346	19.0	a
Calgary	1981	6.1	28.1	248,200	4.0*	35,331	18.0	b
San Diego	1981	15.9	51.7	100,111	6.2	12,006	19.0	
Buffalo	1984	1.2	6.2	19,398	2.5	7,822	12.0	
Portland-MAX	1986	15.1	43.8	97,000	5.2	11,516	19.0	
Sacramento	1987	18.3	37.8	50,088	5.2	6,890	21.0	
San Jose	1987	6.6	41.6	34,837	5.1	4,271	16.7	c
Los Angeles	1990	20.7	54.7	136,000	7.2	17,901	21.0	
Baltimore	1992	22.5	30	18,964	5.7	3,603	22.0	
St. Louis	1994	15.5	46	44,297	7.2	6,933	27.0	
Denver	1994	5.3	34.7	68,784	5.2	10,308	19.0	d
Dallas	1996	10.3	44	62,007	7.4	10,428	21.0	
Salt Lake	1999	15	19	51,952	5.7	15,586	25.0	
Jersey City-Hudson Bergen	2000	7.6	16.6	25,840	3.1	4,826	15.2	e
Minneapolis	2004	7.8	12	34,072	5.5	15,616	14.6	f

Camden-Trenton River Line	2004	34.5	34.5	7,350	4.5	959	na	
Houston	2004	7.5	7.5	38,113	2.4	12,196	14.0	
Charlotte, NC	2007	9.6	9.6	16,000	4.0*	6,667	15.7	g
Oceanside-Escondido	2008	22	22	6,560	10.4	3,101	22.0	h
Phoenix	2009	19.8	19.8	37,000	6.0*	11,212	18.3	i
Seattle	2009	15.6	15.6	14,399	6.0*	5,538	na	j
Streetcar systems that survived to 1970 and were modernized subsequently								
Toronto		na	48.9	162,500	2.7*	8,972	9.0	k
Boston		26.9	26.9	245,236	2.7	24,615	14.0	
Cleveland		10.5	12.7	13,379	5.8	6,110	19.0	
New Orleans 2004		6.5	12.9	24,000	2.0	3,721	9.0	
Newark		4.3	6.1	18,664	2.5	7,649	na	
Philadelphia subway-surface		22.3	22.3	80,994	2.7	9,806	11.0	l
Philadelphia Media/ Sharon Hills		11.8	11.8	7,700	3.6	2,349	16.0	m
Philadelphia-surface streetcars		54.5	8.5	19,992	2.7*	6,350	8.3	n
Pittsburgh		na	23.3	25,884	4.4	4,888	16.0	

Light Rail Transit, Systemic Viability. Table 1 (Continued)

New light rail systems								
Urban area	Opening year	Opening one way miles	Recent one way miles, 2006 unless otherwise noted	Recent light rail average weekday boardings, 2006 unless otherwise noted	Distance traveled by average passenger miles	Average daily density of passengers carried along each mile of route	Scheduled speed, mph	Notes
San Francisco		24.2	31.7	140,426	2.6	11,518	11.0	
Portland streetcar	2001	2.5	4.1	7,800	2.0*	3,805	10.0	o

*Average trip length not reported; authors estimated distance based on similar systems

[a]Reflects April 2010 extension; speeds from [35]; other from: http://www.edmonton.ca/transportation/ets/lrt.aspx, downloaded on 29 June 2010

[b]Average for 2006; speeds from [35]; other from: http://www.calgarytransit.com/html/technical_information.html, downloaded on 29 June 2010

[c,d]2008 figure from source [36], transformed to weekday figure at rate of 300 days per year

[e]2006 figures from source [33]

[f]2008 figure from source [36], transformed to weekday figure at rate 300 days per year

[g]Oct/Nov 2008 average. Taken from: http://www.norfolk.com/2008/12/charlotte-light-rail-ridership-down-november, downloaded on 29 June 2010

[h]Figures are from 2008, taken from: http://www.ridecheckplusburst.com/development/Default.aspx?q=28&pdf=08_NS_WK_CompStatSysWide.pdf, downloaded on 29 June 2010

[i]April 2010 weekday average from press report, found at: http://image.examiner.com/x-11410-Fresno-Transportation-Examiner~y2009m5d28-Valley-METRO-light-rail-reaching-new-heights

[j]November 2009 weekday average, http://seattletimes.nwsource.com/ABPub/2010/01/11/2010767928.pdf, downloaded on 29 June 2010

[k]Newspaper story claiming annual streetcar ridership of 52 million in 2006, http://transit.toronto.on.ca/archives/data/200707150430.shtml, downloaded on 30 June 2010

[l,m,n]From SEPTA Service Planning Department Annual Service Plan, June 2010, http://www.septa.org/reports/pdf/asp11-proposed.pdf

[o]This is a new streetcar line but is included because its stats were mixed with those of Portland MAX, and authors wanted to preserve the stats after extracting them

Sources: References [33–36] unless otherwise noted.

Car," persuaded City Council to scrap the previously secret freeway plan for the city. A year later, the activists presented City Council with a second book, "Light Rapid Transit, the (Immediate) Answer for Edmonton." This book, with a line drawing of the 1968 Frankfurt U2 car on the cover and heavily footnoted with references from *Modern Tramway* and *Traffic Quarterly*, presented the light rail idea. The principal authors had been acquainted with light rail on European trips. "Light Rapid Transit . . . ," then described how the idea could be applied to Edmonton, including diagrams showing how bus routes could be restructured around suburban light rail stations (Fig. 8). Oil royalties then flowing into provincial coffers led to a provincial light rail construction fund available to both Edmonton and Calgary, and Edmonton City Council approved light rail development in 1973. Edmonton opened its first line with turnstiles but

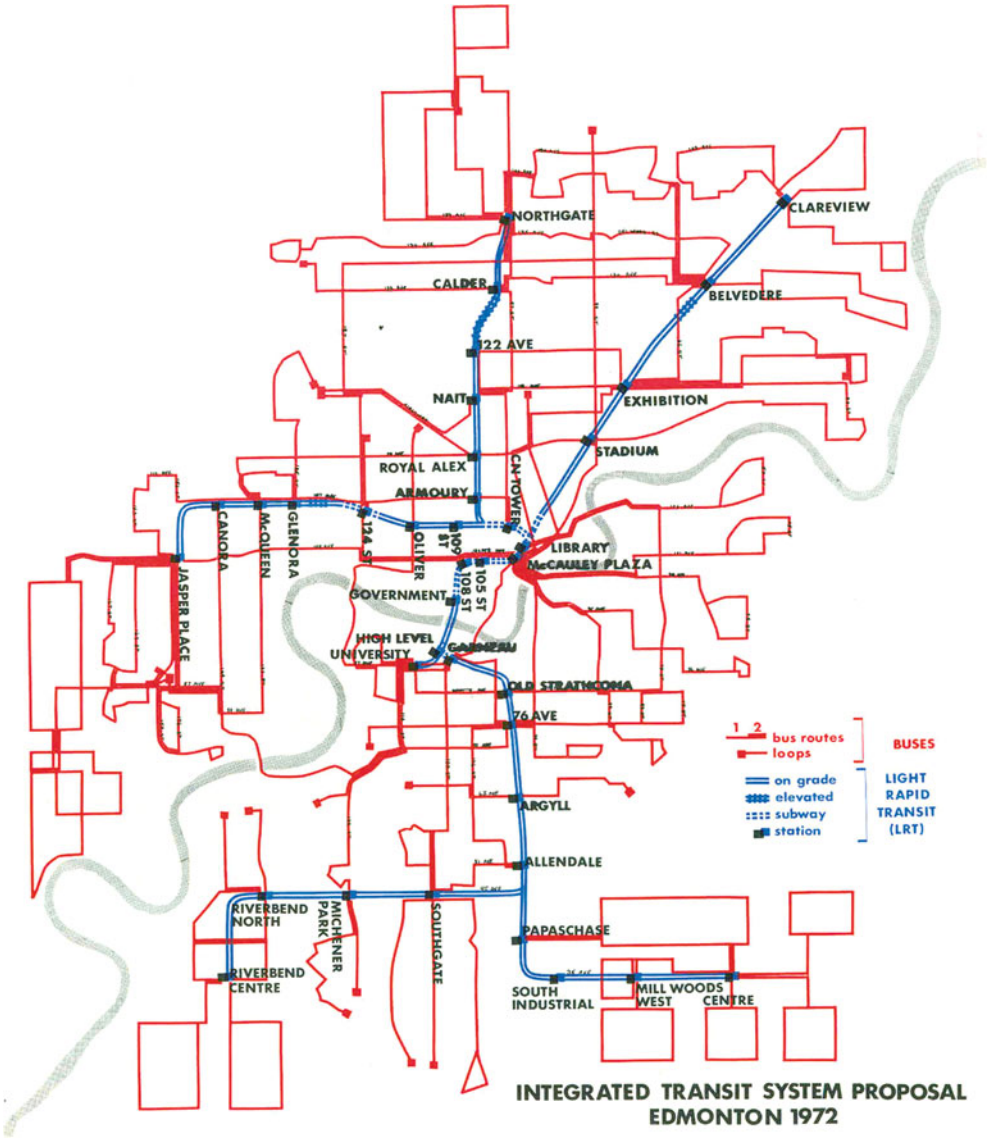

Light Rail Transit, Systemic Viability. Figure 8
Neighborhood activist vision for an integrated bus and light rail network for Edmonton in 1972. Taken from the Practicum on Community Analysis, "Light rapid transit: the (immediate) answer for Edmonton"

within a year replaced them with the proof-of-payment (POP) fare collection system after its successful debut for Vancouver's Seabus. The POP fare collection system made it easier for passengers to transfer between buses and trains, and station designs generally required short walks between modes. Edmonton made the mistake of putting the CBD part of its light rail line in a subway, however, which greatly increased light rail construction cost, thus slowing light rail expansion. Not until 2003 did the line finally break to the surface on its southern face. Since then, it has expanded to the south rapidly, and its patronage more than doubled since 2003 as a consequence [5, 6].

Edmonton's light rail system still lags the light rail impact of Calgary, however. Under the direction of William Kuyt, a Belgian-born traffic engineer who already was familiar with light rail, Calgary put its light rail line comingled with buses on a surface mall through the CBD. With the same amount of money that Edmonton received from the provincial government, Calgary subsequently expanded more rapidly and farther in several directions in the manner described in, "Light Rapid Transit…". The Calgary light rail line directly serves most of the metropolitan area's major destinations, and Kuyt restructured its bus system around its three lines in the manner projected for Edmonton in Fig. 8.

San Diego was the first US urban area to open light rail, and it followed the example of Edmonton (though it avoided subway construction). San Diego's light rail was championed by the President Pro Tempore of the California State Senate, James R. Mills of San Diego. Opponents included the city-owned and federally financed bus system and the federally sanctioned metropolitan planning organization, called the Comprehensive Planning Organization. The bus system's general manager maintained that buses could do anything a rail system could do better and at lower cost. The MPO viewed light rail as interfering with its plans for a Washington Metro-like system. Arguing that the bus system already exhausted the region's financial resources for transit with unproductive bus service and that the MPO's plans were financially and politically infeasible, Senator Mills put forward the German concept of light rail as a feasible alternative to both. An avid reader of *Modern Tramways*, he persuaded the San Diego County Department of Transportation to study the feasibility of the German light rail concept in San Diego. The department's head, Rudy Massman hired an engineer and a planner from the Edmonton Transit System during a window when it looked like political approval for the Edmonton system would not happen. Massmann married the Edmonton transit people with San Diego County roadway department project planning and financing staff to prepare the study. The study found that a regional network of light rail trunk lines, around which bus service in the county was restructured, was a viable transit concept for the highly decentralized and auto-centric San Diego region. On the basis of the report, the Senator carried legislation that stripped the city bus system and the MPO of much of their powers, created a new transit planning, programming, and construction organization (the San Diego Metropolitan Transit Development Board, or MTDB), and gave it access to state and local funding. The legislation creating MTDB envisioned light rail becoming the backbone of a regional transit system, and it gave MTDB the power to make that happen. The first MTDB general manager, Robert Nelson sold the MTDB to business leaders in the region by arguing that light rail was the only way to improve transit productivity in the region by replacing a large number of unproductive bus miles with productive rail miles. Earlier as Deputy General Manager for the Metropolitan Atlanta Transit Authority, Nelson made similar arguments there. With such arguments, MTDB gained local support for its plans, and when Mayor Pete Wilson of San Diego swung on board, the project moved forward. From the opening day, the San Diego Trolley used the POP fare collection systems, and as the LRT network expanded, bus routes have been restructured around light rail stations. The *Verkehrsverbund* form or organization, described earlier, governed the region for over 20 years of light rail expansion [14, 32].

As Edmonton's, but unlike San Diego's, Portland's light rail decision grew out of pro-neighborhood and anti-freeway organizations that coalesced in that city during the early 1970s. The region used Interstate Transfer Funds freed up by a deleted freeway to finance part of the light rail line. As in San Diego, the concept of light rail development in Portland was heavily influenced by Edmonton and incorporated Canadian ideas of light rail forming the armature of a

restructured regional bus system. The first document advocating light rail in Portland was a state Public Utilities Commission examination of the suitability of using rail rights-of-way in the Portland region for rail transit or busways. The author of the document patterned it on, "Light Rapid Transit, the Immediate Answer for Edmonton," which he cited. Most of the major players in the decision to adopt light rail in Portland had been to Europe and seen the concept there. Some were readers of *Modern Tramways*. One of them was the transit system's planner, but the management of the transit system was otherwise opposed to light rail. The governor had to reorganize it, and also change staff at the Oregon Department of Transportation before light rail could move forward. The reorganized transit system (TriMet) took the lead in designing the integrated light rail/bus system. It hired Don MacDonald from Edmonton to manage Portland's first light rail construction as well as to plan for restructuring bus service around proposed light rail trunk lines [24]. The Canadian approach was strengthened in Portland by Tom Matoff, who brought Portland's first light rail line into operation and restructured eastern city and suburban bus lines around it in time for the first day of operation. Matoff had worked with Brian Sullivan in Vancouver on the Vancouver regional rail/bus integration concept and its incorporation into the *Greater Vancouver Regional Plan*. Sullivan brought Matoff to Vancouver, and from Vancouver Matoff moved to San Francisco, where he was director of planning for the San Francisco Municipal Railway. In that capacity, Matoff initiated and secured adoption of a revolutionary plan for restructuring the San Francisco Municipal Railway's bus and trolley bus network around the new light rail transit subway investment in that city. From there, he moved to Portland, San Jose rail operations, and later still to Sacramento.

As did Portland, Sacramento used Interstate Transfer funds to finance part of the construction of its first light rail lines, which also arose out of an anti-freeway, neighborhood revitalization movement. Youthful activists in that movement previously traveled widely in Europe and read *Modern Tramways*. Despite the project's anti-freeway origins, the California Department of Transportation, which had assisted in the San Diego light rail project, contributed significantly to the design of the Sacramento proposal. The bus transit system, run by a regional district, originally was opposed to light rail. However, Bob Nelson, who was the San Diego Metropolitan Transit Development Board's first general manager, and as such led in the design and adoption of San Diego's first light rail line, was appointed general manager of the Sacramento system after leaving San Diego. Nelson was not directly involved in light rail planning in Sacramento, but he and John Schumann, who was (as director of a special agency to plan and construct light rail), sold light rail to the business community there as a means for improving transit productivity by eliminating bus route duplication. Nelson previously used this argument in San Diego (and before that, he used it in Atlanta with its heavy rail system) with success. After opening Portland's light rail system, and a year after Sacramento's first light rail line opened, Tom Matoff became Sacramento Regional Transit's general manager and insured a coordinated light rail/bus system there for its first several years. Unfortunately, more recent extensions have not been supported by bus restructuring, and the old bus people there have dismantled much of the original coordinated rail/bus scheduling from the earlier era [14].

The close linkages between development of five of the pioneer light rail systems result in a commonality of system design between them. In all five cases, light rail was envisioned as the backbone of restructured regional transit systems, and in four of the five cases this idea has been kept as their light rail systems expanded. Four of the five cases now experience high passenger traffic density on their light rail lines, exceeding 10,000 passenger miles per track mile of route. Light rail in Sacramento does not achieve this intensity of use, perhaps because that system's commitment of bus/rail coordination has waned.

Buffalo and San Jose followed different paths to light rail development that resulted in less coordination between their bus systems and light rail lines. Buffalo's light rail line was conceived by the region's transit operator originally as a heavy rail line using Type A right-of-way. The transit authority requested federal and state funding for their project but was turned down. However, the Urban Mass Transit Administration was looking for a light rail demonstration project that it could finance, and it chose Buffalo. To transform

the original proposal from heavy rail to light rail so that it could obtain federal funding, the transit authority redesigned the plans so that rail cars would run for a mile along a transit mall, built on the right-of-way of the downtown's major shopping street. For the remaining 5 miles from the edge of the downtown to a university campus in the northeastern sector of the city, the line ran in a subway, stopping at several underground stations. The cost of the subway made it impossible to extend the line any farther, though a surface extension farther into the suburbs was in the original plans. The line did open with the POP fare systems, and there are unimpeded transfers between bus and rail. However, it does not appear that there was a significant restructuring of the bus network around the light rail investment, even though the same agency in the Buffalo area runs both the bus and light rail lines.

Local business support focused by a political leader, Rod Diridon was the momentum behind light rail development in the San Jose metropolitan area. Diridon held several elected positions but was particularly active as a Santa Clara County supervisor, where he organized a county-wide transit system to develop bus and rail service in the area. With support of the business community leadership, Diridon obtained state funding opportunities for transit made available through the leadership of Senator James Mills of San Diego, and he also obtained federal funding to support light rail plans. The San Jose light rail initiative differed from that in San Diego, however, by not following the transit planning objective of having light rail forming the core of a regional bus system, which was one of the principles around which the legislation creating the MTDB was written. Both light rail and buses now are operated by the same county transit authority in the San Jose area, but the two systems are not well integrated. In many locations, transfers between modes require long walks in pedestrian-hostile environments, and there never was a strategic vision of integrating light rail and bus lines into a regional system in which the heavy investment in light rail would replace the trunk parts of bus routes headed to major destinations. Matoff was brought in to open the first light rail line in San Jose following his successful opening of Portland's first line, but unlike in Portland he was not charged with establishing a coordinated bus and light rail network in San Jose, and there had been no ground work in that direction before he got there. There is another problem, as well. Because of a design flaw of the CBD mall that has proven impervious to correction, the light rail system is plagued with a 10-mph speed restriction through San Jose's CBD, which lengthens travel times between residential districts in the southern part of the county and employment concentrations, which tend to lie north of the CBD [14].

During this period, most of the streetcar lines that survived to 1970s were modernized. All except New Orleans and Toronto received fleets of light rail cars. The Urban Mass Transit Administration wrote specifications for what it intended to be the standard light rail vehicle for the United States, and it encouraged Boston and San Francisco to be the first purchasers of the car. Boeing-Vertol was selected to build it, but the car proved to be complicated and unreliable. No other orders followed. Other systems ordered the U2 car or cars built by different builders but similar to the U2 car. Toronto replaced its PCCs with new vehicles of similar design built in Canada. New Orleans renewed its old pre-PCC traditional streetcars and expanded the fleet with replicas. Changes to the physical plants of the streetcar systems varied widely from city to city. Pittsburgh rebuilt its South Hills lines to light rail standards and placed the CBD part in a new streetcar subway. Cleveland renewed its Shaker Heights lines, which already were mostly on Type B right-of-way. San Francisco placed the CBD portion of its streetcars into a subway, which connects with the two long tunnels extending into the suburbs. The subway was a byproduct of regional rapid transit development. Even with the streetcar subway running beneath Market Street, the city's transit system continues to operate streetcars on tracks in the center of the street as part of an historic streetcar line. In 2007, San Francisco's transit system opened a new light rail line to the southern part of the city using right-of-way Type B. Boston and Philadelphia renewed their already existing subway-surface streetcar lines with Type B right-of-way. Philadelphia made major streetcar cutbacks, however, by eliminating all of its north–south Type C streetcar routes. It since restored one of them using rebuilt PCCs. Route 15 – Girard Avenue intersects both the Broad Street Subway and Market-Frankford Elevated rapid transit lines. Boston also abandoned some Type C

streetcar service. New Orleans renewed its traditional St. Charles Street streetcar operation, and it expanded its streetcar operation by converting its heaviest bus route to streetcar operation. Before Hurricane Katrina temporarily shut the system down in August 2005, the New Orleans streetcar operation remained slow and traditional.

How streetcars function as a part of the overall transit system varies from city to city. Metropolitan Toronto's transit system was one of the few to have been organized as a grid network of north–south and east–west routes from the 1920s. Streetcars serve some of the heavy east–west routes in the grid, and they intersect with north–south bus, subway, and in some cases, other streetcars at every major north–south cross street. The transit system provides many off-street transfer stations that allow passenger to transfer between vehicles, using all doors, without drivers supervising their fare collection [37].

For years, Boston's streetcars have operated as radial routes funneling into the CBD-destined streetcar subway, which intersects with three rapid transit subway lines in the CBD. The streetcar subway then continues out the northern end of the CBD, where it serves a major commuter train terminal before crossing the Charles River and terminating at a streetcar/bus transfer station at Lechmere. Very few bus routes enter Boston's CBD, so almost all bus passengers destined for the CBD transfer to the streetcar subway or the other three rapid transit lines.

During the early 1980s, under the direction of Muni Planning Director Tom Matoff, the San Francisco Municipal Railway extensively restructured bus and trolley bus routes in the central part of the city to better serve non-CBD destinations. The transit system created new crosstown bus routes that intersected with the light rail subway running to the downtown. Parts of the bus routes previously running from the stations to the CBD were discontinued, and passengers heading to the CBD transferred to trains. The change was intended to increase productivity and make more destinations reachable by transit, thus increasing patronage.

In Pittsburgh, Cleveland, and Philadelphia transit service remains organized primarily as radial bus and streetcar (and in the case of Cleveland and Philadelphia, rapid transit lines) operating to the CBD. In some cases, passengers have to pay an additional fare to transfer between routes, and most passengers do not transfer. The subway-surface streetcar lines are not the organizing principle of area-wide route restructuring but function as just other transit routes heading downtown. (However, the 15 – Girard is a crosstown line functioning as part of the North Philadelphia grid system.)

This entry generally does not consider previously all-bus cities that built new streetcar lines during the last two decades. There are several of these. Most of the new streetcar lines are short urban circulator or tourist-oriented loops in central city areas. Table 1 does show one of these streetcars, however, partly because the line is longer than others and functions as a transit line connecting several destinations together. It also is shown, because its statistics had to be disentangled from Portland's light rail statistics in the construction of Table 1.

Analysis of Light Rail Transit Performance

Light rail advocates hoped that their efforts would increase transit use, improve transit productivity, and create North American lifestyles that could be independent of automobiles. There are no comprehensive studies that evaluate the extent to which such objectives have been reached, but there are academic studies that touch on light rail performance. Some are critical of light rail investments for costing a lot while achieving very little, while other studies show that light rail investments have had favorable impacts on transit system performance if the investments were planned to improve transit productivity. This section examines light rail performance. It first considers academic criticisms of light rail investments, followed by examinations of how light rail investments have affected overall transit performance in different metropolitan areas.

The primary conclusion from the various analyses is that light rail investments that have been accompanied by restructuring of bus systems have increased transit riding per capita in their service areas, and they have been more productive and more efficient in this regard than alternative forms of transit investment. Light rail investments accompanied by bus network restructuring have been particularly effective in rapidly growing parts of the country. Light rail investments not

accompanied by bus route restructuring have been less effective. New streetcar investments that eschew light rail productivity enhancements appear to be less effective, as well. Light rail investments have not, however, substituted for auto traffic to a large extent.

Criticisms of Rail Investments

Light rail traffic densities shown in Table 1 suggest that some light rail lines, such as in Salt Lake or Phoenix, are carrying sizable traffic in sprawling, auto-oriented regions where heavy rail transit volumes would not be expected. Examining the patronage consequences of new light rail transit investments throughout the USA, Polzin [38] found that although light rail patronage initially was disappointing, it was growing considerably as various systems expanded in scope. Light rail critics counter, however, that traffic density figures are not an indication of whether light rail investments increased transit ridership or reduced transit costs. They argue that without rail most of the same patronage would occur on buses at lower cost. Some critics argue that patronage actually would be higher without rail. Rail investments and operating expenses, they argue, starves the bus system of funds, resulting in its emaciation and loss of patronage. Without the rail lines, the bus systems would be much healthier and would have more patronage.

Arguments critical of light rail investments stem from the 1966 work of Meyer, Kain, and Wohl [39], which laid out an argument against investing in rail transit. They argued that public transportation was effective in only one market, which was connecting suburbs with CBDs. Unfortunately, CBDs had been in decline for almost a half century, and census data suggested the decline would continue into the foreseeable future. Thus, transit patronage would continue to decline. They also showed that for the suburb to CBD market, under almost all conceivable residential densities in the suburbs and employment densities in the CBD, express buses on freeways were a better choice than rail transit. Express buses could provide faster service with a one-seat ride at lower cost per passenger than rail transit lines. The latter were more expensive to build and operate, they argued, and required passengers to transfer from local buses to rail lines at suburban stations. Even worse, rail transit lines sometimes required a second transfer from rail to bus in the CBD. This type of argument has been used against proposed rail transit investments in numerous cities, and it also is used against restructuring of bus services around rail transit lines. The transit system opponents to light rail in San Diego, for example, appealed to these arguments extensively.

Examining patronage and cost data from recent heavy and light rail investments in the early 1990s, Pickrell [40] argued that rail transit supporters obtained political support for their projects by inflating patronage projections and underestimating cost projections. Kain [41] offered a case study on how such deception was used in Dallas. O'Toole [42] and Richmond [43] also provided empirical evidence showing that the actual costs of rail projects were greater and patronage less than projected. They also claimed that rail investments depressed transit patronage and increased transit costs compared to doing nothing or using similar investments for express buses. Richmond did report that there was one rail investment that improved transit patronage and reduced costs: San Diego.

In a forthcoming article, Giuliano argues that transit investments in the USA fail to achieve their objectives. She argues that the investments are large. In 2006, for example, all levels of government in the USA spent $36 billion for transit capital investments and for subsidizing two-thirds of transit operation expenses for that year. Such large expenditures in that year and in all prior years leading up to 2006 did little to expand transit ridership or influence urban form. She further argues that transit in the USA is useful primarily to the poor, but that government expenditures in transit do little to increase transit's usefulness to the poor. She includes expenditures on light rail development among expenditures that fail to achieve objectives or help the poor [44].

Comparison of Transit Performance in Urban Areas With and Without Light Rail Investments

The criticisms of rail transit investments suggest that metropolitan regions investing in rail transit will have lower overall transit ridership per capita than comparable regions that have bus-only transit systems. While trains might carry substantial patronage, it is suggested

by critics that the overall train plus bus patronage would be lower than the all-bus patronage in a region that did not invest in rail. The criticisms also suggest that the overall transit productivity, measured in passenger miles per vehicle mile, would be lower in urban areas with rail compared to similar regions with only buses. Finally, rail critics imply that the rail plus bus operating expense for moving each passenger 1 mile in urban regions that invested in rail would be higher than the bus-only operating expense for moving each passenger 1 mile in urban regions that did not invest in rail.

Brown and Thompson [45] tested these assertions for US metropolitan areas that contained between 1 and 5 million people. There were 45 of such midsized urban areas. Many light rail new starts were made within this group of metropolitan areas, and other metropolitan areas in this group considered light rail but decided not to implement it, such as Kansas City, Cincinnati, and Columbus. Brown and Thompson divided the 45 metropolitan areas into four categories. The first category contained bus-only metropolitan areas where the transit systems organized bus routes to carry passengers to many destinations. Six metropolitan areas fell into this category (Table 2). The second category contained metropolitan areas that operated both bus and rail routes (light rail in most cases), and the bus and rail routes were organized to reduce duplication of bus routes and to carry passengers to many different destinations. There were 10 metropolitan areas in this category. The third category contained metropolitan areas that operated both bus and rail routes, but most of the routes were radial in nature, focused on the CBD. The fourth, and largest category (20 metropolitan areas), contained metropolitan areas that operated only buses, and the bus routes mostly focused on the CBD.

Having established the categories, Brown and Thompson then calculated median transit performance in 1984 and 2004 for each of the four categories, using three performance measures. One performance measure was annual passenger miles per capita for the region. This measure indicates the degree to which the average inhabitant of the region uses transit. Another performance measures was passenger miles per vehicle mile, which indicates the average number of passengers on board a transit vehicle each mile that it operates. This is a measure of productivity. The remaining performance measure is total transit operating expense per passenger mile, expressed in real dollars that remove inflation. This is a measure of operating efficiency.

Tables 3–5 show the results. The multidestination bus plus rail category outperforms the other three categories by a wide margin. This is the category that includes cities that invested in light rail and reconfigured the bus route structure around new rail lines (San Diego, Portland, Atlanta, Miami, St. Louis as examples). Most of the rail transit investments were light rail, though Atlanta's and Miami's rail investments were rapid transit lines. This is the only category to increase transit patronage per capita (Table 3). It is the category to have the lowest reduction in transit productivity, and three of the light rail/bus systems actually increased their productivity (Portland, St. Louis, San Diego). It also is the category to have the lowest increase in operating costs. By 2004, operating costs in this category were far lower than in the radial bus-only category.

The multidestination bus and rail category performed well despite poor performance of two of its metropolitan areas: Sacramento and New Orleans. As noted earlier, Sacramento partially abandoned coordination between buses and trains that characterized the system in its early years. New Orleans saw the worst change in performance on all three performance indicators. Slow traditional streetcar lines do not appear to be good for transit performance.

Urban areas that invested in rail but operated most of their rail and bus routes to the CBD did not do well. Such urban areas include Pittsburgh, Cleveland, and Buffalo. These metropolitan areas saw declines in most of the performance indicators. Salt Lake and Memphis, however, did well. Memphis is included in the rail category because it invested in a short downtown circulator streetcar. Carrying about 3,400 passengers per day, the Memphis streetcar carries about 10% of transit patronage in the Memphis metropolitan area [36]. Salt Lake operates a long, fast light rail line with a short branch to a university. The two light rail lines serve several important destinations, while the bus system was very sparsely developed before the light rail line was built and changed little with its opening.

The worst-performing category for each performance measure is the radial all-bus category, which is

Light Rail Transit, Systemic Viability. Table 2 Classification of 45 midsized US metropolitan areas into four categories based on mode of transit and orientation of route structure

Multidestination MSAs[a]			
Bus-only (in 2004)[b]	% Non-CBD routes	Bus-and-rail (in 2004)[b]	% Non-CBD routes
Las Vegas	73.58%	Atlanta	75.00%
Milwaukee	48.53%	Dallas	61.08%
Norfolk	49.18%	Denver	58.70%
Phoenix	61.36%	Miami	67.61%
Rochester	45.00%	New Orleans	50.50%
San Antonio	45.00%	Portland	56.82%
		Sancramento	69.05%
		Saint Louis	54.55%
		San Diego	81.87%
		Seattle	53.88%
Radial MSAs[a]			
Bus-only (in 2004)[b]	% Non-CBD routes	Bus-and-rail (in 2004)[b]	% Non-CBD routes
Albany	9.52%	Buffalo	34.92%
Austin	22.86%	Cleveland	39.68%
Birmingham	5.41%	Hartford	6.90%
Charlotte	27.16%	Houston	38.32%
Cincinnati	7.14%	Jacksonville	23.81%
Columbus	24.14%	Memphis	20.90%
Dayton	23.53%	Minneapolis-Saint Paul	34.80%
Grand Rapids	21.74%	Pittsburgh	21.33%
Greensbroo	16.39%	Salt Lake City	42.42%
Greenville	0.00%		
Indianapolis	7.14%		
Kansas City	40.82%		
Louisville	29.63%		
Nashville	0.00%		
Oklahoma City	16.13%		
Orlando	43.75%		
Providence	29.31%		

the category that contains almost half of the transit systems. In 2004, the median metropolitan area in this category had only one-fifth the transit ridership per capita as the median multidestination bus-rail system (Table 3). Over the preceding 20 years, the median decline in ridership per capita for the all-bus radial category was 13%, while the median increase in ridership per capita for the multidestination bus/rail category was 9% (Table 3). Productivity for the median all-bus radial category was about a third worse (Table 4),

Light Rail Transit, Systemic Viability. Table 2 (Continued)

Radial MSAs[a]			
Bus-only (in 2004)[b]	% Non-CBD routes	Bus-and-rail (in 2004)[b]	% Non-CBD routes
Raleigh	22.89%		
Richmond	9.62%		
Tampa	33.33%		

[a]We defined MSAs as multidestination or rail using the variable measuring percent of transit routes that do not serve the CBD. We classified MSAs with 45% or more of the routes not serving the CBD as multidestination MSAs. We classified the remaining MSAs as radial MSAs

[b]We defined MSAs as bus-only or bus-and-rail based on the transit system in 2004. We placed two MSAs (Milwaukee and Tampa) with rail transit routes totaling less than 4 miles in length in the bus-only group

Source: Brown and Thompson [45].

while operating expenses per passenger mile were about a third more than the median for the bus/rail multidestination category (Table 5). Real operating expenses per passenger mile for the median all-bus radial category also increased almost four times faster than real operating expenses per passenger mile for the median multidestination rail/bus system (Table 5). Most if not all of the metropolitan areas in this category invested very little in their bus systems for busways. Over the 20 years of the study, they also tended not to expand bus miles to provide more coverage or greater frequency. In short, there is little evidence that because they did not invest in rail transit that they improved their bus systems instead.

Overall, the results of Brown and Thompson [45] suggest that light rail investments around which bus services are reconfigured into multidestination transit systems increase their ridership more, have greater ridership, have greater productivity, and cost less to operate than all-bus systems and rail plus bus systems that focus most of their routes on CBDs. These results appear to occur, because travel markets are more complex than the simple suburb to CBD model originally postulated by Meyer, Kain, and Wohl in 1966. Residents in metropolitan areas are traveling to multitudes of different destinations in addition to CBDs. The multidestination bus/rail systems appear to be better suited to tapping the more complex travel markets than the radial all-bus and bus/rail transit systems. Another study confirmed this point. It shows that regional employment reachable by bus and train combinations in Atlanta is important for explaining rail ridership on Atlanta's rapid transit lines. Fluctuations of employment in Atlanta's CBD are not important, primarily because CBD employment is such a small part of employment in the rest of the transit system's service area. Employment outside of the transit service area, or which there is much in Atlanta, also affects transit ridership, but negatively [46].

Surveys of passengers on board transit vehicles yield additional insights into transit travel markets. Several of the multidestination bus/rail transit systems administered such surveys, and their results are similar. They show that the bus parts of multidestination rail/bus transit systems attract transit-dependent riders while the rail parts attract both transit dependent and choice riders. The large numbers of passengers who use combinations of buses and trains to complete their trips have characteristics almost identical to the passengers who use only buses [14]. In the context of the multidestination transit system attracting many more riders per capita than the radial systems, these results suggest that much of the added demand captured by the multidestination systems comes from the transit dependent. It appears that the demand for transit by the transit dependent population is highly elastic with respect to directness of transit service between origin and destination. Another study of persons going to work on an all-bus multidestination network in Broward County, Florida, confirms this point. It reveals that almost all of the workers are transit dependent and destined to employment throughout the metropolitan area. Transit travel time between origin and destination is the most important variable for influencing their ridership, and

Light Rail Transit, Systemic Viability. Table 3 Ridership per capita in 1984, 2004 for transit systems in each category

Ridership (passenger miles per capita)							
Multidestination bus-and-rail MSAs	1984	2004	Percent change (1984–2004)	Radial bus-and-rail MSAs	1984	2004	Percent change (1984–2004)
Atlanta	173.06	149.07	−13.86%	Buffalo	82.21	56.53	−31.23%
Dallas	63.33	66.12	4.40%	Cleveland	144.50	94.57	−34.56%
Denver	131.74	149.01	13.11%	Hartford	68.50	59.43	−13.24%
Miami	125.14	163.80	30.90%	Houston	97.41	99.28	1.92%
New Orleans	161.51	94.92	−41.23%	Jacksonville	55.01	48.28	−12.23%
Portland	161.89	223.71	38.19%	Memphis	40.87	55.85	36.66%
Sacramento	74.41	67.66	−9.07%	Minneapolis-Saint Paul	105.62	86.36	−18.24%
Saint Louis	71.66	91.72	28.00%	Pittsburgh	130.46	116.43	−10.75%
San Diego	117.19	148.87	27.03%	Salt Lake City	70.66	80.66	14.15%
Seattle	203.13	198.06	−2.49%	*Median*	*82.21*	*80.66*	*−12.23%*
Median	*128.44*	*148.94*	*8.76%*				
Multidestination bus-only MSAs	1984	2004	Percent change (1984–2004)	Radial bus-only MSAs	1984	2004	Percent change (1984–2004)
Las Vegas	22.67	107.05	372.17%	Albany	53.40	45.90	−14.05%
Milwaukee	143.49	101.99	−28.93%	Austin	60.16	80.02	33.02%
Norfolk	53.06	51.32	−3.26%	Birmingham	21.32	17.13	−19.64%
Phoenix	40.16	53.49	33.20%	Charlotte	22.23	36.68	65.02%
Rochester	53.67	39.13	−27.10%	Cincinnati	81.42	72.40	−11.08%
San Antonio	101.14	82.84	−18.09%	Columbus	82.39	25.15	−69.48%
Median	*53.36*	*68.16*	*−10.68%*	Dayton	85.99	41.61	−51.61%
				Grand Rapids	16.37	17.03	4.04%
				Greensboro	11.67	9.50	−18.65%
				Greenville	4.46	4.94	10.69%
				Indianapolis	44.54	22.82	−48.76%
				Kansas City	33.83	25.74	−23.92%
				Louisville	86.59	40.42	−53.32%
				Nashville	34.97	20.15	−42.39%
				Oklahoma City	12.52	16.75	33.80%
				Orlando	27.24	68.62	151.96%
				Providence	55.51	55.07	−0.78%
				Raleigh	15.96	27.64	73.13%
				Richmond	69.86	29.39	−57.93%
				Tampa	38.64	38.82	0.48%
				Median	*36.80*	*28.51*	*−12.56%*

Source: Brown and Thompson [45].

Light Rail Transit, Systemic Viability. Table 4 Productivity, measured as passenger miles per vehicle mile in 1984, 2004 for transit systems in each category

Service productivity (passenger miles per vehicle mile)							
Multidestination bus-and-rail MSAs	1984	2004	Percent change (1984–2004)	Radial bus-and-rail MSAs	1984	2004	Percent change (1984–2004)
Atlanta	13.88	13.79	−0.72%	Buffalo	10.23	6.49	−36.61%
Dallas	11.86	8.60	−27.50%	Cleveland	14.21	7.97	−43.95%
Denver	9.17	7.47	−18.51%	Hartford	10.24	6.77	−33.93%
Miami	11.38	10.34	−9.13%	Houston	9.81	9.56	−2.62%
New Orleans	14.64	8.68	−40.72%	Jacksonville	7.56	5.64	−25.44%
Portland	8.41	12.25	45.53%	Memphis	6.67	8.18	22.61%
Sacramento	11.35	9.14	−19.52%	Minneapolis-Saint Paul	9.70	8.19	−15.63%
Saint Louis	7.77	9.16	17.92%	Pittsburgh	10.05	7.18	−28.59%
San Diego	10.95	11.15	1.77%	Salt Lake City	6.05	5.56	−8.11%
Seattle	11.21	9.38	−16.29%	*Median*	*9.81*	*7.18*	*−25.44%*
Median	*11.28*	*9.27*	*−12.71%*				
Multidestination bus-only MSAs	1984	2004	Percent change (1984–2004)	Radial bus-only MSAs	1984	2004	Percent change (1984–2004)
Las Vegas	10.90	11.23	3.05%	Albany	9.15	6.97	−23.83%
Milwaukee	9.29	7.19	−22.64%	Austin	7.24	6.98	−3.55%
Norfolk	8.31	7.65	−7.96%	Birmingham	6.83	5.98	−12.50%
Phoenix	8.88	6.29	−29.18%	Charlotte	9.46	6.90	−27.02%
Rochester	8.97	6.59	−26.45%	Cincinnati	9.95	9.11	−8.45%
San Antonio	8.59	8.01	−6.74%	Columbus	12.75	4.81	−62.27%
Median	*8.92*	*7.42*	*−15.30%*	Dayton	12.96	5.56	−57.12%
				Grand Rapids	5.63	5.73	1.79%
				Greensboro	8.57	4.92	−42.63%
				Greenville	5.24	7.00	33.73%
				Indianapolis	10.66	6.31	−40.76%
				Kansas City	6.59	4.74	−28.03%
				Louisville	11.96	6.47	−45.89%
				Nashville	8.53	5.28	−38.13%
				Oklahoma City	4.80	5.11	6.46%
				Orlando	7.22	9.37	29.93%
				Providence	8.72	7.19	−17.55%
				Raleigh	6.18	4.55	−26.29%
				Richmond	11.57	5.96	−48.50%
				Tampa	8.26	5.99	−27.52%
				Median	*8.55*	*5.98*	*−26.65%*

Source: Brown and Thompson [45].

Light Rail Transit, Systemic Viability. Table 5 Cost efficiency, measured as real annual operation expenses per passenger mile in 1984, 2004 for transit systems in each category (all expenses expressed in real 2006 dollars)

Cost efficiency (real operating expense per passenger mile, 2006 dollars)							
Multidestination bus-and-rail MSAs	1984	2004	Percent change (1984–2004)	Radial bus-and-rail MSAs	1984	2004	Percent change (1984–2004)
Atlanta	$0.41	$0.57	40.08%	Buffalo	$0.66	$1.27	91.93%
Dallas	$0.70	$0.71	1.60%	Cleveland	$0.54	$0.88	62.75%
Denver	$0.70	$0.67	−4.61%	Hartford	$0.56	$0.92	63.71%
Miami	$0.62	$0.66	7.03%	Houston	$0.60	$0.55	−8.57%
New Orleans	$0.49	$0.98	97.42%	Jacksonville	$0.60	$0.87	45.16%
Portland	$0.72	$0.60	−16.08%	Memphis	$0.78	$0.65	−15.70%
Sacramento	$0.52	$0.87	66.07%	Minneapolis-Saint Paul	$0.66	$0.83	25.59%
Saint Louis	$0.87	$0.65	−25.92%	Pittsburgh	$0.76	$0.97	27.88%
San Diego	$0.45	$0.52	15.96%	Salt Lake City	$0.60	$0.91	51.56%
Seattle	$0.54	$0.82	51.67%	*Median*	*$0.60*	*$0.88*	*45.16%*
Median	*$0.58*	*$0.66*	*11.49%*				
Multidestination bus-only MSAs	1984	2004	Percent change (1984–2004)	Radial bus-only MSAs	1984	2004	Percent change (1984–2004)
Las Vegas	$0.49	$0.46	−5.40%	Albany	$0.52	$0.84	60.93%
Milwaukee	$0.60	$0.87	43.97%	Austin	$0.99	$0.84	−15.12%
Norfolk	$0.62	$0.59	−5.46%	Birmingham	$0.76	$0.69	−8.33%
Phoenix	$0.64	$0.94	46.67%	Charlotte	$0.52	$0.77	46.67%
Rochester	$0.70	$1.05	49.73%	Cincinnati	$0.64	$0.59	−8.33%
San Antonio	$0.49	$0.57	16.61%	Columbus	$0.45	$1.45	225.23%
Median	*$0.61*	*$0.73*	*30.29%*	Dayton	$0.41	$1.05	156.68%
				Grand Rapids	$0.83	$0.92	10.01%
				Greensboro	$0.47	$1.18	154.39%
				Greenville	$0.60	$0.59	−2.41%
				Indianapolis	$0.50	$0.75	48.08%
				Kansas City	$1.09	$0.16	7.06%
				Louisville	$0.43	$0.84	97.51%
				Nashville	$0.50	$0.95	88.28%
				Oklahoma City	$0.97	$0.77	−20.80%
				Orlando	$0.45	$0.50	12.40%
				Providence	$0.62	$0.91	46.10%
				Raleigh	$0.74	$0.89	20.14%
				Richmond	$0.47	$0.90	92.51%
				Tampa	$0.45	$0.82	83.94%
				Median	*$0.52*	*$0.84*	*46.39%*

Source: Brown and Thompson [45].

every 1% decrease in transit travel time between origin and destination increases transit-dependent riding by 2.7% [47].

These results suggest that metropolitan areas that invest in light rail systems achieve far greater transit performance than metropolitan areas that do not invest in light rail systems, if the metropolitan areas restructure their bus networks around light rail stations to reduce bus miles and achieve multidestination travel capability. Productivity will improve, cost efficiency will improve, and ridership per capita will increase. Added ridership will be a combination of the transit dependent and riders who have a choice for using an auto. Metropolitan areas that invest in light rail but do not do restructure their bus systems will not see such improvements in system performance.

This is a suggestive conclusion and not a hard-and-fast rule. There is the counter example of Salt Lake, which invested in a fast light rail line that connected a number of destinations together while not changing its CBD-radial bus system very much. The bus system was sparsely developed to begin with, and decision makers did not want to be accused of cutting back the already sparse CBD-focused bus system to pay for rail. The result was that the rail system attracted new ridership from previous auto users, and it also attracted about half of the bus system's ridership. The largely empty buses became even emptier. The light rail line looked like a winner, while the bus system looked like a loser [14]. The Salt Lake result is consistent with the thrust of a recent study of variables affecting rail transit ridership. That study concludes that the most important variable for increasing ridership is the magnitude of suburban employment within walking distance of rail stations. Rail lines that serve only employment in CBDs have low ridership, because most employment is located outside of CBDs. Rail lines with high ridership directly serve employment in many locations. The study concludes that multidestination rail networks serving large parts of regional employment are essential for attracting rail ridership but bus connections are irrelevant [48].

Consideration of Capital Investment

An unanswered question from the analysis of transit performance in US midsized metropolitan areas is whether the favorable light rail performance results are worth the investment in light rail systems. If annualized capital expenses per passenger mile were added to operating expenses per passenger mile, would light rail appear so attractive? Brown and Thompson did not include capital investments for either buses or light in their analyses, because there is no source from which to obtain capital investments in US or Canadian transit systems. In the absence of such a data source, one could attempt to estimate capital investment in a metropolitan area's transit system in a given year, but doing so is a huge task and rarely has been attempted [49].

One study that did estimate comparative capital costs between light rail and buses was Kain and Liu's 1999 study comparing transit development in Houston and San Diego [49]. Both metropolitan regions aggressively development transit over a period of years, Houston with express buses on busways and high occupancy vehicle (HOV) lanes on freeways, and San Diego with light rail lines, around which the regional bus system was restructured. Kain and Liu found that both metropolitan regions achieved comparable gains in ridership with comparable investment in transit fixed facilities and rolling stock, measured per passenger mile. In coming to this conclusion, Kain and Liu prorated only a portion of the cost of HOV facilities to transit passengers, because motorists also used the facilities. These results suggest that metropolitan regions that invested heavily in express bus on freeway or busway facilities, such as Houston, Minneapolis-St. Paul, Seattle, and Pittsburgh, may incur capital expenses per passenger mile as high or higher (as was the case in Houston compared to San Diego) as metropolitan areas investing in light rail systems, such as San Diego, Denver, Dallas, St. Louis, or Portland.

One may conclude, then, that light rail capital investment, if it is accompanied by a bus network restructuring, buys a much better-performing transit system than no capital investment over and above what is required to buy buses and bus maintenance facilities. The multidestination transit network resulting from the light rail investment carries many more passengers, and the increment of additional passengers comes from both the ranks of auto users and of the transit dependent, who now use transit much more frequently than when they were forced to use a system focused on downtown. Presumably, the transit dependent who

now use transit much more, and the former auto users experience greater welfare for having made the switch to transit. Are these results worth the capital investment? A benefit-cost analysis is required to answer that question, and at the moment the authors are aware of none to which to turn.

Suppose that it is decided to spend a certain amount of capital in a metropolitan region that would buy either a core light rail system, around which buses could be restructured into a multidestination network, or an express bus network, using busways and HOV lanes on freeways, all focused on the CBD. Many light rail critics claim that money would be much better spent on the latter. How does a light rail investment in fact stack up to an express bus investment? The next section addresses that question by turning to three actual cases.

Comparison of Light Rail and Express Bus Performance

Brown and Thompson [51] examined express bus and light rail performance in three metropolitan areas that operate both modes: San Diego, Minneapolis-St. Paul, and Pittsburgh. In San Diego, light rail has been the center of transit development in the southern part of San Diego County since 1978, but express buses and commuter rail are the enhanced mode in the northern part of the county. Light rail and express buses function quite differently in San Diego County. In the light rail corridors, light rail stations are the focus of transit activity. Local bus routes focus on light rail stations, and passengers transfer not only between buses and trains, but between buses and buses (Fig. 9). Two of the stations shown in Fig. 9, 12th and Imperial and Old Town, also are transfer points between light rail lines, and the Old Town station also accommodates transfers with commuter trains.

The express bus corridors in the San Diego area have much less interaction with the local transit network. Buses operate long distances from northern points to the San Diego CBD. Some of the express buses operate nonstop, but some of them leave the freeway at intermediate locations to serve important destinations and transfer stations with light rail and other bus routes. There is a large time penalty in doing so, because of heavy traffic congestion around the freeway on and off ramps, but the destinations are important enough to warrant the loss of time. Nonetheless, there is much less emphasis on express bus transferring with local bus lines than in the light rail corridors, and because of the time penalty associated with express bus stations, there are far fewer express bus stations than light rail stations.

Figure 9 shows the patronage results in the San Diego area. The area of each of the blue circles is proportional to transit passengers getting on and off vehicles. The figure shows that most passenger activity in the San Diego region is associated with the light rail stations. Express bus stations are considerably less important, even though they serve areas of heavy population and employment. Express buses in each of the two corridors to the north carry about 5,000 daily passengers in each corridor. The light rail corridor running from Old Town through the CBD to the border (the Blue Line) carries about 65,000 passengers per day. (The express bus that operated in the CBD to border part of this corridor until the light rail line opened in 1981 carried about 900 passengers per day.) The light rail line running from the CBD to El Cajon to the east (the Orange Line) carries about 25,000 passengers per day. Not shown in the figure is the eastern half of the newest light rail line in San Diego, which runs from Old Town east to El Cajon (the Green Line, operating through the west–east Mission Valley). Even though the Green Line does not serve the CBD, it does serve many other important destinations, including two regional malls, suburban office buildings, apartment and condominium complexes, complexes of big box stores, San Diego State University (SDSU in Fig. 9), and a sports stadium. It is carrying about 22,000 passengers per day [52]. By far the most heavily patronized transit stop in the region is not in the CBD but is the Old Town Station, where the Green Line intersects with the Blue Line running to the CBD and the south, numerous bus lines running to the northeast, north, northwest, west, and southwest, and a commuter rail line running to the north. A large park and ride lot also is located at the Old Town station. Before the Green Line was completed to El Cajon, the Old Town Station accommodated about 20,000 boarding and alighting passengers per day in 2005; that number increased to 32,000 daily boarding and alighting passengers in 2006 after the Green Line opened in its entirety. The second

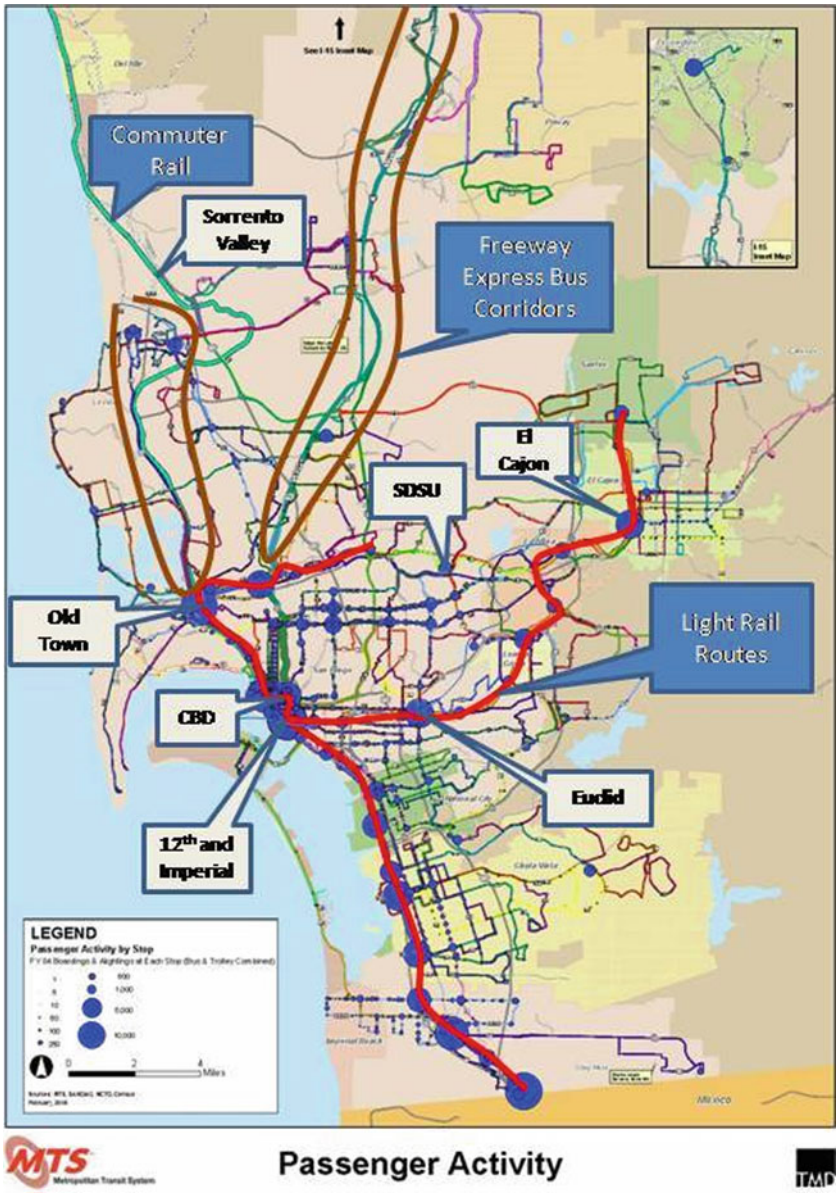

Light Rail Transit, Systemic Viability. Figure 9
Transit lines and daily boardings and alightings at transit stops, San Diego 2005, a year before the full Mission Valley line opened [51]

most heavily patronized station in the region is the 12th and Imperial Station, which is the transfer point between the south (Blue Line) and east (Orange Line) light rail corridors. The 12th and Imperial station (called the Mills Center) handled about 22,000 boardings and alightings per day in 2006, and most of the passengers were transferring between the two light rail routes [14].

The top panel of Table 6 also shows the much greater productivity of light rail compared to express buses in the San Diego area. Express buses account for 12% of the revenue hours of transit service in the region but carry 7% of the transit passengers. The three light rail lines accounts for 7% of the revenue hours of transit service in the region but carry 33% of the transit passengers. These numbers illustrate what is

Light Rail Transit, Systemic Viability. Table 6 Express bus and light rail comparisons in three metropolitan areas. 2006 data

Transit service	Passenger trips	Revenue hours	Revenue miles	Trips per revenue hour[a]	Trips per revenue mile[a]
San Diego					
Express bus	21,606	717	13,839	23.80	1.10
Percent of system total	7%	12%	14%		
Light rail transit	106,087	437	9,552	242.65	11.11
Percent of system total	33%	7%	10%		
Minneapolis-Saint Paul					
Express bus	31,097	742	16,871	39.66	1.77
Percent of system total	13%	15%	22%		
Light rail transit	26,407	142	2,818	186.36	9.37
Percent of system total	11%	3%	4%		
Pittsburgh					
Bus routes using busway	43,582	1,878	33,915	18.62	1.12
Percent of system total	19%	22%	28%		
Light rail transit	26,038	340	4,863	76.54	5.35
Percent of system total	11%	4%	4%		

[a]Performance for express bus routes refers to the median-ranked route
Source: Brown and Thompson [51].

meant by light rail being the backbone of transit service, around which the rest of the transit system is organized. Tables 3–5 show that transit in San Diego is among the best performing of the transit systems in midsized US metropolitan areas.

The San Diego light rail and bus network is organized so that passengers could travel to many destinations in addition to those in the CBD. Most bus routes and one of the three light rail routes do not go to the CBD, and one could infer that most of their passengers are not going to the CBD, either. Even transit routes directly serving the CBD have most of their passengers going to other destinations, as shown in Table 7. Constructing Table 7 was possible, because the San Diego MPO keeps detailed records of passenger boardings and alightings for all stops for all transit routes at different times of the day. During the morning rush period, 65% of the riders of the two light rail lines directly serving the CBD did not get off in the CBD. They got off at other stations. Eighty-five percent of express bus riders, 68% of commuter train riders, and 77% of local bus riders got off at destinations other than the CBD. These figures indicated that a large market does exist for non-CBD transit service. The Canadian approach to transit network design, structuring bus routes around light rail lines serving numerous destinations, thus appears to be an approach to providing transit service that would yield much higher ridership and greater productivity than CBD-focused approaches, such as in the next two examples.

Minneapolis-St. Paul offers a different perspective, in that the region operates both light rail and express buses, but light rail is not the favored mode in that area. Since the 1970s, the area's transit provider, Metro Transit focused on connecting suburban neighborhoods to the CBD with express buses operating on freeways. Metro Transit has done an excellent job expanding the express bus system, and it is considered one of the more

Light Rail Transit, Systemic Viability. Table 7 Weekday morning peak period transit alighting for transit routes serving the San Diego CBD directly. FY 2006 data

Location	Type of service							
	Trolley (LRT)		CBD-serving express bus		Coaster (commuter rail)		CBD-serving local bus	
	Alightings	Percent	Alightings	Percent	Alightings	Percent	Alightings	Percent
Inside CBD	6,687	34%	400	15%	670	32%	2,517	23%
Outside CBD	13,000	66%	2,349	85%	1,447	68%	8,254	77%
Total	19,687	100%	2,749	100%	2,117	100%	10,771	100%

Source: Brown and Thompson [14].

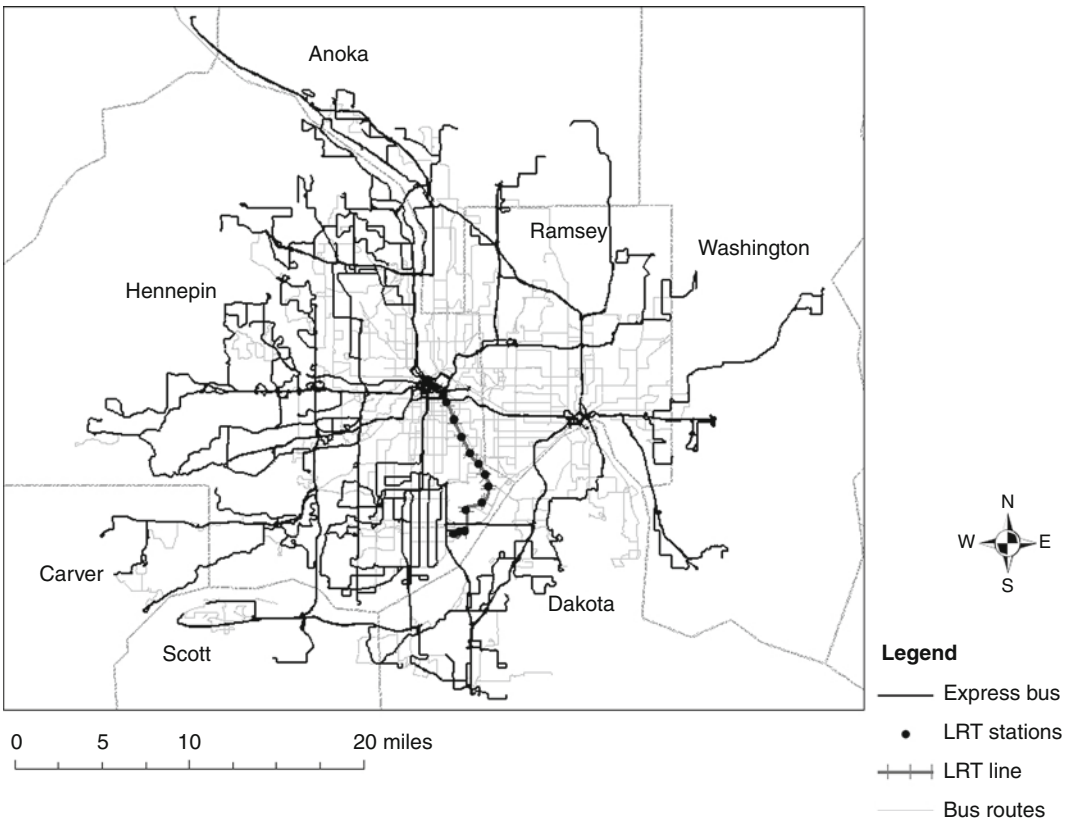

Light Rail Transit, Systemic Viability. Figure 10
Transit routes in Minneapolis-St. Paul [51]

progressive transit systems in the USA for its efforts in this regard. More than 90 of the region's 200 plus bus routes are express bus routes, and 85% of them focus on the Minneapolis or St. Paul CBDs. Figure 10 shows in heavy black lines the area's CBD-oriented express buses and light gray lines other bus routes. There also is a heavy investment in infrastructure to facilitate the express bus service. Express buses make use of 15 miles of busways, 38 miles of high-occupancy vehicle lanes, and 268 miles of bus-only freeway

shoulder lanes [51]. Metro Transit did not open a light rail line until 2004. The agency had opposed light rail transit but acceded to outside political pressures to build a line. To its credit it built a state-of-the art line, around whose stations it restructured local bus lines operating into the light rail corridor. The line serves not only the Minneapolis CBD, but also two stations at the international airport and a terminal station at the Mall of America, perhaps the largest suburban mall in the USA. The Minneapolis light rail line thus is multidestination in character. The light rail line and its stations also are shown in Fig. 10 [14, 51].

Express buses in the Minneapolis-St. Paul region are among the most productive in the nation [14]. Despite this, the express buses are not nearly as productive as the region's light rail line, as shown in the middle panel of Table 6. The express bus system accounts for 15% of the region's hours of transit service and carries 13% of the region's transit passengers. The one light rail line accounts for 3% of the region's hours of service but carries 11% of the region's transit passengers. The percentage may be higher today. The more recent daily light rail patronage figure for Minneapolis of 34,000 daily passengers in 2008, shown earlier in Table 1, indicates light rail passenger growth.

The trend of patronage for the overall transit system, however, has been downward, as shown earlier in Tables 3–5. The downward trend could be caused by decentralization. The transit system is exceptionally well run, and the region is progressive and growing. Service reliability and regional decline are not causes of transit decline. The region continues to decentralize, however, and the CBDs are becoming relatively if not absolutely less important as time passes. Metro Transit recognizes this point and is building more intermediate stations at emerging destinations along its express bus routes to tap new, non-CBD travel demands. Overall, however, the transit system in the Minneapolis-St. Paul region remains CBD-centric.

Pittsburgh also operates both light rail and express buses in a transit system where about 85% of total regional transit service connects suburban neighborhoods with the CBD. The transit system, the Port Authority of Allegheny County (PAT) invested in three busways and a light rail line. The busways are Type A grade-separated facilities that run to the south, east, and west from the CBD. Express buses coming from the suburbs funnel into the busways and head to the CBD. The busways cost several hundred million dollars to build, and each one was designed to serve up to 50,000 passengers per day. Actual usage is much lower, varying between 9,000 and 13,000 daily passengers, depending on the busway. The light rail line is a several hundred million dollar rebuilding of the South Hills streetcar corridor, including a subway in the CBD. Its primary purpose is to connect residential neighborhoods in the south of the city to the CBD. The line does serve a second destination, however, which is South Hills Village, a suburban shopping center. Unlike stations on the light rail line in Minneapolis-St. Paul, Pittsburgh light rail line stations are not focal points for local bus routes. Bus lines tend to parallel the light rail line into the CBD. The south busway also parallels part of the light rail line and uses the light rail Mt. Washington Tunnel to gain access to the CBD. Transferring between buses and light rail trains is difficult at suburban stations. Not only do few bus routes intersect with the rail route, but transferring passengers must pay a second fare on the vehicle to which they transfer [14, 51].

As noted earlier in Tables 3–5, the Pittsburgh transit system has been in decline. Its CBD focus may be the cause. Although population in the overall region has not been growing, it has been decentralizing. The CBD also has been losing employment relative to the rest of the region [14]. The CBD is the only market that the transit system has identified as being important to serve; thus, as the CBD declines, so does the transit system. Because of its isolation from the rest of the transit system, light rail in Pittsburgh is not as well used or productive as light rail is in many other US cities. Table 1 presented earlier shows its passenger density is among the lowest of light rail lines in the USA. Despite that, it still is more productive than the Pittsburgh express bus system, as shown in the bottom panel of Table 6. Express buses account for 22% of daily transit service hours in Pittsburgh and carry 19% of daily transit passengers. Light rail accounts for 4% of daily service hours and carries 11% of daily transit passengers.

Light Rail Traffic Density Related to Strategic Development of Light Rail Systems and to Land Use

Table 1 presents average light rail passenger densities. This section discusses traffic densities in the context of

light rail development strategies and land uses in several of the urban areas listed in the table, coming to conclusions about the relative effectiveness of those strategies in the context of different land uses. Traffic densities, for example, suggest that of the pioneer light rail systems, Edmonton and Calgary are highly successful, and that the systems in San Diego, and Portland are less successful, but on the other hand, they are relatively more successful light rail initiatives than those in San Jose, Sacramento, and Buffalo. The transit systems in Edmonton, Calgary, San Diego, and Portland all developed with similar visions of light rail serving as the core of multidestination light rail/bus networks. Differences in transit development strategy do not explain differences in traffic densities between the Canadian and US light rail systems, but differences in land uses may. Edmonton and Calgary are more compact metropolitan areas than San Diego and Portland, with fewer freeways and more apartment living. Distances between places where people begin and end trips are shorter. Such land use differences may account for the greater light rail traffic densities in the Canadian metropolitan areas compared to their US counterparts employing similar principles of transit development. Jones [11], on the other hand, argues that the higher transit ridership seen in Canadian cities compared to transit use of similar cities in the USA is due largely to lower personal income in Canada.

Higher light rail passenger densities in San Diego and Portland compared to those in San Jose, Buffalo, and Sacramento likely arise as a consequence of the role of the light rail lines in San Diego and Portland as the cores of their multidestination transit networks. Such strategic vision has been less well articulated in San Jose and Buffalo, and it has not been consistently embraced in Sacramento.

The traffic densities of Edmonton, Calgary, San Diego, and Portland light rail lines also equal or exceed the traffic densities of most of the older streetcar operations that have been rebuilt. Boston is the only older streetcar operation whose traffic density exceeds that of most of the modern light rail adoptions, and that is because many passengers use the Boston streetcar subway as a shuttle to their final destination after alighting from rapid transit lines, bus lines, and commuter trains. Hardly any buses serve the Boston CBD, and bus passengers destined to the CBD transfer to light rail or rapid transit lines. The light rail traffic densities of Edmonton, Calgary, San Diego, and Portland light rail lines are much greater to slightly greater than streetcar traffic densities in Toronto and San Francisco, two cities where the streetcars function as important parts of bus/streetcar/rapid transit integrated route networks. Toronto and San Francisco both are densely populated cities, and one would expect that their streetcar traffic densities are greater than they are relative to the lower-density, more sprawling metropolitan areas of Edmonton, Calgary, San Diego, and Portland because of their central city locations. However, streetcars in San Francisco (even in the subway) and in Toronto generally are much slower than the light rail lines, and slow speed may account for the lower-than-expected streetcar traffic densities in Toronto and San Francisco. Similarly, the subway-surface light rail lines in Philadelphia are both relatively slow and are not part of integrated bus/light rail networks.

Light rail traffic densities in Edmonton, Calgary, Portland, and San Diego greatly exceed the light rail traffic densities of Cleveland and Pittsburgh, which are other suburban light rail lines, but where there is no route coordination with buses. Cleveland and Pittsburgh operate CBD-radial transit systems. The light rail traffic densities in Edmonton, Calgary, Portland, and San Diego also greatly exceed the traffic densities of the New Orleans and Portland streetcars.

Similar patterns are exhibited by more recent light rail adoptions. Those that are characterized by bus systems being restructured around light rail lines (Dallas, Denver, Minneapolis, St. Louis) or where the light rail lines have been imbedded into bus grid networks (Los Angeles in the cases of the Blue and Green Lines but not the Gold Line) generally have higher traffic densities than those where bus/light rail integration does not exist (Baltimore, Pittsburgh, Hudson-Bergen).

The importance of the place of light rail in a multidestination bus network for high traffic density is illustrated by the Green Line in Los Angeles. As the Green Line in San Diego, Los Angeles' Green Line does not serve the CBD. It is an east–west crosstown line that runs in the median of huge freeway about 8 miles south of the CBD, and pedestrian access between its stations and surrounding land uses very difficult. The line does not serve directly any major trip generators and is

dubbed locally, "The line from nowhere to nowhere." Yet, it carries between 30,000 and 40,000 passengers per day. It operates entirely on a Type A right-of-way, is very fast, and at every station it intersects with a north–south arterial road, each one of which carries a long, frequent, heavily patronized bus line offering free transfers to and from the rail line. Transfer movements are heavy. The Green Line also connects with the north–south Blue Line, the first light rail line in the region. The Blue Line carries 75,000–85,000 passengers per day (the most heavily traveled single light rail line in the USA) because it is fast and because almost every station serves a major east–west arterial road, each of which hosts a long, frequent, heavily patronized bus line with free transfers to and from trains [53].

There are two light rail applications with lower traffic densities that restructured bus services around the light rail investments. Neither one disproves the proposition that multidestination transit systems achieved by restructuring bus networks around light rail investments improves transit performance. One of these is in St. Louis. St. Louis operates a fast light rail spine through the center of the metropolitan area serving the CBD and several other important destinations. Within the metropolitan area, the transit operator restructured bus routes around light rail stations, primarily to improve transit productivity rather than to create a multidestination network. The line, which originally terminated across the Mississippi River in East St. Louis, later was extended for about 20 miles into Illinois farmland to achieve equity of light rail investment on the Illinois side of the river. The extension dilutes light rail traffic density [33, 54]. Even so, the St. Louis line's patronage density is much higher than that of Pittsburgh and Baltimore. Light rail lines in Baltimore and Pittsburgh (as well as in Cleveland) compete with radial bus lines running to the CBD.

The fact that Cleveland's light rail traffic density is considerably higher than Pittsburgh's and Baltimore's when its service philosophy of serving the CBD is much the same may be related to both speed and land use. Cleveland's light rail line was built in 1920 to serve a series of neighborhoods that were designed concurrently, with the rail line in mind. The neighborhood design objective was the creation of short and attractive walks from all houses in the Shaker Heights development to streetcar stops. This factor may set it apart from light rail line in Baltimore, which is even faster but where favorable urban design around stations does not exist. The Pittsburgh line is somewhat slower than the Cleveland line, and its access to residents may not be as good, either.

The Oceanside-Escondido line is the remaining light rail line, around which bus services are structured, where traffic density is lower. Land uses may be the explanation. The line serves a sprawling, low density and hilly part of San Diego County almost 40 miles north of the CBD, offering service every 30 min with diesel rail cars. The area that it serves is more sparsely settled than the other areas considered, and the frequency of service is much less, as well. These attributes likely result in its low patronage density, even though there are high transfer movements between buses and trains at three transit centers along the line. The three bus transfer stations are the most heavily patronized stations on the line.

The examination of traffic densities in the context of transit service approach and metropolitan context suggests several points. First, it strengthens earlier conclusions that light rail being imbedded in a multidestination transit network is important for achieving high traffic density, which appears to be related to improved overall regional transit performance. The analysis also suggests that faster light rail lines that are backbones of multidestination transit networks perform much better than slower lines in a similar context. The message on the effect of urban form is mixed. Light rail experiences higher passenger densities in Calgary and Edmonton than in San Diego and Portland, even though all four metropolitan areas embraced similar transit development strategies, possibly because the Canadian metropolitan areas are more compact than their US counterparts. On the other hand, lower incomes in the Canadian cities may explain the difference. Urban form may influence higher-than-expected patronage for Cleveland's light rail line. On the other hand, high densities in Toronto and San Francisco do not translate into streetcar traffic densities that are higher than traffic densities for many of the new light rail lines serving much lower density, more sprawling metropolitan areas. The overall conclusion is that where light rail has been employed to take advantage of the high productivity characteristics that were bred into its technology, it has done

extraordinarily well for improving transit performance. Where policy makers have not made use of those characteristics, light rail has had a less favorable effect on transit performance.

Effects of Light Rail Investments on Land Use Patterns

As discussed earlier, growing automobile ownership weakened and all but eliminated the power of streetcar investments to affect metropolitan growth patterns around World War I. Giuliano [55] summarizes theoretical and empirical literature on why automobiles had that effect. Her argument is that transportation investments alter land use patterns when the investments make parcels of land relatively more accessible to jobs and employment than other parcels. More accessible parcels have higher rents and will be developed at higher intensities. When the streetcar era began, extension of streetcar lines into green fields around cities conveyed huge accessibility increases for those parcels. Streetcars thus had a large impact on the pattern of development. The automobile, however, conveyed high levels of accessibility to all parcels in metropolitan areas. After auto ownership in cites was widespread and roads around cities were paved, parcels of land served by streetcars no longer had an accessibility advantage compared to other parcels. All parcels in the metropolitan area had roughly equal accessibility, and so development spread out at low density. The star-shaped city morphed into the blob. Giuliano argues that the condition of relatively uniform accessibility continues today. Parcels proximate to new light rail transit stations are unlikely to have much of an accessibility advantage compared to other parcels and are unlikely to develop much differently if left to the whims of the land market. She then marshals abundant empirical evidence to show that rail transit investments during the post World War II period have had little if any effect on development patterns in US cities. Some other researchers, such as Bernick and Cevero [56] or Knaap, Ding, and Hopkins [57], examined whether property located in proximity to rail stations has fetched higher prices in comparison to similar properties not near rail stations and found that rail transit proximity does bring higher rents, but the effect is marginal. Others have surveyed residents of new transit-oriented developments built adjacent to light rail stations in Washington County west of Portland and Pasadena, California to determine the extent of light rail use. Both studies found that around 10% of residents use light rail stations, which is low but still higher than typical suburban residential areas [58, 59]. The effect appears to be the greatest for inner city parcels near stations on large, comprehensive rapid transit systems operating on right-of-way Type A, of which the Washington Metro is an example [60].

Portland's light rail line often is cited as the best example of light rail investment affecting land uses. The first line extended 16 miles from the CBD through medium to low density blue collar and middle income suburbs to the east and opened in 1986. Its opening was accompanied by planning and zoning policies that allowed higher density development around stations. Little redevelopment happened through the first 15 years of the lines' existence, except in one area called the Lloyd Center. Located across the Willamette River from the Portland CBD, Lloyd's Center was the original suburban mall in the Portland region. By 1986, it was starting to become run-down. After light rail arrived, commercial and government redevelopment started, and over time the Lloyd Center has become an eastside extension of the Portland CBD. It is included in the free fare CBD zone (formerly multimodal, but now limited to LRT and streetcar lines). The extension of light rail 16 miles to the west in 1999 was accompanied by stronger planning and zoning regulations that distinguished between transit-friendly and transit-hostile land uses (authors' terms). Only transit-friendly land uses were permitted near stations. Metro, Portland's regional government, also employed a developer who knew construction techniques for medium density residential complexes (in the range of 20–60 dwelling units per acre). His job was to teach these techniques to local developers, whose expertise was in low density residential or steel-framed high rise building. These changes resulted in some higher density residential redevelopment around stations on the original line and higher density residential development in green field sites along the new western line. Perhaps the biggest decision affecting land use, however, was to take light rail to where growth was happening rather than to naively think that light rail investments, wherever they were made, would attract development.

So, the transit district extended the west line into a region that already was growing very rapidly, both with new employment and new residences. Planners purposefully chose an alignment that offered many green field sites near stations. The net result of all of these actions is the construction of some higher density development connected with pedestrian paths and sidewalks to rail transit stations.

Another slightly different approach to achieving coordination between land use and light rail is to modify auto-oriented commercial development so that light rail can serve it. This also is an example of taking light rail to where growth is happening, rather than trying to entice growth to come to light rail. The City of San Diego and the San Diego MTDB followed this approach with the building of the Green Line through the Mission Valley. Mission Valley, running in an east–west direction about 5 miles north of the San Diego CBD, began attracting intense retailing and commercial development in the 1950s that largely replaced the CBD as the retailing hub of the region and rivaled the CBD as a commercial center. By the time MTDB designed the Green Line in the early 1990s, Mission Valley contained an east–west interstate freeway, an east–west high speed six lane arterial road, and crossings of four north–south freeways built to interstate standards. The valley also contained a regional mall, a mall of big box stores, other scattered big box stores, scattered high rise office building, smaller malls and strip malls, and a sports stadium. San Diego State University rose on the south wall of the valley toward its east end. Another regional mall was located just east of that and already was served by the Orange Line running from the CBD. There also were apartment complexes built on the floor of the valley and on its side. Running through the middle of all of this was the San Diego River, little more than an open storm drain that was dry most of the year but sometimes flooded. Light rail in the Mission Valley was part of a city-led remodeling of the valley. The city rebuilt the river into an attractive, natural-looking wetlands lined on both sides with swales. The light rail line was pieced together from sections of swales, from bits of access street rights-of-way, and from truck alleys serving the backside of mall buildings. The light rail line also used elevated structures liberally. To access San Diego State University, the Green Line dove into the side of the valley in a short subway, with a station directly under the university's bus transfer hub. The city built a pedestrian path along the river and connected it laterally to existing developments. MTDB built pedestrian connections from its light rail stations to the river path. The city also commissioned a nationally known architect, Peter Calthorpe, to design a new apartment complex centered on a light rail station in one of the valley's remaining green field sites. The development is called Rio Vista and is what is known as a Transit-Oriented Development, or TOD. The Green Line, which opened in late 2005, runs from the Old Town station on the west where it connects with numerous bus routes and two rail routes. It connects to another bus transit center at Fashion Valley mall adjacent to one of the freeways coming from the north. Express buses from the north call at this station, as do several local bus routes. It connects with another bus station at San Diego State University, still another bus station as the Grossmont Mall (where it joins the Orange Line from the CBD), and it terminates at still another bus station in El Cajon. The valley still is auto oriented, and most people who go there use autos. The difference is that transit now works there, as well (Fig. 11). The Green Line now is carrying about 22,000 passengers per day to and from valley destinations [52].

Conclusions

Light rail arose during the 1950s and 1960s as a new transit mode in northern European cities that provided higher quality, higher capacity, substantially more productive, and faster transit service than traditional streetcars and local buses. Light rail generally was cheaper to build than traditional subway and elevated railway systems, and as a consequence, it could be afforded by many midsized metropolitan areas that could not afford to build rapid transit lines. These qualities attracted the attention of advocates of transit and urban renewal in Canadian and US cities, leading to light rail's first North American adoption in Edmonton in 1978. Since then, 21 Canadian and US metropolitan areas whose transit systems operated only buses at the beginning of the 1970s opened one or more light rail lines in addition to buses.

The scope of light rail implementation in Canada and the USA also may be responsible for a renewal of

Light Rail Transit, Systemic Viability. Figure 11
The first section of San Diego's Mission Valley Line. Looking east in 2002 along the valley from a high rise building at the Hazard Station. Note train of U2 cars. Author's photo

interest in traditional streetcar investment. Eight Canadian and US metropolitan areas still operated streetcars in 1970 along with large bus systems. Six of these areas subsequently rebuilt their streetcar systems with at least some light rail characteristics, generally leaving out those characteristics that led to productivity improvement. One city with streetcars renewed and expanded its traditional streetcar operation as a traditional streetcar operation (New Orleans), using a mix of historic cars and replicas of historic cars with more modern electromechanical gear. (The eighth city, El Paso abandoned its remaining streetcar line in the early 1970s.) In the last several years, a few other cities built new streetcar lines primarily as tourist-oriented circulator lines in downtown areas. Some of the new lines use restored streetcars, some use replicas of historic cars, and some use modern European-designed articulated streetcars.

Results are mixed. Some of the light rail investments have had strongly positive results. They substantially improved regional transit performance in metropolitan areas such as San Diego, Portland, St. Louis, and Dallas by increasing per capita ridership, improving transit productivity, and stabilizing or decreasing real operating costs per passenger mile. In these metropolitan areas light rail investments have all or most of the following characteristics: light rail lines are significantly faster than local buses, they are long, and their outlying stations are loci of bus route restructuring. Some of the stations in each of these metropolitan areas also have large park and ride lots. In all of these metropolitan areas, light rail lines serve sectors of their respective regions that were experiencing robust growth in both population and employment before the onset of the Great Recession. Zoning and development codes favored denser development around light rail stations. As a consequence, some of the stations in several of these metropolitan areas have been surrounded by dense new development whose residents and employees can and do walk to light rail trains. In each of these metropolitan areas, light rail lines account for between 10% and 20% of the transit service in their respective metropolitan areas but carry 30–50% of the daily passenger miles of transit traffic. These systems clearly are reaping the productivity capability of light rail investments. It also appears that the larger the share of metropolitan area employment directly reached by light rail lines, the more favorable the impact of the light rail investments on all aspects of transit performance.

Light rail lines with such favorable design characteristics have limitations, however. They are powerless

to attract economic growth in depressed areas, for example. They also have not substituted for auto travel on a wide scale. The best performing systems (in San Diego and Portland) have achieved patronage per capita increases in the range of 30–50% over a 20 year period, impressive when compared to the bus patronage magnitudes and trends of most midsized US cities but not impressive when compared to the magnitude of auto use in US metropolitan areas. Autos and light trucks generally account for more than 90% of metropolitan travel, and even a 50% increase in per capita transit use makes little inroads into auto use [61].

Many light rail and streetcar investments result in less favorable results. Results are less favorable where light rail investments cover only limited parts of their metropolitan areas or are placed in depressed parts of metropolitan areas. Light rail and streetcar investments also are less effective where the resulting service is as slow (or slower) than local bus services, where the investments result in the operation of one-car trains (buses on rails), or where the investments result in staff being placed in each car of multicar trains to collect fares. They also are less effective where there has been no coordination of bus and light rail service. If some or all of these qualities are characteristics of the light rail investments, the investments may result in higher real operating expenses per passenger mile, lower productivity, and reduced patronage per capita. (The investments may possess compensating attractive characteristics, such as tourist appeal, or adding cache to a neighborhood.)

Future Directions

Continued light rail investments in US and Canadian cities are consistent with the idea of sustainability if benefits from the investments outweigh the costs of the investments. There are two types of light rail investments to be considered: those that result in improved regional transit performance, and those that do not.

Light rail investments that enhance regional transit productivity have the following characteristics: trains have lots of capacity; trains have lots of wide doors; multicar trains are operated by one person; proof of payment fare systems are used with free transfers to and from buses and between buses; rail routes are long and fast (short routes offer no time advantage over buses); part of the speed is achieved by trains wasting little time at intermediate stops boarding and deboarding large passenger loads, because passengers use all of the wide doors and do not pay fare-collecting personnel; rail stations serve important destinations in addition to CBDs; bus networks are restructured around light rail stations with a substantial part of bus mileage replaced by train mileage; restructured bus routes not only take passengers from residential areas to trains, but train passengers to important destinations located close to but not directly served by stations; rail lines are located to serve growing parts of metropolitan areas, and development in such areas is retrofitted so that passengers can walk between rail/bus stations and adjoining development. In short, light rail works well where planners place it within a region in such a way to make use of its high capacity, productivity, and speed characteristics.

Such light rail investments will enhance regional transit performance. The outstanding and unanswered question is whether they will do so sufficiently to make the light rail investment worthwhile. While the authors do not have quantified benefits from such light rail investments, they can enumerate the categories of benefits and leave it to the reader to judge their significance. To begin with, benefits include consumer surpluses to transit dependent persons who choose to use restructured transit service to reach more quickly destinations throughout metropolitan areas. Benefits also include consumer surpluses to previous auto drivers who find it more convenient to switch to light rail services. Benefits also include fuel savings and pollution reductions resulting from fewer auto trips. There are two categories of fewer auto trips. One category includes previous auto trips made by those who now leave cars at homes or in suburban lots. The other category includes previously chauffeured auto trips of those without cars (perhaps friends and relatives were the chauffeurs). Such trips often involve considerable driving by the chauffeur to pick up the rider at a remote location or to return to the chauffeur's place of residence or work once the rider is dropped off. The elimination of such trips could reduce considerable regional auto and light truck VMT. Another significant saving is the value of time saved by previous chauffeurs. Still other benefits include lower real operating expense per passenger mile carried on the transit systems.

Other benefits include option value to environmentally conscious citizens who value having a multidestination transit network that they might wish to use some day. The aggregate of such benefits, in the authors' opinion, could outweigh resources required to build regional light rail systems that will enhance transit system performance.

The other category of light rail investments does not enhance regional transit performance. Light rail lines belonging to the second category typically are designed as just another slow bus route to the CBD, having no transfer connections with bus lines, no free transfers, displacing no bus miles, and either operating only one-car trains, or having drivers collecting fares on each car of multicar trains. Such lines have little justification. They will not perform well, and neither will the overall transit system. They probably are not consistent with sustainability.

In summary, a midsized metropolitan area into which light rail is introduced to take advantage of its high capacity, productivity, and speed characteristics can achieve substantial patronage growth per capita, improve productivity, and stabilize real costs for moving passengers within a metropolitan area. Stations can be nodes for development if they are located where development activity of the private market is active. Planning intervention in such areas can create attractive development that is accessible by transit, although autos will remain the principle form of access for some years into the future. Accounting for as few as 10% of regional transit service, such light rail lines can carry 30–50% of regional transit passenger miles that continue to grow year by year. Over time auto-less, middle-class subcultures could evolve around such systems. The benefits of such systems might outweigh their construction costs. If they do, this category of light rail investment is consistent with the concept of sustainability.

Abbreviations

APTA American Public Transportation Association, the lobbying organization for transit agencies in the USA

CBD Central business district

FRA Federal Railroad Administration, a division of the US Department of Transportation

FTA Federal Transit Administration, a division of the US Department of Transportation

MTDB The San Diego Metropolitan Transit Development Board, which planned and built light rail in the San Diego region but which organized a Verkerhsverbund arrangement (of which it was the centralized coordinating body) to operate all transit services in its jurisdiction

PCC Presidents' Conference Committee, which conducted basic research to develop a radical new streetcar design between the late 1920s and mid-1930s

POP Proof-of-payment fare collection system. Also called self-service, barrier-free fare collection system

TOD Transit-oriented development

TRB Transportation Research Board, a division of the National Academy of Sciences devoted to expanding knowledge about various transportation systems of all modes

TriMet The tri-county transit district that builds and operates light rail lines and bus services in Portland, Oregon

UMTA The Urban Mass Transit Administration, which is what the FTA was called before 1991

USDOT The US Department of Transportation, headed by the Secretary of Transportation, a member of the President's cabinet

VMT Vehicle miles traveled (generally by autos and light trucks) during a certain time period over a particular road or within a given area, such as a metropolitan area. One can speak of, for example, daily VMT in a metropolitan area, such as Portland, or VMT per capita

Bibliography

Primary Literature

1. Boorse J (2001) This is light rail transit. Transportation Research Circular Issue Number: E-C033. Transportation Research Board, Washington, DC. ISSN: 0097-8515
2. APTA (1994) Glossary of transit terminology. American Public Transit Association, New York
3. Vuchic V (1981) Urban public transportation systems and technology. Prentice Hall, Englewood Cliffs, pp 62–63

4. Vuchic V (2005) Urban transit: operations, planning, and economics. Wiley, Hoboken, pp 380–383
5. Thompson G (2005) The birth of the light rail movement in North America and its results. Transp Serv Telecomun J 8:142–164
6. Thompson G (2003) Defining an alternative future: birth of the light rail movement in North America. Transportation Research E-Circular Number E-C058, ISSN 0097-8515. Transportation Research Board, Washington, DC, pp 25–36. http://gulliver.trb.org/publications/circulars/ec058/ec058.pdf
7. Fielding G (1987) Managing public transit strategically: a comprehensive approach to strengthening service and monitoring performance. Jossey-Bass, San Franciso
8. Post R (2007) Urban mass transit: the life story of a technology. Greenwood, Philadelphia
9. Warner S (1968) The private city: Philadelphia in three periods of its growth. University of Pennsylvania Press, Philadelphia
10. Longstreth R (1997) City center to regional mall: architecture, the automobile, and retailing in Los Angeles, 1920–1950. MIT Press, Cambridge, MA
11. Jones D (2008) Mass motorization + mass transit: an American history and policy analysis. Indiana University Press, Bloomington
12. Longstreth R (1999) The drive-in, the supermarket, and the transformation of commercial space in Los Angeles, 1914–1941. MIT Press, Cambridge, MA
13. Wyse W (1968) The PCC car: a marvel of control engineering of the 1930s, part I: background and general principles. *Modern Tramways*, September, pp 296–303
14. Brown J, Thompson G (2009) The influence of service planning decisions on rail transit success or failure. MTI Report 08-04. Mineta Transportation Institute, San Jose
15. Saltzman A (1992) Public transportation in the 20th century. In: Gray G (ed) Public transportation, 2nd edn. Prentice Hall, Englewood Cliffs, pp 24–45
16. Snell B (1974) American ground transport: a proposal for restructuring the automobile, truck, bus and rail industries. Government Printing Office, Washington, DC
17. St Clair D (1986) The motorization of American cities. Praeger, New York
18. Yago G (1984) The decline of transit: urban transportation in German and U.S. cities, 1900–1970. Cambridge University Press, Cambridge
19. Adler S (1991) The transformation of the Pacific Electric Railway: Bradford Snell, Roger Rabbit, and the politics of transportation in Los Angeles. Urban Aff Q 27:51–86
20. Bianco M (1998) Kennedy, 60 minutes, and Roger Rabbit: understanding conspiracy-theory explanations of the decline of urban mass transit. Discussion paper 98-11. Center for Urban Studies, Portland State University, Portland
21. Black A (1995) Urban mass transit planning. McGraw-Hill, New York, pp 31–39
22. Adams W (1965) The central subway of the Massachusetts Bay Transportation Authority. Traffic Q 19:443–457
23. Smerk G (1991) The federal role in urban mass transportation. Indiana University Press, Bloomington
24. Thompson G (2007) Taming the neighborhood revolution: planners, power brokers, and the birth of neotraditionalism in Portland, Oregon. J Plan Hist 6:214–247
25. Waltking D (1965) The articulated tramcar in West Germany. In: Joyce J (ed) Modern Tramway review. Ian Allen, London, pp 72–88
26. Schmucki B (2003) Cities as traffic machines: urban transport planning in East and West Germany. In: Divall C, Bond W (eds) Suburbanizing the masses: public transport and urban development in historical perspective. Ashgate, Aldershot, pp 149–170
27. Clark R (1978) Light rail vehicles for Edmonton Transit. Presentation at American Public Transit Association rapid transit conference, Chicago
28. Wyse W (1968) Germany goes underground, part 1: Frankfurt's Feiertag. *Modern Tramway*, December, pp 404–409
29. Walker P (1968) The tram subway (a rose by any other name). *Modern Tramway*, May, pp 162–171
30. Quinby D (1962) Major urban corridor facilities: a new concept. Traffic Q 16:242–259
31. Taylor S (1970) The rapid tramway: a feasible solution to the urban transportation problem. Traffic Q 24:513–529
32. Thompson G (2010) Technological change in transit: how the U.S. light rail movement won its first victory in San Diego. Working paper. Department of Urban and Regional Planning, Florida State University, Tallahassee
33. Demrey L (2008) U.S. urban rail transit lines opened from 1980. http://www.publictransit.us/ptlibrary/Railopenings_Feb2008.pdf. Accessed 29 June 2010
34. Schumann J, Francis L (2003) Status of North American light rail transit systems: year 2003 update. Transportation Research E-Circular Number E-C058. Transportation Research Board, Washington, DC, pp 3–24. ISSN 0097-8515. http://gulliver.trb.org/publications/circulars/ec058/ec058.pdf
35. Schumann J (2007) Status of North American light rail transit systems: year 2006 update. Transportation Research E-Circular Number E-C112. Transportation Research Board, Washington, DC, pp 3–20. ISSN 0097-8515. http://onlinepubs.trb.org/onlinepubs/circulars/ec112.pdf
36. Florida Department of Transportation (2010) Florida transit information system. http://www.ftis.org/INTDAS/tableflat.aspx. Accessed 2 July 2010
37. Thompson G (1977) Planning considerations for alternative transit route structures. J Am Inst Plan 43:158–168
38. Polzin S, Page O (2003) Ridership trends of new start rail projects. Report 350-11. National Center for Transit Ridership
39. Meyer J, Kain J, Wohl M (1965) The urban transportation problem. Harvard University Press, Cambridge, MA
40. Pickrell D (1992) A desire named streetcar: fantasy and fact in rail transit planning. J Am Plan Assoc 58:158–176
41. Kain J (1990) Deception in Dallas: strategic misrepresentation in rail transit promotion and evaluation. J Am Plan Assoc 56:184–196

42. O'Toole R (2005) Rail disasters 2005: the impact of rail transit on transit ridership: an update to great rail disasters. Reason Foundation, Los Angeles
43. Richmond J (2005) Transport of delight: the mythical conception of rail transit in Los Angeles. University of Akron Press, Akron
44. Giuliano G (2010, forthcoming) Transportation policy: public transit, settlement patterns, and equity in the U.S. chapter 28. In: Brooks N, Donaghy K, Knaap G, (eds) Oxford University Press handbook of urban economics and planning. Oxford University Press, Oxford
45. Brown J, Thompson G (2008) Service orientation, bus-rail service integration, and transit performance: an examination of 45 U.S. metropolitan areas. Transp Res Rec J Transp Res Board Natl Acad Sci 2042:82–89
46. Brown J, Thompson G (2008) The relationship between transit ridership and urban decentralization: insights from Atlanta. Urban Stud 45:1119–1139
47. Brown J, Thompson G, Bhattacharya T (2010) Evaluation of land use and transportation strategies to increase suburban transit ridership in the short term. Florida Department of Transportation, Public Transit Office, Tallahassee
48. Wood J, Zimmerman M, Poticha S, Center for Transit-Oriented Development (2009) Destinations matter: building transit success. Report FTA CA-26-1007. Federal Transit Administration, U.S. Department of Transportation, Washington, DC
49. Kain J, Liu Z (1999) Secrets of success: assessing the large increases in transit ridership achieved by Houston and San Diego transit providers. Transp Res A 33:601–624
50. Thompson G, Matoff T (2003) Keeping up with the Joneses: planning for transit in decentralizing regions. J Am Plan Assoc 69:296–312
51. Brown J, Thompson G (2009) Express bus versus rail transit: how the marriage of mode and mission affects transit performance. Transp Res Rec 2110:45–54
52. Bates T, Jablonski P (2007) San Diego, California, Trolley's new green line: early success for distinctive service. Transp Res Rec J Transp Res Board Natl Acad Sci 2006:40–49
53. Mieger D, Chu C (2007) Los Angeles, California metro green line: why are people riding the line to nowhere? Transp Res Rec J Transp Res Board Natl Acad Sci 2006:50–59
54. Tennyson E (2005) Analysis of metro-link performance in Saint Louis, Missouri. Transp Res Rec 1930:63–78
55. Giuliano G (2004) Land use impacts of transportation investments, highway and transit. In: Hanson S, Giuliano G (eds) The geography of urban transportation, 3rd edn. Guilford Press, New York, pp 237–273
56. Bernick M, Cervero R (1997) Transit villages in the 21st century. McGraw-Hill, New York
57. Knaap G, Ding C, Hopkins L (2001) Do plans matter? The effects of light rail plans on land values in station areas. J Plan Educ Res 21:32–39
58. Bae CC-H (2002) Orenco station, Portland, Oregon: a successful transit oriented development experiment? Transp Q 56(3): 9–18
59. Lund H, Willson R (2005) The Pasadena Gold Line: development strategies, location decisions, and travel characteristics along a new rail line in the Los Angeles region. Mineta Transportation Institute, San Jose State University
60. Schrag Z (2006) Great society subway: a history of the Washington metro. Johns Hopkins University Press, Baltimore
61. Polzin S, Chu X (2010) A closer look at public transportation mode share trends. Research and Innovative Technology Administration, Bureau of Transportation Statistics. http://www.bts.gov/publications/journal_of_transportation_and_statistics/volume_08_number_03/html/paper_03/. Accessed 8 July 2010

Books and Reviews

Cervero R (1998) The transit metropolis: a global inquiry. Island Press, Washington, DC

Committee for the Study on the Relationships Among Development Patterns, Vehicle Miles Traveled, and Energy Consumption (2009) Driving and the built environment: the effects of compact development on motorized travel, energy use, and CO2 emissions – special report 298. Transportation Research Board, National Research Council, Washington, DC

Downs A (2004) Still stuck in traffic: coping with peak-hour traffic congestion. Brookings, Washington, DC

Mees P (2010) Transport for suburbia: beyond the automobile age. EarthScan, London

Pucher J, Lefevre C (1996) The urban transport crisis in Europe and North America. MacMillan, London

L

Lignocellulosic Energy Crops, Production and Provision

Iris Lewandowski
Department of Biobased Products and Energy Crops, Institute for Crop Science, Hohenheim University, Stuttgart, Germany

Article Outline

Glossary
Definition of the Subject
Introduction
Short Rotation Coppice (SRC)
Energy Grasses
Future Directions
Bibliography

Glossary

C3 Grasses Grasses possessing the C3 photosynthetic mechanism, so called because the first product of carbon fixation contains three carbon atoms.

C4 Grasses Grasses possessing the C4 photosynthetic mechanism, so called because the first product of carbon fixation contains four carbon atoms.

Cellulose Component of plant cell walls made up of chains of D-glucose (C6 sugar) molecules linked via hydrogen bridges consisting of 42% carbon (C), 6% hydrogen (H), and 52% oxygen (O).

Hemicellulose Heteropolysaccharide that contains various different sugar monomers such as glucose, xylose, mannose, galactose, rhamnose, and arabinose. Hemicellulose contains mostly D-pentose or so-called C5 sugars and is found in plant cell walls.

Energy crops Crops grown for the purpose of producing biomass for energetic use.

Energy grasses Perennial grasses with high biomass potential which can preferentially be harvested once a year at low moisture content.

Fischer-Tropsch diesel Biofuel produced from lignocellulosic biomass via a multi-step process. Gasification produces synthesis gas, which is cleaned and then transformed to liquids at high temperature and pressure by Fischer-Tropsch catalysis.

Lignin Complex three-dimensional polymers built from phenylpropane derivatives consisting of 64% carbon, 6% hydrogen, and 6% oxygen.

Rhizomes Underground shoot systems in perennial grasses serving as overwintering organs and for storage of nutrients.

Short rotation coppice (SRC) Fast-growing trees, such as poplar or willow, harvested in cycles of 3–5 years and which regrow from the stools after harvesting.

Definition of the Subject

More than 90% of the dry matter of lignocellulosic biomass consists of the three biopolymers: cellulose, hemicellulose, and lignin. Cellulose is made from chains of D-glucose molecules linked via hydrogen bridges. It is composed of 42% carbon (C), 6% hydrogen (H), and 52% oxygen (O). Cellulose is the most common organic substance found in nature and forms the structural component of cell walls. Hemicelluloses are polysaccharides, which have shorter chains of sugar units than cellulose. They have various functions in the plant including support and holding together the cell membranes. Lignin is a complex three-dimensional polymer built from phenylpropane derivatives, which is stored between the cellulose fibrils to strengthen the cell wall. It consists of 64% C, 6% H, and 6% O.

Lignocellulosic energy crops are characterized by the high lignin and cellulose content of their biomass. Lignin in particular is very suitable for direct combustion due to its high carbon content. Direct combustion as a solid fuel is therefore the preferred use of lignocellulosic biomass so far. But applications based mainly on the use of the cellulose fraction are also promising future energetic applications. These include the production of biofuels such as ethanol produced via enzymatic hydrolysis and diesel produced via gasification and Fischer-Tropsch synthesis.

Introduction

There are two groups of plants that are suitable as energy crops delivering lignocellulosic biomass: trees and grasses.

Forest trees have been delivering firewood for hundreds of thousands of years. The term "energy crops," however, refers to trees that are grown on agricultural land. Compared to forest trees, which are harvested after decades, trees grown as energy crops are harvested in cycles of 3–5 years. After harvesting, they can regrow from the stock up to five or more times. Therefore, this system of wood production is called "short rotation forestry" or "short rotation coppice" (SRC). Trees species suitable for SRC should show three main characteristics: Firstly, they need to be able to regrow from stools after cutting; secondly, they should produce several branches from the stool; thirdly, they need to show the maximum growth increment in the first year to achieve high biomass yields [1]. Tree species most suitable for SRC in temperate climates are willow (*Salix* ssp.) and poplar (*Populus* L).

Grasses suitable for the production of lignocellulosic biomass are characterized by their ability to concentrate high biomass yields in one cut. Many perennial grasses that are used for fodder production have a high

biomass yield potential, but this has to be exploited in multiple harvests (up to five times a year) of green biomass. Energy grasses for the production of lignocellulosic biomass are generally harvested once a year, often at the end of the winter period in early spring. At this time of the year, the harvested biomass is dry and of high quality. This refers to the low content of substances hindering the combustion process, such as ash, chloride, or potassium. These grasses are highly lignified, which allows for the late harvest. Screenings of various perennial grasses have identified three as the most suitable for lignocellulosic biomass production in temperate regions: *Miscanthus*, switchgrass, and reed canary grass.

In the following chapters, the characteristics and systems for the production and supply of lignocellulosic biomass from willow and poplar SRC and the most relevant energy grasses are described.

Short Rotation Coppice (SRC)

Willow and poplar have been identified as the most promising trees for SRC in European temperate climates, mainly due to their high yield potentials. Both belong to the family *Salicaceae*. Most species in the *Salicaceae* family show the characteristics important for SRC plantations. They are pioneer trees with a vigorous juvenile growth, the ability to root from the rods and to regrow from the stools [1].

There are about 300 species of naturally growing willow in the northern hemisphere, but only a few with a growing pattern suitable for SRC willow plantations [2]. Most clones used belong to *Salix viminalis* and *Salix dasyclados*.

The genus *Populus* is separated into six sections, of which *Aigeiros* (Balsam poplar), *Tacamahaca* (Black poplar), and *Leuce* (aspen) are most suitable for SRC.

Presently, there is a maximum of 20,000 ha of willow SRC in Europe, most of which are in Sweden where the biomass is fired in heat or combined heat and power plants. Sweden has the most practical experience with SRC willow, and therefore, the following description of the production and provision of lignocellulosic biomass from SRC is mainly based on the Swedish experiences. The production of poplar as SRC is still at an experimental stage.

Demands and Variety Choice

The main distribution area of *Salicaceae* lies in the temperate zones of the northern hemisphere, but extends from the subpolar area to the north to the subtropical and tropical area to the south.

Willow and poplar can grow on a wide range of soils, but a good water supply is important. To produce high biomass yields, the available rooting zone should be at least 60 cm. Willows prefer cool weather and are therefore most suitable for cool-humid climates. Poplars have higher temperature demands. Although willows have a higher yield potential, poplars can outyield willows on sites with less suitable growing conditions, such as shallow soils or limited water supply.

Black poplars are the most demanding species with regard to nutrient and water supply and temperature but, together with aspen, have the highest yield potential (Table 1).

Breeding activities, mainly performed in Sweden, have resulted in a set of willow varieties for specific conditions. "Tora" is a high-yielding variety that is very frost tolerant. In addition to frost tolerance, varieties were also selected for drier land – which under Swedish conditions means up to 610 mm precipitation. "Todis" and "Inger" are examples of varieties with lower water demands [2]. There are also various varieties that have been bred for resistance to rust or leaf beetles.

A few willow varieties and 71 genotypes again six pathotypes of the fungus *Melampsora larici-epitea* have been tested [3]. Among others, the varieties "Bjorn" and "Tora," were highly resistant.

Propagation and Establishment

SRC are planted from March to June, and planting should take place as early as possible to allow for good establishment. In preparation for planting the fields should be ploughed and harrowed deeply (6–10 cm) to clear the fields from weeds. One-year-old SRC willow rods serve as planting material. These are cut during the winter and stored at −4°C in a cold storage room until they can be planted out. The planting width depends on the harvesting system. The Swedish system stipulates a twin row formation where the distance between the rows alternates from 75 to 150 cm. The distance between the plants in the rows

Lignocellulosic Energy Crops, Production and Provision. Table 1 Agronomic characteristics and demands of *Populus* (poplars and aspen) for SRC according to Kauter et al. (2003) [1] (Data from 0 [low] to ++++ [very high])

		Botanical section		
		Aigeiros (black poplar)	*Leuce*, subsection Trepidae (aspen)	*Tacamahaca* (balsam poplar)
Local characteristics	Soil characteristics	pH > 6, deep soils with good and constant water and oxygen supply	Tolerates stagnant water and hydromorphic soils	pH 4.5–6.5, tolerates water to some degree, lower demands than Aigeiros
	Soil nutrient supply	++++	++	+++
	Water supply	++++	+++	+++
	Mean temperature in vegetation period	++++	+	+++
	Vegetation period (days)	>150	>120	>130
Sensitivity to	Early and late frost	+++	+	+++
	Dense stands	++++	+	0
Increment	Peak mean annual increment at age of (years)	10–15	10–15	4–10

is approximately 59–65 cm. About 13,000 cuttings per hectare are planted. There are two principal planting systems: either cutting and planting the willow rods (1.8–2.4 m long) in one process or planting rods (18–20 cm long) which have already been cut. Once planted, the cutting is pressed down into the ground so that only 1–2 cm protrudes above ground level in order to provide it with good soil contact and minimize the risk of drying out [2].

Fertilization

Various field trials have shown nitrogen fertilization to have little or no effect on biomass yield [4]. Investigation of yield effects of nitrogen fertilization in SRC has shown that willow reacts more strongly to fertilization than poplar and shows increased biomass production [5]. Willow plantations can be fertilized with mineral fertilizers, but also tolerate organic fertilizers. In Sweden, municipal wastewater or sludge is applied to fertilize willows and is thus cleaned in the process [6].

In the plantation year, no nitrogen fertilization should be applied because it strengthens the competing weed. In the following year, it is recommended that fertilizers are applied according to the withdrawal by the harvested biomass, which is about 4–7 kg nitrogen (N), 0.8–1.8 kg phosphorous (P), and 2.5–4 kg potassium (K) per tonne dry matter [7].

The efficient use of nutrients by SRC can be explained by the nutrient cycle in the trees as shown in Fig. 1.

Nutrients accumulated in the leaves are recycled when fallen leaves decay and release these nutrients into the soil. Over winter, parts of the nutrients are also stored in the stems and roots of the trees. Because the vitality of the trees depends on this nutrient cycle, SRC should only be harvested when the leaves have been shed.

Crop Protection

The good establishment of SRC is important to guarantee highest yields. In the first year, establishment is threatened by weed competition, and therefore, intensive weed control needs to be performed. For this purpose, herbicides can be used or weed control can

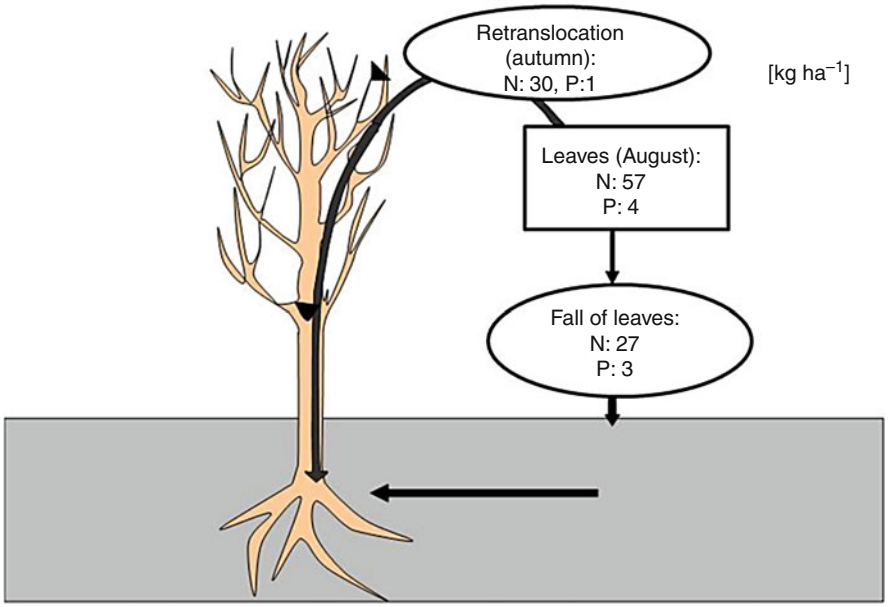

Lignocellulosic Energy Crops, Production and Provision. Figure 1
Nutrient cycling in 4-year-old poplar trees

be performed mechanically at a later stage. If weed competition is strong, weed control may also be necessary in the second year.

Game grazing can damage plantations significantly in the year of establishment. Therefore, planting SRC in the vicinity of forests should be avoided. At endangered locations, fencing may become necessary. Once the plantations are established, grazing is generally limited to the outer rim of the plantation [2].

Of the various insects that feed on SRC (e.g., gall midges, aphids, leaf beetles), leaf beetles can cause the most damage. If necessary, they can be controlled by pesticides. There are also several willow varieties available which show resistance to leaf beetles [2].

The fungal infection, leaf rust, can also lead to significant damage in SRC as it causes leaves to wither and fall prematurely. Through the Swedish breeding program, several varieties with good or total leaf rust resistance have become available.

Harvest and Densification

In the winter, after planting, the shoots have to be cut back to allow the formation of multiple shoots growing from the stools. This measure improves yields and can be performed using a mower.

The harvest can take place once the woody biomass has reached about 25 t dry matter per hectare or the stem diameter at the base is 6 cm. This is usually the case when the shoots are 3–4 years old [2].

To maintain vitality and to improve re-sprouting, harvesting must be performed during winter (November to April) when the leaves have been shed. There are various kinds of harvesting machines. Conventional SRC harvesters can cut and chip the stems in one procedure. For this purpose, a modified forage harvester that cuts and chips the branches through a specified cutting module can be used [8]. Other systems apply a modified sugar-cane harvester or a front hydraulic driven mow-cutter [7]. The chipped material is blown into a trailer alongside the machine as it moves through the crop. In another harvesting system, sticks are cut with one pass of either a self-propelled or trailed machine. The sticks are laid at the field rim from where they are loaded onto a tractor and transported to the store. Because the harvested biomass contains around 50% water, the advantage of this system is that the water content

decreases while the sticks are stored and they can be stored without decomposition.

Yield and Quality

Information on yields from SRC given in publications varies greatly. In Sweden, a yield of 8–10 t dry matter ha^{-1} a^{-1} can be reached in well-managed and pest-free plantations [2]. In field trials at several German locations, large yield differences between locations and varieties were measured. The ten highest yielding varieties produced from 8 t dry matter (black poplar variety Max 2) to 11.5 t dry matter (black poplar variety Raspalje) [9]. But similar to reports from Belgium [10], low yields of 3.5 t ha^{-1} a^{-1} were also measured when less productive varieties or drier sites were employed [9]. Sometimes poplar varieties yielded significantly higher than willow [9]. However, when new willow varieties such as "Tora" are grown on fertile soils with good water supply, dry matter yields of up to 15 t ha^{-1} a^{-1} were harvested [4].

Table 2 gives an overview of the composition of willow and poplar biomass.

Lignocellulosic Energy Crops, Production and Provision. Table 2 Biomass characteristics of willow and poplar

Component in% of dm[a]	Tree species	
	Willow	Poplar
Lignin	20.0	23.2
Cellulose	18.5	22.3
Hemicellulose	20.1	13.8
Carbon (C)	47.1	47.5
Hydrogen (H)	6.1	6.2
Oxygen (O)	44.3	44.1
Ash	2.00	1.85
Nitrogen (N)	0.54	0.42
Potassium (K)	0.26	0.35
Phosphorus (P)	0.09	0.10
Calcium (Ca)	0.68	0.51
Chlorine (Cl)	0.004	0.004
Sulfur (S)	0.045	0.031
Heating value in MJ/kg	18.4	18.5
Sources	[7, 11, 12, 13, 14]	[1, 7, 11, 12, 13, 14]

[a]dry matter

Lifetime of a Plantation and Removal

The economic life of a well-managed SRC plantation is typically up to 20–25 years, which means that an SRC plantation can be harvested about 5–6 times during its lifetime.

To convert land under SRC willow back to agricultural land, spraying the plantation with a mixture of glyphosate and MCPA while the shoots are growing in summer is recommended [2]. This kills the stools which can then be cut up with a heavy disc tool or mulched and ploughed in.

Energy Grasses

Miscanthus, switchgrass, and reed canary grass have been described as the most important energy grasses for temperate regions [15]. They differ from each other in origin, eco-physiological demands, and biomass quality.

The genus *Miscanthus* consists of 17 species and can be divided into four sections [16]. The genetic origin of *Miscanthus* is East-Asia, where it is found throughout a wide climatic range from tropical and subtropical parts of Southeast Asia to warm temperate parts of the Pacific Islands. The genotype widely used in Europe, *Miscanthus x giganteus*, was introduced from Japan to Denmark in 1930. *M. x giganteus* is a triploid (2n = 3x = 57), natural hybrid from *M. sinensis* and *M. sacchariflorus*.

Switchgrass (*Panicum virgatum* L.) belongs to the subfamily Panicoideae of the Gramineae family. It is native to North America where it occurs naturally from a latitude of 55° N down to central Mexico. It is one of the grasses that dominated the North American tallgrass prairie.

Reed canary grass (*Phalaris arundinacea* L.) belongs to the subfamily Pooideae of the Gramineae family. It is native to the temperate regions of Europe, Asia, and North America. In Europe, it can be found throughout the Nordic countries, even in the mountainous areas of the North. It is normally found in wet areas such as lakeshores and along rivers.

There are an estimated 30,000 ha of *Miscanthus* being grown for the production of lignocellulosic biomass in Europe, mainly in the UK, Austria, Switzerland, and Germany. The largest application of *Miscanthus* in Europe is currently the co-firing of *Miscanthus x giganteus* biomass with coal. The world's largest area under production with *Miscanthus* is probably found in China, where 400,000 ha of the species *Miscanthus lutariariparia* growing naturally around the coastal area of Dongting Lake are used for the production of low-quality paper. Reed canary grass is used as a forage crop mainly in North America, but also to some extent in Eastern Europe, Scandinavia, and Japan. Its use as a forage crop is decreasing due to the low feed value of the lignin-rich biomass. But, in more northern and cooler regions of Europe, it is increasingly used to deliver lignocellulosic biomass for solid fuels or pulp and paper production. Switchgrass is the main energy grass in Northern America.

Reed canary grass is a so-called C3 crop, and *Miscanthus* and switchgrass are C4 crops. In contrast to C3 crops, C4 crops are characterized by greater water-use efficiency (WUE) – up to twice that of C3 crops – and a higher biomass production potential [17]. However, this is not the case for very cool regions such as Sweden and Finland where low temperatures limit the photosynthetic process. Here C3 grasses perform better. For this reason, reed canary grass is the most suitable perennial grass for cooler, northern parts of Europe. But in temperate to warmer regions, *Miscanthus* by far outyields reed canary grass.

The processes of production and supply of lignocellulosic biomass from *Miscanthus*, switchgrass, and reed canary grass and the differences in the management of these grasses will be described in the following chapters.

Demands and Variety Choice

The standard genotype *Miscanthus x giganteus* can be grown on a wide range of soils. The highest yields are produced on soils with a good water-holding capacity. Sites with stagnant water are unsuitable. *M. x giganteus* begins growth from the dormant winter rhizome when soil temperatures reach 10–12°C. Leaf expansion occurs at temperatures between 5°C and 10°C, depending on the genotypes [18]. The main problem of *Miscanthus* production in Northern Europe is the poor overwintering of the rhizomes of the productive genotype *Miscanthus x giganteus* in the first winter after planting. Freezing tests have showed that *M. x giganteus* rhizomes removed from the field in January are killed at temperatures below −3.5°C while the rhizomes of *M. sinensis* survived up to −6.5°C [19]. *M. sinensis* genotypes are more winter-hardy than *M. x giganteus*, but they have lower yields than *M. x giganteus* and are therefore only chosen for regions where winter temperatures are too low to secure the survival of *M. x giganteus* plantations. Below, the term *Miscanthus* will be used as a synonym for *M. x giganteus*.

Switchgrasses are divided into upland and lowland ecotypes. The upland ecotypes are most commonly octaploids (2n = 8x = 72) or occasionally hexaploids (2n = 6x = 54). They are shorter, one-stemmed, and are more adapted to drier habitats [20]. The lowland ecotypes are predominantly tetraploid (2n = 4x = 36), coarse-stemmed, tall-growing, and have a more bunchy-type growth. They are more adapted to wetter sites, being found on floodplains, and are later maturing than upland ecotypes [20]. Due to their high yields for bioenergy production, the most promising cultivars for the USA are "Alamo" for the deep South, "Kanlow" for mid-latitudes, and "Cave-in-rock" for the central and northern states [21]. Kanlow and Alamo are lowland ecotypes while Cave-in-rock is an upland ecotype. There is not yet enough field experience with switchgrass in Europe to recommend varieties for specific site conditions, but Kanlow as well as Alamo has performed satisfactorily under European conditions.

Different upland and lowland switchgrass varieties have been tested with respect to their dry matter yields [22]. To this end, 15 varieties in Italy and 10 varieties in Greece were cultivated. In general, the lowland varieties "Kanlow" in Greece and "SL 93-3" in Italy produced the highest dry matter yields with 17.1 t ha^{-1} a^{-1} and 20.0 t ha^{-1} a^{-1} respectively.

Reed canary grass is a highly self-sterile allotetraploid plant (2n = 4x = 28) [23]. There is a large variation in morphological characteristics between, as well as within, different ecotypes. Several commercial varieties for forage purposes are available on the market, mainly in United States, Canada, and Eastern Europe. The recent novel application of this grass for material and energy uses means that

Lignocellulosic Energy Crops, Production and Provision. Table 3 Propagation and establishment methods for selected perennial grasses [15, 25]

		Seed establishment		Rhizome establishment		
		In the field	Pre-culture in greenhouse	In the field	Pre-culture in greenhouse	Micro-propagation
Species	Miscanthus			C	X	C
	Switchgrass	C	X			
	Reed Canary Grass	C				
Estimated costs [Euro ha^{-1}]		120–400	1,500–3,000	3,200	3,000–6,000	3,000–8,000

X = safe method; C = currently performed method for this grass

new types of cultivars need to be developed with lower nitrogen and potassium contents and higher lignin contents [24].

Propagation and Establishment

Establishment of plantations of perennial grasses is often the most expensive and critical step in the production process, because poorly established stand will produce lower yields and are susceptible to weed competition over several years. Table 3 gives an overview of methods for the establishment of the perennial grasses discussed here.

Because *M. x giganteus* is triploid, it cannot form fertile seeds and has to be propagated vegetatively via rhizome cuttings or micro-propagation. Both methods are currently practiced. For rhizome propagation, mother fields have to be "harvested" by cutting the rhizomes mechanically, picking them up by machines (e.g., potato harvesters) and spreading them mechanically over the new fields. Here they have to be ploughed in immediately to prevent them drying out. Rhizome pieces suitable for propagation need a size of 5–8 cm and two living buds. In micro-propagation, apical meristems are transferred into sterile culture and are propagated in vitro in nutrient solutions enriched with phytohormones. Miscanthus fields are planted in April to May – depending on the temperature conditions – with a density of two plants per m^2. Rhizomes can be spread evenly or, as done with the micro-propagated plantlets, planted at a row width of 70 cm.

Switchgrass and reed canary can be established via seeds, which is the establishment method with the lowest costs. Because switchgrass seeds often have a high degree of dormancy, they need to be treated before sowing to break this dormancy. For this purpose, they can be soaked and then stored in a cool place for 24 h to drain. Afterward they are kept in a refrigerator at about 3.5–5.5°C for 4 weeks. Switchgrass can be drilled in a conventional seedbed or no-till seeding methods can be used. Seeds can be broadcast or drilled in rows. As light-seeded species, they should not be placed deeper than 1–2 cm [17]. For no-till planting, less seed (9 kg ha^{-1}) is required than for conventional seeding (11 kg ha^{-1}). A row spacing of 80 cm is recommended.

Best stands of reed canary grass are obtained when sown not deeper than 1–2 cm in a well-prepared, firm seedbed. A row spacing of 12.5 cm and seeding rate of 15–20 kg ha^{-1} is recommended.

Fertilization

As shown in Fig. 2, perennial grasses have an internal system for nutrient recycling. The rhizomes, their overwintering organs, serve also as a nutrient storage. In spring, shoots emerge from these rhizomes and are supplied with nutrients from the rhizome. In autumn, a significant proportion of these nutrients are transferred back to the rhizomes to be stored for the following vegetation period.

Thanks to this nutrient recycling system and the efficient C4 photosynthesis process, the C4 grasses

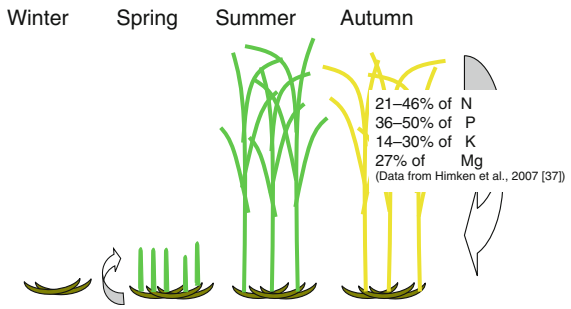

Lignocellulosic Energy Crops, Production and Provision. Figure 2
Nutrient recycling in perennial grasses

Miscanthus and switchgrass have a low demand for nitrogen fertilization. There are reports that nitrogen fertilization has no effect on yields of *Miscanthus* and switchgrass or only up to the first 50 kg nitrogen ha^{-1} a^{-1} [15, 20]. The effect of nitrogen fertilizer, however, is very site specific. It is recommended that nitrogen fertilization, which is effective only on poorer quality sites, should be applied there at levels of 50 to a maximum of 70 kg nitrogen ha^{-1} a^{-1} [15, 26]. In the year of establishment, no nitrogen fertilization should be applied because it mainly leads to higher weed competition. The requirement for potassium (K), calcium (Ca), and phosphorus (P) fertilization should be calculated according to their withdrawal with the harvested biomass, which is about 0.7 kg phosphorous, 0.9 kg calcium, and 1 kg potassium per tonne dry matter.

Experience from Swedish field trials resulted in the following recommendations for the fertilization of reed canary grass for the production of lignocellulosic biomass. In the year of sowing, an amount of 40 kg nitrogen (N), 15 kg phosphorous (P), and 50 kg potassium (K) ha^{-1} is optimal for a good establishment of the crop. The year after sowing, the most economic result is reached by applying 100, 15, and 80 kg ha^{-1} of N, P, and K respectively. In the following years, the fertilization rates can be decreased if the delayed harvest system is applied, due to the translocation of nutrients at the end of the growing season and leaching during the winter. Recommended rates are 50, 5, and 20 kg ha^{-1} of N, P, and K respectively in spring [15].

Crop Protection

Presently, there are no reports on relevant pests or diseases in perennial energy grasses. The main demand for crop protection is the control of weeds in the year of establishment, due to the slow emergence of the seeds of switchgrass and reed canary grass and the large row distances in *Miscanthus*. As a preventive measure, the field should be ploughed before sowing or planting the grasses. There are various herbicides suitable for use in maize or other cereals which could be used, but there are different national regulations on the licensing of these herbicides for use in perennial grasses. Because *Miscanthus* has large row distances of 70 cm, mechanical weed control through hoeing is a common practice. In switchgrass, a reduction of weed competition can also be achieved by occasional clipping at 6–9 cm height [27].

Harvest and Densification

The lignocellulosic biomass from perennial grasses is harvested in early spring to give a dry biomass. The most suitable date for harvest depends on weather conditions and is ideally when the biomass has a moisture content of less than 20%. But harvest should be performed before emergence of the new shoots. Delayed harvest decreases biomass yields by about 30%, mainly due to leaf abscission. As leaves are rich in ash and substances such as nitrogen, potassium, and chlorine, which are deleterious to the combustion or biomass conversion processes, a reduction in the number of leaves improves the quality of the harvested biomass. This improvement is also enhanced by the leaching of water-soluble substances, such as chlorine, by precipitation in winter.

The most common method of harvesting of biomass from energy crops is cutting with a mower and subsequent baling [15]. Switchgrass and reed canary grass can be harvested with conventional haying equipment [28]. If the biomass is to be used or further densified nearby, *Miscanthus* biomass can also be harvested with a maize chopper. Due to the high silica content of *Miscanthus*, an especially hardened steel needs to be used for the knives. However, *Miscanthus* chips have a very low density and are therefore not suitable for transport over large distances. For combustion in small-scale units, *Miscanthus* biomass is harvested as chips and then pressed to briquettes.

Lignocellulosic Energy Crops, Production and Provision. Table 4 Typical ranges for the composition of biomasses from *Miscanthus*, switchgrass, and reed canary grass (winter harvest)

Component in % of dm	Grass species		
	Miscanthus	Switchgrass	Reed canary grass
Lignin	9.3–16.3	5.0–20.0	15.8
Cellulose	36.5–43.3	30.0–50.0	39.7
Hemicellulose	24.3–31.6	10.0–40.0	13.0
Carbon (C)	47.5	47.12	46.0
Hydrogen (H)	6.2	5.60	5.6
Oxygen (O)	41.7	41.2	
Ash	1.6–4.0	4.5–10.5	1.9–11.5
Silicium (Si)	4.53		0.56–3.70
Nitrogen (N)	0.19–0.67	0.71–1.37	0.45–1.54
Potassium (K)	0.31–1.28	0.23	0.06–0.81
Phosphorus (P)	0.06	0.13	0.14
Calcium (Ca)	0.08–0.14	0.28–0.73	0.08–0.32
Chlorine (Cl)	0.10–0 .50	0.07	0.01–0.30
Sulfur (S)	0.04–0.19	0.12	0.06–0.11
Heating value in MJ/kg	17.6	17.0	16.6
Sources	[15, 30, 31, 32]	[15, 23, 33, 34]	[15, 35, 36]

Yield and Quality

The yield of lignocellulosic biomass depends on the site on which the biomass is produced.

As a C3 grass, reed canary grass has the lowest yield potential. For Sweden, a harvestable yield of 8–12 t dry matter ha^{-1} a^{-1} has been determined.

An analysis comparing *Miscanthus* and switchgrass has shown that the yield potential of *Miscanthus* is significantly higher (30–50%) than that of switchgrass [29]. An overview on yields for energy grasses shows that these range for *Miscanthus* from 4 t dry matter ha^{-1} a^{-1} in Northern Europe to 44 t dry matter ha^{-1} a^{-1} harvestable in Southern Europe and from 12 to 26 t dry matter ha^{-1} a^{-1} for switchgrass in the USA – both for one late harvest per year [15].

Whereas reed canary grass stands are nearly fully productive from the first year on, *Miscanthus* and switchgrass stands do not reach their peak yields until the third or fourth year. The oldest productive stands of *Miscanthus* are over 20 years old. Switchgrass stands can reach a productive period of 15 years and reed canary grass 10 years before yields decrease significantly.

The quality of the harvested biomass differs between the grass species and varieties and is strongly influenced by the harvest date. In addition, site conditions (e.g., mineral content of the soil) influence biomass quality. Table 4 gives an overview of the typical ranges in the composition of lignocellulosic biomasses from perennial grasses harvested in a delayed harvest system (i.e., in winter or early spring).

Future Directions

SRC and energy grasses are still very young crops and little breeding has so far been performed. For this reason, not many varieties are available for the biomass producer to match the demands of specific site conditions or specific biomass uses. In order to develop lignocellulosic energy crops successfully, further breeding programs targeting higher and more stable yields,

improved biomass quality, and adaptation to specific site conditions are required.

The major bottleneck in the production of perennial lignocellulosic crops is their establishment in the field. Establishment costs are high when propagation is performed vegetatively via rhizomes or micropropagation and deter farmers from producing these crops. Additionally, the establishment success is hampered by the low competitiveness of the crops in the year of establishment and through other factors, such as frost. Therefore, the development of safe establishment methods is an important prerequisite for large-scale implementation of these crops.

All perennial lignocellulosic energy crops display a good ecological profile because of

- Very low demands for nitrogen fertilization
- Perennity, which leads to long periods of soil rest and soil carbon accumulation
- The very high energy input-to-output ratio and greenhouse gas saving potential due to low nitrogen fertilizer demand and high yields

With the general demand for more sustainable energy-crop production, perennial lignocellulosic energy crops will play a major role in future bioenergy production. Combined electricity and heat production is the main area for which lignocellulosic energy crops are suitable and where they can be applied in the short term. Future options also include the production of next generation biofuels.

Bibliography

Primary Literature

1. Kauter D, Lewandowski I, Claupein W (2003) Quantity and quality of harvestable biomass from populus short rotation coppice for solid fuel use – a review of the physiological basis and management influences. Biomass Bioenergy 24(6):411–427
2. Lantmännen Agroenergi (2011) Manual for SRC willow growers. http://www.agroenergi.se
3. Pei MH, Lindegaard K, Ruiz C, Bayon C (2008) Rust resistance of some varieties and recently bred genotypes of biomass willows. Biomass Bioenergy 32(5):453–459
4. Boehmel C, Lewandowski I, Claupein W (2008) Comparing annual and perennial energy cropping systems with different management intensities. Agric Syst 96(1–3):224–236
5. Guidi W, Piccioni E, Bonari E (2008) Evapotranspiration and crop coefficient of poplar and willow short-rotation coppice used as vegetation filter. Bioresour Technol 99(11):4832–4840
6. Dimitriou I, Rosenqvist H (2011) Sewage sludge and wastewater fertilisation of Short Rotation Coppice (SRC) for increased bioenergy production – Biological and economic potential. Biomass Bioenergy 35(2):835–842
7. Kaltschmitt M, Hartmann H, Hofbauer H (eds) (2009) Energie aus Biomasse, 2nd edn. Springer, Berlin/Heidelberg
8. Lavoie F, Savoie P, D'Amours L, Joannis H (2008) Development and field performance of a willow cutter-shredder-baler. Appl Eng Agric 24(2):165–172
9. FNR (1999) Modellvorhaben schnellwachsende baumarten. GmBH, Verlag, Landwirtschaftsverlag, Münster, 476 pp
10. Vande Walle I, Van Camp N, Van de Casteele L, Verheyen K, Lemeur R (2007) Short-rotation forestry of birch, maple, poplar and willow in Flanders (Belgium) I-Biomass production after 4 years of tree growth. Biomass Bioenergy 31(5):267–275
11. McWilliam EL, Barry TN, López-Villalobos N (2005) Organic matter digestibility of poplar (Populus) and willow (Salix) forage trees and its in vitro prediction. J Sci Food Agric 85(7):1098–1104
12. Tharakan PJ, Volk TA, Abrahamson LP, White EH (2003) Energy feedstock characteristics of willow and hybrid poplar clones at harvest age. Biomass Bioenergy 25(6):571–580
13. Chauvet E (1987) Changes in the chemical composition of alder, poplar and willow leaves during decomposition in a river. Hydrobiologia 148(1):35–44
14. Baertsche SR, Yokoyama MT, Hanover JW (1986) Short rotation, hardwood tree biomass as potential ruminant feed-chemical composition, nylon bag ruminal degradation and ensilement of selected species. J Anim Sci 63(6): 2028–2043
15. Lewandowski I, Scurlock JMO, Lindvall E, Christou M (2003) The development and current status of perennial rhizomatous grasses as energy crops in the US and Europe. Biomass Bioenergy 25(4):335–361
16. Deuter M (2000) Breeding approaches to improvement of yield and quality in Miscanthus grown in Europe. In: Lewandowski I, Clifton-Brown JC (eds) European miscanthus improvement – final Report, Institute of Crop Production and Grassland Research, University of Hohenheim, Stuttgart, pp 28–52
17. Squire GR (1990) The physiology of tropical crop production. CAB International, Wallingford, 236 pp
18. Clifton-Brown JC, Jones MB (1997) The thermal response of leaf extension rate in genotypes of the C4–grass Miscanthus: an important factor in determining the potential productivity of different genotypes. J Exp Bot 48(8):1573–1581
19. Clifton-Brown JC, Lewandowski I (2000) Winter frost tolerance of juvenile Miscanthus plantations: studies on three genotypes at four European sites. New Phytol 148:287–294
20. Sanderson MA (1996) Switchgrass as a sustainable bioenergy crop. Fuel Energy Abstr 37:436–436
21. Elbersen HW (2001) FAIR 5-CT97-3701 Switchgrass (Panicum virgatum L.) as an alternative energy crop in Europe initiation of a productivity network Final Report for the period from 01-04-1998 to 30-09-2001. http://www.switchgrass.nl

22. Alexopoulou E, Sharma N, Papatheohari Y, Christou M, Piscioneri I, Panoutsou C et al (2008) Biomass yields for upland and lowland switchgrass varieties grown in the Mediterranean region. Biomass Bioenergy 32(10):926–933
23. Andersson B, Lindvall E (1999) Canarygrass breeding in Sweden. In: Mela T, Christiansen J, Kontturi M, Pahkala K, Partala A, Sahramaa M, Sankari H, Topi-Hulmi M, Pithan K (eds) Alternative crops for sustainable agriculture. COST 814, European Commission, BioCity, Turku, Finland, pp 53–57
24. Wolf DD, Fiske DA (1995) Planting and managing switchgrass for forage, wildlife, and conservation. Extension agronomist, Forages. Virginia Tech. Virginia Polytechnic Institute and State University, Publication 418–013
25. Atkinson CJ (2009) Establishing perennial grass energy crops in the UK: a review of current propagation options for Miscanthus. Biomass Bioenergy 33(5):752–759
26. Wright LL (1994) Production technology status of woody and herbaceous crops. Biomass Bioenergy 6(3):191–209
27. McLaughlin SB, Bouton J, Bransby D, Conger JB, Ocumpaugh W, Parrish D, Taliaferro C, Vogel K, Wullschleger S (1999) Developing switchgrass as a new crop. In: Janick J (ed) Perspectives on new crops and new uses: proceedings fourth national new crops symposium, Phoenix, AZ. ASHS Press, Alexandria, pp 282–299
28. ATTRA – National sustainable agriculture information service (2006) switchgrass as a bioenergy crop. http://www.attra.ncat.org
29. Heaton EA, Dohleman FG, Long SP (2008) Meeting US biofuel goals with less land: the potential of Miscanthus. Glob Change Biol 14:2000–2014
30. Kaack K, Schwarz K, Brander PE (2003) Variation in morphology, anatomy and chemistry of stems of Miscanthus genotypes differing in mechanical properties. Ind Crops Prod 17(2):131–142
31. Hodgson EM, Lister SJ, Bridgwater AV, Clifton-Brown J, Donnison IS (2010) Genotypic and environmentally derived variation in the cell wall composition of Miscanthus in relation to its use as a biomass feedstock. Biomass Bioenergy 34(5):652–660
32. Monti A, Di Virgilio N, Venturi G (2008) Mineral composition and ash content of six major energy crops. Biomass Bioenergy 32(3):216–223
33. McKendry P (2002) Energy production from biomass (part 1): overview of biomass. Bioresour Technol 83(1):37–46
34. Ogden CA, Ileleji KE, Johnson KD, Wang Q (2010) In-field direct combustion fuel property changes of switchgrass harvested from summer to fall. Fuel Process Technol 91(3):266–271
35. Burvall J (1997) Influence of harvest time and soil type on fuel quality in reed canary grass (Phalaris arundinacea L.). Biomass Bioenergy 12(3):149–154
36. Dien BS, Jung HG, Vogel KP, Casler MD, Lamb JFS, Iten L et al (2006) Chemical composition and response to dilute-acid pretreatment and enzymatic saccharification of alfalfa, reed canarygrass, and switchgrass. Biomass Bioenergy 30(10): 880–891
37. Himken M, Lammel J, Neukirchen D, Czypionka-Krause U, Olfs H (1997) Cultivation of Miscanthus under West European conditions: seasonal changes in dry matter production, nutrient uptake and remobilization. Plant Soil 189(1):117–126

Books and Reviews

Anderson B (1995) Establishing dryland forage grasses – Neb guide B-18, issued in furtherance of cooperative extension work, Acts of May and June 30, 1914, in cooperation with the US Department of Agriculture. University of Nebraska, Institute of Agriculture and Natural Resources

Linear Fresnel Collectors

Andreas Häberle
PSE AG, Freiburg, Germany

Article Outline

Glossary
Definition of the Subject and Its Importance
Introduction
Design of Linear Fresnel Reflectors
Reference Area
Receiver Design
Benefits and Disadvantages
Future Directions
Bibliography

Glossary

Dish Short for point focusing concentrator with circular paraboloid reflector.

Heliostat The reflecting device that is positioned such that it reflects the direct sun light to the receiver.

IAM Incident angle modifier: optical efficiency at a certain angle of incidence in relation to the optical efficiency at normal incidence.

Longitudinal Parallel to the direction of the receiver.

Longitudinal IAM IAM for incident rays with no transversal component.

Receiver The device, usually a tube or a bundle of tubes, that absorbs solar radiation and transfers it to useful heat.

Reflector Here sometimes used synonymously with "mirror" or "heliostat".

Tower Here used as a short form for solar power tower or central receiver system.

Transversal Perpendicular to the direction of the receiver and parallel to the aperture.

Transversal IAM IAM for incident rays with no longitudinal component.

Trough Linear concentrating collector with parabolic reflector trough.

Definition of the Subject and Its Importance

Linear Fresnel Collectors are a subgroup of linear concentrating collectors. They use linear receivers and reflectors, which are segmented in single axis tracking heliostats. The reflector segments are typically aligned horizontally and track the sun such that the receiver is illuminated without need to be moved (see Fig. 1).

Similar to heliostat fields in tower projects Linear Fresnel reflectors allow for a much bigger aperture area per unit of receiver compared to the ideal reflector that is, the parabolic trough. The mechanical size limits of ideal reflectors (due to wind load and weight) are similar for each individual heliostat as for a trough. The beauty of heliostat systems is of course that the aperture size of a complete system is independent of the

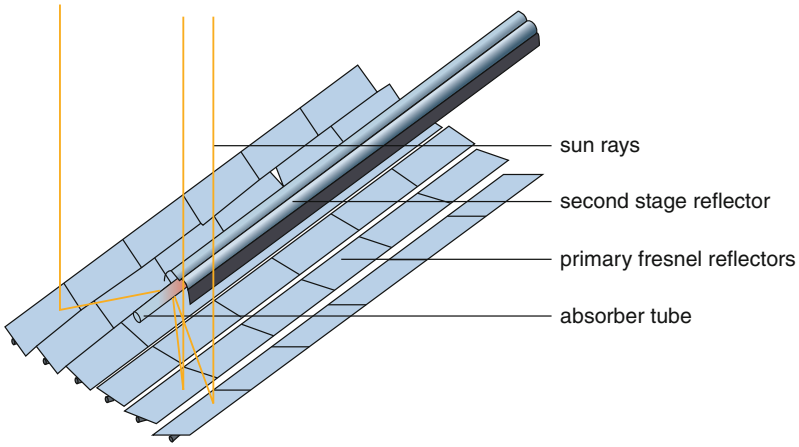

Linear Fresnel Collectors. Figure 1
Schematic of a Fresnel collector with secondary reflector

size of the individual reflectors. This means the individual heliostats can be small but jointly cover a big aperture area. The drawback of heliostat systems is a lower optical efficiency per reflector area, mainly due to interference between individual reflector segments, which by principle can only approach the optical efficiency of an ideal (i.e., non-segmented) reflector geometry.

Whilst solar towers, dishes, and parabolic troughs were subject of continuous research and development during the past decades, it is only since late in the 1990s that linear Fresnel concepts are again on the agenda of a few companies and research groups worldwide.

Introduction

Linear Fresnel Collectors are named after Augustin Jean Fresnel (1788–1827), who among many other things developed refractive lenses, with the same focal length but using a fraction of the material compared to standard lenses. With Fresnel collectors the similar principle of segmenting the optical device is found but applied to a reflecting parabolic mirror rather than a refracting lens.

A first prototype linear Fresnel collector is documented from the Italian researcher Giovanni Francia in 1964 (see Fig. 2).

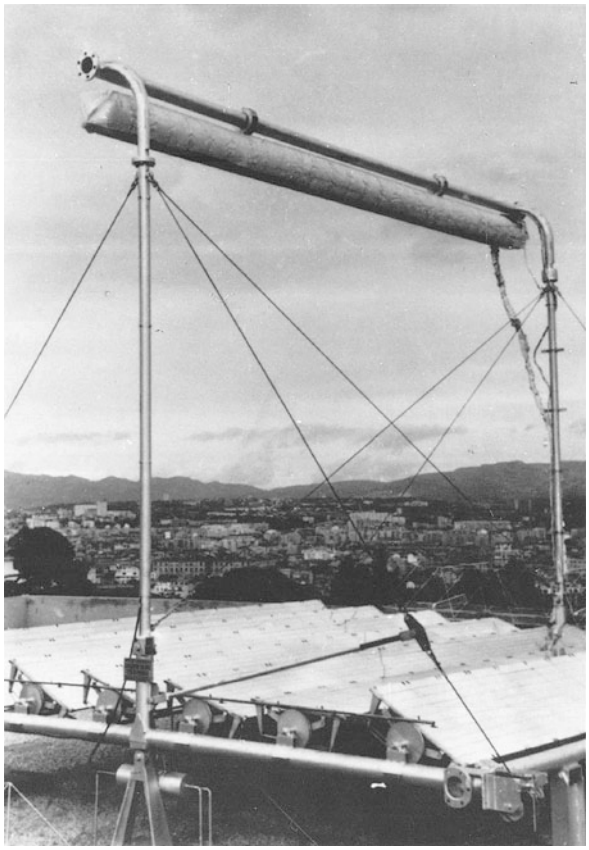

Linear Fresnel Collectors. Figure 2
Prototype linear Fresnel collector (From Giovanni Francia's (1911–1980) private archive)

Francia reported temperatures of 450°C and direct steam generation [1]. A few pilot installations from other groups followed in other parts of the world but none of them are known to be operated for a longer time. Technical problems with these projects are speculative. One might be the underestimation of the efforts to reach and maintain sufficient tracking precision.

At the end of the 1990s, two groups have restarted the development of linear Fresnel collector technology: the Australian Solar Heat and Power (SHP) (SHP was later renamed AUSRA, which was then acquired by the French AREVA Group) and the Belgian Solarmundo (Solarmundo was later transferred to Solar Power Group, which was joined by the German MAN Ferrostaal). A new company called Novatec Biosol (later renamed Novatec Solar and joined by the German ABB Group) entered the field in 2006 and could soon announce the first 1.4 MW linear Fresnel system to feed electricity into the electric grid (see Fig. 3).

The commercial rational behind linear Fresnel collectors compared to parabolic troughs for CSP applications is an expected advantage in cost reduction potential due to their simpler design, which shall compensate for their lower optical performance.

It is now the question whether the big CSP projects that are on their way will prove the commercial viability of the linear Fresnel collector technology.

A different market segment is addressed for the application of concentrating solar collectors in the field of industrial process heat. Here it can be necessary to mount the solar collectors on rooftops, which highlights the importance of low wind loads and high ground usage factors compared to the application in CSP projects. The company Industrial Solar GmbH already installed a number of such rooftop linear Fresnel systems, mostly for solar cooling applications but also for direct steam generation (see Fig. 4).

Linear Fresnel Collectors. Figure 3
Novatec Solar GmbH

Linear Fresnel Collectors. Figure 4
Rooftop mounted Fresnel collector by Industrial Solar GmbH for a Solar Cooling system at the technical university of Seville, Spain

Design of Linear Fresnel Reflectors

The general design idea is to cut a parabolic reflector into pieces, align the pieces horizontally and let them track the sun individually. When looking a little closer it becomes obvious that for an optimum design the reflector segments are not part of the same parabola but belong to parabolas with bigger focal lengths the farer off center the reflector segment is located (see Fig. 5).

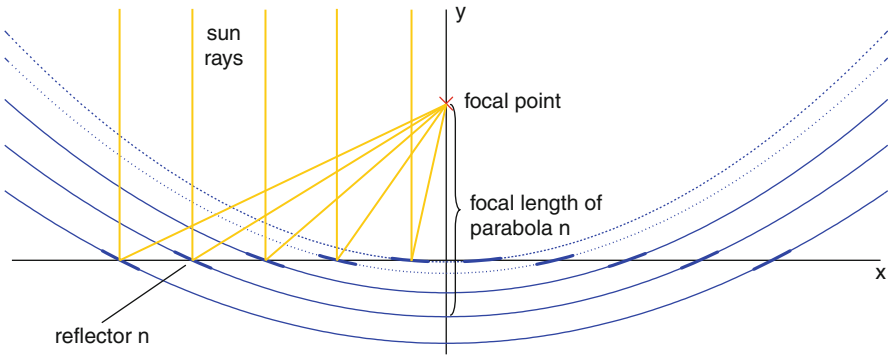

Linear Fresnel Collectors. Figure 5
Ideal Fresnel reflectors for perpendicular irradiation

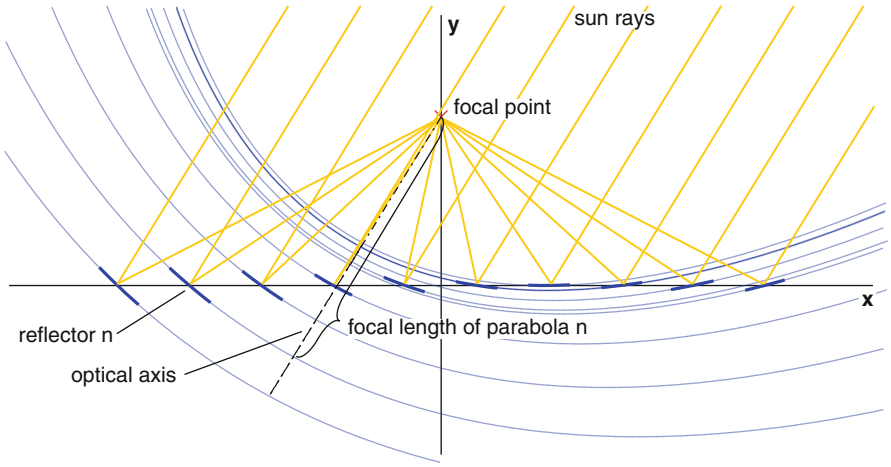

Linear Fresnel Collectors. Figure 6
Ideal Fresnel reflectors for off-normal incidence

Furthermore, the ideal shape of the heliostats changes when tracking the sun, because ideally they are different segments of different parabolas for different sun angles. The parabola segments are close to the optical axis for near normal reflection but far off-center for high reflectance angles. Ideally, each reflector should be able to take on the shape of segments of parabolas with different focal lengths and at a varying distance to the optical axis (see Fig. 6).

When practically constructing a linear Fresnel collector, one needs to compromise with the ideal geometrical design in order to stay within reasonable efforts for realization. It is, e.g., not reasonable to change the shape of reflectors for different inclinations. A fixed shape however will lead to an optical error called astigmatism for any incident angle other than the design angle. In other words, the cross-sectional focal point transforms to a focal area. This would happen anyway due to imperfections of material and assembly. The art of engineering is thus to find the optimum compromise of effort for construction and material and overall performance.

An interesting effect for the sun tracking principle is that for each heliostat the incremental tracking of mirrors is identical as long as the turning axis of the heliostat is in the reflecting plane (see Fig. 7). For practical use this means that with a simple mechanical coupling of neighboring mirrors it is possible to track a complete mirror field with only one actuator.

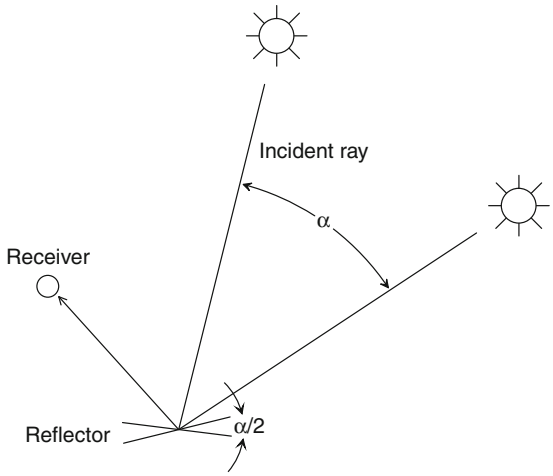

Linear Fresnel Collectors. Figure 7
For a change α of the incident angle each reflector has to be turned by α/2

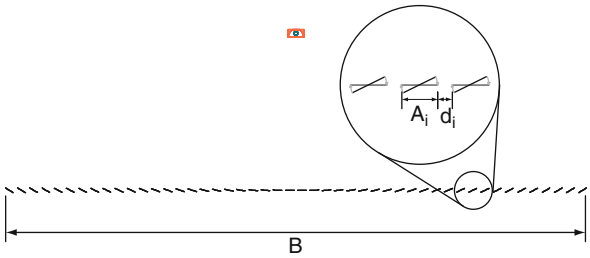

Linear Fresnel Collectors. Figure 8
Aperture area $A = \Sigma A_i$ and gross area B of a Fresnel collector

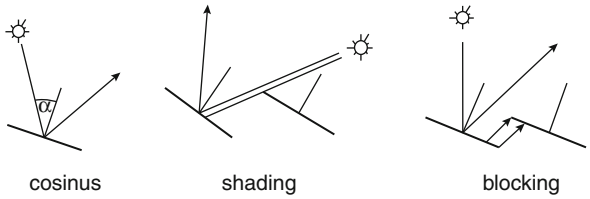

Linear Fresnel Collectors. Figure 9
Cosine losses, shading, and blocking of neighboring reflectors

Reference Area

When discussing performances and efficiencies, it is important to define a reference area. For parabolic trough collectors, the reference area is defined as the projection of the reflector shape. It would be nice to find a similar definition for a linear Fresnel collector. However the projection of the reflector shape of a Fresnel reflector field changes with the incident angle so this definition would not be practical. A compromise was found by defining the aperture of a Fresnel collector as the projections of its reflectors when turned horizontally (see Fig. 8).

The typical optical performance of a Fresnel collector with respect to aperture area as defined above is lower than that of a parabolic trough with identical material parameters. This is not surprising given the approximate character of the Fresnel approach.

Optical losses are caused by the effect that the aperture area is not perpendicular to the incident rays and thus the active area is diminished by the cosine of the incident angle of each reflector. Structural shading by support structures and mutual shading and blocking of the reflectors are the other major optical loss factors (see Fig. 9).

The angular dependence of optical performance is described by the biaxial incident angle modifier (IAM). It is defined as the ratio of optical efficiency at a certain angle of incidence and the optical performance at perpendicular irradiation. Figure 10 gives a typical example of the incident angle modifier in longitudinal and transversal direction.

Receiver Design

The light absorbing receiver of a linear Fresnel collector is typically a selectively coated single steel tube or a bundle of steel tubes.

Many linear Fresnel collector designs use a secondary concentrator above a single receiver tube to reflect those rays to the back of the receiver tube that missed it in the first place. Non-imaging optics [2, 3] allow for an additional concentration via the secondary concentrator by a factor of approximately 2. In other words the target area of the receiver is enlarged, which reduces the requirements on optical precision of the primary reflectors.

Heat losses are reduced by enclosing the receiver in an insulating cavity with a transparent cover facing toward the primary reflectors. Alternatively, a vacuum tube similar to the receivers of parabolic trough collectors can be used.

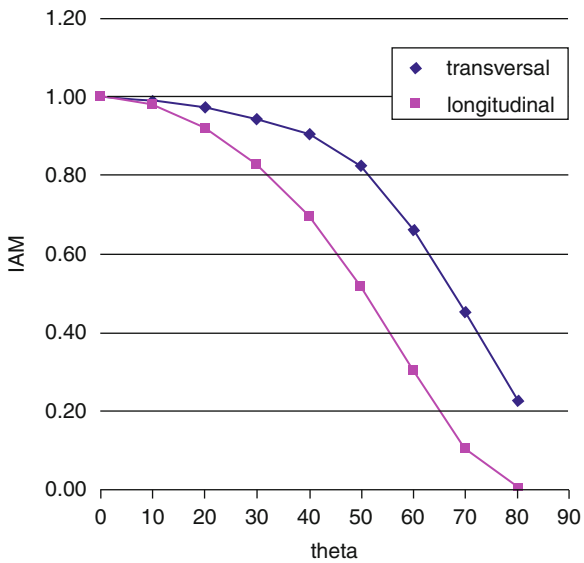

Linear Fresnel Collectors. Figure 10
Incident angle modifier IAM

Benefits and Disadvantages

When discussing pros and cons of different collector technologies, it is important to differentiate between commercial and technical objectives. The following discussion shall look at technical specifics of Fresnel collectors, while presuming a reasonable commercial collector design.

With respect to parabolic trough collectors, the main features of a Fresnel collector are:

- Stationary receiver
  With a stationary receiver, there is no need for flexible hoses or ball joints to connect the receiver. Still the receiver ends will move due to thermal expansion. The maximum movement depends on the maximum operation temperature and the overall length of the receiver. This daily movement can easily be several meters, with a receiver length of many 100 m. However the respective compensators are standard industrial equipment.
- Illumination from underneath
  The receiver is always illuminated from underneath, no matter of the sun angle. This means that the thermal stress to the receiver does not change its direction throughout the day. In particular, there is no thermal stress that leads to a sideward bending of the receiver.
  The illumination from underneath is an important advantage for direct steam generation, at least for those flow patterns where the constant cooling of the upper part of the tube cannot be guaranteed (stratified flow or slug flow).
- Low wind load
  Low wind load is considered an advantage because it directly leads to slimmer and more lightweight mechanical structures, less influence by wind during operation, and fewer damages due to high wind speeds.
- High ground usage
  The optimum design of a Fresnel reflector carefully adjusts all geometrical parameters like height of the receiver, distances between the mirrors, the mirror size itself, the number of mirrors, etc. The resulting design typically has a higher thermal peak power per ground area compared to parabolic trough plants by a factor of approximately 1.5.
- Cleaning of mirrors
  This is one of the most important O&M factors for performance and cost. The basically flat primary mirrors and the possibility to position all primary reflectors horizontally offers the advantage of an easily accessible surface that can also be cleaned by robots with very little water consumption.

Of course also some disadvantages of Fresnel collectors need to be considered:

- Lower optical performance
  Shading/blocking of the primary reflectors lead to a reduced optical performance per aperture area.
- Higher tracking accuracy needed
  The movement of the reflected beam of a heliostat is twice the angular movement of the heliostat itself. This means that for the same concentration ratio a Fresnel reflector needs to be controlled twice as precisely as a trough and also the reflector shape needs to be accordingly more accurate.
- The yearly energy production per installed capacity is lower, which compensates partly the effect of a higher capacity per ground area.

In the end the above mentioned technical advantages translate into commercial benefits, which need to compensate the commercial drawbacks that result from technical disadvantages. It is thus a multidimensional

optimization procedure that finally leads to a highly competitive technology.

Future Directions

There are two target markets for linear Fresnel collector technology.

The presently most interesting market is the large-scale generation of electricity (CSP). Very large collector fields will generate steam to drive turbines in power blocks of many hundreds of MW power. Fresnel companies try to catch up with the prominence of trough technology in terms of operation experience and consequential bankability.

Most probably direct steam generation will be the predestined choice for linear Fresnel collectors but other heat transfer fluids are also worthwhile to be considered for this technology at least until latent or chemical heat storages are available in sufficient commercial scale to provide suitable storage for direct steam generation.

In areas with water scarcity it will be important to use low water consumption technologies, where the cleaning of the basically flat Fresnel mirrors seems advantageous for the implementation of automated cleaning devices.

The other target market is the provision of solar generated process heat in MW scale for industrial production processes and the generation of cold. Also small-scale power generation in Cogeneration or Polygeneration systems can be classified within this market of "industrial process heat" and will become more and more interesting in future.

Industrial process heat is still a much less developed market for solar technologies than CSP but it will eventually offer a substantial commercial potential.

The typical project size will be much smaller than in CSP projects, typically starting in the sub MW scale and up to several MW peak thermal capacities. Also other aspects might become predominant, e.g., the possibility of rooftop installation or the automated operation including the integration into hybrid fossil powered systems. Some of the above mentioned advantages of Fresnel collectors become even more interesting with rooftop applications (e.g., low wind load and high ground usage factor). Also the direct steam generation fits nicely to supplement the steam supply of industry.

Bibliography

1. Silvi C (2009) The pioneering work on linear Fresnel reflector concentrators (LFCs) in Italy. In: Proceedings SolarPACES 2009, Berlin
2. Rabl A (1985) Active solar collectors and their applications. Oxford University Press, New York
3. Welford WT, Winston R (1978) The optics of nonimaging concentrators. Academic, New York

Lithium Battery Electrolyte Stability and Performance from Molecular Modeling and Simulations

Grant D. Smith[1], Oleg Borodin[1,2]
[1]Department of Materials Science and Engineering, University of Utah, Salt Lake City, UT, USA
[2]Electrochemistry Branch, SEDD, AMSRD–ARL–RDRL–SED–C, Adelphi, MD, USA

Article Outline

Glossary
Definition of the Subject
Introduction
Quantum Chemistry Studies of Oxidative Stability of Electrolyte Compounds
Modeling of Reductive Decomposition of Electrolytes
Molecular Dynamics Simulations of Bulk Electrolyte Properties
Modeling of Ionic Liquid Electrolytes
Molecular Dynamics Simulations of Electrode/Electrolyte Interfaces
Summary
Future Directions
Acknowledgments
Bibliography

Glossary

Interfacial impedance The resistance to lithium motion at the interface between the electrolyte and an electrode due to structure imposed on the electrolyte by the electrode, barriers to intercalation into the electrode, lithium desolvation energy, and/or the SEI layer.

Ionic liquid electrolyte An electrolyte comprised of a lithium salt dissolved in a room-temperature ionic liquid.

One-electron reduction The reduction of an electrolyte molecule by a single electron resulting in formation of species believed to be important contributors to the outer part of the SEI.

Organic liquid electrolyte An electrolyte comprised of a lithium salt dissolved in liquid carbonates, esters, ethers, or a mixture thereof.

Oxidative stability The ability of an electrolyte to remain electrochemically stable against oxidation at the surface of the cathode.

SEI layer The layer of electrolyte decomposition products that forms at the interface between an electrode (primarily the anode) and the electrolyte, called the solid electrolyte interphase or solid electrolyte interface. The SEI is believed to be comprised of an inner SEI layer and an outer SEI layer.

Solid polymer electrolyte An electrolyte comprised of a lithium salt dissolved in a polymer matrix.

Two-electron reduction The reduction of an electrolyte molecule by two electrons resulting in formation of species believed to be important contributors to the inner part of the SEI.

Definition of the Subject

Lithium batteries are complex devices whose performance optimization necessitates that they be well understood on multiple timescales and length scales, ranging from systems level to molecular. Optimization of the electrolyte, in particular, requires detailed, fundamental, molecular-level understanding of the chemical features that lead to stable electrolytes with large electrochemical windows – what electrolyte solvents and additives facilitate the formation of stable solid electrolyte interface layers and which features of the electrolyte result in good bulk and interfacial lithium transport properties as well as thermal stability, low-temperature transport, and low volatility/high safety [1, 2]. Molecular modeling has contributed significantly to this fundamental understanding of electrolyte properties and will continue to contribute to it in the future.

Introduction

Electrolytes and electrode/electrolyte interfaces are well suited for molecular modeling studies because important timescales and length scales are accessible to these powerful methodologies, and because gleaning molecular-level information from experiment is intrinsically challenging. While molecular modeling methods have not yet reached the point where they can be used exclusively in the design of electrolytes for improved battery performance, they have provided important insight into electrolyte stability, transport mechanisms, and the nature of the interface between the electrolyte and electrodes. These insights, or more precisely, a subset thereof, are the subject of this chapter.

The primary molecular modeling methods that have been extensively applied to lithium battery electrolytes and electrode/electrolyte interfaces are molecular orbital calculations and molecular dynamics simulations. The former involves ab initio and density functional methods and will be referred to quantum chemistry or QC calculations. In QC methods, atomic centers and electrons are treated explicitly and the optimized molecular orbitals (with corresponding energies and molecular/complex geometries) are obtained. QC methods are extremely powerful and accurate given adequate levels of theory (e.g., electron correlation treatment or density functional used) and adequate atomic basis sets, but quickly become computationally prohibitive with increasing system size. Hence, QC methods are applied to individual molecules or small clusters of molecules and as such do not typically allow for direct inclusion of condensed phase/solvent effects. Furthermore, while it is possible to perform molecular dynamics simulations using QC methods, the computational cost of this approach is such that the size of the system, the length of the trajectory, and the level of theory that can be employed are typically severely compromised. Despite their computational limitations, QC methods provide invaluable information relevant to the stability and performance of lithium battery electrolytes, including properties such as the electron affinity and ionization potential of a molecule or molecular cluster, solvation/complexation energies, and the energetics of various reactions. QC methods are also invaluable in providing information needed in the development of atomistic potential functions, or force fields, for molecular dynamics (MD) simulations.

MD simulations of electrolytes for lithium batteries retain the atomistic representation of the electrolyte molecules but do not treat electrons explicitly. Instead the influence of electrons on intermolecular interactions is subsumed into the description of the interatomic interactions that constitute the atomistic

potential or force field. The interatomic potential used in MD simulations is made up of dispersion/repulsion terms, Coulomb interactions described by partial atomic charges, and in some cases, dipole polarizability described by atom-based polarizabilities. The importance of explicit inclusion of polarization effects is considered below. In the most accurate force fields, interatomic potentials are informed by high-level QC calculations. Specifically, QC calculations provide molecular geometries, conformational energetic, binding energies, electrostatic potential distributions, and dipole polarizabilities that can be used to parameterize atomic force fields.

Because MD simulations use atomic force fields (i.e., do not explicitly include electrons), they are computationally orders of magnitude more efficient than QC methods. Hence, MD simulations can be run to predict bulk liquid properties, understand solvation/coordination structure, elucidate transport mechanisms, and study the interface between liquids and solid substrates, e.g., electrodes and electrolytes. Typical MD simulations involve hundreds of molecules and thousands of atoms, and trajectories of many nanoseconds can be routinely generated. Unlike QC methods, however, most classical MD simulation methodologies do not allow for chemical reactions, specifically the making and breaking of covalent bonds. An exception is MD simulations that involve reactive force fields, such as the ReaxFF, that allow for bond breaking and formation through use of bond order potentials and partial atomic charges that depend upon the bonding environment of an atom. Reactive force fields are computationally more expensive than nonreactive atomistic force fields, resulting in typically smaller simulation systems and shorter trajectories. Furthermore, reactive force fields, in an effort to minimize complexity and number of parameters, are less accurate in the prediction of thermophysical and transport properties than the better nonreactive force fields.

Quantum Chemistry Studies of Oxidative Stability of Electrolyte Compounds

Electrolyte oxidative stability is one of the key parameters for designing electrolytes compatible with a cathode. An electrolyte should be either anodically stable toward the cathode or form a stable passivation layer on the cathode that is capable of conducting lithium ions and accommodating electrode dimensional changes during cycling. QC calculations were used to estimate the oxidative stability of electrolyte solvents [3, 4], additives [5], anions [6–8], and redox shuttle molecules [9]. A free-energy cycle shown in Fig. 1 is used to relate the gas-phase adiabatic ionization potential (IP) to the absolute oxidation potential using the free energy of solvation $\Delta G^0{}_S(M)$ and $\Delta G^0{}_S(M^+)$ for the reduced and oxidized forms of a molecule M. IP is defined as the enthalpy changes of the oxidation reaction in the gas phase at 298 K. QC calculations yield the standard oxidative potential $E^0{}_{abs}(M)$ at the absolute electrochemical scale [10, 11] with the reference vacuum state corresponding to an electron at rest in a field-free vacuum.

Using the free-energy cycle shown in Fig. 1, $E^0{}_{abs}(M)$ is expressed by Eq. 1

$$E^0{}_{abs}(M) = IP + \left[-T\Delta S + \Delta G^0{}_s(M^+) - \Delta G^0{}_s(M)\right]/F \quad (1)$$

where F is Faraday constant 23.061 kcal per volt gram equivalent and $-T\Delta S$ is the entropy difference in the gas phase between M and M^+. Most electrochemical experiments, however, report oxidation potential versus standard hydrogen electrode (SHE) or Li^+/Li in the lithium battery literature instead of using absolute oxidation potential. The SHE at room temperature (25°C) is estimated [11] to have the absolute potential of 4.42 V in aqueous solutions. Older International Union of Pure and Applied Chemistry (IUPAC) recommendation [10] of 4.44 V is often used. The IUPAC recommended values for the absolute SHE potential in nonaqueous solvents are within a few tens of volts of

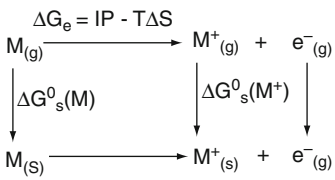

Lithium Battery Electrolyte Stability and Performance from Molecular Modeling and Simulations. Figure 1 Free-energy cycle for the redox reaction $M \rightarrow M^+ + e^-$, $M_{(g)}$ denotes molecule M in gas phase, while $M_{(S)}$ denotes the solvated molecule

the value of the absolute SHE potential in aqueous solutions. For example, it was recommended by IUPAC to use the following absolute potential values for SHE in nonaqueous solvents: 4.13 ± 0.06 V for acetone and 4.60 ± 0.10 for acetonitrile. The Li^+/Li standard absolute electrode potential is −3.04 V versus SHE. Most commonly [4, 5, 7, 9], the aqueous value of 4.44 – 3.04 = 1.4 V is used to convert from the absolute electrochemical scale used in QC calculations to the experimentally measured potential versus Li^+/Li.

An extensive QC study [4] of 160 structurally unrelated organic molecules reported prediction of IPs with a standard deviation of 0.14 V at B3LYP/6-311++G (2df,2p)//B3LYP/6-31+G(d). Such good agreement was achieved after correcting IPs obtained from QC calculations for the systematic underestimation of the experimental data by adding 0.28 V to all QC IP values. At the next step, $E^0_{abs}(M)$ was calculated from IP using Eq. 1. Widely available in QC codes, polarized continuum models (PCM) are commonly used to estimate free energy of solvation of the reduced and oxidized forms of M (see Eq. 1 and Fig. 1). The standard redox potentials of 270 structurally unrelated organic molecules in acetonitrile were predicted with the standard deviation from experiments of 0.17 V [4]. This accuracy is sufficient for guiding the electrolyte solvent development. One caveat, however, should be mentioned. For a number of alkene molecules, the deviation between the experiment and the theory was about 0.5–0.8 V (i.e., 11–18 kcal/mol). No explanation was given for this discrepancy [4].

The other QC studies [5, 9] focused on the redox additives that could be reversibly reduced and oxidized for the overcharge protection. The calculated oxidative potential using B3PW91/6-31 + G(d,p) density functional theory (DFT) level were found in close agreement with the experimental data with the root mean-square deviation is 0.08 V and the maximum deviation is 0.15 V, indicating high fidelity of QC calculations of the solvent oxidation potential using PCMs to account for the solvation effects [5]. The experimental measurements were performed in 1 M lithium hexafluorophosphate ($LiPF_6$) ethylene carbonate (EC)/ethylmethyl carbonate (EMC) (1/2, v/v) supporting electrolyte on Pt wire. The correlation coefficients (R^2) of IP(calc. QC), E_{ox}(calc. QC) with respect to E_{ox}(exp.) were 0.84 and 0.98, respectively. Similarly, Wang, Buhrmester, and Dahn [9] reported an excellent agreement between the calculated values for 17 redox shuttle additives with the root-mean-square deviation between the calculated and measured oxidation potentials being 0.15 V with the maximum deviation of 0.25 V, indicating that DFT calculations at B3LYP/6-31 G(d,p) could be effectively used for screening redox additives.

Comparison of the common electrolyte solvents (EC, propylene carbonate [PC], dimethyl carbonate [DMC], EMC, vinylene carbonate [VC], dimethoxyethane [DME]) oxidative stability with experiments was reported by Zhang et al. [3]. While trends of the oxidative stability were reasonably captured in this study, typical deviations between experiments and simulations were reported to be around 0.5–1.0 V. Note that Zhang et al. [3] did not use the value of 1.4 V to convert from the absolute to Li^+/Li potential scale, instead they used the Li/Li^+ and M/M^+ cycles with a number of calculated/estimated quantities, resulting in the absolute potential versus Li^+/Li being around 2.2 V. Application of the value of 1.4 or 1.54 V derived from SHE potential in water and acetonitrile and using the standard Li^+/Li vs. SHE potential will result in an improved agreement between QC-based values reported by Zhang et al. [3] and experiments.

Ue et al. [6] and Johansson [7, 8] have reported anion oxidative potentials. They found a significant correlation between the predicted single molecule gas-phase QC values and experimental oxidation potential measurements performed on numerous solvents and salt concentrations. Figure 2 and Table 1 shows the vertical (e.g., anion (charge=−1e) geometry was used in the oxidized molecule (charge = 0) energy calculation) ionization energy (ΔE_v) and free energy of anion ionization (ΔG_v) from the Johansson work [8] that employed VSXC DFT functional and 6-311 + G (2df,p) basis set. Johansson [8] used vertical instead of adiabatic energies in calculations to lower the computational cost. QC calculations generally reproduced the order of oxidation potentials with the exceptions of the large anions that have low oxidative stability where deviations up to a few volts were observed. Another case where QC calculations fail to reproduce oxidative potential trends was the comparison of highest occupied molecular orbital (HOMO) calculations and measured oxidative potential of propargyl methanesulfonate (PMS) and EC [12]. Calculations indicated higher HOMO absolute value implying higher oxidative

stability of EC compared to PMS by 0.8–1.0 V, while oxidative stability of PMS on Pt was higher compared to EC by ~0.2 V in the $LiPF_6$-based electrolytes [12]. It is important to note that anodic stability of electrolytes on active cathode surfaces could be significantly (up to a few volts) lower than the electrolyte stability on Pt or glassy carbon; therefore, one would need to include surfaces in the electrolyte calculations in order predict oxidative stability of electrolytes on active materials [1].

While the focus of this section was on the prediction of oxidation potentials, reduction potentials of EC, PC, DMC, VC, and vinylethylene carbonate (VEC) were calculated using quantum chemistry methods and compared with experiments [13–15].

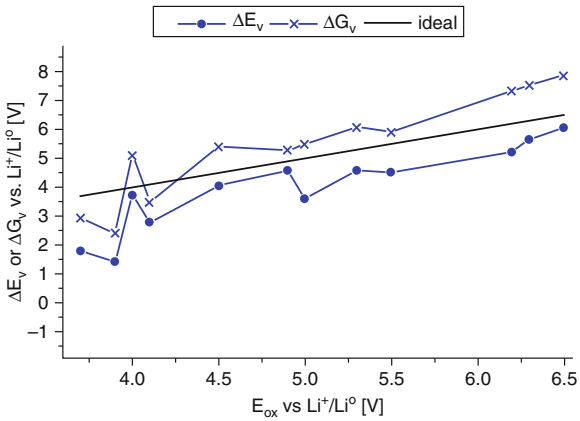

Lithium Battery Electrolyte Stability and Performance from Molecular Modeling and Simulations. Figure 2 Experimental anion oxidation potential compared with the vertical electron transition energy (ΔE_v) and the vertical free-energy difference (ΔG_v) from Johansson [7]. The highest experimental values from Table 1 are shown in this figure (Reproduced with permission of ACS)

Modeling of Reductive Decomposition of Electrolytes

The properties of the solid-electrolyte interface (SEI) that forms as a result of reduction of the electrolyte solvent and lithium salt are key elements in determining the performance of lithium ion batteries [1, 16]. The electrolyte solvent is typically comprised of a mixture of linear and cyclic carbonates, with EC being a major component of most electrolytes. The solvent and lithium salt anion undergo one- and two-electron reduction at the anode, typically Li-intercalated graphite. During the first cycle, the reaction products of electrolyte reduction form a thin SEI film, which in the ideal case protects the electrolyte from further reductive decomposition during subsequent cycles while at the same time contributing significantly to the resistance for Li^+ exchange between the electrolyte and the electrode. There have been number of experimental studies focusing on understanding of mechanisms of the SEI formation, a detail discussion of which can be found in Ref. [1, 17]. In general, the SEI is thought to consist of an inner and an outer layer. The inner layer is believed to be primarily comprised of doubly (two electron) reduced compounds, such as Li_2CO_3, while the outer SEI layer is thought to be comprised largely of reaction products of singly (one electron) reduced electrolyte species [1, 18–21], the nature of which remains controversial.

Lithium Battery Electrolyte Stability and Performance from Molecular Modeling and Simulations. Table 1 Anion oxidation potentials (in V) from experiments and vertical electron transition energy from DFT calculations by Johansson [7, 8]

Anion	Exp	QC	Anion	Exp	QC
AsF_6^-	6.5–6.8	6.05	$[1,3\text{-}BF_3\text{-}(N_2C_3H_3)]^-$; "imidazolide"$^-$	4.9	4.58
PF_6^-	6.3–6.8	5.65	$[(C_2O_4)_2B]$; BOB^-	>4.5	4.05
BF_4^-	6.2–6.6	5.22	$[(1,2\text{-}C_6F_4O_2)_2B]^-$ 4 F-BBB$^-$,	4.1	2.79
$N(SO_2CF_3)_2^-$,TFSI$^-$	6.1–6.3, 5.3	4.52	$N_5C_4^-$; TADC$^-$	>4.0	3.72
$(CF_3SO_2)_3C^-$, methide$^-$	6.1, 5.5	4.57	$(2,3\text{-}C_{10}H_6O_2)_2B]^-$; BNB$^-$	3.9	1.43
$CF_3SO_3^-$	5.9–6.0, 5.0	3.6	$[(1,2\text{-}C_6H_4O_2)_2B]^-$ BBB$^-$	3.7	1.79

Given the importance of the SEI layer in lithium batteries, it is clear that improved understanding of the mechanisms of electrolyte decomposition and the formation of the SEI layer would facilitate optimization of battery performance. The reductive decomposition of organic solvents at the anode–electrolyte interface is largely responsible for the formation of the SEI. The electrochemical reactions leading to the formation of the SEI are complex and not well understood. Fortunately both QC and molecular dynamics simulations have provided some insight into reaction pathways that are believed to be important in the formation of the SEI. Reduction pathways for EC [14, 15, 22–24], PC [15, 23, 25], and VC [15, 23, 24], among others, have been most extensively studied extensively computationally, with the greatest focus on EC. Two schemes have been proposed in the literature for reductive decomposition of solvents at the anode interface. The first involves decomposition after electron transfer to Li^+-solvent complexes, while the latter involves direct decomposition on the electrode surface. Computational insights into both of these schemes for EC are considered below.

Reduction of Li^+–EC Complexes

One-Electron Reduction of EC The most important component of the current generation of electrolytes is EC. The initial step in the commonly accepted single-electron reduction mechanism is shown in Fig. 3a. QC calculations [14] have shown that this reaction is energetically unfavorable in the gas phase and energetically favorable when solvent effects are taken into account through the polarized continuum model approach. However, the reaction becomes dramatically more favorable when Li^+ is complexed to the carbonate molecule, resulting in the cation/anion complex shown in Fig. 3b. The next step in the one-electron reduction process is commonly believed to be the opening of the closed EC radical anion (complexed to Li^+), denoted as c-EC$^-$, to form an open radical, shown in Fig. 3c. This process involves a substantial energy barrier leading ultimately to a substantially lower energy radical anion [14].

The fate of the o-EC$^-$ radical anion formed from one-electron reduction of EC is a matter of central importance in understanding the formation of the SEI in EC-based electrolytes, and is a matter of controversy. Dilithium ethylene dicarbonate $(CH_2OCO_2Li)_2$ has been proposed as a major component of the outer SEI layer [1], resulting from combination reactions of pairs of o-EC$^-$, as shown in Scheme I in Fig. 4. Fourier transform infrared (FTIR) and x-ray photoelectron spectroscopy (XPS) studies of SEI films formed on lithium metal in EC-based electrolytes reveal the presence of alkyl carbonates [19, 26], while FTIR shows the presence of alkyl carbonates in the SEI formed from EC/diethyl carbonate electrolytes on graphite [20]. Hydrolysis of alkyl carbonate species formed from reduction of EC on noble metal electrolytes leads to the formation of ethylene glycol, which has been taken as evidence for the formation of $(CH_2OCO_2Li)_2$ [27]. Nuclear magnetic resonance (NMR) studies of the surface species formed on graphite in EC electrolytes resulted in spectra consist with that of alkyl carbonates, and in particular, the spectrum of $(CH_2OCO_2Li)_2$ [28]. A combined transmission electron microscopy (TEM)/FTIR study of the SEI formed on graphite in a EC/lithium perchlorate ($LiClO_4$) electrolyte revealed the formation of alkyl carbonates, one of whose chemical composition (O/C ratio = 1.5) is consistent with $(CH_2OCO_2Li)_2$ [29].

In addition to experimental investigations, QC studies have provided important insight into single reduction reactions of EC. In one study, DFT studies at B3PW91/6-311++G(d,p) level of theory were performed in order to investigate the energetics of

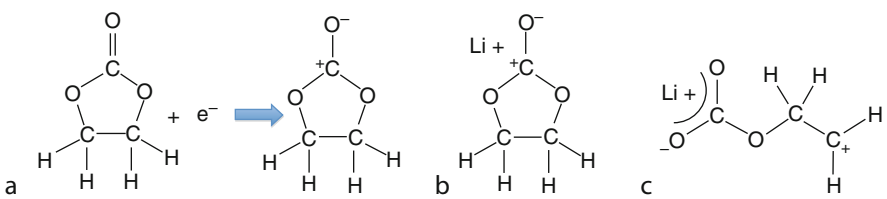

Lithium Battery Electrolyte Stability and Performance from Molecular Modeling and Simulations. Figure 3 (**a**) Reduction of EC by one electron to form the closed radical anion c-EC$^-$; (**b**) Li^+/c-EC$^-$ complex; (**c**) Li^+/c-EC$^-$ complex

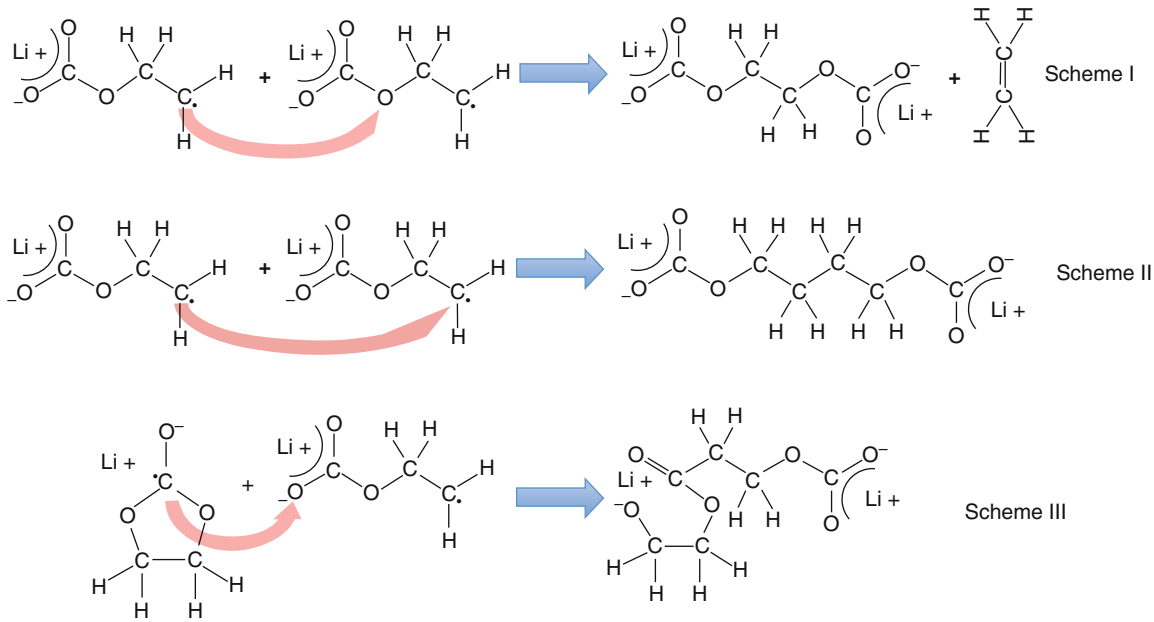

Lithium Battery Electrolyte Stability and Performance from Molecular Modeling and Simulations. Figure 4 Proposed reaction schemes involving singly reduced EC

radical termination reactions of EC^- [14]. Both $(CH_2OCO_2Li)_2$ and dilithium butylene dicarbonate $(CH_2CH_2OCO_2Li)_2$ (Scheme II, Fig. 4) are believed to form by the reaction of two o-EC^-, while an ester-carbonate compound forms from the reaction of o-EC^- with c-EC^- as shown in Fig. 4 Scheme III. In terms of energy and free energy, $(CH_2CH_2OCO_2Li)_2 < (CH_2OCO_2Li)_2 + CH_2 = CH_2 <$ ester-carbonate compound [14]. Furthermore, the DFT study revealed that while Li^+/o-EC^- is much lower in energy than Li^+/c-EC^- (by about 27 kcal/mol), there is a substantial energy barrier for opening c-EC^- to form o-EC^-, around 13 kcal/mol in energy and 11–12 kcal/mol in free energy. For the elementary reaction $A \leftrightarrow A^*$, where A^* represents an activated complex, the Eyring rate equation is given as [30]

$$k = \frac{k_b T}{h} \exp\left[-\frac{\Delta G^*}{k_b T}\right] \tag{2}$$

At room temperature, the estimated lifetime c-EC^-, given as $1/k$, is around 100 μs. Hence, reactions involving the high-energy but long-lived c-EC^- form of the EC radical anion to form the ester-carbonate compound shown in Fig. 4 should be considered as a possible contributor to the outer SEI in EC-based electrolytes.

While the presence of $(CH_2OCO_2Li)_2$ in the SEI formed from EC-based electrolytes is not disputed, there is limited evidence for the presence of $(CH_2CH_2OCO_2Li)_2$ and the ester-carbonate compound. The combined TEM/FTIR study that claimed evidence for the presence of $(CH_2OCO_2Li)_2$ also found evidence for an alkyl carbonate compound with O/C ratio = 1, which the investigators associated with $(CH_2CH_2OCO_2Li)_2$ [29]. This O/C ratio is also consistent with the ester-carbonate compound. However, in their NMR analysis of surface compounds that was consistent with the presence of $(CH_2OCO_2Li)_2$, Xu et al. ruled out the possibility of these compounds [28]. In general, however, studies (e.g., FTIR and XPS) that reveal the presence of alkyl carbonates in the SEI formed in EC-based electrolytes do not allow for the differentiation between $(CH_2OCO_2Li)_2$ and $(CH_2CH_2OCO_2Li)_2$ and the ester-carbonate compound.

In addition to QC studies, reactive molecular dynamics (RMD) simulations using the reactive force field ReaxFF have been used to gain insight into reactions of singly reduced EC in the condensed (solution) phase [31]. In this study the reaction of Li^+/o-EC^- with both Li^+/o-EC^- and Li^+/c-EC^- has been studied in a solution of EC molecules. A snapshot of the system

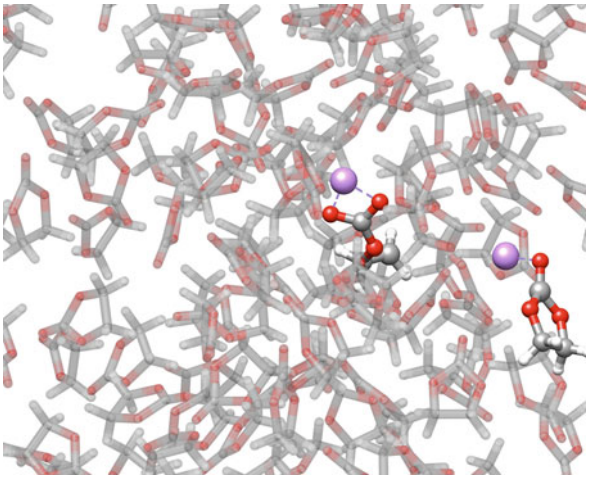

Lithium Battery Electrolyte Stability and Performance from Molecular Modeling and Simulations. Figure 5 Snapshot of a reactive molecular dynamics simulation (ReaxFF) of singly reduced EC species in a solution of EC molecules [31]

is shown in Fig. 5. RMD simulations were used to determine the free energy as a function of reaction coordinate (see below) and to examine the propensity of various radical combination reactions to occur in the condensed phase of an EC solvent.

The free energy in the condensed phase was determined for the reactions of Li^+/o-EC^- with Li^+/o-EC^- according to Scheme I and Scheme II in Fig. 4. ReaxFF simulations predict essentially no barrier for formation of $(CH_2CH_2OCO_2Li)_2$ while a barrier of around 12 kcal/mol is seen for the formation of $(CH_2OCO_2Li)_2 + CH_2 = CH_2$. ReaxFF simulations also predict $(CH_2CH_2OCO_2Li)_2$ to be of lower energy than $(CH_2OCO_2Li)_2 + CH_2 = CH_2$, in qualitative agreement with ab initio predictions [14]. The only reaction observed in an o-EC^-/EC system containing many Li^+/o-EC^- complexes was the rapid combination of o-EC^- radical pairs to form $(CH_2CH_2OCO_2Li)_2$ (Scheme II, Fig. 4). No formation of $(CH_2OCO_2Li)_2 + CH_2 = CH_2$ was observed in simulations of o-EC^-/EC system, indicating the presence of an appreciable barrier to this reaction.

The free energy of the condensed phase reaction path for Li^+/o-EC^- with Li^+/c-EC^-, Scheme III, Fig. 4, as a function of the reaction coordinate (C-O distance) reveals a barrier for this reaction of around 6 kcal/mol, but it is significantly less than that for ring opening reaction as estimated from QC of 11–12 kcal/mol [14]. This barrier is sufficiently large such that no reactions were observed in simulations of the o-EC^-/c-EC^-/EC system at 313 K. At elevated temperature (500 K), the reaction shown in Scheme III, Fig. 4, was observed in ReaxFF simulations on the timescale of a hundred picoseconds. At this temperature, the estimated lifetime (mean time to ring opening) of c-EC^- is, according to Eq. 2, much greater, around 10 ns. At lower temperatures, the separation in timescale between the reaction of Li^+/o-EC^- with Li^+/c-EC^- and the ring opening reaction will become even greater due to the much higher activation energy for the latter reaction. These results imply that the reaction of Li^+/o-EC^- with Li^+/c-EC^- occurs rapidly enough that this reaction could be important in the formation of the outer SEI in EC-based electrolytes.

In summary, a review of experimental and QC studies of compounds present or likely to be present in the outer SEI formed at the anode in EC-based electrolytes leads to the conclusion that these studies cannot be easily reconciled regarding the importance/presence of $(CH_2CH_2OCO_2Li)_2$, $(CH_2OCO_2Li)_2$, and the ester-carbonate compound. Condensed phase ReaxFF simulations have demonstrated that while $(CH_2CH_2OCO_2Li)_2$ and the ester-carbonate compound can easily form through the mechanisms shown in Fig. 4, $(CH_2OCO_2Li)_2$, often suggested as the most important compound of the outer SEI, does not form through the commonly held mechanism of combination of two o-EC^- radicals (Scheme I, Fig. 4). Furthermore, the large barrier for the ring opening reaction leading to formation of o-EC^- from c-EC^-, revealed by previous QC studies, combined with the relatively low barrier for formation of the ester-carbonate compound from reaction of c-EC^- with o-EC^- implies that the presence of the ester-carbonate compound as a component of the SEI in EC-based electrolytes should be given serious consideration. Furthermore, reactions of the relatively long-lived c-EC^- with electrolyte additives such as VC may also be important.

Two-Electron Reduction of EC In addition to participating in the formation of the outer SEI through one-electron reduction, EC can undergo two-electron reduction. The resulting compounds are believed to be

important components of the inner part of the SEI. QC reveals that this is a two-step process involving one-electron reduction to the o-EC radical followed by reduction by the second electron [14]. QC reveals that this an energetically unfavorable reaction in the gas phase but energetically favorable in the presence of Li^+, resulting in the formation of ethylene gas and $LiCO_3^-$. This doubly reduced form of EC can react with an additional Li^+ form lithium carbonate (Li_2CO_3) or with a Li^+/EC complex to form dilithium ethylene dicarbonate, also shown in Fig. 4. Both of these compounds are believed to be present in the inner SEI [16, 32, 33].

Decomposition at Electrode Surfaces Computational investigation of the reduction of carbonate compounds occurring directly on the anode (e.g., lithium metal) surface has received less attention than reactions in the gas phase or bulk electrolyte. In one example, a QC study of a number of important electrolyte compounds, including EC, reacting with lithium clusters, has been conducted [14]. While the level of theory is modest, qualitative trends were clear. Reaction of EC with the lithium cluster results in the formation of ethylene plus Li_2CO_3, a known major component of the inner SEI. The energetics of this reaction is highly favorable, while there was found to be an appreciable activation energy for the reaction. This high activation energy is somewhat surprising due to the known reactivity of lithium metal with carbonate solvents, and may reflect the computational approach and modest level of theory employed. ReaxFF simulations of EC in contact with lithium metal show fast reaction on a timescale of picoseconds (ps) resulting in formation primarily of Li_2CO_3 and ethylene gas [31]. These initial RMD simulations on lithium metal show no signs of formation of dicarbonate compounds or the presence of an appreciable barrier for the formation of Li_2CO_3.

The decomposition of EC on graphitic anode with C = O, C–OH, and C–H terminations was studied at 450 K in ab initio simulations using the Perdew–Burke–Ernzerhof (PBE) functional, with a more accurate PBE0 functional used as for spot checks [34]. Fast EC decomposition on ps timescale occurred upon two-electron reduction at the graphite edge rich in oxidized sites (C = O and C-OH), yielding CO_3^{2-} and $OC_2H_4O^{2-}$. A potential reaction between $OC_2H_4O^{2-}$, or HOC_2H_4OH in the proton rich environment, with CO_2 or CO_3^{2-} was suggested as a possible route to forming $(CH_2CO_2Li)_2$ SEI product but was not observed presumably because of short simulation timescales [34]. The C = O termination was significantly more active in decomposing EC than C–H termination.

Molecular Dynamics Simulations of Bulk Electrolyte Properties

Organic Liquid Electrolytes

Molecular dynamics simulations were used to study a number of electrolytes with potential interest to lithium battery applications: EC:DMC/$LiPF_6$[35], EC/LiTFSI [36, 37], DMC/LiTFSI [38], GBL/LiTFSI [38], oligoethers/Li salts [39–41], acetamide/LiTFSI [42], EC/$LiBF_4$ [43], PC/$LiBF_4$ [43, 44], PC/$LiPF_6$ [44], DMC/$LiBF_4$ [43], oligoethers/$LiPF_6$ [45–47], and PC/LiTFSI [37]. The lithium cation coordination by solvent molecules, cation–anion aggregation, and transport properties were derived from MD simulations. It is important to pay attention to the reported simulation time because some of the earlier simulations by Li et al. [48] and Soeten [43] were only 200 ps and 100 ps long [43, 48], which is less than one EC-lithium residence time (~0.5 ns) [35] and significantly less than the lithium–anion residence time of 2–3 ns found for similar electrolytes at 298 K [35]. Experience indicates that MD simulation trajectories should be longer than the cation–anion or lithium-solvent residence time in order to obtain an equilibrated ion aggregation and the composition of the ion solvation shell. Recent MD simulations [35, 38] were performed for 7–20 ns to ensure a complete equilibration and extraction of the accurate conductivity values.

Early study of one $LiBF_4$ in PC, EC, and DMC by Soeten [43] provided initial insight into the structure of the lithium solvation shell. Four strongly bound solvent molecules in a tetrahedral arrangement around lithium cation were reported [43], which is qualitatively consistent with the recent MD studies [35, 36, 38] and ab initio simulations of Li^+ in 32 EC [34]. MD simulations with polarizable force fields predicted ion diffusion coefficients [35, 36, 38, 49] within 40% of experiments for DMC/LiTFSI, EC/LiTFSI, PC/LiTFSI,

DMC/LiTFSI, (EO_n)/LiTFSI, where EO is ethylene oxide repeat unit, $n = 2,5,12$ and EC:DMC/$LiPF_6$. MD simulations employing nonpolarizable force field [37], on the other hand, predicted ion diffusion a factor of 2–4 slower for EC/LiTFSI and PC/LiTFSI and 5–7 times slower for PC/$LiBF_4$ and PC/$LiPF_6$ [44]. Conductivity was predicted a factor of 5 lower for PC/$LiPF_6$ [50] and a factor of 2 lower for PC/LiTFSI [37] and EC/LiTFSI [37] in MD simulations using nonpolarizable force fields. MD simulations using polarizable force fields predicted electrolyte conductivity within 20–40%. Figure 6 shows conductivity of EC: DMC/$LiPF_6$ as a function of solvent composition and temperature. MD simulations slightly overestimate EC/$LiPF_6$ conductivity but overall quality of the conductivity predictions is satisfactory, especially in light of recent results from the Umebayashi group [44] that reported conductivity of PC/$LiPF_6$ and PC/$LiBF_4$ from MD simulations being a factor of 5–7 lower than experiments.

Many of the practical electrolytes contain a combination of linear and cyclic carbonates doped with $LiPF_6$ salt. Using $LiPF_6$ salt yields electrolytes with high ion dissociation, conductivity and aluminum current collector passivation and SEI formation [1, 2]. EC has high melting point of 36.4°C, a high dielectric constant ($\varepsilon \approx 90$), and an acceptable viscosity (1.9 cP at 40°C) [1]. Its ability to dissociate lithium salts is attributed to its high dielectric constant [1]. The addition of lower viscosity and lower dielectric constant ($\varepsilon \approx 3.1$) to linear carbonate solvents such as DMC decreases electrolyte viscosity, reduces its melting point, and improves conductivity. While EC dissolves lithium salts much better than DMC presumably due to high dielectric constant (90 for EC versus 3 for DMC), the question remains as to the number of EC and DMC molecules contributing to the lithium solvation shell in the mixed EC:DMC electrolyte. Intuitively, one expects EC contribution to dominate over DMC because of the difference in dielectric constants [1]. The issue of the competitive lithium cation solvation in mixed linear and cyclic carbonate solvents was addressed in a recent MD simulation and QC study [35]. Both EC and DMC were found to participate in the Li^+ solvation in mixed EC:DMC (1:1) electrolytes despite a huge difference between their dielectric constants (90 for EC versus 3 for DMC). These results were found in agreement with the reanalyzed [53] Raman spectroscopy experiments. A more detailed examination of the mixed electrolyte MD data revealed that the free lithium cations slightly favor EC solvation, while Li^+ contact ion pairs with PF_6^- anions leads to a preference for DMC in the Li^+ solvation shell. These conclusions are in accord with the quantum chemistry studies that indicated that $LiPF_6$ ion pair binds slightly stronger to DMC compared to EC, while binding energy of Li^+-EC is larger than Li^+-DMC. Analysis of the lithium cation

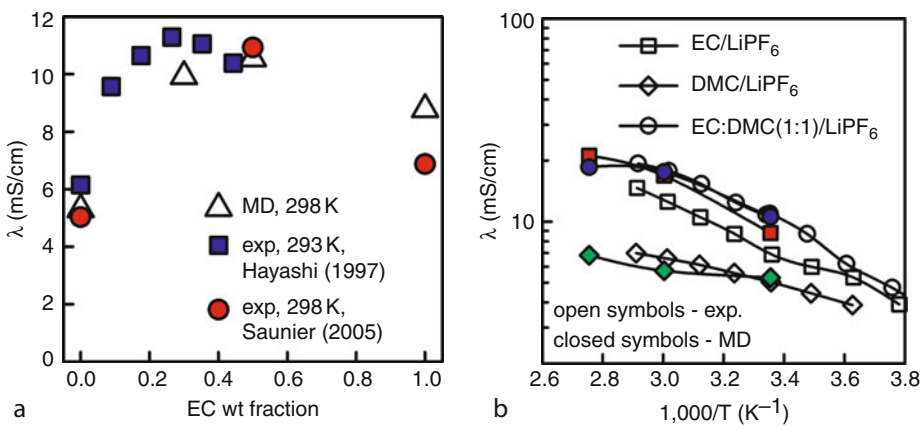

Lithium Battery Electrolyte Stability and Performance from Molecular Modeling and Simulations. Figure 6 Solvent composition (*left*) and temperature (*right*) dependence of ion conductivity from MD simulations [35] and experiments [51, 52]. Solvent: Li ratios were the following: EC:Li = 13, DMC:Li = 10, (EC + DMC): Li =11.8 for EC:DMC mol/mol = 1/1 and (EC + DMC): Li =10.7 for EC:DMC mol/mol = 3/7

coordinated by four solvent molecules (EC and DMC as shown in Fig. 7) indicated that the most stable configuration is not $Li^+(EC)_4$, but $Li^+(EC_3, DMC)$ and energy of the $Li^+(EC_2, DMC_2)$ cluster is only 0.8–1.6 kcal/mol higher than $Li^+(EC_3, DMC)$ depending on the level of theory used.

MD simulations offer a unique opportunity to investigate the degree of ion correlation from both structural and dynamic points of view. The degree of ion dissociation α_s (static) defined as the fraction of Li^+ and PF_6^- with no counterion in their first solvation shell, i.e., r(Li-P) < 4.4 Å for all pairs, is shown in Fig. 8. The fraction of free ions increases near linearly with increasing EC fraction in electrolyte and that increasing temperature slightly decreases the fraction of free ions. Surprisingly, the DMC/$LiPF_6$ 1 M electrolyte, which exhibits a reasonable DC conductivity shown in Fig. 6, has a very low fraction of free ions (1.7% at 298 K). The degree of dynamic correlation (α_d) was extracted from MD simulations using ion self-diffusion

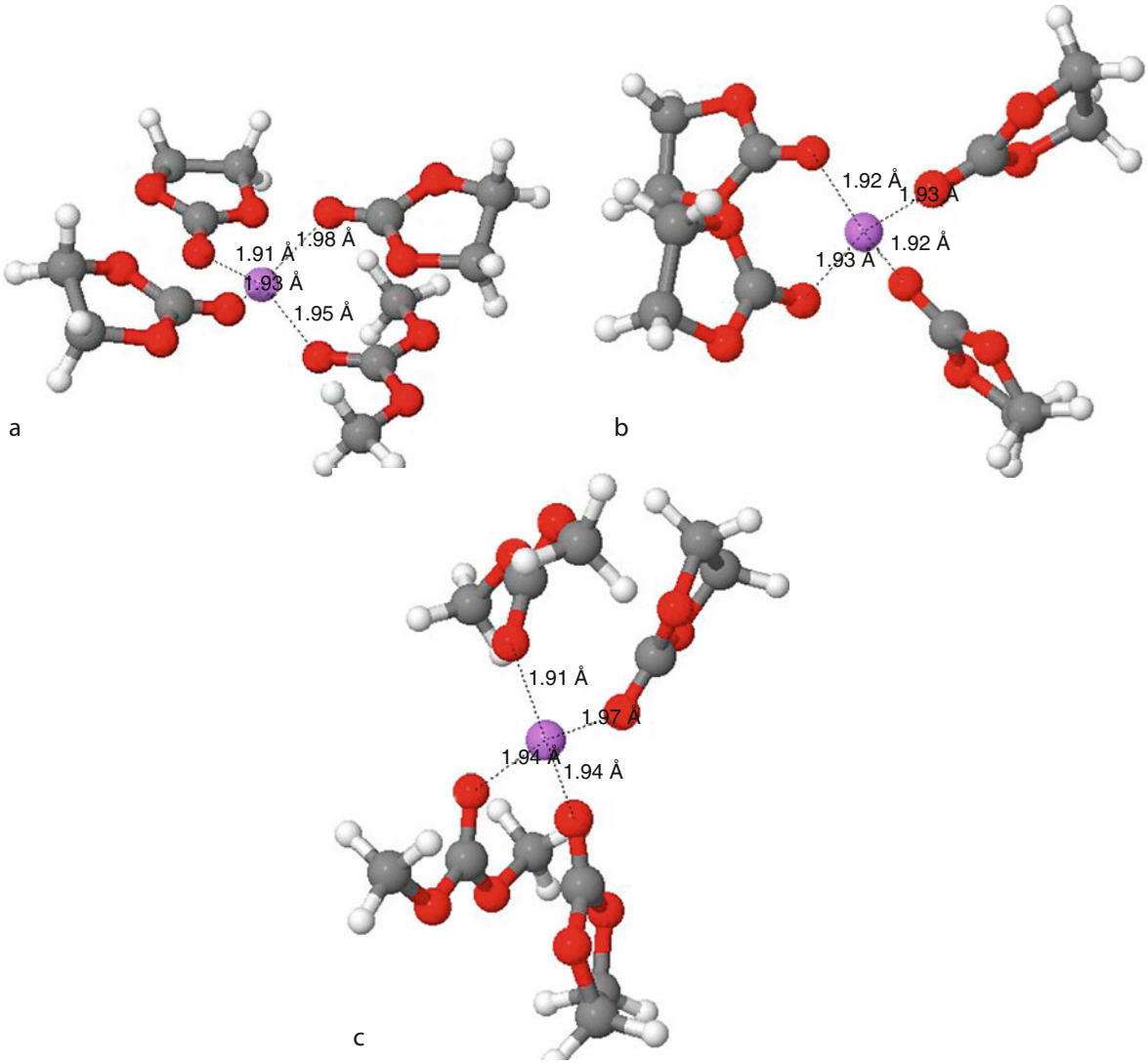

Lithium Battery Electrolyte Stability and Performance from Molecular Modeling and Simulations. Figure 7 Geometry of the three most stable clusters of Li^{4+} coordinated by EC and DMC solvent molecules from M05-2X/6-31 G* geometry optimization

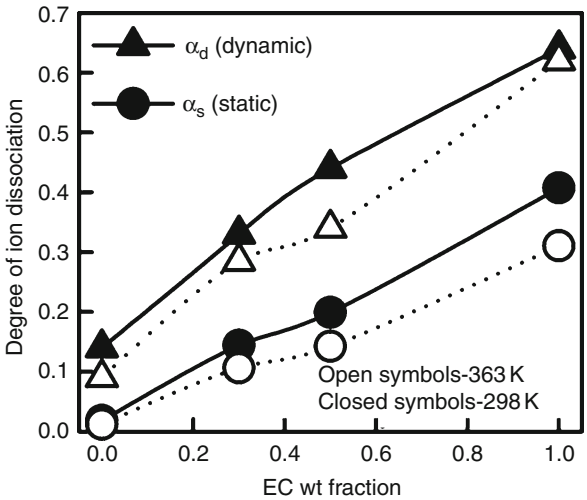

Lithium Battery Electrolyte Stability and Performance from Molecular Modeling and Simulations. Figure 8 The dynamics (α_d) and static (α_s) degree of ion dissociation (fraction of free ions) for EC:DMC/$LiPF_6$ at 298 K at an ~1 M salt concentration

coefficients and conductivity (λ) as given by Eqs. 3–4 in order to compare with α_s (static),

$$\alpha_d = \frac{\lambda}{\lambda^{N-E}} \tag{3}$$

$$\lambda^{N-E} = \frac{e^2}{Vk_BT}(n_+D_+ + n_-D_-) \tag{4}$$

k_B is the Boltzmann constant, T is temperature, V is the volume of the simulation box, and D_- and D_+ are self-diffusion coefficients of the anion and cation, respectively. The degree of ion dynamic correlation α_d is plotted versus electrolyte composition and temperature in Figure 8 together with the static fraction of free ions from the structural analysis α_s. It was found that α_d is always higher than the fraction of free ions from the structural analysis (α_s), indicating an important contribution from the charged ion clusters transport to ion conductivity discussed in details elsewhere [35]. Joint pulsed gradient spin echo (pgse)-NMR and conductivity analysis of LiTFSI in multiple electrolytes at solvent:Li ratio of 20 at 298 K for PC/LiTFSI and DMC/LiTFSI yielded α_d values 0.62 and 0.11 in accord with MD predictions for EC:DMC/$LiPF_6$ shown in Fig. 8 provided $LiPF_6$ and LiTFSI yield similar α_d [54]. This indeed seems to be the case as similar α_d were found for LiTFSI and $LiPF_6$ salts in γ-butyrolactone (GBL) electrolyte from a combination of pgse-NMR and conductivity analysis [55].

Analysis of the solvent residence times relative to the diffusion coefficients allows one to estimate the frequency of the solvent exchange during the time it takes for a solvent to diffuse its own size [49]. For EC:DMC/$LiPF_6$ electrolytes [49], an approximately equal contribution from vehicular motion with the first solvation shell and solvent exchange for Li solvated by EC was found. In contract to the lithium motion in carbonates, in oligoethers, Li^+ moves 3–4 solvent molecules before its solvation shell is renewed, indicating that motion or the Li^+ together with its solvation shell dominates over solvent exchange mode of the lithium transport in oligoethers.

Polymeric Electrolytes

Solid polymer electrolytes (SPEs) are formed by doping a polymer with a lithium salt. SPEs have several advantages over traditional organic solvent–based electrolytes that include negligible volatility, leading to increased safety and reduced environmental impact, and intrinsic mechanical integrity, which could eliminate the need for a separator [56]. However, SPEs suffer from a major disadvantage, namely, dramatically reduced lithium ion conductivity compared to organic solvent-based electrolytes. Consequently, SPEs can currently only be employed at elevated temperatures, typically 60–80°C [56]. Simulation and modeling studies of SPEs have concentrated on elucidating the mechanism of ion motion in SPEs, and in understanding how polymer structure influences ion motion.

Polyethylene oxide (PEO)-based polymers have been investigated most extensively as SPEs both experimentally [56] and in simulations [40, 57–67]. These polymers are very effective at dissolving lithium salts due to strong Li^+-ether oxygen binding. QC [68] and MD simulation studies [58] of oligoethers (low molecular weight PEO) as well as PEO have revealed that Li^+ cations are very strongly coordinated by an average of 5–6 ether oxygen atoms in configurations similar to that shown in Fig. 9. Simulations reveal that coordination of Li^+ usually involves a single oligoether or two segments of a single PEO chain as shown in Fig. 9 [58].

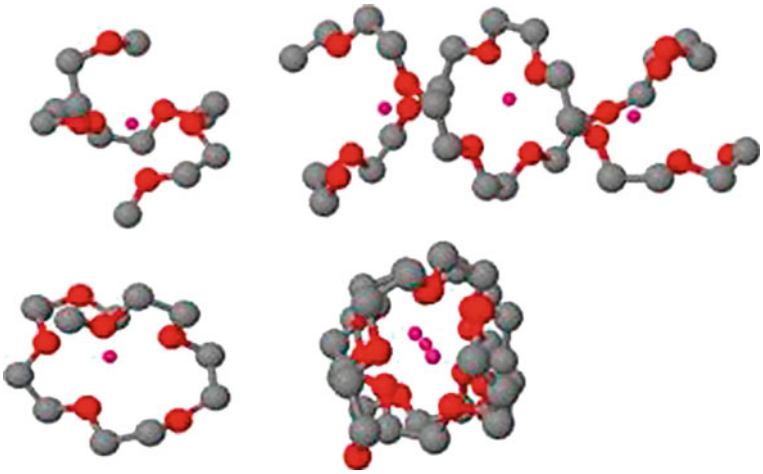

Lithium Battery Electrolyte Stability and Performance from Molecular Modeling and Simulations. Figure 9
A representative configuration of Li^+ cation coordination by an oligoether chain from MD simulations

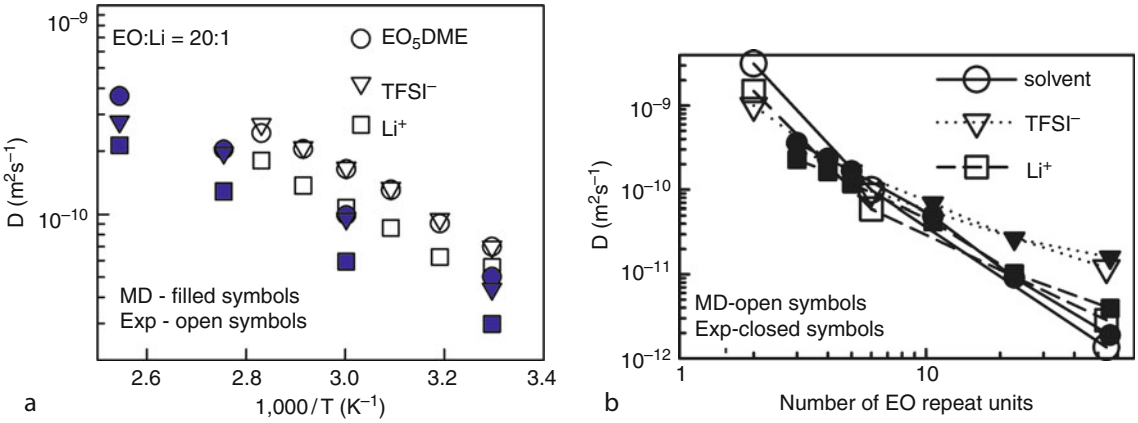

Lithium Battery Electrolyte Stability and Performance from Molecular Modeling and Simulations. Figure 10
Ion diffusion in (**a**) pentaglyme (EO_5DME) and (**b**) oligoethers from MD simulations [49] and pulsed field gradient (pfg)-NMR experiments [69]

The nature of ether-Li^+ binding has a very strong influence on the mechanism for Li^+ conduction in PEO-based SPEs. This can be understood by first comparing the mechanism of Li^+ diffusion in an oligoether versus that in organic solvents. As discussed in Organic Liquid Electrolytes, Li^+ motion in organic liquid electrolytes occurs by a mixture of vehicular (with solvent shell) and structural (exchange of solvent shell) diffusion [49]. In contrast, simulations reveal that Li^+ diffusion in pentaglyme (six repeat unit PEO) + LiTFSI, compared with experiment in Fig. 10, occurs almost entirely by a vehicular mechanism [49]. In other words, a pentaglyme/Li^+ complex diffuses on average distances many times larger than the size of the pentaglyme before Li^+ changes complexation to a different pentaglyme molecule. The residence time of Li^+ with a pentaglyme molecule is around 50 ns, compared to around 1 ns in propylene carbonate [49].

While the lack of an efficient structural diffusion mechanism has relatively little influence on Li^+ motion in pentaglyme because of the fast center-of-mass diffusion of pentaglyme, the situation is quite different in higher molecular weight PEO. Because the center-of-mass diffusion of PEO is negligible, a Li^+ cation

necessarily *must* change coordinating PEO chains, i.e., undergo "jumps" between PEO chains, in order to move distances greater than the size of the PEO chain. Figure 11a shows ion and polymer diffusion in a PEO-LiTFSI SPE as a function of inverse temperature from simulation and experiment [38], while Fig. 11b shows conductivity as a function of salt concentration [58]. In both cases, excellent agreement between simulation and experiment can be seen. Compared with pentaglyme (Fig. 10), it can be seen that Li^+ transport is considerably slower in the SPE, while the diffusion of TFSI is reduced relatively little, indicative of the relative independence of TFSI motion from that of the solvent/polymer. This leads to a significantly lower transference number in the SPE compared to the liquid electrolyte as a significantly greater fraction of charge is carried by TFSI in the former due to the very slow Li^+ motion. Furthermore, while pentaglyme motion is faster than that of Li^+ in the oligoether electrolyte, PEO center-of-mass motion is considerably slower than that of cation, supporting the supposition that the vehicular mechanism, which is so important in the oligoether, does not contribute significantly to Li^+ in the SPE. Note that Li^+ motion in the PEO SPE can be well reproduced by a model that allows for 1-D diffusion along Gaussian chains, motion with a segment of the chain with occasional interchain jumps [59, 66].

Coupling of Ion Motion and Polymer Segmental Motion Figure 12 shows the dependence of Li^+ and $TFSI^-$ motion on salt concentration from both experiment and simulation [58]. Also shown is the time (relative to that at for Li:EO = 0.05) from simulations at which the mean-square displacement of the ether oxygen atoms reaches 50 $Å^2$, the length scale of the cage imposed by neighbor packing. This timescale is directly related to the timescale of conformational transitions. Figure 12 reveals that while TFSI motion remains much faster than that of Li^+ for all salt concentrations, the translational dynamics of both ions follow the same dependence on salt concentration as polymer segmental/conformational dynamics, i.e., a dramatic decrease in mobility with increasing salt concentration. These results show that both cation and anion dynamics are strongly coupled with local polymer relaxation. The slowing of segmental/conformational dynamics of the polymer with increasing salt concentration is due to the strong binding between ether oxygen atoms and Li^+, which greatly restricts conformational motion. The correlation of both cation and anion dynamics with local polymer relaxation is further illustrated by simulations in which the barrier for dihedral/conformational transitions were artificially increased by 1.3 kcal/mol [58]. Simulations of the PEO/LiTFSI SPE at EO:Li = 20:1 at 393 K revealed a decrease in the diffusion coefficient of both $TFSI^-$ and

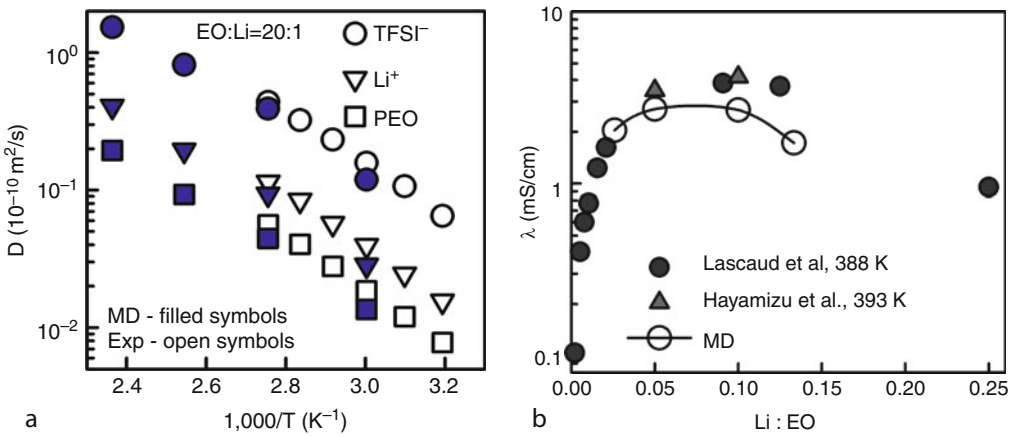

Lithium Battery Electrolyte Stability and Performance from Molecular Modeling and Simulations. Figure 11 (**a**) Diffusion in a PEO/LiTFSI electrolyte from simulation and experiment. (**b**) Ionic conductivity in a PEO/LiTFSI electrolyte from simulation and experiment

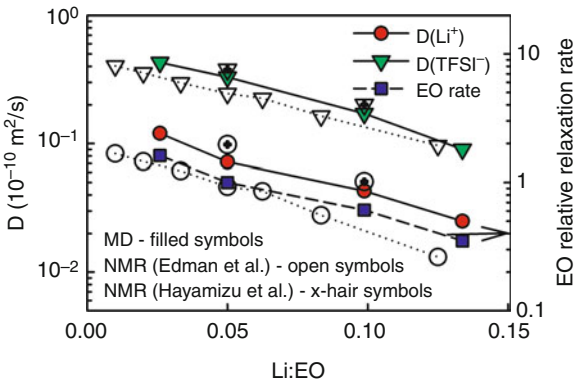

Lithium Battery Electrolyte Stability and Performance from Molecular Modeling and Simulations. Figure 12 Dependence of Li^+ and $TFSI^-$ motion on salt concentration from both experiment and simulation

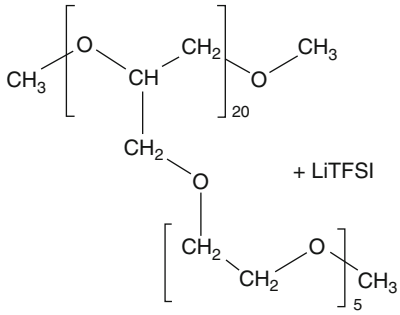

Lithium Battery Electrolyte Stability and Performance from Molecular Modeling and Simulations. Figure 13 Structure of comb-branch copolymers used as SPEs

Li^+ by a factor of 3, and an increase in the polymer segmental relaxation time by about the same factor.

An interesting feature of the PEO SPE is the maximum in conductivity for Li:EO ratio around 0.05, as can be seen in Fig. 11b. Simulations reveal that this is due to two counter effects. On the one hand, ionic conductivity increases with increasing salt concentration due to the increase in the number of charge carriers per unit volume. On the other hand, increasing salt concentration decreases the rate of polymer dynamics dramatically decreasing Li^+ transport as well (to a lesser extent) TFSI transport.

Other Polymer Architectures In summary, simulation studies of SPEs based on linear PEO have revealed that strong binding of ether oxygen to Li^+, while facilitating dissolution of lithium salts, reduces the mobility of Li^+ by suppressing structural diffusion. Furthermore, the vehicular mechanism is eliminated in the polymer due to negligible center-of-mass motion of the coordinating polymer chain, necessitating interchain hopping for transport, which is found to be a rare event. While both anion and cation motion are found to be coupled to local polymer relaxation, the anion mobility is found to be significantly greater than that of the strongly bound Li^+ in the PEO-based SPEs, leading to very low transference numbers. Finally PEO crystallizes at around 60°C, precluding its use at lower temperatures due to very poor transport of Li^+ in the crystalline phase. On the other hand, about 60°C (in the molten state), PEO does not provide any mechanical properties that would allow for elimination of a separator, a major potential advantage of SPEs

Comb-Branched Polyethers Comb-branch polyethers with architectures similar to that shown in Fig. 13 have been investigated in efforts to develop SPEs that take advantage of the ability of oligoethers to coordinate Li^+ while at the same time (1) preventing crystallinity due to use of short side chains and (2) allowing in principle for separate optimization of the backbone properties from those of the side chains. The ideal comb-branch SPE might, for example, use a glassy backbone polymer, thereby resulting in good mechanical properties, while Li^+ transport is carried out by flexible ether side chains. The use of relatively short side chains not only reduced/prevents crystallinity, but may also facilitate interchain hopping, which is necessary for large-scale Li^+ transport in SPEs, due to sharing of Li^+ cations between side chains. The optimization of the properties/chemical structure of comb-branch SPEs would be greatly facilitated by an improved understanding of Li^+ transport mechanisms in these polymers, particularly the roles played by the polymer backbone and side chains in ion transport.

MD simulations of comb-branch polyethers of the structure shown in Fig. 14 ($PEPE_5$) have been performed [60]. SPEs formed from this comb-branch polymer have also been studied experimentally [70–72]. A comparison of the ionic conductivity of SPEs with LiTFSI and this comb-branch polymer from simulation and experiment, along with the conductivity of a linear PEO SPE with same salt concentration is shown

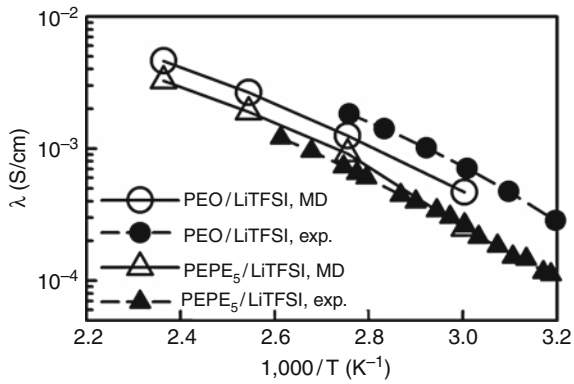

Lithium Battery Electrolyte Stability and Performance from Molecular Modeling and Simulations. Figure 14 Ionic conductivity in comb-branch SPEs from simulation and experiment

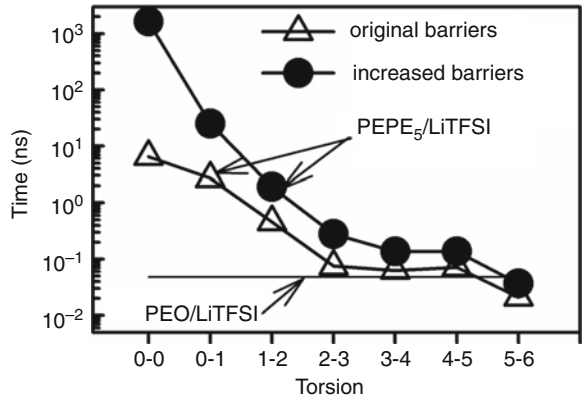

Lithium Battery Electrolyte Stability and Performance from Molecular Modeling and Simulations. Figure 15 Conformational relaxation time as a function of position of the dihedral in comb-branch polymer electrolytes from MD simulation

in Fig. 14 [60]. Good agreement between experiment and simulation is apparent. Furthermore, the conductivity of the comb-branch SPE is very similar to that of the linear PEO SPE. The slightly higher conductivity in the linear PEO SPE is facilitated by the lower molecular weight (2,380 Da) of the linear polymer compared to the comb-branch (around 6,000 Da).

Analysis of the MD simulations of the $PEPE_5$ reveal that Li^+ occurs primarily by hopping of the cation from one side chain to another [60]. The six oxygen atoms of the side chains facilitated coordination of Li^+, as anticipated. However, a fraction of Li^+ cations are partially coordinated by the polyether backbone. These cations have very slow dynamics and do not contribute appreciably to Li^+ motion. The slow dynamics of cations partially coordinated by the chain backbone can be understood by considering conformational dynamics in the comb-branch polymer. Figure 15 shows conformational relaxation time, based on decay of the O–C–C–O dihedral autocorrelation function, as a function of position of the dihedral. "0-0" indicates backbone dihedrals, while "5-6" is the last O–C–C–O dihedral on the side chain. Figure 15 reveals that while conformational transitions near the free end of the side chains are similar to those in the linear PEO SPE, those closer to the backbone, and particularly the backbone itself, are significantly slower due to steric crowding. Those Li^+ complexed by the slowest dihedrals show the lowest mobility.

Interestingly, despite slower dihedral dynamics for the polymer backbone on the comb-branch polymer, the overall Li^+ mobility is comparable to that in the linear PEO SPE. Hence, those Li^+ not complexed by the backbone in the comb-branch SPE exhibit higher mobility than in the linear PEO SPE, indicating that the short side chain architecture does promote interchain hopping, as hoped for. Furthermore, it appears that Li^+ mobility, at least for those not complexed by the backbone, is largely independent of backbone motion [60]. This independence is further demonstrated in Fig. 16, which shows the influence of backbone dihedral barriers in the $PEPE_5$ SPE on ion mobility. When the backbone dihedral barriers are increased, the polymer backbone becomes glassy on the timescale of the simulations. Despite the elimination of backbone conformational dynamics, the mobility of the ions is reduced by less than a factor of 2, less than that observed in the linear PEO SPE when the barriers was increased by only 1.3 kcal/mol (see previous discussion). Furthermore, Li^+ diffusion increased by about 30% when a repulsive interaction between the backbone ether oxygen atoms and Li^+ was introduced, thereby eliminating the role of the backbone in cation coordination. In summary, simulations support the supposition that a comb-branch copolymer with ether side groups and a glassy, noncoordinating backbone would show conductivity comparable to or even

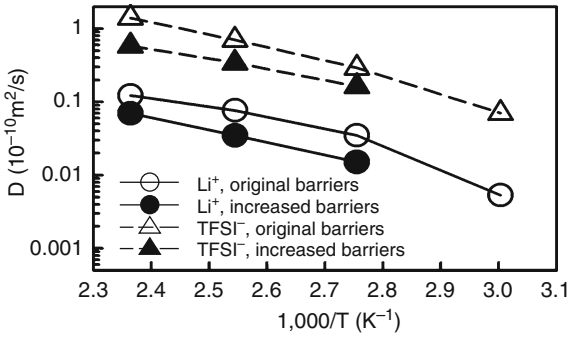

Lithium Battery Electrolyte Stability and Performance from Molecular Modeling and Simulations. Figure 16 Li^+ and anion diffusion in a $PEPE_5$ showing influence of dihedral barriers on ion mobility

superior to ether-based polymers, with improved mechanical properties.

Finally, it may seem reasonable that shortening the ether side chains (to less than six ether oxygen atoms) would support interchain hoping by promoting multiple side-chain coordination of Li^+. Combined with a noncoordinating backbone, however, shorter side chains could be effective in increasing Li^+ mobility.

Single-Ion Conductors As discussed above, one of the disadvantages of PEO-based SPEs is their low transference number due to relatively high anion mobility. Large-scale anion motion in comb-branch SPEs can be eliminated by attaching the anions to the polymer, such as shown in Fig. 17. Here, the TFSI anion of LiTFSI has been attached to the oligoether side chain to form a polyanion with essentially no large-scale mobility, resulting in a single-ion conductor. Here, the ether oxygen to Li^+ ratio is controlled by the length of the side chains. Unfortunately, simulations show that reducing the mobility of the TFSI anion has a deleterious effect on Li^+ mobility, particularly for low temperatures and short side chains/small EO:Li^+ ratios. Simulations reveal that anions play an important role in the ability of Li^+ cations to undergo interchain jumps in PEO-based electrolytes, particularly at higher ion concentrations. Attaching TFSI to the side chain reduces the mobility of the anion and apparently its ability to assist in Li^+ hops. The effect is reduced for longer side chains, due both to decreased importance of anions for the lower salt

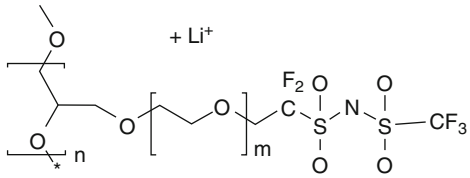

Lithium Battery Electrolyte Stability and Performance from Molecular Modeling and Simulations. Figure 17 Structure of a PEO-based single ion conductor

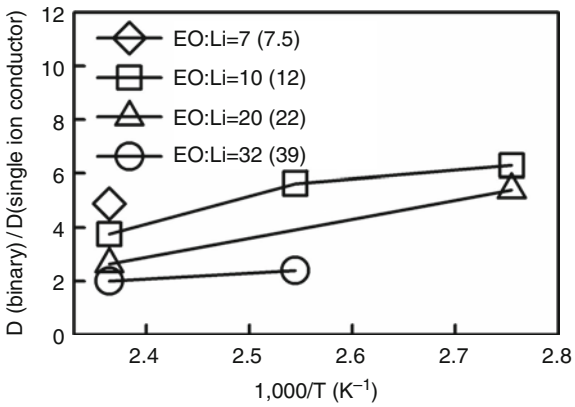

Lithium Battery Electrolyte Stability and Performance from Molecular Modeling and Simulations. Figure 18 A comparison of the lithium diffusion coefficient in PEO-based single ion conductors (Fig. 14) and PEO-based binary comb-branch polymer electrolytes (Fig. 10) from simulations

concentration, and possibility increased anion mobility on the longer tether.

Figure 18 shows the lithium diffusion coefficient in a PEPE binary (free anion) SPE (Fig. 13) and single ion conductors (Fig. 17) from unpublished simulations for various EO:Li ratios. Simulation reveals that the lithium diffusion coefficient in the single ion conductor is about a factor of 2–6 lower than in the binary PEO SPEs. Note that unlike the binary PEO SPEs, the PEPE-based single ion conductor does not show a maximum in conductivity around EO:Li = 20, but increases monotonically with increasing EO:Li, again due to the deleterious effect on Li^+ mobility of attaching the anion as discussed above.

Finally, while attaching the anion to the polymer has the advantage of improving transference number

(all charge is carried by Li^+), reducing the already low mobility of Li^+ is a major disadvantage. Addition of a solvent/plasticizer to form a gel, single-ion conductor electrolyte is a possible solution. Simulations reveal that gel electrolytes formed from 37 wt.% ethylene carbonate plasticizer with a $PEPE_5$:TFSI single ion conductor show dramatic improvement in ionic conductivity over the nonplasticized single ion conductor, particularly at lower temperatures. Here, conductivity, which is due to Li^+, is comparable to that for the comb-branch binary SPE, where the majority of charge is carried by the free anion. Simulations reveal that the primary role of the EC solvent is to "plasticize" the polymer, i.e., increase the rate of polymer conformational transitions, and not to coordinate and transport Li^+; EC does not compete well with oligoethers for coordination of Li^+. These results from unpublished work are consistent with the recent findings for PEO/LiTFSI plasticized with carbonate solvents [37].

Modeling of Ionic Liquid Electrolytes

Room-Temperature Ionic Liquid-Based Binary Electrolytes

Two types of ionic liquid electrolytes have been extensively studied: (1) ionic liquid solvents comprised of ions shown in Fig. 19 doped with lithium salts and called binary room temperature ionic liquid (RTIL) electrolytes; and (2) molten salts, in which the lithium solvating host such as oligoether is attached to an anion such as $TFSI^-$, thus forming an ionic liquid (also called molten salt) without a free solvent. Binary ionic liquid electrolytes have attracted a significant attention because of their negligible vapor pressure; good thermal and electrochemical stability in the range of 5.3 V [73]; good dissolution properties with many organic and inorganic compounds and lithium salts; and low flammability [74]. A wide variety of possible anions and cations offer a potential to tailor RTIL properties to a particular application. The solvent free molten salt electrolytes (type b) are attractive due to their potential to eliminate ion concentration polarization during battery operation. However, low oxidative stability of oligoether solvating host attached to anion and low conductivity counterbalance this advantage.

Hundreds of MD simulation studies of pure RTIL solvents have been reported [75, 79, 80]. Accurate prediction of density, heat of vaporization, conductivity, viscosity, self-diffusion coefficients, structure factors, and crystal structure was reported [75, 80–83] for RTIL comprised of ions listed in Fig. 19, while other MD studies [84] reported ion transport an order of magnitude slower than experiments. An order of magnitude slower prediction of RTIL transport cannot be fully attributed to the absence of polarization in the force field as turning off polarization slowed down ion transport only by a factor of 1.3–3 and not an order of magnitude in published simulations [75, 85]. The relation between ion transport, ion volume, and a combination of the heat of vaporization and the cation–anion binding energy has been reported [76].

Unlike the tremendous interest in simulating pure RTIL solvents, only a very limited number of MD simulations studies of ILs doped with lithium salts have been reported: $[pyr_{11}]$[TFSI] doped with LiTFSI and $[pyr_{13}]$[TFSI] doped with LiTFSI (at 303, 333, 393, and 500 K) [86], [1-ethyl-2,3-dimethyl-imidazolium (emmim)]$[PF_6]$ doped with $LiPF_6$ (at 523 K) [87], and [1-butyl-2,3-dimethyl-imidazolium (bmmim)][TFSI] doped with LiTFSI (at 400 K) [88]. See Fig. 19 for ion notation. MD simulations [86] employing a polarizable force field accurately captured ion self-diffusion coefficients of $[pyr_{13}]$[TFSI] doped with 0.25 mol LiTFSI as shown in Fig. 20, indicating good predictive capabilities of MD simulations for ion transport properties. The lithium self-diffusion was the slowest, while pyr_{13}^+ cation diffusion was the fastest in this IL. In a contrast to this work, MD simulations [88] of [bmmim][TFSI] doped with LiTFSI using the nonpolarizable force field predicted ion transport less than an order of magnitude slower than pfg-NMR data. Such poor ion transport predictive capabilities reported for [bmmim][TFSI] doped with LiTFSI [88] is likely due to inadequate force field development efforts as the nonpolarizable force fields could be designed to have much more accurate prediction of ion transport (within a factor of 2–3) [80, 85].

In $[pyr_{13}]$[TFSI] doped with 0.25 mol LiTFSI the Li^+ cation was found to be coordinated on average by slightly less than four oxygen atoms. The Li^+ coordination by four $TFSI^-$ and by TFSI clusters was observed, in contrast to conclusion of infrared and Raman studies of alkyl-substituted imidazolium-TFSI-based IL doped with LiTFSI [89]. The spectroscopic study found for

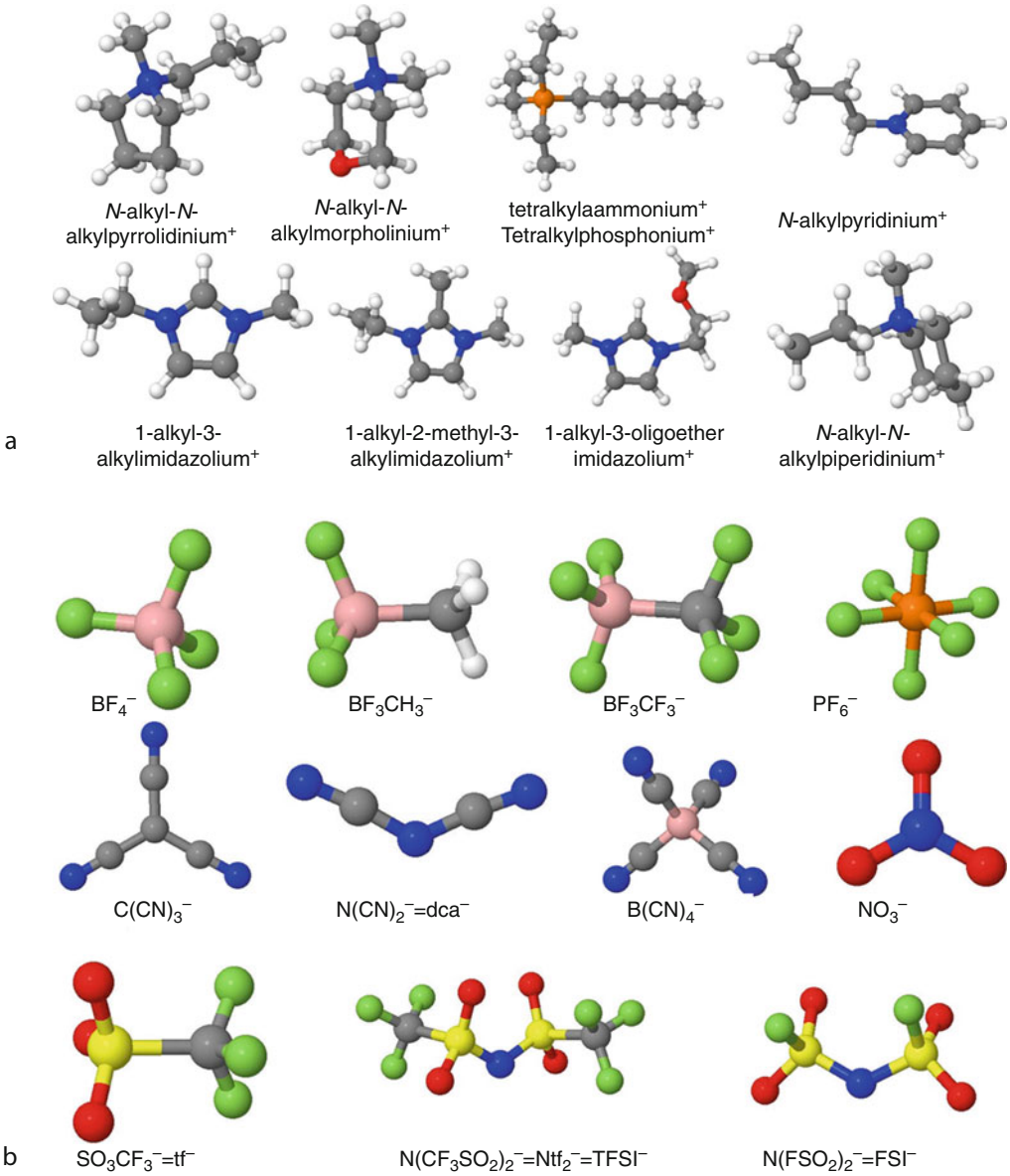

Lithium Battery Electrolyte Stability and Performance from Molecular Modeling and Simulations. Figure 19 A list of representative anion and cations in ionic liquid solvents used in MD simulations [75–78]

low to moderate LiTFSI mole fractions, $0.08 < \times < 0.2$, the $[Li(TFSI)_2]^-$ solvating cage involving bidentate coordinations of Li^+ with two oxygen atoms of one anion in the trans (C_2) conformation and two oxygen atoms of the other anion in the cis (C_1) conformation. It is not clear how to explain the difference between MD results and analysis of the spectroscopic study. Turning off ion polarization in MD simulations dramatically reduced probability of forming extended $(Li^+)_n(TFSI^-)_m$ aggregates but did not result in the Li^+ cation solvation by only two $TFSI^-$.

The mechanism of lithium transport was also studied in $[pyr_{13}][TFSI] + 0.25$ LiTFSI [86]. The Li^+ cation transport was found to occur primarily by exchanging $TFSI^-$ anions in the first coordination shell of a Li^+ with a smaller (~30%) contribution also due to Li^+ cations

diffusing together with their first coordination shell. It is important to note that despite high conductivity of IL-based electrolytes ($\sim 10^{-2}$ S/cm) the lithium contribution to the charge transport remains quite low. In fact, conductivity due to the Li^+ cation transport only in $[pyr_{13}][TFSI]$ + 0.25 LiTFSI was found to be somewhat greater than that for a model poly(ethylene oxide)(PEO-based)/LiTFSI polymer electrolyte but 1–2 orders of magnitude lower than conductivity of ethylene carbonate/LiTFSI liquid electrolyte depending on temperature [86].

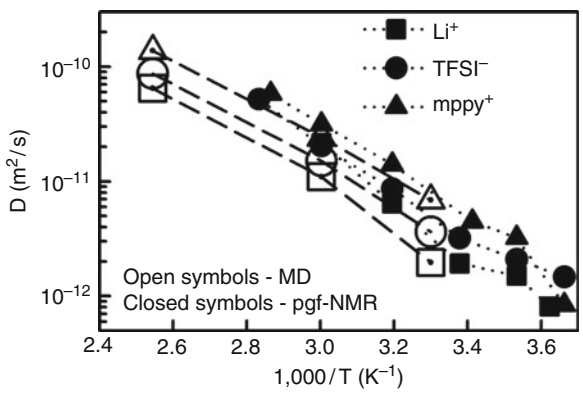

Lithium Battery Electrolyte Stability and Performance from Molecular Modeling and Simulations. Figure 20 Ion self-diffusion coefficients of $0.25Li^+TFSI^-$-$0.75mppy^+TFSI^-$ from MD simulations and pgf-NMR experiments (Used from Ref. [86] with permission of ACS)

Solvent-Free Molten Salts Electrolytes

MD simulations provided insight into the lithium coordination and transport mechanism in the solvent-free molten salt electrolyte comprised of $TFSI^-$ tethered to oligoethylene oxide (EO) ($EO_{12}TFSI^-/Li^+$) [39]. Behavior of $EO_{12}TFSI^-/Li^+$ was contrasted with the ion transport and aggregation in a binary solution of EO_{12} doped with LiTFSI salt (EO_{12}/LiTFSI). It was found from MD simulations and experiments that attaching $TFSI^-$ anion to the chain end of the oligoether resulted in reduction of conductivity by one order of magnitude at 423 K and two orders of magnitude at room temperature, as shown in Fig. 21. The lithium cations were separated from $TFSI^-$ anion by oligoether in most instances (75–90%) for both EO_{12}/LiTFSI and $EO_{12}TFSI^-/Li^+$. For the EO_{12}/LiTFSI binary electrolyte, the fraction of separated $Li^+/TFSI^-$ ions was similar to the degree of ion uncorrelated motion (α_d, see Eqs. 3–4) indicating mostly uncorrelated Li^+ and $TFSI^-$ ion motion in agreement with conclusions the coordinated pfg-NMR and conductivity study [69]. In contrast to this, a significant correlation between lithium and anion motion was found in $EO_{12}TFSI^-/Li^+$ molten salt with a degree of ion uncorrelated motion (α_d) being about ($\sim$45–55%).

The Li^+ cation self-diffusion coefficient in a binary EO_{12}/LiTFSI electrolyte was dominated (90%) by Li^+ vehicular diffusion of the Li^+ with an EO_{12} solvent. In $EO_{12}TFSI^-/Li^+$ molten salt electrolyte, half of the

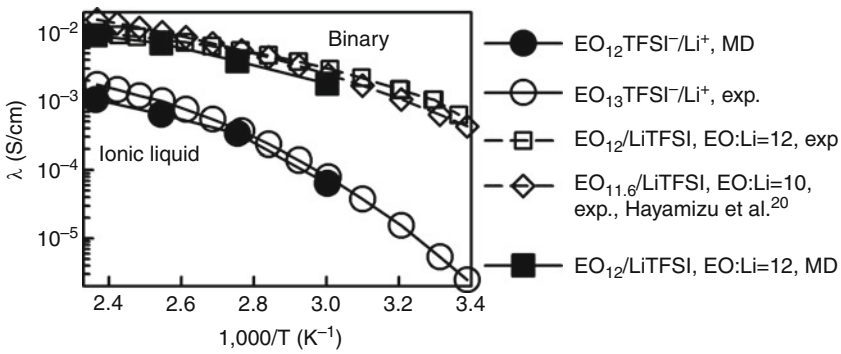

Lithium Battery Electrolyte Stability and Performance from Molecular Modeling and Simulations. Figure 21 Conductivity of binary electrolytes EO_{12}/LiTFSI and EO_nTFSI^-/Li^+ IL from MD simulations (n = 12) and experiments (n = 13). Hayamizy data for binary electrolyte from Ref. [69] are also shown (Reproduced with permission of ACS from Ref. [39])

Li^+ motion was attributed to the Li^+ motion with $EO_{12}TSFI^-$ anion, with the other half being due to the solvating group exchange that involves a Li^+ local motion along the chain, Li^+ motion together with its coordination shell and interchain hopping. Only solvating group (EO and TFSI) exchange contributes to charge transport in $EO_{12}TFSI^-/Li^+$, as vehicular motion results in transport of neutral species accounting for reduction of conductivity by a factor of 2. Interestingly, the Li^+ solvating group exchange rate was found in the binary electrolyte (EO_{12}/LiTSFI) being quite similar to that in $EO_{12}TFSI^-/Li^+$ at high-temperature range (393–423 K). However, as temperature decreased, the Li^+ exchange of oligoether solvating part of anions in molten salts became slower than that the Li-oligoether exchange found in the binary electrolyte.

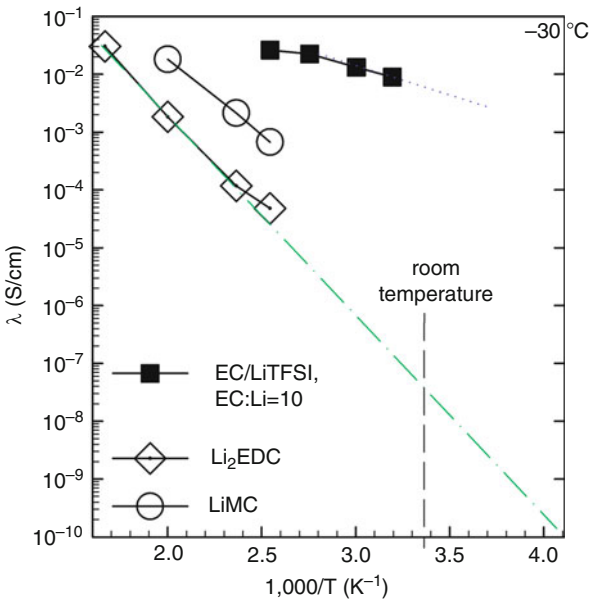

Lithium Battery Electrolyte Stability and Performance from Molecular Modeling and Simulations. Figure 22 Conductivity of lithium dilithium ethylene dicarbonate (Li_2EDC) > lithium methyl carbonate (LiMC) from MD simulations [91] compared to conductivity of EC/LiTFSI from MD simulations [36]

SEI Model Compounds

The ability of an electrolyte to form a stable and conductive SEI on electrodes is paramount for efficient battery operation as discussed previously. Solubility of SEI model compounds by DMC and EC reduction on anode was studied in simulations by Tasaki et al. [90]. They suggested the following order for the SEI forming salts to be soluble in DMC and EC: lithium dilithium ethylene dicarbonate (Li_2EDC) > lithium methyl carbonate (LiMC, $LiOCO_2CH_3$) > LiOH > $LiOCO_2C_2H_5$ > $LiOCH_3$ > LiF > $(LiCO_2)_2$ > Li_2CO_3 > Li_2O. This order agreed with experiments performed in DMC quite well [90]. MD simulations [91] have been used to investigate the structure and transport of two SEI components: Li_2EDC and LiMC. These SEI components are commonly reported in the outer part of SEI [92, 93] and probably exist in a disordered state in it because of the high fraction of other components present, thus inhibiting formation of the crystalline phase.

Ionic conductivity of Li_2EDC and LiMC predicted from MD simulations is shown in Fig. 22. At high temperature, conductivity of alkyl carbonates is comparable to that of liquid electrolytes such as EC/LiTFSI [36]. However, the much stronger temperature dependence of alkyl carbonate conductivity compared to typical liquid electrolytes (e.g., EC/LiTFSI) leads to significantly lower conductivity of alkyl carbonates at lower temperature compared to liquid electrolytes. The extrapolated conductivity of Li_2EDC at −30°C is on the order of 10^{-10} S/cm, suggesting that an SEI comprised primarily of Li_2EDC with typical width of ~10 nm would give rise to significant SEI layer resistance. Conductivity of LiMC is somewhat greater than that for Li_2EDC but also would result in a quite low conductivity of SEI. The extrapolated Li_2EDC conductivity from MD simulations is around 2×10^{-8} S/cm at room temperature in a good agreement with the value 10^{-9} S/cm measured by Phillip Ross group from LBNL [94]. These results are in stark contrast with a dramatically faster ion transport in Li_2EDC predicted by Tasaki et al. [90] at room temperature. The lithium diffusion in Li_2EDC of 8×10^{-12} m^2/s predicted from Tasaki et al. [90] is approximately four and a half orders of magnitude higher than the extrapolated from high temperature D (Li^+) of 2×10^{-17} m^2/s self-diffusion from Borodin et al. [91].

Molecular Dynamics Simulations of Electrode/Electrolyte Interfaces

Graphite Interface

Experimental studies [95–98] of the secondary cells at low temperature (less than −20°C) have consistently found that $R_{ct} > R_{SEI} > R_{bulk}$ for mixed carbonate solvents using conventional $LiBF_4$, $LiPF_6$, and LiBOB salts for a number of tested cells. Thus, the charge transfer resistance (R_{ct}) resistance is the dominant contribution to the secondary lithium cell resistance at low temperature, followed by R_{SEI} (SEI resistance) and R_{bulk} (bulk electrolyte resistance). Similar results have been reported for ionic liquid [99] and polymeric electrolytes [100]. Therefore, the conventional matrix for choosing liquid electrolytes based upon bulk electrolyte conductivity and its ability to form a stable SEI layer needs to be augmented with understanding and optimization of the electrolyte interfacial properties such as interfacial resistance. Intriguingly, the interfacial resistance does not always correlate with the bulk electrolyte resistance creating both opportunities and additional challenges for optimization of electrolyte materials. Importantly, the charge transfer resistance is commonly linked to the Li^+ cation desolvation process from electrolyte and its intercalation into SEI layer or an electrode followed by the actual electron transfer reaction. The length scale for the desolvation process is on the scale of nanometers and, therefore, could be accessed via molecular simulations together with the fundamental electrolyte properties such as conductivity, ion self-diffusion, and the degree of ion aggregation.

MD simulations were performed on EC/$LiPF_6$ and EC:DMC(3:7)/$LiPF_6$ 1 M electrolytes next to the material blocking for anion and solvent but nonblocking to lithium cation and measure the interfacial resistance and free energy due to lithium desolvation from electrolyte. At the initial stage, graphite was chosen as the electrode material and did not include an SEI or controlled voltage between electrodes. MD simulations have been performed at 298 K for two sets of EC/$LiPF_6$ and EC:DMC(3:7)/$LiPF_6$ at 1 M salt concentration next to graphite as shown in Fig. 23 for EC:DMC (3:7)/$LiPF_6$ | Graphite. The electron transfer process has not being included in the simulated model.

The free-energy profile for the lithium desolvation ($\Delta G(z)$) in the range of k_BT could be obtained from equilibrium MD simulations using Eq. 5:

$$\Delta G(z) = -k_b T \cdot \log(\rho(z)) \tag{5}$$

where k_B is the Boltzmann constant, T is temperature, and $\rho(z)$ is the normalized lithium probability profile calculated perpendicular to graphite (z-direction). Figure 24 shows the lithium free-energy profile $\Delta G(z)$ calculated from Eq. 2 using the lithium cation probability profile obtained from 20 ns MD simulations with the first 10 ns omitted as equilibration. The free-energy

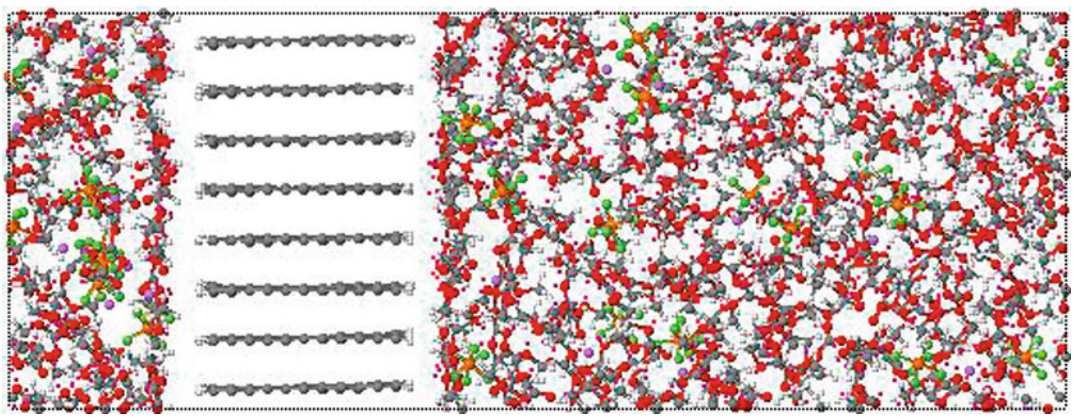

Lithium Battery Electrolyte Stability and Performance from Molecular Modeling and Simulations. Figure 23 A snapshot of the simulation box used for calculating the free-energy barrier of the lithium desolvation energy

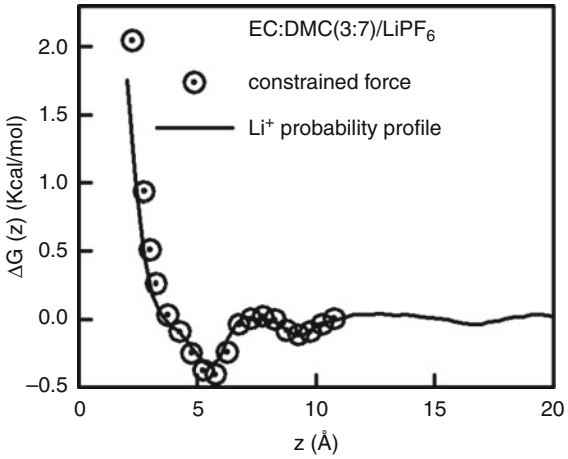

Lithium Battery Electrolyte Stability and Performance from Molecular Modeling and Simulations. Figure 24 The free-energy profile for the lithium cation desolvation from EC:DMC(3:7)/$LiPF_6$ at 1 M electrolyte at 298 K calculated using the Li^+ probability profile from equilibrium MD simulations and the integration of the constrained force method. $Z = 0$ at the position of hydrogen atoms of graphite

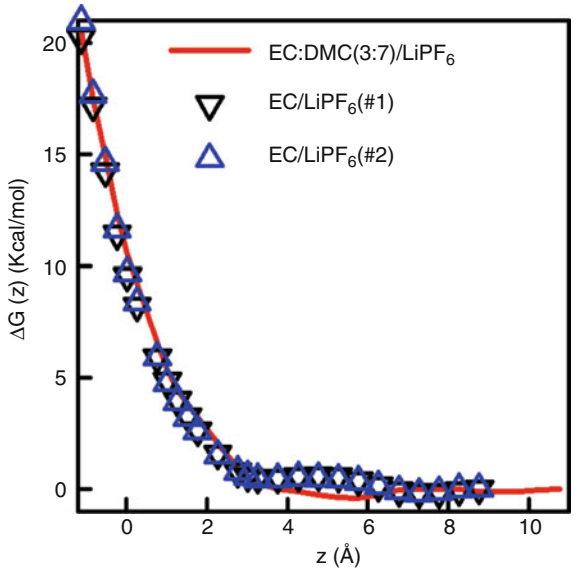

Lithium Battery Electrolyte Stability and Performance from Molecular Modeling and Simulations. Figure 25 The lithium cation desolvation free-energy profile for EC/$LiPF_6$ and EC:DMC(3:7)/$LiPF_6$ 1 M electrolytes next to graphite at 298 K

profile $\Delta G(z)$ shows a local minimum of −0.5 kcal/mol at ~5 Å from the graphite indicative of a preferential lithium position in the Helmholtz plane. The free energy sharply increases as the lithium approaches graphite and is forced to desolvate from electrolytes at distances closer than 4 Å from graphite. Note, that even long (10 ns) simulation trajectory allowed us to sample the free-energy profile only for energies lower than 1.5 kcal/mol, indicating that an advanced sampling technique needs to be used.

The $\Delta G(z)$ was also calculated using the integration of the constrain force technique, in which a Li^+ is constrained at a certain position relative to the surface and the constraining force is calculated (for all points shown in Fig. 24). This methodology was previously used to investigate small molecule permeation through a lipid bilayer [101]. The simulations were 6–12 ns for each constrained distance. The integral of the constrained force gives a free-energy profile that is also shown in Fig. 24. An excellent agreement between two methods of calculating the free-energy profile is observed for free energies below 1 kcal/mol, where the equilibrium MD is expected to provide an adequate sampling.

Two independent sets of simulations of EC/$LiPF_6$ 1 M | graphite for calculating $\Delta G(z)$ have been performed in order to ensure convergence of simulation results and their independence from the state of the lithium coordination shell. In the first simulation, the test-lithium was initially solvated only by EC molecules in the first coordination shell, while in the second set of simulations the lithium (with the constrained distance to graphite) had one PF_6^- anion in its first coordination shell. The free-energy profiles for the lithium desolvation from these electrolytes were calculated by the integration of the constrain force and are shown in Fig. 25.

A similar barrier of $\Delta G(z)$ is observed for EC/$LiPF_6$ and EC:DMC(3:7)/$LiPF_6$ 1 M electrolytes next to graphite is in accord with the experimental evidence. If one assumes that the charge-transfer reaction occurs when a Li^+ is located between outer layer carbon and hydrogen atoms then a value of $\Delta G(z)$ around 12–19 kcal/mol is obtained, which is consistent with the experimental [102] activation energies of 16.4–17 kcal/mol.

$LiFePO_4$/Electrolyte Interface

Lithium iron phosphate ($LiFePO_4$) is an attractive cathode material for lithium-ion batteries for a number of reasons, including good thermal stability, low fabrication costs (from abundant starting materials), nontoxicity, a reasonably high theoretical specific capacity and an inherently flat voltage – time discharge profile [103]. Interfacial impedance for $LiFePO_4$ cells, which includes both anode/electrolyte and cathode/electrolyte contributions, can be an important source of overall cell impedance at rates and temperatures of practical interest, with both conventional solvent–based electrolytes and ionic liquid–based electrolytes [99]. It has long been held that resistance to Li^+ transport through the anode/electrolyte interface contributes significantly to cell impedance due to the presence of a poorly conducting SEI that forms on most anode materials due to reduction of the electrolyte [104]. Recently, more attention has been focused on contributions of Li^+ transport across the cathode/electrolyte interface to cell impedance. Interfacial effects, particularly those associated with Li^+ desolvation during intercalation, are thought to play an important role in determining the impedance of $LiFePO_4$-based cathodes [105, 106].

An atomistic simulation MD simulation of a common carbonate-based organic electrolyte, ethylene carbonate:dimethyl carbonate (EC:DMC = 3:7) with approximately 1 mol/kg $LiPF_6$, referred to as the organic liquid electrolyte or OLE, and an ionic liquid–based electrolyte (ILE), 1-ethyl 3-methyl-imidazolium: bis(fluorosulfonyl)imide ($EMIM^+$:FSI^-) with 1 mol/kg LiFSI, in contact with $LiFePO_4$ has been carried out [107]. Simulations were carried out using quantum chemistry–based polarizable force at 363 K on a 3-D periodic orthorhombic $LiFePO_4$ film + electrolyte systems such as shown in Fig. 26. POMF studies analogous to those for graphite were carried out in order to investigate the free-energy profile of bringing a Li^+ cation from the bulk electrolyte to the $LiFePO_4$ surface.

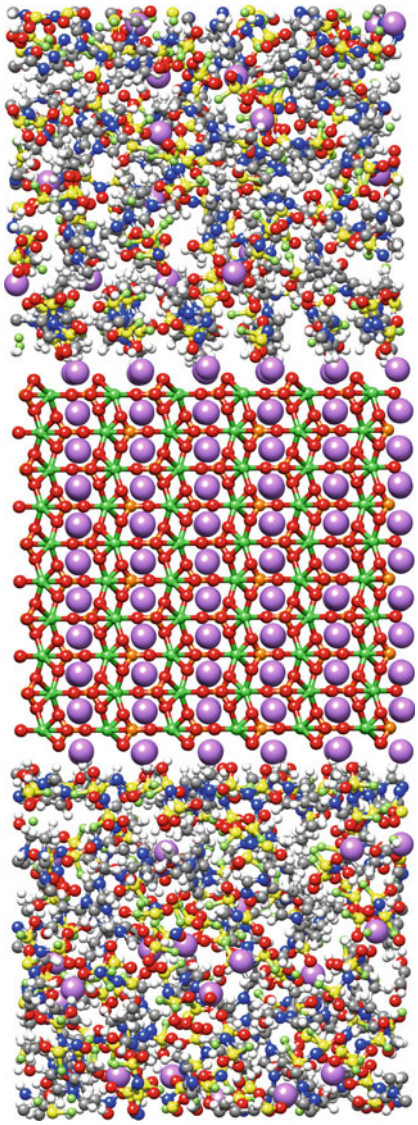

Lithium Battery Electrolyte Stability and Performance from Molecular Modeling and Simulations. Figure 26 Snapshot from an MD simulation of an ionic liquid electrolyte in contact with $LiFePO_4$

Poisson Potential Profile and Double Layer Structure for the ILE The Poisson potential for the ILE is shown in Fig. 27. In addition to the potential for the $LiFePO_4$/ILE system, the potential for the $LiFePO_4$ film alone (in vacuo) is shown. For the $LiFePO_4$ in vacuo, the potential at the outer edge of the $LiFePO_4$ surface, i.e., $y \approx 0.5$ Å ($y = 0$ at the surface lithium layer, with y being the direction of the surface normal) reaches a constant value which is arbitrarily assigned a value of 0 V. For $LiFePO_4$ in contact with the ILE system, the potential exhibits structure with a period of 2.5–3 Å, oscillating between negative and positive values, which

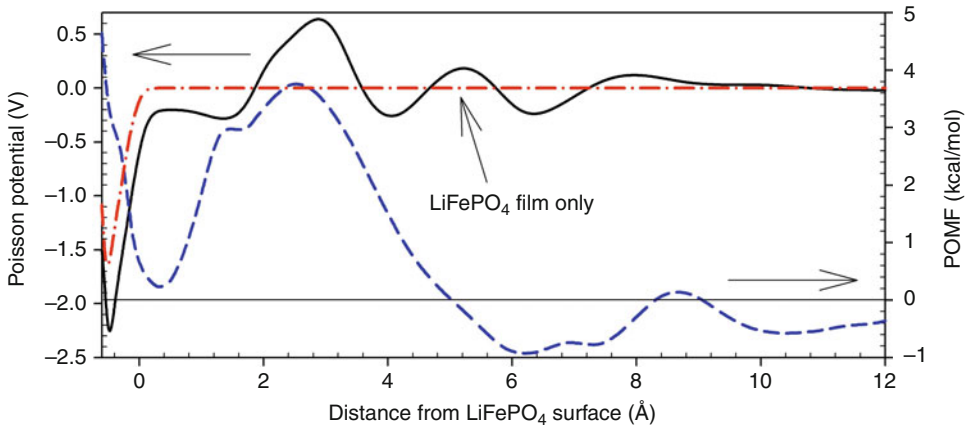

Lithium Battery Electrolyte Stability and Performance from Molecular Modeling and Simulations. Figure 27 Poisson potential and Li^+ free energy as a function of position with respect to the interface with $LiFePO_4$ in an ionic liquid electrolyte

reflects the atomic-scale surface-induced ordering in the electrolyte. The surface-induced local structure in the ILE reflected in the potential is clear in the snapshot of the system (Fig. 26) FSI^- and $EMIM^+$ are strongly segregated in the surface layer, with the former concentrated near surface Li^+ and the latter near surface oxygen atoms. The electrostatic potential reaches the bulk value (arbitrarily set to 0 V) at about 1 nm from the surface, indicating a relatively narrow double layer. The potential at the outer edge of the $LiFePO_4$ surface (the electric surface potential) is about −0.25 V with respect to the bulk electrolyte. Hence, the presence of the ILE results in a negative potential at the $LiFePO_4$ surface. This negative potential is due to the excess negative charge in the electrolyte between 1.5 and 2.5 Å, resulting from excess FSI^- in the interfacial layer. Between the potential minimum near the surface and the next minimum at around 4 Å, there is a large positive potential of about 0.6 V with respect to the bulk electrolyte.

Poisson Potential Profile and Double Layer Structure for the OLE The Poisson electrostatic potential for the $LiFePO_4$/OLE is shown in Fig. 28. Also shown is the potential for the $LiFePO_4$ film alone (in vacuo). The potential at the outer edge of the $LiFePO_4$ surface is negative with respect to the bulk (around −0.8 V). This electric surface potential is much more negative than observed for the ILE because of the propensity of negatively charged carbonyl oxygen atoms from the carbonate molecules to approach the surface and coordinate Li^+ and the lack of a strong positive charge (such as the hydrogen and nitrogen atoms in $EMIM^+$) to offset the resulting negative charge density. Between the negative potential minimum near the surface (around 1 Å) and the next minimum at around 5 Å, there is a positive potential comparable in magnitude to that observed in the ILE. The electrostatic potential reaches a constant (bulk) value at about 1 nm from the surface as was observed for the ILE electrolyte, indicating a narrow double layer.

The carbonyl oxygen atoms of the carbonate molecules, which have an appreciable negative charge (−0.4e to −0.5e) and are principally responsible for solvating Li^+ in bulk EC/DMC electrolytes [35], play the same role for the surface Li^+. Unlike the ILE, however, there are no exposed highly positively charged atoms in the OLE available to solvate the $LiFePO_4$ surface oxygen atoms. The CH_2/CH_3 groups in EC/DMC have a small positive charge in the range of +0.1e to +0.15e and the hydrogen atoms from these groups are the main coordinating atoms for the surface O atoms. This results in a dense layer of EC and DMC centered 3–4 Å from the surface as indicated by atomic and molecular density profiles.

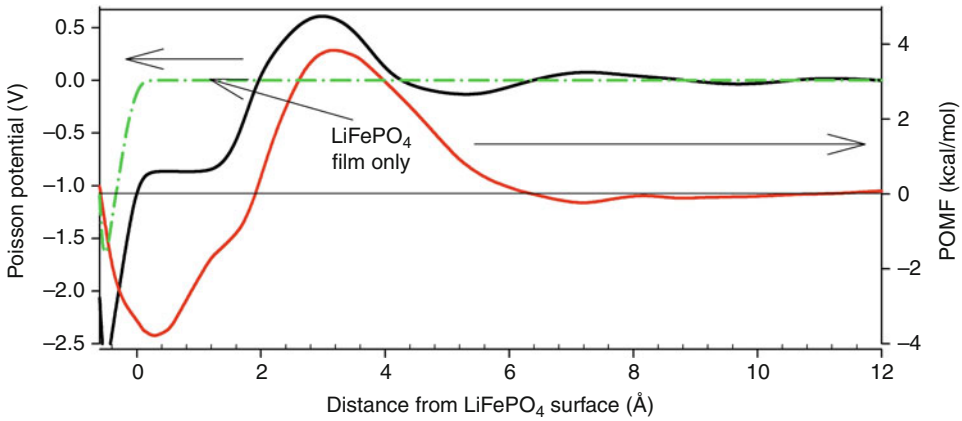

Lithium Battery Electrolyte Stability and Performance from Molecular Modeling and Simulations. Figure 28 Poisson potential and Li^+ free energy as a function of position with respect to the interface with $LiFePO_4$ in an organic liquid electrolyte

Free Energy of Li^+ as a Function of Position Relative to the $LiFePO_4$ Surface The potential of mean force (POMF), i.e., the free energy as a function of the position of a Li^+ relative to the $LiFePO_4$ surface, is shown in Fig. 27 for the ILE/$LiFePO_4$ system and in Fig. 28 for the OLE/$LiFePO_4$ system. For both the OLE and ILE systems the POMF is qualitatively similar to the Poisson potential. First, there is little structure in the POMF beyond 1 nm from the surface. Similarly, both the POMF and Poisson potential exhibit a maximum (in energy and potential, respectively) around 3 Å from the surface and a minimum very near the surface. However, a Li^+ cation interacting with the Poisson potential would experience a much larger positive energy at the barrier (note that the potential is in volts and the POMF in kcal/mol) and a much lower energy near the surface than is indicated by the POMF. In is important to note that the POMF measures the free energy (thermodynamic potential) associated with the actual process of bringing of a Li^+ cation to the $LiFePO_4$ surface while the Poisson potential is a plane-average measure of the equilibrium electrostatic potential. The Li^+ will find the lowest free-energy path to the surface and bring negative charge with it, and its presence results in a local restructuring of the electrolyte and electrolyte/$LiFePO_4$ interface.

Interfacial Impedance The total interfacial impedance from the bulk electrolyte to a point y relative the $LiFePO_4$ surface can be estimated (in units of Ω-cm^2) as the integral of the local resistivity:

$$R_{\text{int}}(y) = \int_{y=14}^{y} -2.71 \times 10^{-9} \frac{kT \exp\left[\frac{\Delta G(y)}{kT}\right]}{D_{Li^+}(y) N_{\text{bulk}} e^2} dy \tag{6}$$

where ΔG is Li^+ free energy, D is the Li^+ diffusion in the y direction, N_{bulk} is the concentration of Li^+ in the bulk electrolyte, and T is temperature. Using values of these quantities as determined from simulation, $R_{int}(y)$ for the ILE and the OLE systems was estimated using Eq. 2 [107]. Results are shown in Fig. 29, where it can be seen that the interfacial impedance for transporting Li^+ from y = 14 Å to about y = 3 Å is very small. In this region, the greater interfacial impedance for the ILE is due to the bulk lower Li^+ diffusion compared to that in the OLE. Beginning at around y = 3 Å, the decrease in Li^+ concentration due to the free-energy barrier observed for both the OLE and the ILE systems results in an increase in resistivity. The free energy of almost 4 kcal/mol, relative to the bulk and the corresponding decrease in Li^+ concentration in this region, does not lead to an appreciable contribution to R_{int}. An important conclusion from this work is that the higher bulk viscosity/lower bulk Li^+ mobility for the ILE compared to the OLE does not appear lead to a significant barrier for transporting Li^+ to the $LiFePO_4$ surface.

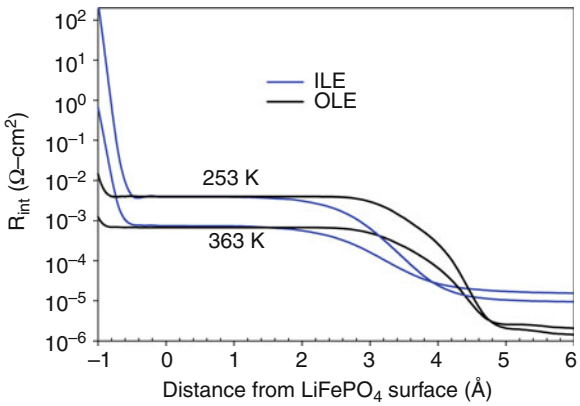

Lithium Battery Electrolyte Stability and Performance from Molecular Modeling and Simulations. Figure 29 Predicted interfacial impedance as a function of position

If/when the resistance for Li^+ transport through the electrolyte/$LiFePO_4$ interface is to make a significant contribution to overall cell impedance (in the absence of an SEI layer at the cathode/electrolyte interface), simulations indicate that it is likely due to the final desolvation process associated with intercalation of Li^+ into $LiFePO_4$. The rapid increase in free energy associated with this process leads to large resistivity according to Eq. 2 and a rapid increase in R_{int}, as shown in Fig. 29. Unfortunately, the range of positions (for $y < 0$) over which the free-energy profile used to estimate $N_{Li^+}(y)$ is accurate is unknown. Furthermore, use of Eq. 2 to estimate the equilibrium $N_{Li^+}(y)$ is questionable for $y < 0$ due to adsorption of Li^+ on the surface and the localization of Li^+ into specific channels (galleries). Nevertheless, assuming that the free-energy profile from simulation is valid to $y = -1$ Å, Fig. 29 indicates that interfacial impedance associated with the initial stages of intercalation from the surface into the $LiFePO_4$ gallery is significantly greater for the ILE than the OLE, but in either case is estimated to be quite small. The greater interfacial impedance for the ILE is not due to differences in the energetics of the desolvation process but rather to the much lower propensity of Li^+ to populate the $LiFePO_4$ surface in the ILE.

While interfacial impedance associated with bringing the cation to the $LiFePO_4$ surface and the initial stages of intercalation appears to be small at 363 K, the situation may be quite different at lower temperatures. Equation 2 can be applied at any temperature of interest assuming that $D_{Li}+(y)$ and $\Delta G_{Li}+(y)$ are independent of temperature. The estimated interfacial impedance at 253 K so calculated is shown in Fig. 29. Certainly $D_{Li}+(y)$ will decrease with temperature, particularly for the ILE, which, combined with increased interfacial structure with decreasing temperature, makes the estimated interfacial impedance at 253 K shown in Fig. 29 lower than would be obtained from direct determination of $D_{Li}+(y)$ and $\Delta G_{Li}+(y)$ at lower temperatures. The estimated contributions of the desolvation process associated with the initial stages of Li^+ intercalation are much greater at the lower temperature than at 363 K, particularly for the ILE. This result is intriguing in light of recent experimental studies that claim that interfacial impedance at the cathode electrode is important at sub-ambient temperatures for OLE-based systems, albeit, desolvation process on the anode was found to have a higher activation energy [108, 109]. Simulation results indicate that this could be exacerbated by the use of ILEs.

Summary

In summary, MD simulations of an OLE and an ILE in contact with $LiFePO_4$ reveal surface-induced structure in the electrolytes that extends about 1 nm from the $LiFePO_4$ surface. The Poisson electrostatic potential was found to be large and negative within about 1 Å of the surface and large and positive in the region of 2–4 Å from the $LiFePO_4$ surface. The negative potential at the $LiFePO_4$ surface results from an excess of negative charge from the electrolyte near the surface that participates in the coordination of the surface Li^+ atoms. The positive potential slightly further from the surface results from the orientation of the electrolyte molecules at the $LiFePO_4$ surface. This positive electrostatic potential is qualitatively consistent with a free-energy barrier for bringing Li^+ cations from the bulk electrolyte to the surface found to be 4 kcal/mol. However, this barrier and the corresponding decrease in Li^+ concentration due to lack of coordinating atoms (carbonyl oxygen atom) in the OLE in this range of distances from the interface, large local positive charge in the ILE, and the highly structured nature of the interfacial electrolyte, which reduces its ability to solvate Li^+, do not contribute significantly to interfacial impedance.

The latter, if and when important, appears to be dominated by the desolvation process associated with intercalation of Li^+ into the galleries of $LiFePO_4$.

Future Directions

The future will see increased reliance on modeling for understanding of electrolyte electrochemical stability, electrolyte/electrode interactions, and the structure and properties of the SEI layer. Particularly valuable will be simulation methods that accurately reproduce reactions between the electrolyte, salts, and electrolyte additives with the electrodes. These methods, which will include QM and reactive molecular dynamics methods, will be invaluable in providing fundamental insight into the mechanisms of electrolyte decomposition, reactions leading to the formation of the SEI as well as in predicting the structure of the SEI. As efforts toward developing high-voltage cathodes increase, simulations will play an important role in the development of electrolytes that are oxidatively stable at the higher voltages as well as in development of strategies for passivating the cathode surface.

Acknowledgments

The authors are grateful to the Department of Energy under Contract grant DE-SC0001912 to University of Utah and Air Force Office of Scientific Research contract number FA9550-09-C-0110 for the financial support of this work. We would also like to thank T. Richard Jow and Phil Ross for their comments and suggestions. This work was partially supported by an Interagency Agreement between the U.S. Department of Energy and the U.S. Army Research Laboratory under DE-IAOI-11EE003413 for the office of vehicle technologies programs including Batteries for Advanced Transporation Technologies (BATT) program.

Bibliography

1. Xu K (2004) Nonaqueous liquid electrolytes for lithium-based rechargeable batteries. Chem Rev 104:4303
2. Armand M, Tarascon JM (2008) Build better batteries. Nature 451:652
3. Zhang XR, Pugh JK, Ross PN (2001) Computation of thermodynamic oxidation potentials of organic solvents using density functional theory. J Electrochem Soc 148: E183
4. Fu Y, Liu L, Yu HZ, Wang YM, Guo QX (2005) Quantum-chemical predictions of absolute standard redox potentials of diverse organic molecules and free radicals in acetonitrile. J Am Chem Soc 127:7227
5. Han YK, Jung J, Yu S, Lee H (2009) Understanding the characteristics of high-voltage additives in Li-ion batteries: solvent effects. J Power Sour 187:581
6. Ue M, Murakami A, Nakamura S (2002) Anodic stability of several anions examined by Ab initio molecular orbital and density functional theories. J Electrochem Soc 149:A1572
7. Johansson P (2006) Intrinsic anion oxidation potentials. J Phys Chem A 110:12077
8. Johansson P (2007) Intrinsic anion oxidation potentials (vol 110, pg 12077, 2006). J Phys Chem A 111:1378
9. Wang RL, Buhrmester C, Dahn JR (2006) Calculations of oxidation potentials of redox shuttle additives for Li-ion cells. J Electrochem Soc 153:A445
10. Trasatti S (1986) The absolute electrode potential – an explanatory note (recommendations 1986). Pure Appl Chem 58:955–966
11. Isse AA, Gennaro A (2010) Absolute potential of the standard hydrogen electrode and the problem of interconversion of potentials in different solvents. J Phys Chem B 114:7894
12. Abe K, Hattori T, Kawabe K, Ushigoe Y, Yoshitake H (2007) Functional electrolytes. J Electrochem Soc 154:A810
13. Zhang XR, Kostecki R, Richardson TJ, Pugh JK, Ross PN (2001) Electrochemical and infrared studies of the reduction of organic carbonates. J Electrochem Soc 148:A1341
14. Wang YX, Nakamura S, Ue M, Balbuena PB (2001) Theoretical studies to understand surface chemistry on carbon anodes for lithium-ion batteries: reduction mechanisms of ethylene carbonate. J Am Chem Soc 123:11708
15. Vollmer JM, Curtiss LA, Vissers DR, Amine K (2004) Reduction mechanisms of ethylene, propylene, and vinylethylene carbonates. J Electrochem Soc 151:A178
16. Verma P, Maire P, Novák P (2010) A review of the features and analyses of the solid electrolyte interphase in Li-ion batteries. Electrochimica Acta 55(22):6332–6341
17. Aurbach D (2000) Review of selected electrode-solution interactions which determine the performance of Li and Li ion batteries. Power Sour 89:206
18. Aurbach D et al (1994) The Correlation between the surface-chemistry and the performance of Li-carbon intercalation anodes for rechargeable rocking-chair type batteries. J Electrochem Soc 141:603
19. Aurbach D, Einely Y, Zaban A (1994) The surface-chemistry of lithium electrodes in alkyl carbonate solutions. J Electrochem Soc 141:L1
20. Aurbach D et al (1995) The study of electrolyte-solutions based on ethylene and diethyl carbonates for rechargeable Li batteries. 1. Li metal anodes. J Electrochem Soc 142:2873–2882
21. Aurbach D et al (1995) The study of electrolyte-solutions based on ethylene and diethyl carbonates for rechargeable Li batteries. 2. graphite-electrodes. J Electrochem Soc 142:2882–2890

22. Li T, Balbuena PB (2000) Theoretical studies of the reduction of ethylene carbonate. Chem Phys Lett 317:421
23. Tasaki K, Kanda K, Kobayashi T, Nakamura S, Ue M (2006) Theoretical studies on the reductive decompositions of solvents and additives for lithium-ion batteries near lithium anodes. J Electrochem Soc 153:A2192
24. Wang YX, Nakamura S, Tasaki K, Balbuena PB (2002) Theoretical studies to understand surface chemistry on carbon anodes for lithium-ion batteries: how does vinylene carbonate play its role as an electrolyte additive? J Am Chem Soc 124:4408
25. Wang YX, Balbuena PB (2002) Theoretical insights into the reductive decompositions of propylene carbonate and vinylene carbonate: density functional theory studies. J Phys Chem B 106:4486
26. Aurbach D, Weissman I, Schechter A, Cohen H (1996) X-ray photoelectron spectroscopy studies of lithium surfaces prepared in several important electrolyte solutions. A comparison with previous studies by Fourier transform infrared spectroscopy. Langmuir 12:3991
27. Aurbach D, Gofer Y, Benzion M, Aped P (1992) The behavior of lithium electrodes in propylene and ethylene carbonate – the major factors that influence Li cycling efficiency. J Electroanal Chem 339:451
28. Xu K, Lam YF, Zhang SS, Jow TR, Curtis TB (2007) Solvation sheath of Li + in nonaqueous electrolytes and its implication of graphite/electrolyte interface chemistry. J Phys Chem C 111:7411
29. Naji A, Ghanbaja J, Humbert B, Willmann P, Billaud D (1996) Electroreduction of graphite in $LiClO_4$-ethylene carbonate electrolyte. Characterization of the passivating layer by transmission electron microscopy and Fourier-transform infrared spectroscopy. J Power Sour 63:33–39
30. Eyring H (1935) The activated complex in chemical reactions. J Chem Phys 3:107
31. Bedrov D, Smith GD, van Duin A (2010) Reactions of singly-reduced ethylene carbonate in lithium battery electrolytes. A molecular dynamics simulation study using the reaxFF. J Phys Chem B (accepted)
32. Aurbach D, Levi MD, Levi E, Schechter A (1997) Fail stabilization mechanisms graphite electrodes. J Phys Chem B 101:2195
33. Aurbach D, Moshkovich M, Cohen Y, Schechter A (1999) The study of surface film formation on noble-metal electrodes in alkyl carbonates/Li salt solutions, using simultaneous in situ AFM, EQCM, FTIR, and EIS. Langmuir 15:2947
34. Leung K, Budzien JL (2010) Ab initio molecular dynamics simulations of the initial stages of solid-electrolyte interphase formation on lithium ion battery graphitic anodes. Phys Chem Chem Phys 12:6583
35. Borodin O, Smith GD (2009) Quantum chemistry and molecular dynamics simulation study of dimethyl carbonate: ethylene carbonate electrolytes doped with $LiPF_6$. J Phys Chem B 113:1763
36. Borodin O, Smith GD (2006) LiTFSI structure and transport in ethylene carbonate from molecular dynamics simulations. J Phys Chem B 110:4971
37. Wu H, Wick CD (2010) Computational Investigation on the role of plasticizers on ion conductivity in poly(ethylene oxide) LiTFSI electrolytes. Macromolecules 43:3502–3510
38. Borodin O, Smith GD (2006) Development of many-body polarizable force fields for Li-battery applications: 2. LiTFSI-doped oligoether, polyether, and carbonate-based electrolytes. J Phys Chem B 110:6293–6299
39. Borodin O et al (2006) Li^+ Transport in lithium sulfonylimide-oligo(ethylene oxide) ionic liquids and oligo(ethylene oxide) doped with LiTFSI. J Phys Chem B 110:24266
40. Siqueira LJA, Ribeiro MCC (2006) Molecular dynamics simulation of the polymer electrolyte poly(ethylene oxide)/$LiClO_4$. II. Dynamical properties. J Chem Phys 125:214903
41. Borodin O, Smith GD (2000) Molecular dynamics simulation study of LiI-doped diglyme and poly(ethylene oxide) solutions. J Phys Chem B 104:8017–8022
42. Li S et al (2008) Molecular dynamics simulation of LiTFSI-acetamide electrolytes: structural properties. J Phys Chem B 112:6398
43. Soetens JC, Millot C, Maigret B (1998) Molecular dynamics simulation of $Li^+BF_4^-$ in ethylene carbonate, propylene carbonate, and dimethyl carbonate solvents. J Phys Chem A 102:1055
44. Takeuchi M et al (2009) Ion-ion interactions of $LiPF_6$ and $LiBF_4$ in propylene carbonate solutions. J Molec Liq 148:99
45. Brandell D, Liivat A, Aabloo A, Thomas JO (2005) Molecular dynamics simulation of the crystalline short-chain polymer system $LiPF_6$ center dot PEO_6 (M-w similar to 1000). J Mater Chem 15:4338–4345
46. Brandell D, Liivat A, Kasemagi H, Aabloo A, Thomas JO (2005) Molecular dynamics simulation of the $LiPF_6$ center dot PEO_6 structure. J Mater Chem 15:1422–1428
47. Borodin O, Smith GD, Jaffe RL (2001) Ab initio quantum chemistry and molecular dynamics simulations studies of $LiPF_6$/poly(ethylene oxide) interactions. J Comput Chem 22:641
48. Li T, Balbuena PB (1999) Theoretical studies of lithium perchlorate in ethylene carbonate, propylene carbonate, and their mixtures. J Electrochem Soc 146:3613
49. Borodin O, Smith GD (2007) Li^+ transport mechanism in oligo (ethylene oxide)s compared to carbonates. J Solution Chem 36:803
50. Newman J, Thomas KE, Hafezi H, Wheeler DR (2003) Modeling of lithium-ion batteries. J Power Sour 119:838
51. Hayashi K, Nemoto Y, Tobishima S, Yamaki J (1997) Electrolyte for high voltage Li/LiMn1.9Co0.1O4 cells. J Power Sour 68:316–319
52. Saunier J, Gorecki W, Alloin F, Sanchez JY (2005) NMR study of cation, anion, and solvent mobilities in macroporous poly (vinylidene fluoride). J Phys Chem B 109:2487–2492
53. Morita M, Asai Y, Yoshimoto N, Ishikawa M (1998) A Raman spectroscopic study of organic electrolyte solutions based on binary solvent systems of ethylene carbonate with low viscosity solvents which dissolve different lithium salts. J Chem Soc Faraday Trans 94:3451–3456

54. Hayamizu K, Aihara Y, Arai S, Martinez CG (1999) Pulse-gradient spin-echo H-1, Li-7, and F-19 NMR diffusion and ionic conductivity measurements of 14 organic electrolytes containing $LiN(SO_2CF_3)_2$. J Phys Chem B 103:519–524
55. Aihara Y et al (2004) Ion transport properties of six lithium salts dissolved in gamma-butyrolactone studied by self-diffusion and ionic conductivity measurements. J Electrochem Soc 151:A119
56. Tarascon JM, Armand M (2001) Issues and challenges facing rechargeable lithium batteries. Nature 414:359
57. Snyder JF, Ratner MA, Shriver DF (2002) Polymer electrolytes and polyelectrolytes: Monte Carlo simulations of thermal effects on conduction. Solid State Ionics 147:249
58. Borodin O, Smith GD (2006) Mechanism of ion transport in amorphous poly(ethylene oxide)/LiTFSI from molecular dynamics simulations. Macromolecules 39:1620–1629
59. Diddens D, Heuer A, Borodin O (2010) Understanding the lithium transport within a Rouse-based model for a PEO/LiTFSI polymer electrolyte. Macromolecules 43:2028
60. Borodin O, Smith GD (2007) Molecular dynamics simulations of comb-branched poly(epoxide ether)-based polymer electrolytes. Macromolecules 40:1252–1258
61. Borodin O, Smith GD, Bandyopadhyaya R, Redfern P, Curtiss LA (2004) Molecular dynamics study of nanocomposite polymer electrolyte based on poly(ethylene oxide)/$LiBF_4$. Model Sim Mater Sci Eng 12:S73
62. Londono JD et al (1997) Cation environment in molten lithium iodide doped poly(ethylene oxide). Macromolecules 30:7151–7157
63. Annis BK, Kim MH, Wignall GD, Borodin O, Smith GD (2000) A study of the influence of LiI on the chain conformations of poly(ethylene oxide) in the melt by small-angle neutron scattering and molecular dynamics simulations. Macromolecules 33:7544–7548
64. Saboungi ML et al (2002) Coherent neutron scattering from PEO and a PEO-based polymer electrolyte. Solid State Ionics 147:225
65. Muller-Plathe F, van Gunsteren WF (1995) Computer simulation of a polymer electrolyte: lithium iodide in amorphous poly(ethylene oxide). J Chem Phys 103:4745–4756
66. Maitra A, Heuer A (2007) Cation transport in polymer electrolytes: a microscopic approach. Phys Rev Lett 98:227802
67. Maitra A, Heuer A (2007) Understanding segmental dynamics in polymer electrolytes: a computer study. Macromol Chem Phys 208:2215
68. Sutjianto A, Curtiss LA (1998) Li+−diglyme complexes: barriers to lithium cation migration. J Phys Chem A 102:968
69. Hayamizu K, Akiba E, Bando T, Aihara Y (2002) H-1, Li-7, and F-19 nuclear magnetic resonance and ionic conductivity studies for liquid electrolytes composed of glymes and polyetheneglycol dimethyl ethers of $CH_3O(CH_2CH_2O)n\ CH_3$ (n = 3-50) doped with $LiN(SO_2CF_3)_2$. J Chem Phys 117:5929
70. Buriez O et al (2000) Performance limitations of polymer electrolytes based on ethylene oxide polymers. J Power Sour 89:149
71. Kerr JB et al (2002) From molecular models to system analysis for lithium battery electrolytes. J Power Sour 110:389
72. Kerr JB (2004) Nazri GA, Pistoia G (eds) Edsin Lithium batteries: sience and technology. Kluwer, Boston
73. Paillard E et al (2009) Electrochemical and physicochemical properties of $PY_{14}FSI$-based electrolytes with LiFSI. J Electrochem Soc 156:A891
74. Fox DM et al (2003) Flammability, thermal stability, and phase change characteristics of several trialkylimidazolium salts. Green Chem 5:724–727
75. Borodin O (2009) Polarizable force field development and molecular dynamics simulations of ionic liquids. J Phys Chem B 113:11463
76. Borodin O (2009) Relation between heat of vaporization, ion transport, molar volume, and cation and anion binding energy for ionic liquids. J Phys Chem B 113:12353
77. Smith GD et al (2010) A comparison of fluoroalkyl-derivatized imidazolium:TFSI and alkyl-derivatized imidazolium:TFSI ionic liquids: a molecular dynamics simulation study. Phys Chem Chem Phys 12:7064
78. Smith GD et al (2008) A comparison of ether- and alkyl-derivatized imidazolium-based room-temperature ionic liquids: a molecular dynamics simulation study. Phys Chem Chem Phys 10:6301
79. Maginn EJ (2009) Molecular simulation of ionic liquids: current status and future opportunities. J Phys Condens Matter 21:17
80. Koddermann T, Paschek D, Ludwig R (2007) Molecular dynamic simulations of ionic liquids: a reliable description of structure, thermodynamics and dynamics. Chemphyschem 8:2464–2470
81. Hooper JB, Borodin O (2010) Molecular dynamics simulations of N, N, N, N-tetramethylammonium dicyanamide plastic crystal and liquid using a polarizable force field. Phys Chem Chem Phys 12:4635
82. Borodin O, Gorecki W, Smith GD, Armand M (2010) Molecular dynamics simulation and pulsed-field gradient NMR studies of Bis(fluorosulfonyl)imide (FSI) and Bis[(trifluoromethyl)sulfonyl]imide (TFSI)-based ionic liquids. J Phys Chem B 114:6786
83. Kelkar MS, Shi W, Maginn EJ (2008) Determining the accuracy of classical force fields for ionic liquids: atomistic simulation of the thermodynamic and transport properties of 1-ethyl-3-methylimidazolium ethylsulfate ([emim][EtSO4]) and its mixtures with water. Ind Eng Chem Res 47:9115–9126
84. Tsuzuki S et al (2009) Molecular dynamics simulations of ionic liquids: cation and anion dependence of self-diffusion coefficients of ions. J Phys Chem B 113:10641
85. Bedrov D, Borodin O, Li Z, Smith GD (2010) Influence of polarization on structural, thermodynamic, and dynamic properties of ionic liquids obtained from molecular dynamics simulations. J Phys Chem B 114:4984
86. Borodin O, Smith GD, Henderson W (2006) Li^+ cation environment, transport and mechanical properties of the LiTFSI doped *N*-Methyl-*N*-alkylpyrrolidinium$^+$TFSI$^-$ ionic liquids. J Phys Chem B 110:16879

87. Niu SA, Cao Z, Li S, Yan TY (2010) Structure and transport properties of the LiPF6 doped 1-ethyl-2,3-dimethyl-imidazolium hexaftuorophosphate ionic liquids: a molecular dynamics study. J Phys Chem B 114:877
88. Monteiro MJ, Bazito FFC, Siqueira LJA, Ribeiro MCC, Torresi RM (2008) Transport coefficients, Raman spectroscopy, and computer simulation of lithium salt solutions in an ionic liquid. J Phys Chem B 112:2102
89. Lassegues JC, Grondin J, Aupetit C, Johansson P (2009) Spectroscopic identification of the lithium ion transporting species in LiTFSI-doped ionic liquids. J Phys Chem A 113:305
90. Tasaki K et al (2009) Solubility of lithium salts formed on the lithium-ion battery negative electrode surface in organic solvents. J Electrochem Soc 156:A1019
91. Borodin O, Smith GD, Fan P (2006) Molecular dynamics simulations of lithium alkyl carbonates. J Phys Chem B 110:22773
92. Xu K et al (2006) Syntheses and Characterization of lithium alkyl mono- and dicarbonates as components of surface films in Li-ion batteries. J Phys Chem B 110:7708
93. Zhuang GV, Xu K, Yang H, Jow TR, Ross PN (2005) Lithium ethylene dicarbonate identified as the primary product of chemical and electrochemical reduction of EC in 1.2 M $LiPF_6$EC:EMC electrolyte. J Phys Chem B 109:17567–17573
94. Ross P (2006), in BATT report
95. Zhang SS, Xu K, Jow TR (2006) EIS study on the formation of solid electrolyte. Electrochimica Acta 51:1636
96. Zhang SS, Xu K, Jow TR (2006) Charge and discharge characteristics of a commercial $LiCoO_2$-based 18650 Li-ion battery. J Power Sour 160:1403–1409
97. Xu K (2007) "Charge-transfer" process at graphite/electrolyte interface and the solvation sheath structure of Li + in nonaqueous electrolytes. J Electrochem Soc 154:A162
98. Abraham DP, Heaton JR, Kang SH, Dees DW, Jansen AN (2008) Investigating the low-temperature impedance increase of lithium-ion cells. J Electrochem Soc 155:A41
99. Kobayashi Y et al (2007) Comparative study of lithium secondary batteries using nonvolatile safety electrolytes. J Electrochem Soc 154:A677
100. Seki S et al (2005) Degradation mechanism analysis of all-solid-state lithium polymer secondary batteries by using the impedance measurement. J Power Sour 146:741
101. Bemporad D, Essex JW, Luttmann C (2004) Permeation of small molecules through a lipid bilayer: a computer simulation study. J Phys Chem B 108:4875
102. Xu K, Lam YF, Zhang SS, Jow TR, Curtis TB (2007) Solvation sheath of Li + in nonaqueous electrolytes and its implication of graphite/electrolyte interface chemistry. J Phys Chem C111:7411–7421
103. Padhi AK, Nanjundaswamy KS, Goodenough JB (1997) Phospho-olivines as positive-electrode materials for rechargeable lithium batteries. J Electrochem Soc 144:1188
104. Aurbach D (2003) Electrode-solution interactions in Li-ion batteries: a short summary and new insights. J Power Sour 119:497
105. He P, Zhang X, Wang YG, Cheng L, Xia YY (2008) Lithium-ion intercalation behavior of $LiFePO_4$ in aqueous and nonaqueous electrolyte solutions. J Electrochem Soc 155:A144
106. Yu DYW et al (2007) Study of $LiFePO_4$ by cyclic voltammetry. J Electrochem Soc 154:A253
107. Smith GD, Borodin O, Russo SP, Rees RJ, Hollenkamp AF (2009) A molecular dynamics simulation study of $LiFePO_4$/electrolyte interfaces: structure and Li + transport in carbonate and ionic liquid electrolytes. Phys Chem Chem Phys 11:9884
108. Jow TR et al (2010) Electrolytes SEI and charge discharge kinetics in Li-ion batteries. ECS Trans 25:3
109. Ogumi Z (2010) Interfacial reactions of lithium-ion batteries. Electrochemistry 78:319

Lithium Ion Batteries, Electrochemical Reactions in

Paul J. Sideris, Steve G. Greenbaum
Department of Physics and Astronomy, Hunter College of CUNY, New York, NY, USA

L

Article Outline

Glossary
Definition of the Subject and Its Importance
Introduction
Electrochemistry
Overview of Experimental Techniques
Diffraction Methods
X-Ray Photoelectron Spectroscopy
X-Ray Absorption Spectroscopy
NMR Spectroscopy
Computational Methods
Survey of Experimental Results and Their Interpretation
Future Directions
Acknowledgements
Bibliography

Glossary

Diffraction A phenomenon which occurs when a propagating wave encounters or interacts with an object. Diffraction techniques have become a standard method for the investigation of the atomic structure of matter.

Nuclear magnetic resonance (NMR) A condition in which magnetic nuclei in the presence of an external magnetic field absorb and reemit electromagnetic radiation (in the radiofrequency regime). The energy absorbed depends on the strength of the magnetic field and a number of chemical and structural properties of the matter under investigation.

Photoelectron The electrons ejected from matter after having absorbed electromagnetic radiation of a particular wavelength.

Relaxation The process by which a system returns to equilibrium after a perturbation, usually characterized by a specific time *t*.

Solid electrolyte interphase (SEI) Electrolyte decomposition products, both organic and inorganic, that form a protective layer on the electrodes (predominantly the anode) of lithium-ion batteries which is necessary for optimal performance and cell longevity.

Definition of the Subject and Its Importance

Despite their spectacular success in portable electronics applications, continued technical advances of lithium-ion batteries are crucial to establishing large-scale storage applications such as electric vehicles and enabling development of renewable intermittent energy sources, i.e., wind and solar. Paramount considerations in realizing scaled-up battery systems are safety, cost, energy density, and service lifetime. Some of these applications also require rapid charge and discharge capability. To move beyond the current generation of lithium-ion batteries, it is necessary to understand some of the outstanding materials issues of the individual components (i.e., electrodes and electrolytes) as well as the battery system as a whole where the components interact under conditions of elevated temperature and electric current flow.

The rational design of compounds, complexes, and systems consisting of them for particular applications is the basis of modern materials science. The advent of powerful computing hardware and software in the last decade has made great strides in predicting material properties without doing a single experiment. On the other hand, the need for experimental verification has often resulted in the discovery of new scientific principles and behavior, and driven the development of not only the materials themselves but also ever more potent and versatile experimental tools. The purpose of this article is to describe several analytical methods with examples of their use in investigating material properties of rechargeable lithium battery cell components and systems, especially in the context of the outstanding technical challenges to further development. In addition, a few examples detailing how computational studies can aid in the interpretation of experimental results and in the development of new materials will be presented.

Introduction

Since their successful commercialization in the 1990s, extensive research has been carried out on lithium-ion batteries. The main material challenges have been recently summarized by Goodenough and Kim [1]. A lithium-ion battery cell consists of three main components: two electrodes – an anode (the negative terminal), and a cathode (positive terminal), as well as a non-aqueous electrolyte which physically separates the two electrodes, but allows conduction of ions between them during cycling (discharging and charging) of the battery. The work of Whittingham on titanium(II) sulfide as a cathode material was a breakthrough in the field and generated a lot of interest in utilizing intercalation chemistry for energy storage applications [2]. Since then, lithium metal oxides –$LiCoO_2$, $LiNiO_2$, $LiMn_2O_4$– have been employed as cathode materials. Due to the high reactivity of lithium metal, safety concerns have prompted the use of lithiated graphitic carbon as a replacement anode. Typical liquid electrolytes include lithium salts dissolved in organic carbonates.

The advancement of battery technology ultimately resides in a fundamental understanding of the structural, chemical, and electronic changes in the component materials that occur upon cycling. Experimental techniques commonly used in battery science can be broadly categorized as probing either the long-range or local structure. For a significant advancement in the field, both sets of techniques need to be utilized effectively to fully understand the chemistry and structure-property relationships of materials.

Electrochemistry

The overwhelming majority of commercially available anode and cathode materials for Li-ion batteries undergo an insertion reaction. The reaction mechanism involves the migration of Li^+ cations into (insertion, intercalation) and out of (extraction, deintercalation) cathode and anode materials, both of which often have a layered or tunnel structural motif. Since Li metal anodes have been largely replaced by graphitic carbon due to safety concerns, the positive electrodes in Li-ion batteries act as a source of lithium. During discharge, Li^+ migrates from the anode, through the electrolyte, to the cathode. Concomitantly, an electron is released for every Li^+ ion involved in the migration to an external circuit where it can power a device and perform work. The half-reactions, or one component of a redox (reduction-oxidation) reaction, of the two electrodes composed of lithium metal oxides of the form $LiMO_2$ (where M is a transition metal) and graphite can be written as,

$$LiMO_2 \leftrightarrow Li_{1-x}MO_2 + xLi^+ + xe^-, \quad (1)$$

for the cathode and

$$xLi^+ + xe^- + 6C \leftrightarrow Li_xC_6, \quad (2)$$

for the anode, respectively. In the $LiMO_2$ case, the transition metal gets oxidized from M^{3+} to M^{4+} during charging, with a subsequent reduction from M^{4+} to M^{3+} during discharge. Initially, layered $LiNiO_2$ was considered a promising cathode material considering it is cheaper and less toxic than cobalt [3], but the delithiated compounds were recognized as being too reactive with the organic electrolyte, posing a significant safety hazard. Moreover, Li–Ni exchange in the material over repeated cycles drastically hindered performance [4]. Issues stemming from environmental concerns and the cost of cobalt have motivated the study of similar layered compounds containing little to no Co as replacement cathode materials, such as $LiNi_{1-y}Co_yO_2$ [5], $LiMnO_2$ [6], $LiNi_{1-y}Mn_yO_2$ [7], and $LiNi_{1-y-z}Mn_yCo_zO_2$ [8, 9]. Structural instability of the electrodes, in conjunction with unavoidable side reactions which occur in the cell, limits the amount of charge and discharge cycles a battery can undergo. The rate of cycling also has a pronounced effect on the structure of many electrode materials and is an important factor in the depletion of performance.

A few classes of materials, such as binary copper compounds (copper sulfide CuS and copper oxide CuO) and metal fluorides ($M^{n+}F_n$), undergo a conversion reaction during cycling. These compounds have generated interest as potential electrode materials due to their high specific capacities (~600–1,000 mAh/g) and excellent cycling reversibility [10]. In this reaction mechanism, lithium compounds (lithium sulfide Li_2S, lithium oxide Li_2O, lithium fluoride LiF) are formed along with metal nano-particles during discharging. The overall reaction can be written as

$$M_xX_y + nyL_i \leftrightarrow yLi_nX + xM^0, \quad (3)$$

where X is either O or F, and M^0 denotes a transition metal in the metallic state. The reaction typically involves micron-sized M_xX_y particles which react to form composite materials composed of nano-sized metallic particles (on the order of 1–10 nm) and Li_nX which occurs on the first cycle. In subsequent redox cycles, the size of these particles remains virtually unchanged. The confinement of these metal particles in the lithium salt matrix is thought to play a crucial role in the electrochemical activity in the material. Of the M_xX_y compounds, only metal fluorides are considered as alternative positive electrodes in lithium-ion batteries. This is due to their ionic character, which in turn necessitates higher operating voltages [11, 12]. Unfortunately, fluorides tend to be large bandgap insulators, prohibiting their use in batteries. To circumvent the inherent issues of the fluorides, Amatucci and coworkers have prepared a mixed conductive matrix (MCM) composed of nanocarbon-metal-fluoride composite materials [13, 14]. In a few instances, a conductive oxide such as MoO_3 can also be used to enhance conductivity [15]. The drastic reduction of the metal fluoride particles, along with the presence of the highly conductive matrix in the nanocomposites results in enhanced electrochemical activity and cycling properties. The smaller particle size decreases the tunneling lengths of the electrons during the redox reaction in addition to increasing the available surface area, facilitating the diffusion of Li. The presence of a conducting matrix between the nanograins of the materials allows the reaction to progress.

The choice of electrolytes highly depends on the operating voltages and nature of the cell, i.e., a polymer or liquid-based battery. Employing a polymer electrolyte imposes further criteria, as electrochemical stability of the backbone and sidechains becomes relevant [16, 17]. Many liquid solvents are available to use as electrolytes, each with a respective viscosity and dielectric constant that can be selected to facilitate the ionic conductivity. Typically, ethylene carbonate and dimethyl carbonate are used. In contrast, only a handful of lithium salts – lithium hexafluorophosphate ($LiPF_6$), lithium triflate ($LiSO_3CF_3$), lithium tetrafluoroborate ($LiBF_4$), lithium perfluorosulfonimide ($Li^+[CF_3SO_2NSO_2CF_3]^-$), among others – have been used for the electrolyte. Additionally, polyethylene oxide (PEO) has been the primary focus of polymer electrolytes. Despite this, details regarding the nature of salt-polymer interactions as well as the local structure of polymer electrolytes remain elusive. Ongoing research is focused on finding new, highly conductive salts with a large electrochemical operating window which dissolves in PEO at low temperature [18].

During charging and discharging, a small amount of the electrolyte separating the two electrodes decomposes, producing a film across the surface of the electrode materials. This film is referred to as the solid electrolyte interphase (SEI). The formation of an SEI is critical in the function and longevity of the battery–it is electrically insulating, which protects the remaining electrolyte from further decomposition, and allows for the diffusion of lithium during the discharging and charging processes. Ethylene carbonate (EC) is present in the overwhelming majority of commercially available electrolyte compositions, due to its ability to form this protective layer on the surface of graphite. In the event that the SEI cracks or flakes off, lithium dendrites could form which could lead to a "chemical short circuit." The end result would be the cell overheating causing flammability and, in the worst case scenario explosions. A thin passivating layer which has some degree of flexibility to expand and contract along with the anticipated volume changes of the electrodes upon intercalation and deintercalation is also desirable. While the capacity of a battery cell is primarily determined by the structure and electronic properties of the electrode materials, the longevity is intricately tied to the frequency of sidereactions that occur between the electrolyte and electrode. Control of the chemistry of this interface is of crucial importance to the longevity and performance of the battery [19].

To date, many of the decomposition products are not fully known. To complicate matters, SEI products depend on several variables, such as degree and rate of cycling, as well as temperature. However, it is well established that achieving a desired thickness of the insulating layers is essential to prolonging cell life and acquiring stable performance. As the thickness increases, the rate-determining step of the charge transfer reaction becomes the migration of the ion across the interphase. Irreversible capacity loss occurs when the lithium ions chemically bind to the components of the SEI or become trapped in the boundaries between SEI components, the layers become too electrically insulating, or if the thickness of the layer prevents lithium intercalation.

Overview of Experimental Techniques

Among the techniques that probe the average or long-range structure, powder X-ray diffraction (PXRD) and neutron diffraction (ND) will be briefly discussed. Techniques that provide local, atomistic information that will be mentioned are nuclear magnetic resonance (NMR) spectroscopy, X-ray photoelectron spectroscopy, X-ray absorption spectroscopy, and pair distribution function (PDF) analysis. A brief introduction to the underlying theory of each technique will be provided along with relevant examples to illustrate the type of information that can be extracted from each measurement. A particular emphasis will be placed in NMR spectroscopy and the various experiments that can be used to extract structural and dynamical information. The section will conclude with a few examples of the successes in first-principles calculations in determining the structure and properties of relevant materials.

Diffraction Methods

Two routine methods to determine the crystal structure, sample phase purity, estimations of atomic disorder, and grain size are through X-ray and neutron diffraction. Initially, these measurements could only be performed ex-situ for cycled battery samples. Currently, diffraction

patterns of relevant materials can be taken in-situ, as the battery is being cycled. Fundamentally, the techniques rely on the measurement of the intensity and angles of scattered X-rays or neutrons after the beams come in contact with a solid. X-ray diffractometers are readily available, allowing for the technique to be routine in the study of condensed matter. In contrast, neutron diffraction measurements require a special facility – either a spallation source or nuclear reactor.

The X-rays and neutrons scatter elastically in these diffraction experiments, meaning the energy of the incident and diffracted radiation is comparable. Bragg reflections occur when the incident and scattered waves of radiation interfere constructively in accordance with Bragg's law. Bragg's law describes the condition whereby you have constructive interference between successive atomic planes in a solid separated by an interlayer spacing d and is given by

$$n\lambda = 2d\sin(\theta), \tag{4}$$

where n is an integer greater than or equal to 1, and θ is the scattering angle. Atoms arranged periodically in a 3-D structure will impose selection rules on the type of reflections that are observed based on the symmetry of the crystal lattice. After considering the various symmetry operations possible in a 3-D arrangement of atoms, it is possible to classify all crystals into 1 of 230 so-called space groups. Additionally, one can define a unit cell, which contains atoms in the appropriate geometry that represents the simplest repeat unit of the crystal structure. The unit cell is parameterized by the lengths of the cell edges as well as the angles between them. The positions of the atoms inside the unit cell are given by a set of coordinates (x_i, y_i, z_i) measured from a specific lattice point known as the origin. Displacement parameters accompany the atomic positions to indicate anisotropic or spatially dependent positional disorder from thermal motions in the crystal. Information about the space group, unit cell parameters, and atomic positions uniquely identifies a material. Figure 1 shows in-situ diffraction patterns of the olivine compound $LiFePO_4$/C composite material collected by Myung et al. as a function of Li content [20]. As Li continues to be deintercalated, reflections due to a secondary $FePO_4$ phase appear, while the intensity of the $LiFePO_4$ reflections diminishes. By the end of the charge, $FePO_4$ becomes the major phase. As Li is introduced into the $FePO_4$ phase, the process is reversed, and the $LiFePO_4$ phase becomes dominant again. The reflections remain at the same 2θ, indicating that the lattice parameters are essentially constant upon cycling, in sharp contrast to the lithium transition metal (Co, Ni, Mn) oxide materials.

One of the main differences between X-ray and neutron diffraction is that X-rays scatter from the electron density of atoms within the crystal, whereas neutrons scatter from atomic nuclei. This implies that heavier elements, those with a larger atomic number, scatter and absorb the X-rays more effectively, making it difficult to detect light elements like lithium. A second implication is that contrast between neighboring elements in the periodic table or two different elements whose oxidations states produce the same electronic configuration will be poor. Neutrons posses spin, which can interact with the magnetic moment of electrons leading to so-called magnetic scattering. In this manner, so-called magnetic reflections can appear in the diffraction pattern, which aid in elucidating the magnetic structure of materials. Unlike X-rays, the neutron-scattering length does not vary in a systematic manner. Consequently, neutrons may diffract relatively strongly with light elements. Additionally, adjacent elements, which would be difficult to discern through X-ray diffraction experiments, may possess nuclear scattering properties that allow for their identification. A relevant example of this contrast is between Fe and Co. An added benefit of neutrons over X-rays is that relatively few elements, or more precisely isotopes, have significant absorption cross-sections. Since neutrons scatter from the nucleus, there is a significant dependence of the diffracted intensity on the particular isotope of the element. The sensitivity of the technique to different isotopes offers the possibility of performing a null scattering experiment, where a specific ratio of two isotopes is chosen, having neutron-scattering lengths of opposite sign, that effectively cancels the contribution of the element to the diffracted intensity.

In X-ray diffraction, the intensity of the diffracted beam I_{hkl} is proportional to the so-called structure factor F_{hkl} given by

$$F_{hkl} = \sum_{n=1}^{N} f_n e^{2\pi i(hx+ky+lz)}, \tag{5}$$

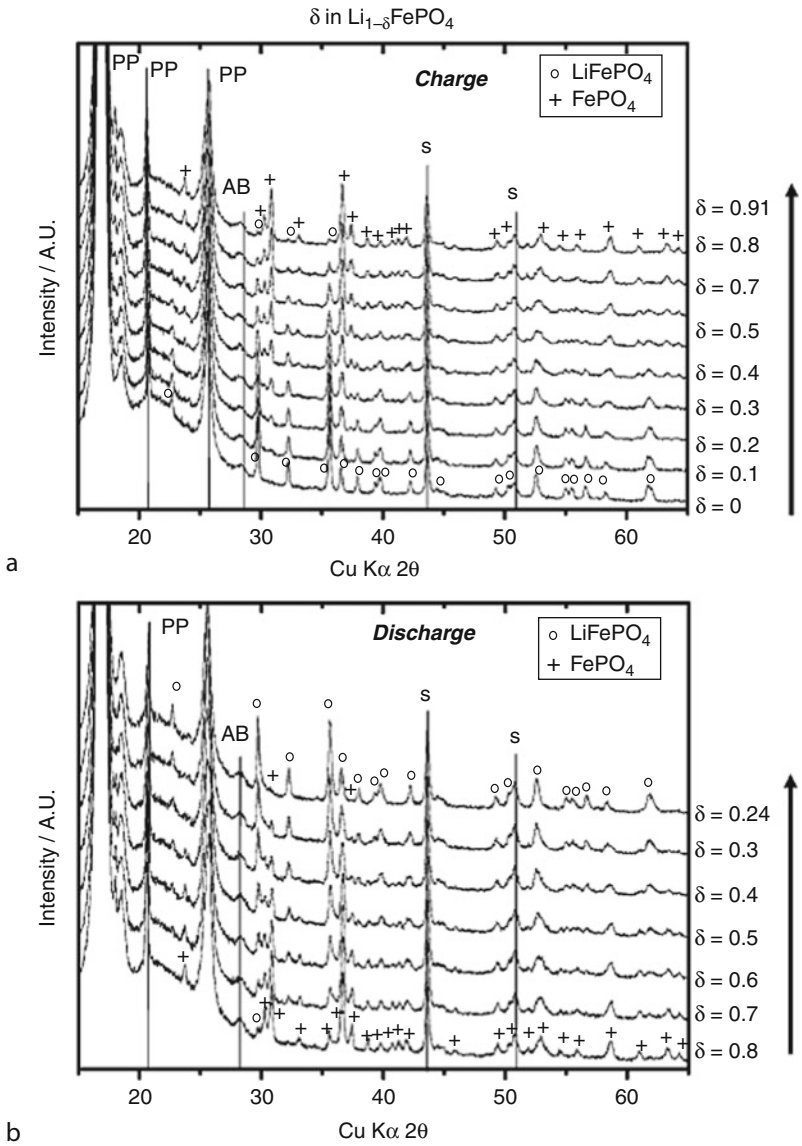

Lithium Ion Batteries, Electrochemical Reactions in. Figure 1
In-situ X-ray diffraction patterns of $Li_{1-\delta}FePO_4$ as a function of lithium content δ (From [20])

where f_n is the scattering factor for atom n within the unit cell (repeat unit of the crystal), and h, k, l are the Miller indices, which describe the virtual planes of atoms in a crystal lattice. For neutron diffraction, a similar expression is obtained for the structure factor, with the exception that the neutron-scattering factor b replaces f. The nuclei of atoms act as pin-point scatterers, unlike the electron clouds which have a finite size relative to the wavelengths of the radiation used in the experiment. The parameter b is independent of the scattering angle, in sharp contrast to f in the analogous X-ray expression which decreases with increasing angle. Thus, d-spacings, atomic positions, and their corresponding thermal parameters are more precisely determined through powder neutron diffraction. A breakthrough in structure analysis using diffraction

techniques was realized with the Rietveld method [21] which allowed the full profile of the diffraction pattern to be refined according to a specific structural model.

One method that is becoming increasingly useful in the study of solid, disordered materials is pair distribution function (PDF) analysis. The PDF can be understood as the distribution of bond lengths in a sample, weighted by the scattering power of the contributing atoms. It provides the probability of finding an atom at a distance r from another atom. The PDF is obtained from the sine Fourier transform of the total scattering pattern $S(Q)$, which includes both the Bragg and diffuse scattering, of a sample. Formally, this is given by

$$\begin{aligned} G(r) &= 4\pi r[\rho(r) - \rho_0] \\ &= \frac{2}{\pi}\int_0^\infty Q[S(Q) - 1]\sin(Qr)dQ, \end{aligned} \tag{6}$$

where $\rho(r)$ is the microscopic pair density, ρ_0 is the average number density, and Q is the magnitude of the scattering vector. For elastic scattering, $Q = 4\pi\sin(\theta)/\lambda$ with 2θ being the scattering angle and λ being the wavelength of the radiation used. A data plot includes $G(r)$ as a function of distance in angstroms. Since data cannot be collected to infinite Q, the real-space resolution of the PDF is decreased; Fourier transformation at a finite Q yields artifacts known as termination ripples. Additionally, the Q resolution results in an exponential dampening of peaks in the PDF with increasing r. As a result, it is desirable to perform experiments at high energy neutron or synchrotron X-ray sources to access high values of Q_{max} in order to enhance resolution. An added benefit of neutron PDF studies is that isotopic substitution can provide chemically specific pair distribution functions. For a sample containing two atoms of interest, say A and B, independent measurements can provide A–A, A–B, and B–B pairwise correlations.

Several analyses are available after obtaining an experimental PDF. Among these are bond length information and coordination number of atoms through a simple fit of the data. Peak widths can provide information regarding bond length distributions or correlated motions of atoms. PDFs are also used to refine or compare structural models of materials at the local- and medium-range length scales. Given a specific structural model, a calculated PDF, $G_c(r)$ is given by,

$$G_c(r) = \frac{1}{r}\sum_i\sum_j\left[\frac{b_i b_j}{\langle b\rangle^2}\delta(r - r_{ij})\right] - 4\pi r\rho_0, \tag{7}$$

where the sum extends over all ij atom pairs in the model crystal separated by an internuclear distance r_{ij}, b_i is the scattering power of atom i, and $\langle b\rangle$ is the average scattering power of the sample. For neutron scattering, b_i is the neutron-scattering length; for X-rays, it is the atomic form factor evaluated for a given Q. At $Q = 0$, the value of b_i in the X-ray scattering case is the number of electrons in the i atom. To model the finite Q in the data, a Q-dependent termination function of the form $\sin(Q_{max}r/r)$ is convoluted with the calculated PDF $G_c(r)$. An exponential damping function can also be multiplied to mimic the loss of resolution in reciprocal space.

A few methods are available for a full profile refinement of the PDF obtained from a structural model. Structural parameters such as lattice constants, atomic positions, atomic displacement parameters, and site occupancies can be refined over a distance r using the program PDFFIT [22]. The program works well in instances where the model structure can be defined with a relatively small number of atoms. For more complex cases, in which many atoms are needed to match a structural model, the Reverse Monte Carlo (RMC) [23] technique can be employed. This algorithm involves the calculation of the PDF from a specific crystal configuration and a corresponding "goodness-of-fit" parameter χ^2 given by,

$$\chi^2 = \sum_{i=1}^{N}\frac{[G_e(r_i) - G_c(r_i)]^2}{\sigma^2} \tag{8}$$

where G_e and G_c are the experimental and calculated PDFs, respectively, and σ is a weighting factor corresponding to experimental uncertainty. The best calculation is that which produces a χ^2 minimum. The algorithm proceeds to a random selection of an atom in the model crystal. The occupancy or displacement of the atom is changed by a random amount. The new PDF and χ^2 are subsequently recalculated, along with the change in the agreement factor $\Delta\chi^2$. If the change made lowers χ^2, then the change is accepted.

On the other hand, if the change increases χ^2 by $\Delta\chi^2$, it is not automatically rejected but accepted with a probability of $P = \exp(-\Delta\chi^2/2)$. This formalism ultimately ensures that the structural model does not get trapped in a local minimum, but converges to a global minimum. An RMC simulation serves to maximize the amount of disorder (entropy) in the atomic configuration while maintaining an agreement with experimental data. It is important to emphasize that this method can produce a range of atomic configurations, each with varying degrees of disorder that are consistent with experimentally obtained PDFs. Therefore, it is essential to have complementary information from other techniques which can place constraints on both local- and long-range structures to minimize the number of plausible configurations.

X-Ray Photoelectron Spectroscopy

X-ray photoelectron spectroscopy (XPS) is a quantitative technique which measures the number and kinetic energy of photoelectrons emitted from a sample that was irradiated with X-ray radiation. It is routinely used to determine the surface elemental composition or empirical formula of materials. XPS requires ultrahigh vacuum (UHV) conditions, on the order of $<10^{-9}$ torr, in order to detect the emitted electrons and minimize contamination or side reactions on the surface of the material. The spectrum involves a plot of electron count versus electron binding energy. The binding energy of electrons is specific to the element, so that peaks in the spectrum occur at characteristic energies corresponding to the electron configuration in a specific chemical bonding arrangement. Two peaks, with various integrated intensity ratios, are observed for electrons residing in *p*, *d*, or *f* orbitals. The separation of the two peaks, known as spin-orbit coupling, and their relative intensity assist in the identification of the elements in the sample. This is due to the fact that these values are characteristic and approximately constant for a core level of a given element, irrespective of the compound.

Variations in the binding energy of a core electron for an element, although small (on the order of a few electron volts eV), are still measureable and form the basis of the determination of the chemical speciation of a particular element, i.e., the bonding arrangement, type of nearest neighbors, and oxidation state. Briefly, the binding energy of an electron is determined primarily by the magnitude of the electrostatic interaction between itself and the nucleus. This interaction strength can be modulated by electrostatic shielding effects from other electrons, which in turn can depend on the removal or addition of charge brought about by chemical bonding. Removal of valence electron charge from an element (oxidation) results in an increase in binding energy; addition lowers the binding energy. This sensitivity to chemical speciation is demonstrated using the results from Dedryvère et al. (see Fig. 2), who studied various organic and inorganic decomposition products of the SEI in a CoO battery [24]. Peaks corresponding to C–C, C–O, O–C═O, and O_2C═O were clearly identified. Given quantitative information about the different carbon local environments, decomposition mechanisms that form the constituents of the SEI can be proposed.

The photoemission process that forms the basis of an XPS measurement can be deconstructed into three basic steps: (1) photon absorption and ionization, (2) atomic response with the generation of a photoelectron, and (3) transport of the ejected electron to the surface. These three steps are often labeled initial state, final state, and extrinsic state respectively. The intensity of an electron emitted at a depth d from the surface of material will be attenuated according to the Beer-Lambert Law. One can define the sampling depth as the minimum distance from the surface in which 95% of all the emitted photoelectrons are scattered. This parameter is intimately tied to the inelastic mean free path of an electron in a solid. The mean free path depends on the kinetic energy of the photoelectron and sample studied. For XPS, typical sampling depths are on the order of a few nanometers, rendering the technique most useful for thin films and surface studies. Composition-depth profiling can be performed by combining XPS with Ar^+ ion sputtering to study species away from the surface. In interpreting the results of XPS depth profiling, it is essential to consider two important factors that can affect the results: (1) the sputtering efficiency is dependent on the type of material being investigated – usually lower for stable inorganic solids and higher for organic matter, and (2) sputtering will induce surface chemical reactions and sample decomposition.

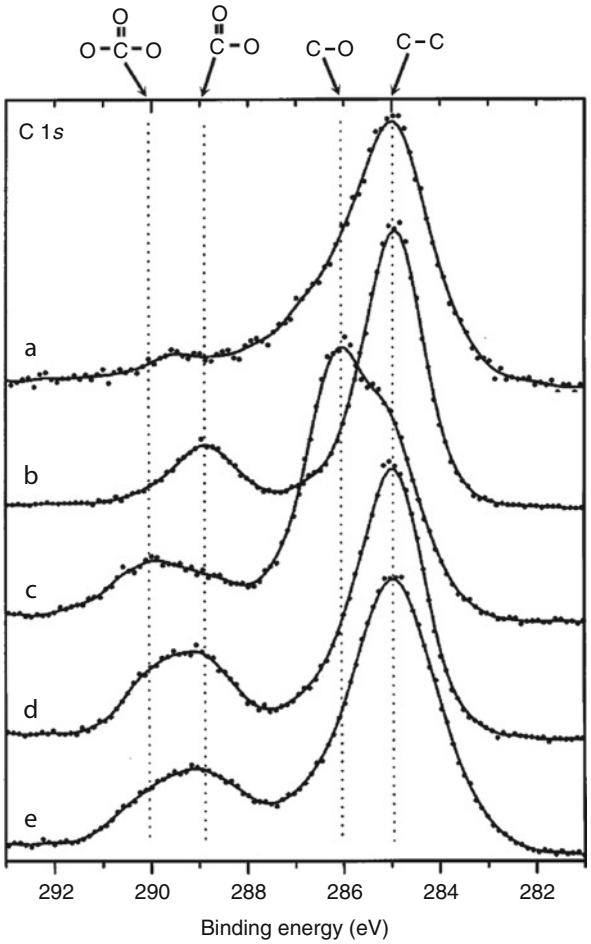

Lithium Ion Batteries, Electrochemical Reactions in. Figure 2
Carbon 1*s* XPS spectra of the first charge/discharge cycle of CoO reacting with Li in a CoO-liquid electrolyte-Li metal electrochemical cell: (**a**) starting CoO powder, (**b**) after insertion of 1 Li per mole ($x = 1$), (**c**) after total discharge at 0.02 V, (**d**) after charge at 1.8 V, and (**e**) after charge at 3.0 V, from [24]. The assignments of the peaks are shown at the *top* of the figure

Quantitative measurements of an element ($\sim \pm 10\%$) can be made by relating the intensity of a specific peak "p" for an element "i" (I_i) using the relation:

$$I_i = CN_i\sigma_i\lambda_i \tag{9}$$

where C represents a constant which captures instrumental factors related to the signal acquisition, N_i is the atomic concentration of element "i," σ_i is the photoelectron cross-section for the element "i" expressed by peak "p" (commonly referred to as the Scofield factor), and λ_i is the inelastic mean free path of a photoelectron emitted by element "i" as expressed by peak "p."

X-Ray Absorption Spectroscopy

X-ray absorption spectroscopy (XAS) is performed using synchrotron radiation sources, where the X-ray energies are tunable and the intensity is large. XAS measurements of transition metals are most often performed at convenient energy ranges, i.e., without the use of ultrahigh vacuum conditions, although a notable exception includes the study of the oxygen K-edge in a lithium cobalt oxide-based cell [25]. The technique is involves tuning the incident X-ray radiation to excite core electrons of a specific element. The primary use of this absorption spectroscopy in battery science is to determine the oxidation state of a metal and bonding configuration between the metal of interest and the nearest neighboring ions or molecules, oftentimes referred to as ligands. Bonding between metals and ligands vary in degrees of covalency, a measure of how electron density is shared among atoms.

The energy profile of a sample depends on several factors: the element, the oxidation state of the element, the specific atomic orbital in which the electron resides, as well as the geometry and strength of the bonding to ligands. Depending on the type of core electron that is excited, the energy is given a specific label, called an "edge." The principal quantum numbers, $n = 1, 2, 3$, correspond to the K-, M-, and L-edges, respectively [26].

An XAS spectrum consists of normalized absorption plotted against the incident energy of the X-ray radiation. There are three main features to the absorption plot. The most prominent feature is called the "rising edge" and corresponds to a pronounced increase in absorption arising from 1*s* to *p* electronic transitions. A second region, known as the "pre-edge," occurs at slightly lower energies with respect to the rising edge. The pre-edge features arise from weak transitions between electrons in 1*s* and *d* atomic orbitals. Spectroscopy using energies in the pre-edge and rising edge regions is often called X-ray absorption

near edge structure (XANES) or near-edge X-ray absorption fine structure (NEXAFS). The third region occurs at higher energies from the rising edge and is referred to as extended X-ray absorption fine structure (EXAFS). The EXAFS region is characterized by oscillations that arise from backscattering events that modulate the amplitude and wavelength of the ejected photoelectron from the source atom. Both the type of neighboring atoms and their distance to the source of the ejected photoelectron affect the degree of backscattering, so that bonding geometry and local coordination chemistry of the sample can be elucidated.

Given a homogeneous sample with a uniform thickness x, the absorption coefficient $\mu(E)$ can be related to the intensity of the incident (I_0) and transmitted (I) radiation using

$$\frac{I}{I_0} = e^{-\mu(E)x} \tag{10}$$

XAS can measure either transmission or fluorescence. The absorption coefficient is typically a smooth function of the energy of the radiation E, with the exception of the behavior at the absorption edge of a particular element. $\mu(E)$ can be approximated by

$$\mu(E) \approx \frac{\rho Z^4}{ME^3}, \tag{11}$$

where ρ is the density of the sample, Z is the atomic number of the element, and M is the corresponding atomic mass.

However, the true power and utility of the technique lies in the fact that the total absorption of the sample is not a simple summation of the atomic absorption coefficients, but is strongly affected by the neighboring atoms – a phenomenon particularly relevant in the EXAFS region. One can express the total absorption coefficient $\mu(E)$ as the absorption coefficient of an isolated atom $\mu_0(E)$ multiplied by a correction factor χ such that $\mu = \mu_0(1 + \chi)$. The parameter χ can be thought of as the fractional change in absorption coefficient induced by the neighboring atoms. In the single scattering approximation, Sayers et al. have introduced [27] an expression for χ – what is now known as the standard EXAFS equation:

$$\chi(k) = \sum_j \frac{N_j f_j(k) e^{-2k^2\sigma_j^2}}{kr_j^2} \sin\left[2kr_j + \delta_j(k)\right] \tag{12}$$

where k is the wave number of the photoelectron ($k = \sqrt{\frac{2m(E-E_0)}{\hbar^2}}$, E is the energy of the electron, E_0 is the absorption edge energy, m is the mass of the electron), N_j is the number of j atoms surrounding the element under investigation, r_j is the distance from the observed element to the nearest neighbors, σ_j^2 is a measure of the disorder in the distance to neighboring j atoms, $f(k)$ is the scattering amplitude of the wave and $\delta_j(k)$ is the corresponding phase shift. In essence, by simply measuring the scattered amplitude and phase shift, the number of neighboring atoms, and their distance, a measure of the atomic disorder can be estimated. Moreover, EXAFS will be sensitive to the type of neighboring element since the scattering amplitude depends on Z.

Figure 3a displays the normalized Ni K-edge absorbance spectrum of $Li_{1-x}Ni_{1/3}Co_{1/3}Mn_{1/3}O_2$ as a function of lithium content as performed by Tsai et al. [28]. Figure 3b shows the corresponding second derivative absorbance. Similar measurements can be made at the Co and Mn K-edges. The energy position of the pre-edge and absorption edge peaks of $LiNi_{1/3}Co_{1/3}Mn_{1/3}O_2$ are similar to those found in the reference compound NiO, consistent with the presence of Ni^{2+} in the pristine material. During delithiation, these peaks shift gradually to higher energies and eventually surpassing the energy position of the absorption edge of $LiNiO_2$ starting at the composition $Li_{0.15}Ni_{1/3}Co_{1/3}Mn_{1/3}O_2$, implying the existence of Ni^{4+} cations. During lithiation, these peaks shift to their original energy positions, indicating that during charging and discharging either a two-step (Ni^{2+}/Ni^{3+} followed by Ni^{3+}/Ni^{4+}) or single step (Ni^{2+}/Ni^{4+}) redox pair reaction with Ni occurs.

The authors then proceeded to analyze the corresponding EXAFS data. The k^2-weighted Fourier transformed spectra of the Ni K-edge of $Li_{1-x}Ni_{1/3}Co_{1/3}Mn_{1/3}O_2$ as a function of x is shown in Fig. 4. A total of four peaks are observed in each sample, which were ascribed to single and multiple scattering events. The first peak at ~1.5 Å is assigned to the shortest Ni-O distance in the octahedral site occupied by Ni. The second peak at ~2.5 Å describes the distance

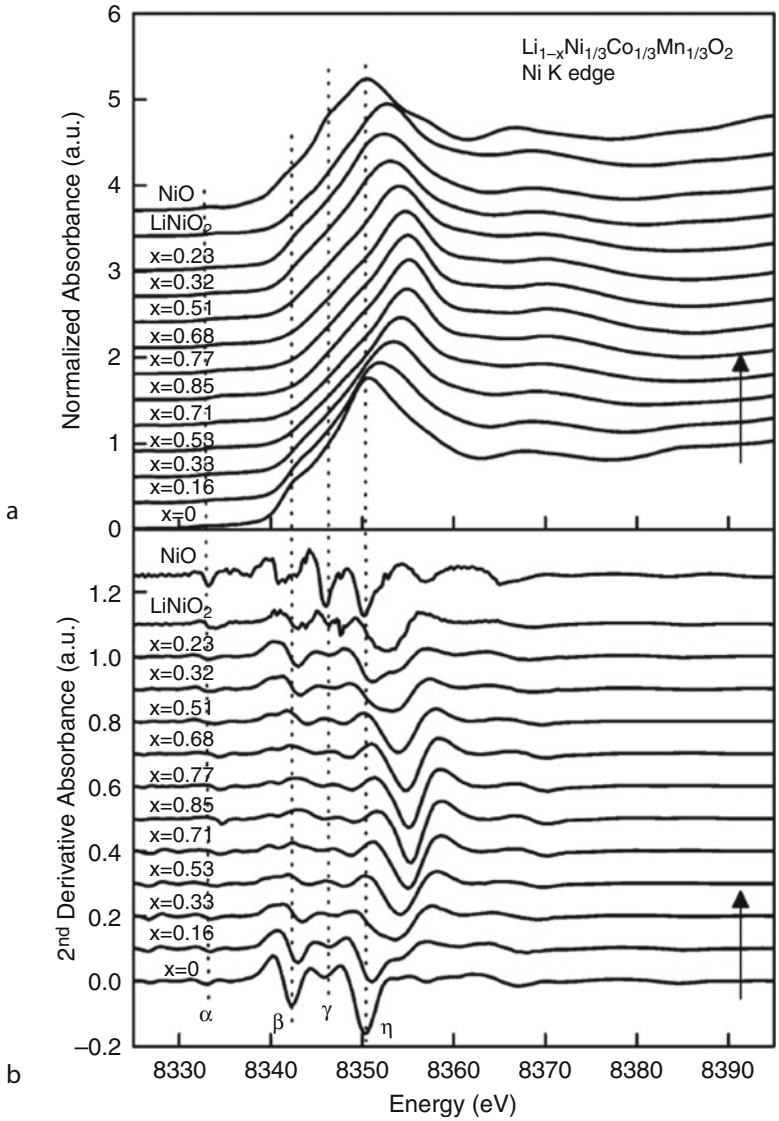

Lithium Ion Batteries, Electrochemical Reactions in. Figure 3

(**a**) Normalized in situ absorbance and (**b**) second derivative absorbance of Ni K-edge for $Li_{1-x}Ni_{1/3}Co_{1/3}Mn_{1/3}O_2$ as a function of Li content *x*. The plots for $LiNiO_2$ and NiO are also presented to provide reference spectra for Ni^{3+} and Ni^{2+} local environments respectively (From [27])

from Ni to the nearest Ni/Co/Mn in the transition metal layer. The weak peak at 4.5 Å is dominated by combined effects of six metal-metal scattering within the transition metal layer, and six metal-metal scattering from two adjacent transition metal layers. The second weak peak at ~5.3 Å is attributed to a focusing effect of 12 collinear multiple metal-metal-metal scattering events, where a second scatterer lies in between the emitting atom and another scatterer. During delithiation of the pristine material the Ni-O decreases, consistent with the electroactivity of the Ni sites. Additionally, the two-step reaction mechanism proposed earlier was also confirmed, since the trends in the experimentally determined Ni-O distances as a function of Li content could not be explained without the incorporation of Ni^{3+}. The differences in bond length are consequence of the various sizes of the Ni^{2+}, Ni^{3+}, and Ni^{4+} cations.

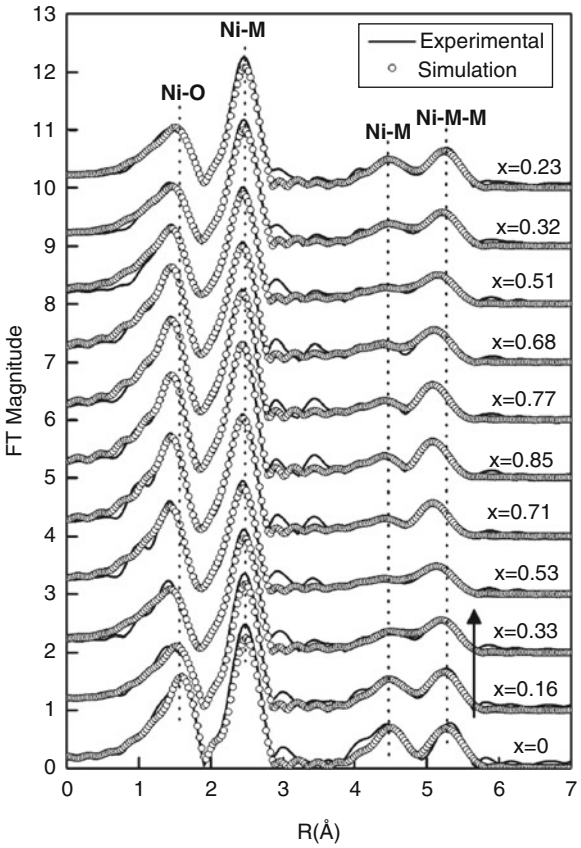

Lithium Ion Batteries, Electrochemical Reactions in.
Figure 4
In situ k^2-weighted Fourier transformed spectra of the Ni K-edge of $Li_{1-x}Ni_{1/3}Co_{1/3}Mn_{1/3}O_2$ as a function of lithium content x during the first charge and discharge cycle. The *dotted lines* correspond to various internuclear distances involving Ni atoms (From [27])

NMR Spectroscopy

Over the years, numerous materials have been investigated as potential electrodes in new generation Li-ion batteries using nuclear magnetic resonance (NMR) spectroscopy [29]. The primary nucleus of investigation for the electrode materials has been lithium. However, any nucleus possessing spin can potentially be studied, such as ^{31}P, ^{51}V, ^{13}C, ^{1}H, ^{19}F, etc. There are two spin-active isotopes of lithium which can be observed using NMR techniques – ^{6}Li and ^{7}Li. The natural abundance of ^{7}Li is approximately 92.41%, while that of ^{6}Li is 7.59%. The gyromagnetic ratio γ, in units $10^7 \mathrm{rad T^{-1} s^{-1}}$, of ^{7}Li and ^{6}Li is 10.40 and 3.94, respectively. Both nuclei are quadrupoles, with spin $I > ½$ ($I = 1$ and $I = 3/2$ for ^{6}Li and ^{7}Li, respectively), and are affected by the quadrupole interaction. The quadrupole moment of ^{7}Li is significantly larger than that of ^{6}Li. Consequently, the effects of the quadrupole interaction are more pronounced in ^{7}Li spectra. The interaction is anisotropic and produces characteristic broadening and line shapes in the static and magic angle–spinning (MAS) spectra, which reflect the local site symmetry of the lithium ion. If sample spinning speeds do not exceed the static line width of the spectra, a series of peaks, termed spinning sidebands, can be observed from the satellite transitions ($\pm\frac{3}{2} \leftrightarrow \pm\frac{1}{2}$) and to a lesser extent, the magnetic dipole broadened central transition ($+\frac{1}{2} \leftrightarrow -\frac{1}{2}$). The chemical shift range of lithium in diamagnetic compounds is relatively small, which may hinder the identification of chemically distinct sites. In contrast, the Li spectra of materials for Li-ion batteries, particularly the paramagnetic transition metal oxide cathode materials, are dominated by interactions involving the nucleus and the electronic spins.

The nucleus can interact with the unpaired electron spins of a nearby paramagnet through hyperfine interactions or with electrons in the conduction band of materials, the latter referred to as the Knight shift. These interactions can lead to significant peak broadening and shifts of the resonances. Nevertheless, these interactions contain information about the electronic structure and local environment of the Li atoms and can be theoretically used to track changes in each contribution upon cycling.

The observed NMR shift, expressed as $\Delta\omega/\omega_0$, induced by the Fermi contact hyperfine interaction in materials containing 3*d*-transition metals is proportional to the unpaired electron spin density at the nucleus site. The magnitude of the interaction is directly proportional to the Fermi constant A_c and the time-averaged electron spin $\langle S_z \rangle$ by

$$\frac{\Delta\omega}{\omega_0} = -\frac{A_c}{\omega_0 \hbar}\langle S_z \rangle \tag{13}$$

The term $\langle S_Z \rangle$ can be expressed as

$$\langle S_Z \rangle = -\frac{B_0}{\mu_0 g N_A \mu_B}\chi_M \tag{14}$$

where B_0 is the strength of the external magnetic field, χ_M is the molar susceptibility, μ_0 is the permeability of

free space, g is the g-factor of the electron, N_A is Avogadro's number, and μ_B is the Bohr magneton.

The Fermi constant is a measure of the amount of spin density that is present at the site of interest, which in this case is the Li ion. The constant also determine the direction of the shift, i.e., whether it is positive or negative. The time average of the electron spin of the paramagnetic ion is of importance since at ambient temperatures, in systems that can be studied by nuclear magnetic resonance spectroscopy, the relaxation of the electrons occurs many orders of magnitude faster than the coupling frequency A_c/h. The formalism presented is strictly true for systems where the orbital angular momentum is sufficiently suppressed so that the magnetic moments could be reasonably calculated using the "spin-only" contributions. For transition metal ions found in battery materials, this is usually a reasonable approximation. The Fermi contact shift in many materials has been found to be additive, so that the total observed shift arises from the summation of individual shift contributions induced by each paramagnetic ion. In this manner, shift scales can be created for the Li ion in different environments using the shifts of model compounds. This scale can then be used to make tentative assignments of Li spectra in battery materials. Figure 5 shows a Li shift scale for Mn-containing compounds compiled by Grey et al. [30].

The Li atoms in $LiMO_2$ (M = Co, Cr, Fe, Mn, Ni) phases, and their respective solid solutions, may interact with transition metal ions in the first and second cation coordination shells. These interactions are termed the 90° and 180° interactions, respectively, and are named according to the angle of the M–O–Li bond. In the discussion of the shift mechanisms, the labeling conventions used by Carlier et al. will be employed [31]. The $3d$ atomic orbitals of a metal in an ideal octahedral site are labeled t_{2g} and e_g. The $2p$ oxygen valence orbitals will be labeled p_σ and p_π,

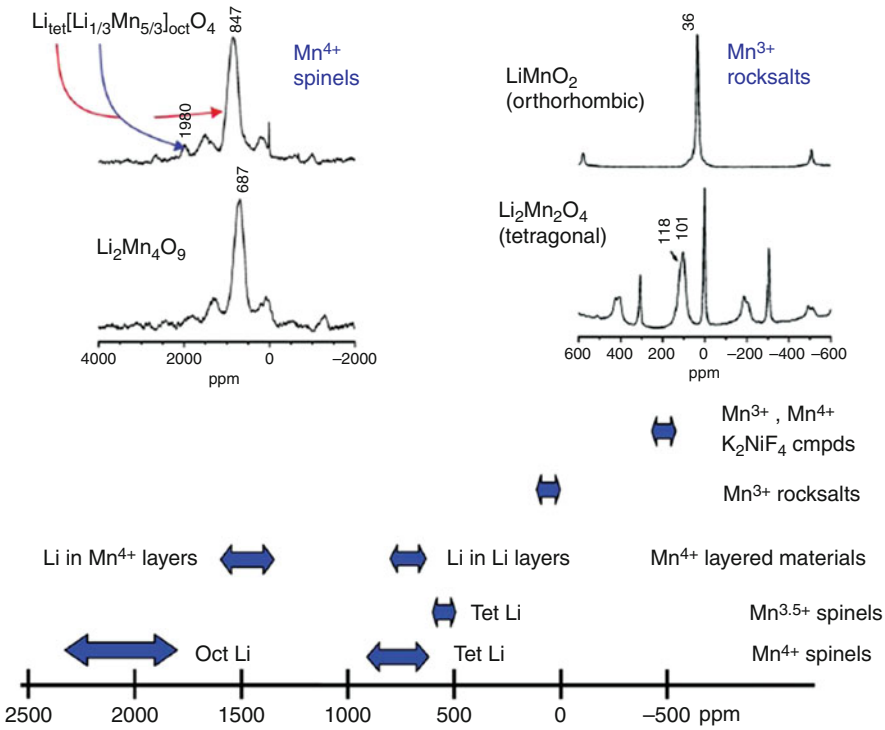

Lithium Ion Batteries, Electrochemical Reactions in. Figure 5
Lithium hyperfine shifts observed in model Mn-containing compounds for four-coordinate and six-coordinate lithium environments (From [29])

depending on the type of overlap between the oxygen and M $3d$ orbitals. If electron density is present along the O-M internuclear axis, it is labeled p_σ. If electron density lies above and below the O-M internuclear axis, the O $2p$ valence orbital is labeled p_π. The Li valence atomic orbital is labeled s. Overlap of the M e_g, O $2p$ and Li s atomic orbitals leads to a bonding and antibonding molecular orbital, e_g-p_σ-s and e_g^*-p_σ -s respectively. The bonding orbital has a large contribution from the oxygen, while the antibonding orbital has a significant contribution from the metal. The M t_{2g} atomic orbitals are nonbonding to a first approximation, though Fermi contact shifts in some materials cannot be explained without mixing of these orbitals with Li s.

The spin transfer from the metal to the Li occurs via two concurrent mechanisms – spin delocalization and spin polarization (see Fig. 6). In the spin delocalization mechanism, the Li, O, and M atomic orbitals of appropriate symmetry overlap in the lattice. Consequently, a positive spin polarization is maintained along M–O–Li, so that the spin transferred from the metal to the lithium ion is aligned with the external magnetic field. The spin polarization mechanism relies on the quantum mechanical effect known as the exchange interaction, which causes unpaired electrons in a metal orbital to polarize the electrons in the other doubly occupied $3d$ orbitals. Thus an electron with the *same* spin as the unpaired electron in a second nonequivalent transition metal orbital is present at the metal site rather than an electron with the opposite spin. Positive spin density increases on the transition metal site while negative spin density is transferred to the oxygen and lithium orbitals.

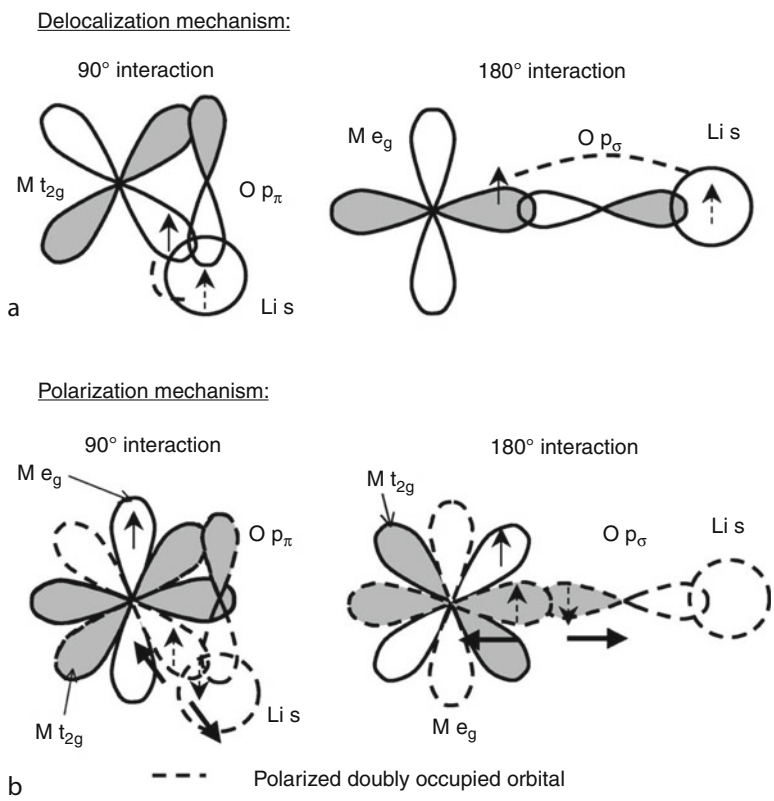

Lithium Ion Batteries, Electrochemical Reactions in. Figure 6
Schematic of the two principle mechanisms of the Fermi contact interaction governing the observed Li shifts in battery materials for both 90° and 180° geometries between the Li nucleus and the paramagnetic transition metal, from [30]. See text for details

The observed ^{6,7}Li shifts depend on the total transfer of spin density to the Li atom by these two mechanisms for every transition metal in the sample. In general, the delocalization mechanism induces larger shifts than the polarization mechanism. However, the geometry of the system must be considered since Jahn-Teller distortions of the MO_6 octahedral units remove the degeneracy of the e_g orbitals, for example, and affect the orbitals involved and the amount of spin density transferred. Since $\langle S_z \rangle$ is proportional to $B_0\chi_M$, the Fermi contact interaction and the magnetic susceptibility of a material should display the same temperature behavior. If the magnetic susceptibility of a material exhibits Curie-Weiss behavior, then it follows that the lithium shift will be inversely proportional to temperature.

The Knight shift results from the interaction of a nuclear spin with the electrons in the conduction band of the material. This shift is often much larger than the chemical shift observed in diamagnetic compounds. For the most part, the frequency shift ($\Delta\omega$) is positive, and the fractional shift, defined as $\Delta\omega/\omega_D$ (where ω_D is the frequency of the metal in a diamagnetic compound) has the following properties: (1) at different magnetic fields, $\Delta\omega/\omega_D$ is constant, (2) the fractional shift is nearly independent of temperature, and (3) the fractional shift generally increases with increasing nuclear charge. Figure 7 shows a series of static in situ ^{7}Li NMR spectra of lithium inserting into disordered carbon in an assembled battery from Letellier and co workers [32]. The initial spectrum is characterized by two peaks – an intense and relatively narrow resonance at approximately −2 ppm arising from diamagnetic lithium in the electrolyte ($LiPF_6$) and SEI, and a second broad resonance at 263 ppm arising from metallic lithium used as the anode. A series of relatively weak and broad resonances appear during cycling of the battery, corresponding to various amounts of lithium inserting into the disordered carbon. These resonances vary smoothly during the charge and discharge cycles. The shifts of the Li metal and the various Li_xC_y compounds, each of which contains varying degrees of metallic character, from the diamagnetic 0 ppm region are due to the Knight shift effects.

NMR spectroscopy is very sensitive to a wide timescale – on the order of seconds to nanoseconds.

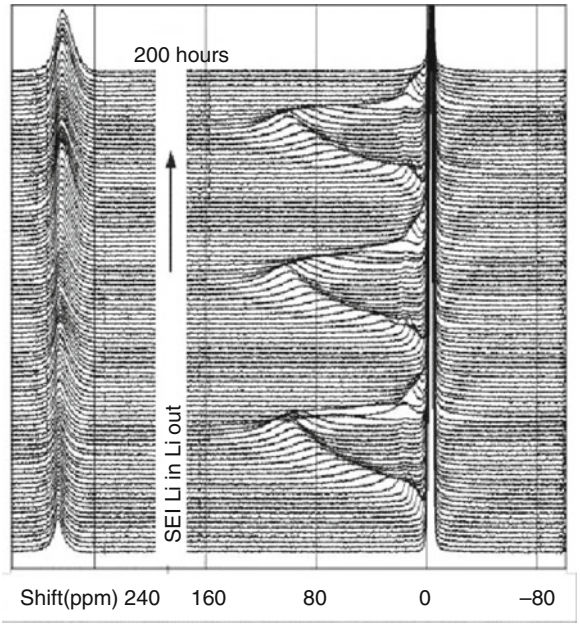

Lithium Ion Batteries, Electrochemical Reactions in. Figure 7
In situ static ^{7}Li NMR of a disordered carbon-Li metal battery cell taken over three charge and discharge cycles. Peaks at ~0 ppm and 260 ppm correspond to lithium in the electrolyte/SEI and Li metal anode respectively. Resonances in the range of 0–140 ppm are assigned to Li environments inserted into the disordered carbon (From [31])

An accurate mathematical treatment of motional averaging in NMR spectroscopy is highly dependent on the relative timescale of the motional process, with respect to the Larmor time scale (the reciprocal of the NMR frequency), since nonsecular Hamiltonian terms (i.e., those that do not commute with the Hamiltonian) are mainly responsible for relaxation. Motional processes that are faster than the Larmor timescale, such as vibrations or librations, average the spin Hamiltonians *before* the secular approximation is made. Motion that is slower than the Larmor timescale, such as rotations and translations, average the spin Hamiltonian *after* the secular approximation has been made.

After the application of a radiofrequency pulse, which manipulates the nuclear magnetization, the spins begin to preferentially align with the external,

static magnetic field, or to state it differently – the populations of spins in the different spin-states reach thermal equilibrium. Three relaxation times are typically measured: (1) the spin-lattice or longitudinal relaxation (T_1), (2) spin-spin or transverse relaxation (T_2), and (3) the relaxation in the rotating frame ($T_{1\rho}$). The rotating frame is a coordinate system which rotates about the z-axis (the direction of the static external magnetic field B_0) at the Larmor frequency of the nucleus under observation. This frame of reference is used to simplify the analysis of the trajectory of nuclear spin magnetization.

The T_1 relaxation refers to the time it takes for the z-component of the magnetization M_z to achieve an equilibrium value M_0. Two different equations could be used to extract T_1 from a series of measurements, depending on whether a saturation-recovery experiment or an inversion recovery experiment (explained in the subsequent section) is used. In the former case, the following equation is used:

$$M_z(t) = M_0\left(1 - e^{-\frac{t}{T_1}}\right) \tag{15}$$

For an inversion recovery experiment, the equation changes slightly to,

$$M_z(t) = M_0\left(1 - 2e^{-\frac{t}{T_1}}\right) \tag{16}$$

The T_2 relaxation time refers to the return of the observable, transverse (xy-plane) magnetization M_{xy} to an equilibrium value. This process could be modeled by a simple exponential

$$M_{xy}(t) = M_{xy0}e^{-\frac{t}{T_2}} \tag{17}$$

Two factors influence the loss of transverse magnetization – magnetic, molecular interactions and inhomogeneity in magnetic field. The observed decay in transverse magnetization is thus a combination of these two effects.

Both spin-lattice and spin-spin relaxation occur simultaneously, with $T_2 \leq T_1$ in the majority of cases. In heterogeneous samples, there are often multiple T_1 and T_2 relaxation times due, in part, to the presence of many local environments. $T_{1\rho}$ magnetization decay can be modeled as a single exponential much like T_2, but oftentimes, the behavior is more complex. Spin-lattice relaxation, evidenced by changes in the characteristic time T_1, occurs when motion is on the Larmor time scale. On the spectral timescale, typically on the order of μs to ms, line shapes of a spectrum are greatly affected, resulting in either line broadening or narrowing. Processes that are relatively very slow – millisecond to second timescales – do not result in line-shape changes. However, they can still be detected by observing their effect on the dynamics of longitudinal magnetization, specifically using a two-dimensional (2-D) exchange experiment [33].

To illustrate the line-shape changes occurring for motion on the spectrum timescale, a two-site symmetrical exchange will be considered. A nuclear spin is transported from site A to site B and back again at a rate k, i.e., A → B and B → A both occur at a rate k. The two sites occur with equal probability, and the exchange is fast enough so that no intermediate chemical states are considered. The two different chemical environments induce two chemical shifts. The angular chemical shift frequencies of the two sites are expressed as ω_A and ω_B for sites A and B, respectively. If the rate constant k is the same order of magnitude as the angular chemical shift frequency, i.e., $k = \omega_{diff} = \omega_A - \omega_B$, the line shapes will change drastically. Under these circumstances, the system is referred to as being in the intermediate exchange regime.

Within this intermediate exchange regime, one can define three regions – the crossover point, slow intermediate exchange, and the fast intermediate exchange regimes. The crossover point occurs when $k = |\omega_{diff}/2|$. For slow and fast intermediate exchange, $k < |\omega_{diff}/2|$ and $k > |\omega_{diff}/2|$, respectively. In the slow intermediate exchange regime, as one approaches the crossover point, motional broadening occurs. In the two-site symmetric exchange example, this would result in broadening of the two peaks along with coalescence as k increases to the crossover point. At the crossover point, a single broad resonance will be present at the average of the two chemical shifts. As k increases past the crossover point to the fast intermediate exchange regime, the line width of the single resonance is reduced – a phenomenon known as motional narrowing. Motional narrowing in this regime occurs because the spins jump so frequently between the two sites, that no significant phase difference in the transverse magnetization is accumulated as a result of the different local environments. The spin experiences

a well-defined average precession frequency, so that the coalesced peak continues to narrow [33].

In ideal cases, the temperature dependent rate constants $k(T)$ display Arrhenius behavior such that the data could be fitted with,

$$k(T) = C\exp(-E_A/(N_A k_B T)) \tag{18}$$

where C is a constant, E_A is the activation energy of the jump, N_A is Avogadro's number, k_B is Boltzmann's constant and T is temperature. For an asymmetric two site exchange, where the rates of A → B and B → A are different, similar phenomena occur, with the exception that in the fast intermediate exchange limit, the coalesced peak is positioned at the average of the chemical shift of the original two peaks, weighted by the equilibrium concentrations of the two species.

Another advantage of NMR spectroscopy is the ability to measure self-diffusion coefficients. Diffusion measurements are overwhelmingly made in the study of liquid electrolytes. The basic principle of the experiment lies in the fact that nuclear spins placed in a nonuniform magnetic field will experience different local fields depending on their spatial location. Differences in the strength of local magnetic fields will induce slightly different procession frequencies of the nuclear spin under investigation.

When a simple Hahn-echo pulse sequence is applied to the sample in a non-uniform magnetic field, the presence of motion can be inferred by the echo signal intensity taken as a function of a delay. If a spin has not diffused, it will have a constant precession frequency so that at the end of the dephasing period 2τ, the spin magnetization is said to have been completely refocused. If a spin moves along a magnetic field gradient the precession frequency will change, resulting in an attenuated echo intensity at 2τ. By performing a series of experiments where τ is varied, the reduced intensity of the resonance could be used to calculate the diffusion coefficient of the nucleus using the equation [34],

$$M(2\tau) = M_0 e^{\frac{2\tau}{T_2}} e^{-\frac{2}{3}\left(\gamma\frac{\delta H}{\delta Z}\right)^2 D\tau^3} \tag{19}$$

where M_0 is some initial magnetization, T_2 is the spin-spin relaxation time, γ is the gyromagnetic ratio of the nucleus under investigation, $(\delta H/\delta Z)$ is the magnetic field gradient, and D is the diffusion coefficient. In the limit where $\tau << T_2$, the reduction of the echo signal intensity is dominated by the diffusion process. In samples with short T_2 values, it is difficult to separate the effects of spin-spin relaxation and diffusion in the attenuation of the echo signal.

These spin-echo experiments are most commonly performed using pulse field gradients, introduced by Stejskal and Tanner [35], or using the so-called "static fringe-field method" [36, 37]. In general, T_2 times greater than 2 ms for each species is required to perform the diffusion measurements and extract precise diffusion coefficients. Pulse-field gradient spin-echo methods require special amplifiers which control the strength, duration, and time interval between gradient pulses. The gradients that can be implemented typically range from 10 to 70 mT/cm. In this experiment, the delay between the Hahn-echo pulses is kept constant, so that the contribution of T_2 relaxation on the attenuation of the echo signal intensity is constant. Since the experiment is performed in the "sweet spot" of the magnet, where the magnetic field is the most homogenous, the spectral resolution is relatively high. The fringe-field method requires the probe to be positioned outside of the sweet spot of the magnet, where large static magnetic field gradients are present – typically greater than 100 mT/cm. The relatively large gradients allow relatively small diffusion coefficients to be measured, usually less than 10^{-12} m^2/s. Unfortunately, the line widths of the resonances are significantly large due to inhomogenous line broadening. Consequently, the sensitivity and resolution decreases. Additionally, the T_2 of the chemical species must be measured independently in a uniform magnetic field.

Conductivity and ionic diffusion could be related using the modified Nernst-Einstein equation

$$\sigma_{calc} = \frac{Nq^2(D_{Li} + D_{an})\alpha}{kT} \tag{20}$$

where σ_{calc} is the calculated ionic conductivity, N is the number of ions per unit volume, q is the charge of the ions, D_{Li} and D_{an} are the diffusion coefficients of the lithium ion and anion respectively, a is the degree of dissociation, k is Boltzmann's constant, and T is temperature. In many instances, the calculated conductivities using the measured diffusion coefficients from pulse-field gradient NMR are much higher than values measured directly [38–43]. The discrepancy could arise

from the differences in the migration distance probed using the two different techniques. Moreover, electrical conductivity detects the motion of charged ions, without discrimination of element or sign of the charge. Diffusion coefficients contain contributions from ions in both charge-neutral and dissociated species of a particular probe nucleus.

The measurement of diffusion coefficients is particularly important in polymer electrolyte research. One of the desired properties of a potential electrolyte material is the selective mobility of the Li^+ cation. Numerous strategies have been implemented to attain this property [1, 44, 45]. One method of quantifying the selective mobility is the calculation of transference numbers, which is the fraction of the total electric current that the anions and cations carry while passing through an electrolyte. Using the notation of Kalita et al. [46], the transference number for lithium, t^+, could be expressed as,

$$t^+ = \frac{D^+}{D^+ + D^-} \tag{21}$$

where D^+ and D^- are the cations and anion diffusion coefficients respectively. As implied above, determining the transference number for free Li^+ is not straightforward using NMR or electrical conductivity measurements.

Computational Methods

Computational methods have advanced significantly over the past few years, allowing for the accurate prediction and explanation of various properties of materials relevant to the battery field, including lithium and electron mobilities [47–49], voltage profiles [50–53], average insertion potentials [50, 54–58], and phase stabilities [59–61], using first-principles calculations. A few methods are available for first-principles calculations of electronic structure – Hartree-Fock, Møller-Plesset Perturbation theory, highly correlated methods, and density functional theory. Typical basis sets used for these calculations include Slater-type functions ($Y_l^m \mathrm{r}^{n-1} \exp(-\xi r/\mathrm{a}_0)$), Gaussian-type functions ($Y_l^m \exp(-(\alpha r)^2)$), or plane waves ($\exp(ig \cdot r)$), where Y_l^m denotes the spherical harmonics and r is the radial distance of the electron from the nucleus. The formalism within which many of these calculations are conducted in condensed matter is typically density functional theory (DFT), using plane waves and pseudopotentials. The intricate details of the theory are beyond the scope of this article. For the purposes of this discussion, it is sufficient to understand DFT as a reformulation of many-body quantum mechanics in terms of the probability density rather than the wave function. Specifically, it is used to investigate the electronic structure of condensed phases using functionals, i.e., functions of another function. The primary challenge in DFT is the expression of functionals to accurately describe the exchange and correlation energies of electrons. Approximations that have yielded accurate molecular geometries and ground-state energies include the generalized gradient approximation (GGA) method [62]. Pseudopotentials, which serve as approximate, effective potential functions to deal with the core electrons of an atom, that have been successful in the calculations of battery materials have been generated from the so-called projector-augmented-wave (PAW) method [63, 64] as utilized from the software package Vienna Ab initio Simulation Package (VASP) [65].

Survey of Experimental Results and Their Interpretation

The following section will summarize additional examples in recent literature which made use of at least one of the experimental techniques outlined above. Clearly, the body of work available in the field cannot be adequately summarized in a single section. Examples will be grouped by the major components of a Li-ion battery – the electrolyte, SEI, cathode, and anode materials. These particular experiments were selected not only to demonstrate how each technique can provide unique information about the structure of a material but also to emphasize the necessity of utilizing multiple techniques to refine a structural model or determine a chemical reaction pathway.

SEI

XPS has been used extensively to study the composition of the SEI and decomposition products of the electrolyte on electrode surfaces. In the overwhelming majority of cases, the binding energy of the C 1*s*

photoelectron peak position is used to identify various carbon-containing decomposition products. Among the most prevalent species to be identified in the SEI are lithium carbonates – $Li_2\mathbf{C}O_3$, $RO\mathbf{C}O_2Li$, and carbonyl carbons (**C**=O) [66]. There have been a few studies using the O 1*s* and F 1*s* positions to identify LiF [67] and ether linkages [68]. The choice of electrolytes and lithium salts has a profound effect on the decomposition products [69]. Ethylene carbonate electrolytes are rich in $(CH_2OCO_2Li)_2$. XPS has been vital in determining the decomposition rate of electrolytes containing various additives [70] and as a function of temperature [71, 72]. Traces of Li_2O and LiOH were observed in a few instances, but could be the result of side reactions caused by Ar+ sputtering or trace amounts of water [66].

Components of the SEI were also investigated using NMR techniques [73]. ^{7}Li studies, while able to distinguish between lithium atoms in the SEI and those in paramagnetic transition metal compounds using the shift of the resonance, does not provide a lot of information regarding the different types of diamagnetic Li environments. This is because the shift range for Li^+ in salts and other compounds present in the solid electrolyte interphase is small and typically around 0 ppm. Nevertheless, Dupré et al. have used ^{7}Li MAS NMR to characterize interphase layers on electrodes as a function of aging [74–76] mostly using relaxation measurements and line-shape analyses. Leifer et al. have used ^{13}C MAS NMR to characterize electrolyte breakdown products using batteries composed of C-13-enriched carbonates stored at various temperatures [77]. Carbon NMR has a larger chemical shift range, relative to Li, rendering the nucleus more sensitive to changes in bonding or chemical speciation. The carbonates used in the study (a mixture of ethylene carbonate and diethyl carbonate) were selectively enriched in the carbonyl carbon position. By incorporating only one enriched carbonate at a time in the electrolyte mixture, the authors were able to identify the source of specific decompositions products. Strong signals emanating from this carbon site on SEI residing on the anode surface demonstrated that the formation of CO_2 is not a unique breakdown product for the carbonyl groups. The results suggested the formation of a new set of electrolyte breakdown products, including acetals, orthocarbonates, orthoesters, and fluorine-containing alkoxy compounds (from reaction with the breakdown products of the $LiPF_6$ salt used in the electrolyte).

Electrolytes

Carbonate-containing liquid electrolytes are primarily chosen for their ability to dissolve lithium salts and their relatively low viscosity (which facilitates Li-ion diffusion between electrodes). Their flammability has in part led to interest in the use of room-temperature ionic liquids (ILs) as replacements. ILs can potentially operate in a higher voltage window relative to carbonates and also have the added benefit of being more thermally stable and having low vapor pressure. The main drawback of this class of compounds is a high viscosity. Additionally, carbonates may have to be introduced at certain voltages to form a suitable SEI for operation.

Fernicola et al. have synthesized and characterized *N*-butyl-*N*-ethylpiperidinium *N*,*N*-bis (trifluoromethane)sulfonimide (PP_{24}TFSI) IL [78]. A lithium bis(trifluoromethane)sulfonimide (Li-TFSI) salt was dissolved in the ionic liquid and was introduced to a polymer matrix. The dynamics of ^{1}H, ^{19}F, and ^{7}Li, as well as the transport properties of the mobile species in neat PP_{24}TFSI, Li-TFSI mixed with PP_{24}TFSI, and Li-TFSI-PP_{24}TFSI mixed in a polymer membrane were studied using NMR. Spin-lattice relaxation measurements as a function of temperature probed short-range motion on small time scales, while diffusion measurements probed long-range motion on a larger time scale. Comparison of the Arrhenius plots of the ^{1}H spin-lattice relaxation time across the sample series indicates an increase in restrictive motion from the neat ionic liquid to the salt mixture and to the mixture in the membrane. This trend is due to the inherent high viscosity of the ionic liquid and IL-membrane interactions. The T_1 minimums shift toward higher temperatures for the Li-TFSI and membrane samples, reaffirming the dramatic change in the dynamics of the systems. Similar trends were observed for ^{19}F and ^{7}Li across the sample series (the ^{19}F relaxation times were assumed to be above the T_1 minimum). The dynamics of the membrane were well described with single relaxation processes, indicating that all the IL was subject to interactions

with the membrane. Diffusion data were consistent with the previous spin-lattice relaxation measurements. The diffusivity of the PP_{24} and TFSI ions was comparable in all samples. The Li diffusivity in the salt mixture was lower than both the PP_{24} and TFSI ions, owing to a relatively stronger electrostatic interaction between Li^+ and TFSI. However, the TFSI/Li self-diffusion coefficient ratios decreased from 2 to approximately 1, going from the salt mixture to the membrane, resulting in a much higher Li transference number in the matrix. This increase in Li transference number is highly desirable in battery applications.

NMR spectroscopy has also been used extensively to study various electrolytes. Challenges and strategies for successful electrolytes have been previously described in literature [1, 17, 79, 80]. In a few instances, these materials consist of solid polymers [17], which are typically of high molecular weight or cross-linked, gel electrolytes, or composite materials containing additives [81–85]. In recent years, nanoscopic additives have gained recent attention [86–88]. A significant contribution of NMR spectroscopy to the polymer electrolyte community arose from line-width measurements of various resonances as a function of temperature [89–92]. The results showed a correlation between ionic conduction and the degree of mobility of the polymer chains. Moreover, the studies demonstrated that ion conduction predominately occurs in the amorphous phase of the electrolyte at temperatures above the glass transition temperature T_g. The proposition of this "segmental motion-assisted transport mechanism" in the amorphous phase has become broadly accepted among the community.

Lithium transport has also been studied in mechanically [93] or magnetically [94] oriented polymers. An analysis of angular dependent line widths in the static NMR spectra of these materials has shown that the induced reordering of the polymers along the stretching direction affects the ordering of the lithium cations. Additionally, lithium diffusion coefficients were shown to increase along the stretched axis [95]. As mentioned previously, lithium transport generally occurs more readily in amorphous polymer phases. This amorphous transport mechanism, mediated through the motion of the polymer chains, is in sharp contrast to the early model of ion transport in polyethylene oxide which asserted that the cations moved through ordered helical channels throughout the material [96]. The faster diffusion in the oriented samples is not unprecedented however. Gadjourova et al. have shown that for certain compositions of polyethylene electrolyte, the more crystalline phase has a higher conductivity above T_g [97]. Though amorphous phase transport is the dominant transport mechanism in randomly oriented polymer chains, the mechanism of conduction in well-ordered, aligned helices may depend on contributions from many other factors, warranting further basic research and a reexamination of previous models.

Cathode Materials

Olivines and their solid solutions have generated considerable interest as replacement cathode materials [98–100]. In particular, $LiFePO_4$ shows great promise as a low-cost, non-toxic alternative to ubiquitous $LiCoO_2$. Aside from facilitating lithium conduction by "opening up" the framework, substituting a XO_4^{n-} anion for an oxygen allows the redox couple to be tuned using the so-called "inductive effect." [101] Tucker et al. have used ^{7}Li MAS NMR at low field to study the nature of the hyperfine fields in pristine polycrystalline $LiMPO_4$ (M = Fe, Co, Ni, Mn) [102]. The temperature dependence of the inverse magnetic susceptibility was determined for all samples using a SQUID magnetometer. All lithium metal phosphates displayed Curie-Weiss behavior. The susceptibility data was fitted using a linear equation to extract Weiss constants and effective magnetic moments. Temperature-dependent NMR measurements revealed isotropic shifts closely following the Curie-Weiss trend of bulk susceptibility for all compositions, confirming the hyperfine coupling between the ^{7}Li nuclei and the paramagnetic transition metals in these materials. Due to the lowering of symmetry of the MO_6 octahedra from O_h to C_s in these materials [100], the d-orbitals of the transition metals split to two sets – one set of three orbitals at relatively higher energy and another for the remaining two. Assuming a high-spin electron configuration for the materials, the shift contribution for all unpaired electrons in both sets of orbitals was estimated. At 37°C, the unpaired electrons in the orbitals at a higher relative energy contribute approximately −24 to −28 ppm to the total shift.

The unpaired electrons in the set containing the remaining two orbitals contribute 70–79 ppm to the shift. The hyperfine coupling constants for each sample were estimated and showed considerable variation with the type of transition metal. Additionally, the constants were of much smaller magnitude than those measured in lithium manganese oxide spinels [103]. These observations were explained on the basis of the longer *M*–O bonds in Li*M*PO_4 and the polarization of the oxygen electrons to the phosphate structural unit, both of which reduce the degree of covalency of the *M*–O bond. Wilcke et al. have reported variable temperature ^{31}P MAS NMR of the Li*M*PO_4 series along with ^{7}Li MAS NMR data of $LiFe_{1-x}Mn_xPO_4$, where $0 \leq x \leq 1$, using fast sample spinning rates and low static magnetic fields [104]. The ^{31}P shifts were much larger than the corresponding ^{7}Li shifts, demonstrating an increased sensitivity to the P-O-*M* bond covalency which may ultimately be correlated with the degree of Jahn-Teller distortions present in the material, electrochemical performance, and mechanisms that lead to failure.

Leifer et al. [105]. used ^{7}Li MAS NMR to study the structure of lithiated silver vanadium oxide, $Li_xAg_2V_4O_{11}$, where x = 0.72, 2.13, and 5.59. This compound is used in biomedical applications as a primary battery, particularly as the power source for implantable cardiac defibrillators (ICDs). Silver vanadium oxide is a vanadium bronze with semiconducting properties. It has been used successfully as a cathode material in the battery of ICDs due to its high rate capability and its high theoretical capacity (315 mAh/g) to 2 V. Electrochemical and structural studies of the average structure were performed by various authors who concluded that the systems undergoes a multistep reduction mechanism and forms silver metal in the early stage of the overall reaction [106–108].

At least three isotropic resonances were identified, two at approximately −1.5 ppm and −4.4 ppm for all samples studied and a third resonance present at −14 ppm in $Li_{0.72}Ag_2V_4O_{11}$ and $Li_{2.13}Ag_2V_4O_{11}$, which shifts to −54 ppm for $Li_{5.59}Ag_2V_4O_{11}$. Many of the spectral features observed were consistent with previously reported Li spectra of lithiated vanadium oxide materials [109–112]. The three plateaus in the electrochemical profile at 3.2, 2.7, and 2.4 V have been attributed to Ag reduction (3.2 V) and V reduction (2.7 V and 2.4 V) [107, 113]. The inserted Li ions reduce and displace the Ag^+ in the oxygen layers of $Li_xAg_2V_4O_{11}$ [114]. The peak at −1.5 ppm was assigned to Li in the solid electrolyte interphase and lithium salts LiF and Li_2CO_3, with the exception of Li_2O, which would have resonated at 2.8 ppm. The resonance at −4 ppm was assigned to Li in octahedral sites, some of which were occupied by Ag. The lack of shift upon lithiation of this resonance is consistent with the assignment, since the octahedral sites are further away from the vanadium ions and would therefore be least affected by changes in V oxidation state. The peak at −14 ppm was assigned to Li ions in tetrahedral sites near the V atoms as found in $\varepsilon - Li_xV_2O_5$ [115]. The broadening and concomitant shift of this resonance was attributed to the formation of V^{4+} or V^{3+} upon lithiation, whose presence is consistent with previous literature [109, 116, 117]. The profound broadening of the resonance is thus attributed to the paramagnetic vanadium ions [118] and shorter Li-V distances in the material that are a consequence of a collapse in the structure after the displacement of silver during discharge. The lithium shifts that occur at high lithiation levels are also consistent with the reduction of the silver prior to reduction of the vanadium. A line shape analysis of the vanadium spectrum from ^{51}V NMR showed that the crystallinity of the materials decreased steadily as they were lithiated. The $Li_{0.72}Ag_2V_4O_{11}$ had features that were close to the pristine material, implying a simple displacement of the Ag atoms with Li, while preserving the structural integrity and order. The spectral broadening and the loss of definition in the line-shape discontinuities were the most profound in $Li_{2.13}Ag_2V_4O_{11}$ and $Li_{5.59}Ag_2V_4O_{11}$.

XAS and XANES measurements at the Ag K-edge confirmed phase segregation of metallic silver from the SVO structure with an increase in lithium content. The XANES data, normalized to a per atom basis, of silver foil, SVO, and lithiated SVO displayed isosbestic points. This demonstrates that the SVO and Ag are related linearly by stoichiometry. In contrast, the normalized XANES data at the vanadium K-edge of SVO and $Li_{5.59}Ag_2V_4O_{11}$ did not display any isosbestic points, implying no linear stoichiometric relationship between vanadium and lithium between the two samples during lithiation. Shifts in the V pre-edge features of the XANES

spectra of samples were consistent with the change in vanadium oxidation state from +5 to +3. Given the full-width half-maximum of the pre-edge peak in the samples, the authors postulated that vanadium could exist in multiple oxidation states, including V^{4+}.

Yamakawa et al. has recently implemented ^{7}Li MAS NMR to study conversion reactions of binary copper-II compounds (CuO, CuF_2, CuS) [119] and iron fluoride [120]. The results of the binary copper compounds will be summarized first. Prior to this work, two separate mechanisms were proposed for the conversion reaction of CuS by Chung et al. [121]. and Debart et al. [122]. The former reaction mechanism proceeded via a two step process. The first is an insertion reaction to form Li_xCuS, which reacts with Li to produce Li_2S and $Cu_{1.96}S$. The second process involves the subsequent conversion of $Cu_{1.96}S$ to Li_2S and copper metal. Debart et al. proposed that Cu_2S is produced as an intermediate phase, before reacting to produce Cu metal and Li_2S. Possible discharge reaction mechanisms for the CuO system have been proposed by various authors, primarily through the analysis of X-ray diffraction data [123, 124].

Based largely on the Li NMR results of Yamakawa et al., in combination with diffraction and electrochemical analysis, the following reaction mechanisms were proposed for the binary copper compounds. In the CuF_2 system, a simple single-step conversion reaction of the form

$$CuF_2 + 2Li^+ + 2e^- \rightarrow Cu + 2LiF, \tag{22}$$

takes place. In CuO, the following reaction could be written based on the preliminary Li NMR studies:

$$CuO + xLi \rightarrow Li_xCuO \tag{23}$$

The CuS system undergoes more complicated processes. In the first step, the reactions

$$xLi + CuS \rightarrow Li_xCuS \qquad (0 < x \leq 0.16) \tag{24}$$

$$Li_xCuS + (y - x)Li \rightarrow Li_yCuS \qquad (y \sim 1) \tag{25}$$

The second process involves the decomposition of the Li_yCuS phase via

$$(1-z)\left(Li_yCuS + Li^+ + e^- \rightarrow \frac{1+y}{2}Li_2S + Cu\right)(y \sim 1) \tag{26}$$

and the concurrent disproportionation reaction

$$z\left(Li_yCuS \rightarrow 0.5Cu_{1.96}S + 0.02Cu + \frac{y}{2}Li_2S\right) \tag{27}$$

Upon charging, assuming $z \sim 3$ and the Li content extracted from the electrochemical data, the reaction could be written as follows:

$$0.85Li_2S + 0.76Cu + 0.15Cu_{1.96}S \rightarrow Li_y, CuS \rightarrow Li_{0.35}CuS + 1.35Li \tag{28}$$

Electrochemical activity of iron-III fluoride (FeF_3) was first reported by Arai et al. [125]. The compound has theoretical capacity of approximately 200 mAh/g in the 4.5–2.5 V region and 400 mAh/g in the 2.5–1.5 V region. Li et al. [12] and Amatucci and co-workers [13, 14, 126] have since proposed reaction mechanisms for the higher and lower voltage windows:

$$FeF_3 + Li \rightarrow LiFeF_3, \tag{29}$$

for the 4.5–2.5 V region and

$$LiFeF_3 + 2Li \rightarrow Fe + 3LiF, \tag{30}$$

for the 2.5–1.5 V region. In the higher voltage region lithium is inserted into FeF_3 in a two-phase reaction to form $Li_{0.5}FeF_3$ and then through a single-phase reaction to form $LiFeF_3$. Badway et al. have proposed that during the conversion reaction the iron metal and lithium fluoride react to form a, "rutile-like FeF_2" structure [14]. Doe et al. have performed first-principles calculations suggesting that intermediate phases could form during the electrochemical process [127].

The ^{7}Li MAS NMR spectra of lithiated FeF_3 samples, taken at cutoff voltages between 3.3 and 1.7 V, display two resonances at approximately 0 ppm and another between 104 and 172 ppm. The resonance at higher frequencies is relatively broader than the peak at 0 ppm. The larger shifts were attributed primarily to the Fermi contact interaction between the Li nuclear spins and the unpaired Fe electrons, which occur via the Li-F-$Fe^{3+/2+}$ bonds. The larger line width of these peaks is attributed to the through-bond and through-space interactions between the ^{7}Li nuclei and rapidly fluctuating electronic dipole moments of the iron, which efficiently relaxes the nuclei and consequently reduces T_1 and T_2. Previous ^{6,7}Li NMR spectroscopy

performed by Grey and co-workers on lithium iron oxides showed that typical shifts for lithium were between 280 and 520 ppm [128, 129]. The smaller shifts observed in the iron fluoride systems was attributed to the presence of Fe^{3+} and Fe^{2+} coordinated to Li and the decreased covalency of the Fe-F bond relative to the Fe-O bond.

The samples arrested at 3.3 and 3.0 V both display a peak at 172 ppm, whose intensity increases with lithium content. The constant shift is indicative of an average Fe oxidation state around the Li coordination environment that remains unchanged. These results are consistent with the proposed two-phase region involving a Li_yFeF_3 ($y \sim 0.5$) phase and an unlithiated FeF_3 phase. The peak at 172 ppm gradually shifts to lower frequency between Li = 0.5 and 0.75, corresponding to voltages of 3.0 and 2.5 V respectively. This observation is in agreement with a solid solution reaction in which Li is inserted to the $Li_{0.5}FeF_3$ phase and a reduction from Fe^{3+} to Fe^{2+} occurs. The resonance does not increase in intensity but noticeably broadens into the baseline at Li = 1.0 (1.7 V), which is ascribed to very fast nuclear relaxation due to the presence of high-spin Fe^{2+} ions.

The ^{7}Li MAS NMR spectra of samples with Li = 1.0–3.0 display a single resonance at 0 ppm with spinning sidebands spanning over 5,000 ppm. Upon discharge, the width of the signal manifold increases as does the broadening of each individual peak. These observations are consistent with the formation of iron nanoparticles. Due to the relative ease of the measurement, it was rationalized that the nano-sized iron metal was not ferromagnetic but superparamagnetic. Liao et al. have shown that particles less than or equal to 6.6 nm display superparamagnetic properties [130].

^{6}Li MAS NMR was performed on the same sample set and revealed a second resonance for the Li = 1.7 sample, at approximately 86 ppm. This peak was assigned to Li in an insertion phase with a higher Fe^{2+}/Fe^{3+} ratio. An additional resonance at 104 ppm was observed in the ^{6}Li spectrum of the Li = 1.0 sample. The relative intensity of the 86 ppm peak was smaller than the 104 ppm peak of the other samples presumably due to the onset of the conversion reaction. Upon charging, the ^{6}Li MAS NMR spectra of Li = 0.5–3.0 revealed resonances in similar positions as the discharged samples, i.e., peaks at 0 ppm and between 80 and 168 ppm, with a gradual shift from 80 to 168 ppm for the Li = 2.0–0.5 samples. The similarity in the peak positions of the charged and discharged samples imply that the Li ions return to very similar local environments and that Fe^{2+} and Fe^{3+} are both present at the end of the charge, having an average iron valence state of $Fe^{2.5+}$. Moreover, the total width of the sideband manifold for the 0 ppm resonance decreases, suggesting that the concentration of superparamagnetic Fe decreases upon charging.

A study by Bréger et al. on $LiNi_{0.5}Mn_{0.5}O_2$, employing X-ray and neutron PDF analysis in conjunction with Li NMR serves as an ideal illustration of employing complementary techniques to obtain clear structural constraints and generate a detailed model of the material [131]. In order to determine the local environment of each transition metal independently, three samples were prepared for neutron diffraction measurements: $^6LiNi_{0.5}Mn_{0.5}O_2$, $^7LiNi_{0.5}Mn_{0.5}O_2$ and $^7Li^{ZERO}Ni_{0.5}Mn_{0.5}O_2$, corresponding to a Li-6-enriched, Li-7-enriched, and a Li-7-enriched sample containing appropriate amounts of ^{62}Ni to natural abundance nickel in order to produce null scattering from the element, referred to as $^7Li^{ZERO}$. The PDF data revealed distributions in the metal-oxygen bond lengths arising from local distortions which were not captured from the average $LiCoO_2$ structure. The PDF data also took into account the superstructure reflections, arising from the non-random distribution of transition metals in the layers, in the scattering data that could not be indexed (labeled) using the $LiCoO_2$ structural model in Rietveld refinements. NMR results and RMC calculations provided further evidence that the cations were non-randomly distributed in the transition metal layers (see Fig. 8). On average, Ni atoms are surrounded by more Mn atoms in the first cation coordination shell (nearest transition metal neighbors) and by Li and Ni atoms in the second coordination shell (next nearest transition metal neighbors). Manganese atoms tend to be surrounded by Li and Ni in the first coordination shell and by other Mn atoms in the second coordination shell. The raw data can be compared to different transition metal–ordering schemes proposed from first-principles calculations, transmission electron microscopy, and previous NMR results [132–135]. The two-ordering schemes proposed were the so-called honeycomb and flower arrangements.

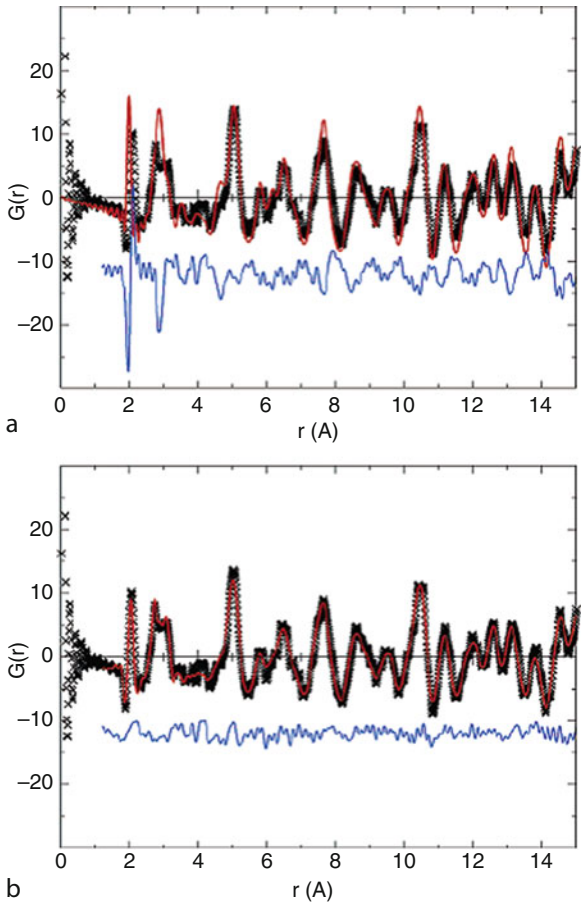

Lithium Ion Batteries, Electrochemical Reactions in.
Figure 8
Neutron PDF data of $^{7}LiNi_{0.5}Mn_{0.5}O_2$ that was fitted (**a**) using an ideal $LiCoO_2$ structural model where the Ni, Mn, and Li atoms are randomly distributed in the transition metal layers and (**b**) after a series of Reverse Monte Carlo (RMC) calculations which accounted for cation ordering. The raw data is shown in *black*, the fit in *red*, and the difference between the two in *blue* (From [131])

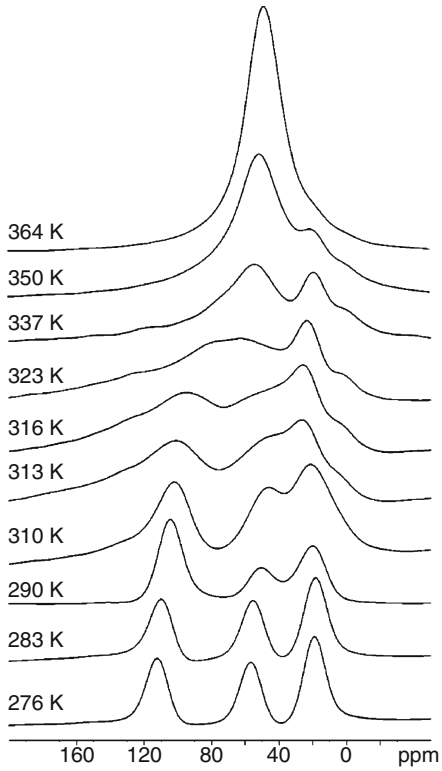

Lithium Ion Batteries, Electrochemical Reactions in.
Figure 9
Variable temperature ^{7}Li MAS NMR spectra of $Li_3V_2(PO_4)_3$ displaying the temperature dependence of the shift and the coalescence of the various lithium environments due to exchange, from [136]. The resonance around 0 ppm is due to a diamagnetic impurity

While the numbers of metal-metal contacts extracted from the experimental data show that a completely random distribution of the transition metals is a poor structural model, it was difficult to distinguish between the flower and honeycomb ordering schemes.

Cahill et al. have used variable temperature ^{7}Li MAS NMR spectroscopy to study the lithium dynamics of monoclinic $Li_3V_2(PO_4)_3$ [136]. The three lithium sites at 103, 52, and 17 ppm (labeled Li3, Li2, and Li1 respectively) are clearly resolved and unambiguously assigned at a sample spinning speed of 25 kHz and a magnetic field strength of 7 T. The relative intensity of the peaks, including contributions from the respective side-band intensities was 1:1:1, as predicted from the crystal structure. One-dimensional ^{7}Li MAS NMR spectra taken from 276 to 364 K (see Fig. 9) display a linear shift dependence with respect to temperature indicative of Curie-Weiss behavior. The electronic insulating nature of the materials as well as the aforementioned Curie-Weiss behavior as a function of temperature confirmed that the origin of the lithium shifts is due to hyperfine interactions. Additionally, the resonances begin to coalesce as the temperature is increased. This implies the hopping of Li atoms between different sites in the crystal lattice. According to the data, Li1 and Li2 begin exchanging first at relatively lower

temperatures. Based on the separation of the peaks before coalescence at 316 K, an estimation of approximately 6.5 kHz (corresponding to a correlation time τ_c of 154 μs) was determined as the lithium hopping rate between the two crystallographic sites. By 364 K, all three Li resonances have coalesced, implying that all lithium atoms are exchanging between the three sites.

Through an analysis of 2D Exchange spectra of the sample as a function of temperature, the authors were able to extract activation energies for lithium conduction between Li1-Li2, Li2-Li3, and Li1-Li3 sites. The activation energies extracted from the NMR measurements can be correlated with structural factors which could affect Li-ion mobility, such as the internuclear distance between the Li sites and bottlenecks in the conduction pathway. The activation energy of the hopping between two Li sites increased when the internuclear distance between Li sites increased and when the distance of the shortest Li-O contact decreased. The lithium ions in $Li_3V_2(PO_4)_3$ can be visualized as existing on sheets along the crystallographic ac plane. The implication of these NMR results is that conduction primarily occurs in one dimension, in a straight line across different Li sites using a series of oxygen atoms along the channel to facilitate the transport. These quantitative measurements are invaluable for rationalizing conduction mechanisms in these materials and understanding transport properties along at small length scales.

Anode Materials

Lithiated graphite has been one of the most widely investigated anode materials [137–139]. The first reported study of lithium intercalated into graphite was by Conard and Estrade [140]. The insertion results in changes in the electronic properties which can be monitored by the Knight shift of the intercalated ^{7}Li using NMR techniques. Increasing the performance of graphitic anodes in Li-ion batteries has been a long-standing research initiative. Partially oxidized or pyrolytic graphite, along with hard carbon, have been investigated to improve performance [141–145]. The chemical and structural modification offered some degree of control over the reversible and irreversible capacity changes in the cell or improving the cycling degradation by facilitating SEI formation.

Most Li NMR studies are performed ex-situ, whereby a material has been investigated at discrete points in the charge-discharge profile. This requires multiple batteries to be made and cycled at those specific points, before being sacrificed for the NMR study. Studies employing such a protocol are time-consuming and can be complicated by sample variability. Moreover, the products of short-lived processes cannot be easily identified or quantified. Recently, Li NMR spectroscopy has been applied in-situ under routine operating conditions. To date, these *in-situ* experiments have been under static conditions, i.e., no magic angle spinning. The first *in-situ* NMR experiment was performed by Gerald et al. [146]. An NMR toroid was used for both spectroscopy and imaging. These initial experiments struggled from poor signal-to-noise ratios, in part due to the incompatibility of a standard lithium ion battery with the toroidal design. Chevallier et al. and Letellier et al. circumvented some of the initial issues by implementing a so-called, "plastic lithium-ion battery" [147, 148] which introduced a flexibility to the battery and eliminated the need for external pressure to maintain contact between the various components of the cell. These initial *in-situ* studies were performed on modified carbonaceous materials designed to replace graphitic carbon as the anode.

Another replacement of graphitic carbon in lithium ion batteries is silicon, due to its large volumetric and gravimetric energy density – 8,322 mAh cm^{-3} (calculated from the original volume of Si) and 3,572 mAh g^{-1} respectively. The high capacitance induces large volumetric changes in the electrode (~300%) which results in issues of capacitance retention, particle fracture and battery design [149]. The Li-Si binary phase diagram contains four reported crystalline lithium silicides – $Li_{12}Si_7$, Li_7Si_3, $Li_{13}Si_4$, and $Li_{21}Si_5$ [150]. These complex materials lie on the border between intermetallic compounds and Zintl phases and contain orbitals delocalized over many lithium ions. Key et al. [149]. have collected ^{7}Li of these model compounds in order to correlate shifts with local environments in silicon based electrodes. The spectrum of $Li_{21}Si_5$ has very broad resonances at approximately 60–100 ppm, owing to the Knight shift. In contrast to $Li_{21}Si_5$, the other lithium silicide phases have single, broad resonances between 6 and 19 ppm, indicative of vastly different electronic properties of each compound.

The authors hypothesized that the various lithium sites in the model compounds were not well-resolved due to a possible combination of factors – slow Li motion, residual ^{7}Li-^{7}Li dipolar coupling, and structural disorder. Nevertheless, a trend toward smaller shifts, implying a greater electron density around the Li atom and more shielded environments, is observed as the Li/Si ratio increases. The resonances with larger shifts in the semi-conductors were found in compounds with Si-Si bonds, whereas smaller shifts were observed in the samples with isolated Si atoms.

The same system was investigated by in-situ ^{7}Li NMR using a plastic battery to monitor real-time changes during a complete charge and discharge at a C/75 rate. The data set largely agrees with the ex situ measurements with slight variations in the shifts of the peaks which were ascribed to the relatively poor resolution of static NMR and small susceptibility effects from metal components in the battery. One striking difference between the in situ and ex situ data was the presence of a new resonance at approximately −10 ppm, at the bottom of the discharge profile (<30 mV), where diffraction measurements displayed evidence for crystalline $Li_{15}Si_4$. The intensity of the −10 ppm resonance decreased rapidly upon charging. A second battery that was fully discharged ex-situ was then monitored using *in-situ* ^{7}Li NMR. The −10 ppm resonance disappeared as the battery relaxed over a period of approximately 10 h. The phenomenon was attributed to a reaction between the metastable $Li_{15}Si_4$ phase with the electrolyte through a "self-charge" mechanism. The reactivity of the amorphous lithium silicides and the self-discharge mechanism may lead to capacity loss or safety concerns. However, the authors noted that the use of carboxymethylcellulose (CMC) as a binder inhibited the discharge process significantly, implicating the reduction of side reactions with the electrolyte and, hence, capacity losses.

Future Directions

In order to meet the ever-increasing demand for energy and portable electronic devices, innovation in the battery community must be a priority. A prerequisite for innovation is a fundamental understanding of chemical reaction pathways and structure determination on a broad length scale. As a natural response to this challenge, there has been a surge of multidisciplinary collaboration. These efforts have been exceedingly successful in elucidating the atomistic details of a plethora of materials and providing a clear direction for future investigations. Breakthroughs are contingent upon a continued and open dialogue between scientists spanning a wide array of expertise. Electrochemical behavior is inextricably related to structure. Consequently, there will be an increasing need to accurately probe and quantify changes in chemical speciation, bond angles, bond lengths, and oxidation state. A particular challenge is to model disordered and nano-sized materials. Implementation and advancement of techniques sensitive to the local environment will be of utmost importance to place structural constraints in these classes of compounds. Such constraints will be invaluable to the computation community in their efforts to predict the phases and electrochemical properties of new materials. Investigation of various room-temperature ionic liquids, for replacement of commonly used carbonate electrolytes, as well as a long-term investment into novel material design and characterization will dominate the battery research community for many years to come. It is only through a concerted effort among materials engineers, analytical, and computational scientists that we are able address the issues of today and those of tomorrow.

Acknowledgments

The authors thank past and present members of the solid-state NMR group at Hunter College for their contributions and gratefully acknowledge support from the US Department of Energy and the U.S. Office of Naval Research.

Bibliography

1. Goodenough J, Kim Y (2010) Challenges for rechargeable Li batteries. Chem Mater 22:587–603
2. Whittingham MS (1976) Electrical energy storage and intercalation chemistry. Science 192(4244):1126–1127
3. Dahn JR, von Sacken U, Juzkow MW, Al-Janaby H (1991) Rechargeable $LiNiO_2$/carbon cells. J Electrochem Soc 138:2207–2211
4. Delmas C, Peres J, Rougier A, Demourgues A, Weill F, Chadwick A, Broussely M, Perton F, Biensan P, Willmann P (1997) On the behavior of the Li_xNiO_2 system: an electrochemical and structural overview. J Power Sources 68(1):120–125

5. Saadoune I, Delmas C (1996) $LiNi_{1-y}Co_yO_2$ positive electrode materials: relationships between the structure, physical properties and electrochemical behaviour. J Mater Chem 6(2):193–199
6. Capitaine F, Gravereau P, Delmas C (1996) A new variety of $LiMnO_2$ with a layered structure. Solid State Ion 89 (3–4):197–202
7. Rossen E, Jones C, Dahn J (1992) Structure and electrochemistry of $Li_xMn_yNi_{1-y}O_2$. Solid State Ion 57(3–4):311–318
8. Liu Z, Yu A, Lee J (1999) Synthesis and characterization of $LiNi_{1-x-y}Co_xMn_yO_2$ as the cathode materials of secondary lithium batteries. J Power Sources 82:416–419
9. Yoshio M, Noguchi H, Itoh J, Okada M, Mouri T (2000) Preparation and properties of $LiCo_yMn_xNi_{1-x-y}O_2$ as a cathode for lithium ion batteries. J Power Sources 90(2):176–181
10. Poizot P, Laruelle S, Grugeon S, Dupont L, Tarascon JM (2000) Nano-sized transition-metaloxides as negative-electrode materials for lithium-ion batteries. Nature 407(6803):496–499
11. Li H, Richter G, Maier J (2003) Reversible formation and decomposition of LiF clusters using transition metal fluorides as precursors and their application in rechargeable Li batteries. Adv Mater 15(9):736–739 (Weinheim, Germany)
12. Li H, Balaya P, Maier J (2004) Li-storage via heterogeneous reaction in selected binary metal fluorides and oxides. J Electrochem Soc 151(11):A1878–A1885
13. Badway F, Cosandey F, Pereira N, Amatucci G (2003) Carbon metal fluoride nanocomposites – high-capacity reversible metal fluoride conversion materials as rechargeable positive electrodes for Li batteries. J Electrochem Soc 150(10):A1318–A1327
14. Badway F, Pereira N, Cosandey F, Amatucci G (2003) Carbon-metal fluoride nanocomposites – structure and electrochemistry of FeF_3: C. J Electrochem Soc 150(9): A1209–A1218
15. Badway F, Mansour A, Pereira N, Al-Sharab J, Cosandey F, Plitz I, Amatucci G (2007) Structure and electrochemistry of copper fluoride nanocomposites utilizing mixed conducting matrices. Chem Mater 19(17):4129–4141
16. Armand M (1994) The history of polymer electrolytes. Solid State Ion 69:309–319
17. Armand M (1986) Polymer electrolytes. Annu Rev Mater Sci 16:245–261
18. Fenton DE, Parker JM, Wright PV (1973) Complexes of alkali-metal ions with poly(ethylene oxide). Polymer 14(11):589
19. Tarascon J-M, Armand M (2001) Issues and challenges facing rechargeable lithium batteries. Nature 414:359–367
20. Myung ST, Komaba S, Hirosaki N, Yashiro H, Kumagai N (2004) Emulsion drying synthesis of olivine $LiFePO_4$/C composite and its electrochemical properties as lithium intercalation material. Electrochim Acta 49(24):4213–4222
21. Rietveld HM (1969) A profile refinement method for nuclear and magnetic structures. J Appl Crystallogr 2:65–71
22. Proffen T, Billinge SJL (1999) PDFFIT, a program for full profile structural refinement of the atomic pair distribution function. J Appl Crystallogr 32:572–575
23. McGreevy RL, Pusztai L (1988) Reverse monte carlo simulation: a new technique for the determination of disordered structures. Mol Simul 1:359–367
24. Dedryvere R, Laruelle S, Grugeon S, Poizot P, Gonbeau D, Tarascon JM (2004) Contribution of X-ray photoelectron spectroscopy to the study of the electrochemical reactivity of CoO toward lithium. Chem Mater 16(6):1056–1061
25. Alamgir FM, Petersburg CF, Daniel RC, Jaye C, Fischer DA (2009) Soft X-ray characterization technique for Li batteries under operating conditions. J Synchrotron Radiat 16:610–615
26. Stern EA (1974) Theory of extended X-Ray-absorption fine-structure. Phys Rev B 10(8):3027–3037
27. Sayers DE, Stern EA, Lytle FW (1971) New technique for investigating noncrystalline structures – Fourier analysis of extended X-ray – absorption fine structure. Phys Rev Lett 27(18):1204–1207
28. Tsai YW, Hwang BJ, Ceder G, Sheu HS, Liu DG, Lee JF (2005) In-situ X-ray absorption spectroscopic study on variation of electronic transitions and local structure of $LiNi_{1/3}Co_{1/3}Mn_{1/3}O_2$ cathode material during electrochemical cycling. Chem Mater 17(12):3191–3199
29. Yoon W, Kim N, Yang X, McBreen J, Grey C (2003) Li-6 MAS NMR and in situ X-ray studies of lithium nickel manganese oxides. J Power Sources 119:649–653
30. Grey CP, Lee YJ (2003) Lithium MAS NMR studies of cathode materials for lithium-ion batteries. Solid State Sci 5(6): 883–894
31. Carlier D, Menetrier M, Grey C, Delmas C, Ceder G (2003) Understanding the NMR shifts in paramagnetic transition metal oxides using density functional theory calculations. Phys Rev B 67 174103:1–14
32. Letellier M, Chevallier F, Beguin F, Frackowiak E, Rouzaud J (2004) The first in situ Li-7 NMR study of the reversible lithium insertion mechanism in disorganised carbons. J Phys Chem Solids 65(2–3):245–251
33. Levitt MH (2001) Spin dynamics: basics of nuclear magnetic resonance. Wiley, New York
34. Slichter CP (1990) Principles of nuclear magnetic resonance. Springer, Berlin
35. Stejskal E, Tanner J (1965) Spin diffusion measurements: spin echoes in the presence of a time-dependent field gradient. J Chem Phys 42:288–292
36. Kimmich R, Unrath W, Schnur G, Rommel E (1991) NMR measurement of small self-diffusion coefficients in the fringe-field of superconducting magnets. J Magn Reson 91(1):136–140
37. Demco D, Johansson A, Tegenfeldt J (1994) Constant-relaxation methods for diffusion measurements in the fringe-field of superconducting magnets. J Magn Reson Ser A 110(2):183–193
38. Gorecki W, Jeannin M, Belorizky E, Roux C, Armand M (1995) Physical properties of solid polymer electrolyte PEO(LiTFSI) complexes. J Phys Cond Matter 7(34):6823–6832
39. Johansson A, Gogoll A, Tegenfeldt J (1996) Diffusion and ionic conductivity in $Li(CF_3SO_3)$PEG(10) and $LiN(CF_3SO_2)$(2)PEG(10). Polymer 37(8):1387–1393

40. Hayamizu K, Aihara Y, Price W (2000) Correlating the NMR self-diffusion and relaxation measurements with ionic conductivity in polymer electrolytes composed of cross-linked poly (ethylene oxide-propylene oxide) doped with $LiN(SO_2CF_3)(2)$. J Chem Phys 113(11):4785–4793
41. Hayamizu K, Aihara Y, Price W (2001) NMR and ion conductivity studies on cross-linked poly(ethyleneoxide-propyleneoxide) and branched polyether doped with $LiN(SO_2CF_3)(2)$. Electrochim Acta 46(10–11):1475–1485
42. Adebahr J, Forsyth M, Gavelin P, Jacobsson P, Oradd G (2002) Ion and solvent dynamics in gel electrolytes based on ethylene oxide grafted acrylate polymers. J Phys Chem B 106(47):12119–12123
43. Gorecki W, Roux C, Clemancey M, Armand M, Belorizky E (2002) NMR and conductivity study of polymer electrolytes in the imide family: P(EO)/Li[N(SO_2CnF2n + 1)(SO_2CmF2m + 1)]. Chemphyschem 3(7):620–625
44. Croce F, Appetecchi G, Persi L, Scrosati B (1998) Nanocomposite polymer electrolytes for lithium batteries. Nature 394:456–458
45. Zhou F, MacFarlane D, Forsyth M (2003) Boroxine ring compounds as dissociation enhancers in gel polyelectrolytes. Electrochim Acta 48(12):1749–1758
46. Kalita M, Bukat M, Ciosek M, Siekierski M, Chung S, Rodriguez T, Greenbaum S, Kovarsky R, Golodnitsky D, Peled E, Zane D, Scrosati B, Wieczorek W (2005) Effect of calixpyrrole in PEO-$LiBF_4$ polymer electrolytes. Electrochimia Acta 50(19):3942–3948
47. Koudriachova MV, Harrison NM, de Leeuw SW (2002) Density-functional simulations of lithium intercalation in rutile. Phys Rev B 65 235423:1–12
48. Kang K, Ceder G (2006) Factors that affect Li mobility in layered lithium transition metal oxides. Phys Rev B 74 094105:1–7
49. Tibbetts K, Miranda CR, Meng YS, Ceder G (2007) An ab initio study of lithium diffusion in titanium disulfide nanotubes. Chem Mater 19(22):5302–5308
50. Aydinol MK, Kohan AF, Ceder G, Cho K, Joannopoulos J (1997) Ab initio study of lithium intercalation in metal oxides and metal dichalcogenides. Phys Rev B 56(3): 1354–1365
51. Courtney IA, Tse JS, Mao O, Hafner J, Dahn JR (1998) Ab initio calculation of the lithium-tin voltage profile. Phys Rev B 58(23):15583–15588
52. Meng YS, Wu YW, Hwang BJ, Li Y, Ceder G (2004) Combining ab initio computation with experiments for designing new electrode materials for advanced lithium batteries: $LiNi_{1/3}Fe_{1/6}Co_{1/6}Mn_{1/3}O_2$. J Electrochem Soc 151(8): A1134–A1140
53. Arroyo-DeDompablo ME, Van der Ven A, Ceder G (2002) First-principles calculations of lithium ordering and phase stability on Li_xNiO_2. Phys Rev B 66 064112:1–9
54. Wolverton C, Zunger A (1998) Prediction of Li intercalation and battery voltages in layered versus cubic Li_xCoO_2. J Electrochem Soc 145(7):2424–2431
55. Hwang B, Tsai Y, Carlier D, Ceder G (2003) A combined computational/experimental study on $LiNi_{1/3}Co_{1/3}Mn_{1/3}O_2$. Chem Mater 15(19):3676–3682
56. Kganyago KR, Ngoepe PE, Catlow CRA (2003) Ab initio calculation of the voltage profile for LiC_6. Solid State Ion 159(1–2):21–23
57. Launay M, Boucher F, Gressier P, Ouvrard G (2003) A DFT study of lithium battery materials: application to the β-VOXO4 systems (X = P, As, S). J Solid State Chem 176(2):556–566
58. Zhou F, Cococcioni M, Marianetti CA, Morgan D, Ceder G (2004) First-principles prediction of redox potentials in transition-metal compounds with LDA + U. Phys Rev B 70 235121:1–8
59. Reed J, Ceder G (2002) Charge, potential, and phase stability of layered Li(Ni0.5Mn0.5)O-2. Electrochem State Lett 5(7): A145–A148
60. Arroyo-DeDompablo ME, Ceder G (2003) First-principles calculations on Li_xNiO_2: phase stability and monoclinic distortion. J Power Sources 119121:654–657
61. Carlier D, Van der Ven A, Delmas C, Ceder G (2003) First-principles investigation of phase stability in the O-2-$LiCoO_2$ system. Chem Mater 15(13):2651–2660
62. Perdew JP, Burke K, Ernzerhof M (1996) Generalized gradient approximation made simple. Phys Rev Lett 77(18):3865–3868
63. Blochl PE (1994) Projector augmented-wave method. Phys Rev B 50(24):17953–17979
64. Kresse G, Joubert J (1999) From ultrasoft pseudopotentials to the projector augmented-wave method. Phys Rev B 59(3):1758–1775
65. Kresse G, Furthmuller J (1996) Efficient iterative schemes for ab initio total-energy calculations using a plane-wave basis set. Phys Rev B 54(16):11169–11186
66. Bar-Tow D, Peled E, Burstein L (1999) A study of highly oriented pyrolytic graphite as a model for the graphite anode in Li-ion batteries. J Electrochem Soc 146(3):824–832
67. Peled E, Tow DB, Merson A, Gladkich A, Burstein L, Golodnitsky D (2001) Composition, depth profiles and lateral distribution of materials in the SEI built on HOPG-TOF SIMS and XPS studies. J Power Sources 97–98:52–57
68. Lu M, Cheng H, Yang Y (2008) A comparison of solid electrolyte interphase (SEI) on the artificial graphite anode of the aged and cycled commercial lithium ion cells. Electrochim Acta 53(9):3539–3546
69. Peled E, Golodnitsky D, Ulus A, Yufit V (2004) Effect of carbon substrate on SEI composition and morphology. Electrochim Acta 50(2–3):391–395
70. Ota H, Kominato A, Chun WJ, Yasukawa E, Kasuya S (2003) Effect of cyclic phosphate additive in non-flammable electrolyte. J Power Sources 119:393–398
71. Andersson AM, Edstrom K (2001) Chemical composition and morphology of the elevated temperature SEI on graphite. J Electrochem Soc 148(10):A1100–A1109
72. Andersson AM, Edstrom K, Rao N, Wendsjo A (1999) Temperature dependence of the passivation layer on graphite. J Power Sources 82:286–290

73. Meyer BM, Leifer N, Sakamoto S, Greenbaum SG, Grey CP (2005) High field multinuclear NMR investigation of the SEI layer in lithium rechargeable batteries. Electrochem Solid State Lett 8(3):A145–A148
74. Dupre N, Martin JF, Degryse J, Fernandez V, Soudan P, Guyomard D (2010) Aging of the $LiFePO_4$ positive electrode interface in electrolyte. J Power Sources 195(21):7415–7425
75. Dupre N, Martin J, Oliveri J, Soudan P, Guyomard D, Yamada A, Kanno R (2009) Aging of the $LiNi_{1/2}Mn_{1/2}O_2$ positive electrode interface in electrolyte. J Electrochem Soc 156(5):C180–C185
76. Dupre N, Martin JF, Guyomard D, Yamada A, Kanno R (2008) Detection of surface layers using Li-7 MAS NMR. J Mater Chem 18(36):4266–4273
77. Leifer N, Smart MC, Prakash GKS, Gonzalez L, Sanchez L, Smith KA, Bhalla P, Grey CP, Greenbaum SG (2011) 13C solid state NMR suggests unusual breakdown products in SEI formation on lithium ion electrodes. J Electrochem Soc 158(5): A471–A480
78. Fernicola A, Weise F, Greenbaum S, Kagimoto J, Scrosati B, Soleto A (2009) Lithium-ion-conducting electrolytes: from an ionic liquid to the polymer membrane. J Electrochem Soc 156(7):A514–A520
79. Scrosati B (1995) Battery technology – challenge of portable power. Nature 373:557–558
80. Gray FM (1991) Solid polymer electrolytes: fundamentals and electrochemical applications. VCH, New York
81. Kalita M, Bukat M, Ciosek M, Siekierski M, Chung SH, Rodriguez T, Greenbaum SG, Kovarsky R, Golodnitsky D, Peled E, Zane D, Scrosati B, Wieczorek W (2005) Effect of calixpyrrole in PEO-$LiBF_4$ polymer electrolytes. Electrochim Acta 50(19):3942–3948
82. Periasamy P, Tatsumi K, Shikano M, Fujieda T, Saito Y, Sakai T, Mizuhata M, Kajinami A, Deki S (2000) Studies on PVdF-based gel polymer electrolytes. J Power Sources 88(2):269–273
83. Pawlowska A, Zukowska G, Kalita M, Solgala A, Parzuchowski P, Siekierski M (2007) The effect of receptor-polymer matrix compatibility on properties of PEO-based polymer electrolytes containing a supramolecular additive. Part 1. Studies on phenomenon of compatibility. J Power Sources 173(2):755–764
84. Bloise A, Donoso J, Magon C, Rosario A, Pereira E (2003) NMR and conductivity study of PEO-based composite polymer electrolytes. Electrochim Acta 48(14–16):2239–2246
85. Masuda Y, Seki M, Nakayama M, Wakihara M, Mita H (2006) Study on ionic conductivity of polymer electrolyte plasticized with PEG-aluminate ester for rechargeable lithium ion battery. Solid State Ion 117(9–10):843–846
86. Dai Y, Wang Y, Greenbaum S, Bajue S, Golodnitsky D, Ardel G, Strauss E, Peled E (1998) Electrical, thermal and NMR investigation of composite solid electrolytes based on PEO, LiI and high surface area inorganic oxides. Electrochim Acta 43(10–11):1557–1561
87. Best A, Adebahr J, Jacobsson P, MacFarlane D, Forsyth M (2001) Microscopic interactions in nanocomposite electrolytes. Macromolecules 34(13):4549–4555
88. Adebahr J, Best A, Byrne N, Jacobsson P, MacFarlane D, Forsyth M (2003) Ion transport in polymer electrolytes containing nanoparticulate TiO_2: The influence of polymer morphology. Phys Chem Chem Phys 5:720–725
89. Berthier C, Gorecki W, Minier M, Armand M, Chabagno J, Rigaud P (1983) Microscopic investigation of ionic conductivity in alkali metal salts-poly(ethylene oxide) adducts. Solid State Ion 11(1):91–95
90. Chung S, Jeffrey K, Stevens J (1991) A Li-7 nuclear magnetic resonance study of $LiCF_3SO_3$ complexed in poly(propylene-glycol). J Chem Phys 94(3):1803–1811
91. Donoso J, Bonagamba T, Panepucci H, Oliveira L, Gorecki W, Berthier C, Armand M (1993) Nuclear magnetic relaxation study of poly(ethylene oxide)-lithium salt based electrolytes. J Chem Phys 98(12):10026–10036
92. Johansson A, Tegenfeldt J (1996) Segmental mobility in complexes of $Pb(CF_3SO_3)(2)$ and poly(ethylene oxide) studied by NMR spectroscopy. J Chem Phys 104(13): 5317–5325
93. Chung S, Wang Y, Greenbaum S, Golodnitsky D, Peled E (1999) Uniaxial stress effects in poly(ethylene oxide)-LiI polymer electrolyte film – a Li-7 nuclear magnetic resonance study. Electrochem Solid State Lett 2(11):553–555
94. Golodnitsky D, Livshits E, Kovarsky R, Peled E, Chung S, Suarez S, Greenbaum S (2004) New generation of ordered polymer electrolytes for lithium batteries. Electrochem Solid State Lett 7(11):A412–A415
95. Golodnitsky D, Livshits E, Ulus A, Barkay Z, Lapides I, Peled E, Chung S, Greenbaum S (2001) Fast ion transport phenomena in oriented semicrystalline LiI-P(EO)n-based polymer electrolytes. J Phys Chem A 105(44):10098–10106
96. Armand MB, Chabagno JM, Duclot MJ (1979) Fast ion transport in solids. Elsevier, New York
97. Gadjourova Z, Andreev Y, Tunstall D, Bruce P (2001) Ionic conductivity in crystalline polymer electrolytes. Nature 412:520–523
98. Padhi A, Nanjundaswamy K, Goodenough J (1997) Phospho-olivines as positive-electrode materials for rechargeable lithium batteries. J Electrochem Soc 144(4):1188–1194
99. Morgan D, Van der Ven A, Ceder G (2004) Li conductivity in Li_xMPO_4 (M=Mn, Fe, Co, Ni) olivine materials. Electrochem Solid State Lett 7(2):A30–A32
100. Yamada A, Chung S, Hinokuma K (2001) Optimized $LiFePO_4$ for lithium battery cathodes. J Electrochem Soc 148(3): A224–A229
101. Padhi A, Nanjundaswamy K, Masquelier C, Okada S, Goodenough J (1997) Effect of structure on the Fe^{3+}/Fe^{2+} redox couple in iron phosphates. J Electrochem Soc 144(5):1609–1613
102. Tucker M, Doeff M, Richardson T, Finones R, Cairns E, Reimer J (2002) Hyperfine fields at the Li site in LiFePO4-type olivine materials for lithium rechargeable batteries: a Li-7 MAS NMR and SQUID study. J Am Chem Soc 124(15):3832–3833

103. Gee B, Horne CR, Cairns EJ, Reimer JA (1998) Supertransferred hyperfine fields at Li-7: Variable temperature Li-7 NMR studies of $LiMn_2O_4$-based spinels. J Phys Chem B 102(50): 10142–10149
104. Wilcke SL, Lee YJ, Cairns EJ, Reimer JA (2007) Covalency measurements via NMR in lithium metal phosphates. Appl Magn Reson 32(4):547–563
105. Leifer N, Colon A, Martocci K, Greenbaum S, Alamgir F, Reddy T, Gleason N, Leising R, Takeuchi E (2007) Nuclear magnetic resonance and X-ray absorption spectroscopic studies of lithium insertion in silver vanadium oxide cathodes. J Electrochem Soc 154(6):A500–A506
106. Crespi A, Skarstad P, Zandbergen H (1995) Characterization of silver vanadium oxide cathode material by high-resolution electron microscopy. J Power Sources 54(1):68–71
107. Takeuchi K, Marschilok A, Davis S, Leising R, Takeuchi E (2001) Silver vanadium oxides and related battery applications. Coord Chem Rev 219–221:283–310
108. Ramasamy R, Feger C, Strange T, Popov B (2006) Discharge characteristics of silver vanadium oxide cathodes. J Appl Electrochem 36(4):487–497
109. Vijayakumar M, Selvasekarapandian S, Nakamura K, Kanashiro T, Kesavamoorthy R (2004) Li-7 MAS-NMR and vibrational spectroscopic investigations of $Li_xV_2O_5$ (x = 10, 12 and 14). Solid State Ion 167(1–2):41–47
110. Holland G, Buttry D, Yarger J (2002) Li-7 NMR studies of electrochemically lithiated V_2O_5 xerogels. Chem Mater 14(9):3875–3881
111. Holland G, Yarger J, Buttry D, Huguenin F, Torresi R (2003) Solid-state NMR study of ion-exchange processes in V_2O_5 xerogel, polyaniline/V_2O_5, and sulfonated polyaniline/V_2O_5 nanocomposites. J Electrochem Soc 150(12):A1718–A1722
112. Nakamura K, Nishioka D, Michihiro Y, Vijayakumar M, Selvasekarapandian S, Kanashiro T (2006) Li-7 and V-51 NMR study on Li+ ionic diffusion in lithium intercalated $Li_xV_2O_5$. Solid State Ion 177(1–2):129–135
113. West K, Crespi A (1995) Lithium insertion into silver vanadium-oxide, $Ag_2V_4O_{11}$. J Power Sources 54(2):334–337
114. Rozier P, Galy J (1997) $Ag_{1.2}V_3O_8$ crystal structure: Relationship with $Ag_2V_4O_{11-y}$ interpretation of physical properties. J Solid State Chem 134(2):294–301
115. Rozier P, Savariault J, Galy J, Marichal C, Hirschinger J, Granger P (1996) Epsilon-$Li_xV_2O_5$ bronzes ($0.33 \leq \times \leq 0.64$) a joint study by X-ray powder diffraction and 6Li, 7Li MAS NMR. Eur J Solid State Inorg Chem 33(1):1–13
116. Kuwabara K, Itoh M, Sugiyama K (1986) Ionic-electronic mixed conduction in $Li_xV_2O_5$. Solid State Ion 20(2):135–139
117. Garcia-Alvarado F, Tarascon J (1994) Lithium intercalation in $Ag_2V_4O_{11}$. Solid State Ion 73(3–4):247–254
118. Stallworth P, Kostov S, denBoer M, Greenbaum S, Lampe-Onnerud C (1998) X-ray absorption and magnetic resonance spectroscopic studies of $Li_xV_6O_{13}$. J Appl Phys 83(3):1247–1255
119. Yamakawa N, Jiang M, Grey CP (2009) Investigation of the conversion reaction mechanisms for binary copper(II) compounds by solid-state NMR spectroscopy and X-ray diffraction. Chem Mater 21(14):3162–3176
120. Yamakawa N, Jiang M, Key B, Grey CP (2009) Identifying the local structures formed during lithiation of the conversion material, iron fluoride, in a Li ion battery: a solid-state NMR, X-ray diffraction, and pair distribution function analysis study. J Am Chem Soc 131(30):10525–10536
121. Chung JS, Sohn HJ (2002) Electrochemical behaviors of CuS as a cathode material for lithium secondary batteries. J Power Sources 108(1–2):226–231
122. Debart A, Dupont L, Patrice R, Tarascon JM (2006) Reactivity of transition metal (Co, Ni, Cu) sulphides versus lithium: the intriguing case of the copper sulphide. Solid State Sci 8(6):640–651
123. Ikeda H, Narukawa S (1983) Behavior of various cathode materials for non-aqueous lithium cells. J Power Sources 9(3–4):329–334
124. Grugeon S, Laruelle S, Herrera-Urbina R, Dupont L, Poizot P, Tarascon J (2001) Particle size effects on the electrochemical performance of copper oxides toward lithium. J Electrochem Soc 148(4):A285–A292
125. Arai H, Okada S, Sakurai Y, Yamaki J (1997) Cathode performance and voltage estimation of metal trihalides. J Power Sources 68(2):716–719
126. Cosandey F, Al-Sharab J, Badway F, Amatucci G, Stadelmann P (2007) EELS spectroscopy of iron fluorides and FeFx/C nanocomposite electrodes used in Li-ion batteries. Microsc Microanal 13(2):87–95
127. Doe R, Persson K, Meng Y, Ceder G (2008) First-principles investigation of the Li-Fe-F phase diagram and equilibrium and nonequilibrium conversion reactions of iron fluorides with lithium. Chem Mater 20(16):5274–5283
128. Nielsen U, Paik Y, Julmis K, Schoonen M, Reeder R, Grey C (2005) Investigating sorption on iron-oxyhydroxide soil minerals by solid-state NMR spectroscopy: A Li-6 MAS NMR study of adsorption and absorption on goethite. J Phys Chem B 109(39):18310–18315
129. Kim J, Nielsen U, Grey C (2008) Local environments and lithium adsorption on the iron oxyhydroxides lepidocrocite (gamma-FeOOH) and goethite (alpha-FeOOH): A H-2 and Li-7 solid-state MAS NMR study. J Am Chem Soc 130(4):1285–1295
130. Liao P, MacDonald B, Dunlap R, Dahn J (2008) Combinatorially prepared [LiF](1-x)Fe-x nanocomposites for positive electrode materials in Li-ion batteries. Chem Mater 20(2):454–461
131. Breger J, Dupre N, Chupas P, Lee P, Proffen T, Parise J, Grey C (2005) Short- and long-range order in the positive electrode material, Li(NiMn)(0.5)O-2: a joint X-ray and neutron diffraction, pair distribution function analysis and NMR study. J Am Chem Soc 127(20):7529–7537
132. Yoon W, Paik Y, Yang X, Balasubramanian M, McBreen J, Grey C (2002) Investigation of the local structure of the $LiNi_{0.5}Mn_{0.5}O_2$ cathode material during electrochemical

cycling by X-ray absorption and NMR spectroscopy. Electrochem Solid State Lett 5(11):A263–A266
133. Yoon W, Iannopollo S, Grey C, Carlier D, Gorman J, Reed J, Ceder G (2004) Local structure and cation ordering in O_3 lithium nickel manganese oxides with stoichiometry Li $[Ni_xMn_{(2-x)/3}Li_{(1-2x)/3}]O_{-2}$ – NMR studies and first principles calculations. Electrochem Solid State Lett 7(7):A167–A171
134. Van der Ven A, Ceder G (2004) Ordering in $Li_{-x}(Ni_{0.5}Mn_{0.5})O_{-2}$ and its relation to charge capacity and electrochemical behavior in rechargeable lithium batteries. Electrochem Commun 6(10):1045–1050
135. Meng YS, Ceder G, Grey CP, Yoon W-S, Shao-Horn Y (2004) Understanding the crystal structure of layered $LiNi_{0.5}Mn_{0.5}O_2$ by electron diffraction and powder diffraction simulation. Electrochem Solid State Lett 7(6):A155–A158
136. Cahill LS, Chapman RP, Britten JF, Goward GR (2006) Li-7 NMR and two-dimensional exchange study of lithium dynamics in monoclinic $Li_3V_2(PO_4)(3)$. J Phys Chem B 110(14):7171–7177
137. Matsumura Y, Wang S, Mondori J (1995) Interactions between disordered carbon and lithium in lithium ion rechargeable batteries. Carbon 33(10):1457–1462
138. Wang S, Kakumoto T, Matsui H, Matsumura Y (1999) Mechanism of lithium insertion into disordered carbon. Synth Met 103(1–3):2523–2524
139. Nakagawa Y, Wang S, Matsumura Y, Yamaguchi C (1997) Li-7-NMR study of lithium charged in carbon electrode. Synth Met 85(1–3):1363–1364
140. Conard J, Estrade H (1977) Résonance magnétique nucléaire du lithium interstitiel dans le graphite. Mater Sci Eng 31:173–176
141. Peled E, Menachem C, BarTow D, Melman A (1996) Improved graphite anode for lithium-ion batteries – chemically bonded solid electrolyte interface and nanochannel formation. J Electrochem Soc 143(1):L4–L7
142. Menachem C, Wang Y, Flowers J, Peled E, Greenbaum S (1998) Characterization of lithiated natural graphite before and after mild oxidation. J Power Sources 76(2):180–185
143. Wang Y, Yufit V, Guo X, Peled E, Greenbaum S (2001) Li-7 nuclear magnetic resonance study of lithium insertion in pristine and partially oxidized graphite. J Power Sources 94(2):230–237
144. Gotoh K, Maeda M, Nagai A, Goto A, Tansho M, Hashi K, Shimizu T, Ishida H (2006) Properties of a novel hard-carbon optimized to large size Li ion secondary battery studied by Li-7 NMR. J Power Sources 162(2):1322–1328
145. Persson K, Sethuraman VA, Hardwick LJ, Hinuma Y, Meng YS, van der Ven A, Srinivasan V, Kostecki R, Ceder G (2010) Lithium diffusion in graphitic carbon. J Phys Chem Lett 1(8):1176–1180
146. Gerald RE, Klingler RJ, Sandi G, Johnson CS, Scanlon LG, Rathke JW (2000) Li-7 NMR study of intercalated lithium in curved carbon lattices. J Power Sources 89(2):237–243
147. Chevallier F, Letellier M, Morcrette M, Tarascon JM, Frackowiak E, Rouzaud JN, Beguin F (2003) In situ Li-7-nuclear magnetic resonance observation of reversible lithium insertion into disordered carbons. Electrochem Solid State Lett 6(11):A225–A228
148. Letellier M, Chevallier F, Clinard C, Frackowiak E, Rouzaud JN, Beguin F, Morcrette M, Tarascon JM (2003) The first in situ Li-7 nuclear magnetic resonance study of lithium insertion in hard-carbon anode materials for Li-ion batteries. J Chem Phys 118(13):6038–6045
149. Key B, Bhattacharyya R, Morcrette M, Seznec V, Tarascon JM, Grey CP (2009) Real-time NMR investigations of structural changes in silicon electrodes for lithium-ion batteries. J Am Chem Soc 131(26):9239–9249
150. Nesper R (1990) Structure and chemical bonding in zintl-phases containing Lithium. Prog Solid State Chem 20(1):1–45

Further Readings

Balbuena PB, Wang Y (2004) Lithium-ion batteries: solid electrolyte interphase. Imperial College Press, London
Linden D, Reddy TB (2002) Handbook of batteries, 3rd edn. McGraw-Hill, New York

L

Lithium-Ion Batteries, Safety

Brian Barnett, David Ofer, Suresh Sriramulu, Richard Stringfellow
TIAX LLC, Lexington, MA, USA

Article Outline

Glossary
Definition of the Subject and Its Importance
Introduction
Basis for Li-Ion Safety Concerns
Triggers for Li-Ion Thermal Runaway
Key Observations from Analysis of Field-Failures
Likely Mechanism of Internal Short Formation in a Field-Failure
Factors Influencing Thermal Runaway from Internal Shorts
Differences Between Abuse Tolerance and Field-Failures
An Overall Framework for Consideration of Li-Ion Battery Safety
Future Directions
Acknowledgments
Bibliography

Glossary

Abuse External stress applied to a battery or cell that is not anticipated to occur under normal operating conditions and may cause the cell to experience thermal runaway.

Cascading Process by which one cell in a battery releases sufficient heat that thermal runaway of one or more neighboring cells in a pack ensues.

Field-failure *Infrequent* safety incident that occurs in lithium-ion cells/batteries in the field under "normal" operating conditions and does not appear to have an obvious external trigger, but is often caused by an internal short circuit. Such internal short circuits are often caused by foreign metal particles.

Safe Zone For a given cell construction and materials, and for a given heat transfer environment, conditions of energy and power associated with an internal short such that a thermal runaway is not possible.

Thermal runaway A process of uncontrolled heat release and rapid temperature rise.

Threshold energy For a given cell design and heat transfer environment, an energy value dissipated in an internal short below which no thermal runaway is possible.

Threshold power For a given cell design and heat transfer environment, an internal short power below which no thermal runaway is possible.

Trigger for thermal runaway A stimulus that initiates thermal runaway in a Li-ion cell. Examples of potential triggers include a variety of abuses as well as internal short circuits created by foreign metal particles.

Definition of the Subject and Its Importance

Safety of lithium-ion batteries is a critical topic that has not received adequate attention in the past, largely due to the fact that data regarding safety failures have been severely restricted. As a result, there are numerous misunderstandings in a field that has not received the same degree of scientific and technical rigor as other areas of lithium-ion battery technology development. However, safety of lithium-ion batteries will become even more important as lithium-ion technology enters transportation markets. Under suitable triggers, Li-ion cells can experience thermal runaway, i.e., the rapid increase in cell temperature accompanied by venting, vent-with-flame, ejection of cell parts, fire, and explosion. Safety failures of lithium-ion cells can result from a variety of triggers including overcharging, overheating, crushing, mechanical impact, and external short circuits. Safety tests have been devised for all these abuses, with varying degrees of fidelity. However, most safety incidents that have taken place with lithium-ion batteries occur due to the slow and rare development in cells of internal short circuits that mature to the point that they result in thermal runaway. Most safety tests carried out in the laboratory or factory do not replicate the conditions by which safety incidents actually occur in the field. These issues are characterized in detail, and an improved overall framework for considering lithium-ion battery safety is suggested.

Introduction

Since their introduction in 1991, lithium-ion batteries have become the dominant rechargeable battery technology for portable products and are beginning to make inroads in transportation and stationary storage applications. Lithium-ion battery technology provides the highest available energy density of any long-cycling rechargeable battery, which has been the most significant factor leading to its widespread adoption. As of this writing, over 4.5 billion lithium-ion cells (almost 40,000 MWh) [1] will be expected to be produced in 2011, the bulk of which are used in consumer electronics applications such as laptop computers and cell phones. While the demand for such cells is increasing at the rate of 15% on a year-on-year basis, emerging applications can significantly increase the Li-ion market. It is anticipated that emerging transportation and stationary storage markets will lead to dramatic increases in the volume of Li-ion production. One recent estimate places automotive Li-ion demand in 2020 at 150,400 MWh, in contrast to 72,500 MWh projected for portable applications in that year. The transportation and stationary applications are expected to use larger capacity cells than those employed for consumer electronics applications [1].

Despite the obvious success of Li-ion technology, safety concerns remain [2]. Under suitable triggers, Li-ion cells can undergo venting, vent-with-flame, ejection of cell parts, fire, and explosion as the consequence

of a process of uncontrolled heat release, termed "thermal runaway." This risk is not surprising given the possible sources of heat release within a cell. Essentially, Li-ion batteries store a very large amount of electrochemical energy, which can be released as heat, for example, through an internal short. The electrochemical energy content of state-of-the-art Li-ion cells is by itself sufficient to raise cell temperature to 700°C if completely dissipated within the cell under adiabatic conditions. But furthermore, Li-ion cells contain energetic materials that can undergo exothermic decomposition reactions within the cell, as well as containing combustible organic solvents (with heat of combustion that is about a third of the heat of combustion of gasoline) and combustible carbonaceous anode materials, both of which can burn in atmospheric oxygen if exposed under suitable ignition conditions. The heat release from such reactions can be as much as ten times the stored electrochemical energy.

Safety failures of lithium-ion cells can result from a variety of triggers. Overcharging, overheating, crushing, mechanical impact, and external short circuit all represent forms of external triggers (often termed "abuse" conditions) that can lead to safety incidents. These external abuses have been extensively studied. Battery engineers have developed several cell-level and pack-level tests to evaluate how a cell/battery responds to the abuse, and they have also developed technologies and approaches to manage the cell and battery response to such external abuses [3–11]. Standardized tests also have been developed to assess cell and battery "tolerance" to external abuses [12, 13]. In general, this chapter shall try to draw distinctions between tests used to screen cells/batteries for their tolerance to a given trigger and the actual tolerance of a cell/battery to the given trigger (i.e., the effectiveness of the test).

Safety concerns have been heightened by highly publicized safety incidents and ensuing widespread recalls of lithium-ion batteries used in laptop computers and cell phones [14, 15]. When these rare safety incidents occur, lithium-ion batteries operating under otherwise normal conditions undergo what appear to be spontaneous thermal runaway events, often with violent flaming and extremely high temperatures. Moreover, these failures usually involve cells and cell designs that have passed extensive abuse testing, including the standardized abuse safety tests. *Most such Li-ion safety incidents in the field are not preceded by any obvious external abuse*. We refer to these spontaneous safety incidents as "field-failures". The fact that cells involved in field-failures generally have passed all standardized safety tests is the first clue that these incidents should be given special consideration. Internal shorts – not external abuses – cause field-failures far more frequently than is generally appreciated. Such shorts are a major focus of this chapter.

Given the near ubiquitous use of Li-ion batteries, field-failures may result in significant property damage and may also prove dangerous to users, not to mention the enormous costs of the recalls they have prompted. Furthermore, the advent of new transportation and stationary applications employing cells larger than those used in portable applications, and often with many cells in series, raises the threat of even more severe outcomes.

Although field-failures and the ensuing recalls have resulted in significant financial losses for the battery industry, relatively little is known or published about them, or the underlying causes of such incidents. Outside of the battery companies and their customers, very few organizations have had an opportunity to carry out careful postmortems of cells and batteries involved in these incidents. As a result, a very large fraction of the lithium-ion battery community, including materials companies, national laboratories, and the worldwide academic community, are not able to approach the lithium-ion battery safety issue with the same scientific and technical rigor that they apply to other aspects of lithium-ion technology. We believe that if better background information were made available to engineers and scientists across the battery community, there would be a profound impact on widely held perspectives regarding safety, how to test for safety, and what actually makes a lithium-ion cell/battery safe. Importantly, most safety tests carried out in the laboratory or factory do not replicate the conditions by which safety incidents actually occur in the field. We will describe this conundrum in greater detail below.

We (at TIAX) are one of the few organizations that have had an opportunity to carry out a significant number of detailed investigations of actual lithium-ion safety incidents [16–21]. Although confidentiality requirements preclude us from showing specific

examples of field-failure cell postmortems, we will describe general observations and conclusions in this chapter. We are hopeful that the lessons learned from such work can enhance the overall perspective of the lithium-ion battery community and support some of the insights developed in this chapter. Finally, an improved overall framework for considering lithium-ion battery safety is suggested.

Basis for Li-Ion Safety Concerns

Li-ion cells are widely understood to have higher energy content than other rechargeable batteries, but this perception is generally focused only on their higher *electrochemical* energy density. While that perception is correct, the heat release associated with the exothermic reactions of all of a cell's contents must also be considered when evaluating safety. In the case of Li-ion technology, this heat release can exceed ten times the stored electrochemical energy content if in the field-failure process, all the cell's combustible contents are reacted with air. For example, Table 1 summarizes the typical contributions to the heat release in a generic Li-ion cell. The table lists the key chemical reactions and provides estimates of the following:

- Temperature range over which the rates of these reactions are significant
- Total heat release from these exothermic reactions
- Heat release that can be attributed to the particular reaction in a 10-Wh 18650 cell (electrochemical energy of 36 kJ)

As can be seen from the table, the anode and cathode reactions with electrolyte and the self-reaction of electrolyte contribute significantly to the heat release relative to the electrochemical energy content of the cell. The mechanism and kinetics of these reactions have been studied extensively in the literature [22–29]. However, complete combustion of the solvent results in much higher heat release. Note that even in Li-ion cells with metal oxide cathodes there is insufficient oxygen available within the cell to completely combust the solvent, a factor not always recognized by many safety investigators. Thus, a major fraction of the solvent combustion can only occur outside the cell. An even greater release of heat occurs if the graphitic anode content of the cell is combusted upon exposure to atmosphere; postmortem audits show that this does in fact occur in many field-failures. Graphite's heat of

Lithium-Ion Batteries, Safety. Table 1 Summary of contributions to heat release in a lithium-ion cell

Process	Temperature range (°C)	Energy release	Energy relaese in a 10 Wh 18650 cell
Anode decomposition and reaction with electrolyte	80–120	~400 J/g-anode[a, b]	~11 KJ
	150–300	~1,300 J/g-anode[a, b]	
Cathode decomposition and reaction with electrolyte	150–300	~1,600 J/g-cathode[a]	~23 KJ
Self-reaction of salt with solvent	250–400	~900 J/g electrolyte[c]	~4 KJ
Complete combustion of solvent[d]	Auto-ignition temperature ~450	~18 KJ/g Solvent	~110 KJ

[a]Values estimated from DSC and ARC measurements of cell components at TIAX, for charged active (graphite and $LiCoO_2$) in contact with standard carbonate electrolyte ($LiPF_6$ in carbonate solvents)

[b]There are two parts to the anode decomposition reactions, a low temperature part typically attributed to the decomposition of SEI film, and a higher temperature reaction involving the reaction of the anode with the electrolyte

[c]Values estimated from DSC and ARC measurements of standard Li-ion electrolyte

[d]There is insufficient oxygen available inside a typical 18650 cell, even with a metal oxide cathode, to effect complete combustion of the solvent that would be present in the cell. However, if vented at high temperatures or vented in the presence of an ignition source, the solvent can burn outside the cell

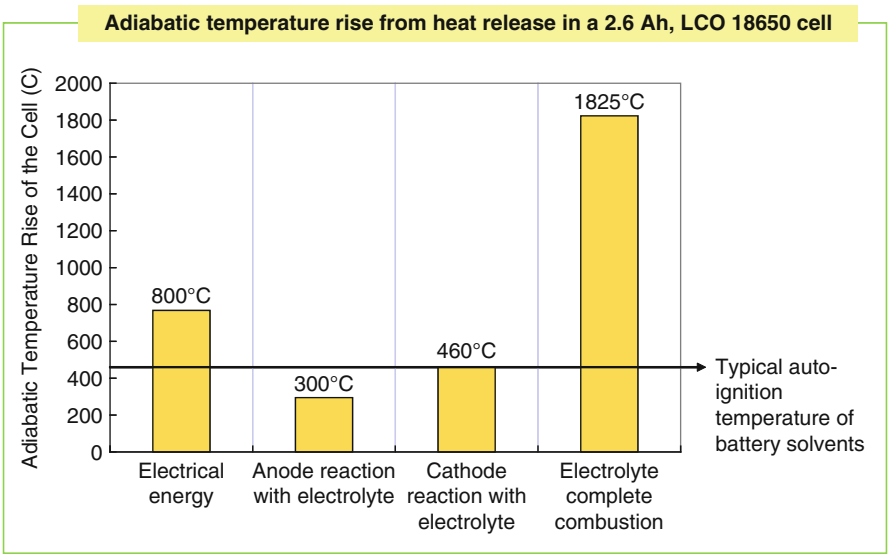

Lithium-Ion Batteries, Safety. Figure 1
Estimate of the adiabatic temperature rise from heat release in a 10-Wh Li-ion 18650 cell

combustion is nearly 33 kJ/g, meaning that complete combustion of a 2.6-Ah cell's graphite content will generate about 260 kJ.

Adding graphite's combustion heat to the energies listed in Table 1, the total energy release by an 18650 cell can exceed 400 kJ. The heat that can potentially be released within the cell absent of atmospheric combustion, shown in Table 1, can itself be significant and can drive severe cell temperature increases. The highest temperatures to which cells might be driven by these processes can be estimated by considering the adiabatic temperature rise associated with the different sources of energy release discussed above, as summarized in Fig. 1. Release of electrochemical energy alone, as by full discharge of the cell through an internal short, can raise the cell temperature by more than 700°C under adiabatic conditions. Furthermore, the anode and cathode exothermal reactions together can also raise the cell temperature by 700°C. These temperatures are significantly higher than the autoignition temperature of the solvent, and hence, if the solvent is ejected from the cell at these temperatures, it is likely to combust outside the cell, further stimulating the development of very high temperatures, and igniting the graphitic anode with explosive combustion.

Table 1 and Fig. 1 illustrate the powerful energetics underlying thermal runaway events. An increase in temperature can stimulate significant heat release from the exothermic anode, cathode, and electrolyte decomposition reactions. If the rate of heat removal is slower than the rate of heat generation, thermal runaway will eventually occur, accompanied by enormous heat release and very high temperatures.

Triggers for Li-Ion Thermal Runaway

In general, some form of trigger, or initiating process, is required to produce a thermal runaway event. The previous section amply illustrates that triggers producing increased temperature of either the whole cell or a significant region of the cell can result in thermal runaway. Table 2 summarizes some common triggers. Ideally, battery developers and implementers can utilize safety tests that specifically screen for a cell's or battery's tolerance to a given trigger.

The triggers that have received the greatest attention include abuse conditions such as external heating, overcharging, external shorting, impact, penetration, etc. Some of these triggers are relatively easy to anticipate as risks, and to study and to develop screening

Lithium-Ion Batteries, Safety. Table 2 Summary of triggers that can lead to thermal runaway of Li-ion batteries

Trigger	Why can this occur?	Is this managed?
Overcharge	Defective connections, failure of charging circuit	Yes, battery management system Yes, cell-level safety devices
Overheating from external sources	Battery back placed too close to a heat source	Yes, cell-level safety devices open the cell at suitable internal pressure
Cell crushing creating massive internal shorts	Physical abuse of battery pack	Yes, design enclosures are built more tolerant to specific abuses
Internal short-circuits (a.k.a., field failures)	Internal-short caused by manufacturing defects	No, new technologies needed
Cascading of thermal energy release	Affected cell can raise the temperature of surrounding cells	No, new technologies needed

tests for, often by selecting a set of abuse conditions that are reasonably plausible. In fact, numerous standardized (or semi-standardized) abuse tests have been developed to assess abuse tolerance (a broader all-encompassing term might be "trigger tolerance"). Examples of such tests include the hot box test, the forced overcharge test, the external short circuit test, etc. [12, 13] These tests are not reviewed in detail, except to point out that they do not generally replicate the conditions in which actual safety events occur in the field. Certain other triggers present more difficult challenges with respect to development of truly effective safety screening tests. In addition, some safety tests can be "gamed," i.e., manipulated to favorably alter the outcome by carrying out the tests under certain conditions, or by modifying cells so that they can pass the tests rather than demonstrate true tolerance to the particular abuse. Situations where definition of plausible screening safety tests may *not* be possible are highlighted. Table 2 identifies (rows 4 and 5) two such triggers.

Technologies and components such as PTCs, CIDs, vents, and safety circuits have been incorporated in today's lithium-ion cells and packs in order to manage safety with respect to many external abuse triggers.

The internal short is yet another trigger that can lead to thermal runaway. Essentially, cell discharge through the internal short causes i^2R heating and high temperatures in the vicinity of the short. High temperatures in the vicinity of the short circuit can stimulate additional heat release from the exothermic decomposition reactions described above, which can then result in thermal runaway. Thermal runaway following internal shorting is discussed in greater detail in a subsequent section describing simulation tools and results. Evidence from investigations of field-failures suggests that they are predominantly triggered by internal short circuits that are very clearly not present or detectable in fresh cells.

Tests (e.g., see Refs. [30–36]) are being developed to simulate an internal short circuit by deliberately placing particles in cells or by controlled pinch tests. There are also some advocates for the use of the nail penetration test or the round bar crush test as means of screening cells for tolerance to internal shorts. However, these tests are not standardized at the moment, and it can be argued that there are fundamental challenges in mimicking the behavior of an internal short circuit that develops only during normal charge/discharge cycling in the field. Later sections will discuss in greater detail the testing issues with respect to internal shorts, and reasons are suggested as to why cells cannot be screened for safety with respect to this trigger. Furthermore, currently there are no strategies to manage internal short-related thermal runaway of Li-ion cells. We will suggest some strategies later in this chapter.

Thermal runaway of a single cell in a lithium-ion pack will frequently stimulate a "cascading" event. In this phenomenon, some time after one of the cells in a pack undergoes thermal runaway consequent to an external or internal trigger, other cells in the battery pack also go into thermal runaway, sometimes as

a series of discrete events. The enormous amount of heat release from a cell undergoing thermal runaway can cause the temperature of one or more nearby cells to rise to the point that they too are stimulated to thermal runaway. Although cascading has been recognized as a risk for Li-ion batteries, adequate cascading screening safety tests have not been developed, and anticascading technologies are not routinely incorporated into battery packs.

The remainder of this manuscript focuses on the internal short and its critical role in triggering thermal runaway. The review of key observations summarized from our audits of field-failure incidents leads to the deduction that the majority of such safety events are due to internal short circuits caused by foreign metal particles in lithium-ion cells, and accordingly, most of this chapter focuses on them. This summary is followed by discussions of the likely mechanism of internal short formation as probed by experimental measurements. Then, simulations are described that elucidate the factors controlling thermal runaway following an internal short circuit, and that provide the basis for a novel construct allowing the first "quantification" of Li-ion battery safety associated with any given cell and its operating environment. The key differences between abuse tolerance and field-failures are then described, followed by discussion of an overall framework to improve the safety of Li-ion batteries.

Key Observations from Analysis of Field-Failures

This section summarizes key observations from our direct investigations of lithium-ion battery field-failures, including work carried out with some of the largest battery and portable device manufacturers in the world. While confidentiality restrictions prevent us from incorporating specific details of these safety incidents, we are able to highlight major observations and insights gained from this work, and from other sources. We have learned that:

- Field-failures occur at a frequency of one failure in 5–10 million cells for the most accomplished manufacturers. Such failures are overwhelmingly attributable to internal short circuits occurring during otherwise "normal" operation, with no outward signs of impending failure.
- These internal shorts are not discernible at the point of manufacture but appear to develop over time. Typically, the failure occurs only after a significant service time in the field (e.g., more than 3 months) and may not occur for 1–3 years. Thus, "fresh" cells do not necessarily exhibit the conditions that lead to a safety event.
- A high proportion of these internal short circuits are caused by extraneous (foreign) metal particles introduced into the cell during the manufacturing process. Evidence for such particles can be found in cell postmortems, except that a high level of destruction often hinders or prevents satisfactory investigation. While metal particles may enter the cell-making activity with incoming materials, they also can be produced by a wide variety of the material processing and metal cutting and shaping operations used in cell manufacturing. The exact composition of the metal causing a given field-failure is often not known with certainty, but iron, nickel, and zinc have all been known to cause field-failures; in typical $LiCoO_2$/graphite cylindrical cells, these elements are not normally present in the jelly roll, and thus have been implicated from postmortem analysis of cells.
- Various processes are employed by battery manufacturers to reduce the frequency of metal particle generation and/or incorporation in cells. These processes include extensive shrouding of key operations, strategic placement of magnets, use of higher grade metals in various operations, and aggressive monitoring of replacement schedules for all cutting and forming tools. Additional measures, such as high-pot and formation aging tests, are employed to catch and reject cells exhibiting internal shorts during cell production and qualification [37, 38].
- A surprisingly high percentage of lithium-ion cells have foreign metal particles in them. Given the rarity of field-failures, it is clear that not all particles in the cells lead to internal shorts or to thermal runaway. In fact, it is likely that the vast majority of internal short circuit defects occurring after some time in the field are manifested as a "dead" cell/pack, rather than as a violent field-failure.
- In field-failures, an induction period lasting on the order of minutes is often reported, during which

self-heating of the battery is discernible by users/observers, prior to violent flaming and explosion.

- Postmortem examinations of actual field-failures indicate that all or portions of a cell have experienced very high temperatures. For example, cells from incidents routinely exhibit multiple localized silver-colored metallic beads. These beads are recondensed aluminum, which melts at 660°C. In some instances, there are areas in which copper current collectors have also experienced melting. Copper melts at 1,085°C.
- Neither the actual mechanism of short circuit initiation nor the mechanism by which an internal short leads to a thermal runaway is fully understood yet. After the fact, postmortems show a level of destruction that renders it impossible to ascertain the exact morphology that existed at the point of thermal runaway. We use experimental and simulation results to discuss the likely mechanism of short formation, and the factors that control thermal runaway following an internal short.

Implications for Managing Field-Failures

Most safety incidents that have been observed and evaluated involved portable computer battery packs. Although some incidents have taken place in mobile phone batteries, computers use many more cells, with cells in series and in parallel. Our discussion of the mechanism of short initiation will show that such failures are also possible in HEV, PHEV, and BEV cells. Without suitable safety technologies in place, safety incidents in HEV, PHEV, and BEV packs are likely to be more severe than those observed in laptops owing to the larger cell sizes employed (approximately 2–30 times on an energy basis) and the lower impedance of the cells. Furthermore, with roughly 75–80 cells per pack (for cells in a single string) and the total energy per pack approximately 20–200 times larger than that of computer packs, the consequences of thermal event "cascading" is a major concern. Field-failure in a vehicle pack could inflict far greater damage than that caused by notebook computer batteries.

Because the consequences of these rare safety events can be so serious, especially with increased use of lithium-ion in transportation applications, it is necessary to recognize that no manufacturing environment can always operate with zero defects. Therefore, given the recognition that foreign particles in cells can never be completely eliminated, there is a need to develop safety technologies that are "on guard" to catch their deleterious effects as early as possible. A useful perspective is to recognize that achieving Li-ion systems which are totally free from the threat of spontaneous safety events is *not* a quality problem. For example, the rate of field-failures for cells produced by the most experienced manufacturers is already at a very low level – one failure in 5–10 million cells produced, which already far exceeds six sigma manufacturing quality guidelines. These manufacturers typically benefit from the most powerful elements of a learning curve – they have produced large numbers of cells (over a billion in several cases) over a very long period of time (more than a decade). It is reasonable to assume that less-experienced manufacturers will eventually approach similar levels, but no manufacturer will achieve zero defects in perpetuity.

Manufacturing improvements should, of course, continue to be implemented whenever possible, but it should be recognized that improvements in the cleanliness or quality control of manufacturing lines are not the fail-safe solution. Manufacturing "quality" is already maintained at a very high level. The defect rate is already very low and not readily correlated with the level of small extraneous metal particles in cells. Greatly reducing the level of particles in cells could probably only be accomplished with significant (and unacceptable) additional processing costs. (For example, consider the manufacturing quality levels that must be achieved in the semiconductor industry, and the associated costs.) Clearly, a new approach is needed to make significant progress toward improving the safety of Li-ion batteries and, in particular, to deal with the insidious role of the internal short circuit in causing lithium-ion safety events.

We have been developing tools and techniques to enable the development of new technologies to manage field-failures. In the following sections, some insights are described that have been gained from exercising these tools; namely, the likely mechanism by which a foreign metal particle forms an internal short, and the mechanism by which an internal short then stimulates thermal runaway.

Likely Mechanism of Internal Short Formation in a Field-Failure

The exact mechanism of field-failure due to foreign metal particles in cells may never be known with certainty, given the rarity of events and the extensive destruction that takes place in affected cells. The realization that field-failures are rare has a number of practical consequences for studies of internal short formation, for attempts to identify electrical signals warning of developing internal shorts, and for development of any safety technology. In particular, a reliable method(s) to generate internal shorts "similar" to those that lead to thermal runaways in the field is essential. Although not discussed in detail in this chapter, we have developed several methodologies to create internal shorts in cells. This section describes the most likely mechanism for initiation of the internal short circuit from metal particle contamination and how we have used internal short implantation methods to investigate that mechanism.

The most likely mechanism for initiation of the internal short involves the formation of a metal dendrite between the anode and cathode. In this process, a metal particle present in or on the cathode (positive) will dissolve by an electrochemical oxidation process, and the resulting metal ions will diffuse to the anode (negative) where they will plate, often over an extended period of time and many charge/discharge cycles, resulting in the formation of a metallic dendrite that eventually makes a durable electrical contact back to the cathode and shorts the cell. In the field, the exact location of the short in a cell is also a critical factor with respect to occurrence of thermal events. We have confirmed this mechanism by implanting particles of iron and nickel in Li-ion cells.

Figure 2 provides experimental evidence supporting this mechanism. The top left panel of Fig. 2 illustrates a cell constructed with a large (oversized relative to particles implicated in field-failures) nickel particle with thickness of either 50 or 100 μm placed on the cathode current collector. The bottom pane of Fig. 2 shows the subsequent cycling of this cell to the point of development of an internal short. Postmortem examination of the cell was very instructive. The top right panel of Fig. 2 shows deposits of plated metal adhered to the separator. Inspection of both sides of the separator shows that the deposit's area is larger on the anode side than on the cathode side, clearly indicating the direction of its growth from the anode to the cathode. Furthermore, EDAX of the anode itself shows deposition of nickel on the anode, which of course was not present prior to cell assembly. Taken together, these results clearly show the operative mechanism for formation of internal shorts. Metal particles on (and possibly in) the cathode dissolve and plate out on the anode, growing back through the separator, leading to an internal short.

It is not surprising that a nickel metal particle present in the cathode would result in shorting of the Li-ion cell. The standard potential for Ni/Ni^{2+} is 2.9 V (vs Li/Li^{+}), implying that Ni will dissolve at typical cathode potentials >3.5 V (vs Li/Li^{+}) and plate at typical anode potentials <1.5 V (vs Li/Li^{+}). Similar behavior is also expected of Fe; the standard potential for Fe/Fe^{2+} is 2.6 V (vs Li/Li^{+}). Separate cyclic voltammetry experiments on Ni and Fe foils in Li-ion battery electrolytes also confirmed this mechanism. This mechanism also explains why internal shorts can develop even on open circuit and explains how the shorts can "grow" over time and not be present for some time after manufacture of the cells. Plating and dendrite growth is a stochastic process, and induction of the overall cell shorting process is also likely to be so. Thus, several factors can limit the rate of dendrite growth and probably even its occurrence.

It has also been experimentally confirmed that metal particles placed on the cathode in 18650 cells can cause internal short circuits capable of inducing thermal runaway (sample result shown in Fig. 3). These experiments will be detailed in a future publication. Using this sort of test platform, the resistance of shorts and the evolution of that resistance during tests can be estimated. It has also been possible to evaluate variations in behavior of various metals and variations in the nature of deposits formed with different metals. Judicious placement of particles can also lead to short formation and cell failure after multiple charge/discharge cycles (as opposed to during the initial charge). The delayed short formation facilitates efforts to identify precursor signals that can warn of development of an internal short in the field.

Several factors can determine how a short might grow from a foreign metal particle, and hence

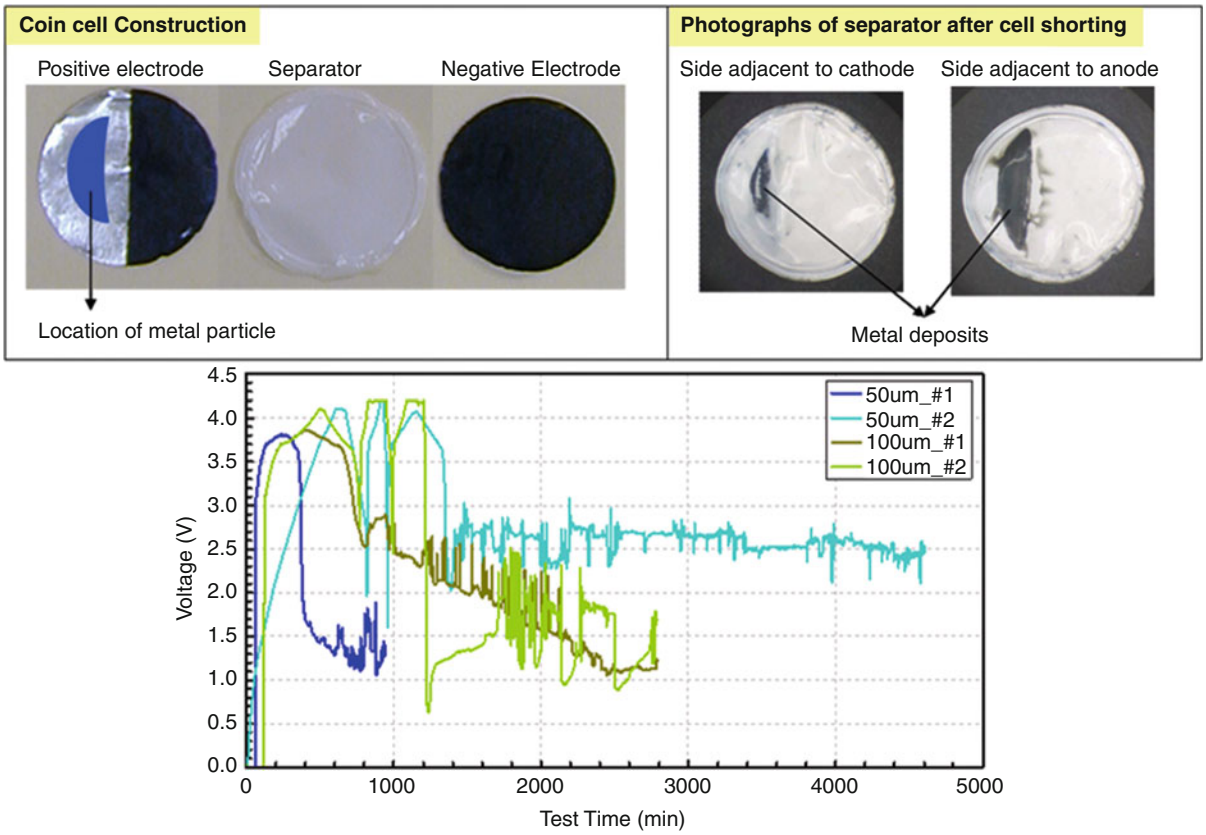

Lithium-Ion Batteries, Safety. Figure 2

Internal short formation in a coin cell. Photographs in the *top left panel* show the coin cell construction for these tests. A crescent-shaped Ni particle was placed on a scraped-off portion of the positive electrode. The cycling data on the bottom panel show the formation of an internal short circuit in the cell during normal charge/discharge cycling, for two different thicknesses of the Ni particle (two different coin cells for each particle thickness). The photographs in the *top right panel* are of the separator from one of the coin cell tests. The metal deposits can be clearly seen. The cathode active material was $LiCoO_2$, the separator was Celgard 2325, and the anode material was MCMB2528

determine the magnitude and rate of local i^2R heating as the cell discharges through the short circuit. These factors include: the nature of the metal, the size and shape of the particle, the rate capability of the cell, separator permeation and thermal properties, charge/discharge history of the cell, and temperature distribution/history. At this moment, there is insufficient experimental data to comment on the relative contributions of these factors in determining the rate and magnitude of heat release through the short circuit. However, we are performing specially designed experiments to probe these factors and will discuss some of them in a forthcoming publication.

Other Possible Mechanisms of Internal Shorting

There are various ways in which an apparently normal cell might develop an internal short in the field [39, 40]. However, the nature of the internal shorts formed by these different routes, and the extent to which they may or may not be likely to induce thermal runaway, might be very different. Mechanisms cited in the literature or generally discussed by battery engineers that implicate foreign metal particles are summarized below:

- *Lithium deposition/dendrites* form during cell operation for a number of possible reasons, including charge processes that drive the anode to the lithium

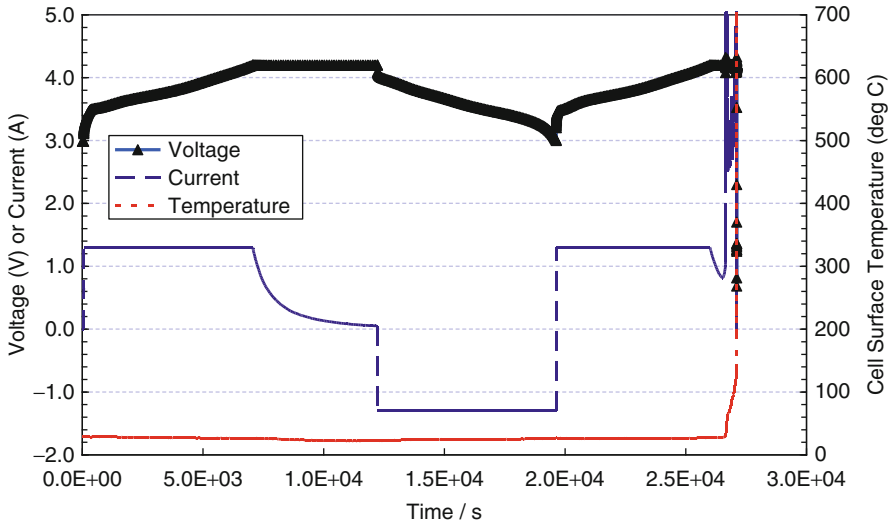

Lithium-Ion Batteries, Safety. Figure 3

Response of an 18650 cell following deliberate implantation of a metal particle on the cathode of the cell. In this experiment, a fully discharged commercial 18650 cell was removed from its can. The jelly roll was partially unwound, and a metal particle was placed on the cathode side. The jelly roll was then placed in a suitably sized can and normally cycled. The cell experienced thermal runaway during normal charge/discharge cycling

potential or as a result of lithium imbalance in the cell. Unintentional overcharge due to a faulty BMU can also result in lithium deposition on the anode, with repeated overcharging leading to lithium dendrite growth. There is also evidence reported for foreign metal particles on the anode surface serving as nucleation sites for lithium deposition. There is no doubt that lithium deposition occurs in lithium-ion cells under a variety of circumstances. We suspect that lithium dendrites can lead to internal shorts, resulting in premature cell failure. However, lithium dendrites are less likely to dissipate sufficient power to enable thermal runaway than are dendrites of higher melting point metals. Our simulations show that the temperature of the dendrite itself can significantly exceed the melting temperature of lithium metal (180°C). Hence, it is less likely that lithium deposits/dendrites could support powers similar to those possible with metal contaminants such as Ni or Fe (melting temperatures >1,400°C).

- *Particle migration and separator puncture.* A metal particle in the cell (presumably in/on the anode) can migrate somewhat as a result of the volume changes that occur during charge and discharge and can translate sufficiently to pierce the separator and create a short. In this mechanism, the nature of the contact between the metal and the cathode could potentially be quite different from that in the mechanism of metal particle dissolution at the cathode followed by plating back to the cathode from the anode. A complex question raised by the formation of internal shorts by metal particles (and a probable driver of the process's highly stochastic nature) is how a durable contact is eventually established between the high voltage cathode and the relatively easily oxidized and dissolved metal. In the dissolution/plating mechanism, the growing dendrite might contact some of the original metal particle remaining on and contacting the cathode, and furthermore, the ongoing dissolution/plating process could result in multiple and repeated contacts being made between the growing dendrite and the cathode, providing many opportunities for a durable short to be established. The mechanism of particle migration and separator puncture might be less likely to yield a durable cathode contact that is capable of supporting a thermal runaway-inducing power dissipation level.

- *Lower power particle short induces separator melting, creating a higher power short.* It has been postulated that a small particle-based internal short, rather than itself dissipating sufficient power to stimulate thermal runaway, generates only enough heat to cause localized separator melting and a larger area face-to-face interelectrode short. This larger short then stimulates thermal runaway.

A number of technologies have been developed to address some of the above scenarios. High puncture strength and high melt strength separators have been developed. Numerous organizations across the battery industry have elected to deploy ceramic layers, implemented as porous coatings on electrodes or separators in cells, as a means of enhancing lithium-ion battery safety. Although such efforts may be effective in preventing the separator puncture or melting scenarios, there is a danger in viewing them as a panacea. These separators and ceramic layers are all necessarily highly porous (otherwise they will compromise a cell's performance), and so the mechanism of particle dissolution and growth of dendrites to the point of internal shorting will still be operative. In our limited testing of cells containing ceramic layers, we have indeed observed formation of internal shorts, including those that mature to thermal runaway, in cells that have been seeded with a particle on the cathode. Therefore, technologies such as ceramic layers may lessen the frequency of internal short occurrence but should not be viewed as eliminating the problem.

Factors Influencing Thermal Runaway from Internal Shorts

As we described earlier, an internal short circuit can cause the local temperature to rise "in the vicinity" of the short, which then stimulates additional heat release due to exothermic anode reaction with electrolyte and cathode reaction with electrolyte. Whether or not thermal runaway follows from such an internal short is a particularly complex problem because:

1. An internal short initiates with a highly nonhomogeneous temperature distribution in the cell due to heat generation in a very small area (a "hot spot")
2. Local temperatures get high enough, fast enough to stimulate exothermic decompositions on a local basis
3. Whether thermal runaway follows from this nonhomogeneous temperature profile is determined by a complex interaction among instantaneous values of temperature, concentrations, and rates of reactions, as well as applicable heat transfer both within the cell and out of the cell through its surface

Simulations allow us to understand this complicated relationship and to identify the critical parameters that can alter this relationship to prevent thermal runaway.

Model Description

We have developed a model that is capable of fully three-dimensional, transient simulations of the thermal response of the cell following an internal short circuit. The model employs a commercial finite element analysis (FEA) code, Abaqus, augmented with our own subroutines. Key features of the model are highlighted in Fig. 4. Abaqus was augmented with subroutines for calculating local heat generation from the short circuit and from anode and cathode decomposition reactions. An effective model must consider not just the total heat release which was discussed earlier but also the kinetics (how fast can the heat be released?). Kinetics submodels for heat generation can be derived from differential scanning calorimetry (DSC) or accelerating rate calorimetry (ARC) measurements of charged anode and cathode materials in contact with standard electrolytes. The measurement techniques and conversion to useful kinetic rate expressions will be detailed in a future publication. The model also incorporates representative thermal properties (specific heat, thermal conductivity, density) for the various components of the Li-ion cell. These were either measured in our labs or taken from the published literature (including Refs. [41, 42]). Dissection of state-of-the-art 18650 cells provided estimates of cell properties such as weights of anode and cathode materials, current collector dimensions, can dimensions, etc. The model also incorporates a submodel for separator shutdown kinetics and is being augmented to incorporate a submodel for electrochemical

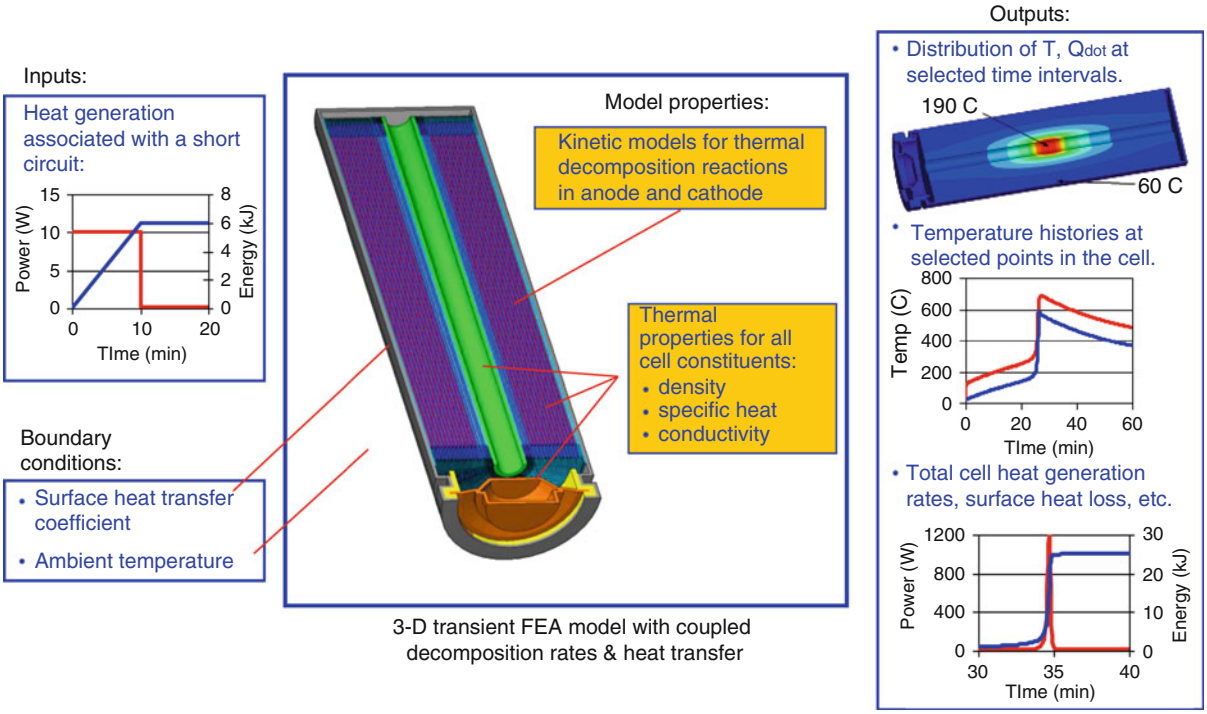

Lithium-Ion Batteries, Safety. Figure 4
Key features of our FEA model to simulate thermal runaway of Li-ion cells

kinetics and pressure, including pressure release from the local temperature rise and decomposition reactions.

The model allows the internal short to be placed anywhere in the cell and typically represents the short as a constant power, localized heat source that acts for a specified period of time. (The ability to terminate the short after an arbitrary period of time is a unique and valuable benefit of a model, for reasons revealed below, that is not available in actual short circuits). Surface heat transfer coefficients and ambient temperatures are specified as boundary conditions. The initial cell temperature is also specified. The transient heat transfer model calculates and keeps track of the local values of temperature, species concentrations, extents of reaction, and heat generation rates at every time step. The model can be two-dimensional or fully three-dimensional, depending on the degree of symmetry afforded by the geometry of the cell and the conditions that are being evaluated, such as the location of the short. For example, for an 18650 cell, if the short is near the center of the cell, the results of a two-dimensional, axisymmetric model are essentially the same as those of a fully three-dimensional analysis of the same conditions. This opportunity for simplification is not available for a short that is located near the outer surface of the jelly roll.

Thermal Runaway Induced by an Internal Short

The following sample simulation illustrates the progression of thermal runaway following an internal short circuit. Consider an 18650 cell which has a 10-W internal short circuit starting at time t = 0 near the center of the cell, and lasting for 1,410 s in this simulation. For this two-dimensional, axisymmetric simulation, Fig. 5 shows the time dependence of temperature in the vicinity of the short and at the cell surface (midway between the top and bottom of the cell). Figure 6 shows the temperature distribution in the cell at select times, and Fig. 7 shows the cumulative heat release and extent of reaction for the anode and cathode decomposition reactions. A surface heat transfer film coefficient of 10 W/m^2-K was employed,

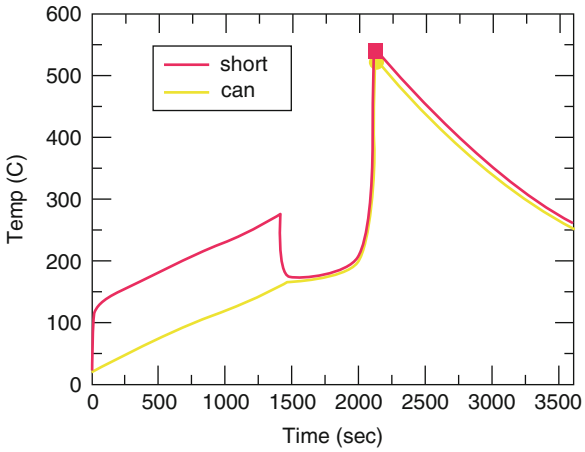

Lithium-Ion Batteries, Safety. Figure 5
Temperature history in the vicinity (~2 mm away) of the short circuit and at the can surface for a 10-W short circuit that is active for 1,410 s in a 2.6-Ah 18650 cell

corresponding to nearly quiescent ambient conditions. The initial temperature and ambient temperature were both set to 20°C.

The results shown in Figs. 5–7 can be considered in terms of three distinct time periods. In the first time period, the temperature in the vicinity of the short circuit is higher than that at the outer extremities of the cell, owing to heat generation from the short circuit (which has been placed near the center of the cell). The internal short is a localized heat source, or hot spot. In practice, this heat source can be driven from other cells in the battery pack or just from the shorted cell itself in the case of an isolated cell. In addition to electrical heating, heat release from the anode and cathode decomposition reactions, occurring wherever critical onset temperatures in the cell have been exceeded, also contributes to the temperature rise. As shown in Fig. 6, the iso-temperature contours are oblong in this

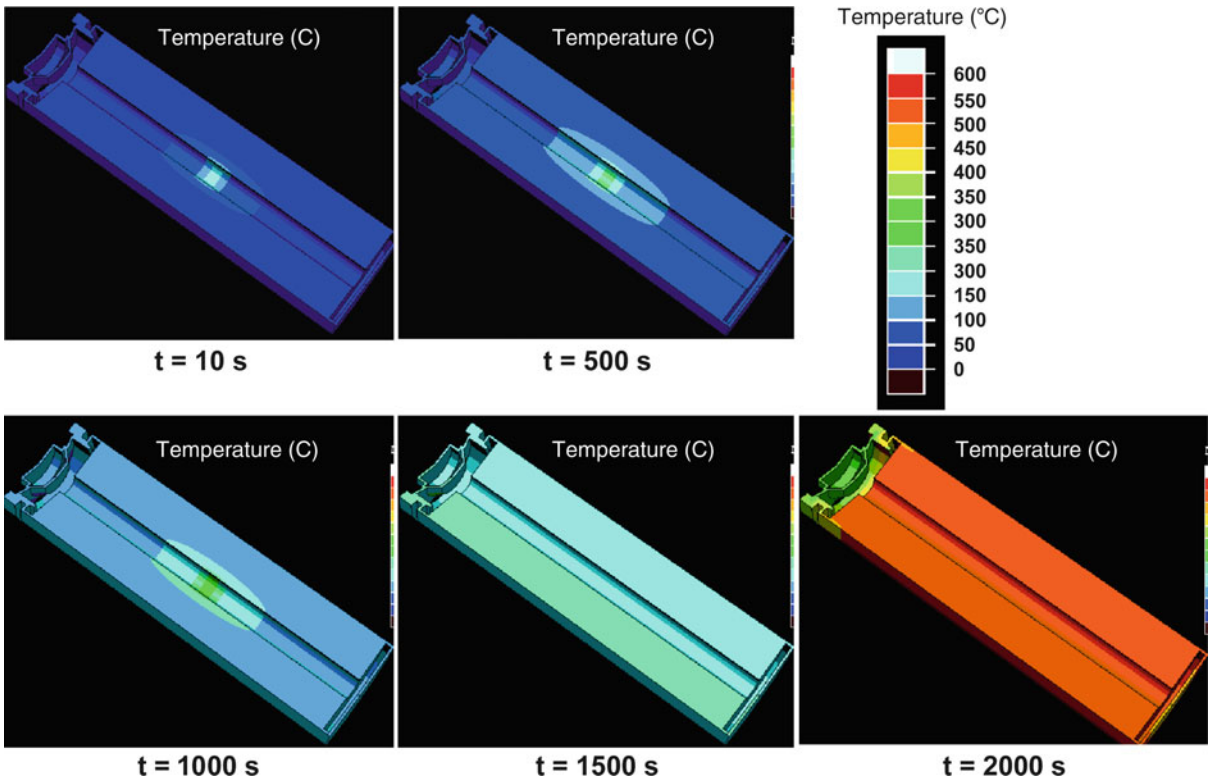

Lithium-Ion Batteries, Safety. Figure 6
Temperature distributions corresponding to the simulation in Fig. 5 showing the progressive change in temperature in a cell following the formation of an internal short circuit that leads to eventual thermal runaway

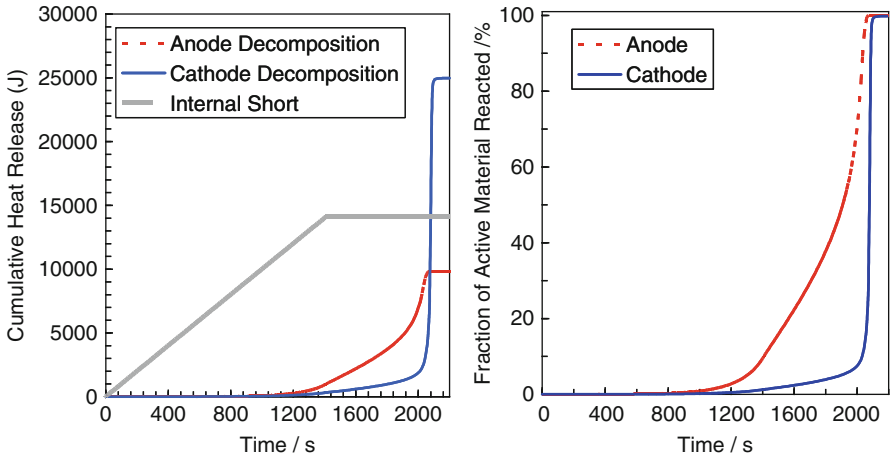

Lithium-Ion Batteries, Safety. Figure 7
Cumulative heat release (plot on the *left*) and the extent of reaction (plot on the *right*) for the anode and cathode decomposition reactions, corresponding to the simulation results in Fig. 5

time frame due to significantly higher thermal conductivity in the axial direction of the jelly roll compared to the radial direction.

Once the short power is reduced to zero at 1,410 s, the cell temperature quickly becomes uniform, as heat transfer internal to the cell equalizes the temperature within the cell.

In the second time period (from about 1,410–2,000 s), there is no longer a contribution from the local heat source because the internal short has been turned off. The temperature continues to increase, albeit at a much slower rate. In this time frame, the rate of heat release from the decomposition reactions is only slightly higher than the rate of heat loss at the cell surface, resulting in a gradual rise of the cell temperature. As can be seen from the results in Fig. 7, it is primarily the exothermal anode decomposition reactions that contribute to this heat release; the energy contributed from the cathode decompositions is insignificant in this time frame. The anode decomposition reactions assume a triggering role because their rates (and hence the associated heat release) become significant at a lower temperature than the cathode decomposition reactions, and hence, the anode reactions proceed to a greater extent than the cathode reactions in this time frame. The particular example and corresponding set of conditions being discussed here have been chosen to illustrate a condition in which a sufficient percentage of the material in the cell has been elevated to a temperature that is just above the "point of no return" on the path toward thermal runaway. In an equivalent simulation in which the internal short is turned off just 10 s sooner at 1,400 s, discussed below and shown in Fig. 8, no thermal runaway ensues. The substantial length of time for which an internal short can be active prior to inducing thermal runaway suggests that there may be sufficient time to intervene and prevent a thermal runaway if adequate signals indicating development of an internal short can be identified.

In the third time period, beyond about 2,000 s, the cell begins to heat up dramatically and goes into thermal runaway. Self-heating of the cell accelerates because the rates of the anode and cathode decomposition reactions accelerate with rising temperature and because the extent of active material in the cell that contributes to this heat generation also increases. The combination of these factors results in an unstable increase in temperature which is known as thermal runaway. The rapid rise in temperature is roughly what witnesses report when they have been in proximity to lithium-ion field-failures. Note not only the very rapid rise in temperature in Fig. 5 once thermal runaway has initiated, but also the general range of temperatures that are realized as a result of the runaway. The latter reflects the general range of temperature

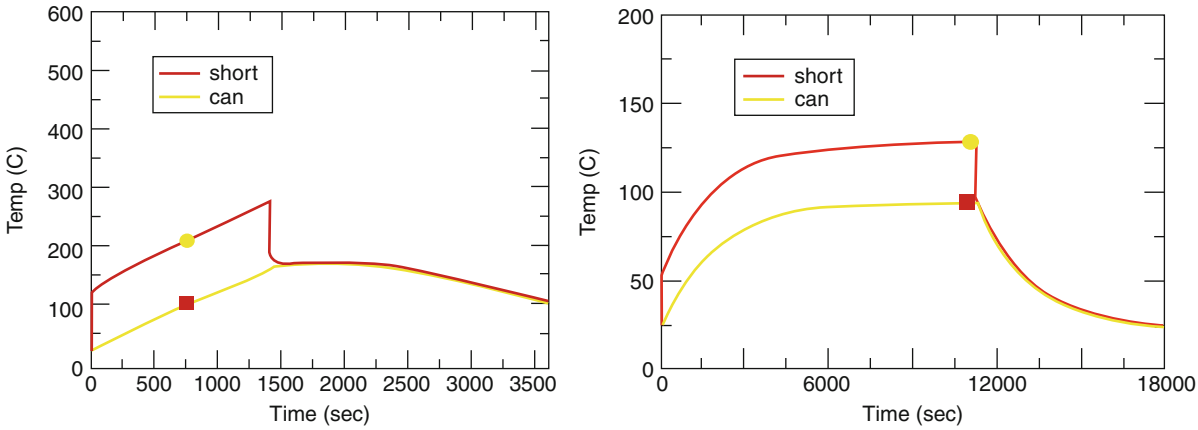

Lithium-Ion Batteries, Safety. Figure 8

Simulated temperature profiles for two conditions where thermal runaway does not occur. The plot on the left corresponds to the case where a 10-W short was active for 1,400 s. The plot on the right corresponds to a short power of 3.5 W, which was active until the cell completely discharged through the short circuit without causing thermal runaway

known to occur in safety incidents because of the evidence (previously cited) that is obtained from cell postmortems.

The above discussion illustrates the complexity of thermal runaway induced by an internal short. Furthermore, the rapid rise in temperature at ~2,000 s illustrates one of the reasons that material-level heat release from DSC or ARC measurements by themselves are not likely to be relevant predictors of relative safety of various cathode materials. Note how in Figs. 6 and 7 the progression to a thermal runaway is inevitable beyond about 1,410 s, at which point the short has been turned off in this simulation, and note how the cell quickly traverses a wide range of temperatures (in this case, from about 150°C to about 550°C) as runaway proceeds.

As mentioned above, this model has also been used to explore the conditions under which thermal runaway will not occur. Figure 8 shows results for two conditions where thermal runaway does not occur. The figure on the left corresponds to a 10-W short, otherwise identical to the one depicted in Fig. 5, which is active for 1,400 s, whereas the figure on the right corresponds to a 3.5-W short that is active until the cell completely discharges through the short. All other conditions are identical to the simulations corresponding to Figs. 5–7.

Comparing the results in Fig. 5 with the left hand plot of Fig. 8 shows that the energy dissipated in the short is a key factor in determining thermal runaway. Essentially, when the 10-W short is active for 1,400 s (Fig. 8), thermal runaway does not occur. But when the 10-W short is active for only 10 s longer (Fig. 5), thermal runaway occurs. Thus, there is a minimum energy (or "threshold energy") that must be dissipated in the short before thermal runaway will occur. The specific value of that threshold energy is related to cell design, materials employed, and operative heat transfer conditions. Of course, slight variations in any of these parameters might result in a different threshold energy.

The right-hand plot in Fig. 8 shows a case in which short power has been reduced in successive simulations until thermal runaway does not occur no matter how long the short is maintained in an active state (a "threshold power"). Note the parallel lines in Fig. 8 beyond about 5,000 s, corresponding to the state in which the rate of heat generation in the cell is exactly equal to the rate of heat loss from the outer surface of the cell. Since the experiment is bounded by the total energy of the cell, the short essentially terminates when there is no capacity remaining in the cell. As can be seen in the figure, the cell temperature then decays to room temperature.

The Concept of a "Safe Zone"

The results presented in Figs. 5, 7, and 8 have been chosen from a larger number of simulations because, in combination, they illustrate how a new figure can be constructed from simulations to demarcate a "Safe Zone" for a given cell construction and cell materials and for the associated heat transfer conditions. Figure 9 illustrates the construct for a generic 18650 cell. In this figure, various short powers are represented on the x-axis. The y-axis corresponds to the relative energy dissipated in the short as a percentage of the total electrochemical energy in the cell.

Figures 5, 7, and 8 represent conditions that can be placed on this chart. The 10-W short begins at t = 0 corresponding to zero energy release on the y-axis and moves vertically with increasing time. At 1,400 s, there has been insufficient energy input to stimulate a thermal runaway, but at 1,410 s, thermal runaway ensues. A threshold energy has been exceeded. Running a series of such simulations, a family of such situations can be constructed, demarcating a threshold energy curve on the plot.

Similarly, Fig. 8 (right) has already demonstrated existence of a threshold power below which no thermal runaway is possible, no matter how long the short is in place. The existence of a threshold power implies that there will be a finite range of short resistance capable of dissipating sufficient localized heat to stimulate thermal runaway. If short resistance is above this critical range, insufficient current is supplied to the short. The critical short resistance range will be defined by the characteristic of the cell and pack.

Note in Fig. 9 how the threshold energy curve rises sharply as short power is reduced to values approaching the threshold power. The resulting cross-hatched area is a "Safe Zone." Internal shorts with power or energy characteristics within this region will not induce thermal runaway. In practice, the threshold power is a more critical parameter, since in the field there are no practical means to interrupt an internal short once it has been initiated. Implications of the threshold energy curve's shape will be discussed in a future publication.

Note that a "Safe Zone" plot can be constructed for any lithium-ion cell, representing the particular cell size and design (i.e., form factor, capacity, electrode dimensions, etc.) and materials employed, as well as the particular heat transfer conditions that apply. One can use

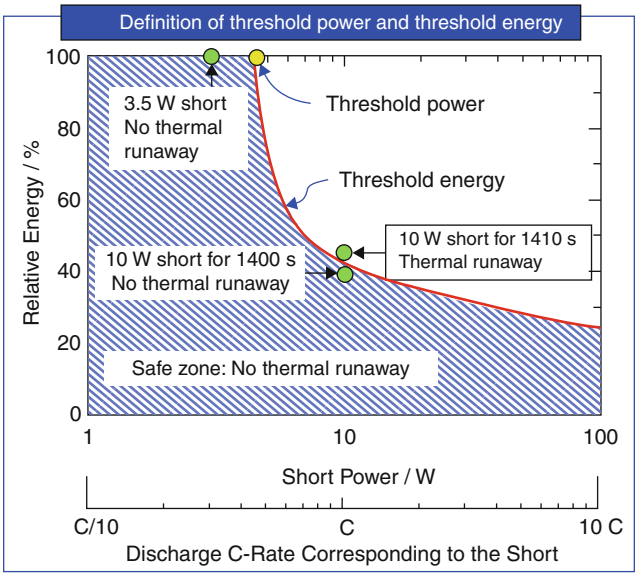

$$RE = \frac{E_s}{E_e}$$

RE: Relative Energy

E_s: Energy dissipated in the short

E_e: Electrical energy stored in the battery

Lithium-Ion Batteries, Safety. Figure 9
The Safe Zone construct

Safe Zone plots to compare the relative safety of various cells and/or materials, as well as to evaluate the relative safety of cells under various heat transfer conditions.

Illustrative Applications of the Safe Zone Concept

The Safe Zone concept allows a quantitative assessment of safety in a way that has not previously been possible. There are numerous ways that the Safe Zone concept may be employed, including as a tool to design safer cells, to assess the safety impact of various system design changes, to assess the impacts of various materials changes, and to consider the relative risk of cascading in a battery pack. The following describes an example of one such use of the Safe Zone concept.

In the last few years, there have been multiple discussions regarding the relative safety of cylindrical cells versus prismatic cells. The subject is attracting a great deal of attention with respect to transportation applications. It has generally been accepted that prismatic cells are safer and will allow superior cooling. But how can this advantage be quantified, and how can it be linked to cooling conditions as well as cooling requirements? The Safe Zone concept, and the associated concept of a threshold power, provides the necessary quantitative basis to allow these problems to begin to be assessed as engineering issues, rather than as a matter of intuition.

Cylindrical and prismatic cell designs with identical capacity (33 Ah, as might be used in PHEV applications) were modeled with identical internal short circuits to assess the threshold power parameters. Figure 10 illustrates the cell designs.

Initial cell temperature was set at 20°C, the surface heat transfer coefficient was set for both cells at 10 W/m^2-K, and the short was assumed to be located near or at the middle of each cell. Simulations were carried out for various short power levels in order to understand and quantify the power levels associated with safety events in these two cells. Figure 11 illustrates the results for an internal short of 12 W, in particular showing the rapid transition of temperatures throughout the cylindrical cell over the critical few seconds when the cell goes into thermal runaway. Similarly, Fig. 12 illustrates the temperature transitions in the prismatic cell with a 53 W internal short around the time at which thermal runaway occurs. Figures 11 and 12 illustrate the rapid temperature increase that accompanies thermal runaway for both cell types;

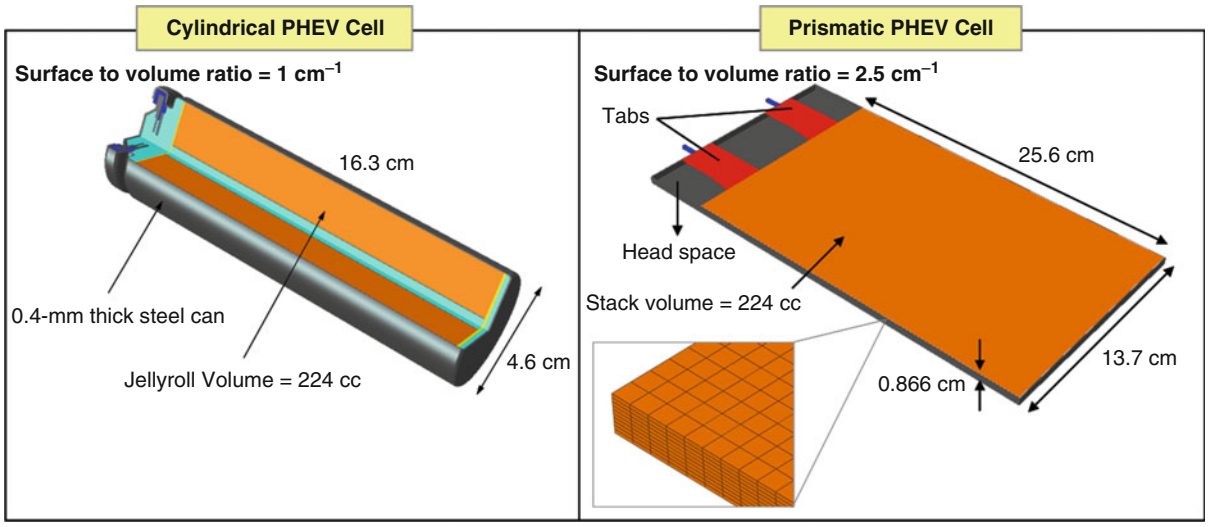

Lithium-Ion Batteries, Safety. Figure 10
Cylindrical and prismatic 33-Ah PHEV cell designs employed for simulating thermal runaway following an internal short circuit

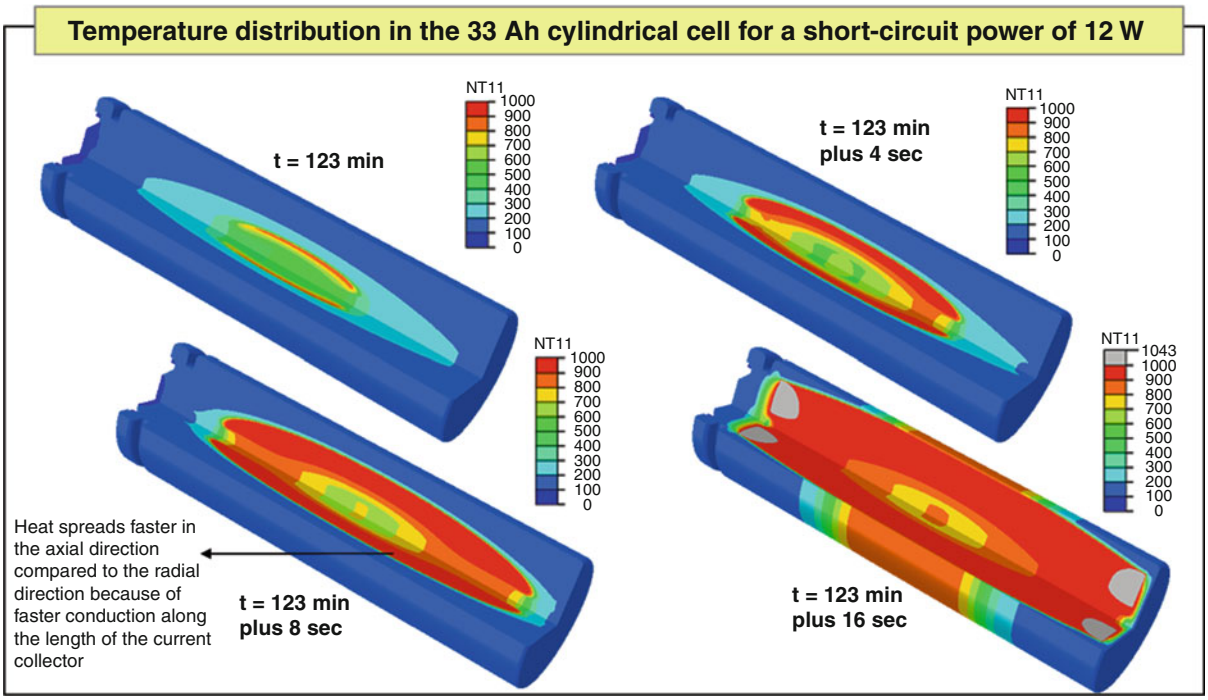

Lithium-Ion Batteries, Safety. Figure 11

Temperature distributions at selected times following a 12-W internal short circuit in the cylindrical PHEV cell

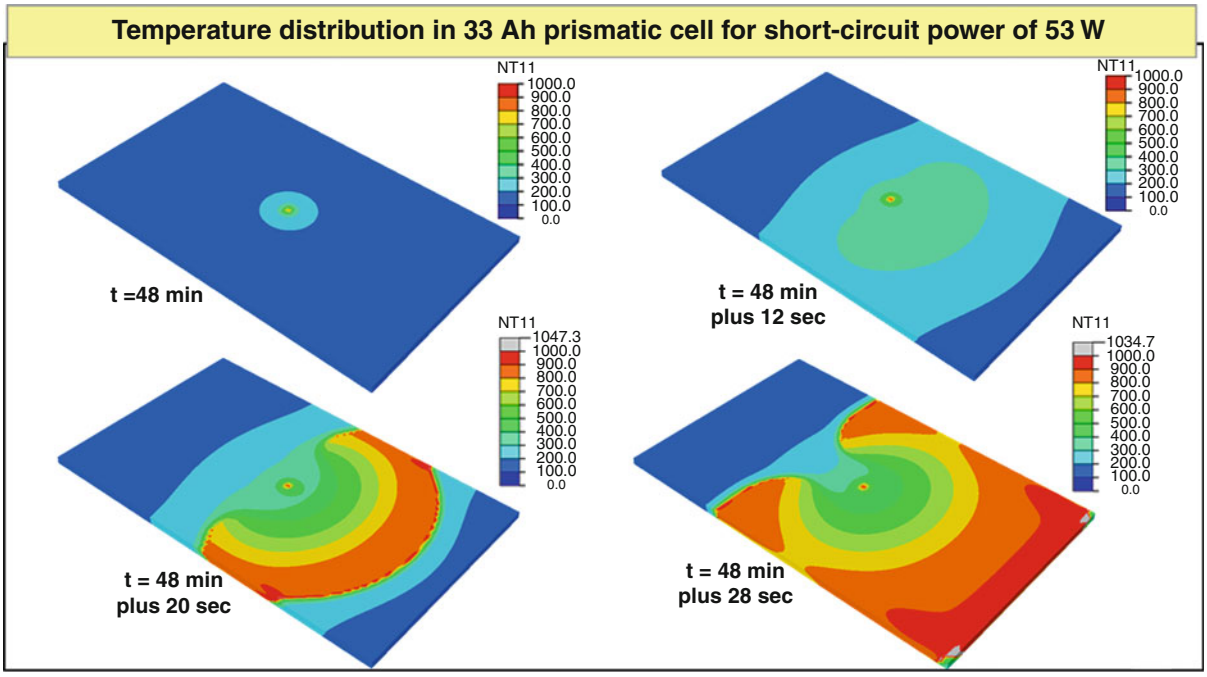

Lithium-Ion Batteries, Safety. Figure 12

Temperature distributions at selected times following a 53-W internal short circuit in the prismatic PHEV cell

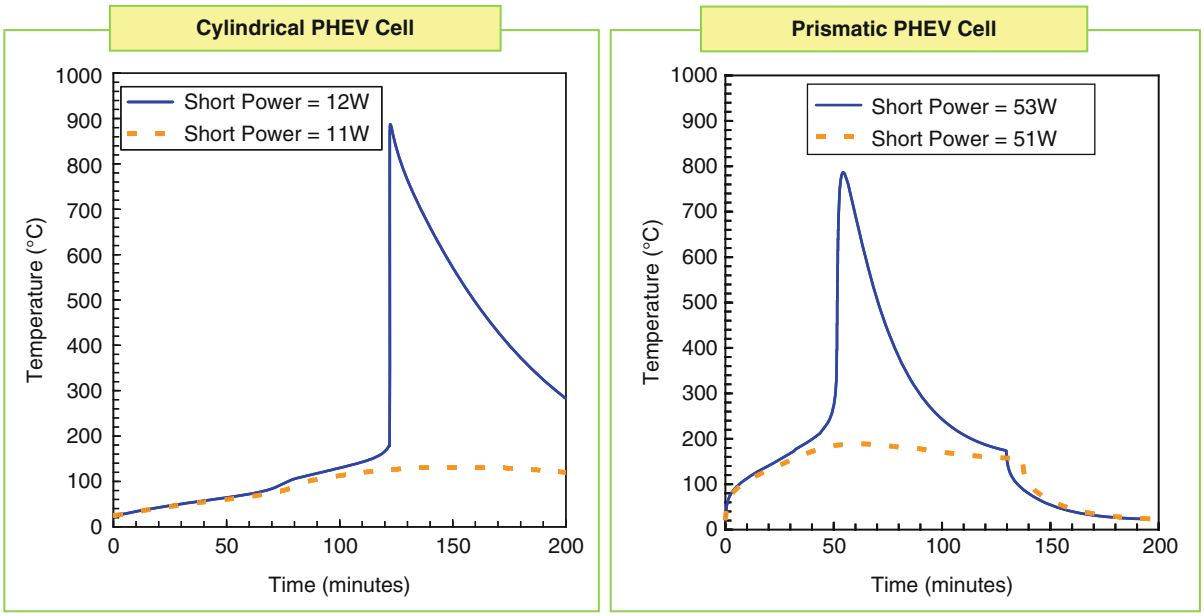

Lithium-Ion Batteries, Safety. Figure 13
Calculation of cell surface temperatures for the cylindrical and prismatic PHEV cells near the threshold power conditions

however, the actual times and short power associated with thermal runaway in these two cell types are quite different.

Figure 13 compares data for the two cell types. For the cylindrical cell, note that a short power of 11 W does not lead to thermal runaway, even at very "long" times. Comparison with the prismatic cell is instructive. For the prismatic cell, with identical capacity and an identical heat exchange environment, a short power of 51 W does not lead to thermal runaway. Short power must be increased to 53 W before a thermal runaway is observed. Thus, a quantitative methodology to evaluate the relative safety of these two cells is demonstrated. The prismatic cell provided a resistance to thermal runaway that is several factors greater than that for the cylindrical cell. Since these calculations incorporate quantitative consideration of the heat transfer conditions, a pathway is available by which it is possible to design a cooling system to prevent thermal runaway events from taking place.

Figure 14 illustrates another use of the Safe Zone construct and the concept of a threshold power. In this assessment, simulations were performed for two otherwise identical 2.6-Ah 18650 cells having different anode materials: one with MCMB 2528 (25 μm mean diameter, low surface area), and one with MCMB 628 (6 μm mean diameter, high surface area). The surface heat transfer coefficient was assumed to be 11 W/m^2-K. The FEA model for this particular set of simulations also accounted for the kinetics of separator shutdown. In this simulation, the short, rather than being modeled as a constant power source, is represented as a constant 25-mΩ resistance in series with the cell's 50-mΩ equivalent series resistance. The total power dissipated in the cell due to the short (both i^2R heating in the short and Joule heating in the jelly roll) was calculated as 220 W initially. The total power dissipated in the short was then set to decrease with time based on a function that includes the relative volume of the jelly roll in which the temperature had risen past the point at which the separator would shut down (130°C).

The right hand charts in Fig. 14 show DSC data for these two anode materials and the associated anode models that were employed in the simulations. The results of the simulations are shown on the left hand side of the figure. The results are striking – a simple change in anode material has a dramatic impact on the safety of this cell, with the cell employing MCMB 628 going into thermal runaway while the cell employing MCMB 2528 does not. DSC data on the

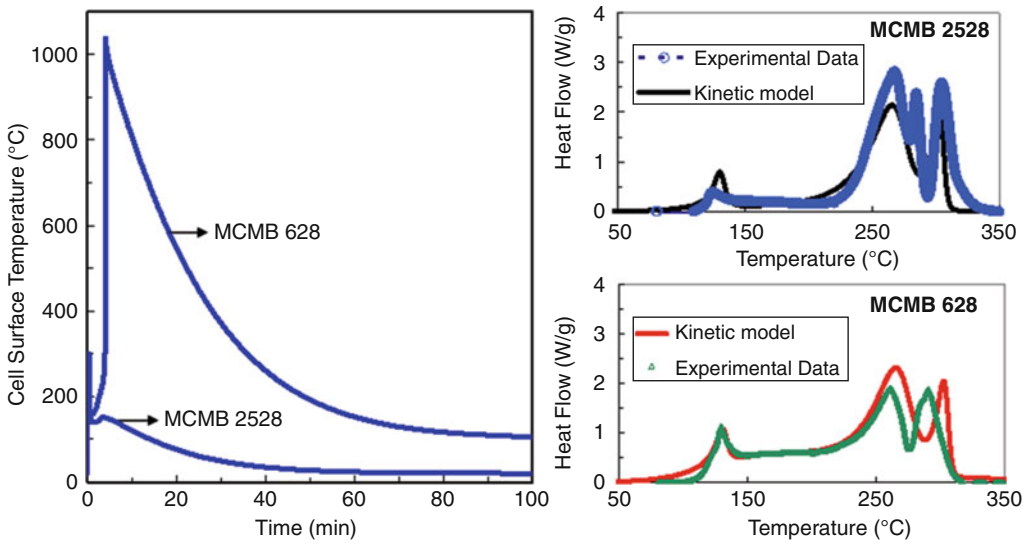

Lithium-Ion Batteries, Safety. Figure 14
Simulation results showing the effect of the choice of anode material on thermal runaway. The plot on the *left* shows the cell surface temperature time dependence for two different anode submodels

right of Fig. 14 suggest the reasons for this result. The MCMB 628 shows significantly higher heat release between 100°C and 200°C than the MCMB 2528. This example shows the extent to which the anode material acts as the trigger for thermal runaway when internal shorts and field-failures occur. Furthermore, the cell surface temperature profiles on the left side of Fig. 14 illustrate another critical factor that is not well appreciated: the cell transitions rapidly into thermal runaway well below 200°C – well before any significant exothermic decomposition of cathode material has taken place.

Differences Between Abuse Tolerance and Field-Failures

The distinction between abuse tolerance and field-failure (internal shorts) is important for a number of reasons. It helps bring into focus the extent to which historic testing for safety is focused on abuse testing, even though the actual safety events that occur in the field are quite different. From a mechanistic perspective, the triggers are fundamentally different and the resulting responses are different. The general distinctions between abuse tolerance and field-failure are summarized in Fig. 15 and discussed below.

Field-failures are overwhelmingly attributable to internal short circuits that occur during otherwise "normal" operation, i.e., there is no external abuse or trigger. In contrast, heat exposure or forced overcharge are examples of an external abuse driving a potentially unsafe situation. The response to these abuse conditions should be identical for all cells of the same cell design employing the same materials.

In response to most abuses (note that penetration- and impact-based abuses are exceptions), a cell's temperature throughout an abuse is homogeneous, until the cell fails or the abuse is terminated. All cells of the same cell design and same materials should respond to an abuse in a roughly identical manner. In contrast, field-failure involves a nonhomogeneous temperature distribution in a cell's response to an internally driven trigger – the internal short, or hot spot.

The internal short represents a particularly insidious failure mechanism not only because it takes place during otherwise normal operation but also because it is self-driven and cannot be protected against by typical safety protection devices such as PTCs, CIDs, etc. It is also how most safety incidents are initiated in the field,

Abuse Tolerance	Field Failures
Predictable	Not predictable, no warning
Common to all cells	One-in-a-million (or less)
Can/should be evaluated at the cell level by standard tests	Difficult to evaluate at the cell level, or through QC
Various chemistries can/should be evaluated for relative abuse tolerance	Cell temperature is non-homogeneous, starting with "hot spot"
Time constants relatively long, entire thermal mass of cell is heated uniformly	Much higher temperatures can occur *quickly, locally*
Can be augmented by protection devices	PTC, CID, shutdown separators, electronic controls are not effective – problem is internally driven.
Externally-driven	

Lithium-Ion Batteries, Safety. Figure 15
Summary of the key differences between abuse tolerance and field-failures

and yet the battery industry does not have adequate tests to "predict" the risk for such failures.

The lack of availability of suitable tests for the internal short should not be a surprise – any event that takes place rarely, is stochastic *and* exhibits some form of incubation process, arguably does not exhibit a detectable precondition at the point of manufacture and certainly does not exhibit a predisposal to the problem *in every cell*. Thus, the practice of removing a few cells from the manufacturing line to test for safety is fine for abuse triggers (for abuse tolerance) but is clearly inappropriate as a measure of susceptibility to development of an internal short in the field.

Perhaps most challenging is the tension between the desire of those in the battery community to have a test that they can use to screen cells for field-failure (the internal short) and the statistical impossibility of picking cells to test that have the necessary preconditions for possible internal short-induced thermal runaway, putting aside the issue of the extent to which actual charge/discharge, voltage/time, and temperature effects may impact the probability of development of an internal short. That tension has led many across the battery and application/user communities to advocate that tests such as nail penetration, round bar crush impact tests, or other custom tests mentioned earlier, be employed to screen cells for tolerance to internal shorts. There are many reasons why this approach is an inappropriate surrogate for field-failure. One reason is that the condition that leads to internal shorts leading to thermal runaway is not present in fresh cells. In addition, it is statistically impossible to identify cells that actually have some form of precondition *and* for which that precondition has matured to the point at which an internal short exists. Most importantly, the nature of the internal shorts produced in such tests is nothing like that of the shorts involved in field-failures. These abuse tests often involve multiple shorts and hard shorts; conditions that are not representative of how internal shorts occur in the field. Both modeling and actual observations have shown that a number of different variable parameters can be critical to whether a given short will cause runaway in a given cell, and thus, the possibility of thermal runaway is a complex, multidimensional response surface. The single protocol, "one size fits all" approach of internal short circuit abuse tests means that such tests fix a number of these parameters and can therefore be gamed. Thus, relative safety under internal short circuit abuse test conditions is not likely to be relevant to the tendency for field-failure.

Nevertheless, the nail penetration test, the round bar crush test, and the drop test do reflect potential triggers (in this case, abuses) that must be considered, especially for transportation applications. In such applications, it is easy to imagine impact conditions that might lead to multiple internal shorts in cells. It is

clearly desirable to understand the tolerance of cells to such abuses. The challenge, however, is to understand how representative such tests may be for the wide variety of impacts (speeds, angles, penetrations, etc.) that might occur in the field (putting aside the issue of potential gaming of the tests). Similar problems have been addressed with regard to transport of large quantities of flammable liquid in vehicles' gasoline tanks.

This abuse tolerance versus field-failure framework is also a useful way to characterize testing work carried out by various researchers, or tests that purport to address safety. For example, various tests can be assessed with respect to whether they reflect or measure a property of all cells of the same design and materials (an abuse), or whether they reflect a rare condition that develops after time in the field.

An Overall Framework for Consideration of Li-Ion Battery Safety

The fact that lithium-ion field-failures (1) are so rare, (2) cannot be completely eliminated, and (3) can cause severe damage has led us to develop an integrated framework for development of lithium-ion battery safety technologies. The framework is especially important in transportation applications. It is clear that field-failures continue to occur in portable computer applications (multiple CPSC and newspaper references can be found) and seem to attract only modest attention. However, a single field-failure in a PHEV or EV is likely to be more violent and represents greater threat to human safety. Thus, it is highly desirable to develop means to assure that such field-failures do not occur and that their impact is minimized.

The overall framework is depicted in Fig. 16 and advocates that several categories be employed to consider lithium-ion safety technologies. These categories help organize specific approaches. First are technologies that preempt thermal runaway, examples of which might include specific cell designs or specific separator types. Next, technologies to detect the earliest stages of development of internal shorts might, for example, involve identification of specific electrical signals and the use of specific sensors. Detection can be of value only if accompanied by access to effective means for intervening and preventing development of a full-blown thermal runaway. When all else fails, it is still very desirable to confine thermal runaway to just a single cell, namely to prevent cascading phenomena.

Figure 16 also captures the difficult challenge of validating any new safety technology that is developed. How can one validate a safety technology intended to address events that occur on the order of once for every 5–10 million cells without producing and testing many

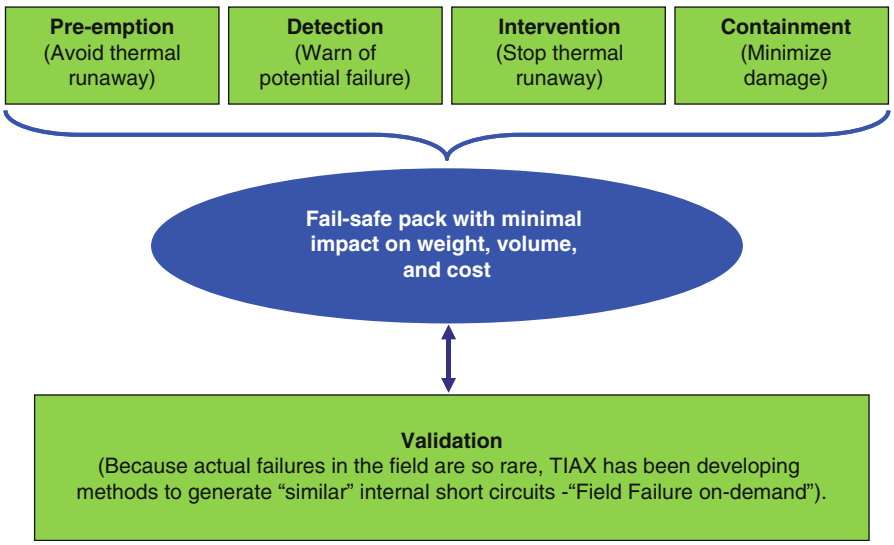

Lithium-Ion Batteries, Safety. Figure 16
Framework for consideration of Li-ion battery safety technologies

millions of cells? The challenge is fundamental, and thus, it is important to have available means of producing cell/battery failures that are arguably "similar" to those that occur in the field. For these reasons, verification of the failure mechanism is also important.

Future Directions

Abuse tolerance in lithium-ion cells is critical to public safety, and a number of screening tests for lithium-ion cells and batteries have been devised. Battery developers and users then test cells and batteries to screen for tolerance with respect to the given abuse, and then design cells and batteries with improved abuse tolerance.

In contrast, safety in lithium-ion cells/batteries requires deliberate new strategies to deal with the possible occurrence of internal shorts that can progress to thermal runaway. These strategies need to recognize the extent to which the safety tests most typically utilized in the battery industry do not reflect the most common and most dangerous mechanism by which safety incidents actually occur in the field – field-failures.

The battery community does not utilize an overall strategy to intervene, for safety's sake, as temperature rises in a lithium-ion cell or battery in advance of a thermal runaway. Although literature publications may consider the relative temperatures at which particular battery materials decompose, there is no consideration given to how these temperatures may be prevented.

The work presented in this chapter clearly shows that when thermal runaway occurs, it proceeds so fast that cell temperature progresses from less than about 150–180°C to over 600°C almost instantly. This result also indicates the fallacy in imputing safety advantages to one battery material that exhibits an onset temperature for decomposition (as captured, e.g., in DSCs) that is somewhat higher than that of another battery material (e.g., a cathode material with an onset temperature of 220°C is suggested to result in a safer cell than one with an onset temperature of 190°C). For example, the assumption is often made that cathode materials with higher onset temperatures will automatically make a cell safer or eliminate safety incidents. This work illustrates why that view has limited validity; first because anode decomposition is generally the lower temperature trigger for initiating thermal runaway subsequent to internal heating generated by an internal short, and second, because higher cathode decomposition temperature can at best increase the threshold energy for inducing thermal runaway (not the threshold power), but cannot eliminate the threat altogether.

Looking to the future, we suggest that abuse tolerance and field-failures be managed as distinct concerns. With both categories, a reasonable strategy involves identifying and pursuing all efforts to prevent the final runaway process from maturing.

In that sense, a new approach to safety should also recognize one additional factor; namely that lithium-ion cells are no longer useful when their temperature exceeds about 100–110°C, and thereafter, they should/must be removed from service. Abuse tolerance can be further enhanced by focusing all efforts on identifying and shutting down all offending safety-related triggers by, for example, discharging the cell as soon as a cell temperature exceeds about 110–120°C. If an abuse/trigger is removed reasonably quickly, the cell simply cools down, and no safety event occurs.

In the case of field-failures (the internal short), this approach does not work because the cell skin temperatures may not reach these levels until thermal runaway is inevitable and/or in progress. Because it can be self-driven, thermal runaway from internal shorts must be detected during charge/discharge cycles prior to the final charge cycle that results in an internal short "mature" enough to lead to a thermal runaway. Therefore, it is imperative to identify early warning signals and to develop sensors that can warn of developing internal shorts well before a thermal runaway initiates and that are capable of integration at low cost into battery management systems.

We hope this chapter encourages the battery community to pursue more fundamental work into safety testing as well as understanding of safety-related processes in lithium-ion batteries. Work is needed to develop more sophisticated models, to measure material properties that contribute to enhanced safety, to develop improved methods of calorimetry, and to develop new safety technologies that will help assure safety of lithium-ion batteries. With greater visibility of the issues, perhaps this field will be taken up in graduate schools as an important topic that should yield rich problems and productive theses.

Acknowledgments

The authors gratefully acknowledge support from the US Department of Energy for portions of this work. In addition, countless discussions with present and past colleagues at TIAX over several years have resulted in many insights regarding battery safety captured in this work. Specifically, the authors gratefully acknowledge Drs. Christopher H. McCoy, Mehmet Rona, Jane Rempel, Ms. Rosalind Takata, Drs. Bookeun Oh, S.K. Singh, Karen Thomas-Alyea, and Per Onnerud. Investigation of various safety incidents also led to very productive discussions with major battery companies and portable product companies which, though anonymous, are gratefully acknowledged.

Bibliography

1. Takeshita H (2011) Worldwide market update on secondary batteries for portable devices, automotive and ESS. Tutorial Presented at the 28th international battery seminar and exhibit, Ft. Lauderdale, FL
2. Zhang J (2011) Li-ion in EDV and safety perspectives. Presentation at the 28th international battery seminar and exhibit, Ft. Lauderdale, FL
3. Roth EP (2008) Abuse testing of high power batteries. Presented at the DOE vehicle technologies peer review, Gaithersburg, MD
4. Nishiyama Y, Tanaka T, Nakajima K (2006) Numerical simulations of thermal behavior with safety improvements of Li-ion battery. Presentation at the 210th ECS meeting, Cancun, Mexico
5. Spotnitz RM, Weaver J, Yeduvaka G, Doughty DH, Roth EP (2007) Simulation of abuse tolerance of lithium-ion battery packs. J Power Sources 163(2):1080–1086
6. Botte GG, Johnson BA, White RE (1999) Influence of some design variables on the thermal behavior of a lithium-ion cell. J Electrochem Soc 146(3):914–923
7. Spotnitz R, Franklin J (2003) Abuse behavior of high-power, lithium-ion cells. J Power Sources 113:81–100
8. Hatchard TD, MacNeil DD, Basu A, Dahn JR (2001) Thermal model of cylindrical and prismatic lithium-ion cells. J Electrochem Soc 148(7):A755–A761
9. Ichimura M (2007) The safety characteristics of lithium-ion batteries for mobile phones and the nail penetration test. In: Proceedings of the 29th international telecommunications energy conference, Rome, IEEE
10. Horn Q, White K, Singh S (2010) Assessing thermal stability of commercial lithium-ion cells. IMLB, Montreal
11. Kim G-H, Pesaran A, Spotnitz R (2007) A three-dimensional thermal abuse model for lithium-ion cells. J Power Sources 170(2):476–489
12. US Automotive Battery Consortium (2005) Freedomcar electrical energy storage system abuse test manual for electric and hybrid electric vehicle applications
13. UL 1642, published by the Underwriters Laboratory
14. Jacoby M (2007) Chem Eng News 85(51):26
15. Hockenberry J (2007) Building a better battery. Wired Magazine, November 2007
16. Stringfellow R, Ofer D, Sriramulu S, Barnett B (2010) New framework for lithium-ion battery safety. IMLB, Montreal, Canada, invited talk (TIAX LLC)
17. Stringfellow R, Ofer D, Sriramulu S, Barnett B (2010) 218th meeting of the Electrochemical Society, Las Vegas
18. Barnett B, Sriramulu S (2010) A perspective on Li-ion safety and opportunities for portable and electric vehicle applications. Presentation at the 27th international battery seminar and exhibit, Ft. Lauderdale, FL
19. Barnett B, Ofer D, Oh B, Stringfellow R, Singh SK, Sriramulu S (2008) On the role of the active materials in thermal runaway from internal short circuits. IMLB 2008 international meeting on lithium batteries, Tianjin
20. Barnett B, Sriramulu S, Singh SK (2007) Influence of active material heat release kinetics on thermal runaway following an internal short circuit. 212th ECS meeting, Washington DC, 7–12 Oct 2007
21. Barnett B, Doughty D, Thomas-Alyea K, Roth P (2006) Safety for lithium-ion: abuse tolerance versus field failure. IMLB 2006 international meeting on lithium batteries, 18–23 June 2006
22. Harris SJ, Timmons A, Pitz WJ (2009) A combustion chemistry analysis of carbonate solvents used in Li-ion batteries. J Power Sources V193:855–858
23. Haik O, Ganin S, Gershinsky G, Zinigrad E, Markovsky B, Aurbach B, Halalay I (2011) On the thermal behavior of lithium intercalated graphites. J Electrochem Soc 158(8):A913–A923
24. MacNeil DD, Dahn JR (2001) Test of reaction kinetics using both differential scanning and accelerating rate calorimetries as applied to the reaction of LixCoO2 in non-aqueous electrolyte. J Phys Chem A 105:4430–4439
25. Maleki H, AlHallaj S, Selman JR, Dinwiddie RB, Wang H (1999) Thermal properties of lithium-ion battery and components. J Electrochem Soc 146(3):947–954
26. Lu W, Belharouak I, Vissers D, Amine K (2006) In situ thermal study of Li1 + x[Ni_1/3Co_1/3Mn_1/3](1 − x)O − 2 using isothermal micro-clorimetric techniques. J Electrochem Soc 153(11): A2147–A2151
27. Yang H, Bang H, Amine K, Prakash J (2005) Investigations of the exothermic reactions of natural graphite anode for Li-ion batteries during thermal runaway. J Electrochem Soc 152(1): A73–A79
28. Arai H, Tsuda M, Saito K, Hayashi M, Sakurai Y (2002) Thermal reactions between delithiated lithium nickelate and electrolyte solutions. J Electrochem Soc 149(4):A401–A406
29. MacNeil DD, Dahn JR (2001) Test of reaction kinetics using both differential scanning and accelerating rate calorimetries as applied to the reaction of LixCoO_2 in non-aqueous electrolyte. J Phys Chem A 105:4430–4439
30. Maleki H, Howard JN (2009) Internal short circuit in Li-ion cells. J Power Sources 191(2):568–574

31. Battery Association of Japan (2008) Activities for safety of Li-ion batteries. Presentation at UN informal working group meeting, Washington, DC, 11–13 Nov 2008
32. Cai W, Wang H, Maleki H, Howard J, Lara-Curzio E (2011) Experimental simulation of internal short circuit in Li-ion and Li-ion-polymer cells. J Power Sources 196(18):7779–7783
33. Orendorff CJ, Roth EP, Nagasubramanian G (2011) Experimental triggers for internal short circuits in lithium-ion cells. J Power Sources 196(15):6554–6558
34. Keyser M (2011) Development of a novel test method for on-demand internal short circuit in a Li-ion cell. Presentation at the 11th international automotive battery conference, Pasadena, CA
35. Zhao F (2007) LIB safety study and improvement. Presentation at the IEEE symposium on product compliance engineering. Denver, CO, USA
36. Mikolajczak C, Harmon J, White K, Horn Q, Wu M, Shah K (2010) Detecting lithium-ion cell internal faults in real time. Power Electronics Technology, March 2010
37. Hayes TA, Mikolajczak C, Horn Q (2010) Key manufacturing practices and techniques to achieve high quality Li-ion cells. Presented at the 27th international battery seminar and exhibit, Ft. Lauderdale, FL
38. Hayes T, Mikolajczak C, Megerle M, Wu M, Gupta S, Halleck P. Use of CT scanning for defect detection in lithium-ion batteries. In: Proceedings, 26th international battery seminar and exhibit for primary and secondary batteries, small fuel cells, and other technologies, Fort Lauderdale, FL, March 16–19, 2009
39. Mikolajczak CJ, Harmon J, Priya G, Godithi R, Hayes T, Wu M (2010) From lithium plating to cell thermal runaway: a combustion perspective. Presentation at the 27th International Battery Seminar and Exhibit, Fort Lauderdale, Florida, March 2010
40. Darcy E (2007) Screening Li-ion batteries for internal shorts. J Power Sources 174:575–578
41. Chen SC, Wan CC, Wang YY (2005) Thermal analysis of lithium-ion batteries. J Power Sources 140:111–124
42. Kawaji H, Oka T, Tojo T, Atake T, Hirano A, Kanno R (2002) Low-temperature heat capacity of layer structure lithium nickel oxide. Solid State Ionics 152–153:195–198

Lithium-Ion Battery Systems and Technology

Zhengming (John) Zhang, Premanand Ramadass
Celgard, LLC, Charlotte, NC, USA

Article Outline

Glossary
Definition of the Subject
Introduction
History of Li-Ion Batteries
Commercial Success
Principle Behind Li-Ion Batteries
Manufacturing Process
Safety
More Details on Cell Components and Modern Trend
Bibliography

Glossary

Active material The material in the electrodes of a cell or battery that takes part in the electrochemical reactions of charge or discharge.

Battery/battery pack An assembly of any number of Li-ion cells, associated electronics, battery packaging, and connector(s).

Capacity The total number of Ampere-hours (Ah) that can be withdrawn from a fully charged cell or battery under specified conditions of discharge.

Cell Basic lithium ion unit providing a source of electrical energy by direct conversion of chemical energy that consists of electrodes, separator, electrolyte, container, and terminals, and that is designed to be charged electrically.

Current collector An inert member of high electrical conductivity used to conduct current from or to an electrode during discharge or charge.

Cycle The discharge and subsequent or preceding charge of a Li-ion cell or battery such that it is restored to its original conditions.

Cycle life The number of cycles under specified conditions which are available from a Li-ion cell or battery before it fails to meet specified criteria as to performance.

Electrolyte The medium which provides the ion transport mechanism between the positive and negative electrodes of a cell.

Negative electrode The electrode acting as an anode when a cell or battery is discharging.

Overcharge The forcing of a current through a Li-ion cell or battery pack after it has been fully charged.

Positive electrode The electrode acting as a cathode when a cell or battery is discharging.

Separator An ionically conductive, electronically insulative material which prevents electronic contact between electrodes of opposite polarity in the same cell.

Thermal runaway The cell condition where the internal cell reactions generate more thermal heat than the cell can dissipate. The condition causes cell venting and premature failure.

Definition of the Subject

Lithium-ion battery (LIB) is one of rechargeable battery types in which lithium ions move from the negative electrode (anode) to the positive electrode (cathode) during discharge, and back when charging. It is the most popular choice for consumer electronics applications mainly due to high-energy density, longer cycle and shelf life, and no memory effect. With Li-ion batteries currently gaining much attraction in electric drive vehicle, the concern for global warming and a clean environment may be well served with advances in such systems.

Introduction

During the last 15 years, lithium-ion batteries have dominated the advanced energy sources by powering the modern portable electronics and replaced many other commercial battery systems in the market. The prime reasons for its rapid success and proliferation in consumer electronic market are its superior characteristics over other battery systems, namely, high voltage, high-energy density, and longer cycle and shelf life with no memory effect. The significant progress of Li-ion batteries is mainly due to numerous innovations and advancements in materials, designs, and safety. This entry is intended to provide an overview of Li-ion batteries on several aspects. Starting with a brief discussion on its history, commercial success, and working mechanism, all the critical components inside the cell have been discussed in adequate detail. The later part of this chapter will primarily focus on manufacturing process, recent advances, and modern trends in Li-ion systems and detailed discussion on Li-ion cell safety.

History of Li-Ion Batteries

The working mechanism of Li-ion cells is often related to that of a rocking chair since within the cell, the lithium ions swing between the negative electrode and the positive electrode through an organic liquid electrolyte, like a rocking chair from side to side. This "rocking-chair" concept was first proposed by M.S. Whittingham at Exxon in 1970s where he discovered the concept of intercalation electrodes using titanium(II) sulfide as the cathode and lithium metal as the anode [1]. The principal concept is based on the intercalation reaction and is rather different from other conventional secondary batteries which are based on chemical reactions.

Goodenough was the first to patent $LiCoO_2$ as a lithium intercalation cathode material in 1980 [2] and H. Ikeda of Sanyo was the first to patent an intercalation material in an organic solvent such as graphite in 1981 [3]. S. Basu of Bell Laboratories filed an US patent in 1982, based on his finding of lithium intercalation in graphite at room temperature [4]. I. Kuribayashi and A. Yoshino developed a new cell design using an intercalation carbon anode and a $LiCoO_2$ cathode and filed patents worldwide [5]. In 1991, Sony Energytec Inc. began to produce commercial lithium-ion cells under the leadership of Yoshio Nishi. Bellcore team under the leadership of J. M. Tarascon pioneered the modern concept of "polymer" (soft pack) Li-ion cells [6–9].

Soon after commercialization, the Li-ion battery (LIB) system became a popular choice because of its high-energy density, good performance, and no memory effect as occurred with nickel-cadmium (Ni-Cd) or nickel-metal hydride (Ni-MH) batteries. LIBs have been primarily used for portable electronics, especially cellular phones and notebook computers. Recently, the application area has been extended to power tools, electric bikes, and energy storage systems. Several companies are now working toward adapting the lithium-ion system for use in electric drive vehicle (EDV) applications.

Li-ion cells are being built in many different shapes and configurations—button, flat, rectangular (also referred as prismatic), and cylindrical. The cell components (electrodes, electrolyte, and separator) are designed to accommodate a particular cell shape and design. The separators are either stacked between the electrodes or wound together with electrodes to form jellyrolls, as shown in Fig. 1. Typical safety features included in cells with metal enclosure are the PTC and CID devices that are usually

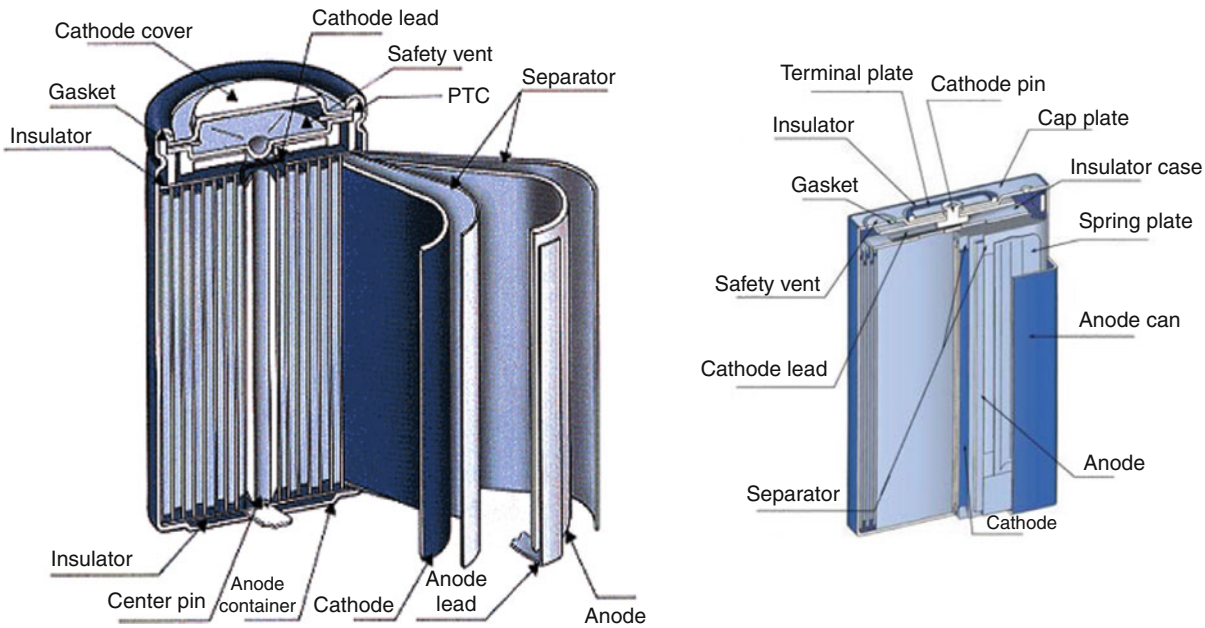

Lithium-Ion Battery Systems and Technology. Figure 1
Typical Li-ion battery configuration: (**a**) spirally wound cylindrical cell, (**b**) wound type prismatic cell

incorporated into the cell top plate and seal. The PTC is a positive temperature coefficient device that changes resistance at a set temperature or current flow and stops a thermal runaway condition from developing. The CID is a current interrupt device that is incorporated into the cell cap, and it interrupts the electrical connection between the cathode tab and the positive terminal when the internal pressure in the cell reaches a given pressure. Another safety feature present in Li-ion cell is the cell vent which activates at pressures just higher than the CID to release the volatile solvent and stops cell action.

Commercial Success

The battery industry has seen enormous growth over the past 15 years in portable, rechargeable battery packs. The majority of this surge can be attributed to the widespread use of cell phones, laptop computers, tablet PCs, video games, and other wireless electronics. At present, this technology is gaining worldwide attention as a battery option for transportation applications, including electric drive vehicles namely HEVs, PHEVs, and BEVs.

The higher volumetric and gravimetric energy storage capability are key characteristics of the Li-ion battery system compared to the conventional sealed nickel-cadmium (Ni-Cd), nickel-metal hydride (Ni-MH), and valve-regulated lead acid (VRLA) battery systems. Figure 2 presents the energy density and specific energy comparisons of small sealed rechargeable battery systems. Some of the distinct advantages of Li-ion system over other commercial rechargeable systems are the choice of chemistry with highest energy and lightest weight, good cycle life, no memory effect, higher energy efficiency, and better high rate capability. Of course there are also certain issues for Li-ion system similar to any other high-energy storage devices that include higher charging times, thermal runaway concerns, relatively more expensive, and requiring advanced protection circuitry for safety and to prevent overcharge and over discharge.

Based on a recent report on rechargeable battery markets that Global Industry Analysts (GIA) announced, the global market for rechargeable batteries is forecast to reach US$16.4 billion by the year 2015 [10]. Factors driving the market growth include growing consumer acceptance of rechargeable battery technologies in various parts of the world, rapid growth in the

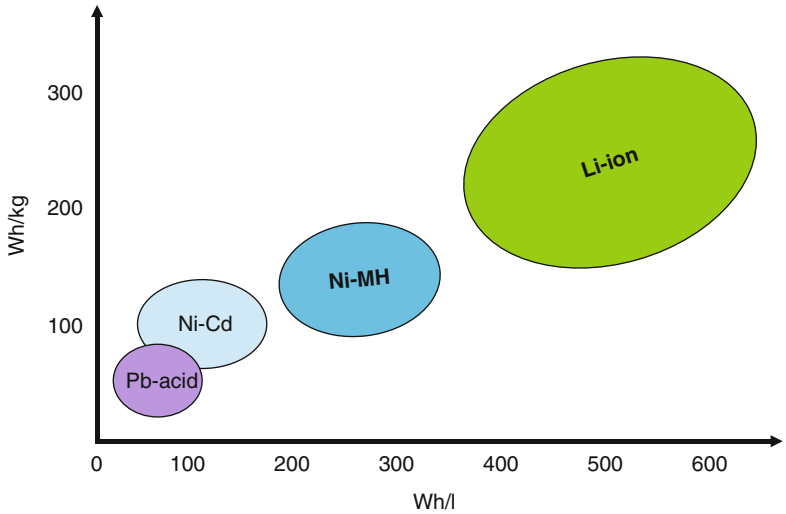

Lithium-Ion Battery Systems and Technology. Figure 2
Volumetric energy density (Wh/l) and gravimetric energy density (Wh/kg) for major rechargeable battery systems

electronics market, and increasing role of rechargeable batteries in the automotive sector. It should be noted that in 2006, the market size of rechargeable battery systems for portable power applications was around US $6 billion out of which Li-ion comprises 75% of the market.

The market survey reports show that the lithium-ion battery is becoming an almighty rechargeable system and in 2010, a whopping sum of around 3.9 billion cells has been supplied all together by cell manufacturers around the world which is about two-fold increase in supply compared to 2006 [11] and the supply is expected to grow by at least 15% during 2011. There is a steady increase in the demand for lithium-ion batteries for all portable electronic devices (almost 100% of cell phones and notebook PCs), and in addition, the Li-ion system also started penetrating more and more in other arenas like power tools, energy storage systems (ESS), and so on. Li-ion system now starts competing with Pb-acid systems in the energy storage systems arena primarily due to its superior cycle life and higher columbic efficiency. For the automotive applications, lithium-ion cells have become a hot topic and are now on the verge of being brought on board vehicles on a massive scale. Although the Li-ion battery for HEV application still has little experience in the real market, research and development activity for it is very dynamic at present worldwide. This fact must surely reflect the common recognition that the technology is one of the most promising for the HEV battery of the coming generation. It is predicted that the HEV will be significantly widespread by 2015 and is expected to take a certain portion of the application market at that time.

The tremendous progress in Li-ion cells is clearly visible with as much as a twofold increase in the volumetric and gravimetric energy density combined with a 50% reduction in price was achieved between 1995 and 2006. Figure 3 depicts the increase in capacity of the cylindrical 18650 cell (18 mm in diameter and 65.0 mm long) from 1992 to 2006. In 1995, an 18650 cell with a capacity of around 1.5 Ah was sold for $8, while in 2006, the same size cell with 2.6 Ah sold for about $4. The early LIBs had a capacity of 800 mAh and an end-of-charge voltage of 4.1 V. The initial cells used hard-carbon anode materials which had a capacity of about 200 mAh/g, and the $LiCoO_2$ had a capacity of nearly 110 mAh/g due to 4.1 V charging voltage. In 2003, the capacity of the 18650 cell reached 2.4 Ah. This corresponds to an energy density of over 200 Wh/kg or 500 Wh/L, respectively. These values were reached in part by increasing the cell-operating voltage higher than 4.2 V due to the availability of improved graphite anode materials, electrolyte additives, and a stabilized $LiCoO_2$.

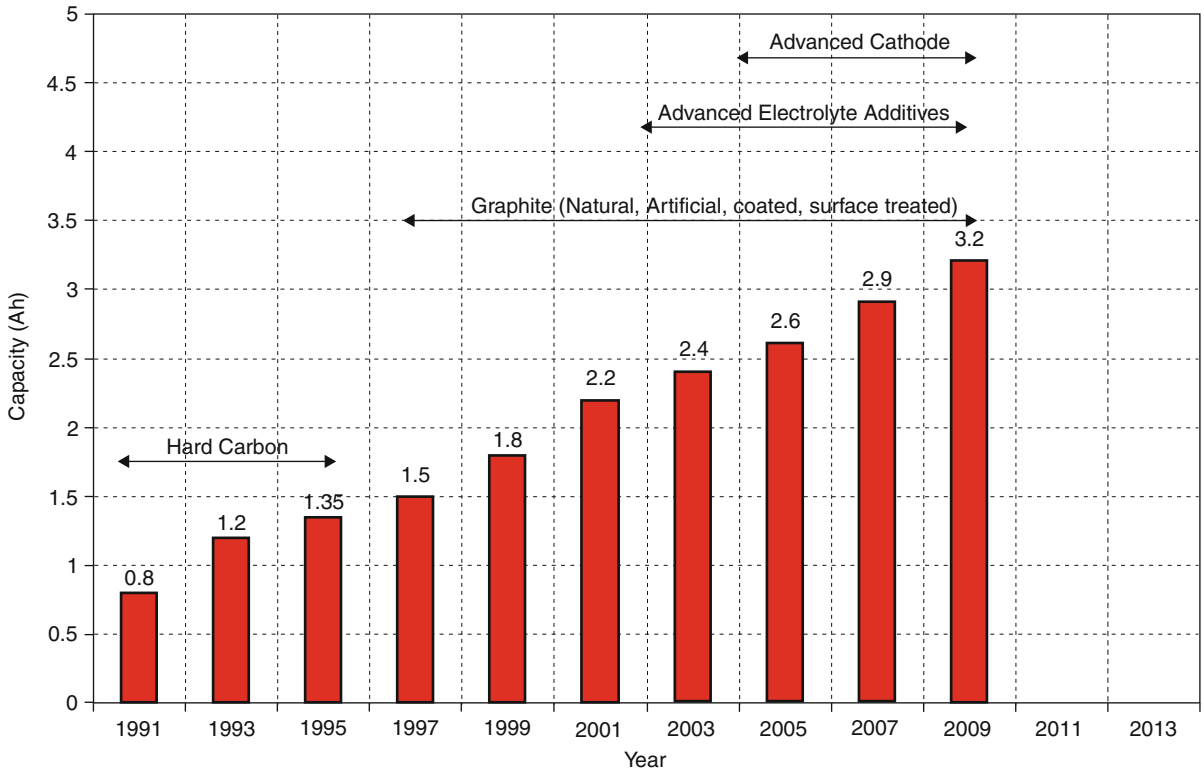

Lithium-Ion Battery Systems and Technology. Figure 3
Capacity (Ah) increase for 18650 lithium-ion cell resulting from advances in active materials and functional additives to electrolyte

The cell producers accomplished the performance improvements through engineering improvements in cell design, new electrode materials, and automated high-speed production to reduce the cost. The capacity of the 18650 cell had reached 2.9 Ah in 2007 based on treated graphite anode and planar-nickel-based cathode and with several kinds of electrolyte additives [12]. With further continuous improvements in all the cell components that includes silicon alloy–type anode materials, lithium-nickel-cobalt-aluminum and nickel-manganese-cobalt cathode materials, novel electrolyte and/or additives, some cell manufacturers are currently able to achieve a maximum capacity of up to 3.4 Ah for the same 18650 cell design.

The major Li-ion cell manufacturers are from Japan, China, and S. Korea. Figure 4 presents the global market share for bare cell shipment volumes from the three countries cell manufacturers for the consumer portable power applications in 2010. Some of the major cell manufacturers include Sanyo, Sony, and Panasonic from Japan; Samsung SDI and LGChem from Korea; and BYD, ATL, and Lishen from China. Figure 5 shows the split-up of small format LIBs supplied for portable power applications namely mobile

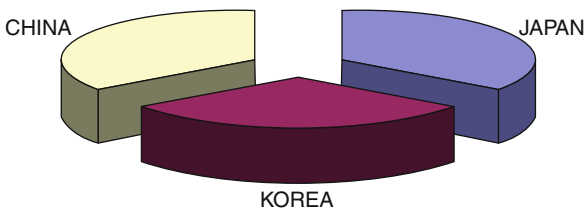

Lithium-Ion Battery Systems and Technology. Figure 4
Major cell manufacturers and their lithium-ion battery movement globally in 2010

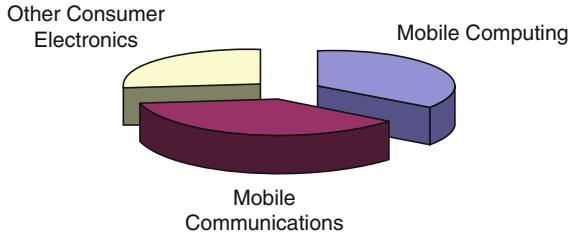

Lithium-Ion Battery Systems and Technology. Figure 5 Movements in cell shipment volumes for each lithium-ion battery application globally in 2010

computing, mobile communications, and other consumer electronics including power tools during 2010. The thin, rectangular polymer/laminate cell construction has been found increasingly favorable in the modern portable consumer electronics market (e.g., Iphone, Ipad smart phones, and so on). Overall, for the consumer electronics market sector, Japan and Korea dominates the production of 18650 type cells and China dominates in prismatic type cell production. There are no major Li-ion manufacturers in the United States or in Europe, even though they constitute large markets for devices powered by Li-ion batteries [13]. Production activity in the United States so far is limited to companies that supply the niche medical and military markets.

There are many emerging market opportunities for Li-ion cells in transportation. Li-ion batteries can provide very high power and are therefore a good candidate for EDV applications. The automotive power market is viewed as the largest future growth opportunity for Li-ion batteries. Their high voltage, low weight, small volume, and potentially long life make them very attractive. Different cell designs and geometries are currently being adapted by cell manufacturers for automotive applications. A few common designs include rectangular flat pouch cell and larger cylindrical cell design.

The cell's capacities for EDV applications are in the range of 25–100 Ah. The typical energy requirement for plug-in hybrid electric vehicle (PHEV) is between 5 and 20 kWh and for all electric vehicle (EV), the energy requirement is more than 20 kWh with a voltage of 300 V or more. A number of modules with energy in the range of 1–2 kWh are necessary. The advantage of Li-ion over Ni-MH for hybrid electric vehicle (HEV) applications that has an energy requirement in the range of 3–5 kWh is still quite not clear, but with decreasing cost as production volume increases, Li-ion cells are considered to be economically competitive. Once Li-ion system finds its place, the transportation market could dominate over the present portable device market.

Principle Behind Li-Ion Batteries

Lithium-Ion Cell

The primary functional components of a typical Li-ion cell are negative electrode (or anode), positive electrode (or cathode), and electrolyte. Most commonly used negative electrode materials include hard carbon, graphitic carbon, and treated graphite. Typical positive electrode materials may include a layered oxide (lithium cobalt oxide, lithium nickel oxide), spinel (like lithium manganese oxide), or a polyanion (such as lithium iron phosphate). The electrolyte in general contains lithium-containing salt such as lithium hexafluorophosphate, lithium tetrafluoroborate, etc. dissolved in a solvent that comprises a mixture of organic carbonates such as ethylene carbonate, diethyl carbonate, etc. Depending upon the material choice, the cell voltage, capacity, performance, and safety can change dramatically. The most common cell design formats of Li-ion cells include cylindrical, prismatic, and pouch. In this section, the working mechanism of Li-ion cells has been discussed along with an overview of each cell component (negative electrode, positive electrode, electrolyte, and separator). Later part of this chapter would add more information on each of them including the modern trend.

Li-ion Cell Mechanism

A typical Li-ion cell consists of a positive electrode composed of a thin layer of powdered metal oxide (e.g., $LiCoO_2$) coated on aluminum foil and a negative electrode formed from a thin layer of powdered graphite, mounted on a copper foil. The two electrodes are separated by a porous polyolefin film called as separator soaked typically in a electrolyte made of LiPF6 salt dissolved in a mixture of organic solvents such as ethylene carbonate (EC), ethyl methyl carbonate (EMC), or diethyl carbonate (DEC).

During cell operation, all the three functional components participate in the electrochemical reaction. Both the negative and positive electrodes are materials into which, and from which, lithium can migrate. During insertion (or intercalation), lithium moves into the electrode and during extraction (or deintercalation), lithium moves back out. During discharge, the lithium ions are deintercalated from the negative electrode moved through the electrolyte and intercalated into the positive electrode. The reverse happens during charging in which lithium ions deintercalate from positive electrode and gets intercalated into the negative electrode. Figure 6 shows the schematic representation of the operation of a lithium-ion cell during discharge process. Useful work can only be extracted if electrons flow through a closed external circuit.

The positive electrode half-cell reaction (with charging being forward) can be represented as:

$$LiCoO_2 \Leftrightarrow Li_{1-x}CoO_2 + xLi^+ + xe^-$$

The negative electrode half-reaction (with charging being forward) is:

$$xLi^+ + xe^- + 6C \Leftrightarrow Li_xC_6$$

where x refer to moles of lithium. The overall cell reaction can thus be represented as:

$$LiCoO_2 + 6C \Leftrightarrow Li_{1-x}CoO_2 + Li_xC_6$$

where the forward reaction corresponds to charging and the reverse reaction occurs during discharge.

Negative Electrode Material (Anode)

The basic requirements for a negative electrode material to be used in lithium-ion cell are that the material should have minimal volume expansion and stress associated with it during charge/discharge process, higher electronic conductivity, lower irreversible capacity loss during first charging or intercalation process, stable under wide operating temperature window in a highly reducing environment, and lower specific surface area (typically <2 m^2/g) for optimal performance and safety.

There are many types of carbonaceous materials being used as negative electrode active material for Li-ion cells. Carbon materials can be broadly classified into amorphous and crystalline. Crystalline or graphitic carbon is a typical layered compound that consists of hexagonal grapheme sheets. Although graphite exists in nature, it can be synthesized artificially by treating a pyrolyzed carbon at high temperatures around 3,000°C.

Amorphous kind carbon includes materials that are heat-treated at lower temperatures of around 1,100–1,300°C and has low crystallinity. They include

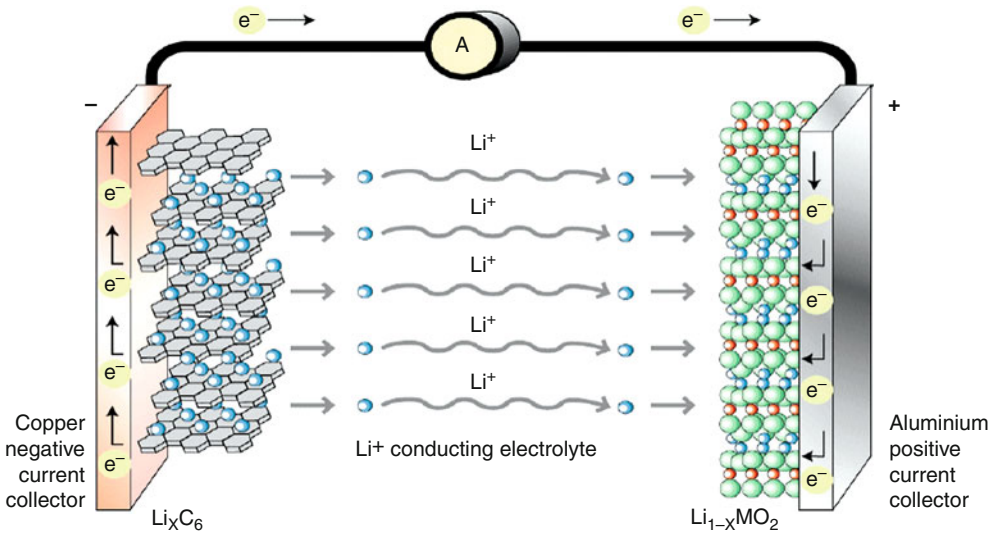

Lithium-Ion Battery Systems and Technology. Figure 6
Schematic representation of Li-ion cell operating mechanism

"soft carbons" (graphitizable carbons) and "hard carbons" (non-graphitizable carbons). In soft carbons, small crystallites are stacked nearly in the same direction, and thereby, subtle diffusion induced upon heating results in graphitization. In contrast, the crystallites of hard carbons do not have such distinct orientation and, hence, are difficult to develop even when heat-treated at high temperatures >3,000°C. Soft carbon material is mostly being used to surface treat the graphite material. The practical materials most widely used in commercial cells include hard carbon, natural graphite, synthetic graphite, and amorphous carbon coated graphite.

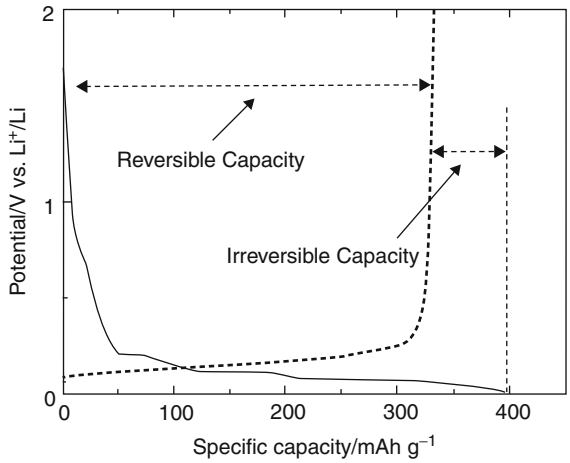

Lithium-Ion Battery Systems and Technology. Figure 7 Typical charge/discharge characteristics of graphitic carbon material

Solid Electrolyte Interface (SEI)

During the first charging after cell assembly, a protective film has been formed on the surface of the negative electrode through reductive decomposition of the electrolytic solution [14, 15]. The passivation film often called as solid electrolyte interface (SEI) acts as an interface between the electrode surface and the electrolyte solution and has the properties of a solid electrolyte with high electronic resistivity. Other favorable properties of the SEI include good mechanical stability/flexibility and good adhesion to the anode. In general, SEI film consists of insoluble and partially soluble reduction products of the electrolyte components. Formation of SEI film suppresses further solvent decomposition and plays a beneficial role in improving the safety and cyclability of lithium ion cells. The SEI formation on negative electrodes thus is a prerequisite for their stable charging and discharging; however, it is the primary cause for the irreversible capacity loss during the first charge through consumption of a considerable amount of lithium. The electrolyte often has additives to enhance SEI formation.

Figure 7 shows a typical charge/discharge characteristic of graphitic carbon material. The solid line represents the intercalation or charging, and the dotted line shows the deintercalation or discharging. During first intercalation (charging), the potential drops rapidly after subtle retardation at ~0.8 V (vs. Li^+/Li). Most of the Li intercalation and deintercalation takes place at potentials <0.25 V (vs. Li^+/Li), accompanied by three potential plateaus. Charge consumed upon first charging is not fully recovered upon discharging and the capacity that cannot be recovered is called irreversible capacity which is observed for any carbonaceous material due to the formation of a passive film over the surface of electrode referred as solid electrolyte interface (SEI). At the second and subsequent cycles, graphite shows good reversibility and the reversible specific capacity ranges from 300 to 370 mAh/g. Table 1 shows the properties of a few commonly used negative electrode materials of Li-ion cells. Graphitic carbons can insert lithium up to a stoichiometry of LiC_6 corresponding to 372 mAh/g.

Positive Electrode Material (Cathode)

In general, positive electrodes in commercially available Li-ion cells utilize a lithiated metal oxide as the active material. Most of the research and commercialization efforts has centered on two classes of materials. The first group includes materials with layered structure that enables two-dimensional diffusion of lithium ions or a spinel structure which enables three-dimensional diffusion as the transition-metal ions are ordered in all layers. Examples include $LiCoO_2$, $LiNiO_2$, $LiNi_{1-y}Co_yO_2$, etc. for layered compounds and $LiMn_2O_4$ for spinel type compound. The second group includes materials with more open structures like vanadium oxide, transition-metal phosphates namely olivine ($LiFePO_4$). The first group, because of their more compact lattices, will have an inherent

Lithium-Ion Battery Systems and Technology. Table 1
for lithium-ion cell

Anode type	First charge capacity (mAh/g)	Irreversible capacity loss	Practical capacity (mAh/g)
Hard carbon	250	25–30%	180–190
Natural graphite	370	16–18%	300–320
Surface treated natural graphite	370	7–9%	340
MCMB graphite	350	10–12%	310–320
Massive artificial graphite (MAG)	360	5–8%	330–340
Mesophase carbon fiber (MCF)	350	10–12%	310

advantage in energy stored per unit of volume, but the second group compound like $LiFePO_4$ is cheaper [16]. Figure 8 shows the charge/discharge characteristics of $LiCoO_2$ material. The theoretical specific capacity of the $LiCoO_2$ cell is relatively low at around 130 mAh/g because only around 0.5 Li/Co can be reversibly cycled without causing cell capacity loss due to changes in the $LiCoO_2$ structure associated with the phase changes that cause low reaction rates and also poor stability of the electrode at low lithium contents. Table 2 shows the properties of a few commonly used positive electrode materials of Li-ion cells.

The ideal requirements for a positive electrode active material used in lithium-ion cell are that the material needs to contain a readily reducible/oxidizable atom, like a transition metal; should react with lithium in a reversible manner without changing the host structure; be a good electronic conductor; be able to react with lithium very rapidly to provide higher power density; should react with lithium with a high free energy of reaction to obtain high voltage, high capacity, and hence high-energy storage; and be stable under

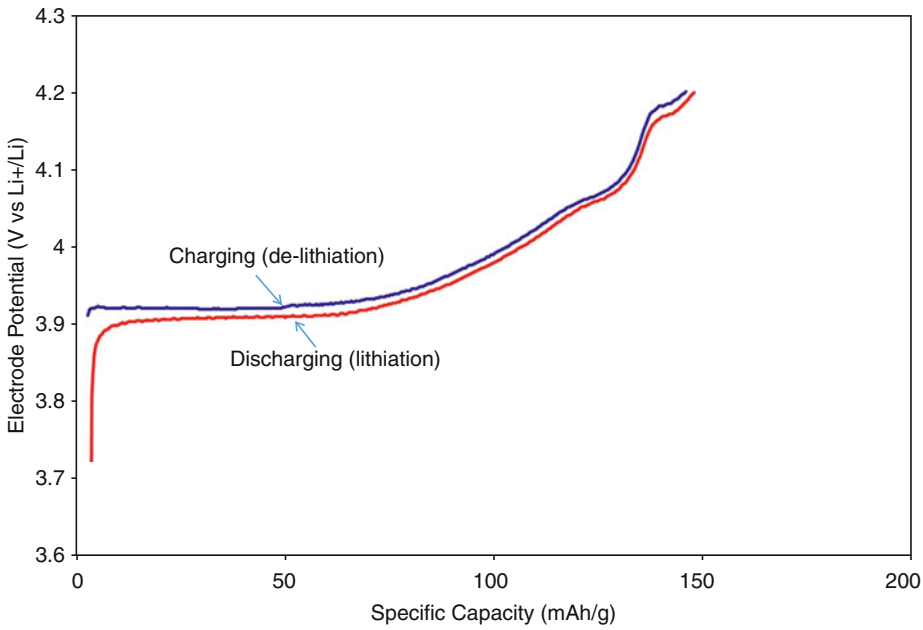

Lithium-Ion Battery Systems and Technology. Figure 8
Typical charge/discharge characteristics of lithium cobalt oxide ($LiCoO_2$) positive electrode material. Charging corresponds to lithium deintercalation, and discharging refers to lithium intercalation

Lithium-Ion Battery Systems and Technology. Table 2 for lithium-ion cell

Positive electrode material	Practical capacity for EOCV 4.2 V (mAh/g)	Density (g/cc)
$LiCoO_2$	140	5.05
$LiNiO_2$	160	4.8
$LiNi_{0.8}Co_{0.2}O_2$	140	4.85
$LiNi_{0.8}Co_{0.15}Al_{0.05}O_2$	160	4.8
$LiNi_{1/3}Co_{1/3}Mn_{1/3}O_2$	165	4.7
$LiMn_2O_4$	100	4.2
$LiFePO_4$	120[a]	3.7

[a]Charge cutoff voltage is ~3.65 V

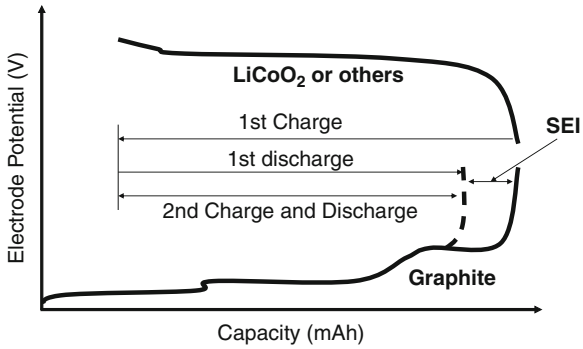

Lithium-Ion Battery Systems and Technology. Figure 9 Schematic showing charge/discharge characteristic of Li-ion cell electrode and state of charge operating window after SEI formation

wide voltage and temperature window. There are several physical properties that determine the quality of positive electrode active material and also influence the battery characteristics. They include particle size, shape, distribution of particle size, water content, tap density, specific surface area, crystallinity, impurity level, and so on.

Cell Balance

Lithium-ion cells operate by cycling lithium ions between two insertion electrode hosts having different insertion energies. Figure 9 shows the schematic of charge discharge characteristics of Li-ion cell electrodes (e.g., $LiCoO_2$ as positive and graphite as negative electrode) [17]. After assembling and filling with electrolyte, the cell will be in a completely discharged state where all the lithium ions are present in the positive electrode. During initial charging, some portion of the lithium ions goes into the irreversible SEI film formation reaction and rest of the lithium ions gets intercalated into the negative electrode. The negative to positive electrode capacity ratio is very critical in determining the cell performance and safety with continuous cycling. Smaller capacity ratios would present safety hazard as the negative electrode can get overcharged as more lithium ions are available for intercalation than is desirable. Higher capacity ratios may prevent optimal utilization of the negative electrode. The typical negative to positive electrode capacity ratio used by most cell manufacturers is around 1.15. The first charge capacity of negative electrode (Li-ion intercalation) needs to be at least 15% greater than the first charge capacity of the positive electrode (Li-ion deintercalation) to accommodate the SEI formation.

Electrolyte

Electrolyte is one of the critical components for any electrochemical device, and the basic function is to serve as the medium for the transfer of charges, which are in the form of solvated ions, between a pair of electrodes. The role of liquid electrolytes in lithium-ion cells is to act as an ionic conductor to transport solvated lithium ions back and forth between positive and negative electrodes as the cells are charged and discharged. Since the electrodes in lithium-ion cells are the porous composite electrodes, consisting of an active material, a conductive material and a polymer binder, the liquid electrolyte must seep into the porous electrodes and transfer lithium ions smoothly at the interfaces between the liquid and solid phases. The minimal requirements of the electrolyte used in Li-ion cells include good ionic conductivity and electronic insulator property, stability over a wide electrochemical voltage window and operating temperature. Most commonly used salt materials for the electrolyte include $LiPF_6$, $LiBF_4$, and the most common solvents are carbonate based, namely, EC, DMC, DEC, EMC, and PC.

An ideal electrolyte solvent for Li-ion cells shall meet the following minimal criteria, namely, high dielectric constant, to be able to dissolve salts of sufficient concentration, lower viscosity for facile ion transport, inert to all cell components, especially the charged surfaces of the electrodes, lower melting point, and higher boiling point to remain liquid in a wide temperature range.

An ideal electrolyte solute in lithium-ion cells completely dissolves and dissociate, in the nonaqueous media, and the solvated ions should be able to move in the media with high mobility, should be stable against oxidative decomposition at the positive electrode, should be inert to electrolyte solvents and other cell components, and should be nontoxic and remain stable against thermally induced reactions with electrolyte solvents and other cell components. LiPF6 is one of the most commonly used salts on commercial Li-ion cells. The success of LiPF6 was not achieved by any single outstanding property but, rather, by the combination of well-balanced properties, namely, conductivity, ionic mobility, dissociation constant, thermal stability, and electrochemical/chemical stability.

Electrolyte Additives Electrolyte additives are compounds that add extra functions to the liquid electrolytes in addition to the fundamental function as an ionic conductor. Examples of role-assigned electrolytes include anode passivation film-forming agents, cathode protection agents, overcharge protection agents, wetting agents, flame retardant agents, and so on. It should be noted that small amount of the electrolyte additives dramatically improves the performances of lithium-ion cells. Since the influence of electrolyte additives depends not only on the electrode materials but also on cell designs, the research and development of the additives is quite challenging.

Separators

A separator is a porous membrane physically placed between electrodes of opposite polarity, permeable to ionic flow but preventing electric contact between the electrodes. As batteries have become much sophisticated, separator function also has become more demanding and complex. The main function of separator in Li-ion cell is to keep the positive and negative electrodes apart to prevent electrical short circuits and, at the same time, allow rapid transport of ionic charge carriers that are needed to complete the circuit during the passage of current in an electrochemical cell. They should be very good electronic insulators and have the capability of conducting ions by soaking electrolyte. Li-ion battery separators can be produced through dry and wet processes. Figure 10 presents the micrographs of separator membrane produced through dry and wet process methods.

A wide variety of properties are required for separators used in Li-ion cells [18]. They include: electronic insulator, minimal electrolyte (ionic) resistance, sufficient mechanical and dimensional stability and physical strength to allow easy handling, chemical stability to degradation by electrolyte, impurities, and electrode reactants and products, readily wetted by electrolyte

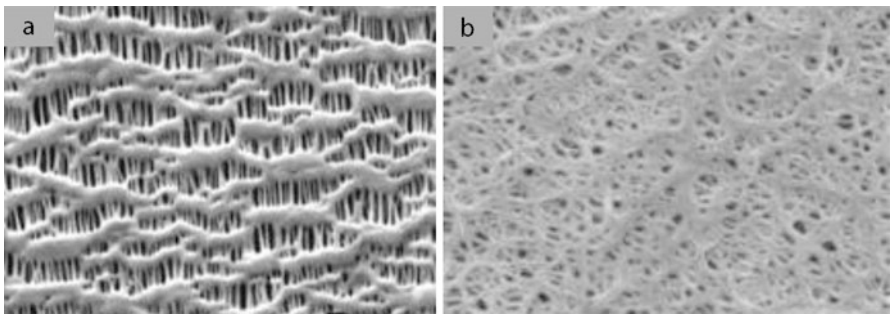

Lithium-Ion Battery Systems and Technology. Figure 10
SEM images of separator membrane produced through (**a**) dry and (**b**) wet process methods

and effective in preventing migration of particles or soluble species between the two electrodes. In order to achieve good performance of Li-ion cells, the separators should have higher ionic conductivity with electrolyte, low shrinkage, and uniform pore structure. Cells with high-resistance separators will perform poorly during high rate discharge and also will increase the cell-charging time.

Microporous polyolefin membranes in current use are thin (<30 um) and are made of polyethylene (PE), polypropylene (PP), or laminates of polyethylene and polypropylene. They are made up of polyolefin materials because they provide excellent mechanical properties, chemical stability, and acceptable cost. They have been found to be compatible with the cell chemistry and can be cycled for several hundred cycles without significant degradation in chemical or physical properties.

Manufacturing Process

The basic principles and processes of cell design and fabrication are well known and quite similar among cell manufacturers. The International Electrotechnical Commission (IEC) has established a common nomenclature for describing the various cell sizes and chemistry. For example, the most common cylindrical Li-ion cell ICR18650 translates into: I is for Li-ion technology, C for cobalt-based cathode, R is for a round cell, 18 is for the cell diameter in millimeters, and 650 is for the cell height in tenths of a millimeter.

The overall manufacturing process for the Li-ion cell can be divided into the five major processes:

1. Mixing, kneading, coating, pressing, and slitting processes of the positive electrode and negative electrode materials
2. Winding process of the positive electrode, negative electrode, and separator
3. Insertion of the wound cell core and electrolyte injection into the battery case
4. Cell closing or sealing process
5. Formation, aging, and cell selection

Electrode Fabrication and Winding Process

Figure 11 shows an outline of the initial process of Li-ion cell manufacturing that includes electrode preparation to winding [19]. In this process, the active materials are coated onto metal foils and calendered for thickness. The positive electrode material consists of active material, such as $LiCoO_2$, $LiNiO_2$, or $LiMn_2O_4$; a carbon-conductive additive like acetylene black; and a binder material namely polyvinylidene difluoride (PVdF). The active material and conductive agent are first dried and are then fed into a ball mill or other mixer along with the previously prepared binder solution (e.g., PVDF dissolved in *N* -methyl pyrrolidone), and then thoroughly stirred. The ball mill contains ceramic balls, e.g., glass, zirconia, about 2–3 mm in diameter, to assist in mixing and the mixing condition can strongly influence the performance of the cell.

The process for the negative electrode follows essentially similar to that of the positive electrode but with different materials. Carbon or graphite is used for the negative electrode-active material. PVDF, carboxymethylcellulose (CMC), or styrene butadiene rubber (SBR) is generally used for the binder that is usually dissolved in solutions like NMP depending on the type of binder.

A better result in mixing may be obtained by first kneading the materials into a stiff paste and then adjusting the viscosity by adding the solvent so that it can be applied easily in the coating process. The electrode slurries (viscosity from 10,000 to 20,000 cps) are uniformly coated onto both sides of the current collector (aluminum foil for the positive and copper foil for the negative) of 10–20 μm thickness. Proper mixing techniques are very critical to obtain uniform distribution of the components of the active mass during the coating operation.

Coating operations can use a slot die, reverse roll coating, or doctor blade coating equipment. Close control of coating thickness is essential to ensure that all the parts fit into the can during final assembly. The coating thickness for different cell designs can vary from 50 to 300 μm, depending on the cell design. The coated material is dried in a continuous process. The coating solvent is collected to prevent emission of toxic vapors. Next, the dried electrodes undergo calendaring process where it is compressed with a roller press machine to provide accurate thickness control of the electrode thickness and to increase the density of the electrode mass. After

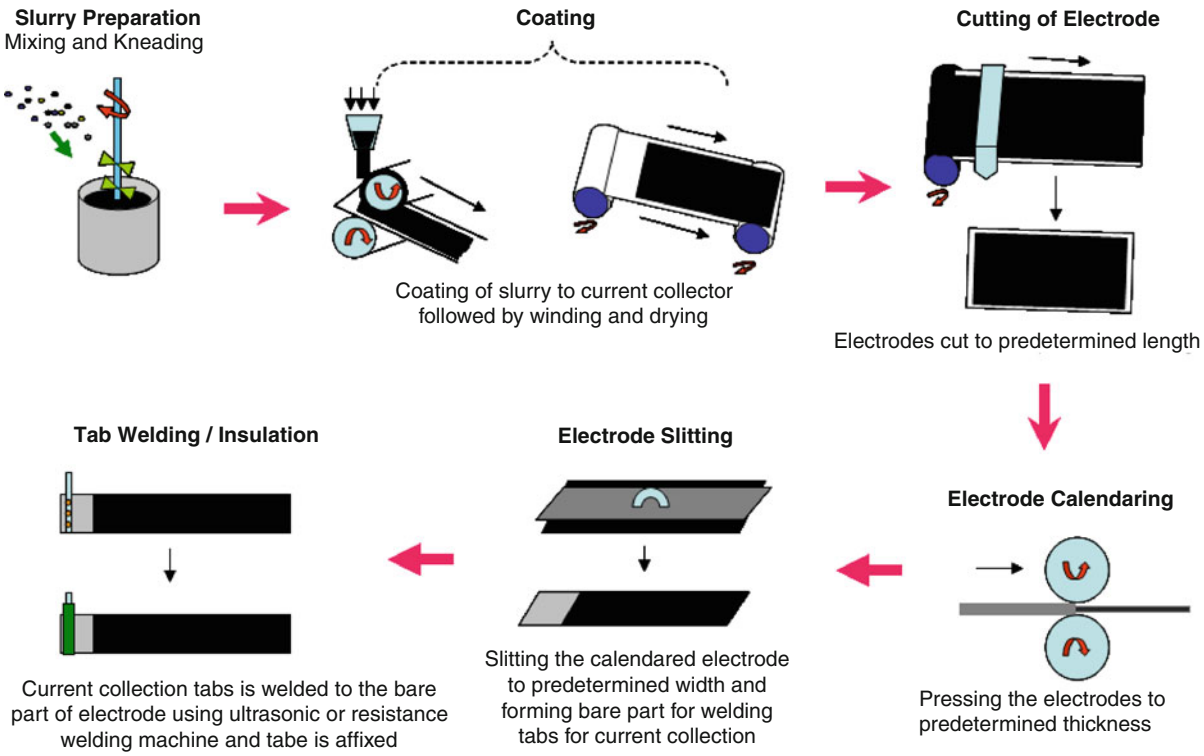

Lithium-Ion Battery Systems and Technology. Figure 11
Schematic of battery electrode fabrication process

calendaring, the master roll is slit to the width specified for cell construction and wound onto a roll for the winding operations.

18650 Cell Fabrication Process

Figure 12 presents the schematic of the assembly of cylindrical cells [19]. The reels of the slit anode, cathode, and separator stock are mounted on the winding machine. The strips have been sized for length, width, and thickness that match the cell design. Once the foils are threaded into the machine, the machine starts and continues to operate automatically until the reels are used up. An aluminum tab is affixed to the bare part of the aluminum foil positive electrode by ultrasonic welding before winding, and similarly, a nickel or copper tab is affixed to the copper negative electrode collector by ultrasonic welding.

The winding machine then combines the two electrodes and separator strip on a mandrel (also referred as pin) and winds the combination in jellyroll fashion into a tight bobbin or cell core. Cylindrical cells are wound on a round mandrel while the prismatic cells use a flat paddle. Winding requires constant tension on the coil as it is formed and grows to the final size. Any irregularity leads to a gap between the separator and electrode, resulting in a nonuniform current distribution that can lead to a malfunction or shortened cycle life. The wound coil is checked for internal shorts before being inserted into the can with a hi-pot or impedance tester. In the last step, the cell core is taped to keep it tightly wound before inserting it into the cell case. It is important that the active material neither peels or sloughs off of the active material nor the separator twists during the winding process. Early rejection of potential cell faults is economical and prevents investing more work on bad/faulty cells.

Following insertion into the cell case, a tubular mandrel with a serration may be inserted in the winding core. The function of this mandrel is to improve the

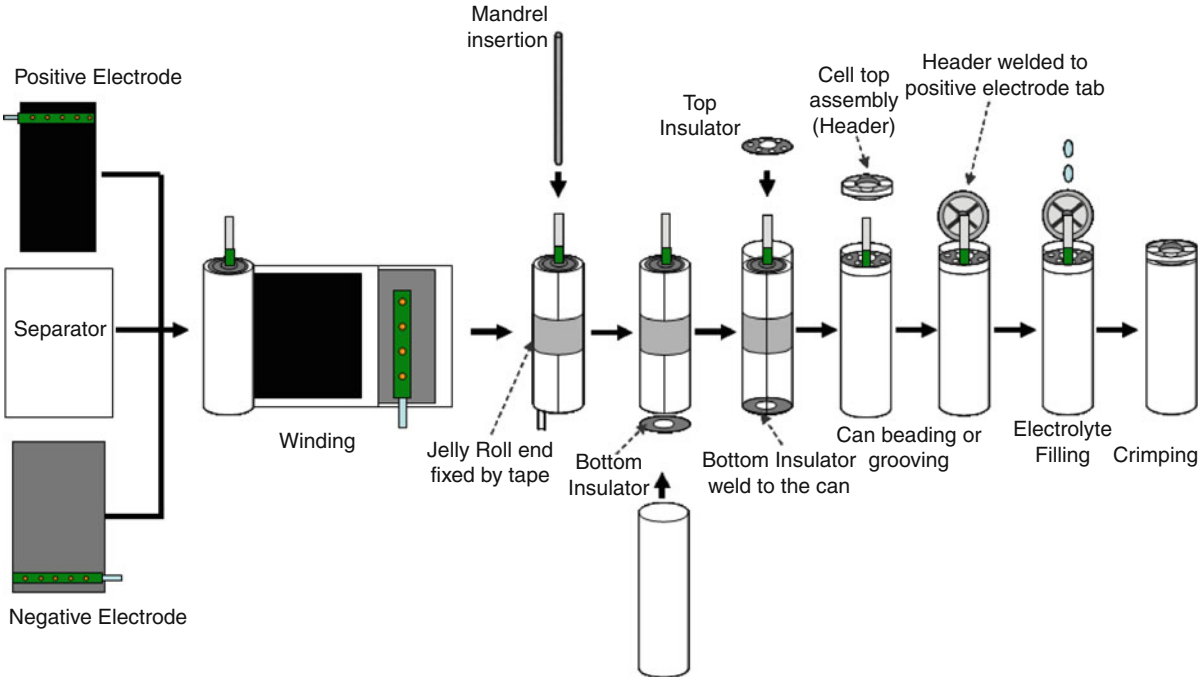

Lithium-Ion Battery Systems and Technology. Figure 12
Schematic of 18650 cell fabrication process

integrity of the cell core and for safety of the battery. When the internal pressure rises, gas has free passage through the hollow center of the mandrel and is released through the vent. When the cell is crushed, the mandrel causes both electrodes to short-circuit and instantaneously discharge. Any moisture contamination of the cell has a deleterious effect on its operation. Therefore, all cell assembly operations are usually carried out in a dry room or dry box. Alternatively, the cell then may be put in a heated vacuum oven for certain durations in order to extract residual water from the cell core before electrolyte filling. In the next process, the cell is filled with the electrolyte using a vacuum injection apparatus.

After filling, the cell cap, also called the header, is welded to the aluminum tab and the cell is finally sealed by crimping the header to the can. The header contains the polymer spacer, vent, PTC, and CID safety devices designed to activate and prevent dangerous temperatures and pressures from developing internal to the cell. After sealing, the cells are completely washed with isopropyl alcohol or acetone in order to remove any adhering electrolyte. An electrolyte leakage test is done using a smell sensor apparatus in order to confirm a good seal. Finally, the cell is subjected to an aging process to select out cells with microshorts and to categorize cells by capacity for assembly into battery packs. The temperature, length of storage, and cell checking methodology vary. This process is designed to identify cells with internal cell faults and microshorts that are not found during cell fabrication.

Large Format Li-Ion Cell Manufacturing Process: Flat Plate Pouch Configuration

Li-ion polymer and flat plate cells are produced in small sizes for cellular phones (about 0.5 Ah and higher) and large sizes (up to 200 Ah) for energy storage and motive power applications. A common characteristic is that the polymer separator holds the electrolyte and forms a physical barrier between the anode and cathode to prevent internal shorting. Most polymer cells are flat plate (prismatic) construction.

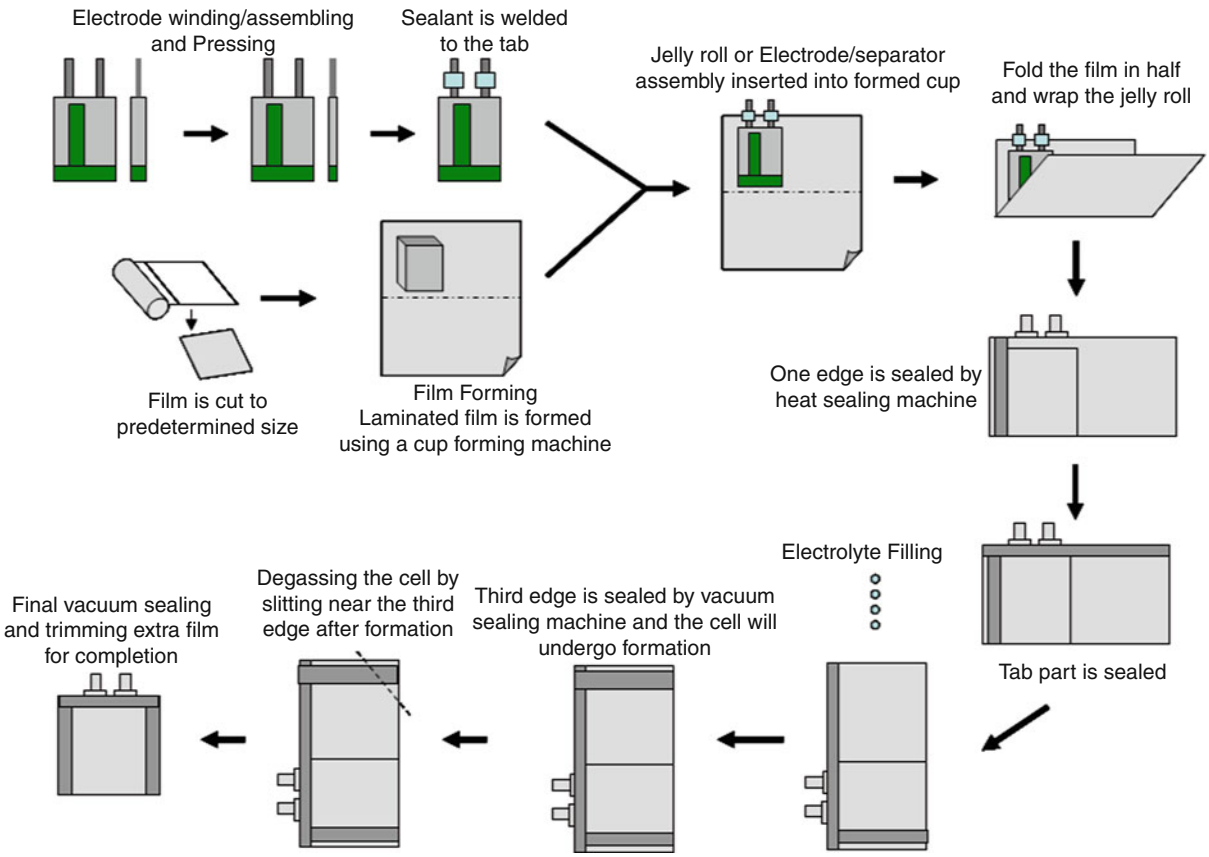

Lithium-Ion Battery Systems and Technology. Figure 13
Schematic of pouch cell fabrication process

There is no one general cell fabrication process for polymer, flat or pouch, cells as there is for the liquid electrolyte cylindrical and prismatic cells. Each manufacturer has a slightly different process flow. Cell designs are essentially laminated constructions produced by several different fabrication processes. A typical example was shown in Fig. 13 [19]. Cell assembly follows the general outline as that for cylindrical cells. The cell assembly could be either a wound design or a stack design. Wound design follows closely to that of cylindrical cell except that the mandrel would be a thin flat plate depending upon the width requirement. In stack design, positive and negative electrodes along with separator are stacked together to give the desired cell capacity. Alternatively, a Z-fold construction may also be used with the electrodes bonded to the separator [20]. The stacks then are bonded together using ultrasonic or heat to ensure uniform bonding and dimensional control.

The cell case is formed from an aluminum-polymer laminated film. The film is fusion bonded, the electrode stack is inserted, and the exterior case is fused by a heat or an ultrasonic sealing apparatus. The assembly then is checked for internal shorts, the moisture is removed by heating in a vacuum dryer, the electrolyte (polymer or conventional electrolyte depending upon the cell kind) is then injected, and the cell is vacuum-sealed in a two-chamber configuration. After formation, any gas formed is removed by a vacuum, the cell resealed, and the gas chamber discarded. Finally, the cell is subjected to top sizing, both side bending, leakage tested with an odor sensor, cleaning and drying, inspection of any coil winding misalignment

using an X-ray apparatus, lot number printing, storage, charging and discharging, and then final inspection.

Formation and Aging

Once the cell assembly process is complete, the final step in the overall production process shifts to the formation and aging of the cells. This applies to cylindrical, prismatic, flat plate, and polymer cell constructions. Li-ion cells are assembled in the discharged condition and must be activated by charging. The first charge is called "formation," which activates the active materials in the cells and establishes their ability to function. The first charge typically starts at a lower current to properly form the protective solid electrolyte interface (SEI) layer on the graphite/carbon anode and then increases to the normal current at about 30% into the charge period.

The cell voltage is measured after the first charge and stored (aged) for a set time period. The storage time and temperature vary from one manufacturer to another. The voltage and capacity measurements are stored for use in the cell-selection/-matching process. These will be used later to sort cells out with internal microshorts or other manufacturing defects. Differences in voltage at the start and end of the storage period can be used to identify problem cells with low voltage and low capacity. Cells with low voltage result from "soft" or "micro" internal shorts and are discarded. The exact first charge regimen and cell-selection procedure may vary with manufacturer. Some manufacturers give the cell one or two cycles after formation to check the capacity for cell matching in assembly of battery packs. Others use the voltage measurement after first charge.

In order to keep up with the market demands, tough quality, performance, and safety requirements, in the cell fabrication methods and process control techniques, are followed. Optical and X-ray systems are currently being used to continuously monitor critical processes like winding, and ensure precise placement of components. The electrolyte-filling process is completely automated by using precision pump combined with advanced multistep vacuum/pressure cycles to ensure that the electrolyte permeates and completely fills the porosity in the separator and electrode structures. The internal construction of every cell produced is inspected by X-ray for proper top cap installation, misalignment of the winding from processing, the improper bending of the tabs, and so forth, which potentially could cause an internal short circuit or cell malfunction.

Safety

Lithium-ion batteries have been commercially available for over 2 decades and currently represent state-of-the-art power source for all modern consumer electronic devices. Due to its advanced chemistry, Li-ion cells exhibit superior performance characteristics over most other rechargeable battery systems. The lithium-ion technology offers a high energy and power density, long life, and reliability that makes it attractive for electric drive vehicle (EDV), military, and aerospace fields, and large format Li-ion cells and battery packs are currently under development for such applications.

Like any other energy storage devices, one of the concerns about the Li-ion technology is the safety associated with the system and is the primary focus for cell/pack manufacturers apart from cost and durability. Li-ion cells can undergo thermal runaway if subjected to unreasonable conditions for which they are not designed as it involves a combination of highly energetic materials with flammable electrolyte solutions.

With several billion Li-ion cells being used to power cell phones, laptops, and other consumer electronics, there are bound to be concerns over field incidents [21–23]. Battery failures that vent with fire are taken very seriously and manufacturers choose a conservative approach by adopting safety recalls. Considering the number of lithium-ion batteries used in the market, this energy storage system has caused little harm in terms of damage and personal injury.

Li-ion cells have had an excellent safety record in the field with very few documented safety events in over one billion cells in the market place. Safety is continuously improving since production rates are increasing. This excellent safety record has come about due to care on the part of manufacturers and due to regulatory standards like IEEE, IEC, and UL governing the safety

of cells. Cell manufacturers are not only trying packing more energy into the pack but also attempting to make it safer. However, there is still room for further improvement in safety as Li-ion system moves into several new arenas like electric cars and trucks, stationary energy storage, military and satellite applications that mostly utilize larger format batteries.

System Level Safety

In general, ensuring a safe product begins at cell level and ends with the user. The IEEE 1625 standard for laptops and the IEEE 1725 standard for mobile phones have recently focused on conveying the concept that Li-ion battery pack safety is a function of the entirety of the cell, pack, system design, and manufacture [24, 25]. A system level approach thus becomes very essential in addressing the safety of Li-ion batteries. System level safety includes the combination of cell, battery pack, host device, power supply, or adapter, end user/environment, and each of these aspects has a role to play in ensuring pack safety. Figure 14 presents the schematic of the system approach to Li-ion design and use. The level of assurance for protection and safety on system level depends on the implementation by the manufacturer/supplier and also on the actions of the end user. This part of system level safety is about understanding the intended use of a product, and mitigating reasonable and foreseeable misuse that may occur. IEEE P1625, the Standard for Rechargeable Batteries for Portable Computing, was the first standard to encompass all levels of the battery manufacturing process and include the customer experience.

Cell Level Safety

The safety of lithium-ion batteries is an essential requirement for commercial use. Cell manufacturers continue to work toward designing safer cells, through modifications of cell components and through improvements in manufacturing practices that ultimately resulted in cells exhibiting excellent safety record in the field. On cell level, thermal runaway failures can occur for a number of reasons, including poor cell design (electrochemical or mechanical), cell manufacturing flaws, external abuse of cells, etc.

The cell level safety can be broadly classified into three categories shown in Fig. 15. The first one

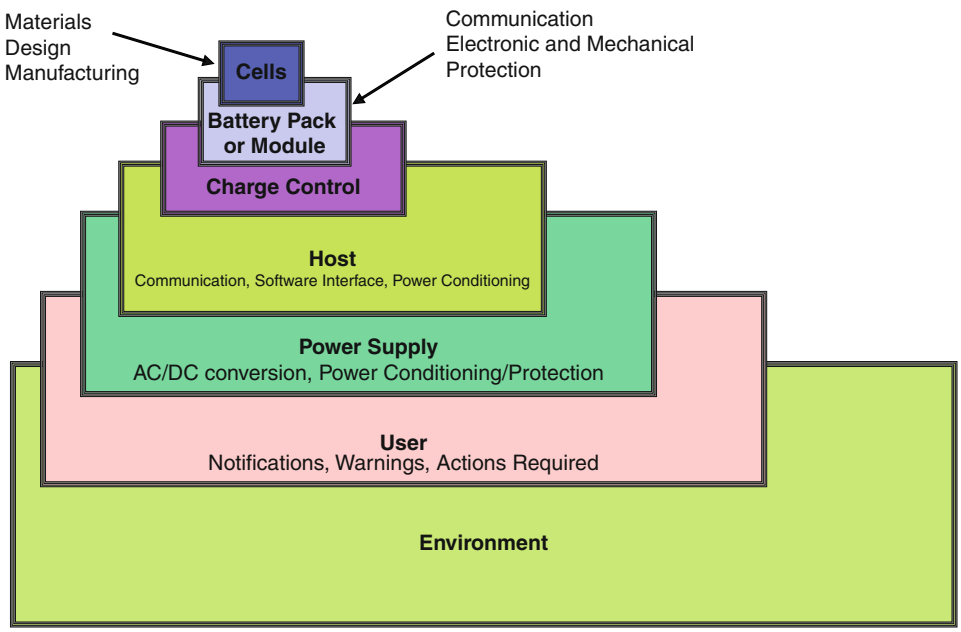

Lithium-Ion Battery Systems and Technology. Figure 14
System approach to Li-ion design and use (IEEE)

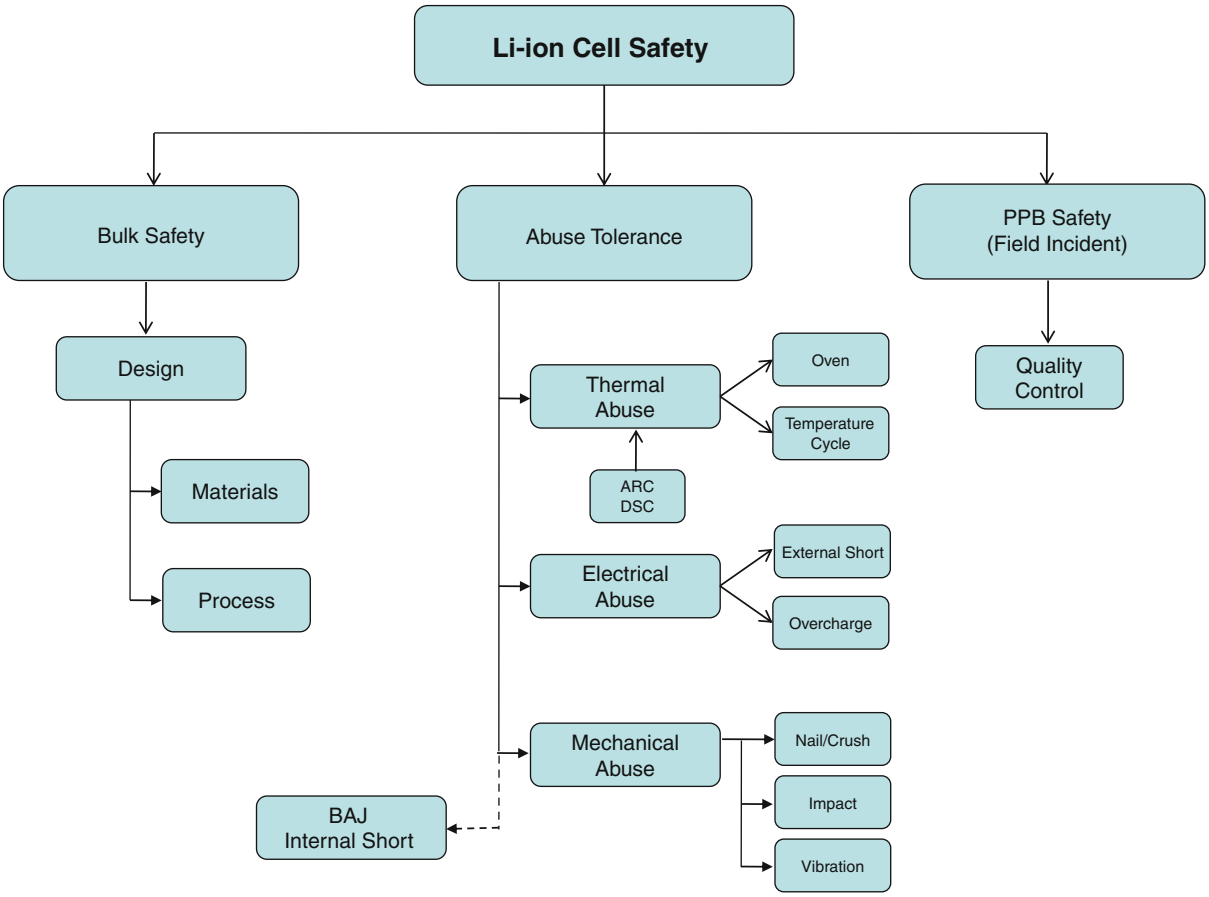

Lithium-Ion Battery Systems and Technology. Figure 15
A schematic flowchart that represents the cell level safety in Li-ion cells for consumer electronics applications

represents safety that depends upon cell design aspects, namely, materials and process conditions. Cell manufacturers around the world are now adapting more sophisticated processes to produce Li-ion cells. The process is highly automated and more efficient with advanced quality control checks based on optical and X-ray inspection techniques to check on several key safety-related factors such as electrode alignment, presence of metal contaminants, presence of burrs in electrode edges, insulation of aluminum current collector next to electrode coating that faces the negative electrode, and so on. Moreover, using advanced electrodes with surface treated and core-shell type materials, very safe electrode capacity ratio, through implementing several cell level safety features, etc., greatly improves the cell level safety. The category can also be referred as bulk safety as almost 99.999% of the cells produced currently for consumer electronics applications by well-experienced cell manufacturers fall into this category. Bulk safety is not a concern with current advanced Li-ion technology as cells are being made with optimized process conditions, with robust design and advanced material choice that when operated under recommended user conditions is much safer and will not result in thermal runaway situations during its operation period.

The second category addressing cell level safety concern is the abuse tolerance. The term "abuse" refers to using of product in a way that is not intended by the supplier but which may result from unreasonable human behavior or unreasonably extreme environmental conditions [24]. Cell designs that are

tolerant to abuse conditions without venting or self-destruction are imperative. Abuse tolerance tests for consumer electronics cells are defined by International Electrotechnical Committee (IEC), Underwriters Laboratories Inc. (UL), and Japan Storage Battery Association (JSBA). The tests are typically classified as thermal, electrical, and mechanical abuse tests. Thermal abuse tests include high-temperature ramp also referred as hot-oven test and temperature cycling test. Characterization test methods, namely, ARC and DSC, are widely used to study the thermal properties of the cell components such as self-heat rate, onset runaway temperature, and so on that are directly linked to the thermal stability of the materials, and these test methods provide insight on thermal abuse tolerance response of Li-ion cells. Overcharge and external short circuit tests are categorized as electrical abuse tests and the most common mechanical abuse tests include crush, nail penetration, crush, impact and vibration tests. For more details regarding each test condition, UL document 1642 could be referred [26]. Cell manufacturers in general adopt a scaling method in quantifying the abuse response of Li-ion cells. The response may be ranging from least severe ones, namely, no change, vent with electrolyte leakage, to the most severe ones like smoke with fire and explosion. For abuse tolerance tests, the criterion for the cell to pass is no fire and no explosion.

The third category is the PPB or parts per billion level safety that refers to the field incidents of Li-ion cells that were subjected to normal recommended operating conditions. Field failures typically represent unprovoked battery explosions, and according to industry experts, such events are rare and it is estimated that one in ten million lithium-ion batteries fail that way [27]. Stringent quality control measures and new safety evaluation methods are being recommended that would help in controlling PPB level. Battery Association of Japan has developed a test methodology to analyze internal short occurring in a Li-ion cell and to characterize the failure associated with it [24]. With this test method, the field incident caused by internal short circuit can be simulated practically [28]. With the increase in the energy of lithium-ion batteries, more advances in safety technology are also necessary to reduce the field incidents still further and gain more consideration from EDV, satellite, and other specialty applications.

More Details on Cell Components and Modern Trend

Negative Electrode Material

Hard Carbon One of the typical examples for hard-carbon materials is the thermal decomposition product of polyfurfuryl alcohol resin (PFA). Hard-carbon materials can offer higher capacity beyond the theoretical limit of LiC_6 at lower potentials but have not achieved broad acceptance because of their higher irreversible capacity and sloping discharge voltages [29]. They are highly sensitive to moisture and are difficult to process; however, the material is practically usable and able to offer around 200 mAh/g capacity. Significant research work has been carried out on hard carbon with the purpose of overcoming the drawbacks through surface modifications and pretreatments. But graphitic carbon is still considered the best choice in practical batteries because of its higher performances.

Graphite Intercalation Compounds (GIC) Theoretically, graphitic carbons can insert lithium up to a stoichiometry of LiC_6 corresponding to 372 mAh/g. The process is called intercalation and Li-ions occupy sites between graphene planes. Morphology of graphitic materials has a strong impact on electrochemical behavior and strongly influences critical stages in the precipitation of the surface films and their passivation properties. In general, graphite particles with some degree of disorder show high reversibility and stability in Li insertion process and are less dependent on solution composition when compared to highly ordered materials.

Graphite intercalation compounds (GIC) have a significant feature called the staging phenomenon, which is characterized by a periodic sequence of intercalant layers (lithium ions) between graphite layers. The nth-stage compound consists of intercalant layers arranged between every n graphite layers. The first-stage lithium graphite intercalation compound has the stoichiometry of LiC_6 with the specific capacity of 372 mAh/g, a theoretical saturated value of lithium

storage for graphite under normal pressure. The staging phenomenon can be easily monitored and controlled by the electrochemical reactions of carbons in Li^+-containing electrolytes, for instance, conducting galvanostatic (constant current) charge/discharge [30] and slow cyclic voltammetric(CV) [31, 32] tests, and analyzing the differential capacity (dQ/dV vs V, where Q is capacity and V is voltage) has proven to be a particularly useful electrochemical method. In conjunction with the electrochemical techniques, some physical methods have been applied to shed light on the stage occurrence and transitions during lithium intercalation into and deintercalation from graphite host. These methods include in situ XRD [30, 33], ex situ XRD [34], in situ laser Raman spectra [35], and STM [36].

Natural Graphite Natural graphite is chosen for lithium-ion battery anode materials mainly because of its low cost, low and flat potential profile, high Coulombic efficiency in proper electrolytes, and relatively high reversible capacity (330–350 mAh/g). On the other hand, it has two main shortcomings, namely, low rate capacity and incompatibility with PC-based electrolytes.

The low rate capacity is primarily due to its high anisotropy causing unfavorable orientation of particles that leads to sluggish of Li^+ intercalation and inadequate electronic contact between graphite particles and copper substrate [37, 38]. To overcome this issue, mechanical millings have been applied to pulverize the natural graphite flakes into small pieces [39], through which the preferred orientation of crystallites within each natural graphite flake particle can be distorted to some extent by separated graphite fragments. One other limitation of natural graphite is its incompatibility with PC-based electrolytes. Studies have been carried out to overcome this through modifying the electrolytes with additives and also modifying the graphite by coating amorphous carbon layers through thermal vapor decomposition technique [40–42].

Synthetic Graphite Synthetic graphite has many properties that are similar to those of natural graphite. Besides, it has many unique merits such as high purity, variety of structures suitable for smooth Li^+ intercalation and diffusion, and so forth. Nevertheless, it is more expensive because of the high-temperature treatment (>2,800°C) on soft carbon precursors, and its reversible capacity is a little smaller than natural graphite.

Graphitized MCMB, mesophase-pitch-based carbon fiber (MCF), and vapor-grown carbon fiber (VGCF) are the representatives of benchmark synthetic graphite anode materials for Li-ion batteries in the market today. Graphitized MCMB has many advantages, namely, high packing density that guarantees high-energy density, and small surface area that decreases the irreversible capacity corresponding to electrolyte decomposition; most surfaces of MCMB spheres are composed of edge-plane surfaces, thus facilitating Li^+ intercalation and higher rate capability, ease of spreading onto copper foil.

Although amorphous carbon and spherical mesophase base graphite have been used mainly as anode materials in Li-ion cells, artificial graphitic carbon also called as massive artificial graphite (MAG) with lower voltage and the higher energy density is being used mainly to fulfill the difficult requirement for mobile equipment in recent years. MAG has been developed for the mass production of unique graphite for the purpose of battery application [43].

The MAG particles consist of spherical aggregation of fine, flat crystals. It has an average diameter of 20–30 μm and an aspect ratio of about one. MAG particles have a pseudo-isotropic texture where primary flat particles are randomly aggregated that also aids in tolerating expansion and shrinkage during charge/discharge operation. The discharge capacity of MAG exhibits a value of 362 mAh/g, which is very close to the theoretical one (372 mAh/g) of graphite. Graphite with a high crystallinity, which has a smaller interlayer spacing in the crystal, has relatively higher discharge capacity. This could be attributed to the fact that the graphite with the higher crystallinity is mainly composed of regular stacking structure, which is suitable for the formation of Li-GIC. Studies also have shown that the movement of Li^+ ions in MAG occurs in the vertical direction to the collector during the charge/discharge and Li^+ insertion into graphite occurring at the edge of graphite crystal, thereby having an easier lithium transfer and hence better high rate performance compared to flaky natural graphite [43].

Lithium Titanate Anode Lithium titanate ($Li_4Ti_5O_{12}$, referred to as LTO) is another promising anode material for certain niche applications that require high C rates, fast charging capability. Some of the challenges for the LTO-based cells include lower voltage (2.5 V vs. LCO and 1.9 V vs. LFP), lower capacity, and excellent high-temperature stability. It has superior high rate performance with very long cycle life. It is being developed for automotive and energy storage applications.

Silicon-Based Anode Existing lithium-ion batteries using graphite anodes have inherent limited Ah capacity. Silicon-based anodes theoretically offer as much as a tenfold capacity improvement over graphite. Silicon, when converted to the compound $Li_{21}Si_5$ by reaction with lithium in an electrochemical cell, has a maximum capacity of 4,200 mAh/g [44]. Due to its relatively low cost, low toxicity, and higher theoretical capacity, silicon is one of the promising candidates to replace graphite anode in Li-ion systems.

However, implementation of Si as an anode material is greatly hampered by several factors such as large volume change, low intrinsic electrical conductivity, and poor cyclability. The loss of capacity on repeated cycling is attributed to mechanical fragmentation and electrical isolation of silicon species due to the volumetric expansion and contraction associated with lithium insertion and extraction [45]. Many experimental techniques were investigated to analyze the cycling behavior and investigate mechanical degradation upon cycling [46, 47]. The reaction of silicon with lithium produces various alloy-type compounds (LixSiy) and causes enormous volume changes of up to 300% during the charge/discharge process, and this, together with the low electrical conductivity of silicon, obstructs the commercial use of silicon as a negative electrode material [48].

There are several approaches used to date for investigating silicon-based anodes. The thin-film approach involves deposition of an active silicon layer as a continuous media on a specially roughened metal or carbon current collector using ion sputtering [49, 50] or vapor deposition techniques [51, 52]. The film formation method, which results in strong adhesion between the current collector and very thin silicon layer, leads to the formation of a stable, self-organized columnar structure during the first volumetric expansion. This structure remains stable over cycles and aids in providing cycling stability of the films. Despite such attractive features of thin silicon film electrodes, they are yet to be commercialized. The thin silicon film electrodes are an order of magnitude thinner than cathodes, which might cause technological problems [53] and does not seem to be easily scalable. Moreover, solid electrolyte interface (SEI) film formation mechanism has yet to be studied in detail [54] and might highlight potential complications for real LIB employing such electrodes, especially during long-term cycling.

The approach is the composite electrode approach that relies on the use of silicon in the form of tiny silicon "cores," uniformly distributed within an electrochemically active or inactive buffering media, which prevents silicon-silicon interaction and the formation of large clusters. The core-shell structured anode materials comprising Si/SiO_2 blended with graphite material are good examples for the composite concept and have been gaining much attention primarily due to its ability to deliver higher capacity with continuous cycling, longer and stable cycling performance with much lower volume change than other silicon-based systems under study. Mixtures of silicon and different blends of graphite were studied and it was found that graphite is important in improving cycling performance [55, 56]. To suppress the volume effects of silicon upon cycling, techniques such as pyrolyzed PVC reactions and high-energy mechanical milling (HEMM) were adopted to disperse ultrafine silicon into a feasible carbonaceous matrix that shows promising results on improving the coulombic efficiency after the first cycle [57]. Further optimization of Si-composite based anodes could lead to practical lithium-ion batteries with high-energy density.

Positive Electrode Material

$LiCoO_2$ Lithium cobalt oxide (LCO) is the primarily used positive electrode–active material of Li-ion rechargeable cells. The simplicity involved in manufacturing and the balanced cell characteristics, namely, cycle performance, rate capability, high and low-temperature performance, safety, and so on, are some of the reasons why LCO is a leading player among

positive electrode–active materials. However, as the Li-ion market is driven by cost reduction both in consumer electronics and in the vehicle and stationary storage segment combined with the present higher market price of cobalt, the application of LCO material is decreasing and focus now shifts more toward nickel, manganese, and iron type materials and cobalt-doped layered mixed oxide materials.

$LiCoO_2$ is obtained using a cobalt compound and a lithium compound as the raw materials and heating. Today cobalt oxide (Co_3O_4) is used as the cobalt compound and lithium carbonate (Li_2CO_3) as the lithium compound due to the stability of their quality and supply, the easiness of handling. The reaction scheme for the $LiCoO_2$ can be indicated as:

$$2Co_3O_4 + 3Li_2CO_3 + 1/2O_2 \rightarrow 6LiCoO_2 + 3CO_2$$

Goodenough recognized that $LiCoO_2$ had a structure similar to the layered structures of the dichalcogenides and showed that the lithium could be reversibly removed electrochemically, thus making it a viable cathode material [58].

$LiNiO_2$ Lithium nickel oxide is isostructural with lithium cobalt oxide and has higher specific capacity. However, it is much more susceptible to thermal runaway and has not been used in commercially lithium-ion cells.

$LiMn_2O_4$ (Spinel) James Hunter of Eveready Battery Co. was the first to patent spinel cathode material. The application of material to Li-ion system has been developed by J. M. Tarascon [59] and extensively studied by M. Thackeray [60]. Generally, lithium spinel oxides suitable for the cathode are limited to those with a normal spinel in which the lithium ions occupy the tetrahedral (8a) sites and the transition-metal ions reside at the octahedral (16d) sites. Currently, spinel is the center of much interest as the cathode material for large format lithium-ion cell for hybrid electric vehicle applications where high power, safety, and low cost are the strongly required features.

Olivine Compound ($LiFePO_4$) A number of researchers have pursued the oxides of iron as potential cathode materials for Li-ion cells. The first cathode material produced in this category is $LiFePO_4$ [61]. Its low cost and environmentally benign characteristics could have a major impact in electrochemical energy storage. Orthorhombic $LiFePO_4$ of the olivine structure forms $FePO_4$ during charging/discharging, and two crystal phases exist during charging/discharging; thus, it exhibits a flat discharge curve with a discharge potential of 3.4 V [62]. The specific capacity of $LiFePO_4$ is lower compared to nickel and cobalt-based materials. Substitution of iron by manganese transforms the shape of the charge/discharge curves, and this proved effective in increasing the energy density [63, 64]. The capacities of the lower voltage (3.5 V) and higher voltage region (4.0 V) correspond to the content of iron and manganese. Modified $LiFePO_4$ material too makes it more stable and compatible with a wide range of electrolyte solvents that greatly enhances performance and rate capability.

Mixed Oxide Cathodes

Nickel Cobalt Dioxide, $LiNi_{1-y}Co_yO_2$, and Nickel Cobalt Aluminum oxide, $LiNi_{1-y-z}Co_yAl_zO_2$ In general, the introduction of cobalt into nickel oxide structures leads to more stability and nickel oxide structures are less likely to lose oxygen than the pure nickel oxide, and studies on the structural details and physical properties of the mixed oxide system showed that there is an increased ordering with increase in the cobalt concentration. An issue with all these layered oxides is their electronic conductivity, which is not uniformly high across the lithium composition range or nickel substitution. For example, cobalt substitution in $LiNiO_2$, as in $LiNi_{0.8}Co_{0.2}O_2$, reduces the electronic conductivity at 4.2 V significantly. These dramatic changes demand that a conductive diluent be added to the cathode-active material, which reduces both the energy storage and the power capabilities.

Substituted nickel oxides, such as $LiNi_{1-y-z}Co_yAl_zO_2$ (NCA), are prime candidates for the cathode of advanced lithium batteries for use in large-scale systems as required for hybrid electric vehicles. They currently are the battery of choice for satellite applications. On charging these mixed oxides, the nickel is oxidized first to Ni^{4+} then the cobalt to Co^{4+} [65]. The significant feature of NCA type material is its increased thermal stability by doping with cobalt and aluminum. The temperature of the exothermic peak with oxygen evolution increased from 200°C of $LiNiO_2$

to 310°C of $LiNi_{0.8}Co_{0.15}Al_{0.05}O_2$ due to the decrease in the nickel content and the aluminum doping [66]. The thermal stability has been considerably improved and there is no oxygen evolution observed below 300°C. Moreover NCA type material has a higher capacity, better cycle life and also rate capability than that of the conventional cobalt-based cathode.

Nickel Cobalt Manganese Oxide, $Ni_xCo_yMn_zO_2$ One other commonly used mixed oxide material as positive electrode is cobalt- and manganese-doped lithium nickel oxide. In general, addition of nickel suppresses manganese dissolution to a great extent, thereby enhancing the cycling performance especially at higher temperature. The most common stoichiometry is the 333 compound $LiNi_{1/3}Mn_{1/3}Co_{1/3}O_2$ synthesized using coprecipitation method by Ozhuku et al. [67] and Jeff Dahn in Canada (3 M). There have been many studies on the 333 compound, which have been made by a number of synthetic techniques over a wide range of temperatures. Most of these studies show similar behavior with the capacity of around 165 mAh/g increasing with increasing charging potential [68–70]. The material attracts much attention because of the large battery capacity of about 200 mAh/g, and is a promising material in future. However, the material has certain disadvantages associated with the physical property, namely, lower tap density, smaller particle size that leads to lower energy density and thus mostly preferred to be used in the mixed cathode material. Similar to NCA type material, for the NMC material also, the DSC peak temperature related to the oxygen evolution shifts to the higher temperature as the increase in manganese doping amount and the amount of heat generation decreases extremely. The thermal stability of the cathode material thus could be improved by manganese doping [71].

High-Energy Structured Type and Layered Cathode Materials There are several approaches currently being pursued to improve the cathode energy density, high rate performance, and cycling performance. One of the means to achieve the trade-off properties, namely, higher capacity and superior thermal stability, is through core-shell structured type electrodes. Higher capacity would be delivered by the core material, and structural/thermal stability would be achieved by the shell material [72–74]. A typical example is NCM type material in core to provide higher capacity surrounded by Ni-/Mn-based layered oxide as shell to offer good thermal stability.

One other approach is a composite layered oxide synthesized through continuous, low-cost highly homogenous coprecipitation process that provides higher capacity and cell voltage. One typical example is $xLi_2MnO_3.(1–x)LiNiO_2$ that claims to deliver around 250 mAh/g with longer cycle life and is able to operate at 4.6 V with surface modification [75, 76]. Other approaches include: surface treated cathode like AlF_3-coated cobalt-doped material to improve cycle life and power when operated at elevated temperatures and pseudo co-crystal-like structure with particle surface doping (e.g., $LiCoO_2$ type core material with the surface being treated with dopants like magnesium) to improve stability of the structure. Coating the positive electrode with materials such as Al_2O_3, $AlPO_4$, and ZrO_2 is also being actively pursued and used in commercial Li-ion cells [77–79]. Such surface coatings provide superior charge discharge characteristics, increased rate capability, long cycle life, and enhancement in structural stability, and this also elevates thermal stability.

Electrolyte and Additives

For the battery electrolyte, more focus is on developing additives to carry out additional functions to improve the performance and safety also referred as role-assigned electrolytes. Sanyo [80] and Saft [81] companies were the pioneers in proposing Vinylene carbonate (VC) as a solvent additive for graphite based electrochemical systems. VC is one of a popular additive for battery electrolytes typically being used as an anode passivation film-forming agent offering excellent stability and improvement in cycle life. The addition of VC has shifted the decomposition temperature of the SEI to a higher temperature, and this enhanced thermal stability can explain the suppression of the reaction between the electrolyte and the anode when the SEI is broken and repaired. It is considered that the relatively thinner homogeneous SEI formed by VC is an origin of the better cell performances, although the quality of its SEI is strongly dependent on the kind of graphitic carbons and charging conditions.

Sulfite compounds, namely, ethylene sulfite (ES), propylene sulfite (PS), dimethyl sulfite (DMS), and diethyl sulfite (DES), were also being used as passivation film-forming agents especially for PC-based electrolyte, and these compounds were reduced at about 2 V versus Li^+/Li to form the passivation layers, which hindered the PC co-intercalation into the graphene layers [82–84]. Cyclic sulfonate compounds, namely 1,3-propane sulfone (1,3-PS), were reported to give a good SEI film, which resulted in improving cycle and storage performances of cylindrical hard-carbon/$LiMn_2O_4$ cells [85].

Some key additive materials used as overcharge protection agents include biphenyl (BP), cyclohexyl benzene (CHB), and hydrogenated *m*-terphenyl (H-mTP). BP polymerizes [86, 87] on the positive electrode during overcharge and the liberated protons migrate to the anode, generating hydrogen gas. This mechanism is used for the overcharge protection: In case of cylindrical cells with pressure-activated current intermitted devices (CID), the internal pressure rise by H_2 evolution helps to operate them and prismatic cells utilize the current shutdown mechanism by the increase in the internal resistance by the polymerized film and the meltdown of polyethylene separators [88].

For protecting the cells from overcharge, one other method is including redox shuttle-type compounds as additives in electrolyte. A compound "R" with a reversible redox potential is added to the electrolyte solution. The R is oxidized to compound "O" on the positive electrode, and then O migrates to the negative electrode and is reduced to the original form R. The requirements for such a compound are that the redox potential should be slightly positive (0.1–0.2 V) to the formal potential of the positive electrode at the end-of-charge and the redox reactions during overcharge should be kinetically reversible on both the electrodes. Some examples include aromatic compounds like 2,4-difluoroanisole (DFA) [87], 4-bromo-1,2-dimethoxybenzene [89], and 2,7-dibromothianthrene [90].

Wetting characteristics are very critical for cell design to obtain optimal performance. In general, one might expect that the solvents and liquid electrolytes will be attractive to hydrophilic surfaces such as cathode materials, but repulsive to hydrophobic ones such as polyolefin separators and carbonaceous anode materials [91]. The separator wettability can limit the performance of batteries by increasing the separator and cell resistance. The contact angle is a good measure of wettability. The uptake of electrolyte can be enhanced by wetting agents such as methyl phenyl carbonate (MPC) [92] and di-octyl carbonate (DOC) [93].

The additives used in electrolyte as a flame-retarding agents include trimethyl phosphate (TMP), phosphazene derivatives, namely, hexamethoxycyclotriphosphazene (HMPN), tris(2,2,2-trifluoroethyl) phosphate (TFP), and hexamethylphosphoramide (HMPA). Due to the passivation layer formed by these flame-retarding additives [94–96], the exothermic peaks were depressed and also the self-heat rate occurring at elevated temperature thereby provided safety during abuse situations. In addition fluorinated ester group materials (e.g., FEC) are also being used as additive to electrolyte to improve upon high-temperature stability [97–99]. There are also several ongoing research activities on molten salt electrolytes to gain the benefits of the nonflammable characteristics, but overcoming the conductivity issues is still challenging.

Separators

The process for making Li-ion battery separators can be broadly divided into dry and wet processes. Both processes usually employ one or more orientation steps to impart porosity and/or increase tensile strength. Dry process involves melting a polyolefin resin, extruding it into a film, thermal annealing to increase the size and amount of lamella crystallites, and precisely stretching to form tightly ordered micropores. In this process, a row lamellar crystal structure is generated in the polymer in the initial extrusion step. This nonporous structure is highly oriented as a result of extrusion and annealing conditions. In the next step, film is stretched to form micropores. This microporous structure is continuous throughout the bulk interior of the membrane. No solvents are required to produce separator membranes through dry process method.

Wet process also called as phase inversion process involves mixing of hydrocarbon liquid or some other low-molecular-weight substance generally with a polyolefin resin, heating and melting the mixture, extruding the melt into a sheet, orienting the sheet either in the

machine direction or biaxially, and then extracting the liquid with a volatile solvent. The structure and properties of the membranes can be changed by controlling the composition of the solutions and the evaporation or subtractions of solvents in the gelation and solidification processes. The separators made by wet process use ultrahigh-molecular-weight polyethylene (UHMWPE). The wet process method is not applicable for polymers such as polypropylene, which do not dissolve in conventional solvents.

Shutdown separators are one of the safety devices inside the cell and act as a last line of defense. The separator shutdown is irreversible, which is fine for polyethylene-based separators, which melt at around 130°C. The impedance of the separator increases by two to three orders of magnitude due to an increase in cell temperature, which results from cell abuse (e.g., short circuit, overcharge). The separator not only should shut down around 130°C, but it also should maintain its mechanical integrity at higher temperatures. The high-temperature melt integrity of separators also is a very important property to keep the cell safe during extended overcharge or during extended exposure to higher temperatures.

Many technology advancements and improvements are achieved for the separators that also enable the Li-ion cell to operate more reliably under wide ranges of voltage and temperature for prolonged cycles. Separators existing in current market exhibit superior uniformity in thickness and pore distribution, higher strength, and dimensionally more stability at elevated temperatures. The separator membrane shows higher thermal stability through blending with high melting polymer resins. Ceramic material coating on top of polyolefin separator is currently becoming a popular choice for large format Li-ion cells for EDV applications to improve safety. Ceramic layer controls the shrinkage of the separator significantly especially at temperatures close to the melting points of polyolefin, thereby enabling the separator to isolate the electrodes for much higher temperatures.

Battery Management Systems

Owing to the fact that no two cells in a battery are exactly identical, their parameters such as capacity, voltage may vary by a fraction even when manufactured under similar conditions with advanced quality control protocols. In the case of a new battery, these factors may not be very noticeable, but play a major role in determining the performance of the pack with continuous charge/discharge cycles. This problem is easier to detect in a battery of up to 6–12 cells as the case in NBPC battery packs. A faulty cell can be easily disguised in a large battery pack consisting of tens or hundreds of series-connected cells as will be used for EDV applications. Thus, it becomes very essential to monitor the batteries individually and detect faults early.

A battery management unit (BMU) monitors and controls a battery pack. To increase the capacity and voltage, cells are connected in series-parallel arrangements. A typical laptop battery pack would contain a total of six 18650 cells where three cells are connected in series and two of the three cell series combination are connected in parallel. This setup is commonly denoted as 3S2P configuration. In the case of electric vehicle applications, it is common to have several hundred cells in series-parallel arrangements to get the desired voltage of 300–400 V and capacity.

The basic functionalities in a BMU consist of safety functions, voltage and current measuring, state of charge (SOC), and temperature monitoring. For Li-ion battery packs, battery management is the most essential as cells are needed to be controlled individually. When all cells are in parallel, the voltages are forced to be equal according to Kirchhoff's circuit laws, and hence, no balancing is needed. When the cells are connected in series, the voltages will differ and hence need balancing.

Cells in a battery pack may have slightly different voltages and capacity after complete charge due to minor differences in capacity, impedance, and rate of self-discharge. Cell balancing has been used to reduce the voltage differences among cells, thereby enhancing capacity and cycle life. Overvoltage safety detection functions will abort charging of the battery when any cell reaches its overvoltage threshold. Therefore, other cells may stay undercharged. One consequence is that the battery's full capacity will not be available for discharge. The same occurs when the weakest cell reaches the lower threshold, resulting in capacity not being

used. Without balancing, the different cell capacities will start to drift with every charge/discharge cycle, leading to a decrease in the battery pack's total performance.

Cell balancing can be carried out using current bypass by burning up energy through a resistor as heat. This is often referred as passive balancing where to even out differences; the lowest cell determines the level of capacity after balancing. Passive balancing shall not be applied during discharge as it reduces the available capacity of the battery. One other means of balancing is active balancing where energy would be passed from a cell with higher voltage to a cell with lower voltage.

In electric vehicle applications, battery management is essential and much more demanding than for portable batteries. It has to interface with a number of other onboard systems, has to work in real time in rapidly changing charge/discharge conditions as the vehicle accelerates and brakes, and it has to work in harsh and uncontrolled environments. Determining the battery state of charge is particularly critical in electric vehicle applications since these batteries require both high-power charge capability (regenerative braking) and high-power discharge capability for start or acceleration. Therefore, they must be maintained at a SOC that allows delivering the required power, while still having enough "headroom" to accept regenerative charge without overcharging the cells.

In addition to current and voltage monitoring, the BMU also monitors the temperature of the cells in all modes of operation (drive, charge, etc.) and controls the pump, fans, and heater to manage the temperature of the battery. Battery thermal management is critical for the battery life and the vehicle performance, and it is done through the battery electronic control unit. The goal is to make a battery pack work at an optimum average temperature (with life and performance trade-off) with even temperature variations in the modules and within the pack.

Bibliography

1. Whittingham MS (1976) Electrical energy storage and intercalation chemistry. Science 192(4244):1126
2. Goodenough JB (1980) U.S. Patent 4,302,518 (Issued 31 Mar 1980)
3. Ikeda H, Narukawa K, Nakashim H (1981) Japanese Patent 1769661 (Issued 18 June 1981)
4. Basu S (1982) U.S. Patent 4,423,125 (Issued 13 Sept 1982)
5. Yoshino A, Jitsuchika K, Nakashima T (1985) Japanese Patent 1989293 (Issued 10 May 1985)
6. Gozdz AS, Schmutz CN, Tarascon JM (1994) U.S. Patent 5,296,318 (Issued 22 Mar 1994)
7. Gozdz AS, Schmutz CN, Tarascon JM, Warren PC (1995) U.S. Patent 5,418,091 (Issued 23 May 1995)
8. Gozdz AS, Schmutz CN, Tarascon JM, Warren PC (1995) U.S. Patent 5,456,000 (Issued 10 Oct 1995)
9. Gozdz AS, Tarascon JM, Warren PC (1995) U.S. Patent 5,460,904 (Issued 24 Oct 1995)
10. Global Industrial Analysts Report. http://www.prweb.com/releases/2011/1/prweb8040051.htm. Accessed Feb 2011
11. Institute of Information Technology, Ltd. (IIT) report, Year 2010, Q4, Chapter 7
12. Brodd RJ (2009) In: Yoshio M, Brodd RJ, Kozawa A (eds) Li-ion batteries: science and technologies. Springer, New York, pp 1–7
13. Takeshita H (2006) 23 rd international seminar on primary and secondary batteries, Ft. Lauderdale, Mar 2006
14. Peled E (1979) The electrochemical behavior of alkali and alkaline earth metals in nonaqueous battery systems—the solid electrolyte interphase model. J Electrochem Soc 126:2047
15. Peled E (1999) In: Besenhard JO (ed) Handbook of battery materials. Wiley-VCH, Weinheim, pp 419–458
16. Whittingham MS (2004) Lithium batteries and cathode materials. Chem Rev 104:4271–4301
17. Zhang ZJ (2011) Li-ion application in EDV and its safety perspectives, Pacific power sources symposium 2011, Hawaii
18. Zhengming (John) Z, Ramadass P (2009) In: Yoshio M, Brodd RJ, Kozawa A (eds) Li-ion batteries: science and technologies. Springer, New York, pp 367–412
19. Tagawa K, Brodd RJ (2009) In: Yoshio M, Brodd RJ, Kozawa A (eds) Li-ion batteries: science and technologies. Springer, New York, pp 181–193
20. Kim J, Hong JJ, Koh S (2006) Proceedings of the 42nd power sources conference, Philadelphia, June 2006
21. Tullo A (2006) Dell recalls lithium batteries. In: Chemical and engineering news: American Chemical Society, 21 Aug 2006
22. Hales P (2006) Dell laptop explodes at Japanese conference. In: The inquirer, June 2006 Staff (27 July 2007). Nokia – Retrieved 15 June 2010
23. N91 cell phone explodes Mukamo. In: Filipino news (blog), July 2007
24. IEEE 1625 (2008) IEEE standard for rechargeable batteries for multi-cell mobile computing devices
25. IEEE 1725 (2011) IEEE standard for rechargeable batteries for cellular telephones
26. UL 1642 (1995) UL standard for safety for lithium batteries, 3rd edn., Dated April 26, 1995
27. Jacoby M (2007) Burning batteries. Chem Eng News 85:26–28

28. Santhanagopalan S, Ramadass P, Zhang Z (2009) Analysis of internal short-circuit in a lithium ion cell. J Power Sources 194:550–557
29. Nishi H (1998) Lithium ion batteries. In: Wakihara M, Yamamoto O (eds) Fundamentals and performances. Codensha/Wiley, New York, pp 181–198
30. Dahn JR (1991) The phase diagram of Li_xC_6. Phys Rev B 44:9170
31. Tatsumi K, Zaghib K, Sawada Y, Abe H, Ohsaki T (1995) Anode performance of vapor-grown carbon fibers in secondary lithium-ion batteries. J Electrochem Soc 142:1090
32. Aurbach D, Levi M, Levi E (1997) The mechanism of lithium intercalation in graphite film electrodes in aprotic media. Part 1. High resolution slow scan rate cyclic voltammetric studies and modeling. J Electroanal Chem 421:79
33. Aurbach D, Ein-Eli E (1995) The study of Li-Graphite intercalation processes in several electrolyte systems using *In Situ* X-ray diffraction. J Electrochem Soc 142:1746
34. Ohzuku T, Iwakoshi Y, Sawai K (1993) Formation of Lithium-Graphite intercalation compounds in nonaqueous electrolytes and their application as a negative electrode for a lithium ion (Shuttlecock) cell. J Electrochem Soc 140:2490
35. Inaba M, Yoshida H, Ogumi Z, Abe T, Mizutani Y, Asano M (1995) *In Situ* raman study on electrochemical Li intercalation into graphite. J Electrochem Soc 142:20
36. Funabiki A, Inaba M, Abe T, Ogumi Z (1999) Nucleation and phase-boundary movement upon stage transformation in lithium–graphite intercalation compounds. Electrochim Acta 45:865
37. Xu K, Zhang S, Poese BA, Jow TR (2002) Lithium bis(oxalato) borate stabilizes graphite anode in propylene carbonate. Electrochem Solid-State Lett 5:A259
38. Kinoshita K (1998) Carbo: electrochemical and physicochemical properties. Wiley, New York, p 70
39. Wang H, Ikeda T, Fukuda K, Yoshio M (1999) Effect of milling on the electrochemical performance of natural graphite as an anode material for lithium-ion battery. J Power Sources 83:141
40. Yoshio M, Wang H, Fukuda K, Hara Y, Adachi Y (2000) Effect of carbon coating on electrochemical performance of treated natural graphite as lithium-ion battery anode material. J Electrochem Soc 147:1245
41. Wang H, Yoshio M (2001) Carbon-coated natural graphite prepared by thermal vapor decomposition process, a candidate anode material for lithium-ion battery. J Power Sources 93:123–129
42. Wang H, Yoshio M, Abe T, Ogumi Z (2002) Characterization of carbon-coated natural graphite as a lithium-ion battery anode material. J Electrochem Soc 149:A499
43. Nishida T (2009) In: Yoshio M, Brodd RJ, Kozawa A (eds) Li-ion batteries: science and technologies. Springer, New York, pp 329–341
44. Wakihara M, Yamamoto O (1998) Lithium batteries-fundamentals and performance. Wiley-VCH, Germany
45. Besenhard JO, Yang J, Winter M (1997) Will advanced lithium-alloy anodes have a chance in lithium-ion batteries?. J Power Sources 68:87
46. Ozhuku T, Tomura H, Sawai K (1997) Monitoring of particle fracture by acoustic emission during charge and discharge of Li/MnO2 cells. J Electrochem Soc 144:3496
47. Ozhuku T, Matoba N, Sawai K (2001) Direct evidence on anomalous expansion of graphite-negative electrodes on first charge by dilatometry. J Power Sources 97–98:73
48. Yoshio M, Wang H, Fukuda K, Umeno T (2002) Carbon-coated Si as a lithium-ion battery anode material. J Electrochem Soc 149:A1598
49. Neudecker BJ, Zuhr RA, Bates JB (1999) Lithium silicon tin oxynitride (Li_ySiTON): high-performance anode in thin-film lithium-ion batteries for microelectronics. J Power Sources 81:27
50. Bordearu S, Brousse T, Schleich DM (1999) Amorphous silicon as a possible anode material for Li-ion batteries. J Power Sources 81:233
51. Green M, Fielder E, Scrosati B, Watchler M, Moreno JS (2003) Structured silicon anodes for lithium battery applications. Electrochem Solid State Lett 6:A75
52. Takamura T, Ohara S, Suzuki J, Sekine K (2002) The 11th international meeting on Lithium batteries, Monterey, 23–28 June 2002, Abs#257
53. Zaghib K, Kinoshita K (2004) 12th international meeting on Lithium batteries, Nara, 27 June–2 July 2004, Abs#7
54. Yonezu I, Tarui H, Yoshimura S, Fujitani S, Nohma T (2004) 12th international meeting on Lithium batteries, Nara, 27 June–2 July 2004, Abs#58
55. Yoshio M, Wang H, Fukuda K, Umeno T, Dimov N, Ogumi Z (2002) Carbon-coated Si as a lithium-ion battery anode material. J Electrochem Soc 149:A1598
56. Dimov N, Fukuda K, Umeno T, Kugino S, Yoshio M (2003) Characterization of carbon-coated silicon: structural evolution and possible limitations. J Power Sources 114:88
57. Liu Y, Hanai K, Yang J, Imanishi N, Hirano A, Takeda Y (2004) Morphology-stable silicon-based composite for Li-intercalation. Solid State Ionics 168:61
58. Mitzushima K, Jones PC, Wiseman PJ, Goodenough JB (1980) Li_xCoO_2 ($0<x<-1$): a new cathode material for batteries of high energy density. Mater Res Bull 15:783
59. Tarascon JM, McKinnon WR, Coowar F, Bowmer TN, Amatucci G, Guyomard D (1994) Synthesis conditions and oxygen stoichiometry effects on Li insertion into the spinel $LiMn_2O_4$. J Electrochem Soc 141:1421
60. Thackeray MM, David WIF, Bruce PG, Goodenough JB (1983) Lithium insertion into manganese spinels. Mater Res Bull 18:461
61. Padhi AK, Nanjundaswamy KS, Goodenough JB (1997) Phospho-olivines as positive-electrode materials for rechargeable lithium batteries. J Electrochem Soc 144:1188
62. Mukerjee S, Yang XQ, Sun X, Lee SJ, McBreen J, Ein-Eli Y (2004) In situ synchrotron X-ray studies on copper–nickel 5 V Mn oxide spinel cathodes for Li-ion batteries. Electrochim Acta 49:3373
63. Yamada A, Chung S-C (2001) Crystal chemistry of the olivine-type $Li(Mn_yFe_{1-y})PO_4$ and $(Mn_yFe_{1-y})PO_4$ as possible 4 V cathode materials for lithium batteries. J Electrochem Soc 148: A960

64. Li G, Azuma H, Tohda M (2002) $LiMnPO_4$ as the cathode for lithium batteries. Electrochem Solid State Lett 5:A135
65. Nakai I, Nakagome T (1998) In Situ transmission X-ray absorption fine structure analysis of the Li deintercalation process in $Li(Ni_{0.5}Co_{0.5})O_2$. Electrochem Solid State Lett 1:259
66. Yoshio M et al (2009) In: Yoshio M, Brodd RJ, Kozawa A (eds) Li-ion batteries: science and technologies. Springer, New York, pp 9–48
67. Ohzuku T, Ariyoshi K, Yamamoto S, Makimura Y (2001) A 3-volt lithium-ion cell with $Li[NiMn_{3/2}]O_4$ and $Li[Li_{1/3}Ti_{5/3}]O_4$: a method to prepare stable positive-electrode material of highly crystallized $Li[Ni_{1/2}Mn_{3/2}]O_4$. Chem Lett 30:1270
68. Ohzuku T, Makimura Y (2001) Layered lithium insertion material of $LiCo_{1/3}Ni_{1/3}Mn_{1/3}O_2$ for lithium-ion batteries. Chem Lett 30:642
69. Yabuuchi N, Ohzuku T (2003) Novel lithium insertion material of $LiCo_{1/3}Ni_{1/3}Mn_{1/3}O_2$ for advanced lithium-ion batteries. J Power Sources 119–121:171
70. Park SH, Yoon CS, Kang SG, Kim H-S, Moon S-I, Sun Y-K (2004) Synthesis and structural characterization of layered $Li[Ni_{1/3}Co_{1/3}Mn_{1/3}]O_2$ cathode materials by ultrasonic spray pyrolysis method. Electrochim Acta 49:557
71. Ohzuku T, Ariyoshi K, Yamamoto S, Makimura Y (2001) A 3-volt lithium-ion cell with $Li[Ni_{1/2}Mn_{3/2}]O_4$ and $Li[Li_{1/3}Ti_{5/3}]O_4$: a method to prepare stable positive-electrode material of highly crystallized $Li[Ni_{1/2}Mn_{3/2}]O_4$. Chem Lett 30:1270
72. Sun YK et al (2005) Synthesis and characterization of $Li[(Ni_{0.8}Co_{0.1}Mn_{0.1})_{0.8}(Ni_{0.5}Mn_{0.5})_{0.2}]O_2$ with the microscale core–shell structure as the positive electrode material for lithium batteries. J Am Chem Soc 127:13411
73. Sun YK et al (2006) Novel core–shell-structured $Li[(Ni_{0.8}Co_{0.2})_{0.8}(Ni_{0.5}Mn_{0.5})_{0.2}]O_2$ via coprecipitation as positive electrode material for lithium secondary batteries. J Phys Chem B 110:6810
74. Sun YK et al (2009) High-energy cathode material for long-life and safe lithium batteries. Nat Mater 8:320
75. Thackeray M (2009) US DOE-VT Annual merit review, Proj ID ES020
76. Amine K (2010) US DOE merit review, Proj. ID ES015
77. Ho-Jin Kweon, Jun-Won Suh, Won Il Jung (2004) U.S. Patent 6, 753, 111 (Issued 22 June 2004)
78. Cho J et al (2001) High-performance ZrO_2-coated $LiNiO_2$ cathode material. Electrochem Solid State Lett 4(10):A159
79. Cho J et al (2000) Novel $LiCoO_2$ cathode material with Al_2O_3 coating for a Li ion cell. Chem Mater 12(12):3788
80. Fujimoto M, Takahashi M, Nishio A (1992) Japan patent 3059832 (Issued 27 July 1992)
81. Simon A, Boeuve J-P (1997) U.S. patent 5,626,981 (Issued 6 May 1997)
82. Wrodnigg GH, Besenhard JO, Winter M (1999) Ethylene sulfite as electrolyte additive for lithium-ion cells with graphitic anodes. J Electrochem Soc 146:470
83. Wrodnigg GH, Wrodnigg TM, Besenhard JO, Winter M (1999) Propylene sulfite as film-forming electrolyte additive in lithium ion batteries. Electrochem Commun 1:148
84. Wrodnigg GH, Besenhard JO, Winter M (2001) Cyclic and acyclic sulfites: new solvents and electrolyte additives for lithium ion batteries with graphitic anodes?. J Power Sources 97–98:592
85. Kusachi Y, Utsugi K (2003) Extended abstracts of the 44th battery symposium in Japan ,Sakai, p 526 4–6 Nov (2003)
86. Xiao L, Ai X, Cao Y, Yang H (2004) Electrochemical behavior of biphenyl as polymerizable additive for overcharge protection of lithium ion batteries. Electrochim Acta 49:4189
87. Kim H-J, Yoo S-I, Cho J-J (2002) Extended abstracts of the 43 rd battery symposium in Japan, Fukuoka, 12–14 Oct 2002, p 78
88. Tobishima S, Ogino Y, Watanabe Y (2002) Effect of electrolyte additives to provide safety and discharge characteristics of lithium batteries. Electrochemistry 70:875
89. Adachi M, Tanaka K, Sekai K (1999) Aromatic compounds as redox shuttle additives for 4 V class secondary lithium batteries. J Electrochem Soc 146:1256
90. Lee D-Y, Lee H-S, Kim H-S, Sun H-Y, Seung D-Y (2002) Redox shuttle additives for chemical overcharge protection in lithium ion batteries. Korean J Chem Eng 19:645
91. Blomgren GE (1999) Electrolytes for advanced batteries. J Power Sources 81–82:112
92. Suzuki H, Shima N, Hasegawa K, Yoshida Y (1996) JP1996–306387A; JP3893627B
93. Noda D, Kotato M, Fuji T, Suzuki H (2002) JP2002–319433A
94. Lee CW, Venkatachalapathy R, Prakash J (2000) A novel flame-retardant additive for lithium batteries. Electrochem Solid-State Lett 3:63
95. Zhang S, Xu K, Jow TR (2003) Tris(2,2,2-trifluoroethyl) phosphite as a co-solvent for nonflammable electrolytes in Li-ion batteries. J Power Sources 113:166
96. Gozales SI, Li W, Lucht BL (2004) Hexamethylphosphoramide as a flame retarding additive for lithium-ion battery electrolytes. J Power Sources 135:291
97. Okuno H et al (1996) U.S. patent 5,525, 443 (Issued 11 June 1996)
98. Yamaguchi et al (2009) U.S. patent 7,491, 471 B2, 17 Feb 2009
99. Abe K et al (2011) U.S. patent application 20110045361 (Pub. Date 24 Feb 2011)

Livestock Somatic Cell Nuclear Transfer

Sergio D. German, Keith H. S. Campbell
School of Biosciences, University of Nottingham, Sutton Bonington, Loughborough, Leicestershire, UK

Article Outline

Glossary
Definition of Cloning and SCNT
Introduction: Embryo Development and Highlights of NT

Nuclear Reprogramming
Factors Affecting Development of Embryos Produced by SCNT
Improving Development
Summary Points
Future Directions
Bibliography

Glossary

Aneuploid An unbalanced number of chromosomes.

Blastocyst A stage of early development where the embryo contains a fluid-filled cavity and two cell populations: an inner cell mass and an outer layer of trophectoderm cells.

Cell cycle The period between the birth of a cell and its division. During a single cell cycle, the cell must duplicate all of its components, including DNA, to form two equal daughter cells.

Chromatin The combination of DNA and proteins, mostly histones.

Cytoplast An enucleated cell used as a recipient for a donor nucleus. Generally in SCNT, the recipient cytoplast is an enucleated oocyte.

Diploid The cell or nucleus contains two complete copies of the genome or a complete complement of chromosomes (2n), in general, a single maternal and a single paternal.

Donor cell The cell that provides the genetic material (nucleus) for SCNT. The resulting animal will be a genomic copy of the animal from which this cell was collected.

Haploid The cell or nucleus contains only a single copy of the genome or half of the chromosome complement (n). Pronuclei are, in general, haploid, containing either a single maternal genome or a single paternal genome.

Karyoplast A cell or a membrane-bound portion of a cell containing the donor nucleus enclosed. In livestock SCNT, the karyoplast is generally an intact cell.

Meiosis The process of reduction in the number of chromosomes that occurs during germ cell formation. Following a round of DNA synthesis, a single cell undergoes two rounds of division resulting in four cells, each containing a haploid genome. During division, independent assortment of parental chromosomes and homologous recombination generate a unique haploid genotype in each of the germ cells.

Metaphase II (MII) Stage during the second meiotic division where the chromosomes are aligned at the metaphase plate prior to segregation of sister chromatids to opposite poles. In most mammalian species, mature oocytes arrest at MII and meiosis is reinitiated and completed upon fertilization.

Parthenote An unfertilized zygote produced by activation of an oocyte. A parthenote may be haploid or diploid for maternal DNA, a gynogenote, or following enucleation and replacement with paternal DNA, an androgenote.

Tetraploid The cell or nucleus contains four haploid copies of the genome (4n).

Zygote The 1-cell stage of development of a fertilized embryo. During most of the first cell cycle, the zygote will contain two pronuclei containing the maternal and paternal DNA.

Definition of Cloning and SCNT

Cloning is the production of genetically identical individuals by the process of asexual reproduction. In animals, the term has been applied to offspring that are produced by the technique of nuclear transfer (NT). The process of nuclear transfer involves the production of an embryo by transferring nuclear genetic material from a donor cell (karyoplast) into a recipient cell from which the genetic material has been removed (cytoplast). Two factors determine the clonality of the resultant offspring. One is the recipient cell, generally an oocyte or unfertilized egg obtained from an unrelated animal. The second is the donor cell, which can be obtained from a variety of sources including embryos, germ line, and somatic tissues of fetuses and adult organisms. When cells from somatic tissues are used, the procedure is termed somatic cell nuclear transfer (SCNT). In most species, transfer of the donor nucleus is primarily carried out by cell fusion with fewer reports of direct injection. In the case of fusion, the complete contents of the donor cell are introduced into the recipient cell, while in the case of injection, the donor nucleus might be accompanied with a proportion of the donor cytoplasm.

While SCNT became publicly known with the creation of Dolly the sheep in 1997, NT was already in the

realm of science since 1928, with the first successful SCNT experiments carried out in frogs in the late 1950s. By creating a genetic copy of a known animal, SCNT opens many opportunities in several fields including biomedical research and agriculture.

Introduction: Embryo Development and Highlights of NT

In animals, reproduction occurs primarily by sexual means, resulting in the creation of a new individual that contains genetic material (DNA) from two contributing parents of different sexes, each parent contributing half of the genetic material. Conception of a new individual occurs by the fusion of specialized cells or gametes, sperm in males and ova in females. Sperm are haploid (n) and contain a single copy of the genome, meanwhile ova, in most species, at the time of fertilization are arrested in metaphase of the second meiotic division and are diploid (2n). After fusion, however, the ovum completes meiosis to become haploid, and the resultant zygote is diploid (2n), containing a full set of chromosomes derived from both parents. The ovum is a large cell that contains sufficient maternally derived proteins and mRNAs to control early development. Following fertilization, during the early stages of development, no net growth occurs (Fig. 1); transcription from the embryonic genome is low but subsequently increases rapidly at a particular stage termed maternal to zygotic transition (MZT) [1]. The timing of the MZT is species dependent, for example, in mice, it occurs at the 1–2-cell stage; in pigs and humans at the 4–8-cell stage; in cattle and sheep at the 8–16-cell stage; while in the amphibian *Xenopus laevis*, it occurs approximately at the 4,000-cell stage [2]. After this transition, the embryonic genome orchestrates its own development. The embryo continues to increase in cell number within the confines of the zona pellucida (ZP), which acts as a protective shell. By the blastocyst stage, a fluid-filled cavity, called blastocoel, has formed and two distinct cell populations have emerged: the inner cell mass (ICM) and the trophectoderm (TE). As the blastocyst expands, build-up pressure together with the secretion of enzymes causes the ZP to break, enabling the blastocyst to hatch. Now the blastocyst is ready to interact with the endometrium and eventually to implant. By cell proliferation and differentiation, the ICM will form the fetus and some extraembryonic tissues while the TE will give rise to most of the placenta (Fig. 1).

The zygote is a totipotent cell, having the capacity to produce the fetus and the placenta. In contrast, sperm and ova are specialized cells. How do they acquire totipotency? Following fertilization, unknown factors present in the ovum's cytoplasm reprogram the paternal and maternal genomes so that their specialized gamete functions are erased to give way to an embryonic totipotent genome. This capacity to reset a specialized genome into a less specialized or totipotent genome is termed nuclear reprogramming. It is this nuclear reprogramming ability of the ovum that is harnessed in NT technology.

The first rudimentary NT experiments were performed by Hans Spemann in 1928. He used a donor nucleus from a 16-cell embryo and a presumptive zygotic cytoplast, resulting in a normal salamander [3]. Interestingly, Spemann had already predicted the possibility of cloning an adult animal by doing NT with an adult donor nucleus in what he termed the "fantastical experiment" [3].

In 1952, Briggs and King used NT to address the question of nuclear equivalence, that is, whether or not the different cells of a multicellular organism have the same genome. They developed the NT procedure by transplanting nuclei from frog blastula cells into enucleated oocytes [4]. Later on, Briggs and King tested the nuclear equivalence of more developmentally advanced frog cells and found that the developmental potential of reconstructed embryos gradually declined with increased donor cell differentiation [5]. However, John Gurdon pushed the field further by generating cloned adult frogs from differentiated epithelial somatic cells at the tadpole stage [6, 7], providing strong evidence for nuclear equivalence. Thus, the first successful SCNT had been achieved, but attempts to clone adult frogs failed [8].

Nuclear transfer in mammals lagged behind, with the first attempt in 1975 using morula-stage blastomere donors and unfertilized rabbit eggs. Even though the extent of reprogramming required for a blastomere, compared with a fully differentiated cell, is quite reduced, the reconstructed cloned embryos did not develop beyond the early cleavage stages [9]. In 1983, McGrath and Solter transplanted zygotic nuclei into

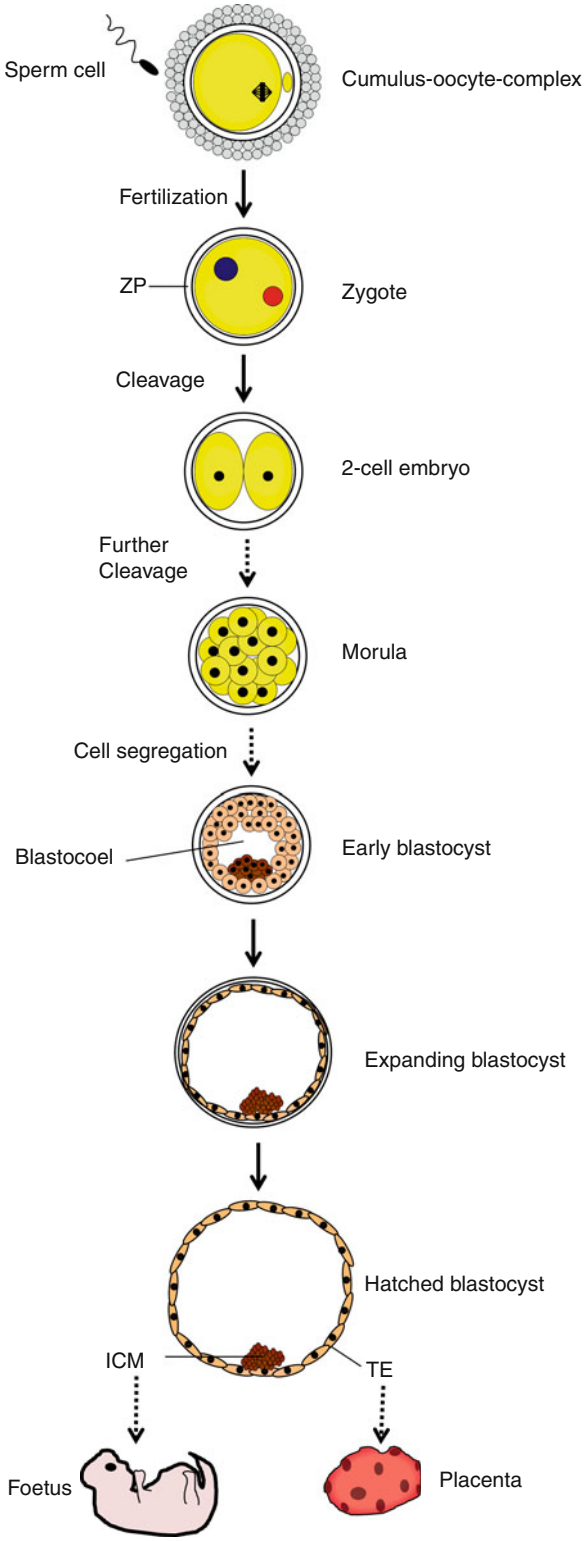

Livestock Somatic Cell Nuclear Transfer. Figure 1 (Continued)

enucleated zygotes resulting in mice developing to term, showing that the technique of nuclear transfer in mammals was feasible [10]. However, such a zygotic nuclei-replacement experiment did not involve any nuclear reprogramming, and when the same approach used more developmentally advanced blastomere nuclei as donors, it failed [11]. This failure in mice NT was followed by several breakthroughs in which enucleated oocytes were used as recipients of blastomere nuclei, leading to the production of cloned animals in sheep [12], cattle [13], and pigs [14]. In contrast to McGrath and Solter's failure in cloning mice, these results suggested that the enucleated oocyte is a better recipient than the enucleated zygote for reprogramming the donor blastomere nucleus.

Ten years passed until another breakthrough advanced the field of mammalian nuclear transfer: Keith Campbell and colleagues at the Roslin Institute succeeded in cloning a lamb by NT using donor nuclei from an established cell line derived from embryos [15]. In this study, cell cycle coordination between the donor cell and recipient oocyte was carried out prior to NT in order to improve the development of reconstructed embryos as previously determined by this group [16, 17]. One year later, this same group, led by Ian Wilmut, used a similar approach and shook the world's news with the creation of "Dolly" the sheep, the first mammal to be cloned from an adult somatic cell [18]. This study showed that an adult somatic cell retains all the information necessary to generate a new organism. After the creation of Dolly, much research has been done in SCNT and several species have been cloned from adult cells. Despite advances in the field,

Livestock Somatic Cell Nuclear Transfer. Figure 1
Flow diagram illustrating mammalian development. Following fertilization of the MII oocyte by sperm, a zygote with the two parental pronuclei is formed. By cleavage, the embryo develops sequentially through the 2-cell, 4-cell, 8-cell, 16-cell, morula, and blastocyst stages. By the blastocyst stage, the first differentiation event has formed the inner cell mass (ICM) and the trophectoderm (TE). These two cell populations will form the foetus and placenta, respectively

the frequency of development of embryos produced by SCNT remains low, with only 1–10% reaching term, depending on the species. Moreover, many cloned animals are born with abnormalities.

Applications of Livestock SCNT

Soon after the arrival of Dolly came the realization that SCNT had several potential applications. For instance, derivation of embryonic stem (ES) cells from human blastocysts was eagerly sought for regenerative medicine research. The rationale was that cells from a patient could be used for SCNT to derive ES cells, which in turn could be induced to differentiate into a specific tissue. Since such a tissue would be genetically identical to the patient, it could replace a damaged tissue in the same patient without the risk of immune rejection. Due to the ethical concerns of destroying human embryos, SCNT for regenerative medicine has been fiercely opposed. Fortunately, this problem seems mostly circumvented with the revolutionary creation of induced pluripotent stem (iPS) cells [19]. These cells have similar properties to ES cells and can also be derived from the somatic cells of a patient without the use of human oocytes or embryos. Since then, much of the field of regenerative medicine research has shifted from SCNT to iPS cell technology. However, recent studies have found genetic and epigenetic abnormalities in iPS cells [20–22], making them potentially unsafe for medical uses. Whether or not iPS cells are inferior to ES cells is currently the focus of heated debate. Since some of the problems found with iPS cells have not been reported with ES cells derived from SCNT embryos [23, 24], the process of nuclear reprogramming occurring in the oocyte appears to be of better quality than the one taking place during the derivation of iPS cells. Very little is known about the mechanism of nuclear reprogramming and the factors present in the oocyte responsible for triggering or carrying out such process. If these factors are found, they could potentially contribute to generate safer iPS cells for regenerative medicine. Thus, further research in the mechanism of nuclear reprogramming following SCNT is needed.

Apart from being a useful tool for basic research with potential indirect applications in regenerative medicine, SCNT has wide applications in agriculture. For instance, an animal of exceptional productivity can be multiplied by SCNT to increase commercial output or to reduce environmental impact. However, caution must be taken with such approach. First, consumption of products derived from cloned animals is not yet widely accepted by the public, and in some countries, there are regulations forbidding their entry into the human food chain. Second, the SCNT technology is so inefficient at present that its application for livestock multiplication might not be economically justified. Finally, it is important to keep in mind that clones are not necessarily true copies of their donor because of epigenetic differences, which result from faulty nuclear reprogramming following SCNT (discussed later). Slight epigenetic differences can affect the physiology of the cloned animal and thus its productivity. Such consideration should especially warn breeders of race-winner horses, as a cloned horse is unlikely to be a winner again.

A more realistic agricultural application of SCNT is to reproduce animals of high genetic value for breeding purposes. For instance, a prizewinning bull could be cloned and subsequently produce thousands of offspring by artificial insemination. To a lower extent, the genetic value of a cow could also be disseminated by SCNT followed by artificial reproductive technologies. While there might be risks associated with consumption of products from cloned animals due to potential epigenetic errors originated during nuclear reprogramming, their offspring should be safe since epigenetic and imprinting errors are normally erased during gametogenesis.

More importantly, SCNT has represented a great technical advance in the production of transgenic animals (this is discussed in detail in the entry ► Nuclear Transfer to Produce Transgenic Mammals, this volume). In turn, transgenic animals have a myriad of other applications, which are discussed throughout this volume. Furthermore, transgenic animals producing pharmaceutical or novel proteins are good candidates for multiplication by SCNT since the cost of using this technology would be relatively small compared to the product harvested from the cloned animals.

SCNT can also be used for cloning individuals from an endangered species population. Examples of this application include the cloning of wild cattle (Gaur and Banteng) and wild sheep (European Mouflon) [25].

These examples resorted to interspecies SCNT in which a close-related species is used as cytoplasmic recipients and surrogates for the donor. Therefore, the resultant offspring will be a hybrid containing a genomic copy of the endangered donor and most mitochondrial DNA (mtDNA) from the close-related recipient. While the physiological consequences for this are unclear, it certainly raises ethical issues. Besides, other efforts such as restoration of the natural habitat and assisted breeding programs are likely to be more effective at helping an endangered population.

Taken together, SCNT has some interesting applications, but the ethical implications surrounding this technology must be fully considered before rushing into implementing SCNT in the field. Rather than an end, SCNT is especially useful when used as a tool in research, production of transgenic animals, and in cloning of prizewinning animals for breeding purposes in agriculture.

NT Techniques

NT is a complex multistep procedure, with several alternatives at some steps, which include oocyte maturation, cumulus cell removal, enucleation, nuclear transfer, activation, and embryo culture. Culture of the donor cells is important and usually accompanied with cell-cycle synchronization prior to NT. Enucleation and nuclear transfer are the most important and difficult steps. To carry out these steps, most laboratories use micromanipulators. A micromanipulator is a relatively complex instrument composed of a microscope, micromanipulators at both sides to hold the holding and injection micropipettes, micromanipulator joysticks to precisely maneuver the micropipettes in three dimensions, and microinjectors to precisely aspirate and expel fluid and cellular material from the micropipettes. For mice cloning, microinjectors are usually equipped with piezoelectric devices to prevent lysis of the fragile mouse oocyte during enucleation and nuclear transfer. An alternative to micromanipulators is a technique called handmade cloning (HMC) and seems equally efficient as micromanipulator-based NT (for a review of HMC, see [26]). Following is a brief discussion of the different steps involved in the entire NT procedure with focus on livestock species unless stated otherwise.

Oocyte maturation is usually required in livestock cloning as immature oocytes are commonly obtained from ovaries collected from slaughterhouses. Alternatively, in vivo–matured oocytes can be obtained by stimulating superovulation, which is followed by oviduct flushing after slaughtering the animal. In vitro maturation (IVM) entails mimicking to some extent the in vivo environmental conditions found in the ovary at the time of the LH (luteinizing hormone) surge. Thus, three key hormones, LH, FSH (follicular stimulating hormone), and estradiol, are added to the IVM medium to stimulate maturation. Oocytes are surrounded by cumulus cells, forming a cumulus-oocyte complex (COC); cumulus cells aid oocyte maturation. COCs are incubated at about 39°C in livestock species and for 24 h (e.g., cow and sheep). Following the required maturation period, oocytes are denuded from the cumulus cells using hyaluronidase to digest the extracellular matrix that holds cumulus cells together. Removal of cumulus cells is necessary to allow visualization of the oocyte's chromatin during enucleation and to prevent inserting a cumulus cell accidentally inside the oocyte during enucleation and cell/nuclear transfer procedures. Now the denuded oocytes are ready for enucleation.

A few enucleation methods exist. The most commonly employed method uses micromanipulators to aspirate the chromatin. In this method, the oocyte is held steady at one side with the holding pipette while the enucleation pipette is inserted from the opposite side to remove, depending on the maturation state, the extruding spindle or first polar body together with the metaphase plate (Fig. 2). In order to confirm enucleation, it is desirable to visualize the chromosomal material. In mice and human oocytes, which have a clear cytoplasm, chromatin can be readily observed under bright field illumination. However, the oocytes of livestock species have high lipid contents that hamper chromatin visualization, and therefore, enucleations must be made "blind" (Fig. 2a). Generally, to aid enucleation of livestock oocytes, they are briefly preincubated with the vital DNA stain Hoechst. The stained karyoplast is confirmed in the enucleation pipette by UV light following enucleation. Although this procedure does not expose the oocyte to direct UV irradiation, conflicting evidence exist whether Hoechst diminishes the developmental competence of the oocyte.

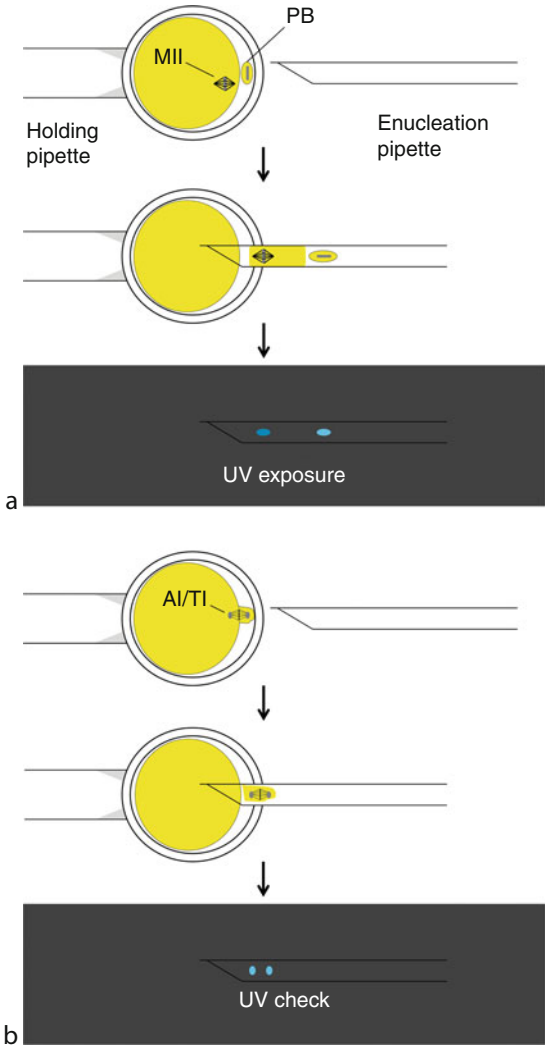

Livestock Somatic Cell Nuclear Transfer. Figure 2 Diagram illustrating enucleation of livestock oocytes. (**a**) When enucleation is carried out at metaphase II (*M*II), the polar body (*PB*) and a portion of cytoplasm is blindly aspirated to remove the underlying MII plate. Chromatin cannot be observed under bright field illumination, thus UV light exposure (*dark field*) is essential to confirm enucleation of the pre-stained chromosomes. (**b**) When enucleation is carried out earlier at anaphase I/telophase I (AI/TI), the extruding spindle is aspirated. In contrast to MII enucleation, the AI/TI spindle can often be observed directly inside the enucleation pipette. However, enucleation of pre-stained DNA can be checked with UV light. In both enucleation methods, the oocyte is removed from the field of view to avoid damage by direct UV irradiation when exposing the enucleation pipette

Alternatively, a blind-enucleation method without DNA staining uses the first polar body as a point of reference to subsequently remove the underlying metaphase II (MII) plate. Unfortunately, the MII plate can shift away from the polar body, rendering its removal inaccurate. However, when blind enucleation is performed earlier at anaphase I/telophase I (AI/TI) stages of the cell cycle, removal of the complete spindle is close to 100% accurate (Fig. 2b) [27]. A newer microscopy technology based on birefringence, the PolScope, allows noninvasive visualization of spindles not only in human oocytes but in other species as well. Probably due to the high cost of the PolScope, this enucleation method has not gained much popularity.

Direct enucleation by aspiration can be chemically assisted with cytoskeleton-relaxing agents, resulting in a protrusion cone containing the oocyte's chromosomes. Drugs used for this purpose include demecolcine and nocodazole, both interfering with microtubule polymerization. Other enucleation methods that have been attempted are centrifugation and laser ablation. In HMC, the zona pellucida is digested, and one third of the oocyte containing the extruding polar body and metaphase plate is manually bisected with a microblade under a stereomicroscope.

Donor cells are usually cultured in vitro and synchronized in a specific phase of the cell cycle prior to NT in order to ensure a known ploidy content. In livestock species, donor cells are preferentially used in G_0 and, to a lower extent, in G_1. Quiescent G_0 cells are arrested in the G_1 phase of cell cycle by either serum starvation or cell-contact inhibition. The advantage of these two methods is that they are drug independent, while methods to arrest cells at G_1 usually require the use of pharmacological agents. Alternatively, actively dividing presumptive G_1 cells can be selected by collecting small-sized cells. A more accurate drug-free method to select for G_1 cells from actively dividing cultures involves using the eukaryotic "baby machine", which briefly consists of an effluent that collects newly divided and floating daughter G_1 cells from the culture medium (this methodology is described in [28]). Such a methodology would be especially useful when it is desirable to clone ES cells in G_1 (discussed further in the section Coordination of Donor and Recipient Cell Cycles). In mice cloning, ES cells are often arrested in metaphase by nocodazole or colcemid treatments.

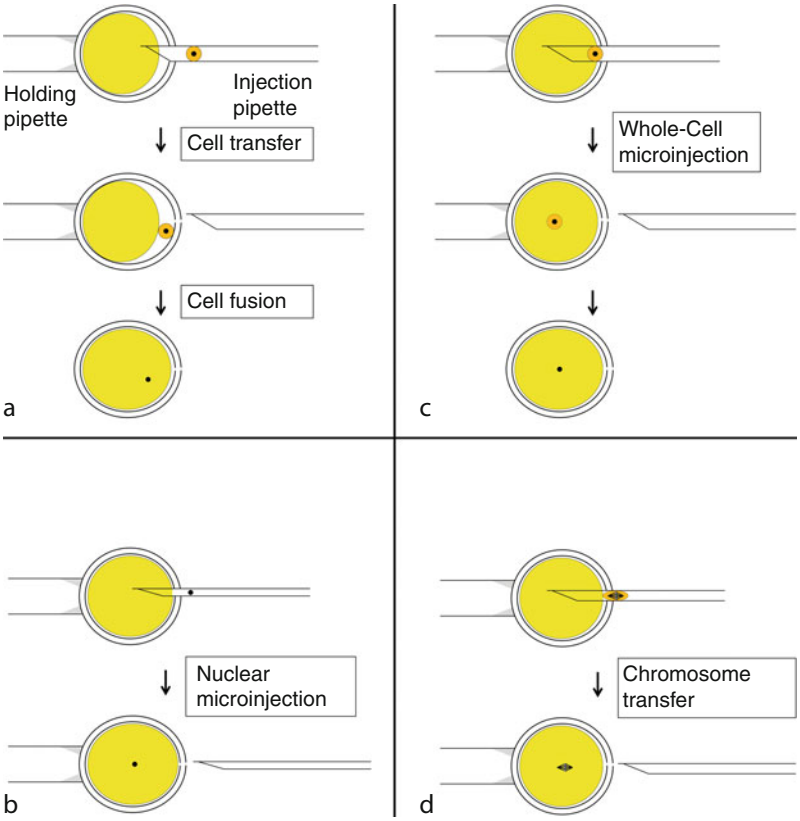

Livestock Somatic Cell Nuclear Transfer. Figure 3
Diagram illustrating different methods for donor genome transfer into recipient enucleated oocytes. (**a**) In cell transfer, an intact donor cell is transferred into the perivitelline space and the genome is then incorporated into the recipient by cell fusion. (**b**) In nuclear microinjection, nuclei are previously isolated and a single nucleus is then microinjected into the recipient. (**c**) In whole-cell microinjection, the whole cell is injected into the recipient. Eventually, incorporation of the genome into the recipient occurs by spontaneous degradation of the donor plasma membrane. (**d**) In chromosome transfer, a broken mitotic cell is microinjected into the recipient to transfer the mitotic spindle

A few alternatives exist for inserting the donor nuclear material into the enucleated oocyte (Fig. 3). In livestock species, the most common method is to insert the whole donor cell (cell transfer) into the perivitelline space to achieve contact between the membranes of donor and recipient cells. The donor DNA is then incorporated into the enucleated oocyte by cell fusion (Fig. 3a) (discussed below). Another method is to directly insert the nucleus (nuclear microinjection) into the enucleated oocyte, a common practice in mice cloning (Fig. 3b). The advantage of this method is that it bypasses the need for fusion. Nuclei are isolated using a micropipette with an inner diameter smaller than the donor cell. Pipetting the cell in and out breaks the membrane and releases the nucleus. Interestingly, it is also possible to microinject the whole cell into the enucleated oocyte cytoplasm, thus bypassing the need for nuclear isolation or fusion (Fig. 3c). Although it is unclear how the donor plasma membrane is degraded, high blastocyst development has been reported with this technique [29]. Another alternative method is to directly microinject a broken cell containing mitotic chromatin and cytoplasm, known as chromosome transfer (Fig. 3d). In HMC, phytohemagglutinin is used to glue the donor cell to the enucleated oocyte, followed by fusion.

When cell transfer is employed, the recipient-donor couplet must be fused to deliver the donor chromatin into the recipient oocyte. This is commonly achieved by electrofusion. In this method, the couplet is placed between two electrodes and short electric pulses are applied to fuse the recipient-donor membranes together. A second method involves the use of inactivated sendai virus (SV). Donor cells are briefly incubated in a solution containing SV prior to cell transfer, achieving oocyte-cell fusion by viral particles. SV-mediated fusion is less laborious and might be less stressful to the reconstructed embryo than electrofusion [30].

Once the donor chromatin has been incorporated into the enucleated oocyte, the reconstructed embryo is activated to begin development. The reconstructed embryo is then ready for embryo culture. Different methods of activation and embryo culture are discussed later in this entry in relation to how they affect NT outcomes. When cloned embryos reach the blastocyst stage in vitro, they are transferred to surrogate females to carry the pregnancy.

Hormonal treatments must be administered to the surrogate so that the "uterine cycle" is synchronized with the developmental stage of the transferred embryo. If this is not properly planned, the uterus will be "out of phase" compared to the blastocyst and implantation will likely fail. To achieve synchrony, in farm animals, the surrogate must be induced to enter estrus on the day of NT. Following transfer to surrogates, care of the embryos is shifted to the hands of the veterinarian. Management of pregnancy includes ultrasonography, to check pregnancy status, as well as measuring maternal levels of pregnancy proteins to assess placental development.

Problems of Cloning

Despite advances in the field, the efficiency of SCNT technology remains very low, with only 1–10% of transferred embryos reaching term, depending on the species. More than 50% of pregnancies are lost in the first trimester, and in contrast to IVF pregnancies, losses of clone pregnancies continue throughout gestation (e.g., [31]). Additionally, developmental abnormalities are commonly observed in cloned fetuses and in their placentas.

During mammalian embryogenesis, the fetus is derived exclusively from the inner cell mass (ICM) while extraembryonic tissues, including the placenta, are mostly derived from the trophectoderm (TE). It is thought that the extraembryonic membranes are the most negatively affected by SCNT, including the placentas of full-term clones. Although cloned fetuses and offspring can present abnormalities as well as large offspring syndrome (LOS), these seem to be secondary to placental dysfunction, which leads to imbalances in placental fluid and in kidney function [32]. In sheep, placental abnormalities include a hypotrophic trophoblastic epithelium, reduced vascularization, and thickening of the trophoblast basement membrane [33]. Placentomegaly (enlarged placenta) is a common occurrence in mice and cattle cloning. Other placental abnormalities in bovine cloning include edema and hydroallantois. Developmental failure can account for fetal losses, stillbirth, and even postnatal mortality of mice, cattle, and sheep. Postnatal mortality is particularly pronounced in cloned sheep [34].

A recent study showed that indeed defects in the trophectoderm lineages rather than in the ICM are the main cause of low cloning efficiencies, at least in mice [35]. This experiment used chimeric aggregates of diploid and tetraploid embryos (Fig. 4). Tetraploid embryos are obtained by fusing the two blastomeres of a two-cell embryo. NT-ICMs were aggregated with tetraploid fertilization-derived (4nFD) early-cleavage-stage embryos. In this diploid/tetraploid "chimera," the 2n NT-ICM cells can only develop into the fetus while the 4n cells can only give rise to the extraembryonic tissues (although minimal cross-contribution was observed). By this approach, a sixfold increase in development to term was obtained compared with the nonaggregated NT control. Moreover, when ICMs from normally fertilized embryos were aggregated with tetraploid NT embryos, the birth rate was similar to that of the NT control, indicating that a normal ICM does not rescue the developmental potential of the reconstructed embryo. However, FD-ICM/4nFD aggregates showed twice the developmental rate than NT-ICM/4nFD. Thus, while trophectoderm defects are mainly responsible for low cloning efficiencies in mice, the ICM has a minor contribution as well.

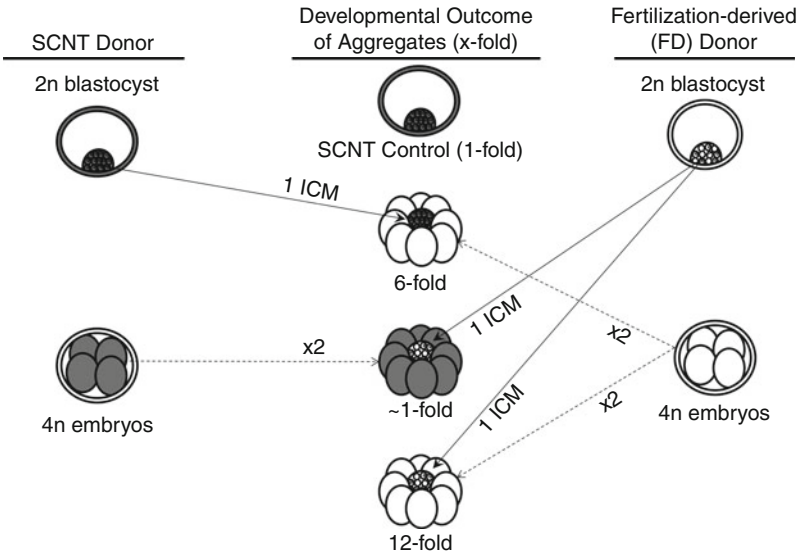

Livestock Somatic Cell Nuclear Transfer. Figure 4
Experimental evidence shows that the trophectoderm lineage is severely affected in mice cloning. A diploid (2n) ICM and two tetraploid (4n) 4-cell embryos were aggregated from cloned and fertilized embryos in different combinations. The ICM forms the embryo while tetraploid blastomeres can only give rise to extraembryonic tissues. Development to term demonstrated that replacing the trophectoderm lineage in cloned embryos dramatically improves development

It is generally thought that the low cloning efficiencies and developmental problems arise from an incomplete reprogramming of the donor nucleus.

Nuclear Reprogramming

Successful NT experiments demonstrated that differentiated cells (with a few exceptions) retain the same intact genome (i.e., nuclear equivalence) within an organism. In other words, these experiments supported that cell differentiation is not achieved through genetic changes or deletions but rather through epigenetic changes. Epigenetics regulates cell identity through chromatin modifications that are heritable through cell divisions, without altering the DNA sequence. Thus, chromatin modifications establish an epigenetic "code" that results in different gene expression programs between cell types.

Chromatin is formed by DNA associated with histone and nonhistone proteins. The chromatin template is epigenetically modified at the DNA and histone levels. DNA modification is limited to methylation (or demethylation), while histone modifications are numerous, including methylation, acetylation, phosphorylation, ubiquitination, ADP-ribosylation, biotinylation, and sumoylation. In turn, such modifications affect gene expression and the overall chromatin structure, which can be described as open or compact. During normal development, global changes in DNA methylation and histone modifications take place; much effort is being dedicated in understanding how these changes are altered or preserved in cloned embryos.

For SCNT to be successful, it is essential that the chromatin of the donor somatic nucleus is remodeled so that it becomes compatible not only with the totipotent gene expression program of development but also with the rapid cell-cycle dynamics of early embryo cleavage.

Nuclear reprogramming, either following fertilization or SCNT, is the result of active and passive processes. For instance, in most mammals after fertilization, the sperm compact chromatin undergoes active remodeling in which protamines are exchanged by

ooplasmic histones followed by global loss of DNA methylation. The sperm pronucleus also acquires distinct histone marks such as histone hyperacetylation. However, it is not clear whether such modification is acquired actively through the action of enzymes or it is the result of passive acquisition from the ooplasmic histone pool already rich in acetylation marks [36].

The timing required for completing nuclear reprogramming is unclear. Some researchers have suggested that the donor nucleus should be reprogrammed upon reaching embryonic genome activation. Such a restrictive reprogramming timing would be consistent with the lower cloning efficiencies usually observed in mice compared to bovine, two of the most cloned animals, the latter having more time for reprogramming the differentiated donor nucleus before genome activation. However, it has also been suggested that reprogramming continues up to the blastocyst stage.

To better understand the nuclear reprogramming process, the dynamics of the most important epigenetic marks and of gene expression during early embryogenesis in fertilized and cloned embryos are discussed next.

Reprogramming of DNA Methylation

DNA methylation is a reversible modification of the chromatin template at the DNA level in which a methyl group is predominantly added to cytosine of the dinucleotide sequence CpG. DNA methylation is a widely used mechanism of epigenetic regulation commonly associated with stable heritable gene silencing, heterochromatin, chromosome stability, genomic imprinting, X-chromosome inactivation, and inactivation of retroviral sequences. It has been shown that DNA methylation is essential for embryonic development, especially at postimplantation stages [37]. DNA methylation is carried out by DNA methyltransferases (DNMTs). DNMT1 maintains DNA methylation patterns after DNA replication by using the old strand as a template to methylate the new strand. De novo DNA methylation is carried out by DNMT3a and DNMT3b.

DNA methylation is dynamically regulated. Removal of methyl groups can be an active process when specific DNA demethylases are involved to remove the methyl groups, or it can be a passive process when failure to copy the methylation marks on the newly synthesized DNA leads to erasure of those marks during cell divisions. In contrast to DNA demethylation of the sperm pronucleus, which is thought to be an active process [38], passive DNA demethylation of the embryonic genome takes place following the zygotic stage.

After SCNT, DNA methylation reprogramming is usually inefficient. Mice and bovine cloned embryos have aberrantly hypermethylated DNA [39]. In sheep, SCNT embryos also tend to be significantly hypermethylated compared to fertilized embryos [40]. Such abnormal hypermethylation was observed from the 1-cell to the 8-cell stage and then at the blastocyst stage, in which the trophectoderm was hypermethylated relative to the fertilized control.

Interestingly, the rate of demethylation is similar in both SCNT and fertilized embryos, suggesting that the hypermethylated DNA pattern of SCNT embryos is probably inherited from the hypermethylated donor cell [38]. Alternatively, it has been suggested that cloned embryos undergo precocious DNA methylation due to the presence of DNMT1 associated with the donor nucleus, thus preventing passive demethylation [39].

DNA methylation reprogramming appears to be an indicator of developmental potential. In sheep, the proportion of SCNT embryos that were normally methylated at the 2-cell stage coincided with the proportion of surviving embryos reaching the 16-cell stage [38]. Similarly in mice, aberrant methylation of early-cleavage cloned embryos was proportionally associated to developmental failure to the blastocyst stage [41].

Reprogramming of Histone Modifications

The tails of the histone subunits H3 and H4 are targets for chromatin modifier enzymes, with histone methylation and acetylation modifications the most extensively studied. These modifications set epigenetic "marks" associated with either gene silencing or gene activity.

Histone acetylation is associated with open chromatin and gene activity. This modification neutralizes positive charges on histone tails and thus increases the overall repulsive negative charge of DNA on the chromatin structure. In turn, an open chromatin favors the binding of transcription factors to DNA.

In contrast, histone methylation can be either repressive or activating, depending in the lysine residue modified. These modifications act as signals that are "read" by proteins, which in turn can trigger downstream chromatin-modulating events. Together with methylated DNA, methylation of lysine 9 of histone 3 (H3K9), H3K27, and H4K20 has been implicated with heterochromatin and gene repression, while methylation of H3K4, H3K36, and H3K79 is associated with active gene expression.

In addition to abnormal DNA methylation, embryos produced by SCNT show aberrant reprogramming of histone modifications. Asymmetry of H3K9me3 fails to be established between ICM and TE in bovine cloned blastocysts compared with fertilized controls [42]. When histone acetylation marks are compared, however, cloned and normal blastocysts look similar [43, 44], suggesting that these marks are well reprogrammed. Yet, at earlier embryonic stages, the same histone acetylation marks show significant differences, with cloned embryos being hyperacetylated [42, 43].

Deregulation of DNA methylation and H3K9 methylation might be major problems during nuclear reprogramming [38, 42]. Their aberrant reprogramming leads to hypermethylated trophectoderm and extraembryonic tissues. As these epigenetic marks promote inactive chromatin, they are likely to cause downregulation of a substantial number of placental genes, explaining the placental abnormalities frequently reported in cloned embryos.

Reprogramming of Gene Expression

After fertilization or SCNT, the ooplasm induces global remodeling of chromatin, genome silencing, erasure of permissive epigenetic marks of differentiation-associated genes, and resetting the genome to an embryonic state [45–47]. Four classes of genes play an essential role to ensure normal embryogenesis following NT: (1) pluripotency-associated genes, (2) trophectoderm genes, (3) imprinted genes, and (4) differentiation-associated genes. Reactivation of pluripotent and trophectoderm genes must take place, whereas differentiation-associated genes must be silenced. Imprinted genes should be reactivated without altering the normal imprinting of somatic cells.

Pluripotent Genes Pluripotency is the capacity to differentiate into all embryonic cells. The cells of the ICM are pluripotent because they form the embryo. To recognize the state of pluripotency, landmarks of the ICM have been sought, such as stage-specific gene expression or antigens. These landmarks should be associated only with those stages and tissues known to have pluripotent potential such as the cleavage-stage embryo and ICM of the blastocyst. They should not be expressed in differentiated tissues of later development. Key genes associated with the ICM vary with species.

In mice, Oct4 is highly expressed and restricted to the ICM. It plays an essential role in early development as Oct4-depleted mouse embryos fail to form the ICM and are developmentally incompetent [48, 49]. Inducing overexpression of Oct4 is key to revert the gene expression profile of an adult differentiated somatic cell to one of embryonic and pluripotent characteristics [19]. Thus, in the mouse, Oct4 appears to be an ICM-specific marker that can be used to assess pluripotency.

Also in mice, other important pluripotent factors restricted to the ICM are Nanog and Fgf4 [50, 51]. Nanog is involved in maintenance of the pluripotent state of ES cells, for instance, by repressing differentiation into primitive endoderm [50]. Fgf4, a target gene of Oct4 [52], is necessary for proliferation and differentiation of both the ICM into embryonic tissues [53] and the TE into placental tissues [54].

In mouse SCNT blastocysts, Oct4 and Oct4-related genes often fail to be reactivated [55, 56]. Frequently, when Oct4 is expressed, aberrant spatial expression in the trophectoderm indicates faulty reprogramming [55]. Interestingly, when ES cells are used as donors, instead of adult somatic cells, Oct4 and related genes were always expressed in cloned blastocysts [56]. Since pluripotent genes are already active in ES cells, these genes do not need to be reactivated in ES-cloned embryos.

In human and large ungulate mammals, however, it is less clear what master regulatory factors are involved in the segregation of the ICM. For instance, Oct4 is expressed in both ICM and TE of bovine, goat, and human blastocysts [57–60]. Thus, for nonmurine species, we are left with less information to assess the extent of ICM-lineage reprogramming. Yet, Nanog does seem to be restricted to the ICM in bovine [61]

and goats [59]. Similarly, Fgf4 is restricted to the ICM of bovine blastocysts [57]. Therefore, Nanog and Fgf4 are preferred ICM markers to Oct4 depending on the species.

To assess reprogramming of ICM, expression of Nanog and Fgf4 has been measured in bovine cloned blastocysts. Differences between studies were found, with similar [62, 63] and lower levels [57, 64] compared with fertilized controls. The disparity of results may reflect differences in nuclear transfer procedures leading to variable success in reprogramming.

Trophectoderm Genes In mice, the transition from morula to blastocyst that results in the segregation of ICM and TE is regulated by the antagonistic activity of Oct4 and Cdx2, respectively [65]. Together with Cdx2, Taed4, Eomes, and Gata3 are required for specification and development of the TE lineage [66, 67]. Tead4 appears to be a master factor in TE-lineage induction since it activates Cdx2 and Gata3 [67, 68].

Less is known about the mechanism of segregation of the trophectoderm lineage in other mammals. Although CDX2 protein seems to be a conserved TE-restricted marker, as observed in bovine and porcine blastocysts [61], transcripts levels of Cdx2 were also found in the ICM [57]. It is possible that a posttranscriptional regulation mechanism accounts for the difference between gene expression and gene product levels. Thus, to assess reprogramming of Cdx2, it might be more appropriate to look at the protein level. In contrast to mice, Cdx2 does not repress Oct4 expression in bovine [69], explaining why OCT4 is detected in the bovine TE [58]. Another difference between these two species is the expression of Tead4 and Gata3 transcripts, which are found in both ICM and TE of bovine blastocysts, and thus, their role in TE lineage segregation is not clear [57]. Further evidence that bovine TE formation is quite different to mice is the observation that Eomes is not detected in trophoblast tissue [70]. Surprisingly, although bovine TE cells will only contribute to the trophectoderm lineage, they are not committed to it before pregastrulation stages since they were observed to contribute to ICM in aggregation assays [69]. Taken together, these observations suggest that differences in expression of lineage markers between species might be the result of different implantation requirements. For instance, while mouse blastocysts implant readily at this stage, domestic blastocysts undergo elongation and have delayed implantations. Indeed, while OCT4 is expressed in both the ICM and TE of the bovine blastocyst, it is restricted to the ICM lineage at a later elongated stage [71].

Few studies have assessed reprogramming of the TE lineage in cloned embryos. In mice, CDX2 protein was frequently expressed normally at the blastocyst stage [72]. A similar result was found in the bovine [57]. Although reprogramming of Taed4 and Gata3 was faulty in bovine cloned blastocysts [57], these are not specific markers of the TE lineage in the bovine. Therefore, in nonmurine species, assessing reprogramming outcome of the TE lineage is currently limited to measuring CDX2 protein.

Imprinted Genes Imprinted genes are genes expressed either from the paternal or maternal chromosomes, but not both. Gene imprinting plays an essential role in development. When androgenetic (two paternal pronuclei) or gynogenetic (two maternal pronuclei) embryos are produced, embryogenesis is arrested shortly after implantation [73]. Thus, the paternal and maternal genomes have different contributions and must complement each other at fertilization for normal development to occur. Imprinting marks originate during gametogenesis and are generally protected from genome-wide reprogramming, such as DNA demethylation/methylation, during embryonic development [36].

Many imprinted genes regulate development, growth, and function of embryonic and extraembryonic tissues. Following SCNT, many imprinting errors can occur during reprogramming of the somatic chromatin. For an imprinted gene, simultaneous expression from the paternal and maternal alleles or lack of expression is the result of aberrant reprogramming. Because of their regulatory growth function, deregulation of imprinted genes might explain several placental abnormalities and "large offspring syndrome" often observed in cloned animals.

Some researchers have proposed that long-term culture of donor cells, the usual scenario for embryonic stem (ES) cells, is an additional source for imprinting

errors, and thus, it has been suggested that ES cells are a poor choice for NT [74]. However, using microarray technologies, Humpherys et al. [75] found no significant difference between ES-NT and noncultured cumulus cell-NT clones in terms of gene expression abnormalities including imprinted genes. Therefore, it is not clear whether extensive in vitro culture is a major problem for NT in terms of imprinting deregulation. Moreover, mammals seem rather tolerant to imprinting errors [76].

Differentiation-Associated Genes Following SCNT, silencing of differentiation-associated genes is often incomplete. For instance, cloned embryos produced with myoblast nuclei still expressed the myoblast marker GLUT4 [77]. Similar somatic epigenetic memory was also observed in Xenopus cloned embryos, which overexpressed endoderm or ectoderm markers according to the origin of the donor cells [78]. While insufficient silencing of differentiation-associated genes may alter metabolic demands, the functional consequences of retaining expression of somatic genes on the developmental potential of cloned embryos are unclear [46].

Several studies have compared global gene expression profiles between cloned and fertilized embryos. At the 1-cell stage of murine embryos, most transcripts (~98%) were similarly abundant between clones and IVF groups [45], although such similarity might be the result of maternal transcripts abundantly present in the oocyte. Nonetheless, similar expression profiles were obtained between cloned and fertilized blastocysts in bovine (e.g., [63, 79]). Thus, overall gene expression of cloned embryos appears normal. However, it is possible that small alterations in gene expression are amplified during postimplantation stages, which would contribute to the low developmental potential of cloned embryos [79].

In summary, perfect gene expression reprogramming may be unlikely following SCNT. Cell-type-specific genes may be incompletely silenced while imprinted genes are subject to deregulation. Reactivation of ICM- or TE-lineage genes might be problematic depending on the species. The mechanism of nuclear reprogramming is still a black box, and much further research is needed to understand where the bottleneck of NT is.

Factors Affecting Development of Embryos Produced by SCNT

Frequently, reports have shown that there is ample room for optimization in NT technology. Major investigated factors affecting NT success include quality of recipient oocyte, time of enucleation, nuclear donor source, cell-cycle coordination of donor and recipient cells, alterations in the timing and inducer of oocyte activation, and culture of reconstructed embryos.

Sources of Recipient Oocytes

Mammal females produce mature oocytes (oogenesis) during the ovarian cycle. The earliest stage of oogenesis is the primary oocyte within the primordial follicle. Primary oocytes are arrested at the first meiotic prophase in a quiescent state. Some of these are regularly recruited for further growth since puberty and thereafter. As primary oocytes resume growth, they increase in size and undergo cytoplasmic maturation. An oocyte must undergo cytoplasmic and nuclear maturation to be developmentally competent. Cytoplasmic maturation involves mRNA synthesis, translation into protein, and posttranslational modifications. Many mRNA and protein molecules are stored in the cytoplasm to function later during early embryo cleavage, before embryonic-genome activation. Some of the proteins produced, such as maturation promoting factor (MPF), are necessary for meiotic progression during nuclear maturation. Within the follicle, oocyte growth is accompanied with follicular growth. Indeed, oocytes obtained from medium- and large-sized follicles are developmentally better than those obtained from small-sized follicles. It seems that oocytes from the latter group have not completed cytoplasmic maturation [80]. Oocytes are surrounded by cumulus cells, and mutual communication is required for complete oocyte maturation.

Oocytes can be matured in vivo or in vitro. In vivo maturation involves collecting oocytes that have naturally matured within the ovary of a live animal. In contrast, in vitro maturation involves aspirating immature oocytes from the ovaries of slaughtered animals and placing them on favorable culture conditions to complete the maturation process in the incubator. Although much understanding has been gained in oocyte maturation, in vitro maturation is still

suboptimal at best. In vitro–matured oocytes have altered energy metabolism [80], higher chromosomal abnormalities [81], and lower developmental competence than in vivo–matured oocytes [82, 83].

For convenience, in livestock cloning, in vitro maturation is widely used as very large numbers of immature oocytes can be obtained from slaughterhouses at low cost. However, the poorer quality of these oocytes is likely to contribute to the low frequency of development usually observed in cloned embryos.

Enucleation of Recipient Oocytes

Nuclear maturation is resumed at the time of the LH surge in vivo or during in vitro conditions. The oocyte continues meiosis to progress from the arrested prophase I to metaphase I, anaphase I, telophase I, and cytokinesis with unequal cytoplasmic distribution, when half of the chromosomes are discarded in the first polar body. The oocyte progresses to meiosis II and is arrested at metaphase II. Following fertilization or artificial activation, the metaphase II–arrested oocyte resumes meiotic progression once more to complete metaphase II, anaphase II, and telophase II, discarding again half the number of chromosomes in a second polar body, achieving a haploid number of chromosomes. Enucleation can be carried out at any of these meiotic stages, although with possible different consequences (discussed later). Table 1 provides some examples of cloning experiments carried out using recipients enucleated at different stages of meiosis or mitosis.

For NT, it is most important that the oocyte undergoes cytoplasmic maturation to construct a developmentally competent embryo, while nuclear maturation is less important because the oocyte DNA is eliminated at enucleation and does not form part of

Livestock Somatic Cell Nuclear Transfer. Table 1 Examples of cloning experiments using recipients at different meiotic and mitotic stages of the cell cycle

Recipient cytoplast	Donor cell type	Species	Offspring	References
Enucleated GV oocytes (subsequently matured)	ES cells	Mouse	No	[84]
Enucleated Pro-MI oocyte (subsequently matured)	ES cells	Mouse	Nd	[84]
Enucleated AI/TI oocyte (subsequently matured)	Fetal	Sheep	Yes	[85]
	Adult	Sheep	Yes	
Enucleated MII oocyte	Embryonic, fetal, adult	Sheep	Yes	[18]
Unenucleated MII oocyte (subsequent enucleation)	Cumulus cells	Mouse	Yes	[86]
Enucleated activated MII oocyte	Blastomeres	Sheep	Yes	[17]
Enucleated PN Zygote	PN karyoplast from zygote	Mouse	Yes	[10]
	PN Karyoplast from first NT embryo	Pig	Yes	[87]
	Blastomeres	Mouse	No	[11]
	Cumulus cells	Mouse	No	[88]
TII enucleated oocyte	Blastomeres	Goat	Yes	[89]
M-phase arrested zygote	ES cells	Mouse	Yes	[90]
	Fibroblast	Mouse	ND	
2-cell embryo	Lymphocyte	Mouse	Yes	[91]

ND not determined

the embryo. Enucleation of prophase I oocytes, also known as germinal vesicle (GV) stage, has been attempted in the mouse, and the resultant recipients were capable of reprogramming donor nuclei [84, 92]. However, the reconstructed embryos are developmentally incompetent even when recipients are further matured in vitro prior to NT [84]. It is possible that GV oocytes are poor recipients because removal of their transcriptionally active chromatin [93] prevents synthesis of new mRNA necessary for completing cytoplasmic maturation. Similarly, enucleation of pro-metaphase I (pro-MI) oocytes also results in poor recipients [84]. Beyond interfering with mRNA synthesis, it is also likely that enucleated GV and pro-MI oocytes are poor recipients because enucleation disaggregates the cumulus-oocyte complex, thus depriving the oocyte of the beneficial communication with cumulus cells for completing cytoplasmic maturation during in vitro maturation.

Enucleation of metaphase II–arrested oocytes is the most common practice in cloning experiments. The rationale of using such recipients is evident as the COC is left undisturbed during the entire in vitro maturation period, thus maximizing the probability of cytoplasmic maturation. However, a practical alternative is to enucleate at anaphase I/telophase I (AI/TI). By doing so, the spindle is more efficiently removed along with less cytoplasm compared to MII enucleation [27]. AI/TI cytoplasts are further cultured to complete the maturation period and have produced lambs after SCNT [85].

Other recipients have been used for NT. Activation of MII oocytes with subsequent enucleation at anaphase II/telophase II has been done for practical reasons similar to those of AI/TI enucleation [89, 94]. Zygotes and two-cell embryos have also been enucleated and used as recipients for NT. These will be better discussed below in relation to the "potential loss of reprogramming factors" during enucleation and later in relation to the "coordination of donor and recipient cell cycles."

Potential Loss of Ooplasmic Reprogramming Factors

Enucleation involves removing the DNA material from the unfertilized or fertilized oocyte plus an unavoidable volume of ooplasm. It has been speculated that loss of ooplasmic volume is accompanied with a reduction of developmental potential, possibly due to the removal of cytoplasmic reprogramming factors. However, fusion of two or more cytoplasts prior to NT did not improve the frequency of development in mice [95]. Apparently, the amount of cytoplasmic factors in the oocyte is not critical for cloning success.

However, the above discussion does not take into account that the content of reprogramming factors in the cytoplast is dependent on the cell-cycle phase. The genome can be removed as interphase pronuclei in zygotes or with the spindle if recipients are mitotic zygotes or meiotic oocytes. In the latter case, the components of the nucleoplasm stay in the recipient as they are diluted in the cytoplasm following nuclear envelope breakdown. Recipient zygotes enucleated at interphase can only support development of nuclei obtained from 1-cell or 2-cell embryos [11] but fail consistently when more differentiated donor nuclei are transferred [11, 96, 97]. Kevin Eggan and colleagues have shown that zygotes and 2-cell embryos at the mitotic phase regain the reprogramming ability [90, 91]. These authors have proposed that reprogramming factors are sequestered in the nucleus during interphase but then redistributed throughout the cytoplasm during M phase [98]. Therefore, reprogramming factors would be lost when enucleation is carried out during interphase [99]. Indeed, Brg1, a component of the Swi/SNF chromatin remodeling complex necessary for embryonic genome activation, was absent in 2-cell cloned embryos when using enucleated interphase zygotes as recipients [99]. Further proof of this idea is supported by the observation that oocyte recipients at the germinal vesicle (GV) stage fail to develop after NT [84]. A possible contributing factor for the low developmental potential of enucleated GV oocytes and interphase zygotes is the low levels of maturation promoting factor (MPF) in these recipients (discussed below). Taken together, while the mechanism of reprogramming remains largely unknown, essential reprogramming factors are present in the recipient's cytoplasm during M phase, but absent during interphase, at least in the mouse model [99].

It is still possible that some unknown factors beneficial for reprogramming might be stably associated with chromatin and lost during enucleation. It is well known that spindle factors are associated with the

meiotic chromosomes, and therefore, enucleation could impair spindle function. Indeed, in human SCNT, it is apparently necessary to leave the recipient genome to achieve development to the blastocyst stage, at the cost of producing a triploid embryo [100]. How spindle function is affected by SCNT in livestock species will be discussed later in this entry.

Coordination of Donor and Recipient Cell Cycles

During a single cell cycle, a cell must double all of its components, segregate its genetic material equally to the two daughter cells, and undergo cell division. One exception occurs during the first few cell cycles of early embryo development where no net growth occurs. However, cell-cycle events associated with duplication and segregation of the nuclear DNA still occur. Another exception to the mitotic cell cycle is meiosis, which results in halving the chromosome number. Only germ cells undergo meiosis, while somatic cells only mitosis.

The mitotic cell cycle has four sequential phases: G_1, S, G_2, and M. During S phase (S for DNA synthesis), replication of DNA takes place. During M phase (M for *mitosis*), the cell divides all its components equally into two daughter cells. Cell growth occurs only during interphase, which constitutes G_1, S, and G_2. In a typical in vitro–cultured mammalian cell, interphase lasts about 23 hours (of a 24-hour cell cycle) while M phase is very short, lasting about one hour. S phase takes about half of the cell-cycle time (reviewed in [101]). The gap phases G_1 and G_2 are designed to provide extra time for the cell to grow and checkpoints for favorable growth conditions as well as for DNA damage.

At fertilization, the oocyte is arrested at MII, in a diploid state, while the sperm cell has completed meiosis and is haploid. Following oocyte activation by the sperm cell, the oocyte resumes meiosis to become haploid, thus matching the chromosome content and forming a viable diploid embryo. In NT, of course, it is not important that the donor chromosome content matches the recipient's since the oocyte chromatin is removed. Rather, the donor's cell-cycle phase should be compatible with the recipient cytoplasmic reprogramming content, which in turn depends on the recipient's cell-cycle phase. An important cytoplasmic reprogramming factor that has been extensively studied and has a profound effect on the donor nucleus is maturation promoting factor (MPF).

Campbell and colleagues, at the Roslin Institute (Scotland), carried out pioneer work in cell-cycle coordination between the donor cell (karyoplast) and recipient cytoplast prior to NT [16, 17, 102]. Their work suggests that cell-cycle coordination is a very important factor that should be taken into account prior to NT experiments to avoid damage of the donor chromatin.

For NT, mature MII cytoplasts are the recipients most frequently used. These contain high levels of MPF (also known as M-Cdk). MPF is a complex of two factors, protein kinase $p34^{cdc2}$ and cyclin B. MPF activity is regulated through synthesis and degradation of cyclin B and through phosphorylation of $p34^{cdc2}$. MPF activity is responsible for nuclear envelope breakdown (NEBD) and premature chromosome condensation (PCC) of the donor nucleus following activation of reconstructed embryos. MPF declines progressively after activation or fertilization and remains low during interphase. Declining MPF levels are followed by nuclear membrane reformation and DNA synthesis. NEBD and PCC occur independent of the cell-cycle stage of the donor nucleus in MII-arrested oocytes. In contrast, when activation precedes NT for a few hours, MPF activity is low and nuclear envelope integrity is maintained because NEBD and PCC do not occur.

An intact nuclear membrane prevents replication of previously replicated DNA [16, 103]. Transferring donor nuclei in S or G_2 phases into MII cytoplasts followed by activation leads to NEBD and eventually to DNA rereplication, likely resulting in ploidy abnormalities. In addition, PCC could also cause chromosomal damage of S-phase nuclear donors. These early observations suggested that only G_1 embryonic donor nuclei should be transferred into unactivated MII cytoplasts. In contrast to unactivated MII oocytes, activated oocytes serve as "universal recipients" since MPF activity is low and NEBD/PCC do not occur, allowing the transfer of any nuclear donor without the risk of DNA rereplication. In these reconstructed embryos, coordinated replication of nuclear DNA should occur. Indeed, unsynchronized sheep blastomere donors developed to the blastocyst stage more frequently when using activated cytoplasts (low MPF) compared with cytoplasts activated following NT (high MPF) [17].

For differentiated cells, however, activated oocytes might be poor recipients because NEBD and PCC are thought to be beneficial for reprogramming the donor nucleus. In bovine, for instance, when activated enucleated MII oocytes were used as recipients for somatic donors at different stages of the cell cycle (except S phase), development did not proceed to the 8-cell stage. However, unactivated MII oocyte recipients resulted in successful in vitro development to blastocyst [104]. Similarly, activated oocytes were shown in mice to be ineffective for development to term when using cumulus cells as donors [105]. These results suggest that activated oocytes, with low levels of MPF, fail to reprogram somatic donor nuclei. Blastomeres, on the other hand, probably require little or no reprogramming and thus can be cloned successfully with activated recipients as in Campbell et al. [17]. Not surprisingly, for somatic nuclei donors, the most common recipient is the unactivated enucleated MII oocyte.

Later research showed that donor genomes at G_0, G_1, and M phases of the cell cycle can be transferred into unactivated oocytes and produce offspring. For instance, embryonic stem (ES) cells arrested at metaphase produced live mice [106]. Metaphase-arrested chromatin donors are ready to segregate and form a pseudo-second polar body, thus eliminating the extra set of chromatin. However, G_2 donors were observed to fail at extruding the pseudo-second polar body resulting in tetraploidy [104], probably because they are "out of phase" with the meiotic cytoplast. This, combined with the rereplication event, could explain the consistent failure to produce viable offspring with G_2 donors (reviewed in [107]). For G_0 and G_1 donors, spindle function inhibitors are required to prevent pseudo-polar body formation and loss of chromosomes.

There is no apparent advantage between nuclei at G_0, G_1, or M phases for NT. Somatic cell donors are routinely synchronized at the G_0 phase of the cell cycle prior to NT. However, synchronized G_0 or G_1 fetal fibroblasts were compared and no clear superiority for either donor was found. Their relative cloning efficiencies were cell-line dependent in cattle [107]. Synchronization of ES cells at G_0 or G_1 might be problematic since they have a very short G_1 phase, and if induced to become quiescent (G_0), they likely differentiate. The most successful studies in cloning mice with ES cells used unsynchronized cell populations [108, 109], but others were less successful [110, 111]. ES cells at presumptive G_1 (by selecting small cells) were used with cloning success [112] and without success [113]. ES cells were also synchronized at M phase with moderate success in several occasions [106, 114, 115].

Taken together, enucleated MII oocytes seem to be the best recipients. However, the cell cycle of the donor nuclei might be less important since cloning success is achieved with G_0, G_1, and M donors, adapting the NT protocol accordingly.

Sources of Nuclear Donor Cells

Donor cells of different ages including embryonic, ES, fetal, and adult cells have been used for NT. It has been suggested that the age of an adult somatic donor cell could be transmitted to the clone. Such belief originated from a study showing that Dolly and other cloned sheep had shorter telomeres compared to age-matched controls [116]. The belief was later emphasized by the premature death of Dolly. However, several studies in cattle and mice showed that telomere length was normal in clones; telomerase activity was found to be reactivated in cloned bovine preimplantation embryos at similar levels to fertilized controls. Yet, further studies in sheep showed that indeed clones have shorter telomeres [117], suggesting that the mechanism of telomerase reactivation differs in this species. Nonetheless, studies have not observed premature aging in clones produced by SCNT.

Beyond age, a more interesting discussion relies on the epigenetic differences between donor cells. Differentiated somatic cell types diverge in their gene expression programs but have similar global chromatin configurations and modifications, or epigenomes. However, the epigenome of differentiated cells contrasts with that of undifferentiated pluripotent cells. It is probably the epigenome features that render one cell more amenable to reprogramming following NT rather than the cell's specific gene expression program.

Epigenomes Differentiated cells are different to pluripotent cells in several epigenetic features. Compared to pluripotent cells, differentiated cells show expansion of repressive domains marked by H3K9me3 and

H3K27me3 [118]. Similarly, differentiated cells show hypermethylated DNA compared to ES cells [119] and have lower levels of histone acetylation, consistent with heterochromatin configurations [120]. In agreement, electron microscopy showed that ES cells have dispersed global chromatin architecture, while the chromatin of the differentiated cells is more compact [121].

The epigenome of a differentiated cell can be reverted to that of an ES cell by overexpression of master-regulatory genes of pluripotency, thus forming iPS cells [19]. It has been shown that iPS and ES cells have similar global DNA methylation [20, 119] and similar global levels of the histone modifications H3K4me3, H3K9me3, and H3K27me3 [118, 119, 122].

Differentiated Versus Undifferentiated Donors It is generally postulated that an inverse relationship exists between the differentiated state of a donor cell and its "reprogrammability." This hypothesis is based on NT efficiencies obtained with different types of donor nuclei ranging in their differentiation status from the totipotent zygote to the terminally differentiated cell.

It has been suggested that a small proportion of somatic stem cells are present in a tissue sample, and these cells, rather than differentiated cells, account for the successful cases of SCNT. Studies were performed to test whether terminally differentiated cells are "clonable." First attempts to clone mice with donor lymphocyte cells failed [123]. Thus, a two-step NT procedure, in which ES cells are derived from cloned embryos and used for embryo tetraploid complementation, was later adopted for lymphocyte and olfactory neurons, resulting in viable mice offspring [124, 125]. Later on, cloned mice were produced by direct NT of T lymphocyte cells, albeit with a very low efficiency [126]. These results show that terminally differentiated cells can be cloned, but does not reject the possibility that less differentiated cells might be better donors.

In contrast to terminally differentiated cells, blastomeres give high frequencies of development after NT. Yet, the developmental potential of donor blastomeres decreases as the cleavage stage of the embryo increases. In mice, a gradual decline is observed from the 1- to the 4-cell-stage embryo followed by a steep decline from the 4- to the 8-cell stage, remaining low thereafter (reviewed in [127]). In cattle, such a significant decline in developmental potential is observed after the 8-cell stage (e.g., [13]). Apparently, the greatest decline in developmental potential after blastomere NT occurs following embryonic genome activation.

Literature reviews on NT generally support that ES cells are better than somatic cells in terms of the developmental potential of the reconstructed embryos. This view is based on experimental evidence gathered from a few early studies in mice, where good outcomes were achieved using ES cells as donors [108, 109, 112]. In these studies, the cloning efficiency (here defined as development to term after blastocyst transfer to surrogate females) ranges from 8% to 21%. These values are much higher than those obtained previously with SCNT by Wakayama and colleagues, where cloning efficiencies ranged from 0.4% to 1.6% using cumulus cells [128] and fibroblasts [129], respectively. Other studies also found similarly low mice cloning efficiencies (0–2.5%) with fibroblast cells (e.g., [130]).

However, lower efficiencies (0–5.4%) were also reported with ES cell donors (e.g., [111, 113–115]). These studies question whether ES cells have indeed better developmental potential than somatic cells following NT and suggest that major reviews are relying too heavily on positive results while overlooking the negative ones. In a critical review, Oback and Wells [127] argue that postimplantation sample sizes are generally small in animal cloning and thus insufficient to draw robust conclusions. Furthermore, they claim that many confounding factors exist in nuclear transfer experiments, rendering comparisons difficult. These factors include cell line and sex, confluency of donor cell culture, cell-cycle, passage number, and nuclear transfer procedure. Oback and Wells conclude that to determine whether ES cells have a better developmental potential than differentiated cells, it is necessary to carry out large NT experiments in which ES cells and the same cells induced to differentiate prior to NT are directly compared while keeping other parameters constant. Taken together, the published data are inconclusive but suggest that ES cells give better cloning efficiencies than somatic cells. Indeed, only one study directly compared the developmental potential of ES cells to somatic cells, resulting in a cloning efficiency of about four times greater with ES cells [112].

According to Jaenisch's group, the cloning efficiencies with ES cells are 10- to 20-fold higher than with somatic cells after embryo transfer [76]. These authors

have proposed that ES cells have better developmental potential following NT because they are undifferentiated and thus require less reprogramming than differentiated cells [76]. For instance, ES cells already express pluripotency-associated genes such as Oct4, Nanog, and Sox2, needed for early embryogenesis. In contrast, these genes need to be reactivated in differentiated cells. A second hypothesis could be that ES cells can be more easily reprogrammed as they have overall open chromatin configurations compared to differentiated cells, which typically have compact heterochromatin. The open and accessible chromatin of ES cells might facilitate the binding of nuclear remodeling factors found in the oocyte's cytoplasm.

Unfortunately, ES cells cannot be stably derived in livestock species yet. However, it is probably a matter of time until the mechanism and factors that govern pluripotency are discovered in these species. When derivation of ES cells in farm animals becomes possible, it would be of interest to further test their developmental potential compared to that of somatic cells following NT.

Differential Organelle Contribution

During fertilization, the oocyte and sperm each contribute a haploid set of chromosomes to form a diploid zygote. However, most of the cytoplasm and organelles are inherited from the oocyte. Among these are mitochondria, with their own genetic material. An exception to this is the centrosome, which is partly contributed by sperm. The differential contribution of the centrosome and mitochondria can affect NT outcomes. These contributions can be altered by the method used to transfer the donor chromatin.

Centrosome Inheritance The centrosome is the main microtubule-organizing center (MTOC) of animal cells involved, among other functions, in assembly of the mitotic spindle for cell division. This organelle is composed of two centrioles surrounded by abundant centrosomal proteins, which are often referred to as pericentriolar material (PCM). The centrosome is replicated during the S phase of the cell cycle from material stored in the cytoplasm. Mammalian oocytes have no centrioles but contain PCM that is recruited by the sperm centriole after fertilization, restoring a functional centrosome. Mice, however, are acentriolar until late preimplantation stages, achieving embryo cleavage by using maternal MTOCs.

In SCNT, the MTOCs associated with the oocyte meiotic spindle are removed while the centrosome from the donor cell is introduced [131]. It is not well understood the composition of the donor centrosome once within the recipient. Also, it is unclear whether the donor centrosome recruits leftover PCM from the recipient oocyte [131]. Nevertheless, it is thought that the donor centrosome needs to be remodeled into a zygotic centrosome for normal embryonic cleavage [131].

Centrosomes from donor cells at S phase might be reduplicated following oocyte activation in the subsequent S phase [132]. This would lead to the formation of extra spindles followed by aberrant segregation of chromosomes, a phenomenon frequently observed with S-phase donors. Even when using G_0 donors, 35% of bovine reconstructed embryos had abnormal cleavage correlated with abnormal centrosome number and distribution [133]. This suggests that providing only one centrosome does not guarantee normal centrosome function following NT.

An early NT study in monkeys suggested that removing the MII meiotic spindle depletes the oocyte of spindle proteins NuMA and HSET [134]. These proteins closely associate with maternal chromosomes and are required for mitotic spindle function. This study showed disorganized spindles with misaligned chromosomes in all reconstructed embryos, which were unable to produce pregnancies. However, in a later study using a different nuclear transfer procedure, NuMA location and spindle formation were normal in most reconstructed monkey embryos [135]. Taken together, these results suggest that different parameters of the NT procedure can affect centrosome function.

Mitochondrial Inheritance The mitochondrion is a special organelle, having a double membrane and containing its own genome (mtDNA). The main function of mitochondria is to produce energy in the form of ATP. Other functions include production of reactive oxygen species (ROS), calcium signaling, and apoptosis. mtDNA encodes for 13 mitochondrial proteins involved in ATP synthesis, for 22 tRNAs, and for

2 rRNA molecules involved in translating mitochondrial proteins [136]. Replication and expression of mtDNA are regulated by the nuclear genome through the expression of transcription and replication factors that translocate into mitochondria.

Mitochondria are maternally inherited because sperm mitochondria are targeted for destruction upon fertilization [137]. In SCNT, the donor cell mitochondria can persist and contribute to the reconstructed embryo, thus resulting in heteroplasmy (two different populations of mtDNA). Donor mitochondrial contribution is quite variable, ranging from 0% to 59% (reviewed in [138]). A bovine oocyte contains about 250,000 mitochondria, a 100-fold compared to a somatic cell [139]. Therefore, high heteroplasmy probably results from preferential amplification of donor mitochondria.

Compatibility between nuclear and the recipient's mtDNA seems to play an important role in SCNT. It has been shown that autologous SCNT (a female donor cell is transferred to its own enucleated oocyte) improves the frequency of pre- and postimplantation development when compared with heterologous SCNT [140]. Likewise, bovine reconstructed embryos developed more frequently as the similarity between the mtDNA haplotype of the donor and of the recipient cell increased [141]. Moreover, it is thought that the developmental block commonly observed in interspecies-SCNT embryos is due to genomic-mitochondrial incompatibilities [142].

Transfer of Donor Nuclei From the above discussion, it is apparent that the method chosen to deliver the donor chromatin into the cytoplast can have implications in terms of organelle inheritance of the reconstructed embryo. By whole-cell fusion, the donor cell contributes the nuclear and cytoplasmic material including mitochondria and centrosome, while nuclear microinjection does not. This would not seem to be problematic in mice since maternal MTOCs suffice to form the spindle-chromosome complex during cell division. In livestock species, however, centrioles function in spindle formation during early embryo cleavage. Nonetheless, pigs have been cloned by nuclear microinjection (e.g., [83]), suggesting that the presence of a centriole is not necessary for embryo cleavage in pigs. While cell fusion contributes mitochondria and cytoplasm, there is no evidence that either heteroplasmy or the amount of somatic cytoplasm contributed by a single donor cell is enough to reduce the developmental potential of the reconstructed embryo.

Cell fusion has been directly compared to nuclear microinjection in cloning experiments. In pigs and cattle, greater preimplantation development with the cell fusion method has been reported [143, 144]. Unless centrioles are often transferred along with residual cytoplasm during nuclear microinjection, these results suggest that centrioles are not strictly necessary for embryo cleavage, although their presence enhance preimplantation development. In mice, conflicting data have been reported when comparing the two methods. These mixed results are consistent with the exception that centrioles are dispensable in mice during preimplantation stages. Interestingly, it has been reported that the quality of blastocyst produced by cell fusion was better; analysis showed that piezo-assisted microinjection can cause DNA damage by shear forces [145].

Activation of Reconstructed Embryos

In mammals, egg activation is achieved when summation of intracellular Ca^{2+} oscillations reach a minimum threshold. Egg activation leading to Ca^{2+} oscillations is thought to be triggered by a sperm-specific isoform of PLC, known as PLC zeta (PLCζ), introduced into the oocyte following fertilization [146]. It has been suggested that summation of these Ca^{2+} oscillations encodes information for directing later development. For instance, few Ca^{2+} oscillations lead to decreased implantation, while excess Ca^{2+} oscillations, to increased postimplantation failure in mice [147].

Maturation promoting factor (MPF) also plays an important role in MII arrest and in regulating Ca^{2+} oscillations (reviewed in [148]). Inhibiting MPF activity enhances oocyte activation. Inhibition of protein synthesis (by cyclohexamide) or inhibition of phosphatases (by 6-dimethylaminopurine [6-DMAP]) can decrease the activity of MPF and induce meiotic progression. These inhibitors are usually combined with stimulation of Ca^{2+} oscillations to efficiently activate reconstructed embryos. However, it is important to bear in mind that these chemicals have broad spectrum actions and can interfere with other cellular processes [148].

In the absence of the natural inducer of egg activation, several artificial methods exist to trigger activation of reconstructed SCNT embryos, including electrical pulses, ethanol, calcium ionophore A23187, ionomycin, strontium, and thimerosal (Thi)/dithiothreitol (DTT). With the exceptions of strontium and Thi/DTT, the other treatments induce a single Ca^{2+} oscillation [149]. Comparisons of several activation methods in mice cloning could not found a preferred method [95].

To mimic more physiological activation events, sperm-mediated activation methods have been used. Fertilized oocytes were used as recipients, but such approach has not produced any significant improvement in developmental potential to term in mice or bovine cloning [150, 151]. To avoid the added complication of removing the sperm chromatin, an alternative activation protocol involved directly injecting the sperm activating factor PLCζ, in the form of mRNA, resulting in long-term Ca^{2+} oscillations [152]. This approach improved gene expression patterns of several genes and reprogramming of the repressive histone mark H3K27me3 [153]. Therefore, mimmicking sperm-activation events might improve reprogramming of the donor nucleus.

Another factor that can be controlled in activation protocols is the timing of activation following embryo reconstruction. It is common practice to delay activation for 1–3 h to extend the time for nuclear remodeling after nuclear envelope breakdown. This "nuclear exposure" has been shown to be beneficial in bovine [104]. However, the effectiveness of this approach likely varies between species since in monkeys, it was shown that development improves by immediate activation [154].

Culture of Reconstructed Embryos

For animal cloning, the reconstructed embryos can be directly transferred to a surrogate female or cultured in vitro to the blastocyst stage followed by transfer. Since in vitro culture functions as a first filter to select growing embryos with exclusion of the developmentally arrested ones, it allows transferring fewer embryos to surrogates and is, therefore, widely used. Many factors can be manipulated in an in vitro culture system to affect the developmental outcome of cloned embryos. These factors include incubation temperature, media composition and osmolarity, oxygen tension, culture substrate, communal or individual culture, embryo concentration, cocultures, medium renewal, and embryo stress. Analyzing each of these factors is outside the scope of this entry, but the reader is encouraged to read Vajta et al. [155] for a comprehensive review on embryo culture. Instead, an eccentric culture preference of cloned embryos will be highlighted.

Usually, NT experiments culture cloned embryos in conditions designed for normal embryos. However, as discussed during *nuclear reprogramming*, a cloned embryo is usually not a normal one. Several reports support that reconstructed embryos have altered metabolism and culture requirements compared to normal embryos (e.g., [77, 156]). For instance, due to incomplete reprogramming of the donor chromatin, mice cloned embryos produced with muscle nuclei overexpress the glucose transporter GLUT4 and thus exhibit enhanced rates of glucose uptake and benefit from somatic cell culture media instead of standard embryo culture media [77]. The benefits of using somatic cell culture media included improved blastocyst formation rate and increased total cell numbers in the resultant blastocysts. These results suggest that normal embryo culture conditions might subject cloned embryos to a harsh selection process, while somatic-like culture media seem to maintain the viability of reconstructed embryos, allowing them more time to complete nuclear reprogramming. Nonetheless, sequential use of different embryo culture media has been shown to dramatically improve blastocyst development of mice reconstructed embryos [156]. Taken together, culture media for reconstructed embryos should be optimized to match the donor cell preferences.

Perinatal/Neonatal Care

Once cloned blastocysts have been transferred to surrogate animals, work is usually limited to monitoring the progress of pregnant surrogates of livestock species. However, it is important to bear in mind that cloned animals are prone to suffer health problems arising from epigenetic errors caused by incomplete nuclear reprogramming of the donor chromatin. Respiratory difficulties seem to be the main problem in cloned

neonates. Other health problems include myoarthroskeletal malformations and metabolic abnormalities. It is advisable that cloned neonates are regarded as being at high risk [157], and thus, intensive care should be provided to increase survival. Some studies suggest that veterinary intervention during the perinatal and neonatal periods can improve the survival rates of cloned livestock animals (for a review, see [158]).

Perinatal care involves monitoring readiness for birth, induced parturition, and induction of final pulmonary maturation. For yet unclear reasons, pregnancies of cloned fetuses often extend beyond the normal gestation period [157]. While this might indicate that cloned fetuses require more time in utero to complete maturation, prolonged gestations are associated with increased birth weight, dystocia, and increased morbidity and mortality [157]. To prevent these problems, induction of parturition is commonly carried out. In parallel, to aid pulmonary maturation, pharmaceutical drugs are often administered to promote production of lung surfactant necessary for alveoli inflation. Due to respiratory deficiencies, cloned neonates can quickly become hypoxic and acidotic. Lack of vigor and weak suckling reflexes are other common symptoms of cloned neonates. Thus, intensive care of the cloned neonate is crucial, even for preventative measures. Good care practice includes providing oxygen for at least one hour, heat, mechanical ventilation for more severe cases, and monitoring blood parameters [158].

Improving Development

From the above discussion, it is clear that veterinary science can play an important role in the management of pregnancy and neonatal care to improve the survival rate of cloned animals. In the laboratory, researchers have attempted many things to improve cloning efficiencies. The two most promising areas that have yielded the best results are chromatin remodeling treatments and embryo aggregation.

Chromatin Remodeling Treatments

Relaxation of the donor chromatin could enhance the reprogramming of the donor nucleus. To this end, a few different approaches have been implemented to treat donor nuclei or SCNT embryos. Well-defined chemical treatments include trichostatin A (TSA) and 5-azacytidine (5-Aza).

Early in the mouse zygote, both parental genomes are rich in histone acetylations, suggesting that these epigenetic marks are important for reprogramming. Treatment of donor cells with TSA, a histone deacetylase inhibitor, has been used to increase histone acetylation and promote opening of the chromatin. Such treatment led to increased development to blastocyst stage in bovine [159]. Later on, optimized TSA treatments resulted in significant increases (up to tenfold) in development to term compared to untreated groups in mice cloning (e.g., [160]). Remodeling of the donor chromatin with TSA has been the single most important innovation for improving consistently the efficiency of SCNT [95, 161].

DNA methylation patterns have been observed to be abnormally high in cloned embryos [36], and therefore, some researchers have attempted to correct this epigenetic abnormality by treating the donor cells with 5-Aza, a DNA demethylating drug. Such treatment, however, has led to poor blastocyst development [159]. A similar decrease in developmental potential was also observed when using 5-Aza in cloned embryos at the 2-cell stage [162]. It is thought that such failure is due to the effects of 5-Aza on massive DNA demethylation and subsequent DNA rearrangements and formation of pronuclei [163]. Chromosomal abnormalities resulting from 5-Aza treatment would be consistent with the regulatory function of DNA methylation on chromosome stability. These unsuccessful results also suggest that following fertilization, active global demethylation of the sperm chromatin must be well regulated to prevent chromosomal damage. Indeed, the sperm genome retains some methylated regions including centromeres, which contribute to chromosomal stability. When 5-Aza and TSA are used together, however, a synergistic effect has been observed in cloned bovine preimplantation development compared to TSA treatment alone [164].

Another approach to induce chromatin relaxation involves using cell extracts from Xenopus eggs to treat differentiated donor cells prior to NT. The rationale is that many of the reprogramming factors present in the mammalian oocyte might also be present in the frog egg. This approach showed a significant increase in development to term in sheep [165]. Treated cells had lower global levels

of the heterochromatic epigenetic mark H3K9me3, thus probably contributing to more relaxed chromatin configurations and to improved cloning efficiencies.

Notoriously, somatic cells have even been preheated at nonphysiological temperatures prior to NT in order to relax higher order chromatin; however, development to term was not significantly higher than nontreated control [166].

Overall, when the "right" treatment is used (such as TSA), remodeling of donor chromatin appears to improve development of cloned embryos. A better understanding of chromatin remodeling following fertilization or NT might help design a "cocktail" of drugs to efficiently remodel the differentiated chromatin of somatic donor cells.

Embryo Aggregation

Two hypotheses exist supporting the rationale of embryo aggregation. One involves the *community effect* in which the ability of a cell to take a specific differentiation pathway is enhanced when more neighboring cells are differentiating in the same way [167]. Since cloned embryos tend to have lower cell numbers than fertilized controls, at least in mice [168], the *community effect* obtained by aggregation might enhance the formation of the ICM and/or TE lineage [169]. The second hypothesis involves *epigenetic embryo complementation* [168, 170]. While the aggregated embryos are genetically identical, reprogramming defects of one embryo can be compensated by another embryo, and vice versa. Although embryo complementation is largely unknown, it is thought that cell-cell communication between blastomeres, by permeable gap junctions or by autocrine and paracrine factors, compensates for deficiencies between blastomeres [170]. It is possible that both hypotheses work together since greater cell numbers will increase the opportunities for epigenetic embryo complementation.

Aggregation of four-cell cloned embryos improved developmental potential and gene expression. In mice, expression of Oct4 increased to normal levels, the number of cells was higher at the blastocyst stage, and development to term was increased eightfold compared to single-clone embryos [168]. In bovine, embryo aggregation resulted in blastocysts with double the number of cells and in upregulation of a subset of differentially expressed genes involved in transcription, biosynthesis, and signaling compared with single-clone embryos [170]. Overall, embryo aggregation is an interesting approach to improve the quality of a cloned blastocyst.

RNA interference

While this entry was in production, an article was published in which mice cloning efficiencies were increased tenfold and the gene expression of the resultant offspring was similar to IVF controls [171]. Such impressive outcome was simply achieved by knockdown of a single gene, Xist, by RNA interference. This study showed that cloned mouse embryos usually undergo permature overexpression of Xist as well as aberrant X chromosome inactivation. Although regulation of X chromosome inactivation differs between mammals [172], cloned bovine embryos were also observed to overexpress Xist [173]. Therefore, the next logical step would be to try the same Xist knockdown approach in livestock species.

Summary Points

- SCNT involves using a somatic donor nucleus and an enucleated oocyte to produce an animal genetically identical to the donor.
- The first NT experiments were carried out in 1928, the first successful SCNTs in the late 1950s, and the first cloned adult mammal (Dolly) in 1996.
- Basic research in the nuclear reprogramming mechanism following SCNT could yield transferable knowledge to produce iPS cells safer for regenerative medicine. Realistic pharmaceutical/agricultural applications of SCNT include production of transgenic animals and cloning prizewinning animals for breeding purposes.
- NT is commonly carried out with micromanipulators, although micromanipulator-free NT is possible and effective. NT steps include oocyte maturation, enucleation, nuclear transfer, fusion, activation, embryo culture, and embryo transfer.
- Common problems in SCNT include low cloning efficiencies and developmental abnormalities. The placenta is mostly affected by the technique.
- Problems in SCNT probably originate from incomplete reprogramming of the donor chromatin.

Faulty chromatin reprogramming in cloned embryos includes hypermethylated DNA and increased H3K9me3, especially in the TE.

- Gene expression reprogramming is usually aberrant in cloned embryos, with differences between species. Pluripotent genes often fail to be reactivated in mice, although reactivation is normal when ES cells are used as donors. Fewer markers exist to assess reprogramming of pluripotency and TE lineage in livestock species, and the existing data are rather conflicting. Imprinted genes are often deregulated and differentiation-associated genes incompletely silenced.
- MII oocytes are the best recipients as they have high MPF levels. Reprogramming factors are lost when enucleating interphase recipients, which also have low MPF levels.
- Donor nuclei can be in G_0, G_1, or M phase of the cell cycle. No specific cell type has been found to be advantageous for NT; however, inconclusive data suggest that ES cells are superior donors than somatic cells.
- Centrosomal structures are recovered by introduction of centrioles along with donor cell in livestock species, although normal spindle function is not always observed in reconstructed embryos.
- Increased compatibility between genomic DNA and mtDNA is beneficial for SCNT.
- In livestock species, cell fusion appears to result in better development than nuclear microinjection, consistent with centrosomal function recovery.
- There is no preferred method for oocyte activation.
- Normal embryo culture media are not optimal for reconstructed embryos.
- Cloned neonates are at high risk, and thus, intensive care should be provided to improve survival.
- Remodeling of the donor chromatin with TSA has been the single most successful innovation for improving consistently the efficiency of SCNT.
- Aggregation of cloned embryos seems to improve embryo quality by two working models: community effect and epigenetic embryo complementation.
- X chromosome inactivation appears to be deregulated in cloned embryos and correcting this by Xist knockdown can dramatically improve development.

Future Directions

Although efforts are being made toward dissecting the mechanism and the factors that bring about nuclear reprogramming of the donor chromatin, scientists are still quite far away from gaining a clear understanding. Even if there is general consensus that the low efficiency of SCNT originates from faulty nuclear reprogramming, there is no common agreement in where the bottleneck is. Does it lie in the reprogramming of the trophectodermal lineage or is the pluripotent lineage to blame? Is deregulation of imprinted genes the culprit of low cloning efficiencies or is it the incomplete silencing of differentiation-associated genes? Is incomplete remodeling of the overall chromatin structure preventing the SCNT technology from thriving? Does the bottleneck lie in the misregulation of X chromosome inactivation? Perhaps all these are contributing factors responsible for the low SCNT outcomes. Unless much further efforts are dedicated toward understanding the mechanism of nuclear reprogramming inside the oocyte, scientists will not have clear answers to such questions. The great improvement in cloning efficiencies observed with TSA treatment and Xist knockdown gives much hope and emphasizes that innovations can radically improve the technology.

In basic science, SCNT is not limited to nuclear reprogramming. For instance, SCNT interferes with centrosomal function in livestock species, and more research is needed to understand donor centrosome behavior, spindle formation, and embryo cleavage following NT in these species. SCNT can also provide insight into genomic-mitochondrial interactions, the effects of heteroplasmy, and preferential mitochondrial amplification. Such studies might warrant a change in technique such as the method by which the donor chromatin is delivered into the cytoplast.

As the science behind SCNT will be better understood through years of research, it is likely that the outcomes of this technology will closely match those of IVF. When that day comes, widespread use of SCNT technology in livestock species would be feasible. However, being an artificial reproductive technology, SCNT is surrounded by ethical issues and regulations that should be fully contemplated to ensure good use of the technology for the benefit of society.

Bibliography

1. Baroux C et al (2008) The maternal to zygotic transition in animals and plants. Cold Spring Harb Symp Quant Biol 73:89–100
2. Newport J, Kirschner M (1982) A major developmental transition in early xenopus-embryos. 1. Characterization and timing of cellular-changes at the midblastula stage. Cell 30(3):675–686
3. Spemann H (1938) Embryonic development and induction, vol 7. Yale University Press, New Heaven, Mrs. Hepsa Ely Silliman Memorial Lectures. Yale University Press, New Haven, London; H. Milford, Oxford University Press, 401 p
4. Briggs R, King TJ (1952) Transplantation of living nuclei from blastula cells into enucleated frogs eggs. Proc Natl Acad Sci USA 38(5):455–463
5. King TJ, Briggs R (1955) Changes in the nuclei of differentiating gastrula cells, as demonstrated by nuclear transplantation. Proc Natl Acad Sci USA 41(5):321–325
6. Gurdon JB (1962) Adult frogs derived from the nuclei of single somatic cells. Dev Biol 4:256–273
7. Gurdon JB, Elsdale TR, Fischberg M (1958) Sexually mature individuals of *Xenopus laevis* from the transplantation of single somatic nuclei. Nature 182(4627):64–65
8. Gurdon JB, Laskey RA, Reeves OR (1975) The developmental capacity of nuclei transplanted from keratinized skin cells of adult frogs. J Embryol Exp Morphol 34(1):93–112
9. Bromhall JD (1975) Nuclear transplantation in the rabbit egg. Nature 258(5537):719–722
10. McGrath J, Solter D (1983) Nuclear transplantation in the mouse embryo by microsurgery and cell fusion. Science 220(4603):1300–1302
11. McGrath J, Solter D (1984) Inability of mouse blastomere nuclei transferred to enucleated zygotes to support development in vitro. Science 226(4680):1317–1319
12. Willadsen SM (1986) Nuclear transplantation in sheep embryos. Nature 320(6057):63–65
13. Prather RS et al (1987) Nuclear transplantation in the bovine embryo: assessment of donor nuclei and recipient oocyte. Biol Reprod 37(4):859–866
14. Prather RS, Sims MM, First NL (1989) Nuclear transplantation in early pig embryos. Biol Reprod 41(3):414–418
15. Campbell KH et al (1996) Sheep cloned by nuclear transfer from a cultured cell line. Nature 380(6569):64–66
16. Campbell KH, Ritchie WA, Wilmut I (1993) Nuclear-cytoplasmic interactions during the first cell cycle of nuclear transfer reconstructed bovine embryos: implications for deoxyribonucleic acid replication and development. Biol Reprod 49(5):933–942
17. Campbell KH et al (1994) Improved development to blastocyst of ovine nuclear transfer embryos reconstructed during the presumptive S-phase of enucleated activated oocytes. Biol Reprod 50(6):1385–1393
18. Wilmut I et al (1997) Viable offspring derived from fetal and adult mammalian cells. Nature 385(6619):810–813
19. Takahashi K, Yamanaka S (2006) Induction of pluripotent stem cells from mouse embryonic and adult fibroblast cultures by defined factors. Cell 126(4):663–676
20. Lister R et al (2011) Hotspots of aberrant epigenomic reprogramming in human induced pluripotent stem cells. Nature 471(7336):68–73
21. Hussein SM et al (2011) Copy number variation and selection during reprogramming to pluripotency. Nature 471(7336):58–62
22. Gore A et al (2011) Somatic coding mutations in human induced pluripotent stem cells. Nature 471(7336):63–67
23. Ding J et al (2009) Embryonic stem cells derived from somatic cloned and fertilized blastocysts are post-transcriptionally indistinguishable: a MicroRNA and protein profile comparison. Proteomics 9(10):2711–2721
24. Brambrink T et al (2006) ES cells derived from cloned and fertilized blastocysts are transcriptionally and functionally indistinguishable. Proc Natl Acad Sci USA 103(4):933–938
25. Loi P, Modlinski JA, Ptak G (2011) Interspecies somatic cell nuclear transfer: a salvage tool seeking first aid. Theriogenology 76(2):217–228
26. Vajta G (2007) Handmade cloning: the future way of nuclear transfer? Trends Biotechnol 25(6):250–253
27. Lee JH, Campbell KH (2006) Effects of enucleation and caffeine on maturation-promoting factor (MPF) and mitogen-activated protein kinase (MAPK) activities in ovine oocytes used as recipient cytoplasts for nuclear transfer. Biol Reprod 74(4):691–698
28. Thornton M, Eward KL, Helmstetter CE (2002) Production of minimally disturbed synchronous cultures of hematopoietic cells. Biotechniques 32(5):1098–1100, 1102, 1105
29. Lee JW et al (2003) Production of cloned pigs by whole-cell intracytoplasmic microinjection. Biol Reprod 69(3):995–1001
30. Song BS et al (2011) Inactivated Sendai-virus-mediated fusion improves early development of cloned bovine embryos by avoiding endoplasmic-reticulum-stress-associated apoptosis. Reprod Fertil Dev 23(6):826–836
31. Heyman Y et al (2002) Frequency and occurrence of late-gestation losses from cattle cloned embryos. Biol Reprod 66(1):6–13
32. Li N et al (2005) Perturbations in the biochemical composition of fetal fluids are apparent in surviving bovine somatic cell nuclear transfer pregnancies in the first half of gestation. Biol Reprod 73(1):139–148
33. Palmieri C et al (2007) Placental abnormalities in ovine somatic cell clones at term: a light and electron microscopic investigation. Placenta 28(5–6):577–584
34. Loi P et al (2006) Placental abnormalities associated with post-natal mortality in sheep somatic cell clones. Theriogenology 65(6):1110–1121
35. Lin J et al (2011) Defects in trophoblast cell lineage account for the impaired in vivo development of cloned embryos generated by somatic nuclear transfer. Cell Stem Cell 8(4):371–375
36. Morgan HD et al (2005) Epigenetic reprogramming in mammals. Hum Mol Genet 14(1):R47–R58

37. Li E, Bestor TH, Jaenisch R (1992) Targeted mutation of the DNA methyltransferase gene results in embryonic lethality. Cell 69(6):915–926
38. Beaujean N et al (2004) Effect of limited DNA methylation reprogramming in the normal sheep embryo on somatic cell nuclear transfer. Biol Reprod 71(1):185–193
39. Dean W et al (2001) Conservation of methylation reprogramming in mammalian development: aberrant reprogramming in cloned embryos. Proc Natl Acad Sci USA 98(24):13734–13738
40. Beaujean N et al (2004) Non-conservation of mammalian preimplantation methylation dynamics. Curr Biol 14(7): R266–R267
41. Shi W, Haaf T (2002) Aberrant methylation patterns at the two-cell stage as an indicator of early developmental failure. Mol Reprod Dev 63(3):329–334
42. Santos F et al (2003) Epigenetic marking correlates with developmental potential in cloned bovine preimplantation embryos. Curr Biol 13(13):1116–1121
43. Wu X et al (2011) Multiple histone site epigenetic modifications in nuclear transfer and in vitro fertilized bovine embryos. Zygote 19(1):31–45
44. Maalouf WE, Alberio R, Campbell KH (2008) Differential acetylation of histone H4 lysine during development of in vitro fertilized, cloned and parthenogenetically activated bovine embryos. Epigenetics 3(4):199–209
45. Vassena R et al (2007) Tough beginnings: alterations in the transcriptome of cloned embryos during the first two cell cycles. Dev Biol 304(1):75–89
46. Oback B (2008) Climbing mount efficiency – small steps, not giant leaps towards higher cloning success in farm animals. Reprod Domest Anim 43:407–416
47. Latham KE, Solter D, Schultz RM (1992) Acquisition of a transcriptionally permissive state during the 1-cell stage of mouse embryogenesis. Dev Biol 149(2):457–462
48. Nichols J et al (1998) Formation of pluripotent stem cells in the mammalian embryo depends on the POU transcription factor Oct4. Cell 95(3):379–391
49. Niwa H, Miyazaki J, Smith AG (2000) Quantitative expression of Oct-3/4 defines differentiation, dedifferentiation or self-renewal of ES cells. Nat Genet 24(4):372–376
50. Mitsui K et al (2003) The homeoprotein Nanog is required for maintenance of pluripotency in mouse epiblast and ES cells. Cell 113(5):631–642
51. Rappolee DA et al (1994) Expression and function of FGF-4 in peri-implantation development in mouse embryos. Development 120(8):2259–2269
52. Dailey L, Yuan HB, Basilico C (1994) Interaction between a Novel F9-specific factor and octamer-binding proteins is required for cell-type-restricted activity of the fibroblast growth-factor-4 enhancer. Mol Cell Biol 14(12):7758–7769
53. Feldman B et al (1995) Requirement of Fgf-4 for postimplantation mouse development. Science 267(5195): 246–249
54. Tanaka S et al (1998) Promotion of trophoblast stem cell proliferation by FGF4. Science 282(5396):2072–2075
55. Boiani M et al (2002) Oct4 distribution and level in mouse clones: consequences for pluripotency. Genes Dev 16(10):1209–1219
56. Bortvin A et al (2003) Incomplete reactivation of Oct4-related genes in mouse embryos cloned from somatic nuclei. Development 130(8):1673–1680
57. Fujii T et al (2010) Aberrant expression patterns of genes involved in segregation of inner cell mass and trophectoderm lineages in bovine embryos derived from somatic cell nuclear transfer. Cell Reprogram 12(5):617–625
58. Kirchhof N et al (2000) Expression pattern of Oct-4 in preimplantation embryos of different species. Biol Reprod 63(6):1698–1705
59. He S et al (2006) Developmental expression of pluripotency determining factors in caprine embryos: novel pattern of NANOG protein localization in the nucleolus. Mol Reprod Dev 73(12):1512–1522
60. Cauffman G et al (2005) Oct-4 mRNA and protein expression during human preimplantation development. Mol Hum Reprod 11(3):173–181
61. Kuijk EW et al (2008) Differences in early lineage segregation between mammals. Dev Dyn 237(4):918–927
62. Rodriguez-Alvarez L et al (2010) Changes in the expression of pluripotency-associated genes during preimplantation and peri-implantation stages in bovine cloned and in vitro produced embryos. Zygote 18(3):269–279
63. Long JE, Cai X, He LQ (2007) Gene profiling of cattle blastocysts derived from nuclear transfer, in vitro fertilization and in vivo development based on cDNA library. Anim Reprod Sci 100(3–4):243–256
64. Beyhan Z et al (2007) Gene expression in bovine nuclear transfer embryos in relation to donor cell efficiency in producing live offspring. Mol Reprod Dev 74(1):18–27
65. Niwa H et al (2005) Interaction between Oct3/4 and Cdx2 determines trophectoderm differentiation. Cell 123(5):917–929
66. Home P et al (2009) GATA3 Is selectively expressed in the trophectoderm of peri-implantation embryo and directly regulates Cdx2 gene expression. J Biol Chem 284(42): 28729–28737
67. Nishioka N et al (2008) Tead4 is required for specification of trophectoderm in pre-implantation mouse embryos. Mech Dev 125(3–4):270–283
68. Ralston A et al (2010) Gata3 regulates trophoblast development downstream of Tead4 and in parallel to Cdx2. Development 137(3):395–403
69. Berg DK et al (2011) Trophectoderm lineage determination in cattle. Dev Cell 20(2):244–255
70. Degrelle SA et al (2005) Molecular evidence for a critical period in mural trophoblast development in bovine blastocysts. Dev Biol 288(2):448–460
71. Vejlsted M et al (2005) Ultrastructural and immunohistochemical characterization of the bovine epiblast. Biol Reprod 72(3):678–686

72. Kishigami S et al (2006) Normal specification of the extraembryonic lineage after somatic nuclear transfer. FEBS Lett 580(7):1801–1806
73. Mcgrath J, Solter D (1984) Completion of mouse embryogenesis requires both the maternal and paternal genomes. Cell 37(1):179–183
74. Inoue K et al (2002) Faithful expression of imprinted genes in cloned mice. Science 295(5553):297
75. Humpherys D et al (2002) Abnormal gene expression in cloned mice derived from embryonic stem cell and cumulus cell nuclei. Proc Natl Acad Sci USA 99(20):12889–12894
76. Rideout WM 3rd, Eggan K, Jaenisch R (2001) Nuclear cloning and epigenetic reprogramming of the genome. Science 293(5532):1093–1098
77. Gao SR et al (2003) Somatic cell-like features of cloned mouse embryos prepared with cultured myoblast nuclei. Biol Reprod 69(1):48–56
78. Ng RK, Gurdon JB (2005) Epigenetic memory of active gene transcription is inherited through somatic cell nuclear transfer. Proc Natl Acad Sci USA 102(6):1957–1962
79. Smith SL et al (2005) Global gene expression profiles reveal significant nuclear reprogramming by the blastocyst stage after cloning. Proc Natl Acad Sci USA 102(49):17582–17587
80. Krisher RL (2004) The effect of oocyte quality on development. J Anim Sci 82(E Suppl):E14–E23
81. Li Y et al (2006) Confocal microscopic analysis of the spindle and chromosome configurations of human oocytes matured in vitro. Fertil Steril 85(4):827–832
82. Rizos D et al (2002) Consequences of bovine oocyte maturation, fertilization or early embryo development in vitro versus in vivo: implications for blastocyst yield and blastocyst quality. Mol Reprod Dev 61(2):234–248
83. Onishi A et al (2000) Pig cloning by microinjection of fetal fibroblast nuclei. Science 289(5482):1188–1190
84. Gao S et al (2002) Germinal vesicle material is essential for nucleus remodeling after nuclear transfer. Biol Reprod 67(3):928–934
85. Lee JH et al (2010) Generation of mtDNA homoplasmic cloned lambs. Cell Reprogram 12(3):347–355
86. Wakayama S, Cibelli JB, Wakayama T (2003) Effect of timing of the removal of oocyte chromosomes before or after injection of somatic nucleus on development of NT embryos. Cloning Stem Cells 5(3):181–189
87. Polejaeva IA et al (2000) Cloned pigs produced by nuclear transfer from adult somatic cells. Nature 407(6800):86–90
88. Wakayama T et al (2000) Nuclear transfer into mouse zygotes. Nat Genet 24(2):108–109
89. Baguisi A et al (1999) Production of goats by somatic cell nuclear transfer. Nat Biotechnol 17(5):456–461
90. Egli D et al (2007) Developmental reprogramming after chromosome transfer into mitotic mouse zygotes. Nature 447(7145):679–U8
91. Egli D et al (2009) Reprogramming after chromosome transfer into mouse blastomeres. Curr Biol 19(16):1403–1409
92. Mohammed AA et al (2010) Enucleated GV oocytes as recipients of embryonic nuclei in the G1, S, or G2 stages of the cell cycle. Cell Reprogram 12(4):427–435
93. Memili E, Dominko T, First NL (1998) Onset of transcription in bovine oocytes and preimplantation embryos. Mol Reprod Dev 51(1):36–41
94. Bordignon V, Smith LC (1998) Telophase enucleation: an improved method to prepare recipient cytoplasts for use in bovine nuclear transfer. Mol Reprod Dev 49(1):29–36
95. Wakayama T (2007) Production of cloned mice and ES cells from adult somatic cells by nuclear transfer: how to improve cloning efficiency? J Reprod Dev 53(1):13–26
96. Robl JM et al (1987) Nuclear transplantation in bovine embryos. J Anim Sci 64(2):642–647
97. Tsunoda Y et al (1987) Full-term development of mouse blastomere nuclei transplanted into enucleated two-cell embryos. J Exp Zool 242(2):147–151
98. Egli D, Birkhoff G, Eggan K (2008) Mediators of reprogramming: transcription factors and transitions through mitosis. Nat Rev Mol Cell Biol 9(7):505–516
99. Egli D, Eggan K (2010) Recipient cell nuclear factors are required for reprogramming by nuclear transfer. Development 137(12):1953–1963
100. Noggle S et al (2011) Human oocytes reprogram somatic cells to a pluripotent state. Nature 478(7367):70–75
101. Alberts B, Wilson JH, Hunt T (2008) Molecular biology of the cell, 5th edn. Abingdon: Garland Science, New York, xxxiii, 1601, 90 p
102. Campbell KH et al (1996) Cell cycle co-ordination in embryo cloning by nuclear transfer. Rev Reprod 1(1):40–46
103. Leno GH, Downes CS, Laskey RA (1992) The nuclear membrane prevents replication of human G2 nuclei but not G1 nuclei in Xenopus egg extract. Cell 69(1):151–158
104. Tani T, Kato Y, Tsunoda Y (2001) Direct exposure of chromosomes to nonactivated ovum cytoplasm is effective for bovine somatic cell nucleus reprogramming. Biol Reprod 64(1):324–330
105. Wakayama T, Yanagimachi R (2001) Effect of cytokinesis inhibitors, DMSO and the timing of oocyte activation on mouse cloning using cumulus cell nuclei. Reproduction 122(1):49–60
106. Ono Y et al (2001) Production of cloned mice from embryonic stem cells arrested at metaphase. Reproduction 122(5): 731–736
107. Wells DN et al (2003) Coordination between donor cell type and cell cycle stage improves nuclear cloning efficiency in cattle. Theriogenology 59(1):45–59
108. Eggan K et al (2001) Hybrid vigor, fetal overgrowth, and viability of mice derived by nuclear cloning and tetraploid embryo complementation. Proc Natl Acad Sci USA 98(11):6209–6214
109. Rideout WM 3rd et al (2000) Generation of mice from wild-type and targeted ES cells by nuclear cloning. Nat Genet 24(2):109–110

110. Gao S et al (2003) Effect of cell confluence on production of cloned mice using an inbred embryonic stem cell line. Biol Reprod 68(2):595–603
111. Humpherys D et al (2001) Epigenetic instability in ES cells and cloned mice. Science 293(5527):95–97
112. Wakayama T et al (1999) Mice cloned from embryonic stem cells. Proc Natl Acad Sci USA 96(26):14984–14989
113. Yabuuchi A et al (2004) Effects of nuclear transfer procedures on ES cell cloning efficiency in the mouse. J Reprod Dev 50(2):263–268
114. Ono Y, Kono T (2006) Irreversible barrier to the reprogramming of donor cells in cloning with mouse embryos and embryonic stem cells. Biol Reprod 75(2):210–216
115. Zhou Q et al (2001) Developmental potential of mouse embryos reconstructed from metaphase embryonic stem cell nuclei (vol 65, pg 412, 2001). Biol Reprod 65(5):1622
116. Shiels PG et al (1999) Analysis of telomere lengths in cloned sheep. Nature 399(6734):316–317
117. Alexander B et al (2007) Telomere length status of somatic cell sheep clones and their offspring. Mol Reprod Dev 74(12):1525–1537
118. Hawkins RD et al (2010) Distinct epigenomic landscapes of pluripotent and lineage-committed human cells. Cell Stem Cell 6(5):479–491
119. Maherali N et al (2007) Directly reprogrammed fibroblasts show global epigenetic remodeling and widespread tissue contribution. Cell Stem Cell 1(1):55–70
120. Meshorer E, Misteli T (2006) Chromatin in pluripotent embryonic stem cells and differentiation. Nat Rev Mol Cell Biol 7(7):540–546
121. Ahmed K et al (2010) Global chromatin architecture reflects pluripotency and lineage commitment in the early mouse embryo. PLoS One 5(5):e10531
122. Guenther MG et al (2010) Chromatin structure and gene expression programs of human embryonic and induced pluripotent stem cells. Cell Stem Cell 7(2):249–257
123. Wakayama T, Yanagimachi R (2001) Mouse cloning with nucleus donor cells of different age and type. Mol Reprod Dev 58(4):376–383
124. Eggan K et al (2004) Mice cloned from olfactory sensory neurons. Nature 428(6978):44–49
125. Hochedlinger K, Jaenisch R (2002) Monoclonal mice generated by nuclear transfer from mature B and T donor cells. Nature 415(6875):1035–1038
126. Inoue K et al (2005) Generation of cloned mice by direct nuclear transfer from natural killer T cells. Curr Biol 15(12):1114–1118
127. Oback B, Wells DN (2007) Donor cell differentiation, reprogramming, and cloning efficiency: elusive or illusive correlation? Mol Reprod Dev 74(5):646–654
128. Wakayama T et al (1998) Full-term development of mice from enucleated oocytes injected with cumulus cell nuclei. Nature 394(6691):369–374
129. Wakayama T, Yanagimachi R (1999) Cloning of male mice from adult tail-tip cells. Nat Genet 22(2):127–128
130. Ogura A et al (2000) Birth of mice after nuclear transfer by electrofusion using tail tip cells. Mol Reprod Dev 57(1):55–59
131. Schatten H, Sun QY (2009) The functional significance of centrosomes in mammalian meiosis, fertilization, development, nuclear transfer, and stem cell differentiation. Environ Mol Mutagen 50(8):620–636
132. Wong C, Stearns T (2003) Centrosome number is controlled by a centrosome-intrinsic block to reduplication. Nat Cell Biol 5(6):539–544
133. Dai Y et al (2006) Fate of centrosomes following somatic cell nuclear transfer (SCNT) in bovine oocytes. Reproduction 131(6):1051–1061
134. Simerly C et al (2003) Molecular correlates of primate nuclear transfer failures. Science 300(5617):297
135. Zhou Q et al (2006) A comparative approach to somatic cell nuclear transfer in the rhesus monkey. Hum Reprod 21(10):2564–2571
136. Anderson S et al (1981) Sequence and organization of the human mitochondrial genome. Nature 290(5806):457–465
137. St John JC, Bowles EJ, Amaral A (2007) Sperm mitochondria and fertilisation. Soc Reprod Fertil Suppl 65:399–416
138. St John JC et al (2004) The consequences of nuclear transfer for mammalian foetal development and offspring survival. A mitochondrial DNA perspective. Reproduction 127(6):631–641
139. Michaels GS, Hauswirth WW, Laipis PJ (1982) Mitochondrial DNA copy number in bovine oocytes and somatic cells. Dev Biol 94(1):246–251
140. Yang XY et al (2006) Improved efficiency of bovine cloning by autologous somatic cell nuclear transfer. Reproduction 132(5):733–739
141. Yan ZH et al (2010) Donor-host mitochondrial compatibility improves efficiency of bovine somatic cell nuclear transfer. BMC Dev Biol 10:31
142. Sansinena MJ et al (2011) Ooplasm transfer and interspecies somatic cell nuclear transfer: heteroplasmy, pattern of mitochondrial migration and effect on embryo development. Zygote 19(2):147–156
143. Kurome M et al (2003) Comparison of electro-fusion and intracytoplasmic nuclear injection methods in pig cloning. Cloning Stem Cells 5(4):367–378
144. Galli C et al (2002) Comparison of microinjection (piezoelectric) and cell fusion for nuclear transfer success with different cell types in cattle. Cloning Stem Cells 4(3):189–196
145. Jouneau A et al (2007) Piezo-assisted nuclear transfer affects cloning efficiency and may cause apoptosis. Reproduction 133(5):947–954
146. Kashir J et al (2010) Oocyte activation, phospholipase C zeta and human infertility. Hum Reprod Update 16(6):690–703
147. Ozil JP et al (2006) Ca^{2+} oscillatory pattern in fertilized mouse eggs affects gene expression and development to term. Dev Biol 300(2):534–544
148. Alberio R et al (2001) Mammalian oocyte activation: lessons from the sperm and implications for nuclear transfer. Int J Dev Biol 45(7):797–809

149. Cervera R et al (2010) Effects of different oocyte activation procedures on development and gene expression of porcine preimplantation embryos. Reprod Domest Anim 45(5):e12–e20
150. Schurmann A, Wells DN, Oback B (2006) Early zygotes are suitable recipients for bovine somatic nuclear transfer and result in cloned offspring. Reproduction 132(6):839–848
151. Kishikawa H, Wakayama T, Yanagimachi R (1999) Comparison of oocyte-activating agents for mouse cloning. Cloning 1(3):153–159
152. Ross PJ et al (2008) Parthenogenetic activation of bovine oocytes using bovine and murine phospholipase C zeta. Bmc Develop Biol 8:16
153. Ross PJ et al (2009) Activation of bovine somatic cell nuclear transfer embryos by PLCZ cRNA injection. Reproduction 137(3):427–437
154. Sparman ML, Tachibana M, Mitalipov SM (2010) Cloning of non-human primates: the road "less traveled by". Int J Dev Biol 54(11–12):1671–1678
155. Vajta G et al (2010) Embryo culture: can we perform better than nature? Reprod Biomed Online 20(4):453–469
156. Zhou Q, Dai XP, Hao J (2009) A modified culture method significantly improves the development of mouse somatic cell nuclear transfer embryos. Reproduction 138(2):301–308
157. Hill JR, Chavatte-Palmer P (2002) Pregnancy and neonatal care of cloned animals. In: Cibelli J, Lanza R, Campbell K, West M (eds) Principles of cloning. Academic, New York, pp 247–266
158. Meirelles FV et al (2010) Delivery of cloned offspring: experience in Zebu cattle (*Bos indicus*). Reprod Fertil Dev 22(1):88–97
159. Enright BP et al (2003) Epigenetic characteristics and development of embryos cloned from donor cells treated by trichostatin A or 5-aza-2′-deoxycytidine. Biol Reprod 69(3):896–901
160. Maalouf WE et al (2009) Trichostatin A treatment of cloned mouse embryos improves constitutive heterochromatin remodeling as well as developmental potential to term. BMC Dev Biol 9:11
161. Loi P et al (2008) Nuclear reprogramming: what has been done. Bioessays 30(1):66–74
162. Tsuji Y, Kato Y, Tsunoda Y (2009) The developmental potential of mouse somatic cell nuclear-transferred oocytes treated with trichostatin A and 5-aza-2′-deoxycytidine. Zygote 17(2):109–115
163. Kiziltepe T et al (2007) 5-Azacytidine, a DNA methyltransferase inhibitor, induces ATR-mediated DNA double-strand break responses, apoptosis, and synergistic cytotoxicity with doxorubicin and bortezomib against multiple myeloma cells. Mol Cancer Ther 6(6):1718–1727
164. Ding X et al (2008) Increased pre-implantation development of cloned bovine embryos treated with 5-aza-2′-deoxycytidine and trichostatin A. Theriogenology 70(4):622–630
165. Rathbone AJ et al (2010) Reprogramming of ovine somatic cells with *Xenopus laevis* oocyte extract prior to SCNT improves live birth rate. Cell Reprogram 12(5):609–616
166. Loi P et al (2002) Nuclei of nonviable ovine somatic cells develop into lambs after nuclear transplantation. Biol Reprod 67(1):126–132
167. Gurdon JB (1988) A community effect in animal development. Nature 336(6201):772–774
168. Boiani M et al (2003) Pluripotency deficit in clones overcome by clone-clone aggregation: epigenetic complementation? EMBO J 22(19):5304–5312
169. Balbach ST et al (2010) Governing cell lineage formation in cloned mouse embryos. Dev Biol 343(1–2):71–83
170. Zhou WL et al (2008) Aggregation of bovine cloned embryos at the four-cell stage stimulated gene expression and in vitro embryo development. Mol Reprod Dev 75(8):1281–1289
171. Matoba S et al (2011) RNAi-mediated knockdown of Xist can rescue the impaired postimplantation development of cloned mouse embryos. Proc Natl Acad Sci
172. Okamoto I et al (2011) Eutherian mammals use diverse strategies to initiate X-chromosome inactivation during development. Nature 472(7343):370–U141
173. Inoue K et al (2010) Impeding Xist expression from the active X chromosome improves mouse somatic cell nuclear transfer. Science 330(6003):496–499

Living Ocean, An Evolving Oxymoron

A. Alonso Aguirre[1,2], E. Scott Weber III[3]
[1]Department of Environmental Science and Policy, George Mason University, Fairfax, VA, USA
[2]Smithsonian-Mason School of Conservation, C/O Smithsonian Conservation Biology Institute, Front Royal, VA, USA
[3]Medicine and Epidemiology: Vet Med Center for Aquatic Biology and Aquaculture, University of California, Davis, Davis, CA, USA

Article Outline

Glossary
Definition of the Subject
Introduction
The Living Ocean
Fish Diversity
Fisheries, Habitat Destruction and Extinction
Aquaculture
Fisheries Interactions
Emerging Infectious Diseases
Aquatic Invasive Species

Predatory Species
Ornamental Fisheries
Threats to Coral Reefs
Global Toxification
Global Environmental Change
Tracking Marine Disturbance and Disease in Marine Ecosystems
Hawaiian Monk Seals as Sentinels of Ocean Health
Sea Turtles as Sentinels of Ocean Health
One Ocean, One Health
Your Everyday Green Choices
Future Directions
Acknowledgments
Bibliography

Glossary

By-catch In fisheries, species that are caught by accident and are discarded dead or alive but injured back into the ocean, a major threat to marine biodiversity.

Conservation medicine The emerging discipline of ecological health in practice.

Global toxification Global toxification can be referred as the deposition of thousands of environmental contaminants in the biosphere that are poorly degraded and can move through water, wind or other transport medium to other countries, regions or continents with catastrophic effects in individuals and populations.

Harmful algal bloom A rapid increase or accumulation in the population of toxic or otherwise harmful phytoplankton in an aquatic system. These events also are known as red tides due to the coloration of the bloom that varies from brown to red. Some examples of harmful toxins include brevetoxin, ciguatera, domoic acid, okadaic acid.

Hypoxia Deprived of adequate oxygen supply.

Invasive species "An invasive species is a nonnative species – including seeds, eggs, spores, or other propagules – whose introduction causes or is likely to cause economic harm, environmental harm, or harm to human health. The term *invasive;* is used for the most aggressive species. These species grow and reproduce rapidly, causing major disturbance to the areas in which they are present." (http://www.invasive.org/101/index.cfm).

Ornamental fisheries Ornamental fisheries is often used as a generic term to describe aquatic animals kept in the aquarium hobby, including fishes, invertebrates such as corals, crustaceans (e.g., crabs, hermit crabs, shrimps), mollusks (e.g., snails, clams, scallops), and also live rock.

Sentinel species Due to their size, movements and behavior, marine mammals, sea birds and sea turtles have been classified as sentinel species because they can provide essential early warning information of damage to the environment and consequently raise concerns for public health. These animal groups can serve as sentinels of marine ecosystem health in relatively pristine habitats or highly degraded or overfished ecosystems.

Taurine An essential sulfonic acid for muscle development in animal species.

Transdisciplinarity (TD) TD thinking employs perspectives and methods that transcend traditional disciplinary boundaries and engage students in addressing real-world problems. TD requires the team members to share roles and systematically cross discipline boundaries. The primary purpose of this approach is to pool and integrate the team expertise so that more efficient and comprehensive assessment and intervention may be provided in a determined field. The communication style in TD involves continuous give-and-take among all members on a regular, planned basis. Assessment, intervention, and evaluation are carried out jointly. TD brings together students, and outside the classroom, the future academic experts, field practitioners, community members, research scientists, political leaders, and business owners among others, to solve some of the pressing problems facing the world, from the local to the global and the natural and social sciences, to address the ecology and health of species and ecosystems.

Definition of the Subject

The ocean, in which life on earth began, is increasingly threatened by human activities. Ecological stresses – including overfishing, transformed coastlines, pollution, sediment loss, introduced species, emerging infectious diseases, altered agricultural runoff, sewage discharges, red tides, increased ultraviolet radiation, and an

apparently changing climate with acidification and increased hypoxia – are together impacting oceans and the health of humans, marine life and ecosystems. The health of the marine environment is at risk. Methods to assess marine ecosystem health are grossly lacking. A system to monitor and assess marine health threats linked to conservation and management policies is needed. This chapter summarizes the state of the oceans, human impacts including fisheries, climate change, globalization, trade, and coastal development, and provides solutions including an integrated health assessment initiative for marine ecosystems, the use of early warning indicator species, and day-to-day green activities that you as a citizen can contribute for a healthier planet.

Introduction

The global loss of biological diversity affects the well being of both animals and people. Human impact on ecosystems and ecological processes is well documented. Habitat destruction and species loss have led to ecosystem disruptions that include, among other impacts, the alteration of disease transmission patterns (i.e., emerging diseases), the accumulation of toxic pollutants, and the invasion of alien species and pathogens [1–3].

Beyond more visible terrestrial systems, growing evidence indicates that the ecological integrity of marine ecosystems is also under increasing threat. Oceanographers have been documenting changes in sea surface and deep core ocean temperatures, ocean acidification and increased hypoxia caused by human activities and global environmental change. The world coastal zones face enormous human developmental and urbanization pressures as most people on the planet live along the coast. Some ecological health symptoms of collective human impacts on the marine environment include increased frequency and intensity of harmful algal blooms (HABs) killing marine organisms. For example, brevetoxicosis in manatees, dolphins, and sea turtles; domoic acid poisoning in sea lions, cetaceans, and brown pelicans; ciguatera in Hawaiian monk seals and sea lions; and brown tide poisoning in humans; are being linked to increased environmental stress on species at higher trophic levels as a result of overfishing, loss of breeding/nursery habitats, and the spread of persistent chemical pollutants such as dioxins and PCBs that bio-accumulate in the food chain [2, 4–7]. Many populations of marine mammals, marine birds, and sea turtles are exposed to pollutants from agricultural runoff, human sewage, and pathogens with a terrestrial origin. Intensive agricultural practices resulting in increased nutrient loading and decreased water quality give rise to concerns of *Cryptosporidium* contaminations and potentially harmful algal blooms [8]. However, methodologies to assess marine ecosystem health are very poorly developed and the scale of monitoring required is well beyond present surveillance capacity. The health consequences of these events require innovative monitoring strategies in order to promote disease prevention, health management, and conservation. Society is ill-equipped to deal with these health impacts at present, lacking professionals with the transdisciplinary skills to link ecosystem, animal, human health issues, and inadequate large scale marine health surveillance capacity [9–11]. But these skills are necessary to change policy and management for improved health. For the past 30 years, human impacts on the health of the planet can be classified within four areas of environmental concern [12]:

1. Increasing biological impoverishment, including loss of biodiversity, habitat destruction and degradation, and modification of ecological processes.
2. Increasing global "toxification" including the spread of hazardous wastes and toxic substances and the impact of low level pollutants such as the pervasive endocrine disruptors.
3. Global environmental change.
4. Global transport of species, including but not limited to pathogens and parasites, into novel environments.

These discrete and cumulative human-induced global impacts have not only diminished the environmental capital of the planet but have also yielded an array of health concerns including the growing physiological impacts on species' reproductive health, developmental biology, and immune systems [13–15].

The Living Ocean

The ocean is the basic source for the hydrologic cycle that makes life on Earth possible, a global thermostat

that regulates entire climates, absorbs carbon dioxide and generates oxygen, a superhighway that carries most globalized trade; and, the playground for millions of people. The ocean comprises approximately 71% of the planet's surface with an area of about 361 million square kilometers (139,400,000 square miles). More than 50% of this area is over 3,000 m (9,800 ft) deep and a total volume of about 1,347,000,000 km^3 (322,280,000 cubic miles). Each cubic mile of seawater weighs 4.7 billion tons and holds 166 million tons of dissolved solids. One of the most unique aspects of ocean water is its salinity, or dissolved salt content. The measurement of salinity is essentially the determination of the amount of dissolved salts in 1 kg of water and is expressed in parts per thousand (‰). Ocean salinities commonly range from 33‰ to 38‰, with an average of 35‰. Six elements (chlorine, sodium, magnesium, sulfur, calcium, and potassium) constitute over 90% of the total salts dissolved in the ocean. The pressure in the ocean increases with depth due to the weight of the overlying water at the rate of 1 atm (=15 lb per square inch), for every 10 m (33 ft). The average temperature of the ocean is 3.9°C (39°F).

Over 230,000 marine species are known to science to date; however, the total could be up to 100–1,000 times that number. However, the extinction threat of marine species is increasing dramatically due to overexploitation and habitat loss. Climate change is becoming an important factor; due to shifting temperatures species ranges are expanding to the poles and into deeper, cooler waters. Shifts in currents and temperatures will affect the food supply of animals. To date, many species have suffered commercial and regional extinction. Entire coral reefs are getting lost within a single generation [16].

Recent studies demonstrate that viruses, despite their small size, are the most abundant biological entity in the ocean (see http://oceanworld.tamu.edu/resources/oceanography-book/microbialweb.htm). Scientists have identified less than 1% of the viruses on the planet; however, there can be three million viruses in 1 ml of water and each one contains 0.2 fg of carbon. That number is larger than the number of stars in the observable universe. Viruses consume the carbon equivalent to 200 million belugas (*Delphinapterus leucas*) if it is estimated that there are approximately 4×10^{30} viruses in the oceans worldwide [17, 18]. Using a molecular technique denominated "shotgun sequencing," Venter et al. (2004) reported 1,800 genomic species based on sequence relatedness, including 148 previously unknown bacterial phylotypes in water samples from the Sargasso Sea [19]. In total, over 1.2 million previously unknown genes were represented amongst these phylotypes and the vast majority of these unknowns have not yet been grown and studied.

Fish Diversity

Fish are the most species-rich class of vertebrates, numbering greater than 56,000 described species and subspecies, of which over 1,100 new species have been added since 2008, with these vertebrates adapted to a diverse range of aquatic habitats from desert to glacial mountain lakes and from deep sea vents to intertidal marshes [20]. Due to their relative abundance, fish and other aquatic animals have played a prominent role in human civilization by:

- Providing an important protein and omega-3 fatty acid source from both fisheries and aquaculture.
- Rapidly becoming one of the most common laboratory animal models for a variety of toxicological, infectious disease, immunologic, and genetic research facilities.
- Remaining the most numerous companion animals, as pets in bowls, aquariums, and ponds.
- Representing the fastest growing vertebrate taxa used for education in public displays at aquaria and zoos.
- Serving as vital sentinel species for marine and freshwater ecosystem evaluation, habitat assessment, conservation medicine, and ecological health.
- Being propagated for stocking natural fisheries for sport and natural enhancement.

Thus, an understanding of fish health and disease is crucial to incorporate a proactive approach when addressing current and future needs in conservation medicine and ecological health. Invertebrate animals will be discussed in brief in this chapter, but have an equally significant role in conservation medicine. Historic and current examples will be used to better illustrate these conservation medicine dilemmas and challenges.

Fisheries, Habitat Destruction and Extinction

Over 30 years ago, it was assumed that the future of humanity was going to be in the ocean due to its magnificent biodiversity and huge biomass, but within three decades humankind has been able to cause severe impacts to a degree that the ocean is in trouble due to ocean acidification, climate change, and overfishing. The ocean provides a primary source (16%) of animal protein (fish) and more than 3.5 billion people depend directly of fish resources. Approximately 110 million tons of fish are removed every year – an amount way above carrying capacity of the ocean – with a value of $50 billion dollars. For example, along the Gulf of Mexico, 5 kg (12 lb) of sea life mostly juvenile fish may be killed for 0.5 kg (1.1 lb) of shrimp. Basically, more than 75% of world fish stocks assessed for several years are over-exploited or depleted from which 60–70% require urgent action (i.e., allow recovery by closing a fisheries). Marine food webs are literally being fished down causing a cascade of trophic effects unknown to human and ecosystem health [21]. These fisheries core problems can be summarized as follows: there are too many fishing fleets with massive government subsidies for fishermen and cooperatives, with millions of tons of unwanted bycatch picturing an unsustainable future for fisheries. Entire fish stocks can be depleted within a single fishing season. Commercial fishing operations target unregulated deep waters where large migratory fish predatory species are exploited with their bycatch consequences. Of course unreliable statistics (i.e., how many fish of a species swim in the ocean and how many can be caught without causing a decline) and habitat destruction including nurseries, coral reefs, and sea floors are major contributing factors.

Recent numbers estimate that less than 1% of marine habitats are protected. Although more than 50,000 species are estimated to live in a coral reef, only the extinction of four snails, five seabirds, and four marine mammals is known in the history of humankind. These numbers provide a sense of how little is known about the ocean [22].

Aquaculture

Although aquatic organisms have been cultivated for centuries, aquaculture production is a relatively new branch of agriculture. US aquaculture in 2008 has decreased slightly from previous peaks in tonnage (2004) and in value (2006), while world aquaculture production for inland and marine animal species has nearly doubled in both tonnage and value from 1998 to 2007 [23]. With an increase in aquaculture production, there are also increased pressures on wild fisheries to help provide broodstock, seedstock, and a nutritional source of protein and fish oils in commercial aquaculture feeds for raising many aquatic species of economic importance. A frequently cited example that well illustrates realized and theoretical pressures on these fisheries is that the ecologic input purported to raise caged salmon in Norway roughly equates to 5 metric tons of food fish to produce each metric ton of farmed salmon [24]. Despite these numbers being calculated over two decades ago, opponents to commercial salmon aquaculture most frequently cite them. Even when dietary inputs for commercial salmon feeds are not double counted for fish meal and for fish oil components, and when increased feed efficiency is noted, the best true feed conversion rates of dry weight to wet weight (1.6–1.8) still require fishery inputs for salmon aquaculture [25]. In 2000, it was recognized that despite dependence on wild fisheries for fishmeal in aquaculture, aquaculture production actually increased world fish supplies, but this earlier publication does not account for a doubling of production since 2000 [26]. Based on increases in feed conversion efficiency for a variety of aquaculture species and scientific improvements in nutrition, some researchers are convinced that aquaculture use of wild fisheries for fish meal and fish oil in aquaculture feeds will continue to decrease [27]; despite an encouraging decrease in use of wild fisheries to all farmed aquaculture of 0.63 and fisheries harvest for fishmeal in aquaculture feeds are well-regulated, others debate that greater economic and regulatory efforts are still needed to protect wild fisheries [28]. One of the greatest limiting factors when rearing marine piscivorous species for food consumption is the need for taurine in the diets for these animals [29]. Taurine is commonly found in fishmeal but often is lacking in soy and poultry replacements. In the US, the Food and Drug Administration (FDA) restricts supplementing taurine to commercial aquaculture diets, which prevents more sustainable dietary formulations for some of the most popularly raised and

consumed fish species and provides a significant hurdle for US offshore aquaculture development.

One of the greatest areas of growth in aquaculture has been the shrimp industry in Central and South America and Southeast Asia. FAO reports show industry growth from 5 million metric tons in 1995, to 40 million tons by 2007 [23], which suggests the reason shrimp are considered "white gold" *oro blanco* in countries such as Ecuador. Problems with such rapid expansion and increasing global demands include habitat use, species protection, and infectious disease. As early as the 1970s in Thailand, shrimp was becoming the fastest growing aquaculture industry, and environmental impacts realized by 1995 were mangrove/wetland destruction, saltwater intrusion, land subsidence, water quality degradation, sediment disposal, abandoned shrimp farms, and displacement of traditional livelihoods [30]. Similar environmental issues including fishery depletion were associated with the shrimp industry in Honduras over a similar time period [31]. Infectious disease problems resulted in major production declines in Taiwan (1988), for China (1993), in Thailand (1996–1997), for Indonesia and the Philippines (1999), and in Ecuador (1999) [32, 33].

The effects of aquaculture on fisheries are multifactorial, including: habitat modification, using wild seed for stocking, impacts on food web interactions, introduction of non-indigenous organisms, and effluent discharge [26]. Understanding the basics for aquaculture health management, biosecurity, and biodiversity are vital to addressing needs of ecological health for aquatic organisms. Aquaculture's effects on biodiversity are seldom recognized as a positive benefit. Instead, aquaculture is viewed as negatively impacting biodiversity through land use, fossil fuel reliance, environmental pollution, antibiotic runoff, exotic species introductions, reliance on fish meal from wild fisheries, broodstock or seed allocation, and water use. However, maintaining biodiversity is essential for current and future aquaculture development [34, 35]. Some realized and potential positive impacts of aquaculture on biodiversity include decreasing exploitation on wild seafood products with cultured livestock, using certain species to enhance wild stocks, and increasing natural production and species diversity [35].

With any type of live organism captive management, there is naturally a direct relationship with disease and production level. As the intensity of production increases, the prevalence of disease also tends to increase. Intensification generally refers to increasing the number of animals raised in confined or restricted areas. For example, the greatest limitations to sustaining development of Asian aquaculture – which accounts for 89% of world aquaculture production [23] – are aquatic animal health concerns, and, without appropriate aquatic animal health management, major disease outbreaks and newly emerging pathogens will continue to dominate costs and socioeconomic development of aquaculture throughout Asia [36].

With optimal aquatic organism health management, advances in technology can be better applied for disease prevention, diagnosis, and amelioration. Increased sophistication of fish health research, advances in molecular diagnostics, and improvements in fish health management will minimize infectious disease in aquaculture (e.g., vaccines and biosecurity) similar to trends noted in production of some terrestrial animals. For example, infectious disease has appeared to have declined in the Atlantic salmon aquaculture industry in British Columbia today than it was 15–20 years ago (Dr. Gary Marty, personal communication).

Aquaculture poses great potential to help feed world populations, improve human health through nutrition, and advance agricultural practices through more practical environmental solutions [37]. As aquatic health practitioners, incorporating a strong foundational aquatic animal health program is essential to the management and future success of aquaculture and the maintenance or restoration of our aquatic ecosystems (including wild fisheries).

Fisheries Interactions

Rapid alterations to the ocean are creating a medium for new disease patterns and health manifestations. For example, new variants of *Vibrio cholerae* have been identified within red tide algal blooms. These toxic blooms are occurring in greater frequency and size throughout the temperate coastal zones of the world.

Intensive aquaculture is a relatively new agricultural practice, and there are several interactions between aquaculture reared animals and wild fisheries. Intensive aquaculture is marked by decreasing needs for natural

inputs for husbandry in order to raise greater biomass (number of fish) in less space, while extensive aquaculture relies on enhancing natural food resources and has a greater dependence on livestock density. In the context of conservation, some prominent concerns are fisheries interactions resulting in disease outbreaks, farm-source antibiotic/chemical resistant pathogens, and environmental contamination caused by effluent. Although aquaculture may contribute to these fisheries interactions, other industries and environmental utilization also make substantial changes to the environment posing a threat to aquaculture and native fish populations. Because of the vast expanse of oceans identifying and quantifying the impact of infectious disease on wild fisheries is compounded by fish mortalities going undetected through natural attrition by predation, sinking to the bottom, or occurrences in remote locations. Understanding infectious diseases in wild fish requires effectively led transdisciplinary teams with expertise in fisheries biology, medicine, pathology, mathematical modeling, and ecology. By including participation of concerned citizens and multiple specialists, fish health professionals will be ultimately equipped to diagnose, treat, and/or mitigate emerging infectious disease outbreaks in fisheries and aquaculture [38].

Emerging Infectious Diseases

Emerging infectious diseases are commonly defined as those that have newly appeared in a population or have existed but are rapidly increasing in incidence or geographic range or appear in new hosts (i.e., canine distemper a disease of dogs has killed tens of thousands of common seals in the North Sea [10]). This rapid trend has been observed in many human populations from AIDS to SARS and from West Nile virus infection to highly pathogenic H5N1 avian influenza. Although current diagnostic methodologies allow the detection of novel pathogens, unprecedented number of emerging and reemerging diseases in marine ecosystems such as brucellosis in dolphins, aspergillosis in coral reefs, fibropapillomatosis in sea turtles, toxoplasmosis in sea otters, and morbillivirus infections linked to large-scale marine mammal die-offs have been documented in recent times [39]. The trends of diseases in the oceans are increasing since 1970 for many taxa including turtles, corals, urchins, and mollusks [40]. The human impacts on the world's oceans have devastated populations, species, and ecosystems at a rapid scale. Some of the emerging pathogens recently documented in the oceans are listed in Table 1. Ancient diseases like mycobacteriosis (tuberculosis) offers some of the greatest health management challenges for managed collections or groups of fish, and have been identified recently in hundreds of freshwater and marine ornamentals, laboratory animals, and also from aquaculture reared striped bass (*Morone saxatilis*) from California [41]. In the last decade mycobacteria infections have been isolated from clinically infected wild striped bass and in juvenile Atlantic menhaden (*Brevoortia tyrannus*) disease prevalence ranged from 2% to 57% in tributaries of the Chesapeake Bay [42] and multiple *Mycobacteria* spp. can colonize numerous species of native fish in this region [43].

Aquatic Invasive Species

Invasive species have a great socioeconomic impact when they negatively impact native species [44]. These alterations can be associated with directly changing the environment such as by eating prey species of fish or invertebrates, eating or disrupting the vegetation and/or phytoplankton, eliminating other important native controls for insects or pests, and changing water flow and water chemistry [45]. Many of these examples can be found on the website for the aquatic nuisance species task force [46]. Some of these examples include (invasive species – probable source):

- Nile perch (*Lates niloticus*), Nile tilapia (*Oreochromis niloticus*), and Water hyacinth (*Eichhornia crassipes*) in Lake Victoria, Africa – developmental projects [47].
- Asian carp in Mississippi Delta and Great Lakes, United States – aquaculture/research.
- *Hydrilla verticillata* in southeast US and *Caulerpa taxifolia* in the Mediterranean – aquarium and water garden trade.
- Zebra mussels (*Dreissena polymorpha*) in watersheds around the world affecting native shellfish populations, water quality, and larval fish – ballast water [48].
- Sea lamprey (*Petromyzon marinus*) parasitism and disease in Great Lakes fishery – possibly Erie and Welland canal projects.

Living Ocean, An Evolving Oxymoron. Table 1 Some emerging and reemerging disease agents recently reported in the marine environment

Disease	Species	Etiologic agent
Adenovirus infection	Walrus	Walrus adenovirus W77R
Arboviral encephalitis	Orca, gray whales, harbor seal [130]	EEE, SLE viruses
Aspergillosis	Marine organisms	*Aspergillus fumigatus*
Black band /white band disease	Corals	Unknown
Bonamiasis	*Ostreaedulis*	*Bonamia ostrea*
Brucellosis in marine mammals	Marine mammals	*Brucella ceti, B. pinnipedialis*
Calicivirus infections	Marine mammals	Caliciviruses (39 serotypes)
Candidiasis	Marine mammals	*Candida albicans*
Canine distemper	Phocids	Canine distemper virus
Chlamydiosis	Sea turtles, Pinnipeds	*Chamydophila psittaci*
Cutaneous viral papilloma	Orca, manatees	Papillomavirus
Disseminated neoplasia/Germinomas	Bivalves	Unknown
Dolphin morbillivirus	*Stenella*	Dolphin morbillivirus
Enterovirus infection	Walrus	Walrus enterovirus 7–19
Erysipelas	Delphinids, little blue penguins [131]	*Erisipelotrix rusiopathiae*
Fibropapillomatosis	Marine turtles	Unknown: Herpesvirus, Retrovirus, possibly Papillomavirus
Hepadnaviral hepatitis	Delphinids	Hepadnavirus
Herpesvirus infection	Phocids; northern fur seals; salmonids, ictalurids, *Cyprinus carpio* [132], *Sardinops sagax*, other fish species	Phocine herpesvirus 1 and 2; Marine herpesvirus 206 CyHV1,2,3; HPV1,2; CCV; Pilchard herpes virus
Immunoblastic malignant lymphoma	*Stenella/Tursiops*	Unknown
Ichthyophoniasis	*Oncorhynchus* spp. [133]	*Ichthyophonus* sp.
Leptospirosis	Pinnipeds	*Leptospira* spp.
Keloidalblastomycosis/ Lobomycosis/Lobo's disease	Delphinids	*Lacazia loboi*
Melioidosis	Delphinids (SE Asia, Australia)	*Burkholderia pseudomallei (Pseudomonas pseudomallei)*
Megalocytisvirus	Numerous fish species [134]	BCIV, ISKNV, RSIV, TRBIV
Metastatic oral squamous cell carcinoma	Delphinids	Possibly papillomavirus
Morbillivirus infection	Mediterranean monk seals	Monk seal morbillivirus

Living Ocean, An Evolving Oxymoron. Table 1 (Continued)

Disease	Species	Etiologic agent
Mycobacteriosis	striped bass; ornamental and tropical marine and freshwater fish species	*Mycobacterium* spp.
Native parasitic sea lice	Salmonid species of genus *Onchorynchus* [135, 136]	*Lepeophtheirus salmonis*
Nocardiosis	Marine mammals	*Nocardia* spp.
Phaeohyphomycosis	Temperate marine teleosts	*Exophiala* spp.
Phocine distemper	Phocids	Phocine distemper virus
Polyps and hyperplasms	Corals	Unknown
Porpoise morbillivirus infection	Porpoises	Porpoise morbillivirus
Pseudomoniasis	Marine mammals	*Pseudomonas* spp
Ranavirus	Amphibians, fish, and chelonian species	FRV-3, numerous others
Rotavirus infection	California sea lion	California sea lion rotavirus A111R
Retrovirus infection	Walrus	Walrus retrovirus T2/19
Salmon fluke	*Salmonid* spp.	*Gyrodactylus salaris Malmberg, 1957*
Salmonellosis	Ornamental freshwater fish and dwarf African frogs	*Salmonella paratyphimyrium* and *S. typhimyrium*
Sea lion transitional cell carcinoma	California sea lions	Herpesvirus??
Seal influenza	Phocids	Influenza virus type A
Seal pox	Pinnipeds	Pox virus
Stress-related necrosis	Corals	High water temperatures
Toxoplasmosis	Pinnipeds, Delphinids	*Toxoplasma gondii*
Vibriosis	Marine mammals, fish, and shellfish [103]	*Campylobacter* spp., *Vibrio* spp., *Photbacterium* ssp.
Viral hemorrhagic septicemia	Marine and freshwater teleosts in northern hemisphere [137]	Viral hemorrhagic Septicemia virus (VHSV)
Whirling disease	Salmonid spp.	*Myxobolus cerebralis*

Invasive species are also detrimental because they *change* predator/prey ecology for ecosystems. These include species that are both predators and prey. Invasive predatory species have an obvious detrimental effect by preying on species that may not have had natural predators in certain habitats. Invasive prey species can have direct or more cryptic effects by consuming resources for native prey species, or through replacing a more nutritious food resource for predators. Some examples are:

Predatory Species

- Pacific Batfish (*Platax orbicularus*) in Molasses Reef in the Florida Keys 2000.
- Lionfish (*Pterois volitans, Pterois miles*) in Northwestern Atlantic and Caribbean, 1992 aquarium escape after hurricane Andrew Biscayne bay [49].
- Snakehead (*Channa argus*), in 2002, this species was discovered in a pond in Crofton, Maryland individual release from aquarium or live food industry.

- Butterfly (*Cichla ocellaris*) and speckled peacock bass (*Cichla temensis*) in Florida by intentional release as game fish 1984.
- Northern Pike (*Esox lucius*) in Davis Lake, California by individual introduction 1994 Prey Species.
- Alewife/Shad (*Alosa pseudoharengus*) 1931 in Great Lakes via Wellend canal.

A greater issue is caused by the release of animals from other geographical locations. Some of these animals may be closely related to native animals separated only by ecological barriers. These species can readily survive in the new location, but given the circumstance for release could pose a greater risk to native relatives. Some examples of this include the release of Maryland diamondback terrapins (*Malaclemys terrapin*) in New York waters from Asian food markets (personal communication with Russell Burke). These terrapins have been exposed to a variety of chelonian species from around the world in poor husbandry conditions that are often unregulated and unhygienic. These animals have potential to become asymptomatic or symptomatic carriers for new diseases that could pose a threat to native threatened and endangered populations. Some examples of sources for these invasives include:

- Aquaculture.
- Live Food Markets.
- Laboratories.
- Collectors.
- Water Gardens/Landscape designers.
- Unwanted Pets – Habitatitude™: (http://www.habitattitude.net/).
- Restoration/Repopulation projects.

New diseases and health problems in native populations can arise from invasives from all the descriptions above. Alterations in the environment can create poor water quality conditions for native species. Well-documented diseases associated with introductions of nonnatives have occurred in fish, invertebrates, reptiles, and amphibians:

- Chytridiomycosis by *Batrachochytrium dendrobatidis* – amphibians globally [50].
- Thiamin deficiency and thiaminase – salmonids Great lakes, alligators Lake Griffin, Florida [51, 52].
- Viral Hemorrhagic Septicemia VHSV – FW and possibly Marine from Great Lakes [53].
- *Hydrilla verticillata*/blue green algae – Avian Vacuolar Myelinopathy Southeastern US [54]
- *Myxobolus cerebralis* causing Whirling Disease Western US [55].
- *Gyrodactylus salaris* from Baltic to North Sea 1974 [56].
- Malpeque and MSX: links between disease and non-indigenous species in *Atla*ntic Canada [57].
- *Trypanosoma acerinae* from Caspian to Lake Superior in Ballast Water 1992 fish pathogen [58]. *Bonamia ostrea* from California to France, Maine, Washington State, and British Columbia [59–62].

As veterinarians and aquatic animal professionals, our role with aquatic invasives is to recognize new and emerging disease threats, including those that might be caused by human actions [63]. This role includes using our skills in education, nutrition, infectious diseases, and public health to help investigate problems associated with the current epidemic of aquatic invasive species. Some of these diseases may have been overlooked because of poor associations or because current husbandry complicate diagnosing new pathogens. Some brief examples of potential threats include:

- *Exophiala* sp. in cold marine and temperate water fishes [64].
- Megalocytisvirus in ornamental freshwater and marine fishes [65].
- *Salmonella* sp. in freshwater fish, amphibians, and turtles [66].
- *Enterococcus* sp. in sea turtles (Innis, Sims, and Weber unpublished data).

Ornamental Fisheries

Marine and freshwater ornamental fisheries are a growing area, and they involve largely unregulated movement of livestock with global implications for potential disease outbreaks [67, 68]. The ornamental aquarium industry includes captive (>90%) and wild freshwater fish with over 632 million animals produced in Malaysia alone as recorded by the Malaysian ornamental fish industry (2010), coupled with a far greater variety of marine ornamental species that are traded

with estimates of close to 8,000 different species of marine animals with only ~25 species captive bred [69–71]. FAO estimates in 2009 suggest 59% of all production of ornamental aquaculture related products were produced in Asian countries. Aquatic animals include fish, reptiles, amphibians, invertebrates (including corals), and live rock (dead coral that becomes encrusted with marine macro- and microorganisms in the wild). Farms in Florida (USA) and Southeast Asia raise many freshwater ornamental varieties with additional inputs from other countries, hobbyists, and wild-caught fisheries. Hobby specialty groups actively trade some of the animals highly prized for appearance, such as African and South American cichlids. The freshwater temperate ornamental industry consists primarily of koi (*Cyprinus carpio*) and goldfish (*Carassius auratus auratus*) with major production in Israel, Arkansas (USA), Japan, and China. There is little marine ornamental production of farm raised stock, and the majority of marine fish for the hobbyist trade come from captured wild stocks in the Caribbean Ocean, Red Sea, and Indo-Pacific Ocean. Methods used for collection in the Philippines for many marine species in the past have included dynamite stunning and potassium cyanide poisoning causing irreparable damage to stock collected as well as the environment and animals caught as bycatch [72]. Zoos and aquariums contribute to these pressures on aquatic animals; they are net consumers of wildlife and are and must maintain high standards of animal care. The increased fishing pressures on these animals have made some species extremely vulnerable. In just the last decade Banggai cardinal fish (*Pterapogon kauderni*) have become one of the first marine ornamentals to be listed on the International Union for Conservation of Nature (IUCN) red list for threatened species [73, 74], and institutions like the Shedd Aquarium in Chicago have sponsored conservation efforts such as *Project Seahorse* to help with education and research of dwindling numbers of sygnathid species. Although restoration projects are proposed to support conservation for many of these species [75], such endeavors can cause catastrophic effects on native populations, and will need to include aquatic animal veterinarians and fish health professionals to develop responsible protocols to help ensure the health status of captive breeding animals and their offspring prior to release with native populations. Restoration efforts should also involve conducting health surveys on wild populations to screen for presence of common and emerging pathogens known to threaten these native organisms [70].

The primary cause of mortality for many ornamental species is from stress associated with transport, resulting in death either immediately from environmental quality issues or later from disease. Mortality for wild caught ornamentals approaches 100% of some shipments. Shipments bring animals together from different geographical locations into holding systems with shared filtration. Geographical strains of common parasites can be deadly for naïve animals using a shared recirculating water source. Emerging infectious disease agents are largely undetected and seldom appear in the peer-reviewed scientific literature despite the existence of a large industry. This lack of knowledge is mostly the result of mortalities in the aquarium and ornamental trade being discarded without any obligation or regulation for movement of these animals, and often, no gross pathology and/or histopathology is performed on fish mortalities.

Threats to Coral Reefs

Destruction of coral reefs and coral diseases are fast outpacing new reef formation [76]. Coral reefs have tremendous species diversity and there are many new resources on conserving coral reefs. Expertise in understanding coral reef destruction through scientific research has uncovered numerous new pathogens and disease syndromes identified in corals, linking environmental quality and climate change to many problems faced by these invertebrates [77]. Corals are being threatened by anthropogenic (human-induced) and environmental variables such as bleaching, infectious disease, climate change, predator plagues, and invasive species [78]. Recently sunscreen was implicated in contributing to causing coral bleaching and promoting viral infections in heavily touristy areas [79].

Global Toxification

Pollution is a common thread for many of these environmental variables and several examples will be highlighted to illustrate the complicated nature of these

interactions. Natural populations of fish in Europe are contaminated with PCBs. Fish from the Rhone River downstream from an incineration plant had high levels of contamination, and that the consequence of this exposure was significant increase in cytochrome P-450 dependent monooxygenase activities [80]. Pollutants can have direct environmental consequences such as the accumulation of halogenated contaminants in farmed salmon, trout, tilapia, pangasius, and shrimp as compared with wild caught marine fisheries, showing salmon as having a greater contaminant level than all other species investigated and Polychlorinated biphenyls (PCBs) being found in the highest concentration [81]. Subsequent studies investigating salmon from Europe and North America in 2004 and 2005 suggested that PCB levels were also significantly higher than levels found in wild Alaskan Chinook salmon but that farms from Eastern Canada had decreased PCB detection in the second year [82–84]. Comparing over 2 metric tons of farmed and wild salmon from around the world for organochlorine contaminants, farmed salmon had significantly higher contaminant levels than wild salmon with Europe having higher levels than both North and South America [85]. However, more recent research showed that much of these differences were a result of lower lipid content in wild Pacific salmon than in farmed Atlantic salmon [86]. Pollutant levels in wild populations of salmonids from the Great Lakes may be improving based on human studies illustrating a decrease of PCBs and DDT among all populations in the Great Lakes region including sport fishers over a 10 year period from 1995 to 2005 [87].

Pollution is also evident from manmade causes and disasters from mines, factories, inadequate wastewater treatment, and oil spills. Fish exposed chronically to petroleum hydrocarbons at the site of the Exxon Valdez oil spill in Alaska had a significant difference in the prevalence and intensity of trichodina parasitism between sculpin originating from an oil-free and an oil-contaminated site, with the oil-contaminated having the greater infection; although extensive environmental differences in both sites were not sufficiently described, as this parasite can also increase rapidly in water temperatures differing by only a couple of degrees C°, especially in eutrophic conditions [88]. After exposure to a variety of pollutants, heavy metals, acid rain, and xenobiotics were shown to cause gross and microscopic lesions of the gill epithelium that were directly linked to osmoregulatory, acid–base, or hemodynamic malfunction, suggesting that toxins may be processed in the gills of fish similar to human pathways found in the kidney, intestine, and liver [89, 90]. Other investigators looking for biomarkers of toxicity caused by crude oil have demonstrated that even at very low exposure the metabolic enzymes citrate synthase and lactate dehydrogenase measured in the gills of Atlantic salmon appeared to be good biomarkers of exposure to the WAF of Bass Strait crude oil, and to chemically dispersed crude oil [90]. Among the many toxins in the aquatic environment, heavy metal toxins are of historical significance. Minamata disease is a disease in humans marked by severe congenital birth deformities that result from eating fish contaminated with methyl mercury waste first characterized in Minamata bay, Japan. Lakes in the Western US such as the Great Salt Lake are reported to have heavy concentrations of mercury and selenium affecting migrating waterfowl [91]. Trends in mercury concentrations in the US Great Lakes from 1969 to 2005 had the greatest downward trends in fish samples from 1969 to 1987, correlating to decreased mercury in sediment and peat cores over that period [92], marking positive news for mitigation of the bioaccumulation of this toxin in this region. Emerging chemicals of concern (ECC) are constantly being investigated such as the effect of endocrine disruptors on fish species [93]. In UK Rivers, a high prevalence of intersexuality and sexual disruption in the roach *Rutilus rutilus* was concomitant with environmental detectable levels of pollutant endocrine disruptors, documenting an initial change in vertebrate behavior related to such compounds [94]. Similar research is investigating fish endocrine disruption in rivers of Virginia and West Virginia.

Veterinarians and the medical profession have the ability to directly mitigate a growing pollutant problem of this century, antibiotics found in the aquatic environment and their possible link to antibiotic resistance of some pathogenic bacteria. Researchers are only beginning to understand the ramifications of antibiotic waste for various ecosystems generated from human and agricultural uses. With improved analytical techniques, antibiotics can easily be identified in waste water and post treatment effluent, and studies suggest that of six antibiotics (ciprofloxacin,

trimethoprim/sulphamethoxazole, tetracycline, ampicillin, trimethoprim, and erythromycin) tested pre- and post-wastewater treatment, some bacteria were resistant to all six antibiotics pretreatment, and posttreatment bacteria were still resistant to two of this antibiotics [95]. In broader surveys conducted on samples from 16 sites in the southern North-Rhine Westphalia of Germany, antibiotics were detected in all watersheds. Both large (Rhine River) and small creeks had some substances (erythromycin and sulfamethoxazole) identified in nearly all samples, and concentrations of these pharmaceutical products ranged from detectable to the limit quantization [96]. Early surveys in Germany also detected antibiotics in groundwater and wastewater, but groundwater in heavy livestock areas was free from antibiotic residues, suggesting that most environmental contamination in Germany is from human medical practices [97]. Although much of this environmental contamination is from human waste or terrestrial agricultural effluent, aquaculture may also contribute the problem of antimicrobial resistance. In a more comprehensive review of the literature, many veterinary treatments are found in the aquatic environment including insecticides, antihelmenthics, and antibiotics [98, 99]. Four Danish freshwater trout farms were investigated comparing inlet and outlet water samples, and assessing levels of antibiotic resistance from bacterial sampling of fish, water, and sediment. Two major fish pathogens (88 *Flavobacterium psychrophilum* isolates and 134 *Yersinia ruckeri* isolates) and 313 motile *Aeromonas* isolates had increased antibiotic-resistant among the culturable microflora that was statistically significant among the motile aeromonads; the study used five MICs from antibiotics commonly used in Danish aquaculture (oxolinic acid (OXA) and sulfadiazine-trimethoprim (S-T), amoxicillin (AMX), oxytetracycline (OTC), and florfenicol (FLO) [100]. In another study, Oxytetracycline-resistant (OTr) mesophilic aeromonads from untreated hospital effluent and from fish farm hatchery tanks in Cumbria shared tetracycline resistance-encoding plasmids identical to a similar plasmid found in *E. coli* even though coming from distinct locations [101]. The long-term consequences of antibiotic resistance in the environment are not fully understood, although some of the work by Costanzo showed certain antibiotics negatively affected bio-nitrification [95]. There are large research gaps for understanding all the implications of antibiotic pollution for ecosystem health and sources of these therapeutants, but this lack of research should not prevent further assessment and proactive approaches to addressing environmental accumulation with these drugs.

Microbes also cause environmental concerns for cultivated and harvested fisheries. Many of these pathogens not only cause disease in aquatic animals, but also pose a health risk for people. Some of the more recent findings include epidemiologic investigations of *Salmonella* outbreaks in Australia. One outbreak was the first to link gastroenteritis outbreaks in humans with identical isolates from home aquaria for multidrug-resistant *S. paratyphi* B dT+ (ApCmSmSpSuTc phenotype) (ampicillin, chloramphenicol, streptomycin, spectinomycin, sulfonamides, tetracycline) containing SGI1 [66]. Subsequent investigations correlated human outbreaks of gastroenteritis with a second multidrug-resistant *S.paratyphi* B biovar Java (*S. Java*) with strains that were resistant to ApCmSmSpSuTc, and this isolate was directly linked with home aquaria maintenance [102]. Aquaculture products can also become incidental vehicles to transmit pathogens as illustrated by a 1991 outbreak of cholera in Guayaquil, Ecuador of multiple antimicrobial resistant *V. cholerae* O1 recovered from a pooled sample of a bivalve mollusk and from 68% of stool samples from case patients [103].

Global Environmental Change

Climate change whether induced by humans or natural, has potential to greatly alter the aquatic landscape in ways poorly appreciated or understood by researchers at present. Climate change may be intimately linked to many issues presented in this chapter from providing sustainable aquaculture to harvesting ornamental fish, from the success or failure of invasive species [104] to natural changes in range for many animals, and from coral reef survival to the ecology of infectious disease organisms [78, 105]. Fish populations at risk to climate change in Northern European countries include disease threats from disease agents occurring in warmer climates such as *Lactococcus garvieae* in farmed trout in the UK [106] and proliferative kidney disease (PKD) in wild Swiss grayling (*Thymallus thymallus*) [107]. Aquatic

biologists and veterinarians must begin to keep records and develop methods of monitoring disease outbreaks in wild fisheries and in managed species globally.

Tracking Marine Disturbance and Disease in Marine Ecosystems

A new model of bridging the growing gap between conservation science and conservation advocacy that now faces the environmental movement is needed. Environmental problems are being defined as more complex interactions. The scale and complexity of issues require novel solution-oriented approaches that are based upon meaningful collaborations among disciplines and institutions. Obviously, the scale of the Ocean makes it difficult to get a handle on the entire health status of this marine environment. And certainly any focal subset of the Pacific Ocean for example the Bering Sea or the Hawaiian Islands does not diminish issues of scale. The ocean is huge by any measure.

An integrated assessment that links together data from ecological, climatic and economic sources was proposed in the late 1990s [108]. This project had the objective of identifying major marine ecological disturbances (MMEDs) through this assessment process. MMEDs can be mapped, using a geographic information system (GIS), to find spatial "hotspots" and temporal clusters of events (e.g., during El Niño years). Data for this effort is derived from peer-reviewed scientific articles, a network of government and academic researchers, existing data sets and, for more current events, mass media sources.

This ocean health framework is similar to traditional epidemiological (population health) models. The model tracks potentially harmful algae, marine pathogens, and other species that respond rapidly to environmental change. Diseases arise from a combination of pathogenicity (degree of disease causing capability), host vulnerability, and a conducive environment. Marine morbidity and mortality (disease) events may be symptomatic of compounding and chronic ecosystem abuse.

A comprehensive survey of instances of marine ecological disturbance, and a methodology for future major marine ecological disturbance (MMED) investigation, is desired by international, federal and state agencies in their efforts to better understand the changes occurring in the world's oceans. The HEED approach drew together the expertise of over 15 separate disciplines, organized historic data in one standard format, assessed the integrity and coverage of data, and provided a method for future standardized data collection and analysis. Events within this morbidity and mortality database served as (eco) indicators of ecologically and economically significant disturbances. The overall framework enabled the assessment of marine ecosystem health.

The six data sets integrated into the HEED (http://heedmd.org/) model include:

- MMED Database: Morbidity/mortality and adverse occurrences among coral, seagrasses, invertebrates, fish, sea turtles, sea birds, marine mammals, and humans, including HABs data.
- Climate Databases: Sea-surface temperature anomalies, precipitation anomalies, unusual weather events, movement of the Gulf Stream, and indices of climatological anomalies, including the NAO and ENSO phenomena.
- Biophysical Databases: Dissolved inorganic and organic nutrients, river flux, metal concentrations, water column stratification, oxygen, salinity, solar radiation, presence/absence and abundance of sentinel species.
- Baseline Ecosystem Datasets: Chlorophyll biomass, plankton abundance and diversity, dynamics and life history for benthic and pelagic species, and their organization in trophodynamic guilds for particular places over time.
- Economic Database: National Marine Fisheries Service fisheries statistics, Federal Emergency Management Agency and Small Business Administration requests for assistance, and other economic and social costs of morbidity and mortality events.
- Mass Media Database: Article searches of MMED-related stories and economic costs, to ensure complete coverage of data too recent to appear in published literature. Case studies include global marine mammal reports.

In HEED study areas which included the Western North Atlantic, Caribbean Sea, and the Gulf of Mexico, major marine ecological disturbances have increased during the last 50 years. Initial findings in the Atlantic Ocean show a rise in marine-related diseases along the USA Atlantic coast, Gulf of Mexico and Caribbean.

This suggests that coastal conditions conducive to illness are widespread. Other findings of note include:

- New diseases are emerging and old diseases are reappearing across a wide range of marine life.
- Humans face increasing health risks associated with seafood consumption and recreation.
- Of deepest concern, infections appear to be spreading among seagrass meadows and coral reefs, the habitat upon which other species depend.
- Disease outbreaks can lead to significant economic losses for seafood industries, fishing communities, trade, travel and tourism.
- Monitoring and supporting communication networks for harmful algal blooms, and combining disease and environmental surveillance, can generate health early warning systems.
- A continuation of the trends described could significantly alter the structure and function of coastal marine ecosystems.

Results from the original HEED effort for the Atlantic Ocean [109] depict a geographic expansion and overall increase in marine ecological disturbances over the last several decades – including unprecedented events, and disturbances of increasing severity. These have had, in some cases, significant human health and economic impacts. Increased understanding of marine ecological disturbances through the use of the tracking methodology provides a justification and basis for a rapid response to public health risks and threats to ecosystems. NOAA's Office of Global Programs and NASA provided support for the Atlantic Ocean monitoring effort (http://www.heedmd.org/).

Hawaiian Monk Seals as Sentinels of Ocean Health

Possibly the best indicator of ecological integrity of Hawaii's regional marine ecosystem, including the Northwestern Hawaiian Islands (NWHI), is the health of marine vertebrates known to be sensitive to system-wide human impacts including fishing. Sea turtles, sea birds, and marine mammals recently have been described as "sentinels" of marine ecosystem health [110, 111]. Hawaiian monk seals (*Monachus schauinslandi*) fall into this category. The Hawaiian monk seal is one of the most endangered marine mammals in the world and the most endangered pinniped in USA waters. Of three species globally, the Caribbean monk seal (*M. tropicallis*) is believed extinct since the late 1950s and the Mediterranean monk (*M. monachus*) seal nearly so with only a few hundred animals remaining. The decline of both species mirrored the development in their respective regions, including increasingly intensive fishing and degradation of coral reef ecosystems [112].

Populations of Hawaiian monk seals have shown a severe decline in recent years and have placed the species in threat of extinction comprising 1,300 individuals in the wild. Although little is known of the pattern of historic decline of the species, precipitous decline in juvenile survival of Hawaiian monk seals since 1990 followed a climate-induced shift in ecosystem carrying capacity together with overharvesting of lobsters, a known prey of juvenile seals. Monk seal-fishing interactions have been documented in all NWHI fisheries. It is highly likely that the cumulative effects of commercial fishing activity negatively impact the monk seal population through both direct and indirect (ecosystem level) mechanisms. It is unlikely this can be determined definitively unless observed by allowing commercial fishing to continue in or adjacent to monk seal habitat [112].

Understanding the potential role of disease and toxins in this recent decline is a high priority. Several natural sources of mortality have been identified or suggested (e.g., ciguatera poisoning, starvation, shark predation, trauma/mobbing and parasites), but the relative significance of these factors and their effect on population trends are poorly understood. Efforts to enhance the recovery of the Hawaiian monk seal will require a better understanding of the health and disease status of the wild population. Thus, health and disease impacts on the population merit a cohesive, well-supported effort to mitigate potential effects [113].

As demonstrated by intensive serologic surveys on a wide number of marine mammal species, it is evident that many diseases known to affect terrestrial species for decades or centuries are now recently being identified in marine ecosystems. Species and disease interactions are resulting in the appearance of mass mortalities and new reservoir hosts in new geographic areas. Examples of these diseases in marine ecosystems include several strains of morbillivirus, *Brucella* spp.

and leptospirosis. NMFS Marine Mammal Research Program has actively investigated Hawaiian monk seal health and disease for more than 30 years. This investigation has included surveillance and analysis, primarily in the Northwestern Hawaiian Islands (NWHI). Veterinarians, marine biologists and other scientists conduct studies including gross necropsy and histopathology, parasitology, hematology, serology, morphometrics, microbiology, epidemiology, scat and spew analysis, population abundance/survival assessment, and reproductive rates. Recent research [114] shows the serologic presence of several infectious agents. The three infectious diseases endemic to the MHI considered to have the highest risk for the Hawaiian monk seal population are morbilliviruses (i.e., canine distemper, seal distemper), *Brucella* spp. and *Leptospira* spp. Fortunately, canine distemper in Hawaii is rarely diagnosed in domestic pets. Leptospirosis is endemic and widespread but public awareness and state monitoring are helpful. Also, Hawaiian monk seals are mostly solitary, reducing the potential for the spread of this deadly disease from seal to seal. The potential for *Brucella* to affect the survival of Hawaiian monk seals is unclear but a cause for concern. *Brucella* is believed to cause reproductive failure in other species and techniques for diagnosis in monk seals are being developed and may be available in the near future.

Data collected regarding morbillivirus, *Leptospira* spp. and *Brucella* spp. need to be analyzed to provide for example: epidemiological trends, morbidity/mortality curves, geographic distribution and prevalence/incidence information. In addition, herpesvirus epidemics and morbillivirus serologic evidence are being reported affecting pinnipeds in the Pacific coast of the USA (http://www.pifsc.noaa.gov/psd/mmrp/health.php). A cooperative initiative has been proposed to systematically address these disease concerns in one of the richest ecosystems of the world.

Sea Turtles as Sentinels of Ocean Health

Habitat destruction, ingestion of plastics, fisheries bycatch, boat collisions, and emerging diseases are among the documented threats to sea turtles in all oceans. Because sea turtles are large and long-lived air-breathing animals that regularly visit the same sites near the coast, they are excellent indicators or sentinels of the health of an ecosystem.

Sea turtles have been threatened by an epidemic of fibropapillomatosis (FP – tumors of skin involving epidermis, dermis and other epithelial tissues) since the mid 1980s. These debilitating tumors are suspected of having a viral etiology. Populations of turtles exposed to agricultural runoff, pollution, HABs or warm water temperatures have been shown to have an increased risk of infection.

FP is a disease characterized by multiple cutaneous masses ranging from 0.1 to more than 30 cm in diameter that has primarily affected green turtles (*Chelonia mydas*), although the condition has been observed in other species including loggerhead (*Caretta caretta*), olive ridley (*Lepidochelys olivacea*), Kemp's ridley (*L. kempii*) and flatback (*Natator depressus*) turtles. The disease has a worldwide circumtropical distribution and has been observed in all major oceans. Where present, prevalence of the disease varies among locations, ranging from as low as 1% to as high as 90%. Although several viruses have been identified associated with the tumors, including several herpesviruses, a retrovirus and a papillomavirus, the primary etiological agent remains to be isolated and identified.

The green turtle nesting population, found at French Frigate Shoals, NWHI, has increased since its protection 18 years ago. No population impacts caused by FP have been observed in the number of nesting females, with the highest season ever being recorded in 1997 (ca. 500 nests); however, less than 100 nests were recorded for 1998. A photograph taken in Kaneohe Bay in 1958 documented the first case of FP for the Hawaiian Islands. This turtle was released to the wild. Between 1989 and 1997, 581 green turtles were captured alive at this Bay. Mild to severe FP was reported in 44% of the turtles handled, of which 17% presented oral tumors. The annual prevalence of the disease has ranged from 42% to 65% with no consistent trend observed. Growth rates for turtles with severe FP were significantly slower than turtles free of FP (1.0 vs. 2.2 cm/year carapace length). To date, FP has not been shown as causing a big impact on the overall population. However, further research is necessary to elucidate the long-term impacts. FP in green turtles has served as an indicator of ocean health at several levels. Although reported since the late 1930s in Florida, it was not until the late 1980s that it reached epizootic

proportions in several sea turtle populations. Long-term studies have shown that pelagic turtles recruiting to near shore environments are free of the disease. After exposure to these benthic ecosystems, FP manifests itself with primary growths in the corner of the eyes spreading to other epithelial tissues. Field observations support that the prevalence of the disease is associated with heavily polluted coastal areas, areas of high human density, agricultural runoff, and/or biotoxin-producing algae. Marine turtles can serve as excellent sentinels of ecosystem health in these benthic environments. FP can possibly be used as an indicator but correlations with physical and chemical characteristics of water and other factors need to be made [115]. Further research in identifying the etiologic agent and its association with other environmental variables can provide sufficient parameters to measure the health of coastal marine ecosystems, which serve not only as ecotourism spots but also as primary feeding areas for sea turtles.

One Ocean, One Health

The idea of the combined health of people, wildlife, and ecosystems – one health – is emerging from this increasingly apparent but still largely overlooked web of linkages. Symptoms of marine ecosystem distress due to nutrient loading with potential contributions of anthropogenic global climate change are associated with the frequency and intensity of HABs and associated toxicity for marine mammals and humans. Many populations of marine animals, marine birds, and sea turtles are exposed to pollutants from agricultural runoff, human sewage, and pathogens of terrestrial origin best described as pathogen pollution [116]. The following example involving a penguin, a pilchard, and a herpesvirus depicts how the terrestrial and aquatic environments are so delicately interconnected.

The Australian pilchard (*Sardinops sagax*) is a schooling fish related to herring that navigates temperate waters in Australia and New Zealand. Australia is also the range for the smallest and more primitive species of penguin referred to as the little blue or fairy penguin (*Eudyptula minor*) which inhabits the beaches of Western Victoria, Australia, Tasmania, and New Zealand. Although they can swim for long distances, *E. minor* do not exhibit the long migrations of Antarctic species. These penguins main food source is the pilchard. A great mass mortality of pilchard with epithelial lesions of the gills that greatly compromised respiratory and osmotic regulation was documented during 1995 off Western Australia. The spread of disease mortality for these animals was 30 km day^{-1} and after a thorough diagnostic investigation, one consistent finding was the presence of novel herpesvirus inclusions in the gills of infected pilchard [117]. The initial introduction of this herpesvirus is currently unknown. Shortly after, little blue penguins on Phillip and St. Kilda islands began experiencing great mortality of adult (86%) and first year birds (14%) with starvation and intestinal parasitism as the only consistent necropsy finding among 1,926 animals [118]. During the subsequent breeding season 1995–1996 these same birds delayed nesting season by 2 weeks and had a decreased chick fledged rate of 0.3 as compared with the mean of 1.0, and researchers concluded increased mortality and subsequent decreased reproduction were associated with the pilchard mortality [118]. Although the origin of the herpes virus is unknown, this example may very well exhibit the devastating consequences of novel pathogens and/or disease-translocation across geographic boundaries can have on multiple trophic levels [119].

Your Everyday Green Choices

Estimates show that marine litter is now 60–80% plastic, and that amount can reach 90% in certain areas. Plastic degrades slowly. Estimates for plastic bag degradation range from 500 to 1,000 years or even longer. Plastic pieces outnumber sea life 6:1 and there are expansive "garbage patches" of broken up plastics in both the Pacific and Atlantic Oceans (see http://marinedebris.noaa.gov/info/patch.html).

- Do your bit to minimize your impact on ocean pollution. Always remember the 3 Rs: Reduce, Reuse and Recycle. *Know what you are buying and how to recycle!!*
- Be a wise consumer. Support companies that are environmentally conscious. Buy products that minimize use of plastic or use degradable materials.
- Consumers choosing to buy sustainably sourced seafood and avoiding threatened species, i.e., Sea Food Watch App for smart phones.

- Follow the National seafood and sushi watch cards or consumer choice cards.
- Put pressure on governments and regulatory bodies to limit fishing subsidies and tighten regulations on industrial, agricultural and domestic pollution.
- Support research projects aimed at understanding pollution better and finding ways to reduce the amount of pollution in our oceans.
- Help support the establishment and expansion of Marine Protection Areas (MPAs). Presently, 1% of the oceans are MPAs.
- Websites for green options and choices: Blueocean.org; Fold-pak.com; Livingoceans.org; Montereybayaquarium.org; Oceanconservancy.org; Ocenaleadership.org; Seakeepers.org; Seathos.org; Sustainablesushi.net

Future Directions

Not all changes in fisheries can be simply ascribed to overfishing or environmental destruction; for example, the non-recovery of Pacific herring populations in Alaska has recently been attributed to natural mortality events caused by several infectious pathogens and subsequent disease, which has been illustrated using an age-structured assessment (ASA) model of disease and population abundance [120]. Box 1 illustrates how research advances when mitigating invasive and emerging pathogens such as *Myxobolus cerebralis* that causes whirling disease in many native species of salmonid fish. With the advent and increasing use of molecular diagnostics, infectious disease modeling, increasing globalization, and changing environmental conditions, marine health scientists will have to rely more heavily on epidemiology irrespective of specialty for the benefit of their clients as well as their patients. This chapter is far from comprehensive, but hopefully it serves to encourage readers, and especially our young readers, to think outside of routine way of life and to become involved with issues that demand a rapid response from consumption to recycling, from advocacy to policy change. Given the vast number of species and current exploitation of our aquatic resources many conservation issues have not been included but are equally relevant to conservation of the ocean, such as the exploitation of sharks and rays in finning fisheries,

Box 1. Whirling Disease: Problems and Solutions

Though speculative, the myxozoan parasite *Myxobolus cerebralis*, likely reached North America in the 1950s with frozen rainbow trout or imported brown trout from Europe [55, 121]. The first recorded epizootic in North America was among brook trout at a hatchery in Pennsylvania, USA. Subsequent episodes were reported in numerous other eastern state trout hatcheries, frequently among rainbow trout, one of the more susceptible species of salmonids [55]. Under conditions of high infectivity, whirling disease may induce severe cranial and spinal deformations and death as parasite stages feed upon and destroy skeletal cartilage prior to bone formation in young fish [122]. The myxospore stages of *M. cerebralis* in the skeletal elements of chronically infected trout may not result in the blackened tail and erratic swimming characteristic of acute disease. If the spores are not detected, the parasite will spread to new geographic regions with the transport of hatchery fish for stocking in rivers and streams for the sport fishery. This mode of parasite movement has facilitated the spread of the parasite to over 25 states in the USA, including most profoundly wild trout in the intermountain west (e.g., Colorado, Montana) where large scale population declines, particularly among rainbow trout have destroyed once highly prized sport fisheries [123, 124]. The two-host life cycle of *M. cerebralis*, which also includes the oligochaete *Tubifex tubifex*, has added to the complexity associated with the control and management of whirling disease. However, a combination of improved diagnostic procedures for parasite detection, in both fish and oligochaetes, and new management procedures in aquaculture are improving the ability to control whirling disease. The advent and now widespread application of PCR can detect the pathogen among fish with no clinical signs of disease, thus preventing the inadvertent movement of infected fish [125]. Improved sanitation in trout hatcheries using both treatments of the water supply with ultraviolet irradiation and several common disinfectants for ponds and equipment including transport vehicles has further reduced the spread of the parasite [126, 127]. Finally, the discovery and exploitation of rainbow trout strains resistant to whirling disease has provided a powerful

management approach to significantly reducing and perhaps eliminating whirling disease from certain hatchery environments and ideally from selected wild trout sport fisheries [128, 129]. The most broadly exploited whirling disease resistant rainbow trout strain is the product of 120 years of selection in a commercial hatchery in Europe. This strain is now being reared in state and commercial fish hatcheries in the USA. It is also being bred with wild trout with the aim to restore selected wild populations of rainbow trout in Colorado.

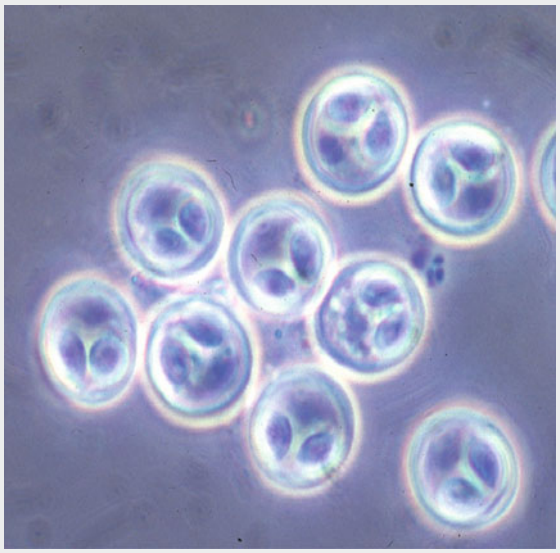

Terminal stage of *Myxobulus cerebralis* found in salmonid fish

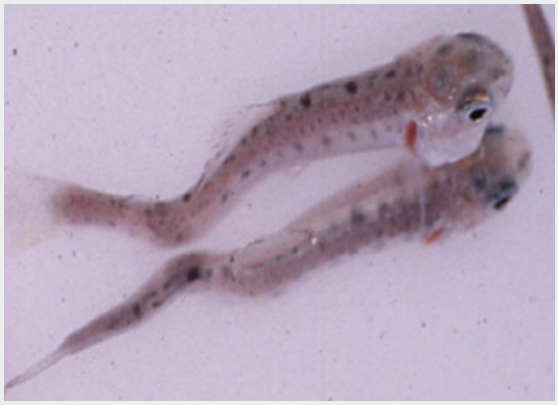

Rainbow trout 2.5 mo post infection showing darker and deformed tail, deformed gill covers and cranium – inability to swim and eat lead to death.

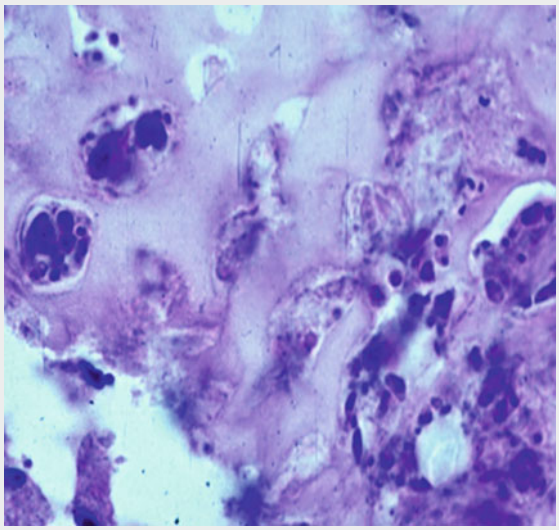

Histopathology section stained with H & E showing trophozoites actively destroying cartilage in the young trout skeleton.

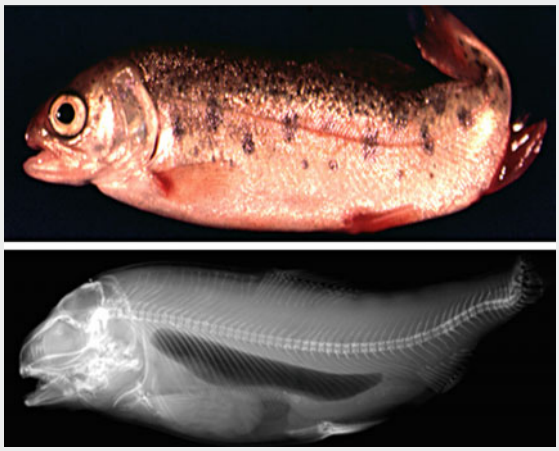

A rainbow trout with chronic deformities caused by whirling disease with a corresponding right lateral radiograph illustrating spinal and skull deformities.

invertebrate aquaculture production, and coral reef conservation.

The conservation of biodiversity in the ocean is becoming increasingly complex because of the intimate role that water has with conserving our terrestrial environs. The vastness of the aquatic world should not be looked at with trepidation, but rather with

excitement for the vast wealth of knowledge it has yet to bestow on us. Although the challenges presented are great, the ocean has been forgiving to anthropogenic transgressions and there is a need to continue striving to leave a smaller wake and help others follow by example.

Acknowledgments

E.P. Weber III wants to thank Dr. Bryon Jacoby for all his patience during the drafting, rewriting, and editing of this chapter and he thanks Dr. Ronald Hedrick for assistance with the whirling disease section and providing images. Dr Hedrick has led Fish Health at the University of California School of Veterinary Medicine in Davis over the last 30 years and has contributed to nearly 300 publications related to Aquatic Animal Health. Ron is a great friend, colleague, and mentor. We are most grateful to H.M. Smith, S. Sgroi and M. DeRario for their thoughtful input and comments for lightening it our scientific jargon up to an enjoyable reading for our K-12 public.

Bibliography

1. Colborn T, Dumanoski D, Meyers JP (1996) Our stolen future. Dutton, New York
2. Epstein PR (1993) Algal blooms in the spread and persistence of cholera. Biosystems 31:209–221
3. McMichael AJ, Bolin B, Costanza R, Daily GC, Folke C, Lindahl-Kiessling K, Lindgren B, Niklasson E (1999) Globalization and the sustainability of human health: an ecological perspective. Bioscience 49:205–210
4. Estes JA, Duggins DO (1995) Sea otters and kelp forests in Alaska: generality and variation in a community ecological paradigm. Ecol Monogr 65:75–100
5. Epstein PR (1999) Climate and health. Science 285: 347–348
6. Bejarano AC, Van Dolah FM, Gulland FMD, Rowles TK, Schwacke LH (2008) Production and toxicity of the marine biotoxin domoic acid and its effects on wildlife: a review. Human Ecol Risk Assess 14:544–567
7. Weber ES (2012) Emerging infectious diseases in fisheries and aquaculture. In: Aguirre AA, Ostfeld RS, Daszak P (eds) New directions in conservation medicine: applied cases of ecological health. Oxford University Press, New York
8. Burkholder JM, Glasgow HB Jr (1995) Interactions of a toxic estuarine dinoflaglellate with microbial predators and prey. Arch Protistenk 145:177–188
9. Meffe G (1999) Conservation medicine. Conserv Biol 13:953–954
10. Aguirre AA, Ostfeld RS, Tabor GM, House CA, Pearl MC (eds) (2002) Conservation medicine: ecological health in practice. Oxford University Press, New York, 407 pp
11. Aguirre AA, Ostfeld RS, Daszak P (eds) (2012) New directions in conservation medicine: applied cases of ecological health. Oxford University Press, New York
12. Tabor GM, Ostfeld RS, Poss M, Dobson AP, Aguirre AA (2001) Conservation biology and the health sciences: defining the research priorities of conservation medicine. In: Soulé ME, Orians GH (eds) Research priorities in conservation biology, 2nd edn. Island Press, Washington, DC, pp 165–173
13. Jones KE, Patel N, Levy M, Storeygard A, Balk D, Gittleman JL, Daszak P (2008) Global trends in emerging infectious diseases. Nature 451:990–994
14. Milligan SR, Holt WV, Lloyd R (2009) Impacts of climate change and environmental factors on reproduction and development in wildlife. Phil Trans R Soc 364:3313–3319
15. Gore A (2010) Disrupting chemicals from basic research to clinical practice. Humana Press, Totowa, 349 pp
16. Rogers AD, Laffoley Dd'A (2011) International earth system expert workshop on ocean stresses and impacts. Summary report. IPSO, Oxford, 18 pp
17. Suttle CA (2005) Viruses in the sea. Nature 437:356–361
18. Weinbauer MG (2004) Ecology of prokaryotic viruses. FEMS Microbiol Rev 28:127–181
19. Venter JC, Remington K et al (2004) Environmental genome shotgun sequencing of the Sargasso sea. Science 304(5667):66–74
20. Eschmeyer WN (ed) Catalog of fishes electronic version (25 Oct 2010). http://research.calacademy.org/ichthyology/catalog/fishcatmain.asp. Accessed 12 Nov 2010
21. Pauly D, Christensen V, Dalsgaard J, Froese R, Torres F (1998) Fishing down marine food webs. Science 279:860–863
22. Myers RA, Worm B (2003) Rapid worldwide depletion of predatory fish communities. Nature 423:280–283
23. Food and Agricultural Organization Aquaculture Production Statistics 1998–2007 (Food and Agricultural Organization, Rome, 2008). http://www.fao.org/fishery/statistics/programme/3,2,1/en. Accessed 15 June 2010
24. Folke C (1988) Energy economy of salmon aquaculture in the Baltic Sea. J Environ Manage 12:525–537
25. Tacon AGJ (2005) Salmon aquaculture dialogue: status of information on salmon aquaculture feed and the environment. Int Aquafeed 8:22–37
26. Naylor RL, Goldberg RJ, Primavera JH et al (2000) Effects of aquaculture on World food supplies. Nature 405:1017–1024
27. Tacon AGJ, Metian M (2009) Fishing for aquaculture: nonfood use of small pelagic forage fish, a global perspective. Rev Fish Sci 17:305–317
28. Naylor RL et al (2009) Feeding aquaculture in an era of finite resources. Proc Natl Acad Sci USA 106:15103–15110
29. Takagi S, Murata H, Goto T, Ichiki T, Munasinghe DMS, Endo M, Matsumoto T, Sakurai A, Hatate H, Yoshida T, Sakai T,

Yamashita H, Ukawa M, Kuramoto T (2005) The green liver syndrome is caused by taurine deficiency in yellowtail, *Seriolaquinque radiata* fed diets without fishmeal. Aquac Sci 53:279–290
30. Dierberg FE, Kiattisimkul W (1995) Issues, impacts, and implications of shrimp aquaculture in Thailand. J Environ Manage 20(5):649–666
31. Dewalt BR, Vergne P, Hardin M (1996) Shrimp aquaculture development and the environment: people, mangroves and fisheries on the Gulf of Fonseca, Honduras. World Development 24(7):1193–1208
32. Kautsky N, Ronnback P, Tedengren M, Troell M (2000) Ecosystem perspectives on management of disease in shrimp pond farming. Aquaculture 191(1–3):145–161
33. Primavera JH (1997) Socioeconomic impacts of shrimp culture. Aquac Res 28:815–827
34. Beveridge MCM, Ross LG, Kelly LA (1994) Aquaculture and biodiversity. Ambio 23:497–502
35. Diana JS (2009) Aquaculture production and biodiversity conservation. Bioscience 59:27–38
36. Bondad-Reantaso MG, Subasinghe RP, Arthur JR, Ogawa K, Chinabut S, Adlard R, Tan Z, Shariff M (2005) Disease and health management in Asian aquaculture. Vet Parasitol 132:249–272
37. Godfray HCJ, Beddington JR, Crute IR, Haddad L, Lawrence D, Muir JF, Pretty J, Robinson S, Thomas SM, Toulmin C (2010) Food security: the challenge of feeding 9 billion people. Science 327:812–818
38. Georgiadis MP, Gardner IA, Hedrick RP (2001) The role of epidemiology in the prevention, diagnosis, and control of infectious diseases of fish. Prev Vet Med 48:287–302
39. Gulland FMD, Hall A (2007) Is marine mammal health deteriorating? Trends in the global reporting of marine mammal disease. Ecohealth 4:135–150
40. Ward JC, Lafferty KD (2004) The elusive baseline of marine disease: are diseases in ocean ecosystems increasing? PLoS Biol 2:542–547
41. Hedrick RP, McDowell T, Groff J (1987) Mycobacteriosis in cultured striped bass from California. J Wildl Dis 23(3):391–395
42. Kane A, Stine CB, Hungerford L et al (2007) Mycobacteria as environmental portent in Chesapeake Bay fish species. Emerg Infect Dis 13(2):329–331, www.cdc.gov/eid
43. Stine CB, Jacobs JM, Rhodes MR et al (2009) Expanded range and new host species of *Mycobacterium shottsii* and *M. pseudoshottsii*. J Aquat Anim Health 21:179–183
44. Lovell SJ, Stone SF, Fernandez L (2006) The economic impacts of aquatic invasive species: a review of the literature. Agric Resour Econ Rev 35(1):195–208
45. McNeely JA, Schutyser F (2003) Invasive species: a global concern bubbling to the surface. In: International conference on the impact of global environmental problems on continental and coastal marine waters. Geneva, Switzerland, 16–18 July 2003, pp 1–14
46. Aquatic Nuisance Species (ANS) task force. http://www.anstaskforce.gov/default.php Accessed 30 March2010. Northeast Aquatic Nuisance Species (NEANS) Panel. http://www.northeastans.org Accessed 15 Dec 2010
47. Njiru M, Nzungi P, Getabu A, Wakwabi E, Othina A, Jembe T, Wekesa S (2007) Are fisheries management, measures in Lake Victoria successful? The case of Nile perch and Nile tilapia fishery. African J Ecol 45:315–323
48. Johnson LE, Padilla DK (1996) Geographic spread of exotic species: ecological lessons and opportunities from the invasion of the zebra mussel Dreissena polymorpha. Biol Conserv 78:23–33
49. Morris JA Jr, Akins JL, Barse A et al (2008) Biology and ecology of the invasive lionfishes, *Pterois miles* and *Pterois volitants*. In: Proceedings of the 61st Gulf and Caribbean Fisheries Institute. Gosier, Goudeloupe, French West Indies, 10–14 Nov 2008, pp 1–6
50. Fisher MC, Garner TWJ (2007) The relationship between the emergence of *Batrachochytrium dendrobatidis*, the international trade in amphibians and introduced amphibian species. Fungal Biol Rev 21:2–9
51. Tillitt DE, Zajicek JL, Brown SB et al (2005) Thiamine and thiaminase status in forage fish of salmonines from Lake Michigan. J Aquat Anim Health 17:13–25
52. Schoeb TR, Heaton-Jones TG, Clemmons RM et al (2002) Clinical and necropsy findings associated with increased mortality among American alligators of Lake Griffin, Florida. J Wildl Dis 38(2):320–337
53. Lumsden JS, Morrison B, Yason C, Russell S, Young K, Yazdanpanah A, Huber P, Al-Hussinee L, Stone D, Way K (2007) Mortality event in freshwater drum *Aplodinotus grunniens* from Lake Ontario, Canada, associated with viral haemorrhagic septicemia virus, Type IV. Dis Aquat Organ 76:99–111
54. Wilde SB, Murphy TM, Hope CP et al (2005) Avian vacuolar myelinopathy linked to exotic aquatic plants and a novel cyanobacterial species. Environ Toxicol 20(3):348–353
55. Hoffman GL (1990) *Myxobolus cerebralis*, a worldwide cause of salmonid whirling disease. J Aquat Anim Health 2:30–37
56. Malmberg G (1957) *Om förekomsten av Gyrodactylus påsvenska fiskar. – Skr. söd. Sver. Fisk För. Årsskr.*1956: 19–76. (In Norwegian, English summary)
57. Needler AWH, Logie RR (1947) Serious mortalities in Prince Edward Island oysters caused by a contagious disease. Transcr R Soc Canada, Ser III 41(V):73–89
58. Pronin NM, Selgeby JH, Litvinov SV, Pronina SV (1998) Comparative ecology and parasite fauna of exotic invaders in the great lakes of the world: amur sleeper (*Percottus glehni*) in Lake Baikal and ruffe (*Gymnocephalus cernuus*) in Lake Superior. Siberian J Ecol 5(5):397–406 (In Russian)
59. Elston RA, Farley CA, Kent ML (1986) Occurrence and signicance of bonamiasis in European flat oysters *Ostrea edulis* in North America. Dis Aquat Organ 2:49–54
60. Friedman CS, McDowell T, Groff JM, Hollibaugh JT, Manzer D, Hedrick RP (1989) Presence of *Bonamia ostreae* among populations of the European flat oyster, *Ostrea edulis* Linne, in California, USA. J Shellfish Res 8:133–137

61. Friedman CS, Perkins FO (1994) Range extension of *Bonamia ostreae* to Maine, USA. J Invertebr Pathol 64:179–181
62. Marty GD, Bower SM, Clarke KR, Meyer G, Lowe G, Osborn AL, Chow EP, Hannah H, Byrne S, Sojonky K, Robinson JH (2006) Histopathology and a real-time PCR assay for detectionof *Bonamia ostreae* in *Ostrea edulis* cultured in western Canada. Aquaculture 261:33–42
63. Crowl TA, Crist TO, Parmenter RR et al (2008) The spread of invasive species and infectious disease as drivers of ecosystem change. Front Ecol Environ 6(5):238–246
64. Nyaoke A, Weber ES, Innis C et al (2009) Disseminated phaeohyphomycosis in weedy seadragons (*Phyllopteryxtae niolatus*) and leafy seadragons (*Phycodurus eques*) caused by species of Exophiala, including a novel species. J Vet Diagn Investig 21(1):69–79
65. Whittington RJ, Chong R (2007) Global trade in ornamental fish from an Australian perspective: the case for revised import risk analysis and management strategies. Prev Vet Med 81:92–116
66. Levings RS, Lightfoot D, Hall RM, Djordjevic SP (2006) Aquariums as reservoirs for multidrug-resistant *Salmonella paratyphi* B. Emerg Infect Dis 12(3):507–510 www.cdc.gov/eid. (Accessed on 21 May 2010)
67. Dentler JL (1993) Noah's farce: the regulation and control of exotic fish and wildlife. University of Puget Sound Law Review 17:192–242
68. Andrews C (1990) The ornamental fish trade and fish conservation. J Fish Biol 37:53–59
69. Helfman GS (2007) Fish conservation: a guide to understanding and restoring global aquatic biodiversity and fishery resources. Island Press, Chicago
70. Smith KF, Behrens MD, Schloegel LM, Marano N, Burgiel S, Daszak P (2009) Reducing the risks of the wildlife trade. Science 324:594–595
71. Food and Agricultural Organization Aquaculture Production Statistics 2010 (Food and Agricultural Organization, Rome, 2010). State of World Fisheries and Aquaculture 2010. http://www.fao.org/docrep/013/i1820e/i1820e.pdf. Accessed 15 June 2011
72. Galvez R, Therese GH, Bautista C, Tungpalan MT (1989) Sociocultural dynamics of blast fishing and sodium cyanide fishing in two fishing villages in the Lingayen Gulf area. 43–62. In: Silvester G, Miclat E, Chua TE (eds) Towards sustainable development of the resources of Lingayen Gulf, Philippines. ICLARM conference proceeding number 17, 200 pp
73. Vagelli AA (2004) Significant increase in survival of captive-bred juvenile Banggai cardinalfish, *Pterapogon kauderni*, with an essential fatty acid enriched diet. J World Aquac Soc 35(1):61–69
74. Lunn KE, Moreau MA (2004) Unmonitored trade in marine ornamental fishes: the case of Indonesia's Banggai cardinalfish (*Pterapogon kauderni*). Coral Reefs 23:344–351
75. Ziemann DA (2001) The potential for the restoration of marine ornamental fish populations through hatchery releases. Aquar Sci Conserv 3:107–111
76. Wilkinson C (2004) Status of coral reefs of the world volumes 1 & 2. Global reef monitoring network. Australian Insititute of Science. http://www.gcrmn.org/status2004.aspx. Accessed 1 May 2011
77. Hoegh-Guldberg O et al (2007) Coral reefs under rapid climate change and ocean acidification. Science 318:1737–1742
78. Goldberg J, Wilkinson C (2004) Global threats to coral reefs: coral bleaching, global climate change, disease, predator plagues, and invasive species. In: Wilkinson C (ed) Status of coral reefs of the world: 2004, vol 1. Australian Institute of Marine Science, Townsville, 301 pp reportscr2004v1-01, pp 68–92
79. Danovaro R, Bongiorni L, Corninaldesi C, Giovannelli D, Damiani E, Astolfi P, Greci L, Pusceddu A (2008) Sunscreens cause coral bleaching by promoting viral infections. Environ Health Perspect 116:441–447
80. Monod G, Devaux A, Riviere JL (1988) Effects of chemical pollution on the activities of hepatic xenobiotic metabolizing enzymes in fish from the Rhone River. Sci Total Environ 73:189–201
81. VanLeeuwen SPJ, van Velzen MJM, Swart CP et al (2009) Halogenated contaminants in farmed salmon, trout, tilapia, pangasius, and shrimp. Environ Sci Technol 43:4009–4015
82. Shaw SD, Brenner D, Bourakovsky A et al (2005) PCBs, dioxin-like PCBs and organochlorine pesticides in farmed salmon (*Salmosalar*) from Maine and eastern Canada. Organohalogen Compounds 67:1571–1576
83. Shaw SD, Brenner D, Berger ML et al (2006) PCBs, PCDD/Fs, and organochlorine pesticides in farmed Atlantic salmon from Maine, eastern Canada, and Norway, and wild salmon from Alaska. Environ Sci Technol 40:5347–5354
84. Shaw SD, Brenner D, Berger ML et al (2007) PCBs, PCDD/Fs, and organochlorine pesticides in farmed Atlantic salmon from Maine, eastern Canada, and Norway, and wild salmon from Alaska (comment/correction). Environ Sci Technol 41:4180
85. Hites RA, Foran JA, Carpenter DO et al (2004) Global assessment of organic contaminants in farmed salmon. Science 303:226–229
86. Ikonomou MG et al (2007) Flesh quality of market-size farmed and wild British Columbia salmon. Environ Sci Technol 41:437–443
87. Knobeloch L, Turyk M, Imm P, Schrank C, Anderson H (2008) Temporal changes in PCB and DDE levels among a cohort of frequent and infrequent consumers of Great Lakes sportfish. Environ Res 109:66–72
88. Khan RA (1990) Parasitism in marine fish after chronic exposure to petroleum hydrocarbons in the laboratory and to the Exxon Valdez Oil Spill. Bull Environ Contam Toxicol 44:759–763
89. Evans DH (1987) The fish gill: site of action and model for toxic effects of environmental pollutants. Environ Health Perspect 71:47–58
90. Gagnon MM, Holdway DA (1999) Metabolic enzyme activities in fish gills as biomarkers of exposure to petroleum hydrocarbons. Ecotoxicol Environ Saf 44:92–99

91. Conover MR, Vest JL (2009) Concentrations of selenium and mercury in eared grebes (*Podiceps nigricollis*) from Utah's Great Salt Lake, USA. Environ Toxicol Chem 28(6):1319–1323
92. Chalmers AT, Argue DM, Gay DA et al (2010). Mercury trends in fish from rivers and lakes in the United States, 1969–2005. Environmental Monitoring and Assessment; published online 10 June 2010. Accessed 05 July 2010
93. Mills LJ, Chichester C (2005) Review of evidence: are endocrine-disrupting chemicals in the aquatic environment impacting fish populations? Sci Total Environ 343:1–34
94. Jobling S, Nolan M, Tyler CR et al (1998) Widespread sexual disruption in wild fish. Environ Sci Technol 32:2498–2506
95. Costanzo SD, Murby J, Bates J (2005) Ecosystem response to antibiotics entering the aquatic environment. Mar Pollut Bull 51:218–223
96. Christian T, Schneider RJ, Farber HA (2003) Determination of antibiotic residues in manure, soil, and surface waters. Acta Hydrochimicaethydrobiologica 31(1):36–44
97. Hirsch R, Ternes T, Haberer K, Kratz KL (1999) Occurrence of antibiotics in the aquatic environment. Sci Total Environ 225(1–2):109–118
98. Boxall ABA, Fogg LA, Blackwell PA et al (2004) Veterinary medicines in the environment. Rev Environ Contam Toxicol 180:1–91
99. Kemper N (2008) Veterinary antibiotics in the aquatic and terrestrial environment. Ecol Indic 8:1–13
100. Schmidt A, Bruun MS, Dalsgaard I et al (2000) Occurrence of antimicrobial resistance in fish-pathogenic and environmental bacteria associated with four Danish rainbow trout farms. Appl Environ Microbiol 66(11):4908–4915
101. Rhodes G, Huys G, Swings J et al (2000) Distribution of oxytetracycline resistance plasmids between aeromonads in hospital and aquaculture environments: implications of TN1 721 in dissemination of the tetracycline resistance determinant Tet A. Appl Environ Microbiol 66(9):3883–3890
102. Musto J, Kirk M, Lightfoot D et al (2006) Multi-drug resistant *Salmonella java* infections acquired from tropical fish aquariums, Australia, 2003–04. Commun Dis Intell 30:222–227
103. Weber JT, Mintz ED, Cañizareset R (1994) Epidemic cholera in Ecuador: multi-drug resistance and transmission by water and seafood. Epidemiol Infect 112:1–11
104. Rahel FJ, Olden JD (2008) Assessing the effects of climate change on aquatic invasive species. Conserv Biol 22(3):521–533
105. Riley SC, Munkittrick KR, Evans AN, Krueger CC (2008) Understanding the ecology of disease in Great Lakes fish populations. Aquat Ecosystem Health and Management 11(3):321–334
106. Bark S, McGregor D (2001) The first occurrence of lactococcosis in farmed trout in England. Trout News 31:9–11
107. Wahli T, Knuesel R, Bernet D, Segner H, Pugnovkin D, Burkhardt-Holm P, Escher M, Schmidt-Posthaus H (2002) Proliferative kidney disease in Switzerland: current state of knowledge. J Fish Dis 25:491–500
108. Sherman BH, Epstein PR (2001) Past anomalies as a diagnostic tool for evaluating multiple marine ecological disturbance. Human Ecol Risk Assess 7:1493–1517
109. Sherman BH (2000) Marine disturbance, a survey of morbidity, mortality and disease events. Mar Pollut Bull 41:232–254
110. Aguirre AA, Tabor GM (2004) Marine vertebrates as sentinels of marine ecosystem health. Ecohealth 1:236–238
111. Tabor GM, Aguirre AA (2004) Ecosystem health and sentinel species: adding an ecological element to the proverbial "canary in the mineshaft". Ecohealth 1:226–228
112. Kittinger JN, Duin KN, Wilcox BA (2009) Commercial fishing, conservation and compatibility in the Northwestern Hawaiian Islands. Mar Policy. doi:10.1016/j.marpol.2009.06.007
113. Aguirre AA, Reif JS, Antonelis GA (1999) Hawaiian monk seal epidemiology plan: health assessment and disease status studies. U.S. Department of Commerce, NOAA Technical report NMFS NWFSC-280, 63 pp
114. Aguirre AA, Keefe TJ, Reif JS, Kashinsky L, Yochem P, Saliki JT, Stott JL, Goldstein T, Dubey JP, Braun R, Antonelis G (2007) Infectious disease monitoring of the endangered Hawaiian monk seal. J Wildl Dis 43:229–241
115. Aguirre AA, Lutz P (2004) Sea turtles as sentinels of marine ecosystem health: is fibropapillomatosis an indicator? Ecohealth 1:275–283
116. Daszak P, Cunningham AA, Hyatt AD (2000) Emerging infectious diseases of wildlife – threats to biodiversity and human health. Science 287:443–449
117. Whittington RJ, Jones JB, Hine PM, Hyatt AD (1997) Epizootic mortality in the pilchard *Sardinops sagax neopilchardus* in Australia and New Zealand in 1995. 1. Pathology and epizootiology. Dis Aquat Organ 28:1–16
118. Dann P, Norman FI, Cullen JM et al (2000) Mortality and breeding failure of little penguins, *Eudyptula minor*, in Victoria, 1995–6, following a widespread mortality of pilchard *Sardinops sagax*. Mar Freshw Res 51:355–362
119. Gaughan DJ (2002) Disease-translocation across geographic boundaries must be recognized as a risk even in the absence of disease identification: the case with Australian Sardinops. Rev Fish Biol Fisheries 11:113–123
120. Marty GD, Hulson P-JF, Miller SE, Quinn TJ II, Moffitt SD, Merizon RA (2010) Failure of population recovery in relation to disease in Pacific herring. Dis Aquat Organ 90:1–14
121. Bartholomew JL, Reno PW (2002) The history and dissemination of whirling disease, pp 3–24. In: Bartholomew JL, Wilson JC (eds) Whirling disease: reviews and current topics. American Fisheries Society, Symposium 29, Bethesda, Maryland
122. Halliday MM (1973) Studies of *Myxosoma cerebralis*, a parasite of salmonids. II. The development and pathology of *Myxosoma cerebralis* in experimentally infected rainbow trout (*Salmon gairdneri*) fry reared at different water temperatures. Nord Vet Med 25:349–358
123. Nehring RB, Walker PG (1996) Whirling disease in the wild: the new reality in the Intermountain West. Fisheries 21:28–30
124. Vincent ER (1996) Whirling disease and wild trout: the Montana experience. Fisheries 21:32–34

125. Andree K, Hedrick RP, MacConnell E (2002) A review of approaches to detect *Myxobolus cerebralis*, the cause of salmonid whirling disease, pp 197–212. In: Bartholomew JL, Wilson JC (eds) Whirling disease: reviews and current topics. American Fisheries Society, Symposium 29, Bethesda, Maryland
126. Hedrick RP, Petri B, McDowell TS, Mukkatira K, Sealey LJ (2007) Evaluation of a range of doses of ultraviolet irradiation to inactivate the waterborne actinospore stages of *Myxobolus cerebralis*. Dis Aquat Organ 74:113–118
127. Hedrick RP, McDowell TS, Mukkatira K, MacConnell E, Petri B (2008) Effects of freezing, drying, ultraviolet irradiation, chlorine and quaternary ammonium treatments on the infectivity of myxospores of *Myxobolus cerebralis* or *Tubifex tubifex*. J Aquat Anim Health 20:116–125
128. Hedrick RP, McDowell TS, Marty GD, Fosgate GT, Mukkatira K, Myklebust K, El-Matbouli M (2003) Susceptibility of two strains of rainbow trout (one with a suspected resistance to whirling disease) to *Myxobolus cerebralis* infection. Dis Aquat Organ 55:37–44
129. Schisler GS, Myklebust KA, Hedrick RP (2006) Inheritance of resistance to *Myxobolus cerebralis* among F1 generation crosses of whirling disease resistant and susceptible strains of rainbow trout. J Aquat Anim Health 18:109–115
130. McBride MP, Sims MA, Cooper RW, Nyaoke AC, Cullion C, Kiupel M, FrascaJr S, Forrester N, Weaver SC, Weber ES (2008) Eastern equine encephalitis in a captive harbor seal (*Phoca vitulina*). J Zoo Wildl Med 39(4):631–637
131. Boerner L, Necvis KR, Hinckley LS et al (2004) *Erysipelthrix*-septicemia in a little blue penguin (*Eudyptula minor*). J Vet Diagn Investig 16:145
132. Hedrick RP, Marty G, Nordhausen RW, Kebus M, Bercovier H, Eldar A (1999) A herpesvirus associated with mass mortality of juvenile and adult koi *Cyprinus carpio*. Fish Health Newsletter, Fish Health Section, American Fisheries Society 27:7
133. Kocan R, Hershberger P, Winton J (2004) Ichthyophoniasis: an emerging disease of Chinook salmon in the Yukon River. J Aquat Anim Health 16:58–72
134. Chinchar VG, Essbauer S, He JG et al (2005) Iridoviridae. In: Fauguet CM, Mayo MA, Maniloff J (eds) Virus taxonomy: 8th report of the international committee on the taxonomy of viruses. Elsevier, London, pp 163–175
135. McVicar AH (1997) Disease and parasite implications of the coexistence of wild and cultured Atlantic salmon populations. ICES J Mar Sci 54:1093–1103
136. Marty GD, Saksida SM, Quinn II TJ (2010) Relationship of farm salmon, sea lice, and wild salmon populations. Proceedings of the National Academy of Sciences of the United States of America for P Natl Acad Sci USA. doi: 10.1073/pnas.1009573108 PNAS December 28, 2010 107(52):22599–22604
137. Hedrick RP, Batts WN, Yun S et al (2003) Host and geographic range extensions of the North American strain of viral hemorrhagic septicemia virus. Dis Aquat Organ 55:211–220

Lodging Resistance in Cereals

Pete M. Berry
Sustainable Crop Management, ADAS UK Ltd, Malton, North Yorkshire, UK

Article Outline

Glossary
Definition of the Subject
Introduction
Impact of Lodging on Grain Yield and Quality
Mechanisms of Lodging
Methods for Controlling Lodging Risk
Future Directions
Bibliography

Glossary

Anchorage failure moment Anchorage failure at the point of failure. Also described as anchorage strength.

Base bending moment Wind-induced force acting on the base of the shoot or the anchorage system. Also described as leverage force.

Brackling Lodging resulting from buckling of the upper half of the stems.

Crop management Agronomic methods of growing crops.

Failure wind speed Wind speed at which a plant will lodge.

Hagberg falling number (HFN) Measure of bread making quality.

Lodging Permanent displacement of cereal stems from their vertical position.

Lodging-proof ideotype Plant dimensions required to achieve a lodging-return period of 25 years.

Necking Lodging resulting from buckling of the stem just below the ear.

Plant growth regulators – (PGRs) Chemical growth regulators that reduce the rate of stem extensions.

Root lodging Lodging resulting from failure of the anchorage system.

Stem failure moment Stem strength at the point of failure. Also described as stem strength.

Stem lodging Lodging resulting from buckling of the lower stems.

Definition of the Subject

Lodging is the process by which the shoots of small grained cereals are permanently displaced from their vertical stance. Lodging limits yield potential and reduces grower profits, but it is difficult to control because it is a complex process that is influenced by many factors including wind, rain, topography, soil type, previous crop, crop management, and disease. Significant progress was made during the 1950s, 1960s, and 1970s to reduce lodging risk by the introduction of semi-dwarf varieties. The reduced lodging risk of these shorter varieties enabled them to respond to greater amounts of fertilizers and this was a significant reason for the steady improvement in global cereal grain yields starting in the late 1960s. However lodging is still a major problem in many countries and there is an urgent need to improve lodging resistance to further increase the yield of cereal species.

Introduction

Lodging is the permanent displacement of cereal stems from their vertical position (Fig. 1) and usually only occurs after the ear or panicle has emerged. This can reduce yield by up to 80% and causes several knock-on effects including reduced grain quality, greater drying costs, and slower harvest. It is a problem that limits cereal productivity in both developed and developing countries.

Lodging Resistance in Cereals. Figure 1
Lodging in wheat

Lodging is a complicated phenomenon that is influenced by many factors including wind, rain, topography, soil type, previous crop, husbandry, and disease. It is frequently associated with conditions that promote plant growth such as an abundant supply of nutrients. Significant progress was made during the 1950s, 1960s, and 1970s to reduce lodging risk by the introduction of semi-dwarf varieties. These shorter varieties had a greater lodging resistance and could respond to greater amounts of fertilizers. For these reasons the introduction of semi-dwarf varieties was one of the most significant reasons for the steady improvement in grain yields starting in the late 1960s, which has resulted in cereal yields increasing by as much as 1 t ha^{-1} per decade in western Europe and 0.5 t ha^{-1} in many American and Asian countries [1]. The continued improvement in yields in some countries has been significantly aided by the use of plant growth regulators (PGRs) that further reduce crop height making cereals even more resistant to lodging. Four major types of PGRs have been introduced including chlormequat chloride during the mid-1960s, ethephon during the late 1980s, trinexapac-ethyl during the mid-1990s, and prohexadione-calcium in the 2000s. In France, Germany, and the UK, which have among the highest cereal yields in the world, PGRs are now applied to more than 70% of wheat area (W. Rademacher 2004, personal communication).

Dwarfing genes and PGRs have been very effective tools for reducing lodging risk and maintaining steady improvements in yield. However, they have not eradicated lodging and there is evidence that farmers will not be able to rely on these tools for further reductions in lodging risk in order to counter the escalating lodging risk resulting from continued yield increases. Several studies have shown that yield is reduced when crops are shortened too much [2–7]. The reduction in yield appears to be exacerbated by high temperatures or drought stress. Several of these studies indicate that the minimum crop height for optimum yield lies between 0.7 m and 1.0 m. Many modern varieties are already within this height range. While there is scope for further shortening with PGRs through sequential applications, pressure may be brought to bear to reduce their use because some PGRs leave residues in the grain [8]. It is therefore clear that new methods of improving lodging resistance in cereals must be developed.

During the 1990s and 2000s collaborative studies by biologists and engineers have elucidated the mechanisms of lodging in cereals [9]. Crucially it has been demonstrated that lodging may occur by two mechanisms: stem lodging and root lodging. These studies have culminated in models of the lodging process which help to understand how the plant interacts with its environment during the lodging process and identifies the most important plant traits that must be targeted to improve lodging resistance. Several studies have also explained how variety, sowing date, seed rate, nitrogen fertilizer, and PGRs affect lodging. This improved understanding offers the prospect of designing a lodging proof ideotype for cereals which may be achieved through a combination of crop management and plant breeding. This entry on lodging resistance in cereals describes (1) the impact that lodging in different cereal species has on crop yield and grain quality, (2) the mechanisms of the lodging process, (3) the effect of cultivar choice and crop management on lodging resistance, and (4) prospects for improving lodging resistance. This entry is intended to be a concise summary of the most important aspects of lodging resistance in cereals, and for a more comprehensive review readers are directed to Berry et al. [10].

Impact of Lodging on Grain Yield and Quality

Grain Yield

Lodging can reduce cereal yield by reducing the grain size and number or through reducing the amount of crop that can be recovered at harvest. This section deals only with physiological reductions in yield associated with lodging. The greatest lodging-induced reductions in grain yield occur when crops are lodged flat at anthesis or early on in grain filling. Yield reductions from this type of lodging have been reported to reduce yields of wheat by [11] 31–80% [12], barley by 28–65% [13–15], oats by 37% [16], and rice by 38% [17]. All of the above studies, apart from Easson et al. [12], artificially lodged the plants. This was achieved by growing the plants through wire netting and then moving the wires to effect lodging. This method has the advantage of lodging the crops at specific dates and at different angles, but may induce damage not normally incurred with natural lodging. Easson et al. [12] compared the yields of crops grown at high seed rate, which lodged naturally, with those at low seed rate, which experienced negligible lodging.

Smaller yield losses have been observed when the angle of lodging is less than 90° from the vertical. Lodging at 45° causes between one quarter and one half of the yield losses incurred from 80° lodging in wheat [18], barley [14], and oats [16]. Smaller yield losses also occur when lodging occurs at a later stage of development. Artificial lodging at the ear emergence, milk, soft dough, and hard dough stages reduced yield by 31%, 25%, 20%, and 12%, respectively [11]. Stapper and Fischer [19] supported these observations by showing that about 0.5% of the potential yield was lost for each day of the grain filling period that a crop was lodged flat. Crops that lodge before anthesis often have smaller yield losses than crops that lodge soon after anthesis [18]. This appears to be associated with the upper one of two internodes bending upward to partially re-erect the crop. Crops that lodge after anthesis have completed stem extension and are unable to re-erect themselves. In natural situations, the re-erected crops are very unstable and are usually re-lodged by unexceptional weather conditions [12].

Grain Quality

Artificial lodging has been observed to cause significant reductions in grain quality in terms of the bread making quality (measured as the Hagberg falling number [HFN]), individual grain weight, and the specific weight of the grain [10]. Lodging increases the likelihood of grain sprouting in the ear due to the more moist environment (Fig. 2) and this reduces HFN. Lodging induced during early grain filling reduced grain quality by reducing the HFN from 289 s to 114 s, reducing individual grain weight from 42.2 mg to 37.2 mg, and reducing specific weight from 70.3 kg/hl to 65.8 kg/hl. Lodging after early grain filling caused smaller effects on quality. A HFN of at least 250 s is required to produce good quality bread. Similar effects on grain weight and specific weight have also been observed in wheat [11, 20], barley [13, 21], and oats [22]. In the UK, the harvest year of 1992 was a severe lodging year with 16% of the wheat area lodged [23]. In this year the national average HFN fell from a 5-year average of 287 s to 254 s, thus significantly reducing the amount of bread making grain produced in this year.

Lodging Resistance in Cereals. Figure 2
Sprouting in a lodged wheat crop

Lodging Resistance in Cereals. Figure 3
Wheat plants leaning as a result of root lodging

Also in this year, the specific weight of wheat grains fell from 77 kg hl^{-1} to 73 kg hl^{-1} and the number of small grains (<2.0 mm) increased from 1.9% to 2.6% [24]. It is likely that at least a proportion of these effects were caused by the greater than usual lodging experienced in this country during this year.

Mechanisms of Lodging

Lodging can either occur through stem buckling (stem lodging) or displacement of the roots within the soil (root lodging) (Fig. 3). During stem lodging the roots are held firmly in a strong soil and the wind force buckles the stem. Stem lodging can occur due to buckling of the lower internodes. Buckling of the middle internodes is commonly known as "brackling" and is often observed in barley (Fig. 4) [25] and oats. Buckling of the peduncle just below the ear is known as "necking" and occurs most frequently in barley [26]. Root lodging becomes more likely when the anchorage strength is reduced by weak soil or poorly developed anchorage roots. Rainfall can reduce soil strength by several fold and has an important influence on the anchorage strength of cereals.

Very few observations have been reported of the lodging process as it occurs and conjecture exists as to whether stem lodging or root lodging predominates in cereals. Wheat and barley have been observed to root lodge [27, 28] and to stem lodge [25]. However, recently a quantitative understanding of root and shoot

Lodging Resistance in Cereals. Figure 4
Brackling in barley

lodging has been developed for wheat and barley showing that both types of lodging are possible depending on the circumstances of a particular crop [29, 30]. This has been confirmed in wheat by direct observations of both mechanisms occurring during wind-tunnel experiments on field-grown winter wheat [31].

The lodging models described by Baker et al. [29] and Berry et al. [30] calculate the wind-induced base bending moment of a shoot from plant characteristics

and meteorological data. The base bending moment is then compared to the failure moments (strength at the point of failure) of the stem base and of the anchorage system. Stem lodging is assumed to occur when the base bending moment of a single shoot exceeds the failure moment of the stem base. Root lodging is assumed when the base bending moment of all the shoots belonging to a single plant exceeds the failure moment of the anchorage system. The following sections describe current understanding about how the components of lodging (base bending moment, stem failure moment, and anchorage failure moment) may be calculated and what factors influence them.

Base Bending Moment

The wind-induced force acting on the upper sections of a shoot or plant results in a bending moment at the plant's base. This can be described as the shoot leverage. The coherent waving of cereal shoots, apparent even in light winds, provides evidence that cereal shoots are subjected to varying forces and illustrates the importance of including the shoot's motion in any calculation of the applied base bending moment. Baker [32] attempted to account for the dynamic nature of shoot movement by considering the forces that act on an idealized shoot and assuming that the shoot's movement could be modeled as damped harmonic oscillator. The theoretical modeling work described in [32] and [29], which was later validated in wind-tunnel experiments using field crops [31], showed that the wind-induced base bending moment of wheat could be calculated from a range of environmental and plant inputs. These include: the wind speed at crop height, the natural frequency of the shoot (rate at which it oscillates), the damping ratio of the shoot (which describes the rate at which oscillations die out), the height at center of gravity of the shoot, and the projected area and drag coefficient of the ear. These parameters can be used to estimate the bending moment at the base of the shoot for a shoot with a stiff stem such as wheat. Additional parameters are required to estimate the bending moment of more flexible stems such as for barley and include the flexural rigidity of the stem and its fresh weight. A method for calculating the bending moment of flexible stems is described in [30].

Anchorage Failure Moment

There is uncertainty about the exact mechanism of anchorage failure in cereals due to the obvious difficulty associated with observing the process in field conditions. Ennos [33] showed that anchorage failure of spring wheat involved bending of the crown roots and resistance to axial movement through the soil. Crook and Ennos [27] showed that the upper portions of the crown root system of winter wheat form a cone (Fig. 5) and anchorage failure occurred when the root-soil cone rotated at its windward edge, the soil inside the cone moved as a block and compressed the soil beneath. This idea supported earlier observations by Pinthus [34], who showed that a wider angle of root spread was related to greater resistance to root lodging. Easson et al. [35] suggested that winter wheat roots acted like ropes to withstand root lodging and that anchorage strength would therefore be a function of the tensile strength of the roots on the windward side of the plant.

The model developed by Crook and Ennos [27] has been tested and calibrated with field experiments on wheat [29] and on barley [30] (Fig. 6). These experiments showed that the anchorage strength was linearly related to the product of the diameter of the root cone cubed, the shear strength of the surrounding soil, and a constant specific to wheat or barley. The size of the

Lodging Resistance in Cereals. Figure 5
Upper portions of the root system of winter wheat

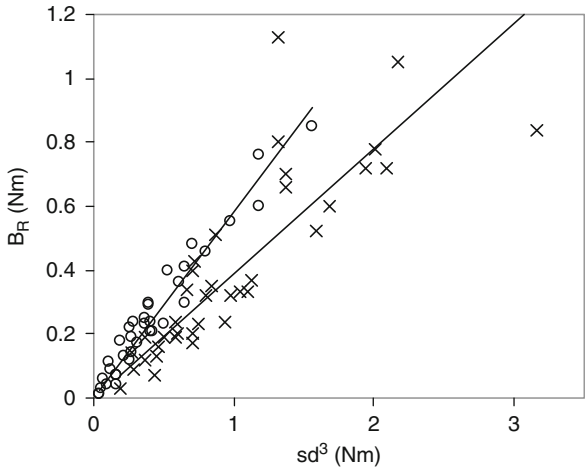

Lodging Resistance in Cereals. Figure 6
The product of soil shear strength (s) and root plate spread cubed (d^3) plotted against failure moment (B_R) for winter barley (o; y = 0.58x, R^2 = 0.95) and for winter wheat (5; y = 0.39x, R^2 = 0.69) (Adapted from [30])

root plate is identified by the parts of the crown roots that are surrounded by a rhizosheath. The rhizosheath is a dense mat of hairs that cover the upper sections of crown roots. These sections of roots have been shown to have an outer ring of lignified tissue in addition to the lignified central stele [27], which is why the rhizosheath can be used to estimate the length of root that provides anchorage.

The observation that anchorage strength was linearly related to the spread of the diameter of the root cone for both wheat and barley strongly suggests that both species have the same mechanism of anchorage failure first described by Crook and Ennos [27]. However, it was apparent that the constant factor was different between species with a value of 0.39–0.43 for wheat [29, 30] compared with 0.58 for barley demonstrating a greater anchorage strength for a given root plate spread for barley. This may have been caused by the greater number of stems per mm of root plate for barley compared with wheat. Up to 20 mm of the stem base is below ground, so it seems likely that a greater number of stems will increase the rotational resistance of the anchorage system.

A model of soil strength developed by Baker et al. [29] showed that variation in clay content, moisture content, and compaction that is normally found within farmer's fields could each be expected to alter the soil shear strength by several fold. This indicates that the state of the soil is likely to be of paramount importance for determining lodging given that it has been predicted in the anchorage model described above to be directly proportional to anchorage strength.

Stem Failure Moment Assuming that a typical stem can be considered to be analogous to a cylinder, Baker [32] showed that the stem failure moment (B_S) can be expressed as:

$$B_S = \frac{\sigma \pi a^3}{4}\left(1 - \left(\frac{a-t}{a}\right)^4\right)$$

where σ is the stem failure yield stress (material strength), a is the external radius of the stem, and t is the wall thickness. This formula assumes that the pith in the center of the stem does not contribute to the structural properties of the stem. Experiments by Neenan and Spencer-Smith [25] have shown that the stems of wheat and barley buckle at a certain critical ratio of radius of curvature to the outside diameter of the stem. Buckling was shown to occur suddenly with negligible amounts of plastic deformation. The Young's modulus of wheat and barley was shown to remain reasonably constant for a range of stem curvatures which indicates that negligible plastic deformation occurs and that the limit of proportionality between the applied stress and corresponding strain is seldom exceeded. It may therefore be concluded that stem lodging occurs abruptly and will result in complete structural failure of the stem.

Influence of Crop and Environmental Characteristics on Lodging Risk

Lodging is a complex process that involves several environmental and plant characteristics. Any assessment of the effect of individual characteristics on lodging risk must account for interrelationships between characteristics. To date the only study to have achieved this involves a sensitivity analysis of the lodging model of Baker et al. [29] and this is described in [9]. This study further developed the model of Baker et al. [29] to account for spatial non-uniformity between plants and temporal changes in plant structure during the growing season. A sensitivity analysis using this

model showed that the risk of stem lodging is influenced most by changes in stem diameter and the risk of root lodging is affected most by changes to the diameter of the root cone (also referred to as the spread of the root plate) (Fig. 7). In these analyses, the risk of lodging is measured in terms of the wind speed required to cause lodging, which is termed the "stem" or "root" "failure wind speed." The large effect on

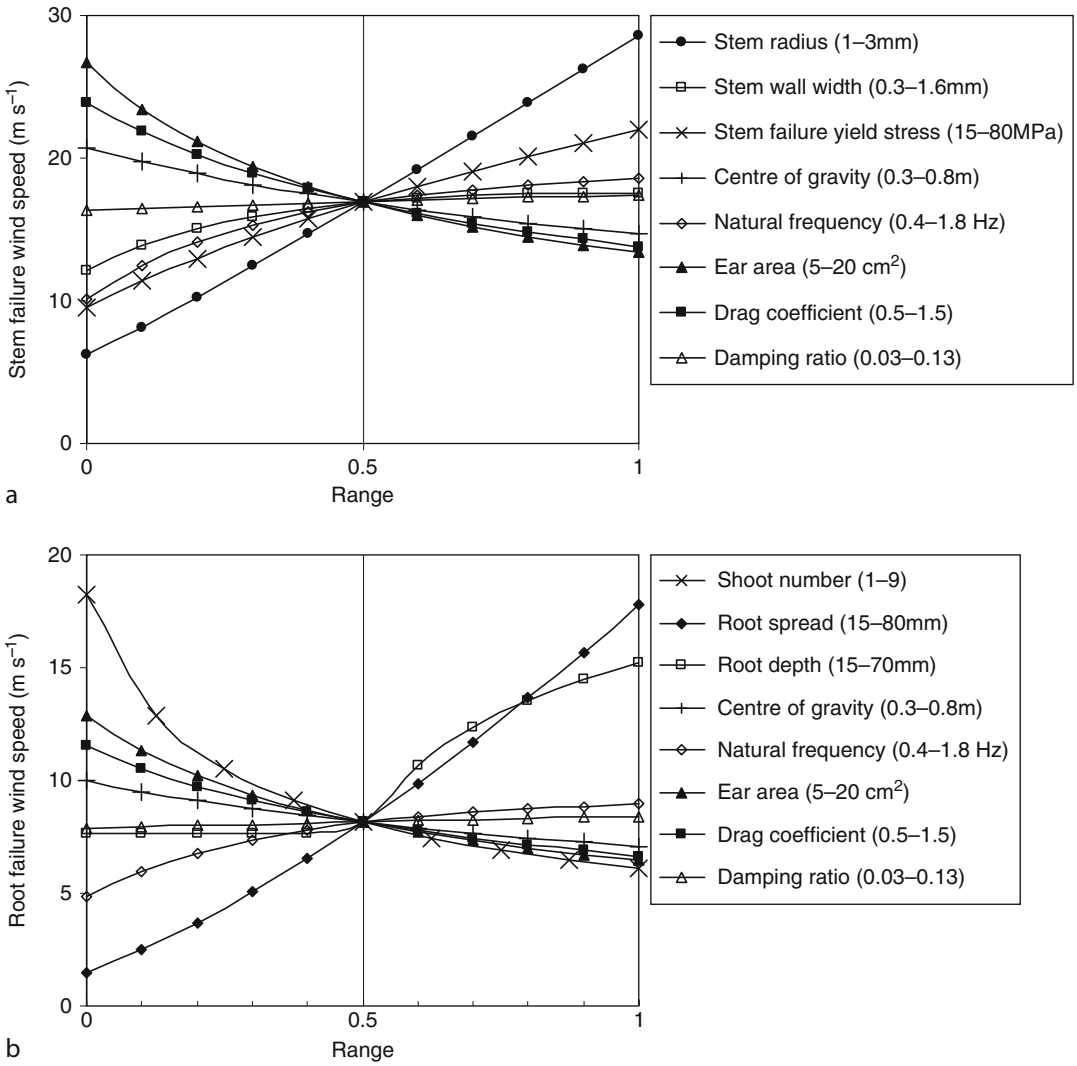

Lodging Resistance in Cereals. Figure 7

Failure wind speeds after 7 mm rain for (**a**) internode 1 and (**b**) anchorage. The ranges (0–1) are judged to represent the combined genetic and environmental range of each parameter within a high yielding wheat crop (Adapted from [9]). Stem radius – radius at the mid-point of the lowest internode; stem wall width – wall width at the mid-point of the lowest internode; stem failure yield stress – material strength of the stem wall of the bottom internode; center of gravity – height at center of gravity of the main shoot; natural frequency – rate at which the shoot oscillates; ear area – projected area of the ear; drag coefficient – resistance offered by the ear to wind; damping ratio – rate at which the shoot's oscillations stop; shoot number – number of fertile shoots per plant; root spread – diameter of the root plate defined by the thickened regions of the crown roots; root depth – depth of the root plate defined by the thickened regions of the crown roots

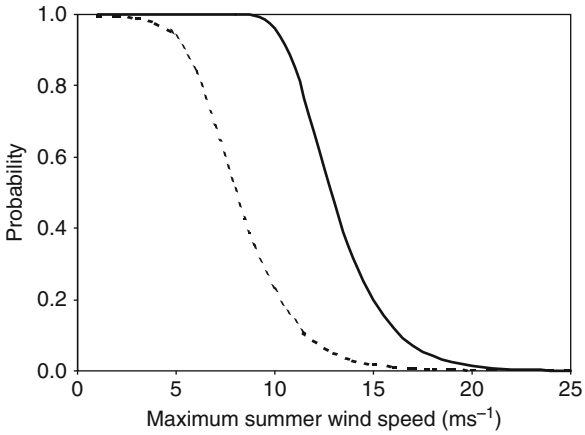

Lodging Resistance in Cereals. Figure 8
Probabilities of experiencing wind gusts independent of rainfall (—) and wind gusts with $\geq$ 7 mm daily rain (---) between mid-June and mid-August within the main wheat-growing regions of the UK (Adapted from [9])

the chance of lodging caused by small changes in the failure wind speed is illustrated by the probabilities of experiencing different wind speeds above a UK wheat crop (Fig. 8).

Methods for Controlling Lodging Risk

Crop Management

Cultivations The use of minimal cultivations or direct drilling to prepare seed beds have been shown to reduce lodging compared with more traditional methods which usually involve plowing to about 20 cm depth [36]. It seems likely that observations for direct drilling or minimal cultivations to reduce lodging are mainly caused directly by increased soil strength resulting from greater bulk density [37, 38]. The common observations for high bulk density to impede root extension and increase root thickness [39, 40] appear to be restricted to sections of the cereal root system that play little part in anchorage, namely, the seminal roots or the distal sections of the crown roots.

Rolling to consolidate the soil is another management practice that has been shown to reduce lodging [34, 41–43]. This can be done immediately after the primary cultivations or can be done in spring to re-consolidate the top-soil after it has been loosened by cycles of freezing and thawing. Berry et al. [43] showed that rolling a sandy loam in the spring increased shear strength in the top 5 cm by 25% and this effect persisted until harvest. No effects were observed on the biomechanical properties of the wheat roots. This study also showed that rolling before growth stage (GS) 30 [44] reduced lodging, but rolling after GS31 had no effect on lodging. It was hypothesized that this treatment damaged the extending stems, which encouraged extra tillering, and these extra shoots countered the effects of the stronger soil. This theory was supported by rolling experiments to break cereal stems by Peltonen and Peltonen-Sainio [45].

Sowing Date and Seed Rate The lodging risk of wheat is almost always reduced by delaying sowing [19, 46–49]. Pinthus [50] cites two studies that show reduced lodging in barley when it is sown later, but [47] observed that early sowings could reduce or increase lodging in barley. Reducing the number of plants established also causes a large reduction in the lodging risk of wheat [12, 19, 48, 51–53], and of barley [54].

The sowing date and seed rate effects described above are caused by changes to the structure of the crop. Berry et al. [48] showed that sowing winter wheat 6 weeks earlier increased both root and stem lodging risk by increasing the base bending moment of the shoot by about 30% and by reducing the strength of the stem base and the strength of the anchorage system by about 50%. Stapper and Fischer [19] have shown that early sowing results in a greater number of extended internodes, and this probably caused the longer stems which gave rise to the greater base bending moment. Establishing 200 plants m^{-2} compared with 400 plants m^{-2} reduced lodging risk by increasing the strength of the anchorage system by more than 50% and the strength of the stem base by 15% [48]. The increase in anchorage strength more than compensated for the increase in shoot number on these plants. The greater anchorage strength has been attributed to several morphological changes including more roots per plant [12], stronger and thicker roots [55], and a wider and deeper root cone [48].

Sowing earlier or establishing more plants resulted in weaker stems because the stems were narrower and had thinner walls [48]. The mechanism by which weak stems develop is thought to be due to a greater number of shoots competing for limited photo-assimilate

during early stem extension, which reduces the dry matter per unit length of the lower internodes [56]. Sparsely populated plants have many tillers [57] each of which develops up to four crown roots from each of their subterranean nodes. Therefore, it should be of no surprise that establishing fewer plants results in plants with more crown roots. Thicker and stronger roots may be caused by the absence of a strong shade avoidance response by the plant, which stimulates a greater proportion of assimilate to be partitioned to the roots [58]. Similar effects on anchorage strength were observed after later sowing as a result of fewer plants established.

Drilling Depth and Seed Treatment Deeper sowing has also been found to reduce lodging in barley [50], but in general published evidence for sowing depth effects is scarce. This is probably caused by the plants ability to adjust its crown depth to about 40 mm for sowing depths of between 40 and 70 mm [59]. This means that sowing depths over this range are unlikely to affect the depth of the structural roots. However, drilling more shallowly than 40 mm may be expected to raise the crown and its structural roots, thus weakening anchorage.

Evidence that altering crown depth can affect lodging can be found from the effect of seed treatments: fluquinconazole [60] and triadimenol [61]. Studies on fluquinconazole showed that it shortened the sub-crown internode linking the seed to the crown (the part of the plant where the crown roots and tillers emerge). This deepened the crown and the depth of the root plate, which in turn increased anchorage strength and the resistance to root lodging. Observed natural root lodging also showed that the plots treated with the triazole seed treatment were less susceptible to root lodging [60].

Disease Scott and Hollins [62] showed that wheat crops with a greater incidence of sharp eyespot (*Rhizoctonia*), brought about through inoculation, had more lodging. It has been shown that severe levels of either disease can reduce the failure moment of the lower internodes by between 30% and 40%, thus increasing the likelihood of stem lodging [10]. Interestingly, slight or medium levels of disease did not appear to weaken the stems. There is no evidence that take-all root disease increases the risk of lodging.

Nutrition An increased supply of available nitrogen from either mineralization of organic matter or from inorganic fertilizer has frequently been shown to increase lodging in wheat [48, 63, 64], barley [26, 65], and oats [66]. In wheat, the greatest increase in lodging is usually observed in response to early applications of nitrogen fertilizer before the onset of stem elongation [22, 23, 67], with applications after anthesis having no effect [52]. Contrary to this, Chalmers et al. [66] found that lodging in winter oats was reduced by applications of nitrogen before the onset of stem extension compared with later applications at GS30/31.

Both Crook and Ennos [68] and Berry et al. [48] showed that increasing the nitrogen supply to winter wheat, through either greater amounts of soil residual nitrogen at sowing or through larger applications of fertilizer in the spring, reduced the strength of the stem base and, to a lesser extent, reduced the strength of the anchorage system. Increases in crop height were generally small. Reductions in stem strength could be as much as 50% when high levels of residual nitrogen were combined with applications of fertilizer early in the spring [48]. Greater nitrogen supply almost always decreases the dry weight per unit length of the basal internodes of wheat [27, 48], barley [26], oats, and rye [22]. In relation to this, stem diameter and stem wall width are also frequently reduced. Berry et al. [48] showed that high levels of residual nitrogen reduced the strength of the stem wall material. These findings were supported by Crook and Ennos [27], who showed that a component of material strength, Young's modulus (which approximates to the stiffness of the stem), was also reduced by more fertilizer in spring. The cause of these effects may have resulted from a reduced amount of lignified tissue within the sclerenchyma zone and the thickness of the sclerenchyma cell walls [22]. Reductions in anchorage strength in response to more nitrogen can be linked with fewer roots, which are thinner with smaller bending and tensile strengths [55, 68]. Mulder [22] showed that the crown roots of oat plants supplied with large amounts of nitrogen were practically free from lignified cells beneath the epidermis, in contrast with plants supplied with moderate amounts of nitrogen.

In the consideration of nutrition, there should be a differentiation between the effects that result from repairing a deficiency and effects resulting from

super-optimal supply. For example, it appears that an increase in nitrogen will increase lodging risk, but the mechanism by which this occurs will depend on the level of nitrogen supply. If a nitrogen deficiency is being repaired then lodging risk increases because the leverage of the shoot and ear increases. It seems likely that the stem strength, and possibly the anchorage strength, will be increased by correcting the deficiency but these effects are outweighed by the greater leverage. Additional nitrogen increases the shoot leverage by progressively smaller amounts, but lodging risk continues to rise because the strength of the stem base and root system begins to decrease as a result of the indirect effects of shading. It is possible that phosphorus behaves in a similar way to nitrogen [67]. However, potassium might be different as the evidence [22, 50, 69] indicates that it can reduce lodging when repairing a deficiency and additional amounts have no effect. This may be due to the important role that this element plays in regulating the turgor of plant tissues.

Plant Growth Regulators Plant growth regulators (PGRs) are synthetic compounds that can be used to reduce lodging in cereal species. They are most commonly used for this purpose in north and western European countries and in North America. In the UK, 89% of the winter wheat is treated with PGRs [70]. PGRs can be classified into two main groups: inhibitors of gibberellic acid biosynthesis and ethylene-releasing compounds. The most commonly used inhibitors of gibberellic acid biosynthesis in cereal crops are chlormequat chloride, mepiquat chloride, trinexapac-ethyl and prohexadione-calcium [71]. Ethephon is the most commonly used ethylene-releasing compound used on cereals [72].

Plant growth regulators have been shown to be a cost-effective method of reducing the incidence of lodging. PGRs applied before the emergence of the ear reduced lodging in almost all of the vast number of published experiments that have studied their effect and in which lodging occurred, with reductions in the percentage area lodged of anything up to 70% [10]. The primary mechanism by which PGRs have been shown to reduce lodging risk is by reducing crop height, with height reductions of up to 40% [10]. The variation on plant height reduction is probably caused by interactions between the type of active ingredient, the cereal species together with the stage of plant development, and the environmental conditions when the chemical is applied. No evidence has been found for PGRs to increase the strength of the stem or of the anchorage system [48, 68], although it must be recognized that only two studies have investigated the effects of PGRs by directly measuring stem and anchorage strength. Chlormequat has been shown to be effective at reducing lodging in winter and spring wheat, oats, and rye, but less effective on barley [73, 74]. Barley undergoes large height reductions in response to a mixture of ethephon and mepiquat chloride [13, 75].

Summary of Crop Management Effects Many crop management practices result in large changes in lodging risk by either affecting the wind-induced leverage of the shoot, the strength of the stem base, the strength of the anchorage system, or a combination of all three mechanisms. Furthermore, the strengths of the stem base and anchorage system are often changed by different amounts for any change in crop management. This means that certain types of crop management would be expected to reduce one type of lodging (stem or root) more than the other. The effects of several crop management practices on the risk of stem and root lodging have been summarized by Berry et al. [76] in terms of changes to the failure wind speed (Table 1). This shows that stem lodging is best reduced by sowing on soils with less residual nitrogen and by reducing and delaying the amount of fertilizer applied in the spring. Root lodging is best reduced by establishing fewer plants, using a seed treatment with growth regulatory properties and by rolling in the spring to consolidate the soil. Delayed sowing and growth regulators were estimated to reduce stem and root lodging by equal amounts.

Plant Breeding

The *Rht* (Reduced height) alleles began to be introduced into wheat varieties during the 1960s and 1970s and are now part of the germplasm of most high yielding semi-dwarf varieties. In UK and German wheats, *Rht*1 and *Rht*2 alleles can reduce height by 14–17% independently of each other and by 42% when in combination [2]. *Rht*3 can reduce height by 59%, but has not yet been used in commercial varieties.

Lodging Resistance in Cereals. Table 1 Effect of crop management on the wind speed required to cause stem or root lodging (Adapted from [60, 76]

Factor	Increase in stem failure wind speed ms^{-1}	Increase in root failure wind speed ms^{-1}
Less soil residual N (116–71 kg N ha^{-1})	2.3 (3.9 [a])	1.3
Seed treatment with PGR activity (e.g., Fluquinconazole [60])	0	0.7
Delayed sowing (per week, between 20 September and 1 November)	0.5	0.5
Less plants established (per 100 plants m^{-2}, between 400 and 200 plants m^{-2})	0.8	1.8
PGRs (split chlormequat @ GS30/31)	1.4	1.4
Delayed and less fertilizer N (Target GAI of 5)	1.4	0.8
Spring rolling (pre-GS30)	0	0.8

[a]At 400 plants m^{-2}

In the UK, the *Rht*1 and *Rht*2 alleles have helped to reduce the height of wheat cultivars from over 1 m to about 0.7–0.9 m between the early 1970s and the mid-1990s. This reduction in height and consequent reduction in leverage has enabled the amount of nitrogen fertilizer applied to wheat to be increased from less than 100 kg ha^{-1} in the early 1970s to nearly 200 kg ha^{-1} in the 1990s [77] without a dramatic increase in the incidence of lodging. Pleiotropic effects have further added to the yield improvements associated with these *Rht* genes in wheat. Reduced stem growth rates allow more resources to be allocated to the developing ear which results in a greater number of fertile florets and grains per year.

In oats, the variety S172, released in 1939, has been reported to be Europe's first dwarf cereal variety [78]. However, dwarfness in this and several derived varieties was associated with small grains and a yield penalty. Recently varieties have been released that contain the *DW-6* dwarfing gene which was discovered in a mutation program in Canada [79] and has been shown to shorten the peduncle [80]. This gene has been shown to reduce height by 20–75 cm, have thicker stems, and to reduce lodging by large amounts [81]. Major dwarfing genes are common in spring barley. The *ari-eGP* dwarfing gene was found in cvs Golden Promise and Midas, which comprised over 70% of the Scottish barley crop from the mid-1970s to early 1980s. The *ari-eGP* gene was then superseded by the *sdw1* dwarfing gene, such that by 1989 the percentages of certified seed carrying the sdw1 and ari-eGP genes were 74 and 8, respectively [82].

There is great potential to continue increasing lodging resistance through further height reductions via the introduction of more extreme dwarfing genes such as *Rht*3 in wheat. However, several studies have shown that yield is reduced when crops are shortened too much [2–7]. The reduction in yield appears to be exacerbated by high temperatures or drought stress. Several of these studies indicate that the minimum crop height for optimum yield lies between 0.7 m and 1.0 m, a height which many modern varieties have already achieved. There is evidence that the same problem could occur in oats because the *DW-6* dwarfing gene has been associated with small grains, low kernel content and poor extrusion of the panicles from the flag leaves in some genetic backgrounds [81]. It therefore seems unlikely that much further improvement in lodging resistance can be made by continuing to shorten wheat crops and there may be only limited further shortening possible in other cereal species. As a result breeders must target other plant traits, namely, stem strength and anchorage strength, to improve lodging resistance and counter greater yields.

The lodging model of Baker et al. [29] has been used with preliminary datasets describing the dry matter costs of improving traits associated with stem strength and anchorage strength to estimate the dimensions of

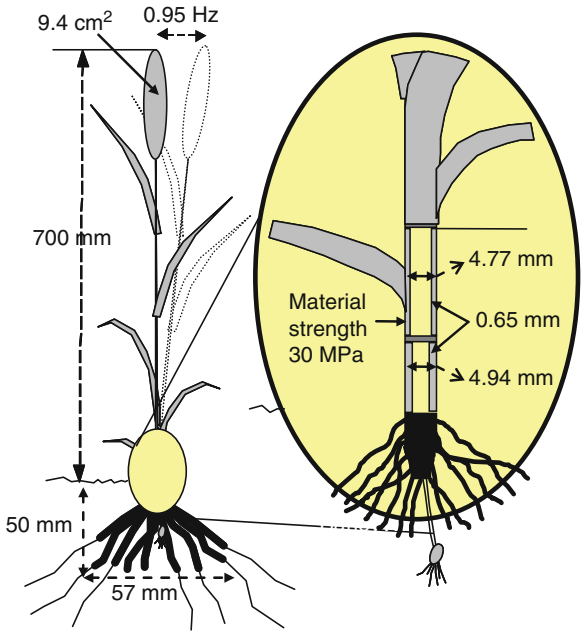

Lodging Resistance in Cereals. Figure 9
Description of a lodging-proof ideotype for wheat grown in a UK environment as defined in [83]

a wheat plant to make it lodging-proof for the least investment of biomass in the supporting stem and root system [83]. The characteristics required to give a crop yielding 8 t ha^{-1} with 500 shoots m^{-2} and 200 plants m^{-2} a lodging return period of 25 years in a UK environment include a height of 0.7 m, a root plate spread of 57 mm, and for the bottom internode a wall width of 0.65 mm, a stem diameter of 4.94 mm, and a material strength of 30 Mpa (Fig. 9). Observations of a range of varieties grown in the UK showed that the root plate of the best variety was 7 mm less than the ideotype target, the widest stem was 0.5 mm below the ideotype target, other stem character targets were achieved but not all in one variety, and the height target was achievable with the use of plant growth regulators.

It is possible that the lodging-proof ideotype traits could be achieved because large differences among wheat varieties have been observed for the traits that determine stem strength and anchorage strength [42, 76, 84]. The latter study showed that anchorage strength could vary from 206 Nmm to 587 Nmm and stem strength could vary from 122 Nmm to 175 Nmm between varieties. These differences were caused by a combination of wider, deeper root plates and stiffer roots for anchorage strength, and wider, thicker walled stems with a greater material strength for overall stem strength. Subsequent studies using more varieties and breeding lines showed even greater genetic variation in the traits which determine stem strength and anchorage strength [83, 85]. In barley, differences in culm wall thickness have frequently been positively correlated with varietal differences in lodging resistance [86–88]. If oats and barley have a similar level of genetic variation in stem and anchorage strength as has been observed in wheat then there appears to be significant scope for breeders to improve the strength of the stems and anchorage systems of cereals. However, these traits are time-consuming to measure; therefore, new technologies will be required to help plant breeders to rapidly select them.

Future Directions

The majority of lodging research has concentrated on wheat. This has enabled models of the lodging mechanism to be developed, which have been used to identify the critical plant characters, to quantify the effects of factors on lodging and to elucidate the mechanisms by which these effects are caused. A rudimentary model of lodging has been developed for barley, but further work is required to fully validate this model, particularly the way in which flexural rigidity of the stem is considered. Understanding about lodging in other cereals, such as rice, maize, and oats, lags far behind wheat. In order to replicate the advances made in wheat the next step must be to model the lodging mechanisms in these cereals. This may require fundamentally different types of lodging model due to the different plant structures of these species.

Historically reducing crop height has been the main avenue by which the lodging risk of wheat has been reduced. However, several studies on wheat indicate that the minimum height compatible with high yields is around 0.7 m. This height has been achieved by many wheat varieties. Crop height also has a major impact on the structural dry matter requirements for lodging resistance with each additional centimeter in height increasing the stem dry matter required by 0.23 t/ha [83]. Further work must investigate why there appears

to be a minimum height for high yield, whether this barrier can be overcome and whether the minimum height for high yield varies between environments.

Preliminary studies with wheat have indicated that increasing stem strength has a significant dry matter cost which could compete with the formation of grain yield [83]. Further work must quantify the dry matter cost of increasing stem strength, understand the optimum combination of stem diameter, wall width, and material that is required to minimize the dry matter cost of increasing stem strength, and quantify the extent to which this competes with yield formation.

It has been predicted that breeders must increase the stem strength and anchorage strength of wheat in order to achieve a lodging-proof ideotype for wheat. These traits are time-consuming to measure; therefore methods must be developed for rapidly assessing these traits. Berry et al. [89] and Keller et al. [90] have identified more than one quantitative trait loci associated with these traits and indicated that they are controlled by several genes. Further work will be required to better understand the genetic control of the traits associated with lodging and to investigate whether reliable genetic markers can be identified which work across a range of genotypes and environments. Phenotypic screens must also be investigated to assess whether they can offer an alternative method to genetic markers for selecting germplasm.

Recent work has shown that although a wide genetic variation for the key lodging traits is present within UK wheat breeding material [85], few of the target traits required for complete lodging proof have been identified. This indicates that a wider range of germplasm must be assessed to find the target traits.

Currently there is not a reliable method predicting the likelihood of lodging from earlier stages of crop development, when growers can alter lodging risk through their crop management (PGRs, fertilizer, rolling). Therefore, further research must study the development of the lodging-associated plant characters with the objective of predicting lodging from early assessments of the crop. Any prediction scheme must predict lodging risk before, or soon after, the onset of stem elongation to enable growers to alter their crop management accordingly.

PGRs reduce lodging risk by shortening crops, but there is little published evidence that they can strengthen the stems and anchorage system. Further research should investigate the effect of existing PGRs on stem and anchorage strength as well as focusing on discovering new chemicals that strengthen these traits.

Bibliography

1. Conway G (1997) The doubly green revolution: food for all in the 21st century. Cornell University Press, Ithaca
2. Flintham JE, Borner A, Worland AJ, Gale MD (1997) Optimizing wheat grain yield: effects of *Rht* (gibberellin-insensitive) dwarfing genes. J Agric Sci 128:11–25
3. Kertesz Z, Flintham JE, Gale MD (1991) Effects of Rht dwarfing genes on wheat grain yield and its components under eastern European conditions. Cereal Res Commun 19:297–304
4. Miralles DJ, Slafer GA (1995) Individual grain weight responses to genetic reductions in culm length in wheat as affected by source-sink manipulations. Field Crops Res 43:55–66
5. Allan RE (1986) Agronomic comparisons among wheat lines nearly isogenic for three reduced height genes. Crop Sci 26:707–710
6. Baylan HS, Singh O (1994) Pleiotropic effects of GA-insensitive *Rht* genes on grain yield and its component characters in wheat. Cereal Res Commun 22:195–200
7. Richards RA (1992) The effect of dwarfing genes in spring wheat in dry environments. I. Agronomic characteristics. Aust J Agric Res 43:517–527
8. Spink JH, Berry PM, Wade AP, White EL (2004) Minimising chlormequat residues in harvested grain. Home-Grown Cereals Authority Research Project No. 332. HGCA, London, p 44
9. Berry PM, Sterling M, Baker CJ, Spink JH, Sparkes DL (2003) A calibrated model of wheat lodging compared with field measurements. Agric For Meteorol 119:167–180
10. Berry PM, Sterling M, Spink JH, Baker CJ, Sylvester-Bradley R, Mooney S, Tams A, Ennos AR (2004) Understanding and reducing lodging in cereals. Adv Agron 84:215–269
11. Weibel RO, Pendleton JW (1964) Effect of artificial lodging on winter wheat grain yield and quality. Agron J 56:487–488
12. Easson DL, White EM, Pickles SJ (1993) The effects of weather, seed rate and cultivar on lodging and yield in winter wheat. J Agric Sci 121:145–156
13. Stanca AM, Jenkins G, Hanson PR (1979) Varietal responses in spring barley to natural and artificial lodging and to a growth regulator. J Agric Sci 93:449–456
14. Sisler WW, Olsen PJ (1951) A study of methods of influencing lodging in barley and the effect of lodging upon yield and certain quality characteristics. Sci Agric 31:177–186
15. Jedel PE, Helm JH (1991) Lodging effects on a semidwarf and two standard barley cultivars. Agron J 83:158–161
16. Pendleton JW (1954) The effect of lodging on spring oat yields and test weights. Agron J 46:265–267
17. Setter TL, Laureles EV, Mazaredo AM (1997) Lodging reduces the yield of rice by self-shading and reductions in canopy photosynthesis. Field Crops Res 49:95–106

18. Fischer RA, Stapper M (1987) Lodging effects on high yielding crops of irrigated semi-dwarf wheat. Field Crops Res 17: 245–248
19. Stapper M, Fischer RA (1990) Genotype, sowing date and plant spacing influence on high-yielding irrigated wheat in southern New South Wales. II. Growth, yield and nitrogen use. Aust J Agric Res 41:1021–1041
20. Laude HH, Pauli AW (1956) Influence of yield on lodging and other characteristics in winter wheat. Agron J 48:452–455
21. Day AD, Dickson AD (1958) Effect of artificial lodging on grain and malt quality of fall sown irrigated barley. Agron J 50: 338–340
22. Mulder EG (1954) Effect of mineral nutrition on lodging in cereals. Plant Soil 5:246–306
23. Berry PM, Spink JH, Griffin JM, Sylvester-Bradley R, Baker CJ, Scott RK, Clare RW (1998) Research to understand, predict and control factors affecting lodging in wheat. Home-Grown Cereals Authority Research Project No. 169. HGCA, London, p 131
24. HGCA (1997) Cereal statistics 1997. Home Grown Cereals Authority, London
25. Neenan M, Spencer-Smith JL (1975) An analysis of the problem of lodging with particular reference to wheat and barley. J Agric Sci 85:495–507
26. White EM (1991) Response of winter barley culivars to nitrogen and a plant growth regulator in relation to lodging. J Agric Sci 116:191–200
27. Crook MJ, Ennos AR (1993) The mechanics of root lodging in winter wheat (*Triticum aestivum* L). J Exp Bot 44:1219–1224
28. Graham J (1983) Crop lodging in British wheats and barleys. Ph.D. thesis, University of Reading, Reading, Berkshire, UK
29. Baker CJ, Berry PM, Spink JH, Sylvester-Bradley R, Clare RW, Scott RK, Griffin JM (1998) A method for the assessment of the risk of wheat lodging. J Theor Biol 194:587–603
30. Berry PM, Sterling MS, Mooney SJ (2006) Development of a model of lodging for barley. J Agron Crop Sci 192:151–158
31. Sterling M, Baker CJ, Berry PM, Wade A (2003) An experimental investigation of the lodging of wheat. Agric For Meteorol 119:149–165
32. Baker CJ (1995) The development of a theoretical model for the windthrow of plants. J Theor Biol 175:355–372
33. Ennos AR (1991) The mechanics of anchorage in wheat (*Triticum aestivum* L.) II. Anchorage of mature wheat against lodging. J Exp Bot 42:1607–1613
34. Pinthus MJ (1967) Spread of the root system as indicator for evaluating lodging resistance of wheat. Crop Sci 7:107–110
35. Easson DL, White EM, Pickles SJ (1992) A study of lodging in cereals. HGCA Research Project No. 52. Home-Grown Cereals Authority, London
36. Ellis FB, Christian DG, Graham JP, Jackson R, Wakel YT (1978) Long-term tillage experiments – agronomic results. Annual Report for 1977, ARC Letcombe Laboratory, Wantage
37. Schjonning P, Rasmussen KJ (2000) Soil strength and soil pore characteristics for direct drilled and ploughed soils. Soil Tillage Res 57:69–82
38. Finney JR, Knight BAG (1973) The effect of soil physical conditions produced by various cultivation systems on the root development of winter wheat. J Agric Sci 80:435–442
39. Wilson AJ, Robards AW (1977) Effects of mechanical impedance on root growth in barley, *Hordeum vulgare* L. J Exp Bot 28:1216–1227
40. Materechera SA, Dexter AR, Alston AM (1991) Penetration of very strong soils by seedling roots from different plant species. Plant Soil 135:31–41
41. Kopecky H (1970) The effect of compacting the soil on the formation of yield and on the quality of malting barley. Rostl Vyroba 16:309–319
42. Crook MJ, Ennos AR (1994) Stem and root characteristics associated with lodging resistance in four winter wheat cultivars. J Agric Sci 123:167–174
43. Berry PM, Spink JH, Sylvester-Bradley R, Pickett A, Sterling M, Baker C, Cameron N (2002) Lodging control through variety choice and management. In: Proceedings of the 8th Home-Grown Cereals Authority R&D Conference on Cereals and Oilseeds. HGCA, London, pp 7.1–7.12
44. Tottman DR (1987) Decimal code for the growth stages of cereals. Ann Appl Biol 110:683–687
45. Peltonen J, Peltonen-Sainio P (1997) Breaking uniculm growth habit of spring cereals at high latitudes by crop management II: tillering, grain yield and yield components. J Agron Crop Sci 2:87–95
46. Green CF, Ivins JD (1985) Time of sowing and the yield of winter wheat. J Agric Sci 104:235–238
47. Fielder AF (1988) Interactions between variety and sowing date for winter wheat and winter barley. HGCA Research Project No. 6. Home-Grown Cereals Authority, London
48. Berry PM, Griffin JM, Sylvester-Bradley R, Scott RK, Spink JH, Baker CJ, Clare RW (2000) Controlling plant form through husbandry to minimise lodging in wheat. Field Crops Res 67:59–81
49. Spink JH, Foulkes MJ, Gay A, Bryson R, Berry PM, Sylvester-Bradley R, Semere T, Clare RW, Scott RK, Kettlewell PS, Russell G (2000a) Reducing winter wheat production costs through crop intelligence information on variety and sowing date, rotational position, and canopy management in relation to drought and disease control. HGCA Research Project No. 235. Home-Grown Cereals Authority, London
50. Pinthus MJ (1973) Lodging in wheat, barley and oats: the phenomenon, its causes and preventative measures. Adv Agron 25:209–263
51. Lowe LB, Carter OG (1972) Response of four wheat cultivars to applications of (2-chloroethyl) trimethyl ammonium chloride (CCC). Aust J Exp Agric Anim Husb 12:75–80
52. Webster JR, Jackson LF (1993) Management practices to reduce lodging and maximise grain yield and protein content of fall-sown irrigated hard red spring wheat. Field Crops Res 33:240–259
53. Spink JH, Whaley JM, Semere T, Wade AP, Sparkes DL, Foulkes MJ (2000b) Prediction of optimum plant population in winter

wheat. HGCA Research Project No. 234. Home Grown Cereals Authority, London
54. Kirby EJM (1967) The effect of plant density upon the growth and yield of barley. J Agric Sci 68:317–324
55. Easson DL, Pickles SJ, White EM (1995) A study of the tensile strength required to pull wheat roots from soil. Ann Appl Biol 127:363–373
56. Berry PM (1998) Predicting lodging in winter wheat. Ph.D. thesis, University of Nottingham, Nottingham, UK
57. Whaley JH, Sparkes DL, Foulkes MJ, Spink JH, Semere T, Scott RK (2000) The physiological response of winter wheat to reductions in plant density. Ann Appl Biol 137:165–177
58. Kasperbauer MJ, Karlen DL (1986) Light-mediated bioregulation of tillering and biosynthate partitioning in wheat. Physiol Plant 66:159–163
59. Kirby EJM (1993) Effect of sowing depth on seedling emergence, growth and development in barley and wheat. Field Crops Res 35:101–111
60. Berry PM (2008) Effects of seed treatments on wheat lodging. In: Proceedings of the Crop Protection in Northern Britain Conference, Dundee
61. Montfort F, Klepper BL, Smiley RW (1996) Effects of two triazole seed treatments, triticonazole and triadimenol, on growth and development of wheat. Pestic Sci 46:315–322
62. Scott PR, Hollins TW (1974) Effects of eyespot on the yield of winter wheat. Ann Appl Biol 78:269–279
63. Bremner PM (1969) Effects of time and rate of nitrogen application on tillering, "sharp eyespot" (*Rhizoctonia solani*) and yield in winter wheat. J Agric Sci 72:273–280
64. Pandey DS, Kumar D, Misra RD, Prakash A, Gupta VK (1997) An integrated approach of irrigation and fertilizer management to reduce lodging in wheat (*Triticum aestivum*). Indian J Agron 42:86–89
65. Widdowson FV (1962) Applying fertiliser for spring barley. Ann Appl Biol 50:356–360
66. Chalmers AG, Dyer CJ, Sylvester-Bradley R (1998) Effects of nitrogen fertilizer on the grain yield and quality of winter oats. J Agric Sci 131:395–407
67. Miller FL, Anderson L (1963) Relationship in winter wheat between lodging physical properties of stems and fertilizer treatments. Crop Sci 3:468–471
68. Crook MJ, Ennos AR (1995) The effect of nitrogen and growth regulators on stem and root characteristics associated with lodging in two cultivars of winter wheat. J Exp Bot 46:931–938
69. Gaspar PE, Reeves DL, Schumacher TE, Fixen PE (1994) Oat cultivar response to potassium chloride on soils testing high in potassium. Agron J 86:255–258
70. Garthwaite DG, Thomas MR, Heyward E, Battersby A (2006) Arable crops in Great Britain 2006, Pesticide Usage Survey Report 213. Department for the Environment Food and Rural Affairs, London
71. Rademacher W (2000) Growth retardents: effects on gibberellin biosynthesis and other metabolic pathways. Annu Rev Plant Physiol Plant Mol Biol 51:501–531
72. Rademacher W (1993) PGRs- present situation and outlook. Acta Hortic 329:296–308
73. Humphries EC (1968) CCC and cereals. Field Crop Abstr 21: 91–99
74. Matthews S, Thompson WJ (1983) New roles for growth regulators in cereal production. In: Wright DW (ed) The yield of cereals. Royal Agricultural Society of England, London, pp 25–31
75. Herbert CD (1982) Growth regulation in cereals- chance or design? In: McLaren JS (ed) Chemical manipulation of crop growth and development. Butterworth Scientific, London, pp 315–327
76. Berry PM, Spink JH, Gay AP, Craigon J (2003) A comparison of root and stem lodging risks among winter wheat cultivars. J Agric Sci 141:191–202
77. Gooding MJ, Davies WP (1997) Wheat production and utilization: systems, quality and environment. CAB International, Wallingford, p 355
78. Valentine J, Cowan S, Howarth C, Langdon T (2003) One hundred years of progress in cereal breeding from Mendel to molecular selection – oats. In: Faccioli P, Marè C, Stanca AM (eds) Proceedings of the EUCARPIA Cereal Section Meeting. From biodiversity to genomics: breeding strategies for small grain cereals in the Third Millennium, Salsomaggiore, pp 21–25
79. Brown PD, McKenzie RIH, Mikaelson K (1980) Agronomic, genetic and cytologic evaluation of a rigorous new semi-dwarf oat. Crop Sci 20:303–306
80. Milach SCK, Rines HW, Philipps RL (2002) Plant height components and gibberelic acid response for oat dwarf lines. Crop Sci 42:1147–1154
81. Valentine J, Jones DM, Jones JE, Griffiths TER, Middleton B (1997) Genetic improvement in oats with specific reference to winter-hardiness and lodging resistance of winter oats and improvement of naked oats. HGCA Research Project No 145. Home-Grown Cereals Authority, London
82. Thomas WTB, Powell W, Swanston JS (1991) The effects of major genes on quantitatively varying characters in barley. 4. The gpert and denso loci and quality characters. Heredity 66:381–389
83. Berry PM, Sylvester-Bradley R, Berry S (2007) Ideotype design for lodging-proof wheat. Euphytica 154:165–179
84. Spink JH, Berry PM, Fenwick R, Gay AP (2003) To establish separate standing power ratings for stem and root lodging in the UK recommended lists for wheat. HGCA Research Project No. 305. Home-Grown Cereals Authority, London
85. Berry PM, Berry S (2008) Breeding for improved lodging resistance in wheat. In: Plant Genetic Resources for Food & Agriculture. AAB, 22 May 2008, Warwick HRI, UK
86. Dunn GJ, Briggs KG (1989) Variation in culm anatomy among barley cultivars differing in lodging resistance. Can J Bot 67:1838–1843
87. Jezowski S (1981) Variation, correlation and heritability of characters determining lodging of spring barley (*Hordeum vulgare* L.). II. Analysis of relationship between lodging grade

and some morphological characters of spring barley varieties. Genet Pol 22:45–61
88. Tandon JP, Jain KB, Singh SB (1973) Relationships between lodging resistance and some morphological characteristics in barley. Indian J Genet Plant Breed 33:347–354
89. Berry PM, Berry ST, Spink JH (2008) Identification of genetic markers for lodging resistance in wheat. Home-Grown Cereals Authority Project Report No 441. HGCA, London, p 16
90. Keller M, Karutz C, Schmid JE, Stamp P, Winzler M, Keller B, Messner MM (1999) Quantitative trait loci for lodging resistance in a segregating wheat x spelt population. Theor Appl Genet 98:1171–1182

Long-Term Ecological Research Network

Robert B. Waide, McOwiti O. Thomas
Long Term Ecological Research Network Office, Albuquerque, NM, USA

Article Outline

Glossary
Definition of the Subject
Introduction
Major Milestones in LTER
The LTER Network Today
Future Directions
Bibliography

Glossary

Biodiversity Variation of life at all levels of biological organization.

Disturbance A relatively discrete event in time and space that alters populations, communities, and ecosystems, including their attendant processes.

Ecology The study of the relationship of organisms or groups of organisms to their environment.

Ecosystem dynamics The observed changes in the characteristics of an ecosystem over time.

Ecosystem The organisms living in a particular area in combination with the physical elements of the environment in which they live.

Episodic Limited in duration or temporary.

Invisible present Relating to an observation whose importance cannot be evaluated for lack of context.

Scale Refers to differences in the spatial or temporal extent of a set of observations or measurements.

Synthesis The creation of new knowledge by combining observations from diverse sources.

Transformative research Scientific investigations whose results lead to radical changes in understanding of fundamental concepts.

Definition of the Subject

The Long-Term Ecological Research (LTER) Network is the largest and longest-lived ecological network in the United States. Designed to provide long-term data from a broad range of key ecosystems, the LTER Network represents a unique national resource to address pressing environmental issues such as climate change, loss of biodiversity, and changes in patterns of land use. LTER is recognized internationally as one of the best organized and most successful large groups conducting research in ecology. With over 1,500 scientists, educators, and students, the network spans 26 sites located in 16 states in the contiguous United States, Alaska in the Arctic, Antarctica, and islands in the Caribbean and the Pacific Ocean (Fig. 1).

The network's formal vision is a society in which long-term ecological knowledge contributes to the advancement of the health, productivity, and welfare of the global environment, thereby advancing human well-being [2]. Within this vision, LTER's mission is to provide the scientific community, policy makers, and society with the knowledge and predictive understanding necessary to conserve, protect, and manage the nation's ecosystems, their biodiversity, and the services they provide. The LTER Network achieves this mission by using long-term observations and experiments to generate and test ecological theory at local to regional scales.

The National Science Foundation (NSF) created the LTER program in 1980. For three decades, the network has generated rigorous, site-based scientific research that has led to important regional and continental syntheses. LTER provides the scientific expertise, research platforms, and long-term datasets necessary to document and analyze environmental change.

Introduction

Because some of the most interesting and important ecological phenomena take place over long periods,

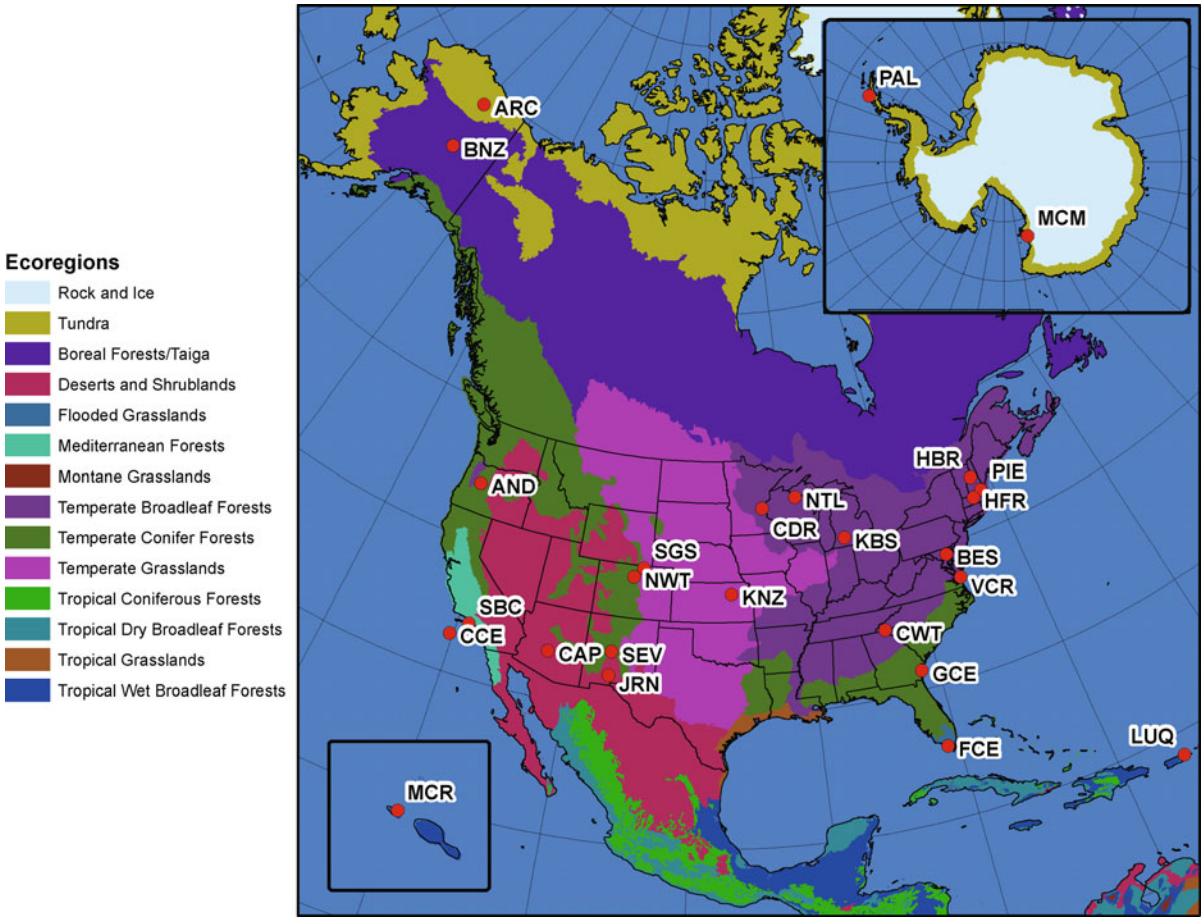

Long-Term Ecological Research Network. Figure 1

Locations of current LTER sites within global ecoregions. Site names, acronyms, and home institutions are as follows: Andrews Experimental Forest LTER (AND) – Oregon State University; Arctic LTER (ARC) – The Ecosystems Center, Marine Biological Laboratory; Baltimore Ecosystem Study (BES) – Cary Institute of Ecosystem Studies; Bonanza Creek LTER (BNZ) – University of Alaska – Fairbanks; California Current Ecosystem (CCE) – Scripps Institution of Oceanography; Cedar Creek Natural History Area LTER (CDR) – University of Minnesota; Central Arizona – Phoenix (CAP) – Arizona State University; Coweeta LTER (CWT) – University of Georgia; Florida Coastal Everglades (FCE) – Florida International University; Georgia Coastal Ecosystems (GCE) – University of Georgia; Harvard Forest (HFR) – Harvard University; Hubbard Brook Experimental Forest LTER (HBR) – Cornell University; Jornada Basin (JRN) – New Mexico State University; Kellogg Biological Station (KBS) – Michigan State University; Konza Prairie LTER (KNZ) – Kansas State University; Luquillo Experimental Forest LTER (LUQ) – University of Puerto Rico; McMurdo Dry Valleys (MCM) – Ohio State University; Moorea Coral Reef (MCR) – University of California-Santa Barbara; Niwot Ridge LTER (NWT) – University of Colorado; North Temperate Lakes (NTL) – University of Wisconsin-Madison; Palmer Station (PAL) – The Ecosystems Center, Marine Biological Laboratory; Plum Island Ecosystems (PIE) – The Ecosystems Center, Marine Biological Laboratory; Santa Barbara Coastal (SBC) – University of California-Santa Barbara; Sevilleta LTER (SEV) – University of New Mexico; Shortgrass Steppe (SGS) – Colorado State University; Virginia Coast Reserve (VCR) – University of Virginia (Courtesy of Jamie Hollingsworth; data from The Nature Conservancy [1])

long-term observations or experiments are necessary to truly understand their impacts. Processes such as climate change, recovery after disturbances such as forest fires, and changes in land cover are ecological processes that must be studied over the time scale of their occurrence (see, e.g., [3, 4]). Consequently, studies over sufficiently long time periods and large geographical scales are necessary to permit generalizations and theory about long-term events – such as deforestation, acid deposition, grazing, fire, and changes in trace gas fluxes [5].

In the concluding summary to a special report entitled "Long Term Ecological Research: An International Perspective," Risser [6] noted that long-term ecological studies are especially useful under four conditions: (1) the phenomena being studied are long term in their dynamics; (2) are episodic in nature, rare, complex, or subtle, such that long-term experiments are needed to isolate their dynamics and the control processes; (3) are poorly understood and cannot be predicted from short time scales; or (4) when long-term records are needed to make policy decisions.

Although important, such long-term studies are generally rare, with only a few examples all across the globe (Fig. 2). According to Risser [6] long-term ecological studies are rare because: (1) long-term studies may not be considered innovative science, making their continuous funding difficult; (2) sites where the measurements are taken may change, making the long-term results meaningless or difficult to interpret; (3) experimental designs may be too ambiguous for consistent long-term measurements or may not include adequate auxiliary studies to unravel controlling processes; (4) resources or incentives may be inadequate for dedicated scientists or research leaders to continue the studies; (5) new instrumentation may render the original methodology obsolete, coupled with insufficient attention to calibrating the old and new technologies; (6) new scientific advances may make the original question or hypothesis uninteresting or may provide a definitive answer, making the studies unnecessary.

It was this dearth of reliable information on key long-term ecological processes that prompted NSF to create the LTER Network in 1980 (see section "Major

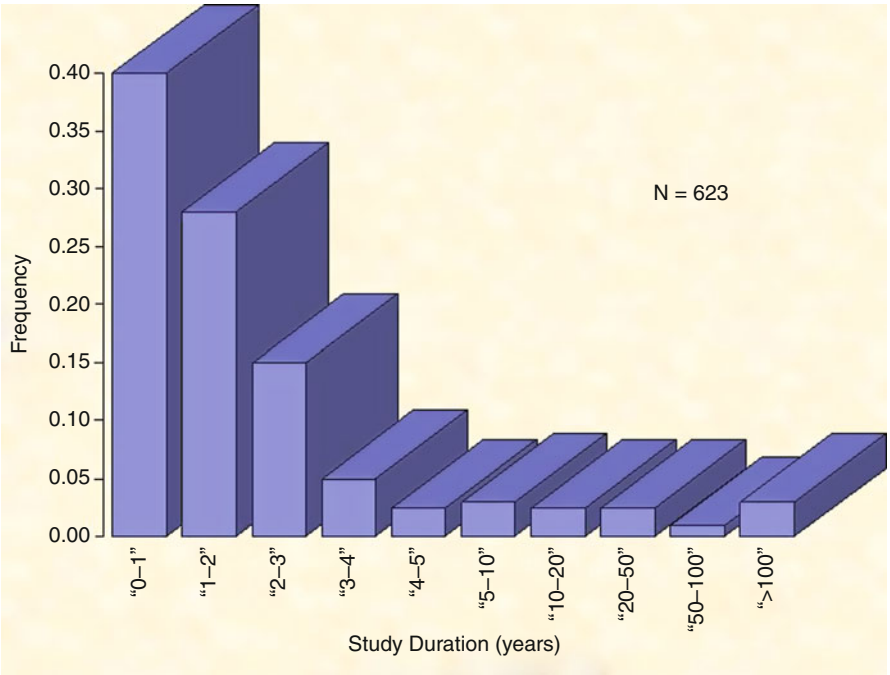

Long-Term Ecological Research Network. Figure 2
Frequency distribution of a random sample of observational and experimental studies published in the journal Ecology between 1977 and 1987 (From Gosz et al. [7]. Data from Tilman [8])

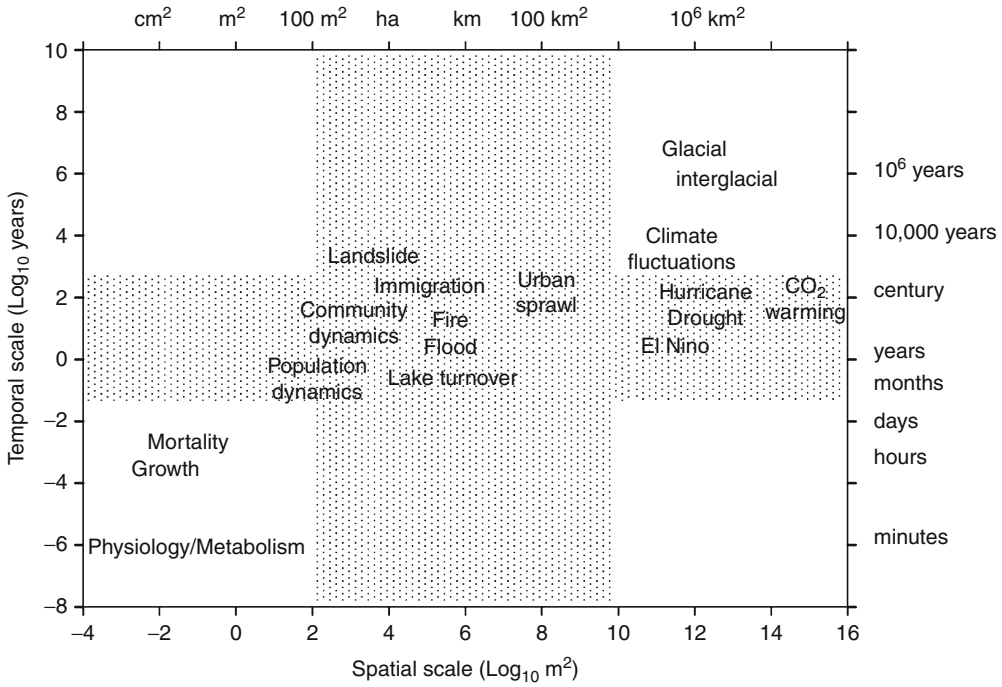

Long-Term Ecological Research Network. Figure 3

Temporal and spatial domains of the LTER program focus on biological phenomena and physical events that operate on year to century time scales and plot to regional spatial scales (Redrawn from Magnuson et al. [13], with permission)

Milestones in LTER" in this document for a brief history of LTER's formation). Acting on the recommendations of three working groups comprising members of the ecological community [9–11], the Division of Environmental Biology at NSF constructed a call for proposals designed to "(1) initiate the collection of comparative data at a network of sites representing major biotic regions of North America and (2) evaluate the scientific, technical, and managerial problems associated with such long-term comparative research" [12]. Although the early emphasis of the LTER program was on expanding the time scale at which ecological research was conducted, a concomitant expansion of the spatial scale of research was also expected (Fig. 3). This broadening perspective led to the twin concepts of the "invisible present" and the "invisible place."

Time and the Invisible Present

Magnuson [4] coined the term "invisible present" to describe ecological processes that result in significant change over decades but are hidden to the investigator conducting short-term studies. Ecologists working in this "invisible present" are not able to place current conditions in perspective without additional data from a longer span of time. Magnuson noted that short-term observations often could not identify cause and effect relationships because of inherent time lags of a year or longer between cause and effect. For example, changes in biomass accumulation in a forest as a result of disturbance may take years or decades to perceive. In short-term observational studies, it is rare to actually observe infrequent but important events. However, it is common to observe responses of an ecological system to an event that occurred long before observations began. Short-term manipulative studies often observe a system in transition rather than the complete trajectory to a new system state.

A good example of the importance of long-term data on the interpretation of ecological processes is given by observations of the ice cover records of Lake Mendota, WI (Fig. 4, [14]). The duration of ice cover in

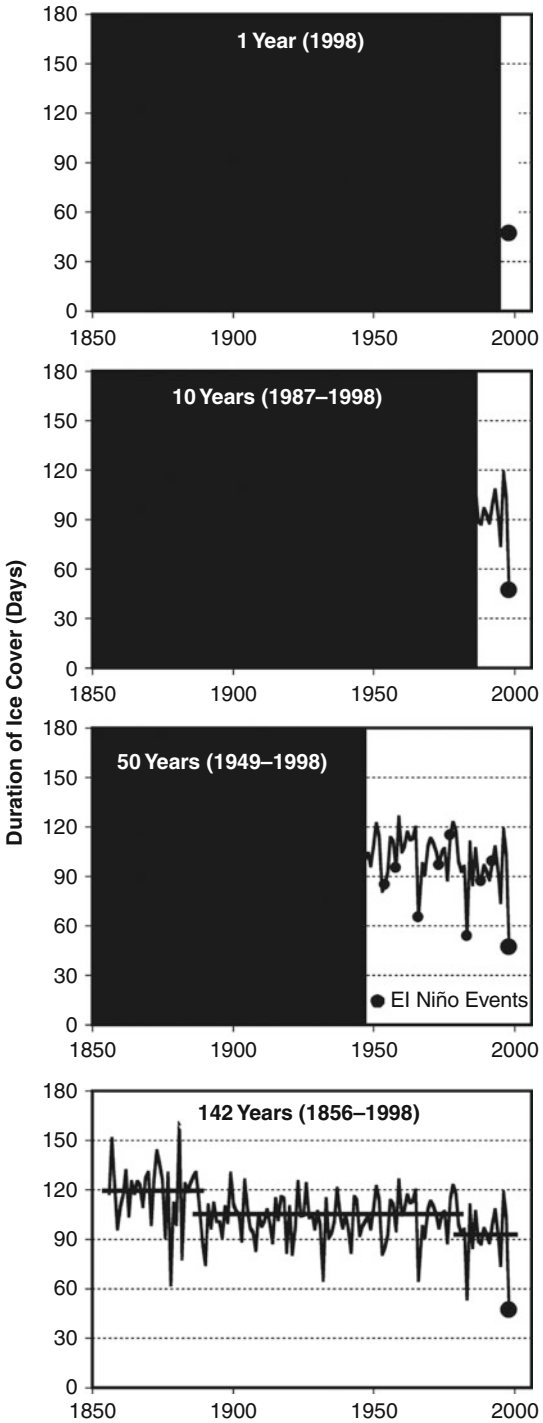

Long-Term Ecological Research Network. Figure 4 Observations of ice cover records of Lake Mendota demonstrate the importance of broad temporal scale in rendering the present visible (From Magnuson et al. [14])

a single winter (1997–1998 in the example) might seem unremarkable without any other context. However, examination of successively longer segments of the 142-plus years of ice duration data provides the context to see the importance of that single year. A 10-year segment of data reveals that duration of ice cover in 1997–1998 was significantly less than the other 9 years of record [15], and that duration of ice cover varies considerably from year to year. A relationship between ice cover and an important feature of global climate, the southern ocean oscillation index [16, 17], is evident in the 50-year data segment, with 1997–1998 and other El Niño years having shorter durations of ice cover. The general warming trend in the data only becomes apparent within the complete record. What's more, the end of the little ice age about 1890 [18, 19] is reflected in the decrease in the duration of ice cover on Lake Mendota. The single observation from 1997 to 1998, viewed in the context of the complete data set, is revealed to be the year of shortest ice duration in the entire 142-year record. Thus, the long-term nature of this set of observations provides a clear context to interpret patterns at multiple temporal scales.

Space and the Invisible Place

In the same way that a point in time requires long-term temporal context for complete understanding, so a point in space requires a broad-scale spatial context [20]. Interpretation of observations at a single site (the invisible place) requires a spatial context that often spans multiple scales. In the LTER Network, observational or experimental studies are often designed and implemented at the plot scale, where the plot may encompass less than 1 m^2 or an entire watershed. Most LTER site research focuses on plot to landscape scales (Fig. 3), but the use of remote sensing and modeling approaches, the steady development of networked interactions among sites [21], and the growth of the long-term approach internationally provides the means to expand the research focus to regional, continental, and global scales [20].

The study of glacial lakes at the North Temperate Lake's LTER site in northern Wisconsin illustrates a typical approach to linking ecological elements in a broader spatial context. Although lakes in this

landscape have many shared characteristics, the relative position of lakes connected along elevation gradients explains much significant dissimilarity, even in areas of slight relief. Lakes that are higher in the landscape are smaller, clearer, more dilute chemically, less diverse, and less affected by human use [22]. This pattern pertains to other lake districts throughout the northern hemisphere.

LTER scientists use two general approaches to extend results from small-scale and short-term studies to regional and broader scales [23]. An empirical approach correlates values of ecological processes with aspects of the physical environment that are measurable at broad spatial scales using specialized tools including remotely sensed imagery. For example, Kratz et al. [24] compared patterns of spatial and temporal variability across 12 LTER sites using normalized difference vegetation indices (NDVI) from Landsat scenes. They found that variability within sites for a given year was considerably greater than variability among sites, indicating that studies of spatial heterogeneity must be coupled with long-term data to achieve an understanding of long-term dynamics at landscape and regional scales.

A second approach uses mechanistic models to simulate interactions among ecological processes measured at sites and predict patterns at broader scales [23]. Data from the LTER Network facilitate construction of mechanistic models in two important ways. Coordination among sites within the network produces consistent, multidisciplinary data sets over a broad geographic range. The existence of data on slow ecosystem processes, which govern long-term ecosystem dynamics, allows estimation of rate constants needed to model these dynamics. One example of the interaction between long-term data and mechanistic models is the photosynthesis and evapotranspiration model (PnET) developed by Aber and colleagues to predict ecosystem processes at regional scales [23]. The PnET models form a nested hierarchy of three models estimating (1) gross and net carbon (C) gain on a daily time step, (2) net C and water fluxes at variable time steps, and (3) biomass, litter fall, decomposition, and nitrogen (N) cycling. Together the three models allow prediction of the integrated function of ecosystems. Predictions from the models have been compared with long-term C, water, and nutrient balance data from the Harvard Forest and Hubbard Brook LTER programs. Discrepancies between predictions and empirical data instruct model improvement and guide site research. The PnET models allow regional scale prediction of integrated ecosystem characteristics over a wide range of future environmental conditions and previous land use histories [23].

Networks of integrated research sites provide the opportunity to examine continental scale ecological patterns and the drivers of those patterns. One multisite, long-term experiment (the Long-Term Intersite Decomposition Experiment or LIDET) manipulated substrate quality across a broad range of vegetation and climate conditions to understand the factors controlling decomposition. Results from standardized measurements at 26 sites (17 LTER sites) indicated that decomposition of low-quality litter across a broad range of environmental conditions was slower than had been previously thought [25] and that significant variability resulted from ecosystem-specific factors such as the composition of the decomposer community. Studies such as these led LTER scientists to develop a conceptual framework for continental-scale research based on connectivity of flows of materials, organisms, and information across scales [26]. This framework emphasizes the importance of coordinated approaches across different research networks at continental and global scales.

Coordination of long-term ecological research at a global scale was initiated in 1993 through the formation of the International Long Term Ecological Research Network [27], which now has research networks in 40 countries. As a founding member of this global network, the US LTER Network continues to play a central role in developing research to address global ecological issues. In addition, many LTER sites perform observations and conduct experiments as part of global networks focused on specific research questions. For example, LTER sites are engaged in global comparisons of forest structure through the Center for Tropical Forest Science at the Smithsonian Tropical Research Institute. This network includes 40 plots in 21 countries encompassing 4.5 million individual trees of 8,500 species.

Major Milestones in LTER

Scientific investigation at and among LTER sites is dynamic and evolves continuously in response to increasing knowledge and new opportunities. The commitment of LTER sites to long-term observations and experiments does not imply rigidity in focus and approach. The ability of LTER researchers to respond nimbly to new opportunities results from a flexible network structure with a minimum of requirements and uniform site activities. This flexibility would not be possible in a more monolithic network design. Thus, during the first decade of LTER (the 1980s), key concepts of long-term ecological research were explored and clarified. In the 1990s, there was an increased emphasis on large spatial scales and multiple interactions of ecological processes, species, and element cycles. In addition, interactions with physical and social scientists also increased. The third decade of the LTER program focused on synthesis. Using data and knowledge gained over the preceding 20 years, the LTER Network sought to reach new levels of understanding of long-term and large-scale ecological patterns and processes. This summary of the intellectual evolution of LTER provides context for a description of the major milestones in the development of LTER research.

Formation of the Network

The seeds of LTER were planted by the National Science Foundation (NSF) when it sponsored three workshops (in 1977, 1978, and 1979) to initiate and maintain close consultation with the ecological sciences community. At these workshops, the philosophy of collaborative research was developed and a centralized working hypothesis approach to collaboration proposed. Five core areas of research (Box 1) were defined to orient long-term ecological research projects toward question/hypothesis formulation and resolution over long time and broad spatial scales.

Box 1. Core Research Areas

The core areas are five research themes that are common to research at all sites and thus central to the coordination of network science. Core areas were originally selected by NSF to ensure appropriate breadth in LTER research programs and to guard against divergence among sites over time. Combined, the five core areas describe most of the major structural components of ecosystems. Although discussions about adding new core areas (e.g., biodiversity, social patterns and processes) have taken place within the LTER Network, none of these have been officially adopted.

The core areas are:

1. *Pattern and control of primary production* – Plant growth in most ecosystems forms the base or "primary" component of the food web. Spatial and temporal patterns of production and the controls of these patterns are major factors in structuring ecosystems.
2. *Spatial and temporal distribution of populations selected to represent trophic structure* – Populations of organisms are dynamic over space and time, and long-term trends in populations can be important indicators of environmental change.
3. *Movement of organic matter* – The sequestration of carbon by primary producers and its eventual fate in ecosystems have important implications for trophic dynamics, nutrient cycling, and global climate.
4. *Movement of inorganic matter* – Nitrogen, phosphorus, and other mineral nutrients are cycled through the ecosystem by way of decay and disturbances such as fire and flood. Availability of these nutrients exerts important controls over ecosystem structure and function.
5. *Disturbance patterns* – Disturbances often shape ecosystems by periodically reorganizing physical or community structure, resulting in significant changes in ecosystem services available to humans.

Major Milestones in the First LTER Decade

1980 – NSF selected an initial set of six sites (North Temperate Lakes, H.J. Andrews Experimental Forest, Coweeta Hydrological Laboratory, Konza Prairie, North Inlet Marsh, and Niwot Ridge) funded at $250,000 per year. Lead scientists from each site met in Washington, DC, and constituted a steering committee to begin the tasks of LTER communication, coordination, and accommodation of mutual goals.

1981 – Dick Marzolf (Konza Prairie) was elected the first Chair of the Steering Committee and NSF awarded

Box 2. The LTER Network Office

The LTER Network Office (LNO) was established in 1983 through a coordination grant awarded by NSF to Oregon State University to support and coordinate network and site activities of the LTER Network. In 1989, NSF awarded another coordination grant to enlarge and establish LNO at the University of Washington-Seattle. The office officially moved to the University of New Mexico in 1997, and added the position of Executive Director. Robert B. Waide, formerly co-principal investigator of the Luquillo LTER program, was the first Executive Director of the LNO. With a core staff of 18 people and an annual budget of $1.5 million, the LNO's current service mandate includes:

- Providing an efficient computational and communication infrastructure for LTER research and education
- Developing and deploying state-of-the-art techniques in information management
- Maintaining a strong public outreach program
- Coordinating interactions with other scientific networks, agencies, and entities
- Providing administrative support
- Contributing to an efficient and effective environment in which site, cross-site, and synthetic research and education can be conducted

Box 3. All Scientists Meetings

Triennial All Scientist Meetings are used by the LTER Network to promote team building for cross-site research and synthesis. These 3–4 day meetings focus the LTER scientific community on new challenges, result in the formation of new research collaborations, help to integrate new sites and scientists into the LTER community, and provide the only opportunity for community-wide discussions of the future of the LTER program. In contrast to the usual scientific conference, an All Scientists Meeting focuses less on the presentation of individual research results and more on brainstorming, discussion, and synthesis of results from researchers addressing similar questions in different ecosystems. Moreover, All Scientists Meetings present excellent opportunities to share expertise, to transfer technology among sites, and to generate new scientific concepts, approaches, and experiments.

The most recent meeting in 2009 was attended by nearly 800 participants including many graduate students and broad representation for the International LTER community. The program included six plenary talks, 75 working group meetings, over 400 posters, four evening mixers, and pre-meetings for information managers, graduate students, education representatives, international attendees, and the LTER Executive Board.

a network coordination grant to Kansas State University (with Marzolf as PI). Subsequently, a second competition added five new sites to the network (Central Plains Experimental Range (now called Shortgrass Steppe), Okefenokee, Illinois Rivers, Cedar Creek Natural History Area, and Jornada Basin).

1982 – LTER held the first Data Management workshop and the first LTER Meteorological Committee (now Climate Committee) meeting, while the Steering Committee created a policy for workshops supported under the coordination grant.

1983 – NSF conducted the first national review of the LTER Program and the LTER Network Office (Box 2) was established through a coordination grant awarded by NSF to Oregon State University (with Jerry Franklin as PI).

1985 – LTER held its first All Scientists Meeting (Box 3) at Lake Itasca, MN.

1986 – NSF announced the third call for proposals for long-term ecological research sites; the LTER Intersite Climate Committee (formerly Meteorological Committee) developed standards for meteorological measurements at LTER sites [28, 29].

1987 – Five new sites (Arctic Tundra, Bonanza Creek Experimental Forest, Hubbard Brook Experimental Forest, Kellogg Biological Station, and Virginia Coast Reserve) joined the network; the LTER Intersite Climate Committee summarized climate information at the first 11 LTER sites [30]; and NSF announced the fourth call for long-term ecological research proposals.

1988 – Three new sites (Luquillo Experimental Forest, Sevilleta National Wildlife Refuge, and Harvard Forest)

Box 4. Evaluation of LTER Sites

NSF funds each LTER site independently for 6-year periods, with renewal of awards based on proposals describing accomplishments and plans for future activities. Renewal proposals are reviewed by special panels of experts convened by NSF. The review panel may recommend continued funding, preparation of an addendum addressing specific points, or probation. An LTER site that is placed on probation receives only 2 years of funding and must write a new proposal addressing shortcomings for the next renewal cycle 2 years later. If the new proposal addresses criticisms successfully, 4 more years of funding are awarded. If not, the site is provided with terminal funding to close operations. The purpose of the probation process is to ensure that NSF's long-term investment is protected from transient problems, such the death or retirement of leading investigators, while still maintaining high standards of rigor in peer review. Four sites have been terminated during the 30-year history of the LTER program.

NSF also conducts mid-term program reviews as an essential part of NSF's ongoing evaluation cycle of the LTER program. Midway through the funding period, external peer review teams visit each site to evaluate the quality of science, education, and outreach as well as how well the site is managed and how integrated the sites are with the entire LTER Network [31]. The site reviews also serve as opportunities for site scientists and staff to get constructive criticism from the review team and to identify potential problems that require correction [32].

were added to the program, while two (Illinois Rivers and Okefenokee) were withdrawn (Box 4); the NSF Advisory Committee on Scientific and Technological Planning for LTER identified scientific issues addressed by the sites and recommended network-wide capabilities to address them; and the minimum standard installation (MSI) for LTER site data management was developed.

1989 – NSF conducted a second national LTER Program review and awarded a coordination grant to enlarge and establish the LTER Network Office at the University of Washington-Seattle (with Jerry Franklin as PI); an LTER working group developed the "Global Change Research Action Plan"; acquisition of satellite imagery and aerial photography for all sites began; an LTER-Chinese Ecological Research Network (CERN) exchange was developed; and the first LTER Network Strategic Plan resulted from the 1989 LTER Coordinating Committee Meeting at Harvard Forest ("A long-range Strategic Plan for the Long Term Ecological Research Network").

Major Milestones in the Second LTER Decade

1990 – The LTER Coordinating Committee developed site data management policy guidelines; LTER held its second All Scientists Meeting at Estes Park, CO.

1991 – Following an NSF Antarctic research proposal competition, a new site, Palmer Station LTER, Antarctica, was added to the network supported by funds from Polar Programs and Environmental Biology divisions; Geographic Information Systems (GIS) working group analyzed the status of LTER Network technical supplements and assessed future technical needs; and Global Positioning Systems (GPS) units were acquired for shared LTER site use and GPS training provided for representatives from all sites.

1992 – The LTER Coordinating Committee, at the request of NSF, developed an 8-year vision ("LTER 2000") for the creation of a global environmental research network based upon approaches established in the LTER Program.

1993 – A second Antarctic site, McMurdo Dry Valleys, was selected for the LTER Network; the NSF commissioned a 10-year review of the LTER Program; the third LTER All Scientists Meeting was held at Estes Park, CO; an International LTER Summit at the Estes Park meeting led to the establishment of the International LTER (ILTER) Network, with Jerry F. Franklin (U.S. LTER Chair) as Steering Committee Chair; the LTER Network Internet (gopher) server was established at the Network Office; the LTER All-Site Bibliography, Core Data Set Catalog, and Personnel Database were developed and put online in searchable form; and the North Inlet LTER site was withdrawn, leaving 18 sites in the network.

1994 – In response to the 10-year review of the LTER Program, NSF conducted a special competition

Box 5. Augmented LTER Sites

In 1996, NSF began an experiment that involved augmenting two LTER sites at a funding level that was double the network standard. The two sites, North Temperate Lakes in Wisconsin and Coweeta in the southern Appalachian mountains, were selected based on competitive proposals [33]. The successful proposals contained significant commitments to involve social and economic sciences and plans for developing regional-scale research.

The increased funding gave these sites the opportunity to focus on complex interactions between humans and ecological processes across a range of scales and to make significant advances in understanding the spatial, temporal, and decision-making components of land use and land-use change, and to build regional, national, and international collaborations.

The site augmentation experiment led to several significant findings by the participating sites. For example, North Temperate Lake researchers found that the economically optimal phosphorus input to lakes is often far less than estimates based on assumptions that lakes are linear, equilibrium systems with no stochastic factors and no time delays. By calculating the net economic value of water quality (based on the economics of farming, value of housing near the lake, and the recreational economy derived from boating, fishing, etc.), the researchers showed that the economically optimal phosphorus loading (which maximizes net costs and benefits to society as a whole) was about one third the current loading rate of the lake. These analyses show that the total economic value (i.e., the net benefit from all uses of the watershed, including agriculture, lakeshore property values, fishing, and other recreation) generated by the Lake Mendota watershed would increase substantially if less fertilizer were used.

At Coweeta, a spatially explicit model of land-use change over a 40-year period (1950–1990) identifying physical and human factors and determining land-use patterns for representative areas across the region showed that land-cover changes were more frequent at lower elevations and near roads. Bird diversity declined with forest patch size, which in turn influenced plant community composition. Some plant groups (e.g., *Liliaceae* and *myrmecochores*) with diaspores dispersed by ants were scarce or absent in patches subjected to intensive past land use. Land-use history was more important than patch size in explaining variation in abundance and composition of seed-dispersing ants. Fish density and diversity, in particular, were more affected by upstream than streamside deforestation. The "legacy effect" and the relative importance of upstream process pointed the way toward large-scale and long-term restoration given the implication that localized efforts often had little effect.

The discovery of these dramatic effects of land-use patterns and environmental heterogeneity on populations and communities led the Coweeta LTER to begin a new 30-year study in 2000 of stream regions forecast to differ over time in type and risk of development.

for cross-site and international comparisons and synthesis; nine grants ranging from $109,353 to $200,000 were made to LTER and non-LTER sites in the United States, Ireland, Scotland, Costa Rica, Argentina, and Russia; NSF announced a special competition for augmentation of LTER projects (Box 5) for regionalization, comprehensive site histories, and increased disciplinary breadth; LTER established a World Wide Web site at the Network Office; the first International LTER (ILTER) Steering Committee meeting was held at Rothamsted, U.K.; and NSF signed Memoranda of Agreement with the U.S. Forest Service and the National Biological Survey to cooperate/collaborate in LTER Program research.

1995 – Jerry Franklin retired after 12 years of service as Chair of the Coordinating Committee and was replaced by James Gosz; LTER established a National Advisory Board; NSF announced 13 new awards for cross-site comparisons and synthesis at LTER and non-LTER sites; the LTER Publications Committee developed a plan for publication of Network research synthesis volumes; and NSF/DOE/NASA/USDA Joint Program Awards, Terrestrial Ecology and Global Change (TECO), were awarded to seven LTER recipients, including researchers at Bonanza Creek, Cedar Creek, Central Plains, Harvard Forest, H.J. Andrews, and Jornada.

1996 – The first LTER site synthesis volume (Palmer LTER) was published by the American Geophysical Union (AGU).

1997 – A special competition resulted in addition of two new urban LTER sites (Central Arizona Phoenix and Baltimore Ecosystem Study); the Network Office officially began operation from the University of New Mexico.

1998 – An NSF competition resulted in a former Land Margin Ecological Research (LMER) site (Plum Island Ecosystem) joining the network; the LTER Network signed a contract to produce a Science Synthesis Series with Oxford University Press; Schoolyard LTER Supplements ($15,000 per year to each site) were added to LTER grants.

1999 – NSF provided funding supplements to enhance Internet connectivity at LTER sites; the LTER Social Science Committee was created; the LTER Network Office, the National Center for Ecological Analysis and Synthesis, the San Diego Supercomputer Center, and University of Kansas collaborated on the "Knowledge Network for Biocomplexity"; and a synthesis volume, "Standard Soil Methods for Long Term Ecological Research," was published by Oxford University Press.

Major Milestones in the Third LTER Decade

2000 – Three new coastal sites joined the network (Georgia Coastal Ecosystem, Florida Coastal Everglades, and Santa Barbara Coastal); the fourth LTER (and first ILTER) All Scientists Meeting was held in Snowbird, Utah, in association with the annual meeting of the Ecological Society of America; and LTER entered into a collaborative relationship with the Organization of Biological Field Stations.

2001 – NSF conducted a 20-year review of the LTER Network; LTER celebrated its twentieth Anniversary; and the LTER Education Strategic Plan was published.

2002 – The first of what became an annual series of NSF-LTER Mini Symposia was held in Washington, DC; the LTER Network Information System Advisory Committee (NISAC) was formed; and the LTER Strategic Plan ("LTER 2000–2010: A Decade of Synthesis") was published.

2003 – The Cooperative Agreement for the LTER Network Office at the University of New Mexico was renewed; the fifth LTER All Scientists' Meeting was held in Seattle, Washington, in association with the Estuarine Research Federation; a Special Issue of *BioScience* focused on the Long-Term Ecological Research Network; the LTER Coordinating Committee approved a formal set of bylaws for the LTER Network; and the U.S. International Committee was formed.

2004 – The first LTER children's book, "My Water Comes from the Mountains," was published; two new sites (California Current Ecosystem and Moorea Coral Reef) joined the LTER Network; and the LTER Network received a grant from NSF to conduct network-level strategic planning.

2005 – The first LTER Graduate Student Collaborative Research Symposium took place at Andrews Experimental Forest; and the LTER Network Office "Strategic Plan" and "Implementation Plan" were published.

2006 – Jim Gosz stepped down after 10 years as Chair of the LTER Coordinating Committee and was replaced by John Magnuson; the Sixth LTER All Scientists' Meeting was held at Estes Park, CO; and the LTER Coordinating Committee approved a new LTER governance structure consisting of a Science Council and an Executive Board (Box 6).

2007 – Phil Robertson was elected Chair of the LTER Executive Board and Science Council; the "Decadal Plan for LTER," incorporating an integrated research plan, a description of the EcoTrends project, a Strategic Plan for Education, a Strategic Plan for Cyberinfrastructure, a new governance plan, and the "Integrative Science for Society and the Environment" document, was published; and "Principles and Standards for Measuring Primary Production" was published as part of the LTER series by Oxford University Press.

2008 – The LTER Network and the National Phenological Network signed a MOU for cooperation in phenological monitoring and assessment.

2009 – The seventh LTER All Scientists Meeting was held at Estes Park, CO; the LTER Network Office core funding was renewed and a separate award was made by NSF to facilitate synthesis and the development of network cyberinfrastructure.

2010 – The LTER Network received the Distinguished Scientist Award from the American Institute of Biological Sciences (AIBS); NSF initiated a 30-year

Box 6. Governance Structure

The Network is governed by bylaws enacted in 2003 by the *Coordinating Committee*, at that time the governing body of the LTER Network. The bylaws established a new governance structure consisting of an elected *Chair* and an *Executive Board* comprising nine rotating site representatives and one non-voting member selected to provide expertise on information management. Site representatives are the lead principal investigators of each LTER site. The Chair and the *Executive Director* of the LTER Network Office are ex officio members of the Executive Board. The *Science Council*, with a membership that includes two representatives from each site and the chairs of each Standing Committee, establishes the scientific direction and vision of the LTER Network. The voting membership of the Science Council (the 26 lead principal investigators from each site) reserves ultimate authority for decisions affecting the network. Ten *Standing Committees* (Climate, Communications, Education, Graduate Students, Information Management, International, Network Information System, Networks Coordination, Publications, and Social and Economic Science) support and inform the governance process. A *Network Office*, (see Box 2) funded separately by the National Science Foundation, facilitates research, education, information management, and governance activities (Fig. 5).

review of the LTER Program; and LTER created a Communications Committee and a Networks Coordination Committee.

2011 – Scott Collins was elected Chair of the LTER Executive Board and Science Council.

The LTER Network Today

Twenty-six research sites and a central coordinating office constitute the LTER Network at present, and more than 1,500 scientists are involved in research at these sites. The annual budget of the LTER program approaches $30 million (Fig. 6). The Network includes a wide range of ecosystem types spanning broad ranges of environmental conditions and human domination of the landscape. The geographic distribution of sites ranges from Alaska to Antarctica and from the Caribbean to French Polynesia and includes agricultural lands, alpine tundra, barrier islands, coastal lagoons, cold and hot deserts, coral reefs, estuaries, forests, freshwater wetlands, grasslands, kelp forests, lakes, open ocean, savannas, streams, and urban landscapes. Collectively, the sites in the LTER Network provide opportunities to contrast marine, coastal, and continental regions, the full range of climatic gradients existing in North America, and aquatic and terrestrial habitats in a range of ecosystem types. All sites are sufficiently large to incorporate moderate to large landscape mosaics, and most sites include human-manipulated as well as natural ecosystems. Most sites embody considerable within-site variability in habitats and ecosystem processes and attempt to characterize this variability in the context of broad regional gradients covering hundreds of kilometers.

In accordance with the factors driving the development of long-term ecological research in the United States, the LTER Network has adopted a central, organizing intellectual aim: to understand long-term patterns and processes of ecological systems at multiple spatial scales. To achieve this aim, the LTER Network focuses on six interrelated goals [7]:

Understanding: Gaining ecological understanding of a diverse array of ecosystems at multiple spatial and temporal scales.

The mission of the LTER Network begins with research based at individual sites, each of which has a unique theme. This site-based focus has allowed for key scientific advances at each of the sites, while the common focus on long-term research in a diverse array of ecosystems and landscapes has facilitated broad comparisons and syntheses across sites. Together the network of sites covers a wide range of subjects at multiple temporal and spatial scales.

Synthesis: Using the network of sites to create general ecological knowledge through the synthesis of information gained from long-term research and development of theory.

The products of LTER research extend beyond the accumulation of knowledge about diverse, individual ecosystem types. At a higher level, synthesis of this site-based knowledge across the network provides the broader scientific understanding from which new theory is derived and general applications can be developed.

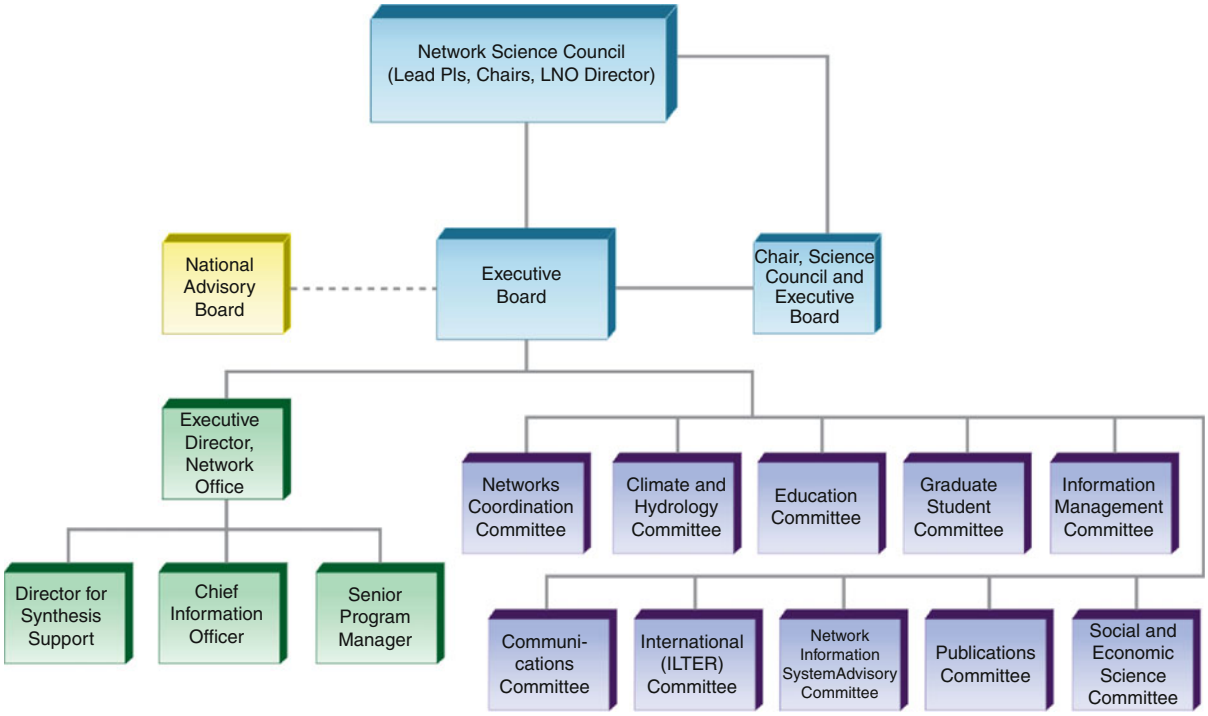

Long-Term Ecological Research Network. Figure 5
Organizational chart for the LTER Network (Courtesy of Phil Robertson)

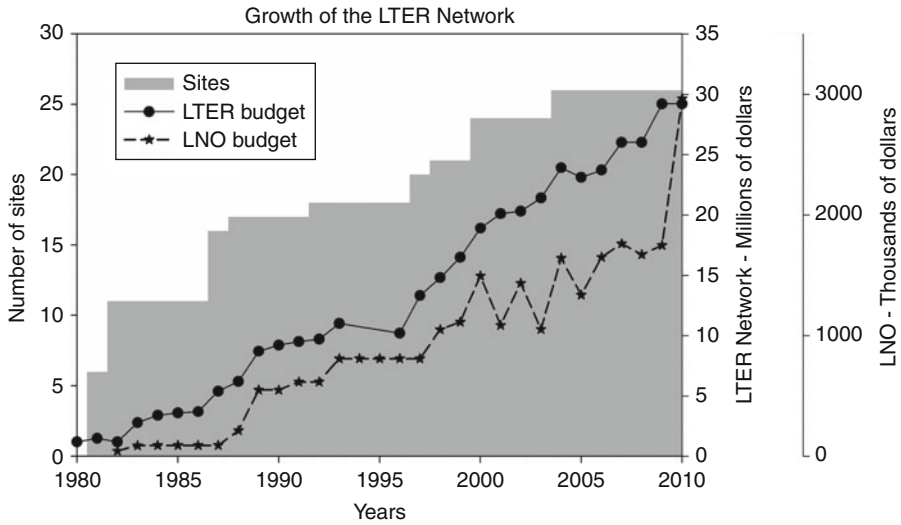

Long-Term Ecological Research Network. Figure 6
Growth of the LTER Network

Information Dissemination: Creating well-designed, documented databases that are accessible to the broader scientific community.

Long-term research demands long-term data. The creation, curation, and dissemination of long-term databases are needed to assure that the data resources

needed by researchers will continue to be available. These databases must include the additional information required to interpret data (i.e., metadata) as well as the data themselves. By adopting policies that promote the timely sharing of data (both inside and outside the LTER Network), the data can be used in a variety of ways not anticipated by the original collector such as regional, national, and global syntheses, thus providing a resource for the broader scientific community.

Legacies: Creating a legacy of well-designed and documented long-term observations, experiments, and archives of samples and specimens.

Many ecological phenomena change at decadal to century and longer time scales, and it is essential to maintain experiments and observations across periods appropriate to the questions addressed. The orderly transfer of experiments and interim results from one generation of scientists to the next requires a research design and setting that allows for multiple samplings (some unanticipated), long-term protection from competing uses, and meticulous documentation of experimental protocols. Also essential is a means to store protocols and observations in a manner that is secure and consistently accessible to the scientific community for use in syntheses and cross-site comparisons (both inside and outside the LTER Network).

Training: Developing a cadre of scientists who are equipped to conduct long-term, collaborative research to address complex ecological problems.

One of the major lessons from the first 30 years of LTER has been that success both within sites and within the network requires a nontraditional approach to ecological research. This approach is characterized by a commitment to long-term measurements that may yield only a few useful initial results but that are essential to understanding long-term change, by a willingness to work as part of large teams that may have priorities that are different than one's own, by a desire to interact closely with others in order to share ideas and data, and by the need to develop a broad interdisciplinary perspective. Disseminating this approach through the involvement of graduate and undergraduate students, postdoctoral and international scientists, and K-12 educators, students, and the general public can ensure the success of long-term ecology in the future.

Outreach: Providing knowledge to the broader ecological community, general public, resource managers, and policy makers to address complex environmental challenges.

Humanity faces increasingly numerous and serious environmental problems that range from local to global in extent, and that must be tackled by institutions at local to international scales. The LTER Network and emerging ILTER networks provide the most comprehensive and diverse system of sites for ecological observations on the globe, and research of the LTER Network has repeatedly demonstrated the ability of long-term ecological science to address these environmental challenges. Increasingly, LTER research is finding applications in the work of federal, state, and local agencies that manage environmental resources. The synoptic and detailed knowledge of individual LTER sites, and the opportunities for multidimensional comparisons among sites, also represents significant opportunities for other disciplines including social sciences, earth sciences, and basic biological sciences that must be pursued. Finally, knowledge from this breadth of views permits us to identify and anticipate new issues and challenges, test existing ideas about causation, and help provide the science that underpins the processes of open, participatory, and forward-looking decision making.

Achievements of the LTER Network

- "At each of the Network's 26 sites we know an extraordinary amount about organisms and processes important at the site, about the way the site's ecosystems respond to disturbance, and about long-term environmental change. A growing number of cross-site observations and experiments is also revealing much about the way that key processes, organisms, and ecological attributes are organized and behave across major environmental gradients. In total, research in the LTER portfolio is contributing substantially to both our basic knowledge of ecological interactions and our ability to forecast change and to test ecological theory." (p(i), [34])

LTER's long-term research and monitoring has led to important new discoveries and had a transformative effect on science and society. Hobbie [35] listed the benefits resulting from the existence of the network: value added to research sites in the network because of long-term stability; value added to ecological science

because long-term sites provide ecology with sustained intellectual attention to fundamental ecological issues; LTER data bases, which are important resources for the broader scientific community; cross-site synthesis, enabling hundreds of scientists to ask similar questions in a wide variety of habitats and increasing the possibilities for creative breakthroughs from interdisciplinary collaboration; education and training of teachers and students as an integral part of research programs; cooperative research with government agencies (e.g., in national parks, wildlife refuges and reserves, and experimental forests); contributions to society through advice on public policy and environmental management; and the establishment of an international LTER Network that now numbers 40 countries, facilitating collaboration in addressing environmental challenges in different parts of the world.

In 2010, the LTER Network received the Distinguished Scientist award from the American Institute of Biological Sciences for its contributions to the biological sciences. LTER research is featured in two of NSF's "Sensational 60" transformative scientific discoveries or advances [36]. Results from LTER research are embodied in over 10,000 peer-reviewed publications [35], a book series from Oxford University Press, and summaries on network (www.lternet.edu) and site web sites. Since 1993, the LTER research model has been adopted by 40 other member countries of the International Long Term Ecological Research Network.

Research Progress in achieving the LTER Mission begins with the work of individual scientists, students, and educators at the 26 LTER sites. It is their work at the site level that forms the foundation of knowledge, data, observational and experimental legacies, and training that will ensure a lasting impact of the overall LTER program. Data and knowledge gained from intensive field experience are also key to development of syntheses of site-level information into models that allow prediction of long-term change and responses to human and other disturbances. Site-level synthesis activities often lead to new insights that feed back to affect the future course and evolution of site-level research.

Network infrastructure also promotes and facilitates cross-site and regional analyses, leading to larger-scale syntheses and to development and testing of ecological theory. In this work, the maintenance of a network database and protocols for data discovery and acquisition are particularly important. These efforts add to the basic body of scientific knowledge of long-term, large-scale ecological phenomena and, because students are deeply involved both at the site level and in intersite and network-level syntheses, they help to increase the numbers of people with appropriate expertise in both research and environmental problem solving.

Ultimately, both site and network-level activities feed back to the development of scientific capital, which includes well-trained scientists, a well-informed citizenry, and the basic data and understanding that underpin them. This accumulation of scientific capital also leads to new research and new applications of LTER research, including new forms of support for both research and education. Growth of scientific capital also includes interactions with new scientific disciplines, leading to expansion of the scope and applications of LTER research.

Research at LTER Sites The LTER Network comprises sites chosen competitively on the basis of research excellence, quality and duration of existing data sets, and strength of the commitment to long-term research and site security. The 26 sites that constitute the network at present represent a wide variety of research emphases and approaches. As part of their commitment to the LTER program, each site conducts a series of measurements and experiments directed toward the understanding of the five core areas as well as studies addressing ecological issues specific to the site. The most common scientific approaches include observation, experimentation, comparative analysis, retrospective study, and modeling, although emphases differ among sites. A sampling of key research results from LTER sites provides an idea of the potential impact of LTER research.

The Ecosystem Value Of Dead Wood – H. J. Andrews LTER scientists revealed the importance of dead trees to diversifying animal habitat and sustaining the flow of vital nutrients in forests and streams by tracking how fallen and standing deadwood changes as forests age. These studies profoundly influenced forest management by prioritizing the retention of dead wood in forests and streams.

Arctic Warming – Arctic LTER scientists discovered how Arctic warming is increasingly thawing frozen ground (permafrost), creating hot spots of erosion, nutrient release into rivers, and decomposition of ancient organic carbon. This information is essential for managers and policymakers grappling with how to mitigate and adapt to future climate change.

Fire and Climate – Through long-term studies of fire cycles and their links to climate, Bonanza Creek scientists have documented an increase in fire severity brought on by climate warming that will likely shift the Alaskan boreal forest from a spruce- to a broadleaf-dominated landscape.

New Climate Pattern – Long-term observations allowed California Current Ecosystem scientists to define a new climate pattern called the North Pacific Gyre Oscillation (NPGO), which links physical ocean changes, such as fluctuations in salinity and nutrients, with biodiversity and ecosystem processes in the eastern North Pacific. This climate pattern may affect marine ecosystems around the world.

Biodiversity Matters – Cedar Creek scientists discovered that the number of plant species in an ecosystem – its biodiversity – has a profound and surprisingly strong effect on ecosystem function. Long-term experiments have shown that ecosystems with greater plant species diversity are more productive and stable.

Integrative Research – Central Arizona-Phoenix scientists spearheaded efforts to integrate ecological and social research in urban ecosystems. Such interdisciplinary research has changed the way scientists and citizens perceive the natural environment in cities, transformed environmental education at all levels, and informed problem solving in cities.

Future Nitrogen Cycling – Drawing on two decades of research, Coweeta researchers discovered that warmer temperatures increase peak nitrate loading to forest streams during the growing season. These findings suggest that climate warming will triple the nitrogen export from forests, reducing water quality and long-term forest productivity.

Productivity Paradox – Florida Coastal Everglades scientists revealed how human-induced nutrient enrichment in the Everglade and Caribbean wetlands affect the "productivity paradox" in which an extraordinarily high level of algal growth supports far fewer aquatic animal consumers than expected. Understanding this dynamic is critical to the restoration of the Everglade ecosystems.

Sea-Level Rise – Georgia Coastal Ecosystem scientists predicted how rising sea levels will impact coastal marshes and reduce the benefits they provide society, such as clean water and fish habitat. Analyses have shown that new marshes created by rising waters do not fully offset the loss of existing marshes.

Legacies Shape Ecosystems – Using its century-long studies, Harvard Forest scientists have documented the persistent influence of human and natural history in shaping modern forest ecosystems. Ancient land use practices and prior forest conditions continue to influence a forest's potential to grow trees, respond to disturbance and stress, and support diverse plants and animals.

Shifting Songbirds – Hubbard Brook scientists have produced the longest continuous songbird record in North America and discovered that changing habitat, land use practices, and climate in eastern forests, tropical forests, and migratory routes drive the abundance of these beloved forest musicians.

Grassland Tipping Points – Jornada LTER scientists discovered that grasslands, shrublands, and other ecosystems have "tipping points," where dramatic and rapid changes can occur once certain thresholds are reached. A better understanding of these thresholds is paramount to management and protection of grasslands and other ecosystems.

Agriculture and Climate Change – Kellogg Biological Station researchers discovered and quantified how different crop management practices can interact to provide novel opportunities for greenhouse gas mitigation by agriculture. These discoveries inform agricultural greenhouse gas policies worldwide.

Sensitive to Change – Using long-term data on plant productivity and novel experiments to manipulate rainfall, Konza Prairie scientists demonstrated that grasslands are among the most sensitive ecosystems to changes in the water cycle. This research helps forecast the impact of climate change on the carbon balance of individual plants to whole ecosystems.

Tropical Carbon Cycling – Luquillo Experimental Forest scientists discovered that carbon cycling in tropical forests is highly sensitive to climate. Relatively small increases in temperature can decrease the ability of tropical forests to store carbon recently

captured by photosynthesis, thus accelerating climate change.

Chain Reaction – McMurdo Dry Valleys scientists documented how even small variations in climate can drive major changes in polar ecosystems: Seemingly slight changes in temperature can set off a cascade of magnified responses that affect stream flow, nutrient cycling, and biodiversity.

Diversity Matters – Coral reef ecosystems are highly sensitive to disturbances and climate change. Moorea Coral Reef research documented how genetic and species diversity among corals and their symbionts helps corals to rapidly adapt to changing environmental conditions such as warming seawater and ocean acidification.

Early Warning Signs – Niwot Ridge research indicates that alpine ecosystems provide important early warning signs of global climate change. Alpine plants and animals survive on the razor's edge of environmental tolerances, making them more sensitive to changes in climate than downstream ecosystems.

Tracking Ice Cover – By synthesizing long-term records of lake and river ice cover throughout the Northern Hemisphere, North Temperate Lake scientists discovered long-term climate-induced reductions in ice cover on freshwater ecosystems over the past 150 years.

Penguins and Climate Change – Palmer Station scientists have documented a 75% reduction in Adélie penguin populations since 1980 and determined the cause to be altered cloud cover, winds, snowfall, sea ice cover, and other climate changes.

Tipping Points – Plum Island Ecosystem scientists discovered regionally specific "tipping points" beyond which marshes can no longer keep up with rising sea levels, and that human alteration of watersheds can either enhance or compromise a marsh's ability to survive in the face of rising sea levels.

Underwater Forests – Giant kelp provides critical food and shelter for a wide diversity of economically important organisms. An interdisciplinary team of Santa Barbara Coastal scientists discovered that kelp plants disperse their reproductive spores over surprisingly great distances, furthering our understanding of how these important ecosystems establish and survive.

Climate and Disease – Long-term observations and experiments by Sevilleta LTER scientists revealed an important link between human hanta virus outbreaks and the population dynamics of small mammals in the southwestern United States as affected by changes in climate systems such as El Niño. The discipline of the ecology of infectious diseases that this research helped to establish is now a transformative area of ecological research.

Plague and Prairie Dogs – For over two decades, Short Grass Steppe scientists have observed black plague spreading through populations of the black-tailed prairie dog, an endangered species candidate. The effects of the resulting die-offs ripple through other populations including other rodents, flowering plants, pollinators, and large herbivores.

Dynamic Coastal Landscapes – By tracking long-term shifts in land cover on undeveloped coastal barrier ecosystems, Virginia Coast LTER scientists have learned how sea-level rise and storms interact to create a highly dynamic landscape. While the locations of lagoons, marshes, and other coastal ecosystems have changed over time, they have not experienced a net reduction in the area they cover.

Cross-Site Research and Synthesis In addition to transformative site–based research, LTER scientists conduct synthetic studies focused on general ecological principles underlying diverse ecosystems [22, 26, 35, 37–47]. Johnson et al. [21] demonstrated the evolution of the LTER program from a collection of research sites with common goals to a highly connected research network. A few examples illustrate the breadth of LTER cross-site research.

EcoTrends – The EcoTrends Project [47] is a collaborative effort among state and federal agencies and institutions in the United States to make long-term ecological data easy to access, analyze, and compare within and across sites (see http://www.ecotrends.info). The project is designed to promote and enable the use and synthesis of long-term data to examine critical trends (e.g., climate, land cover, and habitat availability) in the Earth's ecosystems. In addition to ecological data collected by participating sites, the EcoTrends database includes ancillary data from other sources. For example, LTER investigators obtained human population and economic data from 1790 to 2000, which was one of the four types of data being synthesized in the EcoTrends Project. The "Human

Population and Economy" dataset contains over 200 separate variables suitable for describing changes in population and economic structure since the end of the eighteenth century. The dataset was collected for each of the more than 250 counties associated with the 21 continental North American LTER sites plus the Luquillo site in Puerto Rico. These datasets, tools, and information are available to anyone who would like to view trends in ecological variables for one or multiple sites or pursue additional statistical analyses of within-site and cross-site comparisons.

Climate Database (CLIMDB) and Hydrology Database (HYDRODB) – LTER sites have generally followed established LTER Climate Committee guidelines (see [29]) for collecting baseline meteorological data. Standardized measurements provided a basis for coordinating meteorological measurements at two or more sites and enabled intersite comparisons, but access to comparable datasets from multiple sites was often problematic because most sites, while making climate data accessible online, displayed them in different formats and aggregated them using different methods. Similarly, sites that conducted long-term hydrologic measurements needed to establish access to their long-term datasets for streamflow, precipitation, and ambient air temperature, in addition to the hydrologic data. LTER developed ClimDB and HydroDB in response to the science-based need for standardized measurements, format, and aggregation of these data. LTER sites, along with USGS, and USDA Forest Service sites, contribute climate (http://www.fsl.orst.edu/climhy/) and hydrological (http://www.fsl.orst.edu/hydrodb/) data, which are stored in centralized servers that provide open access to long-term meteorological and stream flow records from these research sites.

Long-Term Intersite Decomposition Experiment Team (LIDET) – Sixteen LTER sites participated in a 10-year, 28-site experiment to test the effect of substrate quality and macroclimate on long-term decomposition and nutrient dynamics – particularly the degree to which these two factors control the formation of stable organic matter and nitrogen after extensive decay. Reciprocal litter transplants of 27 species were conducted at sites in North and Central America. Decomposition rates were strongly affected by substrate quality, but climate also resulted in strong and consistent effects [25]. Large-scale patterns were better explained by variables including both moisture availability and temperature. In general, roots decomposed more slowly than leaves, but ratios of aboveground to belowground decomposition rates varied across ecosystem types. Predictions of decomposition rates were possible using uncomplicated models based on litter quality and climate, but ecosystem-specific factors also contributed to observed differences (see http://andrewsforest.oregonstate.edu/research/intersite/lidet.htm for more information).

Lotic Intersite Nitrogen Experiment (LINX) – The Lotic Intersite Nitrogen Experiment was a collaborative study of nitrogen cycling in streams involving simulation modeling, field tracer (^{15}N) additions, and intersite comparison. The central hypothesis was that the considerable variability among streams in uptake, retention, and cycling of nitrogen is controlled by key hydrodynamic, chemical, and metabolic characteristics that determine water retention, degree of nitrogen deficiency, and energy flow through food webs in stream ecosystems. LINX I ran from September 1996 through August 2001 and resulted in 26 publications, 7 theses and dissertations, and 69 presentations. The study demonstrated that the smallest streams had the highest uptake of inorganic nitrogen, and that small streams were potentially significant sources of atmospheric nitrogen via nitrification.

LINX II was a 5-year project that began in September 2001 and ended in 2006. Data from tracer experiments across 72 streams and eight regions representing several biomes showed that biotic uptake and denitrification were less efficient at removing stream nitrate in streams with high nitrate concentrations. As a result, high nitrate streams export a disproportionate amount of nitrate to receiving waters. In addition, these patterns suggest that small streams become less important as nitrate sinks as nitrate concentration increases [48].

In addition to the specific cross-site and intersite research mentioned above, LTER sites also participate in numerous long-term interdisciplinary and multi-site syntheses with both LTER and non-LTER organizations. These include studies of above- and belowground productivity, carbon dioxide (CO_2) and climate change, biodiversity, disease control, microbial ecology, remote sensing, and geographical information systems, the

adsorption of trifluoroacetate (TFA) in soils, among others.

National and International Networking – As a global leader in long-term and broad-scale ecological research, the LTER Network establishes linkages with existing and developing long-term ecological research programs in the United States and abroad. These relationships range from exchanges at the individual scientist and site research program levels, to participation in national and international meetings, to global-scale research planning and collaboration.

Nationally, LTER develops innovative partnerships with leading ecological research organizations and synthesis centers; facilitates the advancement of current ecological science and innovative research technologies; develops strong multidisciplinary science and public education programs; and pursues a multi-agency approach to develop databases of long-term research in key biomes and along major gradients.

Internationally, LTER assists in the establishment of networks for long-term ecological research worldwide; creates opportunities for collaboration between US and International LTER sites and networks; develops and operates a communication and data-sharing system among an international network of sites; facilitates the establishment of a global network of environmental research sites; and participates in other international scientific efforts.

Education Education and outreach efforts are integral aspects of the LTER program. As a network of sites with a preponderance of academic scientists, graduate and undergraduate education is central to the goals of the network. Students at both graduate and undergraduate levels are routinely engaged in collecting LTER data, performing experiments, and analyzing results. This participation forms an important part of their educational experience, and hence education and research are highly integrated in most LTER programs. The network has many examples of former undergraduate students that have become research scientists in the LTER program.

In addition, LTER provides a unique opportunity to address the educational needs of teachers and students from grades K-12. As a long-term program, LTER has the potential to provide continuous opportunities for students to participate and learn throughout their entire academic life.

The LTER Network has adopted a strategic vision for education and outreach with three components. The first component addresses the structure needed to enable LTER research to have a public impact. This structure includes leadership within the network, a distributed organization that provides resources for sites to implement education programs at the local level, and cyberinfrastructure that enables broad collaboration among local education projects and between researchers and educators. The second element of the LTER vision for education establishes the goal of conducting programs in research and development that address environmental science literacy by respecting and including the diverse perspectives that exist within the LTER Network. The final aspect of the LTER vision addresses inclusion of key constituent groups, including K-12 teachers and administrators, undergraduate and graduate students and professors, and end citizens active in LTER communities.

K-12 Schoolyard LTER Program In 1998, LTER formally expanded its education efforts to include K-12 students and teachers, mainly through the Schoolyard LTER (SLTER – http://schoolyard.lternet.edu/) program, which is funded through supplements by NSF's Division of Environmental Biology (DEB). The SLTER approach emphasizes the connection to local communities, for which an LTER site can serve as a "schoolyard" for understanding ecology and environmental science. The sites design their own programs in relation to the ecological research conducted at the site and the particular needs and resources of the local school district and community ([49], http://schoolyard.lternet.edu/LTEREduHandbook.pdf). SLTER funds support a wide range of education activities, including field trips and lab work for students, teacher professional development workshops, teaching supplies, community outreach, and program and research coordination. The schoolyard approach is particularly consistent with the development of empathy for their local environment ("Environmental Empathy") as discussed by Sobel [50] as a basis for teaching elementary age students. All the 26 LTER sites participate in the SLTER program.

As the SLTER program matured, LTER scientists devised the idea for a Children's Book Series to supplement SLTER activities – thus using children's science literature to overcome "ecophobia" while fostering environmental empathy [51]. The series currently includes three titles: "My Water Comes From The Mountains" by Tiffany Fourment (Note: the title has since been modified to reference specific mountains, e.g., "My Water Comes From The Rocky Mountains" and "My Water Comes From The San Juan Mountains"), "The Lost Seal" by Diane McKnight; and "Sea Secrets" by Mary M. Cerullo and Beth E. Simmons. Each book is richly illustrated with scenes derived from the story, with many artworks and sidebar comments by elementary school children.

Graduate and Undergraduate Education The LTER science community includes academic and government scientists and educators, graduate and undergraduate students, and professional staff. The research conducted at the sites is diverse, encompassing all aspects of ecology and ecosystem science, as well as investigations in atmospheric science, hydrology, and geomorphology. As centers of excellence in ecological research, LTER sites hosted by universities, government agencies, and nonprofit research institutions also provide important training grounds for the next generation of scientists and leaders. LTER offers opportunities for graduate and undergraduate training and education. Many undergraduate and graduate students are supported directly from LTER awards each year and others use LTER facilities and equipment in support of their research programs. In addition, the LTER Network, through its association with other networks worldwide, provides opportunities for the international interchange of students and faculty.

In addition to typical university-based training, many LTER sites are involved in NSF-funded Integrative Graduate Education and Research Traineeship (IGERT) programs, and serve as hosts for Undergraduate Mentoring in Environmental Biology (UMEB) and Research Experience for Undergraduates (REU) site activities. The programs integrate field and laboratory techniques with education, providing the students with deeper understanding of the scientific process in ecology.

Most LTER sites or their home institutions participate in the REU and UMEB programs, which offer opportunities for students at both LTER and non-LTER institutions to work with LTER scientists. Participating sites fund REU students through separate grants and supplements or out of project funds. REU students receive stipends and course credit and work closely with scientist mentors on ongoing site research programs or specially designed projects. The UMEB program provides stipends to minority students during the summer and academic year to undertake independent research projects in environmental biology under the direction of departmental faculty. Students in the program come from a wide variety of disciplines including chemistry, geophysics, and biology. Some sites provide similar opportunities through private foundations and other sources.

LTER Education in the Future The LTER Network has adopted the goal of advancing the theory and practice of ecological and environmental education at all levels and in all areas of LTER expertise. The LTER sites and network are uniquely poised to promote education at the program, institution, state, and national levels. This work builds on, and is linked closely to, LTER scientific expertise in its five core research areas and its long-term, comparative approach. LTER education addresses some of the most important but vexing objectives for ecological and environmental education; that is, it uses outdoor, inquiry-based teaching and learning to build ecological literacy; it creates effective strategies for interdisciplinary and collaborative learning about ecology and it teaches about local ecosystems while fostering an understanding of distant ones as well. Strategic objectives for future LTER education programs [2] include:

1. Expanded resources for education and outreach at both site and network levels by developing new funding sources and improving coordination with existing education and outreach programs
2. Increased participation by LTER sites in education and outreach through collaboration, coordination, training, and exchange of best practices among sites
3. Preparation and dissemination of new instructional materials designed and developed through strategic partnerships with constituent organizations, with

particular attention to the needs of traditionally underrepresented groups
4. Development of metrics to evaluate and guide education and outreach activities at site and network levels
5. Increased use of appropriate cyber technologies to improve indication among partners and to disseminate educational and outreach materials more effectively
6. Regular adaptive assessment by external evaluators to monitor progress of LTER education and outreach programs and to design new approaches when necessary

Data and Information Long-term research and synthesis demands the long-term stewardship and ready accessibility of data. The creation, curation, and dissemination of long-term databases are needed to assure that the data resources needed by researchers will continue to be available. In addition, by adopting policies that promote the timely sharing of data (both inside and outside the LTER Network), scientists can use the data in a variety of ways not anticipated by the original collector, including for regional, national, and global syntheses, thus providing a rich resource for the broader scientific community [2].

LTER has led the ecological community in developing protocols and practices for documenting, curating, and sharing data. The strategic goals for LTER information management are (1) to provide sources of high-quality, well-documented, and error-checked data at each site that support local science, stimulate synthesis and the creation of new knowledge, and facilitate transformative network-wide research at broad scales; (2) to improve existing data practices and information management systems at sites to make them uniformly easy to use, sustainable, and consistent with LTER protocols; (3) to develop a central network-level data discovery and integration platform comprising databases and servers connected through web services for single-portal data publication, discovery, and access; (4) to improve information flow between LTER and other networks; and (5) to evaluate recent developments in computer science, information technology and design, cybersecurity, community standards, and communication and collaboration technology for potential application in LTER Network and site information management.

The recent proliferation of long-term collaborative research programs has created a parallel need for scientific information systems that allow data, information, and knowledge to flow across disciplinary and cultural boundaries [52]. Scientific information systems expand the potential for scientific inquiry and are leading to a paradigm shift in biology [53] most evident to date in the genomic community [54]. Other disciplines, including ecology, are primed for similar dramatic changes driven in part by new tools and approaches to managing data. The success of long-term studies is measured both on the generation of new knowledge and the creation of data and information that will facilitate subsequent studies.

Future Directions

LTER is moving increasingly toward research that integrates ecological and social sciences (Fig. 7), having realized that fundamental questions related to the services that society receives from ecosystems, how these services are perceived, how perceptions affect behavior, and how behavioral changes affect ecosystem form and function are central to understanding the sustainability of ecosystems on which society depends. By blending ecological and social science theories, methods, and interpretations, LTER is better able to understand and forecast environmental changes at a time when no ecosystem on Earth is free from human influence. The *Decadal Plan for LTER* [34] laid out a plan for integrated, network-level research to address crucial long term social-ecological questions in three thematic areas: (1) land and water use change – the dynamics of urban, exurban, and working systems; (2) climate change, variability, and extreme events; and (3) nutrient mobilization and species introductions. These questions are interdisciplinary in nature, and were developed after extensive discussions and consultations among teams of biophysical and social scientists, educators, and

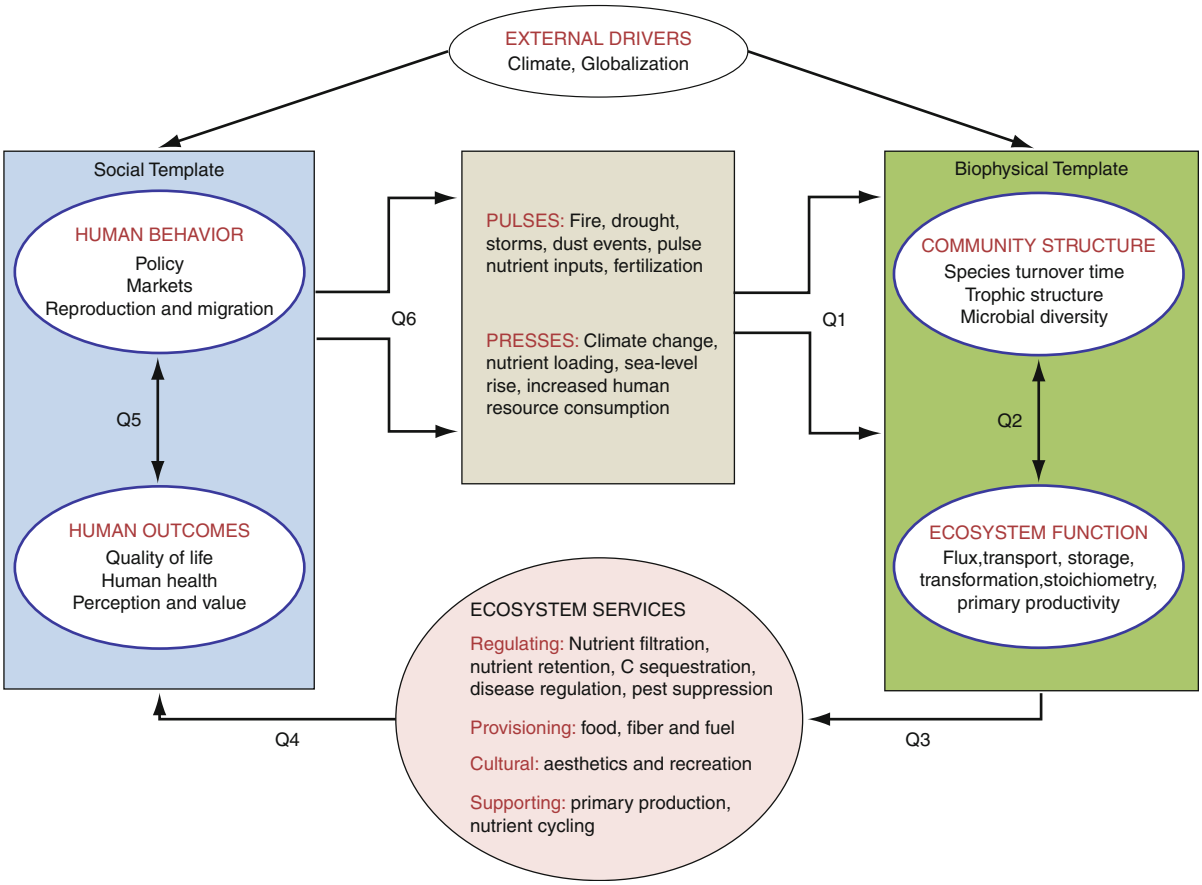

Long-Term Ecological Research Network. Figure 7
Integrated science for society and the environment, a framework for future LTER research (From Collins et al. [55])

information managers. The questions are also multi-scale, and require observations and experiments at multiple sites to test hypotheses at scales ranging from regional to continental.

In fact, LTER is uniquely positioned to address these questions for a variety of reasons related to their long-term nature, the geographic distribution of network sites, the core strength of the network's biophysical science, its considerable and growing strength in the area of coupled human-natural systems, and its commitment to K-12 education and leadership in environmental cyberinfrastructure. Nevertheless, LTER recognized that it will require new long-term social-ecological observations, experiments, and modeling to address these questions effectively; advanced environmental cyberinfrastructure to collect, store, retrieve, visualize, and integrate the resulting complex data streams; partnerships with other environmental observatory networks to achieve this integration and facilitate synthesis; and education initiatives to train the next generation of environmental scientists to address transdisciplinary issues, and to enhance environmental literacy among the public.

Specific details of how the Decadal Plan's goals are to be achieved are constantly being worked out by Network science, education, and cyberinfrastructure teams, who identify individual questions, design observations, experiments, and modeling activities to address them, and the corresponding education

and cyberinfrastructure needs for the resulting transdisciplinary research initiative. Science teams are presently developing four projects to advance the goals of the LTER Decadal Plan. The first of these projects is an effort to develop future scenarios to understand the vulnerability and resilience of regional landscapes to climate and land use change. Vulnerability to future climate change is also the theme of a second working group that will examine the affects of sea-level rise, increased storm surge, ocean acidification, and increases in water temperature, loss of sea ice, and changes in fresh water inflows on coastal LTER sites. Another working group is developing an experimental approach to evaluate the sensitivities of inland social-ecological systems to climate change to be conducted on a continental scale. Finally, a fourth group will examine how changes in the global cryosphere will affect ecosystem services such as planetary cooling, sea-level regulation, carbon storage, soil insulation, and water storage. Together, these four developing projects reflect the future direction of the LTER program.

Bibliography

Primary literature

1. The Nature Conservancy, http://conserveonline.org/workspaces/ecoregional.shapefile/documents/terrestrial-ecoregional-boundaries-tnc/. Accessed 22 Apr 2011
2. Long Term Ecological Research Network (2011) Strategic and implementation plan. University of New Mexico. http://intranet2.lternet.edu. Accessed 13 Mar 2011
3. Likens GE (1983) A priority for ecological research. Bull Ecol Soc Am 64:234–243
4. Magnuson JJ (1990) Long-term ecological research and the invisible present. Bioscience 40:495–501
5. Callahan JT (1984) Long-term ecological research. Bioscience 34:363–367
6. Risser PG (1991) Summary. In: Risser PG (ed) Long term ecological research: an international perspective, vol 47, SCOPE. Wiley, New York, pp 287–290
7. Gosz JR, Waide RB, Magnuson JJ (2010) Twenty-eight years of the US-LTER program: experience, results, and research questions. In: Müller F, Baessler C, Schubert H, Klotz S (eds) Long-term ecological research: between theory and application. Springer, Dordrecht/New York, pp 59–74
8. Tilman D (1989) Ecological experimentation: strengths and conceptual problems. In: Likens GE (ed) Long-term studies in ecology: approaches and alternatives. Springer, New York, pp 136–157
9. National Science Foundation (1977) Long-term ecological measurements: report of a conference, Woods Hole. http://intranet2.lternet.edu
10. National Science Foundation (1978) Pilot Program for long-term observation and study of ecosystems in the United States: report of a second conference on long-term ecological measurements, Woods Hole. http://intranet2.lternet.edu
11. National Science Foundation (1979) Long-term ecological research concept statement and measurement needs: summary of a workshop at the Institute of Ecology, Indianapolis. http://intranet2.lternet.edu
12. National Science Foundation (1979) A new emphasis in long-term research. Washington, DC. http://intranet2.lternet.edu/sites/intranet2.lternet.edu/files/documents/LTER_History/Historical_Documents/LTER_rfp_1980.pdf
13. Magnuson JJ, Kratz TK, Frost TM, Bowser TJ, Benson BJ, Nero R (1991) Expanding the temporal and spatial scales of ecological research and comparison of divergent ecosystems: roles for LTER in the United States. In: Risser PG (ed) Long-term ecological research. an international perspective, vol 47, SCOPE. Wiley, Chichester, p 294
14. Magnuson JJ, Kratz TK, Benson BJ (2006) Long-term dynamics of lakes in the landscape: long-term ecological research on North Temperate Lakes. Oxford University Press, New York, p 400
15. Robertson DM (1989) The use of lake water temperature and ice cover as climatic indicators. PhD dissertation, University of Wisconsin-Madison, Wisconsin
16. Quinn WH, Zopf DO, Short KS, Kuo Yang RTW (1978) Historical trends and the statistics of the southern oscillation, El Niño, and Indonesian droughts. Fish Bull 76:663–677
17. Mysak LA (1986) El Niño, interannual variability and fisheries in the northeast Pacific Ocean. Can J Fish Aquat Sci 43:464–497
18. Wahl EW, Lawson TL (1970) The climate of the mid-nineteenth century United States compared to the current normals. Mon Weather Rev 98:259–265
19. Lamb HH (1977) Climate: present, past, and future. In: Climatic history and the future. Methuen, New York
20. Swanson FJ, Sparks RE (1990) Long-term ecological research and the invisible place. Bioscience 40:502–508
21. Johnson JC, Christian RR, Brunt JW, Hickman CR, Waide RB (2010) Evolution of collaboration within the U.S. Long-Term Ecological Research Network. Bioscience 60:931–940
22. Kratz TK, Deegan LA, Harmon ME, Lauenroth WK (2003) Ecological variability in space and time: insights gained from the US LTER Program. Bioscience 53:57–67
23. Rastetter EB, Aber JD, Peters DPC, Ojima DS, Burke IC (2003) Using mechanistic models to scale ecological processes across space and time. Bioscience 53:68–76

24. Kratz TK, Cunningham GL, Dahlgren RA, Frost TM, Halfpenny JC, Hansen JD, Heisey D, Inouye RS, Kaufman DW, McKee A, Yarie J, Magnuson JJ, Rapport DJ, Gaudet CL, Calow P, Bayley P, Benson BJ, Berish CW, Bledsoe CS, Blood ER, Bowser CJ, Carpenter SR (1995) Temporal and spatial variability as neglected ecosystem properties: lessons learned from 12 North American ecosystems. In: Rapport D, Calow P (eds) Evaluating and monitoring the health of large-scale ecosystems. Springer, New York, pp 359–383
25. Gholz HL, Wedin DA, Smitherman SM, Harmon ME, Parton WJ (2000) Long-term dynamics of pine and hardwood litter in contrasting environments: toward a global model of decomposition. Glob Change Biol 6:751–766
26. Peters DP, Groffman PM, Nadelhoffer KJ, Grimm NB, Collins SL, Michener WK, Huston MA (2008) Living in an increasingly connected world: a framework for continental-scale environmental science. Front Ecol Environ 6: 229–237
27. Franklin JF (1994) The U.S. long-term ecological research program: present, future, and international. In: Nottrott RW, Franklin JF, VandeCastle JR (eds) International networking in long-term ecological research. Proceedings of an international summit. U.S. LTER Network Office, University of Washington, Seattle, pp 22–31
28. Swift LW Jr, Ragsdale HL (1985) Meteorological data stations at long-term ecological research sites. In: Proceedings of the forest environmental measurements conference, Oak Ridge, 23–28 Oct 1983. Reidel, Holland
29. Greenland D (1986) Standardized meteorological measurements for Long-Term Ecological Research sites. Bull Ecol Soc Am 67:275–277
30. Greenland D, Kittel T (1987) A climatic analysis of long term ecological research sites. http://intranet.lternet.edu/archives/documents/Publications/climdes/
31. Crowl TA, Kane M, Gholz H (2010) NSF completes 2009 LTER site reviews and initiates a 30-year review of the LTER program. In: Network news. http://news.lternet.edu/article303.html
32. Corman JR, Gholz H (2008) NSF concludes 2007 LTER mid-term site reviews. In: Network news. http://news.lternet.edu/article152.html
33. Anonymous (2003) The value of LTER site augmentation. Network News 16(1):12–16. http://intranet2.lternet.edu/
34. U.S. Long Term Ecological Research Network (LTER) (2007) The decadal plan for LTER: integrative science for society and the environment. In: LTER network office publication series no. 24, Albuquerque
35. Hobbie JE (2003) Scientific accomplishments of the Long Term Ecological Research Program: an introduction. Bioscience 53:17–20
36. National Science Foundation (2010) NSF sensational 60. http://www.nsf.gov
37. Magnuson JJ, Wynne RH, Benson BJ, Robertson DM (2000) Lake and river ice as a powerful indicator of past and present climates. Verh Internat Verein Limnol 27:2749–2756
38. Carpenter SR, Gunderson LH (2001) Coping with collapse: ecological and social dynamics in ecosystem management. Bioscience 51:451–457
39. Knapp AK, Smith MD (2001) Variation among biomes in temporal dynamics of above ground primary production. Science 291:481–484
40. Foster DR, Swanson FJ, Aber JD, Burke IC, Brokaw N, Tilman D, Knapp AK (2003) The importance of land-use legacies to ecology and conservation. Bioscience 53:77–88
41. Grimm NB, Redman CL (2004) Approaches to the study of urban ecosystems: the case of central Arizona – Phoenix. Urban Ecosyst 7:199–213
42. Seastedt TR, Bowman WD, Caine TN, McKnight DM, Townsend A, Williams MW (2004) The landscape continuum: a model for high-elevation ecosystems. Bioscience 54:111–121
43. Suding K, Collins S, Gough L, Clark C, Cleland E, Gross K, Milchunas D, Penings S (2005) Functional- and abundance-based mechanisms explain diversity loss due to N fertilization. Proc Natl Acad Sci USA 102: 4387–4392
44. Gragson TL, Grove M (2006) Social science in the context of the Long Term Ecological Research Program. Soc Nat Resour 19:93–100
45. Parton W, Silver WL, Burke IC, Grassens L, Harmon ME, Currie WS, King JY, Adair EC, Brandt LA, Hart SC, Fasth B (2007) Global-scale similarities in nitrogen release patterns during long-term decomposition. Science 315:361–364
46. Smith MD, Knapp AK, Collins SL (2009) A framework for assessing ecosystem dynamics in response to chronic resource alterations induced by global change. Ecology 90:3279–3289
47. Peters, DPC, Laney CM, Lugo AE, Collins SL, Driscoll CT, Groffman PM, Grove JM, Knapp AK, Kratz TK, Ohman MD, Waide RB, Yao J (2011) Long-term trends in ecological systems: a basis for understanding responses to global change. In: USDA agricultural research service publication no. XX, Washington, DC (in press)
48. Mulholland PJ, Helton AM, Poole GC, Hall RO Jr, Hamilton SK, Peterson BJ, Tank JL, Ashkenas LR, Cooper LW, Dahm CN, Dodds WK, Findlay S, Gregory SV, Grimm NB, Johnson SL, McDowell WH, Meyer JL, Valett HM, Webster JR, Arango C, Beaulieu JJ, Bernot MJ, Burgin AJ, Crenshaw C, Johnson L, Merriam J, Niederlehner BR, O'Brien JM, Potter JD, Sheibley RW, Sobota DJ, Thomas SM (2008) Stream denitrification across biomes and its response to anthropogenic nitrate loading. Nature 452:202–205

49. Bestelmeyer S, Dailey S, Elser M, Hembree P, Landis C, O'Connell K, Simmons B, Sommer S, Steiner S (2005) Handbook for LTER education. http://schoolyard.lternet.edu
50. Sobel D (1996) Beyond ecophobia: reclaiming the heart in nature education. The Orion Society and the Myrin Institute, Great Barrington
51. McKnight DM (2010) Overcoming "ecophobia": fostering environmental empathy through narrative in children's science literature. Front Ecol Environ 8:e10–e15. http://www.ceeauniba.net/files/e10.pdf. doi:1890/100041
52. Brunt JW, McCartney P, Baker KS, Stafford SG (2002) The future of ecoinformatics in long term ecological research. In: Rishe N (ed) Paper presented at the the 6th world multiconference on systemics, cybernetics and informatics conference, Orlando
53. Baker KS, Benson BJ, Henshaw DL, Blodgett D, Porter JH, Stafford SG (2000) Evolution of a multisite network information system: the LTER information management paradigm. Bioscience 50(11):963–978
54. Robbins RJ (1996) BioInformatics: essential infrastructure for global biology. J Comput Biol 3:465–478
55. Collins SL, Carpenter SR, Swinton SM, Ornstein D, Childers DL, Gragson TL, Grimm NB, Grove JM, Harlan SL, Kaye JP, Knapp AK, Kofinas GP, Magnuson JJ, McDowell WH, Melack JM, Ogden LA, Robertson GP, Smith MD, Whitmer AC (2011) An integrated conceptual framework for long-term social-ecological research. Front Ecol Environ 9:351–357

Books and reviews

American Institute of Biological Sciences (2003) A special section on the US long term ecological research network. Bioscience 53(1):17–98

Bowman WD, Seastedt TR (eds) (2001) Structure and function of an alpine ecosystem: Niwot Ridge, Colorado, Long-Term Ecological Research Network series. Oxford University Press, New York

Chapin FS III, Oswood MW, Van Cleve K, Viereck LA, Verbyla DL (eds) (2006) Alaska's changing boreal forest, Long-Term Ecological Research Network series. Oxford University Press, New York

Coleman DC (2010) Big ecology:the emergence of ecosystem science. University of California Press, Berkeley/Los Angeles

Ecological Society of America (2008) Special issue: continental-scale ecology in an increasingly connected world. Front Ecol Environ 6(5):227–281

Fahey TJ, Knapp AK (eds) (2007) Principles and standards for measuring primary production, Long-Term Ecological Research Network series. Oxford University Press, New York

Foster DR, Aber JD (eds) (2004) Forests in time: the environmental consequences of 1,000 years of change in New England. Yale University Press, New Haven

Gragson TL, Grove M (2006) Social science in the context of the Long Term Ecological Research Program. Soci Nat Resour 19:93–100

Greenland D, Goodin DG, Smith RC (eds) (2003) Climate variability and ecosystem response at long-term ecological sites, Long-Term Ecological Research Network series. Oxford University Press, New York

Havstad KM, Huenneke LF, Schlesinger WH (eds) (2006) Structure and function of a Chihuahuan Desert ecosystem: the Jornada Basin long-term ecological research site, Long-Term Ecological Research Network series. Oxford University Press, New York

Knapp AK, Briggs JM, Hartnett D, Collins SL (eds) (1998) Grassland dynamics: long-term ecological research in tallgrass prairie, vol 1, Long-Term Ecological Research Network series. Oxford University Press, New York

Lauenroth WK, Burke IC (eds) (2008) Ecology of the shortgrass steppe: a long-term perspective, Long-Term Ecological Research Network series. Oxford University Press, New York

Magnuson JJ, Kratz TK, Benson BJ (eds) (2005) Long-term dynamics of lakes in the landscape: long-term ecological research on north temperate lakes, Long-Term Ecological Research Network series. Oxford University Press, New York

Michener WK, Waide RB (2008) The evolution of collaboration in ecology: lessons from the United States Long Term Ecological Research Program. In: Olson GM, Zimmerman A, Bos N (eds) Scientific collaboration on the Internet. MIT Press, Cambridge, MA, pp 297–310

Porter JH (2010) A brief history of data sharing in the U.S. Long Term Ecological Research Network. Bull Ecol Soc Am 91:14–20

Priscu JC (ed) (1998) Ecosystem dynamics in a polar desert: the McMurdo Dry Valleys. American Geophysical Union, Washington, DC

Redman C, Foster D (eds) (2008) Agrarian landscapes in transition: comparisons of long-term ecological and cultural change, Long-Term Ecological Research Network series. Oxford University Press, New York

Robertson GP, Coleman DC, Bledsoe CS, Sollins P (eds) (1999) Standard soil methods for long-term ecological research, vol 2, Long-Term Ecological Research Network series. Oxford University Press, New York

Ross RM, Hofmann EE, Quetin LB (eds) (1996) Foundations for ecological research west of the Antarctic Peninsula, vol 70, Antarctic research series. American Geophysical Union, Washington, DC

Shachak M, Gosz J, Pickett STA, Perevolotski (eds) (2005) Biodiversity in drylands: toward a unified framework, Long-Term Ecological Research Network series. Oxford University Press, New York

Zimmerman A, Nardi B (2010) Two approaches to big science: an analysis of LTER and NEON. In: Parker JN, Vermeulen N, Penders B (eds) Collaboration in the new life sciences. Ashgate, Burlington, pp 65–84

M

MAGLEV Technology Development

James R. Powell[1], Gordon Danby[2]
[1]Maglev-2000 Corporation, Shoreham, NY, USA
[2]Maglev-2000 Corporation, Wading River, NY, USA

Article Outline

Glossary
Definition of the Subject and Its Importance
Introduction
The Physics and Engineering of Maglev
Maglev Applications
Future Directions
Bibliography

Glossary

Gap The physical clearance between a Maglev vehicle and the guideway it travels along.

Guideway The structure that holds Maglev vehicles as they travel. Guideways can be elevated above the local terrain, or on-grade, depending on the design, need for isolation from the local surroundings, and other factors.

Maglev (magnetic levitation) Transport of vehicles that are magnetically levitated above a guideway and magnetically propelled along it.

Magnetic Induction The generation of induced current in a conducting loop by the movement of a magnet past it.

Magnets, electromagnetic The generation of a magnetic field by a current in a loop of conductor, usually wound around an iron core to increase the strength of the magnetic field.

Magnets, permanent A physical object that is the source of a magnetic field, without the need for an electric current to produce the field. The movement of orbiting electrons in the atoms of the permanent magnet is locked in place to create the magnetic field.

Magnets, superconducting The generation of powerful magnetic fields from a loop or loops of zero electrical resistance superconducting wire, usually wound as an air core magnet without iron.

Superconductors Materials that when cooled below a transition temperature completely lose electrical resistance. They can carry very large currents at very high current densities, hundreds of thousands of amps per square centimeter of cross section, indefinitely without any decay in their current and without any voltage being applied to them.

Definition of the Subject and Its Importance

Maglev (magnetic levitation) is the first new mode of Earth-based transport since the invention of the airplane. Maglev vehicles are magnetically levitated and propelled along a guideway, with no mechanical contact and friction, their speed limited only by atmospheric drag. In evacuated tunnels, Maglev vehicles can potentially reach orbital speeds of 8 km/s (18,000 mph). Traveling in the atmosphere, Maglev vehicles have reached 580 km/h (361 mph).

Maglev vehicles have no engines, do not burn oil or other fuels, do not emit pollutants and greenhouse gases, and are quiet, with no rail or engine noise. They are propelled by the interaction between AC currents in the guideway and the magnets on the vehicle. The speed and position of Maglev vehicles on the guideway is determined by the frequency of the AC current that propels them. The distance between individual Maglev vehicles on the guideway can be designed to always remain constant, regardless of what conditions the different vehicles encounter, that is, up or down grades, curved guideways or straight, head or tail winds, etc. The individual vehicles are not

Robert A. Meyers (ed.), *Encyclopedia of Sustainability Science and Technology*, DOI 10.1007/978-1-4419-0851-3,
© Springer Science+Business Media, LLC 2012

controlled by on-board engineers. Instead a central traffic control center views the entire guideway in real time to detect potential hazards, controlling the location and speed of all vehicles by means of the frequency of the AC propulsion current fed to the energized block of guideway that each individual vehicle travels on.

Maglev vehicles can travel as individual single units on the guideway, or during high levels of traffic, can be coupled together to form multi-vehicle consists. Each vehicle is individually propelled by the AC current applied to the energized block of guideway the vehicle, or the multi-vehicle, consist is traveling on.

There are two types of Maglev: electromagnetic and electrodynamic. In electromagnetic Maglev the vehicles are equipped with conventional electromagnets in which a DC current winding energizes an iron structure to create a strong magnetic field. The vehicle's electromagnets are positioned underneath two iron rails attached to the guideway. The magnetic force between the vehicle's electromagnets and the guideways iron rails located above them levitate the vehicle.

Electromagnetic Maglev has three major limitations. First, its magnetic suspension is inherently unstable. As the vehicle electromagnets move closer to the iron rails above them, the attractive force automatically increases. To prevent a crash, the DC current in the vehicle's electromagnets must be reduced by a servo control system that operates on a very fast time scale, that is, thousandths of a second. The servo control system thus continuously adjusts current to maintain a safe gap between the vehicle and the guideway. The second limitation is that to keep the DC magnet power required to levitate the vehicle at an acceptable level, the gap between the vehicle and guideway must be very small, on the order of 1 cm (3/8 in.). This requires a very precise and high cost guideway. The third limitation is that the lifting capability of the Maglev vehicle is small, because of the heavy magnet and power system weights.

The second type, electrodynamic Maglev, uses permanent magnets on the vehicle, not electromagnets. Instead of having iron rails on the guideway, electrodynamic Maglev uses ordinary aluminum loops that are located beneath the vehicle's permanent magnets, not above them. As the Maglev vehicle moves along the guideway, its magnets induce currents in the aluminum loops. These induced currents magnetically interact with the vehicle's permanent magnets, automatically levitating it. The suspension is automatically and inherently stable – the closer the vehicle gets to the aluminum loops beneath it on the guideway, the stronger the levitating force. With appropriate design, Maglev vehicles using electrodynamic forces can be strongly stable in the vertical, horizontal, pitch, yaw, and roll directions, but able to move freely in the longitudinal direction along the guideway.

Electrodynamic Maglev can use either conventional permanent magnets or superconducting magnets. The conventional permanent magnets are much weaker in magnetic strength than superconducting magnets. As a consequence, Maglev vehicles that use permanent magnets have very small gaps between the vehicle and the guideway, on the order of 1 cm (3/8 in.) and are very limited in their capability to lift heavy weights.

In contrast, Maglev vehicles that use superconducting magnets have much larger gaps between the vehicle and the guideway, on the order of 10 cm (4 in.) or more, and have much greater weight-lifting capability. Moreover, they are inherently very strong, stable, and can be designed to resist hurricane force winds and strong earthquakes without contacting the guideway.

The technology for superconducting magnets is commercially well developed. There are thousands of superconducting MRI medical units all around the world, and superconducting magnets are widely used in R&D laboratories. The Large Hadron Collider (LHC) at the CERN Laboratory in Switzerland, for example, has 54 km (31 miles) of superconducting magnets, all of which must function perfectly for the LHC to operate. The same length of magnets on Maglev vehicles would provide half of the highway and airplane passenger miles in the USA, plus half of the intercity truck long distance miles.

Japan is now operating a first-generation passenger Maglev system in Yamanashi Prefecture that has carried well over 80,000 passengers, with accumulated running distances of hundreds of thousands of kilometers. Japan plans to extend their system to become a 500 km (300 miles) route between Tokyo and Osaka that will carry 100,000 passengers daily, with a trip time of 1 h.

Germany has developed a first-generation electromagnetic Maglev passenger system called Transrapid.

A commercial 31 km Transrapid system now operates between the center of Shanghai, China, and its airport.

An advanced second-generation superconducting Maglev system, termed Maglev-2000, is being developed in the USA. The basic components – quadrupole magnets, aluminum loop guideway panels, guideway beam and vehicle – have been fabricated and successfully tested, but as yet funds for operational testing at high speed on a guideway have not been available.

The second-generation Maglev-2000 system will have important new and unique capabilities beyond those already achieved by the present Japanese and German first-generation Maglev systems that will make it a major mode of sustainable transport in the rest of the twenty-first century. These new capabilities include:

- Transport of autos and trucks on Maglev vehicles, enabling electric vehicles to make long trips without the need to consume gasoline
- Much lower cost guideway system that can be privately financed and will not require government subsidies
- High speed electronic skip-stop switching of vehicles to off-line stations for unloading/loading operations enabling high average speeds with many closely spaced stations
- Ability to adapt Maglev-levitated travel to existing railroad tracks at very low cost, enabling Maglev travel inside urban and suburban areas without needing to build new infrastructure
- Ability to greatly reduce highway deaths and injuries by transporting people, autos, and trucks on Maglev rather than on highways
- Ability to use superconducting Maglev for other important applications, including low cost storage of electrical energy from variable wind and solar farms; the long distance, low cost transport of fresh water to drought areas; and very low cost for launching payloads into orbit, particularly space solar power satellites that can beam massive amounts of clean power down to Earth to meet power needs in an environmentally acceptable manner

The implementation of Maglev as a major mode of transport will enable much better sustainable living standards for the world's population, without environmentally damaging the planet by the massive use of fossil fuels.

Introduction

History and Impact of New Modes of Transportation

Over the last 200 years, the development of revolutionary new modes of transport have transformed human society, greatly raising the standard of living and enabling people to do things that were previously undreamed of.

Maglev, magnetic levitation, is such a revolutionary new mode of transport. It will dramatically change how humanity transports people and goods, launch payloads into space, store large amounts of electrical energy generated by wind and solar sources, and deliver billions of gallons of water over long distances to drought stricken regions. Moreover, it will be sustainable for the long term, and not require the use of destructive fossil fuels. In 1800, the only modes of travel were walking, horses, wagons, and sailing ships. In the USA, the per capita annual GDP was only $1,200 (in constant 2007 dollars) and the annual per capita travel distance was just 1,500 miles [1]. Today, the annual per capita GDP is $50,000 (in constant 2007 dollars) and the per capita annual travel distance is 15,000 miles [1].

What happened? A series of revolutionary new modes of travel that made it much faster, better, and cheaper to transport people and goods. During the Constitutional Convention, it took many days to travel from New England to Philadelphia, and to cross the ocean, many weeks. Even in the late 1800s, with steam boats and railroads, it took Phileas Fogg 80 days to go around the world.

The eight major transport revolutions initiated by the USA were (Fig. 1):

1. The Erie Canal (1814)
2. Steamboats on the Hudson and Mississippi (1807 and 1811)
3. The Transcontinental Railroad (1869)
4. The Panama Canal (1914)
5. Henry Ford and the Model T (1908)
6. The Wright Brothers and Kitty Hawk (1903)
7. The Interstate Highway System (1956)
8. The Moon Landing (July 20, 1969)

MAGLEV Technology Development. Figure 1
The eight American transport revolutions

Maglev will be an equally transforming new mode of transport. On Earth, it will move people and goods without being powered by fossil fuels that emit massive amounts of greenhouse gases and pollutants, in vehicles that are very safe, efficient, convenient, quiet, and comfortable. Maglev will also store large amounts of electric energy at very high efficiency and low cost, transport very large amounts of water for long distances over difficult terrain, and launch payloads into space at very low cost, including space satellites that can beam large amounts of power to the Earth.

Why Fossil Fueled Transport Is Not Sustainable

Today's Transport Systems – autos, trucks, airplanes, most trains, and ships – are critically important to present society and its standard of living. All are critically dependent on oil. Without oil, humanity would be back in the 1700s, with only horses and wagons and sailing ships.

Since Edwin Drake started pumping oil in Western Pennsylvania in 1859, the world has consumed approximately one trillion barrels of oil, most of it for transport. How much is a trillion barrels? Visualize a lake of oil that is one square mile in cross section containing a trillion barrels of oil. The oil lake would be 40 miles deep.

Another trillion barrels of oil is still in the ground, but it will not sustain the world for very long. World oil production has plateaued at about 30 billion barrels per year and will soon start to steadily decline. More significant than the arguments over when the "peak oil" crisis will occur is the "oil competition" crisis. As countries like China and India rapidly industrialize, competition with the developed countries for ever scarcer oil will drive up the price of oil. Today, highway traffic in China is increasing 18% annually, and more cars are sold per year in China than in the USA. Today (2010) oil costs about $80 per barrel; in a few years, analysts predict $200 per barrel.

For most of the rest of the twenty-first century, the present world transport systems will not be sustainable, using conventional oil for fuel.

Can society sustain existing autos, trucks, airplanes, trains, and ships with some alternative fuel as the oil runs out? Biofuels? Hydrogen? Synthetic fuels derived from coal, oil shale, tar sands, methane hydrates from ocean beds? No. None of these will be able to maintain society's present transport systems powered by the internal combustion engine. There are a variety of reasons why these alternative fuels are not practical on the scale needed to support a world population of nine billion people in 2050 (Fig. 2).

Biofuels? Not practical for the amounts needed. The acreage required is prohibitively large. In a world

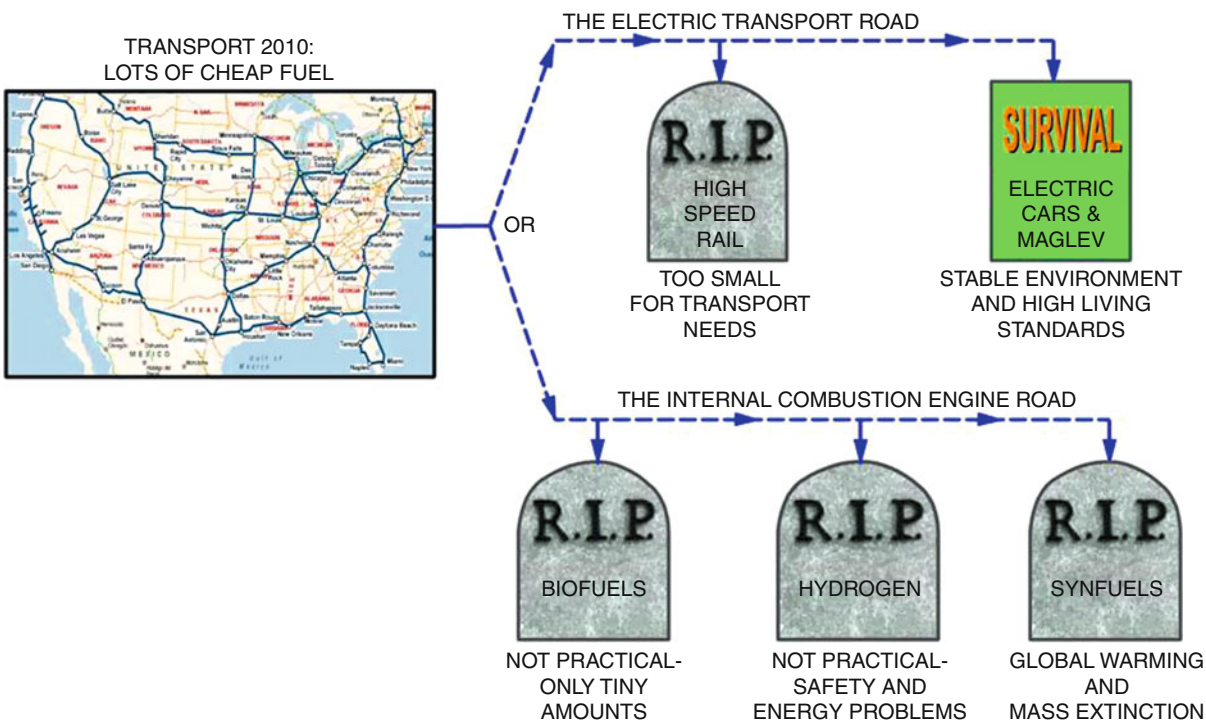

MAGLEV Technology Development. Figure 2
The decision tree for future transport

where there is not enough arable land to adequately feed today's population of 6.6 billion people, which is projected to be 9 billion by 2050, biofuels can supply only a tiny fraction of future transport needs. Not only is the population growing, but the fertility of the world's arable land is declining, due to over use, erosion, increasing acidification due to excessive use of fertilizers, and increasing droughts. Humanity will be lucky to avoid massive famines in the years ahead, even if biofuels are not produced.

Hydrogen fuel would require 1,000 new nuclear reactors, each of 1,000 MW electrical capacity – ten times more than now operated in the USA – to make enough hydrogen fuel to equal the gasoline and diesel fuel currently consumed in USA's transport systems.

Hydrogen cars raise a serious security issue. Over one million cars are stolen in the USA per year. After stealing a hydrogen car, a terrorist need only attach a small bomb with an explosive-driven penetrator to the hydrogen tank, and then park it in a public parking garage, or shopping mall, or on a busy city street. The penetrator bomb could be then remotely detonated by cell phone or an attached timer, releasing the hydrogen gas to cause a massive explosion. Result? Many deaths with no way to prevent them. A terrorist would need no special skills. The penetrator bombs could probably be bought in the black market.

While more expensive than oil, synthetic gasoline and diesel fuel can be manufactured from coal, tar sands, oil shale, and methane at an acceptable cost. The reserves are enormous and could sustain oil-fueled transport for hundreds of years.

The problem with synfuels is not the sustainability of fuel supply, but sustainability of Earth's environment due to the release of carbon dioxide to the atmosphere from the manufacture of the synfuels, and the release of carbon dioxide from the tailpipes of the vehicles that burn the synfuels. Today, the US transport sector emits two billion tons per year of carbon dioxide into the atmosphere [2], roughly one-third of total US emissions. The carbon dioxide emissions from the manufacture of the synfuels needed to replace the oil now consumed by US transport would add another two billion tons per year to the atmosphere, for a total transport emission of four billion tons annually.

Would leaders call for a reduction of 80% in carbon dioxide emissions from today's levels, to be achieved by 2050? This corresponds to a total world emission of five billion tons annually in 2050. Four billion tons of just US transport emissions at today's level of transport would be four-fifth of the world's total.

With synfuels for transport, there is no way to reduce carbon dioxide emissions below today's level, even if all other present sources – coal-fired power plants, industry and home heating, etc. – were to go to zero. In fact, as the developing countries industrialize, their transport needs will greatly increase, making the world's total emissions from transport alone in 2050 much greater than today's total world emissions of 25 billion tons per year [3].

There is no practical way to capture the carbon dioxide emissions from autos, trucks, airplanes, trains, and ships. Inevitably, they will enter the atmosphere.

The climate effects of global warming are very bad – higher temperatures, melting glaciers and ice sheets, increased droughts and food shortages, rising sea levels and flooding, species shifts and extinction, etc. Even worse, at some point, high levels of carbon dioxide emissions risk environmental catastrophe that cannot be stopped, even if all emissions went to zero.

As global warming from the release of greenhouse gases continues, the ocean is becoming more acidic, threatening sea life. Natural carbon dioxide emissions from decaying organic matter in the permafrost regions, plus thermal decomposition of unstable methane hydrates in the sea bed, may cause an irreversible runaway warming of the Earth.

Humanity should not risk global disaster by continuing to emit massive amounts of carbon dioxide from its transport systems. A transition to electrically powered transport must soon start, with the electricity coming from nonpolluting energy sources (Fig. 2).

Maglev and Electric Transport: A Necessity for Long-Term Sustainability

There are three options: electric cars and trucks, electric rail, and Maglev. Electric cars are desirable and practical, but have limitations. The Chevrolet Volt, for example, which will soon be commercially available, has a maximum range of about 40 miles before it must be recharged or shifted to an auxiliary gasoline engine to extend its range [4]. Longer trips almost certainly

will use the gasoline engine because nobody will want to stop every 40 miles or so and wait several hours for a recharge.

There are other limitations. In colder regions, batteries should not be charged or discharged unless they are warmed, as this may degrade them. Heating the car from the battery will reduce the car's range. In hot regions, running the air conditioner from the battery will also reduce range. The battery pack will be very heavy, hundreds of pounds, increasing the weight of the car.

In combination with Maglev, electric cars and trucks can provide practical transport, for both short and long trips. The electric cars can operate locally for trips of a few miles to the nearest Maglev station, there to drive onto a Maglev vehicle that will transport the drivers and their automobiles to any other station in the continental USA at speeds of 300 mph. At the station nearest the destination, the car would be driven off the Maglev vehicle, a few miles by highway to the final destination.

During the trip on the Maglev vehicle, the electric cars would be fully recharged, using on-board power, and ready to travel once driven off. The cost to drivers traveling on a high speed Maglev trip would be less than if driving by highway with a gasoline-powered engine. Maglev would provide the same kind of service for long distance trucks. The average haul distance for intercity trucks, which currently transport 1½ trillion ton miles of freight per year at an annual cost of over $300 billion, is 500 miles. There is no way that electric trucks can make that haul distance if traveling by highway.

With a National Maglev Network, almost all travel could be electrically powered, with long distance travel for autos, trucks, and passengers by Maglev, while electrically powered autos and trucks handled short local trips. There would be little domestic air travel, with most flights being across the oceans and to remote areas not served by Maglev.

Electrically powered conventional rail will still transport bulk freight – grain, cement, etc. – but, the role of high speed rail (HSR) will be limited. This is because HSR only carries passengers, is inherently expensive, and must be subsidized by the government, even in Europe and Japan. Even in countries like France which is much smaller than the USA, with considerably high population density, for example, HSR plays only a small role in transport [1]. Per capita, on average the French travel only 400 miles per year on the TGV, while driving 7,600 miles per year and only taking a 1¼ trip per year on the TGV.

The Physics and Engineering of Maglev

The Physics of Maglev

It has been well known for well over a century, since the beginning of the electrical age, that electromagnetic forces can be very strong, even stronger than gravity. This principle makes magnetic levitation possible. Moving charged particles, which usually means electrons, create magnetic fields. Matter contains atomic electrons perpetually whirling around in orbits. Most materials are largely nonmagnetic because the moving electrons cancel each others' magnetic fields, even when an external magnetic field is applied. A few materials are ferromagnetic. This material responds to external magnetic fields by aligning the electron orbits to produce very strong induced magnetic fields within the ferromagnet that extend beyond it into the surrounding air. When the external magnetic field is removed, the ferromagnetic object essentially returns to the unmagnetized state. It is fortunate that iron, a common and cheap structural material, is strongly ferromagnetic. This enabled the creation of the generators and transformers that made AC electric systems very practical.

It was quickly realized, however, that stable suspension in air is not possible with ferromagnetic materials using static, that is, non-time-varying, external excitation. This is known as Earnshaw's Theorem. The unstable force causes magnetized iron to clamp itself to another piece of iron with a force which gets stronger as it gets closer. This is clearly not suitable for levitation.

Permanent magnets are familiar to people and can be used for levitation. These magnets are made of unusual materials which resist easy magnetization or demagnetization. When exposed to very strong external magnetic fields during manufacture, a large fraction of the electron orbits line up parallel and retain strong magnetization alignment after the charging magnetic field is removed.

Two such permanent magnets will attract each other when the magnets' electron orbits are parallel. However, if one magnet is turned over, the magnets will

strongly repel each together. As the magnets get closer, the repulsive force becomes stronger. At some distance, the repelling force is sufficiently strong to equal that of gravity.

This then leads to suspension at a height where the repulsion force equals that of gravity. However, without additional constraint, this type of suspension is not practical for levitation. The suspended magnet is unstable at right angles to the direction of gravity. A familiar example is two donut-shaped permanent magnets centered on a stick. With the magnetic polarity opposing, the lower magnet will suspend the upper magnet. However, if the lower magnet is moved up on the stick to the point where the upper magnet leaves the top of the stick, the latter will be violently thrown off to the side.

Figure 3 shows how stable levitation can be produced. This is a familiar Maglev model construction for school science projects. The side mounted magnets and the vertically mounted magnets in combination create forces which are highly stable in both directions. For a real Maglev transport system, low cost familiar ferrite magnets can only levitate a very small weight. Moreover, to build many miles of permanent magnet guideway would require an enormous volume of very expensive material to be purchased, installed, and maintained. There is a class of Rare Earth permanent magnets which produce forces at least ten times greater than ferrite magnets. However, this material which weighs as much as iron costs hundreds of times more per pound than iron. In summary, for a robust Maglev system with substantial suspension clearances that can levitate heavy weights, using a permanent magnet approach is not practical.

Let us return to the ferromagnetic circuit which is statically inherently unstable. Figure 4 illustrates that if the applied magnetizing current in a coil is electrically varied over time, the unstable force can be controlled so that a practical suspension is possible. Sensors continually monitor the air gap and signal the power supply to adjust the circuit current in a suitable time-dependent manner so that the air gap is maintained at a constant value. This is the system used by Transrapid [5]. As was the case for permanent magnets shown in Fig. 3, both horizontal and vertical magnets are required for stability in both directions. On each side of the guideway, magnets attached to the vehicle are attracted upward to the bottom of the iron rails on the guideway, providing levitation. Magnets of each side are attracted sideways to the edge of the guideway, as illustrated in Fig. 5, providing lateral guidance. The operating gap between the vehicle magnets and the iron rails on the guideway is typically very small with the electromagnet iron rail system, on the order of 1 cm (3/8 in.).

Another type of magnetic suspension results from applying alternating current (AC) to a current-carrying coil located above a sheet of electrically conductive normal metal, such as copper or aluminum. If the frequency is sufficiently high, currents are induced in the metal sheet that keeps the AC magnetic field from

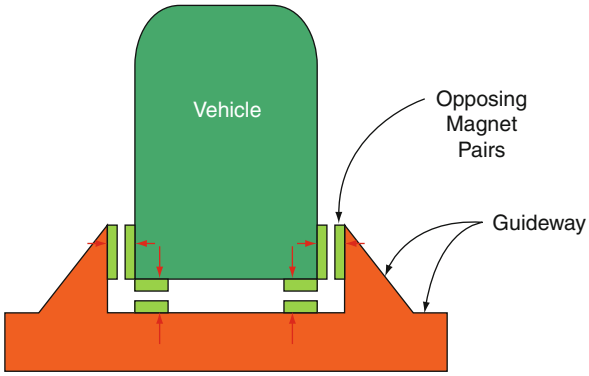

MAGLEV Technology Development. Figure 3
Magnetic suspension based on the repulsive force between permanent magnets on a vehicle

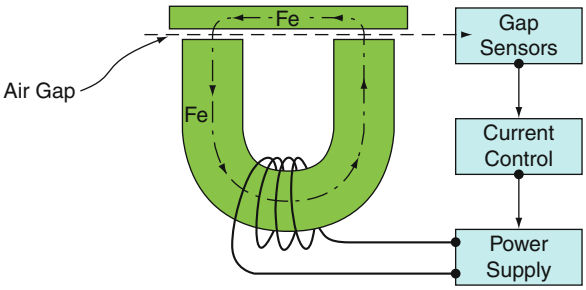

MAGLEV Technology Development. Figure 4
Magnetic suspension based on servo control of the attractive force between an electromagnet and a ferromagnetic sheet

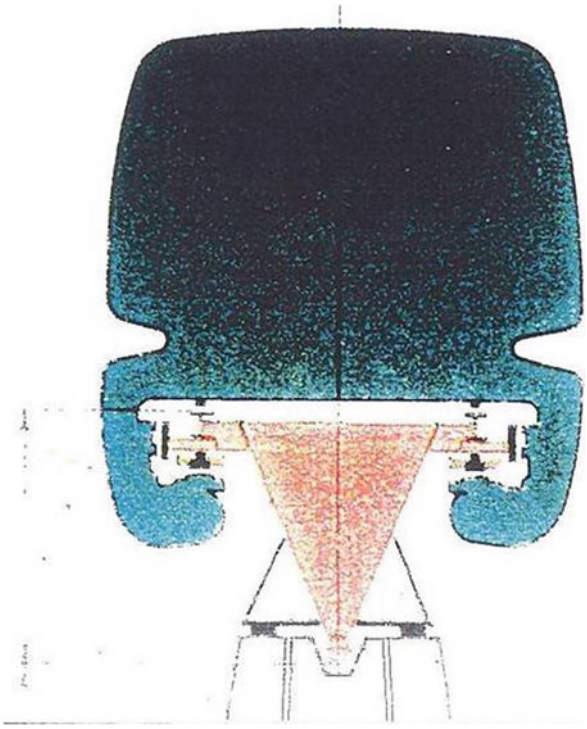

MAGLEV Technology Development. Figure 5
Cross section view of Transrapid Maglev vehicle showing electromagnetic suspension

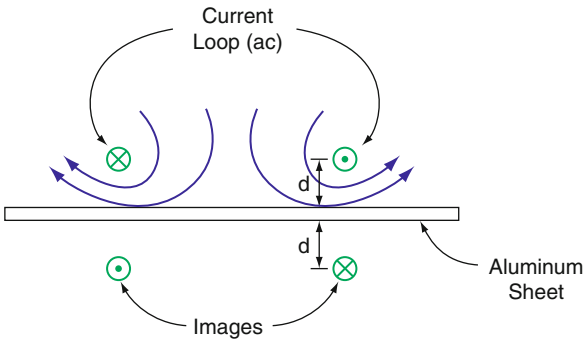

MAGLEV Technology Development. Figure 6
Magnetic suspension based on the repulsive force between a coil carrying alternating current (AC) and a conducting sheet

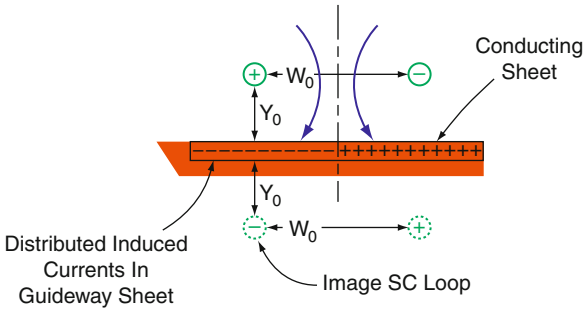

MAGLEV Technology Development. Figure 7
Superconducting (SC) inductive suspension conducting sheet guideway

penetrating the sheet. These induced currents are opposite in direction to the currents in the AC coil above the sheet. The magnetic interaction between the opposing currents produces a repulsive force similar to that of opposing permanent magnets which can levitate the AC coil (Fig. 6). As early as 1912, Batchelet [6] obtained a patent on such a system for vehicle transport. While not practical for transport because of its very inefficient use of energy, it does work from the physics viewpoint.

The concept of induction brings us to electrodynamic Maglev. Note that induction occurs because of time-varying applied magnetic fields. The usual example is an applied AC current, for example, as seen in transformers, which make our electric utility power distribution practical. In the case of Maglev, static (DC) magnets on a vehicle moving along the guideway can also apply a time-varying, that is, AC field to normal conductors that they pass on the guideway.

Powell and Danby shared a house from 1960 to 1962. This was about the time superconducting wires capable of producing strong superconducting magnets were first becoming available. Dr. Powell had studied the use of superconductors positioned on a guideway and the vehicle for Maglev. Then Dr. Danby provided key electrodynamic insights into using induction from superconducting magnets on a vehicle to generate currents in normal conductor loops on the guideway. Together Danby and Powell proceeded to develop and patent superconducting electrodynamic Maglev for which the Benjamin Franklin Medal for Engineering in April 2000 was awarded [7].

These innovations are described on the following figures. Figure 7 shows a superconducting coil moving above a conductive sheet. This configuration, while possible, is less desirable, but is readily visualized.

Figure 8 shows the conductive sheet replaced by a bundle of wire forming a shorted coil. Figures 9–13 illustrate a variety of the many configurations for use of what the authors' term "null flux" loop geometries. These null flux configurations, as discovered by the authors, have proved to be a very desirable approach for superconducting electrodynamic Maglev. The use of strong superconducting magnets enables the vehicle to levitate very heavy loads while at the same time keeping electrical I^2R losses in the normal guideway conductors at a minimum level [7, 8].

In Fig. 9 the superconducting (SC) magnet loop, which is attached to the vehicle, is shown halfway between the guideway loops. The induction in the top and bottom guideway loops is equal and opposite, since these loops are added in series opposing. As a result, no current flows, no force is exerted, and no power is consumed. As the vehicle magnet drops down because of the vehicle weight, a current and force proportional to displacement occurs. The vehicle is suspended with a restoring force as in a spring. In Fig. 10, two loops on the guideway are mounted side by side and connected in series opposition. If the SC loop on the vehicle is centered, there is no net induction or current or force. This gives a strong linear restoring force sideways as the vehicle moves sideways off center. Figure 11 is identical to Fig. 10, but oriented at 90°. Now the force is vertical instead of horizontal. Figure 12 shows another example. When centered there is no induction or sideways force due to the guideway loop. Figure 13 shows canceling of the force between the two sides when the vehicle is centered. In all the above cases, strong restoring forces are developed proportional to the displacement from the ideal position of the vehicle, that is, centered. The figure of 8 configuration is used in the very successful Japanese Maglev [9].

Why is the null flux principle so powerful? For the simple loop of Fig. 8, the geometry and the total ampere turns in the superconducting magnet completely determine the induced current in the shorted guideway loop. With the null flux configuration, the number of ampere turns in the vehicle SC magnets can be much greater than the guideway ampere turns and still have a very strong suspension.

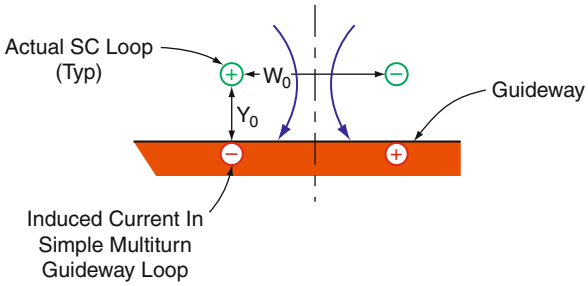

MAGLEV Technology Development. Figure 8
Superconducting (SC) inductive suspension simple loop guideway

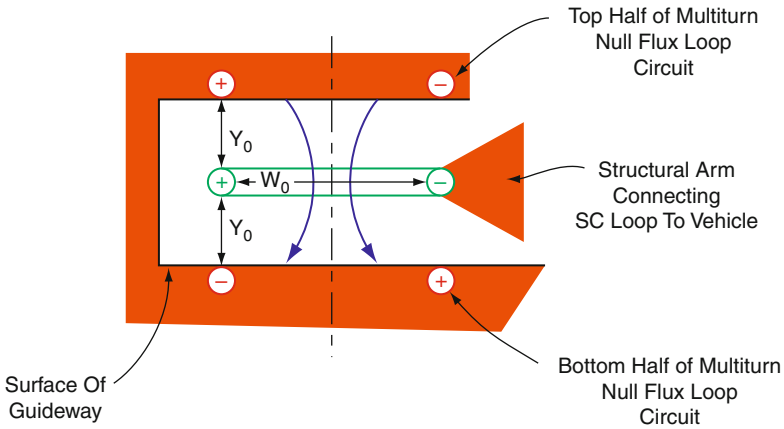

MAGLEV Technology Development. Figure 9
Series opposed loops

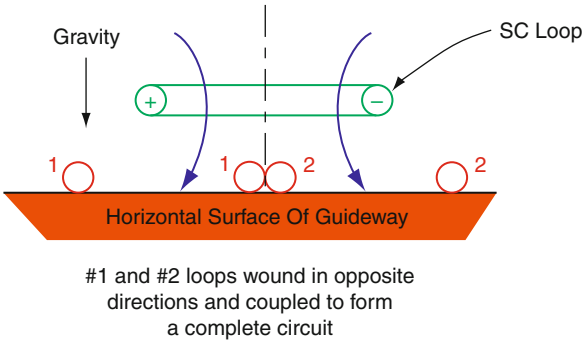

MAGLEV Technology Development. Figure 10
Horizontal figure of 8

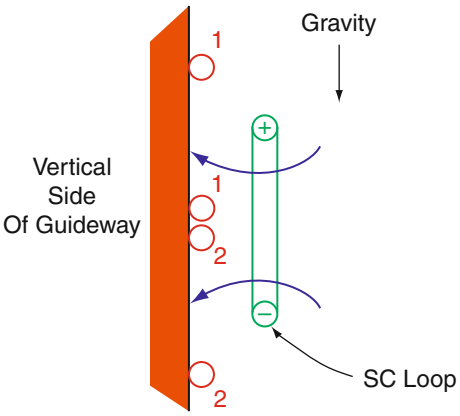

MAGLEV Technology Development. Figure 11
Vertical figure of 8

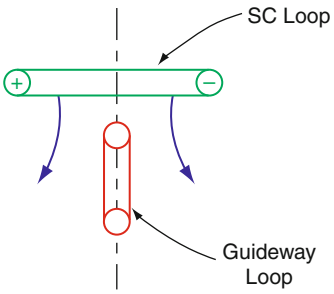

MAGLEV Technology Development. Figure 12
Central orthogonal loop (horizontal or vertical orientation)

This reduces material requirements for the guideway coils and results in low I^2R losses in the guideway. Stronger SC magnets on the vehicles are well within the state of the art. These stronger magnets in turn result in less power needed for the linear synchronous motor discussed later. Moreover, because of the very efficient null flux levitation configuration, most of the propulsion power required for Maglev vehicles at high speeds is due to air drag, not electrical loss.

Throughout the history of technological evolution, ideas that were known in principal had to await new technical advances to make them truly practical. That is the case with Maglev. Early visionaries of Maglev over the last 100 years include Bachelet [6], Goddard [10], and Kemper [11]. Lightweight and strong superconducting magnets provided a great step forward for electrodynamic Maglev. The materials that made this possible appeared about 1960. This in combination with the authors' null flux loop guideway made Maglev eminently practical. Similarly, the development of modern power supplies, controls, and sensors permits fast-acting electronic control of the iron magnets of the Transrapid system which has been demonstrated in Germany and commercially implemented in China.

From the Maglev point of view, a superconducting winding behaves like a very light and strong permanent magnet which is located in a very low temperature container, or cryostat. Superconductivity is now in routine use, especially in the MRI scanners found in hospitals and doctors facilities. Figure 14 shows the history of superconducting development. At the very low temperatures of liquid helium, 4.2 K, Kammerlinge Ohnes [12] discovered that various pure metals had no resistance to current flow. In turn, the flowing electron current generates magnetic fields without the I^2R losses experienced in normal conductors. While the discovery was of great interest to physicists, it was almost 50 years before superconductors were developed which could carry large currents in the presence of high magnetic fields as necessary for magnets. The most common superconducting wire for magnet builders for the last several decades has been Niobium-Titanium (NbTi) followed by Niobium 3-Tin (Nb_3-Sn).

Figure 15 shows the behavior of NbTi alloy. The lower the operating temperature, the greater the superconducting current and magnetic field that can be sustained, that is, the more powerful the magnet capability. Figure 16 shows the behavior of these two most common superconductors at the temperature of boiling helium. Note the much greater current densities

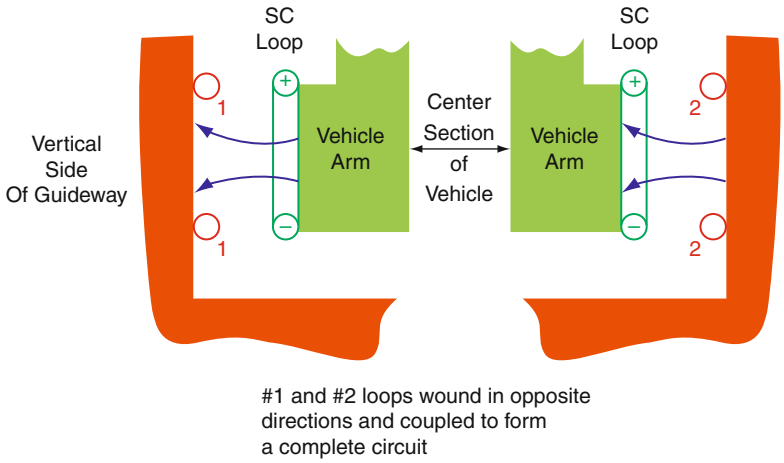

MAGLEV Technology Development. Figure 13
Cross-coupled lateral loops

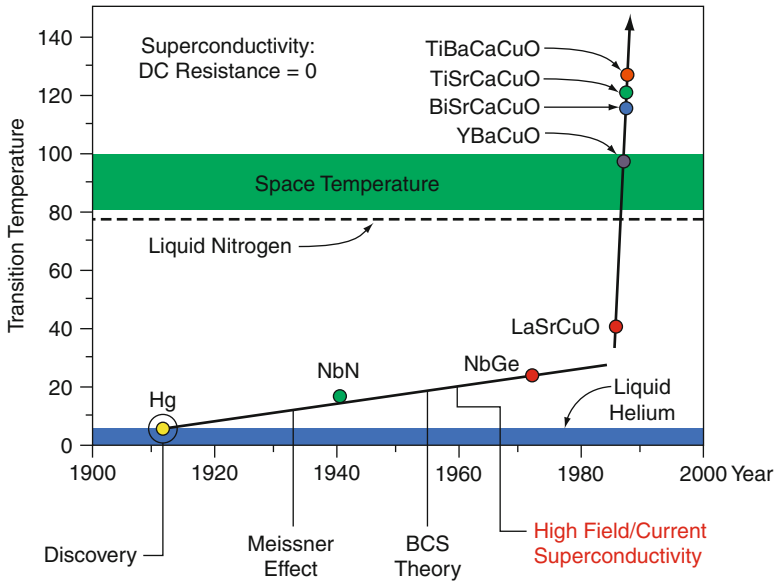

MAGLEV Technology Development. Figure 14
The time evolution of the superconducting transition temperature

and resulting magnetic fields that can be sustained compared to conventional iron electromagnets. Figure 17 shows NbTi wire drawn down to a circular or an approximately rectangular form. The small dots are the NbTi superconductor. The surrounding material is usually copper. This cross section starts out as a short cylinder about 10 in. in diameter. It is then drawn down to a small wire by pulling through orifices of diminishing sizes. The superconducting wire and cryostat technology required for Maglev has existed in the USA for several decades. For example, Fig. 18a shows a large superconducting magnet system which was operated for over a decade as a central part of a high energy physics facility. It was designed and

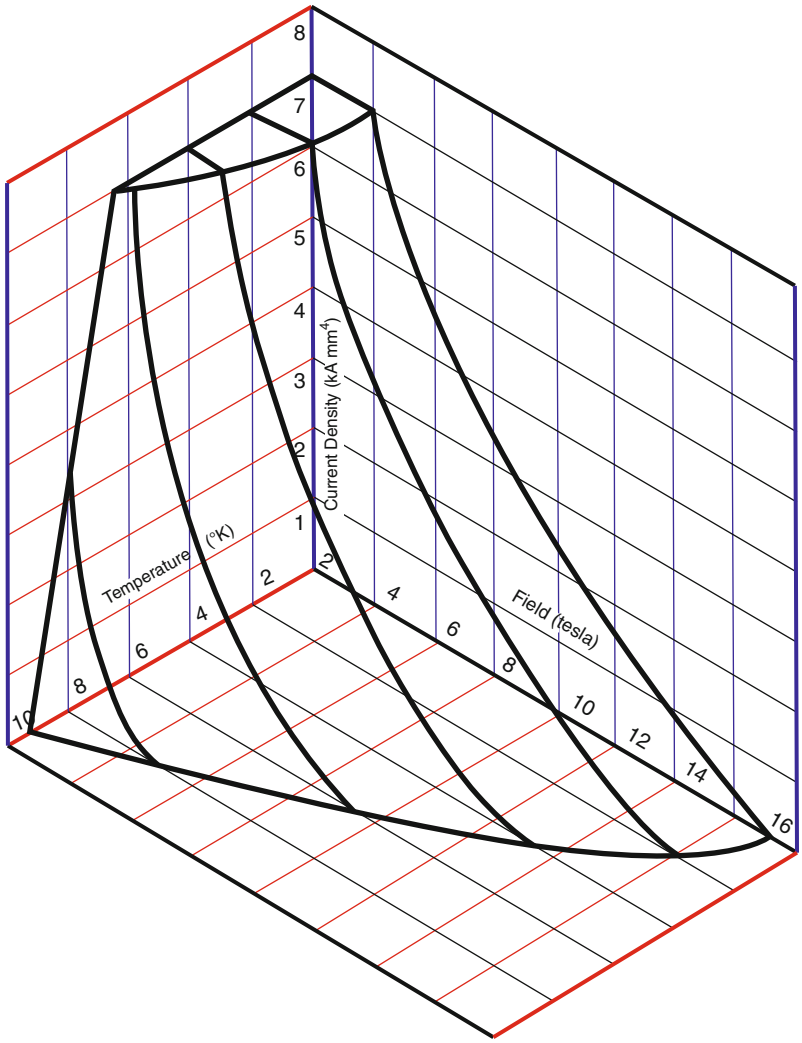

MAGLEV Technology Development. Figure 15
The critical surface for niobium-titanium superconductor

built by Gordon Danby and his group and commissioned in 1973. Figure 18b shows a large superconducting magnet system used as a high energy particle storage ring for a fundamental physics study of the anomalous magnetic moment of the muon, a fundamental point-like particle.

The largest and longest particle accelerator that uses superconducting magnets is the Large Hadron Collider (LHC) now operating at the CERN Laboratory in Switzerland [13]. The LHC has two rings of many thousands of superconducting magnets that accelerate and guide high energy particles for experiments. The total circumferential length of the magnets is 54 km (31 miles). The same length of superconducting magnets on Maglev vehicles could transport half of the 4 trillion passenger miles per year traveled by car, airplane, and rail in the USA, plus half of the 1.5 trillion ton miles per year of freight transported by intercity highway trucks.

The LHC superconducting magnets are much more technically complex and challenging than superconducting Maglev magnets. To achieve maximum field capability, LHC superconducting magnets operate with subcooled liquid helium at 1.7 K, rather than the normal boiling point of 4.2 K, where Maglev magnets operate. The refrigeration requirements at

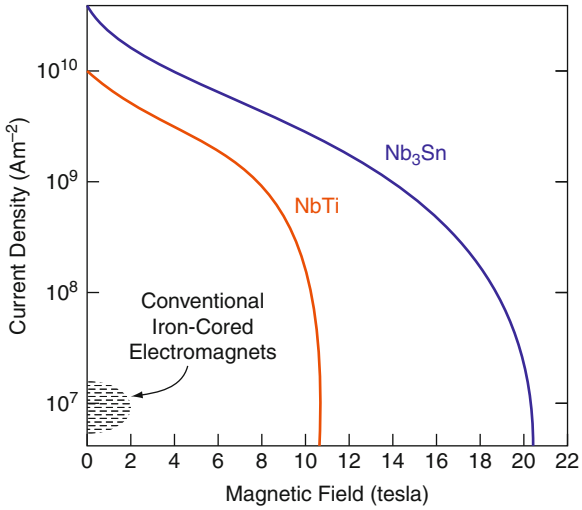

MAGLEV Technology Development. Figure 16
Critical current densities of niobium-titanium and niobium-tin at a constant temperature of 4.2 K

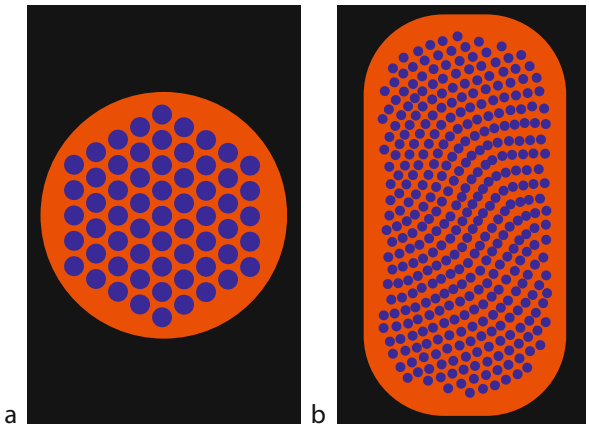

MAGLEV Technology Development. Figure 17
Cross sections of two typical filamentary composites of NbTi in a copper matrix

1.7 K are much more difficult than at 4.2 K. Moreover, the LHC superconductors must operate at higher magnetic field strengths and with much greater spatial precision than Maglev magnets again making them much more challenging. Finally, the many thousands of LHC magnets must all work perfectly for the LHC facility to operate. In Maglev, the vehicles carry multiple independently operating magnets with very high system redundancy and robustness. If one magnet were to fail, a very unlikely event, it would not affect the operation of the other magnets on the vehicle. Several of the multiple independent magnets on the vehicle could fail without compromising safety. If a magnet were to fail, the vehicle would be taken off-line at the next station for repairs. The probability of multiple failures during this time would be many orders of magnitude smaller than the probability of multiple engine failures on commercial jet aircraft, which in turn are extremely small.

Returning to the cost of the magnets for superconducting Maglev, a good measure is the cost of the magnets for the LHC. The total capital cost of the much more complex and difficult LHC magnets was several billion dollars. The equivalent length of magnets on Maglev vehicles would carry half of the annual US passenger and intercity highway freight traffic, which presently costs on the order of $1 trillion per year [14]. The amortized cost of the Maglev magnets is trivial in comparison. Also, the annual cost of the 40,000 deaths and 500,000 serious injuries per year on US highways is estimated at $500 billion annually [1]. The cost of superconducting Maglev magnets is again trivial by comparison, plus the vast amount of human suffering that would be avoided by traveling on much safer Maglev systems.

The newer high temperature superconductors (HTS) shown in Fig. 14 are extremely promising. HTS conductors operate at much higher temperatures than the 4.2°K for NbTi, typically in the range of 30–40 K, with the capability of operating at 77 K, liquid nitrogen temperatures, depending on the desired current capacity. Presently, the most promising HTS conductor is yttrium barium copper oxide (YBCO). Deposited as a very thin film, 1–2 μ in thickness, on a thin tape substrate, YBCO conductors can achieve engineering current densities of 50,000 A/cm^2 or more, depending on operating temperature. Engineering current density is the overall current density of the conductor tape, including the superconductor film, which has a current density of millions of amperes per square centimeter, plus the substrate tape that it is deposited on.

HTS conductors are attractive for Maglev, because their refrigeration systems are simpler and have lower energy requirements. The present Japanese Maglev

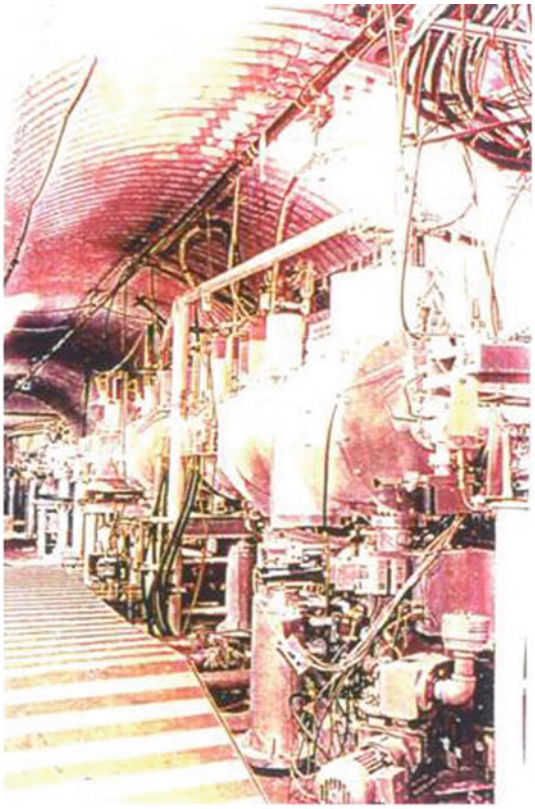

a

b

MAGLEV Technology Development. Figure 18
(**a**) Large superconducting magnet systems for a high energy physics facility. (**b**) Large superconducting magnet system used as a high energy particle storage ring for study of the magnetic moment of muon particles

system uses NbTi superconductor at liquid helium temperatures without problems, and the refrigeration requirements are modest and very acceptable. As HTS conductors come into wider use and larger production, superconducting Maglev will probably shift to their use.

A further question could be raised by people unfamiliar with superconducting technology. Is it too complex for everyday transportation systems? One area where superconductivity is intensively used is MRI medical scanners. The technology of superconducting coils and cryogenics has evolved considerably in scanners over the last 20 years, and thousands of superconducting MRI magnets are now in use all over the world. Figure 19 shows an open MRI, for which Gordon Danby was the leader of the magnet design effort. The important thing for Maglev is that the commercially made superconducting coils in the MRI scanner as yet require elaborate refrigeration systems. Two small cryocoolers approximately a foot in diameter and an arm's length cool the coils. Once a year the cryocoolers are taken off and replaced with another set. The first set is sent back to the manufacturer for reconditioning. No cryogenic fluid has to be added during this year of continuous trouble-free operation. This example shows that superconductivity can be very reliable, just like the refrigerators in people's kitchens. It is definitely ready for efficient, reliable transportation with extremely low maintenance.

Engineering Maglev

If Maglev is to become a major mode of transport in the twenty-first century, as important as road, rail, air, and water have been in the twentieth century, it must be safe, reliable, cost effective, environmentally benign, operate as a nationwide network, not a small number of isolated routes, be readily accessible, and integrate easily with other transport modes. To fulfill Maglev's promise, the proposed Maglev systems must be engineered with respect to the following six development goals.

The first development goal is to have a substantial physical clearance between the Maglev vehicle and the

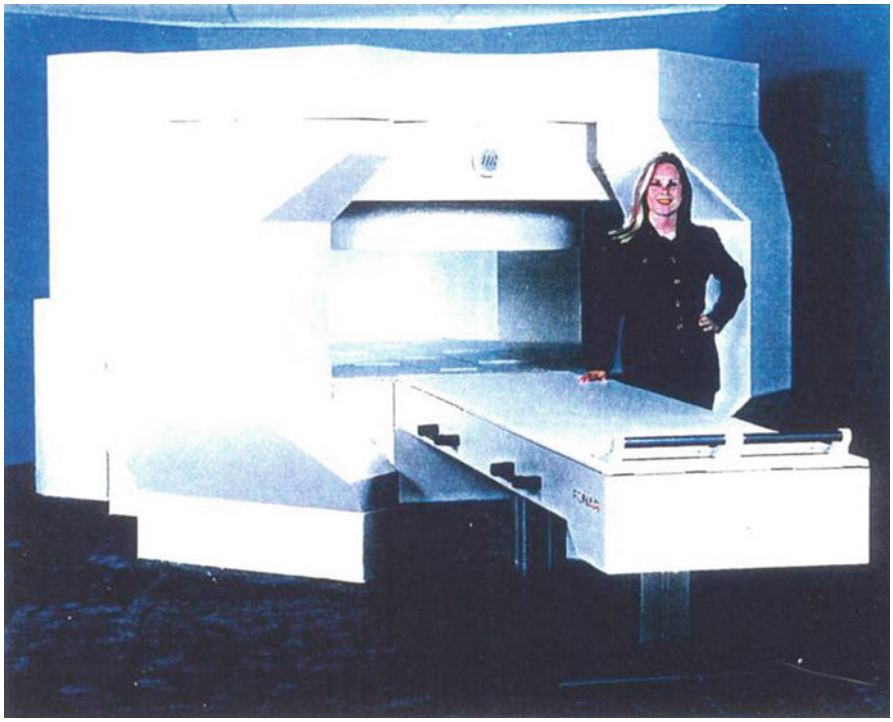

MAGLEV Technology Development. Figure 19
Magnetic Resonage Imaging (MRI) machine for medical diagnostics, using superconducting magnets

guideway. Large clearances are desirable for safe operation, and allow Maglev vehicles to operate in all types of weather, including strong winds, snow, and ice, that are not possible with conventional transport. Superconducting Maglev enables clearances of 10 cm (4 in.) or more between a vehicle and the guideway. Electromagnetic Maglev is constrained to much smaller clearances, on the order of 1 cm (3/8 in.). Also, large clearances reduce guideway cost because construction tolerances are less demanding. Building guideways to a tolerance of ±10% of the vehicle/guideway clearance is much cheaper when the clearance is 4 in., compared to guideways where the clearance is a fraction of an inch.

The second development goal is to have a very stable and safe magnetic suspension. Electromagnetic Maglev systems, such as Transrapid, achieve stability by very fast, for example, thousandths of a second, servo control of the current in the electromagnets on the vehicle. If the gap between the vehicle electromagnets and the iron rails becomes smaller than desired, the magnet current is reduced. If the gap becomes too large, the magnet current is increased. In electrodynamic superconducting Maglev, the vehicle superconducting magnets and the normal conductor guideway loops are arranged so that the moving vehicle will automatically be magnetically suspended at an equilibrium position above the guideway. Any external force on the vehicle – for example, a cross wind or the centripetal force on a curve – that acts to displace the vehicle from its equilibrium position is immediately countered by an inherent, passively generated opposing magnetic force. This opposing magnetic force always acts to push the vehicle back toward its equilibrium position. The magnitude of the displacement from equilibrium is proportional to the strength of the external force. Electrodynamic superconducting Maglev can be designed so that no conceivable external force, even if it were twice the weight of the vehicle, would produce a displacement great enough to make the vehicle contact the guideway. In effect, superconducting Maglev creates a five-dimensional "magnetic well" in which the vehicle is trapped so strongly that any conceivable external force cannot make it climb out of the "well." The five dimensions correspond to vertical ("heave"), lateral ("sway"), pitch, yaw, and roll movements of the vehicle. The vehicle is not constrained in the sixth, or longitudinal, dimension, so that it can move freely along the guideway, with only a small magnetic drag force acting on it.

Electromagnetic Maglev systems, that is, Transrapid, maintain their levitation at all speeds, including zero speed at stations and if the propulsion power to the guideway is cut off, subject to the electrical capacity of the batteries on-board the vehicle.

Superconducting Maglev vehicles can automatically and inherently remain stably suspended as long as they move faster than a transition speed of approximately 20 mph. Below this speed, resistive IR losses in the guideway loops reduce the induced currents in the guideway loops to the point where the magnetic force is insufficient to levitate the vehicle.

Superconducting Maglev vehicles can remain levitated at zero speed and speeds below 20 mph on the short sections, for example, 50 m in length, of guideway at stations where the vehicle is decelerating into a stop at the station or accelerating out of the station. To remain levitated in those special sections, one can power the aluminum guideway loops with DC current or use high temperature superconducting (HTS) guideway loops in place of aluminum loops. The HTS guideway loops will only require a small fraction of the HTS conductor used on the vehicle, and their refrigeration power will be small. Maglev vehicles are magnetically propelled by a set of alternating current propulsion windings in the guideway. In the unlikely event that the electrical power grid that energizes the guideway propulsion windings was to fail, vehicles would simply coast to a safe stop at a special location on the guideway or at the next station where the vehicle remains levitated.

The third development goal is to have the vehicles operate with very low magnetic drag. Low magnetic drag reduces both the energy consumed by the magnetic propulsion system, as well as its capital cost. Because the energy consumed by the superconducting magnets on the vehicle is negligible – the electrical resistance of superconducting windings is zero – low magnetic drag can be achieved by having the magnitude of the currents induced in the guideway loops be much smaller than the magnitude of the currents in the superconducting magnets on the vehicle. The magnetic levitation force on the vehicle is proportional to the product of vehicle magnet current and guideway loop

current. Maximizing vehicle current relative to guideway loop current minimizes magnetic drag since it minimizes the I^2R losses in the guideway loops, the only contributor to magnetic drag. By using a unique configuration of guideway loops and vehicle magnets, termed the null flux suspension, to be described later, the guideway currents can be made very small, resulting in magnetic drag forces that are negligible compared to air drag.

Following publication of Powell and Danby's pioneering 1966 paper [15] on superconducting electrodynamic Maglev, Kolm and Thornton proposed a different Maglev system, called the Magneplane, that also used superconducting magnets on a vehicle to provide levitation and propulsion. Instead of using null flux aluminum guideway loops, the Magneplane [16] used a curved solid aluminum sheet as the guideway underneath the Maglev vehicle. The magnetic fields from the superconducting magnets on the vehicle induced currents in the aluminum sheet guideway. The magnetic interaction between the induced currents in the aluminum sheet guideway and those in the superconducting magnets on the vehicle generated the levitation force.

However, in this configuration, the magnitude of the induced currents in the sheet guideway equaled the magnitude of the currents in the vehicle magnets, resulting in large I^2R losses in the aluminum sheets and strong magnetic drag in the vehicle. Passenger aircraft typically have a lift to drag ratio on the order of 20/1, resulting in high energy consumption per passenger mile. The magnetic lift/drag ratio for the Magneplane is comparable to that for airplanes, again resulting in high energy consumption.

In comparison, by using the null flux guideway configuration [7, 15], the induced currents in the guideway loops are much smaller than those in the vehicle magnets, resulting in much less magnetic drag due to I^2R losses in the in the guideway conductors, and a much larger magnetic lift/drag ratio. Also, the amount of aluminum used in the null flux configuration is much less than in the Magneplane configuration.

The fourth development goal is low capital and operating costs. Most – approximately 80% – of the projected total life cycle cost of a Maglev system is associated with the construction cost of the guideway. A low cost for the guideway appears feasible through the use of prefabricated beams and piers which are mass produced in factories and shipped to the route site where they can be easily assembled into the finished guideway. Not only will the prefabricated, factory-produced beams and piers be substantially lower in cost than if they were fabricated at the construction site, but their quality control and tolerances will be better. The prefabricated guideway loops can be attached to the sides of the beams before they are shipped to the route site, which further reduces cost. The finished prefabricated beams and piers can be shipped by truck, or transported along completed portions of the guideway to where the new sections are being assembled.

The fifth developmental goal is to achieve high revenues from the Maglev system, so as to avoid the need for government subsidies for construction and operation of Maglev routes. Today, as government budgets are tightening and deficits and debt are growing, there is great resistance to having government finance new transportation projects. In the USA, intercity and commuter rail systems all require large subsidies for operation, with fare revenues only accounting for 30–40% of total operating cost. Similarly, the high speed rail (HSR) passenger transport systems in other countries all require major governmental subsidization. For Maglev to be widely implemented, it should require little or no subsidization, and as a goal, be attractive to private investment, without the need for any government funding.

The sixth developmental goal is high speed, nonmechanical switching to off-line stations for unloading/loading operations. Requiring high speed vehicles to operate with online stations greatly limits their convenience and number of stations. Decelerating into and accelerating out of stations greatly reduces the average travel speed unless the stations are far apart, for example, spaced every 50–100 miles or so. Long distances between online stations reduce accessibility and ridership, while short distances negate the benefits of high speed systems. The ability to switch at high speeds to closely spaced off-line stations, when scheduled, and to bypass them at high speeds when not scheduled, enables a high speed transport system to maintain high average speeds while at the same time having many closely spaced stations with easy accessibility.

The nonmechanical contact nature enables a unique new capability not possible with rail systems. Suitably designed, Maglev vehicles can electronically switch at high speeds without the need for mechanically moving long sections of the guideway. Not only does electronic switching avoid the cumbersome mechanical movement, it enables switching at much higher speeds than if the vehicle had to slow down to navigate the mechanical switch section.

Figure 20 lists the superconducting electrodynamic Maglev inventions pioneered by the authors that address the six development goals outlined above.

The first invention is the use of superconducting magnets on the vehicle to induce currents in normal metal – for example, aluminum – guideway loops to levitate and automatically stabilize high speed vehicles [7, 15]. This combination efficiently uses the very strong magnetic fields generated by a small number of superconducting magnets on the vehicle that interact with simple, low cost, low drag normal aluminum guideway loops to levitate the moving vehicles. The combination is ideal, since using normal electrical conductors on the vehicle would require an impractical amount of on-board power for the large clearances involved, and superconducting loops on the guideway would be far too expensive.

The second invention, illustrated in Fig. 21, is the null flux guideway. The principle of the null flux guideway is simple. The guideway loops are arranged so that they have symmetry positions relative to the vehicle magnets. When a vehicle magnet is at the symmetry position, the *net* magnetic flux through the given guideway loop or loop circuit is *zero*. (The null flux condition can be designed to apply to either a simple loop or a circuit of two or more connected loops.) When the net flux through the null flux loop or circuit is zero, the resultant induced current in the loop or circuit is also zero. If the vehicle magnet moves away from its symmetry position, the *net* flux through the loop or circuit becomes *nonzero*, and a current flows that acts to push the vehicle magnet back toward its symmetry position. A wide variety of loops and loop circuits can be used in the null flux guideway. A very useful configuration is the figure of 8 null flux loop circuit, as illustrated in the upper right corner of Fig. 21. The left-hand loop of the figure of 8 circuit is wound in a clockwise direction, while the right hand loop is wound counterclockwise. When the dipole loop vehicle magnet is centered on the figure of 8 loop circuit, the net flux through the circuit is zero. If the dipole loop moves to the left, a net current and force develop to push it back toward the right. Conversely, if it moves to the right, an opposite current and force push it back to the left.

The lower left corner of Fig. 21 shows the guideway and vehicle loops for the narrow beam guideway. The figure of 8 loops, on the sides of the beam, levitate the vehicle. The vehicle magnets move slightly below the symmetry position, generating a current and force that push them upward. The figure of 8 null flux loops, besides levitating the vehicle, also stabilize it against vertical and roll displacement from external forces. The vehicle is stable against pitch displacements by having independent figure of 8 loops along the beam. If the vehicle tends to pitch downward due to an external force, the pitching motion is automatically countered by magnetic forces. A second null flux loop circuit on the narrow beam provides lateral and yaw stability. It consists of two dipole loops, one on each side of the beam, electrically connected to form a null flux circuit. When the vehicle is laterally centered on the beam, the net flux through the null flux circuit is zero. When the vehicle is laterally or yaw displaced from its centered position, a net flux and current develop in the dipole null flux circuit that pushes the vehicle back to the center.

The lower right corner of Fig. 21 shows a fabricated guideway loop assembly for one side of the narrow beam. Besides the dipole and figure of 8 loops, there is also an LSM propulsion loop. The loop assembly is encapsulated in a thin panel of polymer concrete,

Superconducting Electrodynamic Maglev Enabling Inventions

- Magnetic levitation using superconducting magnets and inductive normal guideway
- Null flux guideway
- Linear synchronous motor (LSM)
- Quadrupole vehicle magnets
- High speed electronic switches

MAGLEV Technology Development. Figure 20
Superconducting electrodynamic Maglev-enabling inventions

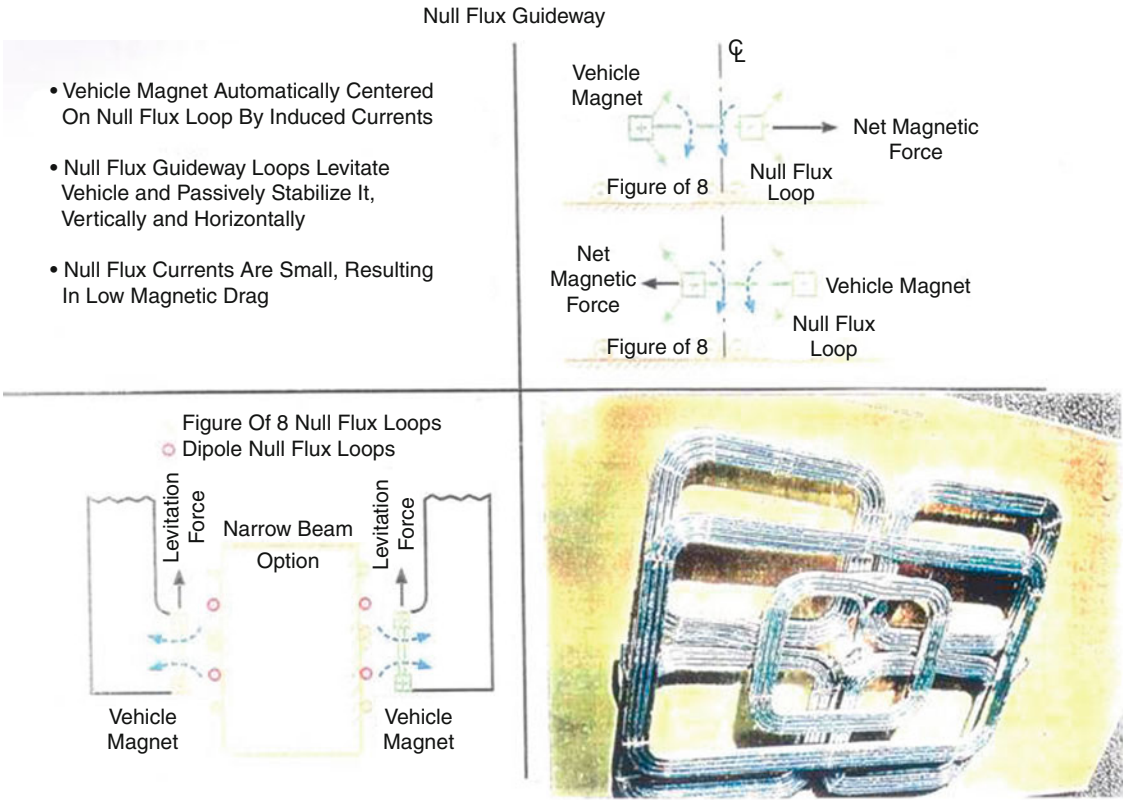

MAGLEV Technology Development. Figure 21
Null flux guideway

a very strong, tough form of concrete, and attached to the sides of the narrow beam and shipped to the construction site. The I^2R losses in the guideway loops, and the corresponding magnetic drag, are much smaller in the null flux guideway than in a guideway that uses a simple conducting sheet or a set of simple dipole, non-null flux loops. Moreover, the magnetic "stiffness" – that is the magnitude of the magnetic restoring force per inch of displacement – is much greater for the null flux guideway.

The third invention is the linear synchronous motor (LSM) [7] illustrated in Fig. 22. Prior to the LSM, a method proposed for the propulsion of high speed ground transport vehicles included conventional steel wheel on rail traction motors, the linear induction motor (LIM), and jet engines. These methods required either on-board engines or collecting power from a high voltage line along the guideway using a sliding contact. In the linear synchronous motor, the superconducting magnets on the vehicle magnetically interact with a traveling wave of AC current in a set of aluminum conductor windings on the guideway, as illustrated in Fig. 22, producing a longitudinal magnetic force that propels the vehicle along the guideway. The vehicle remains locked in phase with the traveling AC current wave, with its speed determined by the frequency of the LSM current wave, in accordance with the relation $v = f\lambda$, where λ is the pitch of the alternating polarity magnets on the vehicle (λ = twice the length of one magnet), f is the frequency of the AC wave, and v is the vehicle speed. Vehicle speed is constant, even if it is subjected to head or tail winds or it climbs or descends grades, as long as sufficient phase margin is maintained by the LSM current wave. As a result, the distance between vehicles on the Maglev-2000 guideway is fixed, even if the external forces on the individual vehicles vary. This is extremely important since it eliminates any possibility of vehicle collisions.

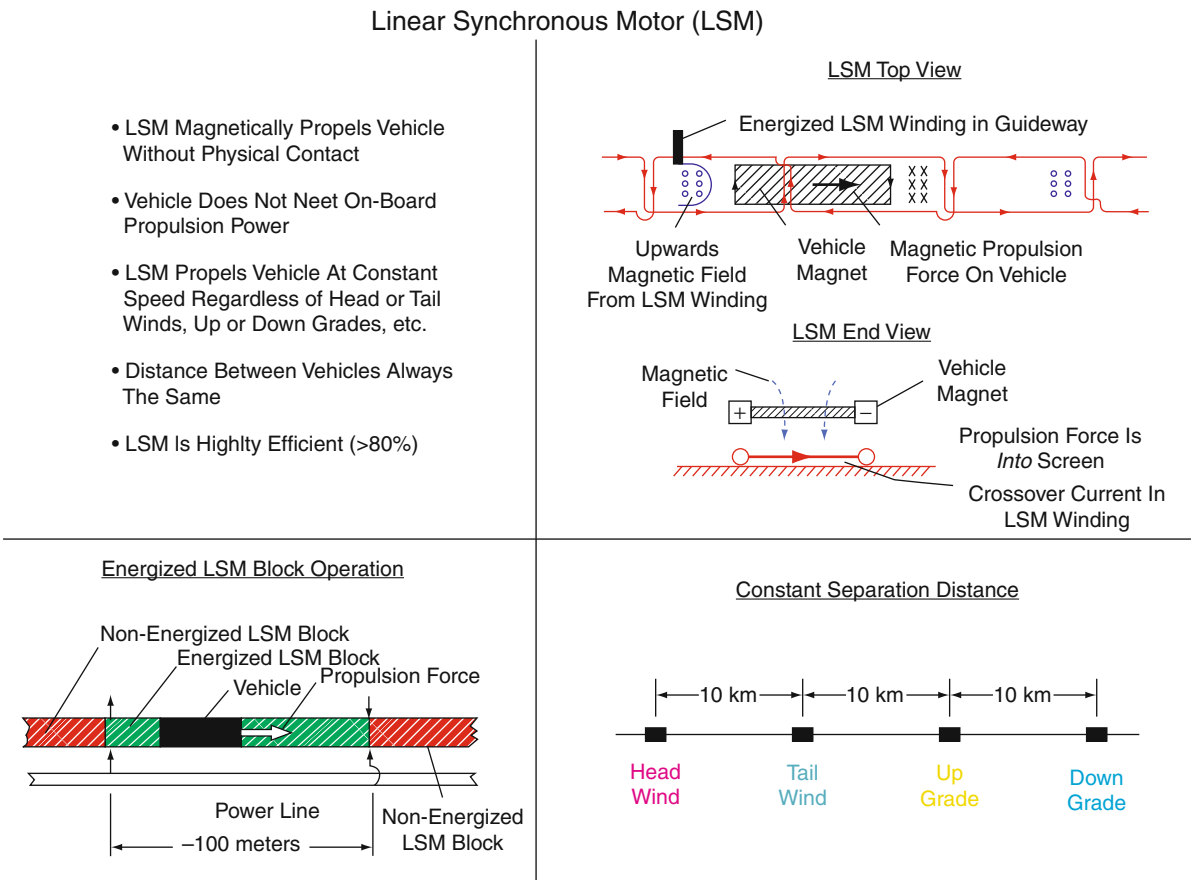

MAGLEV Technology Development. Figure 22
Linear synchronous motor (LSM)

To minimize I^2R losses in the guideway LSM windings, the entire guideway is not energized. Instead, only the section on which the vehicle is traveling is switched on from the DC power line that runs along the guideway, using solid state switches to control local frequency and power flow. The switched-on section length is typically 100–200 m, resulting in high motor efficiency. Approximately 90% of the input electrical power to the switched section is delivered as propulsive power to the Maglev vehicle. As the vehicle leaves the old switched-on section, the electrical power input is transferred to the new section ahead, as illustrated in the drawing in the lower left corner of Fig. 22. By controlling the frequency of the AC power fed to the guideway, the central traffic control facility can speed up or slow down the vehicles if conditions warrant – again, a major advantage for safe operation.

The fourth invention is the Maglev-2000 quadrupole superconducting magnet. It differs from the dipole magnet used in the Japanese Maglev system, and achieves new capabilities. Dipole magnets employ two lines of current that run in opposite directions, forming a simple rectangular loop. Quadrupole magnets employ four lines of current, at the corners of a square, and alternating in direction as shown in Fig. 23. Fringe magnetic fields from quadrupole magnets are much smaller than from dipole magnets, as illustrated in the lower left corner of Fig. 23. A 600 KA dipole magnet has a fringe field of 15 gauss at 6 m, 30 times the Earth ambient field, while the quadrupole magnet fringe field is only 0.07 gauss, one-seventh of Earth ambient, at the same distance. The much smaller fringe fields make it simple to keep the magnetic field strength inside the vehicle passenger compartment and

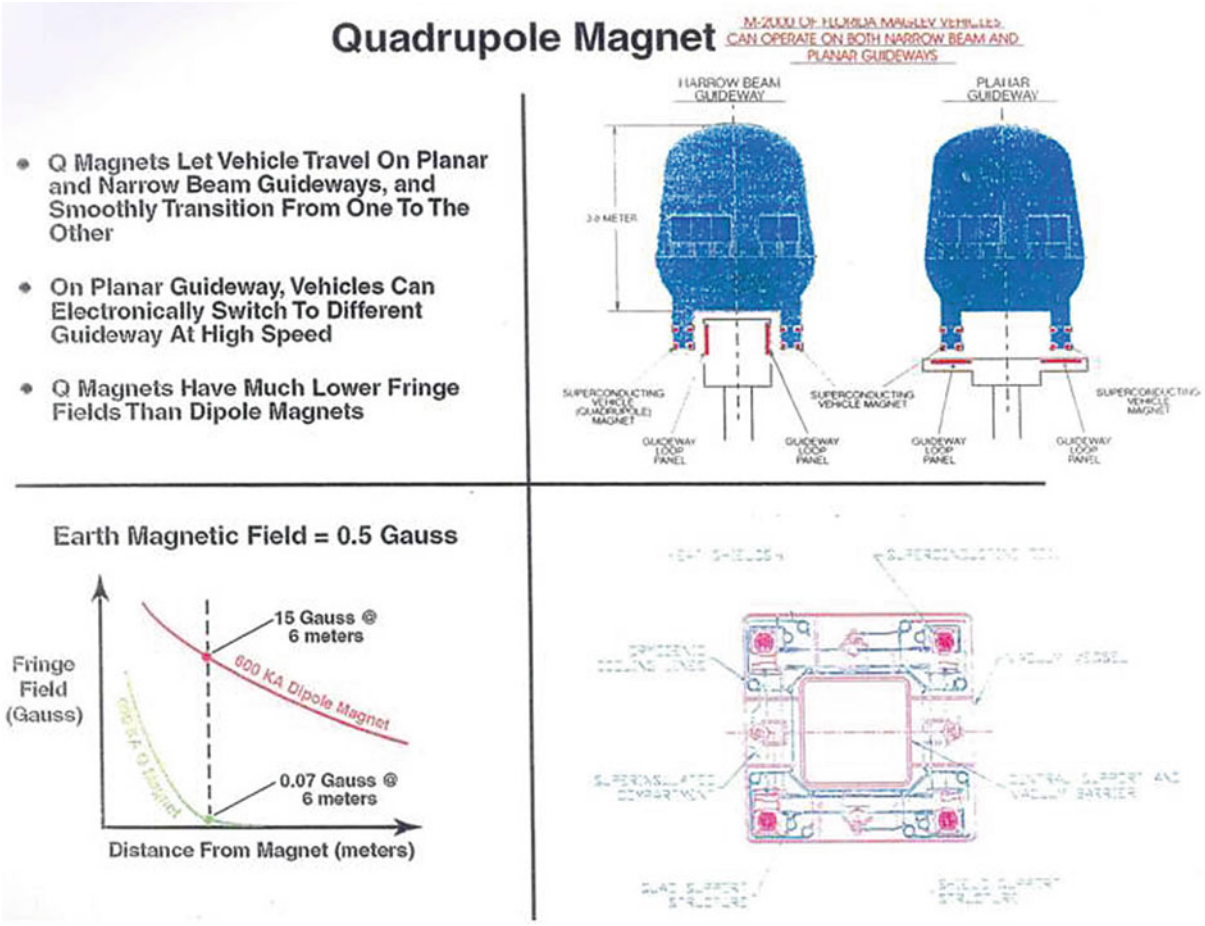

MAGLEV Technology Development. Figure 23
Quadrupole magnet

at stations at Earth ambient level. Quadrupole magnets enable Maglev vehicles to travel on and smoothly transition between both narrow beam and planar guideways. Most of the time, Maglev-2000 vehicles travel on the low cost narrow beam guideway. Near stations, the vehicles transition to the planar guideway where the vehicle can switch from the main guideway to off-line stations to stop and carry out loading/unloading operations. The switch section has two lines of overlapping planar guideway loops, with one line going on as the main high speed route, and the second line directing the vehicle to an off-line station away from the main route. The switching process uses electronic solid state switches to control which line of guideway loops the vehicle will follow. Mechanical movement of the guideway is not required. Depending on schedule, the vehicle may not switch off the guideway, but continue at high speed on the main line to a station further down the line.

The capability to switch at high speed to off-line stations for loading and unloading using an electronic, nonmechanical switching process – the fifth fundamental invention – is very important for countries like the USA, where the population density is relatively low and spread out, not concentrated at a few high density points. High speed switching enables Maglev vehicles to employ "skip-stop" schedules to maintain high average speed, as illustrated in Fig. 24. If vehicles had to stop at or slow down for every station along the route, the average speed would be considerably less than 300 mph, unless stations were a hundred miles apart or more. With "skip-stop" scheduling, stations can be spaced more

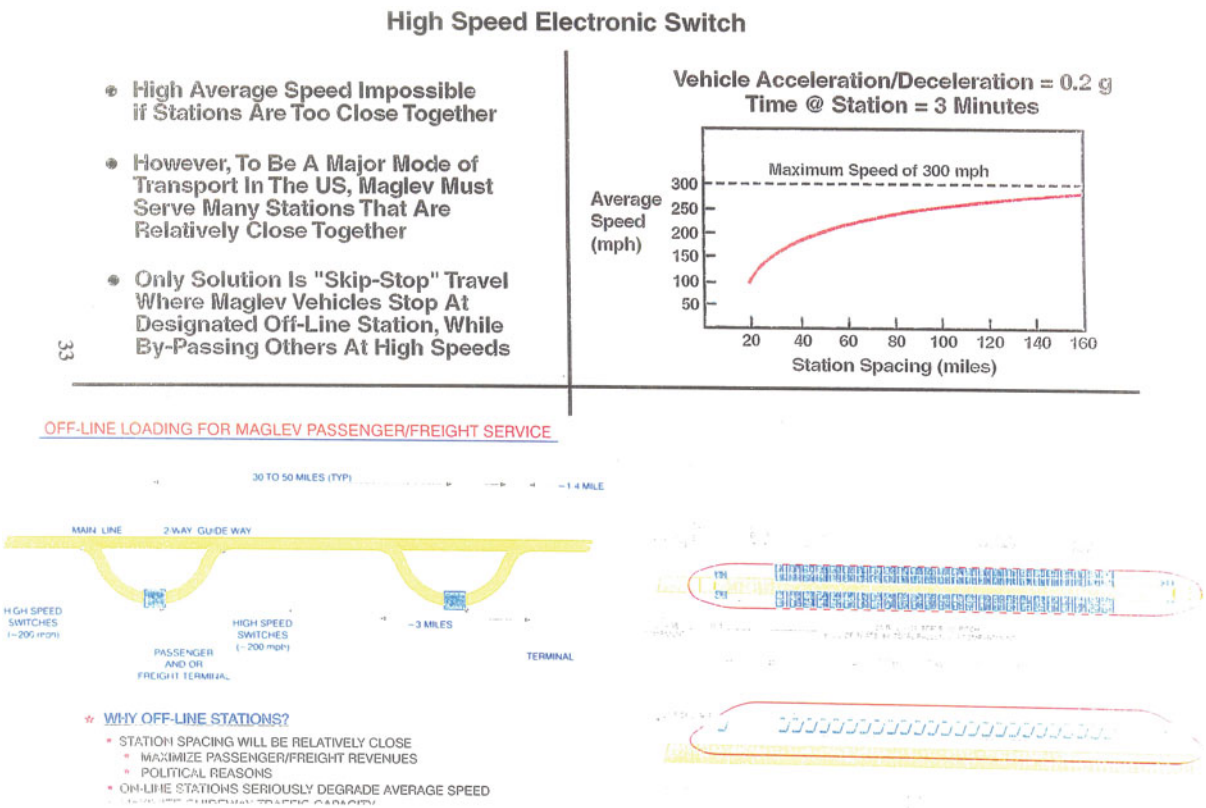

MAGLEV Technology Development. Figure 24
High speed electronic switch

closely to more efficiently serve the spread-out population. Using "skip-stop" travel, a passenger could board a Maglev vehicle at his/her local station and skip all other stations in the area, traveling directly to his/her final destination in some distant city.

Operational First-Generation Maglev Systems

Following the publication of Powell and Danby's 1966 paper on superconducting Maglev [8], a number of countries started Maglev development programs. Japan, and also Germany, visited Powell and Danby to learn about their inventions. Japan chose to focus their Maglev development program on superconducting Maglev because of its large clearance of 10 cm or more – a very important factor in Japan because of the strong earthquakes there – and its strong inherent stability, a very important safety feature.

Germany's Maglev development program focused on both superconducting electrodynamic Maglev and electromagnetic Maglev systems, and tested both approaches. They then selected electromagnetic Maglev as a system that could be commercialized relatively quickly.

Japan and Germany have both achieved technically successful first-generation Maglev systems that have transported many thousands of passengers safely and comfortably at speeds on the order of 300 mph. The Japanese Maglev system presently operates on Japan Railways' 20 km demonstration track in Yamanashi Prefecture [17]. Japan Railways plans to have the Yamanashi track become part of a 500 km (300 mile) Maglev route to be constructed between Tokyo and Osaka that will carry 100,000 passengers daily with a trip time of 1 h [18].

The German electromagnetic Maglev system, called Transrapid, was extensively tested on a 20 km demonstration track at Emsland, Germany [5]. The Transrapid Maglev system now operating in Shanghai,

China [19], has the distinction of being the first commercial Maglev system. The 30 km route runs between the center of Shanghai and its Pudong airport.

Both the Japanese and German first-generation Maglev systems are limited to transporting passengers and lightweight, high-value FedEx-type freight. They cannot transport heavy trucks, autos, and freight containers. They cannot electronically switch from the main guideway to a secondary guideway, but require mechanically moving long sections of the guideway. Guideway construction cost is very high, on the order of $60 million per two-way mile or more [20].

More detailed descriptions of the development and current status of the Japanese and German first-generation passenger Maglev system is given below.

Table 1 [21] lists the significant milestones in the development of the Japanese first-generation Maglev system from its start in 1970 through 2004, the last available update from Japan Railways' Railway Technical Research Institute (RTRI). By 2004, the Yamanashi Maglev Demonstration Line had carried over 80,000 passengers [21] with total accumulated running distances of over 400,000 km (240,000 miles). Since then, the number of passengers and running miles has grown considerably, but data is not available.

The 20 km Yamanashi line located north of Mt. Fuji was dedicated in April 1997. Before then, R&D tests were carried out at the Miyazaki Test site. The first test run of a levitated Maglev vehicle was in 1977. The unmanned ML-500 vehicle (Fig. 25) ran on an inverted T-shaped guideway. In 1977, it attained a speed of 517 km/h [21].

MAGLEV Technology Development. Table 1 Milestones in the development of the first-generation Japan Railways' superconducting Maglev system [21]

Date	Milestone
1970	Study of electrodynamic levitation system (EDS) started
1977	Miyazaki Maglev Test Center opened – test run of unmanned ML-500 vehicle on inverted T-shaped guideway started
1980	Test run of MLU 001 vehicle on U-shaped guideway started at Miyazaki
1982	Manned 2 MLU 001 vehicle set tests started
1986	3 MLU 001 vehicle set achieved 352 km/h
1987	400 km/h achieved by manned MLU 002 vehicle set
1997	First running test of MLX 01 vehicle on Yamanashi Demonstration Line Manned 5 MLX 01 vehicle set attained 552 km/h
1999	Test of 2 MLX 01 vehicle sets passing each other in opposite directions at 1,003 km/h
2003	Manned 3 MLX 01 vehicle set attained 581 km/h (361 mph)
2004	Cumulative number of passengers carried at Yamanashi exceeds 80,000; cumulative distance traveled exceeds 400,000 km

ML-500, 500R

ML-500

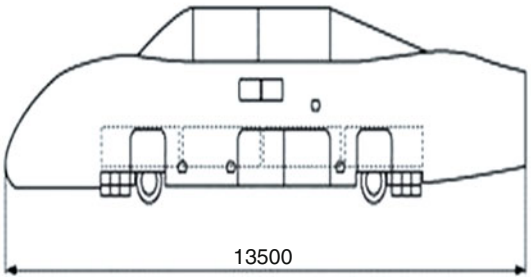

ML-500 (side veiw, dimension in mm)

MAGLEV Technology Development. Figure 25 ML-500, 500R

Japan Railways then transitioned to a U-shaped guideway, which is the configuration for the Yamanashi demonstration route, and the planned line between Tokyo and Osaka. The first test run of the MLU 001 (Fig. 26) vehicle [21] on the U-shaped guideway was carried out in 1980 at the Miyazaki Test site. The U-shaped guideway permitted a more efficient configuration for carrying passengers. Testing of the MLU001 vehicle carrying passengers started in 1982, with a two-car train set. In 1987, the two-car manned vehicle set attained 400 km/h. Also in 1987, test runs of a new Maglev vehicle, MLU002 (Fig. 27), began [21]. It was longer than the MLU001 – 22 m compared to 20 m for the two-car MLUJ001 vehicle set. MLU002 could carry 44 passengers and weighed 17 t. In 1989, it attained a speed of 394 km/h.

In 1991, MLU002 was damaged by a fire started in its braking system caused by excessive heating. MLU002 was then replaced by MLU002N (Fig. 28) which was essentially the same length as MLU001 and slightly heavier, 19 t compared to 17 t [21]. Test runs of MLU002 started in 1993. In 1995, MLU002 attained a speed of 411 km/h with passengers.

By 1996, the Yamanashi Test Center opened, and was officially dedicated in April 1997. A few months later, in December, the new MLX01 vehicle (Fig. 29)

MLU001

MLU001 (3-car train)

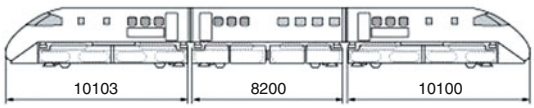

MLU001 (side view)

MAGLEV Technology Development. Figure 26
MLU001

MLU002

MLU002

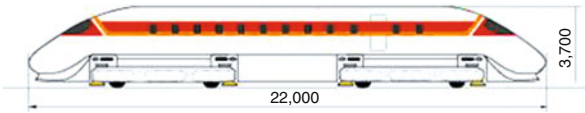

MLU002 (side view, dimensions in mm)

MAGLEV Technology Development. Figure 27
MLU002

MLU002N

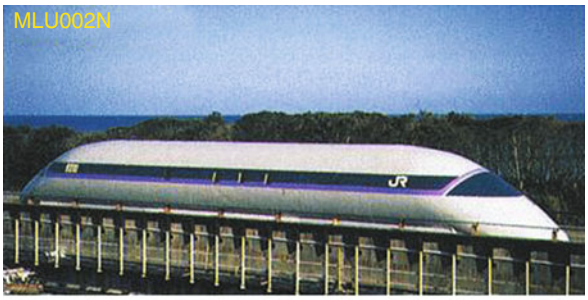

MLU002N

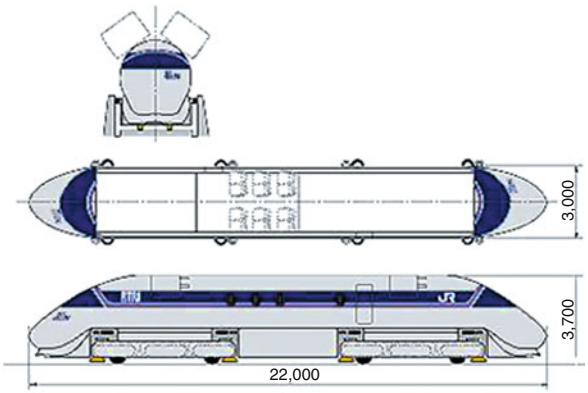

MLU002N (side view, dimensions in mm)

MAGLEV Technology Development. Figure 28
MLU002N

MLX01

MLX01 leading car, aero-wedge

MLX01 leading car, double cusp

MAGLEV Technology Development. Figure 29
MLX01

MLX01-901

New leading car, MLX01-901

MAGLEV Technology Development. Figure 30
MLX01-901

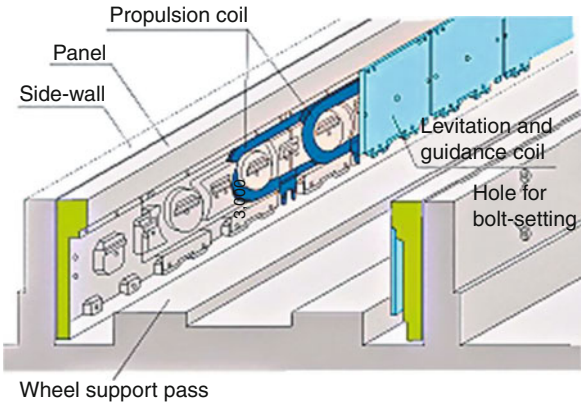

MAGLEV Technology Development. Figure 31
Panel method

attained 531 km/h carrying passengers. In 1999, a five-vehicle MLX01 set reached 552 km/h with passengers [21] and two-vehicle sets passed each other going in opposite directions with a relative speed of 1003 km/h (600 mph). Tests on a new vehicle set, MLX01-901 (Fig. 30) started in 2002. A three-vehicle MLX-01 set attained the world speed record of 581 km/h (361 mph) on December 2, 2003, carrying passengers [21].

The Japanese Maglev system uses a U-shaped guideway, with the aluminum levitation, stability, and propulsion located on the beams at the sides of the guideway (Fig. 31). The concrete panels with their attached aluminum loops are manufactured in a factory and then transported to the construction site [21] where they are bolted to the concrete side beams of the massive field constructed U-shaped guideway. Figure 32 shows a photo of the completed guideway.

Figure 33 shows a photo of the Yamanashi Maglev Demonstration line, with two Maglev vehicles on a bridge that crosses a local highway. In the distance, the JR Maglev guideway enters a tunnel through the mountain. Much of the proposed 500 km (300 miles) Maglev route will be in deep tunnels through the mountains of Central Japan. Three routes are under consideration [22] as illustrated in Fig. 34. Depending on the route, as much as 60% of the Tokyo to Osaka line will be in deep tunnels.

The principal constraints for the first-generation Japanese Maglev system are its high construction cost and its limitation to passenger-only transport. The high field construction cost results from the massive U-shaped guideway, plus the high cost of tunneling for much of the Tokyo to Osaka route. The limitation to passenger-only transport can be a revenue problem in low population countries, like the USA. In the USA, for example, the transport outlay for intercity trucks is much greater than for intercity air and train passengers – the USA spends over $300 billion per year for intercity truck transport, compared to only

MAGLEV Technology Development. Figure 32
Guideway of the Yamanashi Maglev test line

MAGLEV Technology Development. Figure 33
Vehicles crossing bridge over highway on Yamanashi Maglev test line

60 billion for air passengers and three billion for intercity rail passengers.

Turning now to the German electromagnetic Transrapid Maglev system, it is the basis for the first high speed commercial Maglev system in the world. Transrapid is a first-generation electromagnetic (EMS) Maglev system [5] which is levitated by conventional electromagnets on the vehicle that are attracted upward to two iron rails on the guideway. The physical gap between the vehicle's electromagnets is small,

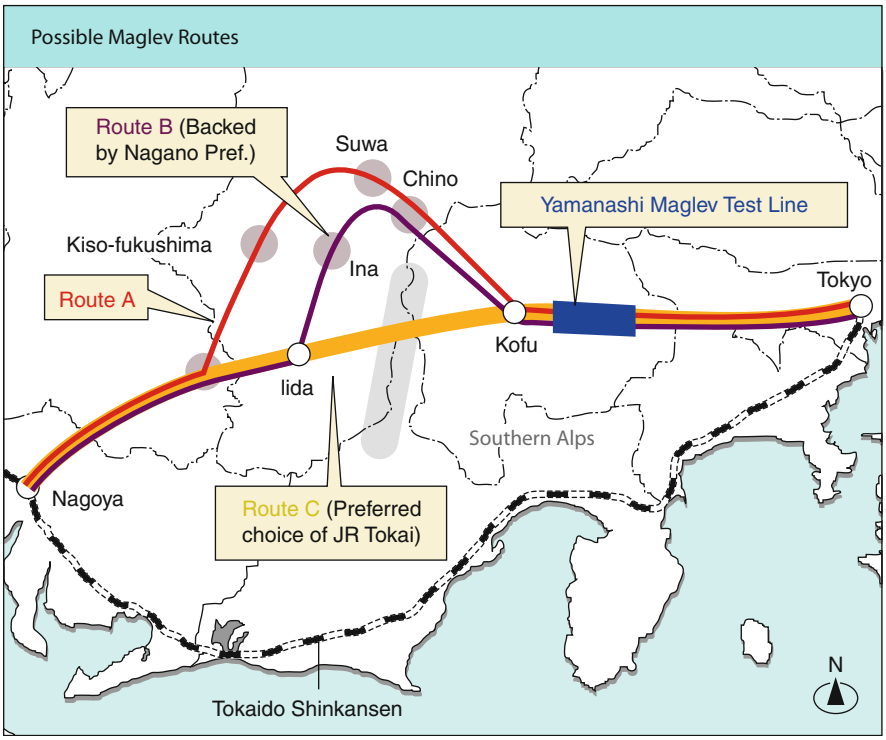

MAGLEV Technology Development. Figure 34
Possible Maglev routes

approximately 1 cm (3/8 in.), necessitating very precise and accurate guideway construction. EMS suspensions are inherently unstable because as the gap between the vehicle's electromagnets and the iron rail decreases, the levitating force on the vehicle increases, acting to pull the vehicle into contact with the rail. The Transrapid system rapidly servo controls the currents in the electromagnets on the vehicle to keep the gap between the vehicle and the guideway constant. If the vehicle moves toward the iron rails above the electromagnets, the servo control system quickly decreases the current in their windings, reducing the levitating force. If the vehicle moves down and away from the iron rails, the current in the electromagnets is quickly raised, increasing the levitating force. The servo control system operates on a time scale of thousandths of a second.

The 30 km long Shanghai Maglev Line runs from the outskirts of Central Shanghai to Pudong Airport. Figure 35 shows a photo of the Transrapid vehicle leaving Pudong Airport, while Fig. 36 shows a photo of the Longyang Road Station at the outskirts of Shanghai. The Transrapid Maglev Line does not service the center of Shanghai. Instead, there is a 20 min subway ride from the center of Shanghai to the Longyang Road Maglev Station [19].

Maglev service on the Shanghai route started on January 1, 2004. Depending on time of day, trip time for the 30 km run is 7.20 min for peak travel hours and 8.10 min for nonpeak hours. The corresponding average speeds are 251 km/h (156 mph) for the faster trip and 224 km/h (139 mph) for the slower trip. Maximum speeds during the trip are 431 km/h (268 mph) and 301 km/h (197 mph). The record speed on the route was 501 km/h (311 mph), achieved on November 12, 2003. The interval between trains is 15 min, except in the evening, when it is 20 min [19].

The 30 km (19 miles) Shanghai Transrapid line cost $1.8 billion (US dollars) and was built in 2½ years. The construction cost was $60 million per kilometer of route ($95 million per mile) [19]. The proposed 200 km (124 miles) extension to Hangzhou was approved in March 2010, with construction planned to start in 2010 [19]. However, given the high cost per kilometer

MAGLEV Technology Development. Figure 35
Maglev train coming out of the Pudong International Airport in Shanghai

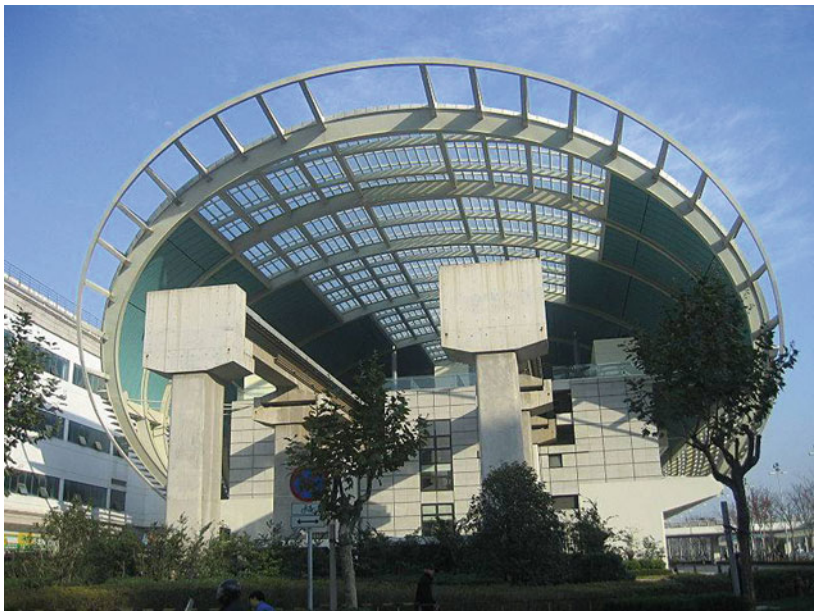

MAGLEV Technology Development. Figure 36
Longyang road Maglev station

and China's plans to build thousands of kilometers of high speed rail, the proposed Maglev extension may be postponed or even canceled.

The development of the Transrapid Maglev System has proceeded through a number of vehicles, as illustrated in Fig. 37, eight during the years 1976–2008. A number of EMS vehicles were tested in Germany in prior years, before 1976, by various companies before settling the final Transrapid system. These included the MBB "Prinzipfahrzeng," the MBB Komet, and the Krauss-Maffei Transrapid TR-02 and TR04 vehicles. In 1974, MBB and Krauss-Maffei joined together to form Transrapid.

The speed records achieved by the various Transrapid vehicles and their predecessors are given below [23]:

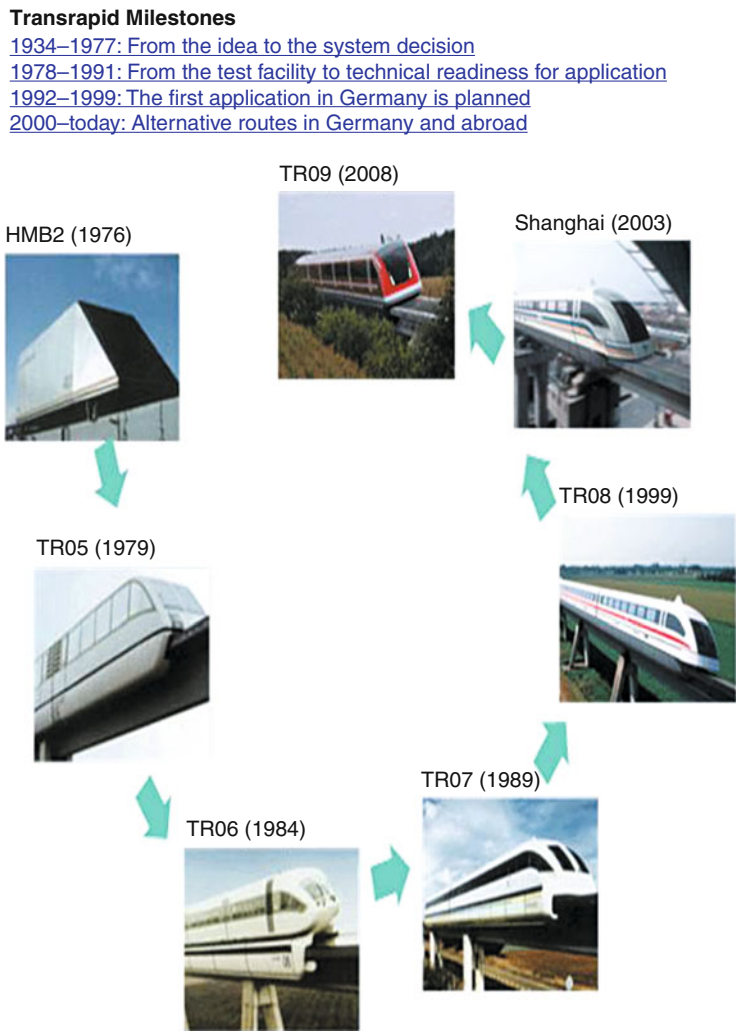

MAGLEV Technology Development. Figure 37
Transrapid milestones. 1934–1977, from the idea to the system decision; 1978–1991, from the test facility to technical readiness for application; 1992–1999, the first application in Germany is planned; 2000–present, alternative routes in Germany and abroad

Year	Vehicle	Speed, km/h
1971	Rinzipfahrzeg	90
1972	TR02	164
1973	TR04	250 (manned)
1975	Komet	401
1987	TR06	406 (manned)
1988	TR06	412 (manned)
1989	TR07	436 (manned)
1993	TR07	450 (manned)
2003	TR08	501 (manned)

For extended testing of the Transrapid vehicles, Germany constructed a 31.5 km test track at Emsland in Germany. The single track had turning loops at both ends, permitting continuous running tests. Construction of the Emsland Facility began in 1980 and was completed in 1984. It was the site of the 2006 accident when a moving Transrapid vehicle collided with

a stopped maintenance vehicle that was working on the guideway [5].

The Transrapid vehicles through TR08 obtained power for levitation and electronics below 80 km/h by physical contact with the track. The new TR09 vehicle (Fig. 38) needs no physical contact with the track at any speed, but receives power by inductive transmission with the track's propulsion system. If the track's propulsion power system fails, TR09 uses on-board batteries for back power to maintain levitation [5].

Application of Transrapid in Germany has been prevented by two factors: (1) the existing network of ICE high speed rail lines, and (2) high construction cost. The proposed Hamburg to Berlin line was canceled because of cost, as was the Munich to its airport route. The 40 km (25 mile) route between Munich Central Station and Munich Airport was originally estimated to cost 1.85 € billion, but later raised to over 3 € billion ($4.7 billion) or almost $200 million per mile. High tunnel and civil engineering costs were significant factors in the 2008 decision to cancel the project [5].

Transrapid has been intensively lobbied in the USA to build Maglev routes between major metropolitan areas, for example, Las Vegas to Anaheim, California, Baltimore to Washington, DC, Pittsburgh to its airport, etc. So far, however, no projects have gone forward.

The Development of the Second-Generation Maglev-2000 System

The first-generation Maglev systems, while technically successful, have two factors that limit their implementation, particularly in the USA.

First, the guideway construction cost is very high, $60 million or more per mile. Second, the first-generation Maglev systems only carry passengers. While useful in densely populated Europe and Japan, passenger-only systems are less useful in lower population density large countries like the USA. US transport outlays for intercity trucks over $300 billion annually; for intercity air passengers, $60 billion per year; and for intercity rail passengers, only $3 billion per year [24]. Maglev or high speed rail passengers only systems in the USA will require major government financing for construction and large subsidies for operation and maintenance. Because of USA's large debt, major government financing is unlikely. Maglev routes will need private investment. To achieve this, they must be profitable, with a short payback time on invested capital, less than a decade.

MAGLEV Technology Development. Figure 38
Transrapid 09 at the Emsland test facility in Germany

The second-generation Maglev-2000 system addresses these two factors. First, the projected guideway construction cost is about $25 million per mile, a factor of 2 or more lower than first-generation systems. Low cost prefabricated monorails are used for the elevated guideway. Figure 39 shows an artist's view of a Maglev-2000 passenger vehicle on the monorail guideway.

The prefabricated monorail beams would be mass produced in factories, with their guideway loop panels, sensors, electronic equipment, etc., attached to them at the factory. The beams and piers would then be transported by truck or rail to the construction site, where they would be quickly erected on pre-poured concrete footings or pilings, using conventional cranes. Low guideway cost would be achieved by the use of conventional box beams for the monorail, which minimizes the materials required, and prefabrication, which minimizes expensive field construction. Disruptions to local infrastructure would also be minimized, which would reduce local opposition to guideway construction.

The superconducting quadrupoles on the vehicles (Fig. 23) have four magnetic poles that alternate in polarity around their circumference. When on the monorail guideway, the vertical sides of the quadrupoles interact with the aluminum loops attached to the adjacent vertical sides of the monorail guideway. When operating on a planar guideway (Fig. 23), the bottom faces of the quadrupoles magnetically interact with aluminum loops located on the guideway beneath the vehicle.

The ability to operate on a planar guideway as well as monorail reduces construction cost. When operating in densely populated urban and suburban areas, Maglev-2000 vehicles do not need a new, very expensive guideway with its accompanying disruptions to existing infrastructure. Instead, the vehicles can transition to, and operate on, existing RR tracks to which aluminum loop guideway panels have been attached on the cross-ties (Fig. 40). Conventional trains can continue to use the RR tracks, given appropriate scheduling. The cost of attaching guideway panels to enable levitated Maglev-2000 operation is very small, only about $4 million per mile, compared to the much higher cost of building a new elevated guideway.

MAGLEV Technology Development. Figure 39
Artist's drawing of Maglev-2000 vehicle on monorail guideway

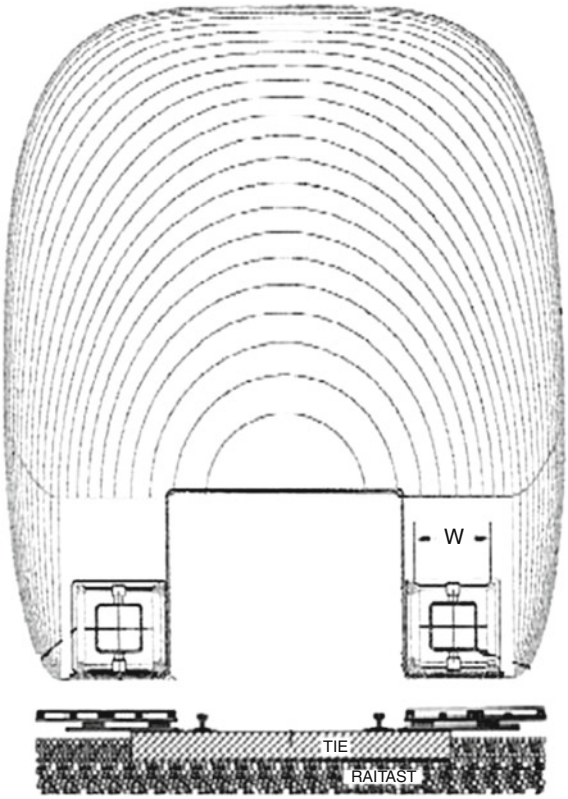

MAGLEV Technology Development. Figure 40
Drawing of levitated Maglev-2000 vehicle traveling on conventional RR tracks to which aluminum loop panels have been attached to the cross-ties

Turning to the second factor affecting Maglev implementation, revenues and net profits, Maglev-2000 can carry heavy trucks as well as passenger vehicles on its dual-use guideway. In contrast to the superconducting dipole loops used in the Japanese first-generation Maglev system, the powerful superconducting Maglev-2000 quadrupoles can be located along the length of a Maglev vehicle, increasing its lifting capability without producing magnetic fields inside the vehicle that significantly exceed the natural Earth ambient value. This is a result of the considerably lower value of the magnetic fringe fields from a quadrupole, compared to a dipole system.

Figure 41 shows a drawing of a passenger and truck carrier Maglev-2000 vehicles on the dual-use Maglev-2000 monorail guideway. The gross revenue from transporting 3,000 trucks daily on a Maglev-2000 route (one-fifth of the daily truck traffic on a typical Interstate Highway) is equivalent to 180,000 passengers per day, assuming a typical US outlay of 30 cents a ton mile for trucks, and 10 cents a passenger mile. The truck revenues alone would pay back the Maglev-2000 guideway in less than 5 years, attractive for private investment.

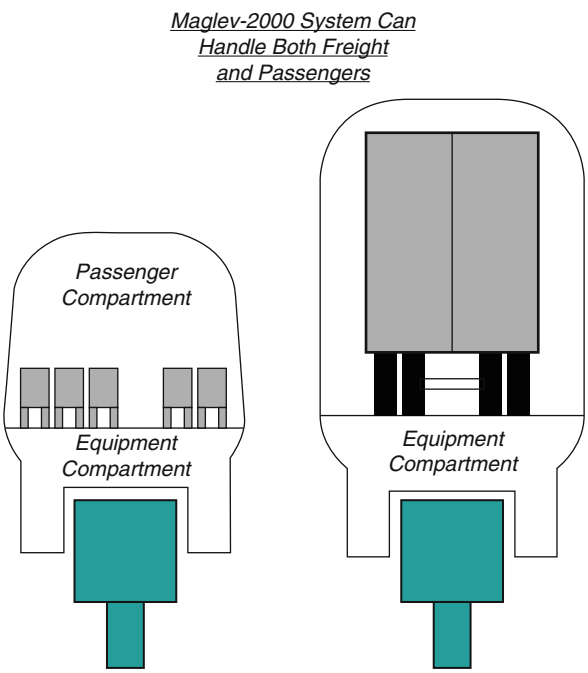

MAGLEV Technology Development. Figure 41
Maglev-2000 passenger and truck carrier vehicles on dual-use guideway

The same Maglev-2000 guideway could also transport personal autos together with their passengers, on long trips at lower cost than by highway. It could also transport high-value freight.

Using Maglev, a trucker could pick up a load, drive a few miles to the nearest Maglev station, travel across the USA in a few hours rather than a few days, and drive off the Maglev vehicle to deliver the load to its destination a few miles away. Wear and tear on the truck would be much less and it could make five deliveries in the time it would take to go by highway.

The ability of Maglev-2000 vehicles to travel on planar guideways also enables high speed electronic switching to off-line stations. Maglev-2000 vehicles can bypass high speed stations they are not scheduled to stop at, enabling stations to be closely spaced for convenient access. This increases revenue potential compared to only a few stations in a metropolitan area.

Figure 42 shows a drawing of the Maglev-2000 aluminum wire loop guideway panel. It has three sets of multi-turn aluminum loops: (1) a sequence of four short figure of 8 loops; (2) a sequence of four short dipole loops; and (3) one long dipole loop.

When the panels are attached on the vertical sides of the monorail guideway beam, the figure of 8 loops provide levitation and vertical stability. The dipole loops on each side of the beam are connected together to make a null flux circuit that maintains the vehicle in a centered position on the beam – when centered no current flows in the aluminum null flux circuit. When an external force (wind, curve, etc.) acts to push the vehicle away from its centered position, a magnetic force develops that opposes the external force. The long dipole loop is part of the linear synchronous motor (LSM) propulsion system, in which the loops on a sequence of panels are connected in series to form an energized block along which the Maglev vehicles travel. The energized block is typically on the order of 100 m in length; as the vehicle leaves an energized block, its AC propulsion current is switched into the next block that the vehicle is entering.

For the planar guideway, the panels are laid flat on the planar surface beneath the line of quadrupoles on the moving vehicle. The figure of 8 loops now provide lateral stability, generating magnetic restoring forces if

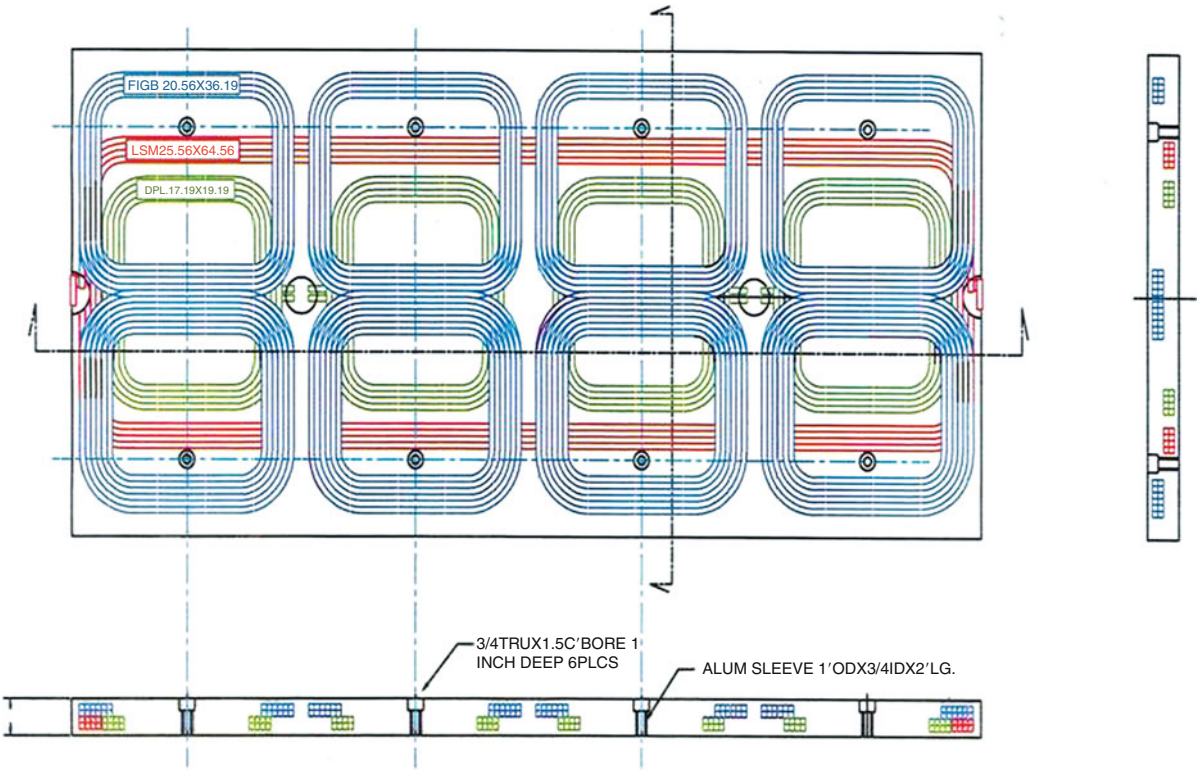

MAGLEV Technology Development. Figure 42
Drawing of aluminum loop guideway panel providing vertical life and stability, lateral stability, and linear synchronous propulsion

an external force acts to displace the vehicle from its centered position on the guideway. The dipole loops act individually, with inductive currents that levitate overhead. The LSM loops function as they do on the monorail guideway.

The planar guideway panel configuration can levitate and propel Maglev vehicles along existing RR tracks, with the panels attached to the cross-ties of the RR tracks.

The planar guideway also enables high speed switching. At a switch section, there are two lines of overlapping guideway loops, which can be either electronically open-circuited or close-circuited, depending on the desired switching action. Line A of guideway loops runs straight ahead on the main line, while the second line (Line B) of loops diverges laterally at a rate acceptable to passengers. If the loops in Line A are close-circuited and those in Line B are open-circuited, the vehicle travels straight ahead on the main route. If Line A is open and Line B is closed, the vehicle diverges laterally from the main route onto a secondary guideway leading to the off-line station. The high speed vehicle then decelerates on the secondary guideway that leads into the off-line station. When the vehicle leaves the station to rejoin the main line, it accelerates on an out-bound secondary guideway to a second switch section where the high speed vehicle reenters the main line.

The Maglev-2000 components discussed above have been fabricated and tested at full scale in order to determine their performance and validate their projected costs.

Figure 43 shows one of the two wound superconducting loops used for the Maglev-2000 quadrupole. The loop has 600 turns of NbTi superconducting wire, supplied by Supercon, Inc. of Shrewsbury, MA [25]. At the design current of 1000 A in the NbTi wire, the Maglev-2000 quadrupole has a total of 600,000 A turns in each of its two superconducting (SC) loops. The SC winding is

MAGLEV Technology Development. Figure 43
NbTi superconductor loop for Maglev-2000 quadrupole

porous, with small gaps between the NbTi wires to allow liquid helium flow to maintain their temperature at 4.2 K, and to stabilize them against flux jumps and micro movements [25].

Figure 44 shows the SC loop enclosed in its stainless steel jacket. Liquid helium flows into the jacket at one end and exits at the end diagonally across from the entrance, providing continuous helium flow through the SC winding. Before insertion of the SC loop into the jacket, it is wrapped with a thin sheet of high purity aluminum (5000 residual resistance ratio) to shield the NbTi superconductor from external magnetic field fluctuations. After closing the jacket, a second layer of high purity aluminum is wrapped around it for additional shielding.

Figure 45 shows a CAD-CAM drawing of the complete Maglev-2000 cryostat that holds two superconducting quadrupoles. The magnetic polarity of the front SC quadrupole is opposite to that of the rear quadrupole. This allows levitation at lower speed than if the two quadrupoles had the same polarity, due to less L/R decay of the currents induced in the aluminum guideway loops. The two SC loops are supported by a graphite-epoxy composite structure that resists the magnetic forces – due both to the forces in a loop from its self current, and to the forces between the two loops – that act on them.

Figure 46 shows the SC loops, support structure, and cooling currents for the Maglev-2000 quadrupole being assembled in Maglev-2000's facility on Long Island. The SC loops have a 10 K thermal shield, which is cooled by helium exiting from the jacket holding the SC loop. The SC quadrupole structure is then enclosed by an outer layer of multilayer insulation (MLI) consisting of multiple alternating layers of glass fiber and aluminum foil. A second thermal shield encloses the SC quad, and maintained at ~70 K by the helium outflow from the 10 K primary thermal shield.

Figure 47 shows the completed SC quadrupole enclosed in its vacuum cryostat, while Fig. 48 shows testing of the quadrupole magnetic levitation and propulsion forces using DC current in the aluminum loop guideway assembly beneath the quadrupole as a stand-in for the induced currents. The quadrupole was successfully tested to its full design current of 600,000 A turns. The magnetic forces between the quadrupole and the guideway loop assembly were measured as a function of vertical separation and lateral displacement from the centered position, and

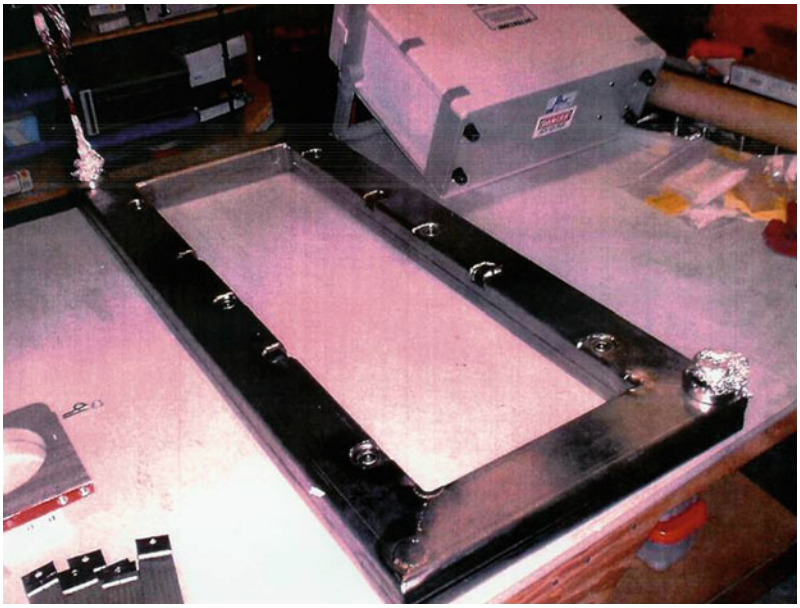

MAGLEV Technology Development. Figure 44
NbTi superconducting loop enclosed in stainless steel jacket

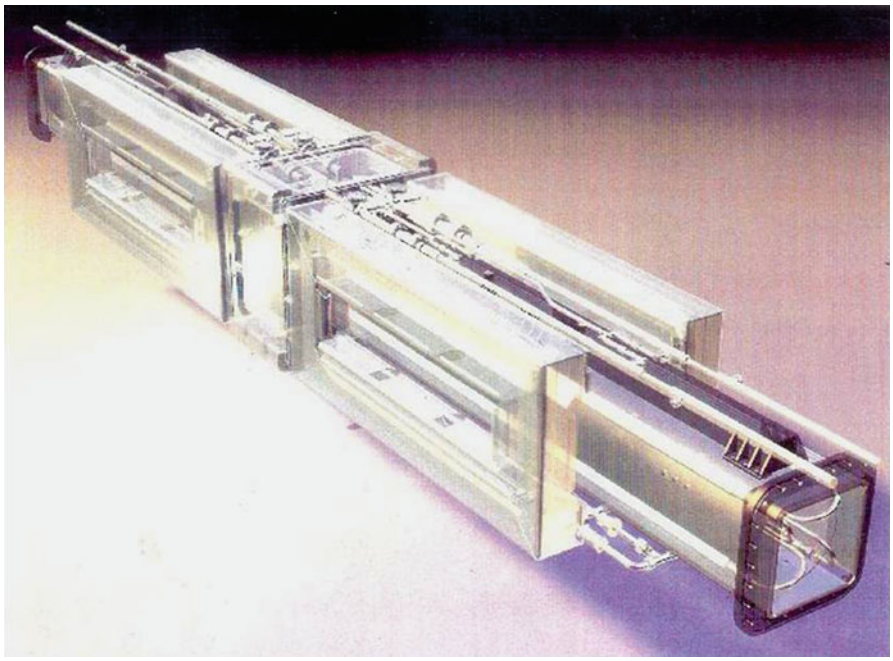

MAGLEV Technology Development. Figure 45
CAD-CAM drawing of Maglev-2000 superconducting quadrupole

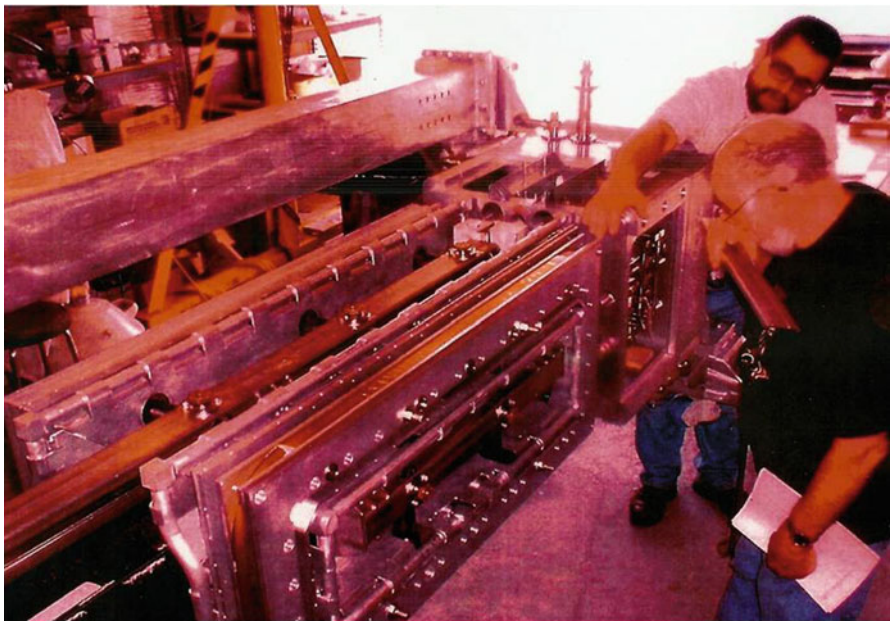

MAGLEV Technology Development. Figure 46
Assembly of Maglev-2000 superconducting quadrupole

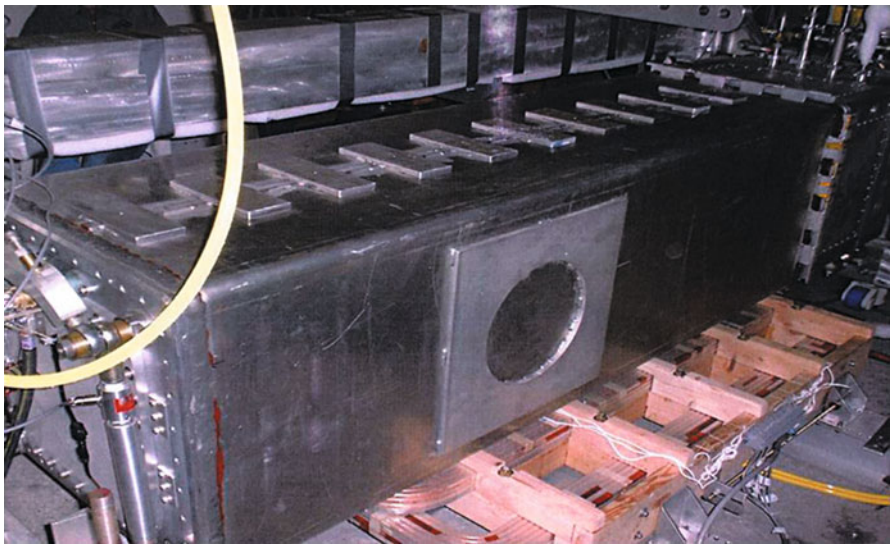

MAGLEV Technology Development. Figure 47
Completed Maglev-2000 quadrupole enclosed in its cryostat

longitudinal position in the direction of movement along the guideway. The measured forces agreed with three-dimensional computer analyses.

In the time following the Maglev-2000 quadrupole tests, high temperature superconductors have become much more capable, and are commercially produced in substantial amounts. Using YBCO high temperature superconductor wire, it appears very possible to fabricate Maglev-2000 quadrupoles that would be much simpler in construction, with much easier refrigeration

MAGLEV Technology Development. Figure 48
Testing of magnetic forces on Maglev-2000 quadrupole using DC current in aluminum loop panel

requirements. The YBCO superconductor would operate at 40 K with a much simpler on-board cryocooler than for NbTi superconductor at 4.2 K. One Maglev-2000 quadrupole requires 3,600 kA turns of superconductor. At $10 per kiloamp meter, which appears achievable with large-scale production of high temperature superconductor, the superconductor for it would cost $36,000. A passenger vehicle with eight quadrupoles would then have a superconductor cost of $288,000, while a truck carrying a vehicle with 16 quadrupoles would then have a superconductor cost of $576,000, both of which are very reasonable for a projected total cost of $5 million per vehicle. Future tests of Maglev-2000 quadrupoles will probably involve high temperature superconductors rather than NbTi superconductor with liquid helium coolant.

As described previously, the guideway loop panels contain three sets of wound aluminum loops, composed of a set of four figure of 8 loops, a set of four dipole loops, and one long LSM propulsion loop. Figure 49 shows a wound dipole loop, to be used in the panel. The aluminum conductor has a ~10 mil layer of nylon using a dip process to coat the conductor. The nylon insulation withstood 10 kV tests without breakdown. Figure 50 shows a completed guideway loop panel with all of its loops.

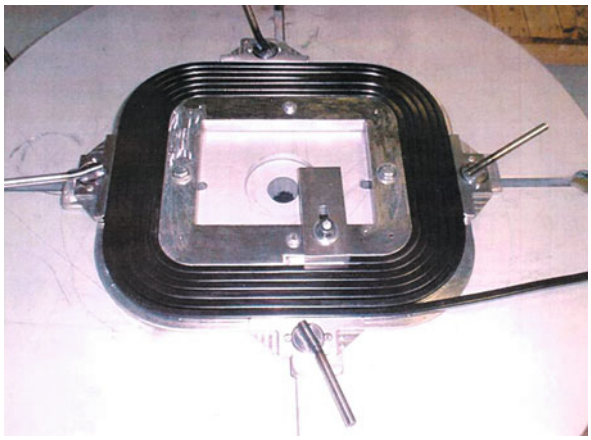

MAGLEV Technology Development. Figure 49
Wound dipole loop for guideway panel using nylon-coated aluminum conductor

The completed panel is then enclosed in a polymer-concrete structure for handling and weather protection (Fig. 51). Polymer concrete – a mixture of aggregate, cement, and plastic monomer – can be cast into virtually any form as a slurry. When the monomer polymerizes (the rate of polymerization is controlled by the amount of added promoter), the resulting concrete-like structure

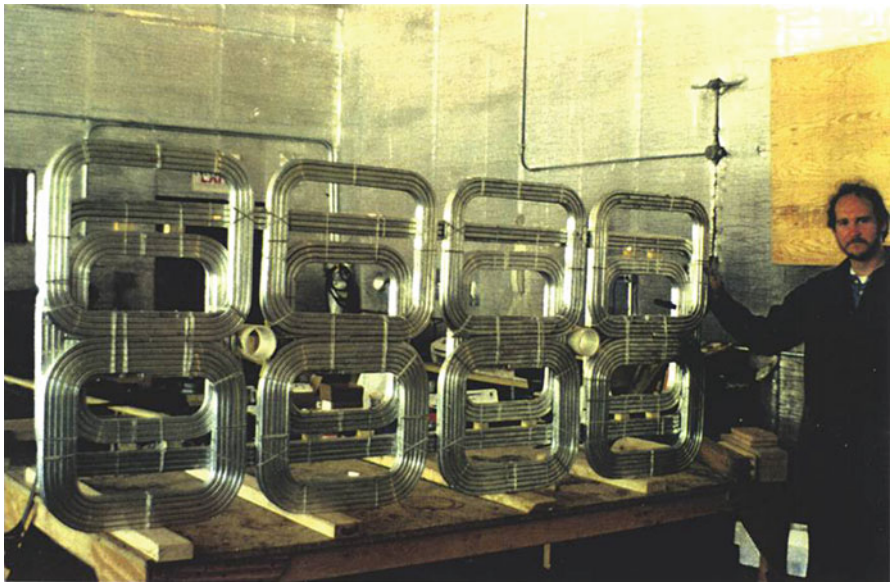

MAGLEV Technology Development. Figure 50
Completed guideway panel with figure of 8 dipole, and LSM propulsion loops

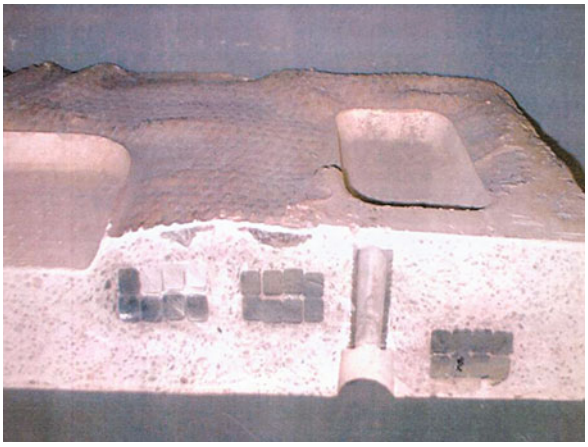

MAGLEV Technology Development. Figure 51
Guideway loop panel enclosed in polymer-concrete matrix

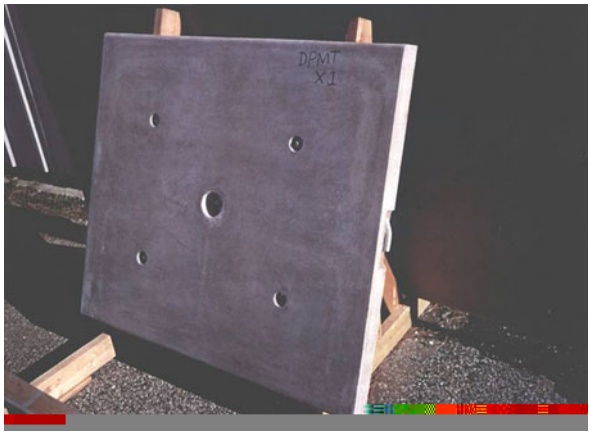

MAGLEV Technology Development. Figure 52
Polymer-concrete panel with enclosed aluminum loop exposed for 2 years to outdoor environment with multiple freeze-thaw cycles

is much stronger – a factor of 4 or greater – than ordinary concrete, and not affected by freeze-thaw cycles, salt, etc. Figure 52 shows a completed polymer-concrete panel left outside of the Long Island facility for 2 years. It was subjected to a wide range of weather conditions and multiple freeze-thaw cycles over the 2 year period, without any degradation.

After being fabricated at the Maglev factory, the guideway panels would be attached to the sides of the monorail or the surface of planar guideway beams to be shipped to a construction site for an elevated guideway, or transported to existing RR trackage that was to be modified for use by Maglev-2000 vehicles.

Figure 53 shows the basic design for the monorail guideway beam. It is a hollow box beam made with reinforced concrete. The beam length is 22 m and weight is 34,000 kg. It uses post-tension construction, which allows the tensioning cables in the base of the beam to be retightened if some stretching were to occur. The beam is tensioned to have a 0.5 cm upward camber at the midpoint of the beam when it is not carrying a Maglev vehicle. When the Maglev vehicle is on the beam, the beam flattens out to a straight line condition, with no vertical dip or camber along its length.

Figure 54 shows a photo of the fabricated beam after transport by highway truck from the manufacturing site in New Jersey to Maglev-2000's facility in Florida. No problems in the 800 mile transport by highway were encountered. The first beam cost $45,000 with a projected large-scale production cost of $25,000 per beam. Since 1999, construction costs have increased. At $50,000 in today's dollars, 140 beams for a two-way monorail guideway would cost $7 million per mile.

Figure 55 shows a CAD-CAM drawing of the aluminum chassis that was fabricated for a 20 m long Maglev-2000 test vehicle, designed to carry 60 passengers in urban and suburban service. Figure 56 shows the fuselage for the test vehicle.

Maglev Applications

High Speed National Maglev Networks

As in other developed nations, USA's three main transport systems – motor vehicles (autos, buses, and trucks), airplanes, and conventional rail – operate as national networks. From any given area in the USA, passengers and freight can drive, fly, or go by bus or train to any other area in the USA. To reach a particular location, it may be necessary to transition from one system to another; for example, one can fly from one airport to another airport, with a short drive to one's final destination. However, such local transitions are usually easily accommodated.

For Maglev to be an important mode of transport in the twenty-first century, it must also function as a national network. A few isolated Maglev routes, while helpful to local travelers, will provide only minor benefits. They will not substantially reduce oil consumption and greenhouse gas emissions, and not significantly increase domestic jobs and exports.

MAGLEV Technology Development. Figure 54
Photo of 22 m long monorail guideway beam delivered to Maglev-2000 facility in Florida from construction site in New Jersey

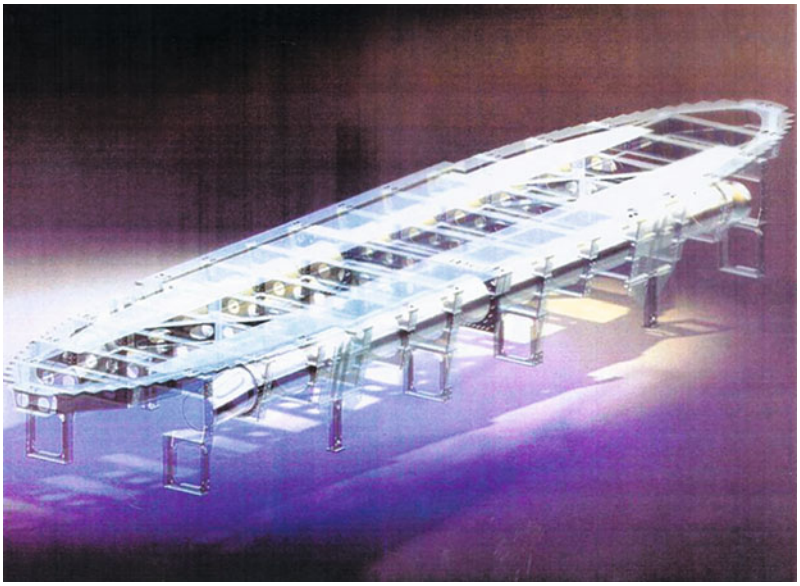

MAGLEV Technology Development. Figure 55
CAD-CAM drawing of aluminum chassis for 60 ft long Maglev-2000 vehicle

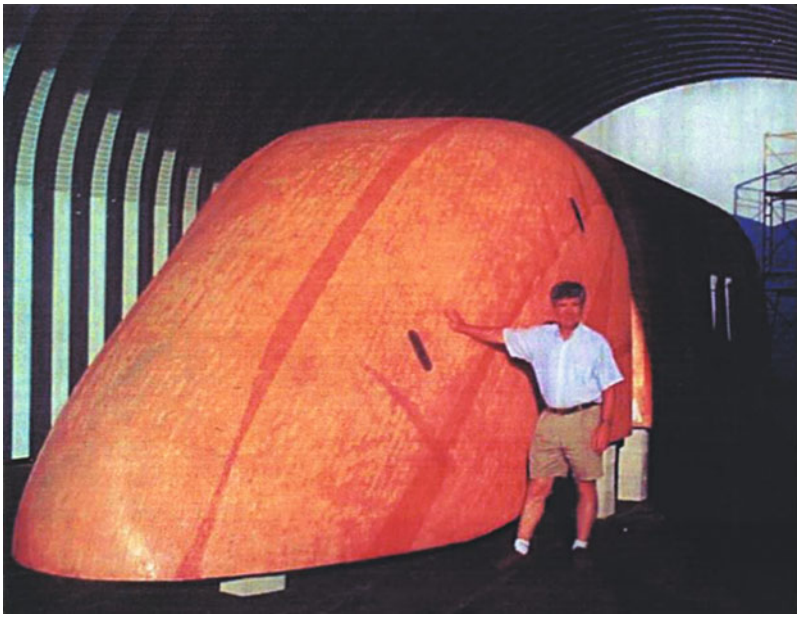

MAGLEV Technology Development. Figure 56
Photo of fuselage for 60 ft long Maglev-2000 vehicle

The potential 25,000 mile National Maglev Network (Fig. 57) would interconnect virtually all major metropolitan areas in the USA. The intercity Maglev routes, following the vision of the late Senator Daniel Patrick Moynihan, would primarily be on the rights of way of the Interstate Highway System [26]. Had his $750 million 1990 Senate passed legislation for a US Maglev R&D program not been killed in the House of Representatives, USA would be well on its way to its National Maglev Network.

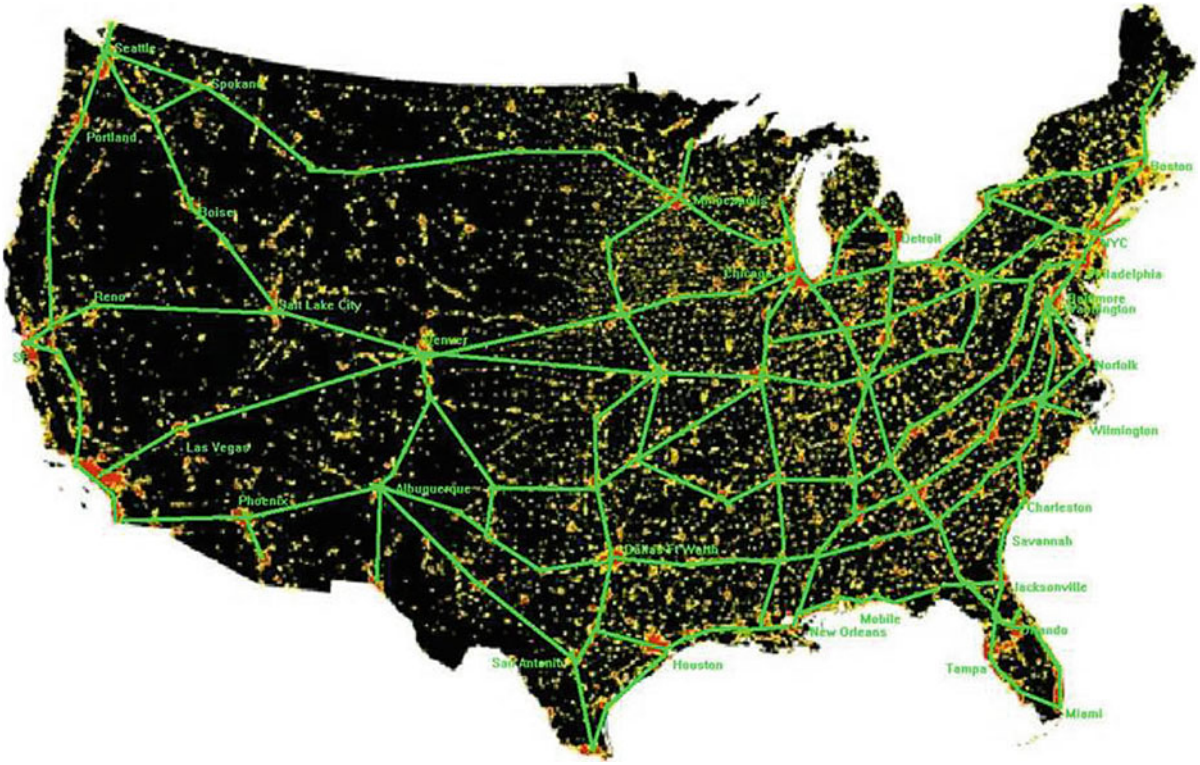

MAGLEV Technology Development. Figure 57
25,000 mile national Maglev-2000 network

One of the unique features of the second-generation Maglev-2000 system is the ability of Maglev-2000 vehicles for levitated travel along existing RR tracks, to which thin panels holding aluminum loops have been attached to the cross-ties.

Conventional trains can continue to use the RR tracks, given appropriate scheduling. This capability to use existing RR tracks enables Maglev-2000 vehicles to travel in densely populated urban and suburban areas, without needing to construct very expensive new infrastructure, with its inevitable disruptions to the existing infrastructure and the local population. Combined with high speed elevated Maglev guideways between metropolitan areas, this would result in fast convenient travel by Maglev, both within a given metropolitan area, and from one metropolitan area to another.

In addition to the attractive transport features and economic benefits of the National Maglev Network benefits and compared to present transport systems, its ability to effectively and cheaply transport passengers and freight without the need for oil will become extremely important in the following decades as world oil runs out.

The desired capabilities for a US National Maglev Network include:

1. Low guideway cost
2. Able to transport passengers, personal autos, highway trucks, and freight containers on dual-use guideways with high energy efficiency in all weather conditions
3. Able to be privately financed without the need for government funding and subsidization for construction and operation
4. Rapid installation of guideways with minimal disruptions and modifications to existing infrastructure
5. High speed electronic switching to off-line stations, with service to multiple convenient stations in metropolitan areas
6. Earth ambient magnetic field levels in passenger cabins

Construction costs for the Japanese and German first-generation Maglev systems are high, for example, $50 million or more per two-way mile [27]. To be widely implemented in the USA, construction cost should be substantially lower (Capability #1).

The National Maglev Network would not just carry passengers, but also intercity highway trucks, personal autos, and freight containers (Capability #2). US transport outlays [24] for intercity highway trucks (over $300 billion) are much greater than those for passenger air ($60 billion annually) and dwarf passenger rail (only $3 billion per year) (Fig. 58).

Intercity highway trucks haul about the same amount of freight, 1.5 trillion ton miles per year as conventional rail, but charge ten times as much per ton mile transported. They are preferred for high-value freight transport over conventional rail because of their much faster delivery and their convenient service, direct from origin to destination. Shipping by rail takes much longer and is much less convenient. The average haul distance for highway trucks is ~500 miles. Truckers would need far fewer trucks to deliver the same volume of goods if they went by Maglev at 300 mph rather than by highway at 60 mph, and at less cost per ton mile delivered (Fig. 59).

Similarly, drivers could take their personal autos with them on Maglev vehicles configured to carry 15–20 autos and their passengers. Travel would be much faster and cheaper than by highway, counting fuel, lodging, and auto maintenance costs.

Private financing is essential for a National Maglev Network (Capability #3) because of the very high government debt levels. Passenger-only Maglev systems will not attract private financing. Figure 60 shows the payback time for a Maglev route as a function of the number of trucks transported daily, for the operating parameters summarized in Table 2 assuming zero passenger revenues (curve A). At 3,000 trucks daily (20% of typical highway truck traffic on an interstate) the payback time is less than 5 years. At 6,000 trucks daily

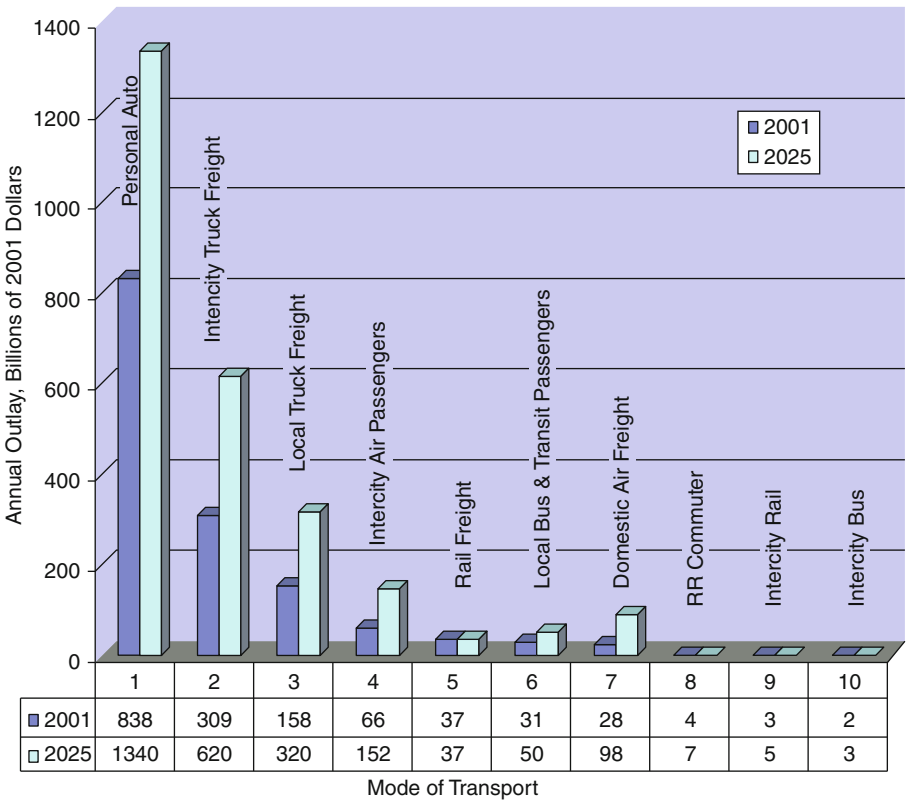

	1	2	3	4	5	6	7	8	9	10
2001	838	309	158	66	37	31	28	4	3	2
2025	1340	620	320	152	37	50	98	7	5	3

MAGLEV Technology Development. Figure 58
Annual outlays current and future, for US transport modes (billions of dollars) (US census Bureau [24])

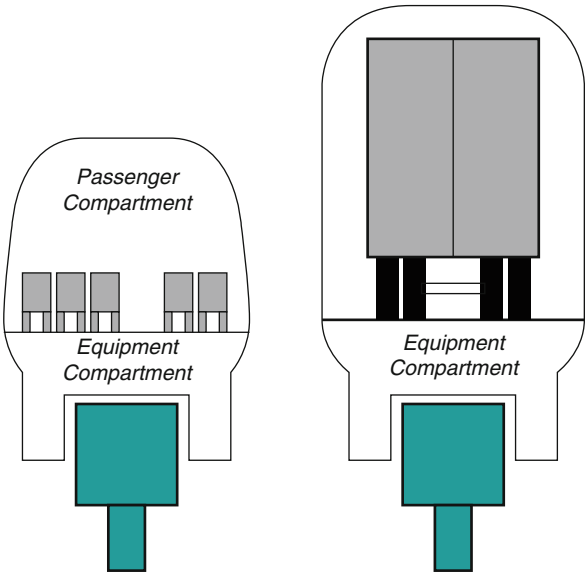

MAGLEV Technology Development. Figure 59
Maglev-2000 system can handle both freight and passengers

(40% of truck traffic) payback time is less than 2.5 years. Without trucks, payback time is many decades for realistic passenger ridership levels of 10,000–20,000 passengers daily (curve B).

Rapidly installing guideways with minimal disruption and modification of existing infrastructure (Capability #4) minimizes the cost and local opposition to the construction of a Maglev route. This is especially important in densely populated urban and suburban areas. Whenever possible, existing infrastructure including existing rail trackage should be used to avoid disruptions to local inhabitants.

High speed electronic switching (Capability #5) is very desirable. Not being able to switch off the main line, or having to mechanically move a long cumbersome guideway switch section significantly reduces average speed. For example, HSR systems, though capable of maximum speeds of ~200 mph, have considerably slower average speeds when station stops and their slow acceleration and deceleration rates are taken into account [28]. Electronic switching to off-line stations will enable Maglev vehicles to bypass at high speed stations they are not scheduled to stop at, maintaining high average speeds. This will allow many

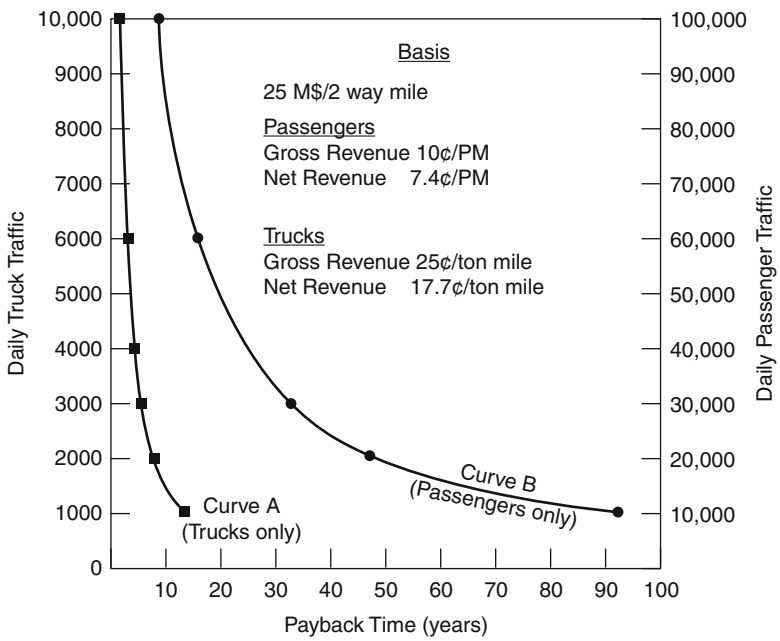

MAGLEV Technology Development. Figure 60
Payback time for Maglev-2000 guideway as a function of truck and passenger traffic

MAGLEV Technology Development. Table 2 Vehicle O&M costs

Revenues and costs	Passengers (cents/pm)	Trucks (cents/ton mile)
Gross rev	10	25
Energy cost	1.2	4.0
Am&M cost	0.9	2.8
Personnel cost	0.5	0.5
Net Rev.	7.4	17.7

$5 million vehicle cost; 10 year amortization; 5%/year maintenance
100 passenger or 30 t capacity; 80% load factor; 12 h op/day
250 mph average speed; 3 MW propulsion power for passenger vehicles
4 MW for trucks; 6 cents/KWH

MAGLEV Technology Development. Table 3 National network and Maglev-2000 system parameters

Network	25,000 miles, 300 mph max
Passenger vehicles	100 passengers
Truck carriers	Two types (one and two trucks)
Auto carriers	15 autos + passengers
Travel	Either as single units or multiunit consists, depending on traffic
Quadrupole magnets	600,000 A turns 18 in. wide, hi temp superconductor, 8 magnets for passenger vehicle, 16 magnets on truck and auto carriers
Magnetic suspension	10 cm gap between vehicle and guideway, 0.3 g/cm automatic magnetic restoring force

closely spaced stations within a metropolitan area, for convenient access.

Earth ambient magnetic field levels in passenger compartments (Capability #6) are not only desirable, but a necessity. The US public strongly resists new technologies that appear to deviate from their normal environment.

There is no evidence that DC magnetic fields of a few gauss have any effect on the body (there is a limit of 5 gauss for people with pacemakers) and people experience much greater fields – at the kilogauss level during MRIs – without problems. However, to avoid possible controversy and opposition to Maglev, it is desirable to keep the magnetic field inside passenger cabins at Earth ambient level.

The guideway panels can also be mounted on the cross-ties of existing RR tracks (Fig. 40), enabling levitated travel of Maglev-2000 vehicles along existing RR tracks in a planar guideway mode. The panels do not interfere with the operation of conventional trains, which could continue to use the tracks for bulk freight transport, given appropriate scheduling, probably at nighttime. The ability of Maglev-2000 vehicles to travel as individual units would enable much more frequent and convenient passenger service, rather as long trains of many RR cars. Also, because the Maglev vehicle loads are distributed along the vehicle and not concentrated at wheels, its local track loading is much less than conventional trains, resulting in much longer track life and reduced maintenance.

The capital cost of the monorail guideway has been examined in detail, based on fabrication experience and costs of magnets, panels, and the guideway beam. In 2000 dollars, the projected cost was $11.4 million per two-way mile for "greenfields" construction (no land acquisition or infrastructure modification costs) [29]. In 2010 dollars, the corresponding construction cost would be ~$25 million per two-way mile. The cost to adapt existing RR tracks for Maglev-2000 operation would be much less, on the order of $4 million per two-way mile, since an elevated guideway would not be required.

Table 3 summaries the nominal operating parameters for the Maglev-2000 system. A key element of the Maglev-2000 system that results in low construction cost is to mass produce its prefabricated components in large factories. The components, beams with attached panels, piers, controls, etc., can then all be shipped to the construction site and quickly erected at low cost on pre-poured concrete footings using conventional cranes. The components can also be readily exported to other countries. A container ship, for example, can carry 20 miles of prefabricated two-way guideway.

The proposed 2000 mile West Coast Maglev Network (Fig. 57) along the I-5 corridor and its branches would connect the metropolitan areas in California, Nevada, Oregon, and Washington State, plus the Vancouver, British Columbia, area into a high speed Maglev

system that would quietly transport many thousands of passengers, highway trucks, and personal autos 6 in. off the rails at speeds of 300 mph and one-fifth the cost of airline travel. Forty-two million persons in California, Nevada, Oregon, and Washington, 85% of the total population of 49 million in the four states, would live within 15 miles of their local Maglev station, from which they could reach any other station in the Maglev Network within a few hours. Another 1.3 million persons in the Vancouver area would be served by the network, making the total population within 15 miles of a Maglev station equal to 43.3 million people. Total government funding is limited to $600 million over 5 years for up front demonstration and certification activities. After that, freight capability enables building the entire network with private financing.

Typical trip times on the Maglev Network, compared to going by highway would be:

San Diego to Seattle	4 h 30 min vs 25 h 15 min
San Francisco to Los Angeles	1 h 45 min vs 9 h 40 min
Portland to San Francisco	2 h 30 min vs 12 h 45 min
Los Angeles to Las Vegas	1 h vs 5 h 30 min

In addition to much shorter trip times by Maglev, the cost of travel by Maglev would be significantly less for passengers, highway trucks, and personal autos as compared to existing transport modes:

Passengers – 3 cents per passenger mile (PM) on Maglev, compared to 40 cents per PM for driving by auto, 15 cents per PM by air, and 50 cents per PM by high speed rail.

Highway trucks – 10 cents per ton mile by Maglev compared to 30 cents per ton mile by highway.

Personal autos – 30 cents per mile by Maglev transport compared to 40 cents per mile by highway.

Table 4 gives data on the vehicle flow and congestion along the I-5 corridor.

Based on the data provided in Table 4 [30], a reference case for the average flow on the West Coast Maglev Network was assumed, with

- 5,000 trucks per day (2 per Maglev vehicle)
- 30,000 passengers per day (100 per Maglev vehicle)
- 20,000 personal autos carried on Maglev per day (10 per Maglev vehicle)

MAGLEV Technology Development. Table 4 Vehicle flow and congestion along the I-5 corridor

Traffic flow on corridor				
	2007		2035	
	Avg.	Max	Avg.	Max
Vehicles/day	71,000	300,000	150,000	~600,000
Trucks/day	10,000	35,000	22,000	~70,000
Urban segments,[a] % congestion	65%		95%	
Rural segments, % congestion	31%		85%	

[a]550 miles of 1,381 mile total length are urban segments

The above traffic flows on Maglev are a significant fraction of the 2035 traffic flow, but could be increased substantially. For the reference case, travels by Maglev results in the major benefits given below:

- $21 billion annual reduction in cost of transport
- 53 billion KWH annual reduction in energy for transport
- 27 million tons annual reduction in CO_2 emissions

The West Coast Maglev Network can be in full operation by 2019, given an aggressive program with adequate funding. Construction ground breaking would start in 2015, following a 5 year program to demonstrate and certify the various types of Maglev vehicles – passenger, auto with passengers carrier, and highway truck carrier on a test guideway at commercial operating conditions. Planning activities, environmental permits, and startup of guideway production plants would also be carried out in parallel with the testing of commercial-type vehicles. The network would be constructed over a 4 year period by simultaneously carrying out construction of nine segments of the 2,000 mile network. Each segment would run between major metropolitan areas on the network, for example, San Diego to Las Angeles would be one segment, Anaheim to Las Vegas another segment, and so on. Each segment of the Network would have one or more guideway beam and pier manufacturing plants. The projected construction cost is on the order of $60 billion, based on an average unit cost of $25 million per two-way mile.

Maglev Energy Storage

Electrical power systems typically experience large swings in power demand, with low demand during the night and high demand during the daytime. Even in the daytime, power demand varies widely, with major peaks during the morning and late afternoon. Existing technologies for electrical power storage are generally too expensive and difficult, for example, batteries, flywheels, superconducting energy storage (SMES), or too limited in siting, for example, pumped hydro. Today, the great majority of peak power demand is supplied by fossil fueled peaking power plants, for example, gas turbine, or by purchase from distant power grids.

A new approach for the storage and rapid delivery of electric power, based on Maglev, is proposed [31]. This new method, termed *MA*glev *P*ower *S*torage (MAPS) uses Maglev technology similar to that employed for the transport of passengers and freight to lift masses a kilometer or more in altitude. In doing so, electrical energy is stored as gravitational potential energy. Raising a 100 t mass 2 km in altitude, for example, stores 0.5 Megawatt Hour (MWH) of energy. Raising 2,000 such masses would store 1,000 MWH of energy, which would be returned to the power grid at appropriate times by simply transporting the masses down to a lower altitude. During periods of electrical storage, Maglev vehicles would transport masses up to a higher altitude storage facility, with the vehicles' magnetic propulsion system operating in the motor mode. During periods of electrical power delivery, the masses would be transported down to lower altitude, with the propulsion system operating in the generator mode.

The total energy delivered is determined by the number of storage masses transported up and down, while the power delivered is determined by the rate at which they are transported. The MAPS system is very flexible and can rapidly alter its power level by changing the rate at which masses are moved up or down the guideway. MAPS power level, for example, could go from zero to 100% of full capability, or from 100% to zero, in less than 2 min. Peak power capabilities of ~1,000 MW(e) can be generated using MAPS. Because of its rapid response capability, in addition to providing peak power, MAPS system could also be used for low cost spinning reserve. Presently, spinning reserve is provided by keeping expensive generator units hot and ready to generate large blocks of power .

While the basic Maglev technology for energy storage is similar to that for passenger and freight transport, there are differences, that is, steeper grades for the MAPS system (up to 45° vs a maximum of ~10° for passenger/freight transport), and considerably heavier vehicles (~100 t vs a maximum of ~50 t for freight transport). The heavier loaded and much shorter vehicles (~6 m for MAPS vs ~30 m for passenger/freight vehicles) use a magnet configuration which maximizes propulsion force relative to I^2R losses in the propulsive windings. To efficiently levitate the short heavy vehicle with minimum I^2R losses, iron plates in the narrow beam guideway provide most of the levitation force, with null flux loops for stability and oscillation damping. The storage masses are simple reinforced large concrete blocks on the flat upper surface of the MAPS vehicle. Typical dimensions for a 100 t storage mass are 3.5 m wide, 2.5 m high, and 4.5 m long. The blocks can be rapidly moved onto or off from the vehicle using a roller bar surface and stored on pads at the guideways high and low altitude points. A 100 m × 600 m long (6 acres) storage facility could handle and deliver 2,000 storage masses, equal to 1,000 MWH of electrical energy at an elevation change of 2 km (6,000 ft). Overall energy efficiency, output electrical energy/input electrical energy, would be well above 90% – much higher than any other electrical storage technology. For a mass unload time of 50 s and a mass load time also of 50 s (both steps are necessary during a vehicle round trip, whether MAPS is operating in the power storage or power delivery mode) a given MAPS vehicle could make 20 round trips per hour. This is quite conservative, since the 50 s intervals could probably be reduced to about 30 s, considering the simplicity of the transfer process. The total number of round trips per hour would then increase.

A very attractive feature is the completely nonpolluting environmentally benign nature of MAPS, and its ability to store power at very low cost from renewable wind and solar energy sources. MAPS facilities could be built in a short time, for example, 3 years or less, to meet increasing peak power demands.

The total land use for a 2,000 MWH facility, including a dual 3 km long guideway, is only about 20 acres. Most MAPS facilities would be sited in remote area and would not impact the environment. At the design speed of 130 mph, the vehicles would be virtually silent.

In locations with flat terrain, MAPS guideways could be installed underground in inclined tunnels or vertical shafts. Many mining tunnels and shafts operate at depths of 1 km (3,300 ft) or more. MAPS would transport its concrete blocks between a storage yard on the surface, and underground storage cavities positioned along a guideway in an underground horizontal tunnel. There are many mines, both coal and hard rock, in the USA that are no longer in use. Such mines would be attractive sites for MAPS facilities in flat regions of the USA.

Maglev Water Transport

The availability of ample clean water is a major concern in many regions, and is expected to be even worse in the decades ahead – in fact, many experts believe it to be the number one problem facing the world. A large fraction of the world's population, most of them poor, already lives in a state of water scarcity. World population is expected to grow to nine billion (mid-range projection) by 2050. This growth, along with increasing industrialization, urbanization, and irrigation, will put even more stress on water resources.

The advanced second-generation Maglev-2000 system described previously is designed to transport passengers and freight at very low cost. With design modifications to the vehicles and guideway, the second-generation Maglev-2000, termed the Water Train [32] system, can transport large amounts of water, that is, on the order of one billion gallons daily (1,000 megagallons/day), for hundreds of miles.

The Water Train vehicles transport a higher load per unit length of vehicle than for passenger and truck transport. The weight of loaded Maglev passenger/freight vehicles is nominally 50 t for a 30 m length. A water transport vehicle will probably weigh 200–300 t for the same length. This much heavier loading requires that the guideway be on-grade, or if it utilizes discrete supports, that they be relatively close together, for example, every 20 ft or so. The Water Train uses the "iron lift" configuration proposed by Danby and Powell [33], in which superconducting magnets on the vehicle are attracted upward to laminated steel plates attached to the guideway. The suspension is designed so there is a vertical equilibrium point at which the vertical lift force from the steel plates equals the weight of the vehicle.

The "iron lift" configuration is vertically stable, since as the vehicle moves upward, the lift force becomes smaller, and as it moves downward, the lift force becomes larger. The iron plates, however, make the "iron lift" configuration horizontally unstable. This horizontal instability is countered by the null flux stability loops on the guideway. The stable restoring force from the null flux loops is greater than the unstable force from the attraction to the steel plates, making the suspension horizontally stable.

An important feature of the Water Train is the flexible "balloon" that carries the water on each vehicle. The "skin" of the balloon is a relatively thick, for example, 1 in., reinforced flexible composite material. When pressurized and filled with water, the container forms a streamlined cylinder that runs the full length of the vehicle. After delivery of the water load and depressurization, the flexible skin is depressurized and collapsed minimizing the frontal area and air drag on the vehicle. The air drag resistance for a long multi-vehicle train will be much smaller than for a single vehicle. The equivalent drag per vehicle of the multiunit train is only 24% of a single vehicle.

The three principal cost components for the Water Train are propulsion energy and amortization of the vehicles and guideway. Energy cost scales as V^2, and vehicle amortization scales as 1/V. The faster the vehicle travels, the more water it can carry in a given period of time, reducing its amortization cost. Guideway cost is independent of vehicle speed, and depends only on the total amount of water carried. For a 1,000 megagallon per day delivery rate – the rate for a large city – amortization of the 300 mile long guideway only costs about 16 cents per 1,000 gal. Adding vehicle amortization and propulsion energy costs, the total cost for a 300 mile delivery is only about $1.50/1,000 gal. If the Water Train delivers water from a higher altitude to a lower one, part or all of the energy cost would be offset by gravitational energy input from the decrease in altitude. A 600 m drop from the origin to its destination would enable the transport of water at zero

energy cost. Over the 500 km delivery distance, this is an average grade of about 1 m/km – less than many natural river systems. A greater drop in altitude would enable the sale of surplus electric power generated by the moving vehicles to the electric grid. Accordingly, the Water Train can also generate large amounts of hydroelectric power at sites where there is substantial water flow and rapid drop in elevation. As an alternative to large dams, such an electric generation system would have significant advantages, including a much lower capital cost and much smaller environmental impact.

Elevation changes in terrain traversed by the Water Train are easily accommodated by small changes in train speed. Even for changes of ±200 m (660 ft), the velocity changes are modest and acceptable, without the need for propulsive power. The Water Train would simply speed up slightly as it coasted downhill, or slow down slightly as it coasted uphill, depending on the local terrain.

Finally, in contrast to long distance pipelines, which require many pumping stations along their length, the Water Train, because of its high kinetic energy and low air drag, can coast for hundreds of miles without additional propulsion. After the Water Train attains an initial velocity of 100 m/s (225 mph), and coasts for a distance of 100 miles, the Water Train velocity has dropped to 80% of the initial value, with the average velocity over the 100 mile segment at ~90% of its initial speed. While the Water Train could coast the entire 300 miles without propulsive input, it probably would be desirable to reaccelerate at intervals of 100–150 miles in order to keep the average velocity close to the optimum for minimizing cost. At its destination, the Water Train would electromagnetically de-accelerate down to zero velocity, and its kinetic energy fed back as electric power into the grid.

Future Directions

Maglev is still at an early stage of development, both in its technology and in its various applications. In the technology area, Maglev will evolve to use high temperature superconductors (HTS) that will enable operating temperatures in the range of 20–40 K, with much lower refrigeration power requirements, that is, W(e) of refrigeration electric power per watt(th) of thermal input through the cryostat insulation, than those for the present liquid helium cooled superconductors that operate at 4.2 K. HTS superconducting Maglev magnets will require only one-tenth as much refrigeration power input as liquid helium cooled magnets.

The lower refrigeration power and greater simplicity of HTS magnets will enable Maglev vehicles to be smaller, carry fewer passengers, and serve a wider range of transport applications. Maglev vehicles can be adapted for levitated travel in existing subways and commuter rail lines, providing faster and more frequent service in urban and suburban areas.

Maglev platforms will be developed to provide faster, easier, and safer movement of heavy objects in industrial plants, and movement of ores dug from open pits and underground mines at lower cost. Maglev vehicles will provide fast, convenient, and nonpolluting movement of heavy freight containers to and from seaports, in place of the thousands of greenhouse gas–emitting trucks that now provide the service.

Bibliography

1. O'Toole R (2009) "Gridlock: why we are stuck in traffic and what to do about it." CATO Institute
2. http://www.eia.doe.gov/bookshelf/brochures/greenhouse/Chapter1.htm
3. http://en.wikipedia.org/wiki/List_of_Countries_by_canbon dioxide_emissions
4. http://en.wikipedia.org/wiki/chevrolet_volt
5. http://en.wikipedia.org/wiki/Transrapid
6. (1914) The Bachelet levitated railway. Nature 93(2324):273
7. Danby G, Powell J (2000) Magnetic levitation: a new mode of transport for the 21st century, lecture given at the award for the Franklin Medal for Engineering, Franklin Institute, 26 Apr 2000
8. Powell J, Danby G (1966) High speed transport by magnetically suspended trains. Paper 66-WA/RR-5, presented at 1966 Winter ASME Meeting, New York City
9. www.rtri.or.JP/rd/maglev/html/english/maglev_frame.E.html
10. http://en.wikipedia.org/wiki/vactrain
11. http://magnetbahnforum.de/index.php?_mf_steering_committee
12. http://en.wikipedia.org/wiki/Heike_Kamerlingh_Onnes
13. http://en.wikipedia.org/wiki/Large_Hadron_Collider
14. Census Bureau (2006) US statistical abstracts, Table 1046, transportation outlays by type of transport: 1970 to 2001. Census Bureau, Washington, DC
15. Powell J, Danby G (1967) High speed transport by magnetically suspended trains. Paper 66-WA/RR-5, presented at 1966 Winter ASME Meeting, New York City; Mech Eng 89:30–35
16. Kolm H et al (1975) The magneplane system. Cryogenics 15:377–384

17. http://en.wikipedia.org/wiki/Maglev_(transport)
18. http://www.upf.org/bering-strait. . ./101. . ./479-Japanese-maglev-technology
19. http://en.wikipedia.org/wiki/Shanghai_Maglev_Train
20. News.smh.com.au ≥ Technology
21. http://www.rtri.or.jp/rd/maglev/html/english/maglev-frame_E.html
22. http://www.digitalworldtokjo.com. . ./500kph_maglev_flying_trains_get_green_light_to_burn_up_japan
23. http://magnetbahnforum.de/index.php?speed-records
24. US Census Bureau (2006) Statistical abstracts of the United States 2006, tables 1046 and 1047. US Department of Commerce, Washington, DC
25. Powell J et al (2008) Fabrication and testing of full scale components for the 2nd generation Maglev-2000 system. In: Maglev 2008 Conference, San Diego
26. Powell J, Danby G (eds) (1989) Benefits of magnetically levitated high speed transportation for the United States, report to United States Senate Committee on environment and public works, Grumman corporation. Bethpage, New York
27. Maglev I (2005) The Pennsylvania project: FRA high speed Maglev deployment program – project description. Transrapid International and Maglev, Pittsburgh
28. http://www.o-keating.com/hsr/tgv/htm
29. Powell J (ed) (1999) Cost projections for the Maglev-2000 system. Report DPMT-20, Maglev 2000 of Florida
30. http://www.thwa.dot.gov/pressroom/dot0795.htm
31. Powell J (2000) Electrical power storage and delivery using Maglev: the Maglev power storage system (MAPS). Report DPMT-14, DPMT Corp., 1 Nov 2000
32. Powell J, Danby G The water train: long distance delivery of water by Maglev. Report DPMT-3
33. Danby GT, Jackson JW, Powell JR (1974) Force calculations for hybrid (ferro-null flux) low drag systems. IEEE Trans Magnetic Mag O:443

Malaria Vaccines

Christopher V. Plowe
Howard Hughes Medical Institute/Center for Vaccine Development, University of Maryland School of Medicine, Baltimore, MD, USA

Article Outline

Glossary
Definition of the Subject
Introduction
The Malaria Life Cycle
Pathogenesis and Disease
Epidemiology
Immunity
Early Malaria Vaccines
Obstacles to Malaria Vaccines
Pre-erythrocytic Vaccines
Blood-Stage Vaccines
Transmission-Blocking Vaccines
Multistage, Multi-antigen Vaccines
Whole-Organism Vaccines
Future Directions
Acknowledgments
Bibliography

Glossary

Adjuvant A substance added to a vaccine to stimulate a stronger or more effective immune response.

Blood stage The stage of the malaria parasite life cycle responsible for clinical symptoms. Vaccines that target the blood stage are intended to prevent disease and death, but they do not prevent infection and may not affect malaria transmission.

Challenge trial Small experimental Phase 1/2 clinical trial in which healthy volunteers receive a malaria vaccine and are exposed to the bites of malaria-infected mosquitoes or injected with malaria parasites under carefully controlled conditions.

Immunogenicity The ability of a vaccine to produce specific immune responses (usually antibodies) that recognize the vaccine antigen.

Pre-erythrocytic Stages of the malaria parasite that are injected by a mosquito and develop in the liver before emerging into the blood where they can cause symptoms. Vaccines targeting pre-erythrocytic stages are intended to prevent infection altogether and, if highly effective, would also prevent disease and block transmission.

Sexual stage The male and female forms of malaria parasites that are responsible for transmission through mosquitoes. Vaccines directed against sexual stages are intended to prevent malaria transmission.

Subunit vaccine A vaccine based on a small portion of the organism, usually a peptide or protein.

Vaccine resistance The ability of malaria parasites to escape strain-specific immune responses by exploiting genetic diversity to increase the

frequencies of non-vaccine-type variants in a population or to evolve new diverse forms.

Whole-organism vaccine A vaccine based on an attenuated or killed whole parasite.

Definition of the Subject

Vaccines are the most powerful public health tools mankind has created, and research toward malaria vaccines began not long after the parasite responsible for this global killer was discovered and its life cycle described more than 100 years ago. But parasites are bigger, more complicated, and wilier than the viruses and bacteria that have been conquered or controlled with vaccines, and a malaria vaccine has remained elusive. High levels of protective efficacy were achieved in crude early experiments in animals and humans using weakened whole parasites, but the results of more sophisticated modern approaches using molecular techniques have ranged from modest success to abject failure. A subunit recombinant protein vaccine that affords in the neighborhood of 25–50% protective efficacy against malaria is in the late stages of clinical evaluation in Africa. Incremental improvements on this successful vaccine are possible and worth pursuing, but the best hope for a malaria vaccine that would improve prospects for malaria eradication may lie with the use of attenuated whole parasites and powerful immune-boosting adjuvants.

Introduction

The malaria parasite is thought to have killed more human beings throughout history than any other single cause [1]. Today, along with AIDS and tuberculosis, malaria remains one of the "big three" infectious diseases, every year exacting a heavy toll on human life and health in parts of Central and South America, large regions of Asia, and throughout most of sub-Saharan Africa, where up to 90% of malaria deaths occur [2].

In the middle of the twentieth century, the availability of the long-acting insecticide dichlorodiphenyltrichloroethane (DDT) and the safe and effective antimalarial drug chloroquine provided the basis for optimism that global eradication was possible. Although malaria was eliminated in several countries around the margins of the malaria map, factors including the emergence of DDT-resistant mosquitoes and chloroquine-resistant parasites, as well as waning economic and political support, led the campaign to stall by the late 1960s, resulting in the rapid resurgence to previous disease levels in many locations [3].

For the next 30 years, the spread of drug-resistant malaria and donor fatigue contributed to an overall lack of progress against the disease. But starting in the late 1990s, new tools, including long-lasting insecticide-impregnated nets and highly efficacious combination drug therapies, led to a wave of successes, including dramatic reductions in disease burden in some areas and complete elimination of malaria in others [4]. These success stories have stimulated a renewed sense of optimism about prospects for global eradication [5].

If it is to succeed, this nascent drive toward country-by-country elimination and possible eventual worldwide eradication of malaria will require powerful new tools, importantly including malaria vaccines that produce protective immune responses that surpass those acquired through natural exposure to malaria [6]. Successful global or regional campaigns to eradicate smallpox, polio, and measles have all relied on vaccines. Those for yellow fever, hookworm, and yaws – and for malaria – which have relied on non-vaccine measures such as vector control or drug treatment have all failed [7]. While the odds of successful global malaria eradication would be very long even with an ideal malaria vaccine, they are virtually nil without one. In the meantime, even a modestly effective vaccine could substantially reduce the continuing heavy burden of malaria-attributable disease (247 million annual cases) and death (881,000 annual deaths) [2].

After nearly a century of malaria vaccine research, today, one modestly effective vaccine based on a parasite surface protein is being tested in a large Phase 3 trial in hopes of licensure within a few years [8]. Many other vaccine candidates have fallen short and been abandoned before reaching this stage, although several are in early stages of clinical development. The chief reasons that it has taken this long to get this far are that malaria parasites replicate and propagate through an extremely complex life cycle involving vertebrate hosts and an insect vector, and that they have evolved a repertoire of mechanisms for evading both natural and vaccine-induced immunity.

This review focuses on key themes that have emerged over 75 years of malaria vaccine research and development and on a few key examples of malaria vaccines that have reached the stage of testing for efficacy in clinical trials in humans. Several recent review articles listed after the primary bibliography explore malaria immunology and preclinical vaccine development in more detail.

The Malaria Life Cycle

Malaria is a potentially fatal parasitic disease transmitted to humans and other vertebrate animals by mosquitoes. Four species of *Plasmodium* cause malaria disease primarily in humans: *P. falciparum, P. vivax, P. ovale* and *P. malariae*. A fifth, *P. knowlesi*, infects mainly nonhuman primates but was recently found also to infect and sicken humans [9], and hundreds of other malaria species infect other mammals, reptiles, and birds. Because it is responsible for most severe malaria and deaths, *P. falciparum* has been the target of most vaccine development efforts and is the main focus of this review. However, in many parts of the world, *P. vivax* is the predominant species, and it causes more severe malaria than has sometimes been appreciated [10]. A vivax malaria vaccine would be highly beneficial, especially if it interrupted transmission.

The malaria life cycle begins when the female *Anopheles* mosquito injects sporozoites from her salivary gland into the skin as she takes a blood meal (Fig. 1). The worm-like sporozoites – about 7 μ in length, or as long as an erythrocyte is wide – invade liver hepatocytes, each sporozoite multiplying over several days into tens of thousands of tiny (about 1 μ in diameter) merozoites packed into a single infected hepatocyte. These pre-erythrocytic stages cause no clinical signs or symptoms. A highly efficacious pre-erythrocytic vaccine would thus completely block infection, preventing parasites from reaching the blood and causing disease, and also preventing transmission.

Rupturing hepatocytes release showers of merozoites into the circulation, initiating the blood stage of malaria infection that is responsible for disease. Merozoites quickly invade erythrocytes and undergo asexual multiplication, dividing, growing, bursting from the erythrocyte, and re-invading in a periodic pattern with each cycle lasting 2 days (3 days in the case of *P. malariae*), until interrupted by host immunity, drug treatment, or death. Malaria vaccines that target the blood stage are thought of as anti-disease vaccines and would be expected to prevent or reduce clinical illness but would not prevent infection.

Some blood-stage parasites develop into male and female gametocytes. These sexual forms are taken up by the mosquito vector during a blood meal, mate to form a brief diploid stage, and then develop through further haploid stages and migrate from the gut to the salivary glands (Fig. 1). Each mating pair of gametocytes yields up to 1,000 infectious sporozoites, which are injected into the host to complete the transmission cycle. Vaccines targeting the sexual stages would prevent neither infection nor disease in the vaccinated individual and are thought of as transmission-blocking vaccines. Highly efficacious pre-erythrocytic or blood-stage vaccines that prevent sexual reproduction would also block transmission, so the term "transmission-blocking" need not refer exclusively to vaccines against sexual or mosquito stages of the parasite. The term "vaccines that interrupt transmission" (VIMT) encompasses all vaccines that interrupt transmission, whatever stage they target [11].

Pathogenesis and Disease

While semi-immune individuals can be chronically infected with malaria and experience no symptoms of illness, malaria infection of a nonimmune person usually causes an acute illness characterized by fever, chills, aches, and other flu-like symptoms. In a minority of cases, for reasons that are not well understood, more severe illness can develop. The clinical syndrome of falciparum malaria originates with changes in the infected erythrocytes. After they invade, blood-stage *P. falciparum* parasites effectively hijack the host cell and its machinery, expressing their own proteins on the surface of the host erythrocyte. Highly variant protein receptors called *P. falciparum* erythrocyte membrane proteins (PfEMP1) are encoded by a large, diverse family of up to 60 *var* genes in each parasite genome [12, 13]. PfEMP1 are expressed on the surface of infected red blood cells in clumps known as knobs, which are responsible for adherence of parasitized erythrocytes to the vascular endothelium, resulting in sequestration in tissue blood vessels [14].

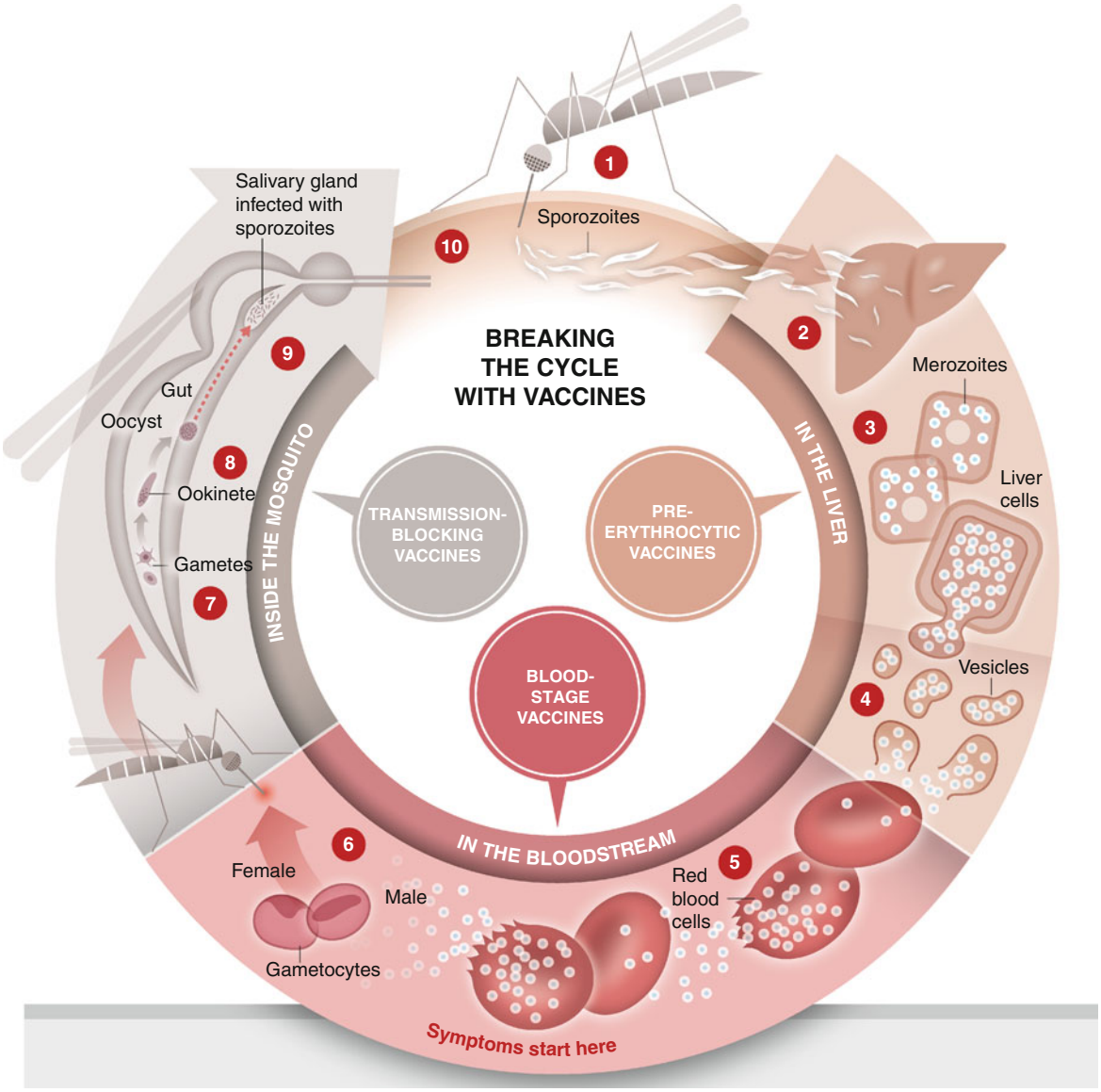

Malaria Vaccines. Figure 1

Life cycle of malaria and stages targeted by vaccines. (Source: PATH – Malaria Vaccine Initiative). 1. Malaria infection begins when an infected female *Anopheles* mosquito bites a person, injecting *Plasmodium* parasites, in the form of sporozoites, into the bloodstream. 2. The sporozoites pass quickly into the human liver. 3. The sporozoites multiply asexually in the liver cells over the next 7–10 days, causing no symptoms. 4. The parasites, in the form of merozoites, burst from the liver cells. 5. In the bloodstream, the merozoites invade red blood cells (erythrocytes) and multiply again until the cells burst. Then, they invade more erythrocytes. This cycle is repeated, causing fever each time parasites break free and invade blood cells. 6. Some of the infected blood cells leave the cycle of asexual multiplication. Instead of replicating, the merozoites in these cells develop into sexual forms of the parasite, called gametocytes, that circulate in the bloodstream. 7. When a mosquito bites an infected human, it ingests the gametocytes, which develop further into mature sex cells called gametes. 8. The gametes develop into actively moving ookinetes that burrow into the mosquito's midgut wall and form oocysts. 9. Inside the oocyst, thousands of active sporozoites develop. The oocyst eventually bursts, releasing sporozoites that travel to the mosquito salivary glands. 10. The cycle of human infection begins again when the mosquito bites another person

The ability of falciparum malaria to sequester plays a critical role in disease severity – the other human malarias do not appear to sequester and, therefore, are not associated with most of the severe manifestations seen with falciparum malaria [15]. Infected red blood cells cytoadhere and sequester in the microcirculatory compartments of organs, most notably in the brain and placenta, leading to disease, and most abundantly in the spleen, causing splenomegaly. Sequestered infected red blood cells not only interfere with microcirculatory blood flow but also hide outside the reach of host defense mechanisms. Infected red blood cells lose their deformability and compromise blood flow in small capillaries and venules [16].

The presence of variant surface antigens leads to immune responses that appear both to harm the human host as well as to lead to the eventual development of protective immunity. Immunity to severe malaria develops rapidly, after only a few infections [17], possibly due to antibody responses that protect against a relatively conserved subset of PfEMP1 variants that are associated with severe malaria. In contrast, the slow acquisition of immune protection against uncomplicated malaria over years of repeated exposure to malaria is thought to represent the accumulation of protective immune responses to a repertoire of diverse antigens, probably including both PfEMP1 and the surface proteins that are the targets of most vaccine candidates [18].

Epidemiology

The epidemiology of malaria is determined primarily by the patterns and intensity of malaria transmission, which in turn drives the prevalence of malaria infection and the incidence of different forms of malaria disease. In low-transmission settings with unstable malaria, there is a potential for epidemic disease when transmission recurs or increases as a result of reintroduction to a population not recently exposed to malaria or to changing climactic or environmental conditions that favor contact between humans and malaria-transmitting *Anopheles* mosquitoes. Outbreaks can occur when malaria-naïve populations such as transmigrants, miners, or soldiers are exposed to malaria, causing high rates of disease [19].

Depending largely on the degree of host immunity, the manifestations of malaria infection can range from completely asymptomatic parasitemia, to mild disease that can be treated on an outpatient basis with oral drugs, to acute catastrophic life-threatening illness requiring intensive care. Very young infants are thought to be protected from malaria disease by maternal antibodies and persistent hemoglobin F. While they may be infected congenitally or by mosquito bites in the first days or weeks of life, infants do not experience clinical disease until they are a few months old. Following this brief period of relative insusceptibility in early infancy, protective immunity against malaria disease is acquired through repeated exposure and is therefore related to transmission intensity.

Where malaria transmission is moderate (average of one or more infected mosquito bites per month) or high (two or more infected mosquito bites per week; up to more than one per day in some areas), the risk period for death from malaria is highest in infants and young children who are in the process of developing acquired immunity. In a typical moderate- or high-transmission setting in sub-Saharan Africa, most severe malaria is experienced by children aged less than 5 years; children aged up to 10–12 years experience frequent episodes of uncomplicated malaria; and older teenagers and adults, while still often infected, rarely experience symptoms of malaria illness. Severe anemia is more frequent in the youngest infants, while cerebral malaria tends to peak in children aged 3–4 years who have experienced previous malaria episodes, suggesting that an overly exuberant immune response contributes to the pathogenesis of cerebral malaria.

In contrast, in low-transmission settings, persons of all ages have a similar risk of infection and uncomplicated malaria, most who are infected become sick, and the risk for severe malaria persists throughout life. Semi-immune adults, although they remain susceptible to asymptomatic parasitemia, are protected against clinical malaria disease, rarely becoming ill even when persistently infected. This protective immunity is lost after a few years in the absence of exposure. Acquired immunity is also diminished in pregnancy, in that women pregnant with their first child are susceptible to severe *P. falciparum* disease from placental malaria because they lack immunity to placenta-specific cytoadherence proteins. As placental immunity develops in subsequent pregnancies, there is

a reduced risk of adverse effects of malaria in pregnancy on the mother and fetus [20].

Based on these epidemiological patterns, the primary populations targeted for malaria vaccines are infants and young children in areas of moderate and high transmission who bear the greatest burden of disease and death, and women of childbearing age in these same areas. Malaria-naïve travelers and military troops would also benefit from a malaria vaccine. As more countries move toward malaria elimination and global eradication is considered [21], the general population of malaria-endemic areas may be vaccinated to drive down transmission [6, 11].

Immunity

Insights into malaria immunity come not only from studies in various animal models including birds, rodents, and nonhuman primates but also from important studies in humans, including classic passive transfer experiments [22, 23] and early studies of malaria therapy for neurosyphilis [24, 25], as well as immunoepidemiological studies that try to identify correlates of clinical protection [26, 27]. Both humoral and cellular factors contribute to acquired immune protection against malaria. Broadly speaking, cellular immune responses are thought to be more important in controlling the pre-erythrocytic stages of malaria infection [28], and antibodies are thought to block erythrocyte invasion to suppress blood-stage infection [22, 26]. For these reasons, cellular immune responses are typically emphasized in the development of pre-erythrocytic vaccines and antibody responses in the development of blood-stage vaccines. However, despite nearly 100 years of human and animal research, the basis of protective immunity against malaria is poorly understood, and no specific immune response has been established as an essential correlate of clinical protection, complicating malaria vaccine development.

New genomic tools have the potential to improve understanding of malaria immunity and may aid in vaccine development. For example, while it has long been known that there is some degree of strain specificity to malaria immunity, the discovery of large families of genes encoding highly variable surface antigens that mediate cytoadherence and immune evasion [14] has led to models for explaining the slow acquisition of protective immunity as a process of building up a repertoire of variant-specific immune responses until protection is in place against the full range of locally prevalent variants. As next-generation sequencing technologies improve their ability to generate sequence from clinical samples and to assemble genomes and map variant sequences to a reference genome, genomic epidemiology studies that relate parasite genotypes to clinical risk and allele-specific immune responses will permit testing of the hypotheses generated by such models. In another new approach, high-density protein arrays permit serological profiling of large numbers of serum samples against thousands of recombinant malaria proteins [29]. When this protein array was used to identify *P. falciparum* proteins that were differentially recognized by the sera of children who were resistant to clinical malaria, several previously unknown antigens were identified as possibly being important in acquired immunity, providing possible new vaccine targets [30].

In addition to acquired immunity, several host genetic factors offer some degree of protection against malaria, generally not by preventing infection but by reducing the risk of clinical illness or severe disease. Sickle cell trait [31] and other hemoglobinopathies [32–34] are more prevalent in populations at risk of malaria because they afford protection against clinical malaria. Various other human genetic polymorphisms associated with the host immune response [35] and with host–parasite binding [36] have also been correlated with susceptibility to clinical malaria in genetic association studies.

Early Malaria Vaccines

In 1880, Charles Louis Alphonse Laveran, a 33-year-old French Army doctor working in Algeria, discovered motile worm-like parasites, later understood to be exflagellating male gametes, in the blood of a feverish soldier [37]. Seven years later, Ronald Ross established that malaria parasites were transmitted to birds by the bites of infected mosquitoes [38]. The tremendous public health benefit that would be provided by an effective malaria vaccine was quickly appreciated, and from the 1930s to the 1970s, malaria vaccine researchers used primarily birds (including ducklings,

canaries, chickens, and turkeys) and occasionally monkeys as model systems, and inactivated or killed whole parasites or parasite extracts as vaccines, often accompanied by immune-boosting adjuvant systems. This wave of vaccine development research crested in the late 1940s as World War II ended and attention shifted to the global campaign to eradicate malaria using drugs and anti-vector methods, and only resurged in the late 1960s when it became apparent that eradication was not possible with existing tools.

Early work focused on attenuated whole-parasite vaccines. Working in India, Russell and Mohan protected chickens from mosquito challenge with *P. gallinaceum* by immunizing them with sporozoites inactivated by ultraviolet light [39]. In 1945, the Hungarian-American immunologist Jules Freund (of Freund's complete adjuvant fame) and colleagues reported that they had successfully protected ducks against intravenous challenge with the avian malaria *P. lophurae* by immunizing them with formalin-inactivated malaria-infected blood cells and an adjuvant system consisting of a lanolin-like substance, paraffin oil, and killed tubercle bacilli [40]. They used a similar vaccine formulation to protect rhesus monkeys against *P. knowlesi* challenge [41]. These pioneering studies demonstrated two important principles that remain highly relevant to contemporary malaria vaccine development efforts, namely that good protective efficacy can be achieved with whole-organism vaccines and that strong immune-boosting adjuvants can achieve levels of protection that match or exceed those acquired through repeated natural exposure.

In a thoughtful and prescient paper published in 1943 describing protection of ducklings when a bacterial toxin adjuvant was added to a killed blood-stage vaccine, Henry Jacobs briefly cited an abstract presented by W. B. Redmond at the 1939 annual meeting of the American Society of Parasitologists, writing that "Redmond. . .noted some protection against bird malaria when he vaccinated with irradiated parasites" [42]. Redmond's abstract described using a frozen killed vaccine but made no mention of inactivation by irradiation [43]. Unfortunately, Redmond never published this work, but one can speculate that he may have described using some form of a radiation-attenuated *P. lophurae* vaccine preparation in his presentation at the 1939 meeting, anticipating subsequent work using this approach, including attenuation by irradiation of both blood stages [44, 45] and later and more famously of sporozoites [46, 47].

Columbia University scientists, who were aware of "inconclusive" earlier studies reported in the German medical literature, described in 1946 their own unsuccessful attempts to protect humans against intravenous challenge with *P. vivax* using a vaccine consisting of formalin-treated and freeze-thawed blood containing 65–150 million blood-stage *P. vivax* parasites [48]. No adjuvant was used in these earliest human studies, which may partially explain the disappointing results.

Several of these historical threads came together in a series of major breakthroughs in the late 1960s and early 1970s. First, Ruth Nussenzweig and Jerome Vanderberg at New York University reported in 1967 that intravenous immunization with irradiated *P. berghei* sporozoites could protect mice against subsequent intravenous challenge with viable sporozoites [46]. This advance was quickly translated into human trials of radiation-attenuated *P. falciparum* sporozoites delivered by the bites of infected, irradiated mosquitoes [49, 50]. In these and subsequent malaria challenge trials, 90% of volunteers who were immunized with radiation-attenuated sporozoites by receiving at least 1,000 infected bites over several sessions were fully protected against infection [51]. All unvaccinated volunteers acquired malaria from the bites of non-irradiated mosquitoes. These pioneering studies, first done by University of Maryland investigators in prisoners [52], provided proof that humans could be protected against infection with deadly *P. falciparum* through immunization, and spurred the identification of specific sporozoite proteins that could serve as antigens for subunit vaccines, as described in the following sections.

At around this time, two major advances ushered in the modern era of malaria vaccine development: the advent of molecular biology and the ability to clone, sequence, and express parasite genes in heterologous expression systems such as bacteria and yeast, and the development of methods for growing *P. falciparum* parasites in continuous in vitro culture [53, 54], providing a reliable and reproducible source of malaria parasites, proteins, and genes.

Obstacles to Malaria Vaccines

Why is there still no licensed malaria vaccine after 75 years of vaccine development research and evaluation of more than 70 vaccine candidates [55] in preclinical and clinical testing? Obstacles slowing progress toward an effective malaria vaccine include the size and complexity of the parasite, its genetic diversity, the efficiency of its amplification, the incomplete and temporary nature of naturally acquired immunity, and the fact that in addition to providing protection, immune responses also contribute to pathogenesis. Furthermore, parasite material must generally be obtained from infected hosts or mosquitoes – only one species, *P. falciparum*, can be grown in continuous culture. Finally, validated immune correlates of protection are lacking, so candidate vaccines can only be down-selected by conducting costly efficacy trials in humans.

The *P. falciparum* genome has about 23 million bases of DNA organized into 14 chromosomes and about 5,000 genes [56]. This is orders of magnitude larger than the genomes of the viruses and bacteria to which vaccines have been successfully developed. This complexity and the large number of gene products provide the means and materials needed for the highly complex life cycle stages in vertebrate hosts and mosquitoes (Fig. 1). Moreover, mutation during mitotic reproduction in the haploid liver and blood stages and genetic recombination during the diploid sexual reproductive stages in the mosquito result in extensive genetic diversity that is driven by selection pressure from the immune system, as well as by drugs and, when they are deployed, potentially by vaccines [57]. All of this complexity and diversity greatly complicates the choice of candidate antigens for vaccine development.

At least 18 different forms of one leading blood-stage antigen [58] and more than 200 variants of another [59] have been documented in a single African village. If vaccines targeting these antigens generate immune responses that are insufficiently cross-protective, vaccines based on just one or two genetic variants are unlikely to be broadly efficacious [57]. To date, the choices of which variants of target antigens to include in malaria vaccines have not been made in consideration of the frequencies of these variants in natural populations. Careful molecular epidemiological studies are beginning to pinpoint which of the many polymorphisms in some of these antigens are the most important determinants of strain-specific natural immunity [58, 59], and this approach may help inform the design of polyvalent or chimeric vaccines that protect against diverse parasite strains [57].

Immunization with whole parasites of a given life cycle stage or with stage-specific proteins typically protects against only that life cycle stage, hence the notion of vaccines that prevent infection, disease, or transmission by targeting the different stages. While a highly efficacious pre-erythrocytic vaccine would prevent not only infection, but by doing so also prevent disease as well as transmission [6], even a single surviving sporozoite could theoretically result in a full-blown infection, severe disease, and transmission. This is because of the parasite's ability to multiply rapidly – one sporozoite gives rise to tens of thousands of merozoites emerging from the liver about a week and a half after a mosquito bite, and each merozoite multiplies roughly tenfold during the 48-h blood cycle, quickly resulting in billions of parasites circulating in the body. In reality, the rate at which parasites amplify their numbers is determined not just by the parasite's maximum reproductive capacity but also by host defenses and other factors. The ability of a partially efficacious pre-erythrocytic vaccine to reduce the risk of clinical malaria illness [60] supports the idea that there is some benefit from slowing the rate of parasite reproduction short of complete prevention of blood-stage infection – a so-called leaky vaccine, perhaps better thought of as an injectable bednet.

Most successful vaccines prevent infection or illness with pathogens that naturally result in strong and long-lasting immune protection after a single exposure. As described above, the naturally acquired protective immunity to malaria is hard won and short lived. An effective malaria vaccine would need to produce stronger immune responses more quickly than those that develop even under intense continuous natural exposure to malaria, and a vaccine intended to prevent infection will need to surpass natural immunity, which gradually protects against clinical illness but does not completely prevent infection.

Because the host immune response contributes to malaria pathogenesis, a vaccine could theoretically increase the risk of harmful inflammatory responses

to subsequent infection, especially for vaccines directed against the blood stages that are responsible for pathology. One blood-stage malaria vaccine based on the *P. falciparum* merozoite surface protein 1 (MSP1) protected monkeys against lethal infection but then resulted in life-threatening anemia following subsequent exposure to malaria [61]. No such post-vaccination anemia has been observed in malaria-exposed adults [62, 63] or children [64, 65] in African trials of a different MSP1 malaria vaccine. A Phase 2 trial of a blood-stage malaria vaccine based on a different antigen, the apical membrane antigen 1 (AMA1), reported a possible increased risk of anemia in vaccinated malaria-exposed children in an unplanned post-hoc analysis [66]. No increased risk of anemia has been seen in trials with a more highly immunogenic AMA1 vaccine tested in similar populations [67, 68]. Vigilance for untoward inflammatory responses to malaria vaccines or to post-vaccination malaria infection will continue to be an important aspect of clinical malaria vaccine development, especially for blood-stage vaccines.

Pre-erythrocytic Vaccines

The vaccine furthest along in clinical development, RTS,S/AS01, targets the pre-erythrocytic circumsporozoite protein (CSP) of *P. falciparum*. The gene encoding CSP was the first *P. falciparum* gene cloned [69], and as the major surface protein coating sporozoites, CSP was immediately of great interest as a vaccine candidate. Thought to be important in sporozoite development and motility [70], CSP contains a central repeat region that elicits antibody responses [71], flanked on each side by non-repetitive regions containing T-cell epitopes [69]. Antibodies directed against the central repeat region cause the protein coat to slough off and block invasion of hepatocytes, suggesting that vaccine-induced antibodies might prevent infection [72]. Early synthetic CSP vaccines based on the repeat region using aluminum hydroxide as an adjuvant were poorly immunogenic, although a few individuals who achieved high antibody titers were protected against experimental challenge with homologous sporozoites [73, 74].

Seroepidemiological studies failed to find an association between anti-CSP antibodies and protection against infection [75], however, and the addition of adjuvants that produced higher antibody levels did not result in improved efficacy [76], leading the developers of RTS,S to include the flanking regions containing T-cell epitopes in subsequent versions of the vaccine. The final form of RTS,S is comprised of the central repeat region (R) and T-cell epitopes (T) using the hepatitis B surface antigen (S) as a carrier matrix, and co-expressed in *Saccharomyces cerevisiae* with additional S, hence "RTS,S." The clinical development of RTS,S has included progressive improvements in adjuvant systems, resulting in improved efficacy both in experimental challenges [77–79] and in clinical trials in malaria-exposed adults [80] and children [60, 81]. The current formulation includes the liposomal-based Adjuvant System AS01, which contains the immunostimulants monophosphoryl lipid A and QS21, a saponin derivative extracted from the bark of the South American soap bark tree *Quillaja saponaria*. The development of RTS,S supports the notion that strong adjuvants are a necessary component for efficacious subunit protein malaria vaccines.

RTS,S/AS01 (and its immediate forebears with oil-in-water versions of the AS0-adjuvant system) was the first malaria vaccine to demonstrate meaningful levels of clinical protection in field trials. Trials in children and infants who are naturally exposed to malaria have demonstrated efficacy against clinical disease in the range of 30–56% and up to 66% against infection, and a good record of safety and tolerability [60, 81, 82]. A large Phase 2 trial in 1,465 Mozambican children showed 26% efficacy against all malaria episodes over nearly 4 years, 32% against first or only episode of clinical malaria, and 38% in preventing severe clinical episodes [83]. After 45 months, the prevalence of parasitemia was significantly lower in vaccines compared to the control group (12% vs 19%). The magnitude of the protective effect after nearly 4 years was thus modest, but importantly, there was no evidence of a post-immunization "rebound" effect – a theoretical concern that the vaccine might interfere with the natural acquisition of protective immunity.

Based on these demonstrations of a level of efficacy that is well below levels of protection expected for vaccines against other common pathogens but rare good news for malaria vaccines, RTS,S/AS01 is currently being evaluated in a large Phase 3 trial of

16,000 children and infants in seven African countries. The cost-effectiveness of licensing and deploying a malaria vaccine with efficacy in the range of 25–50% is debated, but where the malaria burden remains high, as in much of sub-Saharan Africa, such a vaccine is likely to be sought and used. Strategies being investigated to improve on the efficacy of RTS,S/AS01 include adding antigens tested with the same adjuvant system to create a multistage, multi-antigen RTS,S-based vaccine [84] and priming with an adenovirus expressing CSP before boosting with RTS,S/AS01 [85].

Several other pre-erythrocytic vaccine candidates have progressed through various stages of preclinical and early clinical development [55], including recombinant subunit protein vaccines as well as DNA vaccines and viral vectored vaccines [81]. Even though some of these have generated seemingly good humoral and especially cellular immune responses when formulated with strong adjuvants [86], protective efficacy has not been achieved in clinical testing in humans. Prime-boost approaches using DNA vaccines or viral vectors have also resulted in improved immunogenicity including cell-mediated responses in some participants and, in some cases, in measurable delays in time to infection in experimental sporozoite challenge trials [87]. Although prime-boost vaccine strategies have failed to demonstrate meaningful protection in published clinical efficacy trials, recent unpublished reports are more promising, with about 25% sterile protection provided by DNA prime and viral vector boost using both CSP and the blood-stage antigen AMA1 (T. Richie, personal communication). Efforts to improve these approaches to get more consistent cellular immune responses and higher levels of protection may be hampered by variability in host responses to vaccination. Other novel approaches such as a self-assembling polypeptide nanoparticle CSP vaccine are showing promise in preclinical testing [88]. Mining of genomic and proteomic data has led to the identification of new pre-erythrocytic vaccine candidate proteins, some of which have shown promising results in early preclinical testing in animal models [89].

Blood-Stage Vaccines

Most blood-stage malaria vaccine candidates are based on antigens that coat the surface of the invasive merozoites and/or that are involved with the process of erythrocyte invasion, in hopes of generating antibodies that block invasion and curtail parasite replication in the blood, reducing the risk or severity of clinical illness. The merozoite surface protein 1, or MSP1, was the first and best characterized of many proteins on the merozoite surface that are being targeted for vaccine development. MSP1 undergoes cleavage into four fragments that remain on the merozoite surface as a complex. Before erythrocyte invasion, the entire MSP1 complex is shed except for the C-terminal 19-kDa fragment ($MSP1_{19}$), which remains on the surface as the merozoite enters the erythrocyte [90]. Naturally acquired antibodies to $MSP1_{19}$ inhibit erythrocyte invasion and are associated with protection from clinical malaria in field studies [91, 92], supporting its potential as a vaccine candidate. Studies of recombinant MSP1 vaccines in monkeys were encouraging [93]. An $MSP1_{19}$-based vaccine on the same adjuvant platform as RTS,S produced antibodies in Malian adults that recognized MSP1 from diverse strains of *P. falciparum* [62], but had no protective efficacy against clinical malaria in Kenyan children [65]. Comparison of the degree of homology with the vaccine strain of MSP1 sequences in the infections experienced by children in the vaccine and control groups will clarify the extent to which the genetic diversity of MSP1 accounted for this lack of efficacy.

The apical membrane antigen 1, or AMA1, resides in the apical complex of the merozoite [94] before being processed and moving to the surface as the merozoite is released from the infected erythrocyte [95], where it is thought to play a role in erythrocyte invasion [96]. Proteomic studies have shown that AMA1 is also expressed in the sporozoite stage [97], suggesting that it may play a similar role in hepatocyte invasion. People living in malaria-endemic areas produce antibodies to AMA1 that can inhibit erythrocyte invasion in vitro [98] and that are associated with protection in field studies [99]. Studies in animal models show strain specificity in the inhibitory activity of anti-AMA1 antibodies [98], and these results have been corroborated by subsequent allelic exchange experiments [100, 101].

Sequencing of the gene encoding AMA1 in samples from a single Malian village identified more than 200 unique AMA1 variants in about 500 *P. falciparum* infections [59], raising the daunting prospect that

a 200-valent AMA1 vaccine might be required to achieve broad protective efficacy. However, molecular epidemiological analyses showed that a group of just eight polymorphic amino acids lying adjacent to the presumed erythrocyte-binding site on AMA1 were responsible for strain-specific naturally acquired immunity, suggesting that a vaccine comprised of as few as ten "serotypes" of AMA1 might be sufficient to protect against 80% of unique variants.

Two AMA1 vaccines have reached the stage of efficacy trials in humans. A bivalent vaccine with two different forms of AMA1 adjuvanted with aluminum hydroxide failed to provide any protection against parasitemia or clinical malaria [66], and molecular analyses of pre- and post-immunization infections turned up no evidence of strain-specific efficacy or selection of non-vaccine variants [102]. A monovalent AMA1 vaccine formulated with the same adjuvant system as that used with RTS,S was more highly immunogenic [68] in a similar population of African children. Although this vaccine did not prevent infection after experimental sporozoite challenge [103] and showed marginal overall efficacy against clinical malaria, it demonstrated strong strain-specific efficacy, reducing the risk of clinical malaria caused by parasites with AMA1 homologous to the vaccine strain by more than 60% [104]. This encouraging result suggests that it may be possible to develop a more broadly efficacious multivalent or chimeric next-generation AMA1 vaccine, and efforts are being made to do this [105–107].

The *P. falciparum* proteins that are expressed on the surface of infected erythrocytes and that mediate cytoadherence and immune evasion and contribute to pathogenesis would seem to be attractive candidates for anti-disease vaccines. These PfEMP1 proteins are encoded by a large family of diverse *var* genes [14] with up to 60 variants in each parasite genome. Designing a vaccine that would be broadly protective against such an extraordinarily polymorphic target is likely to be very difficult. One possible approach to overcome this difficulty may be the identification of conserved epitopes that are nevertheless immunogenic [108]. Because a single PfEMP1 that is somewhat less polymorphic, VAR2CSA, mediates cytoadherence in placental malaria, prospects for a PfEMP1-based pregnancy malaria vaccine may be better, and research toward this goal is underway [109].

Multistage, multi-antigen vaccines that include blood-stage components are discussed in a subsequent section.

Transmission-Blocking Vaccines

Transmission-blocking vaccines are vaccines that are specifically intended to block transmission by targeting molecules that are unique to gametocytes, the male and female forms that are taken up during a blood meal and that mate in the mosquito midgut, or that target subsequent mosquito stages. Antibodies directed against such targets are capable of blocking the development of mosquito stages, thus interrupting transmission [110]. In a rare example of a vaccine designed to target multiple species, a vaccine based on mosquito-stage proteins in both *P. falciparum* and *P. vivax* was recently shown to produce dose-dependent antibody-mediated transmission-blocking activity [111]. However, the vaccine, which was formulated with the powerful adjuvant Montanide ISA 51, was unacceptably reactogenic. With the recent renewed call for global malaria eradication [5, 21], transmission-blocking vaccines will be increasingly emphasized. In one novel and promising approach, vaccines that target mosquito molecules are being contemplated in hopes of avoiding selection pressure within the host that favors "vaccine-resistant" parasites [112].

Although not traditionally thought of as transmission-blocking vaccines, highly efficacious pre-erythrocytic vaccines that provide sterile immunity would also interrupt transmission. Because they would completely prevent infection, such vaccines would also have the important added benefit of preventing disease caused by the blood stages. In the context of malaria elimination, a highly efficacious pre-erythrocytic vaccine would thus be the product development target for "vaccines that interrupt transmission" [11].

Multistage, Multi-antigen Vaccines

Compared to the viral and bacterial human pathogens for which effective vaccines exist, malaria parasites are big and complex and elicit equally complex and multifaceted immune responses. In retrospect, it may not be surprising that so many candidate vaccines that target just a single variant of a single antigen have failed to demonstrate clinical efficacy, especially against

heterologous natural challenge. Several attempts have been made to improve on the efficacy of single-antigen vaccines by developing multistage, multi-antigen vaccines. One of the earliest was SPf66, a synthetic vaccine consisting of peptides derived from the blood-stage antigen MSP1 linked by the central repeat of the pre-erythrocytic antigen CSP. While reports of efficacy in initial trials in South America generated great excitement [113], subsequent studies in Africa and Asia showed no significant protective efficacy [114–116]. In another approach that yielded disappointing results, vaccinia virus was used as a vector to express seven *P. falciparum* genes, but both immunogenicity and efficacy were limited [117]. Attempts to develop DNA vaccines with from two to as many as 15 *P. falciparum* genes [118] were likewise unsuccessful.

Based on the modest efficacy of RTS,S against clinical malaria and evidence that a blood-stage vaccine using a similar adjuvant system can produce strain-specific efficacy [104], it is reasonable to believe that it may be possible to construct a multistage, multi-antigen recombinant protein that improves on the efficacy of RTS,S [84]. However, it seems not unlikely that vaccines that target 2, 5, or even 15 of the 5,000 gene products will still fall short of the high levels of protection seen with radiation-attenuated whole-organism vaccines when delivered through the bites of infected mosquitoes [51].

Whole-Organism Vaccines

Even though live attenuated vaccines were the earliest and remain some of the best vaccines against other pathogens, and even though birds and monkeys had been protected by live attenuated malaria parasites in the earliest vaccine studies [40, 41], the protection seen with irradiated sporozoites in the early 1970s [49] was interpreted not as a direct path to a malaria vaccine but as proof that a vaccine was possible and as justification for the ensuing decades of research aimed at identifying the "right" vaccine antigen or heterologous expression system. The limited success of these Sisyphean research efforts led to reevaluation of the dogma that it would be impossible to manufacture an attenuated sporozoite vaccine in mosquitoes [51]. A radiation-attenuated, metabolically active, non-replicating sporozoite vaccine has been manufactured in and purified from aseptically raised mosquitoes [47] and was recently evaluated for safety and efficacy in an experimental sporozoite challenge trial in humans. The goal was to administer by needle essentially the same immunogen – albeit aseptic, purified, and cryopreserved – that had previously demonstrated 90% protective efficacy in the form of sterilizing immunity when delivered by the bites of at least 1,000 irradiated infected mosquitoes. When administered by intradermal or subcutaneous routes, the sporozoite vaccine did not have significant protective efficacy [119]. Contemporaneous studies show that the vaccine sporozoites are highly immunogenic in monkeys when administered intravenously but not subcutaneously [119]. The likeliest explanation for this result is thought to be that sporozoites delivered into the skin by needle injection in a comparatively large volume of fluid were unable to reach the liver with efficiency approaching that of sporozoites injected either by a mosquito probing for small blood vessels or intravenously.

The potential for this approach to yield a highly efficacious pre-erythrocytic whole-organism vaccine remains well worth pursuing. Efforts are underway to improve delivery methods to more closely approximate the probing mosquito's efficient delivery of attenuated sporozoites into the circulation, starting with the intravenous route that is clearly superior in animal models. Whole-parasite vaccine experiments in the 1940s showed that adjuvants could boost protection, and this will likely be tried with the sporozoite vaccine. Genetic attenuation of sporozoites as an alternative to radiation is also being explored [120]. In a similar "back to the future" paradigm shift, attenuated whole-parasite blood-stage vaccines are now also back on the table [121, 122] more than 60 years after this approach was shown to work in monkeys.

Future Directions

While about 30 of the more than 100 countries with malaria transmission are actively trying to eliminate malaria, it is generally agreed that global malaria eradication is not possible without either global economic development to the levels that permitted malaria elimination in the United States, Europe, and the former Soviet Union or new tools such as a highly efficacious malaria vaccine that interrupts transmission [11]. A powerfully adjuvanted pre-erythrocytic

single-antigen recombinant protein vaccine, RTS,S/AS01, significantly reduces the clinical burden of malaria in African children [60, 81], but it does not prevent infection, and, somewhat surprisingly, its effect on transmission, if any, has not been reported. While the results of a field trial of a similarly adjuvanted blood-stage vaccine [104] as well as combination of RTS,S with a viral vector in a prime-boost regimen [85] provide a rationale for pursuing improvements on RTS,S and similar vaccines, the dire public health need for a highly efficacious malaria vaccine calls for more than incremental improvements. Whole-parasite vaccines may be the radically different new (and yet very old) approach that is needed. Challenges remain to produce and deliver such a vaccine, but none that are insurmountable.

Research from the 1940s and many more recent studies point to the importance of strong adjuvants for subunit as well as for whole-organism vaccines, and wide access to immunogenic and safe adjuvants will be important for accelerating malaria vaccine development. Researchers are focusing now on the painfully elusive goal of achieving a high degree of efficacy, but the ideal vaccine would be not only safe and efficacious but also thermostable and protective for a long period of time after a single immunization – characteristics that will not be easy to achieve but which might be possible through pharmaceutical technologies such as controlled release formulations.

All predictions of when a malaria vaccine will be available have been overly optimistic, but barring unforeseen setbacks, a vaccine that substantially reduces the malaria burden should be licensed within just a few years. This will be a magnificent accomplishment that will mark not the end of the road for malaria vaccine development but a critical milestone on the path leading toward the malaria vaccine that the world needs.

Acknowledgments

The author is supported by the National Institute of Allergy and Infectious Diseases of the U.S. National Institutes of Health, by the Doris Duke Charitable Foundation, and by the Howard Hughes Medical Institute and wishes to thank Kirsten Lyke, Kavita Gandhi, Matthew Laurens, Mark Travassos, Thomas Richie, and Judith Epstein for critical reading of the manuscript and to acknowledge the U.S. Agency for International Development, the Walter Reed Army Institute of Research, GlaxoSmithKline Biologicals, Sanaria Inc., the U.S. Military Malaria Vaccine Program – Naval Medical Research Center, and the Malaria Research and Training Center of the University of Bamako, Mali, for collaboration on malaria vaccine trials.

Bibliography

Primary Literature

1. Garnham PCC (1966) Malaria parasites and other haemosporidia. Blackwell, Oxford
2. World Health Organization (2008) The global malaria action plan for a malaria free world. World Health Organization, Geneva
3. Rieckmann KH (2006) The chequered history of malaria control: are new and better tools the ultimate answer? Ann Trop Med Parasitol 100:647–662. doi:10.1179/136485906X112185
4. WHO (2007) United Arab Emirates certified malaria-free. Wkly Epidemiol Rec 82:30–32
5. Roberts L, Enserink M (2007) Malaria. Did they really say. . .eradication? Science 318:1544–1545
6. Plowe CV, Alonso P, Hoffman SL (2009) The potential role of vaccines in the elimination of falciparum malaria and the eventual eradication of malaria. J Infect Dis 200:1646–1649. doi:10.1086/646613
7. Henderson DA (1999) Lessons from the eradication campaigns. Vaccine 17(Suppl 3):S53–S55, S0264410X99002935 [pii]
8. Casares S, Brumeanu TD, Richie TL (2010) The RTS,S malaria vaccine. Vaccine 28:4880–4894. doi:10.1016/j.vaccine.2010.05.033, S0264-410X(10)00721–8 [pii]
9. Cox-Singh J, Davis TM, Lee KS, Shamsul SS, Matusop A, Ratnam S, Rahman HA, Conway DJ, Singh B (2008) *Plasmodium knowlesi* malaria in humans is widely distributed and potentially life threatening. Clin Infect Dis 46:165–171. doi:10.1086/524888
10. Price RN, Tjitra E, Guerra CA, Yeung S, White NJ, Anstey NM (2007) Vivax malaria: neglected and not benign. Am J Trop Med Hyg 77:79–87, 77/6_Suppl/79 [pii]
11. The malERA Consultative Group on Vaccines (2010) A research agenda for malaria eradication: vaccines. PLoS Med 8:e1000398
12. Baruch DI, Pasloske BL, Singh HB, Bi X, Ma XC, Feldman M, Taraschi TF, Howard RJ (1995) Cloning the *P. falciparum* gene encoding PfEMP1, a malarial variant antigen and adherence receptor on the surface of parasitized human erythrocytes. Cell 82:77–87
13. Su X, Heatwole VM, Wertheimer SP, Guinet F, Herrfeldt JA, Peterson DS, Ravetch JV, Wellems TE (1995) The large diverse gene family *var* encodes proteins involved in cytoadherence and antigenic variation of *Plasmodium falciparum*-infected erythrocytes. Cell 82:89–100

14. Smith JD, Chitnis CE, Craig AG, Roberts DJ, Hudson-Taylor DE, Peterson DS, Pinches R, Newbold CI, Miller LH (1995) Switches in expression of *Plasmodium falciparum* var genes correlate with changes in antigenic and cytoadherent phenotypes of infected erythrocytes. Cell 82:101–110
15. Miller LH, Baruch DI, Marsh K, Doumbo OK (2002) The pathogenic basis of malaria. Nature 415:673–679
16. Nash GB, O'Brien E, Gordon-Smith EC, Dormandy JA (1989) Abnormalities in the mechanical properties of red blood cells caused by *Plasmodium falciparum*. Blood 74:855–861
17. Gupta S, Snow RW, Donnelly CA, Marsh K, Newbold C (1999) Immunity to non-cerebral severe malaria is acquired after one or two infections. Nat Med 5:340–343
18. Hviid L (2005) Naturally acquired immunity to *Plasmodium falciparum* malaria in Africa. Acta Trop 95:270–275. doi:10.1016/j.actatropica.2005.06.012, S0001-706X(05)00165-8
19. Baird JK, Jones TR, Danudirgo EW, Annis BA, Bangs MJ, Basri H, Purnomo MS (1991) Age-dependent acquired protection against *Plasmodium falciparum* in people having two years exposure to hyperendemic malaria. Am J Trop Med Hyg 45:65–76
20. Duffy PE (2007) Plasmodium in the placenta: parasites, parity, protection, prevention and possibly preeclampsia. Parasitology 134:1877–1881. doi:10.1017/S0031182007000170, S0031182007000170 [pii]
21. Tanner M, de Savigny D (2008) Malaria eradication back on the table. Bull World Health Organ 86:82, S0042-96862008000200002 [pii]
22. Cohen S, McGregor IA, Carrington S (1961) Gamma-globulin and acquired immunity to human malaria. Nature 192:733–737
23. McGregor IA, Carrington S, Cohen S (1963) Treatment of East African *P. falciparum* malaria with West African human gamma-globulin. Trans R Soc Trop Med Hyg 50:170–175
24. Collins WE, Jeffery GM (1999) A retrospective examination of sporozoite- and trophozoite-induced infections with *Plasmodium falciparum* in patients previously infected with heterologous species of Plasmodium: effect on development of parasitologic and clinical immunity. Am J Trop Med Hyg 61:36–43
25. Collins WE, Jeffery GM (1999) A retrospective examination of secondary sporozoite- and trophozoite-induced infections with *Plasmodium falciparum*: development of parasitologic and clinical immunity following secondary infection. Am J Trop Med Hyg 61:20–35
26. Thomas AW, Trape JF, Rogier C, Goncalves A, Rosario VE, Narum DL (1994) High prevalence of natural antibodies against *Plasmodium falciparum* 83-kilodalton apical membrane antigen (PF83/AMA-1) as detected by capture-enzyme-linked immunosorbent assay using full-length baculovirus recombinant PF83/AMA-1. Am J Trop Med Hyg 51:730–740
27. Egan AF, Chappel JA, Burghaus PA, Morris JS, McBride JS, Holder AA, Kaslow DC, Riley EM (1995) Serum antibodies from malaria-exposed people recognize conserved epitopes formed by the two epidermal growth factor motifs of MSP1(19), the carboxy-terminal fragment of the major merozoite surface protein of *Plasmodium falciparum*. Infect Immun 63:456–466
28. Schofield L (1989) T cell immunity to malaria sporozoites. Exp Parasitol 68:357–364
29. Doolan DL, Mu Y, Unal B, Sundaresh S, Hirst S, Valdez C, Randall A, Molina D, Liang X, Freilich DA, Oloo JA, Blair PL, Aguiar JC, Baldi P, Davies DH, Felgner PL (2008) Profiling humoral immune responses to *P. falciparum* infection with protein microarrays. Proteomics 8:4680–4694
30. Crompton PD, Kayala MA, Traore B, Kayentao K, Ongoiba A, Weiss GE, Molina DM, Burk CR, Waisberg M, Jasinskas A, Tan X, Doumbo S, Doumtabe D, Kone Y, Narum DL, Liang X, Doumbo OK, Miller LH, Doolan DL, Baldi P, Felgner PL, Pierce SK (2010) A prospective analysis of the Ab response to *Plasmodium falciparum* before and after a malaria season by protein microarray. Proc Natl Acad Sci USA 107:6958–6963. doi:10.1073/pnas.1001323107, 1001323107 [pii]
31. Allison AC (1954) Protection afforded by sickle-cell trait against subtertian malarial infection. Br Med J 1:290–294
32. Kay AC, Kuhl W, Prchal J, Beutler E (1992) The origin of glucose-6-phosphate-dehydrogenase (G6PD) polymorphisms in African-Americans. Am J Hum Genet 50:394–398
33. Agarwal A, Guindo A, Cissoko Y, Taylor JG, Coulibaly D, Kone A, Kayentao K, Djimde A, Plowe CV, Doumbo O, Wellems TE, Diallo D (2000) Hemoglobin C associated with protection from severe malaria in the Dogon of Mali, a West African population with a low prevalence of hemoglobin S. Blood 96:2358–2363
34. Flint J, Hill AV, Bowden DK, Oppenheimer SJ, Sill PR, Serjeantson SW, Bana-Koiri J, Bhatia K, Alpers MP, Boyce AJ (1986) High frequencies of alpha-thalassaemia are the result of natural selection by malaria. Nature 321:744–750
35. Hill AV, Allsopp CE, Kwiatkowski D, Anstey NM, Twumasi P, Rowe PA, Bennett S, Brewster D, McMichael AJ, Greenwood BM (1991) Common west African HLA antigens are associated with protection from severe malaria. Nature 352:595–600
36. Miller LH, Mason SJ, Clyde DF, McGinniss MH (1976) The resistance factor to *Plasmodium vivax* in blacks. The Duffy- blood-group genotype, FyFy. N Engl J Med 295:302–304
37. Bruce-Chwatt LJ (1981) Alphonse Laveran's discovery 100 years ago and today's global fight against malaria. J R Soc Med 74:531–536
38. Ross R (1897) Observations on a condition necessary to the transformation of the malaria crescent. Br Med J 1:251–255
39. Russell PF, Mohan BN (1942) The immunization of fowls against mosquito-borne *Plamodium gallinaceum* by injections of serum and of inactivated homologous sporozoites. J Exp Med 76:477–495
40. Freund J, Sommer HE, Walter AW (1945) Immunization against malaria: vaccination of ducks with killed parasites incorporated with adjuvants. Science 102:200–202
41. Freund J, Thomson KJ, Sommer HE, Walter AW, Schenkein EL (1945) Immunization of rhesus monkeys against malarial infection (*P. knowlesi*) with killed parasites and adjuvants. Science 102:202–204. doi:10.1126/science.102.2643.202, 102/2643/202 [pii]
42. Jacobs HR (1943) Immunization against malaria. Increased protection by vaccination of ducklings with saline-insoluble

residues of *Plasmodium lophurae* mixed with a bacterial toxin. Am J Trop Med Hyg s1-23:597–606
43. Redmond WB (1939) Immunization of birds to malaria by vaccination. J Parasitol 25:28–29
44. Bennison BE, Coatney GR (1949) Effects of X-irradiation on *Plasmodium gallinaceum* and *Plasmodium lophurae* infections in young chicks. J Natl Malar Soc 8:280–289
45. Ceithaml J, Evans EA Jr (1946) The biochemistry of the malaria parasite; the in vitro effects of x-rays upon *Plasmodium gallinaceum*. J Infect Dis 78:190–197
46. Nussenzweig RS, Vanderberg J, Most H, Orton C (1967) Protective immunity produced by the injection of x-irradiated sporozoites of *Plasmodium berghei*. Nature 216:160–162
47. Hoffman SL, Billingsley PF, James E, Richman A, Loyevsky M, Li T, Chakravarty S, Gunasekera A, Li M, Stafford R, Ahumada A, Epstein JE, Sedegah M, Reyes S, Richie TL, Lyke KE, Edelman R, Laurens M, Plowe CV, Sim BK (2010) Development of a metabolically active, non-replicating sporozoite vaccine to prevent *Plasmodium falciparum* malaria. Hum Vaccin 6:97–106, 10396 [pii]
48. Heidelberger M, Prout C, Hindle JA, Rose AS (1946) Studies in human malaria III. An attempt at vaccination of paretics against blood-borne infection with *P vivax*. J Immunol 53: 109–112
49. Clyde DF, Most H, McCarthy VC, Vanderberg JP (1973) Immunization of man against sporozoite-induced falciparum malaria. Am J Med Sci 266:169–177
50. Rieckmann KH, Carson PE, Beaudoin RL, Cassells JS, Sell KW (1974) Letter: sporozoite induced immunity in man against an Ethiopian strain of *Plasmodium falciparum*. Trans R Soc Trop Med Hyg 68:258–259
51. Luke TC, Hoffman SL (2003) Rationale and plans for developing a non-replicating, metabolically active, radiation-attenuated *Plasmodium falciparum* sporozoite vaccine. J Exp Biol 206:3803–3808
52. Vanderberg JP (2009) Reflections on early malaria vaccine studies, the first successful human malaria vaccination, and beyond. Vaccine 27:2–9. doi:10.1016/j.vaccine.2008.10.028, S0264-410X(08)01414-X [pii]
53. Trager W, Jensen JB (1976) Human malaria parasites in continuous culture. Science 193:673–675
54. Haynes JD, Diggs CL, Hines FA, Desjardins RE (1976) Culture of human malaria parasites *Plasmodium falciparum*. Nature 263:767–769
55. World Health Organization (2010) Initiative for vaccine research: malaria vaccines. WHO, Geneva
56. Gardner MJ, Hall N, Fung E, White O, Berriman M, Hyman RW, Carlton JM, Pain A, Nelson KE, Bowman S, Paulsen IT, James K, Eisen JA, Rutherford K, Salzberg SL, Craig A, Kyes S, Chan MS, Nene V, Shallom SJ, Suh B, Peterson J, Angiuoli S, Pertea M, Allen J, Selengut J, Haft D, Mather MW, Vaidya AB, Martin DM, Fairlamb AH, Fraunholz MJ, Roos DS, Ralph SA, McFadden GI, Cummings LM, Subramanian GM, Mungall C, Venter JC, Carucci DJ, Hoffman SL, Newbold C, Davis RW, Fraser CM, Barrell B (2002) Genome sequence of the human malaria parasite *Plasmodium falciparum*. Nature 419:498–511
57. Takala SL, Plowe CV (2009) Genetic diversity and malaria vaccine design, testing and efficacy: preventing and overcoming 'vaccine resistant malaria'. Parasite Immunol 31:560–573. doi:10.1111/j.1365–3024.2009.01138.x, PIM1138 [pii]
58. Takala SL, Coulibaly D, Thera MA, Dicko A, Smith DL, Guindo AB, Kone AK, Traore K, Ouattara A, Djimde AA, Sehdev PS, Lyke KE, Diallo DA, Doumbo OK, Plowe CV (2007) Dynamics of polymorphism in a malaria vaccine antigen at a vaccine-testing site in Mali. PLoS Med 4:e93
59. Takala SL, Coulibaly D, Thera MA, Batchelor AH, Cummings MP, Escalante AA, Ouattara A, Traore K, Niangaly A, Djimde AA, Doumbo OK, Plowe CV (2009) Extreme polymorphism in a vaccine antigen and risk of clinical malaria: implications for vaccine development. Sci Transl Med 1:2ra5
60. Alonso PL, Sacarlal J, Aponte JJ, Leach A, Macete E, Milman J, Mandomando I, Spiessens B, Guinovart C, Espasa M, Bassat Q, Aide P, Ofori-Anyinam O, Navia MM, Corachan S, Ceuppens M, Dubois MC, Demoitie MA, Dubovsky F, Menendez C, Tornieporth N, Ballou WR, Thompson R, Cohen J (2004) Efficacy of the RTS, S/AS02A vaccine against *Plasmodium falciparum* infection and disease in young African children: randomised controlled trial. Lancet 364:1411–1420
61. Egan AF, Blackman MJ, Kaslow DC (2000) Vaccine efficacy of recombinant *Plasmodium falciparum* merozoite surface protein 1 in malaria-naive, -exposed, and/or -rechallenged *Aotus vociferans* monkeys. Infect Immun 68:1418–1427
62. Thera MA, Doumbo OK, Coulibaly D, Diallo DA, Sagara I, Dicko A, Diemert DJ, Heppner DG Jr, Stewart VA, Angov E, Soisson L, Leach A, Tucker K, Lyke KE, Plowe CV (2006) Safety and allele-specific immunogenicity of a malaria vaccine in Malian adults: results of a phase I randomized trial. PLoS Clin Trials 1:e34. doi:10.1371/journal.pctr.0010034
63. Stoute JA, Gombe J, Withers MR, Siangla J, McKinney D, Onyango M, Cummings JF, Milman J, Tucker K, Soisson L, Stewart VA, Lyon JA, Angov E, Leach A, Cohen J, Kester KE, Ockenhouse CF, Holland CA, Diggs CL, Wittes J, Heppner DG Jr (2007) Phase 1 randomized double-blind safety and immunogenicity trial of *Plasmodium falciparum* malaria merozoite surface protein FMP1 vaccine, adjuvanted with AS02A, in adults in western Kenya. Vaccine 25:176–184
64. Withers MR, McKinney D, Ogutu BR, Waitumbi JN, Milman JB, Apollo OJ, Allen OG, Tucker K, Soisson LA, Diggs C, Leach A, Wittes J, Dubovsky F, Stewart VA, Remich SA, Cohen J, Ballou WR, Holland CA, Lyon JA, Angov E, Stoute JA, Martin SK, Heppner DG (2006) Safety and reactogenicity of an MSP-1 malaria vaccine candidate: a randomized Phase Ib dose-escalation trial in Kenyan children. PLoS Clin Trials 1:e32
65. Ogutu BR, Apollo OJ, McKinney D, Okoth W, Siangla J, Dubovsky F, Tucker K, Waitumbi JN, Diggs C, Wittes J, Malkin E, Leach A, Soisson LA, Milman JB, Otieno L, Holland CA, Polhemus M, Remich SA, Ockenhouse CF, Cohen J, Ballou WR, Martin SK, Angov E, Stewart VA, Lyon JA, Heppner DG, Withers MR (2009) Blood stage malaria vaccine eliciting high

antigen-specific antibody concentrations confers no protection to young children in Western Kenya. PLoS One 4:e4708

66. Sagara I, Dicko A, Ellis RD, Fay MP, Diawara SI, Assadou MH, Sissoko MS, Kone M, Diallo AI, Saye R, Guindo MA, Kante O, Niambele MB, Miura K, Mullen GE, Pierce M, Martin LB, Dolo A, Diallo DA, Doumbo OK, Miller LH, Saul A (2009) A randomized controlled phase 2 trial of the blood stage AMA1-C1/Alhydrogel malaria vaccine in children in Mali. Vaccine 27:3090–3098
67. Thera MA, Doumbo OK, Coulibaly D, Diallo DA, Kone AK, Guindo AB, Traore K, Dicko A, Sagara I, Sissoko MS, Baby M, Sissoko M, Diarra I, Niangaly A, Dolo A, Daou M, Diawara SI, Heppner DG, Stewart VA, Angov E, Bergmann-Leitner ES, Lanar DE, Dutta S, Soisson L, Diggs CL, Leach A, Owusu A, Dubois MC, Cohen J, Nixon JN, Gregson A, Takala SL, Lyke KE, Plowe CV (2008) Safety and immunogenicity of an AMA-1 malaria vaccine in Malian adults: results of a Phase 1 randomized controlled trial. PLoS One 3:e1465
68. Thera MA, Doumbo OK, Coulibaly D, Laurens MB, Kone AK, Guindo AB, Traore K, Sissoko M, Diallo DA, Diarra I, Kouriba B, Daou M, Dolo A, Baby M, Sissoko MS, Sagara I, Niangaly A, Traore I, Olotu A, Godeaux O, Leach A, Dubois MC, Ballou WR, Cohen J, Thompson D, Dube T, Soisson L, Diggs CL, Takala SL, Lyke KE, House B, Lanar DE, Dutta S, Heppner DG, Plowe CV (2010) Safety and immunogenicity of an AMA1 malaria vaccine in Malian children: results of a phase 1 randomized controlled trial. PLoS One 5:e9041. doi:10.1371/journal.pone.0009041
69. Dame JB, Williams JL, McCutchan TF, Weber JL, Wirtz RA, Hockmeyer WT, Maloy WL, Haynes JD, Schneider RD (1984) Structure of the gene encoding the immunodominant surface antigen on the sporozoite of the human malaria parasite *Plasmodium falciparum*. Science 225:593–599
70. Beier JC, Vanderburg JP (1998) Sporogonic development in the mosquito. In: Sherman IW (ed) Malaria parasite biology, pathogenesis, and protection. ASM Press, Washington, DC
71. Ballou WR, Rothbard J, Wirtz RA, Gordon DM, Williams JS, Gore RW, Schneider I, Hollingdale MR, Beaudoin RL, Maloy WL et al (1985) Immunogenicity of synthetic peptides from circumsporozoite protein of *Plasmodium falciparum*. Science 228:996–999
72. Hollingdale MR, Nardin EH, Tharavanij S, Schwartz AL, Nussenzweig RS (1984) Inhibition of entry of *Plasmodium falciparum* and *P. vivax* sporozoites into cultured cells; an in vitro assay of protective antibodies. J Immunol 132:909–913
73. Herrington DA, Clyde DF, Losonsky G, Cortesia M, Murphy JR, Davis J, Baqar S, Felix AM, Heimer EP, Gillessen D et al (1987) Safety and immunogenicity in man of a synthetic peptide malaria vaccine against *Plasmodium falciparum* sporozoites. Nature 328:257–259
74. Ballou WR, Hoffman SL, Sherwood JA, Hollingdale MR, Neva FA, Hockmeyer WT, Gordon DM, Schneider I, Wirtz RA, Young JF (1987) Safety and efficacy of a recombinant DNA *Plasmodium falciparum* sporozoite vaccine. Lancet 1:1277–1281
75. Hoffman SL, Oster CN, Plowe CV, Woollett GR, Beier JC, Chulay JD, Wirtz RA, Hollingdale MR, Mugambi M (1987) Naturally acquired antibodies to sporozoites do not prevent malaria: vaccine development implications. Science 237: 639–642
76. Sherwood JA, Copeland RS, Taylor KA, Abok K, Oloo AJ, Were JB, Strickland GT, Gordon DM, Ballou WR, Bales JDJ, Wirtz RA, Wittes J, Gross M, Que JU, Cryz SJ, Oster CN, Roberts CR, Sadoff JC (1996) *Plasmodium falciparum* circumsporozoite vaccine immunogenicity and efficacy trial with natural challenge quantitation in an area of endemic human malaria of Kenya. Vaccine 14:817–827
77. Gordon DM, McGovern TW, Krzych U, Cohen JC, Schneider I, LaChance R, Heppner DG, Yuan G, Hollingdale M, Slaoui M (1995) Safety, immunogenicity, and efficacy of a recombinantly produced *Plasmodium falciparum* circumsporozoite protein-hepatitis B surface antigen subunit vaccine. J Infect Dis 171:1576–1585
78. Stoute JA, Slaoui M, Heppner DG, Momin P, Kester KE, Desmons P, Wellde BT, Garcon N, Krzych U, Marchand M (1997) A preliminary evaluation of a recombinant circumsporozoite protein vaccine against *Plasmodium falciparum* malaria. RTS, S malaria vaccine evaluation group. N Engl J Med 336:86–91. doi:10.1056/NEJM199701093360202
79. Kester KE, McKinney DA, Tornieporth N, Ockenhouse CF, Heppner DG, Hall T, Krzych U, Delchambre M, Voss G, Dowler MG, Palensky J, Wittes J, Cohen J, Ballou WR (2001) Efficacy of recombinant circumsporozoite protein vaccine regimens against experimental *Plasmodium falciparum* malaria. J Infect Dis 183:640–647
80. Bojang KA, Milligan PJ, Pinder M, Vigneron L, Alloueche A, Kester KE, Ballou WR, Conway DJ, Reece WH, Gothard P, Yamuah L, Delchambre M, Voss G, Greenwood BM, Hill A, McAdam KP, Tornieporth N, Cohen JD, Doherty T (2001) Efficacy of RTS, S/AS02 malaria vaccine against *Plasmodium falciparum* infection in semi-immune adult men in The Gambia: a randomised trial. Lancet 358:1927–1934
81. Bejon P, Lusingu J, Olotu A, Leach A, Lievens M, Vekemans J, Mshamu S, Lang T, Gould J, Dubois MC, Demoitie MA, Stallaert JF, Vansadia P, Carter T, Njuguna P, Awuondo KO, Malabeja A, Abdul O, Gesase S, Mturi N, Drakeley CJ, Savarese B, Villafana T, Ballou WR, Cohen J, Riley EM, Lemnge MM, Marsh K, von Seidlein L (2008) Efficacy of RTS, S/AS01E vaccine against malaria in children 5 to 17 months of age. N Engl J Med 359:2521–2532. doi:10.1056/NEJMoa0807381, NEJMoa0807381 [pii]
82. Alonso PL, Sacarlal J, Aponte JJ, Leach A, Macete E, Aide P, Sigauque B, Milman J, Mandomando I, Bassat Q, Guinovart C, Espasa M, Corachan S, Lievens M, Navia MM, Dubois MC, Menendez C, Dubovsky F, Cohen J, Thompson R, Ballou WR (2005) Duration of protection with RTS, S/AS02A malaria vaccine in prevention of *Plasmodium falciparum* disease in Mozambican children: single-blind extended follow-up of a randomised controlled trial. Lancet 366: 2012–2018
83. Sacarlal J, Aide P, Aponte JJ, Renom M, Leach A, Mandomando I, Lievens M, Bassat Q, Lafuente S, Macete E, Vekemans J,

Guinovart C, Sigauque B, Sillman M, Milman J, Dubois MC, Demoitie MA, Thonnard J, Menendez C, Ballou WR, Cohen J, Alonso PL (2009) Long-term safety and efficacy of the RTS, S/AS02A malaria vaccine in Mozambican children. J Infect Dis 200:329–336. doi:10.1086/600119

84. Heppner DG Jr, Kester KE, Ockenhouse CF, Tornieporth N, Ofori O, Lyon JA, Stewart VA, Dubois P, Lanar DE, Krzych U, Moris P, Angov E, Cummings JF, Leach A, Hall BT, Dutta S, Schwenk R, Hillier C, Barbosa A, Ware LA, Nair L, Darko CA, Withers MR, Ogutu B, Polhemus ME, Fukuda M, Pichyangkul S, Gettyacamin M, Diggs C, Soisson L, Milman J, Dubois MC, Garcon N, Tucker K, Wittes J, Plowe CV, Thera MA, Duombo OK, Pau MG, Goudsmit J, Ballou WR, Cohen J (2005) Towards an RTS, S-based, multi-stage, multi-antigen vaccine against falciparum malaria: progress at the Walter Reed Army Institute of Research. Vaccine 23:2243–2250
85. Stewart VA, McGrath SM, Dubois PM, Pau MG, Mettens P, Shott J, Cobb M, Burge JR, Larson D, Ware LA, Demoitie MA, Weverling GJ, Bayat B, Custers JH, Dubois MC, Cohen J, Goudsmit J, Heppner DG Jr (2007) Priming with an adenovirus 35-circumsporozoite protein (CS) vaccine followed by RTS, S/AS01B boosting significantly improves immunogenicity to *Plasmodium falciparum* CS compared to that with either malaria vaccine alone. Infect Immun 75:2283–2290
86. Cummings JF, Spring MD, Schwenk RJ, Ockenhouse CF, Kester KE, Polhemus ME, Walsh DS, Yoon IK, Prosperi C, Juompan LY, Lanar DE, Krzych U, Hall BT, Ware LA, Stewart VA, Williams J, Dowler M, Nielsen RK, Hillier CJ, Giersing BK, Dubovsky F, Malkin E, Tucker K, Dubois MC, Cohen JD, Ballou WR, Heppner DG Jr (2010) Recombinant liver stage antigen-1 (LSA-1) formulated with AS01 or AS02 is safe, elicits high titer antibody and induces IFN-gamma/IL-2 CD4+ T cells but does not protect against experimental *Plasmodium falciparum* infection. Vaccine 28:5135–5144. doi:10.1016/j.vaccine.2009.08.046, S0264-410X(09)01231-6 [pii]
87. Hill AV, Reyes-Sandoval A, O'Hara G, Ewer K, Lawrie A, Goodman A, Nicosia A, Folgori A, Colloca S, Cortese R, Gilbert SC, Draper SJ (2010) Prime-boost vectored malaria vaccines: progress and prospects. Hum Vaccin 6:78–83, 10116 [pii]
88. Kaba SA, Brando C, Guo Q, Mittelholzer C, Raman S, Tropel D, Aebi U, Burkhard P, Lanar DE (2009) A nonadjuvanted polypeptide nanoparticle vaccine confers long-lasting protection against rodent malaria. J Immunol 183:7268–7277. doi:10.4049/jimmunol.0901957, jimmunol.0901957 [pii]
89. Bergmann-Leitner ES, Mease RM, de la Vega P, Savranskaya T, Polhemus M, Ockenhouse C, Angov E (2010) Immunization with pre-erythrocytic antigen CelTOS from *Plasmodium falciparum* elicits cross-species protection against heterologous challenge with *Plasmodium berghei*. PLoS One 5: e12294. doi:10.1371/journal.pone.0012294
90. Blackman MJ, Heidrich HG, Donachie S, McBride JS, Holder AA (1990) A single fragment of a malaria merozoite surface protein remains on the parasite during red cell invasion and is the target of invasion-inhibiting antibodies. J Exp Med 172: 379–382
91. Egan AF, Morris J, Barnish G, Allen S, Greenwood BM, Kaslow DC, Holder AA, Riley EM (1996) Clinical immunity to *Plasmodium falciparum* malaria is associated with serum antibodies to the 19-kDa C-terminal fragment of the merozoite surface antigen, PfMSP-1. J Infect Dis 173:765–9
92. Riley EM, Allen SJ, Wheeler JG, Blackman MJ, Bennett S, Takacs B, Schonfeld HJ, Holder AA, Greenwood BM (1992) Naturally acquired cellular and humoral immune responses to the major merozoite surface antigen (PfMSP1) of *Plasmodium falciparum* are associated with reduced malaria morbidity. Parasite Immunol 14:321–37
93. Stowers AW, Cioce V, Shimp RL, Lawson M, Hui G, Muratova O, Kaslow DC, Robinson R, Long CA, Miller LH (2001) Efficacy of two alternate vaccines based *on Plasmodium falciparum* merozoite surface protein 1 in an Aotus challenge trial. Infect Immun 69:1536–1546. doi:10.1128/IAI.69.3.1536-1546.2001
94. Peterson MG, Marshall VM, Smythe JA, Crewther PE, Lew A, Silva A, Anders RF, Kemp DJ (1989) Integral membrane protein located in the apical complex of *Plasmodium falciparum*. Mol Cell Biol 9:3151–3154
95. Narum DL, Thomas AW (1994) Differential localization of full-length and processed forms of PF83/AMA-1 an apical membrane antigen of *Plasmodium falciparum* merozoites. Mol Biochem Parasitol 67:59–68
96. Mitchell GH, Thomas AW, Margos G, Dluzewski AR, Bannister LH (2004) Apical membrane antigen 1, a major malaria vaccine candidate, mediates the close attachment of invasive merozoites to host red blood cells. Infect Immun 72:154–158
97. Florens L, Washburn MP, Raine JD, Anthony RM, Grainger M, Haynes JD, Moch JK, Muster N, Sacci JB, Tabb DL, Witney AA, Wolters D, Wu Y, Gardner MJ, Holder AA, Sinden RE, Yates JR, Carucci DJ (2002) A proteomic view of the *Plasmodium falciparum* life cycle. Nature 419:520–526
98. Hodder AN, Crewther PE, Anders RF (2001) Specificity of the protective antibody response to apical membrane antigen 1. Infect Immun 69:3286–94
99. Polley SD, Mwangi T, Kocken CH, Thomas AW, Dutta S, Lanar DE, Remarque E, Ross A, Williams TN, Mwambingu G, Lowe B, Conway DJ, Marsh K (2004) Human antibodies to recombinant protein constructs of *Plasmodium falciparum* Apical Membrane Antigen 1 (AMA1) and their associations with protection from malaria. Vaccine 23:718–728
100. Dutta S, Lee SY, Batchelor AH, Lanar DE (2007) Structural basis of antigenic escape of a malaria vaccine candidate. Proc Natl Acad Sci USA 104:12488–12493
101. Healer J, Murphy V, Hodder AN, Masciantonio R, Gemmill AW, Anders RF, Cowman AF, Batchelor A (2004) Allelic polymorphisms in apical membrane antigen-1 are responsible for evasion of antibody-mediated inhibition in *Plasmodium falciparum*. Mol Microbiol 52:159–168
102. Ouattara A, Mu J, Takala-Harrison S, Saye R, Sagara I, Dicko A, Niangaly A, Duan J, Ellis RD, Miller LH, Su XZ, Plowe CV, Doumbo OK (2010) Lack of allele-specific efficacy of

a bivalent AMA1 malaria vaccine. Malar J 9:175. doi:10.1186/1475-2875-9-175, 1475-2875-9-175 [pii]

103. Spring MD, Cummings JF, Ockenhouse CF, Dutta S, Reidler R, Angov E, Bergmann-Leitner E, Stewart VA, Bittner S, Juompan L, Kortepeter MG, Nielsen R, Krzych U, Tierney E, Ware LA, Dowler M, Hermsen CC, Sauerwein RW, de Vlas SJ, Ofori-Anyinam O, Lanar DE, Williams JL, Kester KE, Tucker K, Shi M, Malkin E, Long C, Diggs CL, Soisson L, Dubois MC, Ballou WR, Cohen J, Heppner DG Jr (2009) Phase 1/2a study of the malaria vaccine candidate apical membrane antigen-1 (AMA-1) administered in adjuvant system AS01B or AS02A. PLoS One 4:e5254
104. Thera MA, Doumbo OK, Coulibaly D, Laurens MB, Ouattara A, Kone AK, Guindo AB, Traore K, Traore I, Kouriba B, Diallo DA, Diarra I, Daou M, Dolo A, Tolo Y, Sissoko MS, Niangaly A, Sissoko M, Takala-Harrison S, Lyke KE, Wu Y, Blackwelder WC, Godeaux O, Vekemans J, Dubois M-C, Ballou WR, Cohen J, Thompson D, Dube T, Soisson L, Diggs CL, House B, Lanar DE, Dutta S, Heppner DG Jr., Plowe CV (2011) A field trial to assess a blood-stage malaria vaccine. N Engl J Med 365: 1004–13
105. Remarque EJ, Faber BW, Kocken CH, Thomas AW (2008) A diversity-covering approach to immunization with *Plasmodium falciparum* apical membrane antigen 1 induces broader allelic recognition and growth inhibition responses in rabbits. Infect Immun 76:2660–2670. doi:10.1128/IAI.00170-08, IAI.00170-08 [pii]
106. Remarque EJ, Faber BW, Kocken CH, Thomas AW (2008) Apical membrane antigen 1: a malaria vaccine candidate in review. Trends Parasitol 24:74–84. doi:10.1016/j.pt.2007.12.002, S1471-4922(07)00328-5 [pii]
107. Dutta S, Dlugosz LS, Clayton JW, Pool CD, Haynes JD, Gasser RA III, Batchelor AH (2010) Alanine mutagenesis of the primary antigenic escape residue cluster, c1, of apical membrane antigen 1. Infect Immun 78:661–671. doi:10.1128/IAI.00866-09, IAI.00866-09 [pii]
108. Klein MM, Gittis AG, Su HP, Makobongo MO, Moore JM, Singh S, Miller LH, Garboczi DN (2008) The cysteine-rich interdomain region from the highly variable *Plasmodium falciparum* erythrocyte membrane protein-1 exhibits a conserved structure. PLoS Pathog 4:e1000147. doi:10.1371/journal.ppat.1000147
109. Avril M, Cartwright MM, Hathaway MJ, Hommel M, Elliott SR, Williamson K, Narum DL, Duffy PE, Fried M, Beeson JG, Smith JD (2010) Immunization with VAR2CSA-DBL5 recombinant protein elicits broadly cross-reactive antibodies to placental *Plasmodium falciparum*-infected erythrocytes. Infect Immun 78:2248–2256. doi:10.1128/IAI.00410-09, IAI.00410-09 [pii]
110. Barr PJ, Green KM, Gibson HL, Bathurst IC, Quakyi IA, Kaslow DC (1991) Recombinant Pfs25 protein of *Plasmodium falciparum* elicits malaria transmission-blocking immunity in experimental animals. J Exp Med 174:1203–1208
111. Wu Y, Ellis RD, Shaffer D, Fontes E, Malkin EM, Mahanty S, Fay MP, Narum D, Rausch K, Miles AP, Aebig J, Orcutt A, Muratova O, Song G, Lambert L, Zhu D, Miura K, Long C, Saul A, Miller LH, Durbin AP (2008) Phase 1 trial of malaria transmission blocking vaccine candidates Pfs25 and Pvs25 formulated with montanide ISA 51. PLoS One 3:e2636. doi:10.1371/journal.pone.0002636
112. Dinglasan RR, Valenzuela JG, Azad AF (2005) Sugar epitopes as potential universal disease transmission blocking targets. Insect Biochem Mol Biol 35:1–10. doi:10.1016/j.ibmb.2004.09.005, S0965-1748(04)00159-6 [pii]
113. Valero MV, Amador LR, Galindo C, Figueroa J, Bello MS, Murillo LA, Mora AL, Patarroyo G, Rocha CL, Rojas M (1993) Vaccination with SPf66, a chemically synthesised vaccine, against *Plasmodium falciparum* malaria in Colombia. Lancet 341:705–710
114. Nosten F, Luxemburger C, Kyle DE, Ballou WR, Wittes J, Wah E, Chongsuphajaisiddhi T, Gordon DM, White NJ, Sadoff JC, Heppner DG (1996) Randomised double-blind placebo-controlled trial of SPf66 malaria vaccine in children in northwestern Thailand. Shoklo SPf66 Malaria Vaccine Trial Group. Lancet 348:701–707
115. D'Alessandro U, Leach A, Drakeley CJ, Bennett S, Olaleye BO, Fegan GW, Jawara M, Langerock P, George MO, Targett GA (1995) Efficacy trial of malaria vaccine SPf66 in Gambian infants. Lancet 346:462–467
116. Alonso PL, Smith T, Schellenberg JR, Masanja H, Mwankusye S, Urassa H, Bastos de Azevedo I, Chongela J, Kobero S, Menendez C et al (1994) Randomised trial of efficacy of SPf66 vaccine against *Plasmodium falciparum* malaria in children in southern Tanzania. Lancet 344:1175–1181
117. Ockenhouse CF, Sun PF, Lanar DE, Wellde BT, Hall BT, Kester K, Stoute JA, Magill A, Krzych U, Farley L, Wirtz RA, Sadoff JC, Kaslow DC, Kumar S, Church LW, Crutcher JM, Wizel B, Hoffman S, Lalvani A, Hill AV, Tine JA, Guito KP, de Taisne C, Anders R, Ballou WR (1998) Phase I/IIa safety, immunogenicity, and efficacy trial of NYVAC-Pf7, a pox-vectored, multiantigen, multistage vaccine candidate for *Plasmodium falciparum* malaria. J Infect Dis 177:1664–1673
118. Kumar S, Epstein JE, Richie TL, Nkrumah FK, Soisson L, Carucci DJ, Hoffman SL (2002) A multilateral effort to develop DNA vaccines against falciparum malaria. Trends Parasitol 18:129–135, S1471492201022073 [pii]
119. Epstein JE, Tewari K, Lyke KE, Sim BK, Billingsley PF, Laurens MB, Gunasekera A, Chakravarty S, James ER, Sedegah M, Richman A, Velmurugan S, Reyes S, Li M, Tucker K, Ahumada A, Ruben AJ, Li T, Stafford R, Eappen AG, Tamminga C, Bennett JW, Ockenhouse CF, Murphy JR, Komisar J, Thomas N, Loyevsky M, Birkett A, Plowe CV, Loucq C, Edelman R, Richie TL, Seder RA, Hoffman SL (2011) Live attenuated malaria vaccine designed to protect through hepatic CD8+ T cell immunity. Science [Epub ahead of print]
120. VanBuskirk KM, O'Neill MT, de la Vega P, Maier AG, Krzych U, Williams J, Dowler MG, Sacci JB Jr, Kangwanrangsan N, Tsuboi T, Kneteman NM, Heppner DG Jr, Murdock BA, Mikolajczak SA, Aly AS, Cowman AF, Kappe SH (2009) Preerythrocytic, live-attenuated *Plasmodium falciparum* vaccine candidates by design. Proc Natl Acad Sci USA 106. doi:10.1073/pnas.0906387106, 13004–13009. 0906387106 [pii]

121. Pinzon-Charry A, McPhun V, Kienzle V, Hirunpetcharat C, Engwerda C, McCarthy J, Good MF (2010) Low doses of killed parasite in CpG elicit vigorous CD4+ T cell responses against blood-stage malaria in mice. J Clin Invest 120:2967–2978. doi:10.1172/JCI39222, 39222 [pii]
122. McCarthy JS, Good MF (2010) Whole parasite blood stage malaria vaccines: a convergence of evidence. Hum Vaccin 6:114–123, 10394 [pii]

Books and Reviews

Bruder JT, Angov E, Limbach KJ, Richie TL (2010) Molecular vaccines for malaria. Hum Vaccin 6:54–77
Desowitz RS (1991) The malaria capers: more tales of parasites and people, research and reality. Norton, New York
Dinglasan RR, Jacobs-Lorena M (2008) Flipping the paradigm on malaria transmission-blocking vaccines. Trends Parasitol 24:364–370
Hill AV, Reyes-Sandoval A, O'Hara G, Ewer K, Lawrie A, Goodman A, Nicosia A, Folgori A, Colloca S, Cortese R, Gilbert SC, Draper SJ (2010) Prime-boost vectored malaria vaccines: progress and prospects. Hum Vaccin 6:78–83
Hviid L (2010) The role of Plasmodium falciparum variant surface antigens in protective immunity and vaccine development. Hum Vaccin 6:84–89
Langhorne J, Ndungu FM, Sponaas AM, Marsh K (2008) Immunity to malaria: more questions than answers. Nat Immunol 9:725–732
Moorthy VS, Kieny MP (2010) Reducing empiricism in malaria vaccine design. Lancet Infect Dis 10:204–211
Richards JS, Beeson JG (2009) The future for blood-stage vaccines against malaria. Immunol Cell Biol 87:377–390
Shah S (2010) The fever: how malaria has ruled humankind for 500,000 years. Farrar, Straus and Giroux, New York
Sherwin IW (2009) The elusive malaria vaccine: miracle or mirage? ASM Press, Washington, DC
Vaughan AM, Wang R, Kappe SH (2010) Genetically engineered, attenuated whole-cell vaccine approaches for malaria. Hum Vaccin 6:107–113
Wykes M, Good MF (2007) A case for whole-parasite malaria vaccines. Int J Parasitol 37:705–712

Mariculture Systems, Integrated Land-Based

Muki Shpigel
Israel Oceanographic and Limnological Research, National Center for Mariculture, Eilat, Israel

Article Outline

Glossary
Definition of Subject
Introduction
History
Nutrient Budget in Land-Based IMTA
Pilot Scale Systems
Future Directions: Challenges and Constraints
Bibliography

Glossary

Detritivores (also known as *saprophages*) They are heterotrophs that obtain nutrients by consuming detritus (decomposing organic matter).

Halophyte Salt-loving plants that can be grown at higher salinities than most traditional crop plants.

IMTA The Integrated Multi-Trophic Aquaculture System (IMTA) is an aquaculture practice in which excretions of one or more organisms are utilized by other cultured organisms from different trophic (nutritional) levels within the system.

Land-based and offshore mariculture systems Two methods of seawater aquaculture (mariculture); the former on land and the latter in the ocean.

Polyculture An aquaculture practice which involves culture of two or more species from the same or different trophic levels in the same water reservoir.

RAS Recirculated Aquaculture System (RAS) is an aquaculture practice for the rearing of aquatic organisms wherein 90% or more of the water is recycled within the system.

Sludge Solid/particulate waste that includes, among other components, feces, uneaten feed, algae and bacteria, which sinks to the bottom of aquaculture water reservoirs.

Definition of Subject

The Integrated Multi-Trophic Aquaculture System (IMTA) is an aquaculture practice in which excretions of one or more organisms are utilized by other cultured organisms from different trophic (nutritional) levels. IMTA systems are distinct from polyculture systems, which involve two or more species from the same or different trophic levels in the same water reservoir. In a typical IMTA, the various species are cultured in separate spatial entities, permitting intensification and optimization of production. The IMTA concept has been increasingly adopted in modern day

aquaculture, including land-based (Fig. 1) [1–5] and offshore mariculture [6, 7].

In land-based IMTA systems, seawater is pumped from the sea to fish or shrimp ponds. A pelleted diet is the only source of nutrients for the animals in the system. Nutrient-rich effluent water from these ponds can take three directions: microalgae ponds, macroalgae ponds, and constructed wetlands with halophyte plants. The microalgae can be utilized by filter feeders such as *Artemia* or/and bivalves. The macroalgae can be utilized by macroalgivores such as abalone or sea urchins, and detritus can be utilized by detritivores such as mullets, sea cucumbers, or polychaete worms (Fig. 1).

Introduction

The concept of polyculture and IMTA systems is not new. Such systems of different species of fish, or combinations of invertebrates and fish, have been existing in ancient Egypt and China for thousands of years. Artificial enclosures or natural ponds in tidal zones were generally used. Extensive traditional IMTA and polyculture systems are still practiced today in various parts of Asia in fresh and salt water. Rice and fish are cultured together in China. Earthen ponds, in association with wild or agricultural plants, are used on a wide scale in fish and shrimp farming in China, Indonesia, Taiwan, Thailand, Japan, Vietnam, India, the Philippines, and Ecuador. In Europe, ducks, fish, and crayfish have been raised together in freshwater ponds. This type of extensive production has proven sustainable, because it utilizes organisms that feed on different levels of the food web, and maintains a clean environment.

The traditional IMTA and polyculture systems are more environmentally friendly than modern intensive mono-aquaculture systems. These systems utilize fewer resources and do not pollute surrounding waters with waste products, because they generally sustain relatively low stocking densities and do not employ fertilizers. Most of them rely on natural production of food.

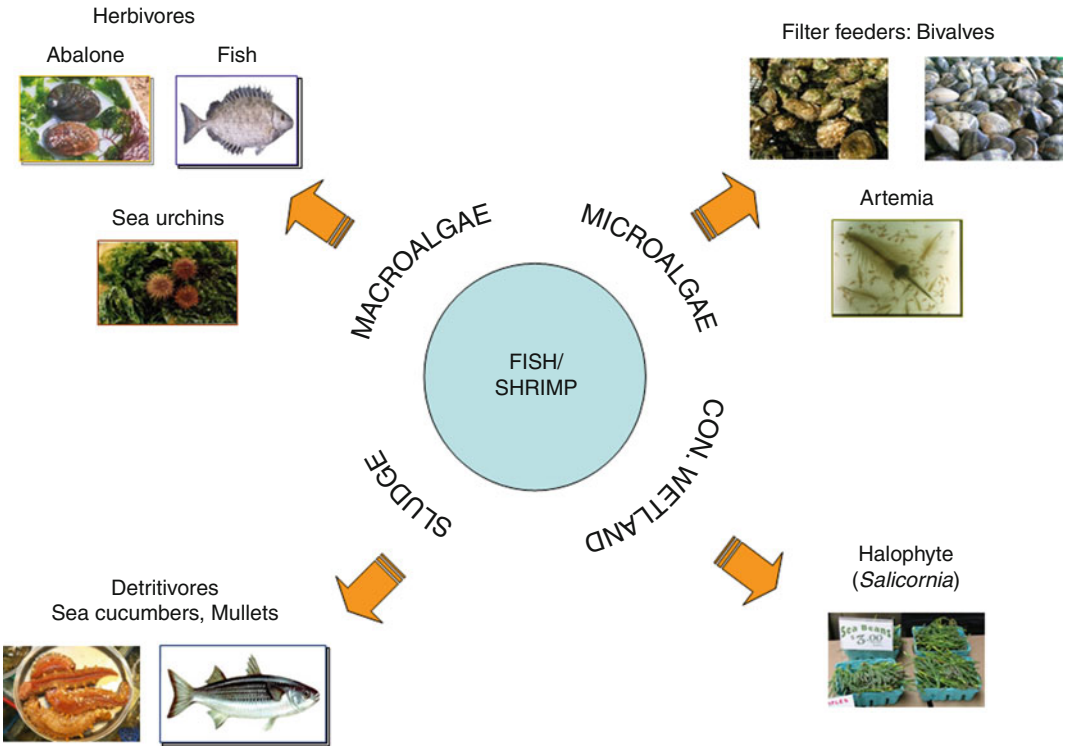

Mariculture Systems, Integrated Land-Based. Figure 1
Schematic design of land-based IMTA systems (con. = constructed)

This concept has increasingly been adopted for modern aquaculture, including land-based and sea-cage mariculture. With dramatic increases in global human population, food demand, and overfishing problems, traditional extensive aquaculture cannot satisfy present demand, and much less so the projected future demand, for sea products.

Modern intensive monoculture systems require high levels of resources and produce undesirable wastes. They are dedicated to a few expensive species and do not generate a large amount of food. Intensive aquaculture uses extensive amounts of resources such as water, feeds, fertilizers, chemicals, and energy, while discharging fecal material, uneaten feed, excretions, and drugs into the environment. In turn, this creates eutrophication of the water, has deleterious effects on marine life, increases the risks of antibiotic resistance in organisms, has an adverse effect on biodiversity, and contributes to habitat destruction. The economic success of intensive monoculture in sea cages or land-based facilities has much to do with the fact that, even today, pollution of the environment involves little or no monetary outlay or penalty for the growers. In most countries, aquaculture does not yet include the cost of effluent treatment. However, in the industrialized nations, this age is coming to a timely end and in Europe, there are already laws and regulations requiring effluent treatment and imposing fines for noncompliance. In some countries, this cost can be as high as €0.5–1 kg^{-1} feed, resulting in an expense of €250,000–350,000 per annum for medium-scale RAS (Recirculating Aquaculture System) farms (250 t/year). Awareness is growing among scientists, industry, the public, and politicians that technologies disregarding environmental impact are neither sustainable nor acceptable.

History

The development of modern land-based IMTA using extractive organisms such as shellfish, microalgae, and seaweeds began in the 1970s with the pioneer work of Goldman et al. [1] and Ryther et al. [2] in the treatment of household effluents. Phytoplankton was cultured in a mixture of domestic wastewater effluent and seawater, fed to suspension-feeder molluscs, and the dissolved remnants of nutrients in the final effluent were assimilated by seaweeds. As the food value of organisms grown on human waste effluents was questionable, adaptations of this principle to the treatment of intensive aquaculture effluents in both inland and coastal areas were proposed [8] and were followed by the integration into a system of carnivorous fish and abalone (e.g., [9]). The first practical and quantitative integrated land-based cultures of marine fish and shellfish, with phytoplankton as biofilter and food for shellfish, were constructed in Israel by Hughes-Games [10] and Gordin et al. [11]. A semi-intensive seabream and gray mullet pond system with silicate-rich green water, located on the coast of the Gulf of Eilat (Red Sea), supported dense populations of diatoms, excellent for feeding oysters [12, 13]. Later, the development of a practical intensive culture of bivalves in phytoplankton-rich effluents was described in a series of articles [3, 14–18]. Lefebvre et al. [19] showed that detritical waste from intensive fish farming can contribute to the growth of bivalves and reduce particulate matter in the water. Jones et al. [20], using the Sydney rock oyster *Saccostrea commercialis*, significantly reduced the concentration of suspended particulates including algae, bacteria, and inorganic particles in integrated systems.

Studies showing the performance of seaweed in land-based IMTA, initially at laboratory scale and later expanded to outdoor pilot scale, began to appear in the 1970s [21, 22]. The theoretical and practical principles of intensive large-scale land-based seaweed culture were studied and developed first at Woods Hole and later at Harbor Branch Oceanographic Institution in Florida – U.S.A. [8, 23–25]. The quantitative aspects of their functioning have been described [14, 16, 26–29]. Fish, abalone, and seaweed IMTA systems were studied by Shpigel et al. [30], Butterworth [31], and Nobre et al. [32]. The aspects of bioeconomics of land-based IMTA are described by Nobre et al. [32], Neori et al. [33], and Bunting and Shpigel [34].

Offshore IMTA system is a relatively new concept that started in the late nineties and is a modification of the land-based IMTA. In coastal integrated mariculture, shellfish and seaweed are cultured in proximity to cage fish culture [6, 7]. Kelp (brown algae) [35, 36] and red algae [37, 38] efficiently take up dissolved inorganic nitrogen excreted by the fish [39], so that seaweed production and quality are often higher in areas surrounding fish cages than elsewhere [6, 40–42].

KEY SPECIES CULTURED IN POLYCULTURE AND MULTI-TROPHIC SYSTEMS

Cold Seawater	Temperate Seawater	Warm Seawater
Oncorhynchus sp.	*Pagrus major*	*Sparus aurata*
Crassostrea sp.	*Sparus aurata*	*Lates calcarifer*
Mytilus edulis	*Dicentrarchus labrax*	*Mugil cephalus*
Haliotis rufescens	*Mercenaria mercenaria*	*Penaeus* sp.
Gracilaria sp.	*Ostrea edulis*	*Crassostrea gigas*
Laminaria sp.	*Ruditapes decussates*	*Tapes japonica*
Macrocystis sp.	*Gracilaria* sp.	*Haliotis diversicolor*
Porphyra sp.	*Ulva* sp.	*Gracilaria changii*
	Penaeus sp.	*Ulva lactuca*
	Crassostrea sp.	

Temperate Brackish Water	Temperate Freshwater	Warm Freshwater
Oreochromis sp.	*Hypophthalmichthys* sp.	*Clarias* sp.
Mugil cephalus	*Macrobrachium rosenbergii*	*Cyprinus carpio*
Sparus aurata		*Oreochromis* sp.
Dicentrarchus labrax		*Mugil cephalus*
Penaeus monodon		*Penaeus* sp.

Mariculture Systems, Integrated Land-Based. Figure 2
Key species cultured in IMTA and polyculture systems for marine and freshwater environment

However, nutrient removal efficiency in offshore IMTA is still relatively low, ranging between 15% and 25% [43].

The concept of IMTA systems is generic and can be applied to cold, warm, and temperate waters, in intensive, semi-intensive, and extensive systems, in sea cages or land-based facilities, in fresh water in land-based facilities or lakes, and all of the above in closed, semi-closed, or flow-through systems.

In recent years, several enterprises and research facilities have begun setting up land-based IMTA; most of the systems are pilot scale or R&D facilities. The IMTA typically include two or three species. In most of the studies, seaweed and microalgae are used as biofilters for the dissolved nutrients (review by Neori et al. [33] and Soto [44]). A broad spectrum list of selected organisms being used in farms and in R&D is presented in Fig. 2. Key species in cold water are salmon, mussels, and the seaweeds *Gracilaria, Laminaria*, and *Porphyra*. For temperate and warm seawater, sea bream, sea bass, oysters, clams, and *Ulva lactuca* are the predominant cultured species (Fig. 2).

Over 200 species are currently the object of R&D projects and in commercial farms and research institutes around the world, in various climate conditions. A significant number of fish and shellfish are cultured in temperate water, and a relatively low number of fish and large number of seaweeds in cold-water climates (Fig. 3).

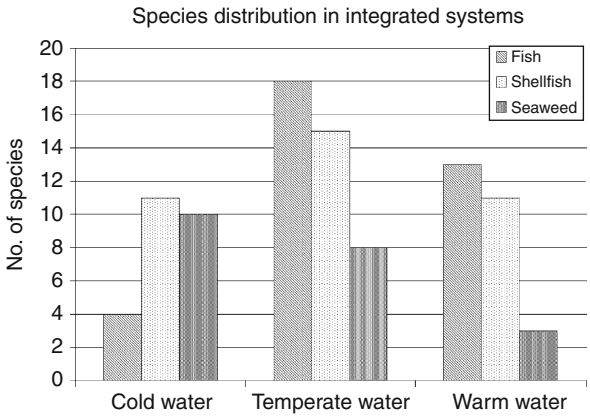

Mariculture Systems, Integrated Land-Based. Figure 3
Fish, shellfish, and seaweed species combination in IMTA systems in different bio-geographical regions around the world

Nutrient Budget in Land-Based IMTA

Protein in fish or shrimp feed is the most expensive component of nitrogen input into the IMTA systems.

In conventional cages or ponds, fish or shrimps assimilate only 20–30% of the nitrogen, while the rest is excreted into the water, mainly as dissolved ammonia, feces, and uneaten feed.

Two main practical approaches are emerging for handling the organic and nitrogenous wastes: bacterial dissimilation into gasses in "Recirculating Aquaculture Systems" (RAS), or plant assimilation into biomass (IMTA). Bacterial biofilters are dissimilative. Through a process of nitrification followed by denitrification, bacteria break down the organic pollutants into N_2 and CO_2 gasses. Bacterial biofilters are technically rather effective for aquaculture and allow significant water recirculation. However, the technology is relatively expensive, and not simple. Bacterial biofilter technologies are suitable for relatively small intensive land-based culture of lucrative organisms. There are no suggestions as to how such technologies can be integrated with large-scale, low cost fish or shrimp production. In addition, this system wastes expensive nitrogen by converting this valuable resource into gas, which is lost into the atmosphere.

Nutrient assimilation by other organisms is a more promising method of water treatment. In land-based IMTA ponds, seawater is pumped from the "nuclear species" (fish or shrimp) into the ponds/tanks of secondary organisms or macro-/microalgae. A pellet diet is the only source of nutrients for the primary animals in the system. Nutrient-rich effluent water from these ponds can take three directions: microalgae ponds, macroalgae ponds, or to irrigate halophyte crops (e.g., *Salicornia* sp.). The microalgae can be utilized by filter feeders such as artemia or bivalves. The macroalgae can be utilized by macroalgivores such as abalone, sea urchins, or herbivorous fish. Halophytes such as *Salicornia* can be used as a food product. The remaining detritus can be fed to detritivores such as mullets, sea cucumbers, or polychaete worms, singly or in combination.

Optimization of the IMTA is typically based on the highest value "nuclear" product at any given time. This "nuclear" product may be shifted according to climatic conditions and economic considerations. For example, in a fish-abalone-seaweed integrated system, abalone is the most valuable species, and the entire system is centered around this species. Abalone will be the first organism to receive the incoming water. From the abalone, the water will drain to the ammonia producers and from there to the biofilters.

The biological and chemical processes in the IMTA system should be balanced between nutrient production by the main organism and nutrient uptake capacity of the micro- and/or macroalgae and downstream by the micro- and macroalgivores. In such systems evaluated in Eilat, Israel, macro-and microalgae were able to assimilate 1–5 g N m^{-2} day^{-1}, while algivores and filter feeders assimilated 0.5–1 g N kg $(WW)^{-1}$ day^{-1} (Table 1 and references therein). However, there will be variation in nutrient uptake depending on season and climate, as algal biomass is influenced by day length (i.e., light hours), water temperature, and the nutrient levels in the water.

Mariculture Systems, Integrated Land-Based. Table 1 Assimilation rates of the uptake organisms in land-based IMTA in Eilat, Israel

	Assimilation rates	References
Microalgae	1–3 g N m^{-2} day^{-1}	Shpigel and Blaylock (1991)
		Shpigel et al. (1993a)
		Shpigel et al. (2007)
Macroalgae/ *Salicornia*	3–5 g N m^{-2} day^{-1}	Neori et al. (1991)
		Boarder and Shpigel (2001)
		Schuenhoff et al. (2003)
		Neori et al. (2004)
Bivalves/ Artemia	0.3 g N kg^{-1} day^{-1} 6 g N kg^{-1} m^{-3} day^{-1} (20 kg m^{-3})	Shpigel and Blaylock (1992)
		Shpigel et al. (1993a,b, 1994, 1996)
		Zmora and Shpigel (2006)
		Neori et al. (2004, 2006)
Abalone/sea urchins	0.5 g N kg WW day^{-1}	Shpigel et al. (1996, 1999, 2005, 2006)
		Neori et al. (2001)
		Stuart and Shpigel (2009)
Salicornia wetland	2–5 g N m^{-2} day^{-1}	Envirophyte (2010)
		Stuart and Shpigel (2009)

For example, in a fish-bivalve-seaweed IMTA system in Eilat, 63% of the nitrogen from the feed was assimilated by edible organisms, 32% sank to the bottom as biodeposit (sludge), and only 4.1% was discharged back to the sea (Fig. 4) [3].

Nitrogen, phosphate, and silicate ratios can vary according to local farm conditions.

Nutrient composition is also affected by additional biochemical processes in the effluent water such as nitrification, denitrification, and ammonification which occurs in the sedimentation pond as well in the pond walls and in the water pipes. These processes can be accelerated or affected by water temperature, nutrient loads, flow rates, and fish feed biochemical composition. Local natural microfauna in the ponds (e.g., zooplankton) and microflora, as well as bloom and crash phenomena, can affect the water quality as well. In most cases, effluent water from fishponds is characterized by a mixture of ammonia, nitrate, and nitrite.

While macro- and microalgae have proven effective components in land-based systems, neither removes 100% of the dissolved matter and they do not remove particulate matter at all. The remaining waste that includes, among other components, feces, uneaten feed, algae and bacteria, sinks to the bottom and becomes what is known as sludge. This sludge contains valuable ingredients, but can also be toxic to the cultured organisms. It can increase stress and disease risk, and reduce the quality of the water both in situ and for reuse. Ignoring the negative effects of the sludge can thus create serious problems and cause financial losses to the farmers. Removing and dumping sludge into the environment would similarly cause damage, even if moderated by dilution, and "foul the fish farmer's own nest" should he use seawater pumped in from the same area. Using detritivores is a novel option for land-based IMTA. Detritivore organisms such as mullets, cockles, and sea cucumbers will assimilate the waste into their bodies, thereby generating a significant saving in treatment costs, while additionally serving as valuable products in their own right, without requiring the purchase of feed for their culture.

The halophyte *Salicornia* sp. as a biofilter in constructed wetlands was evaluated in the "Genesis" and "Envirophyte" EU projects [34, 45, 46]. Using constructed wetlands (CW) planted with halophytes, which would take up the nutrient-rich wastewater and convert it into valuable plant biomass, is a new option for land-based IMTA. This system was developed to a practical stage for cold (UK) and warm (Israel) water. It was found that CW is efficient in clearing water of nutrients and suspended solids, some materials being purified through incorporation into the plants' biomass and others attaching to the substrate or being broken down by bacteria living therein. CW has the benefit of being low cost, is simple to operate, and can be given an aesthetically pleasing appearance. These plants have commercial value as a health food and are potential candidates for the health, beauty, and nutraceutical industries.

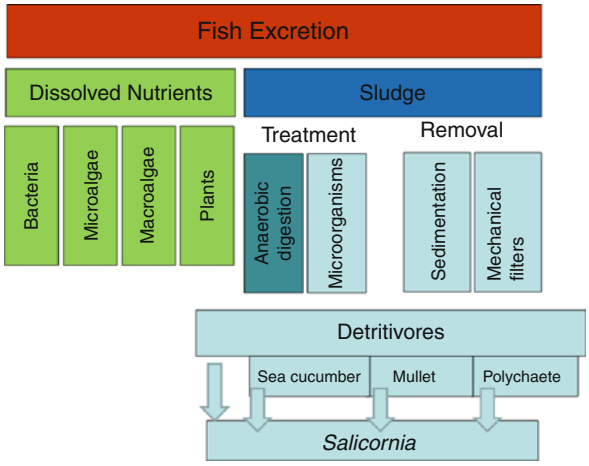

Mariculture Systems, Integrated Land-Based. Figure 4 Different pathways to treat sludge from fishponds

Pilot Scale Systems

In R&D projects in Eilat, Israel, three different types of IMTA systems were developed:

1. Fish (seabream *Sparus aurata*) – seaweed (*Ulva lactuca*)
2. Fish (seabream *Sparus aurata*) – abalone (*Haliotis discus hannai*)/sea urchin (*Paracentrotus lividus*) (macroalgivores) – seaweed (*Ulva lactuca*)
3. Fish (seabream *Sparus aurata*) – bivalve (*Crassostrea gigas* and *Tapes philippinarum*) – seaweed (*Ulva lactuca*)

In the seabream-*Ulva* system, a daily ration of 1.3 t of feed supported 250 t of fish. This amount of food is equivalent to 64 kg of nitrogen. The fish assimilate

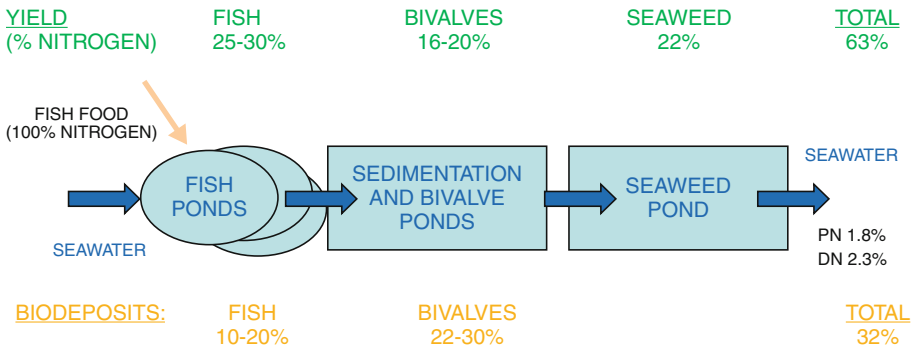

Mariculture Systems, Integrated Land-Based. Figure 5
Nitrogen budget of fish-bivalve-seaweed IMTA system in Eilat, Israel

Mariculture Systems, Integrated Land-Based. Table 2 Expected performance of land-based IMTA (WW = wet weight)

IMTA system	Organism	Pond size Ratio/ha	Yield (WW t year^{-1})	Yield (kg WW m^{-2} year^{-1})
Fish-*Ulva* (500 t feed y^{-1})	Seabream	1	220	22
	Ulva	2.5	1,600	64
	Total		1,820	86
Fish-*Ulva* abalone/sea urchin (500 t feed y^{-1})	Seabream	1	220	22
	Ulva	2.5	1,600	64
	Abalone	1.8	185	10
	Sea urchins	1.8	140	8
	Total		1960–2005	94
Fish-*Ulva*-clam/oyster (500 t feed y^{-1})	Seabream	1	220	20
	Clams/*oysters*	4	140	8
	Ulva	0.5	70	64
	Total		430	92

around 16 kg of nitrogen. About 9.6 kg of the nitrogen is drained as particulate nitrogen, and 38.4 kg is drained as dissolved nitrogen. One hectare (ha) of macroalgae (*Ulva lactuca*) is required to remove most of the dissolved nitrogen from the water. This system using 500 t of food per year would require an area of 3.4 ha, at a ratio of 1 ha fish to 2.5 ha *Ulva*. Expected yield is approximately 220 t of fish and 1,600 t of *Ulva* (modified from [5] and [47]) (Table 2).

In the seabream-*Ulva*-macroalgivores (sea urchins/abalone) IMTA system, 1 ha of macroalgae produces 1,600 t of *Ulva* annually. This *Ulva* supports 133 t (WW) of abalone (*Haliotis discus hannai*) or 200 t of sea urchins (*Paracentrotus lividus*). A seabream-*Ulva*-sea urchins/abalone IMTA system in Eilat, Israel, using 500 t of food per year will need an area of 5.3 ha, at a ratio of 1 ha for fish, 2.5 ha for *Ulva*, and 1.8 ha for the macroalgivores (modified from [5] and [47]) (Table 2).

In the seabream, microalgae, and bivalves (*Crassostrea gigas* and *Tapes philippinarum*) IMTA system, a daily ration of 1.3 t of feed supports 250 t of fish. The fish assimilate around 16 kg of nitrogen; 38.4 kg of nitrogen is drained as dissolved nitrogen. This system using 500 t of food per year would need an area of 2 ha of phytoplankton pond (with assimilation efficiency of

1–2 g N m^{-2} day^{-1}) to support production of 140 t bivalves and 70 t of seaweed (modified from [5] and [47]) (Table 2).

The economics of these types of land-based IMTA systems were summarized in [5]. However, the economics of a land-based IMTA are site specific since they depend on variables including local construction and operating costs and market prices for the farm's products at any given time [34].

Additional anticipated parameters based on the same model of using 500 t feed per year in each of the three IMTA systems tested in Eilat, Israel, with the projected yields as depicted in Table 2, can be seen in Table 3.

Mariculture Systems, Integrated Land-Based. Table 3 Anticipated parameters for organisms in the three IMTA systems tested in Eilat, Israel, based on 500 t feed per year

Seabream
FCR = 1.9; Feed protein content = 49%
Fish stocking density = 200 t ha^{-1}; Annual fish yield −300 t ha^{-1}
Seabream farm gate price = €4 kg^{-1}
Seaweed
Ammonia uptake rate –4 g m^{-2} day^{-1}; ammonia uptake efficiency = 85%
Annual Ulva yield = 900 t ha^{-1}
Seaweed (WW) price = €0.5 kg^{-1}
Abalone
FCR = 12; stocking density = 25 kg m^{-2}
Annual yield = 10 kg m^{-2};
Farm gate price = €35 kg^{-1}
Sea urchins
FCR = 8 t *Ulva* 1 t of production; stocking density = 10 kg m^{-2}
Annual yield = 8 kg m^{-2}
Farm gate price = €10 kg^{-1}
Clams/Oysters
Clam annual yield = 6–8 kg m^{-2}
Clams farm gate price = €4.5 kg^{-1}
Oyster annual yield = 25 kg m^{-3}
Oyster farm gate price = €3.5 kg^{-1}

Future Directions: Challenges and Constraints

Although considerable information is already available for putting land-based IMTA systems into practice, much of it is designed around commercial exploitation of a few high value species that are not affordable for the masses. The challenge for the future is to produce a large quantity of aquaculture products that will be cost-effective for producers, at a reasonable price for consumers, and ecologically sustainable.

Additional studies are required to overcome further constraints, including biological, engineering, and economical aspects:

Biological Aspects

- To acquire the knowledge necessary to maintain the correct balance between nutrient production by the system's core organism, nutrient uptake capacity of microalgae and macroalgae, shellfish filtering efficiency, and macroalgivores' activity in the system
- To acquire the knowledge necessary to maintain steady populations of microalgae (mainly diatoms) for the filter feeders and of macroalgae for the macroalgivores within the system in order to avoid blooms and crashes
- To acquire the knowledge necessary for the efficient regeneration of the biodeposit (sludge) from the bottom back to dissolved nutrients for the macro- and microalgae
- To effectively control diseases of the cultured organisms in IMTA systems and transmission of pathogens between components of the system

Engineering Aspects

- To reduce construction and operating costs by engineering improvements
- To minimize heat loss or gain in downstream components of the system
- To increase the use of greenhouse-covered modular systems, gravitation, low head upwelling, water semi-recirculation and other promising energy-saving methods

Economical Aspects

- To render cost effective the use of the extensive areas required for cultivating micro- and macroalgae

which cannot be done in a fully recirculating system and for which the facilities must thus be located not too far from the sea
- To develop and diversify the market of seaweed for human consumption from IMTA in Europe and North America
- To develop new markets and consumer acceptance of IMTA products

With the dramatic increase in population and food requirements, traditional extensive production systems cannot satisfy present and future market needs. Modern intensive monoculture systems are not ideal for mass production because they focus on few and expensive species, require high levels of resources, and produce undesirable wastes. To achieve high production rates and environmental conservation, food production using land-based IMTA systems is one of the most promising routes. The IMTA method assimilates expensive nitrogen waste into a valuable product that will increase profit for the farmer, improve FCR, diversify the mariculture products, create additional jobs, and, most importantly, reduce environmental pollution.

Bibliography

1. Goldman JC, Tenore RK, Ryther HJ, Corwin N (1974) Inorganic nitrogen removal in a combined tertiary treatment-marine aquaculture system. I. Removal efficiencies. Water Res 8:45–54
2. Ryther JH, Goldman JC, Gifford JE, Huguenin JE, Wing AS, Clarner JP, Williams LD, Lapointe BE (1975) Physical models of integrated waste recycling-marine polyculture systems. Aquaculture 5:163–177
3. Shpigel M, Neori A, Popper DM, Gordin H (1993) A proposed model for 'environmentally clean' land-based culture of fish, bivalves and seaweeds. Aquaculture 117:115–128
4. Shpigel M (2005) The use bivalves as biofilters and valuable product in land based aquaculture systems-review. In: Dame R, Olenin S (eds) The comparative roles of suspension-feeders in ecosystems. Kluwer, Dordrecht, The Netherlands, p 400
5. Shpigel M, Neori A (1996) The integrated culture of seaweed, abalone, fish and clams in modular intensive land-based systems: I. Proportion of size and projected revenues. Aquacult Eng 155:313–326
6. Troell M, Halling C, Nilsson A, Buschmann AH, Kautsky N, Kautsky L (1997) Integrated marine cultivation of *Gracilaria chilensis* (Gracilariales, Rhodophyta) and salmon cages for reduced environmental impact and increased economic output. Aquaculture 156:45–61
7. Troell M, Norberg J (1998) Modelling output and retention of suspended solids in an integrated salmon-mussel culture. Ecol Model 110:65–77
8. Huguenin JH (1976) An examination of problems and potentials for future large-scale intensive seaweed culture systems. Aquaculture 9:313–342
9. Tenore KR (1976) Food chain dynamics of abalone in a polyculture system. Aquaculture 8:23–27
10. Hughes-Games WL (1977) Growing the Japanese oyster (*Crassostrea gigas*) in sub-tropical seawater fishponds. I. Growth rate, survival and quality index. Aquaculture 11:217–229
11. Gordin H, Motzkin F, Hughes-Games A, Porter C (1981) Seawater mariculture pond – an integrated system. Eur Aquacult Spec Publ 6:1–13
12. Krom MD, Erez J, Porter CB, Ellner S (1989) Phytoplankton nutrient uptake dynamics in earthen marine fishponds under winter and summer conditions. Aquaculture 76:237–253
13. Erez J, Krom MD, Neuwirth T (1990) Daily oxygen variations in marine fish ponds, Elat, Israel. Aquaculture 84:289–305
14. Shpigel M, Fridman R (1990) Propagation of the manila clam *Tapes semidecussatus* in the effluent of marine aquaculture ponds in Elat, Israel. Aquaculture 90:113–122
15. Shpigel M, Blaylock RA (1991) The Pacific oyster, *Crassostrea gigas*, as a biological filter for a marine fish aquaculture pond. Aquaculture 92:187–197
16. Shpigel M, Lee J, Soohoo B, Fridman R, Gordin H (1993) The use of effluent water from fish ponds as a food source for the pacific oyster *Crassostrea gigas* Tunberg. Aquac Fish Manage 244:529–543
17. Neori A, Shpigel M (1999) Using algae to treat effluents and feed invertebrates in sustainable integrated mariculture. World Aquac 302:46–51
18. Neori A, Shpigel M, Scharfstein B (2001) Land-based low-pollution integrated mariculture of fish, seaweed and herbivores: principles of development, design, operation and economics. Aquaculture Europe 2001 book of abstracts, European Aquaculture Soc. Special Publ. No. 29, pp 190–191
19. Lefebvre S, Barille L, Clerc M (2000) Pacific oyster (*Crassostrea gigas*) feeding responses to a fish-farm effluent. Aquaculture 187:185–198
20. Jones AB, Dennison WC, Preston NP (2001) Integrated mariculture of shrimp effluent by sedimentation, oyster filtration and macroalgal absorption: a laboratory scale study. Aquaculture 193:155–178
21. Haines KC (1975) Growth of the Carrageenan-producing tropical red seaweed *Hypnea musciformis* in surface water, 870 m deep water, effluent from a clam mariculture system, and in deep water enriched with artificial fertilizers or domestic sewage. In: 10th European Symposium on Marine Biology, 1, pp 207–220
22. Langton RW, Haines KC, Lyon RE (1977) Ammonia nitrogen produced by the bivalve mollusc *Tapes japonica* and its recovery by the red seaweed *Hypnea musciformis* in a tropical mariculture system. Helgoländer wiss Meeresunters 30:217–229
23. Lapointe BE, Ryther HJ (1978) Some aspects of the growth and yield of *Gracilaria tikvahiae* in culture. Aquaculture 15: 185–193

24. DeBusk TA, Blakeslee M, Ryther JH (1986) Studies on the outdoor cultivation of *Ulva lactuca*. L Bot Mar 29:381–386
25. Bird K (1989) Intensive seaweed cultivation. Aquaculure Mag November/December 1989:29–34
26. Vandermeulen H, Gordin H (1990) Ammonium uptake using *Ulva* (Chlorophyta) in intensive fishpond systems: mass culture and treatment of effluent. J Appl Phycol 2:363–374
27. Cohen I, Neori A (1991) *Ulva lactuca* biofilters for marine fishponds effluents. Bot Mar 34:475–482
28. Neori A, Ellne SP, Boyd CE, Krom MD (1993) The integration of seaweed biofilters with intensive fish ponds to improve water quality and recapture nutrients. In: Moshiri GA (ed) Constructed wetlands for water quality improvement. Lewis, Boca Raton, pp 603–607
29. Schuenhoff A, Shpigel M, Lupatsch I, Ashkenazi A, Msuya FE, Neori A (2003) A semi-commercial, integrated system for the culture of fish and seaweed. Aquaculture 2211–4:167–181
30. Shpigel M, Neori A, Marshall A (1996) The suitability of several introduced species of abalone Gastropoda: Haliotidae for land-based culture with pond grown seaweed in Israel. Israeli J Aquaculture/Bamidgeh 484:192–200
31. Butterworth A (2010) Integrated Multi-Trophic Aquaculture systems incorporating abalone and seaweeds. *A report for Nuffield Australia Farming Scholars, Nuffield Australia Project no. 914*
32. Nobre AM, Robertson-Andersson D, Neori A, Sankar K (2010) Ecological-economic assessment of aquaculture options: comparison between abalone monoculture and integrated mult-trophic aquaculture of abalone and seaweeds. Aquaculture 306:116–126
33. Neori A, Chopin T, Troell M, Buschmann AH, Kraemer GP, Halling C, Shpigel M, Yarish C (2004) Integrated aquaculture: rationale, evolution and state of the art emphasizing seaweed biofiltration in modern mariculture. Aquaculture 231:361–391
34. Bunting SW, Shpigel M (2009) Evaluating the economic potential of horizontally integrated land-based marine aquaculture. Aquaculture 294:43–51
35. Subandar A, Petrell RJ, Harrison PJ (1993) *Laminaria* culture for reduction of dissolved inorganic nitrogen in salmon farm effluent. J Appl Phycol 5:455–463
36. Ahn O, Petrell R, Harrison PJ (1998) Ammonium and nitrate uptake by *Laminaria saccharina* and *Nereocystis luetkeana* originating from a salmon sea cage farm. J Appl Phycol 10:333–340
37. Buschmann AH, Troell M, Kautsky N, Kautsky L (1996) Integrated tank cultivation of salmonids and *Gracilaria chilensis* (Gracilariales, Rhodophyta). Hydrobiologia 326(327):75–82
38. Chopin T, Yarish C (1998) Nutrients or not nutrients? That is the question in seaweed aquaculture… and the answer depends on the type and purpose of the aquaculture system. World Aquaculture Mag 29(31–33):60–61
39. Troell M, Rönnbäck P, Halling C, Kautsky N, Buschmann A (1999) Ecological engineering in aquaculture: use of seaweeds for removing nutrients from intense mariculture. J Appl Phycol 11:89–97
40. Ruokolahti C (1988) Effects of fish farming on growth and chlorophyll content of *Cladophora*. Mar Pollut Bull 19:166–169
41. Rönnberg O, Ådjers K, Roukolathi C, Bondestam M (1992) Effects of fish farming on growth epiphytes and nutrient content of *Fucus vesiculosus* L. in the Åland archipelago, northern Baltic Sea. Aquat Bot 42:109–120
42. Chopin T, Yarish C, Wilkes R, Belyea E, Lu S, Mathieson A (1999) Developing *Porphyra*/salmon integrated aquaculture for bioremediation and diversification of the aquaculture industry. J Appl Phycol 11:463–472
43. Folke C, Kautsky N (1989) The role of ecosystems for a sustainable development of aquaculture. Ambio 18:234–243
44. Soto D (2009) integrated mariculture, a global review. *FAO Fisheries and aquaculture technical paper 529*
45. GENESIS (2004) Development of a generic approach to sustainable integrated marine aquaculture for European environments and markets. (European Economic Community; IPS-2000-102)
46. ENVIROPHYTE (2009) Improvement of the cost effectiveness of marine land-based aquaculture facilities through use of Constructed Wetlands with *Salicornia* as an environmentally friendly biofilter and a valuable by-product. (European Economic Community; SME – 37162)
47. Neori A, Ragg NLC, Shpigel M (1998) The integrated culture of seaweed, abalone, fish and clams in intensive land-based systems: II. Performance and nitrogen partitioning within integrated abalone *Haliotis tuberculata* and macroalgae *Ulva lactuca* and *Gracilaria conferta* culture system. *Aquacultural Engineering* 17(4):215–233

Marine and Freshwater Fecal Indicators and Source Identification

Sandra L. McLellan[1], Alexandria B. Boehm[2], Orin C. Shanks[3]
[1]School of Freshwater Sciences, University of Wisconsin-Milwaukee, Milwaukee, WI, USA
[2]Environmental and Water Studies, Department of Civil and Environmental Engineering, Stanford University, Stanford, CA, USA
[3]National Risk Management Research Laboratory, United States Environmental Protection Agency, Cincinnati, OH, USA

Article Outline

Glossary
Fecal Indicator Definition
Introduction
Impact of Fecal Pollution on Coastal Waters

The Link Between Waterborne Disease and Fecal Pollution
Detection of Conventional Indicators
Viruses
Ecology of Pathogens and Indicators in the Environment
Estimating Risk of Pathogen Exposure Using Fecal Indicators
Epidemiological Studies
Rapid Methods for Indicators
Future Directions
Acknowledgments
Bibliography

Glossary

Alternative fecal indicators Fecal indicators that have not been fully validated for standard water quality methods, but show potential for increased sensitivity or specificity over current indicators.

Commensal The general meaning of this word is sharing of food and originates from the Latin word *cum mensa*, meaning "sharing a table." In the context of bacteria and host interactions, the bacteria benefit from the host without causing harm.

Enterococci The term "enterococci" is a general reference to members of the genus *Enterococcus*: however, in the context of water quality standards, enterococci often refers to *E. faecalis* and *E. faecium*, which can be enumerated using selective and differential media.

***Escherichia coli* (*E. coli*)** Gram-negative bacteria found in the gastrointestinal tract of almost all warm-blooded animals. These bacteria are easily cultured and can be enumerated using selective and differential media.

Fecal indicator A chemical or biological constituent that is found in fecal matter that can be used to demonstrate the presence of contamination.

Pathogen A microbe or microorganism such as a bacteria, virus, fungi, prion, or protozoan that causes disease in its animal or plant host.

Polymerase chain reaction (PCR) A scientific technique in molecular biology to amplify a single or few gene copies of a nucleic acid fragment across several orders of magnitude. Amplification results in the generation of thousands to millions of copies of a particular nucleic acid sequence.

Quantitative PCR A technique based on PCR which simultaneously amplifies and quantifies a targeted nucleic acid molecule.

Fecal Indicator Definition

Fecal indicators are organisms or chemical constituents found in fecal material or wastewater that can be measured to demonstrate the presence of fecal pollution. Fecal waste from humans and other animals can contaminant surface waters and pose a serious threat to the environment and human health. Fecal pollution serves as a vehicle for disease transmission including pathogenic bacteria, viruses, or protozoa. Fecal waste also carries with it harmless *commensal* organisms that live in the gastrointestinal (GI) tract and are often used as fecal indicators since they are present in high numbers. The type and amount of pathogens found in fecal pollution is dependent on the host source (human, agricultural animal, wildlife) and the prevalence of illness in the host population. Therefore, employing fecal indicators that provide information about human and other animal contributions is critical for estimating the likelihood that pathogens are present and for directing remediation efforts.

Introduction

Fecal indicators when detected demonstrate the presence of fecal pollution. Fecal indicators play an important role in regulation. Governmental agencies charged with the protection of human health use indicators to assess recreational water quality. In much of the developed world, *Escherichia coli* and *enterococci* are the organisms used for this purpose. Their quantitative link to human health risk in recreational epidemiology studies has led to development of water quality criteria to limit their concentrations in the USA and worldwide.

Conventional indicator methods focus on the cultivation of *E. coli* or enterococci cells isolated from an environmental sample. Culture-based methods are inexpensive and do not require extensive laboratory training to implement. However, these methods are time consuming, requiring 18–24 h to process samples. They also have other limitations such as the inability to

discriminate between different animal sources and the potential of indicator microorganisms to persist and sometimes proliferate in the environment. As new scientific discoveries provide a broader view of the different microbes or chemicals associated with fecal pollution and specific sources, new indicators are being identified. These indicators are often referred to as alternative indicators since they have not been fully validated for use for standard methods in water quality testing, but show promise to address some of the limitations associated with conventional fecal indicator approaches.

Some alternative indicators are common to all sources of fecal pollution and can be used as general fecal pollution indicators. Others are associated with a particular host or group of animals. Host-associated indicators are useful for fecal source identification approaches, which are aimed at improving estimates of potential health risk due to pathogens, or identifying major pollution sources that should be remediated. Alternative indicators may take the place of conventional indicators as technology advances. Technologies such as real-time *quantitative PCR* (qPCR), flow cytometry, and advanced chemical analyses can detect previously uncultured microbes or chemicals associated with fecal pollution.

Impact of Fecal Pollution on Coastal Waters

Coastal waters are a valuable resource. Fecal pollution of beaches is not only a threat to human health [13, 52, 98, 195, 258], but can also result in economic losses to surrounding communities [113, 197]. Within the USA, the ocean and Great Lakes coasts encompass more than 15,000 miles of coastline and are the home of economic and recreational centers and unique and rich ecosystems. Many coastal areas are stressed because of dense development and subsequent anthropogenic impacts (Fig. 1). Studies have shown that with increasing urbanization, there is an increase of fecal pollution in waterways [91, 151, 261]. Agricultural land use in upper reaches of watersheds also contributes to fecal pollution in tributaries that ultimately discharge into the ocean or the Great Lakes [24, 261]. Fecal pollution is the major cause of biological water quality impairment in the USA and is the primary cause of recreational beach advisories and closing [252]. Currently, fecal pollution impacts are determined by measuring fecal indicator bacteria using conventional, culture-based approaches. In 2009, there were 18,682 advisories and closures at 2,876 beaches in the USA that are routinely monitored for fecal pollution.

The Link Between Waterborne Disease and Fecal Pollution

Fecal pollution may contain pathogens that can cause disease in humans. To date, there are more than 150 different agents of disease that can be considered waterborne pathogens. This list grows each year as additional emerging pathogens are identified. Table 1 lists common waterborne pathogens and their major host reservoirs. The primary reservoir of human viruses is humans themselves because viruses by nature are host specific; however, animal viruses may also be a concern if they are able to replicate in human hosts. Recent research has identified pigs as a reservoir of hepatitis E virus [99]. Sewage may contain high concentrations of human viruses and some studies have performed surveillance of the viral diseases in the community by monitoring sewage [213, 214]. Some pathogens are predominately found in nonhuman animal hosts, but if humans become infected, person-to-person or waterborne transmission may occur.

Exposure to contaminated water and potential waterborne pathogens most notably causes enteric illness, but skin, ear and eye, or respiratory illnesses may also occur [27, 39, 65, 141, 195, 258]. Many waterborne disease agents are passed through the fecal-oral route, so any activities that involve ingesting contaminated water present a health risk. Ingesting contaminated seafood may also result in exposure to waterborne pathogens (Table 2). For respiratory diseases, inhalation of water droplets or direct contact with mucus membranes can expose a person to a disease-causing agent. Direct contact of contaminated water with wounds could result in an infection.

Recreational waters are of particular concern because swimmers can come into direct contact with contaminated water. Shellfish beds can also be impacted by fecal pollution and are regularly

Marine and Freshwater Fecal Indicators and Source Identification. Figure 1
Plume of river water released into Lake Michigan from the Grand River (Photo provided by Dr. Philip Roberts, Georgia Institute of Technology)

Marine and Freshwater Fecal Indicators and Source Identification. Table 1 Common pathogens responsible for enteric illnesses

Agent		Major sources	References
Viruses[a]			Reviewed by Fong and Lipp [76]
	Enteroviruses	Human	[32, 91, 122, 125, 167, 178]
	hepatitis A	Human	[86, 91, 122]
	Adenoviruses	Human	[51, 108, 122, 124, 125, 271, 273]
	Norovirus	Human	[17, 91, 263, 273]
	Rotavirus	Human	[85, 202]
	Astrovirus	Human	[47, 194]
Bacteria			
	Pathogenic *E. coli*	Humans and animals[b]	[5, 102, 109, 171, 260]
	Shigella	Humans and animals	[118]
	Vibrio cholerae	Humans and environment	[129, 130, 147]
	Campylobacter	Animals and humans	[8, 33, 112, 183, 254, 260, 270]
	Salmonella	Animals and humans	[21, 100, 144, 254]
	Yersinia enterocolitica	Animals	[104, 205]
	Aeromonas	Environment	[192, 215]
	Plesiomonas	Environment	[11, 166, 203]
	Vibrio parahemolyticus	Environment	[55, 127, 254]
Parasites			
	Cryptosporidium parvum	Animals and humans	[90, 112, 144, 149, 270]
	Giardia lamblia	Animals and humans	[90, 112]
	Entameba histolytica	Animals and humans	[152]

[a]Humans are the predominate source of human viruses, but in some cases, transmission from animals to human is possible. For example, this is suspected to be possible for hepatitis E [99], a calicivirus in the same virus family as norovirus
[b]Animals are the primary reservoir of *E. coli* O157:H7 [46], one strain of shiga-toxin-producing *E. coli*

monitored to assure that harvested shellfish has not been subjected to contamination. In the Great Lakes, nearshore coastal waters are a drinking water source to nearly 40 million people. Stringent treatment requirements provide safe drinking water, but both source water and treated drinking water are closely monitored for evidence of fecal pollution to assure that treatment protocols are adequate. For a more complete discussion of this topic, see Chaps. 3–5 of this volume.

Important Attributes of Indicators. Fecal indicators can either be general indicators of fecal pollution or associated with a particular animal source. Many watersheds and coastal waters have mixed land use; therefore, both general fecal indicators and source-associated indicators have an important role in assessing water quality. Ideally, fecal indicators should be present in high levels in fecal pollution so that they can be used as a sensitive measure of the level of contamination when diluted to small concentrations in the environment. Fecal indicators should provide information about host source contribution when possible, whether it is from humans, or different agricultural animals or wildlife. Detection methods should be relatively simple and affordable considering

Marine and Freshwater Fecal Indicators and Source Identification. Table 2 Common pathogens responsible for respiratory illness and skin infections

Agent		Primary source	References
viruses			
	Adenovirus	Humans	[51, 108, 122, 124, 125, 271, 273]
Bacteria			
	Vibrio parahemolyticus	Environment	[55, 127, 254]
	Vibrio vulnificus	Environment	[187, 264]
	Leptospira	Animals (wildlife)	[96, 236]
	Legionella spp.	Environment	[82, 186, 236]
	Staphylococcus aureus	Humans	[48, 49, 88, 254]

For an expanded list, please see [27, 168]

that much of the hands-on monitoring is done by local health departments. Methods should lend themselves to rapid testing so that beach notification can happen in a timely manner.

Clearly, no single indicator can meet all of these goals. Therefore, it is critical to have multiple indicators that can be used in concert if needed. Different indicators will behave differently in various environments, e.g., marine waters versus freshwater [9, 92, 180, 227, 229]. Certain indicators may be appropriate for investigating sources of fecal pollution, or setting remediation goals, whereas others are better suited for rapid detection for recreational water quality monitoring for any fecal pollution present. Water resource managers, public health officials, and researchers must work together to identify what information is needed and choose the most appropriate indicators. For example, *E. coli* is recommended for freshwater, but it has a very short half-life in the open waters of the Great Lakes [160]; therefore, highly persistent indicators such as *Clostridium perfringens* may be more useful for long-term monitoring [71, 146, 169]. Enterococci qPCR is being developed for rapid beach testing [93, 106], but is a general indicator and host-associated indicators within the order *Bacteroidales* may be more useful for identifying sources [31, 72, 236].

Important Attributes of Fecal Indicators
Routine monitoring: Specific for fecal pollution
Present when pathogens are present
Correlate well to illnesses
Easy to quantify
Simple and cost-effective methodology
Behave in the environment in the same manner as pathogens
No growth outside of the host environment
Amenable to rapid detection methodologies
Investigations: Specific for a source of fecal pollution
Sensitive, e.g., present in high numbers in most animals with a given source
Known or predictable ecology
Known or predictable relationship to pathogens

Detection of Conventional Indicators

Common fecal indicators that are used for water quality monitoring or recreational beaches are listed in Table 3. All of these indicators were originally identified as constituents of fecal pollution using selective and differential culture techniques. The earliest methods data back to late 1800s and early 1900s [14, 66] for coliform bacteria. There are two culture approaches for enumerating bacteria in water samples. The most probable number (MPN) methods involve culture-based detection in liquid broth using a series of dilutions. The dilutions in which organisms are detected can be used to calculate a statistical estimate of *enterococci* concentration for that sample. The second approach involves filtering samples through a membrane filter. The filter is transferred to solid selective media that is optimized for the growth of the target organisms and inhibitory for other organisms. Various chromogenic substrates or pH indicators can be incorporated to make the media differential for fecal indicator microorganisms. A review of conventional and novel indicators can be found in Edge and Boehm [69].

Marine and Freshwater Fecal Indicators and Source Identification. Table 3 Historic and conventional fecal indicators

Organisms	Use	Limitations
Total coliforms	Early indicator used in surface waters, currently in use for drinking water[a] since detection of total coliforms provides information on general sanitation	Not specific for fecal pollution
Fecal coliforms	Used for recreational waters until late 1980s or 1990s in some US states, still in use as a standard for wastewater, recreational waters, and shellfish	Some fecal coliforms can grow in the environment
E. coli	Currently recommended by the USEPA for fresh recreational waters[b]. Replaced fecal coliforms as a more specific indicator of fecal pollution	More specific than fecal coliforms, but has been reported to persist and grow in the environment [7, 117, 134, 265]
Fecal streptococci	Early indicator for surface water quality	Not all are fecal specific
Enterococci	Currently recommended indicator for marine recreational waters. Replaced fecal streptococci	General indicator; some grow in the environment
Clostridium perfringens	Proposed in 1963 as an indicator of wastewater and receiving waters. Used in some European countries but not the USA	May survive for long periods in the environment.

[a]Total coliforms (TC) are used since they are a good measure of bacteriological contamination, regardless of fecal or environmental sources. New proposed rules would change the standard from TC to *E. coli*, e.g., more specific for fecal pollution

[b]Criteria are being revised; new criteria will be based on detection of enterococci by culture or qPCR (total *Bacteroides*)

Culture-based methods continue to be widely used for detection of fecal indicator bacteria; however, the time required to obtain a result is a major limitation of these methods for providing rapid (e.g., 4 h) results of beach water quality to assure timely public notification. Molecular methods such as qPCR can be used for detection of traditional fecal indicators [106, 182, 267].

Coliforms. Coliform bacteria are a group of bacteria that were the first indicators of fecal pollution. Coliforms are gram-negative, rod-shaped, facultatively anaerobic, non-spore-forming bacteria found in warm-blooded animals, as well as in soil, water, and vegetation. Coliforms are not a specific taxonomic group of bacteria, but are classified based on a number of characteristics. These organisms are identified by fermentation of lactose with the production of acid and gas at 35–37°C. Coliforms are also negative for cytochrome oxidase and positive for β-galactosidase. Coliforms are measured by using an MPN [16] or by enumeration of colony-forming units (CFU) using membrane filtration and selective and differential media such as MI [249]. These organisms generally are within the family *Enterobacteriaceae* and include the genera *Citrobacter*, *Escherichia*, *Enterobacter*, *Hafnia*, *Klebsiella*, and *Serratia*. Coliform bacteria were one of the earliest indicators of water quality used in the USA, with individual states setting limits of 50–2,400 coliforms per 100 ml of water as a standard for recreation waters in the 1950s and 1960s [66].

Fecal coliforms. Fecal coliforms are a subgroup of coliforms and refer more specifically to coliforms derived from feces. Like coliforms, they are not a specific taxonomic group; they are based upon several morphological and physiological characteristics. These are defined by the same criteria as coliforms, but are thermotolerant and will grow at 44.5°C. *E. coli* is one of the major fecal coliforms found in feces, in addition to members of *Klebsiella*, *Enterobacter*, and *Citrobacter*. The designation of fecal coliforms was intended to improve specificity; however, some organisms included in this group can be found free living in the environment, most notably *Klebsiella* [42, 83, 177]. Beach water samples have also been found that have evidence of fecal coliforms that have replicated in the environment [158].

The first national water quality criterion for recreational waters was based upon fecal coliforms. In 1968, the National Technical Advisory Committee, commissioned by the Federal Water Pollution Control Administration (now referred to as the Environmental Protection Agency), determined that 400 fecal coliforms per 100 ml corresponded to an adverse GI health effect [66]. Subsequent recommendations stated that for recreational waters, within a 30-day period, the geometric mean should not exceed 200 fecal coliforms per 100 ml, and 10% of the samples should not exceed 400 fecal coliforms per 100 ml. Fecal coliforms are no longer used for recreation waters in most states, but the basis of the 1968 criteria is still used for regulating water quality of wastewater treatment plant effluents and for assessing river water quality. Fecal coliforms are also still used for shellfish testing (water overlying the reefs and oyster meats).

Escherichia coli (E. coli). *E. coli* is a fecal coliform that has been suggested to be more specific for fecal pollution than testing for the group of fecal coliforms and was recommended as an indicator for freshwater in 1986 by the United States Environmental Protection Agency (USEPA) [14, 247]. *E. coli* are present in the GI tract of most warm-blooded animals, and therefore a general indicator of fecal pollution. *E. coli* is a thermotolerant coliform that produces indole from tryptophan and it can be differentiated from other microorganisms based on β-glucuronidase activity. Selective and differential media tests for this activity using methods based on membrane filtration, modified mTEC [248], or MPN approaches such as the Colilert manufactured by IDEXX [68] are commonly used to identify *E. coli* in surface water samples. One testing methodology simultaneously detects coliforms and *E. coli* using β-galactosidase and β-glucuronidase activity, respectively, as discriminators [249]. Some epidemiology studies have shown a relationship between *E. coli* densities and GI illness [65, 195]. *E. coli* has some limitations as a fecal indicator at recreational beaches because it has been shown to persist and even grow in some aquatic environments, thereby potentially interfering with the relationship between *E. coli* and recent fecal pollution events [7, 26, 134, 265].

Enterococci. Enterococci are gram-positive cocci and are nearly universally present as commensal organisms in the intestine of human and nonhuman animal hosts. The most common species in human hosts are *E. faecalis* and *E. faecium* [58, 139]. The enterococci are a subgroup of the fecal streptococci. Fecal streptococci have also been referred to as Group D streptococci according to Lancefield serotyping. The fecal streptococci have historically been used as fecal indicators and include species from two genera: *Enterococcus* and *Streptococcus*. There are two *Streptococcus* species in the fecal streptococci group – *Streptococcus bovis* and *Streptococcus equinus* – that have been shown to survive poorly in water. Hence, in water, fecal streptococci and enterococci are thought to be equivalent [116].

In the USA and the EU, enterococci are used for monitoring marine bathing waters because epidemiology studies have linked their concentration to human health outcomes [256]. The standards are tied to approved culture-based methods for their quantification: multiple-tube fermentation, membrane filtration, and defined substrate assays. Clesceri et al. (1998) describe a multiple-tube method where azide dextrose broth is used followed by confirmation with Pfizer selective *Enterococcus* (PSE) media and brain-heart infusion broth with 6.5% NaCl. Both the EU and the USA have approved the use of defined substrate assays manufactured by IDEXX for the quantification of enterococci (Enterolert and Enterolert-E). The USEPA-approved method 1600 utilizes membrane filtration onto mEI media for quantification [250]. Studies that have compared these culture-based methods for quantifying enterococci often find the methods yield slightly different results [32].

The USEPA has developed a qPCR assay for the enumeration of enterococci which has been compared to membrane filtration results [106, 253]. Enterococci measured via qPCR often yield higher concentrations than culture-based measurements since it enumerates both live and dead bacteria [32]. Enterococci measured by qPCR have been linked to human health outcomes in epidemiology studies of marine and fresh water beaches [257–259]. Ongoing work is focused on better defining these links. As the USEPA formulated new recreational water quality criteria, qPCR for enterococci is expected to be included as a rapid method which allows beach managers and public health

workers to post water quality advisories on the same day the sample is taken.

Clostridium perfringens. *C. perfringens* is member of the phylum *Firmicutes* and is a gram-positive, low GC content organism. *C. perfringens* was suggested as a potential indicator in 1963 [34], and gained acceptance in EU countries, but it was not chosen for use in the USA because it survives for long periods of time in the environment [14, 66]. Epidemiology studies report a relationship between *C. perfringens* and illness [268], while other studies found no relationship [39]. However, *C. perfringens* has been shown to be a useful fecal indicator in certain environments where other indicators are highly modulated by environmental factors. Studies in tropical waters suggested *C. perfringens* is a better indicator compared with fecal coliforms because it is a spore-forming organism and does not replicate in the environment [79, 80]. Because of its spore-forming ability, *C. perfringens* has been used as a tracer of long-term fecal pollution impacts in marine and freshwater systems [36, 54, 70, 110, 169]. *C. perfringens* has also been suggested as a good indicator in the open waters of the Great Lakes because it can serve as a conservative tracer of fecal pollution and may mimic protozoan cyst or oocyst survival [164, 169, 191].

Alternative indicators. Ongoing research studies have identified a broad array of new potential indicators of fecal pollution. Molecular-based methods have made possible the characterization of organisms that previously were either not recognized as associated with fecal pollution, or were difficult to detect due to complex cultivation requirements. Alternative indicators may also employ unique chemical constituents. Alternative indicators are being developed as general detection of fecal pollution, such as total *Bacteroides* [53, 59], as well as source identifiers associated with a particular animal group (Table 4).

Different sources of fecal pollution can contribute different types and concentrations of pathogens (Table 1 and Table 2). For example, human fecal sources, particularly sewage, contain waste from a large number of people and are considered a primary source of human enteric viruses. *Cryptosporidium* may be associated with cattle waste. Fecal indicators that provide information about the source will improve our ability to estimate the health risk due to pathogens as well as direct remediation efforts to major contributing sources of fecal pollution. The development of qPCR methodology has also advanced simple presence/absence detection to quantitative estimates of fecal pollution and provides a platform for the implementation of rapid methods.

16S rRNA gene targets. Many of the alternative indicators that have been described are based on detection of the organisms based on the 16S rRNA gene sequence. This gene is highly conserved among bacteria and has been used extensively to assign taxonomy.

Bacteroidales. Members of the order *Bacteroidales* are potentially useful indicators of fecal contamination because they generally are found in high numbers in fecal material of humans and other warm-blooded animals and are unlikely to survive in the beach environment [74, 136]. Early studies identified unique sequences in the *Bacteroides* 16S rRNA gene from human and ruminant *Bacteroides* species that are associated with respective fecal pollution sources [24, 136]. Sequencing of clone libraries demonstrated that sequences of members of the broader *Bacteroidales* group, rather than exclusively *Bacteroides* spp., are amplified with primers originally targeting total *Bacteroides* spp. [60]. Subsequent studies have used taxon-specific cloning to characterize *Bacteroidales* populations within humans and different animals and have identified a broad range of host-associated genetic markers [25, 60, 75, 78, 121, 133, 137, 138, 153, 165, 184]. Since culture techniques for isolation of these anaerobic bacteria are difficult to perform, molecular techniques have been developed to amplify, detect, and in some cases quantify the 16S rRNA genes of *Bacteroides* spp. from feces and ambient water [53, 59, 133, 153, 218, 262]. Many of these assays utilize the HF183 sequence first reported by Bernhard and Field [25]. The utility of the genetic markers has been tested extensively in fecal impacted environments, including beaches [1, 37, 84, 181, 207, 216]. In addition, numerous studies report information on the distribution of these host-associated genetic markers in target and non-target populations [3, 64, 133, 138, 143, 185, 224, 225, 228], relationship to pathogens [208, 209], and the decay of these genetic markers in marine and freshwaters [20, 61, 184, 210, 261].

Bifidobacterium. This genus represents another group of GI bacteria with particular species reported

Marine and Freshwater Fecal Indicators and Source Identification. Table 4 Examples of biological *alternative fecal indicators* that provide animal host information

	(Notes)	References
Organisms – 16S rRNA gene		
Bacteroidales	*Bacteroidales* associated with hosts have been identified	[25, 60, 75, 78, 133, 137, 138, 153, 165, 184]
Bifidobacterium		[35, 64, 148, 173]
Methanobrevibacterium	Member of Archaea and dominant in the GI	[128, 243–245]
Faecalibacterium		[161, 279]
Lachnospiraceae		[161, 175]
Ruminococcace		[161]
Functional genes		
esp gene in enterococci	Gene responsible for attachment on human epithelial cells	[93, 212]
Toxin genes in *E. coli*		[50, 131]
Beta-glucuronidase	Polymorphisms in this gene have been linked to different host types	[200]
Unknown genes/regions		
Cattle and human markers	Identified by genomic fragment enrichment	[220, 221]
Gull marker	Identified by subtractive hybridization	[101]
Phenotypes		
Antibiotic resistance of standard fecal indicators	Based on the theory that host exposed to antibiotics will have a higher percentage of antibiotic-resistant *E. coli* or enterococci	[97, 105, 188, 269]
Viruses		
F+ coliphage	Type I and IV associated with animals and II and III associated with humans	[114]
Bacteroides phage		[12, 126, 240]
Adenovirus, enterovirus, polyomaviruses	Viruses are host specific by nature, and therefore, detection of human viruses demonstrates human sources are present.	[6, 123, 162, 179, 193]

to be associated with human fecal pollution including *B. adolescentis*, *B. dentium*, and *B. longum* [35, 148, 155, 173]. Several technologies targeting *Bifidobacterium* genes are reported for multiplex PCR detection [35] and qPCR [150, 154]. *Bifidobacterium* typically occur at lower concentrations than *Bacteroidales* making them harder to detect in dilute ambient water samples [219] and exhibit a rapid decay based on bench-scale survival studies [201]. Thus, the detection of a *Bifidobacterium* host-associated genetic marker in a polluted water sample suggests a recent, high concentration contamination event.

Faecalibacterium. This genus of bacteria has been reported in humans and other animals and has been suggested as a potential target for development of host-associated genetic markers [81, 161, 246, 279]. Sewage and cattle have been shown to have a high abundance of *Faecalibacterium* [161, 226]. Additional characterization of this group is needed to characterize phylotypes that are associated with specific animal sources.

Lachnospiraceae. *Lachnospiraceae* are found in high abundance in human fecal samples [57, 77, 242], sewage [161], and cattle [226]. *Lachnospiraceae* are included in the group *Clostridium coccoides* [107, 150].

The proportions of *Lachnospiraceae*, *Bacteroides*, and *Bifidobacterium* of the human microbiota vary among different animal species, and quantification of these proportions has been proposed as a method for fecal pollution source identification [81]. Additional characterizations of this group are needed to characterize phylotypes that are associated with specific animal sources [161].

Gene product targets. Molecular methods have also allowed for detection of genes that serve a functional role in the organism. In some cases, the function may be linked to specific host microbe interactions, making these genetic markers potentially good host-associated alternative indicators [221]. Genetic markers have been identified with a variety of molecular methods, including subtractive hybridization, genome fragment enrichment, and other metagenomic approaches.

Toxin genes *of* E. coli. Specific subpopulations of *E. coli* contain genes coding for toxins, including heat-labile enterotoxin (LT) and heat-stable enterotoxin (ST). *E. coli* carrying toxins are generally clonal populations that are found within certain animal reservoirs and have been suggested as host-associated indicators. Specific sequences of the STII toxin gene were found to be associated with swine, but not present in sewage or dairy farm lagoons [132]. Cattle-associated LTIIa has also been reported [50, 131]. These toxin genes have a worldwide distribution [72]. The occurrence of *E. coli* positive for STII or LTIIa can be low in agricultural animal populations, potentially limiting the use of these genes for the identification of specific animal sources.

Esp *gene*. The enterococcal surface protein (*esp*) gene is a putative virulence factor in *Enterococcus faecium* that has been shown to be associated with enterococci from human origin [212]. Because this gene occurs at a low frequency, original detection methods involved an enrichment step where DNA is extracted from enterococci grown on selective media, followed by PCR. Comparison studies have shown the *esp* gene in enterococci to correlate with other human-associated genetic markers [4, 163] and this alternative indicator has been employed in numerous field studies [275]. Newer methods employ qPCR that can directly detect the *esp* gene [2].

gyrB. The genetic locus *gyr*B is a housekeeping gene (e.g., common to all bacteria because of a central function). Similar to 16S rRNA gene loci, housekeeping genes are generally highly conserved and therefore useful for identifying specific phylotypes. One study employed qPCR targeting *gyr*B in *Bacteroides fragilis* as an indicator of human specific fecal contamination [142].

Methanogens. *Methanobrevibacter smithii* is a dominant Archaea in the human gut [67]. The *nif*H gene of this organism has been used as a human-associated indicator [243]. Similar assays employing the same gene in *Methanobrevibacter ruminantium* have been developed [245]. Assays for quantification of the *nif*H target have also been developed [22, 128]. An Archaea genetic marker may prove useful because it may have a different survival or ecology compared with bacterial indicators and pathogens.

Bacteroides thetaiotaomicron. *B. thetaiotaomicron* is found in high numbers in humans compared with other animals and is described as a niche organism in the human gut [274]. A genomic fragment that was generated with universal primers as a second unexpected amplicon was found to distinguish *B. thetaiotaomicron* from other animal species [241]. PCR primers specific for *B. thetaiotaomicron* were developed based on the sequence of this 547-bp genomic fragment and have been tested against a number of fecal samples from humans and nonhuman sources [45, 241]. A putative gene for complex polysaccharide degradation has also been used as a genetic marker for qPCR since the trait is hypothesized to be involved in host-associated metabolic pathway [277].

Metagenomics. The majority of host-associated genetic markers available to date target the 16S rRNA gene from a limited number of different microorganisms. Advancements in DNA sequencing and sorting technologies now allow researchers to survey the entire genome of all members of fecal microbial community. Different strategies include the use of competitive hybridization approaches [101], microarrays [145, 272], and 454 pyrosequencing [161, 226, 246]. Whole genome and community approaches vastly expand the number of candidate source-associated genetic markers and may allow for the development of even more refined source identification methods.

Viruses

F specific (F^+) coliphages. F^+ coliphage RNA coliphages have serologically distinct groups that predominate in humans (groups II and III) which are distinct from those commonly found in other animals (group I and IV) [114]. Comparison studies of different alternative indicators suggest F^+ coliphage types are reliable indicators of host sources, but the groups are not exclusive to either animal or human sources [28, 180]. Further, differential survival may influence source identification in natural waters and may need to be taken into account in interpreting source identification studies [38, 172]. However, viral indicators may correlate more closely to human viral pathogens as they may have a similar ecology in the environment.

Bacteroides *phages*. Phages infecting *B. fragilis* and *B. thetaiotaomicron* have been used as indicators of human fecal pollution [12, 126, 240]. Differential ability of host strains of *Bacteroides* to detect phages from different sources has been reported [196], as well as geographic variability. Culture methods have been developed to isolate diverse host *Bacteroides* strains [190]. In survival studies, two *B. fragilis* phages were shown to survive longer in seawater compared to MS2 coliphage [157].

Human polyomaviruses. Human polyomaviruses are widespread among human populations and have been suggested as indicators of human waste [6, 162]. This virus is excreted in the urine and therefore may be detected in the absence of human feces. Studies have compared detection of human polyomaviruses with detection of human *Bacteroides* HF183 genetic marker and enterococci carrying the *esp* gene and found a strong correlation [4, 163].

Chemicals. Chemical methods do not detect fecal bacteria. Instead, these methods are designed to detect chemical compounds associated with human activities or sanitary sewage. Chemical indicators may provide additional evidence as to source [87, 95]. These chemicals are often found in sewage treatment facility discharges and septic tank effluent. For example, optical brighteners are commonly found in laundry detergents and have been used to indicate the presence of human fecal pollution in environmental waters [41, 62]. Fecal sterols such as coprostanol are also reported to be associated with human fecal pollution [28, 115, 176, 239]. Other potential chemical fecal indicators include antibacterial compounds, pharmaceuticals, and caffeine [95, 278] (Table 5).

Quantification of Bacterial Indicators Using qPCR. Conventional or endpoint PCR allows for the selective amplification of a particular genetic marker at extremely low concentrations even in the presence of a mixture of heterologous DNA targets making it ideal for environmental applications. The final result of an endpoint PCR method is either the presence or absence of the DNA target. Even though the qualitative determination of fecal pollution in a water sample can be very useful information, researchers quickly recognized the added advantage of generating quantitative data. The ability to estimate the concentration of a DNA target in a known volume of water provides a means to investigate relationships between the concentration of a fecal indicator genetic marker and numerous factors such as illness rates in swimmers or efficiency of waste management practices.

qPCR relies on the continuous monitoring of PCR product accumulation as amplification occurs. Estimation of the concentration of a genetic marker is based on the theoretical premise that there is a log-linear relationship between the starting amount of DNA target in a reaction and the fractional thermal cycle where PCR product accumulation is first significantly detectable (Table 2); for review see [204]. qPCR applications designed to estimate fecal bacteria concentrations in recreational waters are gaining widespread attention due to the rapid nature of these methodologies (same day results), reports linking the occurrence of DNA targets to public health risk [106, 257, 258],

Marine and Freshwater Fecal Indicators and Source Identification. Table 5 Chemical alternative fecal indicators

Chemical constituents
Fecal sterols
Optical brighteners
Caffeine
Personal care products and pharmaceuticals

and the development of host-associated fecal source identification assays [40, 133, 135, 138, 163, 185, 218, 222, 223]. However, there are many technical concerns that must be addressed before these qPCR applications are ready for implementation.

It is important to recognize that a qPCR method consists of several protocols linked in succession including sample collection, sample preparation, nucleic acid purification, target amplification, and data interpretation. Each of these steps plays a critical role in the successful estimation of a DNA target concentration in an environmental sample. In addition, the extremely high level of sensitivity make qPCR methods highly susceptible to cross-contamination during field sampling, nucleic acid purification, and genetic marker amplification (Fig. 2). As a result, numerous studies have been conducted to address issues such as density and distribution of genetic markers in primary and secondary sources [60, 133, 199, 224, 225, 228], sample matrix interference during qPCR amplification [140, 198, 224, 255], estimating decay rates of DNA targets in ambient water [18, 23, 184, 261], loss of target DNA during nucleic acid recovery [106, 170, 238], and selection of a mathematical model to transform raw qPCR data into an estimation of concentration [230, 231].

Microbial Source Identification. Identification of the sources of fecal pollution is important for both developing remediation strategies and for estimating the likelihood of pathogen occurrence. In most cases, the source of fecal pollution in a water body of interest is originally measured because of high amounts of conventional general fecal indicators (i.e., enterococci or *E. coli*). Methods and study designs for source identification, also referred to as "microbial source tracking" (MST) or "fecal source identification" (FSI), has been reviewed extensively [72, 206, 237].

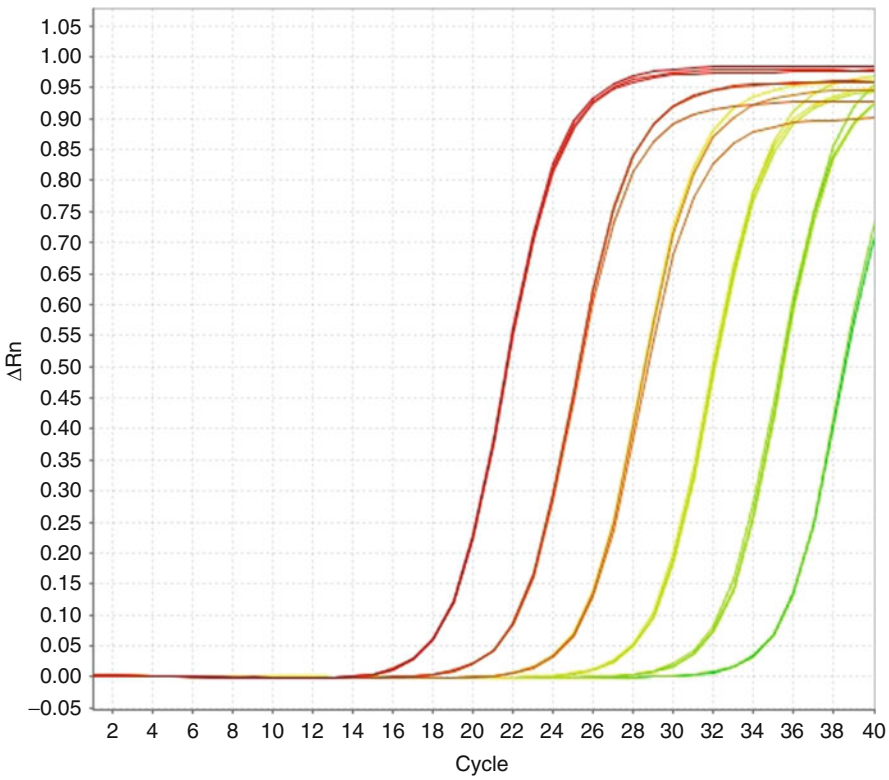

Marine and Freshwater Fecal Indicators and Source Identification. Figure 2
Quantification of real-time polymerase chain reaction (qPCR) product can be achieved by observing an increase in fluorescence, indicating product formation, in relation to cycle number

Identifying fecal pollution sources involves understanding both the physical location of the inputs and the contributing host sources. Most source identification studies begin with spatial and temporal sampling since fecal pollution sources are rarely constant and the locations of inputs are not always obvious. Following release into the environment, the ecology of fecal indicators is greatly influenced by the residence time, type of water body (e.g., marine or freshwater, oligotrophic, or nutrient rich), predation, or even potential growth by some conventional indicators [31, 236]. Therefore, it is very difficult to take one or two samples and determine the major source contributing fecal pollution to an impacted body of water.

Spatial and temporal surveys are complemented by using alternative indicators that can provide information as to the host source of fecal pollution. Often, a first tier assessment will involve distinguishing human versus nonhuman fecal pollution [89, 181]. Cross reactivity needs to be considered, along with geographic relevance of a particular indicator. The possible fecal pollution sources within the watershed need to be considered when choosing the most appropriate alternative indicators. The use of alternative indicators for microbial source identification has been reviewed extensively [20, 72, 73, 206, 211, 235, 237].

Early approaches to microbial source identification focused on library-based methods, where either phenotypic traits or genotypes of indicator bacteria were characterized from a particular source and then compared to what was found in surface waters. Methods for characterizing *E. coli* or enterococci have included antibiotic resistance, ribotyping, and repetitive extragenic palindromic PCR [43, 44, 63, 103, 105, 159, 189, 217, 269]. There are multiple complications in using library-based methods that include applicability of the library across geographic locations, specificity of *E. coli* or enterococci indicators to a particular animal host, and complex genetic relationships among these indicators [10, 72, 159, 206, 236]. Further, creating a library is expensive and multiple water samples need to be analyzed because fecal pollution inputs are usually driven by storm events and can involve multiple animal sources. Most source identification methods have moved to marker-based, or non-library dependent, approaches. Marker-based approaches involve utilizing a chemical or biological constituent that is commonly found in the fecal pollution source of interest, in high abundance so that it can be detected easily and associated with a specific human or animal source (Figs. 3 and 4).

Ecology of Pathogens and Indicators in the Environment

The identification of a host-associated marker of fecal pollution goes beyond microbiology. Once the fecal indicator is discharged into the environment, it becomes necessary to understand the various fate and transport mechanisms that control the concentrations of indicators and pathogens at the point of sampling.

Fate processes include dark or photo-inactivation [32], growth [111], sorption and desorption to sediments [19, 94], and grazing by zooplankton [30]. Inactivation has received the most attention of these fate processes. Although a fair amount of work has examined the interaction of pathogens and indicators with sediments, the work has primarily been focused on porous media, and simplified conditions. More work on the interactions of microbial pollutants and sediments and particles in surface waters is needed, particularly given the widespread occurrence of some indicators and pathogens in sediments and beach sands [7, 26, 56, 117, 265, 275].

Transport processes that control indicator and pathogen transport in surface waters include advection and dispersion of waterborne organisms. These processes are fairly well understood [174] and once determined in a particular surface water, they can be used to model microbial pollution. The resuspension and deposition of sediment-bound organisms is more complicated. Some work has examined these processes for *E. coli* [119, 120] and fecal coliforms [234] in streams and lagoons. Yamahara et al. [275] present a conceptual model for how enterococci in beach sands are suspended into the water column. A better mechanistic understanding of how organisms in the sediment or sand are transported into the water column is warranted.

Of the fate and transport processes described above, perhaps the most important to consider when choosing an indicator for microbial source identification is the time scale of inactivation and its tendency to sorb to sediments. For example, if the goal is enterococci

Marine and Freshwater Fecal Indicators and Source Identification. Figure 3
Stormwater outfalls introduce fecal pollution from domestic pets and wildlife into rivers. Stormwater systems can also become contaminated with human sewage from leaking sanitary sewer systems (Photos provided by Dr. Sandra McLellan, University of Wisconsin-Milwaukee)

Marine and Freshwater Fecal Indicators and Source Identification. Figure 4
Large gull populations are common non-point sources of fecal pollution on beaches (Photos provided by Dr. Sandra McLellan, University of Wisconsin-Milwaukee)

source identification for designing remediation strategies, then ideally, the persistence of the genetic marker will mirror that of enterococci. A health-protective goal may be to have no feces present in a water body. If this is the case, then a source identifier with very long-persistence may be needed. A source identifier that interacts strongly with sediments may be problematic as it may allow sediments to become a secondary, environmental source of the marker. Generally, sediments are believed to be a protective environment for microorganisms, particularly bacteria, where they may persist or even grow [276]. Future work on source identifiers will need to document the importance of sorption and interactions with sediments in general.

Estimating Risk of Pathogen Exposure Using Fecal Indicators

Using fecal indicators to link the presence of fecal pollution to waterborne disease risk is challenging. The types of pathogens that might be present will depend primarily on the source of fecal pollution. For example, sanitary sewer discharges (human sources) may contain high levels of human viruses, whereas wildlife is less likely to carry human viruses, but may contain protozoan and bacteria that can infect humans. Comprehensive models that integrate data from several research fields such as occurrence of pathogens in fecal sources, dose–response relationships, source identifier decay behaviors, acceptable health risk, and route of transmission can be used to estimate risk and are termed quantitative microbial risk assessment (QMRA) [15, 232, 233]. The type of pathogen present will also depend on the prevalence of the disease-causing agent within the population at the time of contamination. Many human viruses are seasonal, and protozoans such as *Cryptosporidium* are prevalent during certain times of the year, such as spring when calves can shed high concentrations of this microorganism.

Factors that Diminish the Relationship Between Indicators and Pathogens
Seasonality of certain pathogens
Rate of infection in the host reservoir (herd, human population)
Differential decay
Differences in transport
Differences in sedimentation rates and partitioning to soil, sand, and sediments

Epidemiological Studies

Epidemiology studies have been conducted around the world to understand the correlative relationship between indicator concentrations and human health. The studies that have been conducted to date, and their methodologies, are summarized by Boehm and Soller (see ► Recreational Water Risk: Pathogens and Fecal Indicators. Most of the studies have focused on the health effects of recreational exposure to human fecal contamination from publicly owned treatment work discharges. These studies generally show a statistically significant correlation between enterococci and GI illness [256] in marine waters and *E. coli* and GI illness at freshwater beaches. Epidemiology studies are the cornerstone of the USA and EU water quality criteria and directives [31]. Acceptable illness rates are anchored to concentrations of indicator organisms in order to set acceptable contaminant levels. In the USA, 19 illnesses per 1,000 people is the acceptable illness level for marine water recreation, and in freshwater, the acceptable level is 8 illnesses per 1,000 people.

There are several important knowledge gaps in the understanding of how fecal contamination in recreational waters affects human health [31]. Few studies have documented the human health effects from exposure to nonhuman sources of fecal contamination including, but not limited to, bird and dog feces and urban and agricultural runoff [52, 98, 156]. A review of these studies suggests the relationship between indicator concentration and recreational waterborne illness risks is equivocal. Current studies with QMRA are trying to more fully understand the risks for exposure to animal feces in recreational waters [233].

Fecal Indicator Applications. There are numerous applications for fecal indicators and indicators need to be chosen that best serve a specific purpose or goal. One primary purpose of an indicator is to evaluate the public health risk for recreational water. In this case, general indicators may be employed since beach managers will need to know if fecal pollution is present and at what

level. Since the presence of pathogens is highly dependent on the source of fecal pollution, adequate protection of public health will depend on assuming that the indicators are derived from sources that carry the highest pathogen burden. Rapid detection of a fecal indicator is more important than the level of information provided by the indicator since water quality can change rapidly in the beach environment [29]. Ultimately, the source of fecal pollution needs to be identified and remediated to remove the health risk.

Fecal indicators also serve as important tools for sanitary survey practices and for prioritizing remediation strategies. While daily monitoring with a general indicator such as enterococci or *E. coli* will provide information on the extent of fecal pollution, the source needs to be identified in order to take corrective actions. Both extensive mapping of the physical location of fecal pollution inputs (where is it coming from?) and determination of the host sources (is it human or nonhuman sources?) are necessary. Host-associated alternative indicators are best suited for these applications.

Source identifiers can also be used to evaluate the success of best management practices and influence of many green infrastructure efforts in agriculture and urban run-off settings. For example, the installation of tile drainage systems or constructed wetlands is commonly used to control the flow of agricultural waste across the landscape during rain events. Host-associated methods provide an excellent metric for estimating the efficiency of these waste management practices.

Rapid Methods for Indicators

Recreational water quality monitoring has traditionally relied upon culture-based methods and therefore test results are not available to the public until, at the earliest, the following day. It is well established that water quality can change in a matter of hours [29, 266]. A high priority for beach managers is to utilize rapid testing methods, many of which are based on qPCR of fecal indicators. Studies have compared different rapid methods [93]. New water quality criteria that are being formulated by the USEPA are expected to include rapid methods for enterococci using qPCR.

BEACH Act Legislation. The Beaches Environmental Assessment and Coastal Health (BEACH) Act of 2000 is an amendment to the Federal Water Pollution Control Act (commonly known as the Clean Water Act). This legislation required states and tribes to adopt new or revised water quality standards by 2004. It also required the USEPA to publish new or revised criteria for pathogens and pathogen indicators. The BEACH Act authorized appropriations for states and tribes to develop and implement water quality monitoring and public notification programs at recreational beaches. The USEPA has identified scientific gaps that need to be filled in order to develop improved water quality criteria [251].

Future Directions

The identification of host-associated source identifiers represents the first step toward the successful implementation of a fecal indicator method. Several additional steps must be taken to complete the method development phase including method optimization, design of appropriate laboratory controls, and defining a data interpretation model. After method development, it is necessary to define the operational parameters of the method. In the case of qPCR, this might include factors such as generation of a calibration curve, defining the range of quantification, precision, and limit of detection. The next step is to characterize the robustness of the method by measuring specificity, host distribution of the source identifier, abundance of source identifier in target group, describing fate and transport mechanisms, establishing links to general fecal indicators, pathogens, and public health outcomes. Once the operational parameters and robustness of the method are adequately described, a multiple laboratory validation study should be conducted to address issues of reproducibility, variability between laboratories, normalization of results, standardization of controls, minimum requirements to establish laboratory efficiency, and requirements for laboratory training. It is important to note that this list is not comprehensive. There may be additional steps required depending on the intended use of the method.

Rapidly advancing technologies will provide new opportunities to expand the number and types

of fecal indicators. Next-generation sequencing technologies have increased our capacity to analyze whole microbial communities, rather than single organisms. Advancing technologies will also allow for more detailed analyses of the dynamics of fecal indicators in the environment. Further, more sensitive, specific, and rapid detection strategies are needed to improve monitoring programs for devising pollution remediation strategies and for the protection of public health.

Acknowledgments

We would like to thank Dr. Alford Dufour for insightful discussion and for providing historical information on the use of traditional indicators and evolution of water quality criteria. The US Environmental Protection Agency, through its Office of Research and Development, funded and managed, or partially funded and collaborated in, the research described herein. It has been subjected to the Agency's peer and administrative review and has been approved for external publication. Any opinions expressed in this entry are those of the author(s) and do not necessarily reflect the views of the Agency; therefore, no official endorsement should be inferred. Any mention of trade names or commercial products does not constitute endorsement or recommendation for use.

Bibliography

1. Ahmed W, Powell D, Goonetilleke A, Gardner T (2008) Detection and source identification of faecal pollution in non-sewered catchment by means of host-specific molecular markers. Water Sci Technol 58:579–586
2. Ahmed W, Stewart J, Gardner T, Powell D (2008) A real-time polymerase chain reaction assay for quantitative detection of the human-specific enterococci surface protein marker in sewage and environmental waters. Environ Microbiol 10:3255–3264
3. Ahmed W, Stewart J, Powell D, Gardner T (2008) Evaluation of Bacteroides markers for the detection of human faecal pollution. Lett Appl Microbiol 46:237–242
4. Ahmed W, Goonetilleke A, Powell D, Chauhan K, Gardner T (2009) Comparison of molecular markers to detect fresh sewage in environmental waters. Water Res 43:4908–4917
5. Ahmed W, Sawant S, Huygens F, Goonetilleke A, Gardner T (2009) Prevalence and occurrence of zoonotic bacterial pathogens in surface waters determined by quantitative PCR. Water Res 43:4918–4928
6. Ahmed W, Wan C, Goonetilleke A, Gardner T (2010) Evaluating sewage-associated JCV and BKV polyomaviruses for sourcing human fecal pollution in a coastal river in Southeast Queensland, Australia. J Environ Qual 39:1743–1750
7. Alm EW, Burke J, Spain A (2003) Fecal indicator bacteria are abundant in wet sand at freshwater beaches. Water Res 37:3978–3982
8. Alonso JL, Alonso MA (1993) Presence of *Campylobacter* in marine waters of Valencia. Spain Water Res 27:1559–1562
9. Anderson KL, Whitlock JE, Harwood VJ (2005) Persistence and differential survival of fecal indicator bacteria in subtropical waters and sediments. Appl Environ Microbiol 71:3041–3048
10. Anderson MA, Whitlock JE, Harwood VJ (2006) Diversity and distribution of *Escherichia coli* genotypes and antibiotic resistance phenotypes in feces of humans, cattle, and horses. Appl Environ Microbiol 72:6914–6922
11. Arai T, Ikejima N, Itoh T, Sakai S, Shimada T, Sakazaki R (1980) A survey of Plesiomonas shigelloides from aquatic environments, domestic animals, pets and humans. J Hyg (Lond) 84:203–211
12. Araujo RM, Puig A, Lasobras J, Lucena F, Jofre J (1997) Phages of enteric bacteria in fresh water with different levels of faecal pollution. J Appl Microbiol 82:281–286
13. Arnone RD, Walling JP (2007) Waterborne pathogens in urban watersheds. J Water Health 5:149–162
14. Ashbolt NJ, Grabow OK, Snozzi M (2001) Indicators of microbial water quality. In: Fewtrell L, Bartram J (eds) Water quality: guidelines, standards, and health. IWA Publishing, London
15. Ashbolt NJ, Schoen ME, Soller JA, Roser DJ (2010) Predicting pathogen risks to aid beach management: the real value of quantitative microbial risk assessment (QMRA). Water Res 44:4692–4703
16. Association, A. P. H. (1999) Standard methods for the examination of water and wastewater, 18th edn. American Public Health Association, Washington, DC
17. Aw TG, Gin KY, Ean Oon LL, Chen EX, Woo CH (2009) Prevalence and genotypes of human noroviruses in tropical urban surface waters and clinical samples in Singapore. Appl Environ Microbiol 75:4984–4992
18. Bae S, Wuertz S (2009) Rapid decay of host-specific fecal Bacteroidales cells in seawater as measured by quantitative PCR with propidium monoazide. Water Res 43:4850–4859
19. Bai S, Lung WS (2005) Modeling sediment impact on the transport of fecal bacteria. Water Res 39:5232–5240
20. Balleste E, Bonjoch X, Belanche LA, Blanch AR (2010) Molecular indicators used in the development of predictive models for microbial source tracking. Appl Environ Microbiol 76:1789–1795
21. Baudart J, Lemarchand K, Brisabois A, Lebaron P (2000) Diversity of *Salmonella* strains isolated from the aquatic environment as determined by serotyping and amplification of the ribosomal DNA spacer regions. Appl Environ Microbiol 66:1544–1552
22. Baums IB, Goodwin KD, Kiesling T, Wanless D, Diaz MR, Fell JW (2007) Luminex detection of fecal indicators in river samples,

marine recreational water, and beach sand. Mar Pollut Bull 54:521–536
23. Bell A, Layton AC, McKay L, Williams D, Gentry R, Sayler GS (2009) Factors influencing the persistence of fecal Bacteroides in stream water. J Environ Qual 38:1224–1232
24. Bernhard AE, Field KG (2000) Identification of nonpoint sources of fecal pollution in coastal waters by using host-specific 16 S ribosomal DNA genetic markers from fecal anaerobes. Appl Environ Microbiol 66:1587–1594
25. Bernhard AE, Field KG (2000) A PCR assay to discriminate human and ruminant feces on the basis of host differences in Bacteroides-Prevotella genes encoding 16 S rRNA. Appl Environ Microbiol 66:4571–4574
26. Beversdorf LJ, Bornstein-Forst SM, McLellan SL (2007) The potential for beach sand to serve as a reservoir for *Escherichia coli* and the physical influences on cell die-off. J Appl Microbiol 102:1372–1381
27. Bienfang PK, Defelice SV, Laws EA, Brand LE, Bidigare RR, Christensen S, Trapido-Rosenthal H, Hemscheidt TK, McGillicuddy DJ, Anderson DM, Solo-Gabriele HM, Boehm AB, Backer LC (2011) Prominent human health impacts from several marine microbes: history, ecology, and public health implications. Int J Microbiol 2011:152815
28. Blanch AR, Belanche-Munoz L, Bonjoch X, Ebdon J, Gantzer C, Lucena F, Ottoson J, Kourtis C, Iversen A, Kuhn I, Moce L, Muniesa M, Schwartzbrod J, Skraber S, Papageorgiou GT, Taylor H, Wallis J, Jofre J (2006) Integrated analysis of established and novel microbial and chemical methods for microbial source tracking. Appl Environ Microbiol 72:5915–5926
29. Boehm AB (2007) Enterococci concentrations in diverse coastal environments exhibit extreme variability. Environ Sci Technol 41:8227–8232
30. Boehm AB, Keymer DP, Shellenbarger GG (2005) An analytical model of enterococci inactivation, grazing, and transport in the surf zone of a marine beach. Water Res 39:3565–3578
31. Boehm AB, Ashbolt NJ, Colford JM Jr, Dunbar LE, Fleming LE, Gold MA, Hansel JA, Hunter PR, Ichida AM, McGee CD, Soller JA, Weisberg SB (2009) A sea change ahead for recreational water quality criteria. J Water Health 7:9–20
32. Boehm AB, Yamahara KM, Love DC, Peterson BM, McNeill K, Nelson KL (2009) Covariation and photoinactivation of traditional and novel indicator organisms and human viruses at a sewage-impacted marine beach. Environ Sci Technol 43:8046–8052
33. Bolton F, Surman SB, Martin K, Wareing DR, Humphrey TJ (1999) Presence of *Campylobacter* and *Salmonella* in sand from bathing beaches. Epidemiol Infect 122:7–13
34. Bonde GJ (1963) Bacterial indicators of water pollution. A study of quantitative estimation. Teknisk Forlag, Copenhagen
35. Bonjoch X, Balleste E, Blanch AR (2004) Multiplex PCR with 16 S rRNA gene-targeted primers of bifidobacterium spp. to identify sources of fecal pollution. Appl Environ Microbiol 70:3171–3175
36. Bothner MH, Takada H, Knight IT, Hill RT, Butman B, Farrington JW, Colwell RR, Grassle JF (1994) Sewage contamination in sediments beneath a deep-ocean dump site off New-York. Mar Environ Res 38:43–59
37. Bower PA, Scopel CO, Jensen ET, Depas MM, McLellan SL (2005) Detection of genetic markers of fecal indicator bacteria in Lake Michigan and determination of their relationship to *Escherichia coli* densities using standard microbiological methods. Appl Environ Microbiol 71:8305–8313
38. Brion GM, Meschke JS, Sobsey MD (2002) F-specific RNA coliphages: occurrence, types, and survival in natural waters. Water Res 36:2419–2425
39. Cabelli VJ, Dufour AP, McCabe LJ, Levin MA (1982) Swimming-associated gastroenteritis and water quality. Am J Epidemiol 115:606–616
40. Caldwell JM, Raley ME, Levine JF (2007) Mitochondrial multiplex real-time PCR as a source tracking method in fecal-contaminated effluents. Environ Sci Technol 41:3277–3283
41. Cao Y, Griffith JF, Weisberg SB (2009) Evaluation of optical brightener photodecay characteristics for detection of human fecal contamination. Water Res 43:2273–2279
42. Caplenas NR, Kanarek MS (1984) Thermotolerant non-fecal source Klebsiella pneumoniae: validity of the fecal coliform test in recreational waters. Am J Public Health 74:1273–1275
43. Carson CA, Shear BL, Ellersieck MR, Asfaw A (2001) Identification of fecal *Escherichia coli* from humans and animals by ribotyping. Appl Environ Microbiol 67:1503–1507
44. Carson CA, Shear BL, Ellersieck MR, Schnell JD (2003) Comparison of ribotyping and repetitive extragenic palindromic-PCR for identification of fecal *Escherichia coli* from humans and animals. Appl Environ Microbiol 69:1836–1839
45. Carson CA, Christiansen JM, Yampara-Iquise H, Benson VW, Baffaut C, Davis JV, Broz RR, Kurtz WB, Rogers WM, Fales WH (2005) Specificity of a Bacteroides thetaiotaomicron marker for human feces. Appl Environ Microbiol 71:4945–4949
46. Center for Disease Control (2011) posting date. *Escherichia coli* O157:H7, General information
47. Chapron CD, Ballester NA, Fontaine JH, Frades CN, Margolin AB (2000) Detection of astroviruses, enteroviruses, and adenovirus types 40 and 41 in surface waters collected and evaluated by the information collection rule and an integrated cell culture-nested PCR procedure. Appl Environ Microbiol 66:2520–2525
48. Charoenca N, Fujioka RS (1993) Assessment of *Staphylococcus* bacteria in Hawaii's marine recreational waters. Water Sci Technol 27:283–289
49. Charoenca N, Fujioka RS (1995) Association of staphylococcal skin infections and swimming. Water Sci Technol 31:11–17
50. Chern EC, Tsai YL, Olson BH (2004) Occurrence of genes associated with enterotoxigenic and enterohemorrhagic *Escherichia coli* in agricultural waste lagoons. Appl Environ Microbiol 70:356–362
51. Choi S, Jiang SC (2005) Real-time PCR quantification of human adenoviruses in urban rivers indicates genome prevalence but low infectivity. Appl Environ Microbiol 71:7426–7433

52. Colford JM Jr, Wade TJ, Schiff KC, Wright CC, Griffith JF, Sandhu SK, Burns S, Sobsey M, Lovelace G, Weisberg SB (2007) Water quality indicators and the risk of illness at beaches with non-point sources of fecal contamination. Epidemiology 18:27–35
53. Converse RR, Blackwood AD, Kirs M, Griffith JF, Noble RT (2009) Rapid QPCR-based assay for fecal Bacteroides spp. as a tool for assessing fecal contamination in recreational waters. Water Res 43:4828–4837
54. Davies CM, Long JA, Donald M, Ashbolt NJ (1995) Survival of fecal microorganisms in marine and freshwater sediments. Appl Environ Microbiol 61:1888–1896
55. DePaola A, Hopkins LH, Peeler JT, Wentz B, McPhearson RM (1990) Incidence of *Vibrio parahaemolyticus* in U.S. coastal waters and oysters. Appl Environ Microbiol 56:2299–2302
56. Desmarais TR, Solo-Gabriele HM, Palmer CJ (2002) Influence of soil on fecal indicator organisms in a tidally influenced subtropical environment. Appl Environ Microbiol 68:1165–1172
57. Dethlefsen L, Huse S, Sogin ML, Relman DA (2008) The pervasive effects of an antibiotic on the human gut microbiota, as revealed by deep 16 S rRNA sequencing. PLoS Biol 6:e280
58. Devriese LLA, van de Kerckhove A, Kilpper-Baelz R, Schleifer K (1987) Characterization and identification of *Enterococcus* species isolated from the intestines of animals. Int J Syst Bacteriol 37:257–259
59. Dick LK, Field KG (2004) Rapid estimation of numbers of fecal Bacteroidetes by use of a quantitative PCR assay for 16 S rRNA genes. Appl Environ Microbiol 70:5695–5697
60. Dick LK, Bernhard AE, Brodeur TJ, Santo Domingo JW, Simpson JM, Walters SP, Field KG (2005) Host distributions of uncultivated fecal Bacteroidales bacteria reveal genetic markers for fecal source identification. Appl Environ Microbiol 71:3184–3191
61. Dick LK, Stelzer EA, Bertke EE, Fong DL, Stoeckel DM (2010) Relative decay of Bacteroidales microbial source tracking markers and cultivated *Escherichia coli* in freshwater microcosms. Appl Environ Microbiol 76:3255–3262
62. Dickerson JW Jr, Hagedorn C, Hassall A (2007) Detection and remediation of human-origin pollution at two public beaches in Virginia using multiple source tracking methods. Water Res 41:3758–3770
63. Dombek PE, Johnson LK, Zimmerley ST, Sadowsky MJ (2000) Use of repetitive DNA sequences and the PCR To differentiate *Escherichia coli* isolates from human and animal sources. Appl Environ Microbiol 66:2572–2577
64. Dorai-Raj S, O'Grady J, Colleran E (2009) Specificity and sensitivity evaluation of novel and existing Bacteroidales and Bifidobacteria-specific PCR assays on feces and sewage samples and their application for microbial source tracking in Ireland. Water Res 43:4980–4988
65. Dufour AP (1984) Bacterial indicators of recreational water quality. Can J Public Health 75:49–56
66. Dufour AP, Schaub S (2007) The evolution of water quality criteria in the United Sates, 1922–2003. In: Wymer LJ (ed) Statistical framework for recreational water quality monitoring. Wiley, New York
67. Eckburg PB, Bik EM, Bernstein CN, Purdom E, Dethlefsen L, Sargent M, Gill SR, Nelson KE, Relman DA (2005) Diversity of the human intestinal microbial flora. Science 308:1635–1638
68. Eckner KF (1998) Comparison of membrane filtration and multiple-tube fermentation by the colilert and enterolert methods for detection of waterborne coliform bacteria, *Escherichia coli*, and enterococci used in drinking and bathing water quality monitoring in southern Sweden. Appl Environ Microbiol 64:3079–3083
69. Edge TA, Boehm AB (2011) Classical and molecular methods to measure fecal indicator bacteria. In: Sadowsky MJ, Whitman RL (eds) The fecal indicator bacteria. ASM Press, Washington, DC
70. Edwards DD, McFeters GA, Venkatesan MI (1998) Distribution of *Clostridium perfringens* and fecal sterols in a benthic coastal marine environment influenced by the sewage outfall from McMurdo Station, Antarctica. Appl Environ Microbiol 64:2596–2600
71. Emerson DJ, Cabelli VJ (1982) Extraction of *Clostridium perfringens* spores from bottom sediment samples. Appl Environ Microbiol 44:1144–1149
72. Field KG, Samadpour M (2007) Fecal source tracking, the indicator paradigm, and managing water quality. Water Res 41:3517–3538
73. Field KG, Bernhard AE, Brodeur TJ (2003) Molecular approaches to microbiological monitoring: fecal source detection. Environ Monit Assess 81:313–326
74. Fiksdal L, Maki JS, LaCroix SJ, Staley JT (1985) Survival and detection of Bacteroides spp., prospective indicator bacteria. Appl Environ Microbiol 49:148–150
75. Fogarty LR, Voytek MA (2005) Comparison of bacteroides-prevotella 16 S rRNA genetic markers for fecal samples from different animal species. Appl Environ Microbiol 71:5999–6007
76. Fong T-T, Lipp EK (2005) Enteric viruses of humans and animals in aquatic environments: health risks, detection, and potential water quality assessment tools. Microbiol Mol Biol Rev 69:357–371
77. Frank DN, St Amand AL, Feldman RA, Boedeker EC, Harpaz N, Pace NR (2007) Molecular-phylogenetic characterization of microbial community imbalances in human inflammatory bowel diseases. Proc Natl Acad Sci USA 104:13780–13785
78. Fremaux B, Gritzfeld J, Boa T, Yost CK (2009) Evaluation of host-specific Bacteroidales 16 S rRNA gene markers as a complementary tool for detecting fecal pollution in a prairie watershed. Water Res 43:4838–4849
79. Fujioka RS (2001) Monitoring coastal marine waters for spore-forming bacteria of faecal and soil origin to determine point from non-point source pollution. Water Sci Technol 44:181–188
80. Fung DYC, Fujioka R, Vijayavel K, Sato D, Bishop D (2007) Evaluation of Fung double tube test for *Clostridium perfringens* and Easyphage test for F-specific RNA coliphages as rapid screening tests for fecal contamination in recreational waters of Hawaii (vol 15, pg 217, 2007). J Rapid Meth Aut Mic 15:411–411
81. Furet JP, Firmesse O, Gourmelon M, Bridonneau C, Tap J, Mondot S, Dore J, Corthier G (2009) Comparative assessment

of human and farm animal faecal microbiota using real-time quantitative PCR. FEMS Microbiol Ecol 68:351–362
82. Gast RJ, Moran D, Dennett MR, Wurtsbaugh WA, Amaral-Zettler LA (2011) Amoebae and *Legionella pneumophila* in saline environments. J Water Health 9:37–52
83. Gauthier F, Neufeld JD, Driscoll BT, Archibald FS (2000) Coliform bacteria and nitrogen fixation in pulp and paper mill effluent treatment systems. Appl Environ Microbiol 66:5155–5160
84. Gawler AH, Beecher JE, Brandao J, Carroll NM, Falcao L, Gourmelon M, Masterson B, Nunes B, Porter J, Rince A, Rodrigues R, Thorp M, Walters JM, Meijer WG (2007) Validation of host-specific Bacteriodales 16 S rRNA genes as markers to determine the origin of faecal pollution in Atlantic Rim countries of the European Union. Water Res 41:3780–3784
85. Gerba CP, Rose JB, Haas CN, Crabtree KD (1996) Waterborne rotavirus: a risk assessment. Water Res 30:2929–2940
86. Gersberg RM, Rose MA, Robles-Sikisaka R, Dhar AK (2006) Quantitative detection of hepatitis A virus and enteroviruses near the United States-Mexico border and correlation with levels of fecal indicator bacteria. Appl Environ Microbiol 72:7438–7444
87. Gilpin B, James T, Nourozi F, Saunders D, Scholes P, Savill M (2003) The use of chemical and molecular microbial indicators for faecal source identification. Water Sci Technol 47:39–43
88. Goodwin KD, Pobuda M (2009) Performance of CHROMagar Staph aureus and CHROMagar MRSA for detection of *Staphylococcus aureus* in seawater and beach sand – comparison of culture agglutination, and molecular analyses. Water Res 43:4802–4811
89. Gourmelon M, Caprais MP, Mieszkin S, Marti R, Wery N, Jarde E, Derrien M, Jadas-Hecart A, Communal PY, Jaffrezic A, Pourcher AM (2010) Development of microbial and chemical MST tools to identify the origin of the faecal pollution in bathing and shellfish harvesting waters in France. Water Res 44:4812–4824
90. Graczyk TK, Sunderland D, Tamang L, Lucy FE, Breysse PN (2007) Bather density and levels of *Cryptosporidium* Giardia, and pathogenic microsporidian spores in recreational bathing water. Parasitol Res 101:1729–1731
91. Griffin DW, Gibson CJ 3rd, Lipp EK, Riley K, Paul JH 3rd, Rose JB (1999) Detection of viral pathogens by reverse transcriptase PCR and of microbial indicators by standard methods in the canals of the Florida Keys. Appl Environ Microbiol 65:4118–4125
92. Griffin DW, Lipp EK, McLaughlin MR, Rose JB (2001) Marine recreation and public health microbiology: quest for the ideal indicator. Bioscience 51:817–825
93. Griffith JF, Cao Y, McGee CD, Weisberg SB (2009) Evaluation of rapid methods and novel indicators for assessing microbiological beach water quality. Water Res 43:4900–4907
94. Grimes DJ (1975) Release of sediment-bound fecal coliforms by dredging. Appl Microbiol 29:109–111
95. Haack SK, Duris JW, Fogarty LR, Kolpin DW, Focazio MJ, Furlong ET, Meyer MT (2009) Comparing wastewater chemicals, indicator bacteria concentrations, and bacterial pathogen genes as fecal pollution indicators. J Environ Qual 38:248–258
96. Haake DA, Dundoo M, Cader R, Kubak BM, Hartskeerl RA, Sejvar JJ, Ashford DA (2002) Leptospirosis, water sports, and chemoprophylaxis. Clin Infect Dis 34:E40–E43
97. Hagedorn C, Robinson SL, Filtz JR, Grubbs SM, Angier TA, Reneau RB Jr (1999) Determining sources of fecal pollution in a rural Virginia watershed with antibiotic resistance patterns in fecal streptococci. Appl Environ Microbiol 65: 5522–5531
98. Haile RW, Witte JS, Gold M, Cressey R, McGee C, Millikan RC, Glasser A, Harawa N, Ervin C, Harmon P, Harper J, Dermand J, Alamillo J, Barrett K, Nides M, Wang G (1999) The health effects of swimming in ocean water contaminated by storm drain runoff. Epidemiology 10:355–363
99. Halbur PG, Kasorndorkbua C, Gilbert C, Guenette D, Potters MB, Purcell RH, Emerson SU, Toth TE, Meng XJ (2001) Comparative pathogenesis of infection of pigs with hepatitis E viruses recovered from a pig and a human. J Clin Microbiol 39:918–923
100. Haley BJ, Cole DJ, Lipp EK (2009) Distribution, diversity, and seasonality of waterborne salmonellae in a rural watershed. Appl Environ Microbiol 75:1248–1255
101. Hamilton MJ, Yan T, Sadowsky MJ (2006) Development of goose- and duck-specific DNA markers to determine sources of *Escherichia coli* in waterways. Appl Environ Microbiol 72:4012–4019
102. Harrison S, Kinra S (2004) Outbreak of *Escherichia coli* O157 associated with a busy beach. Commun Dis Public Health 7:47–50
103. Hartel PG, Summer JD, Hill JL, Collins JV, Entry JA, Segars WI (2002) Geographic variability of *Escherichia coli* ribotypes from animals in Idaho and Georgia. J Environ Qual 31: 1273–1278
104. Harvey S, Greenwood JR, Pickett MJ, Mah RA (1976) Recovery of *Yersinia enterocolitica* from streams and lakes of California. Appl Environ Microbiol 32:352–354
105. Harwood VJ, Whitlock J, Withington V (2000) Classification of antibiotic resistance patterns of indicator bacteria by discriminant analysis: use in predicting the source of fecal contamination in subtropical waters. Appl Environ Microbiol 66: 3698–3704
106. Haugland RA, Siefring SC, Wymer LJ, Brenner KP, Dufour AP (2005) Comparison of Enterococcus measurements in freshwater at two recreational beaches by quantitative polymerase chain reaction and membrane filter culture analysis. Water Res 39:559–568
107. Hayashi H, Sakamoto M, Kitahara M, Benno Y (2006) Diversity of the Clostridium coccoides group in human fecal microbiota as determined by 16 S rRNA gene library. FEMS Microbiol Lett 257:202–207
108. He J, Jiang S (2005) Quantification of enterococci and human adenoviruses in environmental samples by real-time PCR. Appl Environ Microbiol 71:2250–2255
109. Higgins JA, Belt KT, Karns JS, Russell-Anelli J, Shelton DR (2005) *tir*- and *stx*-positive *Escherichia coli* in stream waters in a metropolitan area. Appl Environ Microbiol 71:2511–2519

110. Hill RT, Straube WL, Palmisano AC, Gibson SL, Colwell RR (1996) Distribution of sewage indicated by *Clostridium perfringens* at a deep-water disposal site after cessation of sewage disposal. Appl Environ Microbiol 62:1741–1746
111. Hipsey MR, Antenucci JP, Brookes JD (2008) A generic, process-based model of microbial pollution in aquatic systems. Water Resour Res 44:26
112. Horman A, Rimhanen-Finne R, Maunula L, von Bonsdorff C-H, Torvela N, Heikinheimo A, Hanninen M-L (2004) *Campylobacter* spp., *Giardia* spp., *Cryptosporidium* spp., Noroviruses, and indicator organisms in surface water in southwestern Finland, 2000–2001. Appl Environ Microbiol 70:87–95
113. Hou D, Rabinovici SJM, Boehm AB (2006) Enterococci predictions from partial least squares regression models in conjunction with a single-sample standard improve the efficacy of beach management advisories. Environ Sci Technol 40:1737–1743
114. Hsu FC, Shieh YS, van Duin J, Beekwilder MJ, Sobsey MD (1995) Genotyping male-specific RNA coliphages by hybridization with oligonucleotide probes. Appl Environ Microbiol 61:3960–3966
115. Hussain MA, Ford R, Hill J (2010) Determination of fecal contamination indicator sterols in an Australian water supply system. Environ Monit Assess 165:147–157
116. International Organization for Standardization (2000) Water quality – Detection and enumeration of intestinal enterococci ISO 7899–2:000
117. Ishii S, Ksoll WB, Hicks RE, Sadowsky MJ (2006) Presence and growth of naturalized *Escherichia coli* in temperate soils from Lake Superior watersheds. Appl Environ Microbiol 72:612–621
118. Ishii S, Yan T, Shivley DA, Byappanahalli MN, Whitman RL, Sadowsky MJ (2006) *Cladophora* (Chlorophyta) spp. harbor human bacterial pathogens in nearshore water of Lake Michigan. Appl Environ Microbiol 72:4545–4553
119. Jamieson R, Joy DM, Lee H, Kostaschuk R, Gordon R (2005) Transport and deposition of sediment-associated *Escherichia coli* in natural streams. Water Res 39:2665–2675
120. Jamieson RC, Joy DM, Lee H, Kostaschuk R, Gordon RJ (2005) Resuspension of sediment-associated *Escherichia coli* in a natural stream. J Environ Qual 34:581–589
121. Jeter SN, McDermott CM, Bower PA, Kinzelman JL, Bootsma MJ, Goetz GW, McLellan SL (2009) Bacteroidales diversity in ring-billed gulls (Laurus delawarensis) residing at Lake Michigan beaches. Appl Environ Microbiol 75:1525–1533
122. Jiang SC, Chu W (2004) PCR detection of pathogenic viruses in southern California urban rivers. J Appl Microbiol 97:17–28
123. Jiang S, Noble R, Chu W (2001) Human adenoviruses and coliphages in urban runoff-impacted coastal waters of Southern California. Appl Environ Microbiol 67: 179–184
124. Jiang SC, Nobel R, Chu W (2001) Human adenoviruses and coliphage in urban runoff-impacted coastal waters of southern California. Appl Environ Microbiol 67:179–184
125. Jiang SC, Chu W, He JW (2007) Seasonal detection of human viruses and coliphage in Newport Bay, California. Appl Environ Microbiol 73:6468–6474
126. Jofre J, Blasi M, Bosch A, Lucena F (1989) Occurrence of bacteriophages infecting Bacteroides-Fragilis and other viruses in polluted marine-sediments. Water Sci Technol 21:15–19
127. Johnson CN, Flowers AR, Noriea NF III, Zimmerman AM, Bowers JC, DePaola A, Grimes DJ (2010) Relationships between environmental factors and pathogenic Vibrios in the Northern Gulf of Mexico. Appl Environ Microbiol 76:7076–7084
128. Johnston C, Ufnar JA, Griffith JF, Gooch JA, Stewart JR (2010) A real-time qPCR assay for the detection of the nifH gene of Methanobrevibacter smithii, a potential indicator of sewage pollution. J Appl Microbiol 109:1946–1956
129. Keymer DP, Miller MC, Schoolnik GK, Boehm AB (2007) Genomic and phenotypic diversity of coastal *Vibrio cholerae* is explained by environmental factors. Appl Environ Microbiol 73:3705–3714
130. Keymer DP, Lam L, Boehm AB (2009) Biogeographic patterns in genomic diversity among a large collection of *Vibrio cholerae* isolates. Appl Environ Microbiol 75:1658–1666
131. Khatib LA, Tsai YL, Olson BH (2002) A biomarker for the identification of cattle fecal pollution in water using the LTIIa toxin gene from enterotoxigenic *Escherichia coli*. Appl Microbiol Biotechnol 59:97–104
132. Khatib LA, Tsai YL, Olson BH (2003) A biomarker for the identification of swine fecal pollution in water, using the STII toxin gene from enterotoxigenic *Escherichia coli*. Appl Microbiol Biotechnol 63:231–238
133. Kildare BJ, Leutenegger CM, McSwain BS, Bambic DG, Rajal VB, Wuertz S (2007) 16 S rRNA-based assays for quantitative detection of universal, human-, cow-, and dog-specific fecal Bacteroidales: a Bayesian approach. Water Res 41:3701–3715
134. Kinzelman J, McLellan SL, Daniels AD, Cashin S, Singh A, Gradus S, Bagley R (2004) Non-point source pollution: determination of replication versus persistence of *Escherichia coli* in surface water and sediments with correlation of levels to readily measurable environmental parameters. J Water Health 2:103–114
135. Kirs M, Smith DC (2007) Multiplex quantitative real-time reverse transcriptase PCR for F+ −specific RNA coliphages: a method for use in microbial source tracking. Appl Environ Microbiol 73:808–814
136. Kreader CA (1995) Design and evaluation of Bacteroides DNA probes for the specific detection of human fecal pollution. Appl Environ Microbiol 61:1171–1179
137. Lamendella R, Domingo JW, Oerther DB, Vogel JR, Stoeckel DM (2007) Assessment of fecal pollution sources in a small northern-plains watershed using PCR and phylogenetic analyses of Bacteroidetes 16 S rRNA gene. FEMS Microbiol Ecol 59:651–660
138. Layton A, McKay L, Williams D, Garrett V, Gentry R, Sayler G (2006) Development of Bacteroides 16 S rRNA gene

TaqMan-based real-time PCR assays for estimation of total, human, and bovine fecal pollution in water. Appl Environ Microbiol 72:4214–4224
139. Layton BA, Walters SP, Lam LH, Boehm AB (2010) Enterococcus species distribution among human and animal hosts using multiplex PCR. J Appl Microbiol 109:539–547
140. Leach MD, Broschat SL, Call DR (2008) A discrete, stochastic model and correction method for bacterial source tracking. Environ Sci Technol 42:524–529
141. Leclerc H, Schwartzbrod L, Dei-Cas E (2002) Microbial agents associated with waterborne diseases. Crit Rev Microbiol 28:371–409
142. Lee CS, Lee J (2010) Evaluation of new gyrB-based real-time PCR system for the detection of *B. fragilis* as an indicator of human-specific fecal contamination. J Microbiol Meth 82:311–318
143. Lee DY, Weir SC, Lee H, Trevors JT (2010) Quantitative identification of fecal water pollution sources by TaqMan real-time PCR assays using *Bacteroidales* 16 S rRNA genetic markers. Appl Microbiol Biotechnol 88:1373–1383
144. Lemarchand K, Lebaron P (2003) Occurrence of *Salmonella* spp. and *Cryptosporidium* spp. in a French coastal watershed: relationship with fecal indicators. FEMS Microbiol Lett 218:203–209
145. Lemarchand K, Masson L, Brousseau R (2004) Molecular biology and DNA microarray technology for microbial quality monitoring of water. Crit Rev Microbiol 30:145–172
146. Leung HD, Chen G, Sharma K (2005) Effect of detached/re-suspended solids from sewer sediment on the sewage phase bacterial activity. Water Sci Technol 52:147–152
147. Lipp EK, Huq A, Colwell RR (2002) Effects of global climate on infectious disease: the cholera model. Clin Microbiol Rev 15:757–770
148. Lynch PA, Gilpin BJ, Sinton LW, Savill MG (2002) The detection of Bifidobacterium adolescentis by colony hybridization as an indicator of human faecal pollution. J Appl Microbiol 92:526–533
149. Mac Kenzie WR, Hoxie NJ, Proctor ME, Gradus MS, Blair KA, Peterson DE, Kazmierczak JJ, Addiss DG, Fox KR, Rose JB et al (1994) A massive outbreak in Milwaukee of cryptosporidium infection transmitted through the public water supply. N Engl J Med 331:161–167
150. Malinen E, Rinttila T, Kajander K, Matto J, Kassinen A, Krogius L, Saarela M, Korpela R, Palva A (2005) Analysis of the fecal microbiota of irritable bowel syndrome patients and healthy controls with real-time PCR. Am J Gastroenterol 100:373–382
151. Mallin MA, Williams KE, Esham EC, Lowe RP (2000) Effect of human development on bacteriological water quality in coastal watersheds. Ecol Appl 10:1047–1056
152. Marshall MM, Naumovitz D, Ortega Y, Sterling CR (1997) Waterborne protozoan pathogens. Clin Microbiol Rev 10:67–85
153. Matsuki T, Watanabe K, Fujimoto J, Miyamoto Y, Takada T, Matsumoto K, Oyaizu H, Tanaka R (2002) Development of 16 S rRNA-gene-targeted group-specific primers for the detection and identification of predominant bacteria in human feces. Appl Environ Microbiol 68:5445–5451
154. Matsuki T, Watanabe K, Fujimoto J, Kado Y, Takada T, Matsumoto K, Tanaka R (2004) Quantitative PCR with 16 S rRNA-gene-targeted species-specific primers for analysis of human intestinal bifidobacteria. Appl Environ Microbiol 70:167–173
155. Matsuki T, Watanabe K, Fujimoto J, Takada T, Tanaka R (2004) Use of 16 S rRNA gene-targeted group-specific primers for real-time PCR analysis of predominant bacteria in human feces. Appl Environ Microbiol 70:7220–7228
156. McBride GB, Salmond CE, Bandaranayake DR, Turner SJ, Lewis GD, Till DG (1998) Health effects of marine bathing in New Zealand. Int J Environ Health Res 8:173–189
157. McLaughlin MR, Rose JB (2006) Application of *Bacteroides fragilis* phage as an alternative indicator of sewage pollution in Tampa Bay, Florida. Estuar Coast 29:246–256
158. McLellan SL, Daniels AD, Salmore AK (2001) Clonal populations of thermotolerant Enterobacteriaceae in recreational water and their potential interference with fecal *Escherichia coli* counts. Appl Environ Microbiol 67:4934–4938
159. McLellan SL, Daniels AD, Salmore AK (2003) Genetic characterization of *Escherichia coli* populations from host sources of fecal pollution by using DNA fingerprinting. Appl Environ Microbiol 69:2587–2594
160. McLellan SL, Hollis EJ, Depas MM, Van Dyke M, Harris J, Scopel CO (2007) Distribution and fate of *Escherichia coli* in Lake Michigan following contamination with urban stormwater and combined sewer overflows. J Great Lakes Res 33:566–580
161. McLellan SL, Huse SM, Mueller-Spitz SR, Andreishcheva EN, Sogin ML (2010) Diversity and population structure of sewage-derived microorganisms in wastewater treatment plant influent. Environ Microbiol 12:378–392
162. McQuaig SM, Scott TM, Harwood VJ, Farrah SR, Lukasik JO (2006) Detection of human-derived fecal pollution in environmental waters by use of a PCR-based human polyomavirus assay. Appl Environ Microbiol 72:7567–7574
163. McQuaig SM, Scott TM, Lukasik JO, Paul JH, Harwood VJ (2009) Quantification of human polyomaviruses JC Virus and BK Virus by TaqMan quantitative PCR and comparison to other water quality indicators in water and fecal samples. Appl Environ Microbiol 75:3379–3388
164. Medema GJ, Bahar M, Schets FM (1997) Survival of *Cryptosporidium parvum, Escherichia coli*, faecal enterococci and *Clostridium perfringens* in river water: influence of temperature and autochthonous microorganisms. Water Sci Technol 35:249–252
165. Mieszkin S, Yala JF, Joubrel R, Gourmelon M (2010) Phylogenetic analysis of *Bacteroidales* 16 S rRNA gene sequences from human and animal effluents and assessment of ruminant faecal pollution by real-time PCR. J Appl Microbiol 108:974–984
166. Miller WA, Miller MA, Gardner IA, Atwill ER, Byrne BA, Jang S, Harris M, Ames J, Jessup D, Paradies D, Worcester K, Melli A,

Conrad PA (2006) *Salmonella* spp., *Vibrio* spp., *Clostridium perfringens*, and *Plesiomonas shigelloides* in marine and freshwater invertebrates from coastal California ecosystems. Microb Ecol 52:198–206

167. Mocé-Llivina L, Lucena F, Jofre J (2005) Enteroviruses and bacteriophages in bathing waters. Appl Environ Microbiol 71:6838–6844
168. Moe C (2002) Waterborne transmission of infectious agents. In: Hurst CJ, Crawfod RL, Knudsen GR, McInerney MJ, Stetzenbach LD (eds) Manual of environmental microbiology, 2nd edn. ASM Press, Washington, DC, pp 184–204
169. Mueller-Spitz SR, Stewart LB, Klump JV, McLellan SL (2010) Freshwater suspended sediments and sewage are reservoirs for enterotoxin-positive *Clostridium perfringens*. Appl Environ Microbiol 76:5556–5562
170. Mumy KL, Findlay RH (2004) Convenient determination of DNA extraction efficiency using an external DNA recovery standard and quantitative-competitive PCR. J Microbiol Methods 57:259–268
171. Muniesa M, Jofre J, Garcia-Aljaro C, Blanch AR (2006) Occurrence of *Escherichia coli* O157:H7 and other enterohemorrhagic *Escherichia coli* in the environment. Environ Sci Technol 40:7141–7149
172. Muniesa M, Payan A, Moce-Llivina L, Blanch AR, Jofre J (2009) Differential persistence of F-specific RNA phage subgroups hinders their use as single tracers for faecal source tracking in surface water. Water Res 43:1559–1564
173. Nebra Y, Bonjoch X, Blanch AR (2003) Use of *Bifidobacterium dentium* as an indicator of the origin of fecal water pollution. Appl Environ Microbiol 69:2651–2656
174. Nevers MB, Boehm AB (2010) Modeling fate and transport of fecal bacteria in surface water. In: Sadowsky MJ, Whitman RL (eds) The fecal indicator bacteria. ASM Press, Washington, DC
175. Newton RJ, VandeWalle JL, Borchardt MA, Gorelick MH, McLellan SL (2011) *Lachnospiraceae* and *Bacteroidales* alternative fecal indicators reveal chronic human sewage contamination in an urban harbor. Appl Environ Microbiol 77:6972–6981
176. Nichols PD, Leeming R, Rayner MS, Latham V, Ashbolt NJ, Turner C (1993) Comparison of the abundance of the fecal sterol soprostanol and fecal bacerial groups in inner-shlef waters and sediments near Sydney, Australia. J Chromatogr 643:189–195
177. Niemela SI, Vaatanen P (1982) Survival in lake water of *Klebsiella pneumoniae* discharged by a paper mill. Appl Environ Microbiol 44:264–269
178. Noble RT, Fuhrman JD (2001) Enteroviruses detected by reverse transcriptase polymerase chain reaction from the coastal waters of Santa Monica Bay, California: low correlation to bacterial indicator levels. Hydrobiologia 460:175–183
179. Noble RT, Allen SM, Blackwood AD, Chu W, Jiang SC, Lovelace GL, Sobsey MD, Stewart JR, Wait DA (2003) Use of viral pathogens and indicators to differentiate between human and non-human fecal contamination in a microbial source tracking comparison study. J Water Health 1:195–207
180. Noble RT, Moore DF, Leecaster MK, McGee CD, Weisberg SB (2003) Comparison of total coliform, fecal coliform, and enterococcus bacterial indicator response for ocean recreational water quality testing. Water Res 37:1637–1643
181. Noble RT, Griffith JF, Blackwood AD, Fuhrman JA, Gregory JB, Hernandez X, Liang X, Bera AA, Schiff K (2006) Multitiered approach using quantitative PCR to track sources of fecal pollution affecting Santa Monica Bay, California. Appl Environ Microbiol 72:1604–1612
182. Noble RT, Blackwood AD, Griffith JF, McGee CD, Weisberg SB (2010) Comparison of rapid quantitative PCR-based and conventional culture-based methods for enumeration of *Enterococcus* spp. and *Escherichia coli* in recreational waters. Appl Environ Microbiol 76:7437–7443
183. Obiri-Danso K, Jones K (2000) Intertidal sediments as reservoirs for hippurate negative campylobacters, salmonellae and faecal indicators in three EU recognized bathing waters in North West England. Water Res 34:519–527
184. Okabe S, Shimazu Y (2007) Persistence of host-specific *Bacteroides-Prevotella* 16 S rRNA genetic markers in environmental waters: effects of temperature and salinity. Appl Microbiol Biotechnol 76:935–944
185. Okabe S, Okayama N, Savichtcheva O, Ito T (2007) Quantification of host-specific Bacteroides-Prevotella 16 S rRNA genetic markers for assessment of fecal pollution in freshwater. Appl Microbiol Biotechnol 74:890–901
186. Palmer CJ, Tsai YL, Paszko-Kolva C, Mayer C, Sangermano LR (1993) Detection of *Legionella* species in sewage and ocean water by polymerase chain reaction, direct fluorescent-antibody, and plate culture methods. Appl Environ Microbiol 59:3618–3624
187. Panicker G, Myers ML, Bej AK (2004) Rapid detection of *Vibrio vulnificus* in shellfish and Gulf of Mexico water by real-time PCR. Appl Environ Microbiol 70:498–507
188. Parveen S, Murphree RL, Edmiston L, Kaspar CW, Portier KM, Tamplin ML (1997) Association of multiple-antibiotic-resistance profiles with point and nonpoint sources of *Escherichia coli* in Apalachicola Bay. Appl Environ Microbiol 63:2607–2612
189. Parveen S, Hodge NC, Stall RE, Farrah SR, Tamplin ML (2001) Phenotypic and genotypic characterization of human and nonhuman *Escherichia coli*. Water Res 35:379–386
190. Payan A, Ebdon J, Taylor H, Gantzer C, Ottoson J, Papageorgiou GT, Blanch AR, Lucena F, Jofre J, Muniesa M (2005) Method for isolation of *Bacteroides* bacteriophage host strains suitable for tracking sources of fecal pollution in water. Appl Environ Microbiol 71:5659–5662
191. Payment P, Franco E (1993) *Clostridium perfringens* and somatic coliphages as indicators of the efficiency of drinking water treatment for viruses and protozoan cysts. Appl Environ Microbiol 59:2418–2424
192. Pianetti A, Sabatini L, Bruscolini F, Chiaverini F, Cecchetti G (2004) Faecal contamination indicators, salmonella, vibrio and aeromonas in water used for the irrigation of agricultural products. Epidemiol Infect 132:231–238

193. Pina S, Puig M, Lucena F, Jofre J, Girones R (1998) Viral pollution in the environment and in shellfish: human adenovirus detection by PCR as an index of human viruses. Appl Environ Microbiol 64:3376–3382
194. Pinto R, Abad F, Gajardo R, Bosch A (1996) Detection of infectious astroviruses in water. Appl Environ Microbiol 62:1811–1813
195. Pruss A (1998) Review of epidemiological studies on health effects from exposure to recreational water. Int J Epidemiol 27:1–9
196. Puig A, Queralt N, Jofre J, Araujo R (1999) Diversity of *Bacteroides fragilis* strains in their capacity to recover phages from human and animal wastes and from fecally polluted wastewater. Appl Environ Microbiol 65:1772–1776
197. Rabinovici SJM, Bernknopf RL, Wein AM, Coursey DL, Whitman RL (2004) Economic and health risk trade-offs of swim closures at a Lake Michigan beach. Environ Sci Technol 38:2737–2745
198. Rajal VB, McSwain BS, Thompson DE, Leutenegger CM, Kildare BJ, Wuertz S (2007) Validation of hollow fiber ultrafiltration and real-time PCR using bacteriophage PP7 as surrogate for the quantification of viruses from water samples. Water Res 41:1411–1422
199. Rajal VB, McSwain BS, Thompson DE, Leutenegger CM, Wuertz S (2007) Molecular quantitative analysis of human viruses in California stormwater. Water Res 41: 4287–4298
200. Ram JL, Thompson B, Turner C, Nechvatal JM, Sheehan H, Bobrin J (2007) Identification of pets and raccoons as sources of bacterial contamination of urban storm sewers using a sequence-based bacterial source tracking method. Water Res 41:3605–3614
201. Resnick IG, Levin MA (1981) Assessment of bifidobacteria as indicators of human fecal pollution. Appl Environ Microbiol 42:433–438
202. Rose JB, Mullinax RL, Singh SN, Yates MV, Gerba CP (1987) Occurrence of rotaviruses and enteroviruses in recreational waters of Oak Creek, Arizona. Water Resour 21:1375–1381
203. Saha ML, Khan MR, Ali M, Hoque S (2009) Bacterial load and chemical pollution level of the River Buriganga, Dhaka, Bangladesh. Bangladesh J Botany 38:87–91
204. Sambrook J, Russell D (2001) Molecular cloning: a labortory manual, 3rd edn. Cold Spring Harbor Laboratory, New York
205. Sandery M, Stinear T, Kaucner C (1996) Detection of pathogenic *Yersinia enterocolitica* in environmental waters by PCR. J Appl Bacteriol 80:327–332
206. Santo Domingo JW, Bambic DG, Edge TA, Wuertz S (2007) Quo vadis source tracking? Towards a strategic framework for environmental monitoring of fecal pollution. Water Res 41:3539–3552
207. Santoro AE, Boehm AB (2007) Frequent occurrence of the human-specific *Bacteroides* fecal marker at an open coast marine beach: relationship to waves, tides and traditional indicators. Environ Microbiol 9:2038–2049
208. Savichtcheva O, Okayama N, Okabe S (2007) Relationships between *Bacteroides* 16 S rRNA genetic markers and presence of bacterial enteric pathogens and conventional fecal indicators. Water Res 41:3615–3628
209. Schriewer A, Miller WA, Byrne BA, Miller MA, Oates S, Conrad PA, Hardin D, Yang HH, Chouicha N, Melli A, Jessup D, Dominik C, Wuertz S (2010) Presence of *Bacteroidales* as a predictor of pathogens in surface waters of the central California coast. Appl Environ Microbiol 76:5802–5814
210. Schulz CJ, Childers GW (2011) Fecal *Bacteroidales* diversity and decay in response to temperature and salinity. Appl Environ Microbiol 77:2563–2572
211. Scott TM, Rose JB, Jenkins TM, Farrah SR, Lukasik J (2002) Microbial source tracking: current methodology and future directions. Appl Environ Microbiol 68:5796–5803
212. Scott TM, Jenkins TM, Lukasik J, Rose JB (2005) Potential use of a host associated molecular marker in *Enterococcus faecium* as an index of human fecal pollution. Environ Sci Technol 39:283–287
213. Sedmak G, Bina D, MacDonald J (2003) Assessment of an enterovirus sewage surveillance system by comparison of clinical isolates with sewage isolates from Milwaukee, Wisconsin, collected August 1994 to December 2002. Appl Environ Microbiol 69:7181–7187
214. Sedmak G, Bina D, Macdonald J, Couillard L (2005) Nine-year study of the occurrence of culturable viruses in source water for two drinking water treatment plants and the influent and effluent of a wastewater treatment plant in Milwaukee, Wisconsin (August 1994 through July 2003). Appl Environ Microbiol 71:1042–1050
215. Semel JD, Trenholme G (1990) *Aeromonas hydrophila* water-associated traumatic wound infections: a review. J Trauma 30:324–327
216. Sercu B, Van De Werfhorst LC, Murray J, Holden PA (2009) Storm drains are sources of human fecal pollution during dry weather in three urban Southern California watersheds. Environ Sci Technol 43:293–298
217. Seurinck S, Verstraete W, Siciliano SD (2003) Use of 16 S-23S rRNA intergenic spacer region PCR and repetitive extragenic palindromic PCR analyses of *Escherichia coli* isolates to identify nonpoint fecal sources. Appl Environ Microbiol 69:4942–4950
218. Seurinck S, Defoirdt T, Verstraete W, Siciliano SD (2005) Detection and quantification of the human-specific HF183 *Bacteroides* 16 S rRNA genetic marker with real-time PCR for assessment of human faecal pollution in freshwater. Environ Microbiol 7:249–259
219. Sghir A, Gramet G, Suau A, Rochet V, Pochart P, Dore J (2000) Quantification of bacterial groups within human fecal flora by oligonucleotide probe hybridization. Appl Environ Microbiol 66:2263–2266
220. Shanks OC, Santo Domingo JW, Lamendella R, Kelty CA, Graham JE (2006) Competitive metagenomic DNA hybridization identifies host-specific microbial genetic markers in cow fecal samples. Appl Environ Microbiol 72:4054–4060

221. Shanks OC, Domingo JW, Lu J, Kelty CA, Graham JE (2007) Identification of bacterial DNA markers for the detection of human fecal pollution in water. Appl Environ Microbiol 73:2416–2422
222. Shanks OC, Atikovic E, Blackwood AD, Lu J, Noble RT, Domingo JS, Seifring S, Sivaganesan M, Haugland RA (2008) Quantitative PCR for detection and enumeration of genetic markers of bovine fecal pollution. Appl Environ Microbiol 74:745–752
223. Shanks OC, Kelty CA, Sivaganesan M, Varma M, Haugland RA (2009) Quantitative PCR for genetic markers of human fecal pollution. Appl Environ Microbiol 75:5507–5513
224. Shanks OC, White K, Kelty CA, Hayes S, Sivaganesan M, Jenkins M, Varma M, Haugland RA (2010) Performance assessment PCR-based assays targeting bacteroidales genetic markers of bovine fecal pollution. Appl Environ Microbiol 76:1359–1366
225. Shanks OC, White K, Kelty CA, Sivaganesan M, Blannon J, Meckes M, Varma M, Haugland RA (2010) Performance of PCR-based assays targeting Bacteroidales genetic markers of human fecal pollution in sewage and fecal samples. Environ Sci Technol 44:6281–6288
226. Shanks OC, Kelty CA, Archibeque S, Jenkins M, Newton RJ, McLellan SL, Huse SM, Sogin ML (2011) Community structure of cattle fecal bacteria from different animal feeding operations. Appl Environ Microbiol 77:2992–3001
227. Shibata T, Solo-Gabriele HM, Fleming LE, Elmir S (2004) Monitoring marine recreational water quality using multiple microbial indicators in an urban tropical environment. Water Res 38:3119–3131
228. Silkie SS, Nelson KL (2009) Concentrations of host-specific and generic fecal markers measured by quantitative PCR in raw sewage and fresh animal feces. Water Res 43: 4860–4871
229. Sinton LW, Hall CH, Lynch PA, Davies-Colley RJ (2002) Sunlight inactivation of fecal indicator bacteria and bacteriophages from waste stabilization pond effluent in fresh and saline waters. Appl Environ Microbiol 68:1122–1131
230. Sivaganesan M, Seifring S, Varma M, Haugland RA, Shanks OC (2008) A Bayesian method for calculating real-time quantitative PCR calibration curves using absolute plasmid DNA standards. BMC Bioinformatics 9:120
231. Sivaganesan M, Haugland RA, Chern EC, Shanks OC (2010) Improved strategies and optimization of calibration models for real-time PCR absolute quantification. Water Res 44:4726–4735
232. Soller JA, Bartrand T, Ashbolt NJ, Ravenscroft J, Wade TJ (2010) Estimating the primary etiologic agents in recreational freshwaters impacted by human sources of faecal contamination. Water Res 44:4736–4747
233. Soller JA, Schoen ME, Bartrand T, Ravenscroft JE, Ashbolt NJ (2010) Estimated human health risks from exposure to recreational waters impacted by human and non-human sources of faecal contamination. Water Res 44: 4674–4691
234. Steets BM, Holden PA (2003) A mechanistic model of runoff-associated fecal coliform fate and transport through a coastal lagoon. Water Res 37:589–608
235. Stewart JR, Ellender RD, Gooch JA, Jiang S, Myoda SP, Weisberg SB (2003) Recommendations for microbial source tracking: lessons from a methods comparison study. J Water Health 1:225–231
236. Stewart JR, Gast RJ, Fujioka RS, Solo-Gabriele HM, Meschke JS, Amaral-Zettler LA, Del Castillo E, Polz MF, Collier TK, Strom MS, Sinigalliano CD, Moeller PD, Holland AF (2008) The coastal environment and human health: microbial indicators, pathogens, sentinels and reservoirs. Environ Health 7(Suppl 2):S3
237. Stoeckel DM, Harwood VJ (2007) Performance, design, and analysis in microbial source tracking studies. Appl Environ Microbiol 73:2405–2415
238. Stoeckel DM, Stelzer EA, Dick LK (2009) Evaluation of two spike-and-recovery controls for assessment of extraction efficiency in microbial source tracking studies. Water Res 43:4820–4827
239. Sullivan D, Brooks P, Tindale N, Chapman S, Ahmed W (2010) Faecal sterols analysis for the identification of human faecal pollution in a non-sewered catchment. Water Sci Technol 61:1355–1361
240. Tartera C, Lucena F, Jofre J (1989) Human origin of *Bacteroides fragilis* bacteriophages present in the environment. Appl Environ Microbiol 55:2696–2701
241. Teng LJ, Hsueh PR, Huang YH, Tsai JC (2004) Identification of *Bacteroides thetaiotaomicron* on the basis of an unexpected specific amplicon of universal 16 S ribosomal DNA PCR. J Clin Microbiol 42:1727–1730
242. Turnbaugh PJ, Hamady M, Yatsunenko T, Cantarel BL, Duncan A, Ley RE, Sogin ML, Jones WJ, Roe BA, Affourtit JP, Egholm M, Henrissat B, Heath AC, Knight R, Gordon JI (2009) A core gut microbiome in obese and lean twins. Nature 457:480–484
243. Ufnar JA, Wang SY, Christiansen JM, Yampara-Iquise H, Carson CA, Ellender RD (2006) Detection of the nifH gene of *Methanobrevibacter smithii*: a potential tool to identify sewage pollution in recreational waters. J Appl Microbiol 101:44–52
244. Ufnar JA, Ufnar DF, Wang SY, Ellender RD (2007) Development of a swine-specific fecal pollution marker based on host differences in methanogen mcrA genes. Appl Environ Microbiol 73:5209–5217
245. Ufnar JA, Wang SY, Ufnar DF, Ellender RD (2007) Methanobrevibacter ruminantium as an indicator of domesticated-ruminant fecal pollution in surface waters. Appl Environ Microbiol 73:7118–7121
246. Unno T, Jang J, Han D, Kim JH, Sadowsky MJ, Kim OS, Chun J, Hur HG (2010) Use of barcoded pyrosequencing and shared OTUs to determine sources of fecal bacteria in watersheds. Environ Sci Technol 44:7777–7782
247. USEPA (2000) Improved enumeration methods for recreational water quality indicators: Enterococci and *Escherichia*

coli. EPA 821/R-97/004. US Environmental Protection Agency Office of Water, Washington, DC

248. USEPA (2002) Method 1603: *Escherichia coli* (*E. coli*) in water by membrane filtration using modified membrane-thermotolerant Escherichia coli agar (modified mTEC) EPA-821-R-02-023. US Environmental Protection Agency Office of Water, Washington, DC
249. USEPA (2002) Method 1604: total coliforms and *Escherichia coli* in water by membrane filtration using a simultaneous detection technique (MI Medium). US Environmental Protection Agency Office of Water, Washington, DC
250. USEPA (2006) Method 1600: Enterococci in Water by Membrane Filtration Using MEMBRANE-Enterococus Indoxyl-B-D-Glucoside agar (mEI) EPA-821-R-06-009. US Environmental Protection Agency Office of Water, Washington, DC
251. USEPA (2007) Critical path science plan for the development of new or revised recreational water quality criteria. 823-R-08-002. US Environmental Protection Agency Office of Water, Washington, DC
252. USEPA (2009) National water quality inventory: report to congress 2004 reporting cycle. EPA 841-R-08-001. US Environmental Protection Agency Office of Water, Washington, DC
253. USEPA (2010) Method A: Enterococci in water by TaqMan® quantitative polymerase chain reaction (qPCR) assay. US Environmental Protection Agency Office of Water, Washington, DC
254. Viau EJ, Goodwin KD, Yamahara KM, Layton BA, Sassoubre LM, Burns S, Tong H-I, Wong SHC, Boehm AB (2011) Human bacterial pathogens and fecal indicators in tropical streams discharging to Hawaiian coastal waters. Water Res 45:3279–3290
255. Volkmann H, Schwartz T, Kirchen S, Stofer C, Obst U (2007) Evaluation of inhibition and cross-reaction effects on real-time PCR applied to the total DNA of wastewater samples for the quantification of bacterial antibiotic resistance genes and taxon-specific targets. Mol Cell Probes 21:125–133
256. Wade TJ, Pai N, Eisenberg JN, Colford JM Jr (2003) Do U.S. Environmental Protection Agency water quality guidelines for recreational waters prevent gastrointestinal illness? A systematic review and meta-analysis. Environ Health Perspect 111:1102–1109
257. Wade TJ, Calderon RL, Sams E, Beach M, Brenner KP, Williams AH, Dufour AP (2006) Rapidly measured indicators of recreational water quality are predictive of swimming-associated gastrointestinal illness. Environ Health Perspect 114:24–28
258. Wade TJ, Calderon RL, Brenner KP, Sams E, Beach M, Haugland R, Wymer L, Dufour AP (2008) High sensitivity of children to swimming-associated gastrointestinal illness: results using a rapid assay of recreational water quality. Epidemiol 19:375–383
259. Wade TJ, Sams E, Brenner KP, Haugland R, Chern E, Beach M, Wymer L, Rankin CC, Love D, Li Q, Noble R, Dufour AP (2010) Rapidly measured indicators of recreational water quality and swimming-associated illness at marine beaches: a prospective cohort study. Environ Health 9:66
260. Walters SP, Gannon VPJ, Field KG (2007) Detection of *Bacteroidales* fecal indicators and the zoonotic pathogens *E. coli* O157:H7, *Salmonella*, and *Campylobacter* in river water. Environ Sci Technol 41:1856–1862
261. Walters SP, Yamahara KM, Boehm AB (2009) Persistence of nucleic acid markers of health-relevant organisms in seawater microcosms: implications for their use in assessing risk in recreational waters. Water Res 43:4929–4939
262. Walters SP, Thebo AL, Boehm AB (2011) Impact of urbanization and agriculture on the occurrence of bacterial pathogens and stx genes in coastal waterbodies of central California. Water Res 45:1752–1762
263. Westrell T, Teunis P, van den Berg H, Lodder W, Ketelaars H, Stenstrom TA, de Roda Husman AM (2006) Short- and long-term variations of norovirus concentrations in the Meuse river during a 2-year study period. Water Res 40: 2613–2620
264. Wetz JJ, Blackwood AD, Fries JS, Williams ZF, Noble RT (2008) Trends in total *Vibrio* spp. and *Vibrio vulnificus* concentrations in the eutrophic Neuse River Estuary, North Carolina, during storm events. Aquat Microb Ecol 53:141–149
265. Whitman RL, Nevers MB (2003) Foreshore sand as a source of *Escherichia coli* in nearshore water of a Lake Michigan beach. Appl Environ Microbiol 69:5555–5562
266. Whitman RL, Nevers MB, Korinek GC, Byappanahalli MN (2004) Solar and temporal effects on *Escherichia coli* concentration at a Lake Michigan swimming beach. Appl Environ Microbiol 70:4276–4285
267. Whitman RL, Ge Z, Nevers MB, Boehm AB, Chern EC, Haugland RA, Lukasik AM, Molina M, Przybyla-Kelly K, Shively DA, White EM, Zepp RG, Byappanahalli MN (2010) Relationship and variation of qPCR and culturable Enterococci estimates in ambient surface waters are predictable. Environ Sci Technol 44:5049–5054
268. Wiedenmann A, Kruger P, Dietz K, Lopez-Pila JM, Szewzyk R, Botzenhart K (2006) A randomized controlled trial assessing infectious disease risks from bathing in fresh recreational waters in relation to the concentration of *Escherichia coli*, intestinal enterococci, *Clostridium perfringens*, and somatic coliphages. Environ Health Perspect 114:228–236
269. Wiggins BA (1996) Discriminant analysis of antibiotic resistance patterns in fecal streptococci, a method to differentiate human and animal sources of fecal pollution in natural waters. Appl Environ Microbiol 62:3997–4002
270. Wilkes G, Edge T, Gannon V, Jokinen C, Lyautey E, Medeiros D, Neumann N, Ruecker N, Topp E, Lapen DR (2009) Seasonal relationships among indicator bacteria, pathogenic bacteria, *Cryptosporidium* oocysts, *Giardia* cysts, and hydrological indices for surface waters within an agricultural landscape. Water Res 43:2209–2223
271. Wong M, Kumar L, Jenkins TM, Xagoraraki I, Phanikumar MS, Rose JB (2009) Evaluation of public health risks at recreational beaches in Lake Michigan via detection of enteric viruses

and a human-specific bacteriological marker. Water Res 43:1137–1149
272. Wu CH, Sercu B, Van de Werfhorst LC, Wong J, DeSantis TZ, Brodie EL, Hazen TC, Holden PA, Andersen GL (2010) Characterization of coastal urban watershed bacterial communities leads to alternative community-based indicators. PLoS One 5: e11285
273. Wyn-Jones AP, Carducci A, Cook N, D'Agostino M, Divizia M, Fleischer J, Gantzer C, Gawler A, Girones R, Höller C, Husman AM, Kay D, Kozyra I, López-Pila J, Muscillo M, Nascimento MS, Papageorgiou G, Rutjes S, Sellwood J, Szewzyk R, Wyer M (2011) Surveillance of adenoviruses and noroviruses in European recreational waters. Water Res 45:1025–1038
274. Xu J, Bjursell MK, Himrod J, Deng S, Carmichael LK, Chiang HC, Hooper LV, Gordon JI (2003) A genomic view of the human-*Bacteroides thetaiotaomicron* symbiosis. Science 299:2074–2076
275. Yamahara KM, Layton BA, Santoro AE, Boehm AB (2007) Beach sands along the California coast are diffuse sources of fecal bacteria to coastal waters. Environ Sci Technol 41:4515–4521
276. Yamahara KM, Walters SP, Boehm AB (2009) Growth of enterococci in unaltered, unseeded beach sands subjected to tidal wetting. Appl Environ Microbiol 75:1517–1524
277. Yampara-Iquise H, Zheng G, Jones JE, Carson CA (2008) Use of a *Bacteroides thetaiotaomicron*-specific alpha-1-6, mannanase quantitative PCR to detect human faecal pollution in water. J Appl Microbiol 105:1686–1693
278. Young TA, Heidler J, Matos-Perez CR, Sapkota A, Toler T, Gibson KE, Schwab KJ, Halden RU (2008) Ab initio and in situ comparison of caffeine, triclosan, and triclocarban as indicators of sewage-derived microbes in surface waters. Environ Sci Technol 42:3335–3340
279. Zheng G, Yampara-Iquise H, Jones JE, Carson CA (2009) Development of *Faecalibacterium* 16 S rRNA gene marker for identification of human faeces. J Appl Microbiol 106:634–641

Marine and Hydrokinetic Energy Environmental Challenges

Andrea E. Copping
Marine Sciences Laboratory, Pacific Northwest National Laboratory, Seattle, WA, USA

Article Outline

Glossary
Definition of the Subject and Its Importance
Introduction
Evaluating Environmental Effects of MHK Development
Environmental Challenges Presented by New Technologies
Other Challenges to MHK Energy Development
Conclusions and Future Directions
Bibliography

Glossary

Energy from ocean currents Energy harvested from the continuous and predictable flow of ocean currents near landforms.

Marine and hydrokinetic energy Energy that can be harvested from moving water, specifically from ocean waves, tides and currents, and river flow. Abbreviated as MHK, other ocean-based energy resources are usually included in this definition, including ocean thermal energy conversion and energy derived from osmotic gradients.

Ocean thermal energy conversion Energy harvested from the heat differential from cold deep water to warmer surface waters. Abbreviated as OTEC, this energy capture as presently conceived is viable only when a temperature difference of 20°C or more exists from surface to deep ocean water layers.

Osmotic energy Energy harvested from the gradient of salt content from saline ocean water to freshwater. It is generally thought to be viable only at river mouths that empty directly into the sea.

Receptors Terminology for portions of the aquatic ecosystem that are likely to be affected by MHK devices, generally consisting of aquatic animals, habitats, and ecosystems.

River energy Energy derived from the unidirectional flow of water in natural and managed rivers.

Stressors Terminology for parts of MHK systems that may cause stress or harm to aquatic receptors, including the MHK devices, mooring lines, anchors, floats, power cables, and other equipment that may compromise aquatic receptors during installation, operation, maintenance, and decommissioning of MHK developments.

Tidal energy Energy that can be harvested from the daily tidal prism in estuaries, coastal embayments, and other constrictions in ocean areas.

Wave Energy Energy that can be harvested from the vertical motion of waves in coastal areas and/or in open ocean.

Definition of the Subject and Its Importance

The marine and hydrokinetic (MHK) energy industry in the USA and abroad is moving towards commercial-scale development of devices in the marine environment and major rivers in order to generate carbon-free energy in proximity to major load centers along the coastlines. Laws, regulations, and public sentiment require that these deployments and operations provide minimal risk to the marine and riverine environments, the animals that live in them, and to existing human benefits derived from these systems. Effective siting and permitting of MHK devices can only be done successfully by understanding and measuring the environmental effects of MHK devices on the aquatic animals, habitats, and ecosystems of coastal and riverine areas where cost-effective energy generation is possible.

Introduction

As more ocean energy devices are tested, and plans for commercial-scale developments progress, challenges and potential obstacles presented by environmental siting and permitting must be addressed [1–4]. Environmental laws and regulations require that living organisms and systems be protected [5]. US laws and regulations are particularly stringent and require considerable advance understanding of potential effects before devices are deployed [6]. Oceanographic research can provide insight into the action of tides, waves, ocean currents, and other physical and chemical processes in the oceans. Equivalent information about river systems is also available. However, assessments of biological resources in these areas are generally more limited, particularly in the oceans [7]. And very little useful information is available on potential interactions of marine and hydrokinetic devices on marine and freshwater receptors – the animals, habitats, and ecosystems – in areas of proposed marine and hydrokinetic (MHK) energy development [8, 9]. The scientific literature is very light in this area, with most contributions from government reports, gray (non-peer-reviewed) literature, and industry publications. The very high level of uncertainly surrounding potential adverse encounters between MHK systems and vulnerable receptors drives concerns among regulators and stakeholders, potentially slowing development of the MHK industry [10].

This entry will address the major challenges of identifying, measuring, and setting priorities for environmental effects of MHK devices and arrays. First, the various types of MHK devices and the resources they are designed to harvest will be presented. Next, the challenges are introduced as they apply to each of the specific technology types. In the next section, additional challenges to MHK development are briefly presented. Methods for addressing environmental effects of MHK development make up the next section, including a risk-informed approach under development in a US Department of Energy National Laboratory. Mitigation strategies will be discussed. And finally, a path forward to understand and evaluate the challenges of environmental effects of MHK development will be discussed.

Evaluating Environmental Effects of MHK Development

The challenges of predicting the effects and impacts of MHK energy devices on aquatic receptors are hindered by several factors: (1) the technologies are new, and few appropriate analogues exist that will inform potential interactions with living systems; (2) MHK energy development in the ocean is a new use of ocean space, potentially in conflict with other existing uses; (3) MHK device deployment is often planned for areas of fast currents and large waves where there is little oceanographic knowledge; (4) biological resources that are harvested are better known than those which are not directly consumed; however, in many cases, the resources at risk from MHK are not harvested; and (5) MHK energy devices will often be deployed in areas already affected by anthropogenic stressors so that the effect of these devices may be difficult to distinguish from the cumulative impacts of existing industrial activities. Because other industries face similar in-water challenges, environmental effects associated with the installation, decommissioning, and maintenance phases of MHK deployment can be predicted reasonably well. This experience provides

a record of interactions with aquatic receptors and suggests appropriate mitigation strategies to minimize risk to the marine and riverine environment [11]. However, effects of the operational phase of MHK deployments are not easily compared to analogues.

MHK devices are tailored for the energy source they will harvest. Although certain hybrid technologies are under development, the major MHK devices are those aimed at harvesting energy from tides, waves, river flow, ocean currents, temperature differential, and salinity differential.

Tides – Unlike earlier attempts to create tidal barrages or tidal fences, most tidal MHK devices are turbines, consisting of a rotor with multiple blades that rotate with the flow of ebb and flood tides. A limited number of bays, estuaries, and passes have good tidal energy potential. Most tidal devices are deployed near the seabed.

Waves – Wave energy converters take many forms and configurations, with most encompassing a surface buoy or float and mooring lines through the water column to anchors in the seabed. This technology is potentially viable wherever waves occur, along coastlines and (for specialized technologies) the open ocean.

River Flow – Most devices designed to capture energy from river flow resemble bladed tidal turbines but are unidirectional and generally smaller than tidal turbines.

Ocean Currents – The ability to harvest energy from constant ocean currents will be accomplished with very large rotating turbines. Ocean currents that are sufficiently constant in location and power density lie along the western edges of ocean basins. Within US waters, the most viable candidate for ocean current harvest is the Gulf Stream along the Florida coastline.

Temperature Gradients – Harvest of energy from temperature gradients in the ocean requires a substantial difference in temperature between warm surface and cool water at depth, as is found in tropical waters. Within US waters, the most viable locations are the Hawaiian Islands and Florida, as well as tropical US territories. Temperature gradients can be harvested by large-scale floating OTEC (ocean thermal energy conversion) plants, equipped with deep (1,000 m or more) cold water uptake pipes and shallower warm water uptake and return pipes.

Osmotic Gradients – The difference in salinity found at river mouths entering coastal seas allows for the harvest of energy from osmotic pressure difference. Very large lengths of fine osmotic exchange tubes are needed for this process; however, only the water intake need be deployed in open water, while the osmotic exchange technology can be packed tightly into buildings on land.

Environmental Challenges Presented by New Technologies

Each MHK technology interacts with the marine and freshwater environment in a different way. Each represents a new series of interactions with the living biota, the habitats, and the ecosystems that will become part of the new power generation system. Some suitable analogues exist to help inform predictions of interactions between the various stressors that make up the MHK installations and the many marine and freshwater receptors, such as offshore oil and gas rigs and navigation buoys creating artificial reefs; interaction of fish in conventional hydropower turbines; and offshore wind turbines changing benthic habitats. However, none of these analogue interactions are exactly indicative of the stressor–receptor interactions expected from arrays of MHK devices in the aquatic environment. Many MHK installations have some attachment to the seabed or riverbed; all place some impediment to water flow in the natural circulation; and all require a power cable to carry electricity to the land-based electrical grid [12].

Separate and distinct stressors will act upon aquatic receptors, depending on the phase of MHK development, from installation, operation, maintenance, and decommissioning. Installation may cause a series of high-intensity interactions that result from placing or anchoring the device to the bottom, including pile driving, pinning tidal turbine foundations, and embedding anchors into bottom sediment. In addition, intensive vessel traffic may disturb marine animals and increase the spill risk of petroleum and other hazardous materials. Decommissioning will also result in increased vessel traffic and may cause benthic habitat destruction from the removal of piles or anchors. Maintenance activities increase vessel traffic, potentially disturbing marine animals and increasing spill risks. Operational effects are generally thought to be less destructive but provide the potential for ongoing

interactions between MHK devices and aquatic animals, as well as chronic stressors like acoustic output from turbines and EMF from cables and turbines. Specific environmental interactions for the operational phase of each technology type are summarized here.

Tidal Devices – The most common tidal MHK devices are anchored on or near the seabed with gravity or bottom-piercing mounts. Blades rotate only when the tidal energy reaches the cut-in speed of the device. The benthic habitat onto which the devices are installed is most commonly made up of coarse sediments, as fine sediment particles are carried away by swift currents at the site. Environmental effects of greatest concern for operation of single tidal turbines as well as arrays of devices include: (1) the danger presented by rotating blades to sea life such as marine mammals, fish, and diving birds; (2) acoustic output from rotating turbine blades interrupting marine mammal communication and navigation, as well as disturbing other organisms such as fish and sea turtles; (3) electromagnetic output from turbines and power cables, affecting sensitive organisms, particularly elasmobranchs (sharks and rays); and for large arrays of devices, (4) basin-scale effects from changes in water circulation from the presence of the devices as well as energy removal from power take off, resulting in changes in sediment transport and shore forms, degraded water quality, changes in nearshore habitat quality, and alternation of the base of the marine food web [4, 13, 14]. Maintenance operations generally increase vessel traffic in the area of tidal deployments, potentially disturbing animals and increasing spill risk.

Wave Energy Converters – Wave energy converters (WECs) are most commonly anchored to the seabed with buoys or other structures floating at the surface, attached to the anchors with mooring lines or cables. Environmental effects of greatest concern for operating single WECs as well as arrays of devices include: (1) entanglement of migratory animals such as whales, sea turtles, and diving birds in mooring lines; (2) changes in benthic habitat due to anchors; (3) electromagnetic output from power cables, affecting sensitive organisms, particularly elasmobranchs (sharks and rays) and sea turtles; and for large arrays, (4) changes in benthic habitat and shore forms due to changes in sediment transport, caused by alterations in water circulation around the surface floats [1, 15–17].

River Turbines – Devices planned for river deployment are most commonly turbines similar in design to those used for tidal energy generation, although smaller in size. These devices can be deployed, generally in groups, off bridge abutments, from floating structures, or anchored on foundations above the river bottom. Environmental effects of greatest concern for operation of river turbines include: (1) danger to migratory fish and diving birds from rotating blades; and (2) changes in benthic habitats due to changes in sediment transport, caused by alternations in water circulation around the devices [18].

Ocean Currents – No devices have been tested worldwide; however, these devices are likely to resemble very large tidal turbines and will be deployed at mid-depth in persistent ocean currents, generally at depths of 50–200 m. Surface or subsurface flotation will be needed to keep the turbines at the appropriate depths. Environmental effects of greatest concern for ocean current devices include: (1) entanglement of migratory species particularly whales, dolphins, sea turtles, and large fish in mooring lines, above and below the turbines, as well as avoidance of surface or subsurface floats; (2) changes in benthic habitats due to anchors; and (3) electromagnetic output from turbines and power cables, affecting sensitive organisms, particularly elasmobranchs (sharks and rays) and sea turtles [19].

Temperature Gradients – Pilot-scale OTEC plants were developed several decades ago, and at least one still is in operation in Kona, Hawaii. Full-scale OTEC plants are envisioned as large floating installations anchored to the seafloor in deep water, generally 1,000 m or more. Environmental effects of greatest concern include: (1) changes in the pelagic environment and marine food web due to removal and exchange of warm surface water and cold water from depth; (2) entanglement of migratory species such as marine mammals, fish, sea turtles, and diving birds in mooring lines that reach from the surface installation to the anchors; (3) changes in deep benthic habitats from anchors; and (4) obstructions to migratory pathways due to the large size of the installations [20].

Salinity Gradients – Small-scale osmotic exchange facilities are in operation in Sweden [21] at the mouths of moderate-sized rivers where they enter the sea. To date, the osmotic exchange installations have been

housed in buildings onshore, near the river mouths. Environmental effects are likely to be associated with the withdrawal of freshwater from rivers and nearshore areas and the return of water of altered salinity to these bodies of water.

Other Challenges to MHK Energy Development

In addition to direct environmental risks from MHK energy development, there are other challenges that are inextricably associated with the interaction of MHK devices in the oceans and rivers. These challenges include: the interaction of MHK energy development with existing ocean uses; deployment in high-energy waters; limitations of biological assessments in the target development areas; and cumulative environmental effects of MHK development with other anthropogenic and climate stressors.

Ocean Uses – The coastal and riverine areas that are optimal for energy generation, proximity to a grid connection, and the appropriate distance to a port for construction and maintenance may already be in use for other purposes [22]. Coastal oceans are highly prized for commercial and recreational fishing, navigation, shipping and transportation, national security, boating and surfing, marine conservation, waste disposal, and other uses. As a new industry entering the ocean space, the MHK industry faces the challenge of finding the appropriate space needed for commercial development, within the existing spatial layout and potentially in competition with current users [23].

Energetic Marine and Riverine Locations – The estuarine and nearshore ocean areas where energy is sufficient to generate power are often the areas where the natural resources and physical interactions are least well documented [24]. Oceanographers do not routinely place instruments and deploy gear in areas where the tidal currents and waves are likely to damage or destroy expensive equipment, nor do vessels easily hold station for lengthy deployments or measurements in these areas. For these reasons, our knowledge of the physics, chemistry, and biology of potential MHK sites is often incomplete or lacking altogether.

Biological Assessments – Many of the greatest environmental concerns over the development of MHK energy generation surround interactions with marine and freshwater animals [9]. Robust biological assessments are needed to determine the status of populations prior to MHK deployment and to provide a baseline against which post-installation changes can be evaluated [25]. Populations of commercially and recreationally important species (generally fish, shellfish, and whales) are surveyed with some regularity in some coastal waters and rivers, while bird and other wildlife populations are surveyed episodically by government agencies or nongovernmental organizations. However, in waters preferred for MHK development, many of the populations of concern and their habitats are not well documented.

Cumulative Effects – Coastal areas, estuaries, nearshore marine waters, and major rivers are not made up of untouched wilderness; many commercial, recreational, and industrial activities already use the important ecosystem services supplied by these waters. Sorting out the incremental effects that MHK developments may have on the resilience of aquatic animals, habitats, and ecosystems from the cumulative impacts of other anthropogenic activities, even if robust biological and ecosystems assessment data were available, will prove very challenging [19].

Addressing Environmental Effects

The large number of potential interactions between stressors (those parts of MHK systems that may cause stress on aquatic receptors, including the MHK devices, anchors and mooring lines, cables, and flotation) and receptors (aquatic animals, habitats, ecosystems, or the physical and chemical processes that affect them) requires that one determines which stressor/receptor interactions are most significant, which are likely to cause harm to aquatic receptors and for which appropriate mitigation measures can be developed. MHK development will succeed as a viable renewable energy source in an accelerated fashion if collectively a multipronged approach is pursued, which satisfies the need to be protective of marine and freshwater receptors, while allowing adequate testing of devices, mooring lines and anchors, and electrical systems. The conundrum is the dearth of information on stressor/receptor interactions that makes it difficult to ensure safety for aquatic animals, habitats, and ecosystems, while gaining the performance testing data needed to create viable commercial MHK systems.

The scientific community engaged in evaluating environmental effects of MHK systems appears to be coalescing around two approaches: (1) deploying small numbers of devices as rapidly and safely as possible to gather monitoring data about stressor/receptor interactions and (2) examining each likely stressor/receptor interaction for each class of MHK device (i.e., tidal, wave, river, OTEC) and estimating the relative risk of each receptor encounter.

One risk-based approach is being pursued at Pacific Northwest National Laboratory, in collaboration with other US Department of Energy National Laboratories, university partners, with the cooperation of MHK project developers, regulatory agencies, and stakeholders [26]. Risk is being defined as the potential deleterious consequences of stressor/receptor interactions, as a function of consequence (the seriousness of the effect) and a factor of probability (chance that the encounter will occur) [27, 28]. The risk-based approach, dubbed ERES (environmental risk evaluation system), examines every risk-relevant stressor/receptor pair from MHK projects that are in advanced stages of development, using expert opinion to rank the relative consequences among the pairs, in lieu of field and laboratory data. The semiformal gathering of expert opinion uses a series of biophysical risk factors to rank consequence; regulatory requirements are also taken into consideration to determine the importance of each stressor/receptor pair. As experimental monitoring and modeling data become available, the ranking of these consequences will be re-assessed using these data, replacing the expert opinion with results based on empirical studies. The continuing challenge of the system is that there are insufficient data to carry out probability modeling to create a true risk ranking. The output of an initial ERES screening case for a tidal energy project is shown, for illustration purposes only, in Table 1. Consequence rankings within a tier are considered tied ranks.

Following the expert opinion-based ranking of stressor/receptor pairs for consequences, probability analysis will determine whether some of the highest ranked stressor/receptor pairs represent low probability of encounter and, therefore, a reduced risk despite the potentially high consequences; additionally, further elucidation of the tied ranks will be possible with probability analysis, once sufficient data exist. As more data become available, it will become clear which of the

Marine and Hydrokinetic Energy Environmental Challenges. Table 1 Top tiers of risk based on environmental consequence for stressor/receptor pairs for a tidal case, using the environmental risk evaluation system (ERES). Each receptor group is listed, with an example from Pacific NORTHWEST location in the USA, in brackets. T&E – threatened and endangered animal, listed under the Endangered Species Act (After [26], 53 pp)

Tidal stressor	Tidal receptor
First tier	
Accident/disaster (oil spills)	T&E cetacean (killer whale)
Accident/disaster (oil spills)	T&E pinniped (Steller sea lion)
Physical presence (dynamic)	T&E cetacean (killer whale)
Physical presence (dynamic)	T&E pinniped (Steller sea lion)
Physical presence (dynamic)	T&E bird (marbled murrelet)
Second tier	
Noise	T&E cetacean (killer whale)
Noise	T&E pinniped (Steller sea lion)
Accident/disaster (oil spill)	T&E bird (marbled murrelet)
Leaching of toxic chemicals	T&E bird (marbled murrelet)
Noise	T&E bird (marbled murrelet)
Third tier	
EMF	T&E bird (marbled murrelet)
Physical presence (static)	T&E bird (marbled murrelet)
Fourth tier	
Physical presence (static)	T&E cetacean (killer whale)
Physical presence (static)	T&E pinniped (Steller sea lion)
Fifth tier	
EMF	T&E cetacean (killer whale)
EMF	T&E pinniped (Steller sea lion)
Leaching of toxic chemicals	T&E cetacean (killer whale)
Leaching of toxic chemicals	T&E pinniped (Steller sea lion)

highest ranked stressor/receptor interactions are due to great uncertainty, and which truly constitute risk of adverse impacts to aquatic receptors. Stressor/receptor pairs that rank high due to uncertainty will benefit from additional research and monitoring effort, perhaps allowing some to become less highly ranked. As highly ranked stressor/receptor pairs move to lower tiers with additional information, those pairs that remain highly ranked will be candidates for mitigation. In this iterative manner, ERES will assist MHK developers, regulators, and stakeholders to focus on mitigating the most severe risks and allow renewable, carbon-free MHK energy generation to accelerate.

Regulatory Drivers – In our society, the relative level of concern over environmental effects is determined through the regulatory process. Laws and regulations are enacted to protect natural resources and human health and create de facto value systems for society's use of resources. In order to regulate a new industry, with technologies that have no close analogues, the existing laws and regulations will need to be adapted to cover MHK development. These regulatory drivers often are not well aligned with the realities of new technologies such as MHK and may trigger concerns over risks to the marine and freshwater environment that later are shown to be relatively unimportant. As more experience with MHK devices in the water and more information about environmental effects become available, more impact-appropriate approaches to regulating the industry are likely to emerge, as has happened in many other resource-based industries. Variations on existing regulatory processes that have been implemented in other countries include provisions for early demonstration or small-scale pilot projects that are believed to have minimal impact on the environment; the rationale behind these early deployments is to gather experience and information to better inform commercial-scale environmental risks from MHK devices. However, as the MHK industry emerges, in most countries including the USA, application of existing laws and regulatory pathways will continue to be the major construct for advancing towards commercial development.

Mitigation Strategies

As environmental risks to aquatic animals, habitats, or ecosystems are identified through directed research and monitoring of in-water MHK sites, strategies to mitigate the impacts must be devised and implemented to reduce risks and protect vulnerable living systems. Although little formal investigation of mitigation strategies has been carried out for MHK deployments and operations, they appear to fall into four categories of mitigation, including siting, engineering design, modification of animal behavior, and exclusion of receptors from interaction. Each strategy will be briefly discussed.

Siting as Mitigation Strategy – At a gross level, MHK devices and farms must be located in areas where there is sufficient power resource to allow for generation of power, at whatever level is desired (small distributed systems, utility-scale production, etc.). Siting also requires that attention be paid to distance from shore and capable ports and harbors such that power cables can be laid to shore in proximity to transmission interconnections and to allow for cost-effective and safe installation and maintenance. However, within these constraints, there are generally options for micro-siting and displacement from original plans to lower risk to aquatic animals, habitats, or the ecosystem. For example, if a wave installation is planned for an area where large numbers of seabirds congregate, moving the installation a few kilometers offshore could lower the risk to the birds while causing little disruption to the power-generating potential. Similarly, during preliminary planning, the relocation of the foundation of a tidal turbine or wave anchor from a known crab nursery ground would greatly reduce the environmental risk at little or no increased cost of installation or power production.

Engineering Design Feedback as Mitigation – As environmental studies and risk evaluation of MHK projects proceed in parallel to engineering of deployment, anchoring, and operational systems, there are opportunities for feedback from the environmental risk analysis to engineering teams to reduce stress to the environment with engineering and design solutions. For example, if the leading edge of a river or tidal turbine blade was shown (or even strongly suspected) of causing a threat to a migrating endangered fish species, that knowledge would allow the engineering team to redesign the blade shape or operation to lower that risk. Another example includes the tautness of mooring lines for wave buoys could be shown to affect the frequency with which marine

mammals become entangled, allowing the engineers designing the lines, materials, and operational status to make changes that will protect the animals. And yet another example might be the discovery that EMF from power cables is causing disruptions to feeding and movement of fish such as sharks in marine waters and sturgeon in freshwater; engineering solutions such as cable burial, switching from AC transmission to DC, or specialized shielding, could decrease or eliminate the risk to fish.

Behavior Modification of Threatened Animals – Risk evaluation will help to pinpoint specific aspects of MHK devices and systems that are particularly dangerous to aquatic animals. This knowledge can be used to deter at risk animals from approaching close enough to the devices or systems for that encounter to take place. For example, acoustic deterrents are under investigation on lines of wave buoys to deter migrating whales traveling parallel to the coast, with the desired outcome to move the whales slightly further offshore. Similarly, seabirds can be encouraged to avoid wave platforms with the use of acoustic or visual deterrents. This form of mitigation holds great promise of reducing targeted risk to aquatic animals; however, there are two barriers to its widespread use: (1) predicting the behavior of animals encountering new stimuli in their habitat is very uncertain, leading to potentially unintended consequences, such as animals being preferentially attracted rather than repelled by warnings, or becoming desensitized over time; and (2) harassment of many aquatic animals, which includes injury, death, or alterations in behavior, is not permitted with few exceptions; harassment applies to most protected species (in the USA under the Endangered Species Act or in the EU under Natura 2000), as well as most or all marine mammals (in the USA under the Marine Mammal Protection Act). Additional research is needed into safe deterrents and behavioral reactions of vulnerable animals; this research generally must be carried out under the auspices of the government agencies responsible for protecting these species.

Exclusion of Aquatic Receptors from MHK Devices – Each of the previously discussed mitigation strategies seeks to decrease the risk to aquatic animals, habitats, and ecosystems from stressors created by MHK devices and systems. However, there is an increasing focus from regulatory bodies and stakeholders on taking more proactive steps to ensure the safety of these receptors. Physical barriers and operational changes to prevent the opportunity of encounter are most commonly considered, although other options may be considered as well. Most prominently considered are processes that recognize the threat to an aquatic animal in real time and take action to shutdown a rotating turbine. The pioneering work on the marine current turbine in Strangford Lough in Northern Ireland has involved marine mammal observers, making visual observations during daylight hours to trigger a shutdown of the turbines when endangered pinnipeds approach, and later the use of sonar to provide the approach data to the observer to trigger a shutdown. Another example is the development of the marine animal alert system (MAAS) at PNNL; the MAAS will use passive and active acoustic signals to detect and classify members of an endangered small whale population in Puget Sound and provide a signal to automatically shutdown the nearby tidal turbines when the whales enter a risk envelope developed in partnership and cooperation with the regulatory body. These mitigation strategies, and similar plans to exclude animals from encounters, provide a strong measure of safety for the aquatic receptors but may have sizable deleterious consequences to the ability to develop the MHK industry as a viable renewable energy source.

Conclusions and Future Directions

The MHK industry is emerging in Europe, Asia, North America, and Brazil, based on the extremely large potential for power generation from waves, tides, river flows, ocean current, and other attributes of the world's water resources [29]. There are many MHK technology designs in various stages of development, with a few ready for commercial-scale deployment while most are still in the testing and development stages. As the formidable hurdles of designing robust systems for long-term deployment in harsh ocean and river conditions proceed, the challenges of protecting the natural environment must be given a prominent place in the development sequence. The laws and regulations governing deployment in the water, bringing power cables to land through the nearshore and intertidal/riparian zone, and the activities surrounding installation, operation, maintenance, and

decommissioning of these systems require understanding the baseline conditions where the MHK devices will be placed and the effects and impacts once they are in place. Appropriate mitigation of impacts that cannot be eliminated will become lifelong features of MHK farms. In addition, stakeholders will hold the industry and regulators responsible for adverse outcomes and will press for a high standard of certainty before commercial-scale MHK farms are developed.

Many of the information needs, strategies for collecting cost-effective and accurate monitoring data over long periods of time, and devising effective and efficient mitigation strategies can be assisted with deliberate research programs coordinated among the MHK industry, regulators, funding agencies, and the research community. Early and open coordination of studies, monitoring designs, and mitigation strategies among the interested parties is necessary. The broader the discussions and coordination of these goals and strategies is, and the engagement of all parties, the faster a sustainable and vibrant MHK industry, contributing to the renewable energy portfolio, will become a reality.

Bibliography

1. Boehlert G, McMurray G, Tortorici C (2008) Ecological effects of wave energy development in the Pacific Northwest: a scientific workshop. U.S. Department of Commerce, Seattle, 11–12 Oct 2007
2. Cada G, Ahlgrimm J, Bahleda M, Bigford T, Stavrakas SD, Hall D, Moursund R, Sale M (2007) Potential impacts of hydrokinetic and wave energy conversion technologies on aquatic environments. Fisheries 32:174–181
3. Dadswell MJ, Rulifson RA, Daborn GR (1986) Potential impact of large-scale tidal power developments in the upper Bay of Fundy on fisheries resources of the northwest Atlantic. Fisheries 11:26–35
4. Polagye B, Copping A, Kirkendall K, Boehlert G, Walker S, Weinstein M, Cleve BV (in press) Environmental effects of tidal energy development: a scientific workshop. University of Washington, Seattle, 22–24 Mar 2010
5. Federal Energy Regulatory Commission (2008) White paper on licensing hydrokinetic pilot projects. Federal Energy Regulatory Commission, Washington, DC
6. Michel J, Dunagan H, Boring C, Healy E, Evans W, Dean J, McGillis A, Hain J (2007) Worldwide synthesis and analysis of existing information regarding environmental effects of alternative energy uses on the outer continental shelf. Minerals Management Service, U.S. Department of the Interior, Washington, DC
7. U.S. Commission on Ocean Policy (2004) An ocean blueprint for the 21st century. Final report, Washington, DC
8. Electric Power Research Institute (2008) Prioritized research, development, deployment and demonstration (RDD&D) needs: marine and other hydrokinetic renewable energy. EPRI, Palo Alto
9. U.S. Department of Energy (2009) Report to congress on the potential environmental effects of marine and hydrokinetic energy technologies. Wind and Hydropower Technologies Program, U.S. Department of Energy, Washington DC
10. Copping AE, Geerlofs S (2010) Report on outreach to stakeholders for fiscal year 2009. Pacific Northwest National Laboratory, Seattle
11. Bedard R, Previsic M, Hagerman G, Polagye B, Musial W, Klure J, von Jouanne A, Mathur U, Collar C, Hopper C, Amsden S (2007) North American ocean energy status – Mar 2007. In: European wave and tidal energy conference, Porto, pp 1–8
12. Gill A (2005) Offshore renewable energy: ecological implications of generating electricity in the coastal zone. J Appl Ecol 42:605–615
13. Dacre SL, Bryden IG, Bullen CR (2002) Environmental impacts and constraints of tidal current energy: the Pentland Firth feasibility study. In: Proceedings from MAREC 2002 two day international conference on marine renewable energy, Newcastle
14. El-Geziry TM, Bryden I, Couch S (2009) Environmental impact assessment for tidal energy schemes: an exemplar case study of the Strait of Messina. Proc IMarEST Part A J Mar Eng Technol 13:39–48
15. Bald J, del Campo A, Franco J, Galparsoro I, González M, Liria P, Muxika I, Rubio A, Solaun O, Uriarte A, Comesaña M, Cacabelos A, Fernández R, Méndez G, Prada D, Zubiate L (2010) Protocol to develop an environmental impact study of wave energy converters AZTI-Tecnalia, Herrera Kaia
16. Electrical Power Research Institute (2004) Offshore wave power in the U.S.: Environmental issues. EPRI, Edison
17. Grecian WJ, Inger R, Attrill MJ, Bearhop S, Godley BJ, Witt MJ, Votier SC (2010) Potential impacts of wave-powered marine renewable energy installations on marine birds. IBIS 152: 683–697
18. Cada G, Copping A, Roberts J (in press) The U.S. Department of Energy's efforts to identify and resolve environmental impacts of marine and hydrokinetic energy technologies. Hydrovision
19. Minerals Management Service, Renewable Energy and Alternate Use Program, U.S. Department of the Interior (2006) Technology white paper on ocean current energy potential on the U.S. outer continental shelf. U.S. Department of the Interior, Minerals Management Service, Renewable Energy and Alternate Use Program, Washington, DC
20. Coastal Response Research Center (2010) Ocean thermal energy conversion: assessing potential physical, chemical and biological impacts and risks, Durham
21. Skilhagen SE, Dugstad J, Aaberg R (2008) Osmotic power – power production based on the osmotic pressure difference between waters with varying salt gradients. Desalination 220:476–482
22. Nelson PA, Behrens D, Castle J, Crawford G, Gaddam RN, Hackett SC, Largier J, Lohse DP, Mills KL, Raimondi PT, Robart M,

Sydeman WJ, Thompson SA, Woo S (2008) Developing wave energy in coastal California: potential socio-economic and environmental effects. California Energy Commission, Sacramentro
23. Ehler C, Douvere F (2009) Marine spatial planning: a step-by-step approach toward ecosystem-based management. UNESCO, Paris
24. OEER Association (2008) Fundy tidal energy strategic environmental assessment. Final report, Halifax
25. Shields MA, Dillon LJ, Woolf DK, Ford AT (2009) Strategic priorities for assessing ecological impacts of marine renewable energy devices in the Pentland Firth (Scotland, UK). Mar Policy 33:635–642
26. Copping AE, Van Cleve FB, Anderson RM (2011) Preliminary screening analysis for the environmental risk evaluation system. Evaluating effects of stressors. Environmental effects of marine and hydrokinetic energy. Report to the U.S. department of energy, wind and waterpower program. Pacific Northwest National Laboratory, Seattle, WA, 53 pp
27. US Environmental Protection Agency (1998) Guidelines for ecological risk assessment. US Environmental Protection Agency, Washington DC
28. US Environmental Protection Agency (2003) Framework for cumulative risk assessment. U.S. Environmental Protection Agency, Washington, DC
29. Musial W (2008) Status of wave and tidal power technologies for the United States. National Renewable Energy Laboratory, Golden

Marine Aquaculture in the Mediterranean

Dror L. Angel
Leon Recanati Institute for Maritime Studies, University of Haifa, Mt Carmel, Haifa, Israel

Article Outline

Glossary
Definition of the Subject
Introduction
Sustainable Marine Aquaculture in the Mediterranean
Future Directions
Bibliography

Glossary

Bioassay (BIOlogical ASSAY) A procedure to test the effect of a substance on living organisms, e.g., the effect of plant nutrients on plant growth rate.

Chemotherapeutants The use of chemicals to treat disease.

Dead zones Coastal areas that undergo seasonal hypoxia (low-oxygen), generally related to eutrophication events, whereafter many of the local (mainly benthic) animals die.

Exotic species An introduced or alien species living outside its natural range, which has been introduced by deliberate or accidental human activity.

FCR (feed conversion ratio) The efficiency at which an animal converts its food into biomass (body mass); FCR = mass of food eaten/increase in biomass.

Immunostimulants Chemicals used to stimulate the immune system by inducing activation or increasing activity of any of its components.

Marine protected areas Areas that restrict human activity (e.g., fishing, boating, coastal development) to protect living, nonliving, cultural, and/or historic resources.

NIMBYism "Not In My Back Yard"-ism; the practice of objecting to a human activity (generally commercial or industrial) that will take place near one's home.

Oligotrophic Waters that have low levels of nutrients and algae, high level of dissolved oxygen, and deep light penetration (i.e., clarity).

Prebiotics Food ingredients (e.g., soluble fiber) that stimulate the growth and/or activity of bacteria in the digestive system which are beneficial to the health of the body.

Probiont Living bacteria added to the environment and feed of reared animals and thought to benefit them by improving intestinal microbial balance, thereby inhibiting pathogenic bacteria.

Protista Unicellular (single-cell) eukaryotic organisms, e.g., foraminifera.

Definition of the Subject

Fisheries and aquaculture play an important role in the economies of many countries; yet this fact is often overlooked as the focus, in many nations, is on provision of food primarily, if not exclusively, from terrestrial agriculture. The value of seafood products as a source of foreign currency is especially important in developing countries and in many cases may exceed

the profits from certain agricultural products [1], though this fact also tends to evade common knowledge. The Mediterranean aquaculture sector continues to grow at a rate of close to 9% per year (since 1970) as compared to 3% per year for farmed meat production systems. If the growth of the aquaculture sector can be sustained, it is likely to fulfill the demand for aquatic food supplies by supplying >50% of the total aquatic food consumption within the next 5 years! Therefore, the emphasis here is on the review of the sustainable growth of a commercial activity within an enclosed sea with many conflicting multinational interests. Aquaculture includes the cultivation of finfish, shellfish, crustaceans, and algae; however, this review will focus primarily on Mediterranean finfish farming since many of the sustainability issues revolve around fish farms. There are many different facets (e.g., ecological, social, political, economic) to sustainable commercial activities and this review will touch on several, though not all, of the issues related to aquaculture and its sustainable development in the Mediterranean Sea region.

Introduction

The Mediterranean Sea Environment

Although the term "environment" is often used to mean "ecology," the following description embraces the more holistic meaning, which includes the socioeconomic aspects as well. The Mediterranean is a large, semi-enclosed sea bordered by 22 countries, with two distinct basins divided by a narrow, relatively shallow channel between Sicily in the north and Tunisia in the south. The areal division of the sea between the western and eastern basin is roughly 1/3:2/3. The eastern basin is somewhat more saline than the western basin, especially in the vicinity of the Suez Canal. The Mediterranean Sea has a wide range of seawater temperatures, from as low as 5°C in the Gulf of Trieste in the winter to 31°C off the coast of Libya in the summer [2]. The sea is oligotrophic and phosphorus limited [3] though some limited areas (such as parts of the northern Adriatic) may be eutrophic and it is warmer and more oligotrophic in its southern and eastern areas. Whereas the Mediterranean Sea accounts for only 1% of the world's ocean, it contains 6% of the world's marine species, including >400 endemic species of plants and animals [4]. Despite this impressive biodiversity, biomass is relatively low, mainly due to low primary production.

There are approximately 82 million people in the Mediterranean coastal zone: most in coastal cities and 32% of the population is in North Africa. Levels of development vary widely over the region. Tourism brings >100 million visitors to coastal areas annually, serving as a major source of seasonal population pressure and income and is thus a major competing sector with aquaculture. The Mediterranean Sea is a major shipping route, bridging between Europe and the Middle East and is a base for capture fisheries and mariculture. There are 75 marine protected areas (MPA) in the region, designed to protect unique and threatened resources and habitats such as the seagrass *Posidonia oceanica*, and breeding and nesting sites for endangered species, such as the loggerhead sea turtle (*Caretta caretta*). MPAs were also designated to encourage specific uses, such as sustainable tourism and regenerating fish stocks [5].

A Brief History of Mediterranean Aquaculture

The earliest evidence of aquaculture activity in the Middle East is from the ancient Egyptians. An Egyptian frieze, dated from 2500 B.C., depicted men gathering fish from a pond in what may be the earliest record of such activities in this region [6, 7]. In the sixth and fifth centuries B.C., the Etruscans reared fish in marine farms and the Greeks grew mollusks [8]. Throughout the Roman empire, marine fish (mainly sea bass, sea bream, and mullets) and oysters were reared in special enclosures (e.g., piscines) along the coast [9–11], but this practice seems to have died out with the collapse of the empire and did not appear in the Mediterranean until the middle ages. It is not clear precisely when it began, but there are records of extensive aquaculture in lagoons in Italy, also known as valliculture, starting from around the fifteenth century. Europeans traditionally collected shellfish along the shores, but since the eighteenth century the French oyster industry added a more reliable source – shellfish reared in specialized gear in the intertidal zone. Shellfish aquaculture expanded in the nineteenth century and coastal cultivation spread throughout the Western Mediterranean and the northern Adriatic Sea.

In the second half of the twentieth century, aquaculture developed rapidly, mainly as a result of successful research into the life cycle of the farmed animals (reproduction and larval rearing), as well as physiology, nutrition, and engineering of farming systems [8].

Main Forms of Mariculture (Culture Types and Species) in the Mediterranean

On a global scale, aquaculture production in the Mediterranean Sea is small, but not insignificant – especially with regard to the European demand for fresh seafood. Total aquaculture production in the Mediterranean Sea in 2006 was about 370,000 t [1] with 14% growth from 2000 to 2006, outpacing the growth of capture fisheries. It is noteworthy that the interannual variability in aquaculture production is lower than in capture fisheries (these have reached a plateau in terms of annual harvest), which may be a consideration of prime significance for business and decision-makers concerned with food security, coastal communities, and development.

Within the Mediterranean aquaculture sector, the most striking feature of production is the rate at which finfish have overtaken mussels as the dominant product. In 1990, finfish production accounted for less than 10,000 t as compared to approximately 90,000 t of mussels. In 2003, 180,000 t finfish and 150,000 t mussels were produced (49% and 40% of total production, respectively). Clam and oyster production were only 7% and 2%, respectively, and the remainder of production (~2%) was crustaceans and seaweed. The main cultivated finfish species in the region are gilthead sea bream (*Sparus aurata*), European sea bass (*Dicentrarchus labrax*), and flathead gray mullet (*Mugil cephalus*). Greece, Turkey, Spain, and Italy were the four largest producers of sea bream and bass in 2006, comprising >90% of total Mediterranean production. Sea bream and bass are predominantly reared in net cages in coastal waters, whereas mullets are generally reared in ponds. The major producers of mullets are Egypt and Italy with Egypt generating more than 90% of global mullet production.

A fairly recent development is the farming of bluefin tuna in the Mediterranean, which mainly serves the Japanese sushi market. Tuna farming falls in between the definitions of a standard fishery, which is defined as "capture of wild stock" and aquaculture where fish are both bred and reared in captivity. Because tuna farming is a "postharvest" practice, it is not governed by the regulations of GFCM or ICCAT [12] and as a result there was unregulated growth in this sector, putting heavy pressure on the endangered Mediterranean wild stocks. Concerted efforts are being made to create brood stocks and hatcheries to enable the cultivation of bluefin tuna by the traditional aquaculture methods to release pressure on the endangered Mediterranean wild stocks.

Sustainable Marine Aquaculture in the Mediterranean

One of the features of marine aquaculture in the Mediterranean is that it is developing rapidly in response to a large and ever-growing demand for seafood. This demand was traditionally supplied by fisheries, but the drop in landings in recent decades as a result of overfishing has opened the path for sustainable alternatives to provision of seafood, namely aquaculture. That said, mariculture needs to operate in a manner that will minimize negative impacts on the marine environment, on wild stocks, and on other uses of the seas. Thus, sustainable aquaculture must ensure "*economic viability, social equity and acceptable environmental impacts*" [13].

It is obvious that aquaculture activity must be profitable to succeed, but there are many criteria to profitability and *economic viability* and these may vary considerably in countries that are at different stages of economic development (the process whereby an economic activity develops the technology and experience needed to operate successfully) or that have different interests in mind. In some developing countries, aquaculture may serve as a much needed food and protein source for local consumption, whereas other developing countries may prefer to export their aquaculture production for economic benefit.

Another component of sustainability is *social equity*. Societal equity depends on cultural norms and tendencies of society and varies considerably among the Mediterranean countries. It is probably the most difficult aspect of sustainability to consider because of its intrinsic variability.

Environmental "*acceptability*" is also a difficult issue because of the obvious question: "acceptable by

whom?" In order to address this, one needs to consider where the aquaculture activity takes place, who are the stakeholders and how this activity may be conducted in such a manner that it will be acceptable by as many stakeholders as possible. The first aspect of sustainability, discussed below, is the public perception of aquaculture since public opinion may play an important role in the success or failure of the industry. In addition to the various social ramifications, "environmental acceptability" includes the effects of aquaculture on its surroundings and on the ecosystem. The following sections list several of the environmental issues that affect or are affected by Mediterranean aquaculture and a discussion of what is being done about them to enhance the sustainability of this sector.

Public Perception of Aquaculture

The *image* of fish farming varies considerably among different countries and can have a strong effect on the sustainability of the industry. In some northern European countries, the public considers aquaculture in a positive light as a means to enhance food safety and security. In comparison, many southern European countries have a generally negative attitude toward farmed fish as these are considered inferior in taste and health value in comparison to wild-caught ("natural") fish [14, 15]. Numerous negative connotations are associated with marine aquaculture, including: "pollution causing eutrophication," "discharge of antibiotics and harmful chemicals into the environment," "genetic dilution/pollution of wild fish stocks," and "negative visual impact on the coasts."

The public perception is very important for both producers and coastal zone managers since there are many factors that are stacked against the aquaculture sector [16, 17]. These include lack of knowledge on many aspects of the coastal environment, the weakness of a small industry, competition with tourism and other coastal stakeholders, and increasing political power of local environmental lobbies and associations. These lead to non-sustainable situations, including loss of licenses, leases and markets, and reduced diversity in the coastal economy.

The social acceptability of aquaculture was examined at two Greek islands [18] and revealed that residents were more likely to be opposed to aquaculture if they thought that the fish farms would pollute the environment. A study conducted in Israel [19] evaluated public attitudes toward aquaculture and concluded that although most citizens were not terribly well informed in the implications of aquaculture on tourism and environmental issues, the majority are in favor of marine aquaculture. It is noteworthy that this lack of familiarity with aquaculture and aquaculture implications was also observed among the public surveyed in such countries as Scotland [20], Australia [16], and Germany (Schultz, unpublished).

Although the above focuses on the attitudes of the lay public toward aquaculture, it is possible that the opinion of stakeholders is equally (or more) important, despite the fact that the number of stakeholders is usually smaller. Competition over the coastal zone is one of the major sustainability issues that Mediterranean aquaculture faces on a regular and large-scale basis. The competition is especially severe between aquaculture and tourism since the Mediterranean attracts about 30% of the volume of global tourism annually and this is expected to increase over time. There are many examples of such competition, and one of the more recent clashes between the tourism and aquaculture sectors occurred in Turkey in 2008–2009, resulting in a major shift in legislation and in aquaculture lease requirements.

Measures to Improve the Public Attitudes Toward Aquaculture The negative attitudes toward aquaculture are largely a result of ignorance. The media often presents NGO views and opinions in their description of the fish-farming industry, and many of the facts presented are incorrect. The way to correct some of the misconceptions surrounding aquaculture is by preparing a well-planned outreach and educational program geared to reach as many households as possible. There are myths and misconceptions regarding such things as how fish are reared and the densities at which they are stocked, the safety of the feed used, the quality and healthiness of farmed versus wild fish, etc. Preparation of an aquaculture "module" to be taught at schools is an effective way to reach and educate future stakeholders and decision-makers. Another measure that could reduce conflict between aquaculture and other coastal stakeholders is a search for synergies among the stakeholders that would enable

multiple use of the coastal zone [21]. Promotion of organic and other types of certification programs to increase public confidence in aquaculture practices and products would also improve public attitude toward this sector.

Benthic Impacts

In the 1990s, the study of the interactions of Mediterranean marine aquaculture with the environment focused on the negative impacts of the industry since most of the early research on salmon farms documented heavy benthic loading, which caused serious damage to underlying seafloor communities and in some cases to the water column as well [22–26]. Benthic organic enrichment that often occurs under intensive finfish farms rapidly leads to hypoxia and anoxia in the sediments. Anoxic sediments support bacterial sulfate reduction, generally leading to an increase in sediment hydrogen sulfide [27]; conditions that are noxious, at best and often lethal to macro- and meiofauna [28]. Although abundances of macrofauna in Mediterranean sediments are considerably lower than the abundances found in temperate regions [29–31], defaunation under fish farms strongly reduces benthic bioturbation (i.e., aeration of the sediments) and leads to accumulation of reduced compounds and organic matter therein. If the farm is situated at a site with limited flushing and circulation, the depth and aerial extent of the impacted sediments may grow with time, creating localized "dead zones." Moreover, when methane accumulates in and bubbles out of anoxic sediments, noxious chemicals such as ammonia and hydrogen sulfide may affect the cultivated fish in the overlying cages.

Because the Mediterranean Sea is largely oligotrophic, and fish farming is generally not practiced at sites with poor flushing, the phenomena described above are not common. At a few sites with limited water circulation, for example, some farms in Croatia and Greece, organic enrichment of the seafloor and local impacts were observed, but these were exceptional and sediment conditions under Mediterranean fish farms are generally less impacted.

At those sites that showed evidence of impacted sediments, the visible effects generally did not extend beyond tens of meters from the edge of the perimeter of the farm [32], though the situation at each farm is different as a result of site-specific currents, depth, bathymetry, etc. The determination of the extent of impacted sediments and benthos (distance from the farm) is subjective and may be strongly affected by the method used. Organic matter determinations, visual inspection, and macrofauna indices are often the methods used to assess the state of the sediments and these clearly show a local effect that diminishes with increasing distance from the point source. However, more sophisticated analyses involving stable isotope signatures of farm effluents indicate that the aquaculture effluents may be detected as far away as 1–2 km from the farms [33–35]. It is very important to qualify the meaning of these measurements because they may be used to make a point about the extent of fish farm effects, but the real issue at hand is the extent of "significant impact." The distribution of small suspended particles over great distances will only constitute a significant impact if the flux of these particles is large and in the case of Mediterranean fish farms, the flux of very small suspended particles is small [36]. Therefore – it is essential to emphasize the difference between qualitative and quantitative effects.

Measures to Reduce Benthic Impacts Despite the fact that benthic loading is generally not a major issue in the Mediterranean, a number of different approaches are employed to increase feeding efficiency and reduce benthic loading. Feeding efficiency is not only an environmental issue, but also a major economic consideration since one of the greatest cost factors in intensive fish farming is the formulated feed. Feeding efficiency includes optimizing the composition of the feed (optimal digestibility) to maximize growth and minimize waste at the lowest possible cost, as well as feed delivery. Considerable efforts are invested by feed companies and fish nutritionists to optimize feed for the various strains of cultivated Mediterranean finfish [37, 38] and during recent years, sea bream and sea bass feed conversion ratios (FCR) have been substantially improved, largely (though not exclusively) due to improved diets and feed delivery. Feed delivery includes the optimal feeding regime whereby feed is provided to the caged fish in suitable portions and at the correct intervals to both maximize growth

and health and minimize loss to the surrounding waters. Low-tech feeding involves delivery of pelleted feed to fish either manually by hand, or with the aid of a compressor and regulating the amount according to the response of the fish. High-tech systems include feeding programs that are computerized and customized to each individual cage to optimize delivery of feed to the stock. Another sophistication is the use of submerged Doppler systems (e.g., Doppler Pellet Sensor) that detect when fish stop feeding (increase in the flux of pellets to the bottom of the cages), and send signals to cause the automated feeders to cease feeding (http://www.akvagroup.com/). Many of the above are technologies that were developed outside of the Mediterranean, but as they are also applicable to sea bream and bass production, they are widely used by this sector. One of the more recent developments in Mediterranean aquaculture was the tuna-fattening process, which offered large profits to the farmers. Although it is arguable whether this process should actually be qualified as aquaculture, the environmental ramifications were clear. The penned fish are fed freshly caught or frozen fish rather than pelleted feed and release large amounts of waste (greater than would be released from pelleted food) to the seafloor and have rather high feed conversion ratios (FCRs) 10:1–20:1 as compared to the FCR of sea bream (2:1) or salmon (1:1). Research is currently ongoing to develop artificial diets to create a better FCR for the tuna and to reduce the reliance and fishing pressure on small pelagic fish (e.g., [39]).

Water Quality

The sustainability of any human activity is a function of the nature of the receiving or host environment and in the case of aquaculture this is the basis for estimating the assimilative, holding, or carrying capacity [40]. At a few sites with restricted water exchange, for example, lagoons, there were reports of eutrophication problems [41–43] as the loading of organic and inorganic nutrients clearly exceeded the capacity of the environment to assimilate these [44]. Sites where such self-pollution problems emerge suggest that the preliminary environmental impact assessment and site selection procedures were not carried out properly. In the oligotrophic waters of the eastern Mediterranean, there are generally no reports of eutrophication or degraded water quality related to finfish or shellfish farms [45–47] and this was interpreted as the ability of the oligotrophic system to successfully assimilate the nutrients released by the farms. In an effort to understand whether nutrient release from aquaculture might have large-scale effects on the Mediterranean ecosystem, Karakassis et al. [48] employed a model to examine various production scenarios. They concluded that if aquaculture continues to grow and expand at present rates, farm wastes may increase overall nutrient (mainly N and P) levels by 1%, however, this is a general assessment and does not take into account localized effects. As suggested by Pitta et al. [49] in a study of three different Greek farms, it is likely that dispersion and dilution of the nutrients, combined with efficient herbivore grazing of algae (that develop from the released nutrients) were the reason for the absence of eutrophication around fish farms.

Although water quality is generally not affected, fish farms that operated over or near seagrass beds (especially *Posidonia oceanica*) exerted a clear effect on these [50, 51] and it was proposed that this may be related to the enhanced flux of dissolved and particulate nutrients from aquaculture. In an attempt to identify the effect of the plume of nutrients released from fish farms on water quality, Dalsgaard et al. [52] devised an innovative "bioassay" to measure the effect of dissolved nutrients released from fish farms on micro- and macro-algal production. They determined that primary productivity decreased with distance from the fish farms, yet by comparing bioassays with and without grazer exclusion, Pitta et al. [53] found that planktonic grazers (probably protista) play a key role in transferring nutrients up the food web.

Measures to Reduce Effects on the Water Column

One of the primary considerations when evaluating the suitability of sites for aquaculture is how they will interact with the surrounding marine system [54]. It does not pay, for example, to place net cage farms in shallow, poorly flushed waters (e.g., lagoons) because the organic and inorganic enrichment may affect both the marine ecosystem and the farmed organisms. Nevertheless, some farms have been deployed in unsuitable locations and these need to be relocated to allow the environment to recover and to enable the healthy growth of farmed finfish.

One of the early water quality problems associated with Mediterranean fish farms was the presence of an oily film around the cages. This was generally related to the large percentage of dust (pulverized feed pellets) in the pelleted food, which is not available to the farmed fish. Because this causes considerable loss to the farmers, and reduced water quality (stimulated bacterial growth also depletes the water of essential dissolved oxygen), the problem was rapidly addressed and most of the pelleted feeds are now extruded to improve pellet integrity and reduce feed loss and feed dust is collected and recycled.

A similar problem was identified in the tuna-penning industry. Unlike sea bream and bass that feed on formulated pellets, tuna are fed whole (preferably oily) fish such as sardine, anchovy, and mackerel. When these fish are offered to the tuna, the water around the pens often has an oily film and emits a strong smell. Moreover, in some cases, divers have complained of poor visibility near the pens. As described above, research is ongoing to develop artificial diets for tuna [55] that will address not only the problems related to feeding with fresh fish but also the water quality problems.

Disease

Intensive aquaculture systems are very susceptible to disasters such as loss of the farmed stock. Among the various causes of such disasters, disease outbreaks rank highest [56] and may lead to great losses within a very short period of time.

Most finfish cage farms in the Mediterranean are intensive, that is, they have high stocking density in order to be economically profitable and to compensate for the low profit margin of sea bream and sea bass, the main species reared in this region. Although cage stocking densities are usually <25 kg m^{-3}, in some farms stocking densities are higher and such conditions may cause a reduction in fish growth rates, suppression of immune mechanisms [57–59], and ultimately greater susceptibly to disease agents, including opportunistic bacterial and viral pathogens and eukaryotic parasites [60]. Current estimates of average mortalities for farmed sea bream and sea bass as a result of disease are 10% and 20%, respectively, for growth from juvenile to market size (350 g) fish. In many cases, the profit margin for these fish is not much higher than 10–20%, which has therefore obliged the aquaculture sector to consider various options to address this problem. Moreover, there is concern regarding the potential transmission of disease from the farmed stock to wild fish, based on studies of disease transfer among Atlantic salmon (e.g., [61]). It is noteworthy that although there are numerous examples of disease exchange between caged and wild fish (e.g., [62–64]) in the Mediterranean, and other seas, most of these are not clearly understood [65, 66] and their effect on native stocks is unclear.

Measures to Reduce Disease Outbreaks Numerous antibiotics have been tested against the common farmed fish diseases and there are currently treatments available for most bacterial fish pathogens [67]. However, the routine use of antibiotics in marine aquaculture is problematic and has declined for a number of reasons. First, as specified above, there are concerns related to human and environmental health and safety. Second, although many of these drugs work well in freshwater, some of the major antibiotics, such as quinolones and tetracyclines interact with the divalent cations that are abundant in seawater (mostly Mg^{2+} and Ca^{2+}) which massively reduces their function and efficacy [68, 69]. Moreover, there is no "harmonization" regarding antibiotics use among Mediterranean countries and the list of pharmaceuticals licensed for fish varies from country to country, complicating international trade and marketing.

In addition to bacterial pathogens, there are several parasitic diseases that may stunt growth rates, cause loss of fecundity, and even mortality in Mediterranean fish. These include various protozoa and metazoa, which are classified as ecto- and endoparasites according to their distribution on/in the fish. Pathologists consider the myxosporeans *Myxidium leei*, *Polysporoplasma sparis*, and *Ceratomyxa* sp., isopods, copepods, and monogenean infections among the more problematic parasites.

Athanassopoulou et al. [70] reviewed the drugs used against a variety of parasites and found that amprolium and sanilomycin were the most effective against myxosporans in cultivated breams. Moreover, extracts from oregano revealed anti-myxosporan as well as antibacterial properties. Ivermectin and

deltamethrin – drugs used to combat sea lice, have also been tested against copepod and isopod infections in sea bass and were fairly effective, but they tend to become toxic to the fish at fairly low levels.

In order to limit the use of antibiotics and other chemotherapeutants, the European Union established the "Maximum Residue Limit" (MRL) regulation, which monitors the presence of these drugs in all agriculture and aquaculture products and this has had a dramatic effect on the use of therapeutants. Because the MRL differs among countries insofar as which compounds are regulated and which are not, there is a lot of work ahead, but despite this, the trend looks very promising.

Vaccines are one of the preferred measures for prevention of disease outbreaks, however because the Mediterranean finfish market is still fairly small, only a limited number of vaccines have been developed for commercial use. Moreover, consumer concerns and increasing restrictions regarding their use have led the industry to consider other alternatives to disease "management" [71, 72].

There are other alternatives to the use of chemotherapeutants and vaccines against disease. One of the key factors in the prevention of disease is good husbandry, which focuses on minimizing stress to the farmed stock. This includes proper stocking densities, optimal nutrition, sanitary practices, use of vaccines, and probiotics [66, 73]. The practice of good husbandry ensures fish are healthy and able to resist various disease agents naturally found in their environment. When they become stressed, the dietary requirements of fish for nutrients and vitamins change and a diet that compensates for such needs may optimize the growth of fish in captivity.

In recent years, it has become clear that the integrity of the gastrointestinal tract is essential in defense against pathogen attack as well as in proper endocrine and osmoregulatory activity. In recognition of this, Dimitroglou et al. [74] added the mannan oligosaccharide, Bio-Mos® (Alltech Inc, USA) to the diet of several marine fish including gilthead sea bream and found that this improved the gut morphology.

It is assumed that one of the roles that the mannan plays in protection of the fish is agglutination of pathogenic bacteria, which prevents their colonization of the gut. Indeed, the application of Bio-Mos significantly reduced the bacterial load in fish guts by reducing the biomass of aerobically cultivated bacteria [74]. Torrecillas et al. [75, 76] applied Bio-Mos to sea bass juvenile diets and found that it improved growth rates by 10%. Moreover, challenge trials using *Vibrio alginolyticus* showed that Bio-Mos fed sea bass had fewer of the pathogenic vibrio in their gut.

In recognition of the essential role of healthy gut flora in fish, especially in young fish, the use of immunostimulants, prebiotic, and/or probiotic bacteria have been proposed as a means to reduce gut colonization by pathogens [77], thereby improving the survival of cultured fish. Probiotics involves the addition of nonpathogenic bacteria to the diet and water of fish with the aim of loading the gut with bacteria that will prevent colonization by competing pathogens. The use of prebiotics and immunostimulants focuses on boosting the fish immune system so that the fish may more readily recognize and repel pathogen gut colonization. Although research has been conducted on the use of probiotics in Mediterranean aquaculture, (e.g., [78–80]), this approach has not successfully replaced the use of antibiotics to combat disease. One of the problems related to the use of probiotic bacteria is concern that these may not be as safe as they are supposed to be and their use may lead to other problems rather than a sustainable solution in the battle against disease.

Immunostimulants are commonly used in finfish farming to reduce the risk of disease by stimulating the protective activity of the immune system. The common forms of immunostimulants used in sea bream and sea bass aquaculture include ascorbic acid, a-tocopherol, and glucans [81, 82], which are added to the feed. Their presence appears to enhance antibacterial lysozyme activity and other indicators of disease resistance, but there is considerable discussion about their effectiveness due to the inherently wide range in concentrations and activities of the disease resistance molecules in fish serum.

Another approach to reduce the risk of disease is by means of classical selection/breeding for disease resistance by means of selective breeding programs [83]. The understanding of immune regulatory genes responsible for resistance to finfish pathogens is still in its infancy in Mediterranean aquaculture, but this field is rapidly expanding and it is anticipated that genetically superior lines will dominate the populations of fish reared in intensive aquaculture [84].

Escapes

In addition to problems related to disease and fluctuating profitability of aquaculture operations, fish farmers are also concerned with keeping their fish within the cages so that these can be marketed at the end of the growth cycle. There are many factors that may lead to loss of the farmed stock, including storms that may physically damage the net cages, predators (e.g., sharks, dolphins, bluefish, seals) that may bite the nets in their attempt to eat the enclosed fish, human error (e.g., during replacement of net cages or during harvest), poachers that cut the nets to catch fish, collision of ships with cage farms, etc. All of these generally result in the release of farmed fish to the surrounding environment, involving financial loss to the farmer and potential environmental problems related to genetic and ecological interactions of the escapees with the wild fish. At present, there are an estimated >1 billion fish; mostly sea bream and sea bass in net cage farms throughout the Mediterranean as compared to much smaller stocks of the wild populations of these species [85], so the potential impact of escapees is considerable. Because many Mediterranean countries do not require farmers to report escapes, there are no reliable data on the frequency of escapes, however, it is assumed that the percentages of escapees are similar to those reported in Norway [86], ranging between 0% and 6%. In addition to genetic "pollution" of the wild-stock gene pool, and potential competition between escapees and wild fish over the same habitat and food resources, there is also concern regarding the spread of disease from farmed fish to wild fish populations [87].

Measures to Reduce Escapes and Damage due to Escapes As the volume of aquaculture production increases in the Mediterranean to match demand, and with the anticipated addition of North Africa to the fish-producing countries, there is a growing need for regulation in order to minimize problems related to escapes. In order to appreciate the scale of escapes from Mediterranean aquaculture, there is a need to legislate reporting of escape events, as is currently done in other parts of the world. Moreover, several new finfish species have been domesticated and their potential effect, as escapees, on wild populations and on the ecosystem need to be assessed. In addition, in order to assess escape impacts, it is useful to be able to track the escaped fish, as described by Triantaphyllidis [88].

There are many measures that may be employed to reduce the risk of escapes from fish cages. Storm damage to farm systems is one of the major causes of escapes and employment of a reliable standard, as practiced in Norway (NS 9415 – requirements for design and operation of marine fish farms) is a promising approach to reduce such risks. Even sturdy, reliable cages are occasionally damaged by especially strong storms, but most of the surface wave energy is concentrated in the upper 10 or 15 m of the water column [85]. Submersible cage systems designed for open sea conditions, such as the Sub-flex system (www.subflex.org) and the Ocean-Spar system (www.oceanspar.com/) are an option to reduce mechanical stress to net cages in high-energy environments. Added advantages of submersible cage systems include the reduced risk of collisions with maritime vessels and the reduced visibility following the "out of sight–out of mind" solution to NIMBYism. Human poachers are a problem that may be reduced by vigilance and by cooperation with the local police or security forces. Marine predators that bite net cages from the outside may be deterred by using stronger materials, though this has financial consequences, or by embedding chemical deterrents in the net material. Several farmed species tend to bite the net material from the inside and this may create holes enabling escapes. The biting may be prevented by using taste deterrents, as described for predators, or stronger material that will be more bite resistant. Moe et al. [86] suggest making the cage environment more "appealing" or stimulating to reduce gnawing on the net mesh which they attribute to boredom.

In addition to reducing the risk and frequency of escapes, there is also a need to reduce the impacts caused by the escaped fish. One direction that is being tested is the development of sterile triploid sea bream and sea bass that will not be able to pass on their genes to wild fish. Another possibility is the recapture of the escaped fish, but this direction is still in early developmental stages. The location of fish farms relative to areas of high ecological sensitivity or to spawning grounds should be one of the major

considerations in light of the possibility that some of the stocked fish may escape.

Introduced Exotic Species

Invasive species are probably the cause of the greatest ecological problems identified over the past century, not only in terrestrial but also in aquatic and marine systems [4]. This problem has intensified over the past 20–30 years, as the volume of intercontinental traffic has increased. Aquatic invasive species are a major threat to marine biodiversity and impact human health and the economy [89]. There are numerous examples of the impacts of invasives on human welfare and environmental health, for example, the invasion of the Black Sea by the exotic ctenophore *Mnemiopsis leydi*, which caused the collapse of most of the local fisheries [90]; invasion of the eastern Mediterranean by the Red Sea medusa, *Rhopilema nomadica*, which has heavily impacted Israeli and Turkish fisheries, tourism and coastal facilities [91].

In the eastern Mediterranean, exotic introductions are mainly channeled through the Suez Canal whereas most of the successful invaders in the western Mediterranean have been introduced by ships and via aquaculture [92].

Species introductions via aquaculture activities may be intentional or accidental, though the consequences are generally similar. Intentional introductions generally include the import of an exotic species and its release into the environment, without the intention that it spreads and dominates its new habitat. Examples include shellfish such as the Japanese oyster that was brought to France and spread rapidly throughout French coastal waters and certain species of sport fish that were intentionally released in northwestern US waters. The majority of introductions are not intentional but rather accidental and may occur in a number of ways. One common example of an accidental introduction is the transfer of a local species of oyster from a hatchery to the coast in a restocking program and the accidental release of an associated seaweed with the oysters. In another case, recreational boaters did not thoroughly wash the bottom of their boat after a holiday in a given bay and when they transported the boat back to their own shore, they brought with them a cryptic gastropod which subsequently invaded the new environment and decimated the local clam population.

Measures to Reduce the Invasion of Exotic Aquatic Species and Associated Damages In order to avoid the various risks involved in the use of exotic species, it is essential to rear/grow native species, as a rule. In many cases, the commercially attractive species are not native and farmers prefer to culture nonnative species. Introduced species may only be considered after taking all required precautions as specified in the ICES *Code of Practices on the Introductions and Transfers of Marine Organisms* [93] and the report on *Alien Species in Aquaculture* by Hewitt et al. [94]. Because the introduced species may escape and invade either local or neighboring environments, with implications for marine biodiversity, there is a need for both regional and international collaboration to address transboundary introductions and invasion issues, as discussed in UNEP [92].

The Mediterranean Aquaculture Market

The dominant species currently reared in the Mediterranean Sea are sea bream and sea bass [95]. These are native species that have been traditionally fished and eaten for centuries in many of the Mediterranean countries. Aquaculture has greatly increased the availability of these fish to the public and as production has increased, the price of the farmed fish has dropped dramatically so that in many cases its profitability is questionable. One of the important elements of a sector's sustainability is its economic performance yet the current trend in the Mediterranean is a plateau in profitability, that is, stagnation due to a glut in production of the two main species and a concurrent drop in their market value.

Alternative Aquaculture Species In order to survive and grow, the Mediterranean aquaculture sector needs to diversify its marine finfish production and include species with high market value. There are many native Mediterranean species that have a market because they are caught and sold by fishers and are suitable for cage culture. These include several species that have already been successfully reared in the eastern Mediterranean, such as Grey mullet (*Mugil cephalus*), Dover sole (*Solea solea*), Meagre (*Argyrosomus regius*), Sharp snout sea bream (*Diplodus puntazzo*), White bream (*Diplodus*

sargus), Red porgy (*Pagrus pagrus*), Shi drum (*Umbrina Cirossa*), Striped sea bream (*Lithognathus mormyrus*), Pandora (*Pagellus erythrinus*). Although these fish are commercially available for aquaculture, there are several bottlenecks that prevent large-scale production. These include lack of knowledge regarding their nutritional requirements, lack of farm facilities for production, slow growth rates (may be related to nutrition or other problems), sensitivity to certain pathogens.

Ecosystem Effects

It has been shown that Mediterranean fish farms generally have a local effect, primarily on the underlying benthos, as described above, yet within a short distance from the cages, this effect rapidly dissipates. It has been suggested that the large load of nutrients that pass via the farmed fish into the marine environment are rapidly processed by the biota, yet may exert some ecosystem effects. This hypothesis was tested by comparing the biological/chemical composition of seawater from fish-farming zones (within 2–3 nautical miles of fish farms) versus nonfarm zones (20 nautical miles of fish farms) in three parts of the Aegean sea in May and in September [49]. The data indicate that there is rapid transfer of nutrients up the food web, from the primary producers, via herbivores [53] to fish [96, 97]. These findings may be interpreted in a number of ways and their ramifications are debatable. If the precautionary approach is adopted, it is not clear what sort of implications these ecosystem-level changes may have and so they should be regarded with caution. On the other hand, if fish farms increase the size of natural fisheries, providing fishermen with an increased catch, this may be regarded as a positive externality of aquaculture (positive socioeconomic impact), which should be encouraged.

Seagrasses

One of the unique features in the Mediterranean Sea is the seagrass meadows of *Posidonia oceanica*. This slow-growing seagrass species occurs exclusively in the Mediterranean and grows best in clear, oligotrophic waters [98]. *P. oceanica* provides many ecosystem services, such as seabed stabilization, provision of a complex habitat to many larval and juvenile animals, oxygen production/release and long-term storage of CO_2 as plant tissue. Due to their slow growth rates, there is concern that these seagrass beds will not manage to recover if damaged and this important ecosystem and the services it provides may be lost. Marine botanists have calculated that some clonal colonies of *P. oceanica* may be 100,000 years old, that is, these are probably the largest and oldest-known living "organisms" on earth (http://en.wikipedia.org/wiki/Posidonia_oceanica). Because of their unique features, important ecological role and relatively low resilience to damage there is a strong movement in many Mediterranean countries to conserve and protect seagrass meadows from pollution, coastal development, trawling, and aquaculture. Recent work indicates that *P. oceanica* meadows located near or under fish farms have sustained considerable loss, including reduced meadow density, high shoot mortality rates (50-Diaz-Almela et al. 2008), increased epiphyte cover [99, 100] and very slow recovery rates following farm removal [101]. An analysis of several variables that may cause the observed damage to *P. oceanica*, in the context of the *MedVeg* project, has identified the deposition of particulate organic matter from the farms onto the seagrasses as the main factor leading to seagrass decline [102].

Measures to Protect Seagrass Meadows A set of recommendations were published by Pergent-Martini et al. [103] for the protection of Posidonia from fish farms, guided by the precautionary principle. These specified that: (a) Fish farms should not be situated directly over *P. oceanica* and *Cymodocea nodosa* (another important seagrass) meadows. (b) If seagrasses grow where a farm is planned, cages should be located at least 200 m from the nearest meadow. (c) Because these seagrasses generally occur at depths shallower than 45 m, farms should be set up at depths of 45–50 m where possible. (d) Environmental Impact Studies that relate to all seagrasses in the region should precede all lease requests to set up a fish farm. (e) If there are *P. oceanica* meadows near fish farms, these should be examined every 4 years to assure they have not been affected by the farming activity. On the basis of more recent findings, Holmer et al. [102] recommended to increase the distance between seagrass beds and fish farms to 400 m and to establish permanent seagrass plots to enable annual monitoring and sampling for seagrass health.

Future Directions

In the early 1990s, finfish aquaculture was generally a novelty in most parts of the Mediterranean, but this has changed radically during the past 20 years, as cage culture has spread throughout the region. Aquaculture is one of the fastest growing sectors worldwide and in the Mediterranean and it has many advantages over other food production industries, but in order to maintain a "green" image, aquaculture production and development must be sustainable. Progress has been made in many aspects of aquaculture technology but there are several areas that require attention and improvements in order to make this industry more environmentally and socioeconomically sustainable. Although numerous projects have focused on understanding the environmental interactions of aquaculture, the calculation of a reliable "carrying capacity" for aquaculture in a given water body is still generally beyond our means, that is, there is a need for further study of ecological processes on a variety of different scales with respect to fish farms. Because there are so many different types of habitats and ecosystems within the Mediterranean Sea (e.g., hard vs. soft seafloors, Adriatic vs. Levant, etc.), it is essential that the ecological and socioeconomic research address region-specific issues [45].

As aquaculture expands into new areas and new species, there is added urgency to improve the understanding of fish pathology in Mediterranean systems. In addition to bacterial diseases, there is a need for research into antihelminthic treatments, and better understanding of life cycles and early diagnostics for many of the Mediterranean parasites. In view of EU policies concerning reduction of chemical use in the aquatic environment, the prudent and effective use of chemotherapeutants is essential. This may be achieved by combining therapeutic treatments with such health management strategies as breeding of tolerant fish, improving water quality, and vaccination.

Escaped fish may impact wild fish through competition, predation, habitat displacement, gene pool dilution, etc. In an attempt to reduce the numbers of escapees, progress is being made (e.g., in the EU project "Prevent Escape," which includes several partners from Mediterranean countries) in the design of cages that should be more damage resistant and in devising strategies to track the escapees and to reduce migration away from the breeched cages.

A Need for Legislation

One of the areas that urgently requires attention to enable development of the sector is legislation since this aspect is inadequately addressed in many Mediterranean countries. Moreover, in many countries that are active in aquaculture, there is a policy vacuum with regard to this sector. There is a need for clear rules and standards for licensing, planning, environmental impact assessment (EIA), administrative organization, and coordination. In the absence of clarity and transparency in such matters, investors and entrepreneurs will not take the risks involved in establishing aquaculture operations and the development of the industry will be retarded and sluggish. In a review of the legal obstacles to aquaculture, Van Houtte [104] included: (a) the legal status of water used (public or privately owned), the nature of water used (marine, brackish, or freshwater); (b) the legal status and nature of the land used (coastal vs. inland; private vs. public); and (c) the need for government regulation of aquaculture, and related activities. Moreover, the lack of coordination among public and regulatory agencies with regard to the EIA process, planning, etc. complicates the aquaculture application process. To further complicate matters, the permit application process is complex, cumbersome and very time consuming. The number of laws, regulations, rules, and procedures involved in the application process is large and many different authorities are involved at several levels. On top of that, the application requirements vary widely from country to country and in some countries, aquaculture legislation may vary internally on a provincial or regional basis.

One of the most problematic policy issues has to do with site selection and site allocation for aquaculture. As an economic activity that takes place, and has an effect on the littoral, aquaculture competes with many other uses of the coastal zone and needs to be included in Mediterranean coastal planning and management schemes. In recognition of the rapidly growing sector, in 2002 the European Union acknowledged that planning and coastal management would be among the major challenges facing European aquaculture. This was reinforced by the recent EU [105] communication,

which emphasizes that "area choice is crucial and spatial planning has a key role to play in providing guidance and reliable data for the location of an economic activity, giving certainty to investors, avoiding conflicts and finding synergies between activities and environments with the ultimate aim of sustainable development" and invites all Member States to "develop marine spatial planning systems, in which they fully recognize the strategic importance of aquaculture."

One of the options chosen by some Mediterranean countries is zoning, that is, allocating a specific area for aquaculture as a means to reduce conflicts between coastal activities. In principle, this sort of approach simplifies things, provided: (a) the criteria used for selection of the aquaculture zones were appropriate and (b) the decisions regarding zoning involved the stakeholders and their interests. It is noteworthy that although there is aquaculture zoning in some countries, aquaculture jurisdiction generally falls under regional governance, that is, there are no national zoning plans in the Mediterranean [54]. Although zoning is probably one of the better options for site selection, the lack of national coordination regarding the allocation of space for aquaculture will probably increase conflicts with time, thereby jeapordizing the sustainability of the industry. It would therefore be prudent to promote national zoning policy for aquaculture in the Mediterranean.

The conflict over space is fierce in the coastal zone as there are many competing stakeholders and one of the solutions to this is to go offshore [95, 106]. There have been many initiatives over the past few decades promoting offshore or open-ocean aquaculture, including several international conferences in the Mediterranean; however, a number of obstacles have prevented the realization of this concept. These obstacles include (a) economic feasibility of such ventures; (b) engineering and technological solutions for aquaculture in sites exposed to oceanic conditions; (c) international and national (government) support for an offshore aquaculture industry; (d) investors willing to take the risks involved in offshore aquaculture; (e) lack of understanding of the ecological ramifications (water column and benthos; local and regional effects) of large-scale aquaculture in exposed sites; and (f) the biological effects of cultivation in exposed conditions (storms, currents, predators, etc.) on the farmed stock, and other similar issues. At present, there are a few Mediterranean fish farms situated in exposed, offshore sites, but these are the exception rather than the rule, and most farms are situated in protected or semi-sheltered sites. A move away from the coastal zone into offshore waters will probably become a reality rather than an option in the near future and the aquaculture sector stands to benefit if it can accept this and help establish the scientific basis and technology in advance.

Integrated Aquaculture

Another option that makes considerable ecological and economic sense is an integration of different forms of aquaculture within the same farm. By arranging systems for rearing finfish (a form of "fed" aquaculture) adjacent to systems for growing shellfish and/or seaweeds (extractive aquaculture), it may be possible to increase farm sustainability on a number of levels. On the ecological level, shellfish and algae are called "extractive" because they extract their nutrients or food from within the system (autochthonous), and can therefore help reduce the nutrient loads from fish farms. Finfish are usually "fed" with feed that is manufactured from materials that come from outside the system (allochthonous) and the release of wastes and uneaten feed from the farms may affect water and sediment quality and even cause eutrophication. On the social level, cultivation of different products as compared to monoculture will require greater manpower and expertise and create the opportunity for greater employment, both within the farms and in the form of support services. On the economic level, additional crops should increase farm profitability, provided the filtering organisms are able to absorb the nutrients efficiently and they fetch a good price at market. Moreover, by diversifying the cultured stock, the farmer protects himself from risks related to market fluctuations, storms, and disease. Integrated aquaculture is currently practiced in Canada and in China on pilot to commercial scales but it is not clear how this approach will develop with time. In the Mediterranean Sea, there are no commercial integrated aquaculture farms [21] and this is due to the fact that either the secondary crop is a low-value (not profitable) product or the secondary (extractive) crop is not able to grow in the oligotrophic conditions that characterize Mediterranean waters. The potential for

integrated Mediterranean aquaculture exists, but it must be both ecologically and economically viable to work.

Herbivorous Fish

One of the major challenges for both global and Mediterranean aquaculture is the limited supply of essential fish oil and fish meal [107]. The artificial diets of many farmed fish, including salmon, sea bream, and sea bass rely heavily on fish meal and fish oil, which places considerable pressure on wild fisheries (the source of fish meal and oil), severely jeapordizing the sustainability of the sector [108]. Several strategies have been proposed to address this problem, including the extraction of oils from fish-processing wastes [109, 110] and from fishery by-catch discards (the noncommercial fish and animals that are caught by fishermen and subsequently thrown back to sea), and feeding fish with plant oils. There has been some success in the replacement of fish oils with plant oils [107], but many fish species have reduced survival and growth rates when reared without fish oils.

Another solution that has been proposed to address this problem is the rearing of herbivorous fish that do not require fish oils. Although these are generally not the highest value fish, they are nonetheless commercial species that are profitable to rear. The most common farmed herbivore in the Mediterranean is the diadromous gray mullet, *Mugil cephalus* (www.fao.org/fishery/culturedspecies/Mugil_cephalus/en). A lot of the pond rearing technology of this species was developed in Israel [111] and included polyculture. Egypt, the world leader in mullet production, has recently exceeded 1 million t/y. Although this fish is common in some of the southern Mediterranean countries, it does not have a large market in southern Europe and this is a challenge that needs to be overcome to promote herbivores as more sustainable species for aquaculture. Another problem that exists for *M. cephalus* is the absence of commercial hatcheries. Despite recent breakthroughs in spawning induction [112, 113], juvenile mullets are still collected from river mouths for aquaculture purposes thereby jeapordizing natural populations. These problems need to be addressed if this species is to be seriously considered a sustainable alternative to the common Mediterranean carnivores.

Indicators for Sustainable Aquaculture

The Water Framework Directive establishes the Environmental Quality Standards for European waters, and all activities that may affect environmental quality, for example, aquaculture must comply with these standards. Aquaculture lease applications generally include Environmental Impact Assessments (EIA), which assess risks and predict the impacts of aquaculture. Monitoring is an approach to test if EIA predictions were correct, and to establish a feedback system to protect both the environment and the fish farmer. The Modeling-Ongrowing fish farms-Monitoring (MOM) system [114, 115] was developed for salmon farming in Scandinavia, and includes a feedback process of EIA – monitoring – farm adjustment. Although the MOM concept was developed for Scandinavian farms, this approach has been adopted by the operators of several farms in the Mediterranean Sea to monitor their performance and environmental status. Monitoring generally includes measurement of: (a) physical variables, such as hydrography, weather, water temperature, sediment type, etc.; (b) chemical variables, including dissolved oxygen, nutrients, suspended solids, dissolved and particulate organic matter, etc.; and (c) biological attributes, for example, algal pigments, biomass, productivity, macrofauna abundance, diversity, etc. Fernandes et al. [116] reviewed the science underlying aquaculture monitoring in Europe and found that it was generally motivated by research interests rather than by clear environmental objectives. Whereas comprehensive monitoring of marine environments improves the understanding of the functioning of these systems [117], and thus the ability to predict the response of these waters to anthropogenic perturbations, it is often not necessary to include many of the variables that are monitored [102].

The CONSENSUS project recently established a set of 18 indicators (www.euraquaculture.info/index.php?option%20=%20com_content&task%20=%20view&id%20=%20149&Itemid%20=%20118) to promote "European Best Aquaculture Practice." These indicators are currently being evaluated to examine their practicality and suitability for the sector. In a separate project entitled *ECASA* (www.ecasa.org.uk/), a set of indicators to assess aquaculture–environment interactions were evaluated in order to streamline the farm

monitoring process. This was done for aquaculture in both northern European and several Mediterranean countries (e.g., [118]) yet despite the advances made in that project, there is still a need to further streamline the list of indicators. The main criteria that should be used as a guideline in the quest for optimal indicators have been described in UNESCO [119] and include: (a) relevance, (b) feasibility (amount of effort, expertise, and cost required to obtain the data), (c) sensitivity (to inform on how the environment is responding), and (d) clarity (how easy it is for stakeholders to understand). Although progress has been made toward developing the final list of such indicators for aquaculture, this work is only partially done and further work is needed to achieve this.

Bibliography

1. FAO (2009) Integrated mariculture: a global review. In: Soto D (ed) FAO fisheries and aquaculture technical paper no 529. FAO, Rome, pp 133–183
2. Zveryaev II, Arkhipkin AV (2008) Structure of climatic variability of the Mediterranean sea surface temperature. Part I. Standard deviations and linear trends. Russ Meteorol Hydrol 33:377–382
3. Thingstad TF, Krom MD, Mantoura RFC, Flaten GAF, Groom S, Herut B, Kress N, Law CS, Pasternak A, Pitta P, Psarra S, Rassoulzadegan F, Tanaka T, Tselepides A, Wassmann P, Woodward EMS, Riser CW, Zodiatis G, Zohary T (2005) Nature of phosphorus limitation in the ultraoligotrophic eastern Mediterranean. Science 309:1068–1071
4. EAA (European Environmental Agency), (2006) Priority issues in the Mediterranean environment. EEA Report 4:88
5. Abdulla A, Gomei M, Maison E, Piante C (2008) Status of marine protected areas in the Mediterranean Sea. IUCN, Malaga, p 152
6. Basurco B (2000) Offshore mariculture in Mediterranean countries. In: Muir J, Basurco B (eds) Mediterranean offshore mariculture. Options Méditerranées: Série B. Etudes et Recherches 30, October 20–24 1997, Zaragoza, Spain
7. Bardach JE, Ryther JH, McLarney WO (1972) Aquaculture: the farming and husbandry of freshwater and marine organisms. Wiley-Interscience, New York, p 868
8. Basurco B, Lovatelli A (2003) The aquaculture situation in the Mediterranean sea. In: International conference on sustainable development of the Mediterranean and Black sea environment, Predictions for the Future, Thessalonica, Greece, May 29–31 2003. http://www.oceandocs.org/bitstream/1834/543/1/Basurco.pdf
9. Nun M (1964) Ancient Jewish fishery (in Hebrew). Hakibbutz Hameuchad, Merkhavia, Israel
10. Raban A, Galili E (1985) Recent maritime archaeological research in Israel-a preliminary report. Int J Naut Archeol 14:321–356
11. Cataudella S (1996) Description of main Mediterranean aquaculture systems. Notes from the TECAM advanced course on food and feeding of farmed fish and shrimp, CIHEAM, FAO, NIOF, Alexandria, Egypt
12. Lovatelli A (2005) Report of the third meeting of the ad hoc GFCM/ICCAT working group on sustainable bluefin tuna farming/fattening practices in the Mediterranean. FAO fisheries report no. 779, FAO, Rome, p 108
13. FAO (1997) FAO technical guidelines for responsible fisheries. Fisheries department, aquaculture development. Report no. 5, FAO, Rome, p 40
14. Fish Site (2006) Farmed vs wild salmon? – a comparison. (http://www.thefishsite.com/articles/107/farmed-vs-wild-salmon-a-comparison)
15. Altintzoglou T, Verbeke W, Vanhonacker F, Luten J (2010) The image of fish from aquaculture among Europeans: impact of exposure to balanced information. J Aquat Food Prod Technol 19(2):103–119
16. Mazur NA, Curtis AL (2006) Risk perceptions, aquaculture, and issues of trust: lessons from Australia. Soc Nat Resour 19:791–808
17. Mazur N, Curtis A (2008) Understanding community perceptions of aquaculture: lessons from Australia. Aquac Int 16:601–621
18. Katrandis S, Nitsi E, Vakrou A (2003) Social acceptability of aquaculture development in coastal areas; the case of two Greek islands. Coast Manage 31:37–53
19. Korchenkov I (2010) Mariculture development: public policy, citizen's attitudes and factors affecting them. MA thesis, University of Haifa, Haifa, p 63
20. Whitmarsh D, Wattage P (2006) Public attitudes towards the environmental impact of salmon aquaculture in Scotland. Europ Environ 16:108–121
21. Angel DL, Freeman S (2009) Integrated aquaculture (INTAQ) as a tool for an ecosystem approach to the marine farming sector in the Mediterranean Sea. In: Soto D (ed) Integrated marine aquaculture: a global review. FAO fisheries and aquaculture technical paper no. 529, FAO, Rome, p 133–183
22. Brown JR, Gowen RJ, McLusky DS (1987) The effect of salmon farming on the benthos of a Scottish sea loch. J Exp Mar Biol Ecol 109:39–51
23. Gowen RJ, Bradbury NB (1987) The ecological impact of salmonid farming in coastal waters: a review. Annu Rev Oceanogr Mar Biol 25:563–575
24. Weston DP (1990) Qualitative examination of macrobenthic community changes along an organic enrichment gradient. Mar Ecol Prog Ser 61:233–244
25. Silvert WL (1992) Assessing environmental impacts of finfish aquaculture in marine waters. Aquaculture 107:67–71
26. Hargrave BT (ed) (1994) Modelling benthic impacts of organic enrichment from marine aquaculture. Canadian technical report, fisheries and aquatic science. Report # 1949, DFO, Canada, p 125
27. Holmer M, Kristensen E (1996) Seasonality of sulfate reduction and pore water solutes in a marine fish farm sediment: the

importance of temperature and sedimentary organic matter. Biogeochemistry 32:15–39
28. Pearson TH, Black KD (2001) The environmental impacts of marine fish cage culture. In: Black KD (ed) Environmental impacts of aquaculture. Sheffield Academic, Sheffield, pp 1–31
29. Karakassis I, Eleftheriou A (1997) The continental shelf of Crete: structure of macrobenthic communities. Mar Ecol Prog Ser 160:185–196
30. Karakassis I, Eleftheriou A (1998) The continental shelf of Crete: the benthic environment. PSZNI: Mar Ecol 19:263–277
31. Duineveld GCA, Tselepides A, Witbaard R, Bak RPM, Berghuis EM, Nieuwland G, van der Weele J, Kok A (2000) Benthic-pelagic coupling in the oligotrophic Cretan sea. Prog Oceanogr 46:457–481
32. Karakassis I, Tsapakis M, Hatziyanni E, Papadopoulou K-N, Plaiti W (2000) Impact of cage farming of fish on the seabed in three Mediterranean coastal areas. ICES J Mar Sci 57: 1462–1471
33. Vizzini S, Mazzola A (2004) Stable isotope evidence for the environmental impact of a land-based fish farm in the western Mediterranean. Mar Pollut Bull 49:61–70
34. Vizzini S, Savona B, Caruso M, Savona A, Mazzola A (2005) Analysis of stable carbon and nitrogen isotopes as a tool for assessing the environmental impact of aquaculture: a case study from the western Mediterranean. Aquac Int 13:157–165
35. Sarà G, Lo Martire M, Buffa G, Mannino AM, Badalamenti F (2007) The fouling community as an indicator of fish farming impact in Mediterranean. Aquac Res 38:66–75
36. Cromey CJ, Black KD (2005) Modelling the impacts of finfish aquaculture. In: Hargrave BT (ed) Environmental effects of marine finfish aquaculture. Springer, Berlin, Heidelberg, pp 129–156
37. Askens A, Izquiredo MS, Robaina L, Vegara JM, Montero D (1997) Influence of fish meal quality and feed pellet on growth, feed efficiency and muscle composition in gilthead sea bream (*Sparus aurata*). Aquaculture 153:251–261
38. Lupatsch I, Kissil GWm, Sklan D (2001) Optimization of feeding regimes for European seabass *Dicentrarchus labrax*: a factorial approach. Aquaculture 202:289–302
39. Clarke S, Smart A, van Barneveld R, Carter C (1997) The development and optimization of manufactured feeds for farmed southern bluefin tuna. Austasia Aquacult 11:59–62
40. McKindsey CW, Thetmeyer H, Landry T, Silvert W (2006) Review of recent carrying capacity models for bivalve culture and recommendations for research and management. Aquaculture 261:451–462
41. Porello S, Lenzi M, Persia E, Tomassetti P, Finoia MG (2003) Reduction of aquaculture wastewater eutrophication by phytotreatment ponds system: I Dissolved and particulate nitrogen and phosphorus. Aquaculture 219:515–529
42. Lenzi M, Gennaro P, Mastroianni A, Mercatali I, Persia E, Roffilli R, Solari D, Tomassetti P, Porrello S (2009) Improvement of a system for treating land-based fish-farm effluents. Chem Ecol 25:247–256
43. Sorokin YI, Sorokin PU, Ravagnan G (2006) Hypereutrophication events in the Ca'Pisani lagoons associated with intensive aquaculture. Hydrobiologia 571:1–15
44. Tett P, Gilpin L, Svendsen H, Erlandsson CP, Larsson U, Kratzer S, Fouilland E, Janzen C, Lee J-Y, Grenz C, Newton A, Ferreira JG, Fernandes T, Scory S (2003) Eutrophication and some European waters of restricted exchange. Cont Shelf Res 23:1635–1671
45. Karakassis I (2001) Aquaculture and coastal marine biodiversity. Oceanis 24:272–286
46. Danovaro R, Gambi C, Luna GM, Mirto S (2004) Sustainable impact of mussel farming in the Adriatic Sea (Mediterranean Sea): evidence from biochemical, microbial and meiofaunal indicators. Mar Pollut Bull 49:325–333
47. Sara G (2007) Ecological effects of aquaculture on living and non-living suspended fractions of the water column: a meta-analysis. Water Res 41:3187–3200
48. Karakassis I, Pitta P, Krom MD (2005) Contribution of fish farming to the nutrient loading of the Mediterranean Sea. Sci Mar 69:313–321
49. Pitta P, Apostolaki ET, Tsagaraki T, Tsapakis M, Karakassis I (2006) Fish farming effects on chemical and microbial variables of the water column: a spatio-temporal study along the Mediterranean Sea. Hydrobiologia 563:99–108
50. Diaz-Almela E, Alvarez E, Santiago R, Marba N, Holmer M, Grau T, Danovaro R, Argyrou M, Karakassis Y, Duarte CM (2008) Benthic input rates predict seagrass (*Posidonia oceanica*) fish farm-induced decline. Mar Pollut Bull 56:1332–1342
51. Apostolaki ET, Marba N, Holmer M, Karakassis I (2009) Fish farming enhances biomass and nutrient loss in *Posidonia oceanica* (L.) Delile. Estuar Coast Shelf Sci 81:390–400
52. Dalsgaard T, Krause-Jensen D (2006) Monitoring nutrient release from fish farms with macroalgal and phytoplankton bioassays. Aquaculture 256:302–310
53. Pitta P, Tsapakis M, Apostolaki ET, Tsagaraki T, Holmer M, Karakassis I (2009) "Ghost nutrients" from fish farms are transferred up the food web by phytoplankton grazers. Mar Ecol Prog Ser 374:1–6
54. IUCN (2009) Aquaculture site selection and site management . Guide for the sustainable development of Mediterranean aquaculture. IUCN Gland, Switzerland and Malaga, Spain, p 303
55. Mourente G, Tocher DR (2009) Tuna nutrition and feeds: current status and future perspectives. Rev Fish Sci 17: 373–390
56. Meyer FP (1991) Aquaculture disease and health management. J Anim Sci 69:4201–4208
57. Bonga SEW (1997) The stress response in fish. Physiol Rev 77:591–625
58. Wedemeyer GA (1997) Effects of rearing conditions on the health and physiological quality of fish in intensive culture. In: Iwama GK, Pickering AD, Sumpter JD, Schreck CB (eds) Fish stress and health in aquaculture, vol 62, Society for experimental biology seminar, series. Cambridge University Press, Cambridge

59. Pickering AD (1998) Stress responses of farmed fish. In: Black KD, Pickering AD (eds) Biology of farmed fish. CRC, Boca Raton, pp 222–255
60. Varvarigos P (1997) Marine fish diseases in Greece. Fish Farmer 20:10–12
61. Waknitz FW, Tynan TJ, Nash CE, Iwamoto RN, Rutter LG (2002) Review of potential impacts of Atlantic salmon culture on puget sound chinook salmon and hood canal summer-run chum salmon evolutionarily significant units. US Department of Commerce, NOAA technical memoranda, NMFS-NWFSC-53, p 83
62. Diamant A, Colorni A, Ucko M (2007) Parasite and disease transfer between cultured and wild coastal marine fish. In: Briand F (ed) Impact of mariculture on coastal ecosystems, CIESM workshop monographs, Lisbon no. 32, pp 49–54
63. Breuil G, Mouchel O, Fauvel C, Pepin JF (2001) Sea bass *Dicentrarchus labrax* nervous necrosis virus isolates with distinct pathogenicity to sea bass larvae. Dis Aquat Organ 45:25–31
64. Diaz Lopez B (2006) Bottlenose dolphin *Tursiops truncatus* predation on a marine fin fish farm: some underwater observations. Aquat Mamm 32:305–310
65. Diamant A, Colorni A, Ucko M (2007) Parasite and disease transfer between cultured and wild coastal marine fish. Impact of mariculture on coastal ecosystems. CIESM workshop monographs no: 32, Monaco, pp 49–54
66. IUCN (2007) Interactions between aquaculture and the environment. Guide for the sustainable development of Mediterranean aquaculture, Gland, Switzerland and Málaga, Spain, p 110
67. Austin B, Austin DA (1999) Bacterial fish pathogens: disease of farmed and wild fish. Springer-Praxis, Chichester
68. Barnes AC, Hastings TS, Aymes SGB (1995) Aquaculture antibacterials are antagonized by sea-water. J Fish Dis 18:463–465
69. Smith P, Niland T, O'Domhnaill F, O'Tuathaigh G, Hiney M (1996) Influence of marine sediments and divalent cations on the activity of oxytetracycline against *Listonella anguillarum*. Bull Eur Assn Fish P 16:54–57
70. Athanassopoulou F, Pappas IS, Bitchava K (2009) An overview of the treatments for parasitic disease in Mediterranean aquaculture. Options Méditerranéennes 86:65–82
71. Hansen GH, Olafsen JA (1999) Bacterial interactions in early life stages of marine cold water fish. Microb Ecol 38:1–26
72. Verschuere L, Rombaur G, Sorgeloos P, Verstraete W (2000) Probiotic bacteria as biological control agents in aquaculture. Microbiol Mol Biol Rev 64:655–671
73. Lall SP, Lewis-McCrea LM (2007) Role of nutrients in skeletal development in fish – an overview. Aquaculture 267:3–19
74. Dimitroglou A, Davies S, Moate R, Spring P, Sweetman J (2007) The beneficial effect of Bio-Mos on gut integrity and enhancement of fish health. Alltech technical seminar series, Dublin, November 2007
75. Torrecillas S, Makol A, Caballero MJ, Montero D, Robaina L, Real F, Sweetman J, Tort L, Izquierdo MS (2007) Immune stimulation and improved infection resistance in European sea bass (*Dicentrarchus labrax*) fed mannan oligosaccharides. Fish Shellfish Immunol 23:969–981
76. Torrecillas S, Caballero MJ, Sweetman J, Makol A, Izquierdo MS (2007b) Effects of feeding Bio- Mos on European sea bass (*Dicentrarchus labrax*) juvenile culture. Alltech technical seminar series, Dublin, November 2007
77. Gatesoupe J (2005) Probiotics and prebiotics for fish culture, at the parting of the ways. Aqua Feeds: Formulation & Beyond 2:1–5
78. Gatesoupe FJ (1999) The use of probiotics in aquaculture. Aquaculture 180:147–165
79. Picchietti S, Mazzini M, Taddei AR, Renna R, Fausto AM, Mulero V, Carnevali O, Cresci A, Abelli L (2007) Effects of administration of probiotic strains on GALT of larval gilthead seabream: immunohistochemical and ultrastructural studies. Fish Shellfish Immunol 22:57–67
80. Avella MA, Olivotto I, Silvi S, Place AR, Carnevali O (2010) Effect of dietary probiotics on clownfish: a molecular approach to define how lactic acid bacteria modulate development in a marine fish. Am J Physiol Regul Integr Comp Physiol 298:359–371
81. Jeney G, Galeotti M, Volpatti D (1994) Effect of immunostimulation on the non specific immune response of sea bass *Dicentrarchus labrax*. In: International symposium on aquatic animal health: program and abstracts, Seattle, Washington DC, September 4–8 1994, p 76
82. Bagni M, Archetti L, Amadori M, Marino G (2000) Effect of long-term oral administration of an immunostimulant diet on innate immunity in sea bass (*Dicentrarchus labrax*). J Vet Med 47:745–751
83. Knibb W, Gorshkova G, Gorshkov S (1997) Selection for growth in the gilthead seabream (*Sparus aurata*). Isr J Aquacult/Bamidgeh 49:57–66
84. Chistiakov DA, Hellemans B, Volckaert FAM (2007) Review on the immunology of European sea bass *Dicentrarchus labrax*. Vet Immunol Immunopathol 117:1–16
85. Dempster T, Moe H, Fredheim A, Jensen Q, Sanchez-Jerez P (2007) Escapes of marine fish from sea-cage aquaculture in the Mediterranean Sea: status and prevention. In: Briand F (ed) Impact of mariculture on coastal ecosystems, CIESM workshop monographs, no. 32, Lisboa, pp 55–60
86. Moe H, Dempster T, Sunde LM, Winther U, Fredheim A (2007) Technological solutions and operational measures to prevent escapes of Atlantic Cod (*Gadus morhua)* from sea-cages. Aquac Res 38:91–99
87. Diamant A (1997) Fish to fish transmission of a marine myxosporean. Dis Aquat Organ 30:99–105
88. Triantafyllidis A (2007) Aquaculture escapes: new DNA based monitoring analyses and application on seabass and seabream. In: Briand F (ed) Impact of mariculture on coastal ecosystems, CIESM Workshop Monographs, no. 32, Lisboa, pp 67–72
89. Carlton JT (2009) Deep invasion ecology and the assembly of communities in historical time. In: Rilov G, Crooks JA (eds) Biological invasions in marine ecosystems. Springer, Berlin, Heidelberg, pp 13–56

90. Shiganova TA (1998) Invasion of the Black Sea by the ctenophore *Mnemiopsis leidyi and* recent changes in pelagic community structure. Fish Oceanogr 7:305–310
91. Galil BS (2007) Seeing red: alien species along the Mediterranean coast of Israel. Aquat Invasions 2:281–312
92. United Nations Environment Programme (UNEP)/ Mediterranean Action Plan (2005) Action plan concerning species introductions and invasive species in the Mediterranean Sea. RAC/SPA, Tunis, p 30
93. ICES (2005) ICES code of practice on the introductions and transfers of marine organisms, p 30
94. Hewitt CL, Campbell ML, Gollasch S (2006) Alien species in aquaculture. Considerations for responsible use. IUCN, Gland, Switzerland and Cambridge, p 32
95. Cardia F, Lovatelli A (2007) A review of cage aquaculture: the Mediterranean Sea. In: Halwart M, Soto D, Arthur JR (eds) Cage aquaculture – regional reviews and global overview. FAO fisheries technical paper no. 498, FAO, Rome, pp 159–190
96. Machias A, Karakassis I, Labropoulou M, Somarakis S, Papadopoulou KN, Papaconstantinou C (2004) Changes in wild fish assemblages after the establishment of a fish farming zone in an oligotrophic marine ecosystem. Estuar Coast Shelf Sci 60:771–779
97. Machias A, Karakassis I, Giannoulaki M, Papadopoulou N, Smith CJ, Somarakis S (2005) Response of demersal fish communities to the presence of fish farms. Mar Ecol Prog Ser 288:241–250
98. Holmer M, Perez M, Duarte CM (2003) Benthic primary producers – a neglected environmental problem in Mediterranean maricultures? Mar Pollut Bull 46:1372–1376
99. Balata D, Nesti U, Piazzi L, Cinelli F (2007) Patterns of spatial variability of seagrass epiphytes in the north-west Mediterranean Sea. Mar Biol 151:2025–2035
100. Pérez M, García T, Ruíz JM, Invers O (2008) Physiological responses of the seagrass *Posidonia oceanica* as indicators of fish farm impact. Mar Pollut Bull 56:869–879
101. Delgado O, Ruiz JM, Pérez M, Romero J, Ballesteros E (1999) Effects of fish farming on seagrass (*Posidonia oceanica*) in a Mediterranean bay: seagrass decline after organic loading cessation. Oceanol Acta 22:109–117
102. Holmer M, Hansen P-K, Karakassis I, Borg JA, Schembri PJ (2008) Monitoring of environmental impacts of marine aquaculture. In: Holmer M, Black K, Duarte CM, Marbà N, Karakassis I (eds) Aquaculture in the ecosystem. Springer, Berlin, pp 47–86
103. Pergent-Martini C, Boudouresque CF, Pasqualini V, Pergent G (2006) Impact of fish farming facilities on *Posidonia oceanica* meadows: a review. Mar Ecol 27:310–319
104. Van Houtte A (2001) Establishing legal, institutional and regulatory framework for aquaculture development and management. In: Subasinghe RP, Bueno P, Phillips MJ, Hough C, McGladdery SE, Arthur JE (eds) Aquaculture in the third millennium. Technical proceedings of the conference on aquaculture in the third millennium, NACA and FAO, Bangkok, Thailand, February 20–25 2000
105. EU (European Union) (2009) Building a sustainable future for aquaculture: a new impetus for the strategy for the sustainable development of European aquaculture. Communication from the Commission to the European Parliament and the Council COM (2009), 162, Brussels, p 13
106. Stickney RR (1997) Offshore Mariculture. In: Bardach JE (ed) Sustainable aquaculture. John Wiley & Sons, New York, pp 53–86
107. Turchini GM, Torstensen BE, Ng W-K (2009) Fish oil replacement in finfish nutrition. Rev Aquacult 1:10–57
108. Naylor RL, Hardy RW, Bureau DP, Chiu A, Elliott M, Farrell AP, Forster I, Gatlin DM, Goldburg RJ, Hua K, Nichols PD (2009) Feeding aquaculture in an era of finite resources. Proc Natl Acad Sci 106:15103–15110
109. Raffi SM, (2006) Sustainable Utilisation of Bycatch Resources. In: Kannaiyan S, Balasubramanian T, Ajmalkhan S, Venkataraman K (eds) Biodiversity and Conservation of Marine Bioresources, National Biodiversity Authority, pp 107–113
110. Rubin, S (1993) Fish waste in Japan. Stiftelsen rubin, report no. 007/15, p 22
111. Sarig S (1981) The Mugilidae in polyculture in fresh and brackish water fishponds. In: Oren OH (ed) Aquaculture of grey mullets. Cambridge University Press, Cambridge, UK, pp 391–409
112. De Monbrison D, Tzchori I, Holland MC, Zohar Y, Yaron Z, Elizur A (1997) Acceleration of gonadal development and spawning induction in the Mediterranean grey mullet. Mugil cephalus: preliminary studies. Isr J Aquacult/Bamidgeh 49:214–221
113. Aizen J, Meiri I, Tzchori I, Levavi-Sivan B, Rosenfeld H (2005) Enhancing spawning in the grey mullet (*Mugil cephalus*) by removal of dopaminergic inhibition. Gen Comp Endocrinol 142:212–221
114. Ervik A, Hansen PK, Aure J, Stigebrandt A, Johannessen P, Jahnsen T (1997) Regulating the local environmental impact of intensive marine fish farming I. The concept of the MOM system (Modelling-Ongrowing fish farms-Monitoring). Aquaculture 158:85–94
115. Hansen PK, Ervik A, Schaanning M, Johannessen P, Aure J, Jahnsen T, Stigebrandt A (2001) Regulating the local environmental impact of intensive marine fish farming II. The monitoring programme in the MOM system (Modelling-Ongrowing fish farms-Monitoring). Aquaculture 194: 75–92
116. Fernandes TF, Eleftheriou A, Ackefors H, Eleftheriou M, Ervik A, Sanchez-Mata A, Scanlon T, White P, Cochrane S, Pearson TH, Read PA (2001) The scientific principles underlying the monitoring of the environmental impacts of aquaculture. J Appl Ichthyol 17:181–193
117. Tett P (2008) Fishfarm wastes in the ecosystem. In: Holmer M, Black K, Duarte CM, Marbà N, Karakassis I (eds) Aquaculture in the ecosystem. Springer, Berlin, pp 1–46
118. Borja Á, Germán Rodríguez J, Black K, Bodoy A, Emblow C, Fernandes TF, Forte J, Karakassis I, Muxika I, Nickell TD,

Papageorgiou N, Pranovi F, Sevastou K, Tomassetti P, Angel D (2009) Assessing the suitability of a range of benthic indices in the evaluation of environmental impact of fin and shellfish aquaculture located in sites across Europe. Aquaculture 293:231–240

119. UNESCO (2003) A reference guide on the use of indicators for integrated coastal management – integrated coastal area management dossier 1, Intergovernmental Oceanographic Commission Manuals and Guides No. 45.

Marine Biogeochemistry

Walker O. Smith, Jr.[1], Eileen E. Hofmann[2], Anna Mosby[1]
[1]Department of Biological Sciences, Virginia Institute of Marine Science, College of William & Mary, Gloucester Pt, VA, USA
[2]Center for Coastal Physical Oceanography, Old Dominion University, Norfolk, VA, USA

Article Outline

Glossary
Definition of the Subject and Its Importance
Introduction
Future Directions
Bibliography

Glossary

Autotrophic Organisms whose mode of nutrition is photosynthesis.

Biogeochemistry The biological and chemical processes that transform and cycle elements over various time and space scales and that determine the composition of the environment.

Biological pump The biological processes and transformations that move carbon from the surface to depth.

Cyanobacteria Prokaryotic phytoplankton.

Diatom Phytoplankton which are encased in frustule consisting of silica.

Euphotic zone The surface layer of the ocean where most primary production occurs, generally considered to be the depth to which 1% of surface radiation penetrates.

Heterotrophic Organisms who require reduced organic carbon as an energy and carbon source.

Nutrient Element that is required for biological activity and growth.

Oxidation Chemical reaction in which reactant loses electrons; half-reaction paired with reduction.

Photosynthesis The process by which radiant energy from the sun is transformed into chemical energy that can later be used to reduce carbon dioxide to organic sugars, which in turn are coupled to biochemical pathways to produce all compounds necessary for cell growth.

Phytoplankton Microscopic, often unicellular, floating autotrophs that live in the ocean's surface layer and form the base of nearly all marine food webs.

Reduction Chemical reaction in which reactant gains electrons; half-reaction paired with oxidation.

Definition of the Subject and Its Importance

The biogeochemistry of the world oceans has been studied for many decades, and major advances in understanding have been linked with development of new techniques and tools that allow the accurate representation of various organic and inorganic pools within the water. The classic study of Redfield [1] showed that some critical bioactive compounds (carbon, nitrogen, phosphorus, oxygen) occur in particular ratios to one another that are relatively invariant over space and time and provided a description of the relationship between the ratio of nitrogen to phosphorus (N:P) for inorganic and plankton pools. The processes that control these compounds were assessed, and it was concluded that phosphorus concentrations are largely controlled by terrestrial inputs, whereas nitrogen is under biological control.

Subsequent studies have provided more detailed investigations of the processes controlling these ratios. These studies benefited from the development and standardization of methods for accurately measuring dissolved organic carbon (DOC) and dissolved organic nitrogen (DON). The improved methodology, mostly developed during the 1980s, allowed the spatial (vertical and horizontal) and temporal changes of both DOC and DON to be quantitatively described.

Recognition of the importance of the flux of organic carbon to depth in mediating the marine

response to increased atmospheric carbon dioxide concentrations stimulated development of technical approaches and instruments for assessing and quantifying the biological pump. This component of marine biogeochemical cycles is still a poorly constrained component of numerical models developed for simulation of ocean carbon cycling and climate, and technological approaches that result in better assessment of the flux of organic matter to depth continue to be developed and refined. Also, numerical models of biogeochemical processes are providing insights into critical processes and provide frameworks that allow measurements to be projected over larger space and timescales. Continued measurement and modeling of oceanic biogeochemical cycles is essential for understanding and projecting responses to natural and anthropogenic-induced climate change.

Introduction

The ocean is the dominant surface feature that has controlled much of the evolution, distribution, and success of life on earth, and the changes in ocean chemistry reflect the interaction with biota throughout geological time. The oceans were originally anoxic, but the evolution of organisms with oxygen-generating processes (photosynthesis) resulted in the conversion of the oceans to an oxygenated environment, which greatly altered the availability of some elements for those organisms. The cycling of elements within the earth's oceans and the complex relationships among the biological, chemical, and geological processes are the core of the study of marine biogeochemistry. Understanding these relationships is difficult and is further complicated by the space and time variability of the dominant processes that control the cycling of the different elements. Understanding the interactions and linkages among and between the cycles of biogeochemical elements is critically important for assessing and projecting the nature, degree, and direction of changes in ocean processes that may result from changes induced by natural and/or anthropogenic activities.

Elements in the ocean have characteristic vertical and horizontal distributions that result from the processes that regulate their long-term source/sink relationships. For example, oceanic carbon dioxide (CO_2) distributions are characterized by a horizontal concentration gradient that increases from the equator to the poles, which results from the greater dissolution of CO_2 in colder water. Carbon dioxide concentrations generally increase with depth due to remineralization in the deeper, older waters relative to its removal at the surface. Other elements may be controlled by different factors (e.g., sources from the sediments or hydrothermal vents; atmospheric sources) and have different vertical and horizontal patterns, but all interact to create the observed vertical distributions in the ocean. Understanding marine biogeochemistry requires knowledge not only of specific processes regulating a particular element, but also an understanding of the interdisciplinary aspects that control these cycles.

Nutrients are the biogeochemical elements that are required for biological activity. Some elements are greatly reduced in their concentrations by chemical or biological processes and can reach such low concentrations that they subsequently limit the growth of organisms in the sea. Such elements are thought of as limiting nutrients in the sense of the German agricultural chemist, Justus von Liebig, who suggested that the growth of plants is limited not by the total amount of resources, but by the resource in lowest abundance relative to the others.

Plant growth in the ocean is known to be limited by a small number of nutrients that include nitrogen, phosphorus, iron, silicic acid, and inorganic carbon. The cycling and processes that control the concentrations of these limiting nutrients are critical in the regulation of carbon cycling in the ocean, and hence their study forms the basis for most biogeochemical research.

The biogeochemical cycles described in subsequent sections use carbon as a "common denominator." Carbon is the basic component of organic matter, and with the advent of industrialization is being added to the atmosphere at an unprecedented, rapid rate, which is changing atmospheric temperatures and impacting the thermal equilibrium of the ocean. Also, carbon is absorbed from the atmosphere at the ocean surface where it reacts with ocean water to produce carbonic acid, thereby making ocean waters more acidic (reducing the pH), which has profound impacts on oceanic chemistry and biological activity. Thus, the production and oxidation of organic matter in the ocean has

numerous critical interactions with all other elemental cycles, and is a major regulator of all marine biogeochemical cycles.

The Biogeochemical Cycle of Carbon

Carbon is the primary building block for all life because of its chemical ability to form a myriad of covalent bonds with itself and numerous other elements. As a result, the numerous complex organic compounds that form the basis of life systems are based on carbon. In the present-day ocean, synthesis of organic molecules (photosynthesis) is done largely by phytoplankton, which converts the radiant energy from the sun into chemical energy in the form of adenosine triphosphate (ATP). The ATP, along with reductant, is used to reduce CO_2 into simple sugars, which are in turn modified into all of the compounds required for cellular metabolism, growth, and division. Photosynthesis is dependent on energy from the sun, thereby confining this process to the euphotic zone, which is the part of the upper water column that receives at least 1% of the irradiance that reaches the sea surface. Phytoplankton require energy for the uptake and assimilation of nearly all elements. This dependence on light generally results in vertical distributions of nutrients that are characterized by reduced concentrations in the euphotic zone, where photosynthesis and growth are most active, and increased concentrations at depth, where photosynthesis and growth are reduced or absent (Fig. 1). This vertical profile is a typical of nutrient distributions throughout the oceans. The organic matter generated by photosynthesis and growth has roughly an inverse relationship to that of the inorganic building blocks (Fig. 1).

Redfield [1] suggested that organic matter (carbon, C) production in the sea occurs in relatively constant elemental ratios given by the relationship:

$$106CO_2 + 16H^+ + 16NO_3^- + H_3PO_4 + 122H_2O \leftrightarrow (CH_2O)_{106}(NH_3)_{16}(H_3PO_4) + 138O_2$$

This relationship describes the reaction of CO_2 with hydrogen (H), nitrate (NO_3^-), phosphate (H_3PO_4),

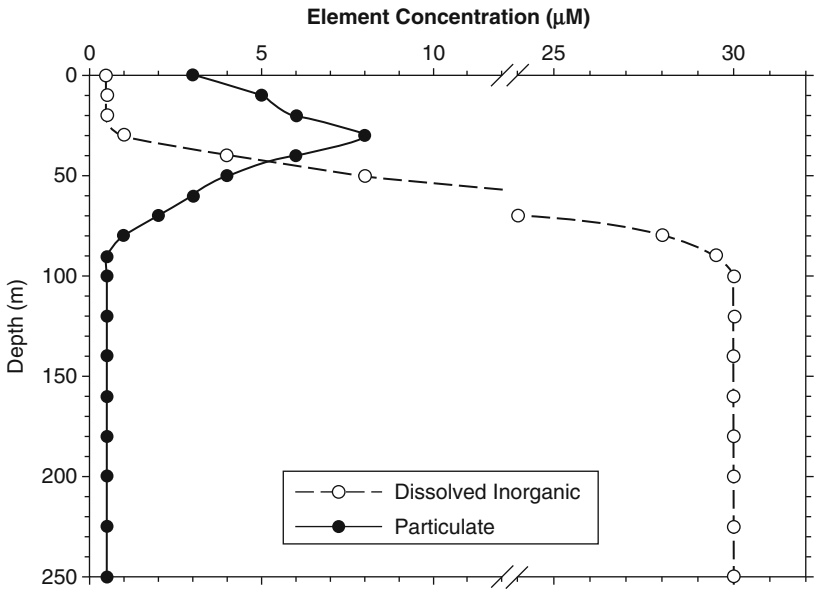

Marine Biogeochemistry. Figure 1
Generalized *vertical* distributions of dissolved inorganic elements and particulate matter produced by phytoplankton photosynthesis. Particulate matter concentrations are less than those expected from the disappearance of inorganic elements because of removal by various processes to depth (see Fig. 2). Similarly, the particulate matter *vertical* distribution is less uniform because the time-scale of redistribution of particles is much faster than that of the inorganic elements

and water (H_2O) within the photosynthetic process to produce (↔) organic carbon-nitrogen-phosphorus compounds $\left[(CH_2O)_{106}(NH_3)_{16}H_3PO_4\right]$ and gaseous oxygen (O_2). The numbers preceding the compounds indicate the amount of each. The relationship is reversible (↔) because metabolism (oxidation) of the organic matter produced by photosynthesis regenerates inorganic C, nitrogen (N), and phosphorus (P) in the same ratio and utilizes oxygen. The C:N:P ratio of 106:16:1 obtained from the above relationship is a basic paradigm of marine biogeochemistry. However, Redfield recognized that the C:N:P ratios vary within plankton types and with time, a fact that has been further established in more recent studies. The departure from the basic ratio provides insights in how marine ecosystems change and/or adapt to modified environmental or biological conditions.

All marine organisms contribute to the carbon cycle by moving carbon between organic and inorganic forms, but some marine organisms are able to use calcification to transform inorganic carbon, using bicarbonate and dissolved calcium from the water column to produce calcium carbonate ($CaCO_3$), which is then used to form a skeleton or protective shell [2]. The dissolution of calcium carbonate back into its original components is one of the primary means by which the particulate components reenter the water column, keeping the inorganic carbon cycle running. Although some of the calcium carbonate dissolved back into the water column comes from dead organisms, a large portion is contributed by phytoplankton from coccolithophorids, the genus coccolithophorid, which produce and shed calcium carbonate shells, making them a major contributor to the inorganic carbon cycle [2]. The calcium carbonate not immediately dissolved back into the water column is removed by sinking, with coccolithophorids comprising a major component of the carbon found in marine sediments. A by-product of calcification is CO_2, which either remains in the water column or reenters the biological pump through photosynthesis [2].

The importance of iron (Fe) and silicic acid ($Si(OH)_4$) in regulating carbon production in oceanic systems has also been established. Iron is required by all living organisms for a variety of metabolic processes, and silicon (Si) is needed by an important phytoplankton functional group, the diatoms, which are characterized by a hard silica shell. Diatoms remove silicic acid in approximately a 1:1 ratio to N, and the P:Fe ratio is approximately 1,000:1. Both ratios show considerable plasticity and their uptake ratios are related to other environmental variables as well [3, 4].

The organic material produced in the upper water column via photosynthesis is used by heterotrophic organisms (e.g., bacteria, zooplankton) and transformed by their metabolism and growth processes. The unassimilated ingestion of these organisms (fecal pellet production) sinks and is oxidized below the euphotic zone by a host of heterotrophic organisms (from bacteria to ciliates to scavenging, mobile animals), thereby converting the organic matter to CO_2. Also, particle aggregates formed from phytoplankton cells, detritus, and dead organisms sink from the euphotic zone and are oxidized. The unidirectional movement of large particles to depth and their remineralization defines the biological pump (Fig. 2), which also contributes to the generation of "nutrient-like" profiles in the ocean. The processes that contribute to the fluxes within the biological pump are critical to understanding the marine carbon cycle.

Atmospheric fluxes of CO_2 into and out of the ocean vary spatially. In general, equatorial waters tend to be large sources of CO_2 (net fluxes are from the ocean to the atmosphere). The equatorial Pacific is a large source because it is the site of large-scale upwelling, a process which brings cold water from depth to the surface. These waters are in turn heated by solar radiation, and because the solubility of CO_2 is strongly temperature dependent (CO_2 is less soluble in warm water), it is lost to the atmosphere. Conversely, polar waters are in general sinks for CO_2. Waters there lose heat to the atmosphere, and thus are able to absorb more CO_2. A topic of intense debate is the possible decrease in carbon flux to the waters of the Southern Ocean resulting from recent increases in wind strength, which may have altered the ocean's ability to remove CO_2 [5]. Such changes potentially would have profound impacts on the global carbon budget. At the present time the ocean is a net sink for atmospheric carbon dioxide, and has sequestered at least 25% of all anthropogenic emissions to date.

Ocean Acidification Recently, great concern has been expressed about the increasing concentrations of CO_2

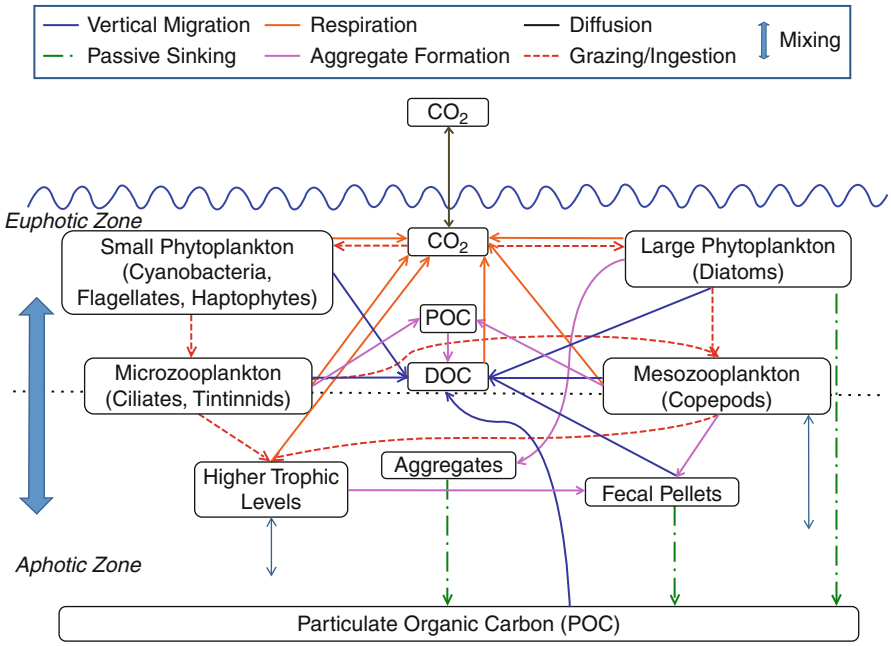

Marine Biogeochemistry. Figure 2
Schematic of the biological pump showing the biological and chemical components and processes involved in the transformation of carbon dioxide (CO_2) to organic matter, and the subsequent transformation, movement, and oxidation of particulate organic carbon (POC) and dissolved organic carbon (DOC). The CO_2 is absorbed from the atmosphere across the air-ocean interface (*wavy lines*) and is transformed by processes in the euphotic (above *dashed line*) and aphotic zone (below *dashed line*). The migration of zooplankton and higher trophic levels within the water column (*light blue lines*) and unidirectional passive sinking of particles of different sizes to depth (*green dot-dashed line*) redistribute organic material. Processes of grazing/ingestion (*red dashed line*), aggregate formation (*red line*), respiration and CO_2 generation (*orange line*), physical mixing (heavy *blue line*), and solubilization, and DOC generation (*dark blue line*) modify the rate at which POC is exported to depth from the surface waters. The POC pool at depth is generally composed of unidentifiable, small particles, whereas the POC pool in the surface is composed of recognizable biota (bacteria, phytoplankton, zooplankton) and variable amounts of detritus

in the ocean, since its absorption decreases the pH, leading to ocean acidification [5, 6]. A decrease in pH would seriously impact calcification, likely increasing dissolution of $CaCO_3$ found in skeletons and shells because the material is unprotected from seawater, and decreasing the rate at which calcification can occur by altering the concentrations of the necessary minerals in the water column. As a result, decreased pH has a great capacity to alter the ecology of marine systems such as coral reefs. In addition, decreased pH levels have been shown to alter the growth, reproduction, efficiency, and survival of those organisms that require $CaCO_3$ to survive, and these effects vary among organisms, suggesting that substantial and unexpected impacts on biodiversity could occur [7].

It is now recognized that many phytoplankton can remove only CO_2 for use in photosynthesis. Under preindustrial pH levels, free CO_2 levels could have been at limiting levels, particularly for conditions that produced high concentrations of algae, because photosynthesis naturally increases the pH level. Decreased pH and increased absolute CO_2 levels arising from current conditions might reduce this limitation. Because there is substantial variability among species of phytoplankton in their response to increased CO_2, planktonic biodiversity is at risk [8]. However, certain algal functional groups, such as nitrogen-fixing cyanobacteria, positively respond to increased CO_2 concentrations by increasing their growth and photosynthesis, whereas others can not. Similarly, at least one

species of toxin-producing dinoflagellate demonstrated increased growth and modified elemental ratios under increased CO_2 conditions [9], suggesting the possibility of an enhancement of occurrences of harmful algal blooms in the future. Because the marine carbon cycle is intimately linked with the biogeochemical cycles of nitrogen, phosphorus, silicon, and iron, these interactive effects make it extremely difficult to predict what future decreases in oceanic pH will generate. Oceanographers have recognized that increased inorganic carbon levels can have subtle effects on the biota, and much work is being done to document and quantify these effects.

The Biogeochemical Cycles of Nitrogen and Phosphorus

Although the early work of Redfield [1] clearly differentiated between the sources of nitrogen and phosphorus and the regulation of their turnover, they are linked in nature by the processes operating in the biological pump (Fig. 2). Despite this coupling, as well as their linkage to carbon, there are a number of features that distinguish them.

Nitrogen occurs in three reactive, inorganic forms in the ocean: nitrate (NO_3^-), nitrite (NO_2^-), and ammonium (NH_4^+) and the processes that transform and modify these forms make up the nitrogen cycle (Fig. 3). The nitrogen cycle has five major pathways that result in changes in the availability of nitrogen that can be used by plants. Nitrogen fixation removes gaseous nitrogen from the atmosphere, which is then converted by a series of reactions to forms that can be used for plant growth. In the ocean this process occurs primarily in tropical and semitropical environments, and the major algal species responsible for this transformation is *Trichodesmium*. Denitrification results in

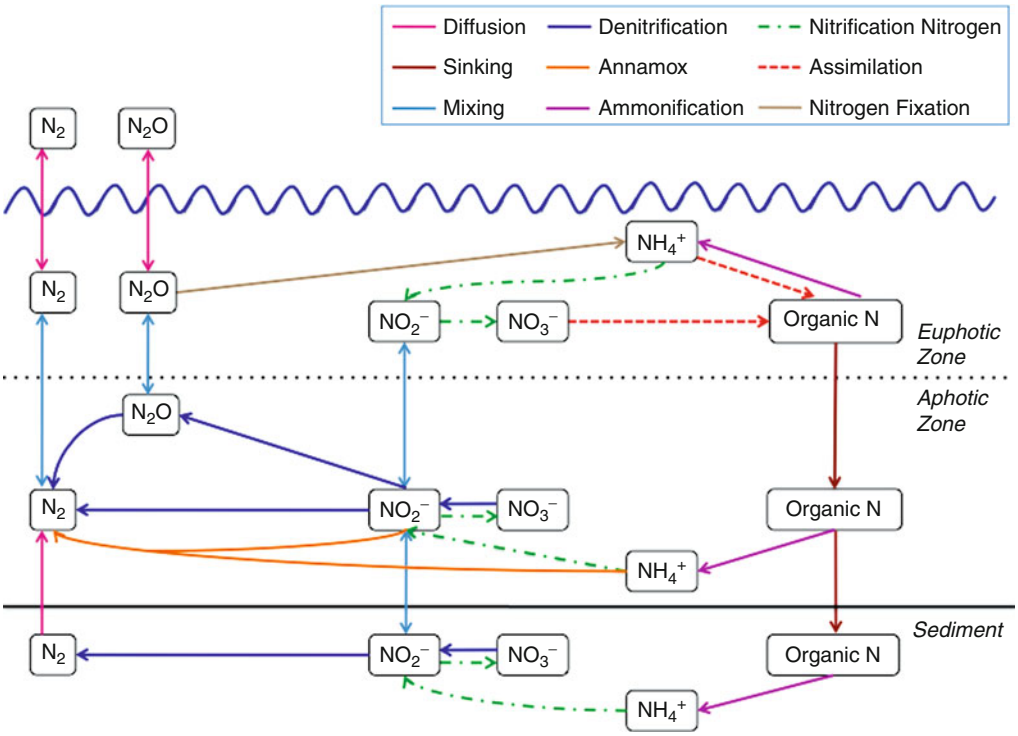

Marine Biogeochemistry. Figure 3
Schematic of the nitrogen cycle showing the nine key mechanisms by which nitrogen moves through the water column, which are denitrification (*dark blue line*), nitrification (*green dash-dot line*), nitrogen assimilation (*red dashed line*), nitrogen fixation (*brown line*), ammonification (*purple line*), annamox (*orange line*), mixing (*light blue line*), diffusion (*pink line*), and sinking (maroon line)

the reduction of NO_3^- to gaseous nitrogen, usually mediated by bacteria, and results in the loss of nitrogen available for phytoplankton in oceanic systems. These two processes are the primary means by which the ocean biota controls nitrogen biogeochemistry.

Nitrogen assimilation is the process by which nitrate (NO_3^-) and ammonium (NH_4^+) are removed from the water by phytoplankton. Ammonium is energetically favored for uptake because it does not have to be reduced intracellularly, but nitrate often occurs in greater concentrations, particularly in areas of upwelling or deep vertical mixing. Ammonium inhibits nitrate uptake, but the degree of inhibition varies with the relative concentration of the two nutrients. Ammonification generates NH_4^+ by the cleaving of amine groups from organic nitrogen. Because many marine organisms excrete ammonium, the vertical distribution of NH_4^+ can depend on the distribution of heterotrophs, such as copepods, which is variable. Nitrification is the production of NO_3^- from ammonium. Earlier work suggested that this was a relatively slow process, but more recent investigations suggest that the oxidation of NH_4^+ and production of nitrate is quite rapid, particularly in tropical waters.

The different transformations result from different organisms and some require specific types of environmental conditions (Table 1). Denitrification and nitrogen fixation are anaerobic processes, which occur only in the absence of oxygen. Oceanic systems, ranging from estuarine to open ocean, provide sites for denitrification and as a result are depleted of oxygen. These oxygen-minimum regions are characterized by large vertical fluxes of organic matter, which heterotrophic bacteria oxidize and release nitrogen, consuming the available oxygen in the process. Anoxic conditions also occur in sediments where oxygen is depleted by aerobic metabolism. An unusual biological adaptation allows for nitrogen fixation (an anaerobic process) to occur in surface waters with high levels of oxygen. Some organisms (e.g., the cyanobacterium *Trichodesmium)* form extensive patches or tufts. These tufts, by virtue of their own metabolism, unusually thick cell walls and biochemical modifications of specialized cells where N_2 fixation occurs, create a microzone of very low oxygen, thus allowing nitrogen fixation to proceed. Other, smaller cyanobacteria have unusual biochemical adaptations that allow them to fix N_2 as well, despite living in oxygen-saturated water.

Recently a new nitrogen transformation, the annamox pathway, has been described in which anaerobic bacteria oxidize ammonium and nitrite directly to gaseous nitrogen, providing a second means by which nitrogen is "lost" from the nitrogen cycle [10]. This pathway has been found to be quantitatively important in regions such as the Peruvian and Arabian Sea oxygen-minimum zones [11, 12]. Because 30–50% of global nitrogen "losses" occur in these types of regions, elucidation of this process, its oceanographic controls, and the absolute rates, have important implications for the global nitrogen cycle.

Marine Biogeochemistry. Table 1 Summary of the major processes in the nitrogen cycle, the organisms responsible for the different processes, and the environmental conditions necessary for each process

Process	Organism(s) responsible	Necessary environmental condition
Nitrogen fixation [N_2(gas)→ reduced N]	Cyanobacteria, nitrogen-fixing bacteria	Absence of O_2; light for cyanobacteria
Denitrification $[NO_3^- \rightarrow N_2(\text{gas})]$	Denitrifying bacteria	Absence of O_2
Ammonification $[N_{org} \rightarrow NH_4^+]$	Heterotrophic organisms	Presence of O_2
Nitrogen assimilation $[NO_3^- \rightarrow N_{org}; NH_4^+ \rightarrow N_{org}]$	Large phytoplankton/diatoms for NO_3^- uptake; small phytoplankton for NH_4^+ uptake	Light
Nitrification $[NH_4^+ \rightarrow NO_3^-]$	Bacteria	Presence of O_2
Annamox $[NH_4^+, NO_2^- \rightarrow N_2(gas)]$	Bacteria	Absence of O_2

The Biogeochemical Cycle of Iron

The understanding of the role of iron in the ocean has undergone a dramatic revision in the past few decades. Until recently data on absolute iron concentrations were seriously compromised by the difficulty of obtaining samples without contamination. As the collection and sampling aspects were greatly improved, the ability to quantify concentrations of iron in the oxygenated waters of the ocean decreased dramatically. Coincident with increased realization and acceptance of the vanishingly low concentrations of iron was the hypothesis that iron could, and does, regulate phytoplankton growth and productivity over large areas of the ocean [13]. Indeed, the hypothesis appeared to explain a number of oceanic features that were only partially explained. For example, large areas of the ocean, such as the Southern Ocean, the equatorial Pacific, and the north Pacific, have substantial standing stocks of nitrate and phosphate, as well as adequate irradiance, but exhibit very low standing stocks of phytoplankton (high-nutrient, low-chlorophyll regions, or HNLCs). During glacial-interglacial periods, atmospheric concentrations of CO_2 showed substantial variations and were strongly negatively correlated with iron deposition [14]. Thus iron limitation could explain CO_2 variations over geological time as well. Given that iron is the fourth most abundant element on earth, how can such low concentrations exist in the ocean, and how did oceanographers unequivocally demonstrate the ecological importance of iron?

Iron is derived from terrestrial and hydrothermal sources, but upon entry into oxygenated, saline waters, it rapidly forms iron oxides. The precipitates are largely insoluble under aerobic conditions, and attach to particles or remain in the water as colloids. The colloids can be solubilized by irradiance, contributing to a pool of dissolved inorganic iron, which consists of two forms, Fe^{+2} and Fe^{+3}. Both of these ions can be removed by plankton for their growth, although Fe^{+2} is generally oxidized to Fe^{+3} and kept at low levels. The mean ocean concentration of dissolved inorganic iron in the upper 200 m of the ocean is 0.07 nmol kg^{-1} [12]. Both forms can also be chelated by organic molecules, and thus become part of the dissolved ferro-organic pool. In general, there are two classes of organic ligands that bind with iron, a strong-binding ligand and a weak-binding ligand. The latter exchanges iron easily with biota, and thus makes iron bioavailable. There is also a class of special ligands called siderophores, which are low molecular weight organics that are produced and excreted primarily by prokaryotic organisms (bacteria, cyanobacteria) and that bind dissolved inorganic iron [15]. The ferro-ligand complex can be assimilated by bacteria, phytoplankton, and cyanobacteria, and the iron incorporated into a variety of cellular processes. Transformations among all of these pools are both biologically and irradiance mediated; entirely different transformations and equilibria are established in anoxic waters and sediments.

Iron in ocean surface waters derives from either atmospheric or deep ocean sources. Atmospheric deposition varies by latitude (proximity to terrestrial sources) and temporally (dependent on source region wind variability). Aerosols can be measured by satellite-borne sensors, which have shown that some oceanic systems receive substantial periodic depositions of iron from industrial sources (the North Atlantic) and from dust derived from terrestrial deserts in China (the western Pacific) and the Sahara in Africa (the coast of North Africa). Dissolution of aerosols in ocean water (fractional solubility) depends on the type of mineral in the aerosol, and can range from <1–90% [16, 17]. Small aerosol particles can rapidly aggregate with biological particles and exit the surface layer by sinking. Residence times for particulate iron can be as short as 6 days [17]. Conversely, other regions are rarely impacted by atmospheric deposition events (e.g., the Southern Ocean, the equatorial Pacific) by virtue of large-scale wind patterns that isolate them from terrestrial sources. These regions have their iron inputs driven by oceanographic processes such as deep vertical mixing and upwelling. Given the spatial and temporal variability in both of these processes, it is not surprising that surface water concentrations of iron are also highly variable.

Mesoscale Iron Fertilization Experiments

In the 1990s a series of large-scale ocean manipulations were undertaken to test the hypothesis that iron limited phytoplankton growth in the tropical Pacific. Two competing hypotheses were offered to explain the

equilibrium concentrations of high concentrations of nitrate and low phytoplankton biomass which were (1) limiting levels of bioavailable iron and (2) rates of loss processes from grazing kept phytoplankton standing stocks at low levels. To test these, in situ additions of iron were planned for limited regions of the ocean. The passive tracer sulfur hexafluoride (SF_6), which can be detected at very low levels, was added with the iron so that the enriched water could be followed over time. The first iron enrichment experiment produced contradictory results. The photosynthetic capacity of phytoplankton showed a clear enhancement that was correlated with iron additions, but nitrate and CO_2 concentrations were unaffected [18, 19]. Further analysis showed that upon initial iron enrichment, the iron dropped to extremely low levels because colloid formation rapidly converted soluble iron to insoluble iron oxides, and the fertilized water patch was subducted to depth, which removed the iron-enriched water from the high irradiance euphotic zone required for nutrient assimilation. To further test the two hypotheses, the experiment was repeated, and this experiment clearly demonstrated the critical role of iron in limiting phytoplankton growth in high-nutrient, low-chlorophyll waters. Iron was added repeatedly to the patch of water at 3-day intervals for almost 2 weeks [20], and the response of the surface water was clear, showing decreased nitrate (which dropped to zero), decreased CO_2, increased phytoplankton biomass and photosynthetic activity, and a quantifiable decrease in iron concentrations. That is, the concentration and supply of iron was nevertheless the essential feature in driving the carbon and nitrogen cycles of the equatorial Pacific Ocean.

Subsequent similar iron enrichment experiments have been conducted in other HNLC regions in the Southern Ocean and the North Pacific. The former is extremely important to global biogeochemical cycles, as it is the site of deep and intermediate water mass formation, and thus regulates the concentrations of inorganic nutrients in much of the world's surface waters. As an example, models suggested that if all the inorganic nutrients were utilized (by iron fertilization) in the Southern Ocean that within 300 years the waters being upwelled in the eastern tropical Pacific would be greatly reduced in nutrient levels, and thus decrease productivity of commercially important higher trophic levels and marine mammals dependent on ecosystem processes in that region [21]. In all iron enrichment experiments to date, substantial and positive responses to additions of inorganic iron were observed, and while the details among experiments differ (and the causes debated), it is now accepted that iron plays a major role in the biogeochemistry of the ocean [22].

The Biogeochemical Cycle of Silicon

Silicon, despite being a nutrient for only one major functional group of phytoplankton (diatoms), is a major factor in regulating other biogeochemical cycles, such as carbon. This is because diatoms are extremely important primary producers, generating approximately as much oxygen on an annual basis as do pine trees in terrestrial systems. In addition, diatoms are among the largest forms of phytoplankton, and hence can sink passively to depth. Diatoms also produce transparent exopolymer particles, which serve as the primary mechanism for aggregating particles in the ocean's surface layer, thus producing large, rapidly sinking particles that are the major component of organic carbon and nitrogen flux to deeper water (Fig. 2). Finally, diatoms are also heavily grazed by herbivorous organisms, and serve as a means to transfer photosynthate to the large organism-based food web. All of these characteristics contribute to the substantial importance of diatoms in the ocean.

Silicon is a major component of rocks and terrestrial minerals, and as a result the inputs to the ocean in riverine waters are substantial. However, silicon is not readily dissolvable, and dissolved silicon, which occurs as $Si(OH)_4$, remains at relatively low levels. Aeolian and oceanic weathering of seafloor rocks also constitutes a significant source of dissolved silicon. Silicon also is found in high concentrations in waters exiting hydrothermal vents, and while quantitative estimates are uncertain, the contribution of this source to total silicon inputs is likely to be significant.

Silicon is incorporated into diatoms and other marine organisms as opal ($Si(OH)_4 nH_2O$), which is slightly more soluble than pure SiO_2 and undersaturated in all ocean waters. Opal is found in the sediments as siliceous deposits of biogenic origin; these deposits are largely focused in the Southern Ocean's polar front region [23]. Silicon is recycled within the water column, but rates of this cycling are modest, and silicon

regeneration is often markedly uncoupled from that of carbon and nitrogen in some regions. The reason for this appears to result from the different controls of each: organic matter regeneration is largely biologically mediated (by heterotrophic processes), whereas silicon regeneration is regulated by temperature [24]. As a result, in polar regions a large fraction of the organic matter that sinks from the euphotic zone is regenerated in the upper 250 m, whereas a substantial amount of silicon sinks to a greater depth as biogenic particles. This uncoupling contributes to the formation of large zones of biogenic silica deposits in polar regions and are reflective of surface layer diatomaceous productivity. In a more recent reanalysis of the global silicon budget, it was concluded that the deposition of silicon in continental margins may have been greatly underestimated [25]. If this were true, then the coupling between the silicon and organic matter budgets would be even stronger than previously thought.

An additional mechanism to couple the biogeochemistry of silicon and organic carbon is the presence of an organic membrane that covers diatom frustules [26]. Silica dissolution does not begin until this membrane is degraded by bacteria, which decreases the time for the dissolution of opal during the transit of a particle through the water column (ca. 3,000 m). Sinking rates of large aggregates are ca. 200 m day^{-1}, so that a reduction in the already low rate of dissolution by the necessity for organic degradation can decrease dissolution of silica markedly. Similar effects of grazing can occur, as fecal pellets are usually composed of an organic pellicle that must be degraded prior to chemical silica dissolution.

As with other nutrients, silicic acid has substantial interactions with other elements, such as nitrate and iron. Under iron-limiting conditions, diatoms continue to assimilate silicon, but because iron is needed in the enzymes used for nitrate assimilation, nitrate uptake decreases [3]. As a result, Si:N ratios increase by nearly an order of magnitude in diatoms under iron limitation and elevated ratios observed in natural systems have been used to infer iron limitation.

The Biogeochemical Cycle of Sulfur

In marine systems sulfur is largely present in its most stable form, which is sulfate (SO_4^{-2}). Sulfate is present in high concentrations in most marine systems, and relatively low concentrations are required by organisms to survive [27]. As a result, sulfur does not normally become growth limiting. Sulfate concentrations in marine systems are primarily controlled by physical rather than chemical processes. Variations in concentration only have a significant biological impact in anoxic zones where sulfate reduction occurs [2]. Sulfur is also present as other inorganic (H_2S) and organic (dimethylsulfoniopropionate (DMSP), dimethylsulfide (DMS), carbonyl sulfide (COS), and methanethiol (MeSH)) forms. Sulfate is transformed into these compounds via the sulfur cycle, which operates primarily in the photic zone of the upper water column, in the sediments, and around hydrothermal vents (Fig. 4).

In aerobic environments sulfur is converted between inorganic compounds (sulfate and hydrogen sulfide) and organic sulfur compounds including DMSP, DMS, COS, and amino acids. Most algae and bacteria use sulfur assimilation to form amino acids, such as cysteine and methionine [27]. Some phytoplankton species, particularly prymnesiophytes and dinoflagellates, use methionine to produce DMSP, a compound with antioxidant properties [28, 29]. DMSP can be released into the water and subsequently used to produce amino acids through assimilation by bacteria or phytoplankton, including some species of diatoms and cyanobacteria, demethylated by bacteria to produce MeSH, or oxidized into DMS and acrylic acid [30]. DMS is either broken down in the water into sulfate through bacterial uptake or photooxidation, or is volatilized into the atmosphere, where it can act as an important aerosol [27].

The sulfur cycle in ocean sediments can be divided into reactions that occur in the upper oxic layer and those that occur in the lower, oxygen-depleted (anoxic) region. In the anoxic sediments, sulfur-reducing bacteria carry out anaerobic respiration using sulfate or sulfur-containing organic compounds to oxidize organic matter, resulting in the production of sulfide, typically as H_2S, a form of sulfur that is highly toxic to most organisms. In the deeper layers of the sediment, sulfide reacts with iron and precipitates as iron sulfides such as pyrite (FeS_2) [30]. Some sulfide remains in the sediment, and, when mixed back into the oxic zone through processes such as bioturbation, is quickly

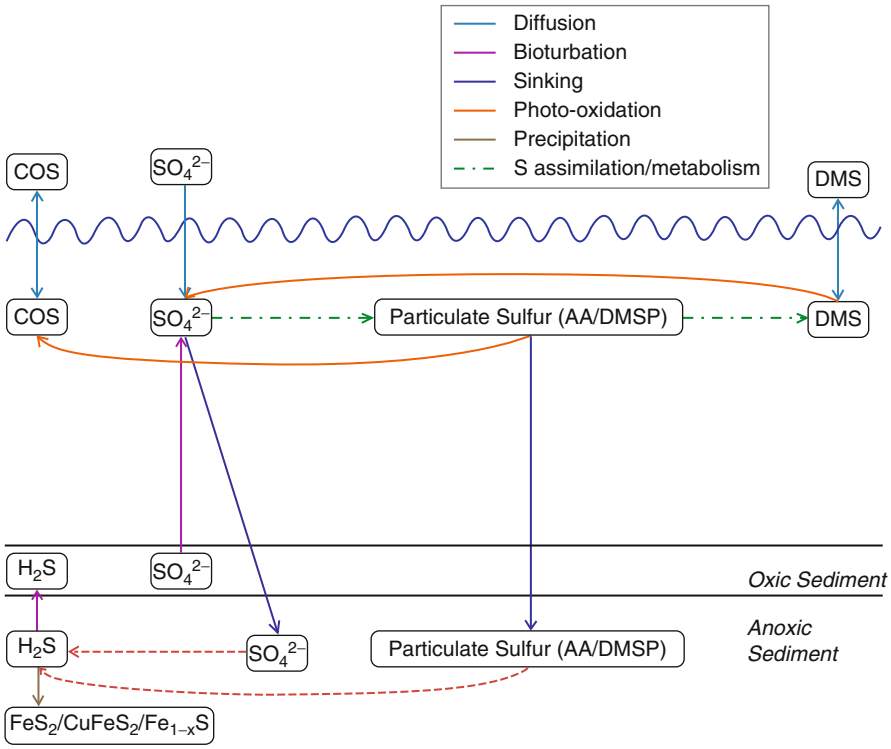

Marine Biogeochemistry. Figure 4

The sulfur cycle involves transformation of sulfur in the water column through physical mechanisms such as diffusion (*light blue line*), bioturbation (*purple line*), and sinking (*dark blue line*); chemical mechanisms of photooxidation (*orange line*), and precipitation (*yellow line*); and biological mechanisms of sulfur assimilation and metabolism by phytoplankton (*green dash-dot line*) and reduction and oxidation by bacteria in the sediment (*orange dashed line*)

oxidized by sulfur-oxidizing bacteria into sulfate, which can then remain in the sediment or be released into the overlying water [31]. Sulfur oxidation and reduction by bacteria in the sediment are also important to the functioning of the nitrogen cycle in oxygen-minimum zones [32]. In these environments, sulfate reduction provides a significant amount of the ammonium used in the anammox reaction in anaerobic environments, and nitrate reduction may be coupled to sulfide oxidation, indicating that the anaerobic mechanisms in the sulfur cycle may also be important in the nitrogen cycle [32].

The presence of hydrogen sulfide around hydrothermal vents has resulted in the development of unique organisms with the ability to use the energy contained in hydrothermal fluids to produce organic compounds through chemoautolithotrophy [33]. At hydrothermal vents seawater comes into contact with magma from the earth's interior, which cools and forms reduced sulfur compounds [2]. The sulfate in seawater then reacts to form hydrogen sulfide as well as sulfur-containing minerals such as pyrite (FeS_2), chalcopyrite ($CuFeS_2$), and pyrrhotite ($Fe_{1-x}S$) [2], which form the surface chimney structure that is characteristic of hydrothermal vents. The hydrogen sulfide provides the energy, rather than light, for the chemoautrophic microorganisms that form the base of the hydrothermal vent food web [33]. Some species of microorganisms can operate in aerobic conditions, using oxygen as the electron acceptor, while others have the ability to carry out this reaction in anaerobic conditions, using nitrate, sulfate, or sulfur as the electron acceptor [2]. These organisms survive in symbiotic relationships with other organisms living near the hydrothermal vents. The microorganisms, which are endemic to hydrothermal vent environments, allow unique

communities to develop and help maintain the oceanic sulfur cycle by transforming hydrogen sulfide released by the hydrothermal vents into sulfate [33].

The Biogeochemical Cycle of Oxygen

Oxygen is involved in all nutrient cycles, and its presence or absence dictates the reactions that will occur in a specific marine environment. Oxygen gas can be introduced into marine environments across the air-sea interface (e.g., by diffusion). However, oxygen concentration is controlled by the biological processes of photosynthesis and respiration, and by physical processes such as mixing within the water column. In the euphotic zone, phytoplankton photosynthesis produces oxygen, which is then used as the electron acceptor to conduct aerobic respiration. This process is carried out by both autotrophic and heterotrophic organisms throughout the water column.

Oxygen concentration generally decreases with depth in the ocean. Photosynthesis can only be carried out in the lighted parts of the water column, but respiration continues throughout the water column. As the organic matter from the surface layers sinks, it is taken up by organisms and used to conduct respiration, depleting oxygen levels. Some marine environments, particularly in marine sediments, are suboxic, with oxygen concentrations less than 0.2 ppm (but still detectable), or anoxic, with oxygen concentrations below detectable levels [2]. Organisms survive in these environments by using anaerobic respiration, in which compounds such a nitrate, sulfate, iron, or even organic matter are used as alternative electron acceptors to oxygen [2].

Anoxic zones are not limited to marine sediments, with increasing attention being paid to decreasing oxygen concentrations in previously oxygen-rich areas of the ocean. Hypoxic zones, marine environments with oxygen concentrations below 2 mg L^{-1}, typically form when primary productivity is high, leading to increased organic matter in the system and increased respiration, and when mixing throughout the water column is low, preventing the oxygen in the upper water column from reaching lower layers [34–36]. Hypoxic zones have been increasing in frequency, including the Gulf of Mexico and Chesapeake Bay [34, 35]. Factors such as eutrophication due to increased fertilizer or wastewater runoff have lead to the development of hypoxic conditions in systems already susceptible due to vertical stratification of the water column [34]. Thus, the disruption in the typical oxygen cycle and the lack of an anaerobic respiration mechanism in most marine organisms can result in serious consequences for the composition and productivity of the marine food web community in these hypoxic zones.

Future Directions

Studies of Biogeochemical Cycles

In the past two decades, a number of large, interdisciplinary programs were conducted to obtain biogeochemical data on appropriate time and space scales so that mathematical models of global climate change can accurately represent the complex processes of elemental cycles. One such program, the Joint Global Ocean Flux Study (JGOFS), which occurred from 1987 to 2003, was international in scope, and undertook coordinated, multidisciplinary, international studies in the equatorial Pacific, the north Atlantic, the Arabian Sea, and the Southern Ocean, and coordinated multidisciplinary national programs in a range of coastal and open ocean environments. The JGOFS project was designed to assess the carbon cycle, but because all elemental cycles are closely linked, insights were gained into the understanding of nitrogen, silicon, and iron cycles as well. The JGOFS program also had a significant synthesis and modeling component that was intended to integrate the data sets from the multidisciplinary studies and to develop mathematical models of increased complexity and biological realism. In addition to providing a wealth of publicly available data, the JGOFS program served as a model for large, multidisciplinary studies of ocean processes.

The results and understanding from the JGOFS program provided the basis for the Integrated Marine Biogeochemistry and Ecosystem Research (IMBER) Project, which was initiated in 2001 by the International Geosphere-Biosphere Program and the Scientific Committee on Oceanic Research. The science goals of the IMBER project extend the investigation of marine biogeochemical cycles to include the influence of feedbacks with marine food webs and the consequences for marine ecosystems. Central to the IMBER goal is the development of a predictive understanding of how marine biogeochemical cycles and ecosystems respond

to complex forcings, such as large-scale climatic variations, changing physical dynamics, carbon cycle chemistry and nutrient fluxes, and the impacts of marine harvesting. IMBER science is making new advances in understanding marine systems by bringing together the natural and social science communities to study key impacts and feedbacks between the marine and human systems. The emerging recognition of human interactions as integral parts of marine ecosystems is providing the direction for future integrative research designed to understand and sustain ocean systems as environmental change and its associated uncertainties occur.

Role of Modeling

Mathematical models provide an approach for integrating and synthesizing the knowledge and understanding obtained from measurements of oceanic biogeochemical processes. The use of biogeochemical models in ocean research has a long history [37, 38] but their use was advanced significantly in the early 1990s when a model that simulated nitrogen cycling through the lower trophic levels in the oceanic mixed layer became generally available [39], which subsequently has provided the basis for the coupled circulation-biogeochemical models that are now embedded in regional, basin, and global scale models.

The skill of the current generation of biogeochemical models is sufficient to allow projections of future states that may result from climate variability and the oceanic uptake of anthropogenic carbon [40–42]. The patterns and distributions emerging from these simulations show shifts in phytoplankton distributions and marine biomes, alteration of phytoplankton species assemblages, and modified lower trophic level community structure [43–45], all of which have direct and important consequences for biogeochemical cycling. Simulations of the effect of increasing atmospheric CO_2 and its uptake by the ocean show reductions in ocean pH and in saturation levels of calcium carbonate, which have serious consequences for many marine organisms [46].

Advances in conceptual understanding, modeling techniques, and data availability have made predictive marine biogeochemical models a feasible goal [47]. However, modeling for prediction is still rapidly developing and much remains to be done in generating appropriate frameworks and in collection of data sets that support predictive modeling for marine biogeochemical cycling [48, 49].

Bibliography

Primary Literature

1. Redfield AC (1958) The biological control of chemical factors in the environment. Am Sci 64:205–221
2. Libes SM (2009) Introduction to marine biogeochemistry. Academic, Amsterdam
3. Hutchins DA, Bruland KW (1998) Iron-limited diatom growth and Si:N uptake ratios in a coastal upwelling regime. Nature 393:561–564
4. Sunda WG, Huntsman S (1997) Interrelated influence of iron, light, and cell size on growth of marine phytoplankton. Nature 390:389–392
5. Le Quéré C et al (2007) Saturation of the Southern Ocean CO_2 sink due to recent climate change. Science 316:1735–1738
6. Doney SC, Fabry VF, Feely RA, Kleypas JA (2009) Ocean acidification: the other CO_2 problem. Ann Rev Mar Sci 1:169–192
7. Ries BR, Cohen AL, McCorkle DC (2009) Marine calcifiers exhibit mixed responses to CO_2-induced ocean acidification. Geology 37:131–134
8. Hutchins DA, Mulholland MR, Fu F (2009) Nutrient cycles and marine microbes in a CO_2-enriched ocean. Oceanogr 22:128–145
9. Fu F-X, Zhang Y, Warner ME, Feng Y, Hutchins DA (2008) A comparison of future increased CO_2 and temperature effects on sympatric *Heterosigma akashiwo* and *Prorocentrum minimum*. Harm Algae 7:76–90
10. Devol AH (2003) Solution to a marine mystery. Nature 422:575–576
11. Lam P et al (2009) Revising the nitrogen cycle in the Peruvian oxygen minimum zone. Proc Nat Aca Sci 106:4752–4757
12. Ward B et al (2009) Denitrification as the dominant nitrogen loss process in the Arabian Sea. Nature 451:78–81
13. Martin JH, Fitzwater S (1988) Iron deficiency limits phytoplankton growth in the northeast Pacific subarctic. Nature 331:341–343
14. Ducklow HW, Oliver JL, Smith WO (2007) The role of iron as a limiting nutrient for marine plankton processes. In: Melillo JM, Field CB, Moldan B (eds) Interactions of the major biogeochemical cycles. Island Press, Washington, DC, pp 295–310
15. Vraspir JM, Butler A (2009) Chemistry of marine ligands and siderophores. Ann Rev Mar Sci 1:43–63
16. Johnson KS, Gordon RM, Coale KH (1997) What controls dissolved iron concentrations in the world ocean? Mar Chem 57:137–161
17. Baker AR, Croot PR (2010) Atmospheric and marine controls on aerosol iron solubility in seawater. Mar Chem 120:4–13
18. Martin JH et al (1994) Testing the iron hypothesis in ecosystems of the equatorial Pacific Ocean. Nature 371:123–129

19. Watson AJ et al (1994) Minimal effect of iron fertilization on sea-surface carbon dioxide concentrations. Nature 371:143–145
20. Coale KH et al (1996) A massive phytoplankton bloom induced by an ecosystem-scale iron fertilization experiment in the equatorial Pacific. Nature 383:495–501
21. Sarmiento JL, Gruber N, Brzezinski MA, Dunne JP (2004) High-latitude controls of thermocline nutrients and low latitude biological productivity. Nature 427:56–60
22. Boyd PW et al (2007) Mesoscale iron enrichment experiments 1993–2005: synthesis and future directions. Science 315:612–617
23. Treguer P, Nelson DM, van Bennekom AJT, DeMaster DJ, Lynaert A, Queguiner B (1995) The silica balance in the world ocean: a reestimate. Science 268:375–379
24. Nelson DM et al (1995) Production and dissolution of biogenic silica in the ocean: revised global estimates, comparison with regional data and relationship to biogenic sedimentations. Global Biogeochem Cycles 9:359–372
25. DeMaster DJ (2002) The accumulation and cycling of biogenic silica in the Southern Ocean: revisiting the marine silica budget. Deep Sea Res II 49:3155–3167
26. Biddle KD, Azam F (1999) Accelerated dissolution of diatom silica by natural bacterial assemblages. Nature 397:508–512
27. Sievert SM, Kiene RP, Schulz-Vogt HN (2007) The sulfur cycle. Oceanography 20:117–123
28. Andreae MO (1990) Ocean-atmosphere interactions in the global biogeochemical sulfur cycle. Mar Chem 30:1–29
29. Sunda W, Kieber DJ, Kiene RP, Huntsman S (2002) An antioxidant function for DMSP and DMS in marine algae. Nature 418:317–320
30. Jorgensen BB (1977) The sulfur cycle of a coastal marine sediment (Limfjorden, Denmark). Limnol Oceanogr 22:814–832
31. Canfield DE, Farquhar J (2009) Animal evolution, bioturbation, and the sulfate concentration of the oceans. Proc Nat Acad Sci 106:8123–8127
32. Canfield DE, Stewart FJ, Thamdrup B, Brabandere LD, Dalsgaard T, Delong EF, Revsbech NP, Ulloa O (2010) A cryptic sulfur cycle in oxygen-minimum-zone waters off the Chilean coast. Science 330:1375–1378
33. van Dover CL (2000) The ecology of deep-sea hydrothermal vents. Princeton University Press, Princeton
34. Diaz RJ, Rosenberg R (2008) Spreading dead zones and consequences for marine ecosystems. Science 321:926–929
35. Scavia D, Justic D, Bierman VJ (2004) Reducing hypoxia in the Gulf of Mexico: advice from three models. Estuaries 27:419–425
36. Lam P, Kuypers MMM (2011) Microbial nitrogen cycling processes in oxygen minimum zones. Ann Rev Mar Sci 3:317–345
37. Riley GA (1946) Factors controlling phytoplankton populations on Georges Bank. J Mar Res 6:54–73
38. Riley GA (1947) A theoretical analysis of the zooplankton populations of Georges Bank. J Mar Res 6:104–113
39. Fasham MJR, Ducklow HW, McKelvie SM (1990) A nitrogen-based model of plankton dynamics in the oceanic mixed layer. J Mar Res 48:591–639
40. Orr JC et al (2001) Estimates of anthropogenic carbon uptake from four three-dimensional global ocean models. Global Biogeochem Cycles 15:43–60
41. Doney SC et al (2004) Evaluating global ocean carbon models: the importance of realistic physics. Global Biogeochem Cycles 18:GB3017. doi:10.1029/2003GB002150
42. Boyd PW, Doney SC (2001) Modeling regional response by marine pelagic ecosystems to global climate change. Geophys Res Lett 29. doi:10.10292001GL014130
43. Follows MJ, Dutkiewicz S, Grant S, Chisholm SW (2007) Emergent biogeography of microbial communities in a model ocean. Science 315:1843–1846
44. Le Quéré C et al (2005) Ecosystem dynamics based on plankton function types for global ocean biogeochemistry models. Global Change Biol 11:2016–2040. doi:10.111/j.1365-2486.2005.1004.x
45. Sinha B, Buitenhuis ET, Le Quéré C, Anderson TR (2010) Comparison of the emergent behavior of a complex ecosystem model in two ocean general circulation models. Prog Oceanogr 84:204–224
46. Orr JC et al (2005) Anthropogenic ocean acidification over the twenty-first century and its impact on calcifying organisms. Nature 437:681–686
47. Friedrichs MAM et al (2007) Assessment of skill and portability in regional marine biogeochemical models: role of multiple planktonic groups. J Geophys Res 112:C08001. doi:10.1029/2006JC003852
48. Anderson TR (2009) Progress in marine ecosystem modeling and the "unreasonable effectiveness of mathematics." J Mar Sys 81:4–11
49. Ducklow HW, Doney SC, Steinberg DK (2009) Contributions of long-term research and time-series observation to marine ecology and biogeochemistry. Ann Rev Mar Sci 1:279–302

Books and Reviews

Baliño BM, Fasham MJR, Bowles MC (2001) Ocean biogeochemistry and global change. IGBP Science no 2, Stockholm (A popular summary of JGOFS main achievements)

Benitez-Nelson CR (2000) The biogeochemical cycling of phosphorus in marine systems. Earth-Sci Rev 51:109–135

Brandes JA, Devol AH, Deutsch C (2007) New developments in the marine nitrogen cycle. Chem Rev 107:577–589

Broecker WS (2009) Wally's quest to understand the ocean's $CaCO_3$ cycle. Ann Rev Mar Sci 1:1–18

Deutsch C, Brix H, Ito T, Frenzel H, Thompson L (2011) Climate-forced variability of ocean hypoxia. Science 333:336–339

Diaz RJ (2000) Overview of hypoxia around the world. J Environ Quality 30:275–281

Doney SC et al (2001) Marine biogeochemical modeling: recent advances and future challenges. Oceanography 14:93–108

Fasham MJR (ed) (2003) The role of the ocean carbon cycle in global change. Springer, Heidelberg, p 297
Gruber N, Galloway JN (2008) An earth-system perspective of the global nitrogen cycle. Nature 451:293–296
Hanson RB, Ducklow HW, Field JG (eds) (2000) The changing ocean carbon cycle: a midterm synthesis of the joint global ocean flux study, IGBP book series no 5. Cambridge University Press, Cambridge, 520 pp
IMBER Science Plan and Implementation Strategy (2005) IGBP Report N°52. IGBP Secretariat, Stockholm, 76 pp
Jickells TD et al (2005) Global iron connections between desert dust, ocean biogeochemistry, and climate. Science 308:67–71
Keeling RF, Kortzinger A, Gruber N (2010) Oxygen deoxygenation in a warming world. Ann Rev Mar Sci 2:199–229
Paulmier A, Ruiz-Pino D (2009) Oxygen minimum zones (OMZs) in the modern ocean. Prog Oceanogr 80:113–128
Ragueneau O et al (2000) A review of the Si cycle in the modern ocean: recent progress and missing gaps in the application of biogenic opal as a paleoproductivity proxy. Global Planetary Change 26:317–365
Sabine CL, Tanhua T (2010) Estimation of anthropogenic CO_2 inventories in the ocean. Ann Rev Mar Sci 2:175–198
Sunda WG (2010) Iron and the carbon pump. Science 327:654–655

Marine Fisheries Enhancement, Coming of Age in the New Millennium

Kenneth M. Leber
Center for Fisheries Enhancement, Mote Marine Laboratory, Sarasota, FL, USA

Article Outline

Glossary
Definition of the Subject
Introduction
Scientific Development of Marine Fisheries Enhancement
Responsible Approach to Marine Fishery Enhancement
Legacy from the Past
Progress in Marine Fisheries Enhancement
Future Directions
Bibliography

Glossary

Anadromous Species that spawn in freshwater, then their offspring gradually make their way into estuaries or the sea, where they remain during much of the subadult and adult stages of the life cycle, before returning to rivers and streams to spawn.

Catadromous Species whose females release their eggs at sea, then the offspring move as larvae or early juveniles into estuaries, rivers, and streams where they spend the juvenile stage of the life cycle.

Marine Species that spawn in sea water, including those that spend most of their lives at sea and catadromous fishes, which spawn in seawater, then enter freshwater nursery habitats.

Marine fisheries enhancement Release of aquacultured marine organisms into seas and estuaries to increase or restore abundance and fishery yields in the wild.

Outbreeding depression Caused when offspring from crosses between individuals from different populations or subpopulations (stocks) have lower fitness than progeny from crosses between individuals from the same population/stock.

Recruitment The process of joining an existing population. Species *recruit* to the juvenile stages in nursery habitats; juveniles subsequently *recruit* to adult stages in adult habitats. Species *recruit* to a fishery when they reach the minimum size fished.

Reintroduction Temporary release of cultured organisms with the aim of reestablishing a locally extinct population.

Restocking Release of cultured juveniles into wild population(s) to restore severely depleted spawning biomass to a level where it can once again provide regular, substantial yields.

Sea ranching Release of cultured juveniles into unenclosed marine and estuarine environments for harvest at a larger size in "put, grow, and take" operations.

Stock enhancement The release of cultured juveniles into wild populations to augment the natural supply of juveniles and optimize harvests by overcoming limitations in juvenile recruitment.

Supplementation Moderate release of cultured fish into very small and declining populations, with the aim of reducing extinction risk and conserving genetic diversity. Supplementation serves primarily conservation aims and specifically addresses sustainability issues and genetic threats in small and declining populations.

Definition of the Subject

Marine fisheries enhancement (aka "stock enhancement") is the use of hatchery-reared saltwater organisms to increase abundance and fishery yields in the wild. "Conservation hatcheries" also produce and stock depleted, threatened, or endangered organisms – to help preserve species in decline. The practice began in the latter part of the nineteenth century when fish hatcheries were first developed but understanding of the ecology and management of wild stocks into which the hatchery-reared organisms where released was very limited. Early stock enhancement thus has gone through a series of fits and starts and misfires. In the century after its birth, the technologies required for scientific inquiry of the effects and effectiveness of stocking hatchery-reared organisms were lacking. The science needed to guide reliable use of cultured aquatic organisms in conservation and resource management remained undeveloped. Then, at the close of the twentieth century, new mariculture, tagging, and genetic technologies surfaced and rapid advances were made in the science underpinning marine stock enhancement.

As growth in human population size approaches the carrying capacity of the planet in this century, and the world increasingly turns to the oceans to farm and harvest food [1], sustainable fishery yields and conservation of natural resources face unparalleled challenges. Over the past two decades, marine fisheries enhancement has been transformed from a tentative, poorly developed management tool to a maturing science. Some believe research funding for this field would be better spent on traditional fishery management. But today's seafood producers, fishery managers, and "...conservationists need all the tools that biology, ecology, diplomacy and politics can muster if endangered species are to survive beyond the next century," [2] and fisheries are to continue to support a viable seafood industry and sport pastime. This entry traces the emergence and progress of marine fisheries enhancement, and offers a prescription for future direction.

The term *stock enhancement* is originally derived from efforts to augment wild fish sub-populations, or "stocks," by releasing cultured fishes into aquatic environments. Stocking cultured organisms is one of the tools available for managing aquatic natural resources. It has been used with varying degrees of success to help increase abundance of habitat- or recruitment-limited stocks to help restore depleted populations, augment fisheries and help recover threatened or endangered species. There has been much debate over the effectiveness of stock enhancement as a fisheries management tool. However, most of the scientific evaluation of stocking is quite recent [3], as is a code of responsible practices that help guide effective application [4–6], and marine fisheries enhancement is finally poised for effective use.

In the USA, from the 1880s through the early 1950s, stocking hatchery-reared marine fishes was a principal approach used by the US Fish Commission (renamed Bureau of Fisheries in 1903, Bureau of Commercial fisheries in 1956, and later the National Marine Fisheries Service) for maintaining fishery stocks. But by the 1950s the practice of stocking marine fishes to manage US fisheries was curtailed for lack of evidence of its effectiveness in fisheries management [7]. Stocking was replaced by harvest management to control total catch and sustain fisheries. Stocking of freshwater habitats continued (particularly with salmonids into rivers), although the scientific basis for many of the management decisions needed for stocking salmonids was clearly lacking and did not begin to be addressed until the mid-1970s.

In the decade following 1975, scientists began to evaluate survival and fishery contributions of stocked salmon enabled by advances in fish tagging technology [8, 9]. Quantitative evaluation of marine fish stocking began in earnest in the 1980s and 1990s. The science underlying fisheries enhancement has since evolved to the point where, in some situations, stocking can be a useful fishery management tool to help restore depleted stocks and increase abundance in recruitment-limited fisheries [6]. Effective use of enhancement, though, requires full integration with harvest and habitat management, and a good understanding by stakeholders and resource managers of the opportunities where enhancement can be used successfully as well as its limitations [5, 6]. Principles for guiding the successful use of marine fisheries enhancement to help sustain aquatic resources are now being employed to design new enhancements and reform existing efforts. What follows is a brief overview of those principles and progress made in using hatchery-reared organisms to help sustain marine resources.

Introduction

Marine fisheries enhancement is happening around the world and in some countries on a massive scale (e.g., China). However, in many countries the careful assessment of genetic and ecological risks is lagging behind implementation, putting wild stocks, the seafood supply, and sport fisheries at risk. The science of marine enhancement is still in its infancy compared to other fields of fisheries science, but now shows good potential to (1) increase fishery yield beyond that achievable by exploitation of the wild stock alone, (2) help restore depleted stocks, (3) provide protection for endangered species, and (4) provide critical information on the natural ecology, life history and environmental requirements of valuable marine species.

Stock enhancement has often been used as a generic term referring to all forms of hatchery-based fisheries enhancement. Bell et al. [3] and Lorenzen et al. [6] classified the intent of stocking cultured organisms in aquatic ecosystems into various basic objectives. Together, they considered five basic types, listed here from the most production-oriented to the most conservation-oriented:

1. Sea ranching – *recurring release of cultured juveniles into unenclosed marine and estuarine environments for harvest at a larger size in "put, grow, and take" operations*. The intent here is to maximize production for commercial or recreational fisheries. Note that the released animals are not expected to contribute to spawning biomass, although this can occur when harvest size exceeds size at first maturity or when not all the released animals are harvested.
2. Stock enhancement – *recurring release of cultured juveniles into wild population(s) to augment the natural supply of juveniles and optimize harvests by overcoming recruitment limitation in the face of intensive exploitation and/or habitat degradation*. Stock enhancements can increase abundance and fisheries yield, supporting greater total catch than could be sustained by the wild stock alone [10]. However, such increases may be offset, at least in part, by negative ecological, genetic, or harvesting impacts on the wild stock component. Stock enhancements tend to attract greater numbers of fishers, which can offset expected increase in each individual's catch-per-unit-effort (CPUE) [5, 11].
3. Restocking – *time-limited release of cultured juveniles into wild population(s) to restore severely depleted spawning biomass to a level where it can once again provide regular, substantial yields* [12]. Restocking requires release number to be substantial relative to the abundance of the remaining wild stock, and close ecological and genetic integration of wild and cultured stocks, combined with very restricted harvesting [6].
4. Supplementation – *moderate releases of cultured fish into very small and declining populations, with the aim of reducing extinction risk and conserving genetic diversity* [13, 14]. Supplementation serves primarily conservation aims and specifically addresses sustainability issues and genetic threats in small and declining populations [6].
5. Reintroduction – *involves temporary releases with the aim of reestablishing a locally extinct population* [15]. Continued releases should not occur, as they could interfere with natural selection in the newly established population. Fishing should also be restricted to allow the population to increase in abundance rapidly [6].

Scientific development of marine fisheries enhancement was lacking throughout most of the twentieth century. Although stocking cultured marine fishes began in the nineteenth century, the technology was limited to stocking only eggs and larvae. There were no published accounts of the fate of released fish until empirical studies of anadromous salmonids began to be published in the mid-1970s [16, 17], followed by the first studies (published in English) of stocked marine invertebrates in 1983 [18, 19] and marine fishes in 1989 [20].

During the past two decades, the field of marine fisheries enhancement has advanced considerably. Science in this field is rapidly growing, in part because of critical examination and debate about the efficacy of enhancement and the need for quantitative evaluation (e.g., [21, 22]), and in part because of advances made in aquaculture, genetics, tagging, and fishery modeling technologies, which have enabled quantitative studies and predictions of stocking effects. A clear process has emerged for developing, evaluating, and using enhancement [4–6]. Together, this process and the rapid growth of knowledge about enhancement effects

should enable responsible and effective use of enhancement in marine fisheries management and ocean conservation.

Scientific Development of Marine Fisheries Enhancement

Scientific and Strategic Development

Since 1989, progress in marine fisheries enhancement has occurred at two levels – scientific advances and adoption of a careful and responsible approach to planning and organizing enhancement programs and manipulating abundance of marine species using aquacultured stocks. Much of the progress made in the 1990s was scientific and involved an expansion of field studies to evaluate survival of released fish and improve the effectiveness of release strategies. The earliest studies on effectiveness of stocking *marine* fishes, published in English in the scientific literature, were in Japan [20, 23–26] and Norway [27–31], followed by studies in the USA [32–39], and Australia [40]. Progress made with invertebrates is well covered by Bell et al. [12].

Following the initial publications of scientific studies of marine fish enhancement, the number of peer-reviewed publications and symposia in this field began to escalate ([41–52], and see abstracts in [53]). It is now clear that stocking marine organisms can be an effective addition to fishery management strategies, but only when certain conditions are met. For stocking to be productive and economical, and help ensure sustainability of wild stocks, careful attention must be given to several key factors and stocking must be thoroughly integrated with fisheries management [6]. It is clear that stocking can be harmful to wild stocks if not used carefully and responsibly.

Aside from scientific gains in this field, the other level of progress made in the past two decades has been the evolution of a strategic "blueprint" for enhancements, such as the principles discussed in "a responsible approach to marine stock enhancement" [4, 6]. By the early 1990s, salmon enhancement in the US Pacific Northwest, which had been underway for a century, was beginning to incorporate reforms that were needed to improve efficiencies and protect wild stocks from genetic hazards that can lead to loss of genetic diversity and fitness. Concerns had been mounting over uncertainty about the actual effectiveness of salmon hatcheries and impacts on wild stocks. Concerns about wild stock impacts were twofold, including ecological effects of hatchery fish, such as competitive displacement, and genetic issues, such as translocation of salmon stocks, domestication and inbreeding in the hatchery and associated outbreeding depression, and loss of genetic diversity related to hatchery breeding practices (e.g., [54, 55]). Meanwhile, special sessions on marine stock enhancement began appearing at major fisheries and mariculture conferences in the early 1990s [41–44]. These sessions took a sharp turn from past approaches, where the principal focus in conference presentations about stock enhancement had been mainly on Mariculture research topics alone. The conveners of the special sessions on stock enhancement in the 1990s recruited presenters who worked on evaluating the effects and effectiveness of stocking hatchery organisms into the sea and interactions of hatchery and wild stocks. The special sessions focused on the "questions of the day" in marine enhancement and fostered debate in the marine enhancement research community about many of the reform issues being considered in salmon enhancement. The early 1990s was a period of rapid developments in enhancements, characterized by engagement of multiple scientific disciplines in a field that had previously been guided largely by a single discipline – aquaculture.

The salmon experience and reforms underway in salmon enhancement made it clear that a careful and multidisciplinary approach was needed in the development and use of marine enhancement. Many involved in developing new marine fisheries enhancement projects were paying close attention to the debate that had emerged over salmon hatcheries. Following the 1993 special session on "fisheries and aquaculture interactions" held at a mariculture conference in Torremolinos, Spain [44], several of the presenters (including scientists from Japan, Norway, the USA, and Italy [United Nations Food and Agriculture Organization, FAO]) met and formed an "International Working Group on Stock Enhancement," and affiliated the workgroup with the World Aquaculture Society. At that inaugural working group meeting, a decision was made to publish a platform paper to frame the question, "what is a responsible approach to

marine stock enhancement?" This paper was presented at the 1994 American Fisheries Society symposium, "Uses and Effects of Cultured Fishes in Aquatic Ecosystems," and published in the 1995 peer-reviewed symposium proceedings [4]. The paper recommended ten principles for developing, evaluating, and managing marine stock enhancement programs. The Responsible Approach paper afforded a model for developing and managing new enhancement programs and refining existing ones. It has also helped frame research questions in the emerging science of marine fisheries enhancement.

The International Working Group on Stock Enhancement (IWGSE) was instrumental in advancing the science of marine fisheries enhancement in the 1990s. The working group focused primarily on highlighting ongoing stock enhancement research around the world and fostering awareness of the Responsible Approach in their publications and presentations. International awareness and new research in the field was aided by the broad international makeup of the working group. Membership grew and soon included scientists from Australia, Canada, China, Denmark, Ecuador, Italy, Japan, Norway, Philippines, Solomon Islands, Spain, the UK, and the USA. Initially, the primary communication vehicle used by the working group was the special sessions on stock enhancement, which it planned and convened annually in various countries at the international conference of the World Aquaculture Society. The working group promoted a synergy among its members and the influence of the group expanded as members planned additional workshops and symposiums in their own countries and brought IWGSE scientists into the planning process.

The period 1990–1997 was a fertile time that gave birth to a rapid expansion of science in marine fisheries enhancement, which continues to this day, aided since 1997 in large part by the International Symposium on Stock Enhancement and Sea Ranching (ISSESR). The first ISSESR, held in 1997 in Bergen, Norway, was the brainchild of the Norwegian PUSH program (Program for Development and Encouragement of Sea Ranching) and the Norwegian Institute of Marine Research (IMR). In 1995, IMR scientists invited IWGSE scientists to become involved in the International Scientific Committee charged with planning the program for the first ISSESR. The first ISSESR, and the series of follow-up symposia that it launched (see www.SeaRanching.org), have encouraged and brought about fundamental advancements in the field of marine enhancement – by networking the scientists working in this specialized field, highlighting their work at the ISSESR, and publishing their peer-reviewed articles in the symposium proceedings. The 3–5 day ISSESR has now become a regular scientific symposium event, hosted by a different country every 4–5 years. Following the first ISSESR in Bergen [47], subsequent symposiums in the series were held in Kobe, Japan in 2002 [49], in Seattle, USA in 2006 [52], and in Shanghai, China in 2011 [53]. The fifth ISSESR will be held in Sydney, Australia in 2015 or 2016. Inquiries from scientists in different countries interested in hosting the sixth one are already being received by the organizing group. Following the first ISSESR, the IWGSE scientists continued the efforts they started in the working group through their involvement in the International Scientific Committees for the ISSESR and steering committees for other stock enhancement symposia (e.g., [46, 48, 51]). In 2010, a refined and updated version of the Responsible Approach was published [6] and presented at the fourth ISSESR.

As in any new science, lack of a paradigm and consensus on the key issues retard progress. The ISSESR and other marine enhancement symposia and working groups have helped to place scientific focus on critical uncertainties and communicate results of new science in this field at symposiums and in the scientific literature. They have also provided a forum for debate on the issues, and increased networking of scientists, resource managers, students, and educators working in this field worldwide. The focus on key issues is nurturing this new field of science.

Technological and Tactical Constraints

Although marine enhancements do show promise as an important tool in fisheries management, why has this field taken so long to develop and why have marine enhancement programs often failed to achieve their objectives? The scientific development of marine fisheries enhancement has long been impeded by lack of the technologies needed to evaluate effects of stocking cultured fish. Although marine enhancements

began in the 1880s, until the advent of the coded-wire tag in the mid-1960s [8], there was no way to identify treatment groups and replicates in experimental releases of juvenile cultured fish [56]; and quantitative marking methods for multiple experimental groups of postlarvae and very small juveniles (<50 mm in length) came much later (e.g., [57]). To make matters worse, scientific development of marine enhancement was also stymied by lack of adequate technology for culturing marine fishes. Rearing methods for larval and juvenile marine fishes, many of which require live feeds during the larval stage, remained undeveloped until the mid- to late 1970s, when breakthroughs finally began to be achieved in rearing a few marine species past metamorphosis [58]. By the mid-1980s mass production of juveniles had been achieved for several species of marine fishes. Even today, though, many marine fishes cannot yet be cultivated to the juvenile stage in the quantities needed for stocking. Without the availability of juveniles grown to a wide range of sizes, fundamental questions about density dependence, hatchery-wild fish interactions and cost-yield efficiency of size-at-release and other release variables cannot be addressed in field experiments. Thus, even the basic technologies needed to develop and understand the potential of marine enhancement have been unavailable until relatively recent times for some fishes and have yet to be developed for others.

Technology has not been the only constraint to successful development of marine fisheries enhancement. The effective use of stocking cultured marine organisms in fisheries management has been hindered by lack of understanding of the effect of releases on fish population dynamics and a lack of related, quantitative assessment tools [10]. Moreover, there has been a lack of essential governance and fisheries management considerations in planning, designing, implementing, and evaluating enhancement programs [6, 59]. A symptom of this is the relentless concern among stakeholders and hatchery managers alike about the numerical magnitude of fish released, rather than on the effective contribution of the hatchery program to fisheries management goals. Certainly, a hatchery needs to meet some release quotas, but the numbers of fish released is a misleading statistic for gauging success or comparing effectiveness among enhancement programs. Yet, from the very beginning, progress has been judged by the number of eggs, yolk-sac larvae or juveniles stocked, rather than by the number of fish added to the catch or to spawning stock biomass. The thinking behind this approach apparently is "grow and release lots of hatchery fish and of course they'll survive and add to the catch," without realizing the need to optimize release strategies (e.g., [39, 60, 61]) (e.g., to know what size-at-release, release habitat and release magnitude combination has the greatest impact on population size, fishery yields, and economics), or that the impact from stocking could in fact be a negative one on wild stocks (such as replacement of wild fish by hatchery fish) if certain precautions are not taken. This attitude has been pervasive and exists even today among many stakeholders and enhancement administrators. In fact, research now shows that survival and recruitment to the fishery following hatchery releases is a complex issue that requires much greater understanding about the fishery, hatchery fish performance, and biological and ecological factors in the wild than simply "the catch is down, thus releasing large numbers of fish will bring it back up." And quite often large release magnitudes are achieved by releasing millions of postlarvae, rather than fewer but larger juveniles. But releases of postlarvae alone may be effective, yet can also be totally ineffective, depending on conditions at the release site [62].

The key to successful use of stocking is to plan enhancement programs from a fisheries/resource management perspective, using a broad framework and scientific approach [6, 59]. The probability of achieving effective results is greatly increased when stakeholders are engaged from the outset in planning *new* programs, using a framework that is structured, multilayered, participatory, and makes good use of science, to design, implement, and analyze enhancement fisheries systems [6]. Incorporating the key principles in the Responsible Approach into the frameworks of *existing* programs as well is likely to improve performance.

Responsible Approach to Marine Fishery Enhancement

In retrospect, the slow development of marine fish culture (a century behind salmonid aquaculture) has helped marine stock enhancement programs avoid some of the mistakes of the past made with salmon

stock enhancement, where lack of understanding of genetic issues during most of the twentieth century led to inadvertent domestication and inbreeding in salmon hatchery populations, leading to reduced fitness in wild stocks. Marine finfish juvenile production technology lagged behind freshwater and anadromous fish culture by a century. Thus, mass release into the sea of juvenile marine fishes large enough to survive and enter the breeding population did not begin until the 1980s. The relatively recent capabilities to conduct marine fisheries enhancement emerged at about the same time that geneticists realized that hatchery practices with salmonids (1) could reduce genetic diversity in the hatchery and ultimately, enhanced wild stocks, owing to inadequate broodstock management, (2) have caused translocations of salmon genes into environments where they are less fit, and (3) have contributed to loss of local adaptations in the wild population. Today, population genetics is much better understood and broodstock genetics and hatchery practices can be better managed to address these concerns (e.g., [63–65]). Thus, marine enhancement programs need careful guidance from qualified geneticists. The Puget Sound and Coastal Washington Hatchery Reform Project in the USA has been instrumental in reforming salmon enhancements [66]. This group affords a model for managing enhancement hatcheries in the twenty-first century.

As progress was being made in the early 1990s to better understand the genetic structure of stocks and how to manage genetics in hatcheries, realizing the need for reform in approaches to enhancing non-salmonids was just beginning. In the mid-1990s, Cowx [67], for enhancements in freshwater systems, and Blankenship and Leber [4], for enhancements in marine and estuarine systems, published papers calling for a broader, more systematic, reliable, and accountable approach to planning stock enhancement programs. Prompted both by the salmonid hatchery reform movement and by the WAS IWGSE, the ten principles presented in Blankenship and Leber ([4] Table 1) gained widespread acceptance as the "Responsible Approach" to stocking marine organisms and provided a platform for subsequent discussions on planning, conducting, and evaluating marine enhancements (e.g., [6, 12, 22, 51, 52, 68–70]). Since 1995, the awareness of the Responsible Approach has steadily increased and has helped guide hatchery and reform processes for marine enhancements worldwide [11, 36, 37, 39, 60, 62, 69–90].

Marine Fisheries Enhancement, Coming of Age in the New Millennium. Table 1 The ten principles of a responsible approach to marine stock enhancement [4]

1	Prioritize and select target species for enhancement by ranking and applying criteria for species selection
2	Develop a management plan that identifies how stock enhancement fits with the regional plan for managing stocks
3	Define quantitative measures of success to track progress over time
4	Use genetic resource management to avoid deleterious genetic effects on wild stocks
5	Implement a disease and health management plan
6	Consider ecological, biological, and life history patterns in forming enhancement objectives and tactics; seek to understand behavioral, biological, and ecological requirements of released and wild fish
7	Identify released hatchery fish and assess stocking effects on the fishery and on wild stock abundance
8	Use an empirical process for defining optimal release strategies
9	Identify economic objectives and policy guidelines, and educate stakeholders about the need for a responsible approach and the time frame required to develop a successful enhancement program
10	Use adaptive management to refine production and stocking plans and to control the effectiveness of stocking

The Responsible Approach provides a conceptual framework and logical strategy for using aquaculture technology to help conserve and increase natural resources. The approach prescribes several key components as integral parts of developing, evaluating and managing marine fisheries enhancement programs. Each principle is considered essential to manage enhancements in a sustainable fashion and optimize the results obtained [4, 6].

A major development since the publication of the original "Responsible Approach" has been increasing interest from fisheries ecologists in understanding and quantifying the effects of hatchery releases from

a fisheries management perspective. This has led to the development of fisheries assessment models that can be used to evaluate stocking as a management option alongside fishing regulations [5, 10]. At the same time, approaches to fisheries governance underwent major changes that allow enhancements to become more integrated into the management framework and in some cases, were driven by interest in enhancement approaches [59].

Walters and Martell [5] discuss four main ways that a marine enhancement program can end up causing more harm than good: (1) the replacement of wild with hatchery recruits, with no net increase in the total stock available for harvest (competition/predation effects); (2) unregulated fishing-effort responses to the presence of hatchery fish that cause overfishing of the wild stock; (3) "overexploitation" of the forage resource base for the stocked species, with attendant ecosystem-scale impacts; and (4) genetic impacts on the long-term viability of the wild stock. They stress that it is critical to monitor the impacts of enhancement as the program develops to have evidence in hand if debate about the efficacy of the program does surface. To help guide developing programs, they provide and discuss a "Code of Responsible Conduct" as critical steps in marine fisheries enhancement program design (Table 2).

Marine Fisheries Enhancement, Coming of Age in the New Millennium. Table 2 Code of responsible conduct for marine stock enhancement [5]

• Make certain that management priorities and acceptable trade-offs are absolutely clear
• Do careful stock assessments to show that the target stock is recruitment overfished or can no longer rear successfully in the wild
• Show that enhanced fish can recruit successfully in the wild
• Show that total abundance is at least initially increased by the hatchery fish contribution
• Show that fishery regulations are adequate to prevent continued overfishing of the wild population, unless there has been an explicit decision to "write off" the wild population
• Show that the hatchery production system is actually sustainable over the long run, when it is to be a permanent component of the production system

In 2010, Lorenzen, Leber, and Blankenship [6] published an updated version of the Responsible Approach to refine the original key principles and include five additional ones (Table 3). The key principles added in the updated version bring stakeholders more firmly into the planning process; place much stronger emphasis on a-priori evaluation of the potential impact of enhancements using quantitative models; place marine fishery enhancements more firmly within

Marine Fisheries Enhancement, Coming of Age in the New Millennium. Table 3 The updated responsible approach (From [6])

Stage I: Initial appraisal and goal setting	
1	Understand the role of enhancement within the fishery system [*new*]
2	Engage stakeholders and develop a rigorous and accountable decision making process [*new*]
3	Quantitatively assess contributions of enhancement to fisheries management goals
4	Prioritize and select target species and stocks for enhancement
5	Assess economic and social benefits and costs of enhancement
Stage II: Research and technology development including pilot studies	
6	Define enhancement system designs suitable for the fishery and management objectives [*new*]
7	Design appropriate aquaculture systems and rearing practices [*new*]
8	Use genetic resource management to maximize effectiveness of enhancement and avoid deleterious effects on wild populations.
9	Use disease and health management
10	Ensure that released hatchery fish can be identified
11	Use an empirical process for defining optimal release strategies
Stage III: Operational implementation and adaptive management	
12	Devise effective governance arrangements [*new*]
13	Define a management plan with clear goals, measures of success, and decision rules
14	Assess and manage ecological impacts
15	Use adaptive management

the context of fishery management systems; emphasize design of appropriate aquaculture rearing systems and practices; and incorporate institutional arrangements for managing enhancements. Lorenzen et al. [6] provide comprehensive discussions for each of the 15 key principles listed in Table 3. Readers are urged to consult Lorenzen et al. [6] for additional detail, as it is beyond the scope, here, to repeat their discussions of each principle.

The 15 principles in the updated Responsible Approach include the broad range of issues that need to be addressed if enhancements are to be developed or reformed responsibly [6]. Clearly, marine enhancement programs are multidisciplinary and their effective use requires specialist knowledge and skills from diverse fields (Table 4). Forming interdisciplinary teams of the various specialists required is an important factor in employing the Responsible Approach in developing, reforming, and executing marine enhancements. For effective design of enhancement programs, specialists in each area of expertise listed in Table 4 should be included in the planning teams.

It should be clear that without a careful monitoring system in place, marine enhancements simply cannot be managed. Monitoring is essential to understand the impacts of enhancement, to manage release strategies so that they are efficient and designed well enough to achieve the goals of the program, to protect against misuse of stocking (as discussed in 5 and 6), resulting in harm to wild stocks, and to document success or failure in meeting enhancement program objectives. Walters and Martel [5] list several key monitoring requirements for managing fishery enhancements well: (1) mark all (or at least a high and known proportion of) fish released from hatcheries; (2) mark as many wild juveniles as possible at the same sizes/locations as hatchery fish are being released; (3) experimentally vary hatchery releases over a wide range from year to year and from area to area, probably in on/off alternation (temporal blocking) so as to break up the confounding of competition/predation effects with shared environmental effects; (4) monitor changes in total recruitment to, production of, and fishing effort in impacted fisheries, not just the percentage contribution of hatchery fish to production; (5) monitor changes in the fishing mortality rates of both wild and hatchery fish directly, through carefully conducted tagging programs that measure short-term probabilities of capture; and (6) monitor reproductive performance of hatchery-origin fish and hatchery-wild hybrid crosses in the wild. Sound management-action design and monitoring is the essence of adaptive management [91] and adaptive management enables refinements, progress, and success in marine enhancement programs [4, 6, 11, 92].

Marine Fisheries Enhancement, Coming of Age in the New Millennium. Table 4 Key areas of expertise needed in marine fisheries enhancement

• Fisheries science
• Fisheries management
• Adaptive management
• Marine aquaculture
• Population genetics
• Aquatic animal health
• Population ecology
• Behavioral ecology
• Community ecology
• Resource economics
• Social science and institutional analysis and design
• Statistics and experimental design
• Tagging technology
• Communications and outreach

Marine fisheries enhancement is a powerful tool that requires careful and interdisciplinary planning to control its effects. The process of transforming marine enhancement from an idea before its time into an effective resource management and sea ranching tool involves adopting a clear prescription for responsible use. As marine enhancement comes of age in this new millennium, agencies and stakeholders have a growing library of protocols for enhancement at their disposal and the responsibility to use them. The Responsible Approach and Code of Responsible Conduct provide healthy prescriptions for controlling the outcome of enhancements. These principles need to be adopted and used well, in order to increase and ensure the readiness of this tool to aid in conservation and to increase fishery yields when it is needed. Growth in human population size is fast approaching a critical

level, and much greater attention will be placed in this century on obtaining food from the sea [1]. It is unwise to not be ready with marine enhancement to help sustain depleted, threatened, and endangered species, help maintain wild stocks in the face of increasing fishing pressure, help sustain sports fisheries, and help increase fishery yields.

Legacy from the Past

Allure of a Quick Fix

Marine enhancement programs are often seen as a "quick fix" for a wide variety of problems in marine resource management. At best, they may be an important new component of marine ecosystem management; if not implemented responsibly, though, they may lull fishery managers into false confidence and thus lead to inaction and delay in the development of other fisheries management and restoration programs [5, 6].

Although marine fisheries enhancement is certainly not a quick fix, it can be a powerful tool for resource management when conditions warrant the use of this tool and if the time and care needed are taken to develop enhancement programs well. Unfortunately, the allure of a quick fix has often prompted stakeholders and managers to skip or ignore several elements needed to allow those programs to succeed, leading to wholesale failure of such efforts. The field of marine fisheries enhancement is littered with examples of enhancement projects that failed to achieve their potential for lack of a careful enough or quantitative approach (e.g., see accounts discussed in [7, 21, 62, 72, 93–95]). Most of the failures can be traced back to attempts to use enhancements when they were not warranted or failure to consider several, if not most, of the principles now incorporated in the "Responsible Approach" and "Code of Responsible Conduct" for marine fisheries enhancement.

Isolation from the Fisheries Science Community

Historically, marine fisheries enhancements have been conducted more or less isolated from other forms of fisheries management. Enhancement hatcheries have often been promoted by stakeholders and government mandates without the necessary funding or authorization behind them to do much more than produce and release fish without funds for monitoring impacts and adaptive management needed to increase the effectiveness of enhancements. Such programs are often built and implemented from a vantage point within resource management agencies that has little or no connectivity with the existing fishery management process. This has stymied development of this field in two ways – first, by compelling hatcheries to operate within resource management agencies largely independent from stock assessment and fisheries monitoring programs, or even worse, within different agencies altogether. Second, such isolation has fostered development of a production-oriented operational mode, and thwarted development of an enhancement-oriented mode [92].

Part of this isolation from fishery management also stems from the poor track record of the early marine hatcheries as an effective way to recover depleted fish stocks, coupled with the lack of scientific development of marine fisheries enhancement for so long into the twentieth century. This has understandably led to bias against fishery enhancements. Many of today's fishery scientists have been schooled to understand that stock enhancement has not worked, based in part on the lingering legacy from past failures and in part on lack of awareness of new marine fisheries enhancement science, as few citations have yet appeared in fisheries science textbooks. With many of the scientific achievements in fisheries enhancement having occurred only over the past decade or so, this is understandable. But in light of the need to couple fisheries enhancement with fisheries management systems, lack of awareness of progress in this field is an obstacle that may be resolved only by compilation of more and more success stories over time. Thus, it is imperative that existing and developing enhancement programs alike incorporate modern concepts about how to plan and conduct enhancements so they are enabled for success.

Progress in Marine Fisheries Enhancement

Lessons Learned from Marine Enhancement Programs

Much progress has now been made in understanding how to manage enhancement more effectively.

Bartley and Bell [96] considered progress made from three decades of stocking initiatives and summarized and discussed lessons learned. These are listed here, below [96], with a brief clarification or caveat on each.

Deciding When and How to Apply the Release of Cultured Juveniles

1. Objective assessment of the need for releases is crucial –and requires an evaluation of the status of the fishery, modeling of stocking impact to determine if stocking can help achieve the goals, coupled with consideration of whether there are recruitment limitations and adequate habitat available for stocking.
2. Releases of cultured juveniles for restocking and stock enhancement need to be made at the scale of self-replenishing populations –releases will not be effective unless the spatial extent of target populations has been identified; thus prior to conducting releases of hatchery organisms, clear identification of genetically discrete stocks should be determined.
3. There are no generic methods for restocking and stock enhancement –largely because of wide variation in life history among different species and variation in ecological conditions among release sites.
4. Very large numbers of juveniles are often needed for effective stock enhancement –this is particularly so for offshore stocks, which can be comprised of a huge number of individuals; more modest releases may suffice for localized enhancement of inshore stocks or those comprised of multiple stocks that occur on relatively small scales.
5. Large areas are needed for stock enhancement of some species –and this can result in user conflict, particularly for sea ranching, where large areas are leased and protected by the enhancement program (e.g., [97]); in other cases, limited dispersal of adults and larvae indicates stocking in smaller areas can be effective, for example, common snook along Florida's Gulf Coast [98].
6. Invertebrates offer good opportunities for restocking and stock enhancement –because invertebrates are often comprised of self-recruiting populations that occur at small scales.

Integrating Interventions with Other Management Measures

7. Problems that caused lower production must be addressed before release of juveniles – particularly in the case of degraded, lost, or insufficient habitat. With better management of the wild resources, the scope for augmentation of total production declines; enhancement becomes a very site specific tool when habitat has been lost, or something needs rebuilding, or there are species of particularly high value [94].
8. Biotechnical research must be integrated with institutional and socio-economic issues – ownership rights and control and use of enhanced stocks need to be well understood by the greater institutional, social, economic, and political environment [99].
9. Successful stock enhancement programs are often run by cooperatives and the private sector – where there is increased incentive in sharing the costs of fisheries enhancement.
10. The costs and time frames involved in restocking programs can be prohibitive – hatchery costs, which can be considerable, are particularly difficult to bear in smaller countries and developing countries.

Monitoring and Evaluation

11. Development of cost-effective tagging methods is critical to efficient evaluation of stock enhancement – refining and monitoring the effects and effectiveness of marine enhancements cannot be done without a way to distinguish hatchery from wild stocks and distinct release groups.
12. Large-scale releases of hatchery-reared juveniles can affect genetic [fitness] of wild populations – genetic hazards can be caused by hatchery-wild fish interactions and these need to be minimized.

Reducing the Cost of Juveniles

13. Costs of stocking programs can be reduced by "piggybacking" production of juveniles for release on existing aquaculture – this could reduce or eliminate the need for expensive new hatchery construction for enhancement programs, as long as appropriate broodstock management protocols are in place for conserving wild-stock genetics.
14. Wild [postlarvae] can provide an abundant, low-cost source of juveniles for stock enhancement

programs – this can sometimes be an effective way to reduce costs and eliminate genetic issues; successful scallop enhancement in Japan is based on collection of wild seed stock.

15. The costs of restocking can be reduced greatly for some species by relocating adults to form a viable spawning biomass – rebuilding spawning aggregations by concentrating broodstock can be effective for depleted stocks with limited larval dispersal, but care must be taken to avoid comingling different stocks (i.e., avoid translocation of exogenous genes).

Improving Survival in the Wild

16. Predation is the greatest hurdle to survival of released juveniles – care must be taken to understand ecology of the species and ecosystem at the release site and pilot experiments are needed to develop optimal release strategies to maximize survival.
17. Excessive releases of juveniles cause density-dependent mortality – density has a strong effect on growth and survival in the wild; planning release magnitude must take into account the carrying capacity at release locations. This requires adaptive management and an experimental framework for releases.
18. Small-scale experiments to test methods for releasing juveniles can give misleading results – "commercial scale" releases are needed to test assumptions made from small-scale release experiments.
19. Good survival of released juveniles at one site is no guarantee that the methods can be transferred to other sites – stocking effectiveness will vary with release location and what works at one site may not be effective at another.

Other Manipulations to Increase Abundances

20. Artificial habitats can be used to increase the carrying capacity for target species – and may enable increased production at release sites where there are resource (food, refuge, space) limitations.
21. Yields of some species can be increased by providing suitable settlement habitat and redistributing juveniles from areas of heavy settlement – for example, redistribution can be used to reduce density effects and increase probability of successful recruitment when moved to a location with greater availability of food, refuge, or settlement habitats. But care must be taken to avoid genetic hazards associated with comingling stocks.

Examples of Progress Made in Marine Enhancement

As science and constructive debate have advanced in this field, there are many signs of progress. Some explicit examples of progress made in marine enhancement over the past couple of decades are presented below, ranging in scale from local experimental investigations of release strategies and density-dependent effects on hatchery and wild stocks (e.g., [100]) to documented replenishment impact in large-scale enhancement efforts (e.g., [101, 102]). This is but a sample of examples and is by no means a comprehensive list. There are many more examples in the peer-reviewed proceedings from the ISSESR and other stock enhancement conferences [41–53] and other journal articles.

1. Adoption of a science-based responsible approach to marine stock enhancement has now become widespread, resulting in a much more assessment-driven and precautionary approach than ever before (a few examples include Refs. [4, 6, 10, 12, 20, 22, 27–29, 33, 37–39, 59–61, 68, 69, 72, 75, 84, 86, 87, 89, 96, 103–106]). This has been enabled, in part, by advances in tagging technology (e.g., [8] and see examples in [9, 56]) and in development of new marine aquaculture technologies that can now provide juvenile fishes for marine enhancement research.
2. Networking of Scientists involved in this rapidly advancing field has been fostered by various symposia and working groups, for example, the World Aquaculture Society Working Group on Stock Enhancement and the scientific committees for the International Symposium on Stock Enhancement and Sea Ranching (www.SeaRanching.org).
3. There is a much better appreciation of the importance of managing marine fishery enhancements from a fisheries management perspective (e.g., [6, 59, 107]).
4. New tools are available for modeling stock enhancement effects and effectiveness [10, 82, 108–110].

5. At least two experimental field studies have now been conducted to evaluate density-dependent interactions of stocked hatchery and wild fish; these provide evidence that increased production can be achieved in juvenile nursery habitats without displacing wild fish, but not necessarily without displacing some of the hatchery fish [33, 100].
6. There is now clear evidence and a prescription of techniques for improving post-release survival (often with a doubling effect or more) of stocked marine fishes, and optimizing release strategies to maximize stocking efficiency and control impacts (e.g., [26, 36, 37, 39, 60–62, 70, 72, 100–115]). There is also ample evidence that in habitats with limited carrying capacity or intense predation, regardless of release strategy used, little can be done to improve survival of hatchery fish and stocking simply cannot increase production [106, 116, 117].
7. It is now fairly clear that marine enhancements may be cost effective only if (a) the supply of recruits is generally limiting, (b) there is adequate habitat to support an increased supply of juveniles, (c) cultured juveniles represent a large portion of recruitment, (d) fishing is regulated appropriately, and (e) other management measures (catch regulations and habitat restoration) are insufficient to restore catch rates [96].
8. Stock enhancement of some species of marine finfish has been successful at the scale of large bays, for example, Hirame flounder and red sea bream in Japan [72, 106] when there is sufficient carrying capacity at release sites. Carrying capacity varies considerably among release sites, and thus must be evaluated and taken into account using monitoring and adaptive management for each release site.
9. Scallop sea ranching has been a large success in Japan, New Zealand, and China, where property rights and large ocean leases have created strong incentives for careful management by fishermen and owners of the sea ranching operations [72, 101, 102, 118]. For example, near Dalian, China, Zhangzidao Fishery Group leases 2,000 km^2 of ocean-bottom-to-ocean-surface for sea ranching. In 2010, Zhangzidao harvested an average of 150 t/day of ocean scallops from their sea ranching operations (over 50,000 t/year) (Wang Qing-yin, personal communication 2011).
10. Property rights have also provided incentives for bivalve culture in the State of Washington, USA, where clam sea ranching operations have remained economically and environmentally sustainable for over three decades [119].
11. Pilot experiments with black bream in an Australian estuary have documented quite good survival and recruitment to the fishery. The latest phase of this project reveals strong rationale for long-term monitoring of enhancement impact [87, 120].
12. Restocking success with red drum in a South Carolina estuary [77, 121]. Pilot experiments revealed surplus productive capacity in the Ashley River in South Carolina, where fishery landings of red drum were doubled over a few years.
13. Pilot experiments to evaluate blue crab enhancement potential in Maryland and Virginia led to improvements in traditional fishery management, with information learned through stocking research [70, 114]. Pilot experiments can be used to provide critical information on the natural ecology, life history, and environmental requirements of valuable marine species [122].
14. Perhaps the largest scale enhancement success for fishes is Japanese chum salmon restocking – a special tool for a circumstance in which the habitat had almost totally been lost [94].

Future Directions

Over the past two decades, there has been a rapid expansion of knowledge about marine fisheries enhancement systems and the effects and effectiveness of stocking a wide variety of marine organisms for sea ranching, stock enhancement and restocking. Many gaps in knowledge have now been filled. Well thought out approaches now provide a roadmap for effective use of enhancements. When models show potential for stocking, efforts to deploy marine enhancements can be successful if the principles in the roadmap are carefully employed. The basic reason that marine enhancement programs do not have more of a track record of success stories yet is that implementing them well is a complex endeavor that demands attention to

multiple factors spanning many disciplines. Rarely have these been pulled together in an enhancement program. The Hatchery Reform Project in the Pacific Northwest USA, which includes an independent scientific review panel ("Hatchery Scientific Review Group") is a good example [123]. Because of their efforts, salmonid hatchery reforms now underway are bringing many of the principles of the Responsible Approach into play. The Norwegian PUSH program is another good example. In that case, information gained from quantitative assessments of enhancement showed that stocking would not be an economical way to enhance cod in Norway, thus saving years of wasteful spending that could have occurred there, had monitoring and adaptive management not been a central part of the enhancement system.

Successful examples of fisheries enhancement are truly group efforts, involving stakeholders, agency officials, and individuals with expertise in the principal sub-disciplines needed. Suffice to say that at this point in time few, if any, marine fisheries enhancement programs have enlisted all of the key elements of the Responsible Approach and Code of Responsible Conduct. But these principles are now well described and laid out in a systematic manner. It is reasonable to expect that if the Responsible Approach is used as the blueprint for planning and executing enhancements, and if the initial appraisal and goal setting stage indicates moving ahead, then there is ample opportunity for success in applying marine fisheries enhancements, as long as dedicated attention is focused on applying each of the key elements.

So how will marine enhancement advance to the next level – emergence of a rapidly growing body of success stories in restocking, stock enhancement, and sea ranching? Listed below are a few factors that are now needed to transition this field to the next level, where marine enhancements are well integrated into resource management systems and used wisely and appropriately.

Enabling Factors for Increasing Successful Marine Enhancements

1. *Greater awareness is needed among all stakeholders of the issues, pitfalls, progress, and opportunities in this field.* The concepts underlying effective enhancements need to be translated into lay language and used to inform stakeholders. This will help all stakeholders recognize the various issues and parameters needed for effective enhancements. Pivotal among stakeholders are public officials who fund enhancement programs, as they need to understand what it takes to develop an effective program or reform existing ones. New enhancement programs that may not be funded well enough to implement all of the key principles in the Responsible Approach would do well to use the results of Stage 1 in Table 3 to document the potential for success, but not proceed beyond Stage 1 until adequate funding is available.
2. *Use of Adaptive management is one of the most important principles for guiding successful enhancement programs.* Active adaptive management [91] is critical for gauging the effectiveness of, improving, and managing fisheries systems in the face of uncertainty. However, it is often dismissed by enhancement programs or given low priority for lack of funding or when enhancement is viewed as a quick fix. But, this important principle is used to optimize release strategies, to identify and deal with ecological or genetic impacts on wild stocks, to refine the enhancement process and identify the results of improvements, to evaluate and improve progress towards goals and objectives, and to monitor and improve economic impact. Active adaptive-management is an essential component of managing enhancement programs; it empowers management teams to understand and control the impacts of enhancements well. Without it, enhancement programs at best rely on hope to achieve their potential (but cannot) and at worst are doomed to failure. Australia is employing active adaptive management principles early in the development stage as part of ongoing work to evaluate enhancement potential for a wide range of species [124].
3. *Adapt the Responsible Approach to local circumstances.* The Responsible Approach is purposely vague on how to implement it. This is partly because not all elements are needed under all situations, but most will be. Fitting the process to particular circumstances is in itself a key part of implementing the Responsible Approach by

engaging the various stakeholders in planning [6]. As progress continues in this field, additional principles will emerge that need to be included, for example, to account for needs of regional fishery management plans in response to climate change.

4. *Seek assistance from established workers in the field.* For new and developing enhancement programs, or existing ones seeking to design and implement reforms, there is a broad and expanding network of workers in this field who could be queried for advice on various enhancement issues. The ISSESR website is a good source for identifying individuals with specific kinds of expertise, by perusing presentation abstracts or locating published proceedings from past ISSESR conferences [125]. If researchers or workers in the field are contacted, but do not have time to provide advice, they usually will help identify others who can.

This entry may help expand awareness among fishery stakeholders, other natural-resource stakeholders, scientists, and fishery managers alike about the pitfalls, challenges, and progress made in using marine hatchery releases as one of the tools in resource management and seafood production. Readers are referred to the articles and symposium proceedings cited herein to gain a better understanding of the issues, lessons learned, and progress.

The debate focused on enhancement is a healthy one, for it is fostering steady improvements and reforms in existing programs, and careful planning and design in new ones. With each advance made, the potential seen by our forefathers to use hatcheries as a tool for recovering depleted stocks, increasing abundance in recruitment-limited stocks, and producing seafood by sea ranching is coming closer to fruition. One of the greatest lessons learned from the past is that the emphasis on expanding hatchery fish production for marine enhancement should not be allowed to take the focus off of the objective – increasing yields in fisheries and recovering stocks in restoration programs. Clearly, marine fisheries enhancement is a strong tool to add to the fishery management toolbox. But only careful analysis of conditions of the wild stock and the fishery will guide when and where it is appropriate to use enhancements in addition to other management options, and when to stop. As Albert Einstein once said, "a perfection of means, and confusion of aims, seems to be our main problem." With the focus shifted to outcomes in marine enhancement programs, the appropriate means should fall into place, aided by healthy debate and prescriptions for a responsible approach to marine fisheries enhancement.

Bibliography

1. Duarte CM, Holmer M, Olsen Y, Soto D, Marbà N, Guiu J, Black K, Karakassis I (2009) Will the oceans help feed humanity? Bioscience 59(11):967–976
2. NOVA (1992) Sex and the single rhinoceros – NOVA examines the high-tech efforts to preserve the world's animal diversity. PBS documentary. NOVA Season 19, Episode 20. Public Broadcasting Service
3. Bell JD, Leber KM, Blankenship HL, Loneragan NR, Masuda R, Vanderhaegen G (eds) (2008) A new era for restocking, stock enhancement and sea ranching of coastal fisheries resources. Special Issue, Rev Fish Sci 16(1–3):402 pp
4. Blankenship HL, Leber KM (1995) A responsible approach to marine stock enhancement. Am Fish Soc Symp 15:167–175
5. Walters CJ, Martell SJD (2004) Fisheries ecology and management. Princeton University Press, Princeton
6. Lorenzen K, Leber KM, Blankenship HL (2010) Responsible approach to marine stock enhancement: an update 2010. Rev Fish Sci 18(2):189–210
7. Richards WJ, Edwards RE (1986) Stocking to restore or enhance marine fisheries. In: Stroud RH (ed) Fish culture in fisheries management. American Fisheries Society, Bethesda, pp 75–80
8. Jefferts KB, Bergman PK, Fiscus HF (1963) A coded-wire identification system for macro-organisms. Nature 198:460–462
9. Blankenship HL, Tipping JM (1993) Evaluation of visible implant and sequentially coded wire tags in sea-run cutthroat trout. North Am J Fish Manag 13:391–394
10. Lorenzen K (2005) Population dynamics and potential of fisheries stock enhancement: practical theory for assessment and policy analysis. Philos Trans R Soc Lond Ser B 260:171–189
11. Leber KM (2004) Marine stock enhancement in the USA: status, trends and needs. In: Leber KM, Kitada S, Blankenship HL, Svåsand T (eds) Stock enhancement and sea ranching: developments, pitfalls and opportunities. Blackwell, Oxford, pp 11–24
12. Bell JD, Rothlisberg PC, Munro JL, Loneragan NR, Nash WJ, Ward RD, Andrew NL (2005) Restocking and stock enhancement of marine invertebrate fisheries. Adv Mar Biol 49:1–370
13. Hedrick PW, Hedgecock D, Hamelberg S, Croci SJ (2000) The impact of supplementation in winter-run Chinook salmon on effective population size. J Hered 91:112–116
14. Hilderbrand RH (2002) Simulating supplementation strategies for restoring and maintaining stream resident cutthroat trout populations. North Am J Fish Manag 22:879–887
15. Reisenbichler RR, Utter FM, Krueger CC (2003) Genetic concepts and uncertainties in restoring fish populations and

species. In: Wissmar RC, Bisson PA (eds) Strategies for restoring river ecosystems: sources of variability and uncertainty in natural and managed systems. American Fisheries Society, Bethesda, pp 149–183
16. Hager RC, Noble RE (1976) Relation of size at release of hatchery-reared coho salmon to age, sex, and size composition of returning adults. Progress Fish Cult 38:144–147
17. Bilton HT, Alderdice DF, Schnute JT (1982) Influence of time and size at release of juvenile Coho Salmon (*Oncorhynchus kisutch*) on returns at maturity. Can J Fish Aquat Sci 39:426–447
18. Appledorn RS, Ballentine DL (1983) Field release of cultured queen conchs in Puerto Rico: implications for stock restoration. Proc Gulf Caribb Fish Inst 35:89–98
19. Appeldorn RS (1985) Growth, mortality and dispersion of juvenile laboratory-reared conchs, *Strombus gigas*, and *S. costatus*, released at an offshore site. Bull Mar Sci 37:785–793
20. Tsukamoto K, Kuwada H, Hirokawa J, Oya M, Sekiya S, Fujimoto H, Imaizumi K (1989) Size-dependent mortality of red sea bream *pagrus major* juveniles released with fluorescent otolith-tags in News Bay. Jpn J Fish Biol 35(Supplement A):59–69
21. Peterman RM (1991) Density-dependent marine processes in north Pacific salmonids: lessons for experimental design of large scale manipulations of fish stocks. ICES Mar Sci Symp 192:69–77
22. Hilborn R (1999) Confessions of a reformed hatchery basher. Fisheries 24:30–31
23. Kitada S, Taga Y, Kishino H (1992) Effectiveness of a stock enhancement program evaluated by a two-stage sampling survey of commercial landings. Can J Fish Aquat Sci 49:1573–1582
24. Sudo HT, Goto R, Ikemoto MT, Azeta M (1992) Mortality of reared flounder (*Paralichthys olivaceus*) juveniles released in Shijiki Bay. Bull Seikai Natl Fish Res Inst 70:29–37
25. Fujita T, Mizuta T, Nemoto Y (1993) Stocking effectiveness of Japanese flounder *Paralichthys olivaceus* fingerlings released in the coast of Fukushima Prefecture. Saibai Giken 22:67–73
26. Yamashita Y, Nagahora S, Yamada H, Kitagawa D (1994) Effects of release size on survival and growth of Japanese flounder *Paralichthys olivaceous* in coastal waters off Iwate Prefecture, northeastern Japanese. Mar Ecol Prog Ser 105:269–276
27. Svåsand T, Jorstad T, Kristiansen TS (1990) Enhancement studies of coastal cod in western Norway. Part I. Recruitment of wild and reared cod to a local spawning stock. J Cons Intl Expl Mer 47:5–12
28. Svåsand T, Kristiansen TS (1990) Enhancement studies of coastal cod in western Norway. Part II. Migration of reared coastal cod. J Cons Intl Expl Mer 47:13–22
29. Kristiansen TS, Svåsand T (1990) Enhancement studies of coastal cod in western Norway. Part III. Interrelationships between reared and indigenous cod in a nearly land-locked fjord. J Cons Intl Expl Mer 47:23–29
30. Svåsand T, Kristiansen TS (1990) Enhancement studies of coastal cod in western Norway. Part IV. Mortality of reared cod after release. J Cons Intl Expl Mer 47:30–39
31. Nordheide JT, Salvanes AGV (1991) Observations on reared newly released and wild cod (*Gadus morhua* L.) and their potential predators. ICES Mar Sci Symp 192:139–146
32. Leber KM (1995) Significance of fish size-at-release on enhancement of striped mullet fisheries in Hawaii. J World Aquac Soc 26:143–153
33. Leber KM, Brennan NP, Arce SM (1995) Marine enhancement with striped mullet: are hatchery releases replenishing or displacing wild stocks. Am Fish Soc Symp 15:376–387
34. McEachron LW, McCarty CE, Vega RR (1995) Beneficial uses of marine fish hatcheries: enhancement of red drum in Texas coastal waters. Am Fish Soc Symp 15:161–166
35. Kent DB, Drawbridge MA, Ford RF (1995) Accomplishments and roadblocks of a marine stock enhancement program for white seabass in California. Am Fish Soc Symp 15:492–498
36. Willis SA, Falls WW, Dennis CW, Roberts DE, Whitechurch PG (1995) Assessment of effects of season of release and size at release on recapture rates of hatchery-reared red rum (*Sciaenops ocellatus*) in a marine stock enhancement program in Florida. Am Fish Soc Symp 15:354–365
37. Leber KM, Arce SM, Sterritt DA, Brennan NP (1996) Marine stock-enhancement potential in nursery habitats of striped mullet, *Mugil cephalus*, in Hawaii. Fish Bull US 94:452–471
38. Leber KM, Arce SM (1996) Stock enhancement effect in a commercial mullet *Mugil cephalus* fishery in Hawaii. Fish Manag Ecol 3:261–278
39. Leber KM, Blankenship HL, Arce SM, Brennan NP (1997) Influence of release season on size-dependent survival of cultured striped mullet, *Mugil cephalus*, in a Hawaiian estuary. Fish Bull US 95:267–279
40. Rimmer MA, Russell DJ (1998) Survival of stocked barramundi, *Lates calcarifer* (Bloch), in a coastal river system in far northern Queensland, Australia. Bull Mar Sci 62:325–336
41. Lockwood SJ (1991) Stock enhancement. Special session at the ecology and management aspects of extensive mariculture. In: ICES marine science symposia 192, Nantes. International Council for the Exploration of the Sea, Copenhagen
42. WAS (1991) Enhancement of natural fisheries through aquaculture. In: Special session at 22nd annual conference and exposition, San Juan, Puerto Rico. Programs and abstracts. World Aquaculture Society, San Juan
43. AFS (1993) Emerging marine fish enhancement and evaluation. In: Special session at 123rd annual meeting of the American Fisheries Society, Portland. Book of Abstracts
44. EAS (1993) Fisheries and aquaculture interactions. In: Special session at world aquaculture'93, Torremolinos. Abstracts. Special Publication No. 19. European Aquaculture Society, Gent
45. Schramm HL Jr, Piper RG (eds) (1995) Uses and effects of cultured fishes in aquatic ecosystems, vol 15, American fisheries society symposium. American Fisheries Society, Bethesda, 608 pp
46. Travis J, Coleman FC, Grimes CB, Conover D, Bert TM, Tringali M (1998) Critically assessing stock enhancement: an introduction to the Mote symposium. Bull Mar Sci 62(2):305–311

47. Howell BR, Moksness E, Svåsand T (eds) (1999) Stock enhancement and sea ranching. Fishing News Books/Blackwell, Oxford
48. Nakamura Y, McVey JP, Leber KM, Neidig C, Fox S, Churchill K (eds) (2003) Ecology of aquaculture species and enhancement of stocks. In: Proceedings of the thirtieth U.S.-Japan meeting on aquaculture, Sarasota, 3–4 Dec 2001. UJNR Technical Report No. 30
49. Leber KM, Kitada S, Blankenship HL, Svåsand T (eds) (2004) Stock enhancement and sea ranching: developments, pitfalls and opportunities. Blackwell, Oxford, 606 pp
50. Nickum M, Mazik PM, Nickum JG, MacKinlay DD (eds) (2004) Propagated fish in resource management, vol 44, American Fisheries Society symposium. American Fisheries Society, Bethesda, 644 pp
51. Bell JD, Bartley DM, Lorenzen K, Loneragan NR (2006) Restocking and stock enhancement of coastal fisheries: potential, problems and progress. Fish Res 80:1–8
52. Bell JD, Leber KM, Blankenship HL, Loneragan NR, Masuda R (2008) A new era for restocking, stock enhancement and sea ranching of coastal fisheries resources. Rev Fish Sci 16(1–3):1–9
53. Loneragan N, Abraham I (2011) The fourth international symposium on stock enhancement and sea ranching, part of the 9th Asian fisheries and aquaculture forum, Shanghai Ocean University, 21–23 April 2011. Book of Abstracts for Oral and Poster presentations, Shanghai. http://www.SeaRanching4.org/documents/4thISSESR2011.pdf. Accessed Aug 2011
54. Allendorf FW, Phelps SR (1980) Loss of genetic variation in a hatchery stock of cutthroat trout. Trans Am Fish Soc 109:537–543
55. Busac CA, Currens KP (1995) Genetic risks and hazards in hatchery operations: fundamental concepts and issues. Am Fish Soc Symp 15:71–80
56. Leber KM, Blankenship HL (2011) How advances in tagging technology improved progress in a new science: marine stock enhancement. In: McKenzie J, Phelps Q, Kopf R, Mesa M, Parsons B, Seitz A (eds) Advances in fish tagging and marking technology, vol 76, American fisheries society symposium. American Fisheries Society, Bethesda
57. Tringali MD (2006) A Bayesian approach for genetic tracking of cultured and released individuals. Fish Res 77:159–172
58. Kirk R (1987) A history of marine fish culture in Europe and North America. Fishing News Books, Farnham, 192 pp
59. Lorenzen K (2008) Understanding and managing enhancement fisheries systems. Rev Fish Sci 16:10–23
60. Leber KM, Brennan NP, Arce SM (1998) Recruitment patterns of cultured juvenile Pacific threadfin, *Polydactylus sexfilis* (Polynemidae), released along sandy marine shores in Hawaii. Bull Mar Sci 62(2):389–408
61. Leber KM, Cantrell RN, Leung PS (2005) Optimizing cost-effectiveness of size at release in stock enhancement programs. North Am J Fish Manag 25:1596–1608
62. Tringali MD, Leber KM, Halstead WG, McMichael R, O'Hop J, Winner B, Cody R, Young C, Neidig C, Wolfe H, Forstchen A, Barbieri L (2008) Marine stock enhancement in Florida: a multi-disciplinary, stakeholder-supported, accountability-based approach. Rev Fish Sci 16(1–3):51–57
63. Waples RS (1999) Dispelling some myths about hatcheries. Fisheries 26(2):12–21
64. Tringali MD, Leber KM (1999) Genetic considerations during the experimental and expanded phases of snook stock enhancement. Bull Natl Res Inst Aquac Suppl 1:109–119
65. Lorenzen K, Beveridge MCM, Mangel M. Cultured fish: integrative biology and management of domestication and interactions with wild fish. Biol Rev (in press)
66. HRP (2011) US Hatchery Reform Program. http://www.HatcheryReform.us. Accessed Aug 2011
67. Cowx IG (1994) Stocking strategies. Fish Manag Ecol 1:15–31
68. Munro JL, Bell JD (1997) Enhancement of marine fisheries resources. Rev Fish Sci 5:185–222
69. Taylor MD, Palmer PJ, Fielder DS, Suthers IM (2005) Responsible estuarine finfish stock enhancement: an Australian perspective. J Fish Biol 67:299–331
70. Zohar Y, Hines AH, Zmora O, Johnson EG, Lipcius RN, Seitz RD, Eggleston DB, Place AR, Schott EJ, Stubblefield JD, Chung JS (2008) The Chesapeake Bay blue crab (*Callinectes sapidus*): a multidisciplinary approach to responsible stock replenishment. Rev Fish Sci 16:24–34
71. Bartley DM, Kent DB, Drawbridge MA (1995) Conservation of genetic diversity in a white seabass hatchery enhancement program in southern California. Am Fish Soc Symp 15:249–258
72. Masuda R, Tsukamoto K (1998) Stock enhancement in Japan: review and perspective. Bull Mar Sci 62(2):337–358
73. Kitada S (1999) Effectiveness of Japan's stock enhancement programmes: current perspectives. In: Howell BR, Moksness E, Svåsand T (eds) Stock enhancement and sea ranching. Fishing News Books/Blackwell, Oxford, pp 103–131
74. Blaylock RB, Leber KM, Lotz JM, Ziemann DA (2000) The U.S. Gulf of Mexico marine stock enhancement program (USGMSEP): the use of aquaculture technology in "responsible" stock enhancement. Bull Aquac Assoc Can 100:16–22
75. Kuwada H, Masuda R, Kobayashi T, Shiozawa S, Kogane T, Imaizumi K, Tsukamoto K (2000) Effects of fish size, handling stresses and training procedure on the swimming behaviour of hatchery-reared striped jack: implications for stock enhancement. Aquaculture 185:245–256
76. Friedlander AM, Ziemann DA (2003) Impact of hatchery releases on the recreational fishery for Pacific threadfin (*Polydactylus sexfilis*) in Hawaii. Fish Bull 101:32–43
77. Smith TIJ, Jenkins WE, Denson MR, Collins MR (2003) Stock enhancement research with anadromous and marine fishes in South Carolina. In: Nakamura Y, McVey JP, Fox S, Churchill K, Neidig C, Leber K (eds) Ecology of aquaculture species and enhancement of stocks. Proceedings of the thirtieth U.S.–Japan meeting on aquaculture, Sarasota, 3–4 Dec 2001. UJNR Technical Report No. 30. Mote Marine Laboratory, Sarasota, pp 175–190
78. Woodward AG (2003) Red drum stock enhancement in Georgia: a responsible approach. Coastal Resources Division,

Georgia Department of Natural Resources, Brunswick. http://www.peachstatereds.org/approach.pdf. Accessed Oct 2010
79. Jenkins WE, Denson MR, Bridgham CB, Collins MR, Smith TIJ (2004) Year-class component, growth, and movement of juvenile red drum stocked seasonally in a South Carolina estuary. North Am J Fish Manag 24:636–647
80. Kuwada H, Masuda R, Kobayashi T, Kogane T, Miyazaki T, Imaizumi K, Tsukamoto K (2004) Releasing technique in striped jack marine ranching: pre-release acclimation and presence of decoys to improve recapture rates. In: Leber KM, Kitada S, Blankenship HL, Svåsand T (eds) Stock enhancement and Sea ranching: developments, pitfalls and opportunities. Blackwell, Oxford, pp 106–116
81. Fairchild EA, Fleck J, Howell WH (2005) Determining an optimal release site for juvenile winter flounder *Pseudopleuronectes americanus* (Walbaum) in the Great Bay estuary, NH, USA. Aquac Res 36:1374–1383
82. Mobrand LE, Barr J, Blankenship L, Campton DE, Evelyn TTP, Flagg TA, Mahnken CVW, Seeb LW, Seidel PR, Smoker WW (2005) Hatchery reform in Washington State. Fisheries 30:11–23
83. Eggleston DB, Johnson EG, Kellison GT, Plaia GR, Huggett CL (2008) Pilot evaluation of early juvenile blue crab stock enhancement using a replicated BACI design. Rev Fish Sci 16:91–100
84. Gardner C, Van Putten EI (2008) The economic feasibility of translocating rock lobsters in increase yield. Rev Fish Sci 16:154–163
85. Karlsson S, Saillant E, Bumguardner BW, Vega RR, Gold JR (2008) Genetic identification of hatchery-released red drum in Texas bays and estuaries. North Am J Fish Manag 28:1294–1304
86. Le Vay L, Lebata MJH, Walton M, Primavera J, Quinitio E, Lavilla-Pitogo C, Parado-Estepa F, Rodriguez E, Ut VN, Nghia TT, Sorgeloos P, Wille M (2008) Approaches to stock enhancement in mangrove-associated crab fisheries. Rev Fish Sci 16:72–80
87. Potter IC, French DJW, Jenkins GI, Hesp SA, Hall NG, de Lestang S (2008) Comparisons of growth and gonadal development of otolith-stained cultured black bream, *Acanthopagrus butcheri*, in an estuary with those of its wild stock. Rev Fish Sci 16:303–316
88. Purcell SW, Simutoga M (2008) Spatio-temporal and size-dependent variation in the success of releasing cultured sea cucumbers in the wild. Rev Fish Sci 16:204–214
89. Støttrup JG, Overton JL, Paulsen H, Mollmann C, Tomkiewicz J, Pedersen PB, Lauesen P (2008) Rationale for restocking the Eastern Baltic cod stock. Rev Fish Sci 16:58–64
90. Taylor MD, Suthers IM (2008) A predatory impact model and targeted stock enhancement approach for optimal release of mulloway (*Argyrosomus japonicus*). Rev Fish Sci 16:125–134
91. Walters CJ, Hilborn R (1978) Ecological optimization and adaptive management. Ann Rev Ecol Syst 9:157–188
92. Leber KM (2002) Advances in marine stock enhancement: shifting emphasis to theory and accountability. In: Stickney RR, McVey JP (eds) Responsible marine aquaculture. CABI Publishing, New York, pp 79–90
93. Grimes CB (1998) Marine stock enhancement: sound management or techno-arrogance? Fisheries 23(9):18–23
94. Hilborn R (1998) The economic performance of marine stock enhancement projects. Bull Mar Sci 62:661–674
95. Serafy JE, Ault JS, Capo TR, Schultz DR (1999) Red drum, *Sciaenops ocellatus*, stock enhancement in Biscayne Bay, FL, USA: assessment of releasing unmarked early juveniles. Aquac Res 30:737–750
96. Bartley DM, Bell JD (2008) Restocking, stock enhancement, and sea ranching: arenas of progress. Rev Fish Sci 16:357–364
97. Arbuckle M, Metzger M (2000) Food for thought. A brief history of the future of fisheries management. Challenger Scallop Enhancement Company, Nelson
98. Tringali MD, Seyoum S, Wallace EM, Higham M, Taylor RG, Trotter AA, Whittington JA (2008) Limits to the use of contemporary genetic analyses in delineating biological populations for restocking and stock enhancement. Rev Fish Sci 16:111–116
99. Garaway CJ, Arthur RI, Chamsingh B, Homekingkeo P, Lorenzen K, Saengvilaikham B, Sidavong K (2006) A social science perspective on stock enhancement outcomes: lessons learned from inland fisheries in southern LAO PDR. Fish Res 80:37–45
100. Brennan NP, Walters CJ, Leber KM (2008) Manipulations of stocking magnitude: addressing density-dependence in a juvenile cohort of common Snook (*Centropomus undecimalis*). Rev Fish Sci 16:215–227
101. Drummond K (2004) The role of stock enhancement in the management framework for New Zealand's southern scallop fishery. In: Leber KM, Kitada S, Blankenship HL, Svåsand T (eds) Stock enhancement and Sea ranching: developments, pitfalls and opportunities. Blackwell, Oxford, pp 397–411
102. Uki N (2006) Stock enhancement of the Japanese scallop *Patinopecten yessoensis* in Hokkaido. Fish Res 80:62–66
103. Stoner AW (1994) Significance of habitat and stock re-testing for enhancement of natural fisheries: experimental analyses with queen conch *Strombus gigas*. J World Aquac Soc 25:155–165
104. Leber KM (1999) Rationale for an experimental approach to stock enhancement. In: Howell BR, Moksness E, Svasand T (eds) Stock enhancement and sea ranching. Blackwell, Oxford, pp 63–75
105. Agnalt AL, Jørstad KE, Kristiansen T, Nøstvold E, Farestveit E, Næss H, Paulsen LI, Svåsand T (2004) Enhancing the European lobster (*Homarus gammarus*) stock at Kvitsoy Islands: perspectives on rebuilding Norwegian stocks. In: Leber KM, Kitada S, Blankenship HL, Svåsand T (eds) Stock enhancement and sea ranching: developments, pitfalls and opportunities. Blackwell, Oxford, pp 415–426
106. Kitada S, Kishino H (2006) Lessons learned from Japanese marine finfish stock enhancement programs. Fish Res 80:101–112
107. Bartley DM (1999) Marine ranching: a global perspective. In: Howell BR, Moksness E, Svasand T (eds) Stock enhancement and sea ranching. Blackwell, Oxford, pp 79–90

108. Lorenzen K (2006) Population management in fisheries enhancement: gaining key information from release experiments through use of a size-dependent mortality model. Fish Res 80:19–27
109. Medley PAH, Lorenzen K (2006) EnhanceFish: a decision support tool for aquaculture-based fisheries enhancement. Imperial College, London. http://www.aquaticresources.org/enhancefish.html. Accessed Aug 2011
110. Ye Y, Loneragan N, Die DJ, Watson R, Harch B (2005) Bioeconomic modeling and risk assessment of tiger prawn (*Penaeus esculentus*) stock enhancement in Exmouth Gulf, Australia. Fish Res 73:231–249
111. Yamashita Y, Yamada H (1999) Release strategy for Japanese flounder fry in stock enhancement programmes. In: Howell BR, Moksness E, Svasand T (eds) Stock enhancement and sea ranching. Blackwell, Oxford, pp 191–204
112. Tsukamoto K, Kuwada H, Uchida K, Masuda R, Sakakura Y (1999) Fish quality and stocking effectiveness: behavioral approach. In: Howell BR, Moksness E, Svasand T (eds) Stock enhancement and sea ranching. Blackwell, Oxford, pp 205–218
113. Brennan NP, Darcy MC, Leber KM (2006) Predator-free enclosures improve post-release survival of stocked common snook. J Exp Mar Biol Ecol 335:302–311
114. Lipcius RN, Eggleston DB, Schreiber SJ, Seitz RD, Shen J, Sisson M, Stockhausen WT, Wang HV (2008) Importance of metapopulation connectivity to restocking and restoration of marine species. Rev Fish Sci 16:101–110
115. Hervas S, Lorenzen K, Shane MA, Drawbridge MA (2010) Quantitative assessment of a white seabass (*Atractoscion nobilis*) stock enhancement program in California: post-release dispersal, growth and survival. Fish Res 105:237–243
116. Smedstad OM, Salvanes AGV, Fosså JH, Nordeide JT (1994) Enhancement of cod, *Gadus morhua* L., in Masfjorden: an overview. Aquac Fish Manag 25:117–128
117. Otterå H, Kristiansen TS, Svåsand T, Nødtvedt M, Borge A (1999) Sea ranching of Atlantic cod (*Gadus morhua* L.): effects of release strategy on survival. In: Howell BR, Moksness E, Svåsand T (eds) Stock enhancement and sea ranching. Fishing News Books/Blackwell, Oxford, pp 293–305
118. Wang Q, Wu H, Liu H, Wang S (2011) Ecosystem based sea ranching in Zhangzidao in northern yellow sea. In: Fourth international symposium on stock enhancement and sea ranching, Shanghai. Abstract, available within pdf file. http://www.SeaRanching4.org/documents/4thISSESR2011.pdf. Accessed Aug 2011
119. Becker P, Barringer C, Marelli DC (2008) Thirty years of sea ranching Manila clams (*Venerupis philippinarum*): successful techniques and lessons learned. Rev Fish Sci 16:44–50
120. Chaplin J, Hesp A, Gardner M, Cottingham A, Phillips N, Potter I, Jenkins G (2011) Biological performance and genetics of restocked and wild black sea bream in an Australian estuary. In: Fourth international symposium on stock enhancement and sea ranching, Shanghai. Abstract, available within pdf file. http://www.SeaRanching4.org/documents/4thISSESR2011.pdf. Accessed Aug 2011
121. Jenkins WE, Smith TIJ, Denson MR (2004) Stocking red drum: lessons learned. Am Fish Soc Symp 44:45–56
122. Miller JM, Walters CJ (2004) Experimental ecological tests with stocked marine fish. In: Leber KM, Kitada S, Blankenship HL, Svåsand T (eds) Stock enhancement and sea ranching: developments, pitfalls and opportunities. Blackwell, Oxford, pp 142–152
123. HSRG (2011) Hatchery scientific review group, puget sound and coastal Washington hatchery reform project: applying the principles of reform to Western Washington's hatcheries. http://www.lltk.org/improving-management/hatchery-reform/hrp/hsrg. Accessed Aug 2011
124. Loneragan N, Jenkins G, Taylor M (2011) Stock enhancement and restocking in Australia and opportunities for finfish, particularly in Western Australia. In: Fourth international symposium on stock enhancement and sea ranching, Shanghai. Abstract, available within pdf file. http://www.SeaRanching4.org/documents/4thISSESR2011.pdf. Accessed Aug 2011
125. ISSESR (2011) The international symposium on stock enhancement and sea ranching, Shanghai. http://www.SeaRanching.org. Accessed Aug 2011

Marine Life Associated with Offshore Drilling, Pipelines, and Platforms

Martin Hovland
Centre for Geobiology, University of Bergen, Bergen, Norway
Statoil ASA, Stavanger, Norway

Article Outline

Glossary
Definition of the Subject
Introduction
The Offshore Hydrocarbon Industry (OHI) and the "Second Surface"
Marine Life Affected by the OHI
Observations Along Pipelines
The Impact of Platforms and Other Fixed OHI-Structures
Future Directions
Bibliography

Glossary

OHI The Offshore Hydrocarbon Industry (OHI) searches for natural accumulations (reservoirs) of

oil and gas (hydrocarbons) and develops the means to extract and distribute (transport) them.

Platform An artificial structure designed to drill for hydrocarbons and/or produce (extract) and distribute hydrocarbons offshore in water depths up to 3 km. A platform can either be floating, semi-submersible, or fixed to the seafloor.

Subsea template A structure normally constructed of steel tubing, designed for a variety of purposes within the OHI. A normal subsea production template has up to four wellheads and has typical dimensions of 20 m × 20 m × 10 m.

ROV Remotely Operated Vehicle (ROV) is a remotely controlled underwater vehicle of variable size (from <1m long, up to about 3 m in length). The vehicle is normally fitted with propellers (thrusters), lights, cameras, manipulator arms, and other sensors and devices depending on its operational task.

Trunk pipeline A pipeline designed to transport large quantities of natural gas or oil over long distances (up to 1000 km). Normally, they have diameters between 20″ and 44″ (inner diameter of the steel pipe). Before laid on the seafloor, they are coated with varying thicknesses of concrete coating for added weight, to prevent them from becoming buoyant.

Umbilical A specially designed flexible, multipurpose cable used for powering underwater equipment (including ROVs and subsea templates) and also used for sending and receiving control and sensor signals. Umbilicals can contain combinations of electrical cables and optical fibers.

Cold-water coral reef A mounded natural structure on the seafloor consisting of live animals and dead remains and sediments. The mound is partly constructed by colonizing corals that are not dependent on sunlight (i.e., ahermatypic corals) such as the most common species: *Lophelia pertusa*.

Cold seep A location on the seafloor where natural fluids (gas and liquids) seep upward from the substratum, into the overlying water column.

Iceberg ploughmark Up to 100 m wide and many kilometer long furrows in the seafloor, produced by the action of drifting grounded icebergs. Off Mid- and Northern-Norway and several other places such (relict) furrows remain from the last glaciation.

Fish sighting The underwater visual detection (recording) of fish (here, larger than 0.5 m in length) using submersible vehicles with lights and cameras, such as ROVs.

Definition of the Subject

The offshore hydrocarbon, "oil," industry (OHI) searches for oil and natural gas by drilling exploration wells as deep as 10 km below the seafloor. When a commercial oil or gas field has been documented by such drilling, the exploitation of the resource will start by developing the field and the construction of production units and transportation infrastructure. Until only 15 years ago, this meant the construction of large, concrete-based or steel "jacket" production platforms. Because of intense research and technological development, many of the new offshore hydrocarbon fields are developed with smaller remotely controlled subsea steel structures placed directly on the seafloor, often without any infrastructure visible above the water. These new fields are produced remotely over distances of up to 150 km, with fiber optical cables, satellite communication, umbilicals, and pipelines.

In contrast to the other main (traditional) offshore industry, for example, the fishery industry, the OHI has employed strict environmental rules and regulations, which are efficiently practiced in most countries. These ensure little harm to sensitive marine organisms during normal field development and production. In addition to obeying the imposed rules and regulations, the OHI is, by tradition, constantly developing new and more cost-effective and environmentally friendly technology and infrastructure.

With knowledge and experience from 30 years of underwater detailed mapping and visual observations, mainly from the North Sea, spanning from predrilling seafloor surveys to annual surveys of pipelines and platforms, it is found that the marine life (the visual mega-fauna, at least) apparently benefits from the OHI-related installations on the seafloor. The reason being improved shelter conditions for large fish and also for spawning fish, and also an increased amount of energy (nutrients and seston) available in the water mass near these human-made structures, some of which act as artificial reefs [1]. The future needs for improved management of the marine biological resources, including the valuable deepwater corals and natural fish stocks, can be done by increased awareness

of underwater life in general, via live video footage released to the public by, for example, the OHI. Furthermore, it also calls for academic scientific research into how best visual documentation of the seafloor can be used for an improved understanding of the complex underwater ecology and biodiversity change.

Introduction

In an increasingly energy hungry society, the quest for finding and exploiting underground oil and gas (hydrocarbon) resources is being continuously improved. Whereas the world's total onshore hydrocarbon production is gradually decreasing, the OHI is currently increasing its production volume. According to Maurer [2], ecological systems are complex and combine both idiosyncratic and unpredictable outcomes with strong constraints on system structure that makes them paradoxically both deterministic and unpredictable at the same time. Because of this, there has been no universal theory to guide research on ecological phenomena.

Over the last 50 years, the OHI has, unfortunately, inflicted several enormous oil-spills on the marine and coastal environments. There have at least been five such episodes that should never have occurred: The blowout and spill in the Santa Barbara basin, off Los Angeles (January, 1969), the Ekofisk Bravo blowout in the Norwegian-sector of the North Sea (April, 1977), the Ixtoc blowout, Mexican-sector of the Gulf of Mexico (GoM) (June, 1979), the Piper Alpha disaster, UK-sector of the North Sea (July, 1988), and lastly, but not least, the Deepwater Horizon blowout and disaster, US-sector of the GoM (May, 2010). Apart from these unfortunate, generally short-lived (less than 2 years), environmental inflictions, the OHI at large appears to be environmentally friendly, as will be discussed herein. This notion has been documented by extensive seafloor mapping and annual visual inspections of platforms, pipelines, and other infrastructure. Thus, rather than representing a threat to marine life in general, the OHI is, at least in the North Sea, a benefit to marine life in general. This is not only because, by its design, it protects numerous fish against industry fishing and trawling, but also because the large artificial underwater steel and concrete constructions represent geometrically complex structures in an otherwise mostly structureless seafloor environment. Furthermore, the industry is continuously improving its methods for underwater mapping, inspection, and monitoring of the environment.

This assessment of marine life associated with normal offshore drilling, pipelines, and platforms stems from over 30 years of unique visual observation by manned submarines (1977–1981) and ROVs (remotely operated vehicles), (1979–2010). It is based on the active participation and responsibility for conducting detailed mapping surveys of the seafloor, visual documentation, coupled with remotely sensed (geophysical data). The current experience covers large expanses of virgin seafloor, stretching from the Shtokman field at 73.6°N, in the eastern Barents Sea, south to 51°N, off Dunkerque, France. A total of 522 fixed production-related structures (platforms and subsea templates) have been installed on the Norwegian Continental Shelf, and over 7,000 km of trunk pipelines have been constructed in these regions during this time-span. Thus, there is a unique variety of first-hand specific knowledge that can be shared from the numerous site surveys of platform locations, pre-lay visual surveys (conducted before the laying of the long, trunk pipelines) of the seafloor, to annual inspections of the constructed pipelines.

However, the main difficulty is how to describe and disseminate this unique visual OHI-related underwater experience and information in a way that can be used by marine scientists in a quantitative manner. This task is envisioned to resemble that faced by the pioneering land-explorers after their long treks across previously unknown parts of the globe, during the "age of discovery," a couple of centuries ago. The narration, therefore, will be fragmentary, as most of what is observed on the seafloor is new, and as most of the water and seafloor bordering onto the visually observed space is virtually unknown, despite it occurring in some of the world's most fished and scientifically studied oceanic regions (the North Atlantic Ocean).

The Offshore Hydrocarbon Industry (OHI) and the "Second Surface"

A Brief History of the OHI

The onshore hydrocarbon industry started moving out into shallow waters sometime in the early 1930s,

offshore Venezuela (Lake Maracaibo), offshore the states of California and Louisiana, USA, and in the Caspian Sea, offshore Baku, Azerbaijan. The first installations were simple steel and wood constructions built in knee-deep waters. However, their size and complexity was gradually increased with increasing water depth, up to several tens of meters. Simple steel jacket drilling towers were constructed and there were bridges and roads built on piled steel and wood foundations, often in a hap-hazard manner. After sometime, there were many accidents and mishaps, before improvements were made and special standards were invoked. The one single event that hit the OHI and aroused the world's environmental conscience was the big blowout oil spill in Santa Barbara, offshore Los Angeles, California on January 29, 1969. This also had immense consequences for the stricter regulations imposed on offshore drilling and the exploitation of offshore oil and gas. Even though no people were killed, this event made such a graphic impression on the population of southern California that in the following spring, "Earth Day" was born. Many consider the publicity surrounding the oil spill a major impetus to the environmental movement.

In Europe, the OHI started with the development of the UK southern gas fields off the east coast of England, in the mid-1960s. Here, the platforms and pipelines met the tough environment of the North Atlantic. New rules and regulations, British North Sea Standards were imposed. In 1967, the OHI moved even further north, in the North Sea, to Norwegian waters. The Norwegian Petroleum Directory (NPD) and The Norwegian state oil company, Statoil, were born, some years later. Although the giant oil field Ekofisk was developed with similar standards as in the UK southern gas fields and the Forties and Piper fields of the mid-UK North Sea, the Norwegian fields still further north, such as Statfjord, Gullfaks, and Troll, had to withstand even tougher environmental conditions. These fields, located at water depths between 130 and 320 m were therefore developed with giant concrete "gravity base" platforms, as the underwater technology evolution was not ready for moving delicate equipment like pumps, electronics, and gauges under water. When the Troll A concrete platform was towed out from Stavanger, and placed on the seafloor over the giant Troll field on May 17, 1995, it became the largest human-made structure ever to be moved. It measures a total of 472 m in height, from the top of the drilling tower to the bottom of the concrete skirts that penetrate 30 m into the soft clays at the location where it is still producing oil and gas, off Bergen, Norway. The platform houses about 200 workers who stay on board for 14 days at a time, rotating in and out by helicopter.

The rotation occurs all year round, even during the darkest and stormiest winter months (December through February). This platform produces about 18% of the total gas consumption of Germany and is, therefore, of immense value both for the owners (Statoil, Shell, and the Norwegian government) and for the consumers in Germany and surrounding countries. The gas is transported through 36″ (36 in.) and 40″ concrete-coated steel pipelines, welded together on board huge offshore pipe-laying vessels and placed carefully onto the seafloor. Such huge "trunk"-pipelines criss-cross from the Norwegian fields to processing plants on mainland Norway, and are re-routed from there, through other gas export pipelines to England, Germany, Belgium, and France. The largest pipe, the Langeled pipeline, was constructed between 2004 and 2006. It is a 40″ and 44″ diameter pipeline of 1,200 km length, which originates from the onshore processing plant at Nyhavna, south of Trondheim. From there, it runs south to the Sleipner field in the middle of the North Sea, and continues to Immingham on the east coast of the UK.

During the last 15 years, subsea technology has developed fast and most modern fields are constructed solely with remote-controlled subsea structures. The Snehvit field in the Barents Sea is, for example, produced through three subsea templates (steel structures) with several production wells in each template. The field lies 135 km from shore and is remotely operated from the onshore production plant at Melkøya near Hammerfest, the world's northernmost city. At present, Norway is the third world's largest exporter of crude oil, and it runs 522 offshore fixed production-related structures of which 365 are subsea and fully submerged. In year 2009, Norway also exported a total volume of 96.6 billion Standard cubic meters (Bn Sm^3) of natural gas to Europe through the trunk pipelines.

The Second Surface of Earth

The seafloor is the "Second Surface" of Earth, indicating that it is hidden in many ways. It covers an area which is about three times larger than the visible land surface. Most of this surface is still unknown – because water is a "black body" substance when it comes to the electromagnetic spectrum. It absorbs most of the visual light that encounters it. Therefore, in contrast to sound waves, the light rays have very low transit ranges through water. The photic zone of the ocean, into which solar rays can penetrate, are reckoned to be down to a maximum of just over 100 m in the clearest waters, that is, water with little seston and other particles. This is not very deep, considering the mean depth of the ocean being about 3,500 m. Because of this lack of efficient visual access, the Second Surface is only beginning to be explored in detail. This surface ranges in depth, from 0 m at the coastlines, to about 300 m on the continental shelves, then down to 5,000 m (5 km) on the great abyssal plains, to over 11 km in the deepest trenches. Because most of Earth's surface is covered by water, the Second Surface represents a very significant and essentially important entity. So far, remotely sensed (acoustic) surveys only cover about 10% of it (i.e., indirectly, with data that needs interpretation by geophysicists) and only less than 1% visually (i.e., directly with cameras). This means there exists more visual documentation of the surfaces of both Moon and Mars, than of the immensely more important Second Surface of Earth. However, from sediment sampling, fishing (trawling), scientific scraping (dredge sampling), and drilling, in all oceans, over time, it is currently known that the Second Surface mostly consists of mud (clay), sand, rock, and in some areas metals and salts. But, because being flooded by water, it is both pressurized, and buoyed at the same time, and behaves accordingly, which is often totally different to the well-known land surface. Furthermore, on average, the Second Surface has a much thinner crust than the onshore continental crust and is more likely to be exposed to high heat flow from the Earth's interior. Along the tectonic plate boundaries (mid-ocean spreading zones and subduction zones), the high heat flow induces underground convection fluid currents and the venting of warm fluids in hydrothermal vent systems [3].

Although academic research institutions and consortia, such as the Integrated Ocean Drilling Program (IODP), perform many types of investigations at water depths to about 6 km, the mining industry is working at depths to about 5 km, and the fishing fleet is gradually trawling to depths greater than 2 km, the OHI is currently working to water depths of about 3 km. However, about 90% of its activity still occurs at water depths between 100 m and 1,500 m. These are the water depths, therefore, which will be addressed herein. From the extensive mapping-, construction-, and visual inspection-work performed by OHI at these depths, several places in the world, there is some general and also specific knowledge about processes and marine life that can be disseminated, including some new discoveries.

Whereas the fishing industry tends to operate in a "blind" mode when it comes to the seafloor, the OHI naturally operates with more caution, partly in order of preventing damage to sensitive and costly equipment and structures, and partly because of law enforcement (at least in US and European, including Norwegian waters). Thus, no drill-site is drilled without a proper predrilling assessment of the seafloor, whereby any significant physical obstructions and known sensitive organisms, including chemosynthetic fauna and coral reefs are documented beforehand. The problem with the bottom trawling of the fishery industry is the insensitivity to what is down there, that is, "indiscriminate obliteration" on the seafloor. As long as such bottom trawling is legal practice, all sessile organisms in the world are actually threatened by trawl-board disturbance, at least those living at water depths shallower than 2,000 m water depth.

The General Background Seafloor Life

In order to set the OHI-related marine fauna observations into perspective, the general background seafloor has to be described. In the depth interval 100–1,500 m, the general background seafloor (about 90% of the total area within this depth range) is drab and appears relatively "uninteresting" (Fig. 1), just like the enormous sand fields of a desert on land. However, in most areas, the drabness is spotted with small hubs of life, like oases in the same desert. There are vast areas with level, muddy bottoms. Several studies have shown,

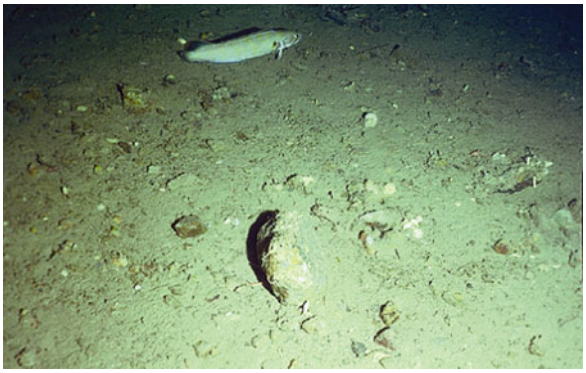

Marine Life Associated with Offshore Drilling, Pipelines, and Platforms. Figure 1
The general seafloor off Mid-Norway looks like this. In the background is a Tusk (*Brosme brosme*). The stones (cobbles and gravel) have been washed out of the underlying clay-dominated till. Some of the larger stones can be seen to be colonized by invertebrates of different colors

Marine Life Associated with Offshore Drilling, Pipelines, and Platforms. Figure 2
A large erratic boulder located inside a pockmark crater at 280 m water depth off the Island of Fugløy off Northern-Norway, north of the Polar Circle. The organisms seen colonizing the boulder are mainly filterfeeders, sea anemones, and serpulid tube worms

however, that, for the deep-sea biota, there is a distinct decrease in population differentiation and species diversity with depth [4, 5]. Any large erratic boulder, rock outcrop, or wreck is colonized by invertebrates, which seem to attract also other marine life, including fish (Fig. 2).

Piepenburg and co-workers [6] used classical marine biological methods to study patterns and determinants of the distribution and structure of benthic faunal assemblages in the northern North Atlantic. Using a suite of sampling methods including corers, trawls, and seabed imaging (benthic spot photography), they managed to "adequately probe various benthic community fractions, such as foraminifers, poriferans, macrobenthic endofauna, peracarid crustaceans, and megabenthic epifauna." The general patterns they found were, not unexpectedly, a depth zonation, and also a significant decline in biomass and abundance by as much as two and three orders of magnitude. These were the most conspicuous general patterns detected. However, in terms of species richness, no common trend for water depth or latitude was perceivable. They especially studied the East Greenland continental shelf margin between 68°N and 81°N at water depths between 40 and 3,700 m. Here they found relatively productive hydrographic zones being the marginal ice zones, polynyas, and anti-cyclonic gyres. They interpret this as being evidence for the importance of water column processes for subsequent food availability being the major determinants for the benthic assemblages and the significance of pelago-benthic coupling in the study in general [6]. This is not surprising, food availability being the most necessary ingredient for life in general. When it came to the distribution of megafaunal species, such as echinoderms, it was found that community patterns on a 10 km scale and the dispersion of organisms on a 100 m scale were best explained by the seafloor properties. This means that macrofauna is dependent on structure and type of the seafloor sediments and topography. Furthermore, they found no evidence for a direct pelago-benthic coupling, irrespective of water depths. These contrasting findings emphasize that the relative importance of potential community determinants can change with both spatial scale and life traits, for example, body size, mobility and feeding ecology, of organisms considered [6]. Thus, the stage is set for a narration of discoveries made by the OHI and the associated biological and physical research performed for this industry by academic researchers and institutions during the period 1980–1998. After 1998, the academic institutions have picked up many of the

research leads pioneered by OHI-activity within marine geophysics and biology.

Unique Processes and Biotypes Initially Studied due to OHI-Activity

Since the late 1960s, new processes and features have been discovered on the Second Surface. Some of them are completely unique to the underwater world at water depths of 100–1,500 m. Perhaps one of the most surprising revelations is that this type of mapping and areal seafloor documentation became instrumental for the discovery of several previously unknown natural conditions of the seafloor. Thus, at least three unique discoveries were made as a result of such surveys: (1) A biological seepage relationship, (2) The discovery of pockmark craters and their potential significance for marine life, and (3) The discovery of myriads of large, cold-water coral reefs (also called deepwater coral reefs). Although the results were not possible without cooperation with academic institutions, especially in the UK, USA, Germany, France, and Norway, the pioneering discoveries were instigated due to OHI-activities, mainly in the Gulf of Mexico and the North Sea. The discoveries are mentioned here, as they sometimes are relevant to the marine life observed on the seafloor. These processes and features are:

1. Venting of reduced organic fluids (fluid flow, or "cold seeps")
2. Crater formation, by fluid flow
3. Bioherms, including the cold-water coral reefs

One of the recent wide-scope books on benthic life in the North Atlantic [7], actually fails to mention the existence of prolific deepwater coral reefs occurring there. In the book, which is aptly titled: "The Northern North Atlantic – A Changing Environment" neither deepwater coral reefs, *Lophelia pertusa*, nor "*Lophelia*-reefs" are found in the index, or at all mentioned in the text. Why is it that thousands of large coral reefs, some known to science for at least 200 years and from the early 1990s published by OHI-related scientists, manage to avoid mention (recognition) in such apparently authoritative scientific literature? Could it be that only "Classical marine biological" results are recognized? The publisher claims that: "the Greenland-Iceland-Norwegian Seas can now be considered one of the best studied subbasins of the world's oceans" [7]. But, even so, the information published in this book is important, as it provides the necessary background knowledge about life in general on the seafloor "desert," outside the coral reefs.

Venting of Reduced Organic Fluids Generally, the ocean floor is covered in thick sediments that deposit by gravitation, with particles sinking through the water column and accumulating in thick layers on the Second Surface. The fluids, including petroleum gas and liquids (hydrocarbons) trapped underneath such sediments are lighter than the solids and, therefore, move upward to surface at discrete locations due to buoyancy. This process is also called "migration" and where the flow penetrates the Second Surface from below, it is called marine fluid flow [8]. The discrete locations where the fluids occur at the surface are called "cold seep" locations. Depending on the geological setting, the distance between each cold seep location on the seafloor varies considerably, from kilometers or miles, to only several meters. However, cold seeps are important for life within, on, and above the Second Surface because they represent transport pathways for dissolved chemical constituents and sustain unique oasis-type ecosystems at the seafloor [9]. Fluids expelled through seeps contain re-mineralized nutrients (silica, phosphate, ammonia, and alkalinity) and hydrogen sulfide, as well as dissolved and free methane from microbial degradation of sedimentary organic matter. Because methane gas molecules (CH_4) have the highest relative hydrogen content (four hydrogen atoms to one carbon atom) of any organic compound, it represents a valuable energy source to certain primary producers: archaea and bacteria, that is, the methanotrophs and the methane oxidizers. Apart from near-cold seep locations, seawater has generally very low concentrations of methane and other light hydrocarbons, such as ethane (C_2H_6), propane (C_3H_8), butane (C_4H_{10}), and pentane (C_5H_{12}). Perhaps the single most important reaction associated with cold seeps is the anoxic oxidation of methane (AOM) by archaea and sulfate reducing bacteria (SRB), with secondary reactions involving the precipitation of carbonate ($CaCO_3$), in the form of inorganic aragonite and calcite [9]. The OHI has long been interested in these

seafloor processes, for various reasons, not least because they contain tell-tale indications of where deep-seated hydrocarbons (reservoirs) may be found.

During a predrilling geophysical site survey, in 1977, at the Tommeliten field in the central North Sea at 78 m water depth, side scan sonar data showed numerous bubble streams emanating from the seafloor, immediately above a buried salt dome [10]. Subsequently, this location was investigated with ROV by Statoil in 1983. The gases leaking naturally through the seafloor were documented to be the reduced organic light hydrocarbon gases (methane to pentane) which also continually charged the upper, porous sediments. An intimate relationship was found between organisms, such as anthozoans and the visual bubbling of gas through the sediments [11]. This visual inspection and sampling of the naturally leaking gas produced several interesting results: (a) documenting small "reefs" or "bioherms" consisting of many kinds of filter-feeders, scavengers, and predators occurring adjacent to the seeps; (b) small depressions (so-called eyed-pockmarks), in the seafloor, with high-density macrofaunal communities in their centers, and (c) white patches of bacterial mats also occurring over relatively large seafloor areas, where the sediments were charged with gas seeping up from deeper layers.

Later studies of this Tommeliten site also showed two other important aspects, relevant to marine life: (1) that the bacterial mats were easily torn apart and carried up into the water column by slight disturbances of the near-bottom water by the ROV and (2) that the seafloor had been partly cemented by methane derived authigenic carbonate rock [8, 11] both within the eyed-pockmarks and elsewhere on the otherwise flat seafloor, near the bacterial mats [12]. Academic research at this active seepage site and also at one similar site near the Gullfaks field, further north, identified a microbial community dominated by sulfur-oxidizing and sulfate-reducing bacteria (SRB) as well as methanotrophic bacteria and archaea. Stable carbon isotope values of specific, microbial fatty acids and alcohols from both the Tommeliten and Gullfaks sites were found to be highly depleted in the heavy isotope ^{13}C, indicating that the microbial community readily incorporated seeping methane or its metabolites [13].

At Tommeliten and Gullfaks there is, therefore, no doubt that the dense bioaccumulations on the seafloor, including, the bioherms, are a direct result of seeping gas (energy and nutrients) from deep below the seafloor. This may also be one of the reasons why there is plenty fish and heavy trawling activity at the Gullfaks location [14]. Although most marine ecologists, environmental scientists, and biologists are used to assess traditional phytoplankton concentrations dependent only on top-down linkages in the food chain, the modern seep studies find more and more bottom-up links [13, 15].

Mud volcanoes are locations where fluids and solids (water, mud, gas, and petroleum) well up through the Earth's surface, driven by overpressures in the subsurface. They both occur on the land surface, as in Azerbaijan [16] and many places on the Second Surface [17, 18]. From studies and surveys at the underwater Håkon Mosby Mud Volcano (HMMV) located at the boundary between the Barents Sea and the Norwegian-Greenland Sea, a relatively prolific and complex ecology has been found. Although only a minor portion of this ecosystem relies directly upon chemosynthetic energy, this portion is probably very important for the sustenance of the system. A simplified food chain for HMMV was published by Vogt et al. [19]: The primary producers are suspected to be methanotrophic bacteria and anoxic methane oxidizers (archae), besides other "conventional" microorganisms relying on added heat and continuous sediment disturbance by the turbid flow of mud from the mud volcanic vent. The secondary consumers were made up of benthic suspension feeders and deposit feeders, such as asteroids, holothurians, etc. In addition, there was a chemosynthetically based food web, relying on symbionts, such as the pogonophoran tube worms, that host endogenic chemosynthetic bacteria [10, 19]. The primary consumers consist of filter-feeders and other predatory invertebrates and vertebrates, such as sponges, crinoids, pycnogonids, basket-stars, and fish, mainly consisting of Eelpout and Skate (Raja spp). A maximum density of one Eelpout for every square meter was documented above portions of the mud volcano [19]. This example also demonstrates the very important influence of substances originating from below the seafloor in modifying and "fertilizing" the immediate seafloor environment, to result in enhanced productivity.

Seabed Pockmarks: Craters Formed by Focused Fluid Flow On the land surface it is often very difficult to detect surface degassing (seepage) events, apart from those associated with water and mud flows, such as at mud volcanoes [20]. On the sediment-covered Second Surface and in some lakes, however, the situation is different. In the late 1960s, numerous craters were found off Nova Scotia. They were called "pockmarks" by their discoverers, Lew King and Brian MacLean of the Bedford Institute of Oceanography (BIO), Canada [21]. Today, it is known that pockmarks occur in certain portions of the seafloor, the world over, and even in some lakes [8, 10]. Also a very close relationship between the pockmarks and local increase in visible seston (including plankton) was found [11]. Although pockmarks ranging in size from the small, "unit-pockmarks" (<5 m diameter, 1 m depth), to normal-pockmarks, complex-pockmarks, and giant-pockmarks (up to 500 m in diameter and 30 m depth), have been found, very little is known about their formation and sustaining mechanisms [8, 22]. Although they are known to be formed as a consequence of buried gas reservoirs and fluid flow, there are only very few pockmarks known to be producing continuous visible bubble streams [23].

After having noticed the marine life occurring inside some of the pockmark explored with ROVs in the North Sea [10], it was recognized that the "classic" (conventional) science of marine geology would probably never have discovered pockmark craters (Fig. 3). The reason being, that this science relied on acquiring numerous spot samples of the seafloor using corers and grab samplers, and determining the nature of the seafloor mainly by measuring the grain-size of the spot sampled sediment grains. Thus, if only one seafloor sample was acquired at 1 km spacing in the Norwegian Trough of the North Sea, where there is an average of 15 pockmarks per square km, it is likely that only one sample out of 100 would happen to sample inside a pockmark crater. This sample would probably turn out to be anomalous (i.e., containing unexpected biota and sediments). Thus, the chances of this sample (one-in-a-hundred) being discarded or recorded as an "anomaly" (or only of "curiosity value") are great. At least it would not turn out in the statistics of the survey, and the chances of it being taken seriously are therefore meager.

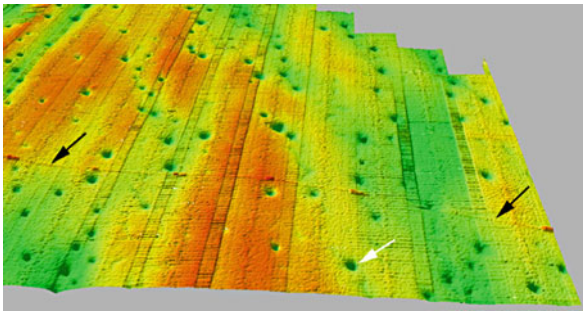

Marine Life Associated with Offshore Drilling, Pipelines, and Platforms. Figure 3
In the 300 m deep Norwegian Trough area of the northern North Sea, there are thousands of normal-pockmarks. They are shown here on a perspective image of a seafloor relief map, with artificial vertical enhancement (x5). The size of the largest pockmark craters is 100 and 8 m depth. The *white arrow* points to a normal-pockmark of about 70 m diameter. The *black arrows* point at a trunk pipeline of 30″ diameter. Lines running north south represent noise in the digital data set, due to inaccuracies in sound velocity and tidal correction

From modern seafloor remote sensing with multibeam (swathe) echo-sounders to long-range side scan sonars, it is known that the seafloor can be covered in a high density of pockmark craters. The density ranges from zero to more than 20 pockmarks per square km of mapped seafloor (Fig. 3). Because recent studies conclude that pockmarks form due to focused fluid flow [22, 23], the seafloor can generally be divided into "hydraulically active" and "passive" areas. Thus, the active seafloor will have seep manifestations, like pockmark craters and the passive areas will be devoid of craters.

There are two important corollaries to this "hydraulic theory": (a) It is valid for all volumes of soil, which have a porosity system partly filled by liquid and partly filled by gas. It is, therefore, also valid for all ocean depths, lakes and swamps, as the driving gas-type (methane, carbon dioxide, hydrogen sulfide, or hydrogen) is immaterial. (b) Because seeping fluids through the seafloor can be regarded as enhanced energy input to the marine fauna (primary producers especially), the enhanced hydraulic activity manifest by seeps and high density of pockmarks indicates the likelihood of enhanced marine biological productivity.

Cold-Water Coral Reefs of the North Atlantic It is known that the presence of solitary corals, sea pens, sea lilies, and sponges on the deep-sea floor offers rare, firm substrates for sessile organisms in an otherwise generally featureless environment. The relative importance of such biotic habitats for the local biodiversity may, therefore, be greater for the deep-sea than for shallower regions [24]. Those modern reef structures that seem to defy all normal reasoning with respect to location and environment are the deepwater coral and cold-water coral reefs (also named "ahermatypic colonial scleractinians"). In the North Atlantic and Gulf of Mexico, the most common types are those built by the *Lophelia* sp. stony coral, found on both sides of the Atlantic Ocean, including the Reykjanes Ridge, south of Iceland (Fig. 4). Because they are also found as far north as the Polar Circle, in the Barents Sea and off Mid- and Northern-Norway, they must somehow be independent of seasonal sunlight variations. Some of these reefs, found off Ireland and on parts of the Norwegian Continental Shelf had been known to fishermen and biologists for over 200 years [25–30].

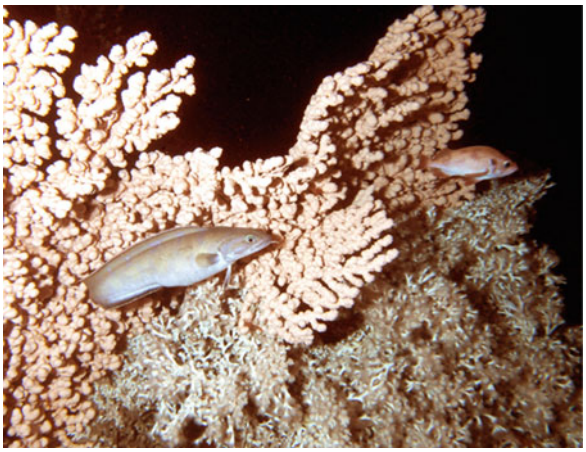

Marine Life Associated with Offshore Drilling, Pipelines, and Platforms. Figure 4
Photograph from a typical Norwegian deep-water coral reef showing two types of corals: the soft-branched octocoral *Paragorgia arborea* (*closest*) and the reef-forming ahermatypic stony coral *Lophelia pertusa*, (*white and pink*). The two most common reef-related fish are also shown here, the Tusk (*Brosme* sp) and the Redfish (*Sebastes* sp) [47]. The height of this coral reef is about 3 m above the surrounding, undisturbed, even seafloor

Even so, the visual documentation by OHI-surveys during the 1980s and mid-1990s of thousands of large, deepwater coral reefs was completely unexpected to most marine biologists [31–36].

Their modern rediscovery with broad-scale geophysical mapping and detailed video footage and photographs became a major eye-opener – a revelation that caused an improved reassessment of the complex and dynamic biological production of the North Atlantic Ocean. This modern documentation actually started in June, 1982, with an OHI-related detailed investigation for a potential pipeline route from the Askeladden field in the Barents Sea to Norway. During which, a 15 m high and 50 m wide *Lophelia*-reef was found and visually documented by Statoil [31, 33]. Further pipeline route surveys off Mid-Norway between 1985 and 1990 documented hundreds of similar reefs, until then unknown to science. Until June, 1991, when Statoil invited researchers from five Scandinavian academic and Norwegian authorities to view their unique data set, consisting of detailed geophysical and photographic/video results, these biotic structures had mainly been treated as curiosities and oddities on the seafloor [37]. But, even after this seminar, it was not the Norwegian scientists who first managed to mobilize an academic detailed visual study of the reefs, but the Germans. Freiwald et al. [34] had previously been studying carbonate secreting algae along the northern Norwegian coast. Having learnt from Statoil where the reefs occurred, they targeted them during their next planned cruise, already in 1992 [34]. The main surge of academic interest in the reefs of the North Atlantic came immediately after the publication of large carbonate reefs off Southwest Ireland. This was also partly based on OHI-related exploration geophysical data [33, 35, 38]. Subsequently, the first International conference on cold-water corals was staged in Canada, 2001 [39].

One of the main and controversial questions still remaining to be answered with respect to these impressive biological structures is why they occur in deep and cold water, even north of the Polar Circle, where there is hardly any photosynthesis occurring during the winter months. Even though there is ample evidence suggesting that they rely on extra nutrients and energy originating from below ground, that is, the "hydraulic theory" [11, 31, 35, 36, 40, 41], modern marine

biological research has still not found sufficient evidence to support this theory. The main theory of the modern marine ecologists is, according to Buhl-Mortensen et al. [24], that they exist in high latitudes and deep waters because this is where the right water masses occur: "...it is not the deep water par *se*, but the distribution of intermediate and deep water masses that controls the bathymetric distribution of these corals. Corals typically create habitats reaching from decimetres to meters above the surrounding seabed and occur on mixed bottoms in areas with relatively high currents." [24], and the argumentation continues: "Colonial scleractinians need hard substrate for settlement. This substrate can be a shell or a pebble, and as soon as one colony is present it provides new hard substrate for subsequent colonisation" [24]. So, the question remains as to why only less than 0.1 per mille (‰) of the total area in the depth zones where they occur is covered by cold-water coral reefs? Why are there, for example, no more of them in the Norwegian and New Zealand fjords where the distribution of intermediate and deep water masses is right, and where there is ample suitable hard substrate (rock bottom) with high current speeds? However, some recent microbial studies seem to point the way further. Yakimov et al. [42], for example, recently found metabolically active microbial communities associated with deepwater corals in the Mediterranean. Also recent OHI-related research of the microbial food chain surrounding the coral reefs off Mid-Norway has provided some interesting new findings. The contrast between coral-associated and free-living bacteria may suggest that few free-living bacteria are directly ingested by the coral and that instead, corals feed on non-bacterial plankton. Small (100–200 μm) zooplankton has been suggested important in the diet of corals [43]. In addition, the tissue-associated bacterial communities potentially provide a direct translocation of nutrients through metabolism of particulate and dissolved organic matter in the seawater. One *Lophelia pertusa* associate was studied in more detail and named "Candidatus Mycoplasma corallicola" [44]. This bacterium was abundant in *L. pertusa* from both sides of the Atlantic Ocean and is considered an organotrophic commensalist [44]. Given the importance of chemosynthesis in deepwater ecosystem development and functioning, cold-water coral reef communities may be linked to a diversity of chemoautotrophic microorganisms that synthesize organic compounds from inorganic compounds by extracting energy from reduced substances and by the fixation of dissolved CO_2. Just a tiny fraction of microorganisms associated with deepwater coral reefs have yet been identified, and even less assigned to a function. Although no nutritional symbiosis based on chemosynthesis [45] are known to have been documented on deepwater coral reefs, primary producers affiliated with chemoautotrophs (utilizing H_2S, NO_2^-) and methanotrophs (utilizing CH_4) have been found associated with the reef animals and their ambient environment [41, 42, 46]. Thus, also light hydrocarbons can probably stimulate the growth and the high biodiversity found on the *Lophelia* reefs associated with some Norwegian hydrocarbon fields [47]. Only further detailed studies of the reefs will be able to answer these important questions.

The cold-water coral reefs and carbonate mounds represent exceedingly valuable habitats for numerous species, besides the corals themselves. Also for fish, they represent shelter and nursing homes for juveniles, as one of the few comparative studies of on-reef versus off-reef fish-counts for deepwater coral reefs documents. Fish species' richness and abundance was found to be greater on the reef than over the surrounding seabed, as 92% of species, and 80% of individual fish were associated with the reef. The results indicate that the reefs have a very important functional role in deepwater ecosystems as fish habitats [48]. In particular, visual monitoring of coral reefs at the Morvin and Kristin fields, off Mid-Norway, has shown that the redfish (*Sebastes* sp.) probably spawns at the *Lophelia* colonies (Fig. 5). During the month of May, numerous fish with wide bellies, obviously ready to spawn (this species spawns live sprats), congregate very close to the *Lophelia* colonies (Fig. 5). The juveniles can immediately after spawning find full protection against predator fish within the complex structure of the live and dead *Lophelia* skeleton mesh-work. Furthermore, the Norwegian coral reefs have long been known to fishermen as "Uer-bakker" [26], meaning "Redfish slopes," and Furevik et al. [49] were the first to report scientific evidence that long-line catches of redfish, ling, and tusk can be significantly greater on the reefs than in off-reef areas. In addition, Husebø et al. [50] set long-lines in coral habitats and found significantly more fish than

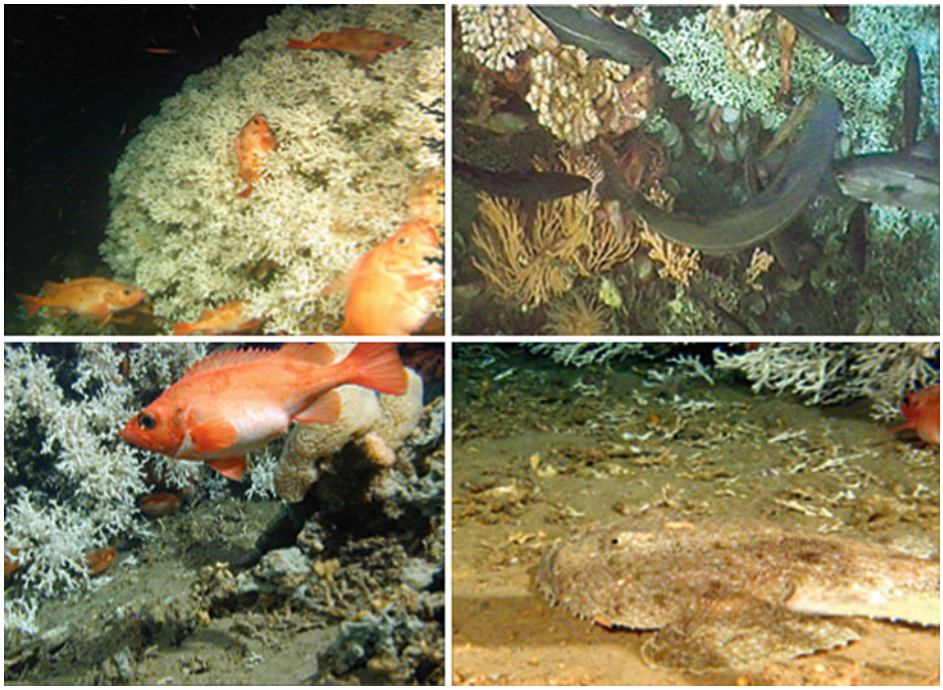

Marine Life Associated with Offshore Drilling, Pipelines, and Platforms. Figure 5
Fish sightings on *Lophelia*-reefs at Norwegian hydrocarbon fields Kristin and Morvin. *Upper and lower left*: *Sebastes* sp. (redfish) congregating for spawning on a 1.5 m tall *Lophelia* colony. Upper right: Seithe feeding near a *Lophelia*-reef at Kristin. The fish often swims around the ROV when operating off Mid-Norway. *Lower right*: A monk fish resting on the seafloor next to a *Lophelia* colony at Morvin. Notice its white protrusions under its head that resemble the *Lophelia* branches. This fish is sometimes found to be resting on top of *Lophelia* colonies, where it is well camouflaged

elsewhere and also that the fish were generally larger than those caught in the non-coral areas. The importance of these habitats and their internal ecological dynamics has been discussed in more detail by Buhl-Mortensen et al. [24].

According to authoritative assessments of possible threats to the cold-water coral reefs, the main threats according to Roberts et al. [51] are: (1) Bottom trawling, (2) Hydrocarbon drilling and seabed mining, and (3) Ocean acidification (i.e., global climate change [52, 53]). In addition, for each individual coral reef, there is always the possibility of dramatic environmental changes by natural causes, such as nearby underwater avalanches (burial), and in the case of the hydraulic theory being viable, that the seepage or venting is naturally depleted or exhausted, and becomes "turned off." However, the OHI seems to come out of such assessments far better than the fishery industry: "Compared with widespread evidence for physical damage to reef structures from bottom trawling, there is little evidence that hydrocarbon exploitation substantially threatens cold-water coral ecosystems. *L. pertusa* colonizes North Sea oil platforms and seems to have a self-seeding population, despite proximity to drilling discharge. Greatest concern is over the potential for drill cuttings to smother reef fauna, but such effects would be highly localized when compared with the extent of seabed affected by bottom trawling" [51]. This latter scenario was carefully tested by a 3-month-long drilling and monitoring campaign of four production wells at the Morvin field off Mid-Norway, where numerous coral reefs exist on-site. The results of this campaign are reviewed in a later chapter.

To sum up the threats, based on OHI-related observations and modern publications, it is found that the coral reefs thrive, despite them being located close to OHI-structures and to sporadic drilling activity. They even colonize parts of the OHI-platforms, as seen

in Fig. 5, from the Statfjord field [47, 54]. The main threats to the deepwater coral reefs are therefore mostly mechanical, as they are delicate structures and cannot sustain the mechanical indiscriminate stress imposed by portions of the fishing industry and to a much lesser extent, the OHI. This has been amply documented off Norway and off New Zealand [55–57]. Furthermore, based on abundant visual and geophysical data mainly acquired from the OHI, it was possible for Norwegian authorities to be first to officially protect and conserve a large portion of cold-water coral reefs. The first area to be protected against bottom trawling was the Sula Reef in the late 1990s and the Haltenpipe reefs off Mid-Norway with a 970 sq km large protected area [36]. Today, awareness of the ecological significance of deepwater corals is growing rapidly, as it is known that colonial corals provide important habitats and could play a critical role in the life history of many marine species, including fish of commercial interest [58, 59]. This awareness has lead to a general call for the establishment of marine protected areas (MPAs) and especially to protect the most important cold-water coral habitats [60].

Marine Life Affected by the OHI

Methods of Observation

Before an offshore hydrocarbon field is developed, rules and regulations say that biological baseline studies shall be carried out. Over the last 2 decades, the focus of such studies has shifted from being purely based on detecting pollution effects from OHI-activity to also include assessments of biodiversity and ecology [61]. A standard outline of a station pattern for sampling seafloor biology is either a grid, covering a large area, or samples obtained along lines forming a cross, with the longest axis downstream with respect to the prevailing current. Several replicate samples are collected at each station. Because this type of sampling was found to be relatively "blind" to any local features on the seafloor, such as pockmarks and cold-water coral reefs, it has now been complemented with an initial seafloor mapping campaign. The macrobenthos fauna of interest in baseline sampling surveys comprises the following main taxonomic groups: Polychaeta, Crustacea, Mollusca, Echinodermata, and Varia (remaining groups). Only animals larger than 1 mm (macrobenthos) are included in such analyses. Subsequent to the development and production at offshore hydrocarbon fields, the sampling of sediments and macrobenthos is repeated perhaps every other year.

The study of benthic communities can provide an indication of pollution from offshore activities. Similarly, the geochemical analysis of sampled sediments can provide levels of pollutants and their distribution around the offshore installations. Any changes in species composition and densities of individuals can also provide tell-tale signals about damaging pollution. Experience from many years of such work has proved that the benthic fauna near OHI-installations can be affected by a number of factors, including the discharges of drilling fluids, cuttings, and others, including the accidental release of oil and also physical disturbances. One of the current challenges of planning future environmental/baseline surveys in the OHI is to improve the cross-departmental communication, as the detailed seafloor mapping is performed by others than those responsible for environmental surveys [61].

During initial mapping and inspection along potential pipeline routes at the Morvin field, off Mid-Norway, numerous coral reefs were found and visually inspected. Here, it was also decided to perform a detailed geochemical investigation prior to the production drilling activity. One of the largest reefs, the MRR ("Morvin Reference Reef") was systematically investigated and sampled (water, sediment, and organisms). This reef is located inside a large (130 m × 80 m × 10 m) pockmark depression (Figs. 6 and 7). The reef occupies about one third of the pockmark, growing from the maximum depth (at 370 m), up along the northern side, to the rim of the depression (at 360 m water depth). The MRR is about 80 m long, 25 m wide, and spans the elevation interval: 360–370 m. *Lophelia pertusa* is the main reef-building coral [47]. The geochemical analyses of sediments at Morvin proved that they contained varying concentrations of light hydrocarbons (methane–butane). Because the sediments in which these hydrocarbons were sampled are located within the oxygenated upper portion of the seafloor (i.e., only 40 cm below surface), any hydrocarbons remaining there over long time would have been reduced (oxidized) relatively rapidly. Therefore, there must be a natural seepage of light hydrocarbons from below, via molecular and fluid migration. This type of fluid flow is called "micro-seepage" of light

Marine Life Associated with Offshore Drilling, Pipelines, and Platforms. Figure 6
Special features on the seafloor attract and protect large fish. Here is an aircraft wreck from World War II off Mid-Norway, which is now utilized as shelter for large Lings. At least five larger than 1 m length can be seen here. The wreck was detected with side scan sonar and inspected by ROV as part of a site survey for exploration drilling

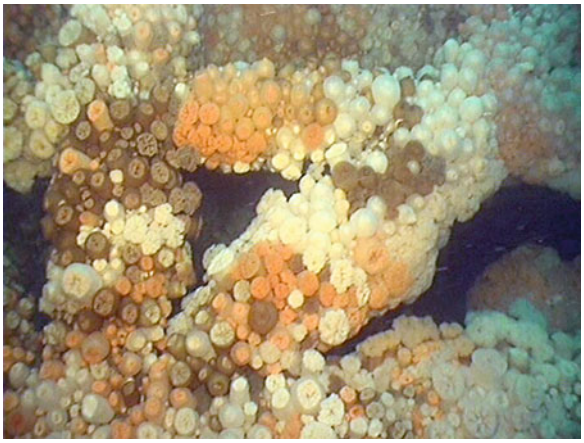

Marine Life Associated with Offshore Drilling, Pipelines, and Platforms. Figure 7
A subsea steel template structure in the central North Sea, Danish Sector. The steel structure has been completely colonized by sea anemones. This is also a perfect hiding place for fish of all sizes

hydrocarbons [8, 62]. However, because no more than eight samples were acquired at Morvin, it is not possible to state any significant statistical variation over a regionally significant area.

The highest interstitial hydrocarbon concentrations were found in the upper sediments at location S8, which is inside a unit-pockmark, located just to the north of MRR (Fig. 4). Combined with modern results from molecular biological methods, there is here factual support for the notion that a nutrient-rich, "fertile" substratum represents one of the keys to understanding the location of this deepwater coral reef. Previous studies of *Lophelia* O-C stable isotopes [63, 64] show that there are relatively large variations in the δC^{13}-value (ranging from −2‰ to −9‰ PDB). For corals, these negative values have so far been interpreted as being caused by ambient pH-variations, among other factors. However, similar variations in stable isotopes in bivalves at seep sites in the Gulf of Mexico were interpreted as being caused by hydrocarbon uptake in microorganisms, subsequently ingested by the bivalves. This suggests that future studies of the coral reefs should also include systematic stable isotope analyses, combined with more geochemical sediment analyses.

The Impact of Exploratory Drilling

Scientific Drilling When the Deep Sea Drilling Project (DSDP) initiated its research with the drilling vessel "Challenger," in 1974, it found indications of oil at nearly 3 km water depth on its second drilling hole on the first exploration leg (DSDP, Leg 1, Hole 2). When the first cores came onto the deck, there was an unmistakable smell of crude, and small droplets of oil could clearly be seen in the carbonate rock sampled. The objective of this hole was to determine the nature of the so-called Challenger Knoll on the abyssal plain of the mid-Gulf of Mexico. By drilling 144 m into this feature, the scientists determined it was a carbonate capped salt dome. However, because the DSDP was a pure scientific drilling project, it should not be looking for oil. A panel of experts was immediately established to make sure that the coming drilling legs should not target hydrocarbon-prone areas. This is how the "Pollution Prevention and Safety Panel" of the DSDP and later the Ocean Drilling Program (ODP) was borne. Today, this panel of experts of the IODP (Integrated ODP) has been re-named to EPSP (Environmental Protection and Safety Panel).

After exploration drilling for oil had come underway, on the Norwegian Continental Shelf (NCS),

during the late 1960s, strict rules and regulations were imposed on the industry. For example, no drilling was allowed on the NCS unless a special "predrilling site survey" was performed. This includes a full seafloor coverage of side scan sonar acoustic images, which is able to detect all types of features on the seafloor larger than about 3 m in extent, such as wrecks, munition, rock outcrops, and many other features, including man-made features on the seafloor.

OHI-Related Drilling On the Norwegian Continental Shelf, it has been normal practice to discharge the sediments produced from drilling ("cuttings") and drill-mud from drilling the first 600–800 m of the well (the "top-hole") directly to the water column, where they are dispersed by currents. The largest particles (about 90% of the cuttings) will then be deposited in a slight mound within about 200 m of the well location and will form a slight mound on the seafloor. Not only do deepwater coral reefs challenge modern science with numerous questions on how they can exist in the middle of a seemingly barren shelf environment [47] – they also present a challenge on how to drill safely without damaging them. At the Morvin field, mentioned earlier, this was a major challenge to field development.

Production Drilling at Morvin, a Special Case The Morvin-field is more densely populated by significant deepwater coral reefs than any other Norwegian offshore field [47]. Whereas pipeline routes and the final location of steel templates could easily be adjusted to avoid the coral reef occurrences, one of the major challenges was how to drill the production wells without harm to the reefs. Because there are significant deepwater coral reefs within 200 m at both the planned Morvin production templates, it was not possible to use the normal practice without incurring damage to some of the reefs. It was therefore decided to seek authorities' permission for discharging top-hole cuttings some distance away from the templates, at locations deemed safe for the coral reefs. The chosen technical solution was to employ a "Cutting Transportation System" (CTS), consisting of two 600 m long flexible tubes installed on the seabed. They were attached to five gravel filled bags ("bigbags") to prevent them from moving on the seafloor and were attached to a manifold placed on the seafloor. This manifold had one exhaust pipe leading from the wellhead where the cuttings were collected and pumped to the CTS. Currents were predicted and numerically modeled, and the optimal discharge locations were found where cuttings would not do harm to the surrounding significant coral reefs. The cuttings were discharged at relatively high speed through recoil dampers placed about 1 m proud of the seafloor at the end of the CTS-hoses.

The cuttings emitting from the recoil damper were found to be heavier and less fine-grained than predicted. This resulted in the discharge plume emitting as a heavy fluid, and spreading along the seafloor as a turbid and heavy cloud. Because this cloud did not spread high up into the water mass most of it accumulated near the end of the CTS hoses without any damage to the corals. Continuous visual monitoring by ROVs of the CTS and the nearest coral reefs was done during the whole top-hole drilling operation at Morvin. This ROV-work also included lifting and repositioning (adjusting) of the recoil dampers, as the heap of cuttings grew to heights of up to 1 m. A total of three sediment traps were also placed on the seafloor in order of documenting the final distribution of any resuspended cuttings. Three of the downstream coral reefs were continuously monitored by using an automatic time-lapse "satellite photo rig" and by ROV-monitoring. This Morvin experience proved that production drilling can also be done near scattered coral reefs without harming them.

Observations Along Pipelines

Prior to the laying of trunk pipelines on the seafloor, detailed visual surveys are performed. The objectives of these "pre-lay" surveys are to make sure the pipeline does not cross any dangerous areas or any features that can hinder the laying. In addition, all features and marine life are also recorded along the pipeline route. Because underwater visibility is restricted, the visually documented corridor is most often no wider than about 10 m. However, the length of the surveyed corridor, which depends on the length of the pipeline to be laid is anything up to several hundred kilometers. During the last quarter century, 1984–2010, several thousands of km long transects were surveyed by Statoil. Thus, trunk gas and oil pipelines have been laid from the Snehvit field in the southern Barents Sea and from

numerous fields offshore Mid- and Southern-Norway. Detailed knowledge about the seafloor and marine life has, therefore, been gathered along transects crossing all ranges of water depths of the North Sea, stretching from Norway to the UK, and from Norway to Germany, Belgium, and France (Dunkerque). In this way, the general seafloor has been imaged, meter for meter, across 50 m iceberg ploughmarks in the Barents and Norwegian Seas, to typically 100 m wide, 5 m deep pockmark craters in the northern North Sea, to wide stretches of rugged sandwave fields off Netherlands and Belgium, to the normal, even, and uneventful seabed in all of the seas. The seabed life pattern always seems to be the same: there is apparently very little variation in macrofaunal life except for when there are special features on the seafloor, such as boulders and rock outcrops, besides the special fluid-flow-related features: pockmark craters and other micro-seeps, and the eventual macro-seeps, which are very rare.

The fact that marine life proliferates wherever there are "special features" on the seafloor means that wherever a new man-made structure is installed on the seafloor, there may be a dramatic impact on the visible macrofaunal life pattern (Fig. 6). On all concrete-coated trunk pipelines laid across the pre-surveyed sections, it is clearly noticed how the pipeline structure introduces new opportunities for benthic life. For example, it only took 1 year before thousands of *Nephrops norvegicus* crustaceans were established along kilometer long stretches of the "Statpipe" pipeline, the first 36″ trunk pipeline laid across the 300 m deep Norwegian Trench (North Sea), in 1985. They were clearly colonizing small sections of the seafloor along the outer, curved wall of the pipeline. Their holes were located snugly inside the sediments nearest to the pipeline wall. The clawed animals had their bodies halfway out of their openings, easily visible during the first thorough visual inspection of the pipe, the so-called as-laid survey, conducted about 1 year after the pipeline was installed. Over time, the annual pipeline inspections, which cover long sections of both sides and the top of pipe, every other year, document not only how the trunk pipelines gradually bury themselves into the seabed, but also how they are colonized by a variety of different invertebrates. Unfortunately, this information is seldom used for quantifiable studies by biologists or marine ecologists, although the data should be fully available for such work. The reason is probably, that this type of visual information is unknown and that it perhaps does not belong in the scientific "vocabulary" of traditional marine biology or ecology.

To illustrate some of the important information content in this unique pipeline inspection data set, there are three particularly noticeable occasions, episodes, and occurrences that are worthy of further description: (1) A temporary anoxic condition recorded in the central North Sea, (2) "Drifts" of dead fish (mackerel) along a pipeline section, and (3) Fish protected by OHI-pipelines.

Temporary Anoxic Conditions

During the annual inspection in 2004, of the Europipe 1 trunk gas pipeline from Kårstø, SW Norway, to Northern Germany, a few dead fish and invertebrates were seen lying on the seafloor along the pipeline about 50 km south of the Draupner platform, central North Sea. There was also some white material, believed to be bacterial mats. This section of the pipe is partly buried into the seafloor and is about 40 cm proud of the smooth seafloor surface. Both sides of the pipeline were affected and, there were also dead invertebrates on top of the pipe itself. Although this anomalous observation could easily have been interpreted as something to do with the pipeline, some further investigations and measurements precluded such a conclusion. Anoxia was obviously the cause of this "mass extinction," – but, what had caused it? Along one short section, it was only the southern side of the pipeline that was affected. This annual inspection was conducted during May, when the expected ambient water temperature should be around 6°C. But, actual measurements showed an ambient water temperature of only 1.1°C near the seafloor. Measurements through the water column showed the lower 20 m of seawater only had between 1.1°C and 2.0°C. This very cold, nearly freezing water apparently occurred as a dome-shaped, dynamically stable water mass occupying the general depression in the seafloor, where the pipeline had been laid. During installation of the Europipe 1 pipeline some years earlier, portions of it were laid into the meandering relict "Elbe valley" on the seafloor of the mid- and southern North Sea. This was obviously where the cold water had accumulated. Investigations

of recorded water temperatures further southeast in the German Bight showed that very cold water had formed during the winter months, January and February when there was a long cold spell. Because there had been no subsequent storms, the cold, dense water mass had since followed the deepest local portions of the seafloor, and gradually flowed toward the central portion of the North Sea, where it engulfed parts of the Europipe 1 pipeline and where it became stagnant and anoxic. During the subsequent annual pipeline inspection, 2 years later, there was neither sign of dead animals nor any other evidence of this temporary "extinction event." These observations clearly demonstrate that great variations in the natural seafloor environment, even in the relatively busy central North Sea can occur without being noticed on the sea surface.

"Drifts" of Dead Fish Along a Pipeline

The fact that large trunk pipelines laid onto the even, flat, featureless seafloor act as barriers for objects drifting across the seafloor is well known. During the early years of trunk pipeline construction in Norwegian waters (1983–1997), quite a lot of garbage, that is, paper, plastic bags, bottles, cans, etc, together with natural debris, such as kelp and sponges, etc, was noted to accumulate along sections of the newly laid pipes. During the last decennium, however, the amount of garbage has decreased markedly, probably as a result of stricter garbage handling rules in general, and Norway in particular. However, such rules are not always obeyed, as the following example proves. During the annual inspection of a section of the 36″ trunk gas pipeline, Europipe 2, in the Norwegian sector of the North Sea, a huge and elongated pileup of dead fish (mackerel) was visually recorded. It formed a ca. 3 km long and nearly 1 m high "drift" along the western side of the pipeline. The volume of dead fish was estimated to about 10,000 m^3. Because this freshly killed mackerel was obviously dumped illegally by one or several of about seven nearby fishing vessels, the Norwegian Fishery Directory was contacted, and on the following evening, live video footage of the drift was broadcast as a news item by the directory on national TV. Although this live footage, from one of OHI's annual pipe inspections surely made a public impression, it is very rare that such information is used for public purposes.

Fish Protected by OHI-Pipelines

The largest pipeline constructed to date, in the North Sea and Norwegian Sea, is the 1,200 km long 40″ and 44″ Langeled pipeline, transporting gas from the giant Ormen Lange field off Mid-Norway, via Nyhavna in Mid-Norway and the Sleipner field in the central North Sea to Immingham on the east coast of the UK. During the initial as-laid survey, immediately after laying, in 2006, a large school of newly spawned fish was documented along a 50–100 km long section of the pipe, in UK waters. This school was also observed to swim along the pipeline about 3 months later, after the individual fish had grown significantly larger in size. Trawling is routinely practiced along exposed trunk pipelines. The intent is to catch fish that swim along and hide beneath free-spanning sections of the pipelines. Because this large school of fish had obviously been spawned near the newly laid pipeline, and because it utilized the opportunity for refuge along the pipeline, it was suggested by OHI-personnel that measures to protect the school should perhaps be taken by British Authorities. To protect a corridor of, say 3 km width, along a 100–200 km long section of the Langeled pipeline could have been feasible. The following annual inspections could also have visually documented the fate of such a school of fish. However, it was soon realized that suggestions of this kind were premature, in 2006, as it was not expected that anybody would actually understand what the problem may be, or what the suggestion was really about. This demonstrates clearly how little is known and currently understood about the subsea world and how difficult it is to convey ideas and impressions from this world, unless the receivers have similar or comparable experience.

The higher abundance of fish sightings (of fish >0.5 m in length) along trunk pipelines was already noticed after the installation of Statoil's first trunk gas pipeline, the over 250 km long and 36″ Statpipe pipeline from the Statfjord field to Kalstø on the SW coast of Norway. This pipeline crosses the 300 m deep Norwegian Trough, where there is a varying density of pockmark craters in the seafloor. During the very first annual survey of this pipeline, a strong correlation between number of fish sightings and the density of pockmarks was noticed. The fish counted in 1987

were either seen swimming along the sides of the pipeline, or occupying some of the space underneath the pipeline where it had intermittent spans over irregular terrain in the seafloor. This comparison was made with fish sightings in 1984, over the same, undisturbed section of seafloor, before the pipeline was installed. The increased number of fish seen, after the pipeline was installed was dramatic and close to tenfold along some of the seafloor sections. Also before the pipeline was installed, there was evidently many more fish in densely pockmarked areas than in areas without pockmarks. This example shows that trunk pipelines attract fish and also likely protects them to some degree.

The question of protection of trunk pipelines against damage by trawl-board impact was assessed prior to installation of the Statpipe pipeline. Carefully designed laboratory studies in test tanks and rigs, however, soon proved that no serious damage would possibly be inflicted on the concrete coated steel trunk pipelines by normal trawl-boards. Therefore, most such pipelines are left on the seafloor without being actively protected by trenching or gravel cover. In some areas, where the seafloor relief is varied, by numerous pockmarks or iceberg ploughmarks, there may be a need to modify the seafloor topography to avoid long free spans in the pipe. Spans longer than about 80 m are unacceptable for two reasons: (1) motions in the pipe caused by water currents may inflict material damage to the pipe, and (2) trawl-boards may snag underneath the pipe, during fishing along the pipeline. Seafloor preparation and intervention is then performed, either by trenching the seafloor highs or by dumping gravel inside seafloor troughs. This type of intervention is performed before installation of pipeline or immediately after installation. In the German sector of the North Sea, where the water depth is not greater than 150 m, all trunk pipelines have to be buried below the seafloor surface. The annual inspection of buried pipelines is done by the use of induced electric currents and magnetic detection of the buried pipe, combined with visual inspection of the seafloor above the buried pipe. During the last 10–15 years, the annual surveys in these waters have not, unfortunately produced many fish sightings, probably as a consequence of lack of protection and intensive fishing activity.

The Impact of Platforms and Other Fixed OHI-Structures

The six giant concrete platforms Statfjord, A, B, C and Gullfaks A, B, C were installed on the seafloor at the Statfjord and Gullfaks fields in the northern North Sea during a 15 year period in the 1980s and 1990s. Apart from the seafloor at the deepest site, Gullfaks C, the seafloor is dominated by sand, gravel, and patches of boulders. Prior to installation, large fish, such as *Brosme* sp., Ling, Cod, and Seithe, were only occasionally seen swimming around. However, during a detailed preinstallation site survey of the deeper Gullfaks C site, a more complex situation was found. The seafloor at Gullfaks C contrasts with the other sites by having a seafloor covered by soft, fine-grained clay-dominated sediments. Furthermore, there are normal-pockmarks in this area. A dedicated visual survey of pockmark craters here revealed that larger fish, most often the *Brosme* sp., were located inside many of these pockmarks. And inside one particular pockmark, of 8 m depth and 120 m length, there were up to 20 large fish located in the deepest end of the pockmark crater [10]. About fifteen of the large fish (Ling, Cod, and Brosme) were swimming against the southward flowing current, whereas about five fish were found inside a tunnel at the deepest portion of the pockmark [10]. This example clearly demonstrates some of the unexpected heterogeneity of the seafloor and that it takes dedicated visual surveying to unravel the true nature of marine life on the undisturbed seafloor.

After about 30 years of operating large fixed structures, it is a well-known fact within the OHI that there are plenty of large fish living near the structures. At some of the hydrocarbon fields in the North Sea special trawl-fenders have been installed on the seafloor to prevent trawlers from fishing within the 500 m forbidden safety zone surrounding all fixed platforms which are over the sea surface. These trawl-fenders are robust, up to 3 m high steel poles driven into the seafloor. They are intended to snag the trawl equipment before it can damage any of the production gear and infrastructure placed on the seafloor within the safety zone. It is also a well-known fact that filter-feeders, such as sea anemones and other sessile animals colonize the legs of both steel and concrete platforms (Fig. 7). However, until for about 15 years ago it was not known that colonizing

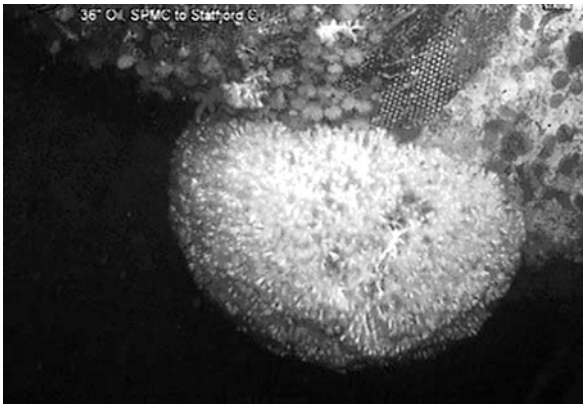

Marine Life Associated with Offshore Drilling, Pipelines, and Platforms. Figure 8
A relatively small *Lophelia* colony seen on a man-made structure at Statfjord, Norwegian sector of the North Sea. The colony cannot be older than about 22 years (age of structure)

ahermatypic corals also lived on these structures (Fig. 8). Thus, OHI-related fixed structures make ideal artificial reefs on the seafloor.

By law, all the OHI-related structures placed on the seafloor shall be decommissioned after use, that is, they shall be dismantled and disposed of in a safe and environmental friendly manner. However, judging from experiences in the North Sea, even some of the large trunk pipelines could perhaps remain until they either buried themselves or corroded into destruction. In the meantime, they would undoubtedly represent an added biologically friendly asset to the normal seafloor, at least in some places (Fig. 9). For the giant concrete structures, the case is also one of cost benefit. These structures are placed firmly into the ground and will require a lot of energy to remove. Because concrete is a very environmental friendly substance and has a high longevity, it should be seriously debated if they could

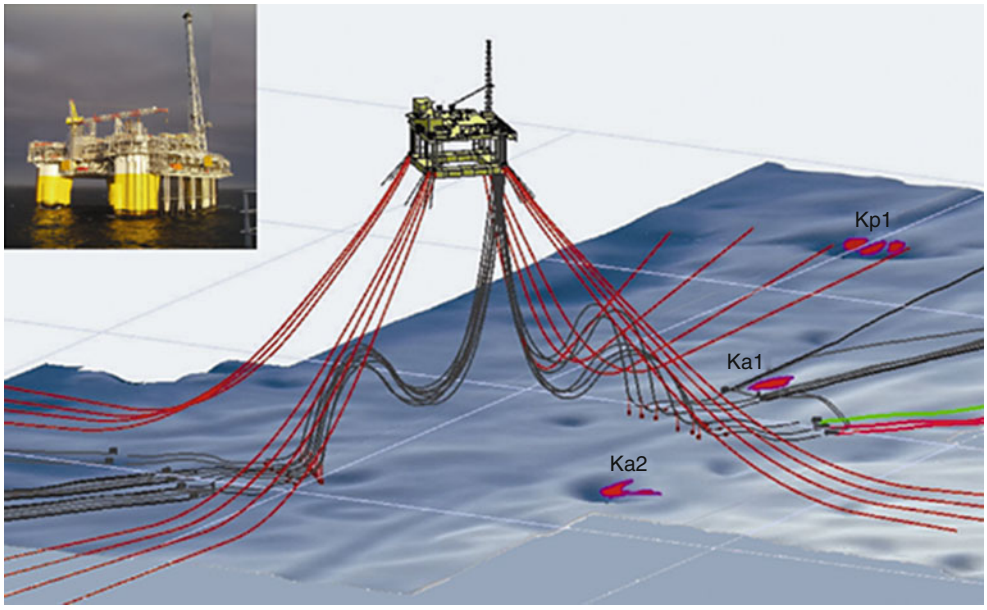

Marine Life Associated with Offshore Drilling, Pipelines, and Platforms. Figure 9
A perspective image of how the Kristin semi-floating platform is located above the seafloor. The water depth below the platform is 305 m. *Red lines* indicate anchor chains and wires. The *black lines* indicate flowlines and risers piping products (gas, condensates, etc.). The chains and wires that hold Kristin in place are attached to "suction anchors," inverted domed steel cylinders sucked into the seafloor clays. The coral reefs, Ka2, Ka1, and Kp1 (in *red*), have been inspected twice before installation and several times after installation of the platform and the other infrastructure on the seafloor. No damage has been found on the reefs. Image is based on true multibeam mapping of the seafloor and digital technical drawings of the platform, shown in a photo *upper left*. This image shows that the platform and infrastructure can be relinquished after use, without any damage to sensitive biology on the seafloor. Courtesy of Statoil ASA and Leslie Austdal

remain in place for 'ever.' They could act as home for plenty of fish, and could even be used by professional fishermen as fish nurseries and fishing grounds.

Future Directions

More dedicated detailed seafloor mapping, combined with visual documentation is undoubtedly needed for improving the understanding and knowledge of life on the seafloor in general. Through the Norwegian "Mareano" project, started by the government in 2005, this type of work has actually started in Norway. Swathe multi-beam detailed seafloor mapping is here combined with up to kilometer long video (visual) transects. In addition to sampling, the seafloor is mapped for biotype and many other parameters. In the long run, such mapping and documentation is necessary for adequate management of the resources in the sea. However, it may take another 100 years for one vessel to map out the whole Norwegian EEZ (Exclusive Economic Zone) in this fashion. This therefore, calls for more technological development and probably also for the use of autonomous robotic systems in the future.

With regard to the OHI-related structures placed on the seafloor, such as trunk pipelines, steel templates, and giant platforms, there needs to be a thorough discussion as to which of them should be relinquished (removed) and which structures could serve to stimulate and protect the marine bio-environment. Judging from the visual documentation over the last 30 years in the North Sea, it can be deemed favorable to let some of the installations remain on the seafloor as artificial reefs and for the future benefit of both marine life and humans.

Bibliography

1. Martin TR, Olsen KR, Cahill MM (2010) Artificial reefs – an important tool for mitigation and restoration. Ocean News Technol 16(4):28–29
2. Maurer BA, McGill BJ (2004) Neutral and non-neutral macroecology. Basic Appl Ecol 5:413–422
3. Humphris SE, Zierenberg RA, Mullineaux LS, Thomsen RE (eds) (1995) Seafloor hydrothermal systems: physical, chemical, biological, and geological interactions. American Geophysical Union, Geophysical monograph 91, 510 pp
4. Etter RJ, Rex MA (1990) Population differentiation decrease with depth in deep-sea gastropods. Deep-Sea Res 37:1251–1261
5. Rex MA (1983) Geographic patterns of species diversity in the deep-sea benthos. In: Rowe GT (ed) The sea. Wiley, New York
6. Piepenburg I et al (2001) In: Schäfer S et al (eds) The northern north Atlantic – a changing environment. Springer, Berlin
7. Schäfer P, Ritzrau W, Schlüter M, Thiede J (2001) The northern north Atlantic – a changing environment. Springer, Berlin, 500 pp
8. Judd AG, Hovland M (2007) Submarine fluid flow, the impact on geology, biology, and the marine environment. Cambridge University Press, Cambridge, 475 pp
9. Suess E (2010) Marine cold seeps. In: Timmis KN (ed) Handbook of hydrocarbon and lipid microbiology, vol 1. Springer, Berlin, pp 187–203 (Part 3)
10. Hovland M, Judd AG (1988) Seabed Pockmarks and Seepages. Impact on geology, biology and the marine environment. Graham & Trotman, London, 293 pp
11. Hovland M, Thomsen E (1989) Hydrocarbon-based communities in the North Sea? Sarsia 74:29–42
12. Hovland M (2002) On the self-sealing nature of marine seeps. Cont Shelf Res 22:2387–2394
13. Wegener G, Shovitri M, Knittel K, Niemann H, Hovland M, Boetius A (2008) Biogeochemical processes and microbial diversity of the ullfaks and Tommeliten methane seeps (northern North Sea). Biogeosciences 5(4):1127–1144
14. Hovland M (2007) Discovery of prolific natural methane seeps at Gullfaks, northern North Sea. Geo-Marine Lett. doi:10.1007/s00367-007-0070-6
15. Seibel BA, Dierssen HM (2009) Animal function at the heart (and gut) of oceanography. Science 323:343–344
16. Moore CJ (1999) Seeps give a peek into plumbing, explorer. Am Assoc Petrol Geol 99:22–23
17. Dimitrov LL (2002) Mud volcanoes – the most important pathway for degassing deeply buried sediments. Earth Sci Rev 59:49–76
18. Dupré S, Woodside J, Klaucke I, Mascle J, Foucher J-P (2010) Widespread active seepage on the Nile Deep Sea Fan (offshore Egypt) revealed by high-definition geophysical imagery. Mar Geol 275:1–19
19. Vogt PR, Crane K, Pfirman S, Sundvor E, Cherkis N, Flemming H, Nishimura C, Shor A (1991) SeaMarc II sidescan sonar imagery and swath bathymetry in the Nordic basin. EOS Trans 72:486
20. Hovland M, Hill A, Stokes D (1997) The structure and geomorphology of the Dashgil mud volcano. Azerbaijan Geomorphol 21:1–15
21. King LH, MacLean B (1970) Pockmarks on the Scotian shelf. Geol Soc Am Bull 81:3142–3148
22. Cathles LM, Su Z, Chen D (2010) The physics of gas chimney and pockmark formation, with implications for assessment of seafloor hazards and gas sequestration. Mar Petrol Geol 27:82–91
23. Hovland M, Heggland R, de Vries MH, Tjelta TI (2010) Unit pockmarks and their potential significance for prediction of fluid flow. J Mar Petrol Geol 27:1190–1199

24. Buhl-Mortensen L, Vanreusel A, Gooday AJ, Levin LA, Priede IG, Buhl-Mortensen P, Gheerardyn H, King NJ, Raes M (2010) Biological structures as a source of habit heterogeneity and biodiversity on the deep ocean margins. Mar Ecol 31: 21–50
25. Gunnerus JE (1768) Om nogle Norske coraller. In: Kongelige Norske Videnskabers Selskabs Skrifter, vol 4, pp 38–73
26. Dons C (1944) Norges korallrev. Norsk Vidensk Selsk Trondheim Forh 16A:37–82
27. Wilson JB (1979) The distribution of the coral Lophelia pertusa (L.) [L. Prolifera (Pallas)] in the north-east Atlantic. J Mar Biol Assoc UK 59:149–164
28. Wilson JB (1979) "Patch" development of the deep-water coral *Lophelia pertusa* (L.) on rockall bank. J Mar Biol Assoc UK 59:165–177
29. Hecker B, Blechschmidt G, Gibson P (1980) Epifaunal zonation and community structure in three Mid- and North Atlantic Canyons. Contract report BLM AA551-CT8-49 prepared by Lamont-Doherty for US Department of Interior
30. Zibrowius H (1980) Les Scléractiniaires de la Méditerranée et de l'Atlantique nord-oriental. Memoires de l'Institute Oceanographique 11:247
31. Hovland M (1990) Do carbonate reefs form due to fluid seepage? Terra Nova 2:8–18
32. Hovland M, Croker PF (1993) Fault-associated seabed mounds in the Porcupine Basin, offshore Ireland. Expanded abstract. In: Proceedings of the 55th EAEG Ann. Mtg., Stavanger, Norway
33. Hovland M, Croker P, Martin M (1994) Fault-associated seabed mounds (carbonate knolls?) off western Ireland and North-West Australia. Mar Petrol Geol 11:232–246
34. Freiwald A, Henrich R, Pätzold J (1997) Anatomy of a deep-water coral reef mound from Stjernsund, west Finnmark, northern Norway. In: James NP, Clarke JAD (eds) Cool-water carbonates. Soc Sediment Geol (SEPM), Special Publ 56:140–161
35. Henriet J-P, De Mol B, Pillen S, Vanneste M, Van Rooij D, Versteeg W, Croker PF, Shannon PM, Unninthan V, Bouriak S, Chachkine P (1998) Gas hydrate crystals may help build reefs. Nature 391:648–649 (Porcupine-Belgica Shipboard Party)
36. Hovland M, Mortensen PB (1999) Norske korallrev og prosesser I havbunnen (Norwegian coral reefs and seabed processes), John Grieg, Bergen, Norway, 167 pp (in Norwegian with English summary)
37. Armstrong CW, van der Hove S (2007) The formation of policy for protection of cold-water coral off the coast of Norway. Internal Report, University of Tromsø
38. Fosså JH, Mortensen PB (1998) Artsmangfoldet på *Lophelia*-korallrev og metoder for kartlegging og overvåkning. The biodiversity on Lophelia-reefs and methods for mapping and monitoring. Fisken og Havet 17:1–95 (in Norwegian)
39. Willison JHM, Hall J, Gass SE, Kenchington ELR, Butler M, Doherty P (eds) (2001) In: Proceedings of the first international symposium on deep-sea corals, Ecology Action Centre and Nova Scotia Museum. Halifax, Canada
40. Hovland M, Risk M (2003) Do Norwegian deep-water coral reefs rely on seeping fluids? Mar Geol 198:83–96
41. Jensen S, Neufeld JD, Birkeland N-K, Hovland M, Murrell JC (2008) Insight into the microbial community structure of a deepwater coral reef environment. Deep-Sea Res I 55:1554–1563
42. Yakimov MM, Cappello S, Crisafi E, Tursi A, Savini A, Corselli C, Scarfi S, Giuliano L (2006) Phylogenic survey of metabolically active microbial communities associated with the deep-sea coral *Lophelia pertusa* from the Apulian plateau, Central Mediterranean Sea. Deep-Sea Res I 53:62–75
43. Sorokin YuI, Sorokin Yu P (2009) Analysis of plankton in the southern Great Barrier Reef: abundance and roles in throphodynamics. J Mar Biol Assoc UK 89:235–241
44. Neulinger SC, Gärtner A, Järnegren J, Ludvigsen M, Lochte K, Dullo W-C (2008) Tissue-associated "*Candidatus Mycoplasma corallicola*" and filamentous bacteria on the cold-water coral *Lophelia pertusa* (Schleractinia). Appl Environ Microbiol 75:1437–1444
45. Tavormina PL, Ussler W, Orphan VJ (2008) Planktonic and sediment-associated aerobic methanotrophs in two seep systems along the North American margin. Appl Environ Microbiol 74:3985–3995
46. Penn K, Wu D, Eisen JA, Ward N (2006) Characteristics of bacterial communities associated with deep-sea corals on Gulf of Alaska seamounts. Appl Environ Microbiol 72:1680–1683
47. Hovland M (2008) Deep-water coral reefs – unique biodiversity hot-spots. Springer Praxis, Chichester, 278 pp
48. Costello MJ, McRea M, Freiwald A, Lundälv T, Jonsson L, Bett BJ, van Weering TCE, de Haas H, Roberts MJ, Allen D (2005) Role of cold-water coral *Lophelia pertusa* coral reefs as fish habitat in the North East Atlantic. In: Freiwald A, Roberts M (eds) Cold-water corals and ecosystems. Springer, Heidelberg, pp 771–805
49. Furevik D, Nøttestad L, Fosså JH, Husebø A, Jørgensen S (1999) Fiskefordeling i og utenfor korallområder på Søregga. Fisken og Havet no 15, 33 pp
50. Husebø A, Nøttestad L, Fosså JH, Furevik D, Jørgensen SB (2002) Distribution and abundance of fish in deep-sea coral habitats. Hydrobiologia 471:91–99
51. Roberts JM, Wheeler AJ, Freiwald A (2006) Reefs of the deep: the biology and geology of cold-water coral ecosystems. Science 312:543–547
52. Turley C, Blackford J, Widdicombe S, Lowe D, Nightingale PD, Rees AP (2006) Reviewing the impact of increased atmospheric CO_2 on oceanic pH and the marine ecosystem. In: Schnellnhuber HJ, Cramer W, Nakicenovic N, Wigley T, Yohe G (eds) Avoiding dangerous climate change. Cambridge University Press, Cambridge, pp 65–70
53. Turley CM, Roberts JM, Guinotte JM (2007) Corals in deep-water: will the unseen hand of ocean acidification destroy cold-water ecosystems? Coral Reefs. doi:10.1007/s00338-007-0247-5

54. Gass SE, Roberts JM (2006) The occurrence of the cold-water Lophelia pertusa (Scleractinian) on oil and gas platforms in the North Sea: colony growth, recruitment and environmental controls on distribution. Mar Pollut Bull 52:549–559
55. Roberts JM, Long D, Wilson JB, Mortensen PB, Gage JD (2003) The cold-water coral *Lophelia pertusa* (Scleractinia) and enigmatic seabed mounds along the north-east Atlantic margin: are they related? Mar Pollut Bull 46:7–20
56. Koslow JA, Gowlett-Holmes K, Lowry JK, O'Hara T, Poore GCB, Willimams A (2001) Seamount benthic microfauna off southern Tasmania: community structure and impacts of trawling. Mar Ecol Prog Ser 213:111–125
57. Fosså JH, Mortensen PB, Furevik DM (2000) *Lophelia*-korallrev langs norskekysten. Forekomst og tilstand. Lophelia coral reefs along the Norwegian coast. Occurrence and conditions. Fisken og havet, 2, 94 pp (in Norwegian)
58. Rogers AD (1999) The biology of *Lophelia pertusa* (Linnaeus 1758) and other deep-water reef-forming corals and impacts from human activities. Int Rev Hydrobiol 84:315–406
59. Mortensen PB, Fosså JH (2006) Species dieversity and spatial distribution of invertebrates on *Lophelia* reefs in Norway. In: Proceedings of the 10th international coral reef symposium. Okinawa, Japan, pp 1849–1868
60. Hall-Spencer J, Allain V, Fosså JH (2002) Trawling damage to Northeast Atlantic ancient coral reefs. Proc Royal Soc Lon Ser B 269:507–511
61. Myhrvold A, Hovland M, Nøland S-A (2004) Baseline and environmental monitoring in deep water – a new approach. In: Seventh international SPE conference on health, safety, and environment, Calgary, 29–31 Mar 2004. Paper no. SPE 86776
62. Etiope G, Feyzullayev A, Baciu CL (2009) Terrestrial methane seeps and mud volcanoes: a global perspective of gas origin. Mar Petrol Geol 26:333–344
63. Mikkelsen N, Erlenkauser H, Killingley JS, Berger WH (1982) Norwegian corals: radiocarbon and stable isotopes in Lophelia pertusa. Boreas 5:163–171
64. Mortensen PB, Rapp HT (1998) Oxygen- and carbon isotope ratios related to growth line patterns in skeletons of *Lophelia pertusa* (L) (Anthozoa: Scleractinia): implications for determination of linear extention rates. Sarsia 83: 433–446

Web Sites

www.mareano.no
www.npd.no
www.nerc.ac.uk
www.iodp.org
www.deepseadrilling.org
www.offshoremagazine.com
www.serpentproject.com
www.diverdiscover.whoi.edu
www.statoil.com
www.eu-hermes.net

Marker-Assisted Breeding in Crops

Roberto Tuberosa
Department of Agroenvironmental Science and Technology, University of Bologna, Bologna, Italy

Article Outline

Glossary
Definition of the Subject
Introduction: Global Food Security and Plant Genomics
Molecular Dissection of the Genetic Control of Traits Governing Crop Performance
Modeling QTL Effects
Marker-Assisted Breeding to Improve Crop Performance
Integrating Marker-Assisted Breeding in Conventional Breeding Projects
Mining Beneficial Alleles in Wild Relatives of Crops
Leveraging the "-Omics" Platforms
Future Directions
Bibliography

Glossary

Backcross Procedure used by plant breeders to introgress an allele at a locus of interest (e.g., disease resistance) from a donor parent to a recurrent parent, usually a successful cultivar. The recurrent parent is crossed several times to the original cross and selection is performed at each cycle to recover the plants with the desired allele and the largest portion of the genome of the recurrent parent.

Candidate gene A coding sequence that is supposed to be causally related to the trait under selection. The candidate-gene approach is best applied with simple biochemical traits when a clear cause-effect relationship can be established between the gene function and the target trait.

Epistasis The interaction between two or more genes to control a single phenotype. Interaction between two or more loci that control the same trait. The presence of epistatic loci makes it more difficult to predict the phenotypic value of progeny derived either from crosses or from selfing.

Forward genetics Approaches to dissect the genetic makeup of traits starting from the observation of the phenotype. QTL mapping and positional cloning are examples of forward genetics to investigate quantitative traits.

Haplotype Chromosome fragment of varying length carrying a common set of marker alleles in close linkage at adjacent loci. When using haplotypes in association mapping studies, the information of several linked bi-allelic markers is combined as a single, multi-locus informative marker.

Heritability The portion (from 0% to 100%) of phenotypic variability that is genetically determined. The additive portion (i.e., not due to dominance) of variability is inherited from one generation to the next and is the main determinant of the gain from selection. Heritability is specific to a particular population in a particular environment.

Introgression library lines (ILLs) A collection of lines (ca. 80–100) obtained by subsequent backcrosses of a recurrent parent (usually an elite cultivar) with a donor parent, usually a line highly diversified from the recurrent parent for one or more traits. Each ILL carries a fragment (from ca. 20 to 40 cM) of the donor genome different from that carried by the other lines. Collectively, the fragments of all ILLs cover the entire genome with partial overlap. ILLs are ideal for the fine mapping and cloning of major loci and to investigate epistatic interactions.

Linkage disequilibrium (LD) The level of nonrandom assortment of alleles at different loci. The level of LD varies greatly according to the species and the mode of reproduction.

Linkage drag The negative phenotypic effects (e.g., lower yield) on the recurrent parent associated with the loci of the donor parent tightly linked to the locus of interest being backcrossed.

Logarithm of the odds ratio (LOD) A logarithmic value (base 10) of the ratio between the probability of the presence of a QTL vs. its absence. A LOD value of 3.0 indicates that the probability of the presence of the QTL is 1,000-fold higher than its absence.

Metanalysis A comprehensive analysis based on the data of several mapping populations of the same species. The objective is to obtain a better resolution of the LOD profile of the QTLs for the traits of interest.

Near isogenic lines (NILs) A set of two or more inbred lines that share most of the genome except for a small portion that contains functionally different alleles at the target locus. NILs are commonly used for the positional cloning of a locus of interest.

Phenotypic selection Selection based on the observation of the phenotype at different levels of functional organization based on the target trait(s). If the selected trait is highly influenced by environmental conditions and has low heritability, the effectiveness of phenotypic selection quickly decreases.

Pleiotropy Condition where a single locus controls more than one trait. It is more common for biochemical traits.

Positional cloning A series of procedures to clone a locus of interest. Positional cloning is based on the joint analysis of phenotypic data and genotyping profiles of near isogenic material with recombination events at the target region.

Quantitative trait locus A portion of DNA that influences the expression of a quantitative trait. The presence of QTLs is determined through appropriate statistical analysis of phenotypic and molecular data of a mapping population (e.g., linkage mapping) or a collection of unrelated genotypes (e.g., association mapping).

Recombinant inbred lines A collection of homozygous lines (usually from 150 up to 400) obtained following subsequent selfings (usually four or five) of an equivalent number of randomly chosen F_2 plants.

Reverse genetics An approach for discovering the function of a locus by analyzing the phenotypic effects of specific sequences obtained by DNA sequencing. Reverse genetics attempts to connect a given genetic sequence with specific effects on the organism.

Synteny The physical colocalization of linked loci on the same chromosome among different species. Study of synteny can show how the genome of phylogenetically related species has evolved from a common ancestor (e.g., rice for cereals) through rearrangements of the genome (e.g., translocations, inversions, duplications, etc.) in the course of evolution.

Definition of the Subject

Attaining global food security by means of increased crop productivity will require an increase in gains from selection achieved through conventional breeding. To this end, the identification of molecular markers associated with loci controlling traits of agronomic interest coupled with the exploitation of marker-assisted breeding (MAB) approaches provides the opportunity to accelerate gain from selection. In particular, marker-assisted selection (MAS) and marker-assisted backcrossing have been widely adopted to improve resistance to diseases and other relatively simple traits. Notwithstanding these remarkable achievements, the improvement of yield and other complex quantitative traits via MAB has been marginal, mainly due to the difficulty in identifying major quantitative trait loci (QTLs) with an adequately stable effect across environments and genetic backgrounds. Additionally, the effect of most QTLs affecting yield is too small to be detected with either biparental mapping or association mapping. Genomic selection (GS) circumvents this problem by using an index for the selection of unmapped QTLs of small individual effects but with otherwise sizable effect at the whole plant level when selected together. GS is already having a positive impact on the improvement of crop yield, mainly in the private sector where high-throughput infrastructures allow breeders to handle the large number of molecular datapoints that are required for effectively deploying GS. Ultimately, an effective exploitation of MAB to enhance crop performance will rely on a closer integration between molecular approaches and conventional breeding.

Introduction: Global Food Security and Plant Genomics

During the past century, plant breeders have been very successful in constantly raising crop yields to a level sufficient to meet the global demand in food, feed, and fiber. For wheat and rice, the two most important staples of humankind, the so-called Green Revolution spearheaded by Norman Borlaug, awarded the Nobel Peace Prize in 1970, provides the most spectacular example of the contribution of science toward an improved food security [1, 2]. Similar progress has been achieved also in maize, particularly following the introduction of hybrids [3]. This notwithstanding, during the past decade, the rate of increase in yield in cereals, especially wheat and rice, has not met the global demand [4] as shown by the substantial decrease in the amount of global cereal reserves. Additionally, during the past two decades the number of chronically hungry people has increased and is fast approaching one billion. A number of reasons have contributed to this worrisome scenario that has already sparked food riots (e.g., during the 2007–2008 food crisis and also in 2009) and social unrest in a number of less-developed countries. An even bleaker picture looms on the horizon, when mankind will reach a projected nine billion in 2050. Consequently, an acceleration in the rate of gain in crop yields is a must in order to keep up with the need of a burgeoning population that increasingly seeks a protein-enriched, nutritionally balanced diet. The challenge faced by modern breeders is even more daunting in view of (1) global warming and the consequent increased frequency of drought, floods, high temperatures, etc., (2) the decreased availability of natural resources (e.g., water, fertilizers, arable land, etc.), (3) the increasing cost of fuels, (4) the necessity to safeguard the remaining biodiversity, and (5) the increased societal awareness of the critical need to improve the long-term sustainability of agricultural practices and decrease its impact on the environment. More simply, agriculture will need to produce more with fewer resources and more sustainably.

In this daunting scenario, genomics has ushered in a new breeding paradigm based on molecular approaches and platforms that in some cases have already contributed to accelerate the yield gain commonly achieved through conventional breeding practices [5–13]. However, a more widespread adoption of genomics-assisted selection will require the definition of new strategies based on a more effective integration of conventional and nonconventional breeding approaches as well as agronomic practices [14]. Clearly, a better knowledge of the genetic factors that determine yield and its variability from season to season will be instrumental in devising effective marker-assisted breeding (MAB) strategies for enhancing crop performance under a broad range of environmental conditions. As compared to conventional breeding approaches, MAB approaches offer unprecedented opportunities to dissect the genetic control of traits,

particularly those that are quantitatively inherited, such as biomass production, yield, and many other agronomic traits selected by breeders.

Molecular Dissection of the Genetic Control of Traits Governing Crop Performance

The first step for the dissection of the genetic control of traits that govern crop performance is the assembly of a linkage (genetic) map based upon the data of the molecular profiles of the marker loci – from as few as 100 up to several thousand – surveyed in a mapping population, usually comprised of ca. 150–200 genotypes such as F_2 plants, F_3 families, recombinant inbred lines (RILs), doubled haploids (DHs), etc., usually derived from the cross of two parental lines differing for the trait(s) of interest. The assembly of a genetic map is based on the level of linkage disequilibrium (LD, i.e., the level of nonrandom assortment of alleles at different loci) among adjacent marker loci on the same chromosome. Accordingly, mapping the loci that control the target trait is also based on the LD between the locus and nearby markers.

The estimated genetic distance between loci (markers or genes) is a function of the average number of recombination events (i.e., crossing-overs) between them at meiosis. The measuring unit used for expressing the distances among loci along a genetic map is the centimorgan (cM), which defines the interval along which one recombination event is expected to occur per 100 gametes produced at each meiotic cycle (i.e., at each sexually reproduced generation). Because a density of one marker per ca. 10–15 cM is usually sufficient to detect the presence of a functionally polymorphic locus with a major effect on the phenotypic variability of a mapping population, the number of well-spaced markers required to adequately sample the targeted species varies from as little as 100–120 as in the case of rice – one of the crops with the smallest genome size (ca. 0.45 billion bp) – to well over 300 for large genomes such as in bread wheat (ca. 16 billion bp). The desired level of genetic resolution will depend on the objective being pursued and the type of genetic materials being used.

For breeding purposes, a density of one marker every 5–10 cM is sufficient for most applications when dealing with elite cultivars. Nonetheless, for the introgression of a particular gene (e.g., a locus for disease resistance) from a wild relative of the crop to the crop itself, a high resolution is desirable in order to avoid the negative effects of the so-called linkage drag caused by negative effects of wild alleles at the loci closely linked to the one being targeted for introgression. A much higher genetic resolution is required when the goal is the cloning of the sequence that affects the target trait. In this case, the screening of several thousands of individuals is required to reach the desired level of resolution.

Cloning the loci that govern a particular trait can be achieved via either forward- or reverse-genetics approaches, or their combination. While forward genetics focuses on the phenotype as starting point, reverse-genetics approaches rely on sequence and functional information of candidate sequences (e.g., expressed sequence tags: ESTs) that are postulated to play a role in the expression of the target trait [15]. Although most results in the dissection of the genetic basis of crop performance and agronomic traits have been obtained via forward genetics, the use of reverse-genetics approaches in *Arabidopsis* and other model species (e.g., resurrection plants, rice, *Brachypodium*, etc.) has been instrumental to elucidate the genetic networks of the signaling pathways that regulate the adaptive response of plants to abiotic and biotic constraints [16–18]. Notably, the spectacular decrease in sequencing costs [19] and the increased availability of sequence information in public databases make the reverse-genetics approach increasingly attractive and feasible.

Following the assembly of the first genetic maps based on the molecular profiling of RFLPs (restriction fragment length polymorphisms; [20, 21]), the introduction of AFLPs (amplified fragment length polymorphisms; [22]), SSRs (simple sequence repeats; [23]), and DArT (diversity array technology; [24]) markers improved substantially the assembly of genetic maps. More recently, high-throughput platforms based on SNPs (single nucleotide polymorphisms), the most frequent polymorphism in living organisms, have enabled a quantum leap in saturating maps with thousands of markers [25–29]. Notably, the spectacular advances obtained with next-generation sequencing (NGS) technology will soon allow for the resequencing of entire mapping populations and association mapping panels of species for which a template sequence is

available, thus providing an almost endless supply of markers [30–34].

Once all the molecular and phenotypic data are available, statistical tests will be applied to verify whether the means of the trait values of the genotypes carrying different alleles at a particular marker are significantly different. A test statistic larger than a threshold value rejects the "null hypothesis" (i.e., the mean is independent of the genotype at a specific marker locus) and implies a significant association between the investigated marker and a linked locus that affects the phenotypic value of the target trait. The exploitation of syntenic relationships among phylogenetically related crops has greatly contributed to the identification of additional markers at target regions [35–37] and, most importantly, candidates for the investigated traits, particularly when the genome sequence of one or more of the syntenic species becomes available. This is the case of cereals, where the annotated sequence for rice, *Brachypodium*, sorghum, and maize has allowed for the identification of conserved orthologous set (COS) markers from ESTs that have maintained their microlinearity throughout evolution and speciation [37]. These markers are particularly valuable to assess the possible role of candidate genes in species not yet sequenced (e.g., wheat) and to identify orthologous sequences that have maintained their functions and colinearity across species. Thus, a good understanding of the syntenic relationships at regions underlining a QTL for rather simple traits can provide excellent clues to pinpoint the most likely candidate.

Notably, mapping loci controlling the target traits allows breeders to implement marker-assisted selection (MAS) on the basis of the polymorphic molecular markers flanking the relevant loci. Traits are usually categorized as monogenic (qualitative or Mendelian traits controlled by a single locus) and polygenic (or quantitative; controlled by many loci), the latter being highly influenced by environmental conditions and considerably more difficult to improve consequent to their lower heritability, [38]. Quantitative traits (e.g., flowering time, plant height, biomass production, yield, etc.) are particularly important for breeding purposes. Although the genetic dissection of both qualitative and quantitative traits relies on similar principles, the latter requires more extensive phenotyping and much larger mapping populations.

The prevailing assumption in the field of quantitative genetics has been that continuous variation in trait performance is caused by the segregation and action of multiple genes with a rather similar effect on the phenotype, together with a major influence of the environment which acts like some sort of "statistical fog" that blurs and limits our capacity to identify the genes that control the target trait. These genes, also referred to as polygenes, are known as quantitative trait loci (QTLs; [39]). Although the original concept – but not the acronym – of QTL mapping was first suggested in 1923 [40], the dissection of quantitative traits became eventually possible in the 1980s and the 1990s with the introduction of molecular marker platforms that allowed for genome profiling with the needed level of genetic resolution [41–45]. Two decades of dedicated experiments indicate that most QTL effects are of small magnitude as originally predicted by the so-called infinitesimal model [38, 46, 47]. This notwithstanding, a limited number of so-called major QTLs have shown a rather large effect and, in a number of cases, have been cloned [48, 49]. Once a QTL has been cloned, both genomics and genetic engineering offer additional opportunities for tailoring improved cultivars and crossing reproductive barriers among species, thus expanding the repertoire of genes available to breeders. In view of the importance of quantitative traits in breeding activities and crop performance, particular attention should be devoted to QTL mapping and the implementation of MAB for this category of traits.

Biparental Linkage Mapping

The early studies in QTL mapping were conducted based on the analysis of the means at single markers using simple test statistics, such as linear regression, *t*-test, and analysis of variance. Because a genome-wide survey typically involves a large number of markers, the probability of detecting one or more false positives at the whole-genome level quickly increases unless the threshold of significance is adequately readjusted according to the number of tested markers [50]. Typically, a threshold level of $P_{0.05}$ entails a false-positive discovery rate (i.e., declaring the presence of a locus able to affect the target trait when actually there is no locus) of approximately 5%. Consequently, a mapping experiment based on 100 markers tested at $P_{0.05}$ will

identify, on average, five markers putatively associated with loci even when no real locus segregates in the population. In order to avoid this problem, the significance threshold is corrected accordingly through a multiple test adjustment (e.g., Bonferroni's or Tukey's) that will adjust the *P* level according to the number of independent statistical tests that are performed. This notwithstanding, a much more critical shortcoming of this single-marker approach is that no information is provided on the most likely position of the locus and its effects on the phenotype. Due to these major limitations, single-marker analysis was quickly replaced by interval mapping and similar methods based on the estimated linear order of markers on a genetic map. In comparison to single-marker analysis, interval mapping provides a much more accurate estimate of the position and genetic effects of each locus [51–53]. In interval mapping, statistical methods are applied to test for the likelihood of the presence of a QTL. The result of the likelihood tests carried out at regular intervals across the ordered markers is expressed as LOD (Logarithm of the ODds ratio) scores, computed as the $\log_{10}$ of the ratio between the chance of a real QTL being present given the phenotypic effect measured at that position, divided by the chance of having a similar effect when no QTL is present. Thus, LOD values of 2.0 and 3.0 indicate that the presence of the QTL is 100- and 1,000-fold more likely than its absence, respectively. The graphical output is an LOD profile that allows one to compute an empirical confidence interval (usually computed as LOD – 1) around the QTL peak. In order to avoid declaring false-positive QTLs (i.e., declaring the presence of a QTL when the QTL is actually absent), a reasonably high threshold value for the LOD score should be set (usually > 2.5). Iterative software based upon resampling procedures provides a more accurate estimate of threshold values according to the size of the mapping population and the number of markers [54].

Epistasis can greatly influence the outcome of interval mapping. This problem can be partially overcome with the use of composite interval mapping, a statistical procedure that can account for the effects of other QTLs inherited independently from the interval (i.e., chromosome region) being considered, thus reducing the possibility of detecting "ghost" (i.e., false) QTLs. Compared to single-QTL interval mapping, statistical approaches for locating multiple QTLs are more powerful because they can differentiate between linked and/or interacting QTLs that will otherwise go undetected when using single QTL interval mapping. Given the potential impact of epistasis on the response to selection, quantifying its influence on target traits is an important component for designing and organizing any MAS strategy [55]. It is likely that the incorporation of epistatic interactions into more properly devised statistical models will play a relevant role in explaining complex regulatory networks governing the expression of quantitative traits.

A major shortcoming of QTL studies is the low accuracy in detecting the real number of QTLs affecting the genetic variation of the investigated traits, particularly with populations of less than 150–200 families, which is the case in the majority of QTL studies reported so far. A simulation study applied to experimental data showed that with populations of ca. 100–200 families only a modest fraction of QTLs was identified; furthermore, the effect of each single QTL was usually overestimated [56]. Another study showed that detection of QTLs of small effect is very difficult with mapping populations with less than 500 families [44]. These predictions were supported in experiments carried out with maize mapping populations large enough (>400 families) to allow for a meaningful subsampling [57, 58]. Therefore, the chance of detecting a QTL in several environments is small even in the absence of QTL × Environment (QTL × E) interaction. Accordingly, inconsistency of QTL detection across environments has been repeatedly reported [59, 60].

Association Mapping

In the past decade, as an alternative to linkage mapping with biparental populations, association mapping based on the evaluation of panels of unrelated accessions (ca. 150 or more) has been adopted as an additional option for trait dissection [61–65]. The assumption underlying the use of association mapping to detect the presence of loci influencing the target trait is that alleles at two closely linked loci share a historical ancestor, and this original co-occurrence will gradually decay in the population due to recombination events during subsequent meioses. Consequently, the relative

allele distributions of an unknown gene and that of a closely linked marker will be nonrandom because the two are in LD. A major factor to be considered for a correct application of association mapping is the presence of population structure, which will significantly bias the results and inflate spurious marker-trait associations (i.e., declaring false positives). Algorithms and methods are being developed to correct for these effects. An important advantage of association mapping is that the linkage is evaluated over the large number of historic meiosis, which in turn entails a much lower LD and higher genetic resolution as compared to linkage mapping with biparental populations. Another advantage is that the genetic variability explored by a large panel of unrelated accessions is much larger than that present in a segregating population derived from two parental lines. Conversely, a major shortcoming of association mapping is that it does not allow for the detection of the effect that a rare, but otherwise agronomically valuable, allele may have on the target trait. In fact, the statistical procedures used for revealing the effects associated to a particular locus/haplotype consider only alleles with a frequency higher than 10% over the entire population; alleles with a frequency lower than 10% are considered rare and as such, are discarded. The cutoff threshold of 10% has been introduced to reduce the ascertainment bias that a small sample (i.e., less than 10%) of accessions would inevitably introduce, being unable to correctly represent the effect of that particular allele at the level of the entire population [62]. Clearly, this is not an issue when dealing with mapping populations where allelic frequencies are expected to be equal to ca. 50%, barring the presence of genetic factors that might influence the transmission of gametes carrying the different parental alleles. In association mapping, the procedure of discarding the individuals carrying rare alleles inevitably reduces the statistical power to identify the role of such loci in controlling the variability measured for the target trait. An example of this has recently been reported in durum wheat, where a locus with a large effect on yield in a biparental cross [162] showed no appreciable effect in a parallel association mapping study where only one of the parental alleles was considered, due to the fact that the other parental allele was present in low frequency [65].

The main factors to be carefully considered for optimizing the effectiveness of association mapping are the level of LD among the investigated accessions and the presence of population structure that could greatly increase the false-discovery rate (i.e., type-I error). Closely related to the concept of LD is the concept of "haplotype," which can be defined as the chromosome fragment carrying a common set of marker alleles in close linkage at adjacent loci [66]. When using haplotypes in association studies, the information of several linked bi-allelic markers is combined as a single, multi-locus informative marker. Haplotypes can be generated *in silico* from sequences deposited in the database, by resequencing target loci (sequence haplotypes) or genetic maps (marker haplotypes). Therefore, haplotypes will extend according to the level of LD, the value of which varies greatly (up to 100-fold or even more) not only among species, but also within a single species according to the frequency of crossing-over events in each chromosome region. As an example, centromeric regions are characterized by very low recombination if compared to subtelomeric, gene-rich regions. Populations characterized by high LD (i.e., extending for > 1 cM, corresponding to several million base pairs (bp) depending on the ratio of the genetic and physical distance) are best suited for a genome-wide search [65]. Alternatively, the utilization of panels with a low LD (i.e., extending < 10,000 bp, typically a small fraction of 1 cM), a condition that is typical of allogamous species like maize [67], allows for a much higher level of genetic resolution and for the validation of a candidate sequence. Clearly, the level of LD influences the number of markers/cM required to obtain meaningful information. As compared to a low LD condition, a high LD level is associated with a proportionally longer haplotype, hence requiring a lower number of markers to conduct meaningful genome-wide surveys. This feature is more prominent in elite materials that have undergone high selection pressure as a result of modern breeding practices, which in most cases has led to a reduction of haplotype diversity as compared to locally grown landraces and, more notably, wild relatives of crops that have not gone through the domestication bottleneck. As an example, LD in wheat – a selfing species that has undergone a very stringent selection mostly due to the importance of quality

parameters required by the food industry – extends up to 5–10 cM [65], while in outcrossing species like maize LD is usually below a fraction of cM or even less than 10,000 bp [68]. An example of the high level of genetic resolution made possible through association mapping is shown by the fine mapping and, in one case, positional cloning of QTLs for flowering time in maize [67, 68]. In particular, association mapping revealed that the most important QTL for flowering time per se (i.e., independently from photoperiod sensitivity) in maize corresponds to a 2.3 kb, noncoding, long-distance enhancer region located 70 kb upstream of a gene known to regulate flowering time also in *Arabidopsis* [49]. Another remarkable example in which the functional polymorphism responsible for phenotypic variability was assigned to a noncoding region far (ca. 5,000 bp) from the structural gene has been reported in sorghum through the cloning of a major QTL for aluminum tolerance [69]. Clearly, only a positional cloning approach is able to unequivocally highlight the role of noncoding regions in controlling the level of expression of a particular gene and the resulting phenotype. To what extent noncoding, long-distance enhancers might be involved in regulating the expression of quantitative traits is presently unknown. Notwithstanding the importance of this issue for a more complete understanding of the regulation of gene expression, this level of genetic dissection is certainly not required from a breeding standpoint, since both MAS and genetic engineering would still allow breeders to fully exploit the beneficial effects linked to either natural allelic variation or the ectopic expression of the structural locus encoding for the target trait.

Despite the clear advantages of association mapping on biparental linkage mapping (e.g., multiallelism, higher genetic variability and genetic resolution, no need to assemble a mapping population, shorter time required to identify relevant loci, etc.), a major limitation of the former is represented by the high rate of false positives (i.e., Type-I error rate), hence spurious association, due to the presence of hidden population structure among the accessions being evaluated [62]. An additional constraint to a more widespread utilization of association mapping for the dissection of physiologically complex traits may derive from factors other than statistical issues. For highly integrative and functionally complex traits such as yield, particularly under adverse conditions, association mapping may quickly lose its effectiveness as the level of functional complexity of the target trait increases. In this case, similar phenotypic values in different genotypes can result from the action of different gene networks and/or trait compensation (e.g., yield components), thus undermining the identification of significant marker-trait association across a broad range of genotypes such are those usually present in the panels used for association mapping. Although a similar limitation also pertains to a mapping population developed from the cross of two divergent lines, its relevance in the case of association mapping for complex traits is greatly increased by the much wider functional variability explored with association mapping. This is particularly the case whenever the investigated trait (e.g., yield under drought conditions) is strongly influenced by differences in phenology, mainly flowering time and/or plant height; in this case, the overwhelming effects on yield of phenological traits will inevitably overshadow the effects due to the action of loci controlling yield per se, i.e., irrespectively of flowering time and plant height.

Comparative QTL Mapping and Metanalysis

A major shortcoming in QTL mapping is the limited accuracy in identifying the most likely position of each single QTL on the chromosome. Unless highly isogenic materials are evaluated, the confidence interval in assigning a QTL is rarely shorter than 10 cM, an interval likely to contain several hundred genes. The availability of QTL data for two or more mapping populations of the same species allows for the comparison of the position of QTLs by means of a metanalysis carried out with dedicated software [70]. This, in turn, provides a better genetic resolution of the QTL interval and reduces the confidence interval around the peak of the LOD profile. This exercise is particularly useful when a reference map with hundreds of well-spaced markers is available and contains "anchor markers" (usually RFLPs, SSRs, and/or SNPs) also used to investigate other mapping populations of the same species. An additional advantage of a reference map is that it allows one to compare the map position of QTLs with that of mutants for the same trait, thus contributing relevant information for the identification of possible

candidate genes causally affecting the investigated trait. Accordingly, Robertson [71] suggested that a mutant phenotype may be caused by an allele with a much more drastic effect in comparison to that of QTL alleles at the same locus, a hypothesis that has been validated in maize for a QTL for plant height colocalized with the mutant *dwarf3* [72]. These results indicate that no real boundary exists between Mendelian and quantitative genetics, while suggesting that loci can be classified in either category based upon the magnitude and heritability of the effect of the alleles being considered. It follows that the information provided by mutants is of great value for QTL studies and breeding applications.

Isogenic Materials for Mapping and Cloning QTLs

A valuable opportunity for investigating the effects of a particular QTL and eventually isolate the functionally polymorphic sequence responsible for its effects is offered by the analysis of pairs of isogenic materials (e.g., near isogenic lines: NILs) contrasted for the parental chromosome regions (usually ca. 10–30 cM long) present at the target QTL. NILs can be obtained through repeated selfings of F_3-F_5 individuals heterozygous at the QTL region prior to isolating the homozygotes for each one of the two parental segments carrying the functionally contrasting QTL alleles [73]. Alternatively, each parental line of the mapping population originally evaluated for discovering the QTL can be used as recurrent parent in a backcross scheme in which a single genotype heterozygous at the QTL in question is utilized as donor of the alternative QTL alleles; in this case, the congenic lines are identified as backcrossed-derived lines [74]. With NILs, it is thus possible to "mendelize" major QTLs characterized by a sizable additive effect. Unlike genome-wide QTL studies where more than 100–150 genotypes are usually screened, experiments conducted with NILs involve few genotypes (two as a minimum), thus allowing for a much more refined and detailed phenotypic evaluation of the effects of the QTL [74, 75]. However, it should always be appreciated that the results of NIL-based studies could to a certain extent be biased by the action of one or more closely linked genes affecting the investigated traits, a particularly likely event when the region flanking the QTL extends for several cM.

A more systematic search of QTLs is made possible with the use of a series of isogenic lines obtained through the introgression, via backcrossing, of a small portion (ca. 20–30 cM) of the genome of a donor line into a common recurrent line, usually an elite cultivar [76]. The final objective is to assemble a collection of so-called introgression library lines (ILLs; at least 70–80 or more lines for each cross), basically a collection of NILs, each one differing for the introgressed chromosome portion and collectively representing the entire donor genome [76]. A major advantage of ILLs is the rapid progress that they allow for the fine mapping and positional cloning of major QTLs [48, 77]. Besides the well-documented effectiveness of ILLs for the mapping and cloning of QTLs in tomato [77, 78], ILLs have been instrumental for mapping drought-adaptive QTLs in rice [79] and maize [163]. Once ILLs are made available and major loci for the target traits are identified, testing for epistasis becomes particularly feasible using a small number of genotypes, unlike with mapping populations, where an accurate testing for epistasis will require the evaluation of at least 200 families.

The availability of NILs for a major QTL is an important prerequisite for undertaking the cloning of the sequence underlying the trait being targeted. Besides contributing to a better understanding of the functional basis of quantitative traits [68, 80], QTL cloning provides an essential opportunity for more effectively mining and exploiting the allelic diversity present in germplasm collections [49, 82]. Recent advances in high-throughput profiling and sequencing of both the genome and transcriptome coupled with reverse-genetics approaches/platforms (e.g., collections of knockout mutants, TILLING, RNAi, etc.) have streamlined the procedures and markedly reduced the time required to identify the sequences governing variation in quantitative traits. Until now, the molecular dissection of a candidate locus has been prevailingly achieved through positional cloning and association mapping. Both approaches exploit LD to identify the most promising candidate gene(s) and benefit from the map information of candidate genes and mutants in the species under investigation and in closely related ones. As sequence information accumulates and our understanding of biochemical pathways improves, QTL cloning via the candidate-gene approach becomes

an attractive alternative to positional cloning, particularly for traits underlined by a known metabolic pathway [83, 84].

Modeling QTL Effects

QTL-based modeling holds promise to allow for a more effective design of "molecular ideotypes" on the basis of estimated QTL effects for growth parameters of response curves to environmental factors revealed by exposing mapping populations to such environmental factors [85–87]. Additionally, crop modeling provides useful clues to unravel the genetic basis of G × E interactions and toward a better understanding of traits' plasticity [88], a feature of increasing importance in view of the effects on crop growth and yield due to the enhanced vagaries in weather conditions consequent to global warming. An accurate estimate of the consistency of QTL effects in a particular genetic background can be obtained through extensive testing of the genetic materials under different environmental conditions as to level of irrigation, nutrients, temperature, etc.

In maize, an ecophysiological model and QTL analysis have been integrated to investigate the genetic basis of leaf growth in response to drought and predict leaf elongation rate as a function of estimated QTL effects at varying air humidity, temperature, and soil water status (Tardieu 2003). QTLs with a limited QTL × E interaction and with a linear response to a particular environmental factor will provide more predictable opportunities to improve crops' performance through MAS. An important issue rarely addressed in view of the inherent difficulty in doing so from an experimental standpoint under field conditions is that crop performance is often constrained by more than one environmental factor (e.g., drought and heat) occurring simultaneously, a condition which greatly undermines the prediction of QTL effects, particularly when considering multiple QTLs.

Marker-Assisted Breeding to Improve Crop Performance

The improvement of crop performance through conventional breeding has for the most part been achieved with little or no knowledge of the genetic basis of the selected traits, particularly yield and its underlying morphophysiological determinants. The main obstacle to raising crop yield via conventional breeding by means of phenotypic selection is represented by the low heritability of yield, particularly under marginal conditions and low-input agriculture (e.g., low supply of nutrients and/or water). As an alternative to phenotypic selection, MAB can be applied to more effectively improve crop performance. The ultimate goal of MAB is to increase the cost-effectiveness of the selection gain per unit time. Although the costs entailed by MAB are still quite high when compared to conventional breeding practices, the sizable reduction in the time required to release an improved cultivar made possible through MAB can justify its application once agronomically valuable alleles at target loci (genes or QTLs) are identified. The convenience of adopting MAB to improve the efficiency of the selection process should be carefully evaluated on a case-by-case basis. The success of MAB will depend on the identification of the agronomically beneficial alleles at target loci, their effect in the different elite genetic backgrounds prevalently grown by farmers and their pyramiding in the correct combinations. MAB could thus be regarded as an extension and evolution of the so-called ideotype breeding, an approach based on phenotypic selection for an ideotype characterized by those morphophysiological features deemed necessary to maximize yield. As compared to ideotype breeding, MAB allows us to dissect the genetic basis of key traits and to piece back together the best alleles in a sort of molecular jigsaw puzzle, the main limitation being that only a very small number of the jigsaw tassels (i.e., genes and QTLs) have been identified. This approach, referred to as "breeding by design" [89], extends the concept of "graphical genotypes" first introduced by Young and Tanksley [90] to portray the parental origin and allelic contribution of each genotype on a genome-wide basis. Although a breeding-by-design approach is technically applicable to all major crops, its impact has been much more tangible for traits with a simple genetic control (e.g., quality, disease resistance; [91–95]) as compared to more complex quantitative traits, such as yield under adverse environmental conditions [60], a result mainly due to our rudimental understanding of the genetic basis of the latter category of traits, their interaction with environmental factors and, most importantly, the difficulty in predicting the phenotypic value of a new

genotype tailored through MAB for several QTLs. Along this line, it should be underlined that the effects of QTL alleles for complex traits (e.g., yield) characterized by a large G × E interaction can drastically change according to the conditions (e.g., water availability along the crop life cycle) present in the environment being targeted.

The molecular profiles obtained with molecular markers provide the basic information required to identify the haplotype of each individual plant at a target locus. Haplotype profiling of collections of elite cultivars released during the past decades and derived from a limited number of founders (i.e., genotypes that in view of their positive features have been frequently used by breeders as parental lines) provides a means to identify the chromosome regions that have been preferentially retained throughout the breeding activities carried out during such time period. It is plausible to hypothesize that these chromosomal regions harbor loci (genes or QTLs) important for the selection of improved cultivars.

The strategies deployed to improve crop performance based on molecular information can be categorized according to the level of knowledge and understanding of the loci that underline the phenotypic traits under selection. While MAS and marker-assisted recurrent selection (MARS) during the past two decades have deployed allelic variation at mapped loci often characterized by a rather large effect on the phenotype, the new paradigm ushered in by genomic selection (GS) via high-throughput profiling has emphasized the selection of unmapped, uncharacterized loci with rather limited individual effects but with otherwise sizable effects when selected together. The next sections will critically analyze some of the main features of these rather different approaches that should not be regarded as antagonistic, but rather complementary.

Marker-Assisted Selection

Once loci are mapped and their effects characterized, the two most common applications of MAS in crop breeding are to (1) accelerate the backcross (BC) procedures required to transfer beneficial alleles at one or more loci into an elite cultivar and (2) facilitate the selection of one or more target traits within a segregating population. The former application is the one that so far has been most frequently adopted in breeding programs and is usually referred to as marker-assisted backcross (MABC). MAS has also been deployed frequently to create isogenic lines (e.g., NILs, introgression libraries, etc.). These materials are used to identify and map genes/QTLs and, as such, usually do not impact directly on the outcome of breeding practices and the release of improved cultivars.

As compared to the conventional BC procedure, MABC based on the use of markers uniformly spaced along the genome (ca. 20–25 cM apart) can save three to four BCs in recovering most of the genome of the recurrent parent, thus reducing the time required for the release via BC of the improved version of the recurrent parent [96]. The advantage is greater for the incorporation via BC of recessive resistance genes, the phenotypic detection of which is only possible for the homozygous individuals carrying recessive alleles at both loci. In this case, phenotypic selection takes twice longer as compared to dominant alleles, since a selfing generation is required after each BC for the phenotypic identification of the homozygous recessive resistant plants to be used for the next BC. The utilization of codominant markers (e.g., SSRs) allows for the identification of heterozygous plants carrying the resistance-encoding allele directly in F_1, thereby saving one generation for each BC cycle. During the past two decades, MABC has been routinely deployed by seed companies to introgress beneficial alleles from unadapted accessions (e.g., landraces or wild, sexually compatible relatives of crops) and particularly to introgress transgenes into elite materials [9, 97, 98]. At each generation, individuals heterozygous at the region flanking the target locus are identified based on the results of molecular profiling. In comparison to conventional BC, MABC provides additional, distinct advantages such as (1) avoiding the vagaries in phenotyping when the conditions do not allow an accurate classification of the progeny segregating for the target trait (e.g., absence of the pathogen when backcrossing an allele for resistance to the disease), (2) reducing the number of plants to be screened in each selection cycle, and (3) identifying plants with the shortest possible chromosome segment introgressed from the donor line. The latter factor is particularly

important when the donor is a wild accession of the recurrent, elite line being backcrossed. In this case, the introgressed chromosome segment flanking the target locus is likely to contain many alleles with a detrimental effect on quality and yield. Therefore, it is necessary to select individuals with the shortest possible chromosomal fragment contributed by the donor parent. An additional benefit is when the phenotyping of the trait under transfer is expensive and/or cumbersome like in the case of genes affecting tolerance to diseases/pests that require artificial inoculation in order to correctly identify those plants carrying the tolerant alleles (e.g., resistance to nematodes; [99]). Other cases where MABC provides a distinct temporal advantage as compared to conventional procedures is when the phenotypic evaluation of the target trait is destructive or when the trait is expressed after flowering. Selection before flowering greatly reduces the number of plants to be selfed or crossed, thus reducing the operating costs, particularly with species with a long life cycle.

During backcrossing, different rates of recovery of the recipient genome are expected at the target region and the nontarget chromosomes. Because each BC reduces by half the percentage of the donor genome at nontarget regions, at least six or seven BCs are required for a satisfactory recovery (ca. 99%) of the recipient genome. However, the number of BCs is frequently higher due to residual linkage drag around the target locus and it is not uncommon that up to nine or ten BCs are implemented before the improved cultivar is finally released. Clearly, the longer the time required to complete the BC procedures, the lower the probability of success of the new cultivar, since other improved, competing cultivars will be released in the meantime. Simulation and practice have both shown that in a moderately sized population of a species with a relatively small genome (<500 million bp, such as rice) using more than two to three well-spaced markers per chromosome arm hardly brings any additional benefit. For a species with large chromosomes (e.g., wheat, ca. 16 billion bp), a larger number of markers in each chromosome are beneficial. With an increasing genome size, more independent recombination events are needed to reduce the contribution of the donor parent, which in turn requires a larger population size. To what extent the contribution of the donor parent should be reduced will depend on the type of alleles carried by such fragments and, most importantly, the genetic distance between the donor parent and the recurrent parent. Nowadays, the availability of large number of SNPs in most of the major crops facilitates the screening of the BC individuals to verify in great detail to what extent the genome of the donor parent has been retained.

Formulas are available to compute the level of concordance between the allelic state at the target locus and the flanking markers during the BC procedures [81]. These formulas values indicate that the level of control made possible with only one marker is insufficient to keep the risk of losing the target allele below 5% throughout five cycles of BC. Conversely, the level of control possible with two flanking markers is considerably higher even when the markers are not tightly linked to the target locus. If the BC procedure targets a QTL instead of a Mendelian locus, the uncertainty about the exact position of the sequence underlining the QTL introduces further complexity. Because the quantity of donor genes on the carrier chromosomes decreases much more slowly in comparison to the noncarrier chromosomes, after six BCs the majority of heterozygous loci with undesirable donor alleles will be on the carrier chromosome, with the vast majority included in the intact fragment flanking the target locus.

At the chromosomes not targeted by the BC procedure, it is expected that after "n" BCs, the probability that any locus remains heterozygous between the donor and the recipient is $(0.5)^n$, which means that each BC halves the residual level of heterozygosity. Consequently, six BCs ensure a level of similarity with the recurrent parent above 99%. Results in different species have shown that there may be a significant deviation from the 75% genomic portion of the recurrent parent expected in the BC_1 generation [100, 101], thus demonstrating the usefulness of genotype-based selection to identify plants with the highest possible portion of the genome from the recurrent parent.

Pyramiding Beneficial Alleles at Multiple Loci

The possibility to rapidly introgress and pyramid into existing cultivars a suite of beneficial alleles allows breeders to more quickly release improved cultivars to

farmers. The best examples are in the area of disease resistance. Monogenic (Mendelian) resistance based on a single major gene is usually nondurable due to the high mutation rate in plant pathogens, which can lead to the selection of new virulent strains able to overcome the physiological barrier of an individual resistance gene. Consequently, the durability of disease resistance can be increased by screening for new sources of resistance followed by marker tagging of the relevant genes and their incorporation in elite cultivars. Pyramiding identifies the procedure for stacking the beneficial resistance alleles in a single line or cultivar, which provides a more durable resistance to pathogens as compared to monogenic resistance based on a single major gene. The advantage of pyramiding multiple alleles for resistance is particularly evident with diseases that require repeated inoculation and when phenotypic selection alone is too cumbersome and fails altogether to detect and combine multiple resistance genes in a single genotype.

Direct disease screening based on phenotypic observations is not always desirable due to a number of factors: quarantine restrictions, lack of routine screening methods and informative pathogen races for discriminating specific resistance genes, host escapes, and/or the inability to identify specific genes or gene combinations due to the occurrence of race or pathogen mixtures in the field. In these cases, MAS of race-specific genes offers a viable alternative for stacking beneficial alleles in improved genotypes which will eventually turn into novel cultivars characterized by more durable resistance to rapidly changing pathogen populations. Along this line, the constant changes in pathogen populations in different environments underline the potential value of previously defeated resistance genes. In this case, MAS offers the only practical solution to maintain such genes in current cultivars since they are masked by the epistatic effects of other resistance genes that are still effective.

In all major crops, the availability of markers tightly linked to resistance loci now allows breeders to tailor new cultivars with a suite of resistance genes able to enhance durable disease resistance to highly variable pathogens [102]. In broader terms, pyramiding is also implemented for combining beneficial alleles at loci (Mendelian or QTLs) that control traits other than disease resistance. In wheat, alleles at major loci that influence quality (e.g., semolina color, protein content, micronutrient concentration, etc.) and tolerance to abiotic stress (e.g., aluminum, boron, salinity, etc.) are routinely introgressed via MABC [94].

When multiple loci are targeted in a BC program, the minimum population size to be considered increases considerably and rapidly becomes a major limiting factor when more than three or four loci are targeted, a number that can be increased to five or six when Mendelian loci are considered. When the targeted loci are QTLs, the uncertainty of the exact location of each selected QTL adds further constraints and reduces the number of loci that can be selected with a population of manageable size. When different lines contribute the beneficial alleles, the easiest strategy is to cross them to produce recombinant progenies and select the desired individuals. Multiple crosses might be required to pyramid all the desired alleles in one single genotype. A more general framework and the underlying theory to optimize breeding schemes for gene pyramiding have been described [103].

Marker-Assisted Selection in a Segregating Population

MAS has been extensively used for the selection of single genes conferring tolerance to diseases/pests [91, 94, 102, 104–106]. Although early simulation studies suggested the effectiveness of MAS for the improvement of biparental populations segregating for moderately complex traits [107], the first applications of MAS in maize were disappointing [57, 108]. Sweet corn is the only exception, the main reason being its much narrower genetic basis as compared to maize used for feed production, a feature that increases the reliability of predicted gains from selection and extrapolation of the effects of different loci to different populations [109]. Another feature that makes the application of MAS particularly attractive in sweet corn is the high costs associated to conventional phenotyping, in view of the large amount of grain that needs to be processed in order to obtain an accurate estimate of the phenotypic values of the progeny to be selected. MAS applications have been more widespread in the private sector as compared to public institutions, most likely owing to a lack in the latter of the infrastructure required for an effective exploitation of MAS.

Notwithstanding the remarkable progress in identifying and in some cases cloning major loci regulating agronomically valuable traits [48, 49], more limited success has been reported for MAS of quantitative traits [110], mainly due to the difficulty in identifying major QTLs with a sufficiently large and stable effect for justifying their deployment via MAS. While true QTL × E interaction due to variable expression of a trait may cause lack of consistency in QTL detection particularly with traits characterized by low to moderate heritability, the interaction between a mapping population of small size – hence with limited power in QTL detection – with variable environments is probably an equally important factor causing inconsistency in QTL detection. This is particularly evident for the improvement of crop yield under drought conditions, one of the most difficult traits to improve not only via MAS [14, 60, 111–113] but also through conventional breeding.

Marker-Assisted Recurrent Selection

Although marker-assisted recurrent selection (MARS) was first proposed in the early 1990s [114], only recently its adoption has provided a tangible contribution to crop improvement, mostly due the difficulty in identifying multiple loci characterized by limited G × E interaction and reasonably consistent effects in different genetic backgrounds other than that in which they were originally identified. The goal of MARS is pretty much similar to that pursued in pyramiding alleles at multiple loci, i.e., accumulating the beneficial alleles at as many as possible, preferably all, loci being targeted. Pyramiding alleles at many loci (e.g., >10) is best achieved with a recurrent selection strategy [115]. In this case, simulation showed that with 50 QTLs and a population of 200 plants the frequency of favorable alleles reached 100% after ten cycles when markers cosegregated with the QTL (i.e., they coincided), but only 92% when the marker-QTL interval was equal to 5 cM, hence increasing the possibility of losing the desired QTL allele due to recombination. In practice, with a higher number of loci under selection the occurrence of plants carrying the desired ideal combination becomes increasingly unlikely and basically impossible when more than 20 loci are targeted simultaneously. This problem can be partially mitigated through successive cycles of crossing individuals carrying complementary combinations of the desired alleles [89]. This concept can be extrapolated to crosses with multiple parents.

MARS can start irrespectively of knowing the map position of the desired loci, which instead can be identified during the selection process. Simulation has clearly shown the superiority of MARS over phenotypic selection (from 5% to 20%), particularly when the selected population is highly heterozygous [116]. In maize, MARS has been applied rather extensively for improving relatively complex traits such as disease resistance, tolerance to abiotic stress, and also grain yield [111, 117–119].

The outcome of both MAS and MARS within a segregating population can be influenced by the genetic makeup of the targeted genetic background in terms of alleles present at other loci that interact epistatically with the target locus, an aspect which becomes particularly relevant for quantitative traits in view of the high number of loci involved in their control. Accordingly, since most evaluations of QTL effects and MAS strategies assume that QTLs act independently [55], it has been argued that MAS has little if any power over traditional phenotypic selection [46]. With maize as a model species, computer simulation showed that gene information is most useful in selection when few loci (<10) control the trait, while with many loci (>50) the least squares estimates of gene effects become imprecise. Based on these results, the typical reductionist approach pursued through QTL discovery strongly limits the outcome of MAS carried out for traits controlled by many QTLs [46].

Genomic Selection

In genomic selection (GS), genetic markers in number sufficient to cover the entire genome according to the level of LD are used so that most QTLs controlling the trait being selected are in LD with at least one neighboring marker. Unlike in MAS, in GS the individual plants are chosen without mapping the underlying QTLs that remain unknown along the entire process. Originally devised for animal breeding, only recently has GS been adopted for improving crop performance [120–122]. This was due to the fact that only in the past few years its application has become technically feasible

in plants thanks to the introduction of SNP profiling with a level of genome saturation sufficient to detect the cumulative effects of the plethora of minor QTLs affecting quantitative traits which, on a single basis, will inevitably remain undetected in a biparental mapping population.

In GS, the breeding values of all the markers distributed across the genome are fitted as random effects in a linear model. The trait values are then predicted as the sum of the breeding values of each individual genotype across all the profiled markers and selection is based on these genome-wide predictions. A simulation study showed that across different numbers of QTLs (from 20 to 100) and levels of heritability, the response to GS was from 18% to 43% higher as compared to MARS. The number of markers that are used to predict the breeding values usually varies from a minimum of ca. 200 up to 500. A higher number of markers are required as the functional complexity of the targeted trait increases and LD decreases. Notably, GS is most effective for complex, low-heritable traits controlled by a large number of QTLs.

Implementation of GS is already having a major impact on the improvement of yield and other complex traits, mainly in the private sector where high-throughput infrastructures and robots allow for the routine creation and handling of millions of datapoints. Clearly, GS is not antagonistic to either MAS or MARS. Rather, they should be deployed in a complementary fashion on a case-by-case basis and according to the availability of mapped major QTLs, the accurate evaluation of their effect, and the frequency of the agronomically desirable alleles in the germplasm under selection.

Integrating Marker-Assisted Breeding in Conventional Breeding Projects

Among other factors, a broader application of MAB in conventional breeding projects will depend on the cost of molecular profiling [123, 124]. SNP markers are ideally suited for this role. In maize, the cost-effectiveness of MAS for the introgression of a single dominant allele into an elite line was compared with that of conventional breeding [125]. In this particular case, neither method showed clear superiority in terms of both cost and speed: Conventional breeding schemes were found to be less expensive while MAS-based breeding schemes were shown to be faster. High-throughput genotyping based on the scoring of markers that do not need the use of gels [126–128] coupled with quick DNA extraction protocols are needed to streamline MAS and lower its cost.

An important factor to be carefully considered prior to embarking in any MAS activity targeting specific loci is the robustness of the marker-locus association and their genetic distance. Clearly, the level of LD of the genetic materials used to investigate the genetic makeup of the target traits plays a pivotal role in determining the level of genetic resolution. Accordingly, biparental F_2 populations have the maximum amount of LD, hence the lowest level of genetic resolution. Although this feature is advantageous for the initial QTL mapping studies in view of the limited number of markers that are required, it clearly limits the accuracy of MAS and usually does not allow us to resolve tightly linked QTLs from pleiotropic ones [129]. This problem can be circumvented by deploying genetic materials that capture a higher recombinational level, either historically (e.g., panels of unrelated genotypes suitable for association mapping; [67, 130]) or through subsequent random matings of the individuals of the original mapping population [131]. Increasing the genetic resolution not only enhances the reliability of MAS but also reduces the list of the possible candidates, an important prerequisite in identifying the sequence responsible for the phenotype of interest. Therefore, prior to undertaking an association mapping study, it is important to acquire a good understanding of the LD patterns in the set of genetic materials to be evaluated. In fact, LD can be caused by factors other than linkage. Spurious associations in a collection of germplasm accessions can be due to LD between unlinked genomic regions (i.e., >50 cM apart) on the same chromosome and/or between genomic regions located on different chromosomes. Dedicated softwares are available to reduce the frequency of false-positive associations due to the bias introduced by preexisting population structure.

One of the most critical steps in any breeding program is the choice of suitable parental lines to create the new segregating populations that will undergo selection. Ideally, such parental lines will contribute beneficial alleles at the loci most critical for the target traits

and, more in general, crop performance and its quality. Molecular profiling can contribute in two major ways to expedite the selection process and increase the response to selection. In autogamous crops, MAS is applied to choose the parental lines that are crossed to generate new mapping populations (mostly biparental) and then to select during the subsequent generations the recombinant progeny that carry the desired alleles at the targeted loci. In wheat, MAS is being deployed in a number of breeding programs both in the public and private sectors [94]. In particular, more than 30 traits have been targeted, mainly for disease resistance, quality, and abiotic stress tolerance. In allogamous crops (e.g., maize) where the populations used to extract new parental lines routinely undergo recurrent selection, MARS can be applied at each selection cycle to increase the frequency of the beneficial alleles within the population until the best performing alleles are fixed within the population and, as such, no longer require selection. By increasing the frequency of beneficial alleles in a breeding population, the probability of recovering a genotype with the combination of desired alleles is increased. As an example, increasing the favorable allele frequency from 0.50 to 0.96 will increase the probability of recovering the ideal genotype for 20 independent regions from one in a trillion to one in five [9]. This change in allele frequency will improve the mean performance for the selected trait of the population and any line derived from it. Breeders can deploy different MARS schemes depending on the selection model and the desired genetic structure (e.g., inbreeding level) of the population obtained after MARS. The MARS schemes require optimization for best managing field and laboratory resources, hence containing the costs, as well as for expediting the selection process, hence the accumulation of favorable allele frequency. When several traits and loci are targeted simultaneously, a multiple trait index is used to combine the values of each individual trait into a single index and different weights are assigned according to the perceived importance of each trait. The output of this process is an estimated genotypic value calculated for each progeny being considered for selection. MARS can also be applied to autogamous crops (e.g., soybean) in order to enhance the performance of the breeding populations used to select improved genotypes that will hopefully outperform the existing cultivars. As compared to conventional breeding practices, the outcome of MARS has clearly indicated its superiority for improving yield in maize, sunflower, and soybean [9]. Of utmost importance for the successful implementation of MARS is that breeders perform phenotypic selection on the lines per se that will be utilized for MARS. Additionally, phenotypic evaluation and selection among and within derived lines should continue after MARS.

Systematic profiling of parental lines is now routinely applied with a different level of genetic resolution, hence according to the level of LD of the target species. SSR profiling is rapidly being replaced by SNP profiling, much more effective than the former to define haplotype structure and much cheaper and amenable to high-throughput profiling. SNP platforms are particularly suited to the high-throughput profiling required by GS.

Once the template sequence of a crop becomes available, resequencing of lines can be used to obtain a far deeper understanding of their genomic architecture, allelic composition, and ultimate haplotype [132–134]. The spectacular reduction in cost that followed the introduction of second-generation sequencers makes resequencing of single genotypes a rather attractive and affordable option [135–137]. Additional progress in sequencing will further reduce the costs in as much direct resequencing of entire mapping populations may soon become more affordable than SNP profiling.

Mining Beneficial Alleles in Wild Relatives of Crops

As compared to their wild counterparts, the domestication bottleneck that all crops went through coupled with the strong selection first empirically practiced by farmers and then more systematically by modern breeders have markedly reduced the level of genetic variability within cultivated species, an aspect even more relevant for traits playing a substantial role in survival under natural conditions [82]. This limitation can be overcome through the implementation of advanced backcross QTL (AB-QTL) analysis [138], an approach that allows breeders to quickly discover and

exploit beneficial QTL alleles present in wild germplasm but otherwise absent from elite germplasm. The AB-QTL approach relies on the evaluation of BC families between an elite cultivar utilized as recurrent parent and a donor accession, usually a wild species that is sexually compatible with the crop. Usually, QTL analysis is delayed until the BC_2 generation and after selection in BC_1 against features known to affect negatively yield (e.g., ear shattering in small-grain cereals). The effectiveness of the AB-QTL approach has been proven in tomato [138, 139], rice [140], and barley [141]. These results are encouraging for using AB-QTL as a germplasm enhancement strategy for identifying wild alleles capable of improving the yield of the related crop, particularly under low-input agriculture and marginal environments where wild alleles may prove more beneficial, particularly for yield per se and disease resistance. An essential prerequisite is that the introgression of such beneficial alleles should bear no negative consequences when crops are grown under more favorable and high-yielding conditions.

Wild relatives of crop species can contribute to the identification of novel alleles for agronomically relevant traits by focusing on those loci that molecular evidence indicates as having been targeted by selection during both domestication and modern breeding [142]. To this end, the comparison of the allelic diversity present in elite accessions, landraces, and the undomesticated wild relatives of each crop allows for the identification of loci devoid of genetic variation within the elite germplasm, most likely as a result of domestication and subsequent man-made selection. The underlying assumption is that the loss of genetic diversity observed from the wild parent to the cultivated crop highlights the strong man-made selection at loci that control the expression of agronomically important traits, particularly those relevant for adaptation to abiotic stress. Therefore, both this "diversity screen" approach and the AB-QTL approach allow for the identification of valuable loci which would otherwise go undetected due to a lack of allelic diversity in the cultivated gene pool. An additional advantage of the diversity screen approach is that it allows for the identification of candidate genes of potential agronomic importance even without prior knowledge of gene function.

Leveraging the "-Omics" Platforms

During the past decade, a number of technologically sophisticated platforms have become available to collect a large amount of data on the dynamics of the transcriptome, proteome, and metabolome. The availability of these "-omics" profiling data facilitates the identification of candidate genes and provides us with a more holistic picture of the molecular events characterizing functions at the cellular, organ, and plant levels and how these are influenced by environmental cues [84, 143–146].

Unlike from the classical QTL positional cloning approach in which an adequately large mapping population is basically "interrogated" in order to identify the genetic determinants of QTLs, the candidate-gene approach capitalizes on gathering experimental evidence to support and validate the causal role of a coding sequence (e.g., glutamine synthetase gene) in governing variation for the putative target trait (e.g., nitrogen-use efficiency). The major advantage of the candidate-gene approach is that it bypasses the tedious and expensive procedures required by positional cloning. Identifying suitable candidate genes and elucidating their function can be expedited by combining different approaches and high-throughput -omics platforms applied to target crops and/or to model species. From a technical standpoint, combining laser-capture microdissection with the -omics platforms offers an unprecedented level of functional resolution at the tissue level, down to a single-cell layer [145]. Among the different platforms available for the mass-scale profiling of the transcriptome, microarrays have been more frequently utilized to investigate the changes in gene expression, particularly in plants exposed to adverse conditions [147–150]. Nonetheless, microarray platforms are quickly being replaced by high-throughput transcriptome sequencing by means of second-generation sequencing platforms [151].

Additional information on the changes in cellular metabolism is provided by the profiling of the proteome [152] and metabolome [153, 154] that, as compared to the transcriptome, are functionally closer to the phenotype, thus reporting also on variability due to posttranscriptional and posttranslational regulation. However, it should be appreciated that both

proteomics and metabolomics report changes for a rather limited portion (ca. 5%) of the expressed genes; additionally, proteomics is often unable to detect the changes in gene products (e.g., transcription factors) that despite their low level are more likely to play an important role in pivotal functions (e.g., signal transduction in response to biotic and abiotic stress) and consequently, to underline QTLs.

Metabolome profiling can also be used to identify loci regulating the level of a particular metabolite and verify its coincidence with QTLs for yield and/or genes involved in metabolic pathways. With the present technology, up to ca. 2,000 different metabolites can be profiled in a single sample [155]. In maize, QTLs for invertase activity have been identified in a population subjected to drought stress [156]. The number of QTLs for invertase activity detected under drought was more than twice the number detected under well-watered conditions, an indirect indication of the important role of this enzyme under drought conditions. One QTL common to both treatments was located near *Ivr2*, an invertase-encoding gene. The colocation reported between the activities of three enzymes (invertase, sucrose-P synthase, and ADP-glucose pyrophosphorylase) involved in sucrose and starch metabolism and a corresponding structural gene suggests its role as a candidate gene for explaining part of the variability in enzyme activity [157]. These studies indicate that invertase activity is an important limiting factor for grain yield in maize exposed to drought during the reproductive phase [158].

The candidate-gene approach is particularly effective when a clear cause-effect relationship can be unequivocally established between the gene product and the target trait. An example of this approach is the cloning of a QTL for cell-wall beta-glucans in barley grains based on a synteny analysis between barley and rice that revealed the presence in the syntenic portion of the rice genome of a cellulose synthase-like *CslF* gene that genetic engineering unequivocally showed to influence beta-glucans content in barley grains as well as in other species, including also *Arabidopsis* [83]. This notwithstanding, identifying suitable candidates for functionally complex traits such as yield and yield components is a much more daunting undertaking given the large number of genes that influence these traits.

Future Directions

The first comprehensive report of DNA-based markers (RFLPs; [20]) in a crop species was published in 1986. Since then, an almost countless number of studies have shed light on the genetic control of plant growth and functions, and, most importantly crop yield. One clear take-home message that has emerged from these studies is the existence of a continuum between Mendelian and quantitative traits that will eventually help in identifying the functional polymorphisms, either of genetic or epigenetic origin that underlie quantitative trait variation. In this respect, QTL cloning will become a more routine and easier practice thanks also to the massive resequencing of mutant collections. This, in turn, will facilitate the identification of the best performing QTL alleles, their pyramiding through MAS, and the identification of novel alleles via TILLING [159] or by means of site-directed mutagenesis at the key functional domains of the encoded proteins. It is under this QTL cloning paradigm that the molecular basis of quantitative traits will be dissected in order to advance our understanding of the genetic makeup of this category of traits and to more accurately tailor crop morphology and productivity with beneficial alleles.

From an applicative standpoint, although conventional selection based on phenotypic evaluation will likely remain the mainstay for most breeding programs, particularly in the public domain, MAB and its applications will increasingly be adopted and will in some cases become prevalent as compared to conventional practices. As the twenty-first century unfolds, a multitude of genomics and postgenomics platforms are at hand to expand our understanding of the genetic basis of crop performance and to improve the efficiency of selection procedures for the release of new, improved cultivars. Resequencing will revolutionize the way breeders deal with their germplasm and will provide unsurpassed opportunities for a deeper mining of allelic diversity and harnessing its full potential. Nonetheless, our understanding of the functional basis of yield and other quantitative traits is likely to remain rudimental. The elusive nature of the QTLs that govern yield and yield stability is a formidable hurdle toward a more effective selection targeting specific loci and a better understanding of quantitative traits. Notably,

GS can and will be applied irrespective of our degree of understanding of the genetic architecture of quantitative traits. Importantly, MAS and GS should be considered as complementary rather than alternative approaches, the utilization of which should be determined on a case-by-case basis. Bioinformatics and user-friendly databases will play a pivotal role for handling and managing the deluge of data produced by the molecular and phenotypic platforms.

In terms of experimental materials utilized for QTL studies, a growing attention will be devoted to the exploitation of multiparental crosses and mini-core collections of germplasm accessions with varying LD levels. In the mapping populations so far utilized for QTL discovery, most QTLs go undetected owing to the small size of the population, the presence of functionally monomorphic alleles and the small effects of many of such QTLs. Along this line, nested-association mapping (NAM) populations provide an interesting option to take advantage of both biparental (linkage) mapping and association mapping [160]. On a finer scale, high-throughput proteome and metabolome profiling will accelerate the identification of the causative mechanisms contributing to adaptive responses to adverse environmental conditions (e.g., drought, flooding, heat, etc.) whose frequency and intensity are expected to increase due to global warming. Nonetheless, the deluge of information originated through the molecular approaches and the -omics platforms will not automatically translate into novel cultivars. A "systems biology"-like approach will be instrumental for optimizing the accurate integration and exploitation in breeding terms of all the -omics information.

From an applicative standpoint, accurate phenotyping often remains the main limiting factor for identifying novel loci [161]. Semiautomated, high-throughput phenotyping under both controlled conditions and in the field promises to streamline gene discovery and narrowing the genotype-phenotype gap that hampers a more widespread deployment of MAB in crop improvement [87]. Along this line, it is important to emphasize that any molecular approach aiming to discover genes/QTLs and test their effects should preferably be carried out in an experimental context whose results are as relevant as possible and readily applicable to the conditions prevailing in farmers' fields [150]. An effective exploitation of genomics approaches to enhance crop performance will depend on their integration with conventional breeding. Although it is not possible to predict to what extent and how quickly the latter will be replaced by MAB, the future release of improved cultivars will be expedited and made more cost effective through a systematic marker-based manipulation of the loci that govern crop performance and the desired features targeted by breeders.

Bibliography

Primary Literature

1. Borlaug NE, Dowswell CR (2005) Feeding a world of ten billion people: a 21st century challenge. In: Tuberosa R, Phillips RL, Gale M (eds) In the wake of the double helix: from the green revolution to the gene revolution, proceedings of the international congress, 27–31 May 2003, Bologna, pp 3–23
2. Borlaug NE (2007) Sixty-two years of fighting hunger: personal recollections. Euphytica 157:287–297
3. Duvick DN (2005) The contribution of breeding to yield advances in maize (*Zea mays* L.). Adv Agron 86:83–145
4. Tester M, Langridge P (2010) Breeding technologies to increase crop production in a changing world. Science 327:818–822
5. Lande R, Thompson R (1990) Efficiency of marker-assisted selection in the improvement of quantitative traits. Genetics 124:743–756
6. Lee M (1995) DNA markers and plant breeding programs. Adv Agron 55:265–344
7. Morgante M, Salamini F (2003) From plant genomics to breeding practice. Curr Opin Biotechnol 14:214–219
8. Varshney RK, Graner A, Sorrells ME (2005) Genomics-assisted breeding for crop improvement. Trends Plant Sci 10:621–630
9. Eathington SR, Crosbie TM, Edwards MD, Reiter R, Bull JK (2007) Molecular markers in a commercial breeding program. Crop Sci 47:S154–S163
10. Yano M, Tuberosa R (2009) Genome studies and molecular genetics-from sequence to crops: genomics comes of age. Curr Opin Plant Biol 12:103–106
11. Flavell R (2010) Knowledge and technologies for sustainable intensification of food production. New Biotechnol 27: 505–516
12. Wei XJ, Liu LL, Xu JF, Jiang L, Zhang WW, Wang JK et al (2010) Breeding strategies for optimum heading date using genotypic information in rice. Mol Breeding 25:287–298
13. Schneeberger K, Weigel D (2011) Fast-forward genetics enabled by new sequencing technologies. Trends Plant Sci 16:282–288
14. Xu YB, Crouch JH (2008) Marker-assisted selection in plant breeding: from publications to practice. Crop Sci 48:391–407
15. Raju NL, Gnanesh BN, Lekha P, Jayashree B, Pande S, Hiremath PJ et al (2010) The first set of EST resource for gene discovery

and marker development in pigeonpea (*Cajanus cajan* L.). BMC Plant Biol 10:45
16. Shinozaki K, Yamaguchi-Shinozaki K (2007) Gene networks involved in drought stress response and tolerance. J Exp Bot 58:221–227
17. Fujii H, Zhu JK (2009) Arabidopsis mutant deficient in 3 abscisic acid-activated protein kinases reveals critical roles in growth, reproduction, and stress. Proc Natl Acad Sci USA 106:8380–8385
18. Yoshida T, Fujita Y, Sayama H, Kidokoro S, Maruyama K, Mizoi J et al (2010) AREB1, AREB2, and ABF3 are master transcription factors that cooperatively regulate ABRE-dependent ABA signaling involved in drought stress tolerance and require ABA for full activation. Plant J 61:672–685
19. Service RF (2006) Gene sequencing – the race for the $1000 genome. Science 311:1544–1546
20. Helentjaris T, Slocum M, Wright S, Schaefer A, Nienhuis J (1986) Construction of genetic linkage maps in maize and tomato using restriction fragment length polymorphisms. Theor Appl Genet 72:761–769
21. Tanksley SD, Young ND, Paterson AH, Bonierbale MW (1989) RFLP mapping in plant breeding: new tools for an old science. BioTechnology 7:257–264
22. Vos P, Hogers R, Bleeker M, Reijans M, Vandelee T, Hornes M et al (1995) AFLP: a new technique for DNA fingerprinting. Nucleic Acids Res 23:4407–4414
23. Senior ML, Chin ECL, Lee M, Smith JSC, Stuber CW (1996) Simple sequence repeat markers developed from maize sequences found in the GENBANK database: map construction. Crop Sci 36:1676–1683
24. Kilian A (2005) The fast and the cheap: SNP and DArT-based whole genome profiling for crop improvement. In: Tuberosa R, Gale M, Phillips RL (eds) In the wake of the double helix: from the green revolution to the gene revolution, proceedings of the international congress, 27–31 May 2003, Bologna, pp 443–461
25. Rafalski A (2002) Applications of single nucleotide polymorphisms in crop genetics. Curr Opin Plant Biol 5:94–100
26. Barbazuk WB, Emrich SJ, Chen HD, Li L, Schnable PS (2007) SNP discovery via 454 transcriptome sequencing. Plant J 51:910–918
27. Akhunov E, Nicolet C, Dvorak J (2009) Single nucleotide polymorphism genotyping in polyploid wheat with the Illumina GoldenGate assay. Theor Appl Genet 119:507–517
28. Close TJ, Bhat PR, Lonardi S, Wu YH, Rostoks N, Ramsay L et al (2009) Development and implementation of high-throughput SNP genotyping in barley. BMC Genomics 10:582
29. McCouch SR, Zhao KY, Wright M, Tung CW, Ebana K, Thomson M et al (2010) Development of genome-wide SNP assays for rice. Breeding Sci 60:524–535
30. Bentley DR (2006) Whole-genome re-sequencing. Curr Opin Genet Dev 16:545–552
31. Nordborg M, Weigel D (2008) Next-generation genetics in plants. Nature 456:720–723
32. Schnable PS, Ware D, Fulton RS, Stein JC, Wei FS, Pasternak S et al (2009) The B73 maize genome: complexity, diversity, and dynamics. Science 326:1112–1115
33. Varshney RK, Nayak SN, May GD, Jackson SA (2009) Next-generation sequencing technologies and their implications for crop genetics and breeding. Trends Biotechnol 27:522–530
34. Deschamps S, Campbell MA (2010) Utilization of next-generation sequencing platforms in plant genomics and genetic variant discovery. Mol Breeding 25:553–570
35. Moore G, Foote T, Helentjaris T, Devos K, Kurata N, Gale M (1995) Was there a single ancestral cereal chromosome? Trends Genet 11:81–82
36. Gale MD, Devos KM (1998) Plant comparative genetics after 10 years. Science 282:656–659
37. Bolot S, Abrouk M, Masood-Quraishi U, Stein N, Messing J, Feuillet C et al (2009) The 'inner circle' of the cereal genomes. Curr Opin Plant Biol 12:119–125
38. Falconer DS (1981) Introduction to quantitative genetics. Longman, London
39. Geldermann H (1975) Investigation on inheritance of quantitative characters in animals by gene markers. I. Methods. Theor Appl Genet 46:319–330
40. Sax K (1923) The association of size differences with seed-coat patterns and pigmentation in *Phaseolus vulgaris*. Genetics 8:552–560
41. Edwards MD, Stuber CW, Wendel JF (1987) Molecular-marker-facilitated investigations of quantitative-trait loci in maize. I. Numbers, genomic distribution and types of gene-action. Genetics 116:113–125
42. Stuber CW, Edwards MD, Wendel JF (1987) Molecular marker facilitated investigations of quantitative trait loci in maize. II. Factors influencing yield and its component traits. Crop Sci 27:639–648
43. Tanksley SD (1993) Mapping polygenes. Annu Rev Genet 27:205–233
44. Beavis WD (1998) QTL analysis: power, precision, and accuracy. In: Molecular dissection of complex traits. CRC Press, Boca Raton, pp 145–162
45. Ribaut JM, Hoisington D (1998) Marker-assisted selection: new tools and strategies. Trends Plant Sci 3:236–239
46. Bernardo R (2001) What if we knew all the genes for a quantitative trait in hybrid crops? Crop Sci 41:1–4
47. Bernardo R (2008) Molecular markers and selection for complex traits in plants: learning from the last 20 years. Crop Sci 48:1649–1664
48. Frary A, Nesbitt TC, Grandillo S, Knaap E, Cong B, Liu J et al (2000) fw2.2: a quantitative trait locus key to the evolution of tomato fruit size. Science 289:85–88
49. Salvi S, Tuberosa R (2007) Cloning QTLs in Plants. In: Varshney RK, Tuberosa R (eds) Genomics-assisted crop improvement-volume 1: genomics approaches and platforms. Springer, Dordrecht, pp 207–226
50. Churchill GA, Doerge RW (1994) Empirical threshold values for quantitative trait mapping. Genetics 138:963–971

51. Lander ES, Botstein D (1989) Mapping mendelian factors underlying quantitative traits using RFLP linkage maps. Genetics 121:185–199
52. Darvasi A, Weinreb A, Minke V, Weller JI, Soller M (1993) Detecting marker-QTL linkage and estimating QTL gene effect and map location using a saturated genetic map. Genetics 134:943–951
53. Kao CH, Zeng ZB, Teasdale RD (1999) Multiple interval mapping for quantitative trait loci. Genetics 152:1203–1216
54. Doerge RW (2002) Mapping and analysis of quantitative trait loci in experimental populations. Nat Rev Genet 3:43–52
55. Podlich DW, Winkler CR, Cooper M (2004) Mapping as you go: an effective approach for marker-assisted selection of complex traits. Crop Sci 44:1560–1571
56. Beavis WD (1994) The power and deceit of QTL experiments: lessons from comparative QTL studies. In: Proceedings of the forty-ninth annual corn and sorghum research conference, Washington, DC, pp 250–266
57. Openshaw S, Frascaroli E (1997) QTL detection and marker-assisted selection for complex traits in maize. In: Annual corn and sorghum research conference American seed trade association. Washington, DC, pp 44–53
58. Melchinger AE, Utz HF, Schon CC (1998) Quantitative trait locus (QTL) mapping using different testers and independent population samples in maize reveals low power of QTL detection and large bias in estimates of QTL effects. Genetics 149:383–403
59. Abiola O, Angel JM, Avner P, Bachmanov AA, Belknap JK, Bennett B et al (2003) The nature and identification of quantitative trait loci: a community's view. Nat Rev Genet 4:911–916
60. Collins NC, Tardieu F, Tuberosa R (2008) Quantitative trait loci and crop performance under abiotic stress: where do we stand? Plant Physiol 147:469–486
61. Buckler ESI, Thornsberry JM (2002) Plant molecular diversity and applications to genomics. Curr Opin Plant Biol 5:107–111
62. Ersoz ES, Yu J, Buckler ES (2007) Applications of linkage disequilibrium and association mapping. In: Varshney RK, Tuberosa R (eds) Genomics-assisted crop improvement-volume 1: genomics approaches and platforms. Springer, Dordrecht, pp 97–120
63. Clark RM (2010) Genome-wide association studies coming of age in rice. Nat Genet 42:926–927
64. Rafalski A (2010) Association genetics in crop improvement. Curr Opin Plant Biol 13:174–180
65. Maccaferri M, Sanguineti MC, Demontis A, El-Ahmed A, del Moral LG, Maalouf F et al (2011) Association mapping in durum wheat grown across a broad range of water regimes. J Exp Bot 62:409–438
66. Buntjer JB, Sorensen AP, Peleman JD (2005) Haplotype diversity: the link between statistical and biological association. Trends Plant Sci 10:466–471
67. Buckler ES, Holland JB, Bradbury PJ, Acharya CB, Brown PJ, Browne C et al (2009) The genetic architecture of maize flowering time. Science 325:714–718
68. Salvi S, Sponza G, Morgante M, Tomes D, Niu X, Fengler KA et al (2007) Conserved noncoding genomic sequences associated with a flowering-time quantitative trait locus in maize. Proc Natl Acad Sci USA 104:11376–11381
69. Magalhaes JV, Liu J, Guimaraes CT, Lana UGP, Alves VMC, Wang YH et al (2007) A gene in the multidrug and toxic compound extrusion (MATE) family confers aluminum tolerance in sorghum. Nat Genet 39:1156–1161
70. Salvi S, Castelletti S, Tuberosa R (2009) An updated consensus map for flowering time QTLs in maize. Maydica 54:501–512
71. Robertson DS (1985) A possible technique for isolating genic DNA for quantitative traits in plants. J Theor Biol 117:1–10
72. Touzet P, Winkler RG, Helentjaris T (1995) Combined genetic and physiological analysis of a locus contributing to quantitative variation. Theor Appl Genet 91:200–205
73. Tuinstra MR, Ejeta G, Goldsbrough PB (1997) Heterogeneous inbred family (HIF) analysis: a method for developing near-isogenic lines that differ at quantitative trait loci. Theor Appl Genet 95:1005–1011
74. Landi P, Sanguineti MC, Salvi S, Giuliani S, Bellotti M, Maccaferri M et al (2005) Validation and characterization of a major QTL affecting leaf ABA concentration in maize. Mol Breeding 15:291–303
75. Landi P, Giuliani S, Salvi S, Ferri M, Tuberosa R, Sanguineti MC (2010) Characterization of root-yield-1.06, a major constitutive QTL for root and agronomic traits in maize across water regimes. J Exp Bot 61:3553–3562
76. Zamir D (2001) Improving plant breeding with exotic genetic libraries. Nat Rev Genet 2:983–989
77. Paran I, Zamir D (2003) Quantitative traits in plants: beyond the QTL. Trends Genet 19:303–306
78. Eshed Y, Zamir D (1995) An introgression line population of *Lycopersicon pennellii* in the cultivated tomato enables the identification and fine mapping of yield-associated QTL. Genetics 141:1147–1162
79. Li ZK, Fu BY, Gao YM, Xu JL, Ali J, Lafitte HR et al (2005) Genome-wide introgression lines and their use in genetic and molecular dissection of complex phenotypes in rice (*Oryza sativa* L.). Plant Mol Biol 59:33–52
80. Takahashi Y, Shomura A, Sasaki T, Yano M (2001) *Hd6*, a rice quantitative trait locus involved in photoperiod sensitivity, encodes the a subunit of protein kinase CK2. Proc Natl Acad Sci USA 98:7922–7927
81. Hospital F (2003) Marker-assisted breeding. In: Newbury HI (ed.) Plant molecular breeding. Blackwell Publishing and CRC Press, Oxford and Boca Raton, pp 30–59
82. Feuillet C, Langridge P, Waugh R (2008) Cereal breeding takes a walk on the wild side. Trends Genet 24:24–32
83. Burton RA, Wilson SM, Hrmova M, Harvey AJ, Shirley NJ, Stone BA et al (2006) Cellulose synthase-like *CslF* genes mediate the synthesis of cell wall (1,3;1,4)-β-D-glucans. Science 311:1940–1942

84. Belo A, Zheng PZ, Luck S, Shen B, Meyer DJ, Li BL et al (2008) Whole genome scan detects an allelic variant of *fad2* associated with increased oleic acid levels in maize. Mol Genet Genomics 279:1–10
85. Yin XY, Stam P, Kropff MJ, Schapendonk AH (2003) Crop modeling, QTL mapping, and their complementary role in plant breeding. Agron J 95:90–98
86. Hammer G, Cooper M, Tardieu F, Welch S, Walsh B, van Eeuwijk F et al (2006) Models for navigating biological complexity in breeding improved crop plants. Trends Plant Sci 11:587–593
87. Tardieu F, Tuberosa R (2010) Dissection and modeling of abiotic stress tolerance in plants. Curr Opin Plant Biol 13:206–212
88. Chapman SC (2008) Use of crop models to understand genotype by environment interactions for drought in real-world and simulated plant breeding trials. Euphytica 161:195–208
89. Peleman JD, van der Voort JR (2003) Breeding by design. Trends Plant Sci 8:330–334
90. Young ND, Tanksley SD (1989) Restriction fragment length polymorphism maps and the concept of graphical genotypes. Theor Appl Genet 77:95–101
91. Young ND (1999) A cautiously optimistic vision for marker-assisted breeding. Mol Breeding 5:505–510
92. Willcox MC, Khairallah MM, Bergvinson D, Crossa J, Deutsch JA, Edmeades GO et al (2002) Selection for resistance to southwestern corn borer using marker-assisted and conventional backcrossing. Crop Sci 42:1516–1528
93. Sørensen AP, Stuurman J, van der Voort JR, Peleman J (2007) Molecular breeding: maximizing the exploitation of genetic. In: Varshney RK, Tuberosa R (eds) Genomics-assisted crop improvement-volume 1: genomics approaches and platforms. Springer, Dordrecht, pp 31–56
94. Gupta PK, Langridge P, Mir RR (2010) Marker-assisted wheat breeding: present status and future possibilities. Mol Breeding 26:145–161
95. Xue SL, Li GQ, Jia HY, Lin F, Cao Y, Xu F et al (2010) Marker-assisted development and evaluation of near-isogenic lines for scab resistance QTLs of wheat. Mol Breeding 25:397–405
96. Randhawa HS, Mutti JS, Kidwell K, Morris CF, Chen XM, Gill KS (2009) Rapid and targeted introgression of genes into popular wheat cultivars using marker-assisted background selection. PLoS One 4:e5752
97. Hospital F, Charcosset A (1997) Marker-assisted introgression of quantitative trait loci. Genetics 147:1469–1485
98. Concibido VC, La Vallee B, McLaird P, Pineda N, Meyer J, Hummel L et al (2003) Introgression of a quantitative trait locus for yield from *Glycine soja* into commercial soybean cultivars. Theor Appl Genet 106:575–582
99. Zwart RS, Thompson JP, Milgate AW, Bansal UK, Williamson PM, Raman H et al (2010) QTL mapping of multiple foliar disease and root-lesion nematode resistances in wheat. Mol Breeding 26:107–124
100. Frisch M, Bohn M, Melchinger AE (1999) Comparison of selection strategies for marker-assisted backcrossing of a gene. Crop Sci 39:1295–1301
101. Frisch M, Bohn M, Melchinger AE (1999) Minimum sample size and optimal positioning of flanking markers in marker-assisted backcrossing for transfer of a target gene. Crop Sci 39:967–975
102. Maccaferri M, Mantovani P, Tuberosa R, DeAmbrogio E, Giuliani S, Demontis A et al (2008) A major QTL for durable leaf rust resistance widely exploited in durum wheat breeding programs maps on the distal region of chromosome arm 7BL. Theor Appl Genet 117:1225–1240
103. Servin B, Martin OC, Mezard M, Hospital F (2004) Toward a theory of marker-assisted gene pyramiding. Genetics 168: 513–523
104. Knapp SJ (1998) Marker-assisted selection as a strategy for increasing the probability of selecting superior genotypes. Crop Sci 38:1164–1174
105. Gebhardt C, Bellin D, Henselewski H, Lehmann W, Schwarzfischer J, Valkonen JPT (2006) Marker-assisted combination of major genes for pathogen resistance in potato. Theor Appl Genet 112:1458–1464
106. Ejeta G, Knoll JE (2007) Marker-assisted selection in sorghum. In: Varshney RK, Tuberosa R (eds) Genomics-assisted crop improvement-volume 2: genomics applications in crops. Springer, Dordrecht, pp 187–206
107. Edwards MD, Johnson L (1994a) RFLPs for rapid recurrent selection. In: Proceedings joint plant breeding symposium series. American Society Horticulture and Crop Science Society America, Corvallis
108. Moreau L, Charcosset A, Gallais A (2004) Experimental evaluation of several cycles of marker-assisted selection in maize. Euphytica 137:111–118
109. Yousef GG, Juvik JA (2001) Comparison of phenotypic and marker-assisted selection for quantitative traits in sweet corn. Crop Sci 41:645–655
110. Chen LM, Zhao ZG, Liu X, Liu LL, Jiang L, Liu SJ et al (2011) Marker-assisted breeding of a photoperiod-sensitive male sterile *japonica* rice with high cross-compatibility with *indica* rice. Mol Breeding 27:247–258
111. Ribaut JM, Ragot M (2007) Marker-assisted selection to improve drought adaptation in maize: the backcross approach, perspectives, limitations, and alternatives. J Exp Bot 58:351–360
112. Reynolds M, Tuberosa R (2008) Translational research impacting on crop productivity in drought-prone environments. Curr Opin Plant Biol 11:171–179
113. Herve P, Serraj R (2009) Gene technology and drought: a simple solution for a complex trait? Afr J Biotechnol 8:1740–1749
114. Edwards MD, Page NJ (1994) Evaluation of marker-assisted selection through computer simulation. Theor Appl Genet 88:376–382
115. Charmet G, Robert N, Perretant MR, Gay G, Sourdille P, Groos C et al (1999) Marker-assisted recurrent selection for cumulating additive and interactive QTLs in recombinant inbred lines. Theor Appl Genet 99:1143–1148
116. van Berloo R, Stam P (2001) Simultaneous marker-assisted selection for multiple traits in autogamous crops. Theor Appl Genet 102:1107–1112

117. Eathington SR, Dudley JW, Rufener GK (1997) Usefulness of marker-QTL associations in early generation selection. Crop Sci 37:1686–1693
118. Eathington SR (2005) Practical applications of molecular technology in the development of commercial maize hybrids. In: Proceedings of the 60th annual corn and sorghum seed research conferences. American Seed Trade Association, Washington, DC
119. Crosbie T, Eathington S, Johnson G, Edwards M, Reiter R, Stark S, et al (2006) Plant breeding: past, present, and future. In: Lamkey KR, Lee M (eds) Plant breeding: the Arnel R. Hallauer international symposium. Blackwell, Ames, pp 3–50
120. Heffner EL, Sorrells ME, Jannink JL (2009) Genomic selection for crop improvement. Crop Sci 49:1–12
121. Bernardo R (2010) Genomewide selection with minimal crossing in self-pollinated crops. Crop Sci 50:624–627
122. Lorenz AJ, Chao SM, Asoro FG, Heffner EL, Hayashi T, Iwata H et al (2011) Genomic selection in plant breeding: knowledge and prospects. Adv Agron 110:77–123
123. Moreau L, Lemarie S, Charcosset A, Gallais A (2000) Economic efficiency of one cycle of marker-assisted selection. Crop Sci 40:329–337
124. Kuchel H, Fox R, Reinheimer J, Mosionek L, Willey N, Bariana H et al (2007) The successful application of a marker-assisted wheat breeding strategy. Mol Breeding 20:295–308
125. Morris M, Dreher K, Ribaut JM, Khairallah M (2003) Money matters (II): costs of maize inbred line conversion schemes at CIMMYT using conventional and marker-assisted selection. Mol Breeding 11:235–247
126. Salvi S, Tuberosa R, Phillips RL (2001) Development of PCR-based assays for allelic discrimination in maize by using the 5′-nuclease procedure. Mol Breeding 8:169–176
127. Canovas A, Rincon G, Islas-Trejo A, Wickramasinghe S, Medrano JF (2010) SNP discovery in the bovine milk transcriptome using RNA-Seq technology. Mamm Genome 21:592–598
128. Mondini L, Nachit MM, Porceddu E, Pagnotta MA (2011) HRM technology for the identification and characterization of INDEL and SNP mutations in genes involved in drought and salt tolerance of durum wheat. Plant Genetic Resources-Characterization and Utilization 9:166–169
129. Graham GI, Wolff DW, Stuber CW (1997) Characterization of a yield quantitative trait locus on chromosome five of maize by fine mapping. Crop Sci 37:1601–1610
130. Darvasi A, Soller M (1995) Advanced intercross lines, an experimental population for fine genetic-mapping. Genetics 141:1199–1207
131. Lee M, Sharopova N, Beavis WD, Grant D, Katt M, Blair D et al (2002) Expanding the genetic map of maize with the intermated B73 × Mo17 (IBM) population. Plant Mol Biol 48:453–461
132. Atwell S, Huang YS, Vilhjalmsson BJ, Willems G, Horton M, Li Y et al (2010) Genome-wide association study of 107 phenotypes in *Arabidopsis thaliana* inbred lines. Nature 465:627–631
133. Bergelson J, Roux F (2010) Towards identifying genes underlying ecologically relevant traits in *Arabidopsis thaliana*. Nat Rev Genet 11:867–879
134. Huang XH, Wei XH, Sang T, Zhao QA, Feng Q, Zhao Y et al (2010) Genome-wide association studies of 14 agronomic traits in rice landraces. Nat Genet 42:961–976
135. Gupta PK (2008) Ultrafast and low-cost DNA sequencing methods for applied genomics research. Proc Natl Acad Sci India 78:91–102
136. Huang XH, Feng Q, Qian Q, Zhao Q, Wang L, Wang AH et al (2009) High-throughput genotyping by whole-genome resequencing. Genome Res 19:1068–1076
137. Lam HM, Xu X, Liu X, Chen WB, Yang GH, Wong FL et al (2010) Resequencing of 31 wild and cultivated soybean genomes identifies patterns of genetic diversity and selection. Nat Genet 42:1053–1059
138. Tanksley SD, Grandillo S, Fulton TM, Zamir D, Eshed Y, Petiard V et al (1996) Advanced backcross QTL analysis in a cross between an elite processing line of tomato and its wild relative *L. pimpinellifolium*. Theor Appl Genet 92: 213–224
139. Bernacchi D, Beck-Bunn T, Eshed Y, Inai S, Lopez J, Petiard V et al (1998) Advanced backcross QTL analysis of tomato. II. Evaluation of near-isogenic lines carrying single-donor introgressions for desirable wild QTL-alleles derived from *Lycopersicon hirsutum* and *L. pimpinellifolium*. Theor Appl Genet 97:170–180
140. Xiao J, Li J, Grandillo S, Ahn SN, Yuan L, Tanksley SD et al (1998) Identification of trait-improving quantitative trait loci alleles from a wild rice relative, *Oryza rufipogon*. Genetics 150:899–909
141. Talame V, Sanguineti MC, Chiapparino E, Bahri H, Ben Salem M, Forster BP et al (2004) Identification of *Hordeum spontaneum* QTL alleles improving field performance of barley grown under rainfed conditions. Ann Appl Biol 144:309–319
142. Yamasaki M, Tenaillon MI, Bi IV, Schroeder SG, Sanchez-Villeda H, Doebley JF et al (2005) A large-scale screen for artificial selection in maize identifies candidate agronomic loci for domestication and crop improvement. Plant Cell 17:2859–2872
143. Tuberosa R, Gill BS, Quarrie SA (2002) Cereal genomics: ushering in a brave new world. Plant Mol Biol 48:445–449
144. Druka A, Druka I, Centeno AG, Li H, Sun Z, Thomas WTB et al (2008) Towards systems genetic analyses in barley: integration of phenotypic, expression and genotype data into GeneNetwork. BMC Genet 9:73
145. Hochholdinger F, Tuberosa R (2009) Genetic and genomic dissection of maize root development and architecture. Curr Opin Plant Biol 12:172–177
146. Urano K, Kurihara Y, Seki M, Shinozaki K (2010) 'Omics' analyses of regulatory networks in plant abiotic stress responses. Curr Opin Plant Biol 13:132–138
147. Ozturk ZN, Talamè V, Deyholos M, Michalowski CB, Galbraith DW, Gozukirmizi N et al (2002) Monitoring large-scale

changes in transcript abundance in drought- and salt-stressed barley. Plant Mol Biol 48:551–573
148. Zinselmeier C, Sun YJ, Helentjaris T, Beatty M, Yang S, Smith H et al (2002) The use of gene expression profiling to dissect the stress sensitivity of reproductive development in maize. Field Crop Res 75:111–121
149. Schnable PS, Hochholdinger F, Nakazono M (2004) Global expression profiling applied to plant development. Curr Opin Plant Biol 7:50–56
150. Talame V, Ozturk NZ, Bohnert HJ, Tuberosa R (2007) Barley transcript profiles under dehydration shock and drought stress treatments: a comparative analysis. J Exp Bot 58:229–240
151. Kofler R, Torres TT, Lelley T, Schlotterer C (2009) PanGEA: identification of allele specific gene expression using the 454 technology. BMC Bioinformatics 10:143
152. Hochholdinger F, Woll K, Guo L, Schnable PS (2005) The accumulation of abundant soluble proteins changes early in the development of the primary roots of maize (*Zea mays* L.). Proteomics 5:4885–4893
153. Fernie AR, Schauer N (2009) Metabolomics-assisted breeding: a viable option for crop improvement? Trends Genet 25:39–48
154. Saito K, Matsuda F (2010) Metabolomics for functional genomics, systems biology, and biotechnology. Annu Rev Plant Biol 61:463–489
155. Sakurai N, Shibata D (2006) KaPPA-view for integrating quantitative transcriptomic and metabolomic data on plant metabolic pathway maps. J Pestic Sci 31:293–295
156. Pelleschi S, Guy S, Kim JY, Pointe C, Mahe A, Barthes L et al (1999) Ivr2, a candidate gene for a QTL of vacuolar invertase activity in maize leaves. Gene-specific expression under water stress. Plant Mol Biol 39:373–380
157. Pelleschi S, Leonardi A, Rocher JP, Cornic G, de Vienne D, Thévenot C et al (2006) Analysis of the relationships between growth, photosynthesis and carbohydrate metabolism using quantitative trait loci (QTLs) in young maize plants subjected to water deprivation. Mol Breeding 17:21–39
158. Boyer JS, McLaughlin JE (2007) Functional reversion to identify controlling genes in multigenic responses: analysis of floral abortion. J Exp Bot 58:267–277
159. Talame V, Bovina R, Sanguineti MC, Tuberosa R, Lundqvist U, Salvi S (2008) TILLMore, a resource for the discovery of chemically induced mutants in barley. Plant Biotechnol J 6:477–485
160. McMullen MD, Kresovich S, Villeda HS, Bradbury P, Li HH, Sun Q et al (2009) Genetic properties of the maize nested association mapping population. Science 325:737–740
161. Zhou M (2011) Accurate phenotyping reveals better QTL for waterlogging tolerance in barley. Plant Breeding 130:203–208
162. Maccaferri M, Sanguineti MC, Corneti S, Ortega JLA, Ben Salem M, Bort J et al (2008) Quantitative trait loci for grain yield and adaptation of durum wheat (*Triticum durum* Desf.) across a wide range of water availability. Genetics 178:489–511
163. Salvi S, Corneti S, Bellotti M, Carraro N, Sanguineti MC, Castelletti S, Tuberosa R (2011) Genetic dissection of maize phenology using an intraspecific introgression library. BMC Plant Biol 11:4

Books and Reviews

Bernardo R (ed) (2010) Breeding for quantitative traits in plants, 2nd edn. Stemma Press, Woodbury, p 400
Costa de Oliveira A, Varshney RK (eds) (2011) Root genomics. Springer, Berlin/Heidelberg, p 318
Guimarães E, Ruane J, Scherf B, Sonnino A, Dargie J (eds) (2007) Marker-assisted selection. current status and future perspectives in crops, livestock, forestry and fish. Food and Agriculture Organization, Rome, p 492
Kole C (ed) (2006) Genome mapping and molecular breeding in plants – cereals and millets. Springer, Berlin/Heidelberg, p 349
Lamkey KR, Lee M (eds) (2006) Plant breeding: the Arnel R. Hallauer international symposium. Blackwell, Ames, p 379
Liu BH (ed) (1998) Statistical genomics: linkage, mapping, and QTL analysis. CRC Press, Boca Raton, p 611
Rao DC, Gu CC (eds) (2008) Genetic dissection of complex traits, 2nd edn. Academic, New York, p 760
Varshney RK, Tuberosa R (eds) (2007) Genomics-assisted crop improvement, volume 1: genomics approaches and platforms. Springer, Dordrecht, p 386
Varshney RK, Tuberosa R (eds) (2007) Genomic-assisted crop improvement, volume 2: genomics applications in crops. Springer, Dordrecht, p 509
Xu Y (ed) (2010) Molecular plant breeding. CABI, Wallingford, p 734

Martin Waste-to-Energy Technology

Johannes J. E. Martin, Ralf Koralewska
Martin GmbH für Umwelt- und Energietechnik, Munich, Germany

Article Outline

Glossary
Definition of the Subject
Introduction
Components of a WTE Plant
Grate Technologies
Combustion Technologies
Combustion Control
Energy Recovery
Process Simulation
NO_x Reduction

Residue Qualities
Reference Plants
Future Directions
Bibliography

Glossary

Reverse-acting grate Grate system, inclined at an angle of 26°, with rows of grate bars moving up and down against the downward flow of solids.

Horizontal grate Horizontal grate system with rows of grate bars moving in opposite directions alternated with stationary rows of grate bars.

SYNCOM *SYN*thetic *COM*bustion using oxygen-enriched underfire air on a reverse-acting grate.

IR camera Infrared camera recording the surface temperature across the width and the length of the bed on the grate for selected bandwidths from the roof of the combustion chamber.

MICC MARTIN Infrared Combustion Control for reverse-acting grate systems including fuzzy logic control, IR camera, operating mode concept, and operational data logging/visualization.

ACC Advanced Combustion Control for horizontal grate systems combining existing standard measurement information to generate the control loops.

LN Low NO_x technology for significant reduction of NO_x concentration downstream of the combustion system by primary measures.

SNCR Selective Non-Catalytic Reduction of NO_x by injection of a reagent into the combustion chamber as a secondary measure without use of a catalytic converter.

T3 Time–Temperature–Turbulence: concept ensuring an efficient post-combustion with good gas burnout.

Definition of the Subject

Waste-to-Energy (WTE) technologies have been confronted with numerous and changing challenges over the last few decades. Various important factors have to be considered, not only the reduction of waste volume and mass and the destruction and capture of pollutants. Environmental concerns have demanded that flue gases are no longer a significant source of emissions, and that the waste, and also residues remaining after thermal treatment, are to be transformed into reusable products. Thermal treatment of waste using a grate-based system has gained acceptance as the preferred system for sustainable treatment of waste worldwide. The reason for this is that the energy content of the waste is utilized and that quality products and residues are produced. Nevertheless grate-based processes must also keep pace with international requirements and proposed alternative thermal treatment technologies by further innovative development.

Recent years have seen significant increases in the average heating values of waste in many countries (Fig. 1). Essentially, this can be attributed to recycling measures, separate recovery of waste streams, as well as pretreatment and processing procedures in modified waste management concepts. As a result of the above and due to the increasingly frequent application of energy recovery schemes for commercial waste, the fuel input to WTE plants combusting household waste has been significantly influenced. In response to the associated increased thermal load, water-cooling of grate bars, using different technical solutions, was developed and used for forward-acting grate systems.

In view of the continual depletion of raw materials, sustainable processes for the recovery of recyclables are becoming increasingly important. Efficient use of the energy recovered (in the form of electricity, process steam, and district heating/cooling) by developing innovative concepts is also in demand. In Europe, there is potential to increase the contribution of WTE to over 10% of the overall renewable energy produced, since over one half of the energy contained in municipal waste is of biogenic origin. All of these aspects have been driven by political and public pressure, regulations, as well as the financial market situation. Any new demand leads to an increase in the overall complexity of the thermal treatment process. Additional skills and competences are needed for plant design, process control, and operation. Nevertheless, cost-benefit and eco-efficiency analyses clearly show that these additional efforts should be made. Modern WTE plants are extremely complex in terms of the technology used. A sound knowledge of the "fuel" waste as well as its effects on design and operation is crucial for successful planning and implementation of WTE plants.

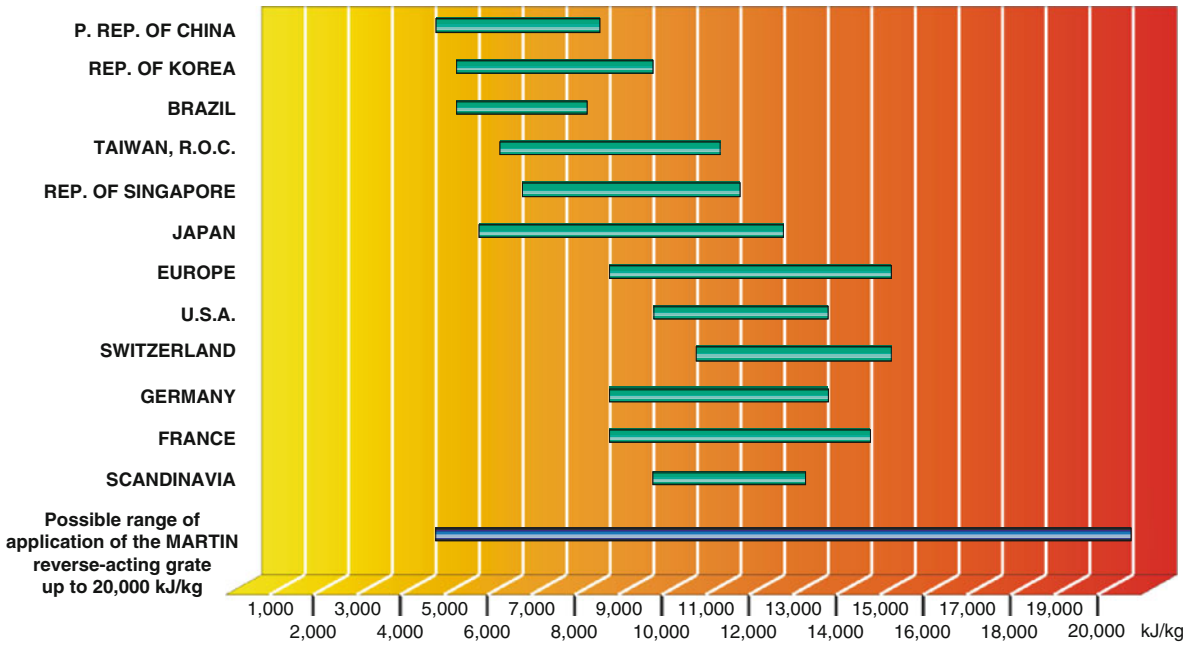

Martin Waste-to-Energy Technology. Figure 1
Typical lower heating values of untreated household waste in different countries

In addition to the environmentally friendly treatment of waste, its use as a source of energy plays an increasingly important role. As discussions on climate change, diminishing sources of fossil fuels and heavy dependence on their supply from potentially unstable regions intensify, waste is progressively being seen as a resource. On a political level, this has led to greater acceptance of combustion as an indispensable component of sustainable waste management.

Introduction

MARTIN GmbH was established in 1925 in Munich, Germany. The founder, Josef Martin, had already been working on various combustion system designs for coal and waste of all types. The invention of the reverse-acting grate is based on the fact that fuel ignites more easily when an already existing glowing mass is pushed back underneath it. The combined effect of gravity and reverse-acting motion resulted in the fuel being circulated and optimally burned out. The reverse-acting grate and the newly invented ram-type discharger were tested in a pilot unit for the WTE plant in Romainville near Paris in 1932. The combustion tests were successfully carried out using waste from Paris, confirming that the principle on which the grate is based can also be successfully applied to the combustion of municipal waste. In 1952, the company was awarded a contract to build its first WTE plant in São Paolo, Brazil. The grate system proved to be capable of ensuring optimum reaction conditions for combusting municipal solid waste (MSW) and high reliability of the overall operation.

In the beginning of the 1980s, waste combustion technology underwent a fundamental technological change. Step by step, the conventional combustion plant was reengineered to become a modern high-tech power station for treating residual waste. The main forces behind this change were growing environmental awareness on the part of the general public, which was reflected in increasingly strict limit values for emissions; great public interest, which focused the attention of politicians and the media on WTE plants; the constantly changing quality of MSW, which led to increasingly higher heating values; and the demand for efficient materials recycling and energy recovery from residual waste.

However, it soon became clear that the most significant innovations for optimizing combustion on the

grate could be achieved through appropriate furnace dimensions and a comprehensive, intelligent combustion control system. Waste is a complex, heterogeneous fuel, the composition and heating value of which fluctuate significantly. Also, the radical change in waste composition in the 1990s, whereby a large fraction of the commercial waste was not recyclable and had a high heat content, necessitated a phase of intense development of existing technologies. Either industrial or biomass waste could be used as fuel.

For over 80 years, MARTIN has been successfully active – as a general contractor, consortium partner, supplier of components, or engineering partner – in the field of combusting difficult fuels such as low-grade coal and waste. Today more than 700 lines for combusting waste have been equipped with MARTIN grates in over 370 plants worldwide [1]. Following restructuring at one of its competitors, MARTIN also took over their horizontal grate technology in 2002.

Components of a WTE Plant

Figure 2 shows the typical components of a WTE plant using the MARTIN technology. A detailed description of the technologies used is provided in the following sections.

In the "tipping" hall, the MSW collection trucks discharge ("tip") their load into the waste bunker, where it is mixed by an overhead crane and is temporarily stored for several days. The tipping hall and waste bunker are totally enclosed buildings to prevent dust and odors from escaping into the environment. In addition, air is continually extracted to maintain a slightly negative pressure and is used as combustion air for the combustion system.

A crane unit lifts the waste from the waste bunker and transports it to the feed system, which consists of a hopper and a feed chute. Feed rams push the waste from the bottom of the feed chute onto the combustion grate. Due to the height of the waste column in the feed chute, unwanted air cannot leak into the combustion system. Microwave level detectors report the height of the waste column in the feed chute to the crane operator. Bridging and obstructions are prevented by the inclined side walls of the hopper and the flaring of the feed chute. A shutoff damper located underneath the hopper is closed when the plant is not operating.

The feed ram changes the direction of waste flow from vertical to horizontal. The waste, compacted in the feed chute, is loosened during this process and pushed onto the grate in amounts determined by the combustion control system. The transition between the feeder and grate can be designed as an inclination or as a drop-off edge. Each feed ram is driven by a hydraulic cylinder. The combustion control system optimizes cycle time, stroke length, and stroke speed to achieve uniform combustion on the grate. The operation of the feed rams is staggered for combustion grates with several parallel grate runs.

The combustion system, consisting of the grate system and furnace, is the heart of the WTE plant. The air required for combustion is fed as "underfire" or primary air from below the grate, passing through the grate bars into the fuel bed. Flue gases emitted from the fuel bed are not completely burned out, therefore "overfire" or secondary air is provided for combustion of the volatile gases rising from the grate. Overfire air is injected into the furnace above the fuel bed via numerous nozzles arranged opposite each other on the front and rear walls of the furnace. The resulting turbulence mixes the flue gas very efficiently, causing complete burnout at temperatures between 1,000°C and 1,200°C. Recirculated flue gas may also be used for secondary combustion. This involves splitting part of the flue gas after the dust removal equipment and returning it to the furnace to replace some of the overfire air. The recirculated flue gas is injected into the furnace via separate nozzles.

The hot, burned-out bottom ash drops from the grate end to a water bath in the ash discharger below the grate where complete quenching occurs. The discharger is filled with water up to the level of the air sealing wall. This creates an air seal against the furnace, thus preventing flue gas and thermal pollution in the basement, on one hand, and air infiltration into the boiler, on the other. The ash discharging ram pushes the bottom ash under the air sealing wall toward the drop-off edge.

Thermal treatment of waste produces energy that is transferred to steam and used in a steam turbine to generate electricity, heat for district heating purposes, or process steam in almost any number of combinations, as described in more detail further on.

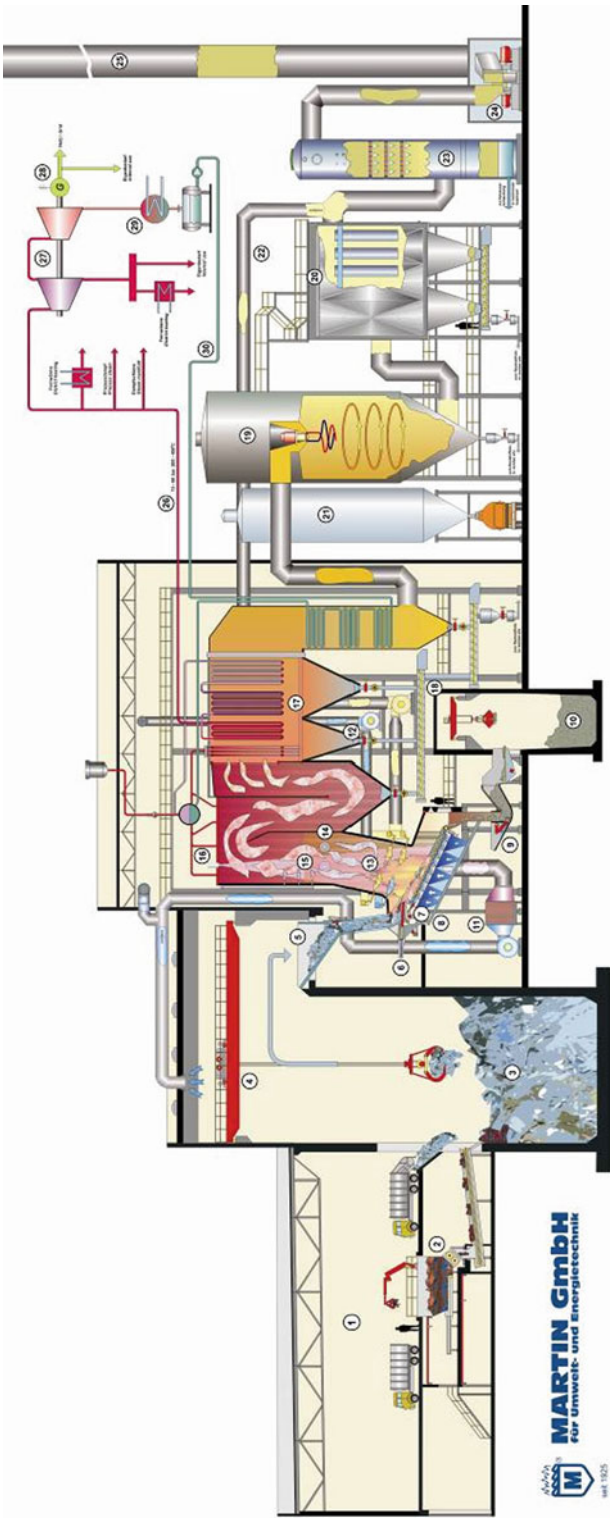

1 Tipping hall
2 Crusher for bulky waste
3 Refuse pit
4 Crane unit
5 Feed hopper
6 Feeder system
7 Reverse-acting grate
8 Grate siftings conveyor
9 Ram-type discharger
10 Bottom ash bunker
11 Underfire air system with air preheater
12 Overfire air system
13 Furnace
14 Oil/gas burners
15 SNCR
16 IR camera
17 Waste heat recovery boiler
18 Fly ash transport
19 Absorber
20 Fabric filter
21 Residue silo
22 Flue gas recirculation
23 Acidic scrubber
24 Induced draught fan
25 Stack
26 Live steam
27 Turbine
28 Generator
29 Condenser
30 Feedwater

Martin Waste-to-Energy Technology. Figure 2
Longitudinal section of a WTE plant

The flue gas cleaning system is an integral and most important part of every modern WTE plant. During combustion, pollutants contained in the waste are released and pass into the flue gas which must be cleaned before it can safely be allowed to enter the atmosphere. Suitable processes and components are combined according to technical and economic requirements. Electrostatic precipitators, fabric filters, spray absorbers, scrubbers, activated coke processes, SCR, or SNCR systems are used in various combinations. The clean gas emissions at the stack are continuously measured, monitored, and documented with state-of-the-art measurement devices. Modern WTE plants respect the strictest emission levels, worldwide, and are trendsetters for the highest environmental standards.

Grate Technologies

The grate system consists of the feed hopper, feeder, combustion grate, bottom ash discharger, and air supply to the furnace (Fig. 3).

Feeding System

The waste feeding system consists of the charging hopper, connected feed chute with shutoff damper and water cooling in the lower part and ram-type feeders (Fig. 3). The waste taken up by the grapple of the waste crane is fed into the feed chute via the hopper. The dimensions of the hopper ensure that the contents of the grapple can be charged without difficulty and that there is always a sufficient stock of fuel in the hopper. By means of the feed chute, the discontinuous charging of the waste into the hopper is transformed to a continuous flow of fuel. The fine metering is done by the ram-type feeding system arranged downstream of the feed chute.

The design of the feed chute must satisfy the following requirements:

- Operational reliability
- Avoidance of damage and operational failures
- Supply of fuel without blockages

Due to the column of waste it contains, a feed chute of sufficient height prevents the ingress of undesirable air into the furnace and provides a certain stock of fuel in the eventuality of failures in preceding systems. The feed chute is provided with a water jacket. By means of natural convection, the water is moved through the warm and cold zones, thereby preventing overheating. The closed water circuit does not lead to any additional

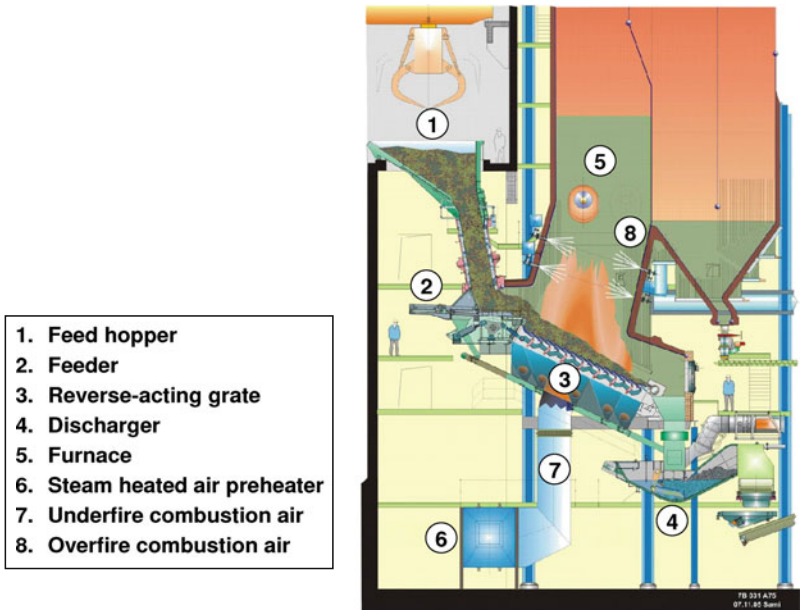

Martin Waste-to-Energy Technology. Figure 3
Typical grate system

water consumption during normal operation. The cooling system for the feed chute is equipped with a thermostat that opens an emergency water connection for cooling, in case the temperature of the water jacket exceeds a certain level, and a warning signal is sent to the control room.

A "bridge" breaking system is provided at the rear side of the hopper to remove any bridging of waste in the transition area between the hopper and the feed chute. Also, in order to be able to take countermeasures in the event of dust formation, an atomized water spray can be generated by means of spray nozzles that are arranged above the upper waste hopper edge. Under the feed hopper, there is a shutoff damper extending over the entire width of the feed chute; this damper is closed when the level in the feed chute drops too low or when the plant is shut down. In order to ensure a sufficiently high waste column in the feed chute, there is a built-in level monitor in the form of microwave sensors.

The direction of movement of the fuel is changed from vertical in the feed chute to horizontal on the feed table. This is done by means of ram-type pushing devices. In the course of charging, a uniform, continuous supply of waste onto the grate is achieved. The design of the combustion grate allows exact fuel metering in accordance with the required thermal output because the feed rams are driven separately for each run via hydraulic cylinders. Cycle time, stroke length, and stroke speed can be varied, independently for each run. The waste transfer zone at the end of the feeding table is designed with a gentle drop-off edge, which has the effect that the fuel is loosened with a minimum of dust formation.

The feeding system is part of the combustion control concept; however, it can also be controlled manually and the feeding ram can be switched from "working" stroke to "clearing" stroke, enabling the feeding system to be emptied within the shortest possible time.

Reverse-Acting Grate

The reverse-acting grate is inclined at an angle of 26° to the horizontal and consists of several stair-like grate "steps" that consist of bars. Every second step is moved up and down against the downward direction of the solids flow (Fig. 4). The moving rows of grate bars are moved forward and backward by a hydraulic cylinder. This constantly rakes and mixes the red hot mass with newly fed waste. In the area of the feeding system, predrying of waste is carried out by radiation from the flame above the grate. The drying process is fully completed in the front grate area. The waste begins to burn already at the front end of the grate and the fuel bed temperature reaches 1,000°C and higher. The waste is combusted fully during its travel over the length of the grate. The combustible constituents of the fuel are converted to gases in the main combustion zone accompanied by the release of energy (primary combustion). Secondary combustion, e.g., the final oxidation of the unburned gases, takes place in the flame above the main combustion zone. Complete gas burnout is achieved by means of overfire air injection that is optimally controlled according to the prevailing furnace conditions.

The number of these agitation cycles, in other words the grate speed, is primarily dependent on the composition of the fuel and only to a minor extent on the combustion throughput. The residence time of the fuel on the grate is typically between 60 and 70 min.

Along its length, the reverse-acting grate is divided into three to six separate air zones, so that underfire air is supplied across the grate in a controlled manner and as needed for combustion. The underfire air flows into the fuel bed through narrow gaps at the head of the grate bars (Fig. 5). These air gaps are kept free of impurities during operation because every second grate bar in a row moves, relatively to its adjacent bars, at the end of each agitation stroke. The effect of the relative stroke is to clear the air gaps, thereby allowing a long period between maintenance outages. The evenly spaced narrow air gaps ensure that the underfire air is distributed evenly over the fuel bed. The grate bars are made of cast chromium steel that is highly resistant to wear.

Combustion on the grate is completed after approximately two thirds of the length of the grate. A clear delimitation between the combustion zone and the end zone is plainly visible. Through its intimate mixing of the fuel, the reverse-acting grate always ensures good thermal protection for the grate bars due to the "insulating" fuel and ash layer on the grate surface. The average operating temperature of the grate bars is approximately 20–50°C above the underfire air

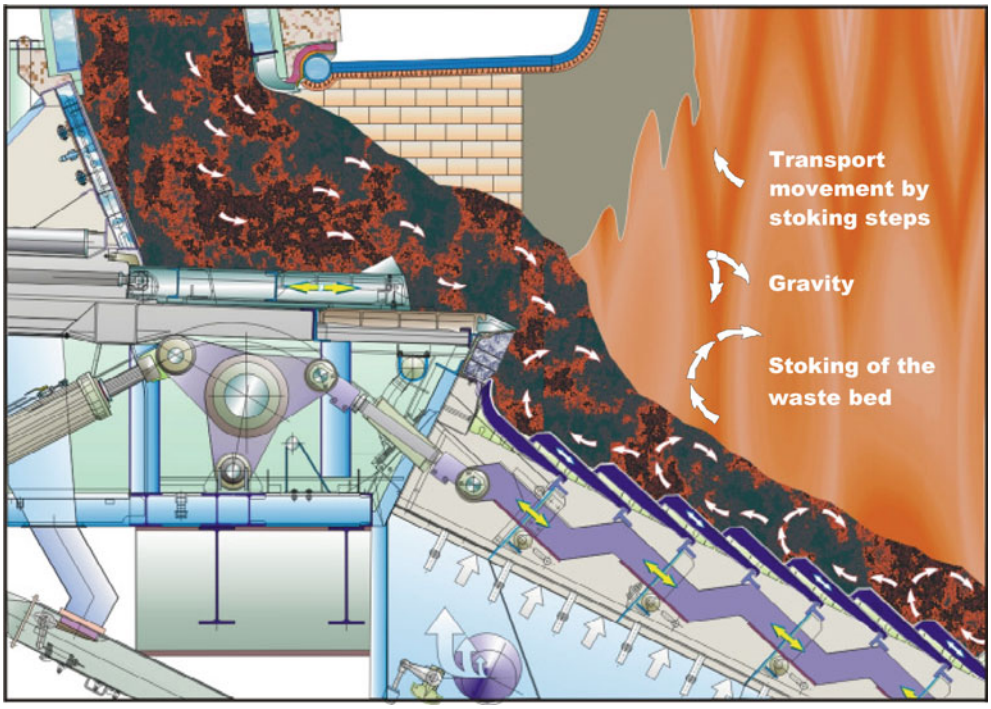

Martin Waste-to-Energy Technology. Figure 4
Mixing of the waste on a reverse-acting grate

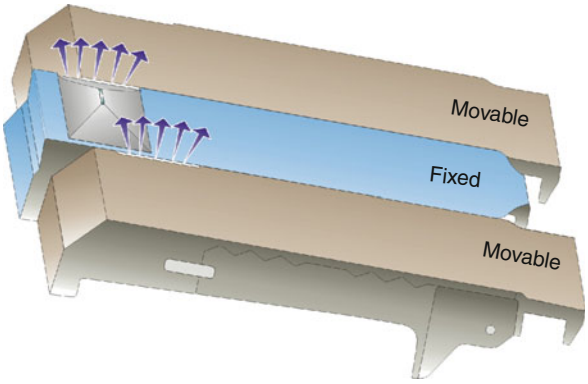

Martin Waste-to-Energy Technology. Figure 5
Underfire air flow/movement of grate bars of a reverse-acting grate

temperature even in the main combustion zone of the grate. This provides a high level of certainty against thermal overloading and makes it possible to achieve a long service life for the grate. The operating experience from numerous plants obtained over many years of continuous service time have conclusively proven that the reverse-acting grate does not require water cooling, even for high heating-value fuel (Fig. 1) [2].

The grate "siftings," i.e., inert particles that may fall through air gaps between the grate bars (mostly in the residue burnout area) are collected in the hoppers under the grate. The particles are discharged from the hoppers by means of pneumatically operated shutoff valves, with no air infiltration. The shutoff valves operate according to a specified timing program to open the ducts and discharge siftings into the bottom ash discharger where they mix with the bottom ash.

The reverse-acting grate is of modular design (Fig. 6). Each module comprises a complete grate run with a width of 1.5–2.5 m. The modules can be fully preassembled at the factory and then shipped to the plant site. Up to eight grate-run modules can be arranged in parallel to produce a total grate width of over 15 m.

A clinker roller, or clinker weir, is installed at the end of the grate to control the height of the fuel bed and bottom ash layer. The roller, or weir, can be adjusted to suit actual combustion conditions. From there, the bottom ash drops into the bottom ash discharger.

Martin Waste-to-Energy Technology. Figure 6
Reverse-acting grate

The reverse-acting grate satisfies the following essential requirements of MSW combustion:

- Wide heating value range and capacity for handling fluctuations in waste composition
- Rapid transition of the fuel from a cold state into the combustion phase in order to prevent smoldering that adversely affects emissions
- High and uniform fuel bed temperature
- Intensive and constant agitation of the fuel bed
- Clear demarcation between combustion zone and burned-out bottom ash over the entire grate width
- Uniform coverage of the grate surface
- Easily definable and controllable supply of underfire air to suit requirements
- No air supply due to mechanical requirements (e.g., cooling of cast-steel parts)
- Low thermal load on grate surface due to covering of the bars with bottom ash
- Small amount of grate siftings
- Low dust emission from the combustion process
- Direct response to control operations
- High equipment availability
- Rapid start-up and shutdown of the grate
- Easy replacement of grate bars

The overall result is long service life for the grate, high availability, ability to recover residues, and compliance with emission requirements.

Reverse-Acting Grate Vario

The reverse-acting grate Vario (Fig. 7) was developed for use with fuels with a high heating value and a low ash content (e.g., a refuse-derived fuel, RDF). This grate uses the same proven and unique reverse-acting principle but its angle of inclination is 24°. The stair-like grate steps are alternately arranged in stationary and moving grate bar rows. The interaction between the upward stoking force and the downward pull of gravity ensures constant mixing of the red hot mass with the fresh fuel. This results in optimal combustion and fully burned-out bottom ash. At the same time, the grate is automatically covered with a thick fuel and ash layer which insulates the grate surface and provides excellent protection against thermal radiation from the furnace (>1,100°C).

The reverse-acting grate Vario is divided into three independent drive zones along its length so that full advantage can be taken of the reverse-acting principle

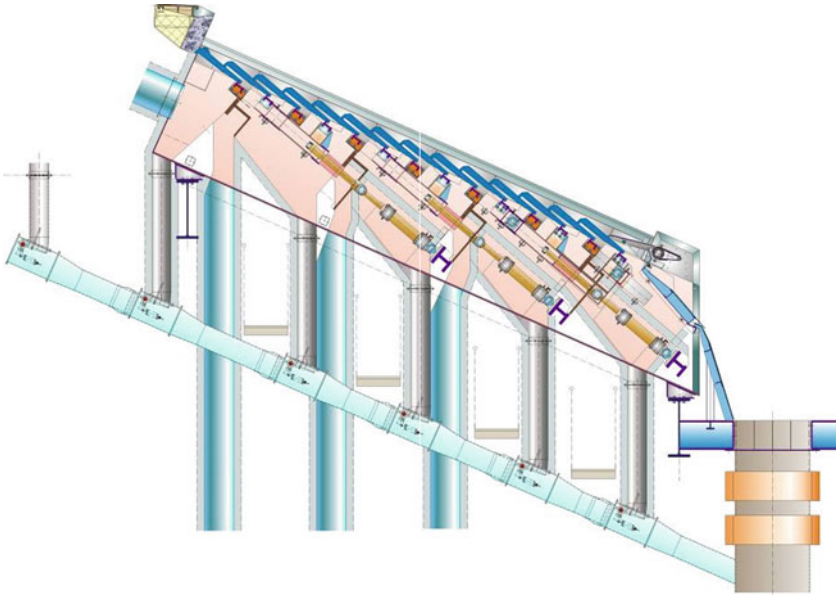

Martin Waste-to-Energy Technology. Figure 7
Reverse-acting grate Vario

even with fuel that has a low inert content. The width of the grate consists of a number of modules, depending on the design capacity of the unit. Each module is driven independently.

The grate Vario satisfies the same requirements as listed earlier for reverse-acting grate. Additionally the following essential requirements are met:

- Grate speed can be individually set per run and zone
- Clear delimitation between combustion zone and burned-out bottom ash over the entire grate width
- Good bottom ash burnout by adjusting the grate speed in the various zones in response to varying waste quality
- Easily controlled supply of combustion air as required
- Small amounts of grate siftings
- Modular design

This design results in the following advantages for combustion system operation: high level of availability, long grate surface service life, recyclable residues, and consistent compliance with emission requirements while at the same time maintaining high efficiency.

Horizontal Grate

The horizontal grate system was originally developed by the Swiss company W + E Umwelttechnik AG. It has been part of the MARTIN technology portfolio since 2002 (Fig. 8). It was developed for the incineration of household waste and combustible industrial residues. The horizontal construction of the combustion grate allows the fuel to be advanced in a well-controlled manner. The grate is modular, providing for the configuration of a variety of different grate sizes, depending on given variables such as:

- Quantity of waste
- Lower heating value of waste
- Type of use (heat evaluation)
- Structural constraints

The waste is pushed forward by rows of grate bars moving in opposite directions, alternated with stationary rows of grate bars (Fig. 9). Moving and stationary horizontally arranged grate-bar supports are located in the solidly built grate support structure. The moving-bar rows are connected to an oscillating crank and move back and forth, working in opposite directions

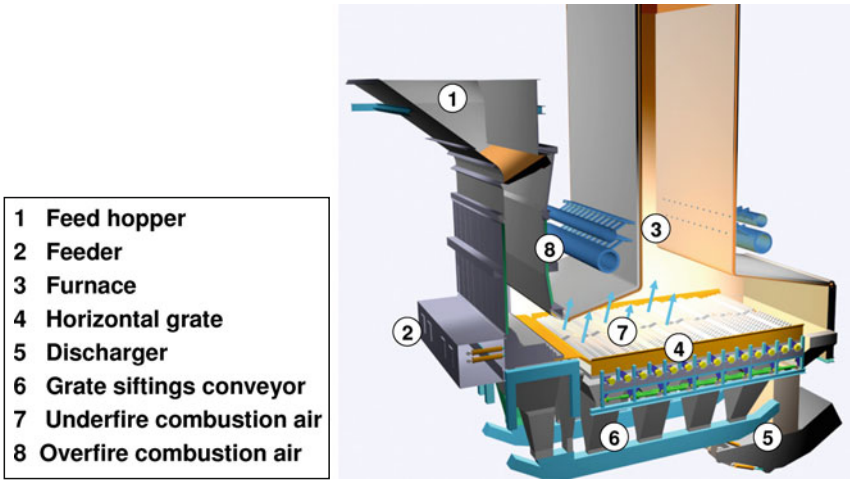

Martin Waste-to-Energy Technology. Figure 8
Horizontal grate system

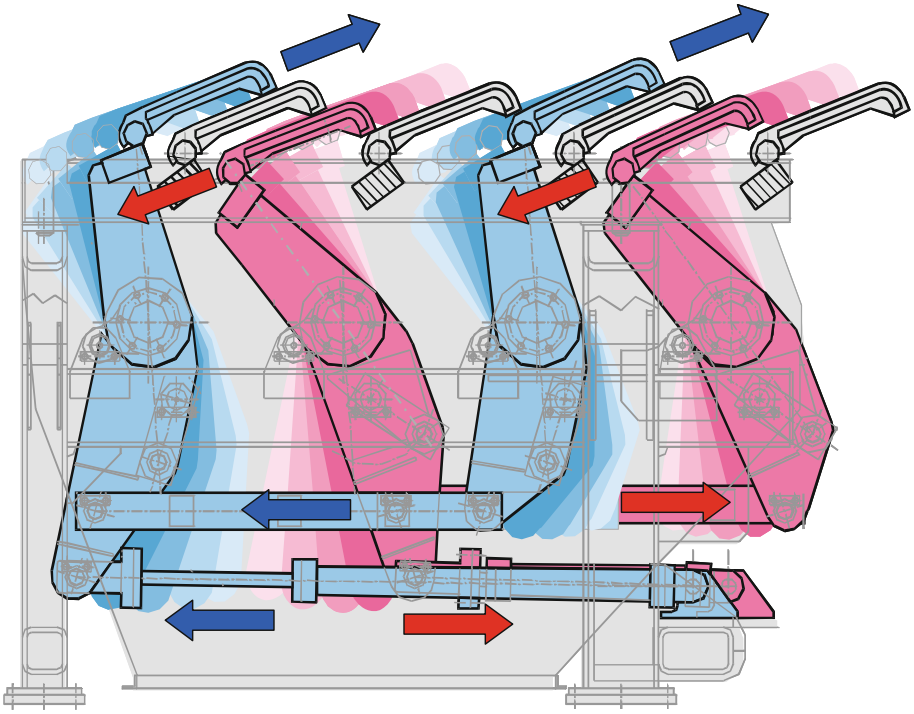

Martin Waste-to-Energy Technology. Figure 9
Movement of grate bars of a horizontal grate

relative to each other. When the rows of grate bars are moved apart in opposite directions, the fuel is dropped down at this point and ignited fuel particles fall down. The grate bars then move toward each other, lifting and igniting the fuel layer. The fuel particles initially ignited as a result of the backward motion of the bars then move forward as a result of the advance feed motion of the bars and drop to the bottom of the fuel layer, where

they become ignition points and accelerate combustion of the fuel above them. On the horizontal grate, ignition takes place not only by radiation and convection of heat from above, but also from within the waste bed. Burning particles are constantly being pushed downward by the intensive stoking and agitation of the waste layer, causing ignition to start from within the bed as well.

The continuous stoking and agitation of the waste results in the waste layer being repeatedly broken up and rearranged. This promotes ignition and combustion by creating a large waste surface area, which favors the admission of combustion air, and effectively transports and mixes the waste to ensure good burnout.

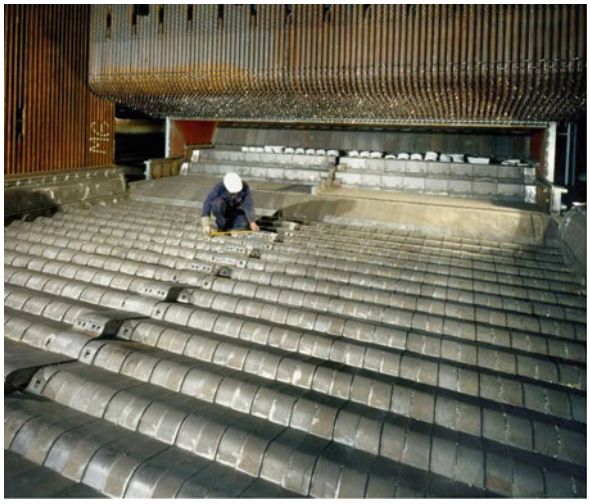

Martin Waste-to-Energy Technology. Figure 10
Horizontal grate

The fuel residence time on the grate (drying, main combustion, and burnout zones) depends on combustion capacity, fuel composition, processes, etc., and takes about 30–120 min. From the grate rear end, bottom ash falls into the water bath of the bottom ash discharger.

The main features of the horizontal grate are:

- Combination of fixed and moving rows of grate bars
- Movement of the grate-bar rows in opposite directions
- Infinitely variable hydraulic drive system
- Slow, continuous movement
- High pressure loss over the grate bars with resultant optimal air distribution
- Low overall height
- No grate steps
- No maintenance of the underfire air area

The horizontal grate is of modular design. The length of each module is fixed but the width may vary according to specific requirements. Each module has its own drive and supply of underfire air, both of which can be controlled separately. A typical grate configuration consists of three modules in the direction of waste flow and there may be between one to three runs in parallel depending on the waste throughput capacity (Fig. 10).

The grate bars are typically air-cooled (Fig. 11) by the flow of underfire air passing through a labyrinth of passages, cooling the bar and promoting a uniform release of heat. The underfire air exits from the front end of the grate bar. The outlet slots have been designed and positioned for an optimal supply of air to the fuel

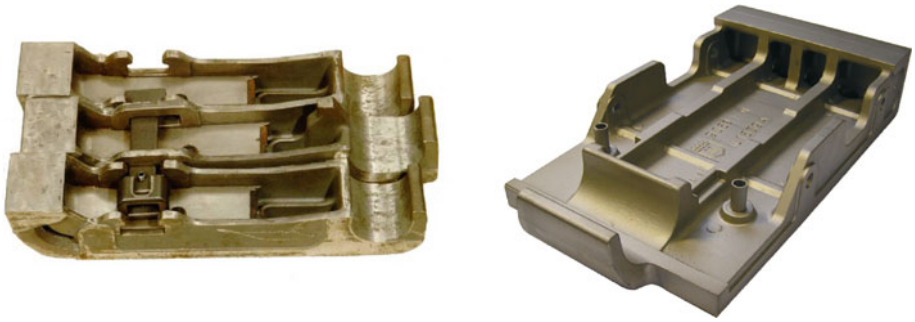

Martin Waste-to-Energy Technology. Figure 11
Air-cooled and water-cooled grate bars

bed. During operation, the air outlet slots are kept clear by the relative motion of adjacent grate bars. The grate bars are made from wear and heat-resistant chromium-nickel alloy steel. The grate bars are an exact fit, which means that the proportion of grate siftings to waste is low. The bottom ash which drops through the grate is collected in ash hoppers and discharged into the bottom ash discharger.

In recent years, there have been significant increases in the heating values of wastes, necessitating the development of water-cooled grate bars (Fig. 11) to achieve acceptable service lives. The solution is a cast-steel construction, where one water-cooled grate-bar block has the width of three air-cooled ones. The cooling circuit is a closed-loop cooling circuit. Two different versions have been installed:

- Medium pressure version (around 7 bar(a)), where the heat removed is then used to either preheat the combustion air or the condensate
- High-pressure version, where the cooling circuit is part of the waste heat boiler circuit; the heat removed is fed to the water–steam cycle

An added benefit of the water-cooled system is that underfire air is no longer needed to cool the grate bars and is controlled only as and when required by the combustion process. The heat dissipated by means of the water-cooling system can be returned in full to the process.

The horizontal grate is notable for a number of beneficial characteristics:

- Controlled transport of the waste due to double-motion overthrust mechanism of the grate bars
- Horizontal construction allows the waste to travel in a controlled manner and precludes sliding of the waste
- Tight-fitting grate bars with high pressure drop producing an even intake distribution of the underfire air over the width of the grate
- Small percentage of combustion products ending up as siftings
- Parts subject to wear are made of a high-tensile cast alloy steel
- A high level of availability and operational safety
- Easy maintenance

Bottom Ash Discharger

From the rear end of the grate, the bottom ash falls into the water bath of the bottom ash discharger (Fig. 12).

The discharging ram pushes the bottom ash under the air sealing wall toward the drop-off edge. As a result, the bottom ash is discharged in a dust-free and odorless manner. Larger pieces of bottom ash

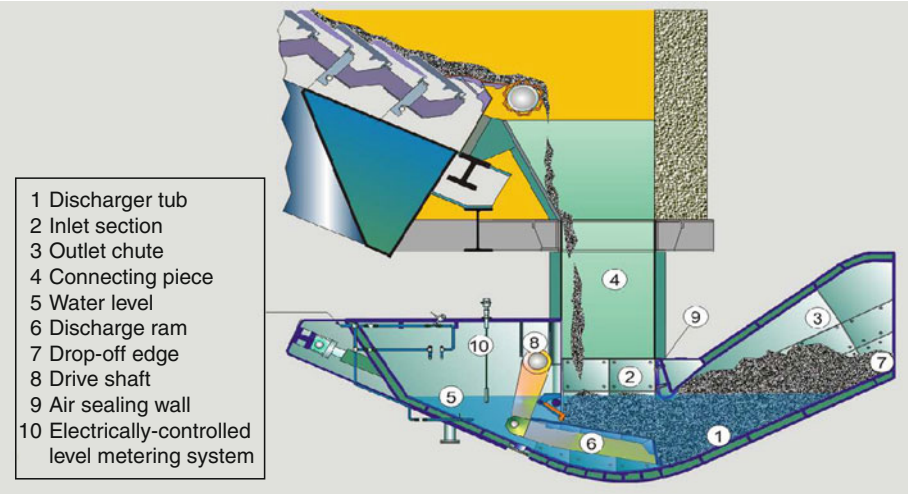

Martin Waste-to-Energy Technology. Figure 12
Bottom ash discharger

become cracked as a result of quenching in the water. They are then broken by the force of the discharging ram.

Because the bottom ash still resides for a while in the chute above the actual water level and during that time is compressed by the discharging ram, most of the water flows back into the discharger tub, with the result that the bottom ash is discharged with only low moisture content. The discharger has no water overflow, so only the small amounts of water escaping through evaporation and taken up by the bottom ash need to be replaced. As necessary, water is added and controlled via a float valve. In normal operation, therefore, the discharger has no water drain and has a very low water consumption. In this way, clean operation is ensured, while at the same time a very sturdy, space-saving, and easily accessible design is obtained.

The interior of the discharger tub and the side walls of the inlet chute are lined with wear plates. The front plate of the discharging ram is protected by easily replaceable slide strips.

A wide range of dischargers is available, the smallest with a discharging capacity of approximately 0.2 m^3/h. Dischargers for coal-based combustion systems have a discharging capacity of approximately 0.2–3.0 m^3/h. Discharging capacities for waste combustion plants range between approximately 4.5 and 12.0 m^3/h.

Combustion Technologies

Using optimal combustion design in terms of thermal efficiency and temperature levels, systems must be applied to limit the specific global and local heat loads to reasonable values for system components, i.e., grate, combustion chamber, and post-combustion chamber, taking design criteria into account:

- Optimal mixing of the flue gases
- Homogeneous temperature and concentration profiles
- Stable combustion and constant heat release
- Minimum formation of pollutants
- Reduction of chemical attack and thermal stress
- Reduction of corrosion and abrasion of materials
- Optimal burnout of bottom ash

A combustion system capable of maintaining stable and uniform operation in terms of thermal load, flue gas flow, bottom ash burnout, and flue gas burnout has major advantages compared with systems in which conditions fluctuate:

- Easier compliance with regulations and limit values
- Smaller design range required for flue gas cleaning components
- Minimum operational effort required for combustion system control
- More uniform thermal and mechanical load and, consequently, longer service life for components such as feeder, grate bars, etc.

Conventional Combustion with Air

The conventional combustion air system essentially comprises the underfire and overfire air systems. Optimum interaction between these systems enables combustion to be as homogeneous as possible with low pollutant emissions.

The underfire air is drawn from the building housing the waste bunker. This is done by means of a frequency-controlled fan through which the underfire air flow rate is adapted to the prevailing requirements of combustion on the grate. The extraction of air from the waste bunker has the positive side effect that a slight negative pressure is maintained in the bunker area, causing fresh air to flow in. This ensures that no odor nuisance occurs outside the plant. After optional preheating, the air flows through the grate and in this way is supplied to the fuel bed in accordance with requirements. Preheating is achieved using a steam-heated air preheater with an air temperature depending on the heating value of the waste and the kind of waste to be burned. Normally for air temperatures up to 120°C, 5 bars process steam is used. Higher air temperatures up to 160°C (e.g., at lower heating values and co-combustion of sewage sludge) are achieved by the second staged supplied with saturated steam from the boiler drum.

The grate is divided lengthwise into five separate air zones. Air is supplied to the individual zones via orifice openings that are covered by adjustable dampers. The shape and size of the orifice openings are determined according to the combustion characteristics and the designed release of heat over the length of the grate. Accordingly, the largest free orifice opening is located

under the grate compartments of the main combustion zone. This concept for underfire air distribution makes it possible to distribute the combustion air to the fuel bed in an individual manner according to requirements. As a result, it is possible to react to differences in the waste quality during combustion.

A vigorous, stable fire, in which all the combustion phases (drying, gasification, ignition, and combustion) occur simultaneously and consecutively, develops at the front end of the grate. The constant stoking motion provides for a uniform heat release and ensures excellent burnout values.

The overfire air is drawn from below the boiler house roof or, alternatively, is extracted from the bottom ash bunker and is injected according to the "stitching method." The overfire air is injected through four rows of nozzles, two rows in the front and two rows in the rear wall of the furnace (Fig. 13). The nozzles in the two rows on each wall are arranged in an offset pattern (stitching). This so-called 4-row stitching arrangement ensures full coverage of the furnace cross section and the turbulence needed for good mixing of the gases, while uniform profiles for temperature and flow are obtained above the injection levels. Gases arising from the fuel bed on the grate are oxidized immediately afterward in the downstream furnace by final mixing of the overfire air with the remaining underfire air at high temperatures. The overfire air is supplied by a frequency-controlled fan, through which the flow rate can be optimally adapted to the prevailing requirements in the furnace.

Conventional Combustion with Recirculation of Flue Gas

Burnout in the fuel bed takes place due to the constant ignition and the supply of underfire air. Most of the unburned gases produced on the grate are oxidized immediately afterward in the furnace after being mixed with the remaining underfire air at high temperatures. However, some unburned gases inevitably escape primary combustion. For this reason, adequate mixing of the combustion gases must be ensured by introducing an additional jet of overfire gas via nozzles. As described above, the "4-row stitching" process for the arrangement of the overfire air nozzles and the recirculated gas nozzles is used (Fig. 13). As a result of this measure, a uniform temperature and flow profile, and optimal mixing of the gases in the furnace is achieved. The residence time of the gases in the high temperature zone is extended and gas burnout improves.

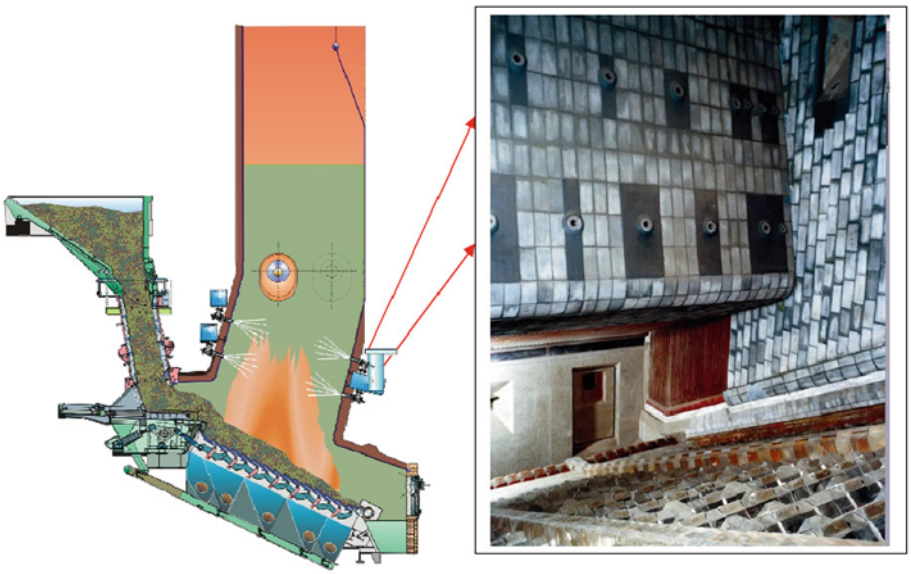

Martin Waste-to-Energy Technology. Figure 13
Positioning of overfire air and/or recirculation flue gas nozzles

In order to reduce the flue gas flow (approximately 20–30%), the excess combustion air and the NO_x content, part of the flue gas flow downstream of the effective pre-deduster (e.g., electrostatic precipitator, baghouse) is extracted with a separate frequency-controlled fan and returned to the furnace as recirculated flue gas. The recirculated flue gas replaces most of the required overfire air. It is injected into the furnace via both rows of nozzles on the rear wall as well as the upper row of nozzles on the front wall.

Since, as described above, unburned gases escape from the fuel, overfire air is injected into the furnace via the lower row of nozzles on the front wall. Sufficient oxygen for the combustion of these gases is provided by the overfire air at this point. The turbulent effect of the overfire air is mainly produced by the recirculated flue gas. The required overfire air could be extracted from the underfire air flow downstream of the air preheater. If the recirculated flue gas is extracted after a baghouse filter, the gas temperature is quite low (about 150°C). In this case, the gas ducts have an electric trace heating system to prevent condensation on the walls. Generally the flue gas ducts are insulated to keep heat loss to a minimum and to protect the outside environment. Since the process requires that the flue gas recirculation system is operated with flue gas, which still contains dust remnants, despite prior dust removal in the pre-deduster (dust content > 20 mg/Nm^3), discontinuous cleaning of the recirculated flue gas nozzles is possible. A fine water jet is injected directly into the nozzles in regular adjustable cycles for short periods, so as to remove any flue gas constituents that may still be present. This system ensures proper functioning of the recirculated flue gas nozzles without having any measurable influences on the operation of the plant (furnace temperature, emissions, etc.).

Combustion with Oxygen-Enriched Air (SYNCOM)

Discussion about how to minimize the level of pollutants produced by WTE plants all over the world has led to many new technological developments, focusing in particular on the treatment of flue gas and residues. Above all, the dioxin input introduced with the waste of about 50 μg TEQ/Mg must be destroyed. Consequently, reduction of pollution burdens, improvement of bottom ash quality and reduction of overall dioxin output to <5 μg TEQ/Mg of waste have been the driving forces behind the development of the SYNCOM process (*SYN*thetic *COM*bustion) [3].

The SYNCOM process is based on the following components, illustrated in Fig. 14:

- Grate-based combustion system using the reverse-acting grate
- Combustion control system using IR thermography
- Overfire air system with four nozzle rows (four-row stitching)
- Flue gas recirculation
- Oxygen enrichment of underfire air

The amount of nitrogen in the combustion air is significantly reduced by replacing part of the underfire air in the main combustion zones 2 and 3 with technically pure oxygen. The oxygen concentration in these zones is then in the range 24–35%. As a consequence, the excess air rate is significantly lower, the flue gas flow is substantially reduced and the pollution burden is clearly decreased compared with conventional combustion. The IR-camera control signal is used to meter oxygen selectively and as required.

One of the core components of the SYNCOM process is the oxygen generation plant. The oxygen is obtained from the ambient air in an air separation plant. In Arnoldstein (Fig. 15), the air separation plant uses the pressure swing adsorption principle, whereby oxygen and nitrogen are separated by means of a zeolitic molecular sieve. The nitrogen is adsorbed on the molecular sieve, while the oxygen flows through the adsorber. The adsorbed nitrogen, water, and CO_2 are then desorbed by reducing the pressure within the adsorber unit.

The surface temperature of the fuel bed is determined using the IR camera in the boiler roof. The temperature is about 100°C higher than when using underfire air without oxygen enrichment. The higher fuel bed temperature means that bottom ash sintering, improved burnout, and destruction of the organic pollutants are achieved.

To reduce the flue gas flow and O_2/NO_x content, the recirculated flue gas is drawn off downstream of the pre-deduster with a separate fan and returned to the furnace. The recirculated flue gas causes turbulence and mixing. Recirculated flue gas is directed to both nozzle rows on the rear wall and to the upper row of the

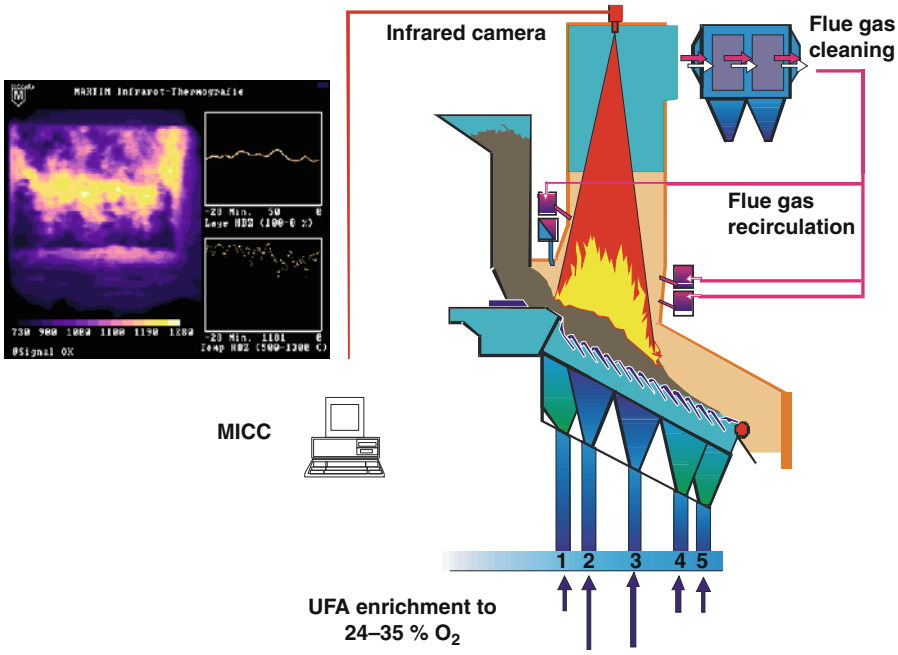

Martin Waste-to-Energy Technology. Figure 14
SYNCOM process

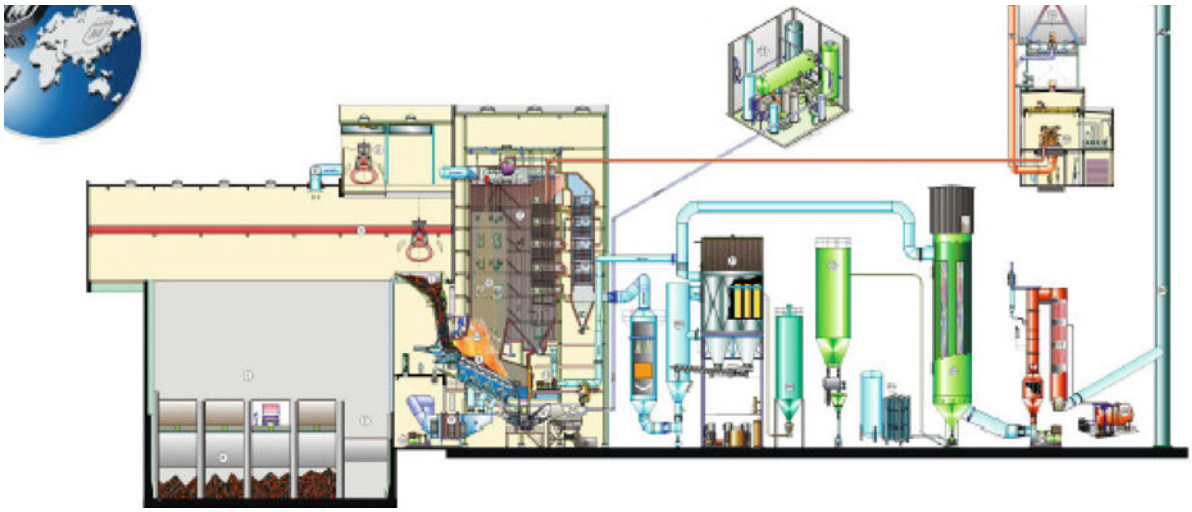

Technical data						
Annual throughput approx.:	80,000 Mg	1 Tipping hall	7 Feed hopper	13 Air separation plant	19 Air-cooled condenser	25 Active coke filter
Number of lines:	1	2 Bulky waste cutter	8 Reverse-acting grate	14 Overfire air nozzles	20 Turbo reactor	26 ID fan
Waste capacity per line:	10.7 Mg/h	3 Waste bunker	9 Discharger	15 Flue gas recirculation fan	21 Fabric filter	27 SCR catalytic converter
Thermal capacity per line:	29.6 MW	4 Waste crane	10 Underfire air fan	16 Burners	22 Additive silo	28 Aqueous ammonia storage
Steam output per line:	35.2 Mg/h	5 Waste crane set down	11 Underfire air preheater	17 Steam boiler	23 Spent active coke silo	29 Stack
Steam pressure:	40 bar	6 Underfire air intake	12 Oxygen distribution	18 Turbine / generator set	24 Nitrogen station	
Steam temperature:	400 °C					

Martin Waste-to-Energy Technology. Figure 15
SYNCOM plant Arnoldstein (AT)

front wall. Due to the use of recirculated flue gas in the overfire air system and the reduction of nitrogen in the underfire air, the gas volume per ton of feed is reduced by up to 35%, as compared with conventional waste combustion.

The smaller flue gas flow has a direct effect on the equipment downstream of the combustion system. As a result, the steam boiler (with the exception of the first boiler pass), any downstream dedusting filter, the ID fan, and the downstream flue gas cleaning equipment can be designed with smaller dimensions than is the case in conventional combustion systems, thereby resulting in lower investment costs and higher energy efficiency. The smaller flue gas volume associated with the SYNCOM process also means that flue gas heat loss is also reduced. The thermal efficiency of the boiler is increased by 3–5%, as compared with conventional thermal waste treatment.

The use of the SYNCOM process results in reducing both capital and operating costs. The additional costs associated with constructing and operating the air separation plant are largely offset by the savings made due to smaller components, a smaller construction volume, better energy utilization, and lower operating costs for the equipment downstream of the combustion system.

In conclusion, the SYNCOM process is characterized by the following features, as compared with conventional combustion using air:

- Intense, uniform combustion
- Minimal CO content in the flue gas
- Temperature in the fuel bed in the main combustion zone approximately 100°C higher
- Partial sintering of the bottom ash and consequently
  - Optimum burnout
  - Minimal heavy-metal leaching in compliance with drinking water quality standards
- Reduction of flue gas flow by approximately 35%
  - Higher boiler efficiency
  - Reduced pollutant burden at stack
  - Reduced fly ash flow

This process was tested extensively in industrial-scale demonstration plants at Coburg (DE), Oita (JP), and Osaka (JP). It was then included in the new WTE plant in Arnoldstein (AT) in 2004 (Fig. 15) and also at the Sendai (JP) WTE plant (three lines).

The WTE plant in Arnoldstein consists of a combustion system with reverse-acting grate (one line, two runs), air separation plant, four-pass vertical boiler, fluidized bed adsorption reactor, fabric filter, lignite-coal fixed-bed filter, ID fan, SCR-DeNO$_x$ unit, stack, turbine, and generator.

Gasification with Post-combustion

Gasification of municipal solid waste has been developed using various technologies, the most widespread being:

- Shaft furnaces (using additional coke)
- Pyrolysis kilns
- Fluidized bed systems

Experience in Europe in the 1990s showed that these processes have their limitations when used for waste due to high cost, low availability, poor energy efficiency, and the need for waste pretreatment [4–7]. Experience has also proven unstable operation under commercial operating conditions. This is why many European waste gasification plants were dismantled after a relatively short period of time. In the 2000s, a large number of gasification systems were built in Japan and continue to operate despite these limitations [8, 9]. All these systems are coupled with post-combustion of the produced gases in furnaces with boilers. The expected advantage of these gasification systems in Japan is the integrated melting of the ash in the post-combustion step, which also leads to reduction of the total dioxin output (through melting of fly ash) [10, 11].

MARTIN has developed a grate-based gasification system since the 1990s. This gasification system has the advantage of controlling the following conversion steps (Fig. 16):

- Drying
- Degassing
- Ignition
- Gasification
- Burnout of carbon

Based on numerous tests with a semi-industrial-scale combustion unit, it has been proven that the reverse-acting grate (Fig. 3) is essentially well suited to gasification. In particular, the reverse-acting grate

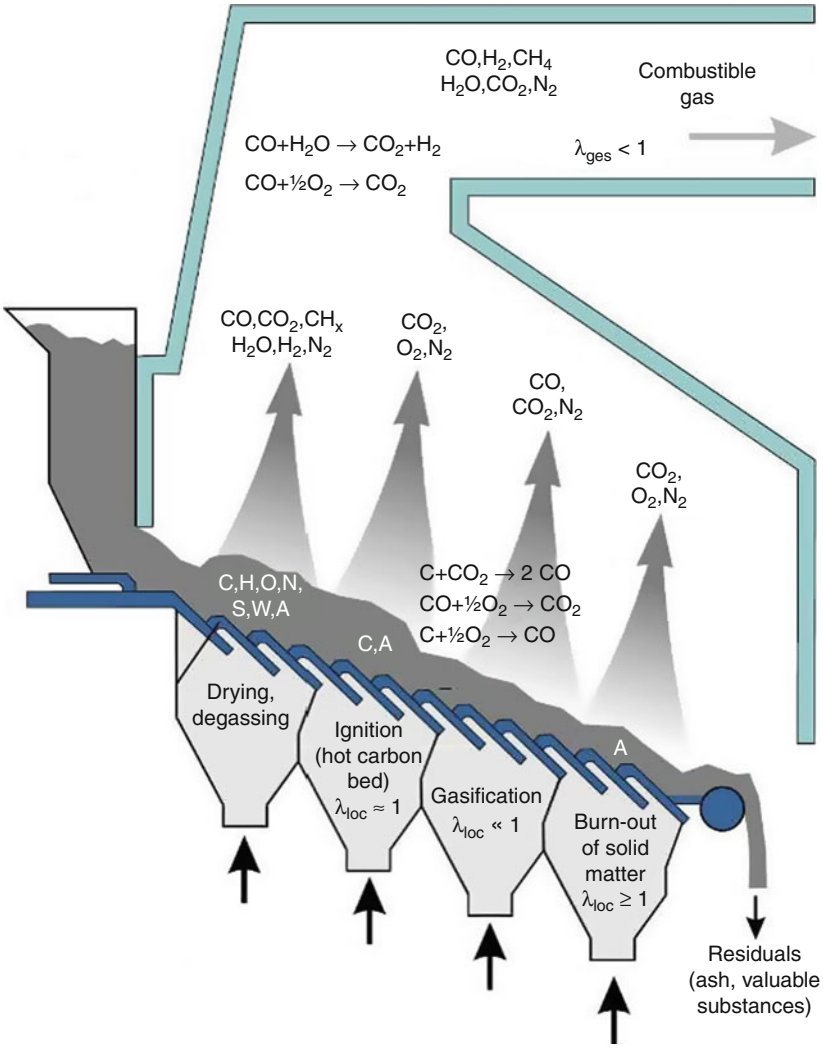

Martin Waste-to-Energy Technology. Figure 16
Conversion steps of grate-based gasification [12]

Vario (Fig. 7) performs well regarding gasification because it has the particular feature that three grate zones can be driven separately and the air compartments are perfectly tight in order to control these conversion steps. Another important advantage of grate-based gasification compared with other gasification systems is its robustness, which makes it possible to use waste that has not been pretreated.

Post-combustion of the gas product of volatilization occurs either in an extension of the membrane wall furnace, or in a following, uncooled separate combustion chamber. Experience with post-combustion chambers is based on the Clausthal test facility (Fig. 17) as well as on the WTE plants in Trieste and Cagliari using T3 (Time–Temperature–Turbulence) controls and Vortex post-combustion chambers (Fig. 18).

Grate-based gasification systems with post-combustion processes are characterized by:

- Reduced excess air rate from 1.8 to 1.4 and thus reduced flue gas flow
- High residence time for sub-stoichiometric flue gas and thus reduced NO_x

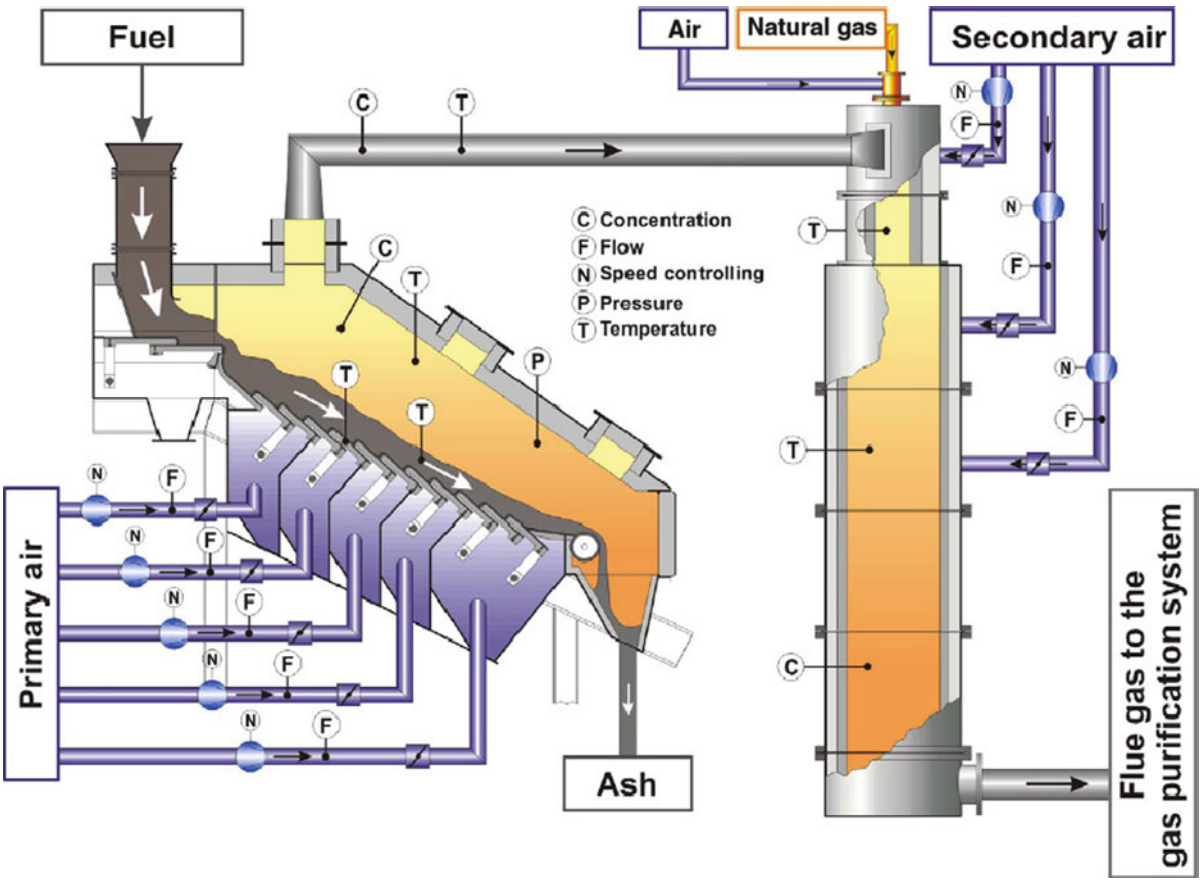

Martin Waste-to-Energy Technology. Figure 17
Clausthal test plant for gasification with post-combustion [13]

- Efficient post-combustion (time, temperature, turbulence), resulting in good gas burnout and reduced dioxin content
- Low gas velocities through waste bed and in the gasification chamber; thus reduced fly ash carryover to the boiler
- Taking advantage of the long experience of traditional grate-based systems: moderate cost, high availability, high energy efficiency, and the possibility of treating waste that has not been pretreated

However, the gasification process requires higher waste heating values for stable reaction conditions on the grate and more sophisticated process control, because changes in waste quality have a much greater influence on the process than in the case for super-stoichiometric combustion.

Combustion Control

Stringent statutory requirements stipulate that the combustion process on grate systems be automatically monitored, regulated, and controlled as far as possible. These tasks are fulfilled by the combustion control system.

The purpose of the combustion control system is to ensure that the combustion process takes place under constant conditions whereby:

- Combustion gases and bottom ash burn out completely
- Flue gas emissions are minimized
- A uniform steam flow is generated

A large number of parameters must be taken into account when controlling a combustion system.

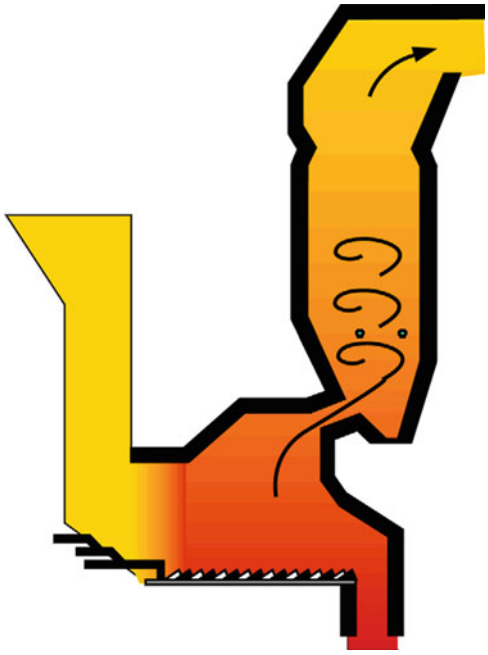

Martin Waste-to-Energy Technology. Figure 18
Vortex post-combustion chamber in T3 plants Trieste/Cagliari

Consequently, only experienced operating staff or, if all available process parameters have been taken into consideration, an essentially automatic combustion control system can achieve stable control.

The goal of modern combustion control systems must, therefore, be to manage the inevitable input fluctuations even at the start of the process, i.e., as soon as the fuel reaches the combustion grate. However, because fluctuations in waste quality (water content, amount of combustible matter, heating value of the combustible matter) cannot be noticeably influenced, an attempt is made to estimate these before fuel starts combusting.

Stable and uniform combustion depends largely on the following factors:

- Uniform, continual feeding (fuel bed on the grate)
- Combustion adjusted to waste quality (combustion air flows, distributions, grate speed, etc.)

A stable combustion process (in terms of the position of the main combustion zone, burnout, heat release, etc.) results when the above factors are managed optimally.

MARTIN Infrared Combustion Control (MICC)

The MARTIN Infrared Combustion Control (MICC) is an innovative, modern combustion control system, developed for the reverse-acting grate and the reverse-acting grate Vario. It is a very flexible, extensible, and independent system that is to be integrated in conventional overall plant control systems. The modular architecture facilitates the use of operating mode concepts, thereby enhancing the functionalities associated with classical combustion control. The purpose of this system is to enable optimization of the entire plant in order to meet different operator-specific requirements such as maximum fuel throughput, maximum service period or maximum energy recovery (in the form of heat or electricity), or minimum gas emission (e.g., NO_x).

Moreover, additional customer requirements can be incorporated, ideally without having to intervene in the overall plant control system. The MICC system comprises hardware and software. All field devices are connected to the overall plant control system to ensure end-to-end visibility between the operator stations and the field (Fig. 19).

The hardware is based on a globally available high-end industrial PC and is installed in a control cabinet. The software comprises various functional modules:

- Fuzzy logic control of the combustion system
- Infrared camera, image analysis, and signal generation for additional optimizing controllers
- Operating mode concept
- Operational data logging and visualization

Other functional modules such as SNCR control can be integrated in the MICC system in line with market requirements.

The term "combustion control" normally includes both the open-loop and closed-loop control functions for the combustion system and grate. Specific closed-loop control system know-how is implemented in the MICC system. The functions of the open-loop control system and a semiautomatic control system (steam flow control) are programmed in the overall plant control system. Consequently, plant operation can be sustained even while maintenance or optimization work is being performed on the MICC system. With the standardized interface and screens generated in the overall plant control system, the closed-loop system

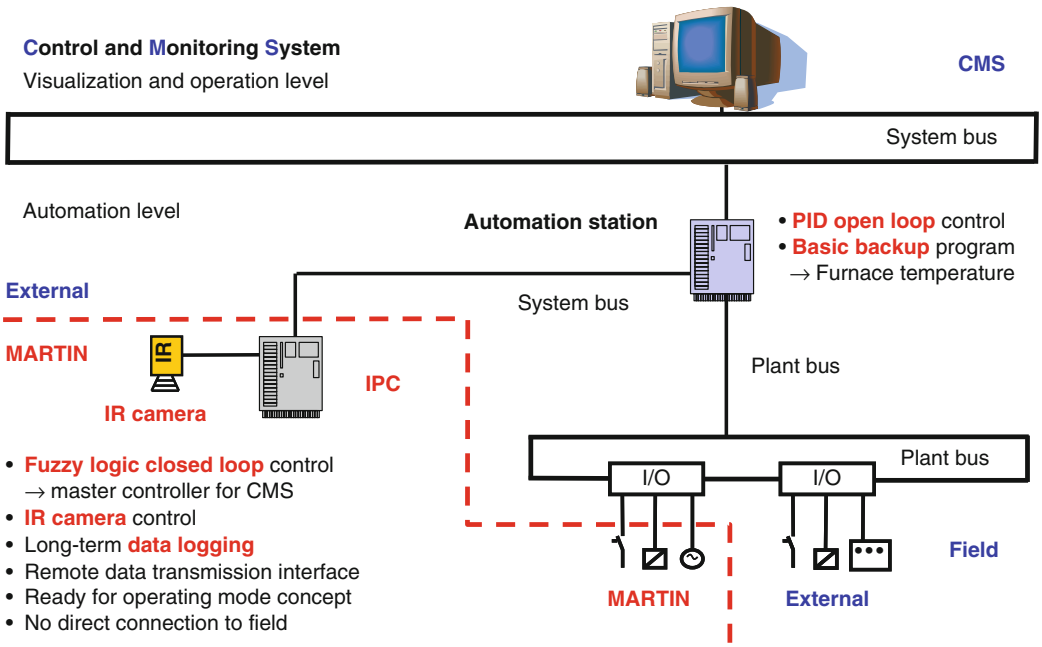

Martin Waste-to-Energy Technology. Figure 19
MICC integration in plant control and monitoring systems (reverse-acting grate/reverse-acting grate Vario)

can be adjusted from the operator consoles in the main control room without requiring expertise in the MICC component.

The MICC combustion control system includes the fuel controller that controls feeding of fuel to the grate; the O_2 controller of underfire air flow for the grate; the overfire air controller that controls flow and distribution of overfire air; and the grate speed controller. Additional controllers receiving signals from the IR camera system influence the distribution of underfire air, ram feeder, and grate movement.

There is a choice of control modes: "steam flow," "furnace temperature," or "steam flow/IR temperature." The quality of steam flow/IR temperature control is significantly improved by the IR camera controller. The combustion controllers are implemented as fuzzy controllers. The actuating variables calculated by the combustion control system are transmitted to the overall plant control system, where they are further processed.

The basic advantage of fuzzy control is its ability to find the "best compromise." Particularly when combusting waste, the process (combustion, boiler, flue gas path, etc.) produces partly contradictory or inexact information for the control system. Fuzzy control processes such information and finds the best solution at that time. Manual intervention is significantly reduced, and on the whole control is very stable. The "if ... then" formulation of control behavior allows every conceivable control case to be formulated simply, which is not possible to the same extent with classical PID control. Compared with classical PID control, the control logic requires less programming, although more complex logical connections can be implemented.

MICC uses specialized infrared camera technology at selected bandwidths. An infrared camera that records the temporal and two-dimensional behavior of the fuel bed surface temperatures from the boiler roof is used to obtain precise additional information from the combustion process (Fig. 20).

Depending on the size of the furnace, the evaluation area of the infrared camera includes (longitudinally for each grate run) grate zones 1–3 up the middle of zone 4, which covers most of the drying, ignition, and combustion stages, and also the entire grate width, which can consist of several grate runs. The infrared camera produces thermographic images of the surface temperature of the fuel bed (Fig. 21).

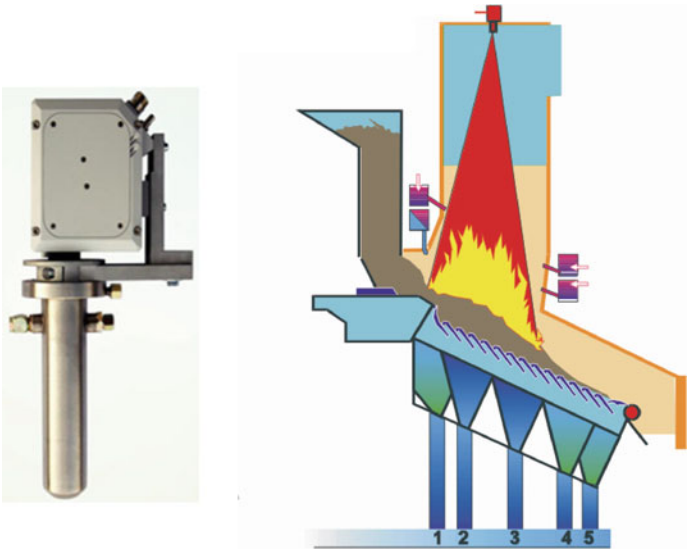

Martin Waste-to-Energy Technology. Figure 20
Infrared camera (photo/position)

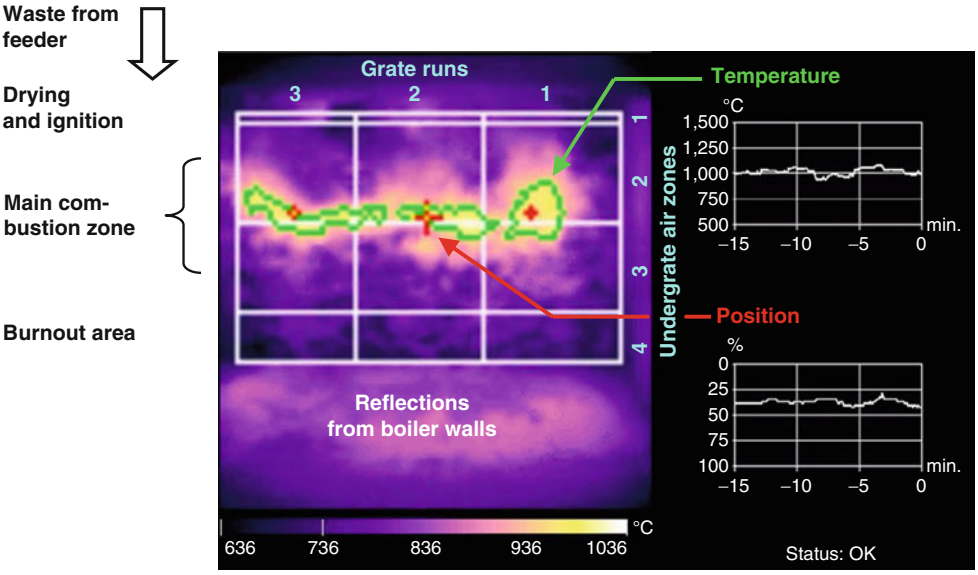

Martin Waste-to-Energy Technology. Figure 21
Image of IR camera

The information delivered by the infrared camera is processed by a specially developed image analysis program using sophisticated mathematical algorithms. Signals for controllers are calculated and transmitted to the combustion control system [14–17]. Operators can see the temporal and two-dimensional distribution of the fuel bed surface temperatures as well as the ash caking distribution on the visible areas of the boiler wall; and also the overfire air nozzles on a separate monitor in the control room. The observer learns to

interpret the infrared images and consequently the temperature distribution over time, as well as the overall combustion behavior on the grate. Further optimization measures can then be introduced ahead of the furnace, such as better mixing of the waste in the bunker, etc. The visual information provided to the operators results in more stable and flexible plant operation.

Modern WTE plants are operated flexibly and many are integrated into power plant parks. This means that the most cost-effective mode of operation may vary from case to case. Different goals may be targeted, such as maximum fuel throughput, maximum energy recovery, minimum pollutant emissions, maximum service period, etc. The "operating mode concept" module supports the different modes of operation required by the different goals (Fig. 22).

The energy input control concept includes the gross heat input operating mode. Here the heating value of the waste and the waste flow are calculated on the basis of various factors: the goal is to automatically regulate the maximum gross heat input as a function of the waste quality and plant condition. The semiautomatic operating mode is a simplified mode for the combustion system, additionally available in all MARTIN plants. There is a choice of control modes: steam flow, furnace temperature, or steam flow/IR pyrometer temperature control. Semiautomatic mode allows the plant, e.g., to be shut down systematically if important components fail, or allows operation to continue with reduced output. It is possible to switch smoothly between operating modes.

The stoker capacity diagram is displayed in the overall plant control system so that the current operating point is visible (Fig. 23). The operating point is indicated by means of a trailing pointer.

In addition to the available modules for the operating mode concept, further modes may be implemented in response to market demand, e.g., the "energy release" module: It will be possible, in the energy input/gross heat input mode, to have a positive influence on individual parameters such as NO_x emissions, residue quality (bottom ash), or residue quantities. The energy input/fuel throughput mode is designed to maximize waste throughput. The limits of the stoker capacity diagram will not be reached in the energy input/service period operating mode. In this mode, it is more important to achieve maximum plant operating time. Plant shutdown for purposes of overhaul is postponed for as long as possible when this operating mode is selected. The energy release/process steam, energy release/electricity, and energy release/district heating operating modes permit additional selection of the appropriate mode of operation to maximize plant profits. The best

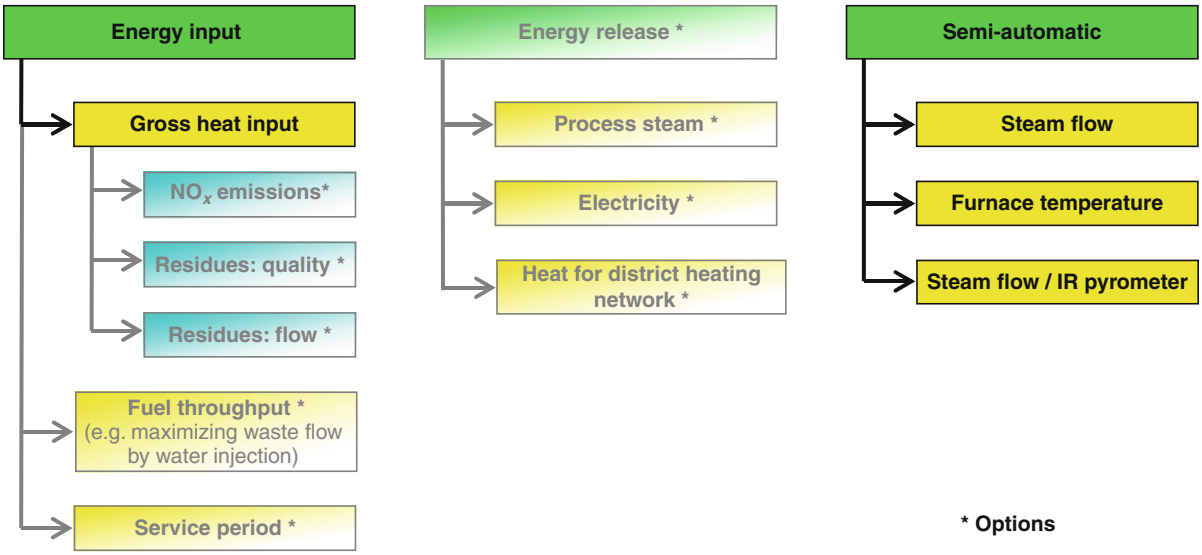

Martin Waste-to-Energy Technology. Figure 22
Diagram of operating modes

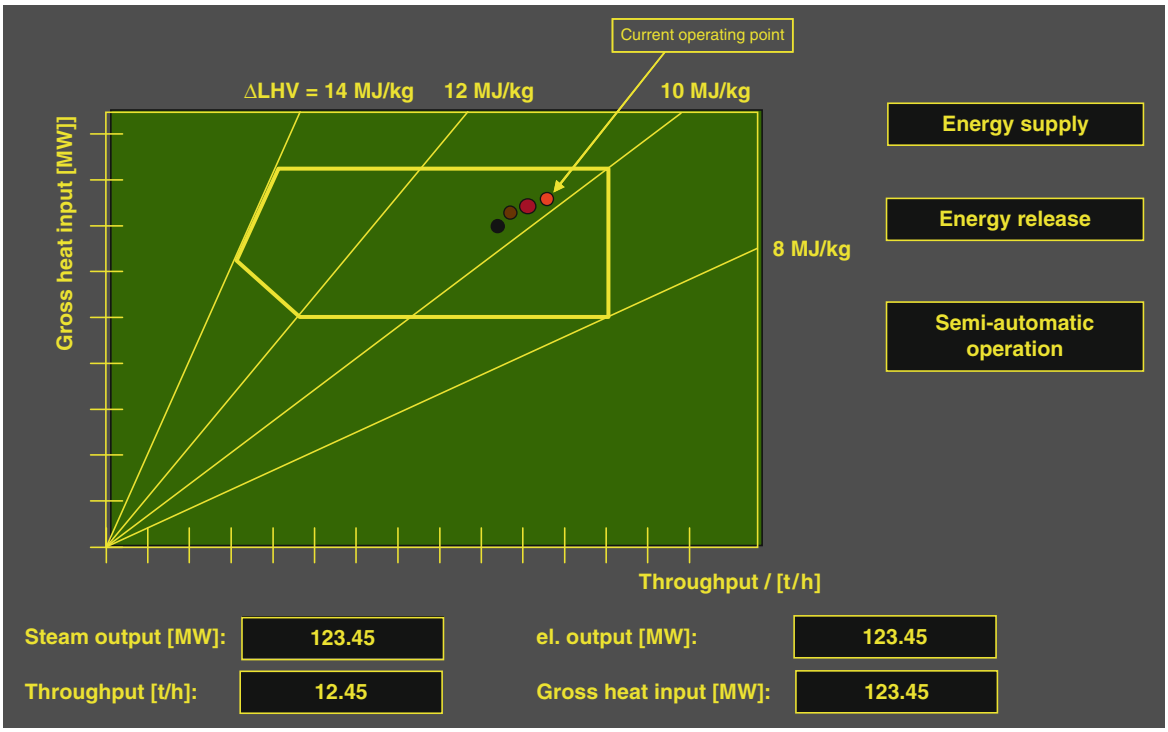

Martin Waste-to-Energy Technology. Figure 23
Stoker capacity diagram

mode can be selected and a constant amount of energy can be supplied to the grid depending on the time of day or year. These operating modes require partial expansion of the fuzzy control system and further observation and start-up phases will be necessary for new parameter settings and optimization measures.

The "operational data logging and visualization" module logs and displays all operating data relevant to the combustion system (Fig. 24). If malfunctions occur or damage is noted, the logged data help identify and eliminate the cause.

The most significant benefits of the MICC component are:

- High flexibility of combustion control
- No dependence on the overall plant control system
- End-to-end visibility from the overall plant control system to the field devices
- Operator strategy can be changed at short notice
- Plant operation in accordance with the plant operator's requirements
- Highly integrated hardware components

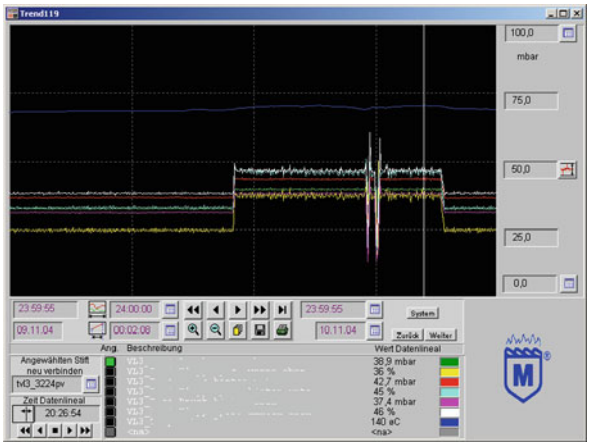

Martin Waste-to-Energy Technology. Figure 24
Data acquisition

- Few interfaces
- Low training costs
- High efficiency
- High level of availability

- Prompt and direct support
- Long-term sustainability through updates

Advanced Combustion Control (ACC)

The horizontal grate uses Advanced Combustion Control (ACC) that can be easily retrofitted to existing plants without additional monitoring equipment.

The ACC consists of four control systems:

- Waste input
- Combustion system output (boiler load or O_2 excess)
- Burnout/calcination
- Combustion air

Figure 25 illustrates the basic principles of the ACC system and shows the actuating and controlled variables.

The waste input area (feeder) and grate zone 1 are used for waste supply and waste transport only. They control loading (fuel bed thickness = flow resistance) of grate zone 2 (constant fuel bed thickness) by providing a uniform supply of fuel to the combustion system, and continuously supply an optimum fuel flow to the fire. The long residence time of the waste in the high-temperature area allows it to dry and become combustible. Consequently, even wet waste can be combusted without any noticeable negative effects. To keep the fire in zone 1 to a minimum in the event of very combustible waste, the underfire air is significantly decreased in the first zone. The waste flow introduced via the feeder to zone 1 is controlled using a three-variable (stroke length, idle time, run-on time) control system with a continuously operating feeder.

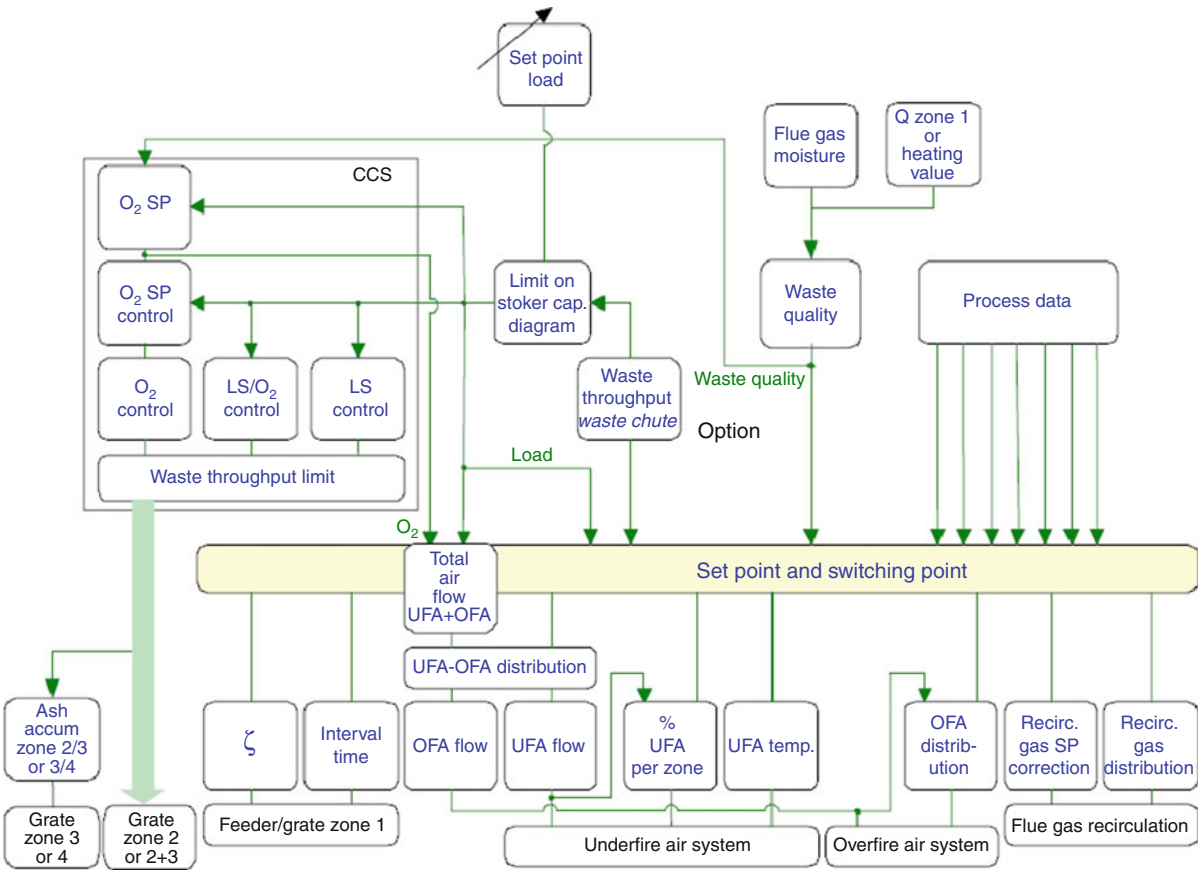

Martin Waste-to-Energy Technology. Figure 25
Advanced combustion control system (ACC, horizontal grate)

The grate zone 2, or in some cases grate zones 2 and 3, directly controls the combustion control system. Either live steam flow or excess O_2 in the flue gas at boiler outlet is used as the reference variable. The percentage O_2 in the flue gas at boiler outlet or the live steam flow can be controlled with a constant combustion air flow via the waste mass flow using the stoking and transporting motion of grate zone 2, or zones 2 + 3.

Grate zone 3, or grate zone 4, is operated so as to increase the residence time of the bottom ash on the grate and, therefore, the burnout quality. If bottom ash transport is slowed down in zone 3, or 4, ash accumulates between zones 2 and 3, or 3 and 4, and its residence time in the furnace is increased.

The total combustion air flow is specified as a function of load and correctively controlled as a function of two modes:

- Live steam control, for which the O_2 control deviation is the controlled variable
- O_2 control, for which the live steam control deviation is the controlled variable

Load, O_2 in the flue gas, and total combustion air flow always correspond in this control system. The air flow can therefore only be influenced if the O_2 set point is changed.

The total combustion air is distributed between underfire and overfire air accordingly at a specified percent distribution. The specified underfire air percentage is determined automatically as a function of waste quality and load.

The underfire air is distributed to the air zones under the grate as a function of load and waste quality. The air flow is reduced drastically in the first zone if the waste is extremely dry. The air not needed for drying the waste is used as overfire air. In this way, a constant air flow is provided to the combustion process in zones 2 and 3 at a steady load.

In an automatic combustion control system, the set points for all control and regulating systems are calculated as a function of the waste quality and current load and then are taken over by the ACC system. Only minimal intervention is required on the part of the operators; the combustion system adjusts continuously to the current operating conditions. CO and NO_x emissions are reduced by this mode of operation and operational effort is reduced. The quality of bottom ash burnout becomes better and more uniform. Automatic adjustment of the controller settings to suit current "waste quality" and load ensures optimized combustion control. As a result, a very stable output and good flue gas and bottom ash burnout can be achieved with minimal operational effort.

Energy Recovery

Thermal treatment of waste produces energy that is used to generate electricity, process steam, or heat for district heating. The first step is to evaporate water and generate steam. The combustion system and steam boiler must be appropriately matched. As early as 1964, MARTIN directly integrated the steam boiler into the combustion system in the Rotterdam and Paris – Issy les Moulineaux – plants. This concept was further developed and used for WTE plants worldwide.

The arrangement, size, and dimensions of the heating surfaces, i.e., radiation chamber, superheater, evaporator, and economizer must be designed carefully. The large volume of furnace and radiation passes result in low flue gas velocities and relatively long residence times. Furthermore, the type and quality of the ceramic lining in the combustion chamber must be specified. The scope of supply includes recommendations regarding the arrangement and type of online cleaning facilities for the heating surfaces and specifications for the measurement and control devices. High availability and long service periods are consequently achieved.

The boilers in the concepts described below are waste-fired water tube boilers with natural circulation; they are designed to generate superheated steam. Depending on the space requirements and desired cleaning system, there are two typical boiler types to choose from:

- Horizontal boiler
- Vertical boiler

In both types, the first radiation pass is made up of the combustion furnace located directly over the grate and the radiation chamber above the furnace. The furnace begins at the grate surface and ends at a height of about 12 m. The membrane walls of the furnace are designed in the lower area to meet the

geometric requirements of the reverse-acting or horizontal grate. Overfire gas nozzles (for overfire air and/or recirculated flue gas) are arranged in the lower area of the front and rear walls for post-combustion and intimate mixing of the volatile flue gas constituents escaping from the grate area.

Ceramic lining is applied to the furnace to protect the boiler tubes against excessive corrosion and to maintain a flue-gas residence time of 2 s at a flue-gas temperature of at least 850°C, as is required in Europe. Studs or anchors suitable to the type of lining used are applied to the wall. The ceramic lining consists of silicon carbide–molded bricks or cast refractory, depending on the location and stress to which the bricks or refractory will be exposed. The walls of the radiation chamber directly over the furnace are protected against corrosion and erosion by applying a weld overlay of nickel alloy (e.g., Inconel 625).

Both boiler types have been designed in many plants for the superheated-steam parameters 40 bar and 400°C. For mixed designs, experience is available for values up to 60 bar and 450°C.

Horizontal Boiler

The horizontal boiler (Fig. 26) consists of three vertical radiation passes and a horizontal pass to accommodate the convective heating surfaces. The three radiation passes are of the same width. The horizontal pass can be up to 30% narrower in order to increase the flue-gas velocity. In the lower area of the second and third radiation passes, the walls are shaped to form a hopper for separating fly ash from the flue gas. The walls of the three vertical radiation passes, the side walls and the roof of the horizontal pass are of the welded, gas-tight tube-fin-tube type (membrane walls). Risers and downcomers connect the membrane walls and convective evaporator(s) in the horizontal pass to the boiler drum, which is arranged transversely across the boiler, forming the natural-circulation evaporator section of the system.

The horizontal pass has convective heating surfaces in the following sequence:

- Evaporator 1 (known as the "cooling trap")
- Superheater (three-stage, with two desuperheaters)
- Evaporator 2 (if required)
- Economizer

All convective heating surfaces consist of aligned bare tubes and the flue gas side is cleaned by means of rapping devices. The energy of the impacts made by the mechanically or pneumatically driven hammers causes the vertically suspended heating surfaces to vibrate,

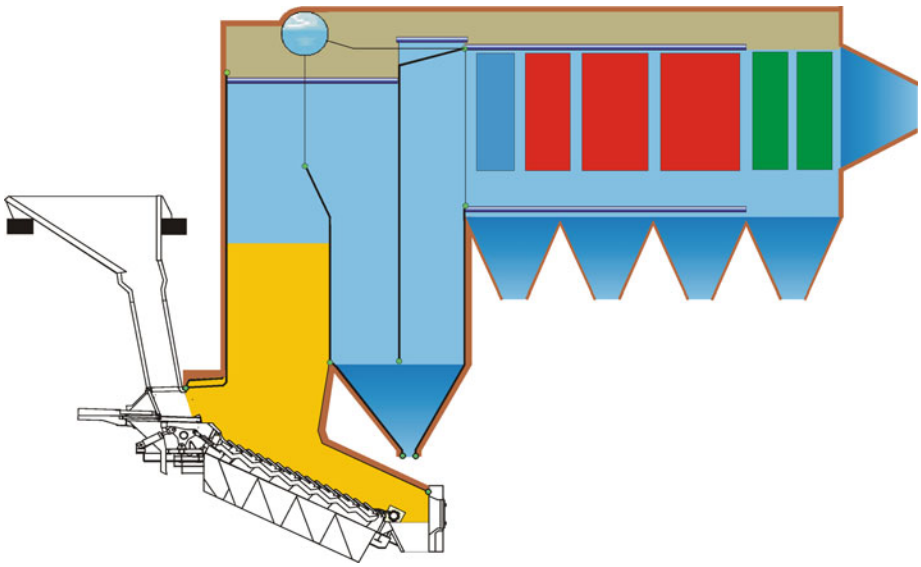

Martin Waste-to-Energy Technology. Figure 26
Horizontal boiler

thereby freeing them of any fouling. The upper heating surface attachment is elastic to prevent cracks due to constant vibration. The bottom sections of the lower headers are specially designed to handle the higher mechanical stress. The economizer is arranged in a gas-tight steel casing and, depending on the space parameters, can either be integrated in the horizontal pass or located in a separate vertical pass. However, a vertical economizer pass requires a different cleaning system (e.g., sootblower or shot cleaning).

Hoppers for collecting fly ash are located below the horizontal pass. The number and form of the hoppers is such that the ash is transported away easily and the flue gases do not unintentionally flow under the heating surfaces.

Vertical Boiler

The convective heating surfaces of the vertical boiler (Fig. 27) are arranged in two vertical boiler passes. The surrounding walls and roofs of the first three vertical passes are of the welded, gas-tight tube-fin-tube type (membrane walls). The convective heating surfaces also consist of aligned bare tubes and are arranged similarly to the convective heating surfaces of the horizontal boiler. However, they are tailored to flue-gas-side cleaning by means of sootblowers due to the tube pitch and depth of the heating surface banks. The economizer is arranged in a welded, gas-tight steel casing and forms the last boiler pass with a hopper for separating fly ash.

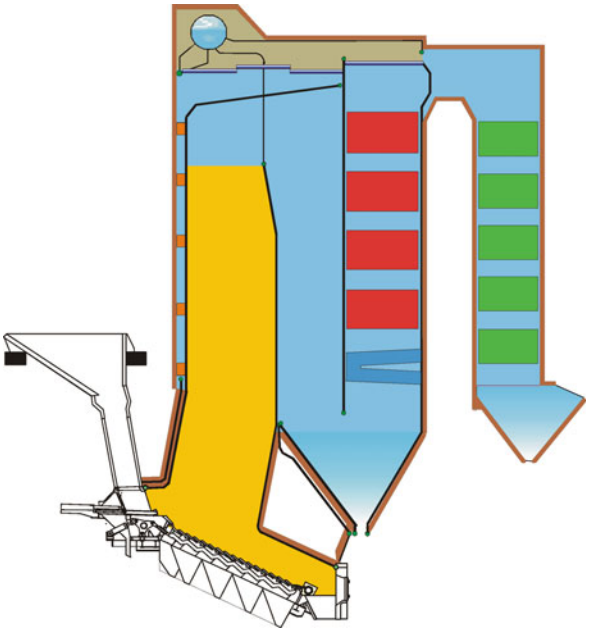

Martin Waste-to-Energy Technology. Figure 27
Vertical boiler

The height of the vertical boiler is largely determined by the size of the convective heating surfaces of the third pass. Under the same boundary conditions, this means that the height is greater than that of the horizontal boiler but that the area required is smaller.

Both boiler types are suspended in a supporting steel structure that allows free thermal expansion downward for all pressure-carrying parts. The transition from the boiler to the stationary reverse-acting grate or horizontal grate is designed accordingly.

Energy Efficiency

Because of concerns about climate change and increasing fuel prices, efficient utilization of energy derived from waste has become more significant. Municipal waste has characteristics that make it particularly suitable for the generation of heat and power. Waste is generally available close to the location of heat and power consumption in towns and densely populated areas. MARTIN investigates and evaluates methods and concepts for increasing efficiency by optimizing the combustion system and water-steam circuit using practice-oriented models for preparing large-scale implementation [18].

The standard WTE technology in Europe consists of grate-based combustion systems. Typically, these, sometimes quite old, plants produce 546 kWh of electricity per Mg of waste, which corresponds to a gross energy efficiency of 18% referred to the gross heat input from waste and additional fuels (basis: heating value of 10.44 MJ/kg and electricity production only). Due to in-plant consumption of an average of 150 kWh/Mg of waste, this results in an average exported electricity of 396 kWh (net efficiency of 13%). Most recent WTE plants use steam parameters of 40 bar/400°C. Typically, these plants produce 650 kWh of electricity per Mg of waste, which corresponds to a gross energy efficiency of 22% (heating value of 10.44 MJ/kg). With an in-plant consumption of 150 kWh, this typically results in exported electricity of 500 kWh (net efficiency of

17%). This data refers to the Best Available Technology document on waste incineration by the EU IPPC directive (BREF) [19].

In some European countries, landfilling of municipal waste is restricted and efforts are being concentrated on further improving the energy efficiency of WTE plants beyond the values mentioned above. The driving force behind the implementation of high-energy systems is usually a premium for renewable electricity from waste.

There is a large potential for improving the use of the energy contained in municipal waste. On the one hand, waste can be diverted from landfilling, on the other hand, the energy efficiency of WTE plants can be improved. In this respect, the main topics apply to power generation: steam parameters (pressure and temperature of superheated steam), flue gas heat losses (temperature at boiler outlet, excess air rate), steam condensation conditions (air or water condensers), thermal cycles (intermediate superheating, external superheating, two or three pressure systems), and in-plant consumption (SNCR/SCR, excess air rate).

Examples of recent innovative WTE plants with MARTIN grate technology and highly efficient power generation can be found in Brescia (IT), Amsterdam (NL), and Bilbao (PT). The Brescia plant has an increased gross efficiency of produced electricity of 27% through increased steam parameters, reduced flue gas losses and minimized in-plant consumption. The new plant in Amsterdam achieves 30% with additional intermediate superheating and water condensers. A further increase in energy efficiency is then only possible by external superheating with natural gas in combined cycle plants, as in Bilbao. However, innovations also took place in the field of heat recovery. The Malmö plant (SE) is an example, where efficiency has been increased by using heat generated from flue gas condensation for district heating. Twence (NL) is another example, where a high degree of energy recovery is achieved by combining heat and power production.

In the case of power generation, the main limitation on increasing energy efficiency is posed by the increased cost and corrosion risk. For the use of heat, climatic limitations and the cost of district heating grids are important considerations. In Europe, potential exists to increase the proportion of WTE to over 10% of the overall renewable energy produced as half of the energy contained in municipal waste is of biogenic origin [20].

Energy performance indicators are plant-specific figures which allow a power/throughput-independent comparison and classification of power plants with respect to their energy efficiency. Efficiency is generally defined as the ratio of useful output and input. In WTE plants, the input is waste and the useful output can be electricity, heat, or even recovered materials. Gross electric efficiency, net electric efficiency, and thermal efficiency are most commonly used. It is essential to define clear system boundaries when comparing the efficiency values of different plants.

In Gothenburg (SE), where the focus is on the production of heat, a large district heating system is installed, where the WTE plant is only one of many heat suppliers. During the summer, the demand for heat is further increased by absorption chillers distributed around the city. The district heating system's feed and return temperature depends to a large extent on the outside temperature. The feed temperature varies from 75°C to 110°C, whereas the return temperature lies between 40°C and 55°C. The yearly averages are 80°C to 45°C. Figure 28 shows the four stages of the heat production system. Due to the low return temperature, it is possible to use the low-temperature heat of the condensing scrubber directly. In the next step, more heat from the scrubber water is extracted by means of absorption heat pumps. These heat pumps are driven by steam extracted at the 5 bar tapping point of the turbine. Depending on the operating conditions, excess heat from the second economizer is used in the following stage. The last stage comprises the back pressure condenser of the turbine operating with floating pressure, depending on the required feed temperature, to maximize electricity production. Nearly 30% of the produced heat is extracted directly from the flue gas, which reduces the loss of electricity production and thereby decreases the power loss coefficient [21].

The new WTE plant in Amsterdam (NL) is designed for maximum electricity production. With a sophisticated water–steam cycle (Fig. 29), the plant achieves an electric efficiency of more than 30%. The turbine can only be operated with elevated pressure of 130 bar at low live steam temperature with a water separator and external reheater system. In 2008,

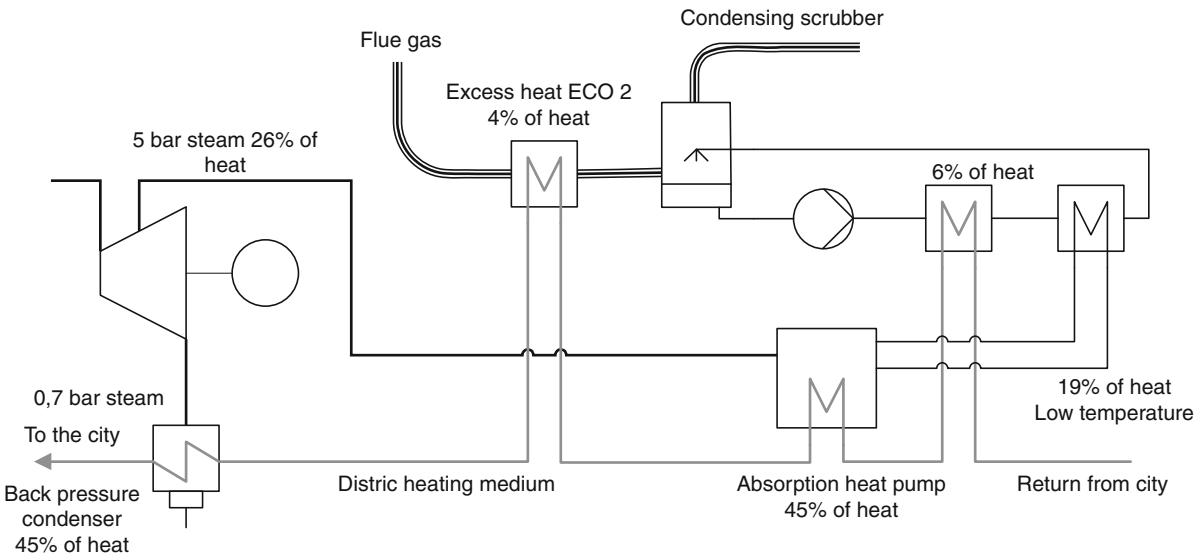

Martin Waste-to-Energy Technology. Figure 28
Heat production Gothenburg (SE) [21]

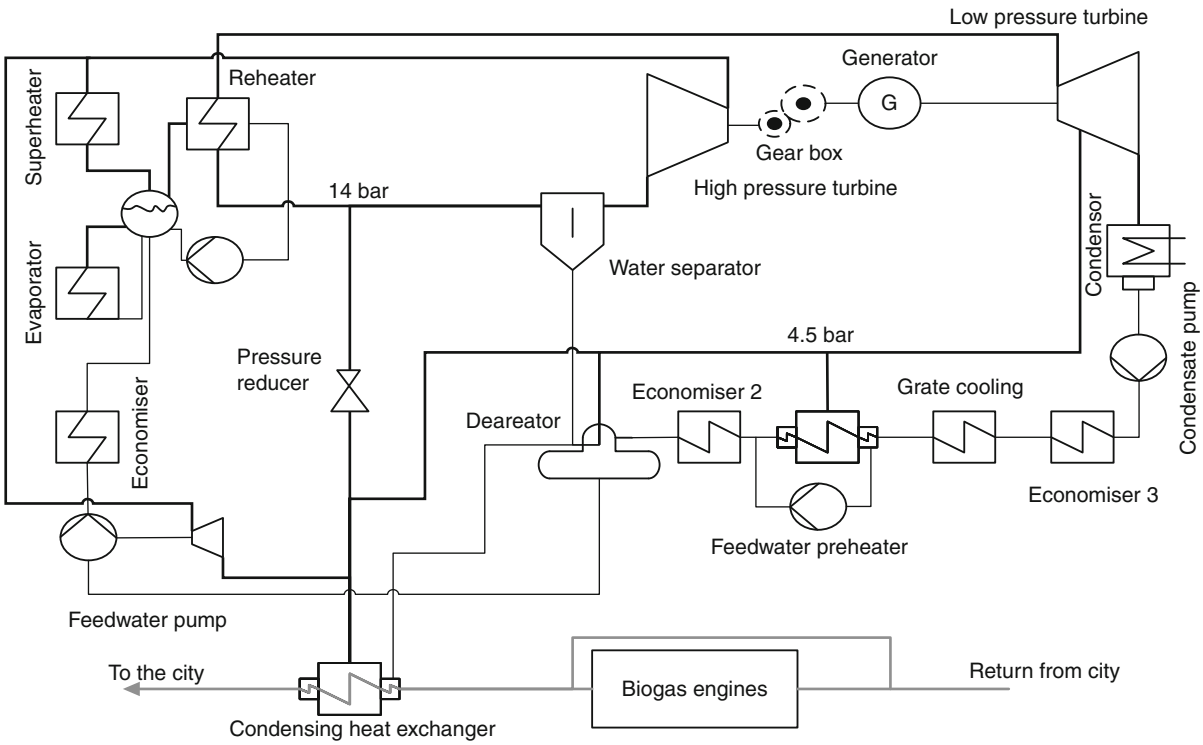

Martin Waste-to-Energy Technology. Figure 29
Plant diagram of new WTE plant, Amsterdam (NL) [21]

the plant was retrofitted with a condensing heat exchanger to produce heat too. The district heating medium is heated up from the return temperature of 50°C to 120°C (design feed temperature) in two stages. In the first stage, waste heat from biogas engines installed in the plant is used to heat part of the district heating medium to 105°C. Upstream of the condensing heat exchanger, the hot stream is mixed with the bypass stream resulting in a temperature of 61°C. Steam extracted from the turbine is condensed in the condensing heat exchanger to reach the final temperature of 120°C. Most of the steam is extracted from the 4.5 bar tapping point, but since the plant was not designed for heat production, not enough steam can be extracted for full load operation of the heat exchanger. Steam from the 14 bar tapping point has to be reduced to 4.5 bar to be used in the heat exchanger. The biogas engines are able to provide 3.5 MW_{th}, while the heat exchanger of the WTE plant is designed for a maximum of 18.3 MW_{th} heat output [21].

Process Simulation

A wide range of simulation tools are used in the WTE sector for the design of new plants as well as for the investigation of operating issues. These tools apply thermodynamic representations of the water–steam cycle to more complex representations such as CFD modeling.

A Boiler Dynamic program is used as a basis for the combustion and boiler/water–steam cycle simulation of a power plant. This program code is designed for engineering complex heat exchangers, e.g., steam boilers and power stations. It allows the user to build a graphical schematic representation of a plant in a graphical user interface by selecting predefined power plant elements from a library and to simulate their operation. Mass and energy balances are calculated for each element, which is considered to be like a black box. The program code makes it possible to simulate different types of boilers such as: natural circulation boiler, force flow boiler, Benson boiler (supercritical), WTE plants, fire tube boilers, fluidized bed combustion etc. It includes static and dynamic modules. The first module will be used to plan a new power plant, to study an existing plant regarding fouling, to analyze the influence of different modifications (fuel, operating point, changing of elements such as heat exchangers). The dynamic modules are useful to analyze the behavior of the boiler in special cases such as start-up, load changes, or shutdown [22].

More complex problems in boilers such as detailed combustion reactions, three-dimensional temperature distributions or formation of emissions are analyzed by means of Computational Fluid Dynamics (CFD). Numeric modeling and simulation to describe the flow processes in waste combustion are regarded as state-of-the-art and are in successful, widespread use. For combustion problems, it has been shown that this software gives accurate results and takes all aspects such as chemical reactions, heat transfer, fluid flow, and thermal radiation into account. CFD works by solving the equations of mass conservation, momentum conservation, and energy conservation over a region of interest, with specified conditions on the boundary of that region.

For boiler design purposes, it is enough to provide a general model including combustion, heat transfer, and radiation. For combustion reactions, there is a wide range of chemical reaction models starting from simple ones for fast chemistry such as the eddy dissipation model or more complex ones for finite rate chemistry such as the eddy dissipation concept model, considering chemical kinetics. For the purpose of investigating unburned carbon monoxide in the flue gas, models with finite rate chemistry are needed, whereas for heat release and heat transfer calculation, simpler models are sufficient to give realistic results.

CFD is also used to investigate more complex problems such as the formation of NO_x (Fig. 30). The CFD software includes numerical models of NO_x reactions from literature for the three NO_x formation mechanisms (fuel, prompt and thermal NO_x). These models can be used to calculate the formation of NO_x for every type of mechanism, showing the different areas in the boiler where this emission is formed. For reduction of NO_x on the other hand, the SNCR mechanism is implemented and can be selected. Ammonia and urea can be injected in gaseous, liquid, or solid form into the boiler to react with NO_x emissions. Different injection models with varying geometries can be chosen to simulate introduction of the reducing agent as realistically as possible [23]. However, these models are used to

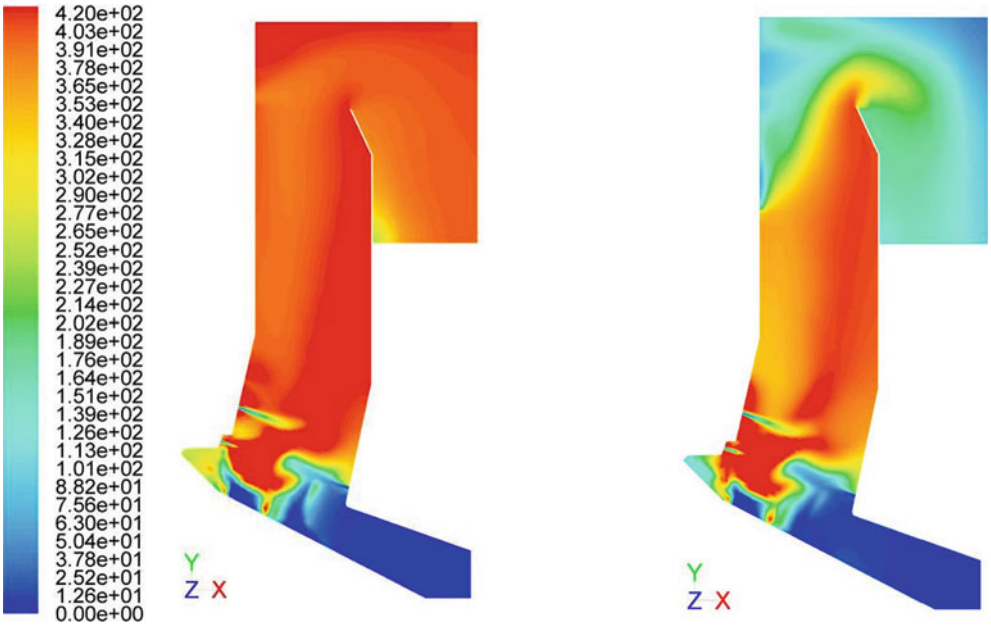

Martin Waste-to-Energy Technology. Figure 30
CFD modeling: NO_x/NO_x – SNCR calculation (NO_x [mg/Nm^3, referred 11% O_2, dry])

optimize the SNCR system and consequently reduce NO_x emissions and additive consumption.

These injection models are further used to investigate the trajectories of fly ash particles and can help to predict deposits or unfavorable flow patterns. Combining particle tracking with other codes, it is possible to numerically observe the growth of the deposit and thereby caused changes in flue gas flow.

A basic precondition for CFD simulation of the gas phase of a boiler is the provision of exact initial values by means of a suitable fuel bed model [24]. A wide range of models is available. This is due to the fact that many different effects occur on the grate bed, which can be modeled in different ways and are considered important by some, while others neglect the same effect. Ensuring transparency and understanding the fuel bed model used are significant when working with CFD. Therefore, it is often easier to develop a new model which is designed to comply with one's needs instead of using other models with a limited capacity for adaptation and tailored for some other purpose.

Instead of modeling the total fuel bed model with motion, gasification, and pyrolysis of the waste, it is sometimes easier to just define the heat or species release along the waste bed to calculate starting values for CFD. These models are more empirical and give no answer to what is happening on the grate, but have proven to be good enough for boiler design calculations or even research topics in the gas-phase combustion [25].

Of primary interest in simulation are the practical implementation and therefore the validity of the model calculations. Validation is not of great importance for thermodynamic water–steam cycle calculation since these models are based on energy and mass balances and therefore give good results. CFD simulations on the other hand are based on a wide range of models simplifying reality. Choosing the right model is important to get realistic results. If there is any possibility, CFD simulations are always validated by measurements. In WTE plants for validation, a mass and energy balance over the boiler is combined with temperature measurements in the flue gas path to perform accurate validations of CFD calculations. For this purpose, grid measurements of temperature are performed in the range of the SNCR level to obtain a two-dimensional temperature profile, which then is compared with the temperature profiles calculated by the CFD software.

In a project covering overall validation on an industrial-scale WTE plant, the development of a fuel bed model yielded improvements in the basic boundary conditions for CFD simulation. Comprehensive measurements of temperatures, flue gas concentrations, and velocities were performed and compared with simulated values. Using the model approaches selected, it was established that the model for CO burnout and for a number of other simplified partial models, such as heat dissipation in the convective area of the heat exchangers, did not permit accurate analysis or forecasting for these subareas. However, good matches were achieved, in particular with regard to temperature and flue gas concentration values for CO_2 and O_2. There were some mismatches in the speed components due, above all, to the turbulence prevailing in the first pass of WTE plants. Nevertheless, it was possible to identify tendencies correctly [26, 27].

NO_x Reduction

Low NO_x Technologies

Most of the waste's nitrogen content is transferred to the flue gas during combustion as nitrogen oxide NO_x. The limit values for NO_x emissions continue to decrease as a result of statutory or regulatory requirements. At the same time, the operators of thermal waste treatment plants are increasingly being put under pressure to reduce investment and operating costs. In the EU, there is a combustion directive that defines a maximum emission limit value of 200 mg/m^3 NO_x as a daily average value referred to 11% O_2. Compliance with this limit value is possible with the SNCR process, which injects ammonia or urea into the furnace. In some cases, SCR catalytic converters are used. However, these involve higher costs (investment/operation) and energy consumptions. Based on the National Emission Ceilings (NEC) defined by the Gothenburg Protocol, it can be expected that the limit values for NO_x in the EU will become even more stringent.

In this respect, various concepts of low NO_x technologies were developed to significantly reduce the NO_x values downstream of the combustion system via primary measures (Fig. 31). This is due to the fact that chemical reactions that convert the primarily formed NO_x back to nitrogen are promoted as a result of the reduced excess air and consequently higher temperatures in the lower area of the furnace.

Figure 31a shows the excess air for a conventional combustion system setting. The underfire air is set to be slightly superstoichiometric. An excess air rate of approximately 1.8 is achieved by supplying overfire air for flue gas burnout. The NO_x content is typically 400 mg/Nm^3. The option in Fig. 31b shows the point at which some of the overfire air is introduced into the upper furnace area being moved. The NO_x content can be reduced to approx. 300 mg/Nm^3. This process option, known as *LN* (*Low NO$_x$*), is extremely suitable for being retrofitted to existing plants. However, it can also be implemented in the design of new plants.

Figure 31c shows the process known as *VLN* (*Very Low NO$_x$*). This process achieves a reduction in the levels of excess air and consequently higher temperatures in the lower area of the furnace by means of internal flue gas recirculation. The internal flue gas recirculation system comprises the extraction of flue gas in the rear area of the combustion chamber and its subsequent use as mixing gas in the upper area of the furnace. This ensures optimal mixing of the flue gases. It has been proven under continuous commercial conditions that NO_x values below 250 mg/Nm^3 are achieved with internal flue gas recirculation. These values are reduced to less than 80 mg/Nm^3 (all NO_x values referred to 11% O_2, dry) by injecting ammonia or urea. A further feature of this process is that a low NH_3 slip is adhered to at the same time. The VLN system is shown and explained in detail in Fig. 32. Both LN and VLN processes have been tested on an industrial scale over longer periods and are offered for new plants, and also within the framework of plant retrofits.

Figure 31d shows a further option, the process known as *VLN-GM* (*Very Low NO$_x$-Gasification Mode*). This option was specially developed for customers preferring gasification to combustion. There is no injection of overfire air in the lower furnace area in this model. Significantly, substoichiometric conditions (gasification) are created in the furnace by simultaneously extracting flue gas in the rear combustion chamber area. Mixing gas and overfire air are supplied to the upper furnace area to ensure complete oxidation of the flue gases.

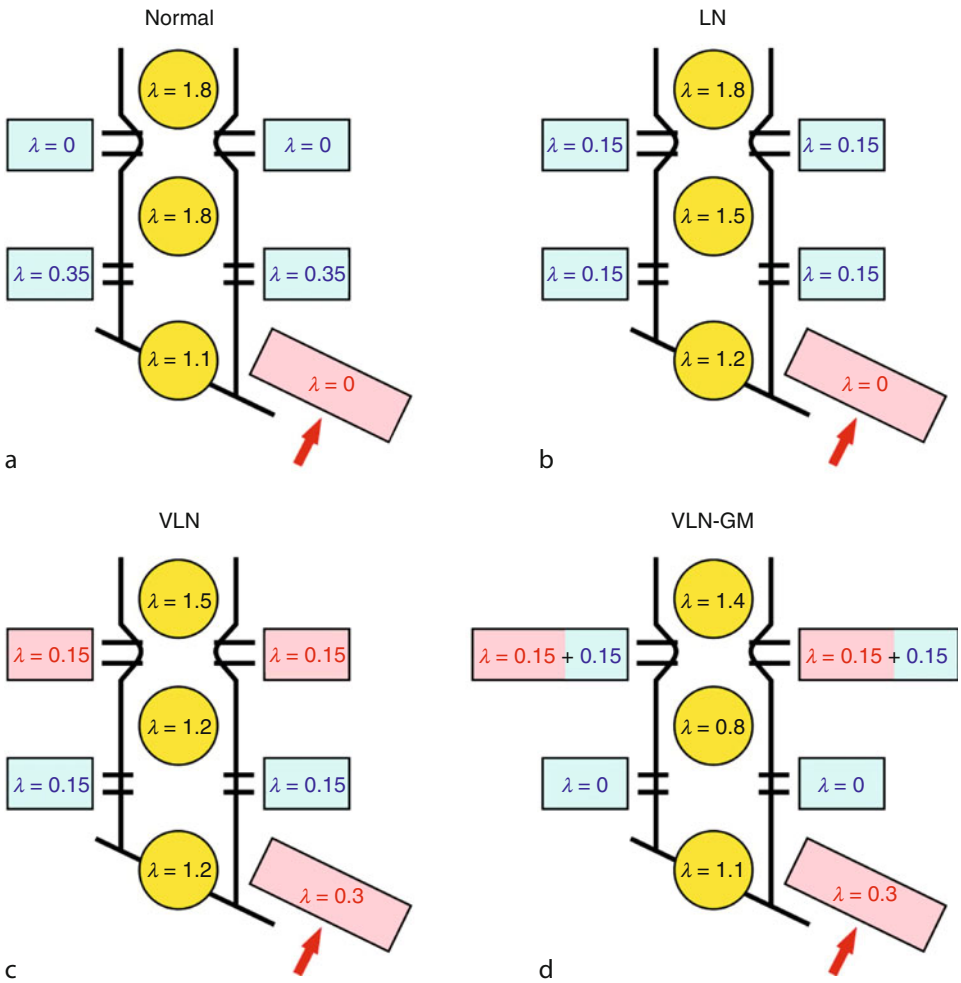

Martin Waste-to-Energy Technology. Figure 31
Various concepts of Low NO_x technologies

The *VLN process* (Fig. 32) is based on a classical grate-based combustion system for municipal waste, where the "VLN gas" is drawn off at the rear end of the grate and is reintroduced into the upper furnace just below the ammonia injection positions. The positive effect of this patented process is twofold: On the one hand, drawing off the VLN gas leads to combustion conditions which promote the inherent NO_x reduction processes such that fuel NO_x is largely reduced to nitrogen. On the other hand, reinjection of the VLN gas cools the flue gases down and enforces their mixing with injected ammonia or urea. This leads to improved efficiency of the SNCR system.

NO_x values of 80 mg/m^3 with an NH_3 slip of less than 10 mg/m^3 have been reached in tests at the WTE plant in Bristol (US). Further industrial-scale tests in Thiverval (FR) and Oita (JP) have confirmed these results. At the Thiverval plant, which has a municipal solid waste throughput of 12 Mg/h, NO_x could be reduced from 190 to 80 mg/m^3 during test operation with the VLN components.

The VLN gas has a temperature below 300°C and is reinjected at a position at which the furnace temperature is around 1,000°C. This typically corresponds to a level of 8–12 m above the grate depending on the capacity of the unit and the type of waste. The overfire air pressures are reduced to around 10 mbar, which is considerably less than in conventional WTE plant design. Nevertheless, superstoichiometric conditions are reached at the overfire air level, which is an

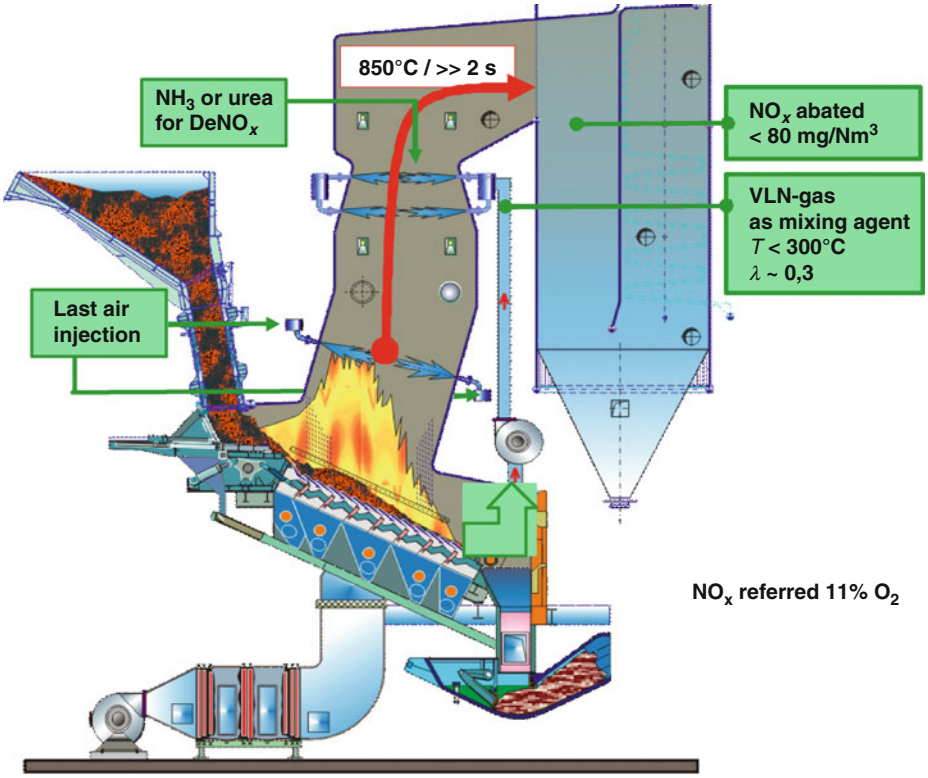

Martin Waste-to-Energy Technology. Figure 32
Very Low NO_x (VLN) process (NO_x [mg/Nm^3, referred 11% O_2, dry])

advantage compared with air-staged or fuel-staged combustion systems. The residence time from the last combustion air injection at the overfire air level to the 850°C level in the furnace is significantly increased. A further advantage of the VLN system is the reduced flue gas velocity in the lower furnace due to internal recirculation via the VLN duct. This leads to a reduction in the fly ash carried over to the boiler.

The VLN gas is reinjected into the front and rear sides of the narrow section of the upper furnace. This leads to an intensive barrier of turbulence, which reduces the flue gas temperature and blocks the passage of flames or unreacted gases. The test plant results give rise to the expectation that corrosion is significantly reduced in the furnace above the VLN level as well as in the superheaters. On the other hand, temperatures between the overfire air and the VLN level are higher than in conventional combustion and higher grades of furnace protection material should be used there. Another advantage of the VLN system is the reduced excess air rate, which allows cost reduction in the boiler and flue gas cleaning and improved boiler efficiency.

Selective Non-catalytic Reduction (SNCR)

Nitrogen oxides are present in the flue gas due to the high nitrogen content of the waste. Their levels can be reduced, on the one hand, by means of primary measures as the various concepts of Low NO_x technologies and on the other hand by secondary measures as Selective Catalytic Reduction (*SCR*) or Selective Non-Catalytic Reduction (*SNCR*).

The nitrogen oxides are reduced to nitrogen (N_2) and water (H_2O) in the SNCR system, based on the principle of selective non-catalytic reduction (SNCR), by injecting aqueous ammonia (NH_4OH) into the furnace. The aqueous ammonia is injected via nozzle lances at two levels within a temperature range of 850–1,050°C. Moreover, the ammonia can be converted to N_2 or even to additional NO_x in secondary

reactions at temperatures above 1,050°C without NO_x participation. Below temperatures of approximately 850°C, the $DeNO_x$ reactions occur only very slowly. Compressed air (on request also softened fresh water or steam) is used as the atomizing medium in order to achieve the finest possible reducing agent distribution.

The compressed-air SNCR system (Fig. 33) requires only one carrier medium (compressed air) for injection and cooling and is adjusted to the specific conditions of the MARTIN combustion system and their flow profiles. Excess ammonia must be supplied due to the dependence on factors such as the temperature window at the injection point, mixing with flue gas and the secondary reactions taking place. In order to remain within the temperature window, the compressed-air SNCR system distributes the aqueous ammonia to two levels as a function of the temperature. This means that there are always two levels in operation at the same time.

The compressed-air SNCR system consists of several system components. The aqueous ammonia storage tank serves as an area for delivery, storage, and drawing off of aqueous ammonia. As specified by regulations, the depressurized storage tank is mostly designed as a double-walled construction. The compressed air supply unit, a screw-type compressor including refrigerant dryer, delivers compressed air continuously. The pumping station includes NH_4OH metering pumps for the upper and lower injection level. Distribution of the mass flows to the individual nozzle rows in the boiler walls takes place in the distributor stations. All lances are required to introduce the aqueous ammonia into the furnace. The compressed air flow ensures an extremely fine distribution of aqueous ammonia droplets.

There are three control concepts that can be optimized using an in situ NH_3 measurement device for

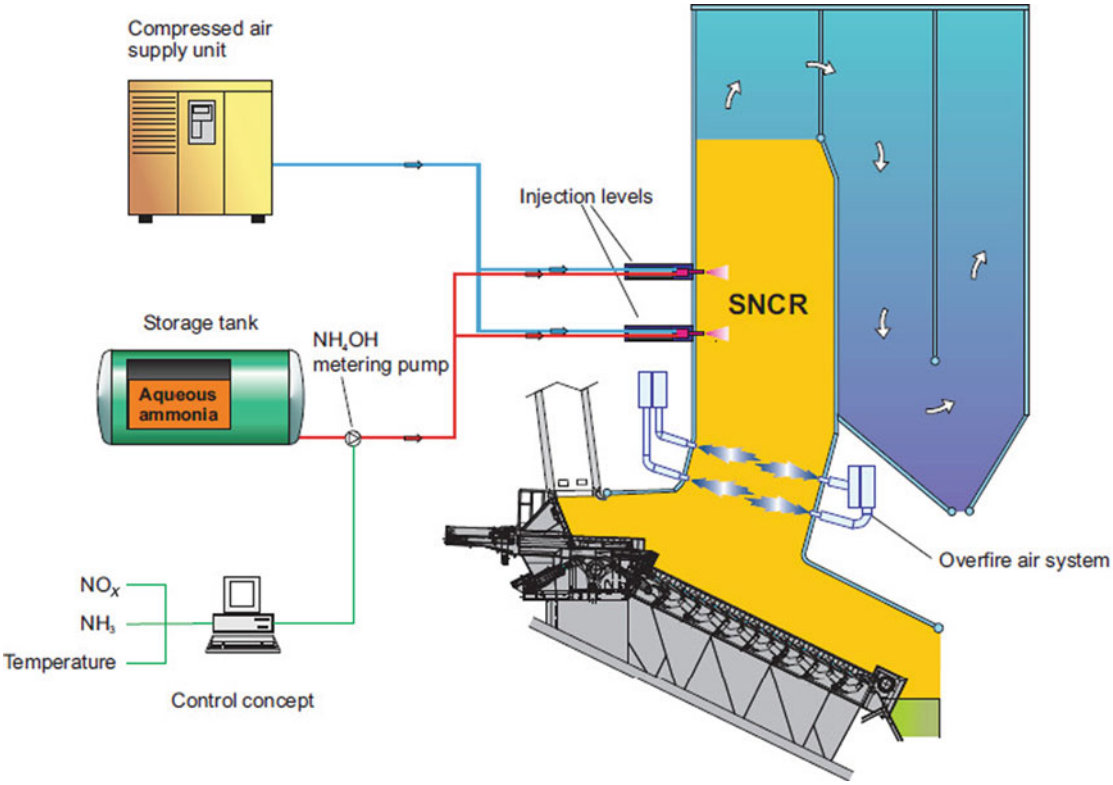

Martin Waste-to-Energy Technology. Figure 33
Compressed-air SNCR system

reducing slip. They can be used to regulate the amounts injected as required and to optimize use of the aqueous ammonia with changing NO_x raw gas concentrations and combustion conditions. In addition, a balance control system steplessly shifts the point at which NH_4OH is injected to the optimum temperature window between the upper and lower injection levels.

NO_x values of up to 70 mg/Nm^3 (referred to 11% O_2, dry) are reliably achieved with a low level of NH_3 slip at the boiler outlet. Features of the SNCR system are:

- Use of cost-effective standard components/easy to replace spare parts
- Stabile spray pattern
- Defined setting of the NH_4OH flow
- Rapid adjustment of the NH_4OH flow when temperature and NH_3 slip change

Within the temperature window, the compressed-air SNCR system can achieve low NO_x emission values. However, the NH_3 slip increases due to the excess aqueous ammonia required for the SNCR reduction method. The system can therefore be equipped with a raw gas catalytic converter. This has the following advantages:

- Use of NH_3 slip for further reducing NO_x
- Only half of the catalytic converter volume is used compared with a complete SCR system in the raw gas area to achieve the same NO_x emission value
- Peripheral plant devices for reheating the raw gas are not required

The NH_3 slip and NO_x emissions remaining in the flue gas flow after the SNCR reaction pass through the raw gas catalytic converter, e.g., downstream of evaporator and upstream of the inlet into the economizer bundles. The converter is equipped with a sootblower system.

At the WTE plant Brescia (IT), a high-dust selective catalytic reduction system has been successfully implemented since 2006 (SNCR + high-dust catalytic converter). The catalytic converter is installed along the gas path where the temperature is already suitable for operation and reheating is not needed. In this way a lower concentration of NO_x (<70 mg/Nm^3) is achieved in the flue gas as well as lower ammonia consumption and lower concentration of ammonia slip (2–6 mg/Nm^3) in the flue gas [28].

Residue Qualities

SYNCOM-Plus

Bottom ash produced during thermal waste treatment accounts for the largest mass flow of the waste input at approximately 25% by weight. In Europe, this bottom ash is currently used as a building material, e.g., in road and landfill construction, or as a mining filler, e.g., in salt or coal mines. However, a considerable percentage is sent to landfills.

In the SYNCOM process, as described earlier, combustion air is enriched with oxygen, so that fuel bed temperatures are considerably higher, thereby causing increased sintering of the bottom ash. To further improve bottom ash quality, the SYNCOM-Plus process was developed, whereby a downstream wet-mechanical treatment process to separate a granulate (Fig. 34) is added to the SYNCOM process [29, 30]. The separated fine fraction and sludge as well as the boiler ash/fly ash are then recirculated to the combustion system for further sintering and the destruction of organic compounds at high fuel bed temperatures of approximately 1,150°C (Fig. 35).

A compact large-scale pilot plant consisting of selected units for the continuous wet-mechanical treatment of bottom ash as well as recirculation of fine

Martin Waste-to-Energy Technology. Figure 34
SYNCOM-Plus granulate

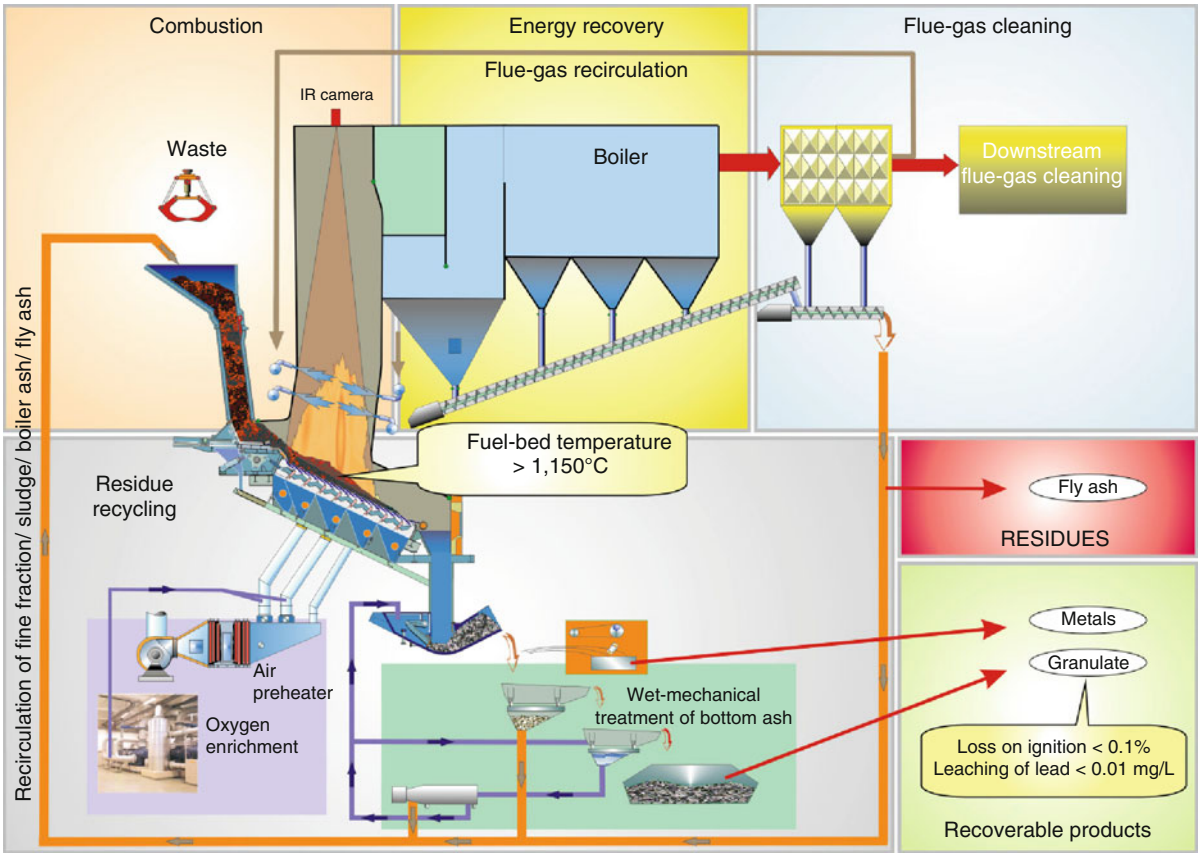

Martin Waste-to-Energy Technology. Figure 35
SYNCOM-Plus concept

particles and boiler ash into the combustion system was implemented in the SYNCOM WTE plant in Arnoldstein (AT). The continuously accumulating bottom ash flow coming from a wet-type discharger was first dry screened to separate a fine fraction of <5 mm, then washed and wet screened to separate a granulate of >2 mm and a suspension in a double deck screening machine. Because the wash water was circulated, any particles <2 mm contained therein had to be completely separated in order to minimize the addition of fresh water. A decanter centrifuge was used for this purpose. The sludge that accumulated was fed into the combustion system; the particle-free wash water was conveyed into a storage tank for washing and wet screening. The pilot plant operated continuously and was always directly connected to the bottom ash discharge.

An average of 428 kg/h fine fraction, 180 kg/h sludge, and 58 kg/h boiler ash were recirculated. In total, this amounted to approximately 6.5% of the entire hourly waste input. No significant accumulation of the fine fraction in the bottom ash total as a result of recirculation could be detected after determining the screening curves (comparison of particle size distribution with/without recirculation). Analysis of the combustion parameters (steam, fuel bed temperatures, etc.) and the raw gas measurements at the boiler outlet indicated no significant influence being exerted by SYNCOM-Plus operation. The granulate meets the criteria for solids and leachates laid down by the recovery regulations and all requirements pertaining to aggregates for unbound materials and anti-frost layers for use in civil engineering and road construction.

Figure 36 shows the entire input and output mass flows in the SYNCOM-Plus process for the SYNCOM WTE plant in Arnoldstein (AT). The greatest residue mass flow is the bottom ash output (3.74 Mg/h). Of this, the SYNCOM-Plus process produces 2.82 Mg/h of a granulate with good recovery qualities. Fine fraction, sludge, and boiler ash are recirculated; the filter ash contains additives from flue gas cleaning and must therefore be disposed of.

Figure 37 is a graphic illustration of the energy flow for the SYNCOM WTE plant in Arnoldstein (AT) showing complete conversion of the waste input into electricity and specifying a value of 2.25 MW for in-plant consumption. However, the components of the SYNCOM-Plus process make only a small contribution in this respect. As an option, heat for district heating and process steam can also be generated. However, this has no influence on the in-plant electricity consumption.

The SYNCOM-Plus trials at the SYNCOM WTE plant in Arnoldstein (AT) demonstrated successful results in continuous operation mode and therefore proved that both, wet-mechanical treatment and recirculation, in continuous operation are feasible. No influence on combustion or the raw gas could be detected [31].

The removed material flows (fine fraction and sludge) and the wash water can be recirculated within the process so that SYNCOM-Plus produces no residues for disposal and the entire process is effluent-free.

The characteristic features of the SYNCOM-Plus process are listed below:

- Wet-mechanical treatment/recirculation feasible in continuous large-scale operation
- Optimized granulate quality with optional recovery
- No vitrification of residues necessary/destruction of dioxins >90%
- Reduced amount of residues for disposal/effluent-free process

Dry Bottom Ash Discharge and Separation

The WTE bottom ash that is discharged from the grate and in particular its metals, can be recycled. Dry discharge of bottom ash offers significant advantages in this respect. Not only are the metals of a better quality, but

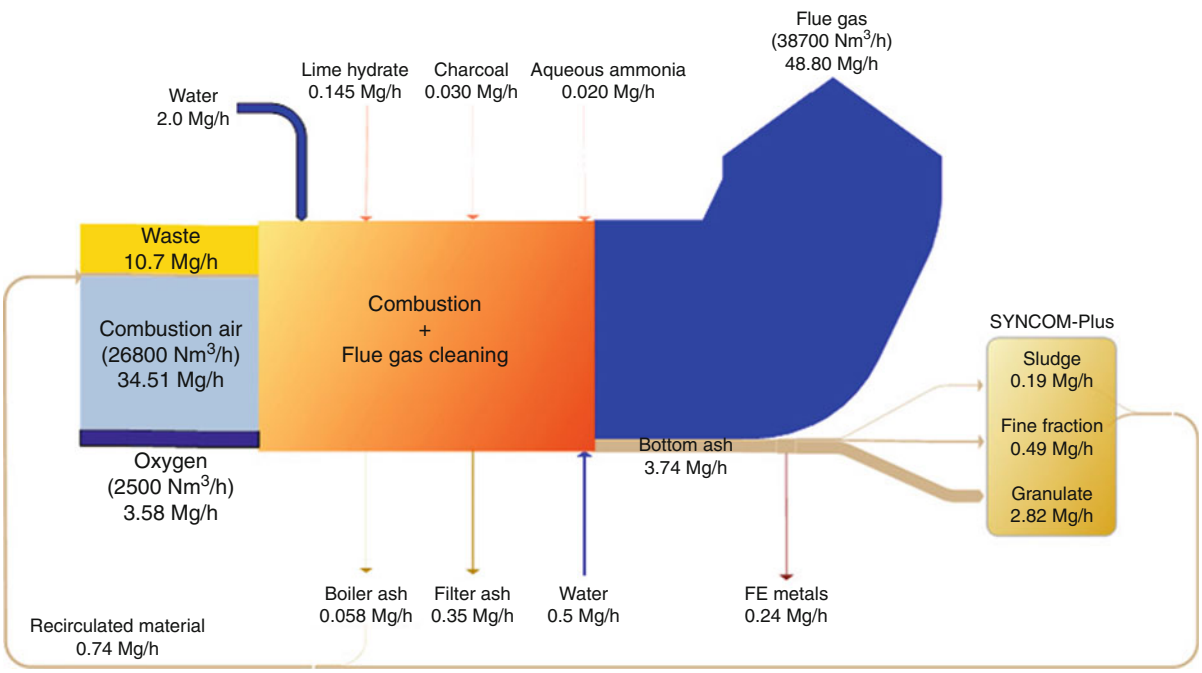

Martin Waste-to-Energy Technology. Figure 36
SYNCOM-Plus – mass flow

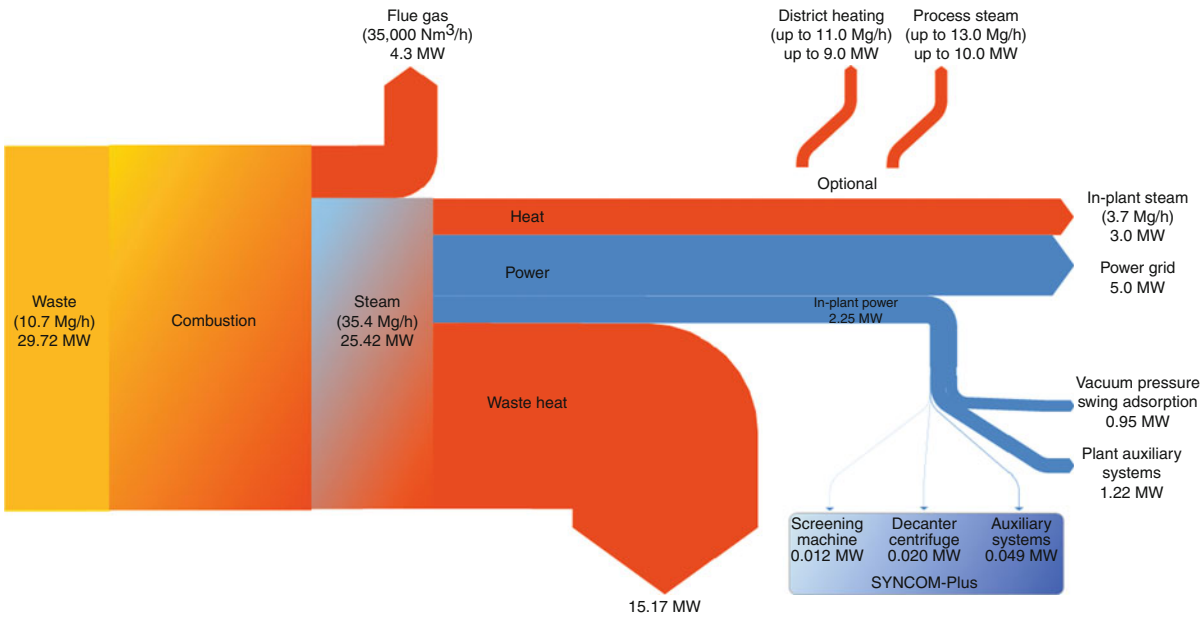

Martin Waste-to-Energy Technology. Figure 37
SYNCOM-Plus – energy flow

the fine fraction that generally contains heavy metals can be separated from the coarse fraction more effectively.

Dry discharge of bottom ash from waste combustion is becoming increasingly important in the context of recycling raw materials from combustion residues. Particularly in Switzerland, but also in numerous other countries, there has been much interest over the last few years in this process. Discharge of graded, dry bottom ash is on the one hand economically interesting because metal is separated more efficiently, returns from metal recovery are maximized and disposal costs are reduced through reductions in weight and lower transport costs. On the other hand, there are advantages due to the better quality of the dry discharged bottom ash and the fact that subsequent treatment, processing, and recycling is easier.

The simple and robust technology used in the dry discharge system is based on generally known process-engineering separation and transport procedures and uses the advantages of a fractioned bottom ash discharge. The ram-type bottom ash discharger is therefore used in unchanged form but with a newly developed and patented air separator and a cyclone separator (Fig. 38).

For dry bottom ash discharge, the ram-type discharger is operated without water. The bottom ash is discharged in dry form from the combustion system. The dry discharged bottom ash is conveyed directly to an air separator (Fig. 39). The fine fraction and bottom ash dust is extracted in a defined manner. Depending on the extraction speed, the fine fraction and dust particle size is set to values <4 mm. The air separation area is enclosed by a housing, in which negative pressure is constantly maintained, thereby preventing false air from entering the furnace or dust from getting into the boiler house. Similar to wet-type discharge, the surface temperature of the discharger lies in the range 40–60°C in the dry discharge mode.

Essentially, three product streams are separated out of the dry bottom ash: coarse fraction, fine fraction, and bottom ash dust. The latter two are discharged out of the air separator with the air flow and conveyed to a cyclone separator, which ensures that they are separated from the air flow. The unburdened air, containing a minimal amount of residual bottom ash dust, is conveyed in a defined manner to the combustion air system via the overfire air. The fine fraction separated in the cyclone separator is sent to a recycling process or landfilled.

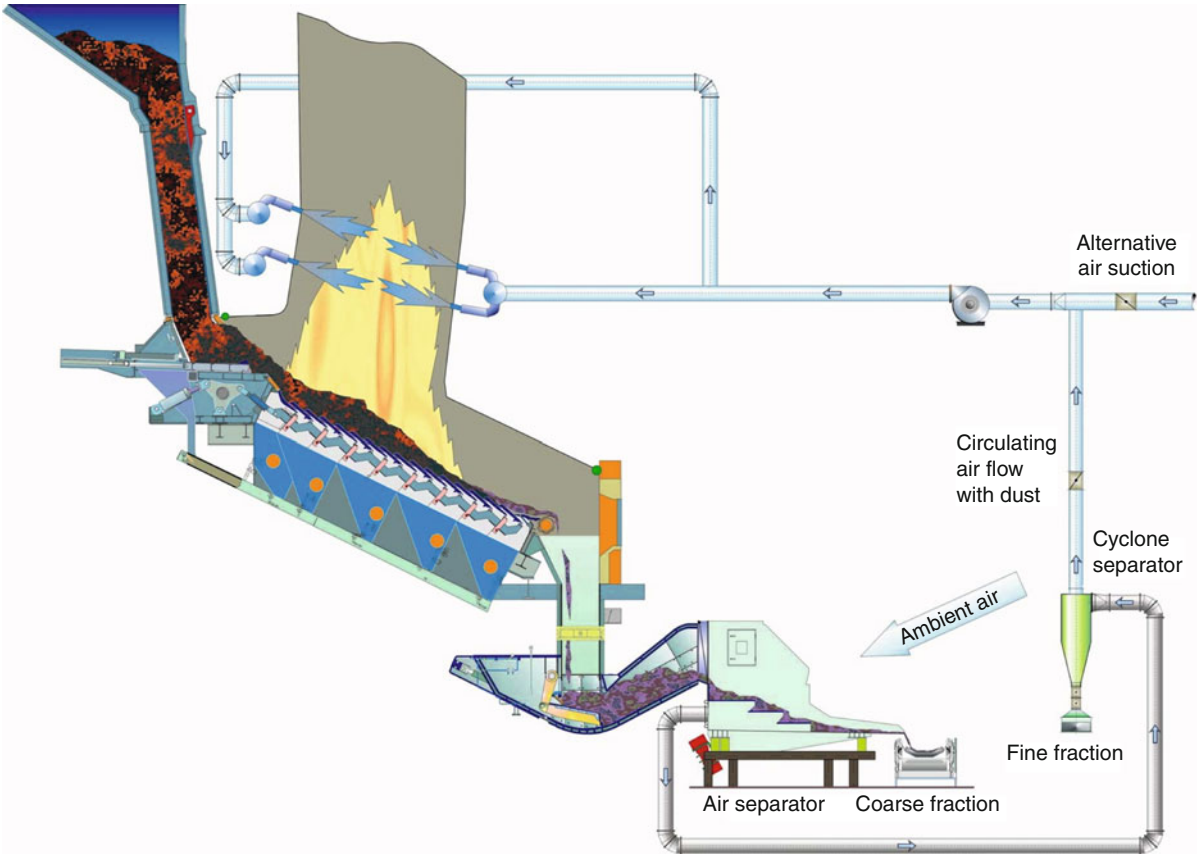

Martin Waste-to-Energy Technology. Figure 38
Dry bottom ash discharge and separation

On the basis of the successful semi-industrial preliminary tests, the operator of the Monthey WTE plant (CH) decided to implement dry discharge systems in both combustion lines for industrial-scale operation.

The characteristic features of the dry bottom ash discharge and separation are listed below:

- Weight reduction (no water!)
- More effective metal separation
- Better quality metals
- Lower water consumption
- Better bottom ash quality

Fly Ash Treatment/Recirculation

In view of the continual depletion of raw materials, sustainable processes for the recovery of recyclables are becoming more and more important. The process of selective zinc recovery from the acid-scrubbed fly ash of thermally treated waste is one example of a cost-effective, process-integrated method for recovering economically profitable heavy metals.

By means of this process, cadmium, lead, and copper are separated and the valuable metal zinc, which is contained in high concentrations in the fly ash, is recovered in pure form (Zn $>$ 99.99%). After acidic fly ash scrubbing, the filter ash cake has an extremely low heavy-metal content. Any organic matter that remains in the cake subsequent to scrubbing is returned to the combustion system so that it can be destroyed (Fig. 40) [32].

The synergies associated with the residues occurring with wet flue gas cleaning are used during the process. During acidic ash extraction, the heavy metals in the fly ash are mobilized and extracted by the acidity of the quench water. At the same time, the excess acid content of the quench water is neutralized by the

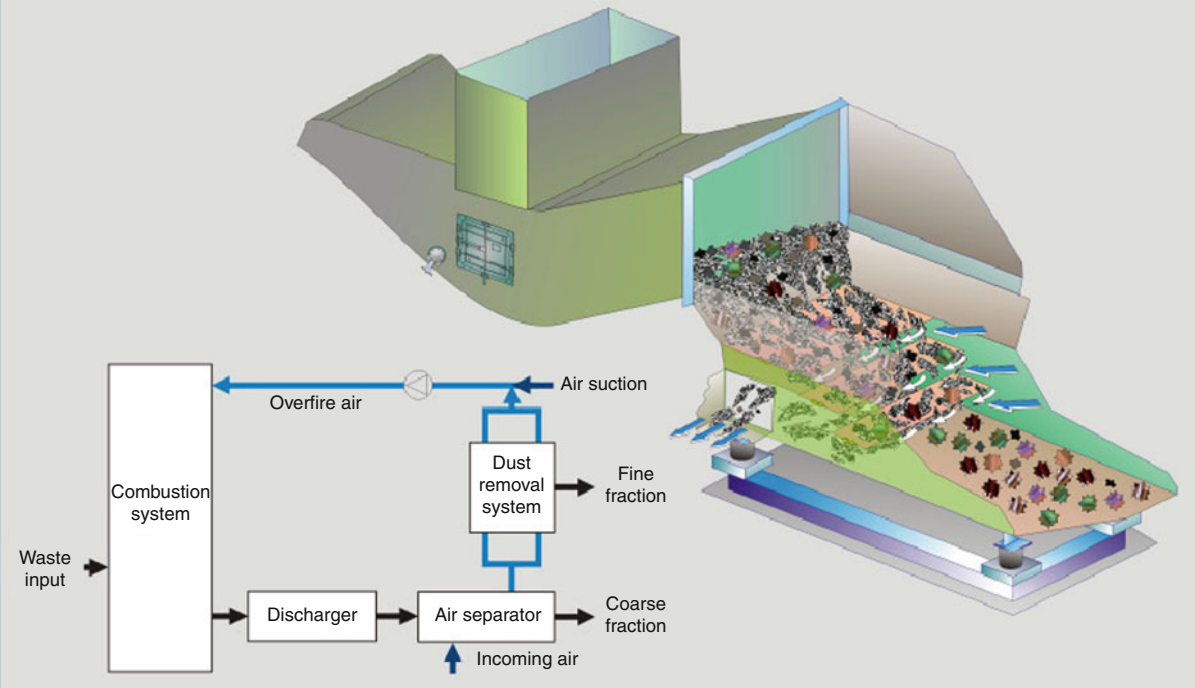

Martin Waste-to-Energy Technology. Figure 39
Concept of dry bottom ash discharge/air separator

alkalinity of the fly ash. In a filtration stage, the filter ash cake, which has an extremely low heavy metal content, is separated from the filtrate containing heavy metals. The filtrate serves as the base material for subsequent targeted heavy metal separation and recovery. Cadmium, lead, and copper are separated using a reductive process and recovered as a metal mixture in lead works. Zinc, which is present in the filtrate in economically interesting concentrations, is separated from the pre-cleaned filtrate using a selective liquid–liquid extraction method, and then concentrated and recovered electrolytically as pure zinc (Zn $> 99.99\%$) [34]. In a waste water treatment plant using lime milk, the filtrate with its extremely low heavy metal content is neutralized, filtered, and freed of all remaining traces of heavy metals using selective heavy-metal ion exchangers. The resulting clean waste water can be supplied directly to the receiving body of water. After filtration, a small amount of residual metal sludge consisting largely of gypsum and alkaline earth metal hydroxides remains and is disposed of.

To destroy the organic matter in the filter ash cake, in particular the dioxins and furans, the filter ash cake with its extremely low heavy-metal content is returned to the combustion system. As proved in several industrial-scale trials at WTE plants, recirculation of the filter ash cake has no effect on plant operation, clean gas parameters and the quality of the resulting bottom ash.

By combining the individual process steps, the residues from flue gas cleaning can be sustainably and efficiently treated. Using the processes described here, thermal waste treatment results in bottom ash and metal fractions containing recyclables that can be selectively returned to the raw materials cycle.

In addition to the sustainable recovery of secondary raw materials and closing of substance cycles, this process also has economic advantages. Value is added through the recovery of zinc and significant cost savings are made in relation to the treatment of waste water with low heavy-metal contents, thereby ensuring the cost efficiency of the overall process. The process could consequently achieve sustainable, ecologically relevant, and economically interesting recovery of residues from flue gas cleaning systems in thermal waste treatment plants.

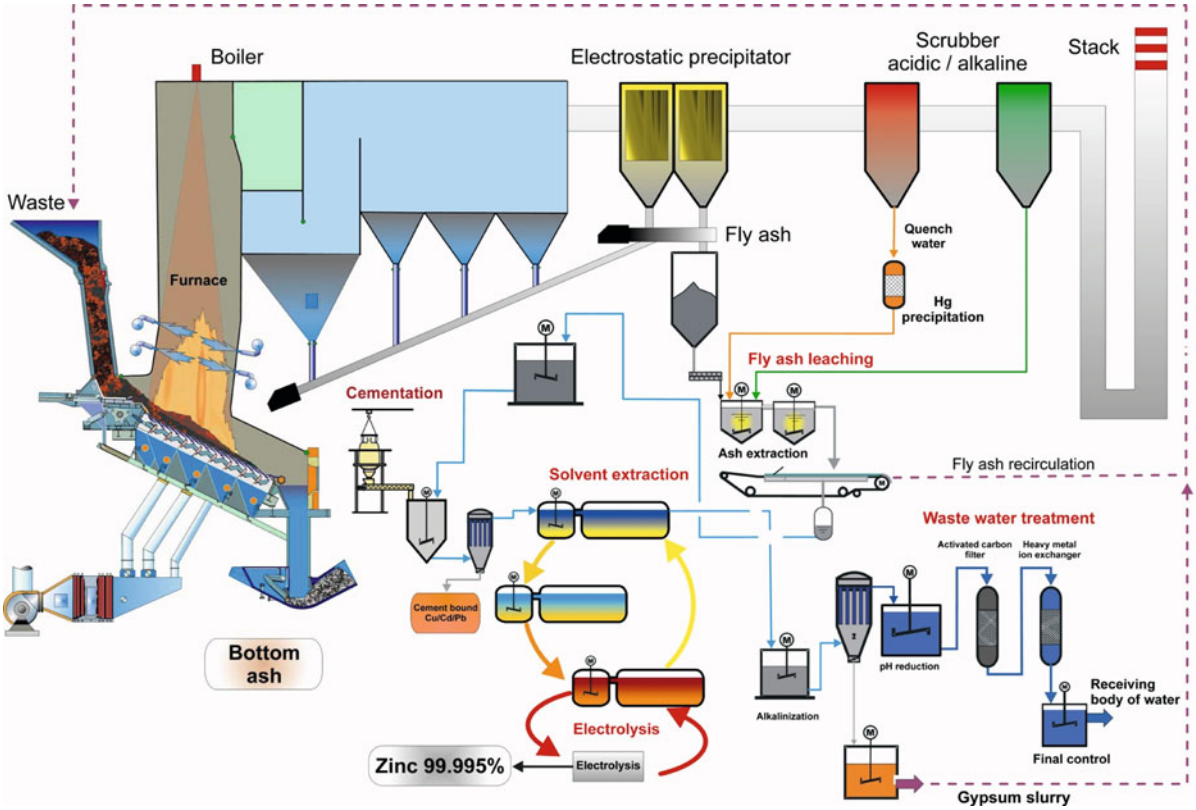

Martin Waste-to-Energy Technology. Figure 40
Fly ash treatment/recirculation/Zn recovery [32, 33]

Together with its cooperation partner, MARTIN has implemented research and development into treatment processes and the recirculation of treated fly ash in industrial-scale WTE plants.

Reference Plants

In Figs. 41–46 some examples of WTE plants using MARTIN technology are provided. A current reference list is available in [1]. In order to provide solutions for customers with small waste volumes, modular and standardized small-scale plants have been specifically developed. These plants are suitable for waste throughputs of 2.5–8 Mg/h per combustion line.

Future Directions

Sustainability, recycling, resource conservation, and global warming are the greatest global challenges facing us today and will continue to occupy our attention in the years to come. Waste combustion is an essential component of all modern waste management concepts and plays a central role in the handling of these issues, which will become increasingly important as time goes on.

Experience and statistics from many countries clearly show that the combustion of residual waste does not conflict with the avoidance, recovery, and recycling of waste in any way. The rate of recycling of secondary raw materials is particularly high in countries predominantly using combustion, while their rate of landfilling of residual waste is low.

There is no doubt that CO_2 is produced and released into the atmosphere with the flue gases generated during waste combustion. However, when assessing the relevance of these emissions to the climate, a difference must be made in terms of where the CO_2 originates. Approximately 50% of this CO_2 is biogenic in origin (paper, cardboard, wood, materials, leather, etc.) and

Reverse-acting grate SYNCOM

Number of lines:	1
Waste capacity per line:	10.7 Mg/h
Thermal capacity per line:	29.6 MW
Steam output per line:	35.2 Mg/h
Steam pressure:	40 bar
Steam temperature:	400°C

Martin Waste-to-Energy Technology. Figure 41
Arnoldstein (AT)

Reverse-acting grate

Number of lines:	2
Waste capacity per line:	15.0 Mg/h
Thermal capacity per line:	38.3 MW
Steam output per line:	46.0 Mg/h
Steam pressure:	35 bar
Steam temperature:	242°C

Martin Waste-to-Energy Technology. Figure 42
Vienna Spittelau (AT)

Reverse-acting grate	
MSW	
Number of lines:	2
Waste capacity per line:	23.0 Mg/h
Thermal capacity per line:	88.3 MW
Steam output per line:	115.0 Mg/h
Steam pressure:	60 bar
Steam temperature:	450°C
Biomass	
Number of lines:	1
Waste capacity per line:	23.0 Mg/h
Thermal capacity per line:	100.0 MW
Steam output per line:	115.0 Mg/h
Steam pressure:	73 bar
Steam temperature:	480°C

Martin Waste-to-Energy Technology. Figure 43
Brescia (IT)

Reverse-acting grate	
Line 3	
Number of lines:	1
Waste capacity per line:	25.0 Mg/h
Thermal capacity per line:	87.0 MW
Steam output per line:	103.5 Mg/h
Steam pressure:	40 bar
Steam temperature:	400°C
Line 4	
Number of lines:	1
Waste capacity per line:	29.0 Mg/h
Thermal capacity per line:	90.0 MW
Steam output per line:	103.5 Mg/h
Steam pressure:	40 bar
Steam temperature:	400°C

Martin Waste-to-Energy Technology. Figure 44
Malmö (SE)

therefore does not increase the global CO_2 balance, similar to the combustion of biomass. The other half, however, is fossil in origin (plastics, paints, varnishes, etc.) and therefore impacts on the climate. Consequently, the technological groundwork must be laid for building highly efficient waste combustion plants and in order that the substitution effect of standard fuels can be maximized to the greatest extent possible. Far-reaching climate policies are basically inconceivable without these plants because their potential for reducing the greenhouse effect and as a source of alternative energies cannot be ignored. Development goals must serve to increase the efficiency of these plants while integrating them into the energy and material flow management systems of individual countries [35, 36].

Further development and optimization of existing technologies and concepts are needed due to international requirements in the field of thermal waste treatment using grate-based combustion systems. It has proven itself repeatedly that innovative technologies

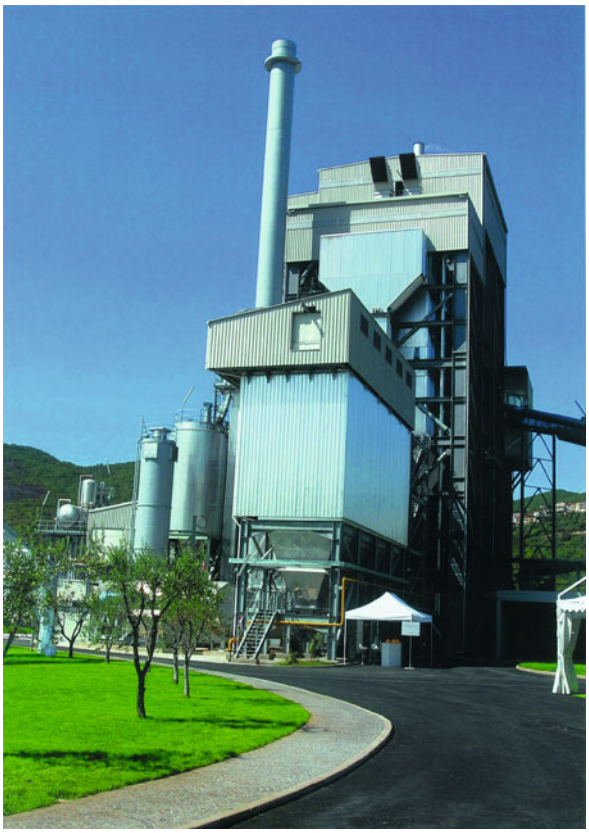

Reverse-acting grate Vario

RDF

Number of lines:	1
Waste capacity per line:	13.4 Mg/h
Thermal capacity per line:	49.9 MW
Steam output per line:	61.2 Mg/h
Steam pressure:	56 bar
Steam temperature:	400°C

Martin Waste-to-Energy Technology. Figure 45
Pozzilli (IT)

Horizontal grate

1994

Number of lines:	4
Waste capacity per line:	30.0 Mg/h
Thermal capacity per line:	73.0 MW
Steam output per line:	77.0 Mg/h
Steam pressure:	43 bar
Steam temperature:	415°C

2007

Number of lines:	2
Waste capacity per line:	33.6 Mg/h
Thermal capacity per line:	93.3 MW
Steam output per line:	102.0 Mg/h
Steam pressure:	130 bar
Steam temperature:	420°C

Martin Waste-to-Energy Technology. Figure 46
Amsterdam (NL)

must first be developed and comprehensively investigated. In the future, MARTIN will continue to reliably ensure treatment of waste under ecological and economic constraints, using innovations and reliable process-engineering technology and taking international statutory requirements into account.

Bibliography

Primary Literature

1. MARTIN GmbH für Umwelt- und Energietechnik (2011) http://www.martingmbh.de
2. Koralewska R (2006) MARTIN Reverse-acting grate system – The challenge of high heating value fuels. In: Proceedings of the 14th NAWTEC, Tampa, 1–3 May 2006
3. Gohlke O, Busch M (2001) Reduction of combustion by-products in WTE plants: O_2 enrichment of underfire air in the Martin Syncom process. Chemosphere 42:545–550
4. Gohlke O, Koralewska R, Zellinger G, Takuma M, Kuranishi M, Yanagisawa Y (2006) Alternatives to ash melting and gasification. In: Proceedings of the 4th i-CIPEC, Kyoto, Japan, 26–29 Sept 2006
5. Gohlke O, Martin J (2007) Drivers for innovation in Waste-to-Energy technology. Waste Manage Res 25:214–219
6. Gleis M (2009) Reliability of new technologies of thermal waste treatment. In: 10th Assises des déchets, Atlantia la Baule, France, 21–22 Oct 2009
7. Gleis M (2010) Ungläubiges Kopfschütteln-Pyrolyse das einst viel gepriesene Abfallbehandlungsverfahren hat sich in Europa nicht durchgesetzt. Steht ihm nun eine Renaissance bevor? RECYCLING Magazine 07, pp 30–31
8. Tadishi O, Hiroyuki H, Kazuaki S (2006) Operation data of MSW gasification and melting plant. In: Proceedings of the 4th i-CIPEC, Kyoto, Japan, 26–29 Sept 2006
9. Whiting K, Schwager J (2006) Why are novel technologies, such as gasification, for MSW processing struggling to make an impact in Europe? In: Proceedings of the 4th i-CIPEC, Kyoto, Japan, 26–29 Sept 2006
10. Vehlow J (2009) Abfallverbrennung in Deutschland. Müllhandbuch digital, ESV Erich Schmidt Verlag, MuA Lfg. 2/09
11. International Energy Agency IEA (2010) IEA Biomass Agreement. Task X, Sub-task 6-Gasification of waste. http://www.ieabioenergy.com
12. Beckmann M, Scholz R, Wiese C, Davidovic M (1997) Optimization of gasification of waste materials in grate systems. In: International conference on incineration & thermal treatment technologies, San Francisco-Oakland Bay, 12–16 May 1997
13. Davidovic M (2007) Gasification and NO_x-reduction with a reverse-acting grate and a multistaged postcombustion chamber. Presentation at Clausthaler Umwelttechnik-Institut GmbH/CUTEC, Clausthal-Zellerfeld, Germany
14. Schreiner R, Jansen A (1997) Infrared cameras guide combustion control. Mod Power Syst 17(9):45–49
15. Meile E, Schreiner R (2002) Gezielte Prozessbeeinflussung durch Aufschalten einer Infrarotkamera am Beispiel der MVA Winterthur. Entsorgungspraxis 5:26–30
16. Zipser S, Gommlich A, Matthes J, Keller H, Fouda Ch, Schreiner R (2004) On the optimization of industrial combustion processes using infrared thermography. In: Proceedings of the 23rd IASTED international conference on modeling, identification and control, Grindelwald, pp 386–391
17. Keller H, Matthes J, Zipser S, Schreiner R, Gohlke O, Horn J, Schönecker H (2007) Kamerabasierte Feuerungsregelung bei stark schwankender Brennstoffzusammensetzung. VGB Powertech 3:85–92
18. Gohlke O (2009) Efficiency of energy recovery from municipal solid waste and the resultant effect on the GHG balance. Waste Manage Res 27:894–906
19. BREF of waste incineration (2005) Integrated pollution prevention and control. Reference document on the best available techniques for waste incineration (BREF), IPPC Bureau. http://eippcb.jrc.es
20. Gohlke O, Seitz A, Spliethoff H (2007) Innovative approaches to increase efficiency in EfW plants – Potential and limitations. ISWA, Amsterdam
21. Murer MJ, Spliethoff H, van Berlo MAJ, de Waal CMW, Gohlke O (2009) Comparison of energy efficiency indicators for EfW plants. Proceedings of the Sardinia 2009 symposium, Sardinia, Italy
22. Mennessier A (2008) Study of an innovative process for NO_x reduction in an energy-from-waste plant, BSc Technische Universität München, München
23. ANSYS Inc (2010) ANSYS FLUENT 12.0 Documentation
24. Wolf Ch (2005) Erstellung eines Modells der Verbrennung von Abfall auf Rostsystemen unter besonderer Berücksichtigung der Vermischung – Ein Beitrag zur Simulation von Abfallverbrennungsanlagen. Dissertation, Universität Duisburg-Essen, Duisburg
25. Martin U (2010) Beschreibung der Brennstoffumsetzung im Brennbett von Rostfeuerungen. Technische Universität München, München
26. Koralewska R (2005) Industrial-scale validation of a CFD simulation in conjunction with a fuel-bed model. Presentation at waste-to-energy research and technology council, Columbia University, New York
27. Koralewska R, Wolf Ch (2005) Industrial-scale validation of a CFD model in conjunction with a fuel-bed model for the thermal treatment of waste in grate-based combustion plants. VDI-Berichte 1888, 22. Deutscher Flammentag, VDI-Verlag, Düsseldorf, pp 613–619
28. Rossignoli P (2010) High-dust selective catalytic NO_x reduction at WTE plant in Brescia. In: Proceedings of the 2nd international conference on biomass and waste combustion, Oslo, Norway, 16–17 Feb 2010
29. Gohlke O, Busch M, Horn J, Takuma M, Kuranishi M, Yanagisawa Y (2003) New grate-based Waste-to-Energy system producing an inert ash granulate. Waste Management World May–June, pp 37–46

30. Martin J, Gohlke O, Tabaries F, Praud A, Yanagisawa Y, Takuma M (2005) Defining inert – a technological solution to minimize ecotoxicity. Waste Management World Sept/Oct, pp 70–73
31. Koralewska R (2009) SYNCOM-Plus: An optimized residue treatment process. In: Proceedings of the 17th NAWTEC, Chantilly, 18–20 May 2009
32. Schlumberger S (2010) Neue Technologien und Möglichkeiten der Behandlung von Rauchgasreinigungsrückständen im Sinne eines nachhaltigen Ressourcenmanagements. In: Proceedings of Bundesamt für Umwelt BAFU: Verbrennungsrückstände in der Schweiz, Bern
33. BSH Umweltservice AG (2011) http://www.bsh.ch
34. Schlumberger S (2005) Entwicklung und Optimierung eines Verfahrens zur selektiven Zinkrückgewinnung aus sauren Ascheextrakten der thermischen Abfallentsorgung. Dissertation, Technische Universität München, München
35. Fleck E (2006) A long-time flame: Waste-to-energy still goes strong in Europe. Waste Management World July–Aug, pp 107–116
36. Martin J (2010) Der Anlagenbau für Abfallverbrennungsanlagen – Strukturen und Märkte im Licht der Globalisierung. In: Thomé-Kozmiensky KJ, Versteyl A (eds) Planung und Umweltrecht, Band 4. TK, Neuruppin, Germany, pp 41–56

Books and Reviews

Chandler AJ, Eighmy TT, Hjelmar O, Vehlow J et al (1997) Municipal solid waste incinerator residues. Elsevier, Amsterdam

Ludwig CB et al (1973) Handbook of infrared radiation from combustion gases. NASA SP-3080, Washington, DC

Ortiz de Urbina G, Goumans JJJM (2003) Proceedings of the 5th International Conference on the environmental and technical implications of construction with alternative materials. WASCON, San Sebastian, Spain, 4–6 June 2003

Spliethoff H (2009) Power generation from solid fuels. Springer, Berlin

Mass Transit Science and Technology, Introduction

Gary L. Brosch
Center for Urban Transportation Research,
University of South Florida, Tampa, FL, USA

Mass transit, or public transportation, has and will continue to play a key function in the shaping of communities. Public transportation plays an enormous role in the economic and social well-being of individuals and societies. Some have said the study and understanding of public transportation is not "rocket science." Indeed, it is much more difficult, as it involves not just science, but also public policy and individual choices.

Mass Transit Science and Technology, Introduction of the *encyclopedia* will examine a wide range of public transportation alternatives from conventional buses and steel wheeled trains to state-of-the-art BRT (bus rapid transit) systems and magnetically levitated trains. It will examine specially designated high-occupancy vehicle lanes (HOT lanes) and the role of bicycle transport. Also examined will be public policy decisions concerning a wide range of issues from parking policy to land use decisions related to transit-oriented development.

Bus Rapid Transit (BRT) combines technological advances and public policy changes to provide a transit system that is faster than conventional buses and often less expensive and more flexible than light rail systems. Development of BRT systems is occurring worldwide as examined in ► Bus Rapid Transit: Worldwide History of Development, Key Systems and Policy Issues. Technological advances such as automated guidance and signal priority are of use only if institutional issues are addressed. Public policy decisions that play a crucial role in the implementation of such systems are addressed in ► Bus Rapid Transit, Institutional Issues Related to Implementation.

As Bus Rapid Transit systems have developed, so has the controversy and debate over choice between Bus Rapid Transit and conventional light rail (LRT) systems. Which is better in the long run, which is more costly, which will attract more riders, which is better for economic development have all been the questions in this ongoing debate. Two articles, such as ► Bus Rapid Versus Light Rail Transit: Service Quality, Economic, Environmental and Planning Aspects and ► Bus Rapid Transit and Light Rail Transit Systems: State of Discussion, provide useful insight into the issues involved. Included in these discussions is a review of the trends of the last 50 years in urban transportation, the differences between developed and developing countries, the characteristics of light rail systems and bus rapid transit systems, and direct comparisons of the alternative modes.

The use of public transportation is determined by a wide array of direct factors including its cost, convenience, travel time, and perceived safety. Ridership also

is affected by external factors such as the cost of alternatives, congestion on roadways, and economic conditions. Public transportation is both affected by land use patterns and affects land use. Suburban versus urban developments clearly affect transit ridership potential. Similarly, transit centers clearly promote greater density. Balancing public policy goals for land use development and for use of mass transit can be facilitated through the use of transit-oriented development (TOD). ► Bus Versus Rail Implications for Transit-Oriented Development examines the differences and opportunities for transit-oriented development when comparing light rail systems and bus rapid transit systems. Urban transport systems clearly affect economic productivity and economic development. It is important to understand the differing implications of bus, bus rapid transit and rail systems on commercial and residential development surrounding transit stations.

Recent technological advances have enabled policy makers the opportunity to consider managing highway express lanes with high occupancy toll (HOT) lanes. Managing congestion and effective throughput of major expressways is a challenge. The use of high-occupancy vehicle lanes is gaining increased acceptance as is the increasing use of toll roads to finance new construction. Finding methods and technologies to combine these two offers the potential to increase the effectiveness of major roadways. Two articles, ► HOT Lanes/Value Pricing: Planning and Evaluation of MultiClass Service and ► High-Occupancy Vehicle and Toll Lanes provide an understanding of the technological advances and policy issues surrounding the potential of HOT lanes. Congestion pricing alternatives, equity issues, and future developments are included.

Light Rail Transit (LRT) is a staple of mass transit systems in both developed and developing countries. Its applications range from streetcars and tramways to modern automated systems. In spite of significant history and experience with light rail systems, understanding the conditions under which new or expanded systems are appropriate remains a challenge. ► Light Rail Transit, Systemic Viability provides important historical background on the development of LRT, a look at over 25 new systems developed in the last 30 years, as well as an analysis of the use of transit in cities with and without LRT.

As new light rail systems have been implemented and existing systems expanded, there have been increasing concerns related to their operation and interaction with pedestrians in urban areas. Light rail is most effective when pedestrian interface is easiest. Yet, this easy access leads directly to greater safety concerns. Technological and policy innovations such as regulatory and warning devices, delineation marking and positive control devices offer potential to reduce pedestrian injuries. ► Light Rail Transit in the US and Abroad, Examination of History and Innovations offers a comprehensive examination of the latest innovations in pedestrian/LRT safety.

Traveling on a cushion of air in high-speed trains is a dream that technological innovation has brought to reality in the form of magnetically levitated trains, both high speed and low speed. ► MAGLEV Technology Development provides the reader with a comprehensive review of magnetically levitated vehicles. The physics, engineering, and costs of magnetic levitation are covered as well as the history and state of the art of its development.

High-Speed Rail systems developed in the last 50 years continue to be expanded and implemented in countries all over the world playing a significant role changing public transport opportunities. Economic changes and technological advances have led to the increasing popularity of high-speed trains, particularly in Europe and Asia. ► High Speed Rail, Technology Development of examines technological developments of high-speed rail as well as the resultant challenges of implementation.

Light rail systems can be effective in moving larger numbers of people from a limited number of origins and destinations. Whereas, moving smaller numbers of people from greater numbers of origins to greater numbers of destinations calls for a smaller-scale system. Personal Rapid Transit (PRT) systems attempt to provide such a smaller-scale system. Sometimes referred to as automated people movers, these systems offer an intriguing concept of quickly moving small groups of people from one place to another. ► Personal Rapid Transit and Its Development looks at the history of PRT in several countries and the current state of PRT development. Also provided is a discussion of the sustainability/energy issues and planning/architectural issues related to the future of personal rapid transit systems.

At the other end of the speed spectrum from high-speed rail is the integration of bicycle transport with mass transportation. Often overlooked, bicycles are an important element of a comprehensive transit system. Finding techniques to successfully integrate the use of bicycles with mass transit bus and rail systems can significantly increase the overall effectiveness of transit systems. A series of case studies and best practices is found in ► Bicycle Integration with Public Transport.

Transit-oriented development, sometimes referred to as "smart growth" seeks to integrate public transportation investments and land use near transit stations to improve the sustainability and effectiveness of both. ► Transit-Oriented Development and Land Use provides a comprehensive look at such developments in countries ranging from Sweden, to Columbia and to the USA. Successful examples of the transportation and environmental benefits of transit-oriented development are presented. Also presented are the challenges, the financing, and the future of transit-oriented development.

► Advanced Public Transport Systems, Simulation-based Evaluation offers the state of the art in computer simulation of transit operations. The use of these simulation techniques is valuable in areas such as fleet management, traveler information systems, electronic fare payments, and transportation demand management systems. Examples are provided of both microscopic transit simulation and mesoscopic transit simulation.

Medical Device Batteries

Michael J. Root
Cardiology, Rhythm and Vascular Research and Development, Boston Scientific Corp., St. Paul, MN, USA

Article Outline

Glossary
Definition of the Subject
Introduction
Electricity as Medicine
Hearing Loss
Future Directions
Bibliography

Glossary

Anode The negative electrode of a discharging cell or battery.

Cathode The positive electrode of a discharging cell or battery.

Electrolyte A solution or material that completes the electrical circuit in a cell by way of ionic conduction.

Hermetic seal A way to seal implantable medical device batteries that is impermeable to fluids and usually includes a terminal feed through that is sealed in glass.

Implantable defibrillator An implanted medical device that functions as a pacemaker and is also capable of delivering high energy shocks to the heart to treat ventricular tachycardia (abnormally fast heart rate) and fibrillation.

Neurostimulation or neuromodulation Electrical stimulation of nerves to modify nerve activity.

Pacemaker An implanted medical device that delivers low level electrical stimulation to the heart for treatment of bradycardia (abnormally slow heart rate).

Primary cell A cell that is intended to be discharged only.

Secondary or rechargeable cell A cell that can be charged following depletion using an external electrical energy source.

Definition of the Subject

Medical device batteries serve an important role in modern health care. They power the devices that allow patients to function more normally by managing and improving their health or even survive life threatening disease conditions.

There are several ways to classify medical devices. Some provide therapeutic functions while others are used for diagnostic purposes. Some provide both functions. For therapeutic devices, devices may be further described as life sustaining or life enhancing (improves the quality of life).

Life sustaining devices provide therapy that keeps a patient alive. An implantable defibrillator is an example of a life sustaining device. Certain cardiac patients experience tachycardia (a very rapid heart beat) or ventricular fibrillation. Either condition limits the ability of the heart to effectively pump blood. Death can result if this type of arrhythmia is sustained and a normal heart rhythm is not restored by a defibrillator.

Life enhancing devices might treat conditions, like severe, chronic lower back pain, that do not threaten a patient's life, but prevent normal function and reduce their quality of life.

Improving the well-being of the patient is the most important use of wearable or implantable medical devices, of course. Medical devices can provide effective treatment or diagnostic information. Although it is not a necessary consideration, treating or monitoring a patient's condition remotely – that is, outside of the hospital or clinic – with such devices can also impact energy sustainability. Patients do not need to be transported to the hospital or clinic as frequently for treatment or monitoring.

In this entry are discussed a few of the specialized batteries for medical devices that are portable or wearable (carried with the patient, like hearing aids), or implantable (surgically placed inside the body as with neurostimulation pain management devices). There is a focus on the batteries designed for a few of the more common applications – implantable cardiac rhythm management (cardiac pacemakers and defibrillators), pain management, and hearing loss devices.

Introduction

Medical Devices that Use Batteries

There are a substantial number of wearable and implantable medical devices powered by batteries. These include devices for cardiac rhythm management (pacemakers, defibrillators, and heart failure devices), hearing loss, bone growth and fusion, drug delivery for therapy or pain relief, nerve stimulation for pain management, urinary incompetence and nervous system disorders, vision, diagnostic measurements and monitoring, and mechanical heart pumps.

This entry will be limited to three major categories of medical devices – cardiac rhythm, neurostimulation, and hearing devices. The first two are devices that apply electrical stimuli to muscle tissues or nerves and the last involves sound amplification. The battery systems used by these devices are used in other devices, as well. Some of these will be noted in the sections describing the batteries.

General Design Considerations for Medical Device Battery Performance

There are several important features that battery developers must consider when designing batteries for medical devices. Many of these are also important for most other battery types, as well.

Medical device batteries are fundamentally the same as any other battery designed for consumer electronics, military, or aerospace applications. All require the same three components to be able to function as an electrochemical power source – a negative electrode (or anode) material to supply electrons, a positive electrode (or cathode) material that takes up electrons, and an electrolyte that completes the electrical circuit through ionic conduction. The other components in a cell are necessary to make the cell perform efficiently, minimize its size, and make it safe and reliable. These components include one or more separators that are electrically insulating to prevent direct contact between the anode and cathode but allow ions to pass through, current collectors to convey electrons to or from the electrodes and various insulators to prevent short circuits.

Medical devices, especially implantable devices, often use batteries that are custom designed and built specifically for that device. Their sizes and shapes may not be standard. The electrode assemblies may consist of pellet or slug electrodes, spirally wound electrode foils, or stacked electrode plates (Fig. 1).

Batteries for implantable medical devices are hermetically sealed. Hermetic seals have long been used for certain cell types, like lithium-sulfur dioxide and lithium-thionyl chloride, where long shelf life is important, or exposure to corrosive and toxic materials could result if the cell leaks.

A feedthrough terminal is used in hermetically sealed cells as a way to connect to one of the battery electrodes to the external device circuit. A glass to metal seal insulates the terminal from the cell case. The glass is specially formulated to create a tight seal against the

battery case and the terminal and resist attack by the cell electrolyte. Glass materials like TA-23 and Cabal-12 are common.

A number of different chemistries have been used for medical device batteries. For example, over 20 years ago there were at least 14 battery chemistries developed and used in implantable cardiac rhythm devices for treating cardiac arrhythmias (Fig. 2). Only a few of these survived and are in use today.

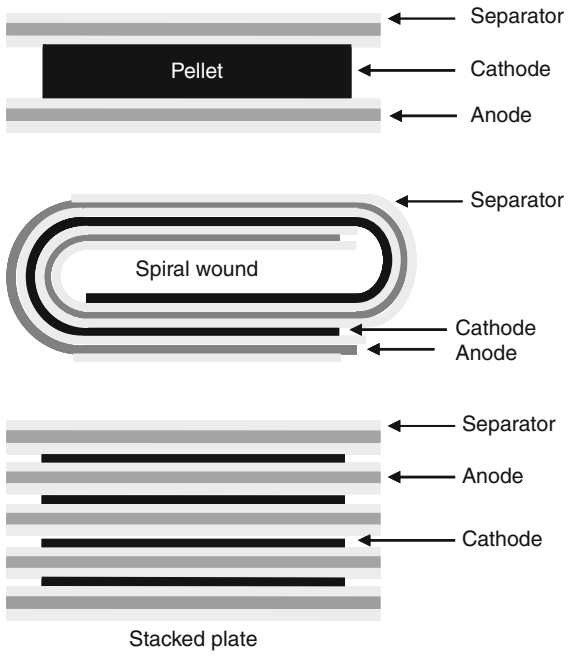

Medical Device Batteries. Figure 1
Electrode assembly designs for prismatic medical device batteries

Electricity as Medicine

Physiological effects of electricity were known by the time Italian scientist Alessandro Volta first invented the battery in 1800. The introduction of the battery meant that a sustained source of electricity was available for the first time. Prior to that, electrostatic sources of electricity and storage devices, like the Leyden jar, were used. Such devices provided only momentary electrical current.

The electrochemical cell, or battery, enabled advances in many areas of research and development involving electricity during the nineteenth century including electrochemistry, electrophysiology, and the use of electricity as medical therapy.

The work of Guillaume-Benjamin-Amand Duchenne (de Boulogne), a French neurologist, was foundational to the advancement of electrophysiology. German neurologist Robert Remak was an early proponent of electrotherapy to treat diseases of the nervous system.

J. Althaus wrote in his 1860 book "A Treatise on Medical Electricity, Theoretical and Practical," [1] "We know that, whatever may be the properties of the nerves, they can be called into action by galvanism. But the effects are widely different according to the form of electricity that is used; again, the quality and intensity of electricity are both of great importance; not less so the mode in which it is transmitted to the human body, and the length of time during which its action is kept up. In fact, we are able, by merely varying modes of applying electricity, to arouse or to kill the vital power of the nerves, and to diminish or to increase

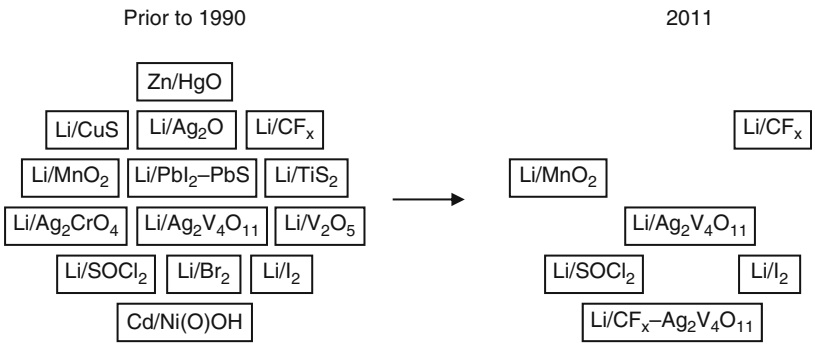

Medical Device Batteries. Figure 2
Types of battery chemistries used for cardiac rhythm devices prior to 1990 and today

their properties. Hence electricity can only be expected to be of service in the treatment of disease, if we are guided in its use by an exact knowledge of the physiological effects which it will invariably produce."

In 1873, Herbert Tibbits wrote, "There will be found here no new ground opened out, but only an earnest endeavor to sift the wheat of our existing knowledge from the chaff, and to make the reader as much at home with his electrical as with his other medical instruments; and further to lead him to estimate electricity at its fair and proved value in therapeutics, as an agent, not to be indiscriminately advocated as a panacea, nor, on the other hand, neglected by the inexperienced, but in appropriate cases to be regarded as one of the most powerful and serviceable weapons with which we can combat disease"[2].

Many claims of treatments using electricity were false, though. H. Lewis Jones in 1892 cautioned the medical community, [3] "One thing is certain, that without a thorough grounding in the physical part of the subject, no satisfactory advances can be made in a field of therapeutics which is at present almost entirely neglected by medical men. A great deal of the quackery which surrounds and discredits medical electricity, is due to the indifference and contemptuous attitude of the medical profession, and we have only ourselves to blame if the public insist on seeking elsewhere for treatment which is refused to them by their medical advisors."

Perhaps, the most prominent and successful use of electrical stimuli in medicine today is for cardiac rhythm management used to treat certain cardiac disease conditions. The American Heart Association reports that nearly 37% of the US population 20 years and older have some form of heart disease. The Heart Rhythm Foundation estimates 325,000 deaths each year in the USA from sudden cardiac arrest making it a leading cause of death.

There are three implantable devices used today to treat cardiac arrhythmias – the pacemaker, the implantable cardioverter defibrillator (ICD), and the cardiac resynchronization therapy (CRT) devices for heart failure patients.

Implantable Cardiac Pacemakers

Blood flow throughout the body occurs because the pumping action of the heart maintains the arterial blood pressure at a higher level than the venous blood pressure. Each heart beat involves the coordinated contraction of cardiac muscle cells as the result of the initiation and propagation of an electrical impulse [4].

Rather than contracting from nerve stimulation like skeletal muscles, cardiac muscle or myocardial cells respond to an electrical signal created by ionic (K^+, Na^+, and Ca^{2+}) concentration differences across their cell membranes. At rest, this potential, called an action potential, is about −90 mV. When the cell is activated, it rapidly depolarizes by redistributing the ionic concentrations across the cell membrane and contraction follows. Specialized muscle cells in the sinoatrial (SA) node of the heart start this process by spontaneously depolarizing once it reaches the critical firing level (CFL) of about −55 mV. The SA node is the primary natural pacemaker in normally functioning hearts. The signal is then quickly conveyed throughout the rest of the heart by way of several conduction pathways [4].

There are a number of conditions that cause the heart to beat abnormally. Electrocardiograms measure changes in potential that occur in the heart. An electrocardiogram of a normal heart rhythm is shown in Fig. 3. Electrocardiograms showing a normal rhythm, bradycardia, tachycardia, and ventricular fibrillation. The beats are regular and the time intervals between them are typical.

Bradycardia is a condition wherein the heart beats too slowly or skips beats altogether (for example, see Fig. 3). This can occur if the electrical impulses through the heart are slowed, too few impulses are transmitted, or they are blocked altogether [4].

Implantable cardiac pacemakers are electronic devices that treat bradycardia. External pacemakers were developed in the early 1950s. These were large devices that were not portable. Introduction of the transistor in the mid-1950s meant that smaller devices could be built. Earl Bakken and coworkers later developed a smaller external pacemaker that could be carried by the patient [5]. The first cardiac pacemakers to be implanted in humans lasted hours to days [6]. In 1960, Wilson Greatbatch developed the first implantable cardiac pacemaker that lasted for longer than a few days [7].

Pacemakers today can pace in one or both chambers (right atrium and right ventricle) on the right side of the heart. The power demand on a pacemaker battery

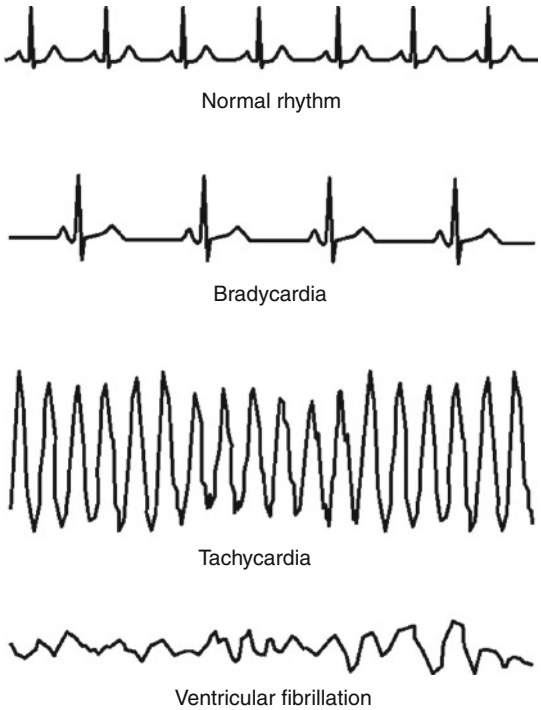

Medical Device Batteries. Figure 3
Electrocardiograms showing a normal rhythm, bradycardia, tachycardia, and ventricular fibrillation

of any individual device varies based on device programming, the number of chambers paced, and the patient's cardiac condition. Cardiac pacing therapy is a relatively low power operation – generally between 20 and 100 μW on average. The amount of electrical energy used to stimulate the heart can be adjusted to meet the needs of the patient. The first pacemakers where asynchronous – meaning they paced at a single rate. Devices today adapt to the patient's activity level to pace more rapidly or more slowly as needed. Additional low power demands on these devices include sensing to detect a natural heart beat and other monitoring features.

Although requiring only low levels of power, it is the frequent application of pacing therapy, as well as the continuous background device operations, that have the most significant impacts on device longevity. Implantable cardiac pacemakers are expected to last up to 10 years or so, depending on the therapy required by the patient; so a battery that has a high energy density is important.

The first devices to be implanted in humans used either rechargeable nickel-cadmium (NiCd) cells or alkaline zinc-mercuric oxide (Zn/HgO) cells [8].

The development of primary lithium batteries for implantable medical devices was a big advance that enabled devices to operate more reliably and longer. Lithium is the lightest metal and has the most negative reduction potential. When combined with any number of positive electrode materials, the result is cells with high energy densities compared to aqueous cells. Most lithium cells have an initial open circuit voltage between 1.8 and 3.9 V, compared to 1.2–1.6 V for most aqueous cells.

A number of lithium cell technologies were developed in the 1970s [9] and some were used clinically, [10] including lithium-copper sulfide (Li/CuS), lithium-silver chromate (Li/Ag_2CrO_4), lithium-thionyl chloride ($Li/SOCl_2$), lithium-lead sulfide-lead iodide ($Li/PbS\text{-}PbI_2$), lithium-titanium disulfide-sulfur ($Li/TiS_2\text{-}S$), lithium-bromine (Li/Br_2), lithium-manganese dioxide (Li/MnO_2), and the lithium-iodine (Li/I_2) cells that are used in most pacemakers today.

Other power sources were developed, as well. Notable were radioactive power sources, principally based on plutonium-238, [11] that were used in the 1970s. Regulations pertaining to the distribution of radioactive devices limited their acceptance.

Implantable Cardiac Pacemaker Batteries

Lithium-Iodine Lithium-iodine (Li/I_2) was proposed as a power source for implantable cardiac pacemakers in 1971 [12]. The first pacemaker run by a Li/I_2 cell was implanted in 1972 [6]. These cells were originally developed as more reliable and longer lived alternative to the zinc-mercuric oxide cells (see below) used in implantable cardiac pacemakers since they were introduced in 1960 and on into the mid-1970s. However, Li/I_2 cells have been the dominant power source for implantable cardiac pacemakers for more than 30 years.

The negative electrode reaction is:

$$Li \rightarrow Li^+ + e^-$$

and the positive electrode reaction is:

$$I_2 + 2e^- \rightarrow 2I^-$$

Iodine is stabilized by mixing it with a polymeric pyridine – poly-2-vinylpyridine (abbreviated P2VP or PVP) – to form an I_2-P2VP charge transfer complex.

The overall cell reaction is:

$$2Li + I_2 \rightarrow 2LiI$$

When a Li/I_2 cell is built and the I_2-P2VP mixture is added, it reacts directly with Li to form in situ a layer of solid LiI between negative and positive electrode materials. This layer serves to protect the Li from further reaction with the I_2. LiI also functions both as an electrolyte and a separator.

The movement of Li^+ is rather slow in solid LiI with conductivities less than 10^{-6} Ω^{-1} cm^{-1} [13]. This limits Li/I_2 cells to low rate applications, like implantable cardiac pacemakers.

The open circuit potential of the Li/I_2 cell is about 2.8 V. As the cell discharges, the thickness of the LiI electrolyte layer increases. This increases the internal resistance of the cell, so the discharge voltage decreases somewhat as the cell becomes depleted. The faster the discharge rate, the more sloped the discharge voltage becomes (Fig. 4).

The gradual voltage and resistance changes during discharge present the means to predict the extent of cell depletion, thereby allowing an accurate prediction of pacemaker longevity. This advanced warning allows sufficient time for the physician and the patient to schedule device replacement well ahead of complete battery depletion and the subsequent inability of the pacemaker to deliver therapy.

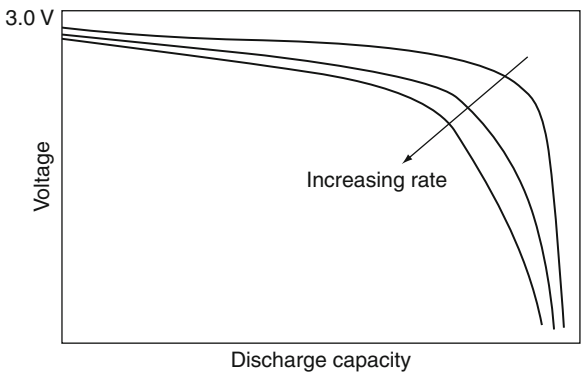

Medical Device Batteries. Figure 4
Discharge voltage of Li/I_2 cells. The voltage is lower for higher discharge loads

A cross section of a Li/I_2 prismatic cardiac pacemaker cell is shown in Fig. 5. In this design, a lithium sheet is placed between two I_2-P2VP electrodes. Energy densities for Li/I_2 cells are 210–280 Wh kg^{-1} and 810–1,030 Wh dm^{-3} [14].

Other devices that use Li/I_2 cells are implantable bone growth stimulators [15] and an implantable electromechanical hearing system [16].

Lithium-Carbon Monofluoride The most common positive electrode materials that have been used in all types of batteries, including those designed for medical devices (I_2 and O_2 notwithstanding), are usually metal oxides, such as silver vanadium oxide ($Ag_2V_4O_{11}$), manganese dioxide (MnO_2), mercuric oxide (HgO), and silver oxide (Ag_2O), or nonmetal oxides, like thionyl chloride ($SOCl_2$). Oxide compounds have a high energy density and can be chemically stable.

A cell pairing lithium (Li) with elemental fluorine (F_2) would have a theoretical open circuit voltage of 5.9 V. It is not practical to build a cell using elemental fluorine, which is a gas at room temperature and highly reactive, but fluoride compounds that retain some of the high energy density could be more realistic positive electrode materials [17].

Carbon monofluoride (CF_x) is one such fluoride compound that today is used as a positive electrode material in Li batteries for a number of different applications. For example, they are used in certain types of heart failure devices – implantable cardiac resynchronization therapy pacemakers (CRT-P). CRT-P devices can pace the right atrium and right ventricle, but they are also capable of pacing the left ventricle. Pacing three chambers requires more power than a Li/I_2 cell can deliver, so a different battery type is needed. Li/CF_x cells were developed in response to the increased power required by CRT-P devices. Vagal nerve stimulator devices also use a Li/CF_x cells.

Li/CF_x cells were first launched/introduced commercially in the mid-1970s and are available as coin cells and spiral wound cylindrical cells in a variety of shapes and sizes.

CF_x used in batteries is synthesized by the direct reaction of fluorine gas with a carbon starting material, such as petroleum coke, at high temperatures – usually between 350°C and 600°C depending on the type of carbon starting material and the fluorination level.

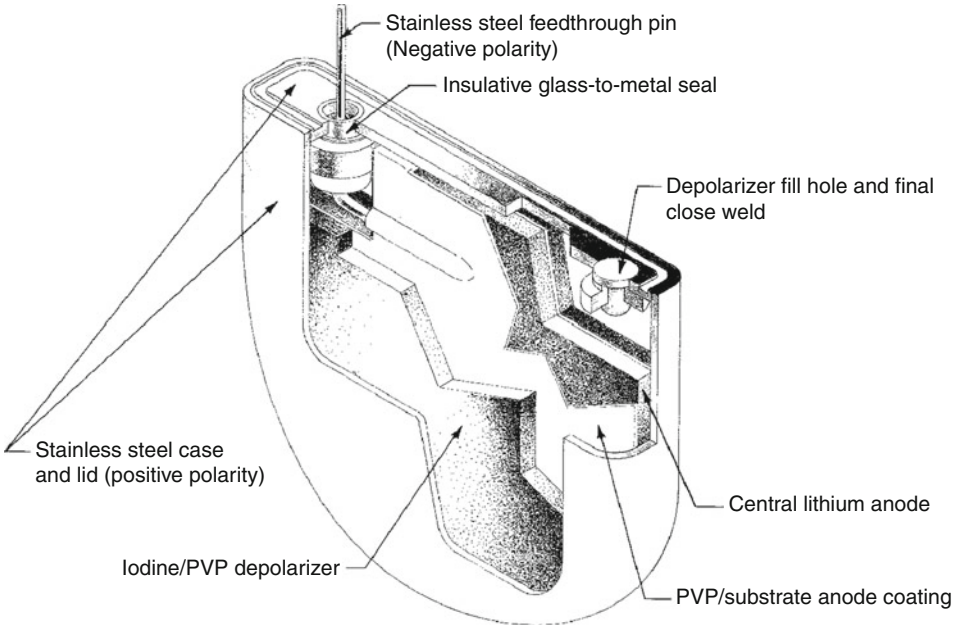

Medical Device Batteries. Figure 5
Cross section of a Li/I_2 prismatic cardiac pacemaker cell. © Greatbatch, Inc (Reprinted with permission)

The value of x in CF_x used in batteries, where x is the average number of fluorine atoms per carbon atom throughout the CF_x material, is usually between 0.9 and 1.2.

Fluorine is a highly corrosive and hazardous gas and so is difficult to handle safely. As a result there are only a few companies that have the ability or desire to manufacture CF_x in large quantities.

The CF_x material is mixed with a conductive carbon, like acetylene black or graphite, and a binder to maintain the mechanical integrity of the electrode. Typical electrolyte solutions are comprised of lithium tetrafluoroborate ($LiBF_4$) dissolved in one or more organic solvents, generally propylene carbonate (PC) or gamma-butyrolactone (GBL) with 1, 2-dimethoxyethane (DME).

The overall cell reaction is:

$$x\mathrm{Li} + \mathrm{CF_x} \rightarrow \mathrm{C} + x\mathrm{LiF}$$

Lithium fluoride (LiF) precipitates as a reaction product and it can limit the utilization of the CF_x.

The nominal open circuit voltage for Li/CF_x is 3.0 V, but the discharge voltage is closer to 2.8 V. The internal resistance of the Li/CF_x cell decreases during the early stages of discharge and remains low throughout discharge (Fig. 6), [18] attributed to the formation of conductive carbon as a reduction product of CF_x.

Energy densities can range between 250–590 Wh kg^{-1} and 635–1,050 Wh dm^{-3} depending on the battery size [19].

CF_x is also now combined with silver vanadium oxide designed for pacemakers and implantable defibrillators (see below).

Lithium Thionyl Chloride Most positive electrode materials are solids. However, among the first lithium cell types to be developed used an inorganic liquid, $SOCl_2$, as the positive electrode material.

Lithium-thionyl chloride ($Li/SOCl_2$) cells have seen a number of uses, including remote monitoring (such as residential water meters), various OEM (original equipment manufacturer) electronic devices, military, aerospace, and down-hole oil well monitoring applications. Medical device uses have included implantable heart monitors, drug infusion pumps, and some of the earliest implantable cardiac pacemakers [9, 10].

The positive electrode reaction is:

$$2\mathrm{SOCl_2} + 4\mathrm{e}^- \rightarrow \mathrm{S} + \mathrm{SO_2} + 4\mathrm{Cl}^-$$

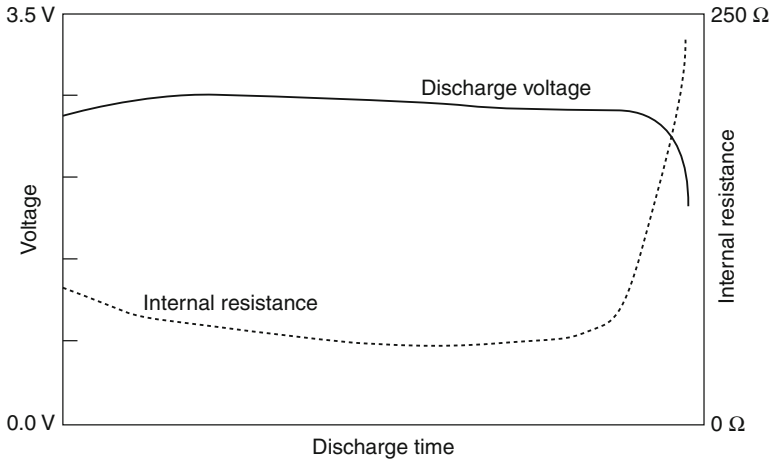

Medical Device Batteries. Figure 6
Discharge voltage and internal resistance for a Li/CF_x coin cell

with the overall cell reaction:

$$4Li + 2SOCl_2 \rightarrow S + SO_2 + 4LiCl$$

Thionyl chloride serves as both positive electrode material and the electrolyte solvent. The electrolyte salt typically is lithium aluminum chloride ($LiAlCl_4$) or, sometimes, lithium gallium chloride ($LiGaCl_4$).

The design of the Li/$SOCl_2$ cell puts $SOCl_2$ in direct contact with the Li anode material. If the direct reaction between Li and $SOCl_2$ continues, the active electrode materials would produce no useful electrical energy. The reaction between Li and $SOCl_2$ is self-limiting, though. Similar to other lithium cell systems, reaction products form a passive layer on the Li that inhibits further reactions from occurring. The passive layer must be both electrically insulating yet ionically conductive for the battery to discharge efficiently.

In systems with solid cathodes, the active positive electrode material is usually mixed with a conductive carbon that conveys electrons from the current collector to the electrode active material. In this case (and similar to the zinc-air cell discussed below), liquid $SOCl_2$ is the active material and needs to come into contact with an electrode site (cathode) where it can take up electrons as the cell discharges. The cathode in Li/$SOCl_2$ cells is a porous carbon, such as acetylene black, and a PTFE binder. An aluminum screen can be used as a current collector to electrically connect the cathode and the positive cell terminal.

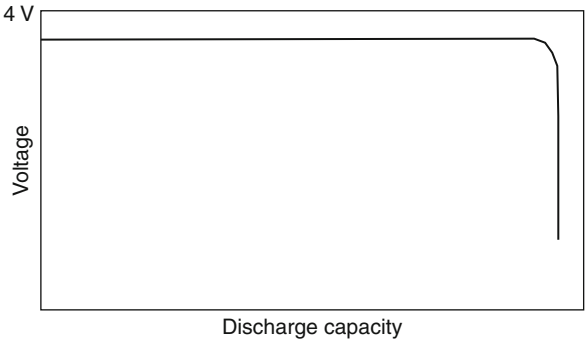

Medical Device Batteries. Figure 7
Discharge voltage for a Li/$SOCl_2$ cell

The lithium chloride (LiCl) and sulfur (S) that form precipitate and build up at the cathode. The cell capacity can be limited by these products if the cathode becomes blocked. Additionally, sulfur dioxide (SO_2) gas forms as a reaction product.

The Li/$SOCl_2$ cell has one of the higher open circuit potentials, 3.65 V, of any primary lithium cell. The voltage is quite flat throughout discharge (Fig. 7). The energy density is about 380 Wh kg^{-1} and 715 Wh dm^{-3}.[14] Li/$SOCl_2$ cells are produced in a wide variety of shapes and sizes for both high and low power applications, including prismatic and spiral-wound cylindrical cells used in pacemakers implanted during the 1970s.

Zinc-Mercuric Oxide Although no longer used, zinc-mercuric oxide (Zn/HgO) cells were the power source of choice for the first commercially viable implantable cardiac pacemakers. More than 3 million Zn/HgO cells were implanted in the 16 years from when the first successful cardiac pacemaker was implanted in 1960 and 1976 [20]. They helped many bradycardia patients until they were eventually supplanted by lithium cells, particularly Li/I_2, so a brief description of Zn/HgO technology is included here. Zn/HgO cells were also once used in wearable hearing aids.

The use of mercuric oxide as a positive electrode material for Zn/HgO cells was patented by British inventor Charles L. Clarke in 1884 [21], and also by others like Danish scientist Johannes N. Brønsted [22] in the early 1900s. A practical Zn/HgO cell was developed in the 1940s by Samuel Ruben with manufacturing support from the Mallory Battery Co [23]. The Zn/HgO cell was designed to replace the Leclanché zinc-manganese dioxide (Zn/MnO_2) cells used in military communications equipment during World War II. The Zn/HgO cell had better storage life and performance compared to Leclanché cells, particularly in the high temperature and high humidity conditions of the South Pacific [24].

Assorted Zn/HgO button and cylindrical cell sizes were produced after the war for military and space applications, as well as a number of consumer applications, including calculators, watches, and cameras. Some of the first implantable cardiac pacemakers that were available commercially were powered by Zn/HgO batteries and they became a popular cell for use in wearable hearing aids.

The Zn negative electrode material, or anode, and electrolyte solution are similar to other primary alkaline battery types, like zinc-air and zinc-silver oxide (Zn/Ag_2O). Zinc powder is mixed with a gelling agent like polyacrylic acid and a $KOH\text{-}ZnO\text{-}H_2O$ electrolyte.

The positive electrode reaction is:

$$HgO + H_2O + 2e^- \rightarrow Hg + 2OH^-$$

The HgO is usually mixed with a conductive carbon powder, like graphite, to improve the electrical conductivity of the cathode. Mercuric oxide forms Hg as it is reduced. Mercury metal is highly conductive, and so it does lower the internal resistance of the cell. It is also a liquid at normal operating conditions, and it tends to coalesce into droplets and pool in a way that can reduce performance. Additives to the cathode like manganese oxides or silver can minimize Hg pooling.

The overall cell reaction may be written:

$$Zn + HgO + 2KOH + H_2O \rightarrow K_2Zn(OH)_4 + Hg$$

or

$$Zn + HgO \rightarrow ZnO + Hg$$

A cross section of a Zn/HgO button cell is similar to that of a Zn/Ag_2O cell and is shown in Fig. 16.

The initial open circuit potential of Zn/HgO cells is about 1.35 V, but can be between 1.40 V and 1.55 V if MnO_2 is added to the cathode. The voltage remains rather constant throughout discharge (Fig. 8).

Energy densities for Zn/HgO button cells are about 100 Wh kg^{-1} and 470 Wh dm^{-3} [14].

Mercuric oxide cells are not readily available any longer. Government regulatory agencies throughout the world forced these cells from the market because of environmental concerns.

For wearable hearing aids, other cells are available, including Zn/Ag_2O and zinc-air discussed below. Lithium-iodine cells replaced Zn/HgO batteries for implantable cardiac pacemakers in the starting, in the early 1970s. The Zn/HgO cells tended to generate gas which is difficult to manage in an implantable device. Further, actual device longevity – generally in the range of 18–36 months – was lower than the expected 5 or more years [20]. Early battery depletion was usually the cited cause; however, some claimed device malfunction was actually responsible [20].

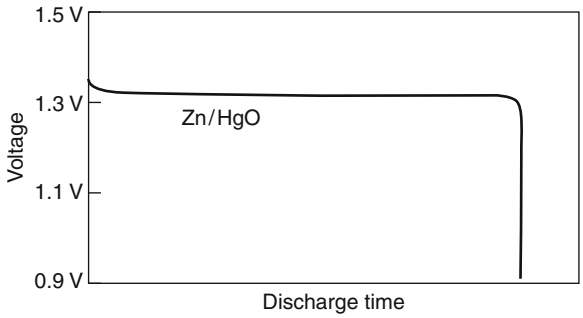

Medical Device Batteries. Figure 8
Discharge voltage behavior for a Zn/HgO cell

Another concern was the voltage characteristics of Zn/HgO cells during use. The end of battery life is difficult to predict because the discharge voltage is flat through battery life then quite rapidly decreases when the battery becomes completely depleted (Fig. 8). The lithium cells developed to take the place of Zn/HgO cells were more reliable, longer lived, and the end of battery life is more easily anticipated.

Implantable Cardioverter Defibrillators and Heart Failure Devices

The implantable cardioverter defibrillator (ICD) is a cardiac pacemaker. It can be used to pace one or both chambers on the right side of the heart. It has an additional feature, though. ICDs can also impart powerful shocks to the heart if it is beating too fast (tachycardia) or goes into ventricular fibrillation. Either condition means that blood cannot be pumped very efficiently, if at all. A number of major clinical studies were done that identified various categories of heart patients who could benefit from the therapies delivered by devices like the ICD.

The cardiac resynchronization therapy defibrillator device (CRT-D) provides the same pacing and defibrillation functions as an ICD, but can also pace the left ventricle for heart failure patients.

The need to deliver energetic shocks to the heart within seconds presents a challenge for battery designers. The battery must provide years of operation for the constant or frequent low power demands of pacing, sensing, and other device functions in the tens of mW range and also the infrequent, but high power, pulses to shock the heart. To deliver a shock, the battery must charge high voltage electrolytic capacitors generally somewhere between 600 and 800 V. The shock is delivered by discharging the capacitors into the heart tissue. Rapidly charging the capacitors requires power on the order of watts. Sometimes multiple shocks are required to get the heart back to a normal rhythm. The balance between energy density for longevity and rate capability for rapidly charging the high voltage capacitors requires careful selection of the chemistry as well as the mechanical design of the battery.

The first clinical studies of ICDs implanted in humans started in 1980 [6] following years of development by Mirowski and coworkers [25]. The first commercially available device was released in 1985. Since then, large clinical studies identified new patient populations that could benefit from ICDs and CRT-Ds.

The first commercial devices were up to 160 cm^3 in volume and needed to be implanted in the abdomen because of their size. Device features were limited and nonprogrammable. Devices typically lasted 2 years before replacement was necessary.

Devices today are about one-fifth the size of the first ICDs. The device industry continued to make improvements by developing smaller devices and while adding more features, such as multichamber pacing, monitoring patient cardiac performance with recorded electrocardiograms, and remote monitoring using radio frequency (RF) telemetry, while providing greater longevity. Devices now are small enough to be implanted in the pectoral area of the chest and can last for 5 or more years.

Improvements in device electronics partially helped to improve device longevities, but new battery systems were also needed. The earliest ICDs were powered by lithium-vanadium pentoxide (Li/V_2O_5) cells [6]. Longevities were insufficient using these cells, so a different battery chemistry, lithium-silver vanadium oxide ($Li/Ag_2V_4O_{11}$ or Li/SVO) was developed [26]. $Li/Ag_2V_4O_{11}$ cell was the cell of choice for ICDs and CRT-D devices since 1985 until recently when other cell chemistries have become more prevalent.

Implantable Cardioverter Defibrillator Batteries

Lithium-Silver Vanadium Oxide The earliest implantable defibrillators used lithium-vanadium oxide (Li/V_2O_5) cells. The chemical stability of this type of cell was unsatisfactory, and they were soon replaced with lithium-silver vanadium oxide ($Li/Ag_2V_4O_{11}$ or Li/SVO) cells. Until only the last few years, $Li/Ag_2V_4O_{11}$ cells were by far the most common cell system used in implantable defibrillators.

Silver vanadium oxide is prepared by the high temperature reaction of V_2O_5 with a silver salt like $AgNO_3$ by a decomposition pathway [27]:

$$2V_2O_5 + 2AgNO_3 \rightarrow Ag_2V_4O_{11} + \text{nitrogen oxides}$$

or with Ag_2O through a combination mechanism [28]:

$$2V_2O_5 + Ag_2O \rightarrow Ag_2V_4O_{11}$$

Reduction to about 1.5 V vs. Li involves up to 7 electrons per mole of $Ag_2V_4O_{11}$:

$$Ag_2V_4O_{11} + 7e^- \rightarrow Ag_2V_4O_{11}{}^{7-}$$

though utilization is less under realistic use conditions.

The $Li/Ag_2V_4O_{11}$ cell discharge reaction occurs in several steps involving sequential reduction of Ag(I) to Ag(O) and V(V) to V(IV) [29]:

$$2Li + Ag^{I}{}_2V^{V}{}_4O_{11} \rightarrow Li_2Ag^0{}_2V^{V}{}_4O_{11}$$

$$4Li + Ag^{I}{}_2V^{V}{}_4O_{11} \rightarrow Li_6Ag^0{}_2V^{IV}{}_4O_{11}$$

Some V(III) may also form, especially if the discharge proceeds beyond $Li_6Ag_2V_4O_{11}$.

Silver(I) is reduced to silver(0) in the first discharge step. Silver metal has a high conductivity, so the resistance of the $Ag_2V_4O_{11}$ positive electrode material decreases rapidly during the early stages of discharge.

The different discharge steps occur at different cell potentials (Fig. 9) that result in a series of voltage steps. The distinct voltage levels offer a means of determining the state of charge for the battery, or at least a set range of states of charge. This, in turn, helps predict battery end of life.

However, a challenge of the $Li/Ag_2V_4O_{11}$ system is the increase in internal resistance that occurs in the middle of discharge. This becomes an issue during the high current demands while charging the high voltage capacitors when it is necessary to deliver high energy shocks to the heart. As the internal resistance increases, the high power pulse voltage decreases (Fig. 9). If the voltage drop is severe enough, it can delay delivery of therapy shocks.

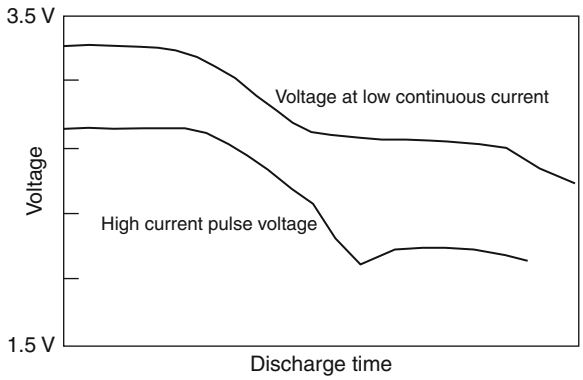

Medical Device Batteries. Figure 9
Low continuous current and high current pulse discharge voltages for a lithium-silver vanadium oxide ($Li/Ag_2V_4O_{11}$) cell

The cause for much of the internal resistance increase is attributed to vanadium that becomes slightly soluble in the middle portion of discharge. The dissolved vanadium diffuses to and deposits on the Li surface. If allowed to build up, the internal resistance increases [30]. The resistance can be lowered by pulling multiple high current pulses from the cell that presumably remove the vanadium as the Li dissolves during the pulse discharge [30].

Silver vanadium oxide is combined with a conductive carbon and a binder like PTFE to make the cathode. The usual electrolyte solution used is lithium hexafluoroarsenate ($LiAsF_6$) in mixed organic solvents, like propylene carbonate and 1,2-dimethoxyethane.

A cross section of a $Li/Ag_2V_4O_{11}$ defibrillator cell is shown in Fig. 10. Energy densities are on the order of about 270 Wh kg^{-1} and 780 Wh dm^{-3} [19].

Lithium-Manganese Dioxide The lithium-manganese dioxide (Li/MnO_2) cell was originally developed and commercialized in the mid-1970s [31] for low power applications such as wrist watches, calculators, and computer memory backup. Later, cells were developed for high power uses like cameras. Today, Li/MnO_2 cells are manufactured in a variety of sizes and configurations for low, medium, and high power consumer; military; and OEM electronic devices. Use of Li/MnO_2 cells in implantable devices was investigated for implantable cardiac pacemakers [32, 33].

Li/MnO_2 cells have a high energy density (230–270 Wh kg^{-1} and 535–520 Wh dm^{-3}) [19] that gives them the ability to provide long life for low current applications. They can also provide high power outputs required for device functions requiring high current levels. This makes Li/MnO_2 an excellent chemistry for implantable cardiac defibrillators. Indeed, Li/MnO_2 cells are now used to power implantable cardiac defibrillators from two manufacturers [34, 35].

The overall cathode reaction may be simply written as:

$$MnO_2 + xLi^+ + xe^- \rightarrow Li_xMnO_2$$

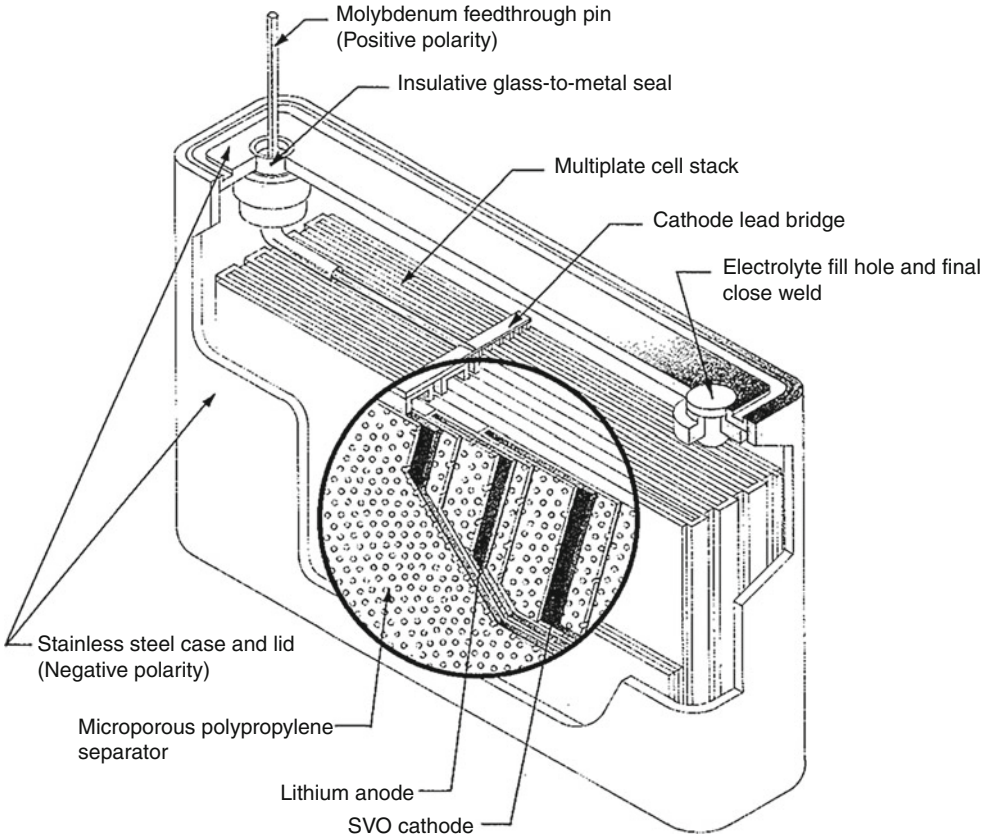

Medical Device Batteries. Figure 10
Cross section of a lithium-silver vanadium oxide ($Li/Ag_2V_4O_{11}$) cell for implantable defibrillators. © Greatbatch, Inc (Reprinted with permission)

The MnO_2 positive material is similar to the type of MnO_2 used in alkaline Zn/MnO_2 cells. However, it must be heat treated at high temperatures, somewhere around 300–400°C to make it suitable for use in lithium cells. Heating removes water and modifies the structure of MnO_2. If this process is not done properly, the Li/MnO_2 cells will generate gas and internal pressure will build up, perhaps to the point where the cells will start to leak.

One or more conductive carbon powders, like acetylene black and graphite, and a binder such as PTFE are added to the MnO_2 to yield the cathode mix.

The discharge voltage of Li/MnO_2 cells exhibits two steps – rather flat during the first part of discharge, but curves downward in the last part of discharge (Fig. 11).

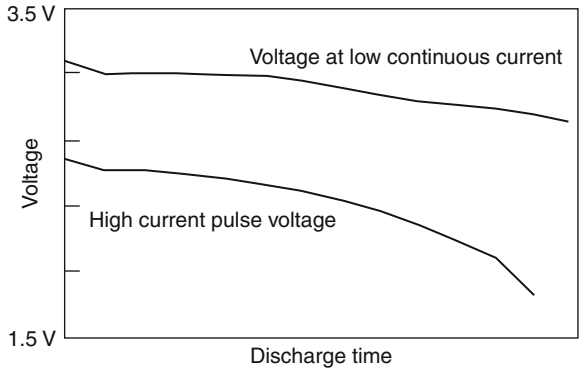

Medical Device Batteries. Figure 11
Low continuous current and high current pulse voltages for a Li/MnO_2 cell

Further, there is no remarkable decrease in pulse voltage as the internal resistance of the cell is relatively low and steady throughout discharge [36, 37].

Lithium-Carbon Monofluoride-Silver Vanadium Oxide One of the challenges of designing batteries for some medical devices is the wide-ranging power requirements to support different device functions. The energy density should be sufficient to provide a long life battery in a small size, yet deliver high power, particularly in ICDs and CRT-Ds.

Pairing two different positive electrode materials – one possessing a high energy density, but a low rate capability and another capable of high rate output, but a lower energy density – is a concept that has been investigated for other applications. It is now starting to be applied to medical device batteries with diverse power requirements.

A straightforward way of accomplishing this (at least from a battery design perspective) is to put together two cells with different rate capabilities, such as Li/I_2 for low rate operations and Li/MnO_2 for high rate functions [38].

Another method is to combine the two positive electrode materials in the same cell. For example, some implantable cardiac defibrillators and pacemakers have started to use lithium cells containing both CF_x (higher energy density but a lower rate capability) and $Ag_2V_4O_{11}$ (high rate capability) positive electrode materials. The CF_x discharges at a voltage that is greater than $Ag_2V_4O_{11}$ throughout most of the cell life, when the device requires only low power from the cell, which is most of the time for implantable defibrillators and pacemakers. When higher power is occasionally required from the cell, such as during RF telemetry or charging high voltage capacitors, the CF_x cannot support the higher load but the $Ag_2V_4O_{11}$ electrode material can.

Dual CF_x-$Ag_2V_4O_{11}$ positive electrodes can be made by mixing the individual CF_x and $Ag_2V_4O_{11}$ materials in the same cathode mix [39] or assembling discrete CF_x and $Ag_2V_4O_{11}$ electrode layers to form the positive electrode [40].

Neuromodulation

Neurostimulators are much like cardiac pacemakers, except they apply small electrical signals to nerve tissue. Devices are available for spinal cord stimulation to manage chronic pain, vagal nerve stimulation to control epilepsy and deep depression, and deep brain stimulation to help relieve symptoms of Parkinson's disease and other neurological disorders.

According to the US Center for Disease Control and Prevention, in 2009 more than 25% of adults, 18 years and older, have experienced low back pain for 24 h or longer [41]. The treatment for chronic pain that does not respond well to drug therapy using implantable electrical neurostimulator devices is growing.

While primary batteries have been used for these devices in the past, the trend is toward using rechargeable batteries to extend the longevity of the device. For implantable devices, the longer the battery lasts, fewer surgeries are required to replace the device, which in turn means lower risks of surgical complications, like infections.

Neuromodulation Batteries

Lithium Ion Secondary, or rechargeable, cells have been used in medical devices for some time. One of the first batteries to be used for implantable cardiac pacemakers was a custom rechargeable nickel-cadmium battery [6]. Systems to recharge the battery transcutaneously using inductive methods were developed starting in the late 1950s [42].

Some implantable medical devices use secondary cells as a way to minimize the number of device replacement surgeries compared to primary cells. An example is neurostimulation for pain management for which primary cells have almost been supplanted entirely by rechargeable cells. The result is longer device longevity in a small size.

Since they were first commercialized in 1991, lithium ion (Li ion) cells now have become the system of choice for high-end portable consumer applications (e.g., laptop and tablet computers, personal multimedia players, and cell phones). They are also seeing increased use in power tools, electric vehicles, and space satellites. Likewise, Li ion cells play an important role in some implantable medical devices.

The chemistry systems in the Li ion cells that are manufactured specifically for implantable medical devices are similar to those developed for consumer applications.

Reliability and safety are utmost concerns when designing Li ion cells for implantable medical devices. They are hermetically sealed and may contain redundant safety features in the batteries (as well as part of the charging circuitry in the device). Also, cell sizes and shapes are often specially designed for a particular device.

The negative electrode material for most Li ion cells is some form of carbon, such as graphite or coke. Cells that use lithium titanate ($Li_4Ti_5O_{12}$) negative electrode material are also available. These cells have cell voltages over 1 V lower than more traditional Li ion cells that use carbon negative electrode materials, though. The advantages are rapid charging, and they can provide thousands of charge–discharge cycles.

Unlike lithium metal, which oxidizes to soluble Li^+ during discharge of lithium primary cells, lithium ions are instead reversibly inserted, or intercalated, between graphite layers during the cell charging process and removed during discharge:

$$C_6 + xLi^+ + xe^- \underset{\text{discharge}}{\overset{\text{charge}}{\rightleftharpoons}} C_6Li_x$$

The value for x is generally between 0 and 1. Carbons intercalated with Li^+ can have electrochemical potentials within tens of millivolts of the lithium metal potential when fully charged.

The structure of the carbon material remains intact after the complete charge and discharge cycle and so is able to repeat the charge–discharge process many times.

Positive electrode materials available for Li ion cells today include metal oxide or phosphate compounds, such as

- Lithium cobalt oxide ($LiCoO_2$)
- Lithium mixed metal oxide, which is a combination of cobalt (Co) and nickel (Ni) and perhaps other metal ions. Examples of mixed metal oxides are $LiNi_{0.8}Co_{0.2}O_2$, $LiNi_{0.8}Co_{0.15}Al_{0.5}O_2$, and $LiNi_{0.33}Co_{0.33}Mn_{0.33}O_2$
- Lithium manganese oxide ($LiMn_2O_4$), sometimes referred to as spinel after its structure type
- Lithium iron phosphate ($LiFePO_4$)

The first commercialized Li ion cells used $LiCoO_2$ as the positive electrode material. It consists of Li^+ inserted between the cobalt and oxygen layers. The charge and discharge reactions are similar to carbon in that Li^+ is removed and inserted leaving the basic $LiCoO_2$ unchanged:

$$LiCoO_2 \underset{\text{discharge}}{\overset{\text{charge}}{\rightleftharpoons}} Li_{1-x}CO_2 + xLi^+ + xe^-$$

where x lies somewhere between 0 and 1.

The overall cell reactions are:

$$C_6 + LiCoO_2 \underset{\text{discharge}}{\overset{\text{charge}}{\rightleftharpoons}} Li_xC_6 + Li_{1-x}CoO_2$$

Some positive electrode materials have three-dimensional rather than layered structures. $LiMn_2O_4$ and $LiFePO_4$ are in this category. Lithium ions are inserted in tunnels rather than between layers.

Positive electrode materials are generally mixed with a conductive carbon powder and a polymer binder. Commonly used binders are polyvinylidene fluoride (PVDF) and a PVDF copolymer with hexafluorpropylene (PVDF-HFP). The positive electrode mix is coated as a slurry onto a thin aluminum foil current collector while the carbon negative electrode material, often using the same binders, is coated onto a thin copper foil current collector.

Cylindrical or prismatic spiral wound cells are assembled by winding the positive and negative electrodes together with a porous membrane separator between them. The electrolyte solution is typically a mixture of organic solvents containing a lithium salt, like lithium hexafluorophosphate ($LiPF_6$).

A related Li ion cell type is the Li ion polymer cell that uses a polymer gel electrolyte. Li ion polymer cells are often designed as flat prismatic cells and can be made quite thin.

The discharge voltage can be sloped or flat depending on the type of cell chemistry used (for example, see Fig. 12).

Maximum voltages at the end of charge are usually in the range of 3.6–4.2 V depending on the chemistry. Energy densities can be as high as 240 Wh kg^{-1} and 640 Wh dm^{-3}.

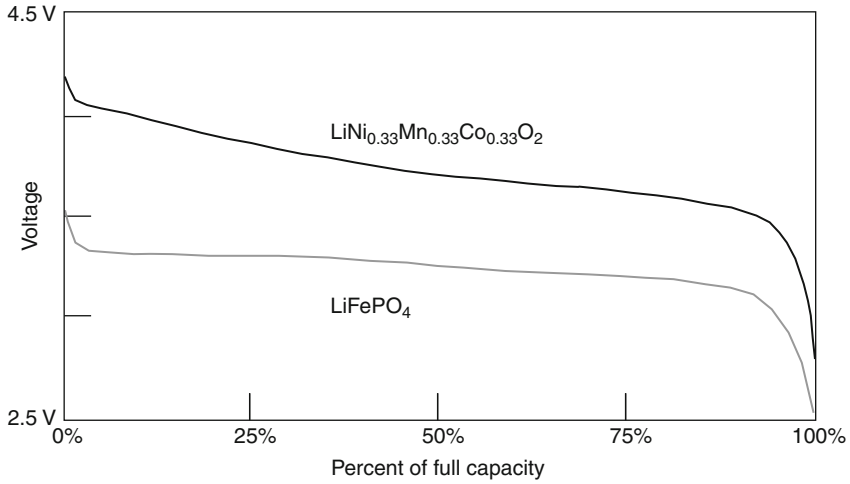

Medical Device Batteries. Figure 12
Discharge voltage for two types of Li ion cells

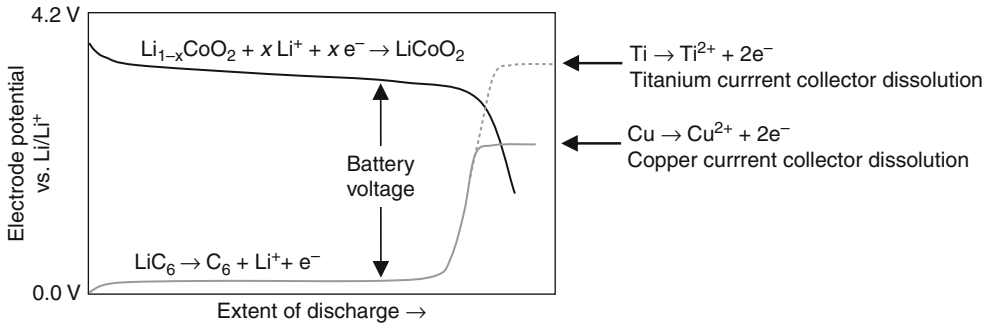

Medical Device Batteries. Figure 13
Individual electrode potentials for a lithium ion cell

Developers of secondary cells for implantable medical devices must consider the possibility of what happens when the battery is not charged for whatever reason in a timely fashion. If the cell becomes over discharged and its voltage is allowed to go below a certain threshold, the cell may not fully recover once it is charged and performance may be reduced.

One reason cell performance may be compromised in the event of the issues with typical Li ion cells is the use of a copper (Cu) current collector for the negative electrode. As a cell is discharged, the positive electrode potential decreases and the negative electrode potential increases. When the cell voltage drops to about 0 V, the potential of the negative electrode is the same as the positive electrode when measured against a reference electrode like Li. If discharge continues, the negative electrode potential could reach the potential at which the Cu current collector oxidizes or corrodes and copper ions dissolve (Fig. 13) [43]. This can lead to loss of cell capacity and degrade cell function. For this reason, the cell anode to cathode capacity balance is a critical design consideration. Cell performance is limited by the cathode capacity.

Selection of a positive electrode material that discharges at a lower voltage can minimize this issue, but an alternative is to replace the Cu current collector with a metal that corrodes at a more positive potential, such as titanium (Ti) [43]. In this case, the capacity of a cell that is held at 0 V for prolonged periods of time can retain more of its capacity [44].

Hearing Loss

The US National Institutes of Health (NIH) reports that 36 million adults in the US report some level of hearing loss [45]. The World Health Organization puts the number at 278 million worldwide in 2005 [46]. Up to 0.3% of children born in the USA are deaf or hard of hearing [45].

Hearing aids are small devices that amplify the sounds picked up by a tiny microphone to enable the hearing-impaired to function. There are several types of hearing aid designs: behind the ear, in the ear, and completely in the canal. NIH finds that 1 out of 5 people in the USA who could benefit from a hearing aid actually wears one [45]. Worldwide, it is less than 1 out of 40 people [46].

The first portable radios operated by batteries were developed in the 1930s. The invention of the first portable hearing aids followed soon after in 1937 [47]. It could be carried by the hearing aid user, but since it used vacuum tubes it was the size of a lunch box. Wearable hearing aids became possible with the development of smaller electronic components that replaced vacuum tubes and the commercialization of small zinc-mercury oxide cells after World War II.

Most hearing aids today run on zinc-air cells because they have a high energy density and so last longer. Depending on the hearing needs of the user and the type of hearing aid, batteries may last from a few days to over 1 month. Recently, rechargeable nickel-metal hydride and zinc-silver oxide cells hearing aid batteries have been introduced.

Hearing Aid Batteries

Zinc-Air The design of a zinc-air cell is different than most other battery types. Nearly all cells store all of the active materials required for the cell to function – negative and positive electrode materials, electrolyte – within a battery case or housing.

However, the positive electrode material for zinc-air cells is atmospheric oxygen, O_2. A thin electrode, or cathode, similar to a fuel cell electrode that provides a site for O_2 to be reduced during cell discharge is all that is necessary. As a result, there is more space within the cell that can be loaded with more of the zinc (Zn) negative electrode material.

The combination of a practically unlimited source of O_2 from the air with more available space inside the cell for additional Zn results in a very high energy density cell. Zinc-air button cells have the highest energy density of all commonly available button cells – up to 370 Wh kg^{-1} and 1,300 Wh dm^{-3} [14]. Of course, using atmospheric O_2 means zinc-air cells cannot be used for implantable devices.

Air was known to improve cell performance early in the nineteenth century, even though the electrochemical mechanism was unknown. Cells that used atmospheric O_2 as the positive electrode material were built in the late 1800s. Practical advances in 1930s through the 1950s made zinc-air cells commercially viable. Prismatic zinc-air cells were developed to operate hearing aids in the early 1950s [48, 49]. The early hearing aid cells were close to 22 cm^3 in volume with energy densities of about 200 Wh kg^{-1} [50].

Improvements in hearing aid electronics resulted in smaller devices that required less power. Lower power demands and advances in battery technology lead to smaller batteries, as well. Typical primary hearing aid cells today are small button cells that range from 5.8 mm in diameter and 2.15 mm in height to 11.5 mm in diameter and 5.4 mm in height (Table 1).

The largest hearing aid cell today is less than about 0.6 cm^3 – almost forty times less volume than the first zinc-air hearing aid batteries.

The zinc is in powder form that is mixed with a compound like polyacrylic acid or sodium carboxymethyl cellulose that is chemically stable and forms a gel in the alkaline electrolyte solution. The gelled anode is more stable mechanically.

The discharge reaction of Zn in aqueous potassium hydroxide (KOH) electrolyte solutions is somewhat complex, but may be simply written as:

$$Zn + 4OH^- \rightarrow Zn(OH)_4{}^{2-} + 2e^-$$

where the zincate product, $Zn(OH)_4{}^{2-}$, is dissolved in the electrolyte. Under certain conditions, especially as the battery is depleted, zinc ions can precipitate as zinc oxide (ZnO):

$$Zn + 2OH^- \rightarrow ZnO + H_2O + 2e^-$$

Typical alkaline, or basic, electrolyte solutions are comprised of 20–50% KOH (typically 28%) by weight

Medical Device Batteries. Table 1 Common primary hearing aid button cell sizes. IEC is the International Electrotechnical Commission and ANSI is the American National Standards Institute

Size designation			Dimensions		Available cells types (IEC, ANSI)
IEC	ANSI	Common	Diameter (mm)	Height (mm)	
63	7012ZD	5	5.8	2.15	Zinc-air (PR63, 7012ZD)
70	7005ZD	10	5.8	3.6	Zinc-air (PR63, 7012ZD)
	1191SO				Zinc-silver oxide (SR70, 1191SO)
41	7002ZD	312	7.9	3.6	Zinc-air (PR41, 7002ZD)
	1135SO				Zinc-silver oxide (SR41, 1135SO)
48	7000ZD	13	7.9	5.4	Zinc-air (PR48, 7000ZD)
	1137SO				Zinc-silver oxide (SR48, 1137SO)
44	7003ZD	675	11.6	5.4	Zinc-air (PR44, 7003ZD)
	1131SO				Zinc-silver oxide (SR44, 1131SO)

in water. A small amount of ZnO, between a few percent up to saturation levels, is added to the KOH electrolyte to help reduce Zn self-discharge. ZnO dissolves to form potassium zincate in the electrolyte.

Zinc is used as the negative electrode material in aqueous primary cells because it has a high energy density. However, Zn is prone to corrosion, particularly when certain impurities are present, that can result in decreased battery life and compromised performance. A common contaminant is iron. When it comes into contact with the Zn and becomes galvanically coupled with it, hydrogen gas (H_2) will form at the iron surface from the reduction of water in the electrolyte. Zinc is oxidized and dissolves into the electrolyte as zincate or precipitates as ZnO.

If Zn corrosion proceeds at a sufficiently high rate for long periods of time, the gas pressure within the cell can build until the seals start to leak gas and electrolyte. This was a common problem in early cardiac pacemakers using Zn/HgO batteries. The gassing cannot be entirely avoided, but the corrosion reactions can be slowed and whatever gas is formed can be controlled to maximize the shelf life and minimize the loss of cell performance.

Alloying Zn with mercury metal to form an amalgam increases the electrochemical overpotential for hydrogen gas formation on Zn. Zinc amalgams in the range of 2–15% Hg by weight of Zn were common.

Since mercury (Hg) and its compounds are toxic, beginning in the early 1990s the European Union, followed by the United States, required battery manufacturers to reduce [51] and then eliminate [52] Hg added to batteries. This requirement addressed genuine concerns that cells discarded in landfills could release Hg into the environment.

Use of battery materials with higher purity levels (including Zn, electrolyte, and cathode), different alloying elements, seals that can withstand higher internal pressures, and cleaner manufacturing processes enabled the elimination of added Hg in batteries.

The positive electrode reaction involves the reduction of O_2 and proceeds in two basic steps:

$$O_2 + H_2O + 2e^- \rightarrow HO_2^- + OH^-$$

and then

$$2HO_2^- \rightarrow 2OH^- + O_2.$$

where HO_2^- is the hydrogen peroxide ion. The second step acts to curb the oxygen discharge reaction, so a catalyst, usually manganese dioxide, may be used to accelerate peroxide decomposition.

The overall cell reaction is:

$$2Zn + O_2 + 4KOH + 2H_2O \rightarrow 2K_2Zn(OH)_4$$

Or

$$2Zn + O_2 \rightarrow 2ZnO$$

The reduction of O_2 is thermodynamically favorable, but the reaction kinetics are relatively slow. Using an electrode material with a high surface area, such as activated carbon powder, can overcome the slow oxygen reduction kinetics by presenting a large number of sites at which O_2 can be reduced. A small amount of a conductive carbon material may also be added to increase the electrical conductivity of the cathode.

While it is important to maximize the electrode area accessible to O_2, the cathode must also allow for contact with the electrolyte. A three-phase boundary comprised of O_2, electrolyte and carbon with catalyst is central to the proper functioning of an air electrode. Maintaining a balance between access to atmospheric O_2 and electrolyte solution is achieved by adequately dispersing just the right amount of a hydrophobic material, polytetrafluoroethlyene (PTFE or Teflon®), in the carbon powder mix. Too little PTFE or it is not dispersed well enough and the electrolyte solution could saturate the cathode. This reduces the area at which O_2 can react with a resulting loss of performance. Too much PTFE and the electrolyte will not sufficiently wet the cathode. Again, this limits battery performance.

A zinc-air cathode must provide a surface at which O_2 can be reduced during battery discharge while not being consumed itself during cell discharge. The zinc-air cathode of today is comprised of multiple layers, each serving an important function. A carbon mix (activated carbon, conductive carbon, and PTFE) is applied to a nickel screen current collector that carries electrons to the cathode during cell discharge. There are two sides to an air cathode – the air side and the electrolyte side. The air side is laminated with a porous PTFE membrane. A polymeric separator sheet is pressed on the electrolyte.

Important considerations for zinc-air cells are air and water management. Air must be allowed to enter the zinc-air cell, which is done by providing holes in the battery can near the cathode (see Fig. 14). There must be an adequate number of holes of a sufficient size to allow enough air to enter the cell such that the discharge reaction is not impeded by lack of O_2. An air diffusion layer may be included just inside the cell to disperse the air more uniformly.

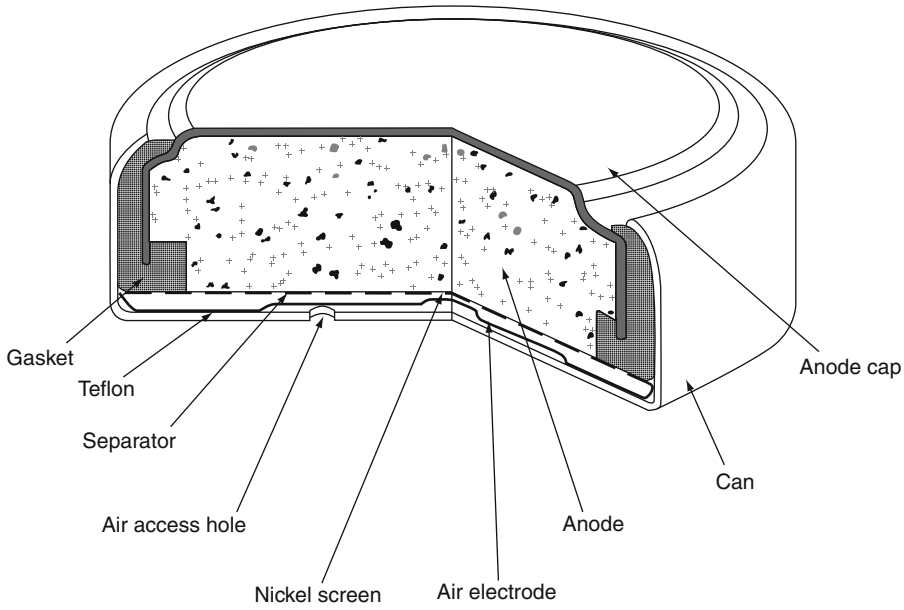

Medical Device Batteries. Figure 14
Cross section illustrating the main components of a zinc-air cathode. © Eveready Battery Company, Inc (Reprinted with permission)

The advantage of zinc-air cells also presents a big challenge for battery designers. Remaining open to the atmosphere renders zinc-air cells exposed to detrimental environmental conditions, especially humidity. Water in humid air can be absorbed by the basic electrolyte solution diluting it and subsequently flooding the cathode. Arid air may evaporate water from the electrolyte and dry the cathode. Both conditions lead to reduced cell performance and battery life. Carbon dioxide in the air can enter the cell, react with the basic electrolyte solution and precipitate carbonates, also decreasing performance.

A simple way to mitigate the effects of environmental exposure is to seal the holes until the cell is needed to operate. The holes are covered, usually with an adhesive tab, after manufacture to curtail exposure to the atmosphere during shipping and storage. The seal is removed prior to use, air enters the cell and it is ready for use. Hearing aid users can also replace the adhesive tab between uses, overnight while sleeping for example, to extend cell life.

The initial open circuit potential of the zinc-air cell is about 1.45 V. The voltage of a zinc-air cell is mostly constant throughout discharge (Fig. 15).

Zinc-Silver Oxide Zinc-silver oxide (Zn/Ag_2O) cells are used in medical applications like hearing aids, but also military, aerospace, watches, cameras, and calculators. Early implanted electrical bone growth stimulators [53] for fracture healing and spinal fusion used Zn/Ag_2O batteries. The Zn/Ag_2O cell is one of the alternatives to Zn/HgO cells (see above) and is used in applications where high energy and power density is required.

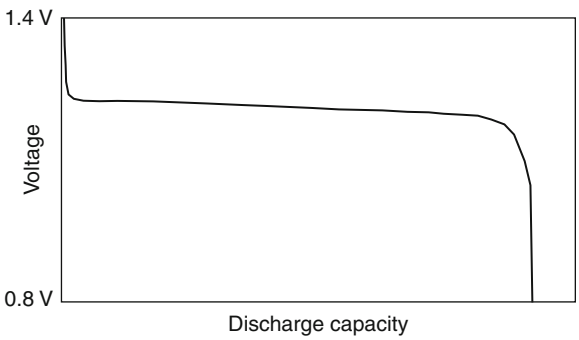

Medical Device Batteries. Figure 15
Discharge voltage behavior for a zinc-air cell

Originally dating back to 1883, [54] alkaline Zn/Ag_2O cells were eventually developed into commercially practical cells in the early 1960s.

The negative electrode material is zinc powder in a gelled $KOH\text{-}ZnO\text{-}H_2O$ alkaline electrolyte solution. NaOH can be used instead of KOH for lower power applications.

The positive electrode reaction is:

$$Ag_2O + H_2O + 2e^- \rightarrow 2Ag + 2OH^-$$

The cathode pellet contains Ag_2O powder and 1–5% of a conductive carbon powder like graphite, to reduce internal resistance and provide good contact to all of the active silver oxide particles, mixed with a PTFE binder to maintain the mechanical integrity of the pellet.

A disadvantage of Ag_2O is its solubility in alkaline electrolyte. Silver ions dissolve into basic electrolyte solutions. The solubility of silver ions (Ag^+) from Ag_2O is on the order of 10^{-4} mol dm^{-3} in concentrated KOH [55]. Dissolved Ag^+ diffuses to the Zn and deposits there as Ag. If this continues, the Ag deposit will grow as dendrites through the separator and eventually create an internal short circuit by directly bridging the positive and negative electrode materials [56]. A big advance toward making this cell chemistry practical came when Henri André developed a cellophane separator that minimized diffusion of Ag^+ through the separator which mitigated this issue [54].

The overall cell reaction is:

$$Zn + Ag_2O + 2KOH + H_2O \rightarrow K_2Zn(OH)_4 + 2Ag$$

or

$$Zn + Ag_2O \rightarrow ZnO + 2Ag$$

The cross section of a Zn/Ag_2O button cell is pictured in Fig. 16.

The open circuit potential of Zn/Ag_2O cells is about 1.60 V and voltage remains relatively constant throughout discharge as seen in Fig. 17. Energy density for Zn/Ag_2O button cells is about 135 Wh kg^{-1} or 530 Wh dm^{-3} [14].

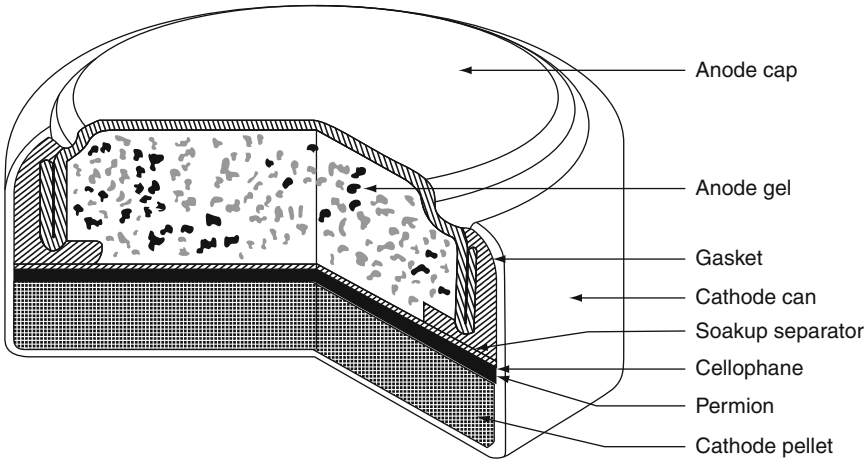

Medical Device Batteries. Figure 16
Cross section illustrating the main components of a Zn/Ag_2O button cell. © Eveready Battery Company, Inc (Reprinted with permission)

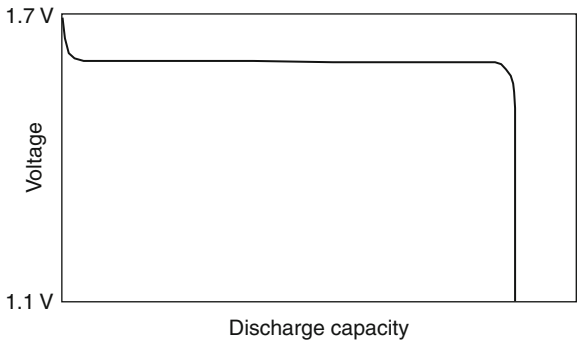

Medical Device Batteries. Figure 17
Discharge voltage behavior for a Zn/Ag_2O cell

Future Directions

A wide variety of wearable, implantable, and even ingestible medical devices are under development or in the early stages of clinical use. Here are just a few.

There is an ongoing need to treat various heart conditions, hearing loss, and chronic pain. Improvements to electronic circuit components and designs, along with the batteries that make them function, will continue. New therapies and device features will be enabled by new battery technologies.

Additionally, there are many emerging indications for wearable or implantable medical devices, particularly new neuromodulation applications such as deep brain stimulation for various movement and neurological disorders [57] and occipital nerve stimulation to treat migraine and cluster headaches [58]. Implantable visual prostheses to restore sight are also under development.

There are ingestible devices for measurement of body core temperature and other sensors to help diagnose gastrointestinal tract disorders. Implantable sensors [59, 60], such as those for blood pH, oxygen, and glucose, along with remote telemetry, are expected to advance as well.

Bibliography

Primary Literature

1. Althaus J (1860) A treatise on medical electricity, theoretical and practical. Lindsay and Blakiston, Philadelphia, pp v–vi
2. Tibbits H (1873) A handbook of medical electricity. P. Blakiston, Son and Co., Philadelphia, p v
3. Steavenson WE, Jones HL (1892) Medical electricity. A practical handbook for students and practioners. P. Blakiston, Son and Co., Philadelphia, pp v–vi
4. Mohrman DE, Heller LJ (1996) Cardiovascular physiology, 4th edn. McGraw-Hill, New York
5. Lillehei CW, Gott VL, Hodges PC, Long DM, Bakken EE (1960) Transistor pacemaker for treatment of complete atrioventricular dissociation. JAMA 172:2006–2010
6. Greatbatch W, Holmes CF (1991) History of implantable devices. IEEE Eng Med Biol:38–41,49

7. Chardack W, Gage A, Greatbatch W (1960) A transistorized, self-contained, implantable pacemaker for the long-term correction of complete heart block. Surgery 48:543
8. Furman S (2003) The early history of cardiac pacing. Pacing Clin Electrophysiol 26:2023–2032
9. Liang CC, Holmes CF (1980) Lithium pacemaker batteries – an overview. In: Owens BB, Margalit N (eds) Proceedings of the symposia on power sources for biomedical implantable applications and ambient temperature batteries, vol 80–84, pp 27–33
10. Bilitch M, Parsonnet V, Furman S (1980) Clinical assessment of pacemaker power sources. In: Owens BB, Margalit N (eds) Proceedings of the symposia on power sources for biomedical implantable applications and ambient temperature batteries, vol 80–84, pp 18–26
11. Greatbatch W (1984) Pacemaker power sources. IEEE Eng Med Biol Mag:15–19
12. Greatbatch W, Lee JH, Mathias W, Eldridge M, Moser JR, Schneider AA (1971) The solid-state lithium battery: a new improved chemical power source for implantable cardiac pacemakers. IEEE Trans BioMed Eng BME 18:317–324
13. Kelly RG, Moran PJ (1987) The rate limiting mechanism of Li/I_2 (PV2P) batteries. J Electrochem Soc 134:25–30
14. Linden D (2002) Ch 7 Primary batteries – introduction. In: Linden D, Reddy TB (eds) Handbook of batteries, 3rd edn. McGraw-Hill, New York
15. Shellock FG, Hatfield M, Simon BJ, Block S, Wamboldt J, Starewicz PM, Punchard WFB (2000) Implantable spinal fusion stimulator: assessment of MR safety and artifacts. J Mag Res Imaging 12:214–223
16. Maurer J, Savvas E (2010) The Esteem system: a totally implantable hearing device. In: Böheim K (ed) Active middle ear implants. S Karger AG, Basel, p 59
17. Root MJ, Dumas R, Yazami R, Hamwi A (2001) The effect of carbon starting material on carbon fluoride synthesized at room temperature – characterization and electrochemistry. J Electrochem Soc 148:A339–A345
18. Spellman PJ, Dittberner KL, Pilarzyk JG, Root MJ (2000) Application of Li/CF_x system in portable electronics. In: Osaka T, Datta M (eds) Energy storage systems for electronics. Gordon and Breach Science, Amsterdam, pp 131–152
19. Linden D, Reddy TB (2002) Ch 14 Lithium batteries. In: Linden D, Reddy TB (eds) Handbook of batteries, 3rd edn. McGraw-Hill, New York
20. Parker B (1978) Obituary: a vindication of the zinc-mercury pacemaker battery. Pacing Clin Electrophysiol 1:148–149
21. Clarke CL (1884) US patent 298,175
22. Brønsted JN (1917) US patent 1,219,074
23. Friedman M, McCauley CE (1947) The Ruben cell – a new alkaline primary dry cell battery. Trans Electrochem Soc 92:195–215
24. Ruben S (1978) The evolution of electric batteries in response to industrial needs. Dorrance, Philadelphia, Ch VI
25. Mirowski M, Reid PR, Mower MM, Watkins L, Gott VL, Schauble JF, Langer A, Heilman MS, Kolenik SA, Fischell RE, Weisfeldt ML (1980) Termination of malignant ventricular arrhytmias with an implanted automatic defibrillator in human beings. N Engl J Med 303:322–324
26. Liang CC, Bolster ME, Murphy RM (1982) US patent 4,310,609
27. Leising RA, Takeuchi ES (1993) Solid-state cathode materials for lithium batteries:effect of synthesis temperature on the physical and electrochemical properties of silver vanadium oxide. Chem Mater 5:738–742
28. Crespi A (1993) US patent 5,221,453
29. Leising RA, Thiebolt WC, Takeuchi ES (1994) Solid state characterization of reduced silver vanadium oxide from the Li/SVO discharge reaction. Inorg Chem 33:5733–5740
30. Syracuse K, Waite N, Gan H, Takeuchi ES (2006) US patent 6,982,543
31. Ikeda H, Saito T, Tamura H (1975) Manganese dioxide as cathodes for lithium batteries. In: Proceedings of the manganese dioxide symposium, vol 1. The Electrochemical Society, Cleveland, pp 384–401
32. Gerbier G, Lehman G (1980) Mangalith: a new lithium pacemaker battery. In: Owens BB, Margalit N (eds) Proceedings of the symposia on power sources for biomedical implantable applications and ambient temperature batteries, vol 80–84. The Electrochemical Society, Pennington, pp 136–143
33. Merritt DR, Schmidt CL (1993) Impedance modeling of the lithium/manganese dioxide battery. In: Surampudi S, Koch VR (eds) Proceedings of the symposium on lithium batteries, vol 93–24. The Electrochemical Society, Pennington, pp 138–145
34. Drews J, Fehrmann G, Staub R, Wolf R (2001) Primary batteries for implantable pacemakers and defibrillators. J Power Sources 97–98:747–749
35. Root MJ (2008) Implantable cardiac rhythm device batteries. J Cardiovasc Trans Res 1:254–257
36. O'Phelan MJ, Victor TG, Haasl BJ, Swanson LD, Kavanagh RJ, Barr AG, Dillon RM (2009) US patent 7,479,349
37. Root MJ (2010) Lithium-manganese dioxide cells for implantable defibrillators – discharge voltage models. J Power Sources 195:5089–5093
38. Drews J, Wolf R, Fehrmann G, Straub R (1999) Development of a hybrid battery system for an implantable biomedical device, especially a defibrillator/cardioverter (ICD). J Power Sources 80:107–111
39. Weiss DJ, Cretzmeyer JW, Crespi AM, Howard WG, Skarstad PM (1993) US patent 5,180,642
40. Spillman DM, Takeuchi ES (1999) US patent 5,935,724
41. National Center for Health Statistics (2010) Health, United States, 2009. US Department of Health and Human Services Center for Disease Control and Prevention, Publication 2010–1232, Hyattsville, p 261
42. Fischell RE, Schulman JH (1976) A rechargeable power system for cardiac pacemakers. Proc 11th IECEC, pp 163–168
43. Tsukamoto H, Kishiyama C, Nagata M, Nakahara H, Piao T (2003) US patent 6,596,439
44. Kishiyama C, Nagata M, Piao T, Dodd J, Lam P, Tsukamoto H (2003) 204th Electrochemical Society Meeting, abstract 425

45. http://wwwnidcdnihgov/health/statistics/quickhtm. Accessed 27 Dec 2010
46. http://wwwwhoint/mediacentre/factsheets/fs300/en/indexhtml. Accessed 3 Jan 2011
47. Wengel AM (1940) US patent 2,192,669
48. Marsal PA, Fox RP (1952) US patent 2,597,116
49. Schumacher EA, Bennett RJ (1952) US patent 2,597,119
50. Brodd RJ, Kozawa A, Kordesch KV (1978) Primary batteries 1951–1976. J Electrochem Soc 125:271C–282C
51. Council Directive 91/157/EEC of 18 March 1991 on Batteries and Accumulators Containing Certain Dangerous Substances
52. "NEMA announces battery industry commitment to eliminating mercury in button cells". https://wwwnemaorg/media/pr/20060302acfm. Accessed 28 Dec 2010
53. Paterson DC, Lewis GN, Cass CA (1980) Treatment of delayed union and non-union with an implanted direct current stimulator. Clin Orthop Relat Res 148:117–128
54. Howard PL, Fleischer A (1971) Ch 1. Milestones in the electrochemistry of zinc-silver oxide batteries. In: Fleischer A, Lander JJ (eds) Zinc-silver oxide batteries. Wiley, New York
55. Amlie RF, Reutschi P (1961) J Electrochem Soc 108:813–819
56. Himy A (1986) Silver-zinc battery phenomena and design principles. Vantage, New York, p 7
57. Pereira EAC, Aziz TZ (2006) Surgical insights into Parkinson's disease. J R Soc Med 99:238–244
58. Schwedt TJ, Dodick DW, Trentman TL, Zimmerman RS (2006) Occipital nerve stimulation for chronic cluster headache and hemicrania continua: pain relief and persistence of autonomic features. Cephalagia 26:1025–1027
59. Van Laerhoven K, Lo BPL, Ng JWP, Thiemjarus S, King R, Kwan S, Gellersen H-W, Sloman M, Wells OW, Needham P, Peters N, Darzi A, Toumazou C, Yang G-Z (2004) Medical healthcare monitoring with wearable and implantable sensors. Proc 3rd international workshop on ubiquitous computing for healthcare applications. http://www.pervasivehealthcare.com/ubicomp2004/papers/final_papers/laerhoven.pdf
60. Fletter PC, Majerus S, Cong P, Damaser MS, Ko WH, Young DJ, Garverick SL (2009) Wireless micromanometer system for chronic bladder pressure monitoring. 6th international conference on networked sensing systems, IEEE, pp 1–4

Books and Reviews

Gabano J-P (ed) (1983) Lithium batteries. Academic, London
Holmes CF (1994) Implantable lithium power sources. In: Pistoia G (ed) Lithium batteries. Elsevier, Amsterdam, pp 377–416
Owens BB (ed) (1986) Batteries for implantable biomedical devices. Plenum, New York
Reddy TB (ed) (2010) Linden's handbook of batteries, 4th edn. McGraw-Hill, New York
Root M (2010) The TAB battery book. McGraw-Hill, New York
Schlesinger H (2010) The battery. HarperCollins, New York
Takeuchi ES, Leising RA, Spillman DM, Rubino R, Gan H, Takeuchi KJ, Marschilok AC (2004) Lithium batteries for medical applications. In: Nazri G-A, Pistoia G (eds) Lithium batteries science and technology. Kluwer, Boston, pp 686–700
Untereker DF, Crespi AM, Rorvick A, Schmidt CL, Skarstad PM (2007) Power systems for implantable pacemakers, cardioverters, and defibrillators. In: Ellenbogen KA, Kay GN, Lau C-P, Wilkoff BL (eds) Clinical cardiac pacing and defibrillation, 3rd edn. Saunders, Philadelphia, pp 235–259
Vincent C, Scrosati B (1997) Modern batteries, 2nd edn. Arnold, London

Medicinal Plants, Engineering of Secondary Metabolites in Cell Cultures

Suvi T. Häkkinen, Anneli Ritala, Heiko Rischer, K.-M. Oksman-Caldentey
VTT Technical Research Centre of Finland, Espoo, Finland

Article Outline

Glossary
Definition of the Subject
Introduction
High-Value Products from Medicinal Plants
Enhancing the Production by Classical Optimization
Metabolic Engineering
Future Directions
Acknowledgments
Bibliography

M

Glossary

Bioreactor A fermentor in which plant cell cultures can be cultivated in sterile, controlled, and contained condition for biotechnological production of cell biomass and/or particular protein or small molecule.

Medicinal plants Plants that are used for medicinal purposes; whole plants or specific plant organs or compounds derived thereof can be utilized.

Metabolic engineering A process to understand metabolic pathways; a targeted alteration of metabolic pathways with the aim of improved yield, quality, and/or spectrum of produced metabolites.

Plant cell culture Process where plant cells are cultivated under controlled conditions; may consist of differentiated tissues or organs (e.g., shoots, roots,

embryos, stems) or undifferentiated cells (e.g., callus, suspension cultures).

Secondary metabolites Low molecular weight compounds with enormous chemical diversity often found in plants in small amounts essential for plants' defense system; many secondary metabolites are used as pharmaceuticals, dyes, flavors, and fragrances by humans.

Transgene A gene that has been transferred from one organism to another.

Definition of the Subject

Plants are the most excellent designers and producers of a variety of small compounds that are beneficial to mankind as foods, medicines, and industrial raw materials. The use of medicinal plants for human health dates back to ancient history of mankind. The first written document of the use of medicinal plants can be found in Papyrus Ebers (1800 BC). Even if the use of certain medicinal plants was known to treat certain diseases – often using the trial-and-error approach – it is only less than 200 years ago the isolation of the first active chemical constituent (secondary metabolite) responsible for its pharmacological effect occurred. Today, many plant-derived compounds are used in pharmaceutical industry, and plants also serve as an important source for new lead compounds.

Many plants containing high-value secondary metabolites are difficult to cultivate or are becoming endangered because of the overharvesting. Furthermore, the chemical synthesis of plant-derived compounds is often not economically feasible due to their highly complex structures and the specific stereochemical requirements of the compounds. The biotechnological production of valuable secondary metabolites in plant cell or organ cultures is an attractive alternative to the extraction of whole plant material. However, the use of plant cell or organ cultures has had only limited commercial success so far. This is explained by the empirical nature of selecting high-yielding, stable cultures and the lack of understanding of how secondary metabolites are synthesized or how their synthesis is regulated.

Introduction

It has been estimated that there are at least 400,000 higher plant species in the world of which only about 10% are characterized chemically to certain extent [1]. There is no doubt that the chemical diversity of plants is much greater than any chemical library made by humans, and thus the plant kingdom represents an enormous reservoir of pharmacologically valuable molecules waiting to be discovered. Plants are thus excellent organic chemists in nature and constantly respond to environmental changes by adjusting their capacity to produce natural products. Functional genomics may open entirely new avenues to screen unexplored medicinal plant species for their pharmacological value. Many pharmaceutical companies have now renewed their interest on plant-derived compounds due to too high expectations on combinatorial chemistry or computational drug design to obtain new drug leads during the past decades [2, 3].

Many secondary metabolites of industrial value are complex in their structures making chemical synthesis very challenging and expensive. Moreover, plants contain usually very low contents of these compounds, and therefore other production processes are essential to be developed. Biotechnological production using plant cells as real green factories is a very promising technology, but currently there are still many limiting factors, mainly related to our poor understanding how the plants synthesize these high-value compounds and how the synthesis is regulated.

In the following sections, an overview is given how secondary metabolites are produced in plant and tissue cultures, how the production can be enhanced by classical optimization methods, and what metabolic engineering has to offer today and in the future. Spectacular advances in plant genomics and metabolite profiling offer unprecedented possibilities to explore the extraordinary complexity of the plant biochemical capacity. State-of-the-art genomics tools can be used to engineer the enhanced production of known target metabolites or to synthesize entire novel compounds by the so-called combinatorial biochemistry in cultivated plant cells. Finally, some future perspectives are given for novel techniques and tools that are just now emerging.

High-Value Products from Medicinal Plants

Medicinal Plants

Many plants such as crops play a central role in our everyday diet. The nutritional value of edible plants

and their constituents has been studied for decades. Besides the edible plants, there is a huge variety of toxic plants in the plant kingdom. These include, for example, many alkaloid or terpene containing medicinal plants such as *Atropa belladonna*, *Camptotheca acuminata*, *Capsicum annuum*, *Catharanthus roseus*, *Erythroxylum coca*, *Papaver somniferum*, *Cannabis sativa*, *Artemisia annua*, and *Taxus* species – just to name a couple of them. These plants have been and still are an important source of pharmaceuticals. Molecules derived from medicinal plants make up a sizable proportion of known drugs currently available on the market. These include compounds such as morphine, codeine, and several anticancer drugs such as paclitaxel, vincristine, and vinblastine, the monetary value of which is very high. In Western medicine, over 25% of prescription drugs sold in pharmacies contain at least one active principle which is directly or indirectly (via semi-synthesis) a natural product. This number does not include the over-the-counter sold drugs or pure phytopharmaceuticals.

According to WHO, 11% of the current 252 drugs considered essential for humans are exclusively derived from flowering plants. Furthermore, plants are also important source of new drug lead compounds. During the past 25 years, 1,010 new drug entities (NDEs) were introduced to the market; 27% of them were either natural products or derived from natural products as semi-synthetic derivatives [3]. In addition, 15% of the drugs were synthesized after the molecule was first discovered from natural resources. Table 1 shows the origin of the 458 NDEs representing the four major therapy groups with anti-infectives (antibacterial, antiviral, antifungal, and antiparasitic), anticancer, antihypertensive, or anti-inflammatory activities discovered between 1981 and 2006. It is remarkable that over 68% of all antibacterial compounds and 51% of all anticancer drugs were directly or indirectly derived from natural resources. Natural sources will undoubtedly continue to play a prominent role in the discovery of pharmaceuticals in the future.

Secondary Metabolism in Plants

Secondary metabolites are low molecular weight compounds found in small quantities throughout the whole plant kingdom. They exhibit many biological functions vital for the survival of the plant such as responding to stress, mediating pollination, or acting as defense compounds. In plant cell, they are accumulated often in the vacuoles. Besides the importance for the plant itself, secondary metabolites have always been of interest to humans as flavors, fragrances, dyes, pesticides, and pharmaceuticals. However, for most of the secondary metabolites, the exact function in plants still remains unknown.

Medicinal Plants, Engineering of Secondary Metabolites in Cell Cultures. Table 1 Number of new drug entities (NDEs) discovered during 1981–2006 belonging to the four most important therapy groups (modified from [3])

Therapy group	Total	N	ND	NS	B	S	V	N+D+NS	%
Antimicrobial	230	12	74	34	13	60	37	120	52.2
Anti-bacterial	109	10	64	1	0	23	11	75	68.8
Anti-fungal	29	0	3	0	1	25	0	3	10.3
Anti-viral	78	0	2	31	12	8	25	33	42.3
Anti-parasitic	14	2	5	2	0	4	1	9	64.3
Anti-cancer	100	9	25	17	17	30	2	51	51.0
Anti-hypertensive	77	0	2	34	0	41	0	36	46.8
Anti-inflammatory	51	0	13	0	1	37	0	13	25.5
Total	458	21	114	85	31	168	39	220	48.0

N natural product, *ND* natural product derivative, *NS* product is synthesized but the original molecule is discovered from natural sources, *B* biotechnologically produced compound (often a large molecule, protein), *S* synthetic molecule, *V* vaccine

More than 200,000 secondary metabolites have hitherto been discovered from the plant kingdom, but only half of them are structurally fully elucidated [4–6]. They are characterized by an enormous chemical diversity, and every plant has its own characteristic set of secondary metabolites. The production of specific alkaloids is often strongly restricted to certain plant families, whereas, for example, flavonoids are abundant in many plant species. Based on their biosynthetic origins, plant secondary metabolites can be structurally divided into five major groups: polyketides, isoprenoids (e.g., terpenoids), alkaloids, phenylpropanoids, and flavonoids [7]. The polyketides are produced via the acetate-mevalonate pathway; the isoprenoids (terpenoids and steroids) are derived from the five-carbon precursor, isopentenyl diphosphate (IPP) produced via the classical mevalonate pathway, or the novel MEP pathway (see the details in section "Targeting the Metabolic Enzymes"); the alkaloids are synthesized from various amino acids; phenylpropanoids are derived from aromatic amino acids phenylalanine or tyrosine; and the flavonoids are synthesized by the combination of phenylpropanoids and polyketides [8].

Since the discovery of the opium alkaloid morphine almost two centuries ago, alkaloids are still one of the most studied groups of plant secondary metabolites although terpenoids are the largest chemical family of secondary metabolites. It is somehow surprising that such an extensive array of different nitrogen-containing organic molecules are known in higher plants even though only 2% of the plant dry weight is composed of the element nitrogen. The largest requirement of nitrogen is the synthesis of amino acids which function as building blocks of proteins as well as precursors to many secondary metabolites. Alkaloids are thus the most prominent nitrogenous compounds with diverse, complex structures and often possessing strong physiological properties leading their wide use as pharmaceuticals. Human use of them dates back to more than 3,000 years. Currently, more than 12,000 alkaloids are known and they are classified into several subclasses based on the amino acids from which they are derived and according to their chemical structures [9].

At the present time, small amounts of plant compounds including alkaloids, for example, morphine, scopolamine, and vincristine are isolated with often some difficulties from natural vegetation or cultivated plants which explain the high price of the raw material. Numerous secondary metabolites have also served as models for modern synthetic pharmaceuticals [3]. However, the biosynthetic pathways leading to their formation in plants are often long, complex multistep events catalyzed by various enzymes, and are still largely unknown in enzymatic and genetic level. The best characterized pathways after the decades' intensive classical biochemical research are the biosynthesis of opium and terpenoid indole alkaloids.

Besides the low quantities of the compounds in plants, the production rates may vary from year to year and secondary metabolites often accumulate in specific plant organs in particular time of the vegetative stage of the plant. Some substances can only be isolated from extremely rare plants which is not a choice for sustainable production. Therefore, alternative production systems for plant-derived compounds are needed. The biotechnological production, that is, producing the plant secondary metabolites in cultured plant cells in large bioreactors may offer an attractive alternative approach.

Biotechnological Production Options

The production of a secondary metabolite of interest for industrial needs is often a challenge. As explained above, these compounds accumulate in plants in small quantities. The biotechnological production of high-value plant secondary metabolites therefore is a viable option to isolation processes from the intact plants or to the total chemical synthesis.

Biotechnology focuses on the exploitation of metabolic properties of living organisms for the production of valuable products of a very different structural and organizational level for the benefit of humans. The organisms vary from microbes (bacteria, fungi, yeast) to plants and animals. Over the decades, many laboratories all over the world have studied the possibilities to produce desired secondary metabolites using plant cell or tissue cultures. Cell cultures have been established from many plants, but often they do not produce sufficient amounts of the required secondary metabolites or the production is unstable. Various classical optimization tools have been applied (see in detail section "Enhancing the Production by Classical Optimization"), but very few success

stories exist contrary to many good examples using microbial production systems.

Molecular biology of plants has emerged enormously during the past decades, but still the plant metabolic engineering has met only limited success, again in sharp contrast to microorganisms. This is due to our limited knowledge on complex biosynthesis of secondary metabolites. Despite the rapid development of not only plant genomics but also of analytical tools, genetic maps of biosynthetic pathways are far from complete. Furthermore, regulation of the individual steps leading to the desired end product is poorly understood (section "Metabolic Engineering").

Plant Cell Cultures Plant cell culture is a method where plant cells are cultivated under sterile conditions *in vitro*. Commonly, cell cultures are established from callus tissues by cultivating callus in liquid medium, and cell aggregates are broken by either mechanically or by orbital shaking in the cultivation vessel. Plant cells are biosynthetically totipotent, which means that each cell in culture retains its complete genetic information and thus is able to produce the same metabolites as the parent plant. Plant cell cultures have been extensively exploited for various biotechnological applications as an alternative to the traditional agricultural cultivation of plants. The use of cell culture systems offers advantages to produce metabolites in a controlled environment, independent of climatic conditions and under conditions in which the different production parameters can be optimized. Plant cell cultures can be categorized in two main classes, differentiated and undifferentiated cell cultures. The former consists of, for example, organs like shoots, roots, or embryos, whereas callus and cell suspension cultures are referred to as undifferentiated cell cultures. Since the first gene transfers in plants in 1983, achieved by four independently working groups [10–13], a number of efficient gene transfer techniques have been developed for genetic engineering of plants. In addition to so-called direct gene transfer techniques (e.g., particle bombardment, electroporation, microinjection), *Agrobacterium*-mediated gene transfer has been the most commonly used method for gene delivery to plants.

Hairy Root Cultures *Agrobacterium* (Rhizobiaceae) is a soil bacterium, which is able to deliver its own plasmid-DNA into the nuclear genome of the plant cell. The bacterium attaches into the wound site of the plant tissue and recognizes certain wound substances, for example, acetosyringone, secreted by the plant [14]. As a result, the *vir* (virulence) region of the plasmid becomes activated and processing of the T-DNA (transferred DNA) for the gene transfer starts [14, 15]. After successful integration of the bacterial DNA into the host plant genome, the tumor formation in the wound site begins as well as the production of low molecular weight tumor substances called opines. The opines are used as a nutrient for the bacterium [16]. The host range of *Agrobacterium* is perhaps broader than that of any other plant pathogenic bacterium, although a number of cultivated monocotyledonous plants and legumes are not natural hosts for this bacterium. The molecular mechanism of the resistance to *Agrobacterium* is not known, although the production of antimicrobial metabolites [17], a lack of *vir* gene inducers [18], inefficient T-DNA integration [19], and *Agrobacterium*-induced programmed cell death [20] have all been suggested. Successful gene transfer in monocot plants via *Agrobacterium* has been performed with maize, rice, wheat, and barley [21].

Hairy root is a plant disease caused by the infection of *Agrobacterium rhizogenes* carrying Ri (root-inducing) plasmid. During infection of the plant, the T-DNA of the Ri-plasmid is transferred and integrated in the nuclear genome of the host. As a result of the transformation, hairy roots appear at the infection site [22]. In the T-DNA, there are four genetic loci, called *rol*A, *rol*B, *rol*C, and *rol*D, which are responsible for the hairy root phenotype. These genes were shown to positively affect the secondary metabolite production in *Nicotiana* [23] and in *Atropa* [24]. Hairy roots are able to grow without externally supplied auxins, and certain *aux* genes from *Agrobacterium* have been shown to provide transformed cells with an additional source of auxin [25]. This is a clear advantage when considering the costs for large-scale cultivation. Hairy roots characteristically lack geotropism and have a high degree of lateral branching. In addition, hairy root cultures have demonstrated their ability to rapidly produce biomass as well as high contents of secondary metabolites, for example, tropane alkaloids [26, 27]. In Table 2, some pharmaceutical compounds produced by hairy

Medicinal Plants, Engineering of Secondary Metabolites in Cell Cultures. Table 2 Examples of metabolites produced by transformed hairy root cultures (adopted mainly from [28, 29])

Metabolite	Species	Activity	Reference
Ajmalicine, ajmaline	*Rauvolfia micrantha*	Antihypertensive	[30]
Artemisinin	*A. annua*	Antimalarial	[31]
Benzylisoquinoline alkaloids	*P. somniferum; E. californica*	Analgesic, antibiotic	[32]
Betalains	*Beta vulgaris*	Antioxidant, colorant	[33]
Camptothecin	*Ophiorrhiza pumila; Camptotheca acuminata*	Antitumor	[34, 35]
Iridoid glycosides	*Harpagophytum procumbens*	Anti-inflammatory, analgesic, and antidiabetic	[36]
3,4-Dihydroxy-L-phenylalanine	*Stizolobium hassjoo*	Therapeutic agent against Parkinson's disease	[37]
Rutin, hispidulin and syringin	*Saussurea involucrata*	Anti-inflammatory, antifungal	[38]
Scopolamine, hyoscyamine and atropine	*A. belladonna*	Anticholinergic	[24, 39]
Scopolamine and hyoscyamine	*Datura innoxia*	Anticholinergic	[40]
Scopolamine and hyoscyamine	*Datura quercifolia*	Anticholinergic	[41]
Scopolamine	*Duboisia leichhardtii*	Anticholinergic	[42]
Scopolamine and hyoscyamine	*Datura candida*	Anticholinergic	[43]
Scopolamine and hyoscyamine	*Datura innoxia*	Anticholinergic	[44]
Scopolamine and hyoscyamine	*H. niger*	Anticholinergic	[40]
Scopolamine and hyoscyamine	*H. muticus*	Anticholinergic	[26]
Scopolamine and hyoscyamine	*H. muticus, Nicotiana tabacum*	Anticholinergic	[45]
Scopolamine	*H. niger*	Anticholinergic	[46]
Solasodine	*Solanum khasianum*	Steroid hormone precursor	[47]
Paclitaxel	*Taxus brevifolia*	Anticancer	[48]
Terpenoid indole alkaloids	*C. roseus*	Antitumor	[49]
Thiarubrine A	*Ambrosia artemisiifolia*	Antifungal, antibacterail, antiviral	[50]
6-Methoxy-podophyllotoxin	*Linum album; Linum persicum*	Anticancer	[51]
Quinine, quinidine	*Cinchona ledgeriana*	Antimalarial	[52]
(+) catechin, (−) epicatechin-3-O-gallate, procyanidin B_2-3′-O-gallate	*Fagopyrun esculentum*	Antioxidant	[53]
Anthraquinone	*Rubia tinctoria*	Antimalarial, antineoplastic	[54]
Thiophene	*Tagetes patula*	Anti-inflammatory precursor	[55]
Valpotriates	*Valeriana officinalis*	Tranquilizing	[56]

root cultures are presented. Unlike crown gall tumors, hairy roots are capable of spontaneously regenerating into plants [57].

Bioreactors The selection of a suitable bioreactor type for the specific process depends on the desired product and the production material, for example, whether the production involves growing undifferentiated cells, hairy roots, or plantlets. Plants cells are larger in size than those of microbial cells, making them more sensitive to shear forces. For this reason, bioreactors have been designed where conventional mechanical impeller stirring have been replaced by bubble or wave-type agitation. Most widely used bioreactors are stirred tanks [58], but also airlift and bubble column reactors have been used in cultivation of plant cells. The classical production of shikonin is performed in airlift type of bioreactors. A balloon-type bubble bioreactor has been successfully used for the cultivation of, for example, ginseng roots [59].

One of the more recent developments in bioreactor design for plant cell applications has been the use of disposable bioreactors, usually plastic bags. Major advantages in these are that the capital costs are much lower than that of common stainless steel tanks. The production of glucocerobrosidase used for treating the enzyme deficiency cased in Gaucher's disease is performed in carrot cells grown in disposable bioreactors by Israeli company Protalix Biotherapeutics (www.protalix.com). The only secondary metabolite of pharmaceutical value, paclitaxel (Taxol®), is commercially produced in *Taxus* cells by German company Phyton Biotech (www.phytonbiotech.com). Moreover, lower expenses allow multiple parallel units to be employed, and high sterility requirements are met when there is no need for costly cleaning processes between runs. Disposable bioreactors may consist of a rigid cultivation container (tube, plate, flask, cylindrical vessel) or a flexible container (bag) [60]. Issues restricting the use of disposable bioreactors arise from a limited experience in their usage, insufficient strength of a plastic material, limited applicability of advanced automatization, and lack of suitable disposable sensors. Wave-mixed bioreactors [61], such as BioWave®, are well suited for small- to middle-scale processes for the production (Fig. 1) of, for example, plant-based secondary metabolites and therapeutic proteins, as well as cultivation of hairy roots [62, 63]. One of the highest productivities reported to date for paclitaxel production in *Taxus baccata* cell suspension cultures was achieved with immobilized cells cultivated in BioWave® system [64, 65].

Important factors when designing the cultivation of plant cell suspension cultures in bioreactors include guaranteed sterility through the whole process and low-shear mixing allowing still efficient nutrient transport without causing sedimentation or a loss in viability of the cells. In addition, the possibility for application of light induction for heterotrophic, photomixotrophic, and photoautotrophic cultures might be relevant [62]. Major physical process parameters regarding cultivation of plant cell and tissue cultures are temperature, viscosity, gas flow rates, and foaming.

Sometimes the lack of end-product formation may be due to the feedback inhibition, degradation of the product in the culture medium, or due to volatility of the substrates or end products. In such cases, adding of extra phase as a site for product accumulation might lead to increased production of the desired substance [66]. For example, addition of amberlite resin and charcoal resulted in increased accumulation of anthraquinones and vanilla, and coniferyl aldehyde, respectively [67–69]. On the other hand, bioconversion of water-insoluble substrates in cell culture systems can be aided by using cyclodextrins. They form inclusion bodies in their cyclodextrin cavity and by this way increase the water solubility of the substrates [70].

Enhancing the Production by Classical Optimization

Selection of High-Producing Lines

Selection of individual plants with desired traits has been a traditional approach in plant breeding. Similarly, high producers have been selected for further use, for example, for cloning and as a starting material for cell cultures. However, cell clones from the same origin may vary considerably in their metabolite production capacities. Selecting high producers is thus a very empirical approach, requiring a huge amount of screening work before good producing individuals are found [71, 72]. In order to obtain good producing cells, mutation strategies or application of various selective

Medicinal Plants, Engineering of Secondary Metabolites in Cell Cultures. Figure 1
Wave bioreactor is used to culture various types of plant cells. This is a 2-L disposable bag in a Wave® reactor containing tobacco hairy roots

agents, such as *p*-fluorophenylalanine [73], 5-methyltryptophan [74], or biotin [75], have been used. Although undifferentiated plant cells can be maintained in an undifferentiated state using phytohormones, they are not genetically or epigenetically stable. The concept of somaclonal variation was introduced by Larkin and Scowcroft in the beginning of 1980s, standing for the genetic variability in tissue culture–derived plants or cell culture clones [76]. These changes causing the variation can occur as large rearrangements in chromosomal level, for example, changes in chromosome number, karyotype modifications, or changes in gene level.

Somaclonal variation can be exploited when searching for high secondary metabolite producers or high producers of biomass, although a clear disadvantage is that these changes cannot be predicted or controlled and moreover, they are not always stable or heritable. The effect of culture age on growth rates were observed with *Nicotiana plumbaginifolia*, which showed higher growth rates with older cultures compared to newer cultures [77]. These differences were thought to appear as a cause of higher proportion of cells in older cultures exhibiting mutations which elevate cyclin-dependent kinases. Changes in ploidy levels are reported to affect regeneration capacity [78], gene silencing [79], and secondary metabolite production [80, 81]. After choosing good-producing cell lines, cultivation over time requires usually continuous selection in order to maintain high production levels. However, a gradual loss of secondary metabolite productivity over time is an obstacle in the development of commercial plant cell culture production systems [82, 83].

Optimization of Culture Medium

One of the major advantages in using plant cell cultures is the possibility of controlled and contained production systems. When attempting to reach high production levels, key roles are played by the composition of nutrient medium and other cultivation parameters, such as temperature, light, phytohormones, and gas exchange.

Because the plant cell is a production factory, the first requirement for obtaining high levels of products

is the generation of high amounts of biomass or at least enough biomass for economic product yields. Plant cell cultures are usually grown heterotrophically using simple sugars as carbon source, sucrose being the most commonly used. Carbon source effects mainly on primary metabolism and by this way affects the overall productivity with either increased or decreased biomass production. Sucrose level may also have an indirect impact on secondary metabolite production, as inverse correlation between sucrose and hyoscyamine production was observed in *Hyoscyamus muticus* hairy root cultures [84]. This was probably due to the increased glycolysis and respiration rate with simultaneous overriding of secondary metabolite production. Sucrose is commonly applied in approximately 3% (w/v) concentration, but levels as high as 8% (w/v) have shown to increase the accumulation of indole and benzophenanthridine alkaloids in cell cultures of *Catharanthus roseus* and *Eschscholtzia californica*, respectively [85, 86].

Phosphate and nitrogen levels are perhaps the most important macronutrient factors effecting the secondary metabolite formation. Phosphate usually promotes cell growth, but often has been accompanied by lower secondary product formation. In fact, very often cell proliferation has been accompanied by decrease in secondary product formation and vice versa. For this reason, a two-stage cultivation system could be considered, where the cells are first cultivated in the medium optimized for cell multiplication and then transferred into medium limiting the biomass growth whereas enabling maximum product formation. As an example, shikonin produced by *Lithospermum erythrorhizon* in commercial scale by this type of two-phase system [87]. Low phosphate levels often have been correlated with high secondary metabolite formation, for example, in case of alkaloids in *Datura stramonium* [88], *Nicotiana tabacum* [89], and *C. roseus* [90]. Nitrogen is an important building block of amino acids, nucleic acids, proteins, and vitamins. Generally, nitrogen is added in the form of nitrate or ammonium, and the ratio of these salts plays an important role in secondary metabolite production of the plant cells. Reducing the levels of nitrogen generally leads to lower biomass production and thus leads to higher secondary metabolite production, as in the case of anthocyanin production by *Vitis vinifera* [91].

Phytohormones have an extensive effect not only on growth of plant cells, but also on differentiation and secondary metabolite production. Both the type and concentration of auxin and cytokinin as well as their ratio alter the growth and metabolite production dramatically in cultured plant cells. High auxin levels are known to inhibit the formation of secondary metabolites in a large number of cases, for example, tobacco alkaloids [92] with the simultaneous activation of polyamine conjugate biosynthesis [93]. Sometimes, replacement of synthetic auxin 2,4-D (2,4-dichlorophenoxy acetic acid) by NAA (naphthalene acetic acid) or natural auxin IAA (indole acetic acid) has shown to enhance the production of anthraquinones, shikonin, or anthocyanins [94–96].

Commonly understanding of cell culture behavior has been relied on the measurements of culture average parameters, such as cell density and metabolite profiles. However, due to the nature of plant cell division, in which daughter cells often remain attached through cell wall, aggregates of various sizes in cell suspension culture are formed. Thus, each aggregate is exposed to different microenvironmental conditions with respect to nutrient and oxygen availability between inner and outer regions of the aggregate [97]. Understanding such subpopulation dynamics and cellular variability using tools such as flow cytometry is important in order to control the culture as a whole.

Effect of Elicitors

The enhanced production of secondary metabolites from plant cell and tissue cultures through elicitation has opened up a new area of research which could have beneficial influences for pharmaceutical industry. Elicitors are compounds, biotic or abiotic, or even physical factors, which can trigger various defense-related reactions, and thereby induce secondary metabolite formation in plant cells. The mechanisms of how elicitors activate the respective genes and the whole biosynthetic machinery in a plant cell are under active investigation. However, it is evident that the gene expression occurs very quickly after the elicitor contact and many hours before the secondary metabolites are accumulated in a plant cell [98].

In general, elicitors can be categorized based on their molecular structure and origin. Biotic elicitors

include compounds such as chitosan, alginate, pectin, chitin or they may contain complex mixtures of compounds like those of fungal or yeast extracts [99]. Abiotic elicitors are chemical compounds of nonbiological origin, for example, heavy metals and vanadate derivatives, or physical factors such as thermal or osmotic stress, UV-irradiation, or wounding. In particular, widely used elicitors for plant cell culture systems are jasmonates and jasmonic acid derivatives, which are naturally occurring hormones involved in the regulation of defence-related genes and act as signaling compounds in these reactions [100]. Application of jasmonates can result in large alterations in desired metabolites in *Catharanthus* [101, 102], in *Taxus* [103], and in *Nicotiana* [98]. Even though plant cells accumulate secondary metabolites typical for species in question independent of the type of elicitor used, the accumulation kinetics may vary greatly with different elicitors. Moreover, elicitors can effect on the release of desired secondary metabolite from the cell to the cultivation medium [104]. This is beneficial when considering the biotechnological production facilitating thus the downstream processing.

Generally, both the elicitor concentration and the length of elicitor application have to be determined for each cell culture individually [104]. Commonly it is thought that the best growth phase for the start of the elicitation is during the exponential growth phase when the enzymatic machinery for elicitor response is most active [105]. In addition, the composition of the culture medium, especially phytohormones, has a major impact on elicitor response. For example, divergent regulation by auxins on the biosynthesis of different metabolites in terpenoid indole alkaloid pathway was observed by *C. roseus* cell cultures [102]. This regulation by auxins was shown to be partly dependent on the presence of methyl jasmonate. Production of various plant-derived medicinal compounds has been successfully induced by using elicitors [106]. Unfortunately, many elicitors also cause a loss of viability of the producing cells, thus a thorough optimization of the whole production process is required when using elicitation.

Metabolic Engineering

Functional genomics tools offer now huge potential to engineer plant metabolic pathways toward the targeted end product or alternatively to form entirely novel structures through combinatorial biochemistry. However, rational engineering of secondary metabolite pathways requires a thorough knowledge of the whole biosynthetic pathway and detailed understanding of the regulatory mechanisms controlling the flux of the pathway (Fig. 2) [7]. Such information is not available for vast majority of secondary metabolites, explaining why only limited success has been obtained by metabolic engineering. New genome-wide transcript profiling techniques combined with up-to-date metabolomics allow us now to establish novel gene-to-gene and gene-to-metabolite networks which facilitate the gene discovery also in non-model plants that include most medicinal plants [102]. The ability to switch on entire pathways by ectopic expression of transcription factors suggests new possibilities for engineering secondary metabolite pathways (Fig. 2). Consequently, the utilization of plant cell cultures for biotechnological production of high-value alkaloids would thus become a true viable alternative.

Gene Discovery

Since the sequencing of *Arabidopsis* genome in 2,000 several other plants are being sequenced but still today very limited information exists for any medicinal plant. Therefore, also the biosynthetic pathways in these plants are largely unknown at the gene level. Several approaches have been developed to identify enzymes and the corresponding genes that are responsible for different biosynthetic pathway steps. One of the classical methods is the identification and isolation of intermediates and enzymes *via* precursor feeding [107]. The other very basic approach is to use cDNA libraries to identify genes by PCR amplification with primers designed to recognize conserved regions on the basis of enzyme homology from other plants with already known sequences [108]. More recently, methods based on differential display comparing mRNA transcripts of elicited and non-elicited cell culture samples have shown their potential in gene discovery. Goossens and coworkers [98] and Rischer and coworkers [102] utilized cDNA-AFLP technique for genome-wide gene hunt, whereas [109] supplemented their search with homology-based analysis of a cDNA library of elicited cells. In addition, the use of random sequencing of

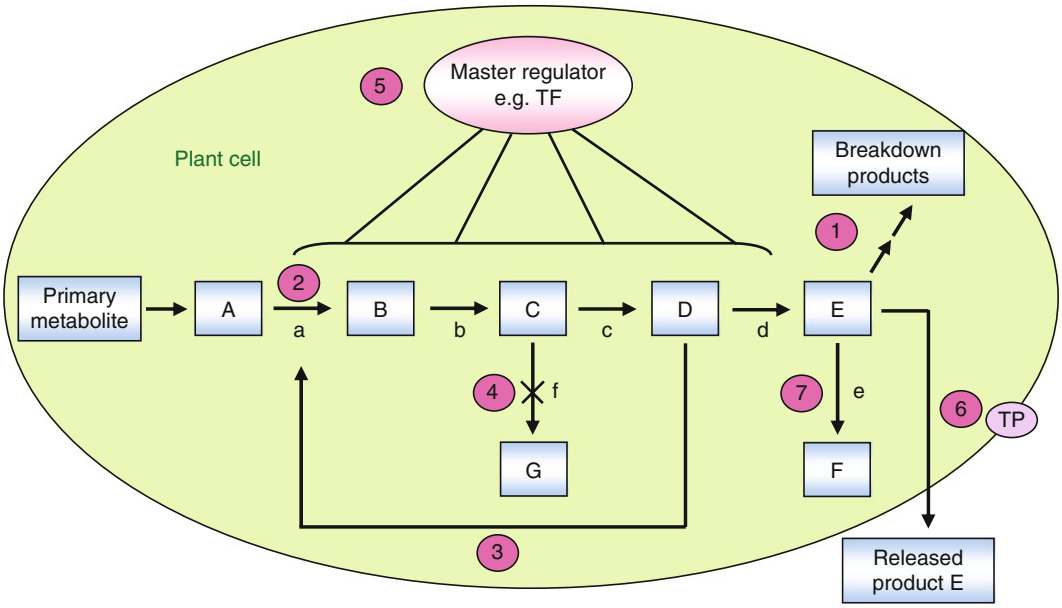

Medicinal Plants, Engineering of Secondary Metabolites in Cell Cultures. Figure 2
The hypothetic scheme how the secondary metabolite E could be formed from primary metabolites via different enzymatic steps and how the biosynthesis could be regulated in a plant cell [7]. Engineering of secondary metabolite pathways is a series of complex events. The following strategies could be used to modify the production of hypothetical plant metabolite E: (1) decrease the catabolism of the desired compound, (2) enhance the expression/activity of a rate limiting enzyme, (3) prevent feedback inhibition of a key enzyme, (4) decrease the flux through competitive pathways, (5) enhance expression/activity of all genes involved in the pathway, (6) compartmentalize the desired compound, and (7) convert an existing product into a new product. *TF* transcription factor, *TP* transporter gene

elicited cDNA library can lead to identification of clones involved in the biosynthetic route in question as proven in case of *Taxus* biosynthesis [110].

The use of microarrays as widely used for model plants such as *Arabidopsis* is usually not applicable to medicinal plants simply because none has been sequenced with the very recent exception of tobacco http://www.pngg.org/tgi/index.html. The rapid advance of deep sequencing, however, will soon result in many important species being investigated at genome scale. The 454 pyrosequencing technique is currently perhaps the most widely used so-called next-generation sequencing technique for the *de novo* sequencing and analysis of transcriptomes in non-model organisms like medicinal plants are. For example, the GS FLX Titanium can generate one million reads with an average length of 400 bases at 99.5% accuracy. This technology was successfully used to discover putative genes involved in ginsenoside biosynthesis [111].

Once the candidate genes are discovered, they are functionally tested alone or in combination to find out their real mode of action, for example, improving or altering the production of desired metabolite. This is time consuming, and therefore new high-throughput systems have been developed, for example, miniaturized cell culture formats and multigene transformations.

Controlling the Expression of Transgenes

In order to be able to modify the metabolite profile of a respective medicinal plant or cell culture, the gene expression of target proteins and enzymes needs to be fine-tuned in an appropriate manner. For that purpose, the elements involved in transcriptional regulation of gene expression should be well characterized and evaluated to ensure correct spatial and temporal display. This also minimizes the potential adverse effects, and

the outcome will be as wanted. Specific DNA sequences upstream of the encoding region of a gene that are recognized by proteins (transcription factors) involved in the initiation of transcription are determined as promoters. It is noteworthy that the promoter sequence itself is present in all tissues and cells, and thus the activity is controlled via transcription factors and their abundance. This opens the possibility to boost a cascade of enzymes and influence in the whole biosynthetic pathway in question by overexpressing transcription factors [112].

Promoters used for the metabolic engineering purposes can be divided into three classes:

1. Constitutive, that is, promoters that are continuously on in most or all of the tissues
2. Organ- or stage-specific, that is, promoters controlling spatiotemporal activity of the transgene
3. Inducible that are regulated by an external trigger of chemical or physical nature [113, 114].

As an example of the constitutive promoters and also the most used one in plant genetic engineering is the *Cauliflower mosaic virus 35S* promoter [115, 116]. The CaMV 35S promoter has been very thoroughly characterized and currently a typical CaMV 35S promoter in plant vectors consists of a bit more than one third of the full-length sequence [117]. It has also been observed that a partial duplication from −343 to −90 amplifies expression up to tenfold [118]. This promoter is also the most used one in metabolic engineering of plant cell cultures [119]. For the secondary metabolite production, the hairy root cultures have shown most potent, and little promise has been found with undifferentiated suspension cultures [120]. Actually there exist no studies for trying to find most suitable callus or suspension culture–specific promoters for efficient expression of target genes. This might be one factor why the success in using undifferentiated plant cell cultures for the production of valuable secondary metabolites has been so poor. However, the main blame for this is the current limited understanding of how the metabolic pathways and fluxes of secondary metabolites work in general.

Nowadays that the multigene transformations [121] are paving the way for more accurate and complex engineering of phenotypes, there is also more need to apply different promoter deployment strategies to reach the wanted goals. The delivery of 10–20 genes at the time is already very demanding, and thus there is no space for failure in running their expression. Roughly, two ways of proceeding can be drawn for promoter choice: utilization of the same promoter to run all the genes or combination of promoters to run different target genes in the generated multigene transformants. The use of same promoter carries the risk of triggering gene silencing. It is very important to increase the promoter diversity via promoter discovery and generation of synthetic sequences to run the expression. Perhaps one of the most interesting ways is to apply bidirectional sequences which allow simultaneous expression of two genes, and thus halves the number of required promoters for multigene engineering [122].

Targeting the Metabolic Enzymes

From the genetic engineering perspective of medicinal plants, one of the key elements is to express the genes in question in right tissues, and even more importantly target the respective enzymes to correct, specific subcellular compartments. A good example of compartmentalization is the biosynthesis of terpenoids that are synthesized from universal five-carbon precursors isopentenyl diphosphate (IPP) and dimethylallyl diphosphate (DMAPP), which in turn are formed via two alternate biosynthetic pathways localized in different subcellular compartments. The cytosolic mevalonic acid (MVA) pathway starts with condensation of two molecules of acetyl-CoA into acetoacetyl-CoA and finally gives rise to IPP. The methylerythritol phosphate (MEP) pathway takes place in plastids and leads to the formation of IPP and DMAPP from pyruvate and glyceraldehyde phosphate. The IPP and DMAPP precursors are then processed with prenyl diphosphate synthases in different compartments giving rise to intermediates that serve as substrates to a large group of terpene synthases resulting in construction of the final terpenoids [123, 124]. However, the picture is never black and white, and the subcellular localization studies as well as the genetic engineering experiments have shown that such a thing as a general rule does not apply to all tissues and species. From the rational genetic engineering point of view, this makes things even far more complex and we still need to reveal several aspects of biosynthetic pathways.

Targeting the biosynthetic enzymes to non-original compartment can also lead to interesting results. Precursors can be available in other compartments, and introduction of the respective enzyme can lead to increased accumulation of target compounds. For example, Wu and coworkers [125] showed that redirecting the sesquiterpene pathway from its natural cytosolic location to chloroplasts increased patchoulol accumulation even up to 10,000-fold when compared to native situation. Another example was given by introducing three different targeting modes: cytosolic, plastid, and ER of limonene synthase in transgenic tobacco plants [126]. Both the cytosolic and plastid targeting resulted in limonene formation, whereas ER targeting gave no response probably due to false folding or instability of the protein.

There has also been discussion on so-called metabolic channeling, which means that enzymes from the same pathway, especially the ones committing successive steps, form a protein complex resulting in efficient reactions and regulation of the pathway [127–129]. Aharoni and coworkers [130] interpreted that this might be a cause why some pathways do not seem to proceed even though substantial amount of substrate seem to be available. As a solution, an artificial channeling is suggested with the help of fusion constructs to be applied in the metabolic engineering. These studies also highlight the need for fluxomics and thorough understanding of metabolic pathways (see Sect. "Controlling the Expression of Transgenes").

Multigene Transformation

The first multigene-carrying transgenic plants were created either with several rounds of crossings between transgenic lines or by transforming transgenic plants with a new set of genes [131, 132]. The current multigene delivery systems are co-transformations with either linked or unlinked genes, that is, genes within a same vector or different vectors, respectively. The transfer itself is carried out either via *Agrobacterium*-mediated or direct transformation techniques. These systems have been developed mainly with crop plants, and the target pathways have been on nutritional composition like in engineering of the carotenoid pathway [133, 134]. These pioneer works have opened the possibility to engineer metabolic pathways of medicinal plants, and the potential in these can be seen almost as limitless. The future aim is the creation of a SMART locus (stable multiple arrays of transgenes), that is, a transgenic locus containing multiple genes, thus avoiding segregation in meiosis and possibly also minimizing rearrangements and silencing [121]. For medicinal plants, the possibility to modify entire metabolic pathways, to introduce completely new pathways, and to study complex metabolic control circuits and regulations are perhaps the main future goals.

New Compounds by Engineered Enzymes/Proteins

In most common approaches, the intention of metabolic engineering is to either overexpress or repress genes leading to the accumulation of certain compounds (Fig. 2). The first successful genetic engineering approach to the medicinal plant was performed already almost 20 years ago. Yun and coworkers [135] introduced the gene-encoding hyoscyamine-6β-hydroxylase (H6H) from *Hyoscyamus niger* to the medicinal plant *A. belladonna*. As a result of the overexpression of *h6h*, the plants produced almost exclusively scopolamine, whereas in the control plants the production of hyoscyamine (precursor of scopolamine) was dominant. Later, the function of the same gene was demonstrated to be different in hairy roots of *Hyoscyamus muticus* [26]. The overexpression of *h6h* caused 100-fold increase in scopolamine production, whereas the hyoscyamine contents were not reduced.

There are also examples where genetic engineering can lead to formation of entirely new metabolites. Classically, this can, for example, be achieved by generating somatic hybrids, that is, by exposing enzymes and regulators derived from different genomes to new environments. A good example is the production of demissidine in somatic *Solanum* hybrids neither parent of which contained this specific metabolite but only a set of different precursors [136].

More recently, the combinatorial biochemistry concept which is based on the fact that enzymes often show relaxed substrate specificity, that is, that they can under certain conditions process substrates which differ from the preferred one is exploited in a stricter sense. Usually, native genes are modified with the aim of creating modified enzymes catalyzing new reactions. Initially, attempts to alter the substrate specificity of

plant-derived terpenoid synthases by rather unspecific methods such as mutagenesis or truncation were quite unpredictable [137]. Meanwhile, however, it could be shown that preselection of a mutant strictosidine synthase with a specific point mutation according to substrate acceptance results in quite predictable events. *C. roseus* hairy roots expressing the gene formed unnatural terpenoid indole alkaloids when were fed with derivatized precursors in contrast to the wild type [138].

Future Directions

Different omics in techniques have opened totally new avenues to discover genes, to learn about their functions, for example, transcription, and to finally map the biosynthetic pathways leading to the formation of important secondary metabolites. Metabolomics, which deals with all cellular metabolites, was first defined in microbiology but has also been recognized as an important sector of post-genome plant science [139]. Even in the absence of any visible change in a cell or individual plant, metabolomics, which allows phenotyping by exhaustive metabolic profiling, can show how cells respond as a system. Plant metabolomics is of particular importance because of the huge chemical diversity in plants compared to microorganisms and animals [140]. The number of metabolites from the plant kingdom has been estimated at 200,000 or even more [6], and each plant has its own complex set of metabolites. By integrating transcriptome and metabolome data, one can build networks and get insight on how particular metabolites are formed in plants [102, 140]. This in turn helps us to identify the key genes that could be engineered for the production of improved medicinal plants.

Since cell physiology involves dynamic rather than static processes, the investigation of fluxes is needed to complement phenotyping by metabolomics which only allows inventory, although time-resolved snapshots. However, in contrast to mammalian and microbial cells, flux quantification in plants is much less advanced. This is mainly due to the high degree of subcellular compartmentation and the complexity which arises from intercompartmental transport. Labeling experiments have been very successfully used already in the past for the elucidation of biosynthetic pathways in plants [141], but flux determination has only recently gained pace due to the fast development of analytical and computational technology. Analytical techniques of choice are nuclear magnetic resonance (NMR) spectrometry and mass spectrometry (MS) [142]. Generally, there are two fundamentally different methods available facilitating flux measurement – steady-state and dynamic analysis – both of which have certain restrictions and benefits [143]. The latter, that is, kinetic approach is particularly interesting in the sense that it potentially could lead to predictive modeling in regard to secondary metabolism, while steady-state analysis is mainly used to measure carbon flux in well-defined pathways of primary metabolism [144].

In conclusion, modern genomic tools allow for mass gene discovery from plants although many biosynthetic pathways are incompletely resolved and medicinal plants have rarely been sequenced. Nevertheless, predictive metabolic engineering remains a goal of the future. This is because transgene integration in higher plants occurs through illegitimate rather than homologous recombination. DNA integration is random with a preference for gene-rich regions. Gene disruptions, sequence changes, and the production of new proteins constitute common consequences resulting in either predictable or unpredictable effects [145]. In this situation, the power of functional genomics tools allowing the comprehensive investigation of biological systems cannot be overemphasized. Genomics identifies all genes of a plant, while transcriptomics and proteomics provide information about their activities in cells or organs under certain conditions, and finally metabolomics and fluxomics account for the accumulation and kinetics of metabolites, that is, the phenotype. The individual techniques as such are thus invaluable to assign functions, but the real advantage lays in their combination, that is, the systems biology approach [140]. Interestingly at the same time, these tools allow not only the investigation of artificial situations generated by man but also for the first time broad assessment of natural variation.

Acknowledgments

This work has been financially supported by the SmartCell project (nr. 222176) from European Commission Framework 7 programme.

Bibliography

Primary Literature

1. Hostettmann K, Terreaux C (2000) Search for new lead compounds from higher plants. Chimia 54:652–657
2. Müller-Kuhrt L (2003) Putting nature back into drug discovery. Nat Biotechnol 21:602
3. Newman DJ, Cragg GM (2007) Natural products as sources of new drugs over the last 25 years. J Nat Prod 70: 461–477
4. Verpoorte R (1998) Exploration of nature's chemodiversity: the role of secondary metabolites as leads in drug development. Drug Discov Today 3:232–238
5. De Luca V, St Pierre B (2000) The cell and developmental biology of alkaloid biosynthesis. Trends Plant Sci 5: 168–173
6. Hartmann T, Kutchan TM, Strack D (2005) Evolution of metabolic diversity. Phytochemistry 66:1198–1199
7. Oksman-Caldentey K-M, Inzé D (2004) Plant cell factories in the post-genomic era: new ways to produce designer secondary metabolites. Trends Plant Sci 9:433–440
8. Verpoorte R (2000) Secondary metabolism. In: Verpoorte R, Alfermann AW (eds) Metabolic engineering of plant secondary metabolism. Kluwer, Dordrech, pp 1–29
9. Ziegler J, Facchini PJ (2008) Alkaloid biosynthesis – metabolism and trafficking. Annu Rev Plant Biol 59:735–769
10. Bevan MW, Flavell RB, Chilton MD (1983) A chimaeric antibiotic resistance gene as a selectable marker for plant cell transformation. Nature 304:184–187
11. Fraley RT, Rogers SG, Horsch RB, Sanders PR, Flick JS, Adams SP, Bittner ML, Brand LA, Fink CL, Fry JS, Galluppi GR, Goldberg SB, Hoffman NL, Woo SC (1983) Expression of bacterial genes in plant cells. Proc Natl Acad Sci 80:4803–4807
12. Herrera-Estrella L, Depicker M, van Montagu M, Schell J (1983) Expression of chimaeric genes transferred into plant cells using a Ti-plasmid-derived vector. Nature 303:209–213
13. Murai N, Sutton DW, Murray MG, Slightom JL, Merlo DJ, Reichert NA, Sengupta-Gopalan C, Stock CA, Barker RF, Kemp JD, Hall TC (1983) Phaseolin gene from bean is expressed after transfer to sunflower via tumor-inducing plasmid vectors. Science 222:476–482
14. Zupan J, Muth TR, Draper O, Zambryski P (2000) The transfer of DNA from *Agrobacterium tumefaciens* into plants: a feast of fundamental insights. Plant J 23:11–28
15. Sheng J, Citovsky V (1996) *Agrobacterium* – plant cell DNA transport: have virulence proteins, will travel. Plant Cell 8:1699–1710
16. Chilton M-D, Tepfer DA, Petit A, David C, Casse-Delbart T, Tempé J (1982) *Agrobacterium rhizogenes* inserts T-DNA into the genomes of the host plant root cells. Nature 295:432–434
17. Sahi SV, Chilton M-D, Chilton WS (1990) Corn metabolites affect growth and virulence of *Agrobacterium tumefaciens*. Proc Natl Acad Sci USA 87:3879–3883
18. Usami S, Morikawa S, Takebe I, Machida Y (1987) Absence in monocotyledonous plants at the diffusible plant factors inducing T-DNA circularization and *vir* gene expression in *Agrobacterium*. Mol Gen Genet 209:221–226
19. Narasimhulu SB, Deng X, Sarria R, Gelvin SB (1996) Early transcription of *Agrobacterium* T-DNA genes in tobacco and maize. Plant Cell 8:873–886
20. Hansen G (2000) Evidence for *Agrobacterium*-induced apoptosis in maize cells. Mol Plant Microbe Interact 13: 649–657
21. Nadolska-Orczyk A, Orczyk W, Przetakiewicz A (2000) *Agrobacterium* -mediated transformation of cereals – from technique development to its application. Acta Physiol Plant 22:77–88
22. Sevón N, Oksman-Caldentey K-M (2002) *Agrobacterium rhizogenes*-mediated transformation: root cultures as a source of alkaloids. Planta Med 68:859–868
23. Palazón J, Cusidó RM, Roig C, Piñol MT (1998) Expression of the *rol*C gene and nicotine production in transgenic roots and their regenerated plants. Plant Cell Rep 17:384–390
24. Bonhomme V, Laurain-Mattar D, Lacoux J, Fliniaux M-A, Jacquin-Dubreuil A (2000) Tropane alkaloid production by hairy roots of *Atropa belladonna* obtained after transformation with *Agrobacterium rhizogenes* 15834 and *Agrobacterium tumefaciens* containing *rol A*, *B*, *C* genes only. J Biotechnol 81:151–158
25. Chriqui D, Guivarch A, Dewitte W, Prinsen E, van Onkelen H (1996) *Rol* genes and root initiation and development. Plant Soil 187:47–55
26. Jouhikainen K, Lindgren L, Jokelainen T, Hiltunen R, Teeri T, Oksman-Caldentey K-M (1999) Enhancement of scopolamine production in *Hyoscyamus muticus* L. hairy root cultures by genetic engineering. Planta 208:545–551
27. Zhang L, Ding R, Chai Y, Bonfill M, Moyano E, Oksman-Caldentey K-M, Xu T, Pi Y, Wang Z, Zhang H, Kai G, Liao Z, Sun K, Tang K (2004) Engineering tropane alkaloid pathway in *Hyoscyamus niger* hairy root cultures. Proc Natl Acad Sci USA 101:6786–6791. doi:6786
28. Georgiev MI, Pavlov AI, Bley T (2007) Hairy root type plant in vitro systems as sources of bioactive substances. Appl Microbiol Biotechnol 74:1175–1185
29. Srivastava S, Srivastava AK (2007) Hairy root culture for mass-production of high-value secondary metabolites. Crit Rev Biotechnol 27:29–43
30. Sudha CG, Obul RB, Ravishankar GA, Seeni S (2003) Production of ajmalicine and ajmaline in hairy root cultures of *Rauvolfia micrantha* Hook F., a rare and endemic medicinal plant. Biotechnol Lett 25:631–636
31. Weathers P, Bunk G, McCoy MC (2005) The effect of phytohormones on growth and artemisinin production in *Artemisia annua* hairy roots. In Vitro Cell Dev B 41:47–53
32. Park S-U, Facchini P (2000) *Agrobacterium rhizogenes*-mediated transformation of opium poppy, *Papaver somniferum* L., and California poppy, *Eschscholzia californica* Cham., root cultures. J Exp Bot 347:1005–1006

33. Pavlov A, Bley T (2006) Betalains biosynthesis by *Beta vulgaris* L. hairy root culture in different bioreactor systems. Process Biochem 41:848–852
34. Saito K, Sudo H, Yamazaki M, Koseki-Nakamura M, Kitajima M, Takayama H, Aimi N (2001) Feasible production of camptothecin by hairy root culture of *Ophiorrhiza pumila*. Plant Cell Rep 20:267–271
35. Lorence A, Medina-Bolivar F, Nessler CL (2004) Camptothecin and 10-hydroxycamptothecin from *Camptotheca acuminata* hairy roots. Plant Cell Rep 22:437–441
36. Georgiev M, Heinrich M, Kerns G, Pavlov A, Bley T (2006) Production of iridoids and phenolics by transformed *Harpagophytum procumbens* root cultures. Eng Life Sci 6:593–596
37. Sung H, Huang S-Y (2006) Medium optimization of transformed root cultures of *Stizolobium hassjoo* producing L-DOPA with response surface methodology. Biotechnol Bioeng 94:441–447
38. Fu C-X, Xu Y-J, Zhao D-X, Ma FS (2006) A comparison between hairy root cultures and wild plants of *Saussurea involucrata* in phenylpropanoids production. Plant Cell Rep 24:750–754
39. Jung G, Tepfer D (1987) Use of genetic transformation by the Ri T-DNA of *Agrobacterium rhizogenes* to stimulate biomass and tropane alkaloid production in *Atropa belladonna* and *Calystegia sepium* roots grown *in vitro*. J Ferment Bioeng 85:454–457
40. Shimomura K, Sauerwein M, Ishimaru K (1991) Tropane alkaloids in the adventitious and hairy root cultures of *Solanaceous* plants. Phytochemistry 30:2275–2278
41. Dupraz JM, Christen P, Kapetanidis I (1994) Tropane alkaloids in transformed roots of *Datura quercifolia*. Planta Med 60: 158–162
42. Mano Y, Ohkawa H, Yamada Y (1989) Production of tropane alkaloids by hairy root cultures of *Duboisia Leichhardtii* transformed by *Agrobacterium rhizogenes*. Plant Sci 59: 191–201
43. Christen P, Robert MF, Phillipson JD, Evans WC (1991) Alkaloids of hairy root cultures of a *Datura candida* hybrid. Plant Cell Rep 9:101–104
44. Dechaux C, Boitel-Conti M (2005) A Strategy for overaccumulation of scopolamine in *Datura innoxia* hairy root cultures. Acta Biol Cracov Bot 47:101–107
45. Häkkinen ST, Moyano E, Cusidó RM, Palazón J, Piñol MT, Oksman-Caldentey K-M (2005) Enhanced secretion of tropane alkaloids in *Nicotiana tabacum* hairy roots expressing heterologous hyoscyamine-6beta-hydroxylase. J Exp Bot 420: 2611–2618
46. Zhang L, Ding R, Chai Y, Bonfill M, Moyano E, Oksman-Caldentey K-M, Xu T, Pi Y, Wang Z, Zhang H, Kai G, Liao Z, Sun X, Tang K (2004) Engineering tropane biosynthetic pathway in *Hyoscyamus niger* hairy root cultures. Proc Natl Acad Sci 1117 USA 101:6786–6791
47. Jacob A, Malpathak N (2004) Green hairy root cultures of *Solanum khasianum* Clarke – a new route to *in vitro* solasodine production. Curr Sci 87:1442–1447
48. Huang Z, Mu Y, Zhou Y, Chen W, Xu K, Yu Z, Bian Y, Yang Q (1997) Transformation of *Taxus brevifolia* by *Agrobacterium rhizogenes* and taxol production in hairy root culture. Acta Bot Yunnanica 19:292–296
49. Palazón J, Cusidó RM, Gonzalo J, Bonfill M, Morales C, Piñol MT (1998) Relation between the amount of rolC gene product and indole alkaloid accumulation in *Catharanthus roseus* transformed root cultures. J Plant Physiol 153:712–718
50. Bhagwath SG, Hjortso MA (2000) Statistical analysis of elicitation strategies for thiarubrine. A production in hairy root cultures of *Ambrosia artemisiifolia*. J Biotechnol 80: 159–167
51. Wink M, Alfermann AW, Franke R, Wetterauer B, Distl M, Windhoevel J, Krohn O, Fuss E, Garden H, Mohagheghzadeh A, Wildi EJ, Ripplinger P (2005) Sustainable bioproduction of phytochemicals by plant *in vitro* cultures: anticancer agents. Plant Gene Res 3:90–100
52. Hamill JD, Robins RJ, Rhodes MJC (1989) Alkaloid production by transformed root cultures of *Cinchona ledgeriana*. Planta Med 55:354–357
53. Trotin F, Moumou Y, Vasseur J (1993) Flavanol production by *Fagopyrum esculentum* hairy and normal root cultures. Phytochemistry 32:929–931
54. Sato K, Yamazaki T, Okuyama E, Yoshihira K & Shimomura K (1991) Anthraquinones production by transformed root cultures of *Rubia tinctorum*: Influence of phytohormones and sucrose concentration. Phytochemistry 30:1507–1509
55. Croes AF, Vander Berg AJR, Bosveld M, Breteler H, Wullems GJ (1989) Thiophene accumulation in relation to morphology in roots of *Tagetes patula*. Effects of auxin and transformation by *Agrobacterium*. Planta Med 179:43–50
56. Granicher F, Christen P, Kapetandis I (1992) High-yield production of valepotriates by hairy root cultures of *Valeriana officnalis* L. var. *sambucifolia* Mikan. Plant Cell Rep 11:339–342
57. Oksman-Caldentey K-M, Kivelä O, Hiltunen R (1991) Spontaneous shoot organogenesis and plant regeneration from hairy root cultures of *Hyoscyamus muticus*. Plant Sci 78:129–136
58. Su WW (2006) Bioreactor engineering for recombinant protein production using plant cell suspension culture. In: Gupta SD, Ibaraki Y (eds) Plant tissue culture engineering. Springer, The Netherlands, pp 135–159
59. Choi YE, Kim YS, Paek KY (2006) Types and designs of bioreactors for hairy root culture. In: Gupta SD, Ibaraki Y (eds) Plant tissue culture engineering. Springer, The Netherlands, pp 161–172
60. Eibl R, Kaiser S, Lombriser R, Eibl D (2010) Disposable bioreactors: the current state-of-art and recommended applications in biotechnology. Appl Microbiol Biotechnol 86:41–49
61. Eibl R, Werner S, Eibl D (2009) Bag bioreactor based on wave-induced motion: characteristics and applications. Adv Biochem Eng Biotechnol 115:55–87
62. Eibl R, Eibl D (2002) Bioreactors for plant cell and tissue cultures. In: Oksman-Caldentey K-M, Barz WH (eds) Plant biotechnology and transgenic plants. Marcel Dekker, Basel, pp 163–199

63. Palazón J, Mallol A, Lettenbauer C, Cusidó RM, Piñol MT (2003) Growth and gingenoside production in hairy root cultures of *Panax ginseng* using a novel bioreactor. Planta Med 69:344–349
64. Bentebibel S, Moyano E, Palazón J, Cusidó RM, Bonfill M, Eibl R, Piñol MT (2005) Effects of immobilization by entrapment in alginate and scale-up on paclitaxel and baccatin III production in cell suspension cultures of *Taxus baccata*. Biotechnol Bioeng 89:647–655
65. Bonfill M, Bentebibel S, Moyano E, Palazón J, Cusidó RM, Piñol MT (2008) Paclitaxel and baccatin III production induced by methyl jasmonate in free and immobilized cells of *Taxus baccata*. Biol Plant 51:647–652
66. Ramachandra Rao S, Ravishankar GA (2002) Plant cell cultures: chemical factories of secondary metabolites. Biotechnol Adv 20:101–153
67. Robins RJ, Rhodes MJC (1986) The stimulation of anthraquinone production by *Cinchona ledgeriana* cultures with polymeric adsorbents. Appl Microbiol Biotechnol 24:35–41
68. Knuth ME, Sahai OP (1991) Flavour composition and method. US Patent 5,068,184, 26 Nov 1991
69. Beiderbeck R, Knoop B (1987) Two-phase culture. In: Constael F, Vasil I (eds) Cell culture and somatic cell genetics of plants, vol 5. Academic, San Diego, pp 255–266
70. Van Uden W, Woedenbag HJ, Pras N (1994) Cyclodextrins as a useful tool for bioconversion in plant cell biotechnology. Plant Cell Tiss Org 38:103–113
71. Oksman-Caldentey K-M, Vuorela H, Strauss A, Hiltunen R (1987) Variation in the tropane alkaloid content of *Hyoscyamus muticus* plants and cell culture clones. Planta Med 53:349–354
72. Mano Y, Ohkawa H, Yamada Y (1989) Production of tropane alkaloids by hairy root cultures of *Duboisia leichhardtii* transformed by *Agrobacterium rhizogenes*. Plant Sci 59:191–201
73. Berlin J (1980) Para-fluorophenylalanine resistant cell lines of tobacco. Z Pflanzenphysiol 97:317–324
74. Widholm JM (1974) Evidence for compartmentation of tryptophan in cultured plant tissues. Free tryptophan levels and inhibition of anthranilate synthetase. Physiol Plant 30:323–326
75. Wataneba K, Yano SI, Yamada Y (1982) Selection of cultured plant cell lines producing high levels of biotin. Phytochemicals 21:513–516
76. Larkin PJ, Scowcroft WR (1981) Somaclonal variation – a novel source of variability from cell cultures for plant improvement. Theor Appl Genet 60:197–214
77. Zhang KR, John PCL (2005) Raised level of cyclin dependent kinase A after prolonged suspension culture of *Nicotiana plumbaginifolia* is associated with more rapid growth and division, diminished cytoskeleton and lost capacity for regeneration: implications for instability of cultures plant cells. Plant Cell Tissue Organ Cult 82:295–308
78. Shiba T, Mii M (2005) Visual selection and maintenance of the cell lines with high plant regeneration ability and low ploidy level in *Dianthus acicularis* by monitoring with flow cytometry analysis. Plant Cell Rep 24:572–580
79. Pikaard CS (2001) Genomic change and gene silencing in polyploids. Trends Genet 17:675–677
80. Hirasuna TJ, Pestchanker LJ, Srinivasan V, Shuler ML (1996) Taxol production in suspension cultures of *Taxus baccata*. Plant Cell Tiss Org 44:95–102
81. Wallaart TE, Pras N, Quax WJ (1999) Seasonal variations of artemisinin and its biosynthetic precursors in tetraploid *Artemisia annua* plants compared with the diploid wild-type. Planta Med 65:723–728
82. Deus-Neumann B, Zenk MH (1984) Instability of indole alkaloid production in *Catharanthus roseus* cell suspension-cultures. Planta Med 50:427–431
83. Qu JG, Zhang W, Yu XJ, Jin MF (2005) Instability of anthocyanin accumulation in *Vitis vinifera* L. var. Gamay Freaux suspension cultures. Biotechnol Bioprocess Eng 10:155–161
84. Wilhelmson A, Häkkinen ST, Kallio P, Oksman-Caldentey K-M, Nuutila AM (2006) Heterologous expression of *Vitreoscilla* hemoglobin (VHb) and cultivation conditions affect the alkaloid profile of *Hyoscyamus muticus* hairy roots. Biotechnol Prog 22:350–358
85. Knobloch KH, Berlin J (1980) Influence of medium composition on the formation of secondary compounds in cell suspension cultures of *Catharanthus roseus* L. G. Don. Z Naturforsch 35C:551–556
86. Berlin J, Forche E, Wray V, Hammer J, Hosel W (1983) Formation of benzophenanthridine alkaloids by suspension cultures of *Eschscholtzia californica*. Z Naturforsch 38:346–352
87. Fujita Y, Tabata M, Nishi A, Yamada Y (1982) New medium and production of secondary compounds with two-staged culture medium. In: Fujiwara A (ed) Plant tissue culture. Maruzen, Tokyo, pp 399–400
88. Payne J, Hamill JD, Robins RJ, Rhodes MJC (1987) Production of hyoscyamine by "hairy root" cultures of *Datura stramonium*. Planta Med 53:474–478
89. Mantell SH, Pearson DW, Hazell LP, Smith H (1983) The effect of initial phosphate and sucrose levels on nicotine accumulation in batch suspension cultures of *Nicotiana tabacum* L. Plant Cell Rep 1:73–77
90. Toivonen L, Ojala M, Kauppinen V (1991) Studies on the optimization of growth and indole alkalooid production by hairy root cultures of *Catharanthus roseus*. Biotechnol Bioeng 37:673–680
91. Do CB, Cormier F (1991) Effects of low nitrate and high sugar concentrations on anthocyanin content and composition of grape (*Vitis vinifera* L.) cell suspension. Plant Cell Rep 9:500–504
92. Ishikawa A, Yoshihara T, Nakamura K (1994) Jasmonate-inducible expression of a potato cathepsin D inhibitor-GUS gene fusion in tobacco cells. Plant Mol Biol 26:403–414
93. Tiburcio AF, Kaur-Sawhney R, Ingersoll R, Galston AW (1985) Correlation between polyamines and pyrrolidine in developing tobacco callus. Plant Physiol 78:323–326
94. Zenk MH, El-Shagi, E, Schulte U (1975) Anthraquinone production by cell suspension cultures of *Morinda citrifolia*. Planta Med 28:79–101

95. Tabata M (1988) Naphtoquinones. In: Constael F, Vasil I (eds) Cell culture and somatic cell genetics of plants, vol 5. Academic, San Diego, pp 99–111
96. Rajendran L, Ravishankar GA, Venkataraman LV, Prathiba KR (1992) Anthocyanin production in callus cultures of *Daucus carota* L. as influenced by nutrient stress and osmoticum. Biotechnol Lett 14:707–714
97. Kolewe ME, Gaurav V, Roberst SC (2008) Pharmaceutically active natural product synthesis and supply via plant cell culture technology. Mol Pharm 5:243–256
98. Goossens A, Häkkinen ST, Laakso I, Seppänen-Laakso T, Biondi S, De Sutter V, Lammertyn F, Nuutila AM, Söderlund H, Zabeau M, Inzé D, Oksman-Caldentey K-M (2003) A functional genomics approach toward the understanding of secondary metabolism in plant cells. Proc Natl Acad Sci USA 100:8595–8600
99. Vasconsuelo AA, Boland R (2007) Molecular aspects of the early stages of elicitation of secondary metabolites in plants. Plant Sci 172:861–875
100. Pauwels L, Barbero GF, Geerinck J, Tilleman S, Grunewald W, Pérez AC, Chico JM, Bossche RV, Sewell J, Gil E, García-Casado G, Witters E, Inzé D, Long JA, De Jaeger G, Solano R, Goossens A (2010) NINJA connects the co-repressor TOPLESS to jasmonate signalling. Nature 464:788–791
101. Lee-Parsons CW, Royce AJ (2006) Precursor limitations in methyl jasmonate-induced *Catharanthus roseus* cell cultures. Plant Cell Rep 25:607–612
102. Rischer H, Orešič M, Seppänen-Laakso T, Katajamaa M, Lammertyn F, Ardiles-Diaz W, Van Montagu MCE, Inzé D, Oksman-Caldentey K-M, Goossens A (2006) Gene-to-metabolite networks for terpenoid indole alkaloid biosynthesis in *Catharanthus roseus* cells. Proc Natl Acad Sci 103:5614–5619
103. Yukimune Y, Tabata H, Higashi Y, Hara Y (1996) Methyl jasmonate-induced overproduction of paclitaxel and baccatin III in *Taxus* cell suspension cultures. Nat Biotechnol 14:1129–1132
104. Sevón N, Hiltunen R, Oksman-Caldentey K-M (1992) Chitosan increases hyoscyamine content in hairy root cultures of *Hyoscyamus muticus*. Pharm Pharmacol Lett 2:96–99
105. Vasconsuelo AA, Giuletti AM, Picotto G, Rodriguez-Talou J, Boland R (2003) Involvement of the PLC/PKC pathway in chitosan-induced anthraquinone production by *Rubia tinctorium* L. cell cultures. Plant Sci 165:429–436
106. Namdeo AG (2010) Plant cell elicitation for production of secondary metabolites: a review. Pharmacogn Rev 1:69–79
107. Bringmann G, Wohlfarth M, Rischer H, Grüne M, Schlauer J (2000) A new biosynthetic pathway to alkaloids in plants: acetogenic isoquinolines. Angew Chem Int Ed 39:1464–1466
108. Wildung MR, Croteau R (1996) A cDNA clone for taxadiene synthase, the diterpene synthase, the diterpene cyclise that catalyzes the committed step of taxol biosynthesis. J Biol Chem 271:9201–9204
109. Kaspera R, Croteau R (2006) Cytochrome P450 oxygenases of taxol biosynthesis. Phytochem Rev 5:433–444
110. Jennewein S, Wildung MR, Chau M, Walker K, Croteau R (2004) Random sequencing of an induced *Taxus* cell cDNA library for identification of clones involved in taxol biosynthesis. Proc Natl Acad Sci USA 101:9149–9154
111. Sun C, Li Y, Wu Q, Luo H, Sun Y, Song J, Lui EMK, Chen S (2010) *De novo* sequencing and analysis of the American ginseng root transcriptome using a GS FLX titanium platform to discover putative genes involved in ginsenoside biosynthesis. BMC Genomics 11:262–273
112. Memelink J, Verpoorte R, Kijne JW (2001) ORCAnization of jasmonate-responsive gene expression in alkaloid metabolism. Trends Plant Sci 6:212–219
113. Potenza C, Aleman L, Sengupta-Gopalan C (2004) Targeting transgene expression in research, agricultural, and environmental applications:promoters used in plant transformation. In Vitro Cell Dev B 40:1–22
114. Yoshida K, Shinmyo A (2000) Transgene expression systems in plant, a natural bioreactor. J Biosci Bioeng 90:353–362
115. Guilley H, Dudley RK, Jonard G, Balázs E, Richards KE (1982) Transcription of cauliflower mosaic virus DNA: detection of promoter sequences, and characterization of transcripts. Cell 30:763–773
116. Odell JT, Nagy F, Chua NH (1985) Identification of DNA sequences required for activity of the cauliflower mosaic virus 35S promoter. Nature 313:810–812
117. Fang RX, Nagy F, Sivasubramanian S, Chua NH (1989) Multiple *cis* regulatory elements for maximal expression of the cauliflower mosaic virus 35S promoter in transgenic plants. Plant Cell 1:141–150
118. Kay R, Chan A, Daly M, McPherson J (1987) Duplication of CaMV 35S promoter sequences creates a strong enhancer for plant genes. Science 236:1299–1302
119. Zárate R, Verpoorte R (2007) Strategies for the genetic modification of the medicinal plant *Catharanthus roseus* (L.) G. Don. Phytochem Rev 6:475–491
120. Weathers PJ, Towler MJ, Xu J (2010) Bench to batch: advances in plant cell culture for producing useful products. Appl Microbiol Biotechnol 85:1339–1351
121. Naqvi S, Farré G, Sanahuja G, Capell T, Zhu C, Christou P (2010) When more is better: multigene engineering in plants. Trends Plant Sci 15:48–56
122. Peremarti A, Twyman RM, Gómes-Galera S, Naqvi S, Farré G, Sabalza M, Miralpeix B, Dashevskaya S, Yuan D, Ramessar K, Christou P, Zhu C, Bassie L, Capell T (2010) Promoter diversity in multigene transformation. Plant Mol Biol 73:363–378
123. Dudareva N, Negre F, Nagegowda DA, Orlova I (2006) Plant volatiles: recent advances and future prospects. Crit Rev Plant Sci 25:417–440
124. Nagegowda DA (2010) Plant volatile terpenoid metabolism: biosynthetic genes, transcriptional regulation and subcellular compartmentation. FEBS Lett 584:2965–2973
125. Wu S, Schalk M, Clark A, Miles RB, Coates R, Chappell J (2006) Redirection of cytosolic or plastidic isoprenoid precursors elevates terpene production in plants. Nat Biotechnol 24:1441–1447

126. Ohara K, Ujihara T, Endo T, Sato F, Yazaki K (2003) Limonene production in tobacco with *Perilla* limonene synthase cDNA. J Exp Bot 54:2635–2642
127. Chappell J, Wolf F, Proulx J, Cuella R, Saunders C (1995) Is the reaction catalyzed by 3-hydroxy-3-methylglutaryl coenzyme A reductase a rate-limiting step for isoprenoid biosynthesis in plants. Plant Physiol 109:1337–1343
128. Winkel BSJ (2004) Metabolic channeling in plants. Annu Rev Plant Biol 55:85–107
129. Kristensen C, Morant M, Olsen CE, Ekstrøm CT, Galbraith DW, Lindberg Møller B, Bak S (2005) Metabolic engineering of dhurrin in transgenic *Arabidopsis* plants with marginal inadvertent effects on the metabolome and transcriptome. Proc Natl Acad Sci USA 102:1779–1784
130. Aharoni A, Jongsma MA, Bouwmeester HJ (2005) Volatile science? Metabolic engineering of terpenoids in plants. Trends Plant Sci 10:594–602
131. Ma JK, Hiatt A, Hein M, Vine ND, Wang F, Stabila P, van Dolleweerd C, Mostov K, Lehner T (1995) Generation and assembly of secretory antibodies in plants. Science 268:716–719
132. Jobling SA, Westcott RJ, Tayal A, Jeffcoat R, Schwall GP (2002) Production of a freeze-thaw-stable potato starch by antisense inhibition of three starch synthase genes. Nat Biotechnol 20:295–299
133. Zhu C, Naqvi S, Breitenbach J, Sandmann G, Christou P, Capell T (2008) Combinatorial genetic transformation generates a library of metabolic phenotypes for the carotenoid pathway in maize. Proc Natl Acad Sci USA 105:18232–18237
134. Fujisawa M, Takita E, Harada H, Sakurai N, Suzuki H, Ohyama K, Shibata D, Misawa N (2009) Pathway engineering of *Brassica napus* seeds using multiple key enzyme genes involved in ketocarotenoid formation. J Exp Bot 60:1319–1332
135. Yun D-J, Hashimoto T, Yamada Y (1992) Metabolic engineering of medicinal plants: transgenic *Atropa belladonna* with an improved alkaloid composition. Proc Natl Acad Sci USA 89:11799–11803
136. Laurila J, Laakso I, Valkonen JPT, Hiltunen R, Pehu E (1996) Formation of parental-type and novel glycoalkaloids in somatic hybrids between *Solanum brevidens* and *S. tuberosum*. Plant Sci 118:145–155
137. Little DB, Croteau RB (2002) Alteration of product formation by directed mutagenesis and truncation of the multiple-product sesquiterpene synthases δ-selinene synthase and γ-humulene synthase. Arch Biochem Biophys 402:120–135
138. Runguphan W, O'Connor SE (2009) Metabolic reprogramming of periwinkle plant culture. Nat Chem Biol 5:151–153
139. Trethewey RN, Krozky AJ, Willmitzer L (1999) Metabolic profiling: a Rosetta stone for genomics? Curr Opin Plant Biol 2:83–85
140. Oksman-Caldentey K-M, Saito K (2005) Integrating genomics and metabolomics for engineering plant metabolic pathways. Curr Opin Biotechnol 16:174–179
141. Wheeler GL, Jones MA, Smirnoff N (1998) The biosynthetic pathway of vitamin C in higher plants. Nature 393:365–369
142. Ratcliffe RG, Shachar-Hill Y (2005) Revealing metabolic phenotypes in plants: inputs from NMR analysis. Biol Rev 80:27–43
143. Kruger NJ, Ratcliffe RG (2007) Dynamic metabolic networks: going with the flow. Phytochemistry 68:2136–2138
144. Kruger NJ, Huddleston JE, Le Lay P, Brown ND, Ratcliffe RG (2007) Network flux analysis: impact of 13C-substrates on metabolism in *Arabidopsis thaliana* cell suspension cultures. Phytochemistry 68:2176–2188
145. Rischer H, Oksman-Caldentey K-M (2006) Unintended effects in genetically modified crops: revealed by metabolomics? Trends Biotechnol 24:102–104

Books and Reviews

Allen DK, Libourel IG, Shachar-Hill Y (2009) Metabolic flux analysis in plants: coping with complexity. Plant Cell Environ 32:1241–1257

Bhagwath SG, Hjortso MA (2000) J Biotechnol 80:159–167

Bonhomme V, Laurain-Mattar D, Lacoux J, Fliniaux M, Jacquin-Dubreuil A (2000) J Biotechnol 81:151–158

Buchanan BB, Gruissem W, Russell LJ (eds) (2000) Biochemistry & molecular biology of plants. American Society of Plant Physiologists, Rockville, p 1367

Christen P, Robert MF, Phillipson JD, Evans WC (1991) Plant Cell Rep 9:101–104

Croes AF, Vander Berg AJR, Bosveld M, Breteler H, Wullems GJ (1989) Planta Med 179:43–50

Dechaux C, Boitel-Conti M (2005) Acta Biol Cracov Bot 47:101–107

Du H, Huang Y, Tang Y (2010) Genetic and metabolic engineering of isoflavonoid biosynthesis. Appl Microbiol Biotechnol 86:1293–1312

Dudareva N, Pichersky E (2008) Metabolic engineering of plant volatiles. Curr Opin Biotechnol 19:181–189

Dupraz JM, Christen P, Kapetanidis I (1994) Planta Med 60:158–162

Fu C-X, Xu Y-J, Zhao D-X, Ma FS (2006) Plant Cell Rep 24:750–754

Georgiev M, Heinrich M, Kerns G, Pavlov A, Bley T (2006) Eng Life Sci 6:593–596

Georgiev MI, Pavlov AI, Bley T (2007) Hairy root type plant in vitro systems as sources of bioactive substances. Appl Microbiol Biotechnol 74:1175–1185

Granicher F, Christen P, Kapetandis I (1992) Plant Cell Rep 11:339–342

Häkkinen ST, Moyano E, Cusidó RM, Palazón J, Piñol MT, Oksman-Caldentey K-M (2005) J Exp Bot 420:2611–2618

Häkkinen ST, Oksman-Caldentey K-M (2004) Regulation of secondary metabolism in tobacco cell cultures. In: Nagata T, Hasezawa S, Inzé D (eds) Biotechnology in agriculture and forestry, vol 53, Tobacco BY-2 cells. Springer, Berlin/Heidelberg, pp 231–249

Hamill JD, Robins RJ, Rhodes MJC (1989) Planta Med 55:354–357

Huang Z, Mu Y, Zhou Y, Chen W, Xu K, Yu Z, Bian Y, Yang Q (1997) Acta Bot Yunnanica 19:292–296

Jacob A, Malpathak N (2004) Curr Sci 87:1442–1447
Jouhikainen K, Lindgren L, Jokelainen T, Hiltunen R, Oksman-Caldentey K-M (1999) Enhancement of scopolamine production in *Hyscyamus muticus* L. hairy root cultures by genetic engineering. Planta 208:545–551
Jung G, Tepfer D (1987) J Ferment Bioeng 85:454–457
Lorence A, Medina-Bolivar F, Nessler CL (2004) Plant Cell Rep 22:437–441
Mano Y, Ohkawa H, Yamada Y (1989) Plant Sci 59:191–201
Nascimiento NC, Fett-Neto AG (2010) Plant secondary metabolism and challenges in modifying its operation: an overview. Meth Mol Biol 643:1–13
Oksman-Caldentey K-M, Barz W (eds) (2002) Plant biotechnology and transgenic plants. Marcel and Dekker, New York, p 719
Oksman-Caldentey K-M, Inzé D (2004) Plant cell factories in the post-genomic era: new ways to produce designer secondary metabolites. Trends Plant Sci 9:433–440
Oksman-Caldentey K-M, Inzé D, Orešič M (2004) Connecting genes to metabolites by a systems biology approach. Proc Natl Acad Sci USA 101:9949–9950
Palazón J, Cusidó RM, Gonzalo J, Bonfill M, Morales C, Piñol MT (1998) J Plant Physiol 153:712–718
Park S-U, Facchini P (2000) J Exp Bot 347:1005–1006
Pavlov A, Bley T (2006) Process Biochem 41:848–852
Rischer H, Oksman-Caldentey K-M (2005) Biotechnological utilization of plant genetic resources for the production of phytopharmaceuticals. Plant Gen Resour 3:83–89
Saito K, Dixon RD, Willmitzer L (2006) Plant metabolomics. In: Nagata T, Lörz H, Widholm JM (eds) Biotechnology in agriculture and forestry, vol 57. Springer, Berlin/Heidelberg, p 347
Saito K, Sudo H, Yamazaki M, Koseki-Nakamura M, Kitajima M, Takayama H, Aimi N (2001) Plant Cell Rep 20:267–271
Saito K, Yamazaki T, Okuyama E, Yoshihira K, Shimomura K (1991) Phytochemistry 30:2977–2980
Samuelsson G (2004) Drugs of natural origin. A textbook of pharmacognocy, 5th edn. Swedish Pharmaceutical Press, Stockholm, pp 473–575
Schäfer H, Wink M (2009) Medicinally important secondary metabolites in recombinant microorganisms or plants: progress in alkaloid biosynthesis. Biotechnol J 4:1684–1703
Sevón N, Oksman-Caldentey K-M (2002) *Agrobacterium rhizogenes*-mediated transformation: root cultures as a source of alkaloids. Planta Med 68:859–868
Shimomura K, Sauerwein M, Ishimaru K (1991) Phytochemistry 30:2275–2278
Srivastava S, Srivastava AK (2007) Hairy root culture for mass-production of high-value secondary metabolites. Crit Rev Biotechnol 27:29–43
Sudha CG, Obul RB, Ravishankar GA, Seeni S (2003) Biotechnol Lett 25:631–636
Sung H, Huang S-Y (2006) Biotechnol Bioeng 94:441–447
Trotin F, Moumou Y, Vasseur J (1993) Phytochemistry 32:929–931
Verpoorte R, Alfermann AW (eds) (2000) Metabolic engineering of plant secondary metabolism. Academic, Dordrecht, p 286
Verpoorte R, Alfermann AW, Johnson TS (eds) (2007) Applications of plant metabolic engineering. Springer, Dordrecht, p 332
Weathers P, Bunk G, McCoy MC (2005) In Vitro Cell Dev B 41:47–53
Wink M, Alfermann AW, Franke R, Wetterauer B, Distl M, Windhoevel J, Krohn O, Fuss E, Garden H, Mohagheghzadeh A, Wildi EJ, Ripplinger P (2005) Plant Gene Res 3:90–100
Zhang L, Ding R, Chai Y, Bonfill M, Moyano E, Oksman-Caldentey K-M, Xu T, Pi Y, Wang Z, Zhang H, Kai G, Liao Z, Sun X, Tang K (2004) Proc Natl Acad Sci USA 101:6786–6791

Membrane Electrolytes, from Perfluoro Sulfonic Acid (PFSA) to Hydrocarbon Ionomers

Kenji Miyatake
Clean Energy Research Center, University of Yamanashi, Kofu, Japan

Article Outline

Glossary
Definition of the Subject and Its Importance
Introduction
Perfluoro Sulfonic Acid Ionomer Membranes
Hydrocarbon Ionomer Membranes
Future Directions
Bibliography

Glossary

Hydrocarbon ionomers Polymers with hydrocarbon backbone (and generally no fluorine groups) and acidic functions.

Hydrophilic/hydrophobic phase separation Phase-separated morphology of ionomer membranes based on the differences in the hydrophilicity (and hydrophobicity) of the components.

Ion exchange capacity Amount of acidic or ion-exchangeable sites per weight or volume unit of ionomer membranes, often abbreviated as IEC. EW (equivalent weight, or weight of ionomer membranes per acidic or ion-exchangeable site) is a reciprocal of IEC.

Ionomers Originally defined as copolymers having one ionic group per polymer repeating unit, where composition of ion-containing copolymer unit is

less than 20%. Nowadays, often used to be synonymous with polymer electrolytes.

Ionic channels Network of acidic groups and water molecules, through which proton and/or hydronium ions can migrate.

Perfluoro sulfonic acid ionomers Copolymers composed of poly(tetrafluoroethylene) and poly (trifluoroethylene) with perfluoro sulfonic acid ether side chains.

Proton exchange membranes Membranes that can exchange protons with other cations or that can transport protons.

Definition of the Subject and Its Importance

Proton exchange membranes (PEMs) are one of the key materials in low-temperature fuel cells; proton exchange membrane fuel cells (PEMFCs); and direct methanol fuel cells (DMFCs). Especially, recent trend in the research and development of low-temperature fuel cells focuses on PEMFCs for transportation (electric vehicle) applications due to the impact on economy and environment. The most important role of PEMs is to transport protons formed as a product of oxidation reaction of fuels at the anode to the cathode, where oxygen reduction reaction takes place to produce water. In addition to this, there are a number of requirements for PEM materials for the practical fuel cell applications, which include

1. Proton conductivity (higher than 0.01 S/cm, hopefully 0.1 S/cm)
2. Chemical, physical (mechanical and dimensional), and thermal stability
3. Impermeability of fuels (hydrogen, methanol) and oxidants (air, oxygen)
4. Water transport capability (high water flux) from the cathode to the anode

   These properties have to be assured under a wide range of temperature and humidity (−30–120°C, nominal 0–100% relative humidity (RH)) considering the fabrication of membrane electrode assemblies (MEAs)
5. Easy processability and compatibility with the electrodes are also crucial factors

   For wide dissemination of fuel cells
6. Environmental adaptability (recyclability or disposability)
7. Low cost (final target for electric vehicle applications would be cheaper than US$ 10/m^2) need to be taken into account. While a number of PEMs have been developed, no single membranes fulfill all of these requirements. Currently, the most promising PEMs are perfluoro sulfonic acid (PFSA) ionomers. Another candidate second to the PFSA ionomers is non-fluorinated (or in some cases only slightly fluorinated) hydrocarbon ionomers. The aim of this chapter is to review the most recent progress on these two classes of ionomer membranes for low-temperature fuel cell applications

US DOE (Department of Energy) has set technical targets in PEMs for transportation applications (Table 1) [1]. The targets are for gas crossover (permeability), area-specific resistance, operating temperature, cost, and durability. In 2015, car companies will make a decision whether they continue their endeavor to commercialize fuel cell vehicles. The membrane scientists are facing a big challenge in order to help them go further with fuel cells.

Introduction

PFSA ionomers are copolymers of poly(tetrafluoroethylene) (PTFE) and poly(trifluoroethylene) with pendant perfluoro sulfonic acid groups. There are several industrial companies that supply the PFSA ionomers as resins, membranes, or solution. Such companies include DuPont, 3M, Asahi Kasei, Asahi Chemical, and Solvay Solexis. A general chemical structure of the PFSA ionomers is shown in Fig. 1. They share the similar chemical structure and the differences in them lie in the copolymer composition and the length of the pendant side chains and/or the presence of trifluoromethyl groups. Originally, DuPont developed the PFSAs in the 1950s. The PFSA membranes have a history as separator membranes in the chlor-alkali electrolysis industry. In this application, the PFSA membranes are used as single ion (Na^+) conductor. Typical PFSA membranes survive electrolysis operation under strongly basic conditions (>30% NaOH aq.) for more than several years retaining high current efficiency (>95%). Due to the hydrophobicity of fluorinated polymer main chains and strong acidity of the flexible side chains, the PFSA ionomer membranes show distinct hydrophilic/hydrophobic phase

Membrane Electrolytes, from Perfluoro Sulfonic Acid (PFSA) to Hydrocarbon Ionomers. Table 1 US Department of Energy (DOE) targets in PEMs for transportation applications

Characteristics	Units	Year 2010	Year 2015
O_2 crossover	mA/cm^2	2	2
H_2 crossover	mA/cm^2	2	2
Area-specific resistance at			
Maximum operating temperature and water partial pressures from 40 to 80 kPa	ohm cm^2	0.02	0.02
80°C water and water vapor partial pressure from 25 to 45 kPa	ohm cm^2	0.02	0.02
30°C water and water vapor partial pressure up to 4 kPa	ohm cm^2	0.03	0.03
−20°C	ohm cm^2	0.2	0.2
Maximum operating temperature	°C	120	120
Unassisted start from low temperature	°C	−40	−40
Cost	\$/m^2	20	20
Durability with cycling			
Mechanical	Cycles with <10 sccm crossover	20,000	20,000
Chemical	mA/cm^2 (H_2 crossover)	200	20

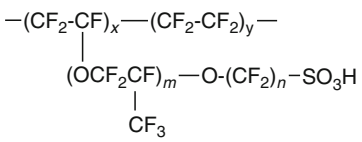

Membrane Electrolytes, from Perfluoro Sulfonic Acid (PFSA) to Hydrocarbon Ionomers. Figure 1 General chemical structure of the perfluoro sulfonic acid (PFSA) ionomers

separation. The sulfonic acid groups aggregate to form hydrophilic domains, while fluorinated main chains form hydrophobic domains with some crystallinity. When hydrated, hydrophilic domains (5–6 nm in diameter) contain water molecules and become interconnected, which are responsible for high proton transport capability or high proton conductivity. The morphology of PFSA membranes has been analyzed by small-angle X-ray scattering (SAXS), X-ray diffraction (XRD), small-angle neutron scattering (SANS), transmission electron microscopy (TEM), atomic force microscopy (AFM), and differential scanning calorimetry (DSC) techniques and well-reviewed in the books and articles. Short side chain and thus, high ion exchange capacity (IEC) and highly proton conductive PFSAs were developed by Dow and the membranes were used by Ballard Power Systems to realize high-performance PEMFCs in the mid-1980s. Since then, the PFSAs have been and will be the most studied PEMs for fuel cells. The recent research trends in PFSA membranes are summarized in Fig. 2. In order to fulfill the above-mentioned requirements, a considerable effort has been consumed especially in the last decade. They can be classified into six items; high-temperature operability, low-humidity operability, proton conductivity, mechanical stability, durability, and cost. Details of each approach can be found in the literature, and because of the limited space, only some of the representative examples are described in the next section.

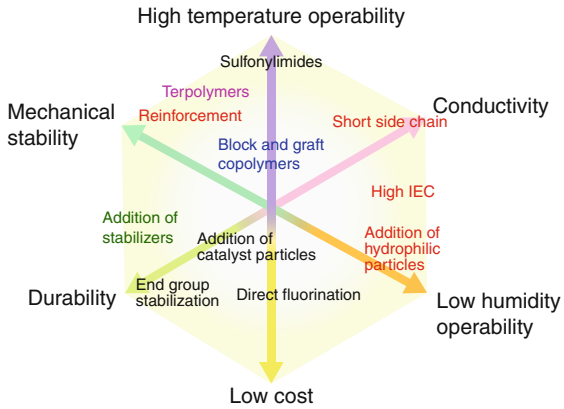

Membrane Electrolytes, from Perfluoro Sulfonic Acid (PFSA) to Hydrocarbon Ionomers. Figure 2 Recent research trends in perfluoro sulfonic acid (PFSA) membranes

Hydrocarbon ionomers have a rather longer history (ca. 100 years) as cation exchange resins. Original hydrocarbon ionomers were based on the sulfonated polystyrenes or phenol resins. In the earliest stage of the PEMFC research, such ionomer membranes were investigated. GE invented PEMFC with hydrocarbon ionomer membranes in the early 1960s. The operation time of the initial PEMFCs was very limited by the membrane durability. PFSA membranes have replaced them in the mid-1960s, and since then they have been the main option. However, the hydrocarbon ionomer materials have been reexamined in more detail in the last decade due to their possible lower production cost, more freedom in molecular design and chemical modification, and better environmental compatibility compared with PFSA ionomers. Hydrocarbon ionomers can be roughly classified into two classes, aromatic and aliphatic ionomers depending on their main chain structure. Most effort has been focused on aromatic ionomers due to their chemical robustness. A number of so-called engineering plastics, such as poly(phenylene)s, polyimides, poly(arylene ether)s, and poly(ether ether ketones)s have been utilized as a base skeleton. Nevertheless, none of the existing hydrocarbon ionomer membranes can compete with the PFSA ionomer membranes. The most critical issues of hydrocarbon ionomer membranes are still insufficient durability and large dependence of the proton conductivity upon humidity. The challenge is to achieve these two conflicting properties within a single ionomer membrane. Recent effective approaches are reviewed below.

Perfluoro Sulfonic Acid Ionomer Membranes

Short Side Chain PFSAs

The simplest way to improve the proton conductivity of ionomer membranes is to increase IEC, either by using monomers with short side chains or by increasing copolymer composition of sulfonic acid-containing units. The former approach seems preferable in terms of the mechanical properties of the membranes. This is the case of Dow membranes, which contain oxytetrafluoroethylene sulfonic acid groups. Due to the synthetic difficulties involving many reaction steps, Dow gave up supplying their short side chain PFSAs. However, due to their high potential as high proton conductive PEMs, a few kinds of short side chain PFSAs are currently available. In Table 2 are summarized chemical structure and molecular weight of representative monomers. Solvay Solexis has developed a simple preparation method of the short side chain vinyl monomers, which enabled them to produce the short side chain PFSAs at the industrial scale [2]. Nowadays, a number of short side chain PFSAs have been produced at the pilot scale from several companies [3, 4].

Figure 3 shows humidity dependence of the proton conductivity of PFSA membranes with different IEC values. In Fig. 4 is plotted proton conductivity of PFSA membranes at 110°C, 20% RH as a function of IEC value. The data shown in both figures clearly demonstrate that the proton conductivity increases with increasing IEC of the membrane material. However, there is still a gap in the conductivity between the current level and the target. The question is how high IEC would be required to reach 0.1 S/cm. Extrapolating the current line gives a rough value of IEC, 2–3 meq/g. Such high IEC membranes probably suffer from low mechanical and dimensional stability, which has to be addressed by appropriate molecular modifications such as cross-linking. Reinforcing with compatible resins (e.g., porous substrates or fabrics of PTFEs) may also be a possible option.

Membrane Electrolytes, from Perfluoro Sulfonic Acid (PFSA) to Hydrocarbon Ionomers. Table 2 Structure and molecular weight of monomers for PFSAs

Structure	Molecular weight (g/mol)	Suppliers
$CF_2 = CF - OCF_2CF - OCF_2CF_2 - SO_2F$ $\vert$ CF_3	446	Du Pont, Asahi Chemical, Asahi Glass, etc.
$CF_2 = CF - O(CF_2CF_2)_2 - SO_2F$	380	3M, Asahi Kasei, etc.
$CF_2 = CF - OCF_2CF_2 - SO_2F$	280	Dow (currently not available), Solvay Solexis, etc.

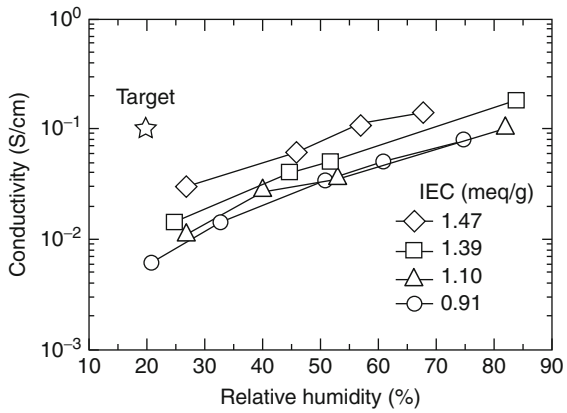

Membrane Electrolytes, from Perfluoro Sulfonic Acid (PFSA) to Hydrocarbon Ionomers. Figure 3
Humidity dependence of the proton conductivity of perfluoro sulfonic acid (PFSA) membranes at 110°C

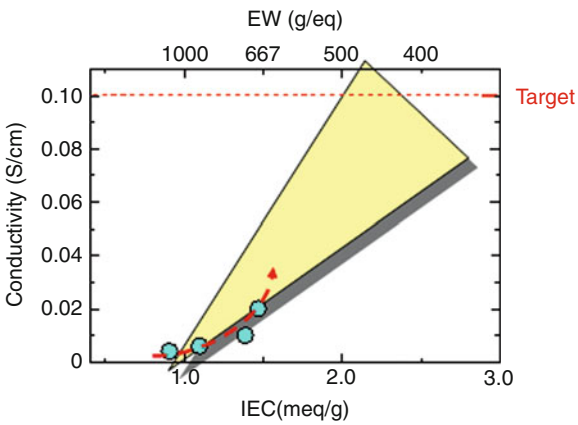

Membrane Electrolytes, from Perfluoro Sulfonic Acid (PFSA) to Hydrocarbon Ionomers. Figure 4
Proton conductivity of perfluoro sulfonic acid (PFSA) membranes at 110°C and 20% RH

In addition to the proton-conducting properties, short side chain provides additional advantages, such as high glass transition temperature and high decomposition temperature. For example, Solvay Solexis's short side chain PFSAs, known as Aquivion, show α relaxation transition at 160°C, which is ca. 50°C higher than that of the conventional long side chain PFSAs. This is a consequence of higher crystallinity of the short side chain PFSAs [5, 6]. Therefore, higher IEC membranes can be prepared from the short side chain

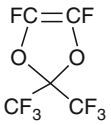

Membrane Electrolytes, from Perfluoro Sulfonic Acid (PFSA) to Hydrocarbon Ionomers. Figure 5
Chemical structure of bulky comonomer for the perfluoro sulfonic acid (PFSA) terpolymers

PFSAs with the same crystallinity (e.g., similar thermal and mechanical properties) with the long side chain PFSAs, or the same IEC membranes with the higher crystallinity.

Terpolymers

Asahi Glass has investigated the effect of third compounds and found that cyclic vinyl compounds, for example, 2,2-bis(trifluoromethyl)-4,5-difluoro-1,3-dioxole, functions well to improve the thermal and dimensional stability (Fig. 5) [7]. Similar to the short side chain ionomers, the terpolymer PFSAs showed higher elastic modulus and ca. 40°C higher softening temperature than those of the conventional long side chain PFSAs. The water absorbability of the terpolymers was nearly half in a wide range of temperature.

There seems to be a number of other candidates suitable as a third comonomer (e.g., trifluorovinyl monomers containing phosphonic acid, sulfonamide, sulfonimide, and/or cross-linkable moieties) [8–12], however, high production cost of these rather complex perfluorinated vinyl compounds may be an obstacle to the practical industrial applications.

Stabilized PFSAs

Despite the established durability of PFSAs as separator membranes in the chlor-alkali electrolysis, they fail to function as proton exchange membranes for longtime fuel cells operation. Typical PFSA membranes degrade and have pinholes within several hundred hours of operation under high temperature, low humidity, and open circuit voltage (OCV) conditions. It is generally recognized that the degradation of PFSA membranes is caused by hydroxide (HO·) radical, which is generated by the homolysis or the Fenton's reaction (catalyzed by Fe^{2+} ions) of hydrogen peroxide. When oxygen

reduction reaction (ORR) occurs via four-electron process, the product is water. Instead, two-electron process provides hydrogen peroxide as the product, which may occasionally form both at the cathode and the anode. At the anode where oxygen permeated through the membrane can react with hydrogen at the lower potential than that of the cathode, the ORR reaction is more likely to proceed via two-electron process. Hydroperoxide (HOO·) radical would also form in the operating fuel cells and cause membrane degradation similarly.

The probable degradation mechanisms (Fig. 6) of the PFSA membranes involving the radicals are

1. Decomposition of the end groups [13–15]

   PFSAs contain carboxylic acid groups at the end of polymer main chains as a result of the initiator in the polymerization reaction. The terminal carboxylic acid groups can be attacked by the radical species to produce shortened carboxylic acid groups and hydrogen fluoride. The repetition of this reaction causes unzipping degradation of polymer main chains.
2. Decomposition of the pendant sulfonic acid groups [16–18].

   In the side chains of PFSA ionomers, the sulfonic acid groups are likely to be attacked by the radicals. Under dry or low humidity conditions, in particular, most sulfonic acid groups are not dissociated and prone to hydrogen abstraction reaction by the radicals. The reaction gives $–CF_2·$ radicals and initiates the unzipping degradation of polymer main chains.

In addition to these mechanisms, there may be another degradation mechanism, in which fluorocarbons ($–CF_2–$) are hydrogenated to $–CH_2–$ with hydrogen gas and then attacked by radicals. It is shown by solid-state NMR spectroscopy that the side chain degradation is severer than the main chain degradation for the stabilized PFSAs.

It has been proposed that the terminal carboxylic acid (–COOH) groups can be converted to trifluoromethyl ($–CF_3$) groups by treating the ionomers with fluorine gas under heated conditions [15]. The degradation could be mitigated significantly with the trifluoromethylated ionomers. However, there remains ca. 10% of the degradation even extraporating the content of terminal carboxylic acid groups to zero. The remaining degradation is considered to be the side chain degradation.

While some transition metal ions promote radical formation and ionomer degradation, other transition metal ions act as radical quencher and mitigate the ionomer degradation (Fig. 7) [16, 17, 19–21]. Such ions include Ce^{3+} and Mn^{2+}, having reduction potential at 1.74 and 1.51 V at 25°C, respectively. These ions can reduce hydroxide radicals or hydrogen peroxide to

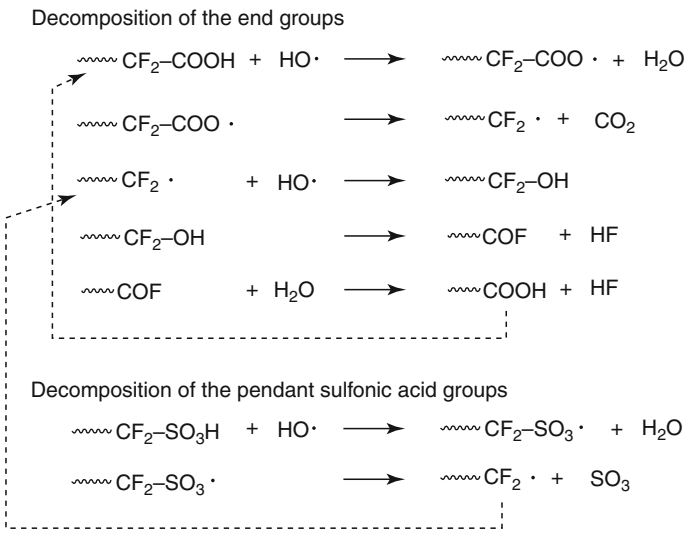

Membrane Electrolytes, from Perfluoro Sulfonic Acid (PFSA) to Hydrocarbon Ionomers. Figure 6
Possible degradation mechanisms of perfluoro sulfonic acid (PFSAs) involving oxidative radical species

water, but not reduce hydrogen peroxide to hydroxide radicals. The oxidized ions, Ce^{4+} and Mn^{3+}, could be reduced to Ce^{3+} and Mn^{2+} by hydrogen permeating through the ionomer membranes from the anode to the cathode. Typically, a few to 10% of sulfonic acid groups are ion-exchanged to such transition metal ions in order to obtain improved durability and acceptable proton conductivity. Some membranes have been claimed to survive OCV test at 120°C and 18% RH and constant current (0.2 A/cm^2) operation at 120°C and 50% RH for several thousand hours. In addition to the role as effective mitigants of chemical degradation, the multivalent transition metal ions function as ionic cross-linkers to render better mechanical properties to the ionomer membranes.

New Synthetic Routes

Synthetic approaches of sulfonated perfluorovinyl monomers are limited and require many steps. Fluorinated cyclic compounds (sultones and epoxides), which are often used as raw materials, need careful attention in handling. Such synthetic complexity is one of the reasons of their high production cost. A unique methodology to produce sulfonated perfluorovinyl monomers has been developed by Asahi Glass (Fig. 8) [7, 22]. The synthetic process, as they name PERFECT (PERFluorination of an Esterified Compound then Thermal elimination) process, involves perfluorination of partially fluorinated aliphatic esters containing sulfonyl fluoride groups. The perfluorination reaction with fluorine (F_2) is carried out in solution. The thermal decomposition of the perfluorinated esters gives acetyl fluorides, which can be converted to the corresponding vinyl monomers via conventional reaction pathway. This process may be applicable to a variety of aliphatic esters to provide new vinyl monomers with fewer steps and at lower production cost.

$$Ce^{4+} + HO\cdot + H^+ \longrightarrow Ce^{3+} + H_2O$$
$$Ce^{4+} + H_2O_2 \longrightarrow Ce^{3+} + HOO\cdot + H^+$$
$$Ce^{4+} + HOO\cdot \longrightarrow Ce^{3+} + O_2 + H^+$$
$$Ce^{3+} + 1/2\ H_2 \longrightarrow Ce^{4+} + H^+$$

Membrane Electrolytes, from Perfluoro Sulfonic Acid (PFSA) to Hydrocarbon Ionomers. Figure 7
Radical quenching mechanism with cerium ions

Hydrocarbon Ionomer Membranes

High IEC Ionomers with Rigid Rod Backbone

Poly(phenylene)s are probably one of the most attractive polymer backbones for hydrocarbon ionomers in terms of chemical stability and long-term durability since their main chains are composed of pure $C_{aromatic}$–$C_{aromatic}$ bonds, which afford rigid rod structure to the polymers. Most other hydrocarbon ionomers suffer from chemical degradation, which

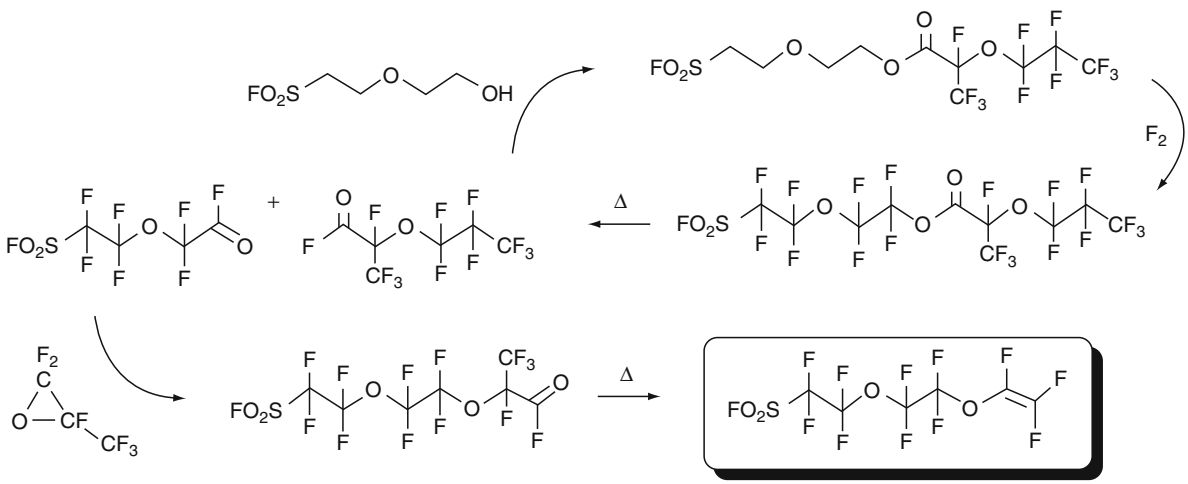

Membrane Electrolytes, from Perfluoro Sulfonic Acid (PFSA) to Hydrocarbon Ionomers. Figure 8
Synthetic route of sulfonated perfluorovinyl monomers via direct fluorination of partially fluorinated compounds

often takes place at hetero linkages, especially electron-donating ether and aliphatic groups, under fuel cell operating conditions. The challenge is how to synthesize soluble high molecular weight poly(phenylene) ionomers (high enough to provide self-standing membranes) and how to introduce ionic groups. There are not many synthetic options available for poly(phenylene) derivatives compared to the other aromatic polymers with heteroatom linkages. Therefore, there have been limited number of reports for poly(phenylene) ionomers. Among them, poly (p-phenylene) ionomers developed by Goto et al. of JSR Corporation, Japan are one of the most successful examples. They have discovered that poly (p-phenylene)s with 3-sulfobenzoyl groups give appropriate properties as fuel cell membranes [23]. A typical synthetic approach is summarized in Fig. 9. The key monomer, neopentyl 3-(2,5-dichlorobenzoyl) benzenesulfonate, synthesized form 2,5-dichlorobenzophenone, was copolymerized with hydrophobic dichloro compounds via nickel-catalyzed coupling reaction. The neopentyl ester groups in the resulting polymers were removed via hydrolysis to obtain the title ionomers.

The striking feature of the poly(p-phenylene)-based ionomers is that the membranes obtained therefrom show well-developed hydrophilic/hydrophobic microphase separation. Such morphology can be controlled by (1) copolymer composition, (2) chemical structure of hydrophobic component, (3) sequenced structure and length of hydrophilic and hydrophobic components, and (4) membrane preparation conditions. Another characteristic of the poly (p-phenylene)-based ionomers is that the IEC can be higher than 3 meq/g without sacrificing good mechanical and chemical stability of the membranes. In Table 3 are summarized properties of typical JSR membranes. According to the disclosed data, the JSR membranes

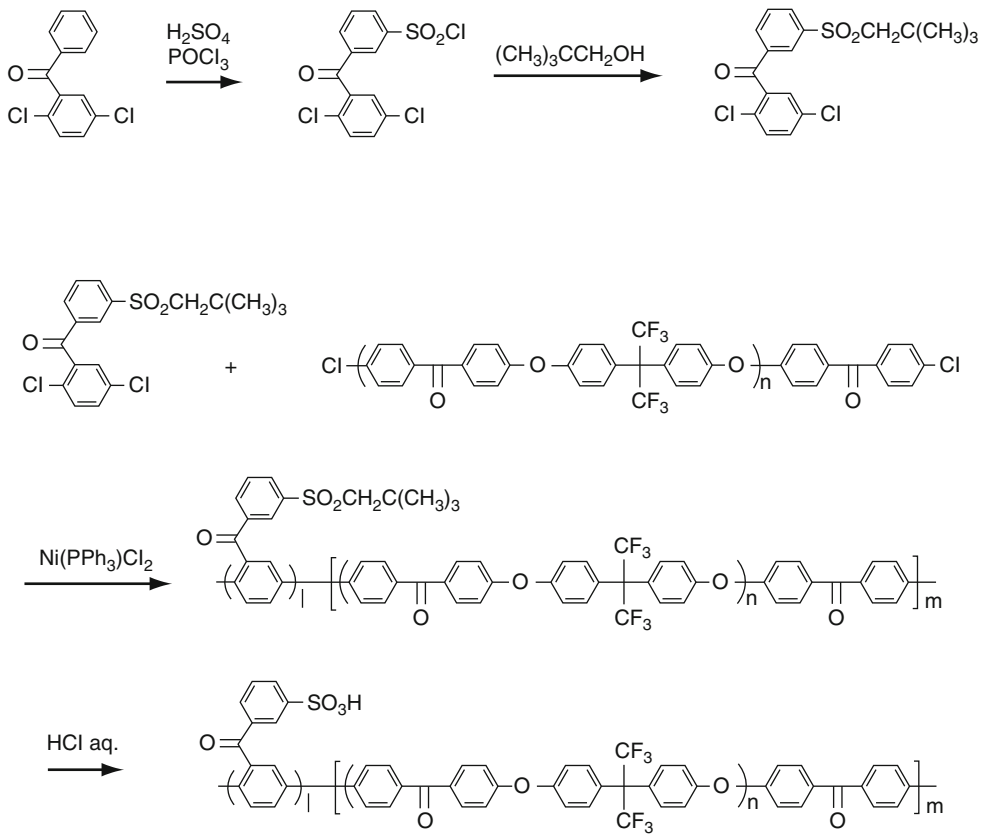

Membrane Electrolytes, from Perfluoro Sulfonic Acid (PFSA) to Hydrocarbon Ionomers. Figure 9
Synthesis of sulfonated poly(p-phenylene) copolymers

Membrane Electrolytes, from Perfluoro Sulfonic Acid (PFSA) to Hydrocarbon Ionomers. Table 3 Properties of the sulfonated poly(p-phenylene) copolymer (JSR) membranes

Proton conductivity	70°C, 80% RH	0.1 S/cm
	95°C, 80% RH	0.16 S/cm
Mechanical strength	Elongation at break at 23°C, 50% RH	100%
	Stress at break at 23°C, 50% RH	130 MPa
Gas permeability	H_2 at 80°C, dry	9 barrer
	O_2 at 40°C, 90% RH	6 barrer
Stability	IEC change after 1,000 h in 95°C water	0%
	Weight change after 1,000 h in 95°C water	0%

absorb more water, show higher proton conductivity, better thermal and mechanical stability, comparable hydrolytic stability, and much lower gas permeability compared to those of the conventional perfluorinated ionomer membranes. It has been recently claimed that the introduction of basic groups such as pyridine and imidazole as a third comonomer component could improve the durability of the poly(p-phenylene)-based ionomers. The JSR membranes have been successfully installed on Honda FCX Clarity fuel cell electric vehicles.

Rikukawa et al. of Sophia University have also developed a series of poly(p-phenylene) ionomers [24–26]. The main differences from the JSR membranes are that sulfophenylene groups are connected with ether bonds in the side chain because of the synthetic reason (Fig. 10). (According to JSR, such extra phenoxy groups do not have positive effect on the properties of the resulting ionomer membranes in terms of the proton conductivity and stability.) Rikukawa's group has applied post-sulfonation method so that the phenyl groups need to be activated with electron-donating ether groups. The advantage is that synthesis of monomers and high molecular weight polymers is easier. Their membranes showed similar properties to the JSR membranes, supporting the validity of the strategy to utilize rigid rod-like main chains.

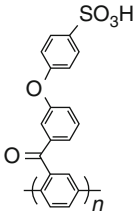

Membrane Electrolytes, from Perfluoro Sulfonic Acid (PFSA) to Hydrocarbon Ionomers. Figure 10 Sulfonated poly(p-phenylene) containing phenoxy side chains

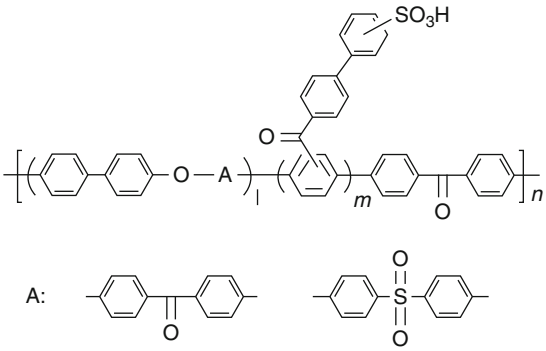

Membrane Electrolytes, from Perfluoro Sulfonic Acid (PFSA) to Hydrocarbon Ionomers. Figure 11 Multiblock copolymer of sulfonated poly(p-phenylene) and poly(arylene ether sulfone)

Sulfonated poly(2,5-benzophenone)s, derivatives of poly(p-phenylene)s with sulfobiphenylenecarbonyl side chains, were synthesized by McGrath and Ghassemi of Virginia Polytechnic Institute and State University [27]. The base (unsulfonated) polymers were thermally stable up to ca. 480°C in air and nitrogen, however, their film-forming capability was insufficient due to rather low molecular weight. They have also synthesized multiblock copolymers composed of the sulfonated oligo(2,5-benzophenone)s and oligo (arylene ether sulfone)s to achieve higher molecular weight and better film-forming capability (Fig. 11) [28]. The block copolymers showed high glass transition temperature (225°C) due to the arylene ether sulfone units. Proton conductivity of the membrane (IEC = 1.20 meq/g) was measured under specific conditions (in water at 30°C) to be 0.036 S/cm.

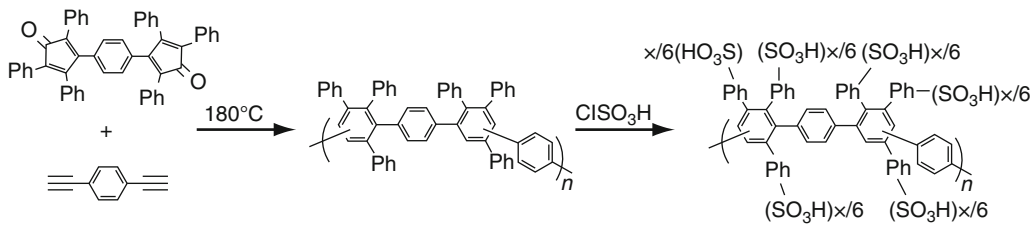

Membrane Electrolytes, from Perfluoro Sulfonic Acid (PFSA) to Hydrocarbon Ionomers. Figure 12
Synthesis of polysulfophenylated poly(phenylene) via Diels–Alder polymerization followed by sulfonation

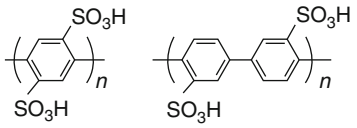

Membrane Electrolytes, from Perfluoro Sulfonic Acid (PFSA) to Hydrocarbon Ionomers. Figure 13
Poly(p-phenylene)s with sulfonic acid groups on the main chains

Cornelius et al. have synthesized a series of unique poly(phenylene)-based polyelectrolytes by Diels–Alder polymerization followed by post-sulfonation (Fig. 12) [29–32]. The ionomers are composed of sulfonated, highly phenylated poly(phenylene)s and do not carry any heteroatoms as their constituents except for the sulfonic acid groups. The complete aryl backbone resulted in a tough rigid-rod material with no Tg below the decomposition temperature. The stiffness of the ionomer backbone did not negatively affect the membrane properties such as water uptake (21–137%, in water) and proton conductivity (13–123 mS/cm, in water at 30°C) with IECs ranging from 0.98 to 2.2 meq/g.

More recently, poly(p-phenylene) ionomers with simpler chemical structure has been proposed by the group of Litt of Case Western Reserve University (Fig. 13). They have synthesized poly(p-phenylene)s with sulfonic acid groups directly attached on the main chains via Ullmann coupling reaction. Their membranes seem promising for high-temperature operable fuel cells in terms of the proton conductivity; the proton conductivity of the membranes was 0.1 S/cm at 75°C and 15% RH, which was approximately 3 orders of magnitude higher than that of Nafion membrane and meets the requirements of DOE for the year of 2015. However, it is difficult to obtain high molecular weight polymers via the Ullmann coupling reaction, which causes poor mechanical properties of the membranes. This issue may be improved by copolymerizing with appropriate hydrophobic comonomers that are more reactive in the Ullmann coupling reaction and also give flexibility to the membranes.

Phosphonic acid containing poly(phenyelne)s were investigated by Kreuer's group of Max-Planck-Institute (Fig. 14) [33, 34]. m-Dichlorobenzene containing phosphonic acid ester was polymerized by nickel-catalyzed polycondensation reaction. The ester groups were hydrolyzed with acid to provide poly (m-phenylene phosphonic acid). Compared to the sulfonated poly(phenylene) ionomers, phosphonated analogues showed lower proton conductivity and better thermal stability due to the lower water affinity. The ionomer membranes are probably not suitable for fuel cells with dry or slightly humidified hydrogen as a fuel but may find applications using liquid fuels such as direct methanol fuel cells. In any case, the ionomers have to be cross-linked or incorporated with hydrophobic moieties in order to prevent excess swelling or dissolving in water.

A new synthetic approach has been developed by the same group to produce poly(phenylene) ionomers containing merely sulfone units connecting the phenylene rings ($SPSO_2$) (Fig. 15) [35, 36]. In the ionomers, each phenylene ring contains one sulfonic acid group (100% degree of sulfonation), which corresponds to very high IEC of 4.5 meq/g. The synthesis was carried out in two-step process, in which bis (sulfophenyl)sulfone was polymerized with sodium sulfide and then the subsequent oxidation reaction of sulfide linkages to sulfone gave the title ionomers. Since phenylene rings in the main chains are connected solely

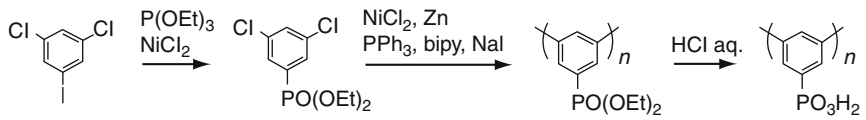

Membrane Electrolytes, from Perfluoro Sulfonic Acid (PFSA) to Hydrocarbon Ionomers. Figure 14
Synthesis of poly(m-phenylene phosphonic acid)

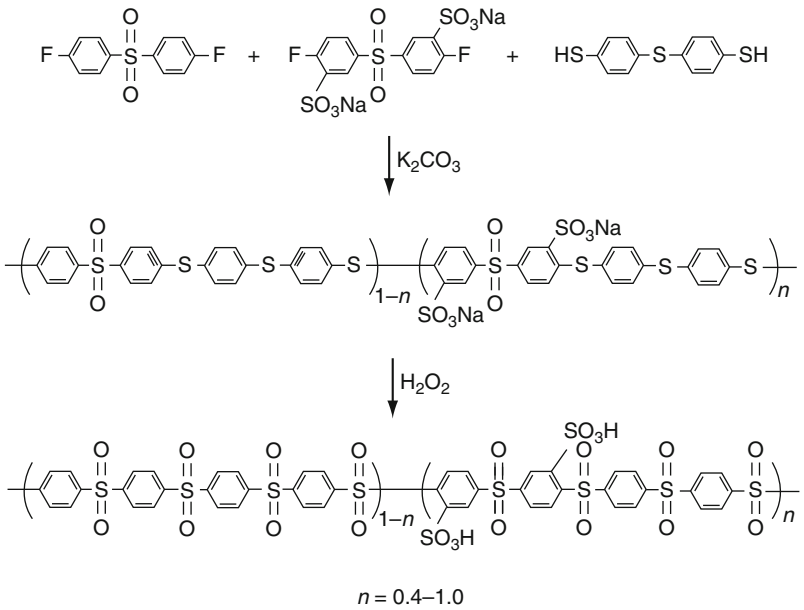

Membrane Electrolytes, from Perfluoro Sulfonic Acid (PFSA) to Hydrocarbon Ionomers. Figure 15
Synthesis of sulfonated poly(phenylene sulfone)s (sPSO2)

with strong electron-withdrawing sulfone groups and not with electron-donating groups such as ether and sulfide, the ionomers show high hydrolytic (no practical desulfonation at 180°C and high water activity) and thermooxidative stability (decomposition in air above 300°C). The high IEC afforded the ionomer membranes very high proton conductivity in the wide temperature range from 110°C to 160°C at a constant water vapor pressure (1 atm), which corresponds to ca. 50% and 15% RH, respectively. The proton diffusion coefficient (calculated from the conductivity data by use of Nernst–Einstein equation) increased with IEC values (Fig. 16). While the conductivity overcomes that of Nafion by a factor of 5–7, the ionomers are soluble in water and become brittle in the dry state. Approaches such as blends, graft-, and block-copolymers are under investigation. The materials have been registered as fumapem S (granular resin, solution, or dispersion) and fumion S (membranes) by fumatech company for commercialization.

Block Copolymers

Block copolymers have been utilized in order for the hydrocarbon ionomer membranes to have well-developed and interconnected ionic domains. The strategy seems to work in many ionomers of different molecular structure. The block copolymers membranes show considerably higher proton conductivity than that of the random copolymer membranes with similar values of IEC. For example, Kawakami et al. of Tokyo Metropolitan University have proved that the block

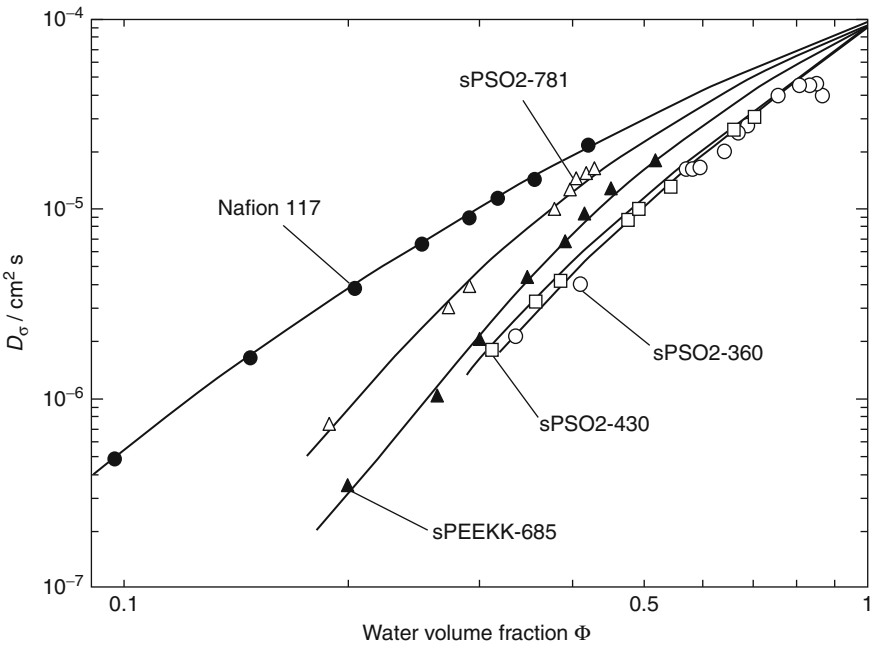

Membrane Electrolytes, from Perfluoro Sulfonic Acid (PFSA) to Hydrocarbon Ionomers. Figure 16
Proton diffusion coefficient of sPSO2, sulfonated poly(ether ether ketone ketone), and Nafion 117 membranes as a function of water volume fraction at 30°C (Reprinted from [36] with permission from the American Chemical Society)

copolyimides containing hexafluoropropylene groups in the hydrophobic segment are much more proton conductive than the random equivalents [37–40]. The differences in the conductivity were much more pronounced at low humidity. The proton conductivity of the block copolyimide membranes depended strongly upon the block chain lengths. The longer the block length was, the higher the conductivity became. They ascribe this effect to ionic channels of which formation depends on the block chain length.

Similar effect was confirmed by the group of Miyatake et al. of University of Yamanashi with other series of sulfonated polyimides of different main chain structure [41]. They have investigated the effect of block copolymer architecture on sulfonated polyimides containing aliphatic segments in the hydrophobic main chains and in the hydrophilic side chains. The block copolymer with longest block segments (the number of repeating unit was 150 for both hydrophilic and hydrophobic blocks) showed the highest proton conductivity of 2×10^{-2} S/cm at 80°C and 48% RH, which was comparable to that of the conventional perfluorinated ionomer membrane (Fig. 17). Well-connected

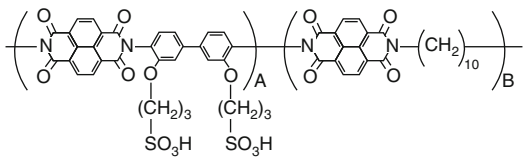

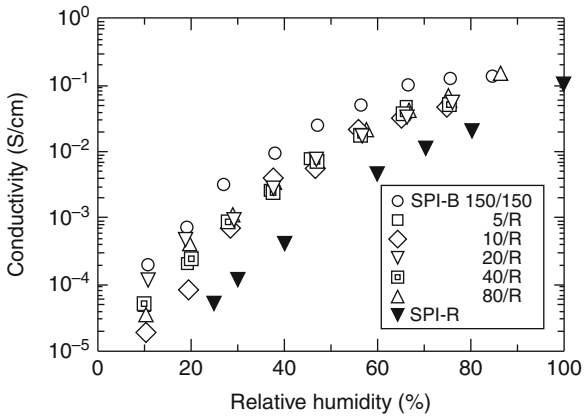

Membrane Electrolytes, from Perfluoro Sulfonic Acid (PFSA) to Hydrocarbon Ionomers. Figure 17
Humidity dependence of the proton conductivity of sulfonated block copolyimide membranes at 80°C

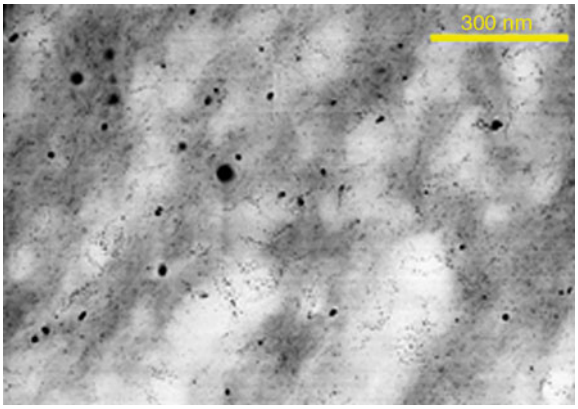

Membrane Electrolytes, from Perfluoro Sulfonic Acid (PFSA) to Hydrocarbon Ionomers. Figure 18
Scanning transmission electron microscopic image of SPI-B 150/150

hydrophilic domains, which looked a cloudlike belt with several hundred nanometers in width, were observed in the transmission electron microscopic images (Fig. 18).

McGrath's group has done an extensive and systematic study on their sulfonated poly(arylene ether sulfone) block copolymers (Fig. 19) [42–51]. The block copolymers are composed of biphenol-based disulfonated arylene ether sulfone (so-called BPSH) units and the unsulfonated equivalents (BPS). The investigated properties of the block copolymer membranes include synthetic details with different main chain linkages, spectroscopic analyses of the chemical structure, water uptake, diffusion of water, proton conductivity at wide range of temperature and humidity, thermal transition and decomposition, morphological analyses (atomic force microscopic (AFM) and transmission electron microscopic (TEM) imaging, and small-angle X-ray scattering (SAXS) profile), mechanical strength, and fuel cell performance. A brief summary is

- High molecular weight block copolymers were obtained when reactive perfluorinated linkage (nonafluorobiphenylene or pentaflurophenylene) groups were attached at the both ends on unsulfonated hydrophobic oligomers.
- The linkage groups had some effect on the membrane properties. The fluorinated biphenylene groups seemed to promote nanophase separation, and thus water uptake and proton conductivity at low humidity than the fluorinated phenylene groups.
- The block copolymer membranes performed much better as proton exchange membranes for fuel cells than the random copolymers with similar IEC, especially in terms of proton conductivity at low humidity (on the order of mS/cm at 80°C and 30% RH, IEC = 1.5 meq/g).
- The block length rather than the IEC was more important to dominate water uptake and proton conductivity, where longer block length led to higher water uptake and higher proton conductivity. So were the nanophase separation (or connection of hydrophilic domains) (Fig. 20) and water diffusion coefficient.
- In the hydrated block copolymers, more freezing water (free and loosely bound water to sulfonic acid groups) existed than in the random copolymers due to the developed morphology (Table 4). The block length should be longer than 10 kDa in order to have noticeable improvement on the morphological order and proton conductivity.
- In addition to the block length and IEC values, casting conditions (such as the solvent and drying temperature or solvent removal rate) did have significant impact on membrane morphology and properties.
- The block copolymer membrane performed in an H_2/air fuel cell at 100°C and 40% RH comparable to Nafion membrane.

These findings are, more or less, applicable to the other hydrocarbon ionomers and useful to tailor the higher order structure and properties of ionomer membranes.

Polymers with Sulfonic Acid Clusters

In order to overcome the trade-off relationship between water uptake and proton conductivity (high conductivity can be achieved with high water absorbing membranes), Hay's group at McGill University has proposed a unique strategy. They have synthesized poly(arylene ether)s containing nanoclusters of up to 18 sulfonic acid groups either tethered on the end groups or distributed in the main chains (Fig. 21) [52–54, 55–58]. Membranes therefrom showed

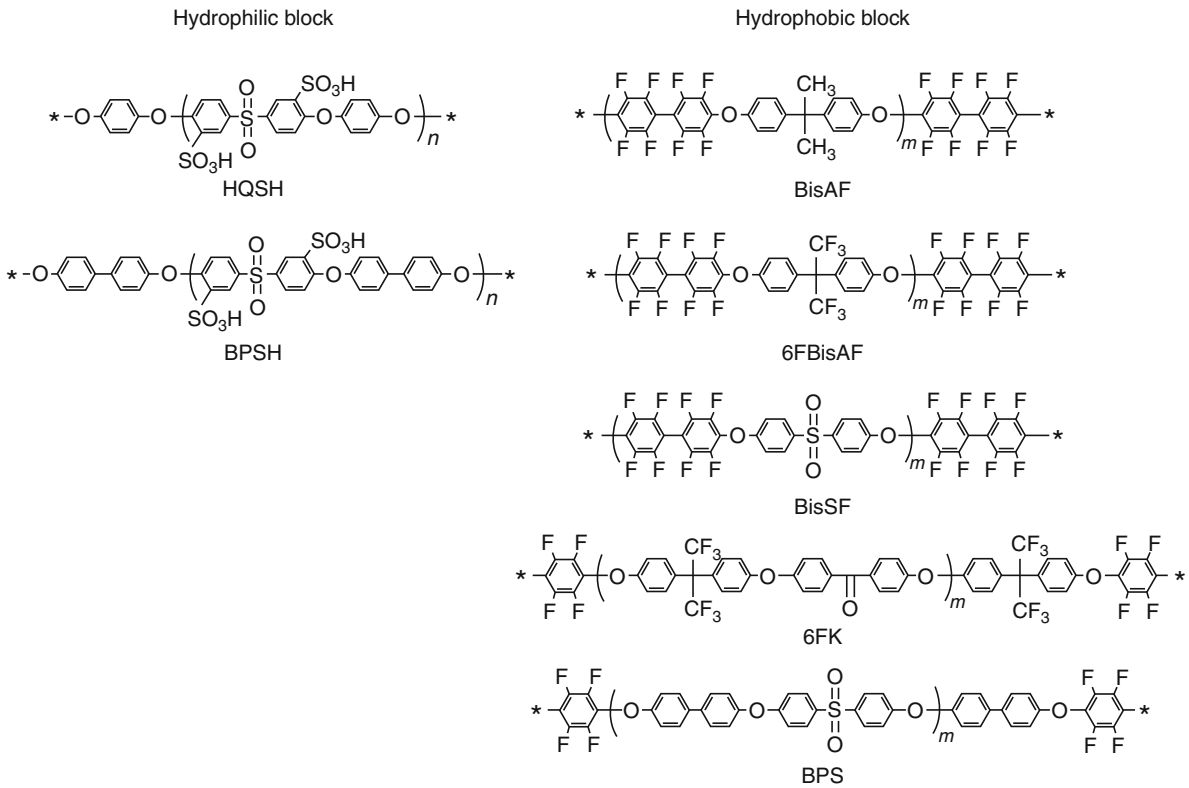

Membrane Electrolytes, from Perfluoro Sulfonic Acid (PFSA) to Hydrocarbon Ionomers. Figure 19
Chemical structure of BPSH block copolymers and their derivatives

significantly phase-separated (worm-like or large hydrophilic domains) and highly connected morphology in the TEM images. The highest proton conductivity at 120°C was 3.1 mS/cm at 10% RH and 10.5 mS/cm at 30% RH for a membrane with IEC = 1.0 meq/g. The reported conductivity values were extremely high compared to those of the other hydrocarbon ionomer membranes with such low IEC and even higher than those of Nafion under the same conditions, 1.7 mS/cm (at 10% RH) and 4.0 mS/cm (at 30% RH), respectively. The membrane absorbed ca. double amount of water compared to the Nafion membrane, which is thought to be responsible for the high proton conductivity.

Ueda and his coworkers of Tokyo Institute of Technology confirmed this strategy with their sulfonated poly(arylene ether sulfone)s (Fig. 22) [59–61]. Their polymers contain highly sulfonated moieties (up to ten sulfonic acid groups per repeating unit) randomly distributed in the main chains. Large difference in the polarity between highly sulfonated units and hydrophobic units caused the formation of defined phase-separated structures and well-connected proton pathways. The proton conductivity of the ionomer membrane with IEC = 2.38 meq/g was comparable to that of Nafion 117 at > 30% RH, 80°C.

Miyatake et al. have combined two strategies in a single polymer architecture (multiblock copolymers containing sulfonic acid clusters in their hydrophilic blocks) [62]. They have successfully synthesized a series of multiblock poly(arylene ether sulfone ketone)s (SPESKs) containing fully sulfonated fluorenylidene biphenylene units (Fig. 23) [63, 64]. The well-controlled post-sulfonation reaction of the precursor polymers enabled preferential sulfonation on each aromatic ring of the fluorenylidene biphenylene groups with 100% degree of sulfonation. The ionomer membranes showed unique morphology with well-developed hydrophilic/hydrophobic phase separation, depending on the block length of each segment. It was concluded that longer block length and/or higher IEC

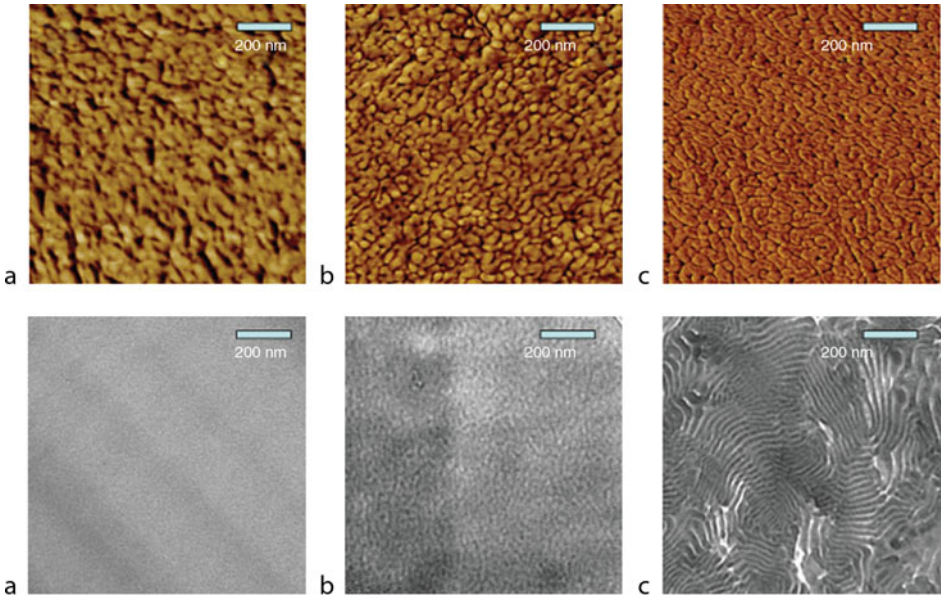

Membrane Electrolytes, from Perfluoro Sulfonic Acid (PFSA) to Hydrocarbon Ionomers. Figure 20
Atomic force microscopy (AFM) (top) and transmission electron microscopy (TEM) (bottom) images of BPSH-6FK multiblock copolymer membranes; (**a**) BPSH5-6FK5, (**b**) BPSH10-6FK10, and (**c**) BPSH10 for AFM or BPSH15 for TEM-6FK15. Numbers represent molecular weight of each block component in kDa (Reprinted from [47] with permission from Wiley Interscience)

Membrane Electrolytes, from Perfluoro Sulfonic Acid (PFSA) to Hydrocarbon Ionomers. Table 4 States of water molecules in the BPSH (random), BPSH-BPS (block), and Nafion membranes

Membrane	IEC (meq/g)	Total water (λ^a)	Tightly bound water (λ^a)	Loosely bound water (λ^a)	Free water (λ^a)
BPSH30	1.34	12	4	8	0
BPSH3-BPS3	1.33	12	7	5	0
BPSH5-BPS5	1.39	13	8	5	0
BPSH10-BPS10	1.28	26	10	8	8
Nafion 112	0.90	17	3	9	5

[a]Number of water molecules absorbed per sulfonic acid group

resulted in larger and better-connected hydrophilic clusters under dry conditions, while the morphology was less dependent on these factors under fully hydrated conditions. The multiblock copolymer membrane with IEC = 1.62 meq/g showed much higher proton conductivity than that of the random copolymer membrane with similar chemical structure and IEC (Fig. 24). The proton conductivity was similar or even higher compared to that of Nafion over a wide humidity range. The membrane retained high proton conductivity at 110°C. The high conductivity resulted from the high proton diffusion coefficient. Longer block length seemed effective in increasing proton diffusion coefficient, which coincided with the morphological observations. The multiblock copolymer membranes were stable to hydrolysis in water at

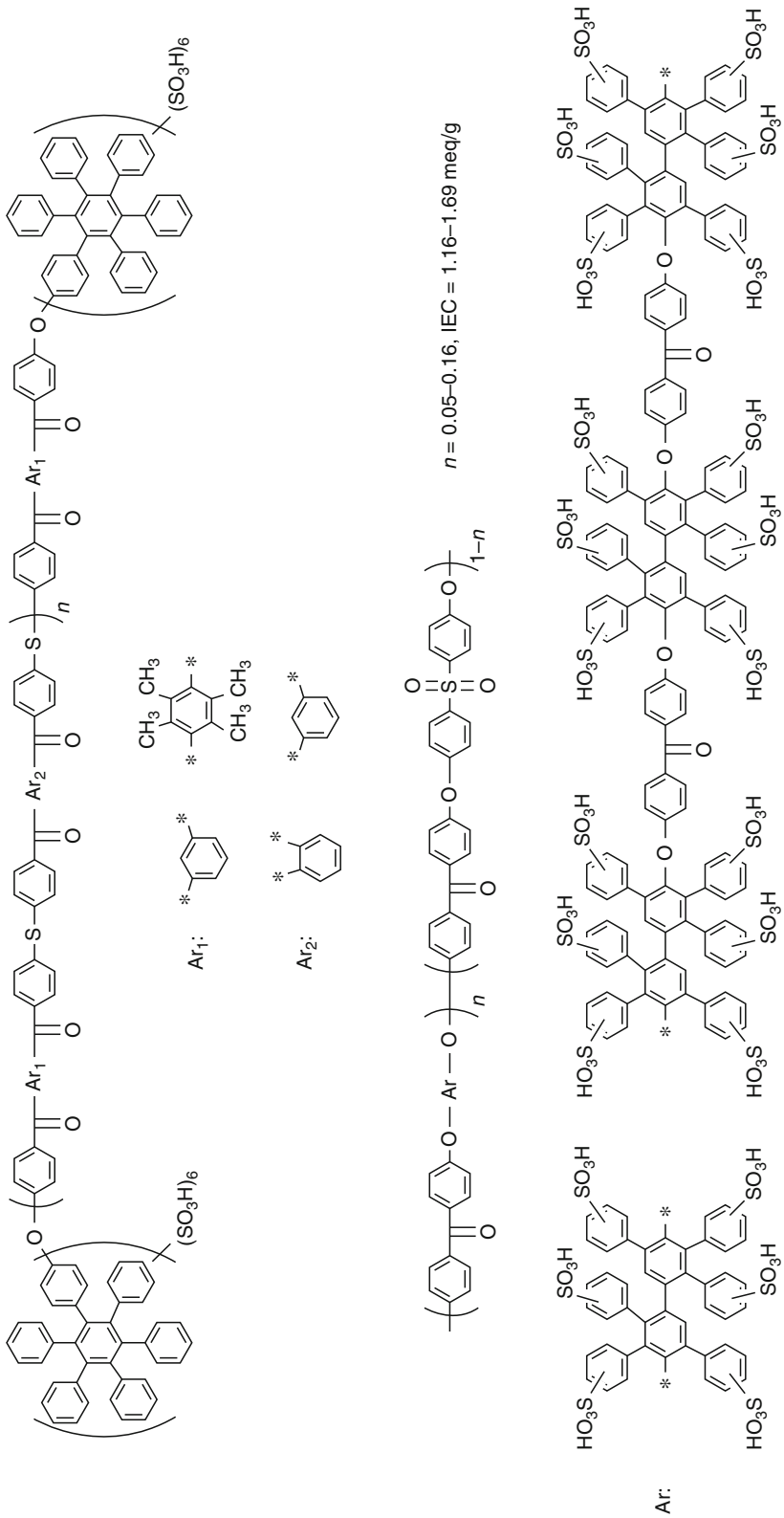

Membrane Electrolytes, from Perfluoro Sulfonic Acid (PFSA) to Hydrocarbon Ionomers. Figure 21
Poly(arylene ether)s containing sulfonic acid clusters

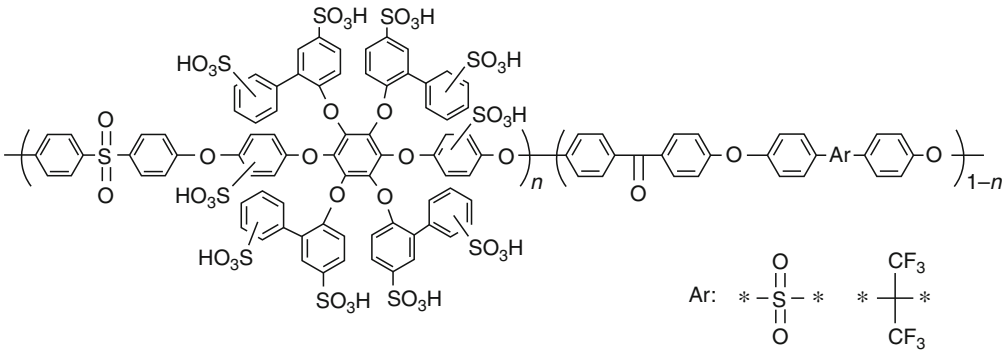

Membrane Electrolytes, from Perfluoro Sulfonic Acid (PFSA) to Hydrocarbon Ionomers. Figure 22
Poly(arylene ether sulfone)s with up to ten sulfonic acid groups per repeating unit

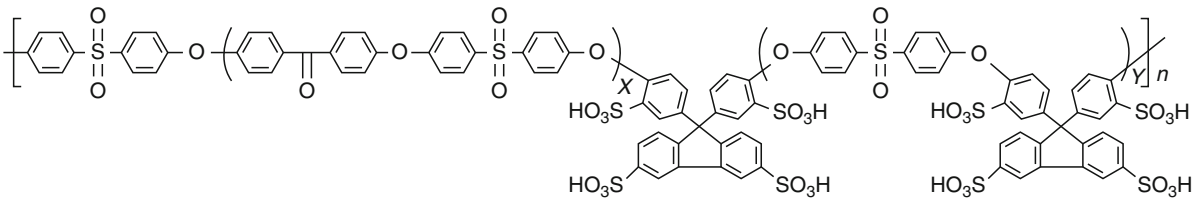

Membrane Electrolytes, from Perfluoro Sulfonic Acid (PFSA) to Hydrocarbon Ionomers. Figure 23
Multiblock poly(arylene ether sulfone ketone)s (SPESKs) containing fully sulfonated fluorenylidene biphenylene units

140°C for 24 h or at 100°C for 1000 h. The membranes degraded to some extent under harsh oxidative conditions (in Fenton's reagent), which is the fate of hydrocarbon ionomer compounds. Oxidative degradation is likely to occur at phenylene carbon atoms *ortho* to the ether bonds by the attack of highly oxidative hydroxyl radicals. The multiblock copolymer membrane showed much lower gas permeability than Nafion while humidity dependence of the permeability was different between hydrogen and oxygen. Hydrogen permeability showed reverse volcano-type dependence on the humidity, decreased slightly with humidification, and then increased with further humidification. Oxygen permeability simply increased with humidity. Such humidity dependency of oxygen permeability was similar to that of Nafion, however, not observed in the random copolymer membranes. The low gas permeability could mitigate their oxidative instability since hydrogen peroxide as a by-product is potentially less produced when the gas permeation through the membranes is low. A fuel cell was successfully operated with the multiblock copolymer membranes at 30% and 53% RH and 100°C (Fig. 25). The current density was 250 mA/cm^2 at 30% RH and 410 mA/cm^2 at 53% RH at a cell voltage of 0.6 V. The high proton conductivity of the membrane at low RH and high temperature was well confirmed in practical fuel-cell operation.

Zhang et al. of Changchun Institute of Applied Chemistry have also confirmed the similar strategy with their unique multiblock copolyimide ionomers, in which hydrophilic blocks were composed of disulfonated dianhydride and disulfonated diamine (each aromatic ring was sulfonated) (Fig. 26) [65]. While they have not done morphological

investigations, the high concentration of the sulfonic acid groups in the hydrophilic block was effective in enhancing water absorbability and proton conductivity of the polyimide ionomer membranes (Fig. 27). For example, their high IEC (2.69 meq/g) block copolymer membranes were much more proton conductive than the random equivalent and the highest conductivity at 50% RH and 70°C was 3.2×10^{-2} S/cm for the multiblock copolyimide with the 50 repeating units in the hydrophilic blocks. The multiblock copolyimides showed lower proton concentration as a consequence of the higher water uptake, however, higher proton mobility compensated the proton concentration. Hydrolysis remains an issue for the polyimides and the block copolymer architecture did not help improve the hydrolytic stability (the fact is that the block copolymers were more susceptible to hydrolysis due to the higher water uptake).

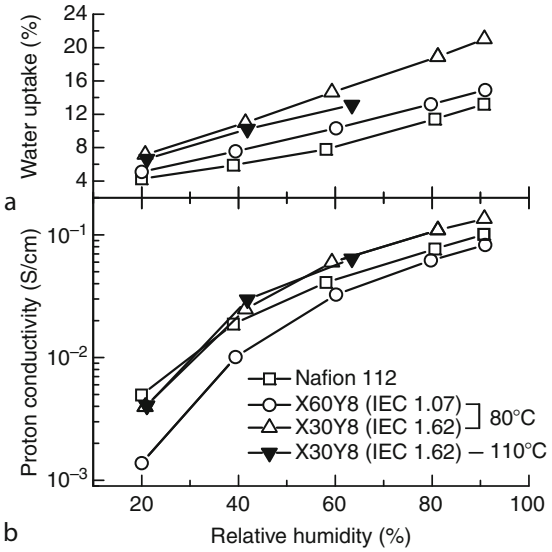

Membrane Electrolytes, from Perfluoro Sulfonic Acid (PFSA) to Hydrocarbon Ionomers. Figure 24
(**a**) Water uptake and (**b**) proton conductivity of Nafion 112 and block SPESKs (where IEC is in meq/g) as a function of relative humidity at 80 and 110°C (Reprinted from [64] with permission from Wiley Interscience)

Polymers with Pendant Acidic Groups

One of the reason for Nafion to have well-developed phase separation and interconnected ionic channels lies on its chemical structure that contains acid groups at the end of flexible perfluoroalkyl ether side chains. The introduction of pendant sulfonic acid groups has been investigated for the aromatic polymers such as polybenzimidazoles, polyimides, and poly(arylene ether)s, to confirm whether a similar effect can be obtained without perfluorinated chains (Fig. 28).

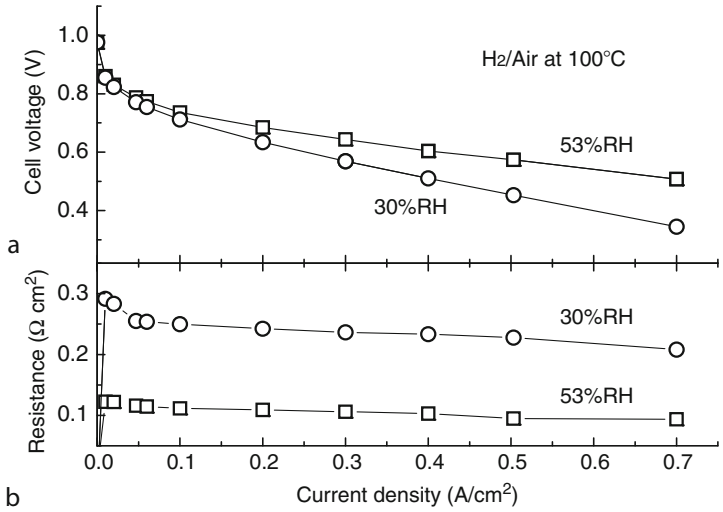

Membrane Electrolytes, from Perfluoro Sulfonic Acid (PFSA) to Hydrocarbon Ionomers. Figure 25
(**a**) H_2/air fuel cell performances including ohmic resistance voltage losses and (**b**) ohmic resistances of SPESK X30Y8 (IEC = 1.62 meq/g) at 100°C with humidification at 53 and 30% RH for both electrodes (Reprinted from [64] with permission from Wiley Interscience)

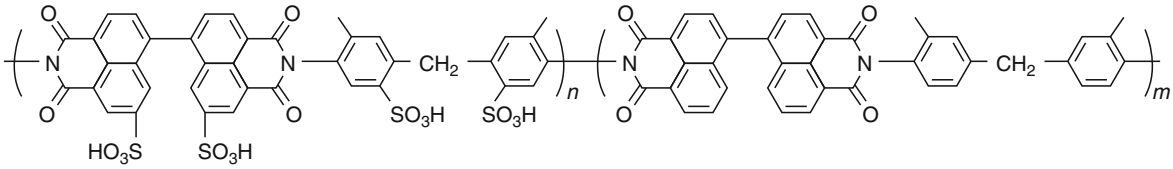

n = 5–150, m = 5–50, IEC = 1.51–2.69 meq/g

Membrane Electrolytes, from Perfluoro Sulfonic Acid (PFSA) to Hydrocarbon Ionomers. Figure 26
Multiblock copolyimides with highly sulfonated hydrophilic block

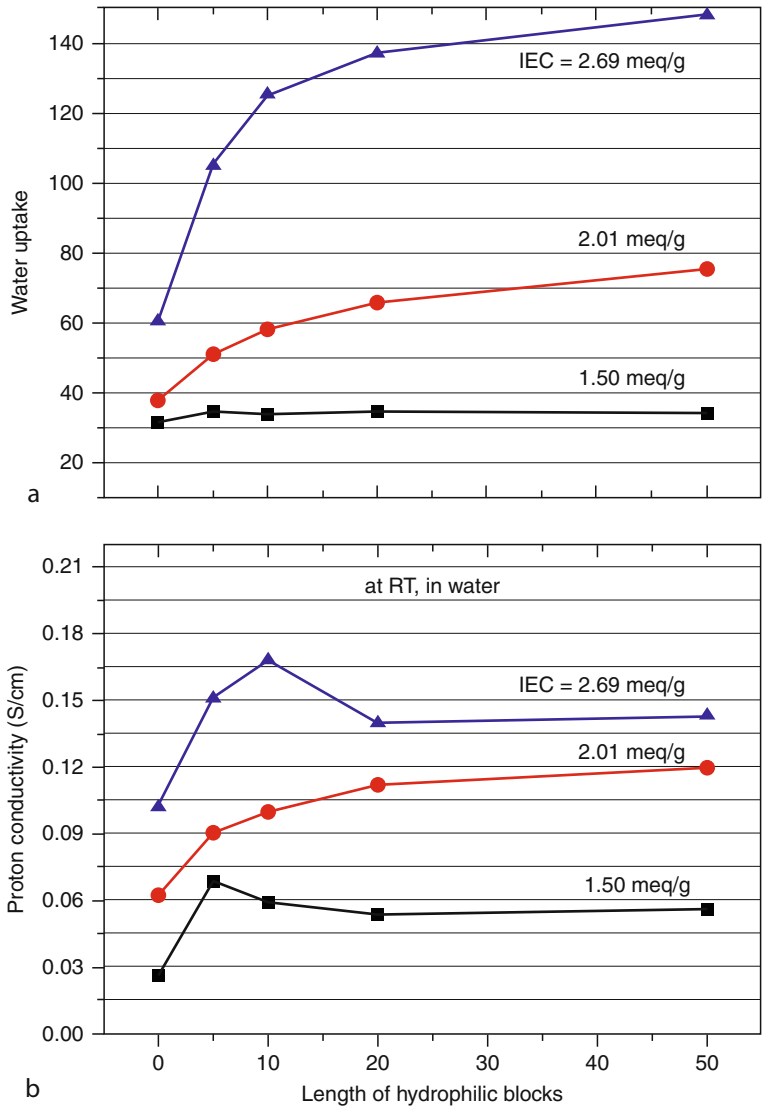

Membrane Electrolytes, from Perfluoro Sulfonic Acid (PFSA) to Hydrocarbon Ionomers. Figure 27
(**a**) Water uptake and (**b**) proton conductivity of multiblock copolyimides with different IEC as a function of hydrophilic block length (Reprinted from [65] with permission from Elsevier)

In most cases, flexible side chains between the aromatic main chains and the acid groups improve morphology and proton conductivity but not as striking as that in Nafion. For example, Jiang et al. of Jilin University have developed a series of poly (arylene ether sulfone)s containing long pendant acidic (sulfopropylbenzoyl, sulfopropoxybenzoyl, or sulfophenoxybenzoyl) groups [66–71] (a), in which membranes ionic clusters of ca. 10–20 nm in diameter were confirmed via TEM observation but rather isolated from one another. When relatively higher sulfonic acid concentration was applied, ionic clusters became larger (ca. 40 nm in diameter) and better interconnected. Poly(arylene ether sulfone)s containing pendant sulfonaphthyl groups (b) were synthesized by Manthiram's group at the University of Texas at Austin [72]. Their membranes outperformed Nafion 115 membrane in DMFC operation, while the effect of pendant naphthyl groups was not well investigated. Jannasch et al. of Lund University proposed poly(arylene ether sulfone)s tethered with hyper-acidified pendant groups (two or more sulfonic or phosphonic acid groups per pendant unit) (c) [73, 74]. By concentrating acidic groups locally onto the side chains, a distinct phase separation between hydrophobic polymer main chains and hydrophilic pendant groups was achieved. The water uptake of these kinds of ionomer membranes seemed rather high, and thus cross-linking or incorporation of inorganic additives may be needed to avoid excess swelling.

Recently, more developed ideas on the pendant acidic groups have been proposed by several research groups. Such include graft copolymers or comb-shaped ionomers, in which ionic grafts were substituted onto aromatic main chains. Jannasch et al. have further developed their above ideas by grafting poly(vinylphosphonic acid) (PVPA) onto poly(phenylene ether sulfone)s (c) [75]. Such molecular architecture caused phase separation and dual glass transition temperature due to the inherent miscibility of the stiff and hydrophobic polymer backbones and strongly hydrogen-bonded phosphonic acid side chains. The membrane with 57 wt% of the PVPA content showed 4.6 mS/cm (dry) and 93 mS/cm (100% RH) at 120°C. Still, the water uptake of the membrane was rather high and should be improved.

Guiver et al. of National Research Council, Canada developed comb-shaped poly(arylene ether) electrolytes containing 2–4 sulfonic acid groups on aromatic side chains (d) [76]. Their membranes showed relatively high proton conductivity and well-developed and continuous ionic domains. However, trade-off relationship between water uptake and proton conductivity of their membranes was not better than that of Nafion. In order to pronounce the hydrophilic/hydrophobic differences, another series of comb-shaped aromatic ionomers with highly fluorinated main chains and flexible poly(α-methyl styrene sulfonic acid) side chains were developed [77]. The membranes seemed to have better properties than their previous version, however, chemical instability of the side chains needed to be improved.

Hydrocarbon Polymers with Superacid Groups

One of the significant differences between hydrocarbon ionomers and perfluorosulfonic acid polymers is acid groups. The *pKa* value of benzenesulfonic acid ($PhSO_3H$) is −2.5 and that of trifluoromethanesulfonic acid (CF_3SO_3H) is −13. The pK_a value was estimated to be ca. −1 for sulfonated polyether ketone and ca. −6 for Nafion membranes [78]. Therefore, the effective proton concentration and proton mobility should be lower in the hydrocarbon ionomer membranes. Without appropriate molecular design such as multiblock copolymer and sulfonic acid clusters as mentioned above, hydrocarbon ionomer membranes lack well-developed ionic channels due to less pronounced hydrophilic and hydrophobic phase separation, which causes the lower proton conductivity at low humidity.

Yoshimura and Iwasaki of Sumitomo Chemical Co. have synthesized aromatic ionomers containing pendant perfluorosulfonic acid groups (Fig. 29) [79]. Poly (arylene ether sulfone) was brominated and then perfluorosulfonated via Ullmann coupling reaction in the presence of copper catalyst. The IEC was controllable up to 1.58 meq/g. The obtained ionomer membranes behaved very differently from the typical sulfonated aromatic ionomer membranes. Characteristic hydrophobic/hydrophilic separation (ca. 3–4 nm) was observed in the small-angle X-ray scattering (SAXS)

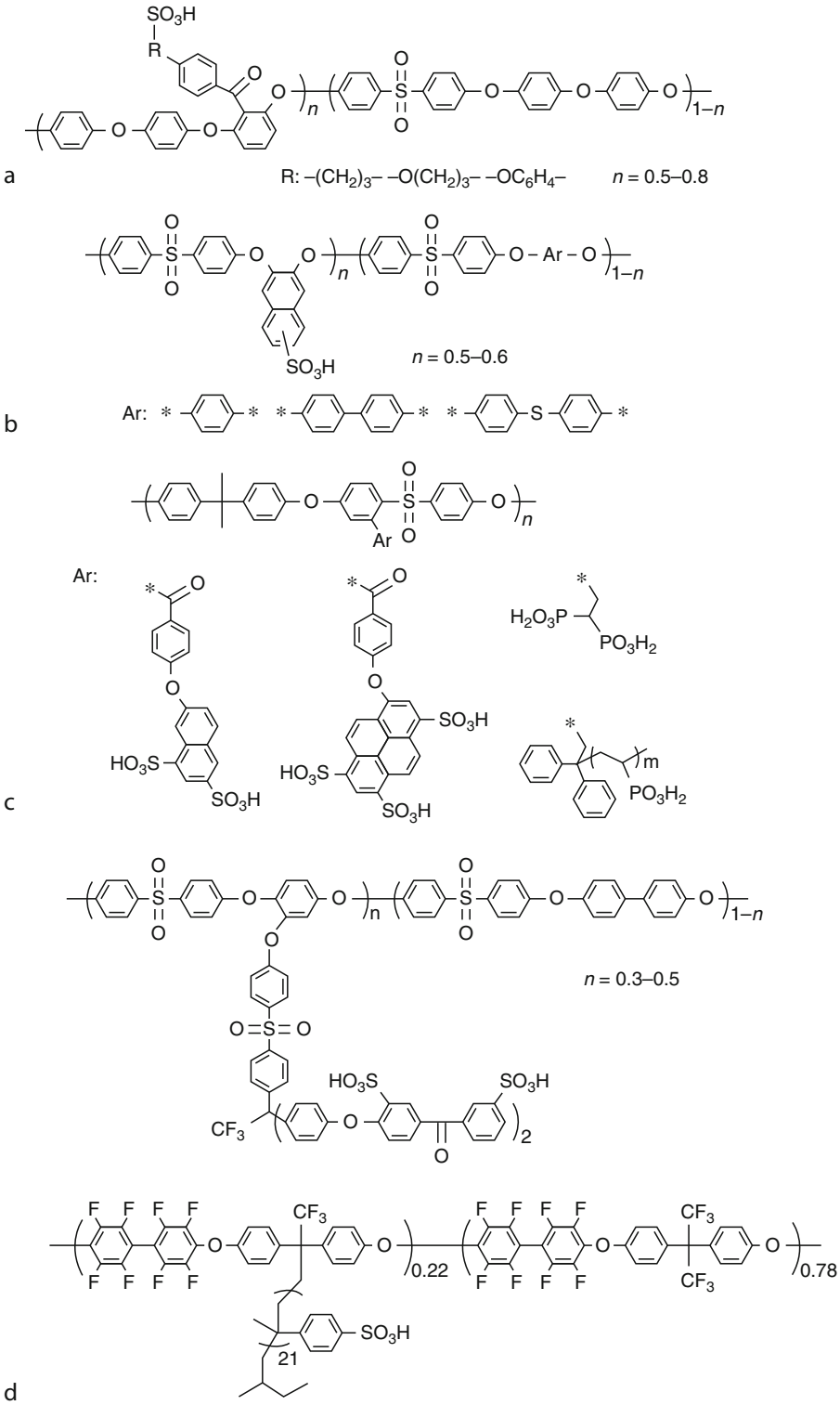

Membrane Electrolytes, from Perfluoro Sulfonic Acid (PFSA) to Hydrocarbon Ionomers. Figure 28
Aromatic polymers with pendant acidic groups

analyses of the hydrated samples. The ionic clusters were slightly smaller than those of Nafion membrane. The superacid groups were effective in improving thermal and mechanical properties of poly(arylene ether sulfone) ionomers as confirmed by dynamic mechanical analyses (DMA) and tensile testings. The superacidified ionomer membranes showed several times higher proton conductivity than that of the typical sulfonated poly(arylene ether sulfone) ionomers with similar IEC at 80°C, 50–90% RH.

Miyatake et al. have also confirmed the positive effect of superacid groups on the properties of the poly(arylene ether) ionomers [80, 81]. They have synthesized poly(arylene ether)s containing pendant superacid groups on fluorenyl groups (FSPEa-c) (Fig. 30) via similar method as that of Sumitomo Chemical Co. The superacid-containing ionomer membranes showed similar thermal and gas permeation properties to those of the conventional sulfonated aromatic ionomers. Instead, their morphology was more similar to that of Nafion. Well-developed hydrophilic/hydrophobic phase separation was observed, while the hydrophilic clusters were somewhat smaller than those of Nafion. More significant difference was observed in water uptake and proton conductivity (Fig. 31). For example, proton conductivity of superacid-containing ionomer membrane (IEC = 1.40 meq/g) was ca. 2 mS/cm at 80°C and 20% RH, which was considerably higher than that (0.02 mS/cm) of conventional sulfonated poly(arylene ether)s (SPE, IEC = 1.59 meq/g) under the same conditions. The two membranes showed very similar water uptake behavior at a wide range of humidity. The results imply that the superacid groups utilize water molecules more efficiently for proton conduction than arylsulfonic acid groups. Their study revealed that the main chain structure seemed to affect the properties and could be optimized for further improvement of the properties. The membrane showed good fuel cell performance at 80°C and 78 or 100% RH, however, the performance became lower under lower humidity conditions.

Hirakimoto et al. of Sony Co. have developed a unique ionomer containing superacid-substituted fullerene groups in the main chain (Fig. 32) [82]. Fullerene was substituted by averaging 7.1–8.4 superacid groups and were polymerized and cross-linked with 1,8-diiodoperfluorooctane to give the polymer with IEC = 1.88 meq/g. The ionomer was thermally stable up to 240°C as confirmed by TG analyses in dry nitrogen and showed high proton conductivity (2×10^{-2} S/cm) at 25°C and 50% RH as a pellet. Since the material did not seem to have good film-forming capability by

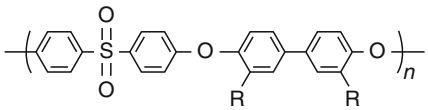

R: H, $-(CF_2)_2O(CF_2)_2SO_3H$ IEC = 0.95–1.58 meq/g

Membrane Electrolytes, from Perfluoro Sulfonic Acid (PFSA) to Hydrocarbon Ionomers. Figure 29
Poly(arylene ether sulfone)s with superacid groups

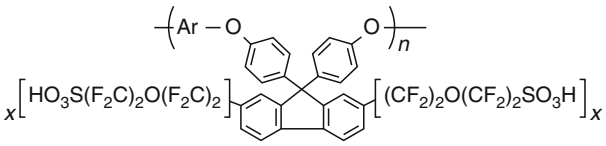

$x = 0.25–0.92$, IEC = 0.51–1.52 meq/g

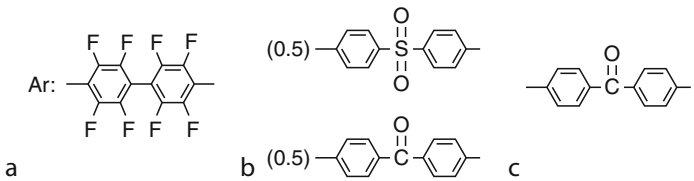

Membrane Electrolytes, from Perfluoro Sulfonic Acid (PFSA) to Hydrocarbon Ionomers. Figure 30
Poly(arylene ether)s containing superacid groups on fluorenyl groups

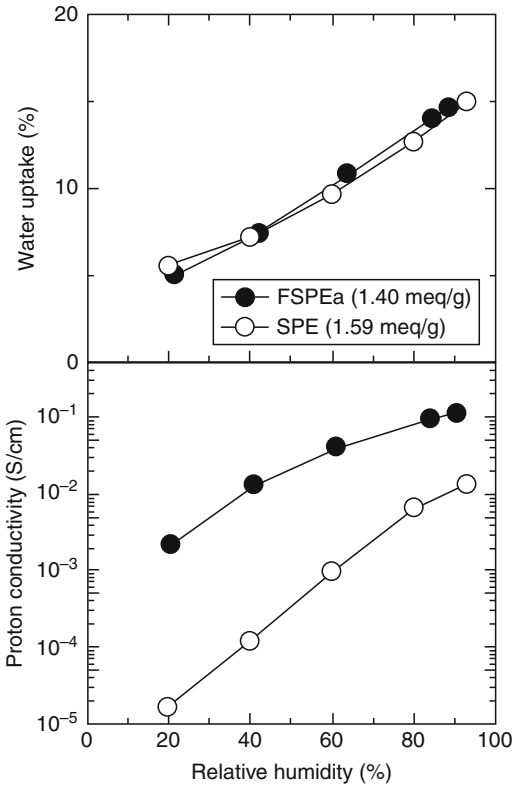

Membrane Electrolytes, from Perfluoro Sulfonic Acid (PFSA) to Hydrocarbon Ionomers. Figure 31
Humidity dependence of water uptake and proton conductivity of fluorene-containing poly(arylene ether)s with superacid groups (FSPEa) and conventional sulfonic acid groups (SPE) at 80°C

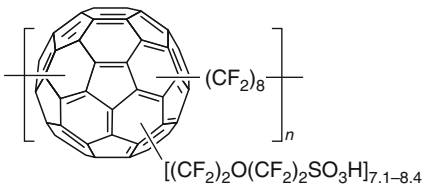

Membrane Electrolytes, from Perfluoro Sulfonic Acid (PFSA) to Hydrocarbon Ionomers. Figure 32
Superacid-modified polyfullerene

itself, composite membranes with poly(vinylidene difluoride) (PVDF) were investigated. The composite membrane containing 20 wt% of PVDF outperformed Nafion membrane in DMFC operation. The maximum power density of ca. 110 mW/cm^2 was achieved.

Composite Membranes

It has been proposed that modification of ionomer materials with hygroscopic oxides such silica, titania, tungsten oxide, zirconia, and zirconia phosphate could improve membrane properties. Introduction of nanoparticles of such oxides has been claimed to increase water affinity and reduce evaporation of water at high temperature and/or low humidity. The original research stems from Nafion composites [83–85] and recently, considerable effort has been devoted to apply the methodology to hydrocarbon ionomers. Some of the composite membranes showed better mechanical properties and lower gas or methanol permeability, however, the composite effect on the proton conductivity was not very obvious or even negative in some cases. In addition to the chemical and physical state of the inorganic additives, membrane fabrication procedure also seems a crucial factor since it affects membrane morphology and miscibility of inorganic additives with the matrix. Therefore, detailed and careful analyses are required to discuss the effect of additives. It is beyond the scope of this chapter to review the composite membranes. A few of the recent examples are introduced.

The group of GKSS Research Center Germany extensively researched the effect of a variety of inorganic nanoparticles on the properties of aromatic ionomer membranes [86–93]. Composite membranes were prepared from silicates and sulfonated poly(ether ketone)s or sulfonated poly(ether ether ketone)s. For DMFC applications, the composite membranes showed promising properties with lower methanol and water permeability and comparable (or higher) proton conductivity compared to the parent polymer membranes. The flux of water and methanol decreased with the increase in content of silicates.

In the case of sulfonated poly(phthalazinone ether ketone)s being used as a matrix, composite membranes showed less swelling in water and methanol, better mechanical and thermal stability, but lower proton conductivity [94, 95]. The results suggest that the amount of inorganic additives have to be optimized for each ionomer material and fuel cell operation conditions. Addition of 5 wt% of silica was optimum for poly(phthalazinone ether ketone)s to obtain high OCV and high power density of DMFC with 3 M methanol at 70°C.

It has been proposed that hybrid membranes are more proton conductive at low humidity than the parent polymer membranes. For example, zirconia phosphate (ZrP) was formed in the sulfonated poly (arylene ether sulfone). Nanoparticles of zirconia phosphate were homogeneously distributed in the membranes as crystalline α-zirconium hydrogen phosphate hydrate [96]. The composite membrane (with ZrP up to 50 wt%) showed 3.7×10^{-3} S/cm of the proton conductivity at 90°C, 30% RH, which was ca. 5 times higher than that of the parent polymer membrane under the same conditions. It is claimed that the composite effect depends upon interfacial contact between the polymer matrix and additives, and inappropriate preparation procedure could result in opposite effects.

In order to take more advantage of the effect of incorporated inorganic additives and to produce highly proton conductive composite membranes, Miyatake et al. have utilized 3-trihydroxysilyl-1-propanesulfonic acid (THOPS) as a precursor of the inorganic component (Fig. 33) [97]. THOPS has a sulfonic acid group covalently bonded to a silicon atom through aliphatic chain. The in situ sol–gel process in the polymer electrolyte matrices gave composite membranes containing sulfopropylated polysilsesquioxane ($\{SiO_{3/2}(CH_2)_3SO_3H\}_n$; SiOPS). Two different ionomer, sulfonated polyimides and sulfonated poly (arylene ether)s, were used as matrices. In the STEM images of the Ag-stained membrane samples, the ionic domains of approximately 5 nm in diameter were observed which were well-connected to each other. The connectivity of the ionic domains was significantly improved compared to that of the parent matrix membrane, while the size of the spherical ionic clusters did not alter. It is thought that the ionic domains result from the aggregation of sulfonic acid groups both from the matrix polymer and SiOPS. EDX analyses of the composite samples support highly dispersed SiOPS. These results suggest that well-dispersed nanocomposite membranes were formed. Nanocomposite membranes thus obtained showed much higher proton conductivity (up to 30 times) than that of the original membranes and accordingly less dependence of the conductivity upon the humidity. The ionomer properties such as thermal, hydrolytic and oxidative stability, and gas permeability were rather unaffected by the SiOPS. The methodology seems to be versatile as confirmed by the two different series of polymer electrolytes, although the miscibility with SiOPS depended on the matrix polymer.

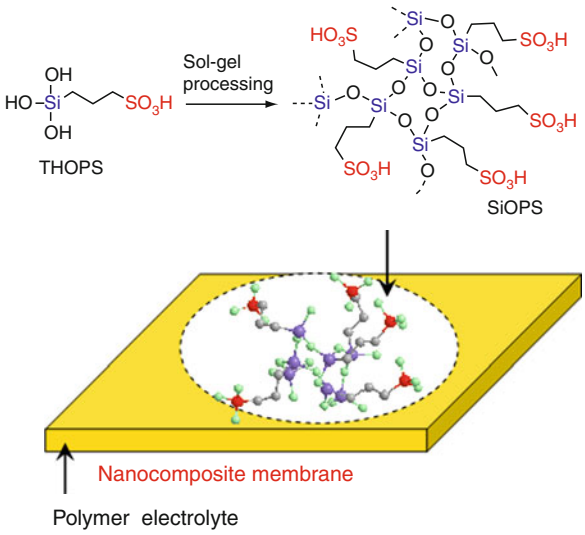

Membrane Electrolytes, from Perfluoro Sulfonic Acid (PFSA) to Hydrocarbon Ionomers. Figure 33 Schematic representation of the proton-conductive nanocomposite membranes composed of ionomer (matrix) and sulfopropylated polysilsesquioxane (SiOPS) (Reprinted from [97] with permission from Wiley Interscience)

Future Directions

The success of fuel cell industry depends greatly on the membrane technology. Since the biggest market of fuel cells will lie in the electric vehicles, most of the effort on the development of proton exchange membranes has been and will be devoted to wide temperature and low humidity (or nominally dry) operable membranes. In the last decade, PFSAs have achieved a significant progress and probably meet most of the requirements for the commercialization of fuel cell vehicles. At least, reasonable performance and durability can be obtained under well-controlled operating conditions using relatively large balance of plant (BOP). On a long-term basis, the current situation is not acceptable and more effort has to be made in developing better (possibly, non-fluorinated) ionomer membranes that fulfill all the above-mentioned requirements. This indicates that investment in such research is essential.

There is no doubt that the PFSA membranes take initiative in this field and contribute a great deal in the commercialization and wide diffusion of fuel cells in the early stage. In terms of environmental compatibility (recyclability or disposability) and production cost, the PFSA membranes would better be replaced with non-fluorinated alternative materials within the next decade. Challenge is how to achieve comparable conductivity and durability with the non-fluorinated membranes. Unfortunately, no alternative materials have overcome the trade-off relationship between these two incompatible properties. Aromatic hydrocarbon ionomers are one of the possible candidates and run next to PFSAs in the race of membrane development. While a number of effective approaches have been proposed, there still remains a significant gap between them. Alternative membranes can show comparable conductivity to PFSAs by absorbing more water, however, such excessive hydrophilicity results in chemical and mechanical instability. All hydrocarbon membranes tend to show severer decrease of proton conductivity with decreasing RH compared to the conductivity of PFSA membranes. A technological breakthrough is certainly required.

Due to the limited space, the other important role of proton-conducting materials as a binder in the gas diffusion electrode has not been mentioned in this chapter. In order to maximize potential activity of catalysts (both for the oxygen reduction and hydrogen oxidation catalysts), the ionomer materials are expected to function differently from the membranes. In addition to the basic properties such as proton conductivity and durability, the binder materials are required to permeate reactant gases and discharge product water. Excess swelling under hydrated conditions often disturb oxygen from diffusing onto the catalyst surface. The membranes are generally flat and rather thick (>10 μm), while the binders cover uneven nanostructured catalysts on carbon black in several nm thickness. The ionomers may behave differently in such thin layers, however, there have been few research works on this topic, particularly for non-fluorinated ionomers. Although some non-fluorinated ionomers are claimed to perform comparably to Nafion as membranes, they show considerably lower performance as a binder in the gas diffusion electrode in most cases. These issues need to be addressed more carefully and extensively in order to realize high-performance fluorine-free fuel cells.

Bibliography

Primary Literature

1. http://www1.eere.energy.gov/hydrogenandfuelcells/mypp/
2. Arenz M, Schmidt TJ, Wandelt K, Ross PN, Markovic NM (2003) The oxygen reduction reaction on thin palladium films supported on a Pt(111) electrode. J Phys Chem B 107:9813–9819
3. Aieta NV, Stanis RJ, Horan JL, Yandrasits MA, Cookson DJ, Ingham B, Toney MF, Hamrock SJ, Herring AM (2009) Clipped random wave morphologies and the analysis of the SAXS of an ionomer formed by copolymerization of tetrafluoroethylene and CF2 = CFO(CF2)4SO3H. Macromolecules 42: 5774–5780
4. Emery M, Frey M, Guerra M, Haugen G, Hintzer K, Lochhaas KH, Pham P, Pierpont D, Schaberg M, Thaler A, Yandrasits M, Hamrock S (2007) The development of new membranes for proton exchange membrane fuel cells. ECS Trans 11:3–14
5. Arcella V, Troglia C, Ghielmi A (2005) Hyflon ion membranes for fuel cells. Ind Eng Chem Res 44:7646–7651
6. Kreuer KD, Schuster M, Obliers B, Diat O, Traub U, Fuchs A, Klock U, Paddison SJ, Maier J (2008) Short-side-chain proton conducting perfluorosulfonic acid ionomers: why they perform better in PEM fuel cells. J Power Sources 178:499–509
7. Yoshitake M, Watakabe A (2008) Perfluorinated ionic polymers for PEFCs (including supported PFSA). Adv Polym Sci, Fuel Cells I 215:127–155
8. Appleby AJ, Velev OA, LeHelloco JG, Parthasarthy A, Srinivasan S, DesMarteau DD, Gillette MS, Ghosh JK (1993) Polymeric perfluoro bis-sulfonimides as possible fuel cell electrolytes. J Electrochem Soc 140:109–111
9. Kotov SV, Pedersen SD, Qiu W, Qiu Z-M, Burton DJ (1997) Preparation of perfluorocarbon polymers containing phosphonic acid groups. J Fluorine Chem 82:13–19
10. Thomas BH, DesMarteau DD (2005) Self-emulsifying polymerization (SEP) of 3, 6-dioxa-Delta 7–4-trifluoromethyl perfluorooctyl trifluoromethyl sulfonimide with tetrafluoroethylene. J Fluorine Chem 126:1057–1064
11. Thomas BH, Shafer G, Ma JJ, Tu M-H, DesMarteau DD (2004) Synthesis of 3, 6-dioxa-Delta 7–4-trifluoromethyl perfluorooctyl trifluoromethyl sulfonimide: bis [(perfluoroalkyl)sulfonyl] superacid monomer and polymer. J Fluorine Chem 125:1231–1240
12. Uematsu N, Hoshi N, Koga T, Ikeda M (2006) Synthesis of novel perfluorosulfonamide monomers and their application. J Fluorine Chem 127:1087–1095
13. Coms FD (2008) The chemistry of fuel cell membrane chemical degradation. ECS Trans 16:235–255
14. Curtin DE, Lousenberg RD, Henry TJ, Tangeman PC, Tisack ME (2004) Advanced materials for improved PEMFC performance and life. J Power Sources 131:41–48

15. Schiraldi DA (2006) Perfluorinated polymer electrolyte membrane durability. Polym Rev 46:315–327
16. Danilczuk M, Perkowski AJ, Schlick S (2010) Ranking the stability of perfluorinated membranes used in fuel cells to attack by hydroxyl radicals and the effect of Ce(III): a competitive kinetics approach based on spin trapping ESR. Macromolecules 43:3352–3358
17. Endoh E (2008) Development of highly durable PFSA membrane and MEA for PEMFC under high temperature and low humidity conditions. ECS Trans 16:1229–1240
18. Ghassemzadeh L, Kreuer KD, Maier J, Muller K (2010) Chemical degradation of nation membranes under mimic fuel cell conditions as investigated by solid-state NMR spectroscopy. J Phys Chem C 114:14635–14645
19. Coms FD, Liu H, Owejan JE (2008) Mitigation of perfluorosulfonic acid membrane chemical degradation using cerium and manganese ions. ECS Trans 16:1735–1747
20. Danilczuk M, Schlick S, Coms FD (2009) Cerium(III) as a stabilizer of perfluorinated membranes used in fuel cells: in situ detection of early events in the ESR resonator. Macromolecules 42:8943–8949
21. Trogadas P, Parrondo J, Ramani V (2008) Degradation mitigation in polymer electrolyte membranes using cerium oxide as a regenerative free-radical scavenger. Electrochem Solid-State Lett 11:B113–B116
22. Okazoe T, Murotani E, Watanabe K, Itoh M, Shirakawa D, Kawahara K, Kaneko I, Tatematsu S (2004) An entirely new methodology for synthesizing perfluorinated compounds: synthesis of perfluoroalkanesulfonyl fluorides from non-fluorinated compounds. J Fluorine Chem 125:1695–1701
23. Goto K, Rozhanskii I, Yamakawa Y, Otsuki T, Naito Y (2008) Development of aromatic polymer electrolyte membrane with high conductivity and durability for fuel cell. Polym J 41:95–104
24. Bae JM, Honma I, Murata M, Yamamoto T, Rikukawa M, Ogata N (2002) Properties of selected sulfonated polymers as proton-conducting electrolytes for polymer electrolyte fuel cells. Solid State Ionics 147:189–194
25. Kobayashi T, Rikukawa M, Sanui K, Ogata N (1998) Proton-conducting polymers derived from poly(ether-etherketone) and poly(4-phenoxybenzoyl-1, 4-phenylene). Solid State Ionics 106:219–225
26. Yanagimachi S, Kaneko K, Takeoka Y, Rikukawa M (2003) Synthesis and evaluation of phosphonated poly (4-phenoxybenzoyl-1, 4-phenylene). Synth Met 135:69–70
27. Ghassemi H, McGrath JE (2004) Synthesis and properties of new sulfonated poly(p-phenylene) derivatives for proton exchange membranes. I. Polymer 45:5847–5854
28. Ghassemi H, Ndip G, McGrath JE (2004) New multiblock copolymers of sulfonated poly(4′-phenyl-2, 5-benzophenone) and poly(arylene ether sulfone) for proton exchange membranes. II. Polymer 45:5855–5862
29. Fujimoto CH, Hickner MA, Cornelius CJ, Loy DA (2005) Ionomeric poly(phenylene) prepared by Diels-Alder polymerization: synthesis and physical properties of a novel polyelectrolyte. Macromolecules 38:5010–5016
30. He L, Fujimoto CH, Cornelius CJ, Perahia D (2009) From solutions to membranes: structure studies of sulfonated polyphenylene ionomers. Macromolecules 42:7084–7090
31. Hickner MA, Fujimoto CH, Cornelius CJ (2006) Transport in sulfonated poly(phenylene)s: proton conductivity, permeability, and the state of water. Polymer 47:4238–4244
32. Stanis RJ, Yaklin MA, Cornelius CJ, Takatera T, Umemoto A, Ambrosini A, Fujimoto CH (2010) Evaluation of hydrogen and methanol fuel cell performance of sulfonated diels alder poly (phenylene) membranes. J Power Sources 195:104–110
33. Rager T, Schuster M, Steininger H, Kreuer K-D (2007) Poly(1, 3-phenylene-5-phosphonic acid), a fully aromatic polyelectrolyte with high ion exchange capacity. Adv Mater 19:3317–3321
34. Steininger H, Schuster M, Kreuer KD, Kaltbeitzel A, Bingoel B, Meyer WH, Schauff S, Brunklaus G, Maier J, Spiess HW (2007) Intermediate temperature proton conductors for PEM fuel cells based on phosphonic acid as protogenic group: a progress report. Phys Chem Chem Phys 9:1764–1773
35. Schuster M, de Araujo CC, Atanasov V, Andersen HT, Kreuer K-D, Maier J (2009) Highly sulfonated poly(phenylene sulfone): preparation and stability issues. Macromolecules 42:3129–3137
36. Schuster M, Kreuer K-D, Andersen HT, Maier J (2007) Sulfonated poly(phenylene sulfone) polymers as hydrolytically and thermooxidatively stable proton conducting ionomers. Macromolecules 40:598–607
37. Kashimura Y, Aoyama S, Kawakami H (2009) Gas transport properties of asymmetric block copolyimide membranes. Polym J 41:961–967
38. Nakano T, Nagaoka S, Kawakami H (2005) Preparation of novel sulfonated block copolyimides for proton conductivity membranes. Polym Adv Technol 16:753–757
39. Nakano T, Nagaoka S, Kawakami H (2006) Proton conductivity of sulfonated long-chain-block copolyimide films. Kobunshi Ronbunshu 63:200–204
40. Niwa M, Nagaoka S, Kawakami H (2006) Preparation of novel fluorinated block copolyimide membranes for gas separation. J Appl Polym Sci 100:2436–2442
41. Asano N, Miyatake K, Watanabe M (2006) Sulfonated block polyimide copolymers as a proton-conductive membrane. J Polym Sci, A: Polym Chem 44:2744–2748
42. Badami AS, Lane O, Lee H-S, Roy A, McGrath JE (2009) Fundamental investigations of the effect of the linkage group on the behavior of hydrophilic-hydrophobic poly(arylene ether sulfone) multiblock copolymers for proton exchange membrane fuel cells. J Membr Sci 333:1–11
43. Badami AS, Roy A, Lee H-S, Li Y, McGrath JE (2009) Morphological investigations of disulfonated poly(arylene ether sulfone)-b-naphthalene dianhydride-based polyimide multiblock copolymers as potential high temperature proton exchange membranes. J Membr Sci 328:156–164
44. Ghassemi H, McGrath JE, Zawodzinski TA (2006) Multiblock sulfonated-fluorinated poly(arylene ether)s for a proton exchange membrane fuel cell. Polymer 47:4132–4139

45. Lee H-S, Lane O, McGrath JE (2010) Development of multiblock copolymers with novel hydroquinone-based hydrophilic blocks for proton exchange membrane (PEM) applications. J Power Sources 195:1772–1778
46. Lee H-S, Roy A, Lane O, Dunn S, McGrath JE (2008) Hydrophilic-hydrophobic multiblock copolymers based on poly(arylene ether sulfone) via low-temperature coupling reactions for proton exchange membrane fuel cells. Polymer 49:715–723
47. Lee HS, Roy A, Lane O, Lee M, McGrath JE (2010) Synthesis and characterization of multiblock copolymers based on hydrophilic disulfonated poly(arylene ether sulfone) and hydrophobic partially fluorinated poly(arylene ether ketone) for fuel cell applications. J Polym Sci Pol Chem 48:214–222
48. Lee M, Park JK, Lee H-S, Lane O, Moore RB, McGrath JE, Baird DG (2009) Effects of block length and solution-casting conditions on the final morphology and properties of disulfonated poly(arylene ether sulfone) multiblock copolymer films for proton exchange membranes. Polymer 50:6129–6138
49. Roy A, Hickner MA, Einsla BR, Harrison WL, McGrath JE (2009) Synthesis and characterization of partially disulfonated hydroquinone-based poly(arylene ether sulfone)s random copolymers for application as proton exchange membranes. J Polym Sci Pol Chem 47:384–391
50. Roy A, Lee H-S, McGrath JE (2008) Hydrophilic-hydrophobic multiblock copolymers based on poly(arylene ether sulfone)s as novel proton exchange membranes - Part B. Polymer 49:5037–5044
51. Yu X, Roy A, Dunn S, Yang J, McGrath JE (2006) Synthesis and characterization of sulfonated-fluorinated, hydrophilic-hydrophobic multiblock copolymers for proton exchange membranes. Macromol Symp 245/246:439–449
52. Matsumura S, Hlil AR, Hay AS (2008) Synthesis, properties, and sulfonation of novel dendritic multiblock copoly(ether-sulfone). J Polym Sci Pol Chem 46:6365–6375
53. Matsumura S, Hlil AR, Lepiller C, Gaudet J, Guay D, Hay AS (2008) Ionomers for proton exchange membrane fuel cells with sulfonic acid groups on the end groups: novel linear aromatic poly(sulfide-ketone)s. Macromolecules 41:277–280
54. Matsumura S, Hlil AR, Lepiller C, Gaudet J, Guay D, Shi Z, Holdcroft S, Hay AS (2008) Ionomers for proton exchange membrane fuel cells with sulfonic acid groups on the end groups: novel branched poly(ether-ketone)s. Macromolecules 41:281–284
55. Matsumura S, Hlil AR, Al-Souz MAK, Gaudet J, Guay D, Hay AS (2009) Ionomers for proton exchange membrane fuel cells by sulfonation of novel dendritic multiblock copoly(ether-sulfone)s. J Polym Sci Pol Chem 47:5461–5473
56. Matsumura S, Hlil AR, Du N, Lepiller C, Gaudet J, Guay D, Shi Z, Holdcroft S, Hay AS (2008) Ionomers for proton exchange membrane fuel cells with sulfonic acid groups on the end-groups: novel branched poly(ether-ketone)s with 3, 6-ditrityl-9H-carbazole end-groups. J Polym Sci Pol Chem 46:3860–3868
57. Tian S, Meng Y, Hay AS (2009) Membranes from poly(aryl ether)-based ionomers containing multiblock segments of randomly distributed nanoclusters of 18 sulfonic acid groups. J Polym Sci Pol Chem 47:4762–4773
58. Tian S, Meng Y, Hay AS (2009) Membranes from poly(aryl ether)-based ionomers containing randomly distributed nanoclusters of 6 or 12 sulfonic acid groups. Macromolecules 42:1153–1160
59. Higashihara T, Matsumoto K, Ueda M (2009) Sulfonated aromatic hydrocarbon polymers as proton exchange membranes for fuel cells. Polymer 50:5341–5357
60. Matsumoto K, Higashihara T, Ueda M (2009) Locally and densely sulfonated poly(ether sulfone)s as proton exchange membrane. Macromolecules 42:1161–1166
61. Matsumoto K, Higashihara T, Ueda M (2009) Locally sulfonated poly(ether sulfone)s with highly sulfonated units as proton exchange membrane. J Polym Sci Pol Chem 47:3444–3453
62. Bae B, Miyatake K, Watanabe M (2009) Synthesis and Properties of Sulfonated Block Copolymers Having Fluorenyl Groups for Fuel-Cell Applications. ACS Appl Mater Interfaces 1:1279–1286
63. Bae B, Miyatake K, Watanabe M (2010) Sulfonated poly(arylene ether sulfone ketone) multiblock copolymers with highly sulfonated block. Synth Properties Macromol 43:2684–2691
64. Bae B, Yoda T, Miyatake K, Uchida H, Watanabe M (2010) Proton-conductive aromatic ionomers containing highly sulfonated blocks for high-temperature-operable fuel cells. Angew Chem Int Ed 49:317–320
65. Li N, Liu J, Cui Z, Zhang S, Xing W (2009) Novel hydrophilic-hydrophobic multiblock copolyimides as proton exchange membranes: enhancing the proton conductivity. Polymer 50:4505–4511
66. Liu B, Robertson GP, Kim D-S, Guiver MD, Hu W, Jiang Z (2007) Aromatic poly(ether ketone)s with pendant sulfonic acid phenyl groups prepared by a mild sulfonation method for proton exchange membranes. Macromolecules 40:1934–1944
67. Liu B, Robertson GP, Kim D-S, Sun X, Jiang Z, Guiver MD (2010) Enhanced thermo-oxidative stability of sulfophenylated poly(ether sulfone)s. Polymer 51:403–413
68. Pang J, Zhang H, Li X, Jiang Z (2007) Novel wholly aromatic sulfonated poly(arylene ether) copolymers containing sulfonic acid groups on the pendants for proton exchange membrane materials. Macromolecules 40:9435–9442
69. Pang J, Zhang H, Li X, Liu B, Jiang Z (2008) Poly(arylene ether)s with pendant sulfoalkoxy groups prepared by direct copolymerization method for proton exchange membranes. J Power Sources 184:1–8
70. Pang J, Zhang H, Li X, Ren D, Jiang Z (2007) Low water swelling and high proton conducting sulfonated poly(arylene ether) with pendant sulfoalkyl groups for proton exchange membranes. Macromol Rapid Commun 28:2332–2338
71. Pang J, Zhang H, Li X, Wang L, Liu B, Jiang Z (2008) Synthesis and characterization of sulfonated poly(arylene ether)s with sulfoalkyl pendant groups for proton exchange membranes. J Membr Sci 318:271–279
72. Lee JK, Li W, Manthiram A (2009) Poly(arylene ether sulfone)s containing pendant sulfonic acid groups as membrane materials for direct methanol fuel cells. J Membr Sci 330:73–79

73. Lafitte B, Jannasch P (2007) Proton-conducting aromatic polymers carrying hypersulfonated side chains for fuel cell applications. Adv Funct Mater 17:2823–2834
74. Parvole J, Jannasch P (2008) Poly(arylene ether sulfone)s with phosphonic acid and bis(phosphonic acid) on short alkyl side chains for proton-exchange membranes. J Mater Chem 18:5547–5556
75. Parvole J, Jannasch P (2008) Polysulfones grafted with poly (vinylphosphonic acid) for highly proton conducting fuel cell membranes in the hydrated and nominally dry state. Macromolecules 41:3893–3903
76. Kim DS, Kim YS, Guiver MD, Pivovar BS (2008) High performance nitrile copolymers for polymer electrolyte membrane fuel cells. J Membr Sci 321:199–208
77. Kim DS, Kim YS, Guiver MD, Ding J, Pivovar BS (2008) Highly fluorinated comb-shaped copolymer as proton exchange membranes (PEMs): fuel cell performance. J Power Sources 182:100–105
78. Kreuer KD (2001) On the development of proton conducting polymer membranes for hydrogen and methanol fuel cells. J Membr Sci 185:29–39
79. Yoshimura K, Iwasaki K (2009) Aromatic polymer with pendant perfluoroalkyl sulfonic acid for fuel cell applications. Macromolecules 42:9302–9306
80. Mikami T, Miyatake K, Watanabe M (2010) Poly(arylene ether)s containing superacid groups as proton exchange membranes. ACS Appl Mater Interfaces 2:1714–1721
81. Miyatake K, Shimura T, Mikami T, Watanabe M (2009) Aromatic ionomers with superacid groups. Chem Commun 42:6403–6405
82. Hirakimoto T, Fukushima K, Li Y, Takizawa S, Hinokuma K, Senoo T (2008) Fullerene-based proton-conductive material for the electrolyte membrane and electrode of a direct methanol fuel cell. ECS Trans 16:2067–2072
83. Watanabe M, Uchida H, Emori M (1998) Analyses of self-humidification and suppression of gas crossover in Pt-dispersed polymer electrolyte membranes for fuel cells. J Electrochem Soc 145:1137–1141
84. Watanabe M, Uchida H, Emori M (1998) Polymer electrolyte membranes incorporated with nanometer-size particles of pt and/or metal-oxides: experimental analysis of the self-humidification and suppression of gas-crossover in fuel cells. J Phys Chem B 102:3129–3137
85. Watanabe M, Uchida H, Seki Y, Emori M, Stonehart P (1996) Self-humidifying polymer electrolyte membranes for fuel cells. J Electrochem Soc 143:3847–3852
86. Dyck A, Fritsch D, Nunes SP (2002) Proton-conductive membranes of sulfonated polyphenylsulfone. J Appl Polym Sci 86:2820–2827
87. Gomes D, Buder I, Nunes SP (2006) Sulfonated silica-based electrolyte nanocomposite membranes. J Polym Sci Pol Chem 44:2278–2298
88. Karthikeyan CS, Nunes SP, Prado LASA, Ponce ML, Silva H, Ruffmann B, Schulte K (2005) Polymer nanocomposite membranes for DMFC application. J Membr Sci 254:139–146
89. Karthikeyan CS, Nunes SP, Schulte K (2005) Ionomer-silicates composite membranes: permeability and conductivity studies. Eur Polym J 41:1350–1356
90. Karthikeyan CS, Nunes SP, Schulte K (2006) Permeability and conductivity studies on ionomer-polysilsesquioxane hybrid materials. Macromol Chem Phys 207:336–341
91. Nunes SP, Ruffmann B, Rikowski E, Vetter S, Richau K (2002) Inorganic modification of proton conductive polymer membranes for direct methanol fuel cells. J Membr Sci 203:215–225
92. Silva VS, Ruffmann B, Silva H, Gallego YA, Mendes A, Madeira LM, Nunes SP (2005) Proton electrolyte membrane properties and direct methanol fuel cell performance. J Power Sources 140:34–40
93. Silva VS, Schirmer J, Reissner R, Ruffmann B, Silva H, Mendes A, Madeira LM, Nunes SP (2005) Proton electrolyte membrane properties and direct methanol fuel cell performance. J Power Sources 140:41–49
94. Su Y-H, Liu Y-L, Sun Y-M, Lai J-Y, Guiver MD, Gao Y (2006) Using silica nanoparticles for modifying sulfonated poly (phthalazinone ether ketone) membrane for direct methanol fuel cell: a significant improvement on cell performance. J Power Sources 155:111–117
95. Su Y-H, Liu Y-L, Sun Y-M, Lai J-Y, Wang D-M, Gao Y, Liu B, Guiver MD (2007) Proton exchange membranes modified with sulfonated silica nanoparticles for direct methanol fuel cells. J Membr Sci 296:21–28
96. Anilkumar GM, Nakazawa S, Okubo T, Yamaguchi T (2006) Proton conducting phosphated zirconia-sulfonated polyether sulfone nanohybrid electrolyte for low humidity, wide-temperature PEMFC operation. Electrochem Commun 8:133–136
97. Miyatake K, Tombe T, Chikashige Y, Uchida H, Watanabe M (2007) Enhanced proton conduction in polymer electrolyte membranes with acid- functionalized polysilsesquioxane. Angew Chem Int Ed 46:6646–6649

Books and Reviews

Colomban P (1992) Proton conductors: solids, membrane and gels – materials and devices. Cambridge University Press, Cambridge

Hickner MA, Ghassemi H, Kim YS, Einsla BR, McGrath JE (2004) Alternative polymer systems for proton exchange membranes (PEMs). Chem Rev 104:4587–4612

Kreuer KD, Paddison SJ, Spohr E, Schuster M (2004) Transport in proton conductors for fuel-cell applications: simulations, elementary reactions, and phenomenology. Chem Rev 104:4637–4678

Rikukawa M, Sanui K (2000) Proton-conducting polymer electrolyte membranes based on hydrocarbon polymers. Prog Polym Sci 25:1463–1502

Scherer GG (2008) Advances in polymer science: fuel cells I & II. Springer, Berlin

Tant BR, Mauritz KA, Wilkes GL (1997) Ionomers – synthesis, structure, properties and applications. Blackie Academic & Professional, New York

Mesoscopic Solar Cells

Michael Grätzel
Laboratory of Photonics and Interfaces, Institute of Chemical Science and Engineering, Ecole Polytechnique Fédérale de Lausanne (EPFL), Lausanne, Switzerland

Article Outline

Glossary
Introduction
Operational Principles of Dye-Sensitized Mesoscopic Solar Cells
Comparison with Conventional p–n Junction Devices
The Virtues of the Nanostructure
Typical Sensitizers Based on Ruthenium Complexes
The Present Status of Dye-Sensitized Solar Cells
Reproducibility of Cell Fabrication and Scale-up
Stability and Commercial Development of the DSC
Ongoing and Future Research
Summary
Acknowledgement
Bibliography

Glossary

AM1.5 Air mass 1.5: Defines position of the sun where the path through the atmosphere is 1.5 longer than at a vertical incidence.

Fill factor of the cell Maximum power output of the cell divided by the product of open circuit photovoltage (Voc) times the short circuit photocurrent density.

IPCE Incident photon to electric current conversion efficiency, presents the ratio of the electric current generated by monochromatic light of a certain wavelength over the incident photon flux.

Mesoscopic Size domain between 2 and 50 nm.

Power conversion efficiency (PCE) the maximal electric power generated by the photovoltaic cell divided by the incident solar light intensity under AM 1.5 standard reporting conditions (Intensity of the sunlight 1000W/m2 and T= 298 K).

Sensitizer Dye molecule generating electric charges from sunlight.

Introduction

Perhaps, the largest challenge for our global society is to find ways to replace the slowly but inevitably vanishing fossil fuel supplies by renewable resources. The problem is compounded by an increase in the worldwide consumption of energy, which is expected to double within the next 40 years from the current level of 500 exajoules/year (exa = 10^{18}) to 1,000 exajoules/year. This additional demand cannot be met by accelerated combustion of fossil fuels, which would entail enhanced environmental pollution and global warming, leave alone the fact that oil production has already peaked and will decline in the future (Fig. 1). Furthermore, the current ongoing disaster at the Fukushima reactor site in Japan along with previous major accidents has exposed to the world the risks and limitations of nuclear energy use, leave alone that the issue of where to store nuclear waste over ten thousands of years in a safe manner and at what cost remains unresolved to date.

The sun provides about 120,000 TW to the earth's surface which amounts to 6,000 times the present rate of the world's energy consumption. However, capturing solar energy and converting it to heat, electricity, or chemical fuels, such as hydrogen, at low cost and using abundantly available raw materials remain a huge challenge. Photovoltaic cells are expected to make pivotal contributions to identify environmentally friendly solutions to this energy problem. One area of great promise is that of a new generation of nonconventional photovoltaic converters generally referred to as mesoscopic solar cells (MSCs), which employ three-dimensional (bulk) interpenetrating network junctions for light harvesting and afford charge carrier transport using structural elements with features in the 2–50-nm size range.

While this field is still in its infancy, it is presently receiving enormous attention, thousands of publications having appeared over the last decade and dozens of industrial enterprises being involved in the commercialization of this new technology. The advantage of the mesoscopic solar cells is that they can be produced at low cost, i.e., potentially significantly less than 1 US$/peak watt. These systems have the potential to deliver solar electricity at a price of 5 cents/KWh, which is competitive with present conventional energy cost. Some, but not all MSC embodiments, can avoid the expensive and energy-intensive high vacuum and

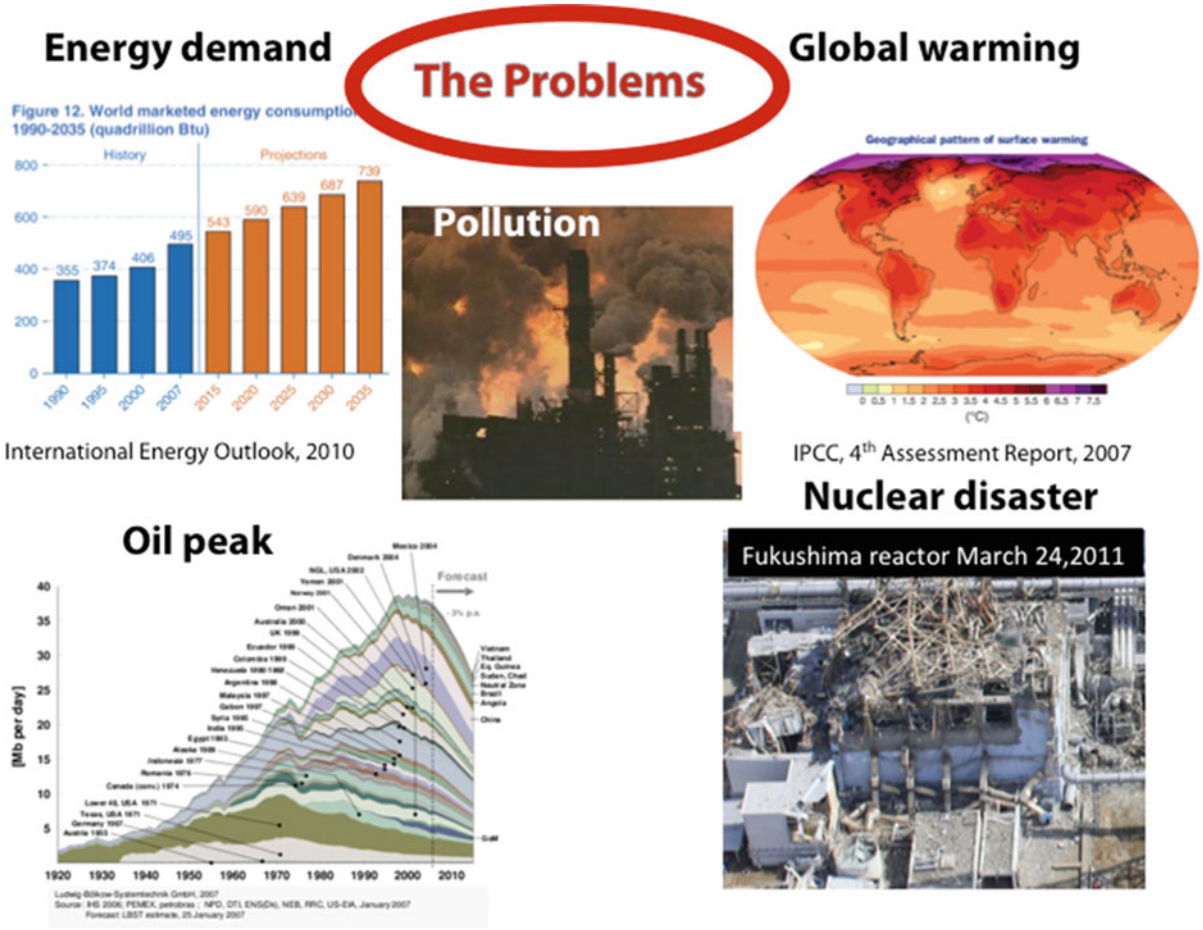

Mesoscopic Solar Cells. Figure 1
Projected growth of future energy demand and problems arising from the use of fossil fuels or nuclear reactors to cover the additional needs of 500 exajoules by 2050

materials purification steps that are currently employed in the fabrication of all other thin film solar cells. They employ materials that are abundantly available so that the technology can be scaled up to the terawatt level without running into feedstock supply problems. This gives mesoscopic solar cells an advantage over the two major competing thin film photovoltaic devices, i.e., CdTe and Cu(In, Ga)Se_2 (CIGS), which are based on highly toxic materials or elements of low natural abundance. While some MSCs do use rare elements such as Ru and Pt the quantities employed are so small that these noble metals are not cost determining and do not limit the scale up of the technology to the terawatt level. However, a drawback of the current embodiment of MSCs is that their efficiency is still lower than that for single and multicrystalline silicon as well as CdTe and Cu(In, Ga)Se_2 (CIGS) cells. Also, MSCs based on conjugated organic compounds, such as blends of C60 with polythiophenes, are very sensitive to water and oxygen and, hence, need to be carefully sealed to avoid rapid degradation. The present entry focuses on dye-sensitized solar cells (DSCs), which are leading this new generation of mesoscopic photovoltaic devices [1]. Research in the DSC field is booming, and the technology is advancing at a very rapid pace. Progress in several important areas related to the sensitization of mesoscopic semiconducting oxides by dyes and quantum dots has been covered by a number of recent reviews and a book [2–23]. Here, we discuss the operational principles of the device and some recent

exciting developments stemming mainly from our own laboratory. We present promising new concepts to boost further the conversion efficiency and stability of the DSC and summarize the status of its commercial applications.

Operational Principles of Dye-Sensitized Mesoscopic Solar Cells

Shown in the upper part of Fig. 2 is the cross section of a typical embodiment for a mesoscopic solar cell based on the sensitization of nanocrystalline titania (TiO_2, anatase) films. The nanoparticles (shown as grey balls) are screen-printed onto a glass sheet covered by a thin film of a transparent conducting oxide (TCO). The latter collects the electrons generated by light excitation of the sensitizer molecules (shown as red dots). The excited state of the sensitizer injects electrons in the conduction band of the TiO_2 particles. The conduction band electrons percolate subsequently across the nanoparticle network, before they reach the TCO front contact. From there, they pass through the external circuit to perform electrical work and reenter the cell through the counter electrode. A redox shuttle, typically the iodide/iodide couple, moves the electrons back to the surface of the nanocrystalline film where it regenerates the sensitizer.

The lower part of Fig. 2 shows a photograph of a dye-sensitized solar cell. The transparent glass module produces electricity from ambient light captured from all spatial angles due to its bifacial character, which is used to drive a fan. The photograph illustrates the transparent character of electricity generating glass which is a unique feature of dye-sensitized mesoscopic solar cells, offering widespread applications as electric power producing window in glass facades of buildings.

Following its inception in 1985 [24], the dye-sensitized mesoscopic solar cells (DSC) were the first device to use a three-dimensional interpenetrating network junction, referred to as "bulk heterojunction" for solar light energy harvesting and conversion. Leading a new generation of solar cells [24–31], the DSC is the only photovoltaic device that uses molecules or semiconductor quantum dots to absorb photons and convert them to electric charges without the need of intermolecular transport of electronic excitation. The conversion of light to electricity does not involve the participation of minority carriers. The role of the sensitizer or quantum dot is to absorb light and generate positive and negative electric charges, which are injected in appropriate charge transport materials, i.e., an n-type conductor such as TiO_2 for the electrons and a p-type conductor or electrolyte for the positive charges (holes).

Figure 3 shows a typical energy band diagram of the DSC. Sunlight is harvested by the sensitizer that is attached to the surface of a large-bandgap semiconductor, typically a film of TiO_2, ZnO, or SnO_2 constituted of nanoparticles, nanorods, nanotubes, or other mesoscopic structures. Photoexcitation of the dye results in the injection of electrons into the conduction band of the oxide, producing the oxidized form of the sensitizer S^+. The dye is regenerated by electron donation from an organic or inorganic hole conductor or a redox electrolyte that is infiltrated into the porous films. Figure 3 shows two typical embodiments of the DSC. The left drawing refers to the version that employs a redox electrolyte while the right configuration employs a solid state hole conductor to shuttle the positive charges generated under light excitation from the oxidized sensitizer to the back contact. The former contains, most frequently, the iodide/triiodide couple as a redox shuttle, although other mediators such as cobalt (II/III) complexes [30–32], the TEMPO/TEMPO + redox couple [33] thiotetrazol [34] tetramethylthiourea [35], and ferrocene [36] have shown promise recently as an alternative to the I^-/I_3^- system. Electron transfer from the reduced mediator to S^+ regenerates the original form of the dye while producing the oxidized form of the mediator. This prevents any significant buildup of S^+ at the surface, which could recapture the conduction band electron. The reduced mediator is regenerated in turn at the counter electrode. Electrons are supplied via migration through the external load completing the cycle. Thus, the device is regenerative producing electricity from light without any permanent chemical transformation. Figure 4 shows two typical embodiments of the DSC using a redox electrolyte or solid hole conductor for charge transport between the working and counter-electrode.

The open-circuit photovoltage V_{oc} produced under illumination corresponds to the difference between the chemical potential (Fermi level), $\mu(e^-)$, attained by the conduction band electrons in the mesoscopic titania

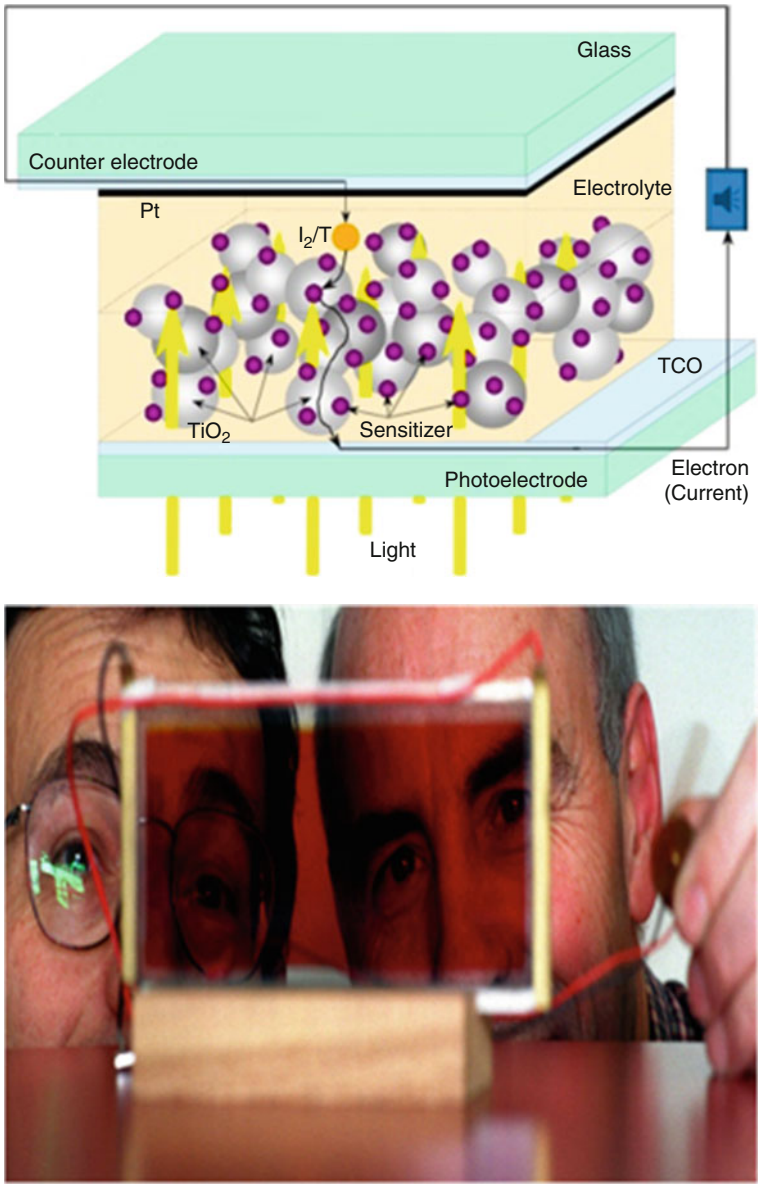

Mesoscopic Solar Cells. Figure 2

Upper part: Cross section of a typical embodiment for a mesoscopic solar cell based on the sensitization of nanocrystalline titania (TiO_2, anatase) films. The nanoparticles (shown as *grey balls*) are screen-printed onto a glass sheet covered by a thin film of a transparent conducting oxide (TCO). The latter collects the electrons generated by light excitation of the sensitizer molecules (shown as *red dots*). The excited state of the sensitizer injects electrons in the conduction band of the TiO_2 particles. The conduction band electrons percolate subsequently across the nanoparticle network, before the reach the TCO front contact. From there, they pass through the external circuit to perform electrical work and reenter the cell through the counter electrode. A redox shuttle, typically the iodide/iodide couple, moves the electrons back to the surface of the nanocrystalline film where the regenerate the sensitizer. *Lower part*: Photograph of a dye-sensitized solar cell. The transparent glass module produces electricity from ambient light from all angles due to its bifacial character, which is used to drive a fan. The photograph illustrates the transparent character of glass which is a unique feature of dye-sensitized mesoscopic solar cells, offering widespread applications as electric power producing window in glass facades of buildings

film under illumination and the chemical potential $\mu(h^+)$ of the holes in the hole conductor. For liquid or solid electrolytes, the latter corresponds to the Nernst potential (E) of the redox couple used as a shuttle to transport positive charges from the sensitizer to the back contact of the cell. Note that in the dark at equilibrium $\mu(e^-) = \mu(h^+)$, i.e., the Fermi level is constant within the whole device.

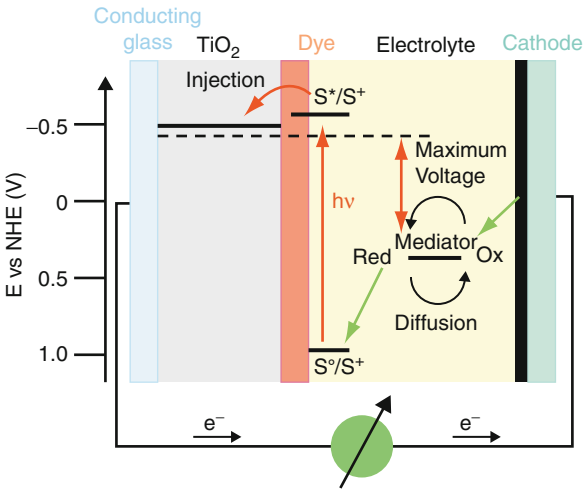

Mesoscopic Solar Cells. Figure 3
Energy band diagram of a typical embodiment of the DSC. The energy levels are presented on the normal hydrogen reference electrode scale for N719 as sensitizer and iodide/triiodide as redox electrolyte

The energy levels in Fig. 3 are drawn to fit a frequently employed embodiment of the DSC based on the N719 ruthenium dye (the di-tetrabutylammonium salt of N3), the iodide/triiodide as a redox couple, and nanocrystalline anatase films as electron collector. The ground state standard redox potential of the N719 as well as that of several other ruthenium complexes and organic sensitizers is around 1 V against the normal hydrogen electrode (NHE) when it is adsorbed at the titania surface, while the Nernst potential of the triiodide/iodide-based redox electrolyte is between 0.3 V and 0.4 V, and the energy of the conduction band edge of anatase is located at −0.5 V. Neglecting entropy changes during the light absorption and using a 0–0 vibronic transition energy of 1.65 eV, the excited state redox potential of N719 is derived to be −0.65 eV. Hence, the driving force for electron injection under standard conditions is 0.15 eV. By contrast, the regeneration consumes an excessive amount of free energy, i.e., between 0.6 and 0.7 eV depending on the exact composition of the iodide-/triiodide-based electrolyte.

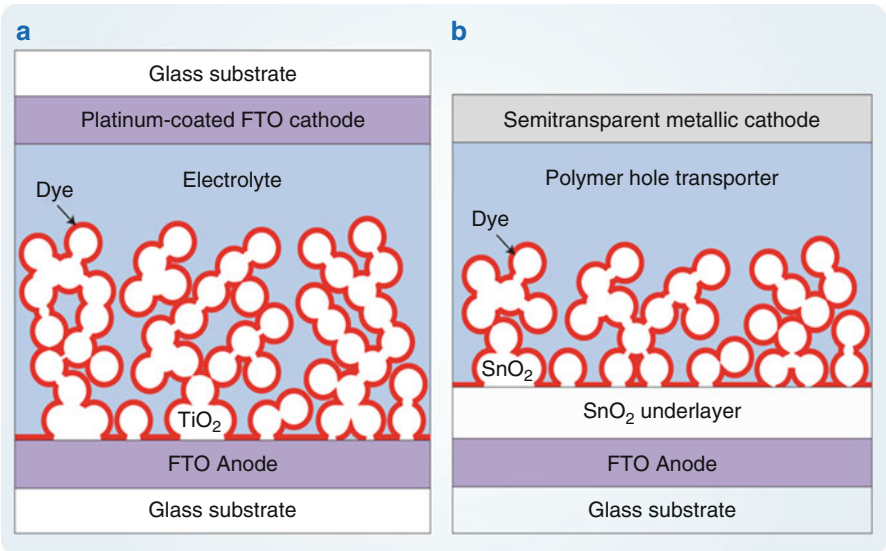

Mesoscopic Solar Cells. Figure 4
Two typical embodiments of dye-sensitized mesoscopic solar cells. (**a**) The dye-loaded mesoscopic TiO_2 film is contacted by a redox electrolyte whose task is to transport positive charges from the sensitized to the counter electrode. (**b**) A polymer or organic molecular hole conductor assumes the role of transporting the positive charge

This mismatch of over 0.6 eV between the redox level of the sensitizer and that of the triiodide/iodide presents the major loss channel for DSCs using this type of electrolyte. Using the black dye (N749) instead of N719, the loss is reduced to 0.4 eV due to its 0.2 eV lower ground-state redox potential [37]. Measurements of a series of ruthenium complexes have shown that the minimum driving force required for the near quantitative interception of the geminate electron recombination with the oxidized sensitizer by oxidation of iodide to triiodide is about 0.3 eV. This relatively high value results from the two-electron character of the iodide oxidation reaction, which passes through I_2^- radicals as intermediates. A recent breakthrough in the DSC field opened up the way to use one electron redox mediators, reducing the losses during the regeneration of the sensitizer to merely 0.2 eV. This has allowed to increase the Voc value of DSCs to over 1 V.

Comparison with Conventional p–n Junction Devices

One of the fundamental advantages of the DSC is that it separates the two functions of light harvesting and charge carrier transport, whereas conventional silicon-based cells and all known organic photovoltaic devices perform both operations simultaneously. This imposes stringent demands on the optical and electronic properties of the semiconductor, i.e., its bandgap and conduction band or valence band position, as well as mobility and the recombination time of photogenerated charge carriers. As a result, the choice of suitable materials that are able to act as efficient photovoltaic converters is greatly restricted. The separation of the functions of light harvesting and carrier transport on the other hand opens up many options for the absorber and charge transport materials. The molecular sensitizer or semiconductor quantum dot is placed at the interface between an electron (n) and hole (p) conducting material (Fig. 5 left side). The former is typically a wide band semiconductor oxide, such as TiO_2, ZnO, or SnO_2, while the latter is a redox electrolyte or a p-type semiconductor. Upon photoexcitation, the sensitizer injects an electron in the conduction band of the oxide and is regenerated by hole injection in the electrolyte or p-type conductor. Alternatively, the excited sensitizer may inject a hole in the valence band of p-type oxide such as NiO [32] and is regenerated from its reduced form by electron transfer to an acceptor in the electrolyte. In both cases, the role of the sensitizer is to absorb light and generate positive and negative charge carriers. The latter are transported to the front and back contacts where they are collected as electric current. The open-circuit photovoltage V_{oc} corresponds to the difference in the Fermi level of the n- and p-type conductor under illumination. This configuration has the following advantages:

- Constraints on individual components of the cell are relaxed, i.e., the electron and hole conductor materials, as well as the sensitizer or quantum dot type, can each be separately selected and tuned for optimal performance.
- Light absorption and charge transport are decoupled avoiding the participation of minority carriers in the light energy conversion process.
- The optoelectronic properties of the mesoscopic semiconductor oxide film, which supports the self-assembled dye monolayer, can be adapted to yield efficient light harvesting and charge carrier collection. Apart from exploiting light scattering and photon containment effects, structures that display photonic bandgaps and plasmonic behavior have shown benefits. These light management strategies allow reducing the oxide film thickness and hence the amount of substances required to harvest solar light, saving materials cost.
- The use of a molecular sensitizer avoids the need for transport of excitons within the absorber material to achieve photoinduced charge separation.
- Finally, the sensitizer itself if present as a well-organized compact monomolecular layer may retard the recombination of photogenerated charge carriers, which has to occur across the interface occupied by the dye molecules.

For comparison, the right side of Fig. 5 shows a schematic illustration of the operational principle for a conventional silicon p–n junction photovoltaic cell. Here, the same semiconductor material, e.g., silicon, assumes the two key functions of light absorption and charge carrier transport. Photoexcitation of the silicon generates electron–hole pairs which need to reach the p–n junction before they recombine.

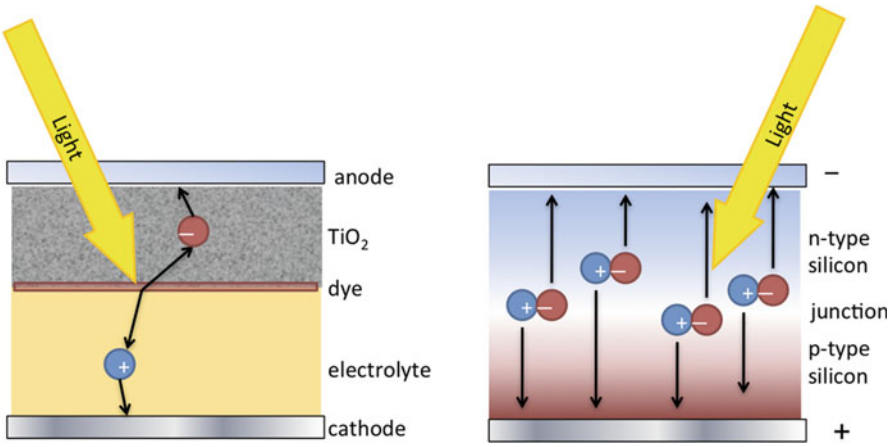

Mesoscopic Solar Cells. Figure 5
Left side: Schematic illustration of the operation principle for dye-sensitized photovoltaic cell. The heart of the device is a sensitizer or quantum dot placed at the interface between an electron (n)-conducting wide bandgap semiconductor material, such as TiO_2, and a hole (p) conductor or electrolyte. Upon photoexcitation, it injects an electron in the conduction band of a wide bandgap semiconducting oxide and is regenerated by hole injection in the redox electrolyte or p-type conductor. The charges diffuse to the front and back contacts where they are collected as electric current. The open-circuit photovoltage corresponds to the difference in the Fermi level of the n- and p-type conductor under illumination. *Right side*: Schematic illustration of the operation principle for conventional silicon p–n junction photovoltaic cell. The same semiconductor material assumes the two key functions of light absorption and charge carrier transport. Photoexcitation of the silicon generates electron–hole pairs which need to reach the p–n junction before they recombine. The local electric field present in the junction separates the charges attracting electrons to the n-doped and holes to the p-doped layer. The diffusion length of the minority carriers, i.e., of the electrons and holes in the p- and n-doped silicon layer, respectively, must be at least ten times larger than the layer thickness to collect more than 99% of the photogenerated charge carriers. This requires precise doping as well as high crystallinity and low levels of defects and impurities imposing stringent conditions on the purity of the semiconductor (>99,999% for silicon)

The local electric field present in the junction separates the charges, attracting electrons to the n-doped and holes to the p-doped layer. The diffusion length of the minority carriers, i.e., that of the electrons and holes in the p- and n-doped silicon layer, respectively, must be at least ten times larger than the layer thickness to collect more than 99% of the photogenerated charge carriers. This requires precise doping as well as a high crystallinity and a low level of defects and impurities imposing stringent conditions on the purity of the semiconductor (>99.9999% for solar grade silicon).

Note that minority carriers, i.e., electrons and positive charges (holes) in p- and n-doped semiconductors, respectively, play no role in the photovoltaic conversion process accomplished by the DSC. Because the sensitizer injects electrons into the n-type and holes into the p-type collector, only majority carriers are generated. These charges move in their respective transport medium to the front and back contacts of the photocell where they are collected as electric current. Therefore, their recombination has to occur across the interface between the electron and hole conducting material.

By contrast, in conventional p–n junction photovoltaic cells, the photocurrent arises from minority carriers generated by the photoexcitation of the semiconductor. The minority carrier must live long enough to reach the junction formed between the p- and n-doped semiconductor material before recombination with the majority carriers takes place. The electric field present in the vicinity of the junction separates the positive and negative charges generated under illumination attracting the electrons to the n-doped and the holes to the p-doped material. In order to impart a sufficiently long lifetime to the

photogenerated electron–hole pairs, the use of very pure materials is required. The chemical purification of the semiconductor contributes largely to the high cost and long energy payback time of silicon photovoltaic cells.

In the DSC, the recombination of charge carriers occurs across the phase boundary separating the electron from the hole conductor medium. This inherent geometry offers the unique prospective to fashion the interface in a judicious manner in order to retard the back electron transfer reaction. One promising approach to accomplish this goal is the molecular engineering of sensitizers forming a self-assembled compact monolayer alone or in conjunction with a coadsorbent at the oxide surface. Such an insulating film would impair the backflow of electrons across the junction reducing the back reaction rate and increasing the overall solar to electric power conversion efficiency of the cell.

The Virtues of the Nanostructure

Figure 6 shows on the top a scanning electron microscopy picture of a mesoscopic TiO_2 (anatase) layer. The particles have an average size of 20 nm, and the facets exposed have mainly (101) orientation, corresponding to the anatase crystal planes with the lowest surface energy (ca. 0.5 J/m^2).

The light harvesting by the surface-adsorbed sensitizer can be further improved by introducing larger titania particles in the film that scatter light. These are either mixed with or printed on top of the film of 15–30-nm-sized TiO_2 nanoparticles. The scattered photons are contained in the film by multiple reflections increasing their optical path length substantially beyond the film thickness. As a result, the absorption of solar light is enhanced, particularly in the red and near IR spectral region where the currently used ruthenium complexes show only weak light absorption. For example, using 200–400-nm-sized anatase particles as light scattering centers increases the Jsc of N719-based DCCs by as much as 3–4 mA/cm^2 due to the enhanced absorption of red or near infrared photons [38]. A scanning electron micrograph of such particles is shown on the bottom of Fig. 6.

A whole range of nanostructures have been tested so far ranging from simple assemblies of nanoparticles to organized mesoporous films [39] nanorods [40] and

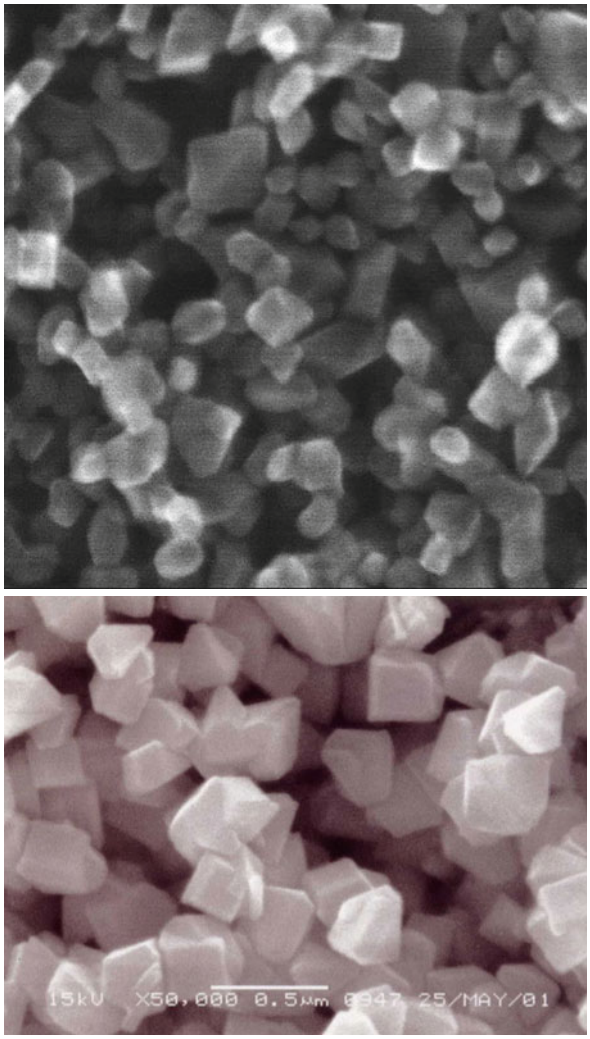

Mesoscopic Solar Cells. Figure 6
Top: Scanning electron microscope picture of a transparent nanocrystalline TiO_2 film formed by ca. 20-nm-sized anatase particles. Note the *bipyramidal* shape of the particles having (101) oriented facets exposed. *Bottom*: Scanning electron microscope image of 200–400-nm-sized anatase particles, which are employed as light scattering centers. The larger particles are either printed as a film on the transparent particles or mixed directly with the 20-nm-sized TiO_2 colloid to augment the optical path by a multiple light scattering effect improving the absorption of sunlight in particular in the red and near IR spectral region where the light absorption by the sensitizer is weak. Scale bars are 200 nm and 500 nm for the *top* and *bottom* SEM photographs, respectively

nanotubes [41, 42]. These studies are motivated by the expectation that the transport of charge carriers along the tubes is more facile than within a random network of nanoparticles where the electrons have to cross many particle boundaries. Hence, one-dimensional nanostructures should produce a lower diffusion resistance than the nanocrystalline films facilitating the collection of photogenerated charge carriers.

The mesoscopic morphology of the oxide semiconductor film is crucial for the efficient operation of a DSC. The key advantages are as follows:

- The mesoscopic structure allows to harvest sunlight efficiently even by a single layer of surface-adsorbed sensitizer. On a flat surface, a monolayer of dye absorbs at most a few percent of the impinging light because it occupies an area that is several hundred times larger than its optical cross section. Employing a mesoscopic structure to support the sensitizer overcomes this notorious inefficiency problem. The real surface area of a 10-μm-thick film formed by 20-nm-sized anatase particles is at least 1,200 times larger than the projected area. This increases dramatically the light-harvesting capacity by the adsorbed monolayer, which for state-of-the-art panchromatic sensitizers is practically quantitative over the whole visible and near IR range.
- The use of oxide nanoparticles to transport the electrons injected by the photoexcited sensitizer into their conduction band avoids space-charge control of the photocurrents as the charge injected is screened by positive ions present in the electrolyte or at the surface of the oxide (Fig. 7). This greatly facilitates electron percolation across the film. The electron charge is screened by the cations present in the electrolyte or on the particle surface, which eliminates the internal field, so no drift term appears in the transport equation.
- The mesoscopic large-bandgap semiconductor oxide films are insulating in the dark. This is an advantage as the presence of significant levels of electrons in the conduction band of the oxide would lead to Auger-type energy transfer quenching of the sensitizer-excited state, reducing the quantum yield of carrier generation. However, under light, the conductivity of the films augments by several orders of magnitude. In fact, a single electron injected in a 20-nm-sized particle produces an electron concentration of 2.4×10^{17} cm^{-3}. This corresponds to a specific conductivity of 1.6×10^{-2} S cm^{-1} if a value of 10^{-4} cm^2 s^{-1} is used for the electron diffusion coefficient. In reality, the situation is more complex because the transport of charge carriers in these films involves trapping unless the Fermi level of the electron is so close to the conduction band that all of the traps are filled and the electrons are moving freely. Therefore, the depth of the traps that participate in the electron motion affects the value of the diffusion coefficient. This explains the observation that the diffusion coefficient increases with the light intensity. Random walk modeling gives an excellent description of the intricacies of the electron transport in such mesoscopic semiconductor films [43].

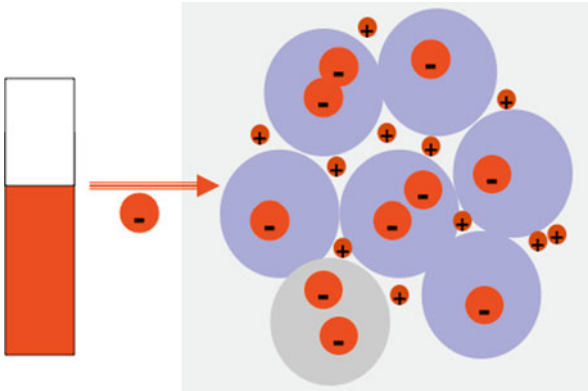

Mesoscopic Solar Cells. Figure 7
Electron transport in nanocrystalline TiO_2 films. Space-charge control of the photocurrent is avoided by screening of the negative charge by the cations present in the electrolyte or at the particle surface

Solids containing periodic pore structures that exhibit photonic bandgaps show also great promise for enhancing the red response of the DSC [44]. The benefits from using such photon capture strategies are unquestionable, as they have been shown to enhance the photocurrent response of the DSC in particular in the near IR and red region of the solar spectrum. The gain in short-circuit photocurrent and overall conversion efficiency achieved by exploiting these optical effects can be as high as 30%.

Typical Sensitizers Based on Ruthenium Complexes

The chemical structures of two typical sensitizers, i.e., the N3 and the black dye (N749), are shown in Fig. 8 together with spectral response of the photocurrent generated by these sensitizers. The incident photon to current conversion efficiency (IPCE), sometimes referred to also as the "external quantum efficiency" (EQE), is plotted as a function of excitation wavelength. The IPCE value corresponds to the photocurrent density produced in the external circuit under monochromatic illumination of the cell divided by the photon flux that strikes the cell. The following product expresses this key parameter:

$$\mathrm{IPCE}(\lambda) = \mathrm{LHE}(\lambda)\phi_{\mathrm{inj}}\ \eta_{\mathrm{coll}} \quad (1)$$

Here, LHE(λ) is the light-harvesting efficiency for photons of wavelength λ, ϕ_{inj} is the quantum yield for electron injection from the excited sensitizer in the conduction band of the semiconductor oxide, and η_{coll} is the electron collection efficiency. Figure 8 shows that the IPCE reaches close to 80% for both sensitizers in the plateau region of the IPCE spectrum. Compared to the N3 sensitizer, the spectral response of the black dye extends further into the near IR, its photocurrent onset being around 900 nm instead of 800 nm for the former dye. This corresponds to a bandgap of 1.4 eV, which is close to the optimum threshold absorption for single-junction photovoltaic cells. However, for both sensitizers, the IPCE curve rises only gradually from the absorption onset to shorter wavelengths due to the low extinction coefficients of the sensitizers in the longer wavelength range. This behavior results in a very significant loss in photocurrent. For example, the photocurrent density obtained currently with the N749 (black) dye

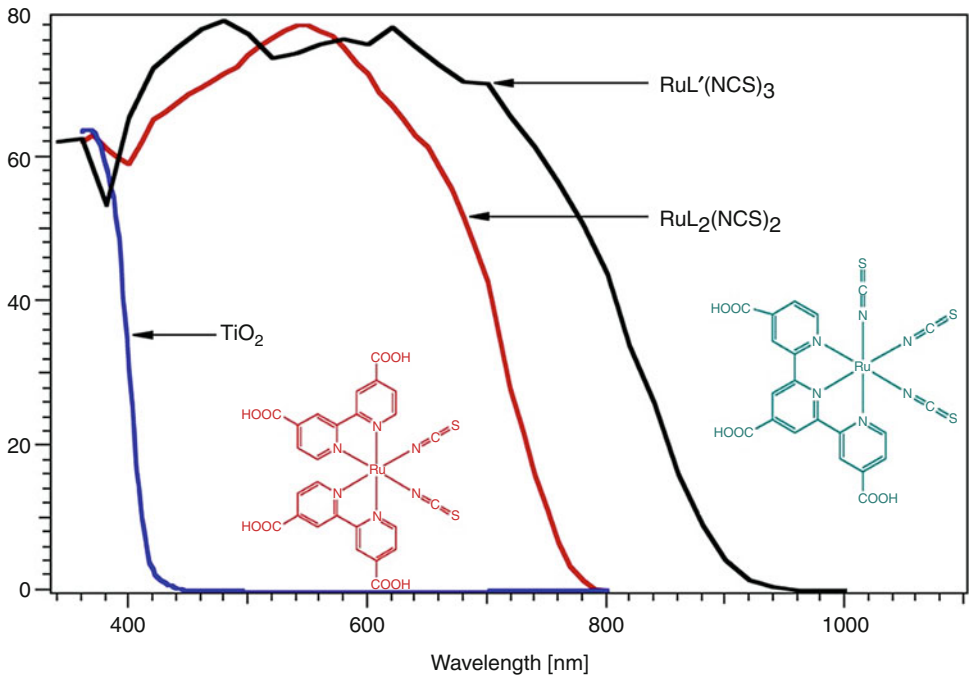

Mesoscopic Solar Cells. Figure 8

Incident photon to current conversion efficiency as a function of wavelength for the standard ruthenium sensitizers N3 (*red line*), the black dye N749 (*black curve*), and the blank nanocrystalline TiO_2 film (*blue curve*). The chemical structure of the sensitizers is shown as *insets*

under standard conditions is close [37, 45] to 21 mA/cm^2, while the maximum J_{sc} for a sensitizer with an absorption onset of 900 nm is 33 mA/cm^2. Even if one concedes an IPCE loss of 10% across the whole spectral absorption domain of the black dye, reducing Jsc to 30 mA/cm^2, the gain in photocurrent would still boost the overall conversion efficiency of the device by a factor of 1.5 to over 15%. Improving the light harvesting in the 650–900-nm domain is therefore one of the greatest challenges faced by present day research in the DSC field. Even moderate improvements in the photoresponse of the sensitizer in red and near IR wavelength region will greatly benefit the conversion efficiency. An amazing advance in this area was recently announced by the Segawa group at the University of Tokyo. By replacing the 3 thiocyanate groups in the black dye with 2 chloride ions and one phosphine ligand a new panchromatic sensitizer, coded DX1, was fashioned that harvests sunlight over the whole visible and near IR range up to 1000 nm generating a short circuit photocurrent close to 27 mA/cm^2 [46].

The Present Status of Dye-Sensitized Solar Cells

The present state of the art of the dye-sensitized solar technology is summarized below in Table 1.

The overall conversion efficiency of the dye-sensitized cell is determined by the photocurrent density measured at short circuit (J_{sc}), the open-circuit photovoltage (V_{oc}), the fill factor of the cell (FF), and the intensity of the incident light (I_s).

$$\eta_{global} = J_{sc} \times V_{oc} \times FF/I_s \quad (2)$$

The fill factor can assume values between 0 and 1 and is defined by the ratio of the maximum power (P_{max}) of the solar cell divided by the open-circuit voltage (V_{oc}) and the short-circuit current (I_{sc}):

$$FF = P_{max}/(I_{sc} \times V_{oc}) \quad (3)$$

P_{max} is the product of photocurrent and photovoltage at the voltage where the cell's power output is maximal. The value of the fill factor reflects the extent of electrical (Ohmic) and electrochemical (overvoltage) losses occurring during operation of the DSC. Increasing the shunt resistance and decreasing the series resistance as well as reducing the overvoltage for diffusion and electron transfer will lead to higher fill factors, thus resulting in greater efficiency and pushing the cells output power closer toward its theoretical maximum.

Under full sunlight corresponding to the standard air mass 1.5 global (AM 1.5 G) spectral distribution, at an intensity I_s = 1,000 W/cm^2, J_{sc} values ranging from 16 to 22 mA/cm^2 are reached with state-of-the-art ruthenium sensitizers, while the V_{oc} attains 0.7–0.86 V, and typical values for the fill factor are 0.65–0.8. Note that the fill factor of a DSC is affected by the transfer coefficient β for the electron transfer from TiO_2 to the electrolyte, whose rate shows exponential voltage dependence, following a Tafel law [47]. For a given Voc, the larger the β value, the better the fill factor. Theoretically, β should be 1 for electron transfer from a semiconductor to a solution redox couple, but smaller values are usually observed due to the participation of surface states in the interfacial charge transfer, whose energy levels lie below the conduction band of TiO_2. A larger β value can be associated with a shallower distribution of these defect states [47].

Until recently, the photovoltaic performance of the black dye measured under full AM 1.5 sunlight was superior to all other known charge-transfer sensitizers. A certified overall power conversion efficiency of 10.4% was reached with N749 already in year 2001 [37]. By 2006, a higher certified efficiency of 11.1% was attained using the same dye [45]. Recently the PCE has been

Mesoscopic Solar Cells. Table 1 Present state of the development of dye-sensitized solar cells. Note the small loss of efficiency encountered on going from a small laboratory cell to an industrially produced module

• *Power conversion efficiency* (PCE) measured under AM 1.5 sunlight (STC): laboratory cells: 12.3% [49], modules: 9.9% [54], tandem cells: 15–16% [50]
• *Stability* >20 years outdoors [59]
• *Energy payback time*: <1 year (3GSolar [60] and ECN [61] life cycle analysis)
• *Industrial development*: has been launched by several industrial companies, mass production of light weight flexible modules started in 2009 by G24Innovation (www.g24i.com)

further improved to 11.4% by the same group using a co-sensitizer along with the black dye [48]. Figure 8 shows that the spectral response of the photocurrent of the black dye is red-shifted by 100 nm with respect to that of the standard N3 dye, resulting in significantly higher short-circuit photocurrents, even though its surface coverage at monolayer saturation and its extinction coefficient are about 30% lower than the respective values obtained for the N3 dye [45].

However, recently new porphyrin sensitizers have been developed, in particular, the YD2-*o*-C8 zinc complex whose PCE exceeds that of the black dye when used in conjunction with Co(II/III)$(bipy)_3$ complexes as redox couple [49]. The Nernst potential of this redox mediator is more positive than that of the iodide/triiodide couple yielding substantial gains in open circuit potential of the cells. The performance of YD2-*o*-C8 is enhanced by judicious substitution of meso-positions at the tetrapyrrol ring with donor and acceptor moieties and the introduction of bulky alkoxy groups. This increases the light harvesting capacity of the porphyrin and blocks the unwanted interfacial electron back transfer. Further gain in efficiency was obtained via the use of a co-sensitizer coded Y123 absorbing strongly in the green spectral region. Figure 9 below shows a plot of the photocurrent density versus voltage for a mixture of the two dyes, co-adsorbed at the surface of the nanocrystalline titania film along with the structure of the sensitizers. The Jsc, Voc, and FF values measured under standard air mass (AM1.5) reporting conditions were 17.8 mA/cm^2, 0.935 V, and 0.74 yielding a power conversion efficiency of 12.3%.

The fact that DSCs are transparent and their optical properties are tunable by varying the type of sensitizer or the thickness of the nanocrystalline film renders them well suited for use in stacked tandem devices. While this development is still in its infancy, promising results have been obtained. Our previous work has shown that efficiencies in the 15–16 % range can be readily obtained in a stacked two-level tandem structure, employing a DSC on top of a CIGS film [50]. Spectral splitting of the solar light flux, e.g., by a heat mirror that passes visible light but reflects IR radiation is another attractive method to improve the efficiency of PV cells. Recent proof-of-concept results suggest that with DSCs as visible light and a silicon cell as IR-absorber system-level efficiencies approaching 20% should be achievable [51].

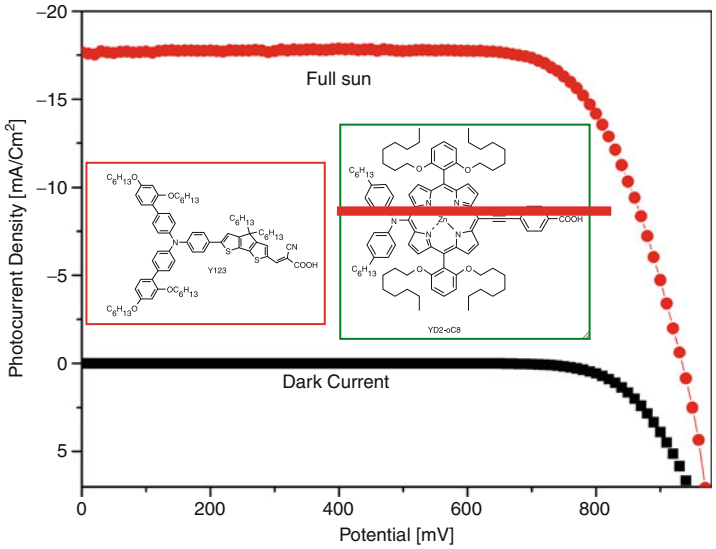

Mesoscopic Solar Cells. Figure 9

Photocurrent density vs voltage curve for a DSC employing the YD2-o-C8 porphyrin and Y123 as a sensitizer and co-sensitizer respectively. The structures of the two dyes are inserted in the diagram. The conversion efficiency achieved under standard reporting conditions, i.e. AM 1.5 sunlight of 1000W/m^2 intensity and 298K temperature is 12.3%

Reproducibility of Cell Fabrication and Scale-up

While the DSC can be produced in a relatively simple way in the laboratory without employing a glove box or high vacuum steps, a rigorous protocol needs to be applied during cell fabrication to achieve high efficiencies in a reproducible manner. By taking the appropriate precautions, relative variations of the efficiency of less than 2–3% can be readily achieved for laboratory cells. Thus, a detailed procedure providing a guide to realize reproducibly cell efficiency values over 10% has been published recently [52]. Reproducible manufacturing of DSC modules on a semiautomated baseline has also been reported [53]. Due to significant industrial upscaling efforts, the conversion efficiency of DSC modules has been steadily rising over the last few years, the certified value measurer under AM 1.5 standard conditions reaching currently 10% [54].

Stability and Commercial Development of the DSC

Long-term stability is a key requirement for all types of solar cell. A vast amount of tests have therefore been carried over the last 15 years to scrutinize the stability of the DSC both by academic and industrial institutions. Most of the earlier work has been reviewed [55, 56]. Long-term accelerated light-soaking experiments performed over many 1,000 h under full or even concentrated sunlight have confirmed the intrinsic stability of current DSC embodiments [57]. Stable operation under high temperature stress at 80–85°C as well as under damp heat and temperature cycling has been achieved by judicious molecular engineering of the sensitizer, the use of a robust and nonvolatile electrolytes such as ionic liquids [58] and adequate sealing materials. In the early development stage of the DSC technology, the quality of device sealing was sometimes not appropriate in laboratory test cells, causing leakage of the volatile nitrile-based solvents, typically used for the electrolytes. While this is occasionally still considered as a problem, most research groups with longer practical experience, including industrial enterprises, have overcome this by improving the sealing methods. Due to the direct relevance to the manufacturing of commercial products, little is published on these processing issues though. Good results on overall system endurance have been reported since several years demonstrating excellent stability under accelerated laboratory test conditions. DSC lifetimes of over 20 years have been projected from continuous light soaking tests performed over 20000 hours [59]. These promising results are presently being confirmed under real outdoor conditions. Thus the Israeli company 3GSolar recently announced that its DSC modules have been operating on the company's rooftop continuously for two years and they continue to perform to the same standard as on the day they were placed outdoors [60]. Importantly, 3GSolar [60] and ECN [61] have also performed life cycle analysis showing the energy pay back time for the DSC to be less than one year in south-European climate as compared to over 3 years for silicon solar cells. From these extensive studies, confidence has emerged that the DSCs can match the stability requirements needed to sustain outdoor operation for at least 20 years. This has paved the way for the recent worldwide surge in the industrial development and commercialization of the DSC.

Ongoing and Future Research

Table 2 lists a number of research topics that are presently under investigation. Below, we illustrate this very active ongoing research with a few examples.

Enhanced light harvesting by advanced nanostructures. Research in this area is presently particularly fertile, and a wealth of new mesoscopic

Mesoscopic Solar Cells. Table 2 A nonexhaustive list of current and future research topics in the field of mesoscopic solar cells

• Enchanced light harvesting by advanced meso-structures
• New sensitizers
• Redox mediators to replace the triidodide/iodide couple
• Alternatives to Pt as electrocatalyst for the counterelectrode
• Solid state sensitized heterojunctions
• Quantum dot injection cells
• Tandem devices
• New solid nanocomposite electrolytes

structures ranging from nanorods composed of oxides having a core shell structure to gyroids and nanotubes are presently under active investigation. Here, we restrict ourselves to a discussion of the very intriguing case of mesoporous semiconductor oxide beads. Figure 10a shows an electron microscopy picture of microscopic particles made of TiO_2 and produced by a hydrothermal method using long-chain amine surfactants as templating agents. The burning of the organic component produces mesopores in the 200–1,000-nm-sized beads whose diameter can be varied between 10 and 25 nm [63]. The internal surface area is about 90 m^2/g providing a suitable host for the adsorption of sensitizers. Solar light harvesting by the dye-loaded beads is enhanced by multiple scattering within the assembly of beads [64] leading to an improved response of the photocurrent in particular in the red wavelength region where the light absorption of many commonly used sensitizers is weak. Using a simple film of these anatase beads in conjunction with the C101 sensitizer, strikingly high power conversion efficiencies exceeding 10% have been readily obtained [62]. Figure 10b compares J–V curves for such mesoporous beads and a layer of conventional TiO_2 nanoparticles using the same C101 sensitizer and a similar film thickness. The inset of Fig. 10b shows a transmission electron micrograph illustrating the interconnection of the titania microbeads within the film. Clearly, the mesoporous beads produce higher photocurrents compared to a conventional nanocrystalline TiO_2 film resulting in better conversion efficiencies.

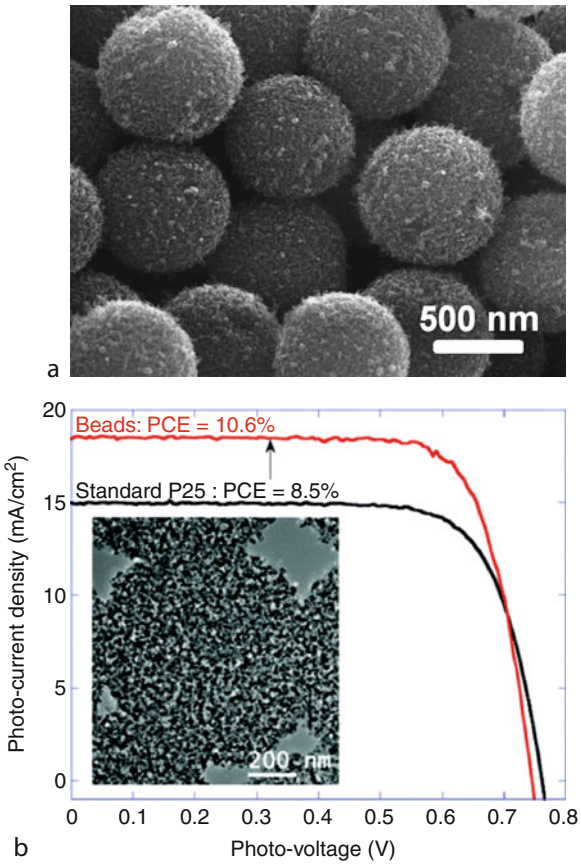

Mesoscopic Solar Cells. Figure 10
(**a**) Scanning electron microscopy picture of an assembly of mesoporous TiO_2 (anatase) beads having an internal surface area of ca. 90 m^2/g. (**b**) Photocurrent voltage curves obtained with similar bead layers using the heteroleptic C101 sensitizer [52]

New sensitizers. Over the last two decades, ruthenium complexes endowed with appropriate ligands and anchoring groups have by far been the preferred choice of charge-transfer sensitizers for mesoscopic solar cells. Recently, however, there has been a surge of interest in organic donor–acceptor dyes [65]. Sensitizers comprising a donor and acceptor group that are bridged by a π-conducting moiety have attracted particular attention. Solar to electric power conversion efficiencies have been sharply increasing, reaching 9.5% in 2008 for the indoline dye D205 [66]. Examples for typical structural elements of such D-p-A dyes are presented in Fig. 11 below. Numerous representatives of this class of compounds have been synthesized [69], and PCE values up to 9.8% have been reported [70].

This rapid development has lead to the discovery of a new class of D-π-A dyes where the π-bridge is constituted by a porphyrin moiety [71]. Power conversion efficiencies of 11% have been reached with the green porphyrin–coded YD-2 whose structure is shown in Fig. 12 along with its IPCE spectrum. Replacing the tert.butyl groups in YD2 by two long chain alkoxy moieties yields the YD2–o-C8 sensitizer reaching a power conversion efficiency of 12.3% as described above in Fig. 9. This is the highest PCE value reported so far rendering this class of D-p-A dyes particularly promising for future applications.

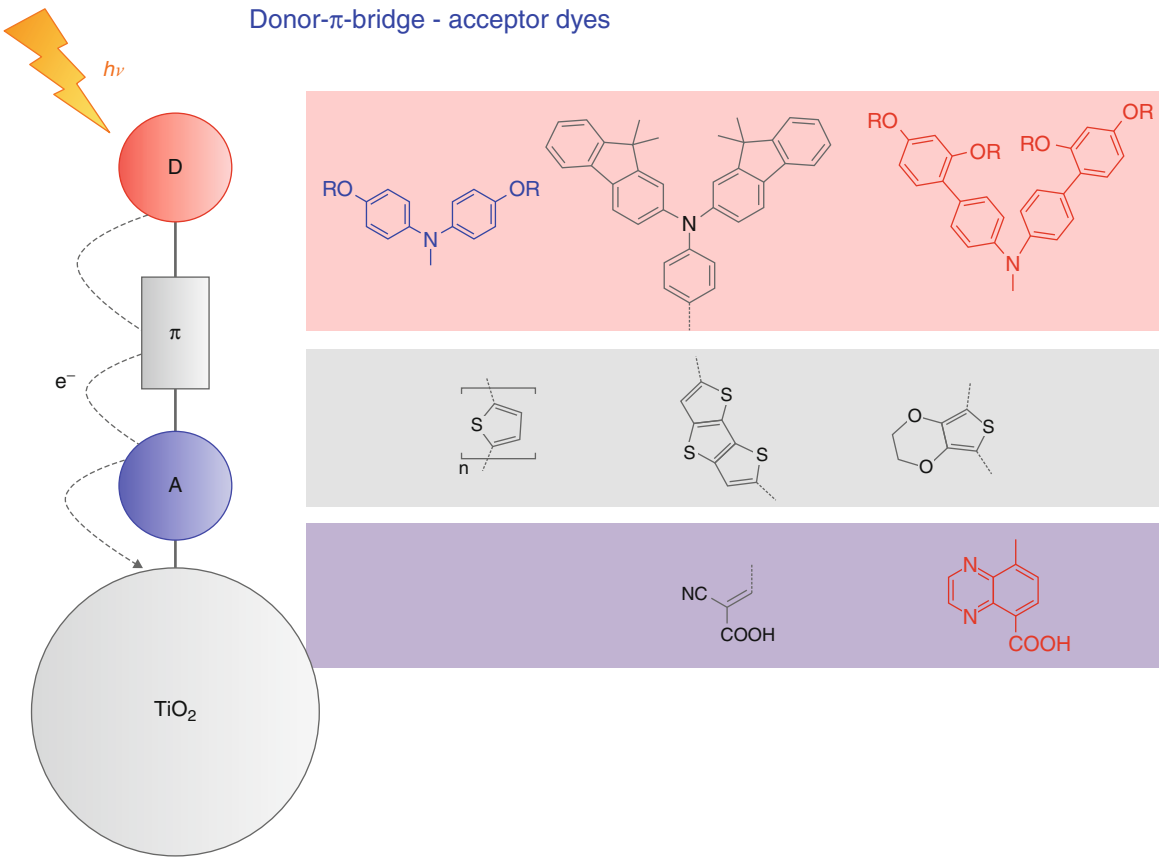

Mesoscopic Solar Cells. Figure 11
Chemical structure for typical molecular components of donor-π-bridge-acceptor (D-π-A) dyes and their linkage to titania nanocrystals through the acceptor group which is coordinatively bound to surface titanium ions

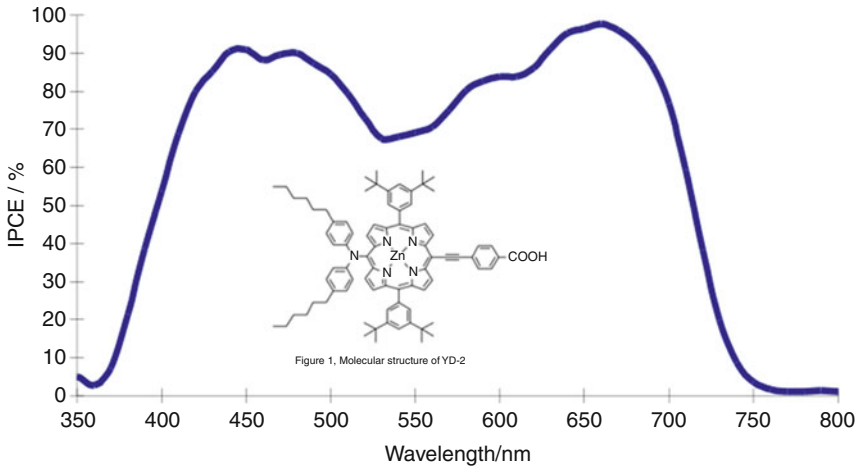

Mesoscopic Solar Cells. Figure 12
Chemical structure and IPCE spectrum of the YD-2 porphyrin, which holds the current power conversion efficiency record of 11% for ruthenium-free sensitizers

The number of suitable options for D-π-A dye structures being very large, state-of-the-art theoretical chemical calculations are being employed as a guide for the selection of the most promising candidates for synthesis. The recently developed scaled opposite-spin configuration interaction singles-doubles technique, abbreviated as SOS-CIS(D) [70], appears to offer great accuracy in calculating the UV–vis spectra of novel D-π-A [71, 72]. This new method will assist the experimentalists in the judicious selection of molecular components to engineer the best-performing push charge-transfer sensitizers.

Summary

The present entry discusses recent research made in molecular photovoltaic cells based on the sensitization of a nanocrystalline wide bandgap semiconductor oxide film by a dye. These cells have now attained efficiencies on the laboratory as well as on the module scale which render them competitive to other thin-film solar cells. Their low cost and ease of production avoiding expensive high vacuum steps should benefit large-scale applications. Impressive stability both under long-term light soaking and high temperature stress has been reached, fostering first industrial applications. These systems will promote the acceptance of renewable energy technologies, not least by setting new standards of convenience and economy.

Acknowledgment

I am grateful to my coworkers and for the support by the organizations listed below. Swiss CTI, CCEM-CH, Swiss National Science Foundation, Swiss Energy Office, US Air Force (European Office of Aerospace Research and Development), FP7 European Joule Program. European Research Council (Advanced Research Grant) GRL Korea (with KRICT) KAUST Center for Advanced Molecular Photovoltaics (CAMP) at Stanford University, Industrial Partners.

Bibliography

1. Grätzel M (2001) Photoelectrochemical cells. Nature 414: 338–344
2. Hagfeldt A, Boschloo G, Sun L, Kloo L, Pettersson H (2010) Dye-sensitized solar cells. Chem Rev 110(11):6595–6663
3. McLeskey JT Jr, Qiao Q (2010) Nanostructured organic solar cells. Nanotechology for Photovoltaics, Loucas Tsakalakos Editor CRC Press 147–185
4. Zhang W, Cheng Y, Yin X, Liu B (2011) Solid-state dye – sensitized solar cells with conjugated polymers as hole-transporting materials. Macromol Chem Phys 212:15–23
5. Mathews N, Varghese B, Sun C, Thavasi V, Andreasson B-P, Sow Ch-H, Ramakrishna S, Mhaisalkar S-G (2010) Oxide nanowire networks and their electronic and optoelectronic characteristics. Nanoscale 2:1984–1998
6. Sekar N, Gehlot VY (2010) Metal complex dyes for dye – sensitized solar cells: recent developments. Resonance 15:819–831
7. Ning Z, Fu Y, Tian H (2010) Improvement of dye – sensitized solar cells: what we know and what we need to know. Energy Environ Sci 3:1170–1181
8. Rowley JG, Farnum BH, Ardo S, Meyer GJ (2010) Iodide chemistry in dye – sensitized solar cells: making and breaking I-I bonds for solar energy conversion. J Phys Chem Lett 1: 3132–3140
9. Halme J, Vahermaa P, Miettunen K, Lund P (2010) Device physics of dye solar cells. Adv Mat 22:E210–E234
10. Wang L, Fang X, Zhang Z (2010) Design methods for large scale dye – sensitized solar modules and the progress of stability research. Renew Sustain En Rev 14:3178–3184
11. Ma BB, Gao R, Wang L-D, Zhu Y-F, Shi Y-T, Geng Y, Dong H-P, Qiu Y (2010) Recent progress in interface modification for dye – sensitized solar cells. Science China: Chem 53:1669–1678
12. Ruehle S, Shalom M, Zaban A (2010) Quantum-dot- sensitized solar cells. Chemphyschem 11:2290–2304
13. Woehrle D, Hild O-R (2010) Energy of the future. Organic solar cells. Chem Unserer Zeit 44:174–189
14. Li X, Wang H, Wu H (2010) Phthalocyanines and their analogs applied in dye – sensitized solar cell. Struct Bond 135:229–274
15. Caramori S, Cristino V, Boaretto R, Argazzi R, Bignozzi C-A, Di Carlo A (2010) New components for dye – sensitized solar cells. Int J Photoenergy 1–17
16. Uzaki K, Nishimura T, Usagawa J, Hayase S, Kono M, Yamaguchi Y (2010) Dye – sensitized solar cells consisting of 3D-electrodes – a review: aiming at high efficiency from the view point of light harvesting and charge collection. J Solar Energy Eng 132:021204
17. Park N-G (2010) Dye – sensitized metal oxide nanostructures and their photoelectrochemical properties. J Korean Electrochem Soc 13:10–18
18. Aguilar RH, Sommeling PM, Kroon JM, Mendes A, Costa CAV (2009) Dye – sensitized solar cells: novel concepts, materials, and state-of-the-art performances. Int J Green Energy 6(3):245–256
19. Desilvestro J (2009) Durability assessment of dye solar cells and modules. In: Miyasaka T (ed) Shin konseputo taiyo denchi to seizo purosesu. Shiemushishuppan, Tokyo, pp 196–205
20. Arakawa H (2009) Weathering resistance of dye – sensitized solar cells. In: Miyasaka T (ed) Shin konseputo taiyo denchi to seizo purosesu. Shiemushishuppan, Tokyo, pp 185–195
21. Yanagida S, Yu Y, Manseki K (2009) Iodine/iodide-free dye-sensitized solar cells. Acc Chem Res 42:1827–1838

22. Grätzel M (2009) Recent advances in sensitized mesoscopic solar cells. Acc Chem Res 42:1788–1798
23. Kalyanasundaram K (2010) Dye-sensitized solar cells. EPFL Press, Lausanne (distributor CRC Press, Boca Raton USA)
24. Desilvestro J, Grätzel M, Kavan L, Moser JE, Augustynski J (1985) Highly efficient sensitization of titanium dioxide. J Am Chem Soc 107:2988–2990
25. Vlachopoulos N, Liska P, Augustynski J, Grätzel M (1988) Very efficient visible light energy harvesting and conversion by spectral sensitization of high surface area polycrystalline titanium dioxide films. J Am Chem Soc 110:1216–1220
26. O'Regan B, Grätzel M (1991) A low-cost, high efficiency solar cell based on dye sensitized colloidal TiO_2 films. Nature 335: 737–740
27. Nazeeruddin MK, Kay A, Rodicio I, Humphrey-Baker R, Müller E, Liska P, Vlachopoulos N, Grätzel M (1993) Conversion of light to electricity by cis-X_2bis(2,2′-bipyridyl-4,4′-dicarboxylate) ruthenium(II) charge transfer sensitizer (X = Cl-, Br-, I-, CN-, and SCN-) on nanocrystalline TiO_2 electrodes. J Am Chem Soc 115:6382–6390
28. Bach U, Lupo D, Comte P, Moser JE, Weissörtel F, Salbeck J, Spreitzert H, Grätzel M (1998) Solid state dye sensitized cell showing high photon to current conversion efficiencies. Nature 395:550
29. Qin P, Linder M, Brinck T, Boschloo G, Hagfeldt A, Sun L (2009) High incident photon-to-current conversion efficiency of p-Type dye-sensitized solar cells based on NiO and organic chromophores. Adv Mat 21:1–4
30. Nusbaumer H, Zakeeruddin SM, Moser J-E, Grätzel M (2003) An alternative efficient redox couple for the dye-sensitized solar cell system. Chem Eur J 9:3756–3763
31. Brugnati M, Caramori S, Cazzanti S, Marchini L, Argazzi R, Bignozzi CA (2007) New components for dye-sensitized solar cells. Int J Photoenergy 2:80756/1–80756/10
32. Feldt SM, Gibson EA, Gabrielsson E, Sun L, Boschloo G, Hagfeldt AJ (2010) Design of organic dyes and cobalt polypyridine redox mediators for high efficiency dye-sensitized solar cells. Am Chem Soc 132:16714–16724
33. Zhang Z, Chen P, Murakami TN, Zakeeruddin SM, Grätzel M (2008) The 2,2,6,6-Tetramethyl-1-piperidinyloxy radical: an efficient, iodine-free redox mediator for dye-sensitized solar cells. Adv Funct Mat 18:341–346
34. Wang M, Chamberland N, Breau L, Moser J-E, Humphry-Baker R, Marsan B, Zakeeruddin S-M, Grätzel M (2010) An organic redox electrolyte to rival triiodide/iodide in dye-sensitized solar cells. Nat Chem 2:385–389
35. Li DM, Li H, Luo YH, Li KX, Meng QB, Armand M, Chen LQ (2010) Non-corrosive, non-absorbing organic redox couple for dye-sensitized solar cells. Adv Funct Mater 20(19):3358
36. Daeneke T, Kwon TH, Holmes AB, Duffy NW, Bach U, Spiccia L (2011) High-efficiency dye-sensitized solar cells with ferrocene-based electrolytes. Nat Chem 3:211–215
37. Nazeeruddin MK, Pechy P, Renouard T, Zakeeruddin SM, Humphry-Baker R, Comte P, Liska P, Cevey L, Costa E, Shklover V, Spiccia L, Deacon GB, Bignozzi CA, Grätzel M (2001) Engineering of efficient panchromatic sensitizers for nanocrystalline TiO2-based solar cells. J Am Chem Soc 123: 1613–1624
38. Rothenberger G, Comte P, Grätzel M (1999) A contribution to the optical design of dye-sensitized nanocrystalline solar cells. Sol En Mat Sol Cells 58:321–336
39. Zukalová M, Procházka J, Zukal A, Yum JH, Kavan L, Grätzel M (2010) Organized mesoporous TiO2 films stabilized by phosphorus: application for dye-sensitized solar cells. J Electrochem Soc 157:H99–H103
40. Galoppini E, Rochford J, Chen H, Saraf G, Lu Y, Hagfeldt A, Boschloo G (2006) Fast electron transport in metal organic vapor deposition grown dye-sensitized ZnO nanorod solar cells. J Phys Chem B 110:16159–16161
41. Shankar K, Bandara J, Paulose M, Wietasch H, Varghese OK, Mor GK, LaTempa TJ, Thelakkat M, Grimes CA (2008) Highly efficient solar cells using TiO_2 nanotube arrays sensitized with a donor-antenna dye. Nano Lett 8:1654–1659
42. Macak JM, Ghicov A, Hahn R, Tsuchiya H, Schmuki P (2006) Photoelectrochemical properties of N-doped self-organized titania nanotube layers with different thicknesses. J Mat Res 21:2824–2828
43. Nelson J, Chandler RE (2004) Random walk models of charge transfer and transport in dye sensitized systems. Coord Chem Rev 248:1181–1194
44. Colodrero S, Mihi A, Haggman L, Ocana M, Boschloo G, Hagfeldt A, Miguez H (2009) Porous one-dimensional photonic crystals improve the power-conversion efficiency of dye-sensitized solar cells. Adv Mat 21:764–770
45. Chiba Y, Islam A, Watanabe Y, Komiya R, Koide N, Han L (2006) Dye sensitized solar cells with conversion efficiency of 11.1%. Jap J Appl Phys Part 2(45):24–28
46. Uchida S (2011) Invited lecture presented at the symposium on nanostructured photosystems at the NTU Singapore symposium on July 26
47. Wang Q, Ito S, Graetzel M, Fabregat-Santiago F, Mora-Sero I, Bisquert J, Bessho T, Imai H (2006) Characteristics of high efficiency dye-sensitized solar cells. J Phys Chem B 110: 25210–25221
48. Han L, Islam A, Chen H, Malapaka C, Chiranjeevi B, Zhang S, Yang X, Yanagida M (2012) High-efficiency dye-sensitized solar cell with a novel co-adsorbent. Energ Environ Sci. Accepted paper. DOI:10.1039/c0xx00000x
49. Yella A, Lee H-W, Tsao HN, Yi C, Chandiran AK, Nazeeruddin MdK, Diau EW-G, Yeh C-Y, Zakeeruddin SM, Grätzel M (2011) Porphyrin-sensitized solar cells with cobalt (II/III)-based redox electrolyte exceed 12 percent efficiency. Science 334:629–634
50. Liska P, Thampi R, Grätzel M, Brémaud D, Rudmann D, Upadhyaya HM, Tiwari AN (2006) Nanocrystalline dye-sensitized solar cell/copper indium gallium selenide thin-film tandem showing greater than 15% conversion efficiency. Appl Phys Lett 88:203103
51. Barber GD, Hoertz PG, Lee S-HA, Abrams NM, Mikulca J, Mallouk TE, Liska P, Zakeeruddin SM, Grätzel M, Ho-Baillie A, Green MA (2011) Utilization of direct and diffuse sunlight in a

dye-sensitized solar cell — silicon photovoltaic hybrid concentrator system. J Phys Chem Lett 2:581–585
52. Ito S, Murakami TN, Comte P, Liska P, Gratzel C, Nazeeruddin MK, Gratzel M (2008) Fabrication of thin film dye sensitized solar cells with solar to electric power conversion efficiency over 10%. Thin Solid Films 516:4613–4619
53. Späth M, Sommeling PM, van Roosmalen JAM et al (2003) Reproducible manufacturing of dye-sensitized solar cells on a semi-automated baseline. Progr Photovoltaics: Res Appl 11:207–220
54. Green MA, Emery K, Hishikawa Y, Warta W (2011) Solar effciency tables (Version 37) Prog. Photovolt: Res. Appl. 19:84–92
55. Lenzmann FO, Kroon JM (2007) Recent advances in dye-sensitized solar cells. Adv Opto-Electr (Recent Advances in Solar Cells) 65073/1–65073/10
56. Grätzel M (2008) Recent applications of nanoscale materials: solar cells. In: Leite RE (ed) Nanostructured materials for electrochemical energy production and storage. Springer, New York, Chapter 1
57. Grätzel M (2006) Photovoltaic performance and long-term stability of dye-sensitized mesocopic solar cells. C. R. Chimie 9:578–583
58. Arakawa H, Yamaguchi T, Okada K, Matsui K, Kitamura T, Tanabe N (2009) Highly durable dye-sensitized solar cells. Fujikura Tech Rev 2009:55–59
59. Harikisun R, Desilvestro H (2011) Long-term stability of dye solar cells. Sol Energ 85:1179–1188
60. http://3gsolar.com/NewsItem.aspx?ID=40
61. De Wild-Scholten MJ, Veltkamp AC (2007) Environmental life cycle analysis of dye sensitized solar devices. www.ecn.nl/publicaties/PdfFetch.aspx?nr=ECN-M–07-081
62. Sauvage F, Chen D, Comte P, Huang F, Heiniger L-P, Cheng Y-B, Caruso RA, Grätzel M (2010) Dye-sensitized solar cells employing a single film of mesoporous TiO_2 beads achieve power conversion efficiencies over 10%. ACS Nano 4(8):4420–4425
63. Chen D, Cao L, Huang F, Imperia P, Cheng Y-B, Caruso RA (2010) Synthesis of monodisperse mesoporous titania beads with controllable diameter, high surface areas, and variable pore diameters (14–23 nm). J Am Chem Soc 132(12):4438–4444
64. Huang F, Chen D, Zhang X-L, Caruso RA, Cheng Y-B (2010) Dual-function scattering layer of submicrometer-sized mesoporous TiO_2 beads for high-efficiency dye-sensitized solar cells. Adv Funct Mat 20(8):1301–1305
65. Qin H, Wenger S, Xu M, Gao F, Jing X, Wang P, Zakeeruddin S-M, Grätzel M (2008) An organic sensitizer with a fused dithienothiophene unit for efficient and stable dye-sensitized solar cells. J Am Chem Soc 130(29):9202–9203
66. Ito S, Miura H, Uchida S, Takata M, Sumioka K, Liska P, Comte P, Pechy P, Gratzel M (2008) High-conversion-efficiency organic dye-sensitized solar cells with a novel indoline dye. Chem Comm 41:5194–5196
67. Yum J-H, Hagberg DP, Moon S-J, Karlsson KM, Marinado T, Sun L, Hagfeldt A, Nazeeruddin MK, Grätzel M (2009) A light-resistant organic sensitizer for solar-cell applications. Angew Chem Int Ed 48:1576–1580
68. Zhang G, Bala H, Cheng Y, Shi D, Lv X, Yu Q, Wang P (2009) High efficiency and stable dye-sensitized solar cells with an organic chromophore featuring a binary π-conjugated spacer. Chem Comm 2198–2200
69. Hsieh C-P, Lu H-P, Chiu C-L, Lee C-W, Chuang S-H, Mai C-L, Yen W-N, Hsu S-J, Diau EW-G, Yeh C-Y (2010) Synthesis and characterization of porphyrin sensitizers. J Mater Chem 20:1127
70. Bessho T, Zakeeruddin SM, Yeh C-Y, Diau EWG, Grätzel M (2010) Highly efficient mesoscopic dye-sensitized solar cells based on donor-acceptor-substituted porphyrins. Angew Chem Int Ed 49:6646–6649
71. Rhee YM, Head-Gordon M (2007) Scaled second-order perturbation corrections to configuration interaction singles: efficient and reliable excitation energy methods. J Phys Chem A 111:5314–5326
72. Casanova D, Rotzinger FP, Grätzel M (2010) Computational study of promising organic dyes for high-performance sensitized solar cells. J Chem Theory Comput 6:1219–1227

Meterology and Wind Power

Erik Lundtang Petersen, Peter Hauge Madsen
Wind Energy Division, Risø DTU National Laboratory for Sustainable Energy, Technical University of Denmark, Roskilde, Denmark

M

Article Outline

Glossary
Definition of the Subject
Introduction
The Local Meteorological Elements
Modeling the Wind Conditions
Assessing Local Wind Conditions for Design and Turbine Safety
Future Directions
Bibliography

Glossary

Atmospheric boundary layer (ABL) Also known as planetary boundary layer (PBL), it is the bottom layer of the atmosphere that is in contact with the surface of the Earth. It extends from 100 m or less in a clear nighttime condition to more the 2 km on a convective sunny day.

Atmospheric surface layer The atmospheric layer closest to the ground up to 50–100 m and where the pressure and Coriolis forces can be neglected in the parameterization of meteorological variables such as the wind profile. The fluxes of the momentum and heat are nearly constant with height.

CFD models Computational Fluid Dynamics models which are mainly used for engineering purposes such as aerodynamic calculations for the flow around a wind turbine blade. They are currently being developed for use for wind studies in very complicated topography.

Climatology The average weather experienced at a place in the course of some chosen run of years.

Coriolis force As air moves from high to low pressure in the northern hemisphere, it is deflected to the right by the Coriolis force. In the southern hemisphere, air moving from high to low pressure is deflected to the left by the Coriolis force. The Coriolis force is caused by the rotation of the Earth.

Downscaling methods The concept of downscaling large-scale analysis and forecasts of weather and climate, such that small-scale features are estimated based on input about large-scale structures of the atmosphere. Two concepts are used: dynamical and statistical.

Dynamic downscaling Use of mesoscale meteorological models to generate high-resolution climate statistics for a specific region and period of time based on, for example, the Global data archive.

Dynamic statistical downscaling Use of mesoscale meteorological models to generate high-resolution climate statistics for a specific region and period of time based on a selected number of weather situations from, for example, the Global data archive.

Geostrophic wind The wind which is in balance between the pressure and the Coriolis forces. It is often close to the wind observed above the PBL by radiosondes and can be calculated from surface pressure measurements.

Global data archive Global or near-global covering climatological and topographic data.

Hub height Height above the ground at the center of the rotor – usually the same as the tower height.

IEC 61400–1 International Standard published by the International Electrotechnical Commission. The Standard specifies essential design requirements to ensure the engineering integrity of wind turbines. Its purpose is to provide an appropriate level of protection against damage from all hazards during the planned lifetime.

Lib files Tables of the two Weibull parameters given for a number of wind direction sectors, heights above ground and terrain roughness classes used in the wind atlas methodology.

Lidar Light detection and ranging. Wind measurement device based on laser – Doppler technology.

Mesoscale model Numerical meteorological models based on the full set of dynamical fluid equations usually covering a region of a few hundred of kilometers and a grid resolution of 2–10 km. An example is the PSU/NCAR mesoscale model (known as MM5) which is a limited-area, nonhydrostatic, terrain-following sigma-coordinate model designed to simulate or predict mesoscale atmospheric circulation.

Microscale model Numerical flow models that can be based on the dynamical fluid equations, for example, CFD models or be based on a linearized version of the fluid equations. An example of a linearized flow model is the BZ (Bessel-zooming-grid) model in WAsP.

Orography The height variations of a terrain.

Power curve Gives the relationship between the net power output of a wind turbine and the wind speed measured at hub height averaged over 10 min.

Reanalysis dataset (Global Data) Time series of the large-scale meteorological situation covering decades. These datasets have been created by assimilating measurement data from around the globe in a dynamical consistent fashion using large-scale numerical models. The primary purpose for the generation of the dataset is to provide a reference for the state of the atmosphere and to identify any features of climate change. For wind energy, the application of the dataset is as a long-term record of large-scale wind conditions.

Reference wind Usually the extreme 10-min average wind speed with a recurrence period of 50 years at turbine hub height. Used in IEC 61400–1 [1] together with the turbulence intensity to define classes for structural loading calculations.

Regional resource assessment Regional resource assessment of wind energy resources means

estimating the potential output from a large number of wind turbines distributed over a region. Ideally, this results in detailed, high-resolution, and accurate resource maps, showing the wind resource (yearly and seasonal), the wind resource uncertainty, and areas of enhanced turbulence.

Roughness length The roughness of a terrains commonly parameterized by a length scale called the roughness length. For the logarithmic wind profile, it is the height where the wind is zero.

Siting Siting is a process that includes estimating the mean power produced by specific wind turbines at one or more specific locations. Proper siting of wind turbines with respect to the wind resource requires proper methods for calculating the wind resource, the turbulence conditions, the extreme wind conditions, and the effects of rotor wakes.

The wind atlas method The conventional method used to produce estimates of wind resource on national scales is to analyze wind measurements made at a number of sites around the country as in, for example, the European Wind Atlas [2]. In order for this method to work there needs to be a sufficient quantity of high quality data, covering the country.

Topography The description of shapes and features of the Earth's surface such as orography, land cover, and buildup areas (especially their depiction in maps).

Turbulence The fast variations of the wind vector in all three directions: longitudinal, lateral, and vertical.

Turbulence intensity The ratio between the mean horizontal wind and the standard deviation of the turbulence fluctuations usually measured over a period of 10 min.

WAsP Wind Atlas Analysis and Application Program. Commonly used computer program for siting and regional resource assessment. Developed for the European Wind Atlas.

Weibull probability density function Two-parameter probability density function which very often fits measured wind speed observations well. Is determined by the scale parameter A, which is close to the mean value and the shape parameter k. For $k = 1$ the function is Exponential for $k = 2$ it is the Rayleigh distribution and for $k = 3$ it is close to the Gaussian distribution.

WENE-048 predictions Prediction of the power output from a wind farm hours and days ahead. This term is treated in a separate chapter.

Wind profile The increase of the wind speed (horizontal component of the wind vector) above terrain. In strong wind in an overcast situation (called thermally neutral conditions), it follows a logarithmic law in the lowest 50–100 m. It deviates from the logarithmic when thermal effects become noticeable (stable and unstable conditions). The industry and the IEC 61400–1 often use a power law to describe the height variation. The power 1/7 may be used to represent neutral conditions and a roughness length of 0.03 m.

Definition of the Subject

The utilization of wind energy requires an ability to assess the wind conditions with a high degree of certainty, being paramount for obtaining low risks and high reliability in wind energy project planning. This in turn requires a profound understanding of how atmospheric motions affect the use of wind energy: From the design and operation of the turbines to the spatial integrated renewable energy systems, say, from the dynamic inflow conditions at the turbine rotor to regional resource assessments. The activities necessary for solving the inherent problems in making use of the kinetic energy available in air that passes through the rotor of a large wind turbine during normal operation – or – respectively minimize the problems, has required a huge effort on analytical formulations, experimental activities, and the creation of dedicated numerical tools. Then, through a close cooperation between scientists and engineers, substantial progress has been achieved in the understanding of the interaction between the wind turbines and the atmospheric motions and has brought it to the practical level of international standards, norms, guidelines, and best practices. The huge advances in information sharing technology, in computer power, and in experimental capability have further aided to the fast progress of the discipline which in a broad term can be called: Wind Power Meteorology.

The current fast development in Wind Power Meteorology can be termed: "From Global to Local" which is synonymous with the process that goes from

catching the relevant data information from Global dataset, applying the data in meteorological models from global to mesoscale, which in turns produces spatial and temporal information to be used by microscale models to produce the relevant information on the wind conditions for design and for power production at a specific site for specific wind turbines. Hence, this can be described as the two parallel chains of respectively models and in- and output statistics. However, the "model chain": Global – mesoscale – microscale is still in its infancy and fundamental problems have to be sorted out. Therefore, most studies of wind conditions for wind power still rely on the use of local measurements in combination with microscale models. This can ensure that local effects are well described but often have the problem of a too short period of measurements, whereas the model chain often can take advantage of the global datasets which covers decades. They have on the other hand the problem of resolution and the computer time necessary for the models to catch the important wind systems on a sufficient small scale.

This chapter treats the two main wind conditions subjects: wind resources and design conditions. The expected power production from a wind turbine is calculated by means of the measured or modeled probability density function of the wind speed at hub height and the power curve for the wind turbine. Determining the design conditions for the turbine is more involved and the wind parameters of interest such as extreme winds and wind gusts, very fast changes in wind direction, and shears across the rotor of wind speed and wind direction are difficult to measure or model with a sufficient accuracy. A complication is that it is not necessarily the magnitude of these inflow conditions that determines the design of a specific turbine but how they impact the turbine's configuration and operational state, such as start-up events, shutdown events, and its control system in general. A wind turbine is a series-produced industrial product, which cannot be designed according to local conditions in all detail. Instead, wind turbines are designed according to reference conditions. Such reference design requirements for land-based wind turbines are specified in the international design standards given by the International Electrotechnical Commission (IEC) 61400–1 [1]. Here a number of wind classes are specified and the designer has to demonstrate that the design is adequate with respect to the loading of the wind turbine in the various classes. Finally, for the specific wind turbine project it has to be demonstrated that the actual conditions are more benign than the reference design conditions or that the resulting loading does not exceed the strength reserves in the turbine components. Hence the design process of a wind turbine for series-production will start with reference conditions and end with assessment of conformity with actual site conditions, while being more complex as shown in the sketch below:

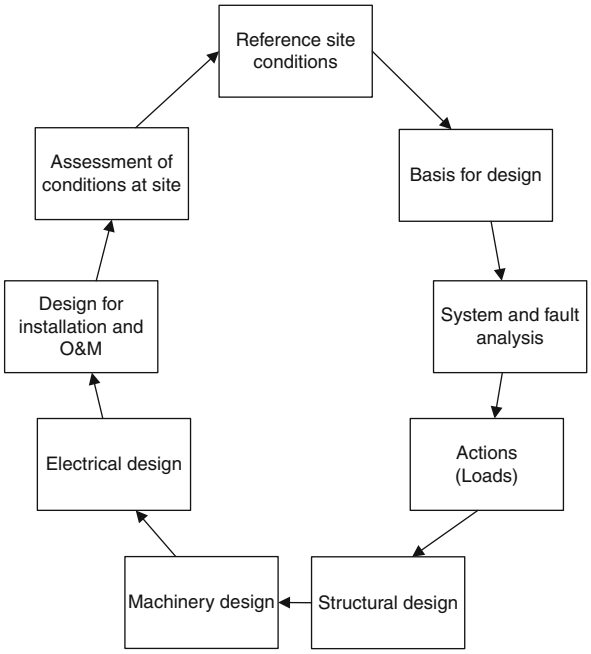

The design aspects of the wind power meteorology are treated in the end of this chapter.

As appetizers, Figs.1 and 2 give, respectively, an overview of the wind resources worldwide and a schematic presentation of many of the concepts that will be treated in this chapter.

Introduction

A recent publication (2009) from the European Wind Energy Association, *The economics of wind energy* [3] states the following:

- *The local wind resource is by far the most important determinant of the profitability of wind energy investments. Just as an oil pump is useless without a sizable oilfield, wind turbines are useless without a powerful*

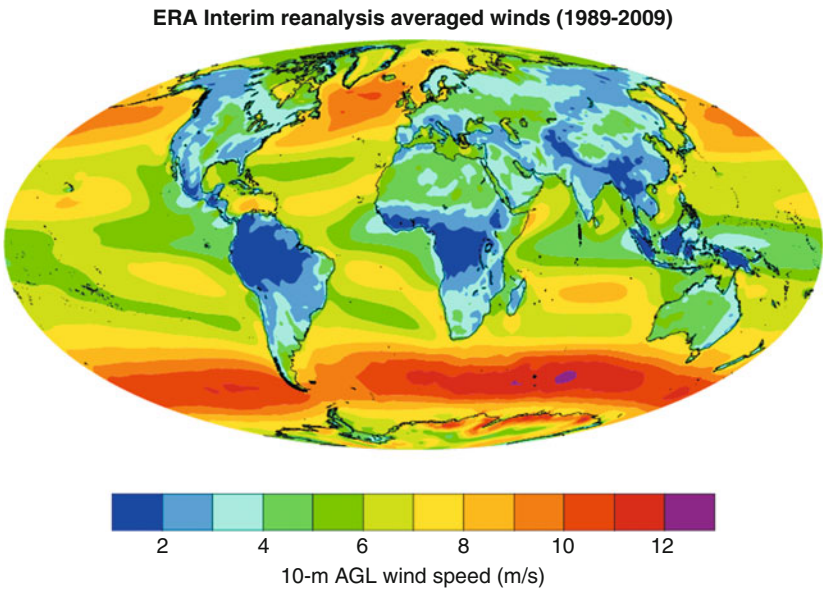

Meterology and Wind Power. Figure 1
The wind climate in terms of the average wind speed at 10 m above ground level was calculated from output from the European Centre for Medium-Range Weather Forecasts (ECMWF; called ERA-Interim) latest reanalysis project. The reanalysis uses a state-of-the-art numerical weather forecast model and techniques that allow taking into account measurement data from around the globe in a consistent fashion from 1989 to the present day. This dataset was generated to provide a reference for the state of the atmosphere and to identify any features of climate change. The dataset is also a long-term record of the large-scale wind climate. Because of the low resolution of the model (1.5° latitude × 1.5° longitude), these data serve only as an indicator for the wind resources of a particular region. To estimate the actual wind energy potential, other higher-resolution models, wind observations, and detailed knowledge of the topography and surface characteristics have to be used. The stronger winds are found between the latitudes of 40° and 50° in both hemispheres; the strongest winds on Earth occur over the southern ocean (sometimes called the "roaring 40s"). Landmasses tend to have weak winds, especially along the equator over the rain forest areas. ECMWF ERA-Interim data used in this project have been obtained from the ECMWF data server (Courtesy Andrea Hahmann)

wind field. The correct micro-siting of each individual wind turbine is therefore crucial for the economics of any wind energy project. In fact, it is beyond dispute that, during the infancy of modern wind industry in 1975–1985, the development of the European Wind Atlas methodology was more important for productivity gains than advances in wind turbine design. The European Wind Atlas method was later formalized in the WAsP computer model for wind resource assessment.

The availability of a suitable wind resource at a turbine site and the ability to accurately calculate it over the 20-year lifespan of the turbine are essential preconditions for the development of wind energy as a major global provider of electricity.

Therefore, the objective for research on wind conditions for wind energy resource and design purposes is to be able to determine the wind conditions with a high accuracy at any place on the Earth which could be a potential site for wind energy exploitation. The wind conditions at a specific site are basically dependent on two factors: the regional climatology and the local topography. Hence, to pursue the objective, one needs climatological and topographical data with global coverage and sufficient resolution in time and space and models which can transform these data into wind energy important key parameters and statistics, which ideally are:

The wind speed probability density functions at relevant heights corresponding to the size of the

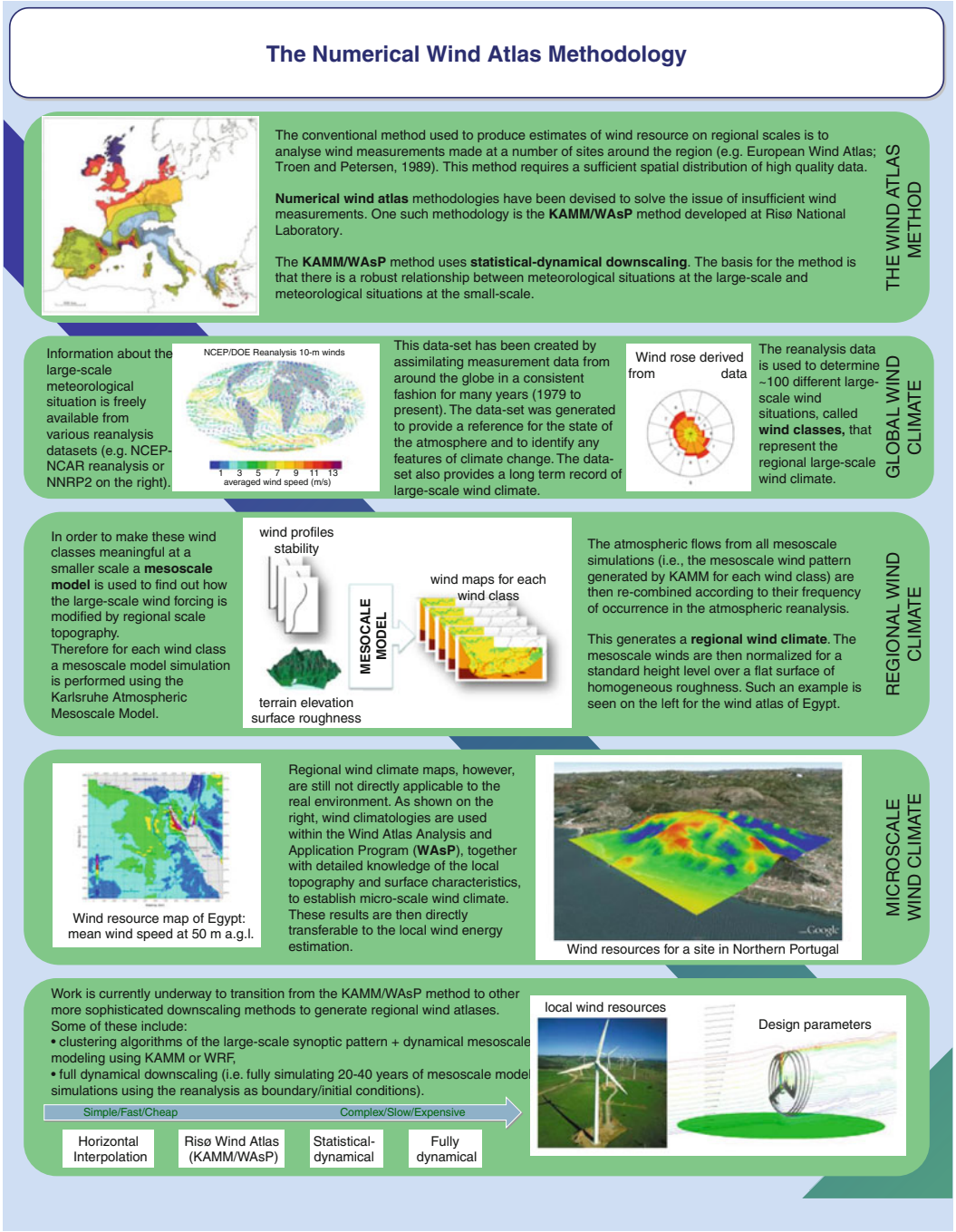

Meterology and Wind Power. Figure 2

The numerical wind atlas methodology. The *arrow* indicates the process from global data to the estimation of local wind conditions for the wind resource and wind turbine design parameters. The *arrow* also indicates the currently undergoing development from the wind atlas method which is based on the use of measured data on a local or regional scale to the fully dynamical mesoscale-, microscale modeling applying data from The Global Archive to determine local wind conditions. The KAMM model (Karlsruhe atmospheric meteorological model) is developed by University of Karlsruhe (Courtesy Andrea Hahmann)

turbines. Together with the power curve, this is used to calculate the power output of the turbine over its lifetime.

The extreme wind speed statistics which is used to determine the reference wind speed used for the structural design of the wind turbine. Usually, this refers to the wind speed that occurs with a recurrence period of 50 years (the reference wind).

The turbulence conditions, such as the turbulence spectra and turbulence intensity used for the structural and aeroelastic design.

The temporal variation of the wind profile, from ground to top of the rotor: Are there anomalies due to topography (e.g., recirculation) and/or the climate (e.g., stability effects).

Statistics and time series of the temporal variations depicting the daily and seasonal variations.

Regional overview of the wind resource, the turbulence conditions, especially areas with adverse conditions which should be avoided due to possible reductions of the turbines lifetime.

The ability to forecast the power production from a wind power installation hours to days ahead.

In the following, the necessary elements for determining the wind conditions for wind energy purposes will be described: The local meteorological elements, the climatological data, the topographic data, the meteorological models, and the tools that finally enable the users to calculate what is described above under the seven items.

The Local Meteorological Elements

The most important meteorological parameters for the siting of a wind turbine are clearly the wind speed and the wind direction (the wind vector) and their variations with time and height above ground. Other parameters such as temperature, precipitation (rain and snow), and pressure are of importance too – but are less dependent of the specific location. The most direct way of determining the wind conditions at a site is to measure the meteorological parameters for an extended period of time and up to a relevant height, which should be at least to the hub height of the wind turbine (the hub height is the height to the center of the rotor). Figure 3 displays the classical way of measuring the meteorological parameters: A lattice tower with instrument-carrying booms at a number of heights. The length of the measuring period depends on how large uncertainty one will accept in, say, the estimated wind resource. For many wind farm projects, there is only very limited time for measurements before the construction phase; often only 1 year, resulting in a sizable uncertainty. This is mainly caused by the large variation over the year of the wind, but also climatological variations, say, from one decade to another, plays a role and finally, a possible global change in the wind climate may have an effect.

There are several ways to reduce the uncertainty in a short-term measured wind resource. One method uses nearby long-term measured data from one of the climatological stations that are part of the synoptic network together with a microscale program such as the Wind Atlas Analysis and Application Program, which is describe later. Another widely used method is called the Measure – Correlate – Predict method (MCP), where the correlation between the measurements at the mast at the site and the climatological measurements are established for the same period of time and then use to extend the data at the site for the period of the climatological measurements, often 10 years or more. A necessary requirement for this method to work is that the correlations for the most prominent wind directions are very high.

A third way to reduce uncertainty and to extend measured data is to use the meteorological models which are described in the following chapters.

Today's large turbines, where the top of the rotor reaches up to 200 m and future wind turbines which may be even higher, constitute a serious challenge to the ability to determine the wind conditions to such heights. First, the cost of erecting meteorological masts of such a height is often prohibitive and second, because of the necessity then to extrapolate lower measured data to these height one encounters the problem, that the theories which have been used and verified for lower heights, say, up to 100 m, are not valid above this level. This is explained in the next section. Presently, a large effort is therefore directed to develop for wind energy purposes what is termed "Remote sensing" to a sufficient degree of accuracy and robustness. The measuring technique that holds the greatest promises for doing measurements up to several hundred of meters is the Lidar technology

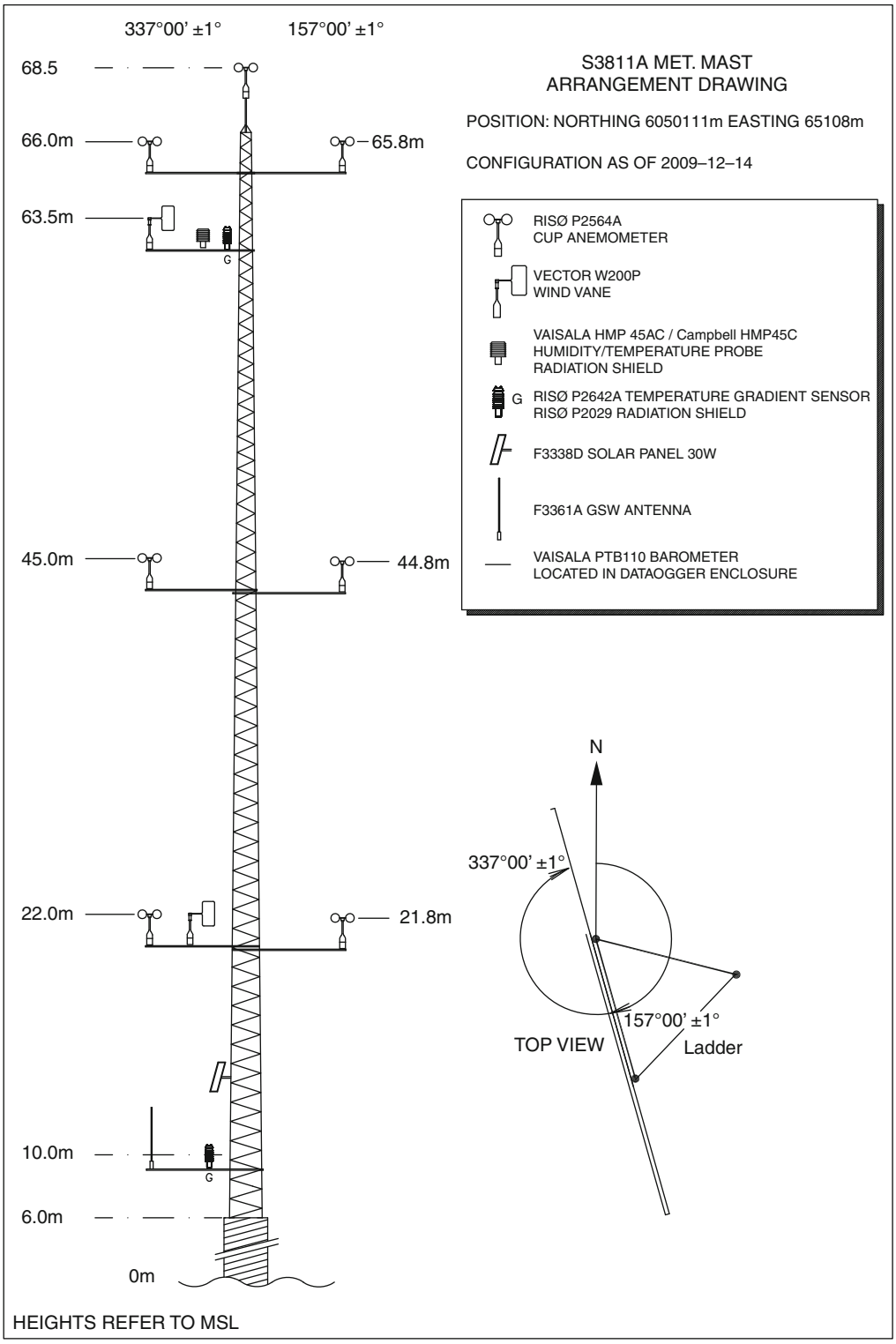

Meterology and Wind Power. Figure 3

Example of an offshore meteorological mast with instrumentation. (*MSL* mean sea level) (Courtesy Anker B. Andersen)

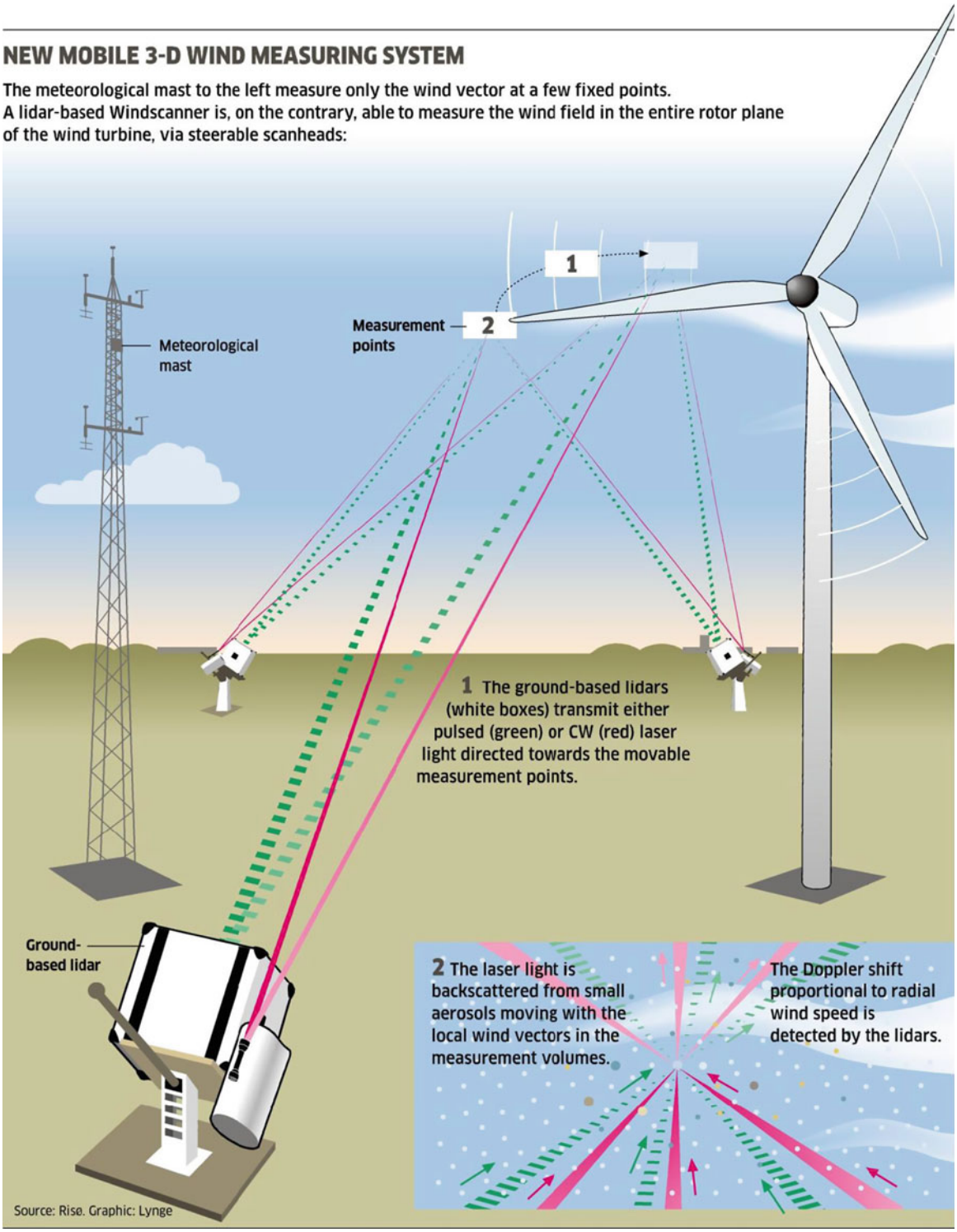

Meterology and Wind Power. Figure 4
The principle for using three lidars (WindScanner) to detect the three-dimensional wind field around a wind turbine (Courtesy Torben Mikkelsen)

(Light Detection and Ranging). The principle is simple: Emitted laser light is reflected by particles in the atmosphere and due to the Doppler Effect, one can deduce the velocity of the particles by the change in the frequency of the reflected light. For a single lidar pointing vertically the technique is "range gating," this is to say that one can look at particles in several layers above ground and thereby establish the vertical variation of the wind speed with height, that is, the wind profile. This technique has been extended such that the lidar measures in many directions and heights almost instantaneously. When three of these instruments are combined, then the three-dimensional wind vector can be measured over the rotor plane and thus can give information for both the resource calculations and the design requirement. The technique is depicted in Fig. 4.

Figure 5 gives a hint to why the height of the large turbines is a problem for the determination of the wind conditions which is actually in the core of the discipline "Boundary Layer Meteorology" which will only be touched briefly here. The reader is referred to the references [4] and [5].

What is depicted in the figure is the diurnal development of the atmospheric boundary layer (ABL) on a clear day over a simple plain topography, for example, an agricultural field with few height variations. This layer is defined as the layer where the underlying surface has a direct influence on the wind and turbulence and other meteorological parameters. Above this layer, the wind is nearly unaffected by the local surface conditions and here blows the free wind, the so-called geostrophic wind.

The geostrophic wind is the theoretical wind that would result from an exact balance between the Coriolis force and the pressure gradient force. This condition is called geostrophic balance. The geostrophic wind is directed parallel to isobars (lines of constant pressure at a given height). This balance seldom holds exactly in nature. The true wind almost always differs from the geostrophic wind due to other forces such as friction from the ground. Thus, the actual wind would equal the geostrophic wind only if there were no friction and the isobars were perfectly straight. Despite this, much of the atmosphere outside the tropics is close to geostrophic flow much of the time and it is a valuable first approximation.

The thickness of the atmospheric boundary layer has a distinct diurnal variation, but is also very dependent on the present weather system: On a sunny day with low wind it can be more than 2 km thick, on a day with high winds it will be around 1 km thick, and during a calm night it can be 100 m or less. The conditions are referred to as convective, neutral, and stable conditions. Close to the ground is the surface layer. Here the wind is dominated by the presence of the ground, that is, the roughness and the temperature of the surface and the resulting heatflux. The fast temporal variations of the wind velocity, called the

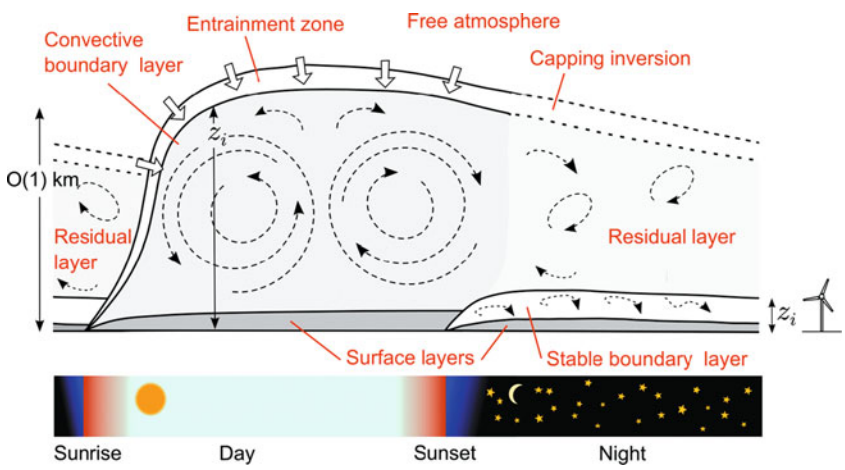

Meterology and Wind Power. Figure 5
The diurnal variation of the planetary boundary layer over not too complicated topography and local climatology (Courtesy Morten Nielsen)

turbulence, transports energy and hence determines the variation of the wind speed with height – the wind shear – which on the other hand is the mechanism for creating turbulence, the so-called mechanically produced turbulence. In this layer, the wind is considered not to be influenced by the Coriolis Effect and the overall pressure gradient. With the wind speed being in the interval of interest for a wind turbine, that is, between 5 and 25 m/s, this layer can be up to 100 m high and the wind profile is logarithmic with height, for example, the variation from 1 to 10 m height is the same as the variation from 10 to 100 m; see Fig. 6.

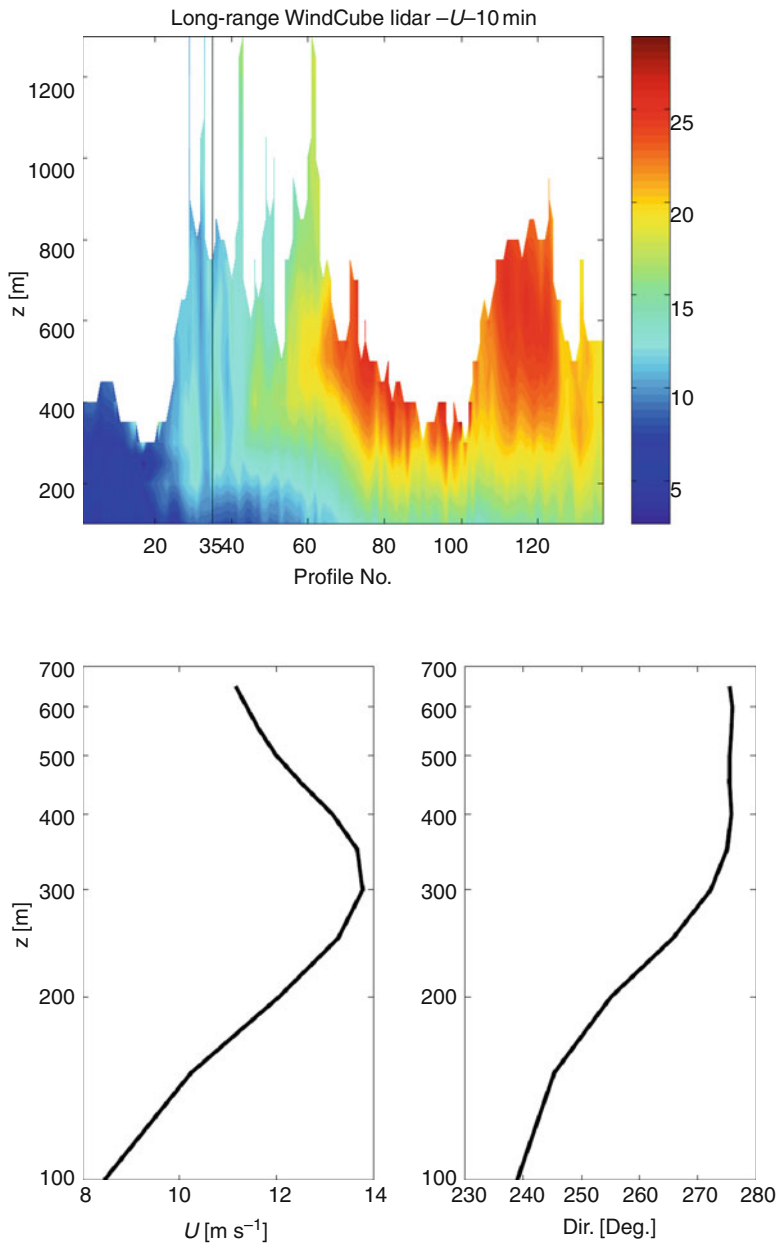

Meterology and Wind Power. Figure 6

Lider measurements (*upper part*) and the derived wind speed and wind direction (*lower part*). The profile is indicated as scan no. 35 (Courtesy Alfredo Peña Diaz)

This is true if the variation of the air temperature is not influencing the production of turbulence, that is, the surface layer is said to be neutral and a parcel of air if moved will stay in equilibrium with the new surroundings. If, on the other hand the temperature decreases fast with height or increases with height there are unstable and stable conditions, respectively, and the turbulence is said to be influenced by thermal effects which in turn deflects the wind profile from the logarithmic height variation. This is well understood and there is a well-founded theory for it called the Monin–Obukov similarity theory [6]. But – and here the problem comes – it only explains what goes on in the lowest 50–100 m. When one moves further up, the wind is also influenced by the Coriolis Effect and the distance to the top of the atmospheric boundary layer. Furthermore, it might be influenced by the variation of the temperature with height above the boundary layer through the processes in the entrainment zone and by creation of internal waves from the action of turbulence on the free atmosphere. Hence the modeling of the wind profile above the surface layer is today far from an established procedure even under well-defined topographic and climatological conditions. For more complicated topography and climatology the knowledge is even less. And the wind conditions over the oceans are turning up to be much more complicated than thought of when the first offshore wind farms were built. Doing meteorological measurements at sea is much more costly and difficult than over land but they are necessary if one shall be able to establish the wind conditions at sea with low uncertainty. For both land and sea the lidar technique holds great promises, but it has it shortcomings: The further away from the instrument the wind is measured, the larger is the volume of air with particles that contributes to the measurement, and therefore this wind is an average over this volume. Figure 6, gives an example of measured wind profiles during a full day up to several hundred meters.

Figure 7 shows examples of measured wind profiles at a Danish North Sea coast together with modeled profiles, where the model takes into account the thermal structure and the height of the atmospheric boundary layer. The boundary layer height is a difficult parameter to determine not to say to get its climatological statistics. For the measured wind speed profiles, the boundary layer height has been determined as the one that gives the best profile fits. For in situ determination of the boundary layer height, remote sensing instruments are required such as lidars, sodars (instrument that emits a sound pulse and listens to the sound reflected from temperature variations with height above ground), and ceilometers, which is a laser-based instrument, basically used to measure the base of clouds. All this is very cumbersome and climatological statistics of the boundary layer height for selected wind farm sites do not exist. Hopefully, satellite measuring techniques will be developed to help out on this.

Now, imagine an ideal sample of wind climatology measured to larger heights, say 200 m, and over a period of 10 years. Definitively, one will be able to perform many of the necessary calculations to determine the wind resource and the wind design conditions at the specific site of the meteorological mast. But how about the conditions at the wind turbines which are to be erected in the large wind farm around the mast? The furthest wind turbine can easily be 10 km away from the mast. If the climatology of the larger scale wind can be considered to be uniform over the wind farm area and if the topography only has small height variations and the roughness is uniform, then it is permissible to use the mast statistics for the whole wind farm. But this is seldom the case; often the topography has variations in orography and land cover such that it is necessary to take this into account when applying the mast statistics to various locations in the wind farm. Even for relatively small wind farms in hilly or mountainous terrain, the variation in the produced power can be more than 25% between the turbines. Therefore, one needs models that can transform the measured wind statistics from the mast location to the locations of all the turbines in the wind farm. Usually this is both a horizontal and a vertical transformation because for economical reasons (and due to some national recommendations) the height of the mast is often chosen to be two-thirds of the hub height. A methodology to perform this task was developed during the creation of the European Wind Atlas (1982–1989) [2] and was made publicly available in 1987 through the PC program WAsP. The basic idea behind the "wind atlas method" is that the wind climatology at a site is "cleaned" from the influence of the surrounding topography to give a generalized regional wind climatology which then could be used at another site, say, tens of kilometers

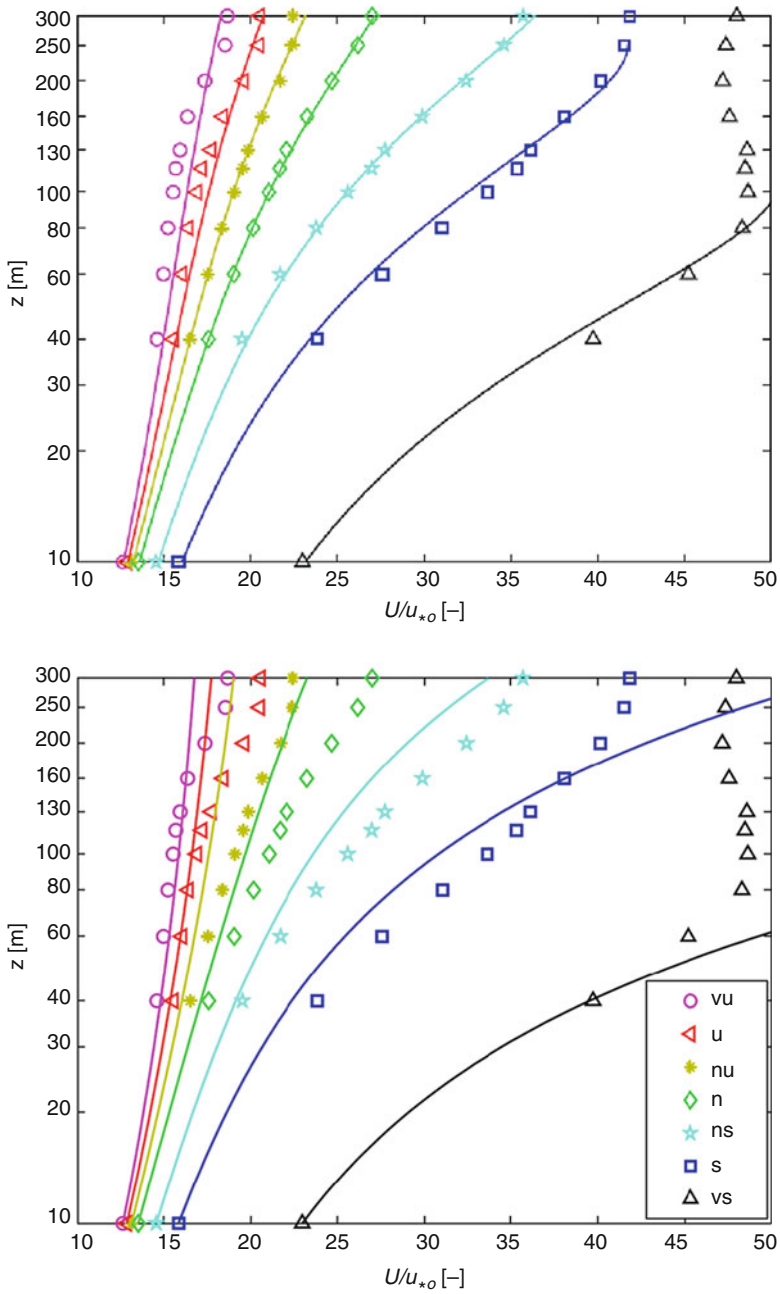

Meterology and Wind Power. Figure 7

Wind profiles measured at the Danish wind turbine test site Høvsøre by means of anemometers up to 165 m and lidars up to 300 m. Both figures show measurements and theoretical derived profiles. At the *top* figure, the height of the boundary layer *Zi* is an important parameter, whereas at the *bottom* figure the conventional theory (Monin–Obhkov) which is only valid up to 50–100 m is applied. Clearly, *Zi* is an important parameter. Stability explanation: *vu* very unstable, *u* unstable, *nu* neutral to the unstable side, *n* neutral, *ns* neutral to the stable side, *s* stable, and *vs* very unstable (Courtesy Sven-Erik Gryning)

away. Then for the new site, the effect of topography at that site is introduced. The procedure is given in Fig. 8 and a short description of its use for the European Wind Atlas is in the next paragraph.

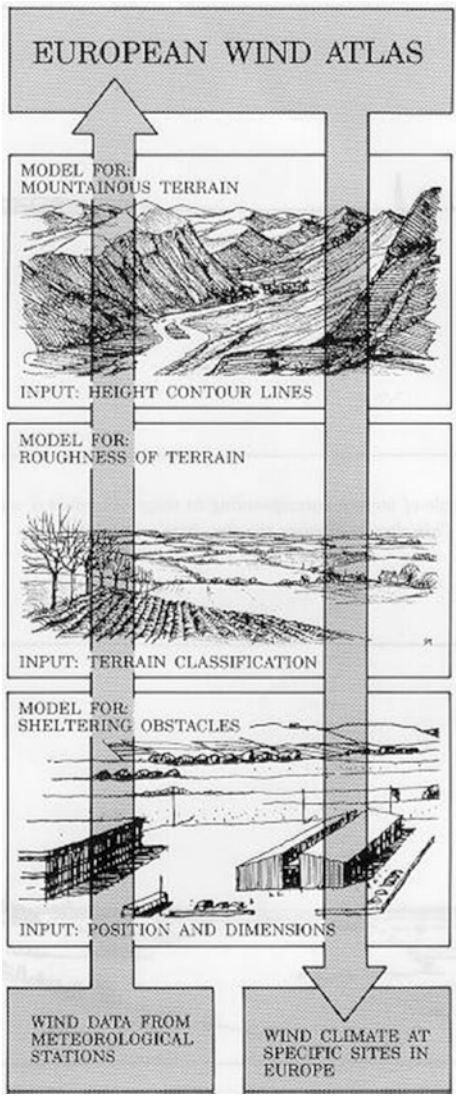

Meterology and Wind Power. Figure 8
A schematic presentation of the wind atlas method used for the transformation of meteorological data. The *left* arrow illustrates the process of "cleaning" the wind data for local conditions. The inverse calculation is illustrated by the *right-hand arrow*: The "cleaned" regionally representative data are used for the calculation of wind conditions at a specific location by introducing the new local conditions

Modeling the Wind Conditions

The state of the atmosphere is well described by seven variables: pressure, temperature, density, water vapor content, two horizontal velocity components, and the vertical velocity component; all functions of time and position. The behavior of these seven variables is governed by seven equations: the equation of state, the first law of thermodynamics, three components of Newton's second law, and the continuity equations for mass and water substance. These equations are mathematical relations between each atmospheric variable and their temporal and spatial derivatives. Mathematical models of the atmosphere can be obtained by integrating the relevant equations with special initial and boundary conditions. The equations can be solved numerically by forward marching in time, using the time rates of change of the variables; the derivatives are replaced by numerical approximations, and changes of the variables over a certain time interval are computed repeatedly as long as needed.

The atmosphere contains motions with scales varying from about 1 mm to thousands of kilometers. Ideally, mathematical models should be constructed from observations with 1 mm spatial and with a fraction of a second temporal resolution. Clearly, this is impossible in practice, and models are constructed separately for systems on different scales. Thus there are models for covering the whole Globe, regional models covering continents, mesoscale models with scales from one to several hundred kilometers and finally microscale models that can resolve topographic and flow features down to a few meters. This is illustrated in Fig. 2 and described in [7].

To solve the differential equations one need a set of initial and boundary conditions. The global models which are run continuously by the large meteorological forecasting centers such as the European Centre for Medium-Range Weather Forecasts (ECMWF) use as initial conditions the millions of measurements from all over the globe shared via the World Meteorological Organization (WMO). There is a great variety of measuring devises covering satellites, ships, radars, buoys, conventional anemometers on masts, etc.; the satellites provide the major part of the data; in all 10^{12} data are collected every hour.

The boundary conditions are provided by global databases of topography (Table 2) and for the oceans, by the sea surface temperature.

In a global circulation model (GCM), the evolution of pressure, wind, temperature, humidity, clouds, rain, and other elements of the weather is computed step by step in a grid with the resolution of approximately 100 km, so as to form a complete, three-dimensional picture of the atmospheric state, evolving with time according to the laws of physics. Such models are used to predict the weather over some days. Another application developed over the last decades is to use such models on a data assimilation setup application of particular interest here.

Model trajectories can be treated in the same way as observations. In particular, averages and other statistical characteristics can be computed for any model variable or combination of variables anywhere within the domain of the model. Similar completeness and coverage cannot be provided by an observation system.

The denser the grid, the smaller is the domain represented by each grid point, and the finer, in general, is the scale of atmospheric motion systems and structures that can be simulated. Still, the model output is not strictly comparable to observations, because the latter will always be influenced by structures and processes beyond the reach of the model – dependent on the distance between grid points. Therefore, in order to resolve atmospheric motions on smaller and smaller scales, it is necessary to operate with a chain of models. In addition, the density in time and space of the observations has a profound influence on the general resolution of the model output. The spatial resolution of topography, that is, land cover and orography also influences what can be resolved by the models.

Still there will always exist processes which have a smaller extent than the size of the computational grid but still are so important for the physics that they have to be taking into account in the modeling process. This is done by the so-called sub-grid parameterization. For example, processes such as convective rain showers of the size of a few kilometers will have to be parameterized in the global models and mesoscale models with a low resolution.

The next step in the model chain is to use the model output from a global model as initial conditions for a regional/mesoscale model. These steps and the resulting higher resolution in the model output are illustrated in Fig. 2. The final step – crucial for wind energy applications is for the mesoscale models to provide the input to a microscale model. Therefore, the core of the downscaling techniques is twofold: First, in the best way to represent the output from the mesoscale model in statistical terms (taking into account thermal stratification, boundary layer structure, and topography) and second to be linked to a microscale model that is capable of using the mesoscale statistics and provide important local siting parameters, such as average and seasonal resource statistics, information on daily and seasonal variability, turbulence and extreme value statistics. An important aspect of the modeling is the validation of the local siting parameters with measurements (if available) and the estimation of uncertainty in the model chain and in the final results.

The output from the mesoscale models is a four-dimensional space – time matrix representing the state of the atmosphere. These data include wind fields at several heights, boundary layer structure parameters, surfaces fluxes, etc. In parallel, the microscale model makes use of the full set of statistics from the mesoscale model and handles effects due to the much more complex topography which generally exist on a scale less than that resolved by the mesoscale model, in order to provide wind characteristics for siting with respect to resource and loads (turbulence, extreme wind, and wind shear). The main problem in the interface between mesoscale and microscale models is to determine the optimal statistical representation of the time series data and important temporal variations, such as seasonal and daily patterns, all dependent on local conditions. Another problem is the ability of the mesoscale model to resolve physical processes on a scale of the order of the numerical grid interval – such as thermally induced flows. Due to the numerical schemes which are used to keep numerical instabilities down, the "true" resolution of a mesoscale model is seldom better than five to seven times the grid length. A typical grid length is 5 km, hence physical processes such as local winds in mountains cannot be resolved and recourse has to be taken to traditional measurements.

The output from the microscale model is validated using available data whenever possible, including data from high masts especially in areas of complex terrain and offshore.

What has been described up to now is the so-called Dynamic Downscaling Method and both this method and the Statistical Downscaling Method are depicted in

Fig. 2. Presently, the latter method is used in most applications, mainly due to a lesser demand on computer power, but the dynamic method is being extensively explored and developed for wind energy purposes due to the much more complete set of wind conditions it can provide.

A large number of mesoscale models are in use, but the most widely used is the WRF (Weather Research Forecast) model developed by the National Center for Atmospheric Research in Boulder, Colorado. It is an open source model and extensive courses are given on its use because it requires highly skilled professionals to run any mesoscale model.

Regional Wind Resource Mapping by Means of the Model Chain

In this paragraph, as a text book example, the concept of The Model Chain is demonstrated by its application in a recent (2010) and very comprehensive study headed by the Finnish Meteorological Institute leading to The Finnish Wind Atlas, illustrated in Fig. 9.

Three different weather prediction models and a microscale model have been used in the production of the Finnish Wind Atlas:

- A Global Model: IFS (Integrated Forecast System) of the European Centre for Medium-Range Weather Forecasts (ECMWF)
- A Regional Model: HIRLAM (High Resolution Limited Area Model of a number of European meteorological institutes, among those FMI: Finnish meteorological Institute)
- A Mesoscale Model: AROME (Applications of Research to Operations at MEsoscale of a number of meteorological institutes and research laboratories, among those, Meteo France)
- A Microscale Model: WAsP (Wind Atlas Analysis and Application Programme of Risø DTU)

The numerical weather prediction models, HIRLAM and AROME, are dynamical forecast models, in which the atmospheric physics is described as accurately as possible for weather forecasting purpose. The WAsP model modifies the wind time series produced by AROME in order to generate the climatological description of wind conditions. WAsP takes into account the effects due to local terrain roughness and topography.

The base material contains 48 months of weather model simulations, in which the winds and other variables are calculated in 2.5×2.5 km^2 grid boxes. Furthermore, the results of the weather model are post-processed in 250×250 m^2 grid boxes in predefined areas by using WAsP model.

All the wind atlas periods were simulated by AROME in 6-h sequential pieces, where atmospheric state is stored after 3 and 6 h of simulation. The initial state of each 6-h subperiod and the required boundary conditions were produced by using weather observations. FMI's weather prediction model HIRLAM was used in this analysis process. The computational domain of HIRLAM covered the Northern Europe with 7.5-km grid spacing. The data required at the edge of the HIRLAM model was taken from ERA-Interim reanalysis that is produced by European Centre for Medium-Range Weather Forecasts (ECMWF). ERA-Interim data covers the whole globe with 80-km grid spacing.

The Web-based Finnish Wind Atlas includes monthly wind statistics and estimates for wind energy production (MWh) for three different sizes of wind turbine (capacities of 1, 3, and 5 MW). These values are given in seven height levels, 50, 75, 100, 125, 150, 200, and 400 m, and in total of 63,550 points each representing 2.5×2.5 km^2 area. Furthermore, the mean wind speed is given also in 250×250 m^2 grid in archipelago, field, and coastal regions and in the chosen land regions. These values are processed from AROME-produced wind information by using mesoscale Lib-software and the WAsP model.

Wind information seen in the wind atlas represents mean monthly and annual wind conditions over last 50 years. Wind conditions of an individual year may deviate considerably from the mean conditions. Furthermore, the actual wind conditions may differ from the mean conditions presented in wind atlas during the lifetime of a windmill. The possible effect of climate change is not taken into account in the values of the wind atlas.

Regional Wind Resource Mapping by means of the Climatological Measurements

As described above mesoscale models may not be applicable in certain topographical and climatological settings due to the grid resolution. Then resource has to be taken to use local measurements (provided they

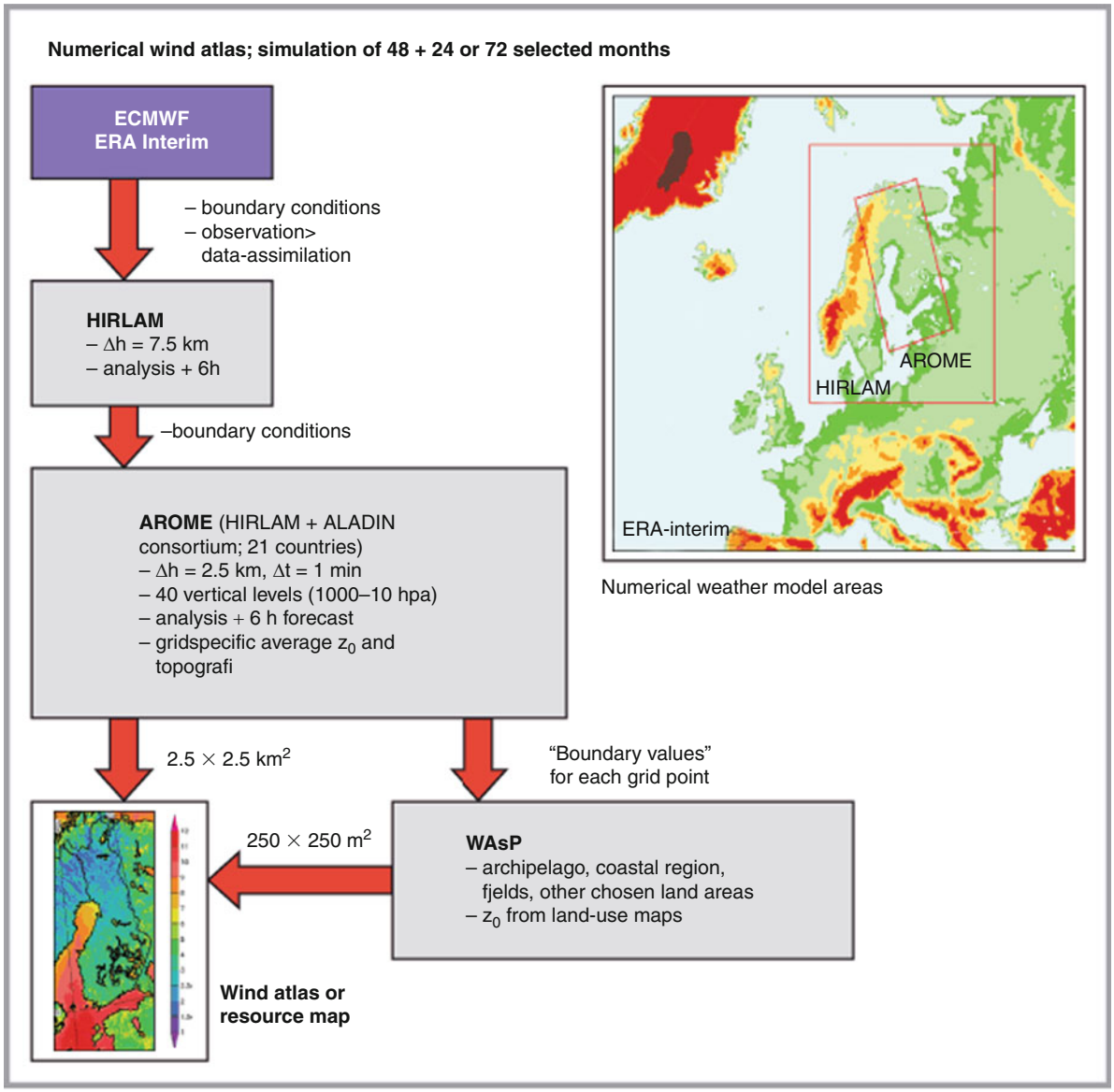

The Finnish Wind Atlas is based on a combination of the FMI's mesoscale numerical weather prediction model AROME and statistical WAsP model that is commonly used in wind atlas applications.

Close

Meterology and Wind Power. Figure 9

The Finnish Wind Atlas showing the way from the global data – ERA Interim – to the microscale model result with a resolution of 250 m. The atlas is based on the combination of FMI's mesoscale numerical weather prediction model AROME and the microscale model WAsP. Finnish Meteorological Institution (FMI) (Courtesy Bengt Tammelin)

exist). During the international project, *The European Wind Atlas* with the aim of establishing the meteorological basis for the assessment of the wind resources of the European Union (1981–1989) a methodology – called the *wind atlas method* – was developed resulting in a comprehensive set of models for the horizontal and vertical extrapolation of meteorological data and estimation of wind resources.

The models are based on the physical principles for flow in the atmospheric boundary layer and they take into account the effect of different surface conditions, sheltering effects due to buildings and other obstacles, and the modification of the wind imposed by the specific variations of height of the ground around the meteorological station in question. Figure 8 illustrates the application of the wind atlas method, following a procedure in which the regional wind climatologies are used as input to the models to produce site-specific wind climatologies. The models and the described methodology constitute the microscale program WAsP.

The European Wind Atlas [2] covers land area of about 2.25 million km^2. It employed surface observations of wind speed and direction, measured over a 10-year period, to determine the wind climate at about 190 European meteorological stations. Then using the wind atlas method, the wind climates were subsequently referenced to a common set of standard topographical conditions, that is, they were expressed as Weibull *A*-and *k*-parameters for five heights and 12 30° sectors over four different values of surface roughness. Wind resource estimates for other sites can then be obtained invoking the same method to introduce the site-specific topography of these sites. Figure 10 shows the overview map from the European Wind Atlas.

The publication of the overview map and the table had a profound influence on European decision makers by showing that it is possible to find location with good wind resources almost everywhere if the right topographical settings are selected. This knowledge has an important implication for any modeling of wind resources, such as mesoscale modeling: The coarser the resolution (large grid cells) the meteorological models work with, the smaller becomes the average wind resource inside the grid cell and this is because that favorable locations such as small hills are smoothed out.

The European Wind Atlas is an example of the use of climatological data from the synoptic network to produce regional wind resource estimations. Another and even earlier example is the creation of the Danish Wind Atlas (1977–1980) [8], which actually builds on the application of a fundamental meteorological concept: The geostrophic wind and its climatology which was determined from long-term pressure measurements at about 55 synoptic stations in and around Denmark (43,000 km^2). The geostrophic wind climate was then used to estimate the wind distributions at a given height over a specific terrain, by means of the geostrophic drag law, which is a relation between the drag force on the surface, the roughness of the surface, and the geostrophic wind. The verification of the atlas was performed by estimating the wind climates of 12 specific sites in Denmark, where long-term wind measurements had been carried out. The procedure follows the right-hand side of Fig. 8, and the geostrophic wind climate is what in the figure is called the generalized regional wind climate. Hence, the development of "the wind atlas method" was initiated during the construction of the Danish Wind Atlas.

Both the Danish and the European Wind Atlas are examples on the use of climatological station of national synoptic networks, many of them located at airports and where routine observations were carried out by the meteorological and other public services. Many of these stations are part of the extensive Global Observing System. Data from satellites form the major part of the data from this system. Data from satellites are used intensively to map wind resources over the ocean. The principle is that the satellite can measure the speed of the capillary waves which then can be transformed into the wind speed [9].

The Global Data Archives

The data sources required for wind resource analysis can be broken into two parts, data about the atmospheric state and flow (known as reanalysis datasets), and data about Earth's surface topography. These two parts are shown below in two tables (Tables 1 and 2). For full information, use a search engine.

The Reanalysis Data Time series of the large-scale meteorological situation covering decades. These datasets have been created by assimilating measurement data from around the globe in a dynamical consistent fashion using large-scale numerical models. The primary purpose for the generation of the dataset is to provide a reference for the state of the atmosphere and to identify any features of climate change. For wind energy, the application of the dataset is as a long-term record of large-scale wind conditions.

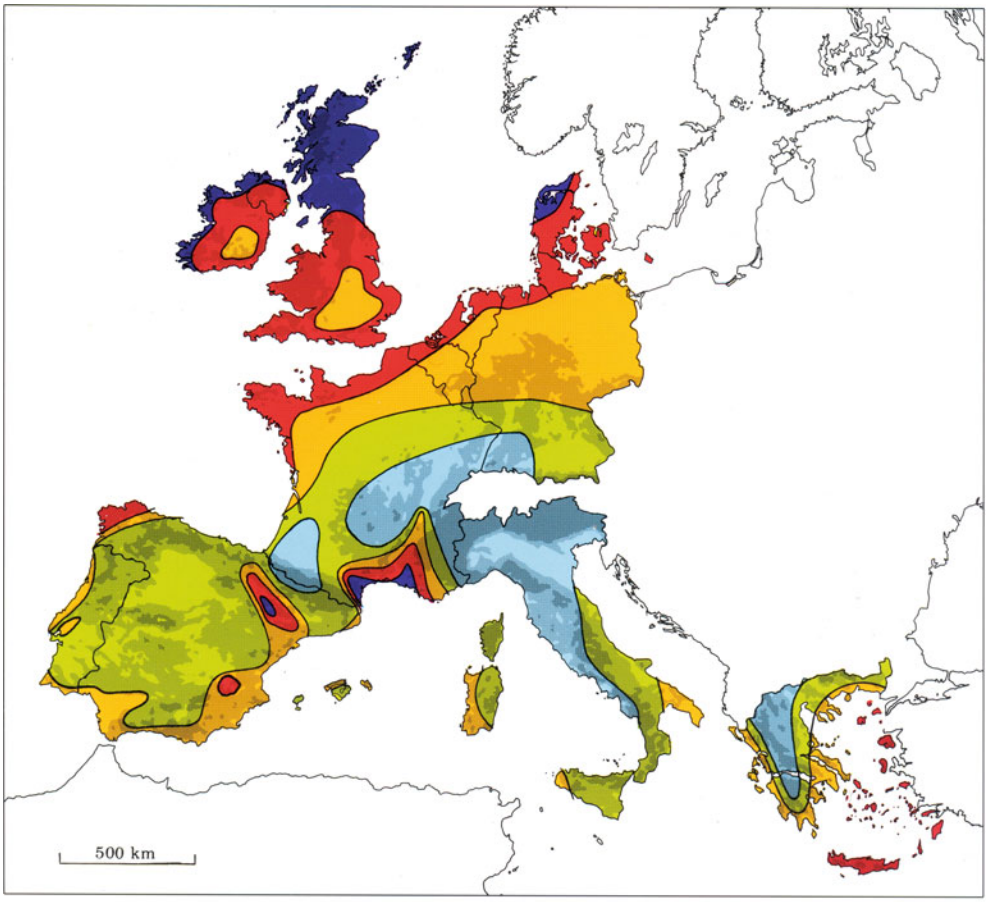

Wind resources[1] at 50 metres above ground level for five different topographic conditions

	Sheltered terrain[2]		Open plain[3]		At a sea coast[4]		Open sea[5]		Hills and ridges[6]	
	$m\,s^{-1}$	Wm^{-2}	$m\,s^{-1}$	Wm^{-2}	$m\,s^{-1}$	Wm^{-2}	$m\,s^{-1}$	Wm^{-2}	$m\,s^{-1}$	Wm^{-2}
	> 6.0	> 250	> 7.5	> 500	> 8.5	> 700	> 9.0	> 800	> 11.5	> 1800
	5.0-6.0	150-250	6.5-7.5	300-500	7.0-8.5	400-700	8.0-9.0	600-800	10.0-11.5	1200-1800
	4.5-5.0	100-150	5.5-6.5	200-300	6.0-7.0	250-400	7.0-8.0	400-600	8.5-10.0	700-1200
	3.5-4.5	50-100	4.5-5.5	100-200	5.0-6.0	150-250	5.5-7.0	200-400	7.0- 8.5	400- 700
	< 3.5	< 50	< 4.5	< 100	< 5.0	< 150	< 5.5	< 200	< 7.0	< 400

1. The resources refer to the power present in the wind. A wind turbine can utilize between 20 and 30% of the available resource. The resources are calculated for an air density of 1.23 $kg\,m^{-3}$, corresponding to standard sea level pressure and a temperature of 15°C. Air density decreases with height but up to 1000 m a.s.l. the resulting reduction of the power densities is less than 10%.
2. Urban districts, forest and farm land with many windbreaks (roughness class 3).
3. Open landscapes with few windbreaks (roughness class 1). In general, the most favourable inland sites on level land are found here.
4. The classes pertain to a straight coastline, a uniform wind rose and a land surface with few windbreaks (roughness class 1). Resources will be higher, and closer to open sea values, if winds from the sea occur more frequently, i.e. the wind rose is not uniform and/or the land protrudes into the sea. Conversely, resources will generally be smaller, and closer to land values, if winds from land occur more frequently.
5. More than 10 km offshore (roughness class 0).
6. The classes correspond to 50% overspeeding and were calculated for a site on the summit of a single axisymmetric hill with a height of 400 metres and a base diameter of 4 km. The overspeeding depends on the height, length and specific setting of the hill.

Meterology and Wind Power. Figure 10

Over view map from the European Wind Atlas – the large-scale variation of the European wind climate. By means of the legend, a range for mean wind speed and mean wind energy at the height of 50 m can be estimated for five topographical conditions. This map sends the important message to politicians, decision makers, and the general public, that even in low wind areas it is possible to find locations for wind farms with a good wind resource

Meterology and Wind Power. Table 1 Global reanalysis datasets (Courtesy Jake Badger)

Product	Model system	Horizontal resolution	Period covered	Temporal resolution
ERA Interim reanalysis	T255, 60 vertical levels, 4DVar	~0.7° × 0.7°	1989–present	Three-hourly
NASA – GAO/ MERRA	GEOS5 data assimilation system (Incremental analysis updates), 72 levels	0.5° × 0.67°	1979–present	Hourly
NCAR CFDDA	MM5 (regional model) + FDDA	~40 km	1985–2005	Three-hourly
CFSR	NCEP GFS (global forecast system)	~38 km	1979–2009 (& updating)	Hourly

Meterology and Wind Power. Table 2 Topographical datasets (Courtesy Jake Badger)

Product	Product description
Elevation – Shuttle Radar Topography Mission (SRTM), version 2.1, released 2009	SRTM data are available as grid point spot heights with a resolution of 1 arc-second (continental USA) and 3 arc-seconds (from 56°S to 60°N, 80% of the Earth's land surface). Derivative datasets exist, where data voids have been filled. The SRTM datasets are used extensively for wind resource assessment already and they are easy to download, process, and transform (e.g., to height contour maps)
Elevation – ASTER Global Digital Elevation Model (ASTER GDEM), version 1, released 2009	ASTER data are available as grid point spot heights with a resolution of 1 arc-second from 83°S to 83°N (99% of the Earth's land surface). Less experience exists using ASTER data for wind resource assessment but they are in principle easy to download, process and transform
Coastline contours – SRTM Water Body Data (SWBD)	Version 2 of SRTM also contains the vector coastline mask derived by NGA during the editing, called the SRTM Water Body Data (SWBD), in ESRI Shapefile format. SWBD data covers the Earth's surface between 56°S and 60°N; the rest of the world is available at lower resolution through the Coastline Extractor hosted by NOAA
Land cover – ESA GlobCover, version 2.1, released 2008	GlobCover is the highest resolution (300 m) global land cover product ever produced and it is made available to the public by the European Space Agency (ESA). The GlobCover land cover map is compatible with the UN Land Cover Classification System (LCCS)
Land cover – regional databases	Several regional and national land cover datasets exist which may be more detailed and sometimes more readily applicable to microscale flow modeling. As an example, the European Environmental Agency (EEA) has produced vector and raster land cover databases – CORINE – for EC Member States and other European countries

Topographical Datasets Modeling of the wind resource requires detailed information on the terrain elevation, water body distribution, and land cover of the terrain. Several global or near-global datasets are available that are used for this purpose.

Assessing Local Wind Conditions for Design and Turbine Safety

The previous paragraphs have focused on the part of the wind conditions which specifically are directed

toward the determination of the wind resource – site dependent or regionally dispersed. Clearly, here the aim is to find the most favorable windy sites or regions for the employment of wind energy. But then the question remains: Are the wind conditions also favorable for operating wind turbines with respect to structural loading and damage to structure and components?

Wind turbine manufacturers offer a range of turbines designed for various wind regimes, characterized in terms of turbulence, mean wind, and extreme wind. The challenge is to select the right turbine for the right site and in order to do this, wind farm developers need to perform verification of design conditions and turbine safety. In this paragraph, a brief introduction to the verification of site conditions is given in accordance with the IEC 61400–1 standard.

Design Standards and Turbine Classes

The International Electrotechnical Commission (IEC) provides standards for electrical equipment including wind turbines. The main principle for ensuring structural safety of wind turbines in the IEC 61400–1 standard, is to design a wind turbine type to a set of design conditions defined for a specific turbine class, and later to verify that site conditions match the turbine class. Turbine classification and design are the responsibility of manufacturers, and site assessment is the responsibility of project developers [10].

To meet the class requirements according to IEC 61400–1, a turbine must be demonstrated to be safe for a range of predefined load cases. In this context, wind conditions are specified by generic models scaled by a reference wind speed V_{ref}, reference turbulence intensity (TI), and turbine hub height. Wind speed and TI are defined for hub height and 10-min averaging periods. The reference wind is the extreme wind with 50-year recurrence, and the reference TI is the average TI at a mean wind speed of 15 m/s. These key wind characteristics at hub height define the wind turbine classes in IEC 61400–1. The wind turbine classes are intended to cover most applications, but the particular external conditions defined for classes I, II, and III are neither intended to cover offshore conditions nor wind conditions experienced in tropical storms such as hurricanes, cyclones, and typhoons (Table 3).

Meterology and Wind Power. Table 3 Basic parameters for wind turbine classes in IEC 61400-1

Wind turbine class		I	II	III	S
V_{ref}	(m/s)	50	42.5	37.5	Values specified by the designer
A	I_{ref} (–)	0.16			
B	I_{ref} (–)	0.14			
C	I_{ref} (–)	0.12			

The turbine class is designated by a roman number (I, II, or III) which refers to the reference wind speed and a suffix letter (A, B, or C) which refers to wind and turbulence, respectively. Thus, a turbine for high wind and medium turbulence is categorized as class I_B.

Atmospheric TI has a variation which is mainly caused by variable atmospheric stability and topographic variations for various wind directions. In general, mean and scatter of the TI decrease with wind speed, though offshore the mean TI will increase when the wind begins to build up waves.

Material damage is not linearly proportional to turbulence, so the IEC standard specifies a design curve, which corresponds to the 90th percentile of the distribution for both extreme and fatigue load estimation. Dynamic loads in operation are estimated by a chain of calculations, which first simulate time series of wind with specified turbulence statistics; then simulate series of aeroelastic responses; and finally evaluate fatigue damage and load extremes.

The simulations are repeated for a range of wind speeds, and the overall fatigue damage is found by an integral weighted by wind speed probability. Vertical wind shear also contributes to fatigue loads, and a somewhat conservative value is prescribed for the aeroelastic simulations. The turbine is considered safe when neither the accumulated material damage over 20 years nor the extreme loads lead to failure. Safe response to severe gust, sudden wind shear, or sudden change of wind direction is verified by special load cases.

As stated above, turbine classification and design are the responsibility of manufacturers, and site assessment is the responsibility of project developers. The purpose of a site assessment is to verify that actual site conditions or resulting loads are less severe than

assumed in the design. In any case, the actual site conditions must be estimated.

There are a number of criteria which apply for the site conditions:

- The 50-year extreme wind must not exceed V_{ref}.
- Flow inclination must not exceed $\pm 8°$.
- Average wind shear must neither be negative nor exceed the design wind shear.
- The wind speed distribution must not exceed the distribution of the turbine class between 0.2 and 0.4 V_{ref}.
- Effective TI must not exceed the TI of the turbine class between 0.2 and –0.4 V_{ref}.

Effective TI is a uniform condition with the same material damage as variable turbulence in winds from various directions. It facilitates comparison of variable field conditions with the uniform TI assumed for the turbine design process. The site-assessment criteria apply to individual turbine sites.

The verification is commonly done by a comparison of the design conditions with conditions at the actual site, determined by a combination of measurements, models, and rules for increasing design parameters, for example TI, if this parameter is not measured. Alternatively, the loads originating from the actual site conditions must be demonstrated to be below the design loads.

An important design parameter is the reference wind speed V_{ref} which is compared with the extreme wind estimated for the site. Extreme winds occur as the highest wind speed during individual storms and they are considered mutually independent. It is possible to fit an extreme wind model to observed extreme winds, and extrapolate to a 50-year recurrence period. Project developers often prefer data from local metmasts installed for resource estimates, but reasonably accurate extrapolation to 50 years obviously requires quite a long time series. The IEC standard recommends a minimum of 7 years, which exceeds most wind energy measurement campaigns. Therefore, recourse is often taken to use data from a nearby reference station. Winds will differ between the reference site and the turbine sites, so it is necessary to correct the observations by a microscale flow model before making the statistical analysis. This can be done using the wind atlas method as previously described.

The measurements at the reference station are then converted to winds over flat terrain with uniform standard surface roughness, and the result is a regional extreme wind atlas. Winds at the potential wind farm sites are then predicted in a second model domain by similar but reverse corrections on the atlas data as it is depicted in Fig. 8.

The reference station could be part of the global meteorological observation network. As a substitute, in case no suitable data are available and with some reservations, a global reanalysis set can be processed for prediction of regional extreme wind climates by means of a mesoscale–microscale combination.

Future Directions

To put "payed" to the problem of determining the right wind conditions for calculating wind resources and structural loads, three things are necessary:

- A body of well-measured data
- A set of models that can reproduce the data
- A theory based on first principles that fully connects measurements and models

Therefore, any advances in this field require an effort on all three components and the fast development in measuring and information technology will continue to contribute. But only advances in theoretical and numerical description of the dynamics of atmospheric motions and the understanding of the interaction with the structural dynamics of wind turbines can secure a significant advancement.

Bibliography

Primary Literature

1. IEC (2005) Wind turbines. Part 1: design requirements, International Standard 61400–1. International Electrotechnical Commission, Geneva
2. Troen I, Petersen EL (1989) European wind atlas. Risø National Laboratory. Published for the EEC, Roskilde, 688 pp (Also in Italian, French, Spanish and German)
3. Krohn S, Poul-Erik Morthorst P-E, Awerbuch S (2009) The economics of wind energy. European Wind Energy Association, Brussels, 155 pp
4. Petersen EL, Mortensen NG, Landberg L, Højstrup J, Frank HP (1998) Wind power meteorology. Part 1: climate and turbulence. Wind Energy 1:2–22

5. Petersen EL, Mortensen NG, Landberg L, Højstrup J, Frank HP (1998) Wind power meteorology. Part 2: siting and models. Wind Energy 1:55–72
6. Kaimal JC, Finnigan JJ (1994) Atmospheric boundary layer flows. Their structure and measurement. Oxford University Press, New York, 289 pp
7. Warner TT (2011) Numerical weather and climate prediction. Cambridge University Press, Cambridge, UK, 526 pp
8. Petersen EL, Troen I, Frandsen S, Hedegaard K (1981) Danish wind atlas. A rational method of wind energy siting. Risø-R-429. Risø National Laboratory, Roskilde, 229 pp
9. Badger M, Badger J, Nielsen M, Hasager CB, Pena Diaz A (2010) Wind class sampling of satellite SAR imagery for offshore wind resource mapping. J Appl Meteor Climatol 49(12):2474–2491, American Meteorological Society
10. Nielsen M, Jørgensen HE, Frandsen ST (2009) Wind and wake models for IEC 61400–1 site assessment, 2009. In: European wind energy conference, Marseilles. 6 p

Books and Reviews

EWEA (2009) Wind energy, the facts. European Wind Energy Association, Brussels

In general: The conference proceedings published yearly by the European Wind Energy Association (EWEA), The American Wind Energy Association (AWEA) and the British Wind Energy Association (BWEA)

Jensen NO, Petersen EL, Troen I (1984) Extrapolation of mean wind statistics with special regard to wind energy applications. Report No. WCP–86. World Climate Programme, WMO, Geneva, 85 pp

Wyngaard JC (2010) Turbulence in the atmosphere. Cambridge University Press, Cambridge, UK, 393 pp

Microbial Risk Assessment of Pathogens in Water

Gertjan Medema
Water Quality & Health, KWR Watercycle Research Institute, Nieuwegein, The Netherlands
Sanitary Engineering, Delft University of Technology, Delft, The Netherlands

Article Outline

Glossary
Definition of the Subject
Introduction
The Safe Water Framework
Risk Assessment
Quantitative Microbial Risk Assessment
Tiered Approach
Good QMRA Practice
Uncertainty Analysis
Applications of QMRA
QMRA for Water Reuse
Future Directions
Bibliography

Glossary

Dose-response assessment The determination of the relationship between the magnitude of exposure (dose) to a microbiological agent and the severity and/or frequency of the associated adverse health effects (response).

Exposure assessment Qualitative and/or quantitative evaluation of the likely intake of microbial hazard via all relevant sources or a specific source.

Exposure Concentration or amount of an infectious microorganism that reaches the target population, or organism usually expressed in numerical terms of substance, concentration, duration, and frequency.

HACCP: Hazard Analysis Critical Control Point A system that identifies, evaluates, and controls hazards that are significant for water safety.

Hazard A biological agent with the potential to cause an adverse health effect.

Hazard identification The identification of microbiological and biological agents capable of causing adverse health effects that may be present in water.

Hazardous event An event that may lead to the presence of a hazard in drinking water.

Health effects Changes in morphology, physiology growth, development or life span of an organism, which results in impairment of functional capacity or impairment of capacity to compensate for additional stress or increase in susceptibility to the harmful effects or other environmental influences.

Infection Colonization of a human (tissue) by a microorganism.

Infectious disease Colonization by a pathogenic microorganism leading to overt symptoms of disease.

Pathogen A microorganism capable of causing disease.

QMRA Quantitative Microbial Risk Assessment.

Risk assessment A scientifically based process consisting of the following steps: (1) hazard

identification, (2) exposure assessment, (3) effect assessment, and (4) risk characterization.

Risk characterization The qualitative and quantitative estimation, including attendant uncertainties of the probability of occurrence and severity of known or potential adverse health effects in a given population based on hazard identification, hazard characterization, and exposure assessment.

Risk The likelihood of occurrence of an adverse health effect consequent to a hazard in drinking water.

Uncertainty Lack of knowledge about specific factors, parameters, or models. Uncertainty includes parameter uncertainty (measurement errors, sampling errors, systematic errors), model uncertainty (uncertainty due to necessary simplification of real-world processes, mis-specification of the model structure, model misuse, use of inappropriate surrogate variables), and scenario uncertainty (descriptive errors, aggregation errors, errors in professional judgment, incomplete analysis).

Variability Intrinsic heterogeneity in a population, process, or parameter.

Water Safety Plan (WSP) A management plan developed to address all aspects of water supply that are under the direct control of the water supplier focused on the control of water production, treatment, and distribution to deliver drinking water.

Definition of the Subject

Water can transmit infectious diseases. Water can be transport vehicle. A range of pathogenic microorganisms is shed into the water cycle by infected hosts (man or animal) and transported to new hosts by the water cycle. Water can also be a niche for (opportunistic) pathogens. These pathogens grow in water ecosystems (natural or man-made) and may infect humans that come into contact with this water. Management of the risk of waterborne disease transmission requires knowledge about the nature of the pathogens, their potential growth, fate and transport in the water cycle, the routes of exposure to humans and the health effects that may result from this exposure in the human population, as well as the effect of potential mitigation measures. The challenge is to combine all this knowledge into information that risk managers can use. Quantitative Microbial Risk Assessment (QMRA) has developed as a new scientific discipline over the last 2 decades as a transparent, science-based approach that allows the risk manager to use the best available scientific evidence as basis for risk management decisions.

Introduction

We run risks. We always have. From being eaten by lions, being slaughtered by a rivaling tribe, to being hit by a car. A principal objective of decision making has always been to reduce risks. From avoiding lions, building walls around cities to regulating traffic. To make wise decisions, it is important to have good information about risks. Risk assessment aims to aid decision makers by collating and evaluating this type of information. Risk assessment is increasingly applied in our society, for a wide range of activities: economy, finance, insurances, traffic, infrastructure, health, and environment. What all these activities have in common is that we want to reduce our risk and need to spend resources on mitigation measures. Our resources are limited, so we need to allocate them wisely and proportionally. Risk assessment helps to keep proportions. Risk assessment as a formal discipline has emerged after World War II, paralleling the developments in air and road traffic, the nuclear power and chemical industries and the need to improve the safety of these activities. The process of risk assessment tries to determine the probability that a hazardous event will occur and the probable magnitude of the adverse effects that such an event will have. In the Netherlands, where a substantial part of the country lies below sea level and is protected against flooding by dikes, the height and strength of the dikes are based on assessing the probability of a storm event and the probable magnitude of the adverse effects of flooding part of the country.

In the health and environment arena, risk assessment science has developed over the last few decades. In environmental health, scientists try to establish the probability of exposure of humans to toxic chemicals or pathogens and the probable magnitude of the health effects of this exposure. Risk assessment has become a dominant tool in environmental policy-making, For chemical risks, this is well established (although not

without debate [52]). Regulatory agencies are using chemical risk assessment to set standards for toxic chemicals in water. For risks of pathogenic microbes via water, the use of risk assessment was first proposed in the early 1990s [60]. The World Health Organization has been instrumental in the introduction of microbial risk assessment as a basis for safety management of the water we use for drinking, recreation, and food crop irrigation [73, 74].

The Safe Water Framework

An international group of experts, assembled by the World Health Organization, discussed the approach to assess and manage the health risk of pathogenic microorganisms in drinking water, recreational water, and wastewater reuse [7]. This group agreed that future guidelines for safe water and sanitation should integrate risk assessment and risk management into a single framework, the Safe Water Framework. The simplest form of the framework is shown in Fig. 1.

The risk that is assessed and managed in this approach is a health risk. It is clearly an iterative cycle in which risk assessment is a basis for decision making in risk management. The four steps of the cycle are described in the next paragraphs, using drinking water safety as an example. In the World Health Organization (WHO) guidelines for the safe use of wastewater, excreta, and grey water [74], these same steps are used for assessing and managing the risk of these water systems.

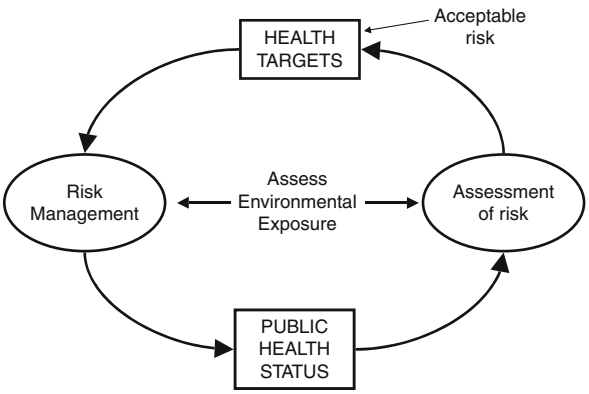

Microbial Risk Assessment of Pathogens in Water. Figure 1
Safe Water Framework for integrated risk assessment and risk management

Health Targets

Health targets are benchmarks for water suppliers, set by the regulator as part of their health policy. Health targets for drinking water are traditionally strict because of the large impact of contaminated tap water and the basic need for safe drinking water. That leads to the question of what level of health risk through drinking water could be tolerated, given the overall health status of the consumer population and the contribution of drinking water to the overall health risk of this population in relation to other routes of exposure, such as food, person-to-person or animal contact, recreational water, etc. This is a question that typically needs answering on the level of the regulator, who can translate this information into a health target for drinking water, considering other factors such as relative contribution of drinking water–transmitted disease to the overall health burden and the economic climate.

The health target is the level of tolerable risk for drinking water, which could be expressed as the tolerable risk of infection through drinking water (i.e., risk of infection $<10^{-4}$ per person per year [61]) or the tolerable amount of disease burden (i.e., $<10^{-6}$ disability adjusted life years per person per year [31, 73]). The health target could be translated into water quality targets for pathogens (analogous to the toxic chemicals). In the latter case, rather than producing a standard and monitoring requirement for all pathogens that could be transmitted through drinking water, the use of a suite of "index pathogens" is advisable. Establishment of adequate control against this suite of pathogens should offer protection against the other known (and even unknown) pathogens.

It is emphasized that the health targets may be different in different health status situations. The question of what is a tolerable level of risk is a judgment in which the society as a whole has a role to play; the decision on the cost-benefit is for each country to decide [71, 73]. It is important that health-based targets, defined by the relevant health authority, are realistic under local operating conditions and are set to protect and improve public health. Health-based targets underpin development of Water Safety Plans [73] and provide information with which to evaluate the adequacy of existing installations, and assist in identifying the level and type of inspection and analytical verifications appropriate.

Risk Management

Managing the safety of drinking water has been the core business of water supply companies for more than a century. Over this period, risk management has evolved into a culture, with codes and specifications of good practice. In the last few decades, quality management systems have been used in the water industry to formalize these practices. Currently, water suppliers in several European Union (EU) countries are using a Hazard Analysis and Critical Control Points (HACCP) based approach for management of (microbiological and other) risks. The basic principles of HACCP are to understand the system and the hazards/hazardous events that may challenge the system and their (health) priority and to ensure that control measures are in place and functioning. HACCP-based systems typically focus on good practice and even more specifically on ensuring that good practice is maintained at all times. HACCP fits within existing quality management systems (i.e., ISO 9001 c.s.). HACCP is the risk management tool that is used in food safety. The Codex Alimentarius (FAO/WHO code for food safety) defines HACCP as a system that identifies, evaluates, and controls hazards that are significant for food safety [10]. The HACCP system is well established in the food industry.

Although there are many aspects of drinking water that are similar to food, there are also differences. Based on experiences of water suppliers with HACCP, the HACCP system has been refined and tailored for application in drinking water abstraction, treatment, and distribution in WHO's Water Safety Plan. The Water Safety Plan is described in the third revision of the Guidelines for Drinking Water Quality [73].

The principal components of the Water Safety Plan are:

System assessment to determine whether the water supply chain (from source through treatment to the point of consumption) as a whole can deliver water of a quality that meets the above targets.

Operational monitoring of the control measures in the supply chain that are of particular importance in securing drinking water safety.

Management plans documenting the system assessment and monitoring, and describing actions to be taken in normal operation and incident conditions, including upgrade and improvement documentation and communication.

In the Water Safety Plan, the risk assessment question: "Do we meet the health target?" is answered in the *System Assessment* and the risk management questions "How do we ensure and demonstrate that we always meet the target?" and "How do we respond to incidents?" are answered in the *Operational monitoring of control measures* and the *Management plans*.

For an overview of the Water Safety Plan and its context, the reader is referred to the WHO GDWQ and the Water Safety Plan guidance documents that are published on the website of WHO Water, Sanitation, and Health.

Public Health Status

The primary objective of drinking water safety management is the adequate protection of public health. The incidence of waterborne illness in the population or the occurrences of waterborne outbreaks are direct triggers for curative risk management. A more preventative incentive for assessing the water-related health risks and the installation of risk management is to demonstrate that the water supply is providing an adequate level of protection of public health.

The installation of health targets in national legislation and the risk management actions of water utilities should result in an improvement of the status of public health. Without addressing this, it is impossible to see if the health targets set and risk management actions taken are effective and if money spent for improving water supply results in a relevant health gain. This step in the process is the place where the health risk of drinking water can be compared to other routes of exposure and to other health risks. It allows comparison of the effort and resources put into the provision of safe drinking water versus resources allocated to manage other health risks.

The risk assessment and management framework is a circular process that can be run in an iterative manner. This fits well with the incremental nature of health decision-making, the efficient use of scarce resources, and the increase of information each time the circle is completed.

Risk Assessment

Risk assessment is used to answer the question: "Is my system able to produce and deliver drinking water that meets the health targets?" The risk assessment process requires quantitative information about the exposure of drinking water consumers to pathogens. This is provided by exposure assessment, one of the components of risk assessment. Quantitative information about pathogens in water sources, their removal by treatment and protection of the distribution network and drinking water consumption is collected and translated into an estimate of the exposure of consumers to pathogens through drinking water. To complete the risk assessment, the potential effect (the risk) of pathogen exposure is estimated through known dose-response models. As will be indicated later, the exposure assessment also provides valuable information to aid risk management in the prioritization of control measures.

An important question in risk management, especially in settings with an already high standard of drinking water safety, is "How far do we need to go with control measures?" This is an optimization that weighs the safety of the consumer against the costs of drinking water.

Quantitative microbial risk assessment (QMRA) can provide an objective and scientific basis for risk management decisions. Water utilities can use QMRA to assess whether they meet the health targets with their water treatment, storage, and distribution systems. This also provides the information to set the critical limits in the Water Safety Plans to ensure good performance. Good performance can now be based on a quantitative assessment of the contribution of the Critical Point (such as a disinfection or filtration process) to the overall safety, and limits can be set to ensure that the multiple barrier chain of water collection, treatment, and distribution as a whole does meet the target.

Risk assessment and risk management should not be regarded as two separate steps in the harmonized framework. To answer the question "Which control measures should be put in place to meet the target?" both the HACCP-based system and quantitative risk assessment provide valuable input: the hazardous events, the most important barriers in the system, the contribution of each of the barriers, target levels for control, the occurrence of weak elements in the chain, the quality of the available information, etc.

Quantitative Microbial Risk Assessment

Quantitative Microbial Risk Assessment (QMRA) is derived from the chemical risk assessment paradigm that encompasses four basic elements:

- A characterization of the problem, including the hazard
- Exposure assessment
- Effect assessment (dose-response)
- Risk characterization

Several QMRA frameworks have been published, such as the generic International Life Sciences Institute (ILSI) framework [8]. Here, most attention is given to exposure assessment and risk characterization of pathogens in drinking water. Therefore, the generic ILSI QMRA framework is expanded to highlight the elements that are important for exposure assessment and risk characterization in drinking water, and put in the overall WHO Safe Water Framework (Fig. 2).

Element 1. Problem Formulation and Hazard Identification

This is the initializing phase of QMRA to establish which specific questions need to be addressed. The scope and the boundaries of the QMRA process are determined in this phase. This requires communication between the risk managers (regulators, public health agencies, water utilities) and the risk assessors. The basic question to QMRA is: "Is my system able to meet the health targets?"

To conduct a QMRA, a good description of the system under evaluation is necessary and the hazards and hazardous events need to be identified.

Step 1. Description of the System from Source to Tap The system for water treatment from catchment to tap is described, identifying the principal control elements and strategies.

Step 2. Hazard Identification Hazard identification is the identification of the microorganisms within the system boundaries that cause human illness, the processes by which each microorganism causes illness and

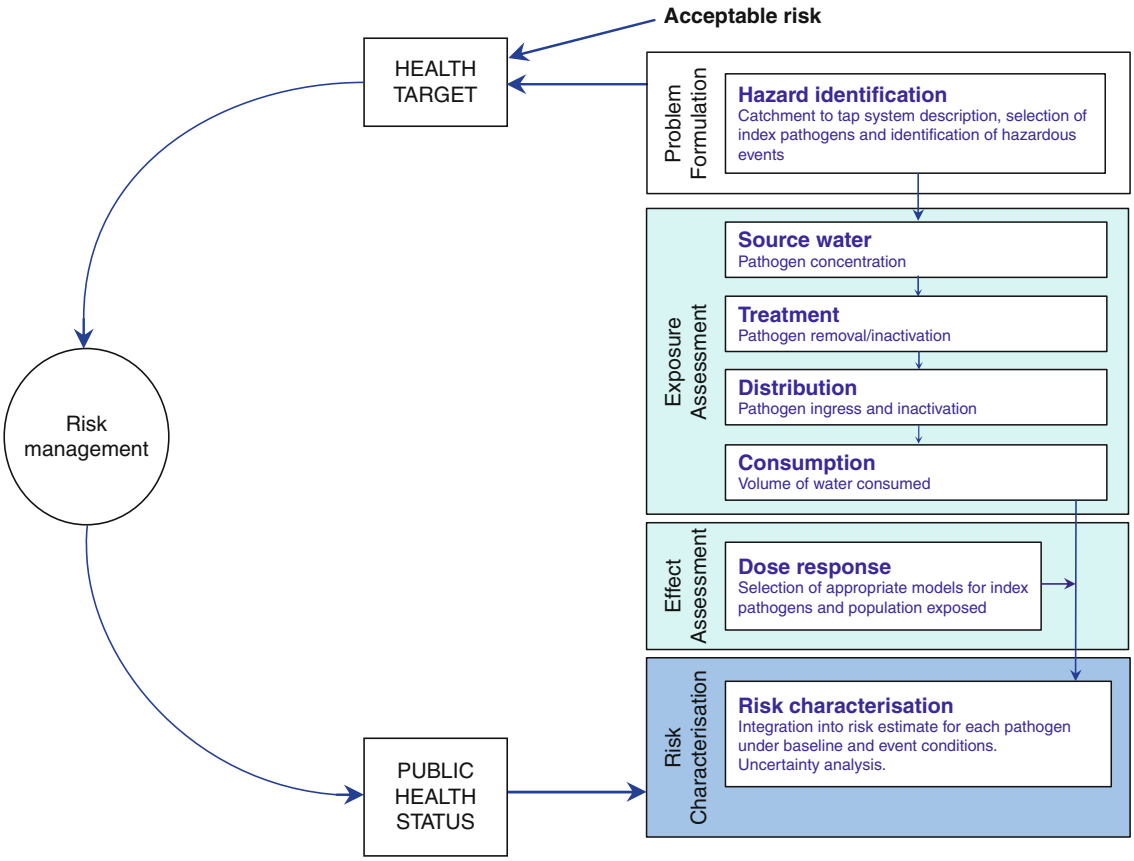

Microbial Risk Assessment of Pathogens in Water. Figure 2
The steps of quantitative microbial risk assessment in the Safe Water Framework

the type of illness(es) caused, and the identification of possible transmission routes and the significance of these routes [26]. QMRA is usually focused on a specific transmission route, in this example drinking water from a surface water source.

The ideal QMRA does not focus on a single pathogen only, but on a suite of "index pathogens" that cover the range of health risks and control challenges for the particular water supply system defined. Adequate control of these index pathogens implies that the health risk of other known pathogens is also adequately controlled by the system and that the system also offers protection against unknown pathogens.

Hazard identification consists of the following steps:

Description of the characteristics of the pathogens, especially those related to waterborne transmission (survival in water, resistance to treatment, etc.).

Description of what is known about the transmission routes of these pathogens and specifically what is known about waterborne transmission, the causes of waterborne outbreaks, and the relative significance of waterborne transmission compared to other routes.

Description of the illness (type, duration, incubation time, etc.) caused by the pathogens in the risk assessment, and available information about sequellae.

Description of what is known about protective immunity and secondary transmission.

Step 3. Description of Hazardous Events In many cases, the majority of the risk is not determined during the normal (baseline) situation, but during hazardous events, such as rainfall leading to a high load of pathogens in source waters, or treatment failure or distribution network failure (or combinations thereof). It is therefore important to ensure that these hazardous

events are incorporated in the QMRA, or that a separate QMRA is conducted to determine the (health) significance of the event.

Element 2. Exposure Assessment

Exposure assessment is the quantitative assessment of the probability that drinking water consumers ingest pathogens. A QMRA of drinking water usually requires the assessment of the levels of pathogens in source water and the changes to these levels by treatment, storage, and distribution, and finally the volume of water consumed.

Step 4. Assess Pathogen Occurrence in Source Water Collect information about the occurrence of pathogens in source water. This is preferably based on a catchment survey, identifying the principal sources of contamination of the catchment and the conditions that may lead to peak events in source water, such as heavy rainfall or resuspension of sediments. Pathogen monitoring in source water can be carried out, using the information of the catchment survey, which needs to include assessment of peak events. The pathogen detection methods are ideally targeted to viable and infectious pathogens. The performance characteristics of the available detection methods for pathogens can have implications for the applicability of the data in risk assessment. These should be identified and evaluated in (the early stages of) the risk assessment process.

Step 5. Assess the Elimination of Pathogens During Treatment Collect information about the removal or inactivation of pathogens during drinking water treatment processes. Ideally, data on removal of pathogens at full scale are used. In practice, however, several other sources of data have to be used to estimate pathogen removal, such as pathogen data of pilot or lab scale systems or data on model parameters (indicator bacteria, phages, spores, particles, etc.) on full, pilot, or lab scale.

The efficacy of treatment processes may vary, depending on feed water composition, operational control, temperature, etc. Moments or periods of poor or suboptimal performance are hazardous events and hence most significant for risk assessment.

Step 6. Assess the Changes in Water Quality During Storage and Distribution Determine the likelihood of recontamination of stored and distributed water (e.g., by the *E. coli* monitoring of water in these reservoirs and pipes or loss of disinfectant residual) and the significance of these contamination events. In well-maintained piped supplies, recontamination events are rare and could be regarded as a result of a hazardous event (heavy rainfall, cross-connection, poor hygiene during repairs, etc.). In other piped and non-piped settings, recontamination events are common and may dominate the health risk.

Step 7. Consumption of Drinking Water The other component of exposure assessment is the volume of water consumed by the population. Not only the average volume of water consumed is important, also the person-to-person variation in consumption behavior and especially consumption behavior of risk groups (in terms of sensitivity to infection or high level of consumption) is relevant. The available data suggest there is considerable difference between drinking water consumption within the population. This variation needs to be captured and incorporated in the risk assessment. Household treatment/point-of-use devices affect the exposure. Hence, consumption data should be on consumption of drinking water without further treatment, such as heating or filters and include water that is drunk directly, but also cold tap water used for food preparation, ice, etc.

Step 8. Dose (Exposure) Estimation Dose (or exposure) is the number of pathogens consumed per unit time. The information obtained in all steps of the exposure assessment needs to be combined into an estimate of the ingested dose. This is preferably a stochastic estimation, including the variability and uncertainty in all steps of the exposure assessment.

Element 3. Effect Assessment

The effect assessment is the determination of the health outcomes associated with the (level of) exposure to waterborne pathogens.

Step 9. Dose-Response Data Dose-response characterizes the relation between dose magnitude, infectivity, and quantitative health effects to an exposed population. The microbial dose-response analysis records the

incidence of a particular effect against dose of the agent. In most cases, this particular effect is infection, rather than symptoms of illness. For *Cryptosporidium parvum* for instance, there is a clear relation between ingested dose and the probability of infection, but not between dose and symptoms of intestinal illness.

Although the dataset is increasing, the number of dose-response studies with human volunteers is limited. Of most pathogens, only one or a few strains are tested in healthy adult volunteers. Information about strain-to-strain variability and the influence of the immune response of the hosts is still limited.

There are several dose-response models available and the type of model can have a very significant impact on the response that is attributed to exposure to low doses. The models and their limitations should be well understood when applying these in QMRA. Synergistic effects between pathogens are not incorporated in the current models.

Step 10. Host Characterization For infectious diseases, the host susceptibility plays an important role in the health outcome of exposure. Exposure of persons with protective immunity will result in lower health outcomes than exposure of risk groups. During "Host Characterization" the characteristics of the potentially exposed populations that are suspected for susceptibility to a particular pathogen are evaluated.

Step 11. Health Outcome Until now quantitative microbial risk assessment has been primarily focused on estimating the risk of infection. The relation between ingested dose and infection is relatively well defined, while the relation between dose and other health outcomes (illness, sequellae) is not available or less clear. This is one of the reasons why it is difficult to establish a direct relation between QMRA (on probability of infection) and epidemiological data (on symptoms of disease). The use of the risk (or probability) of infection is justified by the degree of conservatism in using infection as an endpoint and the inability to quantify the risk of more susceptible subpopulations [43].

However, waterborne diseases differ in nature, severity, and duration. A metric that takes into account the overall health burden of waterborne diseases is necessary. Ideally, this metric can also be used to describe the burden of the disease of chemical compounds, such as carcinogens, so all health risks can be weighed on the same scale.

In the new WHO guidelines for Drinking-Water Quality (GDWQ), the concept of Disability Adjusted Life Years (DALY) [31] is introduced as burden of disease metric in the drinking water guidelines.

The basic principle of the DALY approach is to weigh each health effect for its severity with (usually) death as the most severe outcome, multiply this weight with the duration of the health effect ("duration" of death being the remaining group life expectancy), and with the number of people in a population affected by the particular outcome. Summarizing all the health outcomes caused by a certain agent results in an estimate of the burden of disease attributable to this agent.

To be able to use DALYs in the QMRA, ideally the relation between exposure (dose) and different health outcomes is known. In the absence of sufficient data (which is usually the case), the dose-response relation for infection (as the first step of the disease process) can be combined with data on the fraction of the exposed population falling ill from exposure (for instance, from attack rates in waterborne outbreaks) and data on the fraction of the ill population that contract more severe health outcomes (from health surveillance data).

Element 4. Risk Characterization

In the process of risk characterization, the information obtained in the exposure assessment and the effect assessment are integrated to obtain a risk estimate. This can be done as a point estimation: a point estimate of exposure can be entered into the dose-response relation to compute a point estimate of the risk of infection. The point estimate can be the "best" estimate, to obtain a measure of central tendency of the risk. In the case of computing various risk scenarios, the computed point estimates give a quantitative estimate of the consequences of the circumstances that produce a risk scenario.

An approach that allows the incorporation of the variability and uncertainty in the steps of the risk assessment chain is promoted by [23, 66]. This encompasses the characterization of the distribution of all data used for risk assessment and to combine these distributions into a distribution of the computed risk, for instance, by Monte Carlo analysis. This approach

not only provides the risk manager with important information about the (un)certainty of the risk estimate, but also with the relative contribution of the uncertainty and variability in all steps of the risk assessment. It therefore guides the risk manager to the most appropriate options for efficiently minimizing the risk and the most significant research items to reduce the overall uncertainty of the risk estimate.

With high-level water supply, the baseline risk is usually very low. Under such conditions, hazardous events, such as peak contamination in the source water, treatment failure and especially the combination thereof and contamination events in the distribution network, are responsible for the majority of the risk. Most waterborne outbreaks have been traced to a combination of hazardous events [35] and it is likely that many events result in the presence of pathogens in tap water and hence the transmission of disease. Wherever possible, identify and evaluate these events separately in QMRA to understand the significance of these events. Analysis of events also brings forward opportunities for optimization of the system to prevent these events from occurring or reduce their impact on health.

Tiered Approach

Risk assessment is well suited for a tiered approach and this is also commonly used in risk assessment practice, both in human health risk assessment and in ecological risk assessment. The tiered approach allows an effective interaction between risk assessment and risk management, starting with a crude risk assessment, usually based on limited information to determine the urgency of the perceived problem, to prioritize the risk of different water supply sites or scenarios, and to determine the need of a more detailed study for a particular situation. This allows the effective allocation of resources to the sites or situations that give rise to the highest risk. There is no strict definition of the tiers, only that the initial QMRA is usually generic and simple and the specificity and complexity increase in subsequent tiers.

The most basic (but also most important) QMRA is a screening-level study. Starting with whatever information is available, a crude first evaluation is made. Usually, the available information is not specific to the system that is studied, but has to be extrapolated from the available scientific literature. So, in its simplest form, a QMRA can be performed with only a generic description of the water supply system.

The screening-level assessment may show that the risks are negligible, without much scientific doubt. In that case, the screening-level risk assessment can be used to demonstrate the safety of the system. Setting up a more detailed study is not warranted. Or the screening-level risk assessment may highlight that the risk is unacceptably high, again without much scientific doubt. Such a screening-level risk assessment is also very useful in comparing different scenarios for risk management, for example, different water treatment options.

If the outcome of the screening-level risk assessment is that there may be a health risk that is not negligible, there is an incentive for a next iteration of the risk assessment, the collection of site-specific data, for instance, on the presence of *Cryptosporidium* in the source water or catchment. The QMRA is repeated with the new, site-specific information. The options for the outcome of this second-level QMRA are the same as for the first iteration. In general, a result of any risk assessment is the identification of which information is missing and the prioritization of research needs [21].

The screening-level risk assessments usually work with point estimates of risk. The tendency is to use conservative or worst-case estimates, to "be on the safe side." But worst-case estimates, by nature, may overestimate the risk and it is not clear to the risk manager what the uncertainty of the calculated risk is, only that the uncertainty will be toward the lower risk values (the nature of a worst-case assumption). More helpful for the risk manager is to provide a range of risks (interval estimate) that denote the variability and uncertainty in the risk estimate. In the case of the screening-level risk assessment, this can be achieved by using an average, worst, and best case, to illustrate the range of the risk that can be deduced from the available information and the level of certainty that is embedded in the QMRA.

Interval estimates require information about variability and uncertainty. Variability is the result of intrinsic heterogeneity in the input of the risk assessment, such as the variation in *Cryptosporidium* concentration in source water over time, or the variation in the removal of particles by a filtration process over time. Variability can be characterized if sufficient data points

are collected. Uncertainty is the result of unknown errors in inputs of the risk assessment, such as errors in the measurement of *Cryptosporidium* or the assumption that certain indicator organisms can be used to describe the removal of *Cryptosporidium* by filtration. Uncertainty can be characterized by specific research activities, for example, to determine the recovery efficiency of the *Cryptosporidium* enumeration method or to compare the removal of *Cryptosporidium* to indicator organisms by filtration.

When sufficient data are available, a probabilistic risk assessment can be performed, where the input is described by statistical distribution functions to describe the confidence interval of the input itself and of the calculated risk.

Good QMRA Practice

Food safety has a longer history of employing microbial risk assessment to facilitate risk management. Several international bodies have produced guidance on good microbial risk assessment practice [13, 72]. The principles of good QMRA practice are also applicable to water safety. General principles are:

- Risk assessment should be clearly separated from risk management.
- Risk assessment should be soundly based on science.
- Risk assessment should be transparent: clear, understandable, and reproducible. It should follow a harmonized procedure based on the accepted standards of best practice.
- The scope and objectives of the risk assessment should be clearly defined and stated at the onset, in collaboration with the risk manager who is going to apply the results.
- The data used are evaluated to determine their quality and relevance to the assessment (taking into account their overall weight in the risk and uncertainty). If data are judged irrelevant or of too low quality, this should be justified. All data that are used are referenced.
- If data are variable, the variability should be documented and taken into account in the risk assessment, preferably in a probabilistic manner.
- All assumptions are documented and explained. Where alternative assumptions could have been made, they can be evaluated together with other uncertainties.
- The risk assessment should include a description of the uncertainties encountered in the risk assessment process. Their relative influence on the risk assessment outcome should be described, preferably in a quantitative (probabilistic) manner. Where point estimates are used for uncertain (or variable) quantities, the selected values should be justified and their influence on the assessment included in the uncertainty analysis.
- Conclusions should reflect the objectives and scope of the risk assessment, and include uncertainties and data gaps.

Uncertainty Analysis

Uncertainty is inherent in risk assessment [54]. Many (if not all) data have a degree of uncertainty. Sources of uncertainty in QMRA include:

- Extrapolation from dose-response data (though, unlike with toxic chemicals, many dose-response data are from human exposure)
- Limitations of pathogen detection methods
- Estimates of exposure

It is important to include the uncertainties in all steps of the risk characterization. The uncertainties in the estimates of exposure are usually dominant. Two approaches are used to determine how the uncertainty in the information in individual steps of the risk assessment affect the uncertainty of the overall risk estimate: sensitivity analysis and Monte Carlo simulation. In sensitivity analysis, the value of each parameter in the risk assessment is varied, one at a time, along the uncertainty range of that parameter (e.g., Average and maximum concentration of a pathogen in water) to determine the effect on the final risk estimate. This procedure generates (1) the range of possible values of the final risk estimate and (2) the uncertainty in which of the parameters contribute most to the uncertainty of the final risk estimate. Sensitivity analysis is typically done in screening-level risk assessments. In probabilistic risk assessments, Monte Carlo simulation is the most widely applied method. Monte Carlo simulation needs a deterministic model for the risk assessment. The uncertainty (and variability) in each of the parameters in the risk assessment is expressed in a probability distribution. The simulation computes

a final risk estimate by randomly selecting a value for each parameter in the model from the probability distribution for each parameter. This is repeated many (1,000–10,000) times, each time using a different set of random values from the probability functions. Monte Carlo simulation produces distributions of possible outcome values for the final risk estimate and the shape of the distribution identifies both the general tendency of the risk and the uncertainty of the risk estimate. Also here, the procedure gives information about the contribution of the uncertainty in individual parameters to the uncertainty in the overall risk estimate. While sensitivity analysis evaluates the impact of the uncertainty in each parameter separately and uses few values in the range of possible values of each parameter, Monte Carlo simulation evaluates the impact of the uncertainty in each parameter in combination with all other parameters and uses all possible values and the probability that they occur in the range of each parameter. Burmaster and Anderson [9] published principles of good practice for the use of Monte Carlo simulation in health risk assessments.

Applications of QMRA

The first quantitative microbial risk assessment studies on drinking water were conducted on viruses and *Giardia* [60]. Since the dose-response data from the first human volunteer study on *Cryptosporidium* [12] became available, several authors have performed QMRA for *Cryptosporidium* in water supply (Table 1). This makes the health risk of *Cryptosporidium* through drinking water the most intensively studied object in QMRA studies to date. The overview of QMRA studies for *Cryptosporidium* in water supply illustrates several issues:

1. QMRA studies were conducted to:
   - Evaluate the health risk of *Cryptosporidium* in specific water supply systems or water supply scenarios.
   - Balance the health risk of *Cryptosporidium* in ozonated drinking water to the health risk of bromate formation by ozone [30]. For the assessment of exposure to *Cryptosporidium*, they used raw water monitoring data on *Cryptosporidium*, data on the removal of anaerobic spores by conventional treatment and an ozone disinfection model (the Hom model published by [17]) and a bromate formation model. The ingested dose of oocysts and bromate ions was translated to DALYs to allow comparison of the microbiological and chemical health risk. In their scenario, the health benefits of microorganism inactivation by ozonation outweighed the health losses by bromate formation.
   - Demonstrate the need for additional treatment with UV [1]. They used monitoring data of *Cryptosporidium* in treated water, using a cell-culture-PCR technique to determine the concentration of infectious oocysts in treated water.
   - Demonstrate the need for treatment optimization [46, 48].
   - Illustrate the value of QMRA [47, 48, 59, 66, 68] and relation of QMRA to the Water Safety Plan [49, 65].
   - Evaluate the risk of cryptosporidiosis in different water supply and sanitation scenarios [69].
   - Evaluate the impact of failures in treatment and distribution on the health risk [70]. Failure reports were collected from operational logs/interviews. These failures were translated into an estimate of *Cryptosporidium* (and other pathogen) occurrence (which was the most uncertain step in this QMRA). They indicated that in this system, the health risk associated with normal operation was higher than from the very infrequent and short lasting reported incidents.
   - Prioritize research needs [21], which illustrates how QMRA can be used to determine the relative significance of major, well-controlled and minor, less well-controlled routes of exposure and the impact of moments of reduced treatment performance.
   - Perform a cost-benefit analysis of *Cryptosporidium* regulation that requires additional drinking water treatment for systems with relatively high levels of *Cryptosporidium* in source water [15].
2. Exposure assessment is in many studies hampered by incomplete "site-specific" data. The gaps in the site-specific data are filled by using data from the scientific literature. This is particularly true for the studies in the 1990s. As the use of QMRA progressed, more authors have collected

Microbial Risk Assessment of Pathogens in Water. Table 1 QMRA studies on the risk of *Cryptosporidium* in public water supply

Authors	Exposure assessment	Effect assessment	Outcome	Type	Probability of infection average/95%–range
Medema et al. [47]	*Cryptosporidium* in source water, recovery data [39], viability data [39], removal of oocysts by full scale conventional treatment systems, [39], tap water consumption data [63]	Volunteer study with the Iowa strain [12]	Probability of infection	Probabilistic	3.6×10^{-5} [a] ($3.5 \times 10^{-7} - 1.8 \times 10^{-3}$)
Rose et al. [62]	*Cryptosporidium* in treated water [39]	Volunteer study with the Iowa strain [12]	Probability of infection	Point estimates	5.0×10^{-2} ($4.4 \times 10^{-3} - 1$)
Rose et al. [62]	*Cryptosporidium* in ice prepared from tap water at the time of an outbreak, the latter corrected for the effect of freezing/thawing (90% loss of detectable oocysts) and for the recovery	Volunteer study with the Iowa strain [12]	Probability of infection	Point estimates and comparison of observed and expected illness cases	–
Havelaar et al. [29]	*Cryptosporidium* in source water, recovery data, removal of anaerobic spores by conventional treatment, NL cold tap water consumption data	Volunteer study with the Iowa strain [12]	Probability of infection	Probabilistic	1.3×10^{-4} [a] ($10^{-5} - 10^{-3}$)
Teunis et al. [66]	*Cryptosporidium* in source water, recovery data, viability data [39], removal of anaerobic spores by conventional treatment, NL cold tap water consumption data	Volunteer study with the Iowa strain [12]	Probability of infection	Probabilistic	1.3×10^{-4} [a] ($4 \times 10^{-5} - 4 \times 10^{-4}$)
Teunis and Havelaar [68]	*Cryptosporidium* concentration in source water [5], recovery data [41], viable type morphology [39], removal by storage [66], removal of anaerobic spores by conventional treatment, NL cold tap water consumption data	Volunteer study with the Iowa strain [12]	Probability of infection, illness and DALYs	Probabilistic	No treatment failure: 2.0×10^{-12} 95%: 2.8×10^{-10} Treatment failure: 1.5×10^{-8} 95%: 2.1×10^{-6}

Microbial Risk Assessment of Pathogens in Water. Table 1 (Continued)

Authors	Exposure assessment	Effect assessment	Outcome	Type	Probability of infection average/95%–range
Perz et al. [56]	Assumed concentration of *Cryptosporidium* in tap water, consumption of tap water [63], reduced by 40% for cold tap water consumption and by a further reduction of 33% for AIDS patients	Volunteer study with the Iowa strain [12], assumed threefold higher infectivity for AIDS patients	Probability of infection and illness (probability of illness 0.5 for general population and 1.0 for AIDS patients). Estimated reported cases in general and AIDS population	Point estimates, using two assumed concentrations of *Cryptosporidium* in tap water	$1.0 \times 10^{-3/-2}$ in general population $2.1 \times 10^{-3/-2}$ in AIDS population
Havelaar et al. [30] Gale [20]	*Cryptosporidium* in source water, recovery data, viability data [39], removal of anaerobic spores by conventional treatment, Hom model ozone inactivation [17], NL cold tap water consumption data. The exposure was compared to the exposure to bromate that was formed in the ozonation	Volunteer study with the Iowa strain [12]	DALY	Probabilistic, comparing *Cryptosporidium* to bromate burden of disease	1.0×10^{-3} [a] ($7.6 \times 10^{-4} - 1.5 \times 10^{-3}$)
Haas et al. [24] Haas [26]	*Cryptosporidium* concentration in ice manufactured from tap water during an outbreak, estimation of the inactivation by freezing and thawing, estimation of the duration of the contamination (on onset of cases), attack rate during the outbreak, tap water consumption data [63]	Volunteer study with the Iowa strain [12]	Probability of infection	Point estimate, comparing expected and observed illness	1.1×10^{-2} [b]
Haas et al. [26]	*Cryptosporidium* concentration in distributed water during an outbreak, estimation of the duration of the contamination (on onset of cases), attack rate during the outbreak, assumed 1 L tap water consumption	Volunteer study with the Iowa strain [12]	Probability of infection	Point estimate, comparing expected and observed illness	3.6×10^{-4} [b]

Microbial Risk Assessment of Pathogens in Water. Table 1 (Continued)

Authors	Exposure assessment	Effect assessment	Outcome	Type	Probability of infection average/95%–range
Gale [19, 20]	*Cryptosporidium* in source water [37] and removal of oocysts by full scale conventional treatment systems, [40], data on heterogeneity	Volunteer study with the Iowa strain, including immunity	Probability of infection		1.5×10^{-3} [b]
Haas and Eisenberg [27]	*Cryptosporidium* in different source watersheds, unfiltered system with chlorination, so removal/inactivation by treatment assumed as 0, tap water consumption data [63]	Volunteer study with the Iowa strain [12]	Probability of infection	Point estimate and probabilistic	1.2×10^{-2} 1.2×10^{-3} ($1.2 \times 10^{-4} - 7.7 \times 10^{-2}$)
Medema et al. [48]	*Cryptosporidium* in source water, recovery data, removal of anaerobic spores by conventional treatment, NL cold tap water consumption data	Volunteer study with the Iowa strain [12]	Probability of infection	Point estimate	$1.1 \times 10^{-3} - 3.5 \times 10^{-2}$
	Cryptosporidium in source water, recovery data, removal of bacteriophages by soil passage and of *Cryptosporidium* in soil column studies, NL cold tap water consumption data	Volunteer study with the Iowa strain [12]	Probability of infection	Point estimate	0
	Cryptosporidium in source water, recovery data, viability and genotype data, removal of anaerobic spores by conventional treatment, NL cold tap water consumption data	Volunteer study with the Iowa strain [12]	Probability of infection	Probabilistic	$<1.0 \times 10^{-4}$ with 91% certainty

Microbial Risk Assessment of Pathogens in Water. Table 1 (Continued)

Authors	Exposure assessment	Effect assessment	Outcome	Type	Probability of infection average/95%–range
Westrell et al. [70]	*Cryptosporidium* in source water, removal of particles by conventional treatment, inactivation by disinfection [18, 38], removal of oocysts by membrane filtration [2, 33]	Volunteer study with the Iowa strain [12]	Probability of infection	Probabilistic	Normal operation: 6.0×10^{-4} [a] (6×10^{-6}–4×10^{-2}) Filtration error: 4.0×10^{-5} [a] (6×10^{-7}–2×10^{-3})
	Cryptosporidium in sewage, reports of the water supply on treatment failure and contamination incidents in the distribution network	Volunteer study with the Iowa strain [12]	Probability of infection	Probabilistic	Reservoir contamination: 7×10^{-7} [a] (2×10^{-8}–2×10^{-6})
Masago et al. [46]	*Cryptosporidium* in source water [28], effect of rainfall, viability data [39], failure model for removal by conventional treatment, NL cold tap water consumption data	Volunteer study with the Iowa strain [12]	Probability of infection	Probabilistic	2.0×10^{-4} [a] (2.5×10^{-5} [c] – 2.5×10^{-3})
Gale [21]	Theoretical assumptions in scenario studies of treatment by-pass or failure	Volunteer study with the Iowa strain [12]	Probability of infection	Probabilistic	–
Pouillot et al. [59]	Assumed concentration in distributed water, recovery data, viability data (expert knowledge), French cold tap water consumption	Volunteer study with the Iowa strain for both infection and illness [12], immunodeficient mouse model [75]	Probability of infection and of illness for immunocompetent and immunodeficient persons	Probabilistic	At 2 oocysts/100 L: 1.8×10^{-2} 95%: 5.4×10^{-2}
Pouillot et al. [59]	*Cryptosporidium* in distributed water, recovery data, viability data (expert knowledge), French cold tap water consumption	Volunteer study with the Iowa strain for both infection and illness [12], immunodeficient mouse model [75]	Probability of infection and of illness for immunocompetent and immunodeficient persons	Probabilistic	2.1×10^{-2} 95%: 6.7×10^{-2}

Microbial Risk Assessment of Pathogens in Water. Table 1 (Continued)

Authors	Exposure assessment	Effect assessment	Outcome	Type	Probability of infection average/95%–range
Havelaar et al. [30]	*Cryptosporidium* in source water, recovery data, *Cryptosporidium* challenge study of conventional treatment	–	Quality score of exposure assessment factors	Uncertainty analysis	–
Haas et al. [25] JAWWA 88:131	Calculation of a *Cryptosporidium* concentration that corresponds with the 10^{-4} probability of infection (3.27×10^{-5}) oocysts L^{-1} (95% CI: $1.8-6.4 \times 10$)	Volunteer study with the Iowa strain [12]	Probability of infection	Probabilistic	(1×10^{-4})
Aboytes et al. [1]	*Cryptosporidium* in filtered drinking water, recovery data, infectivity data (cell-culture PCR)	Volunteer studies with the Iowa, UCP and TAMU with Bayesian data-analysis [51]	Probability of infection	Point estimate with confidence interval	8.2×10^{-3} 95%: 1.2×10^{-2}
EPA [15]	*Cryptosporidium* monitoring data (ICR and beyond), recovery data, infectivity fraction, treatment performance credits, USDA consumption data	Volunteer studies with Iowa, TAMU, UCP, using different models	Probability of infection, illness, death and cost	Probabilistic with sensitivity analysis	Scenario evaluation Pre-LT2 filtered: 8×10^{-5} ($<10^{-6} - 0.02$); unfiltered 0.02 (0.002 to ~0.5)

[a]Median
[b]Average daily risk of infection during the outbreak
[c]Minimum annual risk

site-specific information about most if not all steps in the exposure assessment.

3. Most studies used the dose-response data of the Iowa strain of *C. parvum* as published by DuPont and coworkers [12]. Over the years, the dose-response relationships of more *C. parvum* strains have been published. One recent study on the risk of *Cryptosporidium* to fire fighters using recycled water used the dose-response data of the TAMU strain of *C. parvum* as this was the most infective strain [11]. Medema [50] present an approach for the use of a *C. parvum* dose-response relation, that combines the dose-response data that are published for four different isolates of *C. parvum* (Iowa, TAMU, UCP and Moredun).
4. The most frequently used health outcome is the probability of infection; a few studies also determined the probability of illness of the general population and the immunodeficient population [56, 59]. Two studies calculated the DALY resulting from the waterborne transmission of *Cryptosporidium* [67, 30].
5. Using the data of the Milwaukee outbreak [44], the calculated probability of infection/illness with QMRA was compared to the observed probability of illness in the outbreak as observed in the epidemiological investigations [24, 26]. The authors concluded that the results of QMRA and epidemiological investigation were consistent. The analysis of the exposure of the Milwaukee residents to *Cryptosporidium* via tap water was hampered by the lack

of timely measurements of *Cryptosporidium* in the contaminated water. Unfortunately, this is the rule rather than the exception in waterborne outbreaks. The concentration had to be inferred from oocyst concentrations found in samples of ice that was prepared at the time of the water supply contamination and was corrected for the expected loss of detectable oocysts after freezing/thawing. The exposure assessment was therefore not very certain. In addition, the reported magnitude of the Milwaukee outbreak has been criticized by [36]. They claim that the background prevalence of gastrointestinal illness in the USA is much higher (1.2–1.4 episodes per person per year, or 0.10–0.12 per person per month) than the prevalence used by [44] (0.005 per person per month). Use of higher background prevalence would drastically reduce the estimated size of the Milwaukee outbreak.

6. The setup of the QMRAs sometimes used point estimates, but more generally a probabilistic approach is used to be able to estimate the level of uncertainty of the calculated probability of infection or illness.
7. Between the different studies, the calculated probability of infection can differ considerably see (Table 1). Within studies, the uncertainty of the risk estimate toward the higher health risk (illustrated by the difference between the average or median risk and the 95% confidence limit) is limited to around a factor of 10.

In general, it can be seen from these examples that QMRA has become an established tool to evaluate health risks of *Cryptosporidium* in (piped) drinking water supplies. QMRA requires input from data on exposure and dose-response and can be done in different levels of complexity. The next paragraphs give examples of the application of QMRA in water and illustrate the stepwise (tiered) approach that can be taken in QMRA and that QMRA can be conducted and be valuable in the absence of site-specific data and in developing countries.

QMRA to Assess the Safety of a Drinking Water Supply

Suppose that a water utility wants to evaluate if its surface water supply is at risk of significantly transmitting *Cryptosporidium* to its consumers, but has no specific information about *Cryptosporidium* in its source water or removal by its water treatment processes. A first exercise to get an idea of the level of risk could be a screening-level QMRA. The information on *Cryptosporidium* levels in source water can be derived from watershed use (see [50]), and for the water treatment processes default log-credits for the removal or inactivation of *Cryptosporidium* are available [49]. For instance, if the water supply system uses a watershed that can be characterized as moderately polluted and treats this source water with off-stream storage reservoirs and a conventional (coagulation/filtration/chlorination) water treatment system, using the scientific database, the expected concentration of *Cryptosporidium* in source water can be estimated at 0.1/L and the removal by the subsequent water treatment processes can be estimated at 0.5 + 2.5 = 3.0 logs removal. Hence, the estimated concentration of *Cryptosporidium* in drinking water is 1×10^{-4}/L. With a conservative best estimate of consumption of cold tap water of 0.78 L/day (3.49 glasses of 0.25 L, [53]), the average probability of exposure to *Cryptosporidium* is 8.7×10^{-5} per person per day. With the combined dose-response relation of the four *C. parvum* strains, the probability of infection is estimated at 3.8×10^{-5} per person per day, which amounts to 1.4×10^{-2} (=1.4%) per person per year. This is a first estimate of the health risk related to *Cryptosporidium* in this specific water supply system. Similarly, such an exercise can be used to evaluate different scenarios of risk management to reduce this risk (if required) such as measures to improve the catchment or install additional treatment processes. An example of a practical application of such a screening-level risk assessment is given in Medema [50], where a large water supply company uses the screening-level QMRA to prioritize risk management of its water supply systems.

Comparing Water Supply Scenarios with QMRA

Piped and non-piped water supply in Uganda [34].

In Kampala, 72% of the population uses piped water supplies. 20% of the population uses piped water through household connections; the rest collects water at standpipes and stores it in-house. The piped water is produced from Lake Victoria

water through (coagulation/settling) rapid sand filtration followed by chlorination. The rest of the population (28%) uses protected springs for their water supply.

Data on thermotolerant coliforms were available from Lake Victoria and from the protected springs and the household containers. Using an estimate of the percentage of *E. coli* within the thermotolerant coliforms and an estimate of the percentage of pathogenic *E. coli* within *E. coli*, the thermotolerant coliform concentration data were translated to pathogenic *E. coli* concentrations. For the removal of (pathogenic) *E. coli* by the water treatment processes, the authors used a 3-log credit for the physical removal processes and an additional 2-log credit for the chlorination. This was used to calculate the concentration of pathogenic *E. coli* in drinking water. With data or estimates on consumption of unheated drinking water, dose-response for infection, probability of illness when infected, and disease burden (DALY), the concentration of pathogenic *E. coli* in drinking water was translated into the estimated disease burden by exposure (Table 2).

Similar assessments were made for *Cryptosporidium* and Rotavirus exposure for the population using piped water supply. For *Cryptosporidium*, they showed that treatment failure would result in a very significant increase of the disease burden (from 10^{-4} to 4 DALYs per person per year). The authors have compared the calculated levels of disease burden to the WHO reference level of risk (10^{-6} DALY). Upgrading the treatment would be necessary to achieve this health target, but the authors argue that, given the low level of access to piped water in the home and the disease burden associated with the use of alternative (more contaminated) sources, this would not be cost effective. Improving access to piped water supply in homes, sanitation and hygiene would be more effective in reducing the disease burden.

This example illustrates that QMRA is feasible also in settings with limited data. The authors discuss

Microbial Risk Assessment of Pathogens in Water. Table 2 Assessment of disease burden for pathogenic *E. coli* from different water types (adapted from [34])

	Piped water following treatment	Piped water in distribution	Household storage water	Protected spring water
Raw water quality thermotolerant coliforms/L	150		30	140
Raw water quality *E. coli*/L	143		28.5	133
Raw water pathogenic *E. coli*/L	11.5		2.3	10.6
Treatment effect (log)	5		0	0
Drinking water quality (/L)	1.15×10^{-4}	0.18	2.3	10.6
Consumption of unheated drinking water (L)	1			
Exposure (pathogens/day)	1.15×10^{-4}	0.18	2.3	1.06×10^{1}
Dose-response parameter (exponential)	0.001			
Risk of infection (day)	1.15×10^{-7}	1.80×10^{-4}	2.30×10^{-3}	1.06×10^{-2}
Risk of infection (year)	4.20×10^{-5}	6.57×10^{-2}	8.40×10^{-1}	3.87×10^{0}
Risk of diarrheal disease given infection	0.25			
Risk of diarrheal disease	1.05×10^{-5}	1.64×10^{-2}	2.10×10^{-1}	9.67×10^{-1}
Exposed fraction	0.31	0.1	0.42	0.28
Disease burden (DALYs)	1.04×10^{-6}	5.26×10^{-4}	2.82×10^{-2}	8.67×10^{-2}

limitations and assumptions used in their study, but illustrate the value of system assessment to inform risk management of the area where control measures will be most effective.

QMRA to Evaluate the Health Risk of Hazardous Events

Many outbreaks of intestinal illness caused by consumption of contaminated drinking water in affluent nations have been associated with hazardous events, such as heavy rainfall (both for surface and groundwater systems), failures in a treatment process, failures in the integrity of the infrastructure (wells, distribution network), cross-connections in the distribution network, etc. For an overview, see [35]. Additional hazardous events can be identified for non-piped supplies, especially contamination of the water in storage containers. Also, events that lead to a stop in supply of drinking water (due to power or treatment failure, or indeed absence of sufficient quantities of source water) are hazardous events in themselves, since water is essential for life and hygiene.

Water quality testing can help to identify peak events. Often, peak events can be indicated by simple parameters, such as rainfall, river flow, turbidity, etc., and hence their detection does not require advanced equipment or expertise. It does require knowledge of the water supply system, including its catchment. In Microrisk, a European study on microbial risk assessment of drinking water, information was needed about pathogen occurrence in source (surface) water of the water supply systems under study [49]. Knowing the potential importance of peak events, catchment surveys were conducted to identify contamination sources and to identify events that could lead to peak pathogen contamination of the source water. One system used bank filtration and subsequent treatment to produce drinking water from a large river. Historical (50 years) data on the water level of the river showed that an increase of $\geq$3 m within 5 days occurred 1.1% of the time (3.9 days per year on average). This river level rise was used as a criterion to trigger peak event sampling. A dry weather flow sampling scheme was also in place, with monthly pathogen samples. During monitoring, one peak event was encountered and peak event samples were taken, showing a sharp increase in the concentration of *Cryptosporidium* and *Giardia* concentration in the river (Fig. 3). Event samples were also taken from the bank filtrate. The *E. coli* were detected in the bank filtrate only at the time of the peak event (Fig. 4).

Similarly hazardous events may occur in water treatment (i.e., disinfection failure) or distribution (cross-connection, ingress during main breaks, no pressure period or repair). A QMRA to determine the

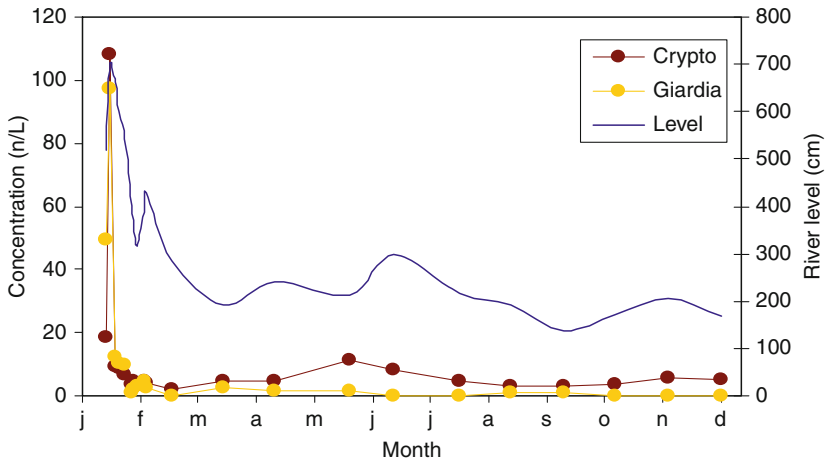

Microbial Risk Assessment of Pathogens in Water. Figure 3
Cryptosporidium and *Giardia* in river water during a peak event (Data from [49])

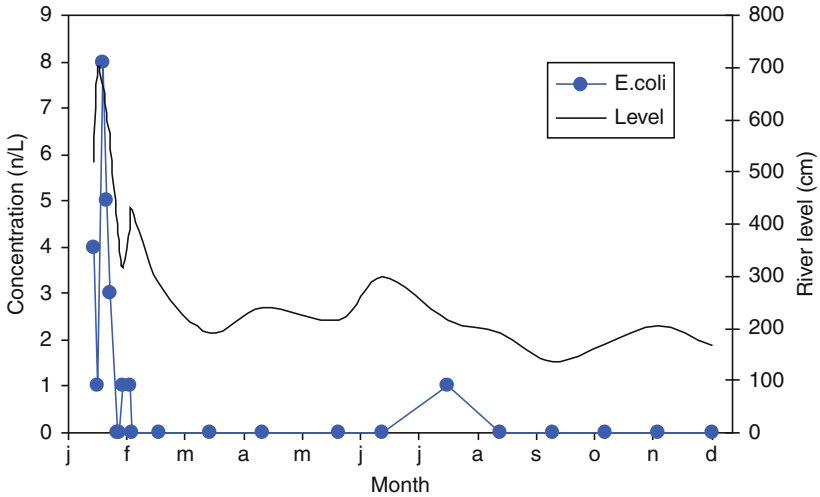

Microbial Risk Assessment of Pathogens in Water. Figure 4
E. coli breakthrough of bank filtration during a peak event in the river see (Fig. 3, data from [49])

health effect of ingress of fecal contamination in municipal piped distribution networks is given in [42]. In the Microrisk project, the health risk associated with several source and treatment hazardous event scenarios in the different water supply systems (called Catchment-to-Tap Systems or CTS) studied was determined and compared to the baseline health risk in these systems in a Monte Carlo simulation [64].

Hazardous events were identified in discussions with local water suppliers and from SCADA data. Of these, five were selected and evaluated with QMRA (Table 3).

In the case of the CTS 1 (a surface water supply) the local managers were concerned about the prospect of a motorway fuel spill and its potential impact on the treatment plant. It was speculated that even small quantities could foul major filters (Rapid Sand Filter and Granular Activated Carbon filters) and reactors (ozone contact tanks) and necessitate cleaning. This led us to simulate a cleanup period of 7 days during which protection was provided by chlorination alone and hence the system was vulnerable to *Cryptosporidium* contamination because of its resistance to chlorine.

It can be seen that the annual risk of infection by *Cryptosporidium* rises by a factor of 1,000 and the estimated probability of infection is much higher than 10^{-4} per person per year. Further, even if the repair period could be reduced to 1–2 days, the additional risk would still be great and hence other action such as a boiled water alert on top of chlorination would need to be considered.

CTS 5 is a surface water supply system with the option to close water intake. If no intake management were in place the average annual risk would have been at least 19 times higher. The impact of a delay in closing the intake was also substantial. This highlighted the need for timely warning of event onset where source extraction is being managed.

CTS 6 included extensive diary and SCADA (Supervisory Control and Data Acquisition) data detailing performance of the chlorination. This information allowed determination whether chlorination failure was occurring. Analysis of the in-line chlorine monitoring data indicated that at worst chlorine dosing failed for a total time of 1.5 h over a 12-month period. The impact of simulated worst-case failure on *Campylobacter* showed a detectable but only small increase in health risk.

The final scenario considered was that of multiple concurrent hazardous events. A concern for CTS 8 and CTS 6 type systems, which draw their supply from a reservoir, is that during high run-off events there can be concurrent polluted input and short-circuiting [32]. Further, storms frequently cause power failures, which could affect treatment plant equipment such as dosing pumps. Two scenarios were considered with

Microbial Risk Assessment of Pathogens in Water. Table 3 Hazardous event impacts on risk

CTS	Pathogen	Hazardous event	Total duration of event	Baseline risk (person^{-1} year^{-1})	Baseline + hazardous event risk (person^{-1} year^{-1})
1	*Cryptosporidium*	Loss of filtration due to petroleum spill necessitating cleanup. Only remaining treatment is chlorination	7 days	1.4×10^{-5}	1.7×10^{-2}
5	*Norovirus*	No intake closures leading to periodic high concentration of virus in source water	57 days	$<5.8 \times 10^{-4}$	2.7×10^{-2}
		Delay in intake closure of 4 h for each of 29 events of high virus concentration in source water per year	4.75 days		3.4×10^{-3}
6	*Campylobacter*	Loss of disinfection capacity: total suboptimal chlorination periods based on analysis of SCADA data – worst case of total loss of disinfection assumed	1.5 h	2.5×10^{-6}	3.2×10^{-6}
8	*Campylobacter*	Short-circuiting leads to reduced (1 log) removal in storage reservoir for 24 h. Nine short-circuiting events occur per year	9 days	1.7×10^{-5}	3.4×10^{-5}
		Short-circuiting leads to reduced (1 log) removal in storage reservoir for 24 h. Nine short-circuiting events occur per year. During one of these periods chlorination loss occurs due to power failure for 2.4 h (0.1 days)	0.1 days		1.8×10^{-4}

The risk estimates in brackets are based on upper 95th percentile uncertainty and are derived from upper limit inputs rather than typical source water concentrations

these events in mind. Concurrent contamination of runoff and short-circuiting of the reservoirs were estimated to double health risk for *Campylobacter*. With the combination of a short duration power failure leading to chlorination loss during a storm could increase annualized risk 11-fold in a short time, confirming the need for avoiding or actively managing periods of concurrent hazardous events.

The value of the hazardous event analyses illustrated lies not only in the actual estimates presented. They also demonstrate how QMRA can be used to evaluate events and other hazardous scenarios to produce risk estimates useful for management. In the case of CTS 1, it was clear that filtration shut down even for a short period posed high risks because of the contamination levels in the source water. Selective water intake at CTS 5 is a beneficial management activity. At CTS 6, chlorine dosing was shown to be maintained at a level sufficient to reduce risks arising from plant failure. The CTS 8 analysis showed that baseline operating conditions provide sufficient barrier protection to mitigate a run-off and short-circuiting event, but with a concurrent event (chlorination failure) pose a significant threat.

QMRA for Water Reuse

In (semi) arid conditions, there is (increasing) water scarcity and competition between agriculture and urban uses of this scarce resource. Wastewater is in most cases a reliable (in terms of quantity) source of water and valuable source of nutrients for agriculture. Wastewater reuse in agriculture is a form of water and nutrient recycling that is practiced worldwide, especially in arid and semi-arid areas. Also the (re)use of gray water in urban areas for applications such as toilet flushing in homes, gardening, etc., is becoming more common.

The new WHO Guidelines for safe use of wastewater, excreta, and gray water are based on the Safe Water

Framework (Fig. 1). QMRA is presented in these WHO guidelines as useful tool to estimate the health risks associated with wastewater reuse in different scenarios and for different pathogens. The guidelines contain several references to the application of QMRA in wastewater reuse. In the next paragraphs, three examples of the use of QMRA in water reuse are given.

Comparing Risks Between Different Uses of Reclaimed Wastewater (California)

The first QMRA to estimate the disease risk associated with the reuse of (treated) wastewater was [3]. They evaluated the risk of an infection with enteric viruses (Poliovirus 1 and 3 and Echovirus 12) when chlorinated or unchlorinated tertiary effluent was used for:

- Irrigation of a golf course
  The exposure scenario was a golf course with night time irrigation with tertiary treated wastewater effluent and person golfing twice a week. Each day this person would be exposed to 1 mL of reclaimed water during handling and cleaning of golf balls. The pathogen concentration in this reclaimed water was calculated from data on enteric viruses in chlorinated and unchlorinated effluent and virus decay on the golf field.
- Spray irrigation of food crops
  After spray irrigation, it was assumed that 10 mL of reclaimed water was left on each portion of crops eaten raw. The spray irrigation was stopped 14 days before harvesting and the virus die-off due to desiccation and sunlight exposure was included in the calculation.
- Swimming in recreational water
  This recreational water was assumed to be an impoundment that was, during summer, completely made up out of reclaimed water. No dilution or die-off was assumed. A swimmer was assumed to ingest 100 mL each swimming day and to swim 40 days in a year.
- Groundwater recharge near domestic wells
  This exposure scenario was based on the proposed Californian groundwater recharge regulations. The nearest domestic well was assumed to receive 50% reclaimed water that had been passing through 3 m of unsaturated soil beneath the recharge basin during a period of 6 months. The people drinking from this well were assumed to consume 2 L/day.

The input data were:

- Concentration of culturable enteric viruses in unchlorinated secondary effluent: 5–734/L (90% and maximum, respectively)
- Concentration of culturable enteric viruses in chlorinated tertiary effluent: 0.01–1.1/L
- Removal of enteric viruses by full tertiary treatment (flocculation, clarification, filtration, chlorination): 5 logs
- Virus decay rate: 0.69/day (first order die-off kinetics)
- Fraction of virus remaining after percolation through the unsaturated soil $c/c_0 = 10^{-0.007\,L}$, where L is the depth of the unsaturated zone in centimeters
- Dose-response parameters for echovirus 12 and poliovirus 1 and 3

The concentration of viruses in reclaimed water was taken from data from surveys of secondary and tertiary effluent. They calculated the exposure to the viruses in the different exposure scenarios. Annual risks were calculated from the maximum concentration found in chlorinated tertiary effluent (1.1 culturable virus unit L^{-1}) and exposure in the different applications (Table 4).

This QMRA showed that the virus risk was highest when reclaimed wastewater was used in recreational

Microbial Risk Assessment of Pathogens in Water.
Table 4 Annual risk of exposure to viruses for different applications of reclaimed water

Exposure scenario	Echovirus 12	Poliovirus 1	Poliovirus 3
Irrigation of golf course	1.0×10^{-3}	3.5 E-5	2.5 E-2
Spray irrigation food crops	4.5×10^{-6}	1.5 E-7	1.1 E-4
Recreational impoundment	7.4×10^{-2}	2.6 E-3	8.4 E-1
Groundwater recharge	5.9×10^{-8}	5.4 E-9	2.3 E-8

impoundments and golf course irrigation. This maximum concentration was found in only 0.1% of the samples (with 99% of the samples with virus concentrations below the detection limit), so they also calculated the risk with a virus concentration of 1/100 L, which were approximately 100-fold (2 logs) lower.

The value of the QMRA was that it provided a comparative basis for addressing the treatment and fate of enteric viruses in wastewater reuse and showed that the risk can further be mitigated by controlling exposure to reclaimed water.

Health Risk of Reuse for Crop Irrigation (Australia; Probabilistic)

In the previous example, the available data and assumptions were used to generate point estimates. This example shows how the variability in available data can be used to determine the uncertainty that is associated with each of the components in a QMRA.

The use of wastewater for irrigation of food crops that are eaten raw is common practice in many arid and semi-arid regions [57] constructed a QMRA-model for evaluating the risks associated with the consumption of wastewater irrigated lettuce crops. The exposure assessment in this model consisted of four process steps:

OCCURRENCE Number of viruses in irrigation water	IRRIGATION Fraction of applied viruses that attaches following irrigation	INACTIVATION Viruses are inactivated on the crop over time	CONSUMPTION Infectious viruses may be consumed with the crops

Exposure to viruses was calculated as:

$$\text{Exposure} = N \times f \times S(t) \times q$$

where

N is the number of viruses in the irrigation water applied to the crop
f is the fraction of those viruses that survive the irrigation process and attach to the lettuce plant
$S(t)$ is the fraction of viruses remaining infectious at consumption
q is the quantity of crop consumed

For each step a best estimate and an extreme estimate were selected (Table 5). This allowed analysis of the sensitivity of the QMRA to each of the model parameters.

Microbial Risk Assessment of Pathogens in Water.

Table 5 Best and extreme estimates for parameters of exposure to viruses in wastewater reused for irrigation of lettuce

Model component	"Best" estimate	"Extreme" estimate
Virus occurrence	2.6 (virus units L^{-1})	470,000 (virus units L^{-1})
Virus attachment (f)	0.024	0.071
Virus inactivation: S(t) Bi-phasic inactivation $Ct = aC_0 * h1 + (1 - a)C_0h2$	$h1 = 2.5\ day^{-1}$ $h2 = 0.5\ day^{-1}$ $a = 0.12\%$	$h1 = 2.0\ day^{-1}$ $h2 = 0.3\ day^{-1}$ $a = 0.96\%$
Consumption per event q	100 g	300 g

Sources: Californian dataset used by [3, 76]. All other data were derived from [57, 58].

The authors calculated the Factor Sensitivity (FS = log ($N_{extreme}/N_{best}$), with N being the number of viruses in the extreme or best estimate) for each of the components. Already obvious from the table above is the high impact of the estimate for the virus concentration in wastewater (FS = 5.49). Less obvious from the table is the high impact of the estimate of virus inactivation (FS = 2.2). This is of course time dependent; the authors used 14 days as the time between final irrigation and consumption. A shorter interval reduces the impact of virus inactivation, since the inactivation is less. The uncertainty associated with virus attachment (FS = 0.45) and consumption (FS = 0.48) was considerably less.

This simple mathematical approach yielded not only the risk estimates associated with wastewater reuse for food crop irrigation, but also the (un)certainty associated with each of the components in the exposure of crop consumers to viruses that remain on the crops at the time of consumption.

Guidelines for Safe Reuse (Australia)

QMRA can be used to estimate health risks from exposure to pathogens via wastewater reuse in agriculture, as illustrated in the above examples. In the National guidelines for water recycling in [6], QMRA is used for a different purpose: to calculate health-based

performance targets for recycled water systems. In these guidelines, the Australians use a health-based target as a benchmark for safety that has to be met by each water reuse system. They use the health-based target that WHO has defined in their GDWQ: 10^{-6} disability adjusted life years per year (DALY, see Box 1 for more information about this disease burden metric) as their tolerable level of risk.

This health-based target is translated to performance targets for the reuse system with respect to microbial hazards. The concentration of pathogens in the source water for the reuse system (raw/treated sewage, gray water, etc.) and the level of exposure of people to the recycled water (via crops, aerosols, ingestion) determine how much reduction of pathogen exposure is required to meet the 10^{-6} DALY/year target.

In formula:

$$PT = \log(C \times E \times N/DALYd)$$

in which

PT is the performance target (required log reduction)
C is the concentration of pathogens in source water (in these guidelines: 95th percentile of concentration data)
E is the exposure (volume (*L*))
N is the average frequency of exposure (number/person/year)
DALYd is the pathogen dose that is equivalent to a DALY of 10^{-6} per year, a translation of the 10^{-6} DALY target to a pathogen dose target, taking into account the pathogen's dose-response relation and the fraction of persons that contract illness when infected.

Since sewage and gray water may contain a wide range of pathogens and it is not feasible to do this QMRA for all, it is more practical to select reference pathogens, pathogens that represent a major group of pathogens. The philosophy is that when risk management is aimed at these reference pathogens, the other pathogens from these groups will also be adequately controlled. For protozoa and helminth eggs, *Cryptosporidium* is selected as reference pathogen because it is reasonably infective and more difficult to control by chlorination and filtration than other protozoa or helminth eggs (DALYd is 1.6×10^{-2}, 95th percentile in sewage: 2,000/L). For bacteria, *Campylobacter* is selected because of its infectivity and high prevalence (DALYd is 3.7×10^{-2}, 95th percentile in sewage: 7,000/L). For viruses, rotavirus is selected because of its high infectivity and the availability of dose-response data. Since no data on rotavirus in sewage were available, but data on adenoviruses occurrence were available, these latter data are used and combined with the rotavirus dose-response data (DALYd is 2.5×10^{-3}, 95th percentile in sewage: 8,000/L).

So with concentration C in source water as known and the DALYd as a constant per reference pathogen, the level and frequency of exposure are needed to determine the performance target for the reuse system.

For a range of intended uses of recycled water the associated level and frequency of exposure was (point) estimated from available scientific and statistic data. For example, for exposure by consumption of commercial food crops irrigated with recycled water the level of exposure was estimated at 5 mL for a service of lettuce and 1 mL for a service of other raw produce, with an annual frequency of 70 and 140 services, respectively. Similar exposure estimates were determined for garden irrigation, municipal irrigation, fire fighting, toilet flushing, washing machine use, and cross-connections.

Now the performance target for the use of recycled wastewater for commercial crop irrigation can be calculated:

Exposure for lettuce is 0.005×70, for other raw produce 0.001×140; this totals to 0.49 L/year

$$\begin{aligned} \mathrm{PT}_{\mathrm{Cryptosporidium}} &= 2,000 \times 0.49/\left(1.6 \times 10^{-2}\right) \\ &= 4.8 \ \log \\ \mathrm{PT}_{\mathrm{Campylobacter}} &= 7,000 \times 0.49/\left(3.7 \times 10^{-2}\right) \\ &= 5.0 \ \log \\ \mathrm{PT}_{\mathrm{Rotavirus}} &= 8,000 \times 0.49/\left(2.5 \times 10^{-3}\right) \\ &= 6.1 \ \log \end{aligned}$$

There are different ways to manage the risk associated with water recycling: prevent pathogens from entering recycled water, remove pathogens from recycled water by treatment processes, and reduce exposure by using restrictions or preventive on-site measures:

restricted access, withholding periods before harvesting, controlled application (drip or subsurface irrigation). The Australian guidelines have assigned default performance credits to a range of treatment processes and on-site preventive measures and give examples of how the combination of these two types of risk management options can be used to achieve safe water recycling.

Box 1. DALY

Disability Adjusted Life Years (DALYs) is as a metric for translating the risk of disease burden a general health burden per case of illness. The DALY accounts for the years lived with a disability (YLD) plus the years of life lost (YLL) due to the hazard (compared to the average expected age of death in a community). One DALY per million people a year roughly equates to one cancer death per 100,000 in a 70-year lifetime [73]. The DALY is calculated as the product of the probability of each illness outcome with a severity factor and the duration (years). Calculation of the DALY contribution per infection is undertaken using:

$$\text{DALY} = \sum_{i=1}^{n} P(\text{ill}|\,\text{inf}) \times P(\text{outcome}_i|\text{ill}) \times \text{Duration}_i \times \text{Severity}_i$$

where n is the total number of outcomes considered

$P(\text{ill}|\text{inf})$ is the probability of illness given infection

$P(\text{outcome}|\text{ill})$ is the probability of outcome i given illness

Duration_i is the duration (years) of outcome i

Severity_i is the severity weighting for outcome i.

The advantage of using DALYs over an infection risk end point is that it not only reflects the effects of acute end points (e.g., diarrheal illness) but also the likelihood and severity of more serious disease outcomes (e.g., Guillain-Barré syndrome associated with *Campylobacter*). Disease burden per case varies widely, but can be focused on a locality. For example, the disease burden per 1,000 cases of rotavirus diarrhea is 480 DALYs in low-income regions, where child mortality frequently occurs. However, it is only 14 DALYs per 1,000 cases in high-income regions, where hospital facilities are accessible to the great majority of the population. Disease burden estimates for different drinking water contaminants is summarized in Table B1.

Microbial Risk Assessment of Pathogens in Water. Table B1 Summary of disease burden estimates for different drinking water contaminants

	Disease burden per 1,000 cases		
	YLD	YLL	DALY
Cryptosporidium parvum	1.34	0.13	1.47
Campylobacter spp	3.2	1.4	4.6
STEC O157	13.8	40.9	54.7
Rotavirus			
High-income countries	2.0	12	14
Low-income countries	2.2	480	482
Hepatitis-A virus			
High-income countries, 15–49 years	5	250	255
Low-income countries	3	74	77

Source: Reproduced from [31].

Future Directions

The examples given in the previous paragraphs illustrate how QMRA can be applied to assess microbial health risks associated with systems where people may be exposed to pathogens through the use of water. QMRA is used to evaluate individual systems (against health-based targets), compare different systems or scenarios and to evaluate the significance of hazardous events and system failures in municipal piped water supply, but also non-piped water supply, and for wastewater and gray water reuse. Others have also demonstrated the use in recreational waters [4].

Risk assessment also allows comparison of the effort and resources put into the provision of safe water systems and resources allocated to manage other health risks. However, given the current state of the art and especially the lack of available quantitative data, QMRA has to rely partly on assumptions. Given the current level of uncertainty in quantitative risk assessments of water systems, the outcome should be regarded as an indication of the level of safety, rather than an absolute assessment of health risk. The outcome can be used to guide the risk management direction to pathogen control and to select the most appropriate control measures.

The benefit of risk assessment is that it gives a better understanding/breakdown of the problems and of important data. Additionally, the risk concept allows us to focus and prioritize research on the areas where important pieces of information are missing.

Improving the Technique of QMRA

The science of risk assessment is increasingly complex; most of the current QMRA work uses the probability of infection as end point. Infection is the first step in the disease process, but does not reflect the severity of the disease, including potential serious health effects that may arise in a particular subpopulation. Some studies have been using burden-of-disease and cost-of-illness measures [45]. This improves the assessment of the magnitude of the adverse effect of pathogens exposure via water and allows balancing pathogen risks with other risks. The dynamics of infectious diseases with secondary transmission and the effect of immunity and sensitive subpopulations have been largely neglected. Several studies are exploring ways to incorporate these disease dynamics into account [14].

The large variability of pathogens in water and the limited availability of data (especially in relation to peak events) and the variability in treatment efficacy are very important issues to take into consideration in QMRA. More data need to be collected, and monitoring programs of water suppliers should be targeted more toward the provision of information for QMRA. Pathogens to be selected for QMRA should be detectable in the water systems with reliable analytical techniques. The use of reference pathogens, pathogens that are critical for the control measures taken in water supply, is recommended. The variability and limited data available will cause uncertainty in the risk assessment, but compared to chemical risk assessment with large uncertainty factors, this is not inhibitive for the implementation of microbial risk assessment.

Improving the Utility of QMRA

QMRA can be done at different levels of sophistication. Sophisticated QMRA can take considerable amounts of time and resources. The level of detail in the QMRA and the extent of the uncertainty analysis that is needed to address a particular problem has to be appropriate only to the extent that is needed to help risk managers decide. QMRA lends itself well for a tiered approach, where the sophistication increases only if the risk manager requires better information to make a decision.

The National Research Council in the USA has advised USEPA to adopt a framework for risk-based decision making to make risk assessments more useful for risk management decisions [55]. In this framework, improved stakeholder involvement should also help to improve the acceptance and utility of risk assessment.

QMRA is a process that requires input from several disciplines. Researchers that are trained in a specific discipline have to learn to combine their data and knowledge with data and knowledge from other disciplines in a (probabilistic) risk assessment framework. And risk assessment is being extended to address broader questions in environment and health: risk-risk trade-offs and cost-benefit analysis. Development of guidance and training on QMRA is needed to strengthen the capacity of QMRA researchers.

Assessing the microbial risks of water systems is a relatively young field of science. It has the capacity to further professionalize safety management in water by providing science-based, objective, credible and proportionate information to help risk managers make informed decisions.

Bibliography

1. Aboytes R, DiGiovanni G, Abrams F, Rheinecker C, McElroy W, Shaw N, LeChevallier MW (2004) Detection of infectious *Cryptosporidium* in filtered drinking water. J Am Water Works Assoc 96(9):88–98
2. Adham SS, Trussel RR, Gagliardo PF, Olivieri AW (1998) Membranes: a barrier to microorganisms. Water Supply 16(1–2): 336–340
3. Asano T, Leong LYC, Rigby MG, Sakaji RH (1992) Evaluation of the California wastewater reclamation criteria using enteric virus monitoring data. Water Sci Technol 26(7–8):1513–1524
4. Ashbolt NJ, Bruno M (2003) Application and refinement of the WHO risk framework for recreational waters in Sydney, Australia. J Water Health 1(3):125–131
5. Atherholt TB, LeChevallier MW, Norton WD, Rosen JS (1998) Effect of rainfall on *Giardia* and *Cryptosporidium*. J Am Water Works Assoc 90:66–80
6. Australia (2005) Australian guidelines for water recycling: managing health and environmental risks (phase 1). Natural Resource Management Ministerial Council, Environment Protection and Heritage Council, Australian Health Ministers' Conference, Australia

7. Bartram J, Fewtrell L, Stenström TA (2001) Harmonised assessment of risk and risk management for water-related infectious disease: an overview. In: Fewtrell L, Bartram J (eds) Water quality: guidelines, standards and health. IWA Publishing, London, pp 1–16
8. Benford D (2001) Principals of risk assessment of food and drinking water related to human health, ILSI Europe concise monograph series. International Life Science Institute, Belgium, pp 1–43
9. Burmaster DE, Anderson PD (1994) Prnciples of good practice for the use of Monte Carlo techniques in human health and ecological risk assessment. Risk Anal 14(4):477–481
10. CODEX (1997) Codex Alimentarius Commission: procedure manual. Joint FAO/WHO Food Standards Programme. FAO, Rome
11. Deere D, Davison A (2004) Health risk assessment of fire fighting from recycled water. Occasional Paper 11. Water Services of Australia, Sydney
12. DuPont HL, Chappell CL, Sterling CR, Okhuysen PC, Rose JB, Jakubowski W (1995) The infectivity of *Cryptosporidium parvum* in healthy volunteers. N Engl J Med 332(13):855–859
13. EFSA (2009) Transparancy in risk assessment – scientific aspects. Scientific opinion. EFSA J 1051:1–22
14. Eisenberg JNS, Soller JA, Scott J, Eisenberg DM, Colford JM (2004) A dynamic model to assess microbial health risks associated with beneficial uses of biosolids. Risk Anal 24(1):221–236
15. EPA (Environmental Protection Agency) (2005) Economic analysis for the final long term 2 enhanced surface water treatment rule. EPA, Office of Water report EPA 815-R-06-001. EPA, Washington
16. Fewtrell L, Bartram J (2001) Water quality: guidelines, standards and health. Risk assessment and management for water related infectious diseases. IWA Publishing, London
17. Finch GR, Black EK, Gyurek L, Belosevic M (1993) Ozone inactivation of *Cryptosporidium parvum* in demand-free phosphate buffer determined by in vitro excystation and animal infectivity. Appl Environ Microbiol 59(12):4203–4210
18. Finch GR, Gyurek LL, Liyanage LRJ, Belosevic M (1997) Effect of various disinfecion methods on the inactivation of *Cryptosporidium*. American Water Works Association Research Foundation, Denver
19. Gale P (1996) Developments in microbiological risk assessment models for drinking water – a short review. J Appl Bacteriol 81:403–410
20. Gale P (2000) Risk assessment model for a waterborne outbreak of cryptosporidiosis. Water Sci Technol 41(7):1–7
21. Gale P (2002) Using risk assessment to identify future research requirements. J Am Water Works Assoc 94(9):30–42
22. Gale P, Stanfield G (2000) *Cryptosporidium* during a simulated outbreak. J Am Water Works Assoc 92(9):105
23. Haas CN (1997) Importance of distributional form in characterizing inputs to Monte Carlo risk assessments. Risk Anal 17(1):107–113
24. Haas CN (2000) Epidemiology, Microbiology, and Risk Assessment of Waterborne Pathogens Including *Cryptosporidium*. J Food Prot 63(6):827–831
25. Haas CN, Crockett CS, Rose JB, Gerba CP, Fazil AM (1996) Assessing the Risk Posed by Oocysts in Drinking Water. J Am Water Works Assoc 88(9):131–136
26. Haas CN, Rose JB, Gerba CP (1999) Quantitative microbial risk assessment. Wiley, New York
27. Haas CN, Eisenberg JNS (2001) Risk assessment. In: Fewtrell L, Bartram J (eds) Water quality: guidelines, standards and health. IWA Publishing, London, pp 161–183
28. Hashimoto A, Hirata T (1999) Occurrence of *Cryptosporidium* oocysts and *Giardia* cysts in Sagami river, Japan. In: Proceedings of the Asian water quallity 1999; 7th reginal IAWQ conference. Taipei, Taiwan, vol 2, pp 956–961
29. Havelaar AH, Teunis PFM, Medema GJ (1996) Risk assessment of waterborne pathogens. Presented at the symposium waterborne pathogens, Bonn, 22–25 May
30. Havelaar AH, den Hollander AEM, Teunis PFM, Evers EG, van Kranen HJ, Versteegh JFM, van Koten JEM, Slob W (2000) Balancing the risks and benefits of drinking water disinfection: disability adjusted-life years on the scale. Environ Health Perspect 108(4):315–321
31. Havelaar AH, Melse JM (2003) Quantifying health risks in the WHO guidelines for drinking water quality. A burden of disease approach. Report 734301022, RIVM, Bilthoven
32. Hipsey MR, Brookes JD, Antenucci JP, Burch MD, Regel R (2004) A three-dimensional model of Cryptosporidium dynamics in lakes and reservoirs: a new model for risk management. Int J River Basin Manag 2(3):181–197
33. Hirata T, Hashimoto A (1998) Experimental assessment of the efficacy of microfiltration and ultrafiltration for *Cryptosporidium* removal. Water Sci Technol 41(7):103–107
34. Howard G, Pedley S, Tibatemwa S (2006) Quantitative microbial risk assessment to estimate health risks attributable to water supply: can the technique be applied in developing countries with limited data? J Water Health 4(1):49–66
35. Hrudey S, Hrudey E (2004) Safe drinking water, Lessons from recent outbreaks in affluent nations. IWA Publishing, London, 486 pp
36. Hunter PR, Syed Q (2001) Community surveys of self-reported diarrhoea can dramatically overestimate the size of outbreaks of waterborne cryptosporidiosis. Water Sci Technol 43(12): 27–30
37. Hutton P, Ashbolt N, Vesey G, Walker J, Ongerth J (1995) Cryptosporidium and Giardia in the aquatic environment of Sydney, Australia. In: Betts WB et al (eds) Protozoan parasites and water. Royal Society of Chemistry, Cambridge
38. Korich DG, Mead JR, Madore MS, Sinclair NA, Sterling CR (1990) Effects of ozone, chlorine dioxide, chlorine, and monochloramine on *Cryptosporidium parvum* oocyst viability. Appl Environ Microbiol 56(5):1423–1428
39. LeChevallier MW, Norton WD, Lee RG (1991) Occurrence of *Giardia* and *Cryptosporidium* spp. in surface water supplies. Appl Environ Microbiol 56:2610–2616
40. LeChevallier MW, Norton WD (1995) *Giardia* and *Cryptosporidium* in raw and finished water. J Am Water Works Assoc 87(9):54–68

41. LeChevalier MW, Norton W, Abbaszadegan M, Atherholt T, Rosen J (1998) Development of a monitoring strategy to determine variations in *Giardia* and *Cryptosporidium* levels in a watershed. In: Proceeding of source water protection international 1998, Dallas
42. van Lieverloo JHML, Blokker EJ, Medema GJ (2007) Quantitative microbial risk assessment of distributed drinking water using faecal indicator incidence and concentrations. J Water Health 5(Suppl 1):131–149
43. Macler BA, Regli S (1993) Use of microbial risk assessment in setting United-States drinking water standards. Int J Food Microbiol 18:245–256
44. MacKenzie WR, Hoxie NJ, Proctor ME, Gradus MS, Blair KA, Peterson DE, Kazmierczak JJ, Addiss DG, Fox KR, Rose JB, David JP (1994) A massive outbreak in Milwaukee of *Cryptosporidium* infection transmitted through the public water supply. N Engl J Med 331(3):161–167
45. Mangen MJJ, Havelaar AH, Bernsen RAJAM, Van Koningsveld R, De Wit GA (2005) The costs of human Campylobacter infections and sequelae in the Netherlands: a DALY and cost-of-illness approach. Food Econ Acta Agric Scand 2(1):35–51
46. Masago Y, Katayama H, Hashimoto A, Hirata T, Ohgaki S (2002) Assessment of risk of infection due to *Cryptosporidium parvum* in drinking water. Water Sci Technol 46(11/12):319–324
47. Medema GJ, Teunis PFM, Gornik V, Havelaar AH, Exner M (1995) Estimation of the *Cryptosporidium* infection risk via drinking water. In: Betts WB et al (eds) Protozoan parasites and water. Royal Society of Chemistry, Cambridge, pp 53–56
48. Medema GJ, Hoogenboezem W, van der Veer AJ, Ketelaars HAM, Hijnen WAM, Nobel PJ (2003) Quantitative risk assessment of Cryptosporidium in surface water treatment. Water Sci Technol 47:241–247
49. Medema GJ, Loret JF, Stenström TA, Ashbolt NJ (2006) Quantitative microbial risk assessment in the water safety plan. Report Microrisk, Kiwa Water Research, Nieuwegein. www.microrisk.com
50. Medema GJ (2009) Risk assessment of *Cryptosporidium* in drinking water. World Health Organization, Geneva, Switzerland
51. Messner MJ, Chappell CL, Okhuysen PC (2001) Risk assessment for *Cryptosporidium*: a hierarchical Bayesian analysis of human dose response data. Water Res 35(16):3934–3940
52. Michaels D (2008) Doubt is their product: how industry's assault on science threathens your health. Oxford University Press, New York
53. Mons MN, van der Wielen JHML, Blokker EJM, Sinclair MI, Hulshof KFAM, Dangendorf F, Hunter PR, Medema GJ (2007) Estimation of the consumption of cold tap water for microbiological risk assessment: an overview of studies and statistical analysis of data. J Water Health 5(Suppl 1):151–170
54. Morgan MG, Henrion M (1990) Uncertainty. A guide to dealing with uncertainty in quantitative risk and policy analysis. Cambridge University Press, New York, 332 p
55. NRC (2009) Science and decisions, Advancing risk assessment. National Research Council. The national Academies Press, Washington, DC
56. Perz JF, Ennever FK, Le Blancq SM (1998) Cryptosporidium in tap water: comparison of predicted risks with observed levels of disease. Am J Epidemiol 147(3):289–301
57. Petterson SR, Ashbolt NJ, Sharma A (2001) Microbial risks from wastewater irrigation of salad crops: a screening-level risk assessment. Water Environ Res 73(6):667–672
58. Petterson SA, Ashbolt NJ (2005) WHO guidelines for the safe use of wastewater and excreta in agriculture. Microbial Risk Assessment Section. www.who.int/wsh
59. Pouillot R, Beaudeau P, Denis J-B, Derouin F (2004) A quantitative risk assessment of waterborne cryptosporidiosis in France using second-order Monte Carlo simulation. Risk Anal 24(1):1–17
60. Regli S, Rose JB, Haas CN, Gerba CP (1991) Modeling the risk from Giardia and viruses in drinking water. J Am Water Works Assoc 83:76–84
61. Regli S, Odom R, Cromwell J, Lustic M, Blank V (1999) Benefits and costs of the IESWTR. J Am Water Works Assoc 91(4): 148–158
62. Rose JB, Lisle JT, Haas CN (1995) Risk assessment methods for *Cryptosporidium* and *Giardia* in contaminated water. In: Betts WB et al (eds) Protozoan parasites and water. Royal Society of Chemistry, Cambridge, pp 238–242
63. Roseberry AM, Burmaster DE (1992) Lognormal distributions for water intake by children and adults. Risk Anal 12:99–104
64. Roser D, Petterson S, Signor R, Ashbolt N, Nilsson P, Thorwaldsdotter R (2006) How to implement QMRA to estimate baseline and hazardous event risks with management end uses in mind. Report Microrisk, Kiwa Water Research, Nieuwegein. www.microrisk.com
65. Smeets P (2008) Stochastic modelling of drinking water treatment in quantitative microbiological risk assessment. PhD thesis, Delft University, The Netherlands
66. Teunis PFM, Medema GJ, Kruidenier L, Havelaar AH (1997) Assessment of the risk of infection by *Cryptosporidium* and *Giardia* in drinking water from a surface water source. Water Res 31(6):1333–1346
67. Teunis PFM, Havelaar AH (1997) *Cryptosporidium* in drinking water. Evaluation of the ILSI/RSI quantitative risk assessment framework. RIVM, Bilthoven, The Netherlands
68. Teunis PFM, Havelaar AH (1999) *Cryptosporidium* in drinking water. Evaluation of the ILSI/RSI quantitative risk assessment framework. Report no. 284 550 006 RIVM, Bilthoven
69. Westrell T (2004) Microbial risk assessment and its implications for risk management in urban water systems. Thesis Linköping University, Linköping
70. Westrell T, Bergstedt O, Stenstrom TA, Ashbolt NJ (2003) A theroretical approach to assess microbial risks due to failures in drinking water systems. Int J Environ Health Res 13:181–197
71. WHO (1993) Guidelines for drinking water quality, 2nd edn. WHO, Geneva
72. WHO (1999) Principles and guidelines for the conduct of microbiological risk assessment. WHO, Geneva, CAC/GL-30
73. WHO (2004) Guidelines for drinking water quality, 3rd edn. WHO, Geneva

74. WHO (2006) Guidelines for the safe use of wastewater, excreta and grey water. WHO, Geneva
75. Yang SS, Benson SK, Du C, Healey MC (2000) Infection of immunosuppressed C57BL/6N adult mice with a single oocyst of *Cryptosporidium parvum*. J Parasitol 86:884–887
76. Yates MV, Gerba CP (1998) Microbial considerations in wastewater reclamation and reuse. In: Asano T (ed) wastewater reclamation and reuse, vol 10, Water Quality Management Library. Technomic Publishing, Lancaster, pp 437–488

Mining and Its Environmental Impacts

Jörg Matschullat, Jens Gutzmer
TU Bergakademie Freiberg, Institute of Mineralogy and Helmholtz Institute Freiberg for Resource Technology, Freiberg, Saxony, Germany

Article Outline

Glossary
Definition of the Subject
Introduction: Sustainable Mining – An Oxymoron?
A Concise Review of Mining History
Environmental Impacts of Mining
Future Directions – Sustainable Mining
Bibliography

Glossary

Biota All life forms.

Decommissioning Removal of something from active status.

Eco-efficiency analysis Analysis of realizing the concept of creating goods and services with fewer resources and less waste and pollution.

Exploitation Act of using something (mineral resources) for any purpose.

Exploration Process of finding mineral resources for the purpose of mining.

Karst A geological feature in relatively soluble rocks, e.g., limestone, where sinkholes, caves, and similar hollows are formed above and below ground.

Lithosphere The outer rocky shell of planet Earth, comprising the oceanic and continental crust and part of the upper Earth mantle.

Long-term effect A change that will last or have an influence over a long period of time.

Nachhaltigkeit German for "sustainability," first used in 1713 in Germany.

Open-pit excavation Process of extracting minerals from surface deposits.

Recultivation Making raw mineral soils (brownfields) fertile again through bioengineering and refertilization.

Rehabilitation Restoring land after some process has damaged it.

Remediation Removal of pollution or contaminants from the environment.

Sinkhole A natural depression at the Earth surface generated by subsurface erosion, particularly in karst areas.

Slag Partially glassy by-product from smelting ore, mostly consisting of a silicate matrix with metal oxides.

Sustainable mining Mining method that does not compromise environmental quality.

Definition of the Subject

The environmental impact of mining is the influence that mining activities have on the natural conditions and world in which humans and all biota live. The impact may involve diverse forms of environmental change or damage, from short- to long-term effects and from highly spatially restricted to long-distance consequences.

Just as any kind of human activity, mining has an inherent and partly unavoidable impact on the environment. From the first steps of exploration via exploitation and (ore) processing to the final stages of decommissioning and rehabilitation, environmental hazards and risks may be encountered and need to be addressed. The potential impacts and long-term aftermath of mining operations are manifold. Whether in fact and to which extent the impacts do lead to detrimental consequences in any one of the environmental compartments (atmosphere, hydrosphere, pedosphere, biosphere, cryosphere, and lithosphere) is difficult to predict. A thorough investigation of local conditions – both boundary conditions and operation-related conditions – is needed to answer that crucial question. Modern mines can be operated in a manner much less detrimental than was the standard up until only recently. Parallel to the mining industry's awareness of issues connected with

the environment, however, new challenges appear: The exploitation of lower concentrations of the valuable constituents (e.g., minerals or metals) presents most demanding challenges that deal with difficult conditions and involve a larger footprint of mining and more complex approaches to beneficiation. Increasing challenges also apply to marine mining, be it nearshore or offshore; be it for diamonds and other placer deposits, oil, and gas; or be it for manganese nodules that are being procured in increasingly deeper marine environments [1].

Developing and implementing sustainable mining practices are tasks that have been high on the agenda of the international mining industry. These need to become the global standard to curtail the most long-lasting and detrimental impacts of mining. Although the necessary knowledge base is rapidly becoming available; there is still a need for basic research to further establish and foster sustainable solutions. Due to its exotic nature and less likelihood to disturb Earth's immediate biosphere and equilibrium, "extraterrestrial mining" is not dealt with here.

Introduction: Sustainable Mining – An Oxymoron?

Environmental impacts of mining appear to be most well known all over the world – almost beyond the necessity of further elucidation and questioning ([2, 3]; Table 1). The mining industry has recognized its impact on the environment and has identified the control and restriction of such impact as one of its key challenges [4, 47])

From a workable standpoint, mining encompasses a very large array of activities. Especially in highly industrialized nations, there is major resistance of societies against mining activities. For the building and construction industry, even aggregate materials from quarries, and sand and gravel from open-pit excavations are increasingly under scrutiny in densely populated areas. Generally, much larger open-pit or underground mines for rock salt, metalliferous ores, or precious stones are often no longer perceived as indicators of economic well-being and development, but rather symptomatic of visual, acoustic, and environmental perturbations with detrimental impact. The same is certainly true for energy resources, namely gas, oil, coal, tar sands, and uranium ores, whether or not these are being mined on land or in marine shelf areas. Not only the general public, but a considerable part of the decision makers in both industry and politics (at least in the western world) has developed a stance that mining is per se a dirty business and that its related activities can be left to (mostly) developing countries.

In the late twentieth century, the idea that "industry and the developed nations would always be able to buy the necessary commodities" prevailed. Since the advent of the twenty-first century, this position has been increasingly under scrutiny, simply because the growing world population demands increasing amounts of raw materials. To find acceptance and support in society, any future mining activity will demand a state-of-the-art environmental management and has to contribute to sustainable development [5]. Furthermore, the role of the mining industry is set to increase, as technological advancement demands rapidly increasing supplies of a rising number of raw materials that have never before found a significant industrial application, e.g., rare earth elements (REE) or lithium (Li).

To clarify current environmental issues connected to mining and to be able to develop alternatives to practices that are currently widely used, an understanding of the history of mining is needed, as well as an overview of the environmental effects of mining, differentiated by its relevant phases: exploration, exploitation and processing, decommissioning, and rehabilitation. Thereby, potentially negative impacts may be largely avoided or significantly abated if intelligent and foresighted precaution is taken. At the end of this contribution, future perspectives and the pathway to sustainable mining shall be evaluated.

A Concise Review of Mining History

Mining has been with mankind for much more than 40,000 years already (Paleolithic), when commodities were procured from surface and even underground deposits from various places on several continents, in order to obtain flint stones for axes and arrowheads, clay and loam for pottery and construction (e.g., [6]), or iron oxide (hematite) for cosmetic purposes [7, 8]. The interest in metals developed later, as the related human activities in metal working became so widespread that entire epochs were named accordingly (Bronze Age, Iron Age, etc.) [9, 10]. With the advent

Mining and Its Environmental Impacts. Table 1 Potential (and real) environmental impact of mining on environmental compartments

Compartment	Potential environmental impact and spatial extent
Atmosphere	Release of (toxic) gases (e.g., SO_2 emissions from sulfide ore roasting, CO_2 and CFC release from aluminum processing), dusts, and aerosols: very-short- (local) to long-range transport may contaminate vegetation cover and other biota, soil, and water. Often, the burning of fossil fuels (e.g., from energy generation) has more detrimental effects than the mining operation itself
	Alteration of local air humidity: effects on local microclimate and thus biota
Hydrosphere	*Surface water*: water level fluctuations, water losses, floods, direct contamination; accidental connection of surface water and soluble ore deposits with local to small regional effects
	Groundwater: direct contamination via seepage water from aboveground or directly from within the mine operation; lowering (due to new permeabilities) or rising of water table (due to ground softening and compression), vertical fluctuations of the water table, causing local underground erosion and loss of rock stability, hydraulic filling of underground cavities and aquifers after stopping the water pumping at mine closure – affects the aquifer extension
	Drainage and seepage water: saline water, acid water, and alkaline water, each with specific toxins – affects surface and groundwaters
	Coastal and marine waters: direct pollution by spills; placer deposit mining disrupts beach systems; use of deep-sea deposits threatens (rare) marine life; mostly local effects
Pedosphere	Soil loss (open-pit and underground operations) – competition for land use; large volumes of waste-rock heaps and tailings deposits; soil contamination (and water) by water spills and seepage of contaminated waters from slag and waste heaps, tailings deposits, improper operation, etc. – local effects
Biosphere	Disturbance of ecosystems, disruption of food chains, eviction of (key) species; silicosis and in general, inhalation of fibers (asbestos mining) as a health hazard to workers and high ambient dust concentrations in the vicinity of operations – local to small regional effects
Lithosphere	Mine structure (surface: collapse, subsidence; underground: pillar breaking, slab breaking), aquifer mine operation: surface overloading, surface vibrations and shaking (blasting), mine sludge, mine tailings, slag heaps – local effects
Anthroposphere	Damage to infrastructure (transport, buildings, etc.) due to surface movements and subsidence – local effects

of even more sophisticated technologies in the Chinese and Roman Empires, the spectrum of sought-after elements had expanded and included components such as silver (Ag), arsenic (As), gold (Au), copper (Cu), iron (Fe), mercury (Hg), lead (Pb), and tin (Sn) minerals [11–13]. There is no doubt that mining has been pursued by man millennia before the Industrial Revolution and on all continents (except for Antarctica), and independent of the global European influences that started with their conquest in the fifteenth century [14]. Following the Industrial Revolution in the late eighteenth to mid-nineteenth centuries, this range of elements not only increased, but new orders of magnitude were reached in the demand for metals and other commodities, including fast-increasing amounts of nonrenewable energy resources (coal, oil, and gas – in that sequence). Today, the timing of Peak Oil is discussed in parallel and just as intensively as the possible shortage of REE and other metals that our modern industrial society technologically and economically depend upon. At the same time, possible causes for the collapse of historical civilizations are examined, and there is evidence that mining may have contributed to such human self-destruction in the past [15].

It was largely not before post-WWII economic recovery that people in the involved industrial countries started to look at the environmental impact of these mining activities. Using European history, the cradle of

the Industrial Revolution, as an example, voices from almost two millennia back deserve mentioning.

Central Europe was mainly forest-covered until the advent of the Early Middle Ages. Mining had remained a rather small-scale business, even though during Roman times (ca. 300 AD), comparatively sophisticated mining and smelting technology is already known from various places (e.g., Harz Mountains, Germany [11]). The push towards the eastern frontier by Gallic and Germanic people under the guidance of Charlemagne (around AD 800) led to new settlements, a subsequent period of significant forest removal and a new period of mining exploration and exploitation. Cities like Annaberg and Freiberg, Erzgebirge in Saxony, Germany; Kutna Hora in Bohemia (Czech Republic); and many others may serve as examples. There, silver (Ag) was found, a key resource for coin making and luxury items – much like today. These successful mining cities developed, and production increased. Around the 1500s, most of the higher-elevation forests had been cut down already, leaving vast stretches of almost tree-barren landscape – much of which was used for agriculture.

In 1557, Georgius Agricola (Latinized version of his name Georg Bauer), a German medical doctor and early allround scientist from Chemnitz in Saxony, published the first and most comprehensive book (12 volumes) on mining and its implications, "De re metallica" (about the metal issues) [46]. His book did not only describe mineral exploration techniques (even touching the use of metallophilic plants), exploitation, and smelting techniques, but also explicitly introduced the reader to the detrimental side effects of mining. He reviewed the "bad smokes" and their effects on biota; he described the barren land where no plants would want to grow and the "dead waters" where fish would no longer live or spawn [16]. Indeed, one has to imagine such metalliferous provinces in Europe as being mainly forest-free areas after a few centuries of steadily increasing mining and smelting activities. The wood was needed and used both to fuel processes and to build support structures and equipment (water wheels, water ducts, etc.) in the mines.

As of the eighteenth century, such evidence on the effects of mining became even more prominent, and more publications related to these issues emerged. In 1713, the first book on sustainability was published to introduce the concept and coin the term "sustainability" (in German *Nachhaltigkeit*) [17, 18]). Hannß Carl von Carlowitz, a Freiberg mining engineer, was also responsible for the wood supply for the local mines and noticed the increasing depletion of this valuable natural resource. Von Carlowitz wrote that a sustainable forest management was then urgently necessary to avoid (and repair) the damage resulting from mining and smelting activities if this business was to continue. As a matter of fact, those days saw a significant decline in mine productivity for various reasons: an increasing lack of wood, a steadily increasing demand for more sophisticated technologies, and permanent wars between the small states and provinces in Central Europe. Until those days, mining and smelting were done as many centuries before, with minor technological advances. This now changed rather rapidly, with first the introduction of stipends for gifted young men (non-aristocrats) to receive a higher education in mining and in 1764 with the foundation of the world's first mining academy (then named *Bergakademie*), today known as the Technical University (TU) Bergakademie Freiberg.

Soon, new technologies were introduced that increased the efficiency of mines by reducing the water and wood (fuel) demand per volume of ore. At the same time, forestry was developed as a scientific field, and in 1811–1816, the world's first forest academy was founded in Tharandt, Saxony. Ever since, it serves to educate future foresters and forest scientists and is today part of the Technical University Dresden. Today, the Erzgebirge is largely forested again (i.e., similar to the Harz Mountains and the Black Forest in Germany, and many other historical mining areas) with a forest cover of about 30%.

Environmental Impacts of Mining

Throughout many historical mining districts, the less noticeable centuries-old legacy of mining is still perceptible to the trained eye. It yields many helpful lessons on avoiding further environmental damage and developing sustainable mining techniques.

In general, the environmental impact of mining takes place on many levels and may affect most environmental compartments – atmosphere, hydrosphere, pedosphere, biosphere, and lithosphere, and under

certain aspects even the cryosphere. Some of the key "priority pollutants" are metals that are being liberated through mining and related activities (Table 2).

Mining requires exploration to identify the exploitation potential of a mineral deposit. Related investigations may include not only geophysical (electric, electromagnetic, gravity, and seismic investigations) and geochemical work at the surface (digging of pits, trenches, or rock cuts) but also drilling activities to verify obtained results. This enables and supports 3D modeling of the ore body, a basis for reducing technical and financial risks. Following a successful exploration phase, and depending on the decision for aboveground (open-pit) or underground mining, the required mining infrastructure will be developed and ensued by rather large surface excavation or the construction of shafts and tunnels. In most cases, extensive aboveground facilities are built concurrently, which encompass infrastructure for processing, workshops, storage, and a general infrastructure of offices, remote control rooms, transport access from helicopter ports and airfields, road and train access to the electrical and water

Mining and Its Environmental Impacts. Table 2 Priority pollutants: metals from natural and mining-related sources[a]

Element	Natural source	Anthropogenic source	Common forms in waste
Ag	Native metal (Ag), chlorargyrite (AgCl), acanthite (Ag_2S); Cu, Pb, Zn ores	Mining	Metallic Ag, Ag–CN complexes, Ag halides, Ag thiosulfates
As	Metal arsenides and arsenates, complex sulfide ores (arsenopyrite, FeAsS), arsenolite (As_2O_3), volcanic gases, geothermal springs	Pyrometallurgical industry, soil heaps and tailings, smelting, mine drainage	As oxides (oxyanions), organo-metallic forms, methylarsinic acid ($H_2AsO_3CH_3$), dimethylarsinic acid ($(CH_3)_2AsO_2H$)
Cd	Zn sulfide ores	Mining and smelting, mine drainage	Cd^{2+} ion, Cd halides and oxides, Cd–CN complexes, $Cd(OH)_2$ sludges
Cr	Chromite ($FeCr_2O_4$)	Pyrometallurgical industry	Metallic Cr, Cr oxides (oxyanions), Cr^{3+} complexes with organic and inorganic ligands
Cu	Native metal (Cu), chalcocite (Cu_2S), chalcopyrite ($CuFeS_2$), bornite (Cu_5FeS_4)	Mining and smelting, pyrometallurgical industry, mine drainage	Metallic Cu, Cu oxides, Cu–humic complexes, alloys, Cu ions
Hg	Native metal (Hg), cinnabar (HgS), degassing from Earth's crust and oceans	Mining and smelting, mine drainage	Organo–Hg complexes, Hg halides and oxides, Hg^{2+}, $(Hg_2)^{2+}$, Hg^0
Ni	Pentlandite ($(Fe,Ni)_9S_8$), Ni hydroxy-silicate minerals	Mining and smelting	Metallic Ni, Ni^{2+} ions, Ni amines, alloys
Pb	Galena (PbS)	Mining and smelting, mine drainage	Metallic Pb, Pb oxides and carbonates, Pb-metal–oxyanion complexes
Sb	Stibnite (Sb_2S_3), geothermal springs	Pyrometallurgical industry, smelting, mine drainage	Sb^{3+} ions, Sb oxides and halides
Se	Polymetallic base metal sulfide ores	Smelting	Se oxides (oxyanions), Se–organic complexes
Tl	Polymetallic base metal sulfide ores	Pyrometallurgical industry	Tl halides, Tl–CN complexes
Zn	Sphalerite (ZnS)	Mining and smelting, pyrometallurgical industry, mine drainage	Metallic Zn, Zn^{2+} ions, Zn oxides and carbonates, alloys

[a]Table modified and focused on mining-related activities after Adriano [49] and Sparks [10]

supply, ore dressing and smelting facilities, and room for waste rocks and tailings deposits. Any one of these units must be seen as an integral part of the mining activity, each with a potential environmental imprint.

Exploration Phase

In the exploration phase, already and depending on the previous land use, land has to be cleared and roads and (minor) infrastructure constructed. Climatological and local conditions define the intensity and duration of exploration activities and thus play a role in the environmental impact. Largely, exhaust fumes and dust emissions may influence air quality during this operation [19]. In general, such works and the related noise emissions have a highly restricted local impact that will stop or rapidly decrease with the end of the exploration activities. Water resources can be impacted during exploration activities by improper handling of equipment and insufficient control of exploration drilling (spillage of drilling additives, oil losses, etc.). Primarily, temporary losses in aquatic biodiversity result; hence, the shorter the operation, the easier is the recovery. Yet, related impacts may remain evident for years and even decades. Soils have a much longer "memory" for human activities. The construction of drilling platforms (pressure and surface sealing) and the drill waste materials (including potentially toxic matter) may leave imprints for many decades or even centuries (arctic environments = potential impact on the cryosphere), albeit again, on a very local scale. Biospheric impact may be of critical importance since it is directly related to all other environmental compartments. Here, environmental impact assessment studies may be helpful prior to starting with the mining phase. Such assessments do not necessarily impede the progress of the exploration project and principally depend on the available ecosystem or site-specific knowledge of biologists or ecologists. These evaluations are in most cases restricted in time, and recovery is possible, provided that state-of-the-art operations and precaution are applied. The crucial and well-known risks related to immediate accidents (fatalities and injuries) and health problems during the mining process itself are not dealt with here. Impact on the lithosphere is restricted to excavations and boreholes themselves and may pose challenges mainly in unstable surface and in karst environments, e.g., triggering unwanted water pathways or rock-mechanical instabilities. In general, and particularly at locations with unsuccessful exploration activities, related legacies of failed prospecting and exploration may impact future land use much later due to non-documented activities in the mining phase that may compromise the free choice of subsequent land use.

While most environmental impacts are small-scale and short-term in the exploration phase, incognizant or careless practices can lead to serious consequences. Therefore, before start-up (and beyond closure) of each mining operation, responsible exploration activities should include a priori environmental assessment studies [20]. Related important work that involves the post-mining operations, such as reclamation and rehabilitation, is an essential source of information and a major support for all subsequent activities, including these post-mining operations. In many cases, it can be responsibly performed by trained personnel of the mining company, ideally jointly with local or regional NGOs and professionals from state agencies who will also accompany the subsequent phases.

Mining or Exploitation Phase

In principle, similar impacts as described above may occur with the establishment of a full mining operation, although these are a lot more extensive and persistent. In addition, a mining phase could result in a suite of considerably more hazardous and long-lasting impacts. For most environmental compartments, the impact duration is at least as important as the strength of the impact. Mines usually have an operating lifetime of at least 10 years to many decades, a period of direct impact. Such a lengthy span of impact has the potential to leave legacies for centuries or even millennia (see A Concise Review of Mining History).

Atmosphere. Both open-pit and underground mines generate exhausts and considerable amounts of dust, even when properly operated [19]. Dust is generated during aboveground and underground mining, drilling, blasting, and all processes involving transferring, dumping, discharging, crushing, hauling, and processing materials. Depending on local heat, humidity, and wind conditions (local climatology), the impact on the

atmosphere may be comparatively large, covering substantial areas with mainly mineral dust and furnace residues (power plants) or even with fine metal aerosols (from smelter operations). Independent of their possible direct toxicity, the settling dusts and aerosols cover plants and soil surfaces, impeding plant respiration and altering the local soil chemistry. Although dusts, aerosols, and other exhausts may travel airborne for up to several thousands of kilometers away from the source, these usually remain within a limited "halo" around the operations. Apart from these, toxic gases may also be released, e.g., sulfur dioxide from mineral sulfides, a major precursor for long-range transport species of key aerosol components (e.g., ammonium sulfate). Very large operations are known to contribute to a great extent to hemispheric pollution, e.g., the Sudbury smelter in Ontario, Canada [21]; the Freiberg smelters in Saxony, Germany [22]; and the Nikel/Zapoljarnyi and Monchegorsk operations on Kola peninsula, Russia [48]. Apart from direct metal emissions, their SO_2 emissions contributed substantially to the atmospheric formation of acidic precipitation and are largely responsible for the related major air pollution with subsequent soil and water pollution in the last decades of the twentieth century [23]. Even the carbon dioxide balance of the operation comes under close scrutiny, since many countries use carbon-trading schemes in order to benefit from implementing smart technology and to penalize big energy wasters. By their very nature, mining activities and equipment can emit high levels of noise and vibration. This usually appears to adversely affect people, including workers, more than most animal species, while no known related impact has been determined on plants.

Hydrosphere. Most mining operations demand comparatively large amounts of energy and water. For some high-volume, high-mass operations, such as coal mining, entire power plants are needed to meet the energy demand of the operations. In addition to cooling water, a water resource is needed in very many parts of the operational stages. The cooling water and its evaporation in cooling ponds or towers may influence the local microclimatology, which involves largely uncritical humidity increases. Open-pit mines may use very large amounts of water for the mining process itself (e.g., high-power water jets, air stripping, machine cooling), and to safeguard infrastructure (e.g., "constant" water spraying to suppress dust generated on haul roads and stockpiles), and particularly for the ore dressing and smelting process (milling, classification and transport as slurries, flotation processes). Additional high water consumption derives from leaching and bioleaching operations. For this reason, water demand itself can pose a major challenge, particularly in dry or semidry environments. The required lowering of groundwater levels around the mining operation (to keep the mine dry, safe, and operable) is another direct imminent impact within the area that is being dewatered throughout the era of active mining. Competition for this water supply with resident people and with terrestrial and aquatic ecosystems can be a contentious issue. In consequence, the water balance at mining sites is altered, and a persistent lowering of water tables or even diminishment of aquifers is often encountered. The described applications lead not only to water losses but potentially to hazardous water contamination. The input of polluted wastewater may directly impact biota – and indirectly, the human body. Acidic mine waters are another big issue, again mostly restricted in their spatial impact – and potentially easy to control. For decades following the 1970s, considerable attention on and inquiry into acid mine drainage (AMD) was triggered by lasting operational and environmental concerns, making it a hot topic [24, 25]. As a consequence of this acidic outflow of water, surface waters (rivers and lakes) and groundwaters may be seriously affected. Sediment pollution needs to be considered [9, 26, 27] since ample examples exist of non-retained mining materials traveling (and contaminating) hundreds of kilometers downstream (e.g., Ok Tedi mine, Papua New Guinea) [28] or of dam failures and subsequent accidents (e.g., Tysa river, Hungary) [29]. Access to clean drinking water remains a challenge in many parts of the world. This issue will remain with us for a long time to come, with a growing world human population exceeding the seven billion humans mark in 2011, and nine billion around the year 2050. While many waterborne pollutants may have a rather limited lifetime (e.g., cyanide from gold mining), persistent organic pollutants (POPs) from drilling operations, ore dressing, and energy conversion and potentially toxic metal species that may reside in aquatic systems for very long periods of time (decades to centuries) pose a lasting challenge.

Such pollutants require particular attention and necessitate safeguarding against any kind of spill, leakage, and loss [30].

Pedosphere. While all mining operations require an initial removal of the natural unconsolidated land surface material (overburden), this is particularly true for open-pit operations. It is common practice to remove and store the nutrient-rich and potentially fertile topsoil separately. The deeper mineral soil material also is removed to free the deposit for active mining and stored separately. This avoids disposal of this subsoil overburden (depending on the operation), which may consist of millions of tons of rock material (usually soft and permeable). In underground mining, the equivalent to this requiring storage is the waste rock from the mining operation. Ore dressing and smelting operations produce partly extensive amounts of tailings, slags, and similar materials that need to be disposed of. Valley filling still appears to be the most sought-after option. As a result and independent of surface or underground mining, comparatively large areas that far exceed the immediate area of the mining facility may become part of the mining operation and of its environmental footprint. Valleys filled or soils covered with such "waste" materials can no longer provide their useful ecological services. Their former habitat function has ended too. While the new morphology and material will attract new life and new ecological equilibria may form (over extended periods of time), the previous ecosystem is no longer functional, and thus, profoundly and permanently impacted. If in addition, the deposited materials contain toxic components, both from the mined raw materials and from chemicals added during the beneficiation processes, these may again further enhance longer-term environmental degradation. Gold-mining legacies with related arsenic toxicity serve as an example [31]. "White mining," the mining of rock salt, further illustrates the challenges: large amounts of impure salt rock debris are being deposited on spoil tips that will persist for centuries. If not covered and not equipped with drain controls (effluent treatment), the easily dissolvable material will deliver excessive amounts of salt into adjacent soils, groundwater, and surface waters. The detrimental effects of excessive amounts of simple mineral salts on plants and many other biota are well known.

Biosphere. With the discussion on ecosystem functions in both the hydrosphere and the pedosphere, it is obvious that the biosphere is strongly impacted too. The first – and often key issue – is habitat loss. This is most certainly the most crucial and critical element of potentially very long-lasting detrimental consequences of mining operations. Although life can re-establish itself even in the most hostile and apparently devastated environments, previous ecosystems may never re-establish. Such consequences could be tolerated if it did not happen at very many places worldwide and if refuge areas did not become increasingly scarcer. Options to protect the biosphere from detrimental impacts are available but often disregarded or considered excessively expensive or demanding. In detail, again a very large array of developments and consequences emerges, depending on biome and local ecosystems. Even if individual species are being extinguished at a specific location, this loss may lead to a domino effect on the web of organisms on all levels – from microbial life via all levels of plants and insects to molluscs, amphibians, fish, reptiles, birds, and mammals. Nutrient supply may become limited due to the mostly fresh rock and overburden materials; the absence of fine materials may further inhibit the growth of higher plants (resettlement). Without further management options, recovery of such sites may take centuries.

Cryosphere. Permanent ice cover and permafrost environments yield potentially attractive mineral resources. These do not only occur at very high latitudes on both hemispheres but also at higher alpine elevations (e.g., Bolivia, Peru). With ongoing global warming, so far mostly inaccessible areas mostly in North America, Siberia, and Greenland as well as in Argentina and Chile become potentially available and feasible for exploration and exploitation. Such environments are extremely sensitive to impacts and will remain sensitive. Their slow biogeochemical cycles retain negative imprints for very long periods of time, and recovery is accordingly extremely slow. Although ice or frozen ground may be compromised, mining will impact exceedingly on the water cycle, the soils (generally very shallow), and the low biodiversity (this low abundance characterizes the rather extreme vulnerability of such environments).

Lithosphere. Even the lithosphere itself can experience a lasting impact, detrimental to future use. Mining subsidence, sinkholes, and drying-up of aquifers are among the most prevalent potential environmental impacts of mining. It is well known that sinkholes may form at the surface over former underground mining operations and that mining subsidence can affect areas of hundreds of square kilometers in size. A notable example (also for a major impact on regional aquifers) is the very densely populated Ruhr area (Ruhrgebiet) in western Germany, where deep coal mining leaves its legacy [32].

Decommissioning and Recultivation Phase

In most modern mines, recultivation commences long before production ceases and the mine is abandoned. An intelligent long-term advance planning may even turn environmental legislation demands into profits. Planning recultivation and handling of environmental issues are key prior to any action. Impressive positive examples can be taken from lignite open-pit mines in the Lusatian basin in Germany (e.g., [33, 34]) and various other places. However, there are still regions where recultivation starts only after decommissioning – if it starts at all. Ever so often, mining companies claim bankruptcy at the end of the operation to save the necessary costs related to recultivation. As leading mining companies, joined in the Global Mining Initiative (GMI; [35]), actively demonstrate their responsibility, a certain fraction of the global mining enterprises still follows a different route – and contributes to the above-mentioned notion of mining being a dirty business. In most countries with a well-developed mining sector, mining companies are forced to put aside funds (usually into trust funds managed by government regulators) that will suffice for recultivation and clean-up of facilities during decommissioning, so that future land use is not compromised. Once the active mining has stopped, all facilities and infrastructures need to be dismantled, removed, and, wherever possible, recycled. Theoretically, the landscape should be returned to its original state prior to the mining-related activities. Water, soils, and biota should be able to recover rapidly. In this phase, however, disturbances are unavoidable, albeit moderate as compared with the active mining phase. The slightly suboptimal reality should be countered by a discussion of some important aspects, namely on the dimensions of scale. An unusual and generally very positive example can be taken from the German superfund site of the Wismut operations, which was a "secret" Russian uranium mining and processing operation in former East Germany. This was one of the world's largest mine closures and remediation projects, "*including five underground mines, and more than 3,700 ha of contaminated areas with ca. 500 million m^3 of solid, radioactively contaminated material*" [36].

Mining enterprises and related activities range from spatially highly restricted small-scale (or artisanal) mining, usually run by local people and often without appropriate training, to very large projects, mostly run by national and international companies with access to highly sophisticated equipment and technology. Such variety cannot be discussed on the same level. Sometimes, small-scale mining may be considerably less environmentally friendly by unit, but if the enterprise remains highly localized, this size restriction at the same time reduces the ecological footprint. At the other end of the scale, a very large operation that manages the site with state-of-the-art techniques may still be making an unsustainably large footprint, simply because of its sheer size. For this reason, it also appears obvious that the boundary conditions of any mine's location play a crucial role in realistically assessing the true impacts of the operation.

The Bottom Line

Mining per se must not be a devastating enterprise as it is ever so often perceived – and undoubtedly often with reason. Only if a comprehensive and open-minded environmental impact assessment is professionally performed from the very beginning and if related recommendations are followed, then the mining operation and its surrounding related activities could be regarded as a rather sustainable enterprise. A skeptic will immediately point out the related assessment costs that may well suppress any entrepreneurial activity and increase financial risks beyond feasibility. That would be a valid argument only if certain boundary conditions are not seen and met.

First and foremost, it has to be acknowledged that the twenty-first century marks the very first human generation that is capable of "seeing the global consequences" of its own activities. Prior to the development

and employment of remote-sensing technologies, this awareness was outright impossible. Still, most people only perceive their immediate habitat and often make far-reaching decisions based on that limited worldview. In 2011, the world human population is the largest ever and is predicted to reach nine billion by 2050. This population increase is but one of the many global change challenges: climate change, soil and biodiversity loss, water scarcity, etc., mark a few other hotspots.

Without mining, however, the growing human population would neither be able to improve its standard of living nor maintain its well-being due to the shortage of primary raw materials essential for developing technology and building houses and infrastructure of any kind. One has only to consider the technological demands of modern medicine. The need for new materials emerges only with scientific and technological advancement. Mining will remain a necessity, since even the very best recycling rates cannot provide the amounts needed of various commodities. To avoid or at least drastically curb the damaging side effects of mining and related activities, a different approach deems necessary and paramount – the approach of sustainable mining.

Future Directions – Sustainable Mining

What Is Sustainable Mining?

The strictly regulated mining industry worldwide may strive for but can never attain a completely sustainable mining scenario. Still, when looking at related publications from the mining industry and authorities (e.g., [20, 37–40]), the notion of sustainable mining has taken a stronghold and increasingly focuses on the social and environmental issues. Sustainability has been clearly defined as having the social, the economic, and the environmental perspective in view [41]. Yet, there is a need for a strong practical bias towards environmental issues when thinking about sustainable mining. Without a "healthy" environment, there would be a rather grim future for both social and economic issues. Rajaram et al. [42] provide a helpful discussion in this respect while shying away from a distinct definition.

Simply spoken, sustainable mining is the kind of mining activity that does not compromise the future long-term well-being of people on or near sites of earlier mining. There may be a discussion on what constitutes "well-being." Hence, a pragmatic, less philosophical approach is suggested by defining "well-being" as the state of a human being where basic social and health needs are met. Since these demand a healthy environment, this three-part perspective is essential to sustainability. How difficult this may be in detail, however, has been addressed by Marker et al. [43] with various multi-scale examples, particularly from the developing world. They argue for a concept of an "*ideal sustainability model as one that minimizes negative environmental impact and maximizes benefits to society, the economy and regional/national development.*" They also acknowledge the long-term character of such an approach, if taken seriously and if broad acceptance is to be achieved.

As a result, the near future will most likely see both conventional mining and also emerging new methods and technologies. These may include phyto-mining and the use of microbial assemblies to access and bring forth desired commodities without large rock and material movement. It will include in situ leaching and in situ processing of ores and will avoid the buildup of waste-rock piles and tailings deposits. It will also see a changing approach from the focus on a single or limited commodity to a broader and more long-term view that avoids producing "wastes" and rather safeguards and leaves future options open. At the same time, however, more surface operations that exploit increasingly lower concentrations of the commodities – with all potential risks involved – are seen. Both underground and surface (open-pit) mining can be done without compromising the environment for future generations. To understand such a claim, an even more complex vision needs to be developed.

The Complete Budget

The term "waste" is purposely accentuated here in quotation marks in order that those unneeded materials not be regarded as waste in the literal sense but rather as a potential future resource. It may be equally necessary not only to look at the entire mining business as an enterprise that will deliver commodities but also to address the issue in a much broader context.

Just like a water reservoir can be seen as a constructed body for the provision of drinking water or water for industrial purposes alone, it can also be seen as a multifunctional construct that

potentially provides hydro energy, flood protection, fish-farming, recreation, and more opportunities and services. Obviously, these additional services may deliver a significant benefit to society. Can mining be seen and interpreted in a similar fashion? It can, although such a perspective demands a rather radical redefinition of the role of mining.

The paradigm change needed demands a complex and holistic long-term view, where a mining company plays a role as a service provider for society at large and not just as an independent private business. As a consequence, a much closer and partnership-based relation would be developed between all stakeholders: the company, the government (local, regional, or national), and the regional populace. A strategy developed by the chemical industry that serves as an example (however, which would need to be adapted to the mining sector) is the concept of eco-efficiency analysis [44, 45]. Adapted for use by the mining industry, a company would benefit from delivering additional services up to the decommissioning and possibly the rehabilitation phases. It would earn its money not only through selling a commodity to the global market but also through the complex added values, hence improving the socioeconomic situation in the region (which is often done already). It might develop post-enterprise industrial activities to ensure the subsequent benefit for the region, and could plan and establish the rehabilitation activities, based not on the minimum but the maximum possible requirements. This includes looking at mining wastes as a potential future commodity that needs to be safeguarded for easy, energy-efficient, and safe retrieval at a later time. All of these added activities generate additional costs, although if done properly, these may save a lot of future costs that are paid by the tax payer and easily excel the monetary benefit of the mining operation itself. One visionary example further illustrates this point where a back-end approach is taken. It is the complex knowledge of an ore body or reserve and its setting that drives the planning for exploiting the mine. The planning is not driven by momentary market prices (that contradict maximum resource efficiency) but by the objective and longer-term necessities and requirements for an efficient, safe, and complete utilization of all commodities in that deposit. "Waste" could be used as construction and building materials, and all toxic components could be extracted as by-products, recycled, or stored in a safe manner to serve future generations as a secondary resource.

Thus, the aim is to establish a long-term partnership and win-win situation for the benefit of all – the company, the employers and residents, and the environment – and to further the development of the region. It basically turns from a single business economy approach to a long-term perspective of political economics. With the most likely future political developments (long-term perspective) in mind, this will translate to international political economy rather than national economy.

The downside, at least as it may be perceived by a company, clearly means a much longer planning phase, the demand for early and truly open communication with all stakeholders (including risk communication), and the necessity of a much more transparent operation throughout as compared to the prevalent current standards. There are quite a few "walls to surmount" and even more prejudice and traditional concepts to overcome. Particularly, the mining industry is still largely characterized by a rather conservative approach.

The benefits are obvious: mining companies and related enterprises can no longer be perceived as obscure omnipotent malevolent entities, interested in basically nothing but the provision of industry with commodities, but as badly needed and responsible partners. Sustainable mining operations will be involved not only in the necessary acquisition and refinement of raw materials but also in the recuperation and delivery of the exploited area to future generations without compromising that future.

Such a vision is nothing short of revolutionary. Yet, it may need truly revolutionary attempts to successfully face the global challenges and to support a still growing human population – without waging wars and without turning a blind eye to extreme socioeconomic disparity.

Bibliography

Primary Literature

1. Schneider J (1998) Environmental impact of marine mining. N Jahrb Geol Paläont Abh 208:397–412
2. Chamley H (2003) Geosciences, environment and man. In: Chamley H (ed) Developments in earth and environmental sciences, 1. Elsevier, Amsterdam, 527 p

3. Ellis D (1989) Environments at risk. Case histories of impact assessment. Springer, Berlin/New York, 329 p
4. IRMA (2011) Documents. The initiative for responsible mining assurance. http://www.responsiblemining.net/documents.html. Accessed 8 Sept 2011
5. Kausch P, Ruhrmann G (2001) Environmental management. Environmental impact assessment of mining operations. Logabok, Köln, 133 p
6. Bednarik RG (1992) Early subterranean chert mining. Artefact 15:11–24
7. Dart RA (1967) The antiquity of mining in Southern Africa. S Afr J Sci 63(6):264–267
8. Dart RA, Beaumont PB (1968) Ratification and retrocession of earlier Swaziland iron ore mining radiocarbon datings. S Afr J Sci 64(6):241–246
9. Matschullat J, Ellminger F, Agdemir N, Cramer S, Liessmann W, Niehoff N (1997) Overbank sediment profiles – evidence of early mining and smelting activities in the Harz mountains, Germany. Appl Geochem 12:105–114
10. Sparks DL (2005) Toxic metals in the environmental: the role of surfaces. Elements 1(4):193–197
11. Klappauf L, Linke FA, Brockner W, Heimbruch W, Koerfer S (1990) Early mining and smelting in the Harz region. In: Pernicka E, Wagner GA (eds) Archaeometry, vol 90. Birkhäuser Verlag, Basel, pp 77–86
12. Rebrik BM (1987) Geologie und Bergbau in der Antike. Deutscher Verlag für Grundstoffindustrie, Leipzig, 183 p
13. Rosman KJR, Chisholm W, Hong S, Candelone JP, Boutron CF (1997) Lead from Carthagian and Roman Spanish mines isotopically identified in Greenland ice dated from 600 B.C. to 300 A.D. Environ Sci Technol 31:3413–3416
14. MHN (1997) The mining history network, http://projects.exeter.ac.uk/mhn/. Accessed 8 Sept 2011
15. Diamond J (2005) Collapse. How societies choose to fail or survive. Penguin, London, 575 p
16. Down CG, Stocks J (1977) Environmental impact of mining. Applied Science, London, 380 p
17. Carlowitz HC von (1713) Sylvicultura oeconomica. Anweisung zur wilden Baum-Zucht. Reprint of the 1713 ed Leipzig, Braun, revised by Klaus Irmer and Angela Kießling, TU Bergakademie Freiberg and Akademische Buchhandlung, Freiberg 2000, ISBN 3-86012-115-4; Reprint of the 2nd ed from 1732, Verlag Kessel, ISBN: 978-3-941300-19-4
18. Grober U (2010) Die Entdeckung der Nachhaltigkeit. Kulturgeschichte eines Begriffs. Kunstmann Antje GmbH, 300 p
19. Plumlee GS, Ziegler TL (2005) The medical geochemistry of dusts, soils and other Earth materials. In: Sherwood Lollar B (ed) Environmental geochemistry. In: Holland HD, Turekian KK (ser eds) Treatise on geochemistry, vol 9, issue 7, pp 263–310
20. PDAC (2009) e3plus – a framework for responsible exploration, 34 p. http://www.pdac.ca/e3plus/. Accessed 8 Sept 2011
21. Gunn JM (ed) (1995) Restoration and recovery of an industrial region, Environmental management. Springer, New York, 358 p
22. Ilgen G, Fiedler HJ (1990) Smelter smoke damage at Freiberg in the 19th century, and its study by Professors Reich (Freiberg) and Stöckhardt (Tharandt) II Explaining the causes of damage by agricultural chemistry methods. Wiss Z TU Dresden 29(6):115–118
23. Last FT, Watling R (1991) Acidic deposition – its nature and impacts. Proc Royal Soc Edinburgh Section B (Biological Sciences) 97:343
24. Blowes DW, Ptacek CJ, Jambor JL, Weisener CG (2005) The geochemistry of acid mine drainage. In: Sherwood Lollar B (ed) Environmental geochemistry. In: Holland HD, Turekian KK (ser eds) Treatise on geochemistry, vol 9, issue 5, pp 149–204
25. Singer PC, Stumm W (1970) Acidic mine drainage: the rate-determining step. Science 167(3921):1121–1123
26. Knittel U, Klemm W, Greif A (2005) Heavy metal pollution downstream of old mining camps as a result of flood events: an example from the Mulde river system, eastern part of Germany. Terr Atmos Ocean Sci 16(4):919–931
27. Ridgway J, Flight DMA, Martiny B, Gomez-Caballero A, Macias-Romo C, Greally K (1995) Overbank sediments from central Mexico: an evaluation of their use in regional geochemical mapping and in studies of contamination from modern and historical mining. Appl Geochem 10:97–109
28. Pernetta JC (1988) Potential impacts of mining on the Fly river, UNEP 99, 191 p
29. Hum L, Matschullat J (2003) Gold kann schmutzig sein. Welche längerfristigen Auswirkungen hatte das Unglück bei Baia Mare auf die Theiss? In: Unland G, Herzog P (eds) Der Bergbaubezirk Baia Mare, Rumänien. Eine komplexe Betrachtung der Lagerstätte, des Bergbaus, der Aufbereitung sowie der Umweltfolgen. TU Bergakademie Freiberg, Freiberg
30. Goudie A (2006) The human impact on the natural environment, 6th edn. Blackwell, Oxford, 357 p
31. Deschamps E, Matschullat J (2011) Arsenic: natural and anthropogenic. In Bundschuh J, Bhattacharya P (ser eds) Arsenic in the environment, vol 4. CRC Press, Balkema, 209 p
32. Bell FG, Stacey TR, Genske DD (2000) Mining subsidence and its effects on the environment: some differing examples. Environ Geol 40(1–2):135–152
33. Hüttl RF (1998) Ecology of post-mining landscapes in the Lusatian lignite mining district, Germany. In: Fox HR, Morre HM, McIntosh AD (eds) 4th International conference of the internat affiliation of land reclamationists. Balkema, Nottingham, UK
34. Krümmelbein J, Horn R, Raab T, Bens O, Hüttl RF (2010) Soil physical parameters of a recently established agricultural recultivation site after brown coal mining in East Germany. Soil Tillage Res 111(1):19–25
35. Littlewood G (2000) The global mining initiative. Address to Mining 2000, Melbourne September 20. www.icmm.com/document/104. Accessed 8 Sept 2011
36. Paul M, Mann S (2010) Environmental clean-up of the East German uranium mining legacy: discussion of some key experiences made under the Wismut remediation program. In: Lam E, Rowson J, Özberk E (eds) Uranium 2010 – Proc 3 rd Internatational conference uranium, vol II, 15–18 Aug, Saskatoon, Saskatchewan, Canada, pp 481–493

37. AusIMM (2011) Australasian institute of mining and metallurgy. http://www.ausimm.com.au/. Accessed 8 Sept 2011
38. CSIRO (2011) Sustainability. Commonwealth Scientific and Industrial Research Organisation. http://www.csiro.au/science/Sustainability.html. Accessed 8 Sept 2011
39. Mining Association of Canada (2011) Towards sustainable mining. http://www.mining.ca/www/Towards_Sustaining_Mining/index.php. Accessed 8 Sept 2011
40. PDAC (2007) Prospectors and developers association of Canada http://www.pdac.com.br/2007/english/index.htm. Accessed 8 Sept 2011
41. United Nation (1987) Report of the World commission on environment and development: our common future. http://www.un-documents.net/wced-ocf.htm (Brundtland Commission)
42. Rajaram V, Dutta S, Parameswaran K (2005) Sustainable mining practices: a global perspective. CRC Press, Baco Raton, 370 p
43. Marker BR, Petterson MG, McEvoy F, Stephenson MH (eds) (2005) Sustainable minerals operation in the developing world. Geological Society Special Publication 250, 249 p
44. Saling P, Kicherer A, Dittrich-Krämer B, Wittlinger R, Zombik W, Schmidt I, Schrott W, Schmidt S (2002) Eco-efficiency analysis by BASF: the method. Int J Life Cycle Assess 7(4):203–218
45. Shonnard DR, Kicherer A, Saling P (2003) Industrial applications using BASF eco-efficiency analysis: perspectives on green engineering principles. Environ Sci Technol 37(23):5340–5348
46. Agricola G (1556) De re metallica. Libri XII. English language version from 1912 by Hoover H and Hoover LH; ISBN 0-486-60006-8; 650 p
47. IIED (2002) Breaking new ground: mining, minerals and sustainable development. 462 p. http://www.iied.org/sustainable-markets/key-issues/business-and-sustainable-development/mmsd-final-report. Accessed 8 Sept 2011
48. Reimann C, Äyräs M, Chekushin V, Bogatyrev I, Boyd R, Caritat P de, Dutter R, Finne TE, Halleraker JH, Jæger Ø, Kashulina G, Lehto O, Niskavaara H, Pavlov V, Räisänen ML, Strand T, Volden T (1998) Environmental geochemical atlas of the Central Barents Region. NGU-GTK-CKE Special Publication, Geological Survey Norway, Trondheim, Norway, 745 pp. http://www.schweizerbart.de/publications/detail/isbn/9783510652631. Accessed 8 Sept 2011
49. Adriano DC (2001) Trace elements in terrestrial environments. Biogeochemistry, bioavailability and risks of metals. 2nd ed. Springer, New York, 867 p

Books and Reviews

Abdelouas A (2006) Uranium mill tailings: geochemistry, mineralogy, and environmental impact. Elements 2(6):335–341

Breitkreuz C, Drebenstedt C (eds) (2009) Sustainable mining and environment – a German – Latin American perspective. TU Bergakademie Freiberg, Freiberg

Einaudi MT (2000) Mineral resources: assets and liabilities. In: Ernst WG (ed) Earth systems: processes and issues, vol 23. Cambridge University Press, Cambridge, pp 346–372

Figueiredo BR (2000) Minérios e ambiente. Editora da Unicamp, Coleção Livro-Texto, 401 p

Fubini B, Fenoglio I (2007) Toxic potential of mineral dusts. Elements 3(6):407–414

Hüttl RF, Heinkele T, Wisniewski J (1996) Minesite recultivation. Springer, New York, 172 p

Maskall J, Whitehead K, Thornton I (1995) Heavy metal migration in soils and rocks at historical mining sites. Environ Geochem Health 17:127–138

Mining, People and the Environment (online magazine) http://www.mpe-magazine.com/. Accessed 8 Sept 2011

Morin G, Calas G (2006) Arsenic in soils, mine tailings, and former industrial sites. Elements 2(2):97–102

Sharma AK (no year) Scientific and sustainable mining. www.fedmin.com/html/goapaper.pdf. Accessed 8 Sept 2011

Woodward J, Place C, Arbeit K (2000) Energy resources and the environment. In: Ernst WG (ed) Earth systems: processes and issues, vol 24. Cambridge University Press, Cambridge, pp 373–401

Mining Industries and Their Sustainable Management

Sandip Chattopadhyay[1], Devamita Chattopadhyay[2]
[1]Tetra Tech Inc, Cincinnati, OH, USA
[2]CH2M Hill, Dayton, OH, USA

Article Outline

Glossary
Definition of the Subject and Its Importance
Introduction
Mining Life Cycle
Coal Mining
Pollution from Coal Mining
Restoration Process
Sustainability and Mining
Irrigation with Lime-Treated Acid Mine Drainage (AMD)
Application of Phytotechnology
Biomining and Bioprocessing
Bioremediation
Metal Recovery: Biotic and Abiotic
Water Quality and Acid Mine Drainage: Pre-mine Predictions and Post-mine Comparisons

Future Directions
Bibliography

Glossary

Abandoned mines Mines for which the owner cannot be found, or for which the owner is financially unable or unwilling to carry out cleanup. They may pose environmental, health, safety, and economic problems to communities, the mining industry, and governments in many countries.

Acid (rock or mine) drainage Many metal ore bodies and coal deposits contain significant quantities of sulfide minerals – often including the ore minerals themselves. When such minerals are brought to the surface, they react chemically with air and water producing sulfuric acid, which may dissolve other minerals containing potentially toxic elements. This *acid drainage* from coal and metal mining around the world can pollute water and the surrounding land, affecting plant and animal life. Acid drainage is known as *acid mine drainage* when it is closely associated with mining activities, and *acid rock drainage* when this phenomenon occurs naturally, without human intervention. Both phrases are in common use, although particular stakeholder groups have particular preferences related to the controversial nature of this issue.

Acidophile An organism that thrives in a relatively acidic environment.

Ammonification The biochemical process whereby ammoniacal nitrogen is released from nitrogen-containing organic compounds.

Amorphous Irregular, having no discernible order or shape. Rocks or minerals that possess no definite crystal structure or form, such as amorphous carbon.

Bioleaching Extraction of metal from solid minerals into a solution is facilitated by the metabolism of certain microorganisms.

Biomining Extraction of specific metals from their ores through biological means, usually bacteria. It is an actual economical alternative for treating specific mineral ores, involving percolation and agitation techniques.

Community The people living around the mine who are directly affected (both positively and negatively) by the mine's activities.

Contaminated land/water Land/water containing concentrations of potentially toxic materials (organic or inorganic) elevated above the natural background concentrations in a particular area. In relation to mining, land or water contamination may occur through fuel spills, run-off from waste rock dumps, leaks from tailings impoundments, windblown dust from tailings and waste rock, smelter emissions, and drainage from mine workings. Contaminated groundwater is caused by the seepage of contaminated waters into aquifers.

Crystalline A substance in which the constituent atoms, molecules, or ions are packed in a regularly ordered, repeating three-dimensional pattern.

Denitrification A microbially facilitated process of nitrate reduction that may ultimately produce molecular nitrogen through a series of intermediate gaseous nitrogen oxide products.

Dissimilatory reduction Sulfate-reducing bacteria reduce sulfate in large amounts to obtain energy and expel the resulting sulfides as waste; this is known as dissimilatory sulfate reduction. They are anaerobes, which use sulfate as the terminal electron acceptor.

Electrowinning The recovery of metal by electrolysis. An electric current is passed through a solution containing dissolved metals, and this causes the metals to deposit on a cathode.

Extractant An immiscible liquid used to extract a substance from another liquid.

Gypsum A sedimentary rock consisting of hydrated calcium sulfate.

Heap leaching To dissolve minerals or metals out of an ore heap using chemicals. For example, a cyanide solution percolates through crushed ore heaped on an impervious pad or base pads during heap leaching of gold.

Macrophyte An aquatic plant that grows in or near water and is either emergent, submergent, or floating. They provide cover for fish and substrate for aquatic invertebrates, produce oxygen, and act as food for some fish and wildlife.

Mesophile An organism that grows best in moderate temperature (typically between 15°C and 40°C). The term is mainly applied to microorganisms. It is also used to describe mesophilic anaerobic digestion, which takes place optimally around 37–41°C

or at ambient temperatures between 20°C and 45°C, where mesophiles are the primary microorganisms present.

Methanogenesis Production of methane by biological processes that are carried out by methanogens. A methanogen is a single-celled microorganism and is a member of the Archaea. Archaea are unique because unlike most life on Earth that rely on oxygen and complex organic compounds for energy, Archaea rely on simple organic compounds (e.g., acetate) and hydrogen for energy.

Mining life cycle The processes of exploration, mining development, extraction, processing, refining, smelting, and mine closure.

Ore Mineral-bearing rock that can be mined and treated profitably under the existing economic conditions, or those conditions which are deemed to be reasonable.

Reclamation Process of converting derelict land (land that requires intervention before beneficial use) to usable land and may include engineering as well as ecological solutions.

Remediation Environmental cleanup of land and water contaminated by organic, inorganic, or biological substances.

Restoration Seeks to artificially accelerate the processes of natural succession by putting back the original ecosystem's function and form.

Tailings Mineral wastes produced from the processing operations after the valuable minerals have been extracted.

Waste rock The mineral wastes produced during mine development – including overburden and barren rock – and those parts of an ore deposit below the economic cutoff grade. Often, and particularly in some metal deposits, the waste rock may contain sufficient sulfide mineral concentrations to generate long-term acid drainage problems.

Definition of the Subject and Its Importance

Mining, minerals, and metals are important to the economic and social development as they are essentials for modern living. However, supplies of minerals, such as coal, are limited, and sustainable management of natural resources requires the maintenance, rational and enhanced use as well as a balanced consideration of ecology, economy, and social justice. Mining industry's recognition and acceptance of its sustainable development is growing. In the mining and metals sector, this means that investments should be:

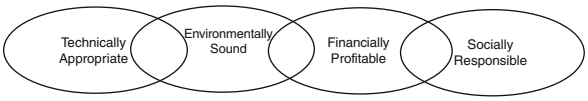

Leaders in the global mining business community have begun to assign a new strategic significance to the term sustainability. No longer confined to the economic realm, sustainability embraces a broad spectrum of organization characteristics related to social and environmental responsibility. Profitability alone is inadequate as a measure of success, and that many of the nonfinancial concerns associated with sustainability are fundamental drivers of long-term shareholder value. Failure to recognize these strategic issues threatens the very survival of a business enterprise.

Large amounts of material are involved in large-scale mining and minerals extraction. The problems arising from the change in the chemistry of million tons of natural ore during the processing steps (such as, grinding, calcining, and roasting operations) and their resultant bioavailabilities are not well understood. Mining produces large volumes of waste, and decisions regarding waste handling and other aspects of operations are often difficult and expensive to reverse; they need to be made correctly initially through mine closure planning. Another challenge is the environmental legacy left by mining. The environmental issues of current mining operations are daunting enough. But in many ways far more troubling are some of the continuing effects of past mining and smelting. The loss of biodiversity is the other great challenge of mining sustainability. The loss of biodiversity is an irreversible loss. Conservation practices that guarantee a minimum impact on biodiversity must be adopted and implemented.

As important as the methods of mining and beneficiation is how the minerals are used for sustainable development. An integrated approach for the use of minerals must be developed. Current patterns of minerals used raise concerns about efficiency and the need for more equitable access to resources worldwide. The environmental and health impacts of different mineral products in use need to be carefully managed.

Where the risks associated with use are deemed unacceptable or are not known, the costs associated with using certain minerals may outweigh the benefits.

The importance of sustainable development in mining industry includes actions at all levels to:

- Support efforts to address the environmental, economic, health, and social impacts of mining throughout the life cycle, including workers' health and safety. A range of partnerships, furthering existing activities at the national and international levels, among interested governments, intergovernmental organizations, mining companies and workers, and other stakeholders to promote transparency and accountability for sustainable mining and minerals development.
- Enhance the participation of stakeholders, including local and indigenous communities, to play an active role in minerals, metals, and mining development throughout the life cycles of mining operations. This includes efforts after mine closure for rehabilitation purposes, in accordance with national regulations and taking into account significant transboundary impacts.
- Foster sustainable mining practices through the provision of financial, technical, and capacity-building support to developing countries and countries with economies in transition for the mining and processing of minerals. This includes small-scale mining, and, where possible and appropriate, improve value-added processing, upgrade scientific and technological information, and reclaim and rehabilitate degraded sites.

Introduction

Mining takes a significant toll on the environment. The intensity of the environmental impact depends on what is being mined, where and how. Unless it is meticulously planned and carefully executed, mining can devastate lands, pollute and deplete water resources, denude forests, wipe out wildlife, and defile the air.

The history of mining has been one of boom and bust periods that were a balance between available natural resources, production costs, and the ability to sustain profitability. In recent years, the mining industry leadership has emphasized that the modern-day mining business has become more complex with the advent of stricter regulations, better-informed stakeholders, and closer in-depth scrutiny of current and/or proposed operations. Increased emphasis is being placed on the importance of sustainable operations that are focused on effectively integrating environment, social, and economic impacts.

The quantity of mining waste produced fluctuates yearly, and as the individual mines and quarries manage their wastes according to local conditions, there are no definitive statistics. After being removed, *waste rock*, which often contains acid-generating sulfides, heavy metals, and other contaminants, is usually stored above ground in large free-draining piles. This waste rock and the exposed bedrock walls from which it is excavated are the primary sources of pollution caused due to mining. The US mining industry produces approximately 8,000,000 tons per year (t/year) of process residue that may contain hazardous species as well as valuable by-products. These process residues are generated by smelter off-gas cleaning at approximately 5,500,000 t/year, and baghouse dust and wastewater treatment at approximately 2,100,000 t/year [24]. Comparable statistics was obtained for other countries. It was estimated that 96.4 million tons of mining and quarrying waste was produced in 2004 in the UK [4]. The Canadian mineral industry typically generates one million tons of waste rock and 950,000 t of *tailings* per day, totaling 650 million tons of waste per year [29]. The right technology may be able to recover marketable by-products from process residues to generate revenue and reduce disposal costs for the mining industry. The process residue that cannot be reused can impact the water resources, and the effect may be manifest throughout the life cycle of the mine and even long after mine closure.

Mining Life Cycle

Minerals are nonrenewable resources, and the mines have finite lives. Mining represents a temporary use of the land, and during this temporary use of the land, the *mining life cycle* can be divided into the following stages: exploration, development, extraction and processing, and mine closure.

Exploration is the work involved in determining the location, size, shape, position, and value of an ore body using prospecting methods, geologic mapping, and field investigations, remote sensing (aerial and

satellite-borne sensor systems that detect ore-bearing rocks), drilling, and other methods. Building access roads to a drilling site is one example of an exploration activity that can cause environmental damage.

The development of a mine consists of several principal activities: conducting a feasibility study, including a financial analysis to decide whether to abandon or develop the property; designing the mine; acquiring mining rights; filing an Environmental Impact Statement (EIS); and preparing the site for production. An example of site preparation impacting the environment is removal of the overburden (surface material above the ore deposit that is devoid of ore minerals) by excavation prior to mining.

Extraction is the removal of ore from the ground on a large scale by one or more of three principal methods: surface mining, underground mining, and in situ mining (extraction of ore from a deposit using chemical solutions). After the ore is removed from the ground, it is crushed so that the valuable mineral in the ore can be separated from the waste material and concentrated by flotation (a process that separates finely ground minerals from one another by causing some to float in a froth and others to sink), gravity, magnetism, or other methods, usually at the mine site, to prepare it for further stages of processing. The production of large amounts of waste material (often very acidic) and particulate emission have led to major environmental and health concerns with ore extraction and concentration. Additional processing separates the desired metal from the mineral concentrate.

The closure of a mine refers to the cessation of mining at a site. Planning for closure is often required to be ongoing throughout the life cycle of the mine and not left to be addressed at the end of operations. It involves completing a *reclamation* plan and ensuring the safety of areas affected by the operation, for instance, sealing the entrance to an abandoned mine. The Surface Mining and Control Act of 1977 states that reclamation must "restore the land affected to a condition capable of supporting the uses, which it was capable of supporting prior to any mining, or higher or better uses." *Abandoned mines* can cause a variety of health-related hazards and threats to the environment, such as the accumulation of hazardous and explosive gases when air no longer circulates in deserted mines, use of these mines for illegal residential or industrial dumping, and others. Many closed or abandoned mines have been identified by federal and state governments and are being reclaimed by both industry and government.

Coal Mining

Mining can affect both air and water. A fossil fuel that has been mined intensively is coal. As an example of environmental impact, effects of coal mining are presented below.

Coal is and will continue to be a crucial element in a modern, balanced energy portfolio, providing a bridge to the future as an important low cost and secure energy solution to sustainability challenges. A review of the Annual Energy Outlook 2010 report from the Energy Information Administration (EIA) indicates that world coal consumption will increase by 56%, from 132 quadrillion BTU in 2007 to 206 quadrillion BTU in 2035. Figure 1 presents the data for coal consumption [6] versus total energy consumption [17] between 1980 and 2030.

The growth rate for coal consumption is uneven, averaging 1.1% per year between 2007 and 2020 and 2.0% per year between 2020 and 2035. The slower growth rate for the earlier period is largely from a decline in coal consumption in 2009 during the global economic recession. With economic recovery, world coal consumption rebounded, and it is expected to return to its 2008 level by 2013. The US energy demand is expected to grow at an average annual rate of 1.1% for the next 25 years. Among the largest consumers of energy are China and India, and together they accounted for about 10% of the world's total energy consumption in 1990 and 20% in 2007. In a separate report by Waddell and Pruitt [31], it is projected that coal utilization will increase worldwide by 44% by 2025.

The process of coal excavation consists of several cycles: the cycle of excavation, disposal, and recultivation. The first step is reconnaissance of the terrain (preliminary survey of ground) that has been identified for mining. Preparation of the terrain may necessitate demolition of constructions, felling of trees, relocation of watercourses, roads, etc. This is usually followed by excavation of the overburden and then transporting and disposing the material using specialized equipment (mining machinery). In present days, bucket wheel excavators, conveyor belts, and

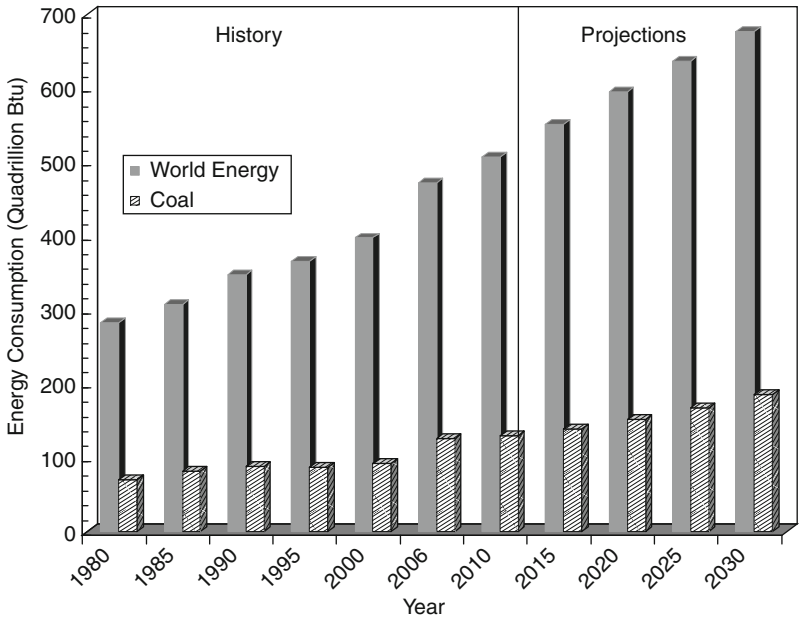

Mining Industries and Their Sustainable Management. Figure 1
Global energy consumption 1980–2030

stackers are mainly used. When the coal seam appears, such a seam is excavated and transported to the crushing plant.

Some of the important characteristics of coal excavation are listed below:

- Notwithstanding the occupancy of large areas and the change in the purpose of the land, end of mining will result in bringing back large portions of the used areas to the previous state. It means that though certain areas are temporarily occupied by mining activities, for example, for a period of 10 or more years, they can be reused as before following this period.
- Area occupied by the external dump, although it is generally higher than the terrain before mining activities, can be brought back to the state so that it can be reused.
- At the end of mining activities, the mine becomes the owner of large areas of agricultural land and forests. The owner of an agricultural land and forest is obliged to work the soil and control forest husbandry.

Pollution from Coal Mining

The process of coal excavation causes deterioration of the original morphological and pedological structure of the terrain and soil, and results in the release of harmful substances and/or mineral dust into the air. Such a release is primarily related to the deterioration of the upper seam structure during mining operations. The negative impact may occur as a result of the excavation of the upper seam and its inadequate disposal, and of mixing the upper seam with the lower one, as well as other barren materials. The impact of lignite excavation also represents a potential contamination of the upper seam due to the precipitation of dust from the air.

In addition to the aforementioned impacts, mining in a particular area will result in an increase in the area population not only due to the increased number of mine workers but also due to the development of related industries. Such development will often result in disappearance of the arable upper seam due to the building up of infrastructure facilities (roads, railroad tracks, waterways, industrial areas, etc.) and of the change in the purpose of the soil in the vicinity of the mine.

Mining can cause physical disturbances to the landscape, creating eyesores such as waste-rock piles and open pits. Such disturbances may contribute to the decline of wildlife and plant species in an area. In addition, it is possible that many of the pre-mining surface features cannot be replaced after mining ceases.

Mine subsidence (ground movements of the earth's surface due to the collapse of overlying strata into voids created by underground mining) can cause damage to buildings and roads.

Opencast coal mining leads to the disturbance of geological layers where different sedimentary products are being mixed, which means that a completely new, anthropogenic land, i.e., substratum, is created, without any resemblance to the original land, which is called a deposol. This is an example of visual pollution where the characteristics of the landscapes' appearance have changed due to mining. The opencast coal exploitation results in morphological modifications of the terrain, such as the creation of large-scale depressions and the formation of outside overburden dumps.

Pollution of Air

Coal mines emit constituents that cause or contribute significantly to air pollution and that may reasonably be anticipated to endanger public health and welfare. In each stage of mining, from exploration to ore recovery to downstream processing, there is the potential for air quality impacts due to emissions of particulates (dust, diesel, and silica). The monochromatic appearance of the mine areas is due to generation of large quantities of fugitive dusts during mining operations. Coal mining areas are black, bauxite and iron-ore rich regions are red, while limestone gives a chalky white hue. Dust results from blasting, handling, processing, or transporting of soil and rock or can arise from bare or poorly vegetated areas in combination with air movements. It is one of the most visible, invasive, and potentially irritating impacts of mining, and its visibility often raises concerns. Many dusts contain metals which are potentially hazardous, and are known to cause certain diseases. It has the potential to severely affect flora and fauna near the mine and to impact the health of mine workers and local residents. Dust also affects the agricultural productivity of the area. The level of dust generated, its behavior (particle size, density, travel distance), and types of health and environmental risks depend on many factors including mine type, local climate, topography, working methods, types of equipment used, the mineralogy and metallurgical characteristics of some ores, and the land use of the area around the mine.

- EIA reported that estimated recoverable reserves of coal in USA stand at 275 billion tons, an amount that is greater than any other nation in the world. All of the energy growth forecasts have major carbon dioxide (CO_2) emission consequences. The world energy outlook [32] indicated that CO_2 emissions will increase from 26.6 gigatonnes (Gt) in 2005 to 34.1 Gt in 2015 and 41.9 Gt in 2030 [10]. In the Alternative Policy Scenario [32], CO_2 emissions rise to 31.9 Gt in 2015 and to 33.9 Gt in 2030. EIA of the US Department of Energy (DOE) in its International Energy Outlook (IEO) 2007 forecasted that CO_2 emissions in the Reference Case will increase from 26.9 Gt in 2004 to 33.9 Gt in 2015 and to 42.9 Gt in 2030. In the past, global CO_2 emissions rose from 23.5 Gt in 2000 to 27.1 Gt in 2005 [11], which is an increase of over 15%. Based on this, one can say that the forecasts made by IEA and IEO are optimistic.
- Methane is the second most emitted greenhouse gas after CO_2, and is more than 20 times more potent than CO_2 in terms of its heat-trapping capabilities. Methane is a by-product of coalification, the process by which organic materials convert into coal. It is stored throughout the surrounding rock strata in varying sized pockets and, due to the greater overburden pressures, often increases in concentration the deeper the coal seam. Because methane can create hazardous working conditions for miners, it must be removed from underground mines. While methane escapes during the processing, transport, and storage of coal, 90% of the emissions come from the actual coal mining process from all three categories of coal mines: surface mines, underground mines, and abandoned mines.

In 2004, methane accounted for 14.3% of the total anthropogenic greenhouse gas emission load. Since pre-industrial times, methane has contributed to 22.9% of the greenhouse gas load in the Earth's atmosphere. Methane is more abundant in the Earth's atmosphere now than it has been at any time during the past 400,000 years, and the average atmospheric concentration of methane has increased 150% since 1750 due to human activities [25]. The US EPA [27] has concluded that recovering methane from coal mines would significantly reduce the amount of greenhouse

gases emitted into the atmosphere because every ton of methane recovered is equal to approximately more than 20 t of carbon dioxide emissions. While methane is a danger in coal mines, it can, if captured, be a valuable commodity: natural gas. To date, underground mines have the most potential to generate a profitable amount of methane. Mines that have adopted a "methane to markets" program as promoted by the US EPA have been successful at methane capture and sale because research has been developing for over three decades to create the best technologies.

- Particulate matters (PM), including total suspended particulates, PM_{10} (particle size less than 10 μm), and $PM_{2.5}$ (particle size less than 2.5 μm), are released during coal mining operations. Coal mining activities that can lead to the release of particulate matter are blasting, truck loading, bulldozing, dragline operation, vehicle traffic, grading, and storage piles.
- Volatile organic compounds (VOCs), including non-methane organic compounds, are often vented along with methane, from coal mining operations. VOCs are precursors to ground-level ozone, a criteria air pollutant, and are regulated under the Clean Air Act.
- Nitrogen oxides (NOx) are a group of gases that are known to be ground-level ozone and $PM_{2.5}$ precursors and that include nitrogen dioxide (NO_2), a criteria pollutant. Sources of NOx at coal mines include fugitive emissions from overburden and coal-blasting events, tailpipe emissions from mining equipment, point source emissions from stationary engines, coal-fired hot water generators, and natural gas–fired heaters.
- For some pollutants, such as sulfur dioxide, the minerals processing industry is the largest source of emissions.
- Certain kinds of ore, for example uranium, are radioactive, and pose health problems to workers and adjacent communities. Radioactivity follows with whatever radioactive materials escape into the atmosphere or water, and accompanies this material to its final destination. Besides targeted minerals that are radioactive, the host rock may be radioactive, and pose problems for workers. Radioactivity is also present in a gas, radon, which can cause problems for workers in underground mines, if it is present.

Impacts of Dust

The impacts of dust, especially from coal mine area are included below:

Effects on animals: Coal dust is a tumorigenic agent in experimental animals. Coal dusts are associated with lymphomas and, at the higher dose, adrenal cortex tumors in rats exposed to 6.6–14.9 mg/m^3 for 6 h/day intermittently for 86 weeks.

Effects on humans: Coal dust causes pneumoconiosis, bronchitis, and emphysema in exposed *community*. Coal workers' pneumoconiosis (CWP) is characterized by development of coal macules, a focal collection of coal dust particles with a little reticulin and collagen accumulation. These lesions may be visible as small opacities (less than 1 cm in diameter) on X-rays. Complicated CWP is characterized by lesions consisting of a mass of rubbery well-defined black tissue that is often adherent to the chest wall. This is associated with decrements in ventilatory capacity, low diffusing capacity, abnormalities of gas exchange, low arterial oxygen tension, pulmonary hypertension, and premature death. The disease may progress after the cessation of exposure.

Effects on plant: Plants exposed to toxic dust exhibit lesser growth, become more prone to disease attack and rodent attack, their stomata and other holes get chocked, and they also gasp for oxygen. Fruits, vegetables, and cereals from these plants contain toxins.

Effects on infrastructure: Biochemical reactions occur when constituents present in the coal dust starts reacting with the constituents of the host surface materials, resulting in increase in the rate of weathering/weakening.

Pollution of Water

The potential impacts of mining on the water [28] are:

- Disruption of hydrological pathways
- Seepage of contaminated leachate into aquifers
- Depression of the water table around the dewatered zone
- Disposal of saline mine water into rivers

The impacts of mining arising from the disruption of hydrological pathways, seepage of contaminated leachate into aquifers, and depression of the water table tend to be relatively localized and limited compared to disposal of mine water. Disposal of mine water

is a worldwide problem, occurring wherever operating mines, both underground and opencast, are found [19]. The quality of the mine water depends largely on the chemical properties of the geological materials that come in contact with the water.

The mining industry is a major producer of acidic sulfur-rich water that typically poses a risk to the environment. Mining increases the exposed surface area of sulfur-bearing rocks allowing for excess acid generation beyond natural buffering capabilities found in host rock and water resources. Pyrite (FeS_2) is the major sulfur mineral in coal. When coal is mined, fresh sulfur-bearing minerals in the coal and rocks are exposed to air and water. Problematic mine drainage is given many names including *acid rock drainage* (ARD), *acid mine drainage* (AMD), and mining influenced water (MIW). AMD forms during metal or coal mining when sulfur-bearing minerals are exposed to water and air, forming sulfuric acid. Heavy metals, leached from rocks, can combine with the acid and dissolve, creating highly toxic runoff. The general distinction between ARD and AMD depends on whether drainage quality has been degraded by mining or is of poor quality due, in part, to natural causes. MIW is the term used to refer all mining-related water because acidic, neutral, and alkaline water can all transport metals and other contaminants.

The origin of acidic metal-rich mine drainage water is the accelerated oxidation of FeS_2 and other sulfidic minerals. The reaction of pyrite with oxygen and water produces a solution of ferrous sulfate and sulfuric acid. Ferrous iron can further be oxidized producing additional acidity. The following reaction shows the reaction of pyrite with oxygen and water to produce hydrogen ions, sulfate ions, and soluble metal ions.

$$2FeS_2(s) + 7O_2 + 2H_2O \rightarrow 2Fe^{+2} + 4SO_4{}^{-2} + 4H^+$$

Further oxidation of Fe^{+2} (ferrous) to Fe^{+3} (ferric) occurs when sufficient oxygen is dissolved in the water or when the water is exposed to sufficient atmospheric oxygen.

$$2Fe^{+2} + {}^1\!/_2O_2 + 2H^+ \rightarrow 2Fe^{+3} + H_2O$$

Fe^{+3} can either precipitate as $Fe(OH)_3$, a red-orange precipitate seen in waters affected by ARD, or it can react directly with pyrite to produce more Fe^{+2} and acidity as per the following reactions:

$$2Fe^{+3} + 6H_2O \leftrightarrow 2Fe(OH)_3(s) + 6H^+$$

$$14Fe^{+3} + FeS_2(s) + 8H_2O \rightarrow 2SO_4{}^{-2} + 15Fe^{+2} + 16H^+$$

In undisturbed natural systems, this oxidation process occurs at slow rates over geologic timescale. Iron- and sulfur-oxidizing bacteria are also known to catalyze these reactions at low pH, thereby increasing the rate of reaction by several orders of magnitude [18]. Bacteria such as *Thiobacillus ferrooxidans* and *Ferroplasma acidarmanus* are known to specifically accelerate such reactions.

A few management options for saline mine water, as summarized by Annandale et al. [1], are:

1. Pollution prevention at source
2. Reuse and recycling of water to minimize the volume of polluted water
3. Treatment of effluents, if the problem cannot be solved through prevention, reuse, and recycling
4. Discharge of treated effluent
5. Utilization of gypsiferous mine water for irrigation

The term "gypsiferous" refers to rocks and soils containing more than 2% *gypsum*, i.e., calcium sulfate ($CaSO_4 \bullet 2H_2O$). There are concerns regarding potential use of mine water for agricultural crops [5], due to the amount of salt that would leach and potentially contaminate groundwater. The next few sections highlight successes and limitations with respect to environmental impact and sustainable use of such waters for irrigation of agricultural crops.

Restoration Process

It is the obligation of the mining company to restore the working cavity in the best possible way, through overburden disposal activities and technical reclamation, to the existing natural environment in terms of functionality and aesthetics. The following measures can be applied for the recultivation of deteriorated surfaces:

- Technical measures – to contribute to the improvement of resistant and deformable characteristics of the dump and directly influence the enhancement of the stability of slopes.

- Bio-technical measures – to contribute to faster achievement and maintenance of the dump stability along with the technical measures.
- Biological measures – that imply the implementation of agricultural and forest improvements that contribute to the stability and maintenance of reclaimed areas, but they are much more significant from the aspect of area revitalization and establishing natural biocenoses (a group of interacting organisms that live in a particular habitat and form a self-regulating ecological community)

The process of reverting an industrial land back to an agricultural terrain is a very slow process and good planning steps are required. Depending on the size of the coal deposit, the process of turning an agricultural, forest, or urban environment into an industrial (mining) one, and then, by the recultivation process, back again into the agricultural or forest one, may require long time, even many decades.

There are ongoing arguments in favor of preventing further expansion of the utilization of fossil fuels, such as coal. One of the restorative measures is to perform the recultivation of a dump even though it has a relatively low impact on the environment. Talking about fertile alluvial lands, it is necessary to preserve the fertile solum (a set of related soil horizons that share the same cycle of pedogenic processes) through selective excavation in order to bring the soil back to agricultural production or other use. The forestation of soil and terrains deteriorated by opencast lignite mining will prevent the further deterioration processes, contribute to the maintenance of the ecological balance in nature, and enhance the absorption of CO_2 from the air and increases the content of the oxygen therein.

The control of particulate emission is a fundamental part of a mine environmental management plan because of the increasing public awareness of human health issues and expectations of environmental performance, and the duty of care required of mine operators by government and the community. Particulate emission management system can result in cost savings, increased profits, and improved government and community relations, as well as easier access to resources and financial support in the future.

There are a number of systems to address emissions of harmful air pollutants from coal mines. It is technologically feasible to capture or flare methane from coal mines, instead of releasing methane directly into the atmosphere. Many mines have already taken steps toward capturing methane emissions for economic reasons. Twenty-three mines in Alabama, Colorado, Pennsylvania, Virginia, and West Virginia have methane drainage facility and they recover methane within the range of 3–88% efficiency [7]. Of these 23 mines, 12 sell recovered methane for natural gas energy use and two mines use the methane to heat mine ventilation air and to generate onsite power. Flaring is an option if capture is not technologically feasible. Although flaring occurs at a small number of mines in the USA, there is a long and safe history of flaring at working coal mines in the UK and Australia. US EPA estimates that nearly 50% of all of the US coal mine methane emissions, or more than 1.25 million tons of methane, can be reduced at a zero net cost, while nearly 90% can be reduced at a cost of less than $15/t. However, the benefit of reducing methane could be as much as $240/t of methane reduced. Any efforts to address methane will most likely also address VOC emissions due to the fact that VOCs and methane are often released together from coal mines.

Examples of particulate matter emission control measures currently in use include, but are not limited to: (a) storing coal in enclosed coal silos or barns; (b) paving coal mine access roads; (c) watering or treating with dust suppressant any unpaved roads; (d) enclosing conveyor transfer points; (e) use of dust collection baghouses or other controls to reduce emissions from transfer points and crushers within processing plants; (f) fitting out-of-pit conveyors with hoods or otherwise containing emissions; (g) fitting out-of-pit dump hoppers with water sprays, a baghouse, or other controls; (h) treating haul roads with dust control chemicals or water; (i) watering short-term haul roads; and (j) regularly maintaining haul roads to reduce dust re-entrainment.

With regard to NO_x, mines have reduced emissions by as much as 75% through the use of borehole liners and changing their blasting agent blends. Other mitigation measures that may be effective at reducing NO_x include reduced blast sizes, changed composition of explosive agents, and changed placement of blasting agents. Reduction of impacts due to radioactivity consists of ventilation for underground mines, dust

control, standard containment measures for solid waste, and standard precautions for discharges from processing.

Sustainability and Mining

The Earth's resources have played a vital role for human communities. Nowadays, the management of our natural resources has become an urgent issue at both national and international level. The extraction and use of natural resources are also causing environmental problems, which require urgent solutions. For mining operations, resource extraction not only has a massive impact on ecosystems, it also releases pollutants contained in the rock, and consumes large amounts of water and energy. The transportation of resources from remote areas requires an ecologically intensive transport infrastructure.

Due to the progressive exploitation of mineral deposits and the availability of new technologies, deposits with lower ore content are now being mined. This means that an increasing amount of ore and other non-usable material has to be extracted to produce the same amount of metal. For example, toward the beginning of the twentieth century, copper ore mined by US mineral industry consisted of about 2.5% of usable metal by weight; today the proportion has dropped to 0.51% [8]. This activity impacts even more severely on ecosystems and water resources and increases the volume of mining waste, resulting in even more radical changes to entire landscapes. The rising global demand for resources accelerates this trend. After extraction, the subsequent stages in the raw materials' life cycle entail further environmental pollution. Comparative analyses of industrial sectors show that the highly resource-intensive industries are associated with above-average levels of emissions of greenhouse gases and other pollutants.

Climate change and the overexploitation of natural resources are two sides of the same coin. Climate change will impact water supplies, exacerbating existing pressures on water resources caused by population and economic growth. Given the combination of these stressors, the sustainability of water resources in future decades is a concern in many parts of the world. The sustainability of water resources is defined as the maintenance of natural water resources in adequate quantity and with suitable quality for human use and for aquatic ecosystems. Human needs for resources, like water, land, continue to grow with increasing population, primarily for direct consumption, but also secondarily for energy production, and agricultural and mining activities.

The privilege of mining can be enjoyed in the best possible way, but there is the responsibility of looking out for the future generations, preserving some of the natural resources by utilizing reserves in compliance with the principles of the sustainable development. There is also a need to reclaim and to revive deteriorated surfaces resulting from mining.

The nine sustainable development challenges that the mining industries face are:

- Ensuring long-term viability of the mining industry
- Controlling, using, and managing the land
- Using minerals to assist with economic development
- Making a positive impact on local communities
- Managing the environmental impacts of mines
- Maximizing the use of minerals so as to reduce waste and inefficiency
- Giving stakeholders access to information to build trust and cooperation
- Managing the relationship between large corporates and small-scale mining companies
- Sector governance: clearly defining the roles, responsibilities, and instruments for change expected of all stakeholders.

Mining, Minerals and Sustainable Development (MMSD) North America has developed an approach to assess how a mining/mineral project or operation contributes to sustainability. The assessment considered tracking the record of mining and minerals in the past and its current contribution to and detraction from economic prosperity, human well-being, ecosystem health, and accountable decision-making. A set of seven questions were developed as a means of assessing whether the net contribution to sustainability over the term of a mining/mineral project or operation will be positive or negative and a way of discovering how current activities can be improved and aligned with the emerging concept of sustainability [12]. The seven-part numbering used by MMSD (see Table 1) has been intended as an aid to

Mining Industries and Their Sustainable Management. Table 1 Seven questions to sustainability – How to assess the contribution of mining and minerals activities

Seven fundamental questions	Framework for guiding a sustainability assessment
1. *Engagement* Are engagement processes in place and working effectively?	Processes of engagement are committed to, designed, and implemented so that they: • Ensure all affected communities of interest have the opportunity to participate in the decisions that influence their own future • Are understood, agreed upon by implicated communities of interest, and consistent with the legal, institutional, and cultural characteristics of the community and country where the project or operation is located
2. *People* Will people's well-being be maintained or improved?	Project/operation lead directly or indirectly to maintenance of people's well-being: • During the life of the project/operation • Post-closure
3. *Environment* Is the integrity of the environment assured over the long term?	Project or operation lead directly or indirectly to the maintenance or strengthening of the integrity of biophysical systems so that they can continue in post-closure to provide the needed support for the well-being of people and other life forms
4. *Economy* Is the economic viability of the project or operation assured, and will the economy of the community and beyond be better off as a result?	Assurance of the financial health of the project/company and contribution of the project or operation to the long-term viability of the local, regional, and global economy in ways that will help ensure sufficiency for all and provide specific opportunities for the less advantaged
5. *Traditional and nonmarket activities* Are traditional and nonmarket activities in the community and surrounding area accounted for in a way that is acceptable to the local people?	Project or operation contribute to the long-term viability of traditional and nonmarket activities in the implicated community and region
6. *Institutional arrangements and governance* Are rules, incentives, programs, and capacities in place to address project or operational consequences?	Institutional arrangements and systems of governance in place that can provide certainty and confidence that: • Capacity of government, companies, communities, and residents to address project or operation consequences is in place or will be built • Capacity will continue to evolve and exist through the full life cycle including post-closure
7. *Synthesis and continuous learning* Does a full synthesis show that the net result will be positive or negative in the long term, and will there be periodic reassessments?	Placement of an overall evaluation and periodic reevaluation based on: • Consideration of all reasonable alternative configurations at the project level • Consideration of all reasonable alternatives at the overarching strategic level for supplying the commodity and the services it provides for meeting society's needs • Consideration of all reasonable alternatives at the overarching strategic level for supplying the commodity and the services it provides for meeting society's needs

communicate and not to imply a particular sequencing of steps or prioritization of topics. These questions follow a hierarchy of objectives, indicators, and specific metrics. In this way a single, initial motivating question cascades into progressively more detailed elements, which can be tailored to the project or operation being assessed for application throughout its full life cycle.

The focus on applying the seven questions to sustainability approach is not so much on how mining can

be sustainable (mining as a discrete activity cannot continue indefinitely) but on how mining can contribute to sustainability [9].

Sustainability Opportunity and Threat Analysis is another simple operational tool addressing the social, economic, and environmental dimensions of the issues under consideration and it can be applied to evaluate the viability of a mining operation and its ability to contribute to sustainable development objectives. An impact-based model of sustainable mine development is shown in Fig. 2. This analysis involves constructing inventory of sources of impacts and following key steps including:

(a) Scoping (addressing the reasons for the mining process and the environment, and agreeing to the scope of the exercise)
(b) Information gathering (to emphasize the importance of collecting and organizing relevant information into a suitable framework)
(c) Identifying risks (systematically reviewing impact areas under consideration, and identifying opportunities or threats)

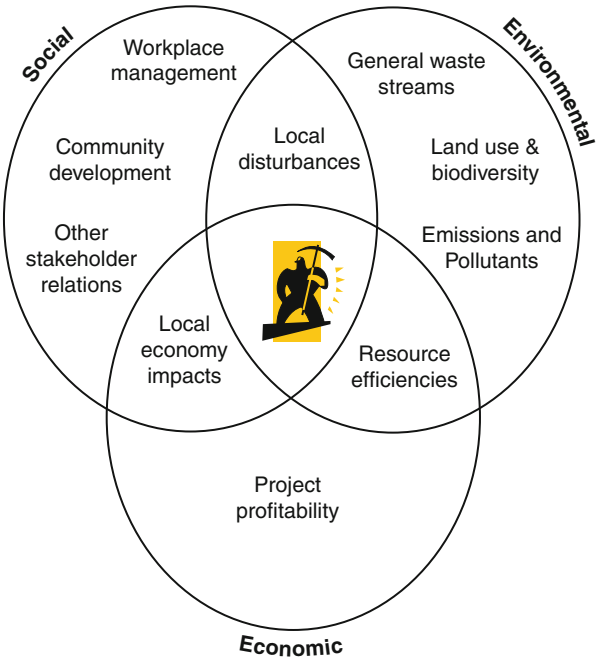

Mining Industries and Their Sustainable Management. Figure 2
Sustainable development model for impact-based mining operations

(d) Analyzing and evaluating the risks (qualitative scales of likelihood and consequence can be assigned to identify opportunity or threat to create overall risk rating and prioritized list)
(e) Treating risks (control measures to address opportunities or threats considered high priority)
(f) Reporting and reviewing to represent a broad, scanning exercise that can be picked up by existing business planning and monitoring processes. It also provides an opportunity for subsequent evaluation of relevant metrics for the issues identified by the process, allowing operations to measure both impacts and progress toward agreed objectives.

Most mine designs are based on traditional mining engineering factors, such as the quality of the commodity being mined, geology, topography, hydrology, land ownership, geography, infrastructure, etc. Environmental compliance and sustainability are to be considered in mine design and operation as a modifying factor to those designs. While practices may become more responsive to sustainability, mine design continues to be governed by established mining engineering approaches.

A review of the available literature on engineering optimization does not reveal any focus on mine design, environmental protection associated with mines, and sustainability. Mathematical multi-criteria optimization approaches, however, have been used in resource management. Mine design optimization would need to consider all constraints, system parameters and characteristics, and desired outcomes in order to build a useful and reliable model. Since optimization of mine design, and in particular coal mine design, to address sustainability along with other parameters has not been widely practiced, identifying the appropriate parameters for measurement and the mathematical or logical relationships between these parameters is not a trivial task.

Another important constraint on mining operations is the statutory and regulatory frameworks within which they are required to operate. Many of these legal and policy structures tend to create an adversarial approach by instituting a system where one or more parties must respond to actions, proposals, decisions, etc. of another party. The participation is often late in the design process, or after design has been completed, and thus any change to mine or reclamation design necessary as a result of public or regulatory agency

input creates a retrofitted design, which cannot possibly be optimal. To optimize the design of mining and reclamation operations, traditional mining engineering considerations and environmental and sustainability goals must be accounted for simultaneously.

Several technologies are discussed that are considered to promote sustainable development.

Irrigation with Lime-Treated Acid Mine Drainage (AMD)

Higher crop yields were obtained under sprinkler irrigation with treated mine water compared to dryland production, without any foliar injury to the crop. Possible nutritional problems, for example deficiencies of potassium, magnesium, and nitrate, occurring due to calcium and sulfate dominating the system, can be solved through fertilization. Such soils need to be managed and fertilized differently to those on which crops are produced under normal farming conditions. Sugar beans, wheat, maize, and potatoes were very successfully produced under irrigation with calcium sulfate and magnesium sulfate-rich mine water. In an experimental setting, soil salinity increased with time, but the values of soil saturated electrical conductivity stabilized at relatively low levels, due to gypsum precipitation [1]. Measurements taken between 1997 and 2007 showed that soil salinity increased from a low base and oscillated around 250 mS m^{-1}.

Land preparation and fertilization management are, however, critical for successful crop production, especially on rehabilitated soil. During short to medium term (up to 8 years) irrigation with gypsiferous mine water, negligible impact was noticed by Annandale et al. [1] on groundwater quality. They operated the system with flexibility and managed with the multiple objectives like maximum crop production, water use, job creation, economic return or maximum gypsum precipitation, and minimum salt leaching. Gypsum precipitation was also shown to be taking place in the soil. The presence of gypsum did not create any physical and/or chemical property changes that could adversely affect crop production and soil management. Crop production under irrigation with coal-mine water, rich in calcium, magnesium, and sulfate is, therefore, feasible, and sustainable if properly managed.

Pasture production with sodium sulfate-rich mine effluent is also feasible, but requires a well-drained profile and a large leaching fraction to prevent unsustainable build up of salt in the soil. Unfortunately, this type of water does not present much of an opportunity for gypsum precipitation, which is able to drastically reduce the salt load of the receiving water in the case of calcium and sulfate-rich mine water. The application of calcium nitrate as a nitrogen source to the crop adds calcium to the soil and removes some sulfate from the water system by enhancing gypsum precipitation. Measurement of the hydraulic conductivity of the soil is recommended to monitor the effect of the water on the infiltration rate of the soil, as high sodium levels are likely to cause deflocculation or dispersion of clay particles.

Application of Phytotechnology

Phytotechnology can be applied to address issues related to stabilization of tailings and hydraulic control for drainage so that human and ecological exposures to contaminants associated with mining solid wastes and mine impacted waters are low. Implementation of phytotechnology is a common component of mining reclamation and *restoration* projects by the establishment of a plant cover as a final remedy. In certain cases, application of phytotechnology can be used for removal of metals from *contaminated media*. Establishing phytotechnology requires careful plant species selection and soil amendments that equates to an initial investment; however, these systems, once established can be maintained with minimal effort.

There are six basic phytoremediation mechanisms that can be used to clean up contaminated sites: phytosequestration, rhizodegradation, phytohydraulics, phytoextraction, phytodegradation, and phytovolatilization (see Table 2).

The particular phytotechnology mechanism used to address contaminants depends not only on the type of contaminant and the media affected, but also on the cleanup goals. Typical goals include containment through stabilization or sequestration, remediation through assimilation, reduction, detoxification, degradation, metabolization or mineralization, or both. Applying phytotechnology to impacted sites entails selecting, designing, installing, operating,

Mining Industries and Their Sustainable Management.
Table 2 Phytotechnology mechanisms to sequester constituents of interest [13]

Mechanism	Description	Cleanup Goal
Phytosequestration	Ability of plants to sequester selected contaminants in the rhizosphere zone through exudation of phytochemicals and on the root through transport proteins and cellular processes	Containment
Rhizodegradation	Exuded phytochemicals can enhance microbial biodegradation of contaminants in the rhizosphere	*Remediation* by destruction
Phytohydraulics	Ability of plants to capture and evaporate water off the plant and take up and transpire water through the plant	Containment by controlling hydrology
Phytoextraction	Ability of plants to take up contaminants into the plant with the transpiration stream	Remediation by removal of plants
Phytodegradation	Ability of plants to take up and break down contaminants in the transpiration stream through internal enzymatic activity and photosynthetic oxidation/reduction	Remediation by destruction
Phytovolatilization	Ability of plants to take up, translocate, and subsequently transpire volatile contaminants in the transpiration stream	Remediation by removal through plants

maintaining, and monitoring planted systems that use the various mechanisms mentioned above. The goal of the system can be broadly based on the remedial objectives of containment, remediation, or both. Furthermore, the target media can be soil/sediment, surface water, or groundwater, and these can be either clean or impacted. In some cases, groundwater transitioning to surface water can be addressed as a riparian situation where target media are combined.

One of the main advantages of phytotechnology is that this technology can be applied to a variety of metals in mining sites and to impacted soil/sediment, surface water, and groundwater. In addition, it can be applied to various combinations of chemical types and impacted media simultaneously. Additional advantages are:

(a) Considered a green and sustainable technology
(b) Does not require supplemental energy, although monitoring equipment may use solar power
(c) Can improve the air quality and sequester greenhouse gases
(d) Minimal air emissions, water discharge, and secondary waste generation
(e) Lower maintenance, resilient, and self-repairing
(f) Inherently controls erosion, runoff, infiltration, and dust emissions
(g) Passive and in situ
(h) Favorable public perception
(i) Improves aesthetics, including reduced noise
(j) Applicable to remote locations, potentially without utility access
(k) Provides restoration and land reclamation during cleanup and upon completion
(l) Can be cost-competitive

The benefits of using the phytotechnology-based techniques are the relative lower costs, labor requirements, and safer operations compared to the more intensive and invasive conventional techniques. Phytotechnology generally provides long-term remedial solutions. Plantations may require irrigation, fertilization, weed control (mowing, mulching, or spraying), and pest control. Establishment of phytotechnology systems include various expenditures, such as earthwork, labor, planting stock, planting method, field equipment, heavy machinery (typically farming or forestry equipment), soil amendments, permits, water control infrastructure, utility

infrastructure, fencing, security, etc. About 10–15% of the initial capital costs can be added as a contingency for replanting [13].

Phytotechnology are appropriate only under specific conditions. The major limitations are depth, area, and time. The physical constraints of depth and area depend on the plant species suitable to the site (i.e., root penetration) as well as the site layout and soil characteristics. Phytotechnology typically require larger tracts of land than many alternatives. Time can be a constraint since phytotechnology generally take longer than many other alternatives and are susceptible to seasonal and diurnal changes. Additional limitations include a plant's tolerance to specific constituents of concern or site conditions, availability of water as irrigation source, climate (challenging for plant establishment in areas with short growing season or in arid environments), and pests, infestations, or other nuisances.

Biomining and Bioprocessing

Mining industries are increasingly aware of the potential of microbiological approaches for recovering base and precious metals from low-grade ores, and for remediating acidic, metal-rich wastewaters that drain from both operating and abandoned mine sites. Biological systems offer a number of environmental and economical advantages over conventional approaches, such as pyrometallurgy, though the microbial application is not appropriate in every situation. *Biomining* (metal extraction) and bioprocessing are currently utilized in full-scale operations to process low-grade deposits and reprocessing earlier metal-containing wastes. This usually results in the production of less chemically active tailings, lower energy inputs, and other environmental benefits (zero production of noxious gases). Recently, there have been major advances in the field of microbiology, which will allow greater control of *bioleaching* operations, resulting in greater efficiencies and faster rates of metal extraction. Mineral processing using microorganisms have been exploited for extracting gold, copper, uranium, and cobalt. Engineering systems ranging from crude *heap leaching* systems to temperature-controlled bioreactors have been used, depending on the nature of the ore and the value of the metal product. A typical example of mineral bioprocessing mechanism is discussed below.

Sulfide minerals may be divided into acid soluble (such as zinc sulfide or sphalerite) and acid insoluble (such as pyrite and arsenopyrite). Two routes (the "thiosulfate" and "polythionate" mechanisms) have been proposed for the biological oxidation of these sulfide minerals [21]. Acid-soluble sulfides are readily degraded by sulfur-oxidizing *acidophiles*. The mineral is first subjected to proton-mediated dissolution, forming the free metal and hydrogen sulfide:

$$MS + 2H^+ \rightarrow M^{2+} + H_2S$$

The hydrogen sulfide so formed is microbially oxidized to sulfuric acid, allowing the process to continue:

$$H_2S + 2O_2 \rightarrow H_2SO_4$$

Acid-soluble sulfides may also be attacked by ferric iron, producing ferrous iron and polysulfide:

$$MS + Fe^{3+} + H^+ \rightarrow M^{2+} + 0.5H_2S_n + Fe^{2+}$$

Polysulfide may be further oxidized by ferric iron to produce elemental sulfur, which, in turn, is oxidized to sulfuric acid, and will further accelerate mineral dissolution via proton attack:

$$0.5H_2S_n + Fe^{3+} \rightarrow 0.125S_8 + Fe^{2+} + H^+$$

$$0.125S_8 + 1.5O_2 + H_2O \rightarrow 2H^+ + SO_4{}^{2-}$$

Sulfides that are resistant to proton attack are oxidized by ferric iron, producing thiosulfate as an initial by-product:

$$FeS_2 + 6Fe^{3+} + 3H_2O \rightarrow 7Fe^{2+} + S_2O_3{}^{2-} + 6H^+$$

Accelerated oxidation can result in low pH, high concentrations of dissolved metals and, in some cases, elevated temperatures. These conditions limit the diversity of life-forms that occurs in commercial bioleaching operations. Single-celled organisms live only in extremely acidic liquors (pH $<$1–4) and are obligate acidophiles, some are thermophilic (to varying degrees) and some can fix carbon dioxide. The primary microorganisms involved in mineral oxidation are those that catalyze the oxidation of ferrous iron and/or reduce sulfur, while others contribute to the process indirectly by, for example, removing materials that accumulate during ore dissolution [14].

Engineering approaches used in biomining are: (a) irrigation-based principles (dump- and heap-leaching,

and in situ leaching) and (b) stirred tank processes [20]. The dump leaching involves gathering low-grade copper-containing ore of large rock/boulder size into vast mounds or dumps and irrigating these with dilute sulfuric acid to encourage the growth and activities of mineral-oxidizing acidophiles, primarily iron-oxidizing *mesophiles*. Copper can be precipitated from the metal-rich streams draining from the dumps by displacement with iron. Other developments on the engineering and hydrometallurgical aspects of biomining have involved the use of thin layer heaps of refractory sulfidic ores (mostly copper, but also gold-bearing material) stacked onto water-proof membranes, and recovery of solubilized copper using solvent extraction coupled with *electrowinning*. In situ bioleaching has been developed to scavenge for uranium and copper in otherwise worked out mines.

Bioremediation

Water draining from active and abandoned mines and mine wastes are acidic and often contain elevated concentrations of metals (iron, aluminum and manganese, and others) and metalloids (arsenic, chromium, selenium, and uranium). The basis of bioremediation of AMD derives from the abilities of some microorganisms to generate alkalinity and immobilize metals, thereby essentially reversing the reactions responsible for AMD.

Microbiological processes that generate net alkalinity are mostly reductive processes, and include *denitrification*, *methanogenesis*, sulfate reduction, and iron and manganese reduction. *Ammonification* (the production of ammonium ion from nitrogen-containing organic compounds) is also an alkali-generating process. Photosynthetic microorganisms, by consuming a weak base (bicarbonate) and producing a strong base (hydroxyl ions), also generate net alkalinity:

$$6HCO_3^-(aq) + 6H_2O \rightarrow C_6H_{12}O_6 + 6O_2 + 6OH^-$$

The reduction of soluble iron (ferric iron) does not decrease solution acidity, however, the reduction of solid phase (*crystalline* and *amorphous*) ferric iron compounds does.

$$Fe(OH)_3 + 3H^+ + e^- \rightarrow Fe^{2+} + 3H_2O$$

where e^- represents an electron donor, which is generally an organic substrate.

Bacteria that catalyze the *dissimilatory* reduction of sulfate to sulfide generate alkalinity by transforming a strong acid (sulfuric) into a relatively weak acid (hydrogen sulfide).

$$SO_4^{2-} + 2CH_2O + 2H^+ \rightarrow H_2S + 2H_2CO_3$$

Besides the ameliorative effect on AMD brought about by the resulting increase in pH, the reduction of sulfate is an important mechanism for removing toxic metals from AMD, since these metals (e.g., zinc, copper, and cadmium) form highly insoluble sulfides.

$$Zn^{2+} + H_2S \rightarrow ZnS + 2H^+$$

The bioremediation technologies, like constructed wetlands and compost bioreactors for AMD, are passive systems. In case of the constructed wetlands, the solid-phase products of water treatment are contained within the wetland sediments. The key major advantages of these passive bioremediation systems are their relatively low maintenance costs. The limitations of these technologies are:

(a) They are often relatively expensive to install.
(b) May require more land area than is available or suitable.
(c) Their performance is less predictable than chemical treatment systems.
(d) The long-term fate and stability (in the case of compost bioreactors) of the deposits that accumulate within them is uncertain [15].

Aerobic wetlands are generally more effective to treat mine waters that are net alkaline. The reaction involves oxidation of ferrous iron, and subsequent hydrolysis of the ferric iron produced, which is a net acid-generating reaction.

$$4Fe^{2+} + O_2 + 4H^+ \rightarrow 4Fe^{3+} + 2H_2O$$

$$4Fe^{3+} + 4H_2O \rightarrow 4Fe(OH)_3 + 12H^+$$

In the event the pH of the mine water decreases significantly as a result of these reactions, additional amendments (such as an anoxic limestone drain) may be required. To maintain oxidizing conditions, aerobic wetlands are relatively shallow systems that operate by surface flow. Though *macrophytes* are planted for aesthetic reasons, they also regulate water flow, accelerate

the rate of ferrous iron oxidation, and stabilize the accumulating iron precipitates.

In contrast to aerobic wetlands, the compost bioreactors (installations that are enclosed entirely below ground level and do not support any macrophytes) are anaerobic. The microbially catalyzed reactions in compost bioreactors generate net alkalinity and biogenic sulfide, and thus can treat mine waters that are acidic and metal-rich. The reductive reactions that occur within compost wetlands are driven by electron donors that derive from the organic matrix of the compost itself. The indigenous iron- and sulfate-reducing bacteria are generally considered to have the major roles in AMD remediation in compost bioreactors.

Metal Recovery: Biotic and Abiotic

Innovative and alternative techniques that facilitate the economic control and recovery of metal values are beneficial not only for protection of human health and the environment, but also for the recovery of these commodities and resource conservation. AMD, rich in metals, should be considered not only as a serious environmental problem, but as an important resource of metals of considerable value to many industrial concerns.

Recently developed metal recovery processes from AMD and other acidic streams enable us to recover and recycle these metals cost effectively. A two-stage process was developed by Tabak et al. [23] to separate the sulfate-reducing bacteria (SRB) from AMD via sulfate reduction and production of biogenic hydrogen sulfide from the four-stage and six-stage metal sequential separation and biorecovery units. The four-stage selective sequential batch-type metal precipitation process was able to separate metal sulfides and hydroxides at reasonably high recovery rate and at high precipitate purities. Copper sulfide and zinc sulfide were precipitated in Stage 1, aluminum hydroxide was precipitated in Stage 2, ferrous sulfide was precipitated in Stage 3, and other metals were precipitated in Stage 4. The effluent water contained only calcium and magnesium in trace concentrations and both sulfate and metal sulfide concentrations were below detectable limits.

von Fahnestock [30] recently developed a breakthrough technology to efficiently remove sulfate ions and metal cations from AMD by using the Acid Mine Drainage Value Extraction Process (AMD VEP), which is a novel adaptation of liquid–liquid extraction process. The process converts AMD to purified water as well as saleable products, such as potassium sulfate and iron sulfate. This technology results in simultaneous cost-effective isolation and concentration of useful metals and sulfate ions from mine pool water. A 30-gpm (113.5-L/m) demonstration plant was built and was operational within 15 months in St. Michael, PA. In this technology, AMD water, laden with sulfate and iron, feeds into the water purification stages where the AMD water is sequentially contacted with an *extractant* solution in a countercurrent flow path. The extractant solution is formulated to efficiently pull the sulfate and iron from the aqueous phase.

The water purification stages are composed as a set of four mixer-settler units, which are two-compartment tanks. The different stages are described below:

1. In the first compartment, the extractant and the AMD are mixed in a chamber. The residence time is between 60 and 90 s.
2. In the second stage, the combined effluent flows from the mixing chamber into the settling chamber where the organic extractant phase disengages from the water phase. The extractant, containing iron and sulfate, overflows an exit weir into the settling chamber, and is separated cleanly from the water phase, which underflows the same weir and exits as a separate stream with proportionately less iron and sulfate.
3. In the recovery stages of the AMD VEP, the extractant, loaded with iron and sulfate, flows sequentially from the water purification stages to the metals recovery and sulfate recovery stages of the process. Iron and sulfate are sequentially recovered as usable products during these stages. The metals-recovery stages are a set of two to three metal cation recovery tanks. The extractant flows counterclockwise with an aqueous sulfuric acid solution to form an iron sulfate concentrate that is harvested for reuse. The sulfuric acid and the extractant are mixed and separated in a similar manner to that in the mixer-settler tanks of the extraction section.
4. The sulfate-recovery stages remove sulfate from the extractant, which again flows through a series of

mixer-settler tanks in a countercurrent fashion. The extractant is contacted with potassium carbonate (a basic aqueous solution) to produce a potassium sulfate concentrate. The extractant exits the last mixer settler of the sulfate-recovery section regenerated and ready to contact a new stream of AMD feedwater in the water purification stages. The potassium sulfate (K_2SO_4) concentrate leaves the sulfate-recovery stages and is collected and stored for sale as fertilizer or reuse in a product tank.

An engineering analysis indicated that the maximum cost to treat and recover metals by AMD VEP process is $8.00 dollars/1,000 gal [3] dependant on product values and reagent pricing. AMD VEP, based on abiotic processes, is one of the few recent technologies to purify AMD water sufficiently to enable its discharge to surface waters. In addition, the product water can be made useful for industrial, municipal, agricultural, residential, and other uses. Importantly, these process products enable the system to focus on meeting seasonal and regional demands. For example, potassium sulfate fertilizer can be produced for 6 months a year for the turf grass industry, and the same system can produce sodium sulfate deicer for highways for 6 months a year, by changing operating conditions and reagent feeds.

Water Quality and Acid Mine Drainage: Pre-mine Predictions and Post-mine Comparisons

Necessity of accurate prediction of acidic drainage from proposed mines is recognized by both industry and government as a critical requirement of mine permitting long-term operation. Substantial emphasis has been placed on prediction of acid drainage associated with coal development in the Eastern USA [2], and metal mining in the Western USA and in Canada [16]. The prediction of acid-generating potential from any geologic formation is dependent on the ability to characterize the presence and quantity of both acid-forming minerals and neutralizing minerals in the materials that are expected to be unearthed during mining operations. Typically, samples are collected by drilling during exploration, analyzed and interpreted with respect to their risk of acid formation. In these analyses, the amount of sulfur present in geologic materials is measured and attributed to being either an acid-forming mineral such as pyrite (FeS_2) or non-acid-forming mineral such as gypsum ($CaSO_4 \bullet 2H_2O$). The relative amount of acid-forming minerals is then contrasted to the amount of neutralizing minerals such as calcite ($CaCO_3$) to develop a prediction of the probability of acid generation.

The acid base accounting (ABA) of a material is the balance between total acid-generating potential (AP), which is the total amount of acidity that would be produced if all sulfide in a material is completely oxidized, and total acid-neutralizing potential (NP), which is the amount of acid that could be consumed by neutralizing minerals. AP and NP are converted to $CaCO_3$ equivalents and reported as grams of $CaCO_3$ per kilogram rock. ABA is typically calculated from analysis of sulfide S and carbonate C, assuming a 1:1 molar ratio of sulfide S (AP) and carbonate C (NP).

Converting chemical analysis for sulfide S (S_{FeS_2}) and carbonate C (C_{CaCO_3}) can be expressed as [26]:

$$AP = S_{FeS_2}(10) \times (3.12)$$

$$NP = C_{CaCO_3} \times (10) \times (8.33)$$

where

S_{FeS_2} = concentration sulfide sulfur in sample (weight% S)

3.12 = molecular weight of $CaCO_3$/molecular weight of sulfur

C_{CaCO_3} = concentration carbonate carbon in sample (wt% C)

8.33 = molecular weight of $CaCO_3$/molecular weight of carbon

The ratio of neutralization potential (NP) to acid potential (AP) is commonly presented in graphical interpretations with the inference that geologic materials with an abundance of NP are unlikely to generate acidic drainage. Skousen et al. [22] reported that NP:AP ratios <1 commonly produce acidic drainage, NP:AP ratios between 1 and 2 may produce either acidic or neutral drainage, and NP:AP ratios >2 should produce alkaline water.

However, this index does not always accurately predict the resultant acid generation from a mine. Out of 56 mines evaluated by Skousen et al. [22], 11% did not conform to the expected results based on NP:AP ratios, including four sites with ratios >2 that eventually produced acidic drainage. Mineralogical

variation between each geologic domain causes dissimilar reactivity to weathering conditions and leads to laboratory variability in assessment. Forecasting future water quality impacts from AMD based on laboratory and field data should not be considered routine and robust, rather they should be considered an area of uncertainty and ongoing research.

Future Directions

The starting point is typically the acceptance of sustainable developmental principles at board-room level as corporate goals, and then informing the workforce, investors, and others of that commitment. Relevant employees need to be engaged as a first step in the practical application of sustainable development principles, followed by the gradual extension of training in sustainable methods of working to the workforce as a whole.

Bibliography

1. Annandale JG, Beletse YG, Stirzaker RJ, Bristow KL, Aken ME (2009) Is irrigation with coal-mine water sustainable? In: Proceedings of international mine water conference, Pretoria, South Africa
2. Brady KBC, Hornberger RJ, Fleeger G (1998) Influence of geology on postmining water quality: Northern Appalachian Basin. In: Brady, KBC, Smith MW, Schueck J (eds) Coal Mine Drainage Prediction and Pollution Prevention in Pennsylvania: Harrisburg, Pennsylvania. Department of Environmental Protection, p. 8–1 to 8–92
3. Conkle HN (2008) Engineering analysis report, value recovery from mine or rock drainage water, with water purity enhancement, using innovative low cost technology. Battelle, Columbus
4. DEFRA (2007) Waste strategy for England 2007. Presented to parliament by command of her majesty. Department for Environment, Food and Rural Affairs, PB12596
5. Du Plessis HM (1983) Using lime treated acid mine water for irrigation. Water Sci Technol 15:145–154
6. EIA (2010) Annual energy outlook 2010 with projections to 2035. U.S. Energy Information Administration, Office of Integrated Analysis and Forecasting, U.S. Department of Energy, Washington, DC. DOE/EIA-0383
7. Earth Justice (2010) Petition for rulemaking under the clean air act to list coal mines as a source category and to regulate methane and other harmful air emissions from coal mining facilities under section 111. Denver, CO
8. Gardner G, Sampat P (1998) Mind over matter: recasting the role of materials in our lives. Worldwatch Institute, Washington, DC, p 18
9. Hodge RA (2004) Mining's seven questions to sustainability: from mitigating impacts to encouraging contribution. Episodes 27(3):177–184
10. IEA (2007a) World energy outlook 2007 – China and India insights. OECD/IEA, Paris
11. IEA (2007b) CO_2 emissions from fuel combustion, 1971–2005, 2007 edition. OECD/IEA, Paris
12. IISD (2002) Seven questions to sustainability: how to assess the contribution of mining and minerals activities. Task 2 work group, mining, minerals and sustainable development North America (MMSD) North America. International Institute for Sustainable Development, Winnipeg
13. ITRC (2010) Technology overview of phytotechnologies. Prepared by The Interstate Technology & Regulatory Council, Mine Waste Team. Washington DC
14. Johnson DB (2001) Importance of microbial ecology in the development of new mineral technologies. Hydrometallurgy 59:147–158
15. Johnson DB, Hallberg KB (2002) Pitfalls of passive mine drainage. Rev Environ Biotechnol 1:335–343
16. MEND (2001) List of potential information requirements in metal leaching/acid rock drainage assessment and mitigation work. Mining environment neutral drainage program. W. A. Price, CANMET, Canada Centre for Mineral and Energy Technology
17. Mishra PC, Jha S (2010) Dust dispersion modeling in opencast coal mines and control of dispersion in Mahanadi coalfields of Orissa. Bioscan 2:479–500
18. Nordstrom DK, Southam G (1997) Geomicrobiology – interactions between microbes and minerals. Mineral Soc Am 35:261–390
19. Pulles W (2006) Management options for mine water drainage in South Africa. In: WISA, mine water division (ed) Mine water drainage-South African perspective. Water Institute Southern Africa, Johannesburg
20. Rawlings DE (2002) Heavy metal mining using microbes. Annu Rev Microbiol 56:65–91
21. Schippers A, Sand W (1999) Bacterial leaching of metal sulfides proceeds by two indirect mechanisms via thiosulfate or via polysulfides and sulfur. Appl Environ Microbiol 65:319–321
22. Skousen J, Simmons J, McDonald LM, Ziemkiewicz P (2002) Acid-base accounting to predict post-mining drainage quality on surface mines. J Environ Qual 31:2034–2044
23. Tabak HH, Scharp R, Burckle J, Kawahara FK, Govind R (2003) Advances in biotreatment of acid mine drainage and biorecovery of metals: 1. Metal precipitation for recovery and recycle. Biodegradation 14:423–436
24. U.S. EPA (1995) Identification and description of mineral processing sectors and waste streams. Office of Solid Waste, Washington, DC. RCRA Docket No. F-96-PH4A-S0001
25. U.S. EPA (2006a) Global mitigation of non-CO_2 greenhouse gases. Office of Atmospheric Programs, Washington, DC. EPA 430-R-06-005
26. U.S. EPA (2006b) Management and treatment of water from hard rock mines. Engineering Issue. Office of Research and

Development National Risk Management, Research Laboratory Cincinnati, OH. EPA/625/R-06/014
27. U.S. EPA (2009) Identifying opportunities for methane recovery at U.S. coal mines: profiles of selected gassy underground coal mines 2002–2006. Coalbed Methane Outreach Program, EPA 430-K-04-003
28. Younger PL, Wolkersdorfer C (2004) Mining impacts on the fresh water environments: technical and managerial guidelines for catchment scale management. Mine Water Environ 23:S2–S80
29. SDWF (2011) Mining and water pollution. Available from safe drinking water foundation. http://www.safewater.org/PDFS/resourcesknowthefacts/Mining+and+Water+Pollution.pdf. Accessed 11 May 2001
30. von Fahnestock M (2010) AMD value extraction process. Water Cond Purificat 52(1):38–40
31. Waddell S, Pruitt B (2005) The role of coal in climate change: a dialogic change process analysis. The generative dialogue project launch meeting, New York, NY, 6–8 Oct 2005
32. WEO (2007) World energy outlook 2OO7: China and India insights. International Energy Agency. 61 2007 01 1 P1, Paris

Mining Solid Wastes

Jaak J. K. Daemen[1], Haluk Akgün[2]
[1]Department of Mining Engineering, University of Nevada, Reno, NV, USA
[2]Department of Geological Engineering, Middle East Technical University (METU), Ankara, Turkey

Article Outline

Glossary
Definition of the Subject
Introduction
Types of Mining Solid Wastes
Sources of Mining Solid Wastes
Quantities of Mining Solid Wastes
Storage/Disposal of Mining Solid Wastes
Environmental and Health Concerns Related to Mining Solid Wastes
Use of Mining Solid Wastes
Remediation of Mining Solid Wastes
Future Directions
Acknowledgment
Bibliography

Glossary

Acid drainage Acidic water (pH < 7, but frequently < 5) released from waste dumps, tailings dams, formed as a result of reactions between inflowing water, e.g., rainwater, and acid-generating minerals, e.g., sulfides, in particular pyrite, present in the dumps. One of the major environmental hazards associated with some types of mining.

Beneficiation Processing of ore, e.g., through crushing, grinding, gravity separation, flotation, in order to recover metals of economic value.

Coal washing Treatment of raw coal to remove noncombustible rocks such as shale and sandstone and to produce clean, washed, coal.

Heap leaching Recovering metal values by leaching the metal out of broken rocks stacked in heap leach dumps.

Reclamation The process of restoring a site, e.g., mine waste dumps, to an acceptable condition for future use, e.g., by controlling and minimizing any environmental impacts the waste might have.

Stripping ratio Ratio of barren overburden ("waste") rock that needs to be removed in a surface mine, e.g., an open pit mine or a strip mine, in order to reach the mineral of economic value (e.g., metal ore, coal seam, limestone bed).

Tailings Leftover very fine particles (typically size ranges <0.1 mm) from mineral processing operations, the recovery of minerals of value from ore after the ore has been crushed and finely ground.

Tailings dams Dams, earth structures, containment embankments, built up from tailings.

Tailings ponds Lagoons in which tailings are dumped, and allowed to settle, after which the water is recovered, preferably recycled.

Waste dumps Earth fill like dams built of broken blasted rock, e.g., overburden, barren rock overlying ore deposits of value, that needs to be removed in order to gain access to the ore deposit.

Definition of the Subject

Miners dig holes in the ground to excavate materials that contain minerals of value to and needed by society. An unavoidable by-product of such mining is the creation of vast amounts of solid wastes. Unavoidable, because the minerals of interest, e.g., copper, platinum,

and gold, typically occur in extremely small concentrations, even in so-called rich ores. One major type of solid waste associated with mining is the barren rock that needs to be removed to gain access to any mineral deposit of commercial interest. A second major type of solid waste created by mining is the solids residue that results from the processing of the ore in order to extract the minerals of economic value. Usually ores need to be broken up, crushed, into relatively small particles, and sometimes need to be ground into even smaller, minute fragments in order to allow the recovery of the minerals of interest. The overwhelming majority of these small particles need to be disposed of as waste, usually referred to as tailings.

In light of the huge volumes, tonnages, generated by mining, solid waste management constitutes a major challenge for mining and for the engineers who design, plan, operate, and close mines. Not only are the amounts of solids vast, but sometimes they are potentially harmful to humans and to the environment. It is an essential and critical responsibility for modern mining to ensure that solid wastes are managed satisfactorily, i.e., with minimal and not more than acceptable detrimental impact to people and to the environment. What is acceptable to people has changed dramatically in recent decades, and as a result the control requirements on solid wastes generated by mining are numerous, stringent, and complex.

Mine wastes have been generated for millennia, although the amounts of waste generated in the distant past were trivial compared to the volumes generated in recent decades, and in the foreseeable future. Mine waste dumps remaining from ancient times now have become archaeological sites of great value for the study of ancient civilizations, and notably for the study of the early development of the use of a variety of metals, as well as of rock, whether for tools (flint, obsidian) or building stone or monument and statue construction. However, some of these ancient sites also have become and remain sources of pollution, notably acid rock drainage, indicating how long such long problems can persist if not treated or addressed adequately.

Although destructive consequences of solid mine waste have been recognized for at least several centuries, it is primarily since the 1970s that a more complete understanding has developed of the environmental and health problems that may be associated with or result from such wastes. By now the seriousness of some of the problems induced by solid mine wastes have become more fully appreciated and more widely recognized. As a result, stringent, and ever more stringent, regulations have been introduced for the management and control of mine wastes. Many mining companies have committed to comply with rigorous homeland regulations even in locations where such regulations may not yet have been legally or formally implemented. In parallel with the regulatory development has been a massive research development aimed at improving the understanding of environmental problems caused by solid mine wastes, and at improving practices for preventing, minimizing, and controlling such problems. As a result, a vast literature now is available, dealing extensively and in detail with virtually any aspect one can think of environmental degradation that might result from solid mine wastes. A major challenge that remains, however, in many parts of the world, is how to deal with a legacy of abandoned mine sites, usually accompanied by mine waste dumps, remaining from the past. In the USA, it has been estimated, although with considerable uncertainty, that such sites, in 12 western states, may number 33,000 ([1], who also provides references to more detailed reports). An obvious prime difficulty in dealing with such sites is that usually no ownership, no responsible party, can be identified, or exists anymore, and hence the responsibility for cleanup and site restoration defaults to society at large, often at considerable cost.

Introduction

Mining provides the raw materials such as base, ferrous, and precious metals; construction materials such as sand, gravel, building stone, and crushed rock; and industrial minerals such as salt, fertilizer (e.g., phosphate), clay (e.g., for ceramics), diatomaceous earth (e.g., for filter applications in the food and beverage industries), and energy, e.g., coal, lignite (brown coal), uranium, on which society critically depends. Associated with mining, unavoidably and intrinsically, is the generation of large volumes and tonnages of waste. Mining generates waste in a variety of ways. For surface mining, e.g., open pit mines, strip mines, or quarries, it usually is necessary to remove overburden, i.e., soil and rock

overlying the deposit to be mined, in order to gain access to the mineral deposit to be mined. Depending on the local geology, this may involve the removal of materials ranging in thickness from meters to tens of meters, occasionally up to hundreds of meters. Overburden removal frequently constitutes a large fraction, often the largest fraction, of solid "waste" associated with surface mining.

A second source of solid wastes is the products that result from the processing of the ore. A fairly extreme and obvious example: a typical gold deposit may contain a few grams of gold per ton of ore. In order to liberate the gold from the ore, the ore needs to be broken up into small particles. Virtually all the crushed and ground rock will be returned to "waste" piles or dumps, except for the minute fraction of gold removed from the ore. While the metal content of base metals may be somewhat higher, e.g., 0.5–1% for copper, that still leaves typically more than 90% and frequently more like 99% of the processed ore to be disposed of as waste. Similarly, inert material removed from coal, in coal washing plants, can generate waste fractions of the order of 5–25% and more of the coal mined.

Given the large quantities of material mined, the volumes and tonnages of waste associated with mining are very large indeed. For reasons briefly touched on in Section Future Directions, it seems highly unlikely that these volumes can be decreased, at least not in the near future – if anything, it is virtually certain that they will increase, probably substantially.

Depending on the methods by which waste is generated, and depending on the controls required to assure that waste does not pose unacceptable hazards to the environment and to people, a variety of methods are used to dispose of solid wastes generated by mining. In strip mining of coal and lignite, by far the major surface mining method of these materials, the mining operations are designed and planned such that the overburden materials, the soil and rock overlying the beds to be mined, are emplaced in previously mined pits or strips. With these types of operations the overburden waste essentially is used and emplaced such that the original, pre-mining, surface contours and topography are restored, more or less, approximately, within a relatively short time after mining, and that reclamation and site restoration can progress simultaneously with, concurrent with, ongoing mining.

In open pit mining, e.g., for precious and base metals, the overburden material typically is emplaced in waste dumps, disposal piles virtually always located at a very short distance from the mine. Depending notably on the geochemical and mineralogical composition of the overburden, such waste piles or dumps may require more or less intensive environmental control measures.

Tailings, finely ground rock particles that result from mineral processing of ores, will require particular care for disposal. Typically, usually, they will be emplaced in tailings ponds and tailings dams. Usually, virtually always, just as for coal slimes, residue from coal washing plants, these types of waste will pose potentially serious environmental risks and hazards. Hence it is imperative that these structures be planned, designed, built, operated, and closed with particular care and with great emphasis on ensuring that any environmental impacts be kept to acceptable levels.

Of particular concern for tailings, and for some types of overburden wastes, is the risk that the materials might contain minerals, most likely sulfides, that, when allowed to react with water and oxygen, might result in the generation of acid releases. Historically, almost certainly, this has constituted the major environmental impact from many mining operations. It is essential, for modern mining operations, to assure that such acid releases be minimized.

For some ores, health hazards are created by the materials mined. This includes notably uranium tailings, often deposited and present in areas where uranium has been or is being mined. The uranium ore virtually always is milled, i.e., processed, near the mine. The milling produces finely ground uranium ore, and not all the uranium can be extracted from the ore. Hence the tailings, the residue, will contain some radioactive particles. Toxic elements such as mercury and arsenic frequently are associated with precious metal, e.g., gold, deposits and may require particular precautions in order to prevent unacceptable health risks associated with these materials, e.g., on waste dumps, in tailings ponds, on tailings dams, etc. Of particular concern in this regard may be dust generated by wind blowing over such structures, especially when dry, and if left without or with minimal surface protection.

Some types of wastes generated by mining have found useful uses, although this certainly is not

common, notably as backfill for underground mines, in order to improve the stability of underground mine excavations, and in order to minimize impacts on the surface, e.g., in the form of surface subsidence, induced by underground mining. While such uses of solid mine waste certainly are important and significant in some mining districts or areas, they remain a relatively minor factor in overall solid mine waste management.

Whatever types of wastes are generated, and whatever waste management approaches are implemented, it is universally accepted good practice today, and a legal and regulatory requirement in most countries, to assure that mining operations, including wastes, be fully restored to an environmentally acceptable condition. Reclamation and site restoration is an integral part of today's mining planning and design practice. This does not imply or suggest that it is trivial or easy or not extremely costly, but responsible mining companies and operators recognize the need to meet society's needs for minerals using methods that are acceptable to society – their customers.

Types of Mining Solid Wastes

Solid mine wastes can be classified according to a number of different schemes, each of which has its own advantages and disadvantages, e.g., in terms of potential health and environmental impacts.

One basic yet important classification is by considering strictly whether or not the waste has a potential detrimental health or environmental impact. For example, a coarsely broken but relatively pure limestone, whether it be removed from above a coal deposit in order to gain access to the coal, or whether it be removed from above a marble deposit, in order to gain access to the marble, is extremely unlikely to, by itself, constitute either an environmental or a health hazard. (Admittedly, even if a relatively pure limestone was dumped in a river, it could have an environmental impact, e.g., resulting in flooding, or acting as an accidental dam.) Conversely, a shale bed, removed for similar purposes, that contains even a fairly small fraction of pyrite (iron sulfide) most certainly could constitute an environmental risk: oxidation of the pyrite, when in contact with water and oxygen, could generate an acidic effluent that could contaminate surface and ground waters.

Solid mine wastes can be classified on the basis of the particle size of the waste products. Both from an environmental control point of view and from a potential health impact point of view, the particle size and the particle size distribution, i.e., the particle grading, are solid waste characteristics of major importance. In addition, particle size and particle size distribution are dominant variables in designing disposal structures in which they are contained, because they are major engineering variables that will enter in stability and in hydrological, i.e., water flow, analyses. The particle size may range from exceedingly fine (e.g., phosphate slimes, <0.01 mm), to very fine, e.g., most tailings that result from metal ore processing, typically <0.1 mm, to very coarse, e.g., typical blasted overburden, where most of the particles will have a size exceeding many centimeters, and a large fraction of the particles will have sizes of the order of 1 m and more, sometimes considerably more. Once dried, dust conditions associated with these different particle size ranges will be very different. Coarse materials will allow ready and easy water drainage, and will not become airborne, even under extreme wind conditions. Fines are likely to be difficult to drain, are likely to have extremely low hydraulic conductivities, and may very easily be blown away by wind, sometimes to considerable distances.

From an environmental impact point of view, it almost certainly is the geochemical composition of the waste, and sometimes, in addition, the chemistry of any products that have been used in the beneficiation of the ore, that will be the major factor. Of prime concern are sulfides, and in particular sulfides that could result in the release of acid drainage, undoubtedly the major environmental problem associated with and generated by solid mine wastes. Equally important, whenever present, if present in sufficient concentration (which may be very low), are heavy metals, e.g., cadmium, selenium, mercury, chromium, and lead. These elements, generally toxic to humans, even in relatively small concentrations, also frequently are toxic to plants and animals. They are naturally present in many metallic orebodies, although in widely varying concentrations and chemical forms, and certainly their release needs to be controlled and limited to acceptable levels.

Solid mine wastes routinely are classified on the basis of the products mined. Hence a clear distinction

is made between coal mine wastes, metal mine wastes, and industrial mineral mine wastes. Not surprisingly, the tailings left from milling uranium ores, and some other radioactive ores, are treated as a class of materials by themselves, given that they release radionuclides. Although such categorizations certainly are helpful, they also are somewhat simplistic, and do not allow for a full accounting for any potential impacts of the wastes: depending on the overburden characteristics, especially chemically, but also physically, coal mine wastes or metal mine wastes may pose significantly different threats or risks, even when resulting from mining the same product of ultimate interest and value.

Sources of Mining Solid Wastes

By far the largest source of solid mine waste is the rock that needs to be removed above minerals of value in order to reach these minerals and allow their recovery. A second major source of solid waste is the residues of the processing that is performed in order to recover the minerals of value. For coal, this frequently involves coal washing. In order to wash the coal, it usually will be ground to a relatively small size (also preferred from a combustion point of view, in burners used for power generation). Similarly in order to allow recovery of precious and base metal values, e.g., platinum, gold, silver, copper, lead, and zinc, it usually is necessary to grind the rock to a very small size (<1 mm, often <0.1 mm), because that is the particle size range in which the metals can be liberated. Iron ore, on the other hand usually does not require sizing to anywhere near such small sizes, whereas phosphate (a major fertilizer source) typically is ground to a much smaller size. In these extremely small size ranges one is concerned about health and about environmental effects. If tailings dams are allowed to dry out, and are not protected, wind is likely to generate a major dust problem, both a potential health and a potential environmental concern. Although the permeability of the very fine particles may be low, the very small particle size greatly enhances the surface area of the particles, and hence the contact area between the particles and any through flowing water: Especially when water flows through the particles at extremely slow rates, over prolonged periods of time (in the extreme, over centuries), it may interact sufficiently with some of the minerals in the particles to generate acidic outflows, as is the case in some districts where mining was conducted millennia ago. Such acidic releases frequently also are carriers of heavy metals dissolved in the liquid.

A third major source of solid mine wastes are spent heap leach dumps. Dump heap leaching is used primarily to recover gold and copper from low-grade ores, ores of which the metal content is insufficient to warrant considerably more expensive processing that requires crushing, usually grinding, and chemical or pyrometallurgical (high temperature) recovery of the metals. In its simplest form heap leach dumps are constructed by dumping run-of-mine ore into large heaps or dumps, on which a solution is sprayed that dissolves the metal of interest from the ore. Unfortunately all practically used leach solutions are toxic and environmentally damaging. The most commonly used solvents are sodium cyanide for gold and sulfuric acid for copper. Even though these are used in extremely diluted solutions, there remains a risk of toxic consequences unless controlled carefully. Once the leach dumps are spent, i.e., all recoverable metal values are removed, the dump material will be disposed of as waste. These materials constitute one of the larger sources of solid waste generated by many open pit gold and copper mines.

Underground mining usually generates only relatively small quantities of waste, at least compared to surface mining operations. One source of barren rock frequently generated in underground mining operations is the rock mined to develop access to ore bodies. This may involve shafts or ramps from the surface. It may involve underground mine development, e.g., drifting in barren rock toward the ore to be mined. It may involve the excavation of support facilities, e.g., underground equipment maintenance rooms, pumping stations, and crusher stations, i.e., the numerous underground space requirements for the efficient operation of a mine. Sometimes it is possible to leave some of this barren rock underground, e.g., in stopes that have been mined out previously as part of the ore production. Usually, this requires careful planning, and further complicates the sequencing of mining operations. Even so, the industry has clearly learned and understood that waste disposal on the surface involves costs, including considerable

public perception costs, visual impact costs. Hence it seems probable that ever more effort will be devoted in the future to minimize the amount of solid waste that needs to be disposed of on the surface.

Quantities of Mining Solid Wastes

Quantities of solid waste are extremely large, voluminous. Consider a typical low-grade copper deposit that contains 0.5% copper (many deposits are being mined that contain significantly less, some that contain significantly more). Assuming a complete recovery, which is never the case, the production of 1 kg of copper requires processing 200 kg of such an ore. Hence 199 kg of the ore processed will remain as solid waste. Assuming a stripping ratio (i.e., ratio of barren overburden rock that needs to be removed in a surface mine in order to reach the mineral of economic value) of 2, a relatively low stripping ratio, 400 kg of overburden needs to be removed in order to access 200 kg of ore. In this case, the 1 kg of copper production results in generating 599 kg of waste.

Given the extreme diversity of the mining industry, it is exceedingly difficult to quantify the amount of waste it actually generates or has generated in the past, for reasons addressed briefly later in this section. In part, certainly, this may be due to the fact that until fairly recently waste management was not a priority for the producers nor for society at large. Only in the last few decades have the problems associated with solid mine waste disposal become fully recognized and appreciated, and, in particular, received extensive public and regulatory attention and scrutiny. Even though it can be assumed and expected that data gathering will improve in the future, for reasons explained in somewhat more detail in section on Future Directions, predicting how much solid waste will be generated by mining in the future also remains fraught with uncertainty.

In 1997, UNEP estimated that the solid waste annually generated by mining a group of selected major metals and industrial minerals amounted to about 2.7 billion tons, resulting from the mining of about 3.2 billion tons of ore [2]. However, this explicitly did not include any overburden mined; hence this almost certainly considerably understates the total amount of "waste" generated by these operations. It also did not include either coal or construction materials such as sand, gravel, dimension (building) stone, or crushed rock.

A reference document by the European Commission [3] estimates that approximately 118,000 kt of solid waste is generated annually by mining and quarrying in the EU-15, or about 20% of the solid waste produced in these countries. It deserves pointing that, as the reference explicitly recognizes, these "statistics on mining waste always bear a level of uncertainty," and, in all probability, this could be strengthened to a "considerable uncertainty." For example, the statistics cited, for 14 countries, are collected from different years, ranging over a 6-year period (1993–1999), because they simply are not available, for many countries, for every year, or even for many years. It needs to be recognized that Western Europe is a relatively minor mining waste producer, certainly compared to most large mining countries, and hence these numbers do not fully suggest the scale of the solid mine waste generated worldwide.

An exceptionally good explanation is given in references [4] and [5] as to why it is so difficult to determine how much solid mine waste exists, and how much is generated. Major data collection agencies come up with vastly different numbers (this holds true not only for solid mine waste, but for most other waste types as well, e.g., municipal solid waste, hazardous waste, demolition waste, etc.). Part of the uncertainty is due to the utter confusion and inconsistencies in waste definitions, e.g., between various governments, government agencies, data collection agencies and groups, etc. This uncertainty reflects rather well how recent it is that the waste problem has received due attention and the fact that people probably only are in the very early stages of dealing with it more or less adequately – given that the problem clearly is not yet fully or well defined. Although efforts are being made toward a more standardized and uniform definition of wastes, these will take time to implement and adopt. Moreover, significant differences exist in definitions and classifications between various governmental and regulatory bodies, and some of them are embodied deeply in legal frameworks, and hence likely to be very difficult to change. On top of that, in many countries and societies, especially poorer ones, waste management tends to remain a fairly low priority.

Storage/Disposal of Mining Solid Wastes

Storage of solid mine waste, i.e., temporary short-term management of solid mine waste, is rather unusual. Much more common is the permanent disposal, even though it may require maintenance. The type of disposal methods implemented will be closely intertwined with the mining method used, and will be influenced strongly by environmental and sometimes health-protection requirements.

In strip mining, a major surface coal mining method, long rectangular strips of coal are mined parallel to each other and directly adjacent to each other. Typically, the overburden from one strip is dumped into the opening left by the mining of the previous strip. Figure 1 illustrates schematically how the overburden is removed from above a coal seam and moved into the parallel pits left void after previous removal of the coal. Relatively shortly after the overburden spoil is dumped into the mined out strips, it is graded, leveled, and shortly thereafter topsoil is placed on the graded spoil. At this time revegetation can start. In these types of operations typically the vast majority of the overburden is replaced in mined out space. This method leaves separate disposal problems and challenges for the disposal of the overburden mined to access the first strip, and the fact that no overburden is available to refill the last strip. Particularly in areas with predominantly flat terrain, e.g., the Midwest of the USA, it has frequently been the practice to re-contour the spoil pile from the first strip into a hill, or hills. It is common practice to allow the last strip to fill with water, and to landscape it as desired, and, e.g., make it into a recreational lake, a reuse of the mined out area that is particularly attractive in areas where lakes are scarce.

The overburden piles, waste dumps, associated with open pit mining typically are left as barren rock piles, and are re-contoured in order to allow reclamation, i.e., revegetation. This usually will require that the slopes not be too steep, that topsoil be replaced and be used to cover the waste dumps, in order to provide a medium for plant growth. In recent decades there has been a growing interest in and movement toward backfilling of open pits, e.g., with overburden materials mined elsewhere in the pit, or sometimes in nearby pits. This somewhat controversial approach raises a serious question of resource conservation: Is it possible that, by this practice, potentially valuable ore resources may be covered up that will be considerably more difficult and expensive to mine at some point in the future? Mining history is replete with examples where further technological developments allowed mining of deposits that previously were abandoned as uneconomical. It is fairly routine, common, for historic mining districts to have gone through repeated mining cycles, sometimes with very lengthy dormant periods in between. But conversely there is no doubt but that pit backfilling reduces the visual impact of mining, and reduces the footprint of the impact left by mining, e.g., by greatly reducing the area occupied by solid waste disposal dumps.

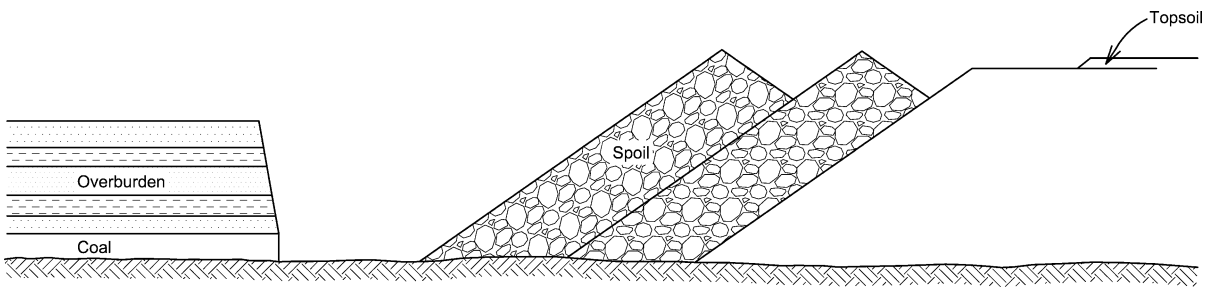

Mining Solid Wastes. Figure 1
Coal mined by strip mining, in which long parallel rectangular strips are mined, perpendicular to this vertical section through the pit. Overburden is stripped from above the coal (*left*) and dumped in the pits where the coal has been removed (*right*). The spoil piles are graded, a layer of topsoil is replaced on top of the graded spoil (*extreme right*), and reclamation can start, and can be performed concurrently with continuing, ongoing, mining (e.g., by seeding and planting)

Tailings disposal poses a particularly serious challenge. Tailings are very finely ground particles. Overwhelmingly they are transported as slurry, i.e., the particles are suspended in water, and pumped through pipes to the disposal dams or ponds. The resulting structures, some of the largest artificial dams in the world, pose major challenges to geotechnical engineers. By definition these structures, consisting of very fine particles, and, for some time after deposition, fully saturated, are intrinsically potentially highly unstable. Hence it is not surprising that these types of structures have resulted in multiple serious failures, including many truly catastrophic ones, with major loss of life, and with large detrimental environmental impacts. There is no doubt that these types of failures have been major contributors to the perception that mining is dangerous and damaging to the environment.

Figures 2 and 3 illustrate typical widely used methods of tailings dam construction. The basic difference between these methods is the sequence, the direction, in which the containment embankment is raised higher. For all three methods, the tailings are slurried to the disposal site, i.e., are carried suspended in water and pumped through pipes. The tailings are discharged a short distance behind the containment embankment. Typically the coarser particles will settle relatively close to the embankment, while the finer ones will travel to greater distances. The result is the formation of "beaches" in the disposal structure. It may be observed that in the second emplacement mode in Fig. 2, the upstream emplacement, subsequent embankments are built on top of these beaches. Hence the strength of the beaches has to be adequate to sustain the later additional loads imposed. In all cases the stability and impermeability of the containment structure are fundamental to assure adequate containment.

In order to minimize the risks associated with tailings dams and tailings ponds it is essential that such structures be planned, designed, constructed, and monitored with extreme care, by highly qualified professionals. There is no doubt that for many decades such structures were slapped together with extremely little if any care, with little understanding of the basic mechanics that determine their stability, or lack thereof, and of the high risk of failure of such structures. Over the last several decades major research efforts in many parts of the world have provided a greatly improved understanding of the failure modes involved, and of the design and construction requirements that need to be imposed in order to prevent future catastrophes. Unquestionably one of the serious challenges in this regard is that waste

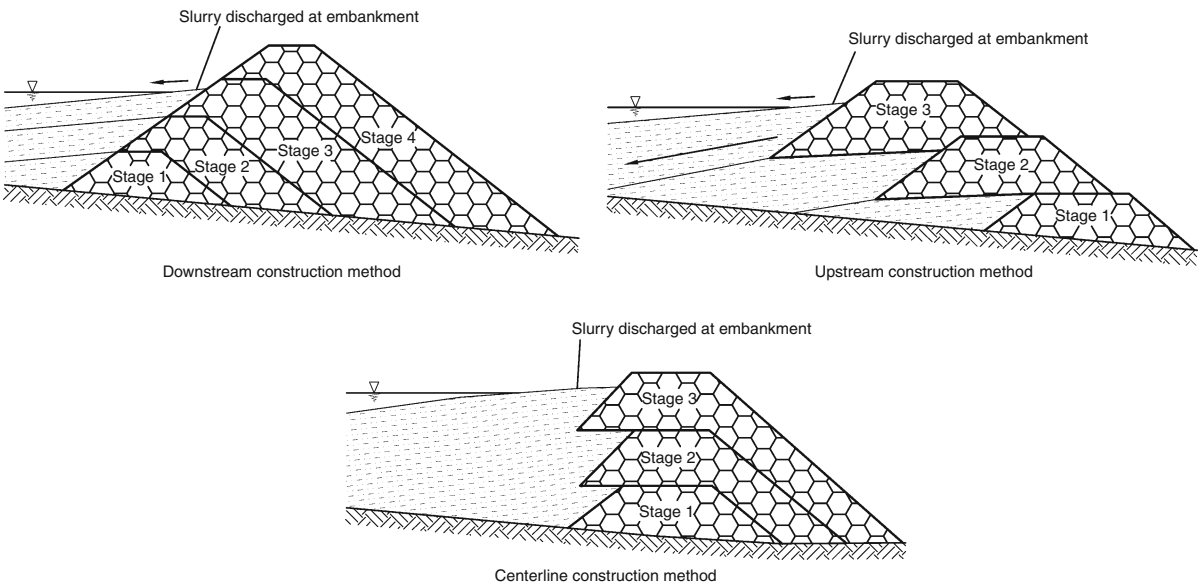

Mining Solid Wastes. Figure 2
Typical refuse facility (tailings dam) construction methods [6, Fig. 2, p. 3]

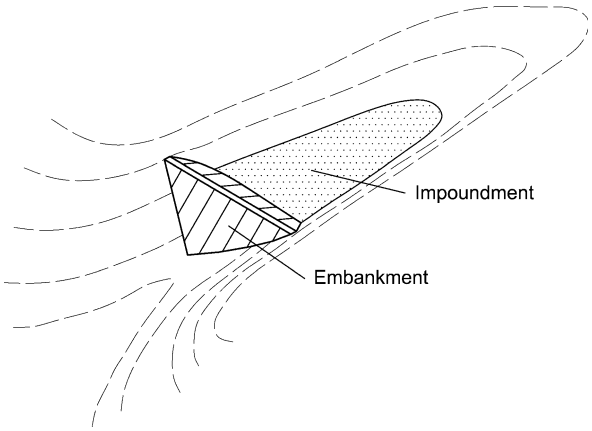

Mining Solid Wastes. Figure 3
Cross-valley tailings dam configuration [6, Fig. 1, p. 2]. A containment embankment is constructed across a valley. Tailings are pumped into the impoundment upstream of the embankment

disposal is a pure cost, and hence may not receive the necessary management attention to assure that it be done correctly. On the other hand, catastrophic failures of the types that have not been uncommon even in the last few decades carry a major penalty that can have a significant impact on the viability of a mining company. Aside from the ethical responsibility for mines to not endanger people or nature, the high visibility and impact of such failures should be an additional strong incentive to provide the necessary engineering to assure that such failures no longer will take place. One hopes. A more detailed and extensive argument and supporting discussion about the necessity and importance for the mining industry as a whole to reduce the number of catastrophic failures that draw great public attention because of their high visibility (and tailings dam failures have been among the most consequential and attention-grabbing disasters) has been given elsewhere [7].

Environmental and Health Concerns Related to Mining Solid Wastes

Depending on the waste characteristics and properties, a variety of environmental and health concerns may be associated with solid mine waste. To a major extent the concerns will be related to the chemical composition of the waste, sometimes to the physical characteristics, especially particle size.

Undoubtedly the major and most widespread, most common, and usually most serious environmental concern created by solid mine waste is the risk of acid drainage. If the mineralogy of the waste is such that some of the constituents of the waste are susceptible to interactions with water and oxygen that might result in the generation and release of acid, this will be of major concern to the public, environmental regulators, and the mine. Although in principle, conceptually, simple, e.g., a simple oxidation reaction of pyrite, the usual experience has been that the actual reactions and interactions taking place are far more complex than seems to be implied by such a simple formula. Particularly complicating dealing with this problem is that the reactions are affected by numerous variables, ranging from the obvious such as temperature and pressure to far from obvious and not yet fully understood synergistic effects between multiple minerals, varieties of water chemistries, and complicating biological and bacterial effects. Acid drainage has been the subject of major research efforts in virtually all major mining countries. Many successful remediation practices have been implemented, but problems still are encountered, and for specific situations further research may be needed.

Frequently closely related to acid mine drainage, associated with acid mine drainage, is the issue of release of heavy metals, some of which are highly toxic to humans, animals, fish, etc. Their immobilization and control will be a high priority objective of solid mine waste management.

In addition to chemical deterioration, physical effects on the environment may be of concern. A major issue in this regard is the presence of fines, especially materials less than 1 mm, in many solid mine wastes. One major concern about fines is that they can enter water streams or bodies, and result in sediment, reduced water clarity, and siltation, i.e., a variety of physical effects that can degrade surface water quality. In order to prevent such problems, it is essential that stringent sediment control and release practices be implemented at all mine waste handling facilities that are prone to sediment releases.

A somewhat related problem, also involving fines, is that of dust generation. Particularly for tailings dams

and ponds, especially some years after they have ceased operations, i.e., after tailings deposition has been terminated, it is likely that the surface will dry out, certainly so in dry or semi-arid climates. Unless adequate preventive measures have been taken, it is rather probable that this might result in severe dust problems, especially in dry windy climates. If, moreover, the dust is contaminated with potentially toxic components, the problem obviously is compounded further. In sum, and as an example, uranium mill tailings in the dry and windy Southwest of the USA (e.g., New Mexico, Utah, Colorado), unless controlled carefully, could be causes of major environmental and health impacts, and over large areas.

Of particular concern, both with regard to environmental impact and with regard to public health and safety, is the question of the stability of tailings dams. Tailings dam failures have been the most catastrophic types of mine waste failures over the last century, both in regard to fatalities, public as well as mine personnel, and with regard to environmental impact. Major tailings dam failures have been associated with coal mine residue wastes (spoil piles), with copper mine tailings, with gold mine tailings, and with a variety of other minerals.

Intrinsically, tailings dams are potentially unstable. They consist of fine particle assemblies, extremely large assemblies, typically, during construction, emplacement, in a high degree of saturation. It is interesting to note in this context that some of the most catastrophic dam failures (civil construction dam failures) occurred at dams that were being or had been constructed as hydraulic fill structures, following a construction method essentially similar to the usual methods of tailings dam construction. While geotechnical engineers have learned a great deal from such failures, it often has been at an exceedingly steep price. Given the inherent potential instability of tailings dams, notably their high susceptibility to liquefaction, of particular concern is the risk that they might be subjected to dynamic earthquake loading. Liquefaction of saturated sandy soils has been a major cause of extensive damage induced by earthquakes on multiple occasions. Therefore it is essential that the dynamic stability of tailings dams be evaluated, certainly in areas with a relatively high earthquake risk.

It certainly can be argued that over the last century a great deal has been learned about the mechanics of tailings dam failures, and that it probably is correct that such structures can be planned, built, operated, and closed today without undue unacceptable risk. One critical factor remains, beyond any doubt: In order for a tailings dam to be safe, it needs to be constructed correctly. No matter how good the planning and design, deviations from the designed construction approaches during operations can easily result in structures that are far weaker, far less stable, than intended. Supervision, inspection, monitoring, observation during construction, by professionals fully and intimately familiar with the details of what makes a tailings dam stable or unstable may well be essential prerequisites to assuring fully satisfactory performance for such delicate structures. While this may seem obvious to outsiders, a self-evident truism, insiders will recognize that in the past, lack of qualified on-site engineering almost certainly has been a major contributing factor, if not a dominant cause of several catastrophic tailings dam failures, including some within the last few decades. It historically has not been perceived as essential, critical, that detailed structural aspects of such containment facilities must be handled correctly, with far less margin of error, uncertainty, than sometimes understood or accepted to be the case.

Use of Mining Solid Wastes

Compared to the overall volumes of waste generated, relatively little use is made of most of the solid waste generated by mining. In general, the volumes are so large, and the locations so remote, that not much use for solid mine waste is readily available.

One very important exception is the use of solid waste for underground mine backfill, although, again, relative to the total waste volumes generated by mining, this undoubtedly is a very minor fraction. Even so, for a number of situations this is an important use of solid mine waste.

Solid waste is backfilled in underground mines for a variety of reasons, but most commonly in order to improve ground control, i.e., to provide greater stability of underground openings. Waste can be backfilled for this purpose in a variety of ways. One common method is to dump relatively coarse rock particles, sized in the order of centimeters, into underground void spaces previously mined out. In order to strengthen the backfill,

a small fraction (of the order of 5%) of cement or fly ash frequently is added to the backfill. The emplaced backfill applies confinement to the walls of the excavations, thereby greatly strengthening them, and reducing the risk of failures of the excavations. In the simplest of concepts, filling up the void space prevents the adjacent rock from bulking into the void space, thereby already greatly improving stability.

Fines, primarily tailings, may be backfilled in the form of a sand slurry, or as a viscous paste. When backfilled as a slurry, drainage of water will be an essential requirement in order to allow densification and strengthening of the backfill. Cement or fly ash here also may be added to give additional strength and stiffness. Backfilling of tailings by pumping them into mined out void space is a relatively simple and straightforward operation, but usually requires extensive preparatory construction of containment barriers that will assure that the tailings remain in place, in the intended locations, and that water can be removed, drained. Tailings emplaced in this fashion have similar geotechnical characteristics as tailings emplaced in dams, and hence raise similar stability concerns, notably with regard to dynamic (e.g., earthquake) loading.

Waste backfill has been used extensively in underground mines, especially in Europe, in order to reduce surface subsidence induced by mining. It was a common practice in coal mines in France, Belgium, and the UK, and still is used widely in Germany. It has been used in salt mines as well. One widely used method to backfill underground voids left by coal mining is to blow in fines with compressed air. Backfilling under these conditions may reduce surface subsidence by up to 50%, possibly more with a very dense (hence even more expensive) backfill.

A major benefit of returning solid mine wastes underground is that it reduces the visual impact of waste disposal on the surface. It reduces the space, e.g., land area, required on the surface for waste disposal. An environmental concern and risk about underground waste disposal is the potential for groundwater contamination. Hence, similarly to surface disposal, a comprehensive understanding of such risks is a prerequisite for decision making with respect to the acceptability of underground waste disposal.

Although there has been considerable research, and there have been efforts at using solid mine waste more widely, this remains the exception, rather than the rule. There have been applications for road construction, for construction fill, and similar applications, but these are not widespread. Unquestionably one of the major reasons is that the major cost for construction materials of this type, aggregates, is transportation. Rarely are large open pit mines in an area where there is great demand for construction materials.

Even for mine wastes that at one time were used, e.g., for road construction, or as fill for housing developments, this frequently is no longer an option, because of the recognition that at least some of these waste rocks contain constituents, e.g., heavy metals, that make their use highly questionable in applications where public exposure might result. It might be too difficult to demonstrate convincingly that no risk or negligible risk is involved, assuming it can be done.

Remediation of Mining Solid Wastes

Given the extremely wide range of materials being dealt with, it is not surprising that the remedial actions required in order to control any detrimental health and environmental effects associated with solid mine waste will be varied, complex, difficult, and expensive. While mining has been going on for millennia, only for a few decades has attention been paid to the need to protect people and the environment from the impacts of solid mine wastes. Considerable progress has been made over the last several decades, and a vast research literature is available on the subject, as well as a considerable data and fact base about a wide range of actual implementation practices of remedial actions that have been taken, although sometimes with mixed success. It seems reasonable to expect that the success rate should continue to improve.

As always when dealing with these types of problems, the first step is to try to minimize any source terms that contribute to potential health or environmental effects. The next step will be to implement control procedures to limit any impacts to an acceptable level.

A fundamental shift has taken place over the last few decades in mine planning and design, driven by the recognized need to minimize negative impacts from solid mine waste. Whereas a few decades ago mine design and planning was aimed primarily at

maximizing profit (although historically other considerations sometimes were taken into account, e.g., maximizing resource recovery, or pursuing energy (partial?) independence, or pursuing self-sufficiency in strategic materials), today mining engineers are taught that mines need to be planned and designed, always, with closure, reclamation, remediation as major objectives, not simply as an afterthought, to be addressed eventually, if and when the need might arise.

This planning and design, taking into account the post-mining fate of the site, greatly affects numerous decisions to be made during the planning and design exercises. Most countries now require, as part of the granting of mine permits or licenses, applications that include environmental impact statements, in which considerable and credible detail needs to be provided about how the operations will be closed and terminated, what the post-mining use of the site will be, and how detrimental environmental impacts will be mitigated.

One important critical first step in such planning and design is site selection of waste emplacement. Whereas in the past the main if not only criterion in this regard was cost, convenience in locating waste disposal dumps, tailings dams, etc., as close as possible to the mining and milling operations, if only to minimize transportation costs, today such site selection needs to performed with great diligence.

For any waste that may incur a risk of water contamination, whether it be surface waters or groundwater, minimizing such risks will be a major site selection criterion. This will require consideration of surface and underground water flow patterns. It may require an environmentally acceptable rerouting of surface water courses. It may require isolating underground water flow, aquifers. Surface topography, permeability, and strength of the ground on which waste is to be emplaced will be investigated, tested, and will be significant factors influencing site selection.

One important aspect of environmental impact control at many mining operations will be waste, and in particular overburden removal and disposal management. For many ore deposits, mining operations, it is possible to consider the overburden as consisting of two primary components (this obviously is a rather considerable simplification): acid-generating waste and acid-consuming waste. An example of the first type might be a shale bed with a large fraction of pyrite. An example of the second type might be a relatively pure limestone bed. By judiciously planning and sequencing overburden mining operations, it might be possible to assure that all potentially acid-generating rock is encapsulated in, embedded by, acid-consuming rock. Such strategies contribute significantly to the reduction of acid generation. Although conceptually simple, following this exceedingly simplified description, in actuality the mine planner will most likely be dealing with a considerable range of rock types, with varying strength and weaknesses. Such mine planning, of necessity, needs to be based on a thorough mineralogical, geochemical, hydrological, etc., understanding of the potential for acid generation at the site. Environmental control planning of this type, unavoidably, fundamentally, requires a deep understanding of the driving factors, the fundamental scientific aspects of what creates environmental problems, in order to be able to mitigate against that potential.

Many solid mine waste disposal facilities will be lined with relatively impermeable liners, and this certainly will be the case for the emplacement of all wastes that have the potential of generating acid drainage. Liners typically will consist of geomembranes, compacted clays, or a combination of both. Less common are asphalt or concrete liners. Installation of such containment structures is critically important for their performance, and hence needs to be conducted, supervised, and inspected with great care. Figure 4 illustrates the approach of using a clay barrier to prevent migration of slimes resulting from coal washing into an underground coal mine located directly underneath and adjacent to the refuse pile.

Closure of heap leach dumps will require first detoxification and next reclamation. Detoxification is performed by rinsing the heap leach dumps with chemicals that neutralize the solvents, react with the solvents, and convert them to innocuous residual chemicals, such as CO_2 and nitrogen gas (the quantities of CO_2 generated by these operations are trivial compared to those generated by, e.g., power production). One of the challenges for engineers closing heap leach dumps is to try to assure that all parts of the dumps have been rinsed and cleaned. It remains difficult, given the complexity of flow paths through such structures, to fully guarantee that no parts of the dump have been

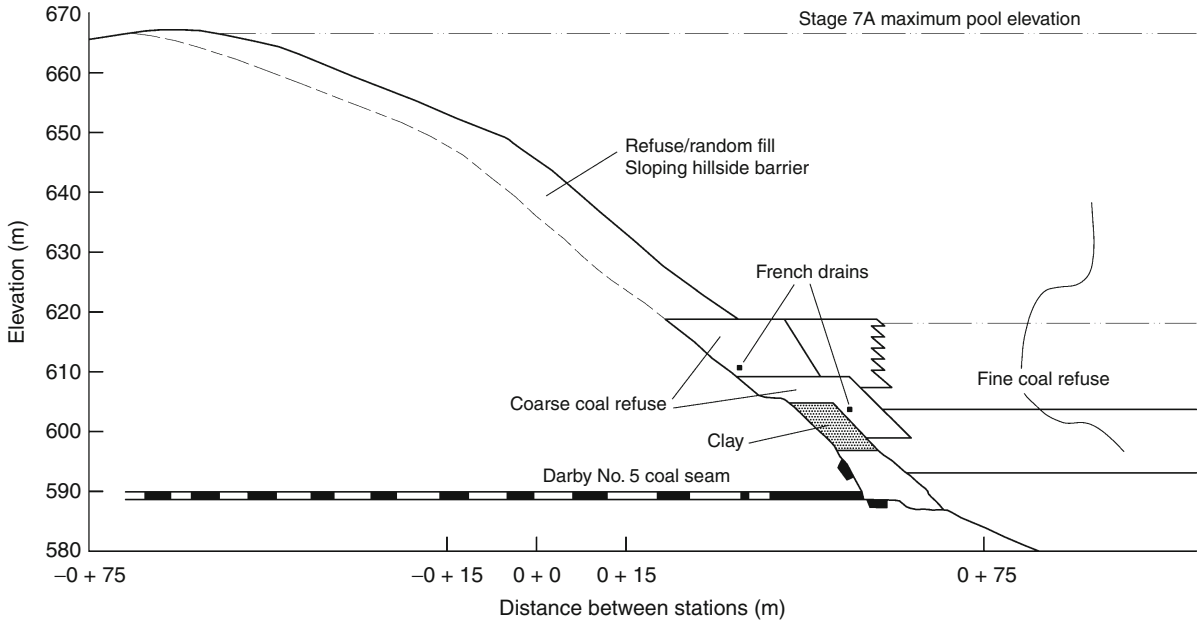

Mining Solid Wastes. Figure 4
Cross section showing earthen liner to be constructed around a refuse impoundment to be installed near an underground mine in order to prevent the slimes, residue from washing the coal, from flowing into the mine (Modified from [6], Fig. 4, p. 7)

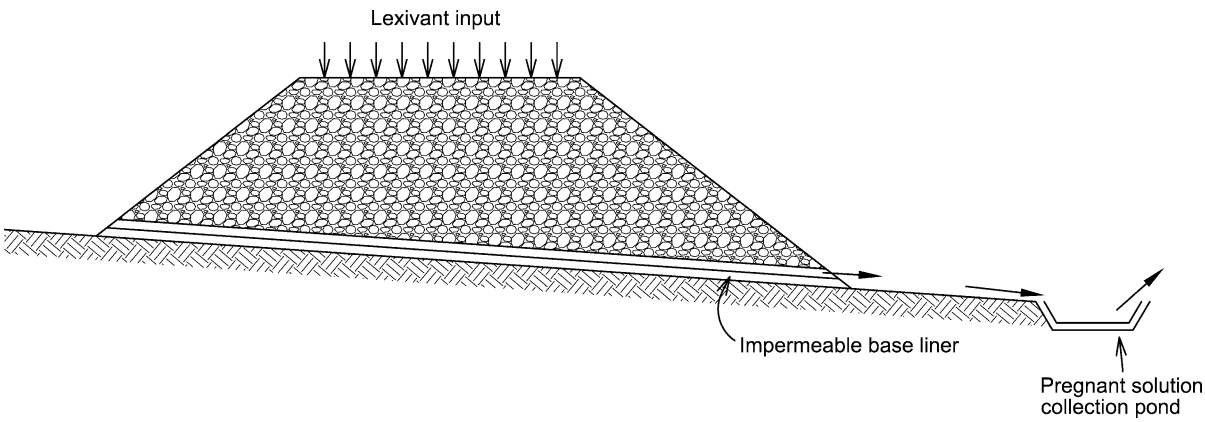

Mining Solid Wastes. Figure 5
Cross section through typical heap leach pad, as used for leaching gold and copper. Broken (blasted, sometimes crushed) rock is stacked in piles, in horizontal lifts of typically about 5 m thick, possibly up to a height of 50 m. Lexivant (leachate) is sprayed, sprinkled, or dripped on top. Pregnant solution is collected at the bottom. An impermeable pad is constructed on the foundation in order to minimize the risk of leachate escape to the groundwater

missed, that no pockets of cyanide or acid have been left behind. The problem is not particularly serious for cyanide, because it relatively quickly decomposes naturally in the presence of oxygen and water. For acid it is relatively straightforward to construct acid-consuming barriers, e.g., lime and limestone, and hence to assure that no acid can exit the site. Figure 5 illustrates a typical heap leach dump operation.

The crushed rock containing the metal to be dissolved (most likely gold, silver, or copper) is stacked loosely on an impermeable base liner. Leach solution is sprinkled, sprayed, or dripped on top of the dump, percolates through the dump, dissolves the metal(s) of interest, and is collected as the pregnant solution, i.e., the metal-bearing solution, in a nearby pond. From the pond it is pumped to a nearby plant where the metal of interest is recovered.

As for all waste containment structures, for heap leach dumps also the first step in minimizing the risk of inducing unacceptable releases will consist of selecting an appropriate site. Clearly attractive are sites where the natural base for the pads to be constructed, i.e., the soil or rock foundation, is impermeable and is sufficiently strong to withstand the load that will be exerted by the dump material in order to prevent, e.g., differential settlement across the base of the pad. Such differential settlement could induce cracking, shear or tensile failures, and thereby facilitate leachate flow through soil as well as through excessively deformed synthetic, i.e., geomembrane type liners. If an adequate site has been found, the next step will be the construction of the base-liner system, which will include an impermeable or very nearly impermeable barrier, above which a drainage system is installed that will allow draining the leachate and collecting it in a pond where the pregnant solution, i.e., the solution loaded with the valuable metal(s), will be gathered and from where it will be pumped to the metal recovery plant. All such leach pad systems installed will be provided with leak detection systems, designed and built in such a way that early warning is provided of any leaks occurring, in order to assure that timely remedial action can be taken.

Subsequent to detoxification of heap leach dumps, the further reclamation steps will be very similar to those of waste or overburden rock dumps. In all likelihood this will involve re-contouring, regrading, reshaping the dumps in order to facilitate revegetation, and in order to make them visually less obtrusive, e.g., by shaping into hill shapes very similar to those naturally occurring in the area. (In areas with flat terrain, it frequently is considered more attractive to maintain a hilly, "mountainous" configuration, and, e.g., provide the local communities with their own "mountain," most likely eventually to be used for recreational purposes.)

Once the desirable shape of the structure has been achieved, the next step will be to grow vegetation, and, e.g., to provide habitat for wildlife. The first step in this direction usually will be the emplacement of a layer of topsoil. In all operations of this type the topsoil, removed during the early stages of site preparation, will have been stored separately, for eventual reuse. Depending on the quality of the topsoil in semi-arid or desert climates, usually very poor and depending on local climatic conditions, the quality of the topsoil may, at the time when it is re-installed, be barely or not at all sufficient to allow plants to grow. Where this is the case, the soil will be amended as required, in order to provide an adequate growth medium. The usual preference today is to reclaim with native vegetation, either with seeding or planting, or a combination of both. It generally is considered desirable to establish a representative mix of plants appropriate for the area. This may require fertilization, and may require watering. In conjunction with the revegetation it is common to provide structures, e.g., an assembly of rock blocks with an arrangement known to be attractive to local wildlife. Wildlife biologists frequently, almost routinely, are employed by mining companies in order to assist with habitat recreation, optimized to accelerate the reestablishment of a diverse wildlife population.

Reclamation of quarries, mines used for the production of construction materials such as crushed rock, e.g., for road base and subbase, for Portland cement concrete or asphalt road concrete, is likely to be very different from that of coal or metal mines in remote isolated locations. In general, most quarries have no problem with chemical reclamation or contamination issues: Rocks that contain sufficient sulfides to be of concern from an acid generation point of view will almost never be acceptable for construction purposes. Hence, most deposits mined for construction material purposes have no associated geochemical contamination issues.

Because typically the major cost component of construction material crushed rock is transportation, many quarries, especially large ones, are started up relatively close to large urban areas. A classical historical pattern, repeated over and over again, is that over the life of the quarry the urban area continues to grow, and eventually totally encroaches on the quarry operation. Eventually the density of nearby population

reaches the point where it becomes ever more difficult to operate the quarry, e.g., as a result of increasingly frequent complaints about noise and dust. The value of the land continues to grow, and reaches a magnitude where the land value exceeds, often by a considerable margin, the value of the remaining "ore" deposit, if any. In many locations around the world at this point the decision is made to convert the mine, the quarry, into a real estate development venture. If the quarry was mined sufficiently deep (and it does not have to be very deep at all), it may be possible to convert the quarry into a lake, e.g., for recreational purposes, or as focal point of urban development, sometimes residential, sometimes commercial, sometimes a combination of both.

Undoubtedly one of the major challenges facing many societies is that of dealing with legacy sites, polluted sites remaining from mining operations in the distant past, that have left major massive contamination problems at a number of locations, in many countries with longstanding mining histories, especially metal mining, but certainly also surface coal, lignite, brown coal, or soft coal operations. In most of these situations remedial actions will require, or have required, massive cleanup efforts, on a vast scale.

Future Directions

As repeatedly stated, the generation of large volumes of solid waste is an unavoidable side effect of mining. Hence the first step in estimating the future of solid mine wastes is to make a brief estimate of the future of mining. For a number of reasons it is to be expected that society at large will need more minerals, and hence that mineral production will expand. The most obvious reason is that a large fraction of the world population continues to live in subsistence poverty levels, and that efforts will continue to improve the standard of living of a larger fraction of the world population. This will require more mineral production. Concurrent with this trend is the growing standard of living for a rapidly growing middle class, worldwide, notably in the largest players, China and India. As the standard of living continues to improve for these hundreds of millions of people, they will need more steel (e.g., for cars and buildings), more construction materials (e.g., for roads, buildings, and houses), more copper (e.g., to wire their houses and cars, and to distribute electrical power), more precious metals (e.g., platinum for car catalytic converters and jewelry, more gold and silver for electronics but especially as jewelry), and more energy (e.g., coal and uranium). In sum, all indications and predictions are that mine production will increase.

Mine production, in volume of materials mined, also will have to increase. For metals this is fairly obvious, as the grades of ore deposits that are being mined continue to decrease, and hence more solid waste needs to be produced per unit of metal recovered. Although for decades professionals have argued that more mining is likely to move underground, the reverse actually has happened: open pit and surface strip mines have continued to grow in size, most notably by going ever deeper, as has been made feasible by ever larger, more powerful, and more efficient surface mining equipment.

The picture is somewhat less clear for coal, one of the major sources of solid mine waste. In the USA as well as in other parts of the world, the future of coal is less obviously one of steady growth than it seemed 10 years ago. The vast expansion of natural gas discoveries and production is putting major price competition in the path of coal growth. Simultaneously, concurrently, in parallel, major efforts are being made to reduce greenhouse gas emissions, and it seems rather likely that this eventually will result in reduced use, or at least in a reduced growth of the use of coal for electrical power generation. Nevertheless, for the foreseeable future, it appears likely that coal will continue to be a major source of electrical power.

All indications are that the revival of nuclear power, most obvious in China and India, will continue, with a concomitant growing demand for uranium. Again, the scale to which this trend may proceed remains difficult to predict, but nevertheless it seems highly probable that uranium mining and milling, with their unique and serious environmental control requirements, will continue to grow.

In light of this high probability of increased solid mine waste production, it is apparent that the need for improvements in the controls on environmental impacts of such waste will increase as well. Major advances have been made over the last few decades in improving the understanding of the causes and mechanics of environmental degradation caused by or

associated with solid mine disposal. Mine planning and design have been fundamentally altered, with as a major objective making mining practices more environmentally acceptable. It seems certain that this trend will continue, probably intensify, and become more widespread, i.e., become more widely adapted.

Although the understanding of the fundamental causes of environmental degradation, e.g., the chemistry of acid drain formation, the physics of particle releases and consequent sedimentation, heavy metal transport, has improved greatly, it also has become clear that many of the fundamentals remain understood only partially, and are in need of further study. Research on this subject continues in virtually all major mining countries, and undoubtedly will result in further improvement in the understanding of the problems, and in the development of technologies for dealing with them.

As experience continues to be gained with control measures, e.g., the use of barriers aimed at containing potential contaminant plumes, such technologies will continue to improve, continue to result in approaches that are more effective, and can be implemented at lower cost. Of particular importance, given that major concerns about these issues have developed only over the last few decades is that as experience is gained over decades, a much better understanding is being developed of the long-term impact of potential health and environmental effects from solid mine waste, about the effectiveness, or lack thereof, of various prevention and control strategies, and of the need for future and further improvements in methods and strategies for dealing with such challenges.

Numerous solid waste disposal facilities have been installed over the last few decades with engineered containment structures and with engineered containment approaches. Many of these facilities have been equipped with monitoring instrumentation. A variety of monitoring methods have been implemented, such as leak detection systems in or below liners, water quality sampling and monitoring wells near dumps, and air sample collection instrumentation. It is certain that over the next few decades a vast experiential database will be collected, an extensive set of factual data at actual disposal operations.

In parallel, ongoing major research efforts aimed at elucidating the fundamental causes of potential environmental impact problems caused by solid mine wastes are seen. This includes detailed laboratory studies of the complex interactions that take place within and on the surface of waste dumps, tailings dams, and spent heap leach pads. Combined with laboratory studies are increasingly sophisticated and detailed numerical modeling studies, computer simulations of the reactions, and water flows that take place in, on, and near such structures. The extensive and intensive full-scale experiments that are being conducted, in many different places, under a wide range of climatic conditions, dealing with a wide variety of solid wastes, will produce comprehensive databases that will allow calibrating and assessing numerical codes and the predictive validity of a variety of laboratory tests and simulations.

It seems virtually certain that the combined and synergistic results of all these efforts will continue to improve the understanding of what takes place inside solid mine waste disposal facilities, and hence will lead to improved approaches to reduce and minimize the detrimental consequences of such wastes, unavoidably generated by mining. The commitment from many major mining companies and from numerous research and regulatory agencies toward such a goal is firm and unequivocal.

Why is all this waste continued to be produced? Is there no alternative? Are there no mining methods that allow recovery without the production of all these massive amounts of waste?

On occasion, although mostly in the somewhat distant past, dreamers, or innovative thinkers have conceptualized mining methods, e.g., in situ mining, that bypass the need for the removal of the vast amount of overburden or barren rock that are typically used in mining. In fact, for a few minerals this is a common mining method. Minerals most commonly mined by in situ mining methods include sulfur and rock salt.

Sulfur is routinely mined by drilling boreholes into the sulfur deposits, injecting hot steam, under high pressure and temperature, thereby melting the sulfur, and then pumping the molten sulfur to the surface. Rock salt frequently is mined by drilling holes into the salt deposit to be mined, injecting water through the hole, allowing salt to dissolve in the water, and then pumping the salt-laden brine to the surface, where the water is evaporated, and the salt crystallized and

recovered. These highly unusual mining practices are possible for these specific minerals because of some unique characteristic (i.e., low melting point, ready solubility). Rarely are such methods feasible for any other materials.

In situ leaching, dissolving metals of interest and value while leaving them in the ground, by accessing ore deposits with boreholes, has been of interest for decades. It is used on an extensive scale for uranium, for which it is a major mining method. It has been practiced on a few occasions for copper, although most commonly in association with conventional mining, e.g., in halos of low-grade ore near mined out richer deposits. It has been discussed for gold. A major concern for in situ mining, especially when considering the use of solvents, is the potential for environmental impact, notably the risk of groundwater contamination. While conceptually feasible, the installation of impermeable barriers around a site to be leached is not easy, certainly is expensive, and confidently assuring that they truly are and will remain impermeable would be a challenge.

In situ coal gasification has been demonstrated to be feasible in several countries. The method essentially consists of starting a controlled fire in a coal seam, and limiting the oxygen available for combustion to assure that useful gases can be recovered, especially methane and carbon monoxide. While technically feasible, the economics clearly have not been convincing for decades, and in this day and age it is likely that far more careful studies would be required of the environmental impacts of such methods.

The technical feasibility of in situ oil shale retorting has been demonstrated convincingly. By this method heavy viscous oil can be recovered from tight impermeable shale formations by inducing a controlled fire, raising the temperature, reducing the viscosity of the oil, increasing the rock permeability, thus allowing oil to flow, and to be recovered. As implemented so far, the method requires developing access along the top and along the bottom of the oil shale layer. This generates some solid waste, but certainly far less than if the shale were mined completely, and the oil recovery implemented on the surface, in surface retorts. Presumably when oil reaches the right price level, this method might be pursued as one option to generate energy, with less solid waste generation.

The most obvious and direct approach to reduce the need for mining, and the associated solid waste generation, is to further enhance and promote recycling. Recycling of metals has been practiced for many centuries, but has become more industrial based in recent decades, and has become driven more strongly by environmental concerns even more recently. Recycling of aluminum, long common and successful, historically has been pursued primarily because of the extremely favorable economics of aluminum recycling: large energy savings for recycling aluminum, as compared to production from raw ore, make it economically very attractive. To a much lesser degree, but nevertheless similarly driven, is the recycling of copper and steel. Recycling of silver and gold from electronic wastes is a well-established practice, as is the recycling of platinum and palladium from catalytic converters. In sum, metal recycling promises to continue to reduce the need for the production of virgin metal, and associated mine solid waste production. To date, it may have slowed the growth of new metal mining, but growth certainly still continues. Considering the large number of people who still live at a metal consumption level far below that of an adequate standard of living, it seems most likely that this trend will continue: recycling can substitute for some fraction of metal demand, but probably a relatively small fraction only, or at least only a fraction that does not yet make it possible to reduce mining new raw materials.

In a similar vein, one approach to reduce the need for energy mining, e.g., coal, uranium, and tar sands, is to strengthen energy conservation efforts. In parallel with the aggressive pursuit of renewable energy, this is likely to result in a reduction in the growth rate of the production of conventional fuels, and associated solid mine waste generation. To date, once again given the worldwide growth in energy demand, it appears that this will result in a reduced growth rate, not in actual reduced production.

Although an argument can be made that recycling of construction materials has been practiced since historical times, in many societies people have dismantled ancient structures, ruins, to reuse building stone, industrial scale recycling of concrete and asphalt is fairly new. Today it is being pursued quite aggressively in many societies. As the impetus for doing so strengthens, and, as a result, as the equipment and the methods for such

recycling keep on being improved, it is likely that recycling of such basic construction materials as crushed rock, sand, and gravel, i.e., aggregates, will expand, and, correspondingly, will result in reduced demand for newly mined materials. This may be a significant contributor to reducing the demand for new quarries, in those societies where recycling of these materials can provide a significant fraction of the demand for such materials. It will have far less impact, if any, in societies where basic infrastructure still needs to be built.

Conceptually, one might conceive of a society less material intensive. And to a significant extent modern societies have achieved this. Modern electronics deliver far more than their far heavier precursors. Far less metal is needed for modern devices of many kinds than used to be the case. To date this is not reflected in a reduced overall demand for metal, energy, or construction rock. While gadgets have become lighter, they also have become more numerous. Houses have become larger, requiring more concrete, copper, and glass. Cars have become larger, at least in some societies, requiring more steel and copper. Unless societal preferences change rather drastically, a move toward a less materials-intensive culture does not appear imminent. As of now, it seems far more likely that the demand for minerals will continue to grow, but it seems equally likely that environmental control requirements will continue to intensify on the producers of the minerals societies desire and need.

According to its 2001 Environment Outlook [8, p. 238] the OECD expects that in OECD countries "...waste from the primary sectors, such as ... mining and quarrying, is expected to grow at a slower rate" (i.e., slower than other wastes, such as municipal waste and manufacturing waste). Even in advanced societies solid mine waste is still expected to grow, not decline. In an updated version of its projections [9, p. 239] OECD estimates that by 2020 metal ore extraction will increase from 5.8 billion tons in 2000 to more than 11 billion tons in 2020. On a per capita base, OECD expects that the solids extraction in OECD countries will reach 22 tons per person by 2020, and 9 tons in the BRIICS countries (Brazil, Russia, India, Indonesia, China, and South Africa). This, combined with the expected population growth in most of these countries indicates why it is virtually certain that the scale of the solid mine waste problem is likely to increase substantially over the next decade, and most likely for several decades beyond that, at least. OECD countries produce about 30% of metal ores, BRIICS countries nearly 40%, and the rest of the world slightly over 30%. Hence the impact of solid waste generated by mining is widespread.

It seems certain and obvious that societies will continue to become less and less tolerant for the types of environmental impacts that mining used to have. In order to successfully provide the minerals needed for people, it is essential that the mineral producers develop mining methods that allow the management of solid mining wastes without unacceptable detrimental consequences.

Acknowledgment

The authors would like to thank Mr. Kıvanç Okalp, Coordinator of Projects, Beray Engineering Consultancy Ltd. for his assistance in drafting the illustrations in this chapter.

Bibliography

Primary Literature

1. Nazzaro RM (2008) Hardrock mining-information on abandoned mines and value and coverage of financial assurances on BLM land, United States Government Accountability Office, Testimony GAO-08-574 T (United States Government Accountability Office, Washington, DC)
2. UNEP (1997) Mining – facts and figures. Ind Environ 20:4–9
3. European Commission (2009) Reference document on best available techniques for management of tailings and waste-rock in mining activities. http://eippcb.jrc.ec.europa.eu. Accessed 8 April 2010
4. Twardowska I, Allen HE (2004) Solid waste origins: sources, trends, quality, quantity, Chapter I.2. In: Twardowska I, Allen HE, Kettrup AAF, Lacy WJ (eds) Solid waste: assessment, monitoring and remediation. Amsterdam, Elsevier, pp 33–88
5. Szczepańska J, Twardowska I (2004) Mining waste, Chapter III.6. In: Twardowska I, Allen HE, Kettrup AAF, Lacy WJ (eds) Solid waste: assessment, monitoring and remediation. Amsterdam, Elsevier, pp 319–385
6. Michalek SJ, Gardner GH, Wu, KK (n.d.) Accidental releases of slurry and water from coal impoundments through abandoned underground coal mines (Mine Safety and Health Administration. Pittsburgh Safety and Health Technology Center, Pittsburgh, PA. www.msha.gov/S&HINFO/ TECHRPT/ MINEWASTE/ASDSO2.pdf). Accessed 6 April 2010
7. Daemen JJK (2009) Geotechnical/geomechanical mine failures. International workshop on winning strategies to

revitalize the mineral sector, August 8–9 2009. Department of Mining Engineering, National Institute of Technology Karnataka, Surathkal, India, Proceedings pp 111–125
8. OECD (2001) OECD Environmental outlook environment (Organisation for Economic Co-Operation and Development, Paris, France)
9. OECD (2008) OECD Environmental outlook to 2030 (Organisation for Economic Co-Operation and Development, Paris, France)

Books and Reviews

Agioutantis Z, Komnitsas K (eds) (2006) In: Proceedings of the 2nd international conference on advances in mineral resources management and environmental geotechnology (AMIREG 2006), 25–27 September 2006. Chania, Crete, Greece, Heliotopos conferences, Athens

Aplin CL (1973) Tailings disposal today. In: Proceedings international tailings symposium (1st, 1972, Tucson, AZ). Miller Freeman Publications, San Francisco

Argall Jr GO (1979) Tailings disposal today. In: Proceedings of the second international tailings symposium, vol 2, May 1978. Denver, CO, Miller Freeman Publications, San Francisco

Aston RL (1999) The legal, engineering, environmental and social perspectives of surface mining law and reclamation by landfilling: getting maximum yield from surface mines. Imperial College Press, London

Azcue JM (ed) (1999) Environmental impacts of mining activities: emphasis on mitigation and remedial measures. Springer, Berlin/Heidelberg/New York

Beedlow PA, Gee GW, Cline JF, Walters WH, Freeman HD (1985) Determination of compliance with criteria for final tailings disposal site reclamation, technical report NUREG/CR-4076, PNL-5324. Prepared by Pacific Northwest labs, Richland, WA (USA) for the US Nuclear Regulatory Commission, Washington, DC

Bell FG (1998) Environmental geology: principles and practice. Blackwell Science, Oxford

Bennett RD, Horz RC, Kimbrell AF (1991) Recommendations to the NRC for soil cover systems over uranium mill tailings and low-level radioactive wastes, NUREG/CR-5432. US Nuclear Regulatory Commission, Washington, DC

Billings Land Reclamation Symposium (2000). In: Proceedings 2000 Billings land reclamation symposium: March 20–24, 2000, Billings, MT. Reclamation Research Center, Water Center, Montana State University, Bozeman

Bouazza A, Kodikara J, Parker R (eds) (1997) Environmental geotechnics. In: Proceedings of the 1st Australia-New Zealand conference on environmental geotechnics-geoenvironment 97, Melbourne, VIC, Australia, 26–28 November 1997. AA Balkema, Rotterdam/Brookfield

Broughton SE (1992) Documentation and evaluation of mine dump failures for mines in British Columbia, mine rock and overburden piles. Review and evaluation of failures, interim report, British Columbia mine waste rock pile research committee. Ministry of Energy, Mines and Petroleum Resources, British Columbia

Cabri LJ, Vaughan DJ (1998) Modern approaches to ore and environmental mineralogy, short course handbook, vol 27. Mineralogical Association of Canada, Ottawa

Chalkley ME, Couard BR, Lakshmanan VI, Wheeland KG (eds) (1989) Tailings and effluent management. In: Proceedings, The metallurgical society of the Canadian Institute of Mining and Metallurgy, vol 14. Pergamon Press, New York

Charles River Associates Incorporated (1985) Estimated costs to the US mining industry for management of hazardous solid wastes. Prepared for US Environmental Protection Agency, Division of Solid Waste Management, Washington, DC. Charles River Associates Incorporated, Boston, MA

Chaudhuri AB (1992) Mine environment and management (an Indian scenario). Ashish Publishing House, New Delhi

Coates DF, Yu YS (eds) (1977) Pit slope manual, Chapter 9-Waste embankments, CANMET (Canadian Centre for Mineral and Energy Technology, formerly Mines Branch, Energy Mines and Resources Canada, CANMET Report 77-1. Ottawa, Canada

Colorado State University Geotechnical Engineering Program (1980) Uranium tailings management. In: Proceedings of the third symposium, November 24–25, 1980, organized by the Geotechnical Engineering Program. Civil Engineering Department, Colorado State University. Colorado State University, Fort Collins, CO

Colorado State University Geotechnical Engineering Program (2001) Tailings and mine waste'01. In: Proceedings of the eight international conference on tailings and mine waste, Fort Collins, CO, 16–19 January 2001. AA Balkema, Rotterdam

Colorado State University Geotechnical Engineering Program (2002) Tailings and mine waste'02. In: Proceedings of the ninth international conference on tailings and mine waste, Fort Collins, CO, 27–30 January 2002. AA Balkema, Rotterdam

Commission of inquiry appointed by his excellency the President of the Republic of Zambia Dr. Kenneth David Kaunda (1971) The Mufulira mine disaster. Republic of Zambia, Lusaka

Commission of the European Communities (2003) Proposal for a directive of the European Parliament and of the Council on the management of waste from the extractive industries, 2003/0107(COD), COM(2003) 319 final. Commission of the European Communities, Brussels

Commission of the European Communities (2006) Directive (2006/21/EC) of the European Parliament and of the Council on the management of waste from the extractive industries, EN, L 102/15-33, 11.04.2006. Commission of the European Communities, Brussels

Committee on Embankment Dams and Slopes (1979) Current geotechnical practice in mine waste disposal. American Society of Civil Engineers, New York

Daniel DE (ed) (1993) Geotechnical practice for waste disposal. Chapman & Hall, London

D'Appolonia Consulting Engineers (1985) Engineering and design manual: Coal refuse disposal facilities. US Department of the Interior, Mining and Safety Administration, Washington, DC

Davies WE, Bailey JF, Kelly DB (1972) West Virginia's Buffalo Creek flood: a study of the hydrology and engineering geology. Geological Survey Circular 667, US Geological Survey, Washington, DC

DeGraff JV (ed) (2007) Understanding and responding to hazardous substances at mine sites in the western United States, reviews in engineering geology XVII. The Geological Society of America, Boulder

Denham DH, Barnes MG, Rathbun LA, Young JA (1985) Monitoring methods for determining compliance with decommissioning cleanup criteria at uranium recovery sites, Technical report NUREG/CR-4118, PNL-5361. Prepared by Pacific Northwest labs, Richmond, WA for the US Nuclear Regulatory Commission, Washington, DC

Dhar BB (ed) (1990) Environmental management of mining operations. Ashish Publishing House, New Delhi

Dhar BB (2000) Mining & environment. APH Publishing Corporation, New Delhi

DHI Water-Environment-Health (2007) Classification of mining waste facilities, European Commission DG Environment Final Report No. 07010401/2006/443229/MAR/G4. Prepared by DHI Environment Health in cooperation with SGI, Swedish Geotechnical Institute and AGH University of Science and Technology, Krakow. http://europa.eu/legislation_summaries/environment/waste_management/128134_en.htm. Accessed 6 April 2010

Doyle FM (ed) (1990) Mining and mineral processing wastes. In: Proceedings of the western regional symposium on mining & mineral processing wastes, Berkeley, California, May 30–June 1, 1990. Society for Mining, Metallurgy, and Exploration, Littleton, CO

Down CD, Stocks J (1976) The environmental impact of large stone quarries and open-pit non-ferrous metal mines in Britain. Department of the Environment and Transport Research Report 21, South Ruislip, United Kingdom

Down CG, Stocks J (1977) Environmental impact of mining. A Halsted press book. Wiley, New York

Environment Protection Agency (1995) Tailings containment. Australian Federal Environment Department, Barton Act, Australia

Erikson KT (1976) Everything in its path-destruction of community in the Buffalo Creek flood. Simon and Schuster, New York

Fourie A (2008) Rock dumps 2008. In: Proceedings of the first international seminar on the management of rock dumps, Stockpiles and heap leach pads, 5–6 March, 2008, Perth, Australia. Australian Centre for Geomechanics, Nedlands, Western Australia

Fourie A, Tibbet M (eds) (2009) Mine closure 2009. In: Proceedings of the fourth international conference on mine closure, Perth, Australia, 9–11 September, 2009. Australian Centre for Geomechanics, Nedlands, Western Australia

Fung R (ed) (1981) Surface coal mining technology: engineering and environmental aspects, energy technology review no. 71, Pollution technology review no. 83. Noyes Data Corp, Park Ridge, NJ

Gadsby JW (ed) (1990) Acid mine drainage: designing for closure. BiTech, Vancouver

Goin P, Raymond CE (2004) Changing mines in America, Center for American Places, Santa Fe, NM. Distributed by University of Chicago Press, University of Chicago, Chicago, IL

Golder Associates (1994) Mined rock and overburden piles. Consequence assessment for mine waste dump failures, Interim report, British Columbia Mine Waste Rock Pile Research Committee. British Columbia Ministry of Energy, Mines and Petroleum Resources, BC

Golder associates (1995) Mined rock and overburden piles. Runout characteristics of debris from dump failures in mountainous terrain, stage 2: Analysis, modelling and prediction, Interim report, British Columbia Mine Waste Rock Pile Research Committee, British Columbia Ministry of Energy, Mines and Petroleum Resources, BC

Hudson-Edwards K, Savage K, Jamieson H, Taylor K, Martin RF (eds) (2009) Minerals in contaminated environments: Characterization, stability, impact, The Canadian Mineralogist, Thematic Issue, Vol. 47, Part 3. Mineralogical Association of Canada, Québec

Hutchison IPG, Ellison, RD (eds) (1992) Mine waste management: a resource for mining industry professionals, regulators, and consulting engineers. Sponsored by California Mining Association, Lewis Publishers, Chelsea, MI

Hustrulid WA, McCarter MK, van Zyl DJA (eds) (2000) Slope stability in surface mining, section 3. In: Tailings and heap leaching. Society of Mining, Metallurgy, and Exploration, Littleton, CO, pp 265–362

Hustrulid WA, McCarter MK, van Zyl DJA (eds) (2000) Stability of waste rock embankments, Section 4. In: Tailings and heap leaching, Society of Mining, Metallurgy, and Exploration, Littleton, CO, pp 363–438

IAEA (2002) Monitoring and surveillance of residues from the mining and milling of uranium and thorium. IAEA (International Atomic Energy Agency), Vienna

IAEA (2004) The long term stabilization of uranium tailings: final report of a coordinated research project 2000–2004. IAEA (International Atomic Energy Agency), Vienna

IAEA (2010) Best practice in environmental management of uranium mining, IAEA Nuclear Energy Series No. NF-T-1.2, IAEA (International Atomic Energy Agency), Vienna

ICOLD (1989) Tailings dam safety: guidelines. International Commission on Large Dams, Paris

ICOLD (1994) Tailings dams design of drainage, review and recommendations. International Commission on Large Dams, Paris

ICOLD (1995) Tailings dams: transport placement and decantation. International Commission on Large Dams, Paris

ICOLD (1995) Tailings dams and seismicity: review and recommendations. International Commission on Large Dams, Paris

ICOLD (1996) A guide to tailings dams and impoundments: design, construction, use and rehabilitation, bulletin 106. International Commission on Large Dams, Paris

ICOLD (1996) Monitoring of tailings dams: review and recommendations. International Commission on Large Dams, Paris

ICOLD (2001) Tailings dams risk of dangerous occurrences: lessons learnt from practical experiences. International Commission on Large Dams, Paris

International Conference on Tailings & Mine Waste (2001) Tailings and mine waste'01. In: Proceedings of the eight international conference on tailings and mine waste'01, Fort Collins, CO, USA, 18–19 January 2001. AA Balkema, Rotterdam

Jacobs Engineering Group, Inc. (1994) Remedial action plan and site design for stabilization of the inactive uranium mill tailings sites at Slick Rock, Colorado, remedial action selection report, preliminary final, DOE/AL/62350-21PF. US Department of Energy, UMTRA Project Office, Albuquerque, New Mexico. www.osti.gov/bridge/servlets/purl/10135330-8eDj6i/.../10135330.pdf

Jambor JL, Blowes DW (eds) (1994) The environmental geochemistry of sulfide mine-wastes, Mineralogical Association of Canada short course series vol 22. Mineralogical Association of Canada, Neapan, ON

Jambor JL, Blowes DW, Ritchie AIM (2003) Environmental aspects of mine wastes, short course series, vol 31. Mineralogical Association of Canada, Ottawa

Koerner RM, Daniel DE (1997) Final covers for solid waste landfills and abandoned dumps. ASCE Press, Reston, VA and Thomas Telford, London

Kreft-Burman K, Saarela J, Anderson R (2005) Tailings management facilities legislation, authorisation, management, monitoring and inspection practices, TAILSAFE, http://www.tao;safe.com. Finnish Environment Institute (SYKE), Helsinki

Lindsey CG, Long LW, Begej CW (1982) Long-term survivability of riprap for armoring uranium mill tailings and covers: a literature review, NUREG/CR-2642. Division of Health, Siting and Waste Management, Office of Nuclear Regulatory Research, US Nuclear Regulatory Commission, Washington, DC

Lottermoser BG (2007) Mine wastes: characterization, treatment and environmental impacts, 2nd edn. Springer, Berlin

Lusher JH (2003) Standard review plan for the review of a reclamation plan for mill tailings sites under Title II of the Uranium Mill Tailings Radiation Control Act of 1978, Final report. NUREG-1620, Rev. 1, Office of Nuclear Material Safety and Safeguards, US Nuclear Regulatory Commission, Washington, DC. http://www.nrc.gov/reading-rm/doc-collections/nuregs/staff/sr1620/sr1620r1.pdf

Marcus JJ (ed) (1997) Mining environmental handbook: effects of mining on the environment and American environmental controls on mining. Imperial College Press, London

McCarter MK (ed) (1985) Design of non-impounding mine waste dumps. Society of Mining Engineers of the American Institute of Mining, Metallurgical, and Petroleum Engineers, New York

Mining Association of Canada (1998) A guide to the management of tailings facilities. The Mining Association of Canada, Ottawa, ON. www.mining.ca/english/ publications/tailingsguide.pdf

Mining Journal Research Services (1996) Environmental and safety incidents concerning tailings dams at mines: results of a survey for the years 1980–1996. United Nations Environment Programme, Industry and Environment, Paris

Montana Department of Natural Resources and Conservation Engineering Bureau (1977) Mine drainage control from metal mines in a subalpine environment-A feasibility study, EPA-600/2-77-224, Environmental Protection Technology Series. US Environmental Protection Agency, Industrial Environmental Research Laboratory, Office of Research and Development, Cincinnati, OH

MSHA (1979) Design guidelines for coal refuse piles and water, sediment, or slurry impoundments and impounding structures, Informational report 1109. US Department of Labor, Mine Safety and Health Administration, Arlington, VA

MSHA (2007) MSHA coal mine impoundment inspection and plan review handbook. US Department of Labor, Mine Safety and Health Administration, Arlington, VA. www.arblast.osmre.gov/.../MSHA%20PH07CoalImpoundmentinspection.pdf

Murray DR (1977) Pit slope manual, supplement 10-1-Reclamation by vegetation: vol 1-Mine waste description and case histories; CANMET (Canadian Centre for Mineral and Energy Technology, formerly Mines Branch, Energy Mines and Resources, Canada, CANMET report 77-31. Ottawa

Murray DR (1977) Pit slope manual, supplement 10-1-Reclamation by vegetation: vol 2-Mine waste inventory by satellite imagery; CANMET (Canadian Centre for Mineral and Energy Technology, formerly Mines Branch, Energy Mines and Resources, Canada, CANMET report 77-58. Ottawa

National Coal Board (1972) Review of research on spoil pile tip materials, Lab. Reference No. S/7307. Wimpey Laboratories, Hayes, Middlesex

Nash JT (2002) Flood deposits of transported mill tailings in Nevada and Utah: evidence for tailings dam failures and implications for risk assessment. US Geological Survey open-file report 02-431. US Department of the Interior, US Geological Survey, Denver, CO

Nash JT (2003) Historic mills and mill tailings as potential sources of contamination in and near the Humboldt River basin, Northern Nevada, USGS Bulletin 2210-D, Version 1.0. US Geological Survey, Denver, CO. pubs.usgs.gov/bul/b2210-d/B2210-D-508.pdf

National Research Council (1974) Rehabilitation potential of western coal lands: a report to the energy policy project of the Ford foundation. Ballinger, Cambridge

National Research Council (1979) Surface mining of non-coal minerals: a study of mineral mining from the perspective of the surface mining control and reclamation act of 1977: a report. National Academy of Sciences, Washington, DC

National Research Council (2002) Coal waste impoundments-risks, responses, and alternatives. National Academy Press, Washington, DC

Nelson JD, Abt SR, Volpe RL, van Zyl D, Hinkle HE, Staub WP (1986) Methodologies for evaluating long-term stabilization designs of uranium mill tailing impoundments, NUREG/CR-4620. US Nuclear Regulatory Commission, Washington, DC

Northwest Mining Association (1990) Environmental compliance. Solutions that work, Northwest Mining Association and

Colorado Mining Association seminar, Denver, May 21–23, 1990. Northwest Mining Association, Spokane, WA

OECD (1978) In: Proceedings of the seminar on management, stabilisation and environmental impact of uranium mill tailings, organized by the OECD Nuclear Energy Agency, Albuquerque, United States. Organization for Economic Co-Operation and Development, Paris

OTA (1992) Managing industrial solid wastes from manufacturing, mining, oil and gas production, and utility coal combustion, Background paper OTA-BP-0-82. Congress of the United States, Office of technology assessment, US Government Printing Office, Washington, DC. www.fas.org/ota/reports/9225.pdf

Oweis IS, Khera RP (1998) Geotechnology of waste management, 2nd edn. PWS, Boston

Paşamehmetoğlu AG, Özgenoğlu A (eds) (1998) Environmental issues and management of waste in energy and mineral production. In: Proceedings, 5th international conference, Ankara, Turkey, 18–20 May, 1998. AA Balkema, Rotterdam

PEDCo (1984) Evaluation of management practices for mine solid waste storage, disposal, and treatment. American Mining Congress, Washington, DC

Peterson SD (1990) RCRA's solid waste regulation and its impact on resource recovery in the minerals industry, Mineral issues, An analytical series. US Department of the Interior, Bureau of Mines, Washington, DC

Pusch R (1994) Waste disposal in rock, developments in Geotechnical Engineering, 76. Elsevier Science, Amsterdam

Puura E, Marmo L, D'Alessandro M (eds) (2003) Workshop on mine and quarry waste-the burden from the past. Official Publications of the European Communities, Luxembourg

Ripley EA, Redmann RE, Crowder AA, Ariano TC, Corrigan CA, Farmer RJ, Jackson LM (1996) Environmental effects of mining. Lucie Press, Delray Beach

Ripley EA, Redmann RE, Maxwell J (1982) Environmental impact of mining in Canada. Centre for Resource Studies, Queen's University, Kingston

Ritcey GM (1989) Tailings management: problems and solutions in the mining industry. Elsevier, Amsterdam

Rockwell RB, McDougal RR, Gent CA (2005) Remote sensing for environmental site screening and watershed evaluation in Utah mine lands-East Tintic mountains, Oquirrh mountains, and Tushar mountains, Scientific investigations report 2004-5421. US Geological Survey, Reston, VA. pubs.usgs.gov/sir/2004/5241/pdf/SIR04-5421_508.pdf

Salomons W, Förstner U (eds) (1988) Chemistry and biology of solid waste: dredged material and mine tailings. Springer, Berlin

Salomons W, Förstner U (eds) (1988) Environmental management of solid waste: dredged material and mine tailings. Springer, Berlin

Sarsby RW, Felton AJ (2007) Geotechnical and environmental aspects of waste disposal sites. In: Proceedings of green4 international symposium on geotechnics related to the environment, Wolverhampton, UK, 28 June – July 1, 2004. Taylor & Francis, London

Sarsby R (2000) Environmental geotechnics. Thomas Telford, London

Sengupta M (1993) Environmental impacts of mining: monitoring, restoration, and control. Lewis, Boca Raton

Serne RJ, Peterson SR, Gee GW (1983) Laboratory measurements of contaminant attenuation of uranium mill tailings leachates by sediments and clay liners, technical report NUREG/CR-3124, PNL-4605. Prepared by Pacific Northwest Lab, Richland, WA for US Nuclear Regulatory Commission, Washington, DC

Sherwood DR, Serne RJ (1983) Tailings treatment techniques for uranium mill waste: a review of existing information, technical report NUREG/CR-2938; PNL-4453. Prepared by Pacific Northwest Lab, Richland, WA for US Nuclear Regulatory Commission, Washington, DC

Singhal RK, Mehrotra AK (eds) (2000) Environmental issues and management of waste in energy and mineral production. In: Proceedings 6th international conference, Calgary, AB, 30th May–2nd June, 2000. AA Balkema, Rotterdam

Soderberg RL, Busch RA (1977) Design guide for metal and nonmetal tailings disposal, Information Circular 8755. US Department of the Interior, Bureau of Mines, Washington, DC

Stanley G, Gallagher V, Mhairtin FN, Brogan J, Lally P, Doyle E, Farrell L (2009) Historic mine sites-inventory and risk classification, vol I. A joint study carried out by The Environmental Protection Agency and The Geological Survey of Ireland. www.dcenr.gov.ie/.../New+Collaborative+Study+by+the+EPA+and+GSI.htm

Symonds Group (2001) A Study on the costs of improving the management of mining waste, report to DG environment by Symonds group, in association with COWI, East Grinstead, Great Britain. http://ec.europa.eu/environment/waste/minng/legis.htm

Symposium on management of uranium mill tailings, low-level waste, and hazardous waste (1984) Management of uranium mill tailings, low-level waste and hazardous waste. In: Proceedings of the sixth symposium, February 1–3. Colorado State University, Fort Collins, CO

Symposium on Management of Uranium Mill Tailings, Low-Level Waste, and Hazardous Waste (1985) Management of uranium mill tailings, low-level waste and hazardous waste. In: Proceedings of the seventh symposium, February 1–3. Colorado State University, Fort Collins, CO

Symposium on uranium tailings management (1978) Uranium mill tailings management. In: Proceedings of a symposium, November 20, 21, 1978, organized by the Geotechnical Engineering Program, Civil Engineering Department, Colorado State University, Fort Collins, CO

Szymanski MB (1999) Evaluation of safety of tailings dams. BiTech, Vancouver

International Conference on Tailings & Mine Waste (2004) Proceedings of the eleventh tailings and mine waste conference, 10–13 October 2004, Vail, CO. AA Balkema, Leiden

Technical Committee on Research and Reclamation (2003) symposium Proceedings 1977–2002, CD-ROM, Digital Archive. Richmond, BC

Thorne PD (1992) Information for consideration in reviewing groundwater protection plans for uranium mill tailings sites. US Nuclear Regulatory Commission, Washington, DC

Trivedy RK, Sinha MP (1990) Impact of mining on environment. Ashish Publishing House, New Delhi

Twardowska I, Allen HE, Kettrup AA, Lacy WJ (2004) Solid waste: assessment, monitoring and remediation, vol 4, Waste Management Series. Elsevier, Amsterdam

United Nations Environment Programme (2001) Environmental aspects of phosphate and potash mining. International Fertilizer Industry Association, Paris

UNEP (2001) APELL for Mining, UNEP DTIE. Division of Technology, Industry and Economics, Paris. www.uneptie.org/pc/apell/publications

COLD US (1994) Tailings dam incidents. US Committee on Large Dams, Denver

US Congress Office of Technology Assessment (1992) Managing industrial solid wastes from manufacturing, mining, oil and gas production, and utility coal combustion-background paper, OTA-BP-O-82. US Government Printing Office, Washington, DC

US EPA (1980) Procedures manual for ground water monitoring at solid waste disposal facilities, SW-611, Office of Water & Waste Management. US Environmental Protection Agency, Washington, DC. nepis.epa.gov/. . ./2000QR04.TXT?. . . EPA. . .pubnumber%5E%22530SW611%22

US EPA (1985) Report to congress: wastes from the extraction and beneficiation of metallic ores, phosphate rock, asbestos, overburden from uranium mining, and oil shale, EPA/530-SW-85-033. US Environmental Protection Agency, Office of Solid Waste and Emergency Response, Washington, DC

US EPA (1994) US Environmental Protection Agency Mine Waste Policy Dialogue committee meeting summaries and supporting materials, EPA 530-R-94-043. US Environmental Protection Agency, Office of Solid Waste, Special Waste Branch, Washington, DC

US EPA (1994) Design and evaluation of tailings dams, technical report EPA530-R-94-038. US Environmental Protection Agency, Office of Solid Waste, Special Waste Branch, Washington, DC

US EPA (1994) Extraction and beneficiation of ores and minerals, vol 1: Lead-zinc, technical resource document EPA 530-R-94-011. US Environmental Protection Agency, Office of Solid Waste, Special Waste Branch, Washington, DC

US EPA (1994) Extraction and beneficiation of ores and minerals, vol 2: Gold, technical resource document EPA 530-R-94-013. US Environmental Protection Agency, Office of Solid Waste, Special Waste Branch, Washington, DC

US EPA (1994) Extraction and beneficiation of ores and minerals, vol 3: Iron, technical resource document EPA 530-R-94-030. US Environmental Protection Agency, Office of Solid Waste, Special Waste Branch, Washington, DC

US EPA (1994) Extraction and beneficiation of ores and minerals, vol 4: Copper, technical resource document EPA 530-R-94-031. US Environmental Protection Agency, Office of Solid Waste, Special Waste Branch, Washington, DC

US EPA (1994) Extraction and beneficiation of ores and minerals, vol 5: Uranium, technical resource document EPA 530-R-94-032. US Environmental Protection Agency, Office of Solid Waste, Special Waste Branch, Washington, DC

US EPA (1994) Extraction and beneficiation of ores and minerals, vol 6: Gold placers, technical resource document EPA 530-R-94-035. US Environmental Protection Agency, Office of Solid Waste, Special Waste Branch, Washington, DC

US EPA (1994) Extraction and beneficiation of ores and minerals, vol 7: Phosphate and molybdenum, technical resource document EPA 530-R-94-034. US Environmental Protection Agency, Office of Solid Waste, Special Waste Branch, Washington, DC

US EPA (1994) Innovative methods of managing environmental releases at mine sites, OSW doc 530-R-94-012. US Environmental Protection Agency, Office of Solid Waste, Special Wastes Branch, Washington, DC

US EPA (1994) Treatment of cyanide heap leaches and tailings, technical report EPA 530-R-94-037. US Environmental Protection Agency, Office of Solid Waste, Special Waste Branch, Washington, DC

US EPA (1994) Acid mine drainage prediction, technical report EPA 530-R-94-036, US Environmental Protection Agency, Office of Solid Waste, Special Waste Branch, Washington, DC

US EPA (1995) Human health and environmental damages from mining and mineral processing wastes. US Environmental Protection Agency, Office of Solid Waste, Special Wastes Branch, Washington, DC. http://www.epa.gov/waste/nonhaz/industrial/special/mining/minedock/damage/index.htm. Accessed February 27, 2010

US EPA (2008) Mineral processing waste. US Environmental Protection Agency, Office of Solid Waste, Special Wastes Branch, Washington, DC. http://www.epa.gov/osw/nonhaz/industrial/special/mineral/index.htm. Accessed February 27, 2010

US EPA (2009) Mining waste. US Environmental Protection Agency, Office of Solid Waste, Special Wastes Branch, Washington, DC. http://www.epa.gov/osw/nonhaz/industrial/special/mining/index.htm. Accessed February 27, 2010

US MSHA (2003) Internal review of MSHA's actions at the Big branch refuse impoundment, Martin County Coal Corporation, Inez, Martin County, Kentucky. US Department of Labor, Mine Safety and Health Administration, Arlington, VA. http://www.msha.gov/MEDIA/PRESS/2003/Report20030113.pdf

US NRC (1980) Final generic environmental impact statement on uranium milling, project M-25. Office of Nuclear Material Safety and Safeguards, US Nuclear Regulatory Commission, Washington, DC

van Zyl D (1993) Mine waste disposal. In: Daniel DE (ed) Geotechnical practice for waste disposal, Chapter 12. Chapman & Hall, London, pp 269–286

van Zyl D, Koval M, Li TM (1992) Risk assessment/management issues in the environmental planning of mines. Society for Mining, Metallurgy, and Exploration, Inc, Littleton

van Zyl DJA, Vick SG (eds) (1988) Hydraulic fill structures: a specialty conference sponsored by the geotechnical engineering division of the American Society of Civil Engineers (ASCE), co-sponsored by the Society of Mining Engineers of AIME, Colorado State University, Fort Collins, CO, August 15–18, 1988. American Society of Civil Engineers (ASCE), New York

Vick SG (1983) Planning, design, and analysis of tailings dams. Wiley, New York

Walters WH, Skagss RL, Foley MG, Beedlow PA (1986) Erosion protection of uranium tailings impoundments, technical report NUREG/CR-4480, PNL-5724. Prepared by Pacific Northwest Lab, Richmond, WA for the US Nuclear Regulatory Commission, Washington, DC

Waters JA, Brink D (eds) (1987) Mining and industrial waste management. In: Proceedings of the international conference, Johannesburg. South African Institution of Civil Engineers, Johannesburg

Whitby-Costescu L, Shillabeer J, Coates DF (1977) Pit slope manual, Chapter 10-Environmental planning; CANMET (Canadian Centre for Mineral and Energy Technology, formerly Mines Branch, Energy Mines and Resources, Canada, CANMET report 77-2. Ottawa

Williams RE (1975) Waste production and disposal in mining, milling, and metallurgical industries. Miller Freeman, San Francisco

Wilson D (ed) (1981) Design and construction of tailings dams: Proceedings of a seminar, November 6–7, 1980, Colorado School of Mines Press, Golden, CO

Yegulalp TM, Kim K (eds) (1990) Environmental issues and waste management in energy and minerals production. In: Proceedings of the first international conference, Battelle Press, Columbus-Richland, Secaucus, NJ, August, 27–29

Modern Nuclear Fuel Cycles

James S. Tulenko
Laboratory for Development of Advanced Nuclear Fuels and Materials, University of Florida, Gainesville, FL, USA

Article Outline

Glossary
Definition of the Subject
Introduction
The Nuclear Fuel Cycle
Uranium History
History of Uranium
Uranium Conversion and Enriching
Nuclear Fuel Fabrication
Nuclear Fuel Operation and Disposal
Future Directions
Bibliography

Glossary

Uranium Occurs in most rocks in concentrations of 2 (sedimentary rocks) to 4 (granite) ppm.

Thorium More readily available nuclear fuel than uranium, being four times more abundant than uranium in the earth's crust.

Uranium dioxide (UO_2) An insoluble oxide of uranium which is the form commonly used in commercial nuclear fuel.

Pitchblende An ore with a very high UO_2 content of up to 70%. Pitchblende also contains radium, thorium, cerium, and lead.

The United States Nuclear Regulatory Commission Regulatory body for radioactive materials and nuclear power plants.

The department of energy Required by law to be responsible for the spent fuel and collects a fee of 1 mill/kWh of nuclear electricity for disposal.

MWD/MTU (mega watt days of energy produced per metric ton of uranium contained) Energy produced per metric ton of uranium (fuel) contained. Current Nuclear Regulatory Commission limits for nuclear power plant fuel is 60,000 MWD/MTU. Normal lifetime of a fuel assembly is 55,000 MWD/MTU.

Definition of the Subject

The Nuclear Fuel Cycle describes the entire process followed to convert uranium or thorium ore to its useful state in nuclear power reactors, and its ultimate and current disposal. The cycle has been followed since the 1960s to produce electrical power safely, and without emissions of environmentally endangering carbon gases.

Introduction

Madame Marie Curie, a pioneer in the field of radioactivity and the first person honored with two Nobel Prizes, discovered radioactivity in 1898, and since then

many radioactive elements have seen various uses. One in particular, uranium, has been used for its fissionable properties. When a uranium (or plutonium) atom fissions, it releases approximately 200 MeV of energy. The burning of a carbon (coal) atom releases merely 4 eV. The difference between the two – a 50 million-times advantage in nuclear energy release – shows the tremendous advantage in magnitude between chemical and nuclear energy. This advantage is used for common good in nuclear power reactors around the world. Currently, the United States lags France in the use of nuclear power with the United States obtaining ~20% of its electrical energy from nuclear power plants, while France obtains ~80% of its electrical energy from nuclear power plants. Worldwide, approximately 18% of all electrical energy is produced by nuclear power plants.

The Nuclear Fuel Cycle

The nuclear fuel cycle uses two naturally occurring elements, uranium and thorium, which are both relatively common metals. Both materials are obtained by mining the earth. Uranium occurs in most rocks in concentrations of 2 (sedimentary rocks) to 4 (Granite) ppm. Uranium also occurs in seawater in a concentration of 0.003 ppm, which corresponds to approximately 4 billion tons of uranium in the oceans. Uranium (1.8 g/t) is more abundant than common materials such as silver (0.07 g/t), tungsten (1.5 g/t) and Molybdenum (1.5 g/t) [1]. It is 800 times more abundant than gold. Natural (as mined) uranium contains in atomic abundance 99.2175% Uranium-238 (U-238); 0.72% Uranium-235 (U-235); and 0.0055% Uranium-234 (U-234). Uranium has atomic number 92, meaning all uranium atoms contain 92 protons, with the rest of the mass number being composed of neutrons. All uranium isotopes are radioactive. This radioactive property makes the detection of uranium deposits relatively easy, even allowing for prospecting by air. Uranium-238 has a half-life of 4.5×10^9 years (4.5 billion years), U-235 has a half-life of 7.1×10^8 years (710 million years), and U-234 has a half-life of 2.5×10^5 years (250,000 years). All the U-234 currently present comes from the decay chain of U-238. Uranium-235 is the only fissile isotope available in nature. Uranium can be a fissionable fuel as mined in pressurized heavy water reactors designed by the Atomic Energy of Canada Limited (AECL). These reactors are termed CANDU for CANada Deuterium Uranium. As a by-product of the operation of a nuclear reactor, uranium-238 absorbs a neutron to form, through radioactve decay, the fissile fuel, plutonium-239. Another fissile isotope, uranium-233 comes from the naturally occurring thorium 232 when it captures a neutron. Finally, as part of the plutonium chain, plutonium-241 is also produced. It is important to note that it is the four odd number isotopes: 233, 235, 239, and 241, which are fissionable.

Thorium is an even more readily available nuclear fuel than uranium, being four times more abundant than uranium in the earth's crust. Thorium is the 39th most common element in the earth's crust and is about as common as lead. Thorium is present in the earth's crust with an average concentration of about 9.6 ppm. Thorium must be converted to a fissile fuel in a nuclear reactor by absorption of a neutron, forming through radioactive decay, the fissionable fuel, uranium-233. Thorium has only one naturally occurring isotope, thorium-232, which is radioactive with a half-life of 1.3×10^{10} years. India, which has large thorium deposits, has been a leader in utilizing thorium to breed uranium-233 to serve as a nuclear fuel. Other countries having major deposits of thorium are Australia, Norway, and the United States.

Uranium History

Uranium was discovered in 1789 by Martin Heinrich Klaproth, a German chemist, in the mineral pitchblende, which is primarily a mix of uranium oxides. No one could identify this new material he isolated, so in honor of the planet Uranus that had just been discovered, he called his new material Uranium. Although Klaproth, as well as the rest of the scientific community, believed that the substance he extracted from pitchblende was pure uranium, it was actually uranium dioxide (UO_2). It was not until 1842 that Eugene-Melchoir Peligot, a French chemist, noticed that "pure" uranium reacted oddly with uranium tetrachloride (UCl_4). He then proceeded to isolate pure uranium by heating the uranium dioxide with potassium in a platinum crucible. Radioactivity was first discovered in 1896 when the French scientist Henri Becquerel

accidentally placed some uranium salts near some paper-wrapped photographic plates and discovered the natural radioactivity of uranium.

Uranium compounds have long been used for centuries to color glass. Uranium trioxide (UO_3) was used in the manufacture of a distinctive orange Fiestaware dinnerware. In 1938, Otto Hahn (1879–1968), Lise Meitner (1878–1968), and Fritz Strassmann (1902–1980) were the first to recognize that the uranium atom under bombardment by neutrons, actually split, or fissioned.

When a uranium or plutonium atom is fissioned, it releases approximately 200 MeV of energy, while the burning of a carbon (coal) atom releases 4 eV. This difference of 50 million times in energy release shows the tremendous difference in magnitude between chemical and nuclear energy.

Thorium was discovered in 1829 by the Swedish chemist Jons Jacob Berzelius, who named the element after the Thor, the mythical Scandinavian god of war. He also was the first to isolate cerium, selenium, silicon, and zirconium. Thorium and thorium compounds have the properties of having very high melting temperatures. As a result, it was used for high-temperature application such as coatings on tungsten filaments in light bulbs and for high-temperature laboratory equipment. However, its use outside the nuclear fuel cycle has been greatly diminished because of state and federal laws concerning the handling and disposal of radioactive materials. Thorium is found in the minerals monazite and thorianite.

History of Uranium

The earliest recovery of uranium was from pitchblende, an ore with a very high UO_2 content of up to 70%. Pitchblende also contains radium, thorium, cerium, and lead. It is mostly found with deposits that contain phosphates, arsenates, and vanadates. Uranium exists in nature in two valence states, U^{6+} and U^{4+}. These properties are key to the geological distribution of uranium. U^{6+} is soluble in water, but changes to the insoluble U^{4+} in a reducing environment. The occurrence of reducing environments in riverbeds and seas have led to the formation of rich uranium deposits. A rich uranium deposit contains 2% uranium and economic deposits are as low as 0.1%. Once the ore is mined, it is sent to a mill, which is really a chemical plant that extracts the uranium from the ore. The ore arrives via truck and is crushed, leached, and approximately 90–95% of the uranium is recovered through solvent extraction. During the processing a large waste stream called tails is formed, which contains approximately 98–99.9% of the material mined. Because this waste stream or tails contains all the radioactive daughter products of uranium, such as radon and radium, this waste stream must be carefully controlled and stabilized. The tailings pile must have a cover designed to control radiological hazards for a minimum of at least 200 years and designed for 1,000 years, to the greatest extent reasonably achievable. It must also limit radon (^{222}Rn) releases to 20 pCi/m^2/s averaged over the disposal area. The end uranium product of the milling process is U_3O_8, better known as "yellowcake," because of its color.

Uranium Conversion and Enriching

The U_3O_8 concentrate must be both purified and converted to uranium hexafluoride (UF_6), which is the form required for the enriching process. At the conversion facility, the uranium oxide is combined with anhydrous HF and fluorine gas in a series of chemical reactions to form the chemical compound UF6. The product UF6 is placed into steel cylinders and shipped as a solid to a gaseous diffusion or gaseous centrifuge plant for enrichment. UF6 is a white crystalline solid at room temperature (its triple point is 64°C (147.3°F) and it sublimes at 56.5°C (133.8°F) at atmospheric pressure). The liquid phase only exists under pressures greater than about 1.5 atmospheres and at temperatures above 64°C. At the enrichment plant, the solid uranium hexafluoride (UF_6) from the conversion process is heated in its container until it becomes a gas. The container becomes pressurized as the solid melts UF_6 gas fills the container. The gaseous diffusion process is based on the difference in rates at which the fluorides of U-235 and U-238 diffuse though barriers. The uranium that has penetrated the barrier side is now slightly enriched in U-235 is withdrawn and fed into the next higher enrichment stage, while the slightly depleted material inside the barrier is recycled back into the next lower stage. It takes many hundreds of stages, one after the other, before the UF_6 gas contains

enough uranium-235 to be used as an enriched fuel in reactor. Each barrier has millions of holes per square inch with each hole approximately 10^{-7} in. in diameter. This gaseous diffusion enrichment process is very energy intensive, as the gas is compressed and expanded at each stage.

The other commercial enriching process, which uses an order of magnitude less energy, is the gaseous centrifuge process. The gas centrifuge uranium enrichment process uses a large number of rotating cylinders in series and parallel formations. Centrifuge machines are interconnected to form trains and cascades. In this process, UF_6 gas is placed in a cylinder and rotated at a high speed. This rotation creates a strong centrifugal force so that the heavier gas molecules (containing U-238) move toward the outside of the cylinder and the lighter gas molecules (containing U-235) collect closer to the center. The stream that is slightly enriched in U-235 is withdrawn and fed into the next higher stage, while the slightly depleted stream is recycled back into the next lower stage. At each stage of the gaseous diffusion process the U-235 is enriched by a factor of 1.004, where at each stage of the gaseous centrifuge process the stage enrichment factor is 1.2. For 1 kg of uranium enriched to 5% U-235, 9.4 kg of natural uranium feed are required and 8.4 kg of depleted uranium (tails) with a U-235 isotope content of approximately 0.2% are produced as a waste stream. The US Nuclear Regulatory Commission has decided that depleted uranium is a low level waste. The Department of Energy has over 560,000 mt stockpile of uranium tails stored as UF_6 in steel cylinders. The tails uranium has minor uses as a shields for radioactive sources, as the penetrator in armor piercing shells, as a yacht hold ballast, and as a weight for the balancing of helicopter rotor tips and passenger aircraft.

Nuclear Fuel Fabrication

The enriched UF_6 is transported to a fuel fabrication plant where the UF_6, in solid form in containers, is again heated to its gaseous form, and the UF_6 gas is chemically processed to form uranium dioxide (UO_2) powder. This powder is then pressed into pellets, sintered into ceramic form, loaded into Zircaloy tubes, pressurized with helium and sealed. The fuel rods are then placed into an array (17×17) which is bound together with guide tubes, spacer grids and top and bottom end fittings, all of which forms the nuclear fuel assembly. Depending on the type of light water reactor, a fuel assembly may contain up to 264 fuel rods and have dimensions of 5–6 in. square by about 12 ft long. The fuel is placed into containers and is trucked to the nuclear fuel plants to generate electricity. A single pressurized water fuel assembly contains about 500 kg of enriched uranium and can produces 200,000,000 kWh of electricity. Since the average national electrical yearly use per person is 11,867 kWh, a single nuclear fuel assembly gives 5,562 people their yearly electric needs during its 3 years of operation.

Nuclear Fuel Operation and Disposal

Every 12–24 months, US nuclear power plants are shut down and the oldest fuel assemblies are removed (approximately ⅓–½) and replaced with new fuel assemblies. The power production of a fuel assembly is measured in MWD/MTU or mega watt days of energy produced per metric ton of uranium (fuel) contained. Currently the normal lifetime of a fuel assembly is 55,000 MWD/MTU and the maximum lifetime currently allowed by the Nuclear regulatory commission is 60,000 MWD/MTU. At the end of its useful life, the spent fuel assembly is placed in a cooled borated water storage pond to allow for removal of the radioactive decay heat. After approximately 5 years of wet storage, the decay heat has been sufficiently decreased that the fuel assembly can be removed to dry storage in concrete or steel containers. Since only approximately 5% of the uranium fuel is destroyed, in Europe and Asia the spent fuel is reprocessed and the 95% of uranium remaining is recycled, with the 5% of radioactive waste products sent to waste storage. At the current time, the United States policy was to store the spent fuel in a waste repository being built at Yucca Mountain in Nevada. Most recently this site has become part of a political struggle and the current administration has moved to halt all licensing of the Yucca Mountain site and to convene a high level committee to revisit the question of nuclear waste disposal. The Department of Energy is required by law to be responsible for the spent fuel and collects a fee of 1 mill/kWh of nuclear electricity delivered, which is paid by consumers of nuclear-generated electricity. The one assembly described above

would generate approximately $200,000 in the waste fund for its disposal.

There is enough uranium and thorium in the world to produce the required amount of fuel to allow nuclear plants to produce the current rate of electrical energy usage for the next 1,000 years.

Future Directions

(A discussion including potential impacts on the development of certain areas of science.) With the dawn of the environmental awareness and new economies of energy production, the nuclear fuel cycle also is undergoing change. Research efforts are continuing to find new and more efficient ways to use the fissionable atom. Also, currently operating nuclear plants are becoming more efficient and cost beneficial. With no greenhouse gases to speak of, nuclear energy is bound to play a role in the nation's future energy needs. More than 100 nuclear reactors nationwide now provide almost 20% of our energy production. The large, proven-safe nuclear plants produce electricity best when running at full power, 24/7.

Bibliography

1. Cochran RG, Tsoulfanidis N (1999) The nuclear fuel cycle: analysis and management. American Nuclear Society, La Grange Park
2. Wilson PD (1996) The nuclear fuel cycle: from ore to waste. Oxford Science Publications, Oxford

Molecular Breeding Platforms in World Agriculture

Jean-Marcel Ribaut, Xavier Delannay, Graham McLaren, Frederick Okono
Integrated Breeding Platform, Consultative Group on International Agricultural Research, Generation Challenge Programme, c/o CIMMYT, Texcoco, Edo. Mexico

Article Outline

Glossary
Definition of the Subject
Introduction
Marker Technologies and Service Laboratories
Analytical Tools, Software, and Pipelines
Information Systems
Cyberinfrastructure and Data Management
Case Study: GCP's Integrated Breeding Platform
Scope and Potential for Molecular Breeding Platforms
Potential Economic Impact of Molecular Breeding Platforms
Future Directions
Conclusion and Prospective Scenarios
Bibliography

Glossary

Analytical pipeline A sequence of data management and statistical analysis algorithms which can be applied to one or more data sets to produce a result which can be interpreted and applied in decision making.

Capacity building Assistance that is provided to entities, usually institutions in developing countries, which have a need to develop a certain skill or competence, or for general upgrading of capability.

Cyberinfrastructure (CI) Computer-based research environments that support advanced data acquisition, data storage, data management, data integration, data mining, data visualization, and other computing and information processing services over the Internet. In scientific usage, CI is a technological solution to the problem of efficiently connecting data, computers, and people with the goal of enabling derivation of novel scientific theories and knowledge.

Gene Segment of DNA specifying a unit of genetic information; an ordered sequence of nucleotide base pairs that produce a certain product that has a specific function.

Information system (IS) An integrated set of computing components and human activities for collecting, storing, processing, and communicating information.

Integrated breeding platform (IBP) Term to describe a Molecular Breeding Platform (see below) in a broader sense including the availability of tools and services suitable for conventional breeding based on phenotypic selection only.

Molecular breeding (MB) Identification, evaluation, and stacking of useful alleles for agronomic traits of importance using molecular markers (MMs) in breeding programs. MB encompasses several modern breeding strategies, such as marker-assisted selection (MAS), marker-assisted backcrossing (MABC), marker-assisted recurrent selection (MARS), and genome-wide selection (GWS).

Molecular breeding platform (MBP) A term that has come to indicate a virtual platform driven by modern information and communication technologies through which MB programs can access genomic resources, advanced laboratory services, and analytical and data management tools to accelerate variety development using marker technologies.

Plant breeding The science of improving the genetic makeup of plants in order to increase their value. Increased crop yield is the primary aim of most plant breeding programs; benefits of the hybrids and new varieties developed include adaptation to new agricultural areas, greater resistance to disease and insects, greater yield of useful parts, better nutritional content of edible parts, and greater physiological efficiency especially under abiotic stress conditions.

Quantitative trait locus (QTL) A region of the genome that contains genes affecting a quantitative trait. Though not necessarily genes themselves, QTLs are stretches of DNA that are closely linked to the genes that underlie the corresponding trait.

Definition of the Subject

In the last decade, private seed companies have benefitted immensely from molecular breeding (MB) [1]. A private sector-led "gene revolution" has boosted crop adaptation and productivity in developed countries, by applying and combining the latest advances in molecular biology with cutting-edge information and communication technologies combined with accurate plant phenotyping.

MB allows the stacking of favorable alleles, or genomic regions, for target traits in a desired genetic background thanks to the use of polymorphic molecular markers (MMs) that monitor differences in genomic composition among cultivars, or genotypes, at specific genomic regions, or genes, involved in the expression of those target traits. The use of MMs generally increases the genetic gain per crop cycle compared to selection based on plant phenotyping only, and therefore reduces the number of needed selection cycles, hastening the delivery of improved crop varieties to the farmers.

In contrast to the private sector, MB adoption is still limited in the public sector, and is hardly used at all in developing countries. This is the result of several factors, among which are the following: (1) scientists from the academic world are more interested in discovering new genes or QTLs to be published than in applied biology; (2) until recently access to genomic resources was limited in the public sector, especially for less-studied crops; (3) public access to large-scale genotyping facilities was not easily available; and (4) although a broad set of stand-alone tools are available to conduct the multiple types of analyses necessitated by MB, no single analytical pipeline is available today in the public sector allowing integrated analysis in a user-friendly mode.

The situation is even more critical in developing countries as additional limitations include shortage of well-trained personnel, inadequate laboratory and field infrastructure, lack of ISs with applicable and flexible analysis tools, as well as inappropriate funding – simply put, resource-limited breeding programs. As a result, the developing world has yet to benefit from the MB revolution, and most of the countries indeed lack the fundamental prerequisites for a move to informatics powered breeding.

Under those circumstances, developing and deploying a sustainable web-based Molecular Breeding Platform (MBP) as a one-stop shop for information, analytical tools, and related services to help design and conduct marker-assisted breeding experiments in the most efficient way will alleviate many of the bottlenecks mentioned earlier. Such a platform will enable breeding programs in the public and private sectors in developing countries to accelerate variety development using marker technologies for different breeding purposes: major genes or transgene introgression via marker-assisted backcrossing (MABC), gene pyramiding via marker-assisted selection (MAS), marker-assisted recurrent selection (MARS) and, in a not too distant future, genome-wide selection (GWS).

Introduction

Since the dawn of agriculture, mankind has sought to improve crops by selecting individual plants with the most desirable characteristics or traits. Agricultural productivity has been progressively enhanced by constant innovation, including improved crop varieties to increase production in specific environments [2]. The major objective of crop improvement is to identify within heterogeneous materials those individuals for which favorable alleles are present at the highest proportion of loci involved in the expression of key traits [3]. The classical plant breeding method is based on increasing the probability of selecting such individuals from populations generated from sexual matings. Selection has traditionally been carried out at the whole-plant level (i.e., phenotype), which represents the net result of genotype and environment (and their interactions). Phenotypic selection has delivered tremendous genetic gains in most cultivated crop species, but is severely limited when faced with traits that are heavily modulated by the environment [4]. In addition, the nature of some traits can make the phenotypic testing procedure itself complex, unreliable, or expensive (or a combination of these).

The recent remarkable development of molecular genetics and associated technologies represents a quantum leap in our understanding of the underlying genetics of important traits for crop improvement. The ongoing revolutions in molecular biology and information technology offer tremendous and unprecedented opportunities for enhancing the effectiveness and efficiency of MB programs. Indirect selection, based on genetic markers, presents an efficient complementary breeding tool to phenotypic selection. Individual genes or QTLs having an impact upon target traits can be identified and linked with one or more markers, and then the marker loci can be used as a surrogate for the trait, resulting in greatly enhanced breeding efficiency [5–8].

Molecular techniques can have an impact upon every stage of the breeding process from parental selection and cross prediction [9], to introgression of known genes [10] and population enhancement. Selection of beneficial alleles of known genes can be done through marker-assisted selection (MAS) – the selection of specific alleles for traits conditioned by a few loci [10] – or through marker-assisted backcrossing (MABC) – transferring specific alleles of a limited number of loci from one genetic background to another, including transgenes [11, 12]. For marker-assisted population improvement, individuals selected from a segregating population based on their marker genotype are intermated at random to produce the following generation, at which point the same process can be repeated a number of times [13]. A second approach aims at direct recombination between selected individuals as part of a breeding scheme, seeking to generate an ideal genotype or ideotype [14]. The ideotype is predefined on the basis of QTL mapping within the segregating population, combined with the use of multi-trait selection indices that can also consider historical QTL data. This variety development approach is commonly referred to as marker-assisted recurrent selection (MARS) [15–17], or genotype construction. An alternative is to infer a predictive function using all available markers jointly, without significant testing and without identifying a priori a subset of markers associated with the traits of interest. This more recent approach coming from genomic medicine [18, 19], and then applied successfully in animal breeding [20] named genome-wide selection (GWS), also appears to be quite promising in crop improvement [7].

Concomitantly with the evolution of marker technologies becoming increasingly "data rich," the amount of data produced by plant breeding programs has increased dramatically in recent years. Increasingly, the critical factor determining the rate of progress in plant breeding programs is their capacity to manage large amounts of data efficiently and subsequently maximize the timely extraction of meaningful information from that data for use in selection decisions. If genotyping has become less of an issue, the efficient management of genotyping data in a broad sense, including sequence information, is increasingly becoming a major challenge in modern plant breeding. This was recognized early on in the private sector where the establishment of platforms or pipelines integrating field and laboratory processes with powerful data management systems (DMS) that merged and analyzed the data collected at every step and guided the process of crop improvement toward the release of improved cultivars has been the key to successful adoption of MB.

A few initiatives have taken place in the public sector to establish efficient data management or ISs [21, 22]. One of these has been led by several centers of the Consultative Group on International Agricultural Research (CGIAR) which have worked over the past decade, along with advanced research institutes (ARIs) and national agricultural research systems (NARS) in developing countries, to develop an open-source generic IS, the International Crop Information System (ICIS), to handle pedigree information, genetic resource, and crop improvement information [23]. Based on some elements of ICIS, the CGIAR Generation Challenge Programme (GCP, http://www.generationcp.org) has invested in integrating crop information with genomic and genetic information and in using existing or developing new public decision-support tools to access and analyze information resources in an integrated and user-friendly way [24]. Another initiative has been led by Primary Industries and Fisheries (PI&F) of the Queensland Government Department of Employment, Economic Development and Innovation in Australia, which recognized that effective data management is an essential element in obtaining maximum benefit from their investment in plant breeding. In conjunction with the New South Wales Department of Primary Industries (NSW DPI) and more recently Dart Pty Ltd (http://www.diversityarrays.com/) they are in the process of developing a linked IS for plant breeding (Katmandoo) that includes applications for capturing field data using hand-held computers, barcode-based seed management systems, and databases to store and link field trial data, laboratory data, genealogical data, and marker data [25].

Although an IS involves far more than a database, the development and implementation of a suitable database system alone remains a real challenge because of the fast turnover in technologies, the need to manage and integrate increasingly diverse and complex data types, and the exponential increase in data volume. Previous solutions, such as central databases, journal-based publication, and manually intensive data curation, are now being enhanced with new systems for federated databases, database publication, and more automated management of data flows and quality control. Along with emerging technologies that enhance connectivity and data retrieval, these advances should help create a powerful knowledge environment for genotype–phenotype information [26].

In addition to efficient data management, advances in statistical methodology [27–29], graphical visualization tools, and simulation modeling [9, 30–32] have greatly enhanced these ISs. The availability of molecular data linked to computable pedigrees [33] and phenotypic evaluation now makes genotype–phenotype analysis a practical reality [34].

In order to realize the full potential of marker technologies and bioinformatics in plant breeding, tools for molecular characterization, accurate phenotyping, efficient ISs, and effective data analysis must be integrated with breeding workflows managing pedigree, phenotypic, genotypic, and adaptation data. The goals of this integration of technologies are to (1) create genotype–phenotype trait knowledge for breeding objectives, and (2) use that knowledge in product development and deployment [4].

This entry generally explores the pace of innovation in world agriculture and the rise of MB. It particularly illustrates the accelerating application of information and communication technologies to the information management challenges of MB and, as a result, the emergence of virtual molecular breeding platforms (MBPs) as a vital tool for accelerating genetic gains and rapidly developing more resilient and more productive cultivars.

This entry reviews the rationale for access to MB technology and services and the status of existing public analytical pipelines and ISs for MB, and offers a detailed case study for the CGIAR GCP Integrated Breeding Platform (IBP) – the pioneer public sector MBP specifically targeting developing country breeding programs. It explores the gaps between countries and between crops in the application of informatics-powered MB approaches, and the potential for adopting MBPs to close these gaps; and it reviews institutional, governmental, and public support for these approaches. The entry discusses the challenges and opportunities inherent in MBPs, and the potential economic impact of MB. Finally, the entry explores the future directions and perspectives of MBPs.

Marker Technologies and Service Laboratories

Markers are "characters" whose pattern of inheritance can be followed at the morphological (e.g., flower

color), biochemical (e.g., proteins and/or isozymes), or molecular (DNA) levels. They are so called because they can be used to elicit, albeit indirectly, information concerning the inheritance of "real" traits. The major advantages of molecular over other classes of markers are that their number is potentially unlimited, their dispersion across the genome is complete, their expression is unaffected by the environment and their assessment is independent of the stage of plant development [35]. During the past two decades, DNA technology has been exploited to advance the identification, mapping, and isolation of genes in a wide range of crop species. The first generation of DNA markers, restriction fragment length polymorphisms (RFLPs), was used to construct the earliest genome-wide linkage maps [36] and identify the first QTLs [37, 38]. During the 1990s, emphasis switched to assays based on the polymerase chain reaction (PCR), which are much easier to use and potentially automatable [39]. The development of simple sequence repeats (SSRs) [40], amplified fragment length polymorphisms (AFLPs) [41], and single nucleotide polymorphism (SNP) [42] opened the door for large-scale deployment of marker technology in genomics and progeny screening.

SNPs are amenable to very high throughput and a wide range of detection techniques has been developed for them, from singleplex systems to high-density arrays. They can be used in fully integrated robotic systems going from automated DNA extraction to automated scoring in high-throughput detection platforms. The combination of increase in throughput and lowering in costs makes SNPs highly suitable to intensive marker applications in plant breeding such as MARS and the emerging approach of GWS. Based on SNP technology, production of molecular marker (MM) data expanded more than 40-fold between 2000 and 2006 at Monsanto, while cost per data point decreased to one sixth of the original cost [43].

With the transition from SSRs to SNPs and the concomitant large increase in the demand for genotyping as markers get more and more widely used in a broad range of applications from medicine to plant breeding, marker genotyping laboratories have evolved from relatively low-tech operations to highly automated, high-throughput laboratories using an array of sophisticated equipment (pipetting robots, high-density PCR, high-throughput SNP detection machines, high-level informatics). Although large private seed companies have had the need and the resources to put in place large-scale genotyping laboratories for their own uses, smaller programs, especially in the public sector, have typically not had the resources or the justification to establish such large operations to respond to their increasing need for SNP genotyping data. In response to this need, a few private marker service laboratories have sprung up over the past few years, which can provide complete genotyping services for their customers, from DNA extraction to generation of large numbers of SNP or other datapoints. Due to their broad customer base (from medical research laboratories to animal and plant breeding operations, both public and private), these laboratories can have a large volume of datapoint production which may lead to low costs for the customer and high throughput. They are able to invest in the most advanced equipment to keep up with the constant evolution of genotyping technologies and are able to pass on the resulting benefits to their customers. Processes have now been put in place for rapid shipment of leaf samples from any location (field or laboratory) around the world without any restrictions. Examples of such companies that can service breeding programs from around the world are DNA LandMarks, Inc. of Saint-Jean-sur-Richelieu, Quebec, Canada (http://www.dnalandmarks.ca/english/) and KBioscience Ltd. of Hoddesdon Herts, UK (http://www.kbioscience.co.uk/). For many public breeding programs and small companies, especially in developing countries, it is now more efficient to use those types of contract genotyping services than to try to support their growing MB needs through the establishment of an in-house laboratory. Functional and reliable SNP laboratories are especially difficult to establish in many developing countries due to the unreliability of the power supply, difficulties in shipping and storing and a low level of resources for the purchase and maintenance of sophisticated equipment. The GCP is facilitating the linkage between users and service laboratories through its marker services, a component of the breeding services offered through the GCP's IBP.

Analytical Tools, Software, and Pipelines

One of the achievements of the plant biotechnology revolution of the last two decades has been the

development of molecular genetics and associated technologies, which have led to the development of an improved understanding of the basis of inheritance of agronomic traits. The genomic segments or QTLs involved in the determination of phenotype can be identified from the analysis of phenotypic data in conjunction with allelic segregation at loci distributed throughout the genome. Because of this, the mode of inheritance, as well as the gene action underlying the QTL, can be deduced [44]. As with the improvement in marker technologies, the statistical tools needed for QTL mapping have evolved from a rudimentary to a very sophisticated level [45]. Previous approaches based on multiple regression methods, using least squares or generalized least squares estimation methods [46, 47], have evolved to composite interval mapping [9], mixed model approaches using maximum likelihood or restricted maximum likelihood (REML) [48], and Markov Chain Monte Carlo (MCMC) algorithms [49, 50], which use Bayesian statistics to estimate posterior probabilities by sampling from the data. In parallel, with progress in the characterization of genetic effects at QTLs and refinement of QTL peak position through meta-analysis [51], advances have also been made in understanding the impact of the environment on plant phenotype. The mapping of QTLs for multiple traits has allowed the quantification of QTL by environment interaction (QEI) [52] and, more recently, approaches using factorial regression mixed models have been applied to model both genotype by environment interaction [53] and QEI [48, 54, 55]. Recent approaches are now implemented to evaluate gene networking [56] and epistasis, based on Bayesian approaches [57, 58] or through stepwise regression by considering all marker information simultaneously [59, 60]. Epistasis and balanced polymorphism influence complex trait variation [61, 62], and classical generation means analyses, estimates of variance components, and QTL mapping indicated an important role of digenic and/or higher-order epistatic effects for all biomass-related traits in model plants [63] and in crops [64–66]. It will be critical to implement the most efficient MB strategies in order to evaluate and include these genetic effects in breeding schemes [60].

All tools necessary to run MB projects, from the simplest to the most complicated approaches, are available today in the public domain. They are based on different algorithms and statistical approaches, from the very simple to the more complex. One challenge is the diversity of tools available for a given analytical function or along the different steps of an analytical pathway, making the choice of the "right" tool difficult and the move from one analytical step to the next very tedious due to the complete lack of common standards and formatting across tools. The number of applications available for QTL analysis illustrates well the multiplicity and diversity of tools that are available for a given analysis. The following software packages have been developed over the past 20 years:

- Mapmaker/QTL [67]
- MapQTL [68, 69]
- QTL Cartographer [9, 70]
- PLABQTL [71]
- QGene [72, 73]
- Map Manager QT [74]
- iCIM [59, 60]

For most of these applications, the first versions were already available 15 years ago and the multiplicity and possible duplication generated by the independent development of these tools were already identified at the Gordon Research Conference on Quantitative Genetics and Biotechnology held in February 1997 in Ventura, California. A main objective of that workshop was to survey participants on the attributes of several software packages for QTL mapping and to define their analytical needs which were not presently met by the existing software packages. The workshop covered software for QTL mapping in inbred and outcrossed populations and the conclusions are available at: http://www.stat.wisc.edu/~yandell/statgen/software/biosci/qtl.html. In those conclusions one can read that "[a] consensus was reached that there is considerable overlap in the kinds of matings handled and statistics produced by the various QTL mapping software packages," clearly identifying the need for better coordinated efforts. Such coordination never took place, as is often the case in public research. As a result, most of those QTL packages are still available today, although in more sophisticated versions. They are all suitable for QTL mapping but use different statistical algorithms, present a different user interface, and necessitate different input and output file formats.

Some specialists in the field realized that the public software packages are usually too specialized and too technical in statistics to permit a thorough understanding by the many experimental geneticists and molecular biologists who would want to use them. In addition, the fast methodological advances, coupled with a range of stand-alone software, make it difficult for expert as well as non-expert users to decide on the best tools when designing and analyzing their genetic studies. Based on this rationale, a few commercial analytical pipelines emerged about a decade ago that include some of the QTL packages mentioned above. Two of them are Kyazma and GenStat®. These applications assist plant scientists by providing easy access to statistical packages for phenotypic and genotypic data. Kyazma was founded in the spring of 2003 (http://www.kyazma.nl/), and offers powerful methods for genetic linkage mapping and QTL analysis. Since 2003 Kyazma has taken over the development of the software packages JoinMap® and MapQTL® from Biometris of Plant Research International. Kyazma handles the distribution and support of JoinMap and MapQTL and, in collaboration with the statistical geneticists of Biometris, Kyazma provides introductory courses on genetic linkage mapping and QTL analysis in order to make the use of the software even more accessible. GenStat encompasses statistical data analysis software for biological and life science markets worldwide. GenStat includes the ASReml algorithm (average information algorithm for REML) to undertake very efficient meta-analyses of data with linear mixed models. The development of GenStat at Rothamsted began in 1968, when John Nelder took over from Frank Yates as Head of Statistics. Roger Payne took over leadership of the GenStat activity when John Nelder retired in 1985 (http://www.vsni.co.uk/). An important feature of GenStat is that it has been developed in (and now in collaboration with) a Statistics Department whose members have been responsible for many of the most widely used methods in applied statistics. Examples include analysis of variance, design of experiments, maximum likelihood, generalized linear models, canonical variates analysis, and recent developments in the analysis of mixed models by REML.

These commercial analytical pipelines offer a set of quality tools to researchers in plant science. However, they cover only a part of the configurable workflow system that is required for integrated breeding activities. In addition, there is a need to have tools and analytical pipelines that are freely available and, if possible, based on open source code to avoid dependence on private companies that might discontinue support and ensure access to the tools even with limited financial resources, which is a critical constraint in the arena of research for development, of which breeding programs of developing countries are key partners. It is important to underline that a version of GenStat that does not include the most advanced version of the different tools but allows users to run most basic analyses is available for breeding programs in developing countries. The web site for the GenStat Discovery Edition is http://www.vsni.co.uk/software/genstat-discovery/, but this version of the pipeline does not include QTL selection based on the mixed model approach, which is available in the commercial version.

The issue of open source code is an important one as, even for freely-available tools, the lack of availability of the source code limits the further expansion and customization of the tools. It also reduces the opportunity of researchers in developing countries to participate in methodology development. Over the last decade, a programming language and software environment for statistical computing and graphics, R, is becoming the reference in open source code for a broad range of biological applications, including genetic analysis (http://www.r-project.org/). Its source code is freely available under the *GNU General Public License* (http://en.wikipedia.org/wiki/GNU_General_Public_License). The R language has become a de facto standard among statisticians for the development of statistical software. It compiles and runs on a wide variety of UNIX, Windows, and MacOS platforms. R is similar to other programming languages, such as C, Java, and Perl, in that it helps people perform a wide variety of computing tasks by giving them access to various commands. For statisticians, however, R is particularly useful because it contains a number of built-in modules for organizing data, running calculations on the information, and creating graphical representations of the data sets. R provides a wide variety of statistical (linear and nonlinear modeling, classical statistical tests, time-series analysis, classification, clustering, etc.) [29] and graphical techniques, and is highly extensible. Close to 1,600 different

packages reside on just one of the many web sites devoted to R, and the number of packages has grown exponentially. However, R is difficult to use directly and procedures based on R must be wrapped in user-friendly menu systems if field biologists are to use them.

Information Systems

A functional IS involves far more than an analytical pipeline; it is a complete system that should include:

- A project planning module
- A germplasm management module
- A robust relational database
- Analytical standards
- Data collection and cleaning tools
- Analytical and decision support tools
- Query tools
- A cyber infrastructure (CI) that links the different tools in a cohesive and user-friendly way

Key elements of an IS are obviously the CI and the DMS as described in the following section. The value of an IS does not only reside in the quality of the individual tools or modules that are part of it, but rather in the CI or middleware that ensures cohesion across tools and efficient communication with databases.

There are not many examples of breeding ISs in the public domain. One example is the ICIS (http://www.icis.cgiar.org, [23]). ICIS is an open source IS for managing genetic resource and breeding information for any crop species. It has been developed over the last 10 years through collaboration between centers of the CGIAR, some NARS, and private companies. The ICIS system is Windows-based, and distributable on CD-ROM or via the Internet. It contains a genealogy management system (GMS, [33]) to capture and process historical genealogies as well as to maintain evolving pedigrees and to provide the basis for unique identification using internationally accepted nomenclature conventions for each crop; a seed inventory management system (IMS); a DMS [75] for genetic, phenotypic, and environmental data generated through evaluation and testing, as well as for providing links to genomic maps; links to geographic ISs that can manipulate all data associated with latitude and longitude (e.g., international, regional, and national testing programs); applications for maintaining, updating, and correcting genealogy records and tracking changes and updates; applications for producing field books and managing sets of breeding material, and for diagnostics such as coefficients of parentage and genetic profiles for planning crosses; tools to add new breeding methods, new data fields, and new traits; and tools for submitting data to crop curators and for distributing data updates via CD-ROM and electronic networks. The community of ICIS collaborators communicates via the ICIS Wiki (http://www.icis.cgiar.org), where all design and development decisions are documented. Feature requests and bug reports are made through the ICIS Communications project and the source code is published through various other ICIS projects on CropForge (http://cropforge.org). A commercial company, Phenome-Networks, has implemented a Web-based IS based on ICIS (http://phnserver.phenome-networks.com/).

Another system available is the Katmandoo Biosciences Data Management System (http://www.katmandoo.org/, [25]), which is a freely available, open source DMS for plant breeders developed by PI&F, NSW DPI, and DArT Pty. Ltd. It comprises linked ISs for plant breeding including applications for capturing field data using hand-held computers, barcode-based seed management systems, and databases to store and link field trial data, laboratory data, genealogical data, and marker data. A particular focus is on the use of whole-genome MM information to create graphical genotypes, track the ancestral origin of chromosomal regions, validate pedigrees, and infer missing data. It includes the applications of the Pedigree-Based Marker-Assisted Selection System (PBMASS) developed by PI&F as well as a seed management system, a digital field book for hand-held computers, and a system for directly recording weights of barcoded samples.

Both ISs struggle with the problem of integrating the different components into a single configurable system which matches the workflows of different breeding projects. Such a workflow should provide the user all tools and analytical means required to run a crop cycle: from germplasm preparation and planting, through the collection of phenotypic and the production of the genotypic data and their analysis, to the identification of genotypes to be

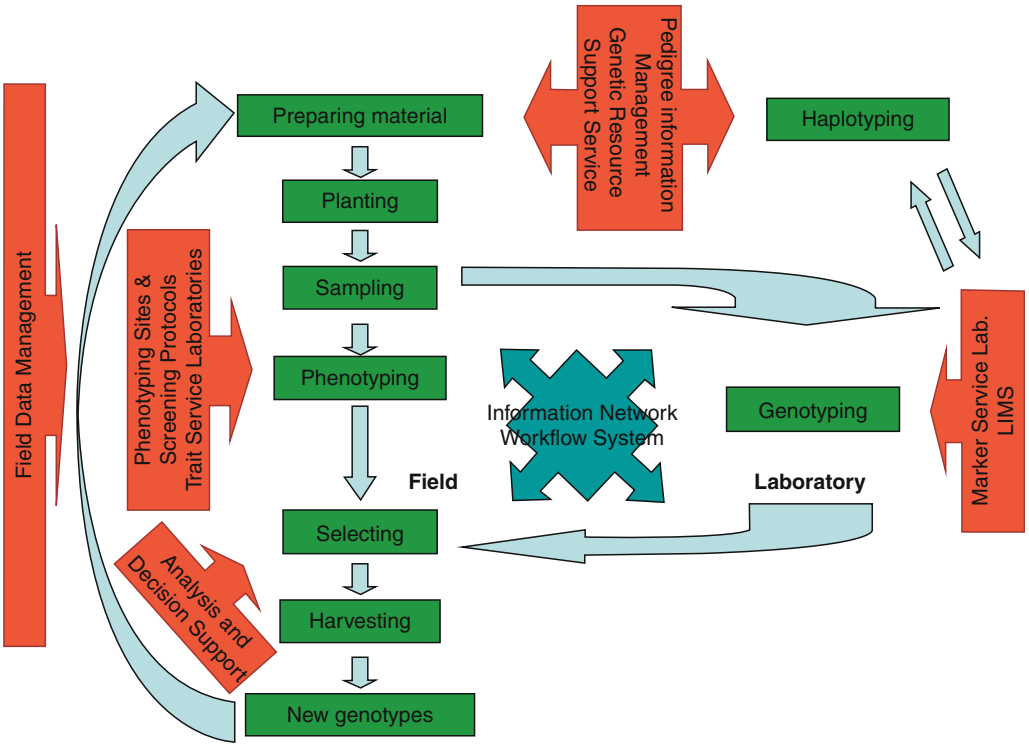

Molecular Breeding Platforms in World Agriculture. Figure 1
Different activities conducted during the crop cycle of an MB experiment presented in a generic way

crossed or the selection of suitable genotypes to be planted in the next cycle (Fig. 1).

In order to do this effectively, a CI is required which allows syntactic linkage between different data resources and applications.

Cyberinfrastructure and Data Management

We have referred to the revolution in Information and Communication Technology and the opportunities it presents for improving the efficiency of plant breeding. However, plant breeding is not the only area of biology being affected by this revolution and, in fact, the successful deployment of MB depends on other fields of information-intensive biology delivering knowledge (markers and methodology) to plant breeding. Even more is expected of the information and communications technology (ICT) revolution in the developing world, as it offers an opportunity for scientists there to overcome some of the constraints of isolation, the "brain drain," and the lack of infrastructure which have prevented them from fully participating in science for development in the past [76].

It is generally recognized that upstream biology is increasingly reliant on networks of integrated information and on applications for analyzing and visualizing that information. Discipline-specific (sequence and protein databases) and model organism ISs such as Graingenes (http://wheat.pw.usda.gov/GG2/index.shtml), Gramene (http://www.gramene.org/), MaizeGDB (http://www.maizegdb.org/), and Soybase (http://www.soybase.org/) have been developed to facilitate exchanges in molecular biology and functional genomics. As noted above, plant breeding depends on these upstream sciences of molecular biology, functional genomics, and comparative biology to deliver the knowledge needed to deploy MB. The bottleneck in the overall network has been the technology needed to integrate diverse and distributed information resources, and many information scientists have been working on this problem [24, 26, 77].

One constraint to integration of scientific information is the necessity to have a standard terminology for biological concepts across species and disciplines. A successful example of such standardization is the Gene Ontology (GO) initiative (http://www.geneontology.org, [78]). Another more specialized ontology initiative, especially pertinent to agriculture, is the Plant Ontology Consortium (POC: http://www.plantontology.org, [79–81]). However, these formal descriptions remain somewhat limited to biology of model plants and controlled environments. A key challenge will be to extend such standards to describe characteristics of plants growing in the unique, stress-prone environments found within the developing world to ensure a wider impact of such standards on international agriculture. The GCP has been working with POC to expand these ontologies to economic traits and farming environments so that they can be used in the field of plant breeding [82].

Another constraint to the efficient utilization of genomic information is the sheer volume of sequence data that can now be generated very cheaply across numerous genotypes. ISs to handle this volume of information are struggling to keep up. In plant biology, some examples of systems aiming to handle these torrents of data are the Germinate database ([83], http://bioinf.scri.ac.uk/public/?page_id=159) and the Genomic Diversity and Phenotype Connection (GDPC, http://www.maizegenetics.net/gdpc/). The primary goal of Germinate is to develop a robust database which may be used for the storage and retrieval of a wide variety of data types for a broad range of plant species. Germinate focuses on genotypic, phenotypic, and passport data, but has been designed to potentially handle a much wider range of data including, but not limited to, ecogeographic, genetic diversity, pedigree, and trait data, and will permit users to query across these different types of data. The developers have aimed to provide a versatile database structure, which can be simple, requires little maintenance, may be run on a desktop computer, and yet has the potential to be scaled to a large, well-curated database running on a server. The design of Germinate provides a generic database framework from which interfaces ranging from simple to complex may be used as a gateway to the data. The data tables are structured in a way that they are able to hold information ranging from simple data associated with a single accession or plant, to complex data sets, images, and detailed text information. Features of the Germinate database structure include its ability to access any information associated with a group of accessions and to relate different types of information through their association with an accession. The GDPC database was designed as a research database to support association genetics applications such as Tassel (http://www.maizegenetics.net/index.php?option=com_content&task=view&id=89&Itemid=119) and is being extended to handle higher and higher densities of genotyping and sequence data. The second version of Germinate seems quite similar to GDPC and if new databases are developed to handle the large data files to be generated soon through high-throughput sequencing, some conversion tools should be easily developed to migrate data from one system to another.

Finally, the problem of integrating all these diverse and widely-distributed information resources is a major informatics challenge, which is being tackled on several fronts at several levels of complexity. The BioMOBY project ([84], http://www.biomoby.org, [85]) and the Semantic Web seek to define standards that will allow computer programs to interpret requests for information or services, find informatics resources capable of fulfilling those requests, and return the results without the authors of the interacting software having specifically collaborated. In the private sector, solutions have been more pragmatic and Enterprise Software solutions have been developed to link data resources and applications with specific services. The iPlant Collaborative (http://www.iplantcollaborative.org/) is a National Science Foundation (NSF)-funded initiative designed to bring these Enterprise Software solutions to the biological sciences in the form of CI which can support any biological data resource and analytical application. iPlant and the GCP are collaborating on integrating plant breeding information resources and applications into the infrastructure. This will automatically link these resources to upstream biological applications using the same infrastructure such as that used by the Systems Biology Knowledgebase initiative (http://genomicscience.energy.gov/compbio/#page=news) of the US Department of Energy which will be producing knowledge needed for crop improvement.

With all the progress achieved in marker technology, software development, analytical pipelines, and DMS, it is time to provide an IS, available through a public platform, that will offer breeding programs in developed and developing countries access to modern breeding technologies, in an integrated and configurable way, to boost crop quality and productivity.

Case Study: GCP's Integrated Breeding Platform

To fill this gap in the public sector and in particular in the arena of research for development, the GCP has been coordinating the development of the IBP (www.generationcp.org/ibp) in collaboration with scientists from ARIs, CGIAR centers, and national research programs since mid-2009. In a first phase the IBP aims at serving the needs of a set of 14 pioneer "user cases" – MB projects for eight crops in 16 developing countries in Africa and Asia. Leading scientists of those user cases help in testing the prototypes developed for the different tools of the analytical pipeline and contribute to the monitoring and evaluation of the platform development. This ensures that IBP development is driven by real breeding needs and its interface is user-friendly.

Objective of the IBP

The overall objective of the IBP project is to provide access to modern breeding technologies, breeding material, and related information and services in a centralized and functional manner to improve plant breeding efficiency in developing countries and hence facilitate the adoption of MB approaches. The short-term objective of the project (the initial phase) is to establish – through a client-centered approach – a minimum set of tools, data management infrastructure, and services to meet the needs and enhance the efficiency of the 14 user cases.

To achieve the overall objective, GCP is developing and deploying a sustainable IBP as a one-stop shop for information, analytical tools, and related services to design, implement, and analyze MB experiments. This platform should enable breeding programs in the public and private sectors to accelerate variety development for developing countries using marker technologies – from simple gene or transgene introgression to gene pyramiding and complex MARS and GWS projects. Hence IBP aims at bringing cutting-edge breeding technologies to breeding programs that are too resource-restricted to invest in the requisite genotyping and data management infrastructure and capacity on their own.

The IBP Partnerships

The primary stakeholders of the platform are plant scientists – at this time specifically breeders leading the selected MB projects of the 14 pioneer user cases. These pioneer user cases are all recently initiated marker-assisted breeding projects with specific budgets, objectives, and work plans. The needs of the projects are defining the user requirements, and hence the design and development prioritization of the different elements of the platform. In selecting the user cases, crop diversity was a primary consideration, since the platform is supposed to address the needs of a broad variety of crops. The platform's reciprocal contribution to these breeding projects is in helping them overcome bottlenecks that would compromise final product delivery and in enhancing their overall efficiency and chances of success by providing appropriate tools and support.

The developmental phase of the IBP brings together highly regarded public research teams – institutes and individuals who have been working on the challenges of crop information management and analysis, biometrics, and quantitative genetics. This team of bioinformaticians, statisticians, and developers aims to design and develop the different elements of the platform, based on needs and priorities defined by the user cases.

A continuous dialogue between users, developers, and service providers ensures a healthy balance between having a user-driven platform on the one hand, with a reasonable degree of "technology push" on the other hand, to ensure that users are kept abreast of technological solutions they may not be aware of but that would facilitate and accelerate breeding work.

The private sector has led the application of MB approaches and utilization of MBPs. The IBP is the first public sector effort of this magnitude aimed at developing and deploying an MBP. Given that MB for complex polygenic traits, and more so MARS, is still in its infancy in the public sector, it is recognized that efficient partnerships with the major private sector

transnational seed companies is a strong prerequisite for the success of the IBP project. Consultations are ongoing with leaders in MB at Limagrain, Monsanto, Pioneer-DuPont, and Syngenta. Partnership with the private sector includes mainly some technology transfer, especially for stand-alone tools, and access to human resources to advise on the development of the platform and contribute to developing new tools or implement data management. The users, tools and services, and partnership of the platform are presented in Fig. 2.

The Platform

The IBP has three broad components (see Fig. 3): a Web-based portal and helpdesk, an open-source IS incorporating an adaptable breeding workflow system, and breeding and support services.

The stepwise development of the breeding workflow includes: (1) access to existing tools, (2) development of stand-alone new tools or adapted versions of existing tools to address the needs of the user cases, and (3) the integration of those tools into a CI (collaboration with the iPlant initiative) or through a thin middleware linking with local database to form a user-friendly configurable workflow system (CWS). A first version of the CWS, including an adequate set of tools, should be available by mid-2012, with full unfettered access scheduled for 2014.

Component 1: The Integrated Breeding Portal and Helpdesk

Inaugurated by mid-2011, the portal is the online gateway through which users access all the tools and services of the IBP. Through the portal, users will select and download tools and instructions, order materials, and procure laboratory services.

The portal's helpdesk facilitates its use and ensures access for users who cannot efficiently use the Web interface by providing the elements they need via email, compact disc, and other offline media.

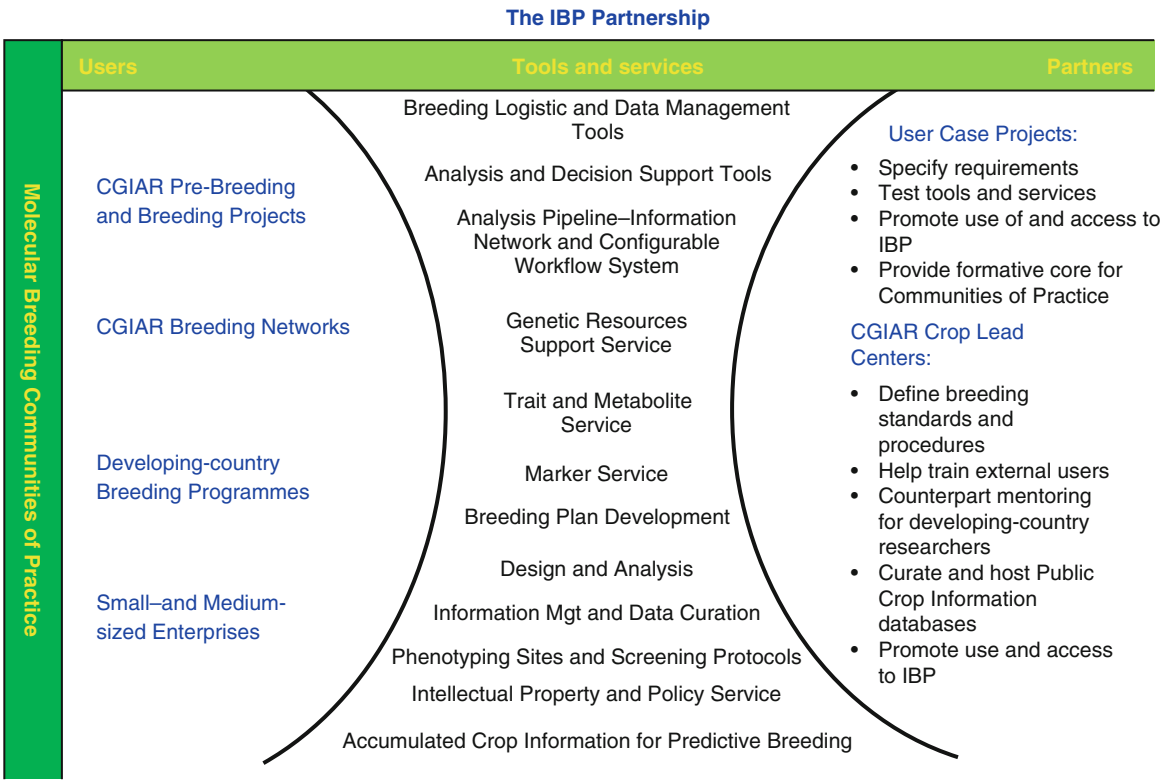

Molecular Breeding Platforms in World Agriculture. Figure 2
The IBP partnership

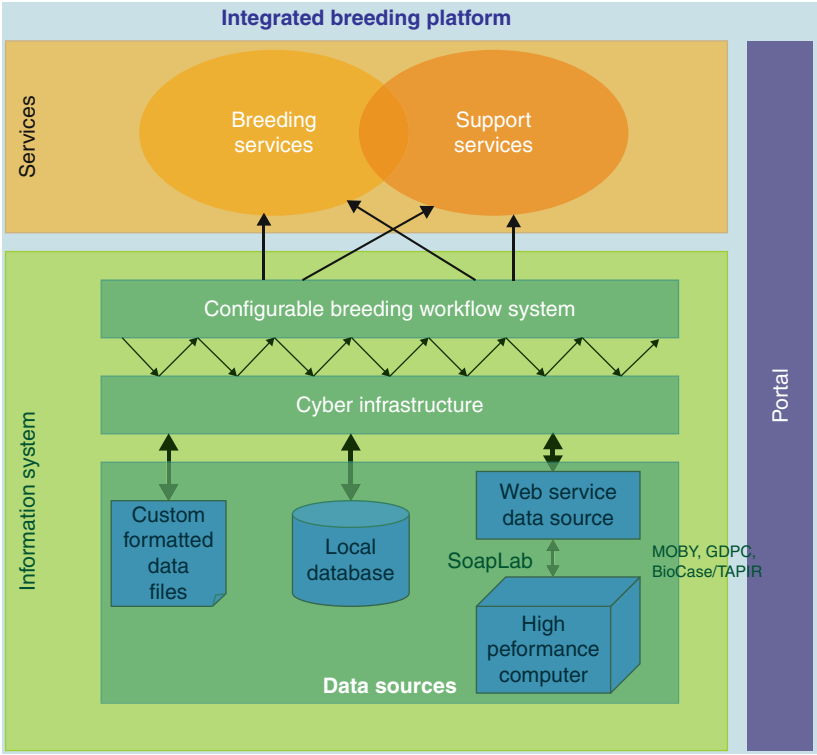

Molecular Breeding Platforms in World Agriculture. Figure 3
The IBP and its three main components

Through their user-friendly networking components, the Portal and Helpdesk will stimulate the development of collaborative crop-based and discipline-based communities of practice (CoPs). The CoPs are expected to promote the application of MB techniques and the utilization of facilitative information management technologies, enhance data and germplasm sharing, and generally advance modern breeding capacity by linking CGIAR Centers and ARIs with developing-country breeding programs and research organizations. There is a strong hope that CoPs will facilitate and accelerate a paradigm shift to a more collaborative, outward-looking, technology-enhanced approach to breeding.

Component 2: The Information System

The IBP IS is structured as a CWS, with access to both local databases and distributed resources, such as central crop databases, molecular databases from GCP partner sites and from public initiatives such as Gramene and GrainGenes.

The Configurable Workflow System This CWS is the operational representation of the IS and will be implemented by assembling informatics tools into applications configured to match specific breeding workflows (e.g., for MAS, MABC, or MARS; Fig. 4). The tools are organized in a series of functional modules comprising the Integrated Breeding Workbench, which is really the background structure that implements the CWS.

The IBP CWS drives the users through the different practical steps or activities of an MB project. The setup of the experiment and the germplasm management are the first steps of any project, to be followed by a set of activities that can be repeated during subsequent crop cycles, depending on the breeding objective of the experiment:

- Germplasm evaluation
- Genetic analysis
- Data management
- Data analysis, and
- Breeding decisions

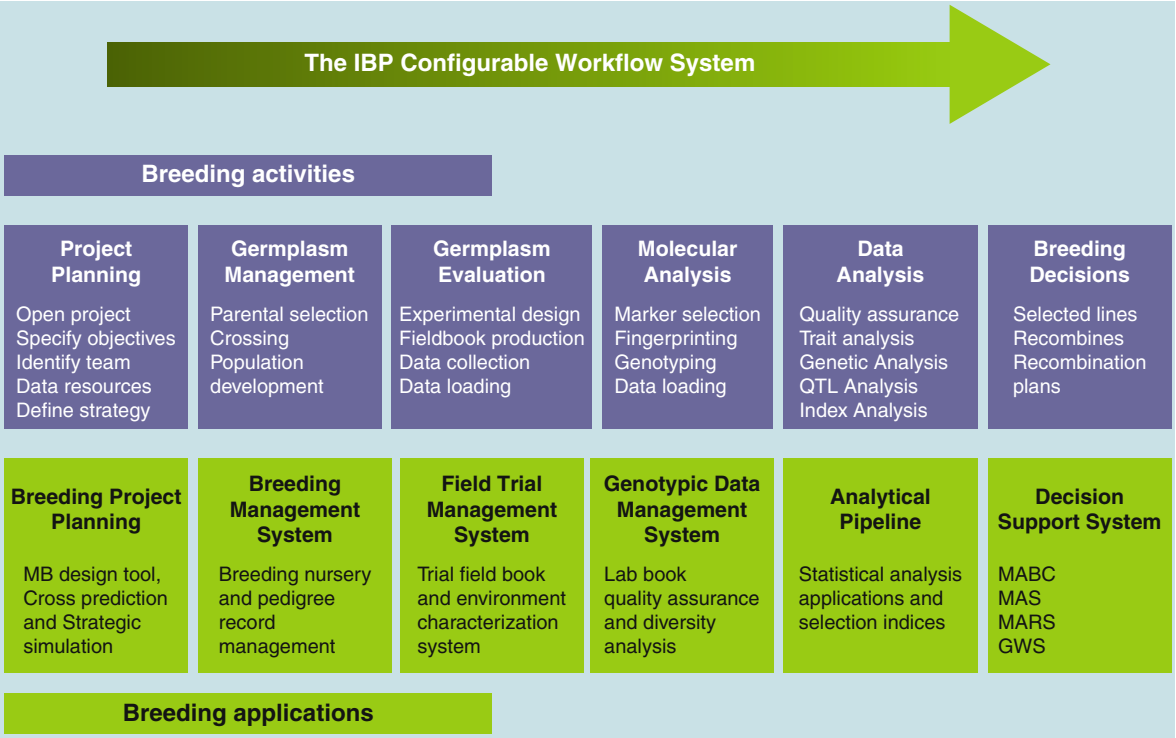

Molecular Breeding Platforms in World Agriculture. Figure 4
The IBP configurable workflow system

The Integrated Breeding Workbench The workbench starts as a blank slate and the first task for the user is to open or create a project. A project manages a breeding workflow for a particular crop and a specified user. The initial sets of tools which should be available are grouped in seven modules: Administration Tools, Configuration Tools, Query Tools, and Workflow Initialization Tools (genealogy, data management, analysis, and decision support; Fig. 5).

The administration module of the workbench specifies the crop, which identifies the central (public) data resources that will be accessible to the project. This includes a central genealogy database, a central phenotype database, a public gene management database, and a central genotype database. Each installation provides access to local (private) data resources. These data resources include a private or local database for the above data types as well as a seed inventory management system. Each installation has at least one user with administrative privileges. Users are identified by authentication codes (username and password) for access to specific private data resources. ("Private" simply means "requiring authentication for access" and several users may have access to the same private data.)

The first functionality of the workbench asks the user to open a project by selecting from a list of available project configuration "files." Once the configuration is selected, the availability of the public data resources should be checked, the user authentication codes verified, and the local data resources checked. Next, the list of modules should be reviewed and checked for availability and, depending on the state of the workflow, icons or menus should be made available for modules and tools.

The configuration tools allow users to:

- Select or specify naming conventions for germplasm, germplasm lists, studies, etc.
- Use and update ontologies such as germplasm methods and the trait dictionary
- Update breeding, testing, or collection locations
- Create and modify study templates

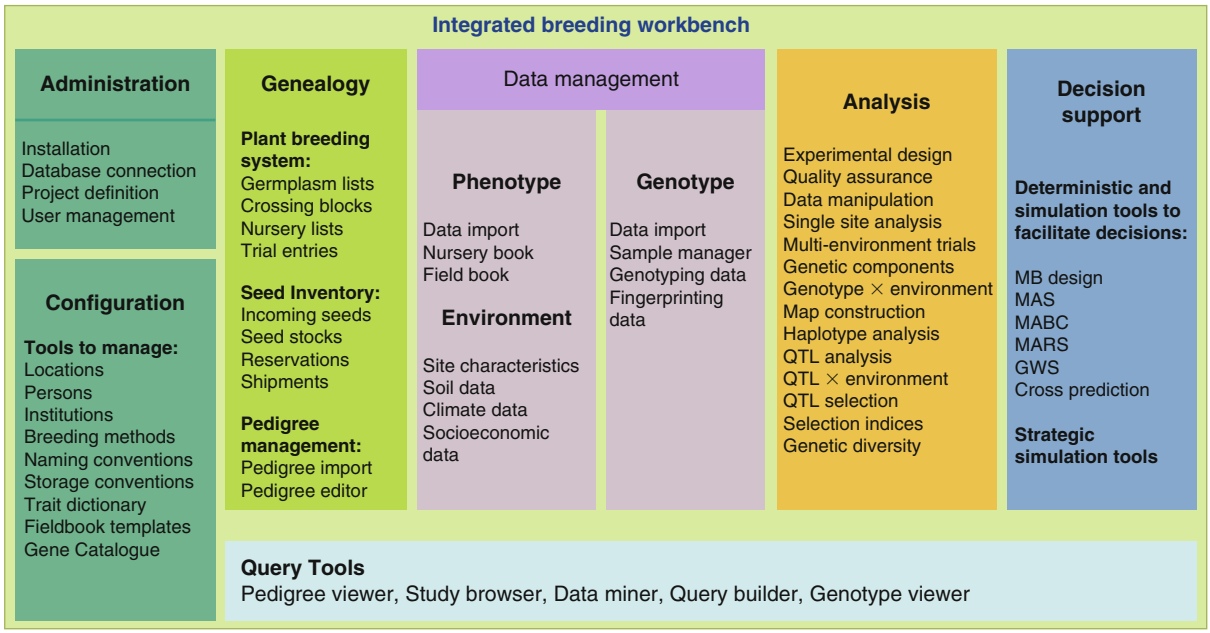

Molecular Breeding Platforms in World Agriculture. Figure 5
The integrated breeding workbench

The query tools will depend on the data resources specified in the project configuration, and examples are:

- A germplasm and pedigree viewer
- A study browser to view phenotype or genotype data
- A data miner for identifying data patterns
- A cross-study query builder for linking different data sets
- A gene catalog viewer for viewing genetic diversity
- A genotype and trait viewer for visualizing graphical genotypes and trait markers

The workflow initialization tools comprise a set of modules (genealogy, data management, analysis, and decision support tools) that provide the user with a choice of different tools to achieve precise breeding objectives. Users might construct different breeding workflows to match their project activities. The user will only see the workbench tools and settings for those tools required to execute the steps in a particular breeding workflow, and at the appropriate step in that workflow.

The development of each tool is overseen by a team of IBP researchers, developers, and users who design, mock up, and prototype the tools of the breeding application and pass the specifications to a software engineering team. They will then monitor the development and test and support the application. For each application, the team develops a description of the application, functional specifications of all the tools, workflow specifications for the application, and an interface mockup. A workflow for a MARS project is shown in Fig. 6.

Component 3: IBP Services

The Services component comprises two modules. The first module, Breeding Services, provides services to conduct MB projects. The second module, Support Services, deals with training and capacity-building, aiming to provide support and improve capacity of NARS breeders to deliver improved germplasm through marker approaches – essential for the adoption of MB approaches and the MBP.

Breeding Services These services provide access to specific germplasm, and assist with contracting a service laboratory to conduct the marker work or to

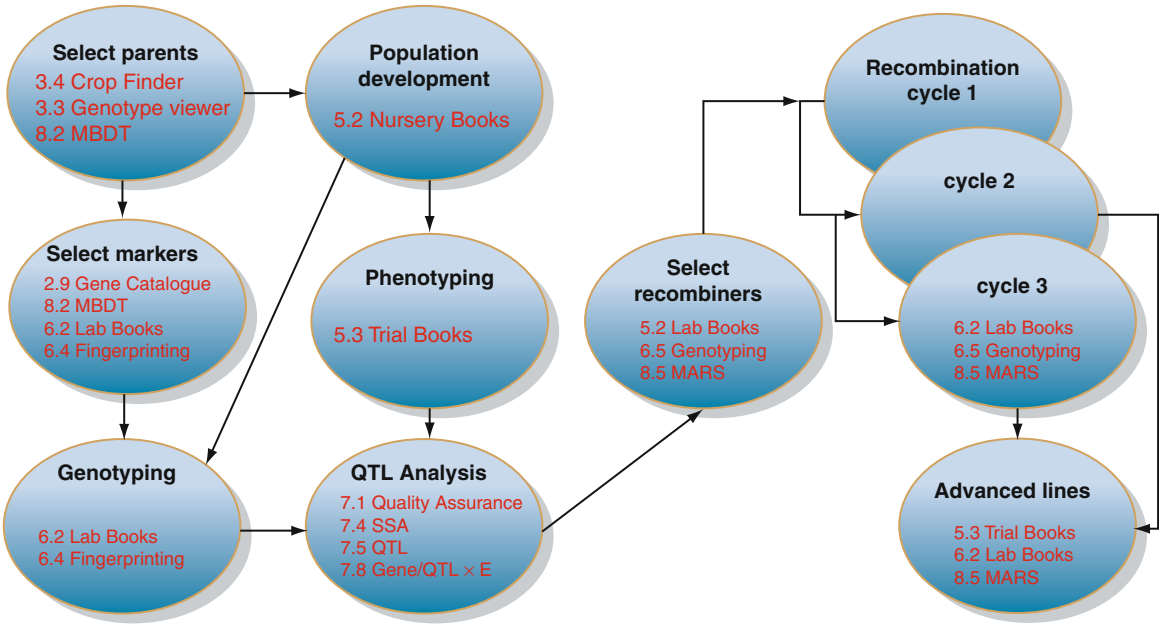

Molecular Breeding Platforms in World Agriculture. Figure 6
Breeding workflow for an MARS experiment

quantify specific traits, such as metabolite profiles or grain quality parameters. The module has three elements (Fig. 7):

Genetic Resource Support Service: Access to suitable germplasm and related information from the different partners is a critical element of the portal. To address this, a Genetic Resource Support Service (GRSS) plans to tap into the CGIAR System-wide Genetic Resources Program (SGRP), a collaborative effort between GCP and existing gene banks in the CGIAR and NARS. The GRSS should ensure quality control, maintenance, and distribution of genetic resources, including reference sets and segregating populations acquired or generated through projects supported by GCP, and material generated from other sources and deposited with the GRSS (e.g., maize introgression lines from Syngenta).

Marker Service: The portal provides a set of online options for users to access different high-throughput marker service laboratories in the public and private sectors with clear contractual conditions. Service Laboratories have been selected on the basis of competitive cost, compliance with quality control requirements, and expeditious delivery, but are currently accessible by offline processes pending deployment of the IBP portal.

Trait and Metabolite Service: The portal provides a set of options for users to access laboratories specialized in the evaluation and analysis of specific traits, such as quality traits, pathology screening, or metabolite quantification. Analyses of certain secondary traits and metabolites that are indicative of plant stress tolerance can potentially provide valuable information to be used in breeding. Such analyses are generally prohibitively expensive if done locally, as it is difficult to maintain assay quality and devote the necessary resources for expertise, quality control, and specialized facilities.

Capacity Development and Support Services
Capacity development is an integral part of the project, encompassing training and support in using MB techniques and markers, designing breeding strategies, quality data management, information analysis and decision modeling, phenotyping protocols, and protection of intellectual property (IP).

The main objective of this set of services is therefore to provide backstopping and training in a broad set of disciplines, to complement the elements of the breeding services and address specific technical and logistical bottlenecks. Such expert assistance is essential for the

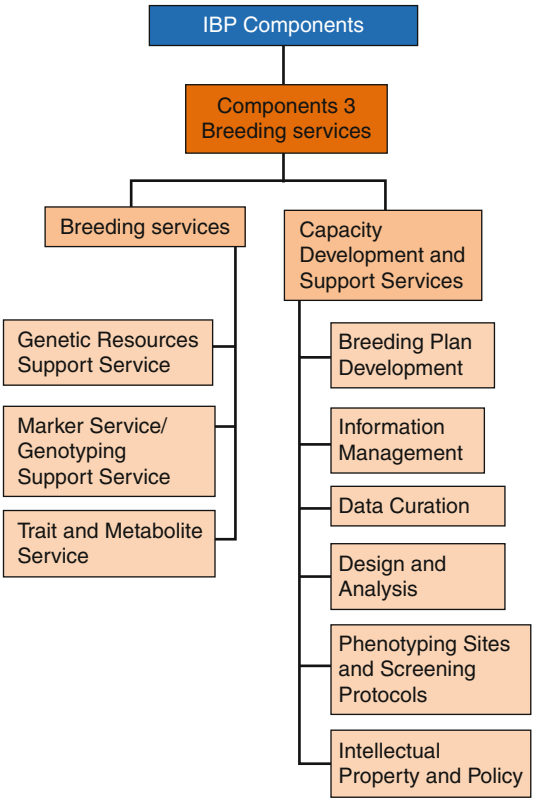

Molecular Breeding Platforms in World Agriculture. Figure 7
Organogram of the services provided by the IBP

adoption and proper use of new technologies. Services that will be available include:

Breeding plan development: It is essential to develop a breeding plan with a cost–benefit analysis before conducting a multi-cycle MB project. Depending on the nature of the experiment, such a plan may be quite simple or very elaborate, from the transfer of a single region (e.g., transgene) to complex selection that can consider the simultaneous transfer of dozens of regions. The critical factor is that the plan must detail all the activities over time, and the costs and benefits of the project to determine if it is worthwhile conducting the experiment. The platform provides templates and associated cost calculation sheets for different breeding schemes.

Information management: Under this service, assistance is provided in installing and parameterizing the platform IS for use by specific breeding projects.

Data curation: This service assists with capturing and curating current data for particular breeding projects, and in entering them into the integrated IS. This step is absolutely critical for quality control and further sharing of the information, and a contact person for each of the pioneer user cases has been identified to ensure good communication between the platform and the users.

Design and analysis: This service provides support on statistics, bioinformatics, quantitative genetics, and molecular biology. It includes training in data generation, handling, processing, and interpretation, as well as experimental design from field planting to MAS and MABC schemes. It provides assistance with the "translation" of the molecular context to the breeding context, and it will ensure that the methodology developed for the design and analysis of breeding trials is rapidly available to the users.

Phenotyping sites and screening protocols: Through this service, users can access information on phenotyping sites, protocols, and potential collaborators to ensure that selection is carried out under appropriate biotic and abiotic stresses and that the adaptation of germplasm is well characterized. Characterization of phenotypic sites includes geographical information, meteorological historical data, soil composition, and field infrastructure.

Genotyping Support Service (GSS): The GSS aims to facilitate access by developing country national agricultural research institutes to genotyping technologies, and bridge the gap between lab and field research. This service provides financial and technical support for NARS breeders to access cost-efficient genotyping services worldwide and supports training activities in experimental design and data analysis for MB projects.

Intellectual property (IP) and policy: This service provides support on IP rights and freedom to operate in the arena of biotechnology and germplasm use. The service is currently being provided on an experimental basis through a virtual IP Helpdesk hosted by the GCP web site at http://www.generationcp.org/iphelpdesk.php.

Integrated Breeding Hubs

If today few question the usefulness of local basic laboratories, it is also generally accepted that large-scale genotyping activities are best outsourced to

cost-effective, high-throughput service laboratories, irrespective of location. Following that rationale, the IBP provides access to marker service laboratories as the main avenue to generate the large amount of genotyping data that will be necessary to support the extensive MABC programs of the future, starting with the user cases, but the GCP also recognizes the need to provide breeders in developing countries with access to some regional hubs. At the beginning of the project four regional hubs are envisioned, covering the needs of the Americas – Centro Internacional de Agricultura Tropical (CIAT, www.ciat.cigiar.org); Africa – BioSciences eastern and central Africa (BecA, http://hub.africabiosciences.org); South Asia – International Crops Research Institute for the Semi-Arid Tropics (ICRISAT, www.icrisat.org); and South East Asia – International Rice Research Institute (IRRI, www.irri.org).

These regional hubs are expected to provide the following services:

- In-house hands-on training (different formats are possible from short- to medium-length periods), with the objective of exposing scientists to new technologies and their applications to breeding.
- Training courses for selected groups of researchers, targeting basic knowledge of marker technologies and their applications, as well as data analysis. These courses can be used for the testing and validation of learning materials, which will then be continuously upgraded.
- Facilitation of small genomic and genotyping projects led by national programs, academia, and small and medium enterprises (SMEs).
- Marker services for "small" and "orphan" crops that do not have mass demand from breeding programs and would therefore not benefit from large service providers, due to the lack of availability of SNP markers and the need to use lower-throughput SSR or other markers that can more easily be handled in lower-tech laboratories.

The Genomics and Molecular Breeding Hubs should help raise the visibility of the IBP and thus help promote the adoption of MB. Collaboration between the IBP and the regional hubs is anticipated to occur through sharing information, guiding users to apply for the appropriate service, organizing training events, and planning other developments of common interest.

Scope and Potential for Molecular Breeding Platforms

Gaps Across Countries and Crops

The application of MB approaches is now routine in developed countries, as is the integration of facilitative information and communication technologies, which are critical given the immense volumes of data necessary for, and generated by, these breeding processes. However, the situation is very different in developing countries, where MB is still far from routine in its application in breeding programs, particularly in Africa. This is especially critical due to the monumental and urgent imperative to rapidly achieve food security and improve livelihoods for a rapidly growing population through breeding for biotic stresses (including weeds, pests, and diseases) and abiotic stresses (including physical soil degradation, nitrogen deficiency, drought, heat, cold, and salinity) – conditions that make accurate phenotyping challenging. Fortunately, the history of modern breeding in developing countries is comparatively short, allowing a larger potential for crop improvement relative to the genetic gains that can be obtained at this time in developed countries, in which extensive breeding has been applied to crops for a longer time.

To address these issues, the capacity of national research institutions in terms of funds, infrastructure and expertise is directly related to the strength of their national economies [86]. This is reflected in the sharp differences in the capacity to conduct and apply biotechnology research as observed across developing countries (FAOBioDeC, http://www.fao.org/biotech/inventory_admin/dep/default.asp), and by the same token in their capacity to establish and/or utilize MBPs. The result is a three-tier typology of developing countries, directly attributable to the level of each country's investment in agricultural R&D [87].

Tier-1 countries, comprising newly industrialized countries (NICs) such as Brazil, China, India, Mexico, South Africa, and Thailand, substantially invest in technology and R&D and are self-reliant in most aspects of marker technologies [88, 89]. These countries have the simultaneous potential to effectively

adopt, adapt, and apply information and communication technologies to enhance research efficiency and outputs. They are therefore naturally at the vanguard in adopting MBPs.

Mid-level developing world economies (tier-2) such as Colombia, Indonesia, Kenya, Morocco, Uruguay, and Vietnam are well aware of MB's importance, and some effectively apply marker technologies for germplasm characterization [90–93] and selection of major genes [94–99]. These countries have a matching potential for a limited utilization of MBPs, a potential that can be enhanced fairly rapidly in the medium to long term.

Low-level developing world economies (tier-3 countries) are struggling to sustain even basic conventional breeding. They have very limited or no application of MB approaches and are unlikely to adopt MBPs except in the long term.

Especially for tier-3 countries, resource-limited breeding programs in many developing countries are severely hampered by a shortage of well-trained personnel, low level of research funding, inadequate access to high-throughput genotyping capacity, poor and inadequate phenotyping infrastructure, lack of ISs and appropriate analysis tools, and by the logistical difficulty of integrating new approaches with traditional breeding methodologies – including problems of scale when scaling up from small to large breeding programs.

Until recently, the scarcity of available genomic resources for clonally propagated crops, for some neglected cereals such as millet, and for less-studied crops such as most tropical legumes, which are all very important crops in developing countries, represented a further constraint to agricultural research for development [100], thereby limiting the application of molecular approaches and hence the potential for MBPs. However, the recent emergence of affordable large-scale marker technologies (e.g., DArT [101]), the sharp decline of sequencing costs boosting marker development based on sequence information [102], and the explicit efforts of national agricultural research programs (e.g., India [103]) and international initiatives such as GCP [104]) have all resulted in a significant increase in the number of genomic resources available for less-studied crops. As a result, most key crops in developing countries now have adequate genomic resources for meaningful genetic studies and most MB applications.

Similarly, international efforts such as GCP's IBP are designed to help overcome the challenges of developing-country breeders – exploiting economies of scale by making available convenient and cost-effective collective access to cutting-edge breeding technologies and informatics hitherto unavailable to them, including genomic resources, advanced laboratory services, and robust analytical and data management tools. Together, this increasing availability of genomic resources and tools for previously neglected but important crops and the access to initiatives targeting the resource-challenged NARS of the developing world will hasten the adoption of MBPs for these countries.

Institutional, Governmental, and Public Support

While corporate and other proprietary MBPs need only meet the specific requirements of a particular corporation or of specific paying clients, the development of platforms targeted at breeding programs in the developing world require a broad consensus among the parties that would use them and support them from multiple overseeing organizations. This is because these platforms are built on the premise of minimizing costs and maximizing benefits through economies of scale generated through collective access by multiple partners.

The public-access MBPs would therefore be critically dependent on well-structured MB programs, which may not be a reality in many developing countries. A good structure would entail compliance with common or compatible:

- Good field infrastructure, including meteo station
- Good agronomical practices at experimental stations
- Crop ontology information system
- Data collection, management, and analysis protocols
- Breeding plan design
- Information and communication technology infrastructure
- Informatics tools for analysis, decision support purposes, and eventually modeling and simulation

Traditionally, developing world breeding programs have largely been poorly funded and poorly supported,

and have been primarily driven by donor organizations [105, 106]. The lack of in-country support has often limited the dependent breeding activities to no more than a basic level. Under such circumstances, it was unrealistic to anticipate the adoption of new biotechnologies – including the utilization of MBPs. Fortunately, this scenario is changing. In 2003, through the Comprehensive Africa Agriculture Development Programme (CAADP, http://www.caadp.net/implementingcaadp-agenda.php), African governments committed to invest more in food security and in agriculture-led growth. Since then, many countries in Africa and elsewhere have developed comprehensive agricultural development strategies.

There is also a growing participation by foundations and nongovernmental organizations, and more recently the emergence of public–private sector partnerships (e.g., US Global Food Security Plan, http://www.state.gov/s/globalfoodsecurity/129952.htm). This governmental and institutional commitment is critical for the adoption of biotechnologies in general [8, 107] and for MB adoption in tier-2 countries in particular, with the attendant establishment and utilization of MBPs.

Challenges, Risks, and Opportunities

Challenges hampering the potential of MBPs in developing countries include both factors applicable generally to MB and those specific to MBPs. These factors encompass infrastructure capacity, human resource, and operational and policy issues. But amidst the challenges there are also actual and potential opportunities.

Human Capacity Human capacity for MB technologies in developing countries is a challenge, and limitations include substandard agriculture programs at universities; difficulties in keeping up to date with relevant developments, including failures by others; poor technical skills in core disciplines; isolation as a result of insufficient peer critical mass in the workplace; and poor incentives to attract and retain scientists, resulting in brain drain and staff turnover [108].

To partially offset the undesirable trend of losing the "champions" and to "generate" more "champions," novel international initiatives like Alliance for a Green Revolution in Africa (AGRA) support high-quality education in the South. Examples include the African Centre for Crop Improvement (ACCI, http://www.acci.org.za/) based at the University of KwaZulu–Natal in South Africa and the University of Ghana-based West African Centre for Crop Improvement (WACCI, http://www.wacci.edu.gh/). Both institutes offer doctorate degrees in modern breeding to African students, with the fieldwork component being carried out in the students' home countries.

While obtaining their Ph.D. in plant breeding, these scientists study the principles of marker technologies, equipping them to undertake MB activities. To retain this much-needed expertise in Africa, the WACCI and ACCI programs also provide post-Ph.D. funds for these scientists to conduct research in their home countries and, in some cases, provide matching funds for their career advancement.

Precise Phenotyping There can be no successful MB program without precise phenotyping of the target traits. Reliable phenotypic data is a must for good genetic studies [109] and most developing countries lack suitable field infrastructure for good trials and collection of accurate phenotypic data. As part of the services of a good MBP, guidelines on best practice must be provided on how to design and run a trial and conduct precise phenotyping for genetic studies under different target environments. Improving access to homogeneous field areas, and paying attention to good soil preparation and homogeneous sowing are critical. The development of new geographic IS tools [102, 110], experimental designs, phenotyping methodologies [111, 112], and advanced statistical methods [113] will facilitate the understanding of the genetic basis of complex traits [114] and of genotype-by-environment (G×E) interactions [48, 115]. Improving phenotyping infrastructure in developing countries must thus be a top priority to promote modern breeding and utilization of MBPs [106].

Laboratories for Markers Services Genotyping can be expensive when it is performed in small laboratories using labor-intensive and low-throughput markers such as SSRs. This has traditionally limited the use of MMs in developing countries beyond the fingerprinting of germplasm with a small number of markers or the use of MAS for a few key traits. Operational

efficiency is also vital, because fundamental timelines must be respected to ensure that no crop cycle is lost. Indeed, at every selection cycle, a service laboratory may have only a few weeks (time between DNA being extracted from leaves harvested on plantlets and the flowering time) to conduct the analysis and return the data to the breeders to enable them to conduct appropriate crosses among selected genotypes.

There is general agreement today that basic local laboratories at national and regional levels can be useful at least to service small local needs such as fingerprinting of limited number of accessions, GMO detection or MAS for specific traits, or for teaching and training purposes. It is also generally accepted that large-scale genotyping activities are best outsourced to advanced, modern, cost-effective high-throughput service laboratories, irrespective of the original location of the needs. This outsourcing is driven by the evolution in marker technologies. The advent of SNP genotyping led the shift from the low-throughput, primarily manual world of SSRs to high-throughput platforms powered by robotics and automated scoring, better handled by dedicated service laboratories [102, 116, 117]. As a result, genotyping costs have decreased by up to tenfold while data throughput has increased by the same magnitude. An example for MARS is provided in Fig. 6. SNP markers are increasingly available for most mainstream crops and for several less-studied crops [118, 119], which are important in developing countries.

A particular effort will be needed to ensure an easy and reliable way to track samples from the field to the laboratory, and back to the field – it will hence be vital to carefully identify DNA samples from material collected in the field. Such documentation should optimally be through bar-coding, and all information pertaining to management of field trials or experiments should be recorded in electronic field books. Marker work would of necessity be subcontracted to a service lab with a good and preferably platform-compatible laboratory information management system (LIMS).

Data Management For breeders to efficiently access relevant information generated by themselves and by other researchers, reliable data management (including sample tracking, data collection and storage, and modern analytical methodologies and tools for accurate decision making, among others) is critical both within a given MB program and across programs. In view of this, it is essential that breeders manage pedigree, phenotypic, and genotypic information through common or mutually compatible crop databases, in keeping with the collective access principle of a public MBP. The format of databases would need to be user-friendly and compatible with field data collection devices and applications to encourage both adoption and compliance. Ultimately, data collection and management processes would need to seamlessly link with a platform-resident analysis, modeling, simulation, and a decision support workbench for full utility of the breeding platform.

Paradigm Shift: Collaborative Work and Data Sharing Access to information and products generated by fellow users is a potentially critical incentive for breeders to use the platform and share their own data with other users. However, this would require a fundamental paradigm shift from the present data-hoarding, inward-looking approach to research common to breeders. This may, however, only be achievable if it is a clear requirement in the terms of engagement for membership of a "platform community," or if distinct financial and other incentives are offered for such sharing.

Technology-Push Versus Demand-Driven An MBP is by nature a high-level technological solution. It carries with it the inherent risk of failing to address fundamental practical problems of developing-world breeding programs, which will often by nature be technology-deficient. Such platforms therefore face the challenge of ensuring that they meet targeted user objectives and address practical constraints.

However, with this challenge comes an opportunity to introduce advanced MB methodologies to developing world breeders, by encouraging change that will enable them to take advantage of the efficiencies and economies of scale offered by the MBP. This opportunity would be particularly reachable with bottom-up platform design and development that actively engages and involves the breeders – including elements of human resource capacity development and support in usage.

Adoption and Use by Breeders An MBP would only make a difference if it is adopted and widely used by the breeders. The most important element influencing this would be credibility – a function of the quality of the technology, the awareness of potential users, the ease of access, and initial incentives. There is a need for successful public sector developing-country examples to demonstrate that the platform can effectively enhance the efficiency of breeders through the use of modern approaches – a clear demonstration of the added value of using the platform.

Sustainability of the Platform Sustainability would be a challenge for MBPs targeting developing world breeding programs, given their resource limitations. These programs may not be able to meet the full cost of platform usage, and the cost of maintaining and updating the different elements of the platform on a regular basis – particularly tools and facilities that must keep abreast with evolving information and communication technologies.

Of course, platform sustainability is directly linked to its adoption by breeders, and sustainability strategies must be adapted to the diversity and financial resources of the potential clients, from developing-world national agricultural research institutes with limited resources to SMEs. Service costs might also be adjusted if clients are willing to share data and release germplasm through the platform.

Platform managers may also have to consider other innovative options like on-platform advertising by agriculture-related commercial enterprises. However, ongoing donor support would most likely still be required in the medium to long term.

Communities of Practice The development of platform-based MB communities of practice, to connect groups of crop researchers, mainly breeders, willing to share experiences and information on modern breeding methods, best field practices, and development of improved varieties, and to practice peer-to-peer mentoring, are an additional potential avenue for platform adoption and sustainability, besides providing means to quickly and efficiently resolve recurring breeding problems. Partnerships between developed and developing-country institutions, and between the private and public sectors, are also an opportunity for realizing the full potential of MB [87, 108].

Many other hurdles limit successful public sector utilization of MB opportunities [120, 121]. However, the potential of virtual MBPs made possible by the revolution in information and communication technologies provides opportunities to counter and overcome many of those shortcomings.

Potential Economic Impact of Molecular Breeding Platforms

By its nature, MB improves the efficiency of crop breeding – progressively increasing genetic gains by selecting and stacking favorable alleles at target loci. The utilization of MBPs accelerates and amplifies the advantages of MB by introducing significant efficiencies in resource and time usage. Predictive or designer breeding, which would be the ultimate result of information-rich MB, attainable through the use of MBPs by numerous different breeding programs that freely share data and germplasm, would particularly bring about these savings in resources and time.

However, a direct comparison of the cost-effectiveness of MB with phenotypic selection is not straightforward. Firstly, factors other than cost – such as trade-offs between time and money – play an important role in determining the selection method. Secondly, this choice is further complicated by the fact that the two methods are rarely mutually exclusive or direct substitutes for each other [122]. On the contrary, under most breeding schemes, they are in fact complementary. Where operating capital is not a limitation, MB maximizes the net present value, especially when strengthened through MBPs [123]. With the increasing ease of accessing marker service laboratories and the declining cost per marker data point, MB costs are shrinking, making it extremely attractive from a purely economic perspective.

However, once the technological hurdles are overcome, the ultimate impact of new technologies (such as MBPs) is often limited by the lack of, or ineffective, seed distribution systems or by distant markets. SMEs are critical in promoting access to, and distribution of, improved seeds, thus helping alleviate a major bottleneck to the impact of improved breeding on smallholder farmers [124, 125].

Few economic analyses have been conducted to objectively assess the potential impacts of MB in the public sector, and none for MBPs that are just now emerging as a tool for breeding in the public sector.

Of the few analyses done to date, one evaluates the economic benefits of MABC using preexisting MMs in developing rice varieties tolerant to salinity and P-deficiency [126] in Bangladesh, India, Indonesia, and the Philippines. Encompassing a broad set of economic parameters, the study concluded that MABC saves an estimated minimum of 2–3 years, resulting in significant incremental benefits in the range of USD 300–800 million depending on the country, the extent of abiotic stress encountered, and the lag for conventional breeding [127].

Future studies are likely to confirm the positive economic benefits of MB and, given that MBPs amplify the benefits of MB, it can be reasonably inferred that the emerging platforms would indeed further enhance those economic benefits.

Future Directions

MBPs will inevitably have a significant impact on crop breeding in developing countries in the medium to long term because of:

- The needs-driven demand for improved crop varieties to counter the global food crisis
- The exponential development of genomic resources
- The ever-declining cost of marker technologies
- The increasing occurrence of public–private partnerships, where the public sector can learn from private companies about best practices for integrating MB into their breeding programs
- The need for innovative solutions to the challenges of resource and operational limitations

The first challenge of MBPs will be to meet the immediate needs of the breeders in developing-country public and private programs. The first step will be to provide them with the tools for enhancement of their current breeding programs, through the implementation of field books, pedigree management, and basic statistical analytical tools necessary to optimally conduct their current breeding efforts. In close succession with these first applications, tools will need to be made available to facilitate the integration of MB into their breeding programs. Databases will need to be developed for storing genotypic and phenotypic data, integrated analytical tools will need to be made available to breeders for analysis of this accumulated data and for the identification of important simple trait loci or QTLs to monitor and recombine in their breeding programs, and decision support tools will need to be developed to help breeders decide on the next steps to engage in based on the data they generated from their MB activities.

In the near future, more complex tools will need to be developed for the storage and analysis of the large amounts of genotypic data that will be generated by new next-generation sequencing technologies and for their application in GWS. A tight linkage will also have to be established with the wealth of information that is being generated and will continue to be generated even faster in the genomics area, leading to the dissection of the genome and to the discovery of the location and function of major genes having an impact upon the performance of crops in environments relevant to developing-country programs.

Eventually, the accumulation of large amounts of genetic information linked to specific haplotypes will lead to the increasing use of predictive breeding in combination with traditional MB usage and appropriate tools will also need to be developed to support those efforts.

Although it is critical for a platform to anticipate all the new possible features of MB, ensuring that new technologies and ISs will find their way in a flexible infrastructure, it is also quite probable that most of the breeding programs in developing countries will work at the short- and mid-term mainly with simple MB approaches as they will never reach the critical size of crosses and germplasm evaluation requested to maximize complex approaches.

Conclusion and Prospective Scenarios

Through international initiatives like the ones coordinated by the CGIAR centers and programs, several notable developing-world MB successes have already been reported.

A well-known example is the development of submergence-tolerant rice cultivars through MABC led by IRRI [128]. The introgression of the Sub1 gene from

FR13A (the world's most flood-tolerant variety) into widely grown varieties like Swarna improved yields in more than 15 million hectares of rain-fed lowland rice in South and Southeast Asia.

MB in general and the use of MBPs in particular have definitely been shown to be an efficient approach for reducing the number of required selection cycles and for increasing the genetic gain per crop cycle to a point where the required human and operational resources can be kept to a minimum.

However, for sustainable adoption, the use of modern breeding strategies requires a breeder-led bottom-up approach. As a start, simple MB approaches adapted to local environments should be tested first by individual breeders to evaluate their success and impact under those breeders' conditions. Once proven, these approaches can then be implemented more widely or integrated to an MBP for enhanced efficiency. In case of individual success the adoption of MB by those breeders should be quite straightforward.

It is clear that the extent, speed, and scope of adoption of MB approaches and of utilization of MBPs will vary somewhat across tier-1, tier-2, and tier-3 countries, depending on the local priorities and on the resources available in given breeding programs. It is unrealistic to expect that large-scale MB breeding activities, including utilization of MBPs, will be widely implemented across the board in developing countries in the near term. However, the prospects are bright for individual breeders in these countries (particularly in tiers 1 and 2) to access germplasm, data, tools, and methodology that will allow them to conduct efficient MB projects by taking advantage of large international initiatives specifically targeting developing-country breeding programs. This will, however, happen in different ways and on different timelines for each tier.

For tier-1 countries, the impact would be evident in the shorter term – say in 3–6 years. These countries will benefit from new tools and platforms by increasing the rate of MB adoption. The biggest change is likely to occur in tier-2 countries, as these countries would be starting MB from scratch, but the impact would realistically be measurable only in the medium term, meaning in about a decade from now. For countries currently in tier-3 to advance to tier-2, basic breeding programs must first be established, which is highly dependent on governmental priorities and on subsequent resource allocation.

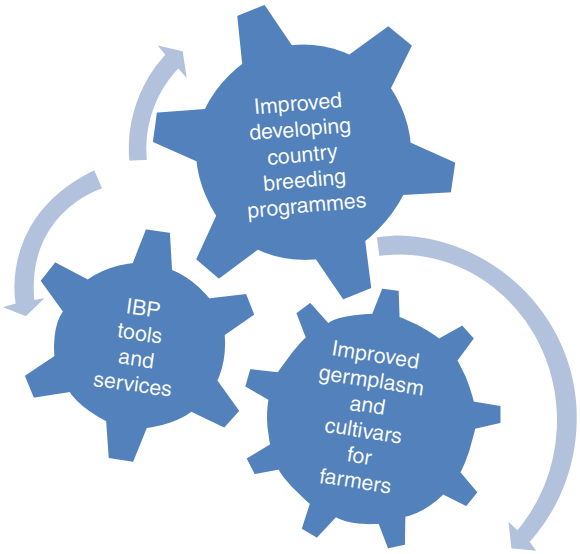

Molecular Breeding Platforms in World Agriculture. Figure 8
IBP as a key component to boost NARS breeding capacities and therefore crop productivity in developing countries

All in all, implementing MB (and catalyzing and accelerating its impact through MBPs) will boost crop production, which will translate into higher farm productivity per unit of land, better nutrition, higher incomes, poverty alleviation, and ultimately improved livelihoods in developing countries (Fig. 8). These gains will be amplified by sustained use, by continuously improving expertise, and by growth and development of homegrown capacity for the application of advanced breeding approaches.

Bibliography

1. Crosbie TM, Eathington SR, Johnson GR, Edwards M, Reiter R, Stark S, Mohanty RG, Oyervides M, Buehler RE, Walker AK, Dobert R, Delannay X, Pershing JC, Hall MA, Lamkey KR (2006) Plant breeding: past, present, and future. In: Lamkey KR, Lee M (eds) Plant breeding: the Arnel R. Hallauer international symposium. Blackwell, Ames, pp 3–50
2. Falck-Zepeda J, Zambrano P, Cohen JI, Borges O, Guimarães EP, Hautea D, Kengue J, Songa J (2008) Plant genetic resources for agriculture, plant breeding, and biotechnology. EPTD Discussion Paper 00762. International Food Policy Research Institute, Washington, DC

3. Goodman RM, Hauptli H, Crossway A, Knauf VC (1987) Gene transfer in crop improvement. Science 236:48–54
4. Cooper M, Smith OS, Merrill RE, Arthur L, Polich DW, Loffler CM (2006) Integrating breeding tools to generate information for efficient breeding: past, present, and future. In: Lamkey KR, Lee MA (eds) Plant breeding: the Arnel R. Hallauer international symposium. Blackwell, Ames, pp 141–154
5. Tanksley SD, Young ND, Paterson AH, Bonierbale MW (1989) RFLP mapping in plant breeding: new tools for an old science. Biotechnology 7:257–264
6. Ribaut J-M, Hoisington DA (1998) Marker-assisted selection: new tools and strategies. Trends Plant Sci 3:236–239
7. Bernardo R (2008) Molecular markers and selection for complex traits in plants: Learning from the last 20 years. Crop Sci 48:1649–1664
8. Moose SP, Mumm RH (2008) Molecular plant breeding as the foundation for 21st century crop improvement. Plant Phys 147:969–977
9. Wang S, Basten CJ, Zeng Z-B (2005) Windows QTL Cartographer 2.5. Department of Statistics, North Carolina State University, Raleigh
10. Collard BCY, Mackill DJ (2008) Marker-assisted selection: an approach for precision plant breeding in the twenty-first century. Philos Trans R Soc B 363:557–572
11. Ribaut J-M, Jiang C, Hoisington D (2002) Efficiency of a gene introgression experiment by backcrossing. Crop Sci 42:557–565
12. Mumm RH (2007) Backcross versus forward breeding in the development of transgenic maize hybrids: theory and practice. Crop Sci 47(S3):S164–S171
13. Hospital F, Charcosset A (1997) Marker-assisted introgression of quantitative trait loci. Genetics 147:1469–1485
14. Stam P (1995) Marker-assisted breeding. In: Van Ooijen JW, Jansen J (eds) Biometrics in plant breeding: applications of molecular markers. Proceedings of the ninth meeting of the EUCARPIA section biometrics in plant breeding, CPRO-DLO, Wageningen, pp 32–44
15. Peleman JD, Van Der Voort JR (2003) Breeding by design. Trends Plant Sci 7:330–334
16. Johnson R (2004) Marker-assisted selection. Plant Breed Rev 24:293–309
17. Bernardo R, Charcosset A (2006) Usefulness of gene information in marker-assisted recurrent selection: a simulation appraisal. Crop Sci 46:614–662
18. Guttmacher AE, Collins FS (2002) Genomic medicine – a primer. N Engl J Med 347:1512–1520
19. de los Campos G, Gianola D, Allison DB (2010) Predicting genetic predisposition in humans: the promise of whole-genome markers. Nat Rev Genet 11:880–886. doi:10.1038/nrg2898
20. Goddard ME, Hayes BJ (2007) Genomic selection. J Anim Breed Genet 124:323–330
21. Tinker NA, Yan W (2006) Information systems for crop performance data. Can J Plant Sci 86:647–662
22. Yan W, Tinker NA (2007) DUDE: a user-friendly crop information system. Agron J 99:1029–1033
23. McLaren CG, Bruskiewich RM, Portugal AM, Cosico B (2005) The international rice information system. A platform for meta-analysis of rice crop data. Plant Physiol 139:637–642
24. Bruskiewich R, Senger M, Davenport G, Ruiz M, Rouard M, Hazekamp T, Takeya M, Doi K, Satoh K, Costa M, Simon R, Balaji J, Akintunde A, Mauleon R, Wanchana S, Shah T, Anacleto M, Portugal A, Ulat VJ, Thongjuea S, Braak K, Ritter S, Dereeper A, Skofic M, Rojas E, Martins N, Pappas G, Alamban R, Almodiel R, Barboza LH, Detras J, Manansala K, Mendoza MJ, Morales J, Peralta B, Valerio R, Zhang Y, Gregorio S, Hermocilla J, Echavez M, Yap JM, Farmer SA, Gary, Lee J, Casstevens T, Jaiswal P, Meintjes A, Wilkinson M, Good B, Wagner J, Morris J, Marshall D, Collins A, Kikuchi S, Metz T, McLaren G, van Hintum T (2008) The Generation Challenge Programme platform: semantic standards and workbench for crop science. J Plant Genom 2008, Article ID 369601, 6 p. doi: 10.1155/2008/369601
25. Rodgers D, Jordan D (2009) Information management systems for plant breeders. Primary Industries and Fisheries (PI&F) of the Queensland Government, Department of Employment, Economic Development and Innovation in Australia, Queensland, Australia
26. Gudmundur A, Thorisson JM, Brookes AJ (2009) Genotype–phenotype databases: challenges and solutions for the post-genomic era. Nat Rev 10:9–18
27. Smith A, Cullis B, Thompson R (2001) Analyzing variety by environment data using multiplicative mixed models and adjustments for spatial field trend. Biometrics 57: 1138–1147
28. Burgueño J, Crossa J, Cornelius PL, Trethowan R, McLaren G, Krishnamachari A (2007) Modeling additive × environment and additive × additive × environment using genetic covariances of relatives of wheat genotypes. Crop Sci 47:311–320
29. Butler D, Cullis BR, Gilmour AR, Gogel BJ (2007) ASReml reference manual, release 2.00. VSN, Hemel Hempstead
30. Hammer G, Cooper M, Tardieu F, Welch S, Walsh B, van Eeuwijk F, Chapman S, Podlich D (2006) Models for navigating biological complexity in breeding improved crop plants. Trends Plant Sci 11:587–593
31. Wang J, Chapman SC, Bonnett DG, Rebetzke GJ, Crouch J (2007) Application of population genetic theory and simulation models to efficiently pyramid multiple genes via marker-assisted selection. Crop Sci 47:580–588
32. Chapman S (2008) Use of crop models to understand genotype by environment interactions for drought in real-world and simulated plant breeding trials. Euphytica 161:195–208
33. DeLacy IH, Fox PN, McLaren G, Trethowan R, White JW (2009) A conceptual model for describing processes of crop improvement in database structures. Crop Sci 49:2100–2112
34. Crossa J, Burgueño J, Dreisigacker S, Vargas M, Herrera S, Lillemo M, Singh RP, Trethowan R, Franco J, Warburton M, Reynolds M, Crouch JH, Ortiz R (2007) Association analysis of historical bread wheat germplasm using additive genetic covariance of relatives and population structure. Genetics 177:1889–1913

35. Lee M (1995) DNA markers and plant breeding programs. Adv Agron 55:265–344
36. Helentjaris T, Slocum M, Wright S, Schaefer A, Nienhuis J (1986) Construction of genetic linkage maps in maize and tomato using restriction fragment length polymorphisms. Theor Appl Genet 72:761–769
37. Edwards MD, Stuber CW, Wendel JF (1987) Molecular-marker-facilitated investigations of quantitative-trait loci in maize. I. Numbers, genomic distribution and types of gene action. Genetics 116:113–125
38. Paterson AH, Lander ES, Hewitt JD, Peterson S, Lincoln SE, Tanksley SD (1988) Resolution of quantitative traits into Mendelian factors by using a complete linkage map of restriction fragment length polymorphisms. Nature 335:721–726
39. Mullis K (1990) The unusual origin of the polymerase chain reaction. Sci Am 262:56–65
40. Senior ML, Heun M (1993) Mapping maize microsatellites and polymerase chain reaction confirmation of the target repeats using a CT primer. Genome 36:884–889
41. Vos P, Hogers R, Bleeker M, Reijans M, Tho L, van der Hornes M, Frijters A, Pot J, Peleman J, Kuiper M, Zabeau M (1995) AFLP: a new technique for DNA fingerprinting. Nucleic Acids Res 23:4407–4414
42. Gilles PN, Wu DJ, Foster CB, Dillon PJ, Chanock SJ (1999) Single nucleotide polymorphic discrimination by an electronic dot blot assay on semiconductor microchips. Nat Biotechnol 17:365–370
43. Eathington SR, Crosbie TM, Edwards MD, Reiter RS, Bull JK (2007) Molecular markers in commercial breeding. Crop Sci 47:154–163
44. Lander ES, Botstein D (1989) Mapping Mendelian factors underlying quantitative traits using RFLP linkage maps. Genetics 121:185–199
45. Borevitz J (2004) Genomic approaches to identifying quantitative trait loci: lessons from *Arabidopsis thaliana*. In: Cronk QCB, Whitton J, Ree RH, Taylor IEP (eds) Molecular genetics and ecology of plant adaptation. Proceedings of an international workshop, December 2002, Vancouver, NCR Research Press, Ottawa, pp 53–60
46. Haley CS, Knott SA (1992) A simple regression method for mapping quantitative loci in line crosses using flanking markers. Heredity 69:315–324
47. Martinez O, Curnow RN (1992) Estimating the locations and the sizes of the effects of quantitative trait loci using flanking markers. Theor Appl Genet 85:480–488
48. Malosetti M, Ribaut J-M, Vargas M, Crossa J, van Eeuwijk FA (2008) A multi-trait, multi-environment QTL mixed model with an application to drought and nitrogen trials in maize (*Zea mays* L.). Euphytica 161:241–257
49. Bink MCAM, Janss LLG, Quaas RL (2000) Markov chain Monte Carlo for mapping a quantitative trait locus in outbred populations. Genet Res 75:231–241
50. Bink MCAM, Boer MP, ter Braak CJF, Jansen J, Voorrips RE, van de Weg WE (2007) Bayesian analysis of complex traits in pedigreed plant populations. Euphytica 161:85–96. doi:10.1007/s10681-007-9516-1
51. Chardon F, Virlon B, Moreau L, Falque M, Joets J, Decousset L, Murigneux A, Charcosset A (2004) Genetic architecture of flowering time in maize as inferred from quantitative trait loci meta-analysis and synteny conservation with the rice genome. Genetics 168:2169–2185
52. Jiang C, Zeng ZB (1995) Multiple trait analysis of genetic mapping for quantitative trait loci. Genetics 140:1111–1127
53. van Eeuwijk FA, Malosetti M, Boer MP (2007) Modelling the genetic basis of response curves underlying genotype x environment interaction. In: Spiertz JHJ, Struik PC, van Laar HH (eds) Scale and complexity in plant systems research. gene-plant-crop relations. Springer, Dordrecht, pp 115–126
54. Boer MP, Wright D, Feng L, Podlich DW, Luo L, Cooper M, van Eeuwijk FA (2007) A mixed-model quantitative trait loci (QTL) analysis for multiple-environment trial data using environmental covariables for QTL-by-environment interactions, with an example in maize. Genetics 177:1801–1813
55. Malosetti M, Ribaut J-M, van Eeuwijk FA (2011) The statistical analysis of multienvironment data: modelling genotype-by-environment interaction and its genetic basis. In: Drought phenotyping in crops: from theory to practice (Monneveux Philippe and Ribaut Jean-Marcel, eds). CGIAR Generation Challenge Programme, Texcoco, Mexico. In press
56. Zhang F, Zhai H-Q, Paterson AH, Xu J-L, Gao Y-M et al (2011) Dissecting genetic networks underlying complex phenotypes: the theoretical framework. PLoS ONE 6(1):e14541. doi:10.1371/journal.pone.0014541
57. Yi N, Yandell BS, Churchill GA, Allison DB, Eisen EJ, Pomp D (2005) Bayesian model selection for genome-wide epistatic quantitative trait loci analysis. Genetics 170:1333–1344
58. Xu S, Jia Z (2007) Genome wide analysis of epistatic effects for quantitative traits in barley. Genetics 176:611–623
59. Li H, Ye G, Wang J (2007) A modified algorithm for the improvement of composite interval mapping. Genetics 175:361–374
60. Li H, Ribaut J-M, Li Z, Wang J (2008) Inclusive composite interval mapping (ICIM) for digenic epistasis of quantitative traits in biparental populations. Theor Appl Genet 116: 243–260
61. Kroymann J, Mitchell-Olds T (2005) Epistasis and balanced polymorphism influencing complex trait variation. Nature 435:95–98
62. Zeng Z-B (2005) Modeling quantitative trait loci and interpretation of models. Genetics 169:1711–1725
63. Kusterer B, Muminovic J, Utz HF, Piepho H-P, Barth S, Heckenberger M, Meyer RC, Altmann T, Melchinger AE (2007) Analysis of a triple testcross design with recombinant inbred lines reveals a significant role of epistasis in heterosis for biomass-related traits in Arabidopsis. Genetics 175:2009–2017
64. Frascaroli CEMA, Landi P, Pea G, Gianfranceschi L, Villa M, Morgante M, Pè ME (2007) Classical genetic and quantitative trait loci analyses of heterosis in a maize hybrid between two elite inbred lines. Genetics 176:625–644

65. Gu X-Y, Foley ME (2007) Epistatic interactions of three loci regulate flowering time under short and long daylengths in a backcross population of rice. Theor Appl Genet 114: 745–754
66. Melchinger AE, Piepho H-P, Utz HF, Muminović J, Wegenast T, Törjék O, Altmann T, Kusterer B (2007) Genetic basis of heterosis for growth-related traits in Arabidopsis investigated by Testcross progenies of near-isogenic lines reveals a significant role of epistasis. Genetics 177: 1827–1837
67. Landers ES, Green P, Abrahamson J, Barlow A, Daly MJ, Lincoln SE, Newburg L (1987) Mapmaker: an interactive computer package for constructing primary genetic linkage maps of experimental and natural populations. Genomics 1:174–181
68. Jansen RC (1993) Interval mapping of multiple quantitative trait loci. Genetics 135:205–211
69. Ooijen V (2004) MapQTL® 5, Software for the mapping of quantitative trait loci in experimental populations. Kyazma BV, Wageningen
70. Zeng Z-B (1994) Precision mapping of quantitative trait loci. Genetics 136:1457–1468
71. Utz HF, Melchinger AE (1996) PLABQTL: a program for composite interval mapping of QTL. J Agric Genom 2:1–5. http://probe.nalusda.gov:8000/otherdocs/jqtl/jqtl1996-01/utz.html (verified 10 September 1999)
72. Nelson JC (1997) QGene: software for marker-based genomic analysis and breeding. Mol Breed 3:229–235
73. Joehanes R, Nelson JC (2008) QGene 4.0, extensible Java QTL-analysis platform. Bioinformatics 24:2788–2789
74. Manly KF, Olson JM (1999) Overview of QTL mapping software and introduction to Map Manager QT. Mamm Genome 10:327–334
75. Portugal A, Balachandra R, Metz T, Bruskiewich R, McLaren G (2007) International crop information system for germplasm data management. In: Plant bioinformatics: methods and protocols. Humana, Totowa, pp 459–471, Chapter 22
76. McLaren CG, Metz T, van den Berg M, Bruskiewich R, Magor NP, Shires D (2009) Informatics in agricultural research for development. Adv Agron 102:135–157
77. Parkhill J, Birney E, Kersey P (2010) Genomic information infrastructure after the deluge. Genome Biol 11:402
78. Gene Ontology Consortium (2008) The Gene Ontology project in 2008. Nucleic Acids Res 36(Database issue): D440–D444
79. Avraham S, Tung CW, Ilic K, Jaiswal P, Kellogg EA, McCouch S, Pujar A, Reiser L, Rhee SY, Sachs MM, Schaeffer M, Stein L, et al (2008) The plant ontology database: A community resource for plant structure and developmental stages controlled vocabulary and annotations. Nucleic Acids Res 36(Database issue): D449–D454
80. Ilic K, Kellogg EA, Jaiswal P, Zapata F, Stevens PF, Vincent LP, Avraham S, Reiser L, Pujar A, Sachs MM, Whitman NT, McCouch SR et al (2007) The plant structure ontology, a unified vocabulary of anatomy and morphology of a flowering plant. Plant Physiol 143(2):587–599
81. Plant Ontology Consortium (2002) The Plant Ontology Consortium and plant ontologies. Comp Funct Genomics 3: 137–142
82. Bruskiewich R, Davenport G, Hazenkamp T, Metz T, Ruiz M, Simon R, Takeya M, Lee J, Senger M, McLaren G, van Hintum T (2006) The Generation Challenge Programme (GCP)—Standards for crop data. OMICS 10:215–219
83. Lee JM, Davenport GF, Marshall D, Ellis TH, Ambrose MJ, Dicks J, van Hintum TJ, Flavell AJ (2005) GERMINATE. A generic database for integrating genotypic and phenotypic information for plant genetic resource collections. Plant Physiol 139(2):619–631
84. BioMoby Consortium (2008) Interoperability with Moby 1.0—It's better than sharing your toothbrush! Brief Bioinform 9(3):220–231. doi:10.1093/bib/bbn003
85. Wilkinson M, Schoof H, Ernst R, Haase D (2005) BioMOBY successfully integrates distributed heterogeneous bioinformatics web services. The PlaNet exemplar case. Plant Physiol 138:1–13
86. Ribaut J-M, Monneveux P, Glaszmann JC, Leung H, Van Hintum T, de Vicente C (2008) International programs and the use of modern biotechnologies for crop improvement. In: Moore P, Ming R (eds) Genomics of tropical crop plants. Springer, New York, pp 21–63
87. Sonnino A, Carena MJ, Guimarães EP, Baumung R, Pilling D, Rischkowsky B (2007) An assessment of the use of molecular markers in developing countries. In: Guimarães EP, Ruane J, Scherf BD, Sonnino A, Dargie JD (eds) Marker-assisted selection: Current status and future perspectives in crops, livestock, forestry and fish. FAO, Rome, pp 15–26
88. Huang J, Rozelle S, Pray C, Wang Q (2002) Plant biotechnology in China. Science 295:674–677
89. Suresh P, Devi SV, Choudhary UN (2008) Resources and priorities for plant biotechnology research in India. Curr Sci 95:1400–1402
90. Ghneim Herrera T, Posso Duque D, Pérez Almeida I, Torrealba Nuñez G, Pieters AJ, Martínez CP, Tohme JM (2008) Assessment of genetic diversity in Venezuelan rice cultivars using simple sequence repeats markers. Electron J Biotechnol. doi:10.2225/vol11-issue5-fulltext-6
91. Khadari B, Oukabli A, Ater M, Mamouni A, Roger JP, Kjellberg F (2004) Molecular characterization of Moroccan fig germplasm using intersimple sequence repeat and simple sequence repeat markers to establish a reference collection. Hortic Sci 40:29–32
92. Onguso JM, Kahangi EM, Ndiritu DW, Mizutani F (2004) Genetic characterization of cultivated bananas and plantains in Kenya by RAPD markers. Sci Hortic 99:9–20
93. Paredes M, Becerra V, González MI (2008) Low genetic diversity among garlic (*Allium sativum* L.) accessions detected using random amplified polymorphic DNA (RAPD). Chil J Agric Res 68:3–12
94. Abalo G, Tongoonaa P, Derera J, Edema R (2009) A comparative analysis of conventional and marker-assisted selection methods in breeding maize streak virus resistance in maize. Crop Sci 49:509–520

95. Danson JW, Mbogori M, Kimani M, Lagat M, Kuria A, Diallo A (2006) Marker-assisted introgression of opaque2 gene into herbicide-resistant elite maize inbred lines. Afr J Biotechnol 5:2417–2422
96. Okogbenin E, Porto MCM, Egesi C, Mba C, Espinosa E, Santos LG, Ospina C, Marin J, Barrera E, Gutierrez J et al (2007) Marker-assisted introgression of resistance to cassava mosaic disease into Latin American germplasm for the genetic improvement of cassava in Africa. Crop Sci 47:1895–1904
97. Leung H, Wu J, Liu B, Bustaman M, Sridhar R, Singh K, Redona E, Quang VD, Zheng K, Bernardo M et al (2004) Sustainable disease resistance in rice: current and future strategies. In: New directions for a diverse planet. Proceedings of the 4th international crop science congress, 26 September–1 October, Brisbane
98. Sagredo B, Mathias M, Barrientos C, Acuña I, Kalazich J, Santosrojas J (2009) Evaluation of a SCAR RYSC3 marker of the RYadg gene to select resistant genotypes to potato virus Y (PVY) in the INIA potato breeding program. Chil J Agric Res 69:305–315
99. Stevens R (2008) Prospects for using marker-assisted breeding to improve maize production in Africa. J Sci Food Agric. doi:10.1002/jsfa.3154
100. Hartwich F, Tola J, Engler A, González C, Ghezan G, Vázquez-Alvarado JMP, Silva JA, Espinoza JJ, Gottret MV (2007) Building public–private partnerships for agricultural innovation, Food security in practice technical guide series. International Food Policy Research Institute, Washington, DC
101. Jaccoud D, Peng K, Feinstein D, Kilian A (2001) Diversity arrays: a solid state technology for sequence information independent genotyping. Nucleic Acids Res 29:e25
102. Ganal MW, Altmann T, Roder M (2009) SNP identification in crop plants. Curr Opin Plant Biol 12:211–217
103. Varshney RK, Penmetsa RV, Dutta S, Kulwal PL, Saxena RK, Datta S, Sharma TR, Rosen B, Carrasquilla-Garcia N, Farmer A et al (2009) Pigeonpea genomics initiative (PGI): an international effort to improve crop productivity of pigeonpea (*Cajanus cajan* L.). Mol Breed 26:393–408. doi:10.1007/s11032-009-9327-2
104. Varshney RK, Close TJ, Singh NK, Hoisington DA, Cook DR (2009) Orphan legume crops enter the genomics era! Curr Opin Plant Biol 12:1–9
105. Ajani EN, Madukwe MC, Agwu AE, Onwubuya EA (2009) Assessment of technology generating institutions in biotechnology innovation system of South-Eastern Nigeria. Afr J Biotechnol 8:2258–2264
106. O'Toole JC, Toenniessen GH, Murashige T, Harris RR, Herdt RW (2001) The Rockefeller Foundation's international program on rice biotechnology. In: Khush GS, Brar DS, Hardy B (eds) Rice genetics IV. Proceedings of the 4th international rice genetics symposium, Los Baños. International Rice Research Institute, pp 39–59
107. Kelemu S, Mahuku G, Fregene M, Pachico D, Johnson N, Calvert L, Rao I, Buruchara R, Amede T, Kimani P et al (2003) Harmonizing the agricultural biotechnology debate for the benefit of African farmers. Afr J Biotechnol 2:394–416
108. Morris M, Edmeades G, Peju E (2006) The global need for plant breeding capacity: what roles for the public and private sectors? Hortic Sci 41:30–39
109. Salekdeh GH, Reynolds M, Bennett J, Boyer J (2009) Conceptual framework for drought phenotyping during molecular breeding. Trends Plant Sci 14:488–496
110. Hyman G, Fujisaka S, Jones P, Wood S, de Vicente C, Dixon J (2008) Strategic approaches to targeting technology generation: assessing the coincidence of poverty and drought-prone crop production. Agric Syst 98:50–61
111. Hamer G, Cooper M, Tardieu F, Welch S, Walsh B, van Euuwijk F, Chapman S, Polish D (2006) Models for navigating biological complexity in breeding improved crop plants. Trends Plant Sci 11:587–593
112. Ribaut J-M, Betran J, Monneveux P, Setter T (2008) Drought tolerance in maize. In: Bennetzen J, Hake S (eds) Maize handbook, vol 1. Springer, New York, pp 311–344
113. Cooper M, van Eeuwijk F, Hammer GL, Podlich DW, Messina C (2009) Modeling QTL for complex traits: detection and context for plant breeding. Curr Opin Plant Biol 12:231–240
114. Mackay TFC, Stone EA, Ayroles JF (2009) The genetics of quantitative traits: challenges and prospects. Nat Rev Genet. doi:10.1038/nrg2612
115. Cooper M, van Eeuwijk FA, Chapman SC, Podlich DW, Löffler C (2006) Genotype-by-environment interactions under water-limited conditions. In: Ribaut JM (ed) Drought adaptation in cereals. Haworth, Binghampton, pp 51–95
116. Chagné D, Batley J, Edwards D, Forster JW (2007) Single nucleotide polymorphism genotyping in plants. In: Oraguzie NC, Rikkerink EHA, Gardiner SE, de Silva HN (eds) Association mapping in plants. Springer, New York, pp 77–94
117. Angaji SA (2009) Single nucleotide polymorphism genotyping and its application on mapping and marker-assisted plant breeding. Afr J Biotechnol 8:908–914
118. Muchero M, Diop NN, Bhat PR, Fenton RD, Wanamaker S, Pottorff M, Hearne S, Cisse N, Fatokun C, Ehlers JD et al (2009) A consensus genetic map of cowpea [*Vigna unguiculata* (L) Walp.] and synteny based on EST-derived SNPs. Proc Natl Acad Sci USA 106:18159–18164
119. Kawuki RS, Ferguson M, Labuschagne M, Herselman L, Kim DJ (2009) Identification, characterisation and application of single nucleotide polymorphisms for diversity assessment in cassava (*Manihot esculenta* Crantz). Mol Breed 23:669–684
120. Dwivedi SL, Crouch JH, Mackill DJ, Xu Y, Blair MW, Ragot M, Upadhyaya HD, Ortiz R (2007) The molecularization of public sector crop breeding: progress, problems, and prospects. Adv Agron 95:163–318. doi:10.1016/S0065-2113(07)95003-8
121. Xu Y, Crouch JH (2008) Marker-assisted selection in plant breeding: from publications to practice. Crop Sci 48:391–407
122. Dreher K, Khairallah M, Ribaut J-M, Morris M (2003) Money matters (I): costs of field and laboratory procedures associated with conventional and marker-assisted maize breeding at CIMMYT. Mol Breed 11:221–234

123. Morris M, Dreher K, Ribaut J-M, Khairallah M (2003) Money matters (II): costs of maize inbred line conversion schemes at CIMMYT using conventional and marker-assisted selection. Mol Breed 11:235–247
124. Delmer DP (2005) Agriculture in the developing world: connecting innovations in plant research to downstream applications. Proc Natl Acad Sci USA 102:15739–15746
125. Guimarães EP, Kueneman E, Carena MJ (2006) Assessment of national plant breeding and biotechnology capacity in Africa and recommendations for future capacity building. Hortic Sci 41:50–52
126. Ismail AM, Heuer S, Thomson MJ, Wissuwa M (2007) Genetic and genomic approaches to develop rice germplasm for problem soils. Plant Mol Biol 4:547–570
127. Alpuerto VE, Norton GW, Alwang J, Ismail AM (2009) Economic impact analysis of marker-assisted breeding for tolerance to salinity and phosphorous deficiency in rice. Rev Agr Econ 31:779–792
128. Septiningsih EM, Pamplona AM, Sanchez DL, Neeraja CN, Vergara GV, Heuer S, Ismail AM, Mackill DJ (2009) Development of submergence-tolerant rice cultivars: the Sub1 locus and beyond. Ann Bot 103:151–160

Molten Carbonate Fuel Cells

Choong-Gon Lee
Department of Chemical Engineering, Hanbat National University, Yuseong-gu, Daejeon, South Korea

Article Outline

Glossary
Definition of the Subject
Introduction
Components of MCFC
Performance Analysis
Future Directions
Bibliography

Glossary

Activation overpotential Voltage loss due to low charge-transfer rate on the electrode surface.

Anode A porous electrode where hydrogen is oxidized with carbonate ions (CO_3^{2-}) to steam and carbon dioxide.

Basicity Log(k_d) of molten carbonates where k_d is the equilibrium constant of the reaction $CO_3^{2-} \overset{k_d}{\rightleftharpoons} O^{2-} + CO_2$ similar to the pH of aqueous solutions.

Cathode A porous electrode where oxygen is reduced with carbon dioxide to carbonate ions (CO_3^{2-}).

Electrolyte Molten carbonates providing ionic paths for the electrode reactions with combinations of Li_2CO_3, Na_2CO_3, and K_2CO_3.

Exchange current density (i_o) An actual current density of an electrode at net zero current indicating catalytic activity of the electrode.

Fuel cell A system of continuous electrochemical energy conversion from chemical energy to electricity mostly by oxidation of hydrogen and reduction of oxygen.

Internal resistance Electrical resistance of cell components.

Mass transfer Access of reactants to the electrode surface and departure of products mainly by diffusion and convection.

Matrix Ceramic porous material holding molten carbonates by capillary forces.

Ohmic loss (η_{IR}) Voltage loss due to electrical resistance of cell components.

Open circuit voltage (E_{OCV}) A cell voltage at net zero current determined by the relation of $E_{OCV} = E^o + \frac{RT}{2F}\ln\left(\frac{p(H_2)p(O_2)^{0.5}p(CO_2)_{ca}}{p(H_2O)p(CO_2)_{an}}\right)$.

Overpotential (η) Voltage reduction from an open circuit voltage due to resistance of electrochemical reactions at an electrode.

Polarization A state of deviation from open circuit voltage due to current flowing in the cell.

Reaction kinetics Charge-transfer rates of electrochemical reactions on electrode surfaces.

Three-phase boundary A site of electrode-carbonate electrolyte-gaseous reactants where electrochemical reactions take place.

Definition of the Subject

Two parts are treated: one is the physical and chemical features of materials of molten carbonate fuel cells (MCFCs), and the other is performance analysis with a 100 cm^2 class single cell. The characteristics of the fuel cell are determined by the electrolyte. The chemical and physical properties of the electrolyte with respect to gas solubility, ionic conductivity, dissolution of cathode material, corrosion, and electrolyte loss in the real cell

are introduced. The reaction characteristics of hydrogen oxidation in molten carbonates and materials for the anode of the MCFC are reviewed. The kinetics of the oxygen reduction reaction in the molten carbonates and state of the art of cathode materials are also described. Based on the reaction kinetics of electrodes, a performance analysis of MCFCs is introduced. The performance analysis has importance with respect to the increase in performance through material development and the extension of cell life by cell development. Conventional as well as relatively new analysis methods are introduced.

Introduction

A fuel cell, as an emerging power source, generates power directly from the chemical energy of fuel. The fuel cell runs with electrochemical reactions at the electrodes where mostly H_2 oxidation at the anode, and O_2 reduction at the cathode occur. The power generation scheme of a fuel cell is very different from that of conventional grid power, where the electricity comes from electromagnetic induction with mechanical rotation. Thus, conventional power is produced by several steps of chemical, mechanical, and electrical energy changes. In contrast, a fuel cell converts chemical energy to electrical energy directly, which allows high energy conversion efficiency and low pollution emission from the fuel cell.

Among the fuel cells, the PEMFC (Polymer Electrolyte Membrane Fuel Cell or PEFC), AFC (Alkaline Fuel Cell), and PAFC (Phosphoric Acid Fuel Cell) are run by H^+ and OH^- movements in the electrolyte. On the other hand, the MCFC (Molten Carbonate Fuel Cell) and SOFC (Solid Oxide Fuel Cell) work with carbonate ions (CO_3^{2-}) and oxide ions (O^{2-}), respectively. The acid (H^+) and base (OH^-) generally run up to 200°C whereas carbonate and oxide ions run at over 600°C. Thus, the PEMFC, AFC, and PAFC have relatively low operating temperatures compared with the MCFC and SOFC.

The MCFC, running with molten carbonate electrolytes, has an operating temperature of about 650°C. This high temperature facilitates electrochemical reactions at the electrodes, allowing inexpensive metal electrodes such as Ni to be used while low temperature fuel cells, that is, PEMFC, AFC, and PAFC, require Pt electrocatalysts. The high operating temperature also gives high efficiency through the bottoming cycle that utilizes exhaust heat. Thus, the MCFC has some merits of high efficiency and system economics over the low temperature fuel cells.

Figure 1 shows current-voltage behaviors of fuel cells. The polarization behavior represents the reaction and performance characteristics of the fuel cells. In principle, the low temperature fuel cell has a larger absolute Gibbs free energy of H_2O formation. Thus, the PEMFC, AFC, and PAFC have a higher open circuit voltage (E_{OCV}) than the MCFC and SOFC. However, the low temperature fuel cells also have a sluggish charge-transfer rate in the electrode reaction, which leads to high activation overpotential. In general, the activation overpotential exponentially decreases voltage due to the applied currents at the early stage of current application (Fig. 1). Moreover, the Pt electrode in a low temperature fuel cell is oxidized at open circuit voltage. Therefore, low temperature fuel cells show an exponential decrease in voltage at around zero current and unclear E_{OCV} values. On the other hand, the MCFC shows a monotonic decrease in voltage even at the early stage of current application. This indicates that the electrode reactions have very small activation overpotential, probably due to the high temperature molten carbonate electrolytes. However, the steep current-voltage behavior of the MCFC shows that it has relatively high internal resistance and electrochemical reaction resistance in the cell compared with other fuel cells.

The carbonate ions (CO_3^{2-}) are supplied by the electrolytes: a combination of Li_2CO_3, K_2CO_3, and Na_2CO_3. Current electrolytes for the MCFC are the

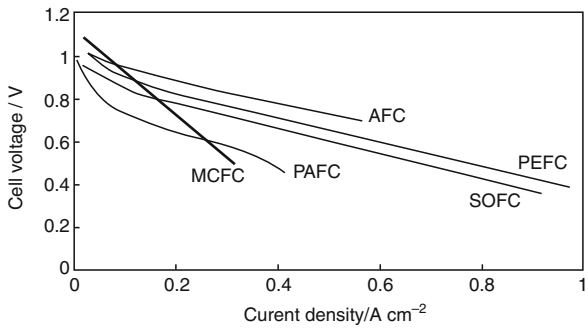

Molten Carbonate Fuel Cells. Figure 1
Current-voltage behaviors of various hydrogen fuel cells (From [46])

eutectics of Li_2CO_3-K_2CO_3 and Li_2CO_3-Na_2CO_3, which have melting temperatures of about 500°C. Then the electrode reactions with H_2 and O_2 in the MCFC are as follows:

$$\text{Anode } H_2 + CO_3^{2-} \rightarrow H_2O + CO_2 + 2e^- \quad (1a)$$

$$\text{Cathode } \frac{1}{2}O_2 + CO_2 + 2e^- \rightarrow CO_3^{2-} \quad (1b)$$

$$\text{Total } H_2 + \frac{1}{2}O_2 \rightarrow H_2O + \text{Heat} + \text{Power} \quad (1c)$$

The molten carbonates also allow the use of CO as a fuel. Then the reactions are as follows:

$$\text{Anode } CO + CO_3^{2-} \rightarrow 2CO_2 + 2e^- \quad (2a)$$

$$\text{Cathode } \frac{1}{2}O_2 + CO_2 + 2e^- \rightarrow CO_3^{2-} \quad (2b)$$

$$\text{Total } CO + \frac{1}{2}O_2 \rightarrow CO_2 \quad (2c)$$

This is a very unique characteristic of a high temperature fuel cell because CO behaves as a fuel in the MCFC while it is a poisonous species for the low temperature fuel cells. It gives fuel diversity to the MCFC. At present, the H_2 fuel is supplied by methane steam reforming as follows:

$$CH_4 + H_2O \rightarrow CO + 3H_2 \quad (3a)$$

$$CO + H_2O \rightarrow CO_2 + H_2 \quad (3b)$$

Methane is a main component of natural gas (over 90 vol.%) and its infrastructure is relatively well built across the world. Thus, natural gas is a main source of H_2 fuel for fuel cells. However, natural gas is much more expensive than coal, and thus fuel cells are economically inferior to coal power. Coal based operations have potential to improve the economics of fuel cells. At present, coal gasification is utilized as a clean coal technology, producing H_2 and CO gases as its main components. Organic materials are also generally decomposed to H_2 and CO. Thus, MCFCs can run with coal and organic wastes, which will enhance the economics of MCFCs.

In the past 35 years, MCFCs have been developed in the world. The primary developer is FCE (Fuel Cell Energy Co.) in the USA, which has developed an internal reforming type MCFC unit stack of up to 300 kW, and provides up to 2.4 MW MCFC systems by combination of the unit stacks. It also reported that a combination of an MCFC and a gas turbine recorded 56% electrical efficiency (based on the lower heating value (LHV) of natural gas) [1]. MTU, a German company, has designed a 250 kW class system, "Hot Module," by adapting FCE's stack. Japan developed MCFC systems of up to 1 MW class during the past 30 years. The 1 MW system was the pressurized external reforming type, and IHI (Ishikawajima-Harima Heavy Industry) produced a 300 kW class external reforming type system. Ansaldo Co. of Italy has developed a 500 kW class MCFC system. A 300 kW class MCFC system is also under development in Korea.

In this work, the characteristics of material for the MCFC such as the electrolyte, electrodes, and matrix are introduced. In addition, the diagnostic tools for MCFC performance are also treated: conventional methods of steady-state polarization, current interruption (C/I), and AC impedance, and novel methods of inert gas step addition (ISA) and reactant gas addition (RA).

Components of MCFC

Electrolytes

The MCFC is an electrochemical reaction system where the anode oxidizes H_2 to H_2O and the cathode reduces O_2 to CO_3^{2-} as shown in Eqs. 1a and 1b. Thus carbonate materials serve as the electrolyte, which is generally a mixture of various alkali metal carbonates of Li_2CO_3, Na_2CO_3, and K_2CO_3. Table 1 shows the melting points (m.p.), surface tension (γ), density (ρ), electric conductivity (κ), and Henry's Law constant of O_2 dissolution (h_{O2}) for various eutectic carbonates.

The table also shows the properties of an aqueous solution (1 M, KCl). It is found that the eutectics are a kind of electrolyte that have about twice the density, about three times the surface tension, and over ten times the electric conductivity of an aqueous solution. Eutectics also have much lower melting points than at single carbonates: Li_2CO_3 (999 K), Na_2CO_3 (1,131 K), and K_2CO_3 (1,172 K).

In general, the molten carbonates have an equilibrium with oxide ions (O^{2-}) and CO_2.

$$CO_3^{2-} \overset{k_d}{\rightleftharpoons} O^{2-} + CO_2 \quad (4)$$

where k_d is the dissociation constant ($= [O^{2-}] \cdot p(CO_2)$). Molten carbonates are also

Molten Carbonate Fuel Cells. Table 1 Properties of eutectic alkali metal carbonates [2]

System	Composition (mol%)	m.p. (K)	γ (mN/m) at 973 K	ρ (g/cm^3) at 973 K	κ (S/cm) at 973 K	h_{O2} (mol/cm^3 atm) at 923 K
Li_2CO_3:Na_2CO_3	53:47		239.0	1.937	2.181	1.83×10^{-7}
	52:48	774				
Li_2CO_3:K_2CO_3	62:38	761	214.1	1.912	1.053	
	50:50	777.5	206.0	1.917		3.26×10^{-7}
Li_2CO_3:Na_2CO_3:K_2CO_3	43.5:31.5:25	670	219.6	1.984	1.476	3.91×10^{-7}
Na_2CO_3:K_2CO_3	56:44	983				
1 M KCl at 298 K [48]			~72[a]		0.108	

[a]Value for water

Molten Carbonate Fuel Cells. Table 2 Dissociation constants (k_d) of carbonate melts [4]

Composition	k_d		
	823 K	923 K	1,023 K
Li_2CO_3	1.01×10^{-6}	2.08×10^{-5}	2.37×10^{-4}
53 mol% Li_2CO_3 – 47 mol% Na_2CO_3	2.58×10^{-9}	1.14×10^{-7}	2.41×10^{-6}
43.5 mol% Li_2CO_3 – 31.5 mol% Na_2CO_3 – 25.0 mol% K_2CO_3	2.04×10^{-10}	1.23×10^{-8}	3.34×10^{-7}
50 mol% Li_2CO_3 – 50 mol% K_2CO_3	9.77×10^{-11}	6.43×10^{-9}	1.86×10^{-7}
56 mol% Na_2CO_3 – 44 mol% K_2CO_3	8.53×10^{-14}	1.38×10^{-11}	8.26×10^{-10}

existing in the form of alkali metal cations (M^{2+}) and carbonate anions (CO_3^{2-}). Thus, the activity of oxide ions in the melt determines the characteristics of the melt as the activity of protons (H^+) in the aqueous solution (pH) represents the acidity of the solution. By adopting the Lux–Flood acid-base theory, the basicity of the molten carbonate can be defined.

In aqueous solution: acid = base + H^+
In carbonate melts: base = acid + O^{2-}

Therefore, the activity of oxide ions indicates the basicity of the melt and CO_2 in the melt behaves as an acid.

Table 2 shows the dissociation constants (k_d) of alkali carbonate melts. The constant rises with Li content and decreases with K and Na contents. Thus the melts become more basic with increasing Li content. The behavior is in agreement with the ionic radius of alkali metals: the smaller ionic radius of alkali metal results in more basic melts. Then the series of basic melts is as follows:

$$Li_2CO_3 > Li_2CO_3 - Na_2CO_3 > Li_2CO_3 - K_2CO_3 > Na_2CO_3 - K_2CO_3$$

The oxygen solubility also becomes higher in more acidic carbonate melts. The behavior can be interpreted from the ionic radius. The larger ionic radius of alkali metal enhances O_2 solubility. This is due to the increased stability of superoxide ions (O_2^-) and peroxide ions (O_2^{2-}) in the carbonate melts, which are produced by the following chemical reactions:

$$O_2 + 2CO_3^{2-} \rightleftharpoons 2O_2^{2-} + 2CO_2 \quad (5a)$$

$$3O_2 + 2CO_3^{2-} \rightleftharpoons 4O_2^{-} + 2CO_2 \quad (5b)$$

The dissociation constants also rise with temperature, indicating that the melts become more basic at a higher temperature.

As another property of molten carbonates, a contact angle is to be introduced. The molten carbonates are transparent liquid and movable. To maintain the molten carbonates in the fuel cell, a porous matrix structure is required. The porous structure holds the carbonate melts by the capillary forces of the pores. The carbonate melts have a very low contact angle with oxide ($\approx 0^{o}$) but very large contact angles with metals [2]. Thus, the cathode of the oxide electrode is very well wetted by the carbonates, while the anode electrode, with a metal state under strong reductants of H_2, is poorly wetted. Based on this concept, a dry agglomerate model for the anode and a well wetted agglomerate model for the cathode have been suggested [3]. According to the different surface tensions of Li-K and Li-Na carbonate melts as shown in Table 1, the melts have different wetting behaviors. The high surface tension of Li-Na carbonate melts causes poor wetting behavior compared with Li-K melts. This results in a steeper overpotential increase in the Li-Na carbonate electrolyte cell than in the Li-K cell at 600°C [4, 5].

Gas solubility is also an important parameter for the electrode reaction because the electrode is covered by carbonates and gas reactants must transfer through the carbonate film. So, higher solubility results in less kinetic and mass-transfer resistances during the electrode reaction. In general, CO_2 and H_2 solubilities are approximately 10^{-5} mole cm^{-3} atm^{-1} and the O_2 solubility is about one tenth of the H_2 solubility in the carbonate melts. The following dependence of gas solubility on the melt compositions at the same gas condition and temperature was reported [6]:

O_2 solubility: Li-K > Li-Na ≈ Li-Na-K
H_2 solubility: Li-K > Li-Na-K
CO_2 solubility: Li-Na > Li-Na-K > Li-K

Electrolyte Loss in the Cell

The carbonate electrolytes are contained in the matrices, which are porous ceramic materials placed between the anode and cathode. Since the matrix is comprised of sub-micron size pores, most of the pores are filled with carbonate electrolytes. Thus, the electrolyte prevents gas leakage between the electrodes. The electrodes are covered by metal separators that provide gas flow paths over the electrodes; the peripheral area of the separators is sealed by matrices and is called the wet seal area. Thus, the matrix prevents gas leaks from the inside to the outside of the cell by wet sealing.

Electrolyte loss weakens the gas sealing and shortens cell life. The molten carbonates are very corrosive materials. Since the separator is made of stainless steel, corrosion takes place on the surface of the separator. To reduce the corrosion, the anode side is coated with Ni and the wet seal area with Al.

According to the report on a 2 MW field test at Santa Clara, the causes and amounts of electrolyte losses are as follows: cathode hardware loss, 73%; fixed losses, 17%; vaporization loss, 7%; and unaccounted loss, 3% [7]. The report pointed out that most of the electrolyte loss was due to corrosion at the cathode because the Ni and Al coatings on the anode and wet seal area respectively prevented serious corrosion. Mitsubishi Electric Co. reported that about half of the electrolyte loss was due to the corrosion at the cathode current collector and the loss was proportional to the area of the current collector [8].

Among the austenitic stainless steels, 316 L and 310 are generally used for the MCFC separator and current collector. The Cr contents of 316 L and 310 are about 17% and 25%, respectively, and thus a denser $LiCrO_2$ layer occurs on the surface of 310 with more corrosion resistivity. However, $LiCrO_2$ has very low conductivity, resulting in a high electrical resistance with 310. Moreover, 310 makes water soluble K_2CrO_4 as a corrosion product, and thus electrolyte loss is more severe with 310 than 316 L [9].

Li-K and Li-Na carbonate melts had different corrosion behaviors with 316 L. These melts showed insignificant corrosion at 650°C but severe pit corrosion was observed only in the Li-Na melt under the present O_2 and CO_2 condition at around 550°C [10, 11]. Mitsubishi Electric Co. reported that an inert gas condition in the temperature range could prevent severe corrosion [10]. IHI in Japan also reported that the corrosion is mitigated by pre-oxidation of the surface by steam [11].

The molten carbonates also react with steam, which produces hydroxides, LiOH, NaOH, and KOH. It was reported that KOH has about twice the vapor pressure of LiOH and the highest vapor pressure among the above hydroxides [12]. However, as reported for the Santa Clara

test [7], the electrolyte loss by vaporization was 7% of total loss, which is still low compared with the total loss.

Anode

In general, H_2 oxidation is a quite fast reaction even in the low temperature fuel cells. The H_2 oxidation in the high temperature molten carbonate is fast enough, as expected. Among the several mechanisms, the following two are mainly discussed.

Ang and Sammells' mechanism [13]

$$\begin{gathered} H_2 + 2M \rightleftharpoons 2M - H \\ M - H + CO_3^{2-} \rightarrow OH^- + CO_2 + M + e^- \\ M - H + OH^- \rightleftharpoons H_2O + M + e^- \end{gathered} \tag{6}$$

Suski's mechanism [14]

$$\begin{gathered} H_2 + 2M \rightleftharpoons 2M - H \\ 2\{M - H + CO_3^{2-} \rightarrow OH^- + CO_2 + M + e^-\} \\ 2OH^- + CO_2 \rightleftharpoons H_2O + CO_3^{2-} \end{gathered} \tag{7}$$

The mechanism of Ang and Sammells was suggested on the basis of experimental results obtained with Ni [13] and Cu [15] electrodes. The other mechanism was supported by the role of OH^- [14], one electron number and double the rate determining step [16]. Although the reaction mechanisms are not yet in agreement, the kinetic values are within an acceptable range: Ni has an exchange current density of about 100 mA cm^{-2} at 923 K in Li-K melts. Moreover, the following reaction orders are in agreement with the experimental results:

$$i_o = i_o^o p(H_2)^{0.25} p(CO_2)^{0.25} p(H_2O)^{0.25} \tag{8}$$

The positive reaction orders of CO_2 and H_2O reflects the fact that CO_2 and H_2O in the anode enhance the reaction kinetics although they are product species.

Owing to the high temperature, H_2 oxidation is largely insensitive to the chosen anode materials. The exchange current densities of Co [13], Cu [15], Pt [16], Ir [16], Au [16], and Ag [16] were about 45, 69, 85, 27, 26, and 19 mA cm^{-2}, respectively at 923 K in Li-K carbonate melts. Considering the possible experimental error, these values indicate that the materials have a similar H_2 oxidation rate at the anode. In addition, the oxidation potential of Ni in molten carbonate is about −0.802 V under a 1 atm O_2 condition at 925 K [2]. Thus, Ni is metallic at open circuit voltage, and is not oxidized up to a certain potential.

The electrodes in the fuel cell should provide solid-liquid-gas three-phase boundary to reduce overpotential. Porous type electrodes are designed and the carbonate electrolytes are dispersed in the electrode by capillary forces. The anode has a higher contact angle and lower wetting with carbonates than the cathode, which allows a smaller pore size at the anode. As mentioned above, the anode has a very high H_2 oxidation rate. So, the active surface area and electrolyte filling in the anode are not critical parameters for its performance. Therefore the anode behaves as an electrolyte reservoir in the MCFC.

The most plausible life-limiting factor is electrolyte depletion in the MCFC. Since the anode serves as electrolyte reservoir, its stable pore structure is very important for the electrolyte management. The Ni-Cr alloy electrodes, however, showed creep behavior, which deforms the pore structure due to Ostwald ripening under the suppression in the carbonate melts. Thus, the anode thickness is reduced with time and electrolyte amounts in the anode are also decreased. Consequently, the cell life can be shortened. It was reported that the addition of Al to Ni-Cr resulted in higher creep resistivity than in Ni-Cr [12].

As alternative anodes, Cu-Al alloy and $LiFeO_2$ were tested, but they had insufficient creep strengths [1].

Cathode Electrode

Oxygen reduction is generally much slower than H_2 oxidation. In particular, low temperature fuel cells have much larger overpotential at the cathode, which is limiting the cell performance. A similar tendency also prevails in MCFCs and most researches on kinetics have focused on oxygen reduction. In the past 35 years, a lot of works on oxygen reduction in molten carbonates have been done and several oxygen reduction mechanisms have been suggested. Among them, two mechanisms, superoxide and peroxide paths, have been mainly suggested from half-cell experiments with plain gold electrodes [17, 18].

Superoxide path [17]

$$3O_2 + 2CO_3^{2-} \overset{k}{\rightleftharpoons} 4O_2^- + 2CO_2 \tag{9a}$$

$$O_2^- + e^- \rightarrow O_2^{2-} \tag{9b}$$

$$O_2^{2-} + 2CO_2 + 2e^- \rightarrow 2CO_3^{2-} \tag{9c}$$

$$i_o = i_o^o p(O_2)^{0.625} p(CO_2)^{-0.75} \tag{9d}$$

Peroxide path [18]

$$O_2 + 2CO_3^{2-} \rightleftharpoons 2O_2^{2-} + 2CO_2 \tag{10a}$$

$$O_2^{2-} + 2CO_2 + 2e^- \rightarrow 2CO_3^{2-} \tag{10b}$$

$$i_o = i_o^o p(O_2)^{0.375} p(CO_2)^{-1.25} \tag{10c}$$

where i_o is the exchange current density, which represents the reaction rate on the electrode surface, and i_o^o is the intrinsic exchange current density. The superoxide path was observed mostly in the acidic carbonate melts of Na-K, whereas the peroxide path was found in the most basic melt of Li_2CO_3. In these melts, general agreements were obtained. However, the two mechanisms were separately suggested by the researchers for the widely used Li-K carbonate melts. This ambiguity probably resulted from experimental difficulties with the very hot corrosive carbonate melts. Among the kinetic works on oxygen reduction, the very high exchange current density in oxygen reduction ($i_o \approx 10$ mA cm^{-2}) was generally accepted. The value is about eight orders higher than that of O_2 reduction in an aqueous solution ($i_o \approx 10^{-7}$ mA cm^{-2} [19]). This very high value allows the expectation of very small activation overpotential at the cathode in the MCFC.

The oxygen reduction characteristics were also investigated with 100 cm^2 class single cells by Japanese and Korean groups. In particular, Uchida's group has suggested that oxygen reduction in Li-K melts is a process of mixed diffusion of superoxide and CO_2 in the melts [20].

$$\begin{aligned} R_{ca,L} &= R_{O_2^-} + R_{CO_2} \\ &= \frac{RTd}{3^2 F^2 D_{O_2^-} \kappa p(O_2)^{0.75} p(CO_2)^{-0.5}} \\ &\quad + \frac{RTdh_{CO_2}}{1.5^2 F^2 D_{CO_2} p(CO_2)} \end{aligned} \tag{11a}$$

$$R_{ca,L} p(CO_2) = A p(O_2)^{-0.75} p(CO_2)^{1.5} + B \tag{11b}$$

where $R_{ca,L}$ is the sum of the diffusion resistance of superoxide ions and CO_2, A and B are constants, $A = \frac{RTd}{3^2 F^2 D_{O_2^-} \kappa}$, $B = \frac{RTdh_{CO_2}}{1.5^2 F^2 D_{CO_2}}$, D is the diffusivity, F is the Faraday constant, κ is the equilibrium constant of Reaction Eq. 9a, d is the film thickness, and h is the Henry constant. The diffusion resistance ($R_{ca,L}$) is the main part of the overpotential, and thus kinetic analysis is available with a full cell. They analyzed cathodic overpotential with respect to the O_2 and CO_2 gas partial pressures and consistently concluded that the superoxide mechanism prevails under a normal condition of the Li-K carbonate single cells [21, 22].

Under the oxidizing conditions of the cathode, oxides are mostly stable. It was suggested that Au, NiO, and SnO_2 have exchange current densities (i_o) of 38.5, 18.3, and 11.2 mA cm^{-2}, respectively, indicating that material species are insignificant for the O_2 reduction rate [23]. Since NiO shows comparable catalytic behavior to Au, NiO is the most popular cathode material so far. In general, Ni is oxidized to NiO inside the cell during the pretreatment procedure of MCFC, which is in situ oxidation. During the oxidation, Li ions in the carbonate melts are doped into the NiO. Reportedly about 2% of Li is doped, and the Li doped NiO has about 33 S cm^{-1} electronic conductivity, which is close to metal conductivity [24].

However, NiO at the cathode dissolves into the carbonate electrolyte (Eq. 12), and the Ni ions are reduced to Ni metal in the matrix by H_2 from the anode. Consequently, Ni deposition in the matrix may cause electrical short circuit between the anode and cathode.

$$NiO + CO_2 = Ni^{2+} + CO_3^{2-} \tag{12}$$

It was reported that NiO dissolution is proportional to CO_2 partial pressure and activity [25]. Thus acidic melts have higher NiO solubility. Several methods have been employed to reduce the NiO dissolution: (1) increased basicity of the melts, (2) finding an alternative cathode material, and (3) modification of the NiO electrode. For the first approach, Li-Na melts were considered instead of widely used Li-K melts. It was reported that Li-Na melts have lower solubility [25] and higher electric conductivity than Li-K melts, as shown in Table 1. A Japanese group also reported that a Li-Na carbonate electrolyte cell showed higher performance than a cell with Li-K carbonates in the temperature range 575–675°C up to 5 atm pressure [5]. The addition of alkali earth metals, MgO, BaO, SrO,

and CaO, to the carbonate melts was attempted because alkali earth metal ions behave as a strong base in the melts [26]. They definitely reduced the NiO solubility. However, alkali earth metal ions were segregated in the matrix and the metal ions were distributed at the anode side. In conclusion, the addition was not effective [27]. As a second approach, oxides such as $LiCoO_2$ and $LiFeO_2$ were developed for the cathode material. Although the solubility of $LiCoO_2$ is about one third of that of NiO [28], the low conductivity and high cost of $LiCoO_2$ are obstructions to its use. $LiFeO_2$ also has low solubility compared with NiO but very low conductivity is also a barrier [29]. As a third method, modification of NiO with MgO and Fe_2O_3 was also attempted. The NiO-MgO-$LiFeO_2$ is a solid solution and the material has lower NiO solubility due to the stable structure [30]. Industrially, thickening the matrix and reducing the CO_2 partial pressure were attempted, and FCE Co. reported that it could ensure a cell life of 5 years using these methods [1].

Performance Analysis

The thermodynamic electromotive force of MCFC, called the open circuit voltage (E_{OCV}), is determined by the following equation according to Eqs. 1a and 1b:

$$E_{OCV} = E^{o} + \frac{RT}{2F}\ln\left(\frac{p(H_2)p(O_2)^{0.5}p(CO_2)_{ca}}{p(H_2O)p(CO_2)_{an}}\right) \quad (13)$$

where E^{o} is the standard potential, the subscripts "an" and "ca" denote the anode and cathode, respectively, and p is the partial pressure of the gases. Other symbols have their usual meanings. E_{OCV} is a voltage at zero current, so it represents a theoretically maximum voltage in the cell. When the current flows in the cell, electrical resistance among the cell components and electrochemical resistance at the electrodes reduce the cell voltage. Thus, the performance of fuel cells is determined by the voltage loss, which is the difference between the open circuit voltage (E_{OCV}) and the voltage (V) at a current load (Eq. 14)

$$V = E_{OCV} - \eta_{IR} - \eta_{an} - \eta_{ca} \quad (14)$$

where η_{IR} is the ohmic loss due to the electrical resistance, and η_{an} and η_{ca} are the overpotential at the anode and cathode electrodes, respectively.

The ohmic loss is relatively easy to understand because the electrical resistance of the cell components behaves as a cause of voltage loss. However, determination of overpotential from the electrochemical reaction resistance at the electrodes has been an interesting research topic. The fuel cell electrodes require a large surface area to increase the reaction rate, and thus porous materials are employed. In addition, the electrode surface is covered by thin electrolyte film to provide the three-phase boundary of gas-liquid-solid where the electrochemical reaction occurs. Thus, the electrochemical resistance in MCFC is comprised of charge-transfer resistance on the electrode surface and mass transfer through the liquid film and gas channel as shown in Fig. 2.

At the anode, the following overpotential relations have been suggested based on the electrode kinetics of Eq. 8 by Selman's group in the USA (Eq. 15a) [31] and CRIEPI (Central Research Institute of Electric Power Industry) in Japan (Eq. 15b) [32].

$$\eta_{an} = a_1 \cdot p(H_2)^{-0.42}p(CO_2)^{-0.17}p(H_2O)^{-1.0} \cdot i \quad (15a)$$

$$\eta_{an} = a_2 \cdot p(H_2)^{-0.5} \cdot i \quad (15b)$$

where a is the constant, and i is the current. Both relations were obtained by the steady-state polarization method. On the other hand, the overpotential relations at the cathode have been reported by Selman's group (Eq. 16a) [31] and the CRIEPI group (Eq. 16b) [33].

$$\eta_{ca} = a_3 \cdot p(O_2)^{-0.43}p(CO_2)^{-0.09} \cdot i \quad (16a)$$

$$\eta_{ca} = \left(a_4 \cdot p(O_2)^{-0.75}p(CO_2)^{0.5} + a_5 \cdot p(CO_2)^{-1}\right) \cdot i \quad (16b)$$

Equation 16a is an empirical relation based on the electrode kinetics of a superoxide path (Eq. 9d). On the other hand, Eq. 16b resulted from the assumptions of mass-transfer resistance of superoxide ions and CO_2 in the carbonate electrolyte film.

Most of the electrode kinetics in molten carbonates has been investigated with half-cell experiments that used smooth surface electrodes. Various experimental techniques could be applied such as the use of rotating disk electrode (RDE) [34], rotating wire electrode [35], ultramicroelectrode [36], potential step [37], AC impedance [37], coulostatic relaxation [37],

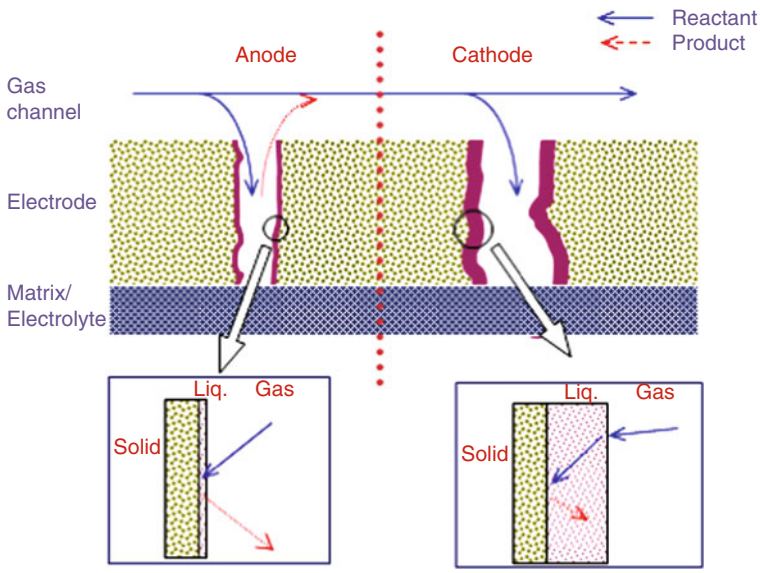

Molten Carbonate Fuel Cells. Figure 2
Schematic drawing of reaction characteristics at the anode and cathode of MCFC

voltammetry [17], and so on. However, the MCFC uses a porous electrode in the cell. Since it is covered by a thin electrolyte film and has a pore volume of over 50%, the behavior of the porous electrode in the cell would be significantly different from that of a plain surface electrode in carbonate melts. A limited number of experimental methods could be applied for the investigation of the reaction characteristics of MCFCs. In general, the voltage loss due to ohmic loss and reaction overpotential in the MCFC has been analyzed with steady-state polarization [31], current interruption [38], and AC impedance methods [39]. As relatively new investigation tools, inert gas step addition (ISA) [22] and reactant gas addition (RA) [40] methods are introduced and the relationship between the methods is treated in this work.

Steady-State Polarization

Steady-state polarization (SSP) is a very simple method that measures voltage by applying currents with sufficient time intervals. Figure 3 shows some results according to different utilizations. An E_{OCV} of 1.07 V is observed. It is very close to the theoretical value according to Eq. 13 because the inlet composition of anode gas is H_2:CO_2:H_2O = 0.69:0.17:0.14 atm and that of cathode gas is air:CO_2 = 0.7:0.3 atm.

Since the utilization (u) is a ratio of consumed gas amounts to supplied amounts, it indicates a gas flow rate at a fixed current density.

$$u = \frac{\text{consumed gas amounts}}{\text{supplied gas amounts}} \tag{17}$$

The utilizations in the figures are based on currents of 15 A. The linear current-voltage behaviors are observed at the utilizations. This indicates that the MCFC has very low charge-transfer resistance as mentioned in the introduction. The difference between E_{OCV} and V at a current load is the total voltage loss according to Eq. 14. As shown in the figures, SSP cannot distinguish between the voltage losses accounted for by η_{IR}, η_{an}, and η_{ca}.

Figure 3 also shows that cell voltage is more severely dependent on the anode utilization than on the cathode one. This indicates that anodic overpotential is more affected by the flow rate than the cathodic one. It is a specific feature of MCFC that flow rate affects cell voltage.

Current Interruption

Current interruption (C/I) is a voltage relaxation method. The measurement is quite simple: the applied currents are rapidly interrupted and the following

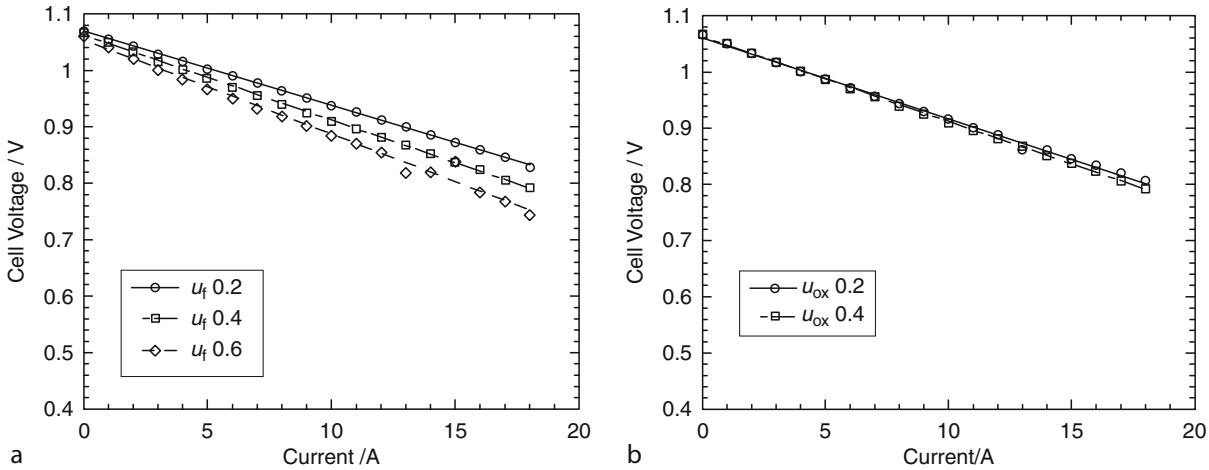

Molten Carbonate Fuel Cells. Figure 3

Steady-state polarization results at various utilizations (15 A current bases) with a 100 cm^2 class MCFC single cell at 650°C, 1 atm. (**a**) anode utilizations at a fixed cathode utilization of 0.4; (**b**) cathode utilizations at a fixed anode utilization of 0.4

voltage relaxation is recorded. Figure 4 presents some results of C/I measurement. In particular, Fig. 4a shows voltage relaxation during 200 μs. At the exact moment of interruption, a voltage jump due to the relaxation of electrical resistance occurs. In the MCFC, most of the electrical resistance is attributed to the ionic resistance in the electrolyte, and thus the voltage jump shows that the ionic resistance is relaxed right after the interruption. Then the flow rate independent time region follows as shown in Fig. 4b. However, voltage relaxation in the time region depends on the oxidant gas composition [38]. This implies that the time region represents the mass-transfer effect through the liquid electrolyte at the cathode. Then the longest time region of 10 s shows that voltage relaxation depends on the anode utilization; higher utilization requires a longer relaxation time. CRIEPI reported that the voltage relaxation for several seconds was ascribed to the relaxation of concentration distribution in the anode electrolyte film [41]. Consequently, the C/I method was found to show ohmic loss and anodic and cathodic overpotential for different time ranges.

AC Impedance

The AC impedance method is a powerful technique for electrode kinetics and mass-transfer investigation. The charge-transfer and mass-transfer resistances are an electrically parallel circuit with an electrochemical double layer that behaves as a capacitor. The parallel circuit of a resistance and a capacitor at a smooth surface electrode has the characteristic behavior of an AC signal: a 90° phase angle between the current and voltage signal at a high frequency AC signal and 0° at a low frequency signal. The phase angle is generally represented in the complex plane where the X axis represents the resistance component and the Y axis the capacitive one. Thus, the impedance of the parallel circuit draws a half circle due to the frequency change, and the diameter of the circle represents the resistance value of the circuit. Interpretation of the AC impedance in the MCFC has not been in agreement, although a lot of theoretical interpretation has been attempted. Difficulties in the interpretation of porous electrode behaviors are major reasons. Figures 5a and b show the results of AC impedance with different flow rates at the anode and cathode, respectively. They were measured in an open-circuit state, and thus electrodes were maintained in an equilibrium state. The length of the X axis from 0 to the high frequency initial point represents the internal resistance of the cell. The high frequency semicircle on the left has a frequency range of 1 kHz–5 Hz, which does not depend on the anode and cathode flow rate. In a previous work, it was reported that the high

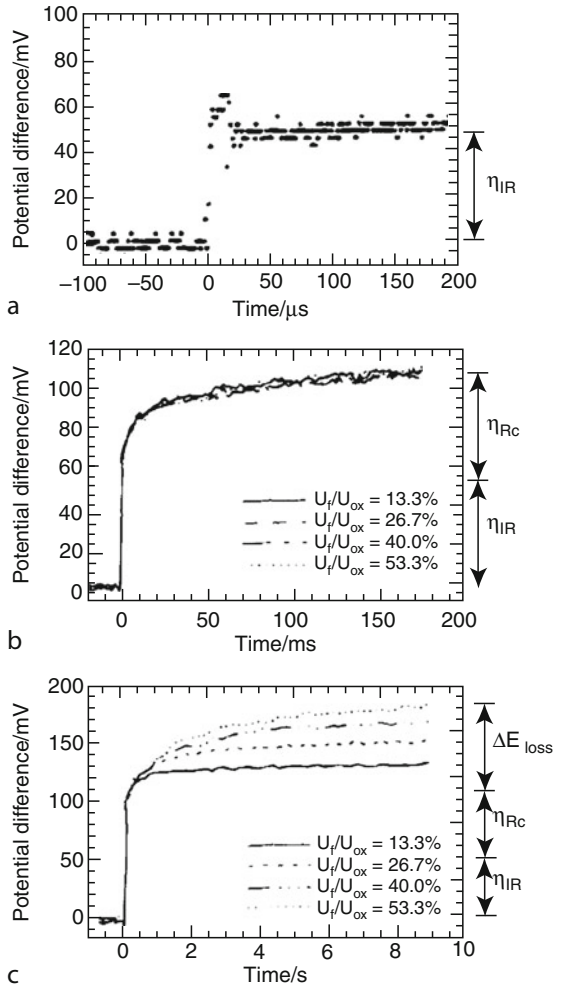

Molten Carbonate Fuel Cells. Figure 4
Voltage relaxations after current interruption of 10 A current loads at a 100 cm^2 class MCFC single cell (From [38]). (**a**) 200 μs time range; (**b**) 200 ms; (**c**) 10 s

frequency semicircle reflected cathodic overpotential due to the mass-transfer resistance through the liquid electrolyte at the cathode [42]. The semicircle on the right has a frequency range of 1 to 0.01 Hz, and is called the low frequency semicircle (LFSC). The LFSC shows a clear dependence on the anode gas flow rate and insignificant change due to the cathode flow rate as shown in the figure. This is in agreement with a previous work [42]. The enlarged LFSC at low flow rate indicates higher resistance in the cell. The CRIEPI group reported that the LFSC represents the effect of gas flow on the concentration distribution along the gas flow path on the electrode; a higher flow rate provides less concentration distribution [43].

Inert Gas Step Addition (ISA)

The above relations of anode overpotential (Eqs. 15a and 15b) and cathode overpotential (Eqs. 16a and 16b) only employ the partial pressure effect of gases. A lot of previous works on the electrode kinetics have been done with a coin type single cell, which had a geometric electrode area of about 3 cm^2. They were carried out with a very low gas utilization that was sufficient to neglect the gas-phase mass-transfer effect. The low utilization, however, was far from the actual condition where the anode utilization is normally over 70%. In addition, the performance of MCFC depends on the gas flow rate even in the 100 cm^2 class single cell as shown in Fig. 3. To investigate the flow rate effect in the MCFC, the inert gas step addition (ISA) method has been developed [22]. ISA can vary the utilization without changing gas compositions, and thus the flow rate effect could be analyzed.

Measurements ISA measurement was mainly carried out with 100 cm^2 class single cells because it had sufficient anode and cathode gas volumes to show the gas flow effect at the electrodes. In fact, the reactant gases flow through the gas channel over the electrode, and thus an electrode has a certain gas volume between the electrode and cell frame. Figure 6 shows the gas flow path of an electrode. When the gas line volume, v_i, is bigger than the gas volume of an electrode, v_c, the added inert gas enlarges the reactant gas flow rate in the electrode during the time range of $t_{i,a}$ of Fig. 7. The flow rates of reactant gases are enhanced without partial pressure change during $t_{i,a}$, which results in a utilization shift. Thus, the voltage variation during the time range represents the utilization effect on the overpotential. The added inert gas flows inside the cell until the step off of inert gas, which varies the gas partial pressures between $t_{i,a}$ and $t_{i,b}$. Therefore, ISA also provides a partial pressure effect on the overpotential. When the inert gas flow is interrupted, the remaining inert gas in the volume, v_i, flows in the cell during $t_{i,b}$. Thus the reactant flow rate is decreased during the time range. The flow rate of inert gas was controlled with a mass flow controller (MFC). During

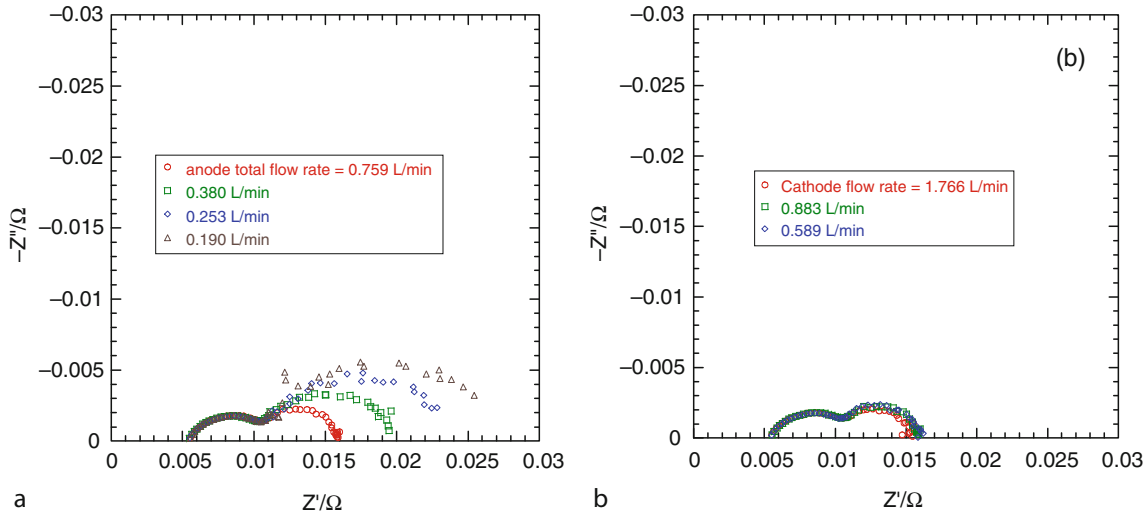

Molten Carbonate Fuel Cells. Figure 5
AC impedance results with various gas flow rates with a 100 cm^2 class MCFC single cell at 650°C, 1 atm, OCV, 5 mV rms signal, 1 kHz–0.01 Hz. (**a**) Various anode flow rates at a fixed cathode flow rate of 0.883 L min^{-1}; (**b**) Various cathode flow rates at a fixed anode flow rate of 0.759 L min^{-1}

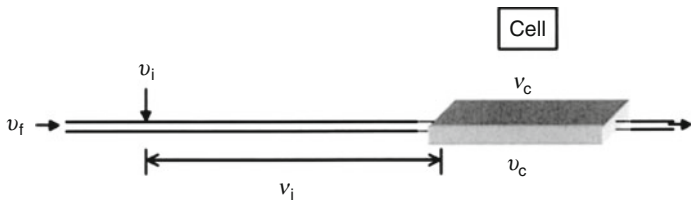

Molten Carbonate Fuel Cells. Figure 6
Schematic drawings of gas flow path of an electrode (From [22]). υ_f is the reactant flow rate, υ_i is the inert gas flow rate, υ_c is the consumed gas rate by the applied currents, v_i is the volume between inert gas inlet port and electrode, v_c is the volume of gas channel

the flow change, the cell voltage and inert gas flow rate were simultaneously recorded with an oscilloscope.

Analysis of Cell Behavior As shown in Fig. 2, MCFC reactions are comprised of charge-transfer reactions on the electrode surface and mass-transfer processes through the gas and liquid phases in series. Resistances in those processes are reciprocal numbers of reaction-rate constant and mass-transfer coefficients that are represented in the overpotential. Thus the overpotential relation is as follows [22]:

$$\eta = \frac{iRT}{n^2F^2ap_0}\left(\frac{h}{k_0}+\frac{h}{k_L}+\frac{1}{k_G}\right) \tag{18}$$

where i is the current, a is the geometrical area, h is the Henry's Law constant, p_0 is the bulk gas pressure, k_0 is the reaction-rate constant, and k_L and k_G are the mass-transfer coefficients through the liquid electrolyte and gas phase, respectively. Other symbols have their usual meanings. As mentioned in the chapter of anode electrode, the H_2 oxidation rate is sufficiently fast ($i_o \approx 100$ mA cm^{-2}) for the charge-transfer resistance to be neglected. In addition, the electrolyte film on the anode electrode can be assumed to be negligibly thin according to the dry agglomerate model [3], and then the mass-transfer resistance through the electrolyte film can be neglected. Consequently, the anode is assumed to be a gas-phase mass-transfer control

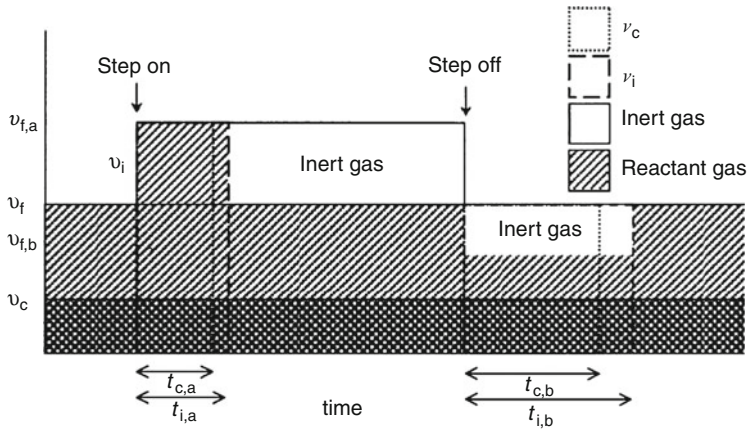

Molten Carbonate Fuel Cells. Figure 7
Schematic drawings of flow rate changes caused by the inert gas addition. The reactant flow rate increases during $t_{i,a}$ and decreases for $t_{i,b}$ (From [22]). υ_f is the reactant flow rate, υ_i is the inert gas flow rate, υ_c is the consumed gas rate due to the applied currents, $\upsilon_{f,a}$ is the flow rate increase due to the inert gas addition, $\upsilon_{f,b}$ is the flow rate decrease by the interruption of inert gas addition, v_i is the volume between inert gas inlet port and electrode, v_c is the volume of gas channel. t_c is the time to fill v_c, t_i is the time of the gas filled in the volume v_i to flow over the electrode

process. The gas-phase mass-transfer coefficient (k_G) was obtained from the mass-transfer coefficient (k_B) of the boundary layer theory in the case of mass transfer between laminar flow and plain substrates [22]. Then k_G is expressed as follows:

$$k_B \cong 0.664\left(\frac{\upsilon_f}{L}\right)^{\frac{1}{2}}(D_G)^{\frac{2}{3}}(v)^{-\frac{1}{6}} \tag{19}$$

For the unit conversion,

$$k_G = \frac{k_B}{RT} \tag{20}$$

where υ_f is the flow velocity, L is the electrode length, D_G is the gas diffusivity, and v is the kinematic viscosity. Other symbols have their usual meanings. Since the gas velocity corresponds to gas flow rate, Eq. (20) can be expressed in terms of utilization (u). Then Eq. (18) becomes:

$$\eta_{an} \cong \eta_G = i\frac{RT}{n^2F^2ap_0}\left(\frac{1}{k_G}\right) = q \cdot u^{0.5} \tag{21}$$

where $q = 1.51\frac{R^2T^2(iLs)^{1/2}v^{1/6}}{(n^3F^3a^2p_0)^{1/2}D_G^{2/3}}$, and s is the cross section area of the gas channel.

Figure 8 shows voltage behaviors with 0.3 L min^{-1} N_2 addition to the anode at various current densities. At the open-circuit state, the voltage increases due to

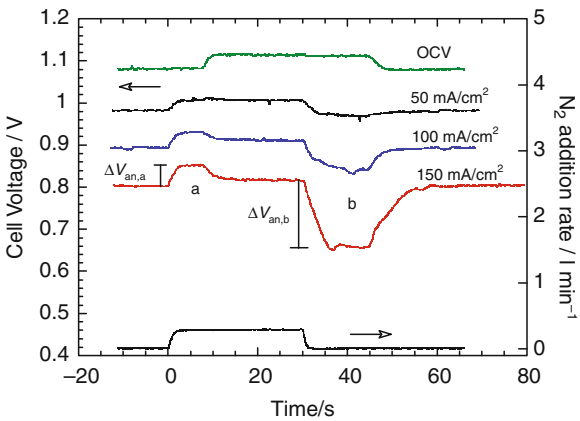

Molten Carbonate Fuel Cells. Figure 8
Voltage shift patterns with an addition of 0.3 L min^{-1} N_2 to the anode at 650°C, u_f = 0.6 (0.253 L min^{-1}) and u_{ox} = 0.4 (0.883 L min^{-1}) of i = 150 mA cm^{-2} (From [47])

the addition because E_{OCV} rises with decreasing partial pressure of anode gases according to Eq. 13. However, at polarization states, a positive peak, "a," and a negative voltage peak, "b," are observed. The peaks are due to the change in the flow rate of reactant gases as shown in Fig. 7. The flow rate increase results in the positive "a" peak while the flow rate decrease leads to the negative

"b" peak. This indicates that the anode reaction is affected by the flow rate of anode reactant gases.

Substituting N_2 with Ar and He gives identical voltage behaviors [22]. This shows that ISA measurements are available regardless of the inert gas species. However, the voltage between the "a" and "b" peaks was affected by the inert gas species; helium showed the highest voltage among them [22]. During the time range, inert gas flows inside the cell and the gas species may affect the diffusivity of H_2. Indeed, helium has the highest diffusivity among them, and thus helium provided the lowest mass-transfer resistance in the anode. This strongly implies that the anode reaction is a gas-phase mass-transfer control process.

Since the height of the positive peak, $\Delta V_{an,a}$, is an overpotential difference at the flow rate change and the flow rate corresponds to the utilization, the peak height can be expressed in terms of anode utilization (u_f).

$$\Delta V_{an,a} = \eta_{an1} - \eta_{an2} = q u_{f,1}^{0.5} - q u_{f,2}^{0.5} = m - q u_{f,2}^{0.5} \tag{22}$$

where subscripts 1 and 2 denote before and after the N_2 addition respectively and m is a constant. Thus the peak height has a linear relation with utilization. Figure 9 shows the peak heights with various N_2 addition rates at different anode utilizations and arranges the heights according to the relation of Eq. 22. The linearity of Eq. 22 at the different anode gas utilizations verifies the validity of the equation, which shows that the anode reaction is a strong gas-phase mass-transfer control process. The slope of q is about 140 mV and the anodic overpotential can be obtained according to Eq. 21.

On the other hand, the linear current-voltage behavior of Fig. 3 and the very high reaction rate of the cathode ($i_o \approx 10$ mA cm^{-2}) allow the assumption of negligible charge-transfer resistance at the cathode. In fact, the cathode has a relatively thick carbonate electrolyte on the surface as shown in Fig. 2. Thus, the following relation has been suggested as the cathodic overpotential [22].

$$\eta_{ca} \cong \eta_{ca,G} + \eta_{ca,L} = i \frac{RT}{n^2 F^2 a p_0} \left(\frac{h}{k_{ca,L}} + \frac{1}{k_{ca,G}} \right) \tag{23}$$

Equation 23 is the sum of overpotential due to the liquid and gas phases, and thus their separate estimation is available. When the overpotential due to the gas-phase resistance is considered, the following relation can be used:

$$\eta_{ca,G} = i \frac{RT}{n^2 F^2 a p_0} \left(\frac{1}{k_{ca,G}} \right) = q \cdot u_{ox}^{0.5} \tag{24}$$

The N_2 addition to the cathode brings about two positive and negative voltage peaks in the "B" and "D" time regions as shown in Fig. 10. The origins of the

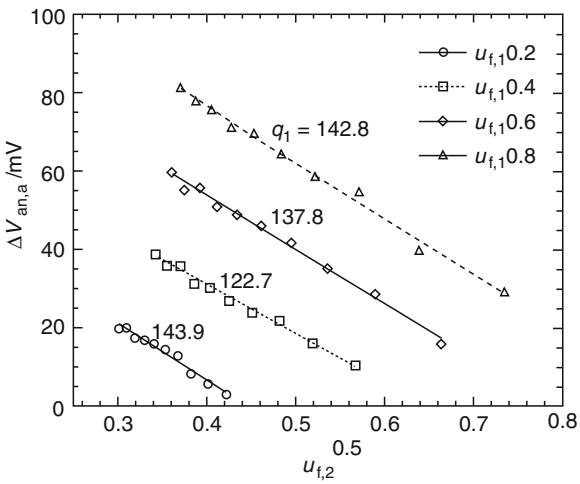

Molten Carbonate Fuel Cells. Figure 9
Rearrangement of the peak height in Fig. 8 with shifted utilization according to Eq. 22 (From [22])

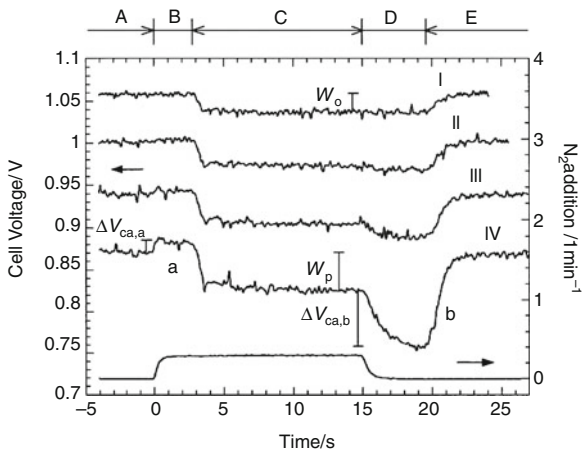

Molten Carbonate Fuel Cells. Figure 10
Cathodic ISA results at different currents with nitrogen addition rate of 0.3 L min^{-1} at a cathode flow rate of 0.589 L min^{-1} and anode flow rate of 0.756 L min^{-1}, 923 K, 1 atm, I/0; II 50; III 100; IV 150 mA cm^{-2} (From [22])

peaks are due to the flow rate and utilization change similar to the anode as shown in Fig. 8. Applying the relation of Eq. 22 to the cathode, we obtain Eq. 25.

$$\Delta V_{ca,a} = \eta_{ca1} - \eta_{ca2} = q u_{ox,1}^{0.5} - q u_{ox,2}^{0.5} = m - q u_{ox,2}^{0.5} \tag{25}$$

Then the q value of the cathode represents overpotential due to the gas-phase mass transfer at the cathode.

Figure 11 shows the results of Eq. 25 at the cathode. The value, q_1, at the cathode equal to q is very small compared with that at the anode of Fig. 9, although the small positive peak height provides deviations in the $\Delta V_{ca,a}$. This means that the cathode has much smaller overpotential due to the gas transport in the cell. In addition, q_1 values are different with cathode utilization; they have larger values at a higher utilization. In general, the cathode showed higher overpotential of over 50% of oxidant utilization [22]. The low diffusivity in the gas phase and low O_2 solubility in the carbonate melts could be the reason. The q_1 value indicates that the cathodic overpotential also depends on the utilization.

On the other hand, the voltage in the "C" time region of Fig. 10 is a steady-state value of voltage at the N_2 flowing in the cathode. The N_2 in the cell varies the gas partial pressures, and thus the region represents some effects of gas partial pressures on the

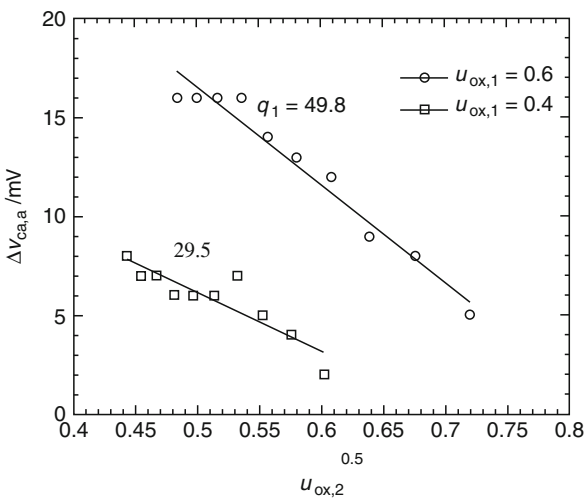

Molten Carbonate Fuel Cells. Figure 11 Rearrangement of the peak heights in Fig. 10 with shifted utilization according to Eq. 25 (From [22])

overpotential. Adding the same amount of N_2 to the various gas partial pressures of O_2:CO_2:N_2 (Table 3) gives overpotential differences ($\Delta W = W_P - W_O$) related to the gas partial pressure. In this case, W_P is the voltage gap at a polarization state and W_O is that at open-circuit state by N_2 addition to the cathode as shown in Fig. 10. Thus, ΔW has the following relations:

$$\Delta W = \eta_{ca,L,2} - \eta_{ca,L,1} = \left(R_{ca,L2} - R_{ca,L1}\right) \cdot i/a \tag{26}$$

where subscripts 1 and 2 represent before and after N_2 addition, respectively, and a is the geometrical electrode area. Then ΔW has a linear relation with gas partial pressure with Eq. (11b).

$$\begin{aligned}(\Delta W \cdot a/i) p(CO_2) &= \left(R_{ca,L2} - R_{ca,L1}\right) p(CO_2) \\ &= A' p(O_2)^{-0.75} p(CO_2)^{1.5} + B'\end{aligned} \tag{27}$$

where $A' = A(\beta^{-0.25} - 1), B' = B(\beta^{-1} - 1)$, $\beta = p(O_2)_2/p(O_2)_1$, A and B are the constants of Eq. 11b, and the subscripts 1 and 2 represent before and after N_2 addition, respectively.

When we assume that the cathode overpotential due to the mass transfer through the carbonate electrolyte is combined diffusion control of superoxide ions and CO_2, the overpotential is a function of gas partial pressure as shown in Eqs. 11a and 11b. Equation 11b shows a linear relation between the ΔW and gas partial pressures. Figure 12 shows linearity of Eq. 11b, indicating that the mass-transfer resistance through the electrolyte film causes cathodic overpotential. From Eq. 26 we can obtain A and B values. Then with Eq. 11b we can have $R_{ca,L}$ and $\eta_{ca,L}$ at normal gas partial pressures of $p(O_2) = 0.15$ atm and $p(CO_2) = 0.3$ atm. The value of $\eta_{ca,L}$ under this

Molten Carbonate Fuel Cells. Table 3 Various compositions of the cathode gases

Gases	Ratio (atm)
O_2:CO_2:N_2	0.9:0.1:0,
	0.7:0.3:0, 0.7:0.1:0.2,
	0.5:0.5:0, 0.5:0.3:0.2, 0.5:0.1:0.4,
	0.3:0.7:0, 0.3:0.5:0.2, 0.3:0.3:0.4,

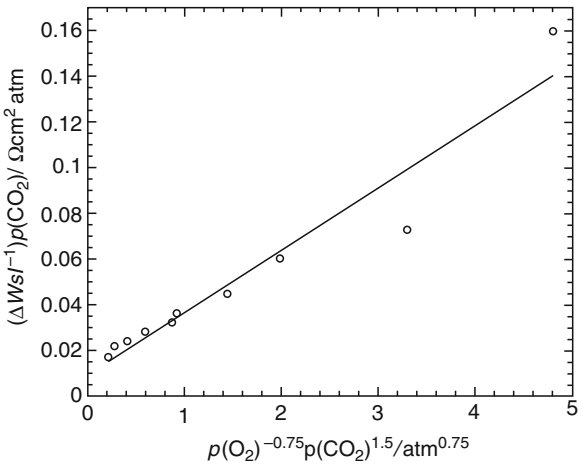

Molten Carbonate Fuel Cells. Figure 12
Relationships of the cathodic overpotentials with partial pressures of oxygen and CO_2 according to Eq. 27 at 923 K, 1 atm (From [22])

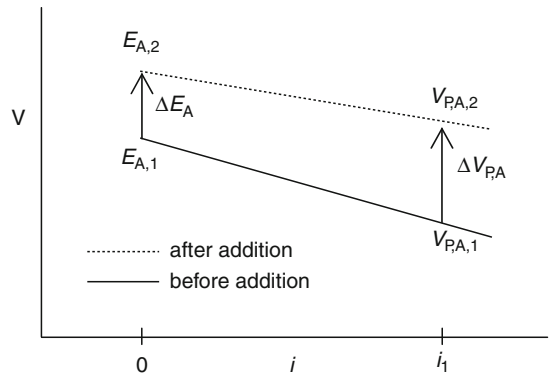

Molten Carbonate Fuel Cells. Figure 13
Schematic drawings of voltage shift behaviors by the addition of a reactant gas at open-circuit (ΔE_A) and polarization states ($\Delta V_{P,A}$) (From [41])

condition is about 62 mV, which is much larger than $\eta_{ca,G}$ ($\approx$18 mV at $u_{ox} = 0.4$) from Eq. 24. This means that overpotential at the electrolyte film is much larger than that at the gas phase and the cathodic reaction is mostly the liquid-phase mass-transfer control process.

The above results show that the anodic overpotential is mostly attributed to the gas-phase mass-transfer resistance and the cathodic one is a sum of overpotential due to gas-phase resistance ($\eta_{ca,G}$) and liquid-phase resistance ($\eta_{ca,L}$). Thus, the following relation can be suggested:

$$\eta_{an} \cong \eta_{an,G} = q_{an} \cdot u_f^{0.5} \tag{28a}$$

$$\eta_{ca} \cong \eta_{ca,G} + \eta_{ca,L} = q_{ca} \cdot u_{ox}^{0.5} + A'' \cdot p(O_2)^{-0.75} p(CO_2)^{0.5} + B'' \cdot p(CO_2)^{-1} \tag{28b}$$

where q_{an} and q_{ca} are the constants q of Eq. 22 and 25, respectively, $A'' = A \cdot i/a$ and $B'' = B \cdot i/a$, and A and B are the constants of Eq. 27.

Reactant Gas Addition (RA) Method

The cathodic overpotential from the ISA method, the sum of $\eta_{ca,L}$ and $\eta_{ca,G}$, is only 80 mV at $u_{ox} = 0.4$. This is smaller than the anodic overpotential from the method at $u_f = 0.4$, which is about 90 mV according to Eq. 21. This is contradictory to the conventional concept that the cathodic overpotential is larger than the anodic one because of the slow oxygen reduction at the cathode.

Meanwhile, the anode and cathode reactions of Eqs. 1a and 1b are multi-component reaction systems. As mentioned regarding the ISA method, the anode and cathode reactions are mass-transfer control processes. Then the mass-transfer of each species would provide overpotential due to the species. To investigate the overpotential attributed to each species, the reaction gas addition method was attempted. This is very similar to the ISA except that a reactant gas is added to an electrode instead of an inert gas [41]. Figure 13 shows the voltage behaviors due to the addition of a reactant gas. Here, the subscript A denotes a reactant gas species.

When a certain amount of a reactant gas is added to an electrode at the open-circuit state, the addition changes the partial pressures of the cell and determines E_{OCV} according to Eq. 13. When the same amounts of reactant gas are added at a polarization state, the voltage is varied by overpotential according to Eq. 14. Thus the gap (ΔV_A) between the voltage shift at the open-circuit state (ΔE_A) and at a polarization state ($\Delta V_{P,A}$) is overpotential variation due to the addition.

$$\Delta V_A = \Delta V_{P,A} - \Delta E_A \tag{29}$$

where $\Delta V_{P,A} = V_{P,2} - V_{P,1}$ and $\Delta E_A = E_{OCV,2} - E_{OCV,1}$. When $\Delta V_A > 0$, the addition mitigates mass-transfer resistance at the electrode. On the

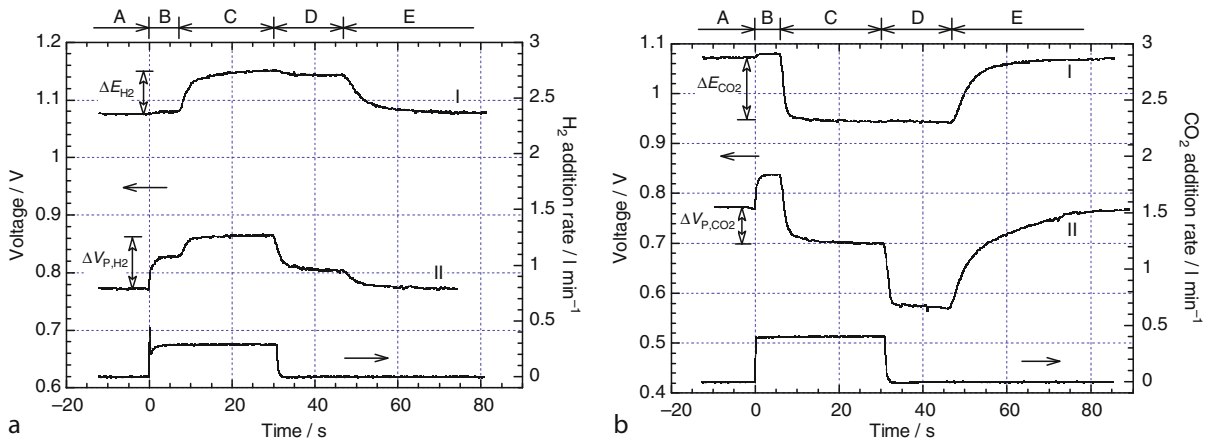

Molten Carbonate Fuel Cells. Figure 14

Results of the RA measurement at the anode with conditions of 923 K, 1 atm at open-circuit state (I) and polarization state of 150 mA cm^{-2} (II), anode feed rate = 0.253 L min^{-1} (u_f = 0.6 at 150 mA cm^{-2}), and cathode feed rate = 0.883 L min^{-1} (u_{ox} = 0.4 at 150 mA cm^{-2}) (From [41]). (**a**) 0.3 L min^{-1} H_2 addition; (**b**) 0.4 L min^{-1} CO_2 addition

contrary, $\Delta V_A < 0$ indicates that the addition enlarges the resistance. When $\Delta V_A = 0$, the addition does not affect the resistance.

Figure 14a shows RA results with H_2 addition to the anode. At the open-circuit state (curve I) the added H_2 flows inside the cell in the "C" and "D" time regions, which results in a partial pressure and E_{OCV} increase in these regions. At a polarization state of 150 mA cm^{-2} (curve II) two positive voltage steps in the "B" and "C" time regions are observed. The step in the "B" region is due to the increase in flow rate of reactant gases due to the H_2 addition, which is the same as the reason for the positive voltage peak obtained with the ISA method. For the "C" region the enlarged H_2 flow rate results in the second voltage step, which involves a change in overpotential due to the addition. The voltage shift of curve II ($\Delta V_{P,H2}$) is larger than that at the open-circuit state (ΔE_{OCV}). In principle, the gas inlet conditions for the two curves are identical. Thus, the difference (ΔV_{H2}) represents variation in overpotential due to the H_2 addition. This results in a positive ΔV_{H2} according to Eq. 29, which shows that H_2 addition reduces the anodic overpotential. It also implies that the anode has overpotential due to the mass-transfer resistance of H_2 species. However, the behavior can provide information on overpotential due to H_2 species through ΔV_{H2}. When the H_2 addition rate was varied from 0.1 to 0.6 L min^{-1}, ΔV_{H2} showed consistency in

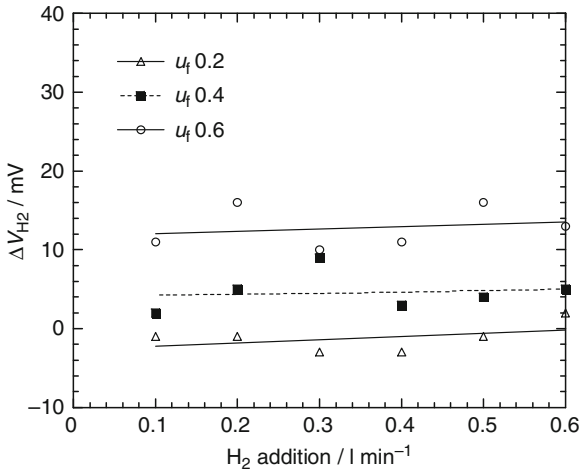

Molten Carbonate Fuel Cells. Figure 15

ΔV_{H2} behavior with respect to the H_2 addition amount at the various anode utilizations at 923 K, 1 atm, cathode feed rate = 0.883 L min^{-1} (From [41])

the rates as shown in Fig. 15. This means that the resistance due to the H_2 species is sufficiently reduced by the addition, and then a consistent ΔV_{H2} is obtained. In addition, when anodic utilization, u_f, is increased, ΔV_{H2} is enlarged [41]. This also implies that anodic overpotential depends on the H_2 flow rate; a lower H_2 flow rate has a larger anodic overpotential.

Figure 14b shows the results of CO_2 addition to the anode. Indeed, CO_2 is a product species of the anode reaction as shown in Eq. 1a. Thus the CO_2 addition reduces E_{OCV} according to Eq. 13. At open-circuit state the reduced E_{OCV} is observed due to the CO_2 addition in the "C" and "D" time regions. At a current density of 150 mA cm^{-2}, two voltage peaks are observed; like the voltage peaks obtained using the ISA method ascribed to the change in flow rate of anode gas. The voltage shift due to the addition at the current density ($\Delta V_{P,CO2}$) is much smaller than that at the open-circuit state (ΔE_{CO2}). Since those values are negative, the difference (ΔV_{CO2}) is a positive value. This indicates that CO_2 addition to the anode reduces anodic overpotential. This can be explained by the reaction kinetics of Eq. 8, where the reaction rate has a positive order for the CO_2 species. Therefore raising the CO_2 partial pressure reduces anodic overpotential [41]. Analysis of overpotential with various anode gas compositions shows identical overpotential behavior, whereby increasing CO_2 partial pressure reduces anodic overpotential [44].

Dissimilar to the H_2 addition, ΔV_{CO2} depends on the amount of CO_2 addition (Fig. 16). Furthermore, ΔV_{CO2} values are much larger than ΔV_{H2}, which implies that CO_2 species has higher mass-transfer resistance than H_2 species and anodic overpotential is more dependent on the CO_2 flow rate. The CO_2 addition reduces the resistance, and thus ΔV_{CO2} rises with CO_2 addition amounts as shown in Fig. 16. At certain amounts, from 0.4 to 0.5 L min^{-1}, ΔV_{CO2} has a maximum value. This indicates that the mass-transfer resistance due to the CO_2 species becomes a minimum. Over the amounts, the CO_2 species rather signifies the resistance probably due to reducing the mass transfer of H_2 species. Then ΔV_{CO2} decreases again. ΔV_{CO2} also depends on the anodic utilization; higher utilization shows larger overpotential. Similar to the H_2 addition, this indicates that the anode reaction is a mass-transfer control process of CO_2.

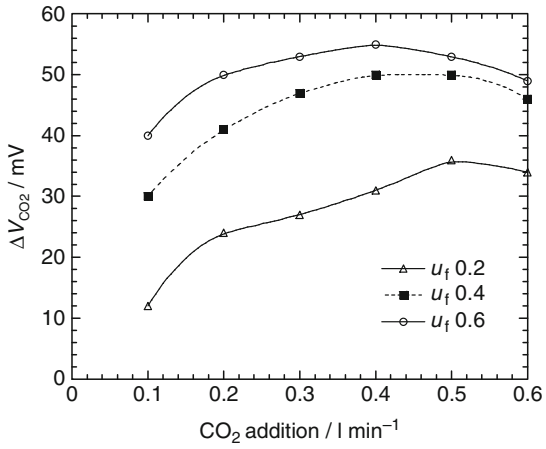

Molten Carbonate Fuel Cells. Figure 16
ΔV_{CO2} behavior with respect to the CO_2 addition amount at various utilizations of anode gas at 923 K, 1 atm, cathode feed rate = 0.883 L min^{-1} (From [41])

The H_2O addition also decreased anodic overpotential [41]. The anode gas was humidified with a bubbler that contained water at a certain temperature. Then the partial pressure of H_2O was controlled by the water temperature in the bubbler. The anodic overpotential decreased monotonously with the increase in H_2O content [41], although the H_2O addition reduced E_{OCV} according to Eq. 13. In addition, ΔV_{H2O} rose with the anodic utilization, which was given larger overpotential by the low H_2O flow rate. The positive order of H_2O partial pressure in Eq. 8 is also the reason for the overpotential behavior.

The above results indicate that anode gases of H_2, CO_2, and H_2O provide overpotential due to their mass-transfer limitations. Moreover, the anodic overpotential rises with utilization. These results indicate that the anode reaction is a mass-transfer control process of the species and that the anodic overpotential is a sum of overpotentials due to the mass-transfer resistance of the species. Interestingly ΔV_{CO2} and ΔV_{H2O} are much larger than ΔV_{H2} under normal operating conditions. The low flow rate of CO_2 and H_2O under the condition (H_2:CO_2:H_2O = 0.69:0.17:0.14 atm) can be a reason [44].

Figure 17a shows RA results with O_2 addition to the cathode. At open-circuit state the O_2 addition slightly enhances E_{OCV}. However, at a current density of 150 mA cm^{-2}, a very high voltage shift ($\Delta V_{P,O2}$) is observed. The small step at 0 s originates from the increase in the flow of reactant gases due to the addition. As mentioned in the section on ISA, the cathode has very small mass-transfer resistance in the gas phase, and thus the height is rather small.

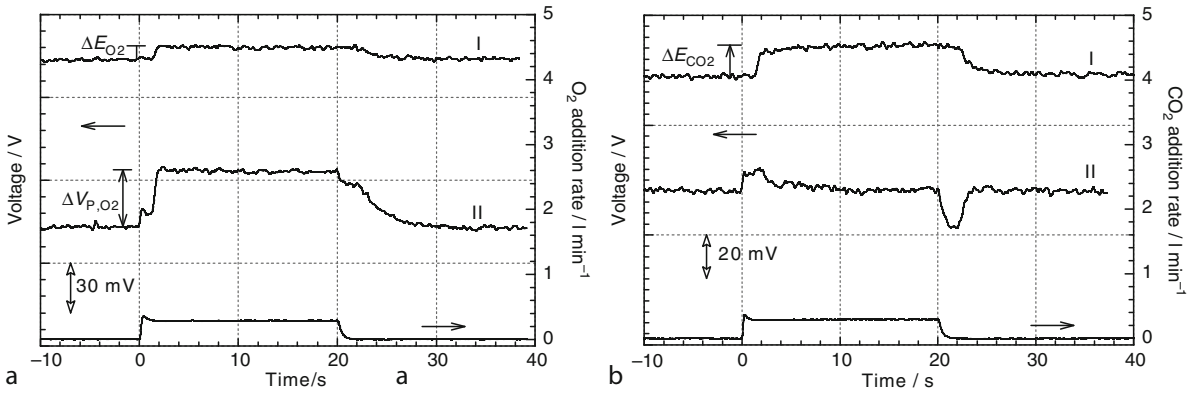

Molten Carbonate Fuel Cells. Figure 17

Results of RA measurement at the cathode with conditions of 923 K, 1 atm at open-circuit state (I) and 150 mA cm^{-2} polarization state (II), anode feed rate = 0.759 L min^{-1} (u_f = 0.2 at 150 mA cm^{-2}), and cathode feed rate = 0.883 L min^{-1} (u_{ox} = 0.4 at 150 mA cm^{-2}) (From [41]). (**a**) 0.3 L min^{-1} O_2 addition; (**b**) 0.3 L min^{-1} CO_2 addition

Therefore, we can expect a large difference ($\Delta V_{O2} = \Delta V_{P,O2} - \Delta E_{O2}$) between voltage shifts at open-circuit state (ΔE_{O2}) and at polarization state ($\Delta V_{P,O2}$). This shows that the cathode has significant overpotential due to the O_2 species and the cathode reaction is an oxygen mass-transfer limitation process. From the half-cell experiments it was also suggested that the mass-transfer limitation of O_2 species prevails at the cathode [45].

The CO_2 addition to the cathode enhances E_{OCV} according to Eq. 13 as shown in Fig. 17b. This is a very similar behavior to the O_2 addition. At a current density of 150 mA cm^{-2}, the CO_2 addition gives rise to the two voltage peaks. As mentioned in the section on the ISA method, these are ascribed to the change in cathode flow rate due to the addition; the positive one is due to the increase in flow rate and the negative one is due to the decrease in flow rate. A dominant feature is that the voltage difference at the current density, $\Delta V_{P,CO2}$, is almost zero. This means that ΔV_{CO2} is a negative value and the CO_2 addition to the cathode enlarges cathodic overpotential. Considering that CO_2 has about ten times the gas solubility of O_2 in the molten carbonate and that the mass-transfer resistance of O_2 species is dominant at the cathode, it is plausible that the CO_2 addition reduces O_2 partial pressure and enhances the resistance of O_2 species in the carbonate electrolyte. Consequently, the CO_2 species may not provide cathodic overpotential under normal operating conditions due to its high solubility.

Future Directions

MCFCs based on natural gas fuel have been commercialized across the world. In general, natural gas MCFCs are economically inferior to coal power electricity. More economic fuels such as decomposition gas of organic waste and coal gas, and so on, are required for wide scale use of MCFC. To investigate the validity of a new fuel, performance analysis tools should be prepared. The methods in this work can be utilized, but some improvements are also necessary. One is the establishment of a theoretical and experimental basis of the AC impedance method for the performance analysis of MCFCs. The strong point of convenient measurement of the method has been weakened by its obscure analytical basis. Another one is the verification of the relationships among the measurement tools listed in this work.

Another point to be mentioned for the dissemination of MCFCs is extending their lifetime. Electrolyte management is strongly related to the problem. The molten carbonate electrolyte is depleted mostly by corrosion with metals and weakening of electrolyte holding in the matrices. Cell design and surface treatment of metal should be considered. It is also necessary to search for appropriate material for the matrix.

Combinations of fuel cells also provide high efficiency. SOFC has been developed as a power system that is comparable to MCFC. SOFC is comprised entirely of solid materials, and thus cracking due to thermal shock is a fundamental problem. The problem confines the SOFC to relatively small power systems, so far. In general, SOFC has higher operation temperatures than MCFC. Thus, series combination of SOFC and MCFC may enhance power generation efficiency.

Bibliography

1. Yuh C, Hilmi A, Farooque M, Leo T, Xu G (2009) Direct fuel cell materials experience. ECS Trans 17:637–654
2. Selman JR, Maru HC (1981) Physical chemistry and electrochemistry of alkali carbonate melts. In: Mamantov G, Braunstein J (eds) Advances in molten salt chemistry. Plenum Press, New York, pp 202–212
3. Yuh CY, Selman JR (1984) Polarization of the molten carbonate fuel cell anode and cathode. J Electrochem Soc 131:2062–2069
4. Hong SG, Selman JR (2004) Wetting characteristics of carbonate melts under MCFC operating conditions. J Electrochem Soc 151:A77–A84
5. Morita H, Komoda M, Mugikura Y, Izaki Y, Watanabe T, Masuda Y, Matsuyama (2002) Performance analysis of molten carbonate fuel cell using a Li/Na electrolyte. J Power Sources 112:509–518
6. Nishina T, Masuda Y, Uchida I (1993) Gas solubility and diffusivity of H_2, CO_2 and O_2 in molten alkali carbonates. In: Saboungi ML, Kojima H, Duruz J, Shores D (eds) Proceedings of the international symposium on molten salt chemistry and technology (The Electrochemical Society PV93-9), pp 424–435
7. Yuh CY, Farooque M, Maru H (1999) Advances in carbonate fuel cell matrix and electrolyte. In: Uchida I, Hemmes K, Lindbergh G, Shores DA, Selman JR (eds) Carbonate fuel cell technology (The Electrochemical Society PV99-20), pp.189–201
8. Fujita Y (2003) Durability. In: Vielstich W, Lamm A, Gasteiger HA (eds) Handbook of fuel cells fundamentals technology and applications. Wiley, New York, pp 969–982
9. Yuh C, Johnsen R, Farooque M, Maru H (1993) Carbonate fuel cell endurance : Hardware corrosion and electrolyte management status. In: Shores D, Maru H, Uchida I, Selman JR (eds) Carbonate fuel cell technology, (The Electrochemical Society PV93-3), pp 158–170
10. Fujita Y, Nishimura T, Hosokawa JI, Urushibata H, Sasaki A (1996) Degradation of materials in molten carbonate fuel cells with Li/Na electrolyte. In the 3 rd FCDIC fuel cell symposium proceedings (Fuel Cell Development Information Center, Japan), pp 151–155
11. Matsumoto K, Yuasa K, Nakagawa K (1999) Protection against localized corrosion of stainless steel below 843 K in molten lithium-sodium carbonate. Denki Kagaku 67:253–258
12. Hoffmann J, Yuh CY, Jopek AG (2003) Electrolyte and material challenges. In: Vielstich W, Lamm A, Gasteiger HA (eds) Handbook of fuel cells fundamentals technology and applications. Wiley, New York, pp 921–941
13. Ang PGP, Sammells AF (1980) Influence of electrolyte composition on electrode kinetics in the molten carbonate fuel cell. J Electrochem Soc 127:1287–1293
14. Jewulski J, Suski L (1984) Model of isotropic anode in the molten carbonate fuel cell. J Appl Electrochem 14: 135–143
15. Lu SH, Selman JR (1984) Electrode kinetics of fuel oxidation at copper in molten carbonates. J Electrochem Soc 131: 2827–2833
16. Nishina T, Takahashi M, Uchida I (1990) Gas electrode reactions in molten carbonate media IV. Electrode kinetics and mechanism of hydrogen oxidation in (Li + K)CO_3 eutectics. J Electrochem Soc 137:1112–1121
17. Appleby AJ, Nicholson SB (1977) Reduction of oxygen in alkali carbonate melts. J Electroanal Chem 83:309–328
18. Appleby AJ, Nicholson S (1974) The reduction of oxygen in molten lithium carbonate. Electroanal Chem Interfacial Electrochem 53:105–119
19. Kinoshita K (1992) Electrochemical oxygen technology. Wiley, New York, p 37
20. Nishina T, Uchida I, Selman JR (1994) Gas electrode reactions in molten carbonate media V. Electrochemical analysis of the oxygen reduction mechanism at a fully immersed gold electrode. J Electrochem Soc 141:1191–1198
21. Yoshikawa M, Mugikura Y, Watanabe T, Ota T, Suzuki A (1999) The behavior of MCFCs using Li/K and Li/Na carbonates as the electrolyte at high pressure. J Electrochem Soc 146: 2834–2840
22. Lee CG, Kang BS, Seo HK, Lim HC (2003) Effect of gas-phase transport in molten carbonate fuel cell. J Electroanal Chem 540:169–188
23. Uchida I, Mugikura Y, Nishina T, Itaya K (1986) Gas electrode reactions in molten carbonate media II. Oxygen reduction kinetics on conductive oxide electrodes in (Li + K)CO_3 eutectic at 650 °C. J Electroanal Chem 206:241–252
24. Baumgartner C (1984) Electronic conductivity decrease in porous NiO cathodes during operation in molten carbonate fuel cell. J Electrochem Soc 131:2607–2610
25. Ota K, Mitsushima S, Kato S, Asano S, Yoshitake H, Kamiya N (1992) Solubilities of nickel oxide in molten carbonate. J Electrochem Soc 139:667–671
26. Doyon JD, Gilbert T, Davies G, Paetsch L (1987) NiO solubility in mixed alkali/alkaline earth carbonates. J Electrochem Soc 134:3035–3038
27. Kunz HR, Bregoli LJ (1990) Ionic migration in molten carbonate fuel cells In: Selman JR, Shores DA, Maru HC, Uchida, I (eds) Carbonate fuel cell technology, (The Electrochemical Society PV90-16), pp 157–168
28. Veldhuis JB, Eckes FC, Plomp L (1992) The dissolution properties of $LiCoO_2$ in molten 62:38 mol% Li:K carbonates. J Electrochem Soc 139:L6–L8

29. Hatoh K, Niikura J, Yasumoto E, Gamo T (1994) The exchange current density of oxide cathodes in molten carbonates. J Electrochem Soc 141:1725–1730
30. Motohira N, Senso T, Yamauchi K, Kamiya N, Ota K (1999) Solubility of nickel in molten carbonates-The effect of Mg addition. In: The 6th FCDIC fuel cell symposium proceedings (Fuel Cell Development Information Center, Japan), pp 237–240
31. Yuh CY, Selman JR (1991) The polarization of molten carbonate fuel cell electrodes I. Analysis of steady-state polarization data. J Electrochem Soc 138:3642–3648
32. Morita H, Mugikura Y, Izaki Y, Watanabe T, Abe T (1997) Analysis of performance of molten carbonate fuel cell V. Formulation of anode reaction resistance. Denki Kagaku 65:740–746
33. Morita H, Mugikura Y, Izaki Y, Watanabe T, Abe T (1998) Model of cathode reaction resistance in molten carbonate fuel cells. J Electrochem Soc 145:1511–1517
34. Ramaswami K, Selman JR (1994) Rotating disk studies in molten carbonates III. Diffusion coefficients and bulk concentration in lithium carbonates. J Electrochem Soc 141:2338–2343
35. Vogel WM, Smith SW, Bregoli LJ (1983) Studies of the reduction of oxygen on gold in molten Li_2CO_3-K_2CO_3 at 650 °C. J Electrochem Soc 130:574–578
36. Malinowska B, Cassir M, Devynck J (1994) Design of a gold ultramicroelectrode for voltammetric studies at high temperature in glass-corrosive media (molten carbonate at 650 °C). J Electrochem Soc 141:2015–2017
37. Uchida I, Nishina T, Mugikura Y, Itaya K (1986) Gas electrode reactions in molten carbonate media I. Exchange current density of oxygen reduction in (Li + K)CO_3 eutectic at 650 °C. J Electroanal Chem 206:229–239
38. Lee CG, Nakano H, Nishina T, Uchida I, Kuroe S (1998) Characterization of a 100 cm^2 class molten carbonate fuel cell with current interruption. J Electrochem Soc 145:2747–2751
39. Yuh CY, Selman JR (1988) Characterization of fuel cell electrode processes by AC impedance. AIChE J 34:1949–1958
40. Morita H, Mugikura Y, Izaki Y, Watanabe T (1999) Analysis of performance of molten carbonate fuel cell VI. Analysis of Nernst Loss on current interrupt wave. Electrochemistry 67:438–444
41. Lee CG, Lim HC (2005) Experimental investigation of electrode reaction characteristics with reactant gas addition measurement in a molten carbonate fuel cell. J Electrochem Soc 152: A219–A228
42. Lee CG, Nakano H, Nishina T, Uchida I, Izaki Y, Kuroe S (1996) Transient response analysis on an 100 cm^2 class molten carbonate fuel cell. Denki Kagaku 64:486–490
43. Morita H, Nakano H, Mugikura Y, Izaki Y, Watanabe T, Uchida I (2003) EIS as a tool to determine fuel flow distribution in molten carbonate fuel cells. J Electrochem Soc 150:A1693–1698
44. Lee CG, Hwang JY, Oh M, Kim DH, Lim HC (2008) Overpotential analysis with various anode gas compositions in a molten carbonate fuel cell. J Power Sources 179:467–473
45. Lee CG, Yamada K, Hisamitsu Y, Ono Y, Uchida I (1999) Kinetics of oxygen reduction in molten carbonates under pressurized Air/CO_2 oxidant gas conditions. Electrochemistry 67:608–613
46. Tomczyk P (2006) MCFC versus other fuel cells—Characteristics, technologies and prospects. J Power Sources 160:858–862
47. Lee CG, Kim DH, Lim HC (2007) Electrode reaction characteristics under pressurized conditions in a molten carbonate fuel cell. J Electrochem Soc 154:B396–B404
48. Lide DR (2007) Handbook of chemistry and physics, 88th edn. CRC Press, Boca Raton, pp 6–143

Monsoon Systems, Modeling of

Chien Wang[1], William K. M. Lau[2]
[1]Department of Earth, Atmospheric, and Planetary Sciences, Massachusetts Institute of Technology, Cambridge, MA, USA
[2]Laboratory for Atmospheres, NASA Goddard Space Flight Center, Greenbelt, MD, USA

Article Outline

Glossary
Definition of the Subject
Introduction
Simulating Monsoon Systems Using Climate Models
Modeling the Impacts of Aerosols on Monsoon System
Climate Change and Monsoon System
Future Directions
Bibliography

Glossary

Aerosol Small particles suspended in the atmosphere in solid or liquid phase.

El Niño and Southern Oscillation (ENSO) Two intimately linked phenomena in tropical regions; El Niño ("the Christ Child" in Spanish) refers to the significant increase in sea surface temperature that irregularly occurs during Christmas time over eastern and central Pacific Ocean; Southern Oscillation refers to the low-latitude oscillation of sea level pressure centered respectively in the eastern Pacific and the western Pacific to Indian Ocean.

General circulation model (GCM) A computer program that solves numerically the time-dependent governing equations describing the evolution of atmospheric or oceanic circulation.

Intertropical convergence zone (ITCZ) A longitudinally extended zone near the equator that separates the northeast wind in the Northern Hemisphere from the southeast wind in the Southern Hemisphere near the Earth's surface.

Madden–Julian oscillation (MJO) An oscillation of zonal wind in both the boundary layer and upper troposphere propagating eastward with an average speed of 5 m/s across equatorial Indian and western and central Pacific Ocean.

Moist static energy (MSE) An atmospheric thermodynamic variable defined as:

$$\mathrm{MSE} = C_p T + gz + L_v q$$

Here C_p is the specific heat of air, T is air temperature, g is gravity, z is height above surface or a given reference level, L_v is the latent heat of water vaporization, and q is the ratio of water vapor to total air in mass.

Tropical biennial oscillation (TBO) A zonal wind oscillation in the equatorial stratosphere.

Definition of the Subject

The word monsoon derives from the Arabic word "mausim," referring to the seasonal reversal of prevailing low-level winds blowing from relatively cold and moist ocean to warm land during the wet season (summer), and from cold and dry land to ocean during the dry season (winter). Monsoon systems are found in tropical regions from Africa, India, East Asia, Australia, and the Americas. Deep convection along with heavy rainfall occurs during the wet monsoon season over land as well as ocean. Typically, in monsoon regions the rainfall in wet season accounts for more than half of the annual surface precipitation. Monsoon evolution heavily influences human activities including agricultural practice and societal habits of billions of people living in monsoon regions. Knowledge and improving prediction of the onset, maintenance, variability, and key drivers are critical to the livelihood of these people. Because the monsoon is an integral part of the global climate system, better understanding of the monsoon is pivotal to predict future climate change and also the response of monsoon systems to such change.

The onset and strength of monsoons are determined by dynamical and thermodynamical processes not only locally over monsoon regions but also remotely over other regions. Computer models combining related dynamical, physical, and chemical processes in various scales are hence important tools to examine the current understanding of monsoon dynamics. These models can be used to test various hypotheses, and to actually simulate and forecast monsoon evolution. Simple models used in the earlier days of monsoon research mostly described the monsoon system from an energy budget perspective. These models could capture very rudimentary features of monsoon energy conversion. However, they lack the capability to go further in revealing the details of rainfall intensity and distribution, and particularly the timing of monsoon onset. Sophisticated three-dimensional regional and global climate models have been used in recent years to simulate monsoon systems, and to study the sensitivity of monsoon circulation and precipitation to various factors, including identification of the anthropogenic impact on monsoon system. These models have also been used to project monsoon evolution under different scenarios of possible future climate change.

Introduction

Over 60% of the world's population lives in monsoon regimes with a clear annual cycle of wind and precipitation. Such a cycle consists of a wet and a dry season. Wind in the lower atmosphere blows poleward from a relatively cold ocean to warm land during the wet season, and goes in the opposite direction during the dry season (Fig. 1). The monsoon regions include a large part of tropical and subtropical Asia and Africa as well as Australia, where some of the most populous nations in the world are located.

Agricultural activities, water resources, and many societal events in regions with a monsoon climate are strongly influenced by the wind reversal and the uneven distribution of rainfall. Forecasting monsoon rainfall and onset, the sudden transition from dry condition into a heavy downpour, has practical meanings to human activities in these places. In addition, whether future climate change would alter the behavior and strength of monsoon is a critical issue in making climate related strategies. The achievement of an adequate skill to forecast future monsoon evolution

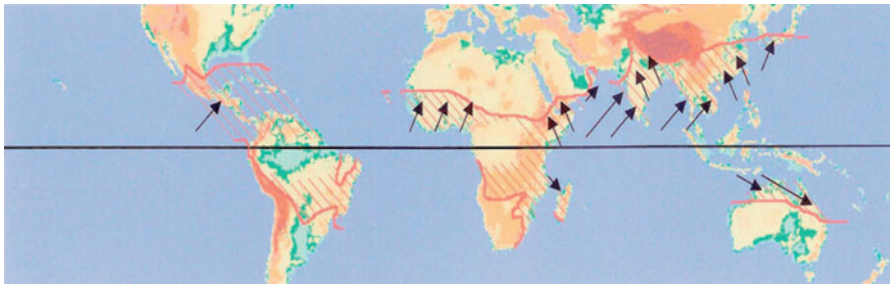

Monsoon Systems, Modeling of. Figure 1
Land areas that have the majority of their rainfall in summer, associated with the poleward motion of deep convection. Where appropriate, low-level wind directions that carry moist warm air are indicated. In areas where there are no arrows, winds are relatively dry, or are weak (as over South America). *Shaded areas* show the normal maximum extent of deep convection (From [1] by J.F.P. Galvin with permissions from the author and Wiley)

relies on a good understanding of fundamental monsoon dynamics along with its variability. This requires knowledge about the formation mechanism and the major driving factors, including both natural and anthropogenic ones, of the monsoon system.

Monsoon Dynamics Fundamentals

Research to identify the driving forces of monsoon onset and strength has been conducted by correlating various diagnostic quantities with monsoon system characteristics. These characteristics include moisture, clouds, precipitation, and the large-scale circulation. With continued advancement of observational technology, from rain gauge stations to satellite monitoring, such effort has gained momentum, leading to improved knowledge. However, improved knowledge often reveals additional complexity of monsoon systems. This will in turn require even better understanding to further improve theory and modeling. This requirement has led to the building of a hierarchy of regional through global climate-system models for monsoon research.

It has long been held that differential heating on land and ocean following solar insolation cycle to be the major formation mechanism of the large-scale monsoon circulation [2, 3]. Such a heating contrast would force wind blow toward warm region, although because of the geostrophic constraint the actual wind direction is altered. Various rather simple models were developed to simulate monsoon systems based on the differential heating concept. These include zonally symmetric and other types of two-dimensional models that describe the zonal circulation and precipitation from ocean to land over monsoon regions, and often include a description of the planetary boundary layer. These simple models along with their limitations have been discussed extensively in literature [4, 5].

Attempts to forecast monsoons have linked monsoon strength with other phenomena or processes, ranging from the snowfall on the hills of Himalaya in the previous winter [6], mountains [7, 8], to the El Niño and Southern Oscillation (ENSO) ([9] and many others). Some of these factors are still within the framework of the large-scale land-sea thermal contrast model while others clearly connect to global climate dynamics.

In recent years, there have been studies suggesting that as a northward extension of the Intertropical convergence zone (ITCZ), the onset of the monsoon could just be a result of a longitudinal sea surface temperature (SST) gradient, not necessarily the traditionally held land-ocean temperature gradient (e.g., [10, 11]). It has also been demonstrated that the poleward boundary of monsoon circulations are co-located with a maximum in sub-cloud layer moist static energy (or entropy; MSE), corresponding to the minimum of vertical meridional wind shear [12–14]. Such a location and extent of the monsoon would also be influenced by the position of subtropical thermodynamic forcing as well as the advection of MSE.

Due to a meteorological phenomenon called the "thermal wind balance," the heating over land to

the north and the cooler ocean to the south during the summer monsoon will produce easterly winds aloft and westerly winds below. When the upper troposphere easterly wind is strong, in the case of a strong monsoon, instability of easterly jet may stimulate the formation of eddies. The formation of these eddies might not always amplify the monsoonal circulation because the northeastward flow from ocean could bring low MSE air to land [5, 12, 13]. A recent proposal [15] actually suggested viewing monsoons as eddy-mediated transitions in the tropical overturning circulation between regimes that are distinct in the degree to which eddy momentum fluxes control the strength of the circulation. In this study, the idealized general circulation model (GCM) simulation on an aqua-planet demonstrated that the role of land in monsoon onset is to just provide a media of low thermal inertia. Whenever such surface differences in heat capacity exist monsoon onset would happen regardless of other surface inhomogeneities. Therefore, interactions between extratropical eddies and the tropical meridional overturning circulation could be essential for monsoons. In addressing the interaction of monsoon and other dynamical system, it was indicated that the feedback of atmosphere to SST forcing might have played a critical role in monsoon evolution [16].

One specific implication of these new hypotheses is on the predictability of the monsoon system. It has been argued that because the dominant forcing of monsoon system are the rather slow processes that control the tropical sea surface temperatures (SST), therefore, the predictability of monsoon rainfall at least in monthly or seasonal scale may be promising [17]. However, should the extratropical eddies and atmosphere to ocean feedback be critical in monsoon onset and evolution, the monsoon predictability issue even on relatively long time scales would be much more complicated. The predictability of the monsoon is further confounded by the ubiquitous presence of monsoon-intraseasonal oscillations (MISO) in both the summer and the winter seasons. These are intrinsic oscillations in the monsoon region, with characteristic timescales of 20–70 days, arising from the organization of tropical convection over the ocean associated, (e.g., planetary scale Madden–Julian Oscillation (MJO); see [18] and many others). MISO are mediated by SST changes as well as the monsoon regional topography, and influence the onset, break, and maintenance of the monsoon as well through interactions with ENSO. Realistic simulations of MISO and MJO have been a challenge even for the state-of-the-art climate models.

Modeling the Monsoon

Because of the complex, multi-scale characteristics of monsoon systems, efforts to understand and to examine various hypotheses about monsoon onset, evolution, and strength have to rely largely on computer models in combination with available data. In order to understand the interaction between this large-scale moist circulation and many other complicated but critical processes, ranging from ocean–atmosphere interaction, extratropical–tropical interaction, MISO, to potential "teleconnection" through synoptic waves between tropical systems in distance, one needs to use a three-dimensional global climate model or a regional climate model interacting with a global climate model.

Simulation of monsoon systems using three-dimensional global models started from the very early stage of atmospheric general circulation models. Typical model used in these early simulations had coarse horizontal resolution (270–540 km) and 11 vertical layers, forced by prescribed seasonal variations of insolation and often sea surface temperature [19]. These simulations were mostly used for exploratory purposes due to their short integration time (often shorter than 3 years), coarse model resolution, and the prescription of some fields of potential importance in modeling the monsoon. Understanding the onset of the monsoon was clearly a far-reach at that stage.

The availability of multi-decadal sea surface temperature data allowed three-dimensional atmospheric general circulation models (AGCM) to simulate monsoon system evolution driven by observed SST time series. This type of simulations follows the procedure of the Atmospheric Modeling Intercomparison Project (AMIP, and AMIP II later; [20]), forced by "real-time" SST data and thus ignored the feedback between the atmosphere and ocean. AMIP models, which generally include interactive land surface models, have the advantage of identifying atmospheric feedback mechanisms without dealing with the

complexity of the coupled ocean–atmosphere system. They were the models of choice in the 1980s–1990s. Nowadays, long-term climate simulations are generally done with coupled ocean–atmosphere models. However, AMIP models are still useful when run at high resolutions to test sensitivity to model atmospheric processes of physics, chemistry, and aerosols, and interaction of the atmosphere with surface vegetation. Some current AMIP runs are conducted at mesoscale resolution (<25 km) globally, and others are configured even at higher resolution for global hurricanes studies. With such configurations, models could explore the onset of the monsoon and aspects of the MJO and MISO [21]. The very high-resolution AMIP models are extremely computationally demanding, and can only be run using high-performance computers at large institutions.

Studies exploring multi-decadal to centennial timescale issues that need to consider the role of atmosphere-ocean feedback in monsoon dynamics, typically utilize moderate-to-low resolution (100–200 km) AGCMs coupled with either mixed-layer ocean model or full ocean general circulation model to reduce the computational demand. Regional climate models have also been used for this purpose. The influence of future climate change on monsoon evolution has also been studied mostly using the ensemble results of three-dimensional climate model simulations included in the Fourth Assessment Report (AR4) of the Intergovernmental Panel of Climate Change (IPCC). A fast growing effort in recent years is to study the impacts of anthropogenic forcings particularly of aerosols on monsoon circulation and precipitation.

This entry will begin by describing efforts to use climate models to simulate monsoon systems. Recent research on the potential role of aerosols in monsoon systems is then described. The projections of monsoon system changes under possible climate change scenarios will also be discussed, concluding with an overview of the future opportunities. The discussion will be focused on the utilization of general circulation models and regional climate models, of moderate-to-low resolution in simulating monsoon systems and the study of the sensitivity of monsoon to various climate dynamical processes as well as anthropogenic impacts on equilibrium climate, or on climate time scales of a century or less.

Simulating Monsoon Systems Using Climate Models

Before attempting to use a computer model to forecast monsoon evolution, one would ask the very question that how well the model might reproduce the major observed characteristics and variability of a monsoon, if some of the known factors controlling monsoons were included in the model (of course this condition itself is somewhat a unsettled issue). This actually leads to a type of modeling study, so-called retrospective modeling. In modeling monsoon systems, a retrospect simulation would be performed by prescribing the time series of sea surface temperature, assuming that the ocean is such a large heat reservoir comparing to the atmosphere so that the change in SST reflect the long-term state of energy balance. This type of modeling allows modelers to concentrate on issues other than the feedbacks from the atmosphere to ocean. With the assumption that historical SST change might well represent the effect of all the long-term forcings, this type of simulations is expected to capture major features of the monsoon systems in the past.

In simulating monsoon systems, it is essential for the model to capture certain representative features of the system. These would at least include the reverse atmospheric circulation between the upper and lower levels, the onset of monsoon rainfall, and total precipitation during monsoon season. In addition, the climatological rainfall patterns including land-ocean partition during monsoon is also among important system characters. A more subtle and difficult task in modeling is to capture the weak correlation between ENSO and Indian summer monsoon rainfall [9], and the correlation between anomaly of Gulf of Guinea SST and the dipole rainfall pattern of the West African monsoon over Guinean coast and the Sahel [22]. Interannual and decadal variability is another important test for both retrospect modeling and for revealing the dependency of monsoon systems on critical forcings. Simulating the intraseasonal variation of detailed rainfall strength and distribution (e.g., [23]) would be an important task for regional or high-resolution global models.

Much progress has been made through years of efforts in modeling the monsoon system. In early stage of such attempt, models typically had low

resolution and prescribed seasonal forcing of SST. Arguably, the physics processes such as clouds and radiation in those models were also poorly treated comparing to models used today. Nevertheless, the early models captured certain basic features of the monsoon system (mostly on Indian summer monsoon due to its rather clearly defined annual cycle and relatively extensive analyses) such as the reverse low-level circulation over northern Indian Ocean (e.g., [19]). Besides, the role of certain hypothesized driving factors of monsoon circulation such as mountains [7] and the anomaly of Arabian Sea surface temperature [24] had been also examined. The simulated onset of monsoon, however, was much delayed and the distribution of rainfall and intensity has large biases compared to observations.

With the availability of decadal-long observed SST dataset, nearly all the major AGCMs in the world joined the effort of Atmospheric Modeling Intercomparison Project (AMIP) in the 1990s. An AMIP configuration is a typical retrospect simulation, where atmospheric general circulation models were driven by a time series of observed SST data to reproduce the past climate. Lau and Yang had used the Goddard Space Flight Center GCM (4 × 5 degree resolution along latitude and longitude, respectively and 17 vertical layers) in an AMIP 1979–1988 simulation to examine the Asian monsoon system [25]. The model was able to capture many broad-scale structures of Asian monsoon system, including evolution of global and regional circulation, rainfall, moisture flux, and intraseasonal and synoptic variability. Interestingly, the model also successfully simulated multiple onset of East Asian monsoon along with the onset of Indian summer monsoon. These onsets were initiated by a sudden jump of the ITCZ from the equator to 10°N, related to a northward shift of the ascending branch of the local Hadley circulation. Clearly, this was a significant advance from the early simulations. On the other hand, the model did not reproduce observed rainfall distribution and quantity over many precipitation centers. Intraseasonal transition of ITCZ between equatorial region (ocean) and monsoon land was not well captured. The East Asian monsoon trough was also severely underdeveloped in the model. These shortcomings actually existed in most AMIP models.

In AMIP-type simulations, the atmosphere-ocean feedback is set aside. The modeling focus is instead on the atmospheric simulation, presuming that the SST time series realistically reflects the forcing of the past. Based on the results of ensemble AMIP simulations, Wang et al. indicated that a lack of the atmospheric feedback in simulations forced by observed SST could lead to serious biases in modeled monsoon precipitation [16]. They found that the atmospheric feedback to SST forcing is more significant than SST to atmospheric forcing. Therefore, coupled model would be critical in even retrospect modeling of monsoon and the atmospheric feedback to tropical SST forcing needs to be included. Meehl et al. further demonstrated an improvement of modeled monsoon features using a higher resolution (T85) coupled atmosphere-ocean model compared to a lower resolution (T42) AMIP configuration model [26]. There have also been reports of significant improvement in modeling monsoon features made simply by using high-resolution atmospheric GCM or regional climate model driven by observed SST (see [27]).

When using coupled model to simulate monsoon system, drifts of SSTs away from observation could become an issue. With a rather coarse-resolution coupled model (4.5 × 7.5 degree and nine layer for the atmospheric model; 5 × 5 degree and four layer for the ocean model), Meehl indicated that without adopting correction terms to force the coupled model to the observed state, model-simulated SSTs in the tropics tend to be too cold. This bias would enhance land-sea temperature contrast in the monsoon region, yet the pattern of mean monsoon seasonal precipitation and the variability of the simulated South Asian monsoon (SAM) were comparable to the observed pattern [28]. One alternative method to the AMIP configuration is to predict SST using a 2½-layer tropical ocean model between 30°S and 30°N and to prescribe SST in other places [16]. The SST-monsoon rainfall correlations indicated by observations (with 1 month lag) were reflected correctly in the simulation conducted by using this method.

Models have also been used to identify certain hypothesized driving factors behind monsoon variability. For instance, it is known that the Tropical Biennial Oscillation (TBO), a variation in precipitation occurring with approximately a 2-year period, affects

monsoon strength. Therefore, identifying the relative importance of various potential conditions leading to TBO transitions could help us to understand the factors that affect monsoon variability. It was found that among three conditions hypothesized to contribute to TBO transitions, tropical Indian Ocean SST anomaly and tropical Pacific Ocean SST anomaly are more effective than anomalous meridional temperature gradients over Asia [29]. The two types of tropical SST anomalies were found to dominate the TBO transitions and thus produce large monsoon response in the model sensitivity results. In addition, the location of the SST anomalies over the tropical Indian Ocean is found to be important. Warm SST anomalies throughout the tropical Indian Ocean enhance rainfall over the ocean and South Asian land areas. Warm SST anomalies near equatorial Indian Ocean produce increased rainfall locally with decreased rainfall over South Asian land areas.

Despite significant progresses achieved, there is still much room for improvement regarding the performance of current climate models in simulating various features of monsoon systems from mean state to variability [30]. For instance, among 18 coupled GCMs that participated the effort of the IPCC Fourth Assessment Report (IPCC AR4), only six of them were found to have realistic representation of South Asian monsoon precipitation climatology in the twentieth century [31]. It is noteworthy that these six models all had large pattern correlation and small root-mean-square differences (RMSD) with observations in modeling June–July–August–September (JJAS) rainfall climatology, both over India (7°–30°N, 65°–95°E) and for the larger monsoon domain (25°S–40°N, 40°E–180°). Only four out of these six, though, exhibited a robust ENSO-SAM teleconnection.

Recent results from the West African Monsoon Model Evaluation (WAMME) project showed that AMIP-type models (both regional and global) generally have reasonable skills in simulating the pattern of the spatial distribution of West African monsoon (WAM) in seasonal mean precipitation, surface temperature, averaged zonal wind in latitude-height cross-section, and low-level circulation [32]. However, there are large differences among models in addition to model biases compared to observations in simulating spatial correlation, intensity, and variability of precipitation.

In a well-designed analysis [22], the abilities of above-mentioned 18 models were evaluated based on whether they can correctly simulate the circulation characteristics that support the precipitation climatology and the physical processes of a prominent mode of WAM variability, that is, the "rainfall dipole" variability that is often associated with dry conditions in the Sahel when SSTs in the Gulf of Guinea are anomalously warm. It was found that each model captured the largest-scale rainfall pattern featuring a zonally oriented precipitation maximum, but about one third of them did not generate the West African monsoon, that is, they did not bring the ITCZ and its associated rainfall onto the African continent during boreal summer. Only three further captured the three precipitation maxima over the continent, that is, the maximum on the west coast, over the eastern portion of the Guinean coast, and over the Ethiopian highlands. It was thus concluded that the current generation of coupled GCMs is much more capable of accurately representing the summer precipitation climatology over North America and Europe than over Africa.

In modeling the Sahel drought during 1970s–1980s, the most pronounced climate signal in WAM regions that had been suggested as a consequence of warm anomalous SST surrounding Africa (e.g., [33]), Lau et al. evaluated the performance of 19 coupled general circulation models (also AR4 models) in twentieth-century simulations [34]. They found that only eight of these models produced a reasonable Sahel drought signal, while others either produced excessive rainfall over the Sahel during the observed drought period or showed no significant deviation from normal. Even the model with the highest prediction skill of the Sahel drought could only predict the increasing trend of severe drought events but not the beginning and duration of the events. Based on the analysis, it was recommended that in order to accurately simulate the Sahel drought, models need to have a strong coupling between Sahel rainfall and the SSTs of both Indian and Atlantic Ocean, in addition to a robust land surface feedback with strong sensitivity of precipitation and land evaporation to soil moisture.

The performance of 12 coupled models in the Coupled Model Intercomparison Project phase 3 (CMIP3; the same group of models that participated in IPCC AR4) in simulating present-day East Asian

monsoon has been examined as well [35]. Almost all of these models were found to be able to reproduce observed interannual variability of summer rain belt and associated circulation. The models can also reproduce the interannual variation of the western North Pacific subtropical high (WNPSH) in the lower troposphere, a parameter closely related to the interannual variation of summer rainfall. However, the predicted quantities of interannual variation of WNPSH from these models differ significantly.

Modeling the Impacts of Aerosols on Monsoon System

Atmospheric aerosols serve as a critical player in the climate system. All aerosols attenuate solar radiation through either scattering or absorption, both leading to cooling at the Earth's surface. In addition, absorbing aerosols warm the atmosphere, affecting atmospheric profile and thus dynamical processes. Aerosols also dominate the cloud formation in the atmosphere, serving as cloud condensation nuclei (CCN) or ice nuclei (IN) to provide preexisting surfaces and thus a superior mean for cloud particles to form than homogeneous nucleation. Therefore, changes in aerosol properties such as number concentration, size distribution, or chemical composition (hygroscopicity) are expected to affect atmospheric systems from regional to global scales including the monsoon.

Human activities produce aerosols containing inorganic matters such as sulfate and nitrate, and organic matter as well as black carbon. These anthropogenic aerosols are regarded as an addition to the natural aerosols that mainly include dust, biogenic, and sea salt particles, and hence exert a forcing to the climate system. Studies suggested that the reduction in Indian monsoon strength in recent decades could be a result of an increase of anthropogenic aerosols over monsoon regions, mostly coinciding with the fastest growing economies including China and India as well as Southeast Asia [36].

On the other hand, a recent analysis of 1951–2003 daily gridded rainfall data over India revealed a decreasing trend in both early and late monsoon rainfall and number of rainy days, implying a shorter monsoon over India [37]. There is also a sharp decrease in the area that receives a certain amount of rainfall and number of rainy days during the season. An increase in the frequency of heavy precipitation in the Indian summer monsoon was also identified [38].

A great deal of attention has been paid to the influence of anthropogenic aerosols (particularly absorbing aerosols) on tropical precipitation in recent years. Absorbing aerosols influence the climate in distinctly different ways from aerosols that primarily scatter energy back to space. Studies using different general circulation models all indicate that direct radiative forcing (DRF) of absorbing black carbon (BC) aerosols can lead to a northward shift of precipitation in ITCZ over the Pacific Ocean [39–41]. Modeling studies also suggest that DRF of aerosols could have a significant impact on the monsoon systems as well [42]. Correlations between estimated precipitation/circulation changes with increasing trend of aerosols have unquestionably fueled the researches toward this direction.

Studies of aerosol-monsoon impact are rapidly growing not only for the Indian summer monsoon, but also for the East Asian monsoon, the West African monsoon, and the Australian monsoon. Most of these studies are conducted by using three-dimensional atmospheric GCMs or coupled climate models. Paired simulations driven respectively by including and excluding aerosol effects, or by including a reference and an altered aerosol profile along with aerosol effects, provide a comparison in climate response between different aerosol forcing assumptions. The aerosol effects would be isolated barring the assumption that model's artifact in simulating the monsoon system would not be significantly amplified by using different aerosol profiles. The descriptions of aerosol and aerosol–climate interaction vary in studies though.

Impacts of Aerosols on the Asian Monsoon

Earlier works focused on impacts of absorbing aerosols (black carbon and dust) on atmospheric water cycle in the Asian monsoon, by using prescribed aerosol distributions from global chemistry transport models and/or observations. These studies excluded the dynamical feedbacks between winds and precipitation features and the aerosol distribution. An early exploratory study tested the climate response to absorbing aerosols over China and India [43]. In this study, a 12-layer and

4 × 5 degree resolution three-dimensional AGCM was used to explore the model response to prescribed aerosol optical depth and single scattering albedo over China and India only. The researchers found that the convection would be enhanced along 20°–30°E in longitude from eastern China to Indian subcontinent in responding to the added aerosol forcing. Despite many discrepancies in detailed results between this study and later ones, perhaps attributed to the regional-only aerosol loading and rather coarse resolution of the model in [43], the general response in large-scale dynamics associated with the monsoon systems caused by the direct radiative effects of absorbing aerosols remains consistent with later studies. For instance, Wang noticed an enhancement of the Indian summer monsoon circulation by the direct radiative forcing of black carbon aerosols in a coupled GCM simulation, though the analysis was done on an annual-mean base so that the seasonal features of the circulation were not discussed [39, 44]. A similar effect of BC aerosols was also found in another study, though where the simulation was driven by prescribed SST [45].

Perhaps the most interesting outcome in recent modeling efforts of aerosol-monsoon studies is the proposals of various hypotheses on the mechanisms of aerosol impact specifically on Indian summer monsoon. The discussions are also centered at the role of absorbing aerosols.

The radiative effects of absorbing (primarily dust and anthropogenic carbonaceous) aerosols in cooling the surface (dimming effect) and in heating the atmosphere can play different roles in affecting the monsoon system. The cooling over land from absorbing aerosols would assist lowering the land-ocean temperature gradient. Ramanathan et al. found that an increase in the BC DRF over Indian Subcontinent and surrounding regions in their model leads to a reduction of monsoon precipitation while an enhancement to the pre-monsoon precipitation of March–April–May (MAM) [36]. Using a coupled atmosphere-ocean general circulation model with prescribed black carbon direct radiative forcing, Meehl et al. found similar circulation and precipitation changes due to BC impact in the pre-monsoon (enhancement) and in monsoon season (reduction) [46]. It was also found that although during the monsoon months the effect of BC is likely to reduce the precipitation over India, it might enhance the precipitation over the elevated Tibetan Plateau. Meehl et al. suggested that BC DRF could weaken the surface temperature gradient between the tropical waters and the land of the Indian Subcontinent. This could serve as the forcing mechanism of BC on the monsoon circulation and precipitation, that is, through the dimming effect.

One specific characteristics of absorbing aerosols is its heating to the atmosphere. How would this effect play a role in aerosol-monsoon impact is also discussed. Lau et al. used an atmospheric GCM driven by prescribed global three-dimensional climatology of aerosol optical depth to examine the direct effects of aerosol on the monsoon water cycle variability [34]. The study suggested that, referred to as an "elevated heat pump" effect (EHP) (Fig. 2), dust mixed with black carbon aerosols that extend against the foothills of the Himalayas over the Indo-Gangetic Plain (IGP) in April and May could heat the air. This would initiate a positive feedback by drawing water convergence from oceans first and then form condensation and thus further heating over the slope of the Plateau. Based on this hypothesis, monsoon precipitation would be suppressed over central India due to aerosol-induced surface cooling. However, precipitation would come earlier and be enhanced over northern India and the southern slope of the Tibetan Plateau. Monsoon rainfall in July and August over the entire India would also be enhanced. Lately, using satellite aerosol index (AI) data and observed clouds and precipitation data, two studies have demonstrated the existence of anomalous absorbing aerosol loading in late spring over IGP [47, 48]. Both works also suggested a correlation of this aerosol anomaly with variation of monsoon evolution. A widespread warming over the Himalayan-Gangetic region and consequent strengthening of the land-sea thermal gradient was also found recently through satellite microwave sounding data [49]. This trend is most pronounced in the pre-monsoon season, resulting in a warming of 2.7°C in the record. All these observation-based analyses appear to be consistent with the EHP effect. The hypothesis involves both atmospheric-heating and surface-cooling effect of absorbing aerosols as well as induced changes in cloudiness. It is different than the hypothesis that only emphasizes surface cooling. The feedback mechanisms introduced by EHP hypothesis are, however, more complicated.

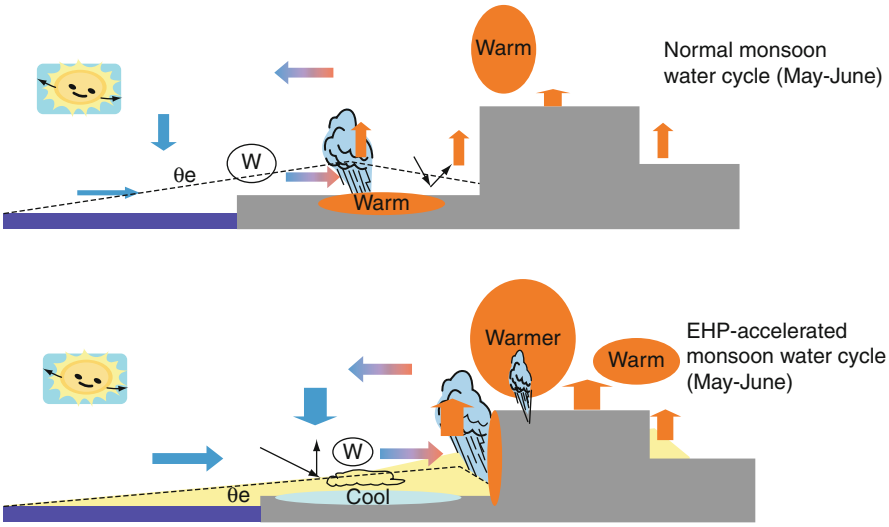

Monsoon Systems, Modeling of. Figure 2
Schematic showing the monsoon water cycle (*top*) with no aerosol forcing and (*bottom*) with aerosol-induced elevated heat pump effect. Low-level monsoon westerlies are denoted by W. The *dashed line* indicates magnitude of the low-level equivalent potential temperature θe. Deep convection is indicated over regions of maximum θe. (See text for further discussions) (Adopted from [42], © American Meteorological Society. Reprinted with permission)

For example, Prive and Plumb indicated that the equatorial oceanic air would have low moist static energy so that the low-level convergence might lead to a negative feedback to monsoon circulation [12, 13].

More recent works include the use of interactive aerosols in the models, that is, the dynamical feedback to aerosol distribution and forcing. For example, the model used in [50] includes a size- and mixing state-dependent aerosol module that is fully coupled with the climate model. Certain sophisticated aerosol microphysical and chemical processes including aging and coating of carbonaceous aerosols with sulfate, along with optical properties of these mixed aerosols are also included. Using this interactive aerosol-climate model coupled with a mixed-layer ocean model, Wang et al. proposed another possible mechanism that absorbing aerosols could affect on Indian summer monsoon [50]. The researchers find that absorbing anthropogenic aerosols, whether coexisting with scattering aerosols or not, can significantly affect the Indian summer monsoon system. This is drawn from a comparison of the results of three simulations. The first two simulations each only included absorbing aerosols (ABS) and scattering aerosols (SCA), respectively; the third one included both types of aerosols (COM). Aerosol-induced climate responses in each of these runs were derived by comparing results to a reference run that excluded the aerosol effect (REF). The similarity in aerosol-induced response between absorbing-aerosol-only case (ABS) and the case with both types of aerosols (COM) was identified. Results of both cases also differ sharply from that of the scattering-aerosol-only case (SCA). The researchers further identified that the influence of absorbing aerosols is reflected in a perturbation to the moist static energy in the sub-cloud layer, initiated as a heating by absorbing aerosols in the planetary boundary layer (Fig. 3). The perturbation appears mostly over land, extending from just north of the Arabian Sea to northern India along the southern slope of the Tibetan Plateau. As a result, during the summer monsoon season, modeled convective precipitation experiences a clear northward shift, coincidently in general agreement with observed monsoon precipitation changes in recent decades particularly during the onset season (Fig. 4). According to previous works, the northward extent of monsoon convection should collocate with the maximum sub-cloud layer MSE [12–14]. Therefore, a small perturbation in such a location could lead to an observable change in distribution of convection and heavy

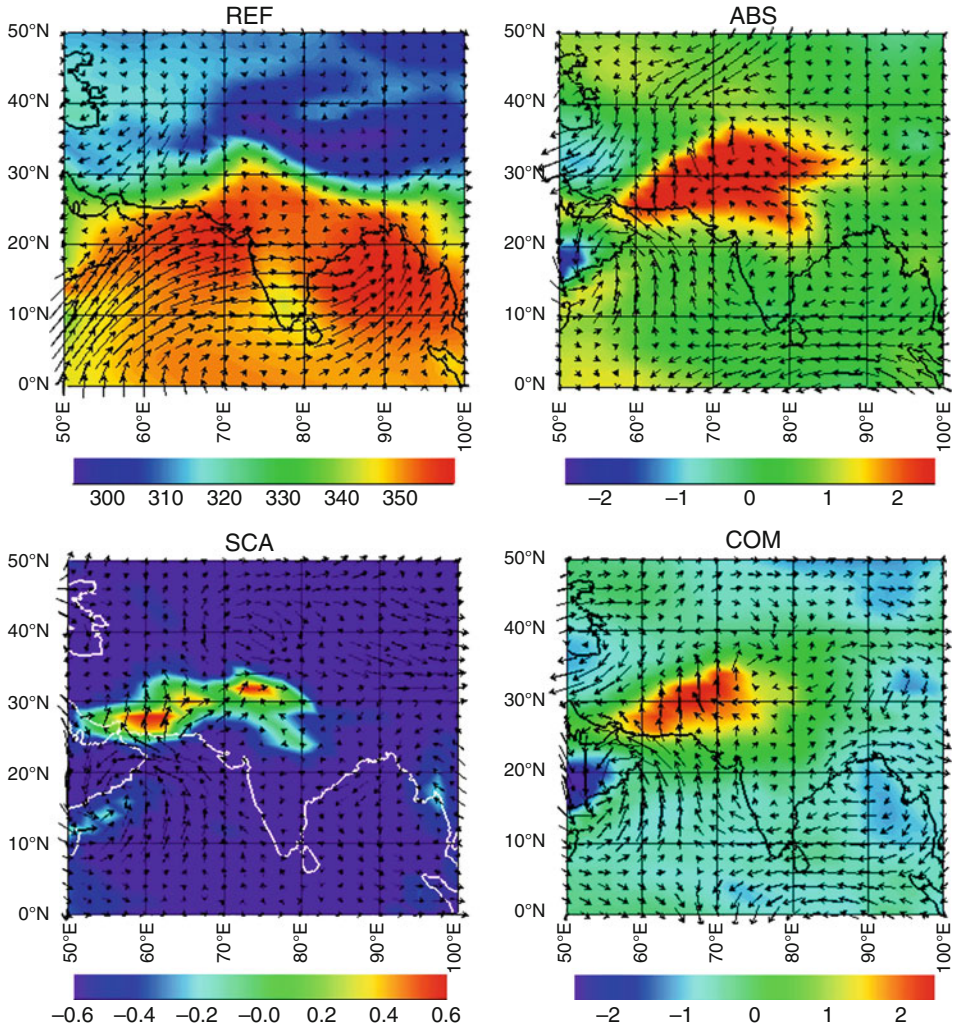

Monsoon Systems, Modeling of. Figure 3

May–June (MJ) mean of wind and moist static energy in the reference run (REF), which excludes the aerosol radiative effect, and anomalies of MJ mean wind and moist static energy derived from three model runs (ABS, SCA, and COM). Data shown are averaged values for the lowermost three atmospheric layers based on year 41–60 means. Unit wind vector = 1 m/s. Moist static energy is in 10^3 J/kg. Note that in the three anomaly plots, a different color scale is used in SCA. A terrain correction has been applied to the REF result (From [50], Copyright 2009 American Geophysical Union. Reproduced/modified by permission of American Geophysical Union)

precipitation. Interestingly, the modeled largest perturbation of absorbing aerosols on sub-cloud layer MSE appeared across this zone. Compared to the forcing required to significantly lower the meridional temperature gradient, the forcing of absorbing aerosols through perturbing MSE to influence monsoon dynamics and precipitation distribution is much more effective. The importance of sub-cloud layer processes, however, does not necessarily preclude the EHP that emphasizes the heating above the boundary layer. It is likely that the heating of the entire atmospheric column from the boundary layer to the upper troposphere could be important in creating the northward shift of the monsoon rainbelt.

At present, there is still a range of opinions about the reasons behind the impact of aerosols on Indian

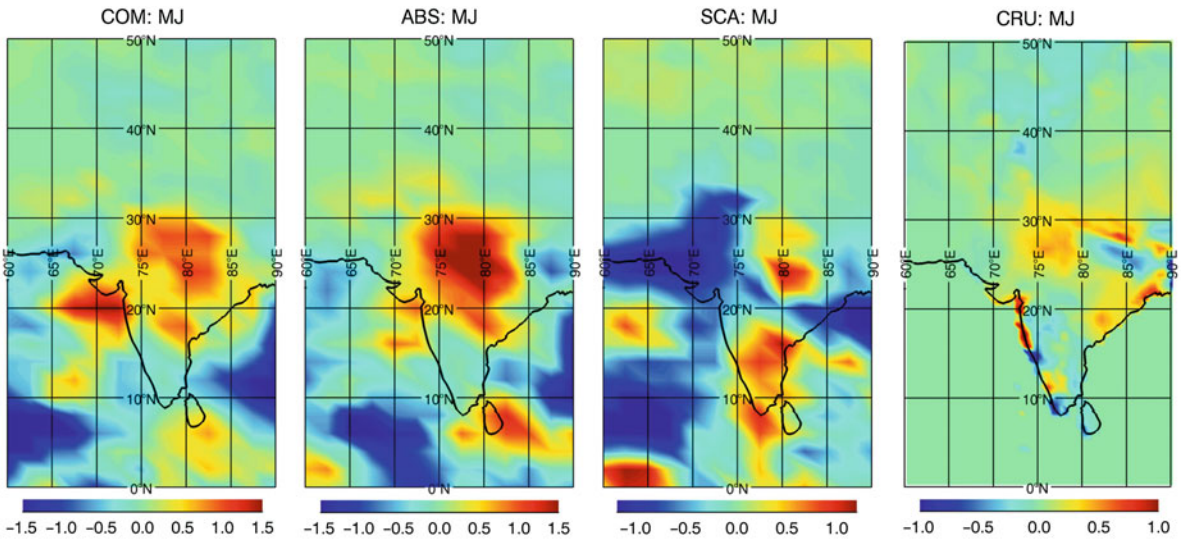

Monsoon Systems, Modeling of. Figure 4

May–June average changes in convective precipitation (dm/season) derived from: COM, ABS, and SCA run for India and surrounding regions, and the observed precipitation change (land-only; dm/season) derived from the data of the Climate Research Unit (CRU) at the University of East Anglia. Model results shown are based on year 41–60 mean differences with REF run. CRU results are derived from differences between 20-year means of 1981–2000 and 1946–1965, and based on the version 2.1 dataset with 0.5° (From [50], Copyright 2009 American Geophysical Union. Reproduced/modified by permission of American Geophysical Union)

summer monsoon [42]. Detailed mechanisms of the aforementioned hypothetical impacts still remain to be examined.

Impacts of Aerosols on the West African Monsoon

Aerosol impacts on another monsoon system, the West African Monsoon (WAM) have also been studied. It is known that aerosols over this region are among the most abundant and persistent on the Earth with distinct seasonal variability. The dominant aerosol type is mineral dust from North Africa through May to August and biomass-burning smoke from southern Africa from July to September. The mixture of dust and biomass-burning smoke appear in November–February due to persistent yearlong dust emission from some North African sources and biomass burning in Sahel region [51–56]. Therefore, this region provides an ideal natural test bed for studying aerosol effects on precipitation. Analyses using satellite data have demonstrated that a high concentration of aerosols can induce a significant precipitation reduction in the WAM region along the coast of the Gulf of Guinea, particularly in the boreal late autumn and winter [57, 58]. A recent study [59] further compared the observational results to a global model simulation including only direct radiative forcing of black carbon [39]. It was found from both observations and model simulations that in boreal cold seasons anomalously high African aerosols are associated with significant reductions in cloud amount, cloud top height, and surface precipitation. This result suggests that the observed precipitation reduction in the WAM region is caused by radiative effect of absorbing BC. The mechanism for this reduction, however, remains to be revealed.

In connection to the hypothesis of aerosol-Indian summer monsoon effect proposed by Wang et al. [50], Eltahir and Gong found a correlation of the strength of the West African monsoon to subtropical meridional gradient of sub-cloud MSE [60]. Therefore, similar mechanism could also exist in aerosol-WAM effect.

Recently, Lau et al. showed from GCM experiment that the EHP effect by Saharan dusts and biomass-burning black carbon has a significant impact on the

climate and water cycle of the North Atlantic and WAM [61]. They found that during the boreal summer, as a result of large-scale atmospheric feedback triggered by absorbing aerosols, rainfall and cloudiness are enhanced over the West Africa/Eastern Atlantic ITCZ while suppressed over the West Atlantic and Caribbean region. As shown in Fig. 5, the elevated dust layer warms the air over West Africa and the eastern Atlantic. As the warm air rises, it spawns an anomalous large-scale onshore flow carrying the moist air from the eastern Atlantic and the Gulf of Guinea. The onshore flow in turn enhances the deep convection over West Africa land, and the eastern Atlantic. The condensation heating associated with the ensuing deep convection drives and maintains an anomalous large-scale east–west overturning circulation, with rising motion over West Africa/eastern Atlantic and sinking motion over the Caribbean region. The response reflects a strengthening of the West African monsoon, manifested in a northward shift of the West Africa precipitation over land, increased low-level westerly flow over West Africa at the southern edge of the dust layer, and a near surface westerly jet underneath the dust layer over the Sahara. The dust radiative forcing also leads to significant changes in surface energy fluxes, resulting in cooling of the West African land and the eastern Atlantic, and warming in the West Atlantic and Caribbean. The EHP effect is most effective for moderate to highly absorbing dusts, and becomes minimized for reflecting dust with single scattering albedo at 0.95 or higher.

Additionally, from the same experiments the authors found strong modulation of the diurnal cycle and a northward shift of the African easterly jet, in conjunction with increased cyclonic vorticity to the south of its axis, and increased rainfall in the Sahel [62]. These modeling results are consistent with recent observations [63] showing that during the periods of a strong Sahara dust outbreak, the Atlantic ITCZ tends to be shifted northward of its climatological position, accompanied by a similar shift of the Africa easterly jet.

Impacts of Aerosols on the Australian Monsoon

The anthropogenic aerosol level in the Southern Hemisphere is lower compared to the condition of Northern

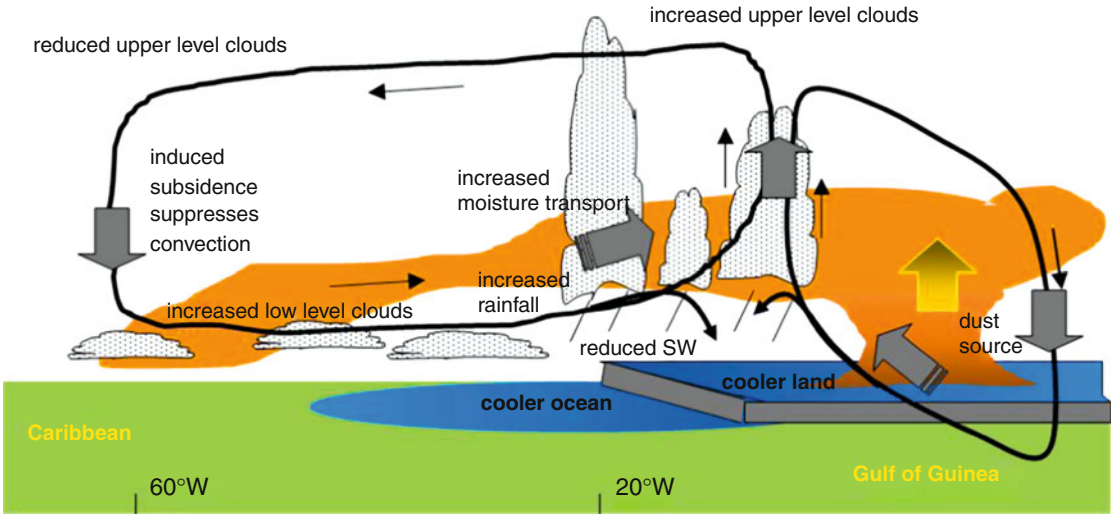

Monsoon Systems, Modeling of. Figure 5
Schematic diagram showing key features in the latitude domain 5–15°N, associated with the "elevated heat pump" mechanism by radiative heating of Saharan dust: anomalous Walker-type and Hadley-type circulations, increased moisture transport from the eastern Atlantic and the Gulf of Guinea to West Africa; enhanced rainfall over the Sahel and the ITCZ off the cost of West Africa; subsidence and suppressed cloudiness in the central Atlantic and Caribbean, and the Gulf of Guinea; cooling of the WAM land, and the upper ocean in the eastern Pacific underneath the dust plume (Adopted from [61] © Author(s) 2009, distributed under the Creative Commons Attribution 3.0 License)

Hemisphere. Therefore, the impact of local aerosols on Australian monsoon system is expected to be insignificant. However, since monsoon systems are closely associated with large-scale circulation, aerosol effects in the Northern Hemisphere could influence southern hemispheric circulation and thus precipitation by altering the general circulation patterns. This has been suggested in a recent modeling study [64]. Drawn from the results of a pair of ensemble simulations conducted using a coupled atmosphere-ocean climate model respectively including and excluding Asian aerosols, the researchers hypothesized that Asian aerosols could lead to an increase in both rainfall and cloudiness particularly over northwest Australia, which coincides with observed rainfall trend in the region since 1950s. The study suggested that this effect could be implemented through an altered latitudinal gradient of temperature (and thus of pressure) over tropical Indian Ocean by Asian aerosols, which would further enhance monsoonal circulation toward Australia. A recent analysis of the twentieth-century modeling results of 24 CMIP3 models, all including either only direct or both direct and indirect aerosol forcing, however, cannot provide support to the above hypothesis [65]. Despite of the inclusion of aerosol effect in these models, their ensembles did not produce the hypothesized rainfall increase in northwest Australia.

Climate Change and Monsoon System

Analyses using oxygen isotope data from Chinese caves providing information about monsoons over millennia suggest that Asian monsoons are influenced by changes in summer insolation in the Northern Hemisphere [66, 67]. However, variability in shorter terms can also be influenced by other factors. Historically, such variation in Asian monsoon system might have triggered social unrest and thus played a key role in causing demise of several Chinese dynasties [68]. Similarly, the persistent drought in Sahel occurred later last century also led to serious food supply problems and could well be responsible for certain conflicts in Africa. It is thus critical to understand these variabilities of monsoon systems and to identify the natural and anthropogenic influences on such variations.

Several persistent trends have been revealed recently. The reconstructed monsoon winds for the past 1,000 years using fossil *Globigerina bulloides* abundance in box cores from the Arabian Sea suggested an increase in strength during the past four centuries while the Northern Hemisphere has been warming [69]. This implies that the Indian summer monsoon strength could be enhanced during the coming century as greenhouse gas concentrations continue to rise and northern latitudes continue to warm. In the most recent decade, the sea surface winds over the western Arabian Sea have been continually strengthening [70]. Such escalation of summer monsoon winds, accompanied by enhanced upwelling, leads to an increase of more than 350% in average summertime phytoplankton biomass along the coast and over 300% offshore, implying that the current warming trend of the Eurasian landmass is making the Arabian Sea more productive.

Over India, analyses based on rainfall data since early 1950 suggest that in the last half century, the frequencies of moderate and low rain days over the entire country have significantly decreased while the frequency and the magnitude of extreme rain events has significantly increased [38, 71]. Decreasing trends were also found in both early and late monsoon rainfall and number of rainy days, implying a shorter monsoon over India [37]. There is also a sharp decrease in the area that receives a certain amount of rainfall and number of rainy days during the season. One study found that the seasonal mean all-India rainfall did not show a significant trend since 1950s [38]. The researchers argued that this is because that the contribution from increasing heavy events is offset by decreasing moderate events. Apparently, should the trend continue, a substantial increase in hazards related to heavy rain would be expected over central India in the future. In another recent study [72], the authors stressed the need to subdivide Indian rainfall geographically and to distinguish early and peak monsoon seasons for the purpose of rainfall trend detection and attribution. They found fingerprints of absorbing aerosols impact on regional rainfall since 1960s featuring increased rainfall in north and northwestern India in May–June and decreased rainfall in central and southern India in July–August since 1960s. However, whether the observed monsoon systems have strengthened or reduced is still very much an open question, limited by the availability of reliable long-term data record. Based on the dramatic decline in ENSO-monsoon correlation

in recent decades, it has been suggested that warming over Eurasia continent might have already led to a favored condition for strong monsoons [9]. Besides the potential cause of global warming behind these trends, anthropogenic aerosols could also be a significant factor based on observation-based and modeling studies discussed in previous sections.

Besides anthropogenic influences, natural variability could also be responsible for decadal to centennial variability of the monsoon. Natural variability in the African monsoon over the past three millennia has been reconstructed using geochemical evidence from the sediments of Lake Bosumtwi, Ghana [73]. It was found that intervals of severe drought lasting for periods ranging from decades to centuries are characteristic of the monsoon and are linked to natural variations in Atlantic sea surface temperatures. The researchers thus believe that the severe drought of recent decades is not anomalous in the context of the past three millennia.

The use of climate models to understand causes and consequences of changes in the past and future monsoon climate system is necessary when complex relationships are under consideration. Patricola and Cook used a regional climate model to study the West Africa monsoon in the African Humid Period (AHP; about 14,800–5,500 years ago) when humidity was increased over Africa based on paleoclimate evidence suggesting that the West African summer monsoon was stronger than today, and the Saharan Desert was green [74]. The model was driven by prescribed changes in insolation, atmospheric CO_2, and vegetation to impose conditions at 6,000 years before present, with SSTs fixed at present-day values. The model simulation produced a precipitation increase across the Sahel and Sahara that is in good agreement with the paleoclimate data. They found the precipitation increase in the Sahel is related to a northward shift of monsoon, the elimination of the African easterly jet, and intensification and deepening of the low-level westerly jet on the west coast. Interestingly, the thermal low-Saharan high system of the present-day climate is replaced by a deep thermal low. Even though solar forcing is the ultimate cause of the AHP, the model responded more strongly to the vegetation forcing, emphasizing the importance of vegetation in maintaining the intensified monsoon system.

Takata et al. carried out a pair of climate model simulations using according land use estimates over China and India in 1700 and 1850 [75]. The comparison between these two runs isolates the climate responses to the two different land use estimations. It was found that land use change over China and India from 1700 to 1850 due to population growth (forest to cropland) led to a reduction of surface roughness and thus a weakening of monsoon circulation and precipitation in India.

Various groups have also studied the influence of projected future climate warming on monsoon evolution. Coupled atmosphere-ocean GCM simulations suggested that the increase of surface temperature due to a doubling of CO_2 concentration could enhance mean precipitation of Indian summer monsoon and, as a partial consequence, interannual variability of area-averaged monsoon rainfall [76]. This is believed to be consistent with the observed large variability associated with warm surface temperature.

The performance of the current GCMs in retrospective modeling of monsoon evolution raises issues on both the capability of these models in projecting monsoon in future climate and certain variabilities used to evaluate the models (e.g., the ENSO-Indian summer monsoon rainfall relation). In a recent study, four out of 18 models participated in IPCC AR4 were selected based on their performance of the twentieth-century modeling of monsoon evolution [31]. An analysis was done then for each of these four models using their results from integrations in which the atmospheric CO_2 concentration doubled over preindustrial values. These selected models in the double CO_2 simulations all projected an increase both in the mean monsoon rainfall over the Indian subcontinent (by 5–25%) and in its interannual variability (5–10%). For each model the ENSO-monsoon correlation in the global warming runs is very similar to that in the twentieth-century runs, suggesting that the ENSO-monsoon connection will not weaken as global climate warms. This result is, however, curiously inconsistent with the finding in [9]. In addition, the diversity as seen in the simulations of ENSO variability of these coupled models suggests that these results should be taken with caution.

In a similar study to explore model performance in simulating twentieth-century WAM climatology, Cook and Vizy selected three best-performing models out of

18 coupled GCMs participated in IPCC AR4 to analyze their twenty-first-century integrations under various assumptions about future greenhouse gas increase [22]. Interestingly, each of these three models behaved differently in the twenty-first-century simulations. Only one model projected wet Guinea coast and more frequent dry year in Sahel that are consistent with predicted warming in the Gulf of Guinea based on known dynamic mechanism of the precipitation dipole. The authors thus concluded that there is no consensus among the models concerning the future of the West African monsoon system under greenhouse gas forcing. In another study based on the results from the CMIP3 models, a similar conclusion was obtained that the outlook for Sahel precipitation in these simulations of the twenty-first century is very uncertain, with different models disagreeing even on the sign of the trends [77]. It is especially surprising because most of these models in the twentieth-century integration reproduced the links of Sahel rainfall anomalies to tropical SST anomalies at interannual time scales as shown in observations. Conversely, such a relationship does not explain the rainfall trend in the twenty-first century in a majority of the models.

Future Directions

A key component that limits modeling of monsoon system is observation. The availability of high-resolution surface precipitation data, based on satellite retrievals and surface rain gauge measurements in recent 2 decades, has generally improved the situation. To analyze the longer-term variability, results derived from such dataset need to be compared more carefully with that from the high-density local meteorological measurements. For certain regions such as India, the latter type of data covers more than half century.

Computational technology is advancing rapidly, providing opportunity to model monsoons at higher resolution. However, the speed or memory gain from hardware or software advancements needs to be harnessed not only to increase model resolution but also for improved treatments of physical, chemical, and biogeophysical processes. For modeling the monsoon systems, previous experience suggests that one might need both. One issue that remains a huge challenge in the field of global climate modeling ever since its earliest day is the parameterization of convection. Because the requirement of a-few-kilometer resolution to resolve convection has been a far stretch for GCMs (and will likely still be the case in the near future), description of convection processes for the monsoon system in these models were empirically formulated using parameters resolved in model grid scale. Though still expensive, today's GCMs are already being run in horizontal resolution much closer to the cloud-resolving scale in exploratory and short tests, and perhaps will reach that scale earlier than one would expect. An immediate issue that would come along with this advancement, however, is the realization that variability of monsoon features will also increase at such a high resolution. Clearly, an accurate characterization of monsoon features at the cloud scale exceeds all the current available measurement networks, providing a challenge in the constraint of the high-resolution global climate models by observations.

Instead of using a global high-resolution climate model, the monsoon system can be also simulated in high resolution by coupling the global model with a regional climate model. The latter model usually has a more realistic description of various physical and chemical processes. When needed, running the regional rather than global climate in cloud-resolving scale would greatly reduce the demand for computation. There are numerous attempts reported in literature of so-called downscaling modeling, mostly done by driving a regional model using the output from a global model with a given increment of time (e.g., 6 h). The two-way coupling of such approach, that is, to include certain feedbacks of regional processes to influence the global model, however, is still rare. For modeling the monsoon system, the two-way coupling would provide a better description in the global model of atmospheric feedback to external forcing such as SST anomalies, presuming that the coupled atmosphere and ocean GCMs will remain dominant type of models to cover the global scale.

Studies in recent years have demonstrated the potential influence of aerosols on monsoon circulation and precipitation. Models need to be improved to include more physical- and chemical-based aerosol descriptions, for example, the mixing of anthropogenic aerosol species with dust by the chemical and physical evolution of those particles. The treatment of

aerosol–cloud interactions (the so-called indirect effect) is currently quite crude and dependence of these interactions on cloud dynamics is also very crude. Both sets of processes need to be improved in next generation models in order to explore their effects on monsoons. The role of absorbing aerosols revealed in recent studies and limited by measurements of aerosol absorption strength and the distribution of absorbing aerosols also remains a challenge and needs to be much improved.

The onset and evolution of the monsoon system can be influenced by both natural and anthropogenic factors, which are often intertwined both in space and time. Future modeling study should work toward unraveling these two major impacts through better simulation design and advanced statistical analysis. Separating anthropogenic impact from natural variability is essential in narrowing uncertainties in projecting future changes of global climate including monsoon system.

Bibliography

Primary Literature

1. Galvin JFP (2008) The weather and climate of the tropics: part 6 – monsoons. Weather 63:129–137
2. Halley E (1686) A historical account of the trade winds and the monsoon, observable in the seas between and near the tropicks, with an attempt to assign the physical cause of the said winds. Phil Trans R Soc London 16:153–168
3. Webster PJ (1987) The elementary monsoon. In: Fein JS, Stephens PL (eds) Monsoon. Wiley, New York, pp 3–32
4. Krishnamurti TN (1987) Monsoon models. In: Fein JS, Stephens PL (eds) Monsoon. Wiley, New York, pp 467–522
5. Plumb RA (2007) Dynamical constraints on monsoon circulations. In: Schneider T, Sobel AH (eds) The global circulation of the atmosphere. Princeton University Press, Princeton, pp 252–266
6. Blanford HF (1884) On the connexion of the Himalaya snowfall with dry winds and seasons of drought in India. Proc R Soc London 37:3–22
7. Hahn DG, Manabe S (1975) The role of mountains in the South Asian monsoon circulation. J Atmos Sci 32:1515–1541
8. Boos WR, Kuang Z (2009) Dominant control of the South Asian monsoon by orographic insulation versus plateau heating. Nature 463:218–223
9. Kumar KK, Rajagopalan B, Cane MA (1999) On the weakening relationship between the Indian monsoon and ENSO. Science 284:2156–2159
10. Chao WC (2000) Multiple quasi equilibria of the ITCZ and the origin of monsoon onset. J Atmos Sci 57:641–651
11. Chao WC, Chen B (2001) The origin of monsoons. J Atmos Sci 58:3497–3507
12. Prive NC, Plumb RA (2007a) Monsoon dynamics with interactive forcing. Part I: axisymmetric studies. J Atmos Sci 64:1417–1430
13. Prive NC, Plumb RA (2007b) Monsoon dynamics with interactive forcing. Part II: impact of eddies and asymmetric geometries. J Atmos Sci 64:1431–1442
14. Emanuel KA, Neelin JD, Bretherton CS (1994) On large-scale circulations in convecting atmospheres. Quart J R Meteor Soc 120:1111–1143
15. Bordoni B, Schneider T (2008) Monsoons as eddy-mediated regime transitions of the tropical overturning circulation. Nature Geos 1:515–519
16. Wang B, Ding Q, Fu X, Kang I-S, Jin K, Shukla J, Doblas-Reyes F (2005) Fundamental challenge in simulation and prediction of summer monsoon rainfall. Geophys Res Lett 32:L15711. doi:10.1029/2005GL022734
17. Charney JG, Shukla J (1981) Predictability of monsoons. In: Lighthill J, Pearce RP (eds) Monsoon dynamics. Cambridge University Press, New York, pp 99–109
18. Lau KM, Walsier D (2005) Intraseasonal variability in the atmosphere-ocean climate system. Springer Praxis, Chichester, 289 pp
19. Manabe S, Hahn DG, Holloway JL Jr (1974) The seasonal variation of the tropical circulation as simulated by a global model of the atmosphere. J Atmos Sci 31:43–83
20. Gates WL et al (1999) An overview of the results of the atmospheric model intercomparison project (AMIP I). Bull Am Meteorol Soc 80:29–56
21. Shen B-W, Tao W-K, Lau WK, Atlas R (2010) Improving tropical cyclogenesis prediction with a global mesoscale model: hierarchical multiscale interactions during the formation of tropical cyclone nargis (2008). J Geophys Res 115:D14102. doi:10.1029/2009JD013140
22. Cook KH, Vizy EK (2006) Coupled model simulations of the West African monsoon system: twentieth- and twenty-first-century simulations. J Clim 19:3681–3703
23. Krishnamurthy V, Shukla J (2007) Intraseasonal and seasonally persisting patterns of Indian monsoon rainfall. J Clim 20:3–20
24. Shukla J (1975) Effect of Arabian sea-surface temperature anomaly on Indian summer monsoon: a numerical experiment with the GFDL model. J Atmos Sci 32:503–511
25. Lau K-M, Yang S (1996) Seasonal variation, abrupt transition, and intraseasonal variability associated with the Asian summer monsoon in the GLA GCM. J Clim 9:965–985
26. Meehl GA, Arblaster JM, Lawrence D, Seth A, Schneider EK, Kirtman BP, Min D (2006) Monsoon regimes in the CCSM3. J Clim 19:2482–2495
27. Christensen JH, Hewitson B, Busuioc A, Chen A, Gao X, Held I, Jones R, Kolli RK, Kwon W-T, Laprise R, Magaña Rueda V, Mearns L, Menéndez CG, Räisänen J, Rinke A, Sarr A, Whetton P (2007) Regional climate projections, in climate change 2007: the physical science basis. In: Solomon S, Qin D, Manning M, Chen Z, Marquis M,

Averyt KB, Tignor M, Miller HL (eds) Contribution of working group I to the fourth assessment report of the intergovernmental panel on climate change. Cambridge University Press, New York
28. Meehl GA (1994) Coupled land-ocean-atmosphere processes and South Asian monsoon variability. Science 266:263–267
29. Meehl GA, Arblaster JM (2002) Indian monsoon GCM sensitivity experiments testing tropospheric biennial oscillation transition conditions. J Clim 15:923–944
30. Shukla J (2007) Monsoon mysteries. Science 318:204–205
31. Annamalai H, Hamilton K, Sperber KR (2007) The South Asian summer monsoon and its relationship with ENSO in the IPCC AR4 simulations. J Clim 20:1071–1092
32. Xue YK et al. (2010) Intercomparision and analyses of the West African monsoon in the West African monsoon model evaluation (WAMME) project: first model intercomparison experiment. Climate Dynamics 35:3–27. doi:10.1007/s00382-010-0778-2
33. Giannini A, Saravanan R, Chang P (2003) Oceanic forcing of Sahel rainfall on interannual to interdecadal time scales. Science 302:1027–1030
34. Lau KM, Kim MK, Kim KM (2006) Asian monsoon anomalies induced by aerosol direct effects. Clim Dyn 26:855–864. doi:10.1007/s00382-006-0114-z
35. Lu R, Fu Y (2010) Intensification of East Asian summer rainfall interannual variability in the twenty-first century simulated by 12 CMIP3 coupled models. J Clim 23:3316–3331
36. Ramanathan V, Chung C, Kim D, Bettge T, Buja L, Kiehl JT, Washington WM, Fu Q, Sikka DR, Wild M (2005) Atmospheric brown clouds: impact on South Asian climate and hydrologic cycle. Proc Natl Acad Sci USA 102:5326–5333
37. Ramesh KV, Goswami P (2007) Reduction in temporal and spatial extent of the Indian summer monsoon. Geophys Res Lett 34:L23704. doi:10.1029/2007GL031613
38. Goswami BN, Venugopal V, Sengupta D, Madhusoodanan MS, Xavier PK (2006) Increasing trend of extreme rain events over India in a warming environment. Science 314:1442–1445
39. Wang C (2004) A modeling study on the climate impacts of black carbon aerosols. J Geophys Res 109:D03106. doi:10.1029/2003JD004084
40. Roberts DL, Jones A (2004) Climate sensitivity to black carbon aerosol from fossil fuel combustion. J Geophys Res 109: D16202. doi:10.1029/2004JD004676
41. Chung SH, Seinfeld JH (2005) Climate response of direct radiative forcing of anthropogenic black carbon. J Geophys Res 110:D11102. doi:10.1029/2004JD005441
42. Lau K-M, Ramanathan V, Wu G-X, Li Z, Tray SC, Hsu C, Sikka R, Holben B, Lu D, Tartari G, Chin M, Koudelova P, Chen H, Ma Y, Huang J, Taniguchi K, Zhang R (2008) The joint aerosol-monsoon experiment, a new challenge for monsoon climate research. Bull Am Meteorol Soc 89:369–383
43. Menon S, Hansen J, Nazarenko L, Luo Y (2002) Climate effects of black carbon aerosols in China and India. Science 297:2250–2253
44. Wang C (2007) Impact of direct radiative forcing of black carbon aerosols on tropical convective precipitation. Geophys Res Lett 34:L05709. doi:10.1029/2006GL028416
45. Randles CA, Ramaswamy V (2008) Absorbing aerosols over Asia: a geophysical fluid dynamics laboratory general circulation model sensitivity study of model response to aerosol optical depth and aerosol absorption. J Geophys Res 113: D21203. doi:10.1029/2008JD010140
46. Meehl GA, Arblaster JM, Collins WD (2008) Effects of black carbon aerosols on the Indian monsoon. J Clim 21:2869–2882. doi:10.1175/2007JCLI1777.1
47. Lau K-M, Kim K-M (2006) Observational relationships between aerosol and Asian monsoon rainfall, and circulation. Geophys Res Lett 33:L21810. doi:10.1029/2006GL027546
48. Bollasina M, Nigam S, Lau K-M (2008) Absorbing aerosols and summer monsoon evolution over South Asia: an observational portrayal. J Clim 21:3221–3239
49. Gautam R, Hsu NC, Lau K-M, Tsay S-C, Kafatos M (2009) Enhanced pre-monsoon warming over the Himalayan-Gangetic region from 1979 to 2007. Geophys Res Lett 36: L07704. doi:10.1029/2009GL037641
50. Wang C, Kim D, Ekman AML, Barth MC, Rasch PJ (2009) Impact of anthropogenic aerosols on Indian summer monsoon. Geophys Res Lett 36:L21704. doi:10.1029/2009GL040114
51. Carlson TN, Prospero JM (1972) The large-scale movement of Saharan air outbreaks over the Northern equatorial Atlantic. J Appl Meteor 11:283–297
52. Prospero JM, Lamb JP (2003) African droughts and dust transport to the Caribbean: climate change and implications. Science 302:1024–1027
53. Dwyer E, Pinnock S, Gregoire JM, Pereira JMC (2000) Global spatial and temporal distribution of vegetation fire as determined from satellite observations. Int J Rem Sens 21:1289–1302
54. Duncan BN, Martin RV, Staudt AC, Yevich R, Logan JA (2003) Interannual and seasonal variability of biomass burning emissions constrained by satellite observations. J Geophys Res 108:4100. doi:10.1029/2002JD002378
55. Ito A, Penner JE (2005) Historical emissions of carbonaceous aerosols from biomass and fossil fuel burning for the period 1870–2000. Global Biogeochem Cy 19:GB2028. doi:10.1029/2004GB002374
56. Huang J, Zhang C, Prospero JM (2009) African dust outbreaks: a satellite perspective of temporal and spatial variability over the tropical Atlantic ocean. J Geophys Res 115:D05202. doi:10.1029/2009JD012516
57. Huang J, Zhang C, Prospero JM (2009) Large-scale effects of aerosols on precipitation in the West African monsoon region. Q J R Meteorol Soc 135:581–594
58. Huang J, Zhang C, Prospero JM (2009) African aerosol and large-scale precipitation variability over West Africa. Environ Res Lett 4:015006. doi:10.1088/1748-9326/4/1/015006
59. Huang J, Adams A, Wang C, Zhang C (2009) Black carbon and West African monsoon precipitation: observations and simulations. Ann Geophys 27:4171–4181

60. Eltahir E, Gong C (1996) Dynamics of wet and dry years in West Africa. J Climate 9:1030–1042
61. Lau KM, Kim KM, Sud YC, Walker GK (2009) A GCM study of the response of the atmospheric water cycle of West Africa and the Atlantic to Saharan dust radiative forcing. Ann Geophys 27:4023–4037, http://www.ann-geophys.net/27/4023/2009/
62. Kim KM, Lau KM, Sud YC, Walker GK (2010) Influence of aerosol-radiative forcing on the diurnal and seasonal cycles of rainfall over West Africa and the Eastern Atlantic using GCM simulations. Clim Dyn. doi:10.1007/s00382-010-0750-1
63. Wilcox E, Lau WKM, Kim KM (2010) A northward shift of the Inter-tropical convergence zone in response to summertime Saharan dust outbreak. Geophys Res Lett 37:L04804. doi:10.1029/2009GL041774
64. Rotstayn LD, Cai W, Dix MR, Farquhar GD, Feng Y, Ginoux P, Herzog M, Ito A, Penner JE, Roderick ML, Wang M (2007) Have Australian rainfall and cloudiness increased due to the remote effects of Asian anthropogenic aerosols? J Geophys Res 112: D09202. doi:10.1029/2006JD007712
65. Cai W, Cowan T, Sullivan A, Ribbe J, Shi G (2011) Are anthropogenic aerosols responsible for the Northwest Australia summer rainfall increase? A CMIP3 perspective and implications. J Climate 24:2556–2564. doi:10.1175/2010JCLI3832.1
66. Wang Y, Cheng H, Edwards RL, He Y, Kong X, An Z, Wu J, Kelly MJ, Dykoski CA, Li X (2005) The Holocene Asian monsoon: links to solar changes and North Atlantic climate. Science 308:854–857
67. Wang Y, Cheng H, Edwards RL, Kong X, Shao X, Chen S, Wu J, Jiang X, Wang X, An Z (2008) Millennial- and orbital-scale changes in the East Asian monsoon over the past 224,000 years. Nature 451:1090–1093
68. Zhang P, Cheng H, Edwards RL, Chen F, Wang Y, Yang X, Liu J, Tan M, Wang X, Liu J, An C, Dai Z, Zhou J, Zhang D, Jia J, Jin L, Johnson KR (2008) A test of climate, sun, and culture relationships from an 1810-year Chinese cave record. Science 322:940–942
69. Anderson DM, Overpeck JT, Gupta AK (2002) Increase in the Asian Southwest monsoon during the past four centuries. Science 297:596–599
70. Goes JI, Thoppil PG, Gomes HDR, Fasullo JT (2005) Warming of the Eurasian landmass is making the Arabian Sea more productive. Science 308:545–547
71. Dash SK, Kulkarni MA, Mohanty UC, Prasad K (2009) Changes in the characteristics of rain events in India. J Geophys Res 114: D10109. doi:10.1029/2008JD010572
72. Lau KM, Kim K-M (2010) Fingerprinting the impacts of aerosols on long-term trends of the Indian summer monsoon regional rainfall. Geophys Res Lett 37:L16705. doi:10.1029/2010GL043255
73. Shanahan TM, Overpeck JT, Anchukaitis KJ, Beck JW, Cole JE, Dettman DL, Peck JA, Scholz CA, King JW (2009) Atlantic forcing of persistent drought in West Africa. Science 324:377–380
74. Patricola CM, Cook KH (2007) Dynamics of the West African monsoon under mid-Holocene precessional forcing: regional climate model simulations. J Clim 20:694–716
75. Takata K, Saito K, Yasunari T (2009) Changes in the Asian monsoon climate during 1700–1850 induced by preindustrial cultivation. Proc Natl Acad Sci USA 106:9586–9589
76. Meehl GA, Washington WM (1993) South Asian summer monsoon variability in a model with doubled atmospheric carbon dioxide concentration. Science 260:1101–1104
77. Biasutti M, Held IM, Sobel AH, Giannini A (2008) SST forcings and Sahel rainfall variability in simulations of the twentieth and twenty-first centuries. J Clim 21:3471–3486

Books and Reviews

Fein JS, Stephens PL (1987) Monsoon. Wiley, New York
Lighthill J, Pearce RP (eds) (1981) Monsoon dynamics. Cambridge University Press, New York
Wang B (2006) East Asian monsoon. Springer/Praxis, Chichester
Webster PJ, Magana VO, Palme TN, Shukla J, Tomas RA, Yanai M, Yasunari T (1998) Monsoons: processes, predictability, and the prospects for prediction. J Geophys Res 103:14451–14510

Mussel Culture, Open Ocean Innovations

Richard Langan
Atlantic Mariner Aquaculture Center, University of New Hampshire, Durham, NH, USA

Article Outline

Glossary
Definition of the Subject
Introduction
Characterization and Selection of Open Ocean Farming Sites
Technologies for and Methods Open Ocean Mussel Farming
Mussel Species in Open Ocean Cultivation
Open Ocean Mussel Farming in Multiuse Facilities
Environmental Considerations for Open Ocean Mussel Farming
Future Directions
Bibliography

Glossary

Suspension culture A production method for mussels and other shellfish that employs ropes, cages, or nets suspended in the water column from either rafts or longlines.

Surface longline An anchored structure consisting of surface floatation supporting one or more horizontal lines from which ropes, cages, or nets can be suspended in the water column.

Open ocean farming Refers to aquaculture production of marine organisms in open ocean or offshore waters that are removed from any significant influence of land masses.

Submerged longline Subsurface structure consisting of anchors and submerged floatation from which ropes, cages, or nets can be suspended.

Site selection The process for selecting farming sites based on specified parameters such as depth, current and wave climate, temperature, and primary productivity.

Environmental effects The effects of farming activities on the physical, biological, and chemical properties of the marine environment *and* the effects of the environment on cultured organisms and consumers of cultured food products.

Seston Particulate material suspended in the water column of water bodies consisting of both living and dead organic material and inorganic particles.

Pseudofeces Suspended particles that have been rejected as food by filter feeding bivalve mollusks. The rejected particles are wrapped in mucus and expelled without being passed through the digestive tract.

Definition of the Subject

Aquaculture production of several species of mussels in sheltered marine waters is well established and occurs in many countries worldwide. The primary method of production of high quality mussels is suspension of ropes with attached mussels from floating rafts or surface longlines that are anchored to the seafloor. While demand for fresh, frozen, and canned mussel products continues to increase, growth in production is hampered by a lack of suitable space for expansion in sheltered waters. For more than a decade, there has been interest in developing production methods suitable for open ocean environments where wind and wave conditions preclude the use of either rafts or surface longlines. Recent advances in the use of longlines that can be submerged below the sea surface and therefore avoid the upper portion of the water column that is most affected by wave energy indicate that open ocean production is feasible. However, additional development in technology and methods to improve production efficiency and insure worker safety, as well as changes to political and regulatory frameworks are needed in order to achieve large-scale production.

Introduction

Population growth and consumer preference have resulted in a growing demand for seafood, a trend that is projected to continue into the future [1]. Production from capture fisheries has leveled off, and by most projections will remain stagnant or decline, depending on management and regulatory measures implemented by fishing nations [2, 3]. In contrast, aquaculture production has increased by nearly 10% each year since 1980, and has played an important role in filling the gap between seafood supply and demand. Only a few decades ago, wild-caught fish and shellfish supplied nearly all edible seafood, though with essentially flat growth since 1980 and the rise of aquaculture over the same time period, capture fishing now accounts for only about half of the total [1]. In the most optimistic scenarios, wild-caught fisheries production will remain stagnant [2]; therefore, growth in the global seafood supply will continue to rely on aquaculture production.

There are signs, however, that the rate of growth for global aquaculture may have peaked for land-based and nearshore marine culture due to political, environmental, economic, and resource constraints [1]. Expansion of land-based culture is limited primarily by economics, particularly in developed countries where costs associated with land, capital equipment, and energy required to pump and treat water are prohibitive. In addition, very few marine species are appropriate for land-based culture. For example, the space and volume of phytoplankton required to produce large quantities of filter feeding mollusks in land-based systems would be enormous, and therefore not economically viable.

For nearshore marine farming, available and suitable space is the primary limiting factor as sheltered coastal waters are for most countries quite constrained to begin with and are already used for a multitude of commercial and recreational activities with which aquaculture must compete for space [4]. Expansion of

large-scale finfish farming in coastal waters is also limited by environmental concerns. While there are also concerns about potential environmental effects of bivalve mollusk culture, they are minor in comparison to net pen culture of finfish and are balanced by recognition of the ecosystem services such as enhanced habitat complexity and filtration capacity provided by mollusks [5]. It is rather the effect of environmental conditions on mollusk culture, and specifically the effects of pollution on product safety that is limiting expansion in nearshore waters. Rapid coastal development and population growth and the resulting increase in human sources of pollution have affected the sanitary quality of nearshore waters, rendering shellfish grown there unsafe for consumption. As a consequence, many otherwise suitable sheltered sites for mollusk culture are off limits due to public health restrictions.

In developed countries, conflict with coastal residents and tourist-related businesses over aesthetic values, primarily over water views from shorefront property, have also affected the establishment of new farming sites. As the demographic of coastal communities continues to change and new residents place more value on views and recreation than food production, these conflicts are likely to increase. Given the constraints on expansion of current methods of production, it is clear that alternative approaches are needed in order for the marine aquaculture sector to make a meaningful contribution to the world's seafood supply.

Farming in open ocean waters has been identified as one potential option for increasing production and has been a focus of international attention for more than a decade. Despite the global interest in open ocean farming, development to date has been measured, primarily due to the significant technical and operational challenges posed by wind and wave conditions in most of the world's oceans [4]. Farming in fully exposed open ocean waters requires a different engineering approach since equipment and methods currently used in sheltered nearshore sites are largely unsuitable for the open ocean. In addition, the scale of investment required to develop and demonstrate new technologies and methods for offshore farming is yet to be determined, though most engaged in this endeavor would agree that it will likely be substantial.

Despite these challenges, there is sufficient rationale for pursuing the development of open ocean farming. Favorable features of open ocean waters include ample space for expansion, tremendous carrying capacity, less conflict with many user groups, reduced exposure to human sources of pollution, the potential to moderate some of the negative environmental and aesthetic impacts of high density coastal farming [6–8], and optimal environmental conditions for some bivalve mollusk species [9, 10]. For many countries, where cost, environmental concerns, limited space, and competing uses have restricted growth of land-based and nearshore marine farming, few other options for significant expansion exist.

Of the many species of finfish and shellfish that have been considered for open ocean farming, several species of mussels have emerged as attractive candidates. There are several reasons for this. Like all filter-feeding mollusks, mussels derive all their nutritional needs from naturally occurring phytoplankton and organic particulates. Therefore, daily visits to deliver formulated feed by service vessels and farm personnel, which may be prohibited for extended periods by sea conditions, are not needed, nor is on-site infrastructure for automated feeding, which is both costly and vulnerable to damage from storms. Unlike many cultured species that have gradually transitioned from wild capture to aquaculture, farming has been the primary means of production for mussels for many decades; therefore, methods used in sheltered waters are well developed, highly automated, and very efficient [11]. Mussels are also relatively fast growers, with production cycles ranging from 12 to 18 months [9, 12].

Production methods in sheltered nearshore waters include bottom culture, which is practiced in some locations such as the Netherlands, Scandinavia, and the USA (Maine), and pole or "bouchot" culture, which is practiced in France; however, suspension culture, because of superior product quality, accelerated growth, and opportunities for mechanization, has emerged as the leading method of production [11]. Techniques and materials used for suspension culture may vary somewhat from place to place; however, in general, culture methodology consists of suspending mussel ropes or "droppers" from either rafts or longlines [13]. Raft culture was pioneered in Spain and from there became established in Scotland and more

recently in Maine USA and in the Pacific Northwest coast of North America [11]. While rafts can be highly productive, they are suitable for use only in very sheltered embayments. Longline technology, which was developed in Japan, consists of either surface or submerged longlines, held in place with anchors and supported by buoys or floats. As with raft culture, surface longlines are only suitable for use in sheltered waters [13]; therefore, in locations where adverse sea conditions or drift ice occur, submerged longlines are the only option. Submerged longlines have been used primarily in locations (e.g., Atlantic Canada) where winter ice would impact buoys and lines [14]. It is only in recent years that the technology has been used in fully exposed open ocean locations [9].

Characterization and Selection of Open Ocean Farming Sites

Before discussing approaches to the development of open ocean mussel culture, it is important to first define what is meant by the term "open ocean." For most engaged in this sector, it is used synonymously with "offshore" and is generally accepted to mean farming in locations that are subjected to ocean waves and currents and removed from any significant influence of land masses rather than a set distance from shore. Clearly, a wide range of sea conditions falls under this broad definition. Ryan [4] reported on a site classification system for marine waters developed in Norway that is based on significant wave height exposure (Table 1).

While this classification method is instructive, knowledge of the full range of conditions at a particular site is needed to develop appropriate technologies and safe and efficient operating procedures.

Mussel Culture, Open Ocean Innovations. Table 1 Norwegian classification of offshore waters based on significant wave heights (From Ryan [4])

Site Class	Significant wave height (m)	Degree of exposure
1	<0.5	Small
2	0.5–1.0	Moderate
3	1.0–2.0	Medium
4	2.0–3.0	High
5	>3.0	Extreme

There are a number of criteria that determine the suitability of open ocean sites for farming, many of which are also considerations for sheltered waters. These include proximity to infrastructure such as ports, processing and distribution centers, as well as physical and biological criteria such as bathymetry, seabed characteristics and contour, current velocities, temperature profiles, dissolved oxygen, turbidity, the quantity of quality of phytoplankton, and the frequency of occurrence of harmful algal blooms. The most important additional feature of offshore sites is wave climate. Significant wave heights, wave periods, the frequency and duration of high energy storm conditions, and the combined forcing of waves and currents must be known in order to determine whether a site is suitable, accessible by service vessels and personnel with reasonable frequency, and if so, what type of technology is required for farming.

It is imperative that a thorough evaluation of the parameters described above be conducted before proceeding with development of a site for farming. The requirements for data and subsequent analysis can be substantial; however, the use of advanced oceanographic technologies can greatly facilitate this task [8]. Multibeam sonar and three-dimensional visualization can generate a wealth of data on seafloor contours and texture to inform mooring system design and placement. Collection of time intensive data on temperature, salinity, dissolved oxygen, turbidity, and fluorescence can be greatly facilitated by strategic deployment of in situ instrumentation at appropriate depth intervals in the water column. Additional instrumentation should include Acoustic Doppler Current Profilers (ADCP) that can measure and record current velocity and direction throughout the water column, wave sensors that can give precise data on wave height, direction, steepness, and period, and meteorological sensors to measure air temperature and wind speed and direction. Many countries have buoy arrays in coastal waters that can provide long-term data on regional climatology to aid site evaluation; however, collection of site-specific data is critical. Assessment of the potential for the effects of global climate change on critical parameters such as water temperature should also be considered.

The data collection period required for site evaluation will vary, depending on local and regional environmental and meteorological conditions. Good baselines for some parameters can be established in a relatively short time frame (1 year), others such as the frequency, duration, and severity of storms or blooms of toxic algae are less predictable and it may take longer to determine the suitability of a particular site.

While most of the focus on open ocean development has been on cage culture of finfish, there has also been growing interest in offshore culture of bivalve mollusks. Some of the same drivers such as ample space and the opportunity to avoid user conflicts are identical to those for finfish culture, though perhaps more importantly, reduced risk of exposure to human sewage and industrial pollution presents a major advantage of open ocean waters over coastal locations.

There are, however, possible limitations as well as advantages. Open ocean waters in many areas of the world are nutrient deficient, so careful attention must be paid during site selection to the quantity, quality, and seasonality of phytoplankton available to dense arrays of filter feeding mollusks. Macroscale information on primary productivity can be obtained from ocean color satellite data generated by instruments such as Sea-viewing Wide Field-of-view Sensor (SeaWiFS) and Moderate Resolution Imaging Spectroradiometer (MODIS). Site-specific data on concentration and composition can be generated by in situ fluorometry and microscopic analysis of the plankton community. Phytoplankton concentration at different depths is also an important factor, as farmers will wish to maximize the use of vertical space for production in deep ocean waters. The frequency and duration of harmful algal blooms (HABs) is also a critical consideration for offshore mollusk farming. In some locations, blooms of toxic algae originate and persist in offshore waters (e.g., *Alexandrium sp.* In the Gulf of Maine, USA) and can result in extended public health closures with severe economic impact on producers.

In addition to physical, chemical, and biological characteristics of a site, other human uses in the vicinity such as shipping, fishing, and mining must be identified in order to avoid conflicts. Involvement of the appropriate permitting authorities in the early stages of development of an open ocean farming site is also critical [15]. Other factors such as use of the area by marine mammals, proximity to foraging areas of predators (e.g., diving ducks), location of sensitive biological communities, presence of parasitic organisms (e.g., pea crabs, trematodes, and copepods), and sediments contaminated by toxic substances must also be considered [16].

Technologies for and Methods Open Ocean Mussel Farming

Technologies for open ocean mussel farming are essentially adaptations of suspension culture methods employed in sheltered marine waters. Designs and prototypes for submersible rafts have been developed [17, 18]; however, submerged longlines are the most commonly used method. This technology was developed in Japan and has been in use there for several decades for deep water suspended scallop culture, though not in fully exposed open ocean conditions. The technology has been successfully adapted for sheltered water mussel culture in Atlantic Canada where winter and spring drift ice can damage surface longlines [14]. More recently, the technology has been shown to be effective for mussel production in very high-energy open ocean conditions (e.g., significant wave heights >10 m) in the northeast USA [9] and at a test site in the German Bight with significant wave heights >8 m, and current velocity up to 1 ms^{-1} [19]. The technology is quite simple and it consists of relatively inexpensive materials. A design currently in use in North America is presented in Fig. 1.

The structural stability of a submerged longline is maintained by the opposing forces of submerged flotation at the ends of a single horizontal backbone, connected by lines set at a 45° angle to seafloor anchors. The most commonly used anchors are large (3–6 tons) deadweight concrete anchors, though both plow type and screw anchors have been used in some locations. Submergence depth of the backbone is dictated by site-specific wave climate and can range from 3 to 15 m. Surface floatation is minimized to prevent the transfer of wave-induced motion the backbone, and consists of nonstructural marker buoys for the anchor lines and a mid-backbone pick-up line that provides access to the crop from a service vessel. Anchors are generally spaced from 100 to 200 m apart, and depending upon the

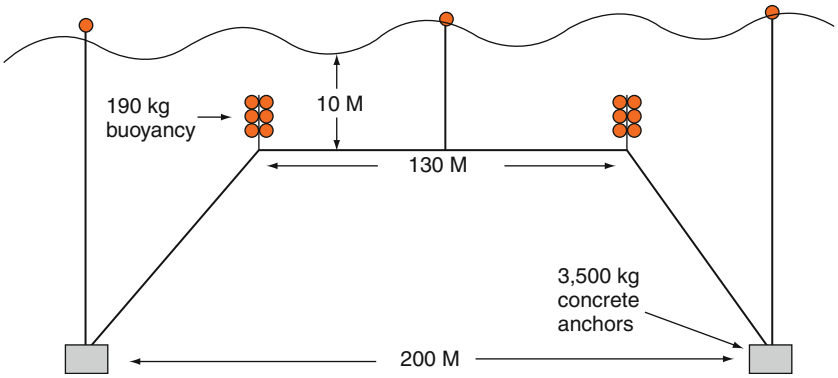

Mussel Culture, Open Ocean Innovations. Figure 1
A schematic of a submerged longline used for suspension culture of mollusks in open ocean environments

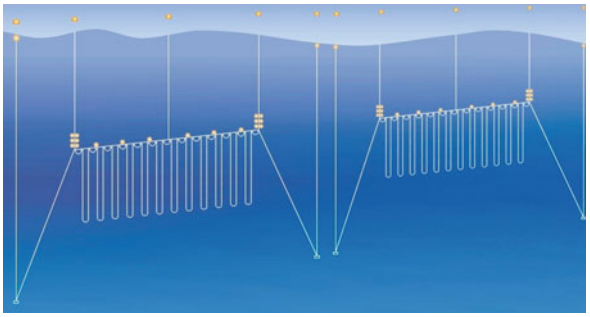

Mussel Culture, Open Ocean Innovations. Figure 2
A diagram of a submerged longlines showing the attachment of mussel growing ropes to the backbone and the placement of floatation added to the backbone as the crop increases in mass during growout (From Langan and Horton [9])

Mussel Culture, Open Ocean Innovations. Figure 3
A forward looking view of the starboard side of a service vessel showing the backbone of a submerged longline set into aft (foreground) and forward starwheels. Growing ropes with seed mussels are attached to the backbone for the growout cycle

depth of the water and desired depth of submergence, the backbone length can range from 70 to 130 m. Ropes or "droppers" of mussels are suspended from the backbone, and additional submerged floatation is added as the crop gains mass during growout (Fig. 2).

At some of the open ocean farms that have been established, converted fishing vessels are currently used to tend offshore longlines. The deck equipment required for tending lines to seed growout ropes and to inspect and harvest crops is similar to that in use for sheltered sites and includes rail mounted starwheels (Fig. 3) and an articulating crane (Fig. 4).

In addition, equipment common to many fishing vessels such as a lobster or crab trap hauler or a rotating boom is needed for lifting the submerged line to the surface. If there is sufficient deck space, bulk processing equipment such as declumping and debyssing machines can be used during harvest operations to reduce the need for extensive processing at shore-based

Mussel Culture, Open Ocean Innovations. Figure 4
A hydraulic articulating crane on a service vessel, shown here being used to unload equipment, is used extensively in mussel farming operations

facilities. Though converted fishing vessels may be used as this sector develops, it is likely that large, seaworthy, specialized vessels that can carry the harvesting and primary processing gear, provide a stable platform for lifting operations and a large load capacity for the harvest will be required to support large-scale operations. Vessels of this nature are in use in France and New Zealand [20].

In addition to submerged longlines, some experimental efforts have employed a submersible ring-like structure attached to a wind turbine tower, which has been used for offshore macroalgae growout [21]. This device could potentially be used for mussel cultivation; however, there may be scaling issues in reaching the desired biomass.

Mussel Species in Open Ocean Cultivation

There are several species of mussels that are cultivated in open ocean waters; however, regardless of species or location, production is currently minor by comparison with well-established nearshore production sites. In North America, small quantities of blue mussels (*Mytilus edulis)* are produced in offshore farms in New England (USA) and Atlantic Canada and Mediterranean mussels (*M. galloprovincialis*) are being grown at an offshore farm off the southern California (USA) coast [22]. In Europe, *M. galloprovincialis* are grown on submerged longlines at exposed locations in the Mediterranean coast of France [23] and in the Turkish Black Sea. Culture trials have been initiated for *M. edulis* in the North Sea off the coast of Germany, [19] and in the Belgian North Sea [24]. Other European countries, including Portugal, Spain, Italy, and Ireland are developing strategies for offshore mussel production.

In New Zealand, where the nearshore greenshell mussel (*Perna canaliculus*) industry is well developed and highly mechanized, there is a great deal of interest in developing large-scale ocean farms, as lease sites in sheltered nearshore waters have become difficult to obtain [25]. Initial efforts at open ocean mussel farming involved moving the double longline surface technology into more exposed sites and some success was achieved in wave conditions up to 2.5 m [26]. However, failure of surface longline systems in higher energy sites has led to the development of submerged technologies and a small number of open ocean mussel farms are operating in New Zealand offshore waters, with many new farms proposed [27]. This scale of expansion is projected to provide a threefold increase in production and export earnings by 2020 [28].

While data is limited to a few locations in North America and France, there are indications that production cycles and product quality for mussels grown in open ocean waters are highly favorable. Open ocean farms off the New Hampshire coast in the northeast USA have consistently produced market-sized (55 mm) blue mussels in 12–14 months from spat settlement with meat yields ranging from 42% to 58% [9]. Similar data has been reported for blue mussels at sites off the coast of Martha's Vineyard [29]. By comparison, rope-grown blue mussels from nearby estuaries and bays can take up to 18 months to reach market size [30]. Mediterranean mussels produced at an open ocean site in California have also demonstrated excellent growth and quality, reaching market size in 6–8 months and nearly 50% meat yield [22]. Trials in the North Sea have shown that the growth conditions in the German Bight

are very favorable for mussel cultivation. Market-size (50–55 mm) can be reached by 12–15 months and infestation by parasites is much lower than in near-shore sites [10]. Faster growth at offshore sites may to be due to a more stable temperature and salinity conditions and therefore lower stress, reduced turbidity, and better water exchange [20].

Open Ocean Mussel Farming in Multiuse Facilities

Open ocean mussel farming can be practiced in isolation of other activities; however, there may be economic or environmental advantages to combining mussel culture with offshore fish farming or energy production. At a nearshore marine farming site in New Brunswick, Canada, Lander et al. [31] demonstrated better growth rates for raft-cultured mussels 100 m down current of a salmon farm than at reference sites, and was able to document that organic wastes, primarily fine particulates from feed emanating from the salmon farm contributed to the diet of the mussels. In open ocean sites, creating mussel culture "zones" in proximity to finfish farms may offset the effects of organic loading to the environment [32].

Energy installations may also provide structure for deployment of mussel culture systems. Mussels (*M. galloprovincialis*) have been harvested from oil platforms in California, USA for many years [33], and there is interest in using decommissioned offshore oil platforms as attachment points for mussel culture infrastructure.

Buck et al. [34] investigated the possibility of integrating suspension culture of oysters and mussels at existing offshore wind energy platforms in the North Sea (Fig. 5).

There are a number of advantages for conducting mussel cultivation activities within the footprint offshore wind farms. The placement of aquaculture production facilities in defined corridors between wind farm turbines eliminates the need for a separately permitted facility and reduces the space required if the two facilities were located separately [34]. Also, infrastructure for regular servicing may be shared. As both industries need a multifunctional service vessel, preferably with lifting capacities to install and change plant components and execute farming operations, and sufficient deck space to carry equipment and stock, the opportunity to share high-priced infrastructure exists [35].

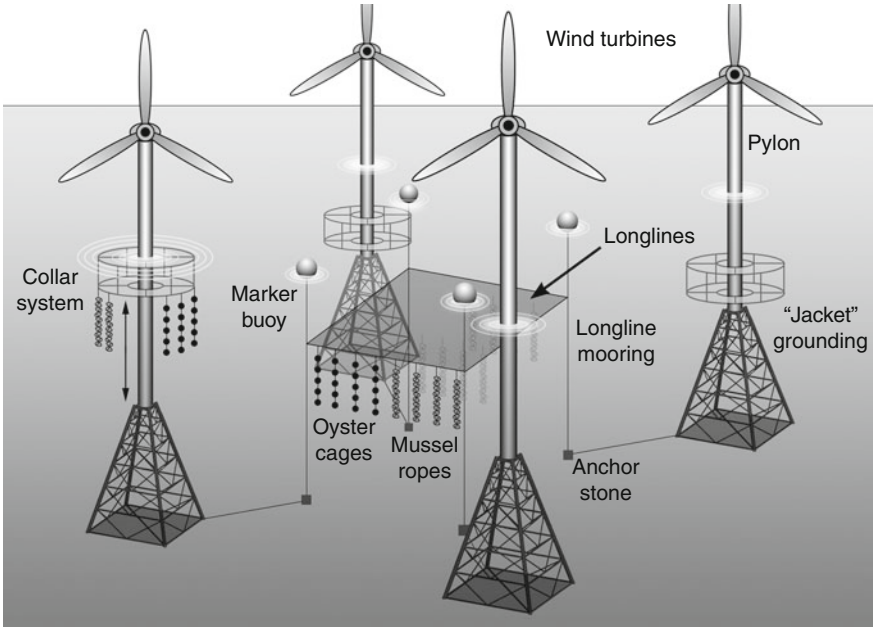

Mussel Culture, Open Ocean Innovations. Figure 5
A schematic of shellfish growing systems associated with wind turbine towers (from Buck et al. [34])

Further, a combined environmental impact assessment for both users may reduce costs.

Environmental Considerations for Open Ocean Mussel Farming

Like all forms of food production, the culture of marine species, whether practiced in land-based, nearshore, or open ocean locations will have some effect on the environment. The effect can be both negative and positive and can vary depending upon the species, location, and farming practices. In the past 3 decades of marine farming in sheltered marine waters, adverse impacts from aquaculture of both molluskan shellfish and finfish have been documented, though most of the concerns and controversy are centered on finfish. Mollusk culture is generally perceived as environmentally benign or even beneficial [5]; however, there have been documented environmental impacts from nearshore mussel farming that merit consideration for development of the offshore sector.

Though mussels feed on naturally occurring seston and no external feed is provided to the organisms, deposition of feces and pseudofeces can enrich bottom sediments beneath culture systems and impact benthic communities [36, 37]. Occurrences of sediment impacts have been associated with very dense culture in shallow embayments; therefore, if offshore farms are sited in locations with sufficient depth and adequate water circulation to disperse wastes, enrichment of bottom sediments should not be an issue [7]. High-density mussel culture can also deplete the water column of planktonic food, affecting both the growth and fitness of the cultured organisms as well as naturally occurring filter feeders in the system [38]. This too, is an impact that has been observed in sheltered embayments with limited circulation and is unlikely to be an environmental issue in open ocean waters [8]. However, in very large, high-density offshore farms, depletion of food within the farm and reduced growth and condition of the stock may be an issue for producers.

Hydrodynamic alteration is another environmental effect that has been documented in sheltered embayments with high-density shellfish culture [39] and has recently been an issue of concern in New Zealand where large-scale open ocean mussel farming is in development. Plew et al. [28] reported significant current and wave attenuation and strong water column stratification at a large (230 longline) mussel farm in Golden Bay, New Zealand. The farm was located in relatively shallow water (10–12 m) and the culture organisms were suspended from the surface to a depth of 8 m, therefore, occupying nearly the entire water column. As it is likely that open ocean development will use submerged culture in much deeper water (30–100 m) with ample space above and below the culture arrays, the severity of flow modifications as observed in this study are improbable.

A legitimate environmental concern for open ocean mussel culture is entanglement of whales and other marine life in seed collection lines [40]. These collectors are either discrete lengths of line or one continuous length of rope suspended from the backbone to provide substrate for settlement of mussel larvae (Fig. 6). As this sector develops, it is important to avoid deployment of seed collection lines in the migratory pathways of endangered marine mammals or to use weak links and electronic alert systems in the farming infrastructure [41].

Mussel Culture, Open Ocean Innovations. Figure 6 Seed collecting rope (*black*) is attached to the backbone of a submerged longline

Future Directions

Developments over the past 2 decades indicate that aquaculture production of mussels in open ocean environments is feasible and that opportunities exist for large-scale production [9, 10]. Conflicts with other uses can be significantly reduced, though they are not totally eliminated [34]. There is also evidence to support the premise that environmental impacts can be reduced by farming in open ocean environments [8, 36]. There is also strong indication that if sites are chosen properly, faster growth and excellent product quality can be achieved [9].

Though some technical challenges remain such as the development of large, purpose built, and highly seaworthy service vessels, obstacles to development of open ocean mussel farming are primarily economic, social, and political in nature. The scale of investment needed to establish and operate large-scale open ocean mussel farms is not well known, though it is assumed that production costs will be higher than for nearshore farming. The additional costs could be partially offset if ocean grown mussels, due to superior quality and greater consumer confidence in product safety can command a higher price [9], however, market prices are subjected to many economic externalities that are difficult to forecast. Space conflicts with the fishing industry may be an issue in some locations, therefore, involvement of local capture fishermen in industry development may be needed to gain acceptance of an alternative use of ocean space. As many countries move toward spatial planning of their territorial ocean waters, it is important to include a future vision of the potential for open ocean mussel farming in the planning process and give due consideration to compatibilities and possible synergies with other uses. Many countries also currently lack the regulatory framework for permitting open ocean farming sites. Until economic and regulatory uncertainties are resolved, entrepreneurs will be reluctant to make the level of investment needed to move this sector forward.

Ideally, development of open ocean farming should take place within the context of overall ocean management and marine spatial planning in order to assure compatibility with other uses and consistency with broader goals to restore and sustain the health, productivity, and biological diversity of the oceans.

Bibliography

1. FAO (2006) State of world aquaculture: 2006. Food and Agriculture Organization of the United Nations, Rome, FAO Fisheries Technical Paper # 500
2. NOAA (2005) Fisheries of the United States – 2003. NOAA, Washington, http://www.st.nmfs.gov/st1/fus/fus03/index.html
3. Worm B, Barbier EB, Beaumont N, Duffy JE, Folke C, Halpern BS, Jackson JBC, Lotze HK, Micheli F, Palumbi SR, Sala E, Selkoe EK, Stachowicz JJ, Watson R (2006) Impacts of biodiversity loss on ocean ecosystem services. Science 314:787–790
4. Ryan J (2004) Farming the deep blue. Board Iascaigh Mhara Technical Report, pp 82
5. Shumway SE, Davis C, Downey R, Karney R, Kraeuter J, Parsons J, Rheault R, Wikfors G (Dec 2003) Shellfish aquaculture – in praise of sustainable economies and environments. World Aquacult 34(3):15–19
6. Buck BH, Krause G, Rosenthal H, Smetacek V (2003) Aquaculture and environmental regulations: the German situation within the North sea. In: Kirchner A (ed) International marine environmental law: institutions, implementation and innovation, vol 64. Kluwer Law International, The Hague, pp 211–229
7. Ward LG, Grizzle RE, Irish JD (2006) UNH OOA environmental monitoring program, 2005. CINEMar/open ocean aquaculture annual progress report for the period from 1/01/05 to 12/31/05. Final report for NOAA grant No. NA16RP1718, interim progress report for NOAA Grant No. NA04OAR4600155, Submitted 23, Jan 2006. http://ooa.unh.edu
8. Langan R (2007) Results of environmental monitoring at an experimental offshore farm in the Gulf of Maine: environmental conditions after seven years of multi-species farming. In: Lee CS, O'Bryen PJ (eds) Open ocean aquaculture – moving forward. Oceanic Institute, Waimanalo, pp 57–60
9. Langan R, Horton CF (Dec 2003) Design, operation and economics of submerged longline mussel culture in the open ocean. Bull Aquac Assoc Can 103-3:11–20
10. Buck BH, Thieltges DW, Walter U, Nehls G, Rosenthal H (2005) Inshore-offshore comparison of parasite infestation in *Mytilus edulis*: implications for open ocean aquaculture. J Appl Ichthyol 21(2):107–113
11. Jeffs AG, Holland RC, Hooker SH, Hayden BJ (1999) Overview and bibliography of research on the greenshell mussel, *Perna canaliculus*, from New Zealand waters. J Shellfish Res 18(2):347–360
12. Island Institute (Sept 1999) The maine guide to mussel raft culture. Island Institute, Rockland
13. Scott N, Tait M (1998) Mussel farming – an expanding industry in shetland North Atlantic fisheries college. Fisheries information note no. 1, October 1998
14. Bonardelli J (1996) Longline shellfish culture in exposed and drift-ice environments. In: Open Ocean Aquaculture: proceedings of an International Conference, Portland, 8–10 May 1996, Marie Polk editor. New Hampshire/Maine Sea Grant College Program Rpt. #UNHMP-CP-SG-96-9, pp 235–253

15. Michler-Cieluch T, Krause G (2008) Perceived concerns and possible management strategies for governing wind farm-mariculture integration. Mar Policy 32(6):1013–1022
16. Brenner M (2009) Site selection criteria and technical requirements for the offshore cultivation of blue mussels. Dissertation. Jacobs University Bremen, Bremen
17. SubSea Shellfish (Dec 2004) Biology and innovation primer project 2004. http://www.freepatentsonline.com/EP1476011.pdf
18. Stanley S (2005) development of a submersible raft for shellfish aquaculture. US Department of Commerce National Oceanic and Atmospheric Administration Small Business Innovation Research (SBIR). Abstracts of Awards for Fiscal Year 2005, pp 12
19. Buck BH (2007) Experimental trials on the feasibility of offshore seed production of the mussel *Mytilus edulis* in the German Bight: installation, technical requirements and environmental conditions. Helgol Mar Res 61(2):87–101
20. Holmyard J (2008) Potential for offshore mussel culture. Shellfish News, 25, Spring Summer 2008
21. Buck BH, Buchholz CM (2004) The offshore-ring: a new system design for the open ocean aquaculture of macroalgae. J Appl Phycol 16:355–368
22. SB Mariculture (2008) http://www.sbmariculture.com/
23. Brehmer P, Gerlotto F, Guillard J, Sanguinède F, Guénnegan Y, Buestel D (2003) New applications of hydroacoustic methods for monitoring shallow water aquatic ecosystems: the case of mussel culture grounds. Aquat Living Resour 16(2003): 333–338
24. Van Nieuwenhove K, Delbare D (2008) Innovative Offshore Mussel Farming in the Belgian North Sea. www.vliz.be/imisdocs/publications/132623.pdf
25. Jeffs AG (2003) Assessment of the potential for mussel aquaculture in Northland NIWA client report: AKL2003-057, NIWA Project: ENT03101. National Institute of Water and Atmospheric Research Ltd, Auckland
26. Thompson NW (1996) Trends in Australasian Open Water Aquaculture. In: Open ocean aquaculture: proceedings of an International Conference. May 8–10, 1996, Portland, ME. Marie Polk editor. New Hampshire/Maine Sea Grant College Program Rpt. #UNHMP-CP-SG-96-9: pp 223–234
27. Stevens C, Spigel R, Plew D, Fredricksson D (Mar/Apr 2005) A blueprint for better mussel farm design. NZ Aquac 04:8–9
28. Plew DR, Stevens CL, Spigel RH, Hartstein ND (2005) Hydrodynamic implications of large offshore mussel farms. IEEE J Ocean Eng 30(1):95–108
29. Lovewell MA (2008) The fisherman. Martha's Vineyard Gazette. 28 Aug 2008. http://www.mvgazette.com/article.php?18129
30. Maine DMR (2009) The blue mussel in maine. Maine Department of Marine Resources. http://www.maine.gov/dmr/rm/bluemussel.html
31. Lander T, Barrington K, Robinson S, Mac Donald B, Martin J (2004) Dynamics of the blue mussel as an extractive organism in an integrated multi-trophic aquaculture system. Bull Aquac Assoc Can 104-3:19–29
32. Langan R (2004) Balancing marine aquaculture inputs and extraction: combined culture of finfish and bivalve molluscs in the open ocean. Bull Fish Res Agency Jpn Suppl 1:51–58
33. Richards JB, Trevelyan GA (Dec 2001) Mussel culture. In: Leet WS, Dewees CM, Kleingbeil R, Larson EJ (eds) California's living marine resources: a status report. California Department of Fish and Game, Yountville
34. Buck BH, Krause G, Rosenthal H (2004) Extensive open ocean aquaculture development within wind farms in Germany: the prospect of offshore co-management and legal constraints. Ocean Coast Manage 47(3–4):95–122
35. Michler-Cieluch T, Krause G, Buck BH (2009) Reflections on integrating operation and maintenance activities of offshore wind farms and mariculture. Ocean Coast Manage 52(1):57–68
36. Hatcher A, Grant J, Schofield B (1994) Effects of suspended mussel culture (*Mytilus spp.*) on sedimentation, benthic respiration and sediment nutrient dynamics in a coastal bay. Mar Ecol Prog Ser 115:219–235
37. Fabia G, Manoukian S, Spagnoloa A (Apr 2009) Impact of an open-sea suspended mussel culture on macrobenthic community (Western Adriatic Sea). Aquaculture 289(1–2):54–63
38. Prins TC, Smaal AC, Dame RF (1997) A review of the feedbacks between bivalve grazing and ecosystem processes. Aquat Ecol 31(4):349–359
39. Grant J, Bacher C (2001) A numerical model of flow modification induced by suspended aquaculture in a Chinese Bay. Can J Fish Aquat Sci 58:1003–1011
40. Lloyd BD (2003) Potential effects of mussel farming on New Zealand's marine mammals and seabirds: a discussion paper. Department of Conservation, Wellington, Vii: 34 p
41. Paul W (1999) Reducing the Risk of Open Ocean Aquaculture Facilities to Protected Species. In: NOAA (Ed.): National Strategic Initiative Project, Summaries 1999, Aquaculture Information Center – DOC/NOAA. 1–11

N

Nanocarbons for Supercapacitors

François Béguin, Encarnación Raymundo-Piñero
Research Centre on Divided Matter,
CRMD-CNRS & Orléans University,
Orléans, France

Article Outline

Glossary
Definition of the Subject
Introduction
Brief Overview of Activated Carbons Properties
General Properties of Electrochemical Capacitors
Carbons for Electrical Double-Layer Capacitors
Carbons for Pseudo-capacitors
Conclusion and Future Directions
Bibliography

Glossary

Carbon structure and texture The structure is the arrangement of the carbon atoms in the space since the texture is the arrangement of the graphene layers in the space for giving porosity or empty space accessible for molecules or ions.

Electric double layer capacitor Electrochemical capacitor in which the charge storage is achieved electrostatically because of the separation of charges in a double layer across the electrode/electrolyte interface.

Nanocarbon Carbon material consisting in more or less disordered graphene layers which can be synthesized with different structures, porous texture, and surface functionality.

Pseudo-capacitor Electrochemical capacitor in which the charge storage is achieved by an electron transfer that produces chemical or oxidation state changes in the electrode materials. As a difference from a battery, the electrode potential varies proportionally to the charge exchanged.

Supercapacitor or electrochemical capacitor Electrochemical energy storage device in which the voltage declines linearly with the extent of charge. A supercapacitor consists of two electrodes separated by a porous membrane immersed in an electrolyte.

Surface functionality Surface groups are ubiquitously present at the edges of graphene sheets in carbon materials, especially the high surface area ones. Oxygen-containing surface groups are the most occurring ones but carbon can contain other heteroatoms, such as nitrogen or sulfur.

Definition of the Subject

Supercapacitors (or electrochemical capacitors) are electrochemical energy storage devices having higher energy density than dielectric capacitors and higher power density than batteries. Actually, they are capable of delivering large amounts of energy in a very short time. These devices rely mainly on the characteristics of the electrical double layer that forms on all polarized conductors when immersed in an electrolyte. The double layer forms in less than 10^{-6} s and responds to changes in a similar time frame. This is about 1,000 times faster than an electrochemical reaction at a battery electrode that has a time constant in the range of 10^{-3} s. These devices find application where high-power delivery is required.

Introduction

Supercapacitors (or electrochemical capacitors or ultracapacitors) represent a relatively new energy storage technology which has known an important development during the recent years. Supercapacitors can be applied for stationary and mobile systems where high-power pulses are requested: cars acceleration, tramways, cranes, lifts, safety systems, etc. Moreover, owing to their low time constant, they can quickly harvest energy, for example during deceleration or

Robert A. Meyers (ed.), *Encyclopedia of Sustainability Science and Technology*, DOI 10.1007/978-1-4419-0851-3,
© Springer Science+Business Media, LLC 2012

braking of vehicles. Although supercapacitors are able to provide high power with a long cycle life compared to accumulators, they suffer of a relatively low energy density. Therefore, the main ongoing research direction concerns the optimization of the existing electrode materials and the development of new materials, both for protic electrolytes and aprotic organic electrolytes.

Industrial supercapacitors are essentially based on nanoporous carbon electrodes. The reasons of the choice lie in the high availability, low cost, chemical inertness, and good electrical conductivity of activated carbons, as well as a high versatility of texture and surface functionality. For these reasons, this chapter will present the capacitance properties of carbon-based electrodes showing optimization strategies playing on the structure/nanotexture of carbon and the nature of the electrolyte.

Brief Overview of Activated Carbons Properties

In industry, activated carbons are essentially produced by carbonization (pyrolysis at temperatures up to 900°C under neutral atmosphere) of various precursors (lignocellulosic, polymers, anthracites, ...), followed by physical and chemical activation [1]. Physical activation is generally realized around 900°C through partial gasification of carbon, using CO_2 or steam, according to Eqs. 1 and 2:

$$C + CO_2 \rightarrow 2\ CO \quad (1)$$

$$C + H_2O \rightarrow CO + H_2 \quad (2)$$

For chemical activation, the main reagents used are KOH, $ZnCl_2$, and H_3PO_4 [1]. KOH activation is a complex process, involving several redox reactions with carbon, followed by potassium intercalation/insertion and expansion of the structure [2, 3]. In the particular case of H_3PO_4, carbonization and activation generally proceed simultaneously at temperatures lower than 600°C [4].

On the nanotextural point of view, activated carbons (AC) are characterized by high values of specific surface area, up to 3,000 $m^2\ g^{-1}$. Depending on the precursor and carbonization/activation conditions, they can be essentially microporous (pores < 2 nm) or microporous and mesoporous (2 nm < pores < 50 nm). Many structural/nanotextural models have been proposed, but none of them gives a perfect description of the properties. The HRTEM 002 lattice-fringe image of an AC in Fig. 1a shows short fringes, few nanometers long, representing graphene-type layers, highly misoriented, some of them forming stacks of few layers. The disorientation of the graphene-type units causes the porosity of the material. According to simulations (Fig. 1b, [5, 6]), the graphene layers are not perfectly planar, and curvatures might be produced by defects such as pentagons and heptagons in their structure.

Based on various observations, Harris et al. proposed a model for the structure/nanotexture of non-graphitizable carbons that consists of discrete fragments of curved carbon sheets, in which pentagons and heptagons are dispersed randomly throughout networks of hexagons, as illustrated in Fig. 2 [7–9]. The size of the micropores in this model would be of

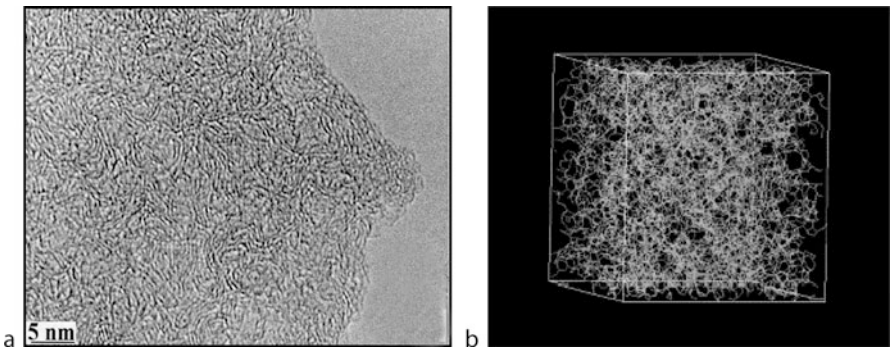

Nanocarbons for Supercapacitors. Figure 1
(**a**) HRTEM 002 lattice fringe image of an activated carbon; (**b**) structure/nanotexture of an activated carbon obtained by coupling HRTEM and numerical simulation [6]

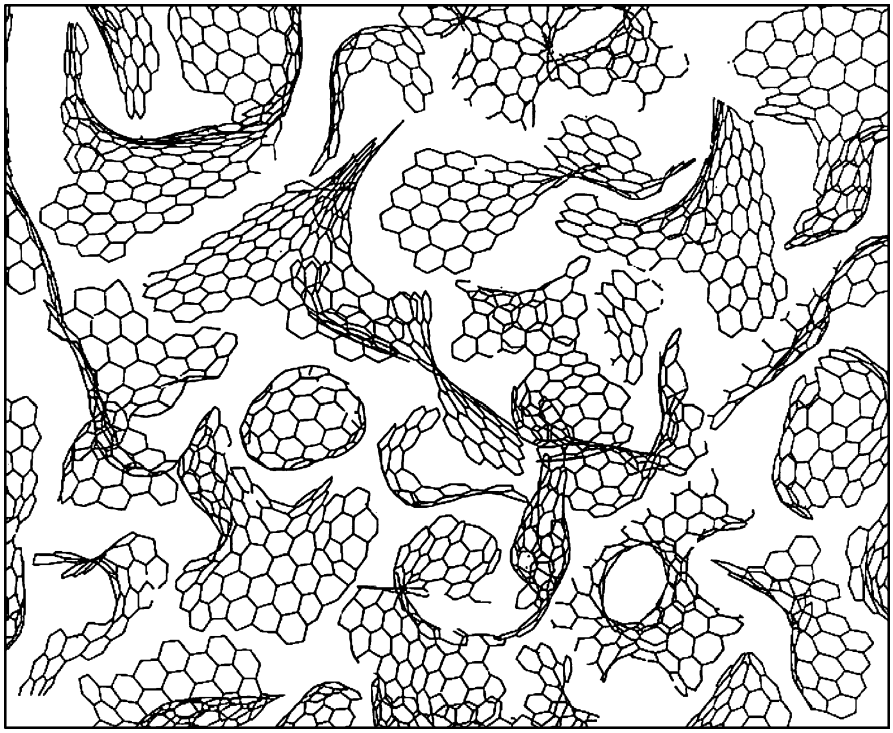

Nanocarbons for Supercapacitors. Figure 2
Schematic nanotextural and structural model of an AC showing fullerene-like elements [7–9]

the order of 0.5–1.0 nm, which is similar to the pore size observed in typical microporous activated carbons. Taking into account that the independent fullerene-like graphene units would be soluble in some solvents and that the thermal stability of activated carbons is high, one has to imagine that, in addition to this representation, the units are connected by bridges which keep the backbone.

Apart of carbon which is the main element constituting nanoporous carbons, heteroatoms (essentially oxygen and nitrogen) in the amount of few atomic percent, generally less than 5 at.%, are always present in activated carbons. These heteroatoms are either remains of the carbon precursor and/or they are introduced during the activation process. Figure 3 shows a representation of the main oxygenated functionalities found at the edge of graphene planes [10]. Beside, free edge sites are present together with unpaired electrons stabilized by resonance. In the case of C/C supercapacitors in organic electrolyte, the later are assumed to be responsible of electrolyte decomposition, leading to capacitance decrease and resistance increase of the systems during cycling [11]. Therefore, specific treatments of carbons are mandatory to partly deplete these sites and get rid of the drawbacks linked to their existence.

In the case of nitrogen, the variety of functionalities (Fig. 4) results both from the position occupied in the ring system and from the extent of association with oxygen, which hardly can be avoided during synthesis. Nitrogen is either substituted to carbon ("lattice nitrogen") or included in the form of functional groups ("chemical nitrogen") at the periphery of polyaromatic structural units [12, 13]. The surroundings of the nitrogen atom in a graphene layer obviously affect its charge, electron donor/acceptor properties, and the contribution to the delocalized π electron system.

For supercapacitor carbon electrodes, it will be further shown that (1) the developed surface area is responsible of an important electrical double-layer capacitance; (2) both the oxygenated and nitrogenated functionalities may be involved in redox reactions with the electrolyte, which enhance capacitance through a pseudo-capacitive contribution.

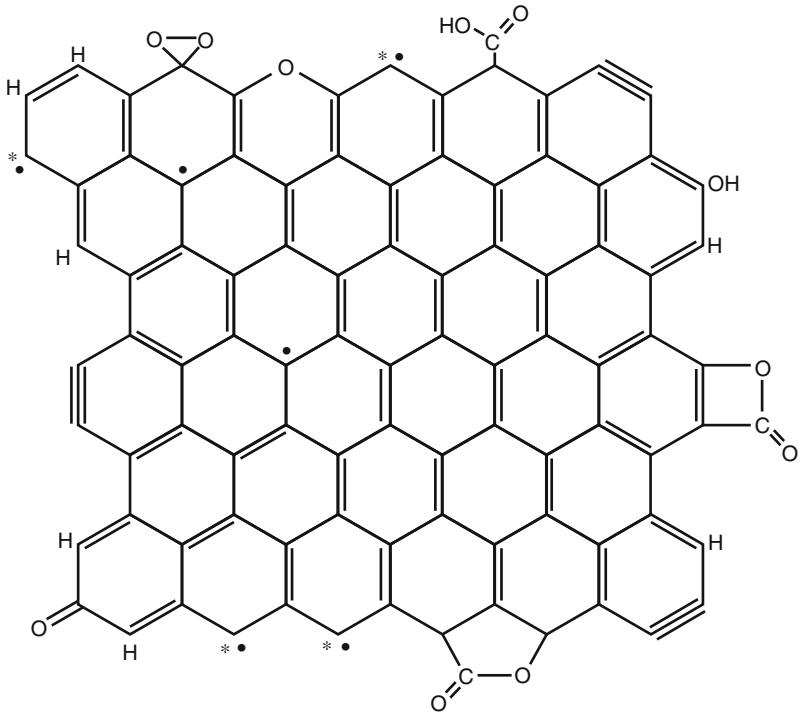

Nanocarbons for Supercapacitors. Figure 3
Schematic representation of some oxygenated functionalities present at the edges of a graphene unit. Free edge sites are present in addition to surface functionalities. In ambient, unpaired electrons are stabilized by resonance on the basal plane [10]

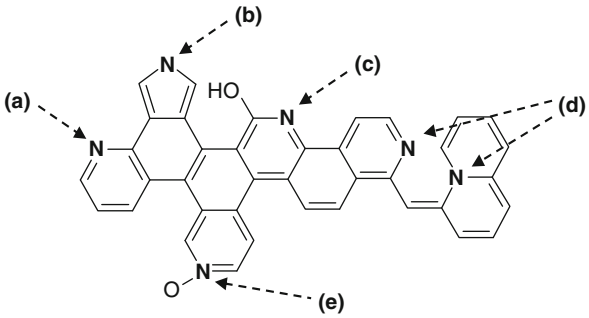

Nanocarbons for Supercapacitors. Figure 4
Nitrogen functionalities in a carbon material. (**a**) Pyridinic (N-6); (**b**) pyrrolic; (**c**) pyridonic (N-5); (**d**) quaternary (N-Q); and (**e**) oxidized nitrogen (N-X)

General Properties of Electrochemical Capacitors

An electrochemical capacitor is generally constituted of two identical carbon electrodes (carbon coating a current collector), separated by a porous membrane, and immersed in an electrolyte (Fig. 5). When the system is charged, the anions of the electrolyte are electrosorbed on the positively polarized electrode and the cations on the negative one, giving rise to an electric double layer at each electrode. As shown in Fig. 5, in its charged state, this system is equivalent to two capacitors of capacitance C_1 and C_2 in series, and the resulting capacitance C is given by the classical relationship (Fig. 3):

$$\frac{1}{C} = \frac{1}{C_1} + \frac{1}{C_2} \tag{3}$$

The capacitance originating itself from the electrical double layer at each electrode/electrolyte interface is given by the formula (Eq. 4) [14]:

$$C_e = \varepsilon A/d \tag{4}$$

where ε is the dielectric constant or permittivity, A the surface area of the electrode/electrolyte interface, and d the distance between the two charged layers of

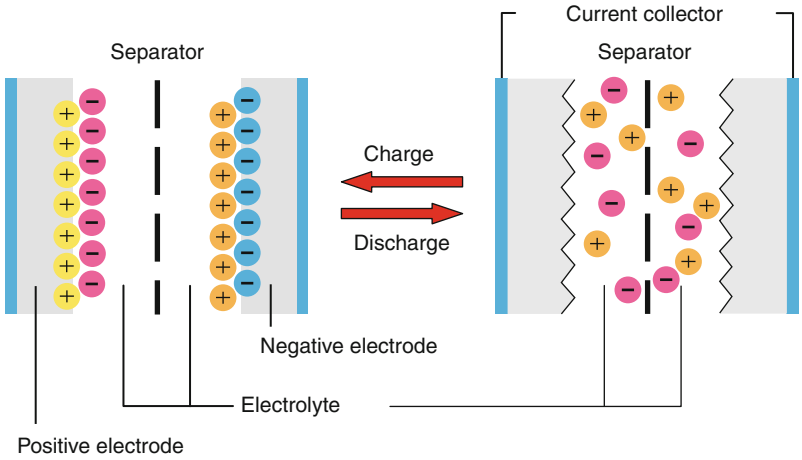

Nanocarbons for Supercapacitors. Figure 5
Discharged (*right*) and charged (*left*) states of an electrochemical capacitor

opposite sign. The value of d is controlled by the size of ions and is of the order of 1 nm. Consequently, the capacitance originating of the electrical double layer is very high, e.g., around 0.1 Fm^{-2}. In electrical double-layer capacitors (EDLC), the electrodes are from high surface area–activated carbons; for this reason, the surface area of the interface is very high and the capacitance C_e reaches values as high as 100 F per gram of carbon.

As said in the introduction, the main research direction on supercapacitors is dedicated to enhancing the energy density of these systems in order to broaden their possible applications. The energy density of supercapacitors is given by formula (Eq. 5):

$$E = \tfrac{1}{2}\, CU^2 \qquad (5)$$

where U represents the operating voltage. In supercapacitors, the later is strongly depending on the stability window of the electrolyte. In water medium, although the thermodynamic value is 1.23 V, practically it ranges from 0.7 to 1 V [15]. In organic electrolyte, the operating voltage can reach 2.7–2.8 V [15], and due to the square dependence of energy with voltage, this medium is definitively preferred for the industrial systems. Hence, the energy density of electrochemical capacitors is mainly controlled by the capacitance of the electrode materials. In aprotic electrolyte (e.g., organic electrolyte), the capacitance originates exclusively from the electrical double-layer formation, whereas an additional pseudo-capacitive contribution, due to fast pseudo-faradic reactions between the electrode surface and the electrolyte, may appear in protic electrolytic media. These two contributions will be considered separately.

Carbons for Electrical Double-Layer Capacitors

Considering Eq. 4 suggests that developing the surface area of activated carbons should lead to an increase of capacitance. For this reason, in the literature, many authors have suggested a proportional dependence between the gravimetric capacitance and the BET specific surface area measured by nitrogen adsorption at 77 K. An example is shown in Fig. 6 for a series of nanoporous carbons obtained by KOH activation of bituminous coal pyrolyzed at various temperatures [16]. Although these carbons were prepared from the same precursor using the same activation process and should be considered of identical nanotexture, the proportionality is observed only for the low values of BET surface area. Above 2,000 $m^2\,g^{-1}$, the observed saturation phenomenon is often interpreted by the fact that the BET model overestimates the values of surface area [17, 18]. Therefore, some plots have been proposed versus the DFT (density functional theory) surface area, but saturation is still observed for the high surface area carbons, i.e., for carbons with increasing activation degree. In order to explain the saturation, Barbieri et al. suggested that due to the decrease of average pore

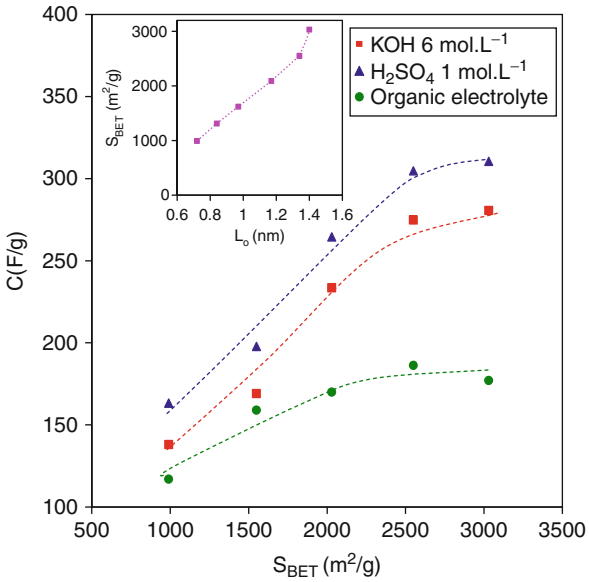

Nanocarbons for Supercapacitors. Figure 6
Gravimetric capacitance in various electrolytes (1 mol L^{-1} H_2SO_4, 6 mol L^{-1} KOH and 1 mol L^{-1} $TEABF_4$ in acetonitrile) vs BET specific surface area for a series of bituminous coal–derived carbons activated by KOH at 800°C. The inset shows the relationship between S_{BET} and the average pore size L_0 (Adapted from [16])

wall thickness in highly activated carbons, the electric field (and the corresponding charge density) no longer decays to zero within the pore walls [19].

Another explanation can be proposed from inset of Fig. 6, showing that the average pore size increases together with the specific surface area, i.e., when the activation degree of carbon increases. In high surface area carbons, with larger pores, one might suggest that the interaction of ions with pore walls is weaker, leading to smaller values of capacitance. Therefore, the normalized capacitance, e.g., the capacitance divided by the DFT surface area, has been plotted versus the average size L_0, both for the series of carbons from bituminous coal (Fig. 7a) [16] and for carbide-derived carbons (Fig. 7b) [20]. In the two cases, an increase of normalized capacitance is observed when the average pore size decreases, the highest values being observed for L_0 smaller than 1 nm. Taking into account the dimensions of solvated and non-solvated ions for tetraethylammonium tetrafluoroborate in acetonitrile, e.g., 1.30 and 0.67 nm for TEA^+, 1.16 and 0.48 nm for BF_{4^-}, respectively, suggests that the ions are at least partly desolvated in the pores [21]. Such property was already suggested for templated carbons which showed

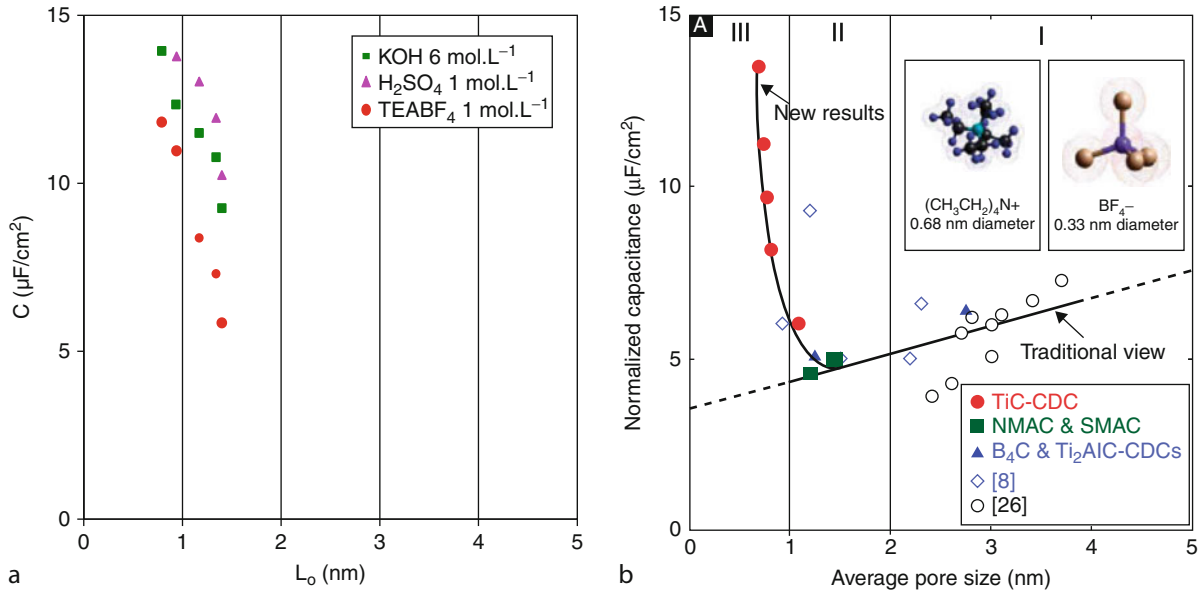

Nanocarbons for Supercapacitors. Figure 7
Normalized capacitance versus average pore size (**a**) for bituminous coal–derived activated carbons in 1 mol L^{-1} H_2SO_4, 6 mol L^{-1} KOH, and 1 mol L^{-1} $TEABF_4$ in acetonitrile (Adapted from [16]) and (**b**) for carbide-derived carbons (CDC) in 1 mol L^{-1} $TEABF_4$ in acetonitrile [20]

proportionality between capacitance and the ultramicropore (<0.7–0.8 nm) volume [22].

At this step, it is now clear that adapting the pore size of carbons to the size of ions is more important than developing the pore volume. Indeed, high surface area carbons display generally broader pores, and according to the data presented above the normalized capacitance is not optimized. Hence, the trend should be to develop carbons with pores ranging between 0.7 and 1 nm, which are able to accommodate desolvated ions, while allowing them to optimally interact with the pore walls. In addition, with such carbons, the useless volume would be reduced, and the volumetric capacitance optimized, fulfilling the industrial requirements for getting compact systems.

However, it has been shown that using carbons with pores in the optimal range, from 0.7 and 1 nm, may lead to porosity saturation before reaching the maximum voltage for the considered electrolyte [23]. Indeed, the comparison of two carbons, named PC (S_{DFT}=1,434 m^2 g^{-1}) and VC (S_{DFT}=2,160 m^2 g^{-1}), with different pore size distribution (Fig. 8), in 1.5 mol. L^{-1} tetraethylammonium tetrafluoroborate in acetonitrile, shows a perfectly rectangular voltammogram in the whole voltage range for VC while the capacitive current dramatically decreases above around 1.5 V for PC (Fig. 9). According to Fig. 8, all pores of PC are narrower than 1 nm and consequently able to optimally interact with ions. However, if one considers the pores larger than the diameter of desolvated TEA^+ cations (0.68 nm), the corresponding DFT values are 198 and 964 m^2 g^{-1}, respectively, for PC and VC. From these values, the maximum theoretical charge able to be accommodated in the pores has been calculated for both carbons and compared to the charge determined by integration of the respective voltammograms [23]. For PC the theoretical and experimental values are almost identical, confirming that the shape of the voltammetry curve is due to porosity saturation. By contrast, in the case of VC, the theoretical value is larger than the experimental one, demonstrating that for this carbon the porosity is not saturated, at least for the maximum voltage value reached in this experiment.

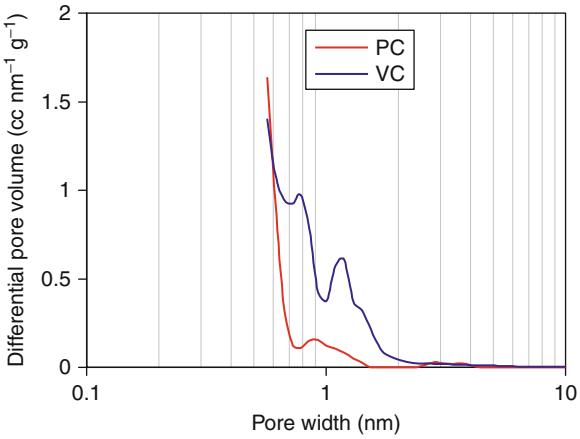

Nanocarbons for Supercapacitors. Figure 8
Pore size distribution of carbons PC and VC [23]

In summary, the porous texture of carbons strongly influences their electrical double-layer properties. With $TEABF_4$ in acetonitrile, the normalized capacitance is optimal in subnanometric pores, which also indicates that ions are partly desolvated in charged electrodes. For obtaining high values of volumetric capacitance, nanoporous carbons should present high values of specific surface area (~2,000 m^2 g^{-1}) with a narrow pore size distribution between 0.7 and 1 nm. Therefore, there is a need of new production techniques enabling to better reach this objective. Beside, taking into account that electrochemical intercalation is possible during charging [24], the structural parameters of carbons should also be more carefully considered in the future.

Carbons for Pseudo-capacitors

In general, two modes of energy storage are combined in electrochemical capacitors: (1) the electrostatic attraction between the surface charges and the ions of opposite charge (electrical double layer); (2) a pseudo-capacitive contribution which is related with quick redox reactions between the electrolyte and the electrode [14, 15]. Whereas the redox process occurs at almost constant potential in an accumulator, the electrode potential varies proportionally to the charge-exchanged dq in a pseudo-capacitor, what can be summarized by formula (Eq. 6):

$$dq = C * dU \tag{6}$$

where dU represents the potential variation.

The electrical response of such a system is comparable to that of a capacitor. Being of faradic origin and

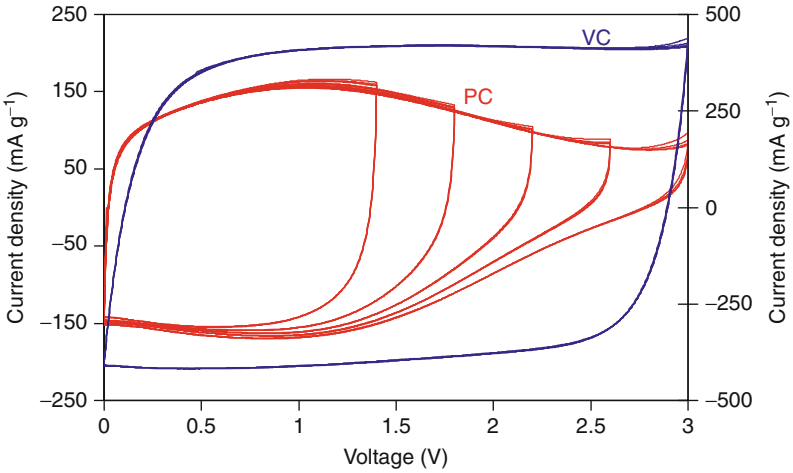

Nanocarbons for Supercapacitors. Figure 9
Cyclic voltammograms for the EDLCs based on PC carbon (*left-hand side* Y-axis for current) and VC carbon (*right-hand side* Y-axis for current) [23]

non-electrostatic, this capacitance is distinguished from the double-layer one and is called pseudo-capacitance. In summary, the electrical double-layer formation is a universal property of a polarized material surface, and pseudo-capacitance is an additional property which depends both on the type of electrode material and electrolyte. Compared to the double-layer normalized capacitance (~10 μF cm^{-2}), it has generally a high value (100–400 μF cm^{-2}), because it involves the bulk of the electrode and not only the surface. From a practical point of view, pseudo-capacitance contributes to enhancing the capacitance of materials and their energy density.

With nanoporous carbon electrodes in organic electrolyte, the double-layer capacitance is the major contribution. By contrast, in protic media (aqueous electrolytes or protic ionic liquids), an important pseudo-capacitive contribution is observed for nanotextured carbons enriched with heteroatoms as nitrogen and oxygen. Reversible hydrogen electrosorption is another kind of pseudo-faradic effect which might be also observed with nanoporous carbons in aqueous medium. In this case, nascent hydrogen formed by water reduction under negative polarization of carbon is adsorbed in the material; polarization reversal provokes its desorption by oxidation. The different types of pseudo-capacitive contributions for nanoporous carbons are reviewed in the following part of this chapter.

Pseudo-capacitance of Heteroatom-Enriched Carbons

The most reported dopants which confer pseudo-capacitive properties to carbons are oxygen (Fig. 3) and nitrogen (Fig. 4). Some other studies described below have recently considered boron or phosphorous as pseudo-capacitive dopants. The nitrogenated and oxygenated functionalities can undergo pseudo-faradic reactions, which can be pH-dependent or not, as presented in Fig. 10. The extent of the thereof extracted pseudocapacitance depends on the number of surface groups, their chemical nature, and accessibility.

Pseudocapacitance due to oxygenated surface functionalities is the most studied. In particular, the quinone/hydroquinone redox pair involves the exchange of one electron per oxygenated group (see Fig. 10a), against 0.18 electron stored per carbon atom in the electrical double-layer [14]. Other functionalities, such as pyrone-like structures (combination of non-neighboring carbonyl and ether oxygen atoms at the edges of the graphene layers – Fig. 10b), have been shown to be electrochemically active in the same potential range as the quinone/hydroquinone pair [26].

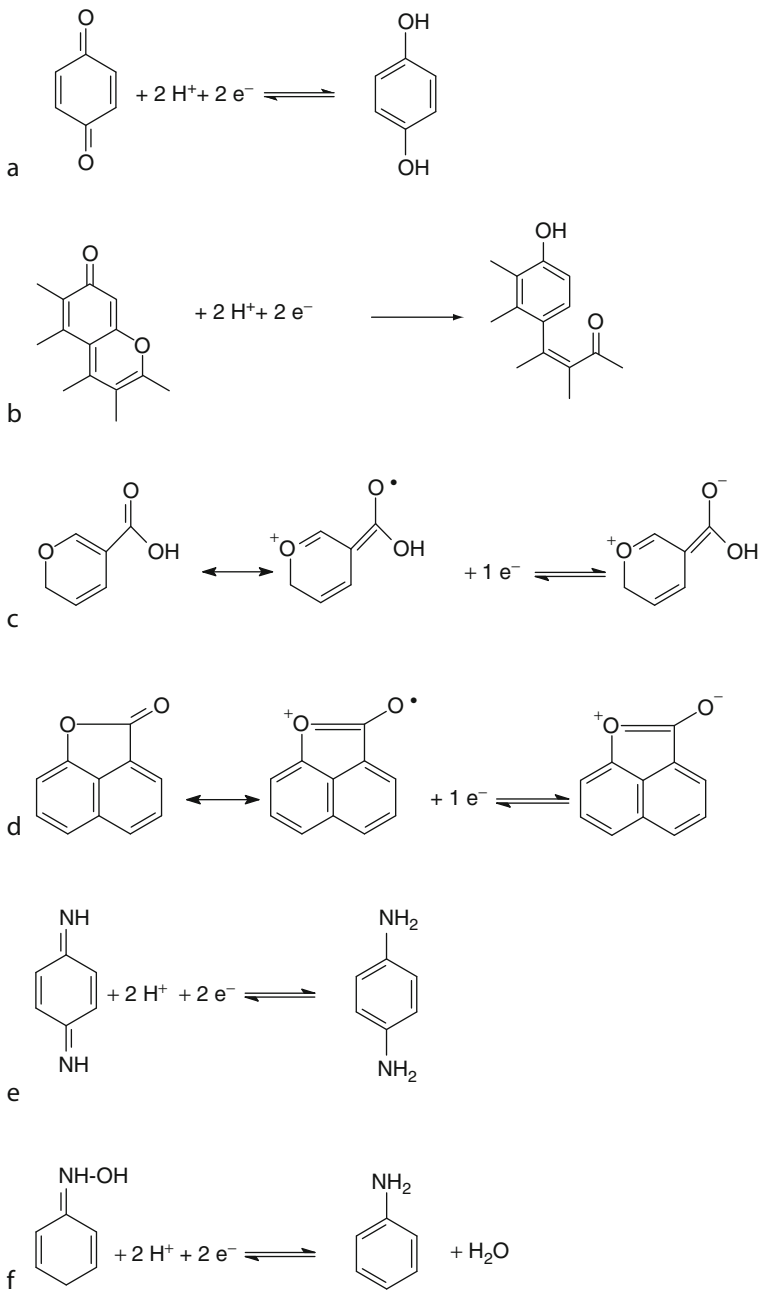

Nanocarbons for Supercapacitors. Figure 10
Possible redox reactions involving oxygenated or nitrogenated surface functionalities

The activity of other functionalities also present in the complex chemistry of a carbon surface is not clear, even if some of them as the carboxylic or lactones could show resonance with other functional groups able to undergo electron transfer reactions (see Fig. 10c, d).

According to the equations in Fig. 10a and b, the electrochemical activity of oxygenated functionalities such as quinones or pyrones depends on the electrolyte pH [27]. The quinone/hydroquinone pair is undoubtedly active at low pH values [27, 28], and it has been claimed that the pyrone-like one is more active at high

than at low pH [27]. Andreas et al. also suggested other unidentified pseudocapacitive reactions occurring on the carbon surface at basic pH. However, any oxygenated surface functionality being electrochemically active at neutral pH has been described. Due to this fact, and taking into account that smaller capacitance values are obtained at neutral pH than at acidic or basic ones [27], the main research efforts on the pseudocapacitive effect of the oxygenated surface functionalities have been focused on using KOH or H_2SO_4 as electrolytes.

Pseudo-capacitance in Basic and Acidic Media

Pseudo-capacitance due to Oxygenated Functionalities The capacitance enhancement of O-enriched carbons in KOH electrolyte has been correlated with the oxygenated functionalities desorbing as CO during a thermal treatment in inert atmosphere, e.g., phenol, ether, carbonyl or quinone groups [29, 30]. A similar correlation between capacitance and the CO-type oxygenated groups has been shown for a series of activated carbons tested in H_2SO_4 [31]. By contrast, the functionalities desorbing as CO_2, e.g., carboxyl, anhydride, or lactone [30], are supposed to hinder the electrolyte migration in the micropores, thus leading to a delay in the electrochemical response.

Although much work is still necessary for determining the exact electrochemical behavior of the individual oxygenated surface functionalities, their contribution in enhancing capacitance of nanoporous carbons in acidic or basic media is a demonstrated fact. However, one of the drawbacks of most nanoporous carbons is their low density which leads to a low volumetric capacitance and consequently to insufficiently compact supercapacitors. Such disadvantage can be circumvented by producing nanotextured carbons through the pyrolysis of seaweed-based biopolymers [32] or seaweeds themselves [33] at mild temperature, e.g., 600°C. The carbons are characterized by a high electrical conductivity and a moderately developed porosity (S_{BET}=200–700 $m^2\ g^{-1}$) and the presence of 10–15 wt% of oxygen. Due to the pseudo-faradic contribution of oxygenated functionalities, the capacitance reaches values as high as 260 $F g^{-1}$ in 1 mol L^{-1} H_2SO_4 with these carbons, despite the poorly developed specific surface area. Figure 11a shows three-electrode cyclic voltammograms of the seaweed-based carbon (LN600) and a commercial-activated carbon AC1 (Norit Super 50; S_{BET}=1,400 $m^2\ g^{-1}$; Oxygen= 4.6 at.%). AC1 shows an almost rectangular voltammogram, demonstrating that charging the electrical double layer is the dominant contribution, whereas LN600 presents very pronounced and reversible humps, at −0.4 and 0.1 V vs Hg/Hg_2SO_4, related with redox reactions probably involving the quinone and the pyrone-like groups. This surface functionality is suggested to enhance capacitance and to shift the irreversible and destructive oxidation of the material toward more positive potentials. On the negative side of the voltammogram, the potential of dihydrogen evolution is shifted to very negative values (ca. −1.2 V vs Hg/Hg_2SO_4) compared to the thermodynamic potential for water reduction, e.g., −0.62 V vs Hg/Hg_2SO_4 at pH=0. Due to this overpotential, hydrogen is sorbed/inserted in the pores during the cathodic scan (hump at around −0.9 V vs Hg/Hg_2SO_4) and further oxidized (hump at around −0.2 V vs Hg/Hg_2SO_4) during the anodic one, giving rise to an additional pseudo-capacitive contribution [34]. This phenomenon will be discussed in detail in section "Pseudo-capacitance Related with Reversible Hydrogen Electrosorption in Nanoporous Carbons". As a result of broadening the stability window, a symmetric capacitor built with LN600 electrodes in 1 mol L^{-1} H_2SO_4 could be charged/discharged at voltage values as high as 1.4 V, whereas only 0.8–1.0 V can be applied with activated carbons [35].

The weakly porous seaweed carbons present a high density, which makes them more interesting than activated carbons in terms of volumetric energy density. Figure 11b shows that the volumetric energy density reached with the carbon LN600 is about one order of magnitude higher than for capacitors based on the commercial-activated carbons AC1 and AC2 (PX21, Kansai, Japan; S_{BET} =2,500 $m^2\ g^{-1}$; Oxygen=5.0 at.%).

When seaweeds are carbonized in the presence of multiwalled carbon nanotubes (CNTs), the resulting composites are mesoporous, and the presence of CNTs dramatically enhances their conductivity [36]. Due to this open mesoporosity and the high conductivity of CNTs, the accessibility of ions to the active mass together with the charge propagation is improved. As it can be observed in Fig. 12, for the

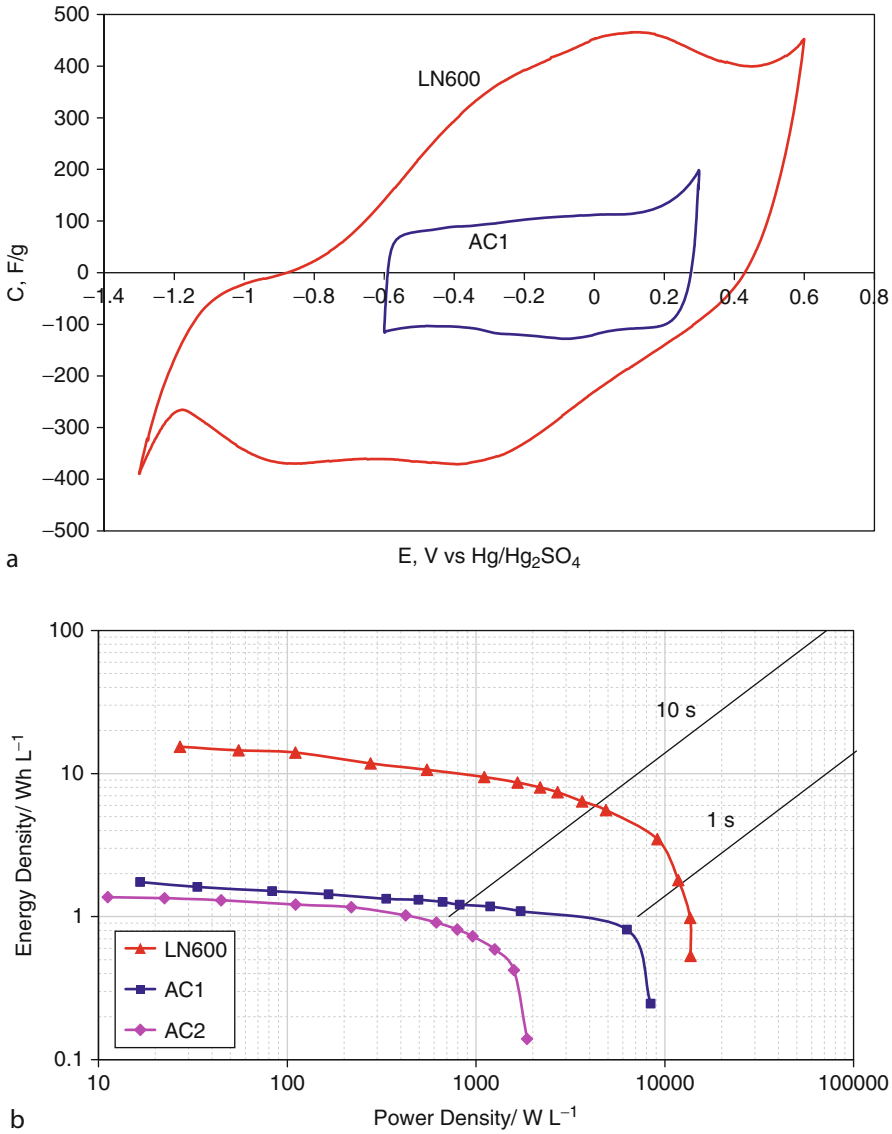

Nanocarbons for Supercapacitors. Figure 11
(**a**) Three-electrode cyclic voltammograms of LN600- and AC1-based electrodes in 1 mol L^{-1} H_2SO_4; (**b**) Volumetric Ragone plots which compare the performance of supercapacitors with LN600-, AC1-, and AC2-based electrodes in 1 mol L^{-1} H_2SO_4 (Adapted from [33])

composites containing 10 wt% of CNTs, specific capacitance values as high as 180 Fg^{-1} can still be obtained at a current density of 50 A g^{-1}, whereas the addition of carbon black does not give any benefit in comparison to the LN600 material alone. As a consequence, the highest extractable energy at high power density is obtained with CNT-based composite electrodes. In addition, the cycle life of the systems is improved owing to the resiliency introduced by the CNTs in the composite electrodes.

Graphene nanosheets are another kind of moderately developed surface area and highly oxygenated carbon material, which has attracted much attention during the last years [37–41]. In literature, perfectly dispersed individual graphene nanosheets are expected to display a high specific surface area, being promising

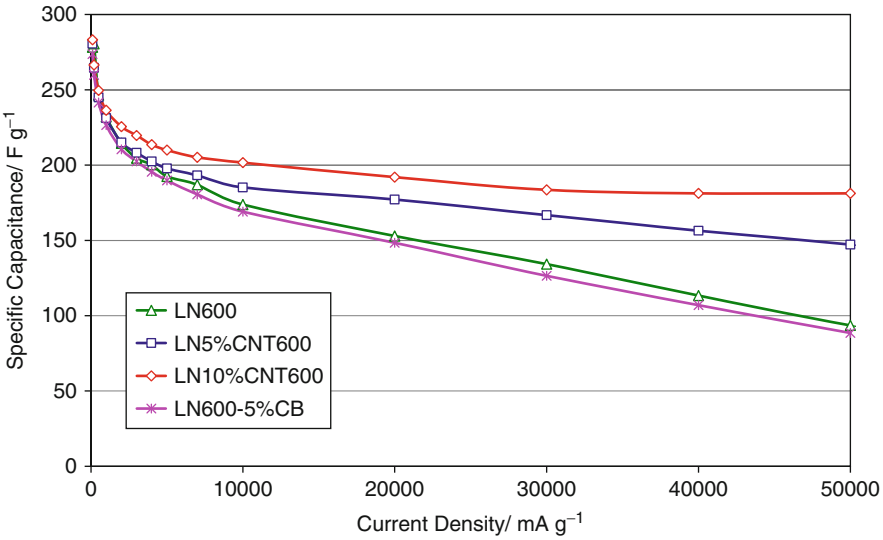

Nanocarbons for Supercapacitors. Figure 12
Specific discharge capacitance vs current density for supercapacitors (charged up to 1.2 V) based on LN600 and its composites with 5 wt% CNTs (LN5%CNT600), 10 wt% CNTs (LN10%CNT600), and 5 wt% carbon black (LN600–5%CB) in 1 mol L^{-1} H_2SO_4 [36]

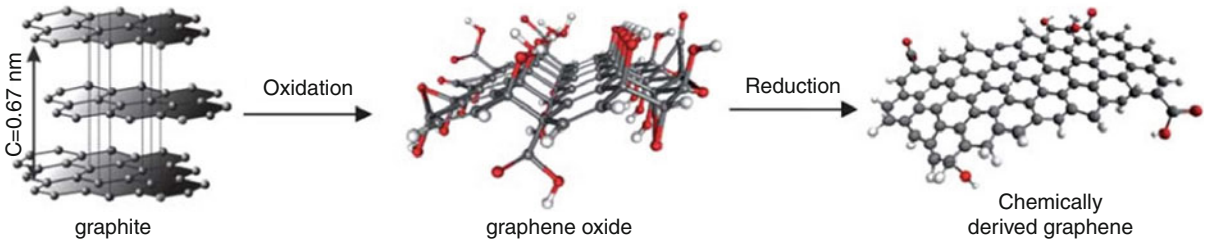

Nanocarbons for Supercapacitors. Figure 13
Illustration of the chemical route to the synthesis of chemically derived graphene [41]

for EDLC. Unfortunately, in practice, the obtaining of stable single graphene sheets with controllable size and morphology remains a great challenge. Among the different synthesis methods, the chemical one based on graphite oxidation giving graphite oxide, which is subsequently reduced by hydrazine (Fig. 13), is the most proposed because of a possible upscaling, even if harmful chemicals are used. Whatever the preparation method, the resulting material consists in an agglomeration of highly functionalized graphene sheets. As a consequence, the specific surface area is relatively low (300–900 m^2 g^{-1}) compared to the theoretical one (2,620 m^2 g^{-1}), and the materials contain 10–20 at.% of oxygen and nitrogen. Obviously, the capacitance values, from 100 to 200 Fg^{-1}, reported for these materials in KOH or H_2SO_4 electrolytes are not related to the nanotexture but mainly to the pseudo-faradic reactions involving the surface functionality at the edges of the graphene sheets. Hence, the literature claims that graphene exhibits good EDL properties are not correct. Moreover, despite the exponential growth of the number of publications on synthesis and applications of graphene for supercapacitors, a cost-effective and environment-friendly mass-production method still remains a challenge [41], and the electrochemical performance should be improved to compete with other existing carbon materials.

Pseudo-capacitance Due to Nitrogenated Functionalities The specific introduction of nitrogen as a dopant of carbon is also extensively reported in the literature. Nitrogen-rich nanocarbons can be obtained either by post-treatment of carbons with N-containing reagents as the NH_3/air mixture [42] and urea [43] or by pyrolysis of N-containing polymers. Such pyrolysis can be performed on the polymer itself, and followed by an activation step for generating porosity [44–46], or on mixtures of polymer and nanotexturing agent as CNTs [47, 48], zeolites [49], or mica [50].

A correlation between capacitance in aqueous KOH or H_2SO_4 electrolytes and the total amount of surface nitrogen has been shown by Frackowiak et al. [45] for a series of N-doped carbons of similar nanoporous texture. The carbons were obtained by pyrolysis of nitrogen-containing precursors as polyvinylpyridine or polyacrylonitrile and their blends with coal tar pitch, followed by steam activation. Among the various nitrogenated functionalities, it seems that the ones located at the graphene edges, as pyridine and pyrrol (see Fig. 4), are the most active [46, 51]. The presence of nitrogen can also influence differently the capacitance of the positive and negative electrodes of a capacitor [43] due to the potential dependence of the pseudo-faradic reactions.

High-performance nitrogen-rich carbons have been developed by applying the "templating technique." Briefly a nitrogen-containing precursor is introduced in a nanoporous scaffold and subsequently pyrolyzed; afterward, the nitrogen-enriched carbon replica is obtained by etching the host with hydrofluoric acid. As an example, a weakly porous carbon material (S_{BET}=400 m^2 g^{-1}) containing 24 at.% of nitrogen was synthesized through melamine intercalation in a lamellar aluminosilicate [50]. The specific capacitance, obtained in three-electrode cell, reaches 200 Fg^{-1} in 1 mol L^{-1} H_2SO_4. Much higher gravimetric capacitance of 340 Fg^{-1} was demonstrated in 1 mol L^{-1} H_2SO_4 by the carbon obtained through pyrolysis of acrylonitrile in NaY zeolite. This carbon displays a higher specific surface area of 1,680 m^2 g^{-1} and a moderate nitrogen amount of 6 at.%. The exceptionally high capacitance comes from the synergy of different contributions: (1) the ordered superstructure inherited from the scaffold which favors the diffusion of ions to the active surface; (2) micropores with a size perfectly adapted to the electrolyte which provide an EDL contribution; and (3) an important pseudo-capacitive effect related with the surface functionality [49]. Moreover, a symmetric capacitor from these carbons could operate up to 1.2 V during 10,000 charge/discharge cycles, which is much higher than the usual maximum voltage for systems based on activated carbon electrodes in aqueous media [35]. Hence, nitrogen enrichment seems to provide a profitable potential shift of the electrodes as it has been observed for oxygen [33].

Following the industrial requirements, the tendency now is to develop heteroatom-enriched carbons enabling to operate at high current density. For example, carbon/CNTs nanocomposites have been prepared by one-step carbonization of polyacrylonitrile/carbon nanotube blends [47] and melamine-formaldehyde/carbon nanotube blends [48]. Although presenting a moderate specific surface area ($S_{BET}\sim$400 m^2 g^{-1}), the later carbons display gravimetric capacitance values of 170 and 130 Fg^{-1} at current densities of 50 and 5 Ag^{-1}, respectively [48]. Such exceptional performance is due, as for the previously presented LN600/CNTs composites, to the synergetic effects of nanotubes and surface functionality. The open mesoporosity of nanotubes and their good electrical conductivity enable good propagation of charges.

Recently, capacitance values around 100–200 Fg^{-1} have been claimed for nonporous (specific surface area ranging from 6 to 86 m^2 g^{-1}) N-enriched carbons prepared by ammonia treatment of an already nitrogenated carbon derived from melamine [52]. However, the data were obtained at very low current density and the study does not provide any information on the performance of these materials in usual operating conditions of supercapacitors.

Even if the previously presented results seem to demonstrate the efficiency of nitrogen as carbon dopant for introducing a pseudocapacitive character, one must take into account that oxygen is always present on the surface of carbons materials. Studies performed on model compounds as crystalline oligomers of 1,5-diaminoanthraquinone (DAAQ) with a 3D-extended π-conjugated structure [53, 54] have shown that the redox peaks corresponding to quinone/hydroquinone and emeraldine/quinone diimide pairs arise in the same potential range. Therefore, the capacitance values

normally assessed only to the nitrogenated functionalities may include a contribution due to the presence of oxygenated surface functionalities.

Conclusion O- and N-enriched nanocarbons demonstrate high capacitance values in KOH or H_2SO_4 due to the contribution of pseudo-faradic reactions. Another positive effect of doping is the broadening of the potential stability window. Composites of these carbons with carbon nanotubes withstand remarkable capacitance values at high current load. Hence, the N- and O-doped carbons open the opportunity of developing high-performance supercapacitors in aqueous electrolytes.

Recently, boron [55] and phosphorous [56] have been tested as dopants for improving the electrochemical performance of carbons in acidic electrolytes. However, since the investigated boron-doped carbons contained also nitrogen and oxygen, the peculiar role of boron is not established. For the particular case of phosphorous, it seems that small amounts affect positively the overall capacitance and improve the capacitance retention ratio at high current load in H_2SO_4.

Pseudo-capacitance in Neutral Medium Neutral electrolytes have been scarcely applied for carbon-based supercapacitors. Indeed, the capacitance values of activated carbons in neutral electrolytes are lower than in other aqueous electrolytes, suggesting that the pseudo-faradic redox reactions of O and N electroactive surface groups are depressed in comparison with acidic or basic electrolytes [25, 27, 57–59]. Therefore, it was concluded that oxygenated or nitrogenated functionalities are electrochemically inactive in neutral electrolytes and that only the formation of the electrical double layer contributes to the capacitance in this media.

Nevertheless, a recent study has shown that a contribution of pseudo-faradic reactions is possible in a neutral electrolyte, e.g., Na_2SO_4, if the carbon material possesses an adequate surface functionality [60]. Figure 14 shows the cyclic voltammograms of supercapacitors built with nanotextured carbons obtained after pyrolysis of seaweeds at 600°C (LN600, S_{BET}=746 m^2 g^{-1}) and at 750°C (LN750, S_{BET}= 1,082 m^2 g^{-1}). Despite the lower specific surface area of LN600 in comparison to LN750, the capacitive behavior is comparable for the two carbons. Taking into account that LN600 and LN750 contain 11.5 at.% and 7.3 at.% of oxygen, respectively, one can conclude that pseudo-faradic reactions contribute more markedly to the capacitance of LN600 in Na_2SO_4. In particular, the fact that quinone-like groups are twice more present in LN600 than in LN750 suggests that the latter are the most active ones at pH=6.4.

Notwithstanding these facts, the most striking result obtained in neutral electrolytes is the ability of symmetric carbon/carbon supercapacitors to operate

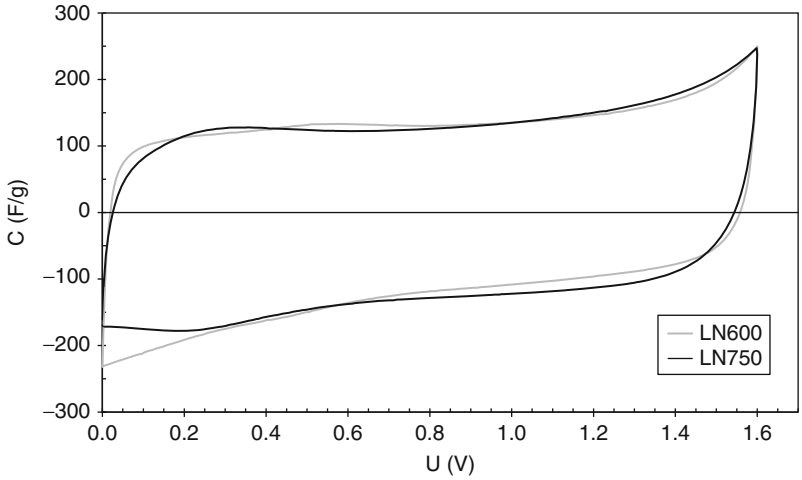

Nanocarbons for Supercapacitors. Figure 14
Cyclic voltammograms of LN600- and LN750-based symmetric capacitors in 0.5 mol L^{-1} Na_2SO_4 [60]

up to voltages as high as 1.6 V during more than 10,000 cycles [60, 61]. According to Eq. 5, the energy density is higher in neutral than in other aqueous electrolytes.

The former result can be understood by comparing the three-electrode cyclic voltammograms of a commercial-activated carbon (AC, S_{BET}=2,250 m^2 g^{-1}, O=2.5 at.%; provided by MeadWestvaco, USA) in acidic (H_2SO_4), basic (KOH), and neutral (Na_2SO_4) electrolytes (Fig. 15) [61]. In Na_2SO_4, the stability potential window is about twice larger than in H_2SO_4 and KOH. Actually, in the neutral electrolyte, it reaches 2.0 V for AC and values of even 2.4 V have been found for seaweed-based carbons [60]. The reason of such a wide stability potential window is the high overpotential for dihydrogen evolution, e.g., 0.6 V, and the better oxidation resistance of carbons in the neutral medium. A pH dependence of the overpotential for H_2 evolution has been also shown with glassy carbon [62] or Pt [63] electrodes. In a neutral pH solution, the overpotential reaches 1.2 V with a glassy carbon electrode, whereas only values of 0.6 V or 0.8 V are attained in acidic or basic pH, respectively. With a Pt electrode, a small overpotential of 0.3 V is found in neutral electrolyte, whereas any overpotential can be detected in acidic or basic solutions. For the particular case of Pt [63], this property is attributed to the fact that the H_3O^+ concentration in neutral electrolyte is too low to induce gas evolution reactions. For nanoporous carbons, it is also related with their storage ability of nascent hydrogen below the thermodynamic potential for water reduction. This pseudo-capacitive contribution related to hydrogen sorption will be discussed in detail in the section "Pseudo-capacitance Related with Reversible Hydrogen Electrosorption in Nanoporous Carbons".

Although 1.6 V is the highest voltage ever claimed for a symmetric carbon/carbon capacitor in an aqueous electrolyte, this value is smaller than the stability potential window of 2.0 V determined for AC in three-electrode cell. The reasons of the potential window underuse in Na_2SO_4 have been demonstrated after experiments using a special two-electrode cell equipped with a reference electrode. Such configuration allows the positive and negative electrode potentials to be recorded separately during cycling the supercapacitor between zero and a given maximum voltage. Figure 16 shows that, if the supercapacitor is charged between 0 V and the maximum stability voltage of 1.6 V, the operating potential window for the negative and the positive electrode is [0.09; −0.61] and [0.09; 0.99] V vs NHE, respectively. According to Fig. 15, in Na_2SO_4 electrolyte, the lowest potential for a negative electrode before dihydrogen production is around −1 V vs NHE and the highest one for avoiding an irreversible

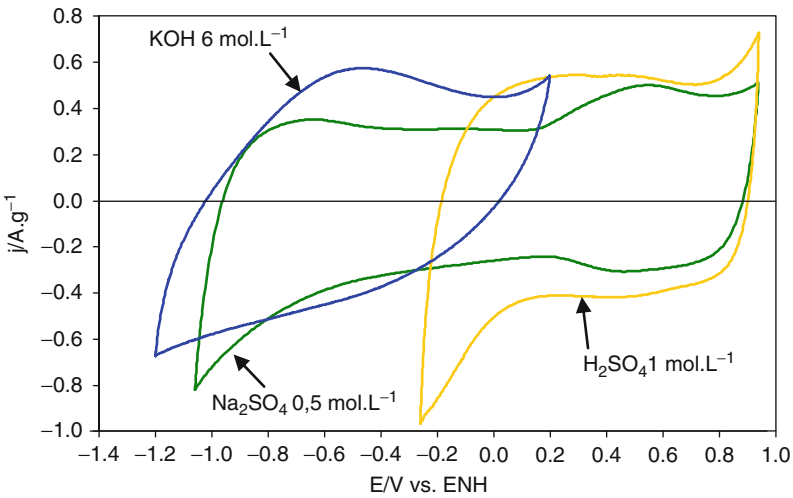

Nanocarbons for Supercapacitors. Figure 15
Three-electrode cyclic voltammograms showing the potential stability window of AC in 6 mol L^{-1} KOH, 1 mol L^{-1} H_2SO_4, and 0.5 mol L^{-1} Na_2SO_4 [61]

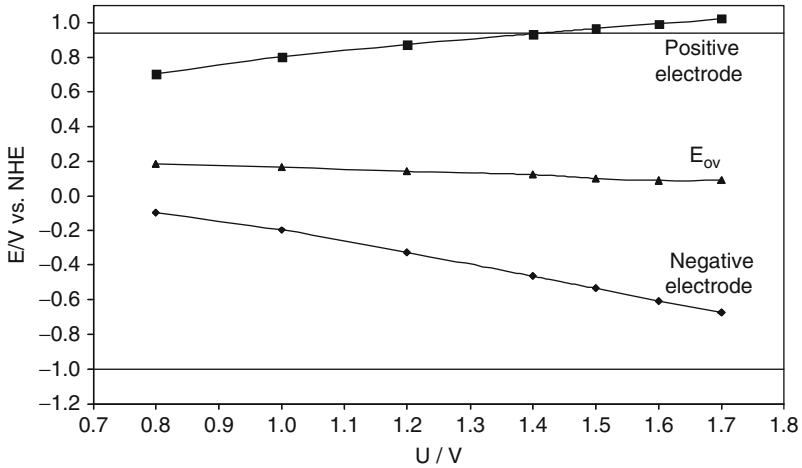

Nanocarbons for Supercapacitors. Figure 16

Potential reached by the positive and negative electrodes during the operation of a 2-electrode cell (equipped with a reference electrode) at different values of maximum voltage. The E_{0V} values correspond to the electrodes potential when the cell voltage U is set to 0 V. Electrolyte: 0.5 mol L^{-1} Na_2SO_4. The *horizontal lines* represent the extreme potential values determined for AC in 3-electrode cell [61]

oxidation of a positive electrode is around 0.95 V vs NHE (see the horizontal lines included in Fig. 16). Hence, Fig. 16 clearly shows that the maximum voltage of the supercapacitor is limited by the positive electrode. In fact, the maximum potential reached by the positive electrode at U = 1.6 V is slightly beyond the oxidation limit, whereas the minimum potential reached by the negative electrode is still far away, ca. 0.4 V, from the limit imposed by dihydrogen evolution. During cycling, the maximum potential of the positive electrode slightly shifts to lower values, allowing a good cyclability of the capacitor.

From the foregoing, even if the AC/AC symmetric capacitor in Na_2SO_4 largely outperforms all the symmetric systems in other aqueous electrolytes, the strategy to follow for taking advantage of the whole stability potential window of 2.0 V, and for enhancing the energy density, would consist to broadening the potential range of the negative electrode. In sulfuric acid medium, it has been shown that this kind of shift of the electrodes potential range is possible by building asymmetric systems combining two different carbon materials with a surface functionality adapted for optimally operating as positive or negative electrode [64].

In conclusion, the nature of the surface functionalities of carbons and the electrolyte pH influence both the capacitance values and stability potential window. Actually, the lately developed supercapacitors in neutral medium are able to compete with the organic electrolyte-based systems while being environment friendly.

Pseudo-capacitance Related with Reversible Hydrogen Electrosorption in Nanoporous Carbons

As it has been introduced in the previous section, hydrogen electrosorption in carbon materials under negative polarization has a direct impact on the energy density of a supercapacitor operating in an aqueous electrolyte. Due to the overpotential of dihydrogen evolution, the electrochemical stability window can be extended to lower potential values. Moreover, the electro-desorption of hydrogen by anodic oxidation gives rise to a pseudo-faradic contribution in addition to the EDL capacitance of the material.

Under negative polarization of a nanotextured carbon electrode in aqueous electrolyte, hydrated cations are first adsorbed forming an electrical double layer. When the electrode potential is lower than the equilibrium value for water reduction, nascent hydrogen is formed (Eq. 7) and adsorbed onto the carbon surface [34] (Eq. 8):

$$H_3O^+ + e^- \leftrightarrow \ <H> + H_2O \tag{7}$$

$$<C> + <H> \ \leftrightarrow \ <CH_x>_{ads} \tag{8}$$

where <H> represents the nascent hydrogen, <C> the carbon host, and <CH_x> hydrogen adsorbed in the later.

It has been demonstrated that the nanoporous texture of the activated carbon plays an important role [22, 34, 65–67]. In particular for carbons prepared by a templating technique, the amount of sorbed hydrogen is proportional to the ultramicropore (0.6–0.7 nm) volume [22]. In this case, straight mesopores are very useful channels for the transport of ions. Galvanostatic charge/discharge experiments in alkaline medium on a series of activated carbons with similar porosity but with different surface chemistry show that the amount of hydrogen reversibly electrosorbed decreases with the increase of the oxygenated surface functionalities [68]. The electrosorption of hydrogen has been extensively studied in alkaline or acidic medium [34]. In such media, the important polarization between reduction and oxidation potentials suggests that the interaction of sorbed hydrogen with the carbon substrate is stronger than physisorption. In the thermo programmed desorption (TPD) analyses realized on carbon samples submitted to galvanostatic charge in KOH medium, a hydrogen peak appears at around 200°C [69]. From this peak, the activation energy was estimated to 110 kJ mol^{-1} for hydrogen desorption, confirming a weakly chemisorbed state of hydrogen.

A recent study demonstrates the effectiveness of a neutral medium for electrochemical hydrogen bonding to the graphene units in nanocarbons [70]. From the galvanostatic charge/discharge curves (Fig. 17), the mechanism for hydrogen sorption seems different in neutral medium and in KOH. In KOH, a single plateau at ca 0.6 V vs NHE characterizes the anodic oxidation of hydrogen [34]. By contrast, in neutral medium (0.5 mol L^{-1} Na_2SO_4), the curve exhibits two different slopes, a first part where the stored hydrogen is oxidized at potentials lower than 0.1 V vs NHE, and a plateau at higher potentials corresponding to more strongly bonded hydrogen. It has also to be noted that the reduction overpotential is more important in neutral than in alkaline medium. The TPD analysis realized after the galvanostatic charge of AC in the neutral medium (Fig. 18) confirms two types of hydrogen bonding with peaks at 125°C and 430°C. The desorption activation energies calculated from these data are 110 and 205 kJ mol^{-1}, respectively. The highest value demonstrates that the main part of nascent hydrogen is strongly bonded to the graphene units in 0.5 mol L^{-1} Na_2SO_4.

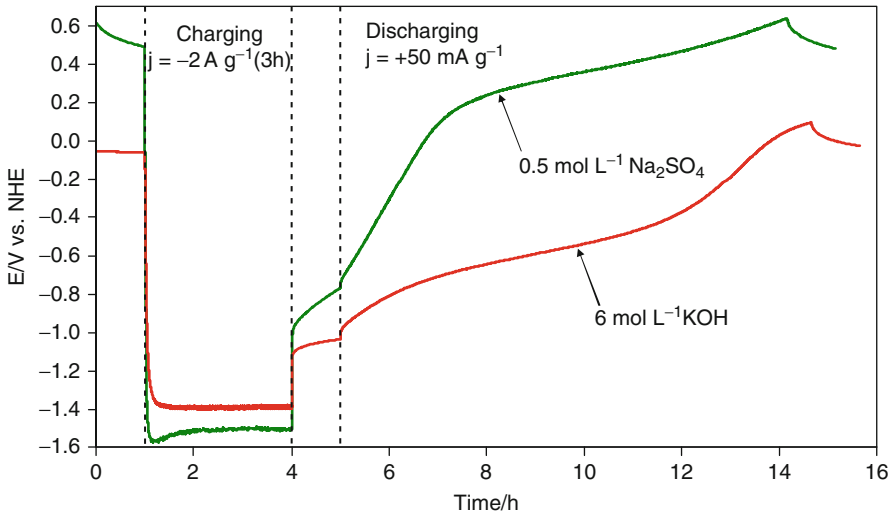

Nanocarbons for Supercapacitors. Figure 17

Galvanostatic charge/discharge of AC in 6 mol L^{-1} KOH (*red curve*) and 0.5 mol L^{-1} Na_2SO_4 (*green curve*). After 1 h relaxation, a negative current of −2 A g^{-1} is applied during 3 h. Then, after 1 h relaxation, a positive current of +50 mA g^{-1} is applied in order to oxidize the sorbed hydrogen [70]

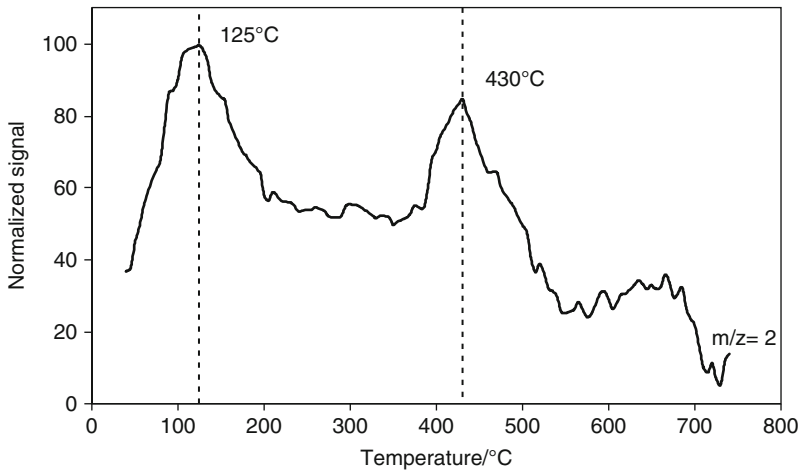

Nanocarbons for Supercapacitors. Figure 18
TPD analysis of dihydrogen evolved from AC power charged at −2 A g^{-1} during 3 h at 50°C in 0.5 mol L^{-1} Na_2SO_4 [70]

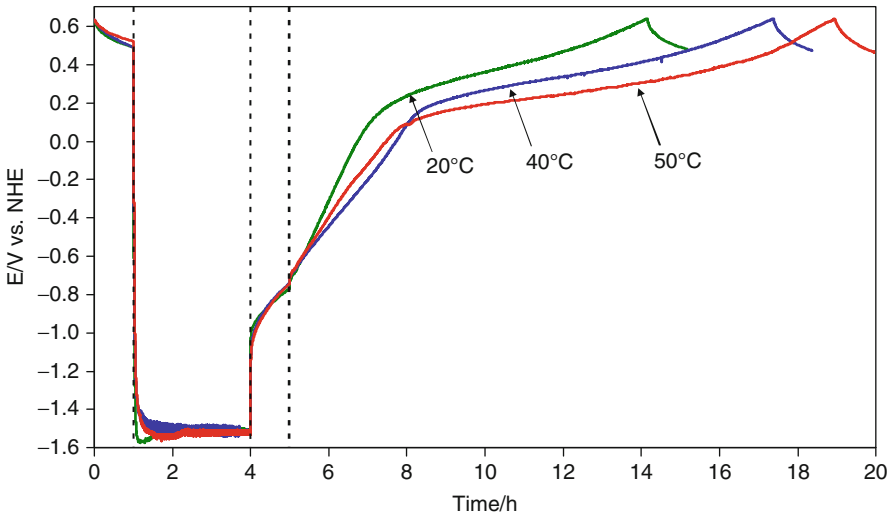

Nanocarbons for Supercapacitors. Figure 19
Galvanostatic charge/discharge of AC in 0.5 mol L^{-1} Na_2SO_4 at 20°C, 40°C, and 50°C [70]

The effect of temperature on the electrochemical performance in 0.5 mol L^{-1} Na_2SO_4 has been evaluated (Fig. 19). The oxidation time of stored hydrogen increases with temperature (1.5 wt% at 20°C, 2.1 wt% at 40°C and 2.4 wt% at 50°C), confirming a weakly chemisorbed state of hydrogen [69]. Meanwhile, the oxidation potential decreases when temperature increases, due to a better conductivity of the electrolytic medium. Hence, the energy density of a cell using activated carbon as negative electrode in neutral aqueous solution will be enhanced by operating at higher values of temperature.

To summarize, in comparison to acidic and basic electrolytes, a neutral medium has two positive impacts for supercapacitor applications: (1) the overpotential for dihydrogen evolution is higher, allowing the stability window to be enlarged; (2) the amount of hydrogen reversibly sorbed is enhanced enabling a higher pseudo-capacitive contribution related with its oxidation.

Protic Ionic Liquids as Electrolytes for Carbon-Based Pseudo-capacitors

Protic ionic liquids (PILs) are relatively cheap and environment friendly electrolytes [71]. Due to their proton-exchanging capabilities, a pseudo-faradaic enhancement of capacitance can be expected, as in aqueous electrolytes, while operating in a larger potential window. For these reasons, they have been proposed as electrolytes in carbon-based supercapacitors [72]. Cyclic voltammograms in Fig. 20 show the electrochemical performance of two pyrrolidinium-based PILs (Pyrrolidinium nitrate [Pyrr][NO3] (IL1) and pyrrolidinium formate [Pyrr][HCOO] (IL2)) [73] in presence of two different carbon electrodes: (1) a commercial-activated carbon (S50 from Norit, S_{BET}=1,400 m^2 g^{-1}, O=4.6 at.%); (2) the same oxidized in order to increase the amount of surface functionalities without modifying the porous texture ($S50_{ox}$, O=9.7 at.%). For IL1 (Fig. 20a), redox peaks are seen at around 0.2 and 0.45 V vs Ag/AgCl(PIL). For activated carbons, peaks in such potential range are traditionally assessed to the electrochemical reactions

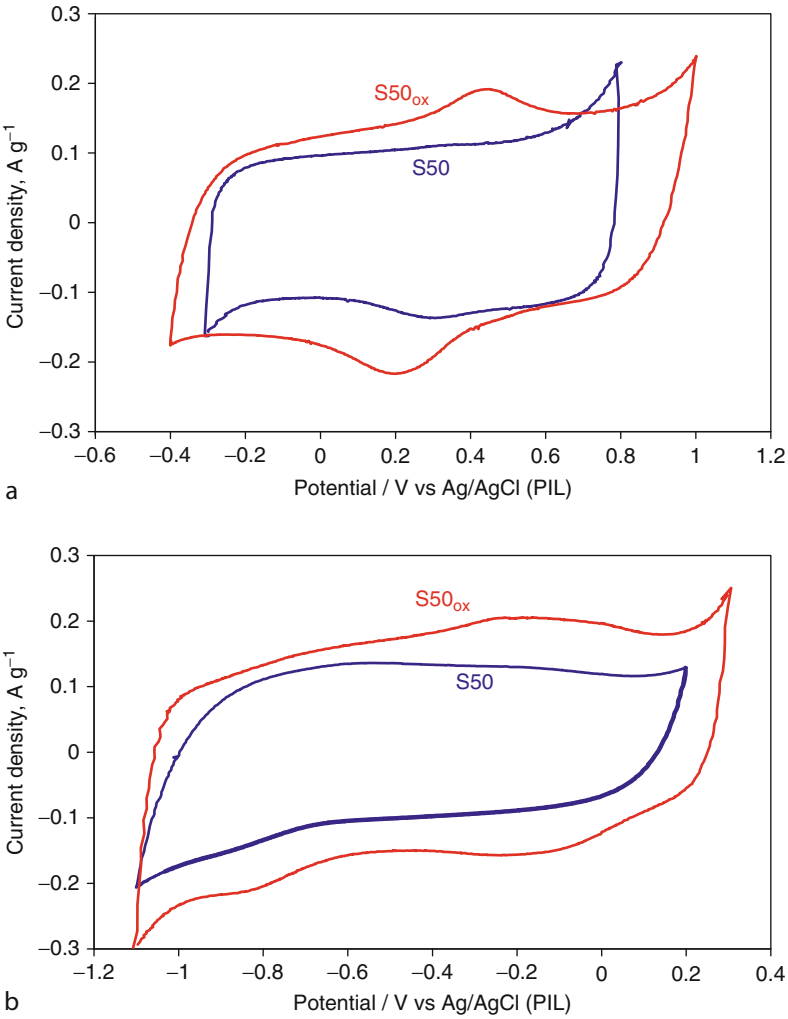

Nanocarbons for Supercapacitors. Figure 20

Three-electrode cyclic voltammograms with activated carbon (S50) or oxidized activated carbon ($S50_{ox}$)-based electrodes in (**a**) pyrrolidinium nitrate and (**b**) pyrrolidinium formate vs the Ag/AgClsat, KClsat (PIL) reference electrode (Adapted from [71])

of oxygenated surface functionalities such as quinone/hydroquinone pairs [14] or pyrone-like structures able to accept two protons and two electrons [26]. For both ILs, the most pronounced redox peaks are observed for $S50_{ox}$ (Fig. 20a, b), that is evidently caused by a stronger pseudo-capacitive effect linked to the higher amount of quinone-type groups and/or pyrone in $S50_{ox}$.

Two-electrode cells based on IL1 and IL2 with the two carbons S50 and $S50_{ox}$ are able to operate up to 1.2 V, which is a substantially higher value than the maximum of 0.7 – 1 V generally observed in aqueous electrolytes [35]. Distinct improvements in capacitance owing to the use of $S50_{ox}$ are noticeable for both ionic liquids; the capacitance increases from 99 to 126 Fg^{-1} in IL1 and from 96 to 130 Fg^{-1} in IL2, when using S50 with $S50_{ox}$, respectively. These values are comparable to those obtained in 1 $mol.L^{-1}$ H_2SO_4 aqueous solution, e.g., 101 Fg^{-1} for S50 and 137 Fg^{-1} for $S50_{ox}$, demonstrating a remarkable pseudo-faradic efficiency of these ionic liquids.

Hence, protic ionic liquids represent a new kind of green electrolyte for developing high-performance capacitors involving both electrical double-layer charging and a pseudo-faradic mechanism. The electrochemical stability and conductivity of protic ILs, the relation between the carbon pore size and the electrolyte ion size, and the design of electrochemical cells are the most important matters for thorough investigations.

Conclusion and Future Directions

Nanocarbons are the most widely used material for supercapacitor electrodes because, among other characteristics, they are cheap, chemically inert, electrically conductive, and their nanoporous texture and surface functionality are highly versatile.

In the case of capacitors in organic electrolyte, it has been demonstrated that the electrical double-layer (EDL) properties are strongly influenced by the pore size. With the tetraethylammonium tetrafluoroborate salt, the largest values of normalized capacitance are observed for pores smaller than 1 nm, with a maximum at around 0.7–0.8 nm, demonstrating that ions are essentially desolvated in the pores. In situ or ex situ techniques, such as small angle neutron scattering or nuclear magnetic resonance, should be applied for better understanding how ions occupy porosity during the charge/discharge of electrodes. Such investigations would help to better defining the optimal porous texture. Beside, taking into account that saturation of porosity can occur with carbons developing essentially subnanometric pores, new processes have to be investigated for developing the surface area of carbons while keeping only such pores. Finally, in light of some literature claims that the EDL properties are not only determined by the porous texture, another research direction should consider the structural parameters of carbons.

In protic media (aqueous electrolytes or protic ionic liquids) a pseudo-faradic mechanism can arise together with the formation of the double layer. In this case, the capacitance and the stability potential window are influenced both by the electrolyte pH and the nature of carbon functionalities. In the future, fundamental studies should be realized on carbons with controlled functionalities, using for example grafting techniques, in order to determine which functionalities are the most effective for pseudo-faradic processes. The demonstration that neutral aqueous electrolytes can offer capacitors with operating voltage values as high as 2 V is an important breakthrough of the recent years. The reasons for the important overpotential of dihydrogen evolution in these media must be elucidated, that could allow developing even higher voltage values. Different neutral electrolytes must also be more systematically screened versus carbons with various functionalities in order to enhance capacitance, electrical conductivity, and the operating temperature range. In this strategy, protic ionic liquids might be a new class of electrolytes opening new insights for optimizing electrochemical capacitors.

In summary, the high versatility of nanocarbons in terms of texture and surface functionality allows to perfectly adapt them to the different mechanisms depending on the electrolyte. Such versatility still offers high potentialities for developing high-performance supercapacitors.

Bibliography

1. Marsh H, Rodríguez-Reinoso F (2006) Activated carbons. Elsevier, London
2. Lillo-Ródenas MA, Juan-Juan J, Cazorla-Amorós D, Linares-Solano A (2004) Carbon 42:1371–1375
3. Raymundo-Piñero E, Azaïs P, Cacciaguerra T, Cazorla-Amorós D, Linares-Solano A, Béguin F (2005) Carbon 43:786–795

4. Jagtoyen M, Derbyshire F (1998) Carbon 36:1085–1097
5. Bandosz TJ, Biggs MJ, Gubbins KE, Hattori Y, Pikunic J, Thomson K (2003) Molecular models of porous carbons. In: Radovic LR (ed) Chemistry and physics of carbon. Marcel Dekker, New York, pp 137–199
6. Pikunic J, Gubbins KE, Pellenq RJM, Cohaut N, Rannou I, Guet JM, Clinard C, Rouzaud JN (2002) Appl Surf Sci 196:98–104
7. Harris PJF, Tsang SC (1997) Philos Mag A76:667–677
8. Harris PJF (1997) Inter Mater Rev 42:206–218
9. Harris PJF (2005) Critical Rev Solid State Mater Sci 30:235–253
10. Radovic LR, Bockrath B (2005) J Am Chem Soc 127:5917–5927
11. Azaïs P, Duclaux L, Florian P, Massiot D, Lillo-Ródenas MA, Linares-Solano A, Peres JP, Jehoulet C, Béguin F (2007) J Power Sourc 171:1046–1053
12. Pels JR, Kapteijn F, Moulijn JA, Zhu Q, Thomas KM (1995) - Carbon 33:1641–1653
13. Kapteijn F, Moulijn JA, Matzner S, Boehm HP (1999) Carbon 37:1143–1150
14. Conway BE (1999) Electrochemical supercapacitors – scientific fundamentals and technological applications. Kluwer/Plenum, New York
15. Kötz R, Carlen M (2000) Electrochima Acta 45:2483–2498
16. Raymundo-Piñero E, Kierzek K, Machnikowski J, Béguin F (2006) Carbon 44:2498–2507
17. Gregg SJ, Sing KSW (1982) Adsorption, surface area and porosity. Academic, London, pp 103–104
18. Kaneko K, Ishii C (1992) Colloid Surf 67:203–212
19. Barbieri O, Hahn M, Herzog A, Kötz R (2005) Carbon 43:1303
20. Chmiola J, Yushin G, Gogotsi Y, Portet C, Simon P, Taberna PL (2006) Science 313:1760–1763
21. Chmiola J, Largeot C, Taberna PL, Simon P, Gogotsi Y (2008) Angew Chem 120:3440–3443
22. Vix-Guterl C, Frackowiak E, Jurewicz K, Friebe M, Parmentier J, Béguin F (2005) Carbon 43:1293–1302
23. Mysyk R, Raymundo-Piñero E, Béguin F (2009) Electrochem Commun 11:554–556
24. Ruch PW, Hahn M, Cericola D, Menzel A, Kötz R, Wokaun A (2010) Carbon 48:1880–1888
25. Frackowiak E, Béguin F (2001) Carbon 39:937
26. Montes-Moran MA, Suarez D, Menendez JA, Fuente E (2004) Carbon 42:1219–1225
27. Andreas HA, Conway BE (2006) Electrochima Acta 51:6510–6520
28. Okajima K, Ohta K, Sudoh M (2005) Electrochima Acta 50:2227–2231
29. Cheng PZ, Teng H (2003) Carbon 41:2057–2063
30. Figueiredo JL, Pereira MFR, Freitas MMA, Orfao JJM (1999) - Carbon 37:1379–1389
31. Bleda-Martínez MJ, Maciá-Agulló JA, Lozano-Castelló D, Morallón E, Cazorla-Amorós D, Linares-Solano A (2005) Carbon 43:2677–2684
32. Raymundo-Piñero E, Leroux F, Béguin F (2006) Adv Mater 18:1877–1882
33. Raymundo-Piñero E, Cadek M, Béguin F (2009) Adv Funct Mater 19:1–8
34. Jurewicz K, Frackowiak E, Béguin F (2004) Appl Phys A 78:981–985
35. Ruiz V, Santamaría R, Granda M, Blanco C (2009) Electrochima Acta 54:4481–4486
36. Raymundo-Piñero E, Cadek M, Wachtler M, Béguin F (2011) ChemSusChem. doi:10.1002/cssc.201000376
37. Stoller MD, Park S, Zhu Y, An J, Ruoff RS (2008) Nano Lett 8:3498–3502
38. Vivekchand SRC, Rout CS, Subrahmanyam KS, Govindaraj A, Rao CNR (2008) J Chem Sci 20:9–13
39. Wang Y, Shi Z, Huang Y, Ma Y, Wang C, Chen M, Chen Y (2009) J Phys Chem C 113:13103–13107
40. Du X, Guo P, Song H, Chen X (2010) Electrochima Acta 55:4812–4819
41. Zhang LL, Zhou R, Zhao XS (2010) J Mater Chem 20:5983–5992
42. Jurewicz K, Babel K, Ziolkowski A, Wachowska H (2003) Electrochima Acta 48:1491–1498
43. Jurewicz K, Pietrzak R, Nowicki P, Wachowska H (2008) Electrochima Acta 53:5469–5475
44. Lota G, Grzyb B, Machnikowska H, Machnikowski J, Frackowiak E (2005) Chem Phys Lett 404:53–58
45. Frackowiak E, Lota G, Machnikowski J, Vix-Guterl C, Béguin F (2006) Electrochima Acta 51:2209–2214
46. Ra EJ, Raymundo-Piñero E, Lee YH, Béguin F (2009) Carbon 47:2984–2992
47. Béguin F, Szostak K, Lota G, Frackowiak E (2005) Adv Mat 17:2380–2384
48. Lota G, Lota K, Frackowiak E (2007) Electrochem Commun 9:1828–1832
49. Ania CO, Khomenko V, Raymundo-Piñero E, Parra JB, Béguin F (2007) Adv Funct Mater 17:1828–1836
50. Hulicova D, Kodama M, Hatori H (2006) Chem Mater 18:2318–2326
51. Hulicova-Jurcakova D, Seredych M, Lu GQ, Bandosz TJ (2009) Adv Funct Mater 19:438–447
52. Hulicova-Jurcakova D, Kodama M, Shiraishi S, Hatori H, Zhu ZH, Lu GQ (2009) Adv Funct Mater 19:1800–1809
53. Naoi K, Suematsu S, Hanada M, Takenouchi HJ (2002) J Electrochem Soc 149:472–476
54. Gao M, Yang F, Wang X, Zhang G, Liu L (2007) J Phys Chem C 111:17268–17274
55. Konno H, Ito T, Ushiro M, Fushimi K, Azumi K (2010) J Power Sourc 195:1739–1746
56. Hulicova-Jurcakova D, Puziy AM, Poddubnaya OI, Suarez-García F, Tascon JMD, Lu GQ (2009) J Am Chem Soc 131:5026–5027
57. Hu CC, Wang CC, Wu FC, Tseng RL (2007) Electrochima Acta 52:2498–2505
58. Subramanian V, Luo C, Stephan AM, Nahm KS, Thomas S, Wei B (2007) J Phys Chem C 111:7527–7531
59. Qu QT, Wang B, Yang LC, Shi Y, Tian S, Wu YP (2008) Electrochem Commun 10:1652–1655
60. Bichat MP, Raymundo-Piñero E, Béguin F (2010) Carbon 48:4351–4361
61. Demarconnay L, Raymundo-Piñero E, Béguin F (2010) Electrochem Commun 12:1275–1278

62. Wang J, Kirgoz UA, Mo JW, Lu J, Kawde AN, Muck A (2001) Electrochem Comm 3:203–208
63. Hong MS, Lee SH, Kim SW (2002) Electrochem Solid State Lett 5:A227–A230
64. Khomenko V, Raymundo-Piñero E, Béguin F (2010) J Power Sourc 195:4234–4241
65. Jurewicz K, Frackowiak E, Béguin F (2001) Electrochem Solid State Lett 4:A27–A29
66. Jurewicz K, Frackowiak E, Béguin F (2002) Fuel Process Technol 77–78:415–421
67. Fang B, Zhou H, Honma I (2006) J Phys Chem B 110:4875–4880
68. Bleda-Martínez MJ, Pérez JM, Linares-Solano A, Morallón E, Cazorla-Amorós D (2008) Carbon 46:1053–1059
69. Béguin F, Friebe M, Jurewicz K, Vix-Guterl C, Dentzer J, Frackowiak E (2006) Carbon 44:2392–2398
70. Demarconnay L, Raymundo-Piñero E, Béguin F (2010) CD Proceedings of the International Carbon Conference, Clemson, USA, 2010
71. Greaves TL, Drummond CJ (2008) Chem Rev 108:206–223
72. Mysyk R, Raymundo-Piñero E, Anouti M, Lemordant D, Béguin F (2010) Electrochem Comm 12:414–417
73. Anouti M, Caillon-Caravanier M, Dridi Y, Galiano H, Lemordant D (2008) J Phys Chem B 112:13335–13343

Nanotoxicology in Green Nanoscience

Leah Wehmas, Robert L. Tanguay
Department of Environmental and Molecular Toxicology, Environmental Health Sciences Center, Oregon State University, Corvallis, OR, USA

Article Outline

Glossary
Definition of the Subject
Introduction
Nanotoxicology's Role in Green Nanoscience
The Embryonic Zebrafish Model
Nanotoxicology and the Zebrafish Model
Future Directions
Bibliography

Glossary

Embryonic development The molecular signaling, cell divisions, cell rearrangements, and cell differentiation that lead to tissues, organs, and structures of an organism.

High throughput A method of stream-lining, often through automation, testing procedures to rapidly conduct thousands of experiments.

Nanotechnology As defined by the National Nanotechnology Initiative, "nanotechnology is the understanding and control of matter at the nanoscale, at dimensions between approximately 1 and 100 nm, where unique phenomena enable novel applications."

Structure activity relationships (SARS) A method of relating how structural and physiochemical properties of a compound influence biological activity.

Tiered approach An approach that optimizes identification of potentially hazardous compounds through testing and systematic interpretation of results [1].

Toxicology testing Testing to examine and understand the adverse effects of physical, biological, or chemical compounds on organisms and the environment with the objective of mitigation or prevention [2].

Definition of the Subject

Nanotechnology holds great promise for future economical and technological advances, yet health and safety concerns regarding nanomaterials persist. As an emerging technology, nanotechnology is in the unique position to proactively address health and safety concerns throughout the product life cycle. Green chemistry aims to create benign compounds in a way that prevents pollution and reduces waste throughout every stage of production. Through green nanoscience, the principles of green chemistry can be applied toward making high performance, yet inherently safe nanomaterials. Successful application of green chemistry principles to assess nanomaterial health and safety requires efficient, predictive, high-throughput nanotoxicity testing. With these approaches, designers and manufacturers of nanomaterials can assess nanotoxicity early in production to redesign or replace hazardous nanomaterials.

Introduction

Nanotechnology is a field of technology, engineering, and science that involves shaping and rearranging matter near the atomic level to make materials, particles,

or structures with at least one dimension on the scale of 1–100 nm [3]. At a size that is approximately one billionth that of a meter, distinctive mechanical, optical, and physiochemical properties emerge [3]. Nanotechnology exploits these novel nanoscale properties for unique applications in electronics, targeted drug delivery, personal care products, textiles, etc. [4–9].

The numerous applications and continued innovation in nanotechnology have contributed to the exponential growth in the industry. Within 5 years nanotechnology is projected to expand from a $3.8 billion industry to a $2.5 trillion industry by 2015 [10] making it a significant contributor to the global economy. This rapid growth indicates that nanotechnology is transitioning from a discovery to production industry [11, 12]. This scale-up in nanomaterial production, while contributing significantly to economic growth and industrial improvement, will also significantly increase the potential for environmental and human exposure to nanomaterials [13]. Therefore, the swift assessment of nano-environmental and human safety (nanoEHS) risks is necessary. While numerous nanomaterial toxicity studies have been conducted, conflicting results make it difficult to adequately assess nanoEHS. The unique properties that make nanomaterials an attractive technology (surface chemistry, surface area, size, shape, core material functionalization, aggregation, etc.) may also contribute to novel biological effects as a result of nanomaterial exposure [12]. Toxicology will play an important role in elucidating the mechanisms of those interactions [14] and will be referred to as nanotoxicology when applied to nanomaterials.

The emergence of nanotechnology occurred in tandem with the introduction of the concepts of green chemistry [15] making it a technology ideally suited for incorporation of the principles of green chemistry (Fig. 1) early in the industry [16]. When nanomaterials are considered for commercialization, collaborative work between the producers of nanomaterials and toxicologists is necessary to prioritize [17] and design comprehensive, efficient, high-throughput nanotoxicity

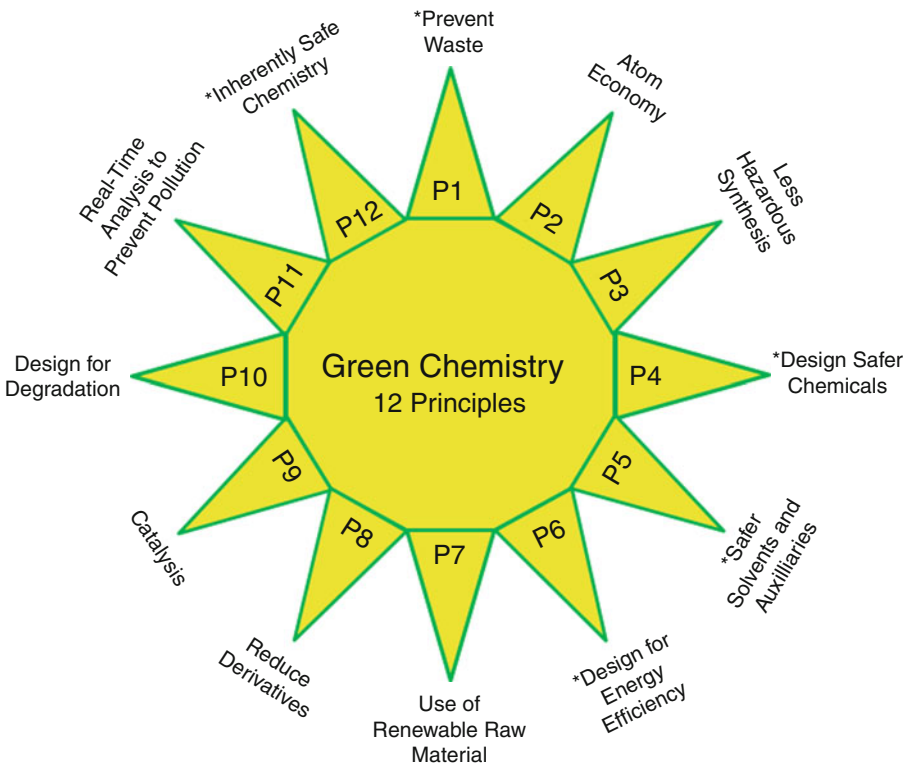

Nanotoxicology in Green Nanoscience. Figure 1
The 12 principles of green chemistry. *Asterisks* designate principles that can be applied to nanotoxicology

tests to address nanoEHS. Faster and predictive nanotoxicity tests will require an in vivo approach at several levels of biological organization including molecular → cellular → tissue → organ → whole organism effects. Toxicity testing implemented early in the nanomaterial design process will allow for refinement or replacement of unsafe nanomaterials earlier in the development pipeline. This will enable the production of inherently safer nanomaterials through the incorporation of the 12 principles of green chemistry [15], a major part of the green nanoscience research approach [16].

This entry will explore the role of toxicology in implementing green nanoscience, the methodology of incorporating nanotoxicology in order to directly and indirectly address the principles of green chemistry in green nanoscience, and the importance of utilizing robust models for nanotoxicity testing.

Nanotoxicology's Role in Green Nanoscience

Application of Green Chemistry

When one thinks of nanotechnology and nanomaterials consumer products such as sunscreens, cosmetics, or antimicrobial socks come to mind, yet there are several innovative nanomaterials that may have environmental remediation applications in oil spill cleanup, water purification, and air filtration [18–20]. As many nanomaterials move closer to commercialization and production levels expand, the potential environmental health applications and economic growth in this field could greatly benefit the society. However, the full benefit and promise of nanotechnology may be greatly impeded, or never realized, until it gains acceptance as safe by the general public and lawmakers. To gain widespread safety acceptance, nanoEHS concerns must be addressed. This will require green nanoscience approaches. Green nanoscience [16] aims to produce inherently safer nanomaterials by combining the 12 principles of green chemistry with nanoscience to provide guidelines to design effective materials with minimized waste and hazard throughout the life cycle [15]. Nanotechnology is a new and evolving industry, and is in the unique position to proactively apply green chemistry principles early in the design and synthesis of nanomaterials.

Material scientists and chemists will not be able to apply all the principles of green chemistry to nanoscience efficiently without collaborations with other scientific disciplines. According to Anastas and Eghbali, there has been a general lack of concern toward addressing principles 4 (P4) of green chemistry which involves designing compounds, such as nanomaterials, in a way to minimize overall hazard [21]. Green nanoscience can avoid the folly of other adopters of green chemistry and alleviate nanoEHS concerns through incorporation of nanotoxicology. The old paradigm of conducting toxicity testing at the end of a development process will be neither sustainable nor suitable to meet the goals of green nanotoxicology. Instead, nanotoxicology must be implemented early and often in green nanomaterial design and synthesis. Nanotoxicology will provide data that can be used in the refinement or replacement of unsafe nanomaterials through direct incorporation of P4 of green chemistry. In addition, it can be used to evaluate the safety of feed stock materials required for the synthesis of nanomaterials such as solvents or other synthesis by-products (P5). This will aid green nanoscience in designing benign nanomaterials (P12). Using nanotoxicology to address P4, P5, and P12 in green nanoscience may be fairly obvious (Fig. 1). What may not be so obvious is how nanotoxicology can be applied to P1 and P6 (Fig. 1) depending on the testing platform and models used which will be covered later in this entry.

Toxicology Models

Traditionally, mammalian toxicity tests are favored and thought to be the most predictive for assessing the human health and safety of compounds. Mammalian models share a high degree of genetic similarity with humans making resulting toxicity data easier to extrapolate to humans [14], thereby addressing P4 of green chemistry. However, concerns about animal welfare have generated a need to restrict mammalian use to only essential testing and to find alternative testing approaches [22]. Maintaining, housing, and testing mammals require significant infrastructure, materials, and time. Cumulatively, these requirements make these tests low throughput, expensive, and impractical for the broad-based nanoEHS research needs. Additionally,

a large amount of test compound is necessary for mammalian toxicity assays making testing nanomaterials particularly challenging as they are often synthesized in small batches during the discovery phase [11]. Larger synthetic needs also create more waste which conflicts with green chemistry P1. Therefore, in vitro assays have become a popular alternative to whole animal tests as infrastructure requirements and maintenance needs are greatly reduced. These assays are also high-throughput and utilize far less test material. While in vitro tests can provide valuable data on a specific pathway or processes, the hazard and risk predictability of these assays for whole animals is quite limited. In vitro assays are inherently less complex as they most often consist of single cell types in cultured dishes. In addition, specific cell types express unique gene products. Since the critical gene products that play roles in nanotoxicological responses are not known in advance, it is a challenge to select the most appropriate in vitro system for nanoEHS research. To increase the sensitivity of in vitro toxicity screens, multiple in vitro assays are assembled to account for routes of exposure, organ effects, chemical deposition, etc. [23]. This reduces the economy of the in vitro approach to toxicity testing as it becomes necessary to conceptually rebuild an organism through numerous assays to obtain the required complexity for predictive results. These caveats will make it challenging to obtain reliable nanoEHS results in the near future. As eluded to in the introduction, the challenges of green nanoscience in conducting nanotoxicity testing for rapid, comprehensive assessment of nanoEHS necessitates the use of a robust and predictive in vivo model that can be adapted to high-throughput screening. Here the embryonic zebrafish (*Danio rerio*) is proposed as the ideal model for nanotoxicity tests.

The Embryonic Zebrafish Model

Background

There are several basic attributes of the embryonic zebrafish model that make it ideal for nanotoxicology and green nanoscience. The husbandry requirements of the zebrafish are minimal. As a small vertebrate model with high fecundity (200–300 eggs per day), short intervals between female spawns (2–3 days), and quick maturation, many zebrafish can be housed in a small area reducing infrastructure costs [24]. Thousands of eggs can be produced daily for experimentation. Aside from ease of care and maintenance, additional benefits of the zebrafish model include transparent eggs and external embryogenesis which facilitates examination of early developmental processes in real time [24].

The transparency of embryos during development make the zebrafish model exceptionally well suited to high-throughput testing platforms which will be necessary to alleviate backlog in demand for quick nanotoxicity evaluations. During early development complex molecular signaling events and organogenesis make the embryo highly susceptible to environmental perturbations [14]. Exposure to nanomaterials at this critical life stage can disrupt organ function, cellular pathfinding, and/or tissue morphology which can be easily tracked in the transparent zebrafish embryos throughout the duration of a 5-day exposure, noninvasively [25].

Molecular Applications What began as a vertebrate model of developmental genetics is now extensively used a model for infectious diseases and immune system function [26–28], to understand hematopoiesis and related diseases [28, 29], for aging [30, 31], oncology [32–34], cardiovascular development [35, 36], kidney development and disease [37–39], for identifying the etiology of diseases of the eye [40, 41] and ear [42, 43], for understanding mechanisms of drug abuse [44–46], and for regenerative medicine [47–49]. Importantly, the zebrafish genome has been sequenced [50] and this information along with the conserved anatomy and physiology between fish and humans is being exploited by the biomedical research community (reviewed in [51–55]). Clearly, there are exciting possibilities to using zebrafish as a model for mechanistic-based nanotoxicity studies.

With the remarkable conservation between the zebrafish and human genome, it is anticipated that nearly all the toxicologically relevant pathways also function in zebrafish. The most well-studied toxicologically relevant pathway in zebrafish is the aryl hydrocarbon receptor (AHR) signal transduction pathway. Over the past few years, the zebrafish AHR pathway has been identified and completely characterized (reviewed in [56–58]). This has served as proof of concept and

demonstrates that toxicology pathways can be efficiently examined in zebrafish.

A first step in elucidating the role of a gene in a biological process or in mediating responses to external stimuli (i.e., toxic responses) is to manipulate the expression level of the gene product. Producing knockout mice using embryonic stem cells has revolutionized biomedical research [59] and has been useful for toxicological studies in rodents [60–62]. Despite extensive efforts, embryonic stem cells for the zebrafish have yet to be developed [63], but a number of approaches have been effectively used to define the role of individual genes in zebrafish. The most common approach is the use of morpholinos which are chemically modified oligonucleotides that are resistant to chemical and enzymatic degradation yet maintain base pairing properties [64]. Morpholinos have been shown to bind to and block translation of mRNA in embryonic zebrafish [65–67]. Morpholinos can also be designed to bind to complement sequences at intron-exon splice junctions to inhibit proper mRNA processing. This approach is especially effective in zebrafish embryos [68–71]. Splice blocking morpholinos are useful to target genes that have alternative translation start sites, and to generate mispliced transcripts that result in dominant-negative proteins [68]. The successful application of morpholinos in zebrafish is evident by the large number of published studies using this approach (http://www.gene-tools.com/Publications).

With the availability of the entire zebrafish genome, conceivably any zebrafish gene can be targeted individually, or in combinations, using morpholinos and other antisense techniques. Thus, the function of mammalian orthologs can be rapidly evaluated in zebrafish. There are, however, limitations to these approaches. The gene repression effects are transient, which are most suitable for evaluating gene functions during development, (up to approximately 3–5 days post fertilization). Efforts to effectively deliver morpholinos to zebrafish at older life stages or to specific cellular targets are not routine. To overcome this limitation, heritable knockout approaches have been developed.

Despite the lack of a technology for gene knockout by homologous recombination, researchers have generated a large number of mutant fish lines. The majority of these were created using the chemical mutagen, ethylnitrosourea (ENU), followed by phenotypic screening for developmental defects [72, 73]. Such screens facilitate the identification of genes essential for biological processes with no prior functional knowledge of the genes. To date, large-scale zebrafish mutant searches have led to the identification of thousands of mutants with unique embryonic and larval development defects [74, 75]. Toxicologists can use available mutants that phenocopy the effects of toxicant exposure to help identify molecular targets. Furthermore, since genome-wide genetic screens are routine in zebrafish, there is a significant untapped potential to use forward genetics to identify modifiers of susceptibility to xenobiotic insult. Since chemical mutagenesis is non-biased, there is a high probability that novel targets can be identified in zebrafish. For instance, a genetic screen for increased susceptibility to nanomaterial exposure could be used to identify suppressor pathways. Screening for resistance to chemical exposure has the potential to identify genes that modulate the toxic response. With the power of comparative genomics, the identification of novel genes can be rapidly evaluated using integrated approaches in mammals. An advantage of ENU-mediated mutagenesis is that small mutations are created; however, the identification of the mutated gene remains a challenge. The once tedious and expensive approach of positional cloning has successfully been used to identify hundreds of the mutated genes [76, 77], and has evolved into a more efficient "targeted" methodology. For example, the Targeting Induced Local Lesions in Genomes (TILLING) method can now be used in zebrafish to identify and/or select for loss-of-function alleles (knockouts) [78]. TILLING is conceptually simple; random mutations are created using traditional chemical mutagenesis followed by high-throughput PCR-based screening to identify point mutations in the gene of interest. Therefore, TILLING is a targeted approach and, in theory, every zebrafish gene can now be knocked out. Insertional mutagenesis is an alternative approach to generate zebrafish mutants and has the benefit that the interrupted gene can be immediately identified [79–81]. An emerging method utilizing zinc finger nucleases (ZFNs) holds promise in bypassing the inability to generate knockout zebrafish by homologous recombination. Zinc finger nucleases are engineered to bind and cleave specific sections of DNA. Application of ZFNs has been successful in

generating targeted germline mutations in the zebrafish [82].

Numerous techniques have been developed to introduce foreign DNA into zebrafish including microinjection [83], retroviral infection [79, 80], biolistic delivery [84], and electroporation [85]. The applications for transgenic zebrafish to unravel mechanisms of toxicity appear limitless. Conditional promoters such as the hsp70 [86] and tetracycline responsive [87] can be used to control transgene expression. Functional analysis in zebrafish can also be achieved using ectopic expression vectors under the control of tissue-specific promoters reviewed in Refs. [88, 89]. The number of transgenic zebrafish lines is rapidly growing with numerous lines useful for toxicological research. For example, transgenic fish that express fluorescent reporter genes in response to stimuli have been used to evaluate estrogenic chemical exposure [90], to visualize calcium signaling in vivo [91, 92], to respond to AHR ligands [93], etc. In addition to assessing the transcriptional responses to xenobiotics, fluorescent transgenes have proven valuable to monitor the dynamic movements of cells. Since embryonic zebrafish are transparent, toxicity targets can be non-invasively monitored, in real time. Examples include the use of transgenic lines with neuronal-specific expression of GFP [94] to assess the impact of nicotine on motor neuron development [45], the use of sonic hedgehog responsive fish to evaluate the impact of TCDD on CNS development [95], and the use of heat shock responsive fish to localize the targets of cadmium toxicity [96]. Finally, transgenic zebrafish lines have been developed to detect mutations in vivo [97].

An emerging area is the use of zebrafish as a model to elucidate the impact of xenobiotics on CNS development and function. Zebrafish possess all typical senses including vision, olfaction, taste, touch, balance, and hearing; and their sensory pathways share an overall homology with humans [98]. Cognitive behavioral tests suggest that anatomic substrates of cognitive behavior are also conserved between fish and other vertebrates. Thus, similar to observations of hippocampal lesions in mammals, lesions of the structural homolog of the hippocampus in fish selectively impair spatial memory [99]. Zebrafish behavior is altered by exposure to ethanol [46, 100, 101], nicotine [45], cocaine [44], antipsychotics [102], pesticides [103, 104], and metals such as mercury [105]. Recent studies indicate that broad-based chemical genetic screens can be used to identify novel, clinically relevant neuroactive compounds [106]. These initial behavioral studies suggest that the zebrafish model may be ideal to investigate the long-term consequences on CNS function following transient exposures to xenobiotics.

Similar to other toxicological models, "omic" based approaches are now routine using zebrafish. With the availability of the genome sequence, custom and commercial cDNA and oligonucleotide microarrays are currently available. These microarrays have been effectively used to define developmental stage and tissue-specific transcriptomes [107–112] and to identify gene expression changes in response to xenobiotic exposure. Microarray technology has been successfully applied to toxicology. For instance, the gene expression changes in response to TCDD [49, 58, 113], hypoxia [114], 4-nonylphenol [115], and chlorpromazine [110] have been reported. Further understanding of genome-wide changes in transcript levels will be possible through application of RNA sequencing technology [116] to examine how the entire zebrafish transcriptome changes with exposure to toxicants. The amenability of the zebrafish to all the molecular biology techniques recently described will be very important in determining the mechanisms by which nanomaterials can cause adverse reactions in humans and other organisms.

High-Throughput Platform The extensive growth in the field of nanotechnology has created a pipeline problem for efficient nanoEHS assessment. High-throughput nanotoxicity testing approaches can alleviate this problem. The embryonic zebrafish model is already a moderate-throughput platform, but readily amenable to high-throughput nanotoxicity testing with the incorporation of robotics and automation.

Zebrafish embryos develop in a chorion, which is an acellular envelope that acts as a protective barrier. Normally, when reared at 28°C, zebrafish hatch at between 48 and 72 hour post fertilization (hpf). To increase the sensitivity of the embryonic assay, it is critical to initiate exposures as early as possible. The earliest feasible stage to remove the chorions from the zebrafish embryos is at 6 hpf via enzymatic digestion. The methods for removing the chorion from large

groups of embryos have been optimized, eliminating a potential barrier to uptake from the surrounding water [25].

A potential bottleneck to high-throughput embryonic zebrafish assays is the placement of dechorionated zebrafish embryos into 96- or 384-well assay plates. For toxicity exposures, it is necessary to sort embryos by identifying and selecting healthy eggs at similar developmental stage. This is a delicate process because the embryos can easily rupture. Incorporation of precision robotic plate loaders with visual systems to sort embryos could greatly increase the productivity of the embryonic zebrafish assay. The development of such a system has recently been achieved [117]. Microinjection of embryos is a molecular technique that introduces exogenous chemicals, nanomaterials, DNA, RNA, protein, or synthetic oligonucleotides into zebrafish embryos. These techniques are powerful investigative tools that are time intensive. Precision robotics with computer vision and control could hasten this arduous task and increase injection success rates [118].

Perhaps the greatest hurdle in developing high-throughput embryonic zebrafish nanotoxicity tests involves screening for sometimes subtle phenotypic changes. Zebrafish embryos can display a wide range of malformations that must be evaluated by laboratory personnel [25]. Experienced toxicologists may require up to 30 min per plate depending on the number of endpoints investigated. Introduction of automated, image-based screening methods would greatly enhance throughput. After devising automated plate preparation and embryo handling, the next step to developing a high-throughput assay is to set up imaging systems that can automatically focus and capture images [119]. There must be sufficient data storage capabilities to save thousands of high content images. In addition, software algorithms are necessary to process the image data [119], and the software must be capable of efficiently evaluating phenotypic changes. Commercial software analyzing in vitro cell cultures is currently available [119]; however, the embryonic zebrafish presents an additional challenge of orientation of the embryo which can influence image content. Finally, data mining and statistical analyses tools are needed to distinguish and report significant results which can then be confirmed and investigated further if necessary [119]. This will require a high amount of computing power. At this point in automation, researchers must pay special attention to the quality of the data analysis such as minimizing the generation of false positives and negatives [120]. Addressing the steps necessary to high-throughput assay development will enhance the efficiency of the zebrafish assay while resulting in more objective data. This will help address the nanoEHS concerns [119]. Currently, there are laboratories that are independently developing such automated systems.

The Zebrafish as a Green Model

Since the development of the 12 principles of green chemistry in the early 1990s [15], the movement toward adopting these principles in research has increased [21]. Many of the aforementioned benefits of the embryonic zebrafish model make it ideal for use in green toxicology and nanotoxicology. This section will discuss how the zebrafish model applies to the principles of green chemistry.

While the principles of green chemistry generally refer to synthesis and design of chemical compounds, they can be adapted to non-chemistry applications. Of the 12 principles of green chemistry (Fig. 1), use of the zebrafish model can help green nanoscience address P1 and P6. Principle 1 of green chemistry pertains to reduction in waste (Fig. 1) and use of the zebrafish as an in vivo, vertebrate model reduces the space, use of materials and equipment, and generation of waste required for maintaining mammals. For example, in our laboratory a standard nanotoxicity assay involves performing a concentration-response exposure in three 96-well plates with 100 μL of solution per well. Each plate contains an n = 16 per treatment and controls that contain no test material. The chemical treatments include a fivefold dilution series; therefore, an exposure with three plates of five treatments uses low milligram quantities of exposure material reducing waste generation (P1). While the zebrafish cannot completely replace the use of mammalian testing, it can be used as a high-throughput screen to prioritize nanomaterials for mammalian tests which will reduce their use.

With the great demand for toxicity testing on many new and existing compounds, mammalian testing cannot keep pace. Therefore, introduction of the zebrafish

assay can increase the energy efficiency of toxicity testing in accord with P6 of green chemistry (Fig. 1). Maintaining and conducting toxicity tests on mammals requires much more energy input than zebrafish toxicity testing. Even with in vitro systems, energy is required in maintaining the cells and conducting the tests. If numerous in vitro tests are required to obtain human-relevant toxicity data, then the energy efficiency of zebrafish testing is superior.

In one assay, the zebrafish model effectively combines the predictability of mammalian toxicity tests with the speed and economy of in vitro assays. Zebrafish embryonic assays are increasingly becoming high-throughput through automation and development. As the molecular signaling cascades, physiology, and anatomy are well conserved between humans and zebrafish, nanotoxicity testing in zebrafish should be highly relevant. To date, many phenotypic endpoints of toxicity in zebrafish can be applied to understanding conditions in humans. For instance, the induction of bradycardia in zebrafish embryos has been applied to identify pre-clinical drugs with risks for heart arrhythmias in humans [121]. Berghmans et al. demonstrated a correlation between the effects of pharmacologically active compounds in humans or mammals with the effects in embryonic zebrafish through cardiac, intestinal, and visual assays [122]. These results support the zebrafish model's predictive capabilities and utility to help green nanoscience achieve the aim of designing inherently safer nanomaterials (P12).

Nanotoxicology and the Zebrafish Model

The zebrafish model has been used to design a high-throughput, three-tiered testing approach that evaluates adverse effects at several levels of organization (Fig. 2). While this tiered testing scheme evaluates the safety of nanomaterials, the major objective of this assay is to understand the physiochemical properties of nanomaterials that result in toxicity. A critical first step is the availability of well-characterized nanomaterials, where the size, number of atoms, agglomeration state, shape, surface chemistry, charge, and purity are precisely known [11, 123]. Tier one involves a waterborne exposure of dechorionated zebrafish embryos to the well-characterized nanomaterials to evaluate effects at the whole organism level. The exposure is continuous for 5 days beginning at 6 hpf and finishing at 120 hpf. During the assay, zebrafish embryos are screened for phenotypic effects at two time points (24 and 120 hpf) which manifest as mortality or phenotypic changes including increased spontaneous movement, developmental delays, or notochord malformations at 24 hpf. At 120 hpf, viable larval fish are screened for pericardial edema; yolk sac

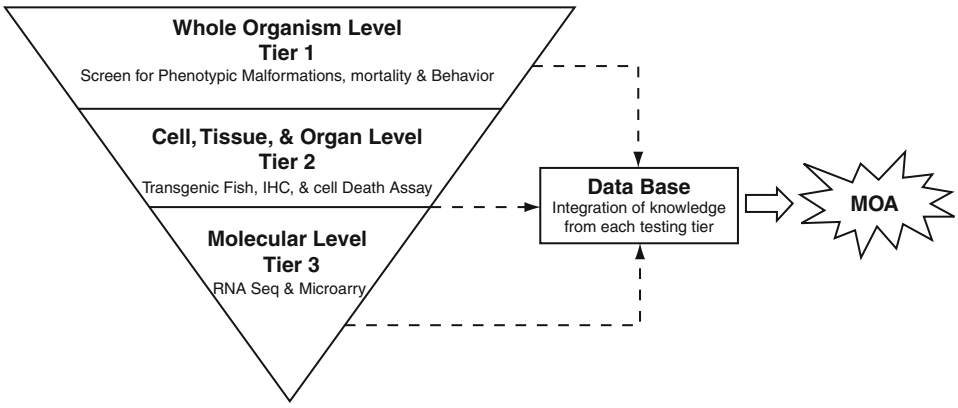

Nanotoxicology in Green Nanoscience. Figure 2
Diagram outlining the tiers of nanotoxicity testing (1–3) and the types the laboratory techniques used to understand effects at the different levels of organization. Data from all three tiers are integrated to determine the mode of action (MOA) of a nanomaterial

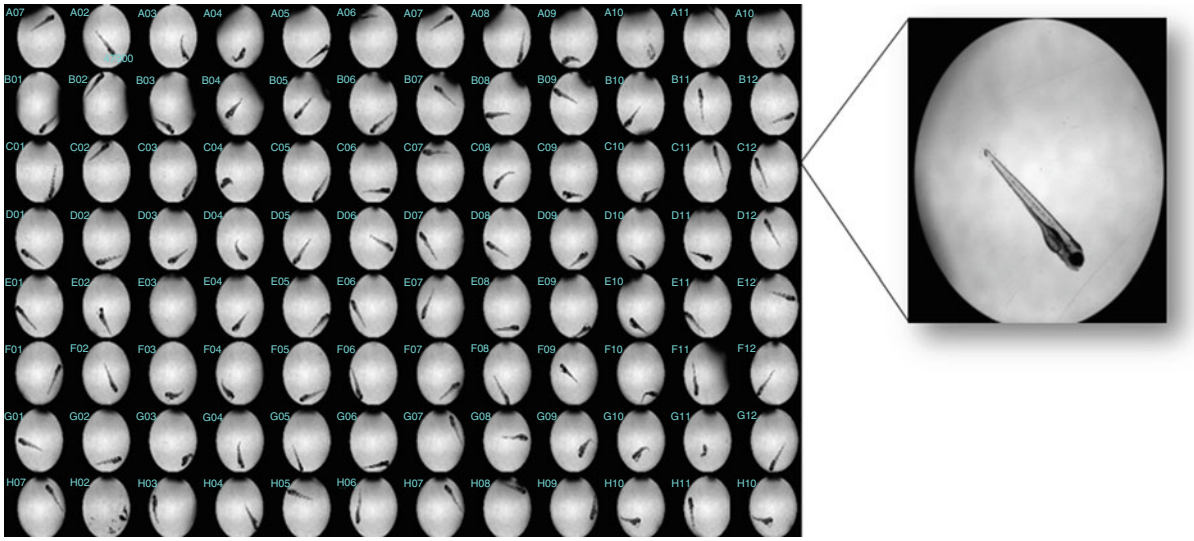

Nanotoxicology in Green Nanoscience. Figure 3
Image of a 96-well plate which is used in the three tiers of zebrafish nanotoxicity assay. The plate contains zebrafish larva (120 hpf) after 5 days of exposure. *Right image* shows an enlargement of a single zebrafish in an exposure well

edema; or eye, nose, snout, jaw, axis, fin, brain, otic, notochord, or circulatory malformations using multi-well microscope imaging (Fig. 3). To evaluate impacts on the CNS development and behavior, two assays have been developed for screening at 120 hpf. The effects on motility and tactile response are evaluated by determining if fish display normal predator avoidance behavior by swimming away from a light touch to the head or tail. The second behavioral assay exploits the well-studied phenomenon of increased larval zebrafish motor activity in the dark [124]. The locomotor activity of nanomaterial exposed zebrafish larvae is recorded using Videotrack V3 software (Viewpoint Life Sciences, Inc., France) for 10 min in the dark following a 10 min rest period in the light. The results reveal whether nanomaterial exposure impacts this complex light-induced behavior.

To understand zebrafish nanomaterial absorption, it is necessary to experimentally measure nanomaterial uptake so that the relationship between in vivo nanoparticle dosimetry and response can be modeled. Determination of the internal dose of nanoparticles in embryonic zebrafish requires the use of Instrumental Neutron Activation Analysis (INAA) or Inductively Coupled Plasma-Optical Emission Spectrometry/Mass Spectrometry (ICP-OES/ICP-MS respectively). Nanomaterials that elicit phenotypic or behavioral responses in the zebrafish advance to tier two of testing to elucidate effects occurring at the cellular, tissue, or organ level. Use of transgenic zebrafish with fluorescent reporters and/or immunohistochemistry can help pinpoint the transport and deposition of a nanomaterial by tracking where adverse effects occur. Examples of two transgenic lines are illustrated in Figs. 4 and 5. Figure 4 illustrates a live 4-day-old zebrafish under non-excitatory light (top panel), and the same live fish images under excitatory light (bottom panel). The green fluorescent protein specifically labels the secondary motor neurons in these fish. Figure 5 illustrates a high magnification view of the spinal cord of a live zebrafish illustrating the detailed structures of the spinal neurons as they innervate into the adjacent muscle. These and other transgenic fish lines are useful tools when nanomaterial exposures are suspected to disrupt either the development or migration of spinal neurons. Another in vivo tier-2 assay is to determine if nanomaterial exposure results in increased cell death (Fig. 6). In this example, exposure to fullerenes leads to an increase in cellular death throughout the live zebrafish embryo [125].

Tier three testing focuses on the molecular effects of nanomaterial exposure. RNA seq or microarrays can be

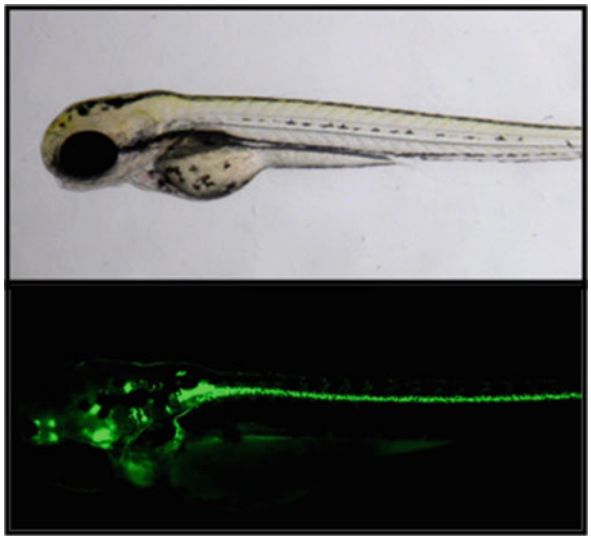

Nanotoxicology in Green Nanoscience. Figure 4
Live 96-hour-old transgenic zebrafish (islet 1-gfp) that expresses the green fluorescent protein expressed specifically in spinal secondary motor neurons (*bottom image*). *Top image* is the transgenic zebrafish imaged under non-excitatory light

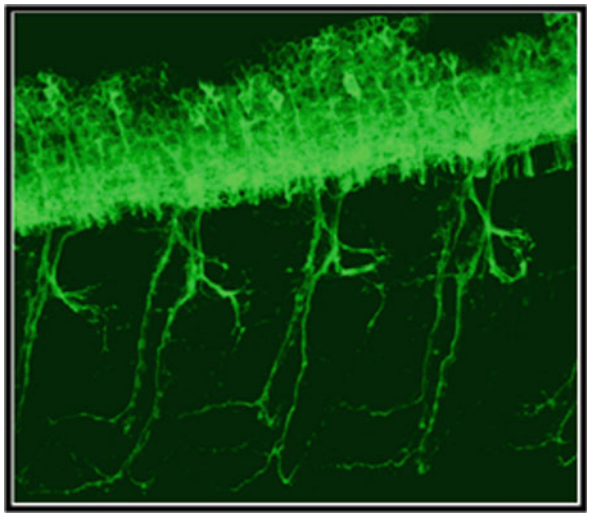

Nanotoxicology in Green Nanoscience. Figure 5
High-resolution confocal image of live transgenic zebrafish (nbt-gfp) expressing the green fluorescent protein in primary motor neurons

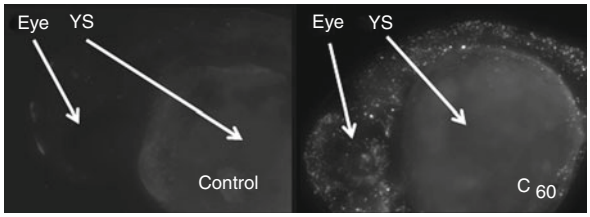

Nanotoxicology in Green Nanoscience. Figure 6
Representative example of live 24-hour-old zebrafish embryos stained with acridine orange (AO). AO stains cells undergoing cellular death assay. AO binds to nucleic acids and fluoresces orange when cells enter lysosomes for degradation. Greater fluorescence in the nanoparticle (carbon 60 fullerene-C_{60}) exposed embryo indicates enhanced cellular death compared to the control.
YS yolk sac

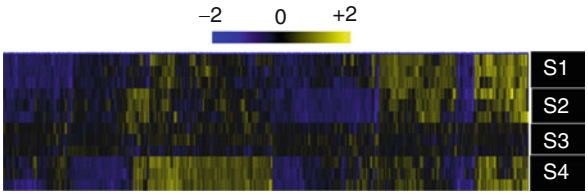

Nanotoxicology in Green Nanoscience. Figure 7
Representative microarray heat map displaying changes in gene expression following exposure to four different chemicals. The *rows* across the heat map (labeled *S1*, *S2*, *S3*, and *S4*) represent three different samples (in triplicate), while each *column* indicates a different gene. *Blue* signifies a decrease in gene expression, *black* signifies no changes, and *yellow* signifies an increase in gene expression

used to evaluate changes in gene expression profiles. Figure 7 illustrates the power and complexity of this approach. Following exposure to four different chemicals, the impact of the exposures on all genes in the genome was assessed, and provided distinct changes in gene expression. Known gene relationships (ontology) can be used to find particular pathways that may be impacted by nanomaterial exposure. The information from tiers two and three also enter the database. Data across all three tiers of nanotoxicity testing are integrated to define the mode of nanomaterial toxicity.

Future Directions

Regardless of the many marketable nanomaterials and nanomaterial-based products poised for industrial production, few have actually been commercialized. A partial explanation for this lag can be assigned to difficulty in scaling up the nanosynthesis process from bench level to production level and still maintaining the quality, purity, and efficiency of the small batches [12]. However, a lack of nanoEHS data for confident assessment of the risks posed by exposure to nanomaterials remains a significant problem. The most critical need is to identify the design rules that define specific physiochemical properties of nanomaterials that predict biologic effects (biotic-nano models based on structure activity relationships) [126].

A major bottleneck to ultra high-throughput screening in the zebrafish assay will be caused by time constraints in data processing resulting from the large volume of data generated from high content imaging and large sample sizes. To avoid increases in total handling time of the screening process, increased computing power and reduction in the time required for data analyses and interpretation of the results are necessary [120]. Improvements in data analyses and interpretation will necessitate improvements and innovations in computer software. Improvements in computer software and whole organism-based imaging technology will also be necessary in augmenting the sensitivity of the zebrafish assay. For example, improvements in and increased dissemination of Cognition Network Technology (CNT) image analysis, a method that attempts to imitate human thought processes, over pixel-based image analysis methods could potentially allow for capturing subtle phenotypes that cannot be seen by the human eye irrespective of the orientation of the embryo [19]. Another method of increasing the sensitivity of the zebrafish assay may be through the addition of a high-throughput adaptation of micro-CT imaging. Micro-CT imaging, which is already used in mammalian research, is able to capture three-dimensional images of an organism noninvasively [127]. This technology could be used to capture slight but perhaps significant morphological responses that are presently not practical to assess on large numbers of animals.

Analysis of the changes in gene expression that occur with toxicant exposure has become a powerful tool in toxicology for determining toxicity mechanisms. With the development of RNA-Seq and organism-wide changes in gene transcripts will allow faster identification of molecular targets of compounds [116]. RNA-Seq also generates large amounts of data which must be processed and analyzed. Future work must be directed at determining the best way to analyze RNA-Seq data and in automating the processing and analysis procedures. This will assist in timely gene expression analysis of effects resulting from nanomaterial exposure in the zebrafish assay.

Adoption of high-throughput embryonic zebrafish assay will alleviate the backlog of nanotoxicity tests necessary for nanomaterial risk assessment, which will not be feasible to evaluate the toxicity of all nanomaterials [128]. Therefore, it is imperative that nanotoxicity screens be conducted in a way to accurately link the physiochemical properties of nanomaterials to toxicological endpoints, effectively creating structure activity relationships (SARS) [126]. By developing nano-SARS, the toxicity of new nanomaterials becomes increasingly predictive of human safety. It is realistic to say that extensive development of nano-SARS will occur over the next decade. There are collaborative efforts ongoing for establishing the foundation for such models [126]. For example, a few nanotoxicity studies have demonstrated that surface chemistry [129, 130] and size [129, 131, 132] may be the most important predictors of nanomaterial activity.

A framework must be also created to organize and curate the data for nano-SARS. To be successful, the framework must include three key guidelines. First, the nanomaterials tested in the toxicity assays must be well characterized [11, 123]. Accurate characterization of nanomaterials remains a major immediate objective in green nanoscience. Second, libraries of well-characterized nanomaterials with systematic variations in structural or physiochemical properties must be assembled. By screening these libraries in the embryonic zebrafish assay and focusing on one property at a time, one can begin to elucidate how nanomaterial core size, core composition, and functionalization influence biological activity [128]. Third, the data gathered from these tests must be assembled into an open database where others can access the information. The success of this framework requires close collaborative

efforts between toxicologists, nanomaterial scientists, regulatory agencies, and industry. With the use of efficient vertebrate toxicological models like zebrafish and the development of accurate SARS, benign by design nanomaterials will be closer to realization.

Bibliography

1. Hushon J, Clerman R, Wagner B (1979) Tiered testing for chemical hazard assessment. Environ Sci Technol 13:1202–1207
2. Society of Toxicology (2005) How do you define toxicology? Soc Toxicol Commun. http://www.toxicology.org/ai/pub/si05/SI05_Define.asp
3. NSET/NEHI (2011) NNI environmental, health, and safety research strategy fact sheet. http://nano.gov/sites/default/files/pub_resource/2011_ehs_strategy_fact_sheet_locked.pdf
4. Forrest DR (2001) Molecular nanotechnology. IEEE Instrum Meas Mag 4(3):11–20
5. Lecoanet H, Wiesner MR (2004) Assessment of the mobility of nanomaterials in groundwater acouifers. Abs Pap Am Chem Soc 227:U1275–U1275
6. Lecoanet HF, Bottero JY, Wiesner MR (2004) Laboratory assessment of the mobility of nanomaterials in porous media. Environ Sci Technol 38:5164–5169
7. Lecoanet HF, Wiesner MR (2004) Velocity effects on fullerene and oxide nanoparticle deposition in porous media. Environ Sci Technol 38:4377–4382
8. Okamoto Y (2001) Ab initio investigation of hydrogenation of C-60. J Phys Chem A 105:7634–7637
9. Sun O, Wang Q, Jena P, Kawazoe Y (2005) Clustering of Ti on a C-60 surface and its effect on hydrogen storage. J Am Chem Soc 127:14582–14583
10. Lux Research (2009) The recession's ripple effect on nanotech. Lux Research Inc., New York
11. Dahl J, Maddux BLS, Hutchison JE (2007) Green nanosynthesis. Chem Rev 107:2228–2269
12. Hutchison JE (2008) Greener nanoscience: a proactive approach to advancing applications and reducing implications of nanotechnology. ACS Nano 2:395–402
13. Thomas K, Sayre P (2005) Research strategies for safety evaluation of nanomaterials, Part I: evaluating the human health implications of exposure to nanoscale materials. Toxicol Sci 87:316–321
14. NRC (2000) Scientific Frontiers in developmental toxicology and risk assessment. National Academy Press, Washington, DC, pp 1–327
15. Anastas PT, Warner JC (1998) Green chemistry: theory and practice. Oxford University Press, Oxford/New York, xi, 135 p
16. McKenzie LC, Hutchinson J (2004) Green nanoscience: an integrated approach to greener products, processes and applications. Chem Today 22:30–33
17. Abbott BD, Perdew GH, Buckalew AR, Birnbaum LS (1994) Interactive regulation of Ah and glucocorticoid receptors in the synergistic induction of cleft palate by 2,3,7,8-tetrachlorodibenzo-*p*-dioxin and hydrocortisone. Toxicol Appl Pharmacol 128:138–150
18. Podgórski A, Balazy A, Gradon L (2006) Application of nanofibers to improve the filtration efficiency of the most penetrating aerosol particles in fibrous filters. Chem Eng Sci 61:6804–6815
19. Savage N, Diallo MS (2005) Nanomaterials and water purification: opportunities and challenges. J Nanoparticle Res 7:331–342
20. Yuan J, Liu X, Akbulut O, Hu J, Suib SL et al (2008) Superwetting nanowire membranes for selective absorption. Nat Nano 3:332–336
21. Anastas P, Eghbali N (2010) Green chemistry: principles and practice. Chem Soc Rev 39:301–312
22. Lein P, Silbergeld E, Locke P, Goldberg AM (2005) In vitro and other alternative approaches to developmental neurotoxicity testing (DNT). Environ Toxicol Pharmacol 19:735–744
23. Oberdorster G, Maynard A, Donaldson K, Castranova V, Fitzpatrick J et al (2005) Principles for characterizing the potential human health effects from exposure to nanomaterials: elements of a screening strategy. Part Fibre Toxicol 2:8
24. Detrich HW, Westerfield M, Zon LI (eds) (1999) The zebrafish biology. Academic, San Diego, 391 p
25. Truong L, Harper SL, Tanguay RL (2011) Evaluation of embryotoxicity using the zebrafish model. Methods Mol Biol 691:271–279
26. van der Sar AM, Appelmelk BJ, Vandenbroucke-Grauls CM, Bitter W (2004) A star with stripes: zebrafish as an infection model. Trends Microbiol 12:451–457
27. Trede NS, Langenau DM, Traver D, Look AT, Zon LI (2004) The use of zebrafish to understand immunity. Immunity 20:367–379
28. Traver D, Herbomel P, Patton EE, Murphey RD, Yoder JA et al (2003) The zebrafish as a model organism to study development of the immune system. Adv Immunol 81:253–330
29. de Jong JL, Zon LI (2005) Use of the zebrafish to study primitive and definitive hematopoiesis. Annu Rev Genet 39:481–501
30. Gerhard GS (2003) Comparative aspects of zebrafish (*Danio rerio*) as a model for aging research. Exp Gerontol 38:1333–1341
31. Keller ET, Murtha JM (2004) The use of mature zebrafish (*Danio rerio*) as a model for human aging and disease. Comp Biochem Physiol C Toxicol Pharmacol 138:335–341
32. Spitsbergen J, Kent M (2003) The state of the art of the zebrafish model for toxicology and toxicologic pathology research – advantages and current limitations. Toxicol Pathol 31:62–87
33. Amatruda JF, Shepard JL, Stern HM, Zon LI (2002) Zebrafish as a cancer model system. Cancer Cell 1:229–231
34. Moore JL, Gestl EE, Cheng KC (2004) Mosaic eyes, genomic instability mutants, and cancer susceptibility. Methods Cell Biol 76:555–568

35. Chen JN, Fishman MC (2000) Genetic dissection of heart development. Ernst Schering Res Found Workshop 29:107–122
36. Beis D, Bartman T, Jin SW, Scott IC, D'Amico LA et al (2005) Genetic and cellular analyses of zebrafish atrioventricular cushion and valve development. Development 132: 4193–4204
37. Drummond IA (2004) Zebrafish kidney development. Methods Cell Biol 76:501–530
38. Hentschel DM, Park KM, Cilenti L, Zervos AS, Drummond I et al (2005) Acute renal failure in zebrafish: a novel system to study a complex disease. Am J Physiol Renal Physiol 288:F923–F929
39. Drummond IA (2005) Kidney development and disease in the zebrafish. J Am Soc Nephrol 16:299–304
40. Bahadori R, Huber M, Rinner O, Seeliger MW, Geiger-Rudolph S et al (2003) Retinal function and morphology in two zebrafish models of oculo-renal syndromes. Eur J Neurosci 18:1377–1386
41. McMahon C, Semina EV, Link BA (2004) Using zebrafish to study the complex genetics of glaucoma. Comp Biochem Physiol C Toxicol Pharmacol 138:343–350
42. Whitfield TT (2002) Zebrafish as a model for hearing and deafness. J Neurobiol 53:157–171
43. Nicolson T (2005) The genetics of hearing and balance in zebrafish. Annu Rev Genet 39:9–22
44. Darland T, Dowling JE (2001) Behavioral screening for cocaine sensitivity in mutagenized zebrafish. Proc Natl Acad Sci USA 98:11691–11696
45. Svoboda KR, Vijayaraghavan S, Tanguay RL (2002) Nicotinic receptors mediate changes in spinal motoneuron development and axonal pathfinding in embryonic zebrafish exposed to nicotine. J Neurosci 22:10731–10741
46. Gerlai R, Lahav M, Guo S, Rosenthal A (2000) Drinks like a fish: zebra fish (*Danio rerio*) as a behavior genetic model to study alcohol effects. Pharmacol Biochem Behav 67:773–782
47. Poss KD, Keating MT, Nechiporuk A (2003) Tales of regeneration in zebrafish. Dev Dyn 226:202–210
48. Akimenko MA, Mari-Beffa M, Becerra J, Geraudie J (2003) Old questions, new tools, and some answers to the mystery of fin regeneration. Dev Dyn 226:190–201
49. Andreasen EA, Mathew LK, Tanguay RL (2006) Regenerative growth is impacted by TCDD: gene expression analysis reveals extracellular matrix modulation. Toxicol Sci 92:254–269
50. Vogel G (2000) Genomics. Sanger will sequence zebrafish genome. Science 290:1671
51. Zon LI (1999) Zebrafish: a new model for human disease. Genome Res 9:99–100
52. Ackermann GE, Paw BH (2003) Zebrafish: a genetic model for vertebrate organogenesis and human disorders. Front Biosci 8:d1227–d1253
53. Rubinstein AL (2003) Zebrafish: from disease modeling to drug discovery. Curr Opin Drug Discov Devel 6:218–223
54. Wixon J (2000) Featured organism: *Danio rerio*, the zebrafish. Yeast 17:225–231
55. Dodd A, Curtis PM, Williams LC, Love DR (2000) Zebrafish: bridging the gap between development and disease. Hum Mol Genet 9:2443–2449
56. Hahn M (2002) Aryl hydrocarbon receptors: diversity and evolution(1). Chem Biol Interact 141:131
57. Tanguay RL, Andreasen EA, Walker MK, Peterson RE (2003) Dioxin toxicity and aryl hydrocarbon receptor signaling in fish. In: Schecter A (ed) Dioxins and health. Plenum Press, New York, pp 603–628
58. Carney SA, Chen J, Burns CG, Xiong KM, Peterson RE et al (2006) AHR activation produces heart-specific transcriptional and toxic responses in developing zebrafish. Mol Pharmacol 70:549–561
59. Muller U (1999) Ten years of gene targeting: targeted mouse mutants, from vector design to phenotype analysis. Mech Dev 82:3–21
60. Ryffel B (1997) Impact of knockout mice in toxicology. Crit Rev Toxicol 27:135–154
61. Rudolph U, Mohler H (1999) Genetically modified animals in pharmacological research: future trends. Eur J Pharmacol 375:327–337
62. Gonzalez FJ (2002) Transgenic models in xenobiotic metabolism and toxicology. Toxicology 181–182:237–239
63. Fan L, Collodi P (2002) Progress towards cell-mediated gene transfer in zebrafish. Brief Funct Genomic Proteomic 1:131–138
64. Summerton J, Weller D (1997) Morpholino antisense oligomers: design, preparation, and properties. Antisense Nucleic Acid Drug Dev 7:187–195
65. Nasevicius A, Ekker SC (2000) Effective targeted gene 'knockdown' in zebrafish. Nat Genet 26:216–220
66. Nasevicius A, Ekker SC (2001) The zebrafish as a novel system for functional genomics and therapeutic development applications. Curr Opin Mol Ther 3:224–228
67. Nasevicius A, Larson J, Ekker SC (2000) Distinct requirements for zebrafish angiogenesis revealed by a VEGF-A morphant. Yeast 17:294–301
68. Draper BW, Morcos PA, Kimmel CB (2001) Inhibition of zebrafish fgf8 pre-mRNA splicing with morpholino oligos: a quantifiable method for gene knockdown. Genesis 30:154–156
69. Yan YL, Miller CT, Nissen RM, Singer A, Liu D et al (2002) A zebrafish sox9 gene required for cartilage morphogenesis. Development 129:5065–5079
70. Knight RD, Nair S, Nelson SS, Afshar A, Javidan Y et al (2003) Lockjaw encodes a zebrafish tfap2a required for early neural crest development. Development 130:5755–5768
71. Imamura S, Kishi S (2005) Molecular cloning and functional characterization of zebrafish ATM. Int J Biochem Cell Biol 37:1105–1116
72. Haffter P, Granato M, Brand M, Mullins MC, Hammerschmidt M et al (1996) The identification of genes with unique and essential functions in the development of the zebrafish, *Danio rerio*. Development 123:1–36
73. Driever W, Solnica-Krezel L, Schier AF, Neuhauss SC, Malicki J et al (1996) A genetic screen for mutations affecting embryogenesis in zebrafish. Development 123:37–46

74. Abdelilah S, Solnica-Krezel L, Stainier DY, Driever W (1994) Implications for dorsoventral axis determination from the zebrafish mutation janus. Nature 370:468–471
75. Stainier DY, Fouquet B, Chen JN, Warren KS, Weinstein BM et al (1996) Mutations affecting the formation and function of the cardiovascular system in the zebrafish embryo. Development 123:285–292
76. Talbot WS, Schier AF (1999) Positional cloning of mutated zebrafish genes. Methods Cell Biol 60:259–286
77. Brownlie A, Donovan A, Pratt SJ, Paw BH, Oates AC et al (1998) Positional cloning of the zebrafish sauternes gene: a model for congenital sideroblastic anaemia. Nat Genet 20:244–250
78. Henikoff S, Till BJ, Comai L (2004) TILLING. Traditional mutagenesis meets functional genomics. Plant Physiol 135:630–636
79. Amsterdam A, Burgess S, Golling G, Chen W, Sun Z et al (1999) A large-scale insertional mutagenesis screen in zebrafish. Genes Dev 13:2713–2724
80. Chen W, Burgess S, Golling G, Amsterdam A, Hopkins N (2002) High-throughput selection of retrovirus producer cell lines leads to markedly improved efficiency of germ line-transmissible insertions in zebra fish. J Virol 76:2192–2198
81. Golling G, Amsterdam A, Sun Z, Antonelli M, Maldonado E et al (2002) Insertional mutagenesis in zebrafish rapidly identifies genes essential for early vertebrate development. Nat Genet 31:135–140
82. Meng X, Noyes MB, Zhu LJ, Lawson ND, Wolfe SA (2008) Targeted gene inactivation in zebrafish using engineered zinc-finger nucleases. Nat Biotechnol 26:695–701
83. Meng A, Tang H, Yuan B, Ong BA, Long Q et al (1999) Positive and negative cis-acting elements are required for hematopoietic expression of zebrafish GATA-1. Blood 93:500–508
84. Torgersen J, Collas P, Alestrom P (2000) Gene-gun-mediated transfer of reporter genes to somatic zebrafish (*Danio rerio*) tissues. Mar Biotechnol (NY) 2:293–300
85. Powers DA, Hereford L, Cole T, Chen TT, Lin CM et al (1992) Electroporation: a method for transferring genes into the gametes of zebrafish (*Brachydanio rerio*), channel catfish (*Ictalurus punctatus*), and common carp (*Cyprinus carpio*). Mol Mar Biol Biotechnol 1:301–308
86. Halloran MC, Sato-Maeda M, Warren JT, Su F, Lele Z et al (2000) Laser-induced gene expression in specific cells of transgenic zebrafish. Development 127:1953–1960
87. Huang CJ, Jou TS, Ho YL, Lee WH, Jeng YT et al (2005) Conditional expression of a myocardium-specific transgene in zebrafish transgenic lines. Dev Dyn 233:1294–1303
88. Linney E, Hardison NL, Lonze BE, Lyons S, DiNapoli L (1999) Transgene expression in zebrafish: a comparison of retroviral-vector and DNA-injection approaches. Dev Biol 213:207–216
89. Linney E, Udvadia AJ (2004) Construction and detection of fluorescent, germline transgenic zebrafish. Methods Mol Biol 254:271–288
90. Bogers R, Mutsaerds E, Druke J, De Roode DF, Murk AJ et al (2006) Estrogenic endpoints in fish early life-stage tests: luciferase and vitellogenin induction in estrogen-responsive transgenic zebrafish. Environ Toxicol Chem 25:241–247
91. Ashworth R, Brennan C (2005) Use of transgenic zebrafish reporter lines to study calcium signalling in development. Brief Funct Genomic Proteomic 4:186–193
92. Higashijima S, Masino MA, Mandel G, Fetcho JR (2003) Imaging neuronal activity during zebrafish behavior with a genetically encoded calcium indicator. J Neurophysiol 90:3986–3997
93. Mattingly CJ, McLachlan JA, Toscano WA Jr (2001) Green fluorescent protein (GFP) as a marker of aryl hydrocarbon receptor (AhR) function in developing zebrafish (*Danio rerio*). Environ Health Perspect 109:845–849
94. Higashijima S, Hotta Y, Okamoto H (2000) Visualization of cranial motor neurons in live transgenic zebrafish expressing green fluorescent protein under the control of the islet-1 promoter/enhancer. J Neurosci 20:206–218
95. Hill A, Howard CV, Strahle U, Cossins A (2003) Neurodevelopmental defects in zebrafish (*Danio rerio*) at environmentally relevant dioxin (TCDD) concentrations. Toxicol Sci 76: 392–399
96. Blechinger SR, Warren JT Jr, Kuwada JY, Krone PH (2002) Developmental toxicology of cadmium in living embryos of a stable transgenic zebrafish line. Environ Health Perspect 110:1041–1046
97. Amanuma K, Takeda H, Amanuma H, Aoki Y (2000) Transgenic zebrafish for detecting mutations caused by compounds in aquatic environments. Nat Biotechnol 18:62–65
98. Scalzo FM, Levin ED (2004) The use of zebrafish (*Danio rerio*) as a model system in neurobehavioral toxicology. Neurotoxicol Teratol 26:707–708
99. Rodriguez F, Lopez JC, Vargas JP, Broglio C, Gomez Y et al (2002) Spatial memory and hippocampal pallium through vertebrate evolution: insights from reptiles and teleost fish. Brain Res Bull 57:499–503
100. Gerlai R (2003) Zebra fish: an uncharted behavior genetic model. Behav Genet 33:461–468
101. Carvan MJ 3rd, Loucks E, Weber DN, Williams FE (2004) Ethanol effects on the developing zebrafish: neurobehavior and skeletal morphogenesis. Neurotoxicol Teratol 26:757–768
102. Giacomini NJ, Rose B, Kobayashi K, Guo S (2006) Antipsychotics produce locomotor impairment in larval zebrafish. Neurotoxicol Teratol 28:245–250
103. Levin ED, Swain HA, Donerly S, Linney E (2004) Developmental chlorpyrifos effects on hatchling zebrafish swimming behavior. Neurotoxicol Teratol 26:719–723
104. Bretaud S, Lee S, Guo S (2004) Sensitivity of zebrafish to environmental toxins implicated in Parkinson's disease. Neurotoxicol Teratol 26:857–864
105. Samson JC, Goodridge R, Olobatuyi F, Weis JS (2001) Delayed effects of embryonic exposure of zebrafish (*Danio rerio*) to methylmercury (MeHg). Aquat Toxicol 51:369–376
106. Kokel D, Bryan J, Laggner C, White R, Cheung CY et al (2010) Rapid behavior-based identification of neuroactive small molecules in the zebrafish. Nat Chem Biol 6:231–237

107. Corredor-Adamez M, Welten MC, Spaink HP, Jeffery JE, Schoon RT et al (2005) Genomic annotation and transcriptome analysis of the zebrafish (*Danio rerio*) hox complex with description of a novel member, hox b 13a. Evol Dev 7:362–375
108. Lo J, Lee S, Xu M, Liu F, Ruan H et al (2003) 15000 unique zebrafish EST clusters and their future use in microarray for profiling gene expression patterns during embryogenesis. Genome Res 13:455–466
109. Linney E, Dobbs-McAuliffe B, Sajadi H, Malek RL (2004) Microarray gene expression profiling during the segmentation phase of zebrafish development. Comp Biochem Physiol C Toxicol Pharmacol 138:351–362
110. van der Ven K, De Wit M, Keil D, Moens L, Van Leemput K et al (2005) Development and application of a brain-specific cDNA microarray for effect evaluation of neuro-active pharmaceuticals in zebrafish (*Danio rerio*). Comp Biochem Physiol B Biochem Mol Biol 141:408–417
111. Mathavan S, Lee SG, Mak A, Miller LD, Murthy KR et al (2005) Transcriptome analysis of zebrafish embryogenesis using microarrays. PLoS Genet 1:260–276
112. Clark MD, Hennig S, Herwig R, Clifton SW, Marra MA et al (2001) An oligonucleotide fingerprint normalized and expressed sequence tag characterized zebrafish cDNA library. Genome Res 11:1594–1602
113. Handley-Goldstone HM, Grow MW, Stegeman JJ (2005) Cardiovascular gene expression profiles of dioxin exposure in zebrafish embryos. Toxicol Sci 85:683–693
114. Ton C, Stamatiou D, Liew CC (2003) Gene expression profile of zebrafish exposed to hypoxia during development. Physiol Genomics 13:97–106
115. Hoyt PR, Doktycz MJ, Beattie KL, Greeley MS Jr (2003) DNA microarrays detect 4-nonylphenol-induced alterations in gene expression during zebrafish early development. Ecotoxicology 12:469–474
116. Wang Z, Gerstein M, Snyder M (2009) RNA-Seq: a revolutionary tool for transcriptomics. Nat Rev Genet 10:57–63
117. Mandrell D, Moore A, Jephson C, Sarker M, Lang C et al (2011) Automated zebrafish chorion removal and single embryo transfer: optimizing throughput of zebrafish developmental toxicity screens. J Lab Autom (submitted)
118. Wang W, Liu X, Gelinas D, Ciruna B, Sun Y (2007) A fully automated robotic system for microinjection of zebrafish embryos. PLoS One 2:e862
119. Carpenter AE (2007) Image-based chemical screening. Nat Chem Biol 3:461–465
120. Mayr LM, Fuerst P (2008) The future of high-throughput screening. J Biomol Screen 13:443–448
121. Milan DJ, Peterson TA, Ruskin JN, Peterson RT, MacRae CA (2003) Drugs that induce repolarization abnormalities cause bradycardia in zebrafish. Circulation 107:1355–1358
122. Berghmans S, Butler P, Goldsmith P, Waldron G, Gardner I et al (2008) Zebrafish based assays for the assessment of cardiac, visual and gut function–potential safety screens for early drug discovery. J Pharmacol Toxicol Methods 58:59–68
123. Grassian VH (2008) When size really matters: size-dependent properties and surface chemistry of metal and metal oxide nanoparticles in gas and liquid phase environments†. J Phys Chem C 112:18303–18313
124. MacPhail RC, Brooks J, Hunter DL, Padnos B, Irons TD et al (2009) Locomotion in larval zebrafish: influence of time of day, lighting and ethanol. Neurotoxicology 30:52–58
125. Usenko CY, Harper SL, Tanguay RL (2007) *In vivo* evaluation of carbon fullerene toxicity using embryonic zebrafish. Carbon 45:1891–1898
126. Harper SL, Dahl JL, Maddux BLS, Tanguay RL, Hutchison JE (2008) Proactively designing nanomaterials to enhance performance and minimize hazard. I J Nanotechnol 5:124–142
127. Holdsworth DW, Thornton MM (2002) Micro-CT in small animal and specimen imaging. Trends Biotechnol 20:S34–S39
128. Harper SL, Usenko C, Hutchinson JE, Maddux BLS, Tanguay RL (2008) *In vivo* biodistribution and toxicity depends on nanomaterial composition, size, surface functionalization and route of exposure. J Exp Nanosci 3:195–206
129. Magrez A, Kasas S, Salicio V, Pasquier N, Seo JW et al (2006) Cellular toxicity of carbon-based nanomaterials. Nano Lett 6:1121–1125
130. Nel A, Xia T, Madler L, Li N (2006) Toxic potential of materials at the nanolevel. Science 311:622–627
131. Colvin V (2003) The potential environmental impact of engineered nanomaterials. Nat Biotechnol 21:1166–1170
132. Jiang W, KimBetty YS, Rutka JT, ChanWarren CW (2008) Nanoparticle-mediated cellular response is size-dependent. Nat Nano 3:145–150

Natural Gas Power

Raub W. Smith, S. Can Gülen
GE Infrastructure-Energy, Schenectady, NY, USA

Article Outline

Glossary
Defining the Subject
Introduction
Gas Turbine Power Plants
Future Directions
Bibliography

Glossary

Brayton cycle The thermodynamic cycle describing the operation of a gas turbine. In a combined cycle, it is the *topping* cycle due to its relative position vis-à-vis Rankine cycle on a temperature–entropy surface.

Carnot cycle Also known as the Carnot engine, it is the embodiment of the second law of thermodynamics in the form of a theoretical cycle comprising two isentropic and two isothermal processes. No heat engine operating in a thermodynamic cycle can be more efficient than the corresponding Carnot engine defined by the constant mean-effective heat addition and heat rejection temperatures.

Cogeneration See combined heat and power (CHP).

Combined cycle power plant A fossil-fired power plant that combines two types of prime movers, usually one or more gas turbines and one or more steam turbines (STs), whose operation are governed by their respective thermodynamic cycles, i.e., Brayton and Rankine.

Combined heat and power (CHP) The term used for fossil-fired power plants, which, in addition to their primary product, electric power delivered to the grid, also supply a secondary product in terms of useful thermal energy.

Combustor A mechanical device to facilitate controlled mixing and reaction of an oxidizer (in almost all cases air) and a fuel (in almost all cases a pure hydrocarbon or a mixture thereof in gaseous or liquid phase) to generate high-temperature gaseous product for expansion in a turbine and useful shaft work generation.

Compressor A mechanical device that increases the pressure of a gas by reducing its volume. There are different types of compressors, e.g., axial, radial, and reciprocating, which are suitable to different types of operating regimes.

Efficiency Unless specified otherwise, the thermal efficiency of a power-generating system, which is the dimensionless ratio of generated kWh of electricity to the amount of energy required to generate it. It is the inverse of the heat rate with a suitable conversion factor.

Emissions Gases and solid particles (usually undesirable) released into the air as by-products of a combustion process (e.g., in the boiler of a fossil-fired power plant, gas turbine combustor, or other internal combustion engine) to create electric power or propel a vehicle.

Firing temperature The temperature of the gas turbine combustor exhaust gas at the inlet to the first stage rotor, which is the starting point of useful shaft work generation.

Gas turbine A prime mover or internal combustion engine comprising a compressor, combustor, and an expander connected via a common shaft, through which air is compressed, burned, and expanded to generate useful shaft work for electric power generation (or thrust in an aircraft jet engine).

Generator A device that converts the mechanical shaft power generated by a prime mover into electrical power.

Global warming The apparent increase in the average temperature of the earth's near-surface air and oceans since the mid-twentieth century and its projected continuation (per *Wikipedia*).

Greenhouse effect The containment of heat from solar radiation striking the earth's surface due to the earth's atmospheric "greenhouse" gases such as carbon dioxide and methane. These gases absorb and emit radiation within the thermal infrared range and are believed to be a primary cause of global warming.

Heat rate Amount of energy required to generate 1 kWh of electricity. It is the inverse of the thermal efficiency with a suitable conversion factor.

Heating value The thermal energy produced by completely burning a unit mass of fuel in a combustor to produce carbon dioxide and water. If the water is in a gaseous phase, the heating value is referred to as net or lower heating value (LHV). If the water is in a liquid phase, the heating value is referred to as gross or higher heating value (HHV).

Heat recovery steam generator (HRSG) Also known as the heat recovery boiler (HRB), HRSG is a cross-flow tubular heat exchanger that recovers the exhaust heat from a prime mover (e.g., a gas turbine) and produces steam at high pressure and temperature that is used in a steam turbine (ST) for additional power generation. HRSG is the key equipment that "combines" gas and steam turbines in a combined cycle power plant.

Rankine cycle The thermodynamic cycle describing the operation of a steam turbine. In a combined cycle, it is the *bottoming* cycle due to its relative position vis-à-vis Brayton cycle on a temperature-entropy surface.

Steam turbine A prime mover or the power-generating part of an external combustion engine comprising one or more sections connected via a common shaft, through which steam flows, expands, and discharges to a condenser to generate useful shaft work for electric power generation or propulsion.

Defining the Subject

Natural gas is an important fossil fuel that has played an increasingly significant role in worldwide electric power generation since the 1980s. The key driver underlying the importance of natural gas as a vital enabler of modern living has been its relative advantage vis-à-vis other fossil fuels in terms of emissions and pollutants. In comparison to coal, the primary fossil fuel used for electric power generation in the world on a constant consumption basis, natural gas emits nearly 45% less CO_2, 80% less nitrogen oxides (NO_x) with negligible amounts of sulfur oxides, particulates, and mercury.

The environmental advantages of natural gas are further amplified by the significantly higher thermal efficiency of the power plants that burn it for electric power generation in comparison to other variants of oil or coal. Natural gas burning modern gas turbines can readily reach efficiencies of 56–57% in combined cycle configurations. This is well above the average efficiency of existing coal burning steam turbine plants (e.g., low 30s) as well as the most advanced ultra-supercritical designs thereof (e.g., low 40s).

With the beginning of the twenty-first century, economic projections pointed to natural gas as the fastest growing fuel for worldwide electric power generation, with an expected average annual rate of growth of about 3.7% between 2005 and 2030. During this period, natural gas will account for almost one-fourth of the world's total net electricity generation [1]. While such long-term forecasts are highly susceptible to uncertainties such as the impact of potential governmental policies or legislation limiting the use of fossil fuels in favor of nuclear and renewable sources of energy (largely driven by concerns over global warming), it is almost a foregone conclusion that natural gas will continue to be an important part of the world's energy and electric power generation portfolio in the foreseeable future.

Given this impact of natural gas on future electrical production, it is important to establish a basic understanding of the history, current state of the art and future possibilities of power generation using natural gas combustion in order to have a complete picture of future energy sustainability.

Introduction

Natural gas is a fossil fuel comprising hydrocarbons, primarily methane (CH_4) up to 90% on a volumetric basis. It differs from the other fossil fuels in that it is naturally available as a gas (hence the name) as opposed to a solid (i.e., coal) or liquid (i.e., oil). Like other fossil fuels, the basic mechanism (thermogenic) of natural gas formation involves the extremely prolonged high-pressure compression of organic matter remains (e.g., plants, animals that lived millions of years ago on earth). The gaseous phase is the result of extremely high temperatures associated with the depth of the organic matter, typically 1–2 miles below the earth's crust. At even deeper levels, natural gas consists almost entirely of pure methane.

Another (biogenic) mechanism for forming natural gas is the chemical transformation of organic matter by microorganisms. The resulting gas contains methane and carbon dioxide. A well-known example of this mechanism is the landfill gas that results from the decomposition of waste materials deposited into large landfills. Other biogas formation mechanisms are sludge digestion in the tanks of sewage treatment plants (sewage gas) and anaerobic fermentation of agricultural waste. Biogas formation takes place near the earth's surface in the absence of oxygen and the resulting gas usually leaks to atmosphere. Controlled capture of landfill gas and other biogases for utilization in electric power generation is a promising technology. (Uncontrolled energy release (explosion) from the trapped landfill gas leading to death and destruction in the poverty-stricken areas of the world is an unfortunate event that appears in the news from time to time.) Biogas utilization is also important because the main constituent, methane, itself is a principal greenhouse gas (GHG). In fact, methane is nearly 20 times more effective than CO_2 in trapping heat emanating from the earth's surface. Therefore, combustion of methane (with resultant CO_2 emissions) that otherwise

would leak into the atmosphere is a preferable trade-off from GHG reduction point of view.

Coal mine gas is another type of natural gas that is released during pit coal mining. Depending on the time of capture and method, there are different types. The most common types are coal bed methane (CBM) and coal mine methane (CMM). The former is largely pure methane and its production is independent of coal mining. The latter is released during active mining and presents a significant danger of violent explosion to miners. Proper ventilation of mine shafts to remove and vent CMM into atmosphere is essential for the safety of mining operation. The methane content of CMM is variable (25–60%) and can change suddenly, which might be problematic for its use as a fuel. A third type of coal mine gas is abandoned mine methane (AMM), which can seep from mines that are no longer active. Annual coal mine methane emissions account for about 8% of total anthropogenic methane emissions or about 28 billion m^3 of carbon dioxide equivalent [3]. Utilization of CMM and AMM for power generation is critical to the prevention of release of a GHG into atmosphere.

Energy content of the natural gas is measured in terms of Btu (kJ or kcal) per lb (kg) or per standard cubic feet (cubic meters). In many practical calculations, natural gas is assumed to be 100% pure methane, which has an energy content of 21,515 Btu/lb (50,044 kJ/kg or 11,953 kcal/kg) on a lower heating value (LHV) basis or 914 Btu/ft^3 (34,050 kJ/m^3 or 8,133 kcal/m^3) at normal (standard) conditions (herein defined as 77°F (25°C) and 1 atm). The actual composition may vary depending on the source and treatment. Based on the mean of over 6,800 samples of pipeline quality natural gas taken in 26 major metropolitan areas of the USA [4], the methane content is 93.1% with a heating value of 930 Btu/ft^3 (8,275 kcal/m^3). A sampling of composition and heating value of most common natural gas variants is given in Table 1.

Production and distribution companies measure natural gas in volumetric terms, i.e., in multiples of cubic feet such as millions of cubic feet, trillions of cubic feet, etc. In power generation calculations, where natural gas is the fuel burned in the combustor of the gas turbine, the more practical approach is to use the mass flow rate (lb/s or kg/s) along with the LHV value or the product of the two, which is referred to as heat consumption (MMBtu/h or kW).

The purpose of a power plant is to generate electric power. Therefore, the key performance metric of an electric power generator is the net thermal efficiency, which is the ratio of the electric power measured at the generator terminals (after subtracting all the power that is spent to keep the plant running) to the plant's fuel energy consumption. The most efficient way to burn natural gas for electric power generation is in a gas turbine combined cycle (GTCC) power plant. Today's state-of-the-art CC power plant has a rated net efficiency of 58% on an LHV basis. In other words, for each 1 lb/s of natural gas (about 23.5 ft^3/s as 100% methane) that enters the combustor of the gas turbine, (using the formula 58% × 21,515 Btu/lb × 1 lb/s × 1.05506 kWs/Btu = 13,166 kW) about 13.2 MW of electric power (net) is delivered to the grid. This is enough power to sustain nearly 13,000

Natural Gas Power. Table 1 Composition and heating values of typical natural gases

Component (%)	Coal bed methane	Coal mine methane	Landfill gas	Biogas	Average NG
O_2	2.1	12.6	0–1	0–2	
N_2	8.2	46.8	2–5	0–10	1.6
CH_4	85.9	40.0	45–60	50–75	93.1
CO_2			40–65	25–50	1.0
C_nH_{2n}	3.8				4.3
LHV, kcal/nm^3 (Btu/scf)	7,762	3,200	3,350–4,775	3,580–5,975	8,275
	872	360	375–535	400–670	930

average homes for 1 h at an average power consumption of 1 kW.

In 2005, natural gas accounted for 3.4 trillion kWh of net electricity production for about 20% of the world total (see Fig. 1). This contribution is projected to reach 8.4 trillion kWh in 2030 or about 25% of the world total corresponding to a total natural gas consumption of 55.5 trillion ft^3 (i.e., 35% of total world production of 158.6 trillion ft^3). Using the calculation above as a rough guide, this translates into an average natural gas–fired power plant thermal efficiency of 56.4%. The natural gas reserves of the world are estimated at about 6,186 trillion ft^3 with top 20 countries contributing nearly 90% of it (see Fig. 2). When one considers the uncertainty in the cited projections, it appears safe to say that there are ample deposits of natural gas to sustain electric power production well into the twenty-first century.

As mentioned in the beginning, natural gas is a superior fossil fuel in terms of emissions and pollutants vis-à-vis other fossil fuels, i.e., coal and oil. This is not to say that natural gas is totally harmless, especially when one considers the emissions of CO_2 – the most abundant anthropogenic greenhouse gas in the atmosphere and, as such, the main culprit suspected in driving global warming. A modern gas turbine combustor generates 2.75 lbs of CO_2 per lb of natural gas burned. In other useful relative terms, this is approximately 129,000 lb (58,500 kg) of CO_2 per billion Btu (1.06 million MJ) of energy input or 1,125 lb/MWh generated by a gas turbine (GT) in simple cycle configuration (cf., 750 lb in combined cycle configuration). Since not all power generation equipment performs at today's higher efficiency level, real averages would be higher, e.g., 1,300 and 800 for simple and combined cycles, respectively. For the projected natural gas–based electric power generation in 2030 cited above, at a rate of 1,300 lb/MWh, this translates into 5 billion metric tons of CO_2 released into earth's atmosphere. (In order to get an idea about the magnitude of this number, consider that the estimated weight of carbon dioxide in the atmosphere was about 2,163 billion metric tons before the industrial revolution.) This is approximately half of the total 2030 projection of CO_2 emission from natural gas combustion, which itself is about 20% of the 42.3 billion metric tons for all fossil fuels.

While an important contributor to the greenhouse effect, natural gas is extremely advantageous from the perspective of two other significant combustion-related pollution phenomena, i.e., smog and acid rain. Smog (whose primary constituent is ozone) is formed

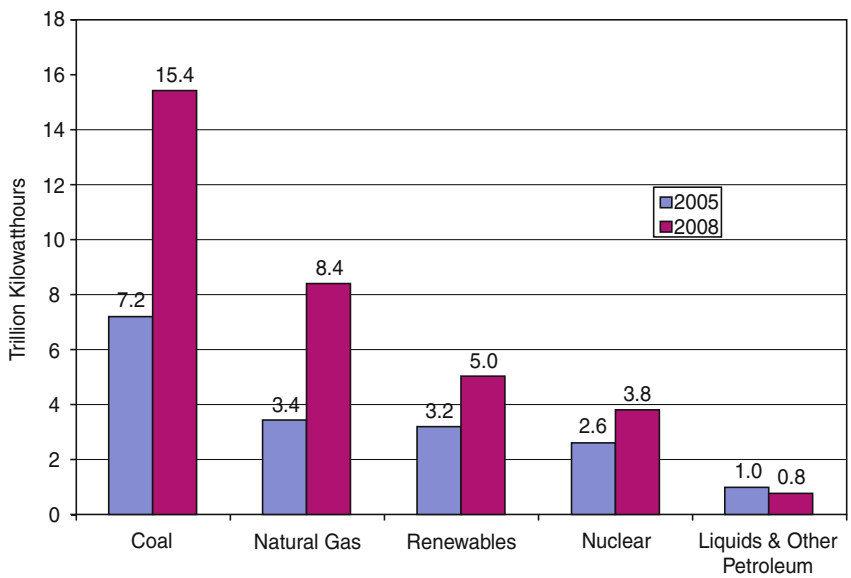

Natural Gas Power. Figure 1

World Net Electricity Generation. Renewables include hydroelectric (Source: Energy Information Administration (EIA) [1])

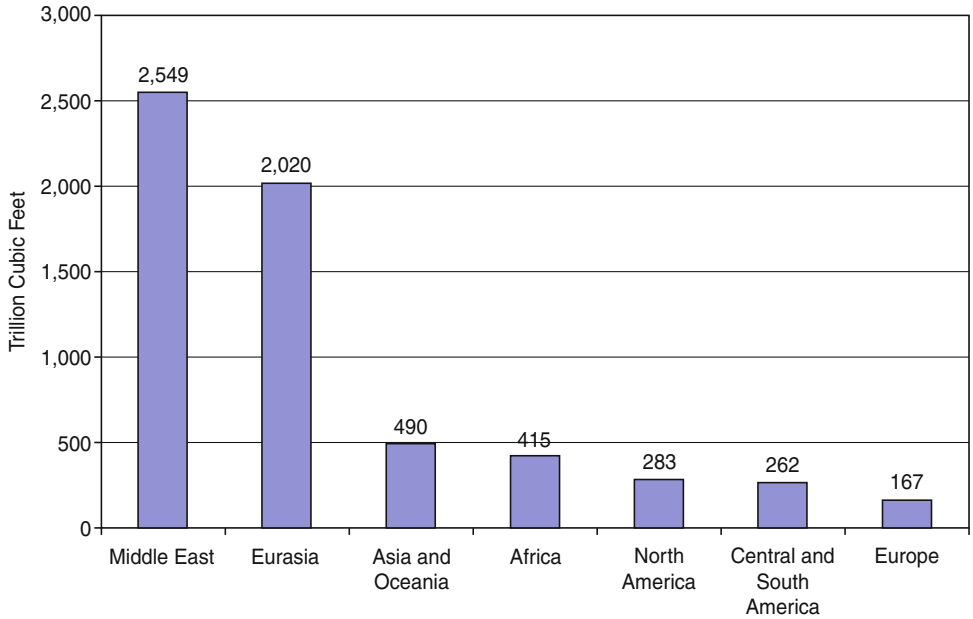

Natural Gas Power. Figure 2

World Natural Gas Reserves, January 2008. Asia, Oceania and Europe exclude countries that were part of the former USSR whereas Eurasia includes only those. Source: Energy Information Administration (EIA) [2]

by a chemical reaction of carbon monoxide, nitrogen oxides, volatile organic compounds, and heat from sunlight [5]. Acid rain is formed when sulfur dioxide and nitrogen oxides react with water vapor and other chemicals in the presence of sunlight to form various acidic compounds in the air [5]. Natural gas combustion products are virtually free of the two main culprits contributing to these severe pollution problems, namely, sulfur oxides (SO_x) and particulate matter, and they have 80% less NO_x than products of coal combustion.

In general (notwithstanding some future fuel cell designs discussed later), the most efficient means to utilize natural gas as a fossil fuel in electric power generation is to burn it in internal combustion (IC) engines. The two most widely used IC engines in electric power generation are gas turbine and reciprocating internal combustion or diesel engine. (Note that the term *diesel* in this context refers to the thermodynamic cycle of the compression-ignition (CI) IC engine and not the fuel.) While possible in theory, natural gas is not used with external combustion technology (e.g., boiler and steam turbine plants) due to the pronounced superiority of the IC engines in efficiency, emissions, power density (i.e., favorable cost vs. size trade-off) and operational flexibility.

Modern gas turbines are large air-breathing turbomachines with extremely large power output. For example, consider a 50-Hz (3,000 rpm) 300+ MW net power output unit as listed in a 2008 trade publication [6]. This machine ingests air at ISO conditions (15°C and 1 atm at 60% relative humidity) at a rate of nearly 1,550 lb/s (705 kg/s), compresses it to a pressure that is 18 times that of the ambient and combusts it with about 35 lb/s (16 kg/s) of natural gas (100% CH_4) generating 312 MW net electric power for a net thermal efficiency of 39.3%. At the inlet to the expander section of the gas turbine, where they produce useful shaft work, the combustion products are at nearly 1,500°C (2,732°F). This is well above the melting point of the most advanced superalloy materials that are used in the manufacture of turbine expander components. In order to ensure the survival of the turbine parts under those extreme conditions for thousands of hours of continuous operation, nickel-based superalloy components are protected by thermal barrier coatings (TBC) and internally cooled by using the "cold" air extracted from the turbine compressor. (Consider that

without cooling and TBC, the first stage vanes of a modern GT would survive barely ten seconds before melting away.) Utilizing those and other technologies, some of which are adopted from the advanced military and civilian aircraft engine–related research and development, land-based heavy-duty industrial gas turbines are true marvels of human engineering.

Diesel or compression-ignition IC engines are no slouches themselves. In fact, the efficiency of a tri-fuel (one that can burn natural gas, light and heavy fuel oils) unit rated at nearly 17 MW net electric output is 47.3% on an LHV basis when operating with natural gas fuel [7]. They are eminently suitable to landfill, biogas, and coal mine gas applications. They are at a disadvantage because of their relatively low power density and cost. The sample multifuel diesel engine cited above has a power density of 0.05 kW/kg of engine weight or 215 kW/m^2 of engine footprint. These numbers compare very unfavorably to the power density of a heavy-duty industrial gas turbine. For a typical advanced machine with the performance similar to the sample cited above, the power density is about 0.8 kW/kg of engine weight or about 3,000 kW or more per m^2 of engine footprint. In order to appreciate the power density of a GT vis-à-vis renewable energy–based systems, consider that the power density of typical wind and solar radiation are 0.4–0.8 (depending on altitude and speed) and 1.4 kW/m^2, respectively [8]. One would need hundreds of acres of wind turbine farms or solar collector fields to replace a single advanced F-Class gas turbine. This gross disparity in the power density of the two IC engine technologies is reflected in the annual unit order numbers displayed in Fig. 3. In terms of the numbers of units ordered in 2005–2006 [9], reciprocating IC engines dominate (nearly 2,700 units vs. 666 for gas turbines) but the significant bulk of the orders are for units rated at 3.5 MW or less. In terms of the total MW rating of the orders, all dual-fuel and natural gas diesel engines add up to 4.4 GW as opposed to more than 40 GW for all gas turbines.

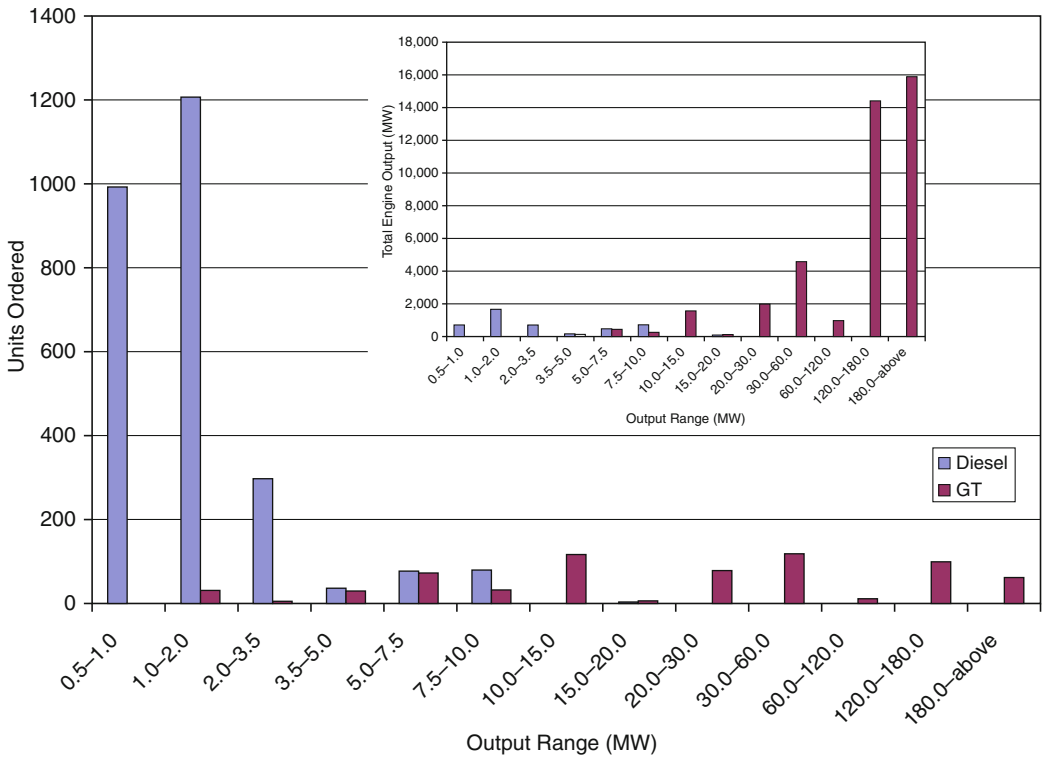

Natural Gas Power. Figure 3

Dual-fuel and natural gas diesel engine and gas turbine orders, June 2005 through May 2006 [9]

At this point, it should be fairly obvious that a treatise on the subject of electric power generation using natural gas is essentially a treatise on modern land-based or heavy-duty industrial gas turbines. This is especially true for the past and the present of the technology. The future of electric power generation using natural gas as a fuel source might have a place for the fuel cell technology (with or without gas turbines). Ongoing research activities include solid oxide (SOFC), molten carbonate (MCFC), and polymer electrolyte (PEFC) technologies. From where one stands today, the most promising use for these technologies seems to be found in the fields of transportation and portable power. With the exception of distributed power generation, in which small-scale (1–500 kW) units power individual residences, office buildings, etc., the prospect of fuel cell–based technologies to replace internal combustion engines and specifically gas turbines as large-scale base load power-generating units in the near term, especially in a cost-effective manner, is practically nil.

A Brief History of Natural Gas

Natural gas has been around for quite a while. In China, nearly 2,500 years ago, early innovators used natural gas escaping naturally from the ground to light their temples and heat brine for distillation. Bamboo sections, split lengthwise, were glued together, and bound with twine, allowing the gas to be transported. In the early seventeenth century, French explorers near Lake Erie reported seeing natives burning gas naturally seeping from the ground. The first industrial use of natural gas can be traced back to England in the late eighteenth century when gas produced from coal was used to light houses and streets. In the USA, the first natural gas well was dug in 1821 in Fredonia, NY, four decades before Colonel Drake hit upon oil and gas at a depth of 69 feet in Lake Erie, PA. The well, dug by William Hart, was 27 ft deep in a creek bed. The extracted gas was transported through hollow log pipes to Fredonia for use in street lamps. Throughout most of the nineteenth century, natural gas was used almost exclusively for the same purpose, i.e., lighting. Following the invention of the Bunsen burner in 1885, natural gas also presented households with a more convenient means of cooking and heating. The main impediment to a wider utilization of natural gas was the lack of a transportation mechanism. The primary method, still in use today, is through an underground pipeline. While the first significantly long pipeline was constructed in 1891 (120 miles long between central Indiana and Chicago), it was only after World War II when technology advances made construction of longer and more reliable pipelines feasible. Until that time, natural gas was either allowed to vent into the atmosphere (intentionally or unintentionally) or burned in flares (as a by-product of coal mining and oil exploration) or just left in the ground when found alone. In fact, when the first astronauts looked at earth from the orbit, the most prominent sights on the earth's surface were the flares from the oil fields in Middle East and Africa. Even now about 150 million m^3 of natural gas, roughly equivalent to annual US residential consumption, is flared to the atmosphere. The contribution of the flared natural gas (NG) to global GHG emissions is about 400 million metric tons, equivalent to nearly one third of the annual US car exhaust emissions.

Today natural gas is used for much more than street lighting or household cooking. In fact, residential use of natural gas accounts for only a fifth of the total US consumption, with more than 60% used by the industrial sector including electric power generation. Until the end of 1980s, high-efficiency fossil fuel (mainly coal) firing or nuclear-powered steam turbine–based power plants supplied the base load electric generation capacity (6,000–8,000 h/year). When newly designed high-efficiency steam plants entered the service, older less-efficient units were relegated to intermediate duty operation (e.g., 4,000 h/year). Early generation, low-efficiency gas turbines, along with old steam plants and hydro pumped-storage plants, were largely limited to short-duration, peak-shaving-type operations. Due to changing economic parameters, introduction of protective environmental regulations, and major technological advances in gas turbine technology, starting in mid-1980s and early 1990s, natural gas became the fuel of choice for new power plants. The steady increase in coal-fired steam plant efficiencies leveled off at the low 40% range, whereas new "F-Class" gas turbines with high firing temperatures, almost exclusively in combined cycle configuration, opened the door for thermal efficiencies easily exceeding 50% and even pushing for 60%. Recently, especially during the so-called energy

boom of early 2000s, a large fraction of new capacity addition in the USA has been in natural gas–fired units, e.g., nearly 95% or 22 GW in 2000. Since then, this rate has tapered off significantly. Natural gas–fired power plant capacity addition in terms of construction starts totaled about the same, i.e., 22 GW, in the years 2005–2007 [10]. Scheduled construction start is about 9 GW for 2010, about the same as in 2009 but lower than the peak year of 2008 with nearly 12 GW. As pointed out earlier, natural gas is projected to be the fastest growing fuel for worldwide electric power generation. Thus, the pace of construction and commissioning of plants burning natural gas might be expected to pick up again. Construction of natural gas–fired power plants scheduled to start between 2011 and 2015 was estimated to be 44.5 GW [10]. Even though some projects will undoubtedly be cancelled or postponed, this is a strong positive sign for the future role of natural gas in electric power production.

The driver of the ascendancy of natural gas as the star of fossil fuels is the gas turbine, which also plays a key role in its transportation and distribution via huge pipeline networks. Heavy-duty industrial and/or aeroderivative gas turbines drive the large centrifugal gas compressors, which increase the pressure of natural gas up to 1,500 psia (∼100 bar). In most cases, these gas turbines burn the natural gas taken from the pipeline. Additional compressor stations, placed at regular intervals along the hundreds of miles long pipelines, maintain line pressures reduced via friction between pipe and gas, which can reach flow velocities up to 40 km/h.

A Brief History of Gas Turbine

When lieutenant colonel Heinz Bär died in a civilian aircraft accident in 1956 in (then) West Germany, he was the world's leading jet fighter ace with 16 victories to his credit. Some five decades after his death and more than six decades after his last aerial exploits, he is still unrivaled. The machine that enabled Bär to permanently enter the annals of military history was the world's first mass production jet fighter, the Messerschmitt Me-262. It was powered, remarked another famous German fighter pilot, "as if pushed by angels" – actually two 1984-lb thrust Jumo-004 gas turbine jet engines.

Developed under the leadership of Franz Anselm, the Jumo-004 was essentially the engine that opened up the jet age. Quite naturally, Dr. Anselm did not conceive Jumo-004 in a vacuum. Paraphrasing Sir Isaac Newton, he was standing on the shoulders of giants such as Sir Frank Whittle and Hans von Ohain, who are widely recognized as the pioneers of modern turbojet engine. Sir Frank and Dr. Ohain themselves almost certainly acknowledged early inventors such as Barber (first GT patent in 1791), Stolze (first GT to be built and tried in 1900–1904), Holzwarth, and others, who showed them the path to the ultimate gas turbine engine design through their patents on air and steam turbines.

It is futile to attempt to plot a straight historical line from Hero's turbine (which had no purpose other than entropy generation) to today's modern 2,600°F firing temperature class steam-cooled H-System™. Countless inventors laid down the building blocks that eventually led to the modern gas turbine engine. For an excellent short history of turbomachinery in general and gas turbines in particular, the reader should consult the relevant chapter in Wilson and Korakianitis [11], who highlight the contributions of lesser known (unfairly) inventors such Aegidius Elling and George Jendrassik. Another good narrative with an emphasis on turbojets and German research and development can be found in Hans von Ohain's foreword to Mattingly's book on gas turbine propulsion [12]. For a detailed look at turbojet development activities of Sir Frank Whittle and Hans von Ohain in their respective countries, three articles by Meher-Homji can be consulted [13–15].

Quite obviously, wars or the prewar atmosphere of the western world in the first half of the last century pushed the development of gas turbines primarily as a military aircraft propulsion device. Starting in the late 1940s and early 1950s, engineers in USA and UK managed to derive robust, land-based power generation and, later, marine propulsion engines from these aircraft designs. Claire Soares essentially came to the conclusion that the involvement of so many people from so many different countries with immense pride in their work led to selective "histories" favoring selected milestones [16]. Her brief summary can be consulted for alternate takes on the development history of gas turbines. For a history of Siemens gas turbine development, a good resource is the paper by Leiste [17].

For a US perspective with an emphasis on GE, the reader should consult Miller and Nemec [18] and Brandt [19]. The paper describing the design and development of the GE MS7001F gas turbine by Brandt [20] is a good reference laying out all design aspects of a modern gas turbine and the trade-offs that are unavoidable in bringing a feasible product into the market.

Even though the development of the modern gas turbine was primarily driven by military and, to a lesser extent, civilian aircraft propulsion considerations, the introduction of stationary (land-based) units dedicated to power production did not lag too far behind. In fact, Aurel Stodola credited Hans Holzwarth with "having built the first economically practical gas turbine [21]." Holzwarth built several types of his "explosion" turbine in the first quarter of the twentieth century. Holzwarth's turbine was, strictly speaking, a hybrid construction combining the spark-ignition (constant volume) combustion process of an Otto cycle with the axial expansion process of a Brayton cycle. Stodola calculated a thermal efficiency of 25.6% for the test of a 1,500-rpm experimental turbine in Mühlheim–Ruhr in 1919 [21]. Burning a gas with 434 Btu/ft^3 heating value the turbine produced about 725 kW. Air and fuel gas was compressed by steam turbine–driven compressors and sequentially injected into the explosion chamber (gas first) at about 30 psia. Stodola reports an average maximum explosion pressure of 160 psia. The combustion products expanded through a two-stage velocity-compounded turbine. Exhaust gas at about 800°F was recovered in an exhaust heat boiler. In that sense, this unit could be considered the first combined cycle. Holzwarth designed and developed several different variants of his turbine between 1907 and 1928. From 1928 on, Brown Boveri Company (BBC) took over the development of Holzwarth turbine and in 1933 installed a blast-furnace gas (BFG)–fired unit in a German steel mill, which was destroyed during World War II.

It is generally accepted that the first commercial stationary gas turbine for electric power generation was erected in Neuchâtel, Switzerland, by the former BBC in 1939, 3 years before the first flight of Me-262 powered by Jumo-004. This fuel oil burning 4 MW machine, primarily used for stand-by and peaking duties, was operational for nearly 70 years (see Fig. 4). The combustion chamber was derived from the

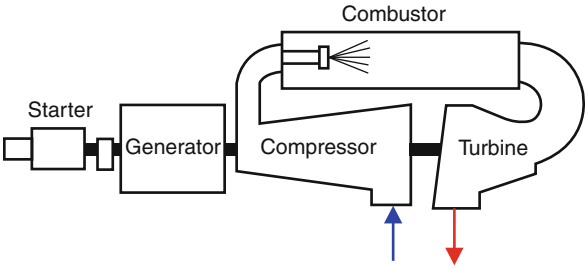

Natural Gas Power. Figure 4
Schematic diagram of Brown Boveri Co.'s Neuchâtel gas turbine (1939)

turbocharged *Velox* boiler, which itself resulted from the BBC work done on the Holzwarth turbine. The BBC turbine was tested under the supervision of Aurel Stodola, who reported an overall thermal efficiency of 17.4%, which is less than half of the efficiency of today's advanced F-Class machines [22]. This machine was designated by the ASME as a *Historic Mechanical Engineering Landmark* in 1988.

The first gas turbine installed in an electric utility in the USA (Oklahoma Gas & Electric, Belle Isle Station, Oklahoma) was a 3.5 MW GE Frame 3 unit that entered service in 1949. In addition to generating power, the exhaust gas of this gas turbine was utilized to heat the feed water of a conventional steam plant. In other words, the first US electric utility gas turbine was in a "combined" cycle configuration [23]. In fact the combined cycle concept goes back to Emmet's mercury-vapor process (1925) [24]. For a brief history of the CC power plants and pertinent references, the reader should consult the 1994 Calvin Winsor Rice Lecture by Sir John Horlock [24].

One can look at the technology history of the land-based gas turbine and combined cycle power plants for electric power production in four generations:

1. Generation 1 (1949–1968)
   (a) Smaller than 30 MW GTs (Frames 3 and 5)
   (b) Firing temperatures 1,500–1,800°F
   (c) For repowering and cogeneration
2. Generation 2 (1968–1990)
   (a) B and E Technology GTs (50–120 MW)
   (b) Firing temperatures ~2,000°F
   (c) NO_x emission control using GT water/steam injection or SCRs
   (d) Non-reheat steam cycles

3. Generation 3 (1990–1998)
   (a) F Technology GTs (75–260 MW)
   (b) Three air-cooled turbine stages
   (c) Firing temperatures ~2,400°F
   (d) Performance fuel heating (365°F)
   (e) DLN combustion system for NO_x control
   (f) Three-pressure, reheat (3PRH) steam cycles
4. Generation 4 (1998–present)
   (a) H technology GTs (400+ MW in CC)
   (b) Closed-loop steam cooling (CL-SC) of the first two turbine stages (both stator and rotor); four turbine stages
   (c) Cooling of cooling air (CAC) for turbine wheel spaces and subsequent stages via a heat exchanger (a kettle reboiler) that generates IP steam to be used in the bottoming cycle
   (d) Active clearance control (compressor and turbine)
   (e) Firing temperatures ~2,600°F
   (f) Performance fuel heating (400+°F)
   (g) DLN combustion system for NO_x control
   (h) Three-pressure, reheat (3PRH) steam cycle integrated with the GT Brayton cycle

The historical advances in GT firing temperature and CC efficiency is summarized in Fig. 5. The data illustrates the significant advance in the thermal efficiency of the GT combined cycle power plants, to the tune of nearly 15 percentage points, which is mainly driven by advances in materials, coatings, and cooling techniques that pushed the firing temperatures by almost 800°F (~450°C). In the following chapters, the reader is introduced to the basic thermodynamic principles that govern the performance of natural gas–burning gas turbine power plants. In addition, also provided is a brief overview of state-of-the-art gas turbine power plants, key economic criteria, and operability considerations. Finally, the future directions in gas turbine–based electric power generation systems are briefly elaborated upon.

Gas Turbine Power Plants

Gas turbine in itself or as a key component of a larger power generation system is a subject that can only be covered in dedicated books. Such books do exist and several selected treatises on the subject, which in the opinion of the authors reflect the best available published work in the field, are listed among the bibliography references. The coverage of the subject in the limited space allotted to the current chapter aims to provide the reader with the fundamental thermodynamic considerations that lead from the Carnot cycle to the present-day advanced gas turbine in a logically coherent manner. There is a reason that the gas turbine combined cycle plant is the most efficient heat engine

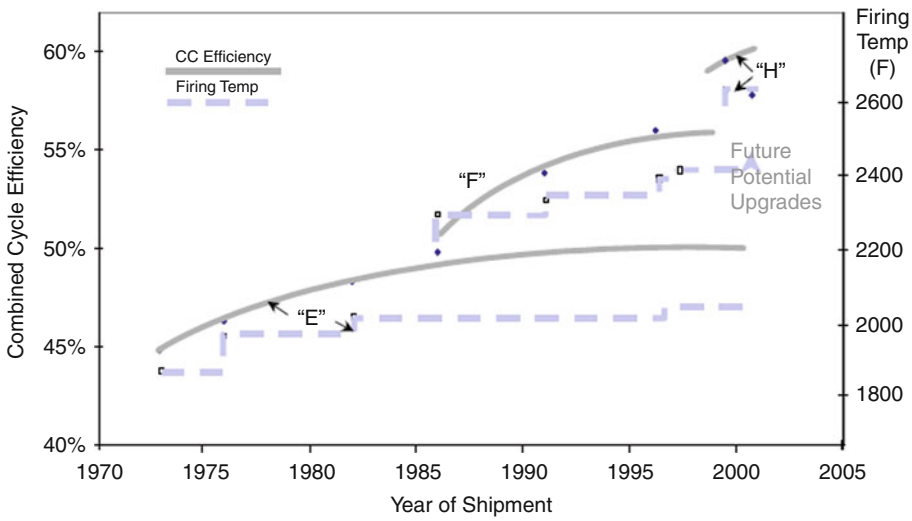

Natural Gas Power. Figure 5
Incremental evolutions of E-, F- and H-Class GT technology (From Ref. [25])

that is commercially available today and, most likely, in the foreseeable future. That reason is embedded in the laws of thermodynamics. Understanding this will enable someone with a basic knowledge of key engineering concepts to grasp the gas turbine design principles and carry out nearly all calculations using simple formulas and a few technology charts. Furthermore, this will also enable the reader to critically evaluate new developments and claims to future improvements in electric power generation systems that employ turbomachines and utilize fossil fuels such as natural gas.

As Descartes wrote in his *Discourse on Method* "one cannot conceive anything so strange and so implausible that it has not already been said by one philosopher or another." As such, in relation to the treatment of the subject in the paragraphs below, a claim of pure originality would be absurd. Nevertheless, the material is wholly original in the sense that key concepts are developed in a unique manner along with all pertinent formulas, representative design parameters and technology curves so that it forms a coherent and compact reference to be used in basic engineering analysis of gas turbine combined cycles. Even then, it must be pointed out that a similar treatment can be found in the excellent brief chapter on gas turbines written by Haselbacher cited in Ref. [26]. Another valuable short reference incorporating the basic fundamental considerations is cited in Ref. [24]. The treatment herein focuses on land-based heavy-duty industrial gas turbines. For a brief introduction to thermodynamic and economic considerations pertaining to aeroderivative gas turbines and pertinent references, the reader should consult Horlock [27].

Basic Thermodynamics

Gas turbine is a relatively simple turbomachine comprising three key components: Compressor, combustor, and expander (Fig. 6). The last one is commonly referred to as a turbine. The compressor and expander are connected through a common shaft. The operation of a gas turbine is described by a thermodynamic cycle comprising four processes: compression, heat addition or combustion, expansion, and heat rejection. A gas turbine can also be classified as an internal combustion engine (just like a car engine), in which the compressed working fluid, i.e., air, mixes with fuel, and the products of the ensuing chemical reaction (i.e., combustion) expand through the turbine. In land-based electric power generation applications, part of the useful mechanical or shaft work, produced by the expanding combustion products (approximately 50% of the total) is consumed by the compressor. The remainder is converted into electric power in a synchronous alternating current (ac) generator, which is connected to the same shaft as the gas turbine.

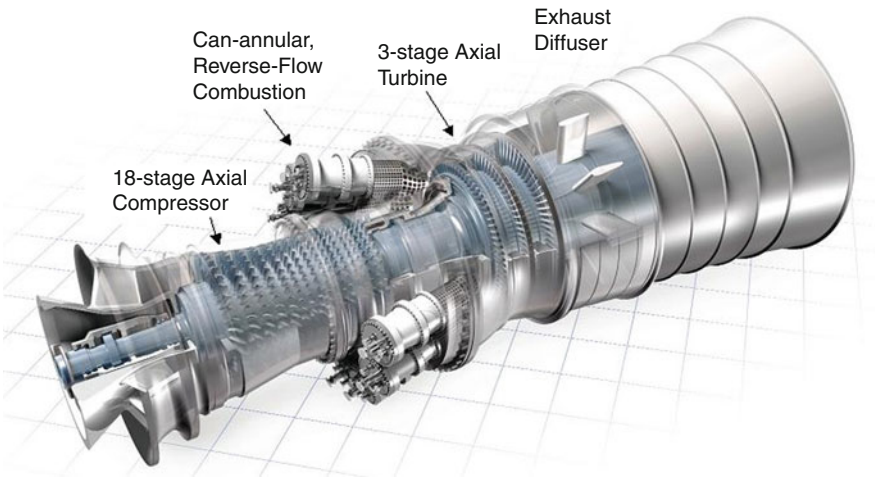

Natural Gas Power. Figure 6
Modern heavy-duty industrial gas turbine (Courtesy: GE Energy)

In aircraft propulsion applications, the entire shaft work generated in the turbine is utilized to drive the engine compressor and fan. The thermal energy in the exhaust gas is converted into kinetic energy in the exhaust nozzle, which generates the net engine thrust.

The thermodynamic cycle that describes the gas turbine operation is the *Brayton* cycle. For simple analytical calculations, which can be found in elementary textbooks on thermodynamics, the ideal or *air-standard* Brayton cycle is used. The classical (and, from an engineering perspective, the most logical) representation of the air-standard Brayton cycle is on a temperature–entropy or T-s surface as illustrated in Fig. 7. The key assumptions in air-standard cycle analysis are:

1. The working fluid is air, which is a calorically perfect gas (i.e., c_p = constant).
2. Isentropic (i.e., adiabatic and reversible) compression and expansion.
3. Constant pressure heat addition and heat rejection.

The two key nondimensional performance metrics for a gas turbine are specific *net* power output and thermal efficiency:

$$w = \frac{\dot{W}_{net}}{\dot{m} \cdot c_p \cdot T_1} \tag{1}$$

$$\eta = \frac{\dot{W}_{net}}{\dot{Q}_{in}} \tag{2}$$

The net power output is the difference between the compressor power consumption and the expander power production. In graphical terms, it is exactly equal to the area encompassed by the cycle 1-2-3-4-1 on the T-s diagram in Fig. 7. Each component's power can be calculated by the application of the *first law of thermodynamics* for steady-state steady-flow (SSSF) successively to their respective *control volumes*:

$$\dot{W}_{comp} = \dot{m} \cdot c_p \cdot (T_1 - T_2) \tag{3}$$

$$\dot{W}_{turb} = \dot{m} \cdot c_p \cdot (T_3 - T_4) \tag{4}$$

$$\dot{W}_{net} = \dot{W}_{turb} + \dot{W}_{comp} \tag{5}$$

From Fig. 7 and (Eqs. 3 and 4) one can easily see that the compressor power consumption is a *negative* number (i.e., work done *on* the control volume) and expander power generation is a *positive* number

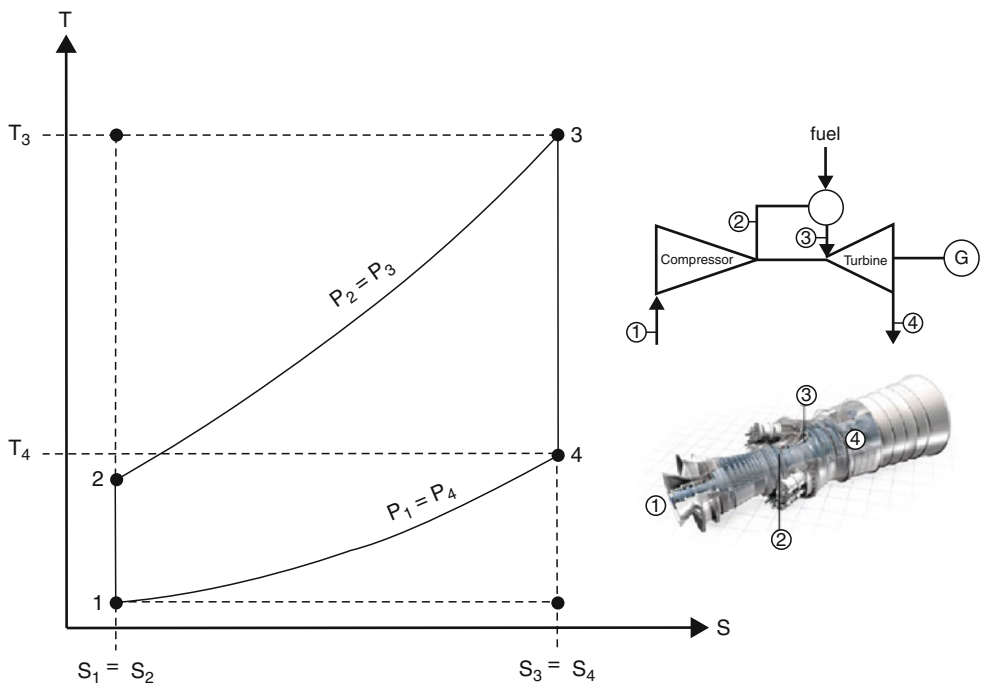

Natural Gas Power. Figure 7
Temperature–entropy diagram of gas turbine Brayton cycle

(i.e., work done *by* the control volume). Application of the first law for SSSF to the heat addition and heat rejection processes, one gets

$$\dot{Q}_{in} = \dot{m} \cdot c_p \cdot (T_3 - T_2) \tag{6}$$

$$\dot{Q}_{out} = \dot{m} \cdot c_p \cdot (T_1 - T_4) \tag{7}$$

From Fig. 7 and (Eqs. 6 and 7), the heat input to the cycle is a *positive* number (i.e., heat supplied *to* the control volume) and heat rejection from the cycle is a *negative* number (i.e., heat taken *from* the control volume).

In addition to the first law of thermodynamics for a SSSF process (or control volume analysis), there is one more key thermodynamic relationship that forms the heart of the GT Brayton cycle calculations: pressure–temperature ratio for an isentropic process:

$$\frac{T_2}{T_1} = \left(\frac{p_2}{p_1}\right)^{\frac{\gamma-1}{\gamma}} \tag{8}$$

where γ is the ratio of constant pressure and constant volume-specific heats. Combining (Eqs.1–7), in nondimensional terms and applying the isentropic formula in Eq. (8) to compression and expansion processes, one ends up with the following two expressions:

$$w = \left(\pi^k - 1\right) \cdot \left(\frac{\tau_3}{\pi^k} - 1\right) \tag{9}$$

$$\eta = 1 - \frac{1}{\pi^k} \tag{10}$$

where $\pi = p_2/p_1$ is the cycle pressure ratio, τ_3 is the cycle maximum temperature (nondimensionalized via division by T_1) and k is the isentropic exponent, $\gamma - 1/\gamma$. The two simple formulas, Eqs. (9) and (10), which are strictly valid only for an ideal air-standard cycle, illustrate almost all of the key facts concerning gas turbine performance:

1. Gas turbine or Brayton cycle performance is controlled by two parameters: Cycle pressure ratio, π, and maximum cycle temperature, τ_3.
2. Cycle efficiency is a function of cycle pressure ratio only; higher cycle pressure leads to higher cycle efficiency.
3. Higher cycle temperature leads to higher cycle specific output.
4. Higher cycle pressure ratio, beyond a certain value, is detrimental to cycle specific output (i.e., $\frac{\partial^2 w}{\partial \pi^2} < 0$ and $\pi = \sqrt[2k]{\tau_3}$ for $\partial w/\partial \pi = 0$).

These observations are also borne out qualitatively by a close examination of the cycle T-s diagram in Fig. 7. As the heat addition isobar moves upward (i.e., higher cycle pressure ratio, π) one can visually verify that the area encompassed by the cycle, 1-2-3-4-1, becomes smaller until, in the limit, it becomes zero. Equation (10) numerically implies that, in the limit when π is sufficiently high, the cycle efficiency will approach 100%, or, $\eta \to 100\%$ as $\pi \to \infty$. This, of course, is impossible, because, as dictated by the *second law of thermodynamics*, the maximum theoretical efficiency attainable by any cycle is given by the Carnot cycle efficiency. The Carnot cycle is a hypothetical power cycle that is represented by two isentropic processes, i.e., compression and expansion; and two isothermal processes, i.e., heat addition and heat rejection. Graphically, it is the rectangle enveloping the Brayton cycle, which is bounded by T_1 and T_3 isotherms and s_1 and s_3 isentropes.

For the cycle in Fig. 7, one can easily visualize the limit of $\pi \to \infty$ as T_3 stays constant. In the limiting case, one will end up with a Brayton cycle that is a rectangle with ~0 area (i.e., zero specific output) and heat addition and rejection at constant temperatures T_3 and T_1, respectively, which essentially defines a Carnot cycle with the efficiency

$$\eta = 1 - \frac{T_1}{T_3} \tag{11}$$

Comparing with Eq. (10), for a cycle maximum temperature of T_3 = 1,500°C and γ = 1.4, this would correspond to a cycle pressure ratio of π = 577 and cycle efficiency η = 87.4%. In other words, as dictated by the second law of thermodynamics, the maximum theoretical cycle efficiency that is attainable by a gas turbine with a "firing temperature" of 1,500°C is 87.4%. Clearly a cycle pressure ratio of 577 is of little practical interest. For the modern heavy-duty industrial gas turbines, the typical value of π is about 18. What does the second law say about a gas turbine for a cycle maximum temperature of T_3 = 1,500°C and π = 18? In order to

find that out, consider the isobaric heat addition process 2 → 3 in Fig. 7. For a reversible and isobaric process, the modified Gibbs equation is

$$h_3 - h_2 = \int_2^3 T \cdot ds \tag{12}$$

One can imagine an (hypothetical) isothermal process that takes place at a constant temperature, whose value lies between T_3 and T_2, and has the same entropy as the actual end states 2 and 3. This process would have exactly the same numerical value of heat addition as the original process, i.e., $h_3 - h_2$, per unit mass. For that process, Eq. (12) can be rewritten as

$$h_3 - h_2 = \bar{T}_H \cdot (s_3 - s_2) \tag{13}$$

Using the calorically perfect gas relationships, the *mean-effective* heat addition temperature can be found from Eq. (13) as

$$\bar{T}_H = \frac{T_3 - T_2}{\ln\left(\frac{T_3}{T_2}\right)} \tag{14}$$

Using the same logic, the mean-effective heat rejection temperature is calculated as

$$\bar{T}_L = \frac{T_4 - T_1}{\ln\left(\frac{T_4}{T_1}\right)} \tag{15}$$

These two mean-effective temperatures are graphically depicted in Fig. 8. Thus, qualitatively any thermodynamic cycle in general, and the Brayton cycle in particular, 1-2-3-4 in Fig. 8, can be represented by its *Carnot-equivalent* cycle, 1′-2′-3′-4′, with mean-effective (constant) heat addition and heat rejection temperatures that are given by Eqs. (14 and 15). The efficiency of that cycle would be given by the well-known relationship for the Carnot efficiency, i.e.,

$$\eta = 1 - \frac{\bar{T}_L}{\bar{T}_H} \tag{16}$$

For an ideal air-standard Brayton cycle, one can show that Eq. (16) is the same as Eq. (10). Thus, for any gas turbine with a cycle pressure ratio of 18, the maximum theoretical efficiency is 56.2%. Using Eqs. (8), (14), and (15), this would be the efficiency of a Carnot cycle with isothermal heat addition and heat rejection at 852°C and 219°C, respectively. It is interesting to note that, changing the cycle maximum temperature from 1,500°C to 1,400°C would change these temperatures to 814°C and 203°C, respectively, but would *not* change the cycle efficiency, i.e., 56.2%, which is only a function of π. This is in contrast to the performance trend of the "real" gas turbines, whose thermal efficiency does indeed increase with increasing cycle maximum or *firing* temperature. Why this is so will be understood below.

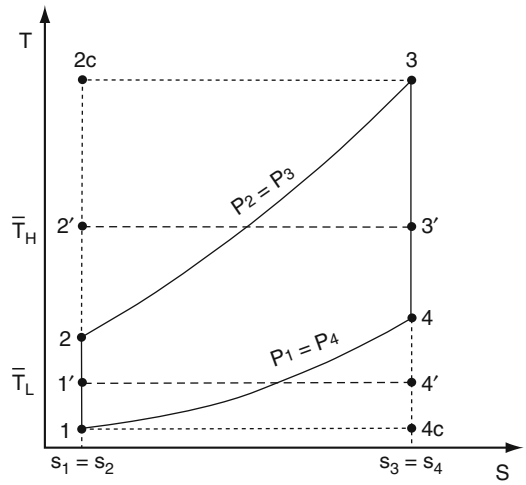

Natural Gas Power. Figure 8
Temperature–entropy diagrams of gas turbine Brayton cycle and its "Carnot equivalent"

One key observation from Fig. 8 is the large thermal efficiency gap between the ultimate Carnot efficiency given by Eq. (11) and the maximum theoretical entitlement level as dictated by the second law, Eq. (10) or Eq. (16), which is nearly 30 percentage points. Graphically, this gap is represented by the two triangular areas in Fig. 8:

1. The upper triangular area 2-2c-3-2, which is equal to the rectangular area 2′-2c-3-3′-2′, and represents the heat addition (i.e., combustion) irreversibility
2. The lower triangular area 1-4-4c-1, which is equal to the rectangular area 1-1′-4′-4c-1, and represents the irreversibility and exergy loss via heat rejection to a heat sink

In terms of cycle temperatures, the upper triangular area is quantified by the gap between the cycle maximum temperature, T_3, and the mean-effective heat addition temperature $\bar{T}_H$. Similarly, the lower

triangular area is quantified by the gap between the cycle minimum or ambient temperature, T_1, and the mean-effective heat rejection temperature $\bar{T}_L$. The latter mechanism of "lost work" associated with heat rejection also points the way to the gas and steam turbine combined cycle power plant concept. This will be explored in some more detail later in the discussion.

The real gas turbine Brayton cycle differs from the ideal, air-standard cycle in the following respects:

1. Non-isentropic compression and expansion (represented by component polytropic or isentropic efficiencies)
2. Pressure losses during heat addition and heat rejection
3. Real gas effects (represented by a suitable equation of state)
4. Change in working fluid composition and properties downstream of combustion process

These nonidealities can be easily incorporated into the simple equations above via polytropic component efficiencies, pressure loss factors, and real gas equation of state. One can refer to one of the available textbooks on the subject for details, e.g., Ref. [29]. For example, Eq. (9) can be rewritten as

$$w = \left(1 - \pi_c^{\frac{k_a}{\eta_c}}\right) + (1+f)\cdot\chi_g\cdot\tau_3\cdot\left(1 - \frac{1}{\pi_t^{\eta_t\cdot k_g}}\right) \tag{17}$$

where π_c and $\pi_t < \pi_c$ are compressor and turbine pressure ratios, respectively, k_a and k_g are isentropic exponents for air and combustion products, respectively, and η_c and η_t are compressor and turbine polytropic efficiencies, respectively. The ratio of the specific heats of combustion products and air is χ_g and f is the fuel–air mass flow ratio. Heat addition can be found from the fuel consumption, i.e.,

$$\dot{Q}_{in} = \dot{m}_f \cdot \mathrm{LHV} \tag{18}$$

where LHV is the net or lower heating value of the fuel at the reference temperature, T_{ref}. The efficiency of the gas turbine is the ratio of Eqs. (17) and (18), i.e.,

$$\eta = \frac{\left(1 - \pi_c^{\frac{k_a}{\eta_c}}\right) + (1+f)\cdot\chi_g\cdot\tau_3\cdot\left(1 - \frac{1}{\pi_t^{\eta_t\cdot k_g}}\right)}{f\cdot\ell} \tag{19}$$

where ℓ is the nondimensional fuel energy content, $\mathrm{LHV}/c_{p,a}\cdot T_1$. Note that for clarity, mechanical and electric losses are omitted from Eqs. (17) and (19), which represent the "shaft" performance. Typically quantified via mechanical and generator efficiencies, η_m and η_g, respectively, these losses should be accounted for the gas turbine generator's net electric output. The fuel mass flow rate (as a fraction of turbine airflow) that is requisite for a specified cycle maximum temperature is given by

$$f = \frac{\chi_g\cdot(T_3 - T_{ref}) - (T_2 - T_{ref})}{\ell\cdot T_1 + \chi_f\cdot(T_f - T_{ref}) - \chi_g\cdot(T_3 - T_{ref})} \tag{20}$$

where the second term in the denominator is the sensible fuel energy input and χ_f is the ratio of the specific heats of fuel and air. Comparing Eq. (19) (along with Eq. (20) that sets the denominator) with Eq. (10), one can easily observe that the GT thermal efficiency, when accounting for the "real" cycle effects, is indeed a function of τ_3. While it is difficult to discern the impact of τ_3 on η just by looking at Eqs. (19) and (20), a sample calculation can illustrate that as shown in Fig. 9.

Typical values that are reasonably accurate for gas turbines burning natural gas fuel (assumed to be 100% CH_4 or methane) are given below (adopted from Ref. [29]) and used in the calculations that resulted in the curves depicted in Fig. 9:

LHV = 21,515 Btu/lb
$c_{p,a}$ = 0.24 Btu/lb-R (1.005 kJ/kg-K)
$c_{p,g}$ = 0.274 Btu/lb-R (1.148 kJ/kg-K) or χ_g = 1.1417
$c_{p,f}$ = 0.60 Btu/lb-R (2.5125 kJ/kg-K) or χ_f = 2.50
γ_a = 1.400
γ_g=1.333
η_c = 87.8%
η_t = 85%
η_m = 99%
η_g = 98.9%
k_a = 0.2857
k_g = 0.2498
T_{ref} = 77°F (25°C)
ℓ = 172.728

Original equipment manufacturer (OEM) data for five 50-Hz (3,000 rpm) heavy-duty industrial gas

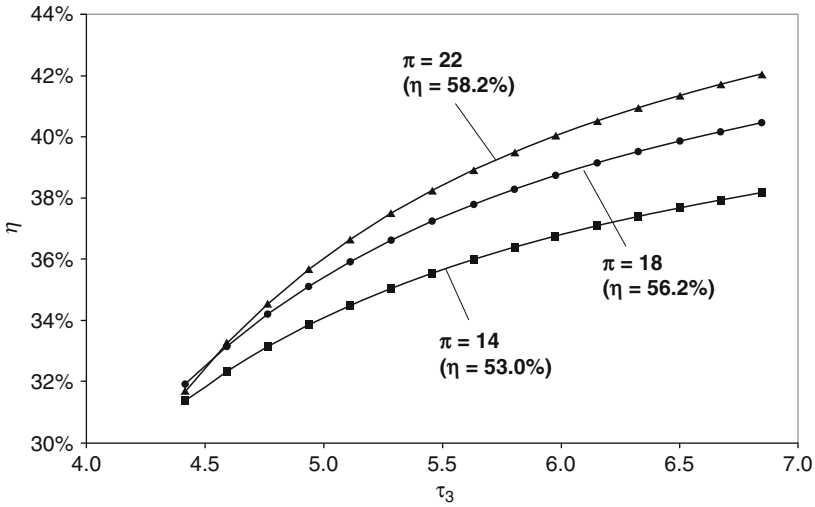

Natural Gas Power. Figure 9
Real Brayton cycle efficiency from Eqs. (19) and (20) as a function of cycle pressure ratio (π) and maximum cycle temperature (τ_3). Also shown (in parentheses) are the ideal, air-standard cycle efficiencies from Eq. (10)

Natural Gas Power. Table 2 OEM data for 50-Hz heavy-duty industrial gas turbines [6]. The maximum cycle temperature, T_3, values are estimated using the published output, efficiency, pressure ratio (PR), and exhaust data with Eqs. (17–20)

	T_3						Exhaust	
Turbine	(°C)	°F	PR	PR_t	Output (MW)	Eff.	(kg/s)	°C
A	1,415	2,579	17.7	15.9	285.0	39.6%	690	572
B	1,443	2,629	17.0	13.5	255.6	36.9%	641	602
C	1,501	2,734	18.3	14.5	279.2	37.8%	655	629
D	1,435	2,616	18.2	16.3	292.0	39.8%	692	577
E	1,476	2,688	18.0	15.5	312.1	39.3%	720	597

turbines from a recent trade publication [6] are given in Table 2.

For an actual gas turbine, the cycle maximum temperature T_3 is equivalent to the turbine inlet temperature (TIT) at the exit of the gas turbine combustor. Another value that is frequently used in the industry is the "firing temperature," which is the temperature at the stage-1 blade row (rotor) inlet. This temperature, also known as rotor inlet temperature (RIT) is the maximum temperature at which the combustion products start producing useful expansion work. The difference between TIT and RIT is about 250°F for modern air-cooled gas turbines and reflects the dilution effect of the stage-1 nozzle and forward wheel space cooling flow. One other cycle maximum temperature definition, favored by European OEMs, is the ISO-TIT, which is a fictitious number as defined by ISO-2314 (typically ~180°F lower than RIT). Obviously, for an uncooled turbine all these definitions are the same.

Gas turbine efficiency as a function of PR is shown in Fig. 10. Specific output, w, in the range covered by the turbines in Table 2 is 400–450 kJ/kg. Carbon dioxide emissions are calculated from the airflow and fuel flow using chemical reaction equations for 100% CH_4 gaseous fuel assumption as 510 kg/h per MW of output

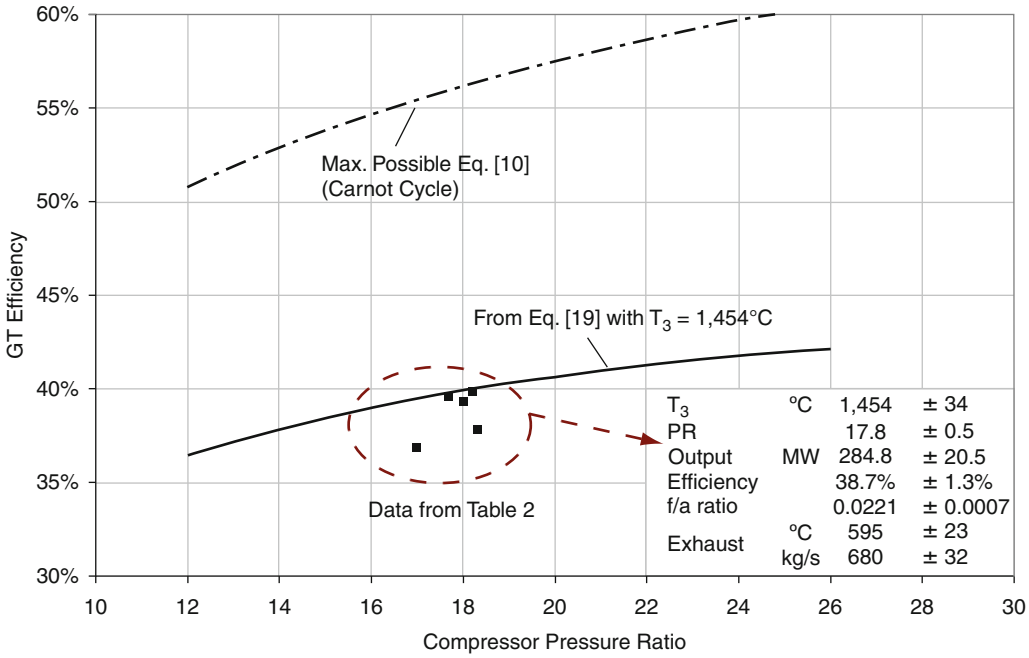

Natural Gas Power. Figure 10
Gas turbine efficiency from Eq. (19) as a function of compressor PR (Data is from Ref. [6] and summarized in Table 2)

at 39% net efficiency. Each one percentage point improvement in efficiency is worth about 15 kg/h per MW reduction in CO_2 emissions. This is equivalent to 27,000 metric tons for a 300 MW GT running at base load for 6,000 h/year.

Figure 10 shows that the gap between the current State of the Art (SOA) in gas turbine technology and the maximum theoretical entitlement level, as dictated by the second law, is more than 15 efficiency points. The GT efficiency – compressor pressure ratio (PR) trend in Fig. 10 (via Eq. (19)) gives the impression that, for a given cycle maximum temperature, the efficiency can be improved indefinitely by increasing the PR. This is *not* true due to a key feature of modern gas turbines that is very difficult to capture in simplified models such as Eqs. (17–20): turbine hot gas path (HGP) component cooling via air extracted from the compressor discharge and/or interstage locations. Since the early days of GT development, the components exposed to the highest temperature environment have been cooled with air drawn from the compressor. The Junkers Jumo-004 jet engine of the German fighter plane Messerschmitt 262, which entered active service in 1944 during the last stages of the World War II, was the first mass production turbojet engine in the history with a turbine inlet temperature (TIT) of 1,427°F [13]. The hollow turbine blades (manufactured by folding flat sheets of 12% Cr alloy called *Cromadur*) were cooled by air extracted from between the fourth and fifth stages of the compressor and introduced to the blade through the holes drilled into the disk. The cooling technology, although unchanged in basic principles, has advanced greatly over the years with the introduction of complex serpentine cooling passages, impingement, film, and transpiration cooling techniques; paced by concurrent advances in superalloys (e.g., nickel-based directionally solidified or single-crystal), manufacturing techniques (e.g., investment casting), oxidation/corrosion (e.g., MCrAlY), and thermal barrier (e.g., yttria-stabilized zirconia, YSZ) coatings. This development supported the advances in TIT, which nearly doubled the standard set by Jumo-004 over the course of the next 50 years (e.g., see Fig. 11 that uses data from Cumpsty [30]). A good overview of the current SOA in advanced GT materials and coatings can be found in Ref. [31].

An alternative to open loop air-cooling (OL-AC) has recently been commercially introduced at the

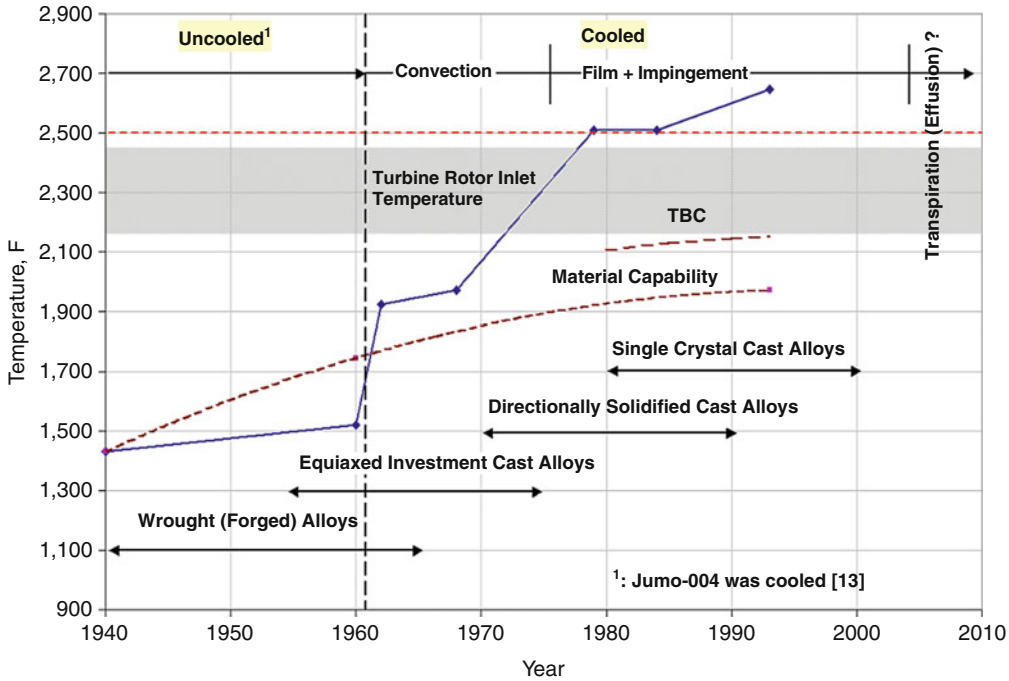

Natural Gas Power. Figure 11

Turbine RIT and bucket alloy capability history [30]. One can add ~250°F to RIT to get a rough idea about TIT of the advanced F-Class units. The shaded region designates the melting point of nickel-based superalloys

480-MW Baglan Bay 109H CC power plant in Wales [32]. This machine employs closed-loop steam cooling (CL-SC) for the majority of the turbine HGP components (the first two stages of the four-stage turbine, to be exact). A "lighter" version of the H-System™ is the G-Class turbine with steam cooling limited to the stationary parts upstream of the turbine HGP [33].

A structural refinement to the basic GT Brayton cycle is the inclusion of a second "reheat" combustor within the turbine expansion. Reheat, or *sequential combustion* as it is referred to by the OEM that successfully commercialized the technology increases the mean-effective cycle heat addition temperature and reduces the combustion irreversibility [34] (the upper triangular area 2-2c-3-2 in Fig. 3). From a fundamental thermodynamic perspective, lower combustion losses give the GT cycle with reheat combustion a higher performance entitlement than a cycle without it. Similarly, there is no doubt that closed-loop (external) cooling is superior to open-loop (internal) cooling but the exact magnitude of that advantage in real machines is difficult to quantify. Chiesa and Macchi [35] quantified the advantages of OL-AC (with and without reheat combustion) and CL-SC technologies via detailed calculations. Using OEM data from GE's 7FB, Siemens V94.3A (now SGT5-4000F), Alstom's GT-26, and MHI's M701G units for calibration, they have developed very detailed cooled GT models and evaluated the CC performances. Their findings are summarized in Table 3, which shows that CL-SC has an advantage of ~1.8 points (%) in net η_{CC} over OL-AC.

A realistic assessment of the gas turbine requires some means to incorporate the cooling penalty into the GT calculations. Cooled turbine expansion models, no matter how much simplified, involve a rather cumbersome system of equations amenable only to a numerical solution. In the open literature, there are numerous published works that range from Holland and Thake [36] and several papers by Elmasri [37–41] during 1980s to the more recent works of Horlock and coworkers [42–45]. Young and Wilcock's comprehensive study [45] and the similar treatment in Ref. [35] incorporate detailed aerothermodynamic calculations.

Natural Gas Power. Table 3 Comparison of CC performances based on four major GT technologies [35]: Air-cooled (OL-AC), air-cooled reheat (OL-AC+SC), steam-cooled (CL-SC), and steam-cooled reheat (CL-SC+SC)

	OL-AC	OL-AC+SC	CL-SC	CL-SC+SC
GT PR	20	30	23	30
HPT RIT (°C)	N/A	1,290	N/A	1,430
HPT RIT (°F)	N/A	2,354	N/A	2,606
RIT (°C)	1,430	1,430	1,430	1,430
RIT (°F)	2,606	2,606	2,606	2,606
Net η_{CC} (%, points)	Base	+0.81	+1.77	+2.74

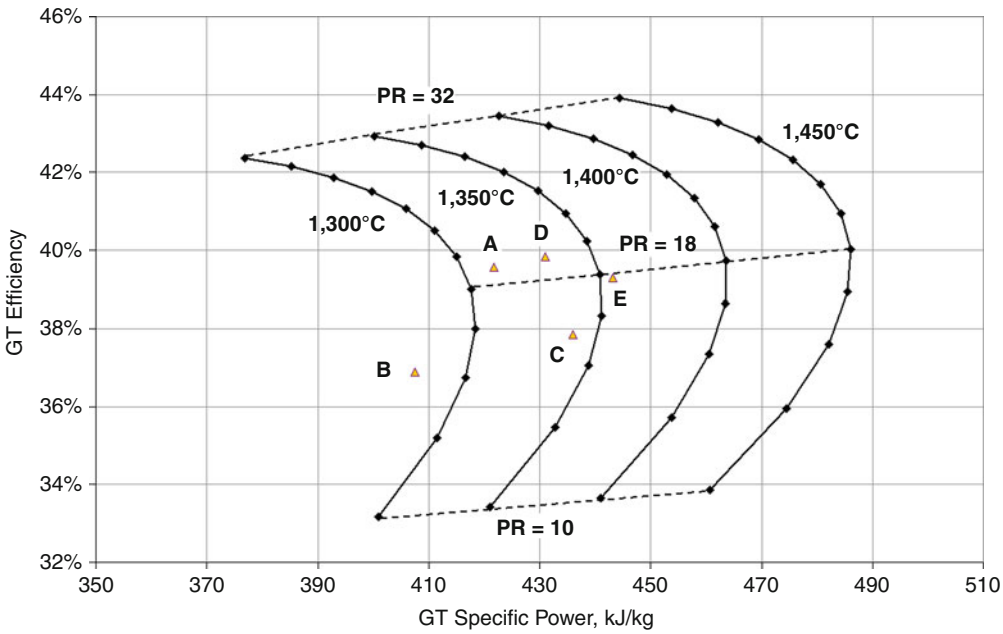

Natural Gas Power. Figure 12
"Real" gas turbine technology curves for different PR-RIT combinations [46] (Also shown is data from Table 2 (as published in Ref. [6]))

On the business side, obviously not available for public consumption, OEMs have their own in-house proprietary codes containing the field-proven knowledge (instead of theoretical approximations) distilled from decades of experience in manufacturing and testing gas turbines. The results from a more realistic GT calculation [46], which includes the impact of turbine cooling with compressor extraction air, are shown in Fig. 12.

Myriad alternate GT design variations have been proposed and entered the literature, some to the extent that they are even covered in elementary textbooks; e.g., compressor intercooling, regeneration (also referred to as recuperation), a combination of both, steam injection (STIG) [47, 48], humid air turbine (HAT) [49], chemical recuperation [50], and closed cycles [51] are among the most well known. For a comprehensive look at those variants and their relative merits, as well as references to the pertinent literature, one can consult the relevant sections in Wilson and Korakianitis [11]. Intercooling and recuperation

technologies have been demonstrated successfully in aeroderivative gas turbines [52,53], whereas the combination of both (ICR) has been incorporated into a ship-propulsion unit [54]. Nevertheless, steam-cooled (G- or H-Class) and reheat machines are the only two commercially proven and successful heavy-duty industrial variants of the basic air-cooled GT, which are suitable to large-scale base load electric power generation.

So far it has been demonstrated that increasing the compressor PR and/or TIT (i.e., maximum cycle temperature) increases the GT efficiency and specific work. The latter reaches a maximum before further increase in PR decreases it. Furthermore, increasing TIT is favorable to CC-specific work and CC efficiency. These trends can be easily visualized and quantified by the ideal cycle diagrams shown in Fig. 13.

The heat rejection "lost work" quantified by the lower triangular area 1-4-4c-1 suggests that a better approximation of the Carnot cycle can be achieved by utilizing the heat source provided by the working fluid at the GT exhaust (i.e., state 4) in a second power generation cycle. At this point, the Rankine cycle presents itself as the ideal choice due to two facts:

1. Good match with GT exhaust (on average about 600°C for SOA F-Class machines) for steam generation at 125–165 bar
2. Constant temperature heat rejection (i.e., in the steam condenser) at a temperature that is much closer to T_1 than $\bar{T}_L$

Earlier in the section, it was shown that the Brayton cycle efficiency is given by the mean-effective cycle heat addition and rejection temperatures, $\bar{T}_H$ and $\bar{T}_L$, respectively, e.g., Eq. (16). Increasing the cycle maximum pressure from p_2 to p_2' increases the cycle efficiency by simultaneously increasing $\bar{T}_H$ and reducing $\bar{T}_L$. It is easy to see that the cycle-specific work, quantified by the area 1-2-3-4, would go through a maximum before approaching zero at which point the cycle efficiency is the Carnot efficiency. The ultimately detrimental effect of continuously increasing the Brayton "topping" cycle (BTC) PR on CC efficiency can also be seen from Fig. 13. The maximum possible CC "bottoming" cycle work, limited by the second law, is equal to the triangular area 1-4-4c-1, which can be shown to be exactly equal to the GT exhaust gas exergy [55]. It is easy to visually appreciate the steady reduction in this maximum with increasing PR (cf. 1-4-4c-1 and 1-4′-4′c-1). The efficiency of the ideal Rankine bottoming cycle (RBC) is given by the equation below:

$$\eta_{RBC} = 1 - \frac{T_1}{\bar{T}_L} \tag{21}$$

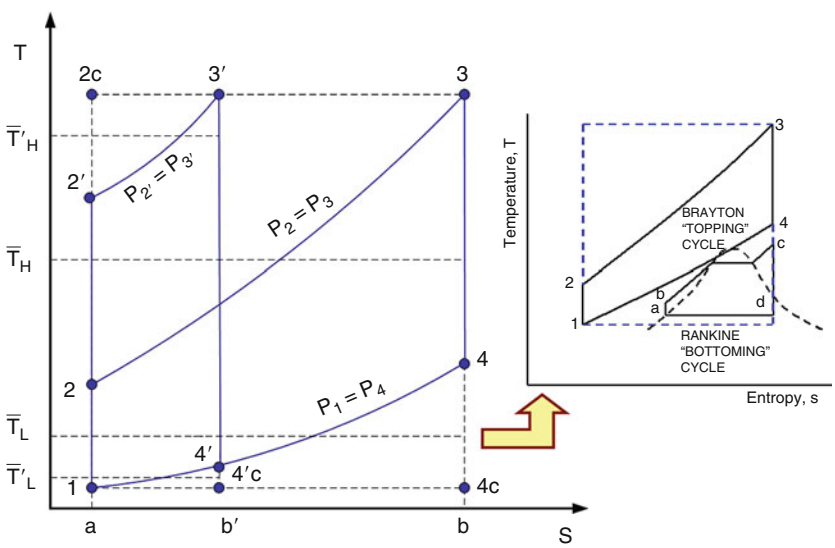

Natural Gas Power. Figure 13

Comparison of Brayton cycles with different PRs on a T-s diagram. Also illustrated is the "combined" cycle concept, in which the Rankine "bottoming" cycle partially recovers the Brayton "topping" cycle heat rejection "lost" work

where $\bar{T}_L$ is from Eq. (15). The formula in Eq. (21) clearly implies that this particular ideal Rankine cycle would be equivalent to a Carnot engine operating between the temperature reservoirs at $\bar{T}_L$ and T_1. Furthermore, the product of Eq. (21) and the total energy content of the GT exhaust $\dot{Q}_{exh}$ can be shown to be exactly equal to the total exergy of the exhaust gas [55]. Exergy is a fluid property that can be calculated using a suitable equation of state with two other known properties (e.g., pressure and temperature) and the composition.

By looking at the cycle T-s diagram in Fig. 13, the ideal CC efficiency with ideal Brayton and Rankine cycles can be deduced to depend on the ratio of the mean-effective Brayton cycle heat addition temperature given by Eq. (14) and the ambient temperature T_1, i.e.,

$$\eta_{CC} = 1 - \frac{\ln\left(\frac{\tau_3}{\pi^k}\right)}{\tau_3 - \pi^k} \tag{22}$$

Ignoring the miscellaneous topping and bottoming cycle losses and minor inputs, a simplified version for the CC shaft efficiency can also be written as

$$\eta_{CC} = \eta_{BTC} + (1 - \eta_{BTC}) \cdot \eta_{RBC} \tag{23}$$

Taking the derivative of both sides with respect to the PR and setting the CC efficiency derivative to zero for the maximum, one finds that (note that the RBC and BTC efficiencies are approximately the same in magnitude)

$$\frac{\partial \eta_{BTC}}{\partial PR} \approx -\frac{\partial \eta_{RBC}}{\partial PR} \tag{24}$$

This relationship states that the maximum *Brayton–Rankine* combined cycle efficiency occurs at the point where the rate of increase of BTC efficiency with PR is the same as the rate of decrease of the RBC efficiency. Using the ideal Brayton cycle formulas, which can be found in any standard thermodynamics textbook such as Ref. [28], the rate of increase of BTC efficiency with increasing PR is

$$\frac{\partial \eta_{BTC}}{\partial PR} = \frac{\gamma - 1}{\gamma} \cdot PR^{\frac{1-2\gamma}{\gamma}} \tag{25}$$

From Eq. (21), once again using the ideal Brayton cycle relationships, the rate of decrease of the RBC efficiency with increasing PR is found as

$$\frac{\partial \eta_{RBC}}{\partial PR} = \frac{\gamma - 1}{\gamma} \cdot \frac{\left(\frac{T_1}{\bar{T}_L}\right) \cdot \left(\frac{T_4}{\bar{T}_L} - 1\right)}{PR \cdot \ln\left(\frac{T_4}{T_1}\right)} \tag{26}$$

Combining Eqs. (21–26) with $\gamma = 1.4$ and $T_1 = 85°F$ (assuming RBC heat rejection at 1.2 in. Hg or 41 mbar of steam condenser pressure) and solving them numerically, the PR of the BTC for maximum CC efficiency can be plotted as a function of T_3 (see Fig. 14). Also plotted in Fig. 14 is the PR corresponding to the maximum BTC specific work, $\pi = \sqrt[2k]{\tau_3}$, with T_1=59°F. For comparison, representative OEM data extracted from a recent trade publication [6] is also shown. It is interesting to note the excellent agreement of the PR-TIT data of actual production machines with values corresponding to maximum GT-specific power output predicted using a rigorous cooled gas turbine model.

Using an uncooled *quasi-ideal* GT model with reasonable assumptions outlined earlier in the section to take into account the real turbine losses, CC efficiencies corresponding to the parameters in Fig. 14 are calculated and plotted in Fig. 15. The key takeaways from the plots in those figures are rather illuminating:

1. Actual OEM designs are at PR values somewhat lower than those for maximum GT-specific output in an uncooled GT but coincide extremely well with the air-cooled GT specific work line, in accordance with the earlier observation made by Horlock [24].
2. This seems to be a reasonable choice from a cost perspective with ~0.50 percentage points sacrifice in performance vis-à-vis the maximum η_{CC} that has a ~50% larger PR. In fact, the proximity of the two maxima is even closer in the presence of turbine cooling so that this is a very reasonable trade-off indeed.
3. 65% and 70% net CC efficiencies require uncooled turbines with TIT of 2,500°F and 3,000°F, respectively.

OEM data for combined cycle performances based on five 50-Hz (3,000 rpm) heavy-duty industrial gas turbines from a recent trade publication [6] (see Table 2) are given in Table 4. The data is for two major combined cycle configurations, which are labeled as 1 × 1 (i.e., one GT and one ST) and 2 × 1 (i.e., two GTs and one ST). Using the GT performance

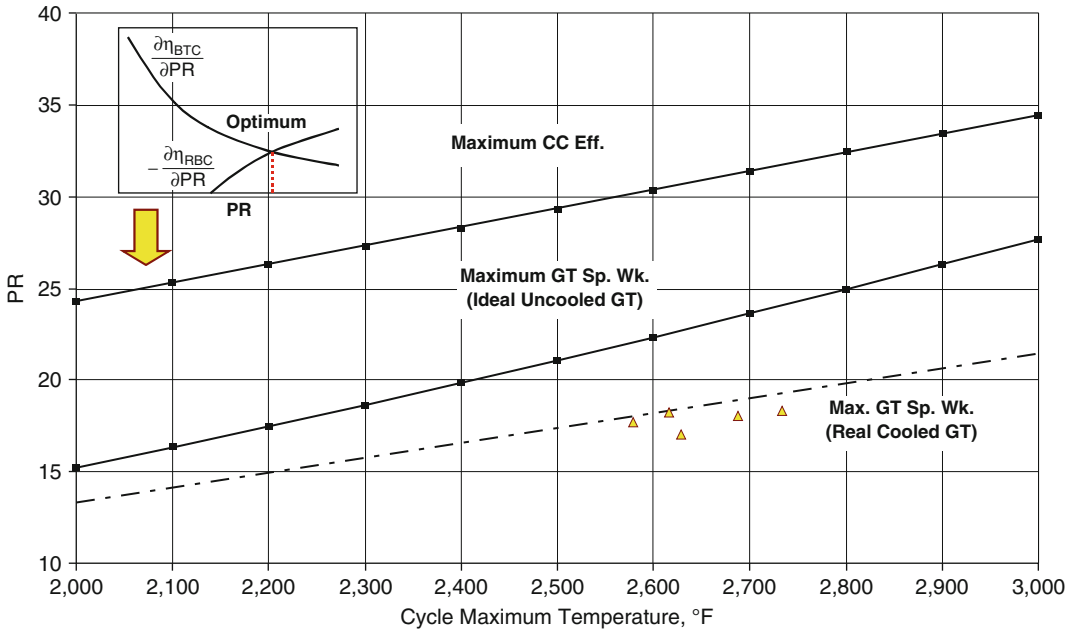

Natural Gas Power. Figure 14

PR for maximum CC efficiency and maximum BTC specific work. Data points are from Ref. [6]. Cycle maximum temperature or T_3 values are from Table 2. The inset illustrates the calculation of maximum η_{CC} point using Eqs. (24–26)

in Fig. 12 as a basis, CC performance curves can be developed using the exergy-based bottoming cycle calculations in Ref. [56] (see Fig. 16).

Today's SOA in CC performance with advanced gas turbines corresponds to a range of 57% to ~60% with TIT values in the range of 2,600–2,800°F. This is a far cry from the theoretically possible values in the absence of turbine cooling as shown in Fig. 15 (by about 10 percentage points). Sponsored by the DOE's National Energy Technology Laboratory (NETL), the *Vision 21* program has a goal to develop, by 2015, the core modules for a fleet of fuel-flexible, multiproduct energy plants that boost power efficiencies to more than 60% (75% on an LHV basis for gas-fueled plants), emit virtually no pollutants, and with carbon sequestration release minimal or no carbon emissions. Lately, several published claims about the future of the CC plant performance at the end of the first quarter of the twenty-first century stated a goal of 65% with the possibility of over 70% with an air-cooled GT [57]. The uncooled GT–based CC efficiency curves and the current SOA data in Fig. 15 underline the significant hurdles to be overcome in terms of cooling flow reduction in pace with increasing firing temperatures in order to achieve those goals. The gap between the uncooled GT TIT (i.e., same as RIT) requirement for 65% η_{CC} and the current material capability is nearly 800°F (~450°C). The current trend in superalloy capabilities, considering the competing tendencies in strength (i.e., creep rupture and fatigue limits) and corrosion resistance, does not seem to be likely to alleviate too much of that [58]. A combination of advanced materials including ceramic matrix composites, metal foams (to enable the upper limit of film cooling, i.e., effusion or transpiration cooling) [59] and external cooling (most likely via steam) accompanied by bottoming cycle advances is imperative to even approach the stated efficiency goals with acceptable NO_x and CO emissions. It is thus fairly obvious that a η_{CC} goal of 65% and higher in a *Brayton–Rankine* CC power plant is a highly unlikely proposition in near future. This is more or less the conclusion reached by Rao et al. [60] who investigated the plant system configurations that might be able to meet the performance and emission goals of Vision 21 program. They concluded that hybrid systems integrating fuel cells with gas turbines,

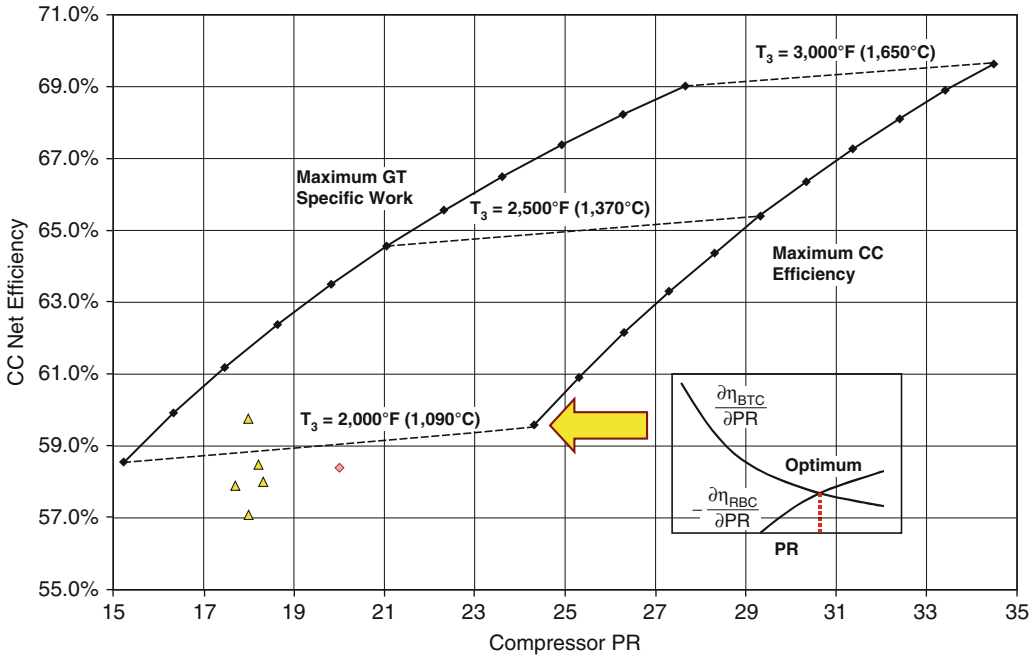

Natural Gas Power. Figure 15
Uncooled GT-based CC efficiencies (note that $T_3 \equiv$ TIT). The data (symbol Δ) is from Table 4. The other data is from Ref. [35] for the SOA air-cooled GT (TIT=2,826°F). The inset illustrates the calculation of maximum η_{CC} point using Eqs. (24)–(26) in the text. Component polytropic efficiencies are assumed to be 92.5% and 90% for the compressor and turbine, respectively

Natural Gas Power. Table 4 OEM data for combined cycle performances (1×1 and 2×1) of 50-Hz heavy-duty industrial gas turbines [6] (Gas turbine data is in Table 2)

		1×1			2×1		
	GT	ST	CC		ST	CC	
Turbine	MW	MW	MW	η (%)	MW	MW	η (%)
A	285.0	141.0	415.1	57.9	282.0	830.2	57.9
B	255.6	141.8	390.8	56.7	289.2	786.9	57.1
C	279.2	157.9	412.9	58.0	315.3	825.4	58.0
D	292.0	144.7	423.0	58.4	290.3	848.0	58.5
E	312.1	157.3	459.0	59.5	317.7	921.1	59.7

e.g., SOFC/GT hybrid system [61], were required to meet the program goals. There's little doubt about the very attractive efficiency of the SOFC/GT hybrid systems, e.g., 65–70% for atmospheric cells and 74–76% for pressurized cells [62]. What is really doubtful is whether they will be competitive with gas turbine–based systems for large-scale electric power generation considering their low power density, e.g., less than 5 kW/m^2 (cf. ~3,000 kW/m^2 for a large GT), and high cost, e.g., about $1,500/kW to $3,000/kW in 2010 dollars [63] (cf., $350/kW to $500/kW for a GT depending on its size).

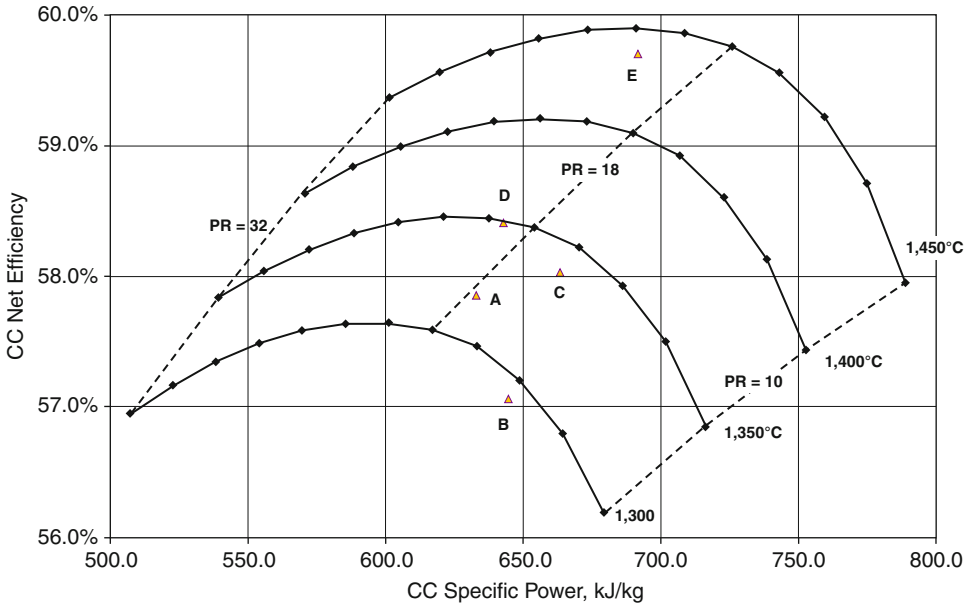

Natural Gas Power. Figure 16
"Real" combined cycle technology curves for different PR-RIT combinations. They are based on the gas turbine technology curves in Fig. 12. (Also shown is data from Table 4 (as published in Ref. [6]))

Today's SOA in CC Power Plants

A schematic diagram of a CC system is shown in Fig. 17, which depicts the four major components: gas turbine, steam turbine, condenser, and the heat recovery steam generator (HRSG). Not shown is the cooling tower (CT), which cools the condenser cooling water. Usually, the heat rejection system (including condenser, CT and circulation pump), and feed pumps along with myriad smaller heat exchangers (such as the GT fuel gas heater in the upper left corner in Fig. 17) are collectively referred to as the "balance of plant" (BOP).

The equipment that combines the GT (i.e., Brayton cycle) and ST (i.e., Rankine cycle) is the HRSG. Hot GT exhaust gas (>1,100°F for modern F-Class units) transfers heat to condensate and generates superheated steam, typically at multiple pressure levels, which is used in the ST for power generation. Current SOA is a three-pressure system with reheat (i.e., heating of HP steam turbine exhaust, referred to as "cold reheat," to the same temperature as the main or HP steam) with steam temperatures of 1,050°F or higher. Highest steam pressure at the ST inlet (throttle) is around 1,800–2,500 psia, beyond which the pressures at the generation point in the HRSG exceed the critical pressure and one would require a "once-through" steam generation system as opposed to the existing "drum type" system. From the fundamental thermodynamics discussed earlier, the theoretically maximum (net)

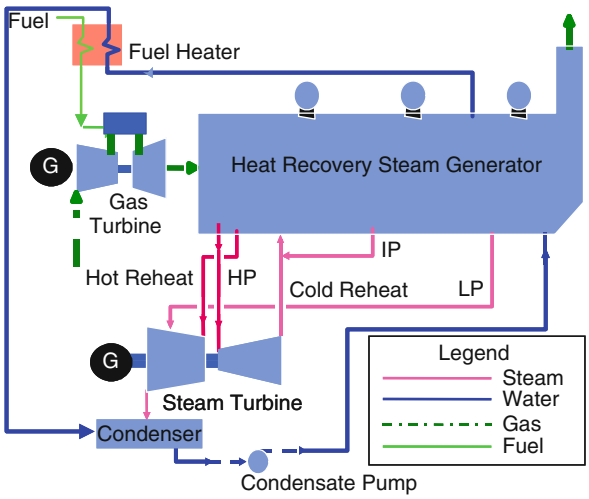

Natural Gas Power. Figure 17
Three-pressure, reheat (3PRH) combined cycle diagram (Source: GE Energy [64])

power output that can be obtained from the Rankine bottoming cycle of the CC plant is exactly equal to the exergy of the GT exhaust gas [55]. Today's most advanced plants with advanced F-, G-, and/or H-Class GTs and 3PRH steam systems, are capable of achieving ~72% of that theoretical maximum, which can only be achieved in a Carnot engine [56]. For rapid estimations, this translates into an ST power output that is about 50% of the combined power output of all GTs in the plant.

As the fundamental CC efficiency relationship, Eq. (23), and the graphical representation in Fig. 13 make it very clear, the cycle's heat rejection temperature is of prime importance. This temperature is dictated by the steam condenser's operation pressure, which is significantly below the atmospheric pressure. For the best performance, lowest possible steam condensation pressures, around 1.5 in. of Hg or even lower, are imperative. Achieving those low-pressure levels requires striking a delicate balance between heat rejection equipment size, cost, type, and site ambient conditions. The key heat rejection system equipment is the steam condenser. There are many types of condensers that are used to handle the heat rejection from the CC plant. Depending on the site ambient conditions, cooling medium availability, environmental regulations and customer-specific economic criteria, a suitable choice can be made. The major options are listed below.

1. Water-cooled surface condenser
   - Once-through or open-loop (utilizing a naturally available cooling water source such as lake, river, ocean)
   - Closed-loop with a natural (very rare for CC plants) or mechanical (forced or induced draft) cooling tower (CT)
2. Dry, air-cooled (also known as the "A Frame") condenser
3. Air-cooled wet surface (hybrid) or "plume abatement" condenser
4. Direct contact condenser with dry CT (Heller) system

In general, water-cooled systems, in particular open-loop systems near a relatively cold natural source of cooling water (e.g., in coastal locations in the northern hemisphere), offer the best performance, i.e., the lowest condenser pressure. How low in condenser pressure one can go is essentially a question of plant economics. Recently, permitting requirements in conjunction with environmental considerations and water scarcity in many geographic locations render water-cooled heat rejection systems infeasible. Significant size and cost of "dry" or air-cooled systems preclude the optimal condenser pressures and optimistic performance projections displayed in Fig. 16.

The key to affordable and sustainable large-scale electric power generation is economies of scale that can be achieved by ever-larger prime movers (gas and steam turbines of 300+ MW) and plant blocks. Modern CC plants include one or more GTs with a single ST; either in a "multi-shaft" or "single-shaft" configuration (e.g., see Figs. 18 and Figure 19). The most common multi-shaft block is 2×1 (i.e., 2 GTs and 1 ST) with power ratings of 600–900 MW. A few larger plants in 3×1 or 4×1 configuration or in multiple blocks of 2×1 are also available (e.g., see Fig. 18). Single-shaft (i.e., 1×1) plants with power ratings of 300–500 MW per "block" can also be combined into very large generating stations via multiple blocks. For a representative selection of modern CC power plant configuration options and performances, the reader is referred to the white papers listed in [64–68].

Even better economies of scale are achieved via the "reference plant" approach, in which OEMs develop pre-engineered modules that can be shipped and installed anywhere in the world with minimal customization to accommodate different site and customer requirements. This ensures that natural gas burning GT-CC power plants are not only the most efficient means of generating electric power available today, but also the most cost-effective (e.g., at a turnkey capital cost of $600–1,000/kW and cost of electricity of a few cents per kWh)) and fastest to build (e.g., less than 24 months of construction time). On top of all that, GTs with modern "dry low NO_x" combustors are also the cleanest fossil fuel burning technology in terms of emissions. This aspect will be explored in detail in the following section.

Cogeneration

Discussion thus far has focused on production of electricity from natural gas. When electricity is the sole product from the thermal cycle the heat rejected to

Natural Gas Power. Figure 18
Illustration of a 2×207FA (two Frame-7 60-Hz GTs with single ST) NG CC power plant. From *left* to *right*, for each GT-HRSG "block" one can see the GT inlet air filter housing and duct (on top of the GT enclosure), HRSG with drums on the top, and the stack. Two STs are located to the right of the GT-HRSG blocks (cross-over pipe and down-flow LP section are clearly visible). Note the elevation of the ST structure to accommodate the steam condenser. Partially visible to the right is the multicell mechanical cooling tower. In the lower right corner are two distillate oil (GT backup fuel) tanks (Courtesy: GE Energy)

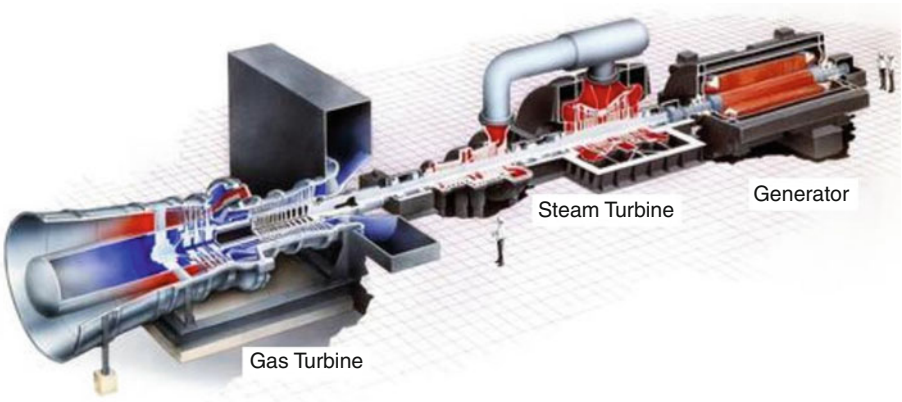

Natural Gas Power. Figure 19
A single-shaft combined cycle train (Courtesy: GE Energy)

ambient is termed "waste heat" because it is no longer economically useful for generation of additional power. In the larger context of a modern industrial society one finds that low temperature heat of the quality least useful for power generation has many economically important uses. It is thus common in industrial and urban settings to integrate a power plant with another process such that heat energy for that process is

provided in whole or in part by the power cycle after the highest quality fuel energy has produced some useful work. Such installations are termed cogeneration systems or Combined Heat and Power (CHP) systems and can be very efficient from an environmental and fuel use perspective. Table 5 provides a sampling of cogeneration opportunities with a synergistic combination of heat and power needs.

In the ideal case, the heat energy available from the prime mover (engine or thermal cycle) will always match the needs of the customer process. In practice, this is challenging since many process heat demands are variable (such as building or district heating). The electrical loads can also be out of phase with process heat demands (e.g., an electric grid with high but unsteady wind or solar renewable power contributions). These variations in electrical load vs. process heat loads can be accommodated with appropriate system design and operating strategies. A variety of cogeneration plant options are available between the extremes of a non-cogeneration facility, e.g., fired heater or boiler, with no power generation at all (e.g., a home heating system capturing the heat content of the fuel but wasting its potential to do work [69]) and the aforementioned power generation combined cycle with no process heat demand, which has accordingly been optimized for production of electricity.

Natural Gas Power. Table 5 A sampling of natural gas Fired cogeneration opportunities [71]

Industrial	
Paper and board manufacture	Pharmaceuticals and fine chemicals
Ceramics	Brewing, distilling, and malting
Textile processing	Food processing
Oil refineries	Minerals processing
Timber processing and paper	Horticulture and glasshouses
Buildings	
Hotels	District heating and cooling
Airports	Hospitals
Supermarkets and large stores	College campuses and schools
Individual houses	Office buildings

Primary considerations in cogeneration system design are the size of the plant, the relative need for heat vs. electrical power, and the electricity and process heat demand variability. The following points summarize the range of system design solutions:

- Large industrial gas turbines ranging from ~20 to 300 MW electrical output are optimized for best combined cycle efficiency, and have exhaust energy of about 60% of heat input with exhaust temperatures between about 1,020°F and 1,160°F (550°C and 625°C). This class of machine is well suited to process heat demands that are large in an absolute sense but small or intermittent in relation to electrical power demand, (0% to ~30% of gas turbine heat input). This level of heat energy supply can readily be accommodated by modifying the power generation combined cycle system to include the capability to extract or divert steam from the bottoming cycle steam turbine to the process. This is a common solution for district heating which may be highly variable and seasonal.
- Aeroderivative gas turbines ranging from ~5 to 60 MW electrical output are optimized for best simple cycle efficiency, and have exhaust energy of about 55% of heat input with exhaust temperatures of about 850°F (455°C). These machines are large enough to support substantial process heat loads and are often configured in a system without a steam turbine to save cost and make a higher portion of gas turbine exhaust energy available to process. In many industrial cogeneration facilities, it is more important to match process heating demand than to meet a specific electric load. The gas turbine load is thus varied to follow process energy demand independent of electric load. Any excess electricity generated is sold to the grid and any power shortfall is purchased. If the design process heat demand is high in relation to electric load, or may occasionally need to be much higher than the unfired gas turbine exhaust energy, the system will need to include a supplemental burner in the HRSG, which can be used to boost process heat export capability. A burner may also be used in combination with part load operation of the gas

turbine to maintain process heat export while reducing electricity production to match its load.

- A micro gas turbine ranging from ~0.03 to 0.3 MW electrical output may be selected if the heat load and/or electric load is small. Micro turbines typically employ uncooled regenerative cycles for best simple cycle efficiency, have exhaust energy of about 75% of heat input, and exhaust temperature of about 530°F (275°C). These units are too small to economically justify a bottoming cycle steam turbine so that they fall into the unfired or supplementary-fired heat recovery–type system configuration.
- In the size range between micro turbines and aeroderivatives, a variety of small industrial gas turbines and other prime movers such as a spark ignition reciprocating engine, or fuel cell, may also be considered. In the range from ~10 to 150 MW, direct-fired steam Rankine systems with steam turbine extraction for process heat can also be an attractive configuration that is well suited to highly variable process heat needs. Power can be varied across a wide range with modulated fuel consumption and heat export can also be widely varied via controlled steam extraction. Efficiency at low process demand is inferior to gas turbine–based systems but fuel flexibility is generally better.

Table 6 shows some examples of gas turbine–based natural gas–fired cogeneration systems. These are presented to elucidate the behavior of such systems and draw conclusions regarding the role of cogeneration in promoting sustainable use of natural gas. Columns tabulate net electric power export, export heat energy to power ratio, quality of export heat expressed as a ratio of its availability to produce work (exergy), electric generation efficiency, cogeneration efficiency expressed on both an energy and exergy basis, and

Natural Gas Power. Table 6 Typical heat-to-power ratios and efficiencies for GT-based CHP systems

							Engine+Burner CO_2 Emissions	
	Net power (MWe)	θ	β	$\eta_{el.}$ (%)	$\eta_{c,I}$ (%)	$\eta_{c,II}$ (%)	*A*	*B*
1. Unfired micro GT	0.1	1.74:1	0.29	25.4	69.6	38.3	284.7	516.9
2. Supplementary fired micro GT	0.1	10.0:1	0.44	8.6	93.0	46.6	212.9	418.3
3. Unfired aeroderivative GT	40	1.13:1	0.41	41.2	87.8	60.4	225.4	327.7
4. Supplementary fired Aeroderivative GT	40	2.63:1	0.44	26.3	93.0	56.6	212.9	349.6
5. Unfired industrial GT	100	1.50:1	0.45	35.6	89.0	59.5	222.5	332.8
6. Supplementary fired Industrial GT	100	2.84:1	0.44	24.8	93.0	55.7	212.9	355.4
7. Gas turbine combined cycle (unfired, industrial GT)	100	0.1:1	0.29	54.3	59.7	55.9	331.8	354.4
		0.5:1	0.34	49.1	73.6	57.4	269	344.7
		1.0:1	0.38	42.4	84.9	58.7	233.3	337.2
8. Gas turbine combined cycle (industrial GT with supplementary firing)	100	1.5:1	0.44	35.2	88.0	58.5	225.1	338.8
		2.0:1	0.44	31.6	93.0	59.4	212.9	333.2

θ is heat to power ratio in kWth/kWe
β is heat quality, which is the ratio of export exergy to export energy
$\eta_{el.}$ is electric generation efficiency
$\eta_{c,I}$ is first law cogeneration efficiency (energy-to-fuel input)
$\eta_{c,II}$ is second law cogeneration efficiency (exergy-to-fuel input)
Emissions are in g/kWh of energy (*A*) and exergy (*B*)

specific CO_2 emissions also expressed on both an energy and exergy basis. Export heat is provided as steam in all cases.

Cogeneration efficiency $\eta_{c,I}$ in Table 6 is the straight ratio of the sum of power (kWe) and heat (kWth) products to the fuel burned in the plant on an LHV basis. This is a commonly used (sometimes with fuel input on an HHV basis) measure, which is ultimately misleading because it does not differentiate between the "quality" of different products. In certain cases, especially with supplementary firing, it can reach improbably high values such as 90% or more.

A more rational measure is the cogeneration efficiency per the second law of thermodynamics, $\eta_{c,II}$, which uses the exergy of the thermal product rather than its energy (i.e., enthalpy) [70]. Exergy, as discussed earlier in the present article, is a direct measure of the work generating ability of a material stream via Kelvin–Planck statement of the second law of thermodynamics. Exergy is a property of a given fluid and, as such, for two given properties (e.g., pressure and temperature), it can be calculated using a suitable equation of state such as ASME steam tables. The relationship between $\eta_{c,II}$ and $\eta_{c,I}$ is given as

$$\eta_{c,II} = \eta_{c,I} \cdot \frac{1 + \beta \cdot \theta}{1 + \theta}$$

where θ is the heat-to-power ratio of the cogeneration plant, and β is the ratio of the exergy to energy (enthalpy). Since $\beta < 1$, $\eta_{c,II} < \eta_{c,I}$ and has typically a value, which is more in line with standard power plant efficiencies. In passing note that the PURPA (*Public Utility Regulatory Policies Act*, a US federal law enacted in 1978 intended to encourage more energy-efficient and environmentally friendly commercial energy production) efficiency, which is another cogeneration plant efficiency definition, is equivalent to $\eta_{c,II}$ with $\beta = 0.5$. Even $\eta_{c,II}$ is an inflated value because β is the efficiency of a hypothetical Carnot engine that converts the thermal energy to useful shaft work.

A realistic turbine that can utilize that thermal efficiency for electric power generation would have a much lower efficiency, which is characterized by the rational efficiency, ε, which is the ratio of actual turbine power output to that of the hypothetical Carnot engine. The most common thermal energy product in cogeneration is steam. Depending on the pressure and temperature of steam, with today's state of the art in ST technology, a reasonably good estimate for ε would be around 0.7. Thus, a more realistic value for $\eta_{c,II}$ would be given as

$$\eta_{c,II} = \eta_{c,I} \cdot \frac{1 + \varepsilon \cdot \beta \cdot \theta}{1 + \theta}$$

Case 1 is a micro turbine–based design with no supplemental fuel addition to exhaust heat recovery. Export energy is high in relation to power production since the engine is only 25% efficient but export heat quality is low since exhaust temperature is a modest 530°F (275°C). This low exhaust temperature also compromises the cogeneration energy efficiency in these examples because only a portion of the unfired exhaust energy is recoverable to steam.

Case 2 adds a supplemental burner fired to 1,600°F (871°C) to boost export energy substantially while also improving its quality. Fuel heat energy is now fully utilized to provide power and process heat (93% cogeneration efficiency, energy basis), but the performance is still modest on an exergy basis since the engine is inefficient. Note also that specific CO_2 emissions (exergy basis) improved because the incremental efficiency due to increased and improved heat export is better than the electrical efficiency of the gas turbine.

Cases 3 and *4* show the corresponding story for a 40 MW aeroderivative gas turbine while *cases 5* and *6* present a 100 MW industrial gas turbine scenario. These gas turbines both improve exergetic performance over the micro turbine cases but when supplemental firing is added the cogeneration efficiency and specific CO_2 emissions (exergy basis) both degrade. The more efficient aeroderivative has slightly higher system performance but lower process heat export capability vs. the industrial gas turbine.

Case 7 shows the 100 MW industrial gas turbine in a combined cycle configuration with increasing steam extraction to process. Electric generation efficiency falls off as more energy is diverted to process while cogeneration efficiencies improve. *Case 8* begins where case 7 left off with power output maintained as supplemental firing is increased. By the time 1,600°F (871°C) supplemental firing

temperature is reached the export heat energy has approximately doubled. As supplementary firing increases the specific CO_2 emissions (exergy basis) stays approximately constant.

Note that the supplementary-fired scenarios presented here stop at 1,600°F (871°C) consistent with uncooled metal ductwork. Firing temperature can be pushed further by application of refractory or water-cooled walls until the excess oxygen is nearly expended; or increased even further if supplemental air is also added. High supplementary firing may be required for some applications but is less desirable from a resource conservation perspective than a design with little (or no) supplementary firing.

The following general conclusions can be drawn from this sampling:

1. Cogeneration efficiency should be expressed on an exergy basis to promote the most sustainable use of fossil fuels. Direct use of fuel for low-quality end uses represents a large waste of the thermodynamic potential inherent in the fuel. Cogeneration efficiency as commonly expressed in relation to export energy gives the false impression that supplementary firing improves the environmental (CO_2) and resource (natural gas) utilization performance.
2. Cogeneration system configuration will be a function of the quality and quantity of heat energy required, its variability, and the relative heat and power needs. A wide range of applications can be served by appropriate system design.
3. Gas turbine–based systems are most efficient when not supplementary fired while gas turbine combined cycle cogeneration systems maintain high cogeneration exergetic efficiency even with supplemental firing. This is because fuel energy can be recovered to power all the way down to the temperature level required by the process user.

Figure 20 shows cogeneration's contribution to electricity production in European Union countries.

The higher penetration seen in four of these countries is attributed to a combination of favorable economics and supportive government energy policy [71].

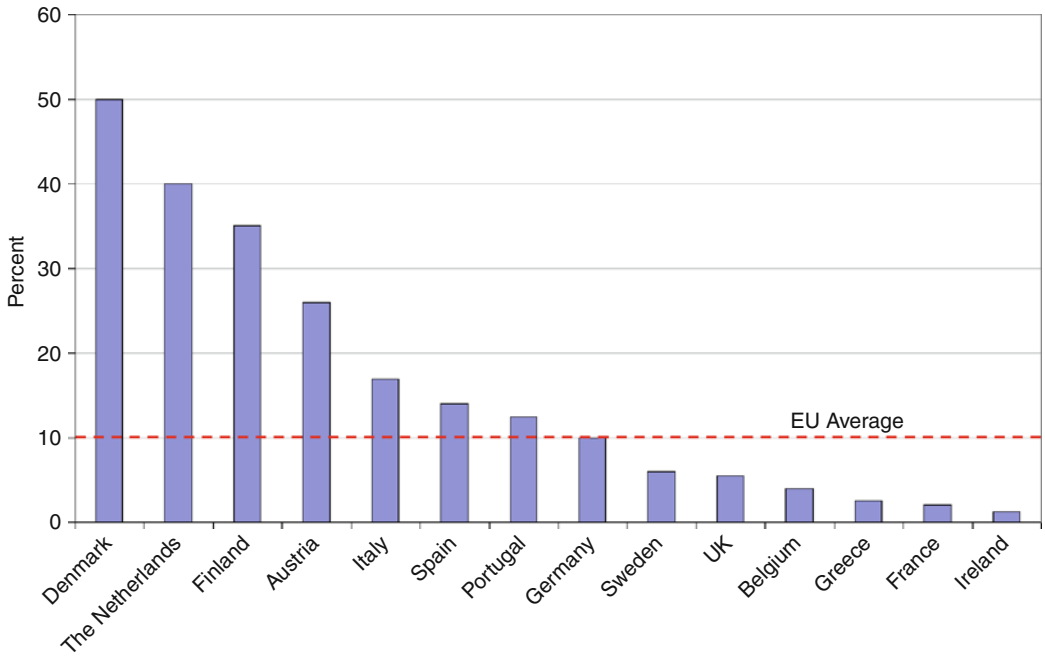

Natural Gas Power. Figure 20
Cogeneration as a share of national power production (1999) (Source: European Association for the Promotion of Cogeneration [71])

Natural Gas Power. Table 7 Annual US thermal energy available supply and rejection, 2008 [72, 73]

	Coal	Petroleum	Natural gas			Nuclear	Total
			Combined cycle	Simple cycle	Cogeneration		
Electricity generation (Billion kWh)	1,986	46.2	562	122	200	806	3,721
Heat rate (Btu/kWh, HHV)	9,884	9,884	7,598	11,526	11,156	10,488	
Heat input (trillion Btu)	19,628	457	4,268	1,402	2,227	8,456	36,062
Approximate heat rejection to ambient or process (trillion Btu)	10,889	254	1,408	847	1,159	5,451	19,730
Heat rejection beta (β)	0.20	0.20	0.20	0.44	0.44	0.20	

In the USA, approximately 4% of electricity production currently comes from cogeneration facilities of which 71% are fueled by natural gas (e.g., see Table 8.2c in [72]).

How far could cogeneration penetrate in the USA and what benefits would accrue? Just as it is possible to look at the utilization rate of renewable energy sources such as wind, hydro, and solar in relation to the size and distribution of these resources, the thermal power plant heat available for low-temperature end users can be quantified to estimate the potential for increased cogeneration and hence its potential to offset other fuel use and emissions.

The annual US thermal power generation totaled 3.7 trillion kWh in 2008 [72]. Factoring in the mix of natural gas–fired systems, nuclear, and direct-fired (mostly coal) plants and their respective thermal efficiencies allow estimation of heat resources available for cogeneration. Table 7 shows an estimated breakdown of heat rejection from thermal power plants in the USA.

While cogeneration with direct-fired or nuclear-fueled Rankine systems is certainly possible, the sheer size of these plants makes it difficult to economically match them to end users that themselves are large enough to benefit from the full heat energy available. For this reason, cogeneration systems tend to be relatively small in terms of electrical output, which in turn aligns well with the NG-fired gas turbine and gas turbine combined cycle. Natural gas accounts for 883 billion kWh or 23.7% of total electricity generation [72, 73]; 199.7 billion kWh or 22.6% of which comes from cogeneration facilities (e.g., see Table 2.1 in [73]). Taking the data in Table 6 for cases 5 and 6 as a typical system configuration, it is possible to estimate the current fuel savings from natural gas–fired cogeneration as follows.

Natural Gas–Fired Cogeneration (GT+Supplemental Firing)

1	Electricity generation (billion kWh, 2008)	200
2	Combined cycle heat rate (Btu/kWh, HHV)	8,305
3	GT heat input (trillion Btu, 2008)	1,658
4	System heat rate (Btu/kWh, HHV)	11,156
5	Burner supplemental heat input (trillion Btu, 2008)	569
6	System heat input (trillion Btu, 2008)	2,228
7	Heat export to process (trillion Btu, 2008)	1,159
8	Equivalent heat input to meet process (trillion Btu, 2008)	1,302
	Cogeneration natural gas savings (trillion Btu, 2008) (Line 8 minus Line 5)	733

The fuel savings from application of cogeneration represents ~24.8% reduction in fuel burn vs. making the power with a gas turbine combined cycle and supplying the heat independently with a fired boiler. CO_2 emissions reductions follow the fuel saving directly if the fuel saving is booked as natural gas. If booked at the current fuel mix for US electricity production, the CO_2 savings are higher by about 33% or higher by 75% if booked as reduced coal fired generation. Looking at the heat rejection from natural gas–fired power generation in the USA in Table 7, in comparison to current heat

export from natural gas-fueled cogeneration, it appears that the amount of cogeneration could perhaps be doubled without a major shift in fuel use patterns. Reaching the electricity contribution levels seen in some small European countries would likely require more distributed generation with replacement of large coal-fired power plants with more small cogeneration systems (likely gas fired) proximate to potential end users.

Turning now to the potential customers for heat energy, Fig. 21 shows the primary energy production by source in the USA for 2008 [72]. Figure 22 shows the incremental retail electric load distributed to each sector and gives a breakdown between residential and commercial sectors. The natural gas contribution to the residential and commercial sectors is 8.2 trillion Btu [72]. Assuming that its primary use is for space heating, it can be seen that it far exceeds the available waste heat from gas-fired power plants tabulated in Table 7. It is difficult to make the case that small (micro) cogeneration systems could be aligned to the heat and power needs at the individual house level, though work on fuel cell systems for this purpose is active. The commercial sector and high-density residential (e.g., apartment complex) does offer real potential for expansion. In either case, the performance of the cogeneration system needs to be high enough to improve on the fuel use and environmental performance of an efficient utility scale power plant in combination with direct use of natural gas for heating.

Combustion and Emissions

There are different types of GT combustors that have been used at one time or another by different OEMs in their products:

1. Silo (obsolete now, once used by Siemens and former ABB)
2. Annular (aero-derivatives such as GE LM6000)
3. Can or tubular (heavy-duty industrial GTs by Siemens, GE)

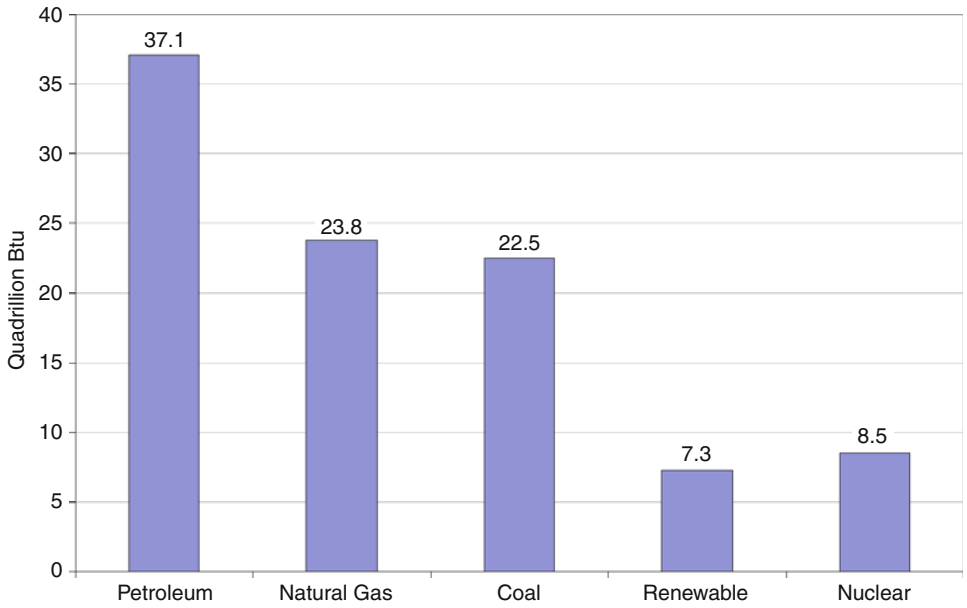

Natural Gas Power. Figure 21
Primary energy production by source, 2008. Total primary consumption is 99.3 quadrillion Btu. Renewable energy sources are hydroelectric power, geothermal, solar/photovoltaic, wind, and biomass. "Petroleum" does not include the fuel ethanol portion of motor gasoline – fuel ethanol is included in "Renewable Energy." "Natural Gas" excludes supplemental gaseous fuels. "Coal" includes less than 0.1 quadrillion Btu of coal coke net imports (Source: Energy Information Administration (EIA) [72])

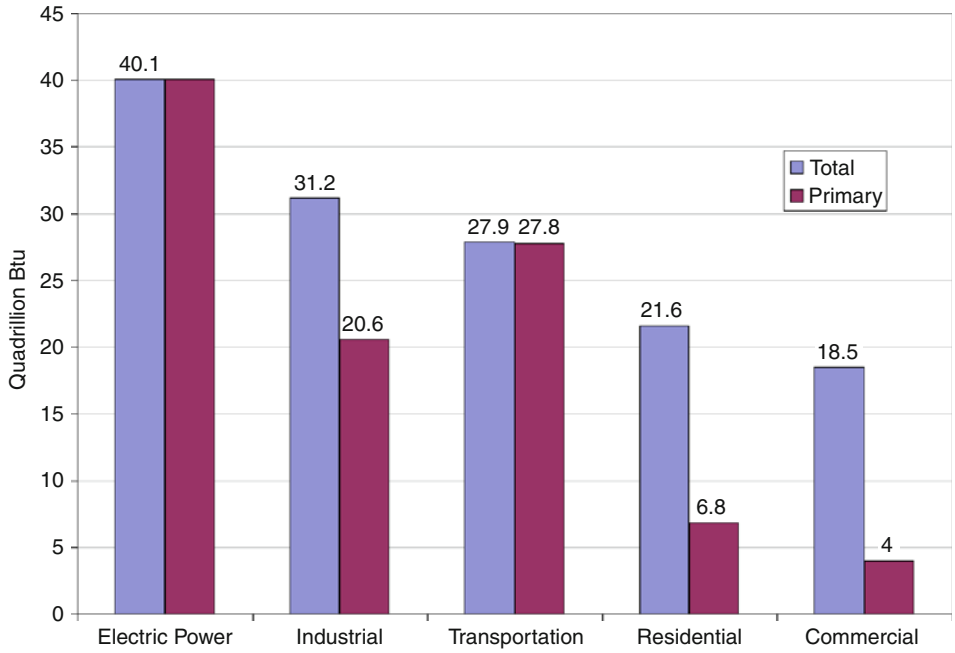

Natural Gas Power. Figure 22
Primary and total consumption by sector, 2008. See Fig. 21 for a breakdown of sources (Source: Energy Information Administration (EIA) [72])

In the following discussion a parameter will appear frequently, i.e., the *equivalence ratio*, ϕ, which is the ratio of the actual fuel-air ratio, *f*, to the *stoichiometric* fuel air ratio. The latter is the theoretical value requisite for complete combustion. Thus,

$$\phi = f_{act}/f_{st}$$

When the equivalence ratio is equal to 1.0, the flame temperature is the highest and the chemical reactions are the fastest. Thus,

1. If ϕ is less than 1.0, the mixture that reacts is referred to as "lean" or "fuel lean."
2. If ϕ is greater than 1.0, the mixture that reacts is referred to as "rich" or "fuel rich."

In either lean or rich combustion, flame temperature is lower and chemical reaction is slower than their stoichiometric counterparts.

The can-type combustor can be divided into three zones (see Fig. 23):

Primary Zone (PZ): This is the combustor *reaction* or flame zone where fuel is injected and mixes with air (about 15–20% of the compressor discharge air is introduced). In order to cap the combustor exit temperatures at a level, which downstream turbine HGP components can tolerate, the requisite value of ϕ is typically 0.4–0.5, which is too lean for stable and efficient burning. This is why only a portion of the combustion air is introduced into the primary zone. High-temperature rapid combustion takes place in the PZ. The design of this part of the combustor must

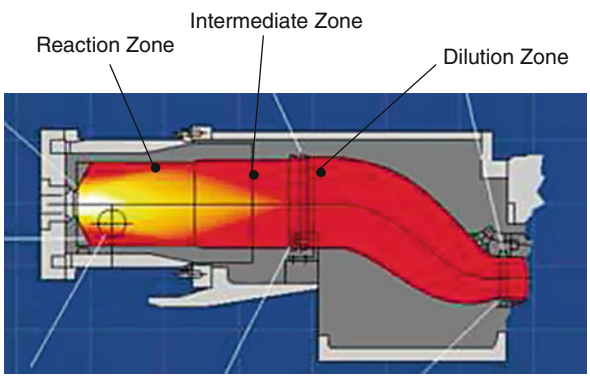

Natural Gas Power. Figure 23
Single-Nozzle Diffusion (SND) Combustor

facilitate highly turbulent and recirculating flow pattern to anchor the flame at the exit of the fuel injector nozzle. This is critical because of the high-speed of the air stream, even at a fraction of its full value, which is an order of magnitude higher than the turbulent flame speed at which the flame propagates into the fuel-air mixture.

Secondary Zone (SZ): This is the *intermediate* zone where a portion of the remaining combustion air (~30% of the total) is introduced in the mid-section of the can through holes or cooling slots in the combustor liner. The hot combustion gas from the PZ gets thermally soaked and the combustion is completed. The air that flows between the liner and flow sleeve and enters the can forms a film to cool the liner wall.

Dilution Zone: This is where the remaining air enters the can through the metering holes and cools the gases to the desired temperature. A design to promote turbulence and thorough mixing of hot and cold streams is essential to ensure a homogeneous temperature distribution and prevent hot streaks.

A successful combustor design should satisfy the following criteria:

1. Efficient and stable operation, which comprises the following characteristics
2. Complete combustion at or near stoichiometric flame temperature
3. Flame stability and reliability at high turndown
   (a) Ignition
   (b) Crossfire (propagation of flame from fired chambers with spark plugs to the unfired chambers via tubes interconnecting the annular combustion chambers or cans)
   (c) Lean blowout
4. Operational stability and reliability at high turndown
   (a) Dynamics (noise), i.e., large-amplitude pressure oscillations in combustion chamber, driven by heat release oscillations; also known as combustion "humming." These oscillations are destructive to engine hardware.
   (b) Pattern factor, which is a measure of the temperature distribution at the combustor exit defined as $PF = \frac{T_{\text{peak}} - T_{\text{mean}}}{T_{\text{mean}} - T_{\text{inlet}}}$
   (c) Pressure drop
5. Low emissions in compliance with regulatory laws

Achieving these goals simultaneously is very difficult due to the counter-acting impacts of design parameters on each criterion. The design history of the GE heavy-duty industrial gas turbine combustors can be found in Ref. [74]. The design evolution can be summarized in three major designs:

1. Single-nozzle diffusion (SND) combustor
2. Multi-nozzle, quiet combustor (MNQC)
3. DLN or Dry-Low-NO_x combustor

The design evolution was primarily driven by the desire to satisfy the increasingly stringent emission control requirements with improved efficiency via higher combustion and turbine inlet temperatures (TIT). In order to clarify this, one must be familiar with the chemical mechanisms of NO_x production, which is one of the most critical pollutants present in GT exhaust gas. Principal pollutants emitted by a GT are as follows [75]:

1. Oxides of nitrogen (NO_x), which are toxic, contribute to chemical smog and lead to depletion of ozone in stratosphere
2. Oxides of sulfur (SO_x), which are toxic and corrosive
3. Carbon dioxide (CO_2), which contributes to greenhouse effect and global warming
4. Carbon monoxide (CO), which is toxic and asphyxiating
5. Unburned hydrocarbons (UHC), including volatile organic compounds (VOC), which contribute to urban smog
6. Particulate matter (PM), which is suspected to cause respiratory diseases

Detailed information on GT emissions and control can be found in Ref. [76]. Some pollutants, i.e., UHC, PM, and SO_x, are generally of no concern for GTs burning gaseous fuel with the exception of coal-gasification SG, which leads to conversion of fuel-contained sulfur to SO_x. (Note, however, that in some cases contamination of fuel in the pipeline, e.g., rust particles, can be a problem for HGP components.) In any event, currently there is no available GT combustion technology to prevent or control SO_x emissions. Similarly, CO_2 is a direct product of the complete combustion process and cannot be controlled or reduced within the GT control volume (except, of

course, increasing the thermal efficiency of the GT, which will reduce the amount of fuel consumed and CO_2 generated for a given power output). Precombustion or postcombustion capture and storage of carbon dioxide, known as carbon capture and storage (CCS), is currently a hot topic of research and development.

A key pollutant emitted by the GT is NO_x. There are two major sources of NO_x:

1. Atmospheric N_2 in post-flame gases, which leads to formation of NO and NO_2 via three principle mechanisms:
   (a) Thermal NO (extended Zel'dovich mechanism)
   (b) Nitrous oxide mechanism
   (c) Prompt NO mechanism
2. Organically bounded nitrogen in fuel or fuel-bound nitrogen (FBN)

The dominant NO_x formation mechanism is the thermal or Zel'dovich mechanism. Although not a significant source of NO_x for NG, FBN in low-quality liquid fuels and LCV gases with hot-gas clean-up (via ammonia) can be high enough to merit attention. NO_x (and CO) formation is a function of three primary parameters:

1. Residence time in the combustion zone
2. Chemical reaction rate
3. Mixing rate

These three reaction parameters can be related to the turbine operating conditions and combustor size [75]. In particular,

$$\text{Residence time} \propto \frac{p \cdot V_c}{\dot{m} \cdot T_{pz}} \tag{27}$$

$$\text{Reaction time} \propto p^n \cdot \exp(kT_{st}) \tag{28}$$

where

- T_{st} is stoichiometric flame temperature (or, equivalently, f or ϕ or firing temperature)
- T_{pz} is the average gas temperature in the reaction or primary zone
- V_c is combustion volume
- p is combustion pressure (raised to a power of n)
- $\dot{m}$ is the combustor mass flow rate

Therefore, NO_x production rate can be expressed in an empirical formula that can be written as

$$NO_x \propto \frac{V_c}{\dot{m} \cdot T_{pz}} \cdot p^{1+n} \cdot \exp(k \cdot T_{st}) \tag{29}$$

The relationship between NO_x production and key parameters per Eq. (29) is shown qualitatively in Fig. 24. In general, NO_x values are reported in parts per million (ppm) on a dry basis (usually expressed as ppmvd) and corrected to 15% O_2 in combustion air. It is extremely important to make sure that the basis of the reported number is clearly defined; otherwise comparisons of data from different sources can be misleading. The expression for correction is as follows:

$$[NO_x]_{15\%O_2} = \frac{[NO_x] \cdot 5.9}{(20.9 - O_{2,meas})} \tag{30}$$

The trends in Fig. 24 show that the impact of pressure on NO_x formation is stronger at high flame temperatures near the stoichiometric value (i.e., $\phi \sim 1.0$) and negligible at leaner mixtures with lower flame temperatures. Consequently, effective control of the NO_x production in the combustion process is a matter of reducing the flame temperature. There are essentially three ways to accomplish this:

1. Design a primary (reaction) zone with leaner fuel-air mixture
2. Injection of a diluent, i.e., water or steam, into the primary zone of the combustor to act as a "heat sink" and reduce the flame temperature

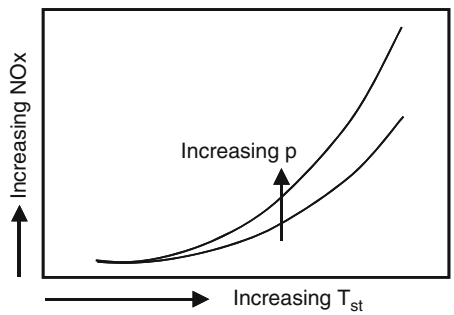

Natural Gas Power. Figure 24
Effect of pressure and stoichiometric flame temperature on NO_x

3. Staged combustion with two distinct reaction zones, which lead to the modern "lean-premixed" designs, which is referred to as *Dry-Low-NO$_x$* (or *DLN*).

The dramatic impact of reducing ϕ, i.e., leaning out the PZ, on flame temperature and NO$_x$ production can be seen in Fig. 25. Leaner fuel-air mixtures lead to lower-value flame and gas temperatures and favorably impact the NO$_x$ production rate via shorter residence and reaction times.

Unfortunately, things get complicated rapidly. For starters, the full operating range of an industrial GT combustor requires significant turn-down ratios, e.g., 40-to-1 in fuel flow, 30-to-1 in air flow, and 5-to-1 in fuel-air ratio. Obviously, the combustor design must ensure stable and efficient combustion across the entire operating range. The early single-nozzle (diffusion flame) combustors, with direct injection of fuel and air into the PZ, were designed for combustion at or near stoichiometric conditions. For a combustor designed for optimal full load operation at $\phi \sim 1$, combustion at lower loads is bound to be very lean. Thus, further leaning out of the PZ for NO$_x$ reduction is a very limited knob. In fact, initial efforts to reduce NO$_x$ via leaning out reaction zone of an SND combustor did not achieve more than 20% reduction [77].

When it became clear that meeting increasingly stringent pollution-control regulations via leaner reaction zones in SND combustors, other methods to reduce flame temperatures were investigated. Injection of water or steam into the PZ to create a "heat sink" for temperature reduction proved successful. Starting in 1979, when regulations required that NO$_x$ emissions be limited to 75 ppmvd, SND combustors with water or steam injection have been successfully used to meet or exceed these requirements successfully [74]. However, SND combustors that use water and steam injection are limited in their ability to reduce NO$_x$ levels below 42 ppmvd on gas fuel (65 ppmvd on oil fuel). The main reason is the practical limit to the amount of diluent injection into the reaction zone before the increase in dynamic pressure oscillations (i.e., noise) start imposing unacceptable penalties in terms of reduced hardware life and increased maintenance frequencies. High levels of water injection excited discrete dynamic pressure tones within the combustor. Frequencies within the range of the hardware's natural frequency resulted in combustor damage. In terms of dynamic pressure response, steam is a better diluent than water, although a larger mass flow rate is needed. Significant reduction in NO$_x$ production is achievable via steam injection, e.g., ~60% at a steam-to-fuel ratio of unity [77, 78].

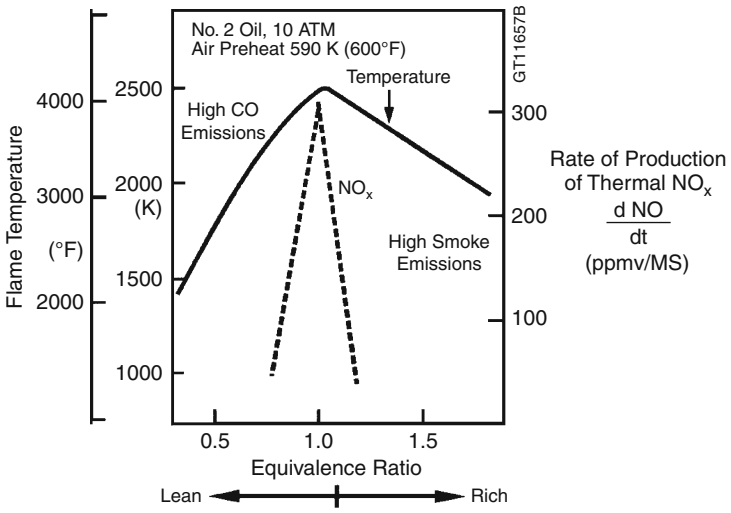

Natural Gas Power. Figure 25
Thermal NO$_x$ production rate (Source: GE Energy [74])

The other significant drawback on water or steam injection for NO_x abatement is the overall simple or combined cycle performance penalty. Even though the turbine output increases via increased mass flow, the associated increase in fuel consumption is detrimental to the heat rate. Furthermore, since the quality of injection water must be high, i.e., of boiler quality, to prevent deposits and corrosion in HGP components, additional *water treatment system* (WTS) cost for simple cycle applications must be considered. In combined cycle applications, where steam from the HRSG or ST (typically *cold reheat* steam) is extracted for injection, increased make-up flow rates and ensuing WTS size increase and water consumption are additional concerns. Even disregarding the combustion noise and life issues, it is easy to imagine that ever-increasing turbine-firing temperatures for improved cycle efficiency would drive the diluent injection flows to such levels where they would literally put the flame out. This is notwithstanding the counterproductive effect of reduced cycle efficiency via higher fuel consumption, which defeats the purpose of increasing the firing temperature in the first place.

Another limit associated with lowering the equivalence ratio and flame temperature for NO_x abatement is the increase in CO emissions. The conflicting emission benefits and harms of lowering or increasing the flame temperature can be seen in Fig. 26. Carbon monoxide is a measure of combustion inefficiency, which becomes more pronounced at leaner combustions. This is due to shorter residence time at leaner mixtures, which does not lend itself to complete CO burnout. Thus, the allowable temperature range for emissions control is limited to a relatively narrow band of ~400°F.

When SND combustors hit a practical limit for NO_x emissions reduction, even with diluent injection, designers responded by developing the "*multi-nozzle quiet combustion*" or MNQC system. For a detailed history of the combustor development, please consult Ref. [74]. Utilizing a multi-nozzle configuration, i.e., six nozzles located peripherally at the combustor head cap, this system eschewed the low-speed ignition and blowout problems associated with excessive leaning out of the PZ in SND systems at low loads (see Fig. 27). Furthermore, the MNQC system also helped with the dynamic pressure oscillation (i.e., noise) problem by

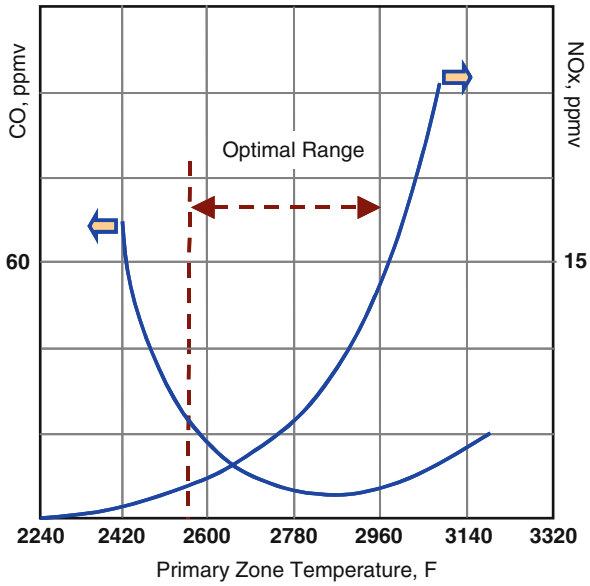

Natural Gas Power. Figure 26
Influence of PZ temperature on CO and NO_x [75]

maintaining a flat dynamic response at increased steam injection levels (that is the reason for the moniker "quiet"), thus enabling the design of combustion systems with higher firing temperatures and compliant NO_x emissions without the problems of increased hardware wear and reduced maintenance intervals. Since 1987, MNQC systems enabled heavy-duty GTs to meet stringent NO_x emission requirements, i.e., 25 ppmvd with gas fuels and 42 ppmvd with liquid fuels. Increase in CO and UHC emissions and combustion stability issues at high injection rates, e.g., steam-to-fuel >2, precluded further improvement with this technology [80].

Reduction in NO_x emissions to even lower levels, the need for balancing the low emissions with ever-increasing firing temperatures and the need to avoid the cycle thermal efficiency penalty associated with steam and water injection lead to the development of DLN combustors. DLN combustion system is the natural next-step in combustor development, i.e., a "staged" combustion system with lean-premixed fuel-air mixture. The primary and secondary combustion zones in the staged combustor are operated at the lowest possible ϕ at high fuel flow conditions (see Fig. 28). During start-up, acceleration, and

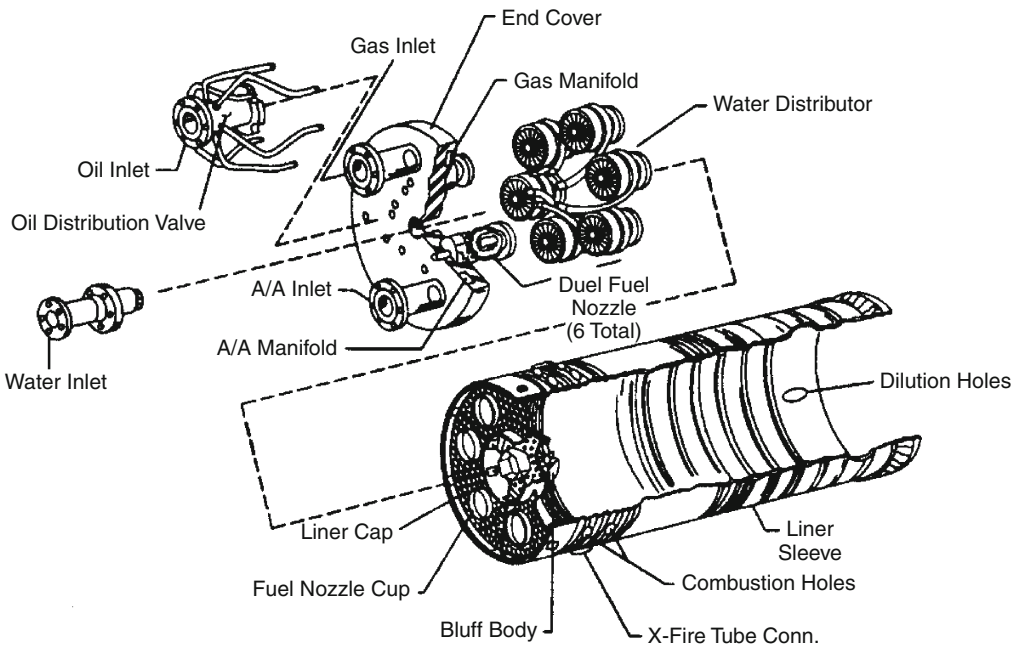

Natural Gas Power. Figure 27
MNQC Combustor (Source: GE Energy [79])

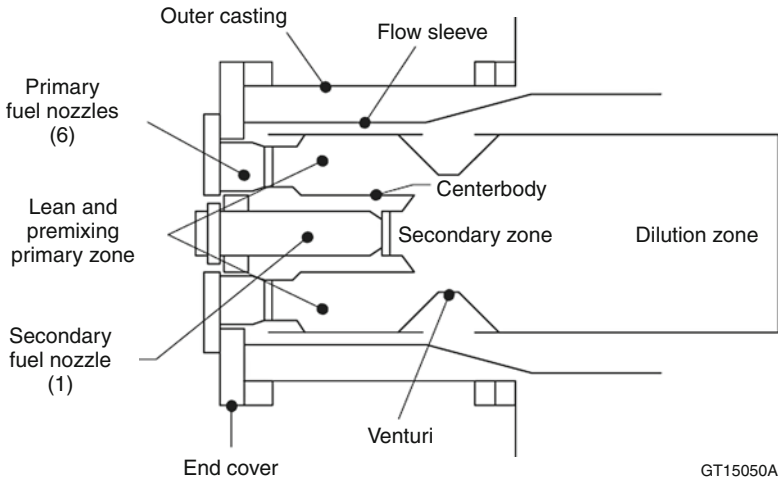

Natural Gas Power. Figure 28
Dry-Low-NO_x (DLN) combustor (Source: GE Energy [80])

low-load conditions, fuel is introduced only in the PZ with good ignition and blowout characteristics. At increasing load levels, fuel is introduced into the SZ at a fuel split to balance the CO and NO_x production at an optimal level, i.e., near the middle of the allowable range shown in Fig. 25. The first successful DLN system, DLN-I, that went into production incorporated a multi-nozzle system similar to that in MNQC for the

PZ and a conventional, large secondary fuel nozzle for the SZ. At normal (50–100% load) operation, fuel and air are "premixed" in the PZ but ignition takes place in the SZ with the flame attached to the secondary nozzle.

DLN technology successfully balanced the requirements for low combustion noise (i.e., dynamic stability) at part-load operation and optimal equivalence ratio for minimum NO_x at acceptable CO levels. DLN achieves this balance without diluent injection (and associated efficiency penalty and cost) while satisfying the requirement for low NO_x emissions, i.e., 25 ppm or lower on gas fuels. A history of the development of DLN-I and DLN-II (for F-Class turbines with high firing temperatures of 2,400+°F) systems can be found in Ref. [74] along with a detailed description of DLN operation modes.

Basic Economics

Natural gas–fired gas turbines and GTCC power plants are the most economic choices for fossil fuel–based electric power generation. This is clearly represented by the data in Table 8. The data in the table reflects 2004 prices. The numbers and the relative position of NG-fired plants should be expected to show a certain variation as a function of changing economic climate (i.e., inflation, demand for generating capacity, absolute and relative fuel prices, labor shortage, raw material prices, etc.) of which the recent worldwide depression that started in the last quarter of 2008 is a very good example. Nevertheless, a dramatic shift in the economic advantages of the CC plants vis-à-vis other nonrenewable large central stations or renewable options (i.e., wind, solar, etc.), which cost nearly ten times per kW capacity and available only in small sizes amenable to distributed power generation, should not be expected near term. A very brief introduction to the key aspects of the CC plant economics, i.e., plant capital (turnkey) cost or price and the cost of generating 1 kWh of electric power, is therefore quite useful.

Turnkey combined cycle plant price levels from 2009 Gas Turbine World (GTW) Handbook are shown in Fig. 29. Note that listed GTW prices are in 2009 US dollars for a basic natural gas–fired combined cycle with gas turbine generator, unfired multi-pressure heat recovery boiler with no bypass stack, condensing multi-pressure steam turbine generator, step-up transformer, water-cooled heat rejection, standard controls, starting system, and plant auxiliaries. Obviously, depending on the scope of equipment, site-specific requirements, geographic location, and competitive market conditions these prices will vary considerably. Also excluded from the prices in GTW are the indirect costs and other commercial

Natural Gas Power. Table 8 Cost and performance of nonrenewable electric power generation plants

	Capital cost per kW	Economic life years	Lead time	Load factor %	Efficiency %	Efficiency % (CHP)	Fuel cost $/MMBtu	Fixed $/kW-year	Variable $/MWh
NG-fired GT	$350–500	30	1.5	5–50	38			9–12	4
NG-fired GTCC	$550–900	30	2	60–85	55		4–5	10–15	2
NG-fired GTCC with CHP	$600–700	30	2	50–85	40–55	79–84		10–15	2
US SCPC	$1,300–1,800	30	4	60–85	35–42			20–25	3
US IGCC	$1,700–2,100	30	4	60–85	39–42		0.75–1.50	30–35	2
Nuclear	$2,000–3,000	40	6	85–92	33		0.5	60–70	1.5

Source: Cambridge Energy Research Associates, MA, USA

Load factor specifies the percent of (equivalent) hours in a year (8,760 h) during which the plant runs at its nominal base load. The data reflects the 2004 prices

CHP Combined Heat and Power (also known as Cogeneration), *SCPC* Supercritical Pulverized Coal, *IGCC* Integrated (Coal) Gasification Combined Cycle

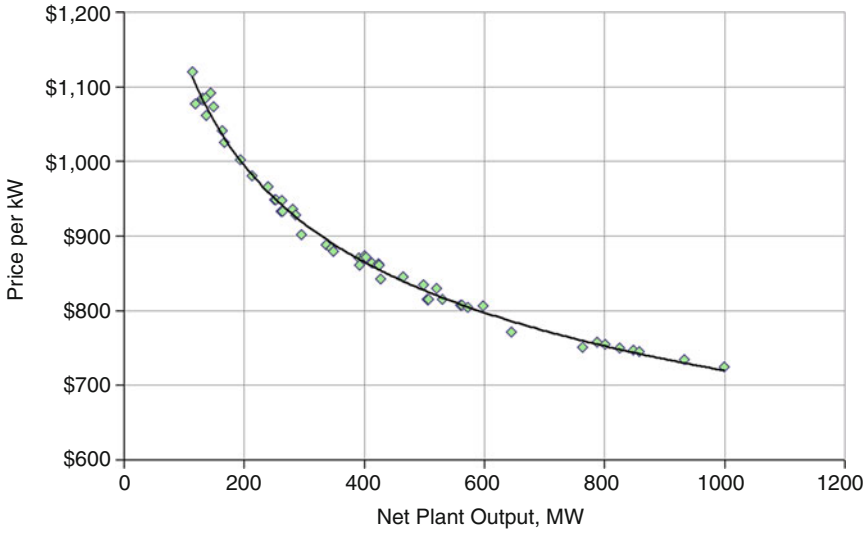

Natural Gas Power. Figure 29
Turnkey CC plant prices from Gas Turbine World 2009 Handbook. An adder of about 60% is applied to the listed price, which is budgetary turnkey equipment package price, to account for items not covered (see Fig. 30 and Table 9 below). Provided for reference only

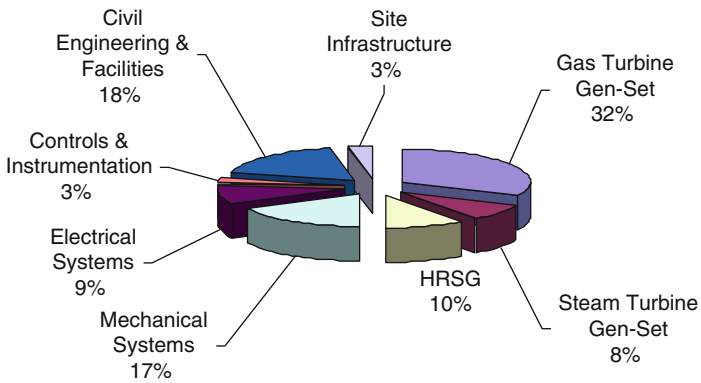

Natural Gas Power. Figure 30
Direct cost breakdown for a typical 400 MW CCPP (Source: Reference [83], pp 16)

outlays. For a more realistic price level, the data in Fig. 29 reflects an adder of about 60% to the listed price, which is based on the assumption that the prices in GTW reflect only 75% of the direct costs, which are 85% of the total installed cost (see Fig. 30 and Table 9 below).

The data plotted in Fig. 29 can be summarized by the power law

$$k = 2,890 \cdot P^{-0.2012} \tag{31}$$

where k is the specific price ($/kW) and P is the net plant output in MW (with R^2=0.994). In general, an exponent of 0.2–0.3 is adequate to estimate the capital cost of a CC plant from a known data point (i.e., price and net output). There are several methods and tools to calculate CC power plant cost (from a plant owner's perspective), which are used within OEMs and A&E firms and not available for public consumption. Well-established cost-estimating techniques, especially those that are adopted by the CPI, are readily available in

Natural Gas Power. Table 9 Typical CC capital cost breakdown between direct and indirect costs. From Energy Issues (World Bank), No. 20 June 1999, which is based on a 350/700 MW CC Plant with a Siemens-Westinghouse V94.3A (now SGT5-4000 F) GT

Integrated services (Indirect costs)	Contribution to total CC cost (%)
Project management and subcontracting	4
Plant and project engineering// software	2
Plant construction, commissioning, and training	8
Transport and insurance	1
Direct costs	**Contribution to total CC cost (%)**
Civil works	15
Gas and steam turbine generators	32
Boiler island	11
BOP	16
Electrical systems	7
Instruments and control	4

textbooks and scholarly articles. For a discussion of those and the underlying details, the reader is referred to Reference [81]. Another valuable source is Reference [82].

Calculation of the final cost of the CC plant requires consideration of many elements. In fact, the total cost of GT and ST generators and the HRSG, which are the major equipments in the CC power plant, comprises about 50% of the total plant cost. A typical distribution is shown in Fig. 30 from Ref. [83]. In addition to these "direct" costs, there are "indirect costs" that can contribute anywhere between 15% and 30% to the final cost of the CC power plant. As an example, consider the representative breakdown in Table 9.

The presented data should suffice to give an idea about the scope of the CC plant capital cost and its importance from a design engineer's perspective. All design performance calculations should be evaluated with an eye to the final plant cost. That final plant cost is the money, i.e., the plant "price," that is going to come out of the plant owner's pockets or his credit sources and thus directly impact the generation cost of 1 kWh of electricity.

Probably the most critical customer criterion for choosing an electric power generation product is the life cycle cost of ownership. The metric that is used to quantify this cost is the unit (per kWh) cost of generating electricity. Cost of electricity (COE), in its most commonly used form, is a simple formula that combines a power generation system's cost (capital and operating) and thermal performance into a single figure of merit that enables comparison of different systems. It is given as:

$$\mathrm{COE} = \frac{\beta \cdot k}{H} + \frac{L \cdot f}{\eta} + \mathrm{OM} \tag{32}$$

where β = Capital charge factor k = Total plant specific cost in \$/kW H = Annual operating hours f = First-year fuel cost in \$/MMBtu(HHV) L = Levelization factor η = Net efficiency of the CC plant OM = Operating & maintenance costs, \$/kWh.

The first term on the right-hand side of Eq. (32) represents the carrying charges, the second term is the cost of fuel, and the last term is the cost of maintaining and operating the plant. Fuel cost and operation and maintenance (O&M) costs are the variable components of the COE whereas carrying charge is the fixed component. COE is typically calculated over the economic lifetime of the plant (typically 30 years).

Levelization factor, L, converts the fuel cost that usually escalates over the plant's economic life due to market conditions and inflation into average annual (constant) values. The formula for L can be found in any financial reference and is a function of discount, escalation, and inflation rates.

The fixed charge rate, β, represents the plant's financial and tax situation and is a function of the economic life of the power plant, debt–equity ratio used in financing the plant, debt and equity rates, corporate tax rate and tax credits, book depreciation, property tax, and insurance. Various methods are available for calculating β, which can be found in plant economic studies. Typical values of β are 16–18% for *Independent Power Producers* (IPPs) and 12–13% for government-owned utilities, depending on the interest and taxation rates.

If the new and clean performance conditions are used within the calculations, the cost of generation as given by the COE formula should be treated as a figure of merit rather than an accurate assessment of the "real" generating cost. Important drivers – such as seasonal variations in ambient conditions, part load operation, recoverable and unrecoverable component deterioration, uncertainty in fuel prices, start-up and shutdown, and unforeseen events – are not considered. Nevertheless, levelized COE is an important metric that provides insight to performance-cost trade-offs for OEMs (system design) as well as customers (system selection).

The exact distribution of the cost of generating 1 kWh of electric energy varies depending on the financial assumptions. Typically, about two-thirds of the COE for an NG-fired, medium-loaded (~6,000 h/year) modern 3PRH CC plant with an F-Class gas turbine is the fuel cost. About one fourth of the COE is the capital cost. The distribution is markedly different (actually, nearly exactly the opposite of NGCC) for the IGCC plant with very high capital expenditure ($2,000/kW or even higher) utilizing a cheaper fuel, coal ($1–2).

Future Directions

At the time of writing of this article, natural gas accounts for about 22% of US electricity generation. The share of natural gas in electricity generation in OECD member countries in Europe is about the same. The share of natural gas is expected to increase in the future to the tune of 25% of total world electricity generation by 2030 [2]. However, recent developments suggest that this projection might in fact be a low estimate. One reason is the new drilling technologies that made extraction of natural gas from shale rocks feasible. The technique is called *hydraulic fracturing* and involves injection of high-pressure water into rock formations to destroy them and enable the trapped gas to be released to the surface for capture. So much so that this development resulted in a 35% jump in US natural gas reserves from about 1,500 trillion ft^3 in 2006 to more than 2,000 trillion ft^3 in 2008 [84]. Note that this number is the total estimated reserves including speculative, possible, and probable sources, and of which only 237 trillion ft^3 is considered to be proven by the Energy Department. According to the same source, shale gas constitutes nearly a third of the total reserves.

Another potential source of natural gas is *gas hydrates* (also known as gas *clathrates*), which are "crystalline solids consisting of gas molecules, usually methane, each surrounded by a cage of water molecules." It looks very much like water ice. Methane hydrate is stable in ocean floor sediments at water depths greater than 300 m, and where it occurs, it is known to cement loose sediments in a surface layer several hundred meters thick. The worldwide amount of carbon bound in gas hydrates is conservatively estimated to total *twice the amount of carbon to be found in all known fossil fuels on Earth*. (Source: US Geological Survey Fact Sheet.) Unfortunately, as of today, commercially feasible production of natural gas from gas hydrates is not a reality.

The dramatic increase in natural gas reserves and actual production via new technology that can extract it from shale rocks, taken at its face value, is a strong driver for its increasing share in electricity generation; at least in the USA. The advantage of natural gas vis-à-vis coal, which roughly accounts for half of US electricity generation, in terms of reduced carbon emissions is thus fortified from lower prices and increased availability. But the situation may not be as simple as it seems. The price of natural gas hit its 7-year low of about $3/1,000 ft^3 in the summer of 2009. This huge drop from a peak of $13 in the summer of 2008 was a direct result of the *great recession* that led to a decrease in demand, coupled with the increase in production. At the time of writing, NYMEX natural gas futures are trading at about $4 per million Btu (about $4.50/1,000 ft^3) and they were as high as $6 per million Btu (about $6.80/1,000 ft^3) at the beginning of 2010. Note that extremely low price levels are not likely to continue for long if they are below the production costs. Extreme price volatility can be expected when demand and supply (or capacity) go neck to neck.

In this context, one should also mention the problems associated with natural gas transportation via pipelines. In January 2009, the price quarrel between Russia and Ukraine ended in Russia cutting off all gas flows through Ukraine for 13 days. This resulted in severe distress in Southeastern Europe, which is nearly completely reliant on Russian gas, and other parts of Europe. While not an issue in North America, political

stability of producer and transit countries is a significant concern for European countries that can make them reluctant in investing in natural gas–fired power plants. Alternate routes between Russia, Azerbaijan, and other countries, such as thousands of miles long *South Stream* and *Nabucco* pipelines, are actively pursued projects to provide answers to such concerns. The only other practical way to transport natural gas is to move it by sea by cooling it to −162°C (−260°F) and converting it to a liquid (liquefied natural gas or LNG), which reduces its volume by 600 times. Specially built, double-hulled cryogenic ships are used to transport LNG from its port of origin to its port of destination, which are purpose-built facilities used exclusively to export or import LNG. From the receiving port, LNG is shipped to its final destination via tanker trucks, trains, or pipelines (after regasification). Expensive infrastructure investment requirements, safety concerns, large "carbon footprint" during liquefaction, transport, and regasification are key concerns associated with LNG, which limit its share in the overall natural gas consumption (currently less than 10% of US imports).

In terms of cost, regulatory costs, and incentives, e.g., those associated with GHG emission caps and cap-and-trade system requirements (e.g., for manufacturers and utilities to purchase pollution permits), should be considered along with straight dollars per Btu. Coal-fired generation can compete with natural gas in terms of GHG and other pollutant emissions only at a significantly high capital cost and reduced efficiency. Currently, there are two major approaches to accomplish this: Postcombustion carbon capture and storage (CCS) technologies that can clean the stack gas of the existing (via retrofit) and new coal-fired plants and precombustion technologies that are a very good fit with *integrated gasification* CC (IGCC) power plants. Note that carbon emission abatement technologies via stack gas treatment are equally applicable to natural gas–fired CC power plants. In terms of both efficiency and cost, detailed studies indicate that NG-fired CC technology is superior to oil or coal-fired plants as well as IGCC [85].

Objectively viewed, these factors are strong incentives for natural gas burning power plants to replace aging, inefficient, and carbon-emitting, coal-fired power plants in the USA. To a certain extent, this can be accomplished even without building new natural gas-fired CC power plants. A recent report estimated that CC power plants had an average 2007 capacity factor of 42% [86]. In comparison, in the same year, coal-fired plants had a much higher capacity factor of 75%. Clearly, at least on paper, the replacement potential by simply switching generation from coal-fired to natural gas-fired plants is pretty big. In reality, factors such as geographical proximity of the power plants to each other and to the locations of highest demand, transmission system limitations and dispatch issues limited this potential severely; i.e., to about 5–9% of total US coal-based electricity generation [86]. While the proposed switch from coal to natural gas would also require an increase of 5–20% in natural gas supply, this should not be a significant problem in the light of recent developments discussed in the earlier paragraphs. A recent article states that several major US utilities have announced that they will replace at least some of their coal-fired plants slated for decommissioning (total capacity of more than 4.5 GW) [10].

Another factor that favors the natural gas–fired gas turbine plants over the coal-fired steam turbine power plants is operational flexibility. The rapid start-up and good turndown characteristics of gas turbine simple and combined cycle power plants, especially with the increase of renewable energy power plants (mostly solar and wind) connecting to the grid, make them eminently suitable to cyclic on-demand duties to compensate for the variability of the renewable generation. Presently, all major OEMs provide CC plants that can reach base load (several hundred megawatts) within 30–60 min without sacrificing base load efficiency, parts life, and RAM. Aeroderivative gas turbines, such as GE's intercooled LMS-100, can provide 100 MW within 10 min in an emergency or for peak shaving in hot summer months. Especially in Europe and to a certain extent in the USA, large, highly flexible natural gas–fired CC power plants that start and shut down daily for up to 250 starts and a total of 4,000 h of operation per year are expected to supplement renewable power generation. These plants are based on advanced F-Class and H-Class gas turbines that are rated at 58–59% efficiency and expected to reach more than 60% in the near future.

Clearly, then, no matter how regional politics in the USA, Europe, and other parts of the world play out, and what kind of legislative packages eventually emerge from governing bodies to control, cap or regulate carbon and other GHG emissions, natural gas–fired electricity generation with advanced gas turbine–based power plants will be an important part of the overall generating technology portfolio. In all likelihood, natural gas–fired advanced CC power plants will be the bridge technology between today's coal-based power generation and tomorrow's renewable (and probably nuclear) power generation to alleviate the lurking problem of global warming. (In fact, this is pretty much the conclusion reached by a recent MIT report, which was made public after the writing of the present article [87].) The question is what will be the primary technologies in the next, say, quarter century?

Without a doubt, gas turbine–based power plants, in simple cycle (both heavy-duty industrial and aeroderivative variants) and combined cycle configurations will be by far the dominant technology in natural gas electric power generation. Today's advanced air-cooled F-Class and H-Class, steam-cooled G-Class, GE's H-System™, and J-Class engines with firing temperatures up to 1,600°C and PRs up to 23 (up to 35 in reheat machines) are currently capable of 58%, have recorded 59%, and are slated for 60% (or even 61% as claimed by one OEM) in 2011–2012 [88]. These are large units with 500–600 MW per block in 1×1 configuration designed not only for base load duty but for operational flexibility as described earlier. (In passing, note that the cited efficiencies are typically ISO rating numbers that reflect the most favorable operating assumptions (e.g., once-through open-loop cooling with water drawn from a natural source such as river, ocean, etc). Depending on site and ambient characteristics, performances of actual installed units will be somewhat lower with wide variability.)

Increasing power plant efficiency is the simplest and arguably the easiest way to reduce carbon emissions without breaking the bank or worrying about what to do with all that CO_2 or where to put it. As mentioned earlier, ambitious targets as high as 65% or even 70% have been in circulation for some time [57–60]. The discussion in the preceding sections of the article hopefully makes it clear that the key to ever-increasing gas turbine combined cycle efficiencies is increasing firing temperatures and commensurate cycle pressure ratios. The factors that prevent easy realization of that simple goal are primarily related to available component materials that can withstand the extreme pressures and temperatures and limits imposed by pollutant emission regulations. State-of-the-art nickel-based alloys used in turbine HGP components require significant amounts of cooling air supplied from extraction ports in the compressor, which is detrimental to performance. Higher flame zone temperatures in DLN combustors result in excessive NO_x and/or CO in flue gas, which is incompatible with increasingly stringent environmental regulations that limit the emissions of those pollutants to low single-digit numbers.

Single-crystal (SC) and directionally solidified (DS) superalloys with TBCs helped push firing temperatures up to 1,500°C. With closed-loop steam cooling and advanced film cooling techniques, J-Class turbines are rated at 1,600°C. Current research efforts focus on advances in materials, e.g., ceramic matrix composites (CMC) [58] or metal foams [59], which can reduce or even eliminate cooling air requirements at extremely high HGP temperatures. Manufacturing techniques have always been a significant driver in the implementation of aforementioned innovations; e.g., TBC application processes (e.g., electron beam physical vapor deposition), casting and machining technologies to produce SC airfoils. In a similar vein, laser-drilling and casting methods to achieve transpiration (effusion) cooling (the ultimate limit of film cooling) are related areas of research and development to further the goal of increasing turbine inlet temperatures. An associated effort is made on the bottoming cycle side, i.e., development of HRSG heat exchanger tubes, steam headers and piping and steam turbine materials (casing, rotor, and buckets) that can withstand increased steam conditions as high as 180 bar and 600–700°C [89].

Closed-looped steam cooling of the combustor transition piece and stage-1 stators (nozzles) is an existing technique to increase the firing temperature without raising the combustor exit (turbine inlet) or flame temperatures [32, 33]. This enables performance improvement without a concomitant increase in NO_x

emissions. Another method to facilitate extreme combustor exit and firing temperatures (up to 1,700°C) is exhaust gas recirculation (EGR), in which a fraction of the stack gas (up to 35%) is recirculated into the compressor or combustor inlet [90]. EGR reduces thermal NO_x production via reduced O_2 in combustion air and peak temperatures in flame. EGR's benefit becomes more pronounced at increased flame temperatures and it can reduce NO_x emissions by up to 50% [91]. EGR is also beneficial for postcombustion CCS because it increases the CO_2 concentration in stack gas (from ~3–4% to ~8–10% by volume), which leads to a reduction in the capital cost of the separation plant [91].

Lean premix or DLN combustion technology is the industry standard for heavy-duty industrial gas turbines for large-scale electricity production. In terms of the ability to meet the stringent emissions requirements, the technology is nearly at its limit at the current turbine inlet temperatures. EGR is one possibility to extend the applicability of DLN or even diffusion combustors to 1,700°C turbine inlet temperatures with low NO_x emissions. Another way to mitigate the NO_x emissions is selective catalytic reduction (SCR) in the HRSG. SCR is an existing postcombustion NO_x reduction technology. Other combustion technologies are being investigated for deployment in IGCC and other low-Btu syngas and blast-furnace gas applications to extend the fuel flexibility of gas turbines. The reader can consult the relevant sections in *The Gas Turbine Handbook* published by NETL (US DOE, Office of Fossil Energy). Various high-hydrogen and oxyfuel combustion technologies are being actively investigated for CO_2-free emissions. Since the subject of the present article is natural gas-burning technologies, the reader is referred to relevant academic journals such as *ASME's Journal of Engineering for Gas Turbines and Power*, which contain a wide selection of recent research papers on the subject.

A potentially promising combustion technology that directly attacks the single largest source of exergy destruction in the GT Brayton cycle is pulse detonation combustion (PDC). Originally proposed for jet engine aircraft propulsion, the technology has been around for more than a half century [92]. Recently, PDC is actively considered for land-based power generation [93]. The technology involves combustion of a fuel-air mixture across detonation waves in tubular devices [94]. Detonation waves are composite waves comprised of a "frozen" shock wave with pressure and temperature jump followed by a relaxation zone where chemical combustion reactions take place. The benefit of the process is temperature *and* pressure rise during the cycle heat addition process with a correspondingly higher mean-effective temperature vis-à-vis the conventional diffusion or DLN combustors with approximately constant pressure (actually a 5–6% pressure loss). Detailed cycle calculations indicate that a PDC gas turbine in CC configuration is potentially 1.5–3 percentage points advantage over standard units at comparable firing temperatures and pressure ratios [95].

SOFC- or MCFC-based hybrid fuel cell plus gas turbine power plants are by far the most efficient future technologies to "burn" natural gas for electric power generation. In these machines, the fuel cell replaces the combustor to oxidize the gaseous fuel. Different configurations are possible. Detailed studies show that fuel cell-GT hybrid plants are capable of thermal efficiencies approaching 70%. Bhargava et al. [96] can be consulted for more information on these and other advanced GT-based power plants such as humid air turbine (HAT) and intercooled recuperated engine (ICR). Almost all variants have been studied in detail and reached various stages of development and commercialization in the past. They have not been able to pass the audition in terms of reliability, operability, capital cost, scalability, and other important considerations (e.g., water consumption) to present viable alternatives to simple Brayton cycle GT in CC configuration. Closed-loop steam cooling and reheat (also known as *sequential combustion*) have been the only successful and commercially accepted variations on the basic cycle. At this time, to the best of the authors' knowledge, there is no reason to expect this situation to change in the foreseeable future; at least in terms of large-scale electric power generation. As always, dual-fuel diesel engines capable of burning gaseous fuels will continue to play a role in small-scale and/or distributed generation applications. The same can be true for very small (several kilowatts) fuel cell–based hybrid units.

Bibliography

Primary Literature

1. Energy Information Administration (EIA) (2009) Annual energy review 2008. http://www.eia.doe.gov/aer. Accessed 29 June 2009
2. Energy Information Administration (EIA) (2008) International energy outlook 2008. DOE/EIA-0484(2008). www.eia.doe.gov/oiaf/ieo/index.html.
3. United States Environmental Protection Agency (EPA) (2010) Methane. www.epa.gov/methane.
4. Liss WH, Thrasher WR (1992) Variability of natural gas composition in select major metropolitan areas of the United States. Gas Technology Institute, Chicago, GRI-92/013
5. Natural Gas and the Environment (2010) From http://www.naturalgas.org/environment/naturalgas.asp
6. Turbomachinery International (2008) 49(6), 10/2008, Handbook 2009. www.turbomachinerymag.com
7. Wärtsilä 50DF generating set (2010) From www.wartsila.com
8. Khan BH (2006) Non-conventional energy sources. Tata McGraw Hill, New Delhi, India
9. McNeely M (2006) Power generation order survey. Diesel & Gas Turbine Worldwide. Article from Oct 2006 issue
10. Burt B, Mullins S (2010) U.S. gas-fired power development: last man standing, POWER. http://www.powermag.com. Accessed Sept 2010, pp 71–73
11. Wilson DG, Korakianitis T (1998) The design of high efficiency turbomachinery and gas turbines, 2nd edn. Prentice-Hall, Uppersaddle River
12. Von Ohain H (1996) Foreword. In: Mattingly JD (ed) Elements of gas turbine propulsion. Tata McGraw Hill, New Delhi, India, Edition 2005
13. Meher-Homji CB (1997) The development of the Junkers Jumo 004B – the world's first production turbojet. J Eng Gas Turb Power 119:783
14. Meher-Homji CB (1998) The development of the Whittle Turbojet. J Eng Gas Turb Power 120:249
15. Meher-Homji CB (2000) Pioneering turbojet developments of Dr. Hans von Ohain – from the HeS 1 to the HES 011. J Eng Gas Turb Power 122:191
16. Soares C (2006) Gas turbines in simple cycle and combined cycle applications. Section 1.1 in The gas turbine handbook. US DOE, Office of Fossil Energy, NETL. http://www.netl.doe.gov/technologies/coalpower/turbines/refshelf/handbook/TableofContents.html
17. Leiste V (1999) Development of the siemens gas turbine and technology highlights. Siemens Power Generation, Erlangen, Germany
18. Miller H, Nemec T (2006) Gas turbines. In: Myer K (ed) Mechanical engineers' handbook, 3rd edn., Energy and power. Wiley, Hoboken, Chapter 24
19. Brandt D (2007) A brief history of GE energy product lines. General Electric Company, New York
20. Brandt D (1988) The design and development of an advanced heavy-duty gas turbine. J Eng Gas Turb Power 110:243–250
21. Stodola A (1927) Steam & gas turbines. Authorized translation from the 6th German edition: Löwenstein LC. McGraw-Hill, New York
22. Langston LS (2010) World's first gas turbine power plant. ASME Mech Eng 132(4):51
23. Tomlinson LO, Lee DT (1985) Combined cycles. In: Sawyer JW, Japikse D (eds) Sawyer's gas turbine engineering handbook, Chapter 7. Turbomachinery International Publications, Norwalk, Conn., USA
24. Horlock JH (1994) Combined cycle power plants – past, present, and future. J Eng Gas Turb Power 117:608–616
25. Gebhardt E (2000) The F Technology experience story, GER-3950C. http://www.gepower.com/
26. Haselbacher H (1989) Gas turbine fundamentals. In: Elliott TC (ed) Standard handbook of power plant engineering. New York, McGraw-Hill Publishing POWER magazine
27. Horlock JH (1997) Aero-engine derivative gas turbines for power generation: thermodynamic and economic perspectives. J Eng Gas Turb Power 119:119–123
28. Moran MJ, Shapiro HN (1988) Fundamentals of engineering thermodynamics. Wiley, New York
29. Cohen H, Rogers GFC, Saravanamuttoo HIH (1987) Gas turbine theory, 3rd edn. Longman, London
30. Cumpsty N (2003) Jet propulsion, 2nd edn. Cambridge University Press, Cambridge
31. Schilke PW (2004) Advanced gas turbine materials and coatings, GER-3569 G. www.gepower.com
32. Pritchard JE (2003) H-System™ technology update. GT2003-38711, ASME turbo expo – power for land, sea & air, 16–19 June 2003, Atlanta
33. Koeneke C (2006) Steam cooling of large frame gas turbines one decade in operation. VDI Ber Nr 1965:33–42
34. Imwinkelried B (1995) Advanced cycle system gas turbines GT24/GT26: the highly efficient gas turbines for power generation. In: Proceedings of the 21st international congress on combustion engines, CIMAC 1995, Interlaken, Switzerland
35. Chiesa P, Macchi E (2004) A thermodynamic analysis of different options to break 60% electric efficiency in CC power plants. J Eng Gas Turb Power 126:770–785
36. Holland MJ, Thake TF (1980) Rotor blade cooling in high pressure turbines. J Aircr 17:412–418
37. Elmasri MA, Pourkey F (1986) Prediction of cooling flow requirements for advanced utility gas turbines. Part 1: analysis and scaling of the effectiveness curve, 86-WA/HT-43, ASME Winter Annual Meeting, Anaheim, 7–12 Dec 1986
38. Elmasri MA (1986) Prediction of cooling flow requirements for advanced utility gas turbines. Part 2: influence of ceramic thermal barrier coatings. ASME Winter Annual Meeting, Anaheim, 7–12 Dec 1986
39. Elmasri MA (1985) On thermodynamics of gas turbine cycles: part 1 – second law analysis of combined cycles. J Eng Gas Turb Power 107:880–889

40. Elmasri MA (1986) On thermodynamics of gas turbine cycles: part 2 – a model for expansion in cooled turbines. J Eng Gas Turb Power 108:151–159
41. Elmasri MA (1986) On thermodynamics of gas turbine cycles: part 3 – thermodynamic potential and limitations of cooled reheat gas turbine combined cycles. J Eng Gas Turb Power 108:160–170
42. Horlock JH, Watson DT, Jones TV (2001) Limitations on gas turbine performance imposed by large turbine cooling flows. J Eng Gas Turb Power 123:487–494
43. Horlock JH (2001) The basic thermodynamics of turbine cooling. J Eng Gas Turb Power 123:583–591
44. Wilcock RC, Young JB, Horlock JH (2005) The effect of turbine blade cooling on the cycle efficiency of gas turbine power cycles. J Eng Gas Turb Power 127:109–120
45. Young JB, Wilcock RC (2002) Modeling the air-cooled gas turbine: parts 1 and 2. J Turbomach 124:207–222
46. Gülen SC (2010) A simple mathematical model for cooled gas turbines. GT2010-22160, ASME turbo expo – power for land, sea & air, 14–18 June 2010, Glasgow
47. Rice IG (1995) Steam-injected gas turbine analysis: steam rates. J Eng Gas Turb Power 117:347–353
48. Cheng DY, Nelson ALC (2002) The chronological development of the Cheng cycle steam injected gas turbine during the past 25 years. ASME International – IGTI Turbo Expo 2002, GT2002-30119
49. Rao A (1989) Process for producing power. U.S. Patent No. 4,289,763
50. Adelman ST, Hoffman MA, Baughn JW (1995) A methane-steam reformer for a basic chemically recuperated gas turbine. J Eng Gas Turb Power 117:16–23
51. McDonald CF, Boland CR (1981) The Nuclear Closed-Cycle Gas Turbine (HTGR-GT) – dry cooled commercial power plant studies. J Eng Gas Turb Power 103:89–100
52. Reale MJ (2004) New high efficiency simple cycle gas turbine – GE's LMS100™, GER-4222A. www.gepower.com
53. Mercury 50, Recuperated Gas Turbine Generator Set, Solar® Turbines (2010) www.solarturbines.com
54. Cox JC, Hutchinson D, Oswald JI (1995) The Westinghouse/Rolls Royce WR-21 gas turbine variable area power turbine design. ASME Paper 95-GT-54, International Gas Turbine and Aeroengine Congress and Exposition, Houston, TX, 5–8 June 1995
55. Hofer DC, Gülen SC (2006) Efficiency entitlement for bottoming cycles. GT2006-91213, ASME turbo expo – power for land, sea & air, Barcelona, Spain, 8–11 May 2006
56. Gülen SC, Smith RW (2008) Second law efficiency of the Rankine bottoming cycle of a combined cycle power plant. ASME Paper GT2008-51381. ASME turbo expo 2008, Berlin, Germany, 9–13 June 2008
57. Bohn D (2006) SFB 561: Aiming for 65% CC efficiency with an air-cooled GT, Modern Power Systems, pp 26–29, Sept 2006
58. Mutassim Z (2008) New gas turbine materials. Turbomachinery International, Sept/Oct 2008 issue, 38–42
59. Bohn D, Dilthey U, Schubert F (2004) Innovative Technologien für ein GuD-Kraftwerk mit 65% Wirkungsgrad. VDI-Berichte Nr 1857:13–25
60. Rao AD, Robson FL, Geisbrecht RA (2002) Power plant system configurations for the 21st century. In: ASME turbo expo 2002, Amsterdam, the Netherlands, 3–7 June 2002
61. Lundberg WL, Veyo SE, Moeckel MD (2003) A high efficiency solid oxide fuel cell hybrid power system using the mercury 50 advanced turbine system gas turbine. ASME J Eng Gas Turb Power 125:51–58
62. Massardo AF, Lubelli F (2000) Internal Reforming Solid Oxide Fuel Cell – Gas Turbine Combine Cycles (IRSOFC-GT); Part I: cell model and cycle thermodynamic analysis. ASME J Eng Gas Turb Power 122:27–35
63. Massardo AF, Magistri L (2003) Internal Reforming Solid Oxide Fuel Cell – Gas Turbine Combine Cycles (IRSOFC-GT); Part II: exergy and thermoeconomic analyses. ASME J Eng Gas Turb Power 125:67–74
64. Chase DL, Kehoe PT. GE combined-cycle product line and performance, GER-3574 g. GE Energy
65. Chris EM, Leroy OT. GE combined-cycle experience, GER-3651. http://www.gepower.com.
66. Tomlinson LO, McCullough S. Single-shaft combined – cycle power generation system, GER-3767c. http://www.gepower.com
67. Matta RK, Mercer GD, Tuthill RS. Power systems for the 21st century – H GT combined-cycles, GER-3935B. GE Energy
68. Smith RW, Polukort P, Maslak CE, Jones CM, Gardiner BD. Advanced technology combined cycles, GER-3936a. GE Power Systems
69. Phylipsen GJM, Blok K, Worrell E (1998) Handbook on international comparisons of energy efficiency in the manufacturing industry. Department of Science, Technology and Society, Utrecht University, The Netherlands
70. Gülen SC (2010) A proposed definition of CHP efficiency, POWER. http://www.powermag.com, pp 58–63, June 2010
71. European Association for the Promotion of Cogeneration (Mar 2001) A guide to cogeneration. http://www.cogeneurope.eu/wp-content/uploads//2009/02/educogen_cogen_guide.pdf
72. Energy Information Administration (EIA) (2009) Annual energy review 2008. http://www.eia.doe.gov/aer. Accessed 29 June 2009
73. Energy Information Administration (EIA) (2010) Electric power annual. http://www.eia.doe.gov/fuelelectric.html. Accessed 20 Jan 2010
74. Davis LB, Black SH (2000) Dry low nox combustion systems for GE heavy-duty gas turbines, GER-3568 g. http://www.gepower.com
75. Lefebvre AH (1995) The role of fuel preparation in low-emission combustion. J Eng Gas Turb Power 117:617
76. Roointon, Pavri, Moore, Gerald D (2001) Gas turbine emissions and control, GER-4211. http://www.gepower.com

77. Hilt MB, Waslo J (October 1984) Evolution of NOx abatement techniques through combustor design for heavy-duty gas turbines. J Eng Gas Turb Power 106:825
78. Touchton GL (1984) An experimentally verified NOx prediction algorithm incorporating the effects of steam injection. J Eng Gas Turb Power 106:833
79. Davi MA (1994) GE gas turbine combustion flexibility, GER-3946. GE Energy
80. Miller HE (1994) Development of the GE quiet combustor and other design changes to benefit quality, GER-3551. http://www.gepower.com
81. Peters M, Timmerhaus K, West R (2004) Plant design and economics for chemical engineers, 5th edn. McGraw-Hill, London
82. Bejan A, Tsatsaronis G, Moran M (1996) Thermal design & optimization. Wiley, New York
83. Kehlhofer R, Warner J, Nielsen H, Bachmann R (1999) Combined cycle gas & steam turbine power plants, 2nd edn. PennWell Corp, Tulsa
84. As reported in the press per Potential Gas Committee report (2008) Potential supply of natural gas in the United States, Potential Gas Agency, Colorado School of Mines, Golden, 31 Dec 2008
85. Gambini M, Vellini M (Jan 2003) CO_2 emission abatement from fossil fuel power plants by exhaust gas treatment. J Eng Gas Turb Power 125:365–373
86. Wagman D (2010) Can natural gas displace coal? Power Eng (Mar 2010 issue): 4
87. The future of natural gas – an interdisciplinary MIT study (2010) Interim report by MIT Energy Initiative, ISBN 978-0-9828008-0-5, Massachusetts Institute of Technology, Boston
88. Robb D (2010) CCGT: breaking the 60 percent efficiency barrier. Power Eng Int 18(3). www.peimagazine.com
89. Review of status of advanced materials for power generation, Technology Status Report, Cleaner Coal Technology Programme, Department of Trade and Industry (Oct 2002) London
90. Tukagoshi K, Muyama A, Uchida S et al (Oct 2005) Latest technology for large capacity gas turbine. MHI Tech Rev 42(3)
91. ElKady AM, Evulet A, Brand A (May 2009) Application of exhaust gas recirculation in a DLN F-class combustion system for postcombustion carbon capture. J Eng Gas Turb Power 131:#034505
92. Kailasanath K (2000) Review of propulsion applications of detonation waves. AIAA J 38(9):1698–1708
93. Goldmeer J, Tangirala V, Dean A (2008) System-level performance estimation of a pulse detonation based hybrid engine. J Eng Gas Turb Power 130:#011201
94. Tangirala VE, Rasheed A, Dean AJ (2007) Performance of a pulse detonation combustor-based hybrid engine, GT2007-28056. ASME turbo expo – power for land, sea & air, Montreal, Canada, 14–18 June 2007
95. Gülen SC (2010) Gas turbine with constant volume heat addition. ESDA2010-24817. ASME 2010 10th biennial conference on engineering systems design and analysis, Istanbul, Turkey, 12–14 July 2010
96. Bhargava R, Bianchi M, Campanari S et al (2010) A parametric thermodynamic evaluation of high performance gas turbine based power cycles. J Eng Gas Turb Power 132:#022001

Books and Reviews

Bejan A (2006) Advanced engineering thermodynamics, 3rd edn. Wiley, New Jersey

Boss M (1996) Steam turbines for STAG™ combined cycle power systems, GER-3582E. http://www.gepower.com

Boyce MP (2006) Gas turbine engineering handbook, 3rd edn. Gulf Professional Publishing, Houston

Chase D (2001) Combined cycle development evolution and future, GER-4206. http://www.gepower.com

Colegrove D, Mason P, Retzlaff K, Cornell D (2001) Structured steam turbines for the combined cycle market, GER-4201. http://www.gepower.com

Constant EW II (1980) The origins of the turbojet revolution. The Johns Hopkins University Press, Baltimore/London

Cotton KC (1998) Evaluating and improving steam turbine performance, 2nd edn. Cotton Fact Inc, Rexford

Denton JD (1993) Loss mechanisms in turbomachines, The 1993 IGTI scolar lecture. J Turbomachinery 115:621–656

Dunn MG (2001) Convective heat transfer and aerodynamics in axial flow turbines. J Eng Gas Turb Power 123:637–686

Elmasri MA (2007) Design of gas turbine combined cycle and cogeneration systems – theory, practice and optimization. Seminar Notes, Thermoflow, Inc., Sudbury, MA. info@thermoflow.com

Han JC, Dutta S, Ekkad SV (2000) Gas turbine heat transfer and cooling technology. Taylor & Francis, New York

Horlock JH (2001) Combined power plants: including Combined Cycle Gas Turbine (CCGT) Plants. Krieger Publishing Company, Malabar

Kehlhofer R, Hannemann F, Stirnimann F, Rukes B (2009) Combined cycle gas & steam turbine power plants, 3rd edn. PennWell Corp, Tulsa

Lakshminarayana B (1996) Fluid dynamics and heat transfer of turbomachinery. Wiley, New York

Lefebvre AH, Ballal DR (2010) Gas turbine combustion: alternative fuels and emissions, 3rd edn. CRC Press/Taylor & Francis, Boca Raton

Nag PK (2006) Power plant engineering, 2nd edn. Tata McGraw-Hill, New Delhi, India

Saravanamuttoo HIH, Rogers GFC, Cohen H, Straznicky PV (2009) Gas turbine theory, 6th edn. Pearson Prentice Hall, England

Traupel W (1977) Thermische Turbomaschinen, Erster Band, Thermodynamisch-strömungstechnische Berechnung, 3, neuarbeitete und erweiterte Auflage. Springer, Berlin/Heidelberg/New York

Natural Resource Flows and Sustainability in Urban Areas

Stefan Anderberg
Lund University Centre for Sustainability Studies, Lund University, Lund, Sweden

Article Outline

Glossary
Definition of the Subject and Its Importance
Introduction
Urban Sustainability Challenges
Urban Planning
Cities as Ecosystems
Urban Metabolism
Future Directions
Bibliography

Glossary

Ecological footprint A measure of the resource consumption of a given unit (e.g., a city and its population) that represents the area of ecologically productive land and water needed for the production and assimilation of wastes generated.

Emergy analysis Emergy is the amount of energy, usually solar, that is directly or indirectly required to generate a given output flow. Emergy analysis allows analysis of the whole embodied environmental work expressed in a single unit and has been applied to flows in cities and other regions as well as different types of products and production processes.

Urban ecology Research on urban ecosystems and applications of ecological principles in connection with urban planning.

Urban metabolism Involves conceptualizing a city as an organism or ecosystem and tracking resources that go into the system and products and wastes that leave it.

Urban mining Recovery of metals and other valuable materials in urban areas. Studies that have identified metal concentrations comparable to mines in cities and urban waste dumps suggested that an increasing share of the raw materials for metal production in the future will be recovered from wastes in urban areas.

Definition of the Subject and Its Importance

Cities and urban areas are of central importance for global sustainable development both as dominating sites of production and consumption and as contexts for developing new, more sustainable practices. All cities depend on large imports of energy and other natural resources to satisfy consumption of their inhabitants as well as local production, trade, and services. These resource flows are closely linked to global and regional sustainability issues, such as resource scarcity, pollution, and competition for land or water, as well as local health, environmental, and distributional issues. How resources are consumed and managed in the expanding cities has strong implications for the global resource flows and related pressures in different scales. The goal of "sustainable development" puts into question many traits of current urbanization and city development and calls for a sustainable urban transformation. Such a transformation needs to rely on sound, efficient, and sustainable resource management and sustainable urban structures in terms of the built environment, transport systems, and green and blue structures. The handling of resource flows in cities and urban areas is the core of this challenge. For increasing the capacity of local strategic action toward a more sustainable use of resources, it is essential to develop improved understanding of the urban resource flows. Studies of urban ecosystems and resource flows as well development of ecological planning approaches connect to this challenge.

Introduction

After centuries of intense urbanization, more than half of the world's population lives in urban areas. The global urban population is expected to grow by more than 50%, or 1.7 billion people, between 2008 and 2030 [1]. Therefore, the cities are increasingly recognized as the most important global sustainability challenge of this century [2]. The urban ecological sustainability challenges are both linked to global resource scarcity, pollution and biodiversity issues,

and local health and environmental problems as well as resource access and distribution among different groups of people. With their central role in connection with manufacturing, trade, and consumption, big cities since long dominate global energy use and material flows [3]. How resource use develops in cities have strong implications for resource flows in different scales and related pressures. How cities are built, heated and cooled; how efficient their infrastructures are, and what urban citizens consume or how they travel in their everyday lives have great influence on greenhouse emissions, and exploitation of scarce land, water and mineral resources in different parts of the world. For increasing the capacity of local action toward a more sustainable use of resources, it is essential to develop improved analysis tools that allow a better guidance for strategic action [4, 5]. A key challenge is to improve the overview and understanding of the environmental linkages of the urban resource flows in different scales and develop urban governance that contributes to a more sustainable use of resources [6, 7]. Studies of urban ecosystems and resource flows as well as development of sustainability planning connect to this challenge. Urban metabolism studies explore the interactions among resource flows, urban transformation processes, waste streams, and quality of life and connect to the challenge of combining urban planning with sustainable resource management. This entry focuses particularly on natural resource flows in urban areas and urban metabolism studies, their results and challenges, and their potential contributions to sustainable urban planning and governance.

Urban Sustainability Challenges

Cities alter their local environments and influence the global environment in several ways. They occupy and modify space and are characterized by intense competition for space between different uses of land [8]. They import vast quantities of food, water, and energy and export emissions and waste, and they depend in various ways on local and global ecological services. Cities have always been a scene for unsafe living conditions and ecological problems [9]. Historically, it is possible to distinguish three different but often overlapping types of urban sustainability crises during the industrial era:

- A *hygienic* crisis connected to unsafe drinking and inadequate sanitation and waste management, and related epidemics in fast growing cities
- A *social* crisis connected to poverty; insufficient, poor, and unhealthy housing; and lacking access to light, fresh air, and green spaces
- An *environmental* crisis particularly connected to severe pollution and health hazards for local people

In cities in industrialized regions, these crises have generally been successfully addressed via development of urban infrastructures, planning, organization, and control, and the most urgent local problems have disappeared [10]. Local pollution problems still remain in most cities, mostly connected to traffic, waste, and diffuse pollution. Figure 1 shows the development in Manchester as an example of the improvement of environmental quality and health in European cities toward the end of the twentieth century. By the end of the nineteenth century, the bronchitis death rate was above 3 per 1,000 inhabitants compared with less than 0.5 in the 1980s.

In fast-growing cities in the developing world, these three types of problems still remain, overlap, and often get worse. In many cities in Africa, Asia, and Latin America, large parts of the inhabitants live under unhealthy conditions in poor housing without access to safe drinking water, sanitation, or other basic services [11, 12]. In great contrast to the desperate needs for basic infrastructure in Third World cities, the emerging sustainable city efforts in Europe, North America, and Australia during recent decades have, to a large extent, been concerned with the unsustainability of the cities in a global context. Global change problems, such as resource scarcity, climate change, land use competition, or biodiversity, put into question the energy use, spatial structures, and infrastructural arrangements of modern society in general and big city regions in particular. In this context, promoting efficient and sustainable management of resource flows in the city has become of central importance.

Urban Planning

Societal development is in different ways reflected in changed flow and flow patterns. Industrialization, increasing wealth, expansion of the city, changed design of buildings and city areas, and changed

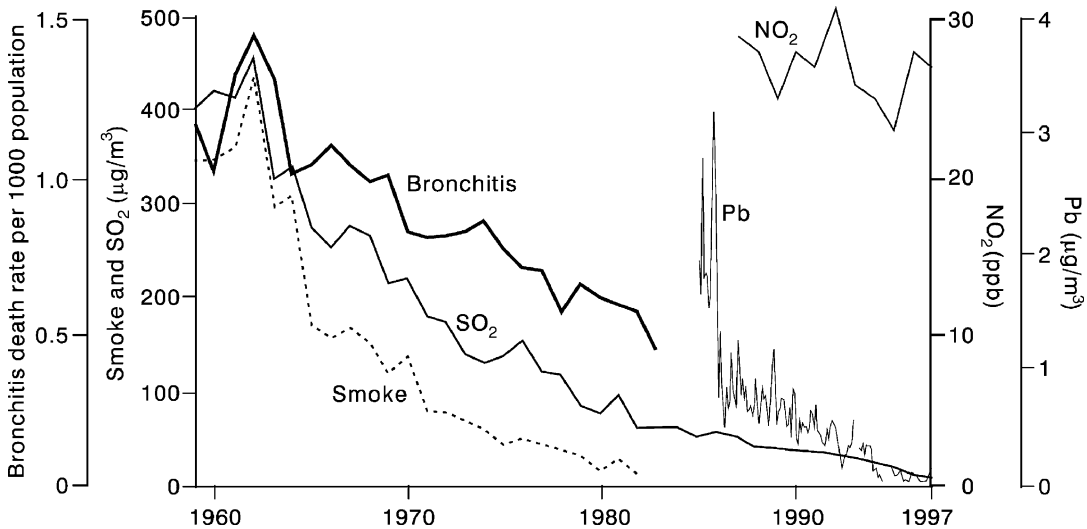

Natural Resource Flows and Sustainability in Urban Areas. Figure 1
Development of air pollution (smoke, SO_2, lead, and NOx) and bronchitis death rate (per 1,000 inhabitants) in Manchester (Source: [10])

patterns of settlement, work, commuting, production, consumption, trade, leisure activities, and use of the urban landscape of the big city all result in changed flows. Resource flows are thus strongly influenced by urban planning and design of urban areas. Urban planning has developed in interaction with different social welfare issues, e.g., local environmental problems. It has traditionally primarily focused on regulating the location and intensity of activities to avoid health problems and environmental degradation and influenced resource flows, but planning has seldom comprehensively and explicitly addressed resource management [13]. Urban planning emerged as a response to the unhealthy and polluted conditions in the fast-growing industrializing European cities in the nineteenth century. The overwhelming problems were gradually overcome by investments in infrastructure and introduction of a system of laws and authorities to take care of waste collection, water, hygienic control, and worker protection. Society took on a growing responsibility for the health and well-being of its citizens, and the major tools have been infrastructural investments and an increasingly ambitious spatial planning. During the twentieth century, the social crisis connected to poor, unhealthy housing conditions was, in European cities, addressed by demolition, renovation and social housing projects, and establishment of parks, green and recreational areas, and separation of industry and housing. Cities were, in the twentieth century, transformed by motorized road traffic and the breakthrough of the private car, but also visions of more human and ecologically sound urban environments influenced the urban development. Both decentralized city visions, such as Howard's "Garden City," and more centralized visions, such as Le Corbusier's "Radiant City," have influenced urban and suburban developments.

With the growing industrial production, increasing use of fossil fuels, cities in general were severely polluted until the mid-twentieth century. From the 1960s to the 1990s, increasing concern for the environment stimulated important infrastructural investments in wastewater treatment, district heating, energy source substitution, which, together with improved pollution control and industrial restructuring, decreased the industrial pollution and health hazards for urban inhabitants in Europe and North America.

Planning for Urban Sustainability

From the 1970s, growing concern about environment and resource use also influenced urban planning. New urban forms, such as the compact city with

high-density settlement and mixed uses, were promoted as a response to urban sprawl and high dependency on cars and fossil fuel consumption after the oil crisis. The real breakthrough for environmental and ecological planning and interest for the relationship between planning and resource management came with the goal of "sustainable development" that became influential from the late 1980s when ecocity or sustainable city visions and ambitions spread rapidly through national, international, and intercity initiatives. UN Habitat, the World Bank, and the EU have launched sustainable urban development programs that, in different ways, support cities in their strive for a more sustainable development. In Europe, more than 2,500 local and regional governments have signed the Aalborg Charter from 1994 and joined the European Sustainable Cities and Towns Campaign. The most ambitious of these local communities have signed the Aalborg Commitments from 2004.

Sustainable urban development ambitions have brought both broader concerns and new ambitions to urban governance and planning. For increasing sustainability, waste and pollution must be minimized, natural resources conserved, and the carrying capacity of ecosystems respected. The sustainable city agenda includes often compact, efficient land use; reduced car use, efficient public transport, efficient resource use, and reduced pollution and waste; restoration of natural systems; good housing and living environments, community participation and involvement, social equity and inclusion, and a sustainable economy [14]. Sustainability planning requires a holistic view of a city or region that includes equal concern for environmental, economic, and social sustainability [15]. It is conceived as a process, and sustainability, as a goal to work toward rather than something soon to be achieved. In order to achieve such goals, comprehensive plans, zoning ordinances, building codes, and planning processes must be revised for incorporating sustainability principles into urban environmental planning [15–17]. This does not only imply that environmental quality or resource conservation goals must be as important as economic but also that other goals, such as social justice and equity, must be addressed in relation to environmental efforts. For realizing such integrative ambitions, it is often stressed that planning and decision processes must become more open and integrated: all levels of government, business, civil society, and individual must work together [17].

Sustainability is a long-term goal, which can only be achieved through consistent strategic action over the long term. Sustainable urban development needs to rely on sound resource management and sustainable urban structures. To realize this and to reduce the demand of resources and flows of energy, water, waste, and materials, it is necessary to develop a more effective, integrated, and flexible infrastructure for water supply, waste, sanitation, heating, electricity, and fuels that is resilient to changes in population, economy, and climate and the hydrological regime. Urban systems should be multifunctional, serving more than one technical purpose and be able to integrate ecological, recreational, and aesthetic values. For increasing the capacity of municipalities to act strategically, an important challenge is to develop systems-based analysis tools in collaboration with stakeholders that allow a better overview and guidance for strategic action [4]. This is the challenge that has inspired many studies of urban ecosystems and urban metabolism.

Cities as Ecosystems

The concept of "urban ecosystems" has proved useful for investigating the relationship between urban areas and the environment [18]. Urban ecosystems are defined by Pickett [19] as "those in which people live at high densities, or where the built infrastructure covers a large proportion of the land surface." Research on urban ecosystems, often called urban ecology research, has grown and broadened during recent decades. This research can be divided into research on *ecological systems in the city* and on *the city as an ecological system* [20]. The former is dominating and includes many specialized study areas that focus on particular ecological aspects in urban areas [19], e.g., urban climates, soils, hydrology, vegetation, animals, nutrient and carbon flows, as well as different human and social urban systems. The latter analyzes the city as a whole ecosystem based on different ecosystem approaches, human ecosystem or sustainability assessment frameworks or watersheds as integrative tools.

Natural resource flows and their transformations are essential for the functional structure and dynamics

of both natural and human ecosystems. From such a flow-based systems perspective, cities can be described as large stocks of accumulated materials stored in buildings and infrastructure, and they are characterized by large and concentrated flows of raw materials, energy, goods, waste, people, and information. In thermodynamic terms, cities are open systems that depend on imported energy and matter. The cities require vast amounts of resources to function. In the past, the amount of accessible resources in the nearest hinterland was a constraint to the growth of cities [21], but with improved transport and development of international trade, cities no longer rely on their immediate hinterlands for a growing share of resources, including food. Most environmental problems are connected to these natural resource flows.

Urban Metabolism

Urban flows and resource management in different cities have been analyzed in various studies since the 1970s. Figure 2 shows the urban metabolism of Brussels from the early 1970s from the study of Duvigneaud and Denayeyer-De Smet [22]. The term "urban metabolism" was launched by Abel Wolman [23] in his study on generalized flows in a "typical" city in the USA. Kennedy et al. [24] defines "urban metabolism" as "the sum total of the technical and socio-economic processes that occur in cities, resulting in growth, production of energy, and elimination of waste." The notion of "metabolism" is based upon analogy with the metabolism of organisms, which is one example of parallels between cities and ecosystems, which are

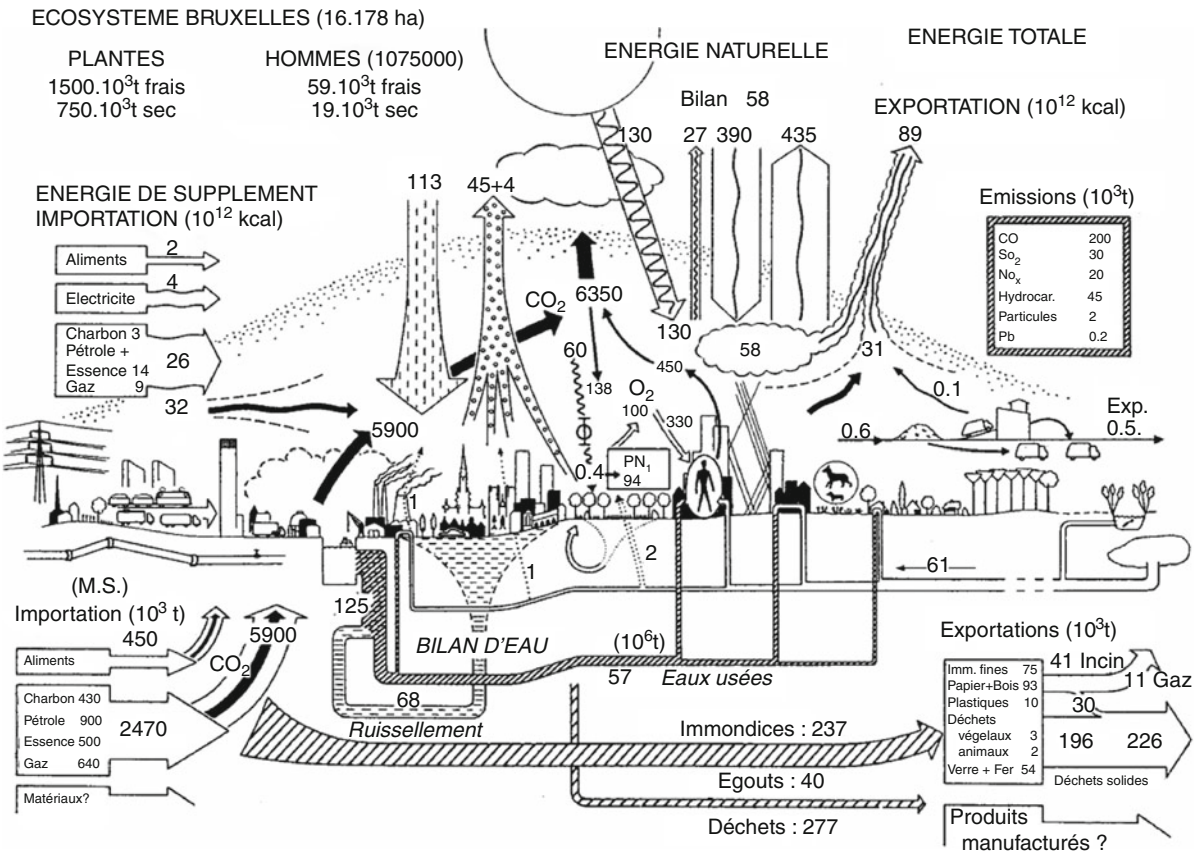

Natural Resource Flows and Sustainability in Urban Areas. Figure 2
The urban metabolism of Brussels, Belgium, in the early 1970s (From: [22])

central in urban ecology. The term "metabolism" has also become established in connection with material and substance flow analysis in other kinds of man-dominated systems, e.g., "industrial metabolism" studies [25] have analyzed material and substance flows in different regions.

The study of the urban metabolism involves in practice a holistic conceptualization of a city as a system of flows and inputs, outputs, and storage of focused flows, e.g., energy, water, nutrients, materials, and wastes that are then quantified for a certain time period. Figure 3 shows an example of a summary of results in terms of inflows and outflows in the metabolism of Sydney in 1990. By looking at the city as a whole system and by analyzing the pathways along which energy and materials, including pollutants, move, the goal is to improve resource management systems, allow assessment of impacts, and identify technological and organizational opportunities to increase the efficiency of resource use through, e.g., recycling of wastes as valuable materials and energy conservation [26].

Different Urban Metabolism Studies

Kennedy et al. [27] identified almost 50 "urban metabolism" studies on more than 30 different cities since the 1970s. After a few forerunners in the 1970s, urban metabolism studies reappeared in the 1990s, and the great majority of studies have been published since the year 2000. Hong Kong, Vienna, Stockholm, Toronto, London, and Paris have been subject for several studies.

Most "urban metabolism" studies have focused on energy, water, food (nutrients), materials (metals), and resulting pollution (typically CO_2, SO_2, NO_x, nutrient releases, or heavy metals) and waste in a limited time period. There are also examples of analyses of the historical development, such as for heavy metals in

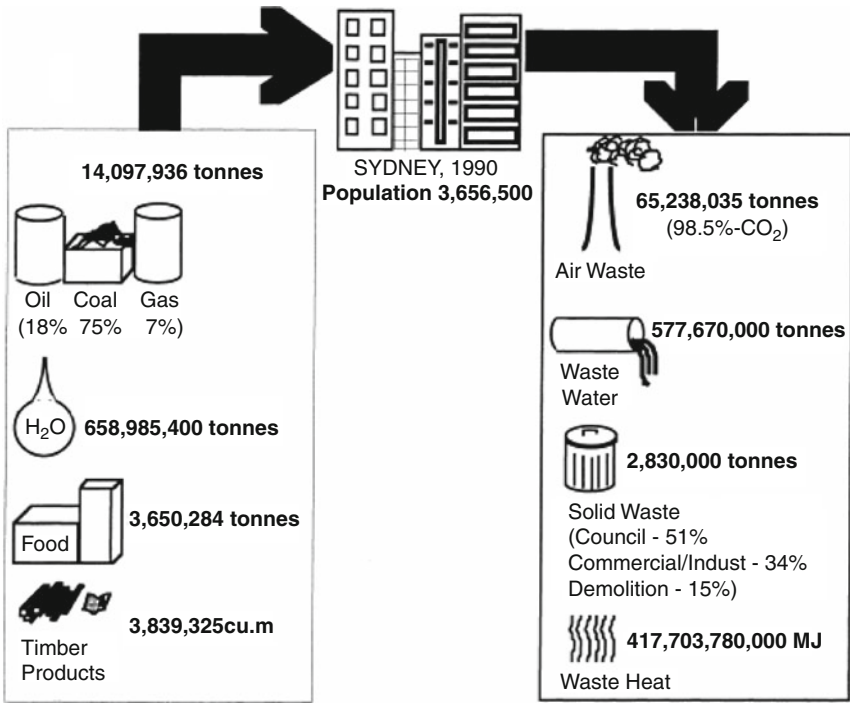

Notes:
Waste water data do not include stormwater
Timber products and food data derived from national per capita data

Natural Resource Flows and Sustainability in Urban Areas. Figure 3
Resource inputs and waste outputs in Sydney, 1990 (From: [7])

Stockholm [28] and nitrogen in food metabolism in Paris [29] and total material flows in Limerick [30]. In some other cities, such as Hong Kong and Toronto, repeated studies have provided some basis for comparison over time [27].

Most studies have been based on mass or energy measurement for different materials and energy flows, respectively. But some studies have sought to use agglomerated measurement units. Several of the earliest studies in the 1970s e.g., [31] described the metabolism in terms of emergy, an approach which more recently has been applied in connection with analyses of Taipei [32], Beijing [33], and Rome [34]. Related to the urban metabolism concept is also the application of the ecological footprint technique to cities [35]. The studies of Vancouver [36], Santiago [37], and cities of the Baltic region of Europe [38] in the 1990s have been followed by many studies. It has also become increasingly popular to describe the urban metabolism in terms of ecological footprints e.g., [39–42].

Many urban metabolism studies have focused primarily on urban material stocks and flows, e.g., of Lisbon [43], Singapore [44], and York [39]. In connection with heavy metal analyses, the urban stocks have been recognized as future environmental risks or potential raw material sources [45–48]. There has also been a growing interest for food flows and related nutrient flows [49–52]. Urban water metabolism has been addressed in several studies [53–57]. In recent years, urban CO_2 emissions in different cities have received growing interest, and many estimations are built on urban metabolism approaches [58]. There are also many broader studies that in different ways connect to urban metabolism, e.g., transportation of materials [59], and urban infrastructure systems [60]. An indication for the renewed and increasing interest in urban metabolism studies is that two projects have recently started under the EU Seventh Framework Programme: SUME [61] and BRIDGE [62].

Contributions by Urban Metabolism Studies

The urban metabolism studies have contributed to the overview and understanding of the flows and stocks of various materials in urban areas, and of pollution risks. They confirm the importance of cities for energy and material flows in different scales. Furthermore, they have shown that large parts of the resource flows accumulate in buildings, wastes, and pollution in urban areas. In some cases, they have indicated that accumulation results in surprisingly high concentrations of hazardous materials "hibernating" in cities, which bring future risks and challenges in connection with demolition and waste, diffuse pollution, and pollution of groundwater (e.g., [28]. Brunner and Rechberger [47] have inspired a growing research on the potentials for "urban mining."

The studies have also contributed to the increase in the understanding of the development of the urban flows in different cities, which often have changed dramatically during the twentieth century. Where city development has been characterized by increasing welfare, consumption, and mobility, the societal flows have grown dramatically and become more diversified, and spatial patterns have changed with the development and expansion of city regions. Most studied cities have, in recent decades, become more energy and material intensive, while other flows, such as water and wastewater, as well as different types of pollution show varying trends in different cities [27]. While Asian cities may still be characterized by increasing levels of traditional pollutants, such as SO_2 and particulates, European cities have generally experienced a dramatic trend break of most of such traditional air pollutants, while emissions of NO_x and CO_2 may remain stable [10]. In parts of East, South, and Central Asia, urbanization has dramatically increased water consumption and water pollution, which adds pressure on scarce water resources in the regions.

Urban Metabolism Studies and Planning

Urban metabolism is often described as "a holistic approach to urban planning" [5] and is fundamental for developing sustainable cities and communities. Such overviews of flows in different cities have, in many cases, been important for informing and stimulating strategic discussions concerning resource provision, resource efficiency, and pollution. Metabolism studies contributed importantly to the development of flow-based ecocycle strategies and related introduction and campaigns for recycling in the 1990s. There are examples of collaboration between authorities and researchers in some studies e.g., [28] and that studies

have been used for developing local sustainability indicators connected to energy or material consumption or ecological footprints. There are also examples of policy frameworks that have been developed for supporting sustainable urban policy development, e.g., the extended metabolism for human settlements from Australia that link the urban metabolism to both socio-economic dynamics and quality of life (Fig. 4). However, it is still rare that urban metabolism studies and perspectives have been fully integrated into local strategies or planning processes.

Kennedy et al. [27] suggest that particularly relevant practical applications of urban metabolism for urban planners and designers include sustainability reporting, urban greenhouse gas accounting, mathematical modeling for policy analysis, and urban design. Urban metabolism studies have often contributed to sustainability reporting and indicators. Indicators based on metabolism studies have many advantages: they are not only indicative of a city's sustainability but also are scientifically valid, relevant to urban planners and dwellers, comparable over time, and understandable. With the growing interest for setting local goals for emissions of greenhouse gases and ecological footprints, metabolism approaches are needed for estimating the emissions in different cities. An increasing number of cities – from the planned city of Masdar in Abu Dhabi to big cities such as Copenhagen and Seattle – have, in the last few years, declared ambitions to become carbon neutral within the next few decades. Partly connected is a trend among "Sustainable Cities" to set targets in terms of decreasing their ecological footprints.

The ambitions of metabolism studies to contribute to regional assessment, modeling, and scenario construction have only seldom been realized, though there are exceptions, such as City Region 2020 [4] and Maastricht 2030 [5], assessment and scenario studies based on metabolism approaches. There are also examples of mathematical models of metal and nutrient flows, such as SIMBOX [63] and STAN [47, 64], that can be used for simulating future changes and identify solutions to perceived problems. Urban metabolism has furthermore been used for development of tools for designing and redesigning urban areas and their infrastructure [27, 65].

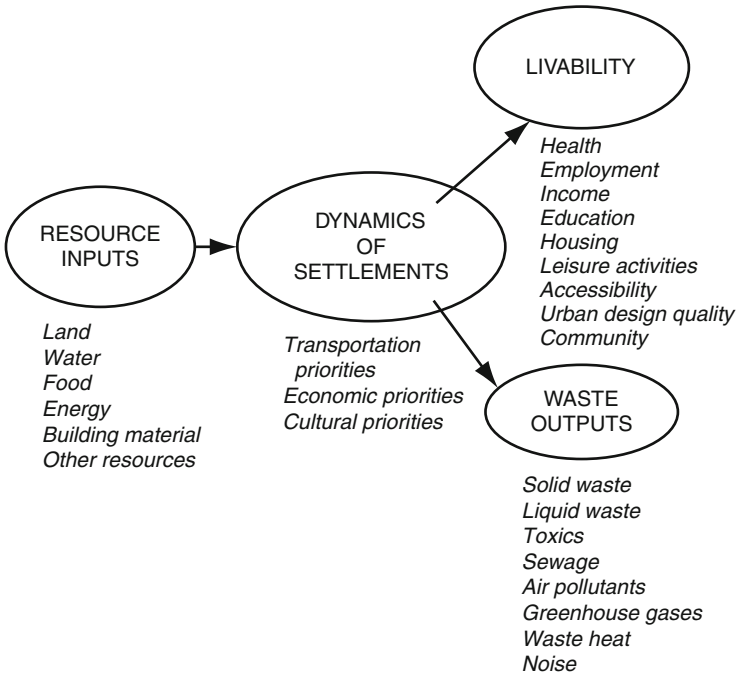

Natural Resource Flows and Sustainability in Urban Areas. Figure 4
Extended metabolism model of human settlements (From: [7])

Limitations and Challenges

The metabolism studies have traditionally limitations that can be connected to data availability, perspectives, and available resources and priority setting in individual projects. Observations and discussion about the difficulties of the studies in terms of data accessibility, missing information, and uncertainties are often neglected in presentations of various studies. Statistics do not adapt very well for following all types of flows and particularly not in a local area. Many types of statistical data and inventories are often only available at the national level, and these data are often used as basis for estimating local flows. Data on water, energy, and waste flows handled by local public organizations are more accessible, which explains the dominance of these in studies. With the exception of very few city areas, such as Hong Kong, which has been subject to repeated studies [66–68], cities are difficult to delimit, which creates problems to estimate inflows to the urban system as well as their international and local exchanges.

Integrating nature and socioeconomic aspects is still an important challenge in connection with ecosystem analysis. The analysis of urban metabolism has largely been dominated by quantification of material inflows and outflows, and the connections to social aspects have often been fairly weak. Only few studies have made efforts to analyze flows in their broader social, economic, and geographical setting, and studies have seldom been able to connect to decision-making or involve stakeholders. Despite increased interest in international aspects of material flows, only limited systematic efforts to evaluate ecological linkages of various cities in more detail than standardized ecological footprints have been made. It is also rare with several levels of scale in the analysis. Summarized flows contribute to an overview but are not adequate for making connections to decision points in society or say much about their qualitative usefulness to society [3].

In making connections to decision-making, planning, and strategy development, it is necessary with closer connections to decision points and institutional structures, and the analysis must become more flexible in scale and detail. A more systematic multilevel analysis and connections between different levels of scale and governance are needed. In many cities, there is a lack of evaluation of local ecocity projects in relation to the whole city and its development. In a discussion paper on how cities can integrate global concerns, Xia Bai [69] presented some thoughts on how scale considerations should be taken into account more systematically when addressing city strategies, which can inspire urban metabolism studies to become more policy relevant.

Future Directions

Many innovative ideas regarding how a city could be planned or developed to minimize its resource consumption have been proposed in recent decades. There are numerous ecocity or sustainable city initiatives in different cities around the world. Cities such as Curitiba, Freiburg, London, Vancouver, Stockholm, Tianjin, and Melbourne can show inspiring examples of initiatives and positive developments. Public planning authorities have developed growing awareness of sustainability issues, and it is difficult to find any comprehensive urban plan that lacks sustainability goals. In local ecocity projects, flow-based initiatives are common in relation to waste, energy, and traffic. Despite this marked increase in awareness and ambitions, there is still a lack of powerful initiatives that decisively shift urban development in a sustainable direction. Even cities that have a high profile as sustainability forerunners, such as Copenhagen and Malmö [70] or Portland [71, 72], may show developments that are fairly inconsistent with declared sustainability ambitions, particularly in terms of road traffic and urban sprawl.

There is generally a need for more comprehensive analysis at the city and big city region level by revitalized urban metabolism efforts. It is, however, possible that the increasing interest among cities concerning climate change mitigation and ecological footprints will stimulate further analysis of the urban metabolism at the city level.

Urban metabolism and ecological footprints have become influential concepts. But it is a bit paradoxical that while urban ecology and sustainable urban development research and actions have grown dramatically, the analysis of urban systems at the city level or big city regional level has played only a marginal role. Efficiency

of energy, problems of traffic flows, and consumption are addressed in an urban setting, but the scale is most often far below the city or city region level (e.g., house, household, city district, infrastructural sector). There exists seldom a sufficiently good information basis for assessing the development of the city and its region and their external exchanges with the surrounding world and for developing comprehensive strategies at the city level.

There are many intriguing questions concerning the development of big city regions, e.g., connected to urban form and location policies that should be systematically analyzed from a metabolic perspective. From studies primarily in the UK and the Netherlands, there is evidence of positive effects in terms of provisions of ecoservices and minimized loss of natural environment and biodiversity from promotion of more compact urban development [73, 74]. However, there is still debate about the desirability and challenges of such compact city ambitions e.g., [75] and need for more empirical evidence [3].

In dynamic big city regions that are characterized by regional enlargement and polycentric developments, such issues are very complex and challenging but need to be analyzed further. In national planning systems all over the EU, the concept of polycentricity is implemented [76]. The European Spatial Development Perspective [77] strongly argued that polycentric urban systems are more equitable, efficient, and sustainable than monocentric or dispersed urban systems and should therefore be actively encouraged, but this hypothesis remains to be tested, and even if polycentric regions have certain potential advantages, these opportunities still need to be identified and used. Major research questions in both the large urban metabolism projects under EU-FP7 connect to these issues. They both focus on urban form, traffic, and land use, and their ambitions to connect to planning and institutional structures are higher and more elaborated than most past urban metabolism projects.

There are many challenges for future urban metabolism studies in relation to developing the overview and understanding of the urban flow systems and to become more policy relevant. Only about 30 cities have been so far analyzed, and there have not been much comparative analysis, generalization, and theoretical development. Kennedy et al. [27] suggested that identification of various classes and comparative analysis of various factors, such as climate, age of city, and development history, should be further focused. Comparative studies are difficult due to very different preconditions in various cities, and comparisons between existing studies are problematic due to inconsistent basic data and lack of standardization of procedures. Even though there has been standardization effort in some study areas (e.g., metal metabolism studies), such challenges are likely to remain. Despite this, comparative studies and comparisons with other cities may still be valuable and almost necessary for developing perspectives on different resource flows and their efficiency in individual cities. Comparative studies can also form a base for looking closer into driving forces of the urban metabolism and effects of different developments or strategies. Besides improving the assessment of linkages of the urban metabolism in different scales, future studies should also aim to improve the overview of storage and accumulation processes in the urban environment. Analysis of urban natural flow systems is of central importance for a more comprehensive understanding of the resource use in the city and for assisting cities to contribute more forcefully to global sustainable development.

Bibliography

Primary Literature

1. UNFPA (2007) State of world population 2007. Unleashing the potential of urban growth. United Nations Population Fund, New York
2. Grimm NB, Faeth SH, Golubiewski NE, Redman CL, Wu J, Bai X, Briggs JM (2008) Global change and the ecology of cities. Science 319:756–760
3. Huang SL, Yeh CT, Chang LF (2010) The transition to an urbanizing world and the demand for natural resources. Curr Opin Environ Sustain 2:136–143
4. Ravetz J (2000) Integrated assessment for sustainability appraisal in cities and regions. Environ Impact Assess Rev 20:31–64
5. Rotmans J, van Asselt MBA, Vellinga P (2000) An integrated framework for sustainable cities. Environ Impact Assess Rev 20:265–276
6. Alberti M (1996) Measuring urban sustainability. Environ Impact Assess Rev 16(4–6):381–423
7. Newman PWG (1999) Sustainability and cities: extending the metabolism model. Landsc Urban Plan 44:219–226
8. Batty M (2008) The size, scale, and shape of cities. Science 319:769–771

9. Luckin B, Massard-Guilbaud G, Schott D (eds) (2005) Environment and the City. Modern European cities and the management of their resources. Ashgate, Aldershot
10. Douglas I, Hodgson R, Lawson N (2002) Industry, environment and health through 200 years in Manchester. Ecol Econ 41(2):235–255
11. Keiner M, Koll-Schretzenmayr M, Schmid WA (2005) Managing urban futures: sustainability and urban growth in developing countries. Ashgate Publishers, Aldershot
12. Ooi GL (2009) Challenges of sustainability for Asian urbanization. Curr Opin Environ Sustain 2009(1):187–191
13. Agudelo-Vera CM, Mels AR, Keesman KJ, Rijnaarts HH (2011) Resource management as a key factor for sustainable urban planning. J Environ Manage 92:2295–2303
14. Roseland M (2005) Toward sustainable communities: resources for citizens and their governments. New Society, Gabriola Island
15. Newman P, Jennings I (2008) Cities as sustainable ecosystems: principles and practices. Island, Washington DC
16. Girardet H (1999) Creating sustainable cities. Green Books/The Schumacher Society, Totnes
17. Register R (2006) Ecocities: rebuilding cities in balance with nature. New Society, Gabriola Island
18. McIntyre NE, Knowles-Yánez K, Hope M (2008) Urban ecology as an interdisciplinary field: differences in the use of "Urban" between the social and natural sciences. In: Marzluff JM (ed) Urban ecology. An international perspective on the interaction between humans and nature. Springer, New york, pp 49–65
19. Pickett STA, Cadenasso ML, Grove JM, Boone CG, Groffman PM, Irwin E, Kaushal SS, Marshall V, McGrath BP, Nilon CH, Pouyat RV, Szlavecz K, Troy A, Warren P (2011) Urban ecological systems: Scientific foundations and a decade of progress. J Environ Manage 92:331–362
20. Hultman J (1993) Approaches and methods in urban ecology. Geograf Ann Ser B, Hum Geogr 75(1):41–49
21. McGranahan G, Marcotullio P, Bai X, Balk D, Braga T, Douglas I, Elmqvist T, Rees W, Satterthwaite D, Songsore J, Zlotnick H, Eades J, Ezcurra E, Whyte A (2005) Urban systems. In: Millennium ecosystem assessment:Conditions and trends assessment. Island, Washington
22. Duvigneaud P, Denayeyer-De Smet S (1977) L'Ecosystéme Urbs, in L'Ecosystéme Urbain Bruxellois. In: Duvigneaud P, Kestemont P (eds) Productivité en Belgique. Traveaux de la Section Belge du Programme Biologique International, Bruxelles, pp 581–597
23. Wolman A (1965) The metabolism of cities. Sci Am 213: 179–190
24. Kennedy CA, Cuddihy J, Engel Yan J (2007) The changing metabolism of cities. J Ind Ecol 11(2):43–59
25. Ayres RU, Simonis UK (eds) (1994) Industrial metabolism. United Nations University Press, Tokyo
26. Newman PWG (1999) Sustainability and cities: extending the metabolism model. Landsc Urban Plan 44:219–226
27. Kennedy C et al (2011) The study of urban metabolism and its applications to urban planning and design. Environ Pollut 159:1965–1973
28. Bergbäck B, Johansson K, Mohlander U (2001) Urban metal flows—a case study of Stockholm, review and conclusions. Water Air Soil Pollut Focus 1(3/4):3–24
29. Barles S (2007) Feeding the city: food consumption and flow of nitrogen, Paris, 1801–1914. Sci Total Environ 375:48–58
30. Browne D, O'Regan B, Moles R (2009) Assessment of total urban metabolism and metabolic inefficiency in an Irish city-region. Waste Manag 29(10):2765–2771
31. Zucchetto J (1975) Energy, economic theory and mathematical models for combining the systems of man and nature. Case study, the urban region of Miami. Ecol Model 1:241–268
32. Huang SL, Hsu WL (2003) Materials flow analysis and energy evaluation of Taipei's urban construction. Landsc Urban Plan 63(2):61–74
33. Zhang Y, Yang Z, Yu X (2009) Evaluation of urban metabolism based on energy synthesis: a case study for Beijing. Ecol Model 220(13–14):1690–1696
34. Ascione M, Campanella L, Cherubini F, Ulgiati S (2009) Environmental driving forces of urban growth and development. An emergy-based assessment of the city of Rome, Italy. Landsc Urban Plan 93:238–249
35. Wackernagel M, Kitzes J, Moran D, Goldfinger S, Thomas M (2006) The ecological footprint of cities and regions: comparing resource availability with resource demand. Environ Urban 18(1):103–112
36. Wackernagel M, Rees W (1995) Our ecological footprint: reducing human impact on the earth. New Society, Gabriola Island
37. Wackernagel M (1998) The ecological footprint of Santiago de Chile. Local Environ 3(1):7–25
38. Folke C, Jansson Å, Larsson J, Costanza R (1997) Ecosystem appropriation by cities. Ambio 26:167–172
39. Barrett J, Vallack H, Jones A, Haq G (2002) A material flow analysis and ecological footprint of York. Technical report. Stockholm Environment Institute, Stockholm
40. Collins A, Flynn A, Weidmann T, Barrett J (2006) The environmental impacts of consumption at a subnational level: the ecological footprint of Cardiff. J Ind Ecol 10(3):9–24
41. Chartered Institute of Wastes Management (2002) A resource flow and ecological footprint analysis of greater London. Best Foot Forward, London
42. Eaton RL, Hammond GP, Laurie J (2007) Footprints on the landscape: an environmental appraisal of urban and rural living in the developed world. Landsc Urban Plan 83:13–28
43. Niza S, Rosado L, Ferrão P (2009) Urban metabolism: methodological advances in urban material flow accounting based on the Lisbon case. J Ind Ecol 13(3):384–405
44. Schulz NB (2007) The direct material inputs into Singapore's development. J Ind Ecol 11(2):117–131
45. Sörme L, Bergbäck B, Lohm U (2001) Century perspective of heavy metal use in urban areas. A case study in Stockholm. J Water Air Soil Pollut Focus 1(3–4):197–211

46. Svidén J, Jonsson A (2001) Urban metabolism of mercury turnover, emissions and stock in Stockholm 1795–1995. J Water Air Soil Pollut Focus 1(3–4):79–196
47. Brunner PH, Rechberger H (2004) Practical handbook of material flow analysis. CRC Press, Boca Raton
48. Obernosterer R, Brunner PH (2001) Urban metal management the example of lead. J Water Air Soil Pollut Focus 1(3–4): 241–253
49. Baker LA, Hope D, Xu Y, Edmonds J, Lauver L (2001) Nitrogen balance for the Central Arizona Phoenix (CAP) ecosystem. Ecosystems 4:582–602
50. Færge J, Magid J, Penning de Vries FWT (2001) Urban nutrient balance for Bangkok. Ecol Model 139:63–74
51. Forkes J (2007) Nitrogen balance for the urban food metabolism of Toronto. Can Resour Conserv Recycl 52:74–94
52. Neset TSS, Lohm U (2005) Spatial imprint of food consumption. A historical analysis for Sweden, 1870–2000. Hum Ecol 33(4):565–580
53. Hermanowicz SW, Asano T (1999) Abel Wolman's the metabolism of cities' revisited: a case for water recycling. Water Sci Technol 40(4):29–36
54. Gandy M (2004) Rethinking urban metabolism: water, space and the modern city. City 8(3):363–379
55. Thériault J, Laroche AM (2009) Evaluation of the urban hydrologic metabolism of the Greater Moncton region, New Brunswick. Can Water Resour J 34(3):255–268
56. Sahely HR, Kennedy CA (2007) Integrated systems flow model for quantifying environmental and economic sustainability indicators: case study of the City of Toronto urban water system. ASCE J Water Resour Plann Manage 133(6):550–559
57. Baker LA (ed) (2009) The water environment of cities. Springer, New York
58. Kennedy C, Steinberger J, Gasson B, Hillman T, Havránek M, Hansen Y, Pataki D, Phdungsilp A, Ramaswami A, Villalba Mendez G (2009) Greenhouse gas emissions from global cities. Environ Sci Technol 43:7297–7302
59. Fischer-Kowalski M, Krausmann F, Smetschka B (2004) Modelling scenarios of transport across history from a socio-metabolic perspective. Rev – Fernand Braudel Center 27:307–342
60. Bettencourt L, Lobo J, Helbing D, Kuhnert C, West GB (2007) Growth innovation scaling and the pace of life in cities. Proc Natl Acad Sci USA 104:7301–7306
61. SUME (Sustainable Urban Metabolism for Europe) FP7 Collaborative Research Project. http://www.sume.at. Accessed 1 Jul 2011
62. BRIDGE programme (sustainaBle uRban plannIng Decision support accountinG for urban mEtabolism). http://www.bridge-fp7.eu. Accessed 1 Jul 2011
63. Baccini P, Bader HP (1996) Regionaler Stoffhaushalt. Spektrum Akad. Verlag, Heidelberg
64. Cencic O, Rechberger H (2008) Material flow analysis with software STAN. J Environ Eng Manage 18(1):3–7
65. Oswald F, Baccini P (2003) Netzstadt: designing the urban. Birkhäuser, Basel
66. Newcombe K, Kalma J, Aston A (1978) The metabolism of a city: the case of Hong Kong. Ambio 7:3–15
67. Boyden S, Millar S, Newcombe K, O'Neill B (1981) The ecology of a city and its people: The case of Hong Kong. Australian National University Press, Canberra
68. Warren-Rhodes K, Koenig A (2001) Escalating trends in the urban metabolism of Hong Kong: 1971–1997. Ambio 30(7):429–438
69. Bai X (2007) Integrating global environmental concerns into urban management – the scale and readiness arguments. J Ind Ecol 2(11):15–29
70. Anderberg S, Clark E (2011) The green and sustainable Øresund region: Eco-branding Copenhagen and Malmö. In: Vojnovic I (ed) Sustainability: a global urban context. Michigan State University Press, Lansing (in press)
71. Redkin A Portland again tops a sustainable cities list, dot earth, the opinion pages, New York Times. http://dotearth.blogs.nytimes.com. Accessed 22 Jun 2011
72. Sustainable Business Oregon Portland's traffic is 16th worst. http://www.sustainablebusinessoregon.com. Accessed 22 Jun 2011
73. Tratalos J, Fuller R, Warrren P, Davies R, Gaston K (2007) Urban form, biodiversity potential and ecosystem services. Landsc Urban Plan 83:308–317
74. Geurs KT, van Wee B (2006) Ex-post evaluation of thirty years of compact urban development in the Netherlands. Urban Stud 43(1):139–160
75. Jenks M, Burton E, Williams K (eds) (2000) The compact city: a sustainable urban form? Oxford Brookes University, Oxford
76. Halbert L, Pain K, Thierstein A (2006) European polycentricity and emerging Mega-City-Regions – "one size fits all" policy? Built Environ 32(2):194–218
77. European Commission (1999) European spatial development perspective. Towards balanced and sustainable development of the territory of the European Union

Books and Reviews

Anderberg S, Prieler S, Olendrzynski K, de Bruyn S (2000) Old sins – industrial metabolism, heavy metal pollution and environmental transition in Central Europe. UN University Press, Tokyo

Baccini P, Brunner PH (1991) Metabolism of the anthroposphere. Springer, Berlin

Bernhardt C (ed) (2004) Environmental problems in European cities in the nineteenth and twentieth centuries. Waxmann, Münster\New York

Odum HT (1996) Environmental accounting: emergy and environmental policy making. Wiley, New York

Tarr JA (2002) The metabolism of the industrial city: the case of Pittsburgh. J Urban Hist 28(5):511–545

Natural Ventilation in Built Environment

Tong Yang[1], Derek J. Clements-Croome[2]
[1]Department of Civil and Building Engineering, Loughborough University, Leicestershire, UK
[2]School of Construction Management and Engineering, University of Reading, Reading, UK

Article Outline

Glossary
Definition of the Subject
Introduction
Vernacular Architecture
Natural Ventilation Principles
Natural Ventilation Design Requirements
Design Guidelines
Selection of Ventilation Strategies
Case Studies
Future Directions
Acknowledgments
Bibliography

Glossary

Air changes per hour (ACH) The volumetric flow rate of supply air, divided by the volume of the ventilated space.

Advanced natural ventilation system (ANV) Integration of basic natural ventilation strategies such as cross ventilation and stack effect with smart controls.

BEMS Building energy management system.

BREEAM Building research establishment environmental assessment method – UK origin.

Exfiltration/infiltration Air flow through unintended leakages out/into buildings.

Hybrid ventilation Combined natural and mechanical ventilation (also called mixed-mode ventilation).

Indoor air quality (IAQ) Indoor Air Quality – broadly defined by the purity of the air but often CO_2 is used as an indicator.

Mixed-mode ventilation See hybrid ventilation.

Natural ventilation Use of natural forces, i.e., pressure differences generated by wind or air temperature, to introduce and distribute outdoor air into or out of a buildings.

Night cooling The use of night air to cool the building using wind towers or a fan to circulate the air.

PAQ Perceived air quality.

Thermal comfort The state of mind that expresses satisfaction with the surrounding thermal environment.

Ventilation Provides fresh air into a building to ensure good air quality for occupant health and well-being.

Ventilation effectiveness The ability of a ventilation system to exchange the air in the room and also the ability to remove airborne contaminants.

Ventilation flow rate The amount of air per unit time into the ventilated space (liter per second or l/s, cubic meters per hour or m^3/h).

Well-being Healthy mind and body.

Definition of the Subject

Natural ventilation uses the natural forces of wind and buoyancy to introduce fresh air and distribute it effectively in buildings for the benefit of the occupants. Fresh air is required to achieve a healthy, fresh, and comfortable indoor environment for people to work and live in. Natural ventilation can ensure or support the supply of adequate breathing air, adequate ventilation of contaminants, adequate thermal conditioning and moisture dissipation, and contribute to well-being through a connection to the dynamics of nature. For natural ventilation to be effective, there has to be a close relationship between the architecture and the air circulation system. This includes the relationship between the built form, the site environment in a particular location, and the layout within the building.

The Natural History Museum in London, designed by Alfred Waterhouse in the Victorian age, is an excellent example of design for natural ventilation. The architect designed the built form to encourage the flow of air through each space in the building by the use of two ventilation towers at the back of the building to induce air flow through stack ventilation [1].

Buildings should be designed to take full advantage of the prevailing natural forces such as wind, outdoor temperature, sunlight, incorporating building elements such as towers, atria, and thermal mass to ventilate and cool occupied spaces. In many climates there is

a growing proportion of naturally ventilated buildings using natural features and forces to reduce a building's *environmental or carbon footprint*.

Introduction

The reasons for ventilating a space with air are as follows:

1. Ventilation air provides oxygen that is needed for human life processes; it takes about 4 s for inhaled air to pass through the respiratory system and transfer oxygen to the blood and then to the brain; poor-quality air deficient in oxygen with consequent high CO_2 levels impedes clear thinking and concentration.
2. Ventilation air dilutes; the contaminants may be CO_2 from respiration, odors secreted through the human skin, cigarette smoke, or emissions from other process such as dust, allergens, aerosols, toxic gases, and particulates in general.
3. Ventilation promotes and directs air movement in the space, removing excessive heat and/or moisture essential for comfort and well-being.

Traditional vernacular architecture has taught us the best of sustainable architecture and ecologically sensitive adaptation, using passive features ranging from building orientation and form, appropriately sized and oriented openings linked with vertical forms, the benefits of local materials and mass for night cooling, and the relationship of buildings in context to ensure effective air flows.

Vernacular Architecture

Vernacular architecture blends buildings into their specific settings, so that there is a natural harmony between the climate, architecture, and people. Vernacular architecture learned from the environmental variations of place relating to local variations in temperature, humidity, sun, wind, rain, earthquakes, and storms. In climates where the diurnal range may be 17°C, vernacular buildings allow a variation in indoor temperature of only some 4°C through time-lag and night cooling. In climates where humidity may be 90%, vernacular buildings support human comfort by allowing air to flow over the many thermo-receptors on the human body. Vernacular architecture also adapted to ensure indoor air quality through natural ventilation through the careful design and placement of indoor pollutant generators from stoves to commodes. Four vernacular solutions are further described: wind towers and courtyards, termite mounds, and igloos, each integrating the conditioning power of natural ventilation in unique responses to local climate.

Wind Towers

The wind towers called *bagdirs* are a distinctive and ancient feature of Islamic architecture. It has been used for centuries to create natural ventilation in buildings. Examples of wind towers (Fig. 1) can be found throughout the Middle East, Pakistan, and Afghanistan and now are sometimes incorporated into Western architecture.

Wind flowing around a building causes separation of flow which creates a positive pressure on the windward side and a negative pressure on the leeward side of the building. Due to its height the wind tower enhances the positive pressure on the windward side; it is then directed through the tower into the building. Airflow follows the pressure gradients within the structure and exits through purposely designed openings and as well as through the leeward side of the tower. The size and location of openings (e.g., windows, doors, etc.) and distribution of internal party walls have a great impact on encouraging cross flow and mixing of the indoor air.

The principal factor is the buoyancy which depends on the temperature difference and the height. During the day the sun heats up the structure warming the internal air which then rises through the wind tower, as illustrated in Fig. 1. At night the cool night air lowers the temperature of the structure and the internal air and the heavier air then flows downward cooling the internal spaces after the heat of the day. Figure 2 shows how wind towers can also provide natural cooling for underground water cisterns.

Courtyards

Courtyards are one of the oldest plan forms for dwellings going back thousands of years and appearing as a distinctive form in many regions in the world. Examples exist in Latin America, China, the Middle East, Mediterranean, and in Europe. Preserving

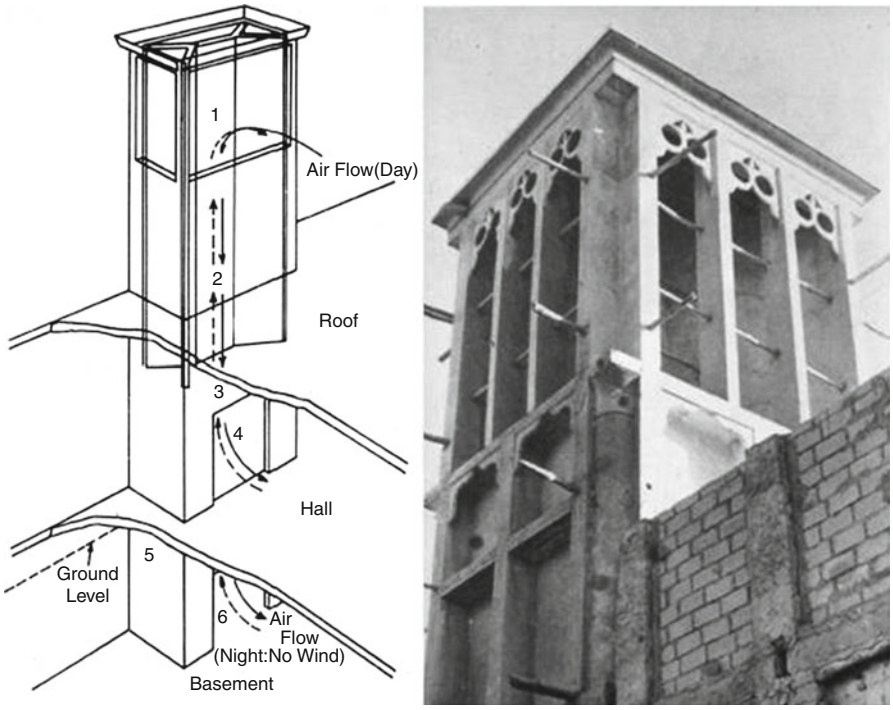

Natural Ventilation in Built Environment. Figure 1
Bagdir in Dubai, in United Arab Emirates [2]

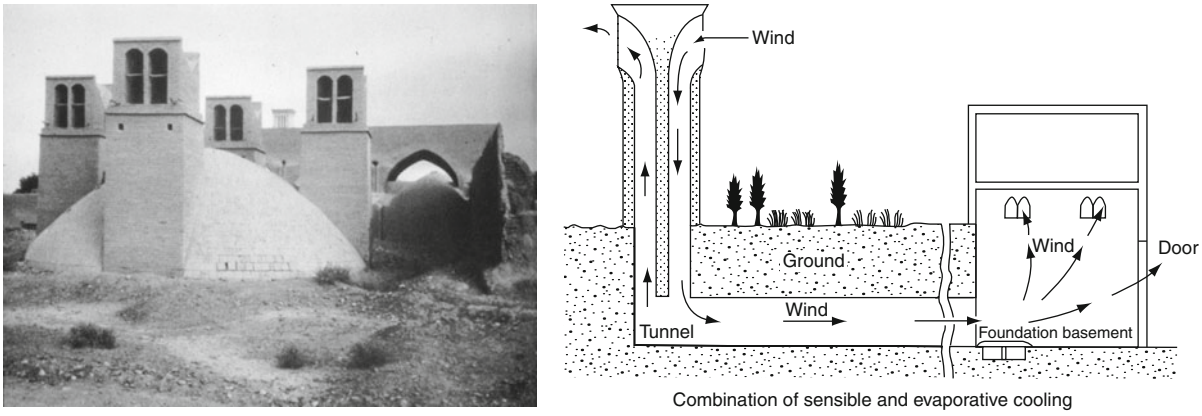

Natural Ventilation in Built Environment. Figure 2
Wind towers in Yazd, Iran to ventilate houses, are also constructed to cool underground cisterns (water reservoir) [3]

the basic typology of the courtyard, local climate and culture has created a unique style for each region.

The Courtyard House (Siheyuan) is a typical form in ancient Chinese architecture, especially in northern China. It offers space, comfort, quiet, and privacy. A Siheyuan consists of a rectangle with a row of houses bordering each side around a courtyard, normally with a southern orientation and having the only gate usually situated in the southeast side. Walls protect the houses from the harsh winter winds and the spring dust storms

that frequently occur in Northern China from the Gobi desert in Mongolia. The house's deep eaves allow the winter sun's warmth to be directed into the rooms, while they also provide cooling shade and protection from the summer rains. Their design reflects the traditions of China, following the rules of Feng Shui and Confucian tenets of order and hierarchy.

All the rooms around the courtyard have doors and large windows facing onto the yard and small windows high up on the back wall facing out onto the street. Ridged roof tops provide shade in the summer and retain warmth in the winter. The verandah divides the courtyard into several big and small spaces that are closely connected, providing a common place for people to enjoy whatever the weather. The courtyard is an open-air living room and garden with plants, rocks, and flowers, for family members to chat and gather.

In cold northern China, courtyards are built broad and large to increase the exposure to sunlight, and there are more open areas inside the courtyard walls for daylight, fresh air, rainwater for plants and gardens to be harnessed. In hot southern China, the courtyard houses (Fig. 3) are built with multiple stories to encourage cross ventilation flow incorporating natural cooling effects. The orientation of houses is not strictly north–south aligned, but follows the local topology of hills and easy access to water sources.

Natural Ventilation in Built Environment. Figure 3
A typical courtyard house in southern China

Lessons from Nature: Termitaries

Termites are an outstanding example in the animal kingdom of ingenious animal architects in the sense of master builders. Over 2,000 species live in tropical and subtropical regions and have shown us by analogy the art of designing for living in a variety of dwelling styles with natural ventilation.

Termites build their nest so as to achieve automatic ventilation to regulate the internal temperature, as well as constantly managing control of gas exchange and moisture level. They do not keep a set temperature, but allow a gradual change between the seasons determined by the external environmental temperature.

In Australia, compass termites build large-sized mounds in the form of huge, flat chisel-shaped blades, with their long axis pointing north–south. This arrangement exposes the minimum possible area to the midday sun but allows the mounds to catch the rays of the early morning and late evening sun, when the termites need warmth, especially in the cold season; peak temperatures can be lowered by about 7°C with N–S orientation and thus maintain a preferred temperature of 30–32°C [4].

There are two main types of termite mounds: (1) The *open ventilation* mounds which let air flow into or out through chimneys or holes built into the mounds; (2) The completely *enclosed mounds* in which gases are exchanged through the porous thin-walled tunnels.

The nest of a termite species *Apicotermes gurgulifex* is shown in Fig. 4a. It is embedded in the soil but clothed by a mantle of air; the nest is constructed from the excrement of the termites so is well insulated. Its outer wall has a pattern of raised, ring-shaped configurations which surround an array of precisely spaced and shaped ventilation slits. These slits link the external and the internal spaces.

The termitary of the fungus cultivating termites, *Macrotermes bellicosus* in Fig. 4b, may reach a height of 3 or 4 m and contain more than two million termites. The fungus chambers are built into complex sponge-like structures with numerous supporting

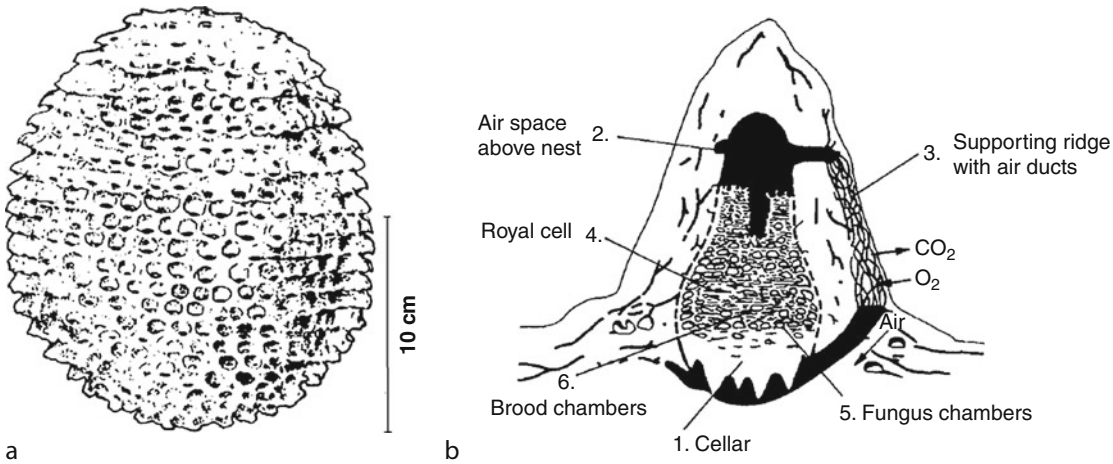

Natural Ventilation in Built Environment. Figure 4
Ventilation of termite molds (**a**) Nest of a termite species *Apicotermes gurgulifex* [4]; (**b**) Longitudinal section through the nest of *Macrotermes bellicosus* from Ivory Coast showing the air being circulated by buoyancy [4]

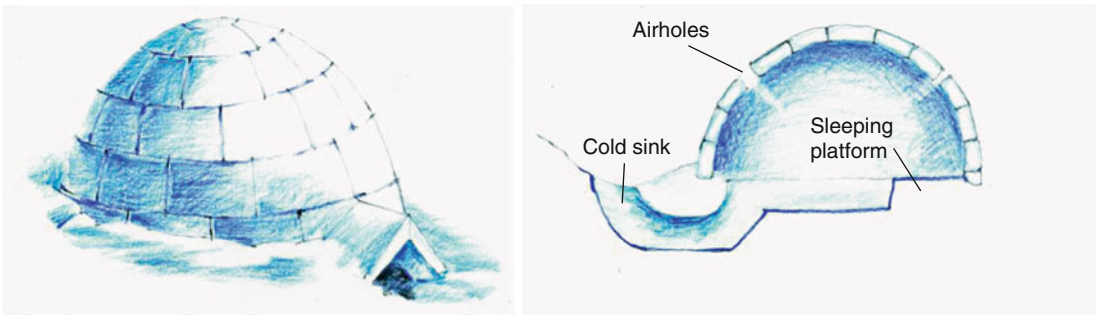

Natural Ventilation in Built Environment. Figure 5
Illustration of an igloo

ridges with air ducts. The air in the fungus chamber is heated by fermentation processes and the metabolic heat generated by the termites. The hot air rises and enters the duct systems in the ridges, the walls of which are porous allowing carbon dioxide to escape from and oxygen to enter the dwelling. The cooler air flows down to the cellar and replaces the rising warmer air.

Igloos

Inuit people build igloos as shelters from the extreme weather conditions in the Arctic. The igloo (Fig. 5) has an excellent thermal performance without mechanical equipment. The hemispherical shape of the igloo provides the maximum resistance to winter gales from all directions, which at the same time exposing the minimum surface area to heat loss. The dome uses packed snow blocks, some 500 mm thick, 1,000 mm long, and 150 mm wide, which are laid in a continuous in sloping pile. Effectively, the shape encloses the largest volume with the least material, so it can be heated by a blubber lamp. Coated by a glaze of ice on the interior surface, the finished dome is made stronger and windproof. The interior surface is also draped with animal skins and furs to prevent radiant and convective heat loss between the cold floor and the walls. Measurements have shown that with no heat source apart from the

small blubber lamp, internal air temperatures are held at levels of −6 to 4°C with external temperatures of −24 and −40°C [5].

General

Traditional building technologies have evolved and been adapted over time by people and animals in all climates to meet specific needs, accommodating the values, economies, and the culture inspired ways of life. However versatile they are all reflect the basic principles described in the next section.

Natural Ventilation Principles

Natural forces to drive ventilation can be wind pressures or pressure generated by the density difference between indoor and outdoor air.

Wind-Driven Ventilation

Wind is caused by pressure differences in the atmosphere. The general flow of wind close to the Earth's surface is subjected to boundary layer effects, so called the atmospheric boundary layer, in which wind speed is influenced by surface friction of the ground. The variation of wind speed in height on different terrains is illustrated in Fig. 6. Wind speed correction coefficients for different terrain conditions in the UK are listed in BS 5925 [6].

When the path of the wind is checked by obstacles, such as trees and buildings, then an energy conversion takes place. Velocity pressure is converted to static pressure, so that on the windward side an overpressure is produced (about 0.5–0.8 times the wind velocity), whereas on the leeward side an under-pressure results (about 0.3–0.4 times the wind velocity). The pressure distribution on the roof varies according to pitch. Figure 7 shows areas of positive and negative pressures generated by wind normal to building front: wind-driven flow through inlets on positive pressure faces and outlets on negative pressure faces [8]. The pressure differentials arising across a building cause infiltration of air through window cracks and other openings.

Relative to the static pressure of the free wind, the pressure on any point on the surface of a building façade p_w can be approximated by the equation:

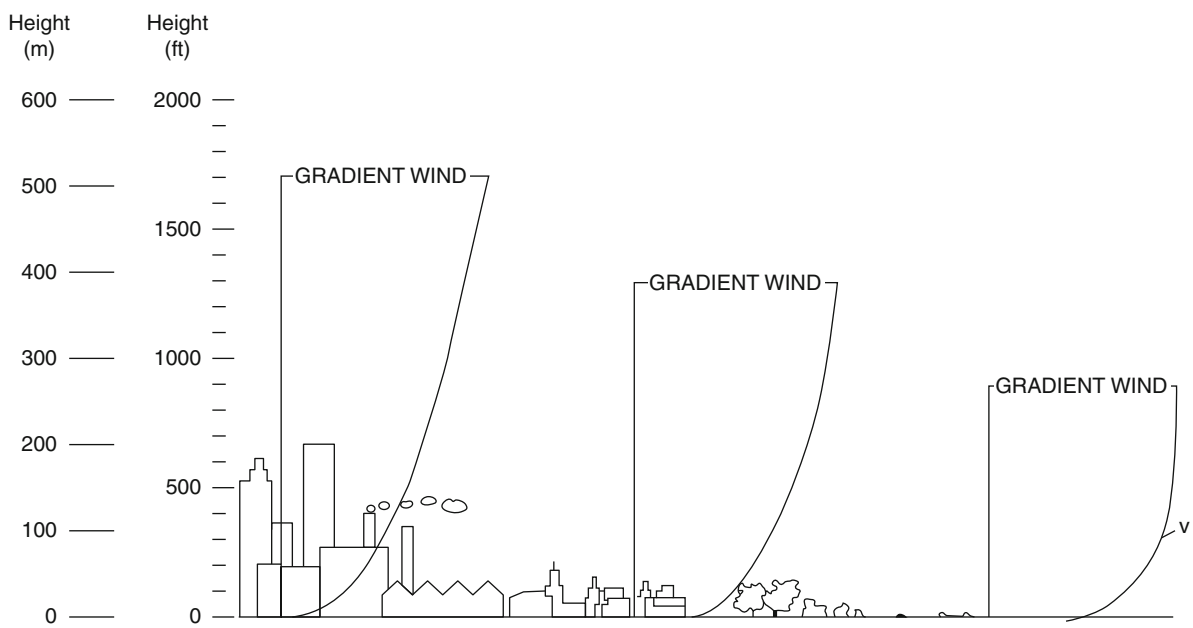

Natural Ventilation in Built Environment. Figure 6
Wind speed variation with height and terrain conditions [7]

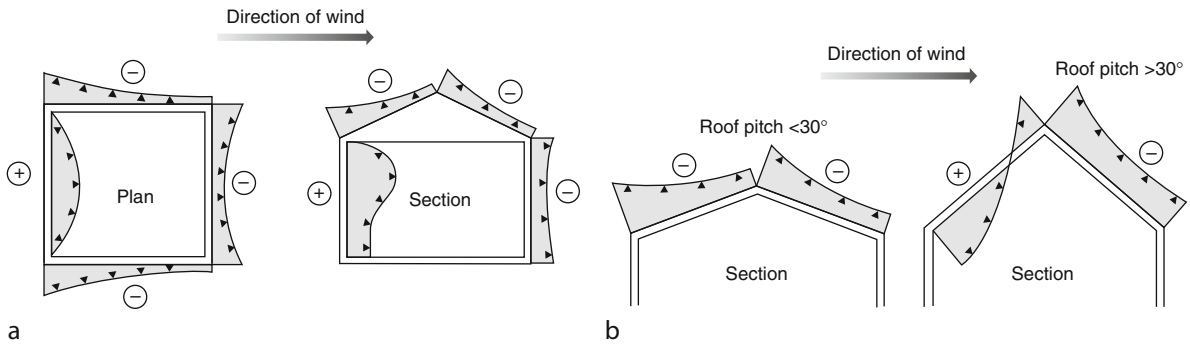

Natural Ventilation in Built Environment. Figure 7
Wind pressure distribution on buildings (**a**) Wind pressure on building; (**b**) Wind pressure on roof [8]

$$p_w = 0.5\rho C_p v_z^2 (P_a) \quad (1)$$

where

C_p = Wind pressure coefficient (dimensionless)
v_z = Local wind speed at a specific reference height z (m/s)
ρ = Air density (kg/m^3)

In order to calculate the ventilation rate due to the wind a knowledge of the wind speed and direction is necessary besides information about the nature of wind-stream patterns developed around the building. Summary of façade-averaged wind pressure coefficient data for simple rectangular-plan low-rise buildings in varying degrees of shelter and wind directions is given in the *AIVC Application Guide: A Guide to Energy Efficient Ventilation* [9].

For buildings with a simple layout, the natural ventilation airflow rate by wind effect can be determined as in the following case, more examples are given in *CIBSE Applications Manual AM 10* [10]:

(a) Wind effect alone for a zone with multi cross flow openings (Fig. 8):

$$q = A \cdot C_d \cdot U \cdot \left[\frac{\Delta C_p}{2}\right]^{0.5} \quad (2)$$

where

U is the wind speed measured at the same height as the building (m/s)
A is the total ventilation area (m^2) – assuming the four openings are identical

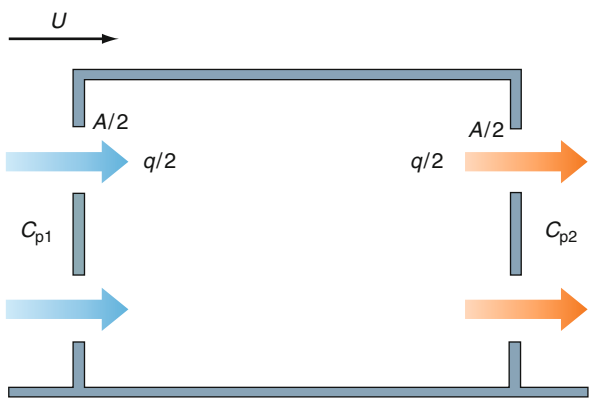

Natural Ventilation in Built Environment. Figure 8
Cross ventilation driven by wind effect alone

C_d is the discharge coefficient (typical value ~0.6)
ΔC_p is the difference between wind pressure coefficient (C_{p1} and C_{p2})

Buoyancy-Driven (Stack) Ventilation

Warm air in a room tends to rise because of its low density. It is replaced by cooler, denser air from outside. There is a neutral pressure plane where the pressure difference is zero as shown in Fig. 9. Since the pressure at the outlet or inlet can be affected by the wind, the extent to which the stack effect operates is governed partly by the wind pressure and partly by the design of the openings and the internal layout.

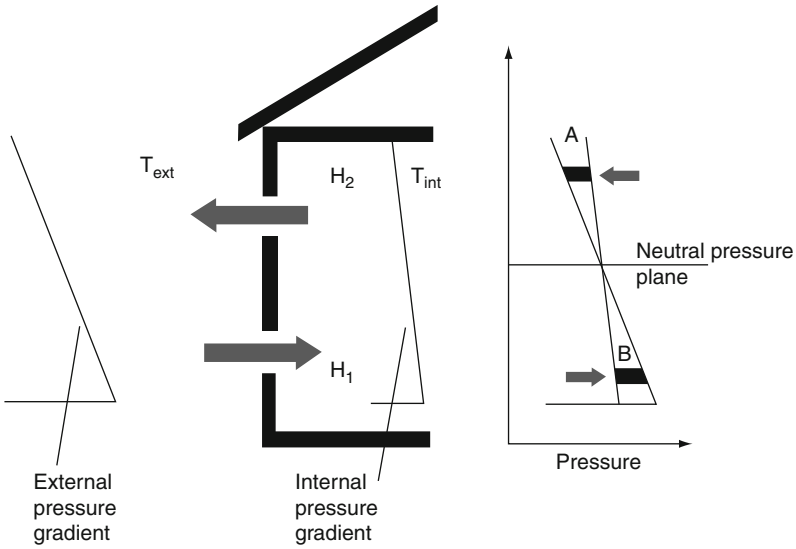

Natural Ventilation in Built Environment. Figure 9
Stack pressure distribution between two vertically placed openings ([9] p. 214)

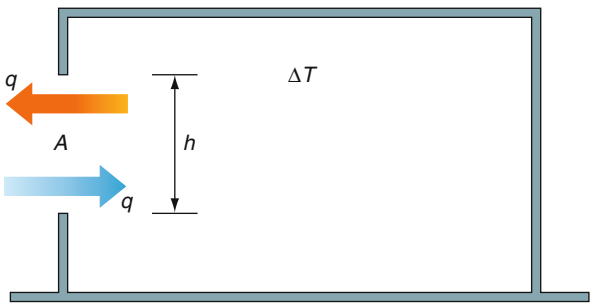

Natural Ventilation in Built Environment. Figure 10
Single-sided ventilation, single-opening, driven by buoyancy alone

For buildings with a simple layout, the natural ventilation airflow rate by buoyancy effect can be determined as in the following case [10]:

(a) Buoyancy effect alone for a single-opening zone (Fig. 10):

$$q = \frac{A \cdot C_d}{\left[\frac{(T_i+273)}{\Delta T \cdot g \cdot h}\right]^{0.5}} \tag{3}$$

where

q is the ventilation flow rate (m^3/s)
T_i is the internal temperature (°C)
ΔT is the difference between the internal and external air temperature (K)
A is the opening area (m^2)
h is the opening height (m)
C_d is the discharge coefficient (~0.25 for single-opening)
g is acceleration due to gravity (m/s^2)

In spaces with high ceilings and where cross ventilation is not feasible, stack ventilation works best (Fig. 11).

An atrium is a variant of stack ventilation principle (Fig. 12). It draws air from both sides of the building toward a central extract point, doubled the natural ventilation effective width in the building.

A well-designed double-skin façade provides buildings with additional protective layer from outdoor environment, improves thermal and visual comfort for occupants and reduce intrusive noise. It can create the circulation and integration of the internal and external space of building, providing views to outside and so achieve the harmonious integration of people and nature.

The Gherkin building (see Fig. 13), 30 St Mary Axe in the city of London, is naturally ventilated in most time of the year, its exterior cladding consists of triangular and diamond shaped glass panels. The glazing

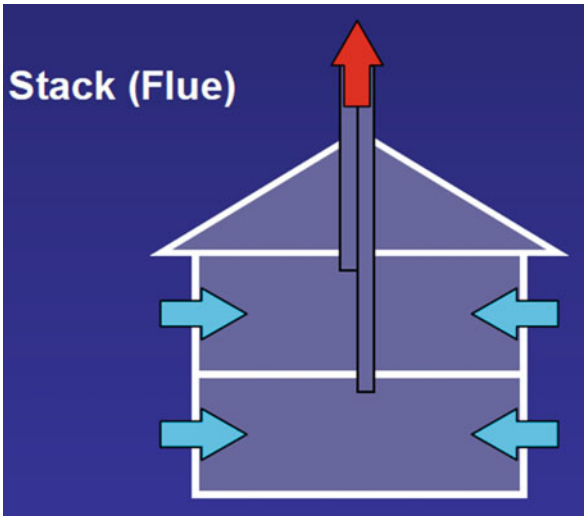

Natural Ventilation in Built Environment. Figure 11
Stack ventilation from vertical chimneys [11]

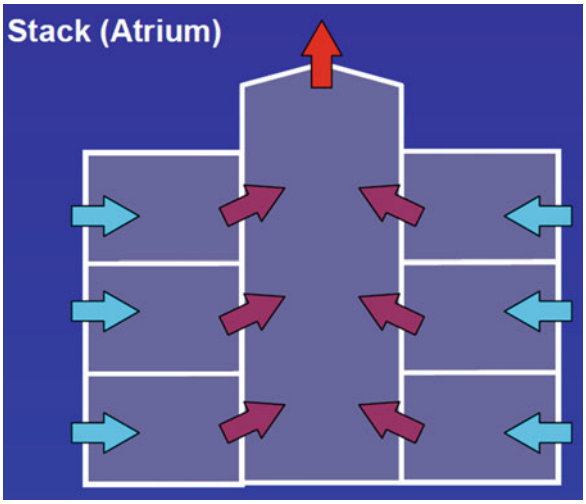

Natural Ventilation in Built Environment. Figure 12
Stack ventilation from Atrium [11]

system contains a double-glazed outer layer and a single-glazed inner screen with solar-control blinds in the central ventilated cavity. Fresh air is drawn up through spiraling light wells which consists of openable double-glazed panels, also effectively reduce the need for additional heating and cooling. The circular tapering shape of the building and the light wells maximized the amount of natural light throughout the building and provide views out across the City from deep inside.

When natural forces cannot provide the required indoor environment conditions, mechanical systems/components, – e.g., fans for increasing ventilation rate, and/or heat exchanger for cooling (or heating) at peak summer (or winter) times – can be used to enhance the natural ventilation through purposely installed openings in the building envelope. *Hybrid ventilation* (mixed-mode) system with pressure sensors and motor-driven dampers are used to give control. Careful considerations in the design and operation as well as end-user education are needed to deliver effective environmental control with ventilation.

Natural Ventilation Design Requirements

Fresh Air

Indoor CO_2 source is primarily generated through human metabolism. Human respiration requires a fresh air rate of 0.1–0.9 l/s per person depending on the activities (metabolic rate) and clothing insulation [14].

Seppänen et al. [15] and Wargocki et al. [16] have made a comprehensive review of over 20 studies with over 30,000 persons and found that ventilation rates below 10 l/s per person results in lower air quality and increase health problems.

Ventilation rates for acceptable indoor air quality are currently assessed by using the ASHRAE Standard 62.1 [17]. In this Standard there are two procedures for estimating the amount of fresh air required. The first is referred to as the ventilation rate and is a prescriptive approach stating that, for office buildings, there is a requirement of 10 l/s per person of fresh air (nonsmoking). A comparison of Standards for the indoor environment is given in the ASHRAE Handbook on Fundamentals [18].

Air Movement in Rooms

It has been well established that air movement is one of the important factors that influence people's perception of thermal comfort [19].

Air movement is a combination of a momentum-induced air flow and buoyancy-induced air flow [20]. A jet air flow is caused by a momentum source, which can either be a fan or the pressure difference across an opening caused by the wind or temperature difference.

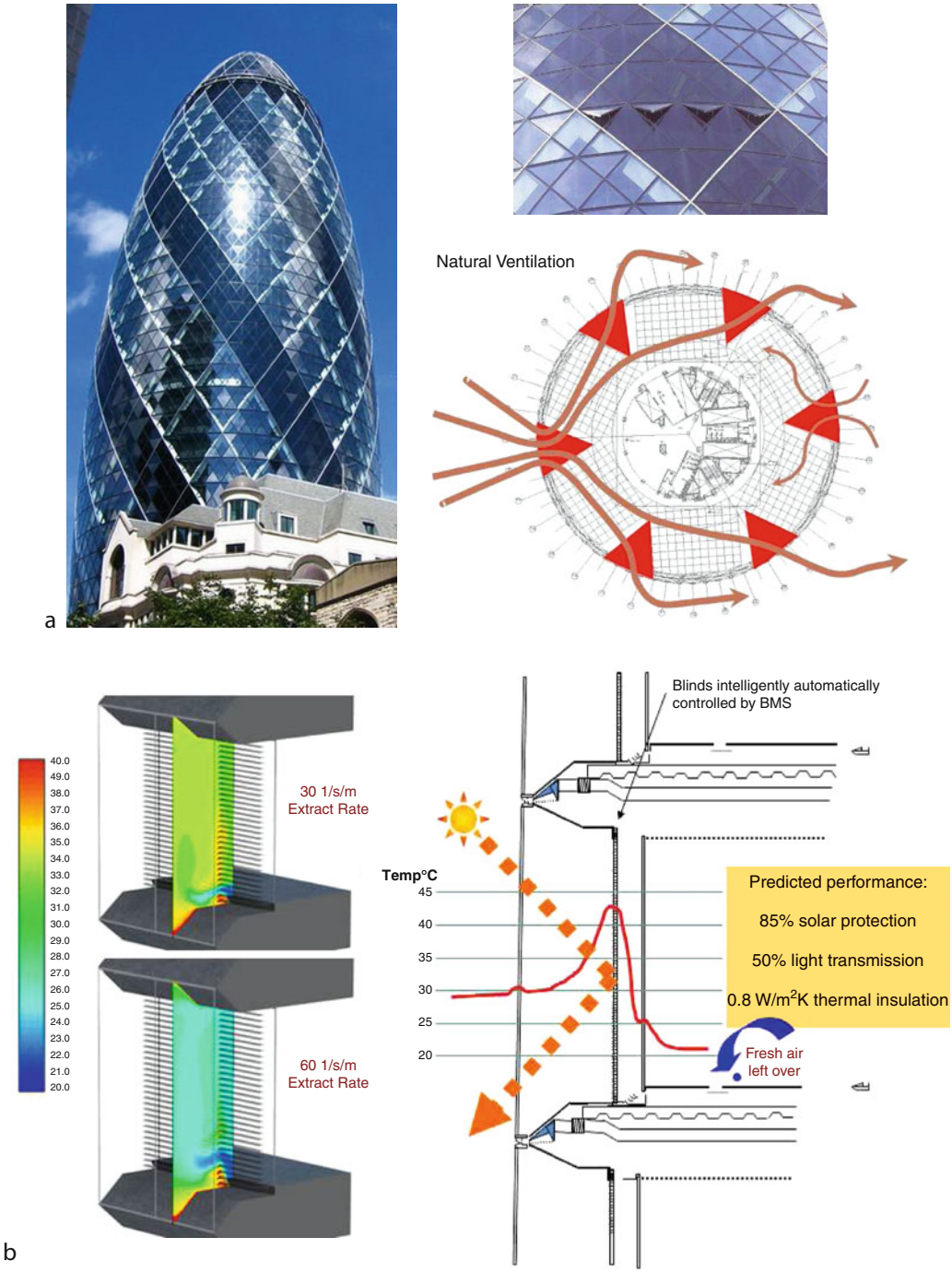

Natural Ventilation in Built Environment. Figure 13
Gherkin London and ventilation through double-skin facade (**a**) Gherkin façade [12] and natural ventilation concept [13]; (**b**) Gherkin double-skin facade design [13]

The other main source of air motion is buoyancy-driven air flow caused by density differences. This type of motion is also called natural convection.

The research work of Linke [21], Mullejans [22], and van Gunst [23] has given clear indications about the air patterns produced by air streams at various velocities and temperatures, when directed through different types of outlet, and also their interaction with the natural convection currents in the space. Optimum air and temperature distribution as well as a satisfactory sound level should be provided from the air streams outlet.

- Air movement should vary in space and time without giving drafts, especially, some parts of the body (i.e., ankles, back of the neck) are more susceptible to drafts.
- Temperatures should vary within a vertical gradient limit, higher level of warmth being preferable at below knee level rather than at head level.
- For freshness higher air velocity are required at higher temperatures, an air velocity change of 0.15 m/s being equivalent to a change of about 1°C in temperature. Air at a lower temperature and relative humidity of 40–60% (i.e., air with a lower enthalpy is perceived as fresher than air with a higher enthalpy [24, 25]).
- Above the head the convection air velocities can be 0.25 m/s or higher depending on the occupancy density and also the amount of artificial lighting.
- Air movement helps to dispel a sense of stuffiness.

Indoor Air Quality and Natural Ventilation

Body Odors A human being's sense of smell permits very low concentrations of odors. The sensitivity varies between individuals. In a typical indoors around 500 out of 6,000 compounds are human bioeffluents [26].

Poor-quality air is usually referred to as being stuffy, stale, close, heavy, or lacking in freshness. Inhaled air comes into contact with the nasal passages and then the respiratory tissue; in each case the motion of the olfactory hairs, and of the cilia on the respiratory membrane, is affected by temperature, humidity, dirt, odors, and also ions [27].

Environmental Tobacco Smoke Environmental tobacco smoke contains more than 4,000 chemicals and at least 50 of these chemicals are known cancer-causing substances [28]. It generates about 2 ppm CO, leads to irritation and discomfort among 20% of those exposed, also suspected increase in the risk of lung cancer [29]. Based on a study on the rates of hospital admissions for heart attacks before and after the smoking ban was introduced in England on July 01, 2007, there was a clear association between the smoking ban and a 2.4% reduction (or 1,200 fewer admissions due to a heart attack) in the 12 months following the ban [30].

Metabolic Carbon Dioxide An average sedentary adult (Metabolic Rate M = 70 W/m^2 and body area A = 1.8 m^2) produces approximately 0.0051 l/s (18 l/h) of CO_2 by respiration when performing light office duties [6]. Younger people such as infants and primary school children have lower emission rates but, they are likely to be more active and may well have CO_2 production at similar levels [29].

Normally, in buildings, CO_2 concentrations below 0.1% (1,000 ppm) are required to avoid discomfort and headaches [31]. According to the Canadian Center for Occupational Health and Safety [32], and also the ASHRAE standard [17], health effects can become acute at higher exposure levels.

Increased CO_2 content of the external atmosphere causes the decreased pH value of the blood [33]. Metabolism is very sensitive to body fluid pH value. Health concerns is another reason, besides global warming why the atmosphere CO_2 concentration should be limited to <426 ppm [27].

Volatile Organic Compounds (VOCs) Thousands of chemical compounds have been identified in the indoor environment. The most common pollutants are given in [17, 34]. Contaminants such as formaldehyde, toluene, volatile organic compounds (VOCs), allergens, and radon can accumulate in poorly ventilated buildings, causing health problems.

Complex mixtures of organic chemicals in indoor air also have the potential to invoke subtle effects on the central and peripheral nervous system, leading to changes in behavior and performance [35]. The latest overview on knowledge and research outcomes concerning the relationships between indoor air

pollutants and health effects highlighted future research directions [36]:

- Development of validated measuring methods
- Establishment of dose–response relationships
- Development of risk indicators for multiple exposures

Natural Ventilation for Cooling

To obtain cooling and remove heat from internal spaces, the incoming air from surroundings must be cooler than indoor temperature. The potential sources for the cool air may be from a shaded or landscaped space or from over a body of water, a labyrinth with heavy thermal mass, underground channels, or other source of cooling.

Cross ventilation is normally the primary strategy for passive cooling. Solar chimneys can be constructed to capture solar radiation to increase the difference in temperature between incoming and out-flowing air to enhance stack ventilation. In moderate and cold climates, nighttime ventilation can be applied to passively cool the building structure and provide a heat sink during the daytime occupancy period to achieve good thermal comfort.

Openable windows, as the most commonly used vents in natural ventilation systems. There are mainly four groups windows, e.g., sliding (sash), horizontal-vane opening, vertical-vane opening, and tilt and turn windows, as illustrated in a summary table in BSRIA guide [37].

Windows selection, integrated with building form and orientation, façade details, and internal layout design contribute to create different indoor airflow patterns and provide different options for the direction and volumetric flow control. In certain conditions, i.e., local drafts, cold radiation in winter, or solar gain in summer, windows can cause localized discomfort. However, occupants of naturally ventilated buildings are generally willing to accept a wider range of internal temperature and prefer more control over their environment.

The design of traditional Mosque in Malacca, Malaysia (Fig. 14) demonstrates the combination of cross ventilation, stack or heat stratification induced ventilation to achieve cooling with natural ventilation.

Daylighting

Daylight is good for health and saving energy. Natural light has a balanced spectrum of colors and wavelengths which vary over the day depending on latitude and seasons (Fig. 15). Studies suggest that daylight has benefits over artificial light sources in regulating circadian rhythms and maintaining overall health [38].

The daylight penetration depends on the room geometry as does the air distribution. Dark colors make the space feel smaller and more enclosed, whereas lighter colors have the opposite effect. In order to create stimulating high quality interior environments, lighting design must consider source intensities, distribution, glare, color rendering, and surface modeling [39]. Improved daylight metrics can be applied in a practical, real-world context to take into account for the temporal and spatial aspects of daylight, as well as meeting design standards for energy and occupants comfort [40].

Urban Pollution, Noise, and Natural Ventilation

In the build-up urban environment, buildings and roads make up the basic geometric form of street canyons. Similar to a natural canyon, which is a steep gorge with very high sides and a minimal valley floor, an urban canyon has narrow street space bordered by very high buildings. Example of an urban canyon is the Magnificent Mile in Chicago as shown in the picture (Fig. 16).

An urban boundary layer rises above the canopy (see Fig. 17). The potential for natural ventilation is seriously affected by the reduction of wind speed, complicated turbulent dispersion patterns, elevated day- and nighttime ambient temperatures due to the urban heat island effect and increased external pollutants as well as noise level.

Based on neural network methodologies, an algorithm calculating the optimum sizes of openings for naturally ventilated buildings located in urban canyons for single-sided and stack-effect configurations was derived by Ghiaus and Allard [43].

Mitigation of the urban heat island effect can be accomplished through the use of green roofs and the use of lighter-colored surfaces in urban areas, which reflect more sunlight and absorb less heat. Green roofs protect the roof materials from intense solar radiation

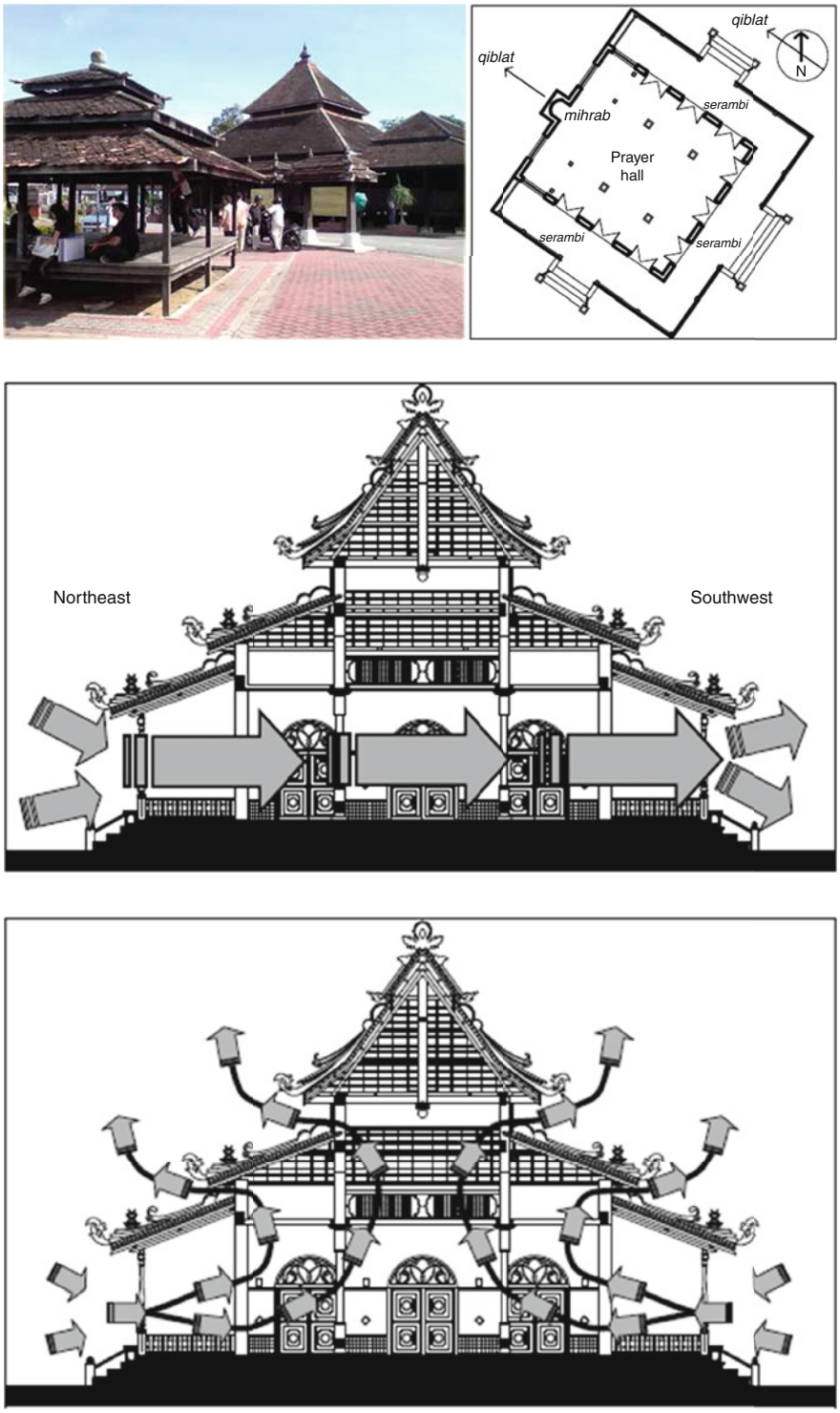

Natural Ventilation in Built Environment. Figure 14
Natural cooling in traditional Malacca Mosque, Malaysia [*Source*: Professor Vivian Loftness at Carnegie Mellon University] (**a**) A traditional Malacca Mosque in Malaysia and typical floor plan; (**b**) Cross ventilation design analysis, viewing toward Southeast facade; (**c**) Stack-effect design analysis

and prolong the service life time. Plants retain and absorb rain improve the microclimate and also reduce the runoff water to drainage systems.

Close to nature, even in urban settings has been long-term inspiration and challenge for architects and engineers. In Japan, Osaka Gas Corporation sponsored an experimental "Open Building" (Fig. 18) project NEXT21 since 1994. The structural and building services have same basic units using resources more effectively through systemized construction [44]. A variety of residential units have been designed by different architects' practices to accommodate varying households. Substantial natural greenery was planted on the "3D streets" formed by different levels of building service pathways connecting different apartments in a high-rise structure. Energy efficient measures included fuel cells and also encouraging occupants to become more aware of how to lead a comfortable life possible without increasing energy consumption.

An early study in climate chamber revealed that a change of 2.4 decipol in the PAQ or a change of 3.9 dB in the noise level has the same effect on thermal comfort as 1°C change in the operative temperature [46]. Recently, a number of newly built schools in the UK with different ventilation strategies have shown that the complex interaction between thermal comfort, ventilation, and acoustics are major challenges for designers [47].

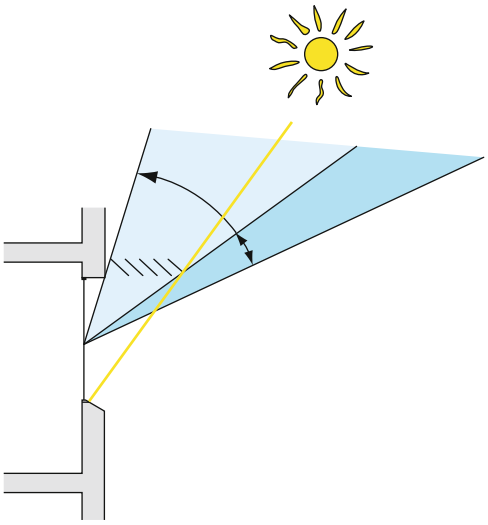

Natural Ventilation in Built Environment. Figure 15
Design to maximize daylight throughout the year [39]

Natural Ventilation in Built Environment. Figure 16
Urban canyon – the magnificent Mile in Chicago [41]

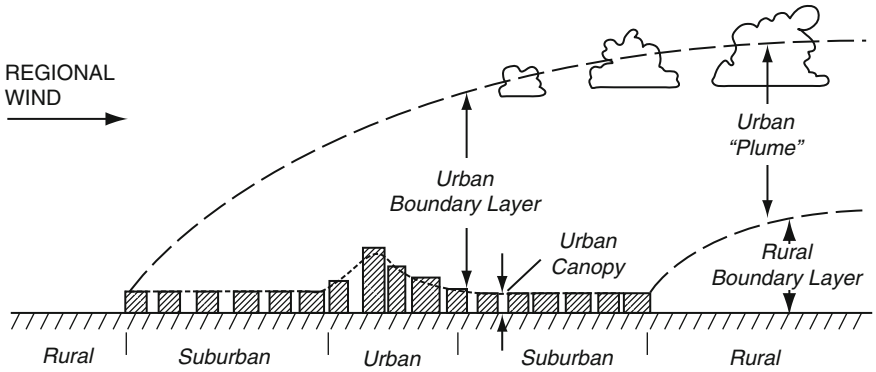

Natural Ventilation in Built Environment. Figure 17
Cross-section of the urban atmosphere [42]

Natural Ventilation in Built Environment. Figure 18
Open building in Japan [45]

The shape of the room and finishing materials of the surfaces affect the sound distribution. For example, concert halls are densely occupied and for music demand high spaces with volumes of 10 m^3 per person. The optimum balance of direct and indirect sound depends on the shape of the space and the boundary surface sound absorption. Combined acoustic and airflow design chart and equations could help designers to achieve both adequate acoustical insulation and airflow rates requirement, especially in the early stages of the design process [48]. The newly completed broadcast center in London has showcased all kinds of sustainable technologies to achieve the world's first naturally ventilated television studios (see detailed in case study).

Humidity and Condensation Management with Natural Ventilation

Ventilation Effectiveness Ventilation effectiveness is an indicator of how efficiently supplied fresh air is mixed and distributed in the occupied space, it related to both the dilution and removal of indoor airborne contaminants [49]. Gan [50] used air flow pattern, air temperature, and local mean age of air (i.e., the average time for air to travel from an inlet to any point in a room and is equal to the room volume divided by the air supply rate) to determine the effective depth of fresh air distribution in a naturally ventilated space. CFD predictions showed that the width and height of window opening, room heat gains, and outdoor air temperature have combined effects in determining the maximum room depth for effective fresh air distribution in single-sided natural ventilation. For summer cooling requirement, thermal comfort is the determine factor compared to indoor air quality. Different from passive contaminants concentration based effectiveness measures [20], Coffey and Hunt [51] proposed three measures of ventilation effectiveness based on the active buoyancy (e.g., the heat or coolth) removal applied on natural displacement and natural mixing flows within a space.

Practical design guidance for naturally ventilated performing arts buildings in an urban context has been outlined in Short and Cook (2005) [52]. Specific space features and operating requirements in designing auditoria were addressed and demonstrated through the presentation of three case studies. The additional technical challenges compared to common natural ventilation space design include:

- Sizing large inlet and outlet areas
- Managing acoustic attenuation
- Configuring building management system to cater for all levels of occupancy density
- Ensuring the stratification of warm, stale air forms above the breathing zone in theaters with raked seating
- Avoiding airflow imbalance generated by wind pressure

In hospital environment, natural ventilation system design need to pay special attention to eliminate the spread of biological (i.e., fungi, bacteria, and virus), chemical, and other contaminants effectively [53].

Humidity and Condensation Prevention Low ventilation rates may lead to high indoor relative humidity. Penetration of rainwater or snowmelt into the building envelope can also cause moisture accumulation into building structures or materials. Damp structures can lead to mold formation and indoor air contamination which has been shown to be strongly associated with adverse health outcomes [54].

Low ventilation rates and moisture accumulation may lead to increased dust mites in residential dwellings; the house dust mite allergen causes asthma. Mold is also associated with exacerbation of asthma and upper respiratory disease in both children and adults [3]. In Nordic residential buildings, monitoring data has shown health risk for the residents with ventilation rates below 0.5 ACH.

Studies of ventilation rate and health effects in public buildings [55] indicate that ventilation rates below 10 l/s per person have significantly associated with health risks and PAQ complaints, increased ventilation rate between 10 and ~20 l/s per person reduce sick building syndromes (SBS) and improve PAQ.

A relative humidity range of 40–60% is generally acceptable. High humidities over 60% gradually increase the risk of mold growth, and other fungal contamination, which may cause allergy and malodors. Increased humidity may also enhance other emissions in buildings, e.g., formaldehyde from furnishings [56]. A low humidity (<30%) may cause dryness and irritation of skin, eyes, and airways of some occupants [29] leading to increased throat infections. Contact lens wearers often experience discomfort in dry environments.

Correct selection of insulation materials in modern more air tight buildings will help to develop low energy buildings in refurbishment and new design but it is important to incorporate ventilation means such as trickle ventilators for example.

Fire Safety

In the event of a fire, smoke can follow natural ventilation paths, natural ventilation system must integrate fire safety strategy and provide solution which facilitates safe occupancy, escape or increased visibility for the fire service [6]. Smoke ventilation designs utilize the buoyancy of hot smoke, operates by opening

automatic opening vents (AOVs) on the fire floor in conjunction with an AOV at the top of the smoke ventilation system to naturally extract smoke from the common escape routes. Depending on the building envelope and structures AOVs should be placed in natural/mechanical smoke shaft, atria, internal glazed screen/façade, escape stair/fire fighting stair, or external wall to achieve the prime objective of keeping common escape routes clear of smoke. Stand by fans should be installed as an emergency safety precaution.

Design Guidelines

The rules of thumb for natural ventilation to be effective are as follows [10]:

- Single-sided single-opening (mainly driven by wind turbulence) effective up to a depth of two times the floor-to-ceiling height, typically 4–6 m (Fig. 19a).
- Single-sided double-opening (mainly driven by buoyancy forces) effective up to a depth of 2.5 times the floor-to-ceiling height, typically 7–8 m (Fig. 19b).
- Cross ventilation with ventilation openings on both sides, generally opposite sides, of a space (mainly driven by wind driven) effective up to a depth of five times of the floor-to-ceiling height, typically 15 m (Fig. 19c).
- Stack ventilation is mainly driven by temperature differences between the hot air in the occupied space and the cooler external air. The effective depth of stack ventilation is up to five times of floor-to-ceiling height. Stack ventilation can also be enhanced by wind effect or through the use of a solar chimney, i.e., solar driven stack ventilation [57].
- Different forms of atrium ventilation are illustrated in Fig. 19d [58].

Figure 20 illustrates various natural ventilation strategies can be integrated into design.

For natural ventilation aim for a heat gain less than 35 W/m^2 to avoid excessive overheating. This means there is a need to reduce internal gains; ensure effective ventilation; select suitable facades and materials. Also provide CO_2 monitors to help occupants know when it is preferable to increase ventilation.

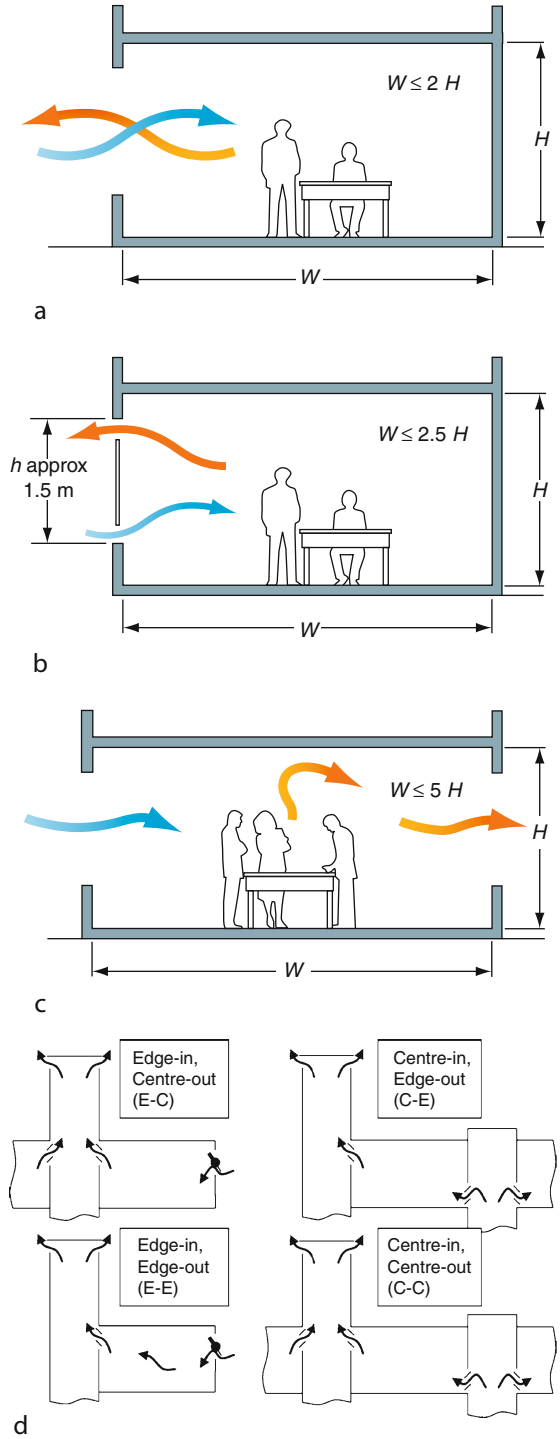

Natural Ventilation in Built Environment. Figure 19 Schematic diagrams of the different forms of natural ventilation (**a**) single-sided single-opening; (**b**) single-sided double-opening; (**c**) cross ventilation (**d**) Atrium ventilation [58]

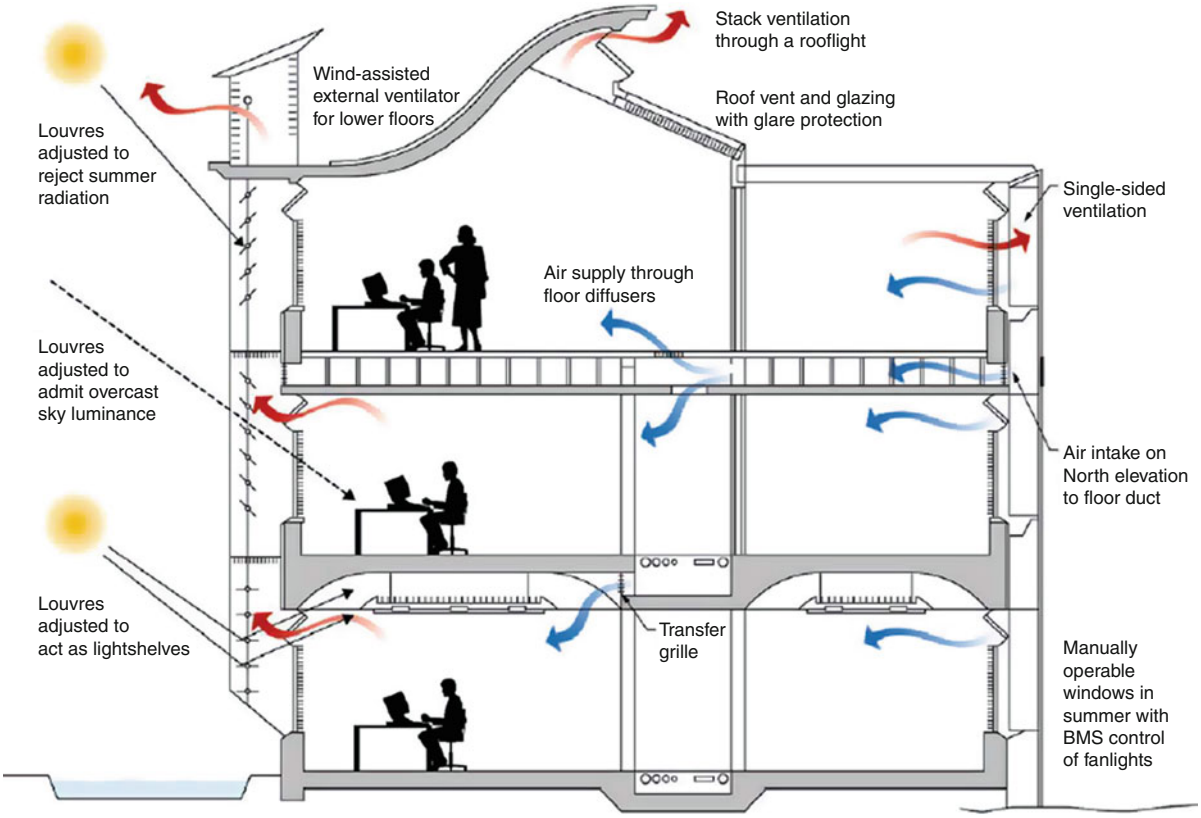

Natural Ventilation in Built Environment. Figure 20
Illustration of various natural ventilation strategies [37]

Passive cooling can be achieved by using:

- Local climate characteristics such as breezes
- Intelligent facades
- Solar protection
- Low energy lighting
- Thermal mass
- Ventilation
- Cloud computing, which can reduce computer heat gains considerably

Evaporative down draft cooling technique [59, 60] involves introducing fresh ambient air at the top of a central lightwell and cooling it so that it flows downward, filling the space with a static reservoir of denser, cooler air.

Benefits of Natural Ventilation

The parameters which affect the air velocity and temperature at a given point in the room are as follows:

1. Air inlet velocity; sound emission must also be accounted for when selecting a value for this
2. Supply to room temperature differential
3. Geometry and position of air supply outlet
4. Position of air extract outlet
5. Room geometry
6. Room surface temperatures; low surface temperature components, such as glass, tend to promote strong convection currents
7. Position, shape distribution, and emission of heat sources (e.g., people)
8. Room turbulence

The advantages of natural ventilation arise because there are no mechanical systems hence:

- Less energy is consumed
- Less plant room space is needed
- Higher level of daylight if well-designed
- Maintenance is simpler

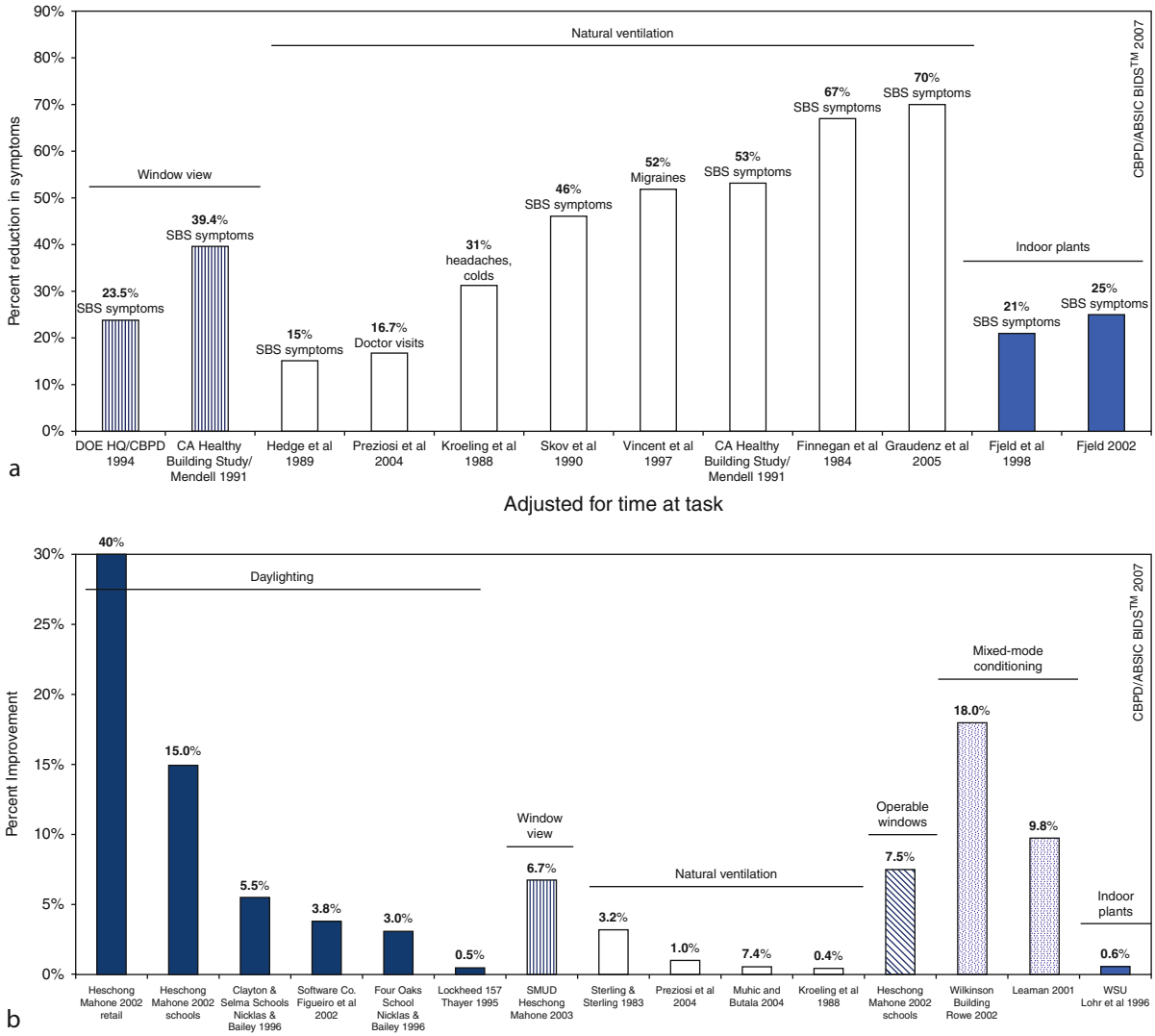

Natural Ventilation in Built Environment. Figure 21

Health and productivity gains from access to the natural environment [61] (**a**) Health gains from access to the natural environment; (**b**) Productivity gains from access to the natural environment

- Increased durability
- No noise
- Good occupant control using windows
- Low cost

The disadvantages are as follows:

- There is no filtration or control of moisture content.
- The driving pressure depends on the wind and/or the stack effect and both are variable and cannot be easily be controlled.
- There has to be an integrated approach to design between the architect and the engineer with regards to built form; orientation; massing; internal layout; selection of window types and their positioning in the façade.
- Internal heat gains are limited to less than 35 W/m^2.

The ventilation rate depends on the strength and direction of wind and/or buoyancy forces and the resistance of the flow path. The uncontrollable feature of natural ventilation can result in the air change rate

varying significantly and being distributed unevenly to internal spaces giving periods of inadequate ventilation, or periods of over ventilation and excessive energy waste.

Health and Productivity

There is a unique relationship between an individual, the environment, and the building they inhabit. The complicated interaction between the "hard" environmental stimuli, such as air and surface temperatures, humidity, air movement, and air purity, and the "soft" interlinked social and psychological factors of individuals and their organization, influences the sense of well-being, consequently the productivity. Task performance is best when the mind is alert at an optimum arousal level with the least distraction [27].

Loftness [61] shows the impact of natural ventilation on health and productivity in the Fig. 18a and b. In addition to the health and productivity benefits brought by design with access to the natural environment, effective daylighting can yield 10–60% reductions in annual lighting energy consumption. There is evidence of potential 40–75% reductions for cooling energy consumption when natural ventilation is interactively supported by mixed-mode HVAC systems.

Sustainable and healthy built environments result from integrating the natural diversity of the region – its unique climate and seasons, textures, sounds, smells, and variety of landscape and species.

Selection of Ventilation Strategies

The CIBSE AM 10 1997 [62] gives the following monograph (Fig. 22) to help the decision process for selecting whether to use natural ventilation, mechanical systems, or air-conditioning.

Design Elements for Natural Ventilation

Natural ventilation can be difficult to control due to the fluctuating indoor and outdoor conditions. As previously stated naturally ventilated buildings have to be inextricably linked to architectural form and fabric; they require holistic design and significant attention to detail.

Well-designed natural ventilation systems need to address the following aspects comprehensively [62–64]:

- *Site design* – building location, orientation, site layout, and landscaping
- *Building design* – building type and function, building form and orientation, envelope, thermal mass, natural ventilation strategy, internal spatial division and functions, internal heat load, solar shading, daylight, passive night cooling potential
- *Vent opening design* – position of openings, clear path of airflow, types of openings, sizing and choice of window opening design, effective area of multiple openings, provision of secure, operable openings, and control strategy

Computer Aided Prediction Models

Chen [65] presented an overview of ventilation performance prediction methods, including analytical models, empirical models, small-scale experimental models, full-scale experimental models, multizone network models, zonal models and Computational Fluid Dynamics (CFD) models. Recent applications of the above simulation tools were also examined in terms of contributions for practical design and research purposes. CFD applications in modeling of wind-driven natural ventilation [66] have shown improved prediction capability for complex naturally ventilated buildings. Walker [67] developed a methodology to evaluate natural ventilation in a multizoned commercial office building by full-scale building monitoring, reduced-scale physical experiment and CFD simulation. Detailed human thermal sensation and comfort models provide more accurate predictions on the dynamics responses of occupants to building environments, also advanced coupling simulation system extends the prediction capability of CFD and brings the human occupancy factor further into the core activities of the design process of buildings [68, 69]. The integration of CFD with dynamic building simulation (BS) models and Geographic information systems (GIS) data would be a practical way to take advantage of the strength of the other models for optimal natural ventilation design and analysis. Figure 23 illustrates CFD application on advanced natural ventilation design in hospital. Lomas and Ji [70] evaluated simple natural ventilation (SNV) and advanced natural ventilation (ANV) design in terms of overheating risk in the current and future

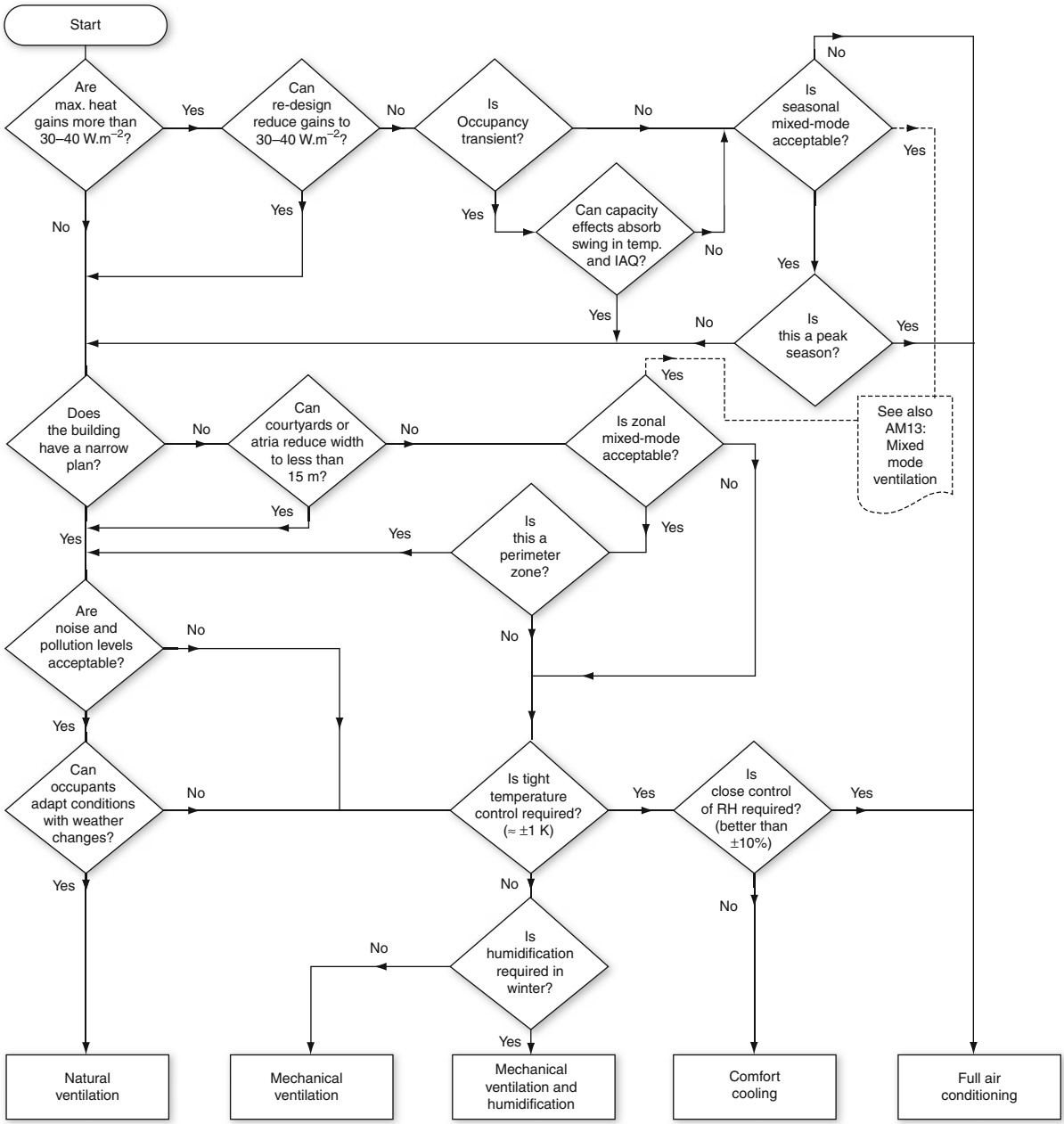

Natural Ventilation in Built Environment. Figure 22
Flowchart for selecting a ventilation strategy [62]

climate in health care buildings. They also proposed an overheating risk criterion compatible with adaptive thermal comfort assessment. Both field monitoring and modeling studies showed that ANV could offer greater resilience to climate change than SNV, particularly as a refurbishment strategy.

The strengths and weaknesses of a wide range design simulation tools are summarized by

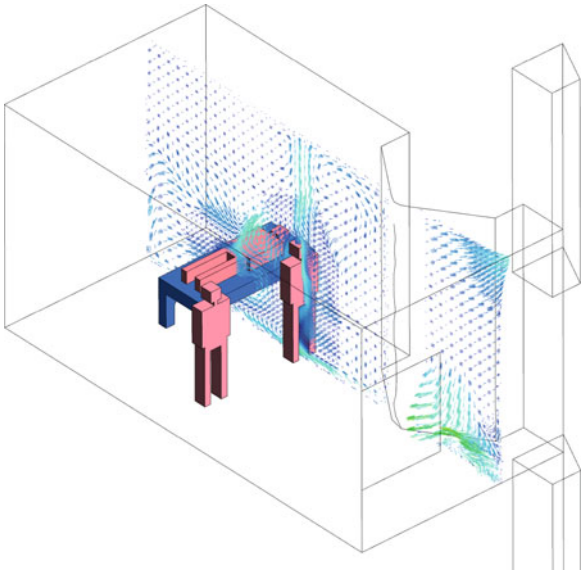

Natural Ventilation in Built Environment. Figure 23 Advanced natural ventilation system design in hospital using CFD [45]

governmental and professional organizations [71, 72]. Educational resources and practical equations for various design stages and step-by-step guided case studies [58, 73–75] would help multidisciplinary professions to design and build sustainable buildings.

The following case studies showcase innovative solution to natural and mixed-mode ventilated buildings in the built environment.

Case Studies

Case Study 1: Liverpool John Moores University, UK

The Liverpool John Moores University art and design academy was designed by award winning Rick Mather Architects and engineered by Whitbybird Engineers and was built by Wates Construction. The building was designed from 2004 and opened in 2008 (see Fig. 24).

The 11,000 m^2 five story university academy building had a number of important environmental initiatives on the client brief including a 25% betterment of UK conservation of fuel and power building regulations; a BREEAM target of Very Good, and a 10% onsite renewable energy target.

Natural Ventilation in Built Environment. Figure 24 LJMU Liverpool façade in nighttime (**a**) LJMU Liverpool exterior; (**b**) LJMU Liverpool façade in nighttime (*Source*: Rick Mather Architects)

To meet these requirements the design team reviewed a number of architectural and structural and services engineering options and concluded that a mixed-mode ventilation scheme utilizing thermal mass with Heat Recovery would of particular benefit to a low energy approach. The building design team used the latest computer modeling techniques to prove compliance with industry standards for thermal

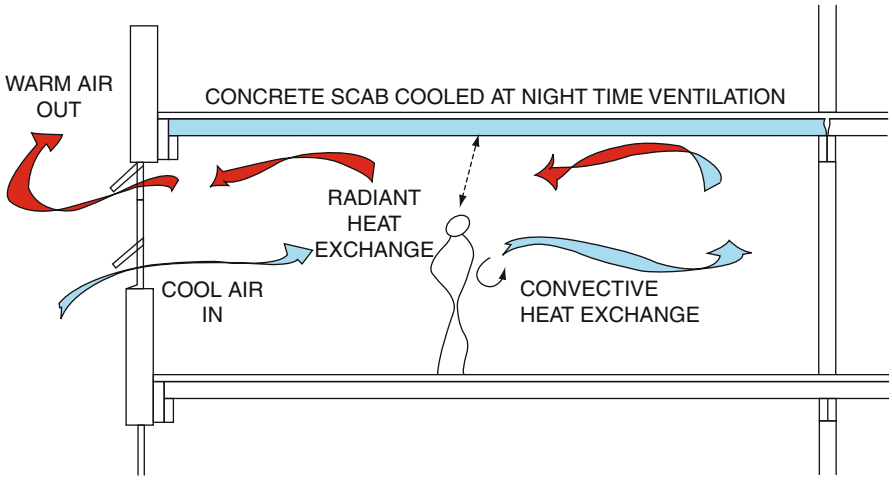

Natural Ventilation in Built Environment. Figure 25
Exposed concrete soffit for thermal mass benefit

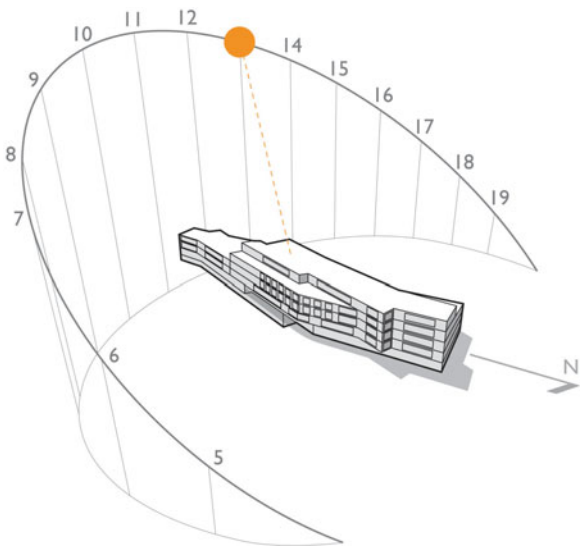

Natural Ventilation in Built Environment. Figure 26
Sun path analysis for external façade design (*Source*: Whitbybird Engineers)

comfort particularly the prevention of overheating (see Figs. 25, 26, 27, and 28).

The building benefits from a heavyweight thermal mass during the spring and summer, utilizes single-sided natural ventilation with mechanical extract during peak summer with nighttime free cooling (see Fig. 25), and during winter operates as a sealed building with heating provided by a biomass pellet boiler. A weather station provides data to the BEMS to ensure the automated windows are aligned with the ventilation strategy.

The building was shortlisted for various awards in 2010.

Case Study 2: Tamworth Academies – Staffordshire, UK

Two secondary school academies were commissioned by Tamworth County Council in 2009. Designed by Aedas architects and engineered by WSP and CTM the buildings were designed in 2009/2010 and are scheduled to open in 2010. Main contractors are Wilmott Dixon Construction.

The two 9,000 m^2 two story buildings (Fig. 29) had to comply with the government's 60% carbon reduction target compared to 2002 UK building regulations. The design team also set a BREEAM environmental target of Excellent.

It was the aim of the architectural and structural and services engineering teams to strive to design a low energy building to ensure the building was future proofed against rising energy costs. In addition the client team wanted a low whole life cost solution.

The selected structural and services strategy was a building that would be designed to operate as a naturally ventilated building but be capable of operating as a highly efficient mechanically ventilated

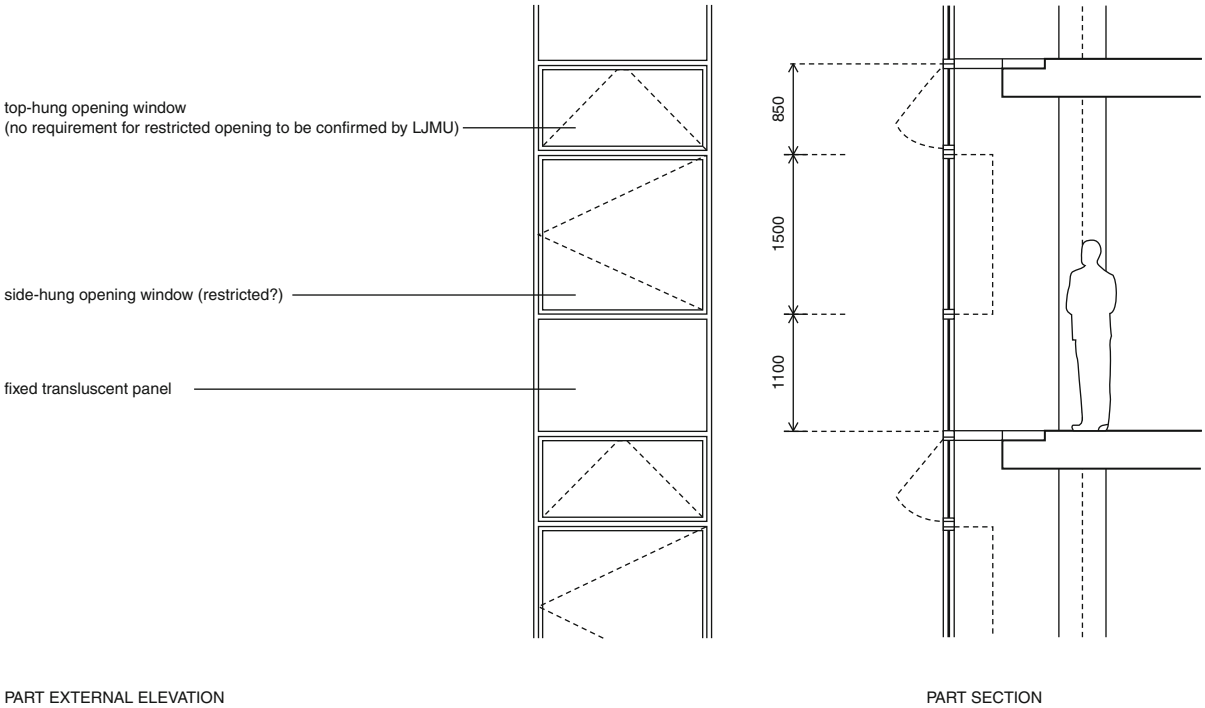

Natural Ventilation in Built Environment. Figure 27
External façade design (*Source*: Rick Mather Architects)

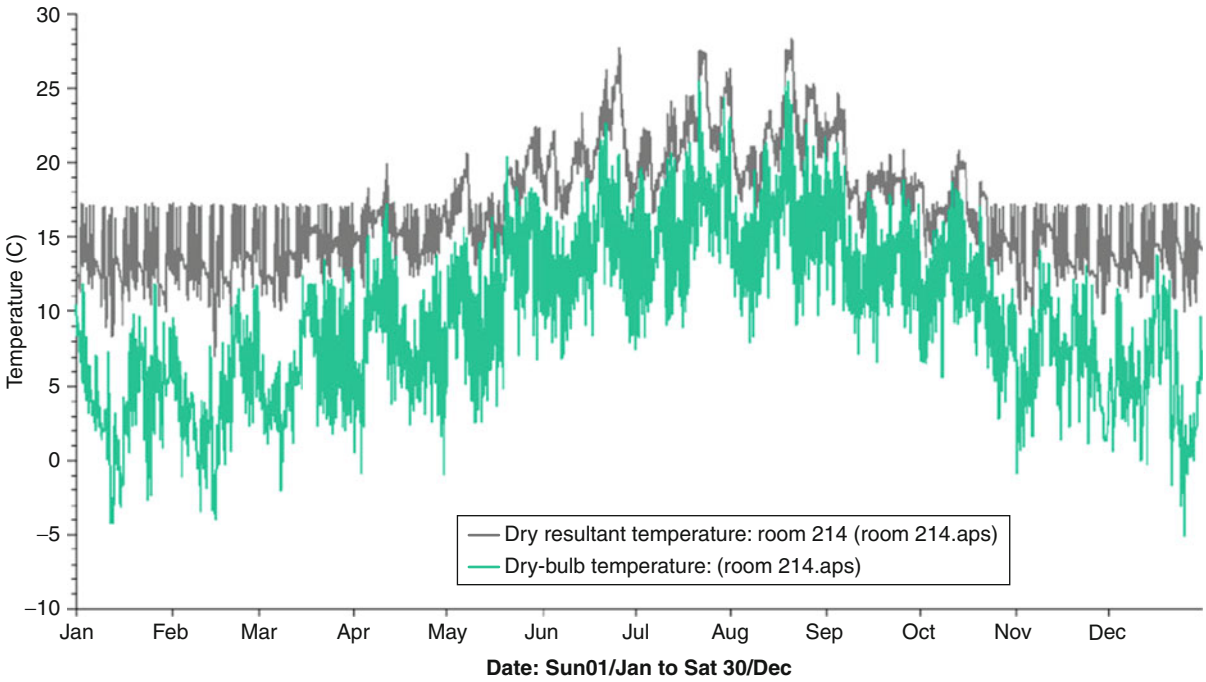

Natural Ventilation in Built Environment. Figure 28
Thermal modeling chart (*Source*: Whitbybird Engineers)

Natural Ventilation in Built Environment. Figure 29
Tamworth landau forte exterior (*Source*: Professor Vivian Loftness at Carnegie Mellon University)

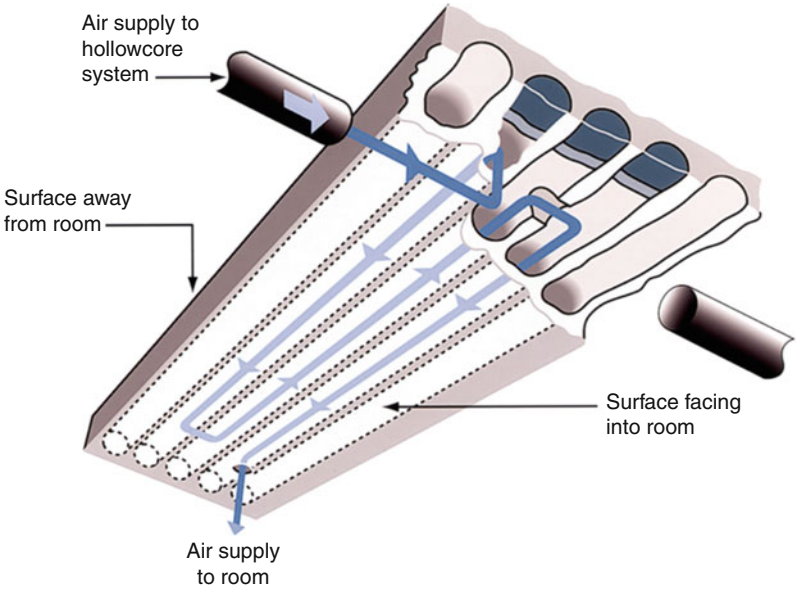

Natural Ventilation in Built Environment. Figure 30
Termodeck concrete plank (*Source*: Tarmac Termodeck)

building during peak summer and extremely cold winters to conserve energy. The client, main contractor, and design team chose Termodeck by Tarmac, an integrated structural mixed-mode ventilation scheme utilizing thermal mass free cooling with energy efficient heat recovery (see Figs. 30 and 31).

Other features of the buildings include areas of the academies where ICT gains are increased provided with chilled water generated by a ground source heat pump. And seasonal operation of the ventilation strategy communicated to the occupants of the academies via building weather station data and LCD flat screen TVs.

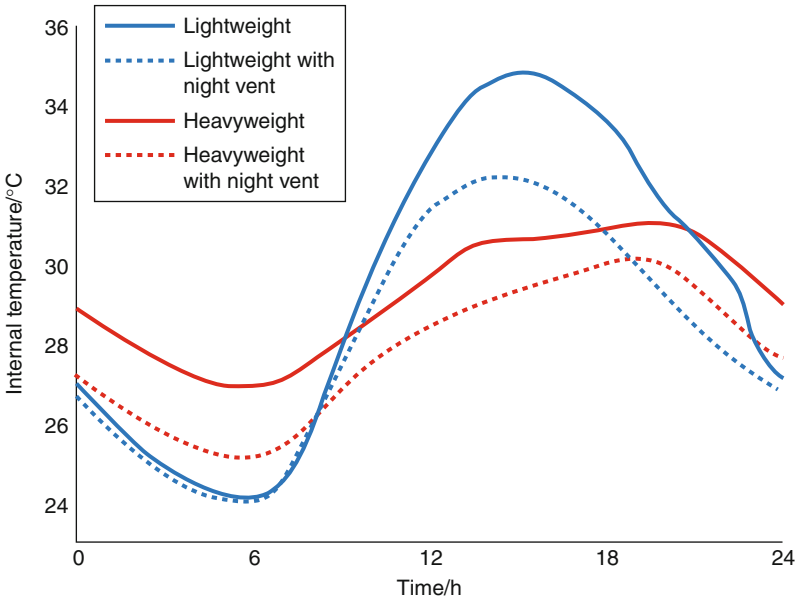

Natural Ventilation in Built Environment. Figure 31
Temperature time-lag for lightweight and heavyweight buildings (*Source*: Tarmac Termodeck)

Case Study 3: BSkyB Broadcast Center – London, UK

Designed by Arup Associates, the BSkyB broadcast center (Fig. 32) located in west London houses the world first naturally ventilated television studios [76]. Thirteen giant ventilation chimneys, nine line the building's eastern elevation and another four appear on the west façade. Concrete boxes within boxes construction provides solution to eliminate external noise as well as naturally ventilate the studios to remove excessive heat generated by studio lights. Fresh air is supplied through acoustically lined labyrinth built in between the underside of the studio's concrete floor and the floor of the surrounding box from street level (see Fig. 33). This construction form allows big air paths to minimize resistance to air movement as well as eliminate all influx of noise.

In order to prevent a common stack ventilation problem – air cooling in the flue and dropping back into a room – the flues are lined and insulated on the inside. In an intermediate mode the ventilation system will run on extract only to pull the air up the chimney and warm it. When the right flue surface temperature has reached, the air's natural buoyancy will take over, the system then switch to natural ventilation mode automatically.

Natural Ventilation in Built Environment. Figure 32
BSkyB broadcast center in west London [76]

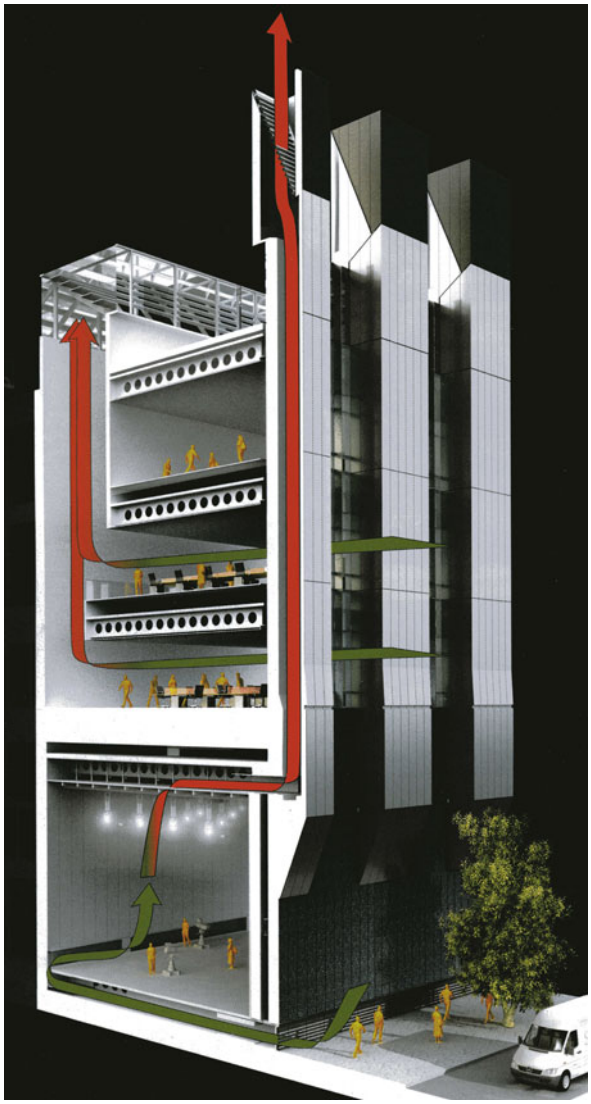

Natural Ventilation in Built Environment. Figure 33 Natural ventilation flow within the BSkyB television studios (*Source*: Arup Associates)

At the south end of the building, a glazed atrium houses a series of meeting rooms, a café, and breakout spaces, which allows access between levels. The office areas (8 m in depth) on the west elevation are ventilated using single-side natural ventilation. The offices (15 m deep) on the eastern side utilize three atrium-line chimneys in the center of the building to help draw air across the floor plates. Natural light through these atriums are additional benefit of the design.

Case Study 4: Commerzbank – Frankurt, Germany

Norman Foster's Commerzbank in Frankurt, Germany (see Fig. 34), demonstrates sustainable urban architecture featured by natural ventilation, vast amount of daylight, and pleasant exterior views within deep building can be achieved at the scale of the skyscraper.

Triangular-shaped plan provide the rigid structural support with high-rise building functional cores located at each corner of this triangle. The center atrium of the buildings provides light both vertically, from the glass roof at the atrium's top, horizontally from the winter garden facades to the office areas. Winter gardens rotate around the façade of the building, allow for ventilation through the atrium being divided into sections. Natural light are brought directly into the center of the buildings, offices facing the center are provided light and outdoor views through these green, natural spaces. The operable layered façade allows natural ventilation through office spaces, while winter gardens provide ventilation for the entire building.

Case Study 5: Queen's Building, De Montfort University, UK

The Queen's Building (Fig. 35) designed by Short Ford Associates and built in 1993 featured with large venting chimneys, heavy thermal mass, shallow floor plan, operable windows, and generous ceiling heights to facilitate natural ventilation and daylighting. This traditional brick building has wide insulation-filled cavity walls and concrete slabs in the ceilings, buffering the indoor from outdoor temperature peaks. Glazed ventilators also help to provide as much natural lighting as possible. In the auditoria fresh air enters through louvers in the north façade by means of plenums below the raked wooden floor and wall inlets which are controlled by the BEMS.

Since being the Green Building winner of the Year 1995, Queen's building has served a great demonstration value for environmental design. It aims to a "Living Lab" to showcase innovative technologies and demonstrate ways of achieving significant carbon reductions in modern buildings through the refurbishment.

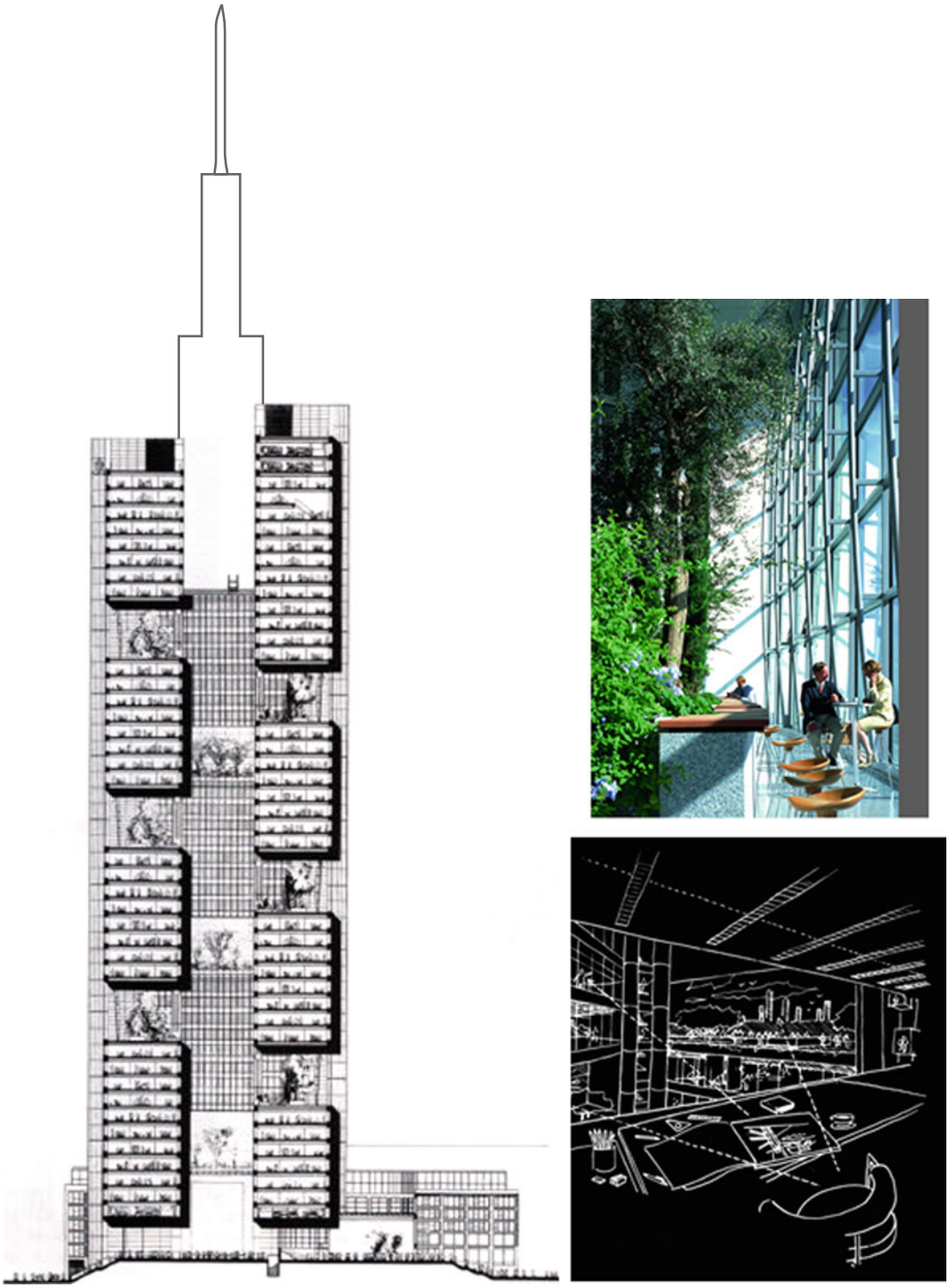

a b

Natural Ventilation in Built Environment. Figure 34
Commerzbank, Frankurt, Germany (**a**) Building section [77] (**b**) Winter garden and interior view design [78]

a

b

c

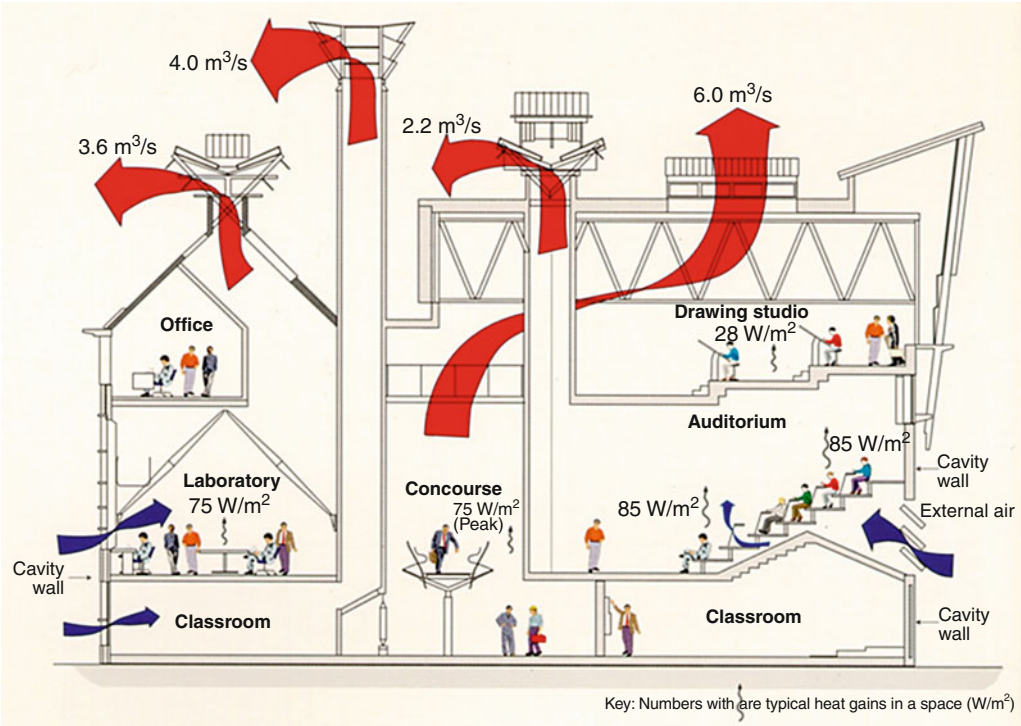

d

Natural Ventilation in Built Environment. Figure 35
The Queen's building, De Montfort University, Leicester, UK (**a**) Exterior view and stack outlets; (**b**) Exterior view and air inlets; (**c**) Interior view of auditorium; (**d**) The Queen's building – natural ventilation strategy

Future Directions

Sustainable design requires a long-term durable approach and passive environmental control offers this. Holistic design and construction is necessary to achieve the sustainable built environment [79, 80], provide the optimum cost-benefit value for all stakeholders in the built environment industry. Natural ventilation should be explored as a possibility for all projects, but various factors can limit its use although, throughout history, vernacular architecture demonstrates it can work effectively in many climates but only if there is a unity of thought between architects and the engineers. However hybrid systems are common in Europe emphasized by the demand for low carbon buildings. Ultimately buildings are for people and systems must provide conditions for enhancing well-being at a time when climates worldwide are showing more variability and change.

Acknowledgments

The authors would like to thank Lee Hargreaves (WSP, UK Ltd.) for his help with researching and organizing some case studies; Mike Beaven of Arup Associates for some case studies; Matt Kitson (Hilson Moran) for providing Gherkin images; Professor Vivian Loftness (Carnegie Mellon University, USA) for providing architectural images and Fig. 21; Beifan Yang and Bin Zhang (Tianjin Weland Landscape Architecture Design Co, Ltd. China) for the architectural drawings; Jin Zhang (JINT Design Consultants Ltd.) for architectural sketch; and Dr Malcolm Cook (Loughborough University) for providing the images of Queens Building.

Bibliography

1. Elliott CD (1992) Technics and architecture: the development of materials and systems for buildings. MIT Press, Cambridge, MA
2. Fathy H (1986) Natural energy and vernacular architecture, principles and examples with reference to hot arid climates. The University of Chicago Press, Chicago
3. Miller JD (2007) Indoor air quality and occupant health in the residential built environment: future directions. In: Yoshino H (ed) Proceedings IAQVEC 2007, Sendai, Japan. ISBN 978-4-86163-069-9, pp 15–22
4. Von Frisch K (1975) Animal architecture. Hutchinson, London
5. Fitch JM (1976) American building: the environmental forces that shape it. Schocken Books, New York
6. BSI (1991) BS 5925:1991 Code of practice for ventilation principles and designing for natural ventilation. BSI, London
7. Texas Tech University (2004) The wind science and engineering (WISE) research center; Available from http://www.wind.ttu.edu/. Accessed 11 June 2004
8. CIBSE (2006) Guide A: environmental design. The Chartered Institution of Building Services Engineers, London
9. Liddament MW (1996) A guide to energy efficient ventilation. Air Infiltration and Ventilation Centre, Coventry
10. CIBSE (2005) AM10: Natural ventilation in non-domestic buildings. The Chartered Institution of Building Services Engineers, London
11. Liddament MW (2010) The applicability of natural ventilation. In: CIBSE Natural Ventilation Group Seminar 2010 – Natural ventilation in the urban environment. RIBA, London
12. The Gherkin (2008) http://www.30stmaryaxe.co.uk/. Accessed 8 Sept 2011
13. Abbas T (2008) MSc intelligent buildings, lecture notes. Hilson Moran, London
14. Hazim A (2003) Ventilation of buildings, 2nd edn. Spon Press, London
15. Seppänen O, Fisk W, Mendell M (1999) Association of ventilation rates and CO_2 concentrations with health and other responses in commercial and institutional buildings. Indoor Air 9(4):226–252
16. Wargocki P, Seppanen O, Anderson J, Boerstra A, Clements-Croome D, Fitzner K, Olaf Hanssen S (2006) Indoor climate and productivity in offices: guide book 6. Federation of European Heating and Air-Conditioning Associations (REHVA), Brussels
17. ASHRAE (2010) Standard 62.1-2010 – Ventilation for acceptable indoor air quality. American Society Heating, Refrigerating and Air Conditioning Engineers (ASHRAE), Atlanta
18. ASHRAE (2009) Handbook – Fundamentals, chapter 9 Thermal comfort. American Society Heating, Refrigerating and Air Conditioning Engineers (ASHRAE), Atlanta
19. Croome DJ, Roberts BM (1975) Airconditioning and Ventilation of Buildings (Pergamon Press); second edition 1981
20. Etheridge D, Sandberg M (1996) Building ventilation theory and measurement. Wiley, Chichester
21. Linke W (1956) Strömungsvorgänge in künstlich belüfteten Räumen, Forschungsberichte des Wirtschafts und Verkehrsministeriums des Landes, NRW Nr 259. Kaltetechnik 18:122
22. Müllejans H (1973) Über die Bedingungen von Modellversuchen in der Klimatechnik. Ki 8/73, Teil 6, S. 63 ff
23. van Gunst E, Erkelens PJ, Coenders WPJ (1967) In 4th congress international du chauffage et de la climatisation, Paris
24. Fang L, Clausen G, Fanger PO (1998) Impact of temperature and humidity on perception of indoor air quality during immediate and longer whole-body exposures. Indoor Air 8:276–284
25. Fang L, Clausen G, Fanger PO (1998) Impact of temperature and humidity on the perception of indoor air quality. Indoor Air 8:80–90

26. Wargocki P (2004) Sensory pollution sources in buildings. Indoor Air 14:82–91
27. Clements-Croome DJ (2008) Work performance, productivity and indoor air. Scand J Work Environ Health Suppl 4:69–78
28. Health Canada (2010) Environmental and workplace health; Available from www.hc-sc.gc.ca. Accessed 15 Aug 2010
29. ECA (1992) Report no. 11 – Guidelines for ventilation requirements in buildings in environment and quality of life, European Collaborative Action – Indoor air quality & its impact on man, EUR 14449 EN
30. Dobson R (2008) Smoking bans reduce heart attack admissions. British Med J 337: a597
31. ISO:7730 (2005) Ergonomics of thermal environments – Analytical determination and interpretation of thermal comfort using calculation of the PMV and PPD indices and local thermal comfort criteria. International Organization for Standardization (ISO), Geneva
32. CCOHS (2002) Health effects of carbon dioxide gas. Canadian Centre for Occupational Health and Safety, Hamilton, Ontario
33. Robertson D (2006) Health effects of increase in concentration of carbon dioxide in the atmosphere. Curr Sci 90(12):1607–1609
34. HSE (1990) Occupational exposure limits – guide note EH 40/90. Health and Safety Executive, HMSO, London
35. Hinds WC (1999) Aerosol technology: properties, behavior, and measurement of airborne particles. Wiley, New York, pp 464
36. Brown T, Holmes P, Harrison PTC (2010) Review: the applicability of epidemiological methods to the assessment of the risks to human health of indoor air pollution: an overview. Indoor Built Environ 19(3):311–326
37. Pennycook K (2009) The illustrated guide to ventilation. In BSRIA guide – BG 2/2009. The Building Services Research and Information Association (BSRIA), Bracknell
38. Boyce PR (2010) Review: the impact of light in buildings on human health. Indoor Built Environ 19(1):8–20
39. RAE (2010) Engineering a low carbon built environment – The discipline of Building Engineering Physics. The Royal Academy of Engineering, London
40. Mardaljevic J, Heschong L, Lee E (2009) Daylight metrics and energy savings. Lighting Res Technol 41(3):261–283
41. Wiki (2010) http://en.wikipedia.org/wiki/Urban_canyon. Accessed 18 July 2010
42. Barlag AB, Kuttler W (1990/1991) The significance of country breezes for urban planning. Energy and Buildings 15(3–4): 291–297
43. Ghiaus C, Allard F (2005) Natural ventilation in the urban environment. Earthscan, London
44. Fukao S (2010) The history of developments toward open building in Japan. Lecture at Loughborough University, UK on 16 July 2010
45. CIB (2010) W104 Open building implementation; Available from http://www.open-building.org/ob/next21.html. Accessed 20 July 2010
46. Clausen G, Carrick L, Fanger PO, Kim SW, Poulsen T, Rindel JH (1993) A comparative study of discomfort caused by indoor air pollution, thermal load and noise. Indoor Air 3:255–262
47. Mumovic D, Davies M, Ridley I, Altamirano-Medina H, Oreszczyn T (2009) A methodology for post-occupancy evaluation of ventilation rates in schools. Building Serv Eng Res Technol 30(2):143–152
48. Coley DA, Hunt S, Mitchell A (2009) Acoustics in schools: explaining the options to architects by the use of approximate formulae and graphs, with a special emphasis on dining spaces. Indoor Built Environ 18(6):505–513
49. Mathisen HM, Moser A, Nielsen PV (2004) Guidebook no. 2 – Ventilation effectiveness. In: Mundt E (ed) Federation of European heating and air-conditioning associations REHVA Journal, Brussels, Belgium
50. Gan G (2000) Effective depth of fresh air distribution in rooms with single-sided natural ventilation. Energy and Buildings 31(1):65–73
51. Coffey CJ, Hunt GR (2007) Ventilation effectiveness measures based on heat removal: part 2 Application to natural ventilation flows. Building Environ 42(6):2249–2262
52. Short CA, Cook MJ (2005) Design guidance for naturally ventilated theatres. Building Serv Eng Res Technol 26(3):259–270
53. WHO (2009) Natural ventilation for infection control in healthcare settings. World Health Organization, Geneva
54. ASHRAE (2009) Indoor Air Quality Guide - Best Practices for Design, Construction, and Commissioning, in ASHRAE Design Guide. American Society of Heating, Refrigerating and Air-Conditioning Engineers, Atlanta
55. Seppänen O, Fisk W (2004) Summary of human responses to ventilation. Indoor Air 14(7):102–118
56. ISIAQ (1996) Control of moisture problems affecting biological indoor air quality. In: Task Force Report. International Society of Indoor Air Quality and Climate (ISIAQ), Austin, TX
57. CIBSE (2005) Guide B: heating, ventilating, air conditioning and refrigeration. The Chartered Institution of Building Services Engineers, London, pp 2–9
58. Lomas KJ (2007) Architectural design of an advanced naturally ventilated building form. Energy and Buildings 39(2):166–181
59. Short CA, Cook MJ, Woods A (2009) Low energy ventilation and cooling within an urban heat island. Renewable Energy 34:2022–2029
60. Ford B, Schiano-Phan R, Francis E (2010) The architecture and engineering of downdraught cooling: a design source book. PHDC Press, London. ISBN 978-0-9565790-0-3
61. Loftness V, Snyder M (2008) Where windows become doors. In: Kellert S, Heerwagen J, Mador M (eds) Biophilic design. Wiley, Hoboken, pp 119–131
62. CIBSE (1997) AM10: natural ventilation in non-domestic buildings. The Chartered Institution of Building Services Engineers, London
63. Cohen R (1997) Environmental criteria for naturally ventilated buildings. In: Clements-Croome D (ed) Naturally ventilated buildings – Buildings for the senses, economy and society. E & FN SPON, London
64. Allard F (1998) Natural ventilation in buildings - a design handbook, James & James Ltd, London, pp. 366. ISBN 9781873936726.

65. Chen Q (2009) Ventilation performance prediction for buildings: a method overview and recent applications. Building Environ 44(4):848–858
66. Jiru TE, Bitsuamlak GT (2010) Application of CFD in modelling wind-induced natural ventilation of buildings – a review. Int J Ventilation 9(2):131–147
67. Walker CE (2006) Methodology for the evaluation of natural ventilation in buildings using a reduced-scale air model. PhD thesis, Department of Architecture, Massachusetts Institute of Technology, USA, p 211
68. Cropper P, Yang T, Cook M, Fiala D, Yousaf R (2010) Coupling a model of human thermoregulation with Computational Fluid Dynamics for predicting human-environment interaction. J Building Perform Simulation 3(3):233–243
69. Zhang H, Arens E, Huizenga C, Han T (2010) Thermal sensation and comfort models for non-uniform and transient environments, part III: whole-body sensation and comfort. Building Environ 45:399–410
70. Lomas KJ, Ji Y (2009) Resilience of naturally ventilated buildings to climate change: advanced natural ventilation and hospital wards. Energ Buildings 41(6):629–653
71. DoE (2010) Building energy software tools directory. Energy efficiency & renewable energy; Available from http://apps1.eere.energy.gov/buildings/tools_directory/. Accessed 12 June 2010
72. IBPSA-Germany (2010) Simupedia - A wiki about building simulation. Accessed 25 Aug 2009
73. Kolokotroni M (2007) Vent dis.course – Development of distance learning vocational training material for the promotion of best practice ventilation energy performance in buildings. European Commission Intelligent Energy – Europe Programme Publishable Final Report (EIE/04/022/S07.38630)
74. Healthheating (2010) Indoor environmental quality – Educational resource of the building and health sciences; Available from http://www.healthyheating.com/index.htm. Accessed 06 March 2010
75. Mumovic D, Santamouris M (eds) (2009) A handbook of sustainable building design & engineering. Earthscan, London
76. Pearson A (2011) Getting on the air . . . naturally. CIBSE Journal, Feb issue, pp 28–32. Available from http://www.cibsejournal.com/issues/2011-02/
77. Noble C (2011) Commerzbank: a sustainable skyscraper. Architecture 489; Available from http://web.utk.edu/~archinfo/a489_f02/PDF/commerzbank.pdf. Accessed 12 Feb 2011
78. Foster + Partners. Commerzbank Headquarters. Frankfurt, Germany; Available from http://www.fosterandpartners.com/Projects/0626/Default.aspx
79. BSI (2010) Constructing the business case – building information modelling. British Standard Institution and Building SMART UK, London
80. Alwaer H, Clements-Croome DJ (2010) Key performance indicators (KPIs) and priority setting in using the multi-attribute approach for assessing sustainable intelligent buildings. Building Environ 45(4):799–807

New Polymers, Renewables as Raw Materials

Richard P. Wool
Department of Chemical Engineering, Center for Composite Materials, Affordable Composites from Renewable Sources (ACRES), University of Delaware, Newark, DE, USA

Article Outline

Glossary
Definition of the Subject
Introduction
Synthetic Pathways for Triglyceride-Based Monomers
Polymers from Plant Oils
Properties of Plant Oil Resins
Castor Oil-Based Polymer Properties
Future Directions
Bibliography

Glossary

Composite materials Are engineered or naturally occurring materials made from two or more constituent materials with significantly different physical or chemical properties which remain separate and distinct at the microscopic scale.

Lignin Is a complex chemical compound most commonly derived from wood and an integral part of the secondary cell walls of plants and some algae.

Triglyceride Is an ester derived from glycerol and three fatty acids. It is the main constituent of vegetable oil and animal fats.

Definition of the Subject

This entry describes how to make high volume materials out of thin-air using CO_2 and sunlight.

Introduction

Recent advances in genetic engineering, composite science, and natural fiber development offer significant opportunities for developing new, improved materials from renewable resources that can biodegrade or be recycled, enhancing global sustainability. A wide range

of high-performance, low-cost materials can be made using plant oils, natural fibers, and lignin. By selecting the fatty acid distribution function of plant oils via computer simulation and the molecular connectivity, chemical functionalization and molecular architecture can be controlled to produce linear, branched, or cross-linked polymers. These materials can be used as pressure-sensitive adhesives, elastomers, rubbers, foams, and composite resins. This entry describes the chemical pathways that were used to modify plant oils and allow them to react with each other and various comonomers to form materials with useful properties.

Polymers and polymeric composite materials have extensive applications in the aerospace, automotive, marine, infrastructure, military, sports, and industrial fields. These lightweight materials exhibit excellent mechanical properties, high corrosion resistance, dimensional stability, and low assembly costs. Traditionally, polymers and polymeric composites have been derived from petroleum; however, as the applications for polymeric materials increase, finding alternative sources of these materials has become critical. In recent years, the Affordable Composites from Renewable Sources (ACRES) program at the University of Delaware has developed a broad range of chemical routes to use natural triglyceride oils to make polymers and composite materials [1, 2]. These materials have economic and environmental advantages that make them attractive alternatives to petroleum-based materials.

Natural oils, which can be derived from both plant and animal sources, are abundant in most parts of the world, making them an ideal alternative to chemical feedstocks. These oils are predominantly made up of triglyceride molecules, which have the structure shown in Fig. 1. Triglycerides are composed of three fatty acids joined at a glycerol juncture. The most common oils contain fatty acids that vary from 14 to 22 carbons in length with 0–3 double bonds per fatty acid. Table 1 shows the fatty acid distributions of several common oils [3]. Exotic oils are composed of fatty acids with other types of functionalities, such as epoxies, hydroxyls, cyclic groups, and furanoid groups [4]. Because of the many different fatty acids present, at a molecular level these oils are composed of many different types of triglycerides with numerous levels of unsaturation. With newly developed genetic engineering techniques, the variation in unsaturation can be controlled in plants such as soybean, flax, and corn; however, some oils are better suited to polymer resin development.

Besides applications in the foods industry, triglyceride oils have been used extensively to produce coatings, inks, plasticizers, lubricants, and agrochemicals [5–11]. In the polymers field, the use of these oils as toughening agents was investigated. Barrett [12] has reviewed an extensive amount of work on using these oils to produce interpenetrating networks (IPNs). It was found that IPNs formed by triglycerides could increase the toughness and fracture resistance in conventional thermoset polymers [13–16]; see also [17–25]. In these works, the functional triglyceride was a minor component in the polymer matrix acting solely as a modifier to improve the physical properties of the main matrix. Consequently, the triglyceride-based materials were low-molecular-weight (M_W), lightly cross-linked materials incapable of displaying the necessary rigidity and strength required for structural applications by themselves.

Synthetic Pathways for Triglyceride-Based Monomers

Triglycerides contain active sites amenable to chemical reaction: the double bond, the allylic carbons, the ester group, and the carbons alpha to the ester group. These active sites can be used to introduce polymerizable

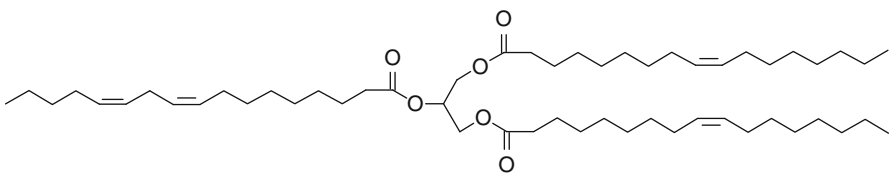

New Polymers, Renewables as Raw Materials. Figure 1 Triglyceride molecule, the major component of natural oils

New Polymers, Renewables as Raw Materials. Table 1 Fatty acid distribution in various plant oils

Fatty acid	# C: # DB	Canola	Corn	Cottonseed	Linseed	Olive	Palm	Rapeseed	Soybean	High oleic[a]
Myristic	14:0	0.1	0.1	0.7	0.0	0.0	1.0	0.1	0.1	0.0
Myristoleic	14:1	0.0	0.0	0.0	0.0	0.0	0.0	0.0	0.0	0.0
Palmitic	16:0	1.1	10.9	21.6	5.5	13.7	41.4	3.0	11.0	6.4
Palmitoleic	16:1	0.3	0.2	0.6	0.0	1.2	0.2	0.2	0.1	0.1
Margaric	17:0	0.1	0.1	0.1	0.0	0.0	0.1	0.0	0.0	0.0
Margaroleic	17:1	0.0	0.0	0.1	0.0	0.0	0.0	0.0	0.0	0.0
Stearic	18:0	1.8	2.0	2.6	3.5	2.5	1.1	1.0	1.0	3.1
Oleic	18:1	60.9	25.4	18.6	19.1	71.1	39.3	13.2	23.4	82.6
Linoleic	18:2	21.0	59.6	51.4	15.3	10.0	10.0	13.2	53.2	2.3
Linolenic	18:3	8.8	1.2	0.7	56.6	0.6	0.4	9.0	7.8	3.7
Arachidic	20:0	0.7	0.4	0.3	0.0	0.9	0.3	0.5	0.3	0.2
Gadoleic	20:1	1.0	0.0	0.0	0.0	0.0	0.0	9.0	0.0	0.4
Eicosadienoic	20:2	0.0	0.0	0.0	0.0	0.0	0.0	0.7	0.0	0.0
Behenic	22:0	0.3	0.1	0.2	0.0	0.0	0.1	0.5	0.1	0.3
Erucic	22:1	0.7	0.0	0.0	0.0	0.0	0.0	49.2	0.0	0.1
Lignoceric	24:0	0.2	0.0	0.0	0.0	0.0	0.0	1.2	0.0	0.0
Average # DB/triglyceride		3.9	1.5	3.9	6.6	2.8	1.8	3.8	1.6	3.0

[a]Genetically engineered high oleic acid content soybean oil (DuPont)

groups on the triglyceride using the same techniques applied in the synthesis of petrochemical-based polymers. The key step is to reach a higher level of M_W and cross-link density, as well as to incorporate chemical functionalities known to impart stiffness in a polymer network (e.g., aromatic or cyclic structures). Figure 2 illustrates several synthetic pathways that accomplish this [1].

In structures **5, 6, 7, 8**, and **11**, the double bonds of the triglyceride are used to functionalize the triglyceride with polymerizable chemical groups. From the natural triglyceride, it is possible to attach maleates (**5**) [6–11] or to convert the unsaturation to epoxy (**7**) [26–28] or hydroxyl functionalities (**8**) [29, 30]. Such transformations make the triglyceride capable of reaction via ring-opening or polycondensation polymerization. These particular chemical pathways are also accessible via natural epoxy and hydroxyl functional triglycerides [12, 14–16] It is also possible to attach vinyl functionalities to the epoxy and hydroxyl functional triglycerides. Reaction of the epoxy functional triglyceride with acrylic acid incorporates acrylates onto the triglyceride (**6**), while reaction of the hydroxylated triglyceride with maleic anhydride incorporates maleate half-esters and esters onto the triglyceride (**11**). These monomers can then be blended with a reactive diluent, similar to most conventional vinyl ester resins and cured by free-radical polymerization.

The second method for synthesizing monomers from triglycerides is to convert the triglyceride to monoglycerides through a glycerolysis (**3A**) reaction or an amidation reaction (**2, 3B**) [31–36]. Monoglycerides are used in surface coatings, commonly referred to as alkyd resins, because of their low cost and versatility [32]. In those applications, the double bonds of the monoglyceride are reacted to form the coating. However, monoglycerides also can react through the alcohol groups via polycondensation reactions with

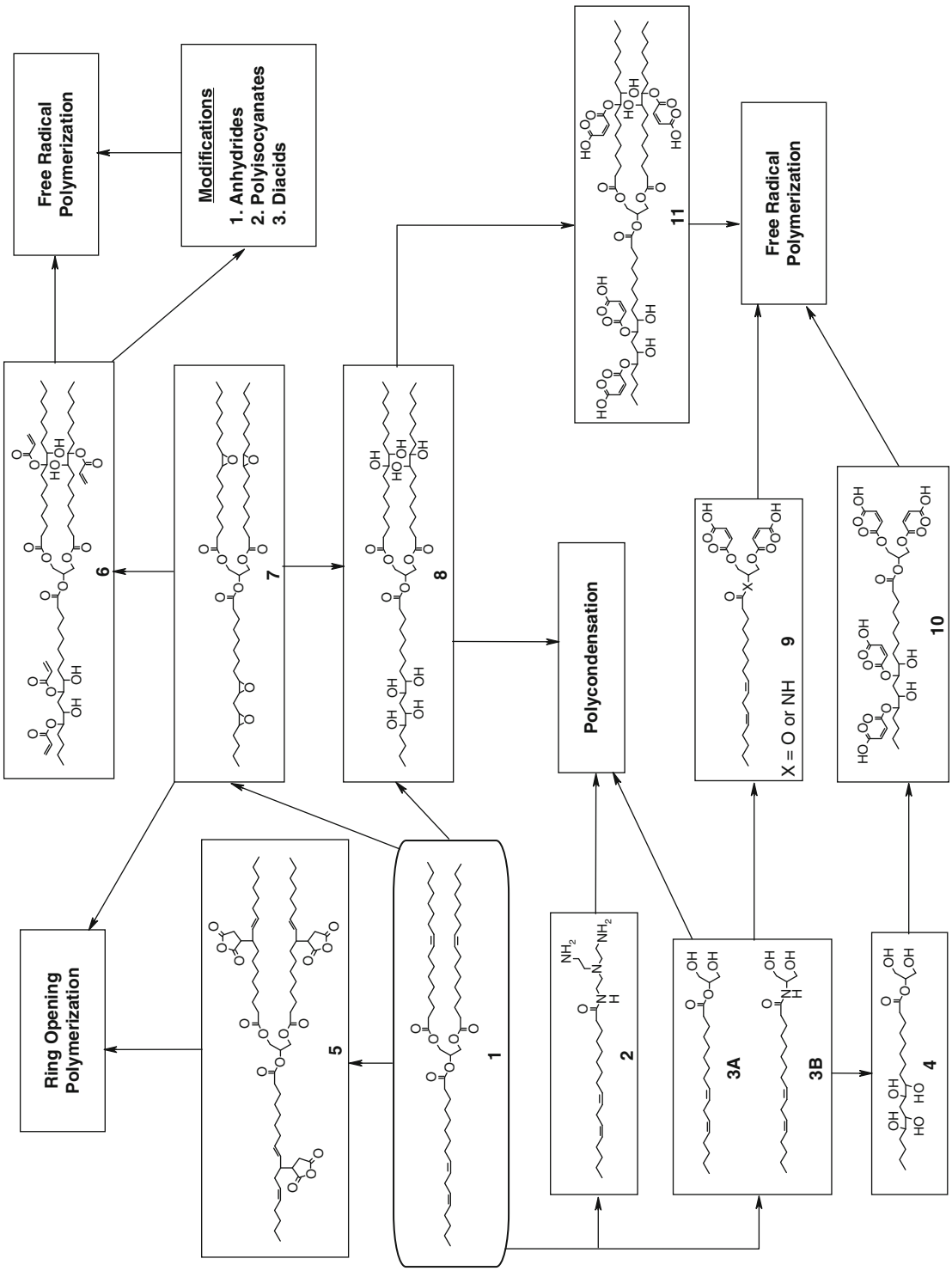

New Polymers, Renewables as Raw Materials. Figure 2
Chemical pathways leading to polymers from triglyceride molecules [1]

a comonomer, such as a diacid, epoxy, or anhydride. Alternatively, maleate half-esters can be attached to these monoglycerides (**9**) allowing them to undergo free-radical polymerization.

The third method is to functionalize the unsaturation sites as well as reduce the triglyceride into monoglycerides. This can be accomplished by glycerolysis of an unsaturated triglyceride, followed by hydroxylation or by glycerolysis of a hydroxy functional triglyceride. The resulting monomer can then be reacted with maleic anhydride, forming a monomer capable of polymerization by the free-radical mechanism [1].

Although the structure of triglycerides is complex in nature, it is possible to characterize some aspects of it using proton nuclear magnetic spectroscopy (^{1}H-NMR) and Fourier transform infrared (FTIR) spectroscopy. A typical ^{1}H NMR spectrum of soybean oil is shown in Fig. 3, with peak assignments. The two sets of peaks at 1.0–1.4 ppm are produced by the four glycerol methylene protons per triglyceride [0]. The triplet set of peaks at 2.3 ppm is produced by the six protons in the alpha position relative to the carbonyl groups. The peak at 0.9 ppm is produced by the nine methyl protons per triglyceride at the end of each fatty acid chain. These three groups of peaks provide a standard by which other peaks can be used to quantitatively characterize functional groups in the triglyceride.

In this entry, the focus is on three triglyceride monomers, shown in Fig. 4, which have been found to be promising candidates for use in the composites and engineering plastics fields. They are acrylated epoxidized soybean oil (AESO), the maleinized soybean oil monoglyceride (SOMG/MA), and maleinized hydroxylated soybean oil (HSO/MA). These monomers, when used as a major component of a molding resin, have shown properties comparable to conventional polymers and composites, and these properties will be presented. In addition, they can be used as a matrix in synthetic and natural fiber-reinforced composites.

Acrylated Epoxidized Soybean Oil

Acrylated epoxidized oils (Fig. 4) are synthesized from the reaction of acrylic acid with epoxidized triglycerides. Epoxidized triglycerides can be found in natural oils, such as vernonia plant oil, or can be synthesized from more common unsaturated oils, such as soybean oil or linseed oil, by a standard epoxidation reaction [37]. The natural epoxy oil, vernonia oil, has

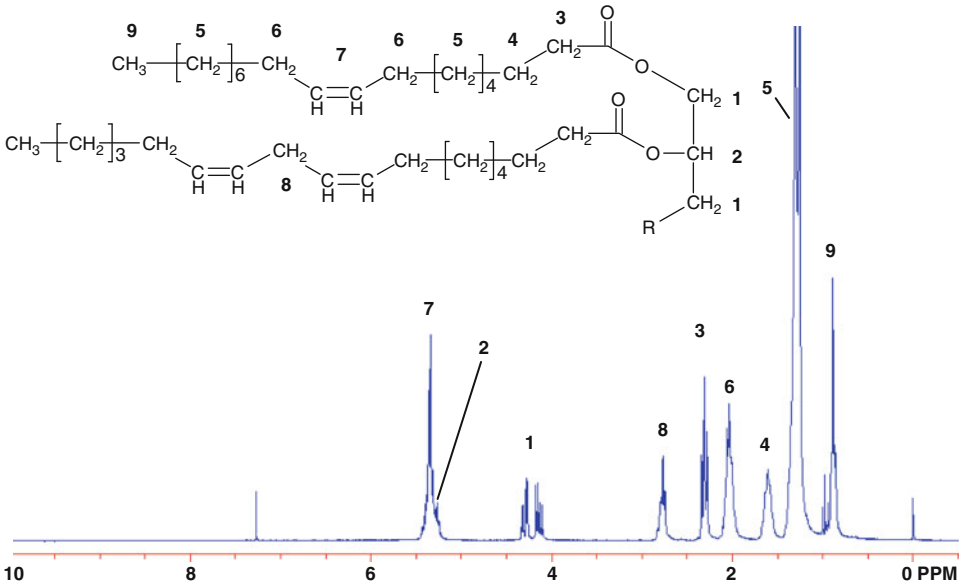

New Polymers, Renewables as Raw Materials. Figure 3
^{1}H-NMR spectrum of soybean oil ($CDCl_3$). R represents a third fatty acid

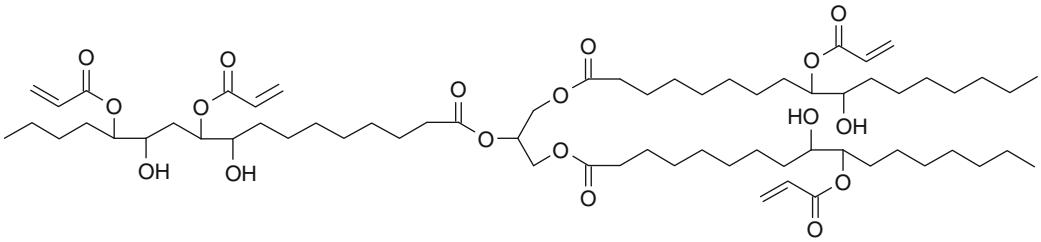
O
O
O

styrene, it is possible to produce polymers with different moduli and glass transition temperatures. Polymer properties can also be controlled by changing the M_W of the monomer or the functionality of the acrylated triglyceride. Consequently, a range of properties, and therefore applications, can be found. Subsequent to the acrylation reaction, the triglyceride contains both residual amounts of unreacted epoxy rings as well as newly formed hydroxyl groups, both of which can be used to further modify the triglyceride by reaction with a number of chemical species, such as diacids, diamines, anhydrides, and isocyanates. The approach presented here is to oligomerize the triglycerides with reagents that have chemical structures conducive to stiffening the polymer, such as cyclic or aromatic groups. Reacting AESO with cyclohexanedicarboxylic anhydride (Fig. 5a) forms oligomers, increasing the entanglement density as well as introducing stiff cyclic rings to the structure. Reaction of the AESO with maleic acid (Fig. 5b) also forms oligomers and introduces more double bonds. Although it is desirable to maximize the conversion of hydroxyls or epoxies, the viscosity increases dramatically at high levels of conversion. Eventually, this can lead to gelation, so the reaction must be carefully monitored. After oligomerization, the modified AESO resin can be blended with styrene and cured in the same manner as the unmodified AESO resin.

Maleinized Soybean Oil Monoglyceride

Maleinized soybean oil monoglyceride (Fig. 4) is synthesized from the triglyceride oil in two steps [33]. The first is a standard glycerolysis reaction to convert the triglycerides into monoglycerides by reacting triglycerides with glycerol; see [31]. The product is generally a mixture of mono- and diglycerides, as illustrated in Fig. 6. Using excess glycerol can aid in conversion. Additionally, the reaction can be run in solvent or in the presence of an emulsifier catalyst [34]. Once the reaction is completed, it is possible to separate a portion of the unreacted glycerol by cooling the product rapidly [33]. The presence of glycerol is not detrimental to the end polymer, because it can be reacted with maleic anhydride in the same manner as the monoglycerides and incorporated into the end polymer network.

The maleinization of the soybean oil monoglyceride (SOMG) mixture at temperatures below 100°C produces monoglyceride, diglyceride, and glycerol maleate half-esters. This reaction makes no attempt to produce a polyester, and the half-ester formation is expected to proceed at low temperatures in the presence of either acid or base catalysts without any by-products. A good indication of the success of this reaction is to follow the signal intensity ratio of maleate vinyl protons to fatty acid vinyl protons ($N_M \backslash N_{FA}$) in the ^{1}H NMR spectrum. The use of 2-methylimidazole and triphenyl antimony as catalysts was shown to be successful when conducting the reaction at temperatures of 80–100°C with a 3:2 weight ratio of glycerides to maleic anhydride ($N_M \backslash N_{FA} = 0.85$) [33, 51]. Once these maleates have been added, the monoglycerides can react via addition polymerization. Because maleates are relatively unreactive with each other, the addition of styrene increases the polymerization conversion and imparts rigidity to the matrix.

To increase the glass transition temperature (T_g) and modulus of the SOMG/MA polymer, more rigid diols can be added during the maleinization reaction. Two such diols are neopentyl glycol (NPG) and bisphenol A (BPA), which may increase the rigidity of the end polymer network. Although their addition to the maleinization mixture will reduce the renewable resource content of the final resin, they should result in higher T_g values for the end polymer. The synthesis of maleate half-esters of organic polyols, including NPG and BPA and the cross-linking of the resulting maleate half-esters with a vinyl monomer such as styrene, has been reported [52, 53]. The literature also abounds with examples of unsaturated polyesters prepared from NPG and maleic anhydride with other polyols and diacids [54–57]. However, the copolymers of NPG and BPA bis maleate half-esters with SOMG maleate half-esters are new.

The properties of the SOMG/MA polymer as well as the effect of adding NPG and BPA on the mechanical properties of the final polymers are presented here. For this purpose, mixtures of SOMG/NPG and SOMG/BPA, prepared at the same weight ratio, were maleinized, and the copolymers of the resulting maleates with styrene were analyzed for their mechanical properties and compared to that of SOMG maleates.

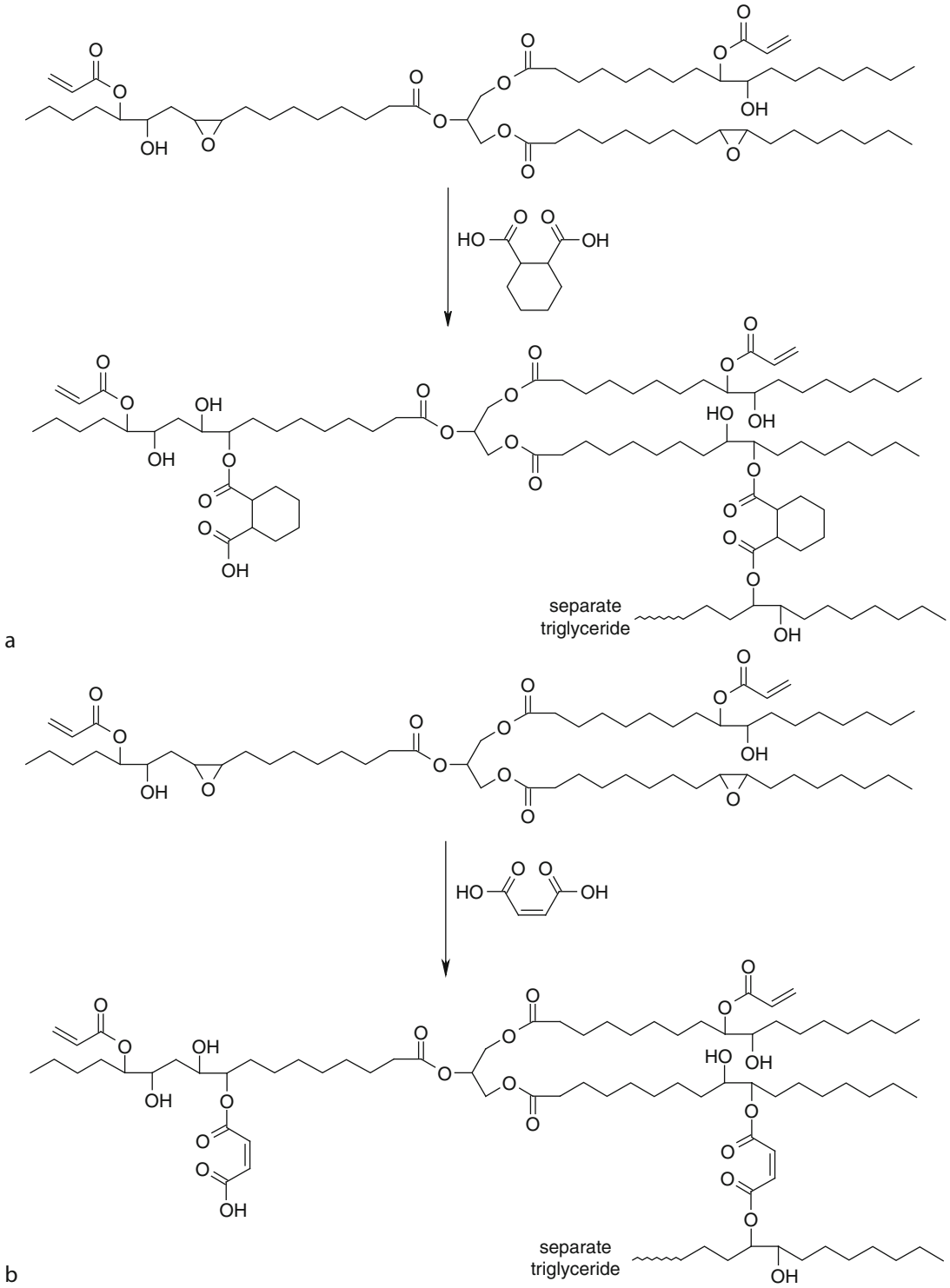

New Polymers, Renewables as Raw Materials. Figure 5
(**a**) Modification of AESO by reaction with cyclohexane dicarboxylic anhydride. (**b**) Modification of AESO by reaction with maleic acid

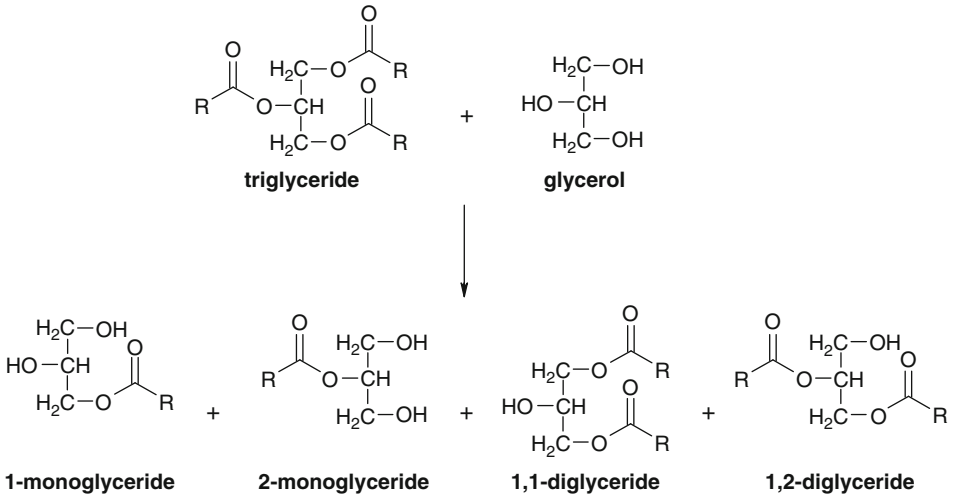

New Polymers, Renewables as Raw Materials. Figure 6
Glycerolysis of triglycerides to form mixtures of mono- and diglycerides

Maleinized Hydroxylated Oil

Maleinized hydroxylated oil (HO/MA) is synthesized in a manner similar to both the AESO and the SOMG/MA monomers. The double bonds of an unsaturated oil are used to attach the polymerizable groups by converting the double bonds of the triglyceride to hydroxyl groups. The hydroxyls can then be used to attach maleates. As shown in Fig. 2, there are two routes to synthesize the hydroxylated triglyceride. The first is through an epoxidized intermediate. By reacting the epoxidized triglyceride with an acid, the epoxies can be easily converted to hydroxyl groups [29, 58]. Alternatively, the hydroxylated oil can be synthesized directly from the unsaturated oil, as described in [1]. After hydroxylation, the oil can be reacted with maleic anhydride to functionalize the triglyceride with maleate half-esters. A molar ratio of 4:1 anhydride to triglyceride was used in all cases, and the reaction was catalyzed with *N*,*N*-dimethylbenzylamine. Once the maleinization reaction is finished, the monomer resin can be blended with styrene similar to the other resins presented here.

SOPERMA: Soybean Oil Pentaerythritol Glyceride Maleates

In the preceding sections, the preparation of soybean oil monoglyceride maleates (SOMG/MA) by E. Can [65] was reported. Soybean oil was reduced to monoglycerides through a glycerolysis reaction, and the glycerolysis product, which was a mixture of mono- and diglycerides as well as unreacted triglycerides and free glycerol, was reacted with maleic anhydride to convert the free hydroxyls to maleate half-esters, thus allowing them to free radically polymerize. The use of pentaerythritol instead of glycerol in the same synthetic route, as shown in Fig. 7, offers certain advantages, such as the presence of more hydroxyl groups and, therefore, more reactive sites for malination, which should result in a higher cross-link density for the resulting polymers. There are no standard conditions for the alcoholysis of the triglyceride oils with pentaerythritol; the reactant molar ratios and reaction conditions change according to the end use of the product. Soybean pentaerythritol molar ratios of SO:PER = 1:2 and SO:PER = 1:3 were used, which should give mixtures of monoglycerides and pentaerythritol monoesters as the main products. Higher amounts of pentaerythritol were avoided because this would further decrease the triglyceride content of the formulation. The idealized reaction scheme for the soybean oil pentaerythritol alcoholysis reaction is shown in Fig. 7.

The soybean oil pentaerythritol alcoholysis reactions were carried out for the first time by E. Can at 230–240°C for 0.5, 2, and 5.5 h. A reaction temperature of 180–190°C was also employed. $Ca(OH)_2$ was used as

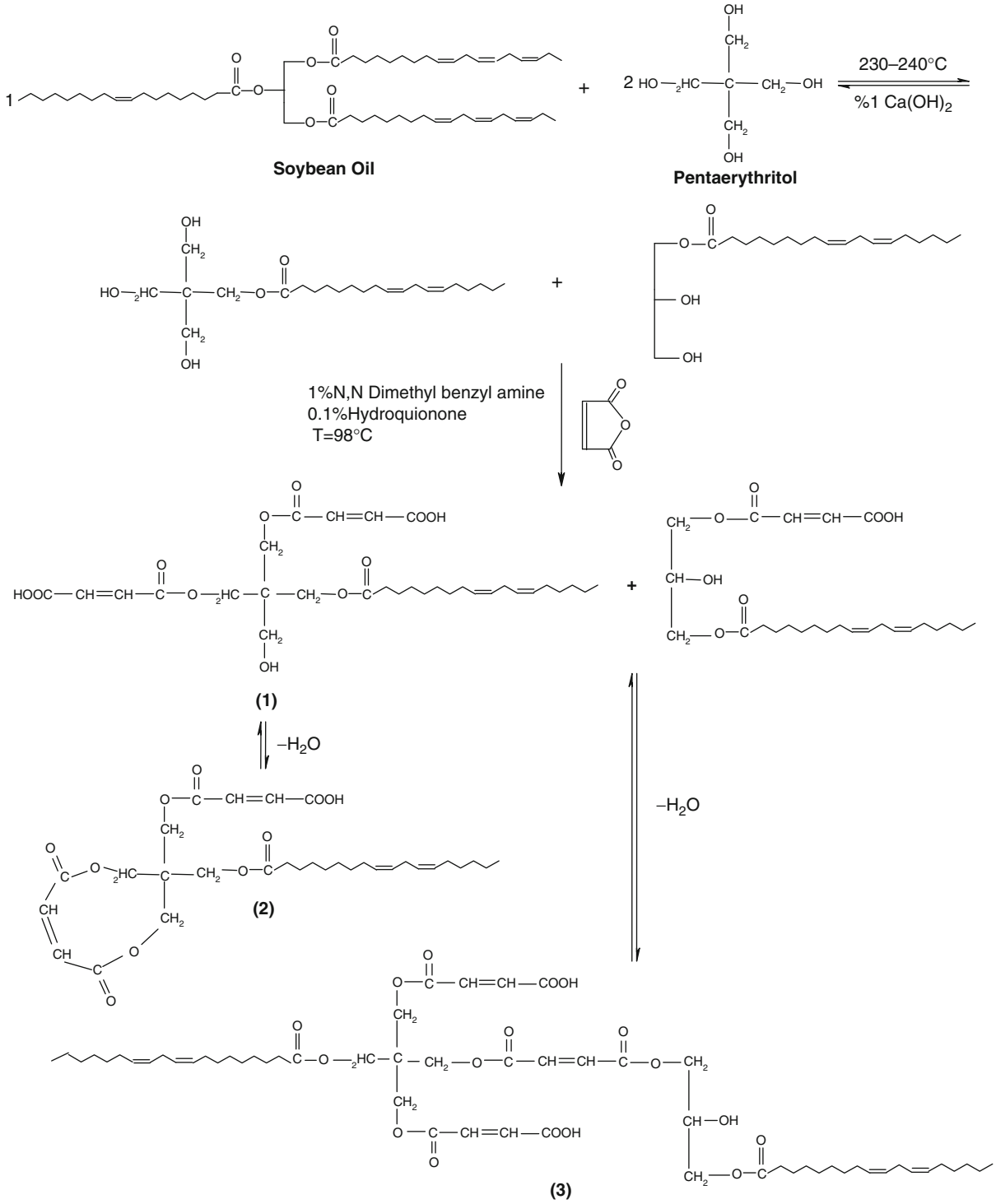

New Polymers, Renewables as Raw Materials. Figure 7

The reaction scheme for soybean oil pentaerythritol alcoholysis and malination reaction (SOPERMA)

a catalyst at a concentration of 1% of the total weight of the oil and the polyol. $Ca(OH)_2$ forms soap with the free fatty acids in the oil and promotes the reaction at least in part by increasing the solubility of pentaerythritol in the oil. $Ca(OH)_2$ was reported to be an effective catalyst for the glycerolysis of soybean oil; it increases the monoglyceride yield and reduces the triglyceride content of the glycerolysis product. The amount of reactants and catalysts used for the soybean oil pentaerythritol alcoholysis reactions and the resulting malination reactions, at different mole ratios, are shown in Table 2.

For the malination of the alcoholysis products, maleic anhydride was in a 1:1 molar ratio with the number of hydroxyls on pentaerythritol used in the alcoholysis reaction, thus molar ratios of SO:PER:MA = 1:2:8 and 1:3:12 were employed. A molar ratio of SO:PER:MA = 1:3:7.62 was also used to reduce the unreacted maleic anhydride content of the latter reaction. A reaction temperature of 95–100°C was used, because when lower reaction temperatures were used, for example, 60°C, the reaction rate was significantly lower and therefore not preferred. Temperatures above 100°C led to gelation of the product due to polyesterification of both the maleate half-esters and maleic anhydride with the free hydroxyls and were therefore avoided. Table 2 shows the amount of the reactants used for the malination reactions done at different SO:PER:MA molar ratios. The product at room temperature was a light brown solid. The SOPERMA (1:3:12) and SOPERMA(1:2:8) products were prepared in a similar manner by changing the molar ratios of the reactants in the formulation.

SOGLYME: Soybean Oil Monoglyceride Methacrylates

Soybean oil monoglyceride methacrylates (SOGLYME) were synthesized by E. Can [66]. Soybean oil monoglyceride methacrylates were prepared in a two-step process. First, soybean oil was glycerolized in the presence of $Ca(OH)_2$ as catalyst at 230–240°C for 5 h. The glycerolysis of soybean oil under these conditions gives a product with an equilibrium mixture containing the monoglycerides, diglycerides, and the two starting materials [63]. The glycerolysis product was then reacted with methacrylic anhydride at 55°C to form the methacrylate esters of the glycerides and methacrylic acid. Pyridine, which is an effective catalyst in the reaction of methacrylic anhydride with alcohols, was used as the catalyst. Hydroquinone was used to inhibit the radical polymerization of the reactive methacrylate esters. The idealized reaction schemes for the glycerolysis and methacrylation are shown in Fig. 8.

The glycerolysis of soybean oil was carried out in a 1:2.4 molar ratio of soybean oil to glycerol. For the following methacrylation reaction, methacrylic anhydride was in a 1:1 molar ratio with the number of hydroxyls on glycerol used in the glycerolysis reaction, thus the molar ratio of soybean oil, glycerol, and methacrylic anhydride was SO:GLYC:ME = 1:2.4:7.2. The amount of reactants and catalysts used for the

New Polymers, Renewables as Raw Materials. Table 2 The amount of ingredients used in the alcoholysis of soybean oil with pentaerythritol and the following malination reactions

Reactants	SO:PER:MA (1:2:8)		SO:PER:MA (1:3:12)		SO:PER:MA (1:3:7.62)	
	Weight of reactant (g)	Moles of reactant	Weight of reactant (g)	Moles of reactant	Weight of reactant (g)	Moles of reactant
Soybean oil	5	0.0057	5	0.0057	5	0.0057
Pentaerythritol	1.554	0.01143	2.331	0.01714	2.331	0.01714
$Ca(OH)_2$	0.0655	–	0.0733	–	0.0733	–
Maleic anhydride	1.479	0.04571	6.720	0.06857	1.267	0.0435
N,N dimethyl benzyl amine	0.1103	–	0.1405	–	0.116	–
Hydroquinone	0.011	–	0.014	–	0.0116	–

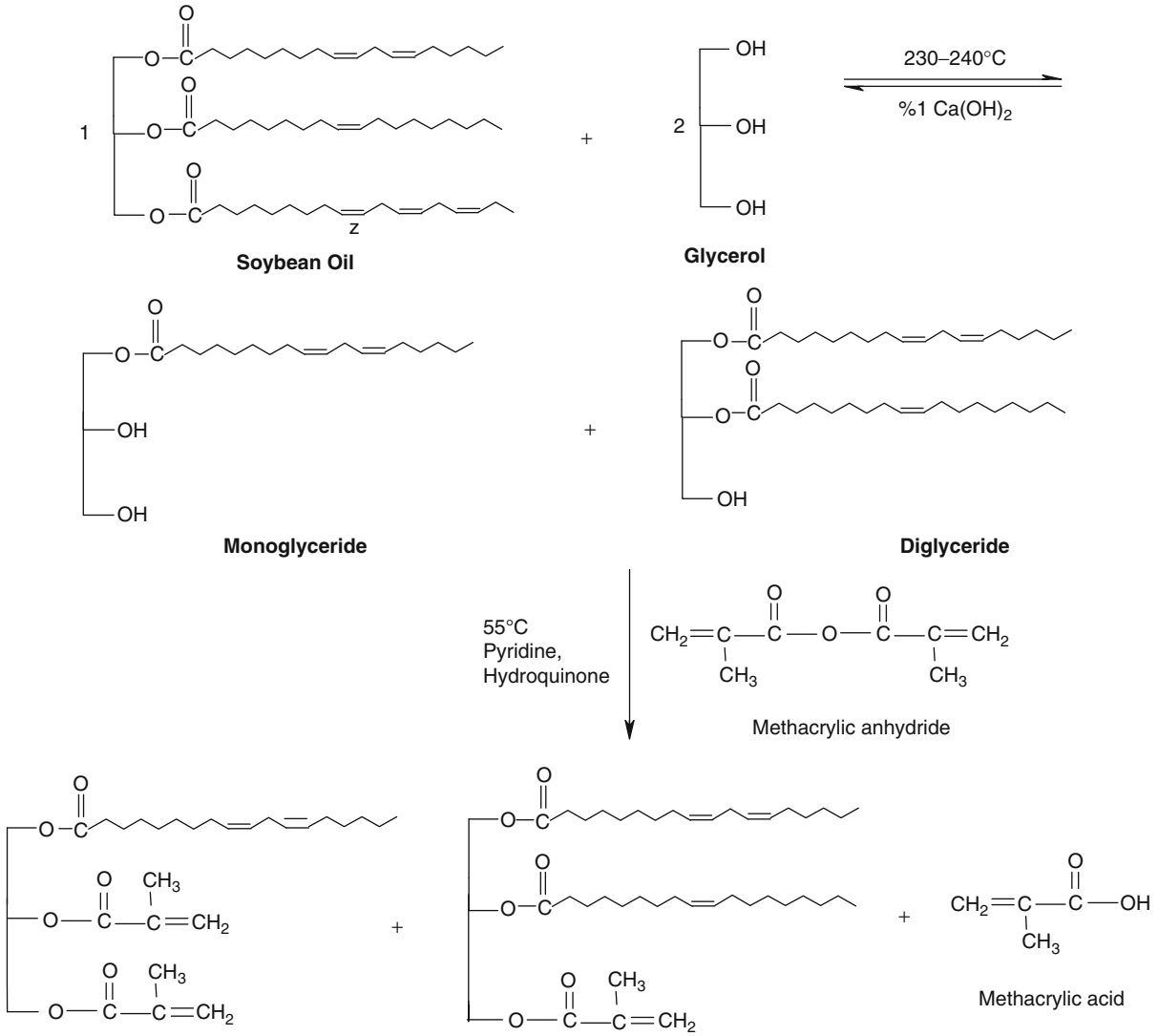

New Polymers, Renewables as Raw Materials. Figure 8
The reaction scheme for soybean oil glycerolysis and methacrylation reactions (SOGLYCMA)

soybean oil glycerolysis and methacrylation reactions are shown in Table 3. The resulting SOGLYME product was a light yellow liquid.

COPERMA: Castor Oil Pentaerythritol Glyceride Maleates

Castor oil is not commonly used in alkyd resin formulations and there are few reports on the alcoholysis of castor oil triglycerides. For the preparation of castor oil-based monomers, castor oil was first alcoholized with glycerol, pentaerythritol, and an aromatic diol; BPA propoxylate and the alcoholysis products were then malinated, as shown in Fig. 9 [66]. Bisphenol A propoxylate was used specifically to introduce the rigid aromatic rings onto the triglyceride structure. The maleate esters of castor oil alcoholysis products have never been synthesized before, thus the castor oil-based monomers presented here are totally new resins. The alcoholysis reactions of castor oil were carried out for 2 h at 230–240°C in the presence of $Ca(OH)_2$ as catalyst, similar to the soybean oil alcoholysis reactions. The malination reactions were carried out for 5 h at

New Polymers, Renewables as Raw Materials. Table 3 Reactant amounts used in soybean oil glycerolysis and methacrylation reactions (SO:GLYC:ME = 1:2.4:7.2)

Component	Weight(g)	Moles
Soybean oil	119.93	0.1371
Glycerol	30.30	0.329
Calcium hydroxide	0.7514	–
Methacrylic anhydride	152.14	0.987
Pyridine	3.024	–
Hydroquinone	0.302	–

98°C to ensure the completeness of the malination of the secondary hydroxyls of castor oil. *N,N*-Dimethylbenzylamine, which is reported to be an effective catalyst for the malination of hydroxylated oils, was used as a catalyst. Castor oil was also directly malinated to see the effect of the alcoholysis step on the mechanical properties of the resulting polymers.

The molar ratio of castor oil to maleic anhydride was 1:3 for malination of castor oil; therefore, the reaction was carried out in an excess of maleic anhydride assuming that 1 mol castor oil contains 2.7 mol of hydroxyls. The reactants used in this reaction as well as their mole numbers and masses are given in Table 1. The COPERMA product was a light brown solid (Table 4).

COGLYMA: Castor Oil Monoglyceride Maleates

The castor oil glycerolysis reaction was carried out in a molar ratio of CO:GLY = 1:2.2 using reactants shown in Table 5. The reaction mixture was heated to 230–240°C and agitated under N_2 atmosphere for 2 h at this temperature. The reaction product at room temperature was a light brown liquid. The idealized structures of both the reactants and products for the glycerolysis reaction are shown in Fig. 10. Both unreacted castor oil and excess glycerol exist as by-products in the reaction.

For the malination of the castor oil glycerolysis product, maleic anhydride was used in a molar ratio sufficient to malinate the hydroxyls of both castor oil and the glycerol used in the glycerolysis reaction. Thus, the molar ratio of castor oil (CO), glycerol (GLY), and maleic anhydride (MA) was CO:GLY:MA = 1:2.2:9.3. The castor oil glycerolysis product as prepared above was heated to 90°C with mechanical stirring, then the specified amounts of maleic anhydride and hydroquinone were added. The mixture was stirred at this temperature until the maleic anhydride melted and mixed with the castor oil glycerolysis product. *N,N*-Dimethylbenzylamine was added and the reaction mixture was heated to 98°C. The mixture was agitated at this temperature for 5 h. The reaction product at room temperature was a light brown solid.

COBPPRMA: Castor Oil Bisphenol a Propoxylate Glyceride Maleates

The castor oil (CO), pentaerythritol (PER) alcoholysis reaction was carried out in a molar ratio of CO:PER = 1:2 [66]. The reaction product at room temperature was a light brown liquid. The idealized structures of both the reactants and products for the alcoholysis reaction are shown in Fig. 11. Both unreacted castor oil and excess glycerol exist as by-products in the reaction. For the malination of the castor oil pentaerythritol alcoholysis product, maleic anhydride was used in a molar ratio to malinate the hydroxyls of both castor oil and the pentaerythritol used in the alcoholysis reaction. Thus, the molar ratio of castor oil (CO), pentaerythritol (PER), and maleic anhydride (MA) was CO:PER:MA = 1:2:10.7. The malinated product at room temperature was a light brown solid.

COMA: Castor Oil Maleates

COMA consists of the castor oil (CO) which was directly maleated on the three hydroxyl groups using maleic anhydride (MA). The ratios of reactants used are shown in Table 6 [66].

Polymers from Plant Oils

Acrylated Epoxidized Soybean Oil Polymers

Acrylated epoxidized soybean oil (AESO), shown in Fig. 4, was examined for its ability to produce high T_g and high modulus polymers. A commercial form of AESO, Ebecryl 860, was blended with various amounts of styrene to determine the effect of blending on mechanical and dynamic mechanical properties. The AESO used had an average functionality of

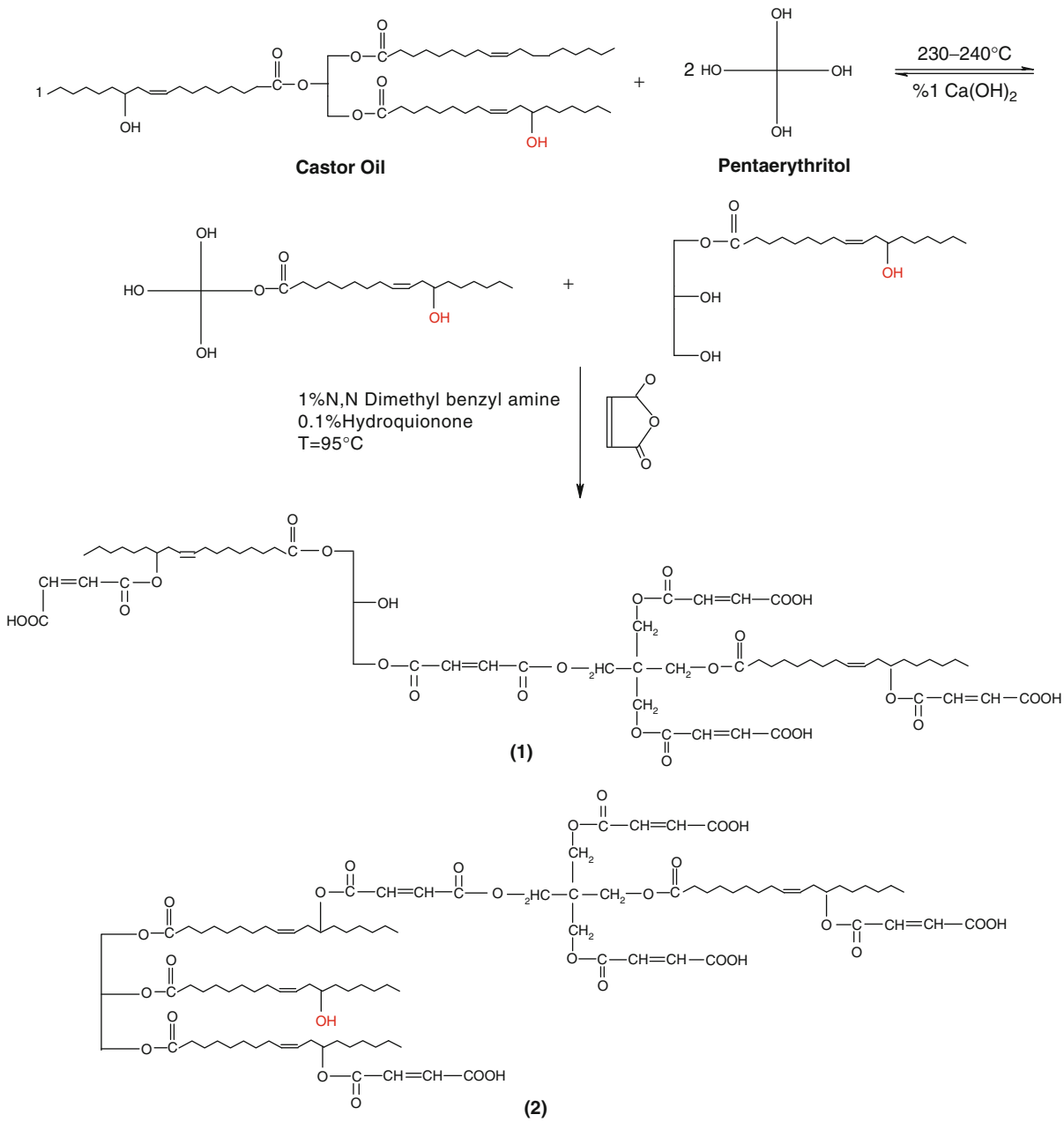

New Polymers, Renewables as Raw Materials. Figure 9
The reaction scheme for castor oil pentaerythritol alcoholysis and malination reactions (COPERMA)

approximately three acrylates per triglyceride as determined by ^{1}H NMR [38]. The optimal number of acrylates per triglyceride to obtain maximum stiffness and strength is about five acrylic acid groups per triglyceride. An example ^{1}H NMR spectrum of AESO is shown in Fig. 12. Similar to soybean oil, the triplet peak at 2.3 ppm can be used as a basis for the protons present alpha to the carbonyls in the triglyceride. The three peaks in the range of 5.8–6.5 ppm represent the three protons of the acrylate group.

Styrene monomer was blended with the AESO along with a free-radical initiator, 2,5-dimethyl-2,5-di

New Polymers, Renewables as Raw Materials. Table 4 Reactant amounts used in castor oil pentaerythritol alcoholysis and malination reactions (CO:PER:MA = 1:2:10.7)

Component	Weight(g)	Moles
Castor oil	120	0.13
Pentaerythritol	35.33	0.26
Calcium hydroxide	0.778	
Maleic anhydride	178.99	1.826
N,N dimethyl benzyl amine	3.35	
Hydroquinone	0.335	

New Polymers, Renewables as Raw Materials. Table 5 Reactant amounts used in castor oil glycerolysis and malination reactions (CO:GLY:MA = 1:2.2:9.3)

Component	Weight(g)	Moles
Castor oil	100	0.108
Glycerol	21.9	0.238
Calcium hydroxide	1.22	–
Maleic anhydride	98.08	1.001
N,N dimethyl benzyl amine	2.20	–
Hydroquinone	0.220	–

(2-ethylhexanoylperoxy) hexane. The addition of styrene to any type of unsaturated polyester is common practice in the composite liquid molding resin field. Its low cost and low viscosity improve the price and processability of the resin. For triglyceride-based polymers, the styrene also imparts a rigidity that the triglyceride does not naturally possess. The amount of initiator used was 1.5 wt% of the total resin weight (AESO plus styrene). For tensile testing of the polymers, samples were prepared in accordance with ASTM D 638. The resin was cured at 60°C for 12 h, followed by 125°C for 1.5 h. Samples for dynamic mechanical analysis (DMA) testing were prepared by pouring resin into a rubber gasket between two metal plates covered with aluminum foil. Samples were cured at 65°C for 1.5 h and postcured at 125°C for 1.5 h.

Synthesis of Modified Acrylated Epoxidized Soybean Oil Polymers

To improve the properties of the AESO-based resins, modified forms of the AESO were synthesized. These modifications involved partially reacting epoxidized soybean oil with acrylic acid and reacting the remaining epoxies with anhydrides or diacids. A more detailed explanation of the synthesis of partially acrylated epoxidized soybean oil can be found in other sources [38]. In summary, a mixture of epoxidized soybean oil was mixed with a stoichiometric amount of acrylic acid (about 1,500 g ESO to 460 g acrylic acid). Hydroquinone was added as a free-radical inhibitor in the amount of 0.07 wt% of the total reactants' weight, as well as 1,4-diazobicyclo[2.2.2]octane to act as a catalyst in the amount of 0.1 wt% of the total reactants' weight. This was reacted at 95°C for about 11 h, after which it was allowed to cool to room temperature. The resulting product had approximately 1.7 acrylates/triglyceride and 0.4 residual epoxy/triglyceride according to ^{1}H NMR. The remaining 2.3 epoxies were lost to epoxy homopolymerization [38].

The first modification was the reaction of AESO with cyclohexanedicarboxylic anhydride (CDCA), as illustrated earlier in Fig. 5a. In a typical reaction, the synthesized AESO was reacted with 7.4% of its weight in CDCA and 0.1% of its weight in 2-methyl imidazole, which catalyzes the reaction [38]. After reacting at 110°C for about 3 h, the majority of the anhydride and epoxy groups was consumed, as indicated by FTIR spectroscopy. The second modification was the reaction of AESO with maleic acid (Fig. 5b). This was accomplished by reacting the synthesized AESO with 11% of its weight in maleic acid [38]. The reaction was held at approximately 80°C for 4 h, during which consumption of the epoxies was again confirmed by FTIR spectroscopy.

The modified resins were then blended with styrene and initiator in the amounts of 66 wt% modified AESO, 33 wt% styrene, and 1 wt% 2,5-dimethyl-2,5-di(2-ethylhexanoylperoxy) hexane initiator. After curing at 65°C for 1.5 h and postcuring at 125°C for 1.5 h, the polymers' dynamic mechanical properties were analyzed and compared to the unmodified AESO resin.

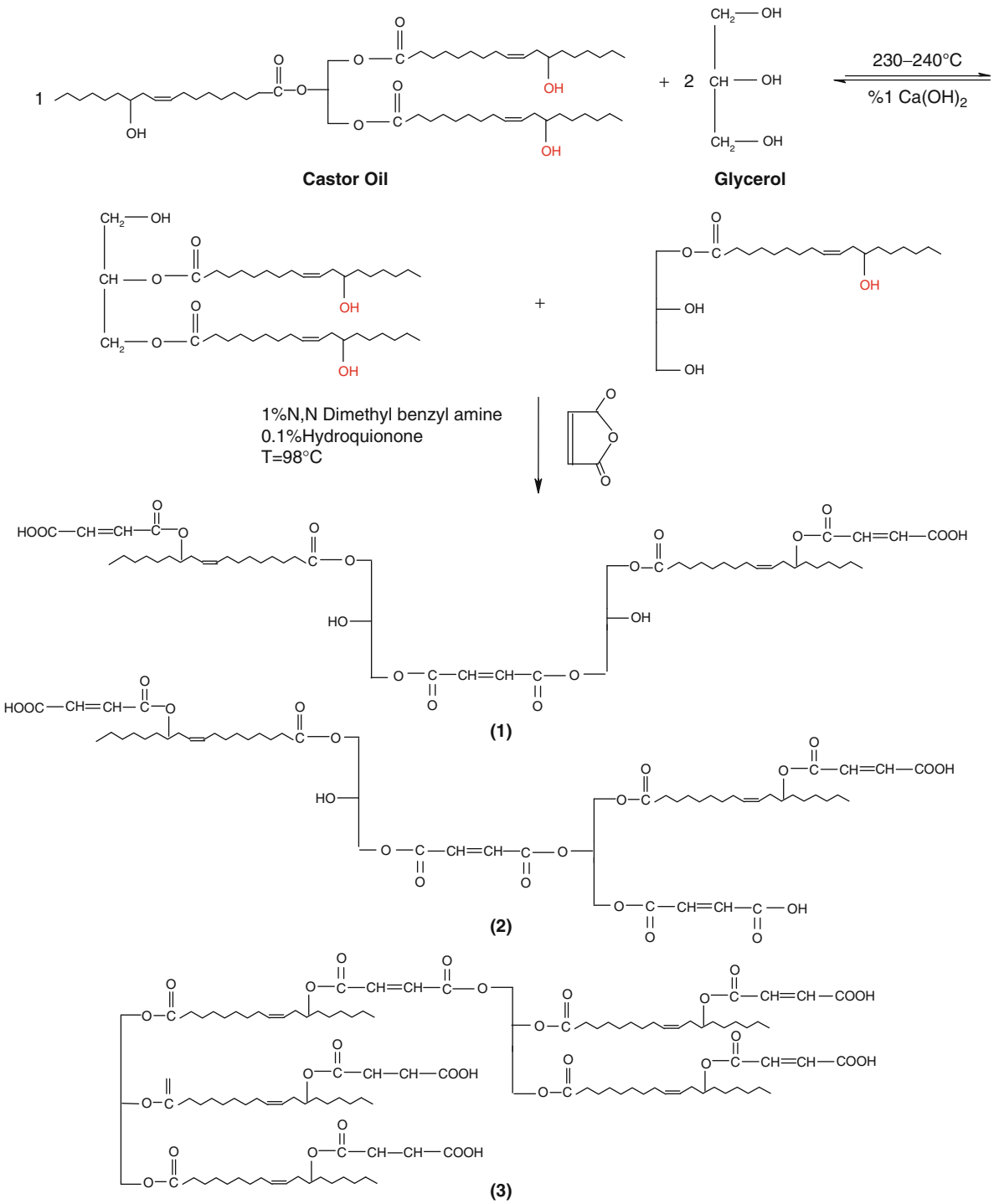

New Polymers, Renewables as Raw Materials. Figure 10
The reaction scheme for castor oil glycerolysis and malination reactions (COGLYMA)

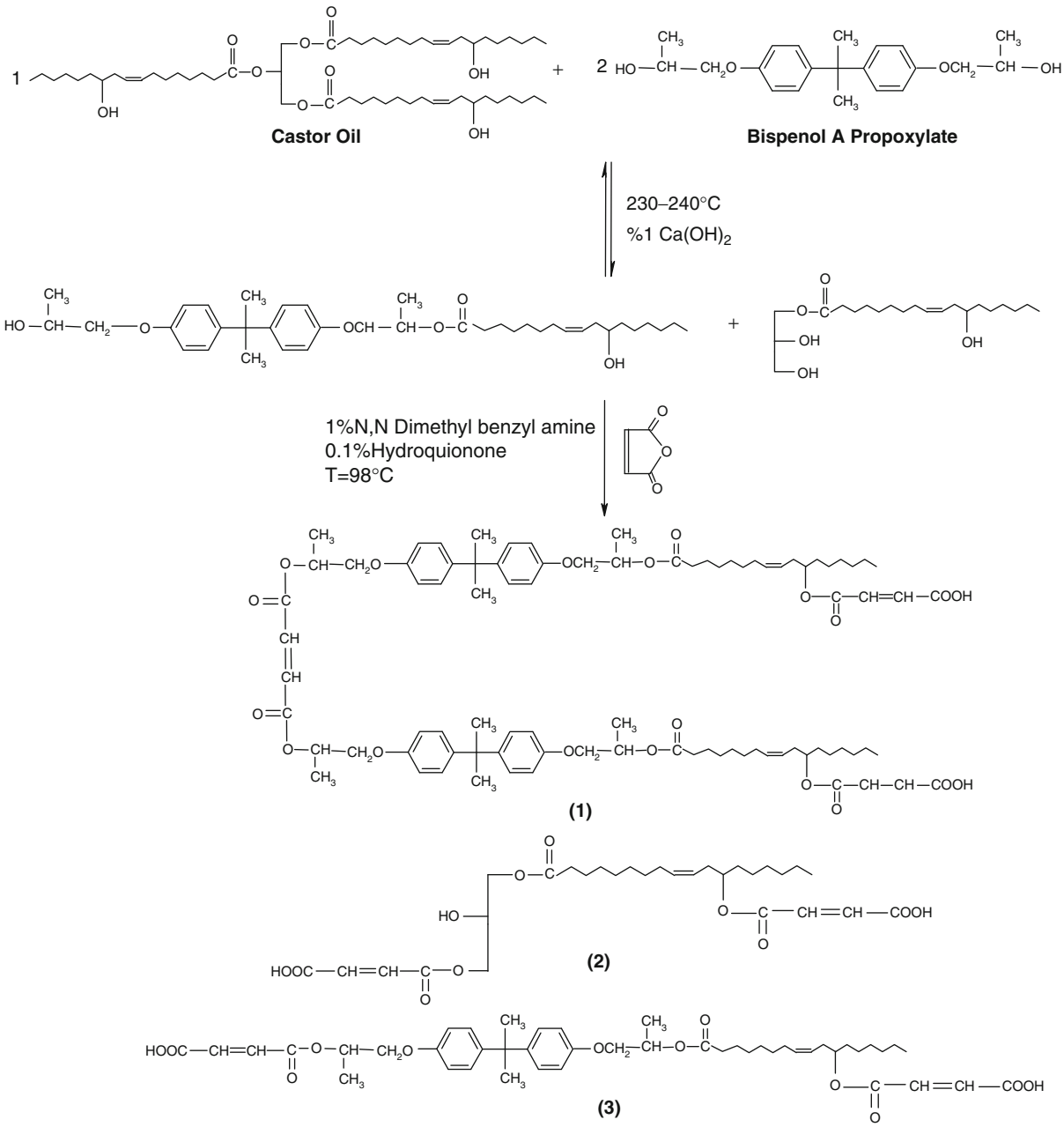

New Polymers, Renewables as Raw Materials. Figure 11
The reaction scheme for castor oil Bisphenol A propoxylate alcoholysis and malination reactions (COBPAPRMA)

Maleinized Soybean Oil Monoglyceride Resin Synthesis

The maleinized soybean oil monoglyceride (Fig. 4) was synthesized by breaking the triglycerides into monoglyceride and then functionalizing the alcohol groups with maleic anhydride. The glycerolysis reaction was done by heating the triglycerides in the presence of glycerol and a catalyst. In a typical reaction, glycerol was heated at 220–230°C for 2 h under an N_2 atmosphere to distill off any water present [33]. The amount

of soybean oil reacted with the glycerol was 4 g soybean oil to 1 g glycerol, a molar ratio of 1.75 mol glycerol to 1 mol triglyceride. The soybean oil was added in five portions to the glycerol, each portion 1 h apart. With the first portion, commercial soap was added in the amount of 1% of the total oil amount to act as an emulsifier and catalyst. The solution was heated at 230°C under N_2 while being stirred. After 5.5 h, the reaction was immediately cooled to room temperature with an ice bath, causing glycerol to separate from the mixture. On removal of this layer, approximately 90% of the reaction solution, consisting of glycerides and glycerol, was recovered.

Maleinization of the mixture was accomplished by heating 60 g of glyceride/glycerol mixture to about 80°C while being stirred. Maleic anhydride was then added in the amount of 40 g. As the anhydride melted, 0.6 g triphenyl antimony was added as a catalyst along with 0.01 g hydroquinone. The reaction was complete after 5.5 h, according to FTIR and ^{1}H NMR, resulting in a mixture of maleinized glycerides and glycerol (SOMG/MA) [33].

New Polymers, Renewables as Raw Materials. Table 6
Reactant amounts used in malination of castor oil (CO:MA = 1:3)

Component	Weight(g)	Moles
Castor oil	100	0.108
Maleic anhydride	31.82	0.325
N,N dimethyl benzyl amine	1.32	–
Hydroquinone	0.132	–

Maleinized Soybean Oil Monoglyceride/Neopentyl Glycol Resin Synthesis

Modifying the procedure given in [53], SOMG/NPG/MA resin was synthesized as follows [51]. Forty-five grams of SOMG was placed into a 250-mL round-bottom flask equipped with a temperature controller and a magnetic stirrer and then heated to 125°C. Fifteen grams of NPG (0.144 mol) was then added to SOMG, and as the NPG melted, 58.3 g maleic

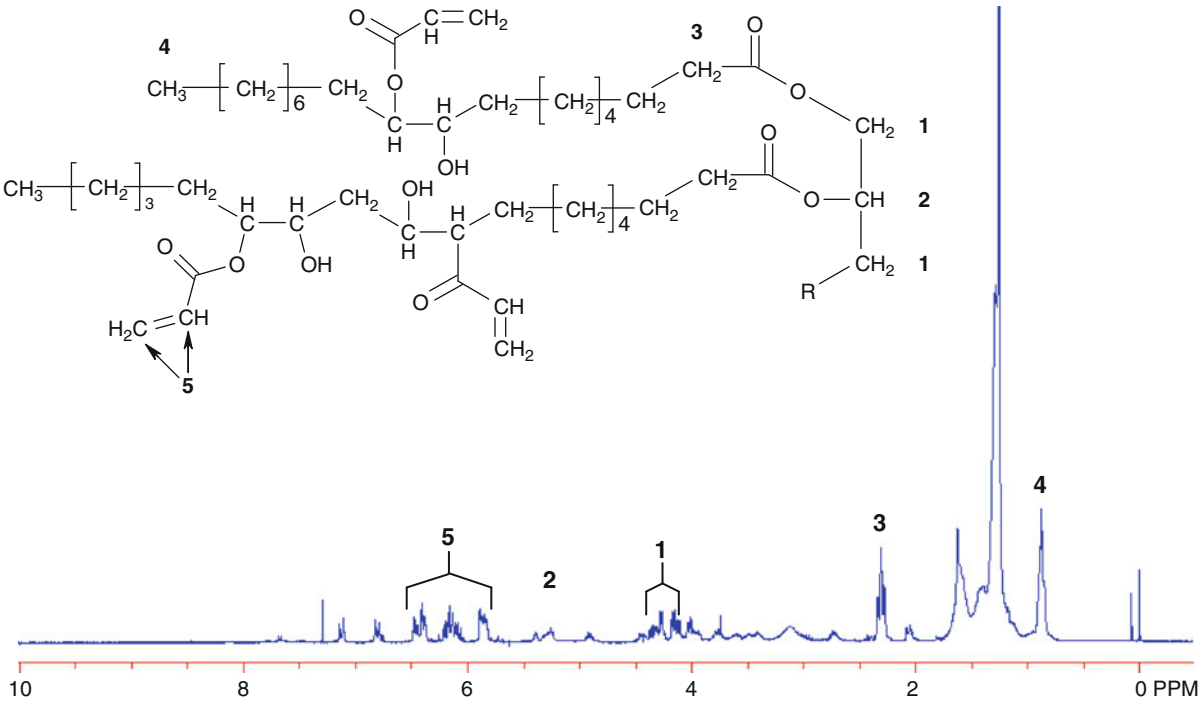

New Polymers, Renewables as Raw Materials. Figure 12
^{1}H-NMR spectrum for acrylated epoxidized soybean oil (Ebecryl 860, UCB Chemicals Co.)

anhydride was added. As the three compounds formed a homogenous solution, 0.06 g triphenyl antimony catalyst and 0.015 g hydroquinone were added. The solution was stirred for 6.5 h at 120°C. ^{1}H NMR analysis of the product showed the formation of both the SOMG and NPG maleate and later fumarate vinyl groups. The product was a light yellow viscous liquid at room temperature.

Maleinized Soybean Oil Monoglyceride/Bisphenol a Resin Synthesis

The preparation of maleates of BPA and ethylene and propylene oxide adducts of BPA was reported in [52]. For this work, SOMG and BPA were maleinized as a mixture [51]. Forty-five grams of SOMG was placed into a 250-mL round-bottom flask equipped with a temperature controller and a magnetic stirrer and heated to 125°C. Fifteen grams of BPA (0.0657 mol) was added to the SOMG, and as BPA dissolved, 42.88 g maleic anhydride (0.4375 mol) was added. As the three compounds formed a homogenous solution, 0.6 g triphenyl antimony and 0.01 g hydroquionone were also added. The solution was then stirred for 9 h at 125°C until maleic anhydride consumption was completed. The ^{1}H NMR analysis of the product showed the formation of both the SOMG and BPA maleate and later fumarate vinyl groups. The reaction product was an orange-colored viscous liquid (98 g) at room temperature.

Copolymerization of the Maleates with Styrene

The copolymerization of SOMG/MA, SOMG/NPG/MA, and SOMG/BPA/MA with styrene were all run under the same conditions for comparison of the mechanical properties of the resulting polymers. For this purpose, a certain weight ratio of the maleate mixture was mixed with 35% of its own weight of styrene in a closed vial. All of the maleate products were found to be soluble in styrene. *tert*-Butyl peroxybenzoate radical initiator, 2% by weight of the total mixture, was added. Nitrogen gas sparging and vacuum degassing were carried out for 5 min. The solution was then transferred to a rectangular rubber gasket mold sandwiched between two steel plates. The resin-filled mold was heated to 120°C at a rate of 5°C/min and was cured at this temperature for 3.5 h. It was then postcured at 150°C for 1 h. Samples were clear, homogeneous, and free of voids or gas bubbles. The polymer samples were polished and prepared for DMA, which was conducted in a three-point bending geometry on a Rheometrics Solids Analyzer II. The temperature was ramped from 30°C to 200°C at a rate of 5°C/min, with a frequency of 1 Hz and strain of 0.01%.

Malinated Hydroxylated Oil Polymer Synthesis

The HO/MA shown in Fig. 4 uses the unsaturation of the triglyceride to incorporate polymerizable groups. This monomer was used in a series of experiments to understand how triglyceride structure can affect the synthesis and dynamic mechanical properties of the end polymer [59]. Olive oil, cottonseed oil, soybean oil, safflower oil, linseed oil, triolein, and a genetically engineered high oleic soybean oil were converted into HO/MA resins. The levels of unsaturation for these oils are shown in Table 1. The fatty acid chain lengths for all of these oils are between 17.5 and 18 carbons, making the unsaturation level essentially the only difference among oils.

Hydroxylation was done by stirring the oil (~100 g) vigorously in the presence of formic acid (150 mL) and 30% (aq) hydrogen peroxide (55 mL) at 25°C [30, 59]. The reaction time was 18 h to reach a maximum conversion of double bonds. Formic acid, peroxide, and water were then removed from the hydroxylated oil by dissolving the reaction mixture in diethyl ether and washing multiple times with water and then saturated (aq) sodium bicarbonate until a neutral pH was reached. The solution was then washed with saturated (aq) sodium chloride and dried over sodium sulfate. Finally, the ether was evaporated off under vacuum. The extent of hydroxylation can be characterized by ^{1}H NMR. An example ^{1}H NMR spectrum is presented in Fig. 13 with corresponding peak assignments [59]. The extent of hydroxylation has a linear dependence on the level of unsaturation. Generally, for every double bond present on the triglyceride, an average of 1.6 hydroxyls can be added [59].

The purified hydroxylated oil was reacted with maleic anhydride in a ratio of 1 mol triglyceride to 4 mol anhydride. The hydroxylated oil was heated to a temperature of about 80°C, and finely ground maleic

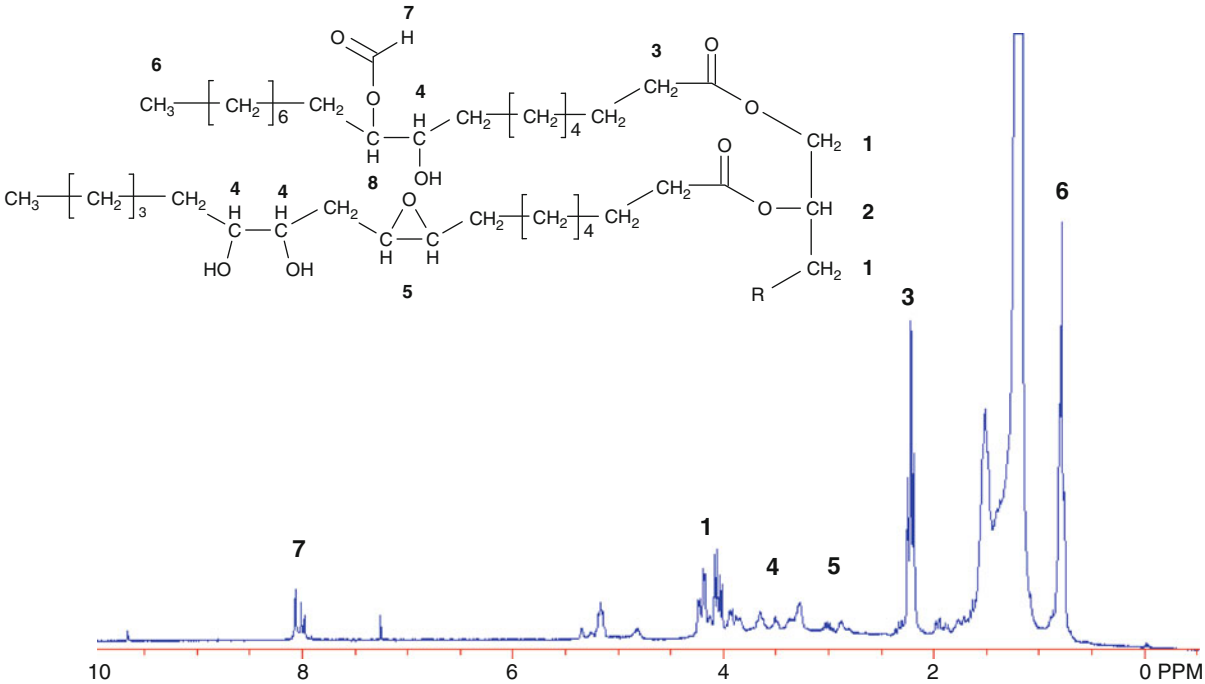

New Polymers, Renewables as Raw Materials. Figure 13
^{1}H-NMR of hydroxylated soybean oil. Treating the oil with formic acid and hydrogen peroxide results in conversion of the double bonds to hydroxy groups

anhydride was then added. Upon dissolving of the anhydride, *N,N*-dimethylbenzylamine was added to catalyze the reaction. The reaction was continued for 3 h, and the extent of maleinization was determined by ^{1}H NMR. An illustrative ^{1}H NMR is shown in Fig. 14 [59]. Under these reaction conditions, the extent of functionalization plateaus in the range of 2.1–2.8 maleates/triglyceride for all oils. Approximately 20–25% of the maleates attached to the triglycerides isomerize to form fumarate groups (*trans* confirmation). Unreacted maleic anhydride remained in the resin and was polymerized during the cure reaction. The HO/MA resins were then dissolved in styrene in a molar ratio of 7:1 styrene to HO/MA. Resins were cured using 2,5-dimethyl-2,5-di-(2-ethylhexanoylperoxy)hexane at 65°C for 1.5 h and postcured at 120°C for 1 h. DMA was conducted in a three-point bending geometry on a Rheometrics Solids Analyzer II. Temperature was ramped from 30°C to 175°C at a rate of 5°C/min, with a frequency of 1 Hz and strain of 0.01%.

SOPERMA and COPERMA Polymer Synthesis

The general-purpose unsaturated polyester (UP) resin is a linear polymer with the number average molecular weights in the range of 1,200–3,000 g/mol. Depending on the chemical composition and molecular weight, they can be viscous liquids or solids. The plant oil-based resins prepared are not linear polymers but similar mixtures of monomers or oligomers with different molecular weights. The number and weight average molecular weights of different species in each of these plant oil-based resins were in the range of ~300–2,000 g/mol as presented in section "Synthetic Pathways for Triglyceride-Based Monomers." With the exception of the COMA and SOGLYME resins, which were liquid at room temperature, all the malinated glyceride-based resins prepared were paste-like solids at room temperature. The melting points of these resins were in the range of 60–70°C, similar to the general-purpose UP resins whose melting points are in the range of 60–77°C.

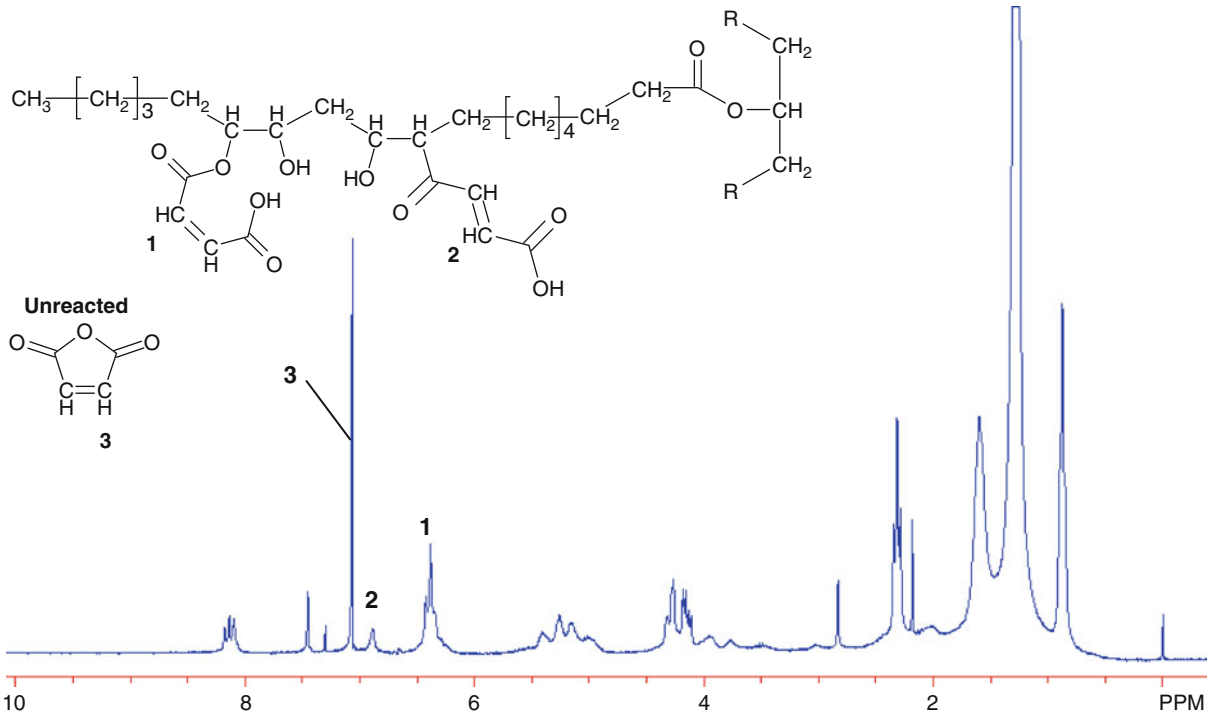

New Polymers, Renewables as Raw Materials. Figure 14
^{1}H-NMR of maleinized hydroxylated soybean oil. Peaks 1 and 2 represent the maleate half esters and fumarate half esters, respectively. Peak 3 represents unreacted maleic anhydride

To prepare the styrenated plant oil-based resins, which were solid at room temperature, the resin was first heated in an oil bath above its melting point (~70°C), then the necessary amount of styrene was added and the mixture was agitated in the oil bath at a temperature of 80°C until styrene and the resin became totally mixed. The resin was then processed at room temperature for polymerization. For the resins that were liquid at room temperature, styrene was added, mixed, and processed at room temperature. Apart from the SOGLYME resin (methacrylated soybean oil monoglycerides), all the styrenated resins showed phase separation in the microscale. Figure 15 shows the optical microscopic pictures of the SOPERMA-styrene mixtures at decreasing SOPERMA concentrations at 500× magnification. The SOPERMA forms nonuniform droplets in the continuous styrene matrix in the 1–5-μm size range. As can be seen in Fig. 15, these droplets become less dense and more uniform in size as the concentration of SOPERMA decreases from 80 to 20 wt%. Similarly, COPERMA, COGLYMA, and COBPAPRMA resins containing 33 wt% styrene were found to be incompatible with styrene and exhibited phase separation.

The general-purpose UP resins based on propylene glycol, phthalic, and maleic anhydride are miscible with styrene. The molecular weights of the general-purpose UP resins have a number average molecular weight of 900 g/mol and a weight average molecular weight of 2,400 g with a polydispersity of 2.7. The acid number of these polyesters is around 50 mg KOH/g. The incompatibility of the malinated plant oil-based resins in styrene can be attributed to both the abundance of the acid groups of the maleate half-esters and the presence of high-molecular-weight species in these resins. The acid number of all the malinated glyceride-based resins was found to be above 200 mg KOH/g. This value is much higher than that of the general-purpose UP resins. The molecular species present in the malinated glyceride-based resins are highly polar compared to styrene, and the strong interactions of these molecules via hydrogen bonding between the acid groups result in

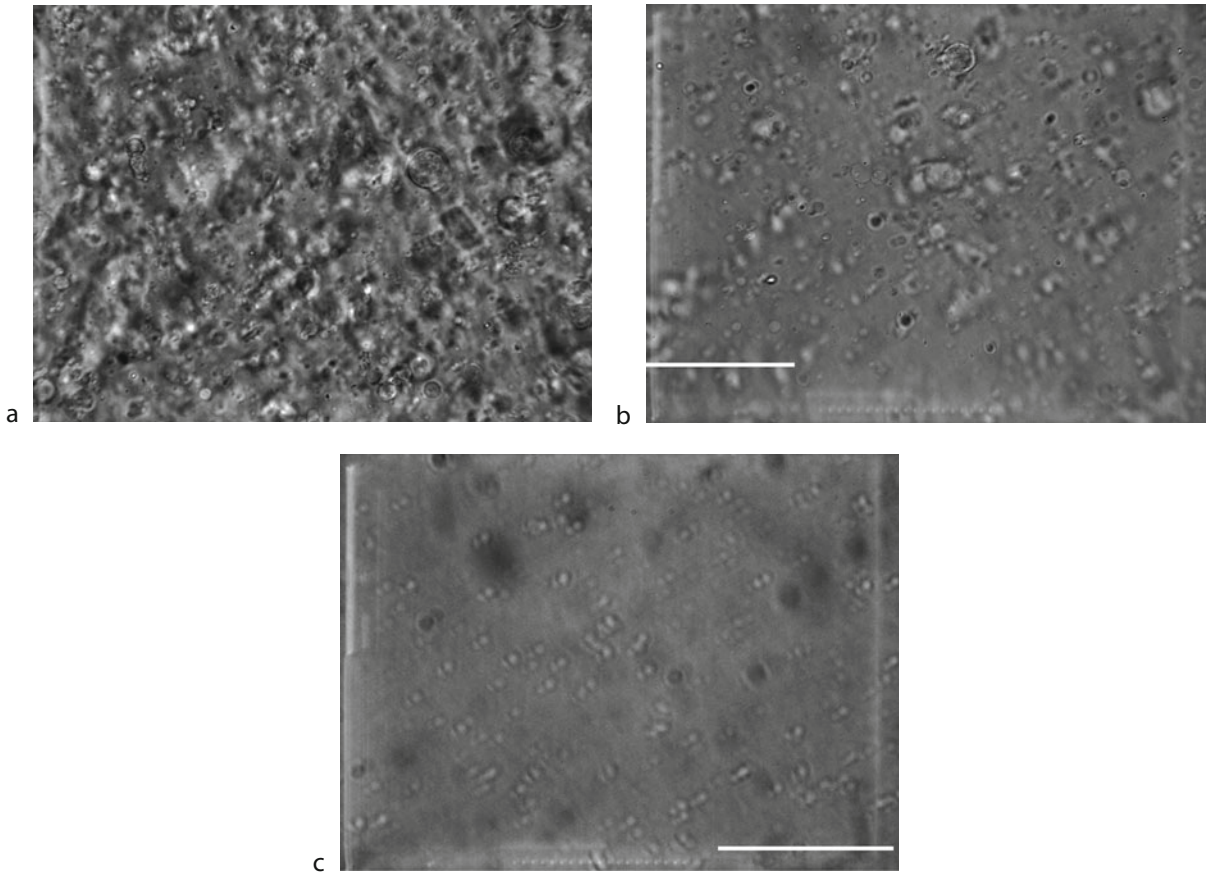

New Polymers, Renewables as Raw Materials. Figure 15
Optical microscopic pictures of the SOPERMA-styrene mixtures (500×) (**a**) 80 wt% (**b**) 60 wt% (**c**) 20 wt% SOPERMA

the insolubility of the malinated glycerides in styrene. Thus, the SOGLYME resin based on methacrylated glycerides, both with the acrylic acid by-product and without acrylic acid, showed no phase separation in styrene. The methacrylate half-esters as shown earlier in Fig. 8 do not carry acid functionality, and oligomer formation during the methacrylation reaction cannot occur. Additionally, these molecules are less polar than maleate half-esters and they cannot interact via hydrogen bonding, which favors their compatibility with styrene. The SOPERMA resin was also found to be insoluble in more polar monomers such as acrylic acid and acrylonitrile. The immiscibility of the SOPERMA resin in these solvents shows that the molecular weight and strong interactions between the malinated glyceride molecules play an important role in the immiscibility of these molecules in polar solvents.

A liquid molding resin should have properties within a certain operating range to be successfully used in molding processes. Possibly the most stringent requirement is the resin's viscosity, which must range between 200 and 1,000 cP. At viscosities lower than 200 cP, air pockets will remain in the mold after injection. At viscosities greater than 1,000 cP, voids may occur in the part, the time required for injection increases, and problems with fiber wetting can arise during composite preparation.

The surface free energy of a liquid, also referred to as *surface tension*, determines most of the surface and interfacial properties such as wetting, adhesion, and adsorption. Surface tension results from an imbalance

of molecular forces in a liquid. At the surface of the liquid, the liquid molecules are attracted to each other and exert a net force, pulling themselves together. High surface tension values mean that the molecules tend to interact strongly; thus, polar materials show high surface energy values. The surface energy of a liquid molding resin may be especially important for reinforcement of the resins by fibers. The wetting of a fiber with a liquid resin can be judged by the difference between the surface energies of the fiber and the resin. For the most desirable condition, proper wetting and spreading in resin transfer molding processes, the surface energy of the fiber should be high, whereas the surface energy of the resin should be low. Table 7 shows the specific gravity, viscosity (η), and surface energy values for the plant oil-based resins and general-purpose UP resins containing 33 wt% styrene.

As can be seen from Table 7, apart from the COMA and the SOGLYME resins, these resins show viscosities that are in a range that is suitable for liquid molding processes. Although the COMA and SOGLYME resins show low viscosities, the viscosities of these resins can easily be increased by decreasing the amount of the styrene diluent. It was found by Can [66] that as the weight fraction of styrene was increased, the viscosity decreased in an exponential manner. This result is very desirable since it shows that a small amount of comonomer can be used to make these resin systems much easier to process.

New Polymers, Renewables as Raw Materials. Table 7 The specific gravity, viscosity, η and surface energy values for the plant oil based resins (33 wt% styrene) and general purpose UP resins

Resin	Specific gravity (g/ml)	Viscosity, η (cP)	Surface energy (mN/m)
SOPERMA	0.94	343	27.38
COPERMA	1.06	363	28.84
COGLYCMA	1.04	213	26.36
COBPAPRMA	0.98	183	27.2
COMA	0.75	92	26.02
SOGLYME	0.87	51	22.7
GP-UP	1.14	200–2,000	24–30

The surface energy values of these resins show values closer to those of UP resins, and are significantly lower than those of vinyl ester resins (32–34 mN/m), which may have difficulty in wetting fiber substrates. Among the malinated resins, the surface free energy value is highest for the COPERMA resin and lowest for the COMA resin in proportion to the maleate content of the resins. A higher maleate content should result in a higher polarity and a higher surface free energy. The SOGLYME resin shows the lowest surface free energy among all the resins. The methacrylated glycerides do not carry an acid functional group as malinated glycerides and, therefore, are less polar than the corresponding maleates.

The curing of UP resin is accomplished via free-radical cross-linking polymerization between the UP molecules and styrene. The UP molecules are the cross-linkers, while the styrene acts as an agent to cross-link the adjacent polyester molecules. Similarly, in the plant oil-based resin systems, the functionalized glycerides act as the cross-linker units, and styrene is the agent that links the adjacent glyceride molecules. Styrene is the most commonly used vinyl monomer in unsaturated polyester resins due to its low viscosity, low cost, and reactivity with the unsaturated sites of polyesters. The unsaturation present on the UP backbone is very sluggish in homopolymerization. The reactivity ratio of styrene and maleic/fumaric acid esters is about 0, indicating that this system has a tendency to form alternating copolymers. Because the malinated plant oil-based resins were found to be insoluble in styrene at room temperature, it was especially important for us to determine the conversion of polymerization for the maleate and styrene monomers.

For the determination of the conversion and kinetics of the polymerization, the styrenated SOPERMA, COMA, and COPERMA resins were prepared as described earlier. The styrene concentration was 33 wt% for each resin. *tert*-Butyl peroxybenzoate was used as the initiator. The initiator concentration was 2 wt% for the SOPERMA and COMA resins and 1.5 wt% for the COPERMA resin. The curing of all resins was carried out at 120°C for 3 h for comparison of conversion and rate of polymerization in different resins. The SOPERMA and COPERMA resins were also postcured

at 150°C and 160°C, respectively, for 1 h after 2 h at 120°C. Although, all the resins showed similar conversion versus time profiles during the isothermal cure, the final conversion values were different for each resin.

Table 8 lists the total conversion (α) and the conversion of maleates (α_{ma}) and styrene (α_{st}) for the COMA, SOPERMA, and COPERMA resins (33 wt% styrene) at the end of 3 h at 120°C. As can be seen, the final maleate conversion decreases as the maleate content of the resin increases from COMA to COPERMA. The styrene conversion and thus the total conversion is also considerably lower for the SOPERMA and COPERMA resins than for the COMA resin. It is expected that the molecular mobility of the resin decreases as the cross-link density increases, resulting in lower total conversion. As a result, styrene monomer as well as some resin can be trapped in the network and cannot participate in polymerization. However, although the COPERMA resin has a higher maleate content and, therefore, a higher cross-link density than the SOPERMA resin, the styrene and thus the final conversions for the SOPERMA and COPERMA resins do not show a significant difference. The maleate conversion was higher than styrene conversion for all of the resins.

The total ultimate conversion of unsaturated polyesters ranges from 0.75 to 0.9 and increases with increasing temperatures. Similarly, the final conversions for the isothermal cure of the plant oil-based resins were lower than the complete conversion. During an isothermal cure, when the increasing glass transition temperature of the resin reaches the reaction temperature and the material evolves from the rubbery state to the glassy state, the rate of propagation becomes diffusion controlled. This process, referred to as *vitrification*, may virtually terminate the polymerization, limiting the conversion that can be reached isothermally. This was true in particular for the SOPERMA and COPERMA resins, which possess glass transition temperatures (T_g) when fully cured [T_g(SOPERMA) = 139°C and T_g(COPERMA) = 146°C] that are higher than the cure temperature. Thus a postcure was necessary for these systems to increase the conversion.

New Polymers, Renewables as Raw Materials. Table 8 The total conversion(α), the conversion of maleates, (α_{ma}), and styrene (α_{st}), for the SOPERMA, COMA and COPERMA resins (33 wt% styrene) at the end of 3 hours at 120°C

Resin	α_{ma}	α_{st}	α
COMA	0.998	0.921	0.967
SOPERMA	0.979	0.828	0.886
COPERMA	0.952	0.835	0.885

Properties of Plant Oil Resins

Viscoelastic and Mechanical Properties of AESO-Styrene Polymers

The storage moduli, E', of the AESO-styrene neat polymers at various temperatures and compositions are shown in Fig. 16. At room temperature, the polymers display moduli proportional to the amount of styrene present, which is expected from the tensile properties presented earlier. Additionally, at room temperature all of the polymers are in the transition phase from the glassy region to the rubbery plateau. Even at temperatures as low as −130°C, it does not appear that these polymers have reached a characteristic glassy plateau. At extremely low temperatures, all compositions exhibit essentially equal moduli of about 4 GPa. At higher temperatures, the compositions show moduli inversely proportional to the amount of styrene present. According to rubber elasticity theory [60], the lower styrene content polymers have a higher cross-link density, as observed in Fig. 16.

The T_g is often designated by either the temperature at which the dynamic loss modulus E'' value is at a peak or the temperature at which the loss tangent tan δ exhibits a peak [61]. As shown in Fig. 17, all of the AESO-styrene copolymers exhibit two peaks in E''. A minor relaxation occurs in the range of −85°C to −95°C, showing little dependence on composition. The much larger relaxation, corresponding to the T_g, occurs in the range of −10°C to 60°C and also becomes sharper in nature with the addition of styrene. These peaks are shown in the tan δ graph in Fig. 18. The temperature at which these peaks occur exhibits a linear dependency on composition, increasing with the amount of styrene present in the system, as illustrated by Fig. 19.

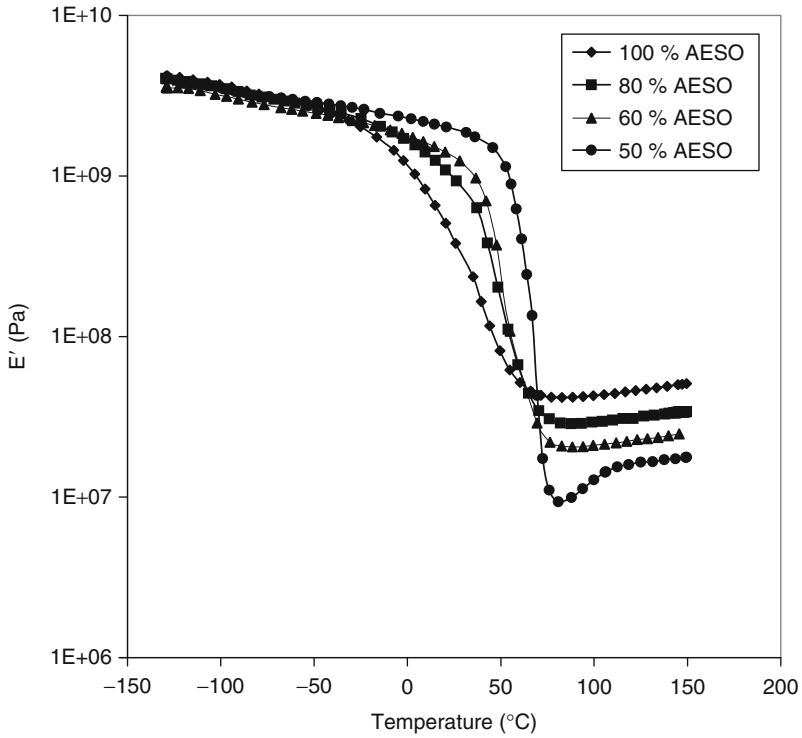

New Polymers, Renewables as Raw Materials. Figure 16
Storage modulus (E′) of AESO-styrene copolymer as a function of temperature

The dynamic mechanical behavior just discussed is a combination of three factors: cross-link density, copolymer effects, and plasticization. As the amount of AESO increases, so does the number of multifunctional monomers. Therefore, the overall cross-link density will be greater with increasing amounts of AESO, as supported by the high-temperature moduli shown in Fig. 16. Increasing the cross-link density slows the transition in E' from glassy to rubbery behavior. Additionally, the tan δ peak broadens and decreases in height [61]. The copolymer effect occurs frequently when there are differences in the reactivity or structure of the different monomers. If one monomer is more reactive, it is depleted faster, causing polymer formed later in the reaction to be composed mostly of the slower reacting monomer. This causes heterogeneity in the composition of the total polymer. If these monomers differ from each other in their physical properties, such as very different T_g′s, a general broadening of the glass–rubber transition is frequently observed, due to this gradient [61].

The other factor in the dynamic mechanical behavior, plasticization, is due to the molecular nature of the triglyceride. The starting soybean oil contains fatty acids that are completely saturated and cannot be functionalized with acrylates. Therefore, these fatty acids act in the same manner as a plasticizer, introducing free volume and enabling the network to deform more easily. The addition of even small amounts of plasticizer to polymers was known to drastically broaden the transition from glassy to rubbery behavior and reduce the overall modulus [61]. This plasticizer effect presents an issue that may be inherent to all natural triglyceride-based polymers that use the double bonds to add functional groups. However, with advances in genetic engineering, it may be possible to reduce this trend by reducing the amount of saturated fatty acids present, thus sharpening the glass–rubber transition. This issue is addressed later in the properties of HO/MA polymers produced from genetically engineered high oleic content oil and synthetic triolein oil. The existence of some saturated fatty acids, though,

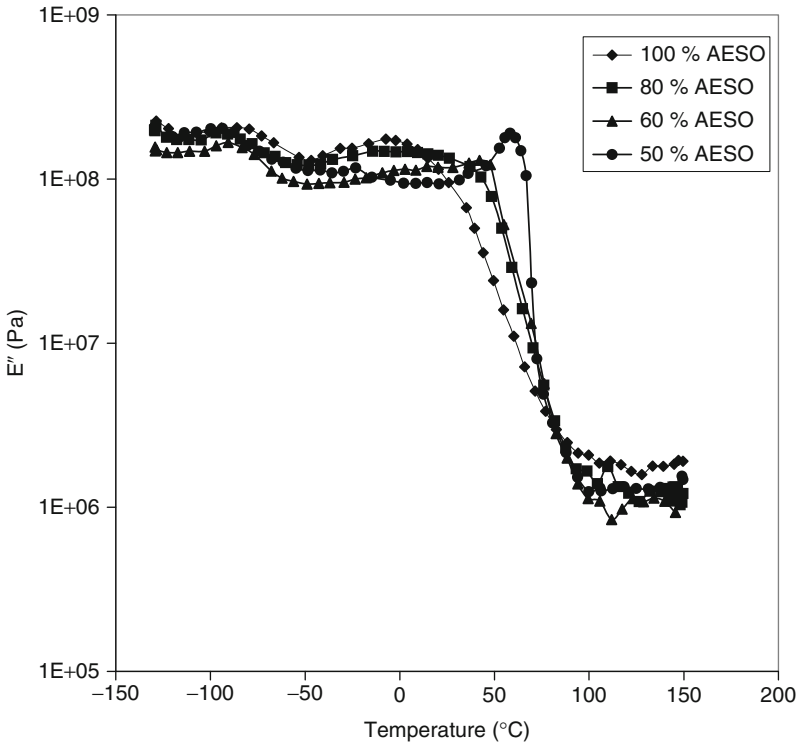

New Polymers, Renewables as Raw Materials. Figure 17
Loss modulus (E″) of AESO-styrene copolymer as a function of temperature

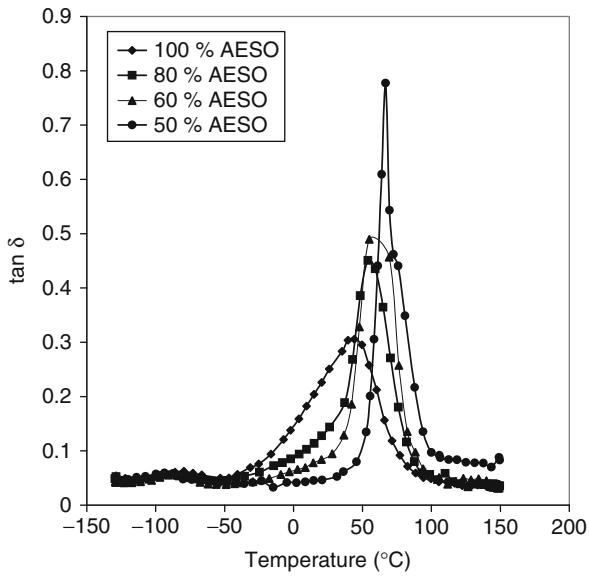

New Polymers, Renewables as Raw Materials. Figure 18
Damping peak (tan δ) of AESO-styrene copolymer as a function of temperature

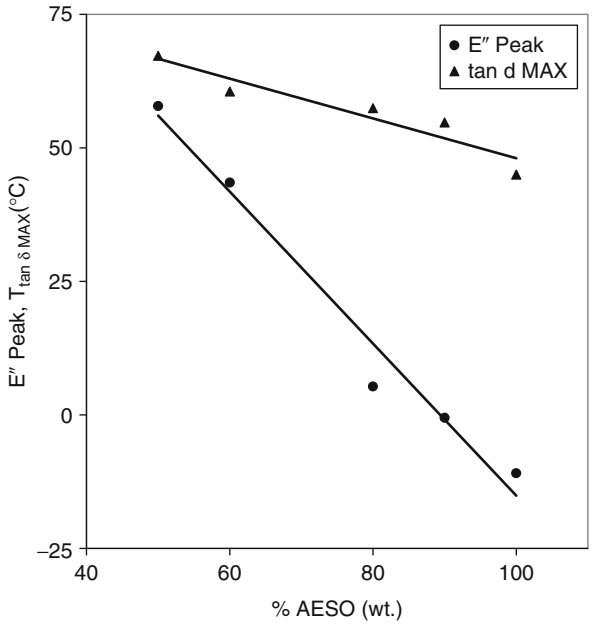

New Polymers, Renewables as Raw Materials. Figure 19
E″ and tan δ peak temperatures of various compositions of AESO-styrene polymer

can contribute to improved toughness and ballistic impact resistance [62].

Tensile Properties of AESO-Styrene Polymers

The tensile moduli of three AESO-styrene copolymers at room temperature are shown in Fig. 20. The pure AESO polymer has a modulus of about 440 MPa. At a styrene content of 40 wt%, the modulus increases fourfold to 1.6 GPa. In this region, the dependency on composition appears to be fairly linear. The ultimate tensile strengths of these materials, as shown in Fig. 21, also show linear behavior. The pure AESO samples exhibited strengths of approximately 6 MPa, whereas the polymers with 40 wt% styrene show much higher strengths of approximately 21 MPa. Therefore, it is apparent that the addition of styrene drastically improves the properties of the end resin.

Dynamic Mechanical Behavior of Modified AESO Resins

The dynamic mechanical properties of the AESO polymers modified by cyclohexanedicarboxylic anhydride (CDCA) and maleic acid were better than the unmodified polymers. As shown in Fig. 22, the storage modulus at room temperature increases with both of these modifications. The storage modulus of the unmodified AESO resin at room temperature is 1.3 GPa, whereas the cyclohexanedicarboxylic anhydride modification increases the modulus to 1.6 GPa. The maleic acid modification provides the most

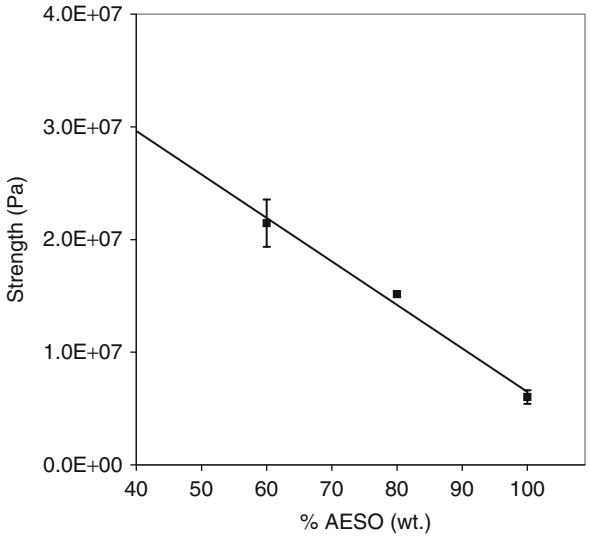

New Polymers, Renewables as Raw Materials. Figure 21 Ultimate tensile strength of AESO-styrene copolymers

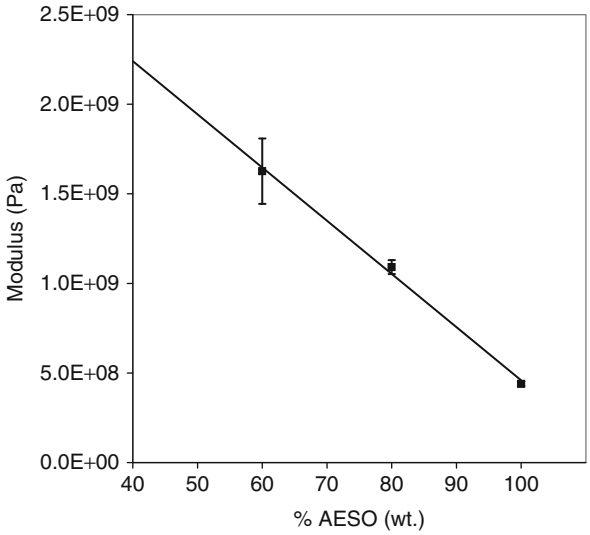

New Polymers, Renewables as Raw Materials. Figure 20 Tensile modulus of AESO-styrene copolymers

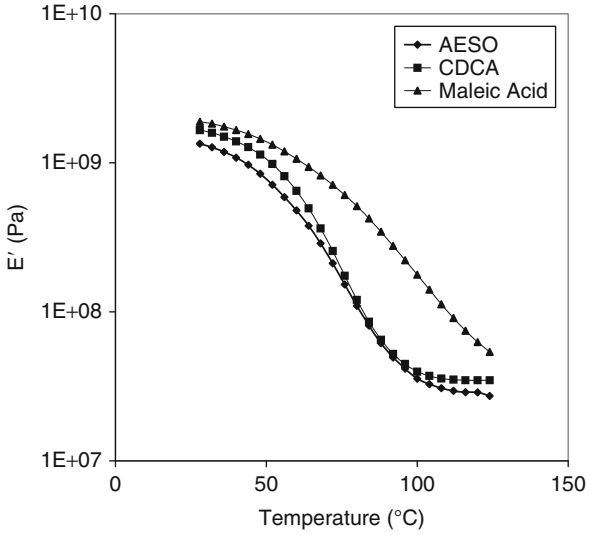

New Polymers, Renewables as Raw Materials. Figure 22 Storage modulus (E′) of modified AESO resins as a function of temperature

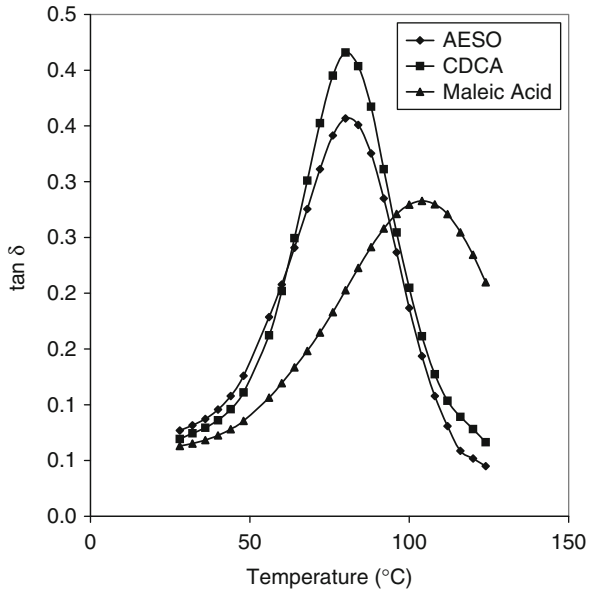

New Polymers, Renewables as Raw Materials. Figure 23 Damping peak (tan δ) of modified AESO resins as a function of temperature. Peaks in tan δ were found at 81°C (CDCA modified) and 105°C (maleic acid modified) compared to 79°C for the synthesized AESO

improvement, raising the storage modulus to 1.9 GPa. The T_g, as indicated by the peak in tan δ, does not show any large increase from the anhydride modification, as shown in Fig. 23. However, the maleic acid modification shifts the tan δ peak by almost 40 °C, showing a peak at 105 °C. The increased broadness of the peak can be attributed to increased cross-link density.

SOMG/MA Polymer Properties

As seen in Fig. 24, the tan δ peak for the SOMG/MA polymer occurs at around 133°C, and the polymer has an E' value of approximately 0.92 GPa at room temperature. It is apparent that the glass transition is rather broad due to the broad molecular weight distribution of the SOMG maleates. The distribution of soybean oil monoglyceride monomaleates, monoglyceride bismaleates, diglyceride monomaleates, and glycerol tris maleates was confirmed by mass spectral analysis, which was reported in a previous publication [63]. The tensile tests performed on the copolymers of SOMG maleates with styrene showed a tensile strength of 29.36 MPa and a tensile modulus of 0.84 GPa as calculated from the force displacement graph.

SOMG/NPG Maleates (SOMG/NPG/MA)

The DMA of SOMG/NPG/MA polymer showed a tan δ peak at approximately 145°C and an E' value of 2 GPa at room temperature. The 12°C increase in the T_g and the considerable increase in the modulus of the copolymers of SOMG/NPG maleates with styrene compared to that of the SOMG maleates can be attributed to the replacement of the flexible fatty acid chains by the rigid methyl groups of NPG. The overall dynamic mechanical behavior of the SOMG/NPG/MA polymer was very similar to that of the SOMG/MA shown in Fig. 21. Despite the higher T_g and modulus, there remained a broad glass transition. The tensile strength of the SOMG/NPG/MA polymer was found to be 15.65 MPa, whereas the tensile modulus was found to be 1.49 GPa.

Maleinized pure NPG polymerized with styrene (NPG/MA) was prepared to compare its properties with the SOMG/NPG/MA polymer [51]. DMA analysis of the NPG/MA showed a tan δ peak at approximately 103°C and an E' value of about 2.27 GPa at 35°C. The high T_g value observed for the SOMG/NPG/MA system (∼145°C) is attributed to a synergistic effect of both the NPG and SOMG together since the T_g value observed for the NPG/MA system (∼103°C) is much lower. This is probably due to the incorporation of the fatty acid unsaturation into the polymer in the SOMG/NPG/MA system. On the other hand, the comparatively higher E' value observed for the NPG maleates explains the increase in the E' observed for the SOMG/NPG/MA system compared to that of the SOMG/MA system. The decrease in tensile strength of the SOMG/NPG/MA system compared to that of SOMG/MA may be attributed to a broader molecular weight distribution of this system compared to that of the SOMG maleates.

SOMG/BPA Maleates (SOMG/BPA/MA)

The DMA of this polymer showed a tan δ peak at around 131°C and an E' value of 1.34 GPa at 35°C. The introduction of the rigid benzene ring on the polymer backbone considerably increased the modulus of the final polymer compared to that of the SOMG

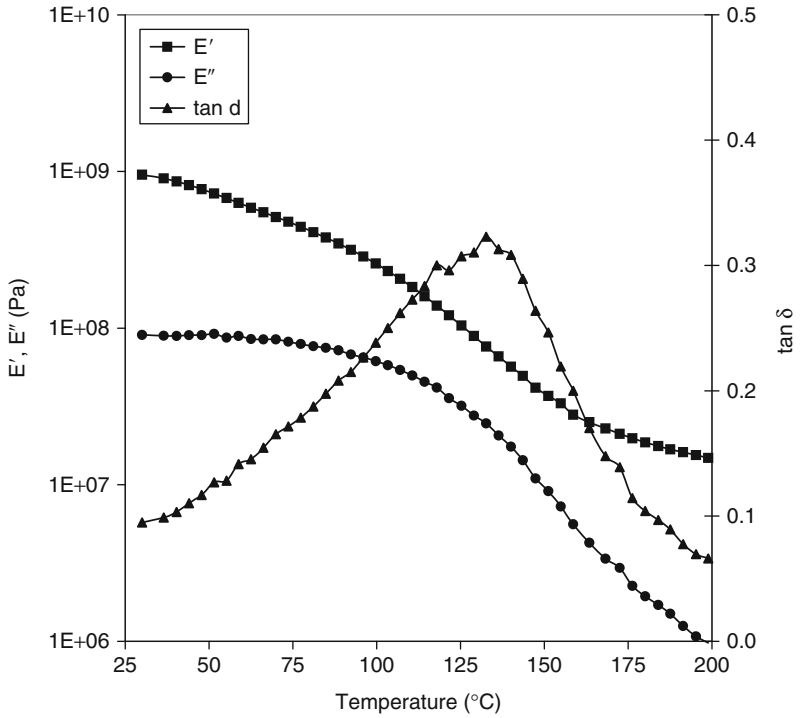

New Polymers, Renewables as Raw Materials. Figure 24
Dynamic mechanical behavior for SOMG/MA polymer

maleates. The T_g of this polymer, however, was not very different from that of the SOMG maleates (133°C). This was attributed to a lower yield in the maleinization of the BPA, as determined from ^{1}H NMR data [51]. Like the SOMG/NPG/MA polymer, the SOMG/BPA/MA displayed the characteristic gradual glass transition shown in Fig. 21.

HO/MA Dynamic Mechanical Polymer Properties

The dynamic mechanical properties of the HO/MA polymers were found to be better than those of the AESO polymers. Little variation was seen between the polymers made from the different oils. At room temperature, the E' for all of the oils existed between 1.45 and 1.55 GPa, showing no dependence on saturation level. The dynamic mechanical behavior was similar between the different oils, with the typical behavior being shown in Fig. 25. The temperatures at which a maximum in tan δ was exhibited ranged from 107°C to 116°C, which are all substantially higher than the AESO base resin. These properties are fairly close to those shown by conventional petroleum-based polymers. However, the distinctive triglyceride behavior still exists, in that the glass transitions are extremely broad and that, even at room temperature, the materials are not completely in a glassy state. Again this is probably due to the saturated fatty acids of the triglycerides that act as a plasticizer.

Although the extent of maleinization was approximately the same from oil to oil, it is possible to see how the slight differences affect the T_g. In Fig. 26, the tan δ peak temperature was plotted as a function of maleate functionality. Within this range, the behavior is linear, suggesting that if higher levels of functionalization are able to be reached, the properties should improve accordingly [64]. However, it is expected that past a certain extent of maleate functionality, the tan δ peak temperature dependence will plateau. Work is currently being pursued to test the limits of this behavior.

It was previously stated that the broadness in the glass transition may be inherent to all triglyceride-based polymers. However, work with genetically engineered oil and synthetic oil has shown that it is

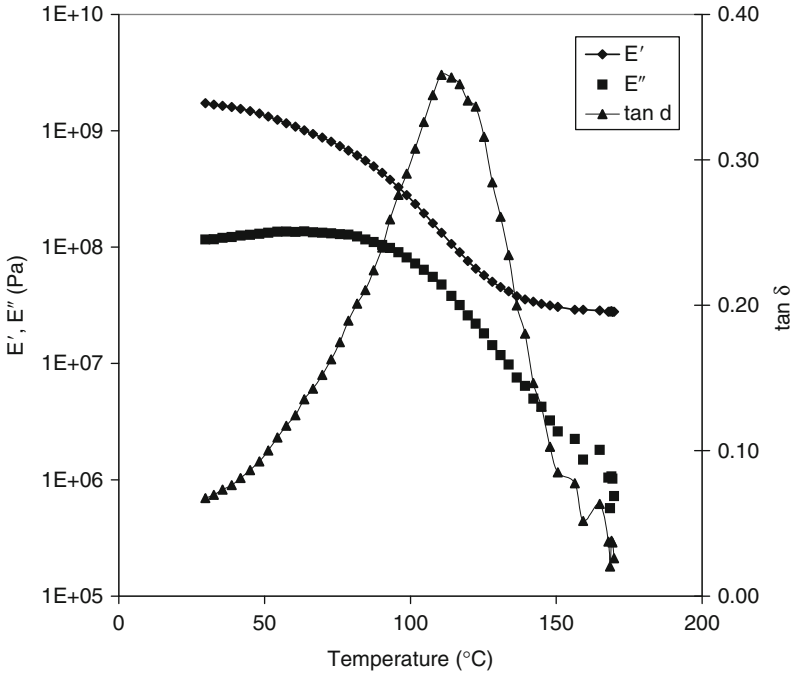

New Polymers, Renewables as Raw Materials. Figure 25
Representative dynamic mechanical behavior for HO/MA polymers

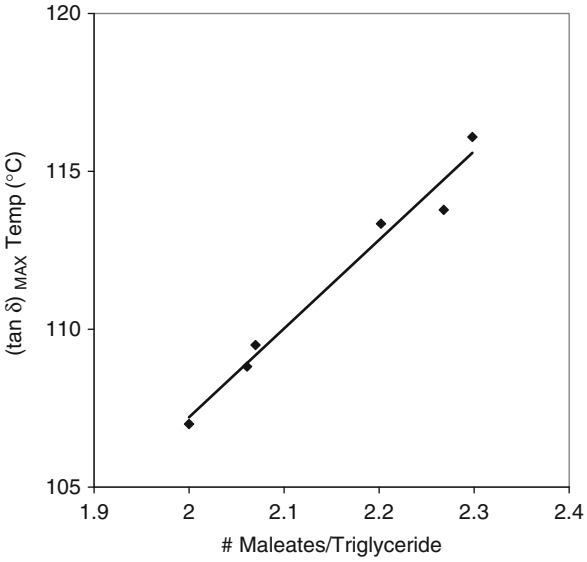

New Polymers, Renewables as Raw Materials. Figure 26
Peak in tan δ as a function of maleate functionality

possible to reduce this characteristic. The genetically engineered high oleic soybean oil has an average functionality of three double bonds/triglyceride and has the fatty acid distribution shown in Table 1. The maleinized form of this oil had a functionality of two maleates/triglyceride. The properties of polymers from this material were compared to polymers from triolein oil, which is monodisperse, consisting only of oleic fatty acid esters (18 carbons long and one double bond). The maleinized triolein oil had a functionality of 2.1 maleates/triglyceride. Thus, the only difference between the two oils is the fatty acid distribution of the high oleic oil versus the monodisperse triolein oil.

The dynamic mechanical properties of polymers made from these oils are shown in Fig. 27. The T_g of these two polymers does not seem to differ much, judging from either their tan δ peak or the inflection in the E'. However, the broadness of the transitions does differ. It is apparent that the triolein polymer has

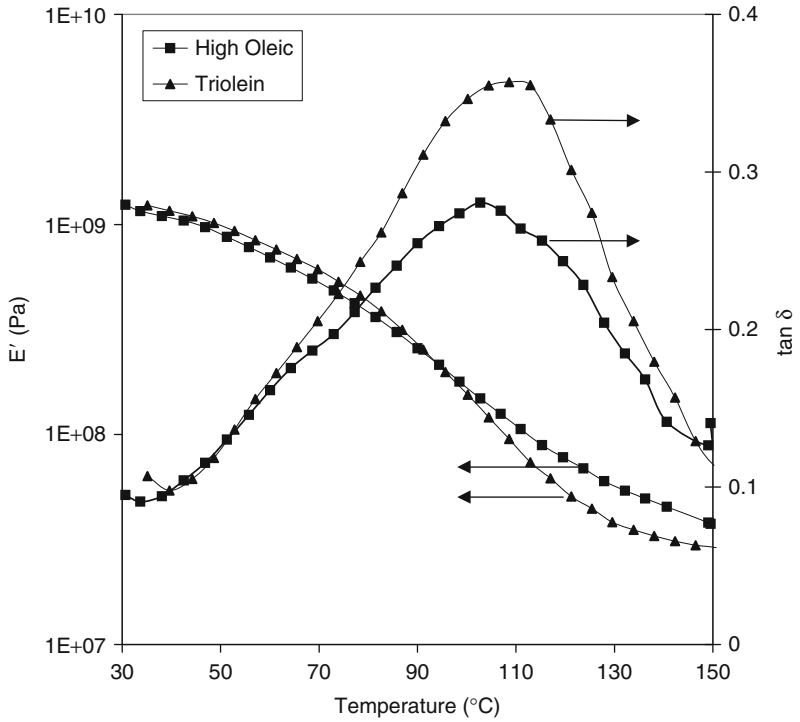

New Polymers, Renewables as Raw Materials. Figure 27
Dynamic mechanical properties of polymers made from maleinized hydroxylated high oleic oil and triolein oil. The monodisperse triolein displays a sharper transition from the glassy region to the rubbery region

a sharper E' transition from the glassy region to the rubbery region. This is evident also in the tan δ peak, which has a higher peak height. The transition is not yet as sharp as petroleum-based polymers. This is probably caused by the triolein monomer having a functionality of only two maleates/triglyceride. Consequently, there is still a plasticizer effect present, but this effect may be reduced by controlling the reaction conditions to reach higher conversions.

SOPERMA Polymer Properties

The typical DMA behavior of the SOPERMA-styrene polymer (40 wt% styrene) is shown in Fig. 28, where it can be seen that, at room temperature, these polymers are already in transition from the glassy region to the rubbery plateau. Most thermoset polymers show a distinct glassy region in which the modulus is independent of temperature. This is not observed for the SOPERMA-styrene polymers. The SOPERMA-styrene polymers show a very broad transition from the glassy to the rubbery state. Because of this broad transition, these polymers do not show a clear peak in the loss modulus E''. Thus, the tan δ curve is also very broad. The broad transition observed for the SOPERMA-styrene polymers is a result of two major effects. One major effect is the phase separation, which results in higher T_g SOPERMA-rich and lower T_g styrene-rich regions in the polymer matrix. Another effect that may result in a broad glass transition is the plasticizing effect of the fatty acids present in the SOPERMA monomer which are not functionalized. The transition from the glassy to the rubbery state broadens significantly with the addition of small amounts of plasticizers to polymers.

Figures 29a and b show the flexural modulus and flexural strength of the SOPERMA-styrene polymers as a function of styrene concentration. As can be seen both the flexural modulus and flexural strength of the polymers increase with increasing concentrations of styrene despite the decrease in cross-link density, ν. Thus, the rigid aromatic structure of the styrene monomer

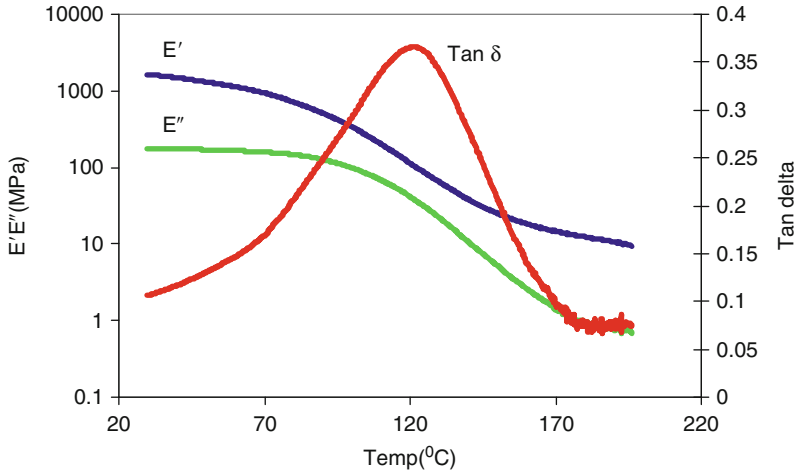

New Polymers, Renewables as Raw Materials. Figure 28
Typical DMA behavior of the SOPERMA-styrene polymer (40 wt% styrene)

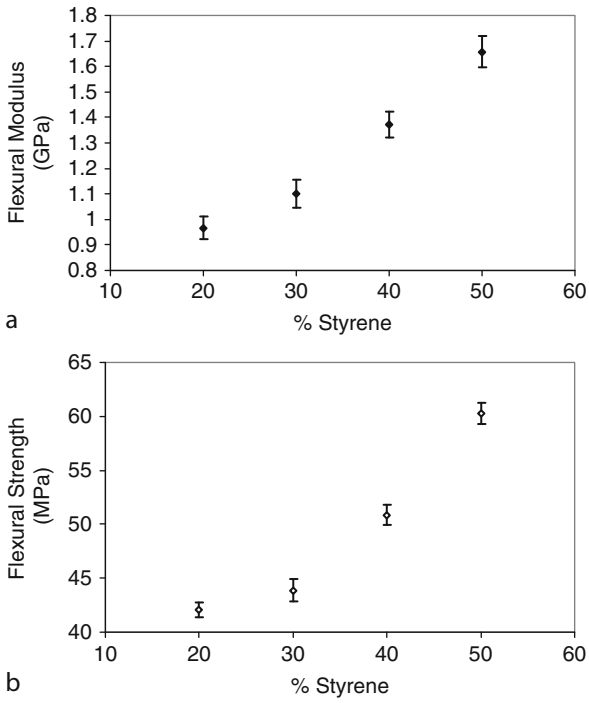

New Polymers, Renewables as Raw Materials. Figure 29
The change of (**a**) flexural modulus (**b**) flexural strength of SOPERMA-styrene polymers at increasing styrene weight percentages

as compared to the SOPERMA monomer with flexible fatty acid chains dominates the effect of cross-link density. The linear dependence of flexural modulus on styrene concentration above 30 wt% styrene follows Eq. 1:

$$E_f = 0.0278\left(W_{\text{styrene}}\right) + 0.2643, \tag{1}$$

where W_{styrene} presents the weight percentage of styrene. This correlation predicts the flexural modulus of 100% polystyrene as 3.04 GPa. The flexural modulus values of standard polystyrenes of different grades are in the range of 2.9–3.8 GPa. In the same manner, the dependence of flexural strength on styrene concentration follows Eq. 2:

$$S_f = 0.6159\left(W_{\text{styrene}}\right) + 27.696 \tag{2}$$

which predicts the flexural strength of the 100% polystyrene as 89.29 MPa. The strength values of standard polystyrene samples are in the range of 70–100 MPa.

The addition of butyrated kraft lignin to SOPERMA had a large effect on the polymer properties. The T_g′s (as determined from the tan δ maximum) of the SOPERMA-styrene polymers as a function of lignin concentration are shown in Fig. 30a. As can be seen, there is a slow increase in T_g at low concentrations and then at 5 wt% lignin the T_g increases significantly.

The T_g of the SOPERMA-lignin composite should be influenced by both the cross-link density of the system as well as the higher T_g of kraft lignin (167°C). The cross-link densities, as determined using the modulus in the rubbery region, are shown in Fig. 30b, where the cross-link density of the network increases with lignin until 5 wt% and then starts to decrease again. The increase in cross-link density with lignin addition may be attributed to specific interactions between the polymer matrix and the lignin molecule. The carboxylic acid groups of the SOPERMA monomer may interact with the available hydroxyl groups or thiol groups of the lignin molecule. Additionally, lignin may have effects on the kinetics of polymerization of both the SOPERMA and styrene monomer due to its inhibition effect on radical polymerization, which may affect the cross-link density. However, more work needs to be done to evaluate this effect. The cross-link density levels off at 5 wt% load and starts to decrease for higher concentrations. Thus, at this point the cross-link density must decrease due to the increase in the volume fraction of lignin, which cannot apparently interact with the matrix any more. The significant increase in T_g at 5 and 7.5 wt% lignin shows that the T_g of the system approaches the T_g of the kraft lignin (167°C) component at these high concentrations.

Figure 31 shows that both the flexural modulus and flexural strength of the SOPERMA-styrene polymers increase continuously with increasing lignin content of the resin. Because butyrated kraft lignin is dissolved in the polymer matrix, it should undergo the same strain as the polymer matrix. Thus, the modulus of the composite should increase with the introduction of the rigid aromatic structure of lignin to the system. Additionally, the cross-link density increase with lignin addition is also expected to increase the modulus. On the other hand, the increase in flexural strength with increasing lignin content may be attributed to both the

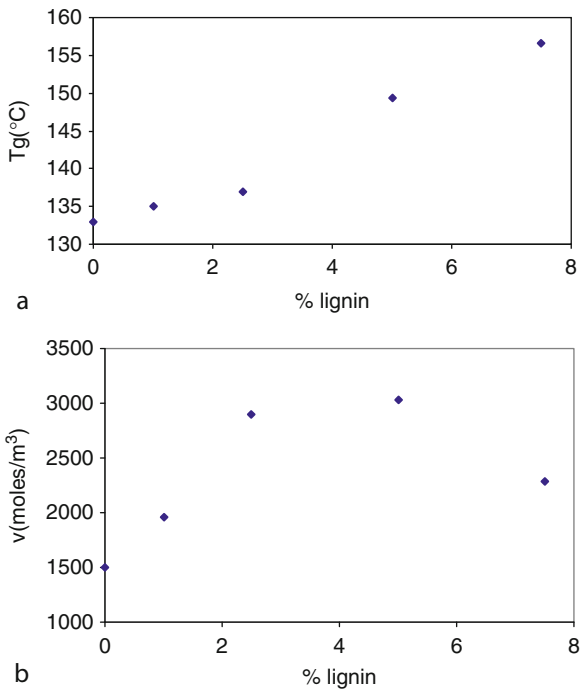

New Polymers, Renewables as Raw Materials. Figure 30 (**a**) Glass transition temperature, T_g, and (**b**) cross-link density (ν) variation of the SOPERMA-styrene polymers as a function of butyrated lignin content

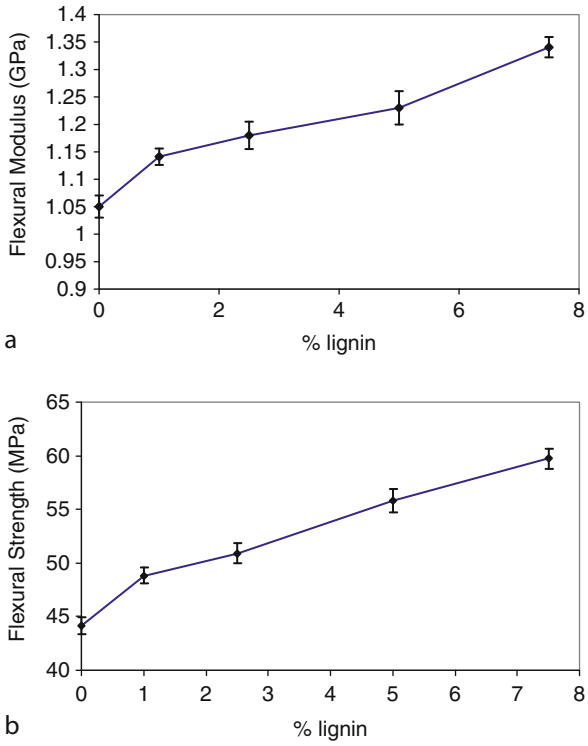

New Polymers, Renewables as Raw Materials. Figure 31 The change of (**a**) flexural modulus (**b**) flexural strength of SOPERMA-styrene polymers at increasing butyrated lignin content

increase in modulus with lignin addition and an increase in cross-link density up to 5 wt% lignin load.

SOGLYME Polymer Properties

As discussed in section "SOPERMA and COPERMA Polymer Synthesis," the soybean oil monoglyceride methacrylates (SOGLYME) were prepared by methacrylation of the soybean oil glycerolysis product by methacrylic anhydride, as shown earlier in Fig. 8. The methacrylated glycerides did not show phase separation in styrene. The crude methacrylated soybean oil monoglycerides contain methacrylic acid as a by-product. Methacrylic acid is itself a reactive diluent and acts as a comonomer in the system. Thus, the mechanical properties of the polymers prepared from this crude product (SOGLYME-MEA) as well as the polymers prepared using styrene as the third comonomer (SOGLYME-MEA-ST) will be examined. Properties of the polymers prepared from the acid extracted product with styrene (SOGLYCME-ST) will also be examined.

Figures 32a and b show the storage modulus (E'), loss modulus (E''), and tan δ values as a function of temperature for the polymers prepared from the crude methacrylated soybean oil monoglycerides that contain

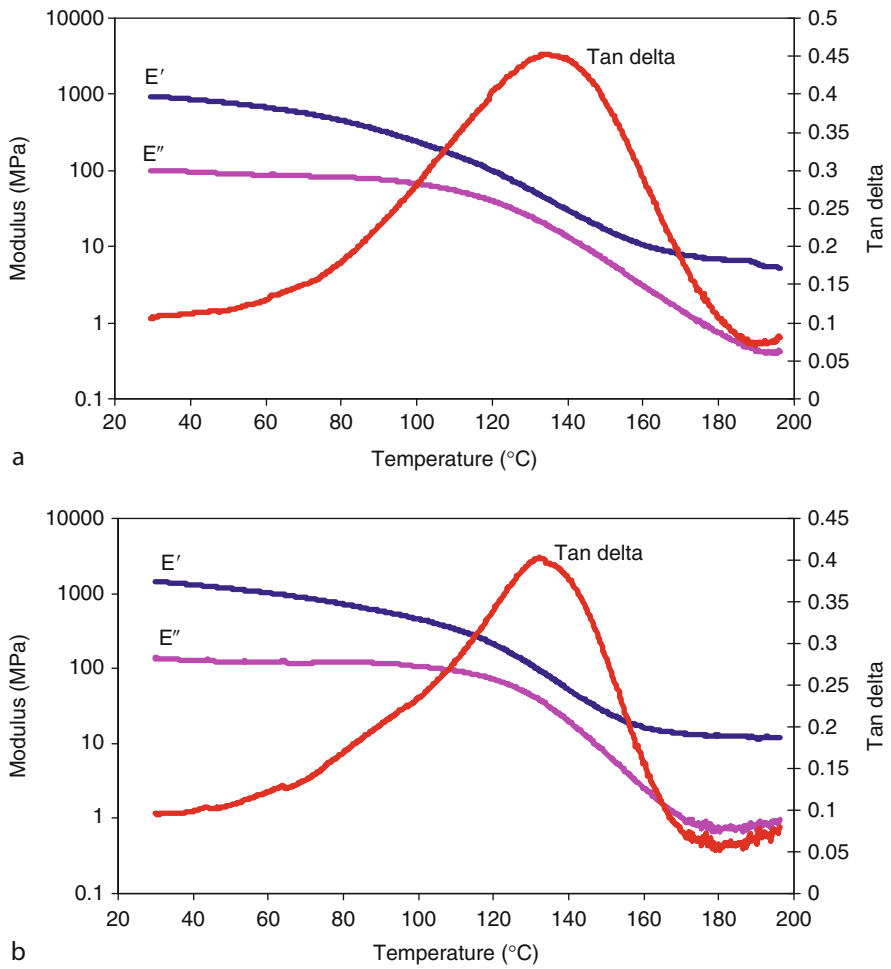

New Polymers, Renewables as Raw Materials. Figure 32
Storage modulus (E′), loss modulus (E″) and tan δ values as a function of temperature for (**a**) SOGLYME-MEA (**b**) SOGLYME-MEA-STpolymers

methacrylic acid as a by-product (SOGLYME-MEA) and the styrenated resin (SOGLYME-MEA-ST) (33 wt%) respectively. As can be seen, these polymers also show a broad transition from the glassy state to the rubbery state, similar to the SOPERMA-styrene polymers. The polymers prepared from these resins did not show phase separation, which means that the phase separation observed in the SOPERMA-styrene polymers is not the only factor responsible for the broad transition observed in these triglyceride-based polymers. The plasticization effect of the long flexible fatty acid chains present in the cross-linked monomer has a significant effect on the observed behavior. Additionally, as can be seen, the tan δ peak is broader for the SOGLYME-MEA polymer compared to the SOGLYME-MEA-ST polymer showing that the higher cross-link density of the former polymer also has a significant effect on broadening the glass transition.

The E' values, T_g values (tan δ maxima) as determined from DMA, flexural moduli, and flexural strengths of the SOGLYME-MEA, SOGLYME-MEA-ST (33 wt% styrene), and SOGLYME-ST (33 wt% styrene) polymers are listed in Table 9. As can be seen, the SOGLYME-MEA-ST polymer has the highest modulus and strength followed by the SOGLYME-MEA polymer. The T_gs of these two polymers do not show a significant difference. The SOGLYME-ST polymer, on the other hand, exhibits considerably lower modulus, strength, and T_g values compared to the other two polymers. The properties of the individual monomers in these polymer systems as well as the cross-link density are both detrimental to the mechanical properties.

New Polymers, Renewables as Raw Materials. Table 9
The 30°C E′ values, T_g values (tan δ maxima), flexural modulus and flexural strength of the SOGLYME-MEA, SOGLYME-MEA-ST (33 wt% styrene) and SOGLYME-ST (33 wt% styrene) polymers

Resin	E′(30°C) (GPa)	T_g (°C)	Flexural modulus (GPa)	Flexural strength (MPa)
SOGLYME-MEA	0.86	131.7	0.80	26.5
SOGLYME-MEA-ST	1.15	132.6	1.04	49.0
SOGLYME-ST	0.23	65.5	0.26	1.0

The cross-link densities as determined by using the modulus values in the rubbery region of these polymers are shown in Table 10.

The cross-link densities of the SOGLYME-MEA and SOGLYME-MEA-ST polymers are in the neighborhood of the SOPERMA-styrene polymer at 50 wt% styrene concentration. The mechanical properties observed for these two polymers, however, are much lower than those observed for the SOPERMA-styrene polymers. The SOPERMA-styrene polymer at 50 wt% styrene has a flexural modulus of 1.65 GPa and a flexural strength of 62 MPa. This fact clearly shows that the maleate comonomer compared to the methacrylates, and the styrene comonomer compared to the methacrylic acid, bring more rigidity and strength to the triglyceride-based polymers. The cross-link density of the SOGLYME-MEA-ST polymer is lower than that of the SOGLYME-MEA polymer, as expected due to the increase in comonomer content. The SOGLYME-MEA-ST polymer, despite its lower cross-link density, still shows superior properties compared to those of the SOGLYME-MEA polymer due to the presence of the rigid styrene molecules in the polymer matrix. The significantly lower modulus, strength, and T_g observed for the SOGLYME-ST polymer is unexpected, especially when considering the properties of the SOGLYME-MEA polymer, and can only be attributed to its lower cross-link density compared to the other polymers. It is shown that the fracture strength σ of all bio-based polymers depends on modulus and cross-link density ν, as $\sigma \sim [E\nu]^{1/2}$.

Castor Oil-Based Polymer Properties

The basic fatty acid constituent of castor oil is ricinoleic acid, which is a hydroxy monounsaturated fatty acid

New Polymers, Renewables as Raw Materials. Table 10
The cross-link densities (ν) of the SOGLYME polymers

Resin	ν (moles/m^3)
SOGLYME-MEA	701
SOGLYME-MEA-ST	609
SOGLYME-ST	520

(12-hydroxy *cis* 9-octodecenoic acid) (~87%). Castor oil was thus first alcoholized with pentaerythritol, glycerol, and an aromatic diol BPA propoxylate, and the alcoholysis products were then malinated with maleic anhydride, introducing maleate functionality to both the polyol hydroxyls and fatty acid hydroxyls. The resulting resins were labeled COPERMA, COGLYMA, and COBPAPRMA, respectively. The reaction schemes and the structures of the final malinated products for the COGLYMA, COPERMA, and COBPAPRMA products were shown earlier in Figs. 9–11, respectively. Additionally, castor oil was directly malinated and castor oil maleates (COMA) were also prepared. In this section, the properties of these castor oil-based polymers are introduced and analyzed with reference to the network structure. The effect of styrene concentration on mechanical properties of the COPERMA-styrene polymers is also explored and compared to the observed trend for the SOPERMA-styrene polymers.

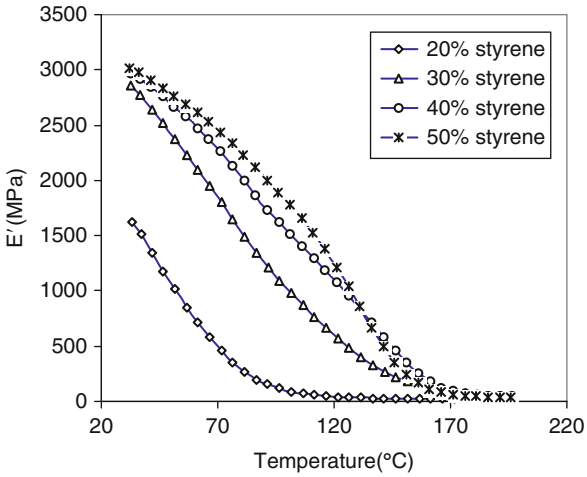

New Polymers, Renewables as Raw Materials. Figure 33 The change of storage modulus (E′) values with temperature for the COPERMA polymers at increasing styrene concentrations

Effect of Styrene Concentration on the COPERMA-Styrene Polymer Properties

Figure 33 shows the storage modulus values, E', of the COPERMA-styrene polymers as a function of temperature at increasing styrene concentrations as determined from DMA. As can be seen, the room temperature modulus values increase significantly, going from 20 wt% styrene to 30 wt% styrene. The increase in styrene concentration has a much less pronounced effect on the modulus at higher concentrations.

The changes in flexural modulus and flexural strength of the COPERMA-styrene polymers at increasing styrene concentrations are shown in Fig. 34a and b, respectively. The increase in flexural modulus and strength with increasing styrene concentrations follows a trend similar to that observed for the storage modulus. A significant increase in both the modulus and strength is observed while going from 20 to 30 wt% styrene, but this increase levels off rapidly at higher concentrations. As discussed in section "Properties of Plant Oil Resins," the SOPERMA-styrene polymers showed a continuous increase in both the modulus and strength, with styrene content in similar concentrations.

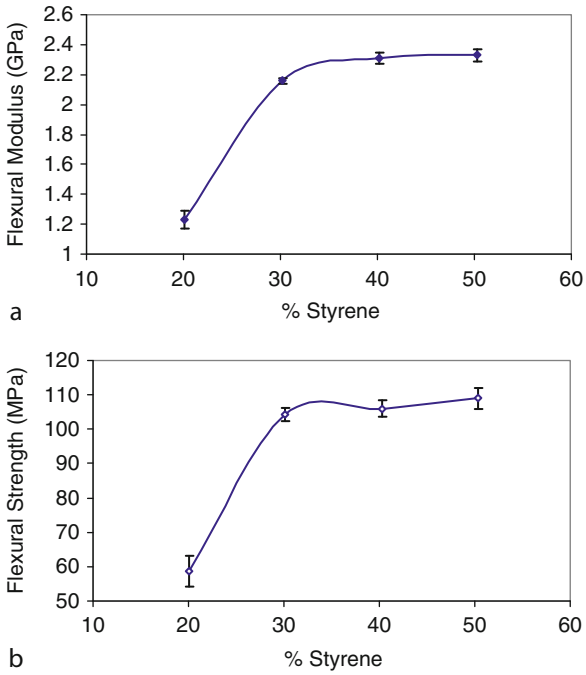

New Polymers, Renewables as Raw Materials. Figure 34 The change in (**a**) flexural modulus and (**b**) flexural strength of the COPERMA polymers with increasing concentrations of styrene

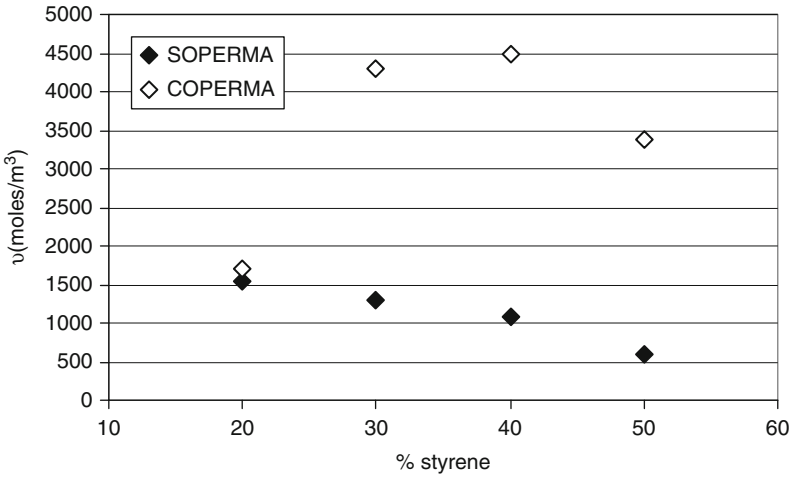

New Polymers, Renewables as Raw Materials. Figure 35
The cross-link densities of the SOPERMA and COPERMA polymers at increasing styrene concentrations

To explain the difference in the effect of styrene concentration on the mechanical properties of these two polymers, it is useful to determine the cross-link densities of the COPERMA-styrene polymers. Figure 35 shows the cross-link densities (ν) of the COPERMA-styrene polymers at increasing styrene concentrations as determined from the rubbery modulus by DMA. The cross-link densities (ν) of the SOPERMA-styrene polymers at the same styrene concentrations are also shown in the same figure, for comparison. For the COPERMA resin, which has a much higher maleate content per triglyceride than the SOPERMA resin, at 20 wt% styrene, the styrene concentration is too low to incorporate all of the maleates into polymerization, since the maleate half-esters do not homopolymerize. The molar ratio of styrene double bonds to maleate double bonds for the 20 wt% styrene COPERMA resin is approximately 0.8, as determined from ^{1}H-NMR analysis. Thus, the 20 wt% styrene COPERMA polymer has the lowest cross-link density. At 30 and 40 wt% styrene, the molar ratio of styrene double bonds to maleate double bonds is 1.3 and 1.8, respectively, thus a significant increase in cross-link density is observed at 30 wt%, and at 40 wt% the cross-link density reaches its optimum value where all the available reactive groups of the COPERMA monomer can react with styrene. At higher concentrations, the cross-link density starts to decrease again since the added styrene increases the length of the segments between the cross-links. Thus, the modulus and strength of the COPERMA polymers at 20 wt% styrene are especially low and show a big increase at 30 and 40 wt% styrene due to the significant increase in cross-link density. After this point, the styrene content does not seem to have a significant effect on the modulus and strength. This behavior is different from that of the SOPERMA polymers, which showed a continuous increase in modulus and strength in the same styrene concentrations, despite the decrease in cross-link density. The introduction of the rigid aromatic rings of the styrene comonomer into the SOPERMA monomer with long flexible fatty acid chains results in a higher net increase in both the modulus and strength of the network than that observed for the COPERMA polymers because the fatty acids present in the COPERMA monomer are malinated and therefore incorporated into the network.

The tan δ curves for the COPERMA-styrene polymers at increasing styrene concentrations, shown in Fig. 36, also reflect the trend observed in cross-link density. As can be seen, the 20 wt% styrene polymer with the lowest cross-link density shows the tan δ maximum at the lowest temperature and therefore has the lowest T_g. The tan δ maximum shifts to higher temperatures with increases up to 40 wt% styrene due to the increase in cross-link density. After this point the increase in styrene concentration decreases the cross-link density and the T_g starts to decrease again.

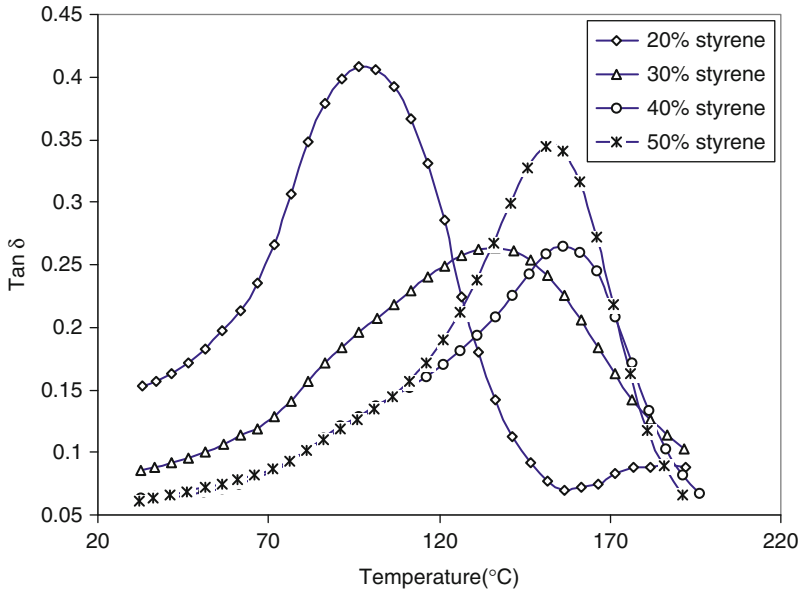

New Polymers, Renewables as Raw Materials. Figure 36
The change of tan δ values with temperature for the COPERMA polymers at increasing styrene concentrations

Thus the highest T_g is observed with 40 wt% styrene at 156°C, for the COPERMA-styrene polymers.

Comparison of COPERMA- and SOPERMA-Styrene Polymer Mechanical Properties

As can be seen in Fig. 35, the COPERMA-styrene polymers show significantly higher cross-link densities than those of the SOPERMA-styrene polymers, especially at 30 wt% and higher weight percentages of styrene. Table 11 shows the properties of the 30 wt% styrene SOPERMA and COPERMA polymers for a direct comparison. It can be seen that the modulus value nearly doubles and the flexural strength shows even a larger increase with the change from soybean oil to castor oil in the formulation. The glass transition temperature of the COPERMA polymer is about 9°C higher than that of the SOPERMA polymer. The incorporation of the fatty acid chains into the polymerization both increases the cross-link density and reduces the plasticization effect of the fatty acid chains in the COPERMA polymer, which in turn leads to a considerable increase in modulus, strength, and T_g compared to those properties of the SOPERMA polymer.

For the COPERMA resin, which has the highest maleate content among all the castor oil-based resins, the styrene concentration should be more than 30 wt% to fully incorporate all of the maleates during polymerization. This level should be lower for the other resins, which show lower maleate contents than the COPERMA resin. Thus 33 wt% styrene concentration is used for the preparation of other castor oil-based polymers, which keeps the renewable content of the resin within a reasonable range and also gives a chance to compare the properties of these materials

New Polymers, Renewables as Raw Materials. Table 11
The mechanical properties of COPERMA and SOPERMA polymers at 30 wt% styrene

Property	COPERMA (30% styrene)	SOPERMA (30% styrene)
Flexural strength (MPa)	101.23	43.86
Flexural modulus (GPa)	1.95	1.10
T_g (°C)	144	135
Storage modulus (GPa)	2.88	1.24

to the commercially available unsaturated polyesters that use similar formulations.

The ratio of the flexural strength of COPERMA/SOPERMA is $\sigma_1/\sigma_2 = 101.2/43.9 = 2.1$. If the square root law for strength is applied, where

$$\frac{\sigma_1}{\sigma_2} = \left[\frac{E_1 v_1}{E_2 v_2}\right]^{1/2},$$

then, theory can be readily compared with experiment. Using $E_1 = 1.95$ GPa and $E_2 = 1.1$ GPa (Table 11), $v_1 = 4{,}300$ mol/m^3 and $v_2 = 1{,}300$ mol/m^3 (Fig. 35 at 30% styrene), then the predicted ratio for strength is $\sigma_1/\sigma_2 = 2.4$, which is in excellent accord with the experimental ratio.

Thermomechanical Properties of Castor Oil-Based Polymers

All of the malinated castor oil-styrene-based polymers exhibited broad transition profiles from the glassy state to the rubbery state, similar to the SOPERMA-styrene polymers. The broad transitions observed were attributed to the phase separation observed on the microscale and the high cross-link density exhibited by these polymers. The plasticization effect of the fatty acids should have a less pronounced effect for the castor oil-based polymers because the hydroxy fatty acids that constitute the majority of the fatty acids (87%) in castor oil were malinated and therefore connected to the network structure. Figure 37 shows the tan δ curves of the castor oil-based polymers as determined by DMA.

As discussed above, the damping peak position is sensitive indicator of cross-linking. As the cross-link density increases, the tan δ maximum shifts to higher temperatures, the peak broadens and a decrease in the tan δ value is observed. The cross-link densities of the malinated castor oil-based polymers (33 wt% styrene) determined by using the value of E in the rubbery region of the polymers as determined by DMA are shown in Table 12. As can be seen, the COPERMA polymer has the highest cross-link density, followed by COGLYMA, COMA, and COBPAPRMA polymers. The COBPAPRMA polymer shows the lowest cross-link density, despite the higher maleate content than both COMA and COGLYMA which can be attributed to the bulkiness of the Bisphenol A propoxylate moiety. As can be seen in Fig. 37, the COPERMA polymer with the highest cross-link density exhibits the highest T_g and shows the broadest peak, with the lowest tan δ value. The COBPAPRMA, which has the lowest cross-link density, shows the highest tan δ values as expected; however, its tan δ max temperature is about 14° C above than that of the COMA polymer. The higher T_g observed for the COBPAPRMA may be explained by the presence of the rigid aromatic backbone of BPA propoxylate, as compared to the aliphatic fatty acid backbone of the COMA polymer. Thus, the monomer chemical structural influence dominates the cross-link density effect on T_g.

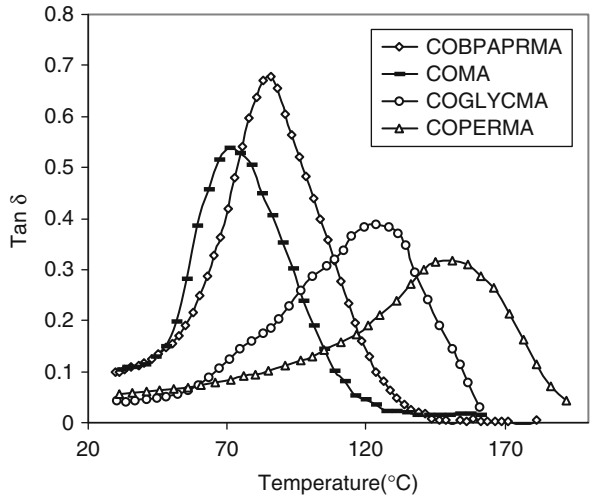

New Polymers, Renewables as Raw Materials. Figure 37 The tan δ values of the castor oil polymers as a function of temperature

New Polymers, Renewables as Raw Materials. Table 12 Crosslink densities of castor oil polymers

Resin type	Mc(g/mole)	v(moles/m^3)
COPERMA	255	4,310
COGLYMA	441	2,494
COMA	732	1,511
COBPAPRMA	783	1,418

Mechanical Properties of Castor Oil-Based Polymers

The storage modulus values at 30°C and the T_g's as determined from DMA, as well as the flexural modulus, flexural strength, and the surface hardness values of the castor oil polymers are given in Table 13. The styrene content of each resin was 33 wt%. The mechanical property hardness is the ability of the material to resist indentation, scratching, abrasion, cutting, and penetration. This property may be important for structural materials that require a high resistance to indentation or abrasion. The hardness of a polymer reflects such other qualities as resilience, durability, uniformity, strength, and abrasion resistance. As can be seen in Table 13, the surface hardness of the castor oil-based polymers changes proportionately with the strength of the polymers.

The observed mechanical properties of the castor oil-based polymers can be explained both in terms of the cross-link density and the chemical structures of the polyols used. The COPERMA polymer, which has the highest cross-link density, shows superior properties to the other castor oil-based polymers. The COPERMA polymer with its T_g around 150°C and flexural modulus of 2.2 GPa and flexural strength of 105 MPa exhibits the highest T_g and strength obtained from any triglyceride-based thermoset resins. The COBPAPRMA polymer's modulus, strength and surface hardness values are higher than those of both COMA and COGLYMA polymers and approach those of COPERMA polymer, although its cross-link density is slightly lower than these two polymers. The aromatic structure of the BPA propoxylate moiety brings both rigidity and strength to the polymer network. Thus, this resin shows both high modulus and strength with a reasonable T_g, despite its lower maleate content, which is beneficial for the formulation since it decreases the nonrenewable content of the polymer. The COMA polymer shows the lowest modulus, strength, surface hardness, and T_g values due to its low cross-link density and also shows that a multifunctional unit at the center of the triglyceride monomer structure is essential for improved properties for these polymers.

Figure 38 gives a comparison between the mechanical properties of these bio-based resins and the properties of two of the most commonly used UP resins: Orthophthalic (Ortho-UP) and Isophthalic (Iso-UP) UP resins. As can be seen, the properties of castor oil-based polymers are in a comparable range with those of the commercially successful UP resins. The properties of these bio-based resins can be significantly improved by the addition of lignin, which introduces the required aromatic groups for high stiffness and high T_g polymers and further increases their bio-based content with low-cost renewable material.

Future Directions

Triglyceride oils are an abundant natural resource that has yet to be fully exploited as a source for polymers and composites. The different chemical functionalities allow the triglyceride to be converted to several promising monomers. These are being commercialized for applications in composite resins, foams, pressure sensitive adhesives, elastomers, coatings with significantly reduced toxicity, and carbon footprint compared to their petroleum-based counterparts. When blended

New Polymers, Renewables as Raw Materials. Table 13 The mechanical properties of castor oil polymers

Resin type	E′ (30°C) (GPa)	T_g (°C)	Flexural modulus (GPa)	Flexural strength (MPa)	Surface hardness (D)
COPERMA (1:2:10.7)	2.94	150	2.21	101.60	89.3
COGLYMA (1:2.2:9.2)	2.40	124	1.76	78.89	86.1
COBPAPRMA (1:2:6.7)	2.69	86	2.17	83.20	88.5
COMA (1:3)	1.15	72	0.78	32.83	77.1
Ortho-UP	–	135–204	3.45	80	–
Iso-UP	–	135–204	3.59	100	–

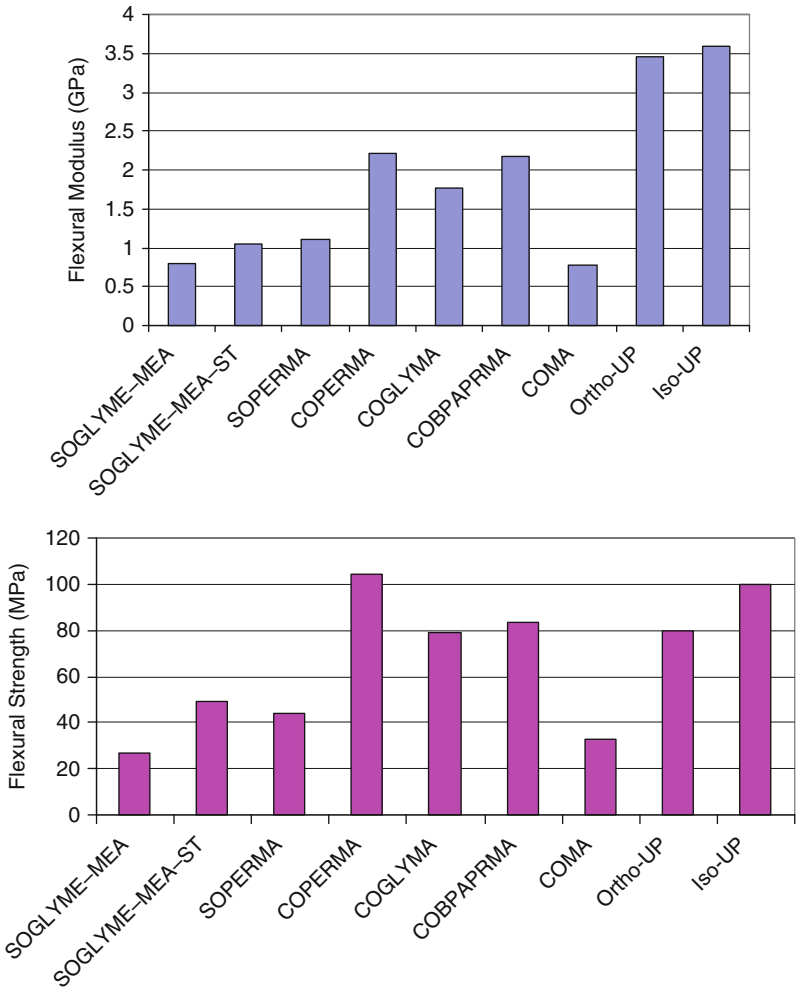

New Polymers, Renewables as Raw Materials. Figure 38
A property comparison of soyoil and castor oil based polymers with commercial petroleum based Ortho and Iso-Unsturated Polyester resins

with comonomers, these monomers form polymers with a wide range of physical properties. They exhibit flexural strength up to 100 MPa and tensile moduli in the 1–3 GPa range, with T_g ranging from 70°C to 150°C, depending on the particular monomer and the resin composition. DMA shows that the transition from glassy to rubbery behavior is extremely broad for these polymers as a result of the triglyceride molecules acting both as cross-linkers and as plasticizers in the system. Saturated fatty acid chains are unable to attach to the polymer network, causing relaxations to occur in the network. However, this transition can be sharpened by reducing the saturation content, as demonstrated with the genetically engineered oil and pure triolein oil. The new design rules for controlling the molecular architecture based on the Twinkling Fractal Theory of the Glass Transition [67–69] will allow the facile development of these materials in future years. When combined with natural fibers (chicken feathers, hemp, flax, straw, etc.), useful high volume applications are made possible in hurricane resistant housing, positive net energy housing, earthquake resistant structures, eco-leather, and wind turbines in support of renewable energy.

This area of research sets a foundation from which completely new materials can be produced with novel

properties. Work continues on optimizing the properties of these green materials and understanding the fundamental issues that affect them. Computer simulation can be used to optimize the choice of the fatty acid distribution function and determine the resulting architecture and mechanical properties for the particular chemical pathways shown in Fig. 2. Use of a computer significantly reduces the number of chemical trials required for a system with a large number of degrees of freedom and suggests the optimal oil most suited to a particular type of resin. In this manner, more renewable resources can be used to meet the material demands of many industries.

Bibliography

1. Wool RP, Kusefoglu S, Zhao R, Palmese G, Khot S (2000) High Modulus Polymers and Composites from Plant Oils. U.S. Patent 6,121,398
2. Wool RP (1999) Chemtech 29:41
3. Liu K (1997) Soybeans: chemistry, technology, and utilization. Chapman and Hall, New York
4. Gunstone F (1996) Fatty acid and lipid chemistry. Blackie Academic and Professional, New York
5. Cunningham A, Yapp A (1971) U.S. Patent 3,827,993
6. Bussell GW (1971) U.S. Patent 3,855,163
7. Hodakowski LE, Osborn CL, Harris EB (1975) U.S. Patent 4,119,640
8. Trecker DJ, Borden GW, Smith OW (1976) U.S. Patent 3,979,270
9. Trecker DJ, Borden GW, Smith OW (1976) U.S. Patent 3,931,075
10. Salunkhe DK, Chavan JK, Adsule RN, Kadam SS (1992) World oilseeds: chemistry, technology, and utilization. Van Nostrand Reinhold, New York
11. Force CG, Starr FS (1988) U.S. Patent 4,740,367
12. Barrett LW, Sperling LH, Murphy CJ (1993) J Am Oil Chem Soc 70:523
13. Qureshi S, Manson JA, Sperling LH, Murphy CJ (1983) In: Carraher CE, Sperling LH (eds) Polymer applications of renewable-resource materials. Plenum Press, New York
14. Devia N, Manson JA, Sperling LH, Conde A (1979) Polym Eng Sci 19:878
15. Devia N, Manson JA, Sperling LH, Conde A (1979) Polym Eng Sci 19:869
16. Devia N, Manson JA, Sperling LH, Conde A (1979) Macromolecules 12:360
17. Sperling LH, Carraher CE, Qureshi SP et al (1991) In: Gebelein CG (ed) Polymers from biotechnology. Plenum Press, New York
18. Sperling LH, Manson JA, Linne MA (1984) J Polym Mater 1:51
19. Sperling LH, Manson JA (1983) J Am Oil Chem Soc 60:1887
20. Fernandez AM, Murphy CJ, DeCosta MT et al (1983) In: Carraher CE, Sperling LH (eds) Polymer applications of renewable-resource materials. Plenum Press, New York
21. Sperling LH, Manson JA, Qureshi SA, Fernandez AM (1981) Ind Eng Chem 20:163
22. Yenwo GM, Manson JA, Pulido J et al (1977) J Appl Polym Sci 21:1531
23. Frischinger I, Dirlikov S (1991) Polymer Comm 32:536
24. Frischinger I, Dirlikov S (1994) In: Sperling LH, Kempner D, Utracki L (eds) Interpenetrating polymer networks. Advances in chemistry series 239. American Chemical Society, Washington, DC, p 517
25. Rosch J, Mulhaupt R (1993) Polymer Bull 31:679
26. Meffert A, Kluth H (1989) Denmark Patent 4,886,893
27. Rangarajan B, Havey A, Grulke EA, Culnan PD (1995) J Am Oil Chem Soc 72:1161
28. Zaher FA, El-Malla MH, El-Hefnawy MM (1989) J Am Oil Chem Soc 66:698
29. Friedman A, Polovsky SB, Pavlichko JP, Moral LS (1996) U.S. Patent 5,576,027
30. Swern D, Billen GN, Findley TW, Scanlan JT (1945) J Am Oil Chem Soc 67:786
31. Sonntag NOV (1982) J Am Oil Chem Soc 59:795
32. Solomon DH (1967) The chemistry of organic film formers. Wiley, New York
33. Can E (1999) M.S. Thesis, Bogazici University, Turkey
34. Bailey AE (1985) In: Swern D (ed) Bailey's industrial oil and fat products. Wiley, New York
35. Hellsten M, Harwigsson I, Brink C (1999) U.S. Patent 5,911,236
36. Cain FW, Kuin AJ, Cynthia PA, Quinlan PT (1995) U.S. Patent 5,912,042
37. Eckwert K, Jeromin L, Meffert A, et al (1987) U.S. Patent 4,647,678
38. Khot SN (1998) M.S. Thesis, University of Delaware
39. Wypych J (1986) Polyvinyl chloride stabilization. Elsevier, Amsterdam
40. Sears JK, Darby JR (1982) The technology of plasticizers. Wiley, New York
41. Carlson KD, Chang SP (1985) J Am Oil Chem Soc 62:931
42. Raghavachar R, Letasi RJ, Kola PV et al (1999) J Am Oil Chem Soc 76:511
43. Pashley RM, Senden TJ, Morris RA, et al (1991) U.S. Patent 5,360,880
44. Likavec WR, Bradley CR (1999) U.S. Patent 5,866,628
45. Bordon GW, Smith OW, Trecker DJ (1971) U.S. Patent 4,025,477
46. La Scala JJ, Wool RP (2002) J Am Oil Chem Soc 79:59
47. Bunker SP (2000) M.S. Thesis, University of Delaware
48. Chu TJ, Niou DYJ (1989) Chin Inst Chem Eng 20:1
49. Betts AT (1975) U.S. Patent 3,867,354
50. Mitch EL, Kaplan SL (1975) In: Proceedings of 33 rd annual SPE technical conference, Atlanta
51. Can E, Kusefoglu S, Wool RP (2001) Rigid thermosetting liquid molding resins from renewable resources: I. Copolymers of soyoil monoglycerides with maleic anhydride. J Appl Polym Sci 81:69
52. Gardner HC, Cotter RJ (1981) European Patent 20,945
53. Thomas P, Mayer J (1971) U.S. Patent 3,784,586
54. Lee SH, Park TW, Lee SO (1999) Polymer (Korea) 23:493
55. ShioneH, Yamada J (1999) Japanese Patent 11,147,222

56. Hasegawa H (1999) Japanese Patent 11,240,014
57. Johnson LK, Sade WT (1993) J Coat Tech 65:19
58. Solomons TWG (1992) Organic chemistry. Wiley, New York
59. La Scala J, Wool RP Polymer. in preparation
60. Flory PJ (1975) Principles of polymer chemistry. Cornell University, Ithaca
61. Nielsen LE, Landel RF (1991) Mechanical properties of polymers and composites. Marcel Dekker, New York
62. Wool RP, Khot SN (2000) In: Proceedings of ACUN-2, Sydney
63. Can E, Kusefoglu S, Wool RP (2001) Rigid thermosetting liquid molding resins from renewable resources: (I) copolymers of soyoil monoglycerides with maleic anhydride. J Appl Polym Sci 81:69
64. Khot SN, La Scala JJ, Can E et al (2001) J Appl Polym Sci 82:703
65. Can E, Kusefoglu S, Wool RP (2002) Rigid thermosetting liquid molding resins from renewable resources. II. Copolymers of soybean oil monoglyceride maleates with neopentyl glycol and bisphenol A maleates. J Appl Polym Sci 83(5):972–980
66. Can E (2004) PhD Thesis, University of Delaware
67. Wool RP (2008) J Polym Sci Part B: Polym Phys 46:2765
68. Wool RP, Campanella A (2009) J Polym Sci Part B: Polym Phys 47:2578
69. Stanzione JF III, Strawhecker KE, Wool RP, doi:10.1016/j.jnoncrysol.2010.06.041

Nickel-Based Battery Systems

Ralph J. Brodd
Broddarp of Nevada, Henderson, NV, USA

Article Outline

Glossary
Definition of the Subject
Introduction
Characteristics of the Nickel Active Materials
Nickel-Iron Batteries (Ni-Fe)
Nickel Cadmium Batteries
Nickel Metal Hydride
Nickel-Zinc Batteries
Nickel-Hydrogen Batteries
Bibliography

Glossary

β-β Transformation The reaction of β-$Ni(OH)_2$ on charge to form β-NiOOH.

α-γ Transformation The reaction of α-$Ni(OH)_2$ on charge to form γ-NiOOH.

Ah Ampere hour 3,600 coulombs, the quantity of current flow in 1 ampere in 1 h.

Charge reserve Additional capacity of the negative or positive electrode to prevent gas evolution when the cell is overcharged or overdischarged.

Electrolyte Electrical conducting liquid flow where charge is carried by positive and negative ions.

Flame-arresting vent A cell vent designed to stop burning discharge from a vent.

Ni-MH Nickel metal hydride cell containing a nickel hydroxide positive and a hydrogen-absorbing metal alloy negative electrode.

Plate Electrode construction containing the active material and a current collector.

Pocket plate electrodes Perforated nickel-plated steel pockets that contain the active materials in a cell with free access of electrolyte.

Self-discharge Loss of capacity due to the chemical instability or a reaction of an active material in an electrode with the electrolyte.

Tubular plate electrodes Perforated nickel-plated steel tubes used to contain the active material in a cell.

Misch metal Containing a mixture of hydrogen-absorbing transition metals, Mm.

Nickel cadmium fiber plate Batteries construction of the positive nickel battery plate that contains nickel metal fibers throughout the plate for more efficient current collection.

Sinter plate cells Sealed battery cells using a nickel current collector structure usually produced by heating to a temperature where powdered nickel metal particles bond together to form a porous structure sinter current collector.

Trickle charging The low-level current flow to maintain full charge in a battery.

Terminal The external connection to the positive and negative electrodes containing the active material inside the battery case.

WH Watt hour, energy content of a battery expressed as the product of ampere-hours times cell voltage.

Zircar Trademark of nonwoven ceramic separator used in some Ni-MH cells.

Definition of the Subject

Nickel batteries are rechargeable batteries that are used in a variety of applications including portable electronic

devices, electric and hybrid vehicles, aeronautics and aerospace and stationary energy storage among others. They operate over a wide temperature range, have a flat discharge curve and are available in sizes ranging from small coin cells to motive power batteries. Nickel batteries are physically and electrically rugged and abuse tolerant including over charge and overdischarge.

Introduction

The nickel electrode serves as cathode for several important commercial rechargeable battery systems. The characteristics of these systems are listed in Table 1. The first commercial nickel battery was the nickel-iron system which provided lighting in railroad cars due to its strong resistance to physical and electrical abuse. The electrode structure has a strong influence on the operating life of a battery system. The nickel systems are robust, both physically and chemically.

Nickel battery systems compete directly with the lead acid battery in many commercial energy storage applications and with Li-Ion in portable electronic applications.

Advantages	Disadvantages
Long cycle life	Heavier than Li-Ion
High reliability	Higher cost than lead acid
Excellent rate capability	
Very robust cell constructions	

Characteristics of the Nickel Active Materials

The family of nickel batteries is based on the utility, strength, and reversibility of the nickel electrode reactions in alkaline media. The nickel active materials for use in batteries are produced, mainly, by chemical precipitation of $Ni(OH)_2$ with the addition of KOH to aqueous nickel sulfate solutions made by dissolving nickel metal in sulfuric acid. The nickel active material is usually produced by a precipitation process wherein a nickel sulfate solution is heated and pumped into hot NaOH. The process produces β-$Ni(OH)_2$. Fine graphite may be added, depending on the application. A small percentage of cobalt, ranging from 3% to 7%, depending on application, is co-precipitated with the nickel sulfate solution to improve charge acceptance, capacity, and operating life. The precipitate is filtered, dried, and ground. Care must be exercised to keep the drying temperature below 200°C as higher temperatures cause formation of electrochemically inactive bunsenite structure. Electrodes for cells used in satellites and other space applications are made by an in situ electrochemical precipitation technique described later.

Nickel Electrode Reaction Characteristics

The battery electrolyte is aqueous KOH solution in a concentration range of 25–30% KOH by weight. The mechanism that best describes the overall nickel electrode reactions in alkaline electrolyte is given in Eqs. 1 and 2 below.

Nickel-Based Battery Systems. Table 1 Characteristics of Nickel batteries (Nominal values)

System	Cell voltage	Wh/kg	Wh/l	Cycle life, 100% DOD	Calendar life, years	Commercial introduction
Ni-Fe	1.37	30	55	2,000–4,000	25	1,898
Ni-Cd, Vented pocket plate	1.29	20	40	500–2,000	25	1,900
Ni-Cd, Vented sintered plate	1.29	30	58	500–2,000	10	1,940
Ni-Cd, Sealed sinter plate	1.29	35	100	300–700	5	1,950
Ni-Cd, Fiber	1.29	10	15	500–10,000	20	1,950
Ni-MH, Sealed sinter plate	1.2	110	430	300–1,000	5	1,980
Ni-H_2	1.4	60	65	1,500–10,000	25+	1,980
Ni-Zn	1.71	60	120	200–500	3–5	1,931, 2,009

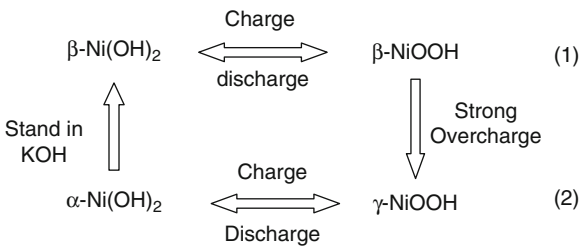

Equation 1 describes the classic β-β transformation reaction of the nickel electrode in alkaline media wherein the valence of the nickel shuttles between divalent Ni^{+2} and trivalent Ni^{+3}. The charged and discharged materials have similar structures and long cycle life. The battery reactions follow this regimen with little or no overcharge. On continued charging after reaching the Ni^{+3} valence state, the high oxygen overvoltage on the electrode surface permits formation of a Ni^{+4} valent nickel in the electrode structure. This transformation stops with oxygen evolution on the electrode surface and a nickel valence of 3.67, resulting in a higher capacity cell. On discharge the γ-NiOOH returns to α-$Ni(OH)_2$. Charge-discharge will continue on this higher capacity regime. However, if the cell is left on open circuit, the $Ni(OH)_2$ slowly transforms back to β-$Ni(OH)_2$. Transition back to the β-β cycle occurs only on open circuit stand as the α structure transforms slowly back to the β structure. The normal materials in electrode construction are produced by chemical or electrochemical precipitation, depending on the application for the cell. The uncharged β-Ni $(OH)_2$ is usually used in electrode fabrication and cells are initially assembled in the discharged state.

The four nickel materials in Eqs. 1 and 2 are distinct phases and have been characterized both-electrochemically and by the XRD patterns exhibited in the chemically precipitated phases. A point defect, nonstoichiometric, structural model correctly describes the structure and interactions of nickel electrode active materials (22). In this model, the intercalated water is incorporated as interlamellar protons, with the oxygen effectively adding to the NiO_2 layers. The model introduces nickel vacancies that explain the empirical Ni/O ratios (less than 1/2). The Raman spectra gives no indication of water in the lattice as the excess protons and alkali cations occupy nickel vacancies or interlamellar sites and three protons can occupy a nickel site for charge compensation. This model correctly explained the empirical observation that Ni has a 3.67 oxidation state observed after overcharge. Raman spectra of these higher oxidation state materials are consistent with the simple rhombohedral space group and the simple γ-NiOOH-type crystal lattice (the ideal, stoichiometric crystal). The spectra are inconsistent with the larger space groups and those which contain molecular water. Thus, the structure is written ideally as γ-NiOOH.

There have been four generations of nickel electrode construction. The first generation included the pocket and tubular electrode structures that were developed independently by Junger in Sweden and Edison in the USA in 1900 for the original system introduction. The Sintered Plate is a second-generation technology and was developed in the 1940s by Varta. The Nickel Cadmium Fiber electrode battery, developed by DAUG, constitutes the third-generation (1985) technology. The nickel cathode electrodes used in nickel-hydrogen batteries for space applications constitute the fourth generation and are produced by an electrochemical deposition of the nickel hydroxide materials directly into the voids in the sintered nickel electrode structure. This is a more expensive process and is used mainly for space and special applications. Because of their ability to withstand physical and electrical abuse, nickel batteries are virtually indestructible. All four electrode constructions are articles of commerce in 2011. Their characteristics will be discussed in more detail below.

Nickel-Iron Batteries (Ni-Fe)

Pocket and Tubular Plate Cells

The iron-nickel battery system is one of the oldest rechargeable systems. It was invented about the turn of the century, independently in Sweden by Junger in 1899, and in the USA by Edison in 1900, each acting without specific knowledge of the other's activity. Common usage today is to call the system the Edison battery. It still finds application today to power materials handling vehicles, underground mining vehicles, miners' lamps, railway cars and signal systems, and emergency lighting. The Edison battery is virtually indestructible and can withstand both physical and electrical abuse situations, discharged stand, and short-circuiting. Edison used tubes for the positive

and pockets for the negative electrode structures for his 1908 battery designs. Disadvantages include low power density, low temperature performance, poor charge retention, and hydrogen evolution on stand.

Both the positive and negative tubular and pocket current collectors are made of perforated nickel-plated steel. They are very robust and are virtually indestructible. The low energy density, poor charge retention, and poor low temperature performance, along with high cost of manufacture, have led to a decline in use of the nickel-iron battery system. The negative electrode, or anode, is iron and the positive electrode, or cathode, is nickel oxide with 6–8 molar potassium hydroxide (KOH) as the electrolyte. The cell reaction occurs in a two-step process. The system has a nominal voltage of 1.37 V.

The two-step cell reaction is:

$$Fe + 2\,NiOOH + 2H_2O = 2Ni(OH)_2 + Fe(OH)_2 \tag{3}$$

$$3\,Fe(OH)_2 + 2\,NiOOH = 2Ni(OH)_2 + Fe_3O_4 + 2H_2O \tag{4}$$

$$\text{Overall: } 3Fe + 8NiOOH + 4H_2O = 8Ni(OH)_2 + Fe_3O_4 \tag{5}$$

On discharge, iron initially forms a divalent hydroxide $Fe(OH)_2$ in the first plateau. Further discharge forms $Fe(OH)_3$, which then further reacts with Fe^{+2} to form Fe_3O_4.

Advantages	Disadvantages
Physically robust	High self-discharge
Long stand and cycle life	Hydrogen evolution on charge and discharge
Withstand electrical abuse	Low voltage and energy density
Very reliable	Poor low temperature performance

The construction of the tubular and pocket plate nickel-iron battery cell is essentially identical to that of the nickel cadmium battery and has not changed over the past 50 years. For good performance, special attention must be paid to use high purity materials and the particle size characteristics of the active materials. The long cycle life is a result of the low solubility of the reaction intermediates. On discharge, supersaturation of the discharge product results in the formation of minute crystallites of Fe_3O_4 near the reaction site. On recharge, these crystals form into a high surface area iron with excellent high rate performance on discharge.

Preparation of Negative Iron Electrode Materials

The active material is produced by dissolution of pure iron in sulfuric acid. The $FeSO_4$ is recrystallized, dried, and roasted at high temperature to produce Fe_2O_3. The materials are washed free of the sulfate, dried, and partially reduced in H_2 to produce a mixture of Fe_3O_4 and iron. The resulting mixture is blended with small amounts of FeS, sulfur, and HgO for use in negative plate assembly.

The anode current collector is an annealed, perforated, nickel-plated steel pocket plate assembly. The tubes for the positive electrode are produced from perforated nickel-plated strips that are wound to produce a tube. One end is crimped and the active material poured into the open end in layers and crimped again to close the tube. A machine automatically introduces the active material and tamps it into the pockets. After filling, the tubes are pressed into openings in the nickel steel electrode frame. The pocket plate follows a similar process. Rectangular pockets of perforated nickel-plated iron strips are filled with active material, crimped, closed, and fixed/bolted in a nickel-plated steel frame. The assembled cells are placed in polyethylene containers and filled with KOH electrolyte. Spacing of the negative and positive electrodes is maintained by the internal assembly structure. There are no separators as are common in the lead acid battery structure.

Preparation of Positive Nickel Electrode Materials

The preparation of the $Ni(OH)_2$ active material starts with dissolving a high purity nickel metal powder, or chips, in sulfuric acid. The hydrogen produced in this step is used in making the negative iron active material. The acidity is adjusted to pH 3 or 4 to remove iron and other insoluble materials. Further conditioning, to remove all of the ferrous iron and copper, may be needed. Cobalt sulfate is added at about the 1.5% level to enhance the charge acceptance of the nickel electrode performance. The resulting solution is heated

and sprayed into hot 50% NaOH to precipitate the $Ni(OH)_2$ active material. The resultant is dried, crushed, and screened to pass 20- but not 200-mesh screen. The construction of the negative plate follows a similar process to that of the positive plate described above. The size of the tubes and configuration of the plates determine the capacity of the finished battery. The battery capacity is designed to be limited by the capacity of the positive plate for longer cycle life.

The nickel-iron battery cell fabrication process is essentially unchanged in over 50 years. Special attention must be paid to use high purity materials and particle size characteristics of the active materials. The iron negative active material is made from pure iron that is dissolved in sulfuric acid. The resulting $Fe(SO_4)_2$ is recrystallized and dried. This is washed free of sulfuric acid and roasted at 915°C to form a mixture of Fe_2O_3 and Fe metal and is, then, blended with small amounts of FeS, sulfur, and HgO for use in the negative plate assembly.

The negative current collector is a perforated nickel-plated steel pocket plate assembly. The tubes are produced from perforated nickel-plated strips that are wound to produce a tube. The tubular construction has one end crimped and the active material is poured into the open end in layers with nickel flakes. Alternatively, a machine automatically introduces the active material and tamps it into the pockets. After filling, the tubes/pockets are crimped and pressed into openings in the nickel-plated steel electrode frame. A similar process is used for the positive electrode.

The positive electrode consists of $Ni(OH)_2$ in alternate layers of nickel flake. High purity nickel metal powder or chip is dissolved in sulfuric acid. Hydrogen is used in making the negative iron active material. The acidity is adjusted to pH 3 or 4 to remove iron and other insoluble materials. Further conditioning to remove all of the ferrous iron and copper may be needed. Cobalt sulfate is added at about the 1.5% level to improve the nickel performance. The resulting sulfate solution is heated and sprayed into hot 50% NaOH to precipitate the $Ni(OH)_2$ active material. The resulting slurry is filtered, washed, dried, and screened to control the particle size to pass 20 but not 200 mesh.

The preferred electrolyte is 25–30% KOH solution with up to 50 g/l of LiOH added. The addition of LiOH improves cell capacity, prolongs cycle life, and facilitates the kinetics of the nickel electrode. It expands the discharge plateau and delays oxygen evolution. It also decreases the carbonate content of the electrolyte as Li_2CO_3 is not very soluble. The negative and positive plates are usually separated by hard rubber pins. The edges of the plates are insulated from the sides and bottom by hard rubber or polymer frames. The spring-loaded, hinged, filler cap protects against carbonation of the alkaline electrolyte by atmospheric CO_2.

The nickel flake is produced by the dissolution of high purity nickel powder in sulfuric acid and the H_2 used in the production of the negative iron active material. The acidity is adjusted to remove soluble iron and copper. A small amount of cobalt sulfate may be added to improve performance. The resulting solution is sprayed into a hot concentrated NaOH solution. The construction of the positive plate follows that for the negative plate.

The size of the tubes and configuration of the plates determine the capacity of the finished battery. The positive and negative electrode frames are bolted together with a spacer to separate the negative from the positive frames for strength and long life. The battery is designed to be limited by the capacity of the positive electrode for longer cycle life. Constant potential charging is not recommended as the system has a tendency to go into thermal runaway. A modified constant voltage with a current limit is acceptable.

Performance

The Ni-Fe batteries range in size from 5 Ah to over 1,200 Ah. The cell open circuit voltage of the Ni-Fe cell is 1.4 which drops quickly to 1.2 V during discharge. Tubular or pocket plate constructions are used. Active materials of high purity are contained inside the perforated nickel-plated steel tubes or rectangular pockets. The active materials are iron for the negative electrode and nickel oxide for the cathode and a KOH electrolyte.

The battery is assembled in the discharged state and a formation charge is used to activate it. The KOH electrolyte is invariant over the charge-discharge regime. The open circuit voltage is 1.4 V that drops quickly to 1.2 V on discharge. The cells vent hydrogen on charge and require a well-ventilated space to prevent

accumulation of hydrogen that could ignite with a spark. The low solubility of iron on discharge results in the formation of minute crystallites of Fe_3O_4 near the reaction site. On charge, these crystallites result in the formation of a high surface area iron electrode deposition that increases the ability to deliver pulse and high current discharge.

Constant potential charging is not recommended as the system has a tendency to go into thermal runaway. A modified constant voltage with a current limit is preferred to prevent thermal runaway situations. The long cycle life of the Ni-Fe battery is a result of the low solubility of the iron electrode reaction intermediates. Series-connected cells require precautions in dealing with high voltage cell assembly connections. Batteries that will be inactive for a month or more should be discharged, short-circuited, and left in that condition. They can be stored in the discharged state with filling caps closed for long periods of time without damage.

Nickel Cadmium Batteries

Nickel Cadmium batteries are available in four different constructions: vented pocket plate, vented tubular plate, sealed sinter plate, and fiber plate constructions. The vented pocket and tubular electrode constructions followed directly from the nickel-iron batteries of Junger and Edison with a substitution of cadmium for iron in the electrode. Like the nickel-iron system, the nickel cadmium pocket and tubular systems are very sturdy, have long life and operate over a wide temperature range with good high rate performance, and require little maintenance. Because they can withstand overcharge, overdischarge, mechanical and electrical abuse, and require little maintenance, they find use in critical industrial applications including switchgear operations, telecommunications, aircraft power, uninterruptible power supplies (UPS), and emergency lighting even though their cost is higher than the lead acid battery system. The cell voltage is 1.29 V and the cell electrolyte is KOH with added LiOH to improve cycle life and high temperature operation.

$$\text{Negative: } Cd + 2OH^- - 2e^- = Cd(OH)_2 \tag{6}$$

$$\text{Positive: } 2NiOOH + 2H_2O + 2e^- = 2\,Ni(OH)_2 + 2OH^- \tag{7}$$

$$\text{Overall: } Cd + 2NiOOH + 2H_2O = 2Ni(OH)_2 + Cd(OH)_2 \quad E = 1.29V \tag{8}$$

Advantages	Disadvantages
Very rugged	Low energy density
Long cycle life	Higher cost than lead acid
Reliable	Contains cadmium
Flat discharge profile	Oxidation of carbon conductor forms CO_2
	Vented cells need regular water service

Nickel cadmium batteries have long life as measured by the number of charge-discharge cycles a battery can sustain and still deliver useful capacity. Under normal conditions a typical Ni-Cd cell can deliver 2,000 cycles or more over a period of 5–20 years depending on application (drain rate, temperature, and ambient conditions of temperature, vibration, duration of high current demand and recharging conditions) as well as the internal design of the cell. Typically, the Ni-Cd cell has a strong internal mechanical design, chemically stable internal ambient and ability to withstand electrical abusive conditions. The sintered electrode cells do have a characteristic termed "memory effect." This arises if the cell has an exact repetitive charge-discharge regime. After a period of time, if the cell is asked to discharge longer than the specified regime, it loses voltage as if it "remembers" the discharge regime. The cell is not damaged. Discharge can continue at a lower voltage and the "effect" eliminated by reconditioning with a series of full capacity charge-discharges.

Nickel Cadmium Pocket and Tubular Plate Cells

Materials fabrication of the Ni-Cd pocket plate and tubular cells follow essentially an identical process to that described for the Ni-Fe cell construction but with cadmium substituted for the iron in the negative electrode construction. The preparation of the cadmium active material uses a co-precipitation process, usually starting with a $CdSO_4$ or $CdCl_2$ solution where KOH is added to precipitate the $Cd(OH)_2$ used in cell fabrication. Here, graphite is used to provide internal

conductivity to contact the positive nickel active mass. On overcharge, the oxygen evolution attacks the graphite conductor to produce CO_2 which, in turn, reacts with the KOH electrolyte to produce K_2CO_3, lowering the concentration of the electrolyte. Each overcharge causes loss of graphite and decreases the available contact to the nickel active mass.

Because they can withstand overcharge, overdischarge, mechanical and electrical abuse, and require little maintenance, the Ni-Cd batteries find use in critical industrial applications including switchgear operations, telecommunications, uninterruptible power supplies (UPS), and emergency lighting even though their cost is higher than the lead acid battery system. The Ni-Cd vented pocket plate battery was used in the world's largest UPS power supply in Anchorage, Alaska.

Nickel Cadmium Fiber Plate Batteries

Fiber Plate Electrode Technology was developed by DAUG in Germany in 1983. The electrodes have an open three-dimensional nickel fiber structure that provides good conductivity throughout the electrode structure to ensure excellent electrical performance. The fibrous nickel matrix current collector matrix forms a lightweight flexible structure with about 90% of the electrode volume available for holding the active material. It is free from graphite and iron, found in other nickel-based cathode battery systems; so reduces water consumption by electrolysis and eliminates carbonation of the electrolyte on overcharge to ensure very long cycle life.

The elastic nature of a NCFP electrode and its fibrous current collector construction enable it to accommodate the volume changes and maintain good contact with the active materials during the charge and discharge cycles, as well as absorb shock and vibration. This feature results in longer cycle life compared to other Ni-Cd battery technologies. The NCFP technology is considerably lighter in weight and has higher energy density than the regular Ni-Cd constructions. Fiber plate batteries can be designed with very thin plates for ultra high rate discharge performance or with thick plates for long duration lower current discharge applications. Other features include no need for change of electrolyte throughout life due to graphite-free electrodes, low water consumption, long shelf life, and flame-arresting vent protection.

Applications include switchgear protection, emergency lighting, motive power, train lighting, instrumentation and process control, UPS, electric vehicles, diesel engine cranking, aircraft and helicopter ground starting.

Nickel Cadmium Sealed Sinter Plate Cells

The present sealed Ni-Cd sinter plate battery technology evolved from the sealed battery technology developed by Varta in the 1940's based on an IG Farben development in the 1930's. The sinter plate construction, developed in the 1940 time frame, has low internal resistance, superior high rate and low temperature performance compared to the pocket plate cell design. The batteries are sealed and can be used in any orientation. This battery powered the Luftwaffe in the 1940s, the early flights in the space program and in the development of portable electronic devices, such as cellular phones and portable notebook computers.

The small sealed sintered plate Ni-Cd cylindrical and prismatic cell constructions have the favorable characteristics of the pocket/tubular plate constructions with increased energy density. The electrodes are thin and the cells have low internal resistance with excellent high rate and low temperature performance. The stem is rugged and can withstand physical and electrical abuse. It requires minimal maintenance.

Advantages	Disadvantages
Sealed, no maintenance	Higher cost than lead acid
Long cycle and shelf life	Lower capacity than Li-Ion and Ni-MH
Excellent high rate performance	Environmental issues with cadmium
Flat discharge profile	
−40°C to +50°C operating range	
Operate in any orientation	

$$\mathrm{Cd} + 2\mathrm{OH}^- - 2\mathrm{e}^- = \mathrm{Cd(OH)2} \tag{9}$$

$$2\mathrm{NiOOH} - 2\mathrm{H2O} = 2\mathrm{Ni(OH)2} + 2\mathrm{OH} \tag{10}$$

$$\mathrm{Cd} + 2\mathrm{NiOOH} + 2\mathrm{H_2O} = \mathrm{Cd(OH)_2} + 2\mathrm{Ni(OH)_2} \quad \mathrm{E} = 1.29\mathrm{V} \tag{11}$$

The electrodes for cell fabrication are produced by vacuum impregnation of the nickel sinter plate. The sinter plates are produced by coating slurry of carbonyl nickel powder in CMC onto a nickel-plated steel or nickel screen current collector and burn off the CMC at high temperature. This process produces a nickel current collector with about 80% porosity. The coils or plates (depending on cell construction) of the sinter plate are vacuum impregnated in an aqueous nickel nitrate solution, dipped into a NaOH bath to convert the nickel nitrate into $Ni(OH)_2$, and then dried. The process is repeated until the desired loading of $Ni(OH)_2$ is obtained. The negative electrode is produced by a similar process except cadmium nitrate solution is used to impregnate the sinter electrode. The impregnated strips of cobalt and nickel electrode stock are cut to size, stacked as plates or wound into a cylinder, and assembled in the appropriate cell container.

The sealed cylindrical and prismatic cells can operate in any orientation. They were instrumental in the electronic revolution that produced the portable computers, cellular phones, digital cameras, and the like. This requires specific design features that prevent pressure buildup from oxygen gas generation on overcharge, with no free electrolyte and no maintenance or servicing. The internal design of each electrode of the cell is critical to long life at full performance. The cell balance, ratio of the capacity of Cd to the capacity of NiOOH electrodes, is carefully controlled to prevent any hydrogen evolution from the cadmium electrode. Sealed cells have a different balance (ratio of the negative and positive electrode capacities) from that for vented cell constructions. In sealed Ni-Cd cells, it is essential to prevent hydrogen evolution on charge as it causes the cell to dry out and develop high internal pressure. This is accomplished by balancing the capacity of each electrode, positive and negative, during cell assembly to ensure that oxygen is the only gas evolved, as depicted in Fig. 1. As the cells reach full charge and enter overcharge, oxygen is evolved from the nickel positive. The oxygen diffuses through/around the porous separator to the cadmium electrode where it reacts directly with the active cadmium metal, just deposited on the negative electrode, to produce $Cd(OH)_2$ with heat evolution. To that end, the negative cadmium plate is designed with an excess of uncharged active mass.

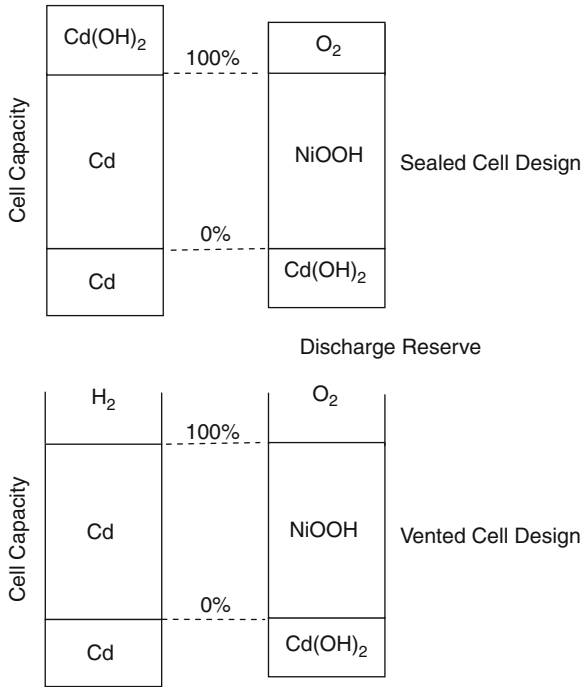

Nickel-Based Battery Systems. Figure 1
Cell balance for vented and sealed nickel cadmium cells. It is important to avoid hydrogen gas evolution in the sealed cell

Nickel Metal Hydride

Nickel metal hydride (Ni-MH) batteries have application in hybrid electric vehicles, portable electronic devices such as cameras, shavers, toothbrushes, etc. They offer a higher energy option than Ni-Cd batteries with the hydrogen-absorbing metal hydride alloy (MH) replacing the cadmium electrode in Ni-Cd cell construction. Like Ni-Cd, the Ni-MH also shows the "memory effect" on repetitive cycle regimes. The nickel metal hydride battery was introduced commercially in 1989. The technology is based on the development of rare earth alloys with nickel that have the ability to reversibly absorb and desorb hydrogen. The nickel metal hydride (MH) electrode replaces the cadmium electrode in the Ni-Cd cell construction. It stores, and can deliver, more energy than an equivalent-sized Ni-Cd cell.

The Ni-MH battery has found wide application as a replacement for rechargeable Ni-Cd cells and primary alkaline manganese cells, especially in portable

electronic devices. It offers a rechargeable replacement for the primary alkaline cell and gives superior performance. Although it initially has a lower voltage, it has a constant voltage discharge as compared to the sloping voltage of the alkaline cell that is very desirable for cameras, portable electronics, etc. More recently, it has found application in hybrid electric automobiles.

$$\text{Negative:}\quad MH + H_2O + 2e^- = M + 2OH^- \tag{12}$$

$$\text{Positive:}\quad 2NiOOH + 2e^- = 2Ni(OH)_2 + 2OH^- \tag{13}$$

$$\text{Overall:}\quad MH + 2NiOOH = M + 2Ni(OH)_2 \qquad E = 1.35V \tag{14}$$

The "metal" M in the equations above refers to the negative electrode of a Ni-MH cell and is an intermetallic alloy or compound capable of storing and releasing hydrogen. These compounds can store many times their volume of hydrogen. The hydrogen atom is much smaller than nickel and can occupy interstices in the nickel alloy anode. In theory, the MH alloy has almost twice the capacity of the cadmium anode material. This gives the Ni-MH battery the capability of about 20% greater energy storage than the Ni-Cd battery. Many different compounds have been developed for this application. The most common is AB_5, where A is a mixture of rare earth elements (chromium, lanthanum, cerium, neodymium, and praseodymium) and B is a mixture of nickel, cobalt, manganese, or aluminum. The metal hydride electrode substitutes for the cadmium electrode in the Ni-Cd cell and makes for a more environmentally friendly system. Many design parameters are similar to those in Ni-Cd.

Alloys used for the negative electrode of Ni-MH secondary batteries function as a hydrogen storage media as well as a catalyst for the hydrogen electrode reaction. The hydrogen-absorbing alloys can be divided into three main types: the AB_5, A_2B_7, and AB_2 types. In the $LaNi_5$ alloys, La is substituted for misch metal, Mm, a mixture of rare earth elements including La, Ce, Pr, and Nd and partially substituted for Ni for Co and Al to increase the hydrogen storage and lengthen the charge-discharge cycle life. The cell balance of the capacity of the positive and negative electrodes for best performance are given in Fig. 2.

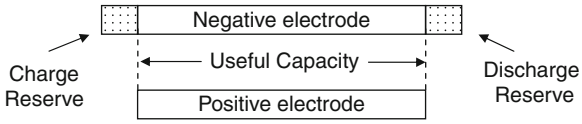

Nickel-Based Battery Systems. Figure 2
Cell balance in sealed nickel metal hydride cells

Ni-MH cells can be practically charged at 1 C rate using a constant current voltage charge regime and discharged at 4 C. Its 1 C charge-discharge cycle life expectancy is more than 500 cycles enabling commercial applications of Ni-MH to a wide variety of cordless equipment. The Ni-MH cells do not have the memory effect characteristic, where cells discharged on the exact same charge-discharge regime "memorize" the cycle and if discharged, further, act as if fully discharged.

As with Ni-Cd, when overcharged at low rates, the oxygen produced at the positive electrode on overcharge diffuses through the porous separator and recombines at the surface of the negative to suppress hydrogen evolution and converts the charging energy into heat. This process prevents internal pressure buildup to allow Ni-MH cells to remain sealed if overcharged during normal operation. Ni-MH cells use a KOH electrolyte and the same hydrophilic polyolefin nonwoven separator materials used in the Ni-Cd cell.

The internal construction of the Ni-MH cell mimics that of the Ni-Cd cells. The Ni-MH cells are available in a wide variety of sizes ranging from the AA-size for digital cameras, up to 50 Ah or larger used in hybrid car applications. Useful discharge capacity is constant up to the 1 h discharge rate and does not differ significantly from the rated capacity.

Nickel metal hydride batteries consist of a positive electrode containing a mixture of carbon/graphite conductive diluent and nickel hydroxide as its principal active material. The negative electrode consists mainly of hydrogen-absorbing conducting metal alloys, a porous polymer separator filled with KOH electrolyte, a metal case and a resealing vent. The anode-separator-cathode foils are wound in a cylinder or stacked in a prismatic format and inserted into a nickel-plated steel can. The prismatic cell construction may also be formed by stacking alternate positive and negative individual electrodes or by winding the electrode strips into a cylindrical form and then

inserted into a prismatic can or wound and inserted into a cylindrical can construction.

A complete discharge of a Ni-MH cell causes permanent damage to the negative electrode. This situation can occur in a group of series-connected cells if one low-capacity cell in the series is completely discharged and driven into reverse due to its lower capacity than surrounding cells. When this happens, the good cells will start to drive the discharged cell in reverse and can cause permanent damage to that cell.

Ni-MH cells have a 5–10% self-discharge rate at the beginning of life but stabilize around 0.5–1% per day. Cooler storage temperatures have lower discharge rate and longer battery life. Continual trickle charging of small Ni-MH cells can cause permanent deterioration in cell performance.

Ni-MH batteries provide a relatively constant voltage during the discharge cycle, unlike a standard alkaline battery where the voltage falls steadily during discharge. This characteristic gives the Ni-MH longer useful service to power portable electronic devices than the standard alkaline zinc manganese cell and can be substituted for the AA-size alkaline cell in most devices.

Ni-MH batteries have application in hybrid electric vehicles and portable electronic devices, such as cameras, shavers, toothbrushes, etc. The Ni-MH battery is also used in hybrid cars to improve stop-start and acceleration performance. It absorbs braking energy to assist the breaking operations and during the acceleration, returns that energy to supplement the gas engine.

Improper disposal of Ni-MH batteries poses less environmental hazard than that of Ni-Cd because of the absence of toxic cadmium.

Nickel-Zinc Batteries

The performance of nickel-zinc (Ni-Zn) batteries lies between that of high-energy silver-zinc and nickel cadmium. The nickel-zinc cells have excellent high rate performance and about twice the energy density of Ni-Cd but the cycle life is severely limited due to "shape change" problems that limit recharge of the zinc electrode. While Junger and Edison were both awarded patents on the rechargeable Ni-Zn battery, the first commercial cell was developed by J. Drumm in Dublin, Ireland, in 1931 to power the lights on a passenger train between Bray and Dublin. It ran until 1949. Later, Yuasa introduced a 10 Ah sealed Ni-Zn battery for use in lawn mowers and light duty electric vehicles without success. Their cells limited cycle life of 200 cycles at the two-hour rate and were not sufficient for a commercial rechargeable battery system. PowerGenix successfully demonstrated that the Ni-Zn battery could substitute for the Ni-MH battery in a Toyota Prius car. A potentially new large application for Ni-Zn is stationary energy storage.

Although the zinc electrode is a difficult system and can deliver excellent high rate performance, it suffers from problems with the surface morphology, dendrite formation on charge, shape change, agglomeration/redistribution and passivation, etc., that limit cycle life. The problems directly result from the characteristics of the reactions of the zinc ions in solution and the reactivity of zinc metal with the electrolyte.

$$\text{Negative: } Zn + 2OH^- - 2e^- = ZnO + 2OH^-$$

$$\text{Positive: } NiOOH + 2H_2O = 2Ni(OH)_2 + 2OH^-$$

$$\text{Overall: } Zn + NiOOH = Ni(OH)_2 + ZnO$$
$$E = 1.73V$$

In 2008, PowerGenex introduced a new sealed cell for the power tool market with a modified KOH electrolyte formulation. The higher voltage of the zinc electrode results in a unit cell voltage of 1.73 versus 1.2 for Ni-Cd, giving the Ni-Zn a distinct advantage in energy density. In addition, the facile kinetics of the zinc electrode gives the system superior performance for high rate applications. The reaction of the active materials with the electrolyte limits the cell life.

$$\text{Zinc electrode: } Zn + 2OH^- - 2e = Zn(OH)_2$$
$$Zn(OH)_2 + 2OH^- = ZnO_2{}^{-2} + 2H_2O$$
$$ZnO_2{}^{-2} + H_2O = ZnO + 2OH^-$$

$$\text{Nickel electrode: } 2NiOOH + 2H_2O + 2e^- = 2Ni(OH)_2 + 2OH^-$$

$$\text{Overall: } Zn + 2NiOOH + H_2O = 2Ni(OH)_2 + ZnO$$

Cell construction for the Ni-Zn cell is similar to that for the sealed spiral wrap cylindrical and prismatic Ni-Cd and Ni-MH cells for portable electronic applications but with some differences. The Ni-Zn cell incorporates a multilayer micro-porous separator

with "wicking" components used to maintain uniform electrolyte distribution, as well as acting as a buffer/barrier to prevent shorting from zinc dendrite formation. The barrier also slows oxygen gas diffusion and lowers the recombination rate that can lead to pressure buildup inside the cell. The KOH electrolyte contains CaO additions to calcium zincate that can control the free zinc ions in solution. In the cell electrolyte, the CaO reacts with zinc ions to form calcium zincate. Other improvements center on the use of fiber (steel wool) current collectors for the zinc electrode. The Ni-Zn cells have excellent high rate and low temperature performance.

Nickel-Hydrogen Batteries

The nickel-hydrogen (Ni-H_2) battery was developed in the late 1960s as a new, long-lived, highly reliable power source to replace Ni-Cd for space applications. It won out over strong competition from regenerative fuel cells mainly due to issues related to life expectancy and system engineering problems in that resulted in increased size, weight, complexity, loss of catalytic activity, and cost to assure the required long life.

The Ni-H_2 system characteristics of its lightweight, extremely long cycle life and simple, yet, accurate state of charge determination based on a pressure measurement, makes it an ideal system for all space applications ranging from low orbits, mid-altitude orbits, to the higher geosynchronous orbits. It replaced the Ni-Cd system because of its lighter weight and longer life. It has powered the space shuttle, space stations, and interplanetary probes including extending planetary exploration stations on the moon and Mars. Ni-H_2 battery cells are by far the longest-lived and most reliable of all sealed rechargeable battery systems.

Advantages	Disadvantages
Long calendar life	Expensive
10+ year's cycle life	Low energy density
Accurate state-of-charge measure	High self-discharge
Abuse-tolerant	

$$\text{Negative:} \quad H_2 - 2e = 2H^+ \tag{14}$$

$$\text{Positive:} \quad 2NiOOH + 2e^- = 2Ni(OH)_2 + H_2O \tag{15}$$

$$\text{Cell:} \quad H_2 + 2NiOOH = 2Ni(OH)_2 + H_2O \qquad E = 1.2V \tag{16}$$

Internal cell design considerations include the depth of overdischarge, positive pre-charge, or negative pre-charge cell designs. The type of pre-charge depends on if there is excess capacity associated with the positive nickel electrodes (positive pre-charge) or the negative hydrogen material (negative pre-charge). In this configuration, there is a capacity loss mechanism caused by the reaction of hydrogen with the cobalt additive in the active material of the positive electrodes. Newer cell designs specify positive pre-charge designs where there is capacity remaining in the positive electrodes of the cell at the end of discharge.

The hydrogen electrodes are Teflon bonded, platinum black catalyzed, supported on a nickel substrate. A high surface area platinum black hydrogen catalyst loading, in the range of 7 mg/cm^2, ensures long life. The electrodes have a porous Teflon backing to stop water loss from the back side while allowing full access for gas transport. The system is designed so that on overcharge, O_2 is forced out of the backside of the electrode to prevent direct contact with the active surface of the hydrogen electrode. Usually, a fibrous Zircar nonwoven ceramic separator holds the KOH electrolyte.

The sintered nickel substrate for the cathode is similar to that used for Ni-Cd and Ni-MH cell constructions. The nickel active materials are loaded into the sinter plate using either an aqueous (Bellcore) or alcoholic-based (Air Force or Pickett) electrochemical impregnation process. A 5–10% cobalt additive is deposited with nickel hydroxide to improve charge acceptance. These electrodes have a significantly longer cycle life over the standard vacuum impregnated or pasted nickel electrodes used in commercial Ni-Cd cells.

In the "pineapple" cell design, two of these nickel sinter electrodes are stacked back-to-back with asbestos cloth separators on each face of the electrodes. The cell construction is named after an exploded view of the slices (electrode components) in a can of pineapple. The recirculating stack design permits a natural concentration gradient across the stack. A thin flame-sprayed zirconium oxide coating on the inner wall of the pressure vessel is contacted by the protruding edges of the separator to redistribute the electrolyte through the diffusive gradient set up by the recirculation

pattern. The hydrogen electrodes are platinum-catalyst-based electrodes with a hydrophilic platinum catalyst on the side facing the separator, and the side facing the gas screen consisting of a hydrophobic porous Teflon layer. The electrolyte is 31% by weight aqueous potassium hydroxide. The cell components are stacked on a polysulfone core that fits into the center hole of the pineapple slice components.

All nickel-hydrogen cell designs have the electrolyte contained within the porous stack components. A hydrophilic wall wick provides a path for diffusion of the electrolyte by capillary forces from wet to dry regions of the stack. The finished Ni-H_2 cell is a sealed pressure vessel with positive and negative terminals.

The second-generation cell, 5.5 in. diameter cell design, has capacities up to 350 Ah. Eagle Picher developed a cell line based on the electrochemical impregnation method for nickel electrodes employing either slurry sinter or dry sinter. The nominal thickness of the nickel electrode was 35 mils, as opposed to the 30-mil thickness of the electrodes used in the COMSAT cells. The cells were built with a back-to-back stacking arrangement that included two layers of Zircar separator, using a 31% potassium hydroxide electrolyte. They were built with about a 15% nickel pre-charge. A nylon compression seal was used to seal the terminals into the pressure vessel. A flame-sprayed zirconium oxide wall wick was included in the design to allow electrolyte gradients to equilibrate by diffusion. The cells had no free electrolyte.

A dual-stack cell design that enclosed two stacks within the same pressure vessel was developed to reduce the number of pressure vessels required in some power systems. This configuration was termed a common pressure vessel. These powered the Iridium constellation of 88 satellites (98 satellites, including orbital spares). While these batteries have functioned reasonably well, there are some difficulties in maintaining all the cells at a similar state of charge. However, these single pressure vessel batteries continue to perform well in orbit.

Bibliography

1. Anderman M, Baker C, Cohen F (1997) Proceedings of the 32nd intersociety energy conversion conference, Honolulu, Hawaii, vol 1, p 97465 Honolulu, Hawaii
2. Anderson B, Ojefors L (1979) In: Thompson JF (ed) Power sources, vol 7. Academic, London, p 329
3. Baker C, Barekatien M (2000) Proceedings of the SAE power systems conference, San Diego, 2000
4. Beauchamp RL (1971) US Patent 3,573,101
5. Beauchamp RL (1972) US Patent 2,653,967
6. Beccu K (1972) US Patent 3,669,745
7. Buzzelli E (1978) Silver-iron battery performance characteristics. In: Proceedings of the 28th power sources symposium, Electrochemical Society, Pennington, p 160
8. (2004) Cadnica sealed type Nickel-Cadmium batteries engineering handbook, Sanyo Electric Company, Osaka
9. Casellato U, Comisso N, Mengoli G (2006) Effects of Li ions on reduction of Fe oxides in aqueous alkaline medium. Electrochemica Acta 51:5669–5681
10. Cook J (1999) Separator-hidden talent Electric and hybrid vehicle technology
11. Corrigan DA, Venkatesan S, Gifford P, Holland A, Fetcenko MA, Dhar SK, Ovshinsky SR (1997) Proceedings of the 14th international electric vehicle symposium, Orlando
12. Corrigan DA, Knight SK (1996) J Electrochem Soc 143(5):1613
13. Ettel V, Ambrose J, Cushnie K, Bell JAE, Paserin V, Kalal PJ (1997) US Patent 5,700,363
14. Falk SU, Salkind AJ (1969) Alkaline storage batteries. Wiley, New York
15. Feduska W, Rosy R (1980) An advanced technology Iron-Nickel battery for electric vehicle propulsion. In: Proceedings of the 15th IECEC, Seattle, p 1192
16. Fetcenko MA, Ovshinsky SR, Chao B, Reichman B (1996) US Patent 5,536,591
17. Fetchenko MA, Venkatesan S, Ovshinsky S (1991) Proceedings of the symposium on hydrogen storage materials, batteries and electrochemistry, Electrochemical Society, Pennington, p 141
18. Fleischer A (1948) J Electrochem Soc 94:289
19. Ford FE (1994) Handbook for handling and storage of Nickel-Cadmium batteries: lessons learned, NASA Ref. Publ. 1326
20. Gutjahr MA, Buchner H, Beccu KD, Saufferer H (1973) In: Collins DH (ed) Power sources, vol 4. Oriel, Newcastle Upon Tyne, p 79
21. Halpert G (1984) J Power Sources 12:117
22. Halpert G (1990) Proceedings of the symposium on nickel hydroxide electrodes, The Electrochemical Society, Hollywood, Oct 1989, J Electrochem Soc, Pennington, pp 3–17
23. Hill TE, Rosy R, Vaill RE (1978) Performance characteristics of iron nickel batteries. In: Proceedings of the 28th power sources symposium, Electrochemical Society, Pennington, p 149
24. Hudson R, Broglio E (1980) Development of nickel-iron battery system for electric vehicle propulsion. In: Proceedings of the 29th power sources conference, Electrochemical Society, Pennington
25. Ishiwa K, Ito T, Miyamoto K, Takano K, Suzuki S (1999) Evolution and extension of NiMH technology. In: 16th international seminar on primary and secondary batteries, Ft. Lauderdale
26. Kanagawa I (1998) 15th international seminar on primary and secondary batteries, Ft. Lauderdale
27. Kruger FJ (1998) 15th international seminar on primary and secondary batteries, Ft. Lauderdale

28. Kulin TM (1998) 33rd intersociety engineering conference on energy conversion, ICECE-98-145, Colorado Springs, 2–6 Aug 1998
29. Reddy TB (2011) Linden's handbook of batteries, 4th edn. McGraw Hill, New York
30. Lindstrom O (1975) In: Collins DH (ed) Power sources, vol 5. Academic, London, p 283
31. McBreen J (1990) The nickel oxide electrode. In: White RE, Bockris JO'M, Conway BE (eds) Modern aspect of electrochemistry, vol 21. Plenum, New York, p 29
32. McRae B, Nary D (1998) Proceedings of the 38th power sources conference, pp 123–126
33. Matsumoto I, Ogawa H, Iwaki T, Ikeyama M (1988) 16th international power sources symposium, 1988, Bournmouth, England
34. Mil-B-81757 (1984) Performance specifications, batteries and cells, storage, nickel cadmium, Aircraft General Specification, Crane Division, NSWC, 1 July 1984
35. Mishima R, Miyamura H, Sakai T, Kuriyama N, Ishikawa H, Uehara I (1993) J Alloys Compd 192:176–178
36. Notten PHL, Hokkeling P (1991) J Electrochem Soc 138(7):1877
37. Notten PHL, Daams JLC, Einerhand REF (1992) Ber Bunsenges Phys Chem 96:5
38. Nickel-Cadmium batteries (2004) charge system guide, Panasonic Industrial Company, Secaucus
39. Ohta K, Matsuda H, Ikoma M, Morishita N, Toyoguchi Y (1996) US Patent 5,571,636
40. Ojefors L, Carlson L (1977) An iron-air vehicle battery. J Power Sources 2:287
41. Oshitani M, Yufu H, Takashima K, Tsuji S, Matsumaru Y (1989) J Electrochem Soc 136:6
42. Oshitani M, Yufu H (1989) US Patent 4,844,999
43. Ovshinsky SR, Dhar SK, Fetcenko MA, Young K, Reichman B, Fierro C, Koch J, Martin F, Mays W, Sommers B, Ouchi T, Zallen A, Young R (2000) 17th international seminar and exhibit on primary and secondary batteries, Ft. Lauderdale, 6–9 Mar 2000
44. Ovshinsky SR (1998) Materials research society fall meeting, Boston
45. Ovshinsky SR, Fetcenko M, Ross J (1993) Science 260:176
46. Ovshinsky SR (1991) In: Adler D, Schwartz B, Silver M (eds) Disordered materials: science and technology. Institute for Amorphous Studies Series/Plenum Publishing Corporation, New York
47. Ovshinsky SR, Corrigan DA, Venkatesan S, Young R, Fierro C, Fetcenko M (1994) US Patent 5,348,822, 14 Apr 1994
48. Pell MB, Blossom RW (1970) US Patent 3,507,699
49. Picket DF, Maloy JT (1978) J Electrochem Soc 12:1026
50. Picket DF (1974) US Patent 3,827,911
51. Picket DF (1975) US Patent 3,873,368
52. Puglisi V (2000) 17th international seminar and exhibit on primary and secondary batteries, Ft. Lauderdale 6–9 Mar 2000
53. Reichman B, Mays W, Fetcenko MA, Ovshinsky SR (1999) Electrochemical society proceedings, vol 97–16, Oct 1999
54. Salkind AJ, Venuto CJ, Falk SU (1964) The reaction at the iron alkaline electrode. J Electrochem Soc 111:493
55. Sapru SR, Reichman B, Reger A, Ovshinsky SR (1986) US Patent 4,623,597
56. Singh D, Wu T, Wendling M, Bendale P, Ware J, Ritter D, Zhang L (1998) Mater Res Soc Proc 496:25–36
57. Souza A, Carlos IA, Lopes M, Finazzi GA, de Almeida MRH (2004) Self-discharge of Fe-Ni alkaline batteries. J Power Sources 132:288–290
58. Stempel RC, Ovshinsky WR, Gifford PR, Corrigan DA (1998) IEEC spectrum 35(11):29–34
59. Takagi S, Minohara T (2000) Society of automotive engineers, 2000-01-1060, Mar 2000
60. Tuomi D (1976) The forming process in nickel positive electrodes. J Electrochem Soc 123:1691
61. van Beek JR, Donkersloot HC, Willems JJG (1984) Proceedings of the 14th international power sources symposium (1984), Waikola, Hawaii
62. Watanabe K, Koseki M, Kumagai N (1996) J Power Sources 58:23–28
63. Weininger JL (1982) In: Gunther RG, Gross S (eds) The nickel electrode, vol 82–84. Electrochemical Society, Pennington, pp 1–19
64. Weizhong T, Guangfei S (1994) J Alloy Compd 203:195–198
65. Young K, Fetcenko MA, Reichman B, Mays W, Ovshinsky SR (2000) Proceedings of the 197th electrochemical society meeting, May 2000
66. Yu X, Licht S (2007) Advances in Fe(VI) charge storage part I, primary alkaline super-iron batteries. J Power Sources 171:966–980
67. Yu X, Licht S (2007) Advances in Fe(VI) charge storage part ii, reversible alkaline super-iron batteries and nonaqueous super-iron batteries. J Power Sources 171:1010–1022

Night Vision Pedestrian Warning in Intelligent Vehicles

Matthias Serfling, Otto Löhlein
Machine Perception Systems and Reliability,
Environment Perception Daimler AG, Ulm, Germany

Article Outline

Glossary
Definition of the Subject and Its Importance
Introduction
Discussion of Fusion Concepts
System Overview
Sensor Configuration
Boosted Feature-Level Sensor Fusion
Global Positioning and Road Course Estimation
Threat Analysis

Experiments
Conclusion
Future Directions
Acknowledgments
Bibliography

Glossary

ACC Adaptive Cruise Control – A cruise control system which controls the vehicle speed in order to keep a set distance to the vehicle in front.

AdaBoost Adaptive Boosting – A supervised machine learning algorithm which combines several weak learners (very simple classifiers) to construct a strong learner classifier.

Baseline The baseline of a stereo camera system defines the distance of the corresponding camera coordinate systems and influences the accuracy of the depth analysis.

Bayes classifier A simple probabilistic classifier based on applying Bayes' theorem from Bayesian statistics.

CAN Controller Area Network – A standard vehicle bus system which is designed to allow microcontrollers and devices to communicate with each other within a vehicle.

CFAR Constant False Alarm Rate – An adaptive algorithm used especially in radar systems to detect targets in noisy measurements.

CMOS Complementary Metal Oxide Semiconductor – A technology for constructing integrated circuits.

CTRV Constant Turn Rate and Velocity – A motion model which assumes an object moves in sample time T with constant velocity and constant turn rate.

Disparity A term in multiple view geometry in computer vision which describes the distance of two points in two different images by identifying the same point in the scene observed from different positions.

Digital map The knowledge database used in automotive navigation systems which provide information about the road network.

Doppler An effect that describes the change in frequency of a wave for an observer moving relative to the source of the wave.

EU European Union

Epipolar line A line describing the positions in a sensor coordinate system, which correspond to a single position in a second sensor coordinate system. Typical term used in stereo camera systems.

False alarm rate A failure measure in detection systems describing the amount or the rate of detections which do not correspond to a proper object.

FIR (far-infrared) A device analyzing the infrared electromagnetic radiation with a wavelength between 0.7 and 300 μm.

Flat world assumption A simple model in the field of computer vision which assumes that all objects perceived by a sensor (e.g., a camera) are positioned in a flat world.

GPS (global positioning system) A space-based global navigation satellite system that provides reliable location and time information of an object on or near the Earth.

Haar wavelets A basic wavelet method to decompose a signal into independent signal parts.

INS Inertial Navigation System – A system that uses motion sensors and rotational sensors installed on a platform to continuously calculate via dead reckoning the position, orientation, and velocity of a moving object without any external references.

MCL Monte Carlo Localization – A method in robotics and sensors to determine the position of a robot given a map of its environment based on Markov localization.

NIR Near-Infrared – A device analyzing the electromagnetic spectrum from approximately 800 nm to 2,500 nm.

NIRWARN Near-Infrared Warning

Particle Filter A probabilistic method in the field of computer vision to track objects using a Monte Carlo approach.

PReVENT Preventive and Active Safety Application, European founded project.

ProFusion ProFusion Subproject of the PReVENT project.

RADAR Radio Detection and Ranging – An object-detection system that uses an electromagnetic wave to identify the range, direction, (and velocity) of a target.

ROI Region of interest – A small region selected for further processing.

ROC Receiver operating characteristic – A graphical plot to show the fraction of true positives vs. the fraction of false positives for a binary classifier system as its discrimination threshold is varied.

Stereo camera system A type of camera system which observes the environment with two lenses in order to simulate human binocular vision, and thus reconstructs the depth information of the environment.

Two-class problem A typical classification problem with an object class and a non-object class.

UTM Universal Transverse Mercator – A grid-based two-dimensional Cartesian coordinate system, which specifies locations on the surface of the Earth.

VGA Video Graphics Array – A standard VGA camera has a resolution of 640 × 480 pixels.

Definition of the Subject and Its Importance

Today's second generation of automotive night vision systems uses near-infrared (NIR) or far-infrared (FIR) cameras combined with integrated pedestrian detection systems. These systems direct the driver's attention by showing all detected pedestrians on a display inside the car. This enables the driver to analyze an imminent situation earlier and react appropriately to prevent a potential hazardous situation, but the driver has to decide on his own whether a detected pedestrian is a potential risk or not. Thus, the next generation of night vision systems needs to integrate an additional warning component which signals to the driver only the relevant objects, that is, all objects on the road or near the road. Such a warning system needs to detect objects more reliably and sooner and has to provide information about the object's position. Moreover, the system has to know the road course in front of the vehicle to do a threat analysis of the detected objects by their position. According to [1] and [2], the brake reaction time under real-life conditions is about 1.5–2 s. Incorporating also the braking time to standstill at a common speed of 100 kph on rural roads, the driver needs to be warned at least 6 s in advance.

In this context, a reliable and robust pedestrian detection system as well as a road course estimation system which covers both factors at a distance up to 120 m is essential for the development of the next generation of night vision warning system.

As shown in a German funded project NIRWARN [3], single NIR sensor systems can provide pedestrian detection reliably up to 90 m. For the enlargement of the detection range to 120 m, the illumination of the road and the camera resolution and sensitivity are limiting factors. Neglecting the cost factor of an automotive FIR camera, which can achieve these ranges, the problem of providing information about the object's position still remains with any kind of single camera sensor system. In fact, a stereo camera system can provide position information, but a large baseline (i.e., at least 0.8 m using a VGA imaging sensor with lenses of focal length 12 mm) is required to realize detection ranges of 120 m. A large baseline is difficult to integrate into a passenger car.

The known approaches for lane or road recognition systems perform well under daylight conditions on motorways [4–9], but these systems mostly fail or have a very limited prediction horizon on rural roads during the night due to high curvature road types, missing lane markings, heavily changing lighting conditions, and varying road surfaces.

This contribution addresses both problems of a reliable and robust pedestrian detection system with enlarged detection range, and also provides information about the object's position and a reliable road course estimation system covering distances up to 120 m in order to carry out a threat analysis and to signal to the driver only the relevant objects. To achieve the full functionality, the presented approach combines the sensor information provided by a NIR camera, an imaging radar, and a digital map.

Unlike other mid- and high-level radar camera fusion approaches [10–15], the proposed system realizes an early feature-level fusion to detect pedestrians at night within 120 m in rural and suburban environment. The presented low-level fusion system shows better results than a camera-only system, outperforms a fusion system on higher levels, and manages the higher computational load of processing raw data.

In order to overcome the drawback of the visibility constraints of an image sensor, a digital map in combination with a new highly sensitive imaging radar is used to provide a reliable prediction of the road course. Unlike an image sensor, the used imaging radar sensor is capable of clearly detecting the road boundary independent of lane markings and for the most part

independent of weather and lighting conditions at least up to 60 m. Reflections from trees, posts, traffic signs, parked cars, and guardrails enlarge the detection range of the road boundary up to 100 m.

Introduction

Many approaches for pedestrian recognition under daylight conditions for vision systems have been developed, especially for shorter detection ranges. Single-sensor pedestrian recognition at night based on image processing is widely discussed in [16–19]. The preferred detection method applied to near-infrared (NIR) images [16, 17] and far-infrared (FIR) images [18, 19] is the cascaded classification using Haar wavelets. Note that [19] uses a pixel classification prestage to reduce the input space and uses in addition to the cascaded classifier, a second classifier based on object shape matching. A particle filter fuses the detection results from both classifiers.

On the other hand, multi-sensor pedestrian recognition has been presented in [20] and [21]. A two-step fusion of a radar sensor and monocular vision sensor is applied in [20]. The first step generates a list of potential targets using the radar sensor. The second step utilizes the images from a vision sensor to verify the targets, applying flexible shape models trained from manually extracted pedestrians. Thus the false alarm rate can be reduced analyzing the image in small regions of interest (ROI), but the detection rate is strictly limited by the radar sensor.

A three-level early fusion system for road user detection including cars and pedestrians is presented in [21]. The fusion process combines raw sensor data provided by a laser scanner, a long and a short range radar, a gray-scale camera, and a FIR camera at an early stage of the data processing chain and performs a joint data interpretation with respect to a common model basis. The first step generates hypotheses for each sensor and merges overlapping hypotheses of different sensors in one hypothesis and assigns the involved sensor measurements. In the second fusion level, different sensor features (e.g., velocity, object dimensions, and FIR image edges) are used to classify the hypotheses. Finally, the third fusion level takes into account the assigned measurements (e.g., object position) of each hypothesis to track the object.

This contribution presents a robust and reliable system for the recognition of pedestrian at night. In contrast to the fusion techniques above, the developed detection system fuses raw sensor data using a boosted classifier. In order to reduce additional costs for new sensors, fusion approach is applied to a scanning ACC radar sensor and an NIR camera sensor, commonly available in modern cars.

The next section gives a general overview of fusion concepts. Moreover, the advantages of feature-level fusion compared with a high-level fusion approach are discussed based on a simple experiment. The developed application of a pedestrian warning system is presented in sections "System Overview" to "Threat Analysis." First, a system overview gives a short description of all components. Section "Sensor Configuration" describes the sensor configuration and the calibration algorithm to associate measurements from different sensors. Section "Boosted Feature-Level Sensor Fusion" presents the developed feature-level fusion approach to detect pedestrians reliably and robustly with an enlarged detection range. The developed road course estimation subsystem is described in section "Global Positioning and Road Course Estimation." The last subsystem, discussed in section "Threat Analysis," combines the two subsystems to realize a threat analysis of detected pedestrians depending on their position on the road. Section "Experiments" analyzes the performance and the results of these subsystems. Finally, section "Conclusion" provides a conclusion and section "Future Directions" discusses the impact on the development of upcoming fusion systems.

Discussion of Fusion Concepts

The special requirements for an automotive pedestrian recognition system can be achieved by means of two strategies. First, enhance the sensing performance of the sensors used in terms of higher spatial resolution and sensitivity and an improved recognition technology. Second, exploit synergistically the electromagnetic spectrum by fusion of different physical sensor technologies.

Sensor fusion allows exploiting the best of all sensors to overcome the shortcomings of one individual sensor. This provides for an enriched knowledge about

the environment in comparison to only one sensor or sensor technology.

The EU projects ProFusion 1 and ProFusion 2 [22] investigated five multiple-sensor data fusion approaches for safety applications, namely, early fusion (also named feature-level fusion), track-level fusion, multilevel fusion, feedback fusion, and grid-based fusion.

Early fusion techniques combine data provided by multiple sensors at an early stage of the data processing chain and perform a joint data interpretation on aggregated data with respect to a common model basis. Two different models for early fusion are possible: pixel-level fusion, only applicable for fusion of images with the same mapping rule, and feature-level fusion, also adaptable for arbitrary sensor combinations. Early fusion techniques demand extensive data processing, which directly requires more complex hardware, and are less flexible compared to high-level fusion methodologies.

The standard approach of sensor fusion in the automotive industry is high-level, or the so-called object-level fusion or decision-level fusion. Each sensor provides high-level track information aligned in space and on a temporal basis, before they are fused by a track-level fusion module. From an economical standpoint [23], there are several advantages. At an object level, it is easy to modify the constellation on the sensor setup, for example, the incorporation of innovative new sensor types, and it is flexible in means that the interface between sensor suppliers can be defined at the object level.

However, one potential drawback is the application-specific definition of objects, leading to an extra effort in adaption. Another disadvantage is a potential loss in raw data or feature information during the object formation process. Subsection "Motivation for Feature-Level Fusion" shows a simple example comparing feature-level fusion and decision-level fusion.

Approaches like multilevel fusion and feedback fusion were investigated in the ProFusion projects [22] and are heavily dependent on the respective applications, incorporating advanced situation refinement techniques.

Grid-based fusion techniques require distance information (e.g., using stereo systems for imaging sensors) for all sensors, attended with additional costs. Nevertheless, this contribution shows in which way it is possible to generate a grid-based representation fusing an imaging sensor with a ranging sensor by feature-level fusion.

The elected fusion approach is the feature level fusion. It uses features extracted from each sensor's data building a composite feature vector to classify the objects. The major advantage of feature-level fusion is that all information, including the sensors, is combined in an optimal manner. Thus, detecting pedestrians can incorporate the information from both sensors at the same time. Even if neither of the two sensors is able to detect any single pedestrian on its own, the fusion approach at the feature level could still be capable of doing the task. Although the advantages are well known, feature-level fusion is rarely used in automotive applications. As mentioned above, this fact can be explained by unavailable low-level sensor data in automotive applications and the higher costs for the transmission with the private CAN or FlexRay link which is generally necessary.

Motivation for Feature-Level Fusion

The following example demonstrates the advantage of feature-level fusion over decision-level fusion. A two-class problem is assumed with a four-dimensional feature space extracted from the measurements of two sensors. The first sensor measures feature 1 and 2. The second sensor observes feature 3 and 4. Two classifiers have been adapted to compare a feature-level fusion approach with a decision-level fusion approach.

The feature-level approach combines all features in one Bayes classifier. The decision-level approach uses two Bayes' classifiers to separate the two classes into their two sensor subspaces of the feature space. The inferences of the two classifiers build a new feature vector, which is then classified by a trained following classifier.

For the experiment, the correlation factor between the features of different sensors is enforced simultaneously, whereas the correlation factor for features of one sensor is held constant. This is done as long as the correlation matrix persists semidefinitely. Figure 1 shows the feature space of a Gaussian distribution. The features are depicted by pairs. For both classes the three-sigma bound is illustrated. The left side

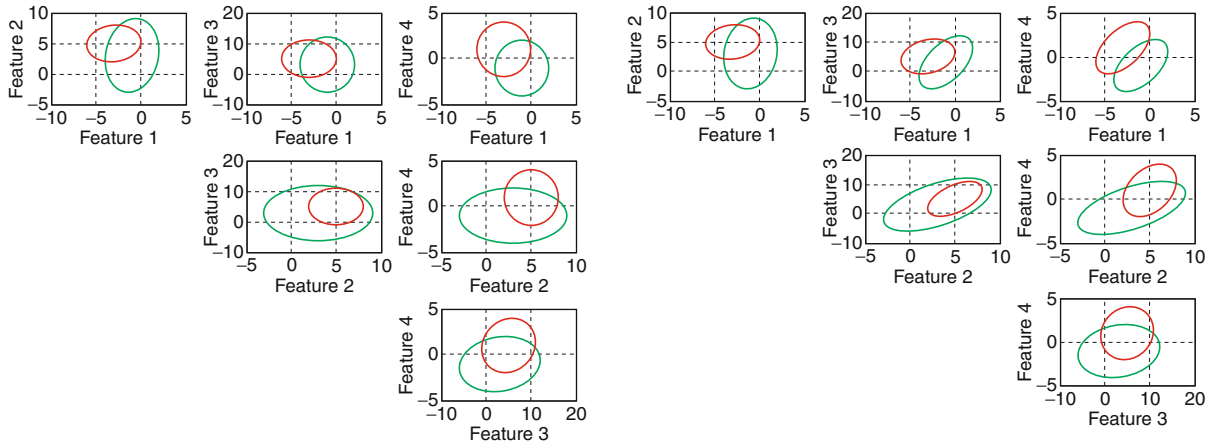

Night Vision Pedestrian Warning in Intelligent Vehicles. Figure 1
Feature space of a Gaussian distribution with dimension four for a two-class problem. The features are depicted by pairs. For both classes, the three sigma standard deviation line is illustrated. The left side presents the distribution with a correlation factor 0. The right side shows it for the maximum correlation

presents the distribution with a correlation factor zero between the features of different sensors. The right side shows the feature space for the maximum simulated correlation.

In Fig. 2 the achieved error rates as a function of the correlation factor are illustrated, whereby the maximum arising correlation factor is scaled to 1. Feature-level fusion clearly outperforms decision-level fusion. The performance enhancement of the feature-level fusion depends strongly on the correlation factor between the features of the two sensors. The risk of applying feature level fusion in place of decision-level fusion is the increased feature space for the classifier. With the expansion of the feature space, the risk of over-adaption in the training stage increases.

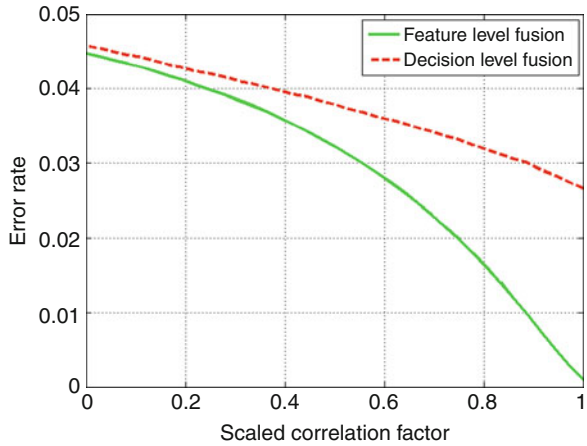

Night Vision Pedestrian Warning in Intelligent Vehicles. Figure 2
Comparison of error rate between feature- and decision-level fusion: The performance enhancement of the feature level fusion depends on the correlation factor between the features of the two sensors

System Overview

Figure 3 shows an overview of the structure and the relations between the information sources and the implemented subsystems necessary to construct a pedestrian warning application. The application is composed of three subsystems.

The first part combines the information provided by the camera sensor and the radar sensor to detect pedestrians reliably and robustly based on the presented feature level fusion approach.

The second part estimates the road course using the information provided by a digital map (i.e., a fixed road shape in front of the vehicle), the radar observations, the inertial vehicle measurements, and the initial position of a GPS receiver. The goal is to fit the road shape

into the radar measurements, which is achieved by testing different global vehicle positions in a local area around the last estimated vehicle position. The GPS receiver provides the first position estimate to initialize the algorithm.

The third part combines the results of the previous subsystems to analyze the relevance of each detected pedestrian depending on their position on the road.

This threat analysis gives the opportunity to direct the driver's attention to a situation of imminent danger.

Sensor Configuration

The presented pedestrian recognition system fuses data from a camera sensor and a radar sensor. Figure 4a shows the sensor mounting positions in the research vehicle: the camera behind the windshield and the radar sensor in front of the radiator grill.

The vision component corresponds to the *Mercedes-Benz Night View Assist*, consisting of an NIR CMOS camera sensor and infrared headlamps providing roughly the same range of visibility as high beam

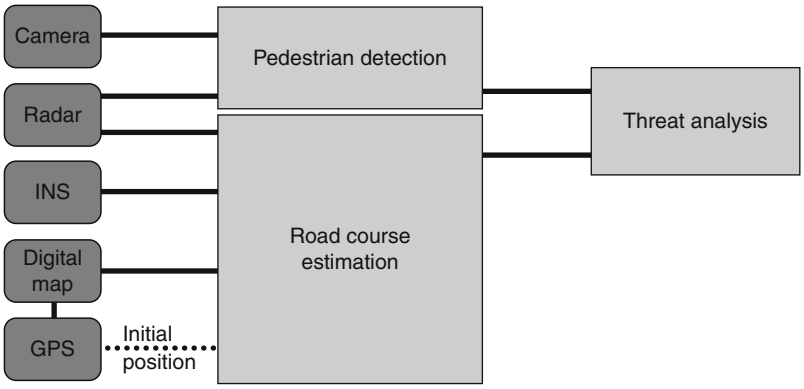

Night Vision Pedestrian Warning in Intelligent Vehicles. Figure 3
System overview: The application is composed of three subsystems, the pedestrian detection, the road course estimation, and threat analysis

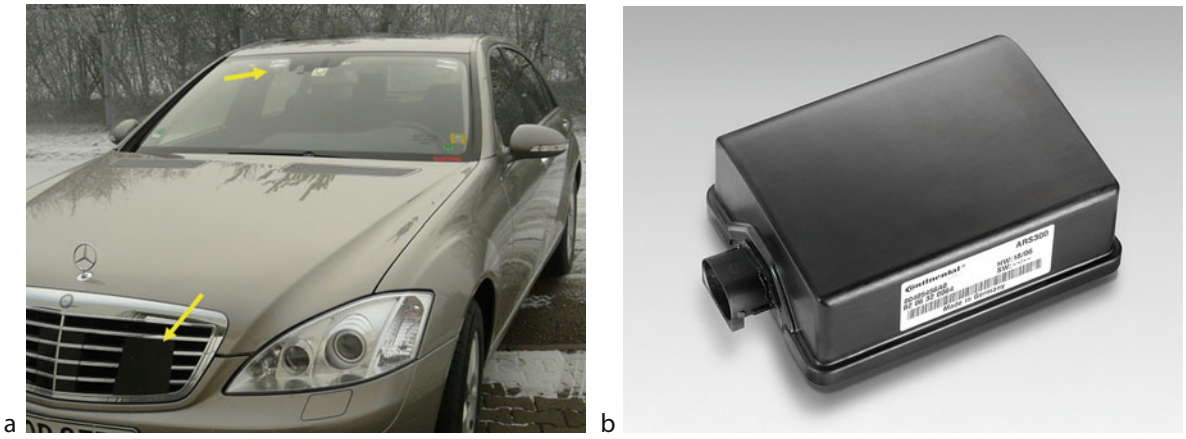

Night Vision Pedestrian Warning in Intelligent Vehicles. Figure 4
(**a**) Research vehicle with sensor mounting positions and (**b**) 3rd generation ACC advanced radar sensor ARS300 from the Continental AG

headlamps – but without impairing the vision of the oncoming traffic. The camera is configured with 12 mm optics and supplies 12 bit gray-scale VGA images.

The advanced radar sensor ARS300 is a new mechanically scanning 77 GHz FMCW radar sensor developed by the Continental AG. Figure 5 gives an impression of the radar measurement raw data which consists of the intensity $i(r, \varphi)$ of the reflected signal in dB and the relative speed $v_{\mathrm{rel}}(r, \varphi)$ of reflecting objects in kph with range $\{r \in \mathbb{Z} | 0\mathrm{m} \leq r \leq 199\mathrm{m}\}$ and azimuthal angle $\{\varphi \in \mathbb{Z} | -8^\circ \leq \varphi \leq 8^\circ\}$. In this configuration each cell (r, φ) has the dimension of 1 m × 1°. The resolution in relative speed is specified with 2.76 kph.

Sensor Alignment

In order to associate measurements from multiple sensors, the alignment of each sensor to the vehicle system (DIN70000) needs to be accurately determined. The radar system is calibrated using the alignment procedure developed by the Continental AG. The centered radar beam is aligned in azimuth and elevation to the longitudinal vehicle axis. However, to calibrate the camera system, the fundamental matrix $\underline{\mathbf{F}} = \underline{\mathbf{F}}_{\mathrm{intr}}\underline{\mathbf{F}}_{\mathrm{extr}}$ containing the intrinsic parameters and the extrinsic parameters needs to be estimated. While the intrinsic camera parameters (e.g., focal length, principal point, skew and distortion coefficients) are estimated using a standard camera calibration technique [24–26], the extrinsic parameters (mounting position and Euler angles) are assessed by solving a nonlinear least-square data fitting problem of the calibration target for N positions:

$$\hat{\underline{\mathbf{F}}}_{\mathrm{extr}} = \arg\min_{\underline{\mathbf{F}}_{\mathrm{extr}}} \sum_{i=1}^{N} \left(\underline{\mathbf{F}}_{\mathrm{intr}}\underline{\mathbf{F}}_{\mathrm{extr}}\underline{\mathbf{x}}(r_i, \varphi_i) - \begin{pmatrix} u \\ v \end{pmatrix}_i \right)^2,$$

where $\underline{\mathbf{x}}(r_i, \varphi_i)$ and $(u, v)^{\mathrm{T}}$ determine the position of the calibration target in the vehicle coordinate system and in the image plane, respectively. An optimal calibration target in the radar plane is a trihedral corner reflector [27], reflecting the emitted electromagnetic wave directly backward to the radar sensor. A 2D Gaussian function is fitted to the intensity data $i(r,\varphi)$ to improve the measured discrete position of the target in the radar frame with $\Delta r = 1$ m and $\Delta\varphi = 1^\circ$. The tip $(u, v)^{\mathrm{T}}$ of each corner position is used as a reference point in the image plane. Figure 6 shows the result of the calibration.

Boosted Feature-Level Sensor Fusion

Fusion Architecture

In order to increase robustness of the pedestrian detection, the system combines the information from complementary sensors (i.e., a camera and a radar sensor) on a feature level using the supervised training algorithm AdaBoost [28]. The sensor fusion architecture consists of three layers (see Fig. 7):

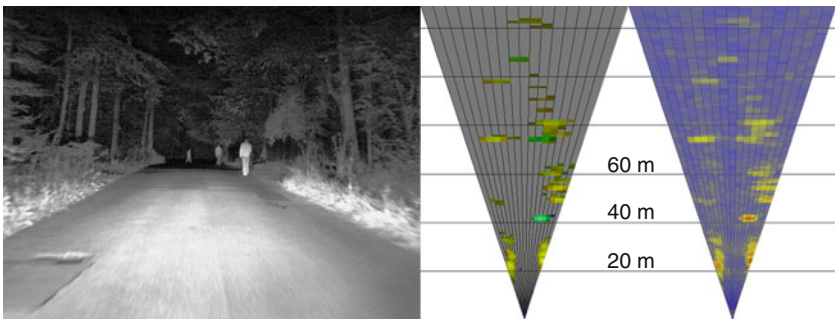

Night Vision Pedestrian Warning in Intelligent Vehicles. Figure 5
Radar measurements: The left image depicts the experienced scene from the camera. The image in the middle shows the radar intensity (value) and relative speed (hue). The three moving pedestrians can be recognized by the green hue component at about 41 m, 75 m, and 108 m. The right image shows all radar intensity values (blue corresponds to low and red to higher intensity)

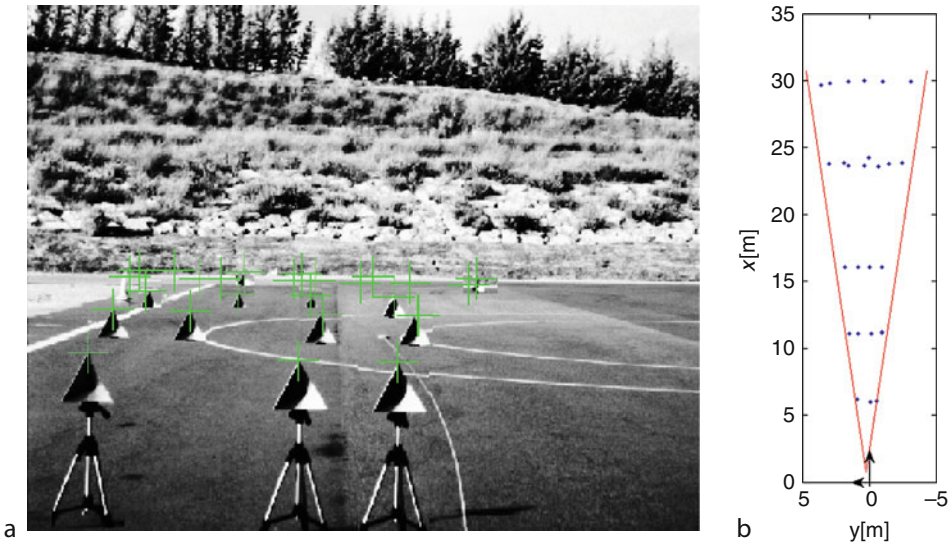

Night Vision Pedestrian Warning in Intelligent Vehicles. Figure 6
Calibration result: (**a**) Composed image of M target positions with $M \subseteq N$ and the projection of N target positions into the image. (**b**) N radar measurements of the trihedral corner reflector in the vehicle coordinate system

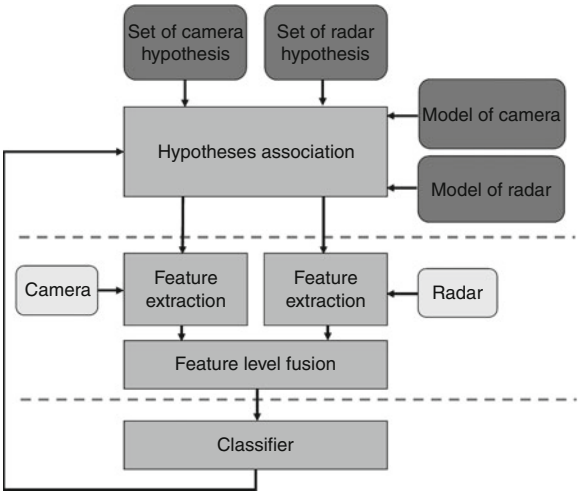

Night Vision Pedestrian Warning in Intelligent Vehicles. Figure 7
Sensor fusion architecture

1. Firstly, hypotheses are generated within the search space. Hypotheses originating from the different sensors are associated based on model information (camera and radar), and eventually on detection results from the previous detection stage (coarse-to-fine search, see section "Multi-Sensor Hypotheses").
2. In the second processing step, the features are calculated and organized in a combined set for both sensors.
3. The classification itself is done in the third processing step based on the calculated features.

The layers two and three are optimized simultaneously. Feature level fusion is achieved in the following way: Features are obtained from each sensor stream simultaneously. These features are held in one set. During the training stage, the source of the individual features and their type do not matter. AdaBoost selects incrementally those features having the lowest weighted error on the training set, until the algorithm achieves a predefined correct and false detection rate. This technique assures an optimal selection and weighting of the features from both sensors for the classification task.

All features are defined within search windows belonging to the different sensors. The tuple of search windows (one for each sensor input) describes a hypothesis presented to the classifier. The latter assumes that both search windows identify the same localization of the scene. This requires an accurate mapping between the camera plane and the radar

plane. However, combining multiple sensors also increases the input space and, consequently, increases the computational effort due to the ambiguous mapping between the camera plane and the radar plane.

The radar measurement $i(r, \varphi)$ defines an ROI in the camera image (see Fig. 8), which is much bigger than the projected object at the measured position (r, φ). Moreover the object height cannot be measured by the radar system. Thus multiple search windows in the image are possible to be associated to a single radar measurement $i(r, \varphi)$. Section "Multi-Sensor Hypotheses" describes the association rule in detail.

In order to realize a real-time detection system, the presented fusion system incorporates cascaded classifiers introduced by Viola and Jones [29], [30]. Such a classifier is capable of separating regions in the input space into two classes, namely, the object and background class using a chain of classifier stages (see Fig. 9). With an increasing number of stages, the complexity of these classifiers rises by the number of

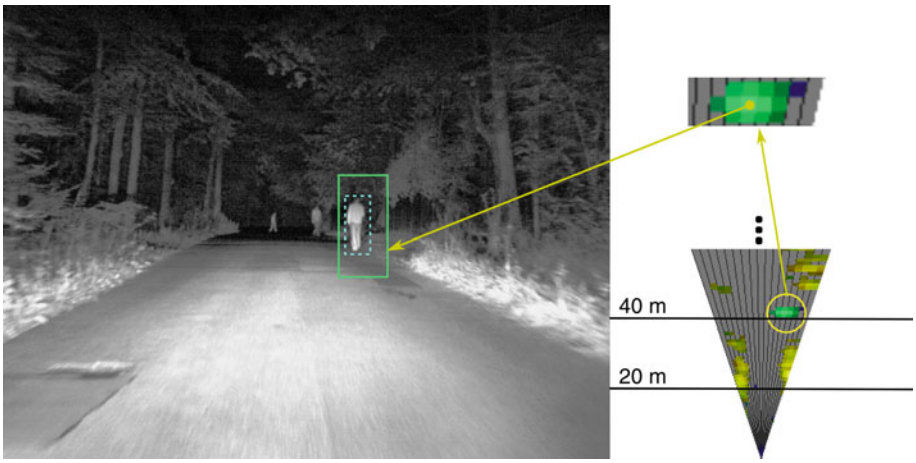

Night Vision Pedestrian Warning in Intelligent Vehicles. Figure 8
Ambiguous mapping between the camera and the radar plane: A radar measurement $i(r, \varphi)$ defines a much bigger ROI (*green*) in the image plane than the corresponding pedestrian object (*dashed blue*). Thus the measurement (r, φ) belongs to multiple search windows in the corresponding image area

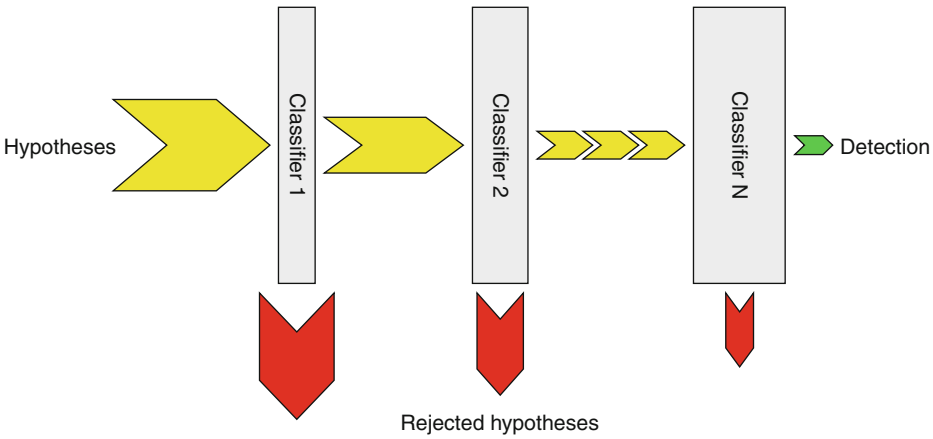

Night Vision Pedestrian Warning in Intelligent Vehicles. Figure 9
Cascaded classifier: Each stage discards hypotheses and passes promising samples onto the successive and more complex stage

features used. Each classifier stage is trained using the AdaBoost algorithm to choose the most significant features from both sensors. Depending on the discriminative power of the features from the camera sensor and the radar sensor, the resulting cascade can perform the classification task very efficiently. Subsection "Radar Features" describes the derived radar features in detail.

The AdaBoost Approach to Machine Learning

Boosted classifiers and the related AdaBoost algorithm introduced by Freund and Schapire [28] are very well described in [31–33]. The basic idea is that a set of weak classifiers build a strong classifier. The decision of the strong classifier is a weighted voting of the decisions of the weak classifiers. The weak classifiers are selected subsequently in the trainings phase. On each round, the weights of incorrectly classified examples increase, the weights of correctly classified examples decrease, so that the next weak classifier focuses more on incorrectly classified samples. The importance of the weak classifier depends on its error on the weighted sample set. A pseudo-code description of the multi-sensor algorithm regarding a two-class classification scenario is given in Fig. 10.

The algorithm requires a multi-sensor training set of N samples with $\left(x_1^{(1)}, x_1^{(2)}, \ldots, x_1^{(M)}, y_1\right), \ldots, \left(x_N^{(1)}, x_N^{(2)}, \ldots, x_N^{(M)}, y_N\right)$ as input where $x_j^{(k)}$ represents the input of the kth sensor and $y_j \in \{-1, +1\}$ the corresponding manually extracted label (i.e., -1 for a background and $+1$ for an object sample). For all iterations $t = 1, \ldots, T$ AdaBoost calls a weak learning algorithm to train the base classifier with importance $\alpha_t \in \mathbb{R}$ on a weighted version of the training set by minimizing the weighted error ε_t:

$$\varepsilon_t = \min_{i,k} \sum_{j=1}^{N} w_{i,j} \left| \frac{h_{t,i}^{(k)}(x_j^k) - y_j}{2} \right|$$

$$\alpha_t = \frac{1}{2} \ln\left(\frac{1 - \varepsilon_t}{\varepsilon_t}\right).$$

Thus each round AdaBoost chooses the best weak learner $h_i^{(k)}$ from the set of specified features of all

Require:

N samples $(x_j^{(1)}, x_j^{(2)}, \ldots, x_j^{(M)}, y_j)$ for M sensors with

$j = 1, \ldots, N$ and $y_j \in \{-1, +1\}$

τ : minum detection rate

T : maximum number of selectable weak classifiers

Ensure:

The final strong learner decision $H(x)$ is composed of the most discriminative weak learners $h_t^{(k)}$ and achieves the required detection rate.

1: initialize $w_j = \frac{1}{N}$

2: **for** feature $t = 1, \ldots, T$ **do**

3: determine weak learner $h_t^{(k)}$ that minimizes the weighted error ε_t on the training data

4: choose α_1, the importance of $h_t^{(k)}$

5: update sample weights and normalize so that w remain a distribution:

$$w_j = \frac{1}{n_t} w_j \exp^{-\alpha_t y_t^{(k)}(x_1^{(k)})}$$

with n_t as a normalizing factor

6: **end for**

7: adjust θ of the final strong learner to realize the minimum detection rate τ:

$$H(x) = \operatorname{sgn}\left(\left(\sum_{t=1}^{T} \alpha_t h_t^{(k)}(x^{(k)})\right) - \theta\right)$$

Night Vision Pedestrian Warning in Intelligent Vehicles. Figure 10
Pseudo-code description of the multi-sensor AdaBoost algorithm

sensors (e.g., an image feature or a radar feature). The final strong learner decision H is a weighted majority vote of the chosen T weak learners:

$$H(x) = \begin{cases} +1 & : \sum_{t=1}^{T} \alpha_t h_t^{(k)}(x^{(k)}) \geq 0 \\ -1 & : \quad \text{else.} \end{cases}$$

Applying this algorithm to each stage of a cascaded classifier, the decision in the first layers with less weak learners can be dominated by one of the sensors with the most discriminative power of their features.

Image Features

In the image plane, an object (e.g., pedestrian) is represented by a rectangular search window, which is defined by its upper left and lower right corner with a fixed width-to-height ratio (e.g., 0.5). The feature set used in the image plane consists of Haar-wavelet filters [34, 35], which vary in size and position within the rectangular search window. These features have been successfully applied in many pedestrian recognition systems [16, 17, 35], and are able to compute efficiently using integral images.

Radar Features

In the radar plane, the feature set is composed of two different filter subsets:

- Subset S_1 consists of filters describing the average value of the reflected object intensity
- Subset S_2 consists of complex signal filters with a structure similar to the radar CFAR (constant false alarm rate) filters [27]

Contrary to the image plane, a pedestrian cannot be distinguished clearly in the radar plane because the radar signal of a typical pedestrian is similar to many other objects, for example, posts, street lamps, and trees. In other words, these filters are not capable of unambiguously classifying a pedestrian. However, they can be used to reject background samples very efficiently. The manually labeled pedestrian in the radar image at position (r, φ) defines the center of the search window with a fixed size 5 m $\times$ 5°. Figure 11 shows the expanded field of view by mirroring the corresponding beam directions at the left and the right border. This allows for apply the filters to all beam directions φ.

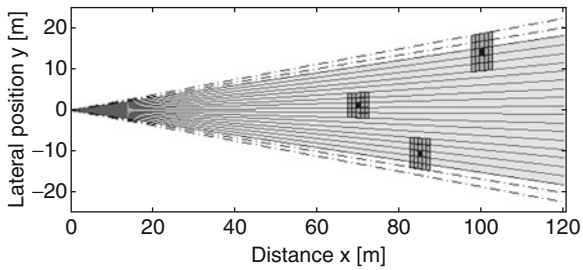

Night Vision Pedestrian Warning in Intelligent Vehicles. Figure 11
Definition of the search window in the radar plane projected onto the Cartesian vehicle plane: Each position (r, φ) indicates the centre of the search window with a fixed size of 5 m $\times$ 5°. The field of view is expanded in φ to apply the filters to all beam directions

1. *Average object intensity filter*: The reflected signal intensity $i(r, \varphi)$ can be used to very efficiently separate between object and background. This can also be seen in Fig. 5 (in the radar intensity measurements). Within the search window, a rectangular filter is used to calculate the mean signal intensity. Thus subset S_1 consists of different rectangular filters varying in position and size within the search window.
2. *Complex signal filter*: The complex signal filter combines the reflected signal intensity $i(r, \varphi)$ and the relative object velocity $v_{\text{rel}}(r, \varphi)$ to detect object clusters of similar velocity. With regard to the theory of radar systems, the measured object intensity and relative velocity represent the highest peak in the Doppler spectrum at the measured position(r, φ). Hence the complex number $z(r, \varphi)$ describes the radar measurement (i, v_{rel}) at position (r, φ) equally:

$$\begin{aligned} &z(r, \varphi) = A_z \exp^{j\pi\omega}, z \in \mathbb{C} \\ &A_z = i(r, \varphi) \\ &\omega = f(v_{\text{rel}}(r, \varphi)) + v_{\text{ego}}, \{\omega \in \mathbb{R} | \ |\omega \leq 1.0|\} \ , \end{aligned}$$

where A_z corresponds to the measured intensity, v_{ego} defines the driving speed, and ω describes the measured absolute velocity of measured objects after the normalization.

A complex signal filter is composed of three rectangular zones (see Fig. 12): a background zone A, a blind

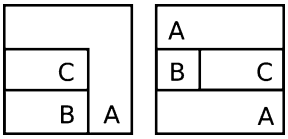

Night Vision Pedestrian Warning in Intelligent Vehicles. Figure 12
A complex signal filter is defined by three zones: a background zone A, a blind zone B and a test zone C with $C \subseteq B \subseteq A$

zone B, and a test zone C with $C \subseteq B \subseteq A$. This corresponds to the CFAR filter structure [27] extended to two dimensions. Arranging the three zones in all positions and sizes within a search window of the size 5 m × 5° results in 44,100 different filters. The real-valued filter value is defined by:

$$\left| \frac{|A \backslash B|}{|C|} \sum_{\forall (r,\varphi) \in C} z(r,\varphi) - \sum_{\forall (r,\varphi) \in A \backslash B} z(r,\varphi) \right|$$

which is equivalent to the norm of normalized differences between the integrated complex values $z(r,\varphi)$ over C and A\B. Figure 13 shows the filter calculation and the resulting filter value which describes a local similarity measure of velocity differences. These filters suppress noisy measurements indicated by a small complex modulus and a random complex argument in $z(r,\varphi)$. However, the defined filters cannot distinguish between moving pedestrians and small stationary objects with a similar intensity pattern (e.g., posts): both result in high filter responses. In contrast, low filter responses are caused by bigger objects with intensity patterns different from pedestrian patterns (e.g., cars, houses).

In order to reduce the computational complexity, the algorithm decomposes the complex number z into their components $\mathrm{Re}\{z\}$ and $\mathrm{Im}\{z\}$ and uses integral images to calculate the filter value components independently.

Multi-Sensor Hypotheses

The presented cascaded classifier requires a tuple of search windows identifying the same scene in the image plane and in the radar plane. Search windows are generated in a range from 20 to 120 m, which corresponds to pedestrian sizes in the image plane from 120 to 21 px. Due to the ambiguous mapping between both sensors (see Fig. 8), this results in multiple search windows in the image plane associated to one search window in the radar plane. In order to efficiently perform on the increased input space, the classifier scans the image plane restricted to the ROI using the relaxed *flat world assumption* presented in [19] that compensates the pitch of the vehicle.

Using the camera model, the search window height of a minimum size and a maximum size pedestrian can be calculated at each distance r of the radar sensor. These heights represent the limits of scaled versions of the minimum search window height at distance r. The combination of the restricted image plane and the set of search window heights define the resulting grid of search windows in the image plane associated to the search windows with distance r in the radar plane.

The resulting amount of hypotheses to be classified remains unmanageable for real-time applications. With a coarse-to-fine search, generating a set of search window grids in the image plane with different position sampling increments the problem can be solved. First, the detector classifies the coarse grid and continues the classification in the fine grid for positive classified search windows.

Global Positioning and Road Course Estimation

The previous sections presented the feature level sensor fusion approach to detect pedestrians at night using an NIR camera and an imaging radar. In order to realize a warning system which directs the driver's attention primarily to the relevant objects, the information about the pedestrian's position is combined with a new road course estimation approach. Instead of estimating the shape of the road, this contribution estimates the position on a digital map and extracts the preceding road course directly from the map. In contrast to loosely and tightly coupled INS/GPS solutions, the main concept of this contribution is based on the method to localize a robot in a known defined environment, also known as Monte Carlo Localization (MCL) [36, 37].

MCL algorithm uses a particle filter approach [38]. Each particle describes a position and an orientation of the robot in a restricted environment which has been mapped using the sensor measurements of the robot (e.g., ultrasonic, radar, laser, and camera). At the beginning, the position of the robot is unknown. Thus each position in the restricted environment is possible,

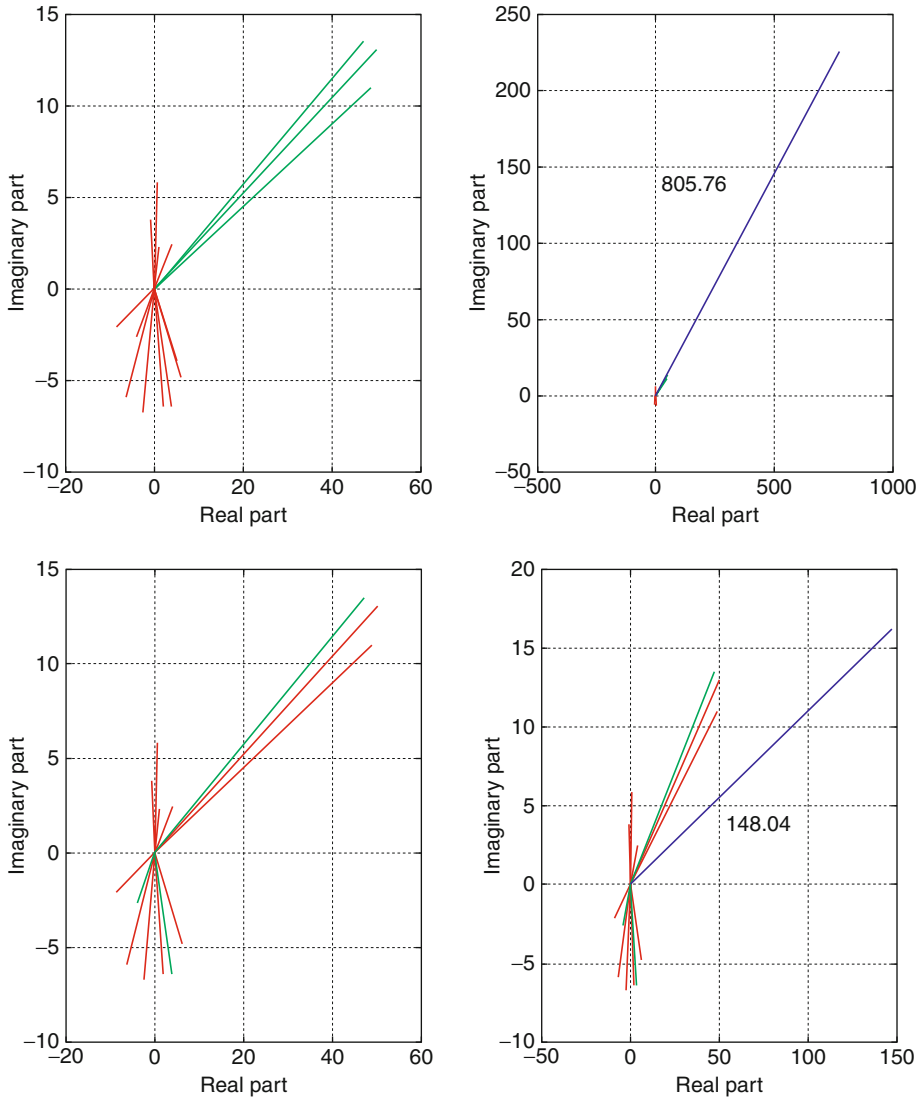

Night Vision Pedestrian Warning in Intelligent Vehicles. Figure 13
Complex signal filter response: Given a search window, the corresponding radar measurements (i, v_{rel}) are assigned to the filter zones (*left figures*): background (*red*), blind (the measurements which are not taken into account) and test (*green*). The upper graphics show the optimal filter and the lower graphics show a suboptimal filter in the complex plane related to the given radar measurements. The filter response (*right graphic*) is shown by the complex number in blue with the corresponding real-valued filter result as text

leading to a uniform distribution of the particles on the map. In order to localize the robot on the map, the algorithm verifies each position based on the local sensor measurements. After a few iterations, the particles will converge to the most likely position and thus the robot is localized.

A significant difference to a robot is that the environment of a passenger car corresponds to an unrestricted network of roads. Thus, the position cannot be uniformly distributed in the initialization cycle. This problem can be solved by means of a low-cost GPS sensor which restricts the area of possible initial

positions to the maximum position uncertainty of ±25 m. The position and the orientation of the ego vehicle are described in UTM (Universal Transverse Mercator) coordinates [39] which project meridian segments into a rectangular plane with negligible distortion error. In order to verify a position hypothesis, the observations of the imaging radar are compared with the extracted road course of an electronic horizon component (e.g., [40]). Note that the electronic horizon component also performs a map matching using the GPS position and a digital map. But the calculated position does not regard the width of the road, and the orientation of the vehicle cannot be estimated precisely. The resulting state vector of a position hypothesis is defined by

$$\underline{\mathbf{q}}_k^{(i)} = \left(e_k^W, n_k^W, \Phi_k^W, b_k^W\right)^{(i)}.$$

The scalar components $e_k^W, n_k^W, \Phi_k^W, b_k^W$ of the particle number (i) denote the position in UTM (east and north coordinate), the orientation of the vehicle, and the width of the road for iteration k.

The main steps of the positioning algorithm using a particle filter approach can be outlined as follows:

1. Sample from the probability density $p(\underline{\mathbf{q}}_{k-1}|\underline{y}_{0:k-1})$ of the previous iteration generates a new set of particles. Each particle $\underline{\mathbf{q}}_k^{(i)}$ describes a vehicle coordinate system in a global UTM coordinate system.
2. Apply a deterministic and a stochastic drift to predict the hypotheses to the most likely position of the current iteration. The deterministic portion corresponds to the egomotion of the ego vehicle during an iteration step which is estimated by an extended Kalman filter (EKF). The stochastic portion models the process uncertainties by an unbiased Gaussian and yields to a random distribution of equally sampled particles.
3. Calculate the likelihood for each particle based on the measurements of the imaging radar sensor. This step is based on an intensity model of the road, which expects that the road itself is free of objects and narrowed by high intensities from stationary objects. Hence a preprocessing step of the radar measurements is required to compensate the high intensities caused by moving objects on the road.
4. The final step is to generate the probability density $p(\underline{\mathbf{q}}_k|\underline{y}_{0:k})$ based on the weighted particle set.

The following subsections discuss the egomotion estimation, the radar preprocessing, and the likelihood function in detail.

Egomotion Estimation

In order to measure the egomotion of the vehicle, an EKF approach is used which considers the inertial sensor measurements providing information about the turn rate $\dot{\Psi}$and the wheel rates $d_{\mathrm{fl,fr,rl,rr}}$ of all four wheels. As discussed in [41], a *Constant Turn Rate and Velocity* (CTRV) motion model is totally sufficient to describe the common movements of a vehicle. The state space and the continuous differential equations are defined by

$$\begin{aligned}
&\underline{\mathbf{x}} = \left[x, y, v, \Psi, \dot{\Psi}\right]^{\mathrm{T}} \quad \text{with}\\
&\dot{x} = v(t)\ \cos\Psi(t),\\
&\dot{y} = v(t)\ \sin\Psi(t),\\
&\dot{v} = 0,\\
&\ddot{\Psi} = 0\,.
\end{aligned}$$

The scalar components x, y, v, Ψ and $\dot{\Psi}$ denote the longitudinal and the lateral (to the left) movement, the longitudinal velocity, the rotation angle, and the turn rate. This curvilinear motion model involves a nonlinear state transition as well as a nonlinear measurement model using a four-wheel vehicle model.The discretized formulation based on the sample time T can be derived by solving

$$\underline{\mathbf{x}}_{k+1} = \underline{\mathbf{x}}_k + \int_t^{t+T} \underline{\mathbf{x}}(\tau)d\tau.$$

This yields to

$$\begin{aligned}
&x_{k+1} = x_k + \frac{v_k}{w_k}\left(-\sin(\Psi_k) + \sin(w_k T + \Psi_k)\right),\\
&y_{k+1} = y_k + \frac{v_k}{w_k}\left(\cos(\Psi_k) - \cos(w_k T + \Psi_k)\right),\\
&v_{k+1} = x_k,\\
&\Psi_{k+1} = \Psi_k + w_k T,\\
&w_{k+1} = w_k \quad (\text{the discrete turn rate}),
\end{aligned}$$

when $|w_k| \to 0$ then use

$$\begin{aligned}
&x_{k+1} = x_k + v_k T\cos(\Psi_k),\\
&y_{k+1} = y_k + v_k T\sin(\Psi_k)\,.
\end{aligned}$$

In order to handle the asynchronous arriving turn rate and wheel rate measurements, the EKF implementation corresponds to the sequential measurement update formulation presented in [42], which is further proved to be efficient and numerically stable. The filter consistency is maintained by testing each measurement innovation against its predicted innovation uncertainty in a three-sigma bound which covers 99.7% of the expected measurements. A failed test will reset the filter to the initial state covariance, which happens when the CTRV process model does not represent the vehicle's motion (occurs mostly in sharp turns and when the vehicle accelerates). The accuracy of the egomotion estimation algorithm is shown in Fig. 14.

The required incremental movement between consecutive radar measurements is provided by a reset operation after each cycle of the positioning algorithm. For this purpose, the scalar components x, y, and Ψ are set to zero and the corresponding entries in the covariance matrix are set to their initial values.

Radar Preprocessing

Moving obstacles in the field of view of the radar sensor have a huge impact on the evaluation of position hypotheses because the algorithm assumes a road model with low intensities on the road and high intensities on the road border. Due to the high radar cross section of vehicles, a moving vehicle on the road violates this assumption. In order to diminish this impact, a preprocessing step is applied replacing the intensity measurements by their corresponding noise level value (measured by the radar sensor for each cell (r, φ)) when the measurement represents a moving object. The moving object decision is based on the measured radial relative velocity $v_{\mathrm{D}}^{\mathrm{R}}$ (Doppler), its direction φ^{R} and the estimated velocity of the ego vehicle v_{ego}.

$$\text{Moving object} \Leftrightarrow \quad \left| v_{\mathrm{D}}^{\mathrm{R}} \cos(\varphi^{\mathrm{R}}) - v_{\mathrm{ego}} \right| \geq \gamma_{\mathrm{v}},$$

where γ_{v} denotes the velocity threshold.

Evaluation of Position Hypotheses

Each hypothesis or particle defines a position and an orientation of the vehicle in UTM coordinates. Given that position and the road course from the digital map, an individual course of the preceding road segment can be described in vehicle coordinates. This provides the possibility to establish a relationship between the digital map data and the radar observations of the environment. The estimation of the road width is used to define two polylines describing the boundary of the road. The next step transforms these two polylines for each particle into the bilinear interpolated Cartesian representation of the preprocessed polar radar intensity measurements (see Fig. 15). Thus, a goodness of fit measure can be computed for each particle. This evaluation is based on

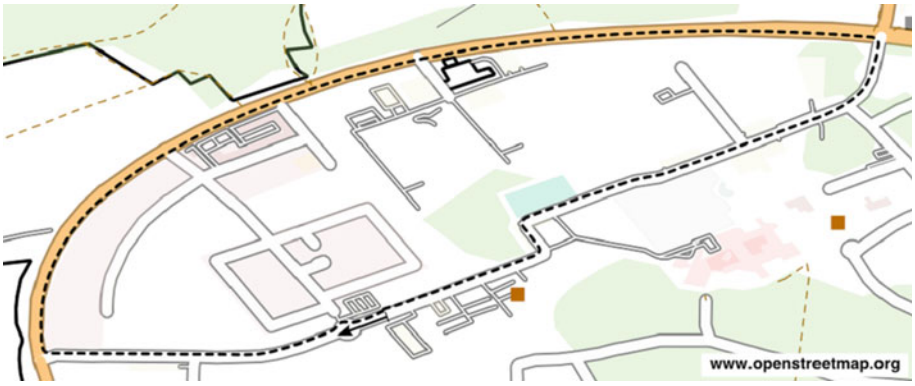

Night Vision Pedestrian Warning in Intelligent Vehicles. Figure 14
Egomotion accuracy analysis: The figure shows the estimated course of a closed-loop scenario of length 4.5 km in UTM coordinates. The resulting estimation error between the starting and the end position (represented by the arrow in driving direction) is about 2.4 m

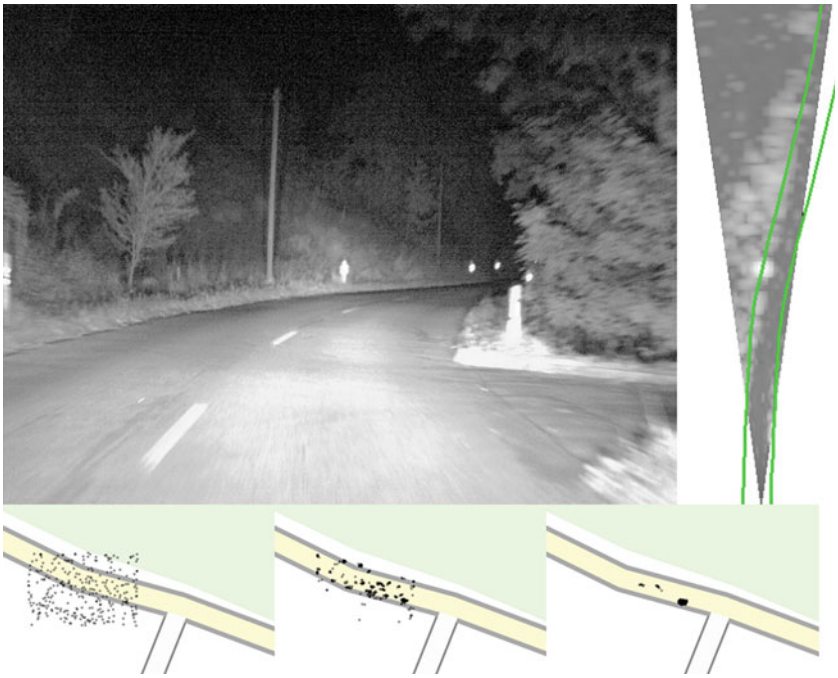

Night Vision Pedestrian Warning in Intelligent Vehicles. Figure 15
Results of the position estimation process: The small maps show the particle distribution at initialization of the algorithm after the 2nd and after the 5th iteration. The sensor observations of the camera and the radar sensor as well as the estimated road course after the 5th iteration step is shown above

the mean intensity value between the polylines $\overline{\Upsilon}_1$ and the mean intensity value below the polylines $\overline{\Upsilon}_2$according to the logistic function

$$g(\overline{\Upsilon}_2 - \overline{\Upsilon}_1) = \beta\,(1 + \exp(-(\overline{\Upsilon}_2 - \overline{\Upsilon}_1 - \alpha)))^{-1}.$$

The inflection point α denotes the barrier to evaluate a hypothesis as a positive road course candidate. The nonlinear characteristic of $g(\cdot)$ improves the convergence behavior. Furthermore, the factor β models the ratio of the estimated road course in the radar's field of view.

Figure 15 shows three iteration steps of the positioning algorithm. The expected road course after the 5th iteration is shown in the Cartesian representation of the radar measurements. Both polylines are partly outside of the field of view which yields to the ratio $\beta < 1.0$.

Threat Analysis

After the detailed description of the pedestrian detection system and the road course estimation system, the final task is to fuse both information sources to realize a pedestrian warning system. A range-dependent object warning is straightforward using the position information provided by the detection system. The more challenging task, discussed here, is to warn the driver about objects depending on their lateral position to the road which requires a threat analysis based on both information sources. Figure 16 shows the desired warning scheme with low ratings on the sidewalk and the highest rating in the center of the right lane. Moreover, a pedestrian on the right sidewalk poses a higher threat to the driver than a pedestrian on the left sidewalk, under the assumption of driving in the right lane.

An advantage of the presented system architecture is the shared usage of the radar data in the detection system and in the road course estimation system. This gives the opportunity to measure directly the relevance of an object. The detection system describes each object position in polar radar coordinates (r_i, φ_j) and in image coordinates (u, v, w, h). The road course estimation system delivers the polylines of the road boundary

in Cartesian radar coordinates which yields to a lateral resolution problem when using (r_i, φ_j) directly. Hence the image position is used to define a more precise object position in (r_i, φ_j). The calculation is based on a linear interpolation between the calibrated left and right image columns of the object beam φ_j.

This refined position defined by (r_i, φ_j^*) is then transformed into the Cartesian view to measure the distance d to the left polyline of the estimated road course. The final warning level of a detected object corresponds to

$$\eta(d^*) = \exp\left(-\frac{(d^* - 0.75)^2)}{2\sigma^2}\right).$$

The distance d^* is normalized by the estimated road width and σ^2 chosen to 0.1 defines the warning focus. Figure 17 shows the result of the realized threat analysis. The warning level changes from red to green for a pedestrian walking from the center of right lane to the left sidewalk.

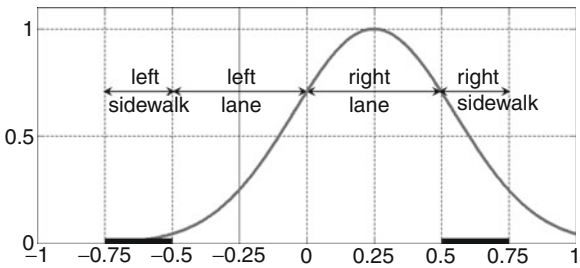

Night Vision Pedestrian Warning in Intelligent Vehicles. Figure 16
The desired warning scheme on a two-lane road: The most threatening object position is in the centre of the right lane. The width of the road is normalized to one

Experiments

Pedestrian Detection System

The following subsections discuss the performance of the feature-level fusion approach used in the pedestrian detection system. This requires methods for ground truth generation, a set of recorded sequences for training and testing and an evaluation criterion.

Defining a Ground Truth Each supervised classification task requires a consistent ground truth for training and evaluating a classifier. With regard to a multi-sensor configuration, consistency is much more important because an object label in one sensor plane has to identify the same object in the other sensor plane. Figure 17 shows a typical scene of pedestrians in a suburban environment. Labeling the pedestrians in

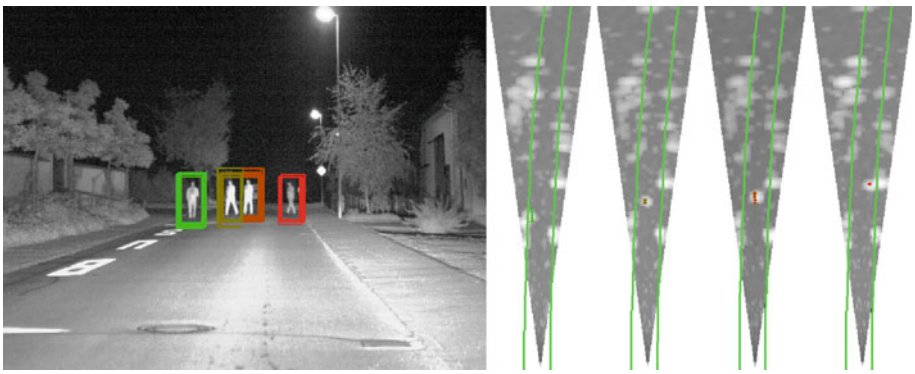

Night Vision Pedestrian Warning in Intelligent Vehicles. Figure 17
Result of the threat analysis: The left image shows a walking pedestrian from the right lane centre at iteration k to the left sidewalk at iteration $k + N$. While the pedestrian is walking to the left sidewalk the warning level of the pedestrian is decreasing from red to green. The figures on the right show the corresponding pedestrian position as well as the estimated road course in the Cartesian radar measurement view

the image is rather simple and easy to learn. However, labeling the same pedestrian in the radar image is much more complicated and requires an expert or some kind of label assistance. Different label assistance options are possible:

1. Monocular distance estimation assuming a fixed pedestrian size of the label in the image plane
2. CFAR detector applied to the projected epipolar line in the radar plane given by an assumed minimum and maximum pedestrian size
3. Stereo distance estimation analyzing the pixel disparity within the label in the image plane

Note that they all utilize the information provided by the pedestrian label in the image plane. While option 1 fails due to poor label accuracy, especially in a high detection range, and option 2 fails due to the fixed structure of the CFAR filter mismatching the pedestrian with other objects on the epipolar line, option 3 achieves the most promising results. Using this assistance the labeler can use the initial conjecture and correct the position if necessary. This method implies also a stereo camera setup with a large baseline in order to achieve good distance estimates of labeled pedestrians up to 120 m.

Training and Evaluation Settings To demonstrate the performance of the presented detection system, two pedestrian detectors were trained: an image-based reference detector using only the Haar-wavelet filters in the image plane and a fusion detector using additionally the defined radar features.

The training set consists of 36,562 images taken from 122 pedestrian sequences and 71 non-pedestrian sequences recorded nightly in the period from July 2007 to June 2008. The collection of images contains 17,833 pedestrian samples and represents a good mixture of pedestrians in rural and suburban environments within 120 m. Both detectors use 30,000 background samples selected randomly in each stage of the cascade from the image set.

The test set contains 7,887 pedestrian samples in 8,449 images. In order to compare the performance of both detectors equitably, an evaluation algorithm analyzes the detections in the image plane restricted by the field of view of the radar sensor. All detections are separated in true and false positives using a coverage measure cov(A,B) between the rectangular detection A and the pedestrian label B:

$$\mathrm{cov}(A, B) = \frac{A \cap B}{A \cup B} .$$

The threshold $\gamma_{\min}$ defines the minimum required coverage to assign detections to the set of true positives.

Detection Results The trained fusion detector significantly outperforms the reference detector while requiring less stages and thus less features (see Table 1). Furthermore, AdaBoost selects up to 38% of the features from the set of radar features which emphasizes their discriminative power. These radar features afford a fast and cost-effective reduction of hypotheses in early stages of the cascaded fusion detector. Figure 18 compares the computational cost of both classifiers in environments of different complexity. Figure 19 shows the ROC curves comparing the performance of the fusion detector and the image based reference detector for $\gamma_{\min} = \{0.5; 0.6\}$. For the fusion detector, the detection rate is higher and the false alarm rate is lower than the performance values of the reference system using only the information provided by the NIR camera. Furthermore, system performance increases with the required minimum coverage $\gamma_{\min}$. This behavior indicates the detection quality in spatial resolution: While the fusion detector uses the information provided by the radar sensor to suppress invalid hypotheses and effectively achieves a grid based fusion approach, the reference classifier cannot distinguish between pedestrian hypotheses at different distances. Hence, the latter produces detection results incapable of localizing the pedestrian in space. Figure 20 shows the precise pedestrian localization of the fusion system compared to the uncertainty of the reference detector.

Road Course Estimation

In order to evaluate the estimated road course, or rather the estimated vehicle position, a ground truth is required.

Night Vision Pedestrian Warning in Intelligent Vehicles. Table 1 Detector characteristics

	Stages	Image features	Radar features
Fusion	28	1061	407
Reference	30	1621	–

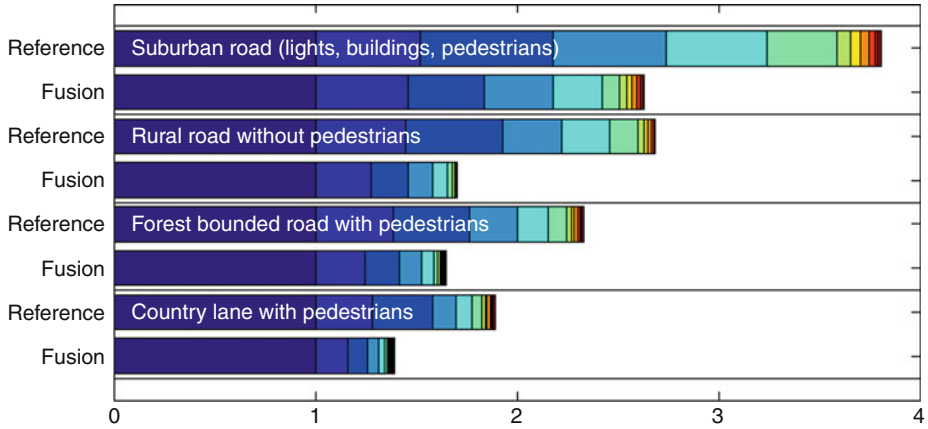

Night Vision Pedestrian Warning in Intelligent Vehicles. Figure 18
Computational cost analysis in the early stages of the cascade up to layer 12: The image based reference detector and the fusion detector classify the same set of hypotheses. In stage one both detectors analyze about 2 million hypotheses using five weak learners (referenced as cost 100%). Due to the combination of radar features and image features, the fusion detector can reject more hypotheses than the image-based reference detector. Thus, the number of weak learner calculations can be reduced more efficiently. The fusion detector also shows similar results in highly structured environments, such as suburban areas with buildings and heavily changing light conditions

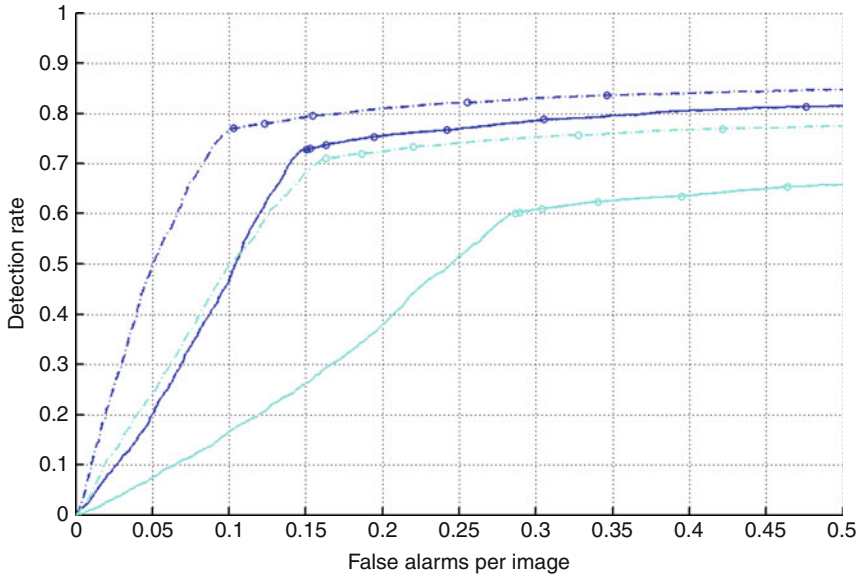

Night Vision Pedestrian Warning in Intelligent Vehicles. Figure 19
Performance comparison between the image based reference detector (solid) and the fusion detector (*dash-dot*) for the coverage 0.5 (*blue*, upper two graphs) and 0.6 (*cyan*, lower two graphs)

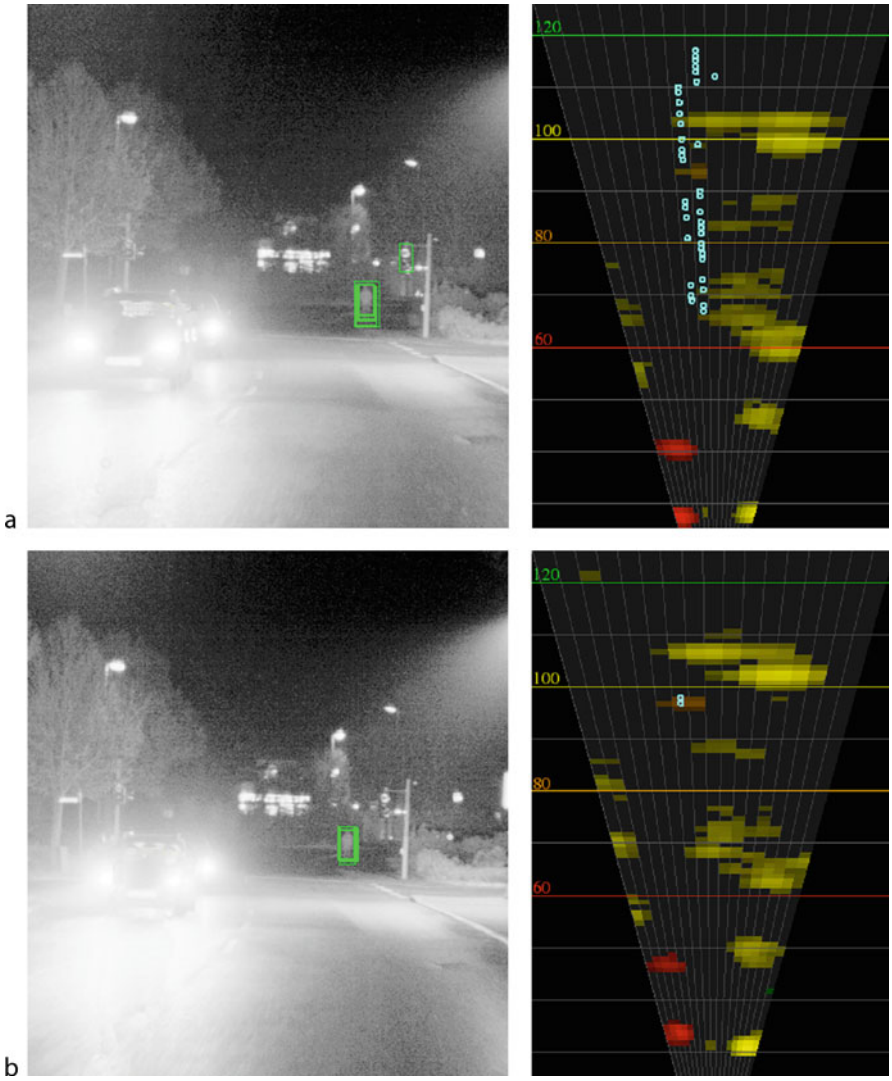

Night Vision Pedestrian Warning in Intelligent Vehicles. Figure 20
Detection examples in a suburban environment (camera image with green detections left and radar data with cyan detections right): (**a**) Typical result of the image based reference detector. The uncertainty in spatial localization is very high using only image features for classification. Figure (**b**) shows the increased performance of the fusion detector incorporating features provided by the radar system too. The result is a precise localization of the pedestrians at 100 m ((a) Image-based reference detector: Typical detection of a pedestrian at 100 m with very imprecise spatial localization (70–120 m). (b) Fusion detector: Accurate detection of a pedestrian at 100 m)

The best, but unfortunately the most expensive, equipment is clearly a RTK GPS measurement unit. It is able to measure the vehicle position with a very high accuracy within a range of a few centimeters. For this examination, such a device was not available.

Nevertheless, the estimated position can also be analyzed considering the position uncertainty in a driving scenario. The position uncertainty calculation transforms each position hypothesis into the vehicle coordinate system of the expected position value of

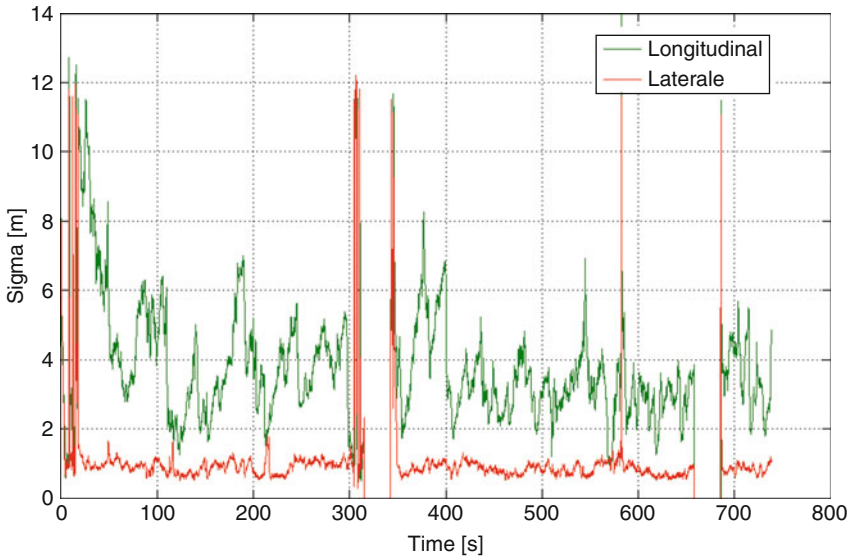

Night Vision Pedestrian Warning in Intelligent Vehicles. Figure 21
Standard deviation of the estimated longitudinal and the lateral position for three driving scenarios

the distribution and determines the standard deviation for longitudinal and lateral position as well as for the orientation angle. Figure 21 shows the lateral and the longitudinal deviation for three scenarios. Whereas the lateral position deviation remains low and nearly constant, the longitudinal position deviation fluctuates more strongly. This behavior is associated with the current road course. A course with frequent curves provides more precise information for longitudinal localization than a straight road, which yields to ambiguous position hypotheses because the digital map fits anywhere along the road.

Moreover, the map-based position estimation can be compared to an approach using only the vehicle data that is the result of the egomotion estimation without resetting the position regularly. The better performance of the presented map matching algorithm against the egomotion approach is shown in Fig. 22.

Note that the collection of investigated scenarios has been checked manually to diminish the impact of errors or outdated information from the digital map which cannot be corrected by the system itself. Correct information of the digital map is a necessary prerequisite condition of the realized road course estimation system.

Threat Analysis of Pedestrians The most interesting part is the evaluation of the warning performance answering the question: How many pedestrian detections have been classified correctly according to their relevance for the driver? This has been investigated on a ground truth of 1,945 labeled pedestrians in a range from 20 to 120 m with manually assigned discrete warning levels. Figure 23 shows the different warning levels. Manual labeling of the warning levels in the camera image is partially very complicated, mostly for detections in the far field of curved roads.

In order to reduce the resulting ground truth errors, the warning levels overlap between adjacent levels by 6%. This corresponds to a tolerance band of 0.4 m for a typical road width of 6.5 m. The evaluation algorithm classifies a detection considered to be correctly warned if at least one detection exists satisfying the following conditions.

1. The calculated warning level $\eta(d^*)$is in the specified range defined by the ground truth label.
2. The coverage between the ground truth label and the detection is at least 80%.

The presented pedestrian warning system achieves 84% correct warnings. The remaining 16% mostly refer to a position error of the presented road course estimation system.

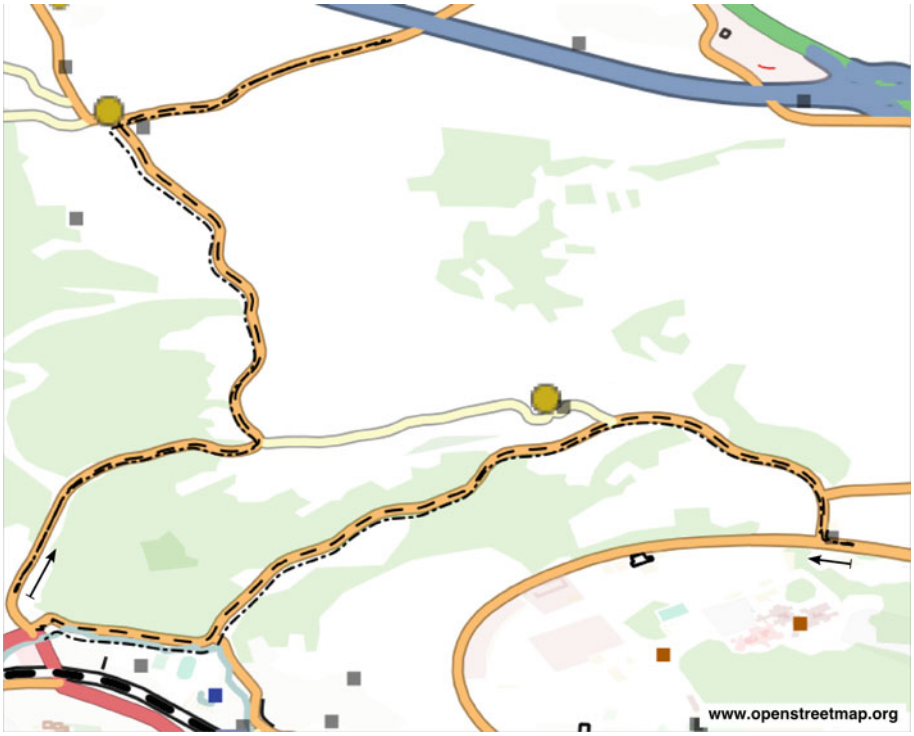

Night Vision Pedestrian Warning in Intelligent Vehicles. Figure 22
Position trajectory with and without localization on the map: The course using only the vehicle data in an egomotion filter (*slash-dotted*) deviates clearly from the course of the map-based positioning algorithm (*dashed*)

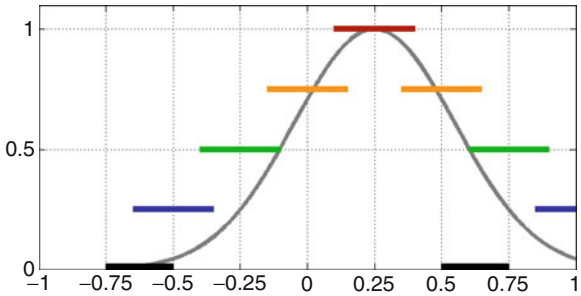

Night Vision Pedestrian Warning in Intelligent Vehicles. Figure 23
The defined discrete warning levels

Conclusion

The described novel pedestrian warning system has been implemented in a test vehicle equipped with an NIR camera sensor, an imaging radar system, and a digital map.

In order to achieve a robust, reliable, and real-time capable detection system, the information provided by the camera sensor and the radar sensor are fused on feature level using a cascade of boosted classifiers. That is, both sensors define a set of features. For the classification task, the relevant feature are selected and parameterized using the supervised training algorithm AdaBoost in multiple stages of increased complexity (number of features). The feature set is composed of Haar-wavelet filters in the image plane and average object intensity as well as complex signal filters in the radar plane. The newly derived radar filters are characterized by their efficiency to separate between objects with a local velocity similarity and background. Experiments have shown that the resulting fusion detector dramatically outperforms a single sensor reference system. Unlike the image-based reference system, the presented multi-sensor fusion approach can reject hypotheses in earlier stages of the cascade and gives a precise spatial localization of the resulting object

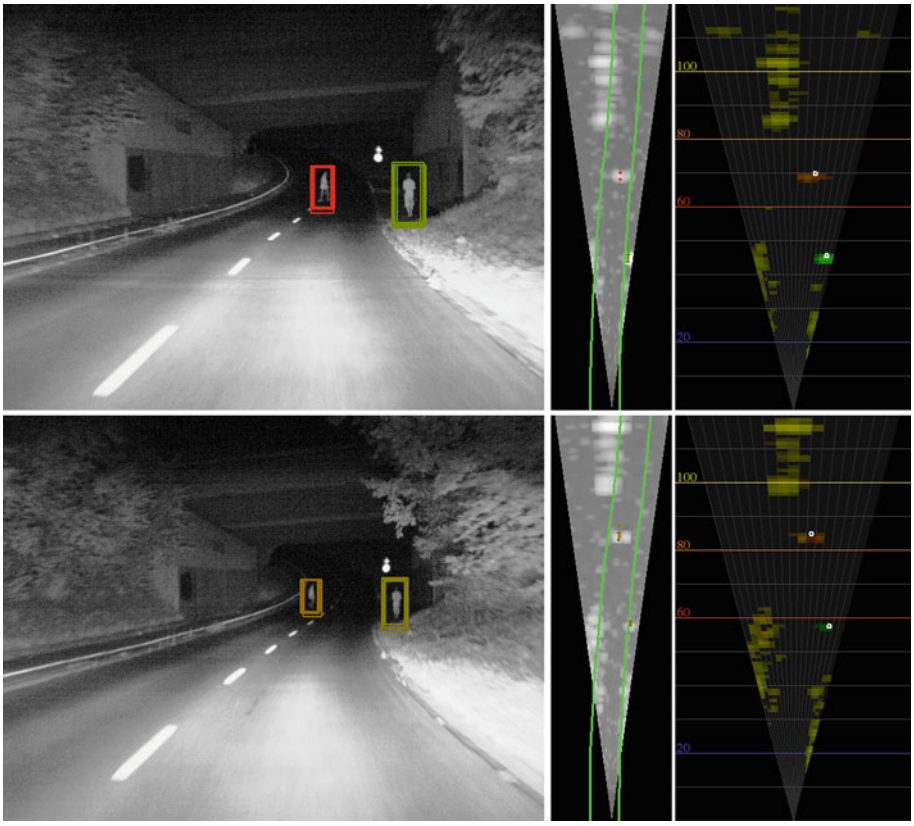

Night Vision Pedestrian Warning in Intelligent Vehicles. Figure 24
Some results of the pedestrian warning system: the *left* camera image with highlighted pedestrians depending on their calculated threat. The next image corresponds to the interpolated Cartesian view of the radar raw data which is the input data to estimate the road course. The *right* image shows the radar raw data including the detected pedestrians

hypotheses. In this way, the fusion system also achieves a grid-based fusion with the digital map and the radar image.

In order to signal to the driver only the relevant objects, a new road course estimation concept has been implemented. The new concept maps the information provided by a digital map to the observations of the radar sensor, similar to the Monte Carlo localization approach in the field of autonomous robotics. Thus this component is more likely a global positioning approach which is apart from the digital map module, independent of inaccurate and error prone GPS measurements. Finally, the implemented threat analysis algorithm combines the pedestrian detection system and the road course estimation system. The evaluation results show a good warning performance. About 84% of detected pedestrians triggered a correct warning. Figure 24 gives an impression of the pedestrian warning system in a rural environment.

Future Directions

Future work will incorporate object classes other than pedestrians and more sensors to improve the environmental perception of vehicles, and will enhance the proposed approach.

The feature-level fusion for sensors of different physical principle is a possible solution to meet the requirements of safety application where high-level fusion is not sufficient. The described method is applicable not only for automotive applications, but also for example in the areas of monitoring, inspection, surveillance, and medicine.

Digital maps are currently the exclusive technology to provide information of the course of road for far distances over 100 m independent of weather conditions, which is necessary to realize a warning system. Today, neither a camera nor a radar sensor can provide this information. This shows that the future development of driver assistance systems should focus more on digital map technologies.

Fusion of local maps with digital maps will offer a lot of applications where a high-precision localization is necessary, and so far no low-cost solution is available.

Acknowledgments

This research was supported by PROPEDES (Predictive Pedestrian Protection at Night), BMBF FKZ 13N9750-13N9754, Germany.

Bibliography

Primary Literature

1. Green M (2000) 'How long does it take to stop?' Methodological analysis of driver perception times. Transp Hum Factors 2(3):195–216
2. Zhang Y, Antonsson E, Grote K (2006) A new threat assessment measure for collision avoidance systems. In: International conference on intelligent transportation systems (ITSC), 2006 IEEE, Toronto, pp 968–975.
3. Beutnagel-Buchner U, Arnon M, Sparbert J, Moisel J, Rode M, Ritter W, Oberländer M, Löhlein O, Serfling M, Strobel M, Graf HG, Valipour H, Müller F, Schweiger R (2007) N I R W A R N Gesamtschlussbericht, BMBF, Forschungsbericht 01M3157A-D
4. Franke U, Loose H, Knöppel C (2007) Lane recognition on country roads. In: Intelligent vehicles symposium (IV), 2007 IEEE, Istanbul, pp 99–104
5. Jung CR, Kelber CR (2005) Lane following and lane departure using a linear-parabolic model. Image Vis Comput 23(13): 1192–1202
6. Apostoloff N, Zelinsky A (2003) Robust vision based lane tracking using multiple cues and particle filtering. In: Intelligent vehicles symposium (IV), 2003 IEEE, Columbus, pp 558–563
7. Southall J, Taylor C (2001) Stochastic road shape estimation. In: International conference on computer vision (ICCV), 2001 IEEE, vol 1. Vancouver, pp 205–212
8. Franke U (1992) Real-time 3D road modeling for autonomous vehicle guidance. In: Johansen P, Olsen S (eds) Theory and applications of image analysis: selected papers from the 7th Scandinavian conference on image analysis, Aalborg, Denmark, vol 2, Machine perception artificial intelligence. World Scientific Publishing Company, Singapore, pp 277–284
9. Dickmanns ED, Zapp A (1986) A curvature-based scheme for improved road vehicle guidance by computer vision. In: Conference on mobile robots, 1986 SPIE, vol 727. Cambridge, pp 161–168
10. Bertozzi M, Bombini L, Cerri P, Medici P, Antonello P, Miglietta M (2008) Obstacle detection and classification fusing radar and vision. In: Intelligent vehicles symposium (IV), 2008 IEEE, Eindhoven, Netherlands, pp 608–613
11. Alessandretti G, Broggi A, Cerri P (2007) Vehicle and guard rail detection using radar and vision data fusion. IEEE Trans Intell Transp Syst 8(1):95–105
12. Haselhoff A, Kummert A, Schneider G (2007) Radar-vision fusion with an application to car-following using an improved AdaBoost detection algorithm. In: Intelligent transportation systems conference (ITSC), 2007 IEEE, Seattle, pp 854–858
13. Dehesa M, Allezard N, Furca L, Kaiser A, Kirchner A, Meinecke MM, Vinciguerra R (2005) SAVE-U: high and low level data fusion algorithms, Public Deliverable 19, 2005. Commission of the European Communities, Brussels
14. Enzweiler M, Gavrila DM (2009) Monocular pedestrian detection: survey and experiments. IEEE Trans Pattern Anal Mach Intell 31(12):2179–2195
15. Milch S, Behrens M (2001) Pedestrian detection with radar and computer vision. In: Symposium on progress in automobile lighting, Darmstadt, Germany, pp 657–664
16. Schweiger R, Hamer H, Löhlein O (2007) Determining posterior probabilities on the basis of cascaded classifiers as used in pedestrian detection systems. In: Proceedings of IEEE intelligent vehicles symposium, Istanbul, Turkey, pp 1284–1289
17. Kallenbach I, Schweiger R, Palm G, Löhlein O (2006) Multi-class object detection in vision systems using a hierarchy of cascaded classifiers. In: Proceedings of IEEE intelligent vehicles symposium, Tokyo, pp 383–387
18. Miyamoto R, Sugano H, Nakamura Y (2007) Pedestrian recognition suitable for night vision systems. Int J Comput Sci Netw Secur 7:1–8
19. Maehlisch M, Oberländer M, Löhlein O, Gavrila D, Ritter W (2005) A multiple detector approach to low-resolution FIR pedestrian recognition. In: Proceedings of IEEE intelligent vehicles symposium, Las Vegas, pp 325–330
20. Milch S, Behrens M (2001) Pedestrian detection with radar and computer vision. In: Proceedings of the symposium on progress in automobile lighting, Darmstadt, Germany, pp 657–664
21. Lindl R, Walchshusl L (2006) Three-level early fusion for road use detection. PReVENT Fusion Forum J 1(1):19–24
22. ProFusion (2004) Subproject of the PReVENT-project (Preventive and Active Safety Applications), founded by European Commission
23. Dickmann J et al (2009) Sensorfusion as key technology for future driver assistance systems. In: Workshop Sensor- und Datenfusion – Architekturen und Algorithmen, Berlin, 20 Nov 2009
24. Zhang Z (1999) Flexible camera calibration by viewing a plane from unknown orientations. In: Proceedings of the

international conference on computer vision, Kerkyra, Corfu, pp 666–673
25. Bouguet J (1999) Visual methods for three-dimensional modeling. Ph.D. dissertation, California Institute of Technology, Pasadena, CA
26. Tsai R (1987) A versatile camera calibration technique for high-accuracy 3D machine vision metrology using off-the-shelf TV cameras and lenses. IEEE J Robot Automation 3(4):323–344
27. Skolnik MI (1990) Radar handbook, 2nd edn. McGraw-Hill, New York
28. Freund Y, Schapire RE (1997) A decision-theoretic generalization of on-line learning and an application to boosting. J Comput Syst Sci 55:119–139
29. Viola P, Jones M (2002) Robust real-time object detection. Int J Comput Vision 57(2):137–154
30. Viola P, Jones M (2001) Rapid object detection using a boosted cascade of simple features. In: Proceedings of IEEE computer society conference on computer vision and pattern recognition, Kauai, HI, vol 1, pp 511–518
31. Freund Y, Schapire RE (1996) Experiments with a new boosting algorithm. In: Proceedings of the international conference on machine learning, Bari, Italy, pp 148–156
32. Freund Y, Schapire RE (1999) A short introduction to boosting. J Jpn Soc Artif Intell 14(5):771–780
33. Schapire RE (2002) The boosting approach to machine learning: an overview. In: MSRI workshop on nonlinear estimation and classification, Berkeley, CA
34. Papageorgiou C, Oren M, Poggio T (1998) A general framework for object detection. In: Proceedings of international conference on computer vision, Bombay, India, pp 555–562
35. Oren M, Papageorgiou C, Sinha P, Osuna Z, Poggio T (1997) Pedestrian detection using wavelet templates. In: Proceedings of IEEE computer society conference on computer vision and pattern recognition, San Juan, Puerto Rico, pp 193–199
36. Dellaert F, Fox D, Burgard W, Thrun S (1999) Monte Carlo localization for mobile robots. In: International conference on robotics and automation (ICRA) 1999, Detroit, vol 2. IEEE, Washington, DC, pp 1322–1328
37. Fox D, Burgard Z, Dellaert F, Thrun S (1999) Monte Carlo localization: efficient position estimation for mobile robots. In: National conference on artificial intelligence (AAAI), Orlando, pp 343–349
38. Isard I, Blake A (1998) Condensation – conditional density propagation for visual tracking. Int J Comput Vis (IJCV) 29(1):5–28
39. Snyder JP (1987) Map projections – a working manual. US Government Printing Office, Washington, DC
40. Ress C, Balzer D, Bracht A, Durekovic S, Löwenau J (2008), ADASIS protocol for advanced in-vehicle applications. In: World congress on intelligent transportation systems (ITS) 2008, New York. IEEE, Washington, DC
41. Schubert R, Richter E, Wanielik G (2008) Comparison and evaluation of advanced motion models for vehicle tracking. In: International conference on information fusion 2008, Cologne, Germany. IEEE, Washington, DC, pp 1–6
42. Bierman GJ (1975) Measurement updating using the U-D factorization. In: Conference on decision and control 1975, Houston. IEEE, Washington, DC, pp 337–346

Books and Reviews

Bar-Shalom Y, Li XR, Kirubarajan T (2001) Estimation with applications to tracking and navigation, 1st edn. Wiley, New York

Blervaque V, Mezger K, Beuk L, Löwenau J (2006) ADAS horizon – How digital maps can contribute to road safety. In: Valldorf J, Gessner W (eds) Advanced microsystems for automotive applications. Springer, Berlin, pp 427–436

Grabham D (2009) Street to screen: how sat-nav maps are made. SatNav News on www.techradar.com, August 2009

Hager JW, Behensky JF, Drew BW (1989) The universal grids: universal transverse mercator (UTM) and universal polar stereographic (UPS). Technical manual DMATM 8358.2, Defense Mapping Agency (DMA), Fairfax, VA

Misra P, Enge P (2006) Global positioning system: signals, measurements and performance, 2nd edn. Ganga-Jamuna Press, Lincoln

Moran T (2008) Tapping mapping for an extra eye on the road. Automotive News: Information Technology, Detroit. July 2008

Non-flame Incineration

Philip H. Taylor
Environmental Engineering Group, University of Dayton Research Institute, Dayton, OH, USA

N

Article Outline

Glossary
Definition of the Subject
Introduction
Thermal Stability–Based (UDRI) Incinerability Ranking
Zone Theory of Formation of Products of Incomplete Combustion
Formation of Chlorinated Polycyclic Aromatic Hydrocarbons
Formation of Polychlorinated Dibenzo-P-Dioxins and Furans
Future Directions
Bibliography

Glossary

De novo synthesis of PCDD/F Synthesis of PCDD/F from native, nonextractable carbon in fly ash.

Molecular growth Molecular growth is defined as the increase in the molecular size and weight of products of incomplete combustion through a

series of radical–molecule reactions typically under oxygen-starved conditions.

Non-flame incineration Thermal destruction of hazardous compounds in the absence of a flame.

Precursor pathway of PCDD/F formation Formation of PCDD/F from the reaction of organic species derived from the combustion process, e.g., chlorophenols, on a transition metal surface.

Thermal stability index The thermal stability of an organic compound, defined by the temperature for a given level of conversion for a constant residence time of exposure, e.g., T_{99} (2)(C) – the temperature for 99% conversion for a two-second gas-phase residence time.

Zone theory of PIC formation States that one can classify the types of reactions occurring within a given zone of a thermal destruction facility and consider their impact on PIC emissions in more detail.

Definition of the Subject

Non-flame incineration is an important and mature area of research pertaining to the thermal destruction of hazardous compounds. Research and field testing was initiated in the mid-1970s and has continued to this day. Non-flame incineration is defined as the "thermal" destruction of hazardous compounds in the absence of a flame. While flame conditions involve very high temperatures and very rapid reaction rates resulting in rapid conversion of organic compounds to thermodynamic end products (CO_2, H_2O, HCl), non-flame incineration is typically defined by temperatures below 1,373 K in flowing air with mean, gas-phase residence times of 2.0 s. Non-flame incineration studies thus typically represent the gas-phase, rate-controlling conditions for pollutant formation in full-scale incinerators, where various failure modes in the flame zones result in the incomplete conversion of parent materials to thermodynamic end products. Non-flame incineration conditions are often similar to the second stage of a liquid injection or rotary kiln incineration system, which is often called an "afterburner."

This review presents an update on non-flame incineration research. Topics covered include the continued development of a thermal stability–based ranking of principal organic hazardous constituents which has been successfully used in full-scale trial burns and an update on research pertaining to the formation of products of incomplete combustion (PIC), with an emphasis on new findings reported over the past 20 years. The majority of the recent research in this latter area pertains to the formation and control of emissions of polychlorinated dibenzo-p-dioxins and furans (PCDD/F) from full-scale facilities. This research has been very successfully translated to full-scale thermal treatment facilities where overall PCDD/F emissions have decreased dramatically over the past 20 years.

Introduction

Controlled, high-temperature incineration, in spite of the associated high costs, is a proven organic waste reduction technology [1]. The current performance requirement states that principal organic hazardous constituents (POHC) designated in each waste must be destroyed and/or removed to an efficiency of 99.99%. The complexity of hazardous organic waste streams often makes correct POHC selection and demonstration of 99.99% destruction and removal efficiency (DRE) a nontrivial task.

To aid the process of POHC selection, the U.S. EPA has limited the number of hazardous organic compounds to those listed in Appendix VIII of 40 CFR Part 261.3 [2] and ranked these substances by their heat of combustion per unit mass (ΔH_c/g) [3]. This scale is based on the premise that the lower the heat of combustion, the more difficult the compound is to incinerate. The heat of combustion approach has undergone considerable policy debate and received criticism on theoretical grounds from the scientific community [4–6].

The destruction efficiency (DE) of POHCs is largely controlled by the temperature, time, and fuel/air stoichiometry (excess air) in the high-temperature zones of incinerators. Calculations and experimental observations have shown that the emissions of undestroyed, residual POHCs are kinetically, not thermodynamically, controlled [5, 7]. Thus, determination of the exact time, temperature, and stoichiometry history of all the molecules in an incinerator is necessary to determine the absolute DE of a POHC. This type of information is not currently available.

However, sufficient information is available to estimate the relative DE of potential POHCs.

Simple conceptual and more complex models suggest that the gas-phase residence time and temperature in the post-flame or thermal zones of incinerators control the relative emissions of most POHCs [6, 8]. The basic theory or advanced hypothesis is that all molecules entering the flame zone of an incinerator are essentially destroyed, and only the minute fraction escaping the flame zone may be emitted from the facility. Various flame zone "failure modes" exist which may cause residual POHCs to be emitted. Once in the post-flame zone, gas-phase, non-flame, thermal decomposition kinetics control the rate of POHC destruction and PIC formation and destruction.

If all POHCs in a given waste stream in a given incinerator are volatilized at nearly the same rate, they will experience the same post-flame gas-phase residence time, temperature, and stoichiometry history. This means that the gas-phase thermal stability of the POHCs (as determined under a standardized set of conditions) may be used to predict their relative incinerability. The temperature for 99% destruction at 2.0 s gas-phase residence time, [T_{99}(2)(C)], is one method of ranking the thermal stability of POHCs. Other residence times or temperatures may be used to develop this ranking. However, laboratory data indicate that although absolute POHC DEs are dependent upon time and temperature, the relative DEs are relatively insensitive to these parameters [9–11]. In contrast, reaction stoichiometry has been shown to be a major variable in determining relative thermal stability [10, 11].

Theoretical considerations suggest that oxygen-starved pathways through the incinerator are responsible for most POHC and PIC emissions. Even though a hypothetical facility is operating under nominally excess air conditions, poor mixing will result in oxygen-deficient pockets where the rate of POHC destruction is low and PIC formation is favored. Consequently, gas-phase thermal stability under sub-stoichiometric reaction conditions becomes an effective predictor of POHC relative incinerability. Dellinger et al. [12] compared the incinerability predictions of seven proposed POHC ranking methods with results of 10 pilot-scale or full-scale test burns. The ranking methods included heat of combustion, autoignition temperature, ignition delay time, flame failure modes, theoretical flame mode kinetics, non-flame thermal stability of pure compounds under excess air conditions, non-flame thermal stability of mixtures under oxidative conditions, and the non-flame, thermal stability of mixtures under oxygen-starved conditions. Rank–order correlations of the prediction of the rankings with field results were poor except for non-flame thermal stability of mixtures under oxygen-starved conditions. Although the laboratory data base used to predict full-scale POHC DREs was limited, statistically significant correlations in seven of ten cases were observed using this ranking approach. The results of this comparison along with theoretical considerations suggest that this type of thermal stability ranking should be used to replace the previously recommended heat of combustion index.

Thermal Stability–Based (UDRI) Incinerability Ranking

Table 1 presents the updated thermal stability–based incinerability ranking of Appendix VIII organic compounds (with thermal stability indices) based on the gas-phase thermal stability under oxygen-starved conditions. The ranking was developed using experimental data generated at the University of Dayton Research Institute (UDRI), limited studies reported in the published literature, and theoretical considerations. The ranking (without thermal stability indices and class divisions) was initially published in 1990 [13]. Subsequent testing added many high-priority compounds including a number of polychlorinated dibenzo-p-dioxins and furans (PCDD/F). The ranking was subsequently validated with pilot and full-scale tests [14, 15].

In total, 86 compounds have been experimentally evaluated under a consistent set of oxygen-starved, low-chlorine experimental conditions. These compounds, where experimental data have been generated which is consistent with available literature data or theoretical consideration, are designated, experimentally evaluated, and are listed in boldface in Table 1. Compounds which have not been experimentally evaluated under these consistent test conditions, but for which experimental data exist within the published

Non-flame Incineration. Table 1 Updated UDRI thermal stability index

Principal organic hazardous constituent	T_{99} (2)(°C)	Rank
Class 1		
Hydrogen cyanide {hydrocyanic acid}[a]	>1,500	1
Cyanogen {ethanedinitrile}	1,500	2
Benzene	1,150	3
Sulfur hexafluoride[b]	1,090	4
Naphthalene	1,070	5
Fluoranthene {benzo[j,k]fluorene}	1,062	6
Benzo[b]fluoranthene {2,3-benzofluoranthene}	1,060	7–11
Benzanthracene (1,2-) {benz[a]anthracene}	1,060	7–11
Chrysene {1,2-benzphenanthrene}	1,060	7–11
Benzo[j]fluoranthene {7,8-benzofluoranthene}	1,060	7–11
Indeno(1,2,3-cd)pyrene {1,10-(1,2-phenylene)pyrene}	1,060	7–11
Benzo[a]pyrene {1,2-benzopyrene}	1,025	12
Dibenz[a,h]anthracene {1,2,5,6-dibenzanthracene}	1,020	13–16
Dibenzo[a,h]pyrene {1,2,5,6-dibenzopyrene}	1,020	13–16
Dibenzo[a,i]pyrene {1,2,7,8-dibenzopyrene}	1,020	13–16
Dibenzo[a,e]pyrene {1,2,4,5-dibenzopyrene}	1,020	13–16
Chlorotrifluoromethane [c, d]	1,010	17
Cyanogen chloride {chlorine cyanide}	1,000	18–19
Acetonitrile {ethanenitrile}	1,000	18–19
Chlorobenzene	990	20
Acrylonitrile {2-propenenitrile}	985	21
Dichlorobenzene {1,4-dichlorobenzene}	975	22–23
Chloronaphthalene (1-)	975	22–23
Cyanogen bromide {bromine cyanide}	970	24–25
Dichlorobenzene {1,2-dichlorobenzene}	970	24–25
Dichlorobenzene {1,3-dichlorobenzene}	960	26–27
Chlorodibenzo-P-dioxin (1-)	960	26–27
Trichlorobenzene (1,2,4-trichlorobenzene)	955	28–29
Tetrachlorobenzene (1,2,3,5-tetrachlorobenzene)[c]	955	28–29
Trichlorobenzene (1,3,5-trichlorobenzene)[c]	950	30–31
Chloromethane {methyl chloride}	950	30–31
Tetrachlorobenzene (1,2,4,5-tetrachlorobenzene)	940	32
Pentachlorobenzene	935	33–35
Hexachlorobenzene	935	33–35

Non-flame Incineration. Table 1 (Continued)

Principal organic hazardous constituent	T_{99} (2)(°C)	Rank
Bromomethane {methyl bromide}	935	33–35
Chlorodibenzo-P-dioxin (2-)	925	36
Dichlorodibenzo-P-dioxin (2,7-)	920	37
Class 2		
Toluene {methylbenzene}	895	38
Tetrachloroethene	890	39
Dde{1,1-dichloro-2,2-bis(4-chlorophenylethylene}	875	40–41
Dichlorodibenzo-P-dioxin (2,3-)	875	40–41
Formic acid {methanoic acid}	870	42–43
Phosgene {carbonyl chloride}	870	42–43
Trichloroethene	865	44–45
Tetrachlorodibenzo-P-dioxin (2,3,7,8-)	865	44–45
Trichlorodibenzo-P-dioxin (1,2,4-)	860	46–48
Dichloroethene (1,1-)	860	46–48
Fluoroacetic acid	860	46–48
Dimethylbenz[a]anthracene (7,12-)	855	49
Aniline	850	50–53
Formaldehyde {methylene oxide}	850	50–53
Methyl chlorocarbonate {carbonochloridic acid, methyl ester}	850	50–53
Methyl isocyanate {methylcarbylamine}	850	50–53
Tetrachlorodibenzo-P-dioxin (1,2,3,4-)	845	54
Dimethylphenethylamine (alpha, alpha-)	840	55–58
Malononitrile {propanedinitrile}	840	55–58
Naphthylamine (1-)	840	55–58
Naphthylamine (2-)	840	55–58
Dichloroethene (trans-1,2-)	835	59
Fluoroacetamide (2-)	830	60
Acrylamide {2-propenamide}	820	61–62
Methyl methacrylate {2-propenoic acid, 2-methyl-,methyl ester}	820	61–62
Dichloromethane {methylene chloride}	815	63–64
Methacrylonitrile {2-methyl-2-propenenitrile}	815	63–64
Chloroaniline {chlorobenzenamine}	810	65
Methylcholanthrene (3-)	805	66
Chloro-1,3-butadiene (2-) {chloroprene}	800	67–70
Diphenylamine {N-phenylbenzenamine}	800	67–70

Non-flame Incineration. Table 1 (Continued)

Principal organic hazardous constituent	T_{99} (2)(°C)	Rank
Pronamide {3,5-dichloro-N-[1,1-dimethyl-2-propynyl] benzamide}	800	67–70
Acetylaminofluorene (2-) {acetamide,N-[9 H-fluoren-2-YL]-}	800	67–70
Class 3		
Aminobiphenyl (4-) {[1,1′-biphenyl]-4-amine}	796	71
Dichlorobenzidine (3,3′-)	795	72–73
Chlorophenol (2-)	795	72–73
Benzidine {[1,1′-biphenyl]-4,4′diamine}	794	74
Dimethylbenzidine (3,3′-)	793	75
Phenylenediamine (1,3-) {benzenediamine}	792	76
Phenylenediamine (1,2-) {benzenediamine}	791	77
Phenylenediamine (1,4) {benzenediamine}	790	78
n-Propylamine {1-propanamine}	789	79
Pyridine	785	80–81
Chlorophenol (3-)	785	80–81
Picoline (2-) {pyridine,2-methyl-}	780	82–85
Dichloropropene (1,1-)	780	82–85
Thioacetamide {ethanethioamide}	780	82–85
Trichloro(1,2,2-)trifluoroethane(1,1,2-) {freon 113}[c]	780	82–85
Phenol {hydroxybenzene}	775	86–90
Benz[c]acridine {3,4-benzacridine}	775	86–90
Dichlorodifluoromethane {freon 12}	775	86–90
Acetophenone {ethanone,1-phenyl-}	775	86–90
Trichlorofluoromethane {freon 11}	775	86–90
Ethyl cyanide {propionitrile}	770	91–93
Benzoquinone {1,4-cyclohexadienedione}	770	91–93
Vinyl chloride (chloroethene)	770	91–93
Dibenz[a,h]acridine {1,2,5,6-dibenzacridine}	765	94–99
Dibenz[a,j]acridine {1,2,7,8-dibenzacridine}	765	94–99
Hexachlorobutadiene (trans-1,3)	765	94–99
Naphthoquinone (1,4-) {1,4-naphthalenedione}	765	94–99
Dimethyl phthalate	765	94–99
Acetyl chloride {ethanoyl chloride}	765	94–99
Acetonylbenzyl-4-hydroxycoumarin (3-alpha-) {warfarin}	760	100–101
Maleic anhydride {2,5-furandione}	760	100–101
Chlorophenol (4-)	755	102–103
Dichloro-2-butene (1,2-)	755	102–103

Non-flame Incineration. Table 1 (Continued)

Principal organic hazardous constituent	T_{99} (2)(°C)	Rank
Dichloropropene (2,3-)	754	104
Dichloropropene (trans-1,2-)	750	105–113
Dibenzo[c,g]carbazole (7 h-) {3,4,5,6-dibenzcarbazole}	750	105–113
Toluenediamine (2,6-) {diaminotoluene}	750	105–113
Toluenediamine (2,5-) {diaminotoluene}	750	105–113
Toluenediamine (2,4-) {diaminotoluene}	750	105–113
Toluenediamine (2,4-) {diaminotoluene}	750	105–113
Toluenediamine (3,5-) {diaminotoluene}	750	105–113
Toluenediamine (3,4-) {diaminotoluene}	750	105–113
Resorcinol {1,3-benzenediol}	750	105–113
Cresol (1,3-) {methylphenol}	749	114
Cresol (1,2-) {methylphenol}	746	115
Cresol (1,4-) {methylphenol}	745	116
Dichlorophenol (2,6-)	740	117
Methyl ethyl ketone {2-butanone}	730	118–119
Diethylstilbesterol	730	118–119
Benzenethiol {thiophenol}	725	120
Isobutyl alcohol {2-methyl-1-propanol}	715	121
Crotonaldehyde {2-butenal}	710	122–123
Dichlorophenol (2,4-)	710	122–123
Chlorocresol {4-chloro-3-methylphenol}	709	124
Methylactonitrile (2-) {propanenitrile,2-hydroxy-2-methyl}	705	125–126
Dihydroxy-alpha-[methylamino]methyl benzyl alcohol (3,4-) {adrenaline}	705	125–126
Dimethylphenol (2,4-)	700	127
Class 4		
Chloropropene (3-) {allyl chloride}	695	128
Tetrachloroethane (1,1,2,2-)	690	129–130
Dichloropropene (3,3-)	690	129–130
Hydrazine {diamine}	685	131–133
Benzyl chloride {chloromethylbenzene}	685	131–133
Dibromomethane {methylene bromide}	685	131–133
Dichloroethane (1,2-)	680	134
Mustard gas {bis[2-chloroethyl]-sulfide}	679	135–137
Nitrogen mustard	679	135–137
N,N-bis(2-chloroethyl)2-naphthylamine {chlornaphazine}	679	135–137
Acrolein {2-propenal}	670	138–141

Non-flame Incineration. Table 1 (Continued)

Principal organic hazardous constituent	T_{99} (2)(°C)	Rank
Bromoacetone {1-bromo-2-propanone}	670	138–141
Chloroethane (ethyl chloride) [4]	670	138–141
Hexachlorophene {2,2′-methylenebis[3,4,6-trichlorophenol]}	670	138–141
Allyl alcohol {2-propen-1-ol}	665	142
Dioxane (1,4-) {1,4-diethylene oxide}	660	143
Chlorambucil	659	144
Nitrobenzene	655	145–146
Chloropropionitrile (3-) {3-chloropropanenitrile}	655	145–146
Dichloro-2-propanol (1,1-)	654	147–148
Ddd {dichlorodiphenyldichloroethane}	654	147–148
Dichloro-2-propanol (1,3-)	652	149
Phthalic anhydride {1,2-benzenedicarboxylic acid anhydride}	650	150–154
Methyl parathion	650	150–154
Nitrophenol (4-)	650	150–154
Trichlorophenol (2,4,6-)	650	150–154
Trichlorophenol (2,4,5-)	650	150–154
Tetrachloromethane {carbon tetrachloride}	645	155–157
Tetrachlorophenol (2,3,4,6-)	645	155–157
Chlorodifluoromethane {freon 22}[c]	645	155–157
Hexachlorocyclohexane {lindane}	640	158–163
Dichlorofluoromethane {freon 21}[c]	640	158–163
Dinitrobenzene (1,3-)	640	158–163
Nitroaniline {4-nitrobenzenamine}	640	158–163
Pentachlorophenol	640	158–163
Pentachloroethane	640	158–163
Dinitrobenzene (1,4-)	635	164–166
Dinitrobenzene (1,2-)	635	164–166
Trichloroethane (1,1,2-)	635	164–166
Isodrin	632	167–169
Dieldrin	632	167–169
Aldrin	632	167–169
Dichloropropane (1,3-)	630	170–174
Dibromoethane (1,2-) {ethylene dibromide}	630	170–174
Nitrotoluidine (5-) {benzenamine,2-methyl-5-nitro-}	630	170–174
Chloroacetaldehyde	630	170–174
Benzal chloride {alpha,alpha-dichlorotoluene}	630	170–174

Non-flame Incineration. Table 1 (Continued)

Principal organic hazardous constituent	T_{99} (2)(°C)	Rank
Trichloromethane {chloroform}	625	175–183
Dichloropropene (trans-1,3-)	625	175–183
Trichloropropane (1,2,3-)	625	175–183
Dinitrotoluene (2,4-)	625	175–183
Dinitrotoluene (2,6-)	625	175–183
Hexachlorocyclopentadiene	625	175–183
Dichloro1-propanol (2,3-)	625	175–183
Ethylene oxide {oxirane}	625	175–183
Dichloropropene (cis-1,3-)	625	175–183
Dimethylcarbamoylchloride	620	184–187
Glycidyaldehyde {1-propanol-2,3-epoxy}	620	184–187
Ddt {dichlorodiphenyltrichloroethane}	620	184–187
Dichloropropane (1,2-) {propylene dichloride}	620	184–187
Auramine	618	188–189
Heptachlor	618	188–189
Dichloropropane (1,1-)	615	190–194
Chloro-2,3-epoxypropane (1-) {oxirane,2-chloromethyl-}	615	190–194
Dinitrophenol (2,4-)	615	190–194
bis(2-Chloroethyl)ether	615	190–194
Trinitrobenzene {1,3,5-trinitrobenzene}	615	190–194
Butyl-4,6-dinitrophenol (2-sec-) {DNBP}	613	195–196
Cyclohexyl-4,6-dinitrophenol (2-)	613	195–196
Dichloroethane (1,1-) {ethylidene dichloride}	610	197–201
bis(2-Chloroethoxy)methane	610	197–201
Chloral {trichloroacetaldehyde}	610	197–201
Trichloromethanethiol	610	197–201
Dinitrocresol (4,6-) {phenol,2,4-dinitro-6-methyl-}	610	197–201
Heptachlor epoxide	609	202
Diepoxybutane (1,2,3,4-) {2,2′-bioxirane}	604	203
Benzotrichloride {trichloromethylbenzene}	600	204–205
Methapyrilene	600	204–205
Class 5		
Phenacetin {N-[4-ethoxyphenyl]acetamide}	593	206–207
Methyl hydrazine	593	206–207
Aflatoxins	590	208
Hexachloroethane	585	209–210

Non-flame Incineration. Table 1 (Continued)

Principal organic hazardous constituent	T_{99} (2)(°C)	Rank
Bromoform {tribromomethane}	585	209–210
Chlorobenzilate	584	211–214
Ethyl carbamate {urethan} {carbamic acid, ethyl ester}	584	211–214
Ethyl methacrylate {2-propenoic acid, 2-methyl-, ethyl ester}	584	211–214
Lasiocarpine	584	211–214
Amitrole {1 h-1,2,4-triazol-3-amine}	580	215–216
Muscimol {5-aminomethyl-3-isoazotol}	580	215–216
Iodomethane {methyl iodide}	567	217
Dichlorophenoxyacetic acid (2,4-) {2,4-d}	565	218–220
Chloroethylvinylether (2-) {ethene, [2-chloroethoxy]-}	565	218–220
Methylene bis(2-chloroaniline) (4,4-)	565	218–220
Dibromo-3-chloropropane (1,2-)	561	221
Propyn-1-OL (2-) {propargyl alcohol}	560	222–223
Tetrachloroethane (1,1,1,2-)	560	222–223
Dimethylhydrazine (1,1-)	555	224–225
N,N-diethylhydrazine {1,2-diethylhydrazine}	555	224–225
Chloromethylmethyl ether {chloromethoxymethane}	550	226–228
Dimethyl-1-methylthio-2-butanone,O-[(methylamino)-carbonyl]	550	226–228
Oxime (3,3-) {thiofanox}		
Dimethylhydrazine (1,2-)	550	226–228
Trichloroethane (1,1,1-) {methyl chloroform}	545	229
Chlordane (alpha and gamma isomers)	533	230
bis(Chloromethyl)ether {methane-OXYbis[2-chloro-]}	530	231–233
Parathion	530	231–233
Dichloropropane (2,2-)	530	231–233
Maleic hydrazide {1,2-dihydro-3,6-pyridazinedione}	525	234
Bromophenyl Phenyl Ether (4-) {benzene,1-bromo-4-phenoxy-}	523	235
bis(2-Chloroisopropyl)ether	520	236–237
Dihydrosafrole {1,2-methylenedioxy-4-propylbenzene}	520	236–237
Methyl methanesulfonate {methanesulfonic acid, methyl ester}	515	238
Propane sulfone (1,3-) {1,2-oxathiolane,2,2-dioxide}	513	239
Saccharin {1,2-benzoisothiazolin-3-one,1,1-dioxide}	511	240
Methyl-2-methylthio-propionaldehyde-O-(methylcarbonyl)oxime (2-)	510	241–242
Methyomyl	510	241–242
Hexachloropropene	505	243
Pentachloronitrobenzene {PCNB}	500	244–248

Non-flame Incineration. Table 1 (Continued)

Principal organic hazardous constituent	T_{99} (2)(°C)	Rank
Diallate {s-(2,3-dichloroallyl)diisopropyl thiocarbamate}	500	244–248
Ethyleneimine {aziridine}	500	244–248
Aramite	500	244–248
Dimethoate	500	244–248
Trichlorophenoxyacetic acid (2,4,5-) {2,4,5-t}	495	249–250
Trichlorophenoxypropionic acid (2,4,5-) {2,4,5-TP} {SILVEX}	495	249–250
tris(2,3-Dibromopropyl)phosphate	492	251
Methylaziridine (2-) {1,2-propylenimine}	490	252–253
Methoxychlor	490	252–253
Brucine {strychnidin-10-one,2,3-dimethoxy-}	470	254–255
Kepone	470	254–255
Isosafrole {1,2-methylenedioxy-4-allylbenzene}	460	256–258
Safrole {1,2-methylene-4-allylbenzene}	460	256–258
tris(1-Azridinyl) phosphine sulfide	460	256–258
Dimethoxybenzidine (3,3′-)	453	259
Diphenylhydrazine (1,2-)	450	260
O,O-diethylphosphoric acid, O-p-nitrophenyl ester	425	261
n-Butylbenzyl phthalate	415	262
O,O-diethyl-O-2-pyrazinyl phosphorothioate	410	263
Dimethylaminoazobenzene	405	264
Diethyl phthalate	400	265–266
Class 6		
O,O-diethyl-S-methyl ester of phosphoric acid	395	265–266
O,O-diethyl S-[(ethylthio)methyl]ester of phosphorodithioic acid	395	267–268
Citrus red No. 2 {2-naphthol,1-[(2,5-dimethoxyphenyl)azo]}	395	267–268
Trypan blue	392	269
Ethyl methanesulfonate {methanesulfonic acid, ethyl ester}	390	270–274
Disulfoton	390	270–274
Diisopropylfluorophosphate {DFP}	390	270–274
O,O,O-Triethyl phosphorothioate	390	270–274
Di-n-butyl phthalate	390	270–274
Paraldehyde {2,4,6-trimethyl-1,3,5-trioxane}	380	275
Di-n-octyl phthalate	380	276
Octamethylpyrophosphoramide {Octamethyldiphosphoramide}	374	277
bis(2-Ethylhexyl)phthalate	370	278–279
Methylthiouracil	370	278–279

Non-flame Incineration. Table 1 (Continued)

Principal organic hazardous constituent	T_{99} (2)(°C)	Rank
Propylthiouracil	360	280
Strychnine {strychnidin-10-one}	320	281
Cyclophosphamide	300	282–285
Nicotine {(s)-3-[1-methyl-2-pyrrolidinyl]pyridine}	300	282–285
Reserpine	300	282–285
Toluidine hydrochloride {2-methyl-benzenamine hydrochloride}	300	282–285
Class 7		
Tolylene diisocyanate {1,3-diisocyanatomethylbenzene}	290	286
Endrin	285	287
Butanone peroxide (2-) {methyl ethyl ketone, peroxide}	260	288
Tetraethylpyrophosphate	255	289
Nitroglycerine [{trinitrate-1,2,3-propanetriol}]	255	290
Tetraethyldithiopyrophosphate	250	291–292
Ethylenebisdithiocarbamic acid	250	291–292
Tetranitromethane	245	293
Uracil mustard {5-[bis(2-chloroethyl)amino]uracil}	246	294
Acetyl-2-thiourea (1-) {acetamide,N-[aminothioxomethyl]-}	240	295–299
Chlorophenyl thiourea (1-) {thiourea,[2-chlorophenyl]-}	240	295–299
N-phenylthiourea	240	295–299
Naphthyl-2-thiourea (1-) {thiourea,1-naphthalenyl-}	240	295–299
Thiourea {thiocarbamide}	240	295–299
Daunomycin	230	300–301
Ethylene thiourea {2-imidazolidinethione}	230	300–301
Thiosemicarbazide {hydrazinecarbothioamide}	225	302–303
Melphalan {alanine,3-[p-bis(2-chloroethyl)amino] phenyl-,L-}	225	302–303
Dithiobiuret (2,4-) {thioimidodicarbonic diamide}	220	304–305
Thiuram {bis[dimethylthiocarbamoyl]disulfide}	220	304–305
AzaserinE {L-serine,diazoacetate [ester]}	200	306
Hexaethyl tetraphosphate	190	307
Nitrogen mustard N-oxide	170	308–310
Nitroquinoline-1-oxide (4-)	170	308–310
Cycasin {beta-D-glucopyranoside, [methyl-ONN-azoxy]methyl-}	170	308–310
Streptozotocin	155	311
N-methyl-N′-nitro-N-nitrosoguanidine	130	312–327
N-nitroso-di-ethanolamine {[2,2′-nitrosoimino]bisethanol}	130	312–327
N-nitroso-di-N-butylamine {N-butyl-N-nitroso-1-butanamine}	130	312–327

Non-flame Incineration. Table 1 (Continued)

Principal organic hazardous constituent	T_{99} (2)(°C)	Rank
N-nitroso-N-ethylurea {N-ethyl-N-nitrosocarbamide}	130	312–327
N-nitroso-N-methylurea {N-methyl-N-nitrosocarbamide}	130	312–327
N-nitroso-N-methylurethane	130	312–327
N-nitrosodiethylamine {N-ethyl-N-nitrosoethanamine}	130	312–327
N-nitrosodimethylamine {dimethylnitrosamine}	130	312–327
N-nitrosomethylethylamine {N-methyl-N-nitrosoethanamine}	130	312–327
N-nitrosomethylvinylamine {N-methyl-N-nitrosoethenamine}	130	312–327
N-nitrosomorpholine	130	312–327
N-nitrosonornicotine	130	312–327
N-nitrosopiperidine {hexahydro-N-nitrosopyridine}	130	312–327
N-nitrososarcosine	130	312–327
Nitrosopyrrolidine {N-nitrosotetrahydropyrrole}	130	312–327
Di-n-propylnitrosamine {N-nitroso-di-n-propylamine}	130	312–327
Oxabicyclo[2.2.1]heptane-2,3-dicarboxylic acid (7-) {endothal}	120	328
endosulfan	100	329

[a]Boldface print indicates compound thermal stability is fully evaluated; ranking based on UDRI experimental mixture data coupled with reaction kinetic theory
[b]Non-appendix VIII compound
[c]NOS listing; ranking is presented based on either UDRI or literature experimental data coupled with reaction kinetic theory
[d]Italicized print indicates compound thermal stability is fully evaluated based on UDRI or literature data coupled with reaction kinetic theory

literature, are listed in italics. The remaining compounds were ranked based on limited experimental data on the actual compound, experimental data on similar compounds, and/or reaction kinetic theory. For this latter group, which includes the majority of the ranking, sufficient data were not available to designate the compounds as experimentally evaluated. Thus, their ranking is considered less accurate than the experimentally evaluated, bold-faced POHCs.

The ranking was devised by assigning $T_{99}(2)(C)$ values to each compound. For some compounds, initially identical values of $T_{99}(2)(C)$ were assigned resulting in identical rankings. For example, there was no clear-cut basis for predicting the relative stability of diphenylamine, 1,1-dichloroethene, and fluoroacetic acid. Hence, the three compounds received a "tie" ranking as the 41st most stable compound. In other instances, the compounds that were initially assigned identical, $T_{99}(2)(C)$ values belonged to a homologous series. In this case, the mechanisms of destruction were similar and relative reaction rates could be assigned. This was generally the case for polycyclic aromatic hydrocarbons (PAHs); consequently, unique rankings could be assigned for most of these compounds. In general, it was not possible to further distinguish the initial ranking when the compounds in question decomposed by different mechanisms. The uncertainty in predicting $T_{99}(2)(C)$ values, the accuracy of field test data, and the variation in the actual pollutant emissions from facility to facility does not justify a more precise 1 to 1 ranking of the Appendix VIII organic compounds.

The ranking includes all individually listed organic compounds included on the Appendix VIII list. Appendix VIII also lists many compounds by class, i.e., not otherwise specified (NOS). These classes of compounds are generally not ranked. However, there are many instances where compounds are listed individually and by class. When this occurs, the ranking

includes the individually listed compounds. Exceptions to this rule were made for 1,2,2-trichloro-1,1,2-trifluoroethane, dichlorofluoromethane, chlorodifluoromethane, ethyl chloride, 1,3,5-trichlorobenzene, and 1,2,3,5-tetrachlorobenzene. Experimental data were available for these compounds, and they have been of interest as frequently selected POHCs or possible incineration surrogates. Sulfur hexafluoride has also been included in the ranking although it is not listed on Appendix VIII, due to interest in its utility as an incineration surrogate [16].

Application of the Updated UDRI Incinerability Ranking

The ranking in Table 1 is also grouped by horizontal lines which separate compounds into nine thermal stability classes, i.e., very stable, moderate stable, fragile, etc. This grouping is generally based on natural divisions in the predicted stability or reaction kinetic theory which suggests significantly different mechanistic pathways for the non-flame thermal decomposition of compounds within different classes.

One may use the thermal stability ranking in the same manner as the previous heat of combustion index, i.e., selection of a group of POHCs for trial burn testing and only allow POHCs to be burned which are lower in the ranking than the most fragile POHC for which 99.99% DRE can be demonstrated. An alternate approach would be to only allow trial burn testing of experimentally evaluated POHCs, but allow incineration of all POHCs lower in the ranking than the least stable POHC for which 99.99% DRE can be demonstrated.

Another alternate approach involves the use of the incinerability class divisions. In this approach, one can demonstrate 99.99% DRE of a group of experimentally evaluated POHCs within an incinerability class and receive approval to burn all other POHCs within and below that class. For example, if 99.99% DRE can be demonstrated for chloromethane, acetonitrile, and chlorobenzene (all class 1 compounds), the facility would be allowed to burn any Appendix VIII compound. As a second example, if 99.99% DRE is demonstrated for 1,3-hexachlorobutadiene, methyl ethyl ketone, and cresol (all class 3 compounds), the facility would only be allowed to burn compounds ranked in class 3 or lower.

It should be noted that reformation of a POHC from its own decomposition products or formation of the POHC as a PIC from another waste feed component is generally not included as a factor in this ranking. Significantly, laboratory studies have shown that both POHC reformation and PIC formation can affect observed DEs [11, 17]. In some instances, laboratory determination of $T_{99}(2)(C)$ is unavoidably affected by POHC reformation (e.g., formation of chloromethane from chlorine atom attack on methane). When it was judged that POHC reformation was inevitable from almost any waste, reformation was included in the thermal stability ranking assignment.

The extensive testing conducted by UDRI has shown that the ranking of most of the compounds is relatively insensitive to composition of the waste mixture. However, a few notable exceptions have been observed in initial tests. This includes aniline derivatives and PAHs in general. Somewhat lesser variability has been observed for benzene, toluene, and pyridine, which were judged to be sufficiently constant to be included as experimentally evaluated compounds. Consequently, it is suggested that the waste composition be carefully considered before these compounds are selected as POHCs. Benzene, toluene, and PAHs are expected to be particularly prone to formation as PICs in full-scale trial burn incineration testing, and observed DREs may be significantly affected. Effects of PIC formation may be minimized by feeding the POHC at a sufficiently high concentration.

Finally, it should be noted that no rankings are given for polychlorinated biphenyls (PCBs) which are listed as NOS in Appendix VIII. An estimate of the stability of individual PCB congeners may be made by assuming that the congener is slightly less stable than the chlorinated benzene corresponding to the least chlorinated ring in the PCB congener of interest. This means, for example, that dichlorobenzene would be a suitable incineration surrogate for 2,2′,3,3′,4-pentachlorobiphenyl. Similarly, chlorobenzene would be a suitable incineration surrogate for 3,3′,4,5-tetrachlorobiphenyl, and pentachlorobenzene a suitable surrogate for decachlorobiphenyl.

Metal-containing compounds listed in Appendix VIII were not included in the ranking. In many cases,

the metal-containing compound is not converted in the high-temperature process and thus does not fit the description of DRE in the regulatory context.

Zone Theory of Formation of Products of Incomplete Combustion

Because of the wide varieties of physical and chemical compositions of hazardous waste, a universal treatment technique must have a very general mechanism of interaction with the waste. While chemical and photolytic treatment methods may be suitable for specific compounds or waste streams which are susceptible to a particular mechanism of chemical attack or absorb incident radiation, they are far from universal. Because all molecules absorb infrared radiation (viz. thermal energy), they are in principle, all susceptible to thermal treatment. It is largely for this reason that incineration has received such broad application. However, each type of molecule decomposes by a different mechanism, and the resulting fragments can undergo further reaction to form a wide variety of products. It is largely because of the potential complexity and toxicity of this "soup" of thermal by-products that incineration has received such intense scientific and regulatory scrutiny. In contrast to metals, which are not destroyed and undergo only a limited number of chemical reactions, it is feared that the situation concerning organic by-products may be too complex to ever solve, and one may unknowingly pollute the atmosphere with these "toxins."

However, chemists have long known that chemicals react by a limited number of elementary mechanisms. Although the situation is still complex due to the number of compounds contained in a typical waste feed, the number of even trace by-products that can be formed is limited by these mechanisms. Thus, if sufficient effort is placed into identifying and classifying these reactions, we can predict most of the potential by-products. Using this same knowledge of chemistry, we can do an even better job of identifying those compounds that are found in the highest yields, are the most thermally stable, and thus most significantly challenge the performance of a given incineration system. Such an approach is highly beneficial because many toxic by-products may escape undetected unless they are targeted for highly sensitive chemical analysis.

There are many ways to categorize reactions that lead to the emission of organic combustion by-products. From an incineration viewpoint, it is most useful to classify reaction pathways in a manner that they can be associated with regions of the incinerator where they are the most significant. Figure 1 depicts a typical rotary kiln/afterburner-type unit with four reaction zones being designated.

Zone 1, the pre-flame zone, is characterized by a wide range of temperatures (near ambient to approaching combustion temperatures), residence times on the order of 0.1 s, and low-excess-air conditions. Because this zone occurs at the front end of the device, it is not considered to be directly responsible for a very large fraction of pollutant emissions. Instead, it can create new reactants, by several low energy pathways that react further in the downstream zones.

Zone 2, the flame zone, is characterized by temperatures of 1,273–2,073 K at which essentially every organic compound will undergo complete conversion to its most thermodynamically stable end products, e.g., CO_2, H_2O, HCl, NO, etc. Numerous studies of premixed and diffusion flames have shown this to be the case, with any observed emissions of organic species being due to flow-paths that pass through the periphery of the flame, follow eddies of poor fuel/air mixing, or circumvent the flame altogether [8, 18, 19]. These flow-paths represent destruction "failure modes" of the flame and generate pockets that are more properly described as high-temperature thermal zones, viz. Zone 3. Although the flame zone probably does not generate significant toxic organic pollutants, it does generate large quantities of some inorganic pollutants, e.g., NO and HCl, as well as other lower concentration species, e.g., Cl_2 and NO_2, that may be very important reactants in subsequent zones.

Zone 3, the high-temperature, non-flame thermal zone, is a chemistry-rich zone where many types of high-energy unimolecular and bimolecular radical–molecule reactions occur. It is characterized by temperatures from 873 to 1,373 K, residence times of a few seconds, and both oxygen-rich as well as oxygen-depleted regions. Experimental as well as modeling studies indicate that the majority of the pollutant formation in this zone occurs in oxygen-depleted pockets of poor waste-air mixing [8, 18–20]. It is within

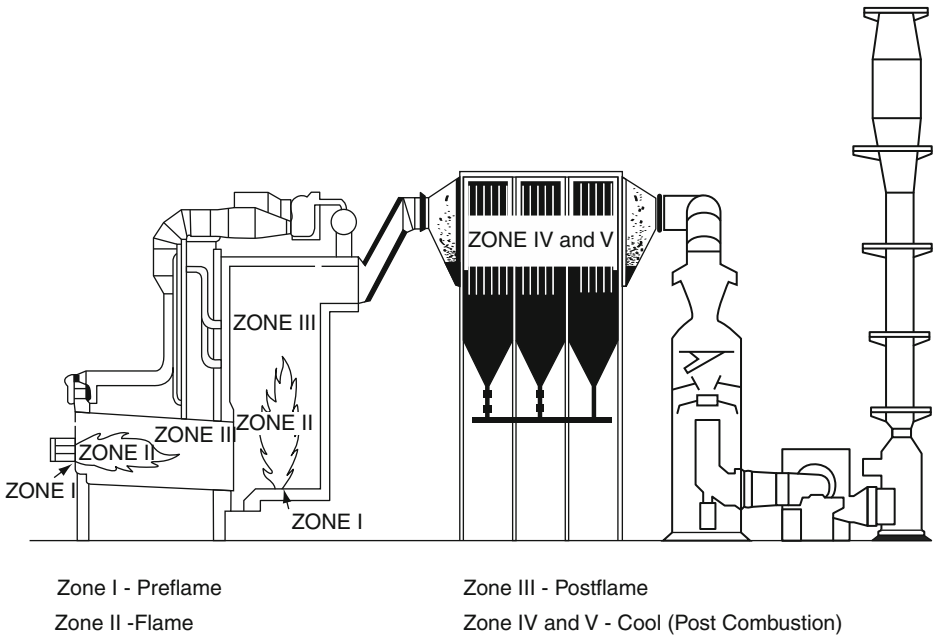

Non-flame Incineration. Figure 1
Chemical reaction zones in a hazardous waste incinerator. *Zone I* – Pre-flame Zone, *Zone II* – Flame Zone, *III* – Post-flame Zone, *Zone IV* & *V* – Post-combustion (cool) zones

this zone that most of the polycyclic aromatic hydrocarbons (PAHs), heteroatom-containing polynuclear aromatic hydrocarbons (PNAs), and some higher molecular weight chlorinated hydrocarbons (CHCs) are formed by radical–molecule, molecular growth pathways.

Zone 4, the gas quench or "cool zone," exists outside the combustion chamber and can be characterized by either gradual or rapid quenching of the gas temperature. Residence times can be very long, up to 10 s, and oxygen concentrations can vary from oxygen depleted, due to combustion in upstream zones, to very oxygen rich if air in-leakage occurs. The "cool zone" has not been well studied, but may in fact be responsible for a significant fraction of observed pollutant emissions from many types of combustors [20]. Partially oxidized products such as formaldehyde, chloroformaldehyde, and phosgene can form by radical–oxygen association reactions [21]. Nitrated products can also form via radical–molecule addition reactions involving NO_x species generated in the upstream, higher temperature zones [22].

Zone 5, the surface catalysis zone, exists at largely the same longitudinal point in the gas flow-path as the "cool zone" (zone 4). However, the distinguishing aspect of this zone that is fundamentally different from zones 1 to 4 is that one must now consider the effects of surfaces. Reaction times for gas-surface reactions can be the same as in zone 4 for entrained particulate; however, reaction times involving deposited particulate matter can be orders of magnitude longer before re-entrainment occurs and even longer if fixed surfaces are involved in the reaction. The temperature range in this zone is about 423–773 K. Below 423 K, sufficient energy is not available for activation of chemisorptions, and above 773 K most reactants are desorbed. This zone has been the subject of somewhat limited study, with the surface-mediated formation of polychlorinated dibenzo-p-dioxins (PCDDs) and polychlorinated dibenzofurans (PCDFs) receiving the only serious attention [23–27]. However, many more pollutants can potentially form as a result of surface catalysis via pathways including *de novo* synthesis of simple and more complex CHCs, partial oxidation of hydrocarbons and CHCs to form carbonyls, alcohols, organic acids, epoxides, etc., and nitration-type reactions to form a range of nitrogen-containing

products [24, 28, 29]. However, most of the reactions necessary to form these products likely require a transition metal catalyst in addition to an adsorption site [26, 30–34].

Table 2 summarizes the conditions and types of reactions (in order of importance) expected in each of five reaction zones. In the most general sense, the mechanisms of pollutant formation and destruction are expected to be relatively consistent within a zone. This "Zone Model" has the advantage that one can classify the types of reactions occurring within a given zone and consider their impact on emissions in more detail [35]. Table 2 also shows how the conditions within each zone may be distinctly different, resulting in different mechanisms of (POHC) destruction and (PIC) formation being dominant in each zone. Four classes of mechanisms of POHC destruction have been defined: (1) concerted molecular elimination, (2) bond fission, (3) bimolecular radical attack, and (4) surface-catalyzed decomposition. Four classes of mechanisms of PIC formation are included: (1) concerted molecular elimination of stable molecules, (2) complex radical–molecule pathways, (3) radical–radical (atom) and radical–molecule association reactions, and (4) surface-catalyzed synthesis.

Although there will be some contribution of each mechanism in zones 1–3, chemical kinetic theory suggests that mechanism 1 will dominate in the pre-flame zone, mechanisms 2 and 3 will dominate in the flame zone, and mechanisms 1 and 3 will dominate in the post-flame thermal zone. The gas quench and surface catalyst zones are somewhat different, due to the much lower temperatures and longer residences describing these zones. Mechanism 1 and 3 will dominate in the gas quench zone, and mechanism 4, by definition, will dominate in the surface catalyst zone. The nature and yield of by-product emissions will depend upon the conditions in a particular incinerator as well as the elemental and molecular chemical composition of the waste/fuel feed.

Non-flame Incineration. Table 2 Dominant mechanisms of pollutant destruction and formation[a] (From [35])

	Zone	Reaction conditions	Decomposition mechanisms[b]	Formation mechanisms[b]
1	Pre-flame	T = 473−1273 K	i	i
		$t_r << 1$ s	ii	ii
		$[O_2] \sim 50\%$ excess air	iii	iii
2	Flame	T = 1273−2073 K	iii	ii
		$t_r \leq 0.01$ s	ii	i
		$[O_2] \sim 50\%$ excess air	i	iii
3	High-temperature thermal (non-flame)	T = 873−1373 K	i	iii
		$t_r = 1-10$ s	ii	ii
		$[O_2] \sim 50-100\%$ excess air	iii	i
4	Gas quench (cool zone)	T = 353−873 K	i	iii
		t_r range: 1–10 s	ii	
		$[O_2] \sim 3-9\%$		
5	Surface catalyst	T = 423−773 K	iv	iv
		t_r range: 10 s–10 min		
		$[O_2] \sim 3$–9%		

[a]Decomposition mechanism: i. concerted molecular elimination; ii. bond fission; iii. bimolecular radical attack; iv. surface-catalyzed decomposition. Formation mechanism: i. concerted molecular elimination; ii. complex radical–molecule pathways; iii. recombination and association reactions; iv. surface-catalyzed synthesis

[b]In decreasing order of importance

PIC Emissions from Full-Scale Facilities

Tables 3 and 4 present specific PIC emissions data calculated from raw data available from field testing of nine hazardous waste incinerators [7, 36]. For each compound, frequency of occurrence, arithmetic mean emission rate, and geometric mean emission rate are presented. In calculation of the arithmetic and geometric mean emission rates, only values greater than analytical detection limits were considered, i.e., detection limit values were not assigned a numerical value.

Inspection of the full-scale incinerator data indicates that chloroform, benzene, tetrachloroethene, toluene, carbon tetrachloride, methylene chloride, 1,1,1-trichloroethane, chlorobenzene, and naphthalene are the most prevalent PICs, emitted in at least 75% of all tests. It should be noted that occurrence frequency in this context excludes the presence of the compound in the waste feed as a POHC. Of these compounds, chloroform, methylene chloride, benzene, toluene, and naphthalene exhibited largest emission rates (>1,000 μg/min). The greater values of arithmetic versus geometric mean emission rates for many of these compounds indicate that absence of a normal distribution of emission data, i.e., the distribution is skewed

Non-flame Incineration. Table 3 Frequently occurring volatile PICs in full-scale research tests

Compound	Frequency of occurrence[a]	Arithmetic mean emission rate[b] (μg/min)	Geometric mean emission rate[c] (μg/min)	Formation mechanism
Benzene	6/6	38396.8	6756.5	Radical–molecule
Chloroform	6/6	31616.3	2549.5	Association
Toluene	3/3	4198.7	1981.7	Radical–molecule
Carbon tetrachloride	1/1	126.3	120.4	Association
Tetrachloroethene	4/4	378.0	107.1	Radical–molecule
Chlorobenzene	4/5	674.0	494.8	Radical–molecule
1,1,1-Trichloroethane	4/5	520.3	84.3	Association
Methylene chloride	3/4	11707.7	1623.0	Radical–molecule
Bromodichloromethane	6/9	4794.7	2295.5	Association
Dibromochloromethane	6/9	1592.8	1059.6	Association
Bromoform	5/9	8254.8	2419.3	Association
Trichloroethene	1/2	762.0	721.1	Radical–molecule
Bromochloromethane	3/9	7334.0	1733.5	Association
Chloromethane	2/8	197481.0	161375.0	Radical–molecule
Methyl ethyl ketone	1/7	172.0	169.0	Radical–molecule
Methylene bromide	1/8	12800.0	12554.0	Association
Bromomethane	1/8	2300.0	2291.3	Association
Chloroethene	1/9	2405.0	2144.0	Molecule elim.
1,2-Dichloroethane	1/9	1946.0	1510.0	Association

[a]Defined as number of occurrences as PIC divided by total number of possible occurrences as PIC; denominator excludes presence in waste feed

[b]Arithmetic mean emission rate for all sites; individual data (per site) consist of an arithmetic mean based on the number of measurements obtained above detection limits

[c]Geometric mean emission rate for all sites; individual data (per site) consist of geometric mean based on the number of measurements obtained above detection limits

Non-flame Incineration. Table 4 Frequently occurring semivolatile PICs in full-scale research tests

Compound	Frequency of occurrence[a]	Arithmetic mean emission rate[b] (μg/min)	Geometric mean emission rate[c] (μg/min)	Formation mechanism
Naphthalene	3/4	2764.3	1461.2	Radical–molecule
Phenol	2/6	4326.5	1633.0	Association
2-Nitrophenol	2/8	4971.5	3398.5	Association
2,4,6-Trichlorophenol	1/8	5867.0	5867.0	Association
2,4-Dimethylphenol	1/8	1600.0	1600.0	Association
Pyrene	1/8	1100.0	1100.0	Radical–molecule
2,6-Toluene disocyanate	1/8	200.0	200.0	Radical–molecule
Hexachlorobenzene	1/8	24.0	24.0	Radical–molecule
2-Chlorophenol	1/8	479.0	479.0	Association
Pentachlorophenol	1/8	340.0	340.0	Association
Fluoranthene	1/8	700.0	700.0	Radical–molecule

[a]Defined as number of occurrences as PIC divided by total number of possible occurrences as PIC; denominator excludes presence in waste feed

[b]Arithmetic mean emission rate for all sites; individual data (per site) consist of an arithmetic mean based on the number of measurements obtained above detection limits

[c]Geometric mean emission rate for all sites; individual data (per site) consist of geometric mean based on the number of measurements obtained above detection limits

towards larger emission rates. Considering the scatter in the data, the geometric mean emission rate is a more representative measure of the actual emission rate for these compounds.

Further inspection of Table 3 indicates that chloromethane, methylene bromide, bromomethane, bromoform, bromodichloromethane, dibromochloromethane, and bromochloromethane also exhibited emission rates comparable to or greater than the more frequently observed compounds. There are at least three potential causes for the intermittent emission of these brominated halomethane PICs: (1) they are formed (via true PIC formation) from bromine-containing precursors in the waste or fuel which were not reliably analyzed for by full-scale sampling/analytical techniques, (2) they are contained in nearly all waste streams yet not reliably analyzed by full-scale analytical techniques, and (3) they are formed by volatile compound stripping from makeup scrubber water. The relative contribution of these sources cannot be ascertained with the available data. However, the fragile nature of these compounds suggests they cannot survive a well-operated incinerator. Thus, their presence in the waste feed in the same chemical form in which they are omitted is unlikely. "Cool zone" formation or stripping from the scrubber water is thus more likely sources.

The Zone Theory of PIC formation delineates three specific PIC formation mechanisms based on an analysis of laboratory-scale PIC formation and destruction behavior. These mechanisms are also listed in Tables 3 and 4 for the specific PICs identified from the incinerator evaluation. For the types of PICs observed, emission mechanisms are divided into three categories: molecular elimination reactions, radical–molecule reactions, and radical association reactions. The relative contributions of these three mechanisms to the observed PIC emissions depend on the relative importance of the following parameters: (1) frequency of occurrence and (2) geometric mean emission rate. Weighting the former as more significant suggests that 67% of the PICs are emitted by a radical–molecule mechanism. However, based on geometric mean emission rate (>1,000 μg/min), the data indicate that both radical–molecule and radical association mechanisms are of equal significant in producing PIC emissions.

An equal weighting of these two parameters indicates that 67% of the PICs are emitted by radical–molecule mechanisms (weighted geometric mean emission rate >1,000 μg/min). The above analysis excludes brominated halomethane compounds because their mechanism of formation may be partially due to stripping of scrubber makeup water. Observed phthalate compounds have also been excluded because their mechanism of formation are at least partially due to ubiquitous sources, e.g., outgassing of phthalates in plasticizers used in analytical laboratories.

In summary, the field data base indicates that the most prevalent class of PICs emitted was the chlorinated methanes. Benzene, toluene, and naphthalene represented the most prevalent aromatic species observed. PICs of secondary prevalence, yet still observed in at least 50% of possible cases, included the chlorinated ethenes and the chlorinated ethanes. Another major observation from the analysis of the specific PIC emissions is related to their mechanism of formation. The data from all types of thermal disposal facilities indicate that radical–molecule reactions and radical association reactions are by far the dominant emission mechanisms. This conclusion is reached independent of the relative weighting of PIC classification parameters. Analysis of specific PICs generated by these two emission mechanisms indicated that radical association reactions varied in significance from ~30% to as high as 50%, depending on the emission source. As discussed in the Zone Theory of PIC Formation, radical–molecule and radical–radical association reactions are the dominant chemical reactions occurring in the post-flame and cool zones of incineration systems. Although the available PIC emissions data base is very limited, the mechanistic implications of this analysis suggest that the cooler region downstream of the flame zone may be responsible for a significant fraction of the observed emissions. The degree to which these types of reactions contribute to the observed emissions is dependent on several facility-dependent factors, the most important perhaps being post-flame zone waste/air mixing and cool zone quenching rates.

Examination of full-scale PIC measurements for more than a dozen incinerator compliance and test burns has resulted in the observation that there are several common or "generic" PICs that tend to be emitted regardless of the waste being fed. With the exception of methyl chloride and vinyl chloride, these are all hydrocarbons that likely result from both waste and fuel combustion. Surprisingly, the yields of these PICs do not seem to vary greatly from incinerator to incinerator. Thus, it has been possible to develop approximate PIC emission factors. Table 5 lists these values in μg of PIC per kg of waste feed. Although one still expects significant variations of actual emission rates from those calculated based on these values, experience has shown them to be accurate to within an order of magnitude. Furthermore, the relative emission rates of each PIC have been found to be quite consistent with these emission factors.

Formation of Chlorinated Polycyclic Aromatic Hydrocarbons

In this section, laboratory studies of the molecular growth reactions of CHCs are reviewed. Mechanisms and rate parameters associated with the formation of chlorinated aromatic compounds are emphasized.

Non-flame Incineration. Table 5 Approximate emission factors for consistently observed PICs

Compound	Emission factor (μg/kg)
Biphenyl	63
Benzene	31
Toluene	30
Naphthalene	22
Phenol	8.7
Benzaldehyde	5.5
Ethyl benzene	5.1
Xylene	4.3
Benzoic acid	2.7
Benzofuran	5.0
Methyl chloride	5.0
Vinyl chloride	0.88
Acenaphthalene	0.50
Acenaphthene	0.50
Fluoroanthene	0.50
Phenanthrene	0.20
Dibenzofuran	0.01

From an environmental perspective, the molecular growth of CHCs is significant because by-products of these reactions include chlorinated aromatic and chlorinated polycyclic aromatic hydrocarbons (ClPAH). The potential emission of these products into the environment is of concern due to their potential health effects [37].

Gas-Phase Molecular Growth Reactions

Nearly 50 years ago, Aubrey and van Wazer [38] showed empirically the existence of an equilibrium between chloro-aliphatic and aromatic compounds:

$$9C_2Cl_6 \rightarrow 12CCl_4 + C_6Cl_6(cy) \qquad (R1)$$

There were several further investigations on thermal reactivity of chloro-aliphatic and aromatic compounds between 1960 and 1980. Most of these early studies were performed using scaled ampoule techniques. For a review, see Choudhry and Hutzinger [39]. Since 1980, modern methods of elucidating reaction mechanisms using hyphenated analytical techniques (typically gas chromatography coupled to specific detectors) interfaced directly to special flow reactors, and drop tube reactors have been used to unravel the complexity of non-flame thermal reactions of chloro-organic compounds under both oxidative and pyrolytic conditions. These more recent studies are updated here.

The oxidative pyrolysis of methylene chloride (CH_2Cl_2), chloroform ($CHCl_3$), and carbon tetrachloride (CCl_4) has been investigated by Tirey et al. [40] and Taylor et al. [41] using a fused silica, tubular flow reactor coupled to gas chromatographic–mass spectrometric (GC–MS) detection. This study first illustrated the dominance of pyrolytic reaction behavior leading to the formation of several thermally stable reaction by-products and the observation of chlorinated molecular growth reactions resulting in the formation of hexachlorobenzene from simple chlorinated methane precursors. The facile formation of C_6CI_6 (cy) from the oxidative pyrolysis of $CHCl_3$ is illustrated in Fig. 2. Key elementary reactions leading to the formation of C_6CI_6 (cy) are presented and discussed by Taylor and Dellinger [42].

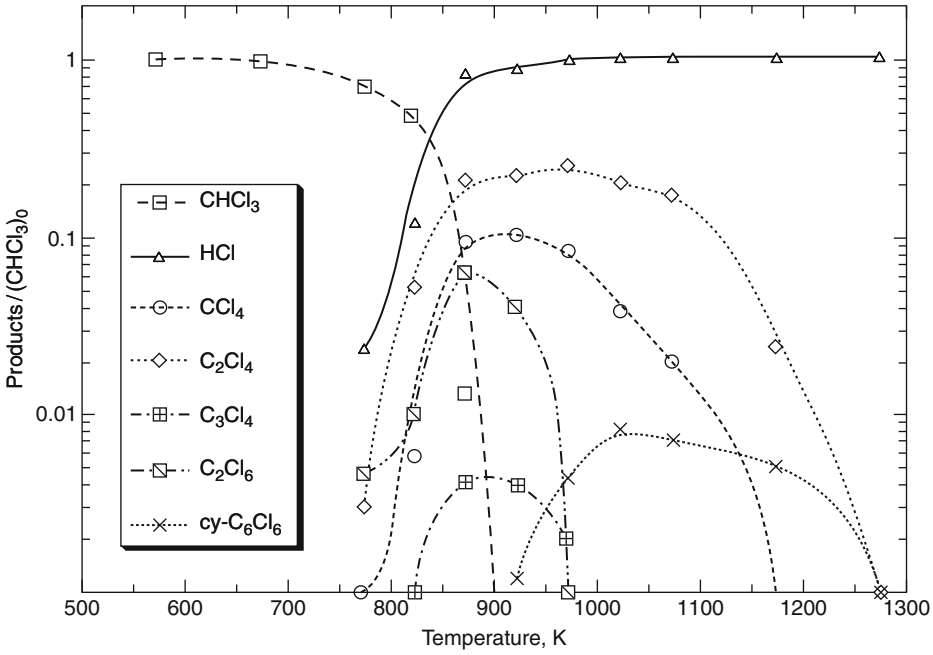

Non-flame Incineration. Figure 2
Product distributions from the oxidative pyrolysis of $CHCl_3$. $CHCl_3/O_2$ equiv. ratio = 3.0, $[CHCl_3]_0 = 2.7 \times 10^{-5}$ mol/L, $t_r = 2.0$ s, P = 1.15 atm. Curves drawn through data based on smoothed interpolated fit (From [41])

The formation of higher molecular weight compounds from the pyrolysis and combustion of CHCs has been observed for the following precursors: $CHCI_3$ [40, 41, 43], CCI_4 [40, 41, 43], dichloroacetylene (C_2Cl_2) [44], trichloroethene (C_2HCI_3), [45–47], tetrachloroethene (C_2CI_4) [48–50], hexachloropropene (C_3Cl_6) [51], and 1,3-hexachlorobutadiene (C_4CI_6) [52, 53]. Tirey et al. [49] proposed a mechanism including the formation of the following intermediate species: C_2Cl_2, C_2Cl_3, C_2Cl_4, C_2HCl_3, C_4Cl_4, C_4Cl_5, and C_4Cl_6 that required further experimental and theoretical analysis. The mechanism was based on mechanisms proposed to account for observed products from the pyrolysis and combustion of unsaturated aliphatic hydrocarbons [54, 55] and methyl chloride [56]. However, based on the absence of production of chlorinated aromatics from CH_3Cl and CH_2Cl_2 as compared with $CHCl_3$ and CCl_4, Dellinger and Taylor [42] proposed that chlorine facilitates condensation reactions resulting in the formation of chlorinated aromatic species. They suggested that the tendency to form high molecular weight species is attributable to the propensity for chlorinated radicals to undergo reversible, addition/elimination (displacement)-type molecular growth reactions:

$$C_2Cl_3 + C_2Cl_4 \leftrightarrow C_4Cl_7{}^* \rightarrow C_4Cl_6 + Cl \qquad (R2)$$

Chlorine substitution can play a major role in the rate of these molecular growth reactions through inductive destabilization of the initially formed adduct (*) and through rapid elimination of chlorine. Chlorine elimination reduces the probability of the reverse decomposition to reactants. The lower C–Cl bond energies in CHCs (vs. C–H bond energies in hydrocarbons) favor these types of molecular growth reactions. Tirey et al. [49] and Dellinger and Taylor [57] presented Quantum RRK calculations illustrating that chemically activated Cl displacement from olefinic and acetylenic species by olefinic radicals is favored for CHCs as compared with the similar displacement of H atoms from hydrocarbons. They proposed that this is in part responsible for the high yields of chlorinated aromatics for the more chlorinated of these species. The following paragraphs summarize recent studies of the pyrolysis and combustion of C_2 unsaturated CHCs and the development of core reaction models describing molecular growth leading to the formation of chlorinated aromatic species.

Measurements of condensed-phase products of C_2HCI_3 pyrolysis in a drop-tube reactor obtained over a temperature range of 1,100–1,500 K were reported by Mulholland et al. [45]. A predominance of perchloroaromatics was found, in sharp contrast to the largely unsubstituted PAHs obtained from the pyrolysis of a mixture of trichloroethylene and toluene under similar conditions. Detailed characterization of product tars from the pyrolysis of C_2HCI_3 using GC–MS analysis revealed the following molecular growth products: C_4Cl_6, C_6HCl_5, C_6Cl_6, $C_8H_4Cl_6$, C_8Cl_6, C_7HCl_7, C_8Cl_8, $C_{10}H_4Cl_6$, C_9Cl_8, $C_{10}Cl_8$, $C_{10}HCl_7$, $C_{12}Cl_8$, $C_{12}Cl_{10}$, and $C_{14}Cl_8$. A reaction mechanism beginning with C_2CI_2 formation from C_2HCl_3 via concerted HCI elimination was proposed. Aromatic ring formation and growth were proposed to occur by successive additions of C_2CI_2 to C_2HCI_3, in a manner similar to that proposed by Dellinger and Taylor [57].

The oxygen-free pyrolysis of C_2HCI_3 was investigated by Taylor et al. [46, 47] using a fused silica, tubular flow reactor coupled to in-line GC–MS detection. The major degradation by-products and molecular growth by-products are summarized in Figs. 3 and 4, respectively. Pronounced molecular growth was observed above 1,000 K as evidenced by the formation of C_2Cl_4, C_4CI_6, and C_6Cl_6 (cy) as major (> 5 mol %) products and dichlorodiacetylene (C_4Cl_2), pentachlorobenzene (C_6HCl_5 (cy)), hexachloroethynylbenzene (C_8Cl_6, (cy)), octachlorostyrene (C_8Cl_8 (cy)), octachloronaphthalene ($C_{10}Cl_8$ (cy)), and $C_{12}Cl_8$ (cy) as minor(< 5 mol %) products. A detailed reaction kinetic model was developed describing molecular growth up to the formation of C_8Cl_6 (cy) and C_8Cl_8 (cy).

A core pyrolysis model that accounts for the major products up to C_8Cl_6 (cy) and C_8Cl_8 (cy) is depicted in Table 6. Sensitivity and production rate analyses indicated that C–CI hand fission is the dominant initiation step. Cl atoms abstract H from C_2HCl_3 yielding C_2CI_3 and HCI. Trichlorovinyl decomposes by C–Cl scission to form C_2Cl_2 or reacts with Cl_2 to give C_2Cl_4. Alternatively, C_2Cl_3 can add to C_2HCI_3, C_2Cl_2, or C_2CI_4 via CI displacement to give C_4HCl_5, C_4CI_4, or C_4CI_6, respectively. Reaction of C_4Cl_5 and C_4CI_3

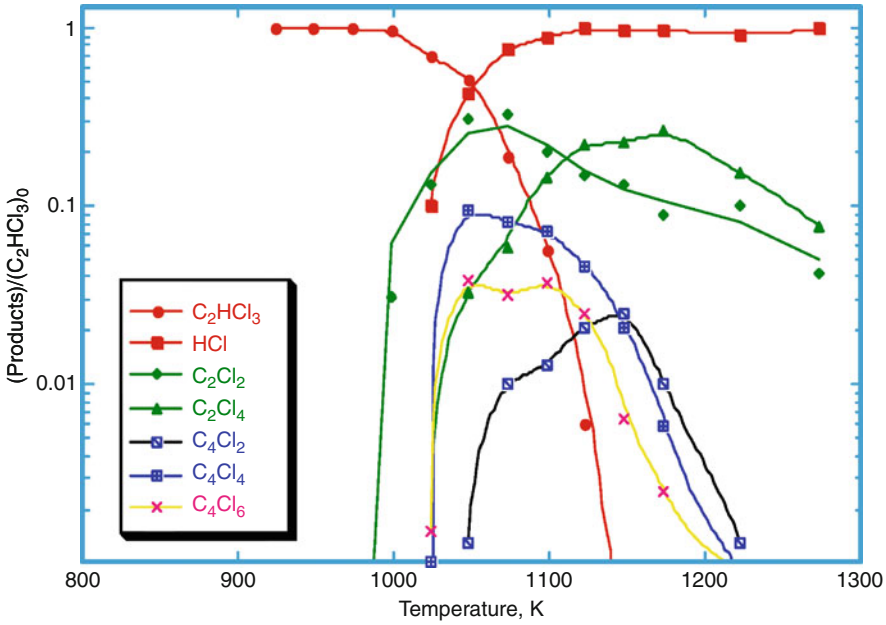

Non-flame Incineration. Figure 3

Major products from the oxygen-free pyrolysis of C_2HCl_3. $[C_2HCl_3]_0 = 5.4 \times 10^{-5}$ mol/L, $t_r = 1.7$ s, P = 1.83 atm

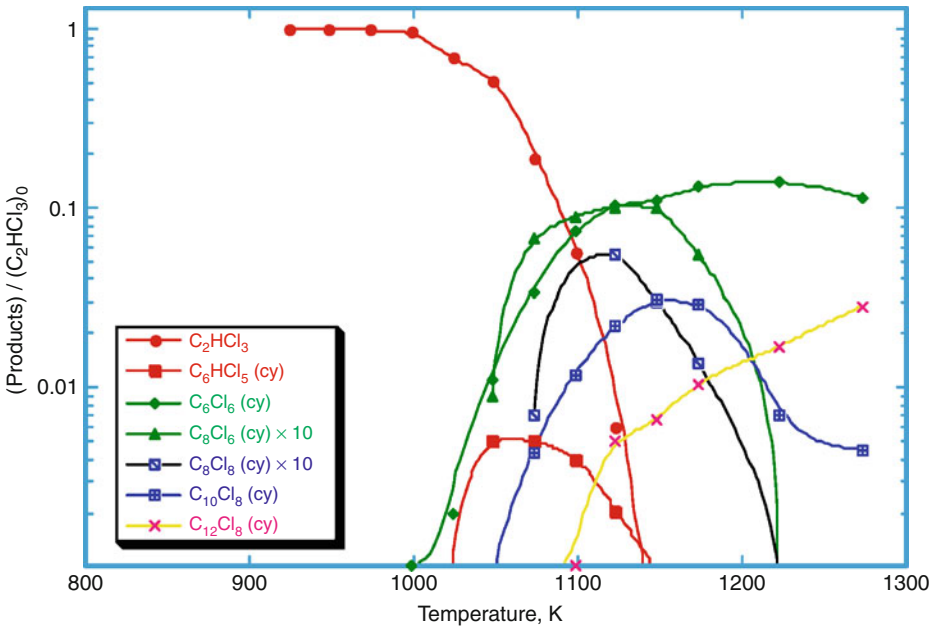

Non-flame Incineration. Figure 4

Chlorinated aromatic products from the oxygen-free pyrolysis of C_2HCl_3. $[C_2HCl_3]_0 = 5.4 \times 10^{-5}$ mol/L, $t_r = 1.7$ s, P = 1.83 atm

Non-flame Incineration. Table 6 C_2HCl_3 Core pyrolysis and molecular growth mechanism (From [47])

Reaction	log k (cm^3/mol/s/kcal)
$C_2HCl_3 \rightarrow C_2HCl_2 + Cl$	15.0-91.0/2.303 RT
$C_2HCl_3 + Cl \rightarrow C_2Cl_3 + HCl$	12.3-9.5/2.303 RT
$C_2C1_3 + M \rightarrow C_2Cl_2 + Cl + M$	15.0-32.8/2.303 RT
$C_2C1_3 + Cl_2 \rightarrow C_2Cl_4 + Cl$	12.5-4.8/2.303 RT
$C_2Cl_3 + C_2HCl_3 \rightarrow C_4HCl_6$	11.0-7.0/2.303 RT
$C_4HCl_6 \rightarrow C_4HCl_5 + Cl$	13.0-18.0/2.303 RT
$C_4HCl_5 + Cl \rightarrow C_4Cl_5$ (i) + HCl	12.3-5.0/2.303 RT
C_4Cl_5 (i) $\rightarrow C_4Cl_4 + Cl$	13.4-43.9/2.303 RT
$C_2Cl_3 + C_2Cl_2 \rightarrow C_4Cl_5$ (n)	12.0-6.0/2.303 RT
C_4Cl_5 (n) $\rightarrow C_4Cl_4 + Cl$	13.4-34.1/2.303 RT
$C_4Cl_4 \rightarrow C_4Cl_3$ (i) + Cl	16.0-68.4/2.303 RT
$C_4Cl_4 \rightarrow C_4Cl_3$ (n) + Cl	16.0-84.0/2.303 RT
C_4Cl_3 (n) + $C_2Cl_2 \rightarrow C_6Cl_5$ (l)	11.7-5.0/2.303 RT
C_6Cl_5 (l) $\rightarrow C_6Cl_5$ (cy)	10.0
C_6Cl_5 (cy) + Cl $\rightarrow C_6Cl_6$ (cy)	12.6 + 1.2/2.303 RT
C_4Cl_5 (n) + $C_2Cl_2 \rightarrow C_6Cl_7$ (l)	12.5-5.0/2.303 RT
C_6Cl_7 (l) $\rightarrow C_6Cl_6$ (cy) + Cl	10.0
C_6Cl_5 (cy) + $C_2Cl_2 \rightarrow C_8Cl_6$ (cy) + Cl	11.7-5.0/2.303 RT
C_6Cl_5 (cy) + $C_2Cl_4 \rightarrow C_8Cl_8$ (cy) + Cl	11.7-5.0/2.303 RT

radicals with C_2Cl_2 are the dominant pathways to formation of C_6Cl_6 (cy). Reaction of C_6Cl_5 (cy) with C_2CI_4 and C_2CI_3 with C_6CI_6 (cy) contribute nearly equally to C_8Cl_8 (cy) formation while the reaction of C_2CI_2 with C_6Cl_5 (cy) dominates C_8CI_6 (cy) formation. The conversion of C_2CI_3 into C_2Cl_4 inhibits both the formation of larger molecular weight species and the destruction of C_2HCl_3.

Except for the very lowest temperatures, model calculations indicate that the C_2CI_3 radical chain is the dominant conversion cycle for C_2HCI_3 under pyrolytic conditions. Rapid abstraction of H from C_2HCl_3 by Cl atoms removes most H-containing species from the reaction system before C_4 species can be formed. Hydrogen-containing C_2 or C_4 species that form at trace levels are rapidly destroyed by additional H abstraction by Cl. When a hydrogen-rich fuel is added, there is competition for the available CI atoms, and H-containing CHCs would be expected to survive and result in the formation of a variety of H-containing molecules. This is in agreement with observations of others working on mixed H and CI systems [45].

Experimental and modeling studies were also carried out by Taylor et al. on other unsaturated CHCs including C_2Cl_4 [50], C_3Cl_6 [51], and C_4Cl_6 [52] under conditions very similar to the C_2HCl_3 experiments. Similar molecular growth reaction products were observed. Attempts to model this data using similar reaction pathways developed for the C_2HCl_3 degradation products were generally successful with some exceptions.

The implication of the results of the experimental and modeling effort on CHC pyrolysis is the manner in which weaker C–Cl bonds (vs. C–H bonds) facilitate certain reactions. Chlorine atom displacement, internal chlorine atom abstractions, and chlorine migrations can all facilitate molecular growth. Formation of perchlorinated aromatic species and ClPAH that are resistant to oxidation may actually be more kinetically favored than formation of PAH from the corresponding hydrocarbons.

Formation of Polychlorinated Dibenzo-P-Dioxins and Furans

In the previous section, it was demonstrated that complex aromatic CHCs readily form from aliphatic CHCs at elevated temperatures. Combustion processes are one of the major sources of PCDD/F in the environment ([58, 59]). The concerns regarding environmental exposure to PCDD/F are well known, see, for example, the US-EPA Dioxin Reassessment by the National Academy of Sciences [60].

Gas-phase molecular growth mechanisms of CHCs leading to the formation of PCDD/F have been unable to account for the PCDD/F concentrations observed in the flue gas of full-scale combustors [61, 62]. As a result, over the past two decades, research on the mechanism of formation of PCDD/F in combustion sources has focused on surface-mediated pathways [23–27, 63, 64]. In this section, we review that state of

knowledge of both low-temperature, surface-mediated formation of PCDD/F and recent efforts to develop a kinetic model that can predict the higher temperature, surface-mediated formation of PCDD/F from chlorophenol precursors.

Current Status of Surface-Mediated (Low Temperature) Studies of PCDD/F Formation

Seventy percent of emissions of PCDD/F from combustion and thermal processes have been estimated to occur via transition metal-mediated reactions, in the post-flame, cool zone [65–67]. Two surface-mediated formation pathways have been proposed: (1) the de novo pathway in which elemental carbon and transition metals in combustion-generated particles react with oxygen and chlorine to liberate PCDD/F from the carbon matrix and (2) the precursor pathway in which organic species such as chlorophenols react on a transition metal surface to form PCDD/F [23–27, 33–35, 39, 61, 63–70].

In the de novo pathway, it has recently been proposed that nonchlorinated dibenzofuran and dibenzo-p-dioxins are first formed from the carbon and then chlorinated to form PCDFs and lesser amounts of PCDDs [71–75]. Research on the precursor pathway has demonstrated that chlorophenols are readily converted to PCDDs and lesser amounts of PCDFs by reaction over a copper oxide surface [23, 76, 77]. The high yields of PCDFs from the de novo process and the high yields of PCDDs from the precursor pathway have led to the suggestion that PCDFs are formed primarily from elemental carbon (or PAHs), and PCDDs are formed primarily from chlorophenols in full-scale incinerators.

In apparent contradiction to the chlorophenol hypothesis, correlations between various incineration parameters and PCDD/F emission concentrations indicated chlorobenzene concentrations, rather than chlorophenol concentrations, were the best predictors of total PCDD/F emissions [24, 27, 67, 78–80]. This finding is complicated by the fact that chlorophenols are difficult to analyze due to their propensity to strongly bind with the surface of particulate matter. However, there is a lack of experimental evidence of formation of PCDD/Fs from chlorobenzenes [81, 82]. In spite of this, it is frequently assumed that chlorobenzenes readily form PCDD/Fs in full-scale systems [24, 27].

Although research has demonstrated copper oxide-mediated reactions can convert simple hydrocarbons such as ethylene and acetylene to chlorobenzenes and ClPAHs [26, 32, 44, 83, 84], chlorophenols have not been detected as intermediates in these experiments. Chlorophenols do not form from chlorobenzenes during gas-phase pyrolysis, as chlorobenzenes undergo ring rupture with a small fraction converting to other substituted aromatic compounds under oxidative conditions [85, 86].

A recent study has attempted to determine if chlorobenzenes can be converted to PCDD/Fs in sufficient yields to make a significant contribution to their emissions from full-scale facilities. Nganai et al. [34] investigated the potential contribution of chlorinated benzenes to the formation of PCDD/Fs using 1,2-dichlorobenzene as a surrogate for reactions of other chlorinated benzenes and CuO/silica (3 wt.% Cu) as a surrogate for fly ash. Results were similar for oxidative and pyrolytic conditions with a slight increase in more chlorinated products under oxidative conditions. Reaction products included chlorobenzene, polychlorinated benzenes, phenol, 2-chlorophenol (2-CP), dichlorophenols, and trichlorophenols with yields ranging from 0.01% to 2% for the phenols and from 0.01% to 10% for chlorinated benzenes. 4,6-Dichlorodibenzofuran (4,6-DCDF) and dibenzofuran (DF) were observed in maximum yields of 0.2% and 0.5%, respectively, under pyrolytic conditions and 0.1% and 0.3%, respectively, under oxidative conditions. In previous studies of the pyrolysis of 2-CP under identical conditions [33], 4,6-DCDF and dibenzo-p-dioxin (DD) were observed with maximum yields of ~0.2% and ~0.1%, respectively, along with trace quantities of 1-chlorodibenzo-p-dioxin (1-CDD). Under oxidative conditions, DD, 1-CDD, and 4,6-DCDF were observed with maximum yields of 0.07%, 0.3%, and 0.1%, respectively. When combined with the fact that measured concentrations of chlorobenzenes are often 10–100 times higher than chlorophenols in full-scale combustion systems, these studies suggest that surface-mediated reactions of chlorinated benzenes can be a significant source of PCDD/F emissions.

Current Status of Modeling of Higher Temperature PCDD Formation from Chlorophenol Precursors

Shaub and Tsang [61, 87] initially explored this issue through the development of a simple 13-step, gas-phase reaction mechanism and a separate heterogeneous catalytic model of dioxin formation and concluded that heterogeneous rates were much faster than homogeneous rates. Furthermore, they concluded that the more rapid heterogeneous rates were necessary to account for full-scale municipal waste incinerator data. Sidhu et al. [88] challenged the kinetic rates used in the gas-phase dioxin model and concluded, based on experimental measurements of PCDD/F formation from 2,4,6-trichlorophenol, that the estimated rate for pre-dioxin formation from trichlorophenol precursors was underestimated by Shaub and Tsang [61]. Grotheer and Louw [89] conducted an experimental study to verify the hypothesis of Sidhu et al. [88] and concluded that the homogeneous rates in the reaction mechanism proposed by Shaub and Tsang [61] were indeed correct and that their experiments and those by Sidhu et al. could be interpreted in terms of a different gas-phase model incorporating phenoxyl radical recombination as the key step in dioxin formation.

With the realization that phenoxyl radicals are exceptionally unreactive with oxygen, a modified gas-phase PCDD model has recently been proposed that could explain the formation of PCDD by purely gas-phase reactions of phenoxyl radicals [90, 91]. Published models have assessed the relative importance of the role of labile chain carriers including H, CI, O, OH, HO_2, and alkyl radicals (R) [90–93]. In the recently published modeling of Khachatryan et al., OH proved to be the dominant chain carrier [90, 92, 93]. However, other recent publications suggest that CI is a highly active chain carrier in the formation of PCDD and chlorinated aromatic pollutants as well as being a chlorinating agent [91, 94]. In these models, the main channel for the decomposition of chlorinated phenoxyI radicals was expulsion of CO (the dominant oxygen-containing product) and formation of chlorinated cyclopentadienyl radical, $C_5H_2CI_3$ [90, 92, 93]. For the sake of simplicity, the further decomposition of $C_5H_2CI_3$ was not considered, which leads to a low steady-state concentration of CI versus OH [91]. To more fully assess the role of CI in overall chain processes over wide temperature ranges, it is important to release CI atoms from $C_5H_2CI_3$ (as one of the major products) using reasonable decomposition pathways and associated reaction kinetics.

The roles of OH and Cl in the formation of 1,3,6,8-tetrachlorodibenzo-p-dioxin (1,3,6,8-TCDD) from 2,4,6-trichlorophenol (2,4,6-TCP) were recently assessed by Khachatryan et al. [95] using an expanded PCDD model that includes several new reaction schemes that were added to the original model [90]. The final model of 132 reactions (given in Scheme 1 of the Supporting Information of Khachatryan et al. [95]) includes updated sub-models for TCDD formation; hydrogen oxidation; hexane oxidation; recombination/decomposition of $C_5H_2CI_3$ and release of CI; generation of CI through reactions of Cl_2 with OH, H, and O; additional reactions for release of CI [96]; and an additional four-step surface-mediated generation of 1,3,6,8-TCDD sub-model (see Table 4 of [95]).

The modifications to the model resulted in improved agreement with experimental results [97] below 900 K as illustrated in Fig. 5. The maximum deviation of calculated and experimental yields for 1,3,6,8-TCDD was less than factor of 4 in the temperature region between 823 and 1,073 K, and the maximum experimental yield of 0.004 wt% at 773 K was very close to the calculated yield 0.006% at 948 K despite an approximate 150 K shift in the maximum. Considering the large uncertainties in some of the thermochemistry and kinetic parameters of key reactions, the agreement is quite remarkable.

The experimentally observed yields of 1,3,6,8-TCDD between 648 and 798 K [97] are still higher than calculated. However, recent publications on the pyrolysis of 2-CP and 2,4,6-TCP reported lower PCDD yields in this temperature regime [98, 99]. PCDDs were not detected below 748 K from the gas-phase pyrolysis of 2-CP [98]. The oxidative pyrolysis of 2,4,6-TCP resulted in the formation of 1,3,6,8- and 1,3,7,9-TCDD between 773 and 1,053 K with a maximum at 898 K [99]. The results of this model agree reasonably well with these experimental results over the temperature range of 823–1,073 K. Khachatryan et al. [95] included very favorable rates for silica-catalyzed reactions in the revised model. It is thus possible that the higher yields of 1,3,6,8-TCDD

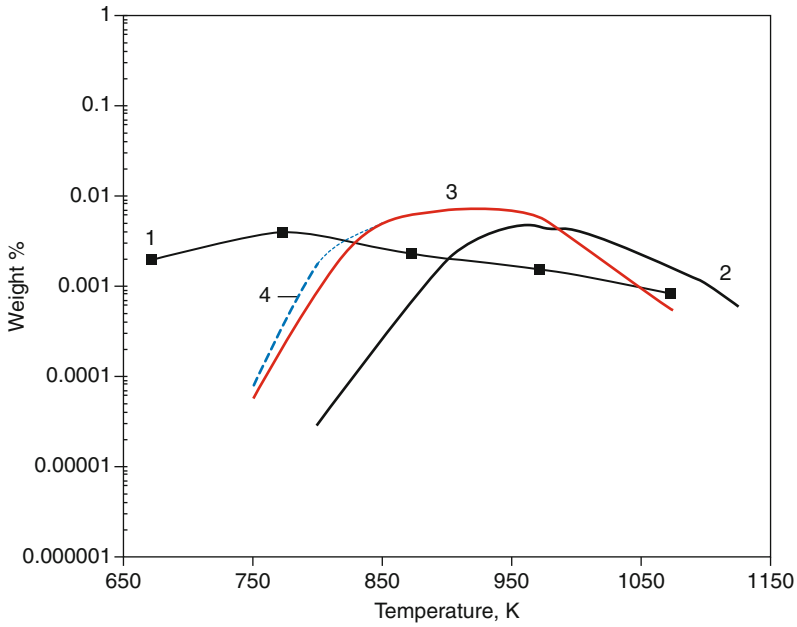

Non-flame Incineration. Figure 5
Comparison of gas-phase experimental and modeling results for 1,3,6,8-TCDD formation. *Curve 1*: experimental results [97]. *Curve 2*: gas-phase model [90]. *Curve 3*: revised gas-phase model – 132 gas-phase reactions [95]. *Curve 4*: combined gas-phase and surface reaction model – 136 reactions including four reaction surface sub-model [95] (From [95])

between 648 and 848 K for the reference experimental study were due to wall deposits of carbon or other impurities [27] that are not accounted for in the current model.

Modeling results indicate that the role of CI is limited during pyrolysis of highly chlorinated phenols because CI is incorporated into the reaction products. Although the OH to CI ratio is <1 in the equilibrium calculations, it is always >1 for the reaction kinetic schemes with 136 reactions considered here. This suggests that OH is the dominant chain carrier below 1,048 K, and CI only participates as a secondary chain carrier at higher temperatures.

Future Directions

Thermal Stability–Based Incinerability Ranking

The thermal stability–based incinerability ranking does not currently have experimental indices for highly chlorinated aromatic compounds with expected high thermal stability and high toxicity. These compounds would include specific isomers of the family of PCBs and PCDD/Fs, in addition to specific ClPAHs of suspected high toxicity. The addition of these compounds would provide expanded utility of this important ranking for full-scale trial burns.

Formation of Products of Incomplete Combustion

Field tests of large scale incinerators yield emissions data that are not readily explainable using flame or post-flame chemistry, exclusively. Many or most of the observed emissions are products that are thermally fragile and are not expected to survive the flame zones of a thermal destruction facility. Thus, "cool zone" chemistry is implicated. As a result of the need to reduce PCDD/F emissions, surface-catalyzed chlorination reactions under "cool zone" conditions have received the most attention to date. This research has been very successfully translated to full-scale thermal treatment facilities where overall PCDD/F emissions have decreased dramatically over the past 20 years. However, recent characterization of combustor effluents using a technique known as multidimensional gas-chromatography–mass spectrometry (MDGC–MS) has shown that a large number of oxygenated PICs are

emitted [100]. These are thermally fragile species that are most likely formed in the "cool zone" of the incinerator. Surface-catalyzed partial oxidation is suspected as the route of formation. If this is true, then these species are likely to be emitted from virtually any combustion system. Since some of the observed pollutants are known endocrine disrupting chemicals (EDCs), their route of formation and their relationship to formation of other pollutant emissions from thermal destruction facilities is meritorious of future study.

CHC Molecular Growth and PCDD Modeling

The limitation in more accurate CHC molecular growth models is the lack of experimental elementary rate measurements for many key reactions. In addition to chlorine isomerizations, =CCI–CI dissociations, H abstraction by CI atoms, Cl atom transfer reactions, and radical addition reactions all represent major classes of reactions for which a lack of accurate rate data exists. Although serious attempts have been made to estimate the rates of these reactions, a larger database of validated CHC reaction rate data are needed to improve the development of extended reaction mechanisms.

The current status of PCDD/F formation modeling is not comprehensive and requires major improvement. For the current high-temperature PCDD model [95], additional PCDD decomposition/oxidation reactions may significantly impact the PCDD yields. Direct condensation reactions of molecular chlorinated phenols can be important at high temperatures [101, 102]. For PCDD/F modeling in general, there is a critical need for high-level calculations of rate constants and polynomials for key reactions as well as new pathways [103] and precursors [104]. The large uncertainties of rate parameters for reactions involving aromatic species as well as calculating thermodynamic parameters of these species may be the most difficult challenge in further improving PCDD/F formation models.

Bibliography

Primary Literature

1. Dempsey CR, Oppelt ET (1993) Incineration of hazardous waste: a critical review update. J Air Waste Manage Assoc 43:25
2. Electronic Code of Federal Regulations (1984) Appendix VIII to Part 261—Hazardous Constituents. http://ecfr.gpoaccess.gov/cgi/t/text/text-idx?c=ecfr&tpl=/ecfrbrowse/Title40/40cfr261_main_02.tpl. Accessed 11 July 2011
3. US-EPA (1983) Guidance manual for hazardous waste incinerator permits. U.S. EPA Office of Solid Waste and Emergency Response, Washington, DC, pp 2.16–2.26, NTIS PB84-100577
4. Lee KC, Morgan N, Hansen JL, Whipple GM (1982) Revised model for the prediction of the time-temperature requirements for thermal destruction of dilute organic vapors and its usage for predicting compound incinerability. In: Proceedings of the seventy-fifth air pollution control association meeting, New Orleans, LA, Paper 82–5.3
5. Tsang T, Shaub W (1982) Chemical process in the incineration of hazardous materials. In: Exner J (ed) Detoxification of hazardous waste. Ann Arbor Press, Ann Arbor, pp 41
6. Dellinger B, Rubey WA, Hall D, Graham JL (1986) Incinerability of hazardous wastes. Hazard Waste Hazard Mater 3:139
7. Trenholm A, Gorman P, and Jungelaus G (1984) Performance Evaluation of Full-Scale Incineration, Volumes I-V, US-EPA Final Report, EPA-600/2-84-181a-e. Cincinnati, OH
8. Clark WD, Seeker WR, Lee CC (1988) Engineering analysis of hazardous waste incineration: energy and mass balance. In: Freeman HM (ed) Incinerating hazardous wastes. Technomic Publishing, Lancaster, p 357
9. Dellinger B, Torres J, Rubey WA, Hall D, Graham JL, Carnes R (1984) Determination of the thermal stability of selected hazardous organic compounds. Hazard Waste Hazard Mater 1:137
10. Graham JL, Hall D, Dellinger B (1986) Laboratory investigation of thermal degradation of a mixture of hazardous organic compounds – I. Environ Sci Technol 2:703
11. Taylor PH, Dellinger B (1988) Thermal degradation characteristics of chloromethane mixtures. Environ Sci Technol 22:438
12. Dellinger B, Graham M, Tirey DA (1986) Predicting emissions from the thermal processing of hazardous wastes. Hazard Waste Hazard Mater 3:293
13. Taylor PH, Dellinger B, Lee CC (1990) Development of a thermal stability based ranking of hazardous organic compound incinerability. Environ Sci Technol 24:316
14. Carroll GJ, Thurnau RC, Lee JW, Waterland LR, Dellinger B, Taylor PH (1992) Pilot-scale evaluation of an incinerability ranking system for hazardous organic compounds. J Air Waste Manage Assoc 42:1430
15. Dellinger B, Taylor PH, Lee CC (1993) Full-scale evaluation of the thermal stability-based hazardous organic waste incinerability ranking. J Air Waste Manage Assoc 43:203
16. Taylor PH, Chadbourne JF (1987) Sulfur hexafluoride as a surrogate for monitoring hazardous waste incinerator performance. J Air Pollut Control Assoc 37:729
17. Dellinger B, Tirey DA, Taylor PH, Pan J, Lee CC (1988) Products of incomplete combustion from the high temperature pyrolysis of chlorinated methanes. In: 3rd Chemical congress of North America and the 195th national meeting of the American Chemical Society, vol 28. Division of Environmental Chemistry Preprints, Toronto, p. 81

18. Chang DPY, Sorbo NW, Law CK, Steeper RR, Richards MK, Huffman GL (1988) Relationships between laboratory and pilot scale combustion of some chlorinated hydrocarbons. In: Proceedings of AIChE national meeting, Denver, CO
19. Cundy VA, Lester TW, Sterling AM, Montestruc AN, Morse JS, Leger CB, Acharya S (1989) Rotary kiln incineration iii an in-depth study – kiln exit/afterburner/stack train and kiln exit pattern factor measurements during liquid CCl_4 processing. J Air Waste Manage Assoc 39:944
20. Dellinger B, Taylor PH, and Tirey DA (1991) Minimization and Control of Hazardous Combustion Byproducts, US-EPA Final Report, EPA/600/52-90/039. Cincinnati, OH
21. Russell JJ, Seetula JA, Gutman D, Senkan SM (1989) Kinetics of reactions of chlorinated vinyl radicals (CH_2CCl and C_2Cl_3) with molecular oxygen. J Phys Chem 93:1934
22. Schuetzle D, Perez JM (1983) Factors influencing the emissions of nitrated Polynuclear Aromatic Hydrocarbons (PNAs) from diesel engines. J Air Pollut Control Assoc 33:751
23. Dickson LC, Lenoir D, Hutzinger O (1992) Quantitative comparison of *de novo* and precursor formation of polychlorinated Dibenzo-p-Dioxins under Simulated municipal solid-waste incinerator postcombustion conditions. Environ Sci Technol 26:1822
24. Addink R, Olie K (1995) Mechanisms of formation and destruction of polychlorinated Dibenzo-p-dioxins and Dibenzofurans in heterogeneous systems. Environ Sci Technol 29:1425
25. Fiedler H (1998) Thermal formation of PCDD/PCDF – a survey. Environ Eng Sci 15:49
26. Taylor PH, Sidhu SS, Rubey WA, Dellinger B, Wehrmeier A, Lenoir D, Schramm K-W (1998) Evidence for a unified pathway of dioxin formation from aliphatic hydrocarbons. In: Proceedings of the Combustion Institute, vol 27, pp 1769. Pittsburgh, PA
27. Stanmore BR (2004) The formation of dioxin in combustion systems. Combust Flame 136:398
28. Konduri R, Altwicker E (1994) Analysis of timescales pertinent to Dioxin/Furan formation on fly ash surfaces in municipal solid waste incinerators. Chemosphere 28:23
29. Gullett BK, Lemieux PM, Dunn JE (1994) Emissions of polychlorinated dibenzo-*p*-dioxins and polychlorinated dibenzofurans from the open burning of household waste in barrels. Environ Sci Technol 28:107
30. Golodets GI (1983) Heterogeneous catalytic reactions involving molecular oxygen. Elsevier, New York Volume 15
31. Pieters WJM, Conner WC, Carlson J (1984) The oxyhydrochlorination of methane on fumed silica-based Cu^{+1}, K, La catalysts: I. Catalyst synthesis. Appl Cat 11:35
32. Wehrmeier A, Lenoir D, Sidhu SS, Taylor PH, Rubey WA, Kettrup A, Dellinger B (1998) Role of copper species in chlorination and condensation reactions of acetylene. Environ Sci Technol 32:2741
33. Nganai S, Lomnicki S, Dellinger B (2009) Ferric oxide mediated formation of PCDD/Fs from 2-monochlorophenol. Environ Sci Technol 43:368
34. Nganai S, Lomnicki S, Dellinger B (2011) Formation of PCDD/Fs from the copper oxide-mediated pyrolysis and oxidation of 1,2-dichlorobenzene. Environ Sci Technol 45:1034
35. Taylor PH, Lenoir D (2001) Chloroaromatic formation in incineration processes. Sci Total Environ 269:1
36. Trenholm A, Lapp T, Scheil G, Coores J, Klamm S, Cassady C (1988) Total mass emissions from a hazardous waste incinerator. J Hazard Mater 18:99
37. Ramamoorth S, Ramamoorth S (1997) Chlorinated organic compounds in the environment: regulatory and monitoring assessment. Lewis, New York
38. Aubrey NE, van Wazer JR (1964) Equilibrium rearrangement of perchlorocarbon compounds. J Am Chem Soc 86:4380
39. Choudry GC, Hutzinger O (1983) Mechanistic aspects of thermal formation of halogenated organic compounds including polychlorinated dibenzo-p-dioxins. Gordon and Breach, New York
40. Tirey DA, Taylor PH, Dellinger B (1990) Products of incomplete combustion from the high temperature pyrolysis of chlorinated methanes. In: Clement R, Kagel R (eds) Emissions from combustion processes: origin, measurement and control. Lewis, Chelsea, p 109
41. Taylor PH, Dellinger B, Tirey DA (1991) Oxidative pyrolysis of CH_2Cl_2, $CHCl_3$, and CCl_4 – I: incineration implications. Int J Chem Kinet 23:1051
42. Taylor PH, Dellinger B (1991) Modeling of molecular growth chemistry from high-temperature chlorocarbon pyrolysis. Chem Phys Process Combust, The Combustion Institute, pp 58/1
43. Dellinger B, Taylor PH, Tirey DA (1989) Pathways of formation of chlorinated PICs from the thermal degradation of simple chlorinated hydrocarbons. J Hazard Mater 22:175
44. Taylor PH, Wehrmeier A, Sidhu SS, Lenoir D, Schramm K-W, Kettrup A (2000) Copper-catalyzed chlorination and condensation of acetylene and dichloroacetylene. Chemosphere 40:1297
45. Mulholland JA, Sarofim AF, Sosthikul P, Monchamp PA, Plummer EF, Lafleur AL (1992) Formation of perchloroaromatics during trichloroethylene pyrolysis. Combust Flame 89:103
46. Taylor PH, Tirey DA, Dellinger B (1993) High temperature studies of the pyrolysis of trichloroethene: formation of perchlorinated PAHs. In: Joint Eastern and Central States Meeting of the Combustion Institute, New Orleans, pp 312
47. Taylor PH, Tirey DA, Rubey WA, Dellinger B (1994) Detailed modeling of the pyrolysis of trichloroethene: formation of chlorinated aromatic species. Combust Sci Technol 101:75
48. Ballschmiter K, Kirschmer P, Zoller W (1986) Experiments in high temperature chemistry of organohalogens. Chemosphere 15:1369
49. Tirey DA, Taylor PH, Kasner JH, Dellinger B (1990) Gas-phase formation of chlorinated aromatic compounds form the pyrolysis of tetrachloroethylene. Combust Sci Technol 74:137

50. Taylor PH, Tirey DA, Dellinger B (1996) A comprehensive kinetic model of the high temperature pyrolysis of tetrachloroethene. Combust Flame 104:260
51. Taylor PH, Tirey DA, Dellinger B (1996) The high temperature pyrolysis of hexachloropropene: kinetic analysis of pathways to formation of perchloro-arylbenzenes. Combust Flame 105:486
52. Taylor PH, Tirey DA, Dellinger B (1996) The high temperature pyrolysis of 1,3-hexachlorobutadiene. Combust Flame 106:1
53. Baillet C, Fadli A, Sawerysyn J-P (1996) Experimental study on the thermal oxidation of 1,3-hexachlorobutadiene at 500–1100°C. Chemosphere 32:1261
54. Cole JA, Bittner JD, Howard JB, Longwell JP (1984) Formation mechanisms of aromatic compounds in aliphatic flames. Combust Flame 56:51
55. Westmoreland PR, Dean AM, Howard JB, Longwell JP (1989) Forming benzene in flames by chemically activated isomerization. J Phys Chem 93:8171
56. Weissman M, Benson SW (1984) Pyrolysis of methyl chloride, a pathway in the chlorine-catalyzed polymerization of methane. Int J Chem Kinet 16:307
57. Dellinger B, Taylor PH (1990) The role of chlorine-induced inductive destabilization versus bond energy reduction on high temperature displacement reactions of chlorinated hydrocarbons. Chem Phys Process Combust, The Combustion Institute, pp 9/1
58. Liem AKD, van Zorge JA (1995) Dioxins and related compounds: status and regulatory aspects. Environ Sci Pollut Res 2:46
59. Thomas VM, Spiro TG (1995) An estimation of dioxin emissions in the United States. Toxicol Environ Chem 50:1
60. US-EPA Dioxin Reassessment, National Academy of Sciences 2004 draft. http://www.epa.gov/ncea/pdfs/dioxin/nas-review/. Accessed 11 July 2011
61. Shaub WM, Tsang W (1983) Dioxin formation in incinerators. Environ Sci Technol 17:721
62. Kilgroe JD, Lanier WS, von Alten TR (1991) Montgomery county incinerator test program: formation, emission, and control of organic pollutants. In: 2nd International conference on municipal waste combustion, Tampa
63. Froese KL, Hutzinger O (1996) Polychlorinated benzene, phenol, dibenzo-p-dioxin, and dibenzofuran in heterogeneous combustion reactions of acetylene. Environ Sci Technol 30:1009
64. Milligan MS, Altwicker ER (1996) Chlorophenol reactions on fly ash. Adsorption – desorption equilibria and conversion to polychlorinated dibenzo-p-dioxins. Environ Sci Technol 30:225
65. Altwicker EH, Schonberg JS, Konduri RKNV, Milligan MS (1990) Polychlorinated dioxin and furan formation in incinerators. Hazard Waste Hazard Mater 7:73
66. Ismo H, Kari T, Juhani R (1997) Formation of aromatic chlorinated compounds catalyzed by copper and iron. Chemosphere 34:2649
67. Olie K, Addink R, Schoonenboom M (1998) Metals as catalysts during the formation and decomposition of chlorinated dioxins and furans in incineration processes. J Air Waste Manage Assoc 48:101
68. Born JGP, Mulder P, Louw R (1993) Fly-ash mediated reactions of phenol and monochlorophenols – oxychlorination, deep oxidation and condensation. Environ Sci Technol 27:1849
69. Ryu JY, Mulholland JA, Kim DH, Takeuchi M (2005) Homologue and isomer patterns of polychlorinated dibenzo-p-dioxins and dibenzofurans from phenol precursors: comparison with municipal waste incinerator data. Environ Sci Technol 39:4398
70. Hatanaka T, Imagawa T, Takeuchi A (2003) Effects of copper chloride on formation of polychlorinated dibenzo-p-dioxins in model waste incineration. Chemosphere 51:1041
71. Altwicker ER (1991) Some laboratory experimental designs for obtaining dynamic property data on dioxins. Sci Total Environ 104:47
72. Milligan MS, Altwicker ER (1993) The relationship between *de Novo* synthesis of polychlorinated dibenzo-p-dioxins and Dibenzofurans and low-temperature carbon gasification in fly ash. Environ Sci Technol 27:1595
73. Stieglitz L, Zwick G, Beck J, Roth W, Vogg H (1989) On the *de Novo* synthesis of PCDD/PCDF on fly ash of municipal waste incinerators. Chemosphere 18:1219
74. Stieglitz L, Zwick G, Beck J, Bautz H, Roth W (1990) The role of particulate carbon in the *de novo* synthesis of polychlorinated dibenzodioxins and dibenzofurans in fly ash. Chemosphere 20:1953
75. Oeberg T, Bergbaeck B, Oeberg E (2007) Different catalytic effects by copper and chromium on the formation and degradation of chlorinated aromatic compounds in fly ash. Environ Sci Technol 41:3741
76. Karasek FW, Dickson LC (1987) Model studies of polychlorinated dibenzo-para-dioxin formation during municipal refuse incineration. Science 237:754
77. Cains PW, McCausland LJ, Fernandes AH, Dyke P (1997) Polychlorinated dibenzo-p-dioxins and dibenzofurans formation in incineration: effects of fly ash and carbon source. Environ Sci Technol 31:776
78. Ballschmiter K, Braunmiller I, Niemczyk R, Swerev M (1988) Reaction pathways for the formation of polychlorodibenzodioxins (PCDD) and -dibenzofurans (PCDF) in combustion processes: II. Chlorobenzenes and chlorophenols as precursors in the formation of PCDD/PCDF in flame chemistry. Chemosphere 17:995
79. Alderman SL, Farquar GH, Poliakoff ED, Dellinger B (2005) An infrared and X-ray spectroscopic study of the reactions of 2-chlorophenol, 1,2-dichlorobenzene and chlorobenzene with model CuO/Silica fly ash surfaces. Environ Sci Technol 39:7396
80. Pandelova M, Lenoir D, Schramm K-W (2006) Correlation between PCDD/F, PCB, and PCBz in coal/waste combustion: Influence of various inhibitors. Chemosphere 62:1196
81. Sommeling PM, Mulder P, Louw R (1994) Formation of PCDFs during chlorination and oxidation of chlorobenzenes in chlorine/oxygen mixtures around 340°C. Chemosphere 29:2015

82. Addink R, Cnubben PAJP, Olie K (1995) Formation of polychlorinated dibenzo-p-dioxins dibenzofurans on fly-ash from precursors and carbon model compounds. Carbon 33:1463
83. Froese KL, Hutzinger O (1996) Polychlorinated benzene and polychlorinated phenol in heterogeneous combustion reactions of ethylene and ethane. Environ Sci Technol 30:998
84. Lenoir D, Wehrmeier A, Sidhu SS, Taylor PH (2001) Formation and inhibition of chloroaromatic micropollutants formed in incineration processes. Chemosphere 43:107
85. Ritter E, Bozzelli JW (1990) Chlorobenzene and dichlorobenzene reactions in hydrogen and in hydrogen oxygen mixtures. Hazard Waste Hazard Mater 7:103
86. Fadli A, Briois C, Baillet C, Sawerysyn J-P (1999) Experimental study on the thermal oxidation of chlorobenzene at 575–825°C. Chemosphere 38:2835
87. Shaub WM, Tsang W (1985) Overview of dioxin formation in gas and solid phases under municipal incinerator conditions. In: Keith LH, Rappe C, Choudhary G (eds) Chlorinated dioxins and Dibenzofurans in the total environment. II. Elsevier, St. Louis, p 469
88. Sidhu SS, Maqsud L, Dellinger B, Mascolo G (1995) The homogeneous gas-phase formation of chlorinated and brominated dibenzo-p-dioxin from 2,4,6-trichloro- and 2,4,6-tribromophenols. Combust Flame 100:11
89. Grotheer H-H, Louw R (1996) The reaction of phenoxy radicals with monochlorobenzene and its meaning for gas-phase dioxin formation in incineration. In: Proceedings of the Combustion Institute, Pittsburgh, PA, 26, pp 2405
90. Khachatryan LA, Burcat A, Dellinger B (2003) An elementary reaction kinetic model for the gas-phase formation of 1,3,6,8- and 1,3,7,9-tetrachlorinated dibenzo-p-dioxins from 2,4,6-trichlorophenol. Combust Flame 132:406
91. Babushok Y, Tsang W (2003) Gas-phase mechanism for dioxin formation. Chemosphere 51:1023
92. Khachatryan L, Asatryan R, Dellinger B (2003) Development of expanded and core kinetic models for the gas phase formation of dioxins from chlorinated phenols. Chemosphere 52:695
93. Khachatryan L, Asatryan R, Dellinger B (2004) An elementary reaction kinetic model of the gas phase formation of polychlorinated dibenzofurans from chlorinated phenols. J Phys Chem A 108:9567
94. Procaccini C, Bozzelli JW, Longwell JP, Smith KA, Sarofim AF (2003) Formation of chlorinated aromatics by reactions of Cl, Cl_2, and HCl with benzene in the cool-down zone of a combustor. Environ Sci Technol 37:1684
95. Khachatryan L, Burcat A, Dellinger B (2010) The role of chlorine atoms and hydroxyl radicals in the formation of PCDDs from the oxidative pyrolysis of 2,4,6-trichlorophenol. Int J Chem Kinet 42:90
96. Babushok V, Tsang W, Noto T (2000) Propargyl-type radicals as precursors for polychlorinated aromatic hydrocarbons during incineration. Proc Combust Inst, Pittsburgh, PA, 28:2691
97. Sidhu SS, Dellinger B (1997) The effect of hydrocarbons on PCDD/F formation in the gas-phase oxidation of 2,4,6-trichlorophenol. Organohalogen Compd 31:469
98. Evans CE, Dellinger B (2003) Mechanisms of dioxin formation from the high-temperature pyrolysis of 2-chlorophenol. Environ Sci Technol 37:1325
99. Shinkura T, Kishi T, Kawakami T, Onodera S (2007) Organohalogen Compd 69:1602
100. Striebich RC, Rubey WA, Klosterman JR (2002) Trace-level measurement of complex combustion effluents and residues using multi-dimensional gas chromatography-mass spectrometry (MDGC-MS). Waste Manag 22:413
101. Okamoto Y, Tomonari M (1999) Formation pathways from 2,4,5-trichlorophenol (TCP) to polychlorinated dibenzo-p-dioxins (PCDDs): an ab initio study. J Phys Chem A 103:7686
102. Mohammednoor A, Bogdan Z, Dlugogorski Z, Kennedy EM, Mackie JC (2007) Theoretical study of reaction pathways of dibenzofuran and dibenzo-*p*-dioxin under reducing conditions. J Phys Chem A 111:7133
103. Okamoto Y (1999) A new dioxin decomposition process based on a hybrid density functional calculation. Chem Phys Lett 310:355
104. Farajian AA, Mikami M, Ordejon P, Tanabe K (2001) Ring closure in dioxin formation process: an *ab initio* molecular dynamics study. J Chem Phys 115:6401

Books and Reviews

Brunner CR (1993) Hazardous waste incineration, 2nd edn. McGraw-Hill, New York. ISBN-10: 0-0700-8595-1

Niessen WR (1995) Combustion and incineration processes, 2nd edn. Marcel-Dekker, New York. ISBN ISBN: 0-8247-9267-X

Roberts SM, Teaf CM, Bean JA (1998) Hazardous waste incineration: evaluating the human health and environmental risks. CRC Press, Boca Raton. ISBN: 1-5667-0250-X

Santoleri JJ, Reynolds J, Theodore L (2000) Introduction to hazardous waste incineration, 2nd edn. Wiley, New York. ISBN-10: 0-4710-1790-6

Waste Incineration and Public Health (2000) Committee on health effects of waste incineration, Board on Environmental Studies and Technology, National Research Council. The National Academies, Washington, DC. ISBN-10: 0-309-06371-X

N

Nuclear Accidents, Chernobyl Fallout in Scandinavian Watersheds

Lars Håkanson
Department of Earth Sciences, Uppsala University, Uppsala, Sweden

Article Outline

Glossary
Definition of the Subject

Introduction, Background, and Aim
A Brief Overview
Key Catchment Characteristics
Remedial Measures for Aquatic Pathways
Future Directions
Bibliography

Glossary

Adsorption The process of attachment on to and release from surfaces.

Algae Simple photosynthetic nonvascular plants; mainly aquatic.

Alkalinity The total amount of weak acid salts (largely bicarbonate) per unit volume of water.

Allochthonous From outside (often used to characterize materials transported from the drainage area to a lake).

Anoxic sediment Sediment devoid of free oxygen.

Autochthonous Originating from inside the lake.

Benthos Organisms living in or on the river or lake bed.

Bioaccumulation The increase in the amount of chemical or compound in the tissues of living organisms.

Biological half-life The time required for the amount of a particular radionuclide in a biological system, such as an animal, to be reduced by one half by biological processes, when the contamination has been terminated.

Biomass Mass of living organisms present at any one time within a given area or volume.

Biota The total flora and fauna of a given area.

Bioturbation Mechanical mixing, e.g., of bottom sediments due to living organisms.

Catchment The drainage basin that channels precipitation into a lake or single outflow.

Compartment Any part of the environment or process that may conveniently be considered as a single entity. Used in developing mathematical models.

Compartment model A model in which a series of compartments is used to represent the system of interest. Material can flow between the compartments. Differential or difference equations often are used to represent the rates of flow in the system.

Conductivity Quantity of electricity transferred across unit area per unit of potential gradient and unit of time (in mS/m). It usually gives an indication of total ionic concentration.

Confidence interval An interval that encompasses the true value for a parameter or measurement with a degree of confidence stated in terms of a probability.

Default value A value prescribed for a model parameter in the absence of data directly relevant to the assessment situation.

Diffusion The movement of atoms or molecules from a region of higher concentration of the diffusing species to regions of lower concentration.

Dimictic A lake having two seasonal overturn periods of mixing and two of thermal stratification (see thermocline).

Dynamic model A model that simulates the changes that occur through time in a system, especially, in the current context, in containment concentrations in the system.

Dystrophic Lake rich in humic matter mainly in the form of suspended plant colloids and larger plant fragments.

Ecological half-life The time required for the amount of a particular radionuclide in a particular organism living in a natural ecosystem to be reduced by one half.

Ecosystem A community of organisms together with the environment they inhabit and with which they interact.

Effective half-life The time required for the amount of a particular radionuclide in a system to be reduced by one half as a consequence of radioactive decay and all other processes.

Epilimnion The upper layer of lake water above the thermocline with a comparatively homogeneous temperature profile.

Eutrophic A lake rich in nutrients, usually resulting in high productivity.

Evapotranspiration Loss of water by evaporation from soil and by transpiration from vegetation over a given area with time.

Food chain Sequence of organisms in an ecosystem occupying specific hierarchical levels (trophic levels) such that organisms belonging to a superior level survive by eating organisms

belonging to inferior levels. The sequence can be represented as compartments in a mathematical model or analysis.

Food web The network of interconnected food chains in an ecosystem.

Generic model A model that is not built on site-specific information.

Hardness (water) A measure of the amount of calcium and magnesium cations in the water.

Hydraulic residence time The ratio of the volume of a water body to water discharge (corresponding to the theoretical time needed for a complete exchange of water).

Hypolimnion The layer of lake waters below the thermocline.

Load (internal/primary) Fallout directly onto the lake surface.

Load (secondary) The flux (transport) from the catchment to the lake.

Macrophytes Large aquatic plants.

Mesohumic Lake with intermediate levels of humic matter.

Monomitic Lake having a single period of free circulation or overturn per year.

Monte Carlo A technique involving the use of random numbers in a computer program or simulation model to represent stochastic events.

Morphometric All the geometric characteristics relative to the shape of the basin (volume, surface, depth, etc.).

Oligohumic A lake poor in nutrients, usually resulting in low productivity.

Oligotrophic A lake with low primary productivity.

Output variables Variables that are produced as model output. Output variables can be state variables or functions of one or more state variables.

Partition coefficient (K_d) The ratio between the amount of radionuclide attached to suspended matter per unit of mass and the amount of dissolved radionuclide per unit of volume of water.

Permeability Rate of passage of water through a given cylindrical section of a sediment core.

Pelagic Pertaining to the water column of the lake; used for organisms inhabiting the open waters of the lake.

Periphyton A community of plants, animals, and associated detritus forming a surface coating on stones, plants, and other submerged objects.

Phytoplankton Plant members of the plankton.

Piscivorous Fish eating.

Plankton Organisms that float or swim very feebly in the water masses of lakes and rivers.

Predator An animal that kills other animals for food.

Primary productivity The total production by photosynthetic and chemosynthetic activity of organic substances.

Resuspension The remobilization of particles from the sediments of a water body by the action of water movement.

Sediment The matter that has fallen to the bottom of a water body.

Sedimentation rate The amount of matter deposited on the bottom of a water body per unit of surface and time.

Sensitivity analysis The analysis of variation of model output with changes in the values of model parameters.

Stratification Division of lake water masses into horizontal layers with different physical and chemical properties.

Suspended matter Matter suspended in lake and river waters.

Thermocline The boundary layer of lake waters in which temperature changes sharply with depth; situated between the epilimnion and hypolimnion.

Tributary A smaller river flowing into a larger river or a lake.

Trophic level The hierarchical level that an organism occupies in the food chain. The group of organisms that occupy the same level in the food chain.

Uncertainty analysis An analysis of the way in which the uncertainty in assessment results is affected by uncertainty in the input data used in the model.

Validation (model) The process of comparing model outputs with independent experimental data sets. A model is considered validated when sufficient testing has been performed to ensure an acceptable level of predictive accuracy over the range of conditions over which the model may be applied.

Volume development The ratio between the lake volume and the volume of a cone having the basis equal to the area of lake surface and the height equal to the maximum depth of the lake.

Zooplankton Animal members of the plankton.

Definition of the Subject

Aquatic radioecology deals with the transport processes of radionuclides in lakes, rivers, and marine areas. During the Chernobyl accident in April/May 1986, large amounts of radionuclides were released as a single pulse. To follow that pulse through ecosystem pathways has meant that many of the complex transportation routes can now the calculated with a much higher level of certainty than before.

Introduction, Background, and Aim

Figure 16 in Ed Waller's contribution "Sources of Radiation in the Environment" shows the fallout map of radiocesium (Cs-137) in soil systems throughout Europe. Note that there is no information from certain countries shown in white, e.g., for several Balkan states. Scandinavia (Norway, Sweden, and Finland) received a relatively large fallout with maximum values around 100 kBq/m^2 in the eastern part of central Sweden. The fallout was very patchy due to the prevailing atmospheric conditions, which were responsible for transporting the two main radionuclides, radiocesium and radiostrontium, from the site of the accident (Chernobyl) to basically all European countries. Figure 16 (Waller – Introduction) gives a spatial perspective to the problem and Fig. 1 a temporal perspective to the Chernobyl accident using data from Scandinavia. This figure exemplifies radiocesium concentrations in cow milk in Sweden from the late 1950s to 2005. One can note the high and broad initial peak with maximum values in 1964 related to the nuclear weapons testing. It should be stressed that there were no such tests in Sweden or Scandinavia and this figure illustrates that radionuclides from these tests were distributed all around the globe. There is also a very pronounced peak from the Chernobyl fallout in April/May 1986. From these two background figures, the following questions will be addressed in this entry:

- "Peak and tail." A fundamental concern in radioecology is to understand, model, and predict the "peak and the tail" concerning radionuclide concentrations in ecosystems related to a given accidental fallout [1]. Peak concentrations are related to short-term conditions (hours to days after the fallout), whereas the "tail" concentrations generally are governed by the long-term conditions in the catchment areas that regulate fixation, percolation, surface and ground water transport, resuspension, and biotic fluxes of radionuclides [1–3].
- The literature related to the transport of radionuclides from the Chernobyl accident from land to water, in rivers, in lakes, and to coastal marine systems is extensive. Excellent compilations have been presented, e.g., for Scandinavia by [4], for the conditions in the Ukraine by [5]; and comprehensive review papers related to countermeasures

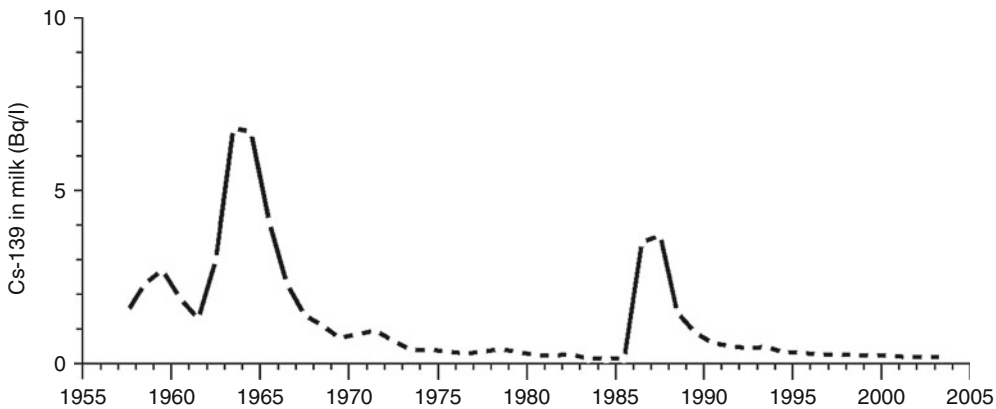

Nuclear Accidents, Chernobyl Fallout in Scandinavian Watersheds. Figure 1
Radiocesium concentrations in Swedish milk between 1955 and 2005. Values in Bq/l (Modified from [98])

by [6], lake processes by [7], catchments by [8], and rivers by [9]. This entry will discuss key factors regulating the fluxes of radiocesium in watersheds and it will draw much from those reviews, but this article does not give a comprehensive literature review. The focus is on ecosystem function.

It should also be noted that during the last 10–15 years, there has been something of a "revolution" in ecosystem modelling. The generality and predictive power of present-day models have increased in a way that was inconceivable 15 years ago. A new generation of predictive models that predict as well as one can measure – if one measures well – have been presented. And yet, they may be run by readily available driving variables and have a general structure that applies to most types of pollutants in aquatic systems. The major reason for this development is, in fact, the Chernobyl accident. Large quantities of mainly radiocesium and radiostrontium were released in April/May 1986 as a pulse. To follow the pulse of these radionuclides through ecosystem pathways has meant that important fluxes and mechanisms, i.e., ecosystem structures have been revealed. It is important to stress that many of these new structures and equations are valid not just for radionuclides, but for most types of contaminants, e.g., for metals, nutrients, and organic radionuclides. This means that many of the models and methods of building and testing models discussed in this entry for aquatic systems should also be of interest to other ecosystem modellers.

Predictive models are fundamental tools for forecasting the consequences of different remedial actions (see [1]). The term "predictive model" is used to indicate models in which one or a few important y-variables are predicted from a few x-variables that can be obtained easily from standard maps or monitoring programs. That is the goal, but that goal is often very difficult to achieve. It is as much a challenge to develop practical models as it is to create comprehensive validated ecosystem models that predict the time-dependent interactions of many y-variables from many x-variables.

It should be stressed that many of the processes regulating the flow and biological uptake of radionuclides in aquatic systems are controlled by hydrological and morphometrical factors, which cannot be influenced by remedies that change the water chemistry, e.g., liming and potash treatment [10–12]. Remedies that could speed up the recovery (e.g., reduction of the substances in fish) must aim at reducing the radionuclide load to the lake, or the uptake in biota by blocking the biouptake, increasing bioproduction and cause a "biological dilution" of the radionuclides in biota, and/or include specific substances, like potash (K), that can be taken up in fish in almost the same way as radiocesium and cause a "chemical" dilution. Time is an important factor in such remediations. The sooner the remedy is launched the better the results generally gained [13]. Lakes suited to potash treatment should have low initial ionic K-concentrations [14].

Predictive models must satisfy some categorical features that make them reliable tools for environmental management:

- They must be characterized by a relevant and simple structure, i.e., involve the smallest possible number of driving variables.
- The values of the necessary driving variables should be easy to access and/or to measure.
- The models must be validated for a variety of circumstances showing a wide range of environmental characteristics.

In broad terms, the variables used in environmental models may be divided into two categories:

1. Variables for which site-specific data must be available, such as lake volume, mean depth, water discharge, and amount of suspended particulate matter in water.
2. Variables for which generic (= general) values are used because of the lack of site-specific data, e.g., the sedimentation rate and/or rates for internal loading (like diffusion and advection rates).

The variables belonging to the first category are often called "site-specific variables," "environmental variables," or "lake-specific variables." They can generally be measured relatively easily and their experimental uncertainty should not significantly affect the overall uncertainty of the model predictions of the target variable(s). The second category, the "model variables" or "model constants," are often difficult to access for each specific system, such as the transfer rates from the

sediment to the water, the deposition velocity of a given radionuclide from water to sediments, and the migration rate from catchment to lake. The model variables may contribute significantly to the model uncertainty unless they have been validated and reliable sub-models for their generic values established from critical tests.

Unfortunately, critically validated widely applicable models showing a high predictive power are difficult to develop. As a consequence, predictive models are generally [15] based on "collective parameters." It has been shown that [16] in many circumstances, the values of such important collective parameters integrate many compensatory effects of the different phenomena occurring in the very complex ecosystem where "everything depends on everything else" [17]. Examples of such collective parameters in the freshwater environment are the "migration velocities" of the metal or radionuclide from water to sediments, the "effective removal" rates, and the "soil permeability coefficients" of a radionuclide from the catchment to a water body [18].

Models based on such "collective parameters" show a unique and important feature: Their predictions are characterized by a relatively low uncertainty, despite the large range of environmental characteristics and the lack of site-specific values of the model variables [19]. The use of models based on collective parameters is the result of a change in the perspective concerning the modelling of natural ecosystems. The main lesson is that in predictive modelling, it is seldom necessary, or wise, to account for "everything." The difficult task is to omit processes that may add more to the model's uncertainty than to the predictive success for the given target variable.

Environmental models based on collective parameters are structured more like a web than a pyramid. Each process is indeed related to a variety of other phenomena and it would be unreasonable to use only a few of them as fundamental starting points for understanding and predicting all the others. A variety of experiences [17, 20, 21] demonstrate that big complex models are often more uncertain, and yield poorer predictive success than simpler models based on collective parameters.

It is often extremely difficult to distinguish cause and effect in natural ecosystems. One cannot base a dynamic ecosystem model on a full understanding of the ecosystem. In complex ecosystems, "understanding" at one scale (e.g., the ecosystem scale) is generally related to processes and mechanisms at the next lower scale (e.g., the scale of individual animals and/or plants), and the explanation of phenomena at this scale is related to processes and mechanisms at the next lower scale (e.g., the scale of the organ), and so on down to the level of the atom and beyond. In radioecology and environmental management, the predictive scientist must often find a balance between answering interesting, often important, questions of understanding, and delivering a practical tool to society. If a model were based on a causal analysis of what takes place at the cellular level, then at levels involving organs, individuals, populations, and finally at the ecosystem level, one would wait an eternity before the model could be developed.

In a strict sense, there is no such thing as a general (= generic) ecosystem model that works equally well for all ecosystems (of a given type) because all models need to be tested against reliable, independent empirical data and the data used in such validations must of necessity belong to a restricted domain. If this domain is equal to the entire population of ecosystems of the given type, then, and only then, is the model generic in the strict sense. The complexities of natural ecosystem always exceed the complexity and size of any model. Simplifications are always needed, and this entails problems. The dynamic mass-balance models discussed in this entry have been tested over such wide ranges that it is tempting to label them generic, but there will always be an ecosystem with properties outside the given domain for which the model would yield poor predictions. This is why modelling can be pictured as a two-sided coin: One needs the equations as well as the range, the domain, within which the equations apply.

The crucial point in ecosystem modelling is the structuring of the model see (Fig. 2 for an outline related to key concepts for lakes). The model structure should include all important processes regulating the transport and biouptake of a given radinuclide – no more, no less. The principles and processes illustrated in Fig. 2 will be further elaborated in the following text.

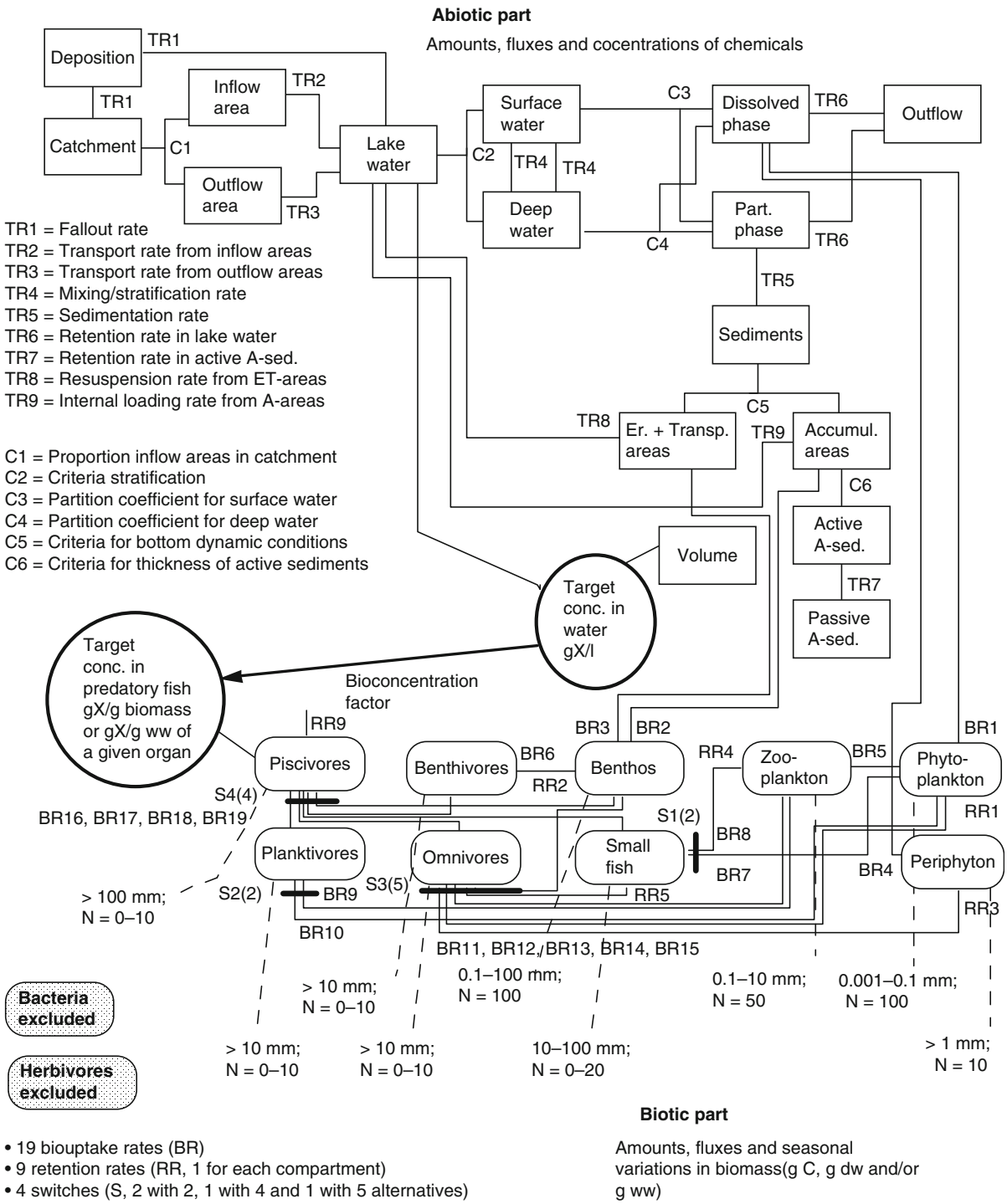

Nuclear Accidents, Chernobyl Fallout in Scandinavian Watersheds. Figure 2
A compilation of fundamental abiotic and biotic processes regulating the spread and biouptake of toxic substances in aquatic ecosystems. The figure also gives typical sizes (mm) and numbers of species (N) in Nordic lakes. This structuring of the aquatic ecosystem will be used in the following model, where the concepts will be further elaborated (Modified from [63])

A Brief Overview

The aim of this section is to give a few empirical examples illustrating the temporal and special development for radiocesium and radiostrontium related to the Chernobyl accident. Figure 3 first shows measured mean levels of radiocesium in mouse shot in Heby commune in central Sweden (close to Uppsala and Stockholm) in the years 1986–2004. This figure illustrates some important principles related to the "peak and tail" problem. First, the recovery is relatively slow and principally governed by the physical half-life for radiocesium (30 years). So, the ecological half-life in this example is close to the physical half-life. Then, there are marked variations in the radiocesium levels in mouse from year to year depending on what the animals have been eating ("you are what you eat"). In years when mushrooms are abundant, the Cs-levels are generally high because many types of mushrooms with mycelium pick up radiocesium from the soils, and vice versa.

Figure 4 exemplifies river data from several European rivers (see Table 1) on annual concentrations of radiocesium from the Chernobyl fallout. One can note that among these river sites and years, the variation is three to four orders of magnitude. The basic aim of the following discussion related to the transport from land to water is to highlight important factors regulating the variation among and within river sites. The first five rivers listed in Table 1 are Scandinavian (Finnish).

Figure 5 gives data on annual concentrations for radiostrontium from the nuclear weapon fallout and the Chernobyl fallout. The variability among the sites and the years is 100 times lower than for radiocesium.

Key Catchment Characteristics

What are the key factors regulating the transport of radionuclides from land to water explaining the three to four orders of magnitude variability for radiocesium concentrations in rivers illustrated in Fig. 4? The first and most evident reason for the variability is the variability in fallout.

Many studies [22, 23] have demonstrated that aquatic systems are affected by catchment characteristics (e.g., area covered by bedrocks, soils, and different land-use activities). This is exemplified in Fig. 6 by river data on radiocesium. This figure gives normalized data (i.e., river water concentrations divided by fallout) and

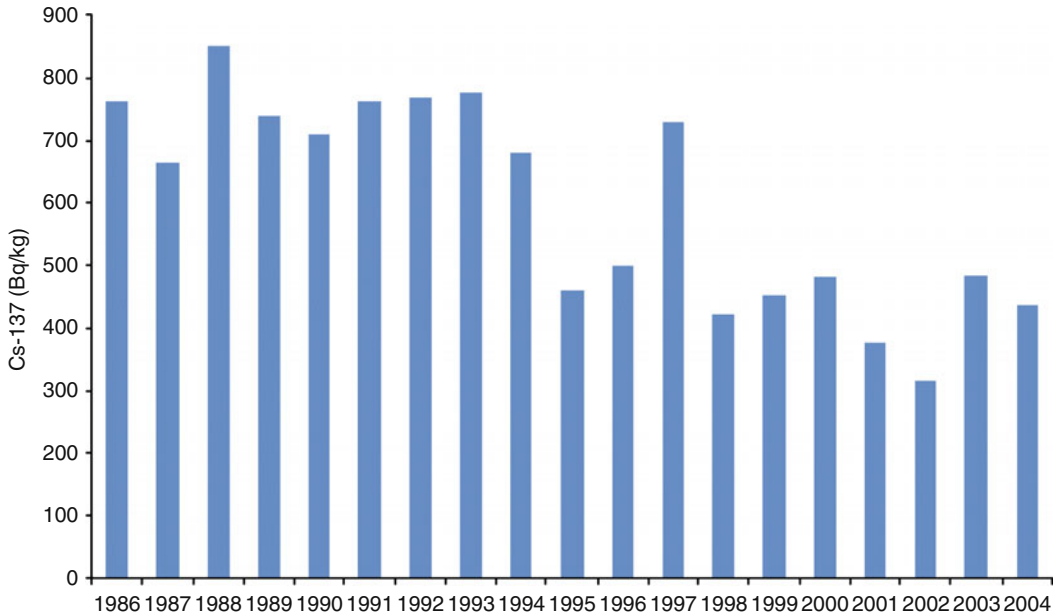

Nuclear Accidents, Chernobyl Fallout in Scandinavian Watersheds. Figure 3
Radiocesium concentrations in mouse from Heby commune (close to Uppsala in Sweden) between 1986 and 2004 (Modified from [99])

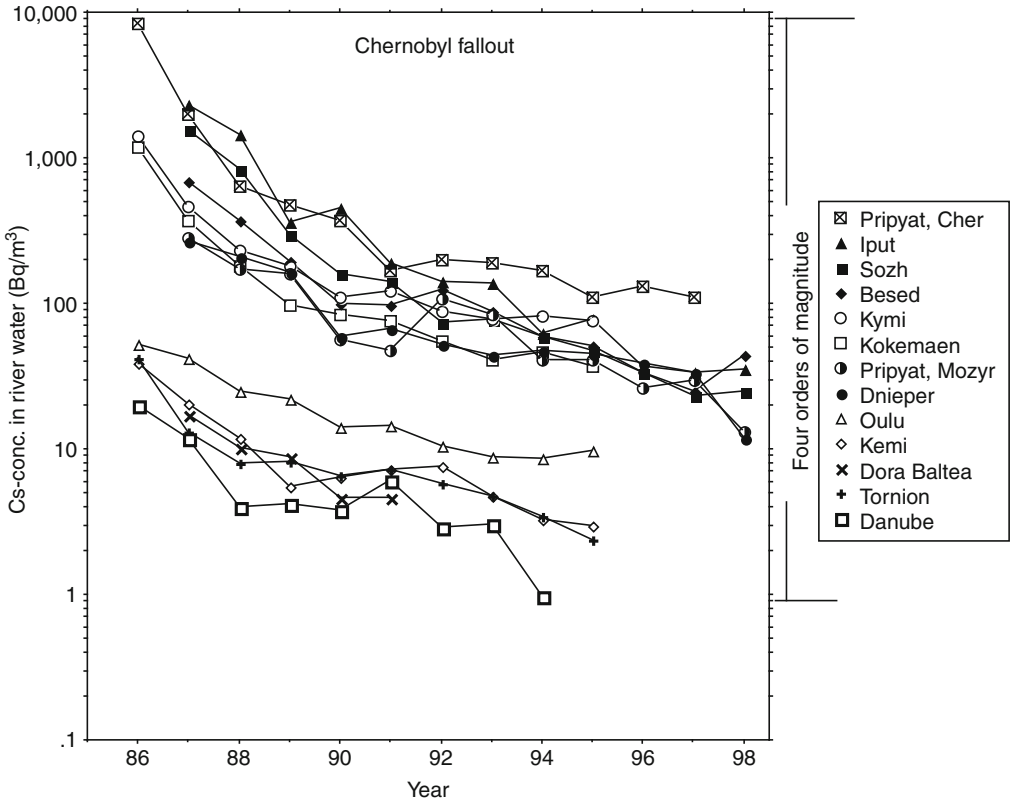

Nuclear Accidents, Chernobyl Fallout in Scandinavian Watersheds. Figure 4
Measured radiocesium concentrations in rivers contaminated by the Chernobyl fallout. Note that these empirical data vary among the rivers sites and with time between 1 and 10,000 Bq/m^3. The basic aim of the river model is to explain the factors regulating these variations (From [41])

one can see that the variations among the rivers sites is 10–100 times lower than in Fig. 4 without normalization for fallout. The remaining variation (a factor of 2) among the river sites depends on differences in catchment area and river characteristics.

There are basically two main factors related to the conditions in the catchment area, [1] the distribution of inflow and outflow areas and [2] fixation.

Figure 7 first illustrates principal aspects related to fixation for radiocesium and radiostrontium in catchment areas. From this figure, one can see that radiostrontium is more mobile, less fixed, than radiocesium. The fixation of any given radionuclide depends on:

1. The soil type.
2. The percentage of outflow areas (OA = wetlands like mires, bogs, upstream rivers, and lakes).
3. The mobility constant, which describes the mobility of a given radionuclide relative to the mobility of radiocesium. The default value for the dissolved fraction (DF) or radiostrontium in river water may often be set to 0.95 and for radiocesium to 0.56 see (Fig. 8). The higher the DF-value, the more mobile the substance, and this is also shown in Figs. 7 and 8.

An important concept in the modelling of radionuclides concerns the equilibrium constant, the K_d-value between the amount of the radionuclide in dissolved and particulate phases [24–27]. The default value for lake K_d for radiocesium is often set to about 800,000 l/kg or 0.8 l/mg suspended solids (from [1]). Another approach for radiocesium (see [28–30]) is to express K_d as a function of the "frayed edge site" concentration of the clay mineral illite (which has a unique

Nuclear Accidents, Chernobyl Fallout in Scandinavian Watersheds. Table 1 Data on radiocesium and radiostrontium fallout after Chernobyl and the nuclear weapons tests (NWT), catchment areas, mean annual precipitation (data from [78]), altitudes, and latitudes for the studied river sites. Data on latitude and altitude have been obtained from an atlas of Europe

River	Catchment area (km^2)	Annual precipitation (mm/year)	Chernobyl fallout (Bq Cs/m^2)	Total NWT deposition (Bq Cs/m^2)	Total NWT deposition (Bq Sr/m^2)	Altitude (m.a.s.l.)	Latitude (°N)
Kymi	33,620	566	29,900	3,500	2,180	0	63
Kokenmaen	26,620	549	34,100	3,400	2,110	0	62
Oulu	24,800	518	3,800	3,200	2,000	0	65
Kemi	42,760	467	1,700	3,060	1,800	0	66
Tornion	56,830	497	1,700	2,900	1,900	0	66
Thames	12,370	719			1,840	0	52
Tirso	3,360	867			3,340	0	44
Ofanto	3,390	847			3,260	0	41
Volturno	7,070	941			3,600	0	42
Tevere	17,290	1,038			4,000	0	42
Arno	11,020	1,119			4,300	0	43
Reno	7,820	1,163			4,478	0	43
Po (Torino)	9,190	987			3,800	240	45
Ticini	8,100	1,301			5,000	50	45
Dora Baltea	4,020	987	6,180			270	46
Pieve	4,890	1,731			6,660	0	45
Garda	13,900	1,380			5,300	100	46
Dnieper	50,610	696	38,900			200	52
Sozh	22,330	709	254,000			250	51
Besed	4,890	701	283,000			1,000	51
Iput	11,050	700	275,000			200	51
Pripyat, Mozyr	63,970	675	31,200			50	52
Pripyat, Che	46,020	694	138,000			100	52
Danube	180,810	962	11,100	5,920	3,700	300	47
Yenisei	2,564,580	487			1,880	0	70
Lena	2,397,580	418			1,600	0	72
Ob	2,950,760	477			1,840	0	67

potential to bind cesium), C_{FES}, the K-concentration of the water, C_K, and the selectivity coefficient between radiocesium and potassium (Kc), where $K_d = Kc \cdot C_{FES}/C_K \cdot Kc$ and C_{FES} are often assumed to be constants since it is generally very difficult to access reliable empirical data for these variables for different lakes. This means that the approach may be written as $K_d = \text{const}/C_K$. On the basis of these arguments, the following may be regarded as a typical "collective" approach, i.e., as a simplification of many complex relationships [16],

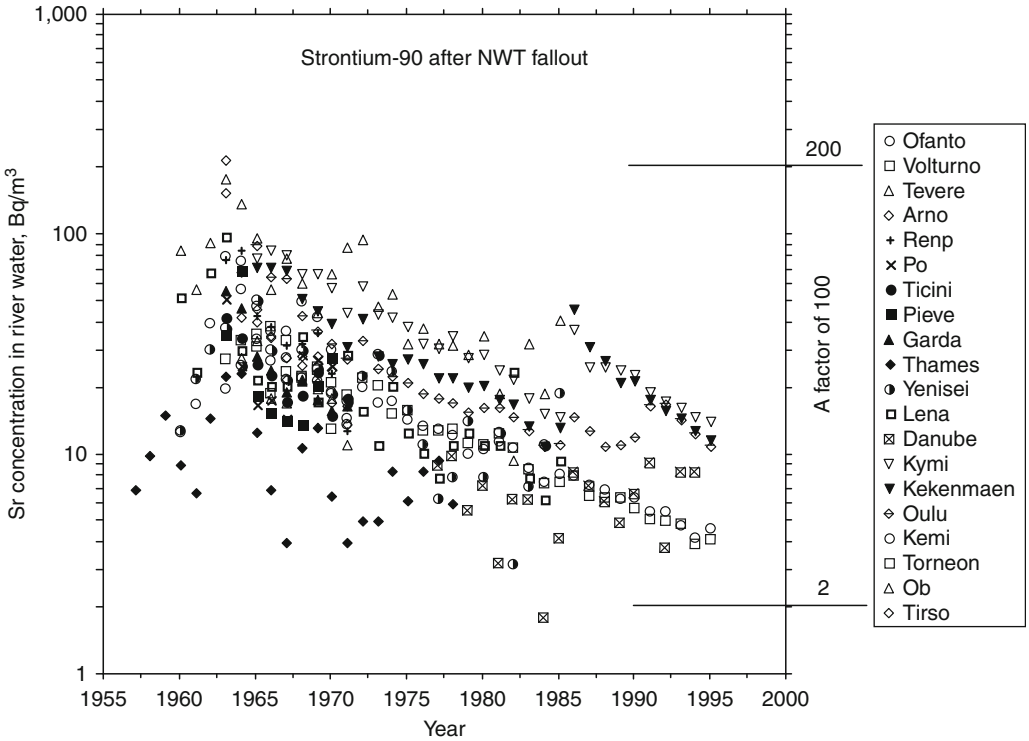

Nuclear Accidents, Chernobyl Fallout in Scandinavian Watersheds. Figure 5
Measured radiostrontium concentrations in rivers contaminated by the NWT (nuclear weapons testing) fallout and the Chernobyl fallout. These data vary among the rivers and with time between 2 and 200 Bq/m^3. The aim of the river model discussed in the text is to account for the factors regulating these variations (From [41])

where positive "errors" are balanced by negative ones. Thus, for Cs-137:

$$K_d = 800,000/C_K \quad (1)$$

where C_K is given in mg K/l (K = potassium). 800,000 is the K_d-constant.

Traditionally, K_d is defined as is the ratio between the particulate (C'_{part} in Bq/kg dw) and the dissolved (C_{diss} in Bq/1) phases, i.e., $K_d = C'_{part}/C_{diss}$. The total amount (in Bq/l) is equal to ($C_{diss} + C_{part}$), where C_{part} is given in Bq/l. Then K_d is given in l/kg. The amount of suspended particulate matter in the lake water, SPM, is given in mg/l. This means that the dissolved fraction (DF) can be written as:

$$DF = 1/\left(1 + K_d \cdot SPM \cdot 10^{-6}\right) \quad (2)$$

Since C_K generally varies in the range from 0.5 to 50 mg/l in aquatic systems [31] and since SPM-values generally also vary in the range between 0.5 and 50 mg/l [32], it is evident that DF varies in the entire range from almost 0–1. For example, for lakes with characteristic C_K– and SPM-values between 1 and 5 mg/l, one can expect DF-values for radiocesium in the range from 0.25 to 0.75. Håkanson et al. [33] have shown that DF for Sr-90 may be given by this approach but that Eq. 1 is replaced by

$$K_d = C_{CsSr} \cdot 800,000/C_{Ca} \quad (3)$$

Where C_{CsSr} is a calculation constant between Cs and Sr set to 10 and C_{Ca} is the Ca-concentration in mg/l, since Ca should work in relation to Sr in the same competing manner as K does to Cs.

Figure 8 also illustrates that the principle of fixation/mobility should be valid not just for radionuclides but also for stable metals. The information of cation exchangeability illustrated for Hg, Pb, Cd, Cu, Zn, Cr, and Ni in Fig. 8 comes from the literature [32, 34, 35].

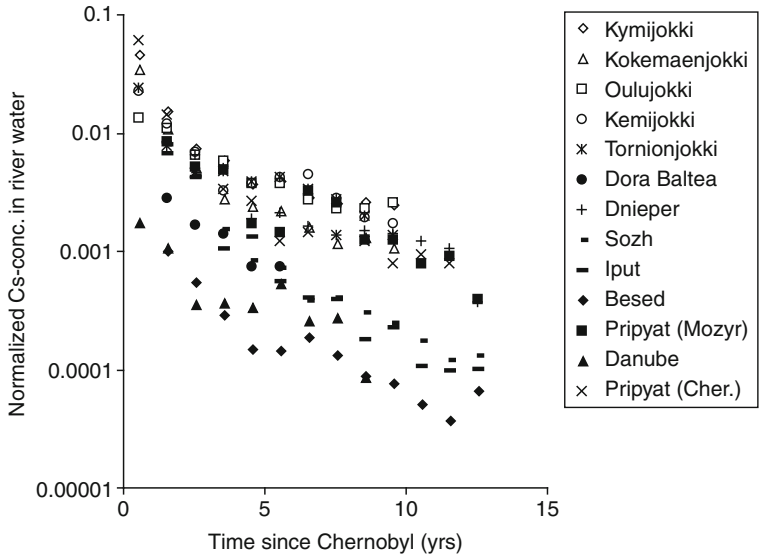

Nuclear Accidents, Chernobyl Fallout in Scandinavian Watersheds. Figure 6
Total concentrations of Cs-137 in water in 13 European rivers after Chernobyl (mean annual values) normalized for fallout (Bq/m^3 to Bq/m^2). These normalized concentrations vary two orders of magnitude due to differences among the rivers sites in catchment area and river characteristics. The aim of the model discussed in the text is to quantify such differences based on mechanistic principles regulating the flow of radionuclides from land to water and the internal factors regulating the retention of radionuclides in rivers. The model gives monthly predictions of the target variable, radionuclide concentrations at defined sites in rivers (From [41])

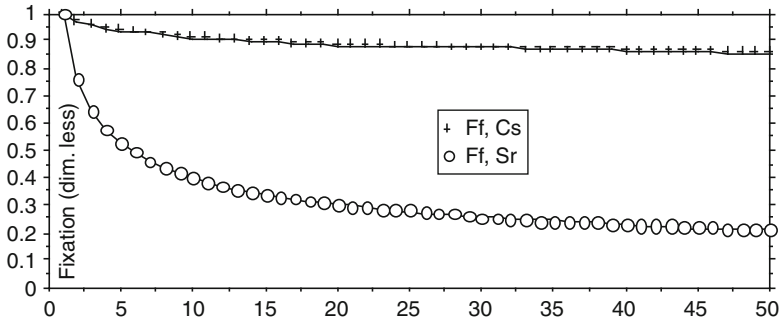

Nuclear Accidents, Chernobyl Fallout in Scandinavian Watersheds. Figure 7
Illustration of fixation in catchment areas calculated for radiocesium and radiostrontium (From [41])

The catchment area is often divided into two parts see (Fig. 9):

1. The outflow areas (i.e., wetlands = upstream lakes, rivers, bogs, and mires), where there may be a relatively quick horizontal transport of the radionuclide from land to surface water, and the remainder.
2. The inflow areas (= the dry land areas), where there is a much slower transport of the radionuclide first vertically to the ground water through several soil layers and then from the ground water to the surface water.

Many papers and textbooks in hydrology treat these topics thoroughly [22, 36–39].

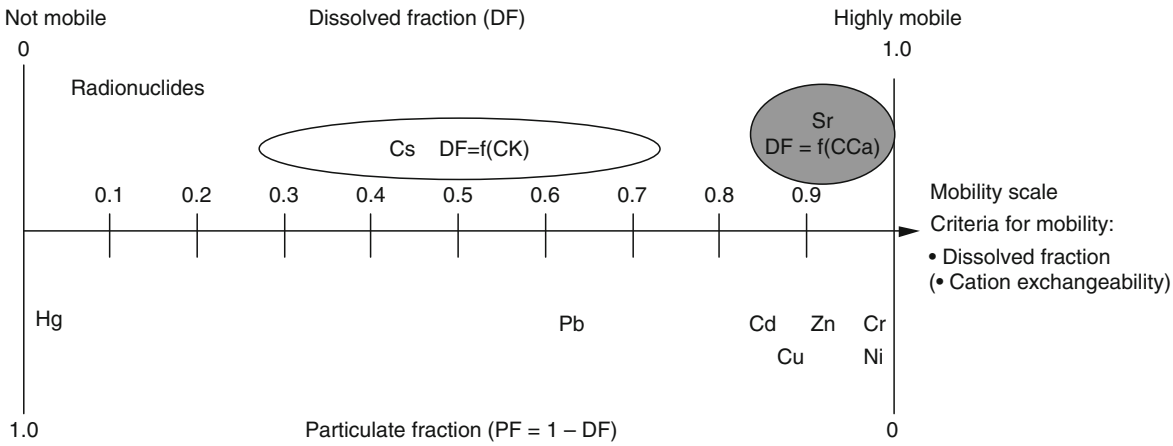

Nuclear Accidents, Chernobyl Fallout in Scandinavian Watersheds. Figure 8
A schematic illustration of the mobility and the dissolved fraction of various substances

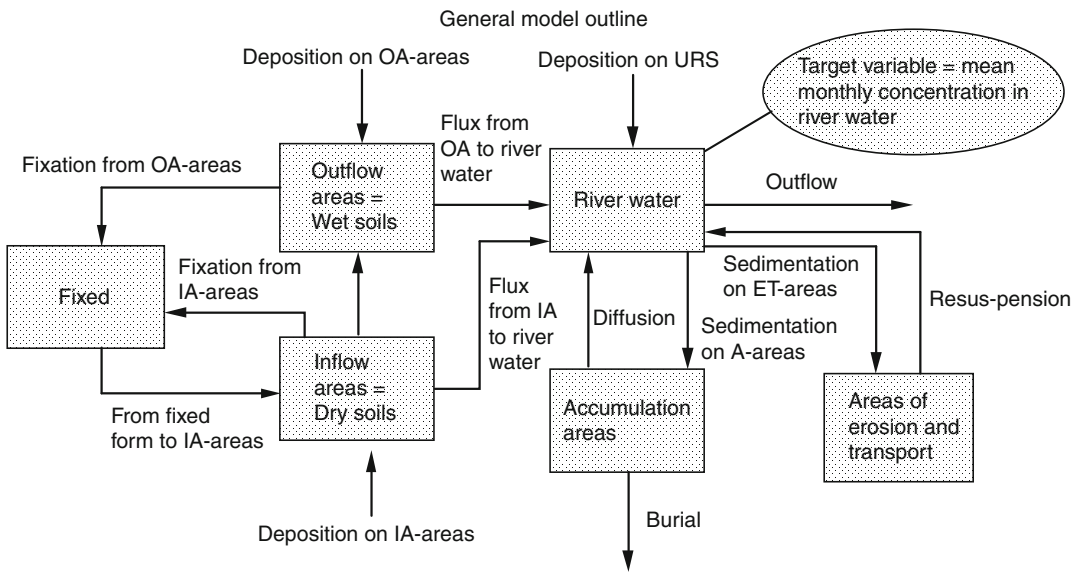

Nuclear Accidents, Chernobyl Fallout in Scandinavian Watersheds. Figure 9
An outline of the river model

Rivers Fluxes

The following processes are important for the river transport see (Fig. 9):

1. Direct fallout onto the river
2. Input from the catchment area (one flux from outflow areas to the river water, another flux from inflow areas)
3. Internal fluxes (sedimentation on ET-areas and A-areas; i.e., areas of fine sediment erosion plus transportation and fine sediment accumulation, respectively; see Section Dynamic Modelling for further explanation)
4. Resuspension of fine sediments and particulate forms of the radionuclides from ET-areas back to river water

5. Diffusion from A-areas back to river water (i.e., the return flow from sediments back to water related to concentrations gradients; see [40]; this is especially important for radiocesium)
6. Outflow to downstream river stretches

Modelling Catchments and Rivers

There are uncertainties in most empirical data used to run and test models, e.g., in the climatological factors regulating precipitation and runoff of the radionuclides from land to water. This is exemplified in Fig. 10 using data for the River Thames. This figure gives the fallout (curve 3), the measured Cs-concentrations related to the fallout from the nuclear weapons test (NWT; curve 2), and the modelled Cs-concentrations in river water (curve 1; from [41]). Note that there is nothing in the fallout curves that would suggest that there should be a small peak in measured river concentrations just before week 280 (week 1 is January of 1955). This should be attributed to, e.g., hydrological/climatological factors. To be able to predict variations of this type, one would need actual data on precipitation and water discharge for the entire period. Such data are often not available, or very difficult to access for many/most rivers. Further, such data add more descriptive power rather than predictive power to the model, since one cannot predict relevant climatological conditions but more than a few days ahead. Given such uncertainties, one can understand that modelling of radiocesium would not predict concentrations in rivers better than a factor of 1.6 compared to the empirical data and not Sr-concentrations better than a factor of 2.2. The characteristic coefficients of variation (CV = SD/MV; SD = standard deviation, MV = mean value), as a measure of the uncertainties in the empirical data for radionuclide concentrations in rivers are generally simply too high and higher for radiostrontium than for radiocesium [41].

A graphical illustration of a traditional compartmental modelling approach for aquatic systems is given in Fig. 11a. This figure illustrates top predator (like pike or large perch), small fish 1 and 2 (e.g., small perch and roach), zooplankton, phytoplankton, algae and zoobenthos, and abiotic compartments (like water and sediments) and the processes regulating the fluxes between these compartments. The figure also gives the fluxes to the given aquatic system (direct lake load and river input related to catchment load) and from the lake (outflow and burial = sediment transport from active to passive sediment layers). This is a general modelling setup applicable for any substance X in a lake. The concentration of X in any biological compartment is defined by the ratio between the amount of

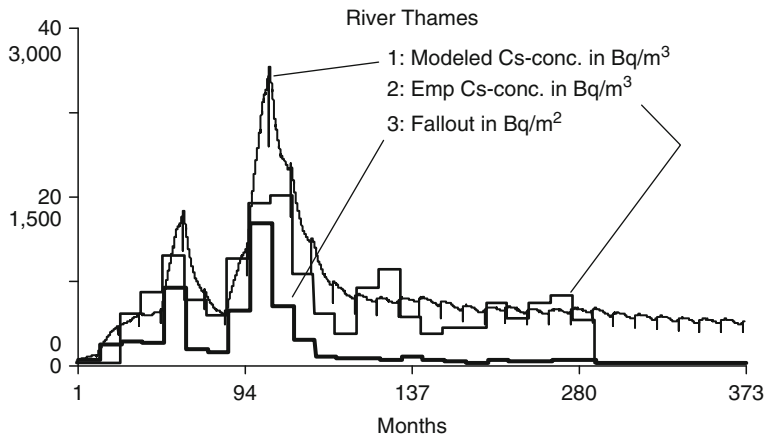

Nuclear Accidents, Chernobyl Fallout in Scandinavian Watersheds. Figure 10
Data from River Thames illustrating the NWT fallout (curve 3), measured mean annual values of Cs-concentrations in river water (curve 2), and modelled Cs-concentrations (curve 1). Note that there are significant variations (a factor of 2) in the empirical data, which cannot be attributed to variations in fallout but must be explained by climatological variations in water discharge, runoff from land, etc. (From [41])

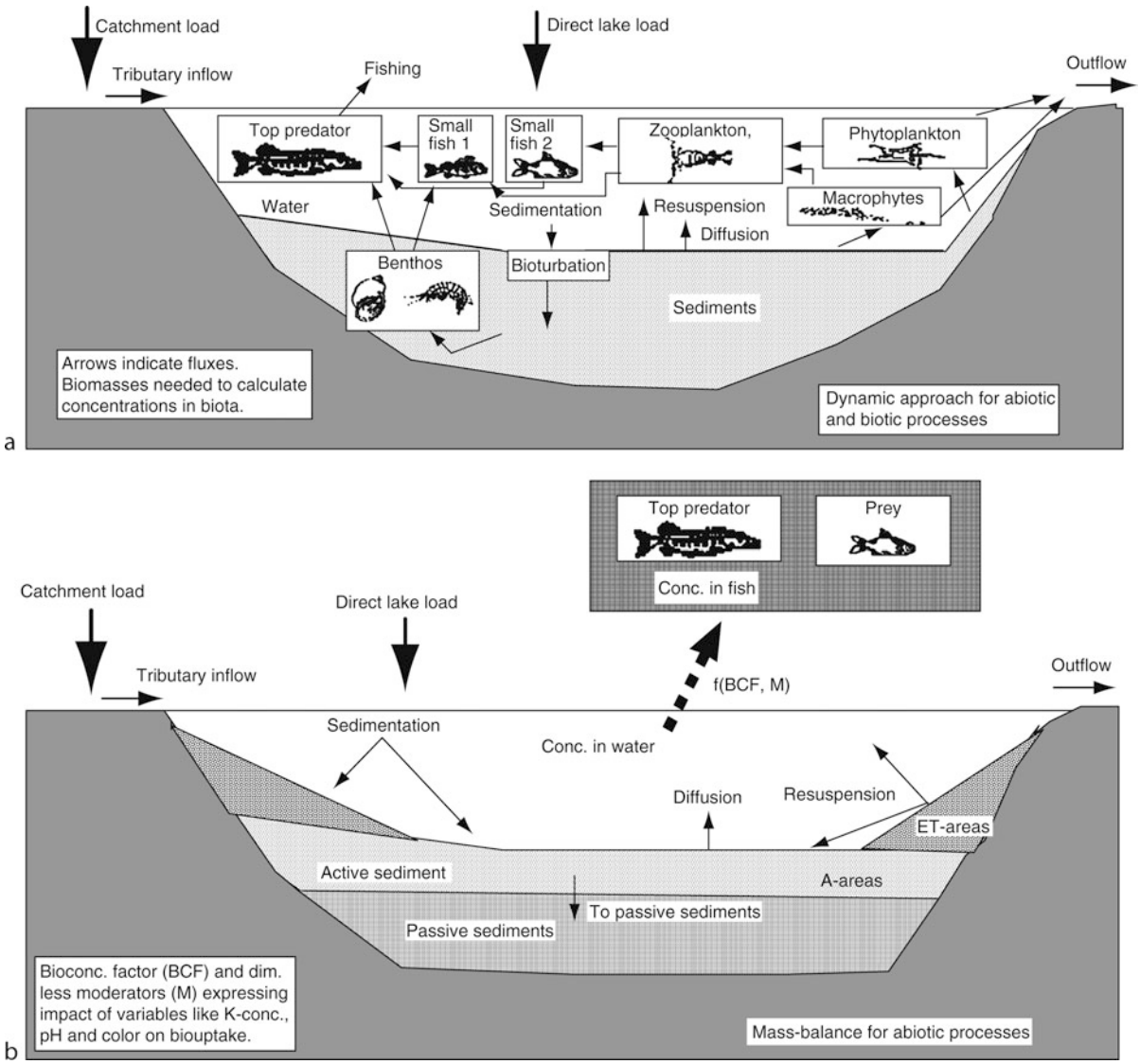

Nuclear Accidents, Chernobyl Fallout in Scandinavian Watersheds. Figure 11
(**a**) Illustration of a traditional compartment model showing the fluxes (arrows; mass per unit time) for a given radionuclide or metal in a lake ecosystem with compartments for top predator, two types of small fish, zooplankton, phytoplankton, algae, benthos, water and sediments. (**b**) Illustration of another modelling approach showing a model based on mass-balance concepts for all abiotic fluxes, a bioconcentration factor, which is used to calculate concentrations of toxic substances in biota (so that one does not need to determine biomasses), and dimensionless moderators used to quantify how different water chemical conditions (pH, color, K-concentration, etc.) affect biouptake via the bioconcentration factor (From [19])

X in the compartment (in g or Bq) divided by the biomass of the species (e.g., kg pike in the lake). One needs biouptake rates and excretion/retention rates for all biological compartments, variables to describe the compartments (like age, sex, organ, weight, and feed habits) and the biomasses of the species in the lake. All these variables are difficult and expensive to access; they vary seasonally and are often based on expert

opinion. This means that models of this kind are often based on many opinions and assumptions, which explain the fact that they generally provide poor predictions (see [17]). Better predictions can often be obtained for models structured in a different way. Then, one would use a dynamic (mass-balance) model for all important abiotic processes, which are relatively easy to handle compared to biological processes, so that the concentration of X in water and/or sediments can be predicted accurately, and then use the bioconcentration factor (BCF) approach to model the biological fluxes so that the concentration of X in biota is calculated directly without having to estimate biomasses. Often there is knowledge about the factors influencing the biouptake, like a lower biouptake for Cs-137 in lakes with high concentrations of potassium. This knowledge can be expressed by dimensionless moderators operating on the BCF-value see (Fig. 11b).

The inherent uncertainty for the Cs-concentrations in rivers, which is 1.6 [41], is illustrated in Fig. 12. Figure 12 gives a direct comparison between modelled concentrations of radiocesium against empirical data for the European rivers listed in Table 1. Most of the data, but not all, are within these two uncertainty bands for the empirical data. This means that the model (from [41]) can explain most of the variability in this situation (related to the Chernobyl fallout for Cs-concentrations in rivers; compare Fig. 4).

Modelling Lakes

Background Many studies have been done on especially radiocesium in lakes after the Chernobyl accident. It is evident that many factors and processes can influence the variability in radiocesium concentrations in water and biota within and among lakes. But what relative importance should one expect for the various factors and processes? It is evident that hundreds of x-variables may be of interest, but they cannot all be of equal importance for the predictions of the target y-variable (generally Cs-137 in fish eaten by man). Only reliable empirical data can be used to provide a quantitative ranking of different x-variables influencing a defined target y-variable. Table 2 may be regarded as an introduction to the following modelling. It gives (based on data from 14 Swedish lakes; see [3, 10, 11]) a ranking based on stepwise multiple regression analysis of the factors influencing a target y-variable, here the concentration of radiocesium in pike (Cs_{pi88}) caught in the spring of 1988 in relation to:

1. One variable for the load of radiocesium to the lake, Cs_{wa87} (Cs-concentration in lake water in 1987 in Bq/l). Accounting for this explains statistically 78% of the variation among the lakes in Cs_{pi88}.
2. Different lake variables (mean annual values for 1987), first and logically, variations among the lakes in K-concentrations (in meq/l); the r^2-value (the coefficient of determination) increases to 0.89 if this is accounted for.

It is evident that the target y-variable in this test, Cs_{pi88}, may also be related to the fallout (Cs_{soil}) after the Chernobyl accident, and several of the given water variables could, potentially, influence the bioavailability and biouptake of radiocesium as well as the biomasses, and hence the concentration of radiocesium in the biomasses. The morphometrical parameters could, potentially, influence the retention of radiocesium in lakes, the resuspension and the internal loading of Cs-137, and the catchment parameters could all, potentially, influence the runoff of radiocesium from land to water, i.e., the secondary load of radiocesium to the lakes. But all these factors cannot be of equal importance in predicting Cs_{pi88}.

It should be stressed that this empirical model only applies for a given year after the Chernobyl accident. The most important water chemical variable in this empirical model is the lake K-concentration – the more ions similar to Cs, like K, the lower the uptake of ^{137}Cs – a case of "chemical dilution" [42–44]. For a "peak emission" like this, the biouptake of Cs-137, and the Cs-concentration in fish, is also lower in lakes with fast water turnover than in lakes with slow water turnover – a case of normal "water dilution." The higher the lake phosphorus concentration, the higher the bioproduction, the greater the biomasses, and the lower the Cs-concentrations in the biomasses – a case of "biological dilution."

Radiocesium is rather reactive [25, 45–47]. This is very important and means that the behavior of radiocesium in lakes is strongly influenced by the chemical and physical properties of the carrier particles (illite clays). In addition, the retention in a lake will be

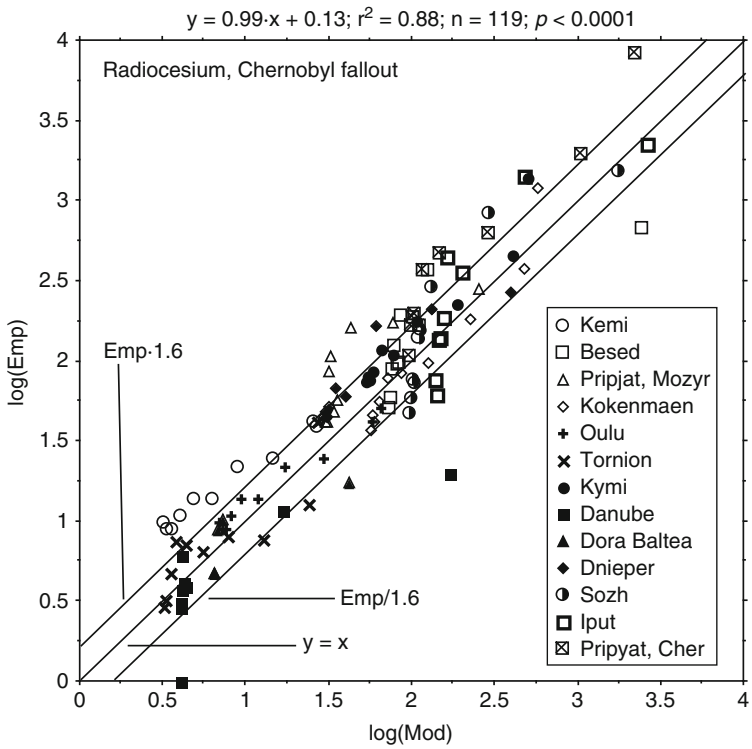

Nuclear Accidents, Chernobyl Fallout in Scandinavian Watersheds. Figure 12
Results for radiocesium concentrations in river water related to the Chernobyl fallout. The figure also gives the ideal line (y = x), the two uncertainty lines related to the uncertainty in the data (measured river concentrations, fallout, and catchment features; note that these lines indicate that one cannot expect that the model should predict better than the interval given by these two *lines*). The slope of the regression line is 0.99, which is very close to the ideal and indicates that the model on average neither overpredicts nor underpredicts the empirical data. Over this wide range of data, the coefficient of determination (r^2) is 0.88. The number of measured data (n) is 119 and the statistical certainty (p) < 0.0001 (From [41])

Nuclear Accidents, Chernobyl Fallout in Scandinavian Watersheds. Table 2 Results from stepwise multiple regression analyses (from [100]) based on data from 14 Swedish lakes. y-variable = radiocesium concentrations in pike caught in 1988 (Cs_{pi88} in Bq/kg ww) tested against different x-variables that could potentially influence the variability among these lakes in Cs_{pi88}

Step	*F*-value	Variable	r^2-value	Model
1	4	Cs_{wa87}	0.78	$y = 9479 \cdot x1 + 769$
2	4	K	0.89	$y = 9559 \cdot x1 - 170.6 \cdot x2 + 2524$
3	2	Open land%	0.92	$y = 9685 \cdot x1 - 249.5 \cdot x2 + 172 \cdot x3 + 2804$
4	1	Total-P	0.93	$y = 9259 \cdot x1 - 226.4 \cdot x2 + 191.6 \cdot x3 - 224.6 \cdot x4 + 4939$

Other tested variables: Area of drainage area; Dm = mean depth in m; Q = mean water discharge in m^3/s; Tw = theoretical water retention time in yr; A-areas = accumulation areas; DR = dynamic ratio; RDA = relief of drainage area; color in mg Pt/l; CaMg (hardness) in meq/l

governed by the turnover time of the lake water; i.e., the longer the water turnover time, the larger the proportion of the initial cesium load retained within the lake (mostly in the sediments).

Table 2 gives statistical results, and a central part in the derivation of the following model was to account for the mechanistic principles expressed by the empirical results given in Table 2. The empirical model is static, i.e., it is only valid for the Cs-concentration in pike caught in the spring of 1988 two years after the Chernobyl fallout. The following model (see section "Dynamic Modelling") is dynamic, i.e., it provides time-dependent predictions not just for pike, but for many species of fish with different feeding habits, for many different types of lakes, and for different fallout scenarios.

Dynamic Modelling The transport processes (sedimentation, resuspension, burial, diffusion, mixing, biouptake, etc.) illustrated in Fig. 13 are general and apply for all substances in all/most aquatic systems, but there are also substance-specific parts mainly related to the particulate fraction, the criteria for diffusion from sediments to water and the fact that some substances (e.g., nitrogen) have a gaseous phase. So, these processes have the same names for all systems and for all substances:

- Sedimentation is the flux from water to sediments or to deeper water layers of suspended particles and radionuclides attached to such particles.
- Resuspension is the advective flux from sediments back to water, mainly driven by wind/wave action and slope processes.
- Diffusion is the flux from sediments back to water or from water layers with high concentrations of dissolved substances to connected layers with lower concentrations. Diffusion is triggered by concentration gradients, which would often be influenced by small-scale advective processes; even after long calm periods, there are currents related to the rotation of the earth, the variations of low and high-pressures, temperature variations between day and night, etc. However, it should be noted that it is difficult to measure water velocities lower than 1–2 cm/s in natural aquatic systems.
- Mixing (or large-scale advective transport processes) is the transport between layers of water, e.g., surface-water layers and deep-water layers related to changes in stratification (variations in temperature or salinity).
- Burial is the sediment transport of matter from the biosphere to the geosphere often of matter from the technosphere.
- Outflow is the flux out of the system of water and everything dissolved and suspended in the water.

Figure 14 shows the basic structure of the model for radionuclides in focus in this section. When there is a partitioning of a flow from one compartment to two or more compartments, this is handled by a partitioning or distribution coefficient. There are five such distribution coefficients (DC) in this model:

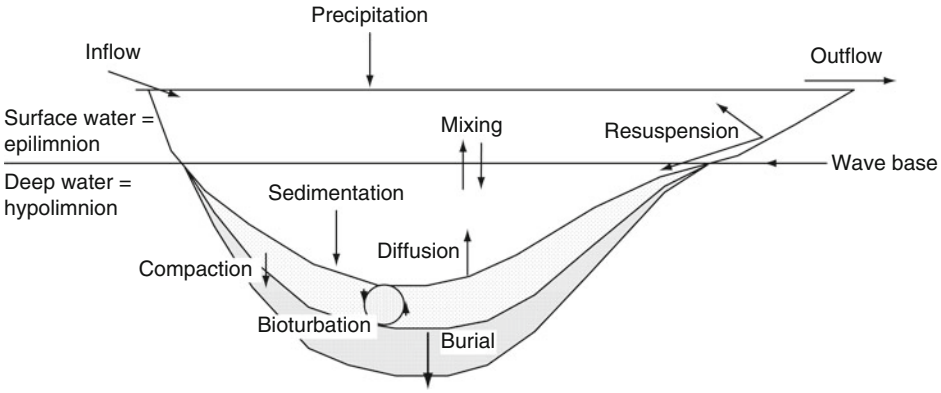

Nuclear Accidents, Chernobyl Fallout in Scandinavian Watersheds. Figure 13
Illustration of fundamental transport processes in lakes

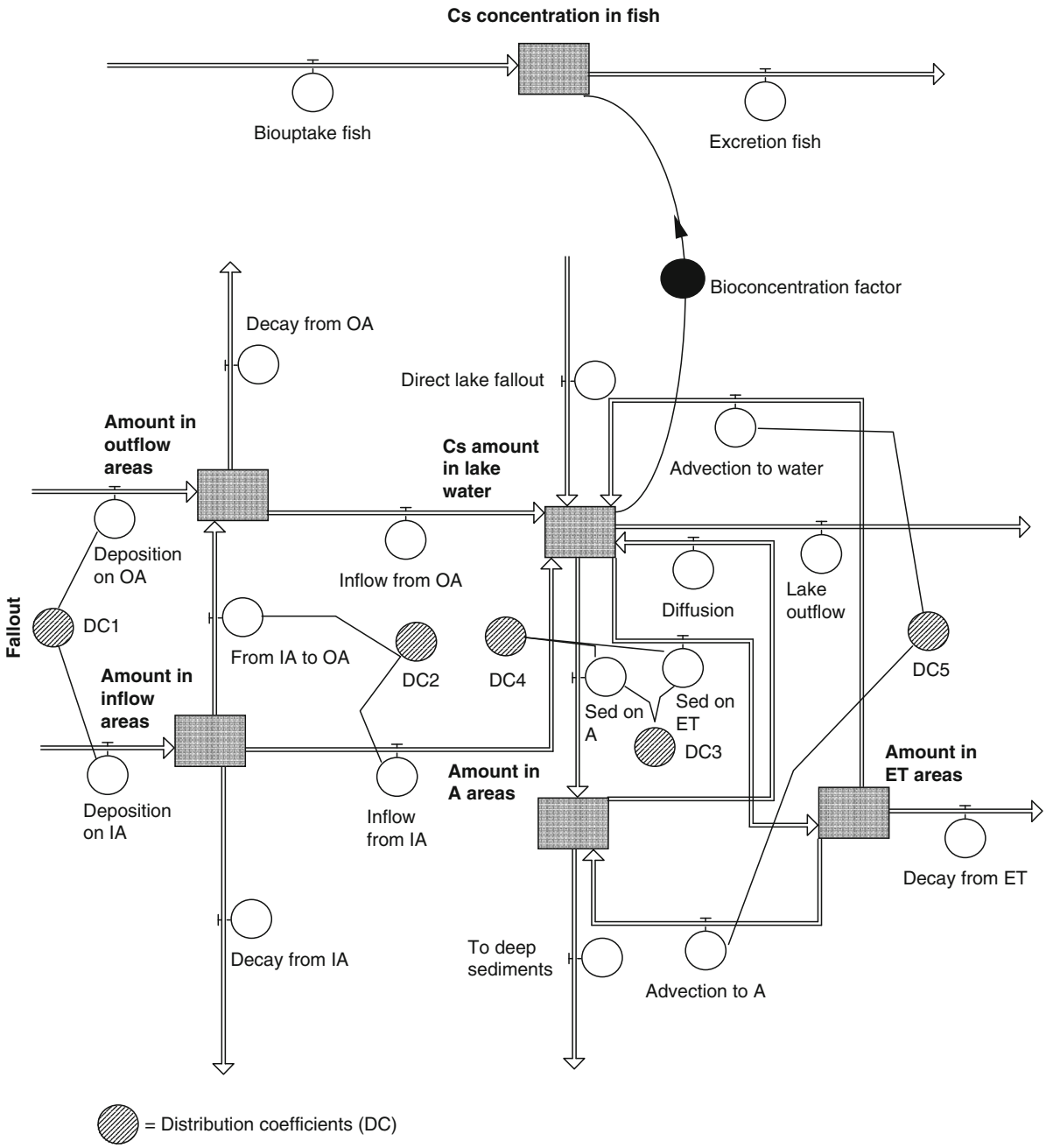

Nuclear Accidents, Chernobyl Fallout in Scandinavian Watersheds. Figure 14
Illustration of the basic structure of the mass-balance model for substances, here radiocesium in lakes

1. The DC to distribute the fallout on the catchment area to inflow and outflow areas. The catchment area is divided into two parts: "outflow areas" (≈ wetlands) dominated by a relatively fast turnover of substances and horizontal (land overflow) transport processes and "inflow areas" (≈ dry land) dominated by vertical transport processes, first through the soil horizons, then ground water transport, and, finally, tributary transport to the lake.

2. The DC handling the partition from inflow areas to outflow areas and lake water.
3. The DC differentiating between dissolved and particulate fractions of the given radionuclide.
4. The DC regulating the sedimentation of the substance to either areas of erosion and transport (ET-areas, i.e., areas where by definition there is a discontinuous deposition of fine particles so that periods of sedimentation and resuspension occur [48] and/or to areas of accumulation (A-areas; areas with continuous sedimentation of fine particles settling according to Stokes' law; from these areas, the substance may be transported back to the water, e.g., by diffusive processes).
5. The DC describing the flux (resuspension = advection) of the substance from ET-areas back to water and/or to A-areas.

Technically, the biotic processes are treated separately from the abiotic fluxes and the two pathways are linked by means of a bioconcentration factor, which in turn is influenced by factors known to regulate the biouptake and concentration of the substance in the target organisms. In the radiocesium model, the target organism is fish eaten by man. This approach is a simplification with many advantages in predictive ecology.

In quantifying sedimentological processes, the lake is divided into four zones: surface water, deep water, ET-areas (areas where processes of fine sediment erosion and transport dominate the bottom dynamic conditions), and accumulation areas (A-areas). The following abbreviations for such fluxes are generally used rather than abbreviations in Greek letters: F for fluxes (Bq/month), C for concentrations (Bq/m^3), R for rates (1/month), and M for masses (= amounts in g or Bq). Fluxes from one compartment to another are denoted, e.g., F_{SWDW} for sedimentation from surface water (SW) to deep water (DW). The resuspended particulate forms of the given radionuclide may be transported either back to the surface water (F_{ETSW}) or to the deep water (F_{ETDW}). How much will go in either direction is regulated by a distribution coefficient (DC) calculated from the form of the lake.

Sedimentation of suspended particles depends on:

1. A default settling velocity, v_{def}, which is substance-specific and related to the type of carrier particle. Examples are 12 m/year for illite clays, the carrier particles for radiocesium [19] or 72 m/year for planktonic materials [49]. The v-value is changed into a rate (1/month) by division with the mean depth for the surface-water areas (D_{SW}) for sedimentation on the ET-areas above the wave base and by the mean depth of the deep-water areas (D_{DW}) for sedimentation in deep-water areas (the A-areas) below the wave base.
2. The concentration of suspended particulate matter (SPM in mg/l) will influence the settling velocity. The greater the aggregation of suspended particles, the bigger the flocs and the faster the settling velocity [50–52].
3. The amount of resuspended matter will settle faster than the primary materials. The resuspended particles have already been aggregated and they have also generally been influenced by benthic activities, which will create a "gluing effect."

The wave base is often determined from the ETA diagram (Erosion–Transportation–Accumulation). This approach see (Fig. 15) focuses on the behavior of the cohesive fine materials settling according to Stokes' law (see Eq. 4). The grain size and/or the composition of the material is often used as criteria to distinguish different sediment types [53]. One can also differentiate between different sediment types by means of functional criteria (like erosion, transportation, and accumulation) of coarse sediments (friction material) or fine sediments (cohesive material). In ecological contexts, it is common to focus on the finer materials most easily set in motion/resuspension and having the highest capacity to bind pollutants [54, 55]. In defining the bottom dynamic conditions (erosion, transportation, and accumulation), this work uses the following definitions (from [56]; see Fig. 15):

- Areas of erosion (E) prevail where there is no apparent deposition of fine materials but rather a removal of such materials, e.g., in shallow areas or on slopes; E-areas are generally hard and consist of sand, gravel, consolidated clays, and/or rocks.
- Areas of transportation (T) prevail where fine materials are deposited periodically (areas of mixed sediments). This bottom type generally dominates where wind/wave action regulates the bottom dynamic conditions. It is sometimes difficult in

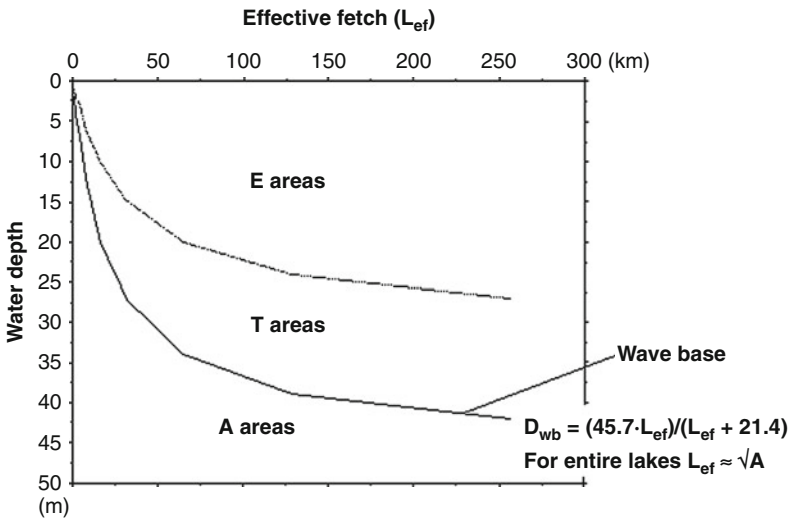

Nuclear Accidents, Chernobyl Fallout in Scandinavian Watersheds. Figure 15
The ETA diagram (Erosion–Transportation–Accumulation; for more information, see [48] illustrating the relationship between effective fetch, water depth, and bottom dynamic conditions. The wave base (D_{wb}) can be used as a general criterion to differentiate between surface water and deep water in lakes

practice to separate areas of erosion from areas of transportation.

- Areas of accumulation (A) prevail where the fine materials are deposited continuously (soft bottom areas). These are the areas (the "end stations") where high concentrations of pollutants may appear.

The generally hard or sandy sediments within the areas of erosion (E) often have a low water content, low organic content, and low concentrations of nutrients and pollutants. The conditions within the T-areas are, for natural reasons, variable, especially for the most mobile substances, such as phosphorus, manganese, iron, and radiocesium that react rapidly to alterations in the chemical "climate" (given by the redox potential) of the sediments. Fine materials may be deposited for long periods during stagnant weather conditions. In connection with a storm or a mass movement on a slope, this material may be resuspended and transported up and away, generally in the direction toward the A-areas in the deeper parts, where continuous deposition occurs. Thus, resuspension is a most natural phenomenon on T-areas.

It should also be stressed that fine materials are rarely deposited as a result of simple vertical settling in natural aquatic environments. The horizontal velocity is generally at least ten times larger, sometimes up to 10,000 times larger, than the vertical component for fine materials or flocs that settle according to Stokes' law [57, 58].

The particles settling on accumulation areas (A-areas) are, by definition, not further resuspended by physical forces. However, such particles with their attached radionuclides may be eaten by zoobenthos, and zoobenthos by fish, so these particles can be transported up to the lake water again in this manner. They can also be transported by migrating zooplankton between the sediments and the water column. The organic fraction of these particles could also be mineralized and decomposed by sediment-living bacteria. The newly formed dissolved phase can then migrate up to the lake water phase by diffusive processes. Bioturbation, i.e., the mechanical mixing of sediments by sediment-living organisms, can also contribute to the transport of settled particles both back to the water and downward to the biologically passive sediments.

Generally, various types of zoobenthos live in sediments down to about 5–15 cm sediment depth. This upper part of the sediment column is biologically active in the sense that the bottom fauna can influence the

physical, chemical, and biological conditions of the sediments and cause bioturbation. However, the larger animals (macro- and meiofauna) generally die if the oxygen concentration becomes lower than about 2 mg/l. This will stop the bioturbation and laminated (layered and unmixed) sediments may appear. The continuous sedimentation will cause the sediment layer to grow upward so that the bioturbation limit, i.e., the limit between the upper biological layer and the lower biopassive (or geological) layer moves upward (see [48] for further information on sedimentary processes).

Many polluting substances have a considerable particle affinity. This means that the behavior of all substances with a particular phase in aquatic systems is influenced by SPM suspended particulate matter; see (Eq. 2). In addition, the retention of a given substance in a system will be governed by the turnover time of the water; i.e., the longer the water turnover time, the larger the proportion of the initial load is retained within the system.

Geochemically, fine, cohesive materials behave differently compared to coarse (friction) materials. From the basic Stokes's equation for settling particles (Eq. 4), as well as for convenience, the limit between coarse and fine materials can be set at a particle size of medium silt.

Stokes' law expresses the settling velocity (v) as

$$v = \left((d_w - d_p \cdot g \cdot d^2)/(18 \cdot AV \cdot FR)\right) \quad (4)$$

wherev is the settling velocity (usually in cm/s)d_p is the particle density (usually in g d_w/cm^3; g d_w = gram dry weight) d_w is the density of the lake water (often set to 1 g ww/cm^3; g ww = gram wet weight) g is the acceleration due to gravity (980.6 cm/s^2)d is the particle diameter (in cm)AV is the coefficient of absolute viscosity (obtained from standard tables; 0.01 P at 20°C) FR is the coefficient of form resistance (set to 1 for spheres)

The behavior of materials that follow Stokes' law (i.e., particles with a diameter between about 0.01 and 0.0001 cm) differs from the coarser friction material and the still finer material. The sedimentological behavior of the friction material is closely linked to the grain size of the individual particles [59, 60]; the sedimentological behavior of the very fine materials is governed by Brownian motion. These latter particles are so small that they will not settle individually, but will do so if they form larger flocs or aggregates that are dense enough to settle according to Stokes' law. The cohesive materials that follow Stokes' law are very important, since they have a great affinity for pollutants. This group includes many types of detritus, humic substances, and plankton. All play significant roles in aquatic systems [35, 61].

So, the settling velocity (v) of a given particle, aggregate, or particulate pollutant, and its distribution in an aquatic system, depends on the density, size, and form of the particle (and on the hydrodynamics of the flow of water in the system). If the particle density, d_p, is close to 1, if the form factor, FR, is large, and if the diameter, d, is small, the settling velocity, v, may be very small. If v is close to 0, the particle or aggregate is conservative in the sense that it may not be deposited in the system. In many lakes (see [48]), Cl and alkalinity are often conservative substances, and color, organic matter, total-P, Si, particulate-P, and SPM are more reactive.

Modelling Biouptake in Fish To predict the concentration of radionuclides such as Cs-137 and Sr-90 in biota (primarily in fish eaten by man), a sub-model added to the main mass-balance model may be used see (Figs. 16 and 19). The sub-model discussed here has been validated (blind-tested) with good results for a great number of lakes. Some of those results are shown in Fig. 17. Empirical data are first directly compared to modelled values for Cs-concentration in 500 g pike in Lake Siggefora, Sweden (Fig. 17a). A statistical correlation of these data (22 fish) gives a r^2-value of 0.51. This regression only covers one lake and one type of fish and, hence, has a limited range. More interestingly for a general model is to see how the model predicts for several fish species for a large number of lakes when the same model setup is used for all systems and there has been no coastal-specific "tuning" of the model variables. This is shown in Fig. 17b. The dataset consists of 185 values for seven fish species covering a very wide range of radiocesium concentrations, from 2 to over 30,000 Bq/kg ww. There are three obvious outliers. If these are omitted, the r^2-value is 0.98 and if they are included, the r^2-value is 0.95. The slope is very close to one. The r^2-value for the actual

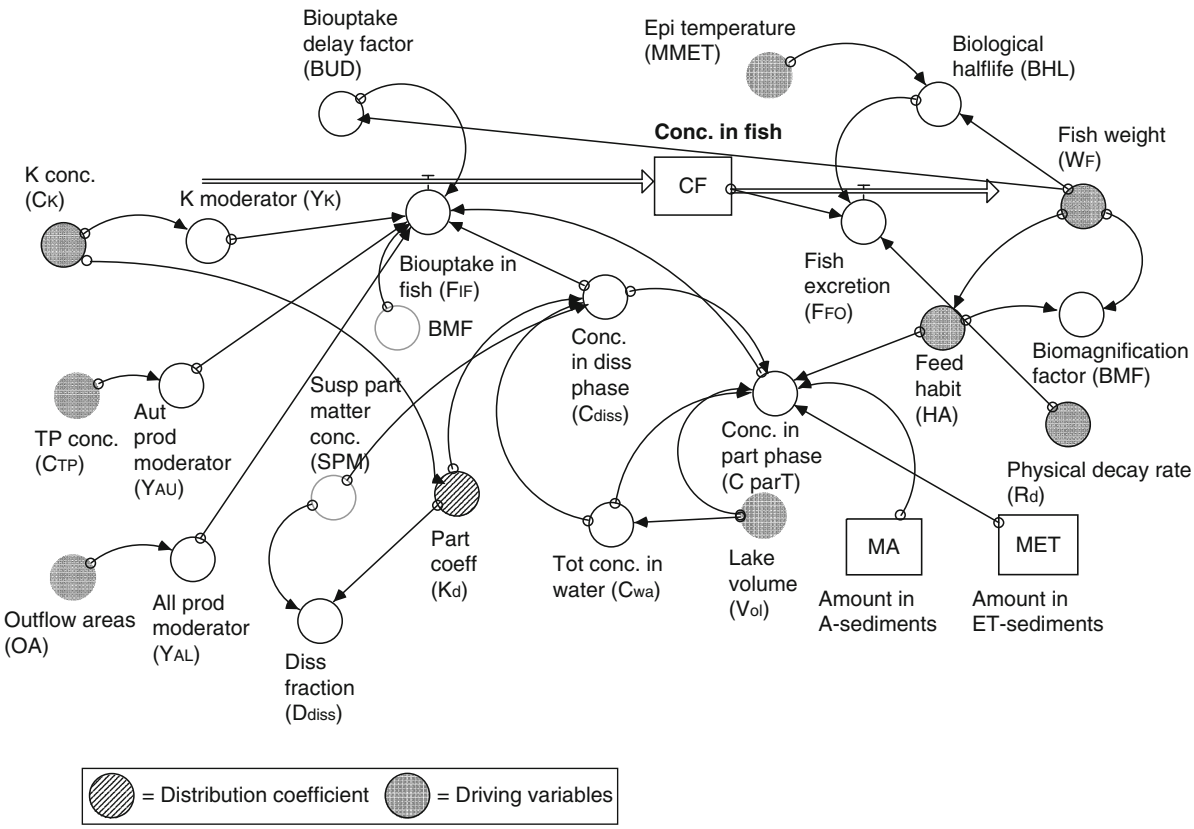

Nuclear Accidents, Chernobyl Fallout in Scandinavian Watersheds. Figure 16
An outline of the biotic part (the sub-model for fish) of the mass-balance model for substances (here radiocesium)

(non-log) data is 0.86. This demonstrates that the basic structure of the sub-model for Cs-137 in biota (fish) in lakes is good. If such good predictions can be obtained for Cs-137 for fish in lakes, this holds great promise also for coastal areas and other types of contaminants in future models.

Basically, the fish model relates the concentrations of a given radionuclide in water, on suspended particles, and in sediments to concentrations in fish. In the model, the bioconcentration factor (BCF; see, e.g., [62]) is influenced by factors known to change the biouptake and retention of radionuclides in biota. Algorithms for this are included in the sub-model for fish and are only briefly described below:

- The concentration of the given radionuclide in dissolved and particulate phases: The concentration in dissolved form will mainly influence planktivorous fish, since they feed on plankton, which are susceptible to the dissolved part of the radionuclide in the lake water; the radionuclide concentration in sediments mainly affects benthivores.
- The feeding habits of the fish (a general algorithm is used for planktivores (eating plankton), piscivores (eating fish), omnivores (eating "everything"), and benthivores (eating bottom fauna), but not for herbivores (eating plants) due to lack of data for model tests for such fish.
- The weight of the fish (a general algorithm where the weight of the fish influences the response time related to biouptake [BUD in Fig. 16] and the biological retention time of the radionuclide in the fish).
- The trophic characteristics of the coastal system: A general algorithm accounting for biological dilution, i.e., the fact that the mean concentration in fish basically is basically defined by the total amount

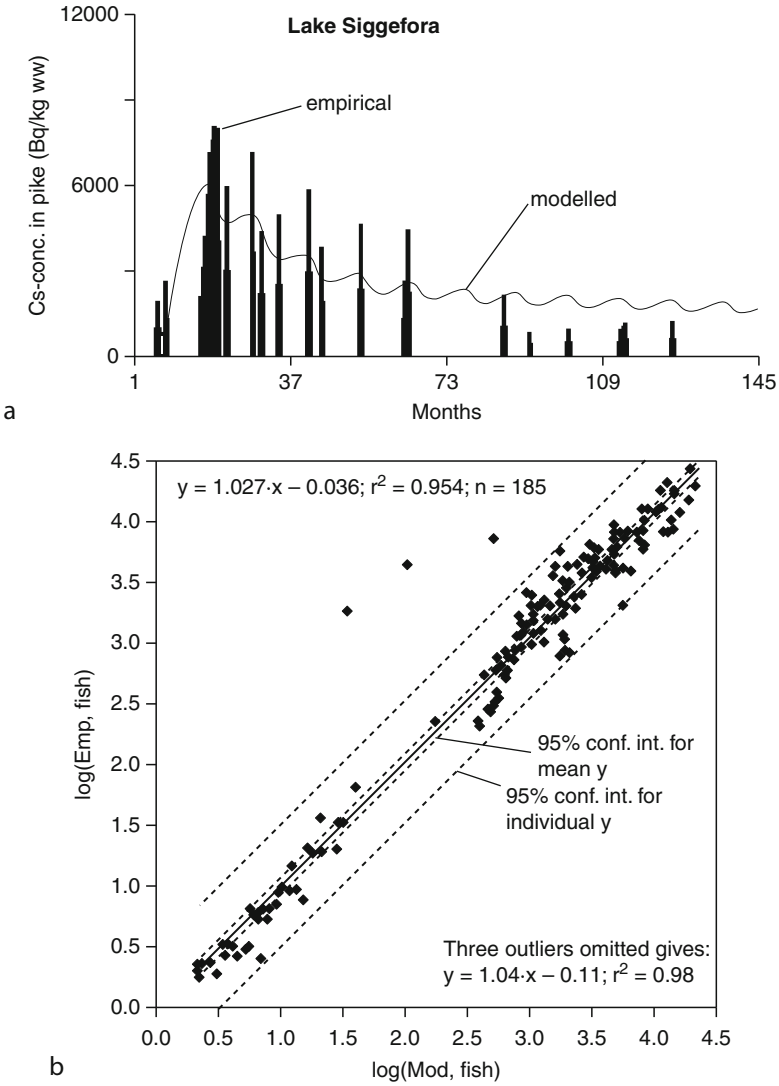

Nuclear Accidents, Chernobyl Fallout in Scandinavian Watersheds. Figure 17
(**a**) The relationship between empirical data and modelled values for radiocesium in 500 g pike in Lake Siggefora, Sweden and (**b**) results of model validation for lake fish from 185 samples from different types of fish from European lakes (Modified from [19])

of the radionuclide in the fish divided by the total biomass of the fish; if the amount of the radionuclide is constant, the concentration will decrease if the fish biomass increases, and vice versa.

- Water temperature: A general algorithm is used where the water temperature influences the biological half-life of the radionuclide in fish, and hence also the excretion of the radionuclide from fish. This model uses an algorithm for the biological half-life that has been tested for water-soluble substances (such as radionuclides), but not for lipophilic substances (such as DDT and PCB), so this approach is substance-specific.
- Chemical dilution: If the water contains a large amount of substances that are taken up by biota in a way similar to the given radionuclide, the biouptake of the radionuclide will be lower. The K-concentration in water specifically influences

the biouptake of Cs-137 and the Ca-concentration specifically the biouptake of Sr-90. There are substance-specific algorithms for this in the model.

So, technically, the biotic processes are treated separately from the biotic fluxes and the two pathways are linked by means of a bioconcentration factor see (Fig. 14). This is a simplification with many advantages in predictive modelling:

1. One can then, as already stressed, predict the target concentrations in biota directly without data on biomasses, which are generally extremely hard to access and predict. This model uses compartments of one mass unit: Cs-137 is transported from one mass unit of lake water to one mass unit of fish. This means that the model automatically yields concentrations of the given substances in fish. Most mass-balance models use the entire lake or a given part of the lake as the unit of size and calculate the concentration of a substance in water as the ratio between the total amount (g or Bq) of material water related to in the total volume of water (l or m^3).
2. One can relatively easy test (calibrate and/or validate) models of this type, since concentrations in biota are easily measured.

This model structure generally gives better predictive success than traditional models using connected or parallel biotic compartments (like phytoplankton, zooplankton, zoobenthos, prey fish, and predator fish models of the type illustrated in Fig. 11a). The uptake of the given substance from water to biota is still modelled dynamically.

These factors are accounted for in this model see (Fig. 16). Such approaches are most relevant in cases when the biotic fluxes of the given substance are much smaller than the abiotic fluxes. This is the case for practically all metals and radionuclides in most lakes (see [63]).

The differential equation for the radionuclide concentration in fish (i.e., C_F in Bq Cs-137 per kg wet weight of fish) is given by

$$C_F(t) = C_F(t - dt) + (F_{IF} - F_{FO}) \cdot d \qquad (5)$$

where

F_{IF} is the biouptake (Bq/month·kg)
F_{FO} is the excretion (Bq/month·kg)

Equation 5 is simple but the model is relatively comprehensive to achieve generality. The number of obligatory driving variables is still small and they are all readily accessible from standard maps and/or monitoring programs (an important demand for the practical utility of the model).

Model Testing The lake model for radiocesium has been validated for a broad set of independent lakes for two target variables, [1] radiocesium concentrations in lake water and [2] radiocesium concentrations in fish see (Fig. 17b). The validation lakes cover a wide range of lake characteristics, although they are all European: sizes are from 0.041 to 1,147 km^2, mean depths are from 2.9 to 90 m, characteristic pHs are from 5.1 to 8.5, trophic levels range from oligotrophic (phosphorus concentrations from 10 μg/l) to highly eutrophic (phosphorus concentrations = 60 μg/l), fallout ranges from 2 to 130 kBq/m^2.

The validations were done in the following manner. Empirical data were first directly compared to modelled values for all lakes individually according to the procedure illustrated in Fig. 17a. All data-series like the one given in Fig. 17a have been compiled for all the validation lakes. The results for the Cs-concentrations in lake water are given in Fig. 18. The r^2-value is 0.92. The figure also gives the 95% confidence intervals for the mean y and the individual y and the regression line. The slope is also almost perfect, 1.087. This regression is based on 61 individual data covering a range from 0.001 to 4.5 Bq/l. This is, of course, a very good result for a validation.

Figure 17b gave the corresponding results for Cs-concentrations in lake fish.

Figure 19 gives the fallout map showing calculated deposition of radiocesium (kBq/m^2) over Sweden from the Chernobyl accident. The figure also shows the boundaries of two provinces (Gäveborgs and Västernorrlands counties) in central Sweden where intensive studies and full-scale experiments were carried after the Chernobyl accident to speed up the recovery related to radiocesium concentrations in lake fish. The map to the right in Fig. 19 shows radiocesium concentrations in lake fish (values in kBq/kg wet substance in one 100 g perch caught in the fall of 1987; small perch is the most abundant fish in Swedish lakes) based on empirical data from 644 lakes. The interesting

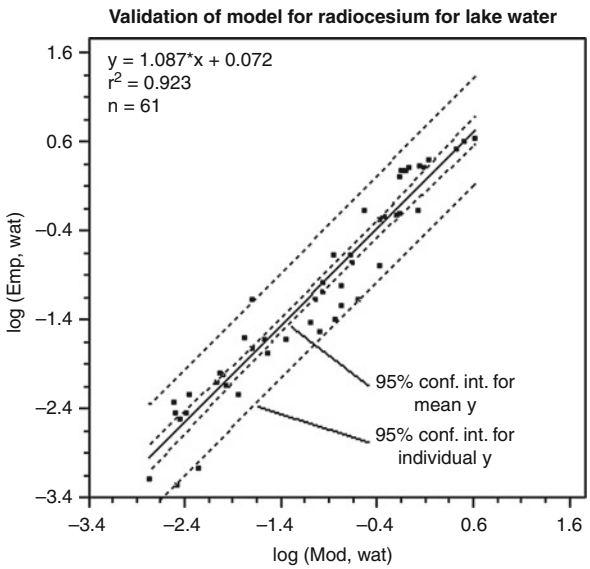

Nuclear Accidents, Chernobyl Fallout in Scandinavian Watersheds. Figure 18
Validation of the radiocesium model for lake water (From [19])

aspect concerns the differences between the fallout map and the map showing concentrations in fish and how to explain this difference. The model discussed here can statistically and causally explain about 90% of this difference, as shown in Fig. 17b.

With this dynamic modelling approach, it is also possible to make realistic predictions on how the situation would likely change in the future – e.g., for how long there will be a radiocesium problem with concentrations of Cs-137 higher than 1,500 Bq/kg in fish in Swedish lakes (the guideline value for consumption and sale) from the Chernobyl accident. Figure 20 gives two maps on modelled radiocesium levels in pike (a top predator). In 1987, 1 year after the Chernobyl accident, there were about 14,000 lakes in Sweden with fish having more than 1,500 Bq/kg. From Fig. 20, one can note that on a regional basis all lakes in Sweden should have fish with radiocesium levels below 1,500 Bq/kg in 2010.

It is often argued that the quality of Science is related to the possibilities to make meaningful predictions. This argument would give Mathematics and Physics a pool position in the scientific community. It has long been argued that due to the complex nature of aquatic ecosystems, it will never be possible to predict important target variables, especially not with more comprehensive dynamic models. Those arguments are no longer valid. The key lies in the structuring of the predictive models.

Modelling Coastal Marine Systems

Introduction, Background, and Aim Coastal areas are target areas for research and environmental management for several reasons:

- The coastal zone may be regarded as a "pantry and a nursery" for the sea and coastal areas can have a very high bioproduction (20 times higher than the most productive areas on land; see [64]). All three functional groups of primary producers, phytoplankton, benthic algae, and macrophytes are present in coastal areas, but not in open water areas. Where there is a high primary production, there is also a high secondary production of zooplankton, zoobenthos, and fish (see [49, 65]).
- The coastal zone is also a zone of conflicts where many different users, such as professional and leisure-time fishermen and people responsible for recreation, shipping, and environmental management and research, place different demands on the coastal waters and apply different criteria to set the value of coastal waters and to define desired conditions (see [49, 65]).
- The coastal zone is also the "recipient" of many types of pollutants, such as radionuclides, nutrients, metals, and organic toxins (see [69, 70]).

Due to the hydrodynamic conditions characterizing a given coastal area, such as the Coriolis-driven coastal jet-zone, tidal effects, and winds, the transport of water pollutants along coasts, the biological value of the coastal zone, and the different demands on the utilization of coastal waters, it is easy to understand why so much interest and research concern this zone. However, in contexts of aquatic radioecology, it is easy to conclude that much more effort has been focused on lakes (see, e.g., [1, 71–74]) and rivers (see, e.g., [75–78]) than on coastal areas. In fact, it is very difficult to find the radionuclide data necessary to test coastal models.

The basic aim of this work is to present a generic coastal model. It is meant to be valid for most coastal

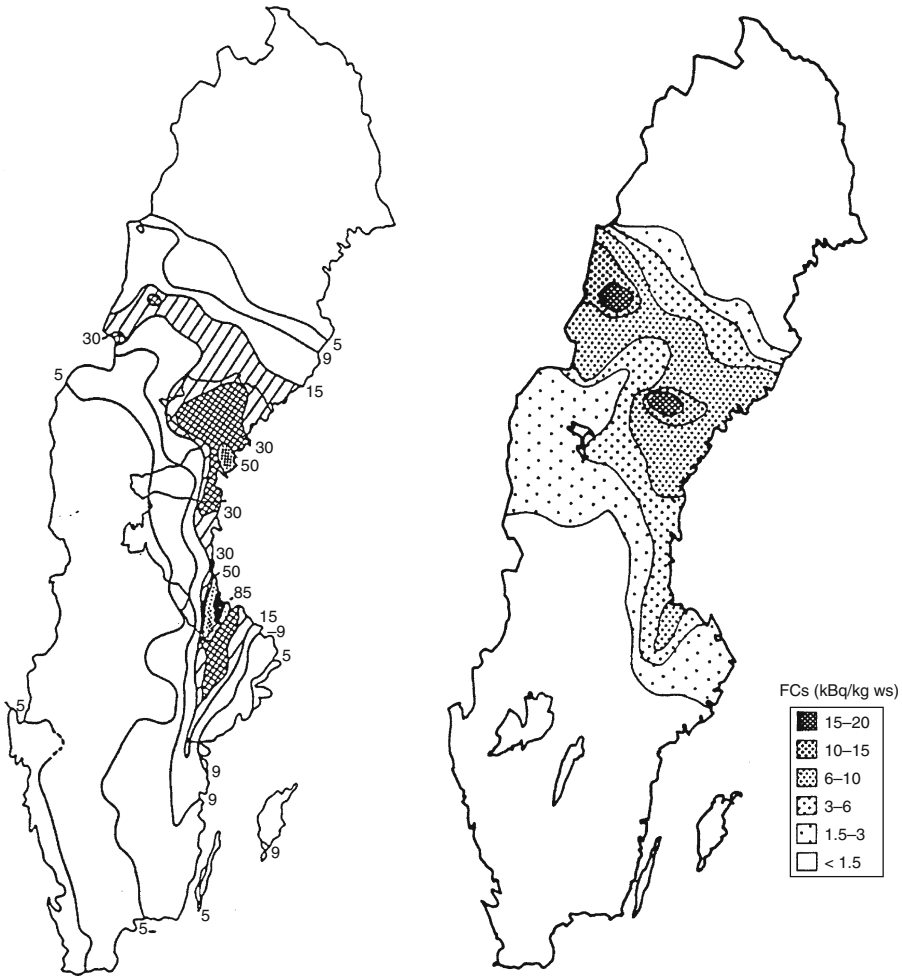

Nuclear Accidents, Chernobyl Fallout in Scandinavian Watersheds. Figure 19
Left; fallout map showing the deposition of radiocesium (kBq/m^2) over Sweden from the Chernobyl accident. *Right*; map showing radiocesium concentrations in lake fish (values in kBq/kg wet substance in 1 hg perch caught in the fall of 1987) based on empirical data from 644 Swedish lakes

areas and for most substances, not only radionuclides. It is dynamic and based on ordinary differential equations (and not on partial differential equations). It is intended to give seasonal (monthly) variations on radionuclide concentrations in water and sediments and not variations at finer temporal or spatial scales. It is meant to be practically useful in radioecology, so the obligatory driving variables should be easily accessed from standard bathymetric maps and monitoring programs. Basically, this model is intended to be analogous in terms of structure and applicability to lake and river models used in the MOIRA decision support system (DSS; see [79]).

In radioecology, there are some coastal models, e.g., Threetox and Coasttox. Unlike the model discussed in this work, these models are distributed 2-d models based on partial differential equations; the model POSEIDON is based on several interlinked boxes. These models are used in the RODOS DSS (see http://www.rodos.fzk.de/) and they are mainly designed to handle short-term (hours to days) spatial variations after accidental fallouts. They are driven by online

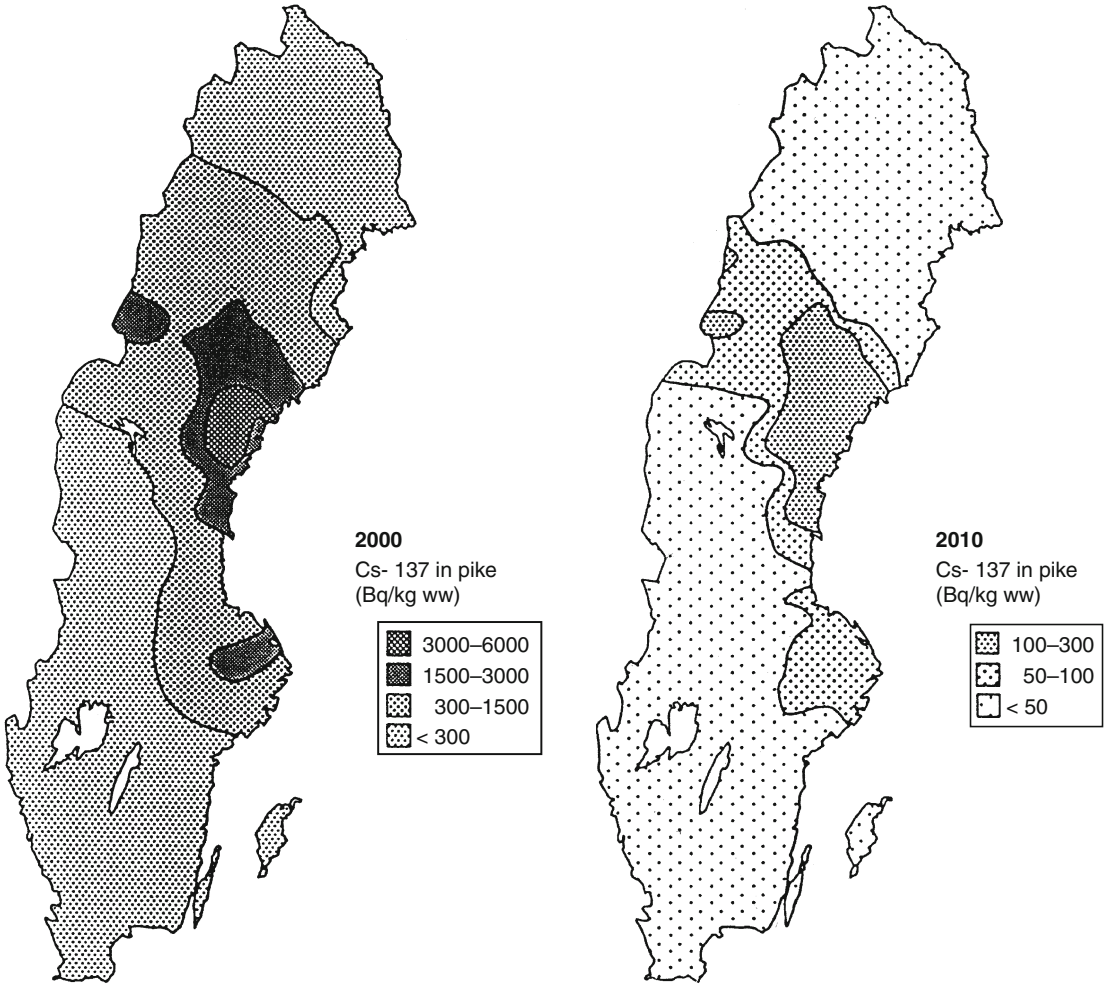

Nuclear Accidents, Chernobyl Fallout in Scandinavian Watersheds. Figure 20
Modelled radiocesium levels in pike in Swedish lakes in the years 2000 and 2010

meteorological data (winds, temperature, and precipitation) and operate over much smaller temporal and spatial scales than the coastal model discussed in this context.

The ideal dataset for coastal modelling would have reliable measured data on several radionuclides and their concentrations in coastal water, sediments, rivers, and the sea outside the coast, as well as relevant co-parameters describing morphometry, water quality, etc., for several coastal areas covering a wide geographical domain. While waiting for that ideal dataset, this section may be regarded as "stepping-stone" for future model validations in coastal radioecology.

The following specific questions will be discussed in this section:

- Which fluxes (Bq/month) to, within, and from a given coastal area can be expected to be large and small? Evidently, it is more important to predict large fluxes with a smaller uncertainty than smaller fluxes. The answer to this question is also fundamental for sensitivity and uncertainty analyses (see [63]).
- The exchange processes between the coast and the sea are often of fundamental importance for the concentrations of radionuclides (and other substances as well) in coastal water, sediments, and biota (see, e.g., 19). For which coast types will the concentration in the coastal water be close to the concentrations in the sea and when and why will there be differences?

- In models of this kind (i.e., process-oriented mass-balance models based on ordinary differential equations and monthly timescales) there are always uncertainties related to the model structure and uncertainties in driving variables – but which uncertainties related to fluxes and driving variables are generally small, and which are important and need to be reduced to increase the predictive power of the model?
- In this model, there are generic parts that apply for all substances/radionuclides and substance-specific components. In applying models of this kind for different radionuclides, it is essential to stress this point. This may be done by using the algorithm for sedimentation as an example. Sedimentation is a general process that applies for all substances with particulate phases. Sedimentation is given in this coastal model by the following algorithm, which gives sedimentation from surface water (SW) to deep water (DW) separated by the wave base:

$$F_{SWDW} = M_{SW} \cdot (v/D_{SW}) \cdot PF \cdot (1 - ET) \cdot [(1 - DC_{res}) + 10 \cdot DC_{res}] \quad (6)$$

M_{SW} is the mass (amount) of the radionuclide/substance in the SW compartment in Bq.

v is the settling velocity of the particulate fraction (PF) of the radionuclide in m/month. The v-value used here is valid for suspended particulate matter (SPM).

D_{SW} is the mean depth of the surface-water compartment in the given coastal area in m.

ET is the fraction of ET-areas (i.e., areas where discontinuous sedimentation of fine particles appear) in the coastal area; these are the areas above the wave base (WB); the deep-water areas are the areas below this water depth (ET is dimensionless).

DC_{res} is the fraction of resuspended particles of the total amount of particles in the surface water compartment; resuspended particles from the ET-areas have a higher settling velocity (a factor of 10 compared to the primary particles) and a shorter distance to settle. C_{res} is calculated automatically in the model.

The only substance-specific part in Eq. 6 is the particulate fraction (PF). The dissolved fraction DF is (1-PF); DF is about 0.95 for Sr-90, about 0.5 for Cs-137 and about 0.05 for Pb-210 in aquatic environments (see [1, 80] and Fig. 8). Radiostrontium is, as already stressed, more mobile than radiocesium and this is expressed by the substance-specific DF-value. From this, the following question will be addressed in this section: How important is the DF-value for predictions of radionuclide concentrations in coastal waters, sediments, and biota?

Other interesting questions that may be addressed using this model are:

- How will coastal morphometry (coastal size and depth conditions and the openness toward the sea) influence concentrations in water, sediments, and biota? Is it possible to find some general guidelines related to the vulnerability of coastal areas to radionuclide contamination?
- How would tidal effects influence radionuclide concentrations in coastal areas?
- If a coastal area is contaminated by radionuclides, can the model be used to simulate realistic responses and feasible remedial measures?

It should be noted that it would be extremely difficult and costly to scrutinize questions like these using more traditional approaches based on field studies in coastal areas. This is an area where process-based modelling can provide an important input to clarify what is happening in natural coastal areas.

To address such questions, this entry is structured in the following way: Section The Coastal Model gives a short model description, Section A Ranking of Fluxes gives a ranking of key fluxes for a defined coastal are in the Baltic Sea, Section Key Factors Influencing the Ranking of Fluxes and Concentrations discusses factors influencing the ranking of fluxes and concentrations and Section Remedial Measures Simulations: A dredging Scenario gives a remediation scenario on dredging.

First, however, Section Defining Coastal Area Boundaries will discuss criteria to define the fundamental unit, the coastal area. It is evidently easy to define what is a lake. A river stretch may be defined by the area between two inflowing tributaries. But where and how should one draw the borderlines toward the sea and/or adjacent coastal areas? If such borderlines are drawn arbitrarily, one would get arbitrary volumes, areas, and mean depths and the mass-balance model would lose predictive power (see [19]).

Secondly, fundamental criteria for the water exchange between the coast and the sea will be briefly discussed based on three coast types with different characteristics. The main model in this section is the coastal mass-balance model handling internal fluxes. This model is a modified version of a model for suspended particulate matter (SPM) presented by [81]. It will be outlined in the following text.

Defining Coastal Area Boundaries Today, there are many modern digitized methods applicable in aquatic studies including Geographical Information Systems (GIS). Those methods enable quick and effective estimations of morphometric variables (see [82]). Special considerations should be given to define the boundaries of coastal areas. After digitizing and interpolation, the area outside the coastal area can be masked, resulting in one vector file containing coordinates for all shore lengths (of islands and the coastline) and openings to the surrounding open water areas, and one raster file containing the pixel size (header) and the digital elevation model of the coastal area. Figure 21 illustrates steps to define a coastal area and the boundaries to the open water areas or adjacent coastal areas at the topographical bottlenecks using GIS-techniques where the exposure ($Ex = 100 \cdot At/A$) attains minimum values when different alternatives for settling the boundary lines are tested (At = section area; A = enclosed coastal area; method from 81). Once the coastal area is defined, one can also define important variables for mass-balance calculations, such as the coastal volume (regulating the concentration of any given substance), and important morphometric parameters for internal fluxes, such as the mean depth and the water surface area, and key variables regulating the water exchange between the coast and the sea, such as the section area, the exposure, and the filter factor see (Fig. 22). This method of defining coastal areas also opens a possibility to use empirical models to estimate, e.g., the theoretical water retention times of the surface water see (Fig. 23) and the deep water, and the bottom dynamic conditions (regulating sedimentation, resuspension, and diffusion) from morphometrical parameters (such as area, mean depth, and section area).

Water Exchange in Different Coast Types Figure 23 shows an overview of the three main coast types, (1) tidal coasts, (2) open coasts, and (3) archipelago coasts and bays, and how the theoretical surface water retention time (T_{SW}) may be calculated for each type and for any given coast that may be a combination of all three (for further details also on these matters, see Table 3 and [19]. From the theoretical surface water retention time (T_{SW} in months), one can calculate the surface water flux (Q_{SW} in m^3/month) as V_{SW}/T_{SW}, where V_{SW} is the surface water volume (m^3) and the flux of the given substance, $Q_{SW} \cdot C_{sea}$ in g/month, where C_{sea} is the concentration of the substance in the sea outside the given coastal area (g/m^3).

As a rule of thumb, one can say that the costs of establishing an empirical value of the theoretical water retention time from traditional field measurements (using dye, current meters, *etc.*) is about US $30,000 for one coastal area in the size range from 1 to 100 km^2 (see [19]). In many contexts, it may not be very meaningful to build a model if it is a prerequisite that such field work first must be carried out to determine the water retention time as a driving variable (x) predicting target y-variables, such as concentrations of radionuclides in water and fish. This means that it is of major importance that water retention time can, in fact, for many coastal areas be predicted very easily from one coastal morphometric variable, i.e., the exposure (Ex).

The Coastal Model The coastal model see (Table 4 for default values for the obligatory driving variables and some calculated model constants) is modified from two validated coastal models (for suspended particulate matter and phosphorus) based on the same modelling principles and structures as discussed for the lake model in this entry. One can note that for all the tested coastal areas, the model, as applied for predicting phosphorus concentrations (see [83]), generally predicts within the uncertainty bands given by the variations in the empirical data. Sensitivity and uncertainty tests of the model have also been presented (see [81]). The model can be used for coastal areas of the types shown in Fig. 23 and combinations of these three coastal types: coasts where the water exchange is dominated by tides, open coasts dominated where the water renewal is governed by coastal current activities, and archipelago coasts. In estuaries (with freshwater inflow), one must

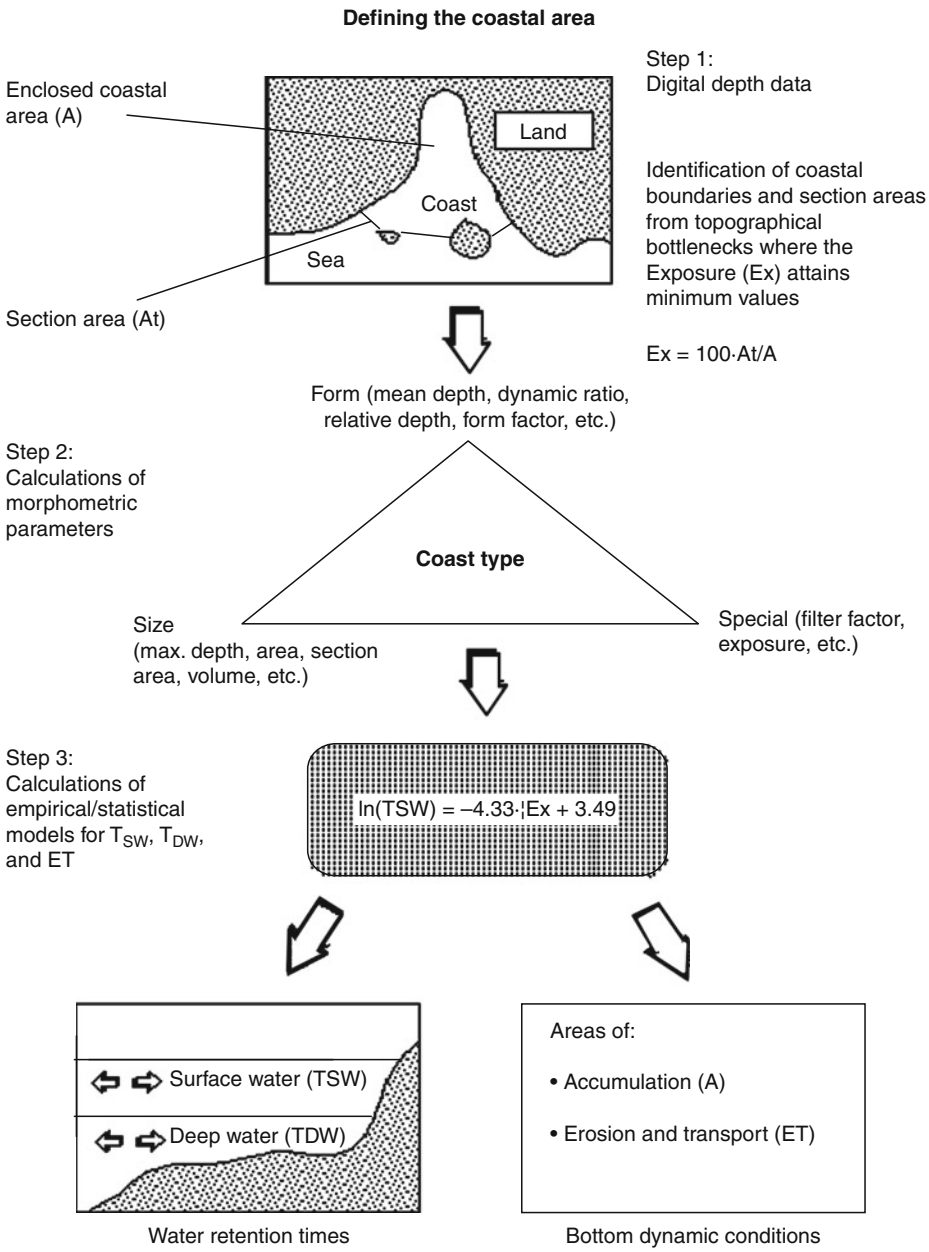

Nuclear Accidents, Chernobyl Fallout in Scandinavian Watersheds. Figure 21
Illustration of the steps to define the boundary lines for a coastal area (step 1) and how to calculate important coastal parameters in contexts of mass-balance modelling at the ecosystem scale, i.e., for defined entire coastal areas (steps 2 and 3).

also evidently account for the inflow of water (and radionuclides) from all major tributaries to the coastal area.

An important demand, related to the practical utility of the model, is that it should be driven by variables readily accessed from standard monitoring programs or maps. The obligatory driving variables include four morphometric parameters (coastal area, section area, mean and maximum depth; see Fig. 22), latitude (to predict surface-water and deep-water temperatures,

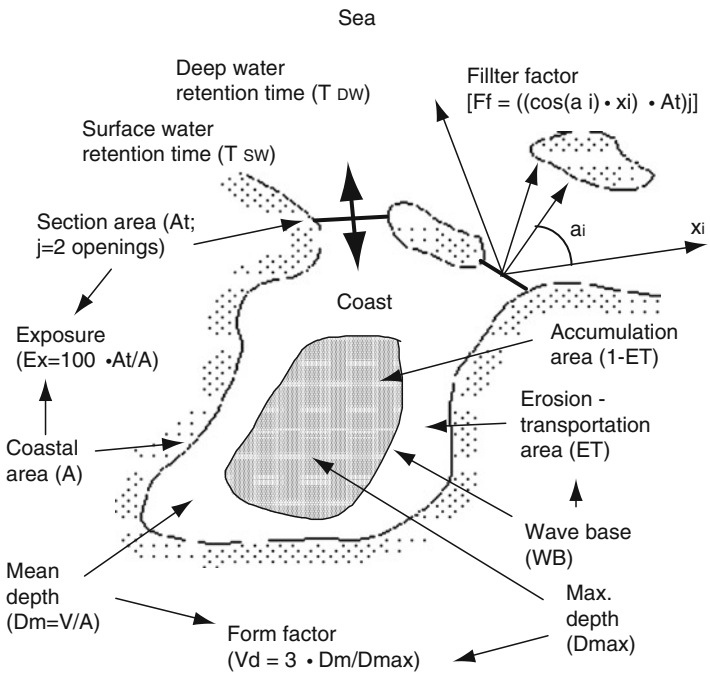

Nuclear Accidents, Chernobyl Fallout in Scandinavian Watersheds. Figure 22
Illustration of key coastal parameters in mass-balance modelling that can be determined quickly from digitized bathymetric maps using GIS-methods (*GIS* Geographical Information System). The most important criteria in this context is to define the boundary lines, i.e., where the coastal area ends and the sea or adjacent coastal area begins. The approach illustrated in this figure is to define the boundary lines so that the topographical openness (the exposure, *Ex*, defined by the ratio between the section area, *At*, and the enclosed coastal area, *A*) attains a minimum value. This is the "topographical bottleneck" method. The filter factor (a measure similar to the fetch) describes how islands and topographical barriers between the defined coastal area and the sea act as energy filter for the wave impact on the coastal area. In this figure, the filter factor is illustrated for one of the two section areas in this coastal area (a_i = the angle between two radials sent out from the opening over open water; x_i = the length of each radial; i = the number of radials at each opening; j = the number of openings; j = 2 in this example)

stratification, and mixing) and the concentration of the given radionuclide in the sea outside the given coastal area, which is estimated in this entry using a simple approach based on the ecological half-life.

Like the lake model, the coastal model has four compartments. Two water compartments, surface water and deep water. The separation between these two compartments is done not in the traditional manner from measured water temperatures but from sedimentological criteria, as the water depth separating transportation areas from accumulation areas (the wave base). The model also has two sediment compartments, the ET-areas, i.e., the erosion and transportation areas where fine sediments are discontinuously being deposited, and the A-areas, i.e., the accumulation areas where fine sediments are continuously being deposited. The processes accounted for are inflow and outflow from the outside sea (and for estuaries also from rivers) via surface and deep water, direct fallout onto the water surface of the coastal area, sedimentation, burial (the transport from surficial A-sediments to underlying sediments), resuspension, diffusion, and mixing between surface and deep water.

A Ranking of Fluxes A ranking of all fluxes to, within and from a "typical" Baltic coastal area, defined here as the default area see (Table 4), is exemplified in Fig. 24 (see [20]). One can note that the fluxes in and out from

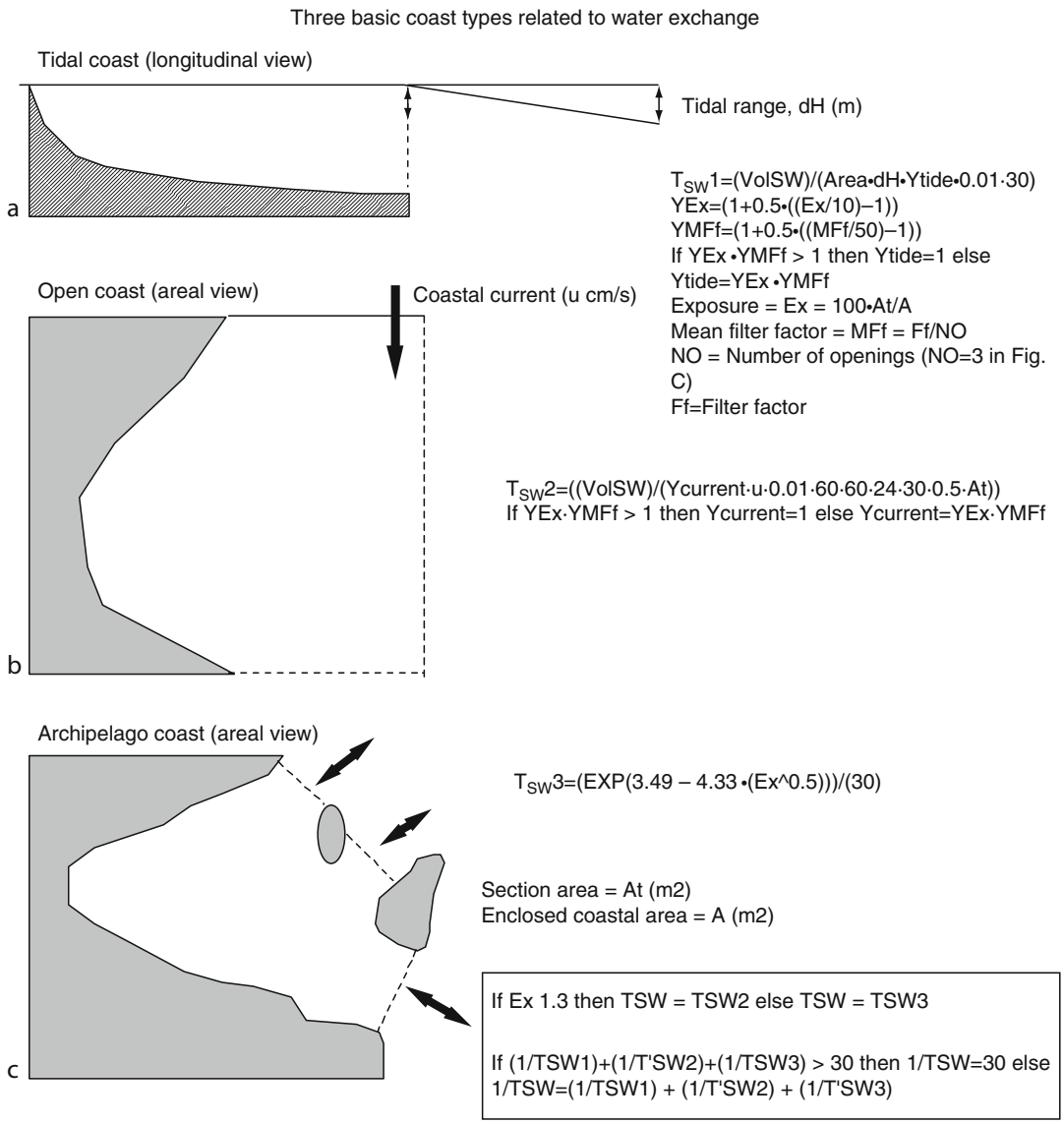

Nuclear Accidents, Chernobyl Fallout in Scandinavian Watersheds. Figure 23
Illustration of the three main coast types and how the theoretical surface water exchange (T_{SW}) may be estimated for each type

the sea are the most dominating fluxes and that burial, diffusion, sedimentation to the deep water, and resuspension to the deep water are the four smallest fluxes. These results are valid for the default coastal area (but not necessarily for other coastal areas) and they imply that for this area, the conditions in the sea are of utmost importance for the conditions prevailing in the given coastal area. Figure 25 compares calculated concentrations in river water (Fig. 25a, curve 1), in coastal water (Fig. 25a, curve 2), and in the sea (Fig. 25a, curve 3), in accumulation area sediments (A-sediments; Fig. 25b) and concentrations in particulate and dissolved phases. From Fig. 25, one can conclude that the short-term changes in concentrations in coastal water the month after the fallout are very significant compared to the long-term changes after the initial month(s) when the water concentrations in the coastal area approach the concentrations in the sea.

Nuclear Accidents, Chernobyl Fallout in Scandinavian Watersheds. Table 3 Empirical models used in this dynamic coastal model to predict theoretical surface water and deep-water retention times (T_{SW} and T_{DW} in days) and the fraction of ET-areas (ET) from morphometric parameters in archipelago areas and bays. Note that if reliable empirical data are at hand for a given coastal area on T_{SW}, T_{DW}, or ET, such data should be used rather than the values predicted by these empirical models (From [81])

Regression	r^2	Number of coastal areas
$\ln(T_{SW}) = (-4.33(\sqrt{Ex}) + 3.49)$	0.95	14
$T_{DW} = (-251 - 138\log(At) + 269\log(Vd))$	0.79	15
$A = 1 - ET = (D_{max} - D_{TA})/(D_{max} + D_{TA} \cdot EXP(3 - Vd \wedge 1.5)) \wedge (0.5\,Vd)$ $D_{TA} = WB = Y_{Ex1}(45.7(Area\,10 \wedge (-6)) \wedge 0.5/(21.4 + (Area\,10 \wedge (-6)) \wedge 0.5)))$ If $D_{TA} \geq D_{max}$ then D_{max} else D_{TA} If $Ex < 0.003$ then $Y_{Ex1} = 1$ else $Y_{Ex1} = (Ex/0.003) \wedge 0.25$		

Model domain: $0.002 < Ex < 1.3$; $0.0006 < At < 0.08$; $0.5 < Vd < 1.5$; data from coastal areas with very little tidal range; note that T_{SW} and T_{DW} are never permitted to be < 1 day and T_{DW} never > 120 days

Ex (exposure) = 100·At/A; Vd (the form factor) = $3 \cdot D_m/D_{max}$; At = section area (km^2); A = coastal area (km^2); D_m = mean coastal depth (m); D_{max} = max. coastal depth (m); A = the fraction of A-areas; ET = the fraction of ET-areas; D_{TA} = WB = the wave base (m)

Key Factors Influencing the Ranking of Fluxes and Concentrations Figure 26 shows how the conditions in the sea influence the calculated concentrations of radiocesium in coastal water under different presuppositions. In Fig. 26a, the ecological half-life regulating the concentration in the sea has been set to 1, 3, and 5 years. This will strongly influence the long-term, but not the short-term, concentrations in the coastal area. Fig. 26b illustrates how three different values of the theoretical surface water retention time (T_{SW}), which regulates the transport between the sea and the coastal area ($Q_{SW} = V_{SW}/T_{SW}$), will influence the calculated water concentrations of radiocesium in the default coastal area. This T_{SW}-value will regulate the "mid-term" conditions more than the short-term and the long-term conditions.

From these results, it is evident that for the default coastal area in the Baltic Sea with a very small tidal amplitude some fluxes and model uncertainties are relatively unimportant. Figure 27 shows that the value used for the particulate fraction (PT set to 0.05, 0.5 and 0.95) is very important for the concentrations in dissolved and particulate phases (Fig. 27a), for the concentration in A-sediments (Fig. 27b) and for the concentrations in fish (Fig. 27c; here calculated for 20 g planktivores; results from [20]). If the PF-value is low and the dissolved fraction high, sedimentation is low and the concentration in the dissolved phase and in small planktivores fish high; and vice versa if the PF-value is high.

Since resuspension, deep-water fluxes, diffusion, and burial are not very important in the default coastal area, the model predictions for the concentrations of radiocesium in water are not very sensitive to the value used for the ET-areas, the theoretical deep-water retention time (T_{DW}), the diffusion rate (R_{diff}), or the age of the A-sediments regulating burial (T_A).

An important point here is that using a process-based model, one can also identify coastal areas where the conclusions for the default coastal area in the Baltic Sea are not valid.

Remedial Measures Simulations: A Dredging Scenario Simulations for one of the few feasible remedial measures for radionuclide contamination of coastal areas, fertilization, have been presented by [19].

Nuclear Accidents, Chernobyl Fallout in Scandinavian Watersheds. Table 4 Default values for the obligatory coast-specific driving variables, some model variables and calculated values for some model constants. The default values have been selected to represent a "typical" Baltic coastal area

Obligatory coastal-area-specific driving variables
Coastal area (= Area) = $10 \cdot 10^6$ m^2
Latitude (= Lat) = 60°N
Max depth (= D_{max}) = 40 m
Mean depth (= D_m) = 10 m
Mean annual precipitation (= Prec) = 750 mm/year
Salinity (= Sal) = 7%
Section area (= At) = 10,000 m^2
Generic default values for some model variables
Age of ET-sediments = 1 month
Organic content of A-sediments (= IG) = 10% dw
Thickness of A-sediment layer = 10 cm
Water content of A-sediments (= W) = 75% ww
Bulk density of A-sediments = 1.26 g/cm^3
Potassium concentration = 1.75 mg/l
Calculated values for the default coastal area for some model constants
Duration of growing season (T_{dur}) = 189 days
ET = 0.73 (the ET-areas constitute 73% of the coastal area)
Exposure (Ex) = 0.1
Form factor (Vd) = 0.75
Mean depth of the SW compartment, D_{SW} = 7.07 m (from the water surface to the wave base)
Mean depth of the DW compartment, D_{DW} = 12.93 m (from the wave base to the maximum depth)
Particulate fraction (PF) = 0.79 (dim. less)
SPM (= concentration of suspended particulate matter) = 4 mg/l
Theoretical surface water retention time (T_{SW}) = 8.3 days
Theoretical deep-water retention time (T_{DW}) = 8.4 days
Wave base, WB = D_{TA} = 14.14 m

The concentration of nutrients in coastal areas can be influenced by emissions from different sources, e.g., from point-source emissions like fish farms and water purification plants. Since the theoretical surface water retention time of Baltic Sea coastal areas in the size range between 1 and 100 km^2 is often 2–10 days [63], it is evidently difficult to maintain high concentrations of nutrients from single additions, and, hence, difficult to use fertilization as an effective remedial measure for radionuclide concentrations in water and biota. Increasing the concentration of nitrogen or phosphorus also means probable changes in water clarity, gross sedimentation, and the amount of suspended particulate matter [81]. If realistic assumptions about possible changes in nutrient concentrations are made, the results given by [19] indicated that coastal water fertilization is not a relevant remedial measure. Firstly, because it would not be very efficient to reduce radionuclides in water, sediments and fish, secondly because it would not be acceptable for ecological reasons to fertilize coastal areas, since many European coastal areas (including the Baltic Sea) are already severely eutrophicated (see [70]), and thirdly because it would be very costly to try to maintain the higher nutrient concentrations.

In the following, results from a dredging scenario will be given, since this is one of the few feasible remaining options (see [1, 84] or Section Remedial Measures for Aquatic Pathways for compilations of remedial measures for aquatic systems).

Figure 28 gives results (see [20]) from a test in which 75% of the radionuclide in the active A-sediments was hypothetically removed month 7 (2 months after the simulated fallout), or months 9 or 12; and month 12 when also 75% of the radionuclides in the active A-sediments in the river were removed. Note that in practice, it is not realistic to remove as much as 75% of the inventory in A-sediments in large coastal areas, and it is not realistic to assume that this can be done shortly after the fallout. Thus, these simulations are meant to give indications as to whether dredging in coastal areas is advisable, and also to provide realistic expectations for such endeavors. The results are given for the concentration

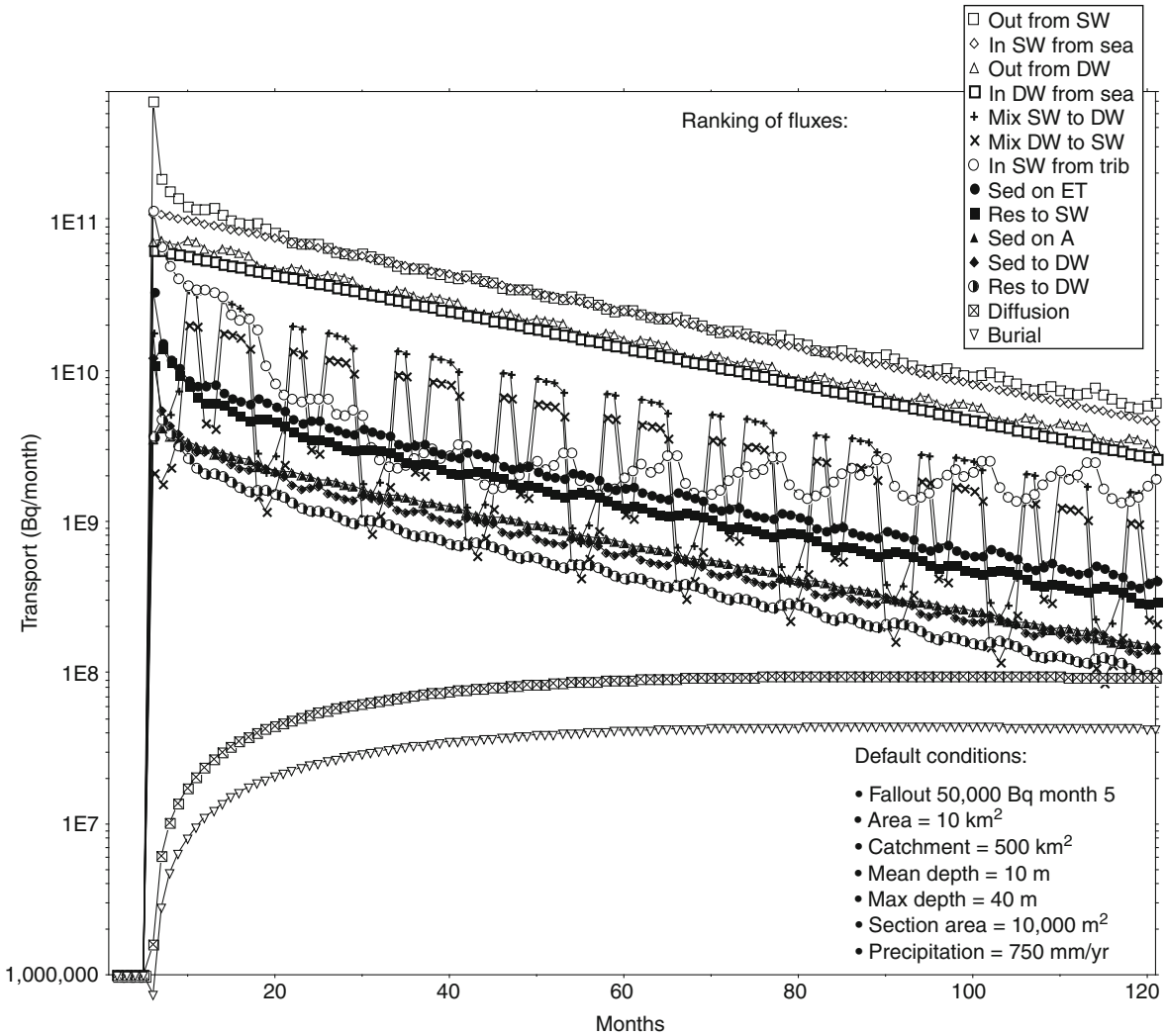

Nuclear Accidents, Chernobyl Fallout in Scandinavian Watersheds. Figure 24
A ranking of the fluxes to, from, and within the given Baltic Sea coastal area under default conditions (From [20])

in coastal water (Fig. 28a) and for the inventory of the radionuclide in A-sediments in (Fig. 28b). From these results, it should be noted that this would probably be a costly and inefficient remedy. Just like fertilization , it cannot be generally recommended in coastal areas. This means that actions like fish bans and domestic food treatment, e.g., salting of fish before consumption (see [1]), are likely to be more efficient than measures like fertilization and dredging (see Section Remedial Measures for Aquatic Pathways).

Discussion and Conclusions It is often stated that the quality of science is related to the possibilities for making meaningful predictions (see [21]). Models for hourly and daily predictions at different sites in coastal areas driven by climatological data on prevailing winds, precipitation, or temperatures may provide good descriptive power (if the necessary driving variables are at hand, which is not generally the case) but poor predictive power since it is difficult to predict winds and temperatures more than a few days ahead. The key

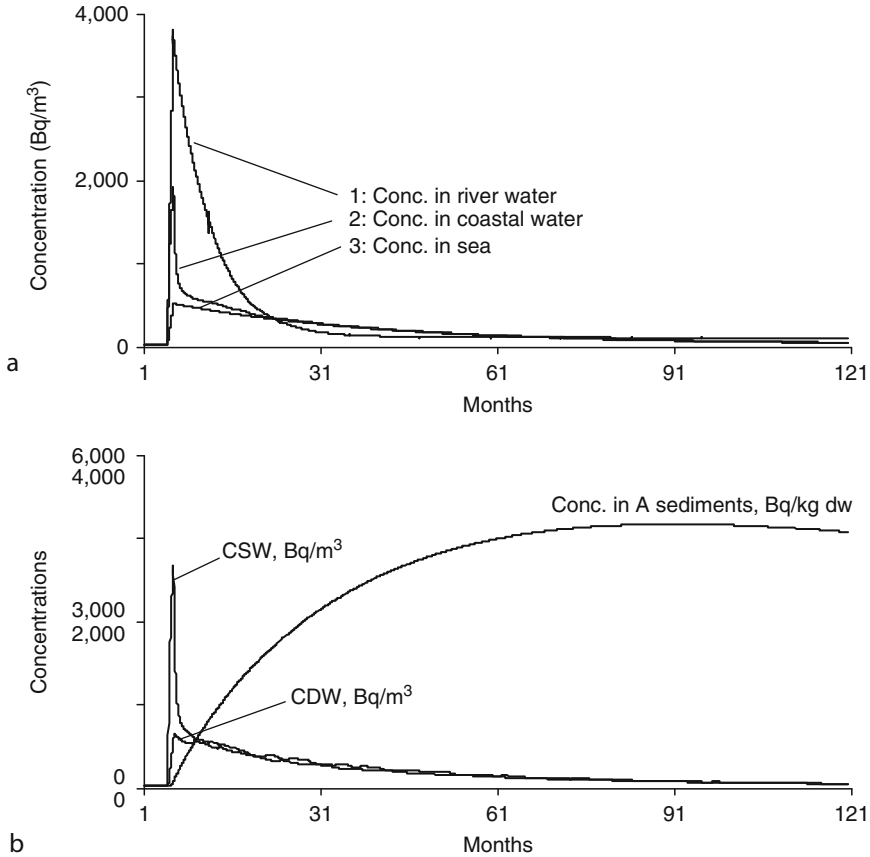

Nuclear Accidents, Chernobyl Fallout in Scandinavian Watersheds. Figure 25
(**a**) A comparison between modelled radiocesium concentrations (Bq/m^3) in river water, coastal water, and sea water (outside the given coastal area) under default conditions. (**b**) A comparison between modelled radiocesium concentrations (Bq/m^3) in surface water, deep water (scale 0–4,000), and accumulation area sediments (A-sediments; scale 0–6,000 on the y-axis) in the default coastal area in the Baltic Sea (From [20])

to obtain predictive power lies in the structuring and equations used for the models, and models based on monthly predictions using ordinary differential equations are likely to be more optimal in contexts where practical applicability and high predictive power are requested.

The coastal model discussed here is based on the same model structuring as the lake and river models, which have shown to yield very good predictive power see (Figs. 12 and 17).

The method to define the coastal area and set the borderlines using the "topographical bottleneck" approach (where the exposure attains minimum values) is very useful and a necessary prerequisite for the determination of three fundamental process variables for mass-balance models for coastal archipelagos and bays, [1] the theoretical surface water retention time (T_{SW}); [2] the theoretical deep-water retention time (T_{DW}); and [3] the bottom dynamic conditions (i.e., to define where resuspension from erosion- and transportation areas, ET, are likely to appear). This means that T_{SW}, T_{DW}, and ET can be estimated easily for such areas from standard bathymetric charts using GIS-methods. To estimate these variables using

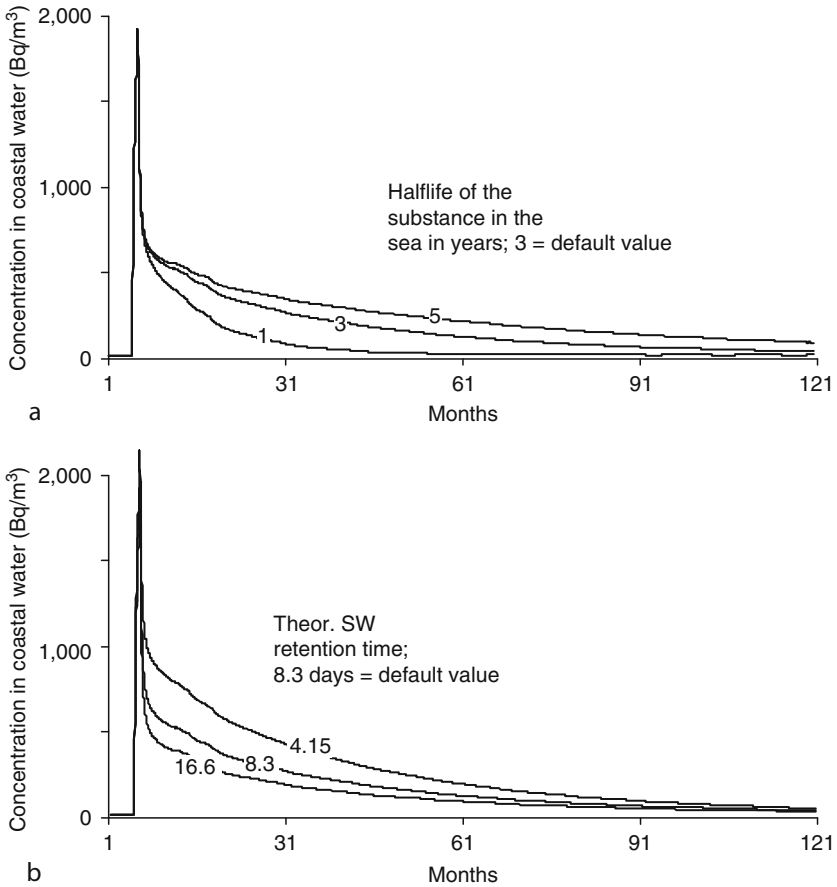

Nuclear Accidents, Chernobyl Fallout in Scandinavian Watersheds. Figure 26
(**a**) Sensitivity analyses illustrating the role of different values for the ecological half-lives (1, 3, and 5 years) of the radionuclide in sea water outside the given coastal area for the concentration in coastal water. (**b**) Sensitivity analyses illustrating the role of different values for the theoretical surface water retention time (4.15, 8.3, and 16.6 days) for the concentration in the default coastal area in the Baltic Sea (From [20])

traditional methods (such as dye tracers, continuous monitoring, and/or field measurements) is very time consuming and expensive (see [19]).

The presented results have indicated that the predictions of radionuclide concentrations in water and fish largely depend on two factors, (a) the concentration in the sea outside the given coastal area and/or adjacent coastal areas and (b) the ecological half-life of the radionuclide in the sea. Uncertainties in these factors may dominate all other uncertainties, e.g., regarding the surface water retention time, the settling velocity of the particulate fraction of the radionuclide, and the distribution coefficient regulating the fluxes in dissolved and particulate phases. This means that the conditions in the sea are of paramount importance for the conditions in the coastal area, even for relatively enclosed coastal areas.

Therefore, for any given coastal area one can produce a simplified version of the coastal model in which the relatively unimportant processes, factors, and sub-models are omitted and/or simplified. The river sub-model and the fish sub-model can be added to the coastal model for all large and open estuaries, and criteria for this have been discussed by [19]. The model can be used for this purpose for any coastal area. If the river sub-model and the

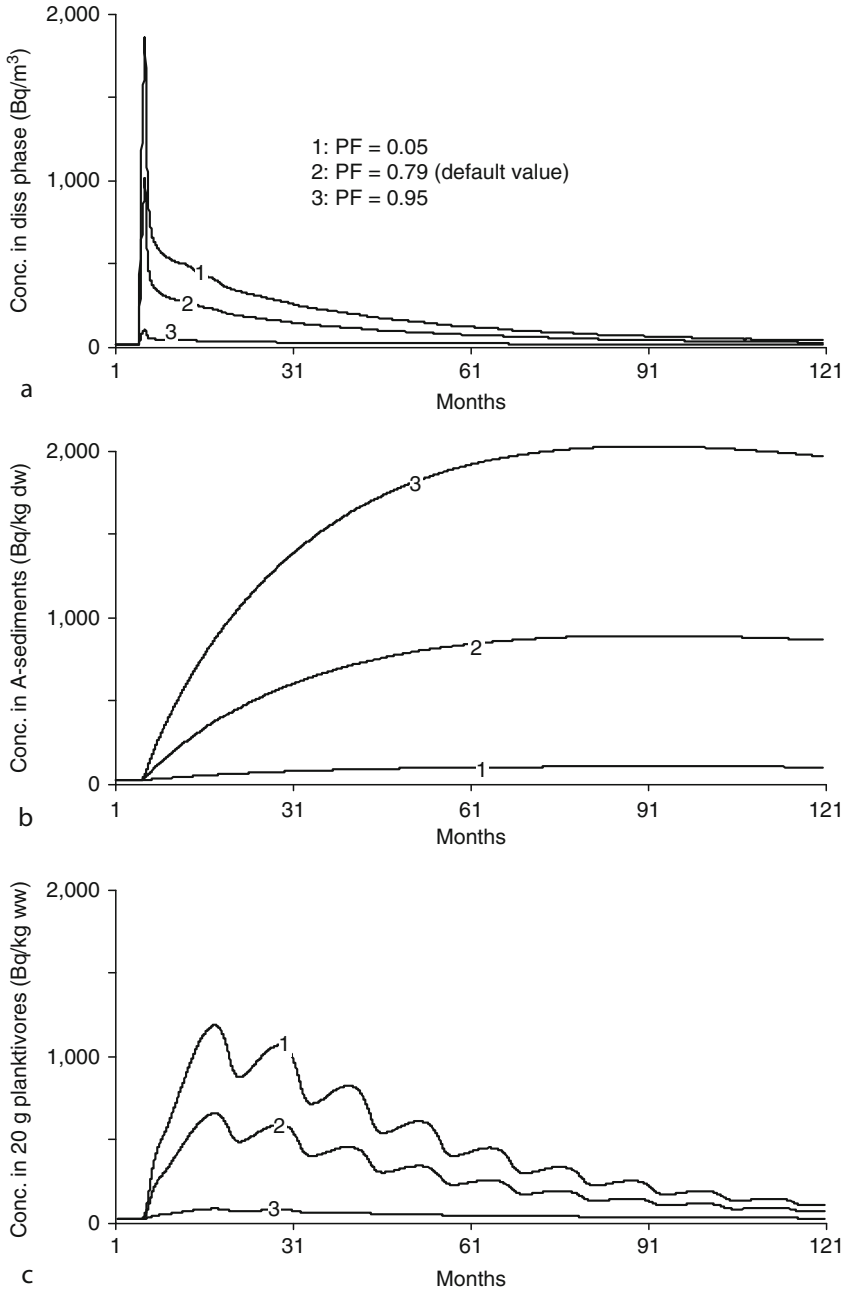

Nuclear Accidents, Chernobyl Fallout in Scandinavian Watersheds. Figure 27
Calculated concentrations in (**a**) dissolved phase in the coastal water, (**b**) in A-sediments, and (**c**) in 20 g planktivorous fish when the particulate fraction (PF) is set to 0.05 (curve 1), 0.79 (curve 2), and 0.95 (curve 3) in the default coastal area in the Baltic Sea (From [20])

fish sub-model are added to the basic coastal mass-balance model, this implies that the catchment area parameters should also be added to the panel of driving variables.

This coastal model may be regarded as a scientific tool for posing and testing working hypotheses on the relative roles of different processes in different coastal areas. Such information may be essential for getting

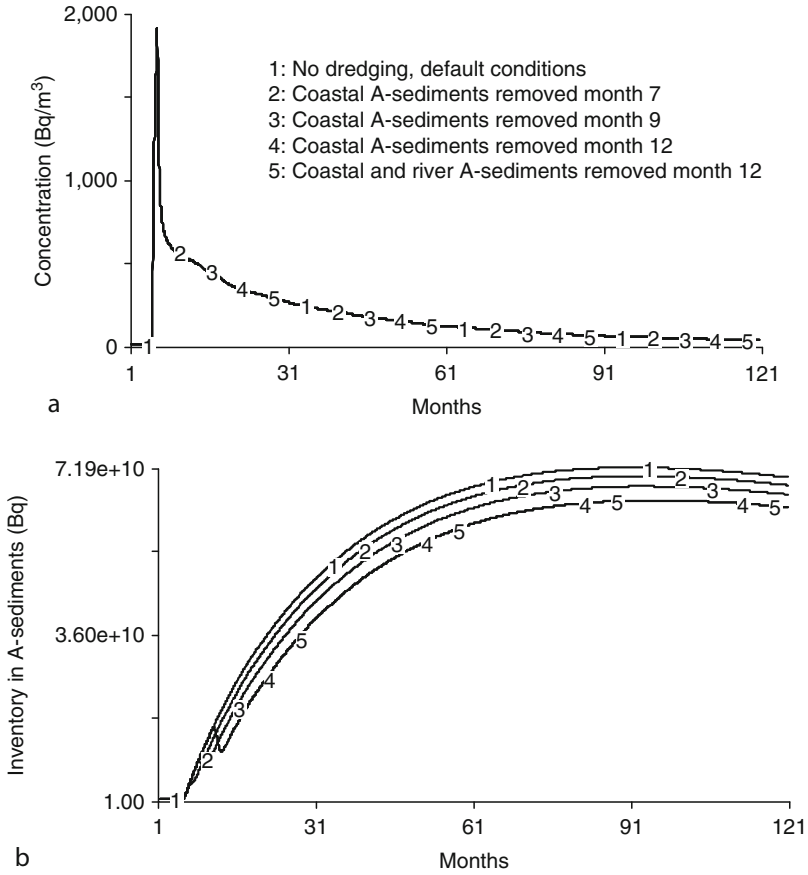

Nuclear Accidents, Chernobyl Fallout in Scandinavian Watersheds. Figure 28
Results of simulated dredging operations when 75% of the radionuclides in the coastal A-sediments have been removed (months 7, 9, and 12; curves 2, 3, 4, and 5) and 75% of the river A-sediments (month 12; curve 5) calculated results for (**a**) the concentration in coastal water and (**b**) for the inventory in coastal A-sediments in the default coastal area in the Baltic Sea (From [20])

realistic expectations of various remedial measures, such as coastal dredging discussed above.

Remedial Measures for Aquatic Pathways

Introduction and Aim

There are a number of possible intervention measures to reduce radioactive doses to the public via the water pathways. Countermeasures may be grouped into two categories: those aimed at reducing radionuclides in drinking water and those reducing doses to man from consumption of aquatic foodstuffs, principally fish. It has been shown [30, 85] that doses to man from terrestrial foodstuffs are generally more significant than doses from drinking water and aquatic foodstuffs. Measures to reduce doses via drinking water may, however, be required in the short term (weeks) after a fallout when radionuclide concentrations in surface waters are relatively high. Measures to reduce doses via fish may be required over longer periods as a result of bioaccumulation of radioactivity through the aquatic food chain. In addition, it was found [85] that after the Chernobyl accident the public perceived that the contamination of water supplies was a much greater problem than it actually was. Thus, measures to protect water supplies were also used as a method of restoring

public confidence. It should be noted that surface waters are important transporters of radioactivity from contaminated zones to populations in less contaminated areas. The use of water supplies for drinking and irrigation generally results in small individual doses, but may lead to significant collective doses.

The purpose of this section is to discuss options available to decision makers in the event of radioactive contamination of surface waters and the results discussed here are mainly derived from a paper by [84]. The framework is the requirement for countermeasures in the context of a large-scale atmospheric release of radionuclides. The following intervention measures will be discussed:

- Drinking water distribution and treatment
- Direct and secondary contamination of surface waters
- Uptake by fish and aquatic foodstuffs from contaminated water
- Preparation of fish prior to consumption

Measures Related to Drinking Water Consumption

Temporary bans on drinking water consumption and provision of alternative supplies may be required immediately after a fallout. Since radionuclide concentrations in rivers tend to decline rapidly (half-life of decline of Cs-137 and Sr-90 in rivers during this early period is typically 2 weeks and of I-131 about 5–6 days), such bans are not likely to be in place for more than a few weeks after fallout.

Switching to less contaminated water supplies may be an accepted and effective countermeasure to radioactive contamination of drinking water. If the water supply system is sufficiently integrated, supplies may rapidly be switched to groundwater sources, or less contaminated surface water sources. The effectiveness of this approach depends on a quick assessment of the extent of the contamination of different water supplies.

Supplementary purification of drinking water in water treatment plants is another option. The mechanism for removal is generally by attachment to and settling of solid particles during flocculation, as well as removal during filtration. It has been found that activiated charcoal was effective in removing I-131 and Ru-106 and zeolite in removing and radiostrontium [86]. These substances were found to be effective for the first 3 months, after which they became saturated and their efficiency declined [86].

Regulation of flow of contaminated water through reservoirs is another viable action. After Chernobyl, surface gates on the Kiev Reservoir dam were opened to let clean water out of the reservoir so that surface runoff water from the contaminated areas could be captured by the reservoir. Because the relative importance of atmospheric fallout and secondary contamination processes to reservoir and lake contamination was not known, the countermeasure had the opposite effect to that intended. In fact, because of atmospheric fallout to the reservoir surface, deep waters in the reservoir were much less contaminated than surface ones.

Measures to Reduce Contamination of Surface Waters

Various measures could be used to reduce runoff of radionuclides attached to eroded soil particles (see, e.g., [87–89]). Typically, suspended solid concentrations in river and lake waters are lower than 50 mg/l and less than 50% of radiocesium and less than 10% of radiostrontium and radioiodine are expected to be in the particulate phase, limiting the potential effectiveness of this method. It should also be noted that the dissolved, rather than particulate, forms of these radionuclides are important in determining concentrations in drinking water and freshwater biota.

Dredging of canal-bed traps to intercept suspended particles in contaminated rivers was carried out after Chernobyl. These traps were found to be inefficient for two reasons: [1] flow rates were too high to trap small suspended particles carrying much of the radioactivity; [2] a significant proportion of the activity (and most of the "available" activity) was in dissolved forms and thus would not have been intercepted by the sediment traps.

Buffer strips adjacent to rivers can be used to trap eroded particles and increase sorption of radionuclides to soil. Buffer strips have been used to reduce runoff of fertilizers and pesticides from agricultural land, but are untested for radionuclides. Removal of radioactivity from water by "filtering" through reed beds is also possible, though probably not feasible on a large scale. Zeolite-containing dykes were constructed on smaller

rivers and streams around Chernobyl in order to intercept dissolved radionuclides. These were found to be ineffective [85]. In addition, the rivers and streams on which they were placed were later found to contribute only a few percent to the total activity load in the Pripyat–Dnieper system.

Measures to Reduce Uptake by Fish and Aquatic Foodstuffs

Bans on consumption of freshwater fish have been applied in the restricted zones of Chernobyl [90]. In some areas, selective bans on the more contaminated predatory fish have been applied. It seems that bans are often ignored by fishermen. Bans on the sale of freshwater fish have been applied in some areas of Norway [91]. Use of farmed fish has been suggested by [92] as an alternative source of freshwater fish in areas affected by fishing bans. Farmed fish, fed with uncontaminated food, do not significantly accumulate radionuclides [92, 93].

Lake liming was tested in 18 Swedish lakes [11]. Different types of lime were used: primary rock lime (PR) was used in ten lakes, sedimentary rock lime in six lakes, and so-called mixed lime (a lime also containing various trace elements and nutrients) in two lakes. The lime was spread over the lakes by different methods, such as helicopters, pontoon boats, and dosers, in the mouth of the tributaries. The amounts of lime supplied were as one or several applications, either on ice or directly into the water. As a result of the liming, the mean pH of the lakes increased and also other parameters that are directly linked to the addition of lime, e.g., hardness and alkalinity. A certain decrease in the color of the lakes was also noted. The results of the experiments showed that liming had no significant effect on uptake of Cs-137 in fish in comparison with control lakes. Although uptake of Sr-90 was not studied in these experiments, it is expected that increased Ca concentration in lakes may reduce S-concentration in fish.

Wetland liming was carried out in the catchment areas of 17 lakes, of which eight were limed with primary rock lime, seven with sedimentary lime, and two with "mixed lime." The amount of lime added followed the recommendations by the Swedish Environmental Protection Agency, which implies 0.3 t/ha totally over the catchment area, 15 t/ha on wetlands where the wetlands make up 2% of the area, and 3 t/ha on wetlands where the wetlands make up 10% of the area (see [19]). The supply was done using helicopters and a single application. In theory, wetland liming has several advantages in comparison with lake liming:

- A considerably prolonged durability.
- A possible "liming shock" in the lake is minimized.
- Improved conditions for animals and plants in streams and rivers; reduced transport of several metals (e.g., Fe and Al) into the lake from the catchment area.

Full-scale drainage area liming was done in two areas using dolomite. Since the dolomite is less soluble than ordinary limestone, the durability should be further prolonged.

Although the mean pH in the limed lakes increased from 6.0 to 6.7, and also other variables, which are directly linked to the liming remedies (e.g., water hardness and alkalinity) showed increased long-term mean values, no effect of the approach was observed in Cs-concentrations in fish.

Addition of potassium to lakes: It is known that the concentration factor of radiocesium in fish is inversely related to the potassium content of the surrounding water (see [94, 95]). After Chernobyl, potassium was added to 13 lakes in Sweden either as potash or as an additive in the mixed lime [11]. In most of the treated lakes, mean potassium concentrations were increased from less than 0.4 mg/l to about 0.8 mg/l. The results of the potash treatment were somewhat inconclusive, with a small reduction in concentrations in perch fry being observed during the 2-year experiment. It was found that in lakes with short water retention times, it was difficult to maintain high levels of potassium in the lake. It is likely that potassium treatment is only feasible in lakes with very long water residence times, allowing increased potassium concentrations to be maintained. In an experiment on Lake Svyatoe in Belarus, Smith et al. (1999) added potassium chloride fertilizer onto the frozen lake surface. This resulted in an increase of the lake-water potassium concentration from 1 to 10 mg/l. Because of the long water residence time of this lake (it has no outflow), potassium concentration was still 8 mg/l 1 year after application. Initial results showed a 50% reduction in Cs-137 concentration in fish during the first year after the experiment [92, 96].

Manipulation of the aquatic food web – intensive fishing and fertilization: Intensive fishing was carried out in four lakes in Sweden [11] and as a complementary measure in three other lakes. This resulted in a reduction of the fish population by about 5–10 kg per hectare. The species reduced were mainly pike, perch, and roach. No effect of intensive fishing on Cs-137 concentrations in fish was observed. Fertilization was carried out in two Swedish lakes using "Osmocoat" (5% P and 15% N). The concentrations of total-P generally showed no significant changes in the long-term mean value: It appears that the fertilization remedy was not conducted sufficiently effectively. No effect was observed on Cs-137 activity concentrations in fish.

Preparation of Fish Prior to Consumption

Different methods of food preparation may affect the quantity of radionuclides in consumed food. Ryabov [90] suggested bans on consumption of smoked and dried fish since these processes increase concentrations of radionuclides (per unit of weight consumed). Other preparation processes may reduce radioactivity in fish.

Although radiocesium is relatively evenly distributed throughout the fish, radiostrontium is strongly concentrated in the bony parts of fish. An effective measure to reduce consumption of radiostrontium is to remove the bony parts of fish prior to cooking.

It has been known for a long time that salting may eliminate Cs-137 from meat. After 2–4 days immersion in concentrated salt solution, the Cs-concentration in a 500 g piece of meat may be reduced by 60–70% [97]. There are, however, at least three severe drawbacks with the salting method:

1. The amount of vitamins (e.g., B6, B12) would decrease significantly with the time of exposure; after 2–4 days most of these vitamins would be lost.
2. The levels of Na (and K) would increase and this would influence the taste of the meat; a large intake of Na and K may also give rise to negative health effects in humans.
3. The color and texture of the meat would change, and most people would probably agree that the grayer and harder meat obtained after 2–4 days in a salt solution would be less appetizing than normal, fresh meat.

Tests were carried out [97] to try to speed up the salting procedure from 2 to 4 days to 2–4 h. Different types of salts were tested, as well as different types of meat, and different forms and sizes of meat. Two different approaches to speed up the salting procedure were also tested: rotating the meat in the salt solution (called centrifugation) or to rotate the salt solution around the meat (called rotation). Both rotation and centrifugation in salted water may reduce Cs-137 in meat (moose, deer, and fish) by 60–70% in 2–3 h. The first round (of centrifugation or rotation) was most efficient in reducing Cs-137: about 30–50% of the Cs-137 may be reduced in the first round (depending on the salt concentration and the type of meat), with about 10–15% reduction in subsequent rounds. There is no significant change in vitamin B6 if the treatment lasts for 2–3 h. There is also no significant change in the texture of the meat, except an increase in the Na concentration. The best results in terms of Cs-137 reduction were obtained for meat that had been frozen: frozen meat showed a 20–40% decrease in Cs-137 compared to unfrozen conditions.

The rotation and centrifugation procedure takes 2–3 h and it requires access to a household machine that could either centrifugate the meat (about 1,000 rotation/min.) or rotate the salt solution. Salting, speeded up by rotation, may be a practical method in areas with heavily contaminated meat, especially for larger kitchens (schools, military, restaurants, etc.). It may also be used in homes, because there may be people who, from primarily a psychological point of view, would like to feel that they are able to do something themselves to reduce their intake of radioactive cesium.

Conclusions

The key to successful implementation of countermeasures is the provision of accurate information to the public. Measures can be counterproductive in increasing the stress people feel in a situation of radioactive contamination. If not accompanied by adequate information, the application of countermeasures may make people overestimate the danger of their exposure to radiation. People may feel that if countermeasures are necessary, the potential exposure must be "dangerous," even when actual radiation doses present only a small

risk. Conversely, countermeasures may also be implemented to increase people's fears of radioactivity. Thus, after Chernobyl, measures were implemented to reduce radioactivity in the Kiev Reservoir even though doses via this pathway to the people of Kiev were relatively low.

This section has discussed a number of measures to reduce doses of radionuclides via the freshwater pathway. These range from simple and well-tested measures (e.g., bans on drinking water consumption) to more complex measures such as lake liming or potassium addition. The most effective and viable measures to reduce radioactivity in drinking water are those that operate at the water treatment and distribution stage. Intervention measures to reduce concentrations of radioactivity in rivers and reservoirs are expected to be less efficient at reducing doses via the drinking water pathway for two primary reasons:

- It is generally only possible to apply intervention measures to reduce concentrations of radioactivity in rivers and reservoirs in the medium term (months) after an accident since they require significant engineering works. Radioactivity concentrations in drinking water tend largely to be a short-term problem – the concentrations in river water decline rapidly during the first days to few weeks after a fallout. Thus, intervention needs to be implemented rapidly and therefore based on accurate monitoring data and modelling.
- Intervention to reduce radioactivity concentrations in rivers and reservoirs necessarily requires manipulation of much larger volumes of water than intervention at the water treatment and supply stage.

Direct measures to reduce uptake of radioactivity by fish, and food preparation measures, are most likely to be effective at reducing doses via consumption of fish. Deboning fish contaminated by radiostrontium is probably the most effective food preparation measure, but salting and freezing can also reduce radiocesium concentrations. Bans on consumption of fish can be effective, but there are few viable measures to reduce radioactivity in fish prior to the preparation stage. Lake liming and biomanipulation were ineffective for radiocesium, though addition of potassium to lake waters appears promising in lakes with long water retention times. Lake liming may be effective in reducing radiostrontium in fish, though this has not, to our knowledge, been tested.

Future Directions

It is essential in radioecology to predict the outcome of remedial measures designed to lower doses of radionuclides to man and ecosystems and evidently also to predict the consequences of future possible accidents, The predictive power of quantitative models in radioecology need to be high and to achieve that goal, it is important to initiate and run international comparative projects. That means that there is a need to continue with projects such as the famous VAMP project and the BIOMOVS project based on large amounts of reliable empirical data and strict model comparisons.

Bibliography

Primary Literature

1. IAEA (2000) Modelling of the transfer of radiocesium from deposition to lake ecosystems. Report of the VAMP Aquatic Working Group. International Atomic Energy Agency, Vienna, IAEA-TECDOC-1143, p 343
2. Sansone U, Voitsekhovitch OV (1996) Modelling and study of the mechanisms of the transfer of radionuclides from the terrestrial ecosystem to and in water bodies around Chernobyl. EUR 16529 EN. European Commission, Luxembourg
3. Strand P, Howard B, Averin V (eds) (1996) Transfer of radionuclides to animals, their comparative importance under different agricultural ecosystems, and appropriate countermeasures. EUR 16539 EN. European Commission, Luxembourg
4. Moberg L (ed) (1991) The Chernobyl fallout in Sweden. The Swedish Radiation Protection Institute, Stockholm, p 633
5. Onishi Y, Voitsekhovich O, Zheleznyak MJ (2007) Chernobyl – what have we learned? Springer, Heidelberg, p 289
6. Monte L, Brittain JE, Håkanson L, Gallego E (1999) MOIRA models and methodologies for assessing the effectiveness of countermeasures in complex aquatic systems contaminated by radionuclides. ENEA,RT/AMP, Rome, p 150
7. Monte L, Brittain JE, Håkanson L, Heling R, Smith JT, Zheleznyak M (2003) Review and assessment of models used to predict the fate of radionuclides in lakes. J Environ Radioact 69:177–205
8. Monte L, Brittain JE, Håkanson L, Smith JT, van der Perk M (2003) Review and assessment of models for predicting the migration of radionuclides from catchments. J Environ Radioact 75:83–103
9. Monte L, Boyer P, Brittain JE, Håkanson L, Lepicard S, Smith JT (2005) Review and assessment of models for predicting the

migration of radionuclides through rivers. J Environ Radioact 79:273–296
10. Andersson T, Håkanson L, Kvarnäs H, Nilsson Å (1991) Remedial measures against high levels of radioactive cesium in Swedish lake fish (in Swedish). SSI Report 91-07, p 114
11. Håkanson L, Andersson T (1992) Remedial measures against radioactive cesium in Swedish lake fish after Chernobyl. Aquatic Sci 54:141–164
12. Abrahamsson O, Håkanson L (1997) Presentation and analysis of a model simulating the response of a potash treatment of a lake. J Environ Radioact 37:287–306
13. Andersson E (1989) Incorporation of Cs-137 into fishes and other organisms. In: Feldt W (ed) The radioecology of natural and artificial radionuclides. Verlag TUV, Köln, pp 312–317
14. Dahlgaard H (ed) (1994) Nordic radioecology, the transfer of radionuclides through nordic ecosystems to man. Elsevier Science, Amsterdam, p 483
15. Monte L, Håkanson L, Brittain J (1997) Prototype models for the MOIRA computerised system. ENEA, ISSN/1120-5555, Roma, p 90
16. Monte L (1996) Collective models in environmental science. Sci Total Environ 192:41–47
17. Håkanson L, Peters RH (1995) Predictive limnology. Methods for predictive modelling. SPB Academic Publishing, Amsterdam, p 464
18. Monte L (1995) A simple formula to predict approximate initial contamination of lake water following a pulse deposition of radionuclide. Health Phys 68(3):397–400
19. Håkanson L (2000) Modelling radiocesium in lakes and coastal areas - new approaches for ecosystem modellers. A textbook with Internet support. Kluwer, Dordrecht, p 215
20. Håkanson L (2005) A new general dynamic model predicting radionuclide concentrations and fluxes in coastal areas from readily accessible driving variables. J Environ Radioact 78: 217–245
21. Peters RH (1991) A critique for ecology. Cambridge University Press, Cambridge, p 366
22. Knoechel R, Campbell CE (1988) Physical, chemical, watershed and plankton characteristics of lakes on the Avalon Peninsula, Newfoundland, Canada: a multivariate analysis of interrelationships. Verh Internat Verein Limnol 23:282–296
23. Rochelle B, Liff C, Campbell W, Cassell D, Church R, Nusz R (1989) Regional relationships between geomorphic/hydrologic parameters and surface water chemistry relative to acidic deposition. J Hydrol 112:103–120
24. Santschi PH, Honeyman BD (1991) Radioisotopes as tracers for the interactions between trace elements, colloids and particles in natural waters. In: Vernet JP (ed) Heavy metals in the environment. Elsevier, Amsterdam
25. Riise G, Björnstad HE, Oughton DH, Salbu B (1990) A study on radionuclide associations with soil components using sequential extraction procedure. J Radioanal Nucl Chem 142:531–538
26. Erel Y, Stolper EM (1993) Modeling of rare-earth element partitioning between particles and solution in aquatic environments. Geochim Cosmochim Acta 57:513–518
27. Gustafsson Ö, Gschwend PM (1997) Aquatic colloids: Concepts, definitions and current challenges. Limnol Oceanogr 42:519–528
28. Comans RNJ (ed) (1998) Modelling fluxes and bioavailability of radiocesium and radiostrontium in freshwaters. Progress report from the ECOPRAQ project. Netherlands Energy Research Foundation
29. Comans RNJ, Hockley DE (1992) Kinetics of cesium sorption on illite. Geochim Cosmochim Acta 56:1157–1164
30. Stone D, Smith JT, Jackson D, Ibbotson AT (1997) Scoping study on the relative importance of freshwater dose pathways following a major nuclear accident. Report to IMC/Magnox Electric 1997
31. Håkanson L (1991) Ecometric and dynamic modelling – exemplified by cesium in lakes after Chernobyl. Springer, Berlin, p 158
32. Lindström M (2000)Predictive modelling of heavy metals in urban lakes. Doctoral thesis, Uppsala University, Sweden
33. Håkanson L, Sazykina TG, Kryshev II (2002) A general approach to transform a lake model for one radionuclide (radiocesium) to another (radiostrontium) and critical model tests using data for four Ural lakes contaminated by the fallout from the Kyshtym accident in 1957. J Environ Radioact 60:319–350
34. Förstner U, Wittmann GTW (1981) Metal pollution in the aquatic environment. Springer, Berlin, p 486
35. Salomons W, Förstner U (1984) Metals in the hydrocycle. Springer, Heidelberg, p 349
36. Kirkby HJ (ed) (1978) Hillslope hydrology. Wiley, Chichester, p 389
37. Hillel D (1982) Introduction to soil physics. Academic, New York, p 364
38. Harper DM, Stewart WDP (1987) The effects of land use upon water chemistry, particulary nutrient enrichment, in shallow lowland lakes: comparative studies in three lochs in Scotland. Hydrobiologia 148:211–229
39. Schofield NJ, Ruprecht JK (1989) Regional analysis of stream salinisation in southwest Western Australia. J Hydrol 112: 19–39
40. Alberts JJ, Tilly LJ, Vigerstad TJ (1979) Seasonal cycling of cesium-137 in a reservoir. Science 203:649–651
41. Håkanson L (2004) A new generic sub-model for radionuclide fixation in large catchments from continuous and single pulse fallouts, as used in a river model. J Environ Radioact 77: 247–273
42. Black VS (1957) Excretion and osmoregulation. In: Brown ME (ed) The physiology of fishes, vol 1. Academic, New York, pp 163–205
43. Fleishman DG (1963) Accumulation of artificial radionuclides in freshwater fish. In: Klechkovskii VM, Polikarpov GG, Aleksakhin RM (eds) Radioecology. Wiley, New York, pp 347–370
44. Carlsson S (1978) A model for the turnover of Cs-137 and potassium in pike (Esox Lucius). Health Phys 35:549–554
45. Madruga MJ, Cremers A (1997) On the differential binding mechanisms of radiostrontium and radiocesium in sediments.

In: Desmet G et al (eds) Freshwater and estuarine radioecology. Elsevier, Amsterdam, pp 207–216
46. Konitzer K, Meili M (1997) Redistribution of sedimentary Cs-137 in small Swedish lakes after the Chernobyl fallout 1986. In: Desmet G et al (eds) Freshwater and estuarine radioecology. Elsevier, Amsterdam, pp 167–172
47. Konoplev A, Bulgakov A, Hilton J, Comans R, Popov V (1997) Long-term kinetics of radiocesium fixation by soils. In: Desmet G et al (eds) Freshwater and estuarine radioecology. Elsevier, Amsterdam, pp 173–182
48. Håkanson L, Jansson M (1983) Principles of lake sedimentology. Springer, Berlin, p 316
49. Håkanson L, Boulion VV (2002) Empirical and dynamical models to predict the cover, biomass and production of macrophytes in lakes. Ecol Model 151:213–243
50. Kranck K (1973) Flocculation of suspended sediment in the sea. Nature 246:348–350
51. Kranck K (1979) Particle matter grain-size characteristics and flocculation in a partially mixed estuary. Sedimentology 28:107–114
52. Lick W, Lick J, Ziegler CK (1992) Flocculation and its effect on the vertical transport of fine-grained sediments. Hydrobiologia 235(236):1–16
53. Sly PG (1978) Sedimentary Processes in Lakes. In: Lerman A (ed) Lakes: chemistry, geology, physics. Springer, Berlin, pp 65–89
54. Thomas RL (1972) The distribution of mercury in the sediments of Lake Ontario. Can J Earth Sci 9:636–651
55. Thomas RL, Kemp ALW, Lewis CFM (1972) Distribution, composition and characteristics of the surficial sediments of Lake Ontaio. J Sediment Petrol 42:66–84
56. Håkanson L (1977) The influence of wind, fetch, and water depth on the distribution of sediments in Lake Vänern, Sweden. Can J Earth Sci 14:397–412
57. Bloesch J, Burns NM (1980) A critical review of sedimentation trap technique. Schweiz Z Hydrol 42:15–55
58. Bloesch J, Uehlinger U (1986) Horizontal sedimentation differences in a eutrophic Swiss lake. Limnol Oceanogr 31: 1094–1109
59. Einstein HA (1950) The bed-load function for sediment transportation in open-channel flowes, Soil Conservation Service. Technical Bulletin, no. 1026. US Department of Agriculture, Washington, DC
60. Allen JRL (1970) Physical processes of sedimentation. Allen & Unwin, London, p 248
61. Wetzel RG (1983) Limnology. Saunders College Publishing, Philadelphia, p 767
62. Walker CH, Hopkin SP, Sibly RM, Peakall DB (2001) Principles of ecotoxicology, 2nd edn. Taylor & Francis, London, p 309
63. Håkanson L (1999) Water pollution – methods and criteria to rank, model and remedi-ate chemical threats to aquatic ecosystems. Backhuys Publishers, Leiden, p 277
64. Rosenberg R (ed) (1984) Biological evaluation of shallow Swedish coastal areas (in Swedish, Biologisk värdering av grunda svenska havsområden). Swedish EPA, report 1911, p 384
65. Mann KM (1992) Ecology of coastal waters – a systems approach. Blackwell Scientific Publications, Oxford, p 322
66. Lundin LC (1999) Water in society. Sustainable water management in the Baltic Sea basin, The Baltic University Programme, Uppsala University, Sweden, p 244
67. Lundin LC (2000) The waterscape. Sustainable water management in the Baltic Sea basin, The Baltic University Programme, Uppsala University, Sweden, p 207
68. Lundin LC (2000) River basin management. Sustainable water management in the Baltic Sea basin, The Baltic University Programme, Uppsala University, Sweden, p 244
69. Meeuwig JJ, Kauppila P, Pitkänen H (2000) Predicting coastal eutrophication in the Baltic: a limnological approach. Can J Fish Aquat Sci 57:844–855
70. Aertbjerg G (ed) (2001) Eutrophication in Europe's coastal waters. European Environment Agency, Topic report 7/2002, Copenhagen, p 86
71. BIOMOVS (1991) Dynamics within lake ecosystems. Scenario A5. Sundblad B (ed) Technical report 12, September 1991, Swedish Radiation Protection Institute
72. Davis P (1999) BIOMOVS II. Special Issue. J Environ Radioact 42:1–304
73. Davis PA, Avadhanula MR, Cancio D, Carboneras P, Coughtrey P, Johansson G, Little RH, Smith GM, Watkins BM (1999) BIOMOVS II: An international test of the performance of environmental transfer models. J Environ Radioact 42: 117–130
74. Smith JT, Konoplev AV, Bulgakov AA, Comans RNJ, Cross MA, Kaminski S, Khristuk B, Klemt E, de Konig A, Kudelsky AV, Laptev G, Madruga MJ, Voitsekhovitch OV, Zibild G (2002) AQUASCOPE Technical Deliverable. Simplified models for predicting ^{89}Sr, ^{90}Sr, ^{134}Cs, ^{137}Cs, ^{131}I in water and fish of rivers, lakes and reservoirs. CEH Centre for Ecology and Hydrology, Natural Environmental Research Council
75. Zheleznyak M, Shepeleva V, Sizonenko V, Mezhueva I (1997) Simulation of countermeasures to diminish radionuclide fluxes from the Chernobyl zone via aquatic pathways. Radiat Prot Dosim 73:181–186
76. Monte L (1997) A collective model for predicting the long-term behaviour of radionuclides in rivers. Sci Total Environ 201:17–29
77. Monte L (1998) Predicting the long term behaviour of ^{90}Sr in lacustrine systems by a collective model. Ecol Modell 106:141–159
78. Smith JT, Wright SM, Cross MA, Monte L, Kudelsky A, Saxen R, Vakulovsky SM, Timms DN (2004) Global analysis of the riverine transport of ^{90}Sr and 1^{37}Cs. Environ Sci Technol 38:850–857
79. Monte L, Van der Steen J, Bergström U, Gallego Diaz E, Håkanson L, Brittain J (2000) The project MOIRA A model-based computerised system for management support to identify optimal remedial straegies for restoring radionuclide contaminated aquatic ecosystens and drainage areas. Final report. ENEA. ISSN/1120-5555, Rome, p 89

80. Appleby PG, Oldfieldd F (1979) Letter on the history of lead pollution in Lake Michigan. Environ Sci Technol 13:263–273
81. Håkanson L (2006) Suspended particulate matter in lakes, rivers and marine systems. The Blackburn Press, New Jersey, p 319
82. Pilesjö P, Persson J, Håkanson L (1991) Digital bathymetric information for calculations of coast morphometrical parameters and surface water retention time (in Swedish with English summary). Swedish Environmental Protection Agency, Report 3916, Stockholm, p 76
83. Håkanson L, Eklund JM (2007) A dynamic mass-balance model for phosphorus fluxes and concentrations in coastal areas. Ecol Res 22:296–320
84. Smith JT, Voitsekhovitch OV, Håkanson L, Hilton J (2001) A critical review of measures to reduce radioactive doses from drinking water and consumption of freshwater foodstuffs. J Environ Radioact 56:11–32
85. Voitsekhovitch OV, Nasvit O, Los'y Y, Berkovski V (1997) Present thoughts on aquatic countermeasures applied to regions of the Dnieper river catchment contaminated by the 1986 Chernobyl accident. In: Desmet G, Blust R, Comans RNJ, Fernandez J, Hilton J, de Bettencourt A (eds) Freshwater and estuarine radioecology. Elsevier, Amsterdam, pp 75–86
86. Tsarik N (1993) 1993, Supplying water and treating sewage in Kiev after the Chernobyl accident. J Am Water Works Assn 85(1):42–45
87. Schwab GO, Frevert RK, Edminster TW, Barnes KK (1966) Soil and water conservation engineering. Wiley, New York
88. Morgan RPC (1986) Soil erosion and conservation. Longman, Harlow
89. Hudson NW (1981) Soil conservation. Batsford, London
90. Ryabov IN (1992) Analysis of countermeasures to prevent intake of radionuclides via consumption of fish from the region affected by the Chernobyl accident. In: Proceedings of international seminar on intervention levels and countermeasures for nuclear accidents, EUR 14469, CEC, Luxembourg, pp 379–390
91. Brittain JE, Storruste A, Larsen E (1991) Radiocaesium in Brown Trout (Salmo trutta) from a subalpine lake ecosystem after the Chernobyl reactor accident. J Environ Radioact 14:181–191
92. Smith JT, Kudelsky AV, Ryabov IN, Hadderingh RH (1999) Aquatic countermeasure against radiocaesium uptake by the ecosystem (AQUACURE) second interim report. European Commission, 1999
93. Smith JT, Leonard DRP, Hilton J, Appleby PG (1997) Towards a generalized model for the primary and secondary contamination of lakes by Chernobyl-driven radiocesium. Health Phys 72:880–892
94. Camplin WC, Leonard DRP, Tipple JR, Duckett L (1989) Radioactivity in freshwater systems in Cumbria (UK) following the Chernobyl accident MAFF fisheries research data report no. 18, MAFF, Lowestoft
95. Fleishman DG, Nikiforov VA, Saulus AA, Komov VT (1973) Cs-137 in fish of some lakes and rivers of the Bryansk region and North-West Russia in 1990-1992. J Environ Radioact 24:145–158
96. Blaylock BG (1982) Radionuclide data bases available for bioaccumulation factors for freshwater biota. Nucl Safety 23:427–438
97. Smith JT, Leonard DRP, Hilton J, Appleby PG (1997) Towards a generalized model for the primary and secondary contamination of lakes by Chernobyl-driven radiocesium. Health Phys 72:880–892
98. Wallström A, Håkanson L (1991) A household method to reduce Cs-137 in meat. Swedish Health and Food Institute, Stockholm (in Swedish)
99. Andersson P (2006) Miljöövervakning före och efter Tjernobylolyckan. Strålskyddsnytt 1:37–38
100. Johansson KJ (2006) Cesium-137 i svamp, bär och vilt. Strålskyddsnytt 1:25–31
101. Håkanson L (1997) Modelling of radiocesium in lakes - on predictive power and lessons for the future. In: Desmet G et al (eds) Freshwater and estuarine radioecology. Elsevier, Amsterdam, pp 3–45

Books and Reviews

Salomons W, Förstner U (1984) Metals in the hydrocycle. Springer, Heidelberg, p 349

Nuclear Energy, Introduction

Nicholas Tsoulfanidis
Department of Nuclear Energy, Missouri University of Science and Technology, Rolla, MO, USA

In terms of technical progress of the human species/society, the second half of the twentieth century is marked by two developments: the computer and nuclear energy. And the two are related since progress in the development and applications of nuclear energy owes a lot to the power of computations made possible by the digital computer.

The whole twentieth century is marked by the ever-increasing use of electricity. The century started with a tiny amount of electricity use and ended with ~30% of the total energy consumed to be in the form of electricity.

Nuclear energy, unfortunately, was released in the world as a weapon. But, fortunately, after the initial shock of Hiroshima and Nagasaki, nuclear energy turned out to be of great benefit to society. First, in a "Faustian bargain," of sorts, the existence of nuclear weapons resulted in having a *cold war* between the two

superpowers of the time (Soviet Union and the USA) instead of a *hot one*. Second, nuclear energy proved to be an excellent method of generating electricity and also provided the means for numerous applications in industry, science, education, and probably most of all medicine. Not even the fiercest critics of nuclear energy deny the benefits of nuclear medicine in correct diagnosis and therapy and, therefore, prolongation of life for millions of people all over the world.

Although, as mentioned above, nuclear energy touches today beneficially many aspects of our lives, the most prominent application is the generation of electricity by using nuclear fission reactors to generate heat that is used to produce steam (or hot gas) that runs a turbo generator and produces electricity. There are many advantages in using nuclear energy for the generation of electricity. Primary among them is the absence of green house gases and other pollutants such as sulfur oxides, nitrogen oxides, heavy metals (mercury etc.).

Probably, the most important difference between nuclear and fossil or any renewable fuels is the concentrated energy release of the former. The fission of one U nucleus releases $\sim 200 \times 10^6$ eV; the burning of one atom/molecule in a chemical reaction releases a few eV; a ratio of many million! A single pellet of nuclear fuel, about the size of a fingertip, contains as much energy as 1,700 ft^3 of natural gas, or 1,780 lb of coal, or 149 gal of oil. As a result of this concentrated energy, the "ashes" of the process, the fission products that are radioactive, constitute a, relatively, small volume. Yes, they have to be safeguarded and be kept away from the biosphere for thousands of years, but the volume of wastes is considered manageable.

Today (2011), there are 441 nuclear power plants operating in the world amounting to a total generating capacity of 375 GWe. The top five countries, in terms of number of operating plants are the USA (104), France (58), Japan (54), Russia (32), and Korea (21). In 2010, there were 62 plants under construction amounting to a capacity of 60.2 GWe. The top countries in numbers of plants under construction are China (25), Russia (11), Korea (5), and India (4); two plants under construction are in the USA, Japan, Bulgaria, Slovakia, and Ukraine.

- Today, ~16% of the electricity worldwide is produced by nuclear power plants; that fraction will increase in the coming years as developing economies (e.g., China and India) and developed ones (Korea, Japan, and Europe) complete their announced ambitious nuclear expansion in order to satisfy their ever-increasing demand for electricity. The World Nuclear Association (WNA) projects that by 2060 at least 1,100 GWe of new nuclear capacity will be added.

What drives this "Nuclear Renaissance"? There are several factors:

1. *Increasing energy demand*: Due to an ever-increasing population and desire of the underdeveloped countries to improve their standard of living. In addition, a need for new plants materializes because old plants reach the end of their life and must be shut down (all types of electricity generating plants, not only nuclear, are designed with a finite operational life).
2. *Climate change concerns*: Increased awareness that fossil fuels release a large amount of greenhouse gases that may lead to a planetary climate change are driving decisions for new plants to be "green," that is, to emit reduced amounts of greenhouse gases and other pollutants or not at all. Nuclear power plants are the only ones generating electricity with, essentially, zero emissions.
3. *Economics*: The main cost component of a nuclear plant is its construction cost; once this cost is overcome, the other two cost components for the generation of electricity (O&M and fuel) favor nuclear over fossil plants. Experience during the past 50 years, especially in the USA, has shown that nuclear is the best plant for generation of base load electricity, both in terms of cost and reliability.
4. *Fuel price stability*: Because the fuel cost constitutes a, relatively, small fraction of the total cost of generating electricity (for nuclear the main cost is the construction cost; fuel cost is between 10% and 16% of the total cost), even if the price of fuel doubles, the effect on the cost of electricity will be minimal. It should be noted that the cost components of the fuel are uranium, conversion, enrichment, fabrication-transportation; of these, only the uranium price fluctuated during the previous

50 years; the cost of the other components has been remarkably stable.

5. *Security of Fuel Supply*: Supply of fossil fuels (oil, gas, and coal) is vulnerable to interruptions of supply due to political turmoil, strikes, weather, etc. On the contrary, uranium is plentiful and available at reasonable prices, for the foreseeable future; more than that, since nuclear plants refuel every 2 years, it is quite likely that short-term upheavals can be settled before they have an effect on nuclear fuel supply.
6. *Nuclear Safety and Public acceptance*: The safety record of nuclear power plants during more than 50 years of operation (195702011) is outstanding. There were three accidents during that period. The TMI accident in the USA in 1979: it was a financial loss to the company operating the plant; not a single injury resulted to any person in or out of the plant and there was no contamination of the environment. The Chernobyl accident in 1986 was a very serious accident: radioactivity was released to the environment and 33 persons are known to have died, mostly firefighters. Some cancers will develop as a result of exposure to the radiation from the accident, making it a difficult task to quantify them. One should note, however, that no plant licensed anywhere today can have the Chernobyl type of accident; it is physically impossible (the Chernobyl design has been abandoned). Considerable area around the plant has been contaminated, but the reports today (2011) indicate that life is returning to normal. On March 11, 2011 a 9.1, Richter scale, earthquake hit Japan and affected the Fukushima nuclear site. There are six reactors on that site. On that day, two reactors were shut down and were not affected by what followed. When the quake hit, the four operating plants shut down, as design dictated. Shutting down means that the fission reaction is stopped; however, heat continues to be generated in the core from fission products, hence cooling must be provided. As per design, cooling continued using emergency diesel generators required by regulation and readily available for such eventuality. Then, 15–20 min later, the tsunami arrived; the waves of the tsunami swept away generators and their fuel supply and cooling of the core was lost. Fuel meltdown of the cores occurred and radioactivity was released to the environment. Two plant workers were killed by the tsunami; these are the only immediate deaths as a result of this event. The tsunami itself and the earthquake resulted in the death of ~22,000 people. The area around the site was contaminated. Definitely the accident was a tremendous financial loss to the company operating the Fukushima plants.

As a result of the accident at Fukushima, two plant workers were killed by the tsunami; these are the only immediate deaths as a result of this event. At Chernobyl, ~33 persons, mostly firefighters, were the reported immediate deaths. Of course as a result of TMI, no deaths occurred; in fact in the USA there are zero deaths from the operation of commercial nuclear power plants from 1957 until today. Compare this, for example, to coal mining fatalities which amount to ~30/year in the USA; in other countries, e.g., China, the direct annual death toll from coal mining is much higher.

Without trying to deemphasize the importance of these three accidents, the net effect is that the world community still recognizes and accepts the generation of electricity using nuclear fission reactors as an indispensable component in the energy portfolio. At about 9 months after the Fukushima accident, there is no report of any country changing nuclear energy policy because of that accident (with the exception of Germany that decided to accelerate the shutdown of its nuclear fleet following a decision taken earlier by its Government). Overall acceptance of nuclear technology is the result of its excellent performance; another factor in favor of nuclear power is the lack of greenhouse gases by this technology or of any environmental effect in the vicinity of the plant. In the USA, acceptance of nuclear power by communities around the plant is ~70% or more favorable.

The nuclear industry, especially in the USA, learned and improved a lot after the TMI accident. I have no doubt that the international nuclear community will apply the lessons learned from Fukushima to make the already safe record of this industry even safer.

This section on Nuclear Energy consists of 19 articles that cover all aspects of the nuclear enterprise. Here is a brief description of each article:

A. *Radiation sources*: It discusses radioactivity and basic radiation sources.
B. *Radiation detection devices*: One characteristic of radioactivity is the fact that it can be detected relatively easily and accurately. This article discusses the devices used to accomplish such measurements.
C. *Dosimetry* and *Health Physics*: Very early in the twentieth century (1920s), it was realized that ionizing radiation may be harmful to humans, therefore measures must be taken to protect people. These measures were based on (a) quantifying the effects of radiation exposure by establishing units of radiation dose and means to measure it and (b) establishing professional bodies that set protection standards [ICRP (1928), NCRP (1964) etc.]. The field of Health Physics was thus born resulting in great benefit for the radiation workers.
D. *Fission reactor physics*: Fission reactors are the major sources of production of radioactive materials. What are the principles of their operation? What are the foundations of their safe operation? These are two of the major items discussed in this article.
E. *Nuclear fuel cycles*: Providing nuclear fuel for a fission reactor is not a simple or straightforward task; it involves many steps (U procurement, conversion, enrichment, fuel rod and assembly fabrication). The users of the fuel are presented with choices, such as discarding the irradiated fuel as waste or reprocessing and recycling it. Also, reactor designers may affect the nuclear fuel "cycle" by building reactors that just produce electricity, or combine electricity production with generation of new fuels (breeders), or generate electricity in combination with burning some of the nasty by-products of the fission process. These are the matters discussed in this article.
F. *Uranium reserves and mining*: How much uranium is there on our planet and at what price? Where is it found? How is it extracted? These are the topics of this article.
G. *Nuclear fission power plants*: Once the fission reactor is designed and ready to operate, how is the fission energy utilized to generate electricity? The reactor core itself is not enough; plenty of other components must operate for the successful transformation of energy released in fission to electricity feeding a lightbulb. The fission reactor core makes a small part of a nuclear power plant. It is this aspect of nuclear power, components and activities outside the core, that is described in this article.
H. *Nuclear reactor materials and fuel*: For a successful and long-term safe operation of a nuclear power plant, the materials used, especially those directly tied to the fuel, must function as designed (as expected) in the very hostile environment of a nuclear fission core. This article describes the pros and cons of the various materials that have been considered and the final choices made.
I. *Nuclear safeguards and proliferation of nuclear weapons materials*: Of great concern to human kind is the acquisition of nuclear materials by groups or governments that may use them to make nuclear weapons, contrary to international treaties. This "proliferation" or rather "nonproliferation" of nuclear materials and possibly weapons is a concern that will never disappear; all that can be done by the international community of nations is to set up treaties, policies, and procedures that diminish the probability of proliferation. It is these aspects of this terrible problem facing humanity that are discussed in this article.
J. *Radiation shielding and protection*: This article is complementary to articles A–C. Having discussed radiation sources, dangers from radiation, and standards of protection, how does one provide the means for a safe radiation environment for the workers and the public? How are relevant computations performed? Measurements? How is an effective radiation shield designed? These are the questions answered in this article.
K. *Isotope separation methods for nuclear fuel*: The two elements found in nature that may be considered as fuels for fission reactors are Th and U. Unfortunately, only certain isotopes of these elements or made with the help of these elements can be manufactured into fuels. Hence, isotope separation methods must be employed for the

production/concentration of the "useful isotope(s)." These methods are discussed in this article.

L. *Reprocessing of nuclear fuel*: Irradiated fuel contains many useful isotopes, primarily U and Pu. Reprocessing is the operation that extracts the useful isotopes from the irradiated (spent) fuel. The reprocessing methods used until today and those under research and development are discussed in this article.

M. *Decommissioning of nuclear facilities*: Every nuclear facility has a finite lifetime; at the end, when operations stop for good, the law says that the site must, eventually, be returned to its preoperational state in terms of the presence of radioactivity. This is what decommissioning means. All the tasks associated with decommissioning are discussed in this article.

N. *Radioactive waste management*: Storage, transport, disposal. The operation of fission reactors results in the production of radioactive materials. Such materials, if they have no further use, they must be safeguarded for long periods of time in order that their release to the biosphere may be prevented. The method of eventual disposal of such materials considered today by their producers is placement in a geologic repository. In the meantime, radioactive wastes must be stored and transported. These activities are discussed in this article.

O. *GEN-IV reactors*: By any measure, current fission reactor designs are successful. However, there is room for improvement in terms of fuel utilization, thermal efficiency, use of the heat generated by the energy released in fission, multifunction of a nuclear plant, etc. There is considerable global effort underway to design fission reactors that will show some, if not all, of the improvements just mentioned. These new designs, collectively named as GEN-IV reactors, are described in this section.

P. *Nuclear fusion*: Fusion reactors offer many advantages over fission reactors. Unfortunately, although fusion became known to man before fission and life on earth owes its existence to a fusion reactor in the sky (our Sun), no fusion plant has been built yet; fusion reactors present some unique challenges/difficulties that have not been resolved yet. But, the world's scientific community is working as a team in an effort to resolve the issues and build an operational fusion plant sometime in the future. All the past and current efforts in fusion research and the expected future developments are presented in this article.

Q. *Nuclear power economics*: In a free market, every plant generating electricity must compete economically with all other options; nuclear is no exception, of course. Nuclear power presents some unique problems, with respect to financing, and these are the problems (and possible solutions) discussed in this article.

R. *Thorium – An excellent 'fertile' nuclear fuel*: In addition to Uranium, Thorium (Th) is the only other element found on earth that can be used as a fuel in fission reactors. The Th properties, relevant to fission reactors, resources, availability and prices are discussed in this article.

Nuclear Facilities, Decommissioning of

David R. Turner
Geosciences and Engineering Division, Southwest Research Institute, San Antonio, TX, USA

Article Outline

Glossary
Definition of the Subject
Introduction
Types of Nuclear Facilities
General Methodologies for Decommissioning
Status of Decontamination and Decommissioning
Future Directions
Bibliography

Glossary

Decommissioning Nuclear decommissioning is a term used to describe the process of removing a nuclear facility or site safely from service and reducing residual radioactivity to a level that permits (1) release of

the property for unrestricted use and termination of the license or (2) release of the property under restricted conditions and termination of the license. Although waste classification and management is an important aspect of decommissioning, the details of radioactive waste management and disposal are not addressed in this article.

Decontamination The removal of undesired residual radioactivity from facilities, soils, or equipment, prior to the release of a site or facility and termination of a license. Also known as remediation, remedial action, and cleanup.

Exposure pathway The route by which radioactivity travels through the environment to eventually cause radiation exposure to a person or group.

Financial assurance A guarantee or other financial arrangement that ensures funds for decommissioning will be available when needed.

Institutional controls Administrative and physical measures to control access to a site and minimize disturbances to engineered measures established to control the residual radioactivity.

Monitoring The measurement of radiation levels, concentrations, surface area concentrations, or quantities of radioactive material and the use of the results of these measurements to evaluate potential exposures and doses.

Nuclear fuel cycle Consists of the different stages necessary to produce nuclear power. Specific stages include (1) the *front end* of the nuclear fuel cycle where uranium is mined and fuel is prepared, (2) the *service period* in which the fuel is used during reactor operation, and (3) the *back end*, which involves safe management, containment, and either reprocessing or disposal of spent nuclear fuel. Because uranium fuel is the most common type of nuclear fuel, this article focuses on the uranium nuclear fuel cycle.

Radiological survey An evaluation of the radiological conditions and potential hazards at a site related to the production, use, transfer, release, disposal, or presence of radioactive material or other sources of radiation. Radiological surveys can be used to provide the basis for acquiring necessary technical information to develop, analyze, and select appropriate cleanup techniques.

Residual radioactivity Radioactivity in structures, materials, soils, groundwater, and other media at a site resulting from activities under the licensee's control, excluding background radiation.

Definition of the Subject

The process of safely shutting down, dismantling, cleaning up, and monitoring nuclear facilities is collectively known as nuclear decommissioning. Nuclear power has been used as a source of energy for more than 50 years, and more than 500 nuclear reactors have been constructed and operated worldwide [1]. In addition to power plants, the nuclear fuel cycle requires different types of facilities to mine uranium, produce fresh nuclear fuel, and manage spent nuclear fuel and associated radioactive wastes after the fuel can no longer be effectively used to produce power. Many of the facilities associated with the nuclear fuel cycle that supports these reactors, as well as the reactors themselves, have either reached or are approaching the end of their planned service life. Also, some countries such as Belgium and Germany have initiated national policies to phase out nuclear power over time [2, 3]. Owners and operators of nuclear facilities, as well as government agencies responsible for their regulation, must evaluate economic and public policy considerations to determine whether to renew facility licenses or to permanently remove facilities from service, and decommission them to release the sites for other potential uses.

Definitions of nuclear decommissioning, radiological dose limits for site release, and even terminology can vary from country to country depending on the nature of the laws and regulations that govern the nuclear fuel cycle. The International Atomic Energy Agency (IAEA) defines decommissioning as "...the administrative and technical actions taken to allow the removal of some or all of the regulatory controls from a facility" [4]. Similarly, the Nuclear Energy Agency (NEA) broadly defines decommissioning as covering "all of the administrative and technical actions associated with cessation of operation and withdrawal from service" [1]. The World Nuclear Association (WNA) defines the two main objectives of decommissioning as rendering the site permanently safe and restoring it, "as far as practicable," for reuse for nuclear or non-nuclear activities. Reuse can apply to different components of a nuclear

facility, including land, water bodies, buildings, equipment, and materials [5].

Some early nuclear facilities were developed without explicit consideration of decommissioning, and these "legacy" sites continue to be identified and cleaned up – often at public expense. As it is currently practiced in most nations with a robust legal and regulatory framework, the decommissioning process begins when a facility is removed from service. Planning for decommissioning should begin at the design stage, before a facility enters operation [4, 6]. For example, early decisions about construction materials, site layout, spill prevention and control measures, waste management, and financial assurance can all influence decommissioning activities at the end of a facility's life cycle and may be made (or be required) before a facility receives an operating license. Similarly, some national nuclear regulatory programs require that decommissioning plans be submitted with the initial license application and periodically reevaluated and updated during the operating life of the facility [6, 7]. Decommissioning is generally considered complete when the facility is removed from regulatory control (e.g., the license is terminated) and the site is made available for reuse.

The processes and technologies are similar to those used for other industrial facilities, but because of the nature of the materials used in the nuclear fuel cycle, nuclear decommissioning tends to be a regulated process that requires special procedures to handle and dispose of radioactive materials safely. The specific methods used in nuclear decommissioning vary widely, depending on factors such as the type, size, age, operational history, and design of a given nuclear facility. National policies differ on detailed objectives, and individual countries are likely to have different issues of concern such as the future use of nuclear power, the continued availability of trained staff, socioeconomic effects on surrounding communities that may result from shutting down a large facility, and financial issues associated with funding decommissioning activities.

For these reasons, there is no unique or preferred "one size fits all" approach to the nuclear decommissioning process. The intent of this article is neither to endorse any particular approach, nor to describe all potential aspects of nuclear decommissioning in detail, but rather to provide a broad overview of generally applicable principles. Further, this article focuses on decommissioning facilities associated with the commercial-scale production of nuclear power. Other processes that use or generate nuclear materials such as military programs, nuclear medicine, and industrial operations that produce radioactive materials as a byproduct are beyond the intended scope of this discussion. The reader is referred to the references identified in the Bibliography for further information and more detailed discussion of the processes described here.

Introduction

In 2007, nuclear reactors provided slightly more than 14% of the world's electricity, with ranges as high as 76.8% in France [8]. Currently (July 2009), 436 nuclear power reactors are in operation, with 5 reactors in long-term shutdown and 48 new reactors under construction [9]. In addition to nuclear reactors, generating nuclear power requires different types of facilities to support the nuclear fuel cycle. For example, as of August 2003, the IAEA reported that there were 423 operating nuclear fuel cycle facilities, with 19 more under construction. Eventually, decisions will need to be made with regard to closing and decommissioning these facilities in a safe manner and potentially returning the land to other uses.

More than 50 years after the first nuclear power reactor went on line, many of the facilities associated with commercial-scale nuclear power generation are now approaching the end of their planned service life. For example, the European Union estimates that at least one-third of the 152 nuclear power plants operating in its member countries will need to be decommissioned by 2025 [2], and the IAEA reported that 297 nuclear fuel cycle facilities were shut down or in the process of being decommissioned worldwide as of August 2003 [4]. An even larger number of manufacturing and research facilities (about 1,600) that use radioactive material will need to be decommissioned "over the coming decades" [10].

At the same time, increased global energy demand, coupled with a growing concern about the effects of carbon emissions from traditional fuel sources, has sparked renewed interest in nuclear power generation. As an example, the U.S. Nuclear Regulatory

Commission (USNRC), the agency responsible for licensing and regulating commercial nuclear activities in the United States, received a total of 17 applications to construct and operate 26 new commercial nuclear reactors during 2007–2008 [11]. Although some countries are deemphasizing nuclear power, other countries in Europe and Asia have indicated a renewed interest in nuclear power as a component of their overall energy portfolio [3, 8, 12].

Together, these developments indicate that all stages of the commercial nuclear fuel cycle will continue to be active or will be expanded in the foreseeable future. For this reason, methods to safely take these facilities out of service and decommission them will continue to be an important component of energy policy. It is these methods that are the subject of this article.

Although primarily developed for nuclear power plants, there are three basic types of alternative decommissioning strategies that may be applicable to other nuclear facilities:

- A strategy of immediate decontamination and dismantlement [1, 7] (also defined as DECON [11, 13]) begins soon after the nuclear facility closes.
- Safe storage [1], deferred or delayed decontamination [7], or SAFSTOR [14, 15] refer to decommissioning strategies where a nuclear facility is left intact after closing, placed in a stable condition, and maintained and monitored until subsequent dismantlement and decommissioning. Similarly, uranium production facilities (mines and mills) may be placed on standby status when uranium prices are low and deposits cannot be produced at a profit.
- A strategy of entombment [1, 7] or ENTOMB [14, 15] involves encasing radioactive materials onsite in a long-lived, structurally sound material such as concrete.

The first two strategies may also be combined. For example, some facilities at a site may be immediately dismantled while other structures are placed in safe storage. Generally, decommissioning activities are anticipated to be completed in a period of decades from the end of operations [14, 15].

Once the decommissioning strategy is selected for a given facility, general activities associated with nuclear decommissioning may include:

- Characterizing the features of the site and conducting radiological surveys to determine radiation background and residual radiation levels
- Developing a site-specific decommissioning plan
- Estimating cost
- Conducting safety and performance assessments
- Decontaminating structures, equipment, and components for reuse or recycling
- Dismantling and removing buildings, structures, and equipment from the site
- Remediating contaminated soils and groundwater
- Performing waste management and disposal
- Conducting final inspections and surveys
- Reclaiming disturbed lands
- Implementing active institutional controls and monitoring

Specific decommissioning activities and technologies are determined on a case-by-case basis and can depend on many things at a given site, such as the duration, type, and scale of operations; the geologic setting of the site; socioeconomic considerations; and the regulatory policies of the government. In addition, a key part of a decommissioning plan is estimating decommissioning costs to establish financial arrangements that ensure resources are available to complete the decommissioning process.

Types of Nuclear Facilities

As described in the "Introduction" section, generating electricity from nuclear power plants is only part of the nuclear fuel cycle [16] and decisions will need to be made with regard to the safe closure and decommissioning of each of these facilities. To understand any unique aspects that will need to be addressed during nuclear decommissioning, it is important to describe the general nature of the activities that are conducted at each type of facility in the nuclear fuel cycle. Because uranium fuel is the most common type of nuclear fuel, this article focuses on the uranium nuclear fuel cycle (Fig. 1).

To support the nuclear fuel requirements of commercial power-generating facilities, there are facilities that

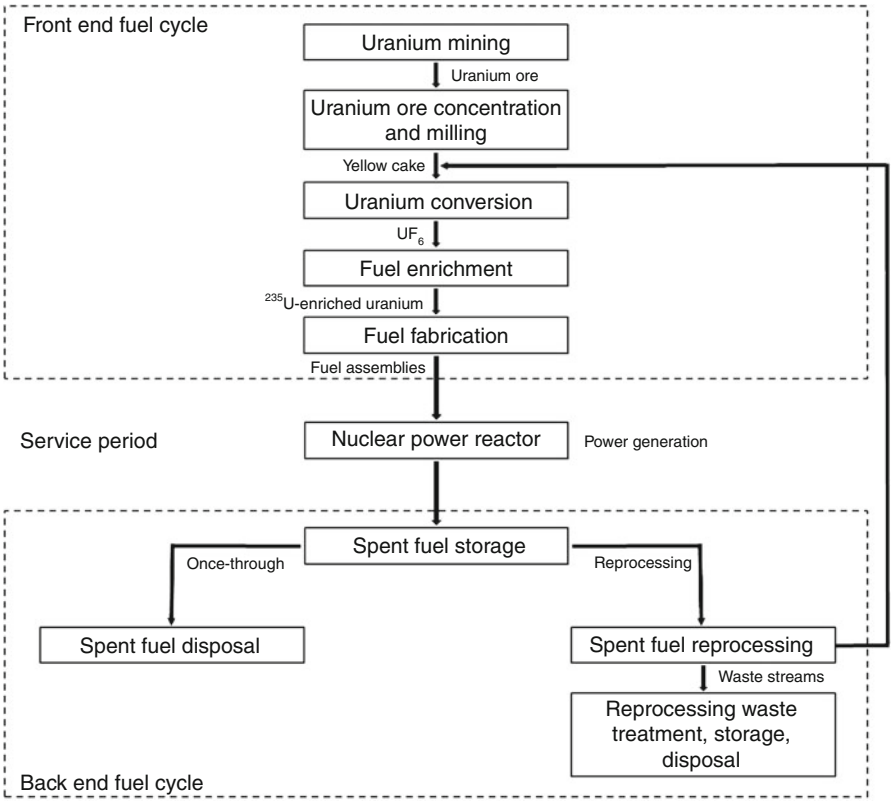

Nuclear Facilities, Decommissioning of. Figure 1
Simplified diagram representing the nuclear (uranium) fuel cycle

- Produce uranium by mining
- Mill ore to concentrate the uranium and package it for transportation
- Purify and transform the uranium concentrate into a form suitable for fuel manufacture through a process called uranium conversion
- Enrich the uranium in isotopes (^{235}U) that produce sustainable nuclear reactions
- Fabricate reactor fuel components and fuel assemblies

These facilities are part of the "front end" of the nuclear fuel cycle. Decommissioning issues for the front end of the fuel cycle are typically associated with naturally occurring radioactivity, such as uranium and radium, and hazards associated with the chemical processing of natural uranium-bearing ores [5].

After the nuclear fuel is used in a commercial reactor to produce electrical power during the service period, the management of the spent nuclear fuel at the "back end" of the nuclear fuel cycle can include facilities that

- Reprocess the fuel to extract nuclear materials and recycle uranium back into the front end of the fuel cycle
- Store or permanently dispose of spent nuclear fuel

At the back end of the fuel cycle, high-level sources of radioactivity and direct irradiation from spent nuclear fuel are decommissioning concerns in addition to natural radioactivity and chemical processing hazards [5]. An example of the typical material balance for the annual operation of a 1,000 Megawatt electric (MWe) nuclear power reactor [17] is included in Table 1.

Each of these facilities will require nuclear decommissioning at the end of its life cycle. Usually, the operator of a facility develops a decommissioning plan (see "Developing a Site-Specific Decommissioning Plan") to identify specific activities, estimate costs, and

Nuclear Facilities, Decommissioning of. Table 1 Material balance for the annual operation of a 1,000 MWe nuclear power reactor [17]

Type of nuclear facility	Material balance[a]
Mining	20,000 metric tons (22,000 t) of 1% uranium ore
Milling	230 metric tons (250 t) uranium oxide concentrate (U_3O_8) containing 195 metric tons (215 t) of uranium
Uranium conversion	288 metric tons (317 t) uranium hexafluoride (UF_6)
Fuel enrichment	35 metric tons (39 t) UF_6, containing 24 metric tons (27 t) enriched uranium (4% U-235), 11 metric tons (12 t) depleted uranium (0.25% U-235) tails
Fuel fabrication	27 metric tons (30 t) UO_2, containing 24 metric tons (30 t) enriched uranium
Reactor operation	8,640 million kilowatt-hour electricity at full output (assuming 100% load factor)
Spent nuclear fuel	27 metric tons (30 t) spent nuclear fuel containing 23 metric tons (25 t) uranium (0.8% U-235 as UO_2), 240 kg (529 lb) plutonium, 720 kg (1,587 lb) fission products, and transuranic elements

[a]Assuming enrichment to 4% U-235 with 0.25% tails assay; core load 72 metric tons (79 t) U, refueling so that 24 metric tons (26 t) U/year replaced; operation – 45,000 MWday/t (45 GWday/t) burn-up, 33% thermal efficiency

lay out a schedule [18–21]. The plan is submitted to the regulatory agency to ensure that it complies with the applicable regulations. Once it is approved, the initial decommissioning plan is periodically updated and becomes more detailed as the facility evolves during its operational life. At the end of the facility life cycle, the decommissioning plan serves as a blueprint for the nuclear decommissioning process. During decommissioning, the regulatory agency may periodically inspect the site to ensure that the decommissioning plan is being implemented correctly.

The following sections introduce the types of nuclear facilities associated with generating nuclear power and identify features that may influence nuclear decommissioning decisions and activities. The listing is not intended to be exhaustive, nor is it intended to provide a detailed discussion of the complex regulatory controls that may apply for a given type of nuclear facility. The reader is referred to the references identified in the Bibliography for further reading.

Front End Fuel Cycle Facilities

Uranium Mining At the start of the nuclear fuel cycle, uranium mining focuses on extracting natural uranium ore from the earth. Uranium mining may be done through a conventional process of excavation by open pit or underground mining techniques. During excavation, uranium ore is segregated from waste rock or overburden, and shipped to a uranium mill for further processing (see "Uranium Milling"). Open pit and underground uranium mines are typically decommissioned and reclaimed in accordance with regulations applicable to the mining industry in general [22]. In many ways, decommissioning a uranium mine is subject to challenges similar to those faced in cleaning up mining operations for other resources such as coal and metals. For example, excavations may need to be backfilled, pit walls and disturbed surfaces recontoured, and revegetated to meet applicable mine reclamation standards. Groundwater contamination plumes with elevated levels of uranium and associated heavy metals (e.g., arsenic, selenium) need to be remediated and monitoring systems installed, as appropriate.

Alternatively, uranium recovery may be through a process called in situ leaching (ISL), where chemical fluids are injected through a series of wells into the subsurface to dissolve uranium from ore minerals. The now uranium-enriched solution is pumped back to the surface for subsequent extraction and processing [13, 22–24]. Decommissioning of ISL uranium facilities is different from cleaning up conventional uranium mining operations. For example, because there are no

large-scale excavations associated with the ISL uranium recovery technology, surface land disturbance is much less than with conventional mining methods, and large amounts of waste rock are not generated. This can simplify the reclamation effort, but impacts to groundwater are potentially greater, and restoration of groundwater quality to premining levels tends to be a focus in decommissioning ISL facilities [13]. In addition, although the surface facilities such as well heads and pump houses necessary to support ISL uranium mining may be small compared to conventional operations, the well fields themselves may be very large. For example, the permitted areas for U.S. ISL operations in Wyoming and Texas may be as large as 6,500 ha (16,000 acres) and individual well fields may contain hundreds to thousands of wells [13].

Uranium Milling While varying depending on the deposit and the type of ore, uranium ores typically have a concentration of about 1% or less uranium (U_3O_8) by weight, although it can be as high as 20%. Decommissioning uranium milling facilities is generally concerned with naturally occurring radioactive elements such as uranium, thorium, and radium. For conventional uranium mining and milling operations (Fig. 2), uranium is concentrated through milling (crushing, grinding, separation) and subsequent chemical processing of the ore using alkaline or acid leaching solutions to produce a product called "yellow cake," a coarse powder that is approximately 70% or more U_3O_8 by weight. Milling operations are similar for ISL uranium, but because the mill input is uranium-bearing solutions instead of solid ore, the crushing and grinding, and leaching circuits are not necessary.

Depending on the economics of the operation, a mill may be colocated with a uranium mine, or it may be separate, charging a "toll" to accept and mill ore (conventional) or uranium-bearing solutions (ISL) from nearby uranium mines. Because of the throughput of uranium-bearing solutions and the handling of yellow cake, some of the buildings, pipes, and equipment in the mill may become radioactively contaminated with natural radioactive elements over time and will need to be decontaminated and/or disposed of during decommissioning. Spills and unintentional releases of uranium-rich solutions can lead to soil and

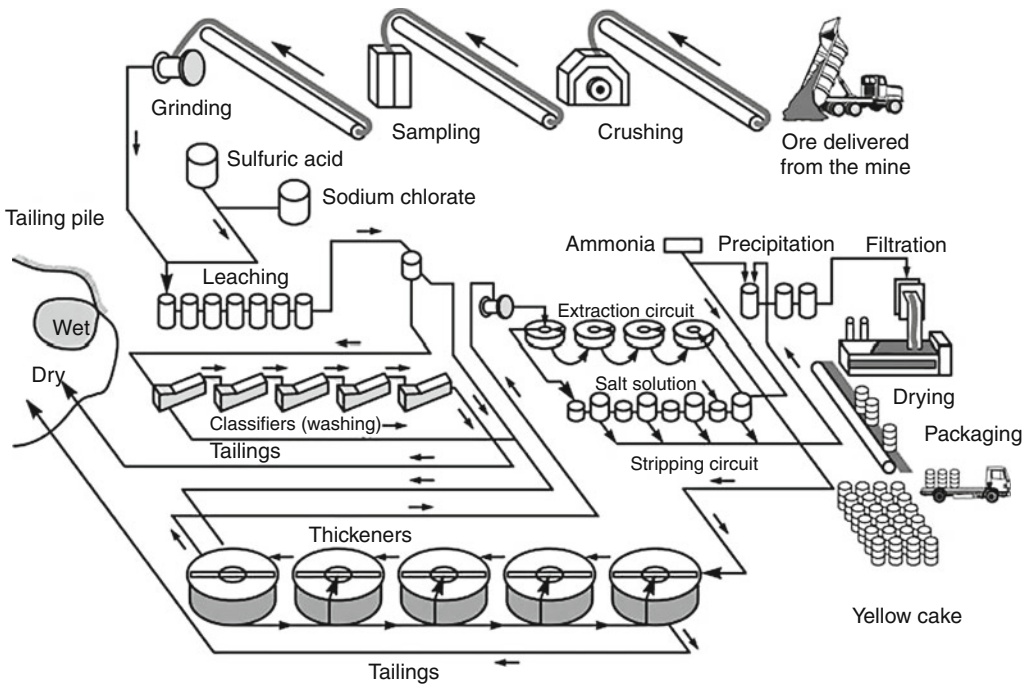

Nuclear Facilities, Decommissioning of. Figure 2
A typical conventional uranium mill [22]

groundwater contamination that may need to be remediated during decommissioning. In addition, during conventional milling, large quantities of waste solids are produced by the crushing, grinding, and leaching circuits. These waste solids, or "tailings," are placed in large impoundments that will also need to be decommissioned at the end of the mill's operational life. ISL facilities do not treat solid rock and therefore produce no tailings. Because these facilities handle large volumes of uranium-rich solutions, however, they may have one or more evaporation ponds that will eventually need to be decommissioned. Although specific activities will vary depending on size, age, operational conditions, and design, decommissioning of a uranium mill (both for conventional and ISL facilities) includes general activities described in the "General Methodologies for Decommissioning" section.

Uranium Conversion Although natural uranium ores are concentrated and purified during milling to produce yellow cake, the uranium must be further purified and converted to a gas state to produce nuclear fuel. The nature of these chemical processes and the size and complexity of these uranium conversion facilities strongly influence the decommissioning process. Uranium conversion facilities are designed to remove impurities from the yellow cake and convert solid uranium into uranium hexafluoride (UF_6), the only uranium compound that exists as a gas at suitable temperatures [4, 17]. The UF_6 gas is then pressurized and cooled to a liquid state [4]. The liquid is stored in cylinders and allowed to solidify for shipment to a fuel enrichment plant (see "Fuel Enrichment"). Some uranium conversion facilities also recycle uranium scrap that may come from manufacturing facilities or other production plants [4].

The uranium conversion process involves strong acids and alkali agents to dissolve the yellow cake powder. As with mining and milling, the operational risks associated with uranium conversion are chemical as well as radiological, and the safe removal and disposal of hazardous chemicals used in the conversion process must be taken into consideration as part of the decommissioning process. Because it is predominantly an industrial chemical facility, the types of decommissioning issues for a uranium conversion facility are similar to those described in the "Uranium Milling" section for buildings, equipment, and land reclamation at uranium mills. No tailings are produced during uranium conversion. Groundwater and soil contamination from spills and leaks are possible and will need to be identified, remediated, and monitored in accordance with applicable regulations [19]. The size and complexity of uranium conversion plants can lead to significant decommissioning costs. For example, alternative decommissioning options for the 243-ha (600-acre) Sequoyah Fuels uranium conversion plant site in Gore, Oklahoma, varied from about US $19 to US $254 million (2006 dollar value), depending on the option selected for disposal of contaminated materials [25].

Fuel Enrichment Natural uranium is composed of ^{238}U (99.274%) and ^{235}U (0.711%) and contains trace amounts of ^{234}U (<0.01%). Nuclear reactor fuel requires increasing (or enriching) the fissionable ^{235}U above these natural levels to sustain the nuclear reactions. During the fuel enrichment process, gaseous UF_6 is gradually enriched in ^{235}U to about 3–5% – levels that are sufficient for fabricating commercial reactor fuel [26, 27]. One product of the enrichment process of special concern during decommissioning is depleted uranium tails, where the ^{235}U content has been reduced to below natural levels (about 0.2–0.35%) [28]. This waste stream is commonly stored at the site in gas cylinders of UF_6, although it may also be converted to solid form such as uranium oxide. Depleted uranium emits low levels of radiation and is also a toxic heavy metal, so during decommissioning, this waste must be managed and disposed in accordance with both radiological and hazardous waste criteria [27, 29].

Gaseous diffusion is the process most widely used for nuclear fuel enrichment. The gaseous diffusion process takes advantage of the different diffusion rates that result from the slight differences in mass for ^{238}U and ^{235}U. Gaseous UF_6 is pumped through a permeable porous barrier media. The lower molecular weight ^{235}U has a higher diffusion rate and moves through the barrier media more readily than the higher molecular weight ^{238}U; the UF_6 gas that passes through the media is therefore slightly enriched in ^{235}U [30]. The process

is repeated through many barriers until the desired enrichment levels are achieved.

These types of plants are large industrial facilities, with a footprint of about 300–600 ha (750–1,500 acres) that contains a large amount of piping and pumps required to move the UF_6 gas through the permeable barrier system [4]. During operations, the primary hazards in gaseous diffusion plants that may influence subsequent decommissioning include the chemical and radiological hazard of a UF_6 release [31]. There is also a potential for mishandling the enriched uranium, which could create a criticality accident (inadvertent nuclear chain reaction). Because these are large facilities, decontamination and decommissioning of inactive buildings and areas may occur while other parts of the facility continue to operate. Surveillance, maintenance, and security will continue for active parts of the facility. Depending on the operating history of the plant, including spills and unintentional releases, decommissioning and cleanup activities at fuel enrichment facilities may include assessing and remediating soil or groundwater and waste management activities, such as disposing of contaminated materials. The size and complexity of a gaseous diffusion plant can lead to large costs for full decommissioning of all facilities. For example, the U.S. Government Accountability Office (GAO) estimated that cleanup activities at three fuel enrichment plants (Paducah, Kentucky; Oak Ridge, Tennessee; Portsmouth, Ohio) cost US $2.7 billion (in 2004 dollars) from 1993 through 2003, and total costs through final decommissioning in 2044 would exceed revenues into the Uranium Enrichment Decontamination and Decommissioning Fund by about US $3.2–6.2 billion (in 2007 dollars) [32]. Newer technologies such as gas centrifuge and laser separation are being considered for the next generation of fuel enrichment facilities, and the decommissioning issues are likely to be different, with perhaps less waste generated during operation [26].

Fuel Fabrication For a typical commercial light water reactor, nuclear fuel is the solid form of uranium oxide (UO_2). Fuel fabrication facilities use chemical processes to convert the ^{235}U-enriched UF_6 into UO_2 in the form of a fine powder [28]. Because many of the materials (such as UF_6) are the same, specific factors that may influence the decommissioning of fuel fabrication facilities will be similar to those identified for uranium conversion and fuel enrichment facilities (see "Uranium Conversion" and "Fuel Enrichment"). This powder is then compacted and sintered (heated at a high temperature to fuse the particles together) to produce fuel pellets. These pellets are loaded into metal tubes to produce fuel rods. Hardware is then used to configure the fuel rods into fuel assemblies of the appropriate dimensions and design for a nuclear power reactor. Although this article focuses on the uranium nuclear fuel cycle, other nuclear fuels can also be fabricated, including mixed oxide (MOX) fuels formed from combining uranium and plutonium oxides, thorium fuels based on the ^{232}Th decay chain with ^{233}U as the fissile fuel element, uranium metal alloy fuels, and microsphere fuel particles [28].

Heavy water (water that contains more than the natural proportion of the hydrogen isotope deuterium, ^{2}H) is used as a moderator in some types of nuclear reactors. Heavy water is extracted from normal water through several chemical processes, the most common of which is distillation through electrolysis or isotopic exchange [24].

Chemical, radiological, and criticality hazards at fuel fabrication facilities are similar to hazards at enrichment plants. Most at risk from these hazards are the plant workers. These facilities generally pose a low risk to the public.

Service Period: Nuclear Power Plants

As indicated, the three decommissioning strategies described in the "Introduction" section were initially developed for nuclear reactors and power plants. The principal concerns during the decommissioning of these reactors and power plants are the safe cessation of operation; the safe management, storage, and disposition of highly irradiated spent nuclear fuel; draining and treatment of water and other fluids from the reactor cooling systems; and the decontamination and disposal of equipment, materials, and other systems that may contain contamination or activation products at the site.

At a very basic level, most nuclear reactors operating today use the heat from the controlled fission of ^{235}U (and perhaps ^{239}Pu in the case of MOX fuel) to boil

water that turns a turbine and produces electrical power. As described previously, there are 436 nuclear power reactors operating worldwide, with 48 new reactors under construction. In addition, there are 287 (as of August 2003) research and test reactors and critical assemblies (i.e., producing little or no power), predominantly located at research universities and government facilities, that are used for research, education, and training purposes [4, 33].

There is no single design that is representative of all reactors. Of the operating nuclear power reactors, about 400 are water cooled and moderated (Energy Information Administration, 2006) and are predominantly pressurized water reactors (PWR), boiling water reactors (BWR), and pressurized heavy water reactors (PHWR). For example, all of the 104 operating commercial nuclear reactors in the United States are either BWR (35 reactors) or PWR (69 reactors) types [34]. Other operating reactor types include gas-cooled reactors, graphite-moderated reactors, and fast breeder reactors.

Early prototype nuclear reactors are sometimes called Generation I reactors. The current nuclear reactor designs are sometimes called Generation II (large central nuclear power plants) and Generation III (advanced LWR) reactors [28, 35]. Current research and development efforts are focused on designing the next generation, or Generation IV reactors, with a goal to provide more efficient and safe nuclear power generation that is also more resistant to nuclear proliferation [28, 36–38]. In the United States, the Next Generation Nuclear Program initiated with the Energy Policy Act of 2005 focuses on developing a very-high-temperature gas-cooled reactor (VHTR) operating at temperatures greater than 950°C for the production of electricity, process heat, and hydrogen [37]. Other designs are also being considered for the next generation of nuclear reactors, predominantly those based on gas-cooled (such as pebble bed modular reactors), water-cooled (super-critical water-cooled reactors), and fast-spectrum technologies (cooled by sodium, lead, or inert gases) [28, 35].

The different current and future design types and sizes of reactors make decommissioning inherently a site- and reactor-specific process. Each current and future reactor design will have its own design-specific decommissioning requirements that must be taken into consideration.

Back End Fuel Cycle Facilities

After the nuclear fuel is irradiated in a reactor and the useful energy has been extracted, it is called spent nuclear fuel. The removal of spent nuclear fuel from the reactor is generally considered part of the transition from the operational phase of the power plant, and not as part of the decommissioning process. The back end of the nuclear fuel cycle consists of facilities that handle spent nuclear fuel. Currently, most commercial nuclear power is based on an open, or "once through" uranium fuel cycle, where the fuel is used in a power plant one time and then removed as spent nuclear fuel [39].

Fuel Reprocessing Facilities When the spent nuclear fuel is removed from the reactor, it is predominantly composed of uranium oxide (96%), other actinides like plutonium and americium (1%), and other fission products such as cesium and strontium (3%) [30]. The spent nuclear fuel must be cooled both thermally and radioactively in a water-filled spent fuel pool and later placed in dry cask storage at the reactor site.

Fuel reprocessing facilities are designed to recover materials such as uranium and plutonium from irradiated spent nuclear fuel. After sufficient cooling, the spent nuclear fuel is dissolved using solvents and the usable components (mostly uranium and plutonium) are separated from waste materials such as other actinides and fission products [4, 40]. The recovered uranium and plutonium are recycled into the front end of the nuclear fuel cycle and refabricated to produce new nuclear fuel (such as MOX) or used for defense purposes. Waste materials, in the form of sludges, salt cake, or calcined wastes, and the reprocessing solutions are collected for disposal. Liquid wastes are generally not suitable for disposal, and decommissioning and cleanup may include vitrification to solidify waste solutions in the form of borosilicate glass.

Because of the high radiological dose rates and contamination levels associated with irradiated spent nuclear fuel, human access is limited for major parts of the facility. This leads to decontamination and decommissioning that is more complicated than facilities such as uranium mills and fuel fabrication facilities at the front end of the nuclear fuel cycle. Facilities tend to be very large, and large volumes of liquid wastes are produced and stored for subsequent disposal.

Examples of fuel reprocessing facilities in the United States include U.S. Department of Energy (USDOE) facilities at Hanford, Washington, and the Savannah River site in South Carolina. The only commercial fuel reprocessing facility in the United States, located at West Valley, New York, ceased operations in 1972. The Carter administration elected to defer reprocessing of commercial nuclear fuel in 1977, and there are no commercial fuel reprocessing facilities currently operating in the United States. The USDOE has completed vitrification of the liquid wastes at West Valley, storing the borosilicate glass logs on site [41, 42]. Decommissioning activities at West Valley are ongoing. Large reprocessing facilities are also located at Sellafield in the United Kingdom and La Hague in France.

Waste Management and Disposal As with many aspects of nuclear decommissioning, the nature and amount of waste produced during cleanup activities will depend on the age and size of a given facility, as well as the nature and history of operations at the site. As described in IAEA [43], four different types of waste or "waste streams," each with different disposal options, are typically produced during nuclear decommissioning. The first three are types that include radioactive waste:

- Primary waste is generated during dismantling activities and may include internal plant components such as a reactor pressure vessel and associated piping, equipment such as pumps and valves, special facilities such as glove boxes and radiation hot cells, and building materials. These components of the primary waste streams may be radioactive through activation by both short- and long-lived radionuclides during plant operations, or by surface contamination. Primary wastes can include a variety of materials, but typically metal and concrete rubble are the largest component by volume of this waste stream [43].
- Secondary wastes are generated during different steps in decontamination and dismantling. These may include solutions, absorbents, and filters used to treat surfaces to reduce radioactive contamination.
- Tools and equipment, such as cutting equipment and protective gear for personnel use during decontamination and dismantling, may become contaminated. To minimize costs and waste volumes, some equipment may be decontaminated so that it can continue to be used.

In addition to these radioactive wastes, decommissioning can potentially produce large volumes of non-radioactive wastes, such as construction debris, sanitary wastes, hazardous chemicals, and asbestos. These wastes are similar to those that might be encountered during the decommissioning of a typical, nonnuclear industrial facility. Some of these materials like furniture, nonirradiated scrap metal, and office equipment can be reused and recycled. The remainder of this waste stream typically has a well-established disposal path through municipal landfills and sanitary disposal systems.

Radioactive waste can occur in a variety of forms, including gases, liquids, and solids, with radiological characteristics that depend on the concentration and half-lives of the different radionuclides. For these reasons, classification of waste is particularly important, as it will determine the methods to be used in handling, segregating, conditioning, packaging, and transporting wastes. Waste classification also establishes the applicable acceptance criteria for different waste storage and disposal options, which in turn can have a strong effect on decommissioning planning and implementation, and ultimately, the total cost of decommissioning [43].

Although it varies from country to country, classification of radioactive waste is typically based on some combination of the types of processes from which the waste was generated, the radionuclide content of the waste, the timing of the waste generation (e.g., legacy wastes generated prior to developing a robust licensing process), as well as chemical, physical, and biological properties of the waste [30, 43, 44]. The following sections provide general descriptions based on waste classifications proposed in IAEA [45]. Note, however, that specific classification of waste streams and the methods for their management, treatment, and disposal are defined by the policies, laws, and regulations that a nation applies to commercial-scale nuclear power generation and subsequent nuclear decommissioning and waste management activities. For these reasons, waste classification is complex and may vary from country to country [44]; the descriptions presented

here are for informational purposes only and are not an endorsement of a particular radioactive waste classification system.

Uranium Mill Tailings and Groundwater Restoration For conventional mining and milling operations, processing the ore results in a waste stream of solid waste material, sands, fine-grained slurries (sometimes called slimes), and processing liquids. These materials are collectively referred to as tailings and are pumped from the mill to a tailings impoundment for disposal (see Figs. 2 and 3).

Generally, there are a number of tailings impoundments and evaporation ponds at each mill site [22], and the total volume can be quite large. The amount and nature of the tailings, however, depend on the capacity of the mill and the length of time the facility is in operation. For example, the former Climax Uranium Company mill in Grand Junction, Colorado, produced 2 million metric tons (2.2 million tons) of tailings that were placed in a 46-ha (114-acre) tailings impoundment [46]. The nature of the material in each impoundment or pond varies, depending on which part of the mill process produced the tailings. In addition, with the approval of the regulatory agency, operators may use tailings impoundments for onsite disposal of wastes associated with decommissioning and dismantling buildings, structures, and equipment, as well as for soils, pond liners, and sludges that have been radiologically contaminated.

Tailings have become a major focus in regulating active uranium mining and milling operations, as well as cleaning up legacy tailings from older, inactive sites. For example, in 1978, the U.S. Congress enacted the Uranium Mill Tailings Radiation Control Act (UMTRCA) to provide government funds to clean up and stabilize tailings from inactive legacy mills [22].

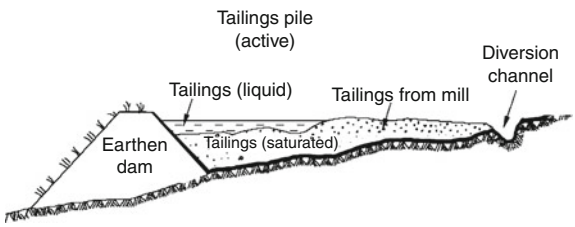

Nuclear Facilities, Decommissioning of. Figure 3
Schematic cross section of a tailings impoundment [22]

In a 1995 summary study of UMTRCA sites, the USDOE noted that tailings reclamation was the costliest aspect of the decommissioning process for conventional uranium mills [22]. During reclamation planning, the operator typically uses computer models to evaluate geotechnical stability. Although site-specific tailings reclamation methods are established in a reclamation plan that is evaluated for compliance with the government regulations that govern the cleanup [22, 24, 47, 48], general steps include:

- Shaping and recontouring the tailings pile and installing drainage diversion systems to minimize erosion hazards from surface runoff.
- Allowing the tailings to settle and dehydrate.
- Establishing survey monuments so that settling can be monitored.
- Installing a low permeability engineered cover to minimize water infiltration into the pile and radon emissions from the tailings. Generally this cover consists of clays and/or geotextiles.
- Installing a final cover for erosion protection.
- Establishing a monitoring system to ensure that the design and construction of the reclaimed tailings work as expected. Long-term stewardship during a period of institutional controls may include active measures to maintain and repair the tailings covers.

For active operations, regulations typically call for lining tailings impoundments and installing monitoring systems to prevent migration of contaminants (e.g., radionuclides and associated heavy metals) from the tailings into underlying aquifers [24, 48]. For older and inactive operations, however, the tailings impoundments may not be lined. This can lead to contaminants leaching into the underlying groundwater system over time; these contaminants need to be remediated when the tailings are reclaimed. Depending on the importance of local groundwater resources to nearby communities and the site and design of the impoundment, the level of effort needed to clean up groundwater may be extensive and long term.

Because uranium milling at an ISL facility does not produce tailings, the amount of material at the surface to be decommissioned and ultimately reclaimed is significantly less. Because there are no large tailings impoundments associated with ISL facilities, contaminated decommissioning wastes (e.g., equipment,

building components, soils, evaporation pond sludges, and liners) must either be transported to a licensed disposal facility, or an onsite disposal cell will need to be built.

The ISL process does, however, alter groundwater chemistry in the production well fields. After uranium extraction from the ore deposit is no longer economically feasible, the groundwater quality is restored to pre-extraction conditions through a series of treatment steps [13, 49]. As with tailings reclamation, site-specific methods are determined with approval of the regulatory agency, but general steps for groundwater restoration include:

- Groundwater sweep, where groundwater is pumped from the production zone to draw in surrounding natural groundwater. The pumped groundwater may be treated to remove contaminants and reinjected.
- Reverse osmosis, where groundwater is pumped from the production zone and passed through a pressurized, semipermeable membrane (reverse osmosis) system to remove dissolved chemicals. The cleaner water is then reinjected, and the more concentrated brines are pumped to evaporation ponds or disposed of by injection in deep wells.
- Stabilization, where chemicals such as hydrogen sulfide may be injected into the production zone to establish chemical conditions that cause dissolved chemicals to precipitate out as minerals.
- Monitoring, where the groundwater quality is tested to ensure that conditions have stabilized and meet the restoration criteria.

Groundwater restoration occurs when the economics for producing a well field are no longer favorable. Because ISL facilities typically have more than one well field, it is common for groundwater restoration to begin in one well field while other well fields are still actively producing uranium [13, 49].

After groundwater restoration, the physical components of the well field are then restored. Piping, well casing, and pipeline materials are hauled to a licensed disposal facility. Surface facilities such as tanks and buildings are dismantled, removed, and disposed. Pumps are removed for reuse in other well fields, and the wells are filled with cement, plugged, and abandoned. Any soils contaminated by well field spills are removed and disposed, and the disturbed land is graded, recontoured, and revegetated.

Spent Nuclear Fuel and High-Level Waste As described previously in "Fuel Reprocessing Facilities" section, after the economic energy has been extracted from nuclear fuel, the fuel is removed from the reactor. At this point, it is referred to as spent nuclear fuel. Spent nuclear fuel is highly radioactive because of the decay of fission and activation products that result from the nuclear reactions that occur when the fuel is inside the reactor core. Although it is no longer hot enough to generate electricity, it is well above ambient temperatures.

For these reasons, spent nuclear fuel must be carefully handled, stored, and shielded to provide both radiation protection to workers and the public, and to manage the thermal heat generated by the cooling fuel. In most cases, spent nuclear fuel is stored at or near the reactor, either in dedicated spent fuel pools that use water to provide both cooling and radiation protection or in air-cooled concrete and steel dry casks [13].

As described in "Fuel Reprocessing Facilities" section, after spent nuclear fuel has been cooled and radioactivity has decreased through decay of short-lived radionuclides, spent nuclear fuel may be reprocessed. The fuel reprocessing process typically produces a liquid waste stream that contains fission and activation products that remain after potentially valuable radioactive elements such as plutonium and uranium are removed. This liquid waste stream is typically stored in large tanks for subsequent treatment. Treatment may include processing the liquid wastes into different forms such as sludges, salt cake, or a calcined solid. These forms still produce radiation and must be shielded to provide protection to workers. Current practice in countries such as France, Japan, the United Kingdom, and the United States involves using high temperature furnaces to vitrify liquid wastes into a solid glass waste form.

In most countries in Europe, Asia, and North America, the ultimate disposal path for spent nuclear fuel and reprocessing high-level radioactive waste (HLW) is permanent geologic disposal in an underground repository [50]. At present, a large number of different geologic settings are under consideration. No country has licensed and constructed a geologic

repository, however, and spent nuclear fuel and reprocessing HLW are typically managed through onsite interim storage.

Intermediate-Level Waste Intermediate-level radioactive waste (ILW) is defined in IAEA [45] as "... waste which, because of its radionuclide content requires shielding but needs little or no provision for heat dissipation during its handling and transportation." This waste may be further classified into components consisting of short-lived radionuclides that will decay to low levels during a period on the order of hundreds of years in which institutional controls such as fencing or access restrictions can be considered to be effective in minimizing radiological dose [45]. Conversely, long-lived ILW is dominated by radionuclides that will not decay to sufficiently low levels. The ILW classification is not used in the United States.

In the United States, a transuranic (TRU) waste stream includes man-made alpha radiation-emitting radionuclides with an atomic number greater than that of uranium (i.e., 92) and a half-life longer than 20 years [51]. TRU is produced during reactor fuel assembly, weapons fabrication, and fuel chemical processing operations [15]. Specifically, TRU is that portion of the waste stream that is not classified as spent nuclear fuel, HLW, or low-level radioactive waste (LLW) [30, 51].

A wide variety of storage options exists for the storage and disposal of ILW and TRU. Storage may be through retrievable burial, underground bunkers, concrete caissons, aboveground concrete pads, and inside buildings [30]. Since 1999 in the United States, the USDOE has been disposing TRU waste in a bedded salt deposit about 700 m (2,300 ft) below the ground surface at the Waste Isolation Pilot Plant (WIPP) in Carlsbad, New Mexico [30].

Low-Level Waste LLW has low radionuclide content. Similar to ILW, IAEA [45, 52] suggests that LLW be further divided on the basis of whether it consists predominantly of short-lived or long-lived radionuclides. LLW tends to be defined by what it is not (i.e., not HLW, ILW, or TRU) rather than what it is, so it can include a broad range of materials and radioactivity levels [30, 51]. For example, LLW may contain small amounts of radioactivity spread through a large volume of material or it may contain sufficiently high levels of radioactivity to require shielding for its safe handling [15, 30, 53]. LLW wastes generated during nuclear decommissioning may involve a wide range of materials including rags, papers, filters, ion exchange resins, discarded protective clothing, contaminated soils and construction rubble, piping, and tanks.

Because of the generally low levels of radioactivity, LLW is typically disposed using near-surface burial. Depending on its physical and chemical properties, LLW may be packaged in drums, casks, special boxes, or other sealed containers [30]. Contaminated soil and construction debris may be disposed directly into the cell without a container. Some large components such as pipes and tanks may be cut up or flattened to reduce the volume.

LLW disposal facilities may be either commercial or government operations, although commercial facilities are still typically governed by government regulation. Similar to municipal landfills, LLW disposal cell designs may include a liner, and an engineered cover system may be installed to reduce water infiltration into the underlying groundwater system [15]. Monitoring systems and institutional controls are installed to ensure waste isolation (air, water, and soil) and to limit access to the disposal facility [51].

Hazardous and Mixed Wastes Depending on their age and size, decommissioning of nuclear facilities may involve management and disposal of hazardous wastes that result from the processes employed during facility operations, or from building standards used during the initial construction of the plant. For example, hazardous chemicals such as acidic, alkaline, and organic solutions used during uranium milling or fuel reprocessing may require special handling, treatment, and segregation prior to disposal. In addition, hazardous materials such as asbestos may be encountered when older buildings are dismantled and may require special treatment and disposal. If these hazardous wastes are free from radioactive contamination, their ultimate disposal path would be based on hazardous waste regulations.

Radioactive wastes may also be mixed with hazardous wastes. The management and disposal of these

wastes can be complicated, as there may be more than one agency with jurisdiction and more than one set of waste handling criteria may apply. For example, in the United States, the U.S. Environmental Protection Agency (USEPA) has authority over hazardous waste through the Resource Conservation and Recovery Act, and the USNRC and USDOE have regulatory authority over radioactive wastes through the Atomic Energy Act. In this case, the management and disposal options to be considered for decommissioning wastes may need to comply with both hazardous and radiation safety requirements [54].

Uncontaminated Wastes As with other industrial operations, nuclear facilities may also produce wastes that contain little or no radioactive contamination. If the radioactivity of these wastes falls below levels established by the applicable regulations and statutes, they may require no additional nuclear regulatory control. Also, as described in "Safety and Performance Assessment" section, some decommissioning wastes can be decontaminated below the applicable "clearance" levels and released from regulatory control [55]. IAEA [45] identifies these as "exempt" wastes and notes that they can be disposed of using conventional methods and systems.

As structures are dismantled and steel, concrete, and other surfaces (e.g., parking lots) are removed, large volumes of construction debris may be generated during nuclear facility decommissioning. Because some of these structures are not associated with nuclear-related activities, construction debris of this nature may meet the requirements of exempt waste. The specific levels of radioactivity that establish the criteria to be used in identifying exempt wastes will typically differ from country to country. As a result, the volume of exempt waste and disposal paths will also vary.

General Methodologies for Decommissioning

Specific decommissioning activities and technologies, as well as the sequence of their application, will vary depending on size, age, operational conditions, and design of a nuclear facility, and on the regulatory framework that governs decommissioning. As indicated previously, this article provides a general discussion of typical decommissioning activities. This discussion is not a recommendation of particular approaches or technologies, and the reader is referred to the references identified in the Bibliography for further reading.

Developing a Site-Specific Decommissioning Plan

Nuclear decommissioning is perhaps most effective when the process is laid out in a decommissioning plan. For the lead organization (either commercial or government) with responsibility for decommissioning, the plan provides the opportunity to develop a strategy that, among other things, identifies specific decommissioning issues at a given site, determines the types of processes and methodologies to be used, specifies the desired end state of the facility, and establishes the schedules and financing mechanisms for decommissioning. For large, complex commercial nuclear fuel cycle facilities such as a power plant or a fuel enrichment plant, the decommissioning plan is an extensive document that is supported by a large number of underlying technical and policy reports and references. Although the specific contents of a decommissioning plan can depend on the type of facility, the regulatory framework, and other policy issues, some of the general topics to be covered include [18]:

- Facility Description and Operational History
- Radiological Status
- Alternate Decommissioning Strategies and Selection of a Preferred Alternative
- Project Management
- Decommissioning Activities
- Surveillance and Maintenance During Decommissioning
- Waste Management
- Cost Estimate and Funding Mechanisms
- Safety and Performance Assessment
- Environmental Impact Assessment
- Health and Safety for Workers and the Public
- Quality Assurance
- Emergency Planning
- Physical Security and Safeguards
- Final Radiation Survey

Typically, a site-specific decommissioning plan is developed and refined in stages. An initial plan describing major structures, systems, and features is developed

as the facility is designed and constructed. The initial plan is designed to provide basic information and establish project baselines prior to facility startup. The initial decommissioning plan is also intended to provide a framework for cost estimates (see "Estimates of Decommissioning Costs") to ensure that the necessary funds will be in place to cover decommissioning when the facility ceases operation. During the operational life of the facility, the initial decommissioning plan is periodically updated to reflect the operator's experience and understanding of the site. As with any large industrial facility, nuclear facilities may change as technology or regulatory oversight develops, or as the economics of the plant change. As the plant approaches the end of its operational life, the decommissioning plan becomes more detailed. The final decommissioning plan is developed just prior to a facility ceasing operations. The regulatory agency typically reviews this plan and must approve it before the operator can implement the decommissioning strategy [18]. Once the decommissioning plan is approved, it then becomes the basis for subsequent activities, although it may continue to be revised throughout a decommissioning process that can extend over decades.

Site Characterization

Site characterization provides the context for nuclear decommissioning. Ideally, site characterization includes a description of the size and location of the facility, buildings and systems, and the operational history of the site, as well as a description of spills or other releases that may affect the decommissioning process. Nonradiological hazardous process chemicals and other materials like asbestos that require special treatment and disposal may also be identified in the site characterization survey.

One objective in undertaking site characterization is to establish the preoperational baselines and background values that may be used to determine criteria for successful decommissioning. For example, an understanding of background water quality is used to establish site-specific levels for groundwater restoration, as well as action levels for monitoring. Site characterization should identify the geographical and geological context of the facility in relationship to important resources for the area such as critical habitat or historical and cultural areas. In addition, site characterization may include a discussion of the socioeconomic impacts of the facility, because this may be an important consideration in selecting among different decommissioning strategies [1]. The site characterization and radiological surveys are intended to be of sufficient detail to provide data for planning the decommissioning effort, including selection of specific remediation techniques, establishing decommissioning schedules, estimating costs and waste volumes, and identifying important health and safety considerations to be considered during decommissioning [20].

For the purposes of nuclear decommissioning, site characterization pays special attention to the radiological status of the site, focusing on establishing the extent to which buildings, systems, equipment, soils, and water may contain residual activity [18]. These radiological "hot spots" can be determined using historical information (e.g., location of historic spills, known storage locations, sites identified by ongoing monitoring during operations), conducting surveys with radiation detection equipment, and collecting soil and water samples for subsequent analysis [18, 20, 56, 57].

A key component of site characterization is locating and maintaining existing records [58, 59]. A lack of information on past activities has been a special challenge for decommissioning Cold War legacy sites.

Selecting a Decommissioning Strategy

The reasons for taking a nuclear facility out of service may be based on economics, national policy decisions about the suitability of nuclear power, safety, or obsolescent technology [60]. As described in "Introduction" section, decommissioning strategies for nuclear facilities generally fall into one of three categories:

- A strategy of immediate decontamination and dismantlement [1, 7, 61, 62] (also defined as DECON [14, 15]) begins soon after the nuclear facility closes. For nuclear reactors, spent nuclear fuel is removed, stored, and cooled, pending permanent disposal or reprocessing, and equipment, buildings, structures, and portions of the facility that contain radioactive contaminants are either removed or decontaminated to meet regulatory requirements for releasing the property. In general, this strategy

imposes the largest requirements for resources (funding) and personnel in the short term. It takes advantage of the existence of a trained workforce with experience in operating the facility.

- Safe storage [1, 61], deferred or delayed decontamination [7, 62], or SAFSTOR [14, 15], refer to decommissioning strategies where a nuclear facility is left intact after closing, placed in a stable condition, and maintained and monitored until subsequent dismantlement and decommissioning. One purpose in choosing this strategy is to allow radioactivity to decay during a period of safe storage, perhaps on the order of decades, potentially reducing the radiological hazards and the quantity of nuclear waste that must be disposed. This strategy may also benefit from continuing developments in decommissioning technology and waste management options.

  This approach places a premium on knowledge management, as the operations workforce may not be available when decommissioning begins years after the end of operations. This decommissioning strategy may be the only option if there are insufficient funds available to cover the costs of immediate decontamination and dismantlement, or if some aspects of the regulatory framework, such as a spent nuclear fuel disposal site, are not available when operations cease [7, 63].

  Safe storage may allow one part of a large facility to be closed while the rest of the facility completes its life cycle. For example, one reactor unit at a nuclear power plant may be closed and the fuel removed while the remaining reactor units continue to produce electricity. When the decision is made to close the remaining portions, all of the components can then be decommissioned together, with accompanying potential benefits from optimizing the use of staff and specialized equipment for decommissioning. An example of this approach is the Peach Bottom Unit 1 reactor in York County, Pennsylvania, which was shut down in 1974 and placed in SAFSTOR. Reactor Units 2 and 3 continue to operate and are scheduled for shutdown in 2034, at which point final decommissioning will begin [64].
- A strategy of entombment [1, 7, 61, 62] or ENTOMB [14, 15] involves encasing radioactive materials onsite in a long-lived, structurally sound material such as concrete. The entombment structures are maintained and monitored as appropriate, with institutional controls (e.g., fencing, security personnel) to limit access. For some facilities, the intent of entombment is permanent encapsulation [7], and computer models are used to simulate performance for thousands of years [19]. Because entombment effectively creates a surface waste disposal site, it is not generally a suitable decommissioning strategy for facilities associated with fuel enrichment, fuel fabrication, and fuel reprocessing [62]. In addition, an entombment strategy may also limit the options for releasing the site for reuse.

The first two decommissioning strategies may also be combined. For example, some facilities at a site may be immediately dismantled while other structures are placed in safe storage. For large sites like fuel enrichment plants, nuclear decommissioning activities may be occurring at some facilities at the same time as active operations [4]. Generally, it is anticipated that decommissioning activities will be completed in a period of decades from the end of operations [14].

Because of the wide variety of nuclear facilities, there is no unique approach to decontamination and decommissioning. Several factors may be considered in selecting the decommissioning strategy [1, 7, 62] for a specific site, including:

- The status of the policies and regulatory framework that establish, among other things, the national direction of the nuclear industry and legal requirements for nuclear decommissioning
- The financial costs (both direct and indirect) associated with a given decommissioning strategy and the amount of funding available
- The availability of waste management and disposal facilities for the types and volumes of waste to be generated during decommissioning
- Risks to health and safety of both workers and members of the public
- Potential environmental impacts associated with a given decommissioning strategy
- Knowledge management concerns and the availability of trained and experienced personnel to conduct the decommissioning activities

- The desired end state for the site, and potential socioeconomic impacts to local communities and other stakeholders, including options for release and reuse of the site after decommissioning is complete

These factors need to be considered within the context of the specific site before selecting the preferred alternative. As described previously, the reasons for selecting one alternative as opposed to another should be discussed in the decommissioning plan.

Estimates of Decommissioning Costs

The facility owner is generally responsible for ensuring that there are sufficient resources to cover activities associated with decommissioning a nuclear facility. These activities may include decontamination, decommissioning, reclamation, and groundwater restoration, as well as surveillance and monitoring that may be necessary for long-term stewardship. Cleanup of government facilities and legacy sites that were established prior to the development of a regulatory framework for nuclear decommissioning are generally the responsibility of the national (or state/provincial) governments. Funds for these government responsibilities may be raised by general appropriations (taxes) or user fees imposed on the beneficiaries of nuclear power.

Methods used to accumulate and manage funds for decommissioning commercial nuclear facilities vary from country to country [1]. One common method to establish a decommissioning fund is to impose a requirement that a portion of business revenues be set aside for decommissioning and waste management. Typically, the types of financial mechanisms that are acceptable for estimating, creating, and maintaining a decommissioning fund are either established by the regulatory agency responsible for the facility license or directly by legislation [1, 21].

In countries with a robust regulatory framework, the owner/operator is commonly required to present estimates for the cost of decommissioning activities as part of the license application. A detailed discussion of estimating decommissioning costs is contained in USNRC [21]. In general, cost estimates are specific to the size, type, and location of the facility, and they incorporate assumptions about:

- The transition between operations and facility shutdown, and the work associated with that process, such as postoperational cleanout
- The definition for the end state of the decommissioning process (e.g., unrestricted release, restricted release)
- The availability and suitability of established approaches to decommissioning methods versus the need for unique and perhaps untested technologies
- Availability and capacity of facilities for managing or disposing of residual spent fuel and radioactive waste

Once the regulatory agency or governing body evaluates and accepts the proposed cost estimates, the type and amount of the financial surety (e.g., letter of credit, prepaid cash, government bond) is established and administered in accordance with government regulations. The regulatory agency (as in Canada, United States, and Sweden) or a waste management body (as in Belgium and Spain) then reviews the fund on a regular basis, generally between 1 and 5 years [1, 21]. As identified during the review, the decommissioning fund may be updated and the amount adjusted either upwards or downwards to account for inflation, changes in technology, or completed decommissioning activities.

As noted previously, the actual costs of nuclear decommissioning can vary substantially. The IAEA provided estimates for median decommissioning costs associated with various types of nuclear facilities based on a combination of expert judgment and decommissioning experience and using assumptions with respect to operating life and time to decommission [4]. These estimates (in US $, 2003 value) are summarized in Table 2. Because the cost of decommissioning will depend strongly on site-specific issues such as local geology, facility age and design, and operational history, the actual costs for a given site may fall outside these ranges.

The estimates reported in IAEA [4] are general in nature and are not intended to bound all potential costs, particularly for very large government facilities. One general conclusion that can be made from these estimates is that management of spent nuclear fuel and radioactive wastes can represent a significant

Nuclear Facilities, Decommissioning of. Table 2 Estimated costs associated with decommissioning different nuclear facilities [4]

Type of nuclear facility	Estimated decommissioning cost (min to max [median] in US $ million, 2003 value)	Operational life (years)	Time to decommission (years)
Uranium milling	0.800	25	1
Uranium conversion/recovery	150	30	3
Uranium enrichment	600	30	10
Fuel fabrication	250	30	2
Nuclear power reactor[a]	250–500 (350)	40	10 (after 5-year transition period)
Fuel reprocessing	800	30	15
Industrial facilities	0.050–3 (0.200)	20	1

[a]Cost estimates for decommissioning nuclear power reactors do not include the processing of operational waste, removal and disposition of spent nuclear fuel, the draining of operational systems, or the development of a waste disposal facility

proportion of the total costs of decommissioning. For example, estimated costs for decommissioning the Sequoyah Fuels uranium conversion site near Gore, Oklahoma, varied from US $19 million for the no-action alternative of long-term stewardship, to about US $36 million for onsite disposal of most contaminated wastes, to as much as US $254 million for transportation and offsite disposal of all contaminated wastes [25]. These cost issues indicate the importance of accurately characterizing a site and identifying appropriate opportunities to decontaminate, recycle, and reuse materials.

Safety and Performance Assessment

Safety is among the highest priority issues in nuclear decommissioning. Safety assessments, typically developed by both operators and regulators, are engineering analyses that involve calculations and computer simulations to evaluate potential radiological doses. The purpose of the safety assessment is to identify and evaluate potential hazards to ensure that nuclear decommissioning can be done in a manner that is safe for workers, members of the public, and the environment [65].

In general, the safety assessment should be systematic and be linked to relevant safety criteria, taking into consideration potential radiological doses to workers and members of the public, discharges to the environment, and exposure to chemical and other nonradiological hazards [18, 57, 65, 66]. To meet these objectives, a safety assessment consists of:

- Estimates of system performance for all the situations selected
- Evaluation of the level of confidence in the estimated performance
- Overall assessment of compliance with safety requirements

The standards and criteria to be used in developing these assessments vary from country to country depending on the regulatory framework that is in place. Also, the nature of the safety assessment may vary depending on the complexity of the decommissioning strategy needed for a given nuclear facility. A general framework proposed by the IAEA [64] includes:

- The scope of the assessment, based on the physical state of the nuclear facility
- The objectives of the assessment
- The applicable safety requirements and criteria to be used in evaluating potential exposures to workers, members of the public, and the environment
- Outputs from the safety assessment, generally in the form of doses that can be compared to the relevant safety requirements and criteria

- A description of the approach used to implement the safety assessment, whether through simplified calculations or complicated computer models, and a discussion of how the approach is appropriate to the magnitude and time frames of the potential hazards
- Time frames for all phases of the decommissioning activities considered in the safety assessment
- A definition of all phases of nuclear decommissioning and the anticipated end points for each phase
- A definition of the final end state of the facility that is anticipated after all decommissioning activities are complete

In practice, a safety assessment starts with a description of the facility and all of the anticipated decommissioning activities that comprise the decommissioning strategy (see "Selecting a Decommissioning Strategy"). To evaluate off-normal scenarios, a safety assessment also includes identification of potential hazards and initiating events (both natural events such as earthquakes and human-made events such as fire), and potential exposure pathways. These are screened, usually on the basis of probability of their occurrence and the resulting consequence should they occur. Plausible scenarios are developed and used in the engineering analysis to quantify the likelihood and magnitude of potential radiological and safety consequences. In addition, the safety assessment should identify relevant experience and lessons learned from the decommissioning of similar facilities, if available.

For disposing of longer lived radionuclides, some regulatory frameworks and decommissioning strategies use a performance assessment that provides a quantitative evaluation of potential releases of long-lived radionuclides over time periods of hundreds to thousands of years or longer. Similar to safety assessments, but with a much longer time horizon, performance assessments typically involve computer simulations based on site-specific features, events, and processes (biological, physical, and chemical) that may affect the long-term performance of engineered barrier systems. A performance assessment also simulates the release of radionuclides from any engineered barrier system and their subsequent migration through the geosphere surrounding the facility. Finally, future potential radiological doses may be calculated for a hypothetical receptor group located away from the facility [38]. Because of the long time frame, it is not possible to include all potential conditions that might affect performance, so simplified models, or abstractions, are used to simulate important aspects of the engineered and geological systems. This can introduce uncertainty into the calculations that should be characterized and evaluated to determine whether there is sufficient confidence that the applicable regulatory criteria will be met [19, 38].

In essence, the idea of safety and performance assessments is intended to answer these questions: What can go wrong? How likely is it? What are the consequences? [38]. Where there is uncertainty in conceptual models of the system or in the model parameters, simplifying assumptions should be chosen in such a way that ensures the models will be transparent, conservative, and not underestimate potential radiological doses. Statistical analysis and sensitivity studies can help to characterize the nature and relative importance of the uncertainty. Depending on the results of the safety and/or performance assessment, the planned decommissioning activities may be modified to reduce risks, or compensate for uncertainty or limited information [66].

Decontaminating Structures, Equipment, and Components for Reuse or Recycling

The objectives of decontamination include reducing the potential radiological exposure of workers and members of the public during decommissioning; minimizing the volume of radioactive waste; and increasing the potential for reusing and recycling equipment, material, and land at the site of a nuclear facility [67].

Although specific technologies to be used during decommissioning activities will vary depending on size, age, operational conditions, and design, general decontamination methods include [68–70]:

- Chemical methods that use agents such as acids, oxidants, or chemical foams and gels to remove contamination fixed to surfaces. The nature of the chemical agent may be determined based on the properties of the surface to be decontaminated. Chemical decontamination methods may generate a liquid waste stream that requires further

treatment to remove radioactive wastes (and generate subsequent secondary waste streams).

- Mechanical methods that rely on cutting, grinding, or other physical techniques to remove contaminated surfaces or layers.

The techniques used for decontamination will vary by material and from site to site, depending on issues such as the operational history of the facility, the level of contamination, and the type of material to be decontaminated [67, 69]. For example, chemical decontamination methods may not be appropriate for porous materials such as concrete, where fluids may migrate into the material.

In addition to technical feasibility, other considerations in selecting decontamination techniques may include the applicable clearance criteria and the potential doses to workers or members of the public to reach these levels. The selection process may also include evaluating the cost of decontamination versus the cost of disposal without decontamination, taking into account estimates of the volume, nature, category, and activity of any primary and secondary wastes that might result. For example, decontamination methods should be selected in such a way as to minimize the amounts of secondary wastes (e.g., cutting fluids or washdown fluids) produced. It is also important to ensure that selected decontamination methods are compatible with and do not compromise existing or planned key treatment, conditioning, storage, and disposal systems [67]. For example, high-pressure jets may not be an appropriate method for cleaning liquid waste storage tanks that are decades old and have experienced some corrosion.

Dismantling and Removing Buildings, Structures, and Equipment from the Site

Equipment removed from buildings (Fig. 4) during the cleanup process is typically categorized as (1) salable for unrestricted use after radiation checks and decontamination; (2) potentially contaminated, but may be salvageable for sale to other nuclear facilities; and (3) contaminated and must be disposed. The responsible regulatory authority generally establishes the levels of contamination for these different categories.

Dismantling and removing buildings, foundations, structures, and equipment from a nuclear facility is sometimes referred to as "construction in reverse," and similar types of heavy equipment (e.g., trucks, cranes, earthmoving equipment) are used during dismantling (see Figs. 4 and 5). In addition, cutting equipment and even demolition explosives may be needed to break large structures down into smaller pieces that can be handled and transported more easily (Figs. 5 and 6). For high-radiation areas, remote techniques such as underwater cutting may be necessary to provide for worker radiation protection [67].

Where salvage is not economically or technically feasible, larger pieces of equipment (e.g., pipes, tanks) may be cut up and flattened, and building materials reduced to rubble to minimize waste volume and make handling for subsequent disposal easier. How much volume needs to be reduced may depend on the

Nuclear Facilities, Decommissioning of. Figure 4
A steam generator is removed from a reactor building [76]

Nuclear Facilities, Decommissioning of. Figure 5
Demolition of a reactor containment building [76]

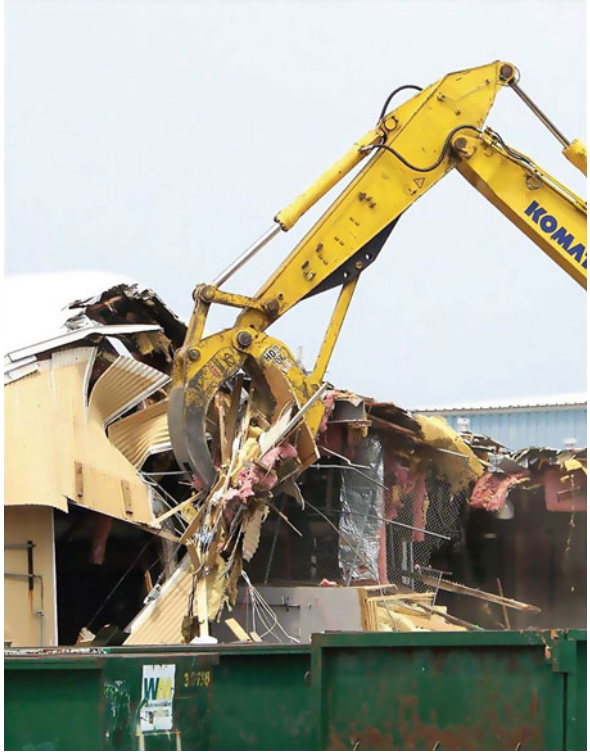

Nuclear Facilities, Decommissioning of. Figure 6 Dismantling industrial buildings at a nuclear facility [42]

Nuclear Facilities, Decommissioning of. Figure 7 Removing uncontaminated soil and debris for offsite disposal [42]

available waste disposal capacity and regulations that govern transportation and disposal. Pavement in roads and parking lots may also be removed for disposal as construction debris.

Remediating Contaminated Soils and Groundwater

Remediating residual radioactivity in soils and water generally uses technologies that are well established in the environmental industry. Evaluating and selecting a specific technique is an important part of decommissioning and depends on many site-specific issues such as the physical and chemical state of the residual radioactive material, the availability of equipment and a trained workforce, the availability of appropriate waste disposal capacity, and stakeholder sentiment. The following discussion is intended only as a brief summary of commonly available methods for remediation.

The most common remediation method used for contaminated soils involves excavating the soil for disposal in a LLW facility (Fig. 7). If the contamination layer is not deep, this may be an economically viable approach. If the contamination is widespread, however, the volume of material to be disposed in this fashion may be quite large and may increase the costs of waste disposal. Alternatively, the soil may be excavated and treated using physical and chemical separation techniques to isolate and reduce the volume of contaminated material [27]. For example, in some cases, residual radioactivity may be more closely associated with fine clay-sized particles in the soil that can be separated by using screens or other physical separation methods. Chemical extraction methods use solutions such as organic acids to bind to the contamination and remove it from the soil. After separation of the contaminated and uncontaminated soil fractions, the uncontaminated soils are used as clean fill, and contaminated soils are treated further or processed for disposal. If chemical methods are used, the leachate may be treated to remove the dissolved radionuclides to meet water standards.

Contaminated surface water and groundwater typically require treatment to meet applicable standards. Widely available technologies for contaminated groundwater include pumping and treating to pull the contaminant plume back toward the extraction well. The contaminated water is then treated through a process such as ion exchange and is either injected back into the aquifer or discharged to a suitable surface water disposal system. A more recent technology for treating contaminated groundwater is the construction of a passive permeable reactive barrier or slurry wall system (Fig. 8). Built below the ground surface so that they intercept the groundwater plume, the reactive materials in the barrier are selected to chemically react with the contaminants and immobilize them in the subsurface. Reactive materials that may be used to remove uranium from groundwater include different forms of iron, such as metallic (zero-valent) or amorphous ferrihydrite [27]. The contamination will remain in place until the barrier is excavated, and barrier longevity and long-term performance are important engineering issues.

Nuclear Facilities, Decommissioning of. Figure 8 Building a slurry wall to remediate contaminated groundwater [42]

Other technologies rely on in place or in situ methods to reduce or immobilize soil and water contamination. For soils, contamination may be reduced or immobilized through mixing in amendments such as apatite or phosphate that will chemically react with the contamination. Alternatively, soil contamination may be immobilized in place by grouting or capping. Bioremediation is a collection of more recent technologies that use biological organisms to preferentially extract or otherwise break down toxic and radiological contamination from both soils and groundwater [71]. For example, sunflowers have been demonstrated to take up uranium from waste at a site in Ashtabula, Ohio, and at a small pond contaminated with uranium near the Chernobyl nuclear power plant site in Pripyat, Ukraine [27, 71].

In addition to active remediation technologies, monitored natural attenuation of contaminated soils and groundwater may be also be applicable, if it can be demonstrated to meet applicable criteria in a reasonable timeframe [72]. This method relies on monitoring soils and groundwater while the natural physical, chemical, or biological processes already occurring at the site contain and reduce volume, mass, and toxicity of the contamination in place. Where site conditions such as soil type and groundwater flow are favorable, monitored natural attenuation can be an attractive option because it is typically less disruptive and costly than more active remediation measures. However, because it can be perceived by stakeholders as "doing nothing," monitored natural attenuation is generally proposed as one part of a broader remediation strategy and combined with active remediation measures [72]. For example, a contamination source may be excavated and removed while monitored natural attenuation is implemented for the associated groundwater contaminant plume.

Waste Management and Disposal

As described in "Waste Management and Disposal" section, decommissioning wastes can fall into several different classes. Waste classification ultimately depends on the type of historical operations at the site and will influence the decommissioning strategy

and waste management options that are selected for a facility. Once the physical, chemical, and radiological properties are characterized and the waste is classified and the applicable criteria are determined, the basic options for waste management are either onsite storage/disposal or transport offsite to an approved waste disposal facility.

For nuclear power plants, one of the final phases of operations before decommissioning is to remove the fuel from the reactor (defuel) and place the spent nuclear fuel in interim storage, either in pools or dry casks. This step would be necessary regardless of the decommissioning strategy selected [69]. As they are generated during operations, other wastes may be collected, segregated, chemically adjusted, and decontaminated onsite, and then placed in temporary monitored storage onsite until a final disposition path is determined [44]. A partial list of examples of the types of wastes that may be encountered during the decommissioning of nuclear facilities is presented in Table 3.

Waste may be treated to prepare it for final disposal. Treatment concepts include volume reduction and separation and removal of radionuclides and other hazardous wastes [44]. Some treatment options include

Nuclear Facilities, Decommissioning of. Table 3 Partial list of the types of waste materials for different nuclear facilities

Type of nuclear facility	Examples of waste materials
Uranium mine	Waste rock
	Fuels and lubricants
	Contaminated soils and groundwaters
Uranium mill	Drums
	Insoluble waste and filter materials
	Liquid effluent
	Tailings and sludges
	Liquid nitrates
	Ion exchange resins
	Tanks, pipes, and equipment
	Contaminated soils and groundwater

Nuclear Facilities, Decommissioning of. Table 3 (Continued)

Type of nuclear facility	Examples of waste materials
Uranium conversion	Solid CaF_2
	CaF_2 sludges with/without minor uranium
	Non-radiological chemical waste
	Tanks, pipes, and equipment
	Contaminated soils and groundwaters
Uranium enrichment	Depleted uranium tails
	Tanks, pipes, and equipment
	Contaminated soils and groundwaters
Fuel fabrication	Uranium scrap material
	Filters
	Wash water and decontamination/cleaning solutions
	Waste oils
	Spent acids and solvents
	Equipment
	Contaminated soils and groundwaters
Nuclear power plants	Reactor vessel and internal components
	Coolant system equipment and components
	Activated concretes and steels
	Evaporator concentrates
	Tanks, pipes, and equipment
	Contaminated debris and soils
Spent fuel reprocessing	Filters
	Activated and contaminated metal components
	Spent solvents, decontamination and metal cleaning agents
	Fuel cladding
	Laboratory analytical equipment and solutions
	Tanks, pipes, and equipment
	Contaminated debris, soils, and groundwater

incineration or compaction to reduce volume, and evaporation or ion exchange to remove radionuclides from liquid wastes. Some of these techniques can generate secondary wastes such as liquids, sludges, and filters that need to be managed as well.

Radioactive wastes may also be conditioned to produce a form that is more suited for handling, transportation, storage, and disposal. Low-level and intermediate-level wastes may be immobilized by mixing with grouts, cements, and bitumen, while liquid high-level wastes from fuel reprocessing may be vitrified into a glass waste form or otherwise modified to produce a solid waste form. These wastes are placed in packages or specially designed containers for interim storage, transportation, and subsequent offsite disposal (Fig. 9). This may be at a licensed disposal site, a specially constructed disposal cell, or an existing tailings impoundment that is being reclaimed and used as a disposal cell. The materials must meet waste acceptance criteria for the disposal facility.

Nuclear Facilities, Decommissioning of. Figure 9 Low-level radioactive waste packages for offsite disposal [42]

Alternatively, waste may be disposed in place with monitoring and an engineered system for long-term disposal [42]. Onsite waste management, including a decommissioning strategy of entombment, must comply with applicable regulations for near- surface storage and disposal facilities [62]. In this case, a performance assessment (see "Safety and Performance Assessment") may be used to evaluate both engineered and natural barrier performance over long times. Depending on the nature of the waste and the site-specific conditions, different design options (backfill, concrete vaults, engineered covers) may be evaluated along with a combination of long-term monitoring and institutional controls [44]. Institutional controls such as fencing, signage, and physical security are generally assumed to be effective only for a period on the order of hundreds of years, while the performance of engineered and natural barriers is evaluated over periods as long as 10,000 years [19, 20].

Conducting Final Inspections and Surveys

During decommissioning, the national regulatory agency will typically conduct onsite reviews and inspections to ensure that the approved decommissioning plan is being followed [19] and the decommissioning activities are being conducted in a safe manner that complies with applicable regulations. After decommissioning is complete, there should be a final survey to evaluate the residual radioactivity that remains at the site. The specific goal of this survey is to determine the extent to which the site complies with the criteria set by the governing regulatory authority for subsequent reuse and/or release of the site [57, 67] – one of the objectives of decommissioning (see "Definition of the Subject").

This survey may be carried out in phases, as decommissioning work is completed, to enable parts of the site to be released from regulatory control. The final survey data are submitted to the regulatory authority, including a description of the applicable reuse/release criteria, the methods and procedures used, and the measurement results. Typically, the sampling and surveys will be focused on areas such as previous waste burial sites or spill locations identified as contaminated during the site characterization survey. These areas are sometimes called Class 1 areas [57],

and sampling and surveys will be more extensive. Areas that are less likely to be contaminated, called Class 2 and Class 3 areas, receive lesser surveying and sample coverage. The results typically include an analysis to demonstrate the statistical significance of the results as compared to natural background radiation levels [20, 56, 57, 67].

Reclaiming Disturbed Land

After decommissioning and dismantlement of buildings and structures is complete, the decommissioning strategy may call for reclaiming disturbed land to preoperational condition. This is generally accomplished by adding clean topsoil, installing drainage and erosion controls if necessary, regrading and recontouring the surface to match the surrounding topography, and revegetating with native vegetation (Fig. 10). In addition, land reclamation efforts should include monitoring to ensure that drainage and erosion controls are functioning as intended, revegetated areas are stable, and invasive species have not become established. Many of these techniques are similar to those used to reclaim surface mines [73].

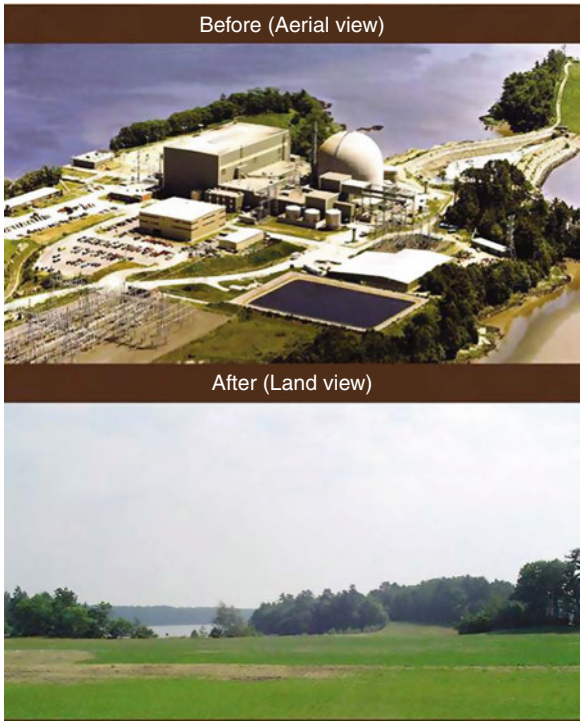

Nuclear Facilities, Decommissioning of. Figure 10 Reclamation and revegetation of site after decommissioning a commercial nuclear power plant [77]

The amount of disturbed land to potentially reclaim can vary significantly for different nuclear facilities, especially conventional uranium mining and milling operations that produce significant quantities of waste rock and tailings covering tens to hundreds of hectares (acres). The type of reclamation will depend, in part, on the intended use of the land once the license is terminated. For example, a site intended for unrestricted release as a recreation area may have a more extensive land reclamation program than a site that will ultimately be released for future industrial uses.

Status of Decontamination and Decommissioning

Because commercial nuclear fuel cycle facilities and nuclear power plants are governed at the national level using different policy, statutory, and regulatory frameworks, the status of nuclear decommissioning around the world is difficult to estimate [4]. A brief summary based on the estimates of international nuclear organizations such as the IAEA, NEA, and WNA is provided here and in Table 4.

- The leading countries for uranium production include Canada, Kazakhstan, and Australia, followed by Namibia, Russia, Niger, Uzbekistan, and the United States [40]. Uranium has been mined for decades, and some of the older mines are small and not well documented. The WNA estimates that more than 100 mines have been "retired from operations," although decommissioning is not complete at all of them [5].
- Uranium mills exist in countries with known uranium ore reserves. As of August 2003, the IAEA reported that 294 uranium mills were operating worldwide, with 231 plants shut down or in decommissioning and 149 fully decommissioned. Eight additional uranium mills were under construction [4].
- Uranium conversion plants to produce UF_6 operate in the United States, Canada, France, United Kingdom, China, and Russia. As of August 2003, the IAEA reports that 29 uranium conversion facilities

Nuclear Facilities, Decommissioning of. Table 4 Decommissioning status for nuclear fuel cycle facilities as of August 2003 ([4], Table 3)

Type of nuclear facility	Operating	Under construction	Shut down/being commissioned	Decommissioned
Uranium milling	294	8	231	149
Uranium conversion/recovery	29	1	14	2
Uranium enrichment	21	2	7	5
Fuel fabrication/heavy water production	66	5	27	23
Fuel reprocessing	13	3	18	13

were operating worldwide, with 14 plants shut down or in decommissioning and 2 fully decommissioned. One additional uranium conversion facility was under construction [4].

- Major enrichment plants are operated in the United States, France, and Russia, with smaller plants located in the United Kingdom, Netherlands, Germany, Japan, and China [28]. As of August 2003, the IAEA reports that 21 fuel enrichment facilities were operating worldwide, with 7 plants shut down or in decommissioning and 5 fully decommissioned. Two additional fuel enrichment plants were under construction [4].
- Fuel fabrication and/or heavy water production facilities operate in most countries with nuclear programs. As of August 2003, the IAEA reports that 66 fuel enrichment and heavy water production facilities were operating worldwide, with 27 plants shut down or in decommissioning and 23 fully decommissioned. Five additional fuel enrichment plants were under construction [4].
- At present, 436 commercial nuclear reactors are operating worldwide in many countries in North America, Europe, and Asia [9]. A total of 112 nuclear reactors have been placed in long-term shut down, and 14 have been completely decommissioned [4, 9]. Russia has the largest number of research and test reactors, followed by the United States, Japan, France, Germany, and China. In addition, research and test reactors are also located in developing countries in Africa, South America, and Asia. After peaking in the mid-1970s at about 370 reactors in 55 countries, the number of research and test reactors worldwide has declined sharply. As of August 2003, the IAEA reported that there were about 287 research and test reactors and critical assemblies in operation worldwide, with 8 more under construction. A total of 214 research and test reactors were shut down or being decommissioned, and 173 were reported as being decommissioned [4].
- As of August 2003, the IAEA reports that 13 fuel reprocessing plants were operating worldwide, with 18 plants shut down or in decommissioning and 13 fully decommissioned. Three additional fuel reprocessing plants were under construction [4].

Future Directions

As noted previously, interest in commercial nuclear power has been revived as a result of concerns with carbon emissions from traditional fossil fuels. As a result, many nations have reported an increase in proposed construction projects for new reactors. Although many of these proposed projects will use current Generation II and III reactor designs, there are research and development programs focused on designing the Next Generation IV reactors [37].

The different current and future design types and sizes of reactors will make decommissioning inherently a site- and reactor-specific process. Each current and future reactor design will have its own design-specific decommissioning requirements that must be taken into consideration. In addition, changes in reactor design or the use of nuclear fuels based on MOX or

thorium may lead to different fuel requirements that will change the nature of decommissioning at the front end of the nuclear fuel cycle.

Much of the decommissioning experience gained to date is focused on an open, or "once through" uranium fuel cycle. Current programs such as the Global Nuclear Energy Partnership are evaluating the potential of a closed fuel cycle, where fuel is reprocessed and used more than once to generate power [39]. This approach, along with changes in ongoing nuclear reactor operations, would change the amount and characteristics of spent nuclear fuel for handling, storage, and disposal. In addition, closing the fuel cycle would require new nuclear fuel cycle facilities and change the waste streams produced at the back end of the fuel cycle. For these reasons, a change from an open to a closed nuclear fuel cycle may need new waste disposal options that will influence the selection of the decommissioning strategy for these types of facilities.

Although new decontamination techniques are continually being developed [27, 69], existing technology that has been previously applied with demonstrated success may continue to be preferred by stakeholders (members of the public, government agencies) to an untried method, particularly if trained staff and specialized equipment are readily available. As decommissioning costs and potential benefits are better understood, newer techniques may be applied more. In addition, many nations are looking at extending the service life of existing nuclear facilities and reactors. At the same time, the nuclear workforce is aging, placing a premium on knowledge management and recordkeeping to ensure valuable information and experience is not lost [58, 74, 75]. Decommissioning decisions are perhaps many decades in the future, but should be taken into consideration as designs are developed for advanced reactors and the nuclear facilities that support them.

Bibliography

Primary Literature

1. NEA (2002) The decommissioning and dismantling of nuclear facilities. Paris, France. Status, approaches, challenges. Report No. NEA 3714. Nuclear Energy Agency/Organisation for Economic Co-Operation and Development, Issy-les-Moulineaux. http://www.nea.fr/html/rwm/reports/2002/3714-decommissioning.pdf. Accessed 28 Apr 2009
2. Commission of the European Communities (Oct 2007) Communication from the commission to the council and the European parliament. Nuclear illustrative programme. Presented under Article 40 of the Euratom Treaty for the Opinion of the European Economic and Social Committee. Commission of the European Communities, Brussels
3. NEA (2009) NEA annual report 2008. Nuclear Energy Agency, Issy-les-Moulineaux. http://www.nea.fr/html/pub/activities/ar2008/AR2008.pdf. Accessed 20 May 2009
4. IAEA (Aug 2004) Status of the decommissioning of nuclear facilities around the world. IAEA, Vienna. http://www-pub.iaea.org/MTCD/publications/PDF/Pub1201_web.pdf. Accessed 20 May 2009
5. WNA (Sept 2006) Safe decommissioning of civil nuclear industry sites. World Nuclear Association, London. http://www.world-nuclear.org/reference/position_statements/decommissioning.html. Accessed 20 May 2009
6. O'Sullivan P, Pescatore C, Tripputi I (2009) Applying decommissioning experience to the design and operation of new nuclear power plants. NEA News 27:13–15, http://www.nea.fr.html/pub/newsletter/2009/applying-decommissioning.pdf. Accessed 8 July 2009
7. IAEA (Nov 2005) Selection of decommissioning strategies: issues and factors. Report by an expert group. IAEA-TECDOC-1478. IAEA, Vienna. http://www-pub.iaea.org/MTCD/publications/PDF/TE_1478_web.pdf. Accessed 20 May 2009
8. IAEA (2008) International atomic energy agency annual report 2007: 50 years of atoms for peace. IAEA, Vienna. http://www.iaea.org/Publications/Reports/Anrep2007/anrep2007_full.pdf. Accessed 20 May 2009
9. IAEA (2009) Latest news related to the power reactor information system and the status of nuclear power plants. IAEA, Vienna. http://www.iaea.org/cgi-bin/db.page.pl/pris.main.htm. Accessed 12 June 2009
10. Reisenweaver D, Laraia M (2000) Preparing for the end of the line. Radioactive residues from nuclear decommissioning. IAEA Bull 42:51–54
11. USNRC (2009) Expected new nuclear power plant applications: updated 4 Feb 2009. U.S. Nuclear Regulatory Commission, Washington, DC. http://www.nrc.gov/reactors/new-reactors/new-licensing-files/expected-new-rx-applications.pdf. Accessed 20 May 2009
12. IAEA (2008) Energy, electricity and nuclear power estimates for the period up to 2030. Reference data series no. 1. IAEA, Vienna. http://www-pub.iaea.org/MTCD/publications/PDF/RDS1-28_web.pdf. Accessed 12 June 2009
13. USNRC (June 2009) Generic environmental impact statement for in-situ leach uranium milling facilities. Final report. NUREG-1910, vols 1 and 2. U.S. Nuclear Regulatory Commission, Washington, DC. http://www.nrc.gov/reading-rm/doc-collections/nuregs/staff/sr1910/. Accessed 5 June 2009
14. USNRC (July 2000) Regulatory guide 1.184. Decommissioning of nuclear power reactors. U.S. Nuclear Regulatory Commission, Washington, DC

15. USNRC (June 2000) Staff responses to frequently asked questions concerning decommissioning of nuclear power reactors. Final report. NUREG-1628. U.S. Nuclear Regulatory Commission, Washington, DC
16. NEA (2005) Decommissioning of nuclear power facilities. It can and has been done. Issy-les-Moulineaux, Nuclear Energy Agency. http://www.nea.fr/html/rwm/reports/2004/nea5728-decom.pdf). Accessed 28 May 2009
17. WNA (Jan 2009) The nuclear fuel cycle. World Nuclear Association, London. http://www.world-nuclear.org/info/inf03.html. Accessed 10 June 2009
18. IAEA (Nov 2005) Standard format and content for safety related decommissioning documents. Safety reports series no. 45. IAEA, Vienna. http://www-pub.iaea.org/MTCD/publications/PDF/Pub1214_web.pdf. Accessed 20 May 2009
19. USNRC (Sept 2006) Consolidated decommissioning guidance. decommissioning process for materials licensees. Final report. NUREG-1757, vol 1, Rev 2. U.S. Nuclear Regulatory Commission, Washington, DC. http://www.nrc.gov/reading-rm/doc-collections/nuregs/staff/sr1757/v1/sr1757v1r2.pdf. Accessed 20 May 2009
20. USNRC (Sept 2006) Consolidated decommissioning guidance. Characterization, survey, and determination of radiological criteria. Final report. NUREG-1757, vol 2, Rev 1. U.S. Nuclear Regulatory Commission, Washington, DC. http://www.nrc.gov/reading-rm/doc-collections/nuregs/staff/sr1757/v2/sr1757v2r1.pdf. Accessed 20 May 2009
21. USNRC (Sept 2003) Consolidated NMSS decommissioning guidance. Financial assurance, recordkeeping, and timeliness. Final report. NUREG-1757, vol 3. U.S. Nuclear Regulatory Commission, Washington, DC. http://www.nrc.gov/reading-rm/doc-collections/nuregs/staff/sr1757/v3/sr1757v3.pdf. Accessed 20 May 2009
22. USDOE (Feb 1995) Decommissioning of U.S. uranium production facilities. DOE/EIA-0592. U.S. Department of Energy, Energy Information Administration, Washington, DC
23. Taylor G, Farrington V, Woods P, Ring R, Molloy R (Aug 2004) Review of environmental impacts of the acid in-situ leach uranium mining process. CSIRO land and water client report. Commonwealth Scientific and Industrial Research Organisation, Clayton South
24. IAEA (Aug 2004) The long term stabilization of uranium mill tailings. Final report of a co-ordinated research project, 2000–2004. IAEA-TECDOC-1403. IAEA, Vienna. http://www-pub.iaea.org/MTCD/publications/PDF/TE_1403_web.pdf. Accessed 20 May 2009
25. USNRC (May 2008) Environmental impact statement for the reclamation of the sequoyah fuels corporation site in Gore, Oklahoma. Final report. NUREG-1888. U.S. Nuclear Regulatory Commission, Washington, DC. http://www.nrc.gov/reading-rm/doc-collections/nuregs/staff/sr1888/sr1888-intro-chaptr11.pdf. Accessed 5 June 2009
26. USNRC (June 2009) Fact sheet: Uranium enrichment. U.S. Nuclear Regulatory Commission, Washington, DC. http://www.nrc.gov/reading-rm/doc-collections/fact-sheets/enrichment.pdf. Accessed 5 June 2009
27. USEPA (Dec 2006) Depleted uranium technical brief. EPA-402-R-06-011. Office of Air and Radiation, U.S. Environmental Protection Agency, Washington, DC. http://www.epa.gov/radiation/docs/402-r-06-011.pdf. Accessed 2 July 2009
28. Bodansky D (2004) Nuclear energy. Principles, practices, and prospects, 2nd edn. Springer/LLC, New York
29. USDOE (Apr 1999) Final programmatic environmental impact statement for alternative strategies for the long-term management and use of depleted uranium hexafluoride. DOE/EIS-0269. U.S. Department of Energy, Office of Nuclear Energy, Science, and Technology, Washington, DC
30. Interstate Technology and Regulatory Council (Jan 2008) Decontamination and decommissioning of radiologically contaminated facilities. Interstate Technology and Regulatory Council, Washington, DC. http://www.itrcweb.org/Documents/RAD5.pdf. Accessed 5 June 2009
31. USNRC (June 2007) Uranium enrichment. U.S. Nuclear Regulatory Commission, Washington, DC. http://www.nrc.gov/materials/fuel-cycle-fac/ur-enrichment.html. Accessed 5 June 2009
32. GAO (Nov 2007) Uranium enrichment: extension of decontamination and decommissioning fund may be needed to cover projected cleanup costs. GAO-08-277T. U.S. Government Accountability Office, Washington, DC. http://www.gao.gov/new.items/d08277t.pdf. Accessed 12 June 2009
33. IAEA (Oct 2004) Research reactors worldwide. IAEA, Vienna. http://www-naweb.iaea.org/napc/physics/ACTIVITIES/Research_Reactors_Worldwide.htm. Accessed 14 June 2009
34. USNRC (Aug 2008) Power reactors. U.S. Nuclear Regulatory Commission, Washington, DC. http://www.nrc.gov/reactors/power.html. Accessed 14 June 2009
35. Lake JA, Bennett RG, Kotek JF (Jan 2003) Next generation nuclear power. new, safer, and more economical nuclear reactors could not only satisfy many of our future energy needs but could combat global warming as well. Sci Am http://www.scientificamerican.com/article.cfm?id=next-generation-nuclear. Accessed 14 June 2009
36. USDOE (Nov 2008) Next-generation nuclear energy. Generation IV program fact sheet. U.S. Department of Energy, Office of Nuclear Energy, Washington, DC. http://nuclear.energy.gov/pdfFiles/factSheets/NextGenerationNuclearEnergy.pdf. Accessed 14 June 2009
37. USDOE (Aug 2008) Next generation nuclear plant licensing strategy. A report to Congress. U.S. Department of Energy, Office of Nuclear Energy, Washington, DC. http://nuclear.energy.gov/pdfFiles/NGNP_reporttoCongress.pdf. Accessed 14 June 2009
38. USNRC (2009) Performance assessment for waste disposal and decommissioning. Updated 11 Feb 2009. U.S. Nuclear Regulatory Commission, Washington, DC. http://www.nrc.gov/about-nrc/regulatory/performance-assessment.html. Accessed 15 May 2009
39. USDOE (Oct 2008) Draft global nuclear energy partnership programmatic environmental impact statement. DOE/EIS-0396.

U.S. Department of Energy, Office of Nuclear Energy, Washington, DC. http://www.gc.energy.gov/NEPA/1003.htm. Accessed 8 July 2009

40. WNA (June 2009) World uranium mining. World Nuclear Association, London. http://www.world-nuclear.org/info/inf23.html. Accessed 5 June 2009
41. Andrews A (27 Mar 2008) Nuclear fuel reprocessing: U.S. policy development. CRS report for Congress, Order code RS22542. Congressional Research Service, Washington, DC. http://www.fas.org/sgp/crs/nuke/RS22542.pdf. Accessed 1 July 2009
42. USDOE (Nov 2008) Revised draft environmental impact statement for decommissioning and/or long-term stewardship at the West Valley demonstration project and Western New York nuclear service center. DOE/EIS-0226-D. U.S. Department of Energy, West Valley
43. IAEA (Dec 2007) Disposal aspects of low and intermediate level decommissioning waste. Results of a coordinated research project 2002–2006. IAEA-TECDOC-1572. IAEA, Vienna. http://www-pub.iaea.org/MTCD/publications/PDF/TE_1572_web.pdf. Accessed 24 June 2009
44. IAEA (Apr 2000) Radioactive waste management profiles: a compilation of data from the waste management database no. 3. IAEA, Vienna. http://www-pub.iaea.org/MTCD/publications/PDF/rwmp-3/RWMP-V3.pdf. Accessed 24 June 2009
45. IAEA (Apr 1994) Classification of radioactive waste. A safety guide. Safety series no. 111-G-1.1. IAEA, Vienna. http://www-pub.iaea.org/MTCD/publications/PDF/Pub950e_web.pdf. Accessed 24 June 2009
46. Environmental Law Institute (1999) Institutional controls case study: Grand junction. Environmental Law Institute, Washington, DC. http://www.elistore.org/Data/products/d9.14.pdf. Accessed 23 June 2009
47. USNRC (2003) Standard review plan for the review of a reclamation plan for mill tailings sites under title II of the Uranium Mill Tailings Radiation Control Act of 1978. Final report. NUREG-1620, Rev 1. U.S. Nuclear Regulatory Commission, Washington, DC
48. USNRC (Nov 2008) Design, construction, and inspection of embankment retention systems at uranium recovery facilities. Regulatory guide 3.11. U.S. Nuclear Regulatory Commission, Washington, DC
49. IAEA (May 2005) Guidebook on environmental impact assessment for *in situ* leach mining projects. IAEA-TECDOC-1428. IAEA, Vienna. http://www-pub.iaea.org/MTCD/publications/PDF/TE_1428_web.pdf. Accessed 20 May 2009
50. National Research Council (2001) Disposition of high-level waste and spent nuclear fuel. The continuing societal and technical challenges. National Academy Press, Washington, DC
51. USDOE (Jan 2007) Radioactive waste management manual. DOE M 435.1-1. U.S. Department of Energy, Office of Environmental Management, Washington, DC. http://www.directives.doe.gov/pdfs/doe/doetext/neword/435/m4351-1c1.pdf. Accessed 24 June 2009
52. IAEA (1999) Near surface disposal of radioactive waste safety requirements. IAEA safety standards series, Safety guide no. WS-R-1. IAEA, Vienna. http://www-pub.iaea.org/MTCD/publications/PDF/P073_scr.pdf. Accessed 29 June 2009
53. IAEA (2008) Managing low radioactivity material from the decommissioning of nuclear facilities. Technical reports series no. 462. IAEA, Vienna. http://www-pub.iaea.org/MTCD/publications/PDF/trs462_web.pdf. Accessed 12 June 2009
54. League of Women Voters Education Fund (1993) The nuclear waste primer. The League of Women Voters Education Fund, Washington, DC
55. IAEA (2004) Application of the concepts of exclusion, exemption and clearance. IAEA safety standards series, Safety guide no. RS-G-1.7. IAEA, Vienna. http://www-pub.iaea.org/MTCD/publications/PDF/Pub1202_web.pdf. Accessed 29 June 2009
56. USNRC (June 2001) Multi-Agency Radiation Survey and Site Investigation Manual (MARSSIM). NUREG-1575, Rev 1/EPA 402-R-97-016, Rev 1/DOE/EH-0624, Rev 1. U.S. Nuclear Regulatory Commission, Washington, DC. http://www.epa.gov/radiation/marssim/obtain.html. Accessed 29 June 2009
57. NEA (2006) Releasing the sites of nuclear installations. A status report. Report no. NEA 6187. Nuclear Energy Agency, Issy-les-Moulineaux
58. IAEA (2008) Long term preservation of information for decommissioning projects. Technical reports series no. 467. IAEA, Vienna, Austria. http://www-pub.iaea.org/MTCD/publications/PDF/trs467_web.pdf. Accessed 12 June 2009
59. IAEA (2002) Record keeping for the decommissioning of nuclear facilities: guidelines and experience. Technical reports series no. 411. IAEA, Vienna. http://www-pub.iaea.org/MTCD/publications/PDF/TRS411_scr.pdf. Accessed 12 June 2009
60. Energy Information Administration (June 2006) When do commercial reactors permanently shut down? The recent record. Energy Information Administration, U.S. Department of Energy, Washington, DC. http://www.eia.doe.gov/cneaf/nuclear/closures/closure16.html. Accessed 14 June 2009
61. European Commission (2009) Decommissioning in short. European Commission, Brussels. http://www.eu-decom.be/about/decominshort/whatis.html. Accessed 7 July 2009
62. IAEA (2007) Decommissioning strategies for facilities using radioactive material. Safety reports series no. 50. IAEA, Vienna. http://www-pub.iaea.org/MTCD/publications/PDF/Pub1281_web.pdf. Accessed 12 June 2009
63. IAEA (2002) Safe enclosure of nuclear facilities during deferred dismantling. Safety reports series no. 26. IAEA, Vienna. http://www-pub.iaea.org/MTCD/publications/PDF/Pub1142_scr.pdf. Accessed 12 June 2009
64. USNRC (2009) Peach Bottom—Unit 1. Updated 16 Apr 2009. U.S. Nuclear Regulatory Commission, Washington, DC. http://www.nrc.gov/info-finder/decommissioning/power-reactor/peach-bottom-atomic-power-station-unit.html. Accessed 12 June 2009
65. IAEA (2008) Safety assessment for the decommissioning of facilities using radioactive material. IAEA safety standards series, Safety guide no. WS-G-5.2. IAEA, Vienna. http://www-pub.iaea.org/MTCD/publications/PDF/Pub1372_web.pdf. Accessed 29 June 2009

66. Interstate Technology and Regulatory Council (Apr 2002) Determining cleanup goals at radioactively contaminated sites: case studies. Interstate Technology and Regulatory Council, Washington, DC. http://www.itrcweb.org/Documents/RAD5.pdf. Accessed 5 June 2009
67. IAEA (1999) Decommissioning of nuclear power plants and research reactors. IAEA safety standards series, Safety guide no. RS-G-2.1. IAEA, Vienna. http://www-pub.iaea.org/MTCD/publications/PDF/P079_scr.pdf. Accessed 29 June 2009
68. USEPA (Apr 2006) Technology reference guide for radiologically contaminated surfaces. EPA-402-R-06-003. Office of Air and Radiation, U.S. Environmental Protection Agency, Washington, DC
69. IAEA (1999) State of the art technology for decontamination and dismantling of nuclear facilities. Technical reports series no. 395. IAEA, Vienna. http://www-pub.iaea.org/MTCD/publications/PDF/TRS395_scr/D395_Part1_scr.pdf. Accessed 12 June 2009
70. NEA (1999) Decontamination techniques used in decommissioning activities. Nuclear Energy Agency/Organisation for Economic Co-Operation and Development, Issy-les-Moulineaux
71. USEPA (Apr 2004) Radionuclide biological remediation resource guide. EPA-905-B-04-001. Region 5, Superfund Division, U.S. Environmental Protection Agency, Washington, DC. http://clu-in.org/download/remed/905b04001.pdf. Accessed 29 June 2009
72. USEPA (Apr 1999) Use of monitored natural attenuation at superfund, RCRA corrective action, and underground storage tank sites. Office of Solid Waste and Emergency Response (OSWER), Directive no. 9200.4-17P. Office of Solid Waste and Emergency Response, U.S. Environmental Protection Agency, Washington, DC. http://www.epa.gov/swerust1/directiv/d9200417.pdf. Accessed 29 June 2009
73. Pennsylvania Department of Environmental Protection (Oct 1998) Coal mine drainage prediction and pollution prevention in Pennsylvania. Pennsylvania Department of Environmental Protection, Harrisburg. http://www.dep.state.pa.us/dep/deputate/minres/Districts/CMDP/main.htm. Accessed 8 July 2009
74. IAEA (2009) Nuclear safety knowledge management. IAEA, Vienna. http://www-ns.iaea.org/coordination/knowledge-mng.htm. Accessed 23 July 2009
75. IAEA (2004) Planning, managing, and organizing the decommissioning of nuclear facilities. IAEA-IECDOC-1394. IAEA, Vienna
76. USNRC (Jan 2008) Decommissioning nuclear power plants. Fact sheet. U.S. Nuclear Regulatory Commission, Washington, DC. http://www.nrc.gov/reading-rm/doc-collections/fact-sheets/decommissioning.pdf. Accessed 14 June 2009
77. USNRC (Jan 2005) U.S. nuclear regulatory commission's decommissioning program. NUREG/BR-0325. U.S. Nuclear Regulatory Commission, Washington, DC. http://www.nrc.gov/reading-rm/doc-collections/nuregs/brochures/br0325/br0325.pdf. Accessed 14 June 2009

Books and Reviews

ASTM International (2005) Standard guide for nuclear facility decommissioning plans. ASTM E1281-89(2005). ASTM International, West Conshohocken

National Research Council (1998) A review of decontamination and decommissioning technology development programs at the department of energy. National Academies Press, Washington, DC

National Research Council (2001) Research opportunities for deactivating and decommissioning department of energy facilities. National Academies Press, Washington, DC

Taboas A, Moghissi A, LaGuardia T (2004) The decommissioning handbook. American Nuclear Society, LaGrange

USDOE (Jan 2000) Decommissioning handbook. Procedures and practices for decommissioning. DOE/EM-0383. USDOE, Office of Environmental Management, Washington, DC

Till JE, Meyer HR (eds) (Sept 1983) Radiological assessment. A textbook on environmental dose analysis. NUREG/CR-3332. U.S. Nuclear Regulatory Commission, Washington, DC

USNRC (Aug 1988) Final generic environmental impact statement on decommissioning of nuclear facilities. NUREG-0586. U.S. Nuclear Regulatory Commission, Washington, DC. http://www.nrc.gov/reading-rm/doc-collections/nuregs/staff/sr0586/initial/index.html

USNRC (Nov 2002a) Generic environmental impact statement on decommissioning of nuclear facilities. Regarding the decommissioning of nuclear power reactors. NUREG-0586, suppl 1, vol 1. U.S. Nuclear Regulatory Commission, Washington, DC. http://www.nrc.gov/reading-rm/doc-collections/nuregs/staff/sr0586/s1/v1/index.html

USNRC (Nov 2002b) Generic environmental impact statement on decommissioning of nuclear facilities. Regarding the decommissioning of nuclear power reactors. NUREG-0586, suppl 1, vol 2. U.S. Nuclear Regulatory Commission, Washington, DC. http://www.nrc.gov/reading-rm/doc-collections/nuregs/staff/sr0586/s1/v2/index.html

Websites

Argonne National Laboratory (USA). Decontamination and decommissioning. http://www.dd.anl.gov/

Atomic Energy Canada Limited. Sustainable development: decommissioning and waste management. http://www.aecl.ca/Development/SD-WMD.htm

Decontamination and Decommissioning Science Consortium (USA). http://www.orau.gov/ddsc/

IAEA. Decommissioning. http://www-ns.iaea.org/tech-areas/waste-safety/decommissioning.htm

IAEA. Nuclear energy handbook. Technologies for the decommissioning of installations and restoration of sites. http://www.iaea.org/inisnkm/nkm/ws/d3/r2531.html

NEA Working Party on Decommissioning and Dismantling (WPDD) http://www.nea.fr/html/rwm/wpdd.html

Nuclear Decommissioning Authority (UK). http://www.nda.gov.uk/

U.S. Department of Energy (USA). Deactivation and decommissioning. http://www.em.doe.gov/EM20Pages/DD.aspx

U.S. Nuclear Regulatory Commission (USA). Decommissioning. http://www.nrc.gov/about-nrc/regulatory/decommissioning.html

World Information Service on Energy Uranium Project. http://www.wise-uranium.org/index.html

Nuclear Fission Power Plants

Ronald Allen Knief
Sandia National Laboratories, Albuquerque, NM, USA

Article Outline

Glossary
Definition of the Subject
Introduction
Principles for Design and Operation
Reactor Systems
Operation, Maintenance, and Control Practices
Nuclear Reactor Safety Features
Nuclear-Power Regulation
Advanced Reactors
Future Directions
Bibliography

Glossary

Blanket Region surrounding the fuel core of a breeder reactor that contains fertile material to increase production of new fuel.

Brayton cycle Method used to transfer fission heat energy to gas (e.g., helium or superheated carbon dioxide) for use in a gas turbine to generate electricity.

Breeder Reactor that produces new fuel from fertile material at a faster rate than it bums fuel for energy production.

Converter Reactor that produces less new fuel from fertile material than it burns for energy production.

Coolant Liquid or gaseous medium used to remove fission heat from a reactor core.

Core Region within a reactor occupied by the nuclear fuel that supports the fission chain reaction.

Critical Condition where a fission chain reaction is stable with neutron production balancing losses at a nonzero power level.

Electron volt (eV) 1 eV is the kinetic energy obtained by an electron moving across 1 V of electric potential 1 eV = 1.602×10^{-19} J. Common multiples are 1 keV = 1,000 eV and 1 MeV = 10^6 eV. Neutron energies from less than an eV through about 10 MeV are important in nuclear fission power plants.

Fast neutrons Neutrons of high energy, particularly those produced directly by the fission reaction (~0.1–10 MeV).

Fertile Material, not itself fissile, capable of being converted to fissile material following absorption of a neutron.

Fissile Material capable of sustaining a fission chain reaction.

Fissionable Nuclei capable of fission by neutrons and of participation in a fission chain reaction (category includes fissile nuclides).

Fission Process in which a heavy-metal nucleus splits into two or more large fragments, releases energy, and emits neutrons and gamma radiation.

Isotopes Different nuclides of the same chemical element, e.g., ^{235}U and ^{238}U are two of the isotopes of uranium.

Moderator Material of low atomic mass included in a reactor for the purpose of reducing the kinetic energy of neutrons.

Multiplication factor Ratio of neutron production rate to neutron loss rate value is unity for a critical system.

Nuclide Atomic nucleus with a specified number of neutrons and protons, e.g., the uranium-235 [$^{235}_{92}$U] nuclide has atomic mass number 235, 92 protons (atomic number), and 235–92 = 143 neutrons.

Reactivity Fractional change in neutron multiplication referenced to the critical condition value is zero for a critical system.

Reactor Combination of fissile and other materials in a geometric arrangement designed to support a neutron chain reaction.

Steam cycle Method used to convert fission heat energy to steam that drives a turbo-generator, thus, generating electricity.

Thermal neutrons Low-energy neutrons at or near thermal equilibrium with their surroundings produced by slowing down or moderating the fast neutrons produced by fission. (Equilibrium thermal energy, e.g., is 0.25-eV at 20°C).

Definition of the Subject

Nuclear fission power plants – or nuclear power reactors – are the instruments for commercial use of nuclear energy, relying on a sustained neutron chain reaction from the fission process. Nuclear fission – splitting of heavy-metal nuclei, most importantly ^{235}U and ^{239}Pu – produces an enormous amount of energy.

Fission was discovered in 1938 on the eve of World War II. The magnitude of the energy release was recognized immediately. However, it was not until after the attack on Pearl Harbor in late 1941 that the USA began serious efforts to develop this energy source for military purposes. Germany conducted research along these same lines, but ultimately was unsuccessful in development efforts.

The USA's ensuing "Manhattan Project" [1] included monumental basic research, development of nuclear reactors for research and nuclear-material production, design of nuclear explosives, and ultimately testing of a nuclear explosive device and development of the two nuclear weapons credited with ending the war. Post war, the next use of nuclear energy was for propulsion in submarines, first by the USA, then other countries. Subsequently nuclear propulsion has been extended to surface vessels as well. About 85% of the world's nuclear electricity is generated by reactors derived from designs originally developed for naval use [2].

Nuclear power for nonmilitary, peaceful uses began in earnest in 1956 with the startup of the world's first full-scale nuclear electric generating plant, at Calder Hall in England, followed in the USA a year later by the initial operation of a 60-MW unit at Shippingport, Pennsylvania [3]. By the middle of the 1960s, there was a growing optimism on the part of US utilities toward nuclear power as well as substantial activity worldwide. Electric generation using nuclear steam-supply systems was economically competitive with fossil-fuel fired plants. The passage in mid-1964 of a US law providing for private ownership of nuclear fuel was hailed as paving the way for an independent nuclear power industry.

By 1970, the combined capacity of US nuclear plants in service, under construction, and on order was over 64 GW, more than twice the total for all other nations combined. Widespread enthusiasm for nuclear power had reached its high-water mark.

Subsequently nuclear technology suffered "growing pains." High interest rates affected the capital-cost-intensive reactors. Then in 1979 came the accident at Three Mile Island. As a result of the accident – and that at Chernobyl in 1986 [4] – over 100 orders for new reactors were cancelled and no new orders were placed in the ensuing three decades.

Despite residual public misgivings over Three Mile Island and Chernobyl, the industry has learned its lessons and established a solid safety record during the past two decades. Meanwhile efficiency and reliability of nuclear plants have climbed to record levels [5]. By 2010, 104 nuclear reactors were producing a fifth of the USA's total electric output.

"Nuclear power supplies a sixth of the world's electricity. Along with hydropower (which supplies slightly more than a sixth), it is the major source of 'carbon-free' energy today" [4]. "Nuclear power now accounts for 73% of the emission-free generation in the USA and is the only technologically mature, non-emitting source of power that is positioned to deliver large-scale CO_2 reduction in the decades ahead" [6].

Growing concern about global warming – and the associated likelihood that greenhouse gas emissions will be regulated in some fashion – has led power providers in the USA and elsewhere, and their governments [4], to recognize that nuclear reactors produce electricity without atmospheric discharge of carbon dioxide, pollutants such as nitrogen oxides, and smog-causing sulfur compounds [5]. With the world demand for energy projected to rise by about 50% by 2030 and to nearly double by 2050, building nuclear power plants appears to be increasingly viable and attractive.

The fossil-fuel alternatives have their drawbacks. Oil and natural-gas supplies are shrinking and their use can have unwanted political consequences [3]. Natural gas – attractive because it has the lowest carbon content of the fossil fuels and advanced power plants have low capital costs – has electricity costs which are

very price-sensitive and can be volatile. Although abundant, coal is difficult to recover, deliver, and burn [3, 4]. As the most carbon-intensive source of electricity, coal's long-term viability will depend on capture and sequestration of carbon dioxide – which is both costly and yet to be demonstrated and introduced on a large scale [4].

Solar, geothermal, wind, and tidal power, while attractive, cannot be expected to supply energy in the vast amounts required in the immediate future. Conservation and tight management of energy consumption are necessary, but not sufficient, parts of the equation [3].

With the future uncertain, energy realists see nuclear power as indispensable for electric generation well past the mid twenty-first century. It can fill uniquely a gap in the spectrum of electricity generation methods.

Designers are adopting novel approaches for new nuclear systems. They are evaluating systems in terms of their sustainability – meeting present needs without jeopardizing the future generations. "It is a strategy that helps to illuminate the relation between energy supplies and the needs of the environment and society. This emphasis on sustainability can lead to the development of nuclear energy-derived products besides electric power, such as hydrogen fuel for transportation. It also promotes the exploration of alternative reactor designs and nuclear fuel-recycling processes that could yield significant reductions in waste while recovering more of the energy contained in uranium" [5].

There are indications of a possible nuclear revival. More than 20,000 megawatts of nuclear capacity have come on-line globally in the early years of the twenty-first century, mostly in the Far East. Nuclear plants have demonstrated remarkable reliability and efficiency recently. The world's ample supply of uranium could fuel a much larger fleet of reactors than exists today throughout their 40- to 50-year life span [4]. The nuclear power industry has been developing and improving reactor technology for more than five decades and is starting to build the next generation of nuclear power reactors to fill orders now materializing [2]. The first firm order for new reactors in the USA was placed in 2009. Nearly 20 more considered "firmly planned" are expected to follow. There are even more prospects worldwide, most notably in pacific-basin countries [7].

Wide-scale deployment of nuclear power technology would seem to offer substantial advantages over other energy sources. However, there also are challenging questions to be addressed regarding the best way to make it fit into the future. These include achievement of economic viability, improved operating safety, efficient waste management and resource utilization, as well as weapons nonproliferation, all of which are influenced by the design of the nuclear reactor system that is chosen and the fuel cycle followed [4, 5].

Introduction

The current nuclear power reactors produce electricity using a steam cycle in much the same way as conventional fossil-fuel power plants. However, special design and operating features are required to address the unique characteristics of the fission-energy source and its associated radiation environment. A wide variety of reactor concepts have been developed to this purpose [8]. (The other major nuclear reaction for energy production, *fusion*, offers the prospect as a future energy source. See ► Nuclear Fusion.)

Fission

Fission reactions occur when a neutron strikes a nucleus of specific heavy-metal isotopes of uranium and plutonium – most notably ^{235}U or ^{239}Pu – and causes splitting into two or more fission fragments, emits additional neutrons and other radiations, and releases a relatively large amount of energy. The energy release from a single fission is between five and six orders of magnitude greater than that from a single chemical reaction (e.g., combustion of carbon and oxygen). This large amount of energy per unit mass of fuel is a major advantage of fission as an energy source. The emission of extra neutrons is a necessary feature to support a sustained chain reaction with steady or accelerated energy release.

The fission reaction also has unique problems in the form of particulate and electromagnetic radiations emitted at the time of fission and from the long-lingering radioactivity (i.e., emission of radiations over time) of the fission fragments and their products. Protection against the effects of these radiations requires shielding and removal of the associated heat.

The fission process produces several hundred different fission fragments, each of which is radioactive and undergoes successive decays prior to reaching stability. Each species has a different characteristic lifetime, described in terms of its unique *half-life* – the average time required for one half of a mass of the radioactive material to decay. The resulting overall radiation levels are substantial, having an energy equivalent to about 7.5% of the total fission output at the time a reactor is shut down, and decreasing roughly inversely as the one-fifth power with time (i.e., $t^{-1/5}$). Handling this lingering decay heat load is a principal consideration in the safe operation of nuclear reactors. Containment of the radioactive material requires both near-term and long-term nuclear waste management strategies. (See ► Health Physics, ► Fission Reactor Physics, and ► Radioactive Waste Management: Storage, Transport, Disposal.)

Fission Chain Reaction

When the chain reaction exactly balances the rates of neutron production from fission with non-fission absorption and leakage from the system boundaries, it is steady and said to be *critical*. When production exceeds losses, it is *supercritical* and power increases. When losses exceed production, the chain reaction is *subcritical* and power decreases, down to and including being shut down. All three states of criticality are necessary to nuclear power reactor operation. These states are quantified with an *effective multiplication factor* k_{eff} or k, defined as

$$k_{\text{eff}} = k = \text{production}/[\text{absorption} + \text{leakage}]$$

or by the change in multiplication, *reactivity* ρ, defined as

$$\rho = (k-1)/k.$$

Thus, $k = 1$ and $\rho = 0$ constitute the critical condition; $k > 1$ and $\rho > 0$ supercritical; and $k < 1$ and $\rho < 0$ subcritical.

The mathematical equations associated with the neutron balance are quite complex since the reaction rates are a strong function of both material (composition, location, and irradiation history) and neutron population (position, direction, and energy) characteristics. Neutron energy is a particularly important parameter. Neutrons emitted in fission are in the 0.1–10 MeV range with an average energy of about 2 MeV. The probability for fission increases dramatically if the neutron energy falls below 1 eV.

For this reason, a *moderator* material of low mass may be added to enhance the slowing down. (The closer the mass of the moderator nuclei to that of the neutron, the larger the potential energy loss in a single collision; thus, hydrogen with essentially the same mass is best in this regard, although it may not be selected for other reasons.) (See ► Nuclear Reactor Materials and Fuels.)

Fissionable Materials

The heavy metals uranium and plutonium each have isotopes that can be caused to fission by neutrons, i.e., that are *fissionable*. Fission occurs under different circumstances among the isotopes.

Fissile nuclides can fission with neutrons of energy, all the way down to essentially zero. The principal fissile materials are those containing significant quantities of ^{233}U, ^{235}U, ^{239}Pu, and/or ^{241}Pu. A fission reactor core contains fissile as well as non-fissile and other materials.

Other isotopes of U, Pu, and Th can be fissioned by neutrons, but only by neutrons with kinetic energy above a minimum threshold. Particularly important examples of such *fissionable* nuclides are ^{238}U, ^{232}Th, and ^{240}Pu. The latter nuclides also have the unique characteristic that upon absorbing a neutron in a non-fission reaction, they will convert to fissile nuclides either directly or via a multi-step process. These *fertile* nuclides produce the new fissile as follows:

$$^{238}\text{U} \rightarrow {}^{239}\text{Pu}:$$
$$^{232}\text{Th} \rightarrow {}^{233}\text{U}: \text{ and}$$
$$^{240}\text{Pu} \rightarrow {}^{241}\text{Pu}.$$

(See ► Fission Reactor Physics)

Reactor Classifications

Nuclear power reactors are designed to achieve a self-sustained chain reaction with a combination of fissile, fertile, and structural materials. The current generation of reactors uses the heat produced by fissions in the core to produce steam and then electricity, employing

a variety of fuel forms, coolants, moderators, and other materials.

Common characteristics useful for classifying reactors are:

1. *Coolant* – principal heat-removal medium.
2. *Steam cycle* – number and configuration of separate coolant "loops" for producing steam to turn a turbine generator and produce electricity.
3. *Moderator* – material (if any) used to "slow down" the neutrons produced by fission.
4. *Neutron energy* – general energy range (typically fast [fission-energy] or thermal) for the neutrons that cause most of the fissions.
5. *Fuel production* – system is referred to as a *breeder* if it produces (i.e., changes from fertile to fissile) more fuel than it consumes; it is said to be a *converter* otherwise.

The first two features relate to the current practice of converting fission energy first to heat and then to electric energy by employing a steam cycle. Coolants include water, heavy water, gases (e.g., CO_2 or helium), and liquid metal (e.g., sodium). The steam cycles may employ from one to three separate loops, including one for primary coolant circulation and one (not necessarily separate from the first) for steam generation. It may be noted that next-generation reactors could bypass steam in favor of direct use of a coolant for electricity, process heat, or hydrogen production.

As mentioned earlier, neutrons emitted from fission are of high energy. However, very low energy neutrons have a higher likelihood of causing fission reactions. Thus, many systems employ a moderator to "slow down" these neutrons. The best moderators are of low mass, allowing maximum energy transfer through neutron collisions (e.g., the limiting case of potentially total energy transfer between a moving cue ball and a stationary billiard ball of equal mass). Typical materials used for this purpose are hydrogen, deuterium (heavy hydrogen), and carbon/graphite. The moderator and coolant may be the same (e.g., water or heavy water) or may be separate (e.g., water, heavy water, or a gas coolant with heavy water or solid graphite moderator). Neutrons with low enough energies to be roughly in thermal equilibrium (<1 eV) with the surrounding materials are said to be *thermal neutrons*. Neutrons at or near fission energies (averaging $\sim$2 MeV) are *fast neutrons*. Fast reactors avoid the use of moderators, such as with a metal coolant like sodium, instead of one of the moderating materials identified above.

All nuclear power reactors contain fertile ^{238}U or ^{232}Th and, thus, produce some amount of new fissile fuel. The ubiquitous light-water reactors (LWR) have slightly enriched uranium fuel which is up to 5 wt% ^{235}U with the remaining 95 wt% ^{238}U. Thus, they produce plutonium during routine operation. Producing about 60% as much new fuel as used for operation, the LWR units are considered to be *converter* reactors. By contrast, a reactor producing more new fuel than it uses is called a *breeder*.

The world's six principal types in the current generation of nuclear power reactors are:

1. Boiling-water reactor (BWR)
2. Pressurized-water reactor (PWR)
3. Heavy-water-moderated reactor (HWR)
4. Gas-cooled reactor (GCR)
5. Light-water-cooled graphite-moderated reactor (LWGR)
6. Fast breeder reactor (FBR)

The section labeled "General" in Table 1 classifies one or more versions of each of these six reactor types in terms of the five categories identified at the beginning of this section [8]. For example, the GCR variation known as the high-temperature gas-cooled reactor (HTGR) is a double-loop, helium-cooled, graphite-moderated, thermal, converter reactor.

Principles for Design and Operation

Nuclear power reactors are complex systems whose design represents a balance among conflicting requirements. Principal among these requirements are nuclear design, materials, thermal design, economics, and control and safety [8, 9].

The nuclear (physics) design seeks to match fissile and fertile constituents with appropriate coolants and moderators (if any) to optimize specific (per unit mass of fuel) fission-energy output and production of new fuel or meet alternative design goals. Materials concern focus on chemical compatibility of components, thermal and radiation stability, and overall mechanical strength. One especially important requirement for

Nuclear Fission Power Plants. Table 1 Characteristics for six representative nuclear steam-supply systems

	BWR	PWR	PHWR	PTGR	HTGR	LMFBR
	Manufacturer					
	General Electric	Westinghouse	Atomic Energy of Canada, Ltd.	(Former) Soviet Union	General Atomic	Novatome
	System (Station)					
	BWR/6	(Sequoyah/ SNUPPS)	CANDU 600	RBMK-1000	(Fulton)	(Superphénix)
General						
Steam cycle						
Loops	1	2	2	1	2	3
Primary coolant	H_2O	H_2O	D_2O	H_2O	He	Liq. Na
Secondary coolant	–	H_2O	H_2O	–	H_2O	Liq. Na/H_2O
Moderator	H_2O	H_2O	D_2O	Graphite	Graphite	–
Neutron energy	Thermal	Thermal	Thermal	Thermal	Thermal	Fast
Fuel production	Converter	Converter	Converter	Converter	Converter	Breeder
Energy conversion						
Gross thermal power, MWt	3,579	3,411	2,180	3,200	3000	3,000
Net electric power, MWe	1,178	1,150	638	950	1,160	1,200
Efficiency,%	32.9	33.7	29.3	31.2	38.7	40
Heat transport						
Primary loops and pumps	2	4	2	2/6 + 2	6	4
Intermediate loops	–	–	–	–	–	8
Steam generators	–	4	4	–	6	8
Steam-generator type	–	U-tube	U-tube	–	Helical coil	Helical coil
No. turbine generators	1	1	1	2	1	2
Fuel						
Particles	Short, cyl. pellets	Short, cyl. pellets	Short, cyl. pellets	Short, cyl. pellets	Coated microspheres	Short, cyl. pellets
Chemical form	UO_2	UO_2	UO_2	UO_2	UC/ThC	Mixed UO_2/PuO_2
Fissile (% by wt.)	2–4% ^{235}U	2–4% ^{235}U	Natural uranium	Natural uranium	93% ^{235}U	10–20% Pu (core)
Fertile	^{238}U	^{238}U	^{238}U	^{238}U	Thorium	^{238}U (core + blanket)

Nuclear Fission Power Plants. Table 1 (Continued)

	BWR	PWR	PHWR	PTGR	HTGR	LMFBR
	Manufacturer					
	General Electric	Westinghouse	Atomic Energy of Canada, Ltd.	(Former) Soviet Union	General Atomic	Novatome
	System (Station)					
	BWR/6	(Sequoyah/ SNUPPS)	CANDU 600	RBMK-1000	(Fulton)	(Superphénix)
Pins	Pellet stacks in Zr-alloy tubes	Pellet stacks in Zr-alloy tubes	Pellet stacks in Zr-alloy tubes	Pellet stacks in Zr-alloy tubes	Microspheres in graphite stick	Pellet stacks in SS tubes
Assembly	8 × 8 sq. pin array	17 × 17 sq. pin array	37-pin concentric circles	18-pin concentric circles	Hex. graphite block with fuel sticks	271-pin hex. array
Core						
Axis	Vertical	Vertical	Horizontal	Vertical	Vertical	Vertical
Assys on axis	1	1	12	2	8	1
Assys radially	748	193	380	1,661	493	364 (core), 233 (blanket)
Performance						
Equil. burnup, MWD/T	27,500	27,500	7,500	18,500	95,000	100,000
Refueling sequence	1/4 per year	1/3 per year	Continuous, on-line	On-line	1/4 per year	Variable
Thermal hydraulics						
Primary system						
Pressure, MPa	7.17	15.5	10.0	7.2	4.90	~0.1
Inlet temp., °C	278	292	267	270	318	395
Avg. out. temp., °C	288	325	310	284	741	545
Core flow, Mg/s	13.1	18.0	7,6	10.4	1.42	16.4
Volume, L	–	3.36×10^5	1.20×10^5	4.0	(9,550 kg)	(3,200 Mg) Na/H_2O
Secondary system						
Pressure, MPa	–	6.89	4.7	54	17.2	~0.1/17.7
Inlet temp., °C	–	227	187	29	188	345/235
Outlet temp., °C	–	285	260		513	525/487
Power density						
Core avg., kW/L	54.1	105	12	4.0	8.4	280
Fuel avg., kW/L	54.1	105	60	54	44	280

Nuclear Fission Power Plants. Table 1 (Continued)

	BWR	PWR	PHWR	PTGR	HTGR	LMFBR
	Manufacturer					
	General Electric	Westinghouse	Atomic Energy of Canada, Ltd.	(Former) Soviet Union	General Atomic	Novatome
	System (Station)					
	BWR/6	(Sequoyah/ SNUPPS)	CANDU 600	RBMK-1000	(Fulton)	(Superphénix)
Linear heat rate						
Core avg., kW/m	19.0	17.8	25.7	29	7.87	29
Core max., kW/m	44.0	42.7	44.1		23.0	45
Design peaking factors						
Radial	1.4		1.21			
(Total)		(2.5)			(2.9)	(1.55)
Axial	1.6		1.41			
Moderator						
Volume, L	(Same as primary coolant)	(Same as primary coolant)	2.17×10^6	(Graphite)	(Graphite in fuel blocks)	–
Inlet temp., °C			43			–
Outlet temp., °C			71			–
Reactivity control						
Control rods						
Geometry	Cruciform	Rod clusters	Rods	Rods	Rod pairs	Hex. pin bundle
Absorber material	B_4C	Ag In Cd	Various	B_4C	B_4C/graphite	B_4C
Burnable poison	Gd. in fuel pellets	Borosilicate glass	–		B_4C/graphite	–
Other systems	Voids in coolant	Soluble boron	H_2O, various		Reserve shutdown	Three bundle secondary
Reactor vessel						
Inside dimension, m	6.05D × 21.6 H	4.83D × 13.4 H	7.6D × 4 L	0.08ID × 8 H tubes	11.3D × 14.4 H	21D × 19.5 H
Wall thick., mm	152	224	28.6	4.0	(4.72 m min.)	25
Material	SS-clad carbon steel	SS-clad carbon steel	Stainless steel	Zr-Nb alloy	Prestressed concrete	Stainless steel
Other features			Pressure tubes	Pressure tubes	Steel liners	Pool-type

Data summarized from [8]. Appendix IV. (Appendix also includes parameters for PWR designs from US manufacturers B&W and CE, France's Framatome, and the former Soviet Union's unique VVER)

reactors that refuel only while shutdown – which is the majority – is that the fuel maintains its general structural integrity throughout up to 4 years or more of in-core residence; unlike other energy production cycles, the fuel is not literally "burned up" with wastes discarded along the way.

Thermal design is concerned with heat removal for effective energy production and maintaining the integrity of the fuel, cladding, and other materials for operational and safety purposes. Reactor thermal operating limits are determined by the most extreme postulated local conditions – to avoid damage anywhere in the reactor core. Temperature limits are established to prevent fuel melting and/or clad damage during power excursions and loss of cooling. Other limits address avoiding coolant-clad temperature mismatch that could lead to local loss of fuel integrity. Both types of limits are established in terms of peak (local)-to-average core conditions. Such factors vary with power level, time in core life, and other parameters.

The primary economic consideration is to minimize overall costs, i.e., initial capital outlay, operating and maintenance costs, and fuel charges. Increasing electric-generation reliability and thermal conversion efficiency are particularly important throughout lifetime.

Power reactor controls must be capable of maintaining the critical condition, increasing and decreasing power, and adjusting to long-term changes such as the conflicting effects from breeding new fuel, depleting existing fuel and burnable neutron poisons, and building in radioactive fission- and transuranic-product neutron poisons. The desired neutron balance is maintained predominately by adjusting neutron absorption using materials designed to remove neutrons from, or "poison," the chain reaction. Methods may include a combination of solid moveable control rods, soluble poisons in the coolant or moderator (PWR), and fixed burnable poisons designed to deplete or be "burned out" by the continuing neutron population. Some reactor designs also change neutron production by on-line fuel exchange. Fission products whose poisoning effects are sensitive to operating conditions also must be subject to control.

Routine control strives to make the power density as uniform as possible throughout the core, while allowing for power changes. In most designs, control-rod movement is used with groups selected for symmetry to maintain uniform, i.e., avoid highly asymmetric, power distribution. Measures are instituted to restrict the speed of movement and reactivity effect of individual rods or groups of rods to prevent excessively rapid power increase. Similarly, the design intends to minimize the likelihood of inadvertent control-rod withdrawal which could lead to unplanned supercritical conditions.

Safety concerns are addressed through a protective system whereby the control rods may be inserted into the core – dropped down or pushed up – into the core quickly; i.e., they "scram" or "trip" the reactor through gravity drop or gas pressure, respectively, when certain predetermined parameter limits (e.g., on pressure, temperature, flow, or power levels) are exceeded.

Reactor safety is enhanced with inherent negative feedback mechanisms, where a power increase tends to be self-limiting. Fuels are designed to have such feedback, with their reactivity decreasing with escalating temperature. Expansion of the coolant and/or moderator (such as with increased temperature) provides negative reactivity feedback in light-water reactors. Reactors with positive reactivity feedback in certain operating regimes may be difficult to control. The essentially instantaneous feedback contributions, along with some long-term ones (such as from time-dependent changes in concentrations of xenon and samarium fission-product poisons), affect the stability of the chain reaction, may limit the ability to change the power level, and are a major consideration in overall reactor safety design.

A fundamental safety feature for all power rectors is multiple-barrier containment of fission products. As may be observed for each reactor type described in the remainder of this article, these barriers include the fuel particles, surrounding cladding, the coolant system boundary, and a containment structure.

An important example of tradeoffs among the design goals is seen in thermal-reactor fuel assemblies (e.g., subsequent Figs. 3 and 8) whose pin arrangement determines the characteristics of the chain reaction, economics, and heat removal [9]. The chain reaction is enhanced by optimum spacing of the fuel in "lumps" with moderator interspersed so that neutrons from fission will undergo a number of scattering collisions for slowing down prior to reentering the fuel; too little and too much spacing can both be detrimental.

The extent of slowing down also determines the amount of conversion of fertile to fissile material and the overall energy production possible from a given amount of fuel. Spacing and coolant flow rate establish heat-removal characteristics (including temperature feedback effects on the fuel's reactivity). Final dimensions generally represent a best-estimate balance among these and other competing concerns.

Reactor Systems

The major nuclear power reactor types were identified at the end of the section "Introduction" noting that characterization of each is provided in the "General" section of Table 1. More detailed descriptions of each of these systems as implemented in the present generation of reactors follow. (As explained in detail in the section "Advanced Reactors," several generations of reactors are commonly distinguished. Of interest here, Generation I (GEN-I) reactors were developed in the 1950s–1960s, while Generation II (GEN-II) reactors are typified by the present US fleet and most in operation elsewhere.) Parameters for selected specific present reactor designs are detailed in the remainder of Table 1.

The main focus of these nuclear power plant descriptions is on the steam cycle, fuel assemblies, reactivity control, and the protective system [8]. General safety-related functions are summarized separately in the section "Nuclear Reactor Safety Features."

Light-Water Reactors

Two light-water reactor (LWR) systems – boiling-water reactor (BWR) and pressurized-water reactor (PWR) – employ ordinary ("light") water as coolant and moderator. The former design produces steam through a direct cycle (Fig. 1), while the latter uses an intermediate steam-generator heat exchanger to maintain an all-liquid primary loop and produce steam in a separate secondary loop (Fig. 2).

The nature of the water coolant/moderator results in similarities between the two LWR designs. The fuel is uranium dioxide pellets enriched to 2–5 wt% ^{235}U; initial core loadings typically span this range with reload cores distinctly at the upper end of the enrichment range. The pellets are clad in sealed zirconium-alloy tubes. Fuel assemblies consist of rectangular arrays of fuel pins with regular spacing (see also ► Modern Nuclear Fuel Cycles).

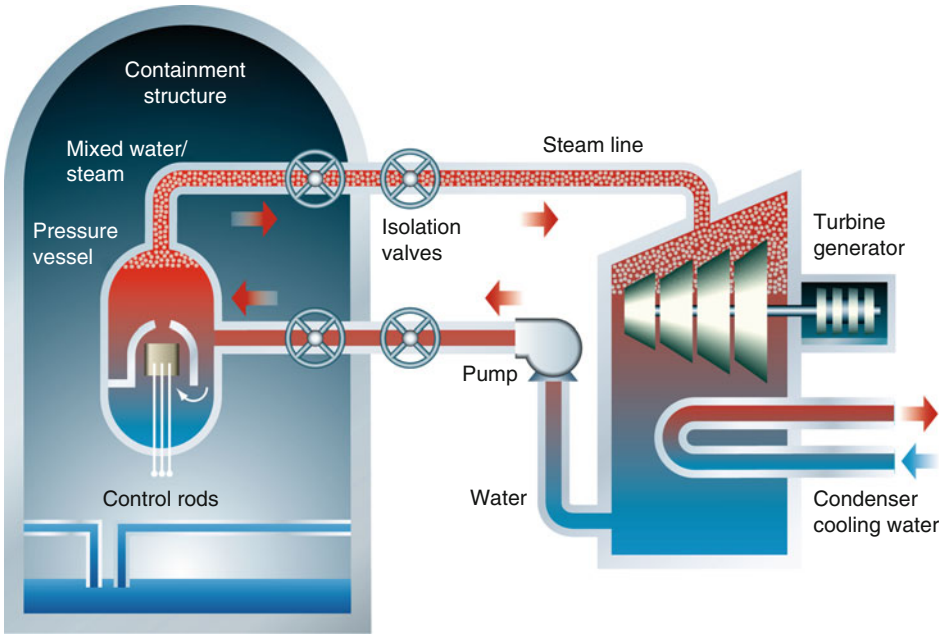

Nuclear Fission Power Plants. Figure 1
Steam cycle for boiling-water reactor (BWR) (Courtesy of Atomic Industrial Forum/Nuclear Energy Institute)

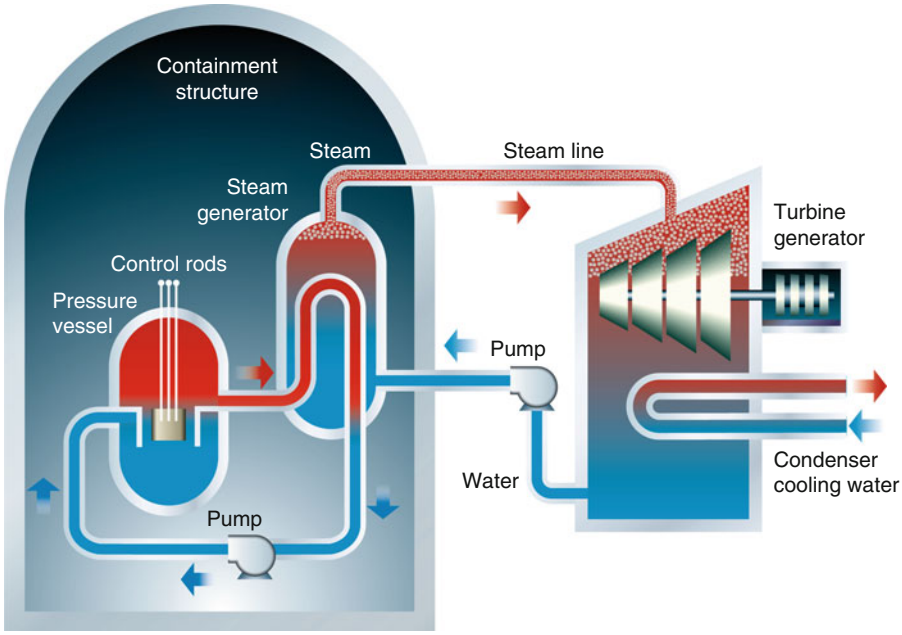

Nuclear Fission Power Plants. Figure 2
Steam cycle for pressurized-water reactor (PWR) (Courtesy of Atomic Industrial Forum/Nuclear Energy Institute)

Since the LWR designs rely on liquid water for moderating neutrons, maximum operating temperatures must remain well below the 706°F (374°C) critical temperature at which pressure increases dramatically and liquid cannot exist regardless of pressure. They, thus, cannot operate at the "modern steam conditions" – nominally 1,000°F (540°C) – typical of fossil-fueled plants. The LWR's saturated steam–water mixture requires a special, more costly "wet steam" turbine.

Boiling-Water Reactors The direct-cycle boiling-water reactor (BWR) was developed in the USA by General Electric and was followed by designs in Western Europe and Japan. It may be noted that the current designs for BWR and other reactors are increasingly characterized by multinational joint ventures. See also the section "Advanced Reactors." For details on historical, current, and proposed units of this and the other designs, see Refs. [7, 8, 10, 11].

Employing the cycle shown in concept by Fig. 1 and in more detail in Fig. 3, feedwater enters the steel reactor vessel, is heated by the fission chain reaction occurring in the fuel pins, and leaves the vessel as steam. The high- and low-pressure turbine stages are employed in concert with the multiple heaters and condensers to enhance energy-conversion efficiency. The more recent BWR designs use jet pumps to recirculate a fraction of the feedwater flow for better control.

Fuel assemblies for the BWR appear as shown in Fig. 4. The 7 × 7 to 9 × 9 square arrays of fuel pins is surrounded by a metal fuel channel, which prevents the water–steam mixture from moving between assemblies (and potentially resulting in inadequate cooling (steam–water mixture) in some assemblies). Fuel assemblies may contain pins of several different enrichments (Fig. 5). The reactor fuel core consists of up to 800 fuel assemblies.

Reactivity control for routine operation is implemented through a combination of control rods and coolant flow adjustment. The bottom-mounted control rods (indicated below the reactor vessel in Fig. 3) are made of long boron carbide–filled pins in a cruciform ("cross") shape that fits between four fuel assemblies as shown in Fig. 5.

Flow adjustment can provide another effective control method, since the water density changes with

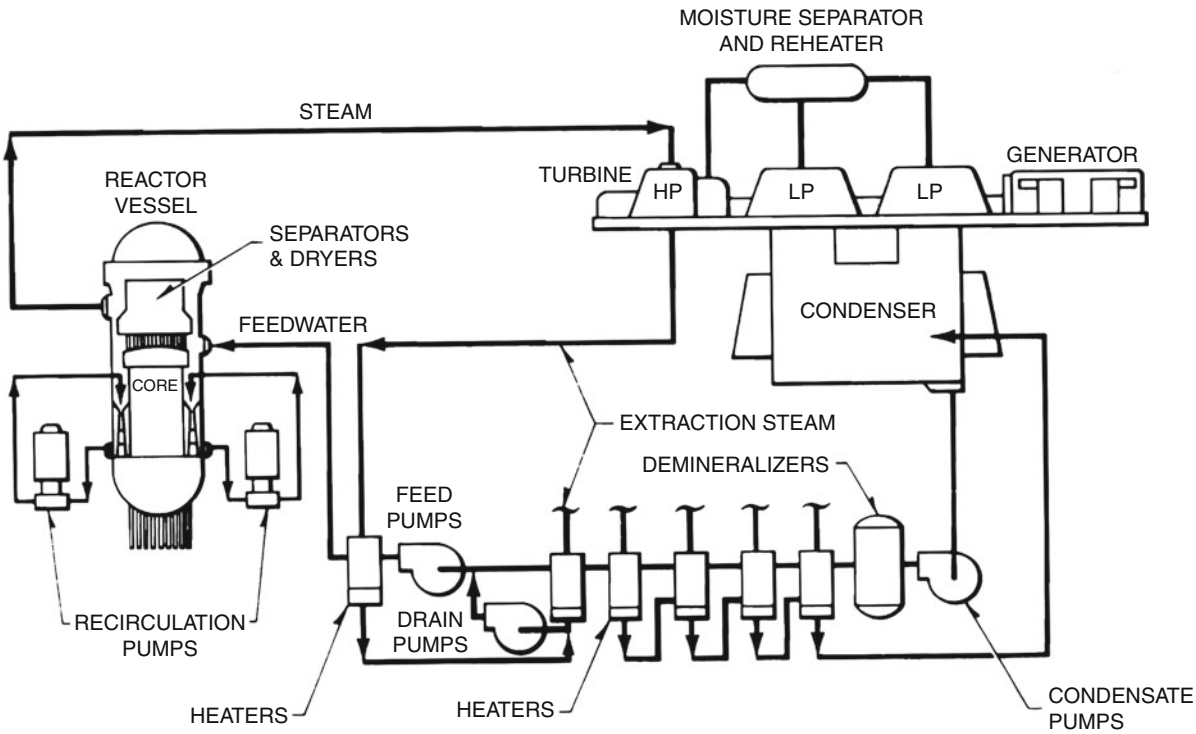

Nuclear Fission Power Plants. Figure 3
Representative steam cycle schematic diagram for a boiling-water reactor (BWR) (Courtesy of General Electric Company)

temperature. At low temperature, the dense water is very effective at moderating neutrons, and thereby encourages fission. With increased temperature, the density decreases (or, equivalently, void content increases as steam is being produced), causing a reduction in moderation and fission rate. Thus, if flow rate is increased, energy removal can be increased without a net change in coolant temperature with a resulting increase in power generation. In practice, power-level changes of up to 40% may be accomplished by flow control. (BWR operational practices are described further in the section "Boiling-Water Reactor.")

Longer-term reactivity control is accomplished using burnable poisons (e.g., "curtains" containing boron placed between fuel assemblies or gadolinium poisons fabricated into the fuel itself) and gradually withdrawing inserted control rods over core lifetime. Reactor shutdown – scram or trip – is accomplished by using gas pressure to insert all of the bottom-mounted control rods into the core.

Table 1 contains parameters for a large BWR and other reactor types. Advanced BWRs are addressed in the section "Advanced Reactors."

Pressurized-Water Reactor The two-loop pressurized-water reactor (PWR) was developed in the USA by Westinghouse Electric Corporation. Other somewhat similar designs have been developed by a pair of US organizations, as well as by others in Western Europe, Japan, and South Korea. A particular unique version has come from the Soviet Union (now by Russia). Water in the primary loop (Fig. 2) is maintained as liquid by using high pressure. The water enters the reactor vessel (Fig. 6) at the inlet nozzle, flows downward along the inner vessel wall, is distributed at the lower vessel plate, flows up through the fuel assemblies removing heat energy, and exits at the outlet nozzle – still as a liquid.

Energy from the primary loop is extracted and converted to steam by two to four U-tube (Fig. 7), once-through, or horizontal (Russian design) steam

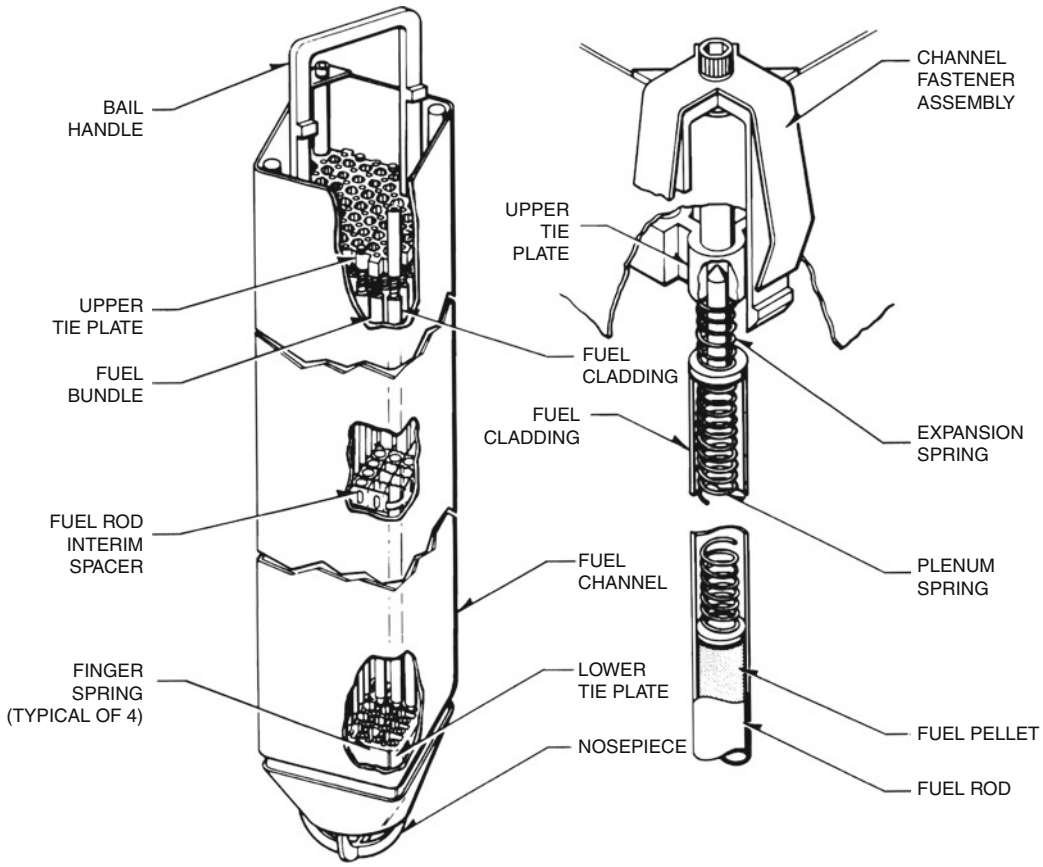

Nuclear Fission Power Plants. Figure 4
Representative fuel assembly for boiling-water reactor (Courtesy of General Electric Company)

generators. Multiple turbine stages, heaters, and a condenser are employed as for the BWR (Fig. 3). A *pressurizer* with a steam–water interface is used to maintain the sensitive pressure/temperature balance in the primary system by using heaters to boil water, increase the amount steam, and thus raise the pressure; conversely spraying "cooler" ("less hot") water condenses steam and reduces the pressure.

Fuel assemblies for the PWR are of 14 × 14 to 17 × 17 square fuel pin arrays (Fig. 8) or a hexagonal array of up to 331 pins (Russian VVER). They are not enclosed in a fuel channel (in part because the single-phase primary fluid is better behaved than the BWR's boiling coolant). These assemblies also have unoccupied pin locations, which can accommodate control rods, burnable poisons, or instruments. The large PWR reactor cores consist of 150–200 or more fuel assemblies.

Like the BWR, the PWR uses control and burnable-poison rods for reactivity control. Uniquely, it also uses the soluble neutron poison, boric acid, for long-term control. The boric acid concentration is adjusted to match general changes from fuel burnup, conversion of fertile material into fissile, and depletion of burnable poisons.

Insertion of control-rod assemblies from the top of the core (by contrast with the bottom-mounted BWR control rods) provides short-term, routine reactivity control. These assemblies consist of 5–24 "fingers," made of boron carbide or of a silver–indium–cadmium mixture, which move in channels within the fuel assemblies (e.g., as shown in Fig. 8). A small group of rods in a symmetric pattern is inserted partially into the fuel (typically >25%) and then moved as needed to compensate for routine

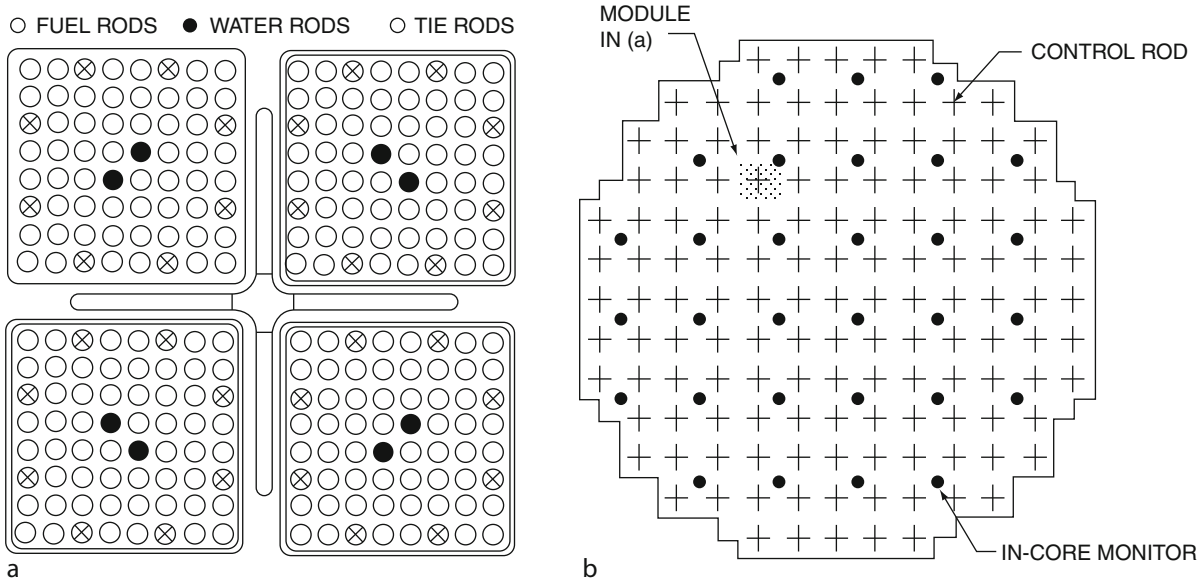

Nuclear Fission Power Plants. Figure 5
Core fuel module (**a**) and control-rod pattern (**b**) for representative boiling-water reactor (Courtesy of General Electric Company)

power fluctuations. Significant power changes up to an including startup and shutdown invoke other, larger groups of control rods. (PWR operational practices are described further in the section "Pressurized-Water Reactor.")

Scram/trip is accomplished in the PWR by dropping the top-mounted control rods (Figs. 6 and 8) into the core under the influence of gravity. The rods are mounted to their drives by electromagnets so that interruption of the current (from power failure or indication that a specific parameter is outside of a predetermined range) causes the rods to fall.

Figure 9 is a cutaway drawing (wallchart) of a representative PWR unit. Other than for the reactor "nuclear island" – also known as the nuclear steam-supply system (NSSS) – the drawing shows features common to the other reactor units, all of which have turbine generator(s), and containment, auxiliary, and support buildings. (Reference [12] contains a Web link to this wallchart, as well as to charts for over 100 other reactors.)

Table 1 contains parameters for a representative PWR and other reactor types. Advanced PWRs are addressed in the section "Advanced Reactors."

Heavy-Water Reactors

Ordinary hydrogen in the form of water is the most effective material for reducing neutron energy, but it also absorbs some of the neutrons that could otherwise participate in the chain reaction. Thus, deuterium as heavy water, which requires more collisions for a given energy change but exhibits much less absorption, is a better moderator in some ways, e.g., allowing use of natural- or other low-enrichment uranium fuel. Deuterium, existing in nature in a ratio of 1:400 with ordinary hydrogen, requires isotopic enrichment prior to use (as does ^{235}U in uranium for many of the reactor applications).

Heavy-water reactors (HWR) have been developed in Canada – their signature CANDU (for Canadian deuterium-uranium) – the UK, West Germany, India, Japan, and South Korea. Pressure-vessel designs (with similar hardware configurations to the PWR) employ the same heavy water volume as coolant and moderator. Pressure-tube designs use heavy water in a separate moderating volume generally with pressurized heavy-water (PHW) coolant, sometimes boiling light-water coolant, and potentially with an organic liquid.

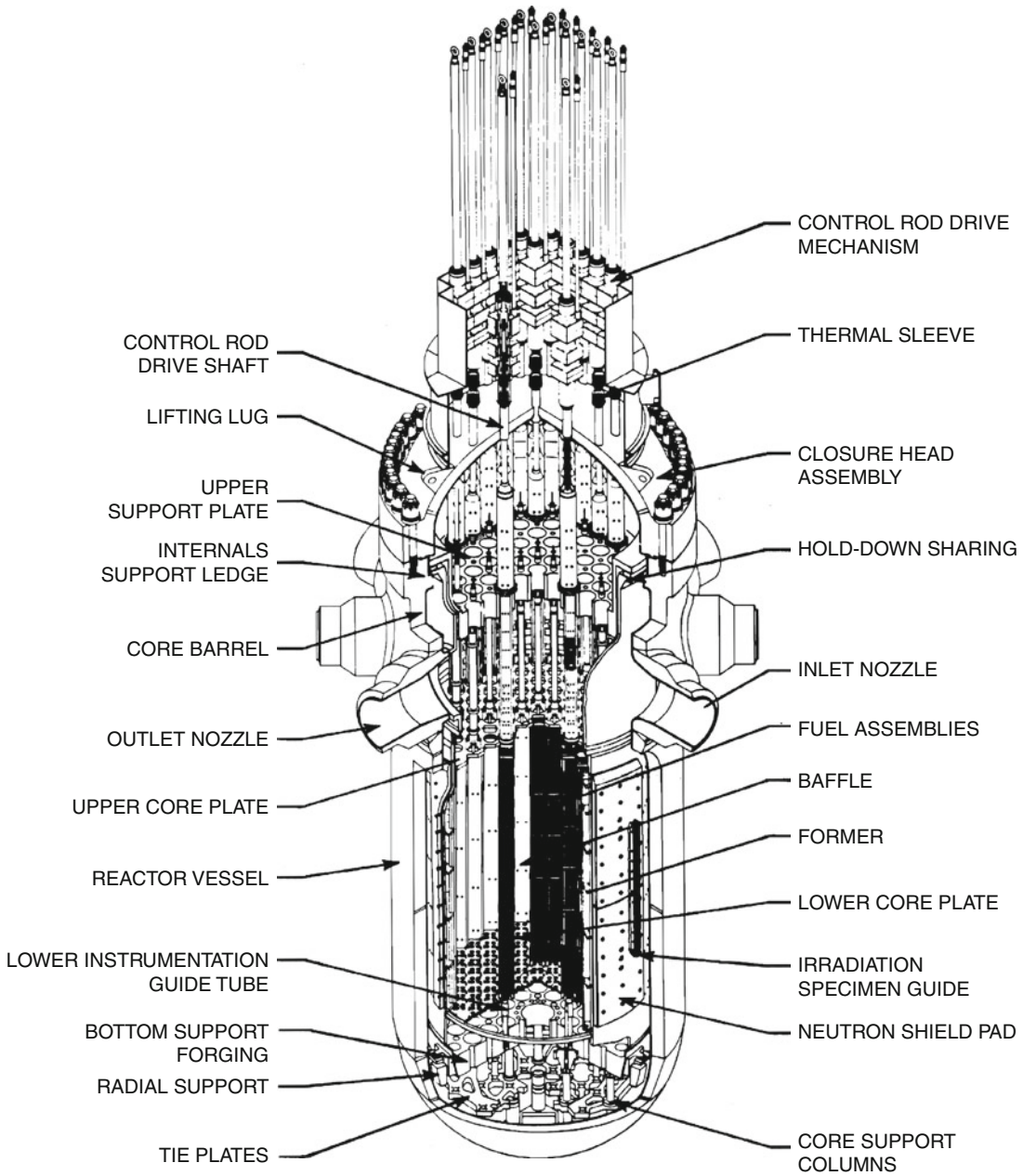

Nuclear Fission Power Plants. Figure 6
Reactor pressure vessel for a representative pressurized-water reactor (Courtesy of Westinghouse Electric Company)

The example of a CANDU-PHW is considered further below.

The CANDU-PHW steam cycle has two loops (Fig. 10), like the PWR, with the primary pressurized heavy-water loop transferring heat energy to a loop of ordinary water for steam production. A major difference, however, is that the primary fluid is distributed among several hundred pressure tubes which pass through a large calandria vessel (Fig. 11) containing the separate heavy-water moderator. The coolant is actually collected in two separate loops, with the fluid in adjacent tubes flowing in opposite directions.

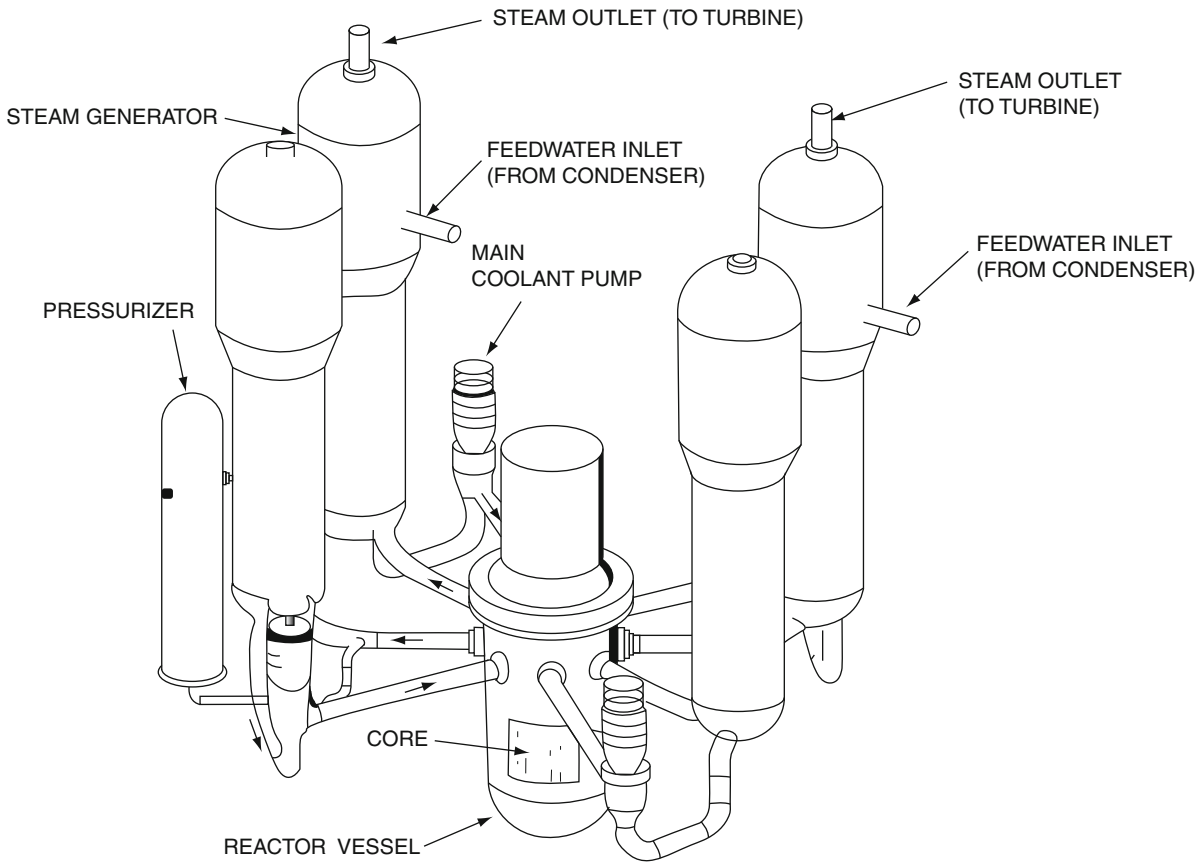

Nuclear Fission Power Plants. Figure 7
Four U-tube steam-generator primary loop configuration for a pressurized-water reactor (Courtesy of Westinghouse Electric Company)

The fuel assemblies consist of natural (i.e., 0.711 wt% ^{235}U) uranium dioxide fuel pellets in zirconium clad, similar to LWR fuel. However, short, cylindrical bundles of fuel pins (Fig. 12) allow a unique on-line fueling scheme whereby a machine attaches to each end of a single coolant tube and inserts one fuel assembly while in effect pushing out another.

A major portion of the reactivity control is accomplished by on-line fueling, which is required to compensate for the low reactivity inherent in the natural uranium fuel. Routine operating adjustments and power shaping are accomplished with neutron-poison control rods, or by introduction of ordinary water (which absorbs more neutrons than heavy water) into special chambers. Other control rods are available for reactor scram/trip. The separation of the coolant and moderator volumes also provides the possibility for moderator "dumping" as an emergency shutdown method.

Table 1 contains parameters for a large CANDU-PHW and other reactor types. Advanced HWRs are addressed in the section "Advanced Reactors."

Gas-Cooled Reactors

The world's first research reactor used natural uranium fuel, graphite moderator, and natural-circulation air cooling. Subsequent systems have also used graphite moderator with natural or enriched uranium and with carbon dioxide or helium coolant. Various commercial gas-cooled reactors (GCR) have operated in France, the UK, the USA, and Germany. Two versions of the helium-cooled high-temperature gas-cooled reactor (HTGR) developed by the USA and Germany are

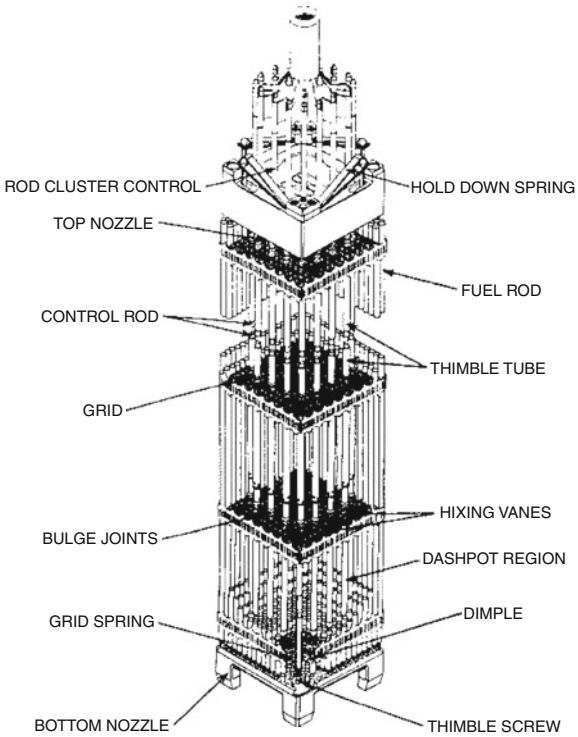

Nuclear Fission Power Plants. Figure 8
Representative fuel assembly for a pressurized-water reactor (Courtesy of Westinghouse Electric Corporation)

described below. (Both are prototypical designs at ~1,000 MWe described for the purpose of comparison with other current large commercial reactors in this section. Evolutionary units of this heritage are addressed in the section "Advanced Reactors".)

The HTGR steam cycle (Fig. 13) employs a primary loop of helium, heat exchangers, and pumps contained within a prestressed concrete reactor vessel (PCRV) – two versions of which are shown in Fig. 14 – and a steam loop. Since the coolant is a single-phase gas, no pressurizer is required (in contrast to the two-loop water-cooled designs). The nature of the coolant also provides the prospect for direct conversion through a gas turbine, e.g., employing a Brayton thermodynamic cycle.

Fuel for the HTGR consists of small microspheres of uranium or thorium carbide (UC/ThC) with coatings of graphite and/or silicon carbide (Fig. 15a). The uranium microspheres, enriched to 20–93 wt%, may be mixed with separate thorium microspheres to an effective fissile enrichment of about 5 wt%.

In the US "prismatic" – hexagonal-block – HTGR system, the microsphere mixture is formed into roughly finger-sized sticks with a carbon-resin binder. The sticks are then loaded into large hexagonal graphite blocks with interspersed coolant holes (Fig. 15b). The blocks are stacked several high and in a roughly cylindrical arrangement to form the reactor core (Fig. 14a). Another version of the HTGR – the thorium high-temperature reactor (THTR) – forms the microspheres into a spherical shape and coats them with hard, thick graphite layers into a 6-cm-diameter "pebble" (Fig. 15c). The reactor core is then formed by loading these fuel units into a hopper in a PCRV (Fig. 14b), from which fueling and defueling can be accomplished on-line. This THTR design feature leads to the alternative designation of the reactor as "pebble bed."

Reactivity control in the prismatic design depends on boron control rods for routine and shutdown functions. Burnable poisons may be used for long-term reactivity control. A reserve shutdown system consisting of small boron-carbide balls backs up the primary systems.

The THTR requires minimal excess reactivity due to its ability to change fuel on-line. Control rods inserted into the pool of pebbles provide the means for routine operational adjustments.

Table 1 contains parameters for a large prismatic HTGR and other reactor types. Advanced GCRs – prismatic and pebble bed – are addressed in the section "Advanced Reactors."

Light-Water Graphite Reactors

Light-water-cooled graphite-moderated reactors (LWGR)/pressure-tube graphite reactors (PTGR) were among the first systems used for purposes of research, plutonium production, and electric power generation. The Soviet Union credits a small unit of this type with generating the first commercial electricity. Current commercial use is limited to the Soviet RBMK pressure-tube graphite reactors (PTGR). The Chernobyl reactor – the site of the catastrophic 1986 accident – was of this type.

The RBMK uses a direct steam cycle (Fig. 16) with boiling-water coolant like the BWR (Fig. 1). However, its complex pressure-tube design with separate coolant

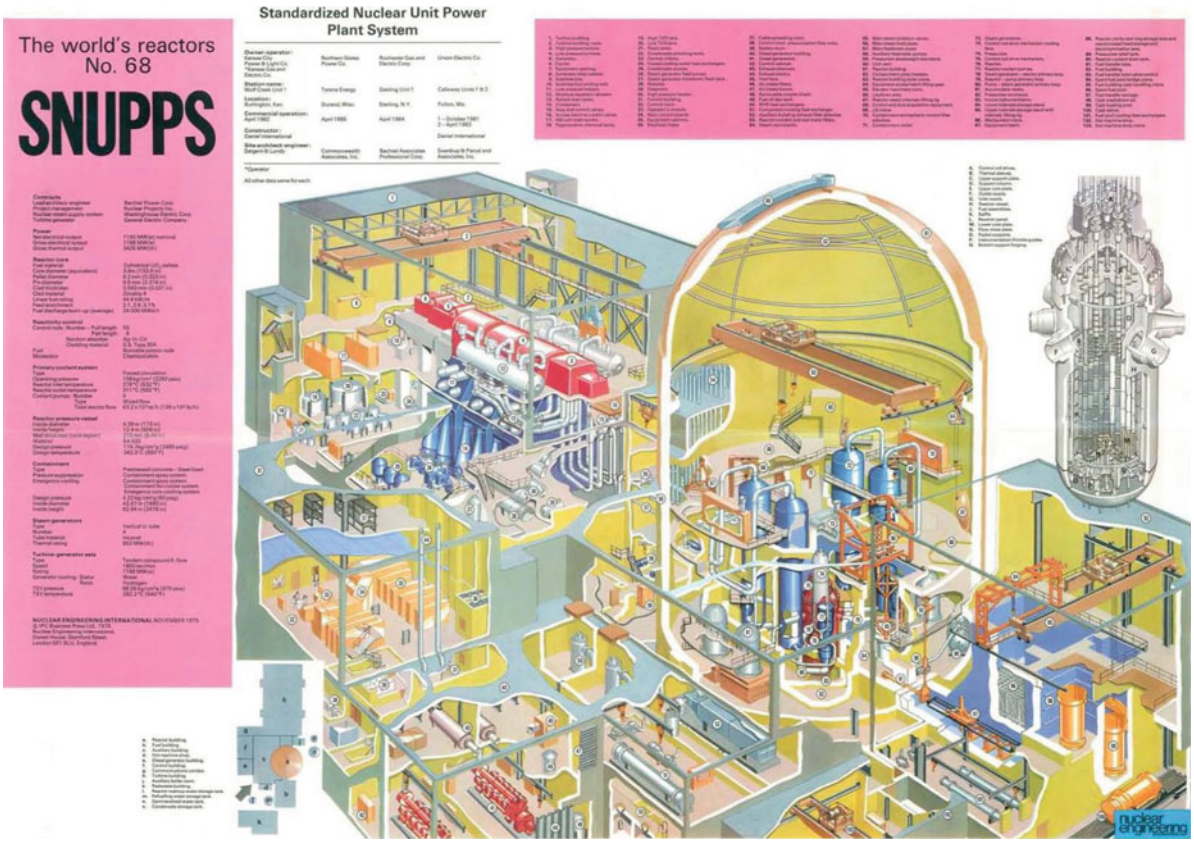

Nuclear Fission Power Plants. Figure 9
Cutaway of a representative PWR station – Standardized Nuclear Unit Power Plant System (SNUPPS) (Courtesy of Nuclear Engineering International)

and moderator also has similarities to the CANDU-HWR (Fig. 11).

The RBMK reactor (Fig. 17) consists of nearly 1,900 vertical pressure tubes – each accommodating a pair of fuel assemblies or a control rod. The pressure tubes are surrounded by an array of long, square graphite blocks – which serve as the system's neutron moderator – set together, side-by-side vertically approximating a cylinder of roughly 12 m diameter and 7 m height. Water introduced at the bottom of the core enters pressure tubes, and then boils in the process of removing fission heat from the fuel pins. Steam is drawn from each tube through a stainless-steel pipe for use in one of two turbine generators.

A steel reactor vessel serves primarily as structural support for the graphite-moderator blocks. This vessel with the pressure tubes and piping constitute the primary-system boundary.

The RBMK fuel assemblies (Fig. 18) each contain two stacked subassemblies of 18 zirconium-clad fuel pins of UO_2 enriched to 1.8 wt% in ^{235}U. Stacked one atop the other, a pair fills a pressure tube to facilitate the on-line refueling paradigm that adjusts reactivity and facilitates plutonium production. Various groups of control rods are moved for routine power adjustment and for full-insertion core shutdown.

Table 1 contains parameters for a large PTGR/RBMK unit and other reactor types. Advanced LWGR/PTGRs, if any, will be of totally different design.

Fast Breeder Reactors

The fast-neutron-spectrum breeder reactor (FBR) design concepts are predicated on breeding more new fuel than that used to sustain the neutron chain reaction (section "Reactor Classifications"). For this

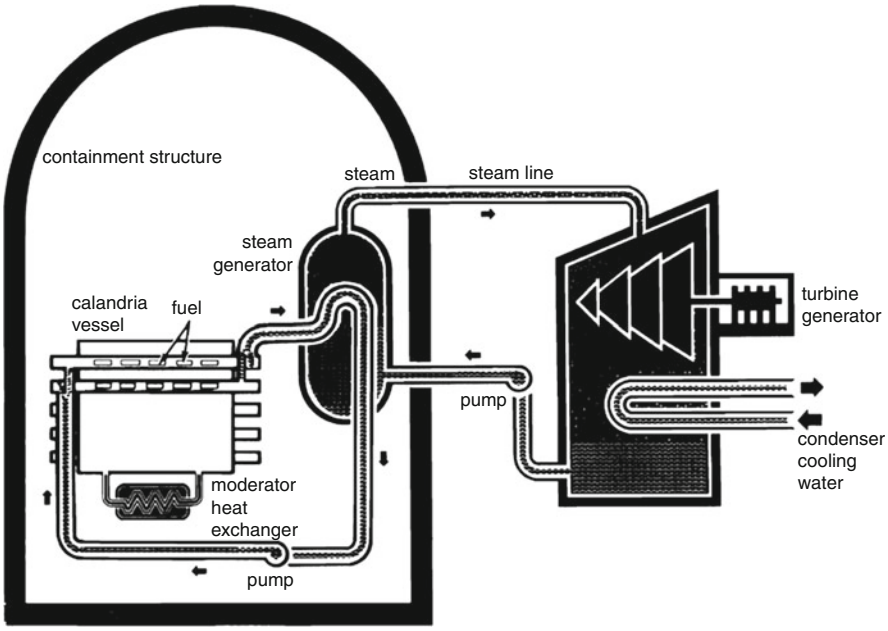

Nuclear Fission Power Plants. Figure 10
Steam cycle for CANDU pressurized heavy-water reactor (Courtesy of Atomic Industrial Forum/Nuclear Energy Institute)

purpose, fissile plutonium (^{239}Pu and ^{241}Pu) and fertile ^{238}U (natural or depleted uranium with, respectively, 0.711 wt% and 2–3.5 wt% in ^{235}U) fuel with a fast-neutron spectrum are most effective. An FBR optimized for breeding, thus, can utilize uranium at least 60 times more efficiently than a normal LWR reactor. (Note that some fast-spectrum reactors – see the section "Advanced Reactors" – may not have actual breeding as a design specification.)

The liquid-metal fast breeder reactor (LMFBR) keeps neutron energy high (in the upper keV to MeV range) by using (non-moderating) liquid sodium as a coolant. The liquid sodium, although not the heaviest coolant available is not too light, has favorable heat transfer properties, and is not an excessively strong absorber of neutrons compared to other choices.

Although experimental fast breeder reactors have operated in the USA since the late 1950s, and subsequently as prototypes in Western Europe, most recent activity has been in Russia, Japan, and India.

The steam cycle has three loops (Fig. 19) with the first two of sodium and the third of water. The intermediate sodium loop is present to isolate the primary from possible direct contact with water in the steam generator. The primary sodium becomes radioactive from neutron absorption and also can pick up fission-product radionuclides from the fuel. If this sodium were to come in contact with water, it would not only precipitate an exothermic reaction but also spread radioactive contamination.

LMFBRs have been implemented in two main configurations – loop-type and pool-type. The former is essentially as shown in Fig. 19 and similar paradigm to LWR and HTGR. The pool-type LMFBR has the reactor vessel, heat exchanger, and associated piping – entire primary loop – immersed in a large pool of sodium. The now shutdown SuperPhenix was a pool-type LMFBR of similar capacity to the current large commercial reactors. The SuperPhenix reactor vessel and layout are shown in Fig. 20.

Fuel for the LMFBR consists of mixed-oxide (PuO_2-UO_2) fuel pellets, which typically combine about 10–30 wt% fissile plutonium with natural or depleted uranium – the remnants of the enrichment process. As shown in Fig. 21a, for a reactor other than SuperPhenix, pellets are loaded into thin stainless-steel cladding tubes, and hence into hexagonal-array subassemblies. Breeding is optimized by surrounding the mixed-oxide core with a *blanket* of depleted uranium. The axial blankets above and below the core are created

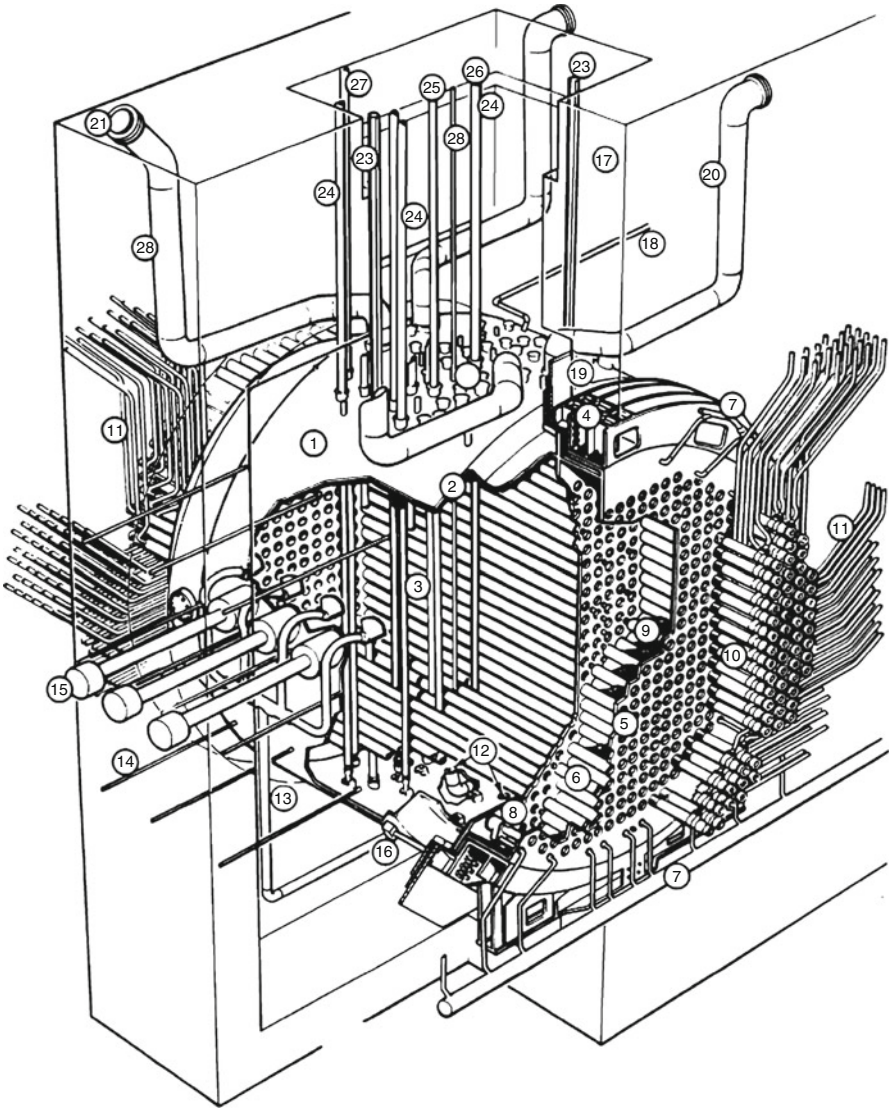

1 CALANDRIA
2 CALANDRIA SHELL
3 CALANDRIA TUBES
4 EMBEDMENT RING
5 FUELLING TUBESHEET
6 END SHIELD LATTICE TUBES
7 END SHIELD COOLING PIPES
8 INLET OUTLET STRAINER
9 STEEL BALL SHIELDING
10 END FITTINGS
11 FEEDER PIPES
12 MODERATOR OUTLET
13 MODERATOR INLET
14 FLUX DETECTOR AND LIQUID INJECTION NOZZLE
15 ION CHAMBER
16 EARTHQUAKE RESTRAINT
17 VAULT WALL
18 MODERATOR EXPANSION TO HEAD TANK
19 CURTAIN SHIELDING SLABS
20 PRESSURE RELIEF PIPES
21 PRESSURE RELIEF DISC
22 REACTIVITY CONTROL ROD NOZZLES
23 VIEWING PORT
24 SHUTOFF ROD
25 ADJUSTER ROD
26 CONTROL ABSORBER ROD
27 ZONE CONTROL ROD
28 VERTICAL FLUX DETECTOR

Nuclear Fission Power Plants. Figure 11
Calandria vessel and pressure tube of CANDU pressurized heavy-water reactor (Courtesy of Atomic Energy of Canada Limited)

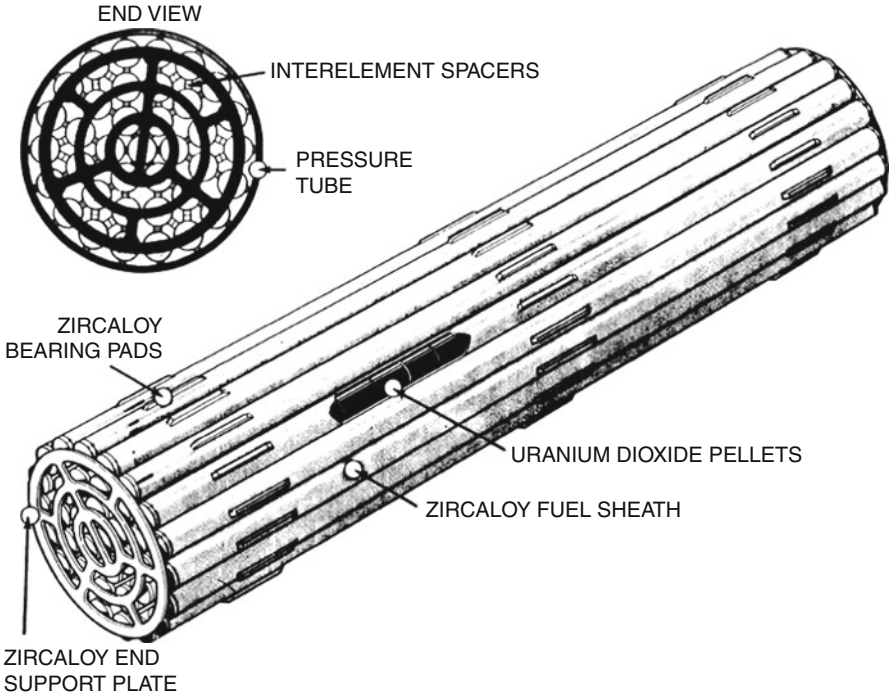

Nuclear Fission Power Plants. Figure 12
Fuel assembly for CANDU pressurized heavy-water reactor (Courtesy of Atomic Energy of Canada Limited)

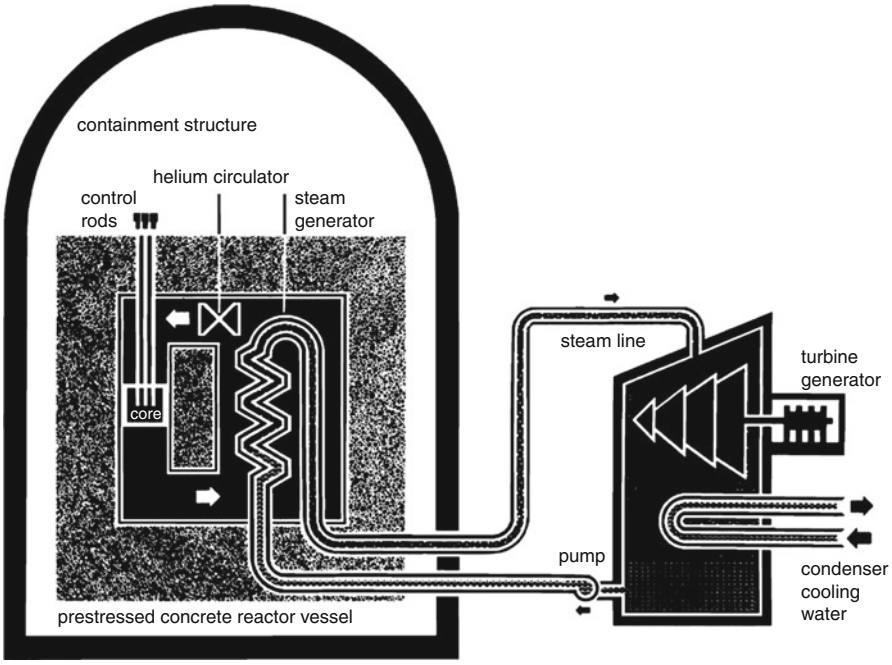

Nuclear Fission Power Plants. Figure 13
Steam cycle for high-temperature gas-cooled reactor (HTGR) (Courtesy of Atomic Industrial Forum/Nuclear Energy Institute)

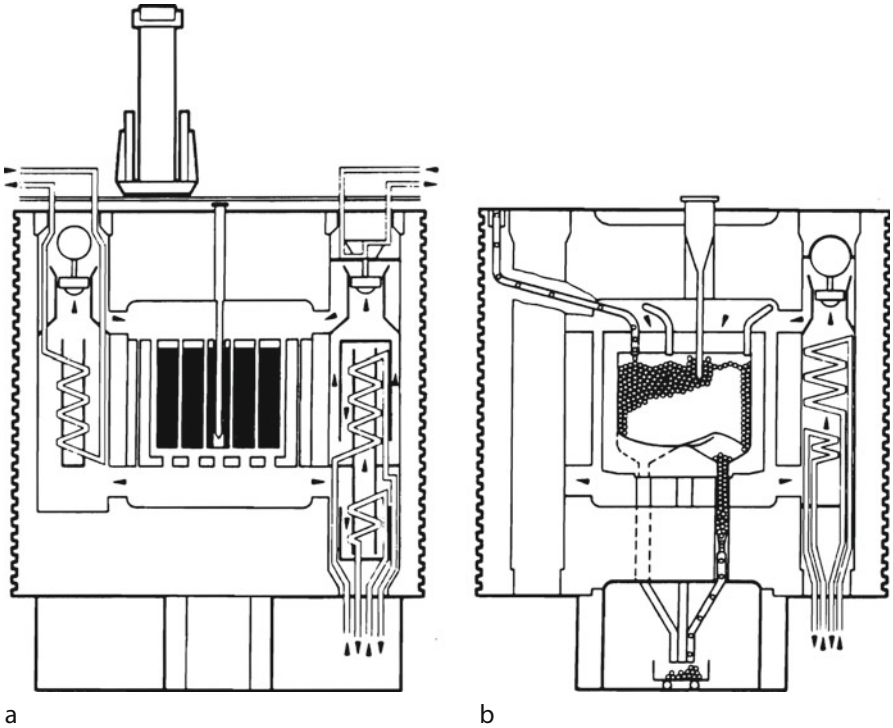

Nuclear Fission Power Plants. Figure 14
Prestressed concrete reactor vessels (PCRV) for (**a**) prismatic high-temperature gas-cooled reactor and (**b**) thorium high-temperature ("pebble-bed") reactor (Courtesy of Oak Ridge National Laboratory)

by loading pellets of natural or depleted uranium at either end of the core fuel pins. The surrounding radial blanket consists of separate subassemblies (Fig. 21b) of natural or depleted uranium, where the pins may be of larger diameter because the power density in the blanket is much lower than it is in the core.

LMFBR reactivity control is accomplished through use of neutron-poison control rods. Since the breeder produces more fuel than it uses, however, the core reactivity does not decrease with fissile burnup and fission-product buildup as dramatically as in the in thermal-neutron-energy converter reactors described previously. This is fortunate, because the traditional neutron poisons are not very effective for fast neutrons.

Rapid shutdown may be implemented with either of two independent sets of control rods. It is typical for one set to consist of solid neutron-poison rods, top-mounted and inserted by gravity – the traditional approach for most of the world's reactors. The second system – providing full redundancy should the first fail – often has features allowing for operation even if core distortion has occurred, e.g., through use of oversized channels and segmented rods. Table 1 contains parameters for a large LMFBR and other reactor types. Advanced fast-neutron reactors are addressed in the section "Advanced Reactors."

Worldwide Perspective

Worldwide nuclear power reactor status is shown in Table 2 as a snapshot circa 2009 of the ever-changing landscape. Reactor data are from Ref. [7], which also provides significant information on essentially each nuclear reactor ever built or even ordered.

The table also shows nuclear generation performance – as both TWe-hr generated and percentage of total national electric energy production – for 2009 and, as a comparison, a decade and a year earlier. It is apparent, e.g., that the USA and many other countries experienced a decade of stagnation at the same as the Pacific-basin nations produced impressive growth.

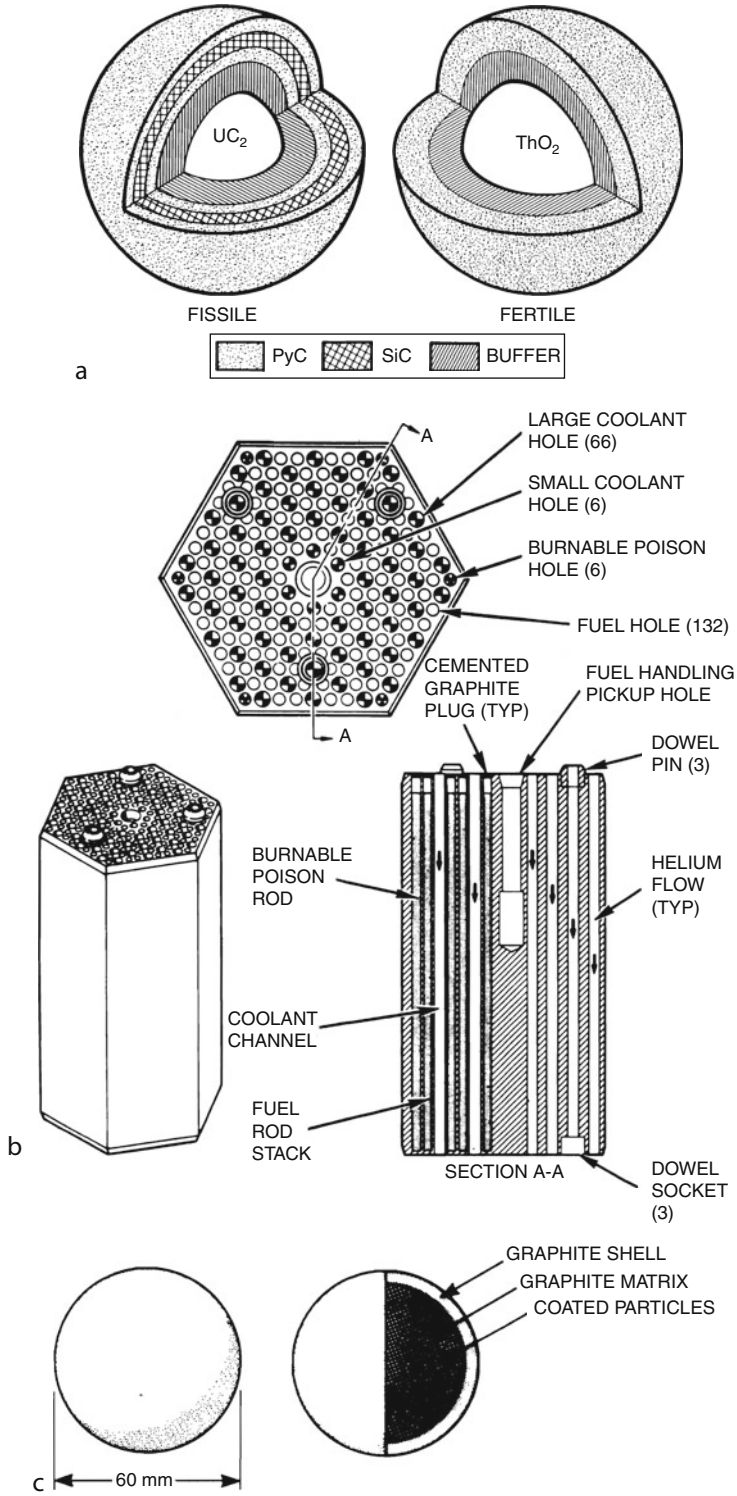

Nuclear Fission Power Plants. Figure 15

Fuel-assembly components for high-temperature gas-cooled reactors: (**a**) microspheres, (**b**) prismatic fuel block (Courtesy of GA Technologies), and (**c**) fuel sphere ("pebble") [8]

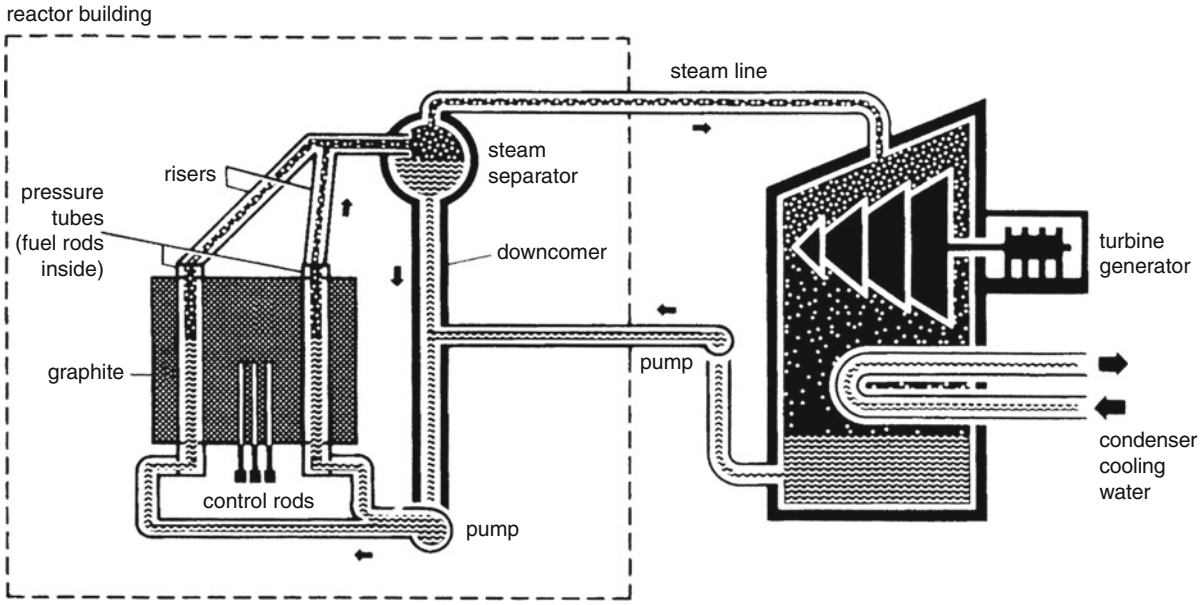

Nuclear Fission Power Plants. Figure 16
Steam cycle for pressure-tube graphite reactor (PTGR) (Courtesy of Atomic Industrial Forum/Nuclear Energy Institute)

Other Reactor Concepts

In addition to the nuclear power reactor designs described above, a wide variety of other possibilities have been built for power production or research purposes. Still others have been researched "on paper." The major approach is to look at viable combinations of fuel, coolant, and moderator. A few examples are identified here and in the section "Advanced Reactors."

CANDU reactors could also be operated with fuel assemblies of enriched uranium, plutonium, ^{233}U/thorium, or a mixture thereof. Potential coolants other than heavy water include light water and organic liquid.

The gas-cooled fast breeder reactor (GCFBR) uses helium coolant and plutonium fuel in a concept similar to the HTGR, except with no graphite moderator. The molten-salt breeder reactor (MSBR) concept includes liquid fuel that circulates through a graphite-block core region in a closed primary loop. The fuel is processed on-line to remove fission products and ^{233}U bred from thorium in the salt.

Many other novel designs that stress enhanced safety and/or compact size also have been proposed. A wide variety of such concepts are identified in the section "Advanced Reactors."

Operation, Maintenance, and Control Practices

Specific characteristics of the fission process and the design of reactors and their fuel result in unique features which affect operations, maintenance, and plant control. With over 50 years of experience for nuclear reactors in general and 30 or more years of experience with the more mature system technologies, an increasingly solid basis for good operating practices is becoming available [13]. Uniformly excellent nuclear plant availability is a key indication of this.

Operation

Routine power operations reflect characteristics of the reactor design – fuel, moderator, coolant, geometry. The BWR, with water boiling in the core, and PWR, with pressurized liquid water in the core – the two plant types dominating the world circa 2010 – show quite different operational characteristics.

Boiling-Water Reactor Startup of a boiling-water reactor begins with running the coolant pumps at minimum speed. The control rods are withdrawn from their initial fully inserted position one at a time in a preset sequence that keeps the power distribution

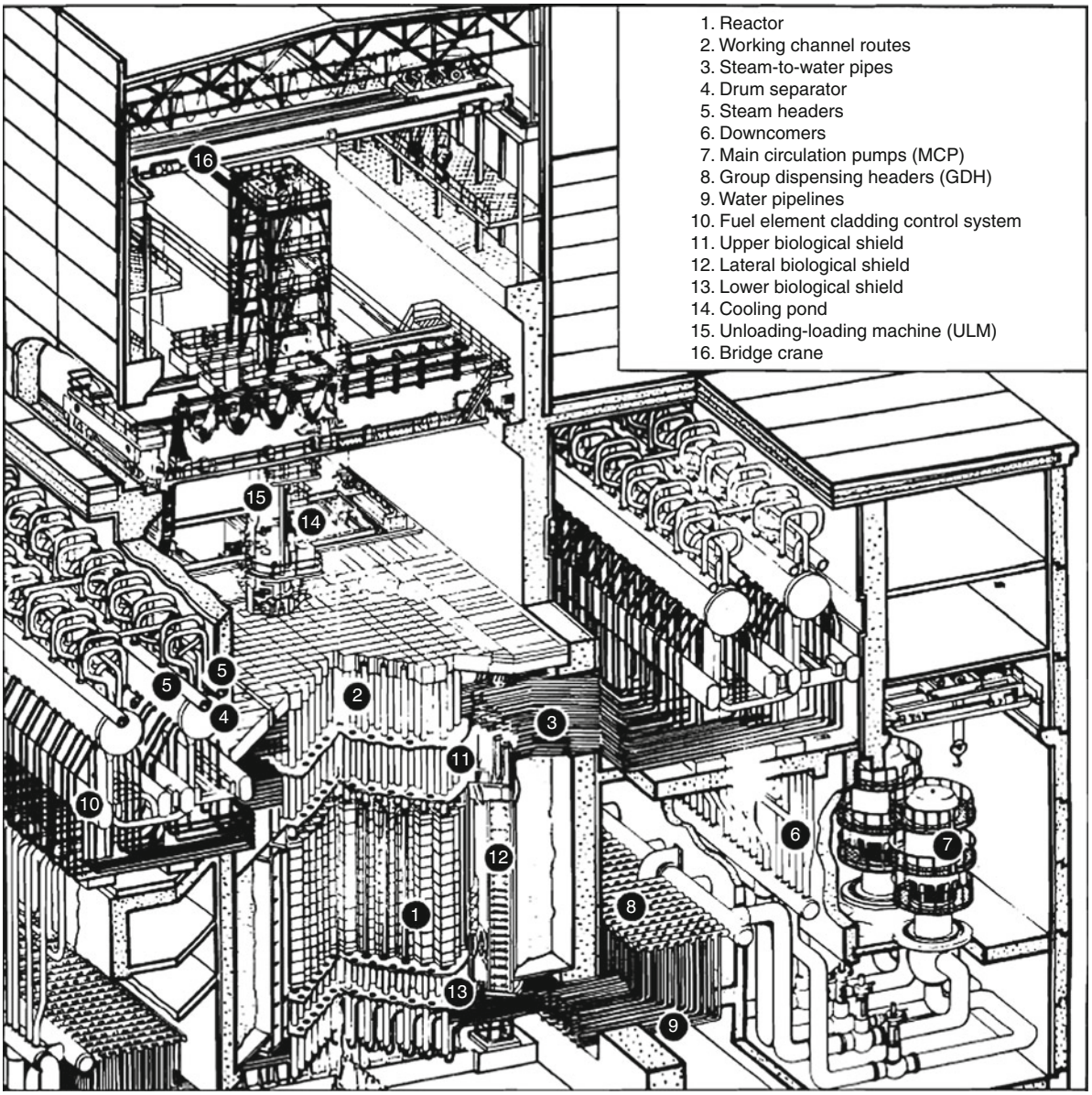

Nuclear Fission Power Plants. Figure 17
Sectional view of a Soviet pressure-tube graphite reactor (PTGR) (From [23])

reasonably uniform. The reactor is brought to critical, and then made slightly supercritical to heat the coolant slowly to the boiling point where steam formation begins to pressurize the vessel. Initially, the steam is dumped to the main condenser (Figs. 1 and 3). When operating temperature and pressure are reached and the steam flow is about 20% of full capacity, the turbine is started and the generator synchronized to the electric power grid. Power level is increased by control-rod withdrawal, flow increase, or a combination (e.g., with flow set for 20% power, rod withdrawal takes the power to 50% and then the pumps are used to achieve full power).

Once at power, an automatic control system is used to change coolant flow for the reactor to *load follow* the turbine steam demand. The control rods are still under

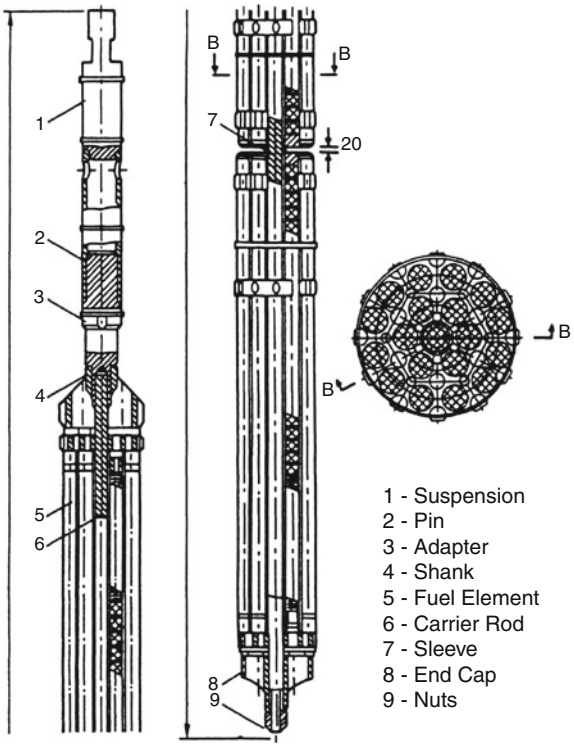

Nuclear Fission Power Plants. Figure 18
Fuel assembly for a Soviet RBMK pressure-tube graphite reactor (PTGR) (From NUREG-1250 [1987])

operator control. For continued steady power operation, control-rod withdrawal or coolant flow changes can be made manually within predetermined power-to-flow limits. Control rods are withdrawn systematically to match fuel-assembly burnup.

Tripping – initiating a scram – of the control rods to shutdown a reactor causes thermal-mechanical stress. Thus, the preferred method for shutdown is essentially the reverse of the startup process. When the power drops too low for production of electricity, the steam is again dumped to the condenser. This is continued until the fission-product-decay heat load is small enough to be handled by a specifically designed residual-decay-heat-removal system.

BWR refueling is similar to that for the PWR – as described in the next subsection. One important difference is that the control rods do not need to be removed with the vessel head (because they are bottom mounted).

Pressurized-Water Reactor Startup of a pressurized-water reactor begins with alignment of support systems and pressurization of the primary reactor coolant system (Figs. 6 and 7). All shutdown (or "safety") rods are "cocked" (i.e., withdrawn fully) to be available for reactor trip if necessary. Designated regulating rods remain fully inserted. The main reactor coolant pumps are started with their inherent heat generation producing a slow heat-up of the reactor coolant system that minimizes mechanical stress. As operating temperatures are approached, a "bubble" (i.e., steam volume) is drawn in the pressurizer, volume control is established, steam may be drawn to warm the steam generators, and final adjustments are made to the reactor coolant system chemistry and the soluble boron concentration. Steady withdrawal of the regulating control rods first takes the core critical and then supercritical to increase the power level at a predetermined rate. The turbine is started and the generator is synchronized to the grid. Manual control of the reactor, turbine, and steam-generator feedwater is maintained until about 15% power when transfer is made to an automatic mode for escalation to full power. In general, the turbine is matched to the reactor's (or actually steam generator's) steaming rate, a *reactor following* mode of operation. (Note: In practice for a PWR the reactor leads turbine, while for a BWR the reactor follows the turbine.)

During routine full-power operation, small movements of the first regulating group balance normal power fluctuations. Larger insertions change the power level.

Boric acid concentration is adjusted to match fuel burnup and allow control-rod positions to remain consistent with the power-dependent insertion limits. This concentration may be as high as 2,000 ppm (parts-per-million) in a fresh core and be reduced to 100 ppm or less by the end of the core's lifetime.

Planned shutdown involves insertion of the rods (with additional boration if cold shutdown, e.g., for defueling, is desired). Decay heat is removed initially by one-pump or natural-circulation operation of the steam generators with the steam dumped to the condenser. When the bulk coolant temperature falls sufficiently, cooling is shifted to a dedicated residual-decay-heat-removal system and the pressurizer bubble is collapsed.

Within a day or two of reactor shutdown, the decay-heat load decreases sufficiently for reactor coolant

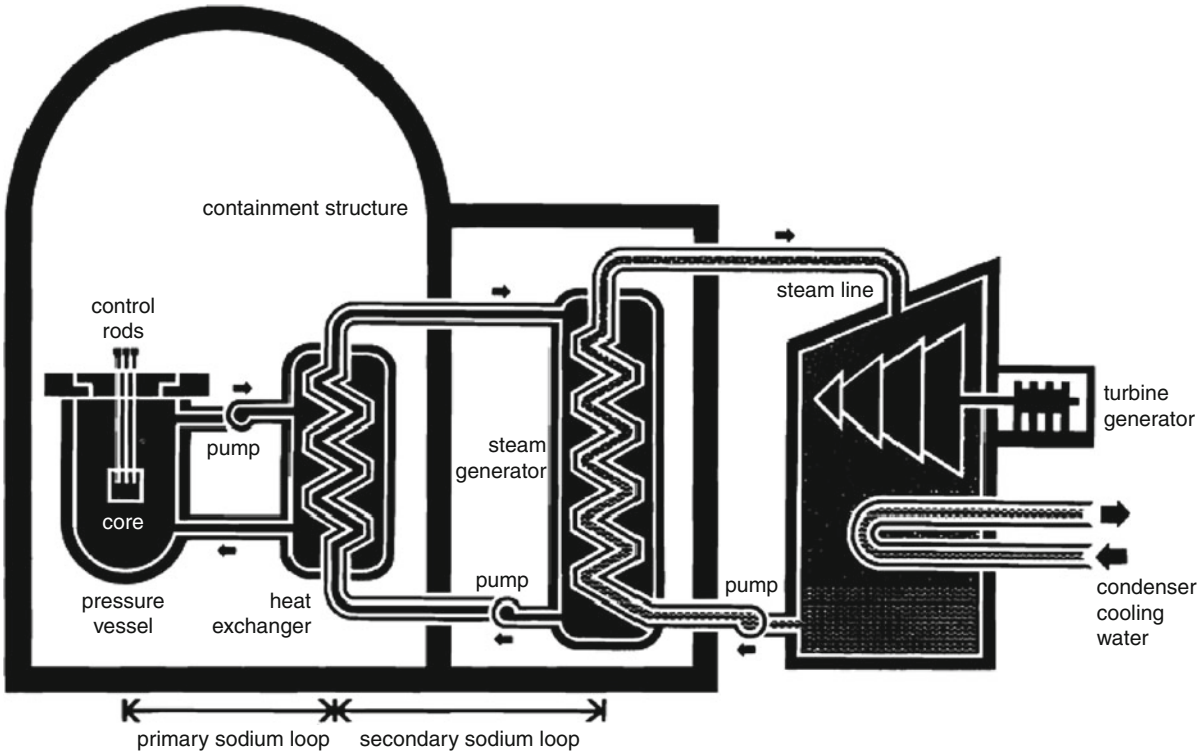

Nuclear Fission Power Plants. Figure 19
Steam cycle for liquid-metal fast breeder reactor (LMFBR) (Courtesy of Atomic Industrial Forum/Nuclear Energy Institute)

system depressurization and refueling. The reactor cavity is flooded with highly borated water to a height of 10 m or more so that the vessel head (with all control rods attached) and the fuel assemblies can be removed while still having enough water above them to provide radiation shielding for operating personnel. Individual spent-fuel assemblies are extracted remotely from the core and moved to a spent-fuel storage rack, usually in a separate building. Fuel not discharged is "shuffled" to new locations. Fresh assemblies are brought in from a fuel handling building.

Refueling itself for an LWR requires only about 4 days. However, "refueling outages" often last up to a month or more when including cool-down and advance preparations, maintenance (corrective and preventive), minor plant modifications, vessel reassembly, and preoperational testing.

Operation Features Four key goals of operations for nuclear power plants – the first two unique and the other two common to all power plants – relate to: (1) nuclear safety, (2) communications, (3) technical results, and (4) operating and fuel costs. Nuclear safety, i.e., prevention of accidents, underlies both technical and economic performance. Good, reliable communications with the public, staff, and company are necessary to counterbalance unfounded fears that may be associated with nuclear energy.

Technical results are judged according to performance indicators, an important one being availability. As for any power plant, availability is enhanced by reducing the length of planned shutdowns and the frequency of unplanned shutdowns. Because reactor fuel assemblies are added and replaced as units, adjustment of cycle length (typically between 1 and 2 years) can affect both availability and reasonable operating and fuel costs.

Where possible, nuclear units run base-loaded due to both high plant capital costs and difficulties in making rapid power-level changes (based on the behavior of certain fission products that poison the chain reaction). France, however, with its large fraction of nuclear

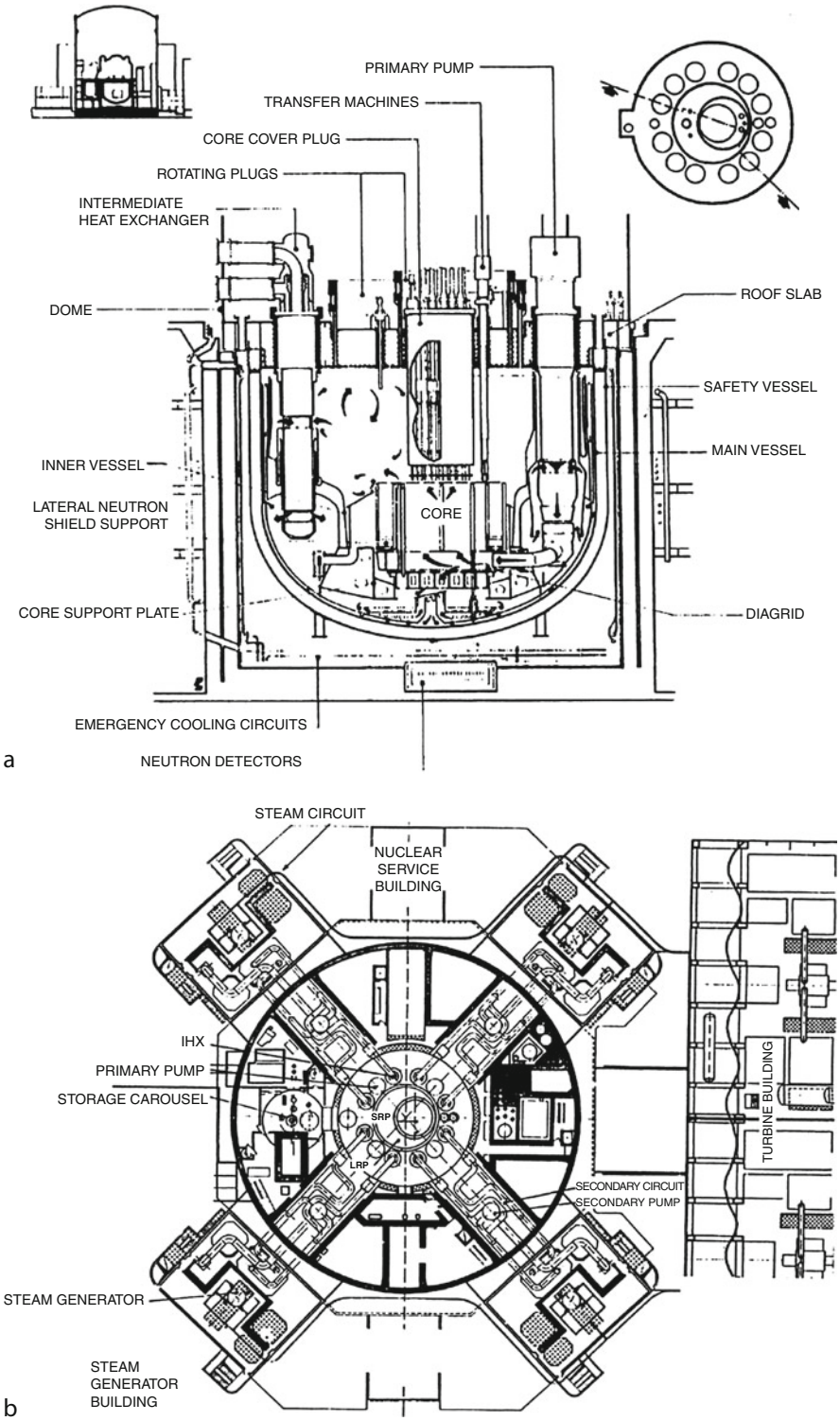

Nuclear Fission Power Plants. Figure 20
Basic features of the pool-type SuperPhenix (**a**) reactor and (**b**) plan-view layout (Reprinted with permission of NOVATOME, a division of Framatome)

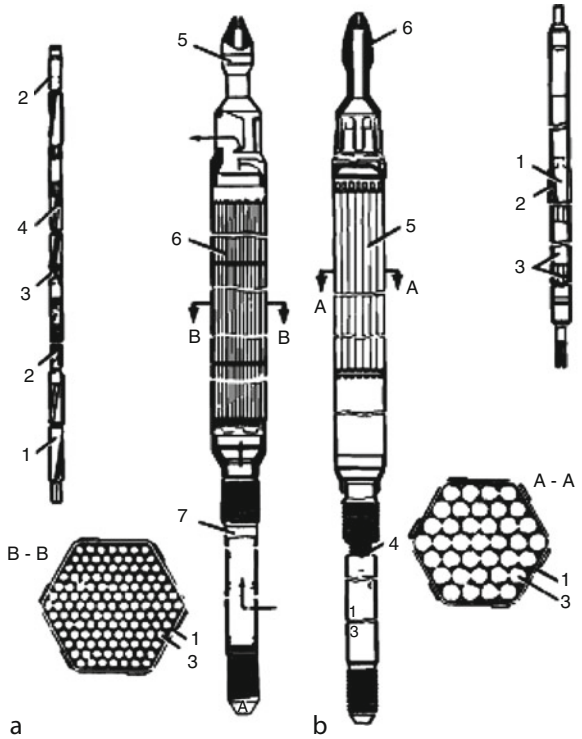

Nuclear Fission Power Plants. Figure 21
Fuel assembly for a representative liquid-metal fast breeder reactor. (**a**) Fuel assembly: *1*, pin cladding; *2*, slugs of depleted uranium; *3*, fuel pellets; *4*, wire-wrapped pin; *5*, fuel assembly head; *6*, fuel-pin assembly; *7*, stem. (**b**) Radial blanket assembly: *1*, pin cladding; *2*, wire-wrapped fin; *3*, depleted uranium; *4*, blanket assembly stem; *5*, blanket pin assembly; *6*, blanket assembly head (Courtesy of *Nuclear Engineering International*)

electricity (e.g., see Table 2) has developed technical ability to facilitate daily load following variations. The latter is also a valued attribute in a number of advanced reactors (e.g., units considered in the section "Advanced Reactors.")

The hazard of nuclear power associated with the large fission-product inventory and the potential severe accident consequences leads to special attention to operator training and to emergency response capabilities. Operators are provided with extensive technical training including substantial use of high-fidelity, plant-referenced control-room simulators which allow practice on routine, anticipated upset, and emergency operating scenarios. Emergency preparedness includes developing procedures, establishing communications, preparing equipment and facilities, and designating an emergency response team personnel.

Maintenance

Due to the presence of fission products and other indirect sources of radioactivity from the neutron chain reaction, many important maintenance and other activities must be conducted in a manner that minimizes the hazards associated with radiation. This has led to the development of remote and other sophisticated radiological control methods. In performing hands-on work, it is challenging to hold radiation exposures of personnel within specified limits on quarterly, annual, and lifetime doses. Overall, however, the requirement that all exposures be kept "as low as reasonably achievable" (ALARA) has resulted in extensive preplanning of all radiological work activities.

Gaseous and liquid wastes are held for as long as practicable to allow maximum radioactive decay. Then, they may be diluted and dispersed to the environment so long as applicable limits for liquid and airborne discharges are not exceeded. Otherwise, solidification, containment, and disposal are required.

Nuclear reactors, like all power plants, require corrective and preventive maintenance that balance the conflicting goals of maximizing short-term profits by deferring work and reducing intervals between regular maintenance activities to assure top performance. The amount of corrective maintenance depends primarily on the initial quality of components and systems, control of operating conditions, and the effectiveness of the preventive maintenance program.

Preventive maintenance for the reactor coolant system (including reactor vessel, reactor coolant pumps, control rod drive mechanisms, instrumentation, and in applicable systems pressurizer and steam generators) must account for neutron irradiation effects on components and systems. The nuclear industry is using methods of reliability-centered maintenance increasingly as sufficient operating experience and data are collected to provide useful statistical reference. In France, where a single utility operates a sizeable number of each of several standardized units, maintenance is considered a lifetime project with integrated goals to guarantee safety, ensure efficiency, assess impact of

Nuclear Fission Power Plants. Table 2 Worldwide nuclear generating capacity by reactor type[a] and summary of reactor performance

Country[c]	Reactors operable		Reactors under construction		Reactors under contract and [planned][b,c]		1998 reactor performance[d]		2009 reactor performance[e]	
	No.	MWe	No.	MWe	No.	MWe	TWe-hr	% of Electric	TWe-hr	% of Electric
Argentina							6.9	10.0	7.6	7.0
PHWR	2	1,005	1	745						
Armenia							1.42	24.7	2.3	45
VVER	1	408			1	1,060				
Belgium							43.9	55.2	45	51.7
PWR	7	6,192								
Brazil							3.3	1.1	12.2	3.0
PWR	2	2,007	1	1,309						
Bulgaria							15.5	41.5	14.2	35.9
VVER	2	2,000								
Canada							67.5	12.4	85.3	14.8
PHWR	17	12,969			[5]	4,800				
China							13.5	1.2	65.7	1.9
PWR	7	5,558	21	23,000	5/[42]					
VVER	2	2,000			[4]					
PHWR	2	1,500								
HTGR	1	2	1	195						
FBR					[3]					
	12		22	23,195	5/[49]					
Cuba										
PWR			2	880 suspend						
Czech Republic							28.5	20.5	25.7	33.8
VVER	6	3,892			[2]					
Finland							21.0	27.4	22.6	32.9
VVER	2	1,020								
BWR	2	1,780								
EPR PWR			1	1,600						
Unspecified					[3]					
TOTAL	4	2,800	1	1,600	[3]					
France							368.4	75.8	391.7	75.2

Nuclear Fission Power Plants. Table 2 (Continued)

Country[c]	Reactors operable		Reactors under construction		Reactors under contract and [planned][b,c]		1998 reactor performance[d]		2009 reactor performance[e]	
	No.	MWe	No.	MWe	No.	MWe	TWe-hr	% of Electric	TWe-hr	% of Electric
PWR	58	63,134	1	1,650	[1]	[1 650]				
Germany							145.2	28.3	127.7	26.1
PWR	11	14,783								
BWR	4	4,526								
	12	19,309								
Hungary					[2]		13.1	35.6	14.3	43
VVER	4	2,000								
PWR										
India							10.2	2.5	14.8	2.2
PWR					[4]					
EPR PWR					[6]					
BWR	2	320			[8]					
PHWR	16	4,140			[4]					
VVER			2	2,000	[4]					
FBR					[1]					
	18	4,460			[27]					
Iran										
VVER			1	1,000						
Japan							306.9	35.9	263.1	28.9
PWR	24	20,278			2	3,076				
BWR	25	23,221	1	1,373	[1][3]					
FBR					[1]	660				
ABWR					2 [6][1]	2,746				
APWR					2	1,590				
	49	43,499	1	1,373	6 [12]					
Kazakhstan							0.1	0.2		
VVER					[3]	1,920				
(Korea, North)										
PWR					[2] cancel	1,000				
Korea, South							85.2	41.4	141.1	34.8
PWR	16	15,643	6	6,800	[2]	2,800				

Nuclear Fission Power Plants. Table 2 (Continued)

Country[c]	Reactors operable		Reactors under construction		Reactors under contract and [planned][b,c]		1998 reactor performance[d]		2009 reactor performance[e]	
	No.	MWe	No.	MWe	No.	MWe	TWe-hr	% of Electric	TWe-hr	% of Electric
PHWR	3	2,189								
	19	17,832								
Lithuania							12.3	77.2	10	76.2
RBMK	2 s/d	2,600								
Unspecified					[1]					
Mexico							8.8	5.4	10.1	4.8
BWR	2	1,364								
Netherlands							3.6	4.1	4.0	3.7
PWR	1	515								
Unspecified					[1]	1,000–1,600				
Pakistan							0.3	0.7	2.6	2.7
PHWR	1	137								
PWR	1	325	1	325						
Unspecified					[1]	600				
	2	462								
Romania							4.9	10.4	10.8	20.6
PHWR	2	1,411			[2]	1,412				
Russian Federation							95.4	13.1	152.8	17.8
VVER	16	12,594	4	4,600	4 [6][19]	4,600				
RBMK	11	11,000	1	1,000						
LWGR (EGP)	4	48			[3]					
KLT (Floating)			2	70						
FBR	1	600	1	880						
BWR (heat)					[4]					
VBER (PWR)					[6]					
	32	14,242	8	6,550	4 [38]	4,600				
Slovakia							11.4	43.8	13.1	53.5
VVER	4	1,896	2	880						
Slovenia							4.8	38.3	5.5	37.9
PWR	1	730								

Nuclear Fission Power Plants. Table 2 (Continued)

Country[c]	Reactors operable		Reactors under construction		Reactors under contract and [planned][b,c]		1998 reactor performance[d]		2009 reactor performance[e]	
	No.	MWe	No.	MWe	No.	MWe	TWe-hr	% of Electric	TWe-hr	% of Electric
South Africa							13.6	7.25	11.6	4.8
PWR	2	1,880			[1]	110				
HTGR										
Spain							56.7	31.7	50.6	17.5
PWR	6	5,912								
BWR	2	6,177								
	8	12,089								
Sweden							70.0	45.8	50.0	34.7
PWR	3	3,002								
BWR	7	6,559								
		9,561								
Switzerland							24.4	41.1	26.3	39.5
PWR	3	1,795								
BWR	2	1,610								
		3,405								
Taiwan									(39.3)	(17.1)
PWR	2	1,914								
BWR	4	3,276	2	2,700						
	6	5,190								
Turkey										
VVER					[2]					
Ukraine							70.6	45.4	77.9	48.6
VVER	15	13,835	2	2,000						
United Arab Emirates										
PWR					2	2,000				
UK							91.1	27.1	62.9	17.9
PWR	1	1,250								
Magnox GCR	4	1,540								
AGR GCR	14	9,112								
EPR PWR					[4]	6,600				
Unspecified					[4]					
	19	11,902			[8]					

Nuclear Fission Power Plants. Table 2 (Continued)

Country[c]	Reactors operable		Reactors under construction		Reactors under contract and [planned][b,c]		1998 reactor performance[d]		2009 reactor performance[e]	
	No.	MWe	No.	MWe	No.	MWe	TWe-hr	% of Electric	TWe-hr	% of Electric
USA							673.7	18.7	798.7	20.2
PWR	69	70,388	1	1,218						
BWR	35	35,903								
AP1000					2 [12]	2,500				
ESBWR					[2]					
ABWR					[2]					
US-EPR PWR					[6]					
US-APWR					[2]					
Unspecified					[6]					
	104	106,291			2 [30]	2,500				
TOTAL[f]										
PWR	214	215,306	31	34,302	9 + [53]					
EPR PWR					[10]					
US-EPR PWR					[6]					
APWR					[2]					
US-APWR					[2]					
AP1000					[12]					
VVER	52	39,645	11	10,480	7 + [40]					
VBER					[6]					
BWR	84	84,736	3	4,073	[12]					
ABWR					2 + [9]					
ESBWR					[2]					
BWR (Heat)					[4]					
PHWR	43	23,351	1	745	[11]					
HTGR	1	2	1	195	[1]					
Magnox	4	1,540								
AGR	14	9,112								
RBMK	11	11,000	1	1,000						
LWGR (EGP)	4	48			[3]					
FBR	1	600	1	800	[5]					

Nuclear Fission Power Plants. Table 2 (Continued)

Country[c]	Reactors operable		Reactors under construction		Reactors under contract and [planned][b,c]		1998 reactor performance[d]		2009 reactor performance[e]	
	No.	MWe	No.	MWe	No.	MWe	TWe-hr	% of Electric	TWe-hr	% of Electric
KLT-Float			2	70						
Unspecified					[17]					
TOTAL	**414**	**385,340**	**51**	**51,665**	**18 + [139]**					

[a]Reactor data current through 2009. Source: *2010 World Nuclear Industry Handbook*, from the publishers of Nuclear Engineering International magazine, www.neimagazine.com. (Note: Reference also contains details on essentially every reactor built or planned)
[b]The source document includes several categories of planned reactors, essentially ranging from very firm to highly speculative. As used in this table, the author's designation "[Planned]" excludes the more speculative categories
[c]World Nuclear Association reported reactors also "planned" and/or "proposed" by Bangladesh, Belarus, Egypt, Indonesia, Israel, Italy, Jordan, Malaysia, Poland, and Thailand – http://www.world-nuclear.org/info/reactors.html – August 1, 2010 (updated periodically)
[d]From *Nuclear Engineering International World Nuclear Industry Handbook 1999*, November 1998
[e]From World Nuclear Association – http://www.world-nuclear.org/info/reactors.html – August 1, 2010 (updated periodically)
[f]Not all countries reporting status distinguished between traditional reactors (e.g., PWR or BWR) and advanced versions (e.g., APWR or ESBWR) thereof

changes in operating conditions, minimize maintenance cost increases, and establish an optimum decommissioning policy (i.e., definition of the end of a reactor's safe and economic lifetime).

Plant Control Systems

Plant instrumentation and control systems are divided among those for normal operation, regulation of parameters through analog or digital technologies, and protection of personnel and equipment by reactor trip and safety feature actuation. Examples of control requirements in the first category may be inferred from discussions earlier in this subsection of operation of boiling- and pressurized-water systems. Specific safety features are described in the next subsection.

Reactors in the USA have tended to continue use of older analog systems for routine reactor control, lacking incentive – and, in some sense, having a *disincentive* associated with time and costs associated with being among the first to develop, test, and license a process – to upgrade to state-of-the-art digital systems. However, significant government-sponsored research and development support in the first decade of the twenty-first century offers the prospect of near-term progress.

Data acquisition and display technology, by contrast, has been upgraded substantially, especially in the aftermath of the accident at the Three Mile Island, Unit 2 reactor. Should the control room become uninhabitable, a remote shutdown panel will allow operators to implement the emergency response functions necessary for safe shutdown of the plant.

France, with its large, dynamic development program, has upgraded controls in early units and developed new systems. Their current and near-future reactor generations have particularly sophisticated reactor operating consoles with state-of-the-art digital systems for control, data acquisition, operator support, and emergency response. Control systems facilitate process monitoring, exchange of information, and self-monitoring and self-diagnosis. Automatic protection systems are designed for reliability with redundancy and diversity (e.g., one of which includes four redundant data acquisition and processing units coupled with two independent safeguard logic units for automatic actuation of the engineered safety features) and include testing and simulation capabilities. Data processing systems are designed to give operators full information on the present state of the reactor, monitor data, store event scenarios and other data changes in memory, and perform calculations.

Advanced reactor controls may facilitate functions such as automatic turbine load shedding, steam level control, (nonreactor, non-safety-related) and trip avoidance – and the consequent thermal-mechanical disruption, and postaccident monitoring and control.

Nuclear Reactor Safety Features

An operating nuclear power reactor accumulates an enormous inventory of radioactive products. Each reactor system has been designed with a multiple-barrier approach to retention of this radioactivity [8]. The first three of these barriers – fuel pellet, metal cladding, and reactor-primary-system – were described in the section "Reactor Systems." The fourth barrier is a containment building supported by safety systems.

A "defense-in-depth" design approach to maintaining the effectiveness of barriers seeks first of all to prevent accidents. But absent this, protective actions – identification and correction – and mitigative actions – long-term response to and control of consequences are provided. Safety analyses address the variety of reactor-related energy sources and their roles in operational abnormalities and in design-basis and more severe accidents. The results of the analyses also define requirements for the engineered safety systems.

Energy Sources

Five distinct energy sources may contribute to an accident in a nuclear power reactor:

1. Stored energy – fuel, coolant, and structures store thermal energy at all times during reactor power operation; redistribution may result in immediate damage and/or prolonged problems.
2. Nuclear transients – positive insertion of reactivity, from configuration or material changes, may add a transient energy source resulting in from an increased power level to a large power pulse.
3. Decay heat – heat from fission-product decay, as high as 7.5% of operating power at the time of shutdown from a lengthy run, dies out slowly, and can be a large energy contribution after dissipation of stored energy and shutdown of the neutron chain reaction; with inadequate heat removal, it may be sufficient to cause fuel melting or other damage.
4. Chemical reactions – fuel, cladding, and coolant materials selected to be essentially unreactive with each other under normal operating conditions at elevated temperatures that may be produced by nuclear transients and/or decay heat may experience energetic chemical reactions.
5. External events – natural (floods, hurricanes, tornadoes, and earthquakes) and man-made (aircraft impacts and industrial explosions) events external to the reactor system have the potential to initiate or otherwise contribute to accidents.

The magnitude and timing of contributions from each category are important to accident progression. Understanding each is necessary to accident prevention and mitigation.

Nearly 98% of all radioactive products are retained by the fuel assemblies when sufficient cooling is provided to prevent fuel melting. Thus, major objectives of nuclear reactor operation and safety are to provide adequate heat removal and control of the energy released in the system to prevent overheating and, in the most severe case, melting of the fuel.

Design-Basis Accidents

Design-basis accidents involve the postulated failure of one or more important systems and an analysis based on conservative assumptions (e.g., pessimistic estimates of fission-product release). The radiological consequences must be shown to be within preestablished limits. In this sense, the accidents serve as the *basis* for assessing the overall acceptability of a particular reactor *design.* Design-basis accidents for light-water reactors (and, by extension, other reactor types) are often classified according to the following general characteristics:

1. Overcooling – excessive heat removal from steam withdrawal, perhaps through a steam-line break or steam-generator overfeeding (PWR and other multi-loop systems).
2. Undercooling – inadequate heat removal occurring when steam flow is decreased, e.g., following a turbine trip or reduction in feedwater flow; a complete *loss of heat-sink accident* (LOHA) – up to and including total loss of heat-removal capability – is the most extreme case of undercooling.

3. Overfilling – increase in reactor coolant inventory, e.g., from malfunction of the volume control system or inadvertent emergency core cooling system (ECCS) – see the section "Safety Systems" – actuation during power operation.
4. Loss of flow (accident (LOFA)) – decrease in reactor coolant system (RCS) flow rate, e.g., follow failure of main reactor coolant pump(s).
5. Loss of coolant (accident (LOCA)) – decrease in reactor coolant inventory resulting from breaches in the reactor coolant pressure boundary; the "classic" LOCA involves rupture of major primary piping, but *steam-generator tube rupture* and inadvertent opening of a relief or safety valve – the proximate cause of the reactor accident at Three Mile Island – are also included.
6. Reactivity-core reactivity and power distribution anomalies – unplanned control-rod withdrawal, other maloperation, and ejection (in a PWR) or drop (in a BWR) of one or more control-rod assemblies; also increased BWR coolant flow rate, and decreased PWR boron concentration, or misleading of a fuel assembly.
7. Anticipated transient without scram (ATWS) – failure to trip (or shutdown) the reactor following a transient such as inadvertent control-rod withdrawal, turbine trip, or loss of feedwater.
8. Spent-fuel and waste system-radioactivity release from a spent-fuel assembly or reactor subsystem or component – events outside of the reactor-primary system.
9. External events-natural or human-caused events that can effect plant operating and safety systems – sequence initiated by an "external event" as identified in the section "Energy Sources."

More severe accidents, sometimes referred to as beyond-design-basis accidents, where multiple safety systems fail to function (or, as in the Chernobyl accident, are disabled), are sometimes considered to evaluate overall responses.

Safety Systems

Safety systems for accident mitigation are highly design-dependent (e.g., based on design and operational differences among fuel form: coolant – water, gas, liquid metal; neutron energy; and other features. The common goals, however, are to prevent overheating, fuel melting and other damage, and subsequent large-scale dispersal of fission products. Reliability is enhanced through redundancy in subsystem function and location.

Reactor safety systems – for the dominant loss-of-coolant accident, but with more general applicability as well – may be classified according to function as:

1. Reactor trip (RT)
2. Emergency core cooling (ECC)
3. Postaccident heat removal (PAHR)
4. Postaccident radioactivity removal (PARR)
5. Containment integrity (CI)

Their basic functions are summarized by Fig. 22 for light-water reactors. The same basic functions apply to all reactor systems, even if in somewhat different form.

Reactor trip for each of the reactor types described in the section "Reactor Systems" includes neutron poison control rods, which can be inserted rapidly into the fuel core to shut down the fission chain reaction. These rods are supplemented by alternative shutdown means including injection of soluble boric acid poison (LWRs); moderator dump (CANDU-PHWR); reserve shutdown spheres (HTGR); and a redundant, independent set of rods (LMFBR).

Emergency core cooling for the light-water, and most other water-cooled, reactors is implemented by injection of borated water – the same medium that provides for emergency reactor trip – into the coolant-starved core region following a LOCA event. Multiple trains of separate systems typically can inject water at high, intermediate, or low pressure to coincide with various needs during the time-history and/or magnitude of the event. The recirculation of coolant that collects in the reactor building sump provides a long-term coolant supply after the initial inventories have been exhausted.

The CANDU-PHWR system also has a unique safety-related design feature with two separate flow circuits configured so that adjacent pressure tubes (Fig. 11) receive coolant from a different source. Thus, a break in a specific pressure tube can affect no more than half of the fuel and no large core volumes are left uncooled. Additionally, the separate moderator volume provided by the calandria vessel provides a huge heat sink for energy removal.

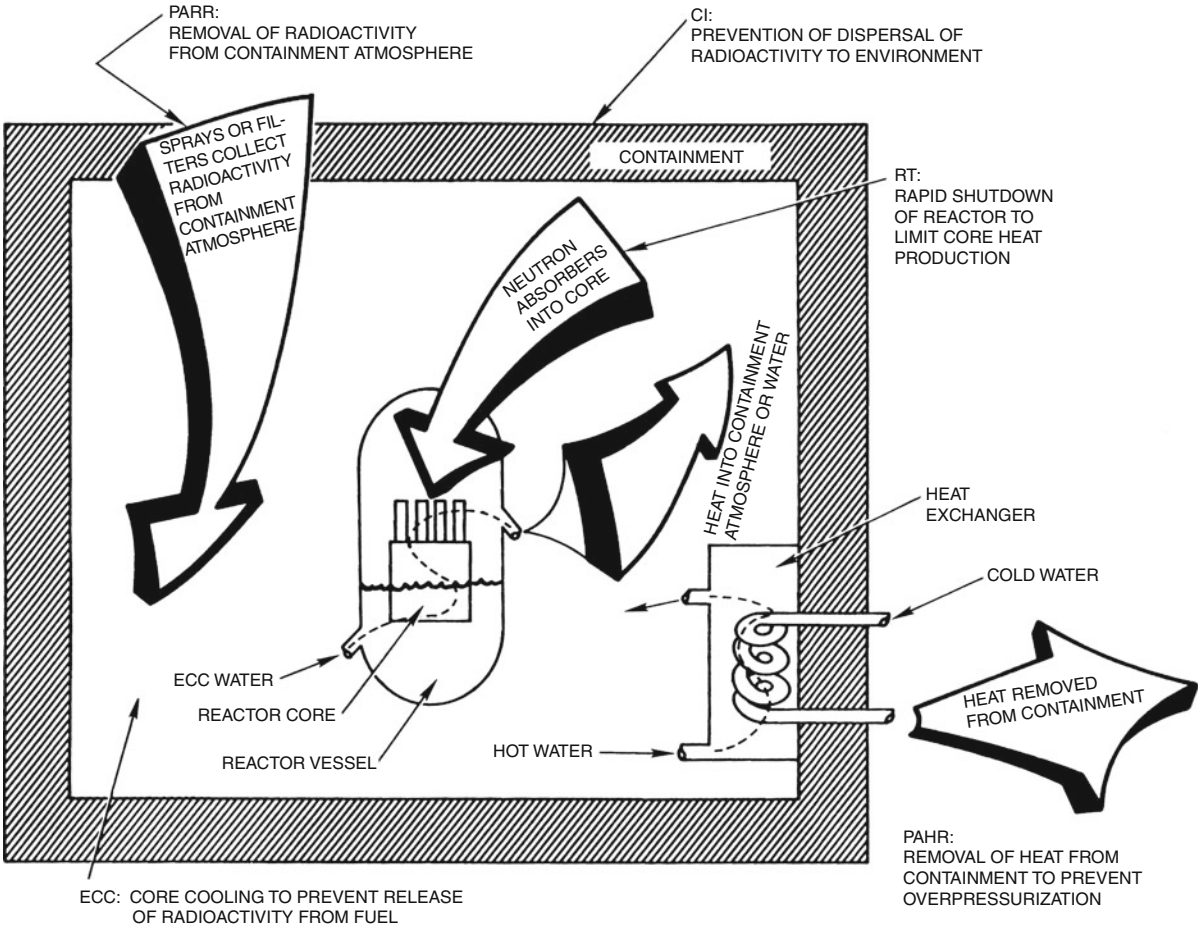

Nuclear Fission Power Plants. Figure 22
Functions of safety systems for light-water reactors (Adapted from WASH-1400 [14], courtesy of US Nuclear Regulatory Commission)

Emergency cooling for the HTGR design is predicated largely on the very high heat capacity of the graphite fuel, supported by auxiliary helium circulation and containment afforded by a steel-lined prestressed concrete reactor vessel (PCRV). The LMFBR, by contrast with the water-cooled reactors, has low-pressure, high-boiling liquid-sodium coolant which would not be voided even during a serious primary-system breach. Thus, long-term, natural-circulation cooling capability is uniquely available. Postaccident heat removal has two components – coolant temperature reduction and containment-building pressure control. The first is accomplished through heat exchangers for ECC water recirculation in the water reactors. For the gas- and liquid-sodium-cooled reactors, continued use of the steam generators can serve a similar function in the primary coolant loops. Pressure control may be accomplished with containment-atmosphere coolers. In water reactors this may be supplemented with steam-condensing water sprays.

Postaccident radioactivity removal of chemically active iodine and aerosol/particulate constituents is accomplished with filtration. The nonreactive noble-gas constituents can only be contained – or released in a controlled manner.

Water-cooled reactors also have provision for containment sprays to remove radioactivity. Although the water sprays used for pressure reduction naturally remove much of the chemically reactive radioactive

material, additives such as sodium hydroxide or thiosulfate increase removal, especially of elemental iodine.

Containment integrity is the last line of defense against fission-product release. Common features of water reactor containments are a leak-tight steel liner surrounded by thick reinforced concrete, including, e.g., that for the pressurized-water and boiling-water reactors in Figs. 23 and 24, respectively. The structure of the HTGR's prestressed concrete vessel (Fig. 14) serves a similar purpose.

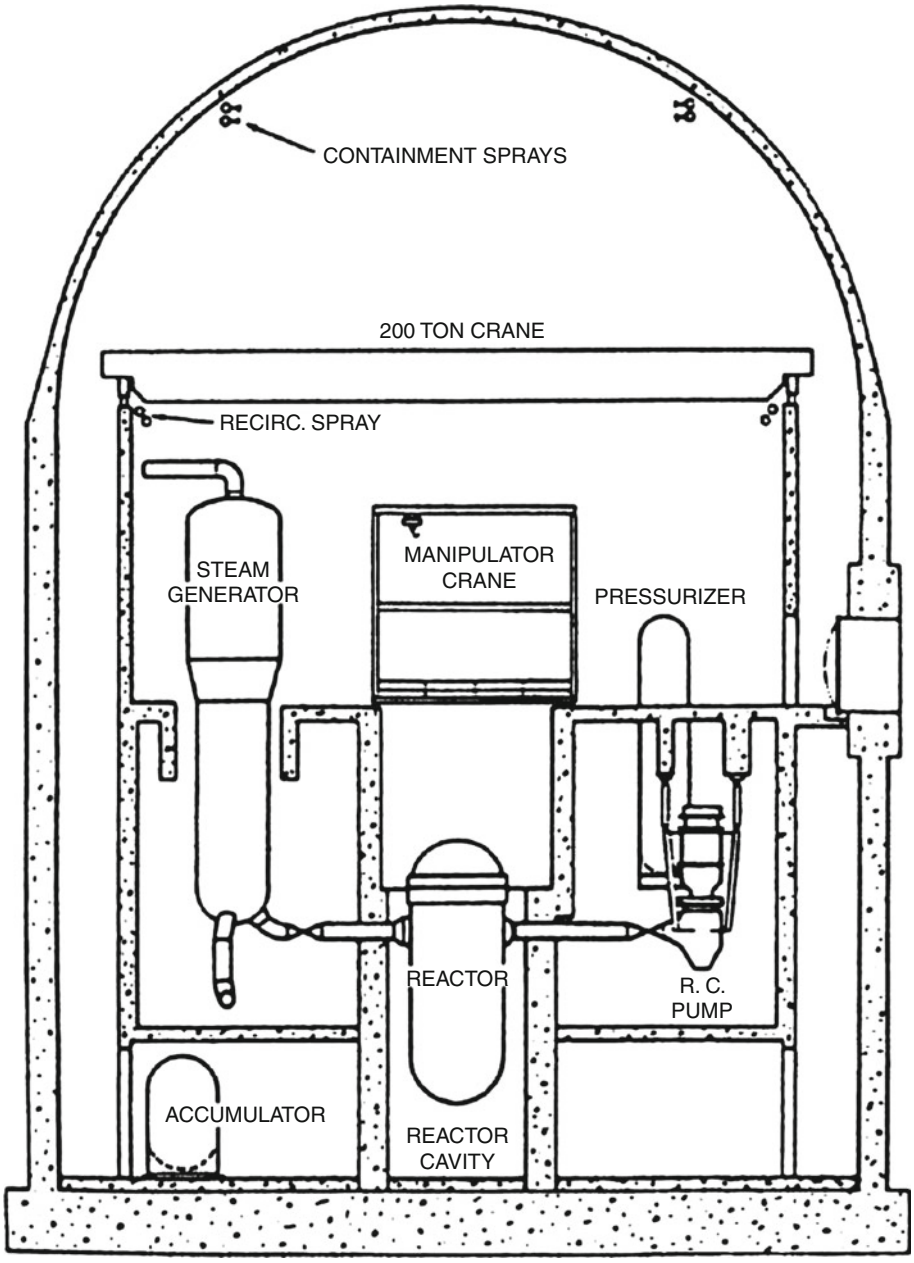

Nuclear Fission Power Plants. Figure 23
Containment structure for a representative pressurized-water reactor (From NUREG-1150 [15], courtesy of US Nuclear Regulatory Commission)

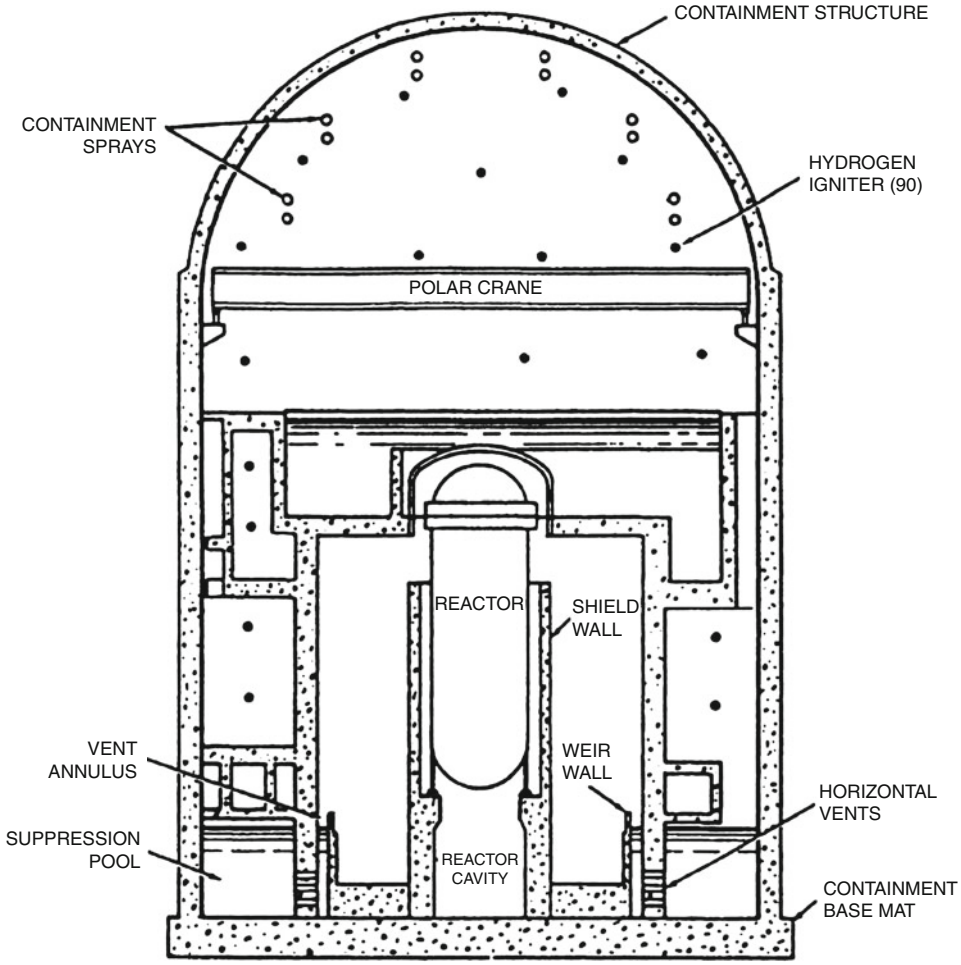

Nuclear Fission Power Plants. Figure 24
Containment structure for a representative boiling-water reactor (From NUREG-1150 [15], courtesy of US Nuclear Regulatory Commission)

Another major element of containment integrity is the ability to isolate penetrations using remotely operated valves or other means. These typically actuate on the predetermined indication of excessive pressure, radiation level, or other related parameters.

Integrity of even the most robust containment, however, depends on having all – or at least a reasonable subset – of the other safety features function as intended. Otherwise there can be excessive pressure buildup and/or severe fuel melting with subsequent dire consequences. The complete lack of a leak-tight containment structure at the Chernobyl PTGR (Fig. 17) was a major contributor to the consequences of the 1986 accident there.

Defense-in-Depth

The previous descriptions of the defense-in-depth approach to nuclear safety have a strong technical emphasis. However, nuclear safety also depends on preventive measures, only a few of which include testing and inspection, safety assessment, deficiency analysis and correction, training, and quality assurance. Protection and mitigation require transient operating guidelines and procedures and detailed emergency planning.

Increasingly important is free and open international exchange of knowledge and experience with proper feedback to reactor design, maintenance, and

operation – the need for which was highlighted dramatically by the TMI-2, Chernobyl-4, and other accidents. Regulatory controls and voluntary peer oversight – e.g., by the US Institute for Nuclear Power Operations (INPO) and the World Organization of Nuclear Operators (WANO) – provide independent verification of safety aspects, but do not replace responsibility of the owner/operators.

Nuclear-Power Regulation

The inherent hazard associated with the radioactive material in reactor systems has led to the nuclear industry being the most regulated in the world [8, 13, 16]. Regulatory bodies include: the US Nuclear Regulatory Commission (NRC); French Commissariat à l'Énergie Atomique et aux Énergies Alternatives (CEA) – up until late 2009, Commissariat à l'Energie Atomique, now with added regulation of alternative energies; Canadian Nuclear Safety Commission (CNSC) – known as Atomic Energy Control Board (AECB) prior to 2000; and the UK Nuclear Installations Inspectorate (NII). Every other nation that operates nuclear-fission reactors also has established a regulatory authority. Requirements for reactor design and operation are established and their implementation is evaluated and monitored. Regulations with the force of law, licenses, or other methods are developed for reactor operation by such bodies, often with significant political and/or public input to the process.

The somewhat recent advent of advanced nuclear power reactors (section "Advanced Reactors") has led to changes in the NRC licensing process. Newly instituted generic certifications are valid for 15 years. Using an exhaustive public process, safety issues within the scope of the certified designs are fully resolved and, hence, will not be open to legal challenge during licensing for specific plants. US utilities will be able to obtain a single NRC reactor license to both construct and operate – as opposed to separate ones previously – before construction begins. A number of reactor types have received design certification [2].

Overall, certification of designs is on a national basis, and is safety based. In Europe, there are moves toward harmonized requirements for licensing. Reactors there may also be certified according to compliance with European Utilities Requirements (EUR) [2].

Quality assurance (QA) requirements focus on methods and procedures to assure proper design, construction, and operation of safety-related components and subsystems. Other requirements address issues from acceptable personnel radiation exposures to analysis methods and acceptance criteria for consequences of design-basis accidents and, in some cases beyond-design-basis accidents.

The accident at the Three Mile Island Unit 2 (TMI-2) PWR in 1979 led to seminal changes in the regulatory process – and nuclear industry as a whole – in the USA and elsewhere in the world. Some of these changes relate to the design, quality assurance, and inspection of modifications to plant safety systems; development and use of preapproved procedures for operation, maintenance, and other activities; administration, including staffing, training, and documentation; emergency planning; technical support, including accident and root-cause analysis; and support services such as radiological controls, chemistry, and maintenance [8, 17].

Training and qualification, in particular, permeates essentially all of the changes. Content for control-room operators and other specialties is developed systematically and formally beginning with intensive job-analysis and moving on through feedback of operating experience. It also represents collaboration among training specialists, incumbents, supervision, management, and subject-matter expertise. Of special significance, operator training is augmented greatly by availability for each reactor of a high-fidelity, replica control-room simulator.

The disastrous 1986 accident at the Chernobyl Unit 4 in the former Soviet Union occurred with a reactor system not used elsewhere in the world. However, it did serve to reinforce many of the designs, operations, and management lessons from the earlier TMI-2 accident. It also provided unprecedented insights into severe-accident behavior and served as a catalyst for completion of post-TMI-2 "action plans," significantly enhanced international cooperation and collaboration in research initiatives and nuclear-power-plant operation and management [8].

Advanced Reactors

The nuclear power industry has been developing and improving reactor technology for more than five decades. Some of the *advanced – next generation* – reactors, which provide hope for revitalizing the nuclear-power option, are starting to be built [2, 3].

Four generations of reactors are commonly distinguished. *GEN-I* reactors were developed in the 1950s–1960s with only a few in the UK still running today. *GEN-II* reactors are typified by the present US fleet and most operated elsewhere worldwide (including those described the section "Reactor Systems" with examples in Table 1). The second-generation nuclear power units have been found to be safe and reliable, but they are being superseded by better designs [2].

GEN-III are the initial "advanced reactors" – the first are in operation in Japan and others are under construction or ready to be ordered. The more cutting-edge units may be termed GEN-III+. Safety-based certification of designs is on a national basis. Many are now under licensing review at the US Nuclear Regulatory Commission with some having received Design Certification. In Europe there is some movement toward harmonized requirements for licensing.

GEN-IV reactors are "still on the drawing board." They will not be operational before 2020 at the earliest [2]. (See the section "Generation IV Nuclear Reactors".)

GEN-III reactors include, conceptually [2]:

- A standardized design for each type which is intended to expedite licensing, reduce capital cost and reduce construction time, and ultimately compete economically with coal-fired and other generation alternatives
- A simpler and more rugged design, making them easier to operate and less vulnerable to operational upsets
- Higher availability and longer operating life – typically 60 years
- Further reduced risk of serious reactor accidents
- Resistance to serious damage that would allow radiological release from an aircraft impact
- Higher fuel burnup lifetime, reduced outage time, and reduced amount of radioactive waste

The signature difference for GEN-III plants is a strong focus on passive, inherent safety features – e.g., gravity, natural convection, or resistance to high temperatures – which require no active controls or operational intervention to avoid accidents in the aftermath of a serious malfunction. This is in contrast to the more traditional (GEN-II, e.g., in the section "Reactor Systems") reactor safety systems which are "active" in the sense of involving electric or mechanical operation on command. Certainly some current features of GEN-II reactors are passive, e.g., negative reactivity feedback and mechanical pressure relief valves which function absent operator action or auxiliary power. However, parallel redundant systems are also necessary. The advanced reactors emphasize inherent or full passive safety depending only on physical phenomena, not on electric power and functioning engineered components. This emphasis is to the extent that some are referred to, probably inappropriately, as *inherently safe*. (See the next section "Conceptual Advanced Reactors" for three distinctly different examples).

Conceptual Advanced Reactors

Since the early 1990s, advanced reactor concepts using light-water, helium, and liquid-sodium coolants have been under development from the experience base of the current "parent" reactors. An early, conceptual version of each is described here. All include enhanced negative power feedback mechanisms to assist in obtaining shutdown and passive postaccident/post-shutdown cooling mechanisms.

Advanced Light-Water Reactor The conceptual advanced light-water reactors differ from the traditional ones (section "Light-Water Reactors) primarily through reduction or elimination of active emergency system components, including large pumps and diesel generators, and implementation of passive features, from reactor control to emergency core cooling functions [18].

Both GEN-III PWR and BWR versions (section "Light-Water Reactor") use conventional uranium-oxide fuel assemblies with negative temperature feedback mechanisms. All combat core damage in the aftermath of a loss-of-coolant accident (LOCA) by flooding the core with sufficient water to last for at

least several days – as compared to the current tens of minutes – without further operator action.

An advanced PWR concept (Fig. 25) features passive emergency core cooling systems (ECCS) with water stored in large tanks above the core. During a large LOCA, injection of water into the core from two of the tanks is initiated by pressurized nitrogen even before the reactor coolant system has a chance to depressurize. Subsequent to depressurization, more water from a massive tank inside the containment structure can flow downward into the core under the influence of gravity alone. Neither of these two ECCS options requires pumps or emergency electric power. If the steam generators are not operable, however, natural circulation of water transfers core thermal energy to a large water storage tank located above the reactor vessel.

Post shutdown, decay heat is ordinarily removed through the steam generators. Heat removal from the steel containment shell is facilitated by

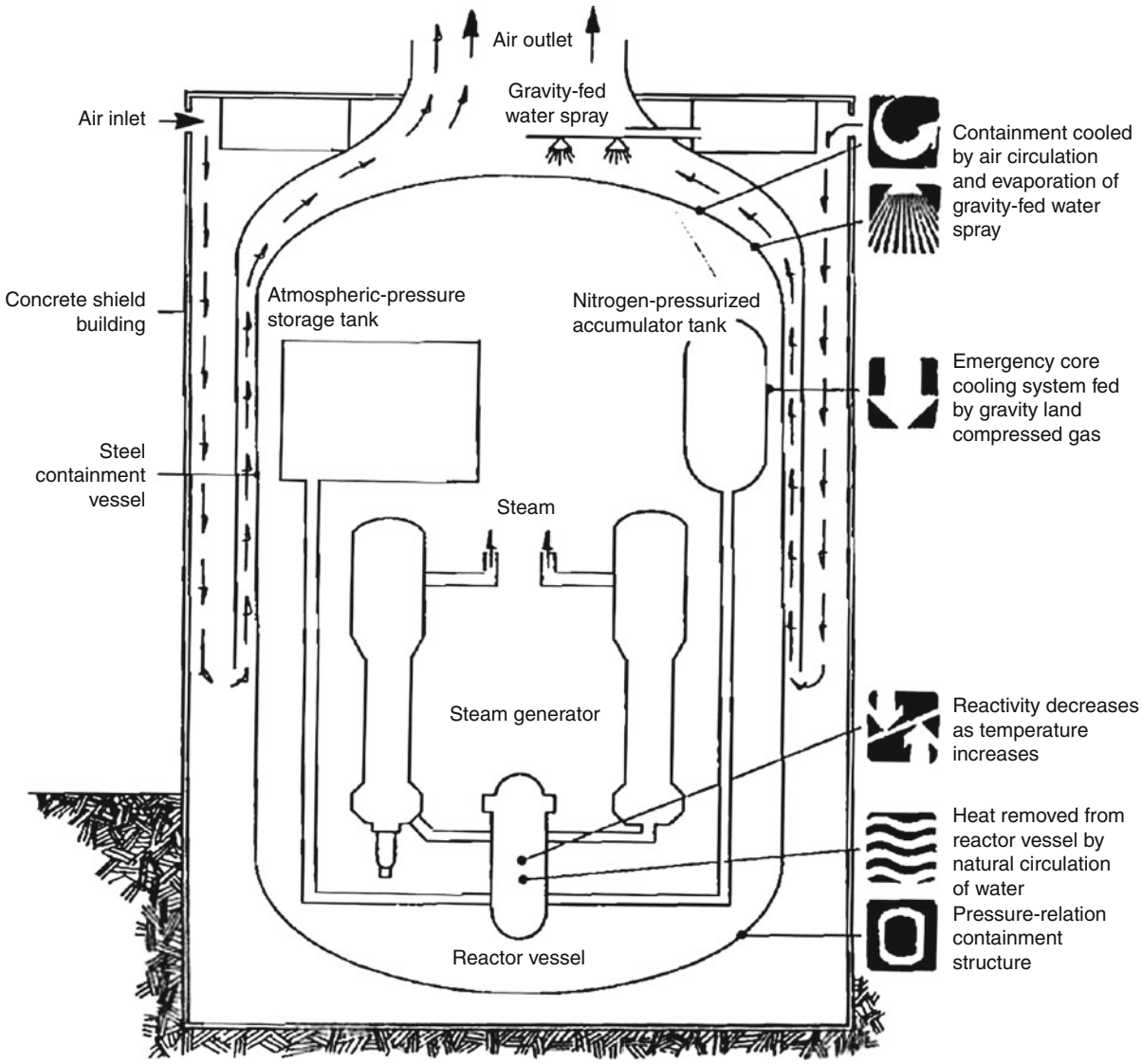

Nuclear Fission Power Plants. Figure 25
Conceptual advanced PWR (Electric Power Research Institute)

a gravity-fed water spray. Natural circulation of air, directed by large baffles, provides passive flow, i.e., without using the large fans and coolers typical of current PWRs.

The passive safety systems also simplify overall plant design. Compared with the active safety systems of a current plant, e.g., there are only half as many large pumps and 40% as much in terms of building volume designed to nuclear-grade seismic standards, number of valves, and amount of piping.

Gas-Cooled Reactors The reference HTGR (section "Gas-Cooled Reactors") combines helium coolant, microsphere fuel, and graphite-moderator blocks to provide uniquely robust safety characteristics. A smaller *modular high-temperature gas-cooled reactor* (MHTGR) design was built upon these same features. The basic MHTGR (Fig. 26) is a 400–600 MWe module intended to be used in groups of four with a pair of turbine generators.

The graphite and fuel core operates at low power density, has a large inherent heat sink, and is very slow to overheat. Even with depressurization of the primary system, fuel failure would be unlikely. Operator response time, thus, is essentially unlimited.

The helium coolant is circulated through the steel – rather than HTGR's prestressed concrete – reactor vessel by an electric blower. It operates at high temperature for high steam cycle electric-generation efficiency or, potentially, a variety of industrial processes including coal gasification, chemical manufacturing, petroleum refining, or desalination of sea water.

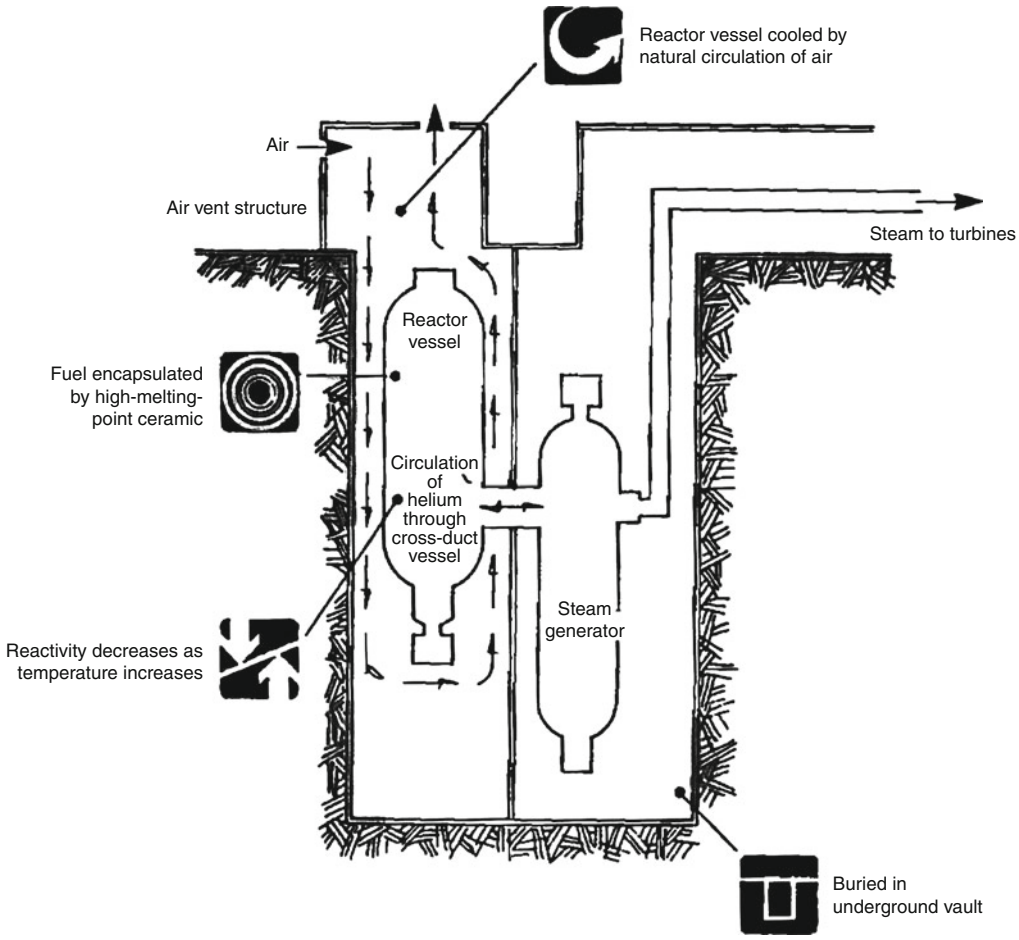

Nuclear Fission Power Plants. Figure 26
Conceptual advanced reactor MHTGR (Electric Power Research Institute)

Each reactor vessel and steam generator is enclosed in an underground silo (Fig. 26). Natural air circulation is sufficient to provide passive silo cooling. Even if said circulation were blocked, direct heat loss to the surrounding earth would keep fuel temperatures well below the melting point. Thus, as with the classic HTGR, an LWR-type containment is unnecessary.

Liquid-Metal Reactor Traditionally, liquid-metal reactors have focused on LMFR-like features (section "Light-Water Graphite Reactors"). The power reactor inherently safe module (PRISM) is a small liquid-metal-cooled module (Fig. 27) which could be used in groups of three connected to a common steam turbine.

Each PRISM module has a pool-type configuration with the liquid-sodium coolant circulated through the core to an intermediate heat exchanger by a pair of pumps. As in an LMFBR, a secondary sodium loop connects to a steam generator.

If pumps fail, sodium flows through the PRISM core by natural convection. If the secondary flow is

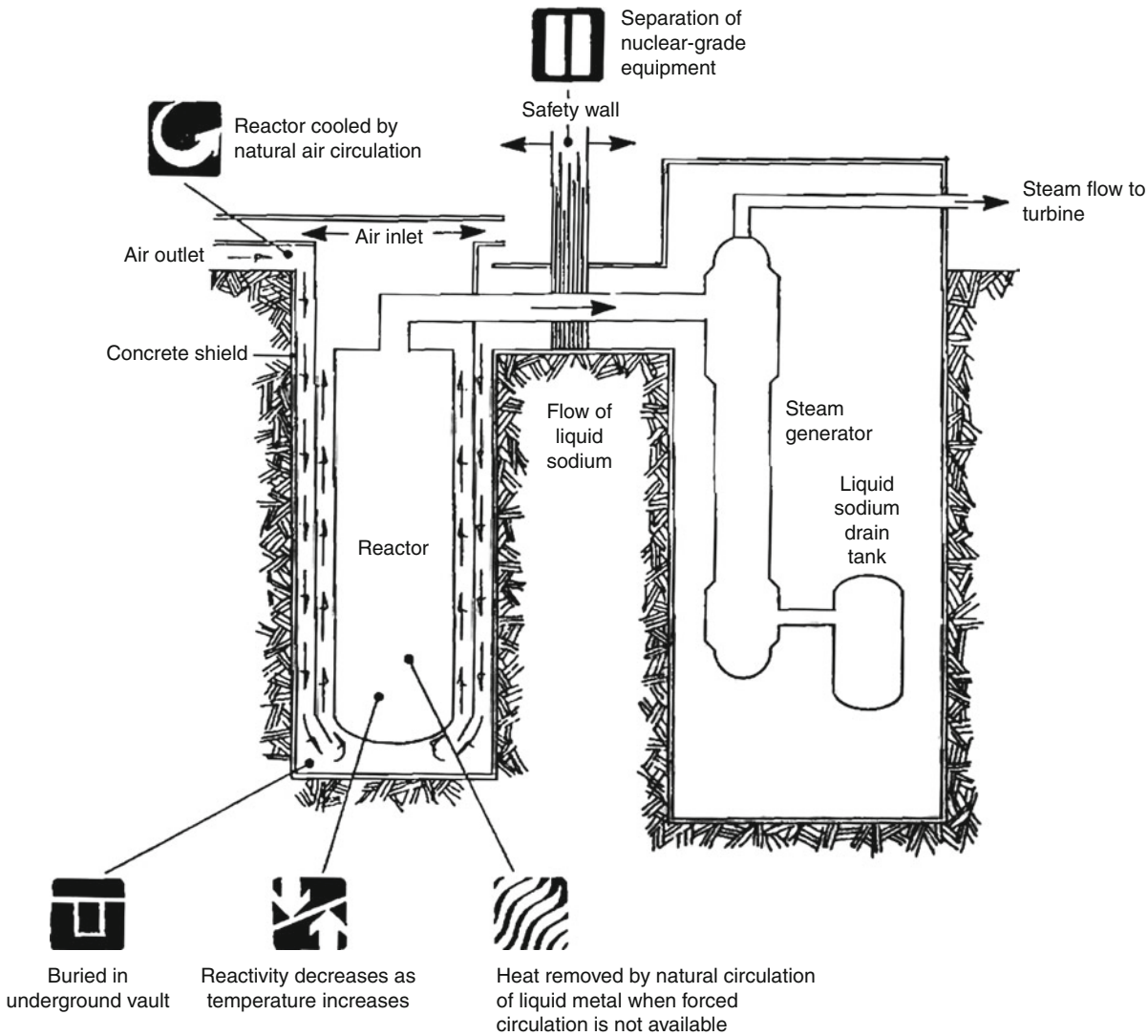

Nuclear Fission Power Plants. Figure 27
Conceptual advanced reactor LMR (Electric Power Research Institute)

interrupted, the primary sodium continues to cool the core by carrying heat to the containment vessel.

Fuel assemblies are made of a pyrometallurgical alloy. Reactor experiments have demonstrated that with loss of liquid-sodium flow, temperature feedback will shut down the neutron chain reaction core and natural circulation of the coolant can remove the decay heat sufficiently to prevent fuel melting.

The PRISM reactor vessel is surrounded by a guard vessel to catch leaking sodium. Both vessels are placed in an underground concrete silo. Air, allowed to circulate freely between the silo wall and guard vessel, can remove core decay heat passively to the outside environment, if necessary. Due to PRISM's passive stability, LWR-type containment is not included in the design.

Generation-III Reactors

The nuclear industry is developing a full product line touted as of clean, safe, secure carbon-free energy sources. Several advanced designs can be ready to meet USA's generating needs by 2015. These fall into the category of "evolutionary," i.e., modifications of existing systems building directly on the experience of operating reactors in the USA, Japan, and Western Europe. These reactors tend to be as large as, or larger than, their predecessors [2, 10].

The industry also is developing more highly advanced nuclear reactors based on new technologies, ready for commercial use by 2020 or later. A revolutionary generation of smaller, passively stable reactors is envisioned [19]. Some could replace older fossil-fired power stations of similar size – and their associated carbon emissions. The infrastructure, cooling water, rail, and transmission facilities already exist at such facilities.

Alternatively, these same small reactors can be a "right size" match for utilities or countries entering the nuclear arena for the first time. They also could be used to generate electricity for remote locations and/or provide process heat for diverse industrial applications. The designs are poised to capitalize on the benefits of modular construction, ease of transportation, and reduced financing. Modules can be added as needed. Units could operate anywhere from 2 to 10 years on an initial fuel load, depending on the design.

Whether the advanced reactor designs are evolutionary or revolutionary, or something in between, almost all involve multi-organizational, multinational collaboration. By the end of 2006, e.g., three major Western-Japanese alliances had formed to dominate much of the world reactor supply market. Subsequently there have been a number of other international collaborative arrangements initiated among reactor vendors and designers. Circa 2010, reactor suppliers in North America, Japan, Europe, Russia, and elsewhere are marketing a dozen new thermal-neutron reactor designs as summarized in Table 3. Others designs, including a number of them based on fast-neutron chain reactions, are, respectively, in advanced planning stages or still in research and development.

Light-Water Reactors Many of the advanced reactors are light-water reactor designs [2]. (See, e.g., Table 3) In the USA, two advanced light-water reactors fall into the category of large "evolutionary" designs, building directly on operating experience in USA, Japan, and Western Europe. Advanced boiling-water reactors (ABWR) derived from a general electric design (section "Boiling-Water Reactors") are in commercial operation and/or under construction in Japan and Taiwan, with others planned in Japan and the USA. It, and the System 80+ advanced PWR, received final design certification from US-NRC in May 1997, noting that they exceeded NRC "safety goals by several orders of magnitude." The ABWR has also been certified as meeting European requirements for advanced reactors. Although the System 80+ itself is not now being promoted for sale, eight System 80 reactors in South Korea incorporate many of its design features and are the basis of the Korean's APR-1400 which has enhanced safety and seismic robustness, and is expected to be in operation by 2013 and is being marketed worldwide.

Another, more innovative US advanced reactor is the smaller AP600 (AP = Advanced Passive) at 600 MWe with highly evolved passive safety features compared to those described in concept in the section "Advanced Light-Water Reactor" (and in concert with Fig. 25). Projected core-damage frequency is nearly 1,000 times less than today's NRC requirements. In 1999, it was the first to gain NRC generic final design certification. Said certifications are valid for 15 years and will allow US utilities to obtain a single NRC

Nuclear Fission Power Plants. Table 3 Advanced thermal-neutron reactors being marketed

Country (developer)	Reactor	Size (MWe)	Design progress	Main features (improved safety in all)
USA-Japan (GE Hitachi, Toshiba)	ABWR	1,300	Commercial operation in Japan since 1996–1997. In USA: NRC certified 1997, FOAKE	• Evolutionary design • More efficient, less waste • Simplified construction (48 months) and operation
South Korea (KHNP, derived from Westinghouse)	APR-1400 (PWR) from System80+	1,450	Design certification 2003, first units expected to be operating c. 2013	• Evolutionary design • Increased reliability • Simplified construction and operation
USA(Westinghouse)	AP-600 AP-1000 (PWR)	600 1,100	AP-600: NRC certified 1999, FOAKE AP-1000 NRC certification 2005, under construction in China, many more planned there	• Simplified construction and operation • 3 years to build • 60-year plant life
USA(GE Hitachi)	ESBWR	1,550	Developed from ABWR, under certification in USA, likely construction there	• Evolutionary design • Short construction time
Japan(Utilities, Mitsubishi)	APWR US-APWR EU-APWR	1,530 1,700 1,700	Basic design in progress, planned for Tsuruga US design certification application 2008	• Hybrid safety features • Simplified construction and operation
France-Germany (Areva NP)	EPR US-EPR (PWR)	1,600	Future French standard French design approval Being built in Finland, France, and China Under certification in USA	• Evolutionary design • High fuel efficiency • Flexible operation
Germany (Areva NP)	SWR-1000 (BWR)	1,200	Under development, pre-certification in USA	• Innovative design • High fuel efficiency
Russia (Gidropress)	VVER-1200 (PWR)	1,200	Under construction at Leningrad and Novovoronezh plants	• Evolutionary design • High fuel efficiency • 50-year plant life
Canada (AECL)	Enhanced CANDU-6	750	Improved model licensing approval 1997	• Evolutionary design • Flexible fuel requirements
Canada (AECL)	ACR	700 1,080	Undergoing certification in Canada	• Evolutionary design • Light-water cooling • Low-enriched fuel
China (INET, Chinergy)	HTR-PM	2 × 105 (module)	Demonstration plant due to start building at Shodaowan	• Modular plant, low cost • High temperature • High fuel efficiency
USA-Russia et al. (General Atomics – OKBM)	GT-MHR	285 (module)	Under development in Russia by multinational joint venture	• Modular plant, low cost • High fuel efficiency • Direct cycle gas turbine

Source: Adapted from World Nuclear Association – http://www.world-nuclear.org/info/inf08.html

license to both construct and operate a reactor before construction begins.

The scaled-up AP1000 was the first GEN-III+ type reactor to receive NRC final design certification from the NRC in December 2005. It also is under active consideration for building in Europe and USA. In comparison to current plants for the same size, AP1000 is about one quarter the size with concrete and steel requirements are less by a factor of five. It is designed for unique modular construction. A single unit has 149 structural modules of five kinds, and 198 mechanical modules of four kinds – equipment, piping and valve, commodity, and standard service modules. These comprise one third of all construction and can be built off site in parallel with the on-site construction. China has four AP-1000 units under construction, with many more to follow.

GE Hitachi Nuclear Energy's ESBWR is a GEN-III+ BWR technology that utilizes passive safety features and natural-circulation principles. It is essentially a larger evolution from a predecessor SBWR.

Mitsubishi's large – advanced – APWR was developed in collaboration with four utilities. It is a simpler four-loop design which combines both active and passive cooling systems. The first two are planned for Japan to come on-line from 2016 and will be the basis for the next generation of Japanese PWRs. US-APWR and EU-APWR versions, respectively, are being developed for USA and European markets.

In Europe, several designs are being developed to meet the European Utility Requirements (EUR) of French and German utilities, which have stringent safety criteria. European pressurized-water reactor (EPR) developed from French and German designs has four separate, redundant safety systems rather than passive safety. The first EPR unit is being built in Finland, with two other slated for France, and another for China. US-EPR – now known as the Evolutionary PWR (EPR) – was submitted for US design certification.

Another evolutionary design, the SWR 1000, is a Siemens BWR now known as Kerena. It is simpler overall and has many passive safety features.

In Russia, several advanced PWR designs with passive safety features have been developed. Late-model VVER-1000 units (see the section "Pressurized-Water Reactor") – one considered GEN-III with enhanced safety – are being built in India and China with two more planned for Bulgaria. A third-generation standardized VVER-1200 reactor is an evolutionary development from the VVER-1000 with longer life, greater power, and greater efficiency. They have enhanced safety including that related to earthquakes and aircraft impact with some passive safety features, double containment, and low core-damage frequency. A Europe-tailored reactor design, MIR-1200 – Modernized International Reactor – has some Czech involvement.

Russia also has a number of other novel small reactor designs [2, 19]. Several *VBER* PWR variations developed from naval power plants may be floating or land-based, modular construction, and/or provide cogeneration. VK-300 – with fuel elements similar to the VVER – have been developed specifically for cogeneration of both power and district heating or heat for desalination. Cooling (by convection) and all safety systems are passive. It has been announced that six would be built in Russia's far east.

Heavy-Water Reactors A pair of GEN-III HWRs are under development based directly on CANDU reactors. Each is to be configured for flexible fuel requirements including standard natural uranium, slightly enriched LWR-like uranium, and mixed-oxide (U and Pu) fuel and from a variety of potential sources, e.g., PWR spent-fuel or even military down-sizing.

Such fuel innovations, combined with the experiences of South Korea and China, suggest that an Enhanced CANDU-6 (EC6) could have a 4.5-year construction and 60-year plant life. This design is under consideration for new build in Canada.

The Advanced CANDU Reactor (ACR) is a more innovative concept using a low-pressure heavy-water moderator with PWR-like light-water cooling for higher thermal efficiency. The resulting compact core would reduce capital cost – an ACR-700 is physically much smaller, simpler, and more efficient as well as 40% cheaper. A larger ACR-1000 – the current focus of attention – has more fuel channels; is designed to run on low-enriched uranium ($\sim$ 1.5–2.0 wt% ^{235}U) with high burnup, MOX fuel, thorium-^{233}U fuels; and extends the fuel life by about three times reducing high-level waste volumes accordingly. Other features include small negative reactivity feedback, other

passive safety features, two independent and fast shutdown systems; and prefabricated modules to cut construction time to 3.5 years. The CANDU X or SCWR – a GEN-IV ACR variant with supercritical light-water coolant – would operate at very high pressure and temperature, and, thus, high thermal efficiency. (See the section "Generation IV Nuclear Reactors".)

Table 3 summarizes key characteristics for the advance HWRs and other advanced reactor types.

For the longer term, India is developing the Advanced Heavy Water Reactor (AHWR) to utilize its plentiful reserves of thorium. The AHWR is a 300-MWe reactor moderated by heavy water in a calandria vessel with about 450 *vertical* pressure tubes. The coolant is boiling light water circulated by convection. A "gravity-driven water pool" near the top of the reactor building with 7,000 cubic meters of water is proposed as a novel heat sink. A unique fuel paradigm calls initially for fuel assemblies each consisting of a mixture of oxide pins of Th-^{233}U and Pu-Th, respectively, with resulting very high net fuel utilization. Once fully operational, the fuel pins would be arranged in three concentric rings each "zoned" with a specific equivalent fissile content based on adjusting Th, ^{233}U, and Pu fractions. The content of ^{233}U – with inherent ^{232}U and its unique high-gamma-active daughter products – is considered to confer a substantial proliferation resistance (i.e., high-capacity fabrication of ^{233}U fuel must be done remotely, a feature not necessary for either ^{235}U or plutonium). (See also the chapter on ► Modern Nuclear Fuel Cycles.)

In 2009, an export version named AHWR-LEU was announced. The major difference is use of low-enriched uranium (LEU) – in lieu of Pu – plus thorium as a fuel. Plutonium production will differ from that in light-water reactors – the fissile proportion will be less and the ^{238}Pu (non-fissile with high radioactivity and associated heat) portion three times as high – giving inherent proliferation resistance. The net result is described as a reactor "manageable with modest industrial infrastructure within the reach of developing countries."

High-Temperature Gas-Cooled Reactors The advanced high-temperature gas-cooled reactors (HTGR) use helium as a coolant at up to 950°C, which for electric generation either makes steam conventionally or directly drives a gas turbine for electricity and a compressor to return the gas to the reactor core. They also are especially well-suited for providing process heat for industrial applications, including hydrogen production and could be used in the development of tar sands, oil shale, and coal-to-liquid applications, reducing the life cycle carbon footprint of all these activities.

The fuel is in the conventional HTGR form of microsphere particles arranged in blocks as hexagonal "prisms" of graphite, or in billiard ball-sized "pebbles" of graphite encased in silicon carbide (Fig. 15) each providing containment for fission products which is stable to 1,600°C or more. Other features are similar to those in Fig. 26.

China's HTR-PM is to have two reactor modules of 105 MWe each and use a steam cycle to drive a single steam cycle turbine at about 40% thermal efficiency. It is expected to pave the way for an 18-unit full-scale power plant also using the steam cycle.

A larger US design, the Gas Turbine–Modular Helium Reactor (GT-MHR), is planned as modules of 285 MWe each directly driving a gas turbine (Brayton cycle) at 48% thermal efficiency. The cylindrical core consists of 102 prism blocks (Fig. 15b) with channels for helium and control rods. It is being developed by General Atomics in partnership with Russia, and supported by Japan. Initially it was to be used to burn pure ex-weapons plutonium in Russia. The preliminary design stage was completed in 2001, but the program has stalled since. Areva's Antares also is based on the GT-MHR.

Table 3 summarizes key characteristics for the first two of the advanced HTGRs and for other advanced reactor types.

South Africa's Pebble Bed Modular Reactor (PBMR) draws on German THTR (section "Gas-Cooled Reactor" and Fig. 14b) expertise. Production units would be 165 MWe, ultimately using a direct-(Brayton) cycle gas-turbine generator with thermal efficiency of about 41%. Power would be adjusted by changing the pressure in the system.

Up to 450,000 fuel pebbles (Fig. 15a and c) recycle through the reactor continuously (about six times each) until they are expended. The reactor will use about 13 fuel loads in a 40-year lifetime. The on-line refueling can facilitate operational cycles with as long as 6 years between shutdowns.

Fast-Neutron Reactors The classic fast-neutron reactor has been the fast breeder reactor (FBR). Current interest centers on their ability to provide unique nuclear fuel-cycle services, such as breeding new fuel, consuming recycled nuclear waste as fuel, and supporting government-sponsored nonproliferation efforts by consuming material from former nuclear weapons [10].

About 20 liquid-metal fast breed reactors (LMFBR), mainly research units, have accumulated some significant operating experience. Several countries have research and development programs for improving their current designs, but generally less as GEN-III efforts and more as a bridge to new GEN-IV reactors [2, 20].

The consummate LMFBR, France's SuperPhenix (section "Light-Water Graphite Reactors"), was optimized to run on plutonium fuel and to "breed" even more plutonium fuel with a depleted uranium blanket around the core. The LMFBRs, however, are expensive to build and could only be justified economically if uranium prices were to rise dramatically above market price circa 2010. For this reason, research work almost ceased for some years. Closure of the SuperPhenix after very little operation over 13 years especially set back developments.

Primarily to address nonproliferation concerns, there apparently are no plans to build any more plutonium-fueled fast reactors with blanket assemblies. Fast-reactor concepts slated for the GEN-IV program simply have a core where both plutonium production and consumption occur [20].

In Russia, the BN-600 – a fast breeder reactor with a conventional core-blanket configuration – has supplied electricity to the grid since 1981 (and has had the best operating and production record of all of the nation's nuclear power units). Its evolutionary BN-800 counterpart originally was fueled with uranium-oxide fuel, but reconfigured to burn the plutonium from military stockpiles. Two BN-800 units have been sold to China with construction slated to start in 2012. Further development of the BN-series is slated to be with an integrated core to meet GEN-IV nonproliferation goals. Russia also has interest in developing lead- and lead-bismuth fast-neutron-reactor designs, having used these coolants in submarines.

Japan is continuing with development of the FBR. The Japan Standard Fast Reactor (JSFR) is a breeder-like concept, but having a breeding ratio less than unity.

Meanwhile in the USA, the modular liquid-metal-cooled inherently safe reactor – PRISM (See the section "Liquid-Metal Reactors" and Fig. 27) – is continuing to receive attention. It is a compact modular pool-type reactor with passive cooling for decay heat removal. PRISM is considered a potential GEN-IV solution to closing the fuel cycle in the USA.

Korea's KALIMER (Korea Advanced LIquid MEtal Reactor) also is pool-type sodium-cooled fast reactor. Having evolved from a smaller unit, it has a core designed to transmute transuranic species and no breeding blanket. Future development of KALIMER for GEN-IV is envisaged.

Research continues in India including on the unique track of using thorium – which it has in abundance – in a breeding scheme with fissile ^{233}U. The Kalpakkam reactor is fueled with uranium-plutonium carbide and has a thorium blanket to breed the ^{233}U.

Generation IV Nuclear Reactors

The GEN-IV International Forum (GIF) was initiated in 2000 as an international collective committed to joint development of the next generation of nuclear technology. Currently six nuclear reactor technologies are under development for deployment between 2020 and 2030 [21, 22].

All six technologies represent advances in sustainability, economics, safety, reliability, and proliferation resistance. Most employ a closed fuel cycle to maximize the resource base and minimize high-level wastes that will need to be sent to a repository.

Collectively, the reactors include thermal-, epithermal-, or fast-neutron spectra. Coolants are light water, helium, sodium, lead-bismuth, and fluoride salt. Temperatures range from 510°C to 1,000°C – compared with less than 330°C for today's LWRs. At the higher temperatures, thermochemical hydrogen production is envisioned. Power ratings range all the way from 20 to 1,500 MWe (or equivalent thermal).

At least four of the systems already have significant operating experience in most respects of their design. This provides a good basis for further research and development and prospects for commercial operation well before 2030.

Table 4 provides a comparison. (See also the following section "Future Directions".) Although six technologies were chosen, development on one of them has gone in two different directions resulting in seven being listed in the table. Summary descriptions of each are provided in the remainder of this section.

Supercritical water-cooled reactors (SWCR) use water coolant at extremely high temperatures and pressures – thermodynamically in the "supercritical" fluid regime. Such fluids are those above the thermodynamic critical point, defined as the highest temperature and pressure at which gas and liquid phases can coexist in equilibrium. They have properties between those of gas and liquid. For water the critical point is at 374°C and 22 MPa, giving it a "steam" density one third that of the liquid so that it can drive a turbine in a similar way to normal steam. A fleet of over 400 supercritical coal-fired plants operating worldwide provides a solid experience base for reactor application [21].

Supercritical water obviates the need for a secondary steam system and drives a turbine generator directly at 44% (and potentially up to 50%) efficiency. Designs call for a high power level and include BWR-like pressure-vessel and CANDU-variant pressure-tube options. Each will have passive safety features with fewer components (e.g., none related to steam separator/driers) and relatively low capital cost. Neutron-spectrum and fuel-cycle options combine in an interesting manner to provide the potential for:

1. Thermal reactors with enriched uranium-oxide fuel and an open fuel cycle
2. Fast reactors with full actinide-element recycle and conventional reprocessing

Very high-temperature gas reactors (VHTR) are thermal-neutron systems with graphite moderator and helium coolant. Fuel can be (1) stacks of prism blocks or (2) a pebble bed (section "Gas-Cooled Reactors" and Fig. 15). The "very high" temperatures result in high thermodynamic efficiency which can be applied for thermochemical hydrogen production with electricity cogeneration or direct high-efficiency driving of a gas turbine (Brayton cycle). Essentially complete passive safety, low operation and maintenance costs, and modular construction are envisioned based on the HTGR (section "Gas-Cooled Reactors") and PBR (section "High-Temperature Gas-Cooled Reactors") heritage.

Gas-cooled fast reactors (GFR) are the fast-neutron counterparts of the VHTR – absent graphite moderator – described above. The design includes a thick steel reactor pressure vessel and helium coolant. It is well suited for conventional steam-electric generation, helium direct-drive gas turbine (Brayton cycle), and thermochemical hydrogen production or other process heat. With the fast-neutron spectrum, fuel of Pu, ^{238}U, and Th can support a blanket-less breeding paradigm.

Sodium-cooled fast reactors (SFR), using liquid-sodium coolant, are progeny of the LMFBR (section "Light-Water Graphite Reactors"). Configurations could be loop-type or pool-type. Passive safety features are augmented by the coolant's low pressure and inherent natural-convection tendency. An initial core plus blanket configuration is likely to be displaced by new core-only breeding designs with depleted uranium integral to the fuel matrix. High-temperature operation is consistent with electricity generation or a supercritical CO_2 turbine. Fuel-related variants include: (1) U-Pu metal fuel with actinide retention and on-site pyrometallurgical processing and (2) conventional mixed Pu-U "mixed-oxide" (MOX) fuel and advanced aqueous reprocessing elsewhere in central facilities.

Lead-cooled fast reactors (LFR) have similarity to the SCFR in terms of fast-neutron spectrum, as well as liquid-metal coolant – here Pb or Pb-Bi eutectic – with low pressure and natural convection. Russia has had multi-decade experience with this technology in its nuclear submarine program. Design power levels range from relatively small for modular units to large for single plants. A novel concept is for a factory-built "battery" unit of 20–180 MWe with 15–20 year life for small grids or developing countries. Operating temperatures are slated to be sufficient for thermochemical hydrogen production. Fuel would be Pu and depleted uranium – with an option to introduce thorium – in metal or nitride form.

Molten-salt reactors (MSR) – the most novel of the technologies – use uranium dissolved in sodium (or zirconium) fluoride salt which serves as both the fuel and the coolant. When the salt circulates through graphite core channels, the neutrons are moderated to epithermal (i.e., average above, or faster than, thermal)

Nuclear Fission Power Plants. Table 4 Generation IV nuclear reactors

	Neutron spectrum (fast/thermal)	Coolant	Temperature (C)	Pressure[a]	Fuel	Fuel cycle	Size(s) (MWe)	Uses
Supercritical water-cooled reactors (SCWR)	Thermal or fast	Water	510–625	Very high	UO_2	Open (thermal)	300–700	Electricity
						Closed (fast)	1,000–1,500	
Very high temperature gas reactors (VHTR)	Thermal	Helium	900–1,000	High	UO_2 prism or pebbles	Open	250–300	Hydrogen and electricity
Gas-cooled fast reactors (GFR)								
Sodium-cooled fast reactors (SFR)	Fast	Sodium	550	Low	U-238 and MOX	Closed	30–150	Electricity
							300–1,500	
							1,000–2,000	
Lead-cooled fast reactors (LFR)	Fast	Lead or Pb-Bi	480–800	Low	U-238[b]	Closed, regional	20–180[c]	Electricity and hydrogen
							300–1,200	
							600–1,000	
Molten salt fast reactors (MSFR)	Fast	Fluoride salts	700–800	Low	UF in salt	Closed	1,000	Electricity and hydrogen
Molten salt advanced high-temperature reactors (AHTR)	Thermal	Fluoride salts	750–1,000		UO_2 particles in prism	Open	1,000–1,500	Hydrogen

Source: Adapted from World Nuclear Association – http://www.world-nuclear.org/info/inf77.html

[a]High 7–15 MPa

[b]With some U-235 or Pu-239

[c]"Battery" model with long cassette core life (15–20 years) or replaceable reactor module

energies and can support a critical chain reaction. Outside of the core and absent proximity to moderator, the salt is very highly subcritical. Similar to the metal-cooled reactors, the molten salt has the inherent safety feature of operating at very low pressure. An appropriately designed secondary loop can provide for electricity generation or thermochemical hydrogen production.

The MSR fuel requires no fabrication per se. Fissile inventory can be kept to a minimal level as the plutonium, depleted uranium, and/or thorium fuel constituents can be inserted at any time as needed. Actinides from outside sources, e.g., to be transmuted by neutron irradiation to less hazardous form, can also be added. Simultaneously, on-line and continuous removal of fission products and recycle of self-generated actinides can be implemented.

There are two separate baseline MSR concepts. One is the (Molten Salt) Advanced High-Temperature Reactor (AHTR) which has a graphite core similar to that of the VHTR (and HTGR Fig. 15b). Use of a neutron-moderating, molten-salt coolant, instead of helium, supports a much higher power density The other version is the Molten Salt Fast Neutron Reactor (MSFR) with a graphite-free "core tank with no internals" and molten-salt compositions which provide less moderation.

Future Directions

The future of nuclear power as a world energy source is a complex part of an overall energy picture, a few aspects of which were summarized in the section "Definition of the Subject." Two recent studies – sponsored, respectively, by the Massachusetts Institute of Technology (MIT) and the Electric Power Research Institute (EPRI) – shed light on both future prospects and problems.

The Future of Nuclear Power

The MIT study, *The Future of Nuclear Power* (2003 report and 2009 update) – in its own words – was "the most comprehensive, interdisciplinary study ever conducted on the future of nuclear energy," and concluded that "The nuclear option should be retained precisely because it is an important carbon-free source of power" [4].

The study examines a growth scenario – characterized as "not a prediction, but rather a study case in which nuclear power would make a significant contribution to reducing CO_2 emissions" – with the current deployment of 360 GWe of nuclear capacity worldwide expanded to 1,000 GWe (1 Terawatt) of "carbon-free" power by mid-century, keeping nuclear's fraction of the electricity market about constant. Correspondingly, the USA would triple its nuclear deployment from about 100 GWe to 300 GWe. (See also the subsequent section "New Nuclear Installations".)

The credibility of such a scenario – and nuclear energy as an option – will be largely determined in the forthcoming decade by the extent to which significant progress is made on four unresolved problems:

1. High relative construction costs
2. Perceived adverse safety, environmental, and health effects
3. Potential security risks stemming from proliferation
4. Unresolved challenges in long-term management of nuclear wastes

The up-front costs associated with nuclear power are higher than those for fossil-fueled plants. However, the study was optimistic about ways to mitigate the costs, and noted that, over time, the societal and environmental price of carbon emissions could dramatically improve the competitiveness of nuclear power. The goal of 1 terawatt of "carbon-free" nuclear power by 2050 is certainly challenging, requiring deployment of about 2,000 MW a month with an associated capital investment of $2 trillion over several decades.

One key economic incentive has been a limited production tax credit – a provision in the 2005 Energy Policy Act – to "first mover" private sector investors who successfully build new nuclear plants. This tax credit is extendable to other carbon-free electricity technologies and is not paid unless the plant operates. The study also suggested the industry-wide cost-reduction options of placing near-term emphasis on the once-through fuel cycle and delaying expensive development projects pending progress on near-term deployments.

Public acceptance turns on the perception of safety, environmental, health effects. Thus, performance, cost, and environmental acceptability of the technology must be demonstrated to the public, political leaders, and investors. Having the government develop

enhanced capabilities to analyze life-cycle health and safety impacts of fuel-cycle facilities is also recommended. It also is essential that NRC regulations are developed and enforced diligently.

Security risks can be addressed by encouraging countries to forego the proliferation-risky nuclear technologies – enrichment and reprocessing – by offering "a preferred position to receive nuclear fuel and waste management services from nations that operate the entire fuel cycle." Near-term emphasis on the once-through fuel cycle also supports this scenario.

Long-term management of nuclear wastes is a huge problem, the solution for which is key to public acceptance. Key to the resolution of this task is the capability of the government to start moving spent fuel from reactor sites and to develop long-term waste management research and development programs. (See also the following section "New Nuclear Installations" with respect to spent-fuel management.)

According to a 2009 MIT update report [4], the initial 2003 study in the years following its publication was credited with a significant impact on the public debate both in the USA and abroad, including influence on the US Department of Energy's (DOE) nuclear energy research and development (R&D) program. Unfortunately, in this same time frame, the challenges to greater nuclear-power deployment were found to have remained largely the same – especially with no new US plants under construction and insufficient progress on waste management – leading to: "The sober warning. . .that if more is not done, nuclear power will diminish as a practical and timely option for deployment at a scale that would constitute a material contribution to climate change risk mitigation."

New Nuclear Installations

An EPRI summer seminar in 2007 entitled "Electricity Solutions for a Carbon-Constrained Future" addressed "New Nuclear Installations" [6]. Whereas the MIT study [4] focused primarily on policy, the EPRI nuclear effort provides a valuable counterpoint on implementation.

At the time, nuclear power accounted for 73% of the emission-free generation in the USA and was described as the only technologically mature, non-emitting source of power that positioned to deliver large-scale CO_2 reduction in the upcoming decades. Employing a study target of 64 GW of new nuclear by 2030 – considered ambitious but achievable – key challenges were identified so as to:

1. Keep the current nuclear power plants running safely and reliably for 60–80 years.
2. Build out the next generation of plants starting around 2015.

   The existing fleet of light-water reactor (LWR) technology – generating approximately 20% of the nation's electricity and operating at an average capacity of 90% – establishes a platform of confidence for the nation to proceed with further life extension of existing plants and to considerably expand the fleet using advanced LWR designs.
3. Achieve consensus on a long-term strategy for spent fuel.

Almost all of the US operating plants have had, or are in the process of having, their operating licenses extended from the initial 40–60 years. It is a reasonable assumption that all units will be granted a 20-year life extension by about 2016.

Even while these life extensions are being finalized, the technical basis must be laid for an additional 20-year extension – from 60 to 80 years – by confirming that ". . .with sufficient maintenance, refurbishment, and upgrades, today's plants could [continue to] operate quite safely . . .." "Ultimately, extending the life of our current fleet an additional 20 years will be a business decision, which means that both continued high safety performance and continued economic competitiveness must be addressed." Key among a wide variety of important milestones are assessing the ability of passive components to continue safe performance, upgrading instrumentation and controls to modern digital technology, and developing of higher-performance fuels to extend the time between refueling outages and reduce spent-fuel volumes.

Design development and prelicensing have produced advanced light-water reactor (ALWR) designs (section "Advanced Reactors") that are approaching the "essentially complete design" status which will enable new plant orders to be based on detailed cost and schedule estimates. ALWRs are already in operation today or under construction around the world.

At least fifteen US companies stated their intent to file for NRC combined construction and operating licenses. Of a total of 30 reactors under consideration, most were slated for sites that have existing units and were developed with such expansion in mind.

The first commercial operation of ALWRs in the USA could begin shortly after 2015. "The first new plants out of the box must be done very, very well. . .. They must be executed thoughtfully, deliberately, and with the highest level of skill." The challenge is daunting. Then, the industry must sustain a much higher build rate out to 2050 and beyond. The research, development, and demonstration (RD&D) – with particular emphasis on the latter – focus for new advanced reactors should/must include:

- Completing, in the short term, engineering work necessary for detailed cost and schedule estimates for plant construction, and resolution of any remaining regulatory issues
- Beginning now to lay the foundation for the high build rates, including bringing capital costs and construction times down, addressing shortfalls in both physical and workforce infrastructure, and dealing with a plethora of other issues
- Helping the US federal government advance the capabilities of the high-temperature gas-cooled reactor (HTGR) from construction of an operational prototype to enabling commercially available units, e.g., to take advantage of the ability to produce electricity, provide process heat for industrial applications, and – especially – cost-effectively generate hydrogen by emission-free methods

Finally, sustained expansion of nuclear generation ultimately requires the resolution of spent-fuel management concerns. Although on-site interim storage in concrete silos has been effective and safe for over two decades, imperatives of economics, security, and sustainability will require establishing an integrated fuel management system for the longer term, i.e., including centralized interim storage, long-term geologic storage, and eventually, a closed fuel cycle. A well-thought-out, deliberate consensus strategy on nuclear fuel storage is needed. Such a consensus will allow for advanced reprocessing and separation technologies, reconditioning, fuel manufacturing facilities, and effective application of GEN-IV fast-reactor technologies.

Notes

Sandia National Laboratories is a multi-program laboratory managed and operated by Sandia Corporation, a wholly owned subsidiary of Lockheed Martin Corporation, for the U.S. Department of Energy's National Nuclear Security Administration under contract DE-AC04-94AL85000.

Bibliography

Primary Literature

1. Rhodes R (1986) The making of the atomic bomb. Simon and Schuster, New York
2. Advanced nuclear power reactors – World Nuclear Association – http://www.world-nuclear.org/info/inf08.html. Accessed 6 July 2011
3. Knief RA (1997) Nuclear steam supply systems. In: Elliott T et al (eds) Standard handbook of power plant engineering, 2nd edn. McGraw-Hill Book, New York
4. Ansolabehere S et al (2003) The future of nuclear power – an interdisciplinary MIT study. Massachusetts Institute of Technology. http://web.mit.edu/nuclearpower/). [Summarized in Deutch JM, Moniz EJ (2006) The nuclear option. Sci. Am, September 2006.] Also "Update of the MIT 2003 future of nuclear power study," Massachusetts Institute of Technology, 2009 – http://web.mit.edu/nuclearpower/pdf/nuclearpower-update2009.pdf
5. Lake JA, Bennett RG, Kotek JF (2009) Next generation nuclear power. Sci Am 286(1):72–79
6. New nuclear installations (from EPRI's 2007 Summer seminar: electricity solutions for a carbon-constrained future), EPRI J (Fall 2007):26–28
7. 2010 World nuclear industry handbook, from the publishers of Nuclear Engineering International magazine, www.neimagazine.com
8. Knief RA (1992) Nuclear engineering – theory and technology of commercial nuclear power, 2nd edn. Taylor & Francis, Washington, DC (Reprinted by American Nuclear Society, 2008; 3rd edition in preparation)
9. Sesonske A (1973) Nuclear power plant design analysis. U.S. Atomic Energy Commission, TID-26241, Washington, DC
10. Nuclear Energy Institute – http://www.nei.org/keyissues/newnuclearplants/ – http://www.nei.org. Accessed 6 July 2011
11. World Nuclear Association – http://www.world-nuclear.org/. Accessed 6 July 2011
12. UNM (University of New Mexico) CEL (Centennial Engineering Library) Nuclear Engineering Wallcharts – http://econtent.unm.edu/cdm4/browse.php?CISOROOT=/nuceng – Nuclear Engineering International – http://www.neimagazine.com/story.asp?storyCode=2055665. Accessed 6 July 2011
13. Rahn FJ, Adamantiades AG, Kenton JE, Braun C (1984) A guide to nuclear power technology: a resource for decision making. Wiley-Interscience, New York

14. U.S. Nuclear Regulatory Commission (1975) Reactor safety study: an assessment of risks in U.S. commercial nuclear power plants. U.S. Nuclear Regulatory Commission, WASH-1400 (NUREG-74/014), Washington, DC
15. U.S. Nuclear Regulatory Commission (1989) Severe accident risks: an assessment for five U.S. nuclear plants. U.S. Nuclear Regulatory Commission, NUREG-1150, Washington, DC
16. Nuclear Engineering International magazine – http://www.neimagazine.com/. Accessed 6 July 2011
17. Walker SJ (2004) Three Mile Island – a nuclear crisis in perspective. University of California Press, Berkeley
18. Catron J (1989) New interest in passive reactor designs. EPRI J 14(3):4–13
19. Small Nuclear Power Reactors – World Nuclear Association – http://www.world-nuclear.org/info/inf33.html. Accessed 6 July 2011
20. Fast Neutron Reactors – World Nuclear Association – http://www.world-nuclear.org/info/inf98.html. Accessed 6 July 2011
21. Generation IV Nuclear Reactors – World Nuclear Association – http://www.world-nuclear.org/info/inf77.html. Accessed 6 July 2011
22. Generation IV Nuclear Energy Systems – U.S. Department of Energy – http://www.ne.doe.gov/genIV/neGenIV1.html. Accessed 6 July 2011
23. Seminov BA (1983) Nuclear power in the Soviet Union. IAEA Bull 25(2):47–59

Books and Reviews

Agnew HM (1981) Gas-cooled nuclear power reactors. Sci Am 244:55–63

American Nuclear Society (+ Nuclear News). www.ans.org

Benedict M, Pigford TH, Levi HW (1981) Nuclear chemical engineering, 2nd edn. McGraw-Hill, New York

Cochran RG, Tsoulfanidis N (1990) The nuclear fuel cycle – analysis and management. American Nuclear Society, La Grange Park

Douglas J (1994) Reopening the nuclear option. EPRI J 19(8):6–17

Electric Power Research Institute (EPRI). http://my.epri.com. Accessed 6 July 2011

Fishetti MA (1987) Inherently safe reactors: they'd work if we'd let them. IEEE Spect 24(4):28–33

Framatome (1992) P4: the 1300 MWe PWR Series. Paris, France, April 1992

Glasstone S, Sesonske A (1994) Nuclear reactor engineering (volume 1: reactor design basics and volume 2: reactor systems engineering), 4th edn. Chapman & Hall, New York

Golay MW, Todreas NE (1990) Advanced light water reactors. Sci Am 262(4):82–89

Hore-Lacy I (2009) Nuclear energy in the 21st century, 2nd edn. World Nuclear University Press, London

International Atomic Energy Agency (IAEA). http://www.iaea.org

Lewis HW (1980) The safety of fission reactors. Sci Am 242:53–65

Lish KC (1972) Nuclear power plant systems and equipment. Industrial Press, New York

Marcus GH (2010) Nuclear firsts: milestones on the road to nuclear power development. American Nuclear Society, La Grange Park

Marshall W (ed) (1983) Nuclear power technology – volumes 1, 2, and 3. Clarendon Press, Oxford

McIntyre MC (1975) Natural uranium heavy-water reactors. Sci Am 233:17–27

MIT: the future of nuclear power. http://web.mit.edu/nuclearpower/. http://web.mit.edu/nuclearpower/pdf/nuclearpower-update2009.pdf. Accessed 6 July 2011

Murray RL (2008) Nuclear energy, 6th edn. Butterworth-Heinemann, Oxford

Nero AV Jr (1979) A guidebook to nuclear reactors. University of California Press, Berkeley

Nuclear Engineering International Special Publications (1989) French PWR technology. Nuclear Engineering International Special Publications, Sutton

Organisation for Economic Co-Operation and Development (OECD) – Nuclear Energy Agency (NEA). http://www.nea.fr/

Rogovin M, Frampton GT Jr (1980) Three Mile Island: a report to the Commissioners and to the public. U. S Nuclear Regulatory Commission, Washington, DC

Todreas NE, Kazimi MS (1990) Nuclear systems (vol 1: Thermal hydraulic fundamentals and vol 2: Elements of thermal hydraulic design). Taylor & Francis/Hemisphere, New York

U.S. Department of Energy (1987) Overall plant design descriptions VVER water-cooled, water-moderated energy reactor. DOE/NE0084, Rev. 1, October

U.S. Department of Energy (DOE) – Office of Nuclear Energy (NE). www.ne.doe.gov. Accessed 6 July 2011

U.S. Nuclear Regulatory Commission (1975) Reactor safety study: an assessment of risks in U.S. commercial nuclear power plants, WASH-1400 (NUREG-74/014). U.S. Nuclear Regulatory Commission, Washington, DC

U.S. Nuclear Regulatory Commission (1987) Report on the accident at the Chernobyl nuclear power station, NUREG-1250, rev.1. U.S. Nuclear Regulatory Commission Washington, DC

U.S. Nuclear Regulatory Commission (1989) Severe accident risks: an assessment for five U.S. nuclear plants, NUREG-1150. U.S. Nuclear Regulatory Commission, Washington, DC

U.S. Nuclear Regulatory Commission (NRC). www.nrc.gov. Accessed 6 July 2011

Vendryes GA (1977) Superphénix: a full-scale breeder reactor. Sci Am 236:26–35

World Nuclear Association (WNA). http://www.world-nuclear.org/info/reactors.html; Advanced Nuclear Power Reactors. http://www.world-nuclear.org/info/inf08.html; Generation IV Nuclear Reactors. http://www.world-nuclear.org/info/inf77.html; Fast Neutron Reactors. http://www.world-nuclear.org/info/inf98.html; Small Nuclear Power Reactors. http://www.world-nuclear.org/info/inf33.html. Accessed 6 July 2011

Nuclear Fuel, Reprocessing of

Michael F. Simpson, Jack D. Law
Fuel Cycle Science and Technology Division, Idaho National Laboratory, Idaho Falls, ID, USA

Article Outline

Glossary
Objective
Introduction
Reprocessing Technology
Future Directions
Bibliography

Glossary

Actinides All elements including and beyond actininium ($Z > 89$) in the periodic table. In spent fuel, the major actinides of interest are uranium, plutonium, neptunium, americium, and curium.

Cathode processor A high-temperature vacuum distillation furnace used to separate salt from metallic actinides deposited on an electrorefiner cathode.

Centrifugal contactors Liquid–liquid extraction equipment used for aqueous solvent extraction that consists of a spinning rotor to intensely mix the different phases.

Ceramic waste The glass-bonded sodalite matrix used to encapsulate waste salt from electrorefiner operation.

COEX™ French process for coextracting uranium and plutonium using extraction methods similar to PUREX.

Electrorefiner An electrochemical system used to separate actinides from spent fuel using a molten salt electrolyte.

Experimental Breeder Reactor-II A sodium-cooled, fast test reactor operational at Argonne National Laboratory-West from 1963 to 1994.

Geologic repository A permanent nuclear waste disposal site located deep within a geological formation.

Metal waste The stainless steel–zirconium matrix used to encapsulate cladding hulls and noble metals left in anode baskets after U electrorefining is completed.

Mixer-settler Liquid–liquid extraction equipment used for aqueous solvent extraction requiring a relatively large footprint.

Minor actinides Actinide elements other than U and Pu. In spent fuel, the primary minor actinides of concern are Np, Am, and Cm.

Noble metals Elements found in spent nuclear fuel that have chloride forms that are thermodynamically less stable than uranium chloride.

Pulsed columns Liquid–liquid extraction equipment used for aqueous solvent extraction involving a single column consisting of trays of perforated plates to promote interphase mass transport.

Pyroprocessing Nuclear fuel treatment technology that uses electrochemical reactors with molten salt electrolytes to separate actinides from fission products.

PUREX Nuclear reprocessing technology that separates actinides from the spent fuel via liquid–liquid extraction involving acidic aqueous and organic liquid phases.

Spent fuel Nuclear fuel that has gone through at least one irradiation cycle in a nuclear reactor. It contains a mixture of actinides and fission products.

Solvent extraction A separations method for extracting species from a liquid phase. In this entry, it refers to a process for removing uranium from spent fuel that utilizes dissolution in acid followed by liquid–liquid extraction between aqueous and organic liquid phases.

UREX A variant of the PUREX process that separates uranium from spent fuel without recovering pure plutonium

V-blender A v-shaped vessel that is designed to efficiently blend two or more different kinds of powders with or without applied heat.

Objective

The objective of this entry is to give a basic overview of the technology elements behind nuclear fuel reprocessing. It should serve as a starting point for more detailed study with the aid of the Bibliography section to obtain more technical details on this subject. Several more process concepts have been proposed, tested, and demonstrated other than those listed in this entry. For the sake of conciseness, only two

fundamentally different technologies have been described here – aqueous and pyrochemical fuel reprocessing. In the case of pyrochemical fuel reprocessing, focus has been placed on the LiCl-KCl electrorefining technology developed originally at Argonne National Laboratory. The overall scope of nuclear fuel reprocessing technology is too broad to cover in this entry.

Introduction

Nuclear reprocessing is the chemical treatment of spent fuel involving separation of its various constituents. Principally, it is used to recover useful actinides from the spent fuel. Radioactive waste that cannot be reused is separated into streams for consolidation into waste forms. The first known application of nuclear reprocessing was within the Manhattan Project to recover material for nuclear weapons. Currently, reprocessing has a peaceful application in the nuclear fuel cycle. A variety of chemical methods have been proposed and demonstrated for reprocessing of nuclear fuel. The two most widely investigated and implemented methods are generally referred to as aqueous reprocessing and pyroprocessing. Each of these technologies is described in detail in Sect. 3 with numerous references to published articles.

Reprocessing of nuclear fuel as part of a fuel cycle can be used both to recover fissionable actinides (primarily U and Pu isotopes) and to stabilize radioactive fission products into durable waste forms. It can also be used as part of a breeder reactor fuel cycle that could result in an almost 70-fold increase in energy utilization per unit of natural uranium [1]. Reprocessing can also impact the need for geologic repositories for spent fuel. The volume of waste that needs to be sent to such a repository can be reduced by first subjecting the spent fuel to reprocessing. The extent to which volume reduction can occur is currently under study by the US Department of Energy via research at various national laboratories and universities. Reprocessing can also separate fissile and nonfissile radioactive elements for transmutation.

The current known reserves of uranium that can be economically harvested are 5.5 million metric tons U at a maximum market price of about $80/lb. At the current usage rate of 65,000 metric tons U/year, this quantity of uranium will last for about 85 years [2]. However, nuclear power expansion in India, China, and other countries will soon lead to a substantial increase in the global usage rate for uranium. Increased investment in uranium exploration will undoubtedly reveal additional recoverable resources. And the inevitable increase in cost of uranium will lead to a higher fraction of economically recoverable resources. Reprocessing of spent fuel and use in light water reactors can also serve to improve efficiency of uranium resource utilization. Estimates range from about 10% to 30% for reduction of natural uranium usage as a result of reprocessing spent fuel and reuse in nonbreeding reactors.

Reprocessing Technology

Aqueous Reprocessing

General Description With this technology, nuclear fuel is dissolved into an acidic solution. The resulting solution is then chemically processed to separate the metals of interest, typically uranium and/or plutonium. Minor actinides as well as other fission products may also be separated using advanced aqueous processes. Specific unit operations utilized in the past primarily consist of precipitation and liquid–liquid extraction. Precipitation was the primary method used in the defense industry initially for the production of plutonium. Liquid–liquid extraction was later developed as an improved method for reprocessing in the defense industry and also became the primary method of reprocessing of commercial nuclear fuel internationally. Since the vast majority of aqueous reprocessing applications continue to utilize liquid–liquid extraction, this will be the primary focus of discussion in this entry.

Liquid–liquid extraction (also called solvent extraction) was initially utilized in the petroleum industry beginning in the 1930s. It has since been utilized in numerous applications including petroleum, hydrometallurgical, pharmaceutical, and nuclear industries. Liquid–liquid extraction describes a method for separating components of a solution by exploiting an unequal distribution of the component(s) between two immiscible liquid phases. In most cases, this process is carried out by intimately mixing the two immiscible phases, allowing for the selective transfer

of solute(s) from one phase to the other, then allowing the two phases to separate. Typically, one phase will be an aqueous solution, usually containing the component(s) to be separated, and the other phase will be an organic solvent, which has a high affinity for some specific components of the solution. The process is reversible by contacting the solvent loaded with solute(s) with another immiscible phase that has a higher affinity for the solute than the organic phase. The transfer of solute from one phase into the solvent phase is referred to as extraction and the transfer of the solute from the solvent back to the second (aqueous) phase is referred to as back-extraction or stripping. The two immiscible fluids must be capable of rapidly separating after being mixed together, and this is primarily a function of the difference in densities between the two phases.

While limited mass transfer can be completed in a single, batch equilibrium contact of the two phases, one of the primary advantages of liquid–liquid extraction processes is the ability to operate in a continuous, multistage countercurrent mode. This allows for very high separation factors while operating at high processing rates. Countercurrent operation is achieved by repeating single-stage contacts, with the aqueous and organic streams moving in opposite directions as shown in Fig. 1.

In this flow diagram, the aqueous feed stream containing the solute(s) to be extracted enters at one end of the process (A_{N+1}), and the fresh solvent (organic) stream enters at the other end (O_0). The aqueous and organic streams flow countercurrently from stage to stage, and the final products are the solvent loaded with the solute(s), O_N, leaving stage N and the aqueous raffinate, A1, depleted in solute(s) and leaving stage 1. In this manner, the concentration gradient in the process remains relatively constant.

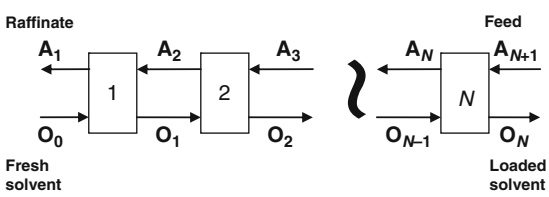

Nuclear Fuel, Reprocessing of. Figure 1 Countercurrent multistage extraction process flow diagram

The organic at stage O_0 contains no solute(s), while the raffinate stream is depleted of solute(s). Streams A_{N+1} and O_N contain the highest concentration of the solute(s).

For the process to be economical, the solvent must be recycled. In order to recycle the solvent, the solute is subsequently stripped from the solvent, and the solvent is then recycled back to the countercurrent extraction process. This allows the solvent to be recycled indefinitely, until it has degraded (due to acid hydrolysis or radiolytic degradation) or the solvent composition has changed due to solubility in the aqueous phase and/or evaporation.

History of Aqueous Separation Technology Aqueous separations processes for nuclear reprocessing evolved from early US defense programs for the separation of Pu for weapons manufacture. The bismuth phosphate process began operation at the Hanford Nuclear Reservation in 1944 for the separation of Pu from irradiated slugs from the B reactor [3]. The first continuous solvent extraction reprocessing plant replaced the bismuth phosphate process at Hanford in 1952. This facility used the reduction oxidation (REDOX) process to separate Pu. The REDOX process utilized methyl isobutyl ketone as an extractant. In the REDOX process, uranium and plutonium nitrate is preferentially extracted from the fission products in a high salting strength aqueous solution [4, 5]. The uranium and plutonium are then selectively stripped from the solvent by adjusting the valence state of the Pu to back-extract it and use a low salting strength strip solution to back-extract U. Additional cycles of extraction were used to decontaminate the products. General Electric's Knolls Atomic Power Laboratory developed the PUREX process in the 1950s. PUREX-based operations at Savannah River F Canyon began in 1954 and replaced the REDOX process at Hanford in 1956 [3]. The PUREX process became the standard method of reprocessing used nuclear fuel throughout the world.

PUREX Process Technology PUREX-based reprocessing consists of leaching the spent fuel from the cladding using a nitric acid solution, chemical adjustment and filtration of the resulting feed solution, several cycles of solvent extraction to separate and purify the uranium and plutonium, solidification of the resulting uranium

and/or plutonium product, as well as the waste solutions. The plutonium oxide product, with or without uranium, is then recycled as mixed oxide (MOX) fuel. This resulting MOX fuel can be used as an alternative to low-enriched uranium in light water reactors. MOX fuel is widely used in Europe, and there are plans for use in Japan. About 40 reactors in Europe (Belgium, Switzerland, Germany, and France) are licensed to use MOX fuel [6]. Existing aqueous commercial reprocessing facilities throughout the world utilize, primarily, the PUREX solvent extraction process or a variant of this process to accomplish the separation of U and Pu. Pure plutonium can also be separated with this process and used to make nuclear weapons.

The front end of the PUREX process involves mechanical chopping of the spent nuclear fuel assemblies into small pieces (1 cm long) followed by leaching of the spent fuel in a nitric acid solution. The chopped pieces of the pins, as well as spacers and other fittings, must then be separated from the leached fuel solution. This has been performed through the use of perforated baskets that hold the hardware, such as in the batch operations performed at the THORP facility in the UK, or through the use of a continuous dissolver, such as the wheel dissolver at the UP2 and UP3 plants in France which holds the hardware in buckets formed in sections of the wheel as the wheel rotates through the nitric acid solution [7]. The dissolver solution, after further clarification and feed adjustment, is then processed through the use of the PUREX technology to separate and purify the uranium and plutonium from the dissolver product solution.

The PUREX process utilizes 20–40 vol% tributyl phosphate in a hydrocarbon diluent to extract uranium and plutonium from the acidic solution resulting from the dissolution of spent nuclear fuel. In general, metals in the +4 and +6 oxidation state are extracted in the PUREX process. The chemical equilibria for U (VI) in a nitrate media is

$$UO_2{}^{2+} + 2NO_3{}^{-} + 2TBP \Leftrightarrow UO_2(NO_3)_2 \cdot 2TBP \tag{1}$$

The chemical equilibria for the actinides in the +4 oxidation state is

$$An^{4+} + 4NO_3{}^{-} + 2TBP \rightleftharpoons An(NO_3)_4 \cdot 2TBP \tag{2}$$

Plutonium maintained in the +4 oxidation state is, therefore, coextracted with the U. Pu (III) and other actinides and lanthanides in the +3 or lower oxidation state are not extracted in the PUREX Process. Neptunium, if maintained in the +6 oxidation state, can be coextracted with the U and Pu. The strong extraction of the +4 and +6 oxidations states, along with the weak extraction of the other oxidations states, results in the effective use of the PUREX process for separation of uranium and plutonium from nearly all of the other metals present in the spent nuclear fuel.

A typical PUREX process first extraction cycle is provided in Fig. 2. The solution resulting from the dissolution of the spent nuclear fuel is the feed to the coextraction section of the flowsheet. The aqueous feed flows countercurrent to the PUREX solvent, and the U and Pu are extracted by the TBP into the normal paraffin hydrocarbon (NPH) organic phase. The loaded organic phase enters the fission product (FP) scrub section in which a nitric acid scrub

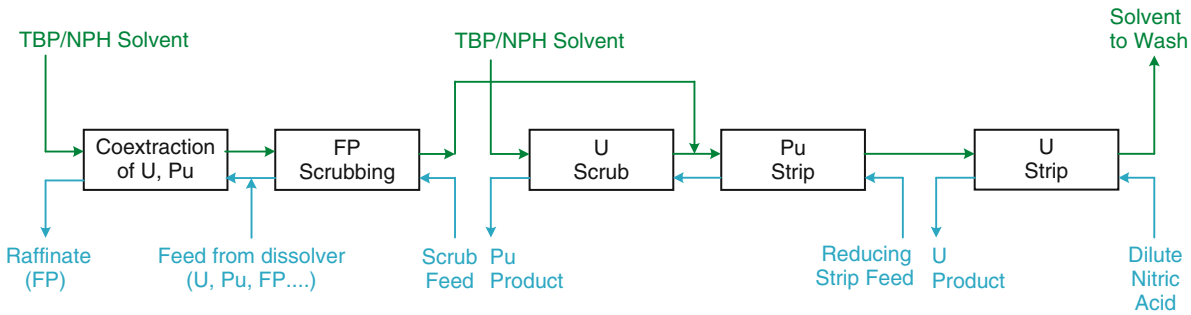

Nuclear Fuel, Reprocessing of. Figure 2
Typical PUREX first cycle flowsheet

solution (approx. 2 M HNO_3) is used to remove coextracted fission products, such as Zr and Ru, from the solvent. The scrub solution containing the Zr and Ru combines with the feed solution entering the extraction section. The solvent then enters a Pu strip section in which the Pu is back-extracted from the organic phase. This is accomplished by reducing the Pu from the extractable +4 oxidation state to the inextractable +3 state. A strip solution containing a reductant, such as hydroxylamine nitrate, U (IV), or ferrous sulfamate, is typically used [8].

Reduction and back-extraction of the Pu also results in back-extraction of a portion of the uranium. The strip product from the Pu strip section therefore enters a uranium scrub section in which the Pu strip solution is contacted with a fresh solvent feed to reextract this uranium into the organic phase. The organic phase containing the reextracted U combines with the loaded solvent from the extraction section which enters the Pu strip section. Once the Pu has been back-extracted from the PUREX solvent, the solvent enters the uranium strip section, which utilizes dilute nitric acid (typically 0.01 M HNO_3) at elevated temperature to back-extract the U into the aqueous phase.

The resulting solutions from the first cycle PUREX extraction process include a solvent solution that is washed with a carbonate or hydroxide solution to remove degradation products and recycled back to the extraction section, a raffinate stream which is depleted of the U and Pu and disposed of as waste, and the Pu and U product streams. The U and Pu product streams are typically further processed with additional PUREX cycles to purify these streams [9].

PUREX Process Waste Treatment The separation of the Pu and U from spent nuclear fuel results in a high-level waste (HLW) requiring immobilization and storage. The immobilization technology currently in use in the UK, France, and Japan is vitrification of the waste to form a stable borosilicate glass waste form suitable for long-term storage [10]. The glass waste produced is poured into canisters and are stored until long-term geological storage is available. Appropriate geological repositories are currently being pursued in these countries. Low (LLW) and intermediate-level wastes (ILW) are also generated from aqueous reprocessing and require treatment and disposal.

Advanced Aqueous Separations Process Technology Advanced aqueous separations processes are being developed throughout the world including the USA, France, UK, Japan, Russia, and China. The goals of the development of advanced aqueous processes include closing the nuclear fuel cycle and reducing the proliferation risk of the technologies. Reduction in proliferation risk is being addressed through development of modified PUREX processes which do not separate pure plutonium. In addition, advanced separation processes are being developed to separate the actinides for reactor recycle to close the fuel cycle.

Advanced Aqueous Reprocessing Strategies Numerous strategies are being developed internationally for advanced aqueous reprocessing processes. The goals of these processes typically are to accomplish separations beyond the Pu and U that is separated with the PUREX process in order to reduce the volume, radiotoxicity, and heat generation of the spent nuclear fuel. The components targeted include the minor actinides as a group, the short-lived fission products (Cs and Sr), and/or individual actinides, such as Am. The minor actinides or Am separated from the spent fuel would be recycled for burning in a fast reactor. If separated, the Cs and Sr could be placed into decay storage.

A wide variety of advanced processes are currently being developed to accomplish these advanced separations. Major research efforts on advanced processing are ongoing in France, Japan, UK, USA, China, and Russia [11–17]. These technologies are at various stages of maturity, and none have been implemented into full-scale reprocessing facilities to date.

Advanced aqueous processing has the potential to significantly reduce the volume, heat load (long and short-term), and radiotoxicity of HLW requiring disposal in a geological repository [18]. These processes, however, will result in the generation of a significant quantity of LLW requiring treatment and disposal. These wastes include spent solvent, solvent treatment solutions, and decontamination solutions, among others. Additionally, solid waste is generated from facility operations (e.g., gloves, shoe covers, cleaning supplies, filters) and will require treatment and disposal.

The primary focus of recent development of advanced PUREX processes is to prevent the separation of pure Pu, thus reducing proliferation risk, as well as

controlling Np and Tc chemistry to allow for the extraction of these metals.

In France, the COEX™ process is being developed which coextracts the U and Pu and produces a Pu/U product instead of a pure Pu product [19]. This is accomplished by adjusting the chemistry of the PUREX process to allow some U to be back-extracted from the solvent with the Pu. The process also uses a coconversion process to produce a (Pu, U) oxide product. Coextraction of Np is also being evaluated with the COEX™ process to produce a (Pu, U, Np) oxide product [19]. The Rokkasho reprocessing plant in Japan, which has been constructed and is currently undergoing operational testing, also uses a PUREX process that has been modified to combine uranium with the separated plutonium in a 50/50 mix prior to denitration [20]. In the USA, the uranium extraction (UREX) process has been developed which separates the uranium from spent nuclear fuel. The UREX process is a modification of the PUREX process in which the Pu is prevented from extracting with the U by adding acetohydroxamic acid as a reductant/complexant [21, 22].

Aqueous Reprocessing Equipment The solvent extraction equipment utilized for industrial-scale aqueous reprocessing must enable continuous processing at high throughputs while efficiently mixing and separating the two phases. In the nuclear industry, specific constraints, such as remote operation and maintenance, must be considered, since the solutions processed are highly radioactive. There are three basic types of equipment used in industrial-scale nuclear solvent extraction processes: mixer-settlers, columns, and centrifugal contactors. A detailed description of the three types of equipment follows.

Mixer-Settlers. This equipment consists of a small mixing chamber followed by a larger gravity-settling chamber as shown in Fig. 3. Each mixer-settler unit provides a single stage of extraction. The two phases enter the mixing section where they are mixed using an impeller. The two-phase solution flows into the settling section where the phases are allowed to separate by gravity due to their density differences. Typical mixer settlers have mixing times on the order of a few minutes and settling times of several minutes. The separate phases exit the settling section by flowing over a weir

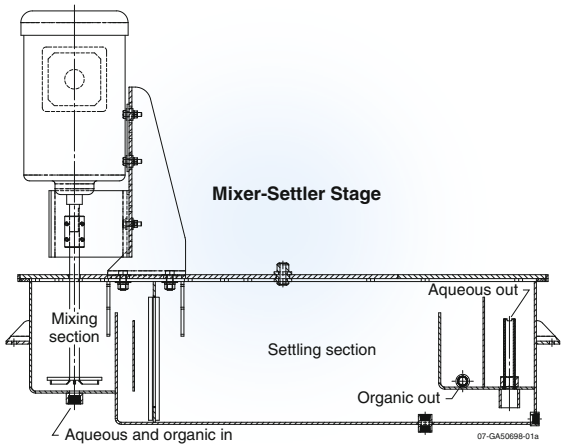

Nuclear Fuel, Reprocessing of. Figure 3
Diagram of a mixer-settler

(less dense phase – typically organic) or through an underflow then over a weir (more dense phase – typically aqueous). The separation interface is controlled by the height of the weirs on the outlets of the settler section. Only minimal instrumentation is required, and mechanical maintenance is limited to occasional mixing motor replacement. In a counter-current process, multiple mixer settlers are installed with mixing and settling chambers located at alternating ends for each stage (since the outlet of the settling sections feed the inlets of the adjacent stage's mixing sections).

Mixer-settlers are best suited for use when a process requires longer residence times and when the solutions are easily separated by gravity. They require a large facility footprint, but do not require much headspace and need limited remote maintenance capability for occasional replacement of mixing motors [23, 24].

Columns. There are two basic types of columns employed industrially, packed columns and pulse columns with plates or trays. Packed columns are filled with some type of packing material, such as Raschig rings, to create a tortuous path for the two solutions as they flow through the column (typically aqueous feed downward and solvent upward), ensuring that the two phases are in constant contact. Packed columns have no moving parts and are relatively simple to operate, but they are not very efficient. Since columns do not have

discrete stages, such as mixer-settlers or centrifugal contactors, the number of stages is determined by the height equivalent of a theoretical stage (HETS) [25]. For most packed columns, this HETS of extraction is usually several feet, meaning that a countercurrent process utilizing several stages to effect a given separation factor would require very tall columns. To reduce the height of a theoretical stage in the column, other packing (trays or perforated plates) is used and mechanical energy is applied to force the dispersed phase into smaller droplets, improving mass transfer. The most common type of column used today, particularly in the nuclear industry, is the pulse column.

In a pulse column, liquids are continuously fed to the column and flow counter – currently, as is done with a packed column; but mechanical energy is applied to pulse the liquids in the column up and down. This is normally done by injecting pressurized air into a pulse leg that pushes liquid into the column, then venting the pulse leg to fill the pulse leg with solution from the column. The pulse action lifts and lowers the solution in the column, usually only a few inches. The column is filled with perforated plates or other plates to promote droplet formation as the dispersed phase is pushed through the plates. This pulsing action reduces droplet size of the dispersed phase and improves mass transfer. A perforated plate pulse column is shown in Fig. 4. There are a number of plate designs used. Early pulse columns used sieve plates, which are flat plates with holes drilled into them. A more effective plate is the nozzle plate, which has different contours on the top and bottom of the plate (making it directional, in that, it must be configured according to the continuous phase in the column). The French and Japanese pulse columns employ a disk and doughnut configuration, where the plates are solid (no openings) but the alternating plates enable effective contacting of the phases [25].

The separation interface is controlled during column operation using bubble probes in the disengaging

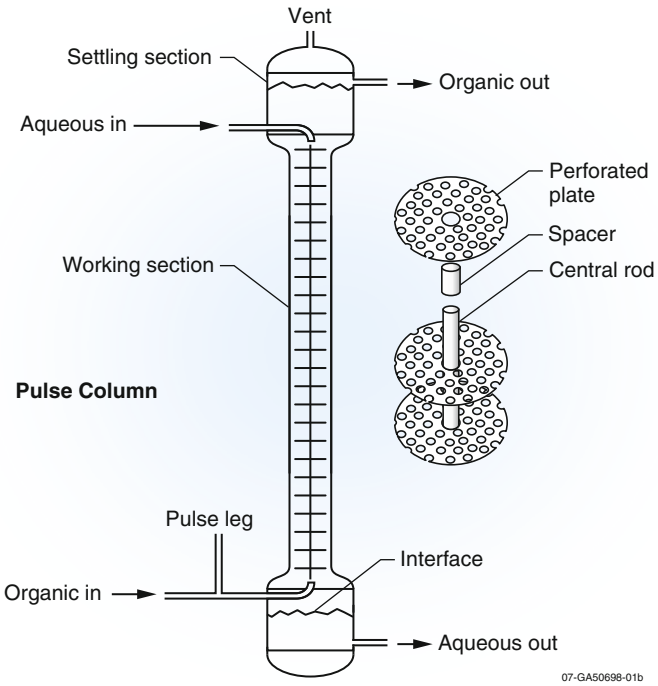

Nuclear Fuel, Reprocessing of. Figure 4
Pulse column with perforated plates

section. The probes are interfaced to a controller that drains heavy phase from the bottom of the column. The bubble probes allow operators to monitor the weight of the column, which gives them a good indication of column performance, by determining the ratio of heavy and light phases in the column. In addition, pulsing devices and pulse speed controllers are required as pulse frequency and amplitude must be controlled during operation. Periodic maintenance is required only for the pulsing equipment, which is located out of cell, above the columns. Pulse columns are used when a process requires intermediate residence times, as adjusting flow rate easily varies residence time. They require a small facility footprint, but do require much headspace (typically 40–50 ft). Pulse columns do not need remote maintenance capability, as all moving parts (pulser equipment) are located outside the shielded cell. Extensive literature has been published on pulse columns [9, 27–29]. Pulse columns are the primary type of aqueous separation equipment utilized in the nuclear industry today.

Centrifugal Contactors. Centrifugal contactors, like mixer-settlers, are discrete-stage units, providing one stage of extraction per unit and are readily linked together as each rotor pumps separated fluids to the next stage inlet in each direction. The primary difference between a centrifugal contactor and a mixer-settler is the separation of the two-phase mixture. Centrifugal contactors employ a spinning rotor that intensely mixes the two phases and separates the two phases inside the rotor where the centrifugal forces can be as high as 300 g. This results in efficient and fast phase separation. The separated phases exit the contactor by overflow and underflow weirs, similar to a mixer-settler. A cutaway view of an operating centrifugal contactor is shown in Fig. 5.

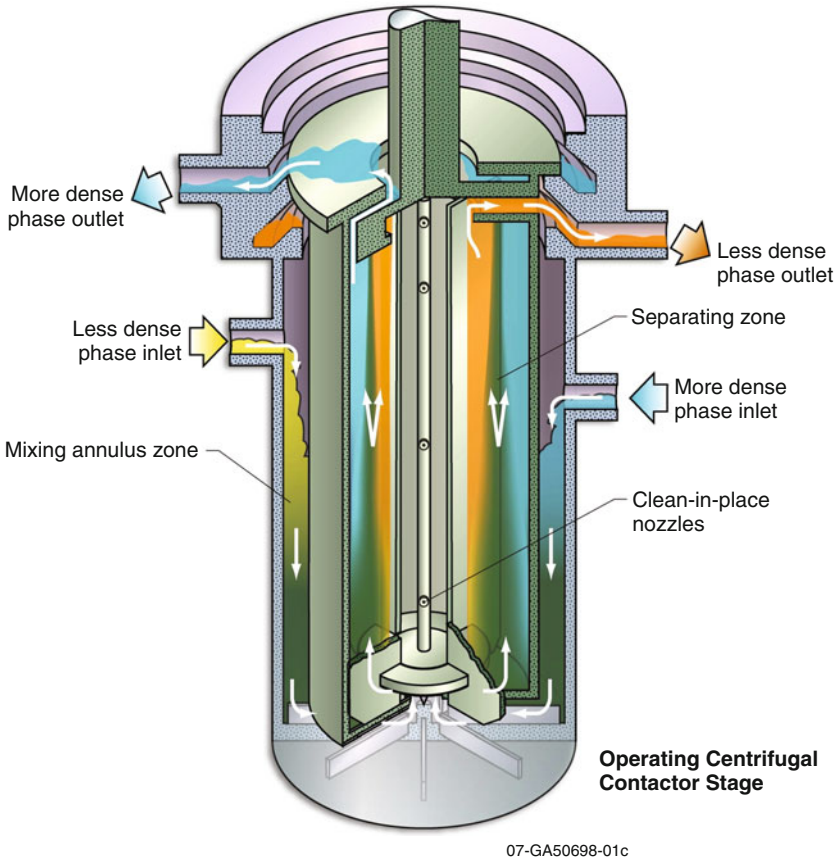

Nuclear Fuel, Reprocessing of. Figure 5
Cutaway view of an operating centrifugal contactor

Centrifugal contactors have high single-stage efficiency (routinely greater than 95% of theoretical for chemical processes with rapid kinetics). Process flow interruptions cause no loss of process concentration profiles if centrifugal contactor rotors are kept spinning. Thus centrifugal contactor-based processes can be paused for a period of time sufficient to reestablish flow or even replace a motor without significant loss of product or rework. Centrifugal contactors require minimal instrumentation for process operation. Computer control via commercial software allows monitoring of motor amperage, rotor rpm, inlet flow rates, temperatures, and many other process parameters. Centrifugal contactors are used when a process requires short residence times, on the order of several seconds. They require a small facility footprint and minimal headspace, but they do require remote maintenance capability for periodic removal of the motor and/or rotor.

Centrifugal contactors have been the subject of much recent development work over the past 40 years, while the designs of pulse column and mixer-settlers has changed little over the same time period [30–32]. Early designs included a paddle wheel to mix the phases below the spinning rotor [33]. This precluded removal of the rotor assembly. The annular centrifugal contactor was subsequently developed, which allowed the motor and rotor assembly to be easily removed [34]. Other designs included multistage units, units for low-mix applications (higher phase separation), and clean-in-place units that have an array of internal spray nozzles to facilitate solids removal as necessary [35–37]. Design of remote operation and maintenance capabilities has also continued, resulting in more efficient remote handling [38, 39].

Pyroprocessing

General Description Pyroprocessing is currently considered an alternative reprocessing technology to the more commonly used aqueous processing technology. Pyroprocessing accomplishes separations by way of high-temperature electrorefining. It is yet to be implemented on a large scale, limited to date to laboratory-scale and engineering-scale experimentation and demonstration. Much of the current state of the art for pyroprocessing was developed during the Integral Fast Reactor (IFR) program, which was carried out at Argonne National Laboratory from about 1984 to 1995 [40, 41]. With the shutdown of Experimental Breeder Reactor-II in 1995, the IFR program was converted into a spent fuel treatment program to safely treat the 25 metric tons of heavy metal from that reactor [42]. Pyroprocessing utilizes molten salt electrolytes as the media rather than acidic aqueous solutions and organic solvents [43]. These electrolytes are principally used to support electrochemical separations such as uranium electrorefining and electrolytic reduction of oxide fuel. The process includes vacuum furnaces that accomplish salt/metal separations and melt metal deposits into ingots for either waste disposal or fuel fabrication. Ceramic and metal waste streams are generated that immobilize fission products and, optionally, plutonium and minor actinides into high-level waste forms. For eventual commercial implementation, it is expected that plutonium and minor actinides will be recycled and used for fast reactor fuel fabrication. While this technology is yet to reach the commercialization stage, it has been the subject of extensive, government-funded research and development worldwide in addition to the EBR-II spent fuel treatment work in the USA. For example, the Republic of Korea is currently pursuing a strategy of developing pyroprocessing technology for treatment of spent fuel from their commercial light water reactors to minimize volume of HLW and possibly extract fissile actinides for eventual fabrication of fast reactor fuel [44, 45]. Russia has already demonstrated production of MOX based on pyroprocessing and plans to develop a closed fuel cycle using the technology by 2020.

While PUREX and related aqueous reprocessing technology has superior maturity, pyroprocessing does have unique benefits that make it a credible alternative and in some cases a preferred alternative. This includes use of process liquids that are more stable than organics in the presence of high radiation fields, improved criticality safety due to the lack of neutron moderators in the process, and waste processing that is integrated with the separations flowsheet.

Process Technology There are many variants of the pyroprocessing flowsheet, but the IFR scheme shown in Fig. 6 can be used as a reference, as it contains all of the key unit operations.

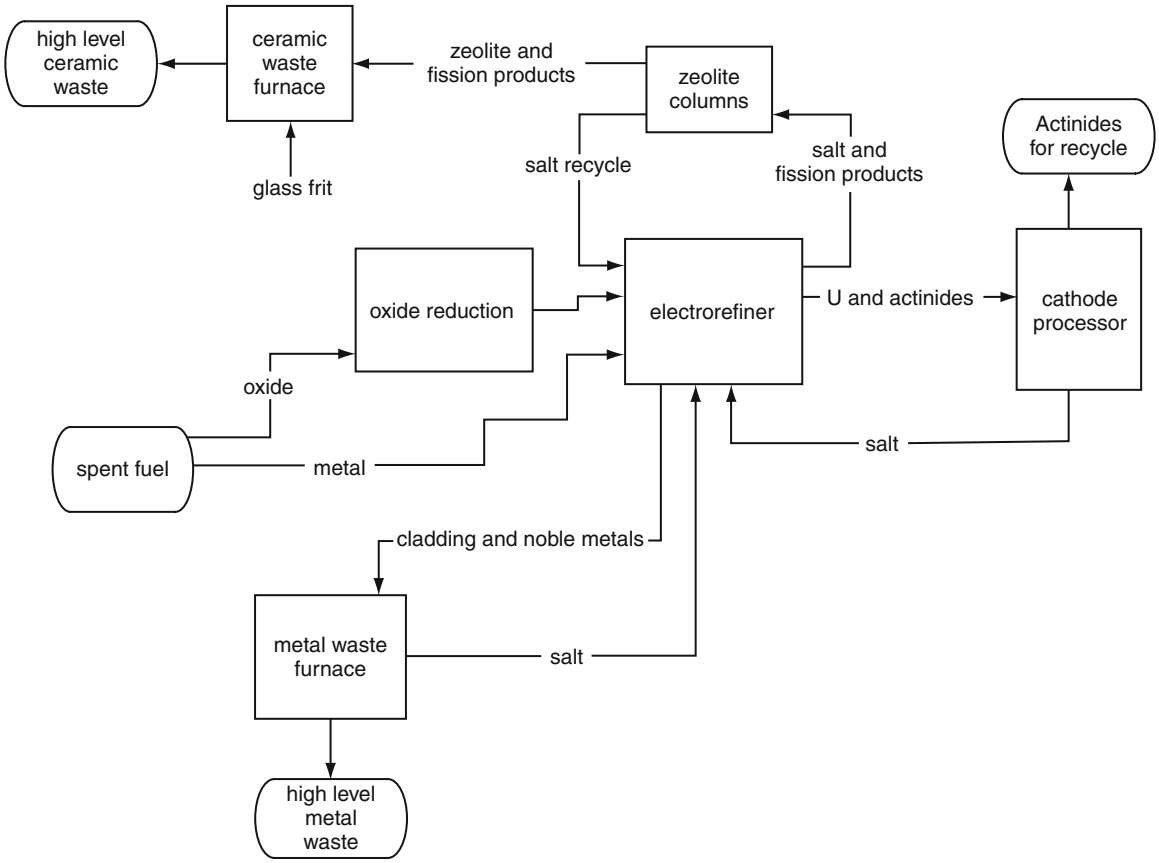

Nuclear Fuel, Reprocessing of. Figure 6
Fuel Processing Flowsheet for the Integral Fast Reactor Program

The electrorefiner is at the center of the flowsheet and is used to perform the primary separation of actinides from fission products [46, 47]. It contains a molten salt electrolyte – typically LiCl-KCl-UCl_3 maintained at 450–500°C. The eutectic composition of LiCl-KCl (44.2 wt% LiCl, 55.8 wt% KCl) is maintained to keep the melting point at approximately 350°C. The UCl_3 content varies depending on desired operating conditions from about 0.5–10 wt%. It is used as a charge carrier for electrotransport through the electrolyte. After the spent fuel is chopped into segments, it is loaded into anode baskets, and the baskets are lowered into the electrorefiner. As current is passed between the anode and cathode, U metal is oxidized to U^{3+} at the anode and reduced back to metallic form at the steel cathode. The deposit contains high purity uranium and is typically dendritic. An example of a U cathode deposit is shown in Fig. 7.

Transuranic (TRU) elements and active metal fission products are oxidized electrochemically or via reaction with uranium chloride in the salt and enter the electrolyte. Under normal conditions, Pu and minor actinides cannot deposit at the cathode, because their back-reaction with UCl_3 is thermodynamically spontaneous. However, codeposition of U and TRU can be achieved via a combination of elevating the TRU to U ratio in the salt and utilizing a liquid cadmium cathode (LCC). In the molten cadmium phase, TRU elements have a very low activity coefficient compared to U. This allows for TRU metals to be present in quantities comparable to that of uranium in the cadmium. Alternative methods are currently being investigated to corecover U and TRU without the need for an LCC.

Fission product elements segregate between the anode basket and the molten salt during the

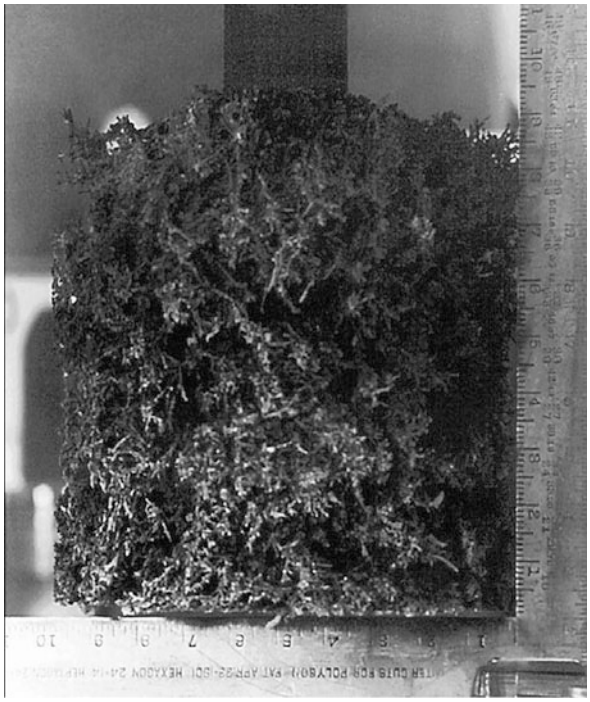

Nuclear Fuel, Reprocessing of. Figure 7
Dendritic uranium deposit on electrorefiner cathode

electrorefining process. Noble metals such as Tc, Ru, and Rh remain with the cladding hulls in the anode basket. Active metals that typically include Group I and II elements in addition to lanthanides are oxidized to chloride form and accumulate in the salt. If sodium metal is used as a bonding agent, as in the case of EBR-II fuel, this sodium is oxidized to sodium chloride, which accumulates in the ER electrolyte.

Note in Fig. 6 that both metal fuel and oxide fuel can be treated via pyroprocessing. Treatment of metallic fuel is relatively straightforward due to the fact that it is already in a state compatible with the ER. Oxide fuel must first be converted to metallic form. This can be accomplished in an oxide reduction step. Various methods have been investigated for reducing spent oxide fuel. Early efforts were focused on chemical reduction via lithium. Similar to electrorefining, a molten salt is used for carrying out this reaction. In this case, it is LiCl saturated with lithium metal at 650°C. The lithium reduction reaction is as follows [47].

$$4Li + UO_2 \rightarrow 2Li_2O \tag{3}$$

More recently, a similar process based on electrochemical reactions has been favored for development. It also uses a vessel containing molten LiCl at 650°C, but it contains lithium oxide in the salt rather than lithium metal. The reactions for the electrolytic process are shown below [49].

$$\begin{aligned} UO_2 + 4e^- &\rightarrow U + 2O^{2-} \\ 2O^{2-} &\rightarrow O_2 + 4e^- \end{aligned} \tag{4}$$

The generated oxygen bubbles out of the salt as a gas and can be sent to an off-gas treatment system to remove any entrained or volatile contaminants. The advantages of the electrolytic method based on the above reactions are that lithium oxide concentration in the molten salt can be kept low (1 wt%), and there is no need for a separate vessel to regenerate lithium metal from lithium oxide.

U or U/TRU product deposited on the cathode in the electrorefiner is transferred to a cathode processor, which is essentially a vacuum distillation furnace. The salt is separated from the metals and recycled to the electrorefiner. The purified metals can be fed into a process for fabricating metallic fuel for fast reactors. For the case of the EBR-II Spent Fuel Treatment process, the cathode processor operates at a temperature up to 1200°C and achieves pressures less than 1 torr.

After an electrorefining run, the anode basket contains the cladding hulls, undissolved actinides, inert fuel matrix material such as zirconium, adhering salt, and noble metal fission products such as Tc, Mo, Rh, and Ru. All of this material is removed from the anode baskets and loaded into an inductively heated vacuum distillation furnace that is used to distill adhering salt and consolidate the metals into an ingot. The metal ingot becomes a waste form that has been tested and shown to be suitable for disposal in an HLW repository [50, 51].

Electrorefiner salt becomes progressively more contaminated with fission product chlorides as well as sodium chloride in the process of treating fuel. Once the contamination level has exceeded a predetermined limit, the salt must be removed from the electrorefiner and either disposed or processed through a purification step and returned to the electrorefiner. The basis for that limit can be fission product decay heat, salt melting point, or criticality limits. Another potential limiting factor is contamination of the metallic actinide

products recovered in the cathode processor. High concentrations of rare earth fission products in the salt, for example, have been shown to lead to high rare earth contamination levels in the actinide product. The process flow sheet shown in Fig. 6 includes zeolite ion exchange columns for achieving this salt purification. Zeolite-A has been shown to exhibit selectivity for the fission product ions when in contact with molten chloride salt [52–55]. Other alternatives that have been considered for treating the salt to remove fission products and other contaminants include selective precipitation, zone freeze refining, and adsorption by nonzeolitic materials [56].

The current baseline technology for dealing with the salt waste from electrorefining EBR-II spent fuel is to nonselectively immobilize the salt into a ceramic waste form consisting of glass-bonded sodalite [57, 58]. In this process, salt is removed from the electrorefiner, sized via crushing and milling to a fine particulate, and absorbed into zeolite-4A in a high-temperature blending operation. A V-blender capable of heating and mixing particulate material to 500°C is used for this absorption step. Prior to being loaded into the V-blender, it is necessary to dry the zeolite to less than 1 wt% water. This drying is used to maximize salt absorption in the zeolite while minimizing evolution of water vapor in a high-temperature, corrosive environment. Drying the zeolite should also minimize pores in the final ceramic waste form. Zeolite drying is accomplished via mechanically fluidizing the zeolite under vacuum at temperatures up to 550°C [57, 58]. Heating the zeolite-4A to temperatures of 600°C or higher has been determined to cause structural damage that inhibits its ability to absorb salt [59]. Final consolidation into the ceramic waste form occurs after borosilicate glass binder has been mixed with the salt-loaded zeolite, loaded into a steel canister, and heated to a maximum temperature of 915–950°C. During the process of consolidation, the zeolite-A phase converts to sodalite. In the glass-bonded sodalite waste form, the fission products are distributed between the glass and sodalite phases [60].

If an ion exchange process with zeolite-A has been used to selectively remove fission products from the salt, the resulting fission product-loaded zeolite-A can be similarly converted into a glass-bonded sodalite ceramic waste form. Zeolite-A used for ion exchange is typically in pelletized form and must be milled to a fine particulate prior to blending with additional dried zeolite-4A and borosilicate glass. The flowsheet shown in Fig. 6 includes zeolite ion exchange followed by conversion of this zeolite into the ceramic waste form.

Future Directions

In the USA, the current focus is on research and development into both aqueous reprocessing and pyroprocessing technology to support a future decision on closing the fuel cycle. The US Department of Energy (2009) has established the Fuel Cycle Research and Development program for carrying out this research in national laboratories and universities. At this time, there are no large-scale demonstration projects planned. Meanwhile, plans to open a geologic repository for spent nuclear fuel and waste in Nevada's Yucca Mountain have been suspended. The government has commissioned a study to evaluate alternative options for disposal of the spent fuel and waste.

In Japan, the main option for reprocessing spent nuclear fuel is based on aqueous process technology. The Rokkasho plant based on such technology is currently operational with a design capacity of 800 tons of spent light water reactor fuel per year, extracting up to 8 tons of plutonium per year for MOX fuel production. Pyroprocessing is considered an option for fast reactors once they have been included in the Japanese energy fleet. A commercial fast reactor is not planned for completion in Japan until about 2050.

In France, advanced aqueous processing technologies are being developed and assessed to support future recycling of Am and Cm or the minor actinides together with U and Pu to fast reactors. Pilot-scale demonstration is planned within the next decade with a goal of industrial deployment to support the deployment of Generation IV fast reactors. France is also in the process of selecting a site for a geological repository for disposal of HLW with a goal to open the repository in 2025. Research related to the study of geological formations and the capacity as a deep geological repository for HLW is being conducted at the Meuse/Haute Marne Underground Research Laboratory located in Bure, France.

Russia is currently reprocessing spent fuel from civilian power reactors as well as spent HEU fuel from naval and other reactors at Mayak's RT-1 aqueous

reprocessing plant. The Experimental-Demonstration Center (EDC), which will be a 100 metric tons/year pilot facility for evaluation of the fuel cycle based on modified PUREX extraction technology, is currently being designed. This facility will also be used to develop other advanced processing technologies for processing used fuel from thermal reactors. The current goal is to support completion of a new aqueous reprocessing facility around 2025. Research is also actively being performed relative to pyroprocessing technologies for the processing of spent fuel from future fast reactors. To this end, the Multipurpose Pyroprocessing Complex (MPC) is being designed at the Research Institute of Atomic Reactors (RIAR) to support molten salt processing development at a capacity of up to 2,500 kg fast reactor used fuel per year.

In South Korea (Republic of Korea), on-site wet storage capacity for spent nuclear fuel at its twenty operating nuclear power plants is rapidly approaching current limits. In December 2008, Atomic Energy Commission of South Korea decided to develop a closed fuel cycle associated with pyroprocessing and sodium fast reactors (SFR) with metallic fuels. A demonstration SFR is planned to operate from 2030 initially with U-Zr metal fuels and later with recycled U/TRU/Zr metal fuels produced from pressurized water reactor (PWR) spent nuclear fuel in a pyroprocessing facility that is planned to be operated from 2025. Pyroprocessing technology research and development continues at Korea Atomic Energy Research Institute with plans to build an engineering scale facility by 2016. Aqueous reprocessing technology is currently not being actively studied and is not considered a candidate for commercialization in the Republic of Korea. The lack of a high-level waste repository is another problem faced by the country due to severely limited land resources. Waste minimization is, thus, a major objective with pyroprocessing technology research and development in South Korea.

Bibliography

1. Cochran RG, Tsoulfanidis N (1993) The nuclear fuel cycle: analysis and management, 2nd ed. American Nuclear Society, Washington, p. 214
2. OECD, IAEA (2008) Uranium 2007: resources, production, and demand. Nuclear Energy Agency, Washington, June 2008
3. Gray LW (1999) From separations to reconstitution – A short history of plutonium in the US and Russia. Lawrence Livermore National Laboratory, UCRL-JC-133802
4. Evans TF, Tomlinson RE (1954) Hot semiworks REDOX studies, Hanford Atomics Products Operations, HW-31767
5. (1951) REDOX technical manual, Hanford Works, HW-18700
6. Hore-Lacy I (2009) Mixed oxide fuel (MOX). World Nuclear Association (Content Partner); Cutler J Cleveland (Topic Editor). In: Cutler J (ed) Encyclopedia of earth. Environmental Information Coalition, National Council for Science and the Environment, Cleveland/Washington, DC
7. Denniss IS, Jeapes AP (2001) Reprocessing irradiated fuel. In: Wilson PD (ed) The nuclear fuel cycle: from ore to wastes. Oxford University Press, Oxford, p 120
8. Poczynajlo A (1988) Studies on reductive back extraction of plutonium in PUREX process. J Radioanal Nucl Chem 125(2):445–465
9. Long JT (1967) Engineering for nuclear fuel reprocessing. Gordon Breach Sci Publ, New York
10. Petitjean V, Fillet C, Boen R, Veyer C, Flament T (2002) Development of vitrification process and glass formulation for nuclear waste conditioning, Proceedings of Waste Management 2002. Tucson, AZ USA
11. Spent Fuel Reprocessing Options (2008) International Atomic Energy Administrations, IAEA-TECDOC-1587, Vienna, Austria 2008
12. Boullis B (2008) Future nuclear fuel cycles: prospects and challenges. In: Bruce Moyer (ed) Solvent Extraction: fundamentals to industrial applications, Proceedings of ISEC 2008 International Solvent Extraction Conference, vol 1., pp 29–42
13. Nash K (2008) Key features of the TALSPEAK and similar trivalent actinide-lanthanide partitioning processes. In: Bruce Moyer (ed) Solvent extraction: fundamentals to industrial applications, Proceedings of ISEC 2008 International Solvent Extraction Conference, vol 1., pp 511–519
14. Laidler J (2008) An overview of spent-fuel processing in the Global Nuclear Energy Partnership. In: Bruce Moyer (ed) Solvent extraction: fundamentals to industrial applications, Proceedings of ISEC 2008 International Solvent Extraction Conference, vol 1., pp 695–701
15. Riddle C, Baker J, Law J, McGrath C, Meikrantz D, Mincher B, Peterman D, Todd T (2005) Development of a novel solvent for the simultaneous separation of strontium and cesium from acidic solutions. Sovent Extr Ion Exch 23(3):449–461
16. Christiansen B, Apostolidis C, Carlos R, Courson O, Glatz JP, Malmbeck R, Pagliosa G, Römer K, Serrano-Purroy D (2004) Advanced aqueous reprocessing in P&T strategies: process demonstrations on genuine fuels and targets. Radiochim Acta 92:475–480
17. Miguirditchian M, Chareyre L, Hérès X, Hill C, Baron P, Masson M (2007) GANEX: adaptation of the DIAMEX-SANEX process for the group actinide separation, Proceedings of GLOBAL 2007 Advanced Nuclear Fuel Cycles and Systems. Bosie, Idaho

18. Wigeland R, Bauer T, Fanning T, Morris E (2006) Separations and transmutation criteria to improve utilization of a geologic repository. Nuclear Technol 154(1):95–106
19. Drain F, Emin JL, Vinoche R, Baron P (2008) COEX process: cross-breeding between innovation and industrial experience. Proceedings from Waste Management 2008, Tucson, AZ
20. Katsuta T, Suzuki T (2009) Japan's spent fuel and plutonium management challenge. Energy Policy doi: 10.1016/j.enpol.2009.05.075
21. Pereira C, Vandegrift G, Regalbuto M, Bakel A, Bowers D, Gelis A, Hebden A, Maggos L (2007) Lab-scale demonstration of the UREX+1a process using spent fuel. Proceedings from Waste Management 2007, Tucson, AZ
22. Nuñez L, Vandegrift G (2000) Evaluation of hydroxamic acid in uranium extraction process: literature review, Argonne National Laboratory, ANL00/35.
23. Colven, TJ Jr, (1956) Mixer-Settler development-operating characteristics of a large-scale mixer-seller. Savannah River Laboratory, DP-140
24. Davidson JK, Shafer AC, Haas WO (1957) Application of Mixer-Settlers to the PUREX Process. In: The Symposium on the Reprocessing of Irradiated Fuels, Book 1. United States Atomic Energy Commission, TID-7534
25. Benedict M, Pigford TH, Levi HW (1981) Nuclear chemical engineering. McGraw-Hill, New York, p 210
26. Milot JF, Duhamet J, Gourdon C, Casamatta G (1990) Simulation of a pneumatically pulsed liquid-liquid extraction column. The Chemical Engineering Journal 45:111–122
27. Sege G, Woodfield FW (1954) Chem Eng Progress 50(8)
28. Geier RG (1954) Application of the Pulse Column to the PUREX Process. USACC, Report TID-7534
29. Richardson GL, Platt AM (1961) Progress in nuclear energy, Series IV, Technology engineering and safety, vol 4. Pergammon Press, New York
30. Leonard RA (1988) Recent advances in centrifugal contactor design. Separation Sci Technol 23:12–13
31. Jubin RT et al (1988) Developments in centrifugal contactor technology. Oak Ridge National Laboratory, ORNL/TM-10768
32. Meikrantz DH, et al (2001) Annular Centrifugal Contactors for Multiple Stage Extraction Processes. Chem Eng Comm 188: 115–127
33. Watts C (1977) Solvent Extraction Equipment Evaluation Study – Part 2. Battelle Northwest Laboratory, BNWL-2186 Pt. 2
34. Bernstein GL et al (1973) A high-capacity annular centrifugal contactor. Nuclear Technol 20
35. Drain F et al (2003) Forty years of experience with liquid-liquid extraction equipment in the nuclear industry. Proceedings from Waste Management Conference 2003, Tucson, AZ
36. Meikrantz DH et al (1996) Rotor sleeve for a centrifugal separator. U.S. Patent # 5,571,070
37. Macaluso LL, Meikrantz DH (1999) Self-cleaning rotor for a centrifugal separator. U.S. Patent # 5,908,376
38. Garn, TG, Meikrantz DH, Law JD (2008) Remote evaluation of a three-stage 5 cm annular centrifugal contactor remote module at the INL. Idaho National Laboratory, INL/EXT-08-13670
39. Meikrantz DH, Garn TG, Law JD, Macaluso LL (2009) Evaluation of a new remote handling design for high throughput annular centrifugal contactors. Idaho National Laboratory INL/EXT-09-16824
40. Chang YI (1989) The integral fast reactor. Nuclear Technol 188(2):129–138
41. Till CE, Chang YI, Hannum WH (1997) The integral fast reactor – an overview. Prog Nuclear Energy 31(1–2):3
42. Benedict RW (1997) EBR-II spent fuel treatment demonstration project. Trans Amer Nuclear Soc 77:75–76
43. Ackerman JP (1991) Chemical basis for pyrochemical reprocessing of nuclear fuel. Industrial Eng Chem Res 30(1):141–145
44. Lee SY et al (2007) A preliminary study on the safeguardability of a Korean Advanced Pyroprocessing Facility (KAPF). Proceedings of Global 2007, Boise, Idaho
45. Lee HS, Hur JM, Ahn DH, Kim IT, Lee JH (2009) Development of Pyroprocessing Technology at KAERI. Proceedings of Global 2009, Paris, France
46. Willit JL, Miller WE, Battles JE (1992) Electrorefining of uranium and plutonium – a literature review. J Nuclear Mater 195(3):229–249
47. Goff KM, Benedict RW (2005) Electrorefining Experience for Pyrochemical Reprocessing of Spent EBR-II Fuel. Proceedings of Global 2005, Tsukuba, Ibaraki (Japan)
48. Karell EJ, Gourishankar KV, Smith JL, Chow LS, Redey L (2001) Separation of actinides from LWR fuel using molten-salt-based electrochemical processes. Nuclear Technology 136:342–353
49. Gourishankar K, Redey L, Williamson M (2002) Electrochemical Reduction of Metal Oxides in Molten Salts. Light Metals 2002, TMS
50. Westphal BR, Keiser DD, Rigg RH, Laug DV (1994) Production of Metal Waste Forms from Spent Fuel Treatment. Proceedings of the DOE Spent Nuclear Fuel Meeting: Challenges and Initiatives, Salt Lake City, Utah; December 13–16, 1994
51. Abraham DP, McDeavitt SM, Park J (1996) Metal waste forms from the electrometallurgical treatment of spent nuclear fuel. Proceedings of the Embedded Topical Meeting on DOE Spent Nuclear Fuel and Fissile Material Management, Reno, Nevada, June 16–20, 1996
52. Pereira C, Hash MC, Lewis MA, Richmann MK, Basco J (1999) Incorporation of Radionuclides from the Electrometallurgical Treatment of Spent Fuel into a Ceramic Waste Form. Materials Research Society Symposium Proceedings 556 (1999), 115–120
53. Ahluwalia RK, Geyer HK, Pereira C, Ackerman JP (1998) Modeling of a zeolite column for the removal of fission products from molten salt. Ind Eng Chem Res 37:145
54. Lexa D, Johnson I (2001) Occlusion and Ion Exchange in the Molten (Lithium Chloride-Potassium Chloride-Alkali Chloride) Salt + Zeolite 4A System with Alkali Metal Chlorides of Sodium, Rubidium, and Cesium. Metallurgical Mater Trans 32B:429
55. Phongikaroon S, Simpson MF (May 2006) two site equilibrium model for ion exchange between multivalent cations and Zeolite-A in a molten salt. AIChE J 52(5):1736–1743

56. Kim EH, Park GI, Cho YZ, Yang HC (2008) A new approach to minimize pyroprocessing waste salts through a series of fission product removal process. Nuclear Technol 162(2):208–218
57. Simpson MF, Sachdev P (2008) Development of electrorefiner waste salt disposal process for the EBR-II spent fuel treatment project. Nuclear Eng Technol 40(3), April 2008
58. Simpson MF, Goff KM, Johnson SG, Bateman KJ, Battisti TJ, Toews KL, Frank SM, Moschetti TL, O'Holleran TP (2001) A description of the ceramic waste form production process from the demonstration phase of the electrometallurgical treatment of EBR-II spent fuel. Nuclear Technol 134:263–277
59. Thomas JL, Mange M, Eyraud C (1971) Molecular Sieve Zeolites-I., R.F. Gould, Ed., Amer Chem Soc (1971), 101:443–449
60. Ebert WE (2005) Testing to evaluate the suitability of waste forms developed for electrometallurgically treated spent sodium-bonded nuclear fuel for disposal in the Yucca Mountain repository. Argonne National Laboratory, ANL-05/43, September 2005

Nuclear Fusion

Thomas J. Dolan
Department of Nuclear, Plasma, and Radiological Engineering, University of Illinois, Urbana, IL, USA

Article Outline

Glossary
Definition of the Subject
Introduction
Fusion Reactions
Magnetic Confinement
Inertial Confinement Fusion (ICF)
Challenges of Plasma Theory
Fusion Technology Issues
Fusion Reactor Design Studies
Fusion–Fission Hybrids
Future Directions
Acknowledgments
Bibliography

Glossary

COE Cost of electricity

EAST Experimental Advanced Superconducting Tokamak

ECRH or ECH Electron cyclotron resonance heating – heats plasma electrons at the natural rotation frequency of electrons in a magnetic field

EFDA European Fusion Development Agreement

FRC Field-reversed configuration

ICRH or ICH Ion cyclotron resonance heating – heats plasma ions at the natural rotation frequency of ions in a magnetic field

ICF Inertial confinement fusion

IFMIF International Fusion Materials Irradiation Facility

ITER International Thermonuclear Experimental Reactor

LHCD or LH Lower hybrid resonance wave heating or current drive – Microwaves injected into the plasma induce a plasma current

Magnetic shear Variation of magnetic field direction from one layer to the next – helps to preserve plasma stability

MHD Magnetohydrodynamic model – treats plasma as a conducting fluid

MTF Magnetized target fusion

NBI Neutral beam injection – injection of high-energy neutral atoms into plasma to heat it, and to help control the plasma current and rotation

OH Ohmic heating – resistive heating caused by a current flowing through the plasma

PF Poloidal magnetic field – The magnetic field component that runs the short way around the torus (donut-shaped vessel). See Fig. 6

Q Fusion energy gain ratio or fusion power gain ratio = (fusion energy)/(input energy) or (fusion power)/(input power)

RF, rf Radiofrequency

SC Superconducting magnet coils – Coils that have zero resistance at very low temperature ($T \sim 4$ K), usually made of Nb_3Sn or NbTi in a copper matrix

TF Toroidal magnetic field – The magnetic field component that runs the long way around the torus (donut-shaped vessel). See Fig. 6

Symbols

Symbol	Units	Meaning
a	m	Minor plasma radius at plasma edge (for circular plasma cross section) (Fig. 4)
B	T	Magnetic field
beta, β	None	Ratio of (plasma pressure)/(magnetic field pressure)

D		Deuterium or deuteron
I_p	MA	Maximum plasma current
L	m	Plasma length
m_e	kg	Electron mass
m_i	kg	Ion mass
n	m^{-3}	Plasma electron density (electrons per m^3)
r	m	Minor plasma radius (Fig. 4)
R, R_0	m	Major plasma radius, and its value at the center of the plasma (Fig. 4)
T	C, K, or keV	Temperature. 1 keV = 11.6 MK (Mega-Kelvin)
T		Tritium or triton
T_e	keV	Electron temperature
T_i	keV	Ion temperature
$v_{\|\|}$	m/s	Particle velocity component along B field direction
$v_\perp$	m/s	Particle velocity component perpendicular to B field

Definition of the Subject

Nuclear Fusion of hydrogen isotopes into helium and heavier elements is the energy source of our sun and the other stars. The goal of nuclear fusion research is to build "miniature suns" on earth that will provide clean energy for electricity generation, production of hydrogen for fuel, and industrial applications.

Introduction

The joining together of two light elements to produce a heavier element is called a "nuclear fusion reaction." For example, a deuteron plus a triton can produce ^{4}He plus a neutron

$$\mathrm{D} + \mathrm{T} \rightarrow {}^4\mathrm{He}\ (3.5\mathrm{MeV}) + n\ (14.1\mathrm{MeV}),$$

where D = deuteron, T = triton, n = neutron, the reaction product kinetic energies are given in parentheses, and 1 MeV = 1.602×10^{-13} J. (Deuterium and tritium are isotopes of hydrogen having one neutron or two neutrons, respectively.)

The positively charged atomic nuclei repel each other, so they must have high speeds in order to approach close enough for reactions to occur, which correspond to high temperatures. Temperatures are usually expressed in keV, where 1 keV = 11.6 MK (Mega-Kelvin).

One liter of water contains 0.034 g of deuterium. When burned in a nuclear fusion reactor, this deuterium could yield as much energy as burning 300 liters of gasoline. Thus, there is enough deuterium in the rivers, lakes, and oceans of the world to provide the world's energy needs for millions of years. The first generation of fusion power plants will use deuterium and tritium fuels. Tritium is unavailable on earth, but it can be bred by neutron absorption in lithium, so deuterium and lithium are the primary fuels. Table 1 lists some potential benefits of such fusion reactors.

Although the fuel for fusion reactors would be cheap, the reactor capital costs would be very high, so the cost of electricity could still be expensive (to be discussed later).

Fusion Reactions

Tritium has negligible abundance on earth, but it can be bred from lithium via the reactions

$$n + {}^6\mathrm{Li} \rightarrow \mathrm{T}(2.73\,\mathrm{MeV}) + 4\mathrm{He}(2.05\,\mathrm{MeV}) \cdots \quad \text{(exothermic} - \text{energy is released)} \tag{1}$$

$$n + {}^7\mathrm{Li} \rightarrow \mathrm{T} + {}^4\mathrm{He} + n - 2.47\,\mathrm{MeV} \cdots \quad \text{(endothermic} - \text{high neutron energy input is required)} \tag{2}$$

The fusion reactions with the highest probabilities at $T < 80$ keV are

$$\mathrm{D} + \mathrm{D} \rightarrow \mathrm{H}(3.02\ \mathrm{MeV}) + \mathrm{T}(1.01\ \mathrm{MeV})$$

$$\mathrm{D} + \mathrm{D} \rightarrow \mathrm{n}(2.45\ \mathrm{MeV}) + {}^3\mathrm{He}(0.82\ \mathrm{MeV}) +$$

$$\mathrm{D} + \mathrm{T} \rightarrow {}^4\mathrm{He}(3.52\ \mathrm{MeV}) + \mathrm{n}(14.1\ \mathrm{MeV})$$

$$\mathrm{D} + {}^3\mathrm{He} \rightarrow {}^4\mathrm{He}(3.66\ \mathrm{MeV}) + \mathrm{H}(14.7\ \mathrm{MeV})$$

where H = proton, D = deuteron, T = triton (distinguish from T meaning temperature), n = neutron, and the energies of the reaction products are shown in parentheses. The TT reaction has a probability similar to those of the DD reactions. The two branches of the DD reaction have roughly equal probabilities. If the

Nuclear Fusion. Table 1 Potential benefits of fusion reactors

• Abundant fuels (deuterium and lithium) – enough for millions of years		
• Cheap fuel		
	D fuel cost $\approx 3 \times 10^{-14}$ \$/J	(assuming D at \$10,000/kg)[a]
	Lithium fuel cost $\approx 10^{-12}$ \$/J	(assuming Li at \$300/kg)[a]
	Coal cost $\approx 2 \times 10^{-9}$ \$/J	(assuming \$150/t)
	Gasoline cost $\approx 2 \times 10^{-8}$ \$/J	(assuming 1.00 \$/l)
• Fuel available to all nations, could reduce conflicts over fossil fuels		
• Fuel has low mass, easy to transport		
• Clean – avoids pollutant emissions, less waste than fission or coal		
• Safe – no supercriticality hazard or meltdown hazard		
• Does not require expensive energy storage		
• No high-level radioactive waste		
• Neutrons from fusion reactors could be used to de-activate high-level radioactive waste from fission reactors or to breed fission reactor fuel		

[a]Assuming a price of \$10,000/kg of D and an energy yield of 7.2 MeV per deuteron in a catalyzed DD fuel cycle (described below), this corresponds to a fuel cost of 3×10^{-14} \$/J. Early fusion reactors will use lithium to breed tritium, because it greatly enhances the fusion reaction rate. In 2008, the average price of lithium carbonate was about 4–6 \$/kg in the USA, so the cost of the lithium itself was about 20–40 \$/kg [1]. Future demand for lithium batteries might escalate this price as high as 300 \$/kg. Assuming 17.6 MeV released from each tritium bred from lithium, this corresponds to a fuel cost of about 10^{-12} \$/J, as shown in the table

^{3}He and T produced by the DD reactions are recycled as fuel in the other two reactions (dashed arrows), the sum of these four reactions yields

$$6\mathrm{D} \rightarrow 2\,{}^4\mathrm{He} + 2\mathrm{H} + 2n + 43.2\ \mathrm{MeV} \tag{7}$$

which is called the "catalyzed DD" fuel cycle, having an average energy yield of 7.2 MeV per deuteron. The only fuel input would be deuterium, avoiding the need to breed tritium from lithium, but the fusion power density would be much lower than from the DT fuel cycle using tritium bred from lithium.

Other reactions, such as H + ^{6}Li and H + ^{11}B, have lower reaction probabilities at $T < 100$ keV, so they are more difficult to use, but they would have the potential advantage of emitting fewer (or no) neutrons, which lead to the production of radioactive materials.

Fusion Reactor Requirements

In order to build a fusion reactor two requirements must be met, heating and confinement:

Heating Requirement The fuel must be heated to $T \sim 15$ keV (170 Million Kelvin) for the D + T reaction, and $T \sim 40$ keV (460 MK) for the D + D fuel cycle. Ions with more positive charge, such as lithium and boron, repel each other more strongly, so higher temperatures would be required to use them as fuels. (At such high temperatures, hydrogen is in the *plasma state* [a sea of positive ions and negative electrons]. The five states of matter are solid, liquid, gas, plasma, and "dark matter." Other familiar forms of plasmas [some of them only partially ionized gases] include lightning, welding arcs, hot flames, and fluorescent lights.)

Table 2 lists some plasma heating methods.

Confinement Requirement The fuel must be confined long enough for part of it to "burn" (to fuse) before it is lost or cools off.

The heating and confinement requirements for a DT reactor may be expressed in the "triple product" parameter

$$n\tau_{\mathrm{E}}T > 4 \times 10^{21}\,\mathrm{m}^{-3}\mathrm{s\ keV} \tag{8}$$

where n is fuel ion density (ions/m^3), τ_{E} is their energy confinement time (s), and T is their temperature (keV). (The required product of density and confinement time is often referred to as the "Lawson criterion.") The energy gain ratio is defined to be

$$Q = (\text{fusion energy per pulse})/(\text{input energy per pulse})$$

or

$$Q = (\text{fusion power})/(\text{input power})$$

if the reactor operates steady state.

Nuclear Fusion. Table 2 Plasma heating methods

Ohmic heating	OH	Ohmic heating power density $P_{oh} = \eta J^2$ (W/m^3), where J = current density (A/m^2) and η = plasma resistivity (ohm-m). At high temperatures η is very low, and ohmic heating is ineffective.
Neutral beam injection	NBI	Ions accelerated to high energies (typically 0.04–1 MeV) pass through a gas cell where some of them are neutralized. The neutral atoms can then penetrate across the magnetic field into the plasma, where they become ionized and trapped, depositing their energy in the plasma.
Ion cyclotron resonance heating	ICRH	Radio waves are injected into the plasma at approximately the frequency of the ion spiral motion around the magnetic field lines, accelerating their motion. Frequency $f = eB/2\pi m_i$ (Hz), where e = electronic charge, B = magnetic field, m_i = ion mass.
Electron cyclotron resonance heating	ECRH	Microwaves injected into the plasma with near the frequency of electron spiral motion around the magnetic field lines. $f = eB/2\pi m_e$ (Hz), where m_e = electron mass.
Lower hybrid wave heating	LH	Waves are injected at the lower hybrid frequency, which is between the ECRH and ICRH frequencies.
Compression		If the plasma is compressed, such as by increasing the magnetic field or by squeezing a metallic shell around the plasma, its temperature and pressure increase.

For the DT fusion reaction Q is given approximately by the equation [2]

$$Q \approx 5(n\tau_E T)/[5 \times 10^{21} - n\tau_E T] \quad (9)$$

which is illustrated in Fig. 1.

Thus, to attain $Q > 10$, values of $n\tau_E T \sim 4 \times 10^{21}$ m^{-3} s-keV are needed. (This equation and graph are only approximate, varying with the type of plasma confinement system.)

When confinement is very good, the alpha particles (^{4}He ions) produced by fusion reactions can deposit enough energy in the plasma to sustain its temperature. Then the input power for heating may be turned off. (Some input power may still be needed to drive a plasma electrical current.) This self-sustainment condition, called "ignition," corresponds to the right side of Fig. 1, where Q reaches very high values. The precise value of the triple product that produces ignition varies from one type of confinement system to another and with plasma impurity content.

For DD reactions, higher values of $n\tau_E$T are required, so the DT reaction will probably be used in the first generation fusion power plants.

Everything in nature tends toward a state of *thermodynamic equilibrium*, in which the temperatures of various bodies are uniform and equal to each other. Since we want to keep the chamber wall temperature below about 1,200 K and the fuel ion temperature

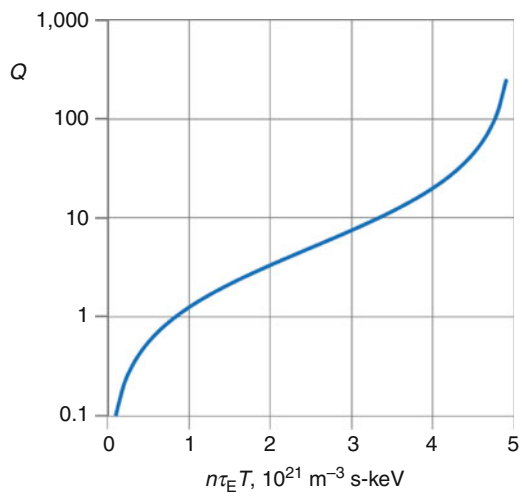

Nuclear Fusion. Figure 1
Energy gain ratio Q versus triple product

$>10^8$ K, the plasma confinement system must retard the establishment of thermodynamic equilibrium. Coulomb collisions and plasma instabilities bring the plasma closer to thermodynamic equilibrium, so avoiding it is a difficult problem.

Plasma Confinement Methods

Plasma confinement methods are listed in Table 3.

Nuclear Fusion. Table 3 Plasma confinement methods

Solid walls	Low-temperature plasmas, such as fluorescent lights, may be contained by glass or metal tubes. Hot plasma confinement in magnetic fields may be augmented by solid walls for brief periods of time, but prolonged contact cools the plasma rapidly by heat conduction and may overheat the wall.
Gravity	Although stellar plasmas, such as the sun, are confined by gravity, the mass of a laboratory plasma is far too small for self-gravitational attraction to be significant. (The mass density and temperature at the center of the sun are about 150 g/cm^3 and 1.3 keV).
Inertia	If a DT fuel pellet is quickly compressed to ultrahigh densities, significant fusion burn can occur before the compressed pellet expands. The inertia of the pellet limits the expansion rate of the internal plasma. At $n = 10^{30}$ m^{-3}, and $T = 10$ keV, a confinement time $\tau_E \sim 4 \times 10^{-10}$ s would yield a triple product $n\tau_E T \sim 4 \times 10^{21}$ m^{-3} s-keV. The compression may be produced by laser beams or by particle beams.
Radiofrequency waves	Radiofrequency waves and microwaves can confine low-pressure plasma, but enormous power inputs would be required to confine high-pressure plasmas. These waves can augment magnetic confinement.
Electrostatic fields	Electrostatic potential peaks can be established with high-voltage grids or by creating local regions of higher plasma density. Positive peaks can inhibit ion motion, and negative peaks can inhibit electron motion. Purely electrostatic plasma confinement has only succeeded in confining low-pressure plasmas, but such electrostatic potential peaks can be used to augment magnetic confinement.
Magnetic fields	Confinement by strong magnetic fields is the most promising means for prolonged containment of high-pressure plasmas. It is based on the fact that ions and electrons cannot travel across a magnetic field easily. Instead, they tend to travel in helical paths along the field lines.

Magnetic Confinement

Magnetic fields may be either "open" (Figs. 2 and 3) or "closed" (Fig. 4).

A plasma ion starting out at the center with velocity components $v_{\|o}$ parallel to magnetic field and $v_{\perp o}$ perpendicular to the magnetic field would experience a higher magnetic field as it moves toward the magnet coil. In the higher field, its rotational velocity component $v_\perp$ would increase, and its parallel velocity component $v_\|$ could decrease gradually to zero, where it would be reflected back toward the center (hence, the name "magnetic mirror"). The ion would oscillate back and forth between points a and b, restrained by a magnetic field gradient force

$$F = -(m_i v_\perp{}^2/2B)\nabla B \tag{10}$$

Electrons would also be confined in the same way. Although electrons and ions are reflected by high magnetic fields, those with high velocities $v_{\|o}$ along the field

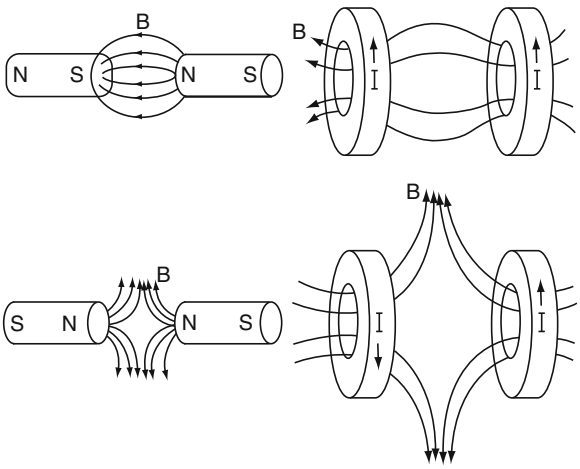

Nuclear Fusion. Figure 2
Simple magnetic "mirror" fields **B** (*top*) and "spindle cusp" fields (*bottom*) produced by bar magnets (*left side*) or by a pair of circular magnet coils carrying currents I (*right side*). Plasma could be confined in the central regions

lines will escape, and confinement is limited by the time it takes for Coulomb collisions to increase their parallel velocities. The end loss problem can be eliminated by using a closed magnetic field, Fig. 4.

It might appear that electrons and ions could be confined forever as they spiral along the closed magnetic field lines, but the magnetic field gradient and curvature cause a drift velocity across the magnetic field. This drift can be compensated by twisting the magnetic field lines, producing a helical closed magnetic field, Fig. 5.

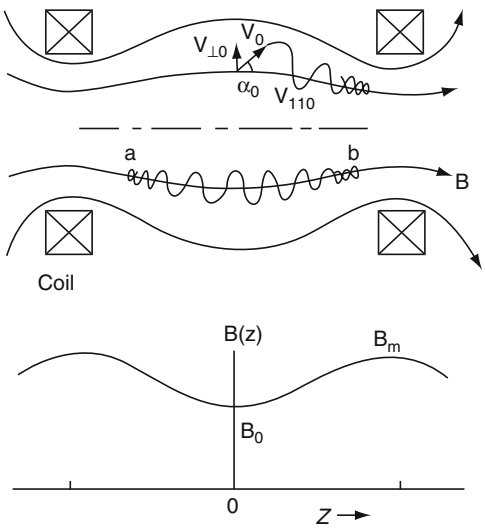

Nuclear Fusion. Figure 3
A simple magnetic mirror (*top*) and axial variation of magnetic field strength (*bottom*)

This twisting of the magnetic field, called "rotational transform," may be produced by inducing a plasma electrical current in the toroidal direction (a "tokamak"), or by using specially shaped magnetic field coils (a "stellarator").

There are many processes that cause plasma energy loss, Table 4.

In what follows, we describe tokamaks, stellarators, compact toroids, and open magnetic confinement systems, then inertial confinement systems, other fusion concepts, plasma theory issues, fusion technology issues, and fusion reactor design studies.

Tokamaks

The name "tokamak" is an acronym for the Russian "**т**ороидальная **к**амера с **м**агнитными катушками"

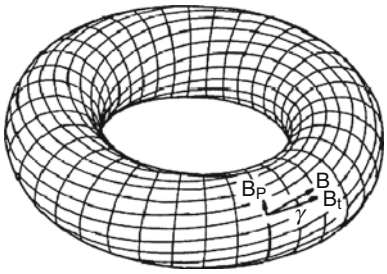

Nuclear Fusion. Figure 5
A helical magnetic field. The field lines B have components B_t in the "toroidal" direction (the long way around the torus) and B_p in the "poloidal" direction (the short way around the torus). Twisting the magnetic field compensates for the tendency of particles to drift across the magnetic field

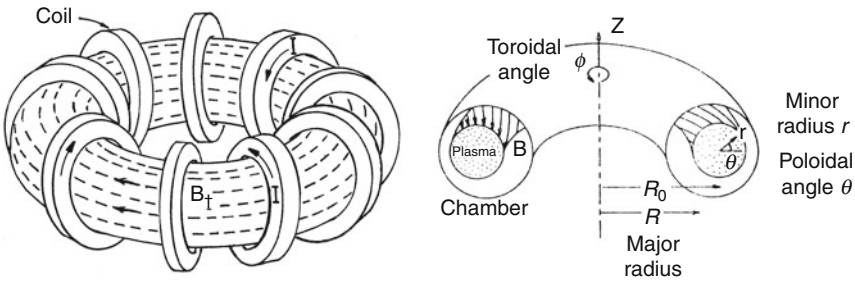

Nuclear Fusion. Figure 4
"Closed" (toroidal) magnetic field lines B_t (*dashed lines*) generated by circular magnet coils carrying currents I, and the definitions of "major radius *R*" and "minor radius *r*." The value of *r* at the plasma edge is called "a", and the value of *R* at the plasma center is called "R_o"

N

Nuclear Fusion. Table 4 Plasma energy loss mechanisms

1. Particle and energy *loss along magnetic field lines* (open magnetic systems) In simple magnetic mirrors, the loss time is roughly the time for collisions to increase the ion velocity along the field lines. If electrostatic potential barriers are used, then the loss time is roughly the time for collisions to increase the particle energies over the barriers.
2. Particle *driftvelocities* across the magnetic field, driven by magnetic field gradient and curvature and by an electric field.
3. *Magnetohydrodynamic (MHD) plasma instabilities*, whereby the plasma boundary, affected by gradients of pressure, current density, and magnetic field, pushes through the magnetic field toward the chamber wall.
4. *Radiation losses* from line radiation, bremsstrahlung radiation (radiation from electrons during deceleration by collisions), cyclotron radiation, and recombination radiation. Radiation losses can be high when the plasma contains many impurity ions (such as iron), when the temperature is very high, or when the magnetic field is very strong (cyclotron radiation).
5. *Energy transport* across the magnetic field by heat conduction and convection.
6. Interaction of electrons and ions with plasma waves can enhance energy transport. Such "*microinstabilities*" have required many decades of plasma theory, experiment, and computer simulation to be understood.
7. Ion energy loss by *charge exchange*. (A hot ion grabs an electron from an atom, becomes neutralized, and is no longer confined by the magnetic field, which does not confine neutral atoms.)

(**to**roidal'naya **ka**mera s **ma**gnitnymi **k**atushkami – toroidal chamber with magnetic coils). Figure 6 shows the main components of a tokamak.

Pulsing a current in the primary winding of the transformer induces a high current in the plasma, which generates the poloidal magnetic field. (Although this figure shows an iron core transformer, most modern tokamaks use air core transformers.) When the transformer saturates, the current gradually dies away. A "current drive" system, such as electromagnetic waves or neutral beam injection, is needed to sustain the current for long periods. Although Fig. 6 shows a plasma with circular cross section, most modern tokamaks have noncircular cross sections, in order to facilitate higher beta values (ratios of plasma pressure to magnetic field pressure).

Over 200 tokamaks have been built worldwide. Table 5 shows the parameters of a few of them.

Figure 7 shows the interior of the European Fusion Development Agreement (EFDA) Joint European Torus (JET), which has a noncircular cross section.

The walls are lined with refractory tiles to withstand high heat fluxes. Using DT fuel JET briefly generated 16 MW of heat from fusion reactions. JET has also demonstrated the feasibility of using beryllium tiles on the walls.

The National Spherical Torus Experiment (NSTX) and Mega Ampere Spherical Torus (MAST) are smaller, with very low aspect ratios $R_o/a \sim 1.4$, which facilitates high values of β (the ratio of plasma pressure to magnetic field pressure). They are called "spherical tokamaks."

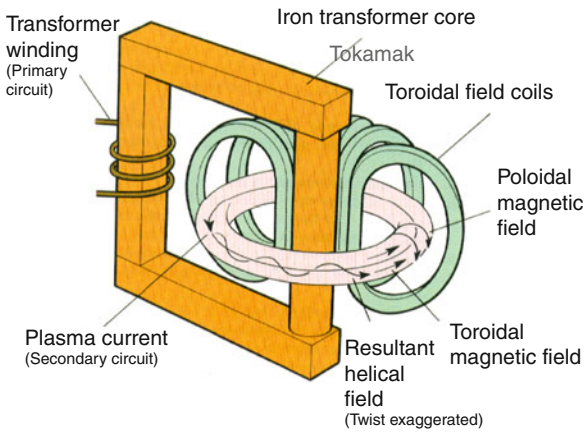

Nuclear Fusion. Figure 6
Simplified diagram of a tokamak with circular plasma cross section (Courtesy of Culham Centre for Fusion Energy, UK)

In order to attain higher triple product values, larger experiments are needed. The International Thermonuclear Experimental Reactor (ITER) Joint Project began construction in 2008 with an estimated cost of about 5 billion Euro. It is to begin operation in about

Nuclear Fusion. Table 5 Parameters of some tokamaks. SC means superconducting coils. Parameters of future experiments are planned values [3]

Name	Country	Years	R_0/a, m/m	B, T	I_p, MA	ECRH + ICRH + LH, MW	NBI, MW	Remarks
TFTR	USA	1982–1997	2.4/0.8	6	3	11	39	Circular cross section plasma; achieved 10 MW fusion power for fraction of a second
DIII-D	USA	1986–	1.66/0.67	2.2	3	11	20	Beta = 12%, graphite walls, plasma shaping
Tore Supra	France	1988–	2.25/0.7	4.5 SC	2	16	1.7	Pulses lasting many minutes
T-15	Russia	1988–1995, 2009–	2.43/0.42	3.5 SC	1	11	9	5 s pulses
JT 60U	Japan	1991–2010	3.4/1.0	4.2	5	24	50	Record fusion triple product, would yield $Q = 1.2$ if DT fuel were used
JET	UK	1992–	3/1.25	4	6	29	24	Generated 22 MJ of DT fusion energy in 4 s. Has used Be wall tiles
MAST	UK	1999–	0.85/0.6	0.5	1.4	1	4	Spherical tokamak
NSTX	USA	1999–	0.85/0.6	0.6	1.4	3	7	Spherical tokamak
EAST	China	2006–	1.75/0.43	5 SC	0.5	8		First fully superconducting tokamak with noncircular cross section
KSTAR	Korea	2008–	1.8/0.5	3.5 SC	2	13	14	Fully superconducting coils
SST-1	India	2012–	1.1/0.2	3 SC	0.2	3	0.8	1,000 s pulses
JT 60 SA	Japan	2014–	3.16/1.02	2.7 SC	5.5	7	34	100 s pulses, startup 2014
ITER	France	2019–	6.2/2.0	5.3 SC	15	40	33	Startup 2019. 400 MW, 400 s pulses in 2023

2019, reaching full power operation in about 2027. Figure 8 shows how the experimentally attained values of the triple product have increased over the years of fusion research.

ITER should demonstrate a power gain ratio $Q > 10$ for hundreds of seconds, and $Q > 5$ for longer periods. The next step planned after ITER will be a technology demonstration fusion power plant called "DEMO" that generates electricity for commercial use.

Stellarators

Stellarators (including "heliotrons" and "torsatrons") produce rotational transform by shaping the magnet coils, Figs. 9 and 10.

The Large Helical Device at the National Institute for Fusion Sciences in Japan, Fig. 11, is a "heliotron" (torsatron) with two helical coils.

Figure 12 shows the Wendelstein 7-X experiment, which uses modular coils to achieve a magnetic field shape suitable for plasma confinement.

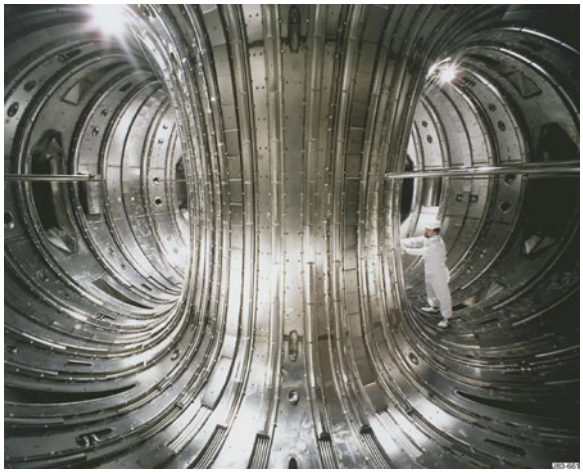

Nuclear Fusion. Figure 7
The interior of the Joint European Torus (JET) (Courtesy of Culham Centre for Fusion Energy, UK)

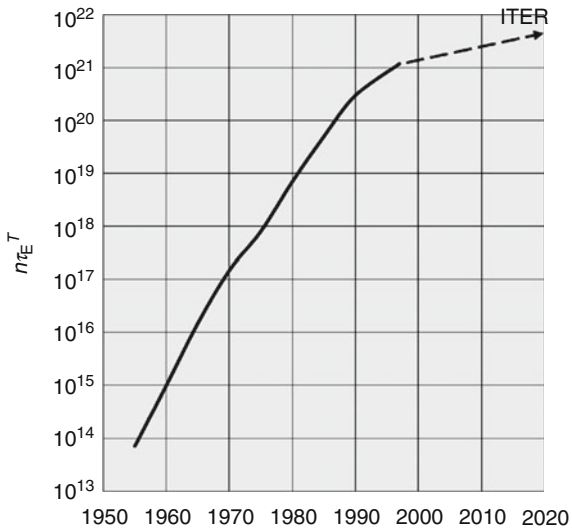

Nuclear Fusion. Figure 8
Triple product $n\tau_E T$ (m^{-3} s-keV) attained by tokamak experiments versus year. The dashed arrow points to planned ITER values [4]

Table 6 shows some parameters of these stellarators.

Since stellarators do not require a strong plasma current, they have the following advantages over tokamaks:

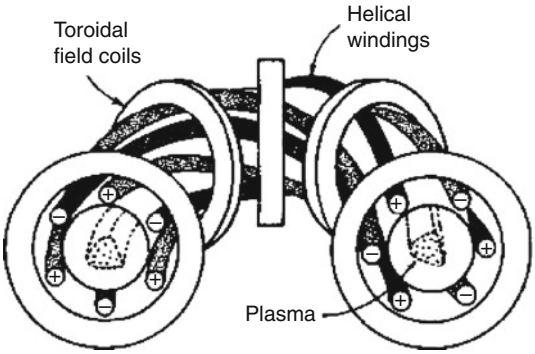

Nuclear Fusion. Figure 9
Magnet coils of a stellarator with three pairs of helical windings, which have currents in alternating directions (indicated by + and – signs). Other numbers of helical windings are also possible

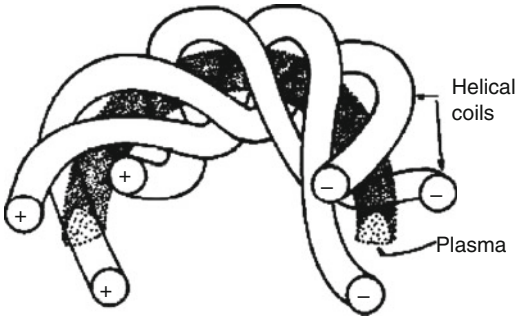

Nuclear Fusion. Figure 10
A torsatron with three helical coils and no toroidal field coils

- No strong disruptions of the plasma.
- Current drive is not required, so the input power is lower, and the energy gain ratio Q can be higher.
- Potentially less plasma turbulence and better energy confinement.

One the other hand, the coils of stellarators are difficult to wind, join, support, and align, and space for energy recovery blankets is limited.

Reversed Field Pinch (RFP)

A reversed field pinch is a toroidal plasma with a relatively weak toroidal field and a strong plasma current. The plasma currents evolve into a stable

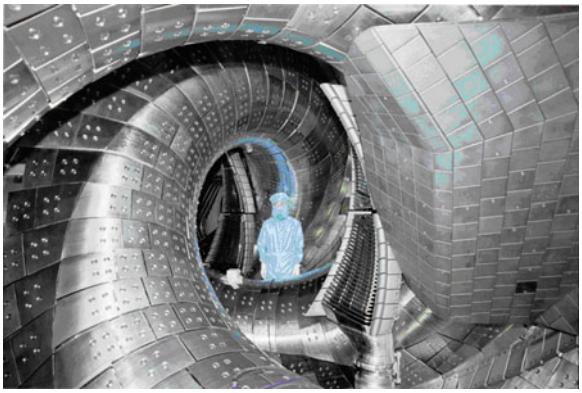

Nuclear Fusion. Figure 11
The two helical superconducting coils inside the Large Helical Device, operating since 1998 (Courtesy of the National Institute for Fusion Science, Japan)

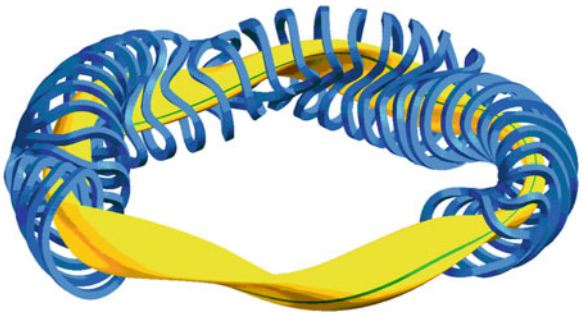

Nuclear Fusion. Figure 12
The coils (*blue*) of the Wendelstein 7-X experiment in Greifswald, Germany, and the resulting plasma shape (*orange*), expected to begin operation in 2014 (Courtesy of the Max-Planck-Institut fuer Plasmaforschung, Greifswald, Germany)

configuration in which the direction of the toroidal component of the magnetic field at the plasma edge is in the opposite direction from the internal toroidal field, Fig. 13.

This strong variation of magnetic field direction with radius, called magnetic shear, helps preserve plasma stability. This type of experiment has been operated in Italy, Japan, the UK, the USA, and elsewhere. It offers the potential of a compact reactor with a simpler toroidal field system than tokamaks, but plasma energy confinement times may be shorter, and efficient current drive to sustain the RFP is difficult to achieve.

Nuclear Fusion. Table 6 Main parameters of the LHD and Wendelstein 7-X experiments. The LHD values shown here were not all attained simultaneously. The Wendelstein 7-X parameters are planned values

Parameter	Units	LHD	Wendelstein 7-X
Startup		1998	2014
Major radius R	m	3.7	5.5
Approximate minor radius a	m	0.64	0.53
Magnetic field on axis	T	2.8	3
Heating power	MW	20	15
Average plasma density n	m^{-3}	4×10^{19}	$\sim 10^{20}$
Ion temperature	keV	13.6	(Several)
Electron temperature	keV	10	(Several)
Energy confinement time	s	0.36	0.15
Beta	%	5	

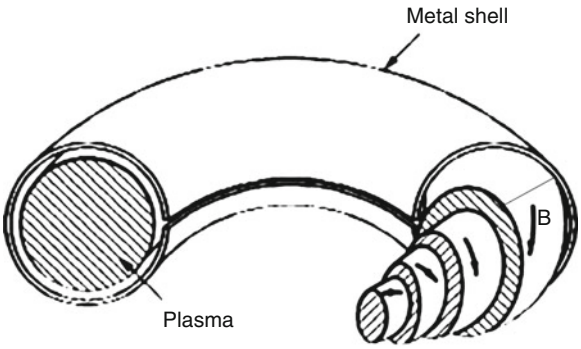

Nuclear Fusion. Figure 13
A reversed field pinch, showing how the direction of the magnetic field varies with radius [5]

Compact Toroids

Figure 14 compares a field-reversed configuration (FRC) and a spheromak.

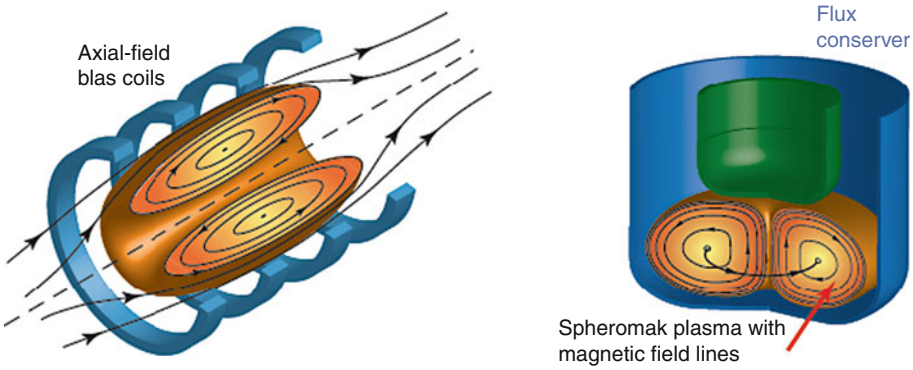

Nuclear Fusion. Figure 14
A field-reversed configuration (*left*) and a spheromak. Neither has any structure on the axis of the torus [6]

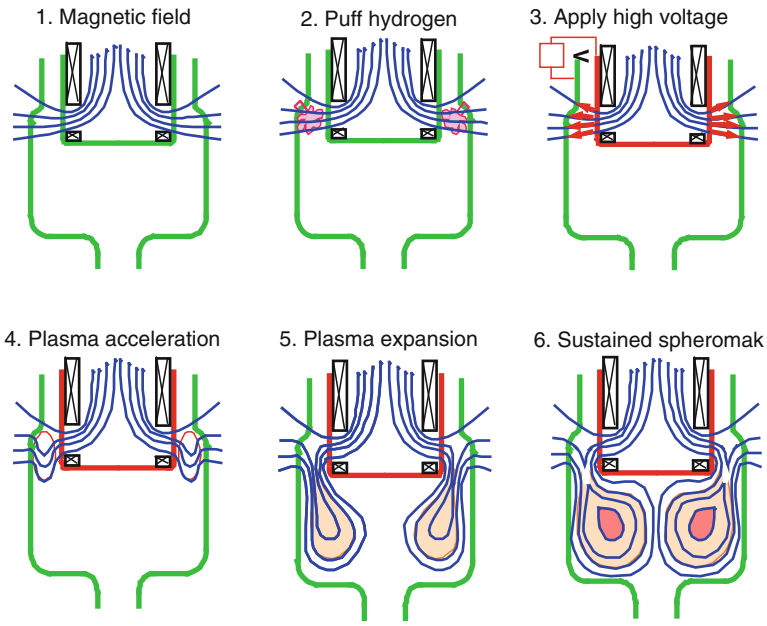

Nuclear Fusion. Figure 15
Formation of a spheromak by coaxial plasma gun injection into a flux conserving chamber (Courtesy of Lawrence Livermore National Laboratory)

The FRC has only poloidal magnetic field components, with zero (or nearly zero) toroidal field. The spheromak is a naturally stable configuration having both toroidal and poloidal magnetic field components. Figure 15 illustrates one way of generating a spheromak, by using a coaxial plasma gun.

In step (1). A coil (black) generates a magnetic field (blue). (2) A puff of hydrogen is admitted into the vacuum (pink cloud). (3) A high voltage is applied between the inner and outer cylinders, ionizing the gas. (4) The plasma current flowing interacts with the magnetic field to produce a thrust that accelerates the plasma downward. (5) The plasma (pink) expands into the metal chamber (green). (6) Image currents in the walls create an opposing magnetic field that retards the plasma penetration into the wall. This is

called a "sustained spheromak" configuration with quasi-closed field lines similar to tokamaks. The plasma has both toroidal and poloidal magnetic fields without the need for toroidal field coils. It is therefore simpler than tokamaks, and potentially less expensive. Some parameters of the Sustained Spheromak Physics Experiment (SSPX) are shown in Table 7.

Spheromak experiments generally last only a few milliseconds, with electron temperatures less than 1 keV. Larger spheromak experiments with more heating auxiliary power and longer duration would be needed to test this concept adequately.

Nuclear Fusion. Table 7 Typical SSPX parameters (SSPX is now decommissioned) (Courtesy of Lawrence Livermore National Laboratory)

Flux conserver radius and height	0.5 m × 0.5 m
Radius of magnetic axis	0.31 m
Plasma minor radius	0.17 m
Peak discharge current	0.45 MA
Toroidal current	0.6 MA
Peak toroidal field	0.6 T
Edge poloidal field	0.35 T
Plasma duration	4.5 ms
Plasma density	5×10^{19} m^{-3}
Peak electron temperature	0.35 keV

Field-Reversed Configuration (FRC) A field-reversed configuration may be formed by a theta pinch coil, as shown in Fig. 16.

A theta pinch coil is usually a one-turn coil with a sudden current flowing in the theta (azimuthal) direction. The coil current may rise to its peak value in microseconds, squeezing the plasma, hence the name "pinch." With careful programming of the coil current, the plasma may form into an elongated torus with the internal magnetic field in the opposite direction from the external magnetic field (indicated by the small arrows in Fig. 16), hence the name "field reversed." FRC plasmas can also be generated and sustained by rotating magnetic fields. They appear to be stable, in spite of their weak or zero toroidal magnetic fields. After formation, an FRC plasma may be moved axially to another chamber, where it can be compressed by a converging magnetic field or by an imploding metallic liner [7]. FRC experiments have been conducted at Los Alamos National Laboratory, University of Tokyo, Osaka University, University of Washington, and TRINITI Laboratory (Troitsk, Russia).

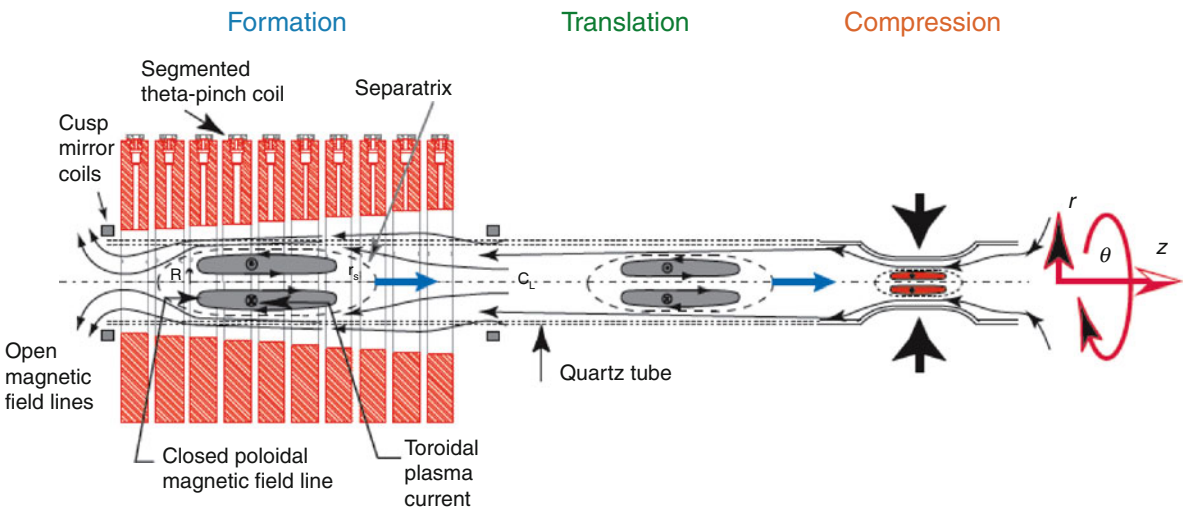

Nuclear Fusion. Figure 16
Formation of an FRC by a theta pinch coil, translation to another chamber, and compression by a metallic liner (Courtesy of Los Alamos National Laboratory)

Magnetized Target Fusion (MTF) MTF target plasma parameters could be $n \sim 10^{23}$ m^{-3}, $T \sim 0.3$ keV, $B \sim 3$ T, and duration $t \sim 10$ μs before compression. The target plasma could be moved axially into another chamber (Fig. 16), where a metallic liner would compress it to thermonuclear temperature ($T \sim 10$ keV). Intense DT fusion burn could occur until the configuration disassembled, and it might be possible to achieve energy gain ratios $Q > 5$ in a less expensive device than tokamaks or stellarators.

Pulsed, High-Density Fusion A similar concept would accelerate an FRC axially to very high velocity, then inject it into a converging magnetic field, which would compress the plasma up to thermonuclear burn conditions. It would flow through the burn chamber, then continue on into an expansion and exhaust chamber [8].

Open Magnetic Confinement Systems

Open magnetic confinement systems can avoid MHD instabilities if the magnetic field pressure is lower in the plasma confinement region than around the outside, a so-called "minimum-B" confinement system.

Tandem Mirror Due to rapid particle loss along the magnetic field lines, a simple magnetic mirror can only achieve a power gain ratio $Q \sim 1$, which is inadequate for a power plant. This loss can be reduced by creating an electrostatic potential variation along the magnetic field with hills and valleys, as illustrated in Fig. 17.

The positive peaks ϕ_c confine ions in the central cell, and the negative wells ϕ_b confine electrons. The plasma density, temperature, and electrostatic potential in tandem mirrors can be controlled by injection of neutral atom beams, by electron cyclotron resonance heating (ECRH), and by radiofrequency (RF) wave heating at selected axial locations. Such electrostatic potential control could make it possible to reduce the required length of a power plant with $Q \sim 10$ from kilometers to less than 200 m. There have been tandem mirror experiments in Japan, Russia, Korea, and the USA. The Gamma-10 experiment in Japan with length $L = 6$ m, $a = 0.36$ m, and central cell $B = 0.41$ T has confined plasma with $n \sim 10^{18}$ m^{-3}, $T_e \sim 0.3$ keV, $T_i \sim 1$ keV. It has achieved values of $\phi_c > 2$ kV [9].

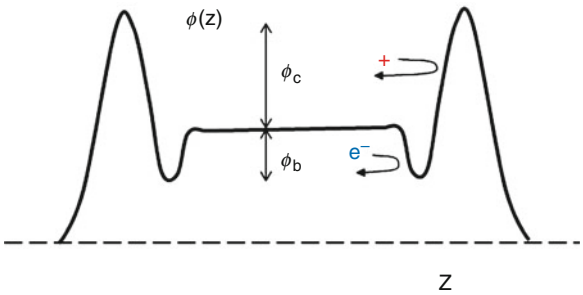

Nuclear Fusion. Figure 17
Electrostatic potential versus axial position in a tandem mirror

Electrostatically Plugged Cusps High-voltage electrodes can also produce electrostatic potential hills and valleys along magnetic field lines, similar to those of a tandem mirror. The electrons are confined by the magnetic field and the negative electrodes, and the ions are confined in a negative electrostatic potential well created by the electrons' negative charge. For example, the Jupiter-IIM electrostatically plugged magnetic cusp experiment in the Ukraine demonstrated low diffusion rates of plasma across the magnetic field [10].

Rotating Plasmas Rotating plasmas can be formed by putting high-voltage electrodes in the ends of a magnetic mirror to create a strong radial electric field, which causes the plasma to rotate azimuthally at high speed. This rotation can accelerate ions up to keV energies, and the angular momentum reduces end losses from the magnetic mirror. Figure 18 shows the Maryland Centrifugal Experiment

This experiment has a central $B \sim 0.3$ T, $a \sim 0.2$ m, $L \sim 1.4$ m, $n \sim 3 \times 10^{20}$ m^{-3}, $T \sim 20$–60 eV, applied voltage 5–20 kV, pulse length 1–10 ms, and has achieved rotational speeds of 100 km/s.

Other Concepts

Plasma Focus The plasma focus uses a coaxial plasma gun to accelerate a blob of plasma to high velocities, as illustrated in Fig. 19.

At time t_1, high voltage breakdown along the insulator forms a plasma that is accelerated axially by the $J \times B$ force. At t_2 the plasma reaches the end of the gun, and at t_3 electromagnetic forces cause it to collapse into a high-density blob, causing a brief burst of fusion

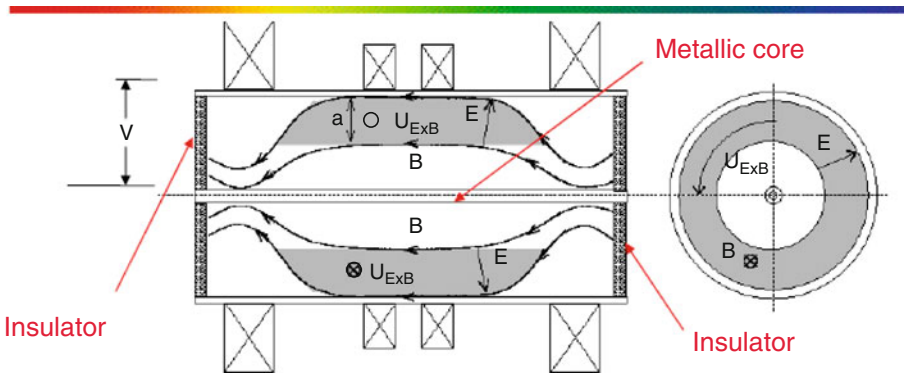

Nuclear Fusion. Figure 18
The Maryland centrifugal experiment (Courtesy of the University of Maryland)

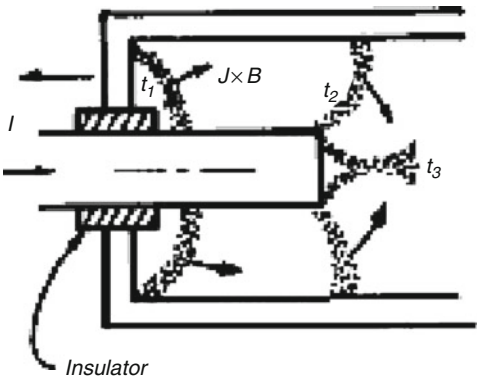

Nuclear Fusion. Figure 19
Plasma acceleration by a coaxial gun

reactions before the plasma expands and cools. At low currents (<0.3 MA), the fusion yield increases proportional to I^4, where I is the plasma current, but this favorable scaling saturates at high currents, and economical power production appears to be unlikely at reasonably attainable currents ($\sim$10 MA). Plasma focus devices are useful as sources of neutrons and x-rays, and many have been built around the world.

Levitated Dipole Experiment The Levitated Dipole Experiment magnetically levitates a superconducting coil ring, Fig. 20.

The resulting magnetic surfaces are good for plasma confinement. This experiment has a low-density background plasma plus a hot electron plasma produced by absorption of microwaves. The superconducting ring gradually absorbs heat, so it must be periodically shut down and recooled. If this scheme were used for a fusion reactor, heating and radiation damage to the ring would be significant issues.

Inertial Electrostatic Confinement (IEC) Plasma may also be confined by concentric spherical grids, Fig. 21.

With tens of kilovolts applied and deuterium plasma, small devices of this type have produced DD fusion reaction neutron emission rates $\sim 10^7$ neutrons/s. In a high-power fusion reactor, however, the electrodes would tend to melt. IEC devices are useful as sources of neutrons and energetic charged particles.

RF Plasma Confinement Potential wells in standing radiofrequency (rf) fields can contain low-pressure plasmas effectively, but for high-pressure plasmas of a fusion reactor excessively high rf power levels would be required. Rf fields have been used to reduce end losses from open magnetic confinement systems, as in the RFC-XX experiment in Japan. High-voltage rf electrodes accelerated ions to higher rotational energies, which inhibited their ability to escape through the point cusps and line cusps.

Polywell The Polywell concept has a spherical array of six or more point cusps, with electron injection creating a negative potential well that focuses ions into the center of the sphere. It is a form of electrostatic plugging of a cusped magnetic field. Good ion focusing to small radii would be required to achieve satisfactory fusion power density.

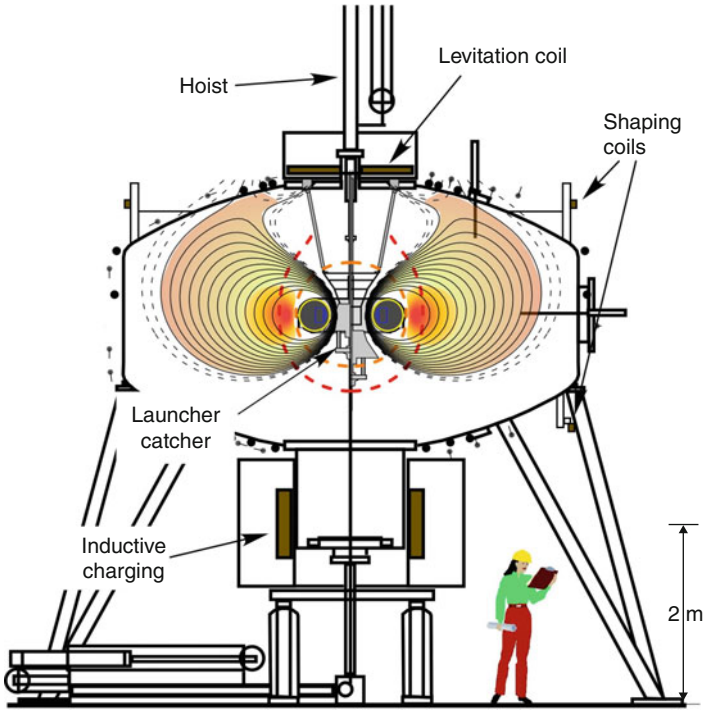

Nuclear Fusion. Figure 20
The Levitated Dipole Experiment, showing the magnetic surfaces surrounding the levitated coil. The dotted curves indicate the resonant surfaces for ECRH with frequencies 2.45 and 6.4 GHz (Courtesy of Columbia University and Massachusetts Institute of Technology [11]

Muon-Catalyzed Fusion Negative mu mesons (muons) produced by accelerators can bind to deuterons to form atoms. Since the muon is 207 times heavier than an electron, the radius of its orbit is 207 times smaller. This small atomic size allows the shrunken deuterium atom to approach very close to another deuteron or triton, close enough for a nuclear fusion reaction to occur. After a fusion reaction occurs the muon is released, and it can bind to another deuteron (or triton) and catalyze a second fusion reaction. The muon may also be captured by other nuclei, such as by an alpha particle (^{4}He nucleus), which stops the reaction chain. This "helium sticking" problem has limited the number of experimentally attained fusion reactions to about 100 per muon, which is not enough to achieve an energy gain, since about 6 GeV energy are required to generate each muon by an accelerator, and the DT fusion reaction yields only 17.6 MeV.

Cold Fusion Evidence for low-energy nuclear reactions (LENR) has been reported from many types of experiments: electrolysis of water, gas discharges, gas diffusion through thin films, electron beam impact, exploding wires, and laser irradiation. The evidence includes apparent heat generation, x-rays, and transmutations. Such phenomena were once called "cold fusion" after the 1989 hypothesis by Fleischmann and Pons that the energy generation by their electrolysis cell was a result of nuclear fusion reactions [12]. Many theories have been proposed to explain the LENR phenomena, but so far, no theory has gained widespread acceptance.

Inertial Confinement Fusion (ICF)

Target Compression

Figure 22 shows the general idea of an inertial confinement fusion (ICF) power plant.

The goal is to ignite frequent small explosions in a blast chamber. The target injector shoots fuel capsules ("targets") into the chamber several times per second.

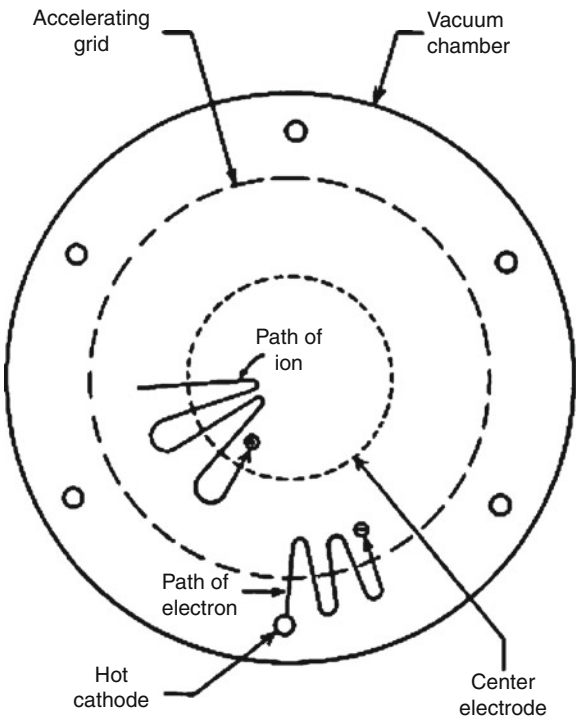

Nuclear Fusion. Figure 21
Plasma confinement by spherical grids. In this configuration, the accelerating grid is positive, and the center electrode is negative

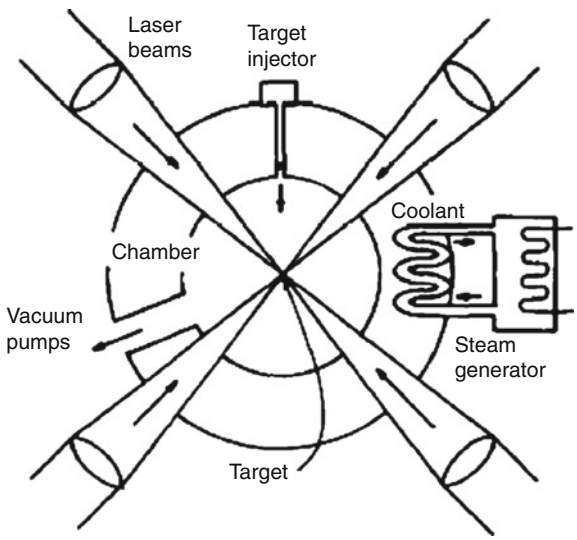

Nuclear Fusion. Figure 22
The general idea of a laser ICF power plant

When the target reaches the center of the chamber laser beams ablate its surface, which causes an inwards force that compresses the target to ultrahigh density. Then a high-power laser pulse raises part of the compressed target to ignition temperature, and a thermonuclear burn wave causes a miniature explosion. The explosion energy is deposited in the chamber walls and absorbed in a blanket and coolant, which could be liquid metal, molten salt, or helium gas. The hot coolant boils water in a steam generator, and the steam drives a turbine to generate electricity. (Helium gas coolant could drive a gas turbine directly without needing to make steam.) Instead of using laser beams, the target compression could also be done with heavy ion beams or exploding wires and x-rays. Figure 23 shows the steps of target compression and burn.

The laser beam heats the plasma surrounding the target shell (Step a of Fig. 23). The plasma ablates the target surface away, causing an inward pressure similar to the forward thrust of a rocket caused by rearward expulsion of burning fuel (Step b). The heating to ignition (Step c) may be done by a shock wave to the center of the volume (Step c) or by a sudden PetaWatt laser beam impact on the outside ("fast ignition"), which requires less heating energy. Then a thermonuclear burn wave can spread to surrounding fuel (Step d).

The National Ignition Facility at Lawrence Livermore National Laboratory, California; the Laser MegaJoule facility in France; and the GEKKO-XII in Japan are all large laser facilities approaching ignition of targets. Figure 24 shows the National Ignition Facility (NIF) in Livermore, California.

Figure 25 shows a man inside the spherical NIF target chamber.

The NIF experiment is expected to demonstrate target ignition and energy gain $Q > 5$ in 2010–2011. It uses glass lasers with low efficiency, and it requires hours between shots to replace the target, which is suspended on a thin quartz fiber. For "ignition campaign" experiments, the target holder must also provide cryogenic refrigeration. The repetition rate is limited by replacement of the target, by evacuation of the chamber, and by cooling of the walls.

If the target capsule irradiation is not extremely uniform, a Rayleigh-Taylor instability [13] can break up the shell before compression is complete, as in Fig. 26.

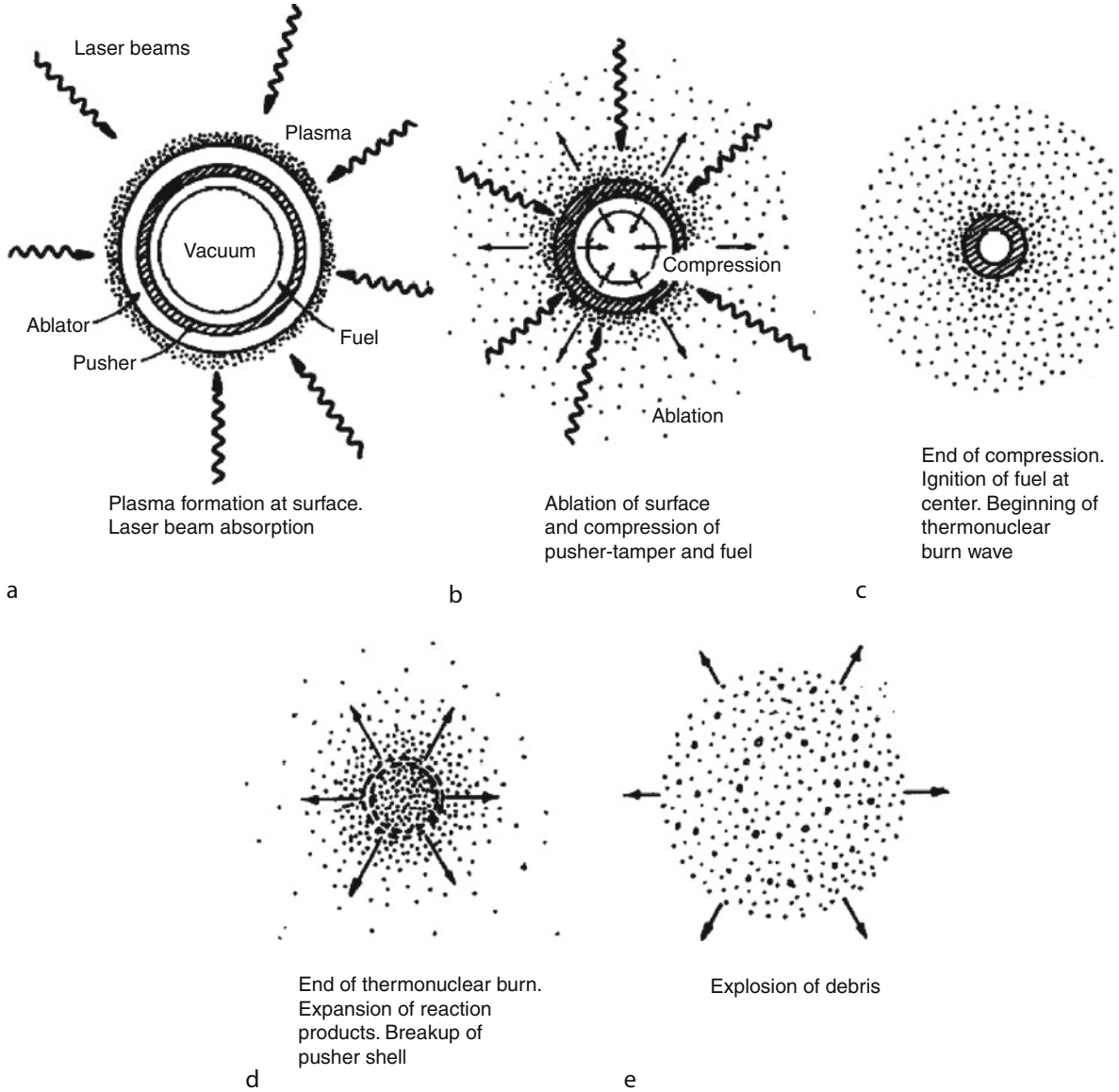

Nuclear Fusion. Figure 23
Ablation, compression, and burn of an ICF target

Target pellets may be irradiated directly by the laser beams, or they may be mounted inside a hollow cylinder, called a "Hohlraum," Fig. 27, to achieve more uniform compression.

The laser beams would enter through holes in the ends of the cylinder and irradiate the inside walls of the Hohlraum, causing them to emit intense x-rays. The x-rays would illuminate the 2.2 mm diameter target capsule, ablating its surface and compressing the frozen DT fuel to ultrahigh density. This "indirect drive" may provide better compression than the "direct drive," where the laser beams interact directly with the target surface, but the Hohlraum targets are more complex and more difficult to inject into a chamber and align with the laser beams.

Table 8 shows that many issues must be resolved before ICF reactors can become practical.

Potential solutions are available for most issues, but technology development has not yet been completed, especially for efficient, reliable, cost-effective drivers.

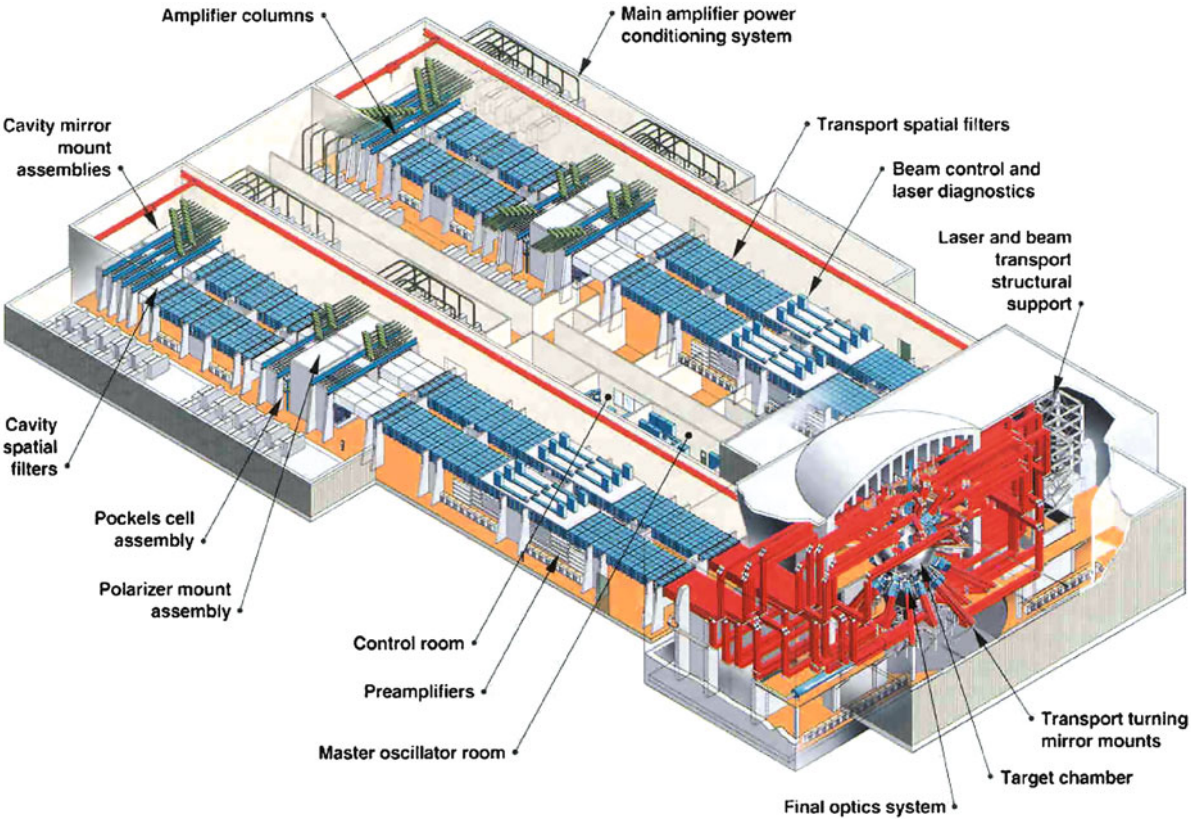

Nuclear Fusion. Figure 24
The National Ignition Facility, USA. 192 laser beams (in *red* tubes) go to the target chamber (Courtesy of Lawrence Livermore National Laboratory)

Nuclear Fusion. Figure 25
The NIF target chamber, with holes where the laser beams enter. (The wide angle photo makes the 10-m diameter chamber appear to be larger.) (Courtesy of Lawrence Livermore National Laboratory)

Table 9 lists some issues of target design and manufacture.

Laser Development

Great improvements are needed in laser efficiency, pulse repetition rate, and target injection rates. In the USA, two experiments are aimed at high average power lasers: Electra and Mercury.

The *Electra KrF laser* experiment at the Naval Research Laboratory is illustrated in Fig. 28.

Electron beams in vacuum from the cathode pass through the foil into the Kr and F_2 gases in the laser cell, where they cause excitation, resulting in a laser beam that exits through the amplifier window. Electra will run at 5 Hz with a laser output of 400–700 J. This will be large enough to develop technologies that can be scalable to the 50–150 kJ needed for a fusion power plant beam line.

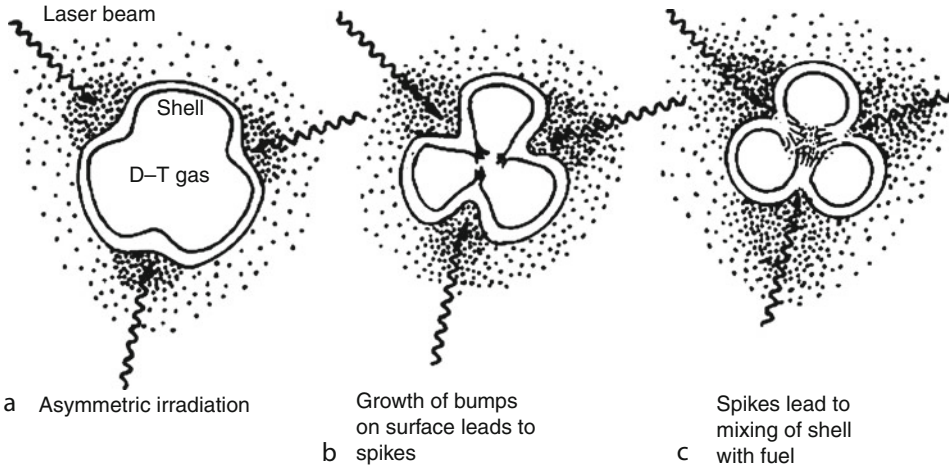

Nuclear Fusion. Figure 26
Growth of the Rayleigh-Taylor instability, causing breakup of the target shell (exaggerated for clarity)

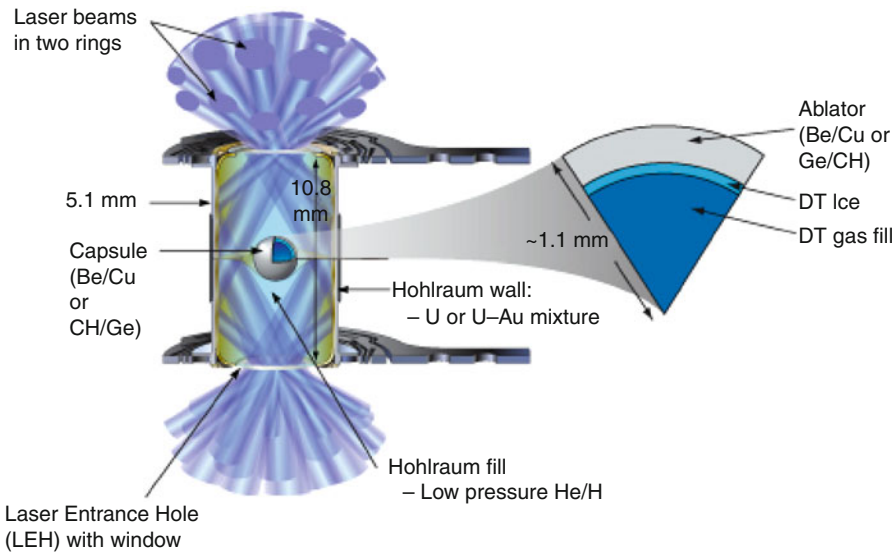

Nuclear Fusion. Figure 27
A Hohlraum target (Courtesy of Lawrence Livermore National Laboratory)

Figure 29 shows the *Mercurydiode-pumped solid state laser.*

The material in which light amplification occurs is crystalline strontium fluoro-apatite doped with ytterbium (Yb:S-FAP), which has a long excited state lifetime and high saturation fluence. High-power diodes inject 900 nm wavelength light into the Yb:S-FAP, which emits near 1,047 nm. About 15–20% of the diode energy is dissipated as heat in the Yb:S-FAP, which is removed by turbulently flowing helium gas [14]. The Mercury laser should deliver 100 J pulses at a rate of 10 Hz. If successful, this could be scaled up by using many units to MJ energies for a power plant. With mass production of diodes, their cost may fall to pennies per Watt, as needed for an economical power plant.

Nuclear Fusion. Table 8 Technical issues of ICF reactor development

Theory	Understand the physics of energy absorption, reflection, heat transport, compression, instabilities ignition, and burn
Experiments	Attain satisfactory values of the critical elements for high energy gain • Beam-to-fuel coupling efficiency • Avoiding fuel preheating before compression is complete • Implosion symmetry • Driver energy per unit fuel mass
Target manufacture	Develop an automated system to manufacture high-gain spherical targets accurately and cheaply. Select target materials to avoid production of long-lived radioisotopes.
	Use cryogenic refrigeration to keep the DT fuel frozen.
Target shelf life	Tritium decay heat can damage the cryogenic target, so targets have a finite shelf life.
Target injection	Develop a target injection and guidance system to ensure that the target is at the focus of the beams when the driver is fired.
Diagnostics	Measure the parameters of experiments, such as implosion velocity, density distributions, energy distributions, ablated matter, laser beam reflection, implosion symmetry, and fusion reaction products, with fine spatial and temporal resolution.
Chambers	Develop reactor chambers to withstand repeated ($>3 \times 10^8$) explosions without failure. (A 1,000 MJ yield has the explosive energy of 240 kg of TNT, but less momentum).
Chamber Clearing	Remove debris and gases rapidly between explosions, in order to avoid attenuating the incident driver beams.
Drivers	Develop laser or ion beams with high-energy (l–10 MJ), high-pulse repetition rate (l–10 Hz), proper pulse shape (duration 10–20 ns), suitable wavelength (lasers), good efficiency ($\geq$8%), and low enough cost.
Reliability	Develop power supplies, power conditioning equipment, diodes, and optical components to operate reliably for $>10^9$ shots.

Nuclear Fusion. Table 9 Target design and manufacture issues

Hydrodynamic stability and high compression
Good sphericity
Fast fill and layering
Uniform thickness shells
Very smooth surfaces
Minimum preheat of fuel
High-Z material to stop electrons and x-rays
Minimum production of long-lived radioisotopes
Easy handling and storage
Capable of high-velocity acceleration and injection without damage
Cheap materials, like plastics
Simple, inexpensive fabrication
Target cost goal typically $<$10 cents per target

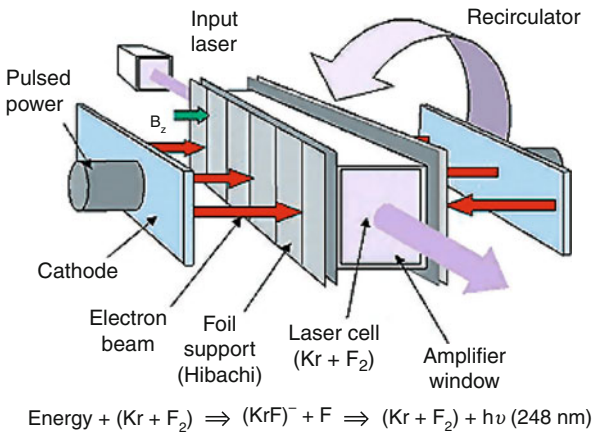

Nuclear Fusion. Figure 28
The Electra KrF laser (Courtesy of Naval Research Laboratory)

Hypervelocity Impact Fusion Small pellets (mass $\sim$1 g) would be accelerated to velocities $>10^5$ m/s and shot at a solid target. Either the projectile or the target would contain DT fuel. During impact, intense compression and shock heating would occur, igniting some of the fuel. The compression could be

made nearly three-dimensional by shaping the projectile and target, Fig. 30.

If compression is great enough, a high energy gain ratio $Q > 30$ may be attained. The fusion yield should be low enough that the blast chamber is not destroyed and high enough for economical power generation. The required projectile energy is about 25 MJ. Possible means of acceleration include electromagnetic rail guns, electrostatic accelerator, light gas guns, traveling electromagnetic wave accelerator, and laser ablation.

Challenges of Plasma Theory

In order to model fusion reactor behavior plasma physics theory must take into account many phenomena, Table 10.

Many of these models are based on simplifications of the Boltzmann transport theory and Maxwell's equations. Because these phenomena are diverse and often involve nonlinear differential equations, there is no unified theory that encompasses all of them. Instead, these phenomena may be modeled separately and the models stitched together to get an approximate picture of plasma behavior. Analytic theories are useful to understand how individual phenomena vary with input parameters, but are limited by the simplifying assumptions that are needed to make the equations solvable.

Large-scale computer simulations are widely used to model these effects. Three-dimensional models can be used to predict plasma behavior. The successful modeling of many phenomena lends confidence to predictions of the behavior of future experiments, such as ITER, but experimental data will still be needed to confirm the predictions.

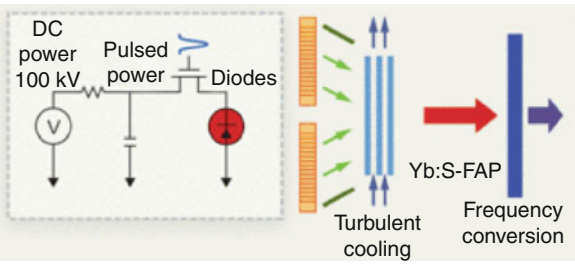

Nuclear Fusion. Figure 29
The Mercury diode-pumped solid state laser (Courtesy of the Lawrence Livermore National Laboratory)

Fusion Technology Issues

Many areas of technology are required for successful development of fusion power, Table 11.

Most of these issues have been successfully resolved during the 6 decades of fusion research. The ITER experiment should demonstrate the successful combination of many of these technologies, but will not demonstrate much tritium breeding, durable wall materials, high availability, or electrical power generation.

ITER must deal with transient heat loads caused by "edge localized modes" (ELMs) and disruptions, which can potentially damage the first wall or divertor. A robotic system to replace damaged wall tiles will be tested under high radiation levels in ITER. Development of first wall or divertor materials that can resist high heat fluxes and are resistant to damage by 14-MeV neutrons will not be completed by ITER, which uses more conventional structural materials.

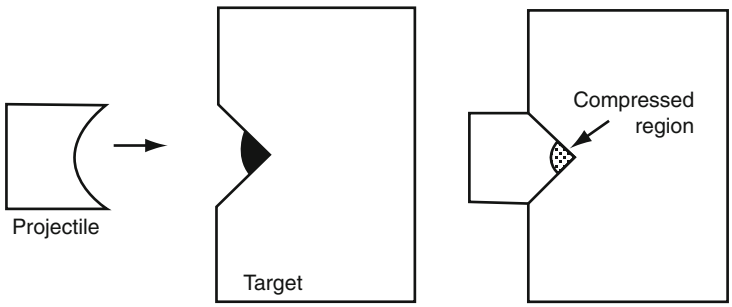

Nuclear Fusion. Figure 30
Hypervelocity impact projectile and target shaped to provide good compression

Nuclear Fusion. Table 10 Some phenomena to be modeled by plasma theory

Magnetohydrodynamic (MHD) instabilities	Motion of plasma boundary, driven by plasma pressure and Lorentz force
Radiation losses	Line radiation, bremsstrahlung, cyclotron radiation
Coulomb collision effects on velocity distributions	Boltzmann or Fokker-Planck equation
Plasma wave generation, cutoffs, and resonances	Maxwell equations coupled to plasma current density and magnetic field
Wave-particle interactions and microinstabilities	Anisotropic or non-Maxwellian distributions; kinetic theory (based on Boltzmann equation)
Nuclear fusion reactions	Cross sections averaged over ion velocity distributions
Particle and energy transport	Transport coefficients in conservation equations; scaling laws derived from experimental data
Plasma–wall interactions	Sputtering, vaporization
Impurity transport and control	Edge plasma and divertor theory
Plasma heating and current drive	Neutral beam injection, wave heating

In parallel with the ITER project, the International Fusion Materials Irradiation Facility (IFMIF), planned to be built in Japan, will bombard a flowing lithium target with 40 MeV deuteron beams to produce an intense flux of energetic neutrons for testing small samples of candidate fusion reactor materials. Figure 31 shows a drawing of IFMIF [15].

Use of high-temperature superconductors is becoming feasible for fusion devices [16]. They could operate near liquid nitrogen temperature (77 K), instead of near liquid helium temperature (4 K). This would simplify the design of the coils, cryostats, and instrumentation, and greatly reduce the refrigeration power and cost of refrigeration systems.

Coating the plasma chamber walls with lithium may help improve plasma performance. Usually, many of the deuterons escaping from the plasma hit the wall, where they are neutralized. Some of them re-emerge from the wall as cold neutral gas, which keeps the plasma edge temperature low, making a steep temperature gradient, which causes rapid heat conduction. Lithium absorbs escaping deuterium, reducing back-flow of cold deuterium gas, and flattening the temperature profile, which can reduce plasma electron turbulence and heat conduction rates [17].

Fusion Reactor Design Studies

Electric power utility companies have many criteria for power plant selection and siting [18] including:

- Output of power plant, compatibility with power grid
- Grid stability
- Required transmission lines
- Capital cost per kW
- Simplicity of plant
- Construction time
- Reliability and availability of power plant
- Ease and speed of maintenance
- Plant lifetime
- Load-following (ability to vary output to meet demand)
- Seismic activity and flood danger
- Availability of fuel, and fuel cycle costs
- Decommissioning costs
- Adequacy of resources, such as helium, lithium, and niobium
- Feasibility of shipping large, heavy components
- Staff numbers, skills, and costs
- Security requirements and costs
- Government laws and regulations
- Ease of licensing
- Intervener lawsuits
- Safety
- Environmental issues
- Plant emissions and waste products
- Willingness of financial institutions to invest
- Public acceptance

The availability of fusion power plants is difficult to predict, because current experiments often have equipment failure rates that would be unacceptable to utilities. The availability of some systems can sometimes be

Nuclear Fusion. Table 11 Fusion technology issues

Component	Issues
Magnet coil systems	High magnetic field, superconducting cable, stresses, quench protection
Plasma heating, fueling, current drive	Plasma compression Magnetic induction Electromagnetic waves Particle beam injection Plasma guns
First wall	Low-Z (atomic number), high heat flux, heat removal, radiation damage, tritium trapping
Blanket, shield	Tritium breeding ratio, neutron and gamma shielding, heat removal, radiation damage
Divertors (channels that remove plasma impurities)	High heat flux, sputtering, vaporization, tritium trapping, vacuum pumping
Energy conversion	Efficient conversion of fusion energy into electrical energy, such as with a steam cycle or helium gas turbine. High efficiency requires high coolant temperature, which causes materials problems
Materials issues	Stress, embrittlement, swelling, creep, fatigue, tritium trapping
Vacuum systems	Pumping speed, conductance, cryopanels
Cryogenic systems	Coolant flow, refrigeration, liquefaction, heat shields
Plasma diagnostic systems	Space-time mapping of magnetic field, electric field, plasma density, temperature, impurities, waves
Control systems	Plasma control, heating, current drive, magnets, fusion burn, electrical power plant
Maintenance	Magnets, first wall, heating systems, diagnostics, heat transfer systems
Safety and environmental systems	Routine emissions, accident scenarios, decommissioning, waste disposal
Power plant designs	Criteria for attractive power plants Reliability, availability, and maintenance Economics Fusion–fission hybrids

improved by providing redundant components, with slight increases in cost. Repair of large superconducting magnets would be difficult, if not impossible, so designers try to ensure that they will last for the life of the plant.

Fusion reactors have an economy of scale, which means that a 3,000 MWe power plant would probably have a much lower COE than a 300 MWe plant, but utilities may not wish to build very large power plants, to avoid large grid perturbations during outages [19].

The electricity from a fusion power plant could also be used to make hydrogen by high-temperature electrolysis. The hydrogen could be used as fuel for transportation and industrial processes. If the fusion reactor blanket could operate at $T > 800°C$, then the heat could be used directly for hydrogen production by a thermo-chemical system, such as one using a sulfur-iodine cycle [20].

Fusion–Fission Hybrids

Present light water fission reactors burn mainly the fissile isotope ^{235}U, which is only 0.711% of natural uranium. ("Fissile" means that it can be fissioned easily by slow neutrons.) The other 99.27% is mostly ^{238}U, which does not fission easily. A strong neutron source is needed in order to convert the ^{238}U into ^{239}Pu, which is

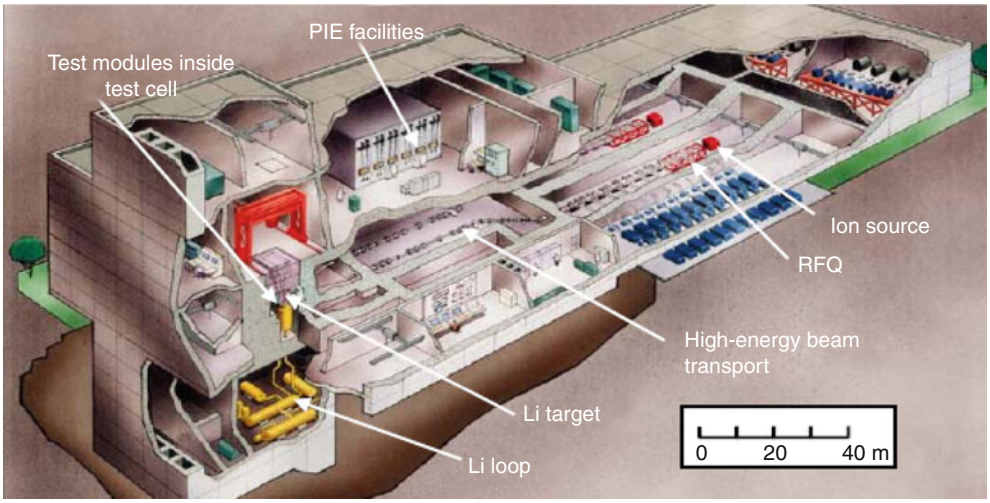

Nuclear Fusion. Figure 31
The international fusion materials irradiation test facility (Courtesy of the International Energy Agency)

another fissile fuel, if we are to generate energy from the other 99% of the uranium resources.

That strong neutron source could be a "fast" fission reactor, such as a liquid metal fast breeder reactor, but it takes years for such a reactor to generate enough fuel to start up a second reactor. The neutron source could be a high-power accelerator beam (like IFMIF), but fusion plasma neutron sources would be better where large quantities of materials are to be irradiated.

A fusion–fission hybrid would use uranium or thorium in the fusion reactor blanket, in addition to lithium. The blanket could be optimized either to produce more heat and electricity from the hybrid plant or to breed fissile fuel (^{239}Pu or ^{233}U) for use in satellite fission reactors. Hybrid blanket design studies indicate that one hybrid reactor could provide fuel for about five light water reactors. An "Energy Park" could have a fusion reactor plus several fission reactors and a fission reactor fuel reprocessing plant. With modern reactor designs, much of the spent fuel radioactive wastes could be recycled in the fission reactors or "incinerated" (transmuted to stable isotopes) in the fusion reactor blanket [21].

Future Directions

Most past magnetic fusion experiments have had small minor radii, so energy confinement times were short ($<$0.1 s), and impurities from the wall prevented optimum performance. The fusion research field needs bold investment to build large, high-power devices, such as ITER, in several other areas:

- Large compact toroid experiments (FRC and spheromak)
- A high-power accelerator neutron source for materials testing
- A plasma-based volumetric neutron source for materials testing
- Tokamak demonstration power plant construction during ITER operation
- Two reactor-sized stellarators following LHD and W 7-X
- A reactor-sized tandem mirror following Gamma-10
- Rapid-pulse, high-gain laser fusion demonstration power plants
- Full-scale heavy ion beam driver demonstration

Fusion reactor design teams in Europe, Japan, and the USA have done many design studies of tokamaks, stellarators, inertial fusion, and other types of fusion power plants. The capital costs of most fusion reactors are very high, but the fuel costs are very low. The resulting cost of electricity (COE) is typically predicted to be about 1.5–2 times as high as the COE from coal plants and nuclear fission reactors. Fusion power plants could become competitive

- If cheaper fusion reactors were developed, such as from compact toroids
- If fusion–fission hybrids were developed
- If carbon emissions were taxed
- If public opposition made it difficult to build new fission reactors or coal power plants

Acknowledgments

The following provided helpful comments on this article: Ralph Moir, Chan Choi, Lee Cadwallader, Nicholas Tsoulfanidis, Alex Parrish, and the Institute for Plasma Research (Gandhinagar, India). Charlou Dolan drew many of the figures.

Bibliography

Primary Literature

1. Jaskula BW (2010) Lithium. USGS 2008 Minerals Yearbook, United States Geological Survey
2. Freidberg J (2006) Plasma physics and fusion energy. Cambridge University Press, Cambridge
3. "All-the-world's tokamaks" (2010) http://www.toodlepip.com/tokamak
4. Bolt H (2001) Materials for Fusion. European White Book on Fundamental Research in Materials Science, Max-Planck-Gesellschaft, Munich, Section 2.9, Figure 2.17. (See also http://www.mpg.de/bilderBerichteDokumente/dokumentation/europWhiteBook/)
5. Hazeltine R et al (2009) Research needs for magnetic fusion energy sciences. Report of the Research Needs Workshop (ReNeW), Bethesda, 8–12 June, 2009, U.S. Department of Energy, p 203
6. Hazeltine R et al (2009) Research needs for magnetic fusion energy sciences. Report of the Research Needs Workshop (ReNeW), Bethesda, 8–12 June, 2009, U.S. Department of Energy, p 213
7. Tacetti JM et al (2003) FRX-L: a field-reversed configuration plasma injector for magnetized target fusion. Rev Sci Instrum 74(10):4314–4323
8. Slough J et al (2007) The pulsed high density experiment: concept, design, and initial results. J Fusion Energy 26:199–205
9. Ichimura M et al (2006) CRF experiments and potential formation on the GAMMA 10 tandem mirror. Plasma Sci Technol 8(1):87–90
10. Dolan TJ (1994) Magnetic electrostatic plasma confinement. Plasma Phys Controlled Fusion 36:1539–1593
11. Boxer AC et al (2010) Turbulent inward pinch of plasma confined by a levitated dipole magnet. Nature-Physics 6:207–212, Supplementary Information
12. Storms E (2007) The science of low energy nuclear reaction: a comprehensive compilation of evidence and explanations. World Scientific, Hackensack
13. Dolan TJ (1982) Fusion research. Pergamon, Elmsford, Chapter 15
14. Ebbers C, Caird J, Moses E (2009) Laser Focus World 45, No. 3, March 1
15. IFMIF International Team (2004) International Fusion Materials Irradiation Facility (IFMIF) Comprehensive Design Report. International Energy Agency, Paris
16. Hazeltine R et al (2009) Research needs for magnetic fusion energy sciences. Report of the Research Needs Workshop (ReNeW), Bethesda, 8–12 June, 2009, U.S. Department of Energy, Thrust 7, pp 285–293
17. Zakharkov LE et al (2004) Ignited spherical tokamaks. Fusion Eng Des 72:149–168
18. Kaslow J et al (1994) Criteria for practical fusion power systems: report from the EPRI fusion panel. J Fusion Energy 13(2/3):181–183
19. Dolan TJ (1993) Fusion power economy of scale. Fusion Technol 24:97–111
20. Terada A et al (2007) Development of hydrogen production technology by thermochemical water splitting IS process, pilot test plan. J Nucl Sci Technol 44(3):477–482
21. Freidberg J et al (2009) Research needs for fusion-fission hybrid systems. Report of the Research Needs Workshop (ReNeW), Gaithersburg, Maryland, September 30–October 2, 2009, U.S. Department of Energy

Books and Reviews

Braams CM, Stott PE (2002) Nuclear fusion: Half a century of magnetic confinement fusion research. Institute of Physics, Philadelphia

Chen FF (1984) Introduction to plasma physics and controlled thermonuclear fusion. Plenum, New York

Dinklage A et al (2005) Plasma physics – confinement, transport, and collective effects. Springer, Berlin

Dolan TJ (1982) Fusion research. Pergamon, Elmsford

Freidberg J (2006) Plasma physics and fusion energy. Cambridge University Press, Cambridge

Nuclear Power, Economics of

M. R. Deinert
Department of Mechanical Engineering,
The University of Texas at Austin, Austin, TX, USA

Article Outline

Glossary
Definition of the Subject
Introduction

Present and Future Value of Money
Levelized Costs
Lead and Lag Times in Cost Calculations
Estimating Uncertainties
Costs and Their Uncertainties
Discount and Interest Rates
Cost Comparisons and External Costs
Future Directions
Acknowledgments
Bibliography

Glossary

c Onetime costs [$]
E_c Cost of electricity [$]
FV Future value [$]
HM Heavy metal, refers to the uranium and or transuranic component of fuel
kg Kilogram
kW Kilowatt
kWh Kilowatt hour
kWh(e) Kilowatt hour electric
mill $0.001
n Number of years
MOX Mixed oxide fuel
MWh(e) Megawatt hour electric
p(t) Distributed costs [$/year]
Pu Plutonium
PV Present value [$]
r Yearly rate of return in discrete discounting
$r(x_i,x_j)$ Correlation coefficient
SD Standard deviation
SF Spent fuel
SW Separative work
t Time [year]
U Uranium
UOX Uranium dioxide fuel
VHLW Vitrified high-level waste
x_i Denotes a cost component
α Linear cost escalation rate [$/year^2]
β Linear cost escalation intercept [$/year]
δ Delta function
ρ Discount or interest rate [1/year]

Definition of the Subject

Financial viability is an important consideration when deciding whether to proceed with any large-scale engineering project. Many studies of nuclear power economics have been undertaken in an attempt to predict its overall costs or competitiveness (e.g., [1–4]). While these studies tend to differ in their assumptions about construction and operating expenses, they all use similar frame works for the analysis. In essence, the idea is to predict the total cost of producing electric power over the lifetime of a facility and compare that to the market value of the electricity produced. All other things being equal, the larger the ratio of revenue to cost the better the project.

Introduction

Economic assessments of nuclear power tend to be complicated, and not just because of the number of components that have to be factored in, Fig. 1. The costs of any large project also depend on how it is financed, and whether this is done through the issuing of bonds by the entity undertaking the project, borrowed money, allocation of liquid assets, and/or the use of complex financial instruments such as derivatives. Tax rates, both federal and local, can also play an important role. The revenue stream from a nuclear power facility itself depends on whether the markets into which the electricity is fed are regulated or unregulated and whether arrangements exist that involve the sale of electricity at fixed rates to municipalities where the facilities reside. The effect of hard to predict market forces can affect the price of electricity itself.

In addition, nuclear power has some peculiarities that are unique to the industry. Among these is the need to safely store the radioactive waste products that are contained in spent nuclear fuel, for extended periods of time. At present, only the US Waste Isolation Pilot Plant, in Carlsbad NM, is actively used for this purpose, and then only for transuranics (a very specific class of high-level waste) from the US nuclear weapons program. Because of this, *interim* storage facilities exist at civilian nuclear power facilities to handle spent nuclear fuel, but the final disposal costs remain uncertain (e.g., [2]). In addition, most modern reactors run on a uranium fuel that has been enriched to contain more of the uranium 235 isotope than is present in natural uranium (natural uranium is made up of two isotopes: ^{238}U and ^{235}U. The ^{238}U isotopes comprises

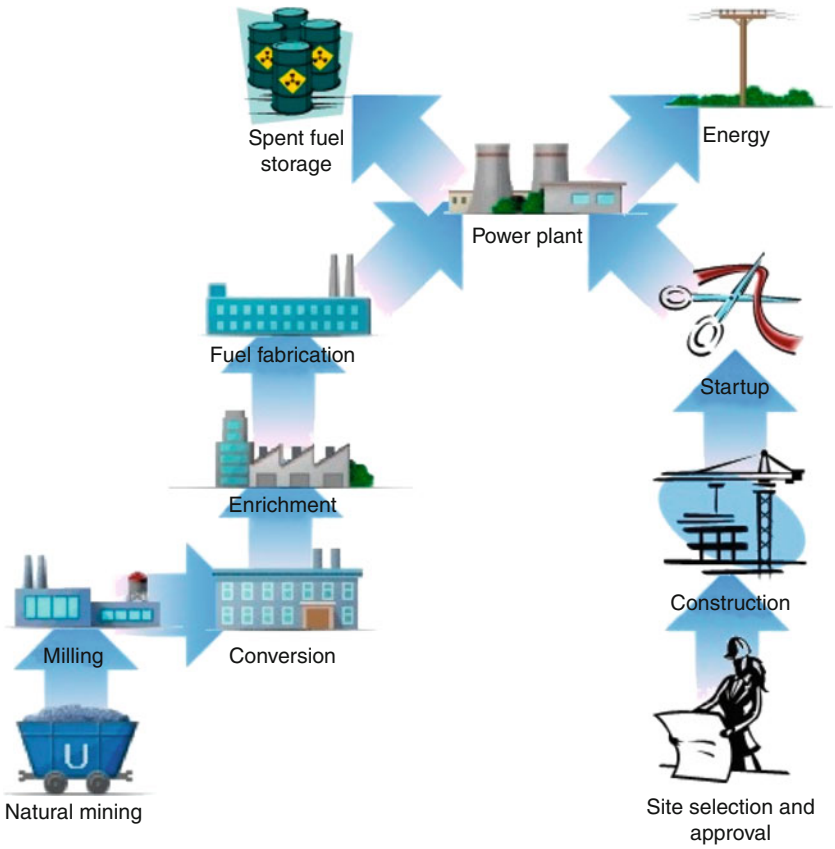

Nuclear Power, Economics of. Figure 1

Components of a nuclear power facility. Construction of a nuclear power facility begins with site selection and approval. Facility construction (reactor and related facilities) comes next, with final startup typically coming 6–12 years after the start of construction activities. The process of producing uranium fuel typically starts 2 years prior to fuel placement in a reactor with uranium mining, milling, conversion enrichment, and fuel fabrication. Finally, fuel is transported to the reactor site. The fuel pipeline will function continuously as the reactor operates. Interim on-sight storage is common until permanent storage facilities are established (Figure courtesy of Robert Bell, The University of Texas at Austin)

99.3% of the uranium atoms and ^{235}U 0.7%. It is the ^{235}U isotope that readily undergoes fission in the thermal reactors that dominate the civilian nuclear power industry.). Because this isotope can also be used in the manufacture of nuclear weapons, concerted efforts have been undertaken to limit the development of enrichment facilities outside of a few highly industrialized countries (e.g., [5, 6]). This of course has the effect of forcing nuclear power facilities in less industrialized countries to buy fuel from external sources. Consequently, a common concern is that the fuel supply could be restricted for political reasons (e.g., [7]).

Uncertainties in fuel availability and spent fuel disposal introduce an element of financial risk that is difficult to quantify. Another potential complication comes from uncertainty in whether construction of a nuclear power plant will actually lead to an operational facility. It has in fact happened that facilities have been undertaken whose construction has been halted, or which have been completed but closed before becoming commercially operational. The Shoreham Nuclear Power Plant in Long Island, NY, is an example of this. The facility was completed in the mid-1980s, but public protest resulted in its closure before it produced commercial power.

Nuclear Power, Economics of. Table 1 *Life-cycle cost estimates for electricity produced from nuclear, coal, and gas.* The different costs of electricity reflect different life-cycle assumptions between the two studies [4, 11]. Costs were adjusted to $2,007

Production	MIT [4] [cents/kWh(e)]	University of Chicago [11] [cents/kWh(e)]
Nuclear	8.4	5.6
Coal	6.2	4.5
Gas	6.5	3.4

Because of the above factors, and others, it is difficult to make blanket statements about the economics of nuclear power, and facilities need to be evaluated on an individual basis. However, several recent studies have taken a look at nuclear power relative to competing technologies, see Table 1, with somewhat mixed results that reflect the different assumptions that went into the analyses. In the current article, the focus is largely on a discussion of how the cost of a nuclear power facility would be computed when taking into consideration factors such as its construction, operation, maintenance, and decommissioning.

Many of the elements that contribute to the life-cycle cost of a nuclear power plant are common to other types of facilities as well. These include:

Capital costs – The costs associated with building the plant and its components.

O&M – The cost to operate and maintain facilities.

Depreciation – This is a charge recorded against earnings that takes into consideration the lifetime of capital components and the fact that they must be replaced as a part of operating expenses. Depreciation of capital components is typically added to the yearly operations and maintenance costs.

Interest – The money paid for the use of borrowed capital or for bonds that have been issued.

Taxes – Both federal and local may apply.

Interest rate – The annual amount of money paid to a lender or bond holder for the use of capital as a percentage of the amount to be repaid.

Discount rate – Effectively the same as the interest rate, see section on discount rates.

Several other factors that affect the cost of nuclear power are particular to the industry. These include:

Fuel costs – A peculiarity of nuclear power facilities is that they do not always buy the fuel that is used to run them. Instead, they will often lease it, sometimes from a company that was created explicitly for the purpose of doing this. The reason has to do with accounting practices, and it is sometimes cost effective for a utility to acquire its fuel in this way [8].

Nuclear waste fund fee – This is a fee levied in the United States to cover the Federal Government's obligation to take possession of spent nuclear fuel and dispose of it [8]. The current rate is $0.001/kWh of electricity produced, which is paid into the Nuclear Waste Fund (The Nuclear Waste Fund was established under US Code Title 42, Chapter 108, Subchapter III, 10222 – i.e., The Nuclear Waste Policy Act of 1983). This monetary unit is so common within the utility industry that it is often given a special unit called a "mill," where 1 mill = $0.001 [8].

On site spent fuel storage cost – The cost to store spent nuclear fuel on site.

Decommissioning costs – The costs associated with removing the power plant and its components along with returning the site to an unrestricted use.

By far the dominant cost for a typical nuclear power plant is that of constructing the facility itself [4]. From the perspective of the people who are building a facility, the cash flows that are required for construction depend not only on the facility cost, and the time required to build it, but also on how it is financed. For example, cash flows associated with a facility financed with cash will be different than those for one financed with a loan that is to be paid back over a fixed period of time, or a bond. Once a facility is built, there are operation and maintenance charges to keep it in working order, and these are spread out over the operating life of the facility. Taxes on property begin as soon as land is acquired, and those on the facility itself depend on the location and municipality, but are likely to be yearly as are taxes on income. Depreciation too is spread out over the operating life of a component (a discussion of common depreciation methods can be found in [4]), and decommissioning costs are

incurred at the end of a facility's life. However, it is typical that money must be set aside for decommission costs well in advance of them.

Present and Future Value of Money

The variable nature of the cash inflows and outflows complicates the cost analysis for any industrial facility, but especially those with long lifetimes as is typical with nuclear power plants. When undertaking a life-cycle cost study, it is also important to recognize that not all money is equivalent. Specifically, a dollar paid or earned today has a different value than does one paid or earned a year from now. The reason for this stems from the fact that money can devalue due to inflation, but also because money held today can be invested and earn interest. Conversely, money received in the future has less value, both because it may have devalued but also because of the inability to invest it until it is received. These concepts are captured in what is often referred to as the "time value of money" [9]. For example, \$100 invested today, at a yearly return of 5%, will yield \$105 in 1 year. In the parlance of financial engineering, \$100 invested this way has a *future value* of \$105, and \$105 received in 1 year has a *present value* of \$100. From the perspective of an investor who expects a yearly return of 5%, both are equivalent.

The relationship between *future value* (FV) and *present value* (PV) is simple:

$$\mathrm{FV} = \mathrm{PV}(1 + r)^n \tag{1}$$

Here r is the yearly rate of return, and n is the number of years over which the investment takes place (not necessarily an integer), and PV is said to be *compounded* over n years. Conversely, the *present value* of FV (received in n years) is given by:

$$\mathrm{PV} = \mathrm{FV}/(1 + r)^n \tag{2}$$

An important point that is often overlooked is that PV = FV when the expected rate of return is zero. This situation can effectively arise in environments, where the rate of return is equal to the inflation rate. Equation 2 is an example of *discounting*. When the effects of inflation are taken into consideration Eqs 1, 2 become:

$$\mathrm{FV} = \mathrm{PV}(1 + r - i)^n \tag{3}$$

and

$$\mathrm{PV} = \mathrm{FV}/(1 + r - i)^n \tag{4}$$

Here i is the yearly inflation rate. Equations 3, 4 give the present and future values in constant, or inflation adjusted, dollars. The quantity $\rho = r–i$ is referred to as the "real rate of return" as opposed to the "nominal rate of return" r, and ρ, r, and i all range between 0 and 1. Most economic analyses are done assuming a real rate of return, and that convention is adopted here.

Equations 1–4 are discrete representations of simple compounding and discounting, and there are several very good descriptions of how they can be extended to more complex situations in general (e.g., [10]), and to the nuclear power industry in particular [1, 8]. However, as these references quickly show, applying discrete financial models becomes cumbersome when the system being analyzed is complex. An alternative is to use continuous approximations to Eqs 3, 4, which then become:

$$\mathrm{FV} = \mathrm{PV}e^{\rho t} \tag{5}$$

and

$$\mathrm{PV} = \mathrm{FV}e^{-\rho t} \tag{6}$$

Here ρ is again the rate of real rate of return per unit time t.

Levelized Costs

Nuclear power facilities typically operate over extended time periods, and some in the United States are even in the process of receiving license extensions that will bring their operating life spans to 60 years (e.g., [11]). As a result, the present value of funds that are used to build, maintain, fuel, or decommission a nuclear facility will depend significantly on when the costs occur. Therefore, the only way to accurately estimate the total cost of a facility is to compute its total *present value* relative to a specific date (usually the date of startup of the facility). This process is called *levelizing*. In fact, in the United States, all large-scale government projects are required to perform this type of levelized cost analysis [12]. Expenses that take place before the reference date have what is called a *lead time* as they happen *ahead of* the reference time. Expenses that take place after the reference time have a *lag time* as they happen behind the reference time [1, 13]. A framework for how

to levelize the costs for nuclear power facilities in terms of lead and lag times was given in a study done by the Organization for Economic Cooperation and Development (OECD) in collaboration with the Nuclear Energy Agency (NEA) [1]. Continuous discounting can be used within this framework to levelize all costs, as well as the revenue from electricity production, to the date at which fresh fuel is loaded into a reactor. Continuous discounting is mathematically simpler than its discrete alternative and often introduces negligible error relative to the large variances for unit cost predictions.

With this approach, levelized costs are easily obtained by multiplying the time-dependent costs, $p(t)$, by the discounting factor, $e^{-\rho(t)t}$, and integrating the product:

$$\mathrm{PV} = \int_{t_1}^{t_2} p(t) e^{-\rho(t)t} dt \tag{7}$$

where PV [\$] is again the present value of a cash outflow, $p(t)$ [\$/year], ρt is the real interest or discount rate [1/year], and t is time [year]. It is common in many studies to assume that ρt is constant, though this is not necessary. The total cost of a system over its life is given by the sum over the costs incurred from its construction to its decommissioning:

$$E_c = \sum_i \mathrm{PV}_i \tag{8}$$

The life-cycle cost in \$/kWh(e) is calculated by dividing E_c by the total kWh's of electricity produced. Some economists argue that the electricity production should itself be discounted using Eq. 7 to factor in the temporal nature of the revenue stream (e.g., [14]). It might seem counter intuitive that a unit of energy, being immutable, should be discounted. However, economists who advocate this approach argue that energy (like money) can be viewed as having greater value when it is available in the near term than if its availability is off in the distance. Another interpretation was given by Hannon [14] who suggested that the energy discount rate reflects a society's desire to convert "a present surplus energy into an energy-transformation process so that a greater surplus of energy can be created in the future, rather than consuming the energy now." While energy discounting is used (e.g., [4, 8]), the approach is not universal.

Examples. Figure 2 shows several distributions for $p(t)$ that are relevant to nuclear power systems and out of which any cost or revenue distribution can be built. Equation 7 is easy to apply to each situation when it is done systematically.

(a) The present value of a onetime cost, c_0, that occurs at time, t_0, is easy to derive using Eq. 7. One starts by noting that:

$$\begin{aligned} p &= 0 \quad 0 \le t < t_0 \\ p &= c_0 \quad t = t_0 \\ p &= 0 \quad t > t_0 \end{aligned} \tag{9}$$

Assuming a constant discount rate, Eq. 7 becomes:

$$\mathrm{PV} = \int_0^{t_0} c_0 \delta(t_0) e^{-\rho t} dt \tag{10}$$

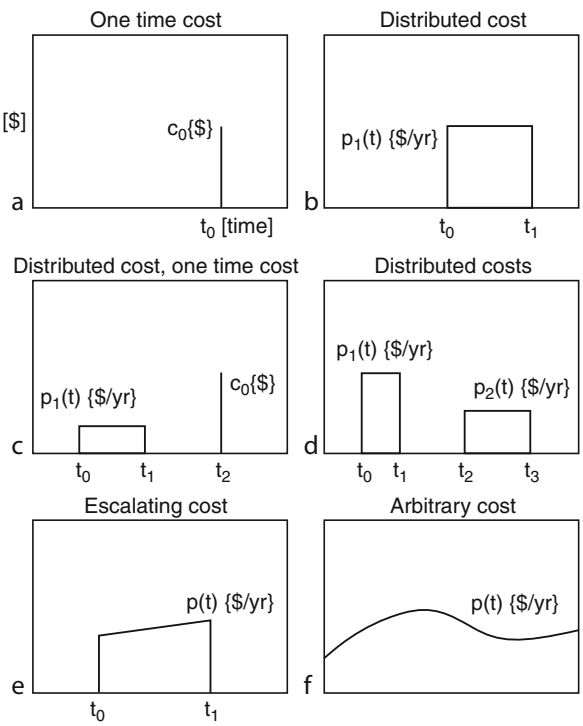

Nuclear Power, Economics of. Figure 2
Common payment, cost, and revenue distributions. Common distributions for $p(t)$ applicable to Eq. 7 are shown. In the figure, c_0 stands for one time cost, and $p(t)$ for distributed cost. The left-hand side of the time axis is assumed to represent $t = 0$

where $\delta(t_0)$ is the delta function (zero everywhere but t_0). Equation 10 then just gives:

$$\mathrm{PV} = c\mathrm{e}^{-\rho t_0} \tag{11}$$

which is just Eq. 6 again.

(b) The present value of a uniformly distributed cost is only slightly more complicated to calculate. Here:

$$\begin{aligned} p &= 0 \quad 0 \le t < t_0 \\ p &= c_1 \quad t_0 \le t \le t_1 \\ p &= 0 \quad t > t_1 \end{aligned} \tag{12}$$

Equation 7 then becomes:

$$\mathrm{PV} = \int_{t_0}^{t_1} c_1 \mathrm{e}^{-\rho t} \mathrm{d}t \tag{13}$$

which has the simple solution:

$$\mathrm{PV} = \frac{c_1\left[\mathrm{e}^{-\rho t_0} - \mathrm{e}^{-\rho t_1}\right]}{\rho} \tag{14}$$

(c) The present value of a distributed cost *and* a onetime cost is just the sum of the results given in Eqs. 11, 14:

$$\mathrm{PV} = c_0 \mathrm{e}^{-\rho t_2} + \frac{c_1\left[\mathrm{e}^{-\rho t_0} - \mathrm{e}^{-\rho t_1}\right]}{\rho} \tag{15}$$

It is implicit in Eq. 15 that the discount rate is the same for both distributions; however, this is not always the case, and not a necessary restriction.

(d) The present value of *two* uniformly distributed costs is just obtained using the result in Eq. 14 twice:

$$\mathrm{PV} = \frac{c_1\left[\mathrm{e}^{-\rho t_0} - \mathrm{e}^{-\rho t_1}\right]}{\rho} + \frac{c_2\left[\mathrm{e}^{-\rho t_2} - \mathrm{e}^{-\rho t_3}\right]}{\rho} \tag{16}$$

Here c_1 and c_2 are the uniform cost rates for the respective distributions. It is again implicit that the discount rate is the same for both distributions, though this is again not a necessary restriction.

(e) Linearly escalating costs are also easy to deal with. Here the cost function is given by:

$$\begin{aligned} p &= 0 \quad 0 \le t < t_0 \\ p &= \alpha t + \beta \quad t_0 \le t \le t_1 \\ p &= 0 \quad t > t_1 \end{aligned} \tag{17}$$

where α has units of [\$/year^2] and β [\$/year]. In this case, Eq. 7 becomes:

$$\mathrm{PV} = \int_{t_0}^{t_1} (\alpha t + \beta)\mathrm{e}^{-\rho t} \mathrm{d}t \tag{18}$$

Equation 18 has the simple solution:

$$\mathrm{PV} = \alpha\left(\frac{\mathrm{t}}{\rho} - \frac{1}{\rho^2}\right)\left(\mathrm{e}^{-\rho \mathrm{t}_1} - \mathrm{e}^{-\rho \mathrm{t}_0}\right) + \frac{\beta}{\rho}\left(\mathrm{e}^{-\rho \mathrm{t}_1} - \mathrm{e}^{-\rho \mathrm{t}_0}\right) \tag{19}$$

In general, Eq. 7 is integrable as long as $p(t)$ is known. While the formulas above may seem at first glance to be complicated, they are far simpler and more compact than their discrete discounting alternatives.

Lead and Lag Times in Cost Calculations

A critical factor in using the above equations, and when performing economic analyses in general, is to know when costs occur relative to a specified date. As already pointed out, this is captured in what are referred to as "lead" and "lag" times, and the reference time is typically taken to be the date of the facilities' first operation. Components that affect the cost of nuclear power are shown schematically in Fig. 1. In very general terms, the costs associated with nuclear power production can be broken into *capital costs* (which include the construction of physical infrastructure such as the reactor plant, spent fuel storage facilities, or facilities involved in producing nuclear fuel, etc.), *operating costs* (which include operations and maintenance costs, taxes, fuel costs, as well as spent nuclear fuel disposal costs), and *decommission costs* (which include dismantling of physical infrastructure and site remediation).

Power Facility Construction

Historically, this has been by far the dominant factor affecting the cost of nuclear power (e.g., [3, 4]). The lead time is highly variable, Fig. 3, but 8 years or more is typical for modern large-scale facilities. How this cost is distributed depends on how a facility is financed, Fig. 2f.

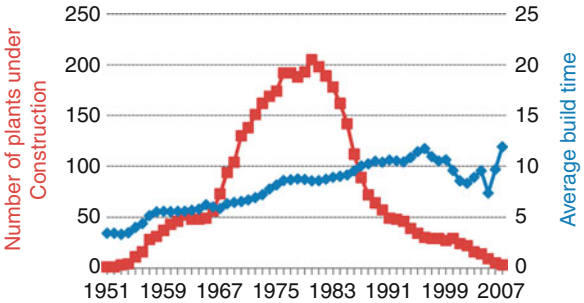

Nuclear Power, Economics of. Figure 3
Reactors under construction and build times. The total number of nuclear power facilities under construction and the time for facility completion (from start of construction to date of first operation) are shown (The data are from the International Atomic Energy Agency Data Center)

Power Facility O&M

Operations and maintenance costs for the facilities are usually computed on a yearly basis and can be approximated with a uniform distribution as in Fig. 1b. Large capital outlays for replacement of major components can often be assumed to be onetime costs as in Fig. 2a (e.g., [3, 4]).

Cooling Water

Availability of cooling water has become a potential constraint for nuclear power plants in some locations. A facility's water use depends on its efficiency, as well as how it is cooled (open loop, closed loop, evaporation pond, etc.). A typical range of water withdrawals for modern Rankine cycle power plants is 2,000–4,000 l/MWh(e), for closed loop systems, and 100,000–220,000 l/MWh(e) for open-loop systems. Water consumption rates are considerably smaller. In this context, water consumption describes water that is taken from a source (ground or surface water), used, and not returned to that source. A cooling tower consumes water through evaporation for example. Water withdrawal describes water that is taken from a source, used, and then returned to that source. Cost estimates for water vary widely, but \$25 per 1,000 m^3 has been reported and can be based on consumption, or withdrawal, rates and will depend on local water markets and regulatory structures (e.g., [15]).

Uranium Mining

The extraction of uranium ore typically occurs 2 years prior to its use as fuel in a reactor. Uranium is mined as U_3O_8 and is typically sold in this form. Modeled as a onetime cost that would recur with the refueling schedule of a reactor.

Uranium Conversion

The U_3O_8 requires conversion into UF_6 if the uranium is to be enriched to a higher ^{235}U content that occurs in natural uranium. Uranium must be enriched for use as fuel in most commercial light water reactors worldwide [16]. The lead time for conversion is typically 1.5 years. Modeled as a onetime cost that would recur with the refueling schedule of the reactor.

Enrichment

Enrichment typically occurs 1 year before fuel placement in the reactor. Modeled as a onetime cost that would recur with the refueling schedule of the reactor.

Fuel Fabrication

Most reactors worldwide use uranium dioxide fuel that is surrounded by a protective "cladding" and configured in assemblies that can be placed into a reactor. Fabrication usually takes place 0.5 years before fuel emplacement. Modeled as a onetime cost that would recur with the refueling schedule of the reactor.

Leasing or Buying Nuclear Fuel

Not all nuclear utilities buy their fuel. Instead, many lease it, and sometimes from a company or trust that has been created specifically for the purpose of doing this. The lease company covers all expenses for the fuel (mining, conversion, enrichment, fuel manufacture transportation and storage) until it is onsite to be loaded into the core. During this time, the utility pays nothing. Once the fuel begins producing power, the utility will pay the lease company a prorated amount that covers the lease company's expenses plus some degree of profit. In some situations, this arrangement is financially advantageous, though this depends on the accounting practices of the utility and possible constraints from regulatory agencies. Typically, the total

cost obligation is met when the fuel has been used to completion. The cost function for the leased fuel can be linearly decreasing, Fig. 2e, or of some other shape [8].

Interim Spent Fuel Storage

When the fuel reaches the end of its useful life, it is discharged from the core and is stored on site either under water or in air-cooled vaults until it is removed for final disposal or reprocessing. The residence time in interim storage is highly variable, and the spent fuel from some US reactors has remained in this type of onsite storage for decades. Spent fuel storage is typically calculated per unit time and per unit mass, and it is therefore a linearly increasing cost, Fig. 2e, at most reactor facilities, (e.g., [3, 4]).

Spent Fuel Recycle

Some countries, notably France, reprocess spent nuclear fuel and use the plutonium that it contains to manufacture what is called *mixed oxide fuel* (MOX – a mixture of plutonium oxide and uranium oxide) that can be used in addition to standard enriched uranium fuel, Fig. 4. In countries where this is done, spent fuel will cool in storage pools for 6–12 years before being sent to reprocessing. The distribution of this cost depends on whether funds are continuously set aside to meet this obligation or whether it is considered to be a series of onetime costs that occur as spent fuel is sent to recycle.

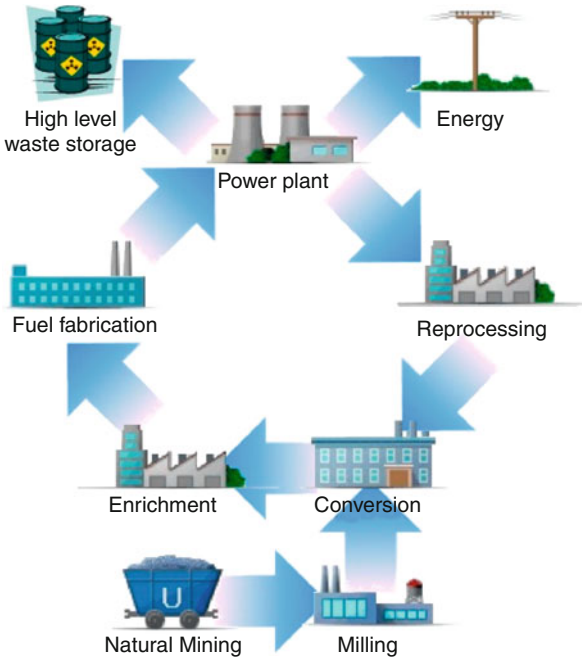

Nuclear Power, Economics of. Figure 4
Recycle-based fuel cycle. A schematic representation of a reprocessing-based fuel cycle is shown. Instead of spent fuel going to storage, it is sent to reprocessing, and the plutonium, and possibly other *transuranic* elements (such as neptunium, americium, and curium) are recycled to make new fuel. The recycled transuranics would not, however, require enrichment. The high-level waste is comprised of byproducts of reprocessing (Figure courtesy of Robert Bell, The University of Texas at Austin)

Spent Fuel Disposal

Most countries with domestic nuclear power assume that long-lived nuclear waste products will go into some form of geological storage. At present, only the US Waste Isolation Pilot Plant, in Carlsbad NM, is actively used for this purpose, and then only on a scale sufficient to handle transuranic waste from past US nuclear weapons efforts. As a result, the actual time at which spent fuel will leave interim storage for final disposal is unclear at most power plants (the final disposal of high-level waste from reprocessing is similarly unclear in countries where this is undertaken). Many reactor facilities whose spent fuel pools are nearing capacity have begun to transition fuel assemblies to onsite dry storage. In the United States, the Nuclear Waste Policy Act of 1987 gives responsibility for the disposal of spent nuclear fuel to the Federal government [17]. In order to cover the associated expenses, US nuclear power facilities pay 1 mill/kWh(e) into the Nuclear Waste Fund for the purpose of covering the final disposal costs [17, 18]. The cost is incurred quarterly and, as a result, constitutes a series of recurrent one time costs for nuclear utilities in the United States, i.e., Fig. 2a.

Estimating Uncertainties

Equation 8 has the convenient feature of being linear with respect to the total cost of each fuel-cycle component. As a result, E_c can be scaled to account for changes in unit cost, provided that time points for the integral

in Eq. 7 remain fixed. Uncertainty in unit costs causes a corresponding uncertainty in the prediction of E_c. These effects can be accounted for by using the well-known formula for error propagation, where the variance of $E_c(x_i)$ is given by:

$$\mathrm{var}(E_c) = \sum_i \left(\frac{\partial E_c}{\partial x_i}\right)^2 \mathrm{var}(x_i) + 2\sum_i \sum_{j \neq i} \left(\frac{\partial E_c}{\partial x_i}\right)\left(\frac{\partial E_c}{\partial x_j}\right)\sqrt{\mathrm{var}(x_i)}\sqrt{\mathrm{var}(x_j)}\,r(x_i,x_j) \tag{20}$$

Here the inputs, x_i, represent the PV_i in Eq. 8 with respective variances $\mathrm{var}(x_i)$. The term $r(x_i,x_j)$ is the correlation coefficient, 1 for fully correlated, –1 for anticorrelated and 0 for uncorrelated. The maximum and minimum variances are given by assuming that $r = 1,-1$ respectively with uncorrelated, $r = 0$, typically giving a variance that falls into the midrange. Equation 20 is much simplified in the case of $r = 0$. The electricity cost is assumed to have a Gaussian distribution which can be justified by the Central Limit Theorem [19], with the standard deviation of E_c being the square root of the variance. It should also be pointed out that Eq. 20 can be used for cost-sensitivity studies.

Costs and Their Uncertainties

Numerous studies have investigated the economics of nuclear power, notably the series of reports produced between 1987 and 2002 by the Organization for Economic Cooperation and Development and the Nuclear Energy Agency (OECD/NEA) [1, 13, 20–22] along with recent reports from groups at MIT and the University of Chicago. The 1994 OECD/NEA study [1], in particular, developed a framework for assessing the economics of nuclear fuel cycles. The study derived the expected levelized cost of a fuel cycle over the lifetime of a reactor, including transients (at startup and shutdown). The fuel cycle was divided into front-end components (uranium ore requirements, conversion to UF_6, enrichment, fuel fabrication and transport) and back-end components (spent fuel transport, reprocessing, direct disposal, or high-level waste (HLW) vitrification and disposal). Cash outflows to meet these obligations were discounted to a reference date using a discrete model as was revenue from electricity, and the subsequent expected cost in \$/kWh (e) was calculated.

The 1994 study [1] gave the most comprehensive cost estimates available at the time. Data were obtained from the literature and through survey of OECD member states and gave reliable results where industries were well established. Because no actual disposal facility existed for SF or vitrified HLW, these estimates were considered to be particularly uncertain [1]. The cost data were updated in the 2002 OECD/NEA study and estimated standard deviations were added [13]. Because no permanent repository is in operation, it is difficult to estimate what it would cost. However, the experience and cost studies at Yucca Mountain in the United States provides some indication. Here the cost estimates for the repository rose in constant dollars from \$32.2 billion to \$57.5 billion between 1989 and 2001, Fig. 5 [18, 23–26], for a repository that was designed to

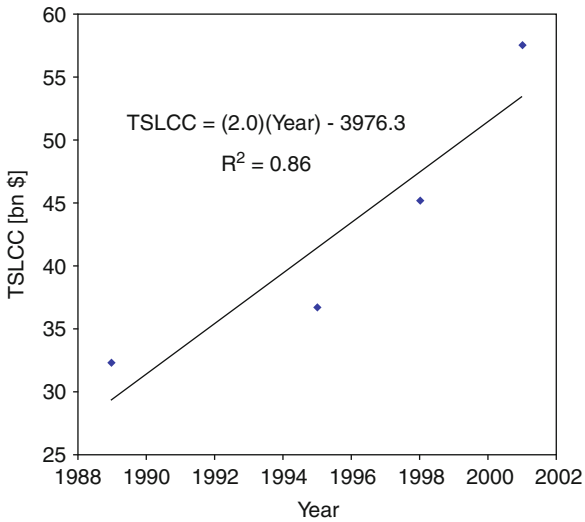

Nuclear Power, Economics of. Figure 5
Yucca Mountain Life Cycle Cost over time. The Total System Life Cycle Cost (TSLCC) predicted for Yucca Mountain is shown over the period between 1985 and 2001 in year 2000 dollars (inflation adjustment done using GDP deflator). In that time, the predicted cost has nearly doubled from \$32.2 to \$57.5 billion in constant dollars, with the repository intended to hold 86,000 metric tons of spent fuel heavy metal [18, 23–26]. In this context, "heavy metal" refers only to the mass of uranium and transuranics within the spent uranium dioxide fuel

hold 86,000 metric tons of spent nuclear fuel. Representative costs, lead/lag times, and standard deviations for nuclear power systems are given in Table 2.

Discount and Interest Rates

The values of ρ that are used in discounting will have a significant effect on an economic analysis. As a result, discount rates have been widely discussed in the context of decision theory, and in cost-benefit analyses of things that can have intergenerational effects such as environmental damage, resource allocation, or nuclear waste disposal. For economic comparisons, or cost studies, discounting accounts for the fact that payments made could instead have been invested and earned a rate of return. Alternately, future payments could be met by setting aside a smaller amount of money today and letting compound interest make up

Nuclear Power, Economics of. Table 2 *Unit costs of various components of the fuel cycle for a light water reactor with and without spent fuel recycle.* For the variables listed U denotes uranium; Pu – plutonium; HM – heavy metal; SD – standard deviation; SW – separative work; % loss – the percentage of material lost during a particular fuel cycle step; SF – spent fuel; MOX – mixed oxide fuel; VHLW – vitrified high-level waste; and led/lag refers to the time at which a particular cost is incurred relative to loading of a fuel batch into the reactor. The lead time for construction is relative to the first startup of the reactor. References are given for each data column in order from *left to right*, NA designates "not applicable." All costs are adjusted to year 2000 dollars. The standard deviation for the reactor facility construction cost was calculated from the cost data for seven reactors whose capital costs were given in [3]. It should be noted that many of the above costs are highly speculative, and other estimates are given in other studies, see for example [31]. Lag times for spent fuel recycle were estimated by assuming that SF_{UOX} remained in storage for 5 years and that fuel reprocessing occurred 1.5 years prior to MOX placement in the reactor. All other times are obtained by applying the time line for UOX fuel. The data in Fig. 4 suggests that the standard deviation for SF disposal is larger than that given in [13]

Fuel cycle component	Basis	$	SD (%)	% loss	lead/lag (years)	References
Reactor facility construction	$/kW(e) installed	3,560	15		−12 > −8	[11], [13], NA, see text
Reactor operations and maintenance	$/kW installed/year	142	15			[13], same as capital costs, NA, NA
Uranium mining and milling	$/kgU	30	33		−2.0	[13], [13], NA, [1]
U_3O_8 to UF_6 conversion	$/kgU	5	40	0.5	−1.5	[13], [13], [29], [1]
Enrichment	$/kgSW	80	37.5	0.5	−1.0	[13], [13], [29], [1]
UOX fabrication	$/kgU	250	20	0.5	−0.5	[13], [13], [29], [1]
Onsite interim SF_{UOX} storage	$/kgHM/year	30	5		+5	[13], [13], NA, NA
SF_{UOX} conditioning and disposal	$/kgHM	668	24		+40	[13], [13], NA, [1]
Spent fuel recycle						
SF_{UOX} transport to reprocessing	$/kgHM	50	20		+10.5	[13], [13], NA, see caption
SF_{UOX} reprocessing	$/kgHM	800	12.5	2.0	+11	[13], [13], [13], see caption
MOX Fabrication	$/kgHM	1,100	18	1.0	+12.5	[13], [13], [30], see caption
Onsite interim SF_{MOX} storage	$/kgHM/year	30	5		+17.5	[13],[13], NA, NA
SF_{MOX} transport to disposal site	$/kgHM/	50	20		+22.5	[13], [13], NA, see caption
SF_{MOX} conditioning and disposal	$/kgHM	668	24		+57.5	Same as UOX, [13], NA, see caption
VHLW conditioning and disposal	$/kgHM	288	12.5		+56	[13], [13], NA, see caption

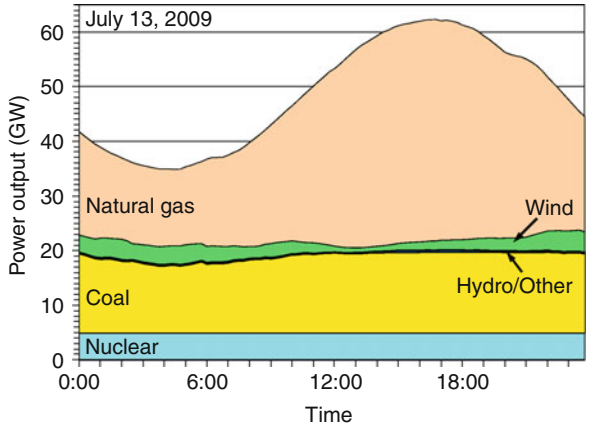

Nuclear Power, Economics of. Figure 6
Electricity load curve and generation source. The figure shows the variation in electricity demand over a 24 h period, and the sources used to meet that demand (The data are from the Electricity Reliability Council of Texas, for July 13, 2009) (Figure courtesy of Stuart Cohen, The University of Texas at Austin)

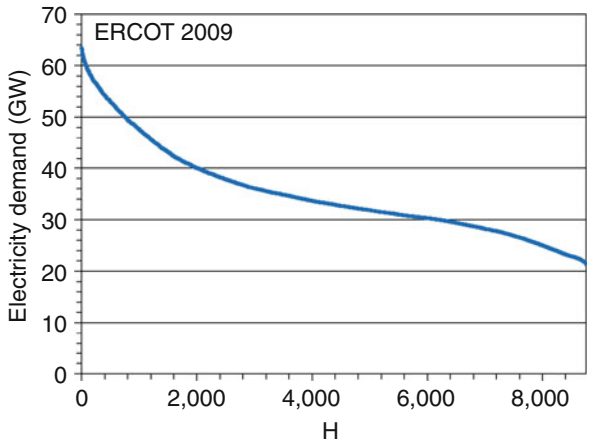

Nuclear Power, Economics of. Figure 7
Load duration curve. The figure shows the number of hours during 2009 during which a given electric demand needed to be met. The base load for the year is shown at the far *right* (The data are from the Electricity Reliability Council of Texas, for July 13, 2009) (Figure courtesy of Stuart Cohen, The University of Texas at Austin)

the difference. In both cases, the appropriate discount rate would be one that reflects what one could obtain by investing the funds in bonds, stocks, or other investments, and receiving the market rate of return.

There is no single discount rate that is accepted for near-term analysis of utilities, nuclear power included, but values between 5% and 10% (in real terms) are common and reflect the historical range of return by the US utility sector (e.g., [4]). However, there are problems in using this discount rate for projects that run on intergeneration time scales. The dominant concerns are well summarized in several different studies (e.g., [27, 28]), but the main point is that a discount rate that is this high would suggest that money so invested would eventually grow to be larger than the domestic product of any country where the investment was made. As a result, some economists suggest that discount rates appropriate for intergenerational projects would have to tend toward a country's real rate of GDP growth and can be assumed to be around 1–2% (e.g., [27, 28]).

The question of which discount rate to use in evaluating nuclear power facilities is far from academic. Cost studies are often used to compare different systems or management strategies. A high discount rate can make the present value of far-off costs appear negligible. In other words, using a high discount rate in a costs-benefit study of a politically divisive issue, such as spent fuel disposal, can have the perverse effect of suggesting that it would always be cheaper to delay action. In fact, this type of argument has been advanced in the United States to advocate for pushing off the development of reprocessing or permanent geological disposal.

Cost Comparisons and External Costs

Using Eq. 8, or similar, one can calculate the cost associated with the generating electricity by various means. Results of such studies are shown in Tables 1 and 2. However, making true comparisons for the "cost" of generating electricity between different types of power systems can be complicated by the effect of externalities that are often difficult to capture in an economic analysis. Factoring in the true cost of carbon dioxide emissions would be an example. Carbon dioxide emissions from fossil-fueled plants are obvious. They are not so obvious for nuclear, wind, or solar power facilities. While nuclear power facilities have no direct emissions, there are carbon signatures associated with the materials out of which they are made,

the processes involved in facility construction, as well as for operations, maintenance, and decommissioning. The same is true for wind and solar power systems. Where one draws the boundary for an analysis (i.e., does one include the carbon dioxide needed to produce, say, the machinery for the processing of facility materials) can have a significant effect on the total carbon signature that is associated with a specific power source, and through this, its total potential cost. Because of the complexity of handling externalities (and the cost of carbon emissions is only one example), how best to do this remains an area of active research and debate.

Future Directions

Electricity demand varies with location, time of day, and time of year. The minimum demand at any point within a year is referred to as *base load*. The utility industry typically gauges demand requirements with what are called *load demand* and *load duration curves*, Figs. 6 and 7. Commercial nuclear power plants have historically been designed to operate at their maximum licensed power. The fraction of time that these facilities are in operation has also increased steadily over the years to an industry average of around 90%. As a result, commercial nuclear power is used to meet base-load requirements, along with coal, hydroelectric, and to a smaller extent wind. Additional load requirements are met with smaller-scale facilities (called *peaking power plants*) that typically run on oil or gas.

Because of perceived economies of scale, nuclear power plants have been built on an increasingly large scale. Recently though, this idea has begun to be been revisited, and there are calls for the development of smaller-scale facilities with peak power outputs of as little as a few tens of megawatts. Such plants, known as *Small Modular Reactors*, could be used to meet local base-load requirements or as peaking plants. A shift in the industry to include smaller-scale facilities could have dramatic effects on the economics of nuclear power. Smaller facilities would likely have shorter build times and far lower capital costs. Many utilities also charge different rates, depending on when electricity is used, and this too would affect the economics of nuclear package plants that might be used to meet peak load requirements. (The first-generation light water reactors were designed for power outputs of 300–600 MWE. In the United States, today most nuclear power facilities are rated for 800–1,000 MWe, but it expected that the next generation of reactor will produce between 1,100 and 1,400 MWe.)

Acknowledgments

Special thanks to Andrew Osborne, Brady Stoll, and Geoff Recktenwald for editorial comments. Thanks to Eric Bickel and Michael Webber for useful discussions and to Nick Tsoulfanidis for editorial comments and for acting as Editor for this series.

Bibliography

1. OECD/NEA (1994) The economics of the nuclear fuel cycle. Technical report, OECD/NEA, Paris
2. Bunn M, Fetter S, Holdren JP, van der Zwaan B (2003) The economics of reprocessing vs. direct disposal of nuclear fuel. Technical report DE-FG26-99FT4028, Harvard University, Boston
3. Anolabehere S, Deutch J, Driscoll J, Holdren PE, Joskow PL, Lester RK, Moniz EJ, Todreas NE, Beckjord ES (2003) The future of nuclear power. MIT Press, Boston (Technical report)
4. Tolley GS, Jones DW (2004) The economic future of nuclear power. Technical report 2004, University of Chicago, Chicago
5. Garwin RL, Charpak G (2002) Megawatts and megatons – the future of nuclear power and nuclear weapons. The University of Chicago Press, Chicago
6. Goldschmidt P (2010) Multilateral nuclear fuel supply guarantees & spent fuel management: what are the priorities? Daedalus 139:7–19
7. Stern R (2007) The Iranian petroleum crisis and United States national security. PNAS 104:377–382
8. Cochran R, Tsoulfanidis N (1990) The nuclear fuel cycle: analysis and management, 1st edn. American Nuclear Society, La grange Park
9. Brealey R, Myers S, Allen F (2002) Principles of corporate finance, 9th edn. McGraw-Hill Higher Education, New York
10. Schneider EA, Deinert MR, Cady B (2009) The cost impact of delaying the US spent nuclear fuel reprocessing facility. Energy Econ 31:627–634
11. Deutch J, Forsberg C, Kadak A, Kazimi M, Moniz E, Parsons J (2009) Update of the MIT 2003 future of nuclear power. MIT Press, Cambridge
12. White House (1993) Executive order #12866: regulatory planning and review. Washington, DC
13. OECD/NEA (2002) Accelerator driven systems and fast burner reactors in advanced nuclear fuel cycles. Technical report, OECD/NEA, Paris

14. Hannon B (1982) Energy discounting. Technological Forecasting Soc Change 21:281–300
15. Stillwell AS, King CW, Webber ME, Duncan IJ, Hardberger A (2011) The energy-water nexus in texas. (Special feature: the energy-water nexus: managing the links between energy and water for a sustainable future), Ecol Soc 16(1):2. http://www.ecologyandsociety.org/vol16/iss1/art2/
16. Benedict M, Pigford TH, Levi HW (1981) Nuclear chemical engineering, 2nd edn. McGraw-Hill, New York
17. Nuclear Waste Policy Amendments Act (1987)
18. DOE (2002) Nuclear waste fund fee adequacy: An assessment. DEO/RW-0534, DOE, Office of Civilian Radioactive Waste Management, Washington, DC
19. Shapiro SS (1990) Selection, fitting, and testing statistical models. In: Wadsworth HW (ed) Handbook for statistical methods for scientists and engineers. McGraw Hill, New York
20. OECD/NEA (1987) Nuclear Energy and its fuel cycle-prospects to 2025. Technical report, OECD/NEA, Paris
21. OECD/NEA (1993) The cost of high-level waste disposal in geological repositories – An analysis of factors affecting cost estimates. OECD/NEA, Paris
22. OECD/NEA (1996) Future financial liabilities of nuclear activities. Technical report, OECD/NEA, Paris
23. GAO (1990) Changes needed in DOE user-fee assessments to avoid funding shortfall. Technical report RCED-90-65, United States General Accounting Office, Washington, DC
24. DOE (1995) Analysis of the total system life cycle cost of the civilian radioactive waste management program. Technical report DOE/RW 0479, DOE, Office of the Civilian Radioactive Waste Management Program, Washington, DC
25. DOE (1998) Analysis of the total system life cycle cost for the civil radioactive waste management program. Technical report DOE/RW-0510, DOE, Office of Civilian Radioactive Waste Management Program, Washington, DC
26. DOE (2001) Analysis of the total system life cycle cost of the civilian radioactive waste management program. Technical report DOE/RW-0533, DOE, Office of Civilian Radioactive Waste Management, Washington, DC
27. Rabl A (1996) Discounting of long term costs: what would future generations prefer us to do? Ecol Econ 17: 137–145
28. Arrow K (1999) Discounting, morality, and gaming. In: Portney PR, Weyant JP (eds) Discounting and intergenerational equity. RFF Press, Washington, DC
29. Rasmussen N, Burke T, Choppin G, Croff G, Garrick J, Grunder H, Hebel L, Hunter T, Kazimi M, Kintner E et al (1996) Nuclear wastes: technologies for separations and transmutation. National Academy, Washington, DC
30. Shropshire D, Williams K, Boore W, Smith J, Dixon B, Dunzik-Gougar M, Adams R, Gombert D (2007) Advanced fuel cycle cost basis. US DOE, The Idaho national laboratory INL/EXT-07-12107

Nuclear Reactor Materials and Fuels

James S. Tulenko
Laboratory for Development of Advanced Nuclear Fuels and Materials, University of Florida, Gainesville, FL, USA

Article Outline

Glossary
Definition of the Subject: Nuclear Reactor Materials and Fuels
Introduction to Nuclear Reactor Materials and Fuels
Nuclear Fuel Materials
Nuclear Clad Materials
Nuclear Moderator Materials
Nuclear Coolant Materials
Nuclear (Neutron) Poison Materials
Nuclear Structural Materials
Future Directions
Bibliography

Glossary

Austenitic stainless steel Austenitic steels contain alloys of chromium and nickel (sometimes manganese and nitrogen), structured around the Type 302 stainless steel composition of iron, 18% chromium, and 8% nickel. Austenitic steels are not hardenable by heat treatment. The most common austenitic stainless steel is type 304.

Burnup A measurement of the energy generated by fuel atoms that undergo fission. It is normally quoted in megawatt–days per metric ton of uranium metal or its equivalent (MWd/MTU).

Core plate In a reactor the upper and lower core plates supports the fuel, channels the cooling water into the fuel bundle, and assures each fuel bundle is maintained equidistant from each other.

Fertile fuel A material capable of creating a fissile fuel upon capture of a neutron. Examples are U^{238} and Th^{232}, which create Pu^{239} and U^{233} respectively.

Fissile fuel Capable of undergoing fission by thermal neutrons. The four primary nuclides are U^{233}, U^{235}, Pu^{239}, and Pu^{241}.

Fissionable fuel A material capable of undergoing fission, via the absorption of a neutron with kinetic

energy above a certain level. Examples are U^{238} and Th^{232}.

Half-life The time it takes for the mass of a substance undergoing decay to decrease by half.

Inconel Refers to a family of austenitic nickel-chromium-based high performance alloys trademarked by the Special Metals Corporation. Inconel metal is typically used in high temperature applications and is generally known for its resistance to oxidation and a superior ability to maintain integrity in high temperature conditions.

Isotopes Isotopes are different forms of atoms (nuclides) of the same chemical element, each having a different number of neutrons. Isotopes differ in mass number (the number of neutrons plus protons in the nucleus) but not in atomic number (total number of protons). All isotopes of an element have the same chemical properties, but frequently they have very different nuclear properties.

Martensitic or ferritic steels The major alloying addition in martensitic stainless steels is chromium in the range of 11–17%. The carbon levels can vary from 0.10% to 0.65% in these alloys. The high carbon enables the material to be hardened by heating to a high temperature, followed by rapid cooling (quenching). Martensitic steels offer a good combination of corrosion resistance and superior mechanical properties, offering maximum hardness, strength, and resistance to abrasion and erosion.

Neutron capture cross section The neutron cross section of an isotope is a measure of the probability of neutron capture by that element. It is the effective area that a particular atom of that isotope presents to absorb a neutron, and is measured by a unit (of area) called "barn," which is 10^{-24} cm^2.

Nuclear fuel clad or cladding The outer layer of the fuel rods, a barrier between the coolant and the nuclear fuel. It is made of a corrosion-resistant metal that has a low absorption cross section for thermal neutrons. In today's modern commercial reactors, cladding is made usually of Zircaloy.

Passivating layer In the context of corrosion, passivation is the formation of a nonreactive surface film which inhibits further corrosion.

Plutonium (Pu) Man-made element with atomic number 94. Of the many Pu isotopes, the most noteworthy is ^{239}Pu because is a fissile isotope and may also be used to make a nuclear weapon. ^{238}Pu has found a great application in space missions powering electronic equipment.

Thermal conductivity Property of a material that describes its ability to conduct heat.

Thorium (Th) Naturally occurring element with atomic number 90; the only isotope found in nature is ^{232}Th. Th is more abundant than U. Upon capture of a neutron and subsequent radioactive decay, it forms ^{233}U, which is a fissile isotope.

Uranium (U) Naturally occurring element with atomic number 92; three isotopes are found in nature: U^{238}, U^{235}, and U^{234} with an abundances respectively, of 99.28%, 0,711%, and 0.00057%. The isotope ^{235}U is the only naturally occurring fissile isotope.

Uranium dioxide (UO_2) An oxide of uranium; a black mildly radioactive, crystalline material that is used in nuclear fuel rods in nuclear reactors.

Zircaloy Is a group of alloys, mostly consisting of zirconium, with minor additions of tin (often about 1.5%), iron and chromium, used as a fuel rod clad material in light water thermal reactors.

Definition of the Subject: Nuclear Reactor Materials and Fuels

Nuclear reactor materials and fuels can be classified into six categories:

- Nuclear fuel materials
- Nuclear clad materials
- Nuclear coolant materials
- Nuclear poison materials
- Nuclear moderator materials
- Nuclear structural materials

The materials unique to nuclear reactors are the nuclear fuel materials. All the other materials are used in other applications. Because nuclear fuel materials are radioactive, they require specialized handling. Additionally, because of the connection of nuclear energy with the atom bomb, security in its tightest form is required for nuclear fuel.

Introduction to Nuclear Reactor Materials and Fuels

The first nuclear reactor was the famous "Chicago Pile" (CP-1) which was built under the west stands of Stagg

Field at the University of Chicago on a squash court and went critical on December 2, 1942. The first nuclear materials were uranium in both a metal and an oxide form as the fuel, carbon in a graphite form as the moderator, atmospheric air as the coolant (since the reactor power was essentially zero), cadmium as the control material, and wood as the structural material. Nuclear power plant designs have come a long way since then, particularly with regard to cooling. However, the fuel form remains basically the same.

Nuclear Fuel Materials

There are three basic nuclear fuel materials which can be utilized in many different forms: uranium, plutonium, and thorium. The most utilized fuel material is uranium and it is most often utilized in the oxide form in pellet form (see Fig. 1). That one pellet held in the tweezers has the energy equivalent of 1 t of coal. Natural uranium is composed of uranium 238 (99.3%) and uranium 235 (0.7%). Uranium 238 is classified as a fertile material, which produces the fissile Plutonium 239 when it captures a neutron. It is necessary to enrich the uranium in the uranium 235 isotope in order to run the light water reactors (LWRs). The uranium for commercial power reactors is normally enriched to ~5% U^{235}. The methods used to enrich the uranium are the gaseous diffusion process in which the isotopes of different molecular weights diffuse differently through a porous barrier and the gaseous centrifuge process, where the different masses are centrifuged in a fast rotating cylinder with the heavier molecules moving toward the periphery of the centrifuge, thus separated from the lighter ones. For both processes a gaseous compound is necessary, that compound is uranium hexafluoride (UF_6) which is a solid at room temperature but becomes a gas at 56.4°C. As a gas, uranium hexafluoride becomes very suitable for a variety of processes to enrich the material in uranium 235. Lastly, and still in development, the laser method where laser radiation is used to excite, ionize, or dissociate one isotopic species without affecting the other may be used for enrichment. The current favored method of enrichment is the gaseous centrifuge.

Nuclear Reactor Materials and Fuels. Figure 1 Uranium dioxide (UO_2) fuel pellet (Courtesy AREVA)

Uranium as a fuel is also utilized in the metallic form as an alloy with either zircaloy or aluminum in Sodium Fast Reactors (SFRs) and in research reactors. Experimental developmental work is researching the carbide and nitride forms of uranium as a useful fuel form for SFR reactors and Gas Cooled Reactors (GCRs) because of their excellent thermal conductivity properties and higher uranium density. Research is also under way to utilizing uranium or plutonium in either the oxide or metal form with materials such as silicon carbide or zircaloy to form inert matrix fuel forms with improved thermal conductivity properties. Uranium dioxide (UO_2) is a good fuel because it has a high melting point (2,865°C) and does not dissolve in water. However, in an oxidizing environment UO_2 can be oxidized to U_3O_8, which does dissolve in water. The major drawback of uranium dioxide as a fuel form is that it has a relatively low thermal conductivity, which continues to decrease with temperature until approximately 2,000°C. Additionally, the thermal conductivity of uranium also decreases with burnup as the fuel produces power. Since the Nuclear Regulatory Commission does not permit reactors to operate in a condition where centerline melting of the fuel pellet may occur, the high melting temperature of the uranium dioxide does tend to offset its low thermal conductivity. However, the high temperatures in the uranium oxide pellet during operation does lead to thermal stresses, which result in cracking in the pellet both in the radial and circumferential directions. The uranium carbide (UC) and uranium nitride (UN) fuel forms have the benefits of a very high thermal conductivity and a higher density than UO_2 of uranium. However, they dissolve in water and therefore cannot be considered for use in the water cooled

Nuclear Reactor Materials and Fuels. Table 1 Comparison between UO_2, UZr, UC, and UN fuel for key material characteristics

Fuel comparison	Uranium oxide (UO_2)	Metallic fuel (UZr)	Carbide fuel (UC)	Nitride fuel (UN)
Density (g/cm^3)	9.75	14	13.58	13.53
Melting point (°C)	2,750	1,080	2,420	2,780
Thermal conductivity (W/mK)	2.9	14	16.5	14.3

reactors. The metal fuel form has a higher thermal conductivity and a higher density of uranium than UO_2, but does have a lower melting temperature. The material properties of the various uranium fuel forms are shown in Table 1.

Plutonium does not exist in nature, but is a totally man-generated fuel. Plutonium 239 is a fissile isotope generated from a neutron being captured in U^{238} and has a larger fission cross section than that of uranium 235. However, plutonium 239 has a smaller half-life of 24,200 years versus the half-life of uranium 235 of 7.04×10^8 years, so it is far more radioactive and cannot be handled like uranium. Additionally, plutonium 239 in reactor forms a whole family of fertile and fissionable isotopes: Pu^{240}, Pu^{241}, and Pu^{242}. These isotopes have similar short half-lives of 6,537 years for Pu^{240}, 14.4 years for Pu^{241}, and a long half-life of 376,000 years for Pu^{242}. Plutonium metal melts at approximately 640°C, a much lower temperature than uranium, and has a thermal conductivity at 300 K of 6.74 W/mK versus a value of 27.5 W/mK for uranium metal. Plutonium fuel is normally used as an oxide and is mixed with natural or depleted uranium oxide. This mixed oxide fuel form is termed MOX.

Thorium is a fertile fuel containing only the single thorium isotope Th^{232}, which upon capture of a neutron forms Th^{233}. Th^{233} is transmuted by beta decay with a half-life of 22.3 min into Pa ^{233}, which beta decays with a half-life of 27 days into the fissile uranium isotope U^{233}. Thorium dioxide's advantage over uranium dioxide as a fuel form is that it has both a higher thermal conductivity ($\sim$5.25 Wm^{-1} K^{-1} at 800 K), a higher melting point (3,350°C), 80°C higher than uranium, and is insoluble in water under all conditions, having only the single oxidation state (O_2). Thorium oxide with enriched uranium oxide was the fuel in the very first full-scale nuclear power reactor (the Shippingport Atomic Power Station), which was built by Admiral Rickover for the Duquesne Light Company. This reactor went critical on December 12, 1957.

Nuclear Clad Materials

The clad materials, which enclose the nuclear fuel, are really the first line of defense to retain the radioactive materials within its boundaries and to protect the fuel from the moderator. In additional to these tasks, the clad also provides structural integrity for the fuel assembly and a surface for heat transfer from the fuel to the coolant. The fuel clad and the guide tubes, which connect the upper and lower end fittings of the fuel assembly, are normally made of the same material. The cladding material must be chemically compatible with the fuel and it must be corrosion resistant with the coolant material. Additionally, it is important that the cladding and the guide tube material have a very small neutron capture cross section so as to not interfere with the fission process. Stainless steel has excellent corrosion properties and an excellent resistance to neutron irradiation. However, it has a relatively high thermal neutron absorption cross section. Until a material could be developed which had a low neutron absorption cross section and good corrosion and structural properties under irradiation, stainless steel was used as both the cladding material and the guide tube for both thermal and fast reactors. However, in thermal reactors, the stainless steel neutron absorption cross section is relatively large and the resulting penalty in neutron economy forced a search for a replacement material which would have the required mechanical strength, corrosion resistance in the water moderator, and a low neutron absorption cross section. This search lead to the development of zircaloy, a zirconium alloy material made with minor additions of tin, oxygen, iron, and chromium. The zircaloy family of materials was developed out of the US Naval Reactors program and was quickly picked up by the commercial industry to replace stainless steel as a cladding material and guide

tube material (and shroud for BWR reactors) both for pressurized and boiling water reactors. The Shippingport Reactor, mentioned earlier, utilized zircaloy clad for its fuel rods. It should be noted that the light water reactor (LWR) concept was developed for the nuclear navy be Admiral H. Rickover and that he helped to shape the nuclear industry. Zircaloy had the required mechanical strength, a small neutron cross section, and good corrosion resistance. While zircaloy reacts with oxygen, it does form a passivating layer that protects the remaining zircaloy from further oxidation. Recent zircaloy alloy developments have added niobium and eliminated the chromium to give better oxidizing and hydriding resistance. Zircaloy is still the material of choice for the nuclear commercial industry. The upper and lower end fittings are made either of stainless steel or of inconel, since they are outside of the active nuclear portion of the core. Different inconels have widely varying compositions, but all are predominantly nickel, with chromium as the second element and iron as the third element. Nickel has a large thermal capture cross section for neutrons. The spacer grids which hold the fuel rods in place were originally either inconel or stainless steel, but were subsequently also changed to zircaloy. Figure 2 displays a schematic of a nuclear fuel rod showing the fuel pellets, top insulator pellet, and the fuel hold down spring which keeps the fuel pellets from moving during shipping and handling. Figure 3 shows a fuel assembly structure with end fittings, guide tubes, and spacer grids, but no fuel rods. The fuel guide tubes provide the vertical structure for the fuel assemblies and serve as channels for the control rods to enter into the fuel assemblies. The spacer grids provide the horizontal structure for the fuel assemblies. Figure 4 shows a fuel assembly with fuel rods in place.

Stainless steel continues to be used as the cladding for fast reactors, since stainless steel tends to have low capture cross sections in the fast neutron energy region. However, even here, as coolant temperatures have been increasing in reactor designs in order to obtain ever higher thermal efficiencies, improved steel alloys have been required to be developed. First, austenitic stainless steels replaced the 304 stainless, and now oxide dispersion strengthened (ODS) martensitic or ferritic steels are under development to replace the austenitic stainless steels. Even more recently, silicon carbide cladding has been being researched as a cladding for the future. The silicon carbide cladding is made from a silicon carbide weave which is then impregnated with a silicon carbide vapor and in the latest designs a metal liner is placed on the inner surface of the clad. As a ceramic, silicon carbide would be resistant to oxidation and would have an extremely high melting temperature, so as to render the loss of coolant accident (LOCA) a nonevent.

Nuclear Moderator Materials

With the advent of nuclear reactors, the nuclear fission process was found to proceed more easily if the neutrons were moderated in energy into the thermal range ($E < 1.0$ eV). The ideal moderator would have a very low thermal neutron capture cross section and a low atomic number in order to increase the neutrons energy loss on each collision. The very first nuclear reactors used graphite (carbon) to slow the fission neutrons down to the thermal energy regime. Carbon had a very small neutron absorption cross section and an atomic weight of 12. With the advent of the power reactors, water was used as both the moderating and the coolant material. Hydrogen, with an atomic weight of 1, equal to that of a neutron, could slow the neutrons down with very few collisions, and moreover, water is inexpensive. However, hydrogen does have a relatively high thermal neutron capture cross section, turning the hydrogen into deuterium. This capture cross section of ordinary water requires that light water reactors must use enriched uranium as a fuel. Deuterium oxide, or heavy water,

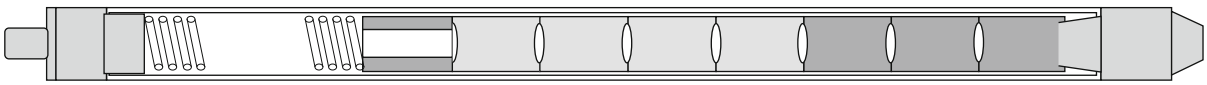

Nuclear Reactor Materials and Fuels. Figure 2
Schematic representation of a fuel rod showing fuel pellets, upper fuel spacer, fuel clad, fuel hold down spring, and upper and lower fuel end plugs

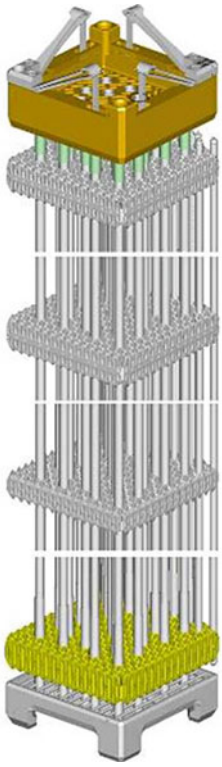

Nuclear Reactor Materials and Fuels. Figure 3
Pressurized water nuclear fuel assembly structure showing upper and lower end fittings, fuel guide tubes, and fuel spacer grids – without fuel rods in place (Courtesy AREVA)

Nuclear Reactor Materials and Fuels. Figure 4
Shows a fuel assembly with fuel rods in place (Courtesy AREVA)

would be an ideal moderator and coolant because of its very low capture cross section for neutrons. However, its very high price makes it a very expensive material to use. The Canadians utilize heavy water as their moderator and coolant in their Canadian-Deuterium-Uranium (CANDU) reactors. The extremely low absorption cross section of deuterium allows the CANDU to construct and operate nuclear power plants without the need for enrichment, utilizing natural uranium fuel. But they had to build plants to separate the heavy water (deuterium) out of ordinary water. Hydrogen has also been used in solid form in zirconium hydride (ZrH) as a moderator for space applications and for the TRIGA (*T*raining, *R*esearch, *I*sotopes, *G*eneral *A*tomics) research reactors of General Atomics. Lithium, a liquid metal, can also be used as a moderator. Beryllium has been used as a moderator in research reactors and in many ways is superior to graphite and lithium. However, beryllium is a very toxic material which limits its usefulness because of Environmental Protection Agency restrictions on its use.

Nuclear Coolant Materials

Nuclear coolant materials should be marked by a low melting temperature and a high boiling point. The obvious coolant which has been used in fossil boilers for years is water or steam. However, its low boiling point requires that it be pressurized to allow for a high heat content. Thus, the pressurized water reactor (PWR) has a system pressure of approximately 2,200 psi and the Boiling Water Reactor (BWR) has a pressure of approximately 1,100 psi. As mentioned earlier, the Canadians utilize heavy water as their coolant in the CANDU reactor. However, the Canadians are developing new reactors which utilize ordinary water as the coolant, while retaining heavy water as the moderator. The British for their reactors went with graphite as

the moderator and pressurized carbon dioxide (CO_2) as the coolant in their Advanced Gas Reactor (AGR). The United States has researched using pressurized helium cooled, graphite moderated reactors at the Peach Bottom Reactor (in Pennsylvania) and the Fort Saint Vrain Reactor (in Colorado). The fast reactors utilize either sodium or helium as a coolant. Various experimental reactors have utilized exotic coolants such as fluoride salts, lithium, sodium-potassium alloy (NAK), and a lead-bismuth eutectic. Lead-bismuth (Pb-Bi) eutectic has a low melting point, a high boiling point, and does not react with water or oxygen. The Russians have operated lead cooled reactors in their nuclear navy. The heavy density of lead may generate erosion in its container pipes, particularly bends in its flow path. Molten salts have the advantage of having a very high boiling point and containing the fuel right in the molten salt mixture, thereby doing away with a need to fabricate the fuel.

Nuclear (Neutron) Poison Materials

Nuclear engineers use the term "poison" to describe any material that steals neutrons away from the fission process. Nuclear reactors use poison materials to control the fission chain reaction. These poison materials must have a high neutron capture cross sections. Poison materials are of two types: burnable and nonburnable. In the burnable poison type, the poison material upon capturing a neutron, loses its large neutron capture cross section. In the nonburnable poison type, the poison materials, upon capturing a neutron, convert into a similar high-absorbing neutron cross section material. Three typical control materials used in control rods are (1) hafnium, (2) an alloy of silver, indium, cadmium, and (3) boron. Boron is not a nonburnable poison, like the other control materials, because the main neutron-absorbing isotope ^{10}B, upon capturing a neutron, converts to ^{4}He and ^{7}Li. Boron control rods must be replaced at regular intervals, unlike control rods made with hafnium or the alloy of silver, indium, and cadmium. Soluble boron is added as a poison material into the coolant of pressurized water reactors, where it can be adjusted to keep the reactor in a critical condition. When used in the coolant, the boron is called a chemical shim or "chem shim." The use of boron in the coolant allows pressurized water reactors to keep the control rods out of the core during operation. In a PWR, control rods are used only to shut down the reactor. Boiling water reactors cannot use boron in the coolant because of the boiling action which would lead to boron plate ousting and also that the boron could reach the turbines and ruin the blades. For these reasons, they must utilize control rods in the core during operation in order to control the reactivity of the core.

Boron is also used as a burnable poison in burnable poison rod assemblies (BPRAs), which are inserted into the unoccupied control rod guide tubes and changed at each refueling. The boron is depleted during the cycle, such that at end of cycle the poison effect has been exhausted. Boron is also placed inside the fuel rods in Westinghouse reactors where a thin layer of zirconium diboride (ZrB_2) is coated on the fuel pellets. Gadolinium and erbium are also used as burnable poison materials and are mixed with the uranium dioxide (UO_2) fuel when forming the fuel pellets. BWR reactors use gadolinium extensively in the fuel in order to control the reactivity because of their inability to utilize boron in the coolant. The advantage of the burnable poison in the fuel, as opposed to BPRAS, is that there is less nuclear waste and the displacement of the water in the guide tube by the BPRAs does result in an end-of-cycle reactivity penalty for the BPRAs.

Nuclear Structural Materials

As mentioned, the very first reactor (CP-1) used wood as the structural material. However, today the nuclear structural materials are steel and concrete. The nuclear-fueled core is contained inside a steel vessel which has steel core support plates, top and bottom, upon which the core is held in place. The steel vessel is approximately 6 in. thick. In new designs, the steel vessel may be inside a concrete shield wall. In pressurized water reactors, steel baffles surround the core and separate the incoming colder water in the down comer from the heated water in the open core. In the boiling water reactor, each fuel assembly is contained in a zircaloy fuel shroud that isolates the water being heated in each fuel assembly. In both the PWR and the BWR, the steel pressure vessel is contained inside a steel reinforced concrete containment structure with a steel liner. Figure 5 shows a PWR reactor vessel with the fuel core, upper core internals, and upper and lower grid assemblies.

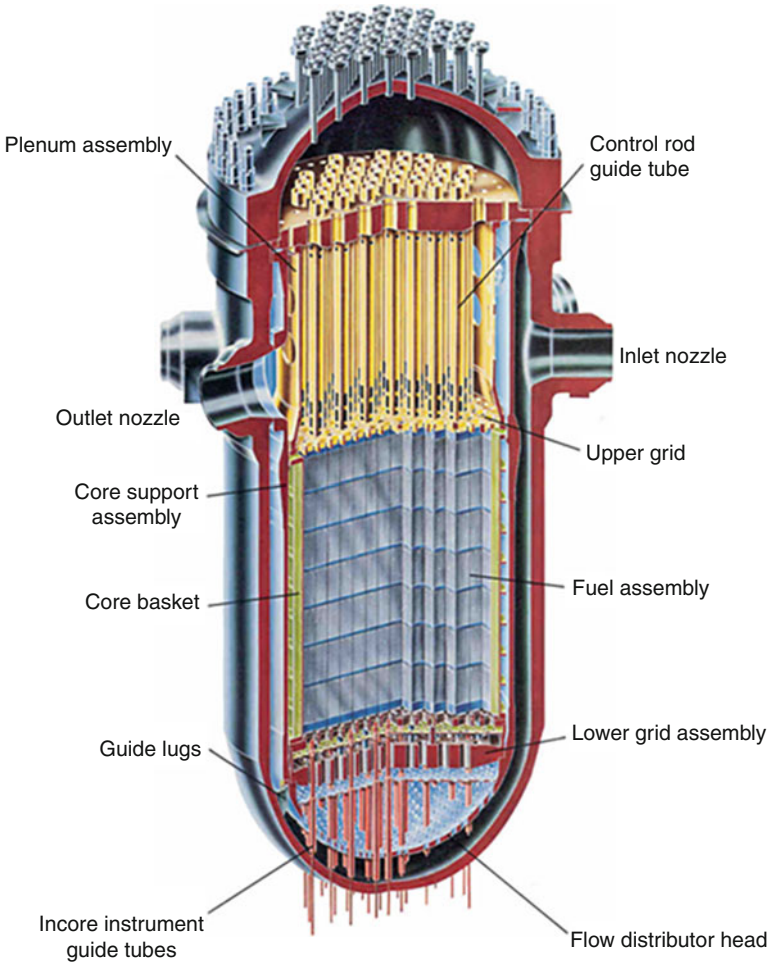

Nuclear Reactor Materials and Fuels. Figure 5
Pressurized water reactor vessel showing fuel core, upper and lower grid assembly, and core internals (Courtesy AREVA)

Future Directions

For light water reactors, the future directions for the thermal reactors include the development of a crushable fuel pellet design and a ceramic cladding, such as the silicon carbide clad mentioned. This crushable pellet is needed because ceramic clad materials do not do well in tension. Thus, it is necessary for the pellet to give when interacting with the cladding, to prevent creating excessive tension forces on the clad. This development would also eliminate concerns regarding the pellet clad interaction (PCI) which currently limits power-transitions during operation of light water reactors.

The successful development of the molten salt reactor would offer many benefits by eliminating the fuel fabrication step, allowing for online reprocessing and fueling, and also allowing for higher temperature operation with a resultant increase in thermal efficiency. In the long run, future reactors will most likely be fast breeder reactors, either using sodium or helium as the coolant, and fueled with uranium carbide and clad with silicon carbide.

Bibliography

1. Cochran RG, Tsoulfanidis N (1999) The nuclear fuel cycle: analysis and management, 2nd edn. American Nuclear Society, La Grange Park. ISBN 0-89448-451-6
2. Knief R (1992) Nuclear engineering: theory and technology of commercial nuclear power, 2nd edn. Hemisphere, Washington, DC. ISBN 978-0-89448-458-2
3. Glasstone S, Sesonske A (1994) Nuclear reactor engineering: reactor design basics, vol 1. Chapman & Hall, New York. ISBN 0-442-20057-9

Nuclear Safeguards and Proliferation of Nuclear Weapons Materials

Michael C. Baker
Advanced Nuclear Technology Group, Nuclear Nonproliferation Division, Los Alamos National Laboratory, Los Alamos, NM, USA

Article Outline

Glossary
Definition of the Subject
Introduction: Historical Development of Nuclear Safeguards and Nonproliferation Policy
Technologies for Safeguarding Nuclear Materials
Detection of Nuclear Proliferation and Treaty Verification
Detection and Prevention of Illicit Trafficking and Terrorism
Future Directions
Bibliography

Glossary

Calorimetry Calorimetry is a nondestructive assay technique for determining the thermal power output of heat-producing nuclear materials. Calorimeter systems are used to determine the power output (Watts) of various radionuclides over a broad range of power levels and sample types (Pu, highly enriched uranium, and Tritium).

Destructive assay Destructive Assay (DA) aims at the measurement of the nuclear material content, the isotopic composition, or other chemical properties of a sample. The analysis introduces a significant change to the physical form of the test sample.

Detection time The maximum time that may elapse between diversion of a given amount of nuclear material and detection of that diversion by a safeguards authority.

Direct-use material Nuclear material that can be used for the manufacture of nuclear explosive devices without transmutation or further enrichment. It includes plutonium containing less than 80% ^{238}Pu, highly-enriched uranium, and ^{233}U.

Diversion The undeclared removal of nuclear material from a safeguarded facility or the use of a safeguarded facility for the production or processing of undeclared nuclear material.

Dual-use technology Technology that can be used for both military and peaceful purposes.

Highly enriched uranium (HEU) Uranium containing 20% or more of the isotope uranium-235.

Holdup The amount of nuclear material remaining in process equipment and facilities after the in-process material, stored materials, and product have been removed.

Nondestructive assay Nondestructive Assay (NDA) techniques allow analysis of a sample in its own physical/chemical form without any modification of its properties and characteristics. The most common NDA techniques applied in nuclear safeguards include gamma spectroscopy, neutron counting, and calorimetry.

Nuclear material (NM) Any source or special fissionable material.

Safeguards An integrated, layered system of physical protection, material accounting, and material control measures designed to deter, prevent, detect, and respond to unauthorized possession, use, or sabotage of nuclear materials.

Significant quantity (SQ) The approximate amount of nuclear material for which the possibility of manufacturing a nuclear explosive device cannot be excluded. The International Atomic Energy Agency uses 8 kg of plutonium, 25 kg of ^{235}U in highly enriched uranium, and 75 kg of ^{235}U in low enriched or natural uranium.

Source material Uranium containing the mixture of isotopes occurring in nature; uranium depleted in the isotope 235; thorium; or ore concentrate.

Special fissionable material Plutonium-239; uranium-233; uranium enriched in the isotopes 235 or 233; and any material containing one or more of the foregoing; and such other fissionable material as the International Atomic Energy Agency Board of Governors shall from time to time determine; but the term "special fissionable material" does not include source material.

Special nuclear material (SNM) Plutonium, uranium-233, uranium enriched in the isotope 235, and any other material which, pursuant to

Section 51 of the United States Atomic Energy Act of 1954, as amended, has been determined to be special nuclear material, but does not include source material; it also includes any material artificially enriched by any of the foregoing, not including source material.

Definition of the Subject

Nuclear technology, by its very nature, may be used for peaceful or harmful ends. From its birth, efforts have existed to control access to, as well as the spread of, nuclear technology for destructive purposes, while at the same time attempting to provide access to its multitude of beneficial applications. Nuclear safeguards refers to the system of legal, institutional, and technical mechanisms used to control the use of nuclear materials, detect nuclear material misuse, and if the material is misused, to provide domestic and international responses in a timely fashion. Proliferation refers to the spread of weapons usable or direct-use materials, nuclear weapons technology, and the knowledge and skills necessary for the design and manufacture of such weapons. Nonproliferation policy and technology, including nuclear safeguards, has traditionally been centered on the spread between nation states. In the past decade, that focus has broadened to include the spread of materials, technology, and knowledge to criminal and terrorist entities. Nuclear safeguards must be viewed as a multilayered system, no single layer being self-sufficient, which as a whole, provides deterrence, detection, and response to theft, diversion, or misuse of nuclear material and nuclear weapons knowledge and skills.

Introduction: Historical Development of Nuclear Safeguards and Nonproliferation Policy

Before the end of World War II, diplomats and scientists familiar with nuclear weapons technology and its early development during the war were struggling with how to control the technology while sharing its benefits. Early efforts were largely focused on international control and the development of an international authority for management of the control regime and nuclear materials. In June 1946, following the formation of the United Nations Atomic Energy Commission (UNAEC) in January, the US representative, Bernard Baruch, proposed a plan for such an international control regime. The Soviet Union and other countries opposed the significant transfer of state authority to an international body, as would be required, and the Baruch plan quickly came to pass. However, it did provide the conceptual framework and foundation for subsequent discussions between nation states.

By mid 1953, three nations (USA, United Kingdom, and Soviet Union) had conducted nuclear tests, Dwight Eisenhower had been elected President of the USA, and Joseph Stalin had died. These events set the stage for President Eisenhower's address to the United Nations on December 8, 1953. This address outlined the President's Atoms for Peace initiative, which included the creation of an international agency responsible for the peaceful expansion of nuclear technology and the control of nuclear materials that in accordance with the President's plan would be contributed by nation states. The President's initiative also called for states receiving assistance with the peaceful application of nuclear technology to allow inspections that would ensure that the technology and materials were not used for military purposes. The President's speech was the genesis of the International Atomic Energy Agency (IAEA).

In 1956, 81 nations unanimously approved the charter of the IAEA. At the same time, international cooperation related to the peaceful application of nuclear technology was rapidly expanding. By the end of 1959, the USA had cooperative bilateral agreements with 42 countries for collaborative nuclear technology development. Within the next decade, the Soviet Union would have similar agreements with another 26 countries. In most cases, both the USA and Soviet Union included at least a minimal acknowledgement of the dual-use capabilities of the nuclear technologies to be shared. The Soviet cooperative agreements typically required the return of spent nuclear fuel to the Soviet Union as a nuclear material control measure, as well as a pledge to use the material only for peaceful purposes. Most of the US agreements foresaw the need for nuclear safeguards to be applied by the USA that would eventually be turned over to the IAEA. The safeguards experience gained as a result of these bilateral agreements, as well as that obtained following the establishment of Euratom safeguards by the European community in 1957, provided a useful experience base and context for the establishment of specific IAEA safeguards agreements and protocols. In 1959,

IAEA safeguards were applied for the first time at the Japanese JRR-3 research reactor running on natural uranium fuel from Canada. [1]

The political history of the early 1960s included France and China joining the club of countries that had conducted nuclear tests and the Cuban Missile Crisis in 1962. This later event, one of the major confrontations of the Cold War, is the closest the world has come to a nuclear war. During the crisis, US armed forces were at their highest state of readiness and Soviet commanders were prepared to use nuclear weapons to defend Cuba against an invasion [2]. As a result, both superpowers came to the realization that greater cooperation on nuclear arms and nuclear safeguards were necessary for their mutual national security and that of their allies. This recognition and associated efforts to seek common ground were also seen in other countries. For example, in 1967, the Treaty for the Prohibition of Nuclear Weapons in Latin America was signed. By 1968, negotiations regarding the Treaty on the Non-Proliferation of Nuclear Weapons (NPT) were well underway. Although the idea of such a treaty had been proposed ten years earlier by Ireland, the NPT was not opened for signature until 1970. This marked a major milestone in the evolution of nonproliferation policy and nuclear safeguards. One of the significant requirements that resulted from the NPT is that nonnuclear weapons states place all of their peaceful nuclear programs under IAEA safeguards. As of 2007, the NPT had been ratified by 189 nations.

After the NPT had established a legal framework for international safeguards in 1970, the next twenty years saw the rapid development of both destructive and nondestructive measurement technology in support of nuclear safeguards, as well as the continued development of procedures and protocols used for international inspections. Formal training programs were established in multiple countries, as well as by the IAEA, to train and develop a cadre of professional safeguards inspectors. Some would argue that safeguards programs, personnel, and international policy had reached a state of maturity by the mid 1980s. However, in 1991, the international community was shocked with the revelation of a clandestine nuclear weapons program in Iraq. This program had developed under the noses of international inspectors that had been reviewing the declared activities in Iraq but were unaware of the clandestine program.

The international community responded with a reevaluation of safeguards and nonproliferation policy that included an acknowledgment of the need for IAEA safeguards to be significantly strengthened. Specifically, the IAEA needed the capability to detect undeclared nuclear activities in countries that were parties to the NPT. In 1997, the IAEA Board of Governors approved the "Additional Protocol" which allows for the use of environmental sampling to detect clandestine activities, earlier provision of design information on nuclear facilities to the IAEA, complementary access to additional locations within a country, and a broader use of open source, satellite imagery, and third party information to access nonproliferation performance in a particular nation. As of 2009, implementation of the Additional Protocol was complete or at a minimum underway in countries with significant nuclear programs.

Until the terror attacks on September 11, 2001, the diversion of nuclear material for a nation state's weapon program was the primary threat that nuclear safeguards programs were designed to mitigate and international policy experts had been focused. Those attacks demonstrated a higher level of sophistication than previously expected and brought the realization to international security professionals that nuclear terrorism sponsored by substate actors must also be considered as a significant threat to be addressed by nuclear security programs. In the last decade, the proliferation of nuclear materials and nuclear weapons to substate groups has replaced a potential nuclear confrontation between dominant superpowers as the preeminent global security concern. This has shifted emphasis in the nuclear security community to border monitoring, event attribution, and consequence management. In 2009, with the election of a new President in the USA, focus of international security policy and programs is returning to the threat from nations with large nuclear arsenals; however, it is certain that the terrorist threat will remain a greater concern than it was before 2001. Significant events that impacted the development of international nonproliferation and safeguards policy are shown in Table 1.

Technologies for Safeguarding Nuclear Materials

To properly secure nuclear materials, a state must know how much material it possesses and where it is located. This baseline is used to plan protection strategies,

Nuclear Safeguards and Proliferation of Nuclear Weapons Materials. Table 1 Influential events in the development of international safeguards and nonproliferation policy

Date	Event
1945	USA's first nuclear test at the Trinity Site.
	Nuclear bombing of Hiroshima and Nagasaki.
1946	Formation of the United Nations Atomic Energy Commission (UNAEC).
	Baruch Plan presented.
1949	Soviet nuclear test.
	UNAEC dissolves.
1952	United Kingdom nuclear test.
1953	President Eisenhower presents Atoms for Peace.
1955	USA and Turkey conclude the first "Atoms for Peace" cooperative agreement for the peaceful uses of nuclear energy.
1956	International Atomic Energy Agency (IAEA) charter is approved.
1957	European Atomic Energy Community (Euratom) is established.
1959	First application of IAEA safeguards.
1960	French nuclear test.
1962	Cuban Missile Crisis.
1964	Chinese nuclear test.
1967	Treaty for the Prohibition of Nuclear Weapons in Latin America established.
1968	Treaty for the Non-Proliferation of Nuclear Weapons (NPT) established.
1974	Indian nuclear test.
1979	Three Mile Island nuclear accident.
1986	Chernobyl nuclear accident.
1991	Iraqi clandestine nuclear weapons program discovered.
1995	NPT is made permanent.
1997	IAEA approves the Additional Protocol.
1998	Pakistan's nuclear test.
2001	September 11, 2001 terrorist attacks in the USA.
2003	Disclosure of the A. Q. Kahn clandestine nuclear trade network.
2006	North Korean nuclear test.

which mitigate the risks from both insider and outsider threats. The fundamental system that both provides this baseline information and allows the tracking and maintenance of the information as it changes over time is the nuclear material accounting system. To be effective, this system must be supported by a nuclear material measurement program, which provides accurate and precise information on the material being protected.

Nuclear material accounting and nuclear material measurements must be closely coupled with a physical protection system that ensures that access to the material is controlled and the materials stay in their intended locations. The physical protection system consists of people, procedures, and technology, which are designed and implemented following a careful evaluation of system vulnerabilities against predicted threats. Each facility is unique; therefore, a systematic planning effort is required to manage risks appropriately.

Nuclear Material Accounting

Nuclear material accounting is not that different from managing inventory for a complicated manufacturing and warehouse operation or the accounting involved in today's banking systems. Matter of fact, initial nuclear materials accounting developed from procedures and tools, which had been developed for financial and materials management. Today, nuclear material accounting is defined as the use of statistical and accounting measures to maintain knowledge of the quantities of SNM present in each area of a facility. It includes the use of physical inventories and material balances to verify the presence of material or to detect the loss of material after it occurs.

The quality of nuclear material accounting data and therefore the quality of the entire safeguards system is dependent on

- A measurement system that provides accurate, repeatable data on nuclear material quantities involved in both storage and internal or external transfers;
- Operating records that document nuclear material movements, locations, item identities, item histories, and links to the measurement data; and

- Accounting control procedures that include frequent cross-checking of data to detect inconsistencies, which may be indications of human error, unidentified measurement errors, or an attempt to divert or steal material.

The accounting system may divide a facility or process into sections, which are frequently called material balance areas (MBA) for monitoring and tracking of nuclear material (NM). Measurement, storage, and transfer records are maintained for each MBA. The choice of MBA boundaries will impact detection probabilities and should be carefully considered. The MBA will include defined key measurement points (KMP), where NM is in a form that can be measured to determine material flow or inventory. KMPs include, but are not limited to, all of the inputs and outputs to the MBA. Selection of appropriate KMPs is a fundamental requirement for timely detection of diversion or theft attempts. Ideally these KMPs would be identified during facility or process design to optimize their effectiveness while minimizing the impact on operational efficiency.

One of the primary goals of an accounting system is to monitor the inventory difference (ID) or material unaccounted for (MUF) within a facility or a specific area within a facility, such as an MBA, over a given period of time. The period of time used is typically the time between physical inventories of SNM within the facility, usually one or two months. The ID for SNM over this time period of interest, represented by t, is defined as:

$$ID_t = BI_t + R_t - EI_t - S_t \tag{3.1}$$

where BI is the beginning inventory of SNM, R is receipts of SNM during the inventory period, EI is the ending physical inventory of SNM, and S is shipments out of SNM during the inventory period. Note that all terms may have multiple individual components and include some uncertainty due to measurement and sampling errors. IDs are charted as a function of time and monitored for trends that may indicate a loss of nuclear material. If the safeguards practitioner understands the uncertainties in the components of each of the inputs to equation 3.1, the practitioner may propagate these uncertainties to determine the variance of the ID, σ_{ID}. The monthly ID may then be compared to statistical limits to determine whether or not an indicator of theft or diversion may exist. An ID in excess of a significant quantity (SQ) indicates an abrupt loss of NM. Trends including systematic, smaller losses of NM over a period of time indicate a protracted loss of material. In some cases, protracted losses may be referred to as a trickle diversion.

A common performance measure for an accounting program is the magnitude of the ID variance, σ_{ID}. IDs must be maintained at a level sufficiently small to detect abrupt diversions, while a sequential test or alternative statistical test for trend detection may be used to detect both abrupt and protracted diversions [3–6]. Specific statistical tests are well documented in the literature and beyond the scope of this section. Safeguards practitioners must understand several issues that complicate the evaluation of IDs, including (1) the impact of holdup on σ_{ID}; (2) serial correlation in successive IDs; (3) poorly characterized measurement quality and its impact on estimates of σ_{ID}; and (4) time delays in the measurement results that are input components to the terms in equation 3.1. Without a detailed understanding of these effects, the practitioner will not be sensitive to the subtle variations and trends, the impact of nuclear process changes, or the impact of safeguards policy changes.

Nuclear Material Measurement Technology

The accurate quantification of nuclear material is essential to nuclear safeguards and as noted previously, the minimization of precision and bias in these measurements of NM is vital to the system's ability to detect abrupt and protracted diversion attempts. Measurement of NM is typically accomplished by either destructive wet chemistry techniques or nondestructive measurement of radiation or heat output. Nuclear material is found in multiple chemical forms, a wide range of quantities, and a variety of packaging configurations. Each of these variables introduces uncertainty into measurement results that must be carefully managed and considered when determining whether or not nuclear material is present and accounted for appropriately without evidence of diversion, theft, or misuse.

Destructive Analysis Analytical chemistry typically provides the most accurate techniques for the

quantification of pure metals and compounds of safeguards interest. These techniques require the destruction of a small sample of the nuclear material item, which must be homogenous to prevent the introduction of significant uncertainties from a sample that is not representative of the bulk item. The nature of these destructive analysis (DA) techniques requires ready access to the material to be analyzed. Finished material, such as a fuel rod, is not a candidate for DA for this reason. Some of the more common techniques, which are described below, are gravimetry, titrimetry, and mass spectrometry [7, 8].

Mass spectrometry is a mature technology used for the determination of the isotopic composition of nuclear material samples. Samples to be analyzed in a thermal ionization mass spectrometer (TIMS) are deposited on a filament that is then inserted into the spectrometer and slowly heated by an electrical current. This results in ions of the sample "boiling off" after which they are accelerated by an electric field through a magnetic field, which is orthogonal to their trajectory. This results in a deflection of the ions, the magnitude of which is a function of the weight of the ion. Following the deflection, ions are collected at positions of interest that allow the analyst to infer the isotopic mass of each ion. The precision of this technique for the analysis of plutonium or uranium isotopics is better than 0.05% [7, 8]. Gas mass spectrometers and Isotope Dilution Mass Spectrometers (IDMS) are also in use and in many cases may lead to even better precision than TIMS.

Plutonium or Uranium can be burned to PuO_2 and U_3O_8, respectively, and then accurately weighed. This technique, called gravimetry, can be performed in the laboratory with random and systematic errors of less than 0.05% [7, 8]. Nonvolatile impurities must be accurately determined and the gravimetric results then corrected accordingly.

Titration procedures are used to assay the amount of uranium or plutonium in solution through the careful addition of a reagent that reacts with the nuclear material. The measured amount of reagent to produce a particular endpoint is then related to the amount of NM. A typical endpoint is detected by a color change or electrical response of the solution. One of the most common techniques in use by the IAEA and other laboratories is the Davies–Gray method [7]. The precision for these techniques can be as good as 0.02% for uranium and 0.04 % for plutonium [7, 8].

DA techniques in use by the IAEA's Safeguards Analytical Laboratory (SAL) and its network of approved analytical laboratories are summarized in Table 2. In addition to requiring access to the material and destruction of a sample, DA techniques, in general, are more costly and time consuming than nondestructive techniques.

Nondestructive Assay Many nuclear materials that one may encounter, such as a fuel assembly or a radioisotopic heat source, are technologically complex and have high economic value. Nevertheless, to

Nuclear Safeguards and Proliferation of Nuclear Weapons Materials. Table 2 IAEA destructive analysis techniques [7]

Technique	NM	Material Type	Random Error (%)	Systematic Error (%)
Davies–Gray	U	U, MOX	0.05	0.05
MacDonald–Savage	Pu	Pu materials	0.1	0.1
Controlled Potential Coulometry	Pu	Pure Pu	0.1	0.1
Ignition Gravimetry	U, Pu	Oxides	0.05	0.05
K X-ray Flouresence	Pu	Pu materials	0.2	0.2
Isotope Dilution Mass Spectrometry (IDMS)	U, Pu	Pu, MOX, spent fuel	0.1	0.1
Pu(IV) Spectrophotometry	Pu	Pu, MOX	0.2	0.2
Alpha Spectrophotometry	Np, Am, Cm	Spent fuel	5.0	5.0
Thermal Ionization Mass Spectrometry (TIMS)	U, Pu	Pure U, Pu	0.05	0.05

adequately track and account for these materials, they must be quantified accurately. This necessitates the use of methods that do not alter their physical form or integrity of the item. Nondestructive assay (NDA) techniques can provide the necessary information and, although the precision and accuracy is generally poorer than DA, NDA is usually less expensive and can be performed within quicker time periods. DA and NDA should be viewed as complimentary techniques that are both necessary for a quality safeguards measurement program.

Most NDA techniques measure spontaneous or stimulated radiation or heat generated as a result of the radioactive decay process. Passive NDA methods measure radiation that is spontaneously emitted, while active techniques measure radiation that is stimulated by external neutron or gamma ray irradiation. Of the principal radiations, alpha and beta particles do not penetrate bulk material sufficiently to be of use to the NDA professional. On the other hand, x-rays, gamma rays, and neutrons are all electrically neutral, penetrate bulk materials, and are regularly used for NDA applied to nuclear safeguards.

Gamma rays and x-rays are photons with energies above that of the visible light spectrum. X-rays are emitted as result of changes in the electronic structure of the atom, while gamma rays are emitted when there is a change in the state of the nucleus. In commonly assayed nuclear materials, x-rays in the energy range 80–120 keV or gamma rays from 60–2,600 keV may be used for quantitative measurements. Since every isotope emits radiations at very precise energies and at well-characterized intensities, it provides a signature that is unique to that specific isotope and related to the amount of material present.

One of the most common NDA measurements is to determine the isotopic composition of plutonium or uranium by measuring the intensity of specific gamma rays produced by one isotope of interest relative to those from other isotopes present in the sample. For example, Fig. 1 shows spectra from two types of plutonium. If the spectra are carefully examined, one can see that the characteristics of each spectrum are highly dependent on the isotopic composition of the plutonium. Common instruments for the measurement of gamma ray spectra are scintillators, such as NaI, or semiconductors, such as high-purity germanium. Scintillators are materials that produce optical light pulses when the detector material interacts with a gamma-ray photon. The production of light is proportional to energy deposited in the detector material by the interacting gamma ray. Alternatively, when a gamma

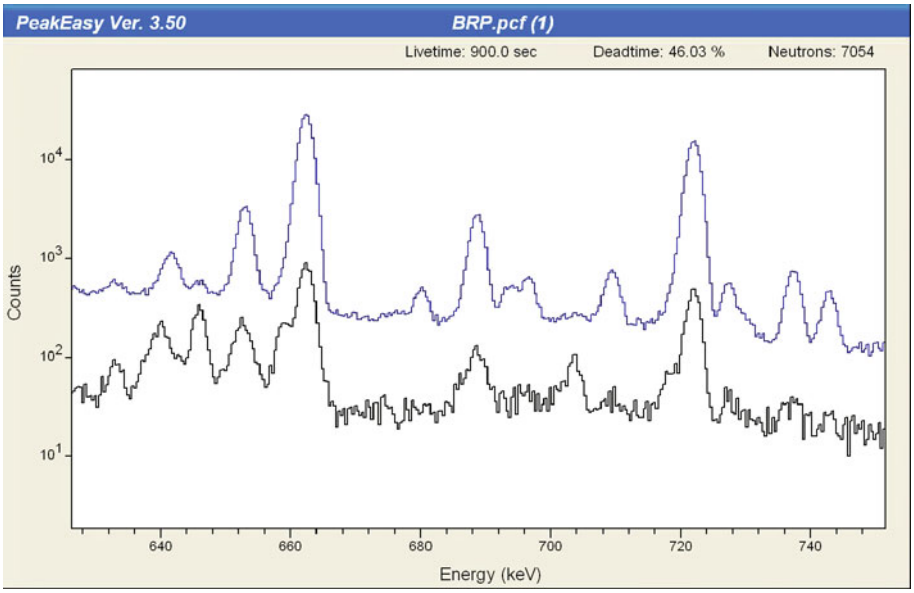

Nuclear Safeguards and Proliferation of Nuclear Weapons Materials. Figure 1
Simulated High Purity Germanium spectra for weapons-grade and reactor-grade plutonium [9]

Nuclear Safeguards and Proliferation of Nuclear Weapons Materials. Table 3 Commonly used gamma detector materials [10]

Material	Type	Average Z	Density (g/cm^3)	Resolution % FWHM @ 662 keV	Resolution % FWHM @ 122 keV
$Bi_4Ge_3O_{12}$ (BGO)	Scintillator	28	7.1	12	28
NaI:Tl	Scintillator	32	3.7	7	13
$LaCl_3$:Ce	Scintillator	28	3.9	3.3	8
$LaBr_3$:Ce	Scintillator	41	5.3	2.8	7
Xe	Gas	54	0.4–0.5	2	7
CdZnTe	Solid-state	49	6.0	3.2	6.3
CdTe	Solid-state	49	6.1	0.6	1.5
Ge (thick planar)	Solid-state	32	5.3	0.2	0.4

photon interacts with a semiconductor (solid-state) material, it creates electron–hole pairs in proportion to the deposited energy. The characteristics of commonly used detector materials are delineated in Table 3. Resolution describes how well a given spectrometer can distinguish one gamma ray from another as a function of energy.

Under some conditions, the measurement of gamma rays may be used to determine the mass of NM present. Most nuclear materials have high atomic numbers and densities and therefore readily scatter and absorb their own radioactive emissions. By measuring the transmission of known gamma-ray intensities at one or more energies, the NDA professional may calculate correction factors to account for the scatter and absorption in the item. It is common practice to use the 413.7 keV gamma ray from plutonium or the 185.7 keV gamma ray from uranium for mass measurements. It should be noted that the self-attenuation factor for plutonium is smaller than that for uranium, since the plutonium gamma ray of interest has a higher energy. This means that self-attenuation corrections for mass measurements of plutonium items are generally smaller than those required for uranium items.

Since many items to be assayed may have the nuclear material dispersed nonuniformly in a matrix that may also be nonuniform, systems that make attenuation correction frequently have to divide the measured item up into a number of elements that are measured individually and have attenuation correction factors determined for each individual element. Early systems used a technique called Segmented Gamma Scanning (SGS) [11]. The SGS measured the item as a series of horizontal slices; each slice was characterized individually and then summed to arrive at an overall result. With the powerful computers that became economically available in the early 1990s, a tomographic gamma scanner (TGS) was developed that divides an item up into a large number of volume elements [12]. The techniques used to calculate the absorption-corrected mass of nuclear material following the TGS measurement are similar to those used in computed tomography for medical applications. The accuracy of assay results for low-density matrices, such as combustible waste, is as good as 2–3%, but may be as high as 15–18% for higher density matrices such as sludge.

Like gamma rays, neutrons are electrically neutral, but they penetrate high-Z, high-density materials further than a gamma ray of the same energy. Therefore, the measurement of neutrons for the assay of special nuclear material is advantageous for large items and items in high-density matrices. At this point in time, neutron detectors in use around the world do little to distinguish one neutron from another of a different energy. However, neutron intensity and the time correlation of multiple neutron detections provide information that can be used to determine the amount of nuclear material present in a sample if the isotopic composition of the sample is already known. Most nuclear material assay applications in use today using

neutrons, measure coincident neutrons that result from induced or spontaneous fission.

Most neutron detectors use ^{3}He gas proportional counters embedded in polyethylene. The ^{3}He has a large cross section (probability) for capturing thermal neutrons. The polyethylene acts as a moderator to slow down the neutrons, produced by fission or (α, n) reactions, to thermal energies where they have a higher probability of interaction with the ^{3}He gas. The capture interaction then results in the release of a triton and proton that share 765 keV of energy, which then ionize the gas and create an associated electronic pulse that can be measured. Passive detector systems developed using this basic technique have been installed in nuclear facilities for nuclear safeguards of plutonium that have demonstrated precisions of better than 2% [8, 13]. Plutonium measurement is the primary application of passive neutron counting since plutonium has a high rate of spontaneous fission from the decay of its even-numbered isotopes. Counters using higher-order coincident neutrons from fission have also been developed and are in widespread use [14, 15]. Such multiplicity counters are advantageous for the measurement of impure plutonium-bearing items [16]. In general, the precision and accuracy of the measurements using multiplicity counting can be as good as 1–3% [8].

Uranium, due to its long radioactive decay half-lives, emits very few neutrons from spontaneous fission or (α, n) reactions, unlike plutonium. Therefore, effective assay of uranium via neutron measurement requires that the fission rate in the item be externally enhanced. By placing an external neutron source near the item, fissions will be induced in the sample. If the external source used to interrogate the sample produces uncorrelated neutrons, such as those from an AmLi source, they can be distinguished from those produced by the induced fissions in the sample, since these later neutrons will be correlated in time. Alternatively, one can use an external fission source, such as a small ^{252}Cf source, that can be moved away from the sample after inducing fissions or be turned off, such as a small accelerator. In these later two cases, the measurement of neutrons from the induced fissions is then conducted after the external source is no longer present.

The Active Well Coincidence Counter (AWCC), which is in common use around the world, uses AmLi sources to induce fissions in a uranium sample [17]. Its precision and accuracy have been reported to be better than 5% for the measurement of uranium [8]. Another advantage of using AmLi sources is that it produces neutrons with a mean energy of 0.5 MeV, which is below the fission threshold of ^{238}U. This allows the effective assay of ^{235}U in a sample of uncertain enrichment.

The Californium Shuffler is an example of an instrument that rapidly moves a spontaneous fission source away from a sample to allow subsequent measurement of the induced fissions [18, 19]. This instrument measures the delayed neutrons from fission. Approximately 1.6% of neutrons from fission reactions are produced a few seconds to minutes after the fission. For materials that are well represented with appropriate calibration standards, the shuffler technique has been reported to accuracy as good as 1–2%.

The differential die-away technique (DDT) was developed to use a pulsed accelerator producing 14 MeV neutrons as the external source. This technique has been successfully applied to the assay of both uranium- and plutonium-bearing wastes [20–22]. The combined thermal epithermal neutron (CTEN) method is similar to the DDT method, but interrogates the sample with both thermal and epithermal neutrons [23]. This is achieved partly by the addition of ^{4}He detectors, which have a faster response than the ^{3}He detectors and can detect fast fission neutrons in the presence of the epithermal interrogating flux. ^{4}He detectors rely on the recoil of light nuclei to ionize the gas in the detector tube, which is dependent on the elastic scattering cross section. Because epithermal neutrons are more penetrating in fissile material than thermal neutrons, the differential response can be analyzed to detect the occurrence of self-shielding by fissile material and measure the size of the effect. Self-shielding occurs when discrete lumps of fissile material are present, and can result in assay errors of several hundred percent. The DDT and CTEN methods have been applied to the measurement of SNM in waste containers and for the detection of the potentially smuggled SNM in packages [24].

Many nuclear materials, including plutonium and to some extent uranium, emit heat produced as a result of alpha particle absorption in the sample following radioactive decay. Plutonium produces 2–12 W of heat

for each kilogram of material in the sample depending on the specific isotopic composition of the plutonium. Radiometric calorimeters measure the heat output of nuclear materials [25]. This method has seen wide application to plutonium and tritium samples, as well as large (kilogram) quantities of uranium and neptunium [26, 27]. Calorimetry is generally considered the most accurate and precise NDA technique for plutonium measurement since it is not subject to many of the biases that effect both gamma-ray and neutron measurements. Accuracy and precisions better than 1% are generally reported in the literature [28]. As is required for neutron-based NDA, the calorimetry data must be combined with isotopic data from gamma-ray or mass spectroscopy to obtain the total amount of plutonium in a specific item. Although calorimeters are the most accurate technique, it usually requires long measurement times (typically 4–8 h) and is not generally portable. These disadvantages make the application of calorimeters to international safeguards and inspection efforts very limited.

Detection of Nuclear Proliferation and Treaty Verification

There is a well-established historical record of states pursuing nuclear weapon development, even after accepting international obligations through treaties not to develop weapons. In recent years, those countries have included Iraq, Libya, and North Korea. It is likely that such trends will continue in the future. This necessitates that the international community have the capability to detect, deter, and even dismantle undeclared nuclear capabilities. It should be noted that Libya agreed to abide by the NPT in 2003 and following negotiations with the USA and Great Britain, the USA airlifted out of Libya components of the abandoned nuclear weapons program in 2004.

Open Source Information and Satellite Imagery

The analysis of open source information and commercial satellite imagery are two methods currently in use by the IAEA and state intelligence assets. Open sources of information include such things as publically available data, media reports, published scientific literature, business reports, information on technical conferences and meetings, and patent applications. Open sources of information are numerous and continuously changing. Each type of information must be assessed in relationship to the others in an attempt to establish an integrated picture of a state's legal nuclear programs, undeclared activity, and potential to breakout and quickly establish a nuclear weapons capability. The open source analyst, which should have a broad technical background, must understand the potential quality pitfalls from the large volume of data available and then formulate useful search, query, and analysis strategies. This type of analysis requires sustained efforts over time, personnel with excellent research skills, and teams with multidisciplinary backgrounds [29].

Another open source is commercial satellite imagery, which has recently become available for anyone with modest computer access to view, identify, and monitor facilities that may be used in a nuclear weapons program. Commercial satellite images have been available since the 1970s, although at that time resolution was as poor as 80 m. Today, commercial images with resolution better than 0.5 m are becoming widely available for panchromatic data [30, 31]. Commercial satellites typically acquire images in the visible and/or near-infrared parts of the electromagnetic spectrum. Multispectral satellites, which collect data from more than one electromagnetic band, generally have poorer resolution (~2.5 m) than those collecting panchromatic data (black and white). An image that results from the fusion of the multispectral data and a panchromatic overlay is generally the best for facility and infrastructure analysis.

Imagery analysis is the process of identifying, analyzing, and attaching significance to the image data. An analyst's effectiveness requires

- Size – an ability to assess true and relative size of the objects being imaged
- Shape – an ability to determine physical characteristics
- Shadows – an ability to use the sun angle and orientation on the imaged objects
- Shade – an ability to use tonal brightness and contrast of objects of interest
- Surroundings – an ability to use context and setting of the objects including topographic and geographic information

- Signatures – an ability to use cultural or manmade features to help separate objects from their surroundings and to uniquely identify them
- Time – an ability to monitor temporal changes to provide insight on functionality, operating histories, or facility changes [32]

These techniques have been used multiple times in the detection and monitoring of clandestine nuclear activities. They are complementary to direct access inspections, open source analysis, and traditional nuclear safeguards (nuclear material accounting and measurements) in the detection and deterrence of nuclear weapons development.

Seismic and Hydroacoustic Monitoring

As a nation tries to develop new nuclear weapons, whether or not it already possesses one or more earlier generation nuclear weapons, they are likely to test new designs. It is probable that such tests would be conducted underground to both contain the fission products and conceal the exact nature of the test from other countries. Hence, seismic monitoring is an important tool in the nonproliferation regime [33]. Monitoring requires the detection of the signal, separation of the signal from background and natural events (earthquake vs. explosion), as well as estimating the location and size of the event. There are more than 200,000 seismic events that are similar in magnitude to a small nuclear explosion every year. These events are either earthquakes or chemical explosions associated with peaceful applications, such as mining.

The energy released by a sudden movement of the earth's crust produces two types of elastic body-waves. The first to arrive at a monitoring station are the high velocity P-waves, which move in a direction parallel to the direction of the wave energy. S-waves move as transverse waves with motion perpendicular to the direction of wave propagation and arrive at the monitoring station at a later time relative to the P-wave. An explosion produces little S-wave energy relative to that produced by an earthquake. Therefore, the shape of the wave recorded by a monitoring station can be used to distinguish between an explosion and earthquake. The Comprehensive Test Ban Treaty, which was opened for signature in 1996, specifies a minimum detection level for explosions of 1 kiloton. This level, which is currently exceeded by international monitoring capabilities, corresponds to a seismic event of approximately 4.0 on the Richter scale. At some locations around the globe, monitoring capability is better than 2.5 on the Richter scale. How this relates to the size of a nuclear explosion is dependent on the geology between the event and the monitoring stations [34, 35].

Since more than 65% of the earth's surface is water, it is also important to monitor for explosive events in the world's oceans. Underwater explosions produce extremely powerful broadband acoustic signals. A sensitive hydrophone either suspended from a moored buoy or anchored to the ocean floor can be used to monitor low frequencies (1–100 Hz). Such low-frequency monitoring is optimal for detecting explosions over long distances. Today's hydrophones can detect signals more than 15,000 km from their source. The waveform detected can be used to differentiate explosions from underwater earthquakes or volcanoes.

Environmental Surveillance and Monitoring

Another tool that can be used to monitor treaty compliance or breakout activity by a proliferant is the surveillance of radionuclides present in the environment [36]. The fission products produced by nuclear fission and their isotopic ratios are an unambiguous and well-characterized indicator. However, unlike seismic or acoustic monitoring, it is not done in real time. Atmospheric and underwater explosions release particles carrying radionuclides as well as noble gases, while underground explosions release noble gases. In either case, the nuclides are then transported by air or water to monitoring stations. At that point in time, which may be several days or even weeks following the event, the analysis of the sample can confirm the nuclear event but not pinpoint the location. Combining seismic and acoustic monitoring with the atmospheric surveillance, with meteorological data, can provide definitive evidence of a nuclear explosion and its location.

Most of the energy of a nuclear explosion is transformed into the immediate blast or the radiation released during the blast. Approximately 10% of the energy is released as residual radiation, which is emitted over time, through the decay of fission products generated during the nuclear blast. Fission products are produced in both gaseous and particulate form and

most are radioactive. Following an atmospheric explosion, solid fission products attach to dust particles, which may then be propagated by winds over significant distances. Underwater explosions also release particles into the atmosphere. Underground explosions may be conducted in such a way that particles carrying radionuclides are contained. However, some fission products, particularly xenon, are noble gases that are much more difficult to contain and can be collected and analyzed by monitoring stations thousands of kilometers from the explosion site [37].

A radionuclide particulate monitoring station contains an air sampler and detection equipment. At the air sampler, air is forced through a filter, which typically retains 85% or more of all particles that reach it. The used filter is usually first cooled for a period of 24 h and then measured for another 24 h in the detection device at the monitoring station. The result is a gamma ray spectrum that the analyst can use to identify specific radionuclides. The analyst can use the spectrum to determine characteristics of the device tested and the nuclear material used in the device.

Detection and Prevention of Illicit Trafficking and Terrorism

Since the attacks in the USA on September 11, 2001, terrorism's threat against a country's national security has come under increased scrutiny. Although few terrorist organizations will implement acts of such devastation, it is considered by many experts that nuclear terrorism cannot be ruled out, and, because the devastation of a nuclear attack would be unmatched, the risks must be mitigated regardless of the low probability [38–40]. To mitigate these risks, one may increase security at the storage locations (strengthen nuclear safeguards), dispose of the nuclear materials in such a way that they are unavailable to the terrorists, strengthen methods to detect their misuse and transport once they have fallen into the wrong hands, and also develop methods through which illegal activity may be attributed to a particular national or subnational group.

Rigorous nuclear safeguards, which have been described previously, are only one layer in a defensive system against the use of nuclear materials by a subnational or terrorist organization. In addition to nuclear safeguards, the other layers of mature protection system would include monitoring of nuclear material in transit, robust intelligence collection and analysis, consequence management, and a vigorous response capability to a nuclear emergency or event to mitigate it prior to a detonation. Each of these layers relies on, at least in part, the ability to detect and characterize nuclear or radiological materials at various points in their life cycle.

Nuclear smuggling is difficult to stop due to the small size of the materials required by the terrorist to make a nuclear bomb; the weak radiation many of these materials emit; the large number of smuggling routes; the large amount of legitimate traffic crossing these borders every year; and the existence of established smuggling networks for other contraband, such as illegal drugs. A recent analysis of 174 illicit radiological material trafficking incidents that have occurred since 1991 found little evidence of clear trends that can be used by nuclear security personnel [41]. It did note that the incidents involved a variety of radionuclides; however, approximately 60% of the cases involved Cesium-137, which happens to be an attractive isotope for radiological dispersal devices.

Border and Port Monitoring

Studies of illicit trafficking of nuclear and radiological materials have indicated that whether by auto, bus, train, or air, smugglers have consistently used transportation methods and routes that were most convenient to them, maintaining a close physical proximity to the materials [42]. During the past decade, one of the areas that has received international emphasis for this very reason is the improvement of border and port detection capability and protocols.

In the USA, one such effort is the Second Line of Defense program at the Department of Energy's National Nuclear Security Administration. This program seeks to interdict illicit trafficking of nuclear and radiological material through airports, seaports, and border crossings in Russia and other key transit states. This is to be accomplished by helping other nations install and use radiation detection equipment at these sites and by providing associated training and support. It is worth investing in improved border detection systems, but this line of defense will inevitably be porous, and one should not place undue reliance on it.

Fixed portal monitors have been installed at land, sea, and air facilities with the goal of detecting smuggled radioactive materials. Typically, these detectors use passive gamma measurement, which in its simplest and least expensive configuration utilizes gross gamma counting with little discrimination of the gamma-ray energy. Plastic scintillators are the most common detector material for this application and are inexpensively available in large sizes. Pedestrians, vehicles, or cargo pass through one or more pairs of these detectors. The number of gamma rays detected over the time interval during which the object is between the detectors can be used to trigger an alarm requiring the intervention of a guard or similar security personnel. There is a significant trade-off between the sensitivity of this method and the permissible duration that the object can be measured. Also, if the sensitivity is set such that frequent false alarms occur, security personnel may ignore alarms in order to keep traffic moving efficiently. Most of the radiation emitted by highly enriched uranium (HEU) is weak, which means it is both easy to shield by the smuggler and difficult to detect through passive means. The detectors being deployed in the Second Line of Defense program simply detect gamma-ray radiation, without attempting to zero in on particular energy levels, and therefore have almost no ability to detect HEU above the background of natural radiation if the terrorist or smuggler uses even modest radiation shielding.

Efforts are underway to develop "advanced spectroscopic portal monitors" (ASPs) that do examine the energy ranges of different gamma rays. This will theoretically allow them to not only detect nuclear or radiological material, but also to identify the type of material. The ASPs are expected to reduce the rates of false alarms caused by naturally radioactive materials in legitimate shipment; however, they are significantly more costly than nonspectroscopic detectors and can only be manufactured with much lower detection probabilities. Thus, substantial controversy exists over whether there is a true benefit to their deployment.

Active detectors, such as neutron sources coupled with detectors to detect induced fission, may offer higher confidence of detecting HEU, even in a shielded configuration. Several methods are under active research and development that have been demonstrated to be highly effective at detecting shielded SNM. These detection methods are based on the active neutron techniques developed for nuclear safeguards discussed previously. Other development efforts are underway to use high-energy photons to induce fission. In both cases, neutron or photon sources, systems are in the developmental stages and not yet ready for wide-spread deployments.

Nuclear Forensics

In response to nuclear smuggling, which was first reported in 1991, a new branch of science was developed: "nuclear forensics" [43]. Analytical methods were initially borrowed from nuclear safeguards and supplemented with techniques developed for material science investigations. Over several ensuing years, techniques were standardized, new methods developed, and extensive databases of nuclear information compiled to guide the analysis and attribution of nuclear materials. As in other forensic fields, the analyst relies on the fact that certain measureable parameters in a sample are characteristic of the nuclear material and can be used to draw conclusions on the intended use or origin of the materials. Such attribution is an important deterrent to a nation state's participation, whether willingly or not, in smuggling activity.

The first category of characteristics to be exploited for nuclear forensics was major elemental and macroscopic composition of the interdicted nuclear material. Physical dimensions and isotopic composition of the major nuclear materials, usually uranium and plutonium, may be used to identify the intended use of the material. For example, plutonium with less than 7% ^{240}Pu is considered to be weapons grade and likely produced for that purpose. The isotopic composition may also indicate the origin of the material. Since different types of nuclear reactors have different fuel loadings and neutron energy spectra, they generally produce plutonium of differing isotopic composition [44]. The concentration of the nuclear material may indicate stoichiometry of the compound or the presence of impurities, both of which may be indicators of the materials' source or status in a known nuclear fuel cycle. Fuel additives, which are used in the fuel cycle or material processing steps, such as gadolinium as a nuclear reactor burnable poison, may also be used by the analyst to narrow down

the type of nuclear material present. In the case of manufactured items, such as nuclear fuel elements or pellets, the physical dimensions may allow the identification of the intended reactor type or design.

Further developments in the nuclear forensics field lead to the use of minor elemental as well as microscopic composition of the nuclear material in investigations initiated in the late 1990s [42]. This included chemical and isotopic analysis of individual particles as part of the forensic toolbox. Techniques such as secondary ionization mass spectrometry and scanning electron microscopy coupled with electron dispersive x-ray analysis allow for the isotopic composition of particles or powders to be determined. With powder samples, the analyst also gains information related to the sample homogeneity with regard to the isotopic composition and the particle size distribution.

In the past decade, analysts have also developed geolocation techniques and methods. Trace elements can be found in uranium at all stages of its mining, milling, and enrichment. Each processing step reduces the concentration of these trace elements and may introduce new trace contaminants. However, it has been noted that the pattern of certain impurities does not vary through the processing and may be used as a characteristic of the starting material. For example, the distribution of lead isotopes in the sample may be used as an indication of the age of the ore body and its initial U/Th ratio. The ratio of $^{18}O/^{16}O$ in a uranium oxide sample may be used to determine the temperature, latitude, and distance to the sea for the water used in the wet processing of the uranium [42].

The challenge in the interpretation of the many data sources discussed above is the accessibility of reference data. Efforts are underway to develop databases of reference forensic information. Data on nuclear materials produced for commercial applications, such as power production, are generally available with the various manufacturers and to some extent in open literature. However, some of the data is commercially sensitive and its availability is limited. Also, similar data on nuclear materials developed for weapons applications is generally protected for national security reasons.

Terrorism Response and Consequence Management

If a terrorist succeeds in smuggling nuclear or radiological material through the layers of nuclear safeguards and security at the source and subsequent national or international monitoring (such as the Second Line of Defense) it may then be readied for use as a weapon. If monitoring stations, intelligence, or criminal investigations lead to the discovery of the material or weapon, a response is required to mitigate the threat. That response requires personnel familiar with weapons design, device characterization, weapon defusing and disposal, and consequence management.

To assist the response or management of the consequences of the event, small portable instruments are required for identification and quantification of the materials involved. Many responders, including those that may be on the incident scene first, such as police officers, today use hand-held or backpack size instruments called radioisotope identification devices (RIIDs). These instruments have undergone significant advancements over the past several years in both hardware and algorithms.

The algorithm used for isotope identification by a RIID plays a key role in obtaining a correct identification of the radioisotope. Correct ID is perhaps the most essential step in determining whether or not a true threat exists that requires a more extensive response for mitigation. The majority of RIIDs deployed around the world are based on NaI spectrometers. Their performance in isotope identification is generally poor and therefore secondary analysis of spectra by a trained spectroscopist is frequently necessary to resolve problems in the isotope identification. A trained spectroscopist is capable of identifying complicated, multiple-line sources with even the poorest resolution detectors, such as NaI. Many factors in detector performance, such as energy resolution, play an important role in isotope identification and are active areas of research [45–47].

Future Directions

World energy demand continues to grow and along with it does the demand for nuclear power, a carbon-free energy source. Some are predicting that world energy demand growth will exceed 50% over the next 20–25 years [48]. This expansion presents both

challenges and opportunities to nuclear safeguards and nonproliferation. Challenges include the timely detection of diversion at large throughput fuel cycle facilities, new types of fuel cycles that may present challenges to accurate measurement of the fuel at appropriate KMPs, and the detection of nuclear material misuse in the background of activity required for a large-scale nuclear fuel cycle. Finally, significant expansion of nuclear power will also include increased nuclear material shipping, which creates its own issues related to continuity of knowledge and monitoring of the material in transit.

Addressing these future challenges will require advances in instrumentation, safeguards system analysis, modeling techniques, and data mining. On-line, near real-time monitoring methods using both radiation and nonradiation signatures will be required as part of integrated process monitoring schemes for new facilities. There will also be opportunities to incorporate nuclear safeguards and physical protection into the design of new facilities. This will allow the efficacy of the safeguards system to be maximized while minimizing cost and impact to the facility.

Improvements in the detection of shielded nuclear material is one of the most active areas of research to improve border monitoring and other efforts related to illicit nuclear trafficking. As worldwide commerce continues to increase, so will the movement of goods around the world. This will necessitate that the false alarm rates of the current generation of portal monitors be significantly improved to avoid considerable negative impacts to commerce. Although this is another area of active research, implementable solutions are likely still several years away.

Bibliography

Primary Literature

1. Fischer D (1997) History of the International Atomic Energy Agency: the first 40 Years. IAEA, Austria
2. Kennedy RF (1968) Thirteen days: a memoir of the cuban missile crisis. McCall, New York
3. Jaech J (1973) statistical methods in nuclear materials control, U.S. Atomic Energy Commission
4. Burr T, Coulter C, Hakkila E, Ai H, Kadokura I, and Fujimaki K (1995) Statistical methods for detecting loss of materials using near-real time accounting data. 36th Annual Meeting of the Institute of Nuclear Materials Management, Palm Dessert, California
5. Picard R (1987) Sequential analysis of materials balances. J Nuclear Mater Manage 15(2):38–42
6. Zrdecki A, Armstrong J, Longmire V, and Strittmatter R (1997) Inventory difference analysis at Los Alamos Plutonium Facility. 38th Annual Meeting of the Institute of Nuclear Materials Management, Phoenix, Arizona
7. IAEA (2003) Safeguards Techniques and Equipment – 2003 Edition. IAEA/NVS/1 (revised), International Nuclear Verification Series No. 1, Austria
8. Aigner H, Binner R, Kuhn E, Blohm-Hieber U, Mayer K, Guardini S, Pietri C, Rappinger B, Mitterrand B, Reed J, Mafra-Guidicini O, and Deron S (2002) International target values 2000 for Measurement uncertainties in safeguarding nuclear materials. ESARDA Bulletin, No. 31
9. Garner S, (2009) personal communication, July 28, 2009
10. Russo P and Vo D (2005) Gamma-Ray Detectors for Nondestructive Analysis, Los Alamos National Laboratory, LA-UR-05-3813
11. Martin R, Jones D, Speir L, and Walker A (1974) Field assay of plutonium with a new computerized segmented gamma scan instrument, Los Alamos Scientific Laboratory, LA-UR-74–924
12. Estep R, Prettyman T, Sheppard G (1993) Tomographic gamma scanning to assay heterogeneous waste. Nuc Sci Eng 118:145–152
13. Menlove H, Swansen J (1985) A high-performance neutron time correlation counter. Nuclear Technol 71:497–505
14. Krick M, Swansen J (1984) Neutron multiplicity and multiplication measurements. Nucl Inst Methods 219:384–393
15. Langer D, Krick M, Ensslin N, Bosler G, and Dytlewski N (1991) Neutron multiplicity counter development, Proceedings of the 13th Annual ESARDA Symposium, Avignon, France
16. Stewart J, Krick M, Langer D, and Wenz T (1998) Neutron multiplicity assay of impure materials using four different neutron counters, 39th Annual Meeting of the Institute for Nuclear Materials Management, Naples, Florida
17. Menlove H, Foley J, and Bosler G (1980) Application of the active well coincidence counter to the measurement of uranium, 2nd Symposium on Safeguards and Nuclear Material Management, Edinburgh, Scotland
18. MacMurdo K, Bowman W (1977) Assay of fissile materials by a cyclic method of neutron activation and delayed neutron counting. Nucl Inst Methods 141:299–306
19. Menlove H, Crane T (1978) A ^{252}Cf Nondestructive assay system for fissile material. Nucl Inst Methods 152:549–557
20. Kunz W, Atencio J, and Caldwell J (1980) A 1-nCi/g Sensitivity transuranic waste assay system using pulsed neutron interrogation, 21st Annual Meeting of the Institute for Nuclear Materials Management
21. Caldwell J, Hastings R, Herrera G, and Kunz W (1986) The Los Alamos second-generation system for passive and active neutron assays of drum-sized containers, Los Alamos National Laboratory LA-10774-MS
22. Rinard P, Coop K, Nicholas N, Menlove H (1994) Comparison of shuffler and differential die-away technique instruments for the assay of fissile materials in 55-gallon waste drums. J Nuclear Mater Manage 22(3):4–28

23. Coop K and Hollas C (1996) Epithermal interrogation of fissile waste, Institute of Nuclear Materials Management Annual Meeting, Naples, Florida
24. Rooney B, York R, Close D, and Williams H (1998) Active interrogation package monitor, IEEE Nuclear Science Symposium, Toronto, Canada
25. Bracken D, Biddle R, Carillo L, Hypes P, Rudy C, Schneider C, Smith M (2002) Application guide to safeguards calorimetry, Los Alamos National Laboratory LA-13867-M
26. Walsh T, Hamilton R, Baker E, Hurlbut S, Fazzari D, Delegard C, McRae L, Liebetrau A, Lemaire R, and DeRidder P (1996) Plutonium assay for safeguards purposes: material heterogeneity and application of calorimetry, 37th Annual Meeting of the Institute for Nuclear Materials Management, Naples, Florida
27. Thornton M, Vassallo G, Miller J, Mason J (1995) Design and performance testing of a tritium calorimeter. Nucl Inst Methods A363:598–603
28. Guardini S (2003) Performance Values for Nondestructive Assay (NDA) techniques applied to safeguards: The 2002 evaluation by the ESARDA NDA Working Group, ESARDA Bulletin 31
29. Wallace R, Anzelon G, Essner J (2009) Safeguards information from open sources. J Nuclear Mater Manage 37(4):30–40
30. Hitchens T (2006) European eyes in the sky: strategic independence is focus as security comes to the forefront. Imaging Notes 21(3):20–24
31. Niemeyer I (2009) Safeguards information from satellite imagery. J Nuclear Mater Manage 37(4):41–48
32. Pabian F (2008) Commercial satellite imagery: another tool in the nonproliferation verification and monitoring toolkit, Chapter 12 of nuclear safeguards, security, and nonproliferation. Elsevier, New York
33. Hannon W (1985) Seismic verification of a comprehensive test ban. Science 227(4684):251–257
34. Bache T (1982) Estimating the yield of underground nuclear explosions. Bull Seismol Soc Amer 72(6B):S131–S168
35. Taylor S, Dowla F (1991) Spectral yield estimation of NTS explosions. Bull Seismol Soc Amer 81(4):1292–1308
36. Yutaka M, Tetsuzo O, Hiroshi N, Hideo N (1998) Overview of atmospheric radionuclide monitoring techniques for CTBT International Monitoring System, Proceedings of the Annual Meeting of INMM Japan Chapter, 19:129–130
37. Carrigan C, Heinie R, Hudson G, Nitao J, Zucca J (1996) Trace gas emissions on geological fualts as indicators of underground nuclear testing. Nature 382:528–531
38. Ferguson C, Potter W, Sands A, Spector L, Wehling F (2005) The four faces of nuclear terrorism. Routledge, New York
39. Jenkins BM (2008) Will terrorists go nuclear? Prometheus Books, New York
40. Allison G (2005) Nuclear terrorism: the ultimate preventable catastrophe. Holt Paperbacks, New York
41. Kerst R (2009) Trends and patterns in illicit trafficking of radioactive sources, LLNL-GS-0052-2009, Lawrence Livermore National Laboratory
42. Battelle Memorial Institute (2009) Nuclear smuggling handbook: case studies and detection methods
43. Mayer K, Wallenius M, Fanghanel T (2007) Nuclear forensic science – from cradle to maturity. J Alloys Compounds 444–445:50–56
44. Wallenius M, Lutzenkirchen K, Mayer K, Ray I, Aldave de lss Heras L, Betti M, Crombroom O, Hild M, Lynch B, Nicholl A, Ottmar H, Rasmussen G, Schubert A, Tamborini G, Thiele H, Wagner W, Walker C, Suleger E (2007) Nuclear forensic investigations with a focus on plutonium. J Alloys Compounds 444–445:57–62
45. Sullivan C, Garner S, Lombardi M, Butterfied K, Smith-Nelson M (2007) Evaluation of key detector parameters for isotope identification. IEEE Nuclear Sci Symposium Conf Record 2:1181–1184
46. Keyser R, Rwomey T, Upp D (2005) A Comparison of an HPGe-based and NaI-based Radioisotope Identifier (RIID) for radioactive materials. ESARDA Symposium, London
47. Sullivan C, Garner S, Blagoev K, Weiss D (2007) Generation of customized wavelets for the analysis of gamma-ray spectra. Nuclear Instruments Methods A 579(1):275–278
48. Energy Information Administration (2007) International Energy Outlook 2007, DOE/EIA-0484

Books and Reviews

Doyle JE (ed) (2008) Nuclear safeguards, security, and nonproliferation: achieving security with technology and policy. Elsevier, New York

Hakansson A, Jonter T, (2007) An Introduction to Nuclear Non-Proliferation and Safeguards. SKI Report 2007:44

IAEA, (2007) Combating illicit trafficking in nuclear and other radioactive material: reference manual, IAEA Nuclear Security Series No. 6. International Atomic Energy Agency, Vienna

Moody K, Hutcheon I, Grant P (2005) Nuclear forensic analysis. CRC Press, Boca Raton

Mozley RF (1998) The politics and technology of nuclear proliferation. University of Washington Press, Seattle/London

Nuclear Transfer to Produce Transgenic Mammals

Alexander Kind, Angelika Schnieke
Chair of Livestock Biotechnology, Technical University of Munich, Freising, Germany

Article Outline

Glossary
Definition of the Subject
History and Introduction

Nuclear Transfer
Future Directions
Bibliography

Glossary

Cell cycle The sequence of stages between one cell division and the next. These are: gap 1 (G1) DNA synthesis (S), gap 2 (G2), and mitosis (M).

Chimera An organism composed of a mixture of genetically distinct cells that originate from two individuals.

Chromatin The natural form of genomic DNA within the nucleus. A highly structured multi-coiled fiber composed of a complex of DNA, RNA and proteins.

Clone (a) Molecular clone, an isolated DNA fragment propagated artificially in bacteria. (b) Cell clone, a group of genetically identical cells descended from a single individual. (c) Animal clone, an animal produced by embryo splitting or nuclear transfer.

Cytoplasm The portion of a eukaryotic cell outside the nucleus.

Differentiation A process by which a cell takes on a more specialized role or function.

Epigenetic regulation Regulation of gene expression by modification of chromatin not involving changes to the DNA sequence, e.g., by methylation of cytosine bases.

Locus A defined position in the genome.

Metaphase A stage of cell division when chromosome pairs are condensed and ready to be divided between the daughter cells.

Pluripotent The ability of a single cell to generate all cell types of the body. Pluripotent cells are distinct from totipotent cells in that they cannot make extraembryonic structures, such as the amniotic sac or the placenta.

Promoter trap A method of enriching gene-targeted cell clones against a background of random integrants. Expression of a selectable marker is conditional on integration at the desired location and driven by the promoter of the target gene.

Pronuclei Two structures formed from the sperm and oocyte genetic material following fertilization. Pronuclei later fuse to form the nucleus of the zygote.

Reprogramming A general term describing a radical change in the pattern of gene expression by a nucleus. This may be in response to a change in cytoplasmic factors, for example, after transfer of a nucleus from a somatic cell into an oocyte.

Somatic cell Cells of an organism other than the germ line.

Transcription The first stage in the expression of a gene, in which an RNA copy, or transcript, is made from a DNA template.

Transfection Term covering a variety of chemical, electrical and mechanical methods of introducing nucleic acids into cells.

Undifferentiated Relating to a cell that is capable of differentiation but has not generated specialized characteristics.

Zygote The one-cell embryo formed after fusion of the male and female pronuclei.

Definition of the Subject

Over the last 3 decades, researchers in molecular genetics and developmental biology have generated a repertoire of powerful biological techniques that allow genes to be isolated, analyzed, modified at will, then transferred and studied in cultured cells and live animals. This technology has revealed the functions of thousands of genes and dramatically advanced the knowledge of normal and disease states, providing the basis for numerous practical benefits especially in biomedicine. This entry tracks one strand within this interconnected and ever-broadening field: the use of nuclear transfer to generate transgenic mammals.

Transgenic animals were originally defined as those that contain additional DNA, such as a gene introduced from another species. The term "transgenic" is now commonly used to encompass a range of experimentally engineered genetic modifications including DNA deletion, rearrangement, and replacement. Here the word is used in this broader sense.

Nuclear transfer is the replacement of the nuclear genetic material of an oocyte or zygote with the nucleus of another cell. The technique has been applied in three main areas:

1. Therapeutic cloning – the generation of embryos and stem cells from differentiated cells.

2. Reproductive cloning – the replication of animals from cells, for example, where sexual reproduction is difficult or impossible, or to preserve valuable genetic material.
3. Cell-mediated transgenesis – the production of transgenic animals from genetically modified cultured cells.

The production of transgenic animals was a principal motivation for the development of nuclear transfer in mammals and is the focus of this entry.

This entry is structured as follows: Section "History and Introduction" gives some historical background to the conception and development of nuclear transfer. Section "Nuclear Transfer" outlines the current state-of-the-art and related transgenic technologies. Section "Future Directions" describes possible developments in the near future. This entry can however provide only an overview of this diverse and expanding subject. Interested readers can gain more detailed information by accessing the key papers, reviews, and books cited.

History and Introduction

Cloning animals by nuclear transfer is not a new idea. The first recorded reference is attributed to Yves Delage, a French marine biologist who wrote in 1895: "if, without any deterioration, the egg nucleus could be replaced by the nucleus of an ordinary embryonic cell, we should probably see this egg developing without changes" [1]. There is however no evidence that Delage actually carried out such an experiment. Hans Spemann described the first nuclear transfer in 1928 [2]. In a remarkable piece of microsurgery using micro-tweezers and a loop of hair from his baby daughter, he constricted a single-cell salamander embryo into two parts, one of which contained the cell nucleus. Left to develop, the portion with the nucleus divided and formed an embryo, while the other side remained a pouch of clear cytoplasm. As the embryo developed further, Spemann allowed a single nucleus to pass back into the empty cytoplasm; this reconstructed single cell then developed into another normal embryo.

In the early 1950s, Robert Briggs and Thomas King performed a series of nuclear transfer experiments with frogs. They removed the nucleus from an activated frog oocyte using a glass needle. A single cell dissected from a later stage embryo was then drawn up into a fine glass pipette connected by rubber tubing to a syringe. The cell broke open as it was squeezed within the pipette, and the free nucleus was then injected into the enucleated egg. Culturing the reconstructed embryos further, they found that cell nuclei from blastula stage embryos could support normal development to tadpoles. But nuclei from later stage embryos, in which the major embryonic cell lineages were already established, were unable to do so.

Transfer of nuclei following this basic scheme was continued by various researchers for several decades. The work was at first restricted to the large eggs of amphibians, but in the late 1970s, embryo culture and micromanipulation techniques improved sufficiently to use the far smaller and more vulnerable eggs of mammals. The overwhelming finding was that the developmental capacity of transplanted nuclei decreased with the age and extent of differentiation of the donor cell. Nuclei of very early embryonic cells had equivalent potential, but at some stage in development, it seemed that the fate of different cells became determined, "hard wired" in some way. The mechanism was unknown, but some form of irreversible modification or loss of nuclear DNA was viewed as a likely explanation. The concept of cell determination thus became widely accepted among developmental biologists. In 1984, James McGrath and Davor Solter seemed to put an end to the possibility of nuclear transfer in mammals. They systematically transferred nuclei from one-, two-, four-, eight-cell and blastocyst stage mouse embryos into enucleated one-cell stage embryos, zygotes. Nuclei from one-cell embryos supported development to blastocysts, but success dropped off sharply using two-cell stage nuclei and failed entirely with later stages. They interpreted this as a rapid loss of nuclear capability during development and concluded their paper with the categorical statement: "the cloning of mammals by simple nuclear transfer is biologically impossible" [3].

However, strict cell determination remained difficult to reconcile with the well-known capacity for organ regeneration shown by various vertebrates, including most fish and some types of amphibian. If for example a newt loses a limb, cells from surrounding tissues migrate into the wound and undergo a process of reverse development, changing their identity to form

a mass of rapidly dividing undifferentiated cells termed a blastema. Cells within the blastema then organize and undergo processes similar to those in embryo development to form a replacement limb [4]. This was good evidence that some adult differentiated cells are not determined in their fate and can radically change their identity. So, despite the repeated failure of experimental nuclear transfer, there remained the tantalizing possibility that the limitations were essentially technical rather than biological. This provided sufficient motivation for some researchers to continue testing.

In retrospect, it was unfortunate that early efforts focused on mice, because they are now known to be one of the more difficult species to clone by nuclear transfer. So, somewhat unusually, the major breakthroughs were made with livestock. The first indication that nuclear transfer from later stage cells might be possible came ironically just a few months before McGrath and Solter's paper was published. Steen Willadsen produced three Suffolk sheep by merging single cells from eight-cell embryos with enucleated unfertilized eggs [5]. It later emerged that the reason for the discrepancy with the mouse work was because McGrath and Solter had used enucleated zygotes for nuclear transfer, because mouse oocytes are too fragile to survive nuclear transfer. Willadsen had been able to use unfertilized oocytes, which are more robust in sheep. Years of work have subsequently shown that unfertilized oocytes are successful recipients for nuclear transfer in numerous species, while zygotes can only be used at a very particular stage.

In the decade that followed Willadsen's achievement, nuclear transfer remained restricted to cells of the very early embryo. While this was potentially useful in increasing the number of embryos of valuable animals such as prize cattle, there were few other practical applications. However, developments in transgenic technologies over the same period led to increasing pressure to improve nuclear transfer.

In 1980, it was reported that naked DNA microinjected into the pronuclei of fertilized mouse eggs could stably integrate into the host genome [6]. Microinjection by the same procedure was extended to livestock 5 years later [7]. A host of practical applications for transgenic livestock species were soon envisaged, including enhanced production characteristics, disease resistance, and the production of pharmaceutical proteins. However as time went on, it became apparent that DNA microinjection suffered numerous drawbacks. The process was inefficient and offered no control over where a transgene would integrate in the host genome. Randomly integrated transgenes exhibited a very wide range of expression, and this was a major problem for biotechnology companies seeking to make useful transgenic products, such as pharmaceuticals.

A quite different means of generating genetically modified animals, based on the use of cultured cells, was also developed during the 1980s. In 1981, Martin Evans and Gail Martin independently isolated embryonic stem (ES) cells from early mouse embryos [8, 9]. ES cells can be grown indefinitely in culture and then be incorporated back into a developing embryo. In 1984, it was found that these cells could also contribute to the germ line and produce functional sperm or oocytes [10]. This provided a means of establishing mouse strains derived from the ES cell genotype, including any experimental modifications. In 1987, a method of introducing predefined alterations into genes in situ, originally developed in tumor cell lines [11], was applied to ES cells by Thomas and Capecchi [12]. This technique, termed gene targeting, made it possible to engineer and study precise genetic alterations in whole animals. The phenomenal power of gene targeting in ES cells has provided an abundance of knowledge about the function of genes in mammals, and was recognized by the 2007 Nobel Prize for Medicine, awarded jointly to Mario Capecchi, Martin Evans, and Oliver Smithies.

Mice are vital for basic research, but by the late 1980s, it was apparent that many practical applications in areas such as biomedicine and animal agriculture required ES technology or a functional equivalent in other species, particularly livestock. Despite considerable efforts, fully functional ES cells had not (and still have not) been derived from livestock. Despite the difficulties, transfer of nuclei from "ordinary" somatic cells was seen as a possible alternative means of transferring engineered genetic modifications from cells to whole animals. However, this would not be possible if nuclear transfer was restricted to cells obtained directly from early embryos. Genetic modification and powerful techniques like gene targeting require cells to be cultured for several weeks.

The breakthrough in nuclear transfer came in the 1990s, when it became clear that the cell-cycle stage of the nuclear donor cell must be correctly matched to the state of the recipient cytoplasm. Keith Campbell and Ian Wilmut of the Roslin Institute near Edinburgh made the key insight that only nuclei in G1 phase (prior to DNA replication) would support normal development in unfertilized oocytes. Transfer of nuclei at other stages in the cell cycle leads to aberrant chromosomal replication and inviable embryos. The method they developed and which is still widely used is to block cycling in the donor cells before DNA replication by reducing the amount of serum in the culture medium.

In 1995, two live lambs, Megan and Morag, were produced by transfer of nuclei from cells that were derived from a day 9 sheep embryo and then grown in culture for 6–13 passages [13]. The following year a similar experiment was performed that also included cultured adult sheep mammary cells. On 5 July 1996, a lamb was born from these cells and named Dolly [14]. Her birth showed that previous difficulties with nuclear transfer had indeed been technical. Adult cell nuclei were not irreversibly determined in their developmental potential and could be radically reprogrammed to adopt a new fate. Shortly after, transgenic and gene-targeted animals were produced, demonstrating that nuclear transfer from somatic cells was a practical means of generating genetically modified animals [15, 16].

Nuclear Transfer

Choice of Transgenic Methods

As mentioned in the introduction, the development of nuclear transfer in livestock mammals was largely inspired by the power of ES cell–mediated transgenesis in mice. The aim was to gain more precision and control over the type of genetic modifications that could be carried out. This section reviews nuclear transfer within the overall context of transgenic technology.

Methods of producing transgenic mammals can broadly be divided into two categories:

1. Direct transgenesis – the transfer of transgene DNA directly into embryos. Methods include DNA microinjection, viral transduction, transposon-mediated transgenesis, and sperm-mediated DNA transfer.
2. Cell-mediated transgenesis – the engineering of genetic alterations in cultured cells that are then converted to whole animals. Nuclear transfer falls within this category. The other major method is the incorporation of ES, or induced pluripotent stem cells, into developing embryos to produce chimeric animals.

Methods of direct transgenesis are more straightforward than cell-mediated transgenesis. However, at present these allow only transgene addition. Earlier techniques, such as DNA microinjection, are also very inefficient. Although not a significant drawback in mice, this is an important factor in livestock because gestation and maturation times are longer and maintenance costs far higher. For example, cattle have a generation interval between 2 and 3 years and each cow bears either one or two calves, while the generation time of mice is 3 months and litter size is between 6 and 12 pups. There has therefore been a strong incentive in livestock programs to reduce the number of animals gestating non-transgenic fetuses. Transgenic fetuses can be identified in utero by analysis of cells shed by the developing fetus and obtained by amniocentesis or allantocentesis. However, these procedures carry a significant risk of inducing abortion. Some efforts have also been made to detect and analyze fetal cells or DNA in the maternal circulation, but with little success. Definitive analysis of the integrated transgene must therefore be carried out in animals shortly after birth using small samples taken from blood, tail, or ear tips.

Methods of cell-mediated transgenesis share the important feature that genetic manipulation and analysis of the transgenic genotype are carried out in cells in the laboratory, rather than in animals "on the farm." These cells are then used to transfer the modified genotype to whole animals. While cell-mediated transgenesis is more labor intensive than direct transgenesis, it offers significant advantages. Cells can be analyzed in detail so that only those with the desired genotype are converted to whole animals. Far larger numbers of independent transgene integration or other events can be screened and investigated in cells than in whole animals. This allows the selection and isolation of cells carrying rare integration events resulting from homologous recombination, the basis of gene targeting.

Nuclear transfer is currently the only practical form of cell-mediated transgenesis in mammals other than mice.

Nuclear Transfer Basics

The standard nuclear transfer procedure is to prepare a recipient cytoplast by removing the genomic DNA from an unfertilized oocyte. This is usually carried out by microsurgical withdrawal of a portion of cytoplasm containing the second metaphase plate using a micromanipulator. A low-tech option is to split the oocyte under a microscope using a thin blade, dye is then used to identify the half containing the metaphase chromosomes, a procedure termed "hand made cloning." The donor nucleus, or a whole cell, is then introduced into the enucleated oocyte by microinjection or electrofusion. Reconstructed embryos are activated with an electrical pulse to simulate fertilization, cultured if possible to identify viable embryos, and then transferred to the oviduct of foster mothers to complete gestation. Readers interested in detailed protocols are referred to a book by Verma and Trounson [17].

As mentioned in the introduction, the key insight that led to the success of nuclear transfer from a wide variety of cells was recognizing the importance of matching the cell-cycle stage of the donor nucleus and the oocyte cytoplasm. Oocytes of most mammalian species pause twice during the meiotic cell divisions that form the gametes: once before the first meiotic metaphase, and again at the second metaphase, at which stage the oocyte is mature and can be fertilized. Oocyte maturation and arrest are induced by a high level of a protein complex termed maturation-promoting factor (MPF). Fertilization causes a chain of events that result in proteolytic cleavage of MPF, breaking the arrested state and allowing the fertilized oocyte to complete meiotic division.

The level of MPF in the oocyte has a profound effect on the outcome of nuclear transfer. If a nucleus is transferred into oocyte cytoplasm with high MPF, the nuclear envelope breaks down and chromatin undergoes chromosome condensation, followed by nuclear reformation and DNA replication. A nucleus from a cell in G1 phase of the cell cycle will undergo normal DNA replication and can support normal development. However, a donor nucleus in S, or G2, phase undergoes aberrant re-replication of DNA, causing chromosomal damage or an abnormal chromosome number with consequent failure of development. Nuclear transfer into unfertilized oocytes can therefore be improved by synchronizing donor nuclei in G1 phase. This can be achieved by depriving donor cells of serum, blocking the cell cycle before DNA replication.

It has been proposed that the key to successful reprogramming of a transferred nucleus is the free availability in the recipient cytoplasm of factors necessary for regulating the program of gene transcription [18]. These are normally associated with DNA within the nucleus, but dissociate from the genome during cell division, and are released into the cytoplasm when the nucleus breaks down, ready to be distributed with the chromosomes into the new daughter nuclei. These factors reassociate with the DNA in G1 phase to reestablish the transcriptional program. Unfertilized oocytes have an abundance of such free factors, being paused part way through meiotic metaphase. Consistent with this model, if the genome of a zygote is removed during cell division, the resulting cytoplast can successfully reprogram an incoming cell nucleus to embryonic gene expression, but if the zygote nucleus is removed during interphase, it cannot [18].

Nuclear transfer from somatic cells opened a new route to produce transgenic livestock, and lifted the requirement for ES cells for cell-mediated transgenesis. Cells such as primary fetal fibroblasts can be obtained in large quantities, manipulated in culture, and then converted into whole animals by nuclear transfer. The initial work carried out in Edinburgh was inspired by the possibility of producing large numbers of genetically modified animals without conventional breeding, termed "instant flocks," for applications such as biopharmaceutical production in milk [19]. The first large animal produced in this way was a Poll Dorset sheep "Polly" that carried a human clotting factor IX transgene, randomly introduced into the genome by in vitro transfection of fetal fibroblasts [15]. Shortly after, an α1-antitrypsin transgene was placed by gene targeting into a site chosen as likely to favor expression [16]. Somatic cell nuclear transfer has since been used to generate transgenic and gene-targeted animals in several other species.

From the outset, comparative data indicated that nuclear transfer requires fewer experimental animals than DNA microinjection to produce a useful transgenic animal [15], reducing costs and benefiting animal welfare. Techniques continue to improve gradually; for example, bovine nuclear transfer data from 1998 to 1999 showed an efficiency of 6.3% calves born per reconstructed embryo, while in 2003–2004 this increased to 15% [20].

Fetal and perinatal mortality and morbidity are the most serious issues that face nuclear transfer. The severity of the problem varies between species, cell types, and experimental regimes and is unrelated to genetic manipulation of the cultured cells. Rather, it is believed to be a consequence of defective epigenetic reprogramming of the donor nucleus and possibly incompatibility between the cell-derived nuclear genome and the oocyte-derived mitochondria. Cumulative data for cattle collected up to 2005 indicate that more than 1,500 cloned calves were born, of these, 60–70% survived normally to adulthood. The performance of these, including reproduction, was similar to non-cloned animals. Evidence is also accumulating that ill effects are limited to the first generation. Offspring, including those from two nuclear transfer parents, exhibit no increased morbidity or mortality.

Nuclear Transfer with Differentiated Cells

Transgenesis by nuclear transfer began with the use of abundantly available somatic cells such as fetal fibroblasts, mainly as a matter of convenience [15]. It is desirable to characterize as fully as possible cell clones used to generate whole animals. However, most primary cell types have a short lifespan in culture, allowing little time for transfection, selection, and the expansion of individual cell clones. Furthermore, prolonged growth in culture risks genetic and epigenetic alterations that may reduce their ability to support normal development.

A number of precautions can be taken to minimize the total time cells spend in culture. Genetic manipulation should ideally be carried out using primary cells at very early passage. Samples of each cell clone can be cryopreserved and retained as a frozen stock for nuclear transfer, while a replicate sample is expanded for further analysis. Determination of the modal chromosome number of cell clones is also useful because it allows those that have undergone gross changes in chromosome complement to be excluded. Frozen samples of cell clones identified as most suitable as nuclear donors can be thawed and used to generate whole animals. The viability and lifespan of primary cells can vary considerably between different isolates and are affected by factors such as the age of the donor animal and the method of preparation. It is therefore important to identify a suitable cell isolate before commencing a transgenic project.

The problem of short lifespan can also be overcome by "rejuvenating" cells by nuclear transfer and re-derivation from resulting fetuses. This allows successive rounds of in vitro genetic manipulation to be carried out relatively quickly, but does introduce a possible risk that genetic aberrations occur in the cultured cells, but remain undetected until animals are born. Serial nuclear transfer has been used to carry out multiple genetic manipulations in large animals. Three successive rounds of cloning were used to inactivate both alleles of the α1,3-GT gene in pigs [21]. In cattle, serial nuclear transfer has been used to inactivate immunoglobulin genes and the prion protein gene PrP [22, 23]. Some researchers have described a progressive decrease in the efficiency of development over successive clonal generations (e.g., [24]). However, there has been a recent report of 15 successive generations of recloned mice produced with no decrease in success rate using a chromatin-modifying reagent trichostatin A [25], suggesting that animal cloning can in principle be repeated indefinitely.

Nuclear Transfer and Gene Targeting

As mentioned in Section "History and Introduction," a major motivation for the development of nuclear transfer in mammals was to circumvent the need for embryonic stem cells and enable gene targeting in species other than mice [16] In brief, gene targeting exploits the ability of a cell to support recombination between an exogenous DNA molecule and chromosomal DNA at regions of shared homology, as part of the DNA repair process. It can be used to inactivate individual endogenous genes by insertion or deletion, replace whole genes, precisely place transgenes in the host genome, introduce subtle gene modifications, and carry out large-scale modifications such as the deletion

of megabase-sized DNA fragments. There are many variations and technical refinements, and the reader is referred to a review by Capecchi [26] for further details. Typically, cells are transfected with a DNA construct carrying an engineered modification flanked by DNA "arms" homologous to the target locus. At a certain frequency, homologous recombination occurs between the construct and the target gene and the engineered modification is seamlessly incorporated. The frequency of homologous recombination events varies by locus, vector, and the cell type used. Identifying cell clones carrying a targeted event among a large background of random integrants is key to success. Various methods have been devised to aid their isolation, the most powerful of which is to use a drug resistance marker gene that is expressed only if the vector recombines correctly at the chosen target site. Variations of this technique are referred to as "promoter trap," "intron trap," or "polyA trap" selection.

Nuclear transfer is currently the only practical method of producing gene-targeted livestock; however, it has become clear that gene targeting in somatic cells is considerably more difficult than targeting in mouse ES cells, and relatively few gene-targeted large animals have been generated. Genes so far targeted in livestock are: *COL1A1* in sheep [16], *PRNP* in cattle, sheep and goats [22, 27, 28], *GGTA1* in pigs [29, 30], *IGH* in cattle [22], and *CFTR* in pigs [31]. The main problems are the short lifespan of primary somatic cells in culture, as discussed above; the overall lower frequency of homologous recombination relative to random integration events in somatic cells; and the difficulty of targeting genes not expressed in the host cells.

Although direct comparisons are hard to find, it is generally understood that homologous recombination events are less frequent in somatic cells than in mouse ES cells [32]. Methods such as promoter trapping can enrich rare cell clones bearing targeted events, but lack of transcriptional activity in the host cell precludes their use. There is also evidence that spontaneous homologous recombination events are particularly rare for non-expressed genes [33]. This has made targeting of many potentially important genes difficult. There are however promising strategies to enhance the proportion of homologous recombination events in somatic cells, such as the synchronization of cells in late S phase so that vector transfection can be optimally timed [34], but these have yet to be fully evaluated. Current progress and a review of the field are provided by Laible and Alonso-González [35].

An entirely new approach to mammalian gene targeting is now emerging, based on the use of highly specific nuclease enzymes. This promises to overcome many of these problems and possibly supplant nuclear transfer for some applications, as discussed in Section "Beyond Nuclear Transfer – Direct Manipulation of Early Embryos."

Multipotent and Pluripotent Stem Cells as Nuclear Donors

The main advantage of multipotent cells, such as mesenchymal stem cells (MSCs), and pluripotent cells, such as ES cells, over more differentiated cell types is their longer lifespan and greater stability in culture. This facilitates genetic manipulation procedures and the isolation of cell clones for the generation of transgenic animals.

One of the defining characteristics of ES cells is that they can grow indefinitely as undifferentiated cells in culture while retaining the ability to form all tissues of the body. However, experience gained in mice is not always applicable to other species. From the few species investigated, it is clear that not all ES cells are as easy to handle as those from mouse. For example, human ES cells survive electroporation and dissociation to single cells poorly and this has made derivation of stable transfected human ES cell clones difficult [36]. Despite considerable efforts over more than a decade, few gene-targeted human ES lines have been reported [37].

However, the main problem is that ES cells are simply not available for most mammals. Artificial induction of pluripotency by the expression of key transcription factors [38, 39] offers an alternative to classical ES cells that is rapidly being extended to other species. Induced pluripotent stem (iPS) cells can be cultured for long periods, and mouse iPS cells have already been used for nuclear transfer [40]. At the time of writing, the detailed characteristics of iPS cells from most species however remain unknown. It is perhaps cautionary to note that although candidate pig iPS cells have been reported by several authors, in each case, the reprogrammed pluripotent state was not stable in culture and relied on continued expression of exogenous transcription factors.

Multipotent mesenchymal stem cells (MSCs) are attractive alternatives to ES cells for generating transgenic animals. MSCs can be readily derived from bone marrow or adipose tissue. They proliferate well for long periods in culture and have been used successfully for nuclear transfer in cattle and pigs [41–44]. MSCs can be transfected and retain their multipotent identity and support preimplantation development of nuclear transfer embryos at rates similar to non-manipulated MSCs [42, 43]. Figure 1 shows an illustrative transgenic experiment in which a green fluorescent protein reporter gene was introduced into pig MSCs and whole animals derived by nuclear transfer.

Studies of reconstructed embryos produced by nuclear transfer indicate that an important cause of developmental failure is incomplete reprogramming of the transferred nucleus. This leads to deficient expression of early embryonic genes and failure to establish a normal embryonic pattern of epigenetic regulation and chromatin structure. It has been suggested that the epigenetic state of the donor nucleus influences reprogramming efficiency, and cells with a high degree of developmental plasticity, such as multipotent and pluripotent stem cells should be more successful nuclear donors than differentiated cell types (e.g., [45]). In mice, a higher fraction of embryos derived from ES cells were found to develop to term than those from differentiated donor cells [46]. Evidence from other species is however less clear, although some studies in pigs describe higher rates of development to blastocyst with bone marrow MSCs than fetal fibroblasts [47, 48]. These findings were supported by analysis of gene expression, which revealed that porcine MSC-derived cloned embryos

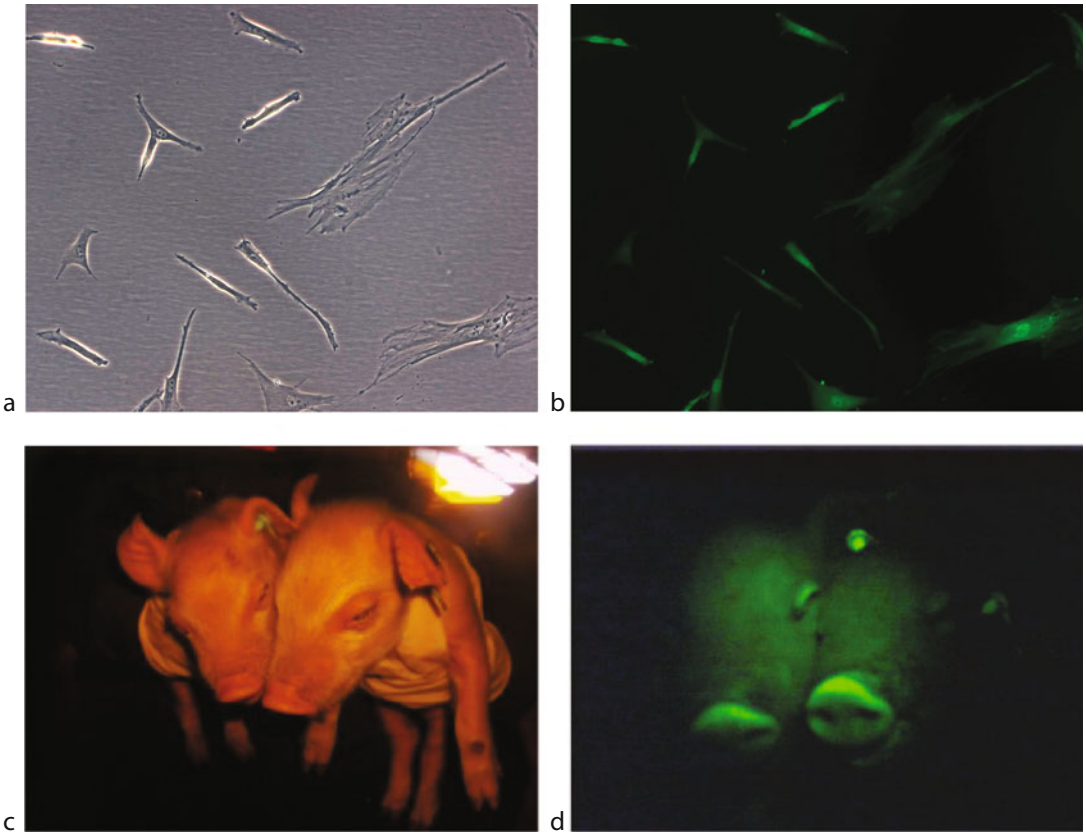

Nuclear Transfer to Produce Transgenic Mammals. Figure 1
Legend (**a**) gfp-transfected porcine MSCs; (**b**) gfp-transfected porcine MSCs under UV light; (**c**) nuclear transfer piglets generated from gfp MSCs; (**d**) nuclear transfer piglets under UV light

resembled normal embryos more closely than did those from fetal fibroblasts [48].

As mentioned in the previous section, another advantage of stem cells is that they may support homologous recombination more efficiently than other cell types, enabling gene targeting. There is insufficient data regarding MSCs, but evidence from mice indicates that iPS cells support homologous recombination at rates similar to ES cells [49]. Human ES cells also seem to support homologous recombination at a rate similar to mouse ES cells [50].

Beyond Nuclear Transfer: Direct Manipulation of Early Embryos

Sequence-specific DNA endonuclease enzymes that recognize long target sequences are new tools that promise to revolutionize genetic manipulation in many species. Enzymes of this type include naturally occurring homing endonucleases, often termed meganucleases, and artificially engineered enzymes such as zinc finger nucleases (ZFN), please see review by Cathomen and Joung [51]. Recent years have seen particular interest in the use of ZFNs in mammals.

ZFNs are artificial enzymes produced by fusing the cleavage domain of the FokI restriction endonuclease with a series of DNA-binding domains known as zinc finger motifs. Each ZFN is a heterodimer that can be produced to recognize a specific DNA target sequence of 18–24 base pairs. An appropriately designed ZFN can create a double-strand break at a single predetermined site in the genomic DNA. In eukaryotes, the error-prone non-homologous end-joining DNA repair pathway is often mutagenic, creating small insertions and deletions at the break site. Thus, careful choice of break site provides a means of inactivating a chosen gene, an alternative to gene knockout by classical gene targeting. ZFNs must be designed and custom made for each individual target site. A critical goal of enzyme design is to ensure that it does not produce double-strand breaks at sites other than that intended. Such off-target activity is likely to be toxic or mutagenic.

Perhaps the most important feature of this technology is that the frequency of gene inactivation can be so high that selection or enrichment of cells carrying the targeted event is unnecessary, effectively removing the need for cell culture. In 2008, ZFN-mediated gene inactivation was achieved directly in vertebrate embryos. Viable gene-targeted zebra fish were created by injecting mRNAs encoding ZFNs directly into one-cell embryos [52, 53]. This approach has now been extended to mammals, with the report of rats carrying inactivated IgM and Rab38 genes produced by ZFN targeting in embryos [54].

At present, ZFNs are expensive and have yet to be widely tested, but on present evidence, it seems likely that this approach could replace somatic cell nuclear transfer as a means of generating knock out animals in many mammal species. The exception being mice, where ES cells already provide a simple means of producing gene-targeted animals. ZFNs also promise to facilitate gene-targeted insertion or substitution of defined sequences in cultured somatic cells. As mentioned in Section "Nuclear Transfer and Gene Targeting," the low frequency of homologous recombination is a problem, and some genes have been difficult to target. Evidence indicates that a double-strand break at the target site dramatically increases the frequency of targeting events [55]. It has recently been shown that ZFNs facilitate gene targeting by homologous recombination in human ES and iPS cells, which had proved difficult [56]. It remains to be seen whether gene-targeted insertions or substitutions can also be achieved directly in embryos, this is a fascinating possibility that will undoubtedly be explored in the near future.

Future Directions

Science can be very unpredictable, and history is littered with authoritative, but inaccurate forecasts of future progress. So these comments are necessarily tentative.

What is already clear is the attention that nuclear transfer has brought to questions of cell identity and fate. The year 1997 marked a radical change in experimental biology; the concept of cell determination was overturned and replaced by the possibility of complete reprogramming of cell identity. This inspired many talented people to embark on projects that were previously inconceivable, with perhaps the most notable outcome being the derivation of induced pluripotent stem cells. The production of primitive stem cells essentially at will, coupled with increasing knowledge of the normal development of many cell types, is fuelling intense research activity in regenerative medicine and will undoubtedly bring significant advances in medicine and benefit to human health.

The efficiency of nuclear transfer has improved, but advances have been incremental rather than dramatic. There is still considerable mortality during gestation and around birth. First generation nuclear transfer animals sometimes face health difficulties, probably as a consequence of epigenetic defects. These may be resolved or mitigated by the use of pluripotent stem cells as nuclear donors, but supporting evidence has so far been restricted to mice. At least for a while, somatic cell nuclear transfer remains the preferred option for the production of genetically modified livestock, and the next decade will likely see gene-targeted animals of many kinds being generated, especially for biomedicine. However, while nuclear transfer remains technically difficult and inefficient, alternative methods will continually be sought. It is possible that efficient methods of embryo incorporation such as laser-assisted injection [57] could supersede nuclear transfer, with iPS cells used to generate 100% chimeras.

Another notable new technology is the use of zinc finger nucleases in early embryos. It already seems likely that this approach might take over from nuclear transfer for the production of gene knockout animals. There is also the promise that the use of ZFNs in combination with gene replacement vectors in cultured cells will significantly improve the efficiency of conventional gene targeting and give access to more difficult genes.

The availability of an enabling technology is in itself insufficient reason to produce genetically modified animals. Any transgenic project requires an objective risk to benefit analysis in which the well-being of the animal is given a high priority. But, where there are real long-term benefits to the environment, or for animal or human health, then nuclear transfer and its successor technologies can offer powerful and precise tools.

Bibliography

1. Beetschen JC, Fischer JL (2004) Yves Delage (1854–1920) as a forerunner of modern nuclear transfer experiments. Int J Dev Biol 48:607–612
2. Spemann H (1928) Die Entwicklung seitlicher und dorsoventraler Keimhälften bei verzögerter Kernversorgung. Zeitschr für Wiss Zool 132:105–134
3. McGrath J, Solter D (1984) Inability of mouse blastomere nuclei transferred to enucleated zygotes to support development in vitro. Science 226:1317–1319
4. Gilbert SF (2006) Developmental biology, 8th edn. Sinauer, USA, pp 573–579
5. Willadsen SM (1986) Nuclear transplantation in sheep embryos. Nature 320:63–65
6. Gordon JW, Scangos GA, Plotkin DJ, Barbosa JA, Ruddle FH (1980) Genetic transformation of mouse embryos by microinjection of purified DNA. Proc Natl Acad Sci USA 77:7380–7384
7. Hammer RE, Pursel VG, Rexroad CE Jr, Wall RJ, Bolt DJ, Ebert KM, Palmiter RD, Brinster RL (1985) Production of transgenic rabbits, sheep and pigs by microinjection. Nature 315:680–683
8. Evans MJ, Kaufman MH (1981) Establishment in culture of pluripotential cells from mouse embryos. Nature 292:154–156
9. Martin GR (1981) Isolation of a pluripotent cell line from early mouse embryos cultured in medium conditioned by teratocarcinoma stem cells. Proc Natl Acad Sci USA 78:7634–7638
10. Bradley A, Evans M, Kaufman MH, Robertson E (1984) Formation of germ-line chimaeras from embryo-derived teratocarcinoma cell lines. Nature 309:255–256
11. Smithies O, Gregg RG, Boggs SS, Koralewski MA, Kucherlapati RS (1985) Insertion of DNA sequences into the human chromosomal beta-globin locus by homologous recombination. Nature 317:230–234
12. Thomas KR, Capecchi MR (1987) Site-directed mutagenesis by gene targeting in mouse embryo-derived stem cells. Cell 51:503–512
13. Campbell KH, McWhir J, Ritchie WA, Wilmut I (1996) Sheep cloned by nuclear transfer from a cultured cell line. Nature 380:64–66
14. Wilmut I, Schnieke AE, McWhir J, Kind AJ, Campbell KH (1997) Viable offspring derived from fetal and adult mammalian cells. Nature 385:810–813
15. Schnieke AE, Kind AJ, Ritchie WA, Mycock K, Scott AR, Ritchie M, Wilmut I, Colman A, Campbell KHS (1997) Human factor IX transgenic sheep produced by transfer of nuclei from transfected fetal fibroblasts. Science 278:2130–2133
16. McCreath KJ, Howcroft J, Campbell KHS, Colman A, Schnieke AE, Kind AJ (2000) Production of gene-targeted sheep by nuclear transfer from cultured somatic cells. Nature 405:1066–1069
17. Verma PJ, Trounson A (2006) Nuclear transfer protocols: cell reprogramming and transgenesis. Humana Press, New Jersey
18. Egli D, Birkhoff G, Eggan K (2008) Mediators of reprogramming: transcription factors and transitions through mitosis. Nat Rev Mol Cell Biol 9:505–516
19. Kind A, Schnieke A (2008) Animal pharming, two decades on. Transgenic Res 17:1025–1033
20. Heyman Y (2005) Nuclear transfer: a new tool for reproductive biotechnology in cattle. Reprod Nutr Dev 45:353–361
21. Phelps CJ, Koike C, Vaught TD, Boone J, Wells KD, Chen SH, Ball S, Specht SM, Polejaeva IA, Monahan JA, Jobst PM, Sharma SB, Lamborn AE, Garst AS, Moore M, Demetris AJ, Rudert WA, Bottino R, Bertera S, Trucco M, Starzl TE, Dai Y, Ayares DL (2003) Production of alpha 1, 3-galactosyltransferase-deficient pigs. Science 299:411–414

22. Kuroiwa Y, Kasinathan P, Matsushita H, Sathiyaselan J, Sullivan EJ, Kakitani M, Tomizuka K, Ishida I, Robl JM (2004) Sequential targeting of the genes encoding immunoglobulin-mu and prion protein in cattle. Nat Genet 36:775–780
23. Kuroiwa Y, Kasinathan P, Sathiyaseelan T, Jiao JA, Matsushita H, Sathiyaseelan J, Wu H, Mellquist J, Hammitt M, Koster J, Kamoda S, Tachibana K, Ishida I, Robl JM (2009) Antigen-specific human polyclonal antibodies from hyperimmunized cattle. Nat Biotechnol 27:173–181
24. Kubota C, Tian C, Yang X (2004) Serial bull cloning by somatic cell nuclear transfer. Nat Biotechnol 22:693–694
25. Thuan NV, Kishigami S, Wakayama T (2010) How to improve the success rate of mouse cloning technology. J Reprod Dev 56:20–30
26. Capecchi MR (2005) Gene targeting in mice: functional analysis of the mammalian genome for the twenty-first century. Nat Rev Genet 6:507–512
27. Denning C, Burl S, Ainslie A, Bracken J, Dinnyes A, Fletcher J, King T, Ritchie M, Ritchie WA, Rollo M, de Sousa P, Travers A, Wilmut I, Clark AJ (2001) Deletion of the alpha(1, 3)galactosyl transferase (GGTA1) gene and the prion protein (PrP) gene in sheep. Nat Biotechnol 19:559–562
28. Yu G, Chen J, Yu H, Liu S, Chen J, Xu X, Sha H, Zhang X, Wu G, Xu S, Cheng G (2006) Functional disruption of the prion protein gene in cloned goats. J Gen Virol 87:1019–1027
29. Dai Y, Vaught TD, Boone J, Chen SH, Phelps CJ, Ball S, Monahan JA, Jobst PM, McCreath KJ, Lamborn AE, Cowell-Lucero JL, Wells KD, Colman A, Polejaeva IA, Ayares DL (2002) Targeted disruption of the alpha1, 3-galactosyltransferase gene in cloned pigs. Nat Biotechnol 20:251–255
30. Lai L, Kolber-Simonds D, Park KW, Cheong HT, Greenstein JL, Im GS, Samuel M, Bonk A, Rieke A, Day BN, Murphy CN, Carter DB, Hawley RJ, Prather RS (2002) Production of alpha-1, 3-galactosyltransferase knockout pigs by nuclear transfer cloning. Science 295:1089–1092
31. Rogers CS, Hao Y, Rokhlina T, Samuel M, Stoltz DA, Li Y, Petroff E, Vermeer DW, Kabel AC, Yan Z, Spate L, Wax D, Murphy CN, Rieke A, Whitworth K, Linville ML, Korte SW, Engelhardt JF, Welsh MJ, Prather RS (2008) Production of CFTR-null and CFTR-DeltaF508 heterozygous pigs by adeno-associated virus-mediated gene targeting and somatic cell nuclear transfer. J Clin Invest 118:1571–1577
32. Arbonés ML, Austin HA, Capon DJ, Greenburg G (1994) Gene targeting in normal somatic cells: inactivation of the interferon-gamma receptor in myoblasts. Nat Genet 6:90–97
33. Thyagarajan B, Johnson BL, Campbell C (1995) The effect of target site transcription on gene targeting in human cells in vitro. Nucleic Acids Res 23:2784–2790
34. Zaunbrecher GM, Dunne PW, Mir B, Breen M, Piedrahita JA (2008) Enhancement of extra chromosomal recombination in somatic cells by affecting the ratio of homologous recombination (HR) to non-homologous end joining (NHEJ). Anim Biotechnol 19:6–21
35. Laible G, Alonso-González L (2009) Gene targeting from laboratory to livestock: current status and emerging concepts. Biotechnol J 4:1278–1292
36. Costa M, Dottori M, Sourris K, Jamshidi P, Hatzistavrou T, Davis R, Azzola L, Jackson S, Lim SM, Pera M, Elefanty AG, Stanley EG (2007) A method for genetic modification of human embryonic stem cells using electroporation. Nat Protoc 2:792–796
37. Elefanty AG, Stanley EG (2009) Reshaping pluripotent stem cells. Nat Biotechnol 27:823–824
38. Takahashi K, Yamanaka S (2006) Induction of pluripotent stem cells from mouse embryonic and adult fibroblast cultures by defined factors. Cell 126:663–676
39. Takahashi K, Tanabe K, Ohnuki M, Narita M, Ichisaka T, Tomoda K, Yamanaka S (2007) Induction of pluripotent stem cells from adult human fibroblasts by defined factors. Cell 131:861–872
40. Kou Z, Kang L, Yuan Y, Tao Y, Zhang Y, Wu T, He J, Wang J, Liu Z, Gao S (2010) Mice cloned from induced pluripotent stem cells (iPSC). Biol Reprod (Epub ahead of print)
41. Kato Y, Imabayashi H, Mori T, Tani T, Taniguchi M, Higashi M, Matsumoto M, Umezawa A, Tsunoda Y (2004) Nuclear transfer of adult bone marrow mesenchymal stem cells: developmental totipotency of tissue-specific stem cells from an adult mammal. Biol Reprod 70:415–418
42. Bosch P, Pratt SL, Stice SL (2006) Isolation, characterization, gene modification, and nuclear reprogramming of porcine mesenchymal stem cells. Biol Reprod 74:46–57
43. Colleoni S, Donofrio G, Lagutina I, Duchi R, Galli C, Lazzari G (2005) Establishment, differentiation, electroporation, viral transduction, and nuclear transfer of bovine and porcine mesenchymal stem cells. Cloning Stem Cells 7:154–166
44. Faast R, Harrison SJ, Beebe LF, McIlfatrick SM, Ashman RJ, Nottle MB (2006) Use of adult mesenchymal stem cells isolated from bone marrow and blood for somatic cell nuclear transfer in pigs. Clon Stem Cell 8:166–173
45. Oback B, Wells D (2007) Donor cell differentiation, reprogramming, and cloning efficiency: elusive or illusive correlation? Mol Reprod Dev 74:646–654
46. Rideout WM, Eggan K, Jaenisch R (2001) Nuclear cloning and epigenetic reprogramming of the genome. Science 293:1093–1098
47. Kumar BM, Jin HF, Kim JG, Ock SA, Hong Y, Balasubramanian S, Choe SY, Rho GJ (2007) Differential gene expression patterns in porcine nuclear transfer embryos reconstructed with fetal fibroblasts and mesenchymal stem cells. Dev Dyn 236:435–446
48. Jin HF, Kumar BM, Kim JG, Song HJ, Jeong YJ, Cho SK, Balasubramanian S, Choe SY, Rho GJ (2007) Enhanced development of porcine embryos cloned from bone marrow mesenchymal stem cells. Int J Dev Biol 51:85–90
49. Hanna J, Wernig M, Markoulaki S, Sun CW, Meissner A, Cassady JP, Beard C, Brambrink T, Wu LC, Townes TM, Jaenisch R (2007) Treatment of sickle cell anemia mouse model with iPS cells generated from autologous skin. Science 318: 1920–1923
50. Cathomen T, Joung JK (2008) Zinc-finger nucleases: the next generation emerges. Mol Ther 16:1200–1207
51. Zwaka TP, Thomson JA (2003) Homologous recombination in human embryonic stem cells. Nat Biotechnol 21:319–321

52. Doyon Y, McCammon JM, Miller JC, Faraji F, Ngo C, Katibah GE, Amora R, Hocking TD, Zhang L, Rebar EJ, Gregory PD, Urnov FD, Amacher SL (2008) Heritable targeted gene disruption in zebrafish using designed zinc-finger nucleases. Nat Biotechnol 26:702–708
53. Meng X, Noyes MB, Zhu LJ, Lawson ND, Wolfe SA (2008) Targeted gene inactivation in zebrafish using engineered zinc-finger nucleases. Nat Biotechnol 26: 695–701
54. Geurts AM, Cost GJ, Freyvert Y, Zeitler B, Miller JC, Choi VM, Jenkins SS, Wood A, Cui X, Meng X, Vincent A, Lam S, Michalkiewicz M, Schilling R, Foeckler J, Kalloway S, Weiler H, Ménoret S, Anegon I, Davis GD, Zhang L, Rebar EJ, Gregory PD, Urnov FD, Jacob HJ, Buelow R (2009) Knockout rats via embryo microinjection of Zinc-finger nucleases. Science 325:433
55. Smih F, Rouet P, Romanienko PJ, Jasin M (1995) Double-strand breaks at the target locus stimulate gene targeting in embryonic stem cells. Nucleic Acids Res 25:5012–5019
56. Hockemeyer D, Soldner F, Beard C, Gao Q, Mitalipova M, DeKelver RC, Katibah GE, Amora R, Boydston EA, Zeitler B, Meng X, Miller JC, Zhang L, Rebar EJ, Gregory PD, Urnov FD, Jaenisch R (2009) Efficient targeting of expressed and silent genes in human ESCs and iPSCs using zinc-finger nucleases. Nat Biotechnol 27:851–857
57. Poueymirou WT, Auerbach W, Frendewey D, Hickey JF, Escaravage JM, Esau L, Doré AT, Stevens S, Adams NC, Dominguez MG, Gale NW, Yancopoulos GD, DeChiara TM, Valenzuela DM (2007) F0 generation mice fully derived from gene-targeted embryonic stem cells allowing immediate phenotypic analyses. Nat Biotechnol 25:91–99

O

Ocean Acidification

Maria Debora Iglesias-Rodriguez
School of Ocean and Earth Science, National Oceanography Centre, University of Southampton, Southampton, UK

Article Outline

Glossary
Definition of the Subject and Its Importance
Introduction
Biogeochemical Considerations: The Marine Carbon Cycle
Chemical Changes Associated with Ocean Acidification
Biological Effects of Ocean Acidification
Changes in pH over the History of the Earth
Geographic Variability in pH
Seasonal Upwelling Events
Future Directions
Bibliography

Glossary

Acclimation Organisms' physiological, morphological, and behavioral changes associated with environmental selection pressure. These are typically changes in size, growth rates, production rates of metabolites, or reproduction rates.

Adaptation Change in population composition and numbers in response to environmental selection pressure. Adaptation is largely driven by the inherent genomic properties of a population (e.g., gene richness, genomic complexity, genetic diversity). In order for a population to adapt, a subset of its members (genotypes/ecotypes) may change in relative abundance.

Anthropocene Period since the beginning of industrialization when the release of CO_2 and other by-products of human activities have had a profound effect on the Earth's ecosystems.

Biological pump The biological processes (e.g., photosynthesis, calcification) that contribute to the downward flux of carbon from the ocean surface to the deep sea.

Biota Animals and plants associated with a specific geographical region.

Calcification Deposition of the soluble mineral phase of calcium carbonate ($CaCO_3$). In the marine environment, calcifiers include plants (e.g., coccolithophores, green and red algae, calcareous dinoflagellates) and animals (e.g., foraminifera, pteropods, fish, bivalves, gastropods, corals, echinoderms, crustacea, sponges).

Calcium carbonate saturation horizon The depth of the ocean below which the saturation state of calcium carbonate is below 1, and therefore dissolution increases dramatically. This depth is also termed lysocline and it is dependent upon temperature and pressure.

Ocean acidification Period of accelerated decline in ocean pH as a result of increasing formation of carbonic acid from rising dissolved carbon dioxide in seawater as a result of human activities.

pH pH is defined as $-\log_{10}[H^+]$ and represents a measure of the acidity of a solution. A pH of 7 is neutral, a pH below 7 indicates that the solution is acid, and a pH above 7 indicates that the solution is alkaline. The pH scale is logarithmic, which means that each unit change in pH equals a tenfold change in acidity. The average surface ocean pH is ~8.1.

Saturation state of calcium carbonate (Ω) The product of the concentration of dissolved calcium and carbonate ions in seawater divided by the stoichiometric solubility product ($\Omega = [Ca^{2+}][CO_3^{2-}]/K^*_{sp}$) of the biomineral produced by an organism, that is, aragonite or calcite. When $\Omega>1$, the water is in supersaturated state with respect to calcite or aragonite, and carbonate precipitates; when $\Omega<1$

Robert A. Meyers (ed.), *Encyclopedia of Sustainability Science and Technology*, DOI 10.1007/978-1-4419-0851-3,
© Springer Science+Business Media, LLC 2012

the water is in undersaturated state with respect to calcite or aragonite and these minerals dissolve; when Ω=1 the water is in saturated state with respect to calcite or aragonite and there is no precipitation or dissolution of carbonate.

Definition of the Subject and Its Importance

The oceans play a central role in the maintenance of life on Earth. Oceans provide extensive ecosystems for marine animals and plants covering two-thirds of the Earth's surface, are essential sources of food, economic activity, and biodiversity, and are central to the global biogeochemical cycles. The oceans are the largest reservoir of carbon in the Planet, and absorb approximately one-third of the carbon emissions that are released to the Earth's atmosphere as a result of human activities. Since the beginning of industrialization, humans have been responsible for the increase in one greenhouse gas, carbon dioxide (CO_2), from approximately 280 parts per million (ppm) at the end of the nineteenth century to the current levels of 390 ppm. As well as affecting the surface ocean pH, and the organisms living at the ocean surface, these increases in CO_2 are causing global mean surface temperatures to rise. As CO_2 increases in the atmosphere, the concentration of CO_2 in seawater increases proportionally as the gas diffuses into the ocean. Part of the dissolved CO_2 reacts with water (H_2O) to form carbonic acid (H_2CO_3) in a process termed ocean acidification [1, 2]. While the levels of CO_2 are not exceptional in the history of the Earth, the rate of increase in CO_2 is thought to be at least an order of magnitude faster than has occurred for 65 million years [3]. This rapid rate of change requires marine biota to adapt rapidly and a concern is whether, to what extent, and how marine animals and plants will be able to adapt (evolutionary selection of individuals) to changes in carbon chemistry as a result of ocean acidification. Changes in acclimation such as adjustments of physiology in marine biota (e.g., changes in photosynthesis, respiration, nitrogen fixation, and calcification) in response to ocean acidification have the potential to alter marine biogeochemical cycles. For example, changes in carbon acquisition via photosynthesis will affect the efficiency of the biological pump to sequester carbon. While the chemistry of ocean acidification is relatively well characterized and there is conclusive evidence that oceans have experienced increases in CO_2 parallel to those in the atmosphere, much less is known about the biological effects of these changes. The effects of ocean acidification are already seen in corals and other marine organisms but the responses appear to be species-specific and in some cases strain-specific (see [4] and references herein). Given that ocean acidification is a global-scale phenomenon, identifying its effects presents a challenge to science and requires joint coordinated international efforts across physical, chemical, and biological oceanography.

Introduction

The oceans provide services to humans, which are of great value to the functioning of societies. Oceans are a major ecosystem providing a significant global food source, for example, fisheries provide up to 20% of protein in Southeast Asian countries, western coastal Africa, and western and northern Europe [5]. The oceans have absorbed about one-third of the anthropogenic carbon emissions, which in part ameliorates global warming induced by human activity. However, this capacity to absorb CO_2 is challenged by the accelerated increase in human activities such as the increasing burning of fossil fuels, cement production, agriculture, and deforestation. These activities have influenced atmospheric CO_2 concentrations significantly since the beginning of industrialization. Over this period, known as the Anthropocene, the speed of CO_2 increase is thought to be at least ten times faster than that experienced by the Earth for 65 million years [3]. As a result, the concentration of CO_2 in the atmosphere has been increasing from preindustrial levels of ~280 parts per million (ppm) to about 390 ppm at present. Projections according to the Intergovernmental Panel on Climate Change (IPCC) business-as-usual emission scenarios suggest that by the end of the century, atmospheric CO_2 could reach 800 ppm.

Observations in the geological record show that some marine biota have been able to adapt and thrive during fluctuations in atmospheric CO_2 while others have been severely affected by CO_2 changes [6–8]. Major extinction events have been associated with drastic changes in CO_2 and other climate-related

factors. For example, during the Cretaceous-Tertiary (K/T) event, which took place ~65.5 million years ago, there was a large-scale mass extinction in a geologically short time period associated with major environmental changes including dramatic increases in temperature and CO_2 [9, 10]. However, to what degree CO_2 and temperature drive the observed extinctions remains an open question.

The accelerated rate of increase in the concentration of atmospheric CO_2 and the parallel rise in dissolved CO_2 in seawater (and the associated chemical changes) (Fig. 1) can affect marine life. For example, increases in CO_2 can potentially disrupt the acid base balance in tissues, fluids, and cells of marine organisms. In organisms relying on building calcium carbonate ($CaCO_3$) structures like shells or skeletons, CO_2 increases can interfere with carbonate mineralization (please see section "Chemical Changes Associated with Ocean Acidification"). The extent to which marine biota can adapt to changes in carbonate chemistry and pH by evolutionary selection of individuals is critically dependent upon the genetic and physiological make up of their populations. Under IPCC carbon emission scenarios, surface ocean pH could decline by 0.3–0.4 units from preindustrial values to the end of this century [2]. Therefore, these fast changes (on geological terms, a century is a short time) may impede species to adapt to the new conditions. In coastal ecosystems the range of variation in CO_2 and temperature can be very broad, depending on biological activity and physical changes such as photosynthesis, respiration, tides, wave effect, etc. For example, an increase in bacterial respiration rates consumes oxygen and produces CO_2 such that acidity increases, sometimes dramatically. Therefore organisms living in these fast-changing environments (e.g., on sediments, where biological activity changes depending on the amount of organic carbon deposition) must be adapted and able to switch their physiology as pH and chemistry changes in their immediate environment. However, offshore and open ocean ecosystems are likely to be particularly susceptible to ocean acidification given that their exposure to fluctuations in pH and carbonate chemistry is much less pronounced than in coastal ecosystems. Therefore,

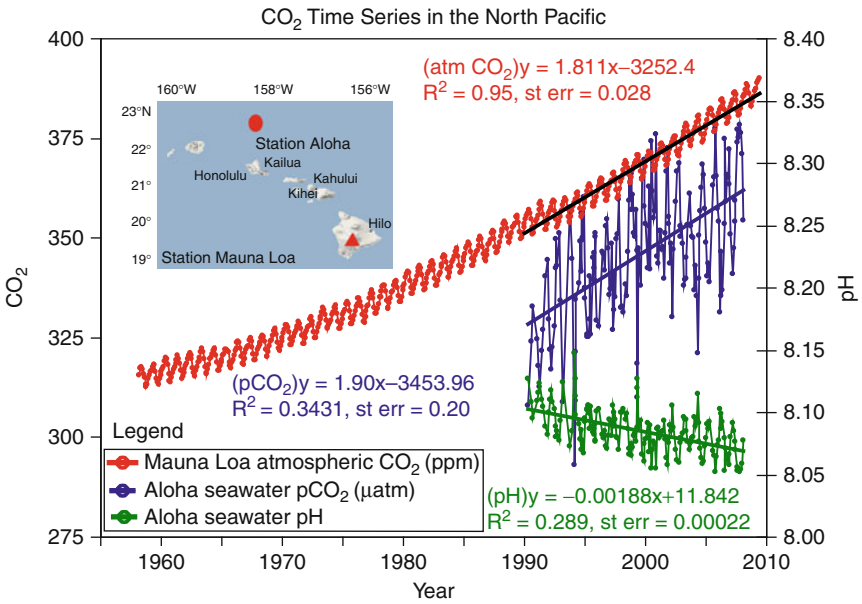

Ocean Acidification. Figure 1

Time series of atmospheric CO_2 at Mauna Loa (in ppm) and surface ocean pH and pCO_2 (µatm) at Ocean Station ALOHA in the subtropical North Pacific Ocean. Mauna Loa data: Dr. Pieter Tans, NOAA/ESRL (http://www.esrl.noaa.gov/gmd/ccgg/trends); HOTS/Aloha data: Dr. David Karl, University of Hawaii (http://hahana.soest.hawaii.edu) (Modified after Feely et al. [11])

abrupt changes in pH due to ocean acidification caused by human activities might occur more rapidly than the ability of some organisms to adapt while others will maintain their population numbers and health.

Biogeochemical Considerations: The Marine Carbon Cycle

The oceans represent the largest reservoirs of carbon in the Earth [12, 13]. In marine ecosystems, the magnitude and direction of carbon fluxes between the atmosphere, the upper ocean, and the ocean interior are critically dependent upon physical and chemical, as well as biological processes such as photosynthesis, which consumes CO_2, and respiration, decomposition, and calcification (CO_2-producing processes) (please see section "Chemical Changes Associated with Ocean Acidification") (Fig. 2). Photosynthesis also contributes to a large fraction of the annual global supply of oxygen, and removes nutrients (e.g., nitrate, phosphate, silicate, iron), which can be limiting in different parts of the ocean. Any change in functional properties of marine systems such as photosynthesis is going to have a profound effect on biogeochemical feedbacks and the ecosystem structure. Additionally, there is a vertical zonation of CO_2 sequestration at the surface and acidification of the deep sea because the organic matter produced by photosynthesis at the ocean surface is transferred to the deep sea where it is reoxidized into CO_2 by respiration, therefore increasing acidity. A change in photosynthetic activity will therefore impact upon the rates of consumption of CO_2 but also the rate of O_2 production. Additionally, a decline in oxygen is predicted as a consequence of expected

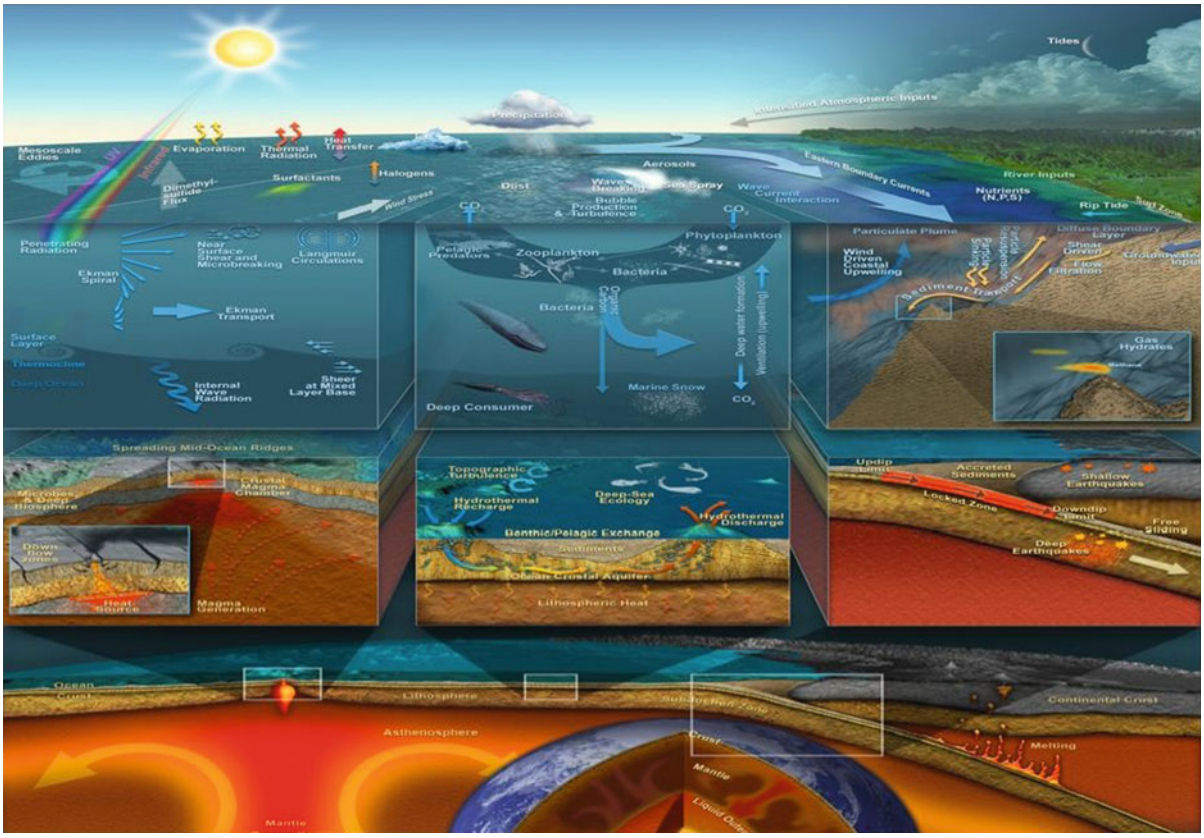

Ocean Acidification. Figure 2
The biological, chemical, and physical complexity of the oceans. Illustration designed by John Delaney and Mark Stoermer, and created by the Center for Environmental Visualization (CEV) for the NEPTUNE Program

increases in temperature driven by climate change and altered ocean circulation [14–16] (O_2 solubility declines by ~6% for a 1°C increase in temperature). If the oceans experience a decrease in oxygenation, it will likely have an effect on respiration rates of marine animals and plants and on biological processes, which rely on oxygen. For example, any changes in the O_2:CO_2 ratios are likely to impact upon the functioning of enzymes catalyzing oxygenation and/or carboxylation reactions. One such example is the enzyme ribulose-1,5-biphosphate carboxylase/oxygenase, the most abundant enzyme on Earth, which controls fluxes of carbon at the ocean surface. Loss of oxygen from the oceans caused by warming could therefore have severe effects on marine biota, particularly those populating future oxygen minimum zones [16].

Chemical Changes Associated with Ocean Acidification

Since the beginning of industrialization, rising atmospheric CO_2 has caused increasing dissolution of CO_2 in seawater, which has lowered the average surface ocean pH by about 0.1 units [1]. Although a change in 0.1 pH units may seem small, this number represents ~30% increase in the concentration of hydrogen ions [H^+], which cause acidification of the seawater. The surface waters of the oceans are in fact alkaline (pH > 7), with an average pH of about 8.1, although there are spatial and seasonal variations due to inherent properties of the water, biological impacts, and weather and ocean physics. Carbon dioxide plays an important role in controlling the seawater pH, and any increases in the atmospheric CO_2 reach equilibration with the seawater phase in timescales of months. The main components of the carbonate system of seawater, the sum of which constitutes dissolved inorganic carbon (DIC), are CO_2, bicarbonate (HCO_3^-), carbonate (CO_3^{2-}), and carbonic acid (H_2CO_3) (Fig. 3), and their relative proportions are controlled by chemical equilibria, which are influenced by exchanges of CO_2 across the air-sea interface, and these are critically dependent upon changes in biological activity at the surface, and physical

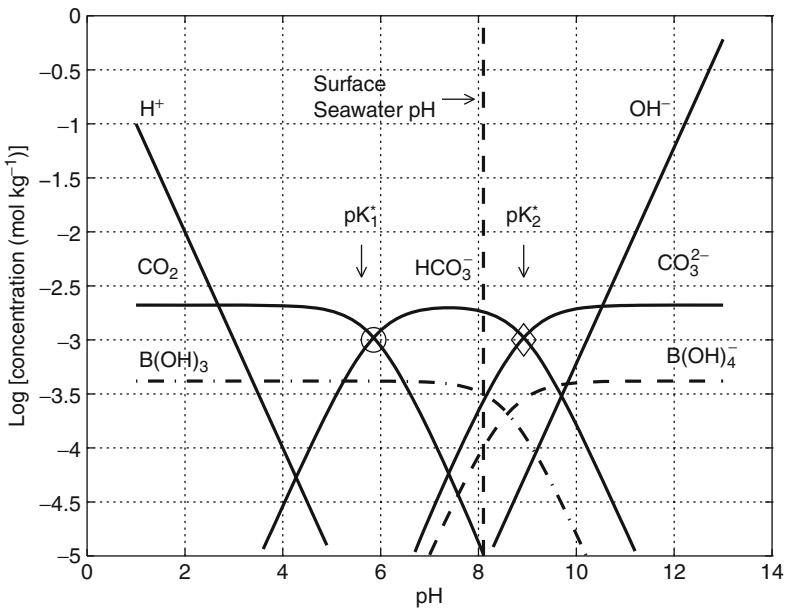

Ocean Acidification. Figure 3
Typical concentrations of dissolved inorganic carbon species in seawater as a function of pH. In addition to CO_2, HCO_3^-, CO_3^{2-}, H^+, and OH^-, this figure includes boric acid [$B(OH)_3$] and tetrahydroxyborate [$B(OH)_4^-$], as they contribute to the alkalinity of seawater (From [17])

processes (e.g., wind, temperature changes) (Fig. 2) [18]:

$$CO_{2(aq)} + H_2O \Leftrightarrow H_2CO_3 \Leftrightarrow H^+ + HCO_3^- \Leftrightarrow 2H^+ + CO_3^{2-}$$

The relative proportion of these components of the DIC of seawater changes in response to increasing atmospheric CO_2 levels. Ocean acidification is a well-recognized consequence of rising atmospheric CO_2 as seen in the well-documented time series of the Hawaii Ocean Time-Series (HOT) station ALOHA, which illustrates the direct impact of changes in atmospheric CO_2 partial pressure (pCO_2) on seawater pCO_2 in parts per million (ppm) (Fig. 1). For surface open ocean conditions, about 93% of the total carbon is in the form of the bicarbonate ion (HCO_3^-), ~6% as carbonate (CO_3^{2-}), and ~1% remains as $CO_{2(aq)}$ and H_2CO_3. While the formation of H_2CO_3 is extremely slow (tens of seconds), the interconversion between HCO_3^- and CO_3^{2-} is extremely fast. These equilibria are shifted when atmospheric CO_2 concentrations increase and CO_2 dissolved in seawater forms a weak acid called carbonic acid (H_2CO_3), therefore causing the acidity of seawater to increase. A major fraction of this weak acid dissociates into hydrogen ions (H^+) and bicarbonate ions (HCO_3^-) ($H_2CO_3 \Leftrightarrow H^+ + HCO_3^-$). A small portion of the H^+ reacts with carbonate ion (CO_3^{2-}) to produce HCO_3^- ions. Therefore, an increase in dissolution of CO_2 in seawater causes a rise in the concentrations of H^+, H_2CO_3, and HCO_3^- and a decline in pH and in the concentration of CO_3^{2-}.

Three major biological processes affect the fluxes and direction of CO_2 between the sea surface and the atmosphere: photosynthesis, respiration, and calcification. Photosynthesis acts as a sink of CO_2 to produce organic carbon and oxygen ($6CO_2 + 6H_2O \Rightarrow C_6H_{12}O_6 + 6O_2$), while respiration produces CO_2 as a by-product ($C_6H_{12}O_6 + 6O_2 \Rightarrow 6CO_2 + 6H_2O$). The process of calcification uses CO_3^{2-} ($CO_3^{2-} + Ca^{2+} \Rightarrow CaCO_3$). However, given that the seawater concentration of HCO_3^- is more than an order of magnitude greater than that of CO_3^{2-}, it is likely that organisms lacking a mechanism for concentrating CO_3^{2-} may use HCO_3^- as their ultimate carbon source for calcification ($2HCO_3^- + Ca^{2+} \Rightarrow CaCO_3 + CO_2 + H_2O$). Therefore, calcification is a source of CO_2 to the surrounding environment (about 0.6 moles of CO_2 are released for each mole of $CaCO_3$ precipitated) [19].

The process of calcification has received great attention over the last decade because a decline in carbonate ions could affect the health of organisms dependent on the use of these ions for the formation of their $CaCO_3$ plates and skeletons. The term $\Omega = ([Ca^{2+}][CO_3^{2-}]/K'_{sp}$, where K'_{sp} is the solubility product constant for $CaCO_3$, defines the saturation state of $CaCO_3$ and controls the formation and dissolution of calcium carbonate:

$$CaCO_3 \underset{\text{biomineralization}}{\overset{\text{dissolution}}{\Leftrightarrow}} Ca^{2+} + CO_3^{2-}$$

Given that the concentration of Ca^{2+} is five times that of DIC in seawater, Ω is largely dependent upon the concentration of CO_3^{2-}. Both $CaCO_3$ and CO_2 solubility increase with decreasing temperature and increasing pressure, and there is a critical depth controlling the formation and dissolution of $CaCO_3$: the saturation horizon or lysocline. Below the lysocline, seawater is undersaturated and $CaCO_3$ will start to dissolve, and above the lysocline $CaCO_3$ will be preserved. Waters are considered to be undersaturated when Ω is below 1 and supersaturated with respect to $CaCO_3$ when Ω is above 1. As temperature and pressure affect Ω, because increasing CO_2 dissolution at the surface decreases the carbonate ion concentration, the saturation horizons become shallower with increasing human activities releasing CO_2 to the atmosphere.

Biological Effects of Ocean Acidification

By the end of the century atmospheric CO_2 levels could reach more than 800 ppm [20], such that by 2100, the acidity of the ocean surface would have increased by about 150% relative to the beginning of industrialization. Although these levels are not unprecedented in the history of the Earth, the fast rate of change over the last 250 years [3] may affect some marine animals and plants in adapting to these abrupt changes in climate. When the carbonate saturation in seawater drops below 1 some $CaCO_3$ producing animals and plants may no longer be able to sustain calcification.

Metabolic Considerations: Advantages and Constraints of Elevated CO_2

Metabolically, CO_2 is not toxic but the shifts in carbonate chemistry associated with ocean acidification require organisms to regulate their physiology, and this adjustment is often associated with some metabolic cost [8, 21, 22]. An extreme case scenario of elevated CO_2 is termed hypercapnia, which has been investigated experimentally in marine organisms although some of these experiments were carried out with unrealistically high CO_2 concentrations (much higher than those projected up to 2100). An analog in humans is respiratory hypercapnia (caused by buildup of CO_2 caused by hypoventilation) and metabolic acidosis, a condition whereby human blood, which is maintained at pH 7.35–7.50, drops below 7.35 (alkalosis occurs when blood pH increases to values above 7.45). A drop below the 7.35 is life threatening in humans despite pH being alkaline. It is however unlikely that marine organisms will suffer from acute poisoning due to a drastic drop in pH at expected future CO_2 levels.

In the metabolic compartments of organisms, CO_2, HCO_3^-, CO_3^{2-}, and oxygen (O_2), among other molecules, are maintained at different ratios depending on the rates and the energetic and catalytic requirements at the sites of photosynthesis (which uses CO_2 and/or HCO_3^-), calcification (which uses HCO_3^- and/or CO_3^{2-}), and respiration (which uses O_2). Therefore, while changes in the relative proportions of the carbon sources will exert a control on key metabolic processes, the balance between photosynthesis, respiration, and the resulting effects on food web feedbacks are also dependent upon other climate-relevant factors (e.g., temperature, light, nutrient availability, group competition, evolutionary processes).

Metabolically, elevated CO_2 could represent an advantage in CO_2 transfer across membranes. Typically, the average pH inside the cell and its compartments (e.g., the cytosol, nucleoplasm, mitochondria, and plastid stroma) is between 7.1 and 7.8 [23], which is lower than the mean surface open ocean pH ($\sim$8.1). As molecules crossing the plasma membrane need to be converted into the preferred electrochemical form, a decreased pH could arguably be energetically beneficial in CO_2 or HCO_3^- utilization across the external membrane of the cell. While the increase in CO_2 and HCO_3^- caused by ocean acidification seems to enhance photosynthetic carbon fixation, the parallel decrease in CO_3^{2-} ions requires the coordinated action of a consortium of enzymes at the site of calcification, internally (e.g., inside marine phytoplanktonic $CaCO_3$-producing cells called coccolithophore) and externally (e.g., in corals). The extent to which organisms can maintain calcification rates is critically dependent upon the efficiency of membrane processes transferring ions to maintain [Ca^{2+}], pH, and, thus, [CO_3^{2-}] and [HCO_3^-] at levels that promote calcification.

Generally, increasing dissolved CO_2 has been found to enhance its removal by photosynthetic carbon fixation in phytoplankton by about 10% [24]. Increases in photosynthesis have been observed in diatoms [25, 26], coccolithophores [8, 27, 28]. Sea grasses [29, 30] seem to be in most cases either unaffected or enhanced by ocean acidification. However, different phytoplankton groups exhibit different sensitivities to increased CO_2 concentrations and this is likely due to whether CO_2 and/or bicarbonate are used for photosynthesis, to the cellular carbon requirements, and to other factors such as temperature. An example of this is a field manipulation experiment varying both temperature and CO_2, which appeared to control phytoplankton population composition [26]. Ocean acidification appears to cause a decline in Fe availability to phytoplankton [31] and shifts in the proportion of nutrients in seawater driven by ocean acidification can influence community structure, nutrient utilization, and productivity [32, 33]. Nitrogen fixation, a functional property of cyanobacteria appears to be enhanced by elevated CO_2 in *Trichodesmium* sp. [34, 35].

Effect of Ocean Acidification on Calcifiers

Calcification, together with photosynthesis, is probably the most important physiological process affected by the increase in seawater CO_2 concentrations. Calcification is a widespread and resilient phenomenon in the history of Earth that is essential to most life forms. Calcification refers to the deposition of the soluble mineral phase of $CaCO_3$ and, in the marine environment, calcifiers include photosynthetic organisms (e.g., coccolithophores, green and red algae, calcareous dinoflagellates) and animals (heterotrophs (foraminifera),

pteropods, fish, bivalves, gastropods, corals, echinoderms, crustacea, sponges). This process represents a source of CO_2 to the surrounding water and potentially to the atmosphere via the following equation: $Ca^{2+} + 2HCO_3^- \Rightarrow CaCO_3 + CO_2 + H_2O$ (please see section "Chemical Changes Associated with Ocean Acidification" for details). However, the effect of calcification (CO_2 source) can be counteracted by that of photosynthesis (CO_2 sink) in photosynthetic organisms like coccolithophores. It has been proposed that if the ratio of $CaCO_3$ to particulate organic carbon (the latter a product of photosynthesis) is below 1.5, then the calcifier is a sink of CO_2, but if this ratio increases to values above 1.5, the calcifier is considered a source of CO_2 to the environment [19]. While calcification is one mechanism by which carbon is exported to depth and it is a carbon sink as the formation of $CaCO_3$ removes carbon from the seawater into solid phase, it is however a source of CO_2.

Polymorph mineralogy and elemental chemistry of marine carbonates should be considered in predicting the responses of marine calcifiers to ocean acidification [36]. In the marine environment there are two main polymorphs of $CaCO_3$: calcite and aragonite. It is well established that aragonite is more soluble than calcite, and that the solubility of calcite increases with its Mg-content. Magnesium tends to substitute for calcium in the calcite lattice, forming "low-Mg calcite" when $\%MgCO_3$ is less than 4, and "high-Mg calcite" when it is greater than 4 [37]. There are other forms of pelagic carbonates, for example, magnesium carbonate ($MgCO_3$) and strontium carbonate ($SrCO_3$), although most carbonate is buried in the form of $CaCO_3$. Although these additional carbonate forms make a smaller contribution to the $CaCO_3$ budget, they should be taken into account to assess the susceptibility of marine carbonates to CO_2-induced ocean acidification and whether or to what extent these proportions change.

In calcifiers, any change in the saturation state of the two main polymorphs of $CaCO_3$ – calcite and aragonite – is of particular concern because the making of their shells and skeletons is dependent on the availability of CO_3^{2-}. Calcifying organisms include planktonic plants and animals that drift in the water (e.g., coccolithophores, foraminifera, pteropods, and fish) and benthic organisms, which live at the bottom of the ocean (e.g., green and red algae, bivalves, gastropods, corals, echinoderms, crustacea, foraminifera, serpulid worms, bryozoa, and sponges). Generally, marine calcification seems to decline with decreasing carbonate ions although there is significant variability in the magnitude and direction of the slope (e.g., [8, 21, 22, 27, 28, 38–55]). However there are varying physiological responses to ocean acidification. For example, manipulations of CO_2 in seawater showed enhanced productivity under CO_2 up to 560 ppm, but severely reduced productivity under CO_2 regimes approaching 1,000 ppm [56]. The calcification response to ocean acidification remains unresolved in a group of $CaCO_3$-producing microscopic plants, the coccolithophores where significant variation has been observed between and even within species [8, 27, 28, 41, 44, 52, 57, 58]. Interestingly, studies suggest that increases in calcification in response to CO_2 occur with a metabolic cost. For example, in an investigation of susceptibility of calcifiers to ocean acidification, 6 of 18 species investigated actually began to dissolve (on a net basis) under high CO_2 and the gross morphology (and presumably function) of many of the shells was modified under high CO_2 [22]. In another study, growth rates of coccolithophores declined significantly under elevated CO_2 [8], suggesting that energetic demand may be significant, for example, in maintaining elevated pH at the site of calcification.

Calcifiers must adapt to the rapid rates of change in $CaCO_3$ saturation because the formation of their skeletons is critically dependent upon the availability of CO_3^{2-}, which is favorable when the seawater is supersaturated with calcium carbonate. This is why increasing CO_2 concentration and declining pH are detrimental to calcification [24]. This is particularly important in polar ecosystems, given that the solubility of CO_2 in seawater increases with decreasing temperature. Undersaturation with respect to aragonite by the year 2032 in the Arctic Ocean [59], and by 2050 in the Southern Ocean [60], may cause additional disruptions to many components of the marine food web. An increase in temperature associated with rising CO_2 will undoubtedly have consequences on metabolic rates. Although there are limited experiments on the combined effects of CO_2 and temperature (and other climate-related variables), it is known that their combined impacts can be different from those on its

own [47, 61, 62]. One example is the relative effect of temperature and CO_2 on coral bleaching, the process by which the photosynthetic organisms living in symbiosis with corals, zooxanthellae, decline in numbers or produce less pigments [63, 64]. Therefore, understanding better the synergistic effects of climate-driven variables is central to managing ecosystems and making robust predictions to future climate scenarios.

Changes in pH over the History of the Earth

Marine organisms have adapted to fluctuations in atmospheric CO_2 throughout their evolutionary history. One of the best preserved calcifying groups, the coccolithophores, exhibits high diversities and abundances within a wide range of pCO_2, temperature, and Mg:Ca regimes, suggesting that they are an ecophysiologically versatile group [65]. Other groups including corals, mollusks, brachiopods, foraminifera, bryozoans, and echinoderms appear to have experienced changes in diversity and abundance though since their onset in the geological record [66–72]. Using coccolithophores as an example of one of the best preserved groups in the geological record, their identification in the late Triassic suggests that these algae evolved coccolithogenesis soon after their genetic differentiation at the Permian-Triassic (P/T) boundary [65, 73]. Their origin and further fast diversification is associated with a long-term decline in atmospheric pCO_2 [73] and a decrease in seawater Mg:Ca that - promoted their predominantly low-Mg calcitic mineralogy [22].

During their evolution, deep sea dwellers have adapted to unique living conditions, with typically very stable temperatures and pressures, and relatively constant CO_2 concentrations (with the exception of volcanic CO_2 vents and zones of exceptionally high respiration rates). While deep sea ecosystems are generally exposed to little fluctuations in environmental factors including pH, the ocean surface and coastal regions are subjected to seasonal variations in pH, exposures to corrosive waters due to seasonal upwelling, and other short-term and often small-scale perturbations (e.g., [53, 74]). These unique ecosystems provide a natural laboratory where to test environmental impacts and adaptation of organisms to environmental selection pressure.

Distinct adaptations are reflected in the geological record revealing that organisms have been relatively resilient to changes in ocean pH [6] and Ca^{2+} levels [7]. However there have been periods of rapid environmental change, such as at the Cretaceous/Tertiary (K/T) boundary, which was accompanied by mass extinction of calcareous phytoplankton [9], and at the P/T boundary, which is associated with selective extinction of a range of calcifying marine organisms [10]. Whether marine calcifiers will adapt (evolutionary selection of specific groups) to future carbonate chemistry conditions (and associated changes in temperature and other factors) is presently at the centre of the debate in the ocean acidification community. At present, there is insufficient information to even speculate about possible biogeochemical shifts originating from distinct adaptations (evolutionary selection) or changes in the functional properties of organisms (acclimation) (e.g., change in photosynthetic carbon fixation, calcification, fertilization success, and larval development).

Geographic Variability in pH

While ocean acidification is a global-scale phenomenon, there are areas that already have naturally low pH conditions representative of projected scenarios. These include polar regions (Arctic and Southern Oceans), coastal zones exposed to river inputs, effects of terrigenous material, and near-coastal seasonal upwelling.

There is plenty of evidence showing ocean acidification although there is temporal and spatial variability in carbonate chemistry [1, 2, 42, 60, 74–81]. It is also well established that the uptake of anthropogenic CO_2 is a major cause for long-term increases in DIC and decreases in $CaCO_3$ saturation state [4, 82]. However, temperature is one important factor determining the solubility of CO_2 in seawater as CO_2 solubility increases with decreasing temperature. Therefore, polar waters have inherently higher CO_2 content and polar ecosystems are potentially more vulnerable to further increases in CO_2 caused by ocean acidification. It has been suggested that the high latitude oceans (Arctic and Southern Oceans) will experience aragonite undersaturation by the middle of the century [36, 60, 83, 84]. Saturation of $CaCO_3$ is also affected by pressure such that deeper waters tend to have lower Ω. Shoaling of the aragonite and calcite saturation horizons is

another effect associated with ocean acidification. Shallower undersaturated waters have been observed in the North Pacific [85], and Chukchi Sea and Arctic Ocean [86, 87], which makes organisms living in them potentially more vulnerable. Many of the organisms producing skeletons or body parts of solid-phase $CaCO_3$ are known to be sensitive to the concentration of CO_3^{2-} in ambient seawater, which determines $CaCO_3$ saturation. At present, most surface waters in the global ocean are supersaturated with respect to aragonite and calcite ($\Omega>1$), but a decrease in these values will affect organisms with optimal carbonate precipitation rates above these saturation states.

Seasonal Upwelling Events

Upwelling is a process by which cold, dense, and typically nutrient-rich waters move toward the ocean surface, replacing warmer and nutrient-poor waters. Therefore, during these events, large areas and the organisms inhabiting them experience exposure to high CO_2. In 2008, Feely and colleagues [74] showed results indicating that the continental shelf of the west coast of North America may already be undersaturated with respect to aragonite resulting from the combined impacts of coastal upwelling and ocean acidification (Fig. 4). In this region, the seasonal upwelling of

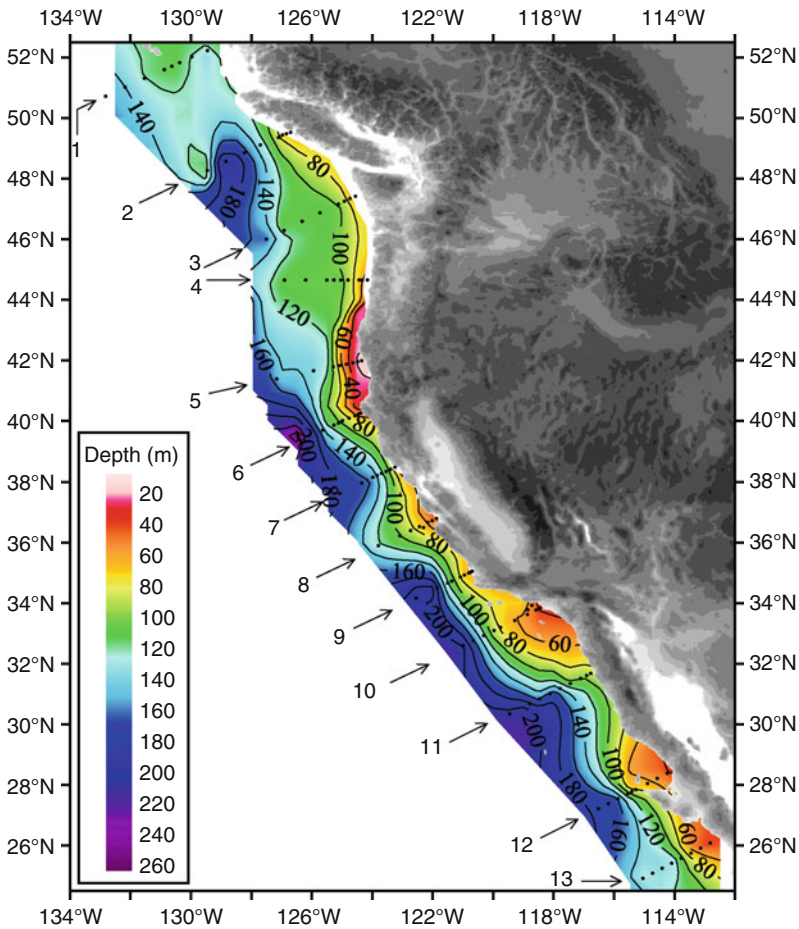

Ocean Acidification. Figure 4

The depths of undersaturated water (aragonite saturation < 1.0; pH < 7.75) on the continental shelf of western North America from Queen Charlotte Sound, Canada to San Gregorio Baja California Sur, Mexico. On transect lines 5 the corrosive water reaches all the way to the surface in the inshore waters near the coast. The *black dots* represent station locations [74]

subsurface waters along the coast brings CO_2-enriched waters from depth to the surface ocean. The observations of this study suggest that these upwelled waters are enriched with anthropogenic CO_2 from gas exchange and vertical mixing as well as being inherently high in CO_2. Therefore, the CO_2 concentrations in these upwelled waters is much greater than those in preindustrial times. These acidified waters could have a detrimental effect on aragonite-producing organisms as these waters are undersaturated with respect to aragonite. Given that upwelling is a seasonal common phenomenon in many coastal regions, the enhanced acidity of upwelled waters could be affecting coastal ecosystems in other upwelling regions. What remains to be tested is whether organisms experiencing these events seasonally have local adaptations to overcome these pronounced alterations in carbonate chemistry.

Future Directions

An international effort in monitoring changes in atmospheric and oceanic CO_2 concentrations, the ocean uptake of anthropogenic CO_2 and the natural CO_2 exchange under climate change and rising atmospheric CO_2 is already underway. This represents a huge step forward in assessing local, regional, and global effects, and identifying regions of particular susceptibility to changes in pH in coastal and open ocean environments.

The majority of studies on the causes and effects of ocean acidification have focused on short-term laboratory experiments with just a few field manipulations. Longer-term experiments that represent more realistic adaptations are needed to validate measured responses to abrupt exposures to acidified conditions, which are typically used in the laboratory. The emerging molecular technology will determine the extent to which organisms adapt to changes over long timescales, for example, by making use of existing and ongoing genome projects. Information at the most fundamental level of biological organization – the genome level – will provide first-hand information about how organisms evolve and how some functions are acquired and some others are lost. Information at all levels of organization, from global through ecological to molecular (genes, proteins), will enhance our ability to predict the fate of the ocean and the organisms inhabiting them a high CO_2 world.

Bibliography

Primary Literature

1. Caldeira K, Wickett ME (2003) Anthropogenic carbon and ocean pH. Nature 425:365
2. Caldeira K, Wickett ME (2005) Ocean model predictions of chemistry changes from carbon dioxide emissions to the atmosphere and ocean. J Geophys Res 110:C09S04, doi:10.1029/2004JC002671
3. Ridgwell A, Schmidt DN (2010) Past constraints on the vulnerability of marine calcifiers to massive carbon dioxide release. Nat Geosci 3:196–200
4. Doney SC, Fabry VJ, Feely RA, Kleypas JA (2009) Ocean acidification: the other CO_2 problem. Ann Rev Mar Sci 1:169–192. doi:10.1146/annurev.marine.010908.163834
5. Cooley SR, Doney SC (2009) Anticipating ocean acidification's economic consequences for commercial fisheries. Environ Res Lett 4:024007. doi:10.1088/1748-9326/4/2/024007
6. Gibbs SJ, Bown PR, Sessa JA, Bralower TJ, Wilson PA (2006) Nannoplankton extinction and origination across the Paleocene-Eocene thermal maximum. Science 314:1770–1773
7. Tyrrell T, Zeebe RE (2004) History of carbonate ion concentration over the last 100 million years. Geochim Cosmochim Acta 68:3521–3530
8. Iglesias-Rodrıguez MD, Halloran PR, Rickaby REM, Hall IR, Colmenero-Hidalgo E, Gittins JR, Green DRH, Tyrrell T, Gibbs SJ, von Dassow P, Rehm E, Armbrust VE, Boessenkool KP (2008) Phytoplankton calcification in a high CO_2 world. Science 320:336–339
9. MacLeod N, Rawson PF, Forey PL, Banner FT, Boudagher-Fadel MK, Bown PR, Burnett JA, Chambers P, Culver S, Evans SE, Jeffret C, Kaminski MA, Lord AR, Milner AC, Milner AR, Morris N, Owen E, Rosen BR, Smith AB, Taylor PD, Urquart E, Young JR (1997) The Cretaceous-tertiary biotic transition. J Geol Soc 154:265–292
10. Knoll AH, Bambach RK, Payne JL, Pruss S, Fischer WW (2007) Paleophysiology and end-Permian mass extinction. Earth Planet Sci Lett 256:295–313
11. Feely RA et al (2008) PICES Press 16(1):22–26
12. Sarmiento JL, Gruber N (2002) Sinks for anthropogenic carbon. Phys Today 55:30–36
13. Archer D (2005) Fate of fossil fuel CO_2 in geological time. J Geophys Res 110: C09S05, doi:10.1029/2004JC002625
14. Garcia HE, Boyer TP, Levitus S, Locarnini RA, Antonov JI (2005) Climatological annual cycle of upper ocean oxygen content anomaly. Geophys Res Lett 32:L09604. doi:10.1029/2004GL022286
15. Brierley AS, Kingsford MJ (2009) Impacts of climate change on marine organisms and ecosystems. Curr Biol 19:R602–R614. doi:10.1016/j.cub.2009.05.046
16. Keeling RF, Körtzinger A, Gruber N (2010) Ocean deoxygenation in a warming world. Ann Rev Mar Sci 2:199–229
17. Zeebe RE, Wolf-Gladrow D (2001) CO_2 in seawater: equilibrium, kinetics, isotopes. Elsevier Oceanography Series, 65, Amsterdam, pp 346

18. Sabine CL, Feely RA, Gruber N, Key RM, Lee K, Bullister JL, Wanninkhof R, Wong CS, Wallace DWR, Tilbrook B, Millero FJ, Peng T-H, Kozyr A, Ono T, Rios AF (2004) The oceanic sink for anthropogenic CO_2. Science 305:367–371
19. Frankignoulle M, Canon C, Gattuso J-P (1994) Marine calcification as a source of carbon dioxide: positive feedback of increasing atmospheric CO_2. Limnol Oceanogr 39:458–462
20. Intergovernmental Panel on Climate Change (2001) Climate change 2001: impacts, adaptation and vulnerability. In: McCarthy JJ et al (eds) Contribution of Working Group II to the Third Assessment Report of the Intergovernmental Panel on Climate Change. Cambridge University Press, New York
21. Wood HL, Spicer JI, Widdicombe S (2008) Ocean acidification may increase calcification rates, but at a cost. Proc Roy Soc Lon B 275:1767–1773
22. Ries JB, Cohen AL, McCorkle DC (2009) Marine calcifiers exhibit mixed responses to CO_2-induced ocean acidification. Geology 37:1131–1134
23. Venn AA, Tambutté E, Lotto S, Zoccola D, Allemand D, Tambutté S (2009) Imaging intracellular pH in a reef coral and symbiotic anemone. Proc Natl Acad Soc 106:16574–16579
24. Raven JA, Caldeira K, Elderfield H, Hoegh-Guldberg O, Liss P, Riebesell U, Shepherd J, Turley C, Watson A (2005) Ocean acidification due to increasing atmospheric carbon dioxide. The Royal Society policy Document 12/05, London
25. Tortell PD, Rau GH, Morel FMM (2000) Inorganic carbon acquisition in coastal Pacific phytoplankton communities. Limnol Oceanogr 45:1485–1500
26. Tortell PD, Payne CD, Li Y, Trimborn S, Rost, B, Smith, WO, Riesselman, C, Dunbar, RB, Sedwick, P, and DiTullio, GR (2008) CO_2 sensitivity of Southern ocean phytoplankton. Geophys Res Lett 35: L04605, 5 pp, doi:10.1029/2007GL032583
27. Riebesell U, Zondervan I, Rost B, Tortell PD, Zeebe RE, Morel FMM (2000) Reduced calcification of marine plankton in response to increased atmospheric CO_2. Nature 407:364–367
28. Shi D, Xu Y, Morel FMM (2009) Effects of the pH/pCO_2 control method on medium chemistry and phytoplankton growth. Biogeosciences 6:1199–1207
29. Palacios SL, Zimmerman RC (2007) Response of eelgrass Zostera marina to CO_2 enrichment: possible impacts of climate change and potential for remediation of coastal habitats. Mar Ecol Prog Ser 344:1–13
30. Zimmerman RC, Kohrs DG, Steller DL, Alberte RS (1997) Impacts of CO_2 enrichment on productivity and light requirements of Eelgrass. Plant Physiol 115:599–607
31. Shi D, Xu Y, Hopkinson BM, Morel FMM (2010) Effect of ocean acidification on iron availability to marine phytoplankton. Science 327:676–679
32. Tortell PD, DiTullio GR, Sigman DM, Morel FMM (2002) CO_2 effects on taxonomic composition and nutrient utilization in an equatorial Pacific phytoplankton assemblage. Mar Ecol Prog Ser 236:37–43
33. Blackford JC (2010) Predicting the impacts of ocean acidification: challenges from an ecosystem perspective. J Mar Syst 81:12–18. doi:10.1016/j.jmarsys.2009.12.016
34. Barcelos e Ramos J, Biswas H, Schulz KG, LaRoche J, Riebesell U (2007) Effect of rising atmospheric carbon dioxide on the marine nitrogen fixer. Trichodesmium Glob Biogeochem Cycles 21: GB2028, 6 pp, doi:10.1029/2006GB002898
35. Hutchins DA, Fu F-X, Zhang Y, Warner ME, Feng Y, Portune K, Bernhardt PW, Mulholland MR (2007) CO_2 control of Trichodesmium N2 fixation, photosynthesis, growth rates, and elemental ratios: Implications for past, present, and future ocean biogeochemistry. Limnol Oceanogr 52:1293–1304
36. Feely RA, Orr J, Fabry VJ, Kleypas JA, Sabine CL, Landgon C (2009) Present and future changes in seawater chemistry due to ocean acidification. In: McPherson BJ, Sundquist ET (eds) Carbon sequestration and its role in the global carbon cycle. AGU Monograph, Washington, DC
37. Morse JW, Andersson AJ, Mackenzie FT (2006) Initial responses of carbonate-rich shelf1369 sediments to rising atmospheric pCO_2 and "ocean acidification": role of high Mg-calcites. Geochim Cosmochim Acta 70:5814–5830
38. Gattuso J-P, Frankignoulle M, Bourge I, Romaine S, Buddemeier RW (1998) Effect of calcium carbonate saturation of seawater on coral calcification. Glob Planet Change 18:37–46
39. Kleypas JA, Buddemeier RW, Archer D, Gattuso J-P, Langdon C, Opdyke BN (1999) Geochemical consequences of increased atmospheric carbon dioxide on coral reefs. Science 284:118–120
40. Kleypas JA, Buddemeier RW, Gattuso J-P (2001) The future of coral reefs in an age of global change. Int J Earth Sci 90:426–437
41. Zondervan I, Zeebe RE, Rost B, Riebesell U (2001) Decreasing marine biogenic calcification: a negative feedback on rising atmospheric pCO_2. Glob Biogeochem Cycles 15:507–516
42. Feely RA, Sabine CL, Lee K, Millero FJ, Lamb MF, Greeley D, Bullister JL, Key RM, Peng T-H, Kozyr A, Ono T, Wong CS (2002) In situ calcium carbonate dissolution in the Pacific Ocean. Glob Biogeochem Cycles 16:1144
43. Leclercq N, Gattuso J-P, Jaubert J (2002) Primary production, respiration, and calcification of a coral reef mesocosm under increased CO_2 partial pressure. Limnol Oceanogr 47:558–564
44. Zondervan I, Rost B, Riebesell U (2002) Effect of CO_2 concentration on the PIC/POC ratio in the coccolithophore Emiliania huxleyi grown under light-limiting conditions and different daylengths. J Exp Marine Biol Ecol 272:55–70
45. Guinotte JM, Buddemeier RW, Kleypas JA (2003) Future coral reef habitat marginality: temporal and spatial effects of climate change in the Pacific basin. Coral Reefs 22:551–558
46. Langdon C, Broecker WS, Hammond DE, Glenn E, Fitzsimmons K, Nelson SG, Peng T-S, Hajdas I, Bonani G (2003) Effect of elevated CO_2 on the community metabolism of an experimental coral reef. Glob Biogeochem Cycles 17:1–14. doi:10.1029/2002GB001941

47. Reynaud S, Leclercq N, Romaine-Lioud S, Ferrier-Pages C, Jaubert J, Gattuso JP (2003) Interacting effects of CO_2 partial pressure and temperature on photosynthesis and calcification in a scleractinian coral. Glob Chang Biol 9:1660–1668
48. Langdon C, Atkinson MJ (2005) Effect of elevated pCO_2 on photosynthesis and calcification of corals and interactions with seasonal change in temperature/irradiance and nutrient enrichment. J Geophys Res 110: C09S07, doi:10.1029/2004JC002576
49. Guinotte JM, Orr J, Cairns S, Freiwald A, Morgan L, George R (2006) Will human induced changes in seawater chemistry alter the distribution of deep-sea scleractinian corals? Front Ecol Environ 4:141–146
50. Kleypas JA, Feely RA, Fabry VJ, Langdon C, Sabine CL, Robbins LL (2006) Impacts of ocean acidification on coral reefs and other marine calcifiers: a guide for future research, report of a workshop, St. Petersburg, FL, USA, 18–20 Apr 2005, sponsored by NSF, NOAA, and the US Geological Survey http://www.ucar.edu/communications/Final_acidification.pdf
51. Gazeau F, Quiblier C, Jansen JM, Gattuso J-P, Middelburg JJ, Heip CHR (2007) Impact of elevated CO_2 on shellfish calcification. Geophys Res Lett 34: L07603, doi:10.1029/2006GL028554
52. Fabry VJ, Seibel BA, Feely RA, Orr JC (2008) Impacts of ocean acidification on marine fauna and ecosystem processes ICES. J Mar Sci 65:414–432
53. Hall-Spencer JM, Rodolfo-Metalpa R, Martin S, Ransome E, Fine M, Turner SM, Rowley SJ, Tedesco D, Buia M-C (2008) Volcanic carbon dioxide vents show ecosystem effects of ocean acidification. Nature 454:96–99. doi:10.1038/nature07051
54. Nienhuis S, Palmer AR, Harley CDG (2010) Elevated CO_2 affects shell dissolution rate but not calcification rate in a marine snail. Proc Roy Soc B: Biol Sci 277(1693):2553–2558. doi:10.1098/rspb.2010.0206
55. Rodolfo-Metalpa R, Martin S, Ferrier-Pages C, Gattuso J-P (2010) Response of the temperate coral *Cladocora caespitosa* to mid- and long-term exposure to pCO_2 and temperature levels projected for the year 2100 AD. Biogeosciences 7:289–300
56. Anthony KRN, Kline DI, Diaz-Pulido G, Dove S, Hoegh-Guldberg O (2008) Ocean acidification causes bleaching and productivity loss in coral reef builders. Proc Natl Acad Soc 105:17442–17446
57. Langer G, Nehrke G, Probert I, Ly J, Ziveri P (2009) Strain specific responses of *Emiliania huxleyi* to changing seawater carbonate chemistry. Biogeosciences 6:2637–2646, http://www.biogeosciences.net/6/2637/2009/
58. Müller MN, Schulz KG, Riebesell U (2010) Effects of long-term high CO_2 exposure on two species of coccolithophores. Biogeosciences 7:1109–1116
59. Steinacher M, Joos F, Frölicher TL, Plattner G-K, Doney SC (2009) Imminent ocean acidification in the Arctic projected with the NCAR global coupled carbon cycle-climate model. Biogeosciences 6:515–533, www.biogeosciences.net/6/515/2009/
60. Orr JC, Fabry VJ, Aumont O, Bopp L, Doney SC et al (2005) Anthropogenic ocean acidification over the twenty-first century and its impact on calcifying organisms. Nature 437: 681–686
61. Findlay HS, Wood HL, Kendall MA, Spicer JI, Twitchett RJ, Widdicombe S (2009) Calcification, a physiological process to be considered in the context of the whole organism. Biogeosciences Discuss 6:2267–2284, www.biogeosciences-discuss.net/6/2267/2009/
62. Walther K, Sartoris FJ, Bock C, Pörtner HO (2009) Impact of anthropogenic ocean acidification on thermal tolerance of the spider crab *Hyas araneus*. Biogeosciences 6:2207–2215
63. Kleppel GS, Dodge RE, Reese CJ (1989) Changes in pigmentation associated with the bleaching of stony corals. Limnol Oceanogr 34:1331–1335
64. Herfort L, Thake B, Taubner I (2008) Bicarbonate stimulation of calcification and photosynthesis in two hermatypic corals. J Phycol 44:91–98
65. Bown PR, Lees JA, Young JR (2004) In: Thierstein HR, Young JR (eds) Coccolithophores –from molecular processes to global impact. Springer, Berlin, p 481
66. Vinogradov AP (1953) The elementary chemical composition of marine organisms. Sears Foundation for Marine Research, New Haven
67. Weber JN (1969) The incorporation of magnesium into the skeletal calcites of echinoderms. Am J Sci 267:537–566
68. Lipps JH (1970) Plankton evolution. Evolution 24:1–21
69. Comperse EL, Bates JM (1973) Determination of calcite: aragonite ratios in mollusc shells by infrared spectra. Limnol Oceanogr 18:326–331
70. Wilkinson BH (1979) Biomineralization, paleoceanography, and the evolution of calcareous marine organisms. Geology 7:524–527
71. Zhuravlev AY, Wood RA (2008) Eve of biomineralization: controls on carbonate mineralogy. Geology 36:923–926
72. Zhuravlev AY, Wood RA (2009) Controls on carbonate skeletal mineralogy: global CO_2 evolution and mass extinctions. Geology 37:1123–1126
73. de Vargas C, Aubry M-P, Probert I, Young J (2007) In: Thierstein HR, Young JR (eds) Coccolithophores – from molecular processes to global impact. Springer, Berlin, p 251
74. Feely RA, Sabine CL, Hernandez-Ayon JM, Ianson D, Hales B (2008) Evidence for upwelling of corrosive "acidified" water onto the continental shelf. Science 320:1490–1492
75. Bates NR (2007) Interannual variability of the oceanic CO_2 sink in the subtropical gyre of the North Atlantic Ocean over the last 2 decades. J Geophys Res 112:C09013. doi:10.1029/2006JC003759
76. Bates NR, Peters AJ (2007) The contribution of atmospheric acid deposition to ocean acidification in the subtropical North Atlantic Ocean. Mar Chem 107:547–558
77. Chung SN, Lee K, Feely RA, Sabine CL, Millero FJ, Wanninkhof R, Bullister JL, Key RM, Peng T-H (2003) Calcium carbonate budget in the Atlantic Ocean based on water column inorganic carbon chemistry. Glob Biogeochem Cycles 17:1093

78. Feely RA, Sabine CL, Lee K, Berelson W, Kleypas J et al (2004) Impact of anthropogenic CO_2 on the $CaCO_3$ system in the oceans. Science 305:362–366
79. Sabine CL, Feely RA (2007) The oceanic sink for carbon dioxide. In: Reay D, Hewitt N, Grace J, Smith K (eds) Greenhouse gas sinks. CABI, Oxfordshire, pp 31–49
80. Santana-Casiano JM, Gonzalez-Davila M, Rueda MJ, Llinas O, Gonzalez-Davila EF (2007) The interannual variability of oceanic CO_2 parameters in the northeast Atlantic subtropical gyre at the ESTOC site. Glob Biogeochem Cycles 21:GB1015. doi:10.1029/2006GB002788
81. Watson AJ, Schuster U, Bakker DCE, Bates NR, Corbière A, González-Dávila M, Friedrich T, Hauck J, Heinze C, Johannessen T, Körtzinger A, Metzl N, Olafsson J, Olsen A, Oschlies A, Padin XA, Pfeil B, Santana-Casiano JM, Steinhoff T, Telszewski M, Rios AF, Wallace DWR, Wanninkhof R (2009) Tracking the variable North Atlantic sink for atmospheric CO_2. Science 326:1391–1393
82. Dore JE, Lukas R, Sadler DW, Church MJ, Karl DM (2009) Physical and biogeochemical modulation of ocean acidification in the central North Pacific. Proc Natl Acad Soc USA 106:12235–12240
83. Cao L, Caldeira K (2008) Atmospheric CO_2 stabilization and ocean acidification. Geophys Res Lett 35:L19609, 5 pp, doi:10.1029/2008GL035072
84. Gehlen M, Gangstø R, Schneider B, Bopp L, Aumont O, Ethe C (2007) The fate of pelagic $CaCO_3$ production in a high CO_2 ocean: a model study. Biogeosciences 4:505–519
85. Feely RA, Byrne RH, Acker JG, Betzer PR, Chen CTA et al (1988) Winter summer variations of calcite and aragonite saturation in the northeast Pacific. Mar Chem 25:227–241
86. Bates NR, Mathis JT, Cooper L (2009) The effect of ocean acidification on biologically induced seasonality of carbonate mineral saturation states in the Western Arctic Ocean. J Geophys Res Oceans 114:C11007, doi:10.1029/2008JC004862
87. Yamamoto-Kawai M, McLaughlin FA, Carmack EC, Nishino S, Shimada K (2009) Aragonite undersaturation in the Arctic Ocean: effects of ocean acidification and sea ice melt. Science 326:1098–1100

Books and Reviews

Feely RA, Fabry VJ, Dickson AG, Gattuso J-P, Bijma J, Riebesell U, Doney S, Turley C, Saino T, Lee K, Anthony K, and Kleypas J (2010) An international observational network for ocean acidification, OceanObs white paper (https://abstracts.congrex.com/scripts/jmevent/abstracts/FCXNL-09A02a-1664525-1-Feely-cwp2c04.pdf)

Houghton JT, Ding Y, Griggs DJ, Noger M, van der Linden PJ, Xiaosu D (2001) Climate change 2001: the scientific basis. In: Contrinbution of Working Group I to the Third Assessment Report of the Intergovernmental Panel on Climate Change 2001. Cambridge University Press, Cambridge, 944 p

Kleypas JA, Feely RA, Fabry VJ, Langdon C, Sabine CL, Robbins LL (2006) Impacts of ocean acidification on coral reefs and other marine calcifiers: a guide for future research. Report of St. Petersburg Workshop, FL, sponsored by NSF, NOAA, and U.S. Geological Survey, 88 p

Schubert R, Schellnhuber H-J, Buchmann N, Epiney A, Grieβhammer R, Kulessa M, Messner D, Rahmstorf S, Schmid J (2006) The future oceans – warming up, rising high, turning sour. German Advisor Council on global change, Special Report, Berlin, 110 p

Zeebe RE, Zachos JC, Caldeira K, Tyrrell T (2008) Oceans: carbon emissions and acidification. Science (Perspectives) 321:51–52

Documents

EPOCA. http://epoca-project.eu/

European geosciences union position statement on ocean acidification http://www.egu.eu/statements/egu-position-statement-on-ocean-acidification.html

IMBER. http://www.imber.info/

JSOST (Joint Subcommittee on Ocean Science and Technology; National Science and Technology Council). http://ocean.ceq.gov/about/jsost.html

National oceanic and atmospheric administration ocean acidification website. http://www.pmel.noaa.gov/co2/OA/

NSTC Joint subcommittee on ocean science and technology (2007) Charting the course for ocean science in the United States for the next decade, An ocean research priorities plan and implementation strategy, 26 Jan 2007, 84 p

Ocean Carbon and Biogeochemistry (OCB). http://www.us-ocb.org/ and http://www.whoi.edu/sites/oceanacidification

The Ocean Acidification Network. http://www.ocean-acidification.net/

Ocean Energy, Introduction

Luis A. Vega
Hawaii Natural Energy Institute, School of Ocean And Earth Science And Technology, University of Hawaii at Manoa, Honolulu, HI, USA

There are sufficient petroleum resources to meet current worldwide demand for almost 50 years. In addition, coal and natural gas resources could meet current worldwide demand for 100–120 years, respectively. Production, however, is peaking and demand increasing, due to emerging economies like Brazil, Russia, India, and China, such that humanity will face a steadily diminishing supply of fossil fuels.

Given that it takes decades for new technologies to reach maturity, it seems sensible to consider ocean energy resources as some of the replacement "fuels"

for the future energy technologies. Based on decades of analyses and small-scale testing, it is concluded that the resources with the most promise, for practical applications, are ocean thermal, offshore wind, waves, tides, and marine currents. In this section the state-of-knowledge of technologies that can convert the wind, thermal, and tidal resources into a useful form of energy is presented. Sorely missing, unfortunately, are wave energy conversion and non-tidal marine current conversion summaries. It must be noted that only the ocean thermal resource is always available while all other ocean energy resources are intermittent.

The issues associated with integrating large amounts of ocean energy into the overall supply will have to be addressed. It is expected that electrical load management, smart grid technology, and system wide energy storage will be required. To bring large amounts of power onshore, dedicated offshore electrical transmission hubs will be needed. At first, ocean technologies providing electricity, via submarine power cables, to shore stations could be implemented. These would be followed, in about 30 years, with factories deployed beyond the 200 nautical miles exclusive economic zones (EEZs) producing energy-intensive products, like ammonia and hydrogen as the fuels that would support the post-fossil fuels era.

A major challenge to implementation continues to be the requirement to finance relatively high capital investments that must be balanced by the expected but yet to be demonstrated low operational costs. Perhaps a lesson should be learned from the successful commercialization of terrestrial wind energy due to the decades long and consistent government funding of pre-commercial projects that led to appropriate and realistic determination of technical requirements and operational costs in Germany, Denmark, and Spain. In this context, commercialization means that equipment can be financed under terms that yield cost-competitive energy. This, of course, depends on specific conditions at the end-user location.

As summarized in the ► Offshore Wind Energy Technology Trends, Challenges, and Risks entry, offshore wind energy holds significant potential for increasingly greater use. Offshore wind energy consists of the use of wind turbines, deployed in groups or "wind farms," which convert the energy in the winds offshore shore to electricity. That electricity is transmitted to shore via submarine cables where the electricity is introduced into conventional transmission systems for delivery to end users.

Currently, all commercial offshore wind turbines are supported by the seabed. There are some floating offshore wind turbine concepts which are being investigated, and it is anticipated that in the foreseeable future a number of commercial floating offshore wind turbines will be used. A floating offshore wind turbine may be defined as an offshore wind turbine whose substructure is vertically supported by the buoyancy of the structure itself and for which the horizontal forces induced by the wind, waves, and current are resisted by mooring lines and anchors.

The extraction of energy from either the rise or fall of the sea surface under the influence of tides or the extraction of energy from tidally driven currents is discussed in the entry entitled ► Tidal Energy. It is shown that theoretical tidal energy resources are considerable on a global scale, but the geographic conditions necessary for significant tidal ranges, or current velocities, do tend to be restricted to a relatively small number of sites worldwide.

Tidal current systems may not have the strategic potential of barrage systems, but, in the short term at least, they do offer opportunities for supplying energy in rural coastal and island communities. In a future in which energy costs are likely to rise, tidal barrage schemes could prove to be major providers of strategic energy in the mid-twenty-first century and beyond.

As postulated in the ► Ocean Thermal Energy Conversion entry, the ocean thermal resource, defined as the difference between surface water and water from about 1,000 m depth, could be used to generate most of the energy required by humanity. What is pending, however, are realistic determinations of the costs and the potential global environmental impact of OTEC plants, and this can only be accomplished by deploying and subsequently monitoring operations with first-generation plants.

In the ► Marine and Hydrokinetic Energy Environmental Challenges entry, the major challenges of identifying, measuring, and setting priorities for environmental effects of ocean energy devices and arrays are addressed. Laws, regulations, and public sentiment require that these devices provide minimal environmental risk. Effective siting and permitting can

only be done successfully by understanding and measuring the environmental effects on the aquatic animals, habitats, and ecosystems of areas where cost-effective energy generation is possible. A risk-informed evaluation approach under development by the U.S. Department of Energy is presented along with mitigation strategies.

OTEC, tidal energy conversion, and wave energy conversion systems are in the pre-commercial phase with several experimental projects having already demonstrated that the technology works but is lacking the operational records required to proceeding into commercialization. Ideally, adequately sized pilot projects must be operated in situ and for one to two continuous years to obtain these records. In the case of offshore wind energy conversion, the foundation provided by decades of land based systems and the ocean engineering state of knowledge already provide the information required to proceeding into commercialization.

It is essential to assure that ocean energy technologies are an environmentally benign and safe alternative to conventional power generation. It is reasonable to expect that detrimental effects on the environment can be avoided or mitigated by proper design and that their impact is less than that of conventional power technologies. While it is certain that physical, chemical, and biological impacts would occur during the construction and operation of ocean energy facilities, the precise magnitude and extent of these impacts are not known. In addition, the cumulative or secondary impacts are largely undeterminable without long-term monitoring.

Current US laws and regulations are particularly stringent and require considerable advanced understanding of potential effects before energy devices are deployed. Oceanographic research can provide insight into the action of tides, waves, ocean currents, and other physical and chemical processes in the oceans. However assessments of biological resources are generally more limited. Minimal useful information is available on potential interactions of energy devices on marine receptors – the animals, habitats, and ecosystems – in areas of proposed marine energy development. The uncertainty surrounding potential adverse encounters between devices and vulnerable receptors drives concerns among regulators and stakeholders, slowing development of the industry.

It is of extreme importance to educate regulatory agencies into understanding that what is important is to determine the differences between ocean energy technologies and other well-established human activities and industries to be able to concentrate in the assessment of the impact of these differences (i.e., their differentiators). For example, the only process that differentiates OTEC from other well-established human activities and industries is the use of ocean water drawn from ~1,000 m depths and its return to the ocean below the photic zone. Given the intricate and dynamic nature of ocean processes, it is nearly impossible to determine at priori and with a high degree of certainty what would be the effect of such differentiator by relying on basic research or the development of ecological theory. The only way to evaluate the OTEC environmental differentiator is to obtain field data with a pilot plant operating with flow rates that are measurable and representative. Such plant must be operated and monitored through ongoing and adaptive experience for one to two continuous years, that is, an adaptive management process. Similar comments apply to the other ocean energy technologies.

Ocean Evaporation and Precipitation

Luis Gimeno, Raquel Nieto, Anita Drumond, Ana María Durán-Quesada
Environmental Physics Laboratory (EPhysLab), Universidade de Vigo, Ourense, Spain

Article Outline

Glossary
Definition of the Subject and Its Importance
Introduction
Distribution of Evaporation from the Ocean and Precipitation
Oceanic Heat Reservoirs (Warm Pools) and Evaporation
Oceanic Evaporation and Monsoonal Precipitation Regimes
Response of the Relationship Between Evaporation and Precipitation to the Forcing of the ENSO

Future Research Directions
Acronyms
Bibliography

Glossary

Atmospheric rivers The analysis of timescales shorter than climatic reveals that there are three to five major conduits of atmospheric circulation in each hemisphere, each of which is responsible for the transport of large amounts of water in narrow streams from the tropics through the midlatitudes toward the higher latitudes. These conduits were termed "atmospheric rivers" [10] because the way that the moisture that is transported is comparable with the way that water is transported in a terrestrial river such as the Amazon.

Clausius–Clapeyron equation This is an equation that relates the saturation vapor pressure of air over liquid water as a function of temperature.

The El Niño–Southern Oscillation (ENSO) *The El Niño–Southern Oscillation* is a quasiperiodic climatic pattern that occurs throughout the tropical Pacific Ocean. It is characterized by variations in the temperature of the surface of the tropical eastern Pacific Ocean (El Niño) coupled with variations in air pressure at the Earth's surface in the tropical Pacific (the Southern Oscillation). Warmer (colder) waters than normal over the eastern Tropical Pacific characterize an El Niño (La Niña) event, and this anomalous oceanic phenomenon is accompanied by a higher (lower) air pressure at the Earth's surface in the western Pacific.

Evapotranspiration Evapotranspiration is a term that describes the transport of water into the atmosphere from different surfaces, including from the soil (soil evaporation), and from vegetation (transpiration).

Feedback mechanisms These are processes such that when a system generates output, that output serves as input to an earlier stage in the operation of the system. This input to earlier stages causes a system to behave in a self-controlling manner. Feedback mechanisms can either amplify ("positive feedback") or diminish ("negative feedback") the effects of a change.

Hadley cell This is a pattern of circulation that occurs in the tropical atmosphere, and involves a rising motion near the equator, a poleward flow at the upper troposphere (about 10–15 km above the surface), descending motion in the subtropics, and equatorward flow near the surface, which then completes the cell.

Inter tropical convergence zone This is a band of cloudiness and precipitation that encircles the Earth near the equator where the northerly and southerly trade winds converge.

Low-level jet This is the name given to a narrow zone of strong winds above the boundary layer (about 1,500 m above the surface), and is responsible for most of the moisture that is transported in tropical areas.

Monsoon Seasonal precipitation caused by changes in atmospheric circulation associated with the asymmetric heating of land and sea.

South Pacific convergence zone This is a band of low-level convergence, cloudiness, and precipitation that extends southeastward from the Indian–Pacific warm pool.

Surface freshwater flux The difference between rates of evaporation and precipitation per unit area

Teleconnections The relationship between, and the influence of, weather patterns in distant locations.

Thermocline The oceanic depth at which the rate of decrease of temperature with depth is at a maximum. The thermocline may be considered to be the zone of separation between the oceanic mixed layer, which is influenced by atmospheric fluxes, and the deep ocean.

Walker circulation This is a conceptual model of the zonal/vertical airflow in the tropical troposphere, caused by differences in the distribution of heat over the Earth's surface. Over the Pacific Ocean, low-level winds flow from the Eastern Pacific (characterized by high pressure) toward Indonesia (lower pressure), where the air then ascends to the high troposphere, before it then flows from Indonesia toward the Eastern Pacific, where it descends again.

Definition of the Subject and Its Importance

In view of the threat of global climate change, the proper understanding of the intensity of the hydrological cycle and of its development over time is one of the

most important challenges of the century, at least in the area of the geosciences. The hydrological cycle can essentially be summarized to be the evaporation of moisture in one location, offset by precipitation elsewhere. The rate of evaporation exceeds the rate of precipitation over the oceans, which are therefore a net source of moisture; this moisture is then transported to the landmasses, which are a net sink for moisture, where precipitation exceeds evapotranspiration. In consequence, surface runoff enters rivers and other watercourses, which discharge into the ocean, thereby completing the cycle. Taken as a whole, the hydrological cycle is characterized by the evaporation of about half a million cubic kilometers of water per year, the bulk of which (86%) is from the ocean, with only 14% originating in the continents [1]. The vast majority of the water that evaporates from the oceans (90%) is precipitated back into them, while the remaining 10% is transported to the continents, where it precipitates. About two-thirds of this precipitation is recycled over the continents and only one-third runs off directly into the oceans. Ultimately, despite the small continental recycled component, all the water used in natural ecosystems and in human activity originates in the oceans. Because societies depend for their continued existence on the security of water resources, it is extremely important to understand the processes that govern the evaporation of water from the oceans (in the domain of oceanography) [2], the transport of moisture in the atmosphere (meteorology) [3], and the effects of these processes on the hydrological cycle (hydrology) [4], all within the context of the current paradigm of global climate change [5].

Introduction

Oceanic evaporation occurs when water molecules change phase from liquid to vapor at the air–sea interface. The rate at which this process occurs depends essentially on three variables: the available heat energy, the difference in humidity between the air and the surface, and the wind speed. The heat energy permits the water molecules to escape from the liquid with a latent energy that is then released during condensation. A gradient in humidity between the air and the surface of the sea is also necessary, because evaporation can only occur when the humidity of the air is lower than that of the evaporating surface of the sea. The wind influences the evaporation through the removal of water vapor from the evaporating surface by the turbulent movement of air, which then facilitates the evaporation by maintaining a vertical humidity gradient from the surface to the overlying air.

An assessment of the major oceanic sources of evaporation may be made conceptually using bulk parameterization and similarity theory [6]. The rate of evaporation (Evp) may be computed using

$$Evp = CeUdq$$

where dq is the difference between the saturation specific humidity at the sea surface and the near-surface atmospheric specific humidity; U is the near-surface wind speed; and Ce is a turbulent exchange coefficient that is controlled by the wind speed, the atmospheric stability, and the difference in temperature between the air and the sea. Evaporation should be prevalent in those oceanic regions with a high sea surface temperature, in sharp contrast with the air temperature, and where strong winds allow the humidity produced by the evaporation to be removed quickly, thereby preserving a clear contrast in the humidity between the air and the surface.

It is very difficult to estimate rates of evaporation, due to the very great uncertainties involved and because the rates themselves are so seldom measured. Usually, these rates are instead estimated from bulk flux formulae, which mean that it is possible to check the global distribution of evaporation over the oceans and to compare rates between different areas. One of the best estimates of evaporation is provided by the OAFlux data [7], which is produced by combining several reanalysis and satellite data sets. Figure 1 shows a picture of the annual and seasonal global distribution of evaporation. The global distribution of evaporation is approximately zonally oriented, with greater evaporation over the subtropical latitudes of the global oceans and less over the equatorial cold tongues and at higher northern and southern latitudes. It is also clear that more evaporation takes place over the regions of the oceanic western boundary currents and their extensions, including the Gulf Stream, the Kuroshio, the eastern Australian Current, the Agulhas Current, and the Falkland/Brazilian Current. These patterns show seasonal intensifications/reductions as

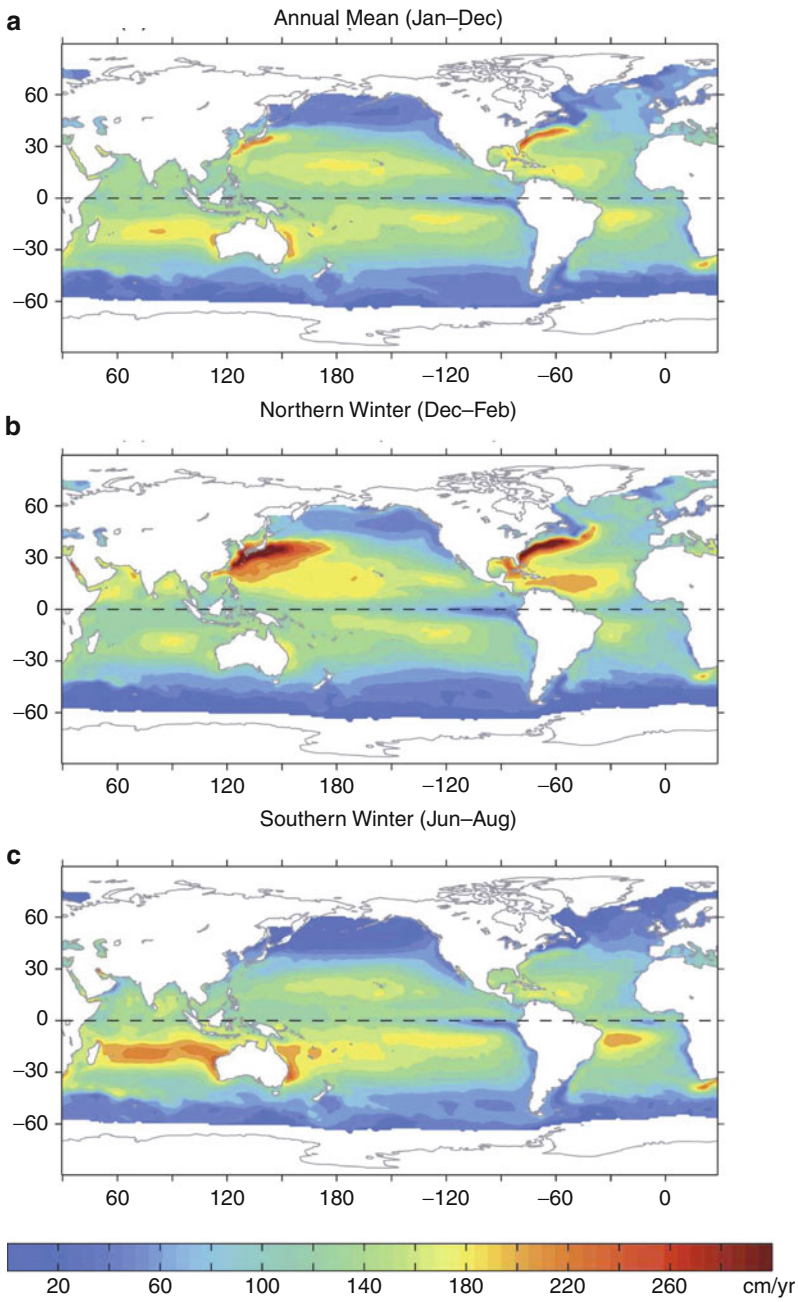

Ocean Evaporation and Precipitation. Figure 1
Mean global evaporation showing (**a**) the annual mean values, and the mean values for (**b**) the northern winter (December–March), and (**c**) the austral winter (June–September). The mean values were constructed using data from the period 1958–2005 (From Yu [3])

a result of differences in wind speed, air–sea humidity gradient, and temperature.

Regions with the highest rates of evaporation coincide neither with those with the greatest amount of atmospheric water vapor nor with those with the highest precipitation. This is because water vapor has a residence time in the atmosphere of about 10 days [8] and can be transported fairly efficiently by general

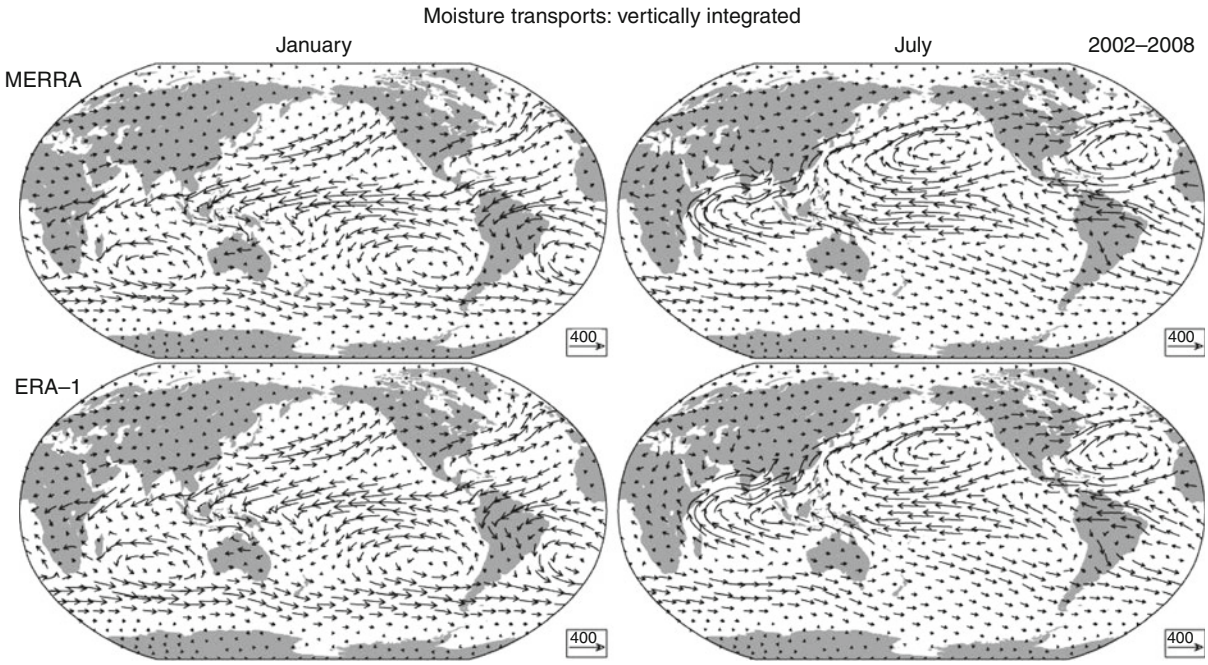

Ocean Evaporation and Precipitation. Figure 2
Vertically integrated atmospheric moisture (including liquid and ice) transport for 2002–2008 from MERRA (*top*) and ERA-I (*bottom*) for January (*left*) and July (*right*). The units are kg m^{-1} s^{-1}; the *vector* key is given in the insert (From Trenberth et al. [9])

circulation. Figure 2 shows the main atmospheric fluxes of water vapor. An understanding of the processes of moisture transport requires a knowledge of the ways in which water vapor, which accounts for approximately 0.25% of the total mass of the atmosphere, is distributed (Fig. 3). The concentration of water vapor varies greatly, both in space and over time. The general global distribution of water vapor largely mirrors that of temperature because the equilibrium vapor pressure depends on temperature (Clausius–Clapeyron equation, C–C). Therefore, the greatest variations in the amount of water vapor occur with increasing height above the surface; specifically, concentrations of water vapor decrease markedly with increasing height. Important variations also occur close to the surface, where the concentrations vary by more than three orders of magnitude, from 10 ppm by volume in the coldest parts of the Earth's atmosphere, to as much as 5% by volume in the warmest [1]. Most of the Earth's water vapor is concentrated in the tropical atmosphere, which contains more than three times as much water as the extratropical atmosphere. The C–C equation describes the water-holding capacity of the atmosphere as a function of temperature, so the largest average values of total column water vapor (TCWV) occur over the tropical Pacific warm pool, where the highest large-scale values of sea surface temperature (SST) are typically found, and a strong gradient of TCWV occurs with latitude (typically, a 7% change in TCWV results from 1°C change in temperature).

Just as the distribution of evaporation differs from that of atmospheric water vapor, so it is also dissimilar to the distribution of precipitation (Fig. 4), which depends both on the supply of moisture and on the atmospheric instability that forces the air to rise. The distribution of precipitation is thus more similar to that of TCWV, especially in the tropics where atmospheric convergence tends to occur at low levels, in close association with the highest SSTs, although with much more structure due to known overturning circulations such as those associated with the Hadley cell and monsoons. In extratropical regions, the similarities between the distributions of TCWV and precipitation are much less clear. In these regions, precipitation is

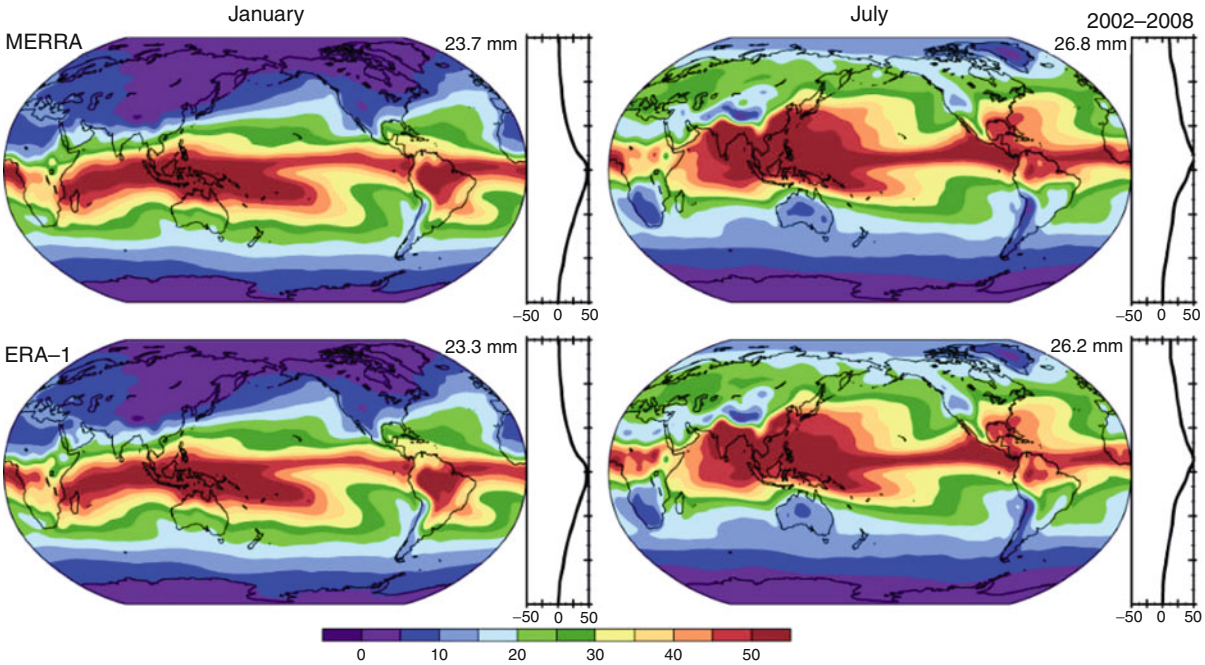

Ocean Evaporation and Precipitation. Figure 3
Maps of total column atmospheric water for January (*left*) and July (*right*) for MERRA (*top*) and ERA-I (*bottom*) in mm for 2002–2008 (From Trenberth et al. [9])

controlled by baroclinic instability due to strong meridional gradients of air temperature and the supply of moisture to strong, relatively narrow streams from the tropics through the mid- to the higher latitudes, which are sometimes referred to as "atmospheric rivers" [10]. It is these streams that provide most of the long-distance transport of moisture, accounting for 95% of the meridional flux of water vapor at 35° latitude [11].

In the following sections, the path of the atmospheric moisture is traced from its evaporation in the oceans to its precipitation in the continents, where water is needed to supply ecosystems and human socioeconomic activities.

Distribution of Evaporation from the Ocean and Precipitation

Once in the atmosphere, moisture is transported by general circulation and then falls to the surface as precipitation. In order to quantify this process of the transport of atmospheric water vapor, it is essential to identify the sources of the evaporation. Unfortunately, however, few direct measurements of evaporation have ever been made. In the absence of reliable measurements from around the globe, indirect methods must instead be used. One means of measuring evaporation involves a diagnosis of the vertically integrated moisture flux by referring to atmospheric data. Global maps that show the flux of moisture can provide a good indication of the major movements of the main moist air masses. Moreover, any divergence or convergence of that flux must reflect a net evaporation or precipitation, and indicate regions that act as sources of or sinks for atmospheric moisture [12].

Figure 5a shows the distribution of the vertically integrated flux of moisture, and its divergence, during the boreal summer (June, July, and August; JJA) and winter (December, January, and February; DJF). The primary sources of moisture for the whole atmosphere (reddish colors) are found over the subtropical oceans, where evaporation takes place continuously, associated with the quasipermanence of the high-pressure cells. Several smaller regions also make significant contributions as sources of moisture in the Northern Hemisphere, such as the Caribbean, Mediterranean, and Red Seas. The major sinks (bluish colors) are in

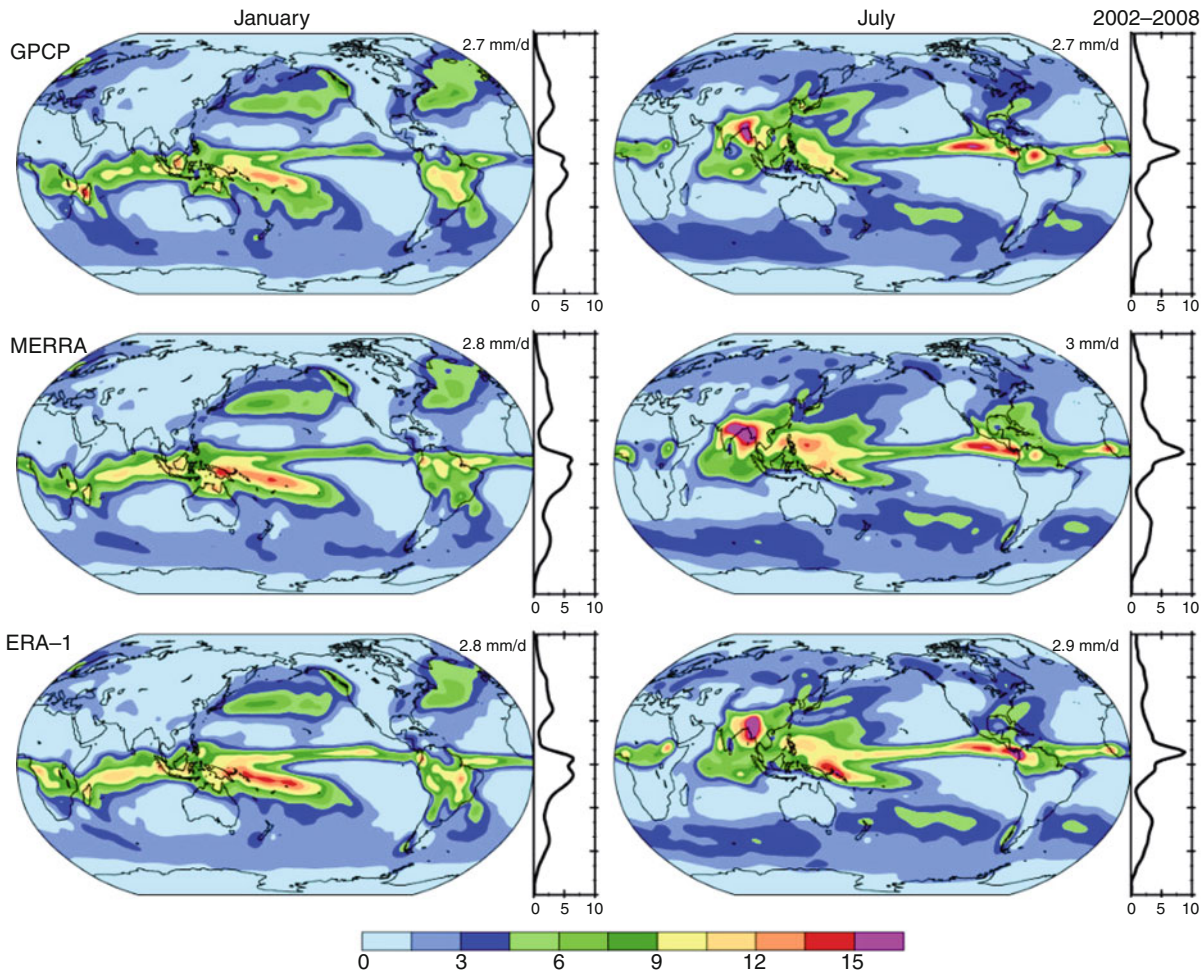

Ocean Evaporation and Precipitation. Figure 4

Maps of precipitation for January (*left*) and July (*right*) for GPCP (*top*), MERRA (*middle*), and ERA-I (*bottom*) in millimeter per day for 2002–2008. The values shown at the *top right* of each map are the global means, and the zonal means are given to the *right* of each map (From Trenberth et al. [9])

the tropical/subtropical convergence zones, the ocean storm tracks of the high latitudes, and the summer monsoonal rains (South America, India, the Sahel, and South Africa).

As a whole, the Southern Hemisphere exhibits a weak divergence (i.e., evaporation exceeds precipitation), and normally supplies moisture to the Northern Hemisphere [13]. The mains sources of moisture are found in the regions of the subtropical anticyclones on the western sides of South America, Africa, and Australia. Over the Indian Ocean, the divergence extends eastward from Africa to Australia in a continuous belt. Two cells of divergence dominate this belt, one located close to Madagascar, and another, stronger, cell located to the west of Australia. Another nucleus of divergence is located over eastern Africa, near the equator. Two divergent cells are prominent over the Pacific Ocean, one to the east of Australia and the other in the central part of the eastern Pacific. The divergence over the high-pressure cells is stronger during the austral winter months (JJA), but their areal domain expands poleward with the displacement of the cells to the south during the austral summer (DJF), a season characterized by a lower hemispheric supply of moisture from the oceans to the atmosphere.

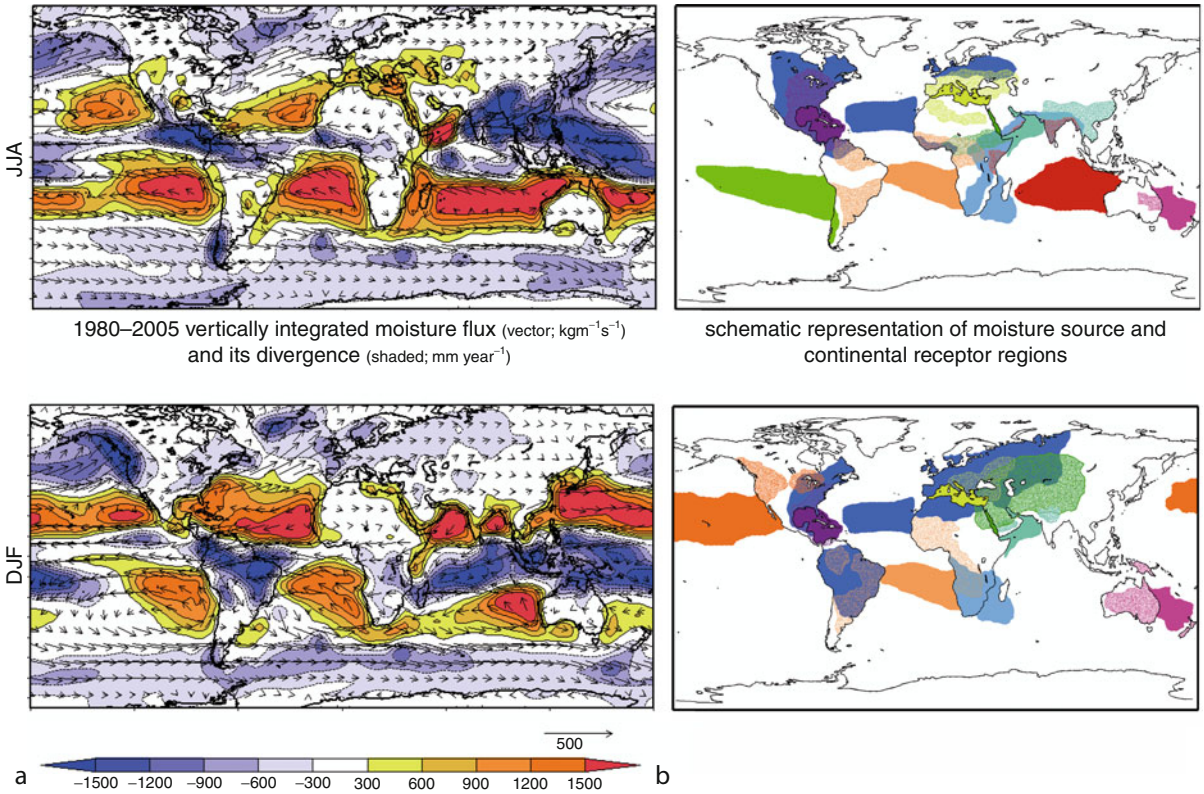

Ocean Evaporation and Precipitation. Figure 5
Column **A**: 1980–2005 vertically integrated moisture flux (*vectors*; kg m^{-1} s^{-1}) and its divergence (*shaded contours*; mm year^{-1}) for JJA and DJF. (Data obtained from http://www.cgd.ucar.edu/cas/catalog/newbudgets/index.html#AtD). Column **B**: Schematic representation of moisture source and continental receptor regions shown in the same colors as the corresponding oceanic source regions for JJA and DJF. Overlapping regions are shown with *shaded texture* (From Gimeno et al. [75])

The distributions of vertically integrated moisture flux reflect the planetary behavior of the general circulation in the lower half of the troposphere, because the specific humidity acts as a weighting factor for the wind field [14]. The transport of moisture is thus characterized by westerlies in the midlatitudes and by easterlies in the tropical belt. Although the values of the meridional component of the transport of moisture are smaller than those of the zonal component, they still play an essential role in maintaining the global water balance. The meridional flux of moisture over the midlatitudes varies considerably with season, but it is predominantly poleward throughout the year. The transport is accomplished mainly by baroclinic lows associated with the polar front and by stationary eddies, such as subpolar lows and subtropical anticyclones, together with their transient pulsations. The largest variability during the year is associated with variations in the Hadley cells, whose lower branches are most effective in transporting moisture to the Inter Tropical Convergence Zone (ITCZ). In the tropics, the mean annual transports are northward to the south of the equator and southward to the north of it. The cross-equatorial flow in the Hadley cells changes direction with season, leading to a flux of water vapor into the Northern Hemisphere during JJA and a flux into the Southern Hemisphere during DJF.

Over the Southern Hemisphere, the patterns of the transport of moisture are predominantly zonal [15]. Although the central pressures are slightly greater during JJA, the high-pressure band in the subtropics is more extensive and the pressure gradient between the

oceans and the continents is reduced. During DJF, the pressure gradients are strengthened because of the thermal lows that develop over the continents, resulting in a stronger meridional circulation [16]. From the maps of moisture flux, one may observe the strong northward transport of moisture in the eastern margin of the semipermanent subtropical high-pressure centers, particularly over the Pacific and Atlantic Oceans. In contrast, the major regions of southward transport are located over eastern South America and East Africa, and over almost the whole of the Pacific Ocean.

Lagrangian transport models have recently been used to provide more precise information about the relationship between the source regions of evaporation and remote precipitation. Figure 5b summarizes the main oceanic sources and the associated continental receptor regions of the evaporated moisture, obtained using the Lagrangian method of Stohl and James [17]. The figure shows that the productivity of the major oceanic sources of moisture for continental precipitation is not evenly distributed and that some specific oceanic sources generate more continental precipitation than others [18]. For example, the subtropical North Atlantic Ocean provides moisture for precipitation over vast geographical areas (from Mexico to large parts of Eurasia) in DJF. The North Atlantic Ocean is a relatively significant source of water vapor through net evaporation, in contrast to the North Pacific Ocean, which produces a higher surface salinity in the Atlantic subregion than in the Pacific [19]. The absence of large mountains along the Atlantic coast in Europe favors the transport of moisture (mainly at low levels) from the Atlantic Ocean into the Eurasian continent and the Mediterranean region. In contrast, the existence of the Rocky Mountains (Andes) parallel to the west coast of North (South) America prevents moisture from the Pacific Ocean from penetrating very far into the American continent [14].

The Red Sea is the ocean basin that has the highest net evaporation [19], and provides large amounts of moisture that precipitate between the Gulf of Guinea and Indochina (JJA) and between the African Great Lakes and Asia (DJF). Although South Africa is surrounded by the Atlantic and Indian Oceans and is also located close to the vast Southern Ocean, the only air masses that cause net precipitation there are those that reach it from the Indian Ocean [19]. It is only the air masses from the Pacific Ocean that cause net precipitation over Australia, even though the landmass is surrounded by the Indian and Pacific Oceans.

Some landmasses receive moisture evaporated in the same hemisphere (e.g., Northern Europe or eastern North America), while others receive moisture from both hemispheres with large seasonal variations (e.g., northern South America). Monsoonal regimes in India, tropical Africa, and the North American Great Plains are fed by moisture provided from a large number of source regions, which highlights the complex nature of precipitation. Vast continental areas lack any appreciable direct transport of moisture from any of the major oceans, particularly those that correspond to some of the most arid inland regions (e.g., inner Asia), unless the recycling of continental moisture can compensate (albeit partly) for the absence of a direct oceanic source of moisture (e.g., in Eastern Siberia) [18].

Despite the points made in the foregoing discussion, not all the oceanic regions can be considered always to be sources of moisture. Air masses that originate in the high-latitude oceans (Hudson Bay, the Arctic, and the Southern Ocean) are extremely strong sinks for moisture when the associated air masses are transported toward lower latitudes [19]. Air masses tracked from the Atlantic, Pacific, and Indian Oceans are a significant source of moisture for the air masses of the Arctic and Southern Oceans. Even the air masses of the Mediterranean Sea, which are a strong source of water for all the Eurasian rivers that lie to the north of it, receive moisture from the river basins over Africa and India (Niger, Nile, Indus), especially during JJA.

Oceanic Heat Reservoirs (Warm Pools) and Evaporation

The term "warm pool" may be used to delineate in general terms those oceanic regions characterized by sea surface temperatures (SSTs) that exceed a fixed threshold. The vertical extent of a warm pool is relatively easy to stipulate precisely, through the use of a selected isothermal layer. However, the horizontal extent of a warm pool is much more difficult to characterize precisely.

In physical terms, a warm pool contains tropical surface water, which by definition is warm and has relatively low salinity. Because of its low density,

it forms a lens of light water that floats on the denser waters below, which are subtropical in origin and therefore cooler and have higher salinity [20]. The clear correspondence of the presence of warm pools with the maxima of atmospheric total heating indicates the role of these pools in setting atmospheric global heating gradients and, by extension, the importance of warm pool for the general circulation of the atmosphere. A variety of phenomena occur both in the ocean and in the atmosphere within the tropical warm pools [21]. The warm pool is a region of net freshwater input into the ocean. Much of the moisture that is precipitated is evaporated locally from the sea surface. However, part is imported by large-scale circulation [21].

The Indian–western Pacific contains the highest SSTs in the open oceans, and has the largest annual precipitation and release of latent heat in the atmosphere [21, 22]. The Indian–western Pacific warm pool (IPWP) has been the subject of much scientific interest in recent years, due to its relationship with the development of El Niño–Southern Oscillation (ENSO) extreme events [20].

Many authors have used the 28°C isotherm as a practical compromise in their characterizations of the horizontal extent of IPWP [20]. By considering this isotherm to define the horizontal extent of the IPWP, it is possible to observe large annual variations in its boundaries. The northerly extreme of the pool is reached in September, whereas in March the pool barely reaches 10°N (Figs. 6 and 7). The annual fluctuations are less pronounced in the Southern Hemisphere, but the pool doubles in size between

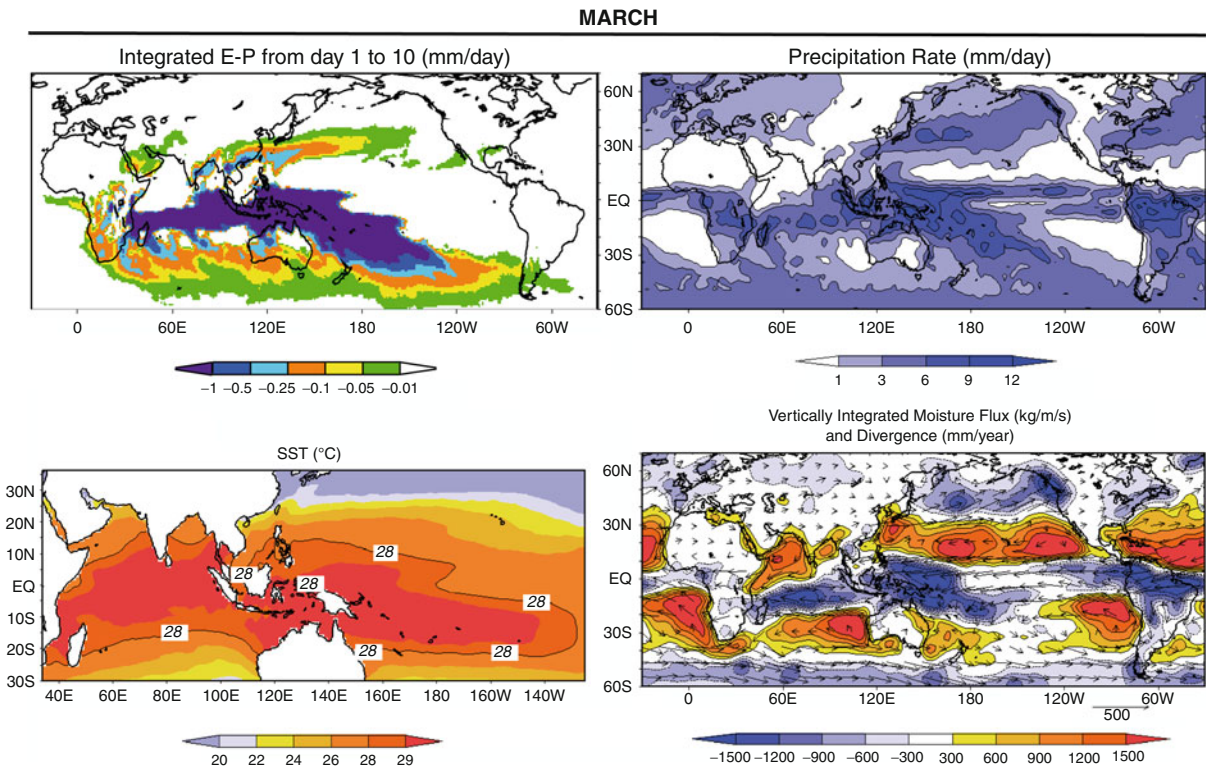

Ocean Evaporation and Precipitation. Figure 6

Surface freshwater flux (E–P) integrated over a 10-day period for the month of March for the period 2000–2004 (*top left*), calculated by forward tracking from the IPWP source of moisture, indicated by the *black line* in the field of SST (*bottom left*). (*Top right*) precipitation rate and (*bottom right*) vertically integrated moisture flux (VIMF) and its divergence. Only negative values of (E–P) are shown, indicating where there is a net loss of moisture. Units of (E–P) and precipitation rate are mm day^{-1}, of SST are °C, of *vectors* of moisture flux are kg m^{-1} s^{-1}, and of *contours* of divergence of moisture are mm year^{-1}

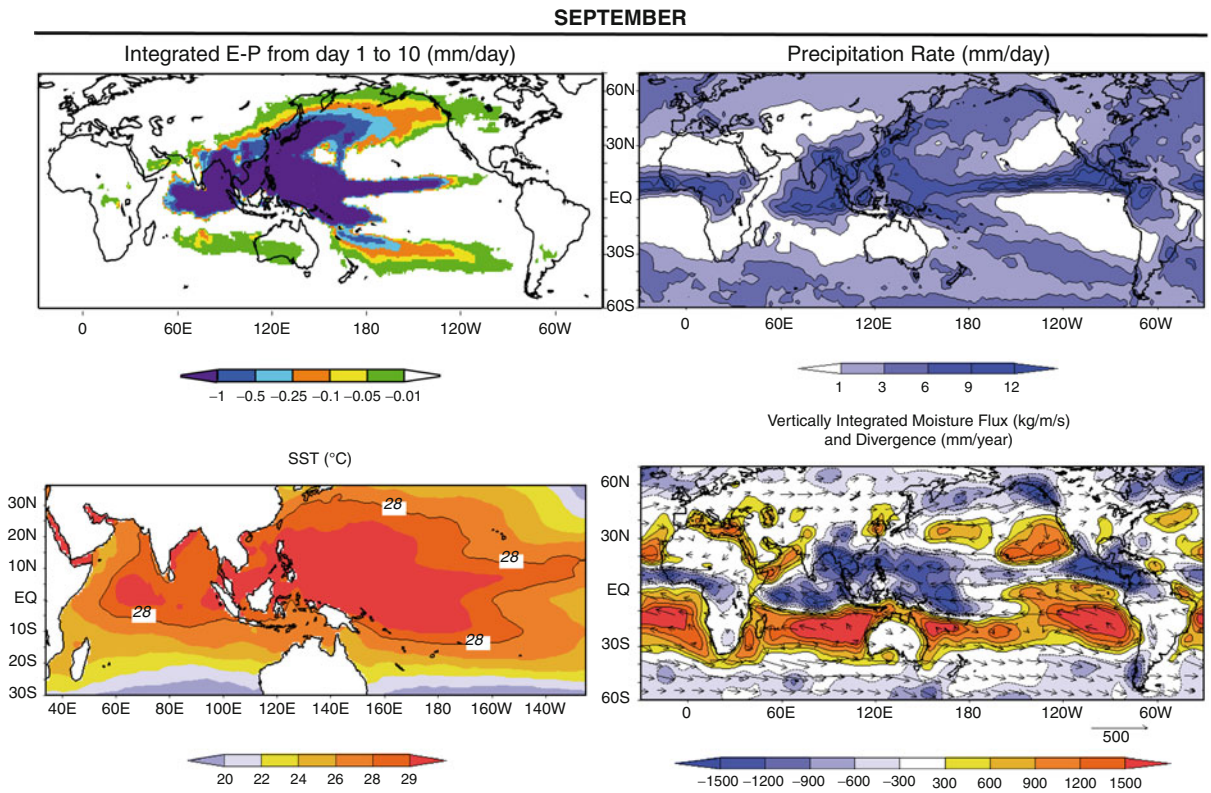

Ocean Evaporation and Precipitation. Figure 7
As Fig. 6, for September

September and March. The area permanently covered by the pool is relatively small, from about 10°N to 10°S and from Indonesia to 170°W, and comprises only about half its average area. These large annual fluctuations in the boundaries of the pool make characterizing its size and volume rather difficult and subject to a degree of uncertainty. Its depth changes little with season. However, its horizontal extent varies considerably [20].

Air–sea interaction in the western tropical Pacific is dominated by the large-scale atmospheric convergence that is associated with the ascending branch of the Walker circulation, with the major tropical ascent occurring over the Pacific–Indian Ocean warm pool (e.g., [23]). The convergence of air and moisture from the Pacific and Indian Oceans leads to vigorous convection and heavy precipitation, together with the release of latent heat in the atmosphere, which drives the Walker circulation [24] (Figs. 6 and 7). The maximum SST of the warm pool is probably associated with the convergence of the oceanic circulation in the western tropical Pacific and the production of a relatively deep thermocline forced by the general atmospheric convergence of the Walker circulation in the area [21].

The hydrological characteristics of the region are also a matter of some interest. Along the equator from 140°E to the date line, a band of minimum evaporation coincides approximately with a region of light winds, and evaporation gradually increases to the north and south, associated with enhanced southeasterly and northeasterly trade winds [25]. The distribution of rainfall is variable in space and over time (e.g., [26–28]). Annual mean distributions of rainfall typically reveal an east–west Inter Tropical Convergence Zone (ITCZ) across the Pacific and a band that extends southeastward from the warm pool into the Southern Hemisphere along the South Pacific convergence zone (SPCZ) (e.g., [29]) (Figs. 6 and 7). In addition, convection varies considerably over time in

the western Pacific, which includes interannual, annual, seasonal, and intraseasonal oscillations (e.g., [30]).

Although less intense, the IPWP may also act as a source of moisture by providing humidity evaporated locally to remote regions via atmospheric circulation throughout its annual cycle. In March (Fig. 6), the IPWP (shown by the 28°C isotherm in SST) is located between 15°N and 25°S. The negative values of surface freshwater flux (E–P) that are obtained along the 10-day trajectories of the air parcels that emanate from the IPWP (selected using a Lagrangian approach) indicate that the moisture transported from this source may contribute to precipitation in remote regions, such as the Equatorial Atlantic and Southern Africa, apart from the contribution to the warm pool area itself and to the Subtropical Indian and Pacific oceans. In September (Fig. 7), the IPWP is displaced to the north, to cover the area between 30°N and 15°S. The net loss of moisture of the air parcels from the IPWP is high over the warm pool and Pacific ITCZ, associated with a strong convergence of tropospheric vertically integrated moisture flux (VIMF) that is observed over the region. The contribution of moisture from the IPWP is predominantly toward the subtropical northern Pacific Ocean during September, and even reaches East Asia and North America. However, the transport of moisture from the IPWP toward the Southern Hemisphere during September is less than it is in March.

Another region of high SSTs is also noteworthy. The tropical Western Hemisphere warm pool (WHWP) may be considered to be the second largest tropical warm pool on Earth, after the IPWP [31] (Figs. 3 and 4). In this case, the compromised threshold in their horizontal characterization extends is the 28.5°C isotherm. So, the WHWP extends over the eastern North Pacific and the west of Central America, the Intra-Americas Sea (i.e., the Gulf of Mexico and the Caribbean), as well as the western tropical North Atlantic [32]. This threshold reflects a temperature that has a significant impact on tropical convection (e.g., [33]), and on the depth of the isotherm of this temperature, which is closest to the average depth of the mixed layer in the WHWP. Differently from the IPWP, the WHWP usually disappears at the start of the boreal winter, but surface heat fluxes warm the pool throughout the spring, which leads to a maximum SST, and a maximum extent of the WHWP, in late summer/early autumn. Apart from the clear seasonal cycle, the interannual fluctuations of area and intensity are significant because the anomalies of the WHWP (in terms of SST and extent) occur at high temperatures at which small changes can have a pronounced effect on the tropical convection [34].

The characteristics of the Pacific side of the WHWP can be related directly to the variability of the ENSO, while the Atlantic side of the warm pool (Atlantic warm pool, AWP) may be considered to be a potential means of predicting summer rainfall in the United States, Mexico, the Caribbean, and Central America, including the large-scale meteorological conditions related to Atlantic hurricanes [35]. The WHWP provides a greater contribution of moisture to North America from June onward, when warmer waters may be observed over the AWP and the transport of moisture may be increased by the Great Plains low-level jet (GPLLJ) [35–38]. During the Boreal Summer, the contribution from the WHWP extends toward western Europe, probably as a result of the transport of moisture by the warm conveyor belts [38].

By using the same Lagrangian approach as mentioned earlier, it is possible to identify the role of the WHWP in providing moisture to the atmosphere throughout its annual cycle, as shown in Figs. 8 and 9. A comparison with the results presented for the IPWP (Figs. 6 and 7) may reveal the relative importance of the largest warm pools to global precipitation. In May (Fig. 8), a warm pool (isotherm of 28.5°C) extends over the eastern North Pacific, a phenomenon that characterizes the onset of the WHWP [32]. The negative values of (E–P) indicate that the WHWP contributes locally to moisture in the ITCZ in the Pacific, and that some moisture is transported toward North America in an anticyclonic flow centered over the Gulf of Mexico. These results are associated dynamically with the convergence of the VIMF over the Pacific ITCZ, as well as with the transport of moisture from the WHWP toward North America, possibly via the GPLLJ [38]. In September (Fig. 9), although the size of the warm pool in the eastern North Pacific is reduced, the spatial expansion of the 28.5°C isotherm over the Intra-America Seas is at a maximum [32]. The values of (E–P) indicate a rather lower contribution of moisture to the precipitation in the Pacific ITCZ and a higher contribution to the Atlantic ITCZ, which is probably

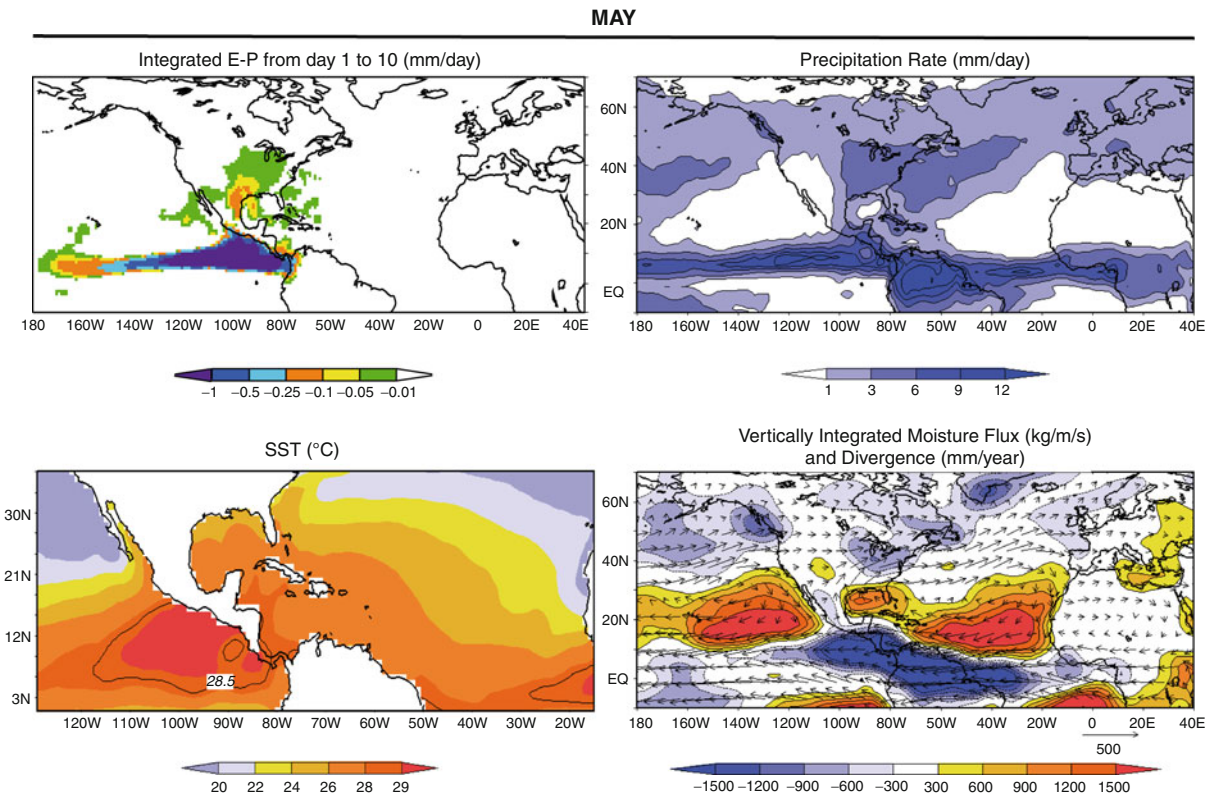

Ocean Evaporation and Precipitation. Figure 8
As Fig. 1, but considering WHWP as source of moisture during May (From Drumond et al. [38])

associated with the spatial expansion of the warm pool toward the equatorial Atlantic. A higher contribution of moisture to the Gulf of Mexico and to southeastern North America may also be observed in the precipitation, and is associated with the convergence of the VIMF over the area. The highest contribution of moisture to the Iberian Peninsula from the air masses that leave the WHWP occurs during September [38].

Oceanic Evaporation and Monsoonal Precipitation Regimes

Within the global distribution of precipitation, some regions are characterized by episodes of intense precipitation. Those regions, which are known to be affected by monsoonal circulations, have been studied extensively. The West African [39], the Asian [40], the Australian [41], and the American monsoonal systems [42] are now considered. To characterize these regions, Fig. 10 presents the seasonal patterns of precipitation and the vectors of low-level wind (925 mb) for both hemispheric summers.

The seasonal characteristics of the monsoons are well known, and the active phase of each can be distinguished easily. Despite both their intensity and seasonality, all have in common the large amount of moisture involved. The sources of moisture for these systems are fundamental to their understanding, and both continental and oceanic regions have been found to be important in this respect. As part of the American monsoon system (AMS), the North American monsoon (NAM) approximately accounts for at least 40% of the summer rainfall in western Mexico and the southern United States. Various authors have suggested that the dominant sources of monsoonal precipitation are the local continental evaporation and the transport of vapor from adjacent oceanic regions [43–45]. This is

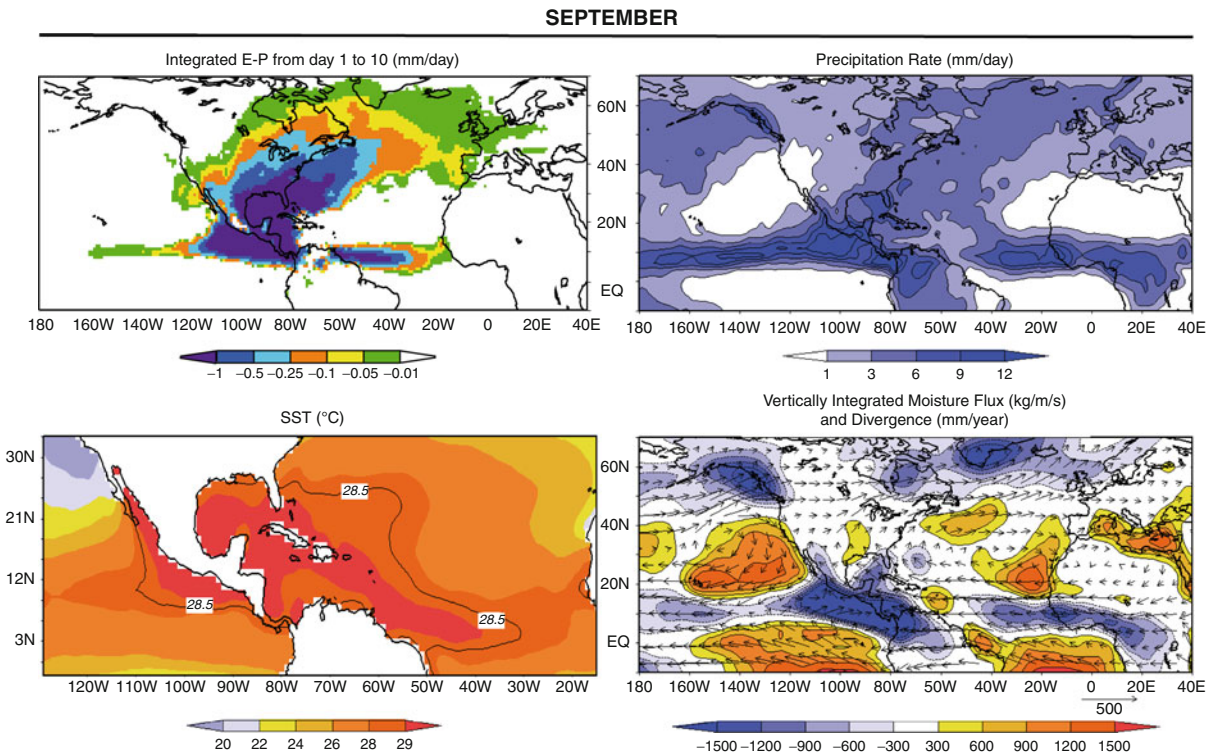

Ocean Evaporation and Precipitation. Figure 9

As Fig. 1, but considering the WHWP as source of moisture during September (From Drumond et al. [38])

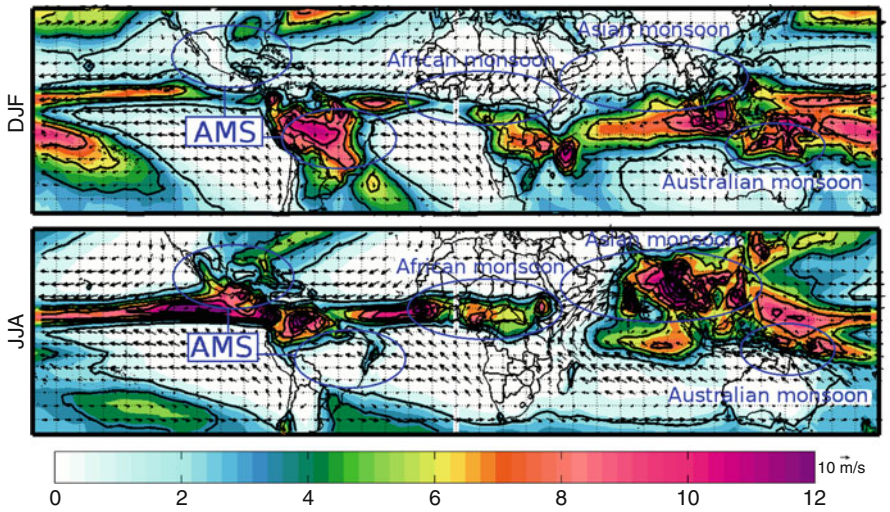

Ocean Evaporation and Precipitation. Figure 10

GPCP precipitation (*shaded contours*) millimeter per day and wind speed at 925 mb (*vectors*), 1989–2008

similar to the case for the Southern American counterpart of the AMS, namely, the SAM. Here, the intensification of precipitation during the boreal summer is related to the presence of strong low-level winds and an intense convergence of moisture related to the interaction between the Chaco Low and the trade winds from the northeast [46]. This supply of moisture from low levels corresponds to the transport of moisture due to the South American low-level jet (SALLJ) [47]. The transport of moisture is also relevant in the case of the West African monsoon, the activity of which is linked with the thermal contrast between the ocean and the surface of the land [48]. Cadet and Nnoli [49] proposed that the Gulf of Guinea and Central Africa act as sources of moisture in this case. In addition, the Mediterranean has been proposed to be a source of moisture for West Africa [50]. The African easterly jet (AEJ), which is associated with easterly fluxes of moisture, has been studied extensively in this regard [49], and is also thought to be a factor of inertial instability [51]. Furthermore, the Asian monsoon has been analyzed extensively in terms of its southwesterly and northeasterly flows. The dynamics of the Asian monsoon are of particular interest. A good description of the wind reversal circulations and of the system as a whole was provided by Wang [52]. Variations in the low-level jet (which include variations in a low-level jet over the Arabian Sea), and changes in the distribution of SSTs, are both associated with variations in precipitation, and are the basis of ocean–atmosphere coupling during the development of this monsoonal pattern. The importance of the moisture evaporated from the Arabian Sea and the South Indian Ocean has been determined and recognized, as have the contributions from the western Pacific Ocean [53]. The Australian monsoon, which is strongly connected with the Asian monsoon [54], has similar characteristics with respect to the Indian Ocean, in that this is an important source of moisture. For the purpose of summarizing this discussion, Fig. 11 shows the distribution of mean evaporation obtained from the OAFlux data [3], together with the vertically integrated moisture flux vectors of wind. The distribution seen during the active phase of the monsoons (see Fig. 10) shows the importance of evaporation from the surface of the oceans for the transport of moisture to regions influenced by monsoons.

The link between evaporation from the ocean and the transport of moisture has already been discussed. However, the importance of oceanic evaporation to monsoonal circulation is not constrained to the transport of moisture alone. In this case, evaporation from the ocean also plays a dynamic role, which has been found to be extremely important in some of the monsoons described above. This dynamic behavior may be considered in terms of the interaction between the process of convection and the water vapor itself [55]. The monsoons provide a clear example of this

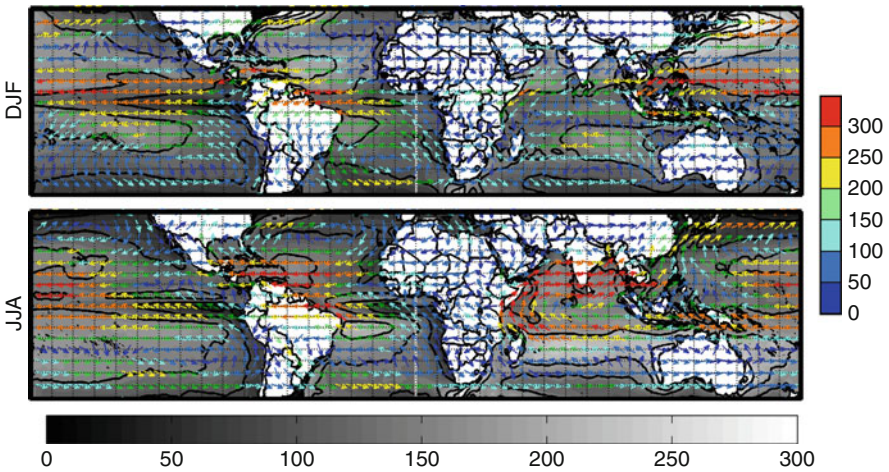

Ocean Evaporation and Precipitation. Figure 11
OAFlux evaporation (*shaded contours*) in centimeter per year and ERA Interim Vertically Integrated water vapor flux (*vectors*), 1989–2008

interaction due to their rapid changes in wind speed, moisture content, and precipitation. As a result of this significant intraseasonal fluctuations may be observed. The relationship between SST and evaporation from the ocean has a number of different interpretations. The warming of the surface increases the rate of evaporation, leading to an increase in the amount of water vapor in the atmosphere. As the contribution to moisture transport increases, the cumulus convection is intensified [56]. This ocean–atmosphere coupling is extremely important, in the case of the West African monsoon the supply of moisture to the atmosphere is led by an intense convergence of moisture flux in the boundary layer [51] and a strong wind–evaporation–SST feedback mechanism [57]. A conceptual model of the moisture-advection feedback in the monsoons was recently developed [58]. In general terms, increases in SST speed up the rate of evaporation, and the ensuing decrease in evaporation from the surface of the ocean then contributes to an increase in SST. The relationship is quite complex, but the importance of evaporation in the development and maintenance of monsoon systems is beyond question.

Response of the Relationship Between Evaporation and Precipitation to the Forcing of the ENSO

The distribution of evaporation from the ocean has been described and it has been explained that this is related strongly to the distribution of SST, in order to show the connection between the atmosphere and the ocean, and the extreme importance of these mechanisms for precipitation. It therefore follows that any change in SST affects the distribution and rate of evaporation, leading to changes in the distribution of precipitation. The SST is affected significantly by El Niño–Southern Oscillation (ENSO) events, which are the main mode of variability of the climate system [59]. The influence of the ENSO on the climate system that has received the most attention to date is that on precipitation. An increase in rainfall has been documented during cold ENSO phases (La Niña) while the warm phase (El Niño) is characterized by a reduction [60]. The regional variability in precipitation has been analyzed by several authors, who showed that the ENSO has a clear influence on the phenomenon (e.g., [61–64]). The variability of surface winds has also been observed to be related to the ENSO, in that the easterly flow of wind over the surface has been found to strengthen during warm ENSO events, while an equivalent weakening has been observed for the opposite phase. Evaporation also varies during ENSO events, as a result of variations in both SST and the surface wind fields [65], and the link between evaporation and the convergence of moisture flux [66] is reflected in the precipitation. Trenberth et al. [67] showed how, under the influence of the ENSO, warmer areas are associated with wetter regions, as suggested by the correspondence between the distributions of precipitation and surface temperature. These authors suggested that this finding may imply the importance of local evaporation for the distribution of precipitation during ENSO events. However, while it is clear that a relationship of this type applies over the land, the nature of the equivalent relationship over the ocean is less clear. Klein et al. [68] undertook a study in which they analyzed changes in SST and evaporation from the ocean by referring to the ENSO index. They determined the importance of evaporation from the ocean (and cloud cover) in leading the SST anomalies related to the ENSO. Furthermore, Yu and Mechoso [69] highlighted the dominance of wind-driven surface evaporation in the response of the surface heat flux to the ENSO in the tropics. A number of different authors have focused on the response of the monsoonal circulations to the ENSO and have discussed the importance of the changes to the distribution of evaporation from the oceans (e.g., [70]). The conditions produced by the ENSO have meant that the importance of evaporation from the ocean is still not fully understood, due to the complexity of the feedback mechanisms involved. These mechanisms are important not only near the surface, but also for the vertical atmospheric column. A good example of this is the "tropospheric temperature mechanism," in which it is proposed that the warming of the oceans' surface might be a response to the tropospheric warming observed in the tropics during El Niño, which causes a reduction in evaporation and therefore in precipitation [71]. The main response of the evaporation from the ocean to the ENSO is the increase of its coupling with the atmosphere through the strength of the feedback mechanisms involved [72, 73].

Future Research Directions

The scenarios associated with climate change suggest that the high sensitivity of saturation vapor pressure to temperature will result in an intensified hydrological cycle, with increased rates of evaporation and precipitation in a world that is warmer than it is today [5, 74]. Changing patterns of circulation will also lead to significant regional changes in the moisture budget. Furthermore, our best estimates of evaporation, such as those derived from the OAFlux data [7], have revealed strong increasing trends in evaporation from the oceans since 1978 (see Fig. 12), with the upward trend being most pronounced during the 1990s. The spatial distribution of these trends ([2]; not shown herein) show that while the increase in evaporation has occurred at a global scale, it has primarily been observed during the hemispheric winter accompanied by spatially coherent structures. Most important among these are the reduction in evaporation in the subtropics, the strong increase in evaporation along the paths of the global western boundary currents, and the increase over the Indo-Pacific warm pools.

In addition, climate change is likely to have effects beyond changes in evaporation. It is clear that changes in atmospheric circulation in a warming climate will result in changes in circulation between source and sink, which will redirect moisture in different ways. The general conclusion drawn by Gimeno et al. [75] was that "Those continental regions receiving moisture from only one or two source region(s) may be exposed more strongly to changes in the water cycle due to a changing climate than regions that draw on multiple moisture sources."

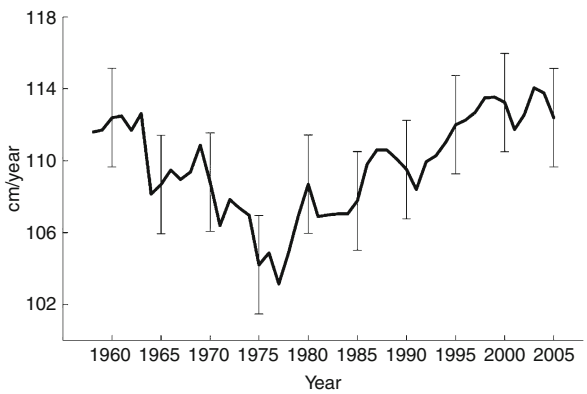

Ocean Evaporation and Precipitation. Figure 12 Variations in annual mean evaporation averaged over the ice-free oceans. The error bars indicate 1 std dev from 1958 to 2005 mean (From Yu [2])

A further reason for understanding the source-to-sink relationships in the atmospheric water cycle in more detail lies in the role they play in extreme weather events. Convergence and transport from regions of high water vapor may trigger extreme rainfall and cause flooding [76], and the persistence of droughts could be due, in part, to the absence of transport of moisture to the continents [77, 78]. This coupling of the ocean–land–atmosphere system via the atmospheric water cycle needs to be understood in view of the potentially severe consequences for humanity that could result from changes to these relationships.

Acronyms

AEJ	African easterly jet.
AMS	American monsoon system.
AWP	Atlantic warm pool.
C-C	Clausius−Clapeyron equation.
Ce	Turbulent exchange coefficient controlled by the wind speed, the atmospheric stability, and the difference in temperature between the air and the sea.
dq	Difference between the specific humidity of saturation at the sea surface and the near-surface atmospheric specific humidity.
DJF	The months of December, January, and February.
E–P	Surface freshwater flux, defined to be the difference between the rates of evaporation (E) and precipitation (P), per unit area.
Evp	Rate of evaporation.
ENSO	El Niño–Southern Oscillation.
ERA-I	European Reanalysis Interim.
GPLLJ	Great Plains low-level jet.
GPCP	Global Precipitation Climatology Project.
JJA	The months of June, July, and August.
ITCZ	Inter Tropical Convergence Zone.
IPCC	Intergovernmental Panel on Climate Change.

IPWP	Indian–western Pacific warm pool.
NAM/NAMS	North American monsoon (system).
MERRA	Modern Era Retrospective-analysis for Research and Applications.
OAFlux	Objectively analyzed air–sea fluxes.
SALLJ	South American low-level jet.
SAM	South American monsoon.
SPCZ	South Pacific Convergence Zone.
SST	Sea surface temperature.
TCWV	Total column water vapor.
U	Near-surface wind.
VIMF	Vertically integrated moisture flux.
WAM	West African monsoon.
WHWP	Western Hemisphere warm pool.

Bibliography

Primary Literature

1. Quante M, Matthias V (2006) Water in the Earth's atmosphere. J Physique IV 139:37–61
2. Yu L (2007) Global variations in oceanic evaporation (1958–2005): the role of the changing wind speed. J Clim 20(21):5376–5390
3. Trenberth KE, Dai A, Rasmussen RM, Parsons DB (2003) The changing character of precipitation. Bull Am Meteor Soc 84:1205–1217. doi:10.1175/BAMS-84-9-1205
4. Bales RC (2003) Hydrology, overview. In: Anderson MG (ed) Encyclopedia of atmospheric sciences, 2nd edn. Elsevier, London, pp 968–973. doi:10.1016/j.physletb.2003.10.071
5. Intergovernmental Panel on Climate Change (IPCC) (2007) Summary for policymakers. In: Solomon S et al (eds) Climate change 2007: the physical science basis contribution of working group I to the fourth assessment report of the intergovernmental panel on climate change. Cambridge University Press, Cambridge, UK, pp 1–18
6. Liu WT, Katsaros K, Businger JA (1979) Bulk parameterization of air–sea exchanges of heat and water vapor including the molecular constraints at the interface. J Atmos Sci 36:1722–1735
7. Yu L, Weller RA (2007) Objectively analyzed air–sea heat fluxes for the global ice-free oceans (1981–2005). Bull Am Meteor Soc 88:527–539
8. Numaguti A (1999) Origin and recycling processes of precipitating water over the Eurasian continent: experiments using an atmospheric general circulation model. J Geophys Res 104:1957–1972
9. Trenberth KE, Fasullo JT, Mackaro J (2010) Atmospheric moisture transports from ocean to land and global energy flows in reanalyses. J Clim. doi:10.1175/2011JCLI4171.1
10. Newell RE, Zhu Y, Scott C (1992) Tropospheric rivers? A pilot study. Geophys Res Lett 19(24):2401–2404. doi:10.1029/92GL02916
11. Ralph FM, Neiman PJ, Rotunno R (2005) Dropsonde observations in low-leveljets over the northeastern Pacific Ocean from CALJET-1998 and PACJET-2001: mean vertical- profile and atmospheric- river characteristics. Monthly Weather Rev 133(4):889–910. doi:10.1175/MWR2896.1
12. Trenberth KE, Guillemot CJ (1998) Evaluation of the atmospheric moisture and hydrological cycle in the NCEP/NCAR reanalysis. Clim Dyn 14:213–231. doi:10.1007/s003820050219
13. Howarth D (1986) An analysis of the water vapor flux divergence field over the southern hemisphere. Ann Assoc Am Geograph 76(2):190–207
14. Peixoto JP, Oort AH (1992) Physics of climate. American Institute of Physics, New York, 520 pp
15. Howarth D (1983) Seasonal variations in the vertically integrated water vapor transport fields over the southern hemisphere. Monthly Weather Rev 111(6):1259–1272
16. van Loon H (1972) Pressure in the southern hemisphere. In: Newton CW (ed) Meteorology of the southern hemisphere. Meteorological monographs 35. American Meteorological Society, Boston, pp 59–86
17. Stohl A, James P (2004) A Lagrangian analysis of the atmospheric branch of the global water cycle. Part I: method description, validation, and demonstration for the August 2002 flooding in central Europe. J Hydrometeorol 5:656–678
18. Gimeno L, Drumond A, Nieto R, Trigo RM, Stohl A (2010) On the origin of continental precipitation. Geophys Res Lett 37: L13804. doi:10.1029/2010GL043712
19. Stohl A, James P (2005) A Lagrangian analysis of the atmospheric branch of the global water cycle. Part II: Earth's river catchments, ocean basins, and moisture transports between them. J Hydrometeorol 6:961–984. doi:10.1175/JHM470.1
20. Wyrtki K (1989) Some thoughts about the West Pacific warm pool. In: Western Pacific international meeting and workshop on TOGA COARE proceedings, Nouméa, New Caledonia, pp 99–109
21. Webster PJ, Lukas R (1992) TOGA COARE: the coupled ocean-atmosphere response experiment. Bull Am Meteor Soc 73:1377–1416
22. Lukas R (1990) Freshwater input to the western equatorial Pacific Ocean and air-sea interaction. In: Proceedings of the US-PRC international TOGA symposium on air-sea interaction in tropical Western Pacific. Ocean Press, Beijing, pp 305–327
23. Webster PJ (1983) The large scale structure of the tropical atmosphere. In: Hoskins BM, Pearce R (eds) General circulation of the atmosphere. Academic, London, pp 235–275
24. Cornejo-Garrido AG, Stone PH (1977) On the heat balance of the walker circulation. J Atmos Sci 34:1155–1162
25. Lin X, Johnson RH (1996) Heating, moistening and rainfall over the western pacific warm pool during TOGA COARE. J Atmos Sci 53(22):3367–3383
26. Taylor R (1973) An atlas of Pacific rainfall. Report HIG-73-9, Hawaii Institute of Geophysics, University of Hawaii at Manoa, Honolulu, Hawaii, 7 pp +13 plates

27. Legates DR, Wilmott CJ (1990) Mean seasonal and spatial variability in gauge-corrected, global precipitation. Int J Climatol 10:111–127
28. Spencer RW (1993) Global oceanic precipitation from the MSU during 1979-91 and comparisons to other climatologies. J Clim 6:1301–1326
29. Kiladis GN, von Storch H, van Loon H (1989) Origin of the South Pacific convergence zone. J Clim 2:1185–1195
30. Madden RA, Julian PR (1971) Detection of a 40-50 oscillation in the zonal wind in the tropical Pacific. J Atmos Sci 28: 702–708
31. Weisberg RH (1996) On the evolution of SST over the PACS region. In: Abstracts of 76th AMS annual meeting. American Meteorology Society, Atlanta, 378 pp
32. Wang C, Enfield DB (2001) The tropical western hemisphere warm pool. Geophys Res Lett 28:1635–1638
33. Graham NE, Barnett TP (1987) Sea surface temperature, surface wind divergence, and convection over tropical oceans. Science 238:657–659
34. Wang C (2002) Atlantic climatic variability and its associated atmospheric circulation cells. J Clim 15:1516–1536
35. Wang C, Enfield DB, Lee SK, Landsea CW (2006) Influences of the Atlantic warm pool on western hemisphere summer rainfall and Atlantic hurricanes. J Clim 19:3011–3028. doi:10.1175/JCLI3770.1
36. Ruiz-Barradas A, Nigam S (2005) Warm season rainfall variability over the U. S. Great Plains in observations, NCEP and ERA-40 reanalyses, and NCAR and NASA atmospheric model simulations. J Clim 18:1808–1830. doi:10.1175/JCLI3343.1
37. Wang C, Lee SK, Enfield DB (2008) Climate response to anomalously large and small Atlantic warm pools during the summer. J Clim 21:2437–2450. doi:10.1175/2007JCLI2029.1
38. Drumond A, Nieto R, Gimeno L (2011) On the contribution of the tropical western hemisphere warm pool source of moisture to the northern hemisphere precipitation through a Lagrangian approach. J Geophys Res 116:D00Q04. doi:10.1029/2010JD015397
39. Janicot S, Harzallah A, Fontaine B, Moron V (1998) West African monsoon dynamics and eastern equatorial Atlantic and Pacific SST anomalies (1970–88). J Clim 11:1874–1882
40. Lau KM, Kim KM, Yang S (2000) Dynamical and boundary forcing characteristics of regional components of the Asian summer monsoon. J Clim 13:2461–2482. doi:10.1175/1520-0442
41. Taschetto AS, Haarsma RJ, Gupta AS, Ummenhofer CC, Hillk KJ, England MH (2010) Australian monsoon variability driven by a Gill–Matsuno-type response to central West Pacific warming. J Clim 23(18):4717–4736. doi:10.1175/2010JCLI3474.1
42. Vera C, Higgins W, Amador J, Ambrizzi T, Garreaud R, Gochis D, Gutzler D, Lettenmaier D, Marengo J, Mechoso CR, Nogues-Paegle J, Silva-Dias PL, Zhang C (2006) Toward a unified view of the American monsoon systems. J Clim 19:4977–5000
43. Higgins RW, Yao Y, Wang XL (1997) Influence of the North American monsoon system on the U.S. summer precipitation regime. J Clim 10:2600–2622. doi:10.1175/1520-0442(1997)010
44. Castro CL, McKee TB, Pielke RA (2000) The climatology and interannual variability of the North American monsoon as revealed by the NCEP/NCAR reanalysis. Preprints, 11th symposium on global change studies, Long Beach. Am Meteor Soc 2000:168–171
45. Dominguez F, Praveen K, Vivoni ER (2008) Precipitation recycling variability and ecoclimatological stability—a study using NARR data. Part II: North American monsoon region. J Clim 21:5187–5203. doi:10.1175/2008JCLI1760.1
46. Lenters JD, Cook KH (1999) Summertime precipitation variability in South America: role of the large-scale circulation. Monthly Weather Rev 127:409–431
47. Falvey M, Garreaud R (2005) Moisture variability over the SouthAmerican Altiplano during the SALLJEX observing season. J Geophys Res 110:D22105. doi:10.1029/2005JD006152
48. Thorncroft CD, Nguyen H, Zhang C, Peyrillé P (2011) Annual cycle of the West African monsoon: regional circulations and associated water vapour transport. Quart J Roy Meteor Soc 137:129–147. doi:10.1002/qj.728
49. Cadet DL, Nnoli NO (1987) Water vapour transport over Africa and the Atlantic Ocean during summer 1979. Quart J Roy Meteor 113:581–602
50. Fontaine B, Roucou P, Trzaska S (2003) Atmospheric water cycle and moisture fluxes in the West African monsoon: mean annual cycles and relationship using NCEP/NCAR reanalysis. Geophys Res Lett 30:1117. doi:10.1029/2002GL015834
51. Hagos SM, Cook KH (2007) Dynamics of the West African monsoon jump. J Clim 20:5264–5284
52. Wang B (2006) The Asian monsoon. Springer/Praxis, New York
53. Lim YK, Kim KY, Lee HS (2002) Temporal and spatial evolution of the Asian Summer monsoon in the seasonal cycle of synoptic fields. J Clim 15:3630–3644. doi:10.1175/1520-0442(2002)
54. Gu D, Li T, Ji X, Zheng B (2010) On the phase relations between the Western North Pacific, Indian, and Australian Monsoons. J Clim 23(21):5572–5589. doi:10.1175/2010JCLI2761.1
55. Sherwood SC, Roca R, Weckwerth TM, Andronova NG (2010) Tropospheric water vapor, convection, and climate. Rev Geophys 48:RG2001. doi:10.1029/2009RG000301
56. Kuo HL (1965) On the formation and intensification of tropic cyclones through latent heat release by cumulus convection. J Atmos Sci 22:40–63
57. Xie SP, Philander SG (1994) A coupled ocean-atmosphere model of relevance to the ITCZ in the eastern Pacific. Tellus 46A:340–350
58. Schewe J, Levermann A, Cheng H (2011) A critical humidity threshold for monsoon transitions. Clim Past Discuss 7: 1737–1765. doi:10.5194/cpd-7-1737-2011
59. Trenberth KE, Stepaniak DP (2001) Indices of El Nino evolution. J Clim 14:1697–1701
60. Dai A, Wigley TML (2000) Global patterns of ENSO-induced precipitation. Geophys Res Lett 27:1283–1286
61. Ropelewski CF, Halpert MS (1987) Global and regional scale precipitation patterns associated with the El Niño/Southern oscillation. Monthly Weather Rev 115:1606–1626

62. Webster PJ, Yang S (1992) Monsoon and ENSO: selectively interactive systems. Quart J Roy Meteor Soc 118:877–926
63. Giannini A, Kushnir Y, Cane MA (2000) Interannual variability of caribbean rainfall, ENSO, and the Atlantic Ocean. J Clim 13:297–311
64. Lau NC, Nath MJ (2000) Impact of ENSO on the variability of the Asian-Australian monsoons as simulated in GCM experiments. J Clim 13:4287–4309
65. Ueki I (2011) Evidence of wind-evaporation-sea surface temperature (WES) feedback in the western Pacific warm pool during the mature phase of the 1997-98 El Niño. Geophys Res Lett 38:L11603. doi:10.1029/2011GL047179
66. Chikamoto Y, Tanimoto Y (2005) Role of specific humidity anomalies in Caribbean SST response to ENSO. J Meteor Soc Jpn 83:959–975
67. Trenberth KE, Caron JM, Stepaniak DP, Worley S (2002) Evolution of El Nino Southern oscillation and global atmospheric surface temperatures. J Geophys Res 107(D8):4065. doi:10.1029/2000JD000298
68. Klein SA, Soden BJ, Lau NC (1999) Remote sea surface variations during ENSO: evidence for a tropical atmospheric bridge. J Clim 12:917–932
69. Yu JY, Mechoso CR (2001) A coupled atmosphere-ocean GCM study of the ENSO cycle. J Clim 14:2329–2350
70. Chou C, Neelin JD, Su H (2001) Ocean-atmosphere-land feedbacks in an idealized monsoon. Quart J Roy Meteor Soc 127:1869–1891
71. Chiang JCH, Sobel AH (2002) Tropical tropospheric temperature variations caused by ENSO and their influence on the remote tropical climate. J Clim 15:2616–2631
72. Chiang JCH, Lintner BR (2005) Mechanisms of remote tropical surface warming during El Niño. J Clim 18:4130–4149
73. Lintner BR, Chiang JCH (2007) Adjustment of the remote tropical climate to El Niño conditions. J Clim 20:2544–2557
74. Held IM, Soden BJ (2006) Robust responses of the hydrological cycle to global warming. J Clim 19(21):5686–5699. doi:10.1175/JCLI3990.1
75. Gimeno L, Nieto R, Drumond A, Durán-Quesada AM, Stohl A, Sodemann H, Trigo RM (2011) A close look at oceanic sources of continental precipitation. Eos Trans Am Geophys Union 92(23):193–194. doi:10.1029/2011EO230001
76. Stohl A, Forster C, Sodemann H (2008) Remote sources of water vapor forming precipitation on the Norwegian west coast at 60°N: a tale of hurricanes and an atmospheric river. J Geophys Res 113:D05102. doi:10.1029/2007JD009006
77. Seneviratne SI, Lüthi D, Litschi M, Schär C (2006) Land-atmosphere coupling and climate change in Europe. Nature 443:205–209. doi:10.1038/nature05095
78. Hoerling M, Kumar A (2003) The perfect ocean for drought. Science 299(5607):691–694. doi:10.1126/science.1079053

Books and Reviews

Gleick PH (1989) Climate change, hydrology, and water resources. Rev Geophys 27(3):329–344

Huntington TG (2006) Evidence for intensification of the global water cycle: review and synthesis. J Hydrol 319:83–95

Liu WT (1993) Evaporation from the ocean. In: Gurney RJ, Foster JL, Parkinson CL (eds) Atlas of satellite observations related to global change. Cambridge University Press, Cambridge, pp 265–278

Li T, Wang B (2005) A review on the western North Pacific monsoon: synoptic-to-interannual variabilities. Terrest Atmos Oceanic Sci 16:285–314

Schott FA, Xie SP, McCreary JP (2009) Indian Ocean circulation and climate variability. Rev Geophys 47: RG1002. doi:10.1029/2007RG000245

Trenberth KE, Caron JM, Stepaniak DP (2001) The atmospheric energy budget and implications for surface fluxes and ocean heat transports. Clim Dyn 17:259–276

Ocean Farming and Sustainable Aquaculture Science and Technology, An Introduction to

Barry A. Costa-Pierce
Graduate School of Oceanography, Rhode Island Sea, Grant College Program, University of Rhode Island, URI Bay Campus, Narragansett, RI, USA

Aquaculture is closely tied to enhanced fisheries; indeed, marine fisheries enhancement by using the "aquaculture toolbox" is happening around the world and in some countries on a massive scale, e.g., in China. The science of marine enhancement is still in its infancy compared to other fields of fisheries science, but now shows potential to (1) increase fishery yield beyond that achievable by exploitation of the wild stock alone, (2) help restore depleted stocks, (3) provide protection for endangered species, and (4) provide critical information on the natural ecology, life history, and environmental requirements of valuable marine species (► Marine Fisheries Enhancement, Coming of Age in the New Millennium). The key to successful use of stocking is to plan enhancement programs from a fisheries/resource management perspective, using a broad framework and a transdisciplinary scientific approach where stakeholders are engaged from the outset in planning new programs.

Marine fisheries enhancement is a powerful tool that requires careful and interdisciplinary planning to

control its effects. Marine enhancement will come of age in this new millennium as agencies and stakeholders align in truly group efforts. Few marine fisheries enhancement programs have enlisted all of the key elements of the Responsible Approach to Marine Stock Enhancement and the Code of Responsible Conduct for Marine Stock Enhancement. But these principles are now well described and laid out in a systematic manner. It is reasonable to expect that future, more sustainable fisheries enhanced by aquaculture will be successful as long as dedicated attention is focused on applying each of the key elements of the Approach and Code.

Polyculture is a sophisticated ecological precept illustrating the "niche concept." In aquaculture, it is ancient practice originating in China where the production of two or more noncompetitive species are cultured in the same physical space at the same time, often with the objective of producing multiple products from one system, and thus multiplying production and adding value. Polyculture is used primarily to enhance total production within an aquaculture facility while maintaining, and in many cases, enhancing water quality. Species used may be a combination of animals and plants, or aquatic and terrestrial species (► Polyculture Ocean Farming). In the modern context, polyculture systems have evolved to incorporate hydroponic systems (aquaponics).

Aquaculture may be an ancient practice, but until recently, the field has developed mainly on a trial and error basis. Modern aquaculture developments are organized principally in a traditional, compartmentalized manner designed to maximize financial returns. However, macroeconomic factors are not the sole drivers of success in aquaculture. Advancing sustainable aquaculture science and technology requires innovation in multiple fields, plus must incorporate innovative participatory processes that engage scientists, extension professionals, policy-makers, and the public. Aquaculture has advanced rapidly in many economically developing countries due to the formation of multidisciplinary teams that have worked together over 10–20-year periods not only to incorporate the latest biophysical and engineering advances but also to evolve innovative, socioecological, and ecosystem governance approaches to management and civil society (► Aquaculture, Sustainability Science in). In the twenty-first century, the environmental and social costs of aquatic food production cannot be externalized, and "social profit" is as important as economic. It is well recognized that the development of sustainable aquaculture is dependent not only on the technical needs for hatcheries to produce seed and feed mills to produce feeds but also on markets, equipment, and the overall capabilities of the entire "seafood infrastructure." Aquaculture is evolving rapidly and has a real chance to be a shining example of sustainable foods production for millions of people both rich and poor. A new development paradigm is needed, one that uses the principles and practices of ecology to break through disciplinary bounds and tie together real-world knowledge, combining the findings of disparate, applied research disciplines in the ecological and social sciences in order to create a new, knowledge-based infrastructure and social-ecological support system (► Aquaculture, Ecological). FAO has developed guidelines for an ecosystems approach to aquaculture which can be used to design "aquaculture ecosystems" at many scales. Until recently, there were few commercial examples of successful models of these advanced aquatic food ecosystems, especially in marine waters, but the basis and content of two commercial operations are described here (► Aquaculture, Integrated Multitrophic (IMTA), and ► Sustainable Ecological Aquaculture).

IMTA and SEA systems incorporate innovative engineering and ecological design components that demonstrate a clear transition from single to multiple species aquaculture production in the ocean. The concept is simple, but the practices are elegant. The farming of aquatic species from different trophic levels in proximity allows one species' uncontaminated (no toxicants used), uneaten feed and nutrient wastes to be recaptured and converted into fertilizers, feeds, and energy for other aquatic crops. IMTA and SEA systems combine "fed aquaculture" (e.g., finfish) with "extractive aquaculture," which utilizes inorganic waste nutrients (absorbed by seaweeds) and organic waste nutrients (filtered by shellfish) from the fed aquaculture system. The aim is to design and operate a balanced farming ecosystem for improved environmental sustainability, greater economic profit (improved outputs, lower costs, product diversification, reduction of risks, value added, ecolabeled

products), and societal acceptability (job creation, improved governance, safe products, no contaminants).

Production of finfish species from coastal aquaculture systems has been limited until recently to the use of open, net pen cage systems. These systems are the most available (inexpensive in terms of cost/volume) and, thus, have proliferated where the regulatory environment has allowed their use inshore. Surface gravity cage systems are also the most controversial of all engineered aquaculture systems. They can be more easily destroyed in storms. And they are capital and labor intensive, requiring large and expensive hydraulic and feeding equipment for management, maintenance, net handling, washing, and cleaning.

In the Mediterranean, coastal finfish aquaculture in surface gravity cages has spread throughout the region. Progress has been made, but there is still a poor understanding of the environmental interactions of aquaculture in such a unique sea. Scientists remain unable to calculate the carrying capacity of areas of the sea for aquaculture (► Marine Aquaculture in the Mediterranean). There are many different types of habitats and ecosystems within the Mediterranean Sea so that it is essential that ecological and socioeconomic research address regionally specific issues. There is a special urgency to improve the understanding of fish pathology in Mediterranean aquaculture systems, especially in view of EU policies concerning the reduction of chemical use in the aquatic environment. Sustainable aquaculture within the Mediterranean Sea may be achieved by combining therapeutic treatments with health management strategies as breeding of tolerant fish, improving water quality, and vaccination.

Aquaculture in the open ocean or in high-energy coastal areas is predicted to grow rapidly in the twenty-first century due to space and resource conflicts in crowded coastal areas where most of the world's population resides. There are few commercial examples of successful models of well-studied commercial finfish cage operations in marine waters off islands, so the example of 5 years experience at the Kona Blue farm site, the evaluation of actual data, and observations recorded there are globally important (► Environmental Impacts of an Open Ocean Mariculture Operation in Kona, Hawaii). Baselines and evaluation of impacts of commercial aquaculture at such sites, their context, and their interpretations give invaluable insights into the future trajectory of sustainable open ocean aquaculture for many tropical nations.

Escaped fish may impact wild fish through competition, predation, habitat displacement, gene pool dilution, etc. In an attempt to reduce the numbers of escapees, rapid progress is being made throughout the world in the design of new, submersible containment cages that are easier to manage in difficult environments and are more storm resistant. One globally important aquaculture engineering innovation is the development of a modular "Aquapod™ cage system" which utilizes individual triangular net panels fastened together to construct a rigid sphere as a secure enclosure. The Aquapod™ panels are made of simple structural members (plastic lumber from mainly recycled bottles) and wire mesh netting. Some individual panels or groups of panels have other functions, such as access, feeding, fish transfer and grading, harvest, mooring, and mortality recovery. Other individual panels may have pneumatically controlled flotation devices which allow an almost infinite orientation of the Aquapod™ in the water (► Aquapod Systems for Sustainable Ocean Aquaculture).

The rationale placement of aquaculture systems in the ocean is now being considered as an essential part of coastal and marine spatial planning (CMSP) efforts, and for some countries, the movement toward development of offshore renewable energy systems (wind, tidal, wave) has been viewed as a opportunity to examine closely the opportunity to site multiple, compatible uses in the ocean, such as the integration of offshore aquaculture with renewable energy systems. Analyses and field experiments have been conducted that merge submerged finfish cages and shellfish growing structures with offshore wind energy structures, and some important logistical, economic, and environmental advantages have emerged (► Aquaculture and Renewable Energy Systems, Integration of). Offshore windmills use the wind above the surface to produce energy, and their fixed pylons, concrete foundations, metal jackets, tripods, or tripiles offer excellent potential for a wide range of aquaculture systems. Pioneering studies conducted in Germany have examined the colocation of offshore wind farms and off-bottom offshore aquaculture for shellfish and algae. In addition,

a broad-based stakeholder process involving all concerned in the multifunctional uses of offshore wind farms for aquaculture has been conducted which has helped dispel the many mistaken perceptions, concerns, and doubts about these ideas.

Engineering advances for open ocean shellfish aquaculture worldwide, initially adapted from deep water suspended scallop culture systems in Japan, push the frontier of shellfish production away from the multiple user conflicts of the world's coast and offer enormous potential for the production of low trophic level grazing shellfish species that could provide massive amounts of new, high protein, and fatty acid rich seafood for humanity. Advances have not been limited to new types of lines, moorings, buoys, but also in shellfish management and innovative extension methods to move capture fishermen into shellfish aquaculture (► Mussel Culture, Open Ocean Innovations). Offshore deepwater shellfish farming technologies have been shown to be effective for mussel production in very high-energy open ocean conditions (e.g., significant wave heights >10 m) in the northeast USA, and at a test site in the German Bight with significant wave heights >8 m and current velocities up to 1 ms^{-1}.

Shellfish and seaweed aquaculture are considered by many marine stakeholders to be best choices due to the elimination of many of the environmental concerns over feeds plus their beneficial impacts on particulate and nutrient pollution (► Seaweed Aquaculture for Human Foods in Land-Based and IMTA Systems). The sustainable expansion of seaweed aquaculture is also being driven by the needs for additional sources of high quality, nutrient-dense human foods (sea vegetables with high levels of omega-3's). Expansion of seaweed aquaculture is being considered in offshore and coastal areas but also in land-based systems. Land-based cultivation of seaweeds reduces the pressure on wild harvests, particularly those which are unsustainable and ecologically damaging, assists in the evaluation of numerous species that are unsuitable candidates for traditional, open water systems, and allows for increased environmental and input controls. High levels of control in land-based settings provide the necessary traceability, security of supply, high quality standards, and safety standards required not just for human consumption but also for nutraceutical and pharmacological applications (► Mariculture Systems, Integrated Land-based).

Shellfish aquaculture is one of the fastest growing sectors of the food industry, raising concerns about the influence of the activity on the environment. The sustainability of shellfish aquaculture and assessments on its trajectory toward sustainability involve a detailed review of the ecological impacts – both positive and negative – on nutrients, particles (filtration), exotic species, biodiversity, structure (habitats), and opportunities for incorporating best practices and developing innovative culture systems (► Shellfish Aquaculture, Methods of Sustainable). The concept of "acceptability" of impacts is critical to determining the sustainability of shellfish aquaculture in the marine environment. Since the term "acceptable" is governed primarily by social values, the social carrying capacity of aquaculture should be the basis of a sustainability program to assess the sum of activities, not only including aquaculture, within a defined area. The mechanism toward identifying sustainable activities in the marine environment will progress when clear policies are elucidated and an inclusive approach is adopted reflecting legislative requirements and the views of all stakeholders.

Sustainable shellfish aquaculture will depend upon a strong but reasonable regulatory system, responsible farmers adhering to best management practices so that they raise do not deplete resources in a given area to such an extent that bivalve production is decreased, and a society that judges if shellfish aquaculture has an acceptable impact on the environment and is sustainable. Since there is intense competition for space and use in many coastal zones, the siting of shellfish aquaculture farms can be contentious. Thus, many organizations have stressed the importance of determining the carrying capacity of different areas for shellfish aquaculture. There are a number of ways that "carrying capacity" may be defined, including physical, production, ecological, and social, and the first three categories are to lesser or greater degrees related to social expectations and standards. A number of methods have been developed to calculate these different categories of carrying capacity for bivalve culture. Advances to estimate the different categories of carrying capacity have been made (► Carrying Capacity for Sustainable Bivalve Aquaculture). Scientific advances

in modeling for shellfish aquaculture have encouraged the rapid development of a sustainable shellfish aquaculture industry, with excellent case studies from throughout the world (► Carrying Capacity for Aquaculture, Modeling Frameworks for Determination of).

There have been concerns that aquaculture has been moving away from its global responsibility to be more sustainable and to realize its altruistic goals of providing net benefits (additional foods) for a protein-hungry planet. Whether the word sustainability has become overused or not, it has catalyzed a forum for oversight of the growth and development of sustainable aquaculture on a global scale. The challenges to aquaculture sustainability are numerous from the biological, environmental, economic, technological, engineering, regulatory, and societal perspectives. Appropriate species need to be selected based on their biology, growth, and harvesting technologies, all adapted to local environmental conditions. Cost-effective, safe, and full containment engineering innovations will be required. Growing multiple species in an ecosystem sense will require aquatic farmers to develop additional "skill sets" since multiple farming practices are oftentimes completely different activities. There is one view that high value markets will have to be found for these additional "janitorial" species to justify their culture. There are also issues with permitting and regulatory authorities and not so trivial opposition from coastal and riparian land owners.

Sustainable aquaculture will also have to incorporate at the outset, and not as an afterthought, planning for not only the sustainable production of aquatic foods but also for innovative participatory social processes, community development, and the wider social, economic, and environmental contexts of aquaculture at diverse scales, both large and small. To judge the sustainability of new models of ecological aquaculture will require the development and use of new, more comprehensive models for decision-making for the evaluation of aquaculture production, such as life cycle assessments, an ISO-standardized accounting framework that allows for multicriteria environmental and social performance assessments (► Life cycle assessment and its application to aquaculture production systems). Such comprehensive methods will help a new cadre of innovators see the opportunities to evolve the next generation of sustainable practices in aquaculture. With an increase in ecological innovations coming to aquaculture, a higher level of sustainable intensification could be achieved. Important flows of natural resources will be increasingly understood, measured, used, and allocated more efficiently globally, regionally, and locally, which could result in the reallocation of resources more consciously into the most efficient animal and plant production systems for humanity. Such a sustainable intensification of ecological aquaculture will be essential in order to maintain and preserve aquatic ecosystems while providing additional high-energy aquatic foods for people by 2050.

Ocean Fertilization for Sequestration of Carbon Dioxide from the Atmosphere

Philip W. Boyd
Department of Chemistry, NIWA Centre for Chemical and Physical Oceanography, University of Otago, Dunedin, New Zealand

O

Article Outline

Glossary
Definition of the Subject
Introduction
Evaluation of OIF in Relation to Other Proposed Geoengineering Schemes
Conclusions and Future Directions
Bibliography

Glossary

Carbon sequestration Is the removal of carbon by physical, chemical, and/or biological processes, and its long-term storage (i.e., decades to millennia) such that the carbon cannot return to the atmosphere as carbon dioxide.

Ocean fertilization Is the purposeful modification of the chemical characteristics of the surface ocean, by the addition of plant macronutrients including phosphate and/or iron, or the deployment of equipment such as ocean pipes to enhance the

supply of nutrient rich deep water to surface waters. This fertilization has the potential to enhance upper ocean productivity, some of which may eventually settle into the ocean's interior, thereby increasing carbon sequestration.

Global warming potential (GWP) Provides a relative index between greenhouse gases, such as carbon dioxide or nitrous oxide, using their specific radiative properties to estimate the effect of anthropogenic emissions of each gas, over a specified time period relating to their atmospheric lifetime, on global climate.

Surface mixed layer Refers to the less dense layer of seawater in the upper ocean (10–200 m thick) that overlies more dense (i.e., colder and/or saltier) waters. This mixed layer is persistently stirred by upper ocean processes such as turbulence and wind mixing.

Free-drifting sediment traps Are devices deployed, usually in the upper 1 km of the ocean, designed to intercept settling particles that are the conduit of carbon sinking into the deep ocean as part of the biological pump.

Definition of the Subject

The ocean is a major sink for both preindustrial and anthropogenic carbon dioxide. Both physically and biogeochemically driven pumps, termed the solubility and biological pump, respectively (Fig. 1) are responsible for the majority of carbon sequestration in the ocean's interior [1]. The solubility pump relies on ocean circulation – specifically the impact of cooling of the upper ocean at high latitudes both enhances the solubility of carbon dioxide and the density of the waters which sink to great depth (the so-called deepwater formation) and thereby sequester carbon in the form of dissolved inorganic carbon (Fig. 1). The biological pump is driven by the availability of preformed plant macronutrients such as nitrate or phosphate which are taken up by phytoplankton during photosynthetic carbon fixation. A small but significant proportion of this fixed carbon sinks into the ocean's interior in the form of settling particles, and in order to maintain equilibrium carbon dioxide from the atmosphere is transferred across the air–sea interface into the ocean (the so-called carbon drawdown) thereby decreasing atmospheric carbon dioxide (Fig. 1).

The strength of the biological pump therefore relies upon the global ocean inventory of plant macronutrients, and its impact on atmospheric carbon dioxide concentrations can only be altered under three scenarios [2]. These scenarios involve either a more efficient carbon fixation for each unit/mole of plant nutrient that is taken up, or additional carbon fixation fueled by either uptake of macronutrients in the open ocean that are currently not utilized, or by another source of macronutrients (such as from nitrogen fixation) that add to the preformed nutrient inventory of the upper ocean [2].

In this entry, the focus is only on the topic of iron fertilization and carbon sequestration as it has received considerable attention over 3 decades, whereas other forms of ocean fertilization including purposeful upwelling [3–5] and stimulation of nitrogen fixation [6–8] have received considerably less scrutiny, and only in the last few years. Iron plays a role in driving the uptake of ocean nutrients that are currently not utilized. In around one-fourth of the world ocean, residual nutrients in the surface ocean are present at significant concentrations (Fig. 2). These so-called HNLC (High Nitrate Low Chlorophyll) waters paradoxically have low stocks of microscopic plants called phytoplankton. Such cells are anemic in these low iron HNLC waters and cannot utilize fully the surface inventories of plant macronutrients such as nitrate. In summary, iron fertilization can potentially enhance the strength of the biological pump by driving down the inventory of plant macronutrients that are currently not taken up in surface waters, in up to a quarter of the World Ocean. By doing so, they can potentially enhance carbon sequestration and hence reduce atmospheric carbon dioxide concentrations.

Introduction

The assembly of the history of atmospheric carbon dioxide concentrations in the geological past from core records such as Vostok [9] reveals that carbon dioxide is not constant over time but ranges between ca. 280 and 180 ppmv. The timing of these changes is clearly associated with the glacial–interglacial transitions (Fig. 3). This record of paleoclimate has led to much discussion regarding the underlying mechanism(s) behind such changes in atmospheric carbon dioxide. Candidate mechanisms for observed

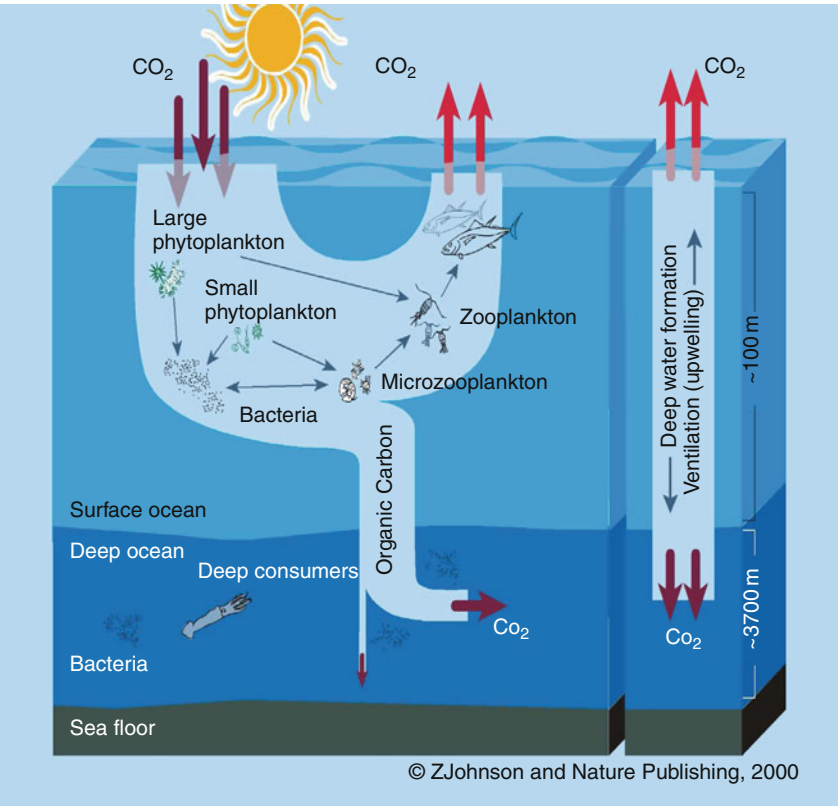

Ocean Fertilization for Sequestration of Carbon Dioxide from the Atmosphere. Figure 1
Cartoons of the biological (*left panel*) and solubility (*right panel*) pumps that drive carbon sequestration in the ocean (from Chisholm [65]). From [65]: "Together with the 'solubility pump', which is driven by chemical and physical processes, it maintains a sharp gradient of CO_2 between the atmosphere and the deep oceans where 38×10^{18} g of carbon is stored. Using sunlight for energy and dissolved inorganic macronutrients, phytoplankton convert CO_2 to organic carbon, which forms the base of the marine food web. As the carbon passes through consumers in surface waters, most of it is converted back to CO_2 and released into the atmosphere. But some finds its way to the deep ocean where it is remineralized back to CO_2 by bacteria. The net result is transport of CO_2 from the atmosphere to the deep ocean, where it stays, on average, for roughly 1,000 years. The food web's structure and the relative abundance of species influence how much CO_2 will be pumped to the deep ocean. This structure is dictated largely by the availability of inorganic macronutrients such as nitrogen, phosphorus, silicon and iron. Iron is the main limiting nutrient in the Southern Ocean, which is why the SOIREE experiment [37, 38] was conducted there (Figure modified from a graphic by Z. Johnson.)"

alterations in paleoclimate which were proposed included a shift in the latitude of winds in the Southern Ocean [10] (i.e., less communication between deep carbon dioxide–rich waters and the atmosphere) greater sea-ice extent [11] (i.e., reduced air–sea exchange due to capping of more of the polar ocean by sea ice) and iron supply to the ocean [12].

In 1990, John Martin [12] published the iron hypothesis which conflated trends in ice core records from Vostok (East Antarctica) with contemporary biological oceanographic studies. The former revealed a striking anti-correlation between atmospheric carbon dioxide and aerosol iron supply (Fig. 3), which Martin interpreted using evidence of phytoplankton in HNLC regions being stimulated rapidly by iron enrichment, leading to significant drawdown of the previously unutilized plant nutrients. Based on these combined observations, Martin hypothesized that increased dust supply during the windier and more arid glacial periods were responsible for a natural fertilization of

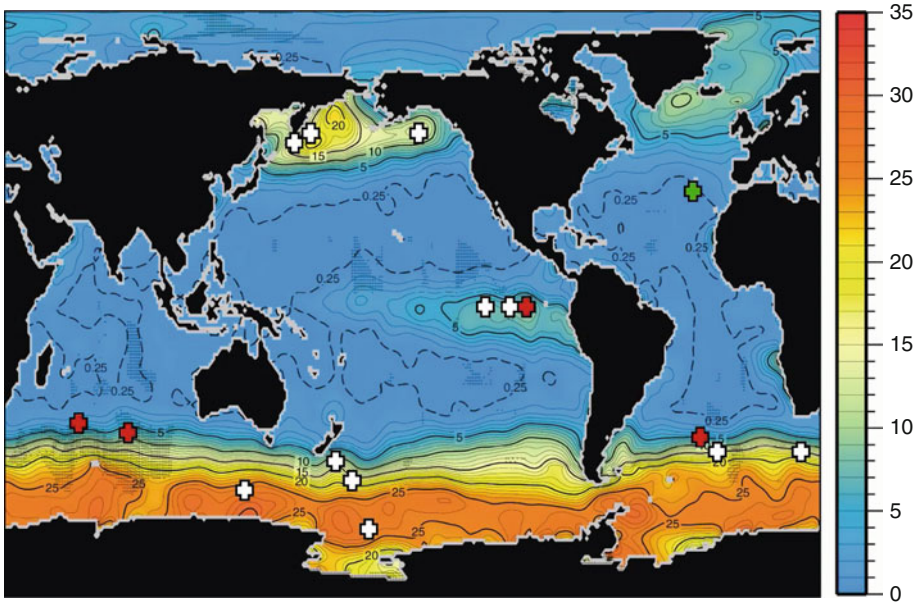

Ocean Fertilization for Sequestration of Carbon Dioxide from the Atmosphere. Figure 2
Annual surface mixed-layer nitrate concentrations in units of μmol liter^{-1}, with approximate site locations of FeAXs (*white crosses*), FeNXs (*red crosses*), and a joint Fe and P enrichment study of the subtropical LNLC Atlantic Ocean (FeeP; *green cross*). FeAXs shown are SEEDS I and II (northwest Pacific; same site but symbols are offset), SERIES (northeast Pacific), IronEX I and II (equatorial Pacific; IronEX II is to the left), EisenEx and EIFEX (Atlantic polar waters; EIFEX is directly south of Africa), SOIREE (polar waters south of Australia), SOFEX-S (polar waters south of New Zealand), SOFEX-N (subpolar waters south of New Zealand), and SAGE (subpolar waters nearest to New Zealand). FeNX sites shown are the Galapagos Plume (equatorial Pacific), Antarctic Polar Front (polar Atlantic waters), and the Crozet and Kerguelen plateaus (Indian sector of Southern Ocean; Crozet is to the left of Kerguelen). (Reproduced from Boyd et al. [19].)

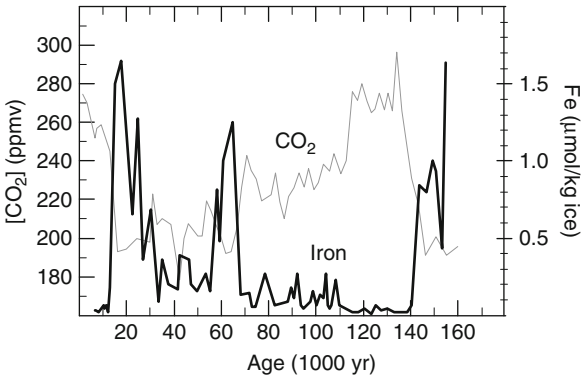

Ocean Fertilization for Sequestration of Carbon Dioxide from the Atmosphere. Figure 3
Fe concentration versus mean CO_2 concentrations in air trapped in ice from the Antarctic Vostok ice core over the last 160 Ma (Reproduced from Martin [12].)

the HNLC waters, in particular the Southern Ocean which is the greatest repository for unused upper ocean plant macronutrients in the World Ocean (Fig. 2). The consequent iron-mediated uptake of plant macronutrients enhanced the strength of the biological pump resulting in a gradual drawdown, over millennia, in atmospheric carbon dioxide of up to 80 ppmv (Fig. 3).

This iron hypothesis stimulated sustained scientific interest in the nature and magnitude of this potential causal mechanism in altering carbon dioxide in the geological past and hence as a drive of paleoclimate. However, Martin's hypothesis also aroused media interest in the application of ocean iron fertilization (OIF) as a "potential climate fix" for rising carbon dioxide concentrations in the Anthropocene [13].

Not long after the publication by Martin and his coworkers of their ship-based iron enrichment

studies [14], and of his iron hypothesis [12], the attendant publicity led to ocean iron fertilization (OIF) making front-page headlines in the Washington Post [13]. This media attention raised awareness of OIF sufficiently to result in considerable interest in this approach as a climate fix by a range of commercial parties. These commercial groups adopted a range of approaches that are summarized elegantly as a timeline by Strong et al. [13]. They ranged from application for patents on OIF, to exploring the potential leasing of large tracts of the open ocean to conduct OIF trials. By the mid-1990s – just a few years after the first mesoscale (i.e., at least 10 km length scale) scientific iron enrichment experiments were conducted (Fig. 2; see next section) – the first trials of OIF by commercial operators had taken place in the Gulf of Mexico [15] and another followed off the Hawaiian island chain [16]. A major distinction between these trials and the scientific studies into the biogeochemical impacts of OIF is that the latter were not reported in detail in the peer-reviewed literature [15], and in some cases they consisted only of a series of photographs [16].

Since these preliminary OIF trials, the advocacy for OIF as a carbon sequestration tool has mainly been driven by selective use of the datasets from the scientific OIF experiments that were readily accessible as peer-reviewed literature in the public domain (see next section), with no further trials being conducted by commercial parties [13]. This potential carbon sequestration strategy is unique among other proposed geoengineering schemes in that there is a suite of scientific research studies into OIF, to examine both its paleoclimatic and contemporary ecological and biogeochemical influences, that commercial parties have been able to tap into and use for advocacy for this biogeoengineering scheme [17].

Over the period from 1993 to 2009 there have been 13 mesoscale iron enrichment studies [18, 19] and three large-scale investigations of regions of the oceans in which high iron supply occurs naturally [20–22]. Such studies were necessary to both overcome the artifacts/limitations of small volume shipboard OIF incubations (1–25 L) [14] and to provide a more realistic and holistic approach to study the ramifications of OIF on oceanic biogeochemistry and ecology [13]. These mesoscale studies were conducted at sites which straddled HNLC waters from polar to tropical (Fig. 2), and hence provide a comprehensive assessment of the range of ecological and biogeochemical responses of OIF that inform questions such as: Could sustained natural OIF over millennia be responsible for the observed 80–100 ppmv decreases in atmospheric carbon dioxide during the glacial–interglacial transitions [3, 19]?; How might changes in iron supply in the coming decades, mediated by a changing climate, alter ocean productivity and ecosystem dynamics [19]?

Several syntheses [18, 19] of the findings of these open ocean OIF experiments clearly reveal that iron supply results in increased phytoplankton stocks and growth rates, rates of net primary production, and concomitant uptake of more plant macronutrients such as nitrate (Fig. 4). These trends were also noted by investigators at all three sites of natural iron enrichment [20–22], and together confirmed the first tenet of Martin's iron hypothesis [12] – that iron supply to HNLC regions such as the Southern Ocean would increase phytoplankton growth rates, productivity, and nutrient uptake.

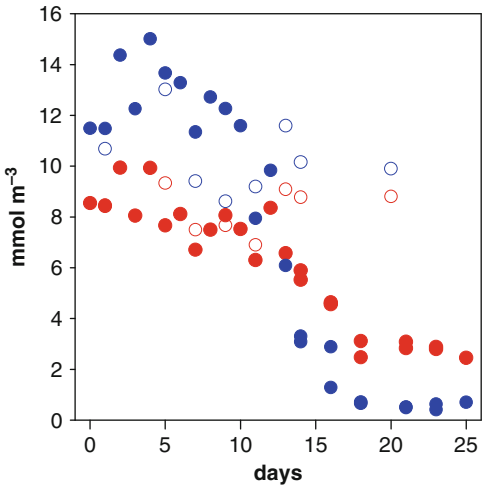

Ocean Fertilization for Sequestration of Carbon Dioxide from the Atmosphere. Figure 4
Time series of observed decreases in the mixed-layer concentrations of silicate (*blue solid symbols*) and nitrate (*red solid symbols*) within the iron-labeled SERIES patch in the NE subarctic Pacific. Day 0 is when the iron was first added, and the open symbols denote the mixed-layer nutrient concentrations in the surrounding HNLC waters (Reproduced from Boyd et al. [43].)

Another striking outcome of these scientific research studies was the pronounced drawdown in upper ocean carbon dioxide (conventionally expressed as the partial pressure of carbon dioxide – pCO_2) by up to 70 μmol during the iron-mediated phytoplankton bloom [18, 19]. The OIF experiments also revealed changes in the concentration of other climate-reactive gases during the resulting phytoplankton blooms, which could potentially either offset or enhance the effect of the drawdown of carbon dioxide. For example, increases in DMSP (dimethyl sulfoniopropionate), and subsequently in DMS (dimethyl sulfide) – a precursor of the sulfate aerosol hypothesized to enhance in increase cloud albedo by increasing cloud condensation nuclei [23] – were observed in experiments such as SOIREE in the Southern Ocean [24] but not in others such as SERIES in the NE Pacific [25] (see Fig. 2). Such an iron-mediated enhancement of cloud reflectance (i.e., albedo) could alter radiative forcing and along with concurrent carbon dioxide drawdown might enhance the ability of OIF to mitigate climate warming by both sequestering carbon and reducing incoming solar radiation (but only in the Southern Ocean where cloud condensation nuclei are undersatuarated [26]). Subsequent modeling studies have pointed to the complex interplay between surface mixed-layer dynamics, meteorological forcing, photochemistry, and microbial activity in determining whether DMS increases or remains unaltered following OIF [27]. The findings of this model [27] suggest that a wider extrapolation of the results of OIF at any particular site or region may be difficult.

Other climate-reactive gases that have been investigated and tracked during OIF scientific experiments include two gases with global warming potential (GWP, see Glossary) far in excess of carbon dioxide. Both N_2O and CH_4 production have been investigated in a small subset of scientific OIF studies which are summarized by Law [28]. As was the case for DMS, in some experiments there was a slight increase near the base of the surface mixed layer, thought to be associated with particle remineralization [29], whereas in other OIF studies there was no or a negligible change in the concentrations of these dissolved gases [19, 28, 30]. The SOFEX-South study (see Fig. 2) provided perhaps the best opportunity to study the impact of OIF on a wide range of gases, but despite this improved sampling coverage there were few significant changes in most of the biogenic gases sampled [26]. Given their high GWP, a relatively small increase in the concentration and subsequent efflux of either gas associated with the evolution of an iron-stimulated bloom, could readily offset the CO_2 mitigation effects that might result from OIF [28, 30].

Thus, these largely unanticipated changes in other climate-reactive gases following OIF, and their potential impact on radiative forcing, must also be factored into any estimation of the net outcome of OIF on climate mitigation.

This suite of scientific mesoscale OIF experiments also revealed a range of other unanticipated side effects, that ranged from physical (dilution of the iron-enriched patch of water [31] (Fig. 5); enhanced upper ocean heating due to more light absorption by the phytoplankton bloom [32]), biological (production of a neurotoxin – domoic acid – by some of the blooms of pennate diatoms [33]), to ecological (importance of the initial conditions with respect to the zooplanktonic grazers to the outcome of the bloom [13, 34] (Fig. 5).

Two of the most striking conclusions to come out of the syntheses of the scientific OIF experiments [18, 19] were the all-pervasive influence of iron supply of ocean ecology and biogeochemistry, and that even mesoscale experiments of an initial areal extent of 100 km^2 were still prone to artifacts [31]. Together these outcomes were indicative of the complex interplay of physical, chemical, optical, biological, and ecological factors in determining the overall biogeochemical signature of OIF experiments. Such a signature has important ramifications for both carbon sequestration, and how additional iron-mediated processes, such as the production of climate-reactive gases, other than carbon dioxide, might either amplify or counteract the impact of such carbon sequestration on climate.

The supply of iron resulted not only in an increase in the stocks of phytoplankton, but in a change of the dominant phytoplankton groups. In HNLC waters, the resident small phytoplankton cells were rapidly replaced by other larger-sized phytoplankton (Figs. 5, 6). Some of these larger cells – the prymnesiophytes – produce a precursor of the sulfate aerosol that is hypothesized to play a key role in the CLAW hypothesis [23]. CLAW proposes a link between the production of these phytoplankton compounds and enhanced

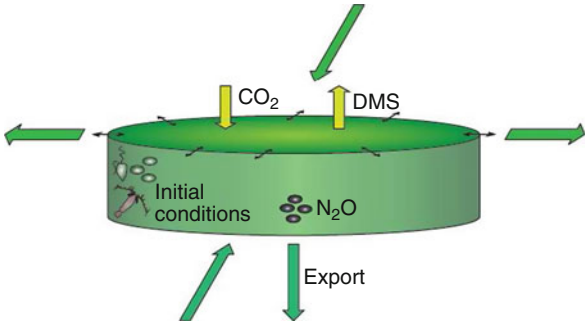

Ocean Fertilization for Sequestration of Carbon Dioxide from the Atmosphere. Figure 5
A schematic of the interactions between the iron-enriched patch of upper ocean and the surrounding HNLC waters redrawn after Boyd and Law [31]. Solid *black arrows* denote diffusion of waters both to and from those at the edge of the patch. The solid *green arrows* denote the impact of strain – due to horizontal currents – which stretch the patch laterally. The effects of the physics can increase the areal extent of the initial patch from < 100 km^2 to $>$ 1000 km^2 in several weeks [43]. CO_2, DMS, and export-labeled arrows represent the drawdown of atmospheric carbon dioxide into the iron-enriched waters; the potential efflux of elevated upper ocean concentrations of DMS; and the enhanced export of biogenic particles at the termination of the bloom (see Fig. 6 for more details on the timing), respectively. In some ocean iron fertilizations (OIFs) [34], the initial conditions – the biological composition of the iron-enriched waters (i.e., phytoplankton and zooplankton community structure) played a pivotal role in determining the bloom signature. As the bloom evolved in most OIFs there was shift from small phytoplankton to diatoms and in some studies the particles sinking to the base of the mixed layer later in the bloom were linked with increased nitrous oxide concentrations [28]

cloudiness which in turn reduces incoming solar radiation – a potential natural form of SRM (Solar Radiation Management [26,35]). However, the prymnesiophytes may only dominate the iron-stimulated bloom for a few days, after which they are rapidly removed by grazing [36]. This grazing in turn helps transform the DMSP into DMS, the ultimate precursor of the sulfate aerosol. By this route, other climate-reactive gases are produced.

During the rise and fall of the stocks of prymnesiophytes, another group of larger phytoplankton – the diatoms – are increasing from very low initial stocks, and soon will come to dominate the phytoplankton bloom (Figs. 5 and 6), carbon fixation, and the drawdown of carbon dioxide – in some studies by as much as 80 μatm. Hence, different phytoplankton groups, with differing biogeochemical signatures, dominate these iron-stimulated blooms at different times (Fig. 6). Interpretation of these signatures is further confounded by three factors, the oceanographic conditions – the mixed-layer depth [18] (see Glossary) – which characterize the site for the experiment (Fig. 3), the seed stock of phytoplankton and zooplankton [34] (Fig. 5), and the role of upper ocean physics in exchanging the surrounding HNLC waters with those of the iron-fertilized patch [31] (Fig. 5).

Site-specific oceanographic conditions can influence the timing and the magnitude of the biological trends and the resultant biogeochemical signatures – outlined in Fig. 6 – which vary considerably between experiments. For example, the initial biological conditions – in particular the seed stock of phytoplankton and zooplankton – also appear to be key drivers of the outcome of scientific OIF experiments [19]. Although our interpretation of the role of seed stocks is restricted to just two of the thirteen OIF studies – SEEDS I and II in the NW Pacific [34] (Fig. 2), this comparison reveals marked differences in the characteristics of each iron-mediated bloom. Both SEEDS experiments took place at the same site, and season but in different years. SEEDS I was a diatom-dominated bloom that resulted in high phytoplankton stocks, whereas SEEDS II was characterized by a mixed community of many different phytoplankton groups and much lower phytoplankton stocks, relative to that recorded during the development of the SEEDS I bloom. Careful analysis of the bloom datasets revealed that unlike SEEDS I, in SEEDS II there were much higher initial stocks of zooplankton which probably kept the bloom in check and which provides the most compelling explanation for the different bloom signature [34]. This example, again points to the difficulty in generalizing on either the ecological or biogeochemical outcome of these iron-stimulated blooms and also provides insights into the complex array of factors contributing to the resultant bloom signature.

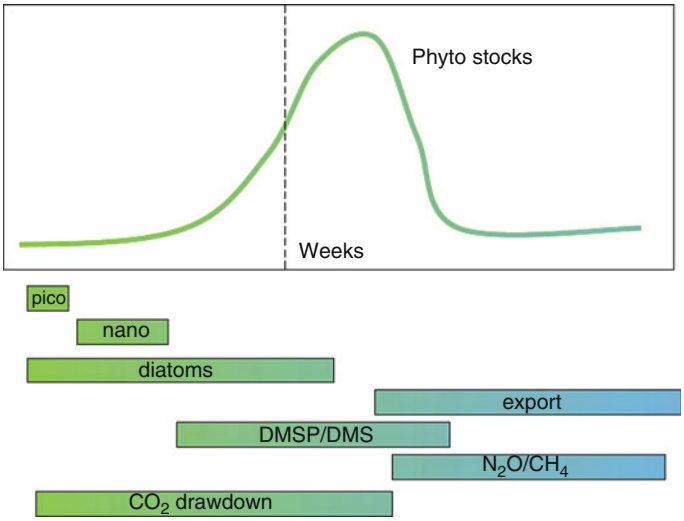

Ocean Fertilization for Sequestration of Carbon Dioxide from the Atmosphere. Figure 6
A generic timeline of biogeochemical events overlaid on the pattern of bloom development, termination, and decline (based on the SERIES OIF [43]). The vertical dashed line denotes the bloom phase attained when most studies terminated, as the vessel had to depart the iron-enriched patch. Hence, only a few studies [41–43] sampled the biogeochemically important termination and decline phases of the iron-mediated blooms. Pico and Nano denote pico- (<2 μm) and nano- (2–20 μm) phytoplankton. The former dominate under low iron HNLC conditions, and are stimulated by iron supply, but are rapidly grazed down to low levels by microzooplankton. The nanophytoplankton also have a transient increase following iron supply, but are also grazed down, in some cases resulting in increased DMSP (dimethyl sulfoniopropionate) followed by elevated DMS (dimethyl sulfide) concentrations

One of the most perplexing outcomes from this suite of scientific OIF studies was that the progression from shipboard experiments in 25 L incubation vessels to enriching 100 km^2 of HNLC ocean with iron did not overcome the issue of experimental artifacts [31]. It was evident from a comparison of the initial area of HNLC waters that were enriched with the areal extent at the end of the experiment that there was up to a tenfold increase in the bloom dimensions. Also, satellite imagery of the blooms – using ocean color (a proxy for phytoplankton stocks) revealed that the blooms had become elongated in one direction/plane and were often ellipsoidal [37, 38]. The analysis of Abraham et al. [38] revealed that the labeled waters interacted with the surrounding HNLC ocean via the strain and rotation of the patch and the dilution of the iron-enriched high chlorophyll patch with the surrounding low chlorophyll low iron waters (Fig. 5). Such dilution was reported to act like a chemostat [37] – an approach used in lab cultures of phytoplankton in which the culture is maintained under steady-state conditions by matching the phytoplankton growth rate with an equal rate of dilution with nutrient-enriched seawater. The so-called chemostat effect explains why some of these iron-stimulated blooms had a longevity not observed for natural blooms from the same ocean basins, for example, the Southern Ocean [39]. Perhaps the most significant effect of dilution of the OIF study by the surrounding HNLC waters was the delay of the bloom termination [40] (Fig. 6), and hence few studies were able to explore one of the key issues – how much of the iron-mediated increase in phytoplankton carbon sank out of the upper ocean and was sequestered within the ocean's interior.

This issue relates to the second tenet of the iron hypothesis of John Martin [12], and is central to assessing the contribution of the candidate mechanism of increased iron supply during the glacial–interglacial periods for the observed 80–100 ppmv decrease in atmospheric carbon dioxide over millennia. Despite its importance, few of the scientific OIF studies were able to measure whether any additional export or

sequestration, over and above that occurring under ambient HNLC conditions, of carbon resulting from purposefully iron-stimulated blooms. Several reasons were responsible for this dearth of C export or sequestration measurements. First, most studies were of too short a duration to capture the transition from bloom development to termination and decline (Fig. 6) – as it is during this phase that the majority of export from the bloom will take place [19]. Second, because of the relatively slow phytoplankton growth rates in the cold waters of the Southern Ocean, the physical dilution of the iron-stimulated phytoplankton bloom was at a comparable rate in these waters [40]. This prolonged the development of the bloom and thus in most of these studies the bloom decline phase was never observed, for example, SOIREE, EisenEX, and SOFEX-South (see Fig. 2).

There are only two published scientific OIF experiments in which the duration of the experiment was sufficient to encompass the bloom termination and decline phase. In IronEX II, in tropical HNLC waters of the equatorial Pacific [41] (Fig. 2) the bloom evolution, termination, and decline took <20 days, and export was measured [42]. However, due to lack of space on the vessel, these export flux measurements were done opportunistically and hence are too sparse to construct a budget to resolve how much of the enhanced phytoplankton stocks from the bloom were exported to depth [42]. In the SERIES study in the NE subarctic Pacific (Fig. 2) water, temperatures were intermediate between tropical and polar HNLC waters and hence the length of the evolution, termination, and decline phases was within the duration of SERIES and enabled this study to conduct the most detailed assessment of the bloom decline to date [43].

The decline of the SERIES bloom occurred relatively rapidly – within 10 days of the bloom peak [43, 44] – and was evident both from several remotely sensed images of the bloom and from detailed vertical profiles from ships within the bloom. Together, these measurements provided an accurate inventory of the enhanced particulate organic carbon (POC) driven by the iron-stimulated diatom bloom. This inventory could then be compared with the export of POC that was intercepted by free-drifting sediment traps (see Glossary) directly below the surface mixed layer and deeper in the water column (i.e., below the depth of the permanent pycnocline below which the carbon will be sequestered on timescales of decades to centuries). Although, shallow sediment traps are widely viewed as imperfect tools to reliably estimate export flux [45], these traps had been carefully calibrated (using thorium), had fluorometers located on the upper part of the array (to ensure the traps always underlay the waters of the bloom), and such traps are thought to be most reliable at sampling export when settling phytoplankton from a bloom dominate this flux [46]. Again, such refinements to this sediment trap sampling approach illustrate the difficulties in making reliable estimates of export flux from such blooms.

During the SERIES OIF study, the comparison of the proportion of phytoplankton carbon fixed in the iron-mediated bloom that exited the upper ocean was around 18%, and around 6% of the phytoplankton carbon settled deeper than the depth of the permanent pycnocline – i.e., was sequestered on long timescales into the ocean's interior [43]. A coupled budget of C and Si revealed that much of the settling phytoplankton carbon was consumed by both zooplankton and in particular by heterotrophic bacteria. These fluxes of iron-mediated POC export and sequestration can be used to provide estimates of C flux per unit iron added – a valuable ratio required by biogeochemical modelers to assess the role of increased iron supply in the geological past [19, 47]. Significantly, the Fe:C molar ratios of 2×10^{-3} and 6×10^{-2} were considerably lower than those used by early models (i.e., 1×10^{-5} summarized by de Baar et al. [47]) – and based upon data from lab culture flasks of iron-replete diatoms – to estimate the role of iron in influencing atmospheric carbon dioxide concentrations in the geological past.

Since the SERIES study, two studies [21, 22] in regions of the Southern Ocean (Fig. 2) where natural iron supply each year stimulates phytoplankton blooms have provided additional estimates of carbon export per unit iron. The advantage of estimates from these natural iron supply laboratories is that their estimates of carbon export per unit iron are based on in situ iron supply c.f. a purposeful addition of an iron salt in OIF, as the latter are reported to overestimate the supply of iron as much of it is rapidly removed by transformations to non-accessible forms of iron for the biota [21]. The disadvantage of such natural laboratories is

that it is difficult to assess the winter inventory of iron available to drive such natural blooms unless these waters are sampled in winter or early spring at the latest. Thus, it is possible to underestimate the winter iron supply and hence overestimate how much carbon export per unit iron supply occurs in each region.

There are wide disparities between the estimates of carbon export per unit iron supplied between the OIF study SERIES [43] and the CROZEX [22] and KEOPS [21] studies of natural laboratories. Even allowing for corrections to improve the reliability of each of these estimates (e.g., Chever et al. [48]) still results in a more than order of magnitude difference between them. Such a disparity between these estimates has major ramifications for assessing the role of increased iron supply in the geological past, with the estimate from KEOPS [21, 48] pointing to iron playing a major biogeochemical role in shaping paleoclimate, whereas the CROZEX [22] and SERIES [43] estimates, if broadly applicable suggest that increased iron supply played a much lesser role in altering the paleoclimate.

Thus, the present information from both a limited number of OIF's and natural laboratories of high iron supply provides too wide a range of estimates, and each with associated uncertainties, to resolve whether OIF sequestered sufficient carbon, on timescales of millennia, can play a pivotal role in the observed decreases in atmospheric carbon dioxide during the glacial terminations over the last 800,000 years [49].

Evaluation of OIF in Relation to Other Proposed Geoengineering Schemes

There have been only a few commercial trials [15, 16] to explore whether OIF is a potential tool in mitigating increasing emissions of anthropogenic carbon dioxide, and as stated none of these tools have been published in the peer-reviewed literature or is in any way comprehensive relative to the suite of scientific research OIF studies to address the role of increased iron supply in paleoclimate. Private sector interest in OIF for geoengineering has therefore based on scant data from any commercial trials, and thus has relied heavily on, and selectively used, datasets from the scientific OIF research studies. This presents problems in trying to do any initial assessment of how OIF compares with the pros and cons of other equally poorly resolved geoengineering schemes. Nevertheless, some attempts have been made at ranking OIF in relation to other schemes [17, 35, 50, 51]. Such ranking schemes have focused on criteria such as efficiency, cost, safety and side effects, mitigation speed, and emergency stop.

The estimates of the carbon exported per unit iron from scientific studies, to better quantify how much additional carbon was sequestered in the geological past due to enhanced iron supply over millennia, can be adopted cautiously to explore this criterion. The greater than an order of magnitude range in C exported per unit iron supplied will prevent refining the efficiency of OIF as a geoengineering tool but can be used to constrain the efficiency of OIF. Model estimates – summarized by Denman [52] range from 5 to 100 ppmv CO_2 (over decades to centuries), but are also subject to many unknowns, some of which – including the fate of the added iron (is it recycled or does it sink out) which several model outcomes are particularly sensitive to [53, 54]. Thus, it is presently difficult to relate the potential efficiency of OIF to other proposed geoengineering schemes. One issue that has also been overlooked is that even if enhanced iron supply was responsible for the majority of the decrease in atmospheric carbon dioxide, this probably took place over millennia in the Southern Ocean – and hence the rate of C sequestration would be 80 ppmv/5,000 years [55] (see later).

Following the banner headlines on OIF as a potential climate fix [13], it became further attractive to investors, etc., as it was reported to be a cheap climate fix – with estimates by one of the first commercial parties interest in OIF – Michael Markels Jr. publishing an estimate of 2$ US per ton of C sequestered [56]. Careful scrutiny of this estimate reveals it to have been based on erroneous and upper bounds for export efficiency [55, 57]. Again, some of the datasets derived from the OIF/paleoclimate scientific studies can be used to reevaluate the claims of 2 $ US per ton of C sequestered that were put forward by Markels. Boyd (2008) [55] rescaled these estimates by simply replacing the upper bound on C exported per unit iron used by Markel's (he had based his 2 $ per ton C estimate on the C:Fe ratio in a lab flask of iron-replete diatoms) with those measured during OIF experiments such as SERIES. The revised estimates increased to between 30 and 300 $ per ton of carbon sequestered when

more realistic estimates from scientific research were applied. Such a range of costs suggests that OIF is not the cheap carbon fix that was originally claimed, indeed the upper bound for OIF C sequestration is comparable to some of the most expensive approaches [35] – "artificial tree" atmospheric carbon dioxide scrubbers – currently being discussed. It should also be noted that the $30–$300 per ton C sequestered estimates for OIF based on the rescaling by Boyd [55] did not include the additional costs associated with verification (Fig. 7) and implementation nor the hidden costs of any unknown side effects.

Insights into potential side effects of OIF have again been obtained from scientific research into the relationship between OIF and paleoclimate. These side effects include the concurrent production of other more potent greenhouse gases (Fig. 5), and the release of neurotoxins by some pennate diatom species that have been reported to bloom [33], upon supply of iron. There are likely to be other side effects if OIF was to be implemented as a large scale – basin scale – geoengineering scheme, which would have to be the approach if it was to have any significant mitigation effects [58] (Fig. 8). Such findings are beyond the

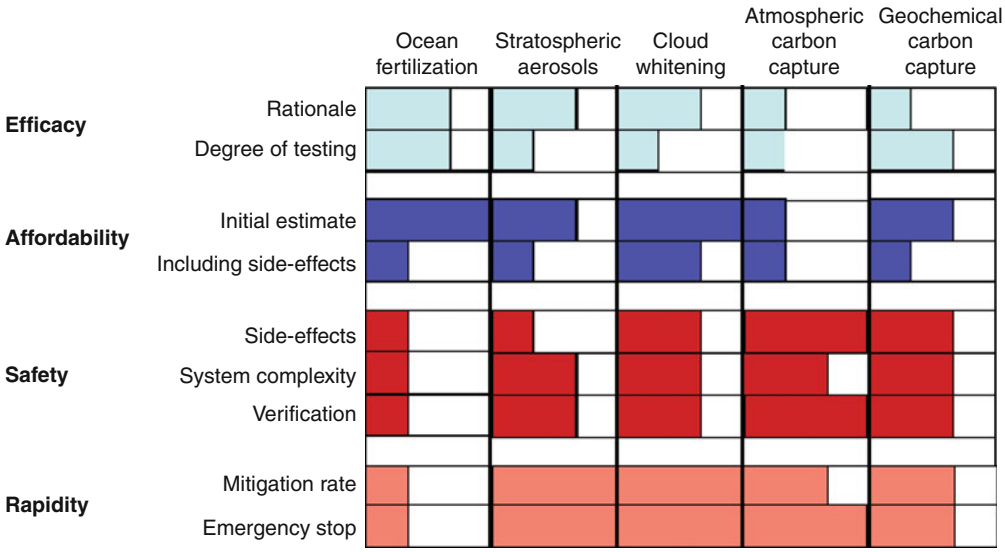

Ocean Fertilization for Sequestration of Carbon Dioxide from the Atmosphere. Figure 7
Comparison of aspects of five geoengineering proposals. The schemes span both carbon storage and reductions of solar radiation, and have been prominent in both the popular and scientific media. The figure highlights schematically some facets of the four criteria: efficacy, cost, risk, and time. The assessment gives scores relative to other schemes. For each facet, more color denotes a higher ranking. Efficacy is assessed in the first line according to the provenance of a scheme, with those based on historical precedents rated higher than those derived from theory and/or models. The extent of testing is shown in the second line, with related observations from experiments or pilot studies scoring higher than model simulations, which in turn rank above a proposal with accompanying technical details. The full degree of efficacy is too uncertain at present to depict as a facet in this intercomparison and will need further research. Affordability is categorized as initial cost assessment from the designer of a scheme in the upper line and a more realistic cost assessment including additional costs that come with a scheme's risks in the lower line. Safety provides an assessment of risk, which is related to known side effects, with unknown side effects represented here by system complexity (biogeochemical complexity is larger than geochemical complexity, which is larger than physicochemical complexity) and the verification of both efficacy and side effects. Other important but very uncertain aspects of risk, such as geopolitical and economic changes, require further research. Relevant aspects of time include the rate of climate mitigation in the top line (higher rates are better), and the rapidity with which to halt any unanticipated deleterious effects, based on residence time of the agent of perturbation in the environment (shortest residence scores highest, reproduced from Boyd [17])

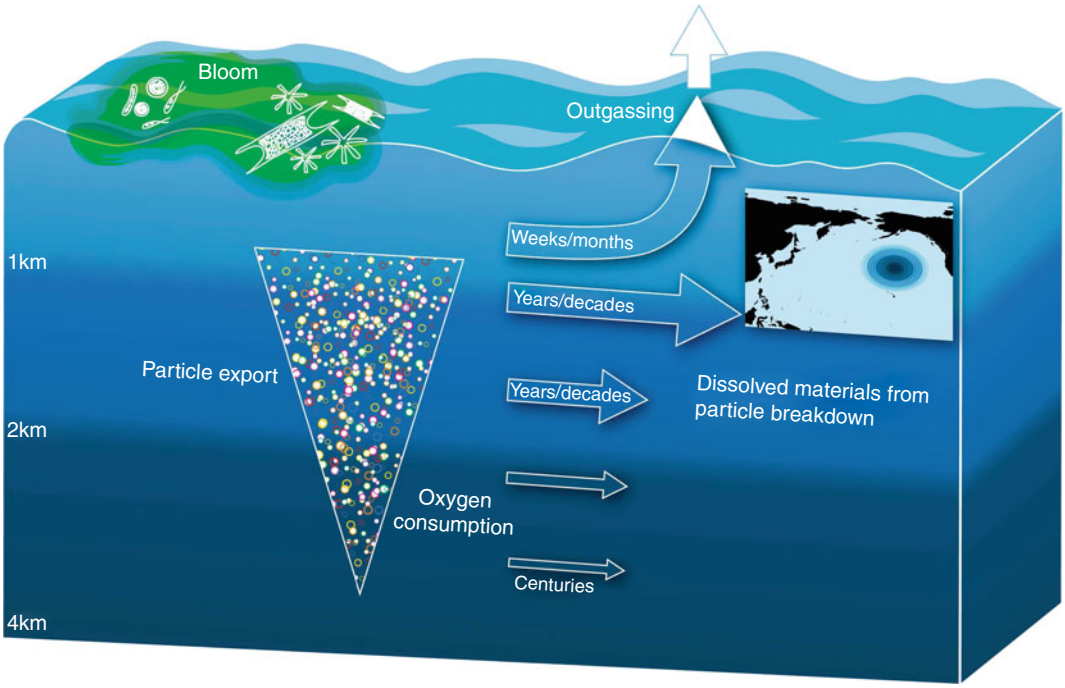

Ocean Fertilization for Sequestration of Carbon Dioxide from the Atmosphere. Figure 8
Vertical (i.e., particle settling and remineralization) and horizontal (ocean circulation) transport processes over a range of timescales affect the fate of biologically fixed carbon in the ocean. The inset map of the NE Pacific denotes the likely initial size of commercial OIF as they would have to be large if they were to have any biogeochemical effect whatsoever [58]. The concentric rings represent the rapid spreading of the perturbed ocean waters due to ocean circulation, with major ramifications for detection and attribution issues (see main text)

length scale of scientific OIF studies (10 km) and are derived from global and basins scale circulation models with embedded biogeochemistry [52–54]. One such side effect would be the potential removal (termed "nutrient robbing" [35]) of much of the northward supply of plant macronutrients from the Southern Ocean to the N hemisphere [53, 54]. The S Ocean is reported to supply around 75% of the macronutrients which drive the productivity of waters – and hence of fisheries – in the N hemisphere [59]. Another potential side effect that has until recently been overlooked is that of OIF resulting in ocean acidification of the ocean's interior due to the purposeful increase in net carbon storage in the deep ocean [60]. In a recent ranking [17], due to the lack of detailed information, geoengineering schemes which had biological aspects such as OIF were ranked as more complex with more unknowns and hence less safe and with the likelihood of more side effects relative to schemes that were based on geochemical or physical–chemical foundations only.

If geoengineering schemes are to be applied, then they must be rapid and effective as it is thought that the time to mitigate climate change is short [61–63] – of the order of decades. However, based on the sustained OIF of the Southern Ocean over millennia in the geological past – it appears that at best OIF would have a mitigation rate of the order of 80 ppmv/millennia [55], which is several orders of magnitude too slow, relative to one of the stabilization wedges of 1 gT C proposed by Paccala and Soccolow [63] to mitigate rising atmospheric carbon dioxide concentrations on a timescale of decades.

A further important criterion, given the lack of pilot studies of trials of potential geoengineering schemes by the private sector, is what happens if some previously unknown and deleterious side effect(s) becomes apparent shortly after an ocean basin scale pilot study and/or

scheme has commenced. How rapidly can such a scheme be shut down – what is the timescale for emergency stop? (Fig. 7). Again, due to the lack of information, on key issues such as what is the fate of the added iron – is it rapidly recycled or does it sink out – perhaps the best proxy to differentiate between a wide range of terrestrial, atmospheric, and oceanic reservoirs is the residence time in them [17]. This is relatively short for the atmosphere relative to the ocean and so suggests that oceanic schemes may well have longer emergency stop times – which would put them at a disadvantage when ranking with other schemes.

The detection of increased carbon sequestration and its attribution to purposeful OIF is not trivial [13, 58] (Fig. 8). Such detection and attribution issues are also pertinent to side effects such as the inadvertent production of other biogenic gases that are climate reactive [58]. There are also issues with increased anoxia in ocean waters [50] that could confound or mask detection and attribution of any decrease in dissolved oxygen due to OIF [13]. Detection of large-scale changes in ocean biogeochemical signatures such as in the concentrations of biogenic gases must overcome a wide range of hurdles, including the dynamic nature of the ocean, where large volumes of waters are rapidly transported both laterally and vertically [64]. Any such changes due to geoengineering must also be detected over and above other concurrent changes to the oceanic environment, such as by climate variability, and climate change [58]. Clearly, detection and attribution issues will help to frame the development of policy on geoengineering [50].

Conclusions and Future Directions

- *"The histories of the scientific and commercial interests in ocean iron fertilization (OIF) are intimately connected—co-evolving and transforming over time* [13]."

OIF is perhaps unique within the fledgling geoengineering debate, in that 13 relatively large-scale (10 km length scale) scientific research experiments have been conducted into better understanding the role of altering iron supply on paleoclimate, and how iron supply influences ocean ecosystems and in turn ocean biogeochemistry. The results from these experiments also have value for a wide range of disciplines surrounding geoengineering from policy formulation to implementation. For example, the results of these experiments point to a wide range of inextricably linked changes in ocean physics, chemistry, biology, and ecology that have both anticipated (increased productivity) and unforeseen (ocean acidification) consequences. The dynamic nature of the perturbed regions of ocean, and their interactions with surrounding waters, raises issues about implementing larger-scale schemes and in tracking such perturbed waters to both assess whether any additional carbon has been sequestered, and also if any chemical or biological side effects that might offset any additional carbon sequestration have occurred. Taken together, this research forms a body of rigorously conducted and communicated science that is indicative of the need to apply the precautionary principle when considering any future development of policy both into regulating future research into OIF and legislating any pilot bio-geoengineering schemes.

Bibliography

Primary Literature

1. Volk T, Hoffert MI (1985) The Carbon Cycle and Atmospheric CO_2, Archean to Present. AGU Geophysical Monograph 32. Sundquist ET, Broecker WS (eds). Am Geophys Union, Washington, DC, pp 99–110
2. Denman KL, Hofmann EE, Marchant H (1996) Marine biotic responses to environmental change and feedbacks to climate. In: Houghton JT, Meira Filho LG, Callander BA, Kattenberg A, Maskell K (eds) Climate change 1995. IPCC/Cambridge University Press, Cambridge, pp 483–516
3. Lovelock JF, Rapley CG (2007) Ocean pipes could help the Earth to cure itself. Nature 449:403
4. White A, Björkman K, Grabowski E, Letelier R, Poulos S, Watkins B, Karl D (2010) An open ocean trial of controlled upwelling using wave pump technology. J Atmos Oceanic Technol 27:385–396
5. Oschlies A, Pahlow M, Yool A, Matear RJ (2010) Climate engineering by artificial ocean upwelling: channelling the sorcerer's apprentice. Geophys Res Lett 37:L04701. doi:10.1029/2009GL041961
6. Rees AP, Law CS, Woodward EMS (2006) High rates of nitrogen fixation during an in situ phosphate release experiment in the Eastern Mediterranean Sea. Geophys Res Lett 33:L10607
7. Karl DM, Letelier RM (2008) Nitrogen fixation enhanced carbon sequestration in low nitrate, low chlorophyll seascapes. Mar Ecol Prog Ser 364:257–268
8. Mills MM, Ridame C, Davey M, La Roche J, Geider RJ (2004) Iron and phosphorus co-limit nitrogen fixation in the eastern tropical North Atlantic. Nature 429:292–294
9. Petit JR, Jouzel J, Raynaud D, Barkov NI et al (1999) Climate and atmospheric history of the past 4,20,000 years from the Vostok ice core, Antarctica. Nature 399:429–436

10. Toggweiler JR, Russell JL, Carson S (2006) Midlatitude westerlies, atmospheric CO_2, and climate change during the ice ages. Paleoceanography 21:PA2005. doi:10.1029/2005PA001154
11. Stephens BB, Keeling RF (2000) The influence of Antarctic sea ice on glacial-interglacial CO_2 variations. Nature 404: 171–174
12. Martin JH (1990) Glacial–interglacial CO_2 change: the iron hypothesis. Paleoceanography 5:1–13
13. Strong AL, Cullen JJ, Chisholm SW (2009) Ocean fertilization: reviewing the science, policy, and commercial activity and charting a new course forward. Oceanography 22(3):236–261
14. Martin JH, Fitzwater SE, Gordon RM (1990) Iron deficiency limits phytoplankton growth in Antarctic waters. Glob Biogeochem Cycles 4:5–12
15. Markels M, Barber R (2001) Sequestration of CO2 by ocean fertilization. Paper presented at the first national energy and technology laboratory conference on carbon sequestration, Washington, DC
16. Schiermeier Q (2003) Climate change: the oresmen. Nature 421:109–110. doi:10.1038/421109a
17. Boyd PW (2008) Ranking geo-engineering schemes. Nat Geosci 1:722–724
18. de Baar HJW, Boyd PW, Coale KH, Landry MR et al (2005) Synthesis of iron fertilization experiments: from the Iron Age in the Age of Enlightenment. J Geophys Res 110:C09S16
19. Boyd PW, Jickells T, Law CS, Blain S et al (2007) Mesoscale iron enrichment experiments 1993–2005: synthesis and future directions. Science 315:612–617
20. Gordon RM, Johnson KS, Coale KH (2009) The behavior of iron and other trace elements during the IronEx-I and PlumEx experiments in the Equatorial Pacific. Deep Sea Res I 56:1230–1241. doi:10.1016/j.2009.01.010
21. Blain S, Quéguiner B, Armand L, Belviso S et al (2007) Effects of natural iron fertilisation on carbon sequestration in the Southern Ocean. Nature 446:1070–1074
22. Pollard R, Sanders R, Lucas M, Statham P (2007) The Crozet natural iron bloom and export experiment (CROZEX). Deep Sea Res II 54:1905–1914
23. Charlson RJ, Lovelock JE, Andreae MO, Warren SG (1987) Oceanic phytoplankton, atmospheric sulfur, cloud albedo and climate. Nature 326:655–661
24. Turner SM, Harvey MJ, Law CS, Nightingale PD, Liss PS (2004) Iron-induced changes in oceanic sulfur biogeochemistry. Geophys Res Lett 31:L14307
25. Levasseur M, Scarratt MG, Michaud S, Merzouk A et al (2006) DMSP and DMS dynamics during a mesoscale iron fertilization experiment in the Northeast Pacific. I: temporal and vertical distributions. Deep Sea Res II 53:2353–2369
26. Wingenter OW, Haase KB, Strutton P, Friederich G, Meinardi S, Blake DR, Rowland FS (2004) Changing concentrations of CO, CH_4, C_5H_8, CH_3Br, CH_3I, and dimethyl sulfide during the Southern Ocean Iron Enrichment Experiments. Proc Natl Acad Sci U S A 101:8537. doi:10.1073
27. LeClainche Y, Levasseur M, Vézina A, Bouillon RC et al (2006) Modeling analysis of the effect of iron enrichment on dimethyl sulfide dynamics in the NE Pacific (SERIES experiment). J Geophys Res 111:C0101
28. Law CS (2008) Predicting and monitoring the effects of largescale ocean iron fertilization on marine trace gas emissions. Mar Ecol Prog Ser 364:283–288
29. Law CS, Ling RD (2001) Nitrous oxide fluxes in the Antarctic Circumpolar Current, and the potential response to increased iron availability. Deep Sea Res II 48:2509–2528
30. Jin X, Gruber N (2003) Offsetting the radiative benefit of ocean iron fertilization by enhancing N2O emissions. Geophys Res Lett 30(24):2249
31. Boyd PW, Law CS (2001) The Southern Ocean Iron RElease Experiment (SOIREE) – introduction and summary. Deep-Sea Research II 48:2425–2438
32. Manizza M, LeQuere C, Watson AJ, Buitenhuis ET (2008) Ocean biogeochemical response to phytoplankton-light feedback in a global model. J Geophys Res 113:C10010. doi:10.1029/2007JC004478
33. Trick CG, Cochlan WP, Wells ML, Trainer VL, Pickell LD (2010) Iron enrichment stimulates toxic diatom production in high-nitrate, low-chlorophyll areas. PNAS. doi:/pnas.0910579107
34. Takeda S, Tsuda A (2005) An in situ iron-enrichment experiment in the western subarctic Pacific (SEEDS): introduction and summary. Prog Oceanogr 64:95–109
35. Geoengineering the climate: science, governance and uncertainty (2009) UK Royal Society report. RS Policy document 10/09, September 2009 RS 1636. ISBN 978-0-85403-773-5
36. Hall JA, Safi K (2001) The impact of in situ Fe fertilisation on the microbial food web in the Southern Ocean. Deep Sea Res 48:11–12
37. Boyd PW, Watson A, Law CS, Abraham E, Trull T, Murdoch R, Bakker DCE, Bowie AR, Charette M, Croot P, Downing K, Frew R, Gall M, Hadfield M, Hall J, Harvey M, Jameson G, La Roche J, Liddicoat M, Ling R, Maldonado M, McKay RM, Nodder S, Pickmere S, Pridmore R, Rintoul S, Safi K, Sutton P, Strzepek R, Tanneberger K, Turner S, Waite A, Zeldis J (2000) A mesoscale phytoplankton bloom in the polar Southern Ocean stimulated by iron fertilization. Nature 407:695–702
38. Abraham ER, Law CS, Boyd PW, Lavender SJ, Maldonado MT, Bowie AR (2000) Importance of stirring in the development of an iron-fertilised phytoplankton bloom. Nature 407:727–730
39. Boyd PW (2004) Ironing out algal issues in the Southern Ocean. Science 304:396–397
40. Boyd PW, Jackson GA, Waite AM (2002) Are mesoscale perturbation experiments in polar waters prone to physical artefacts? Evidence from algal aggregation modelling studies. Geophys Res Lett 29(11):1541. doi:10.1029/2001GL014210
41. Martin JH, Coale KH, Johnson KS, Fitzwater SE et al (1994) Testing the iron hypothesis in ecosystems of the equatorial Pacific Ocean. Nature 371:123–129
42. Bidigare RR, Hanson KL, Buesseler KO, Wakeham SG, Freeman KH, Pancost RD, Millero FJ, Steinberg P, Popp BN, Latasa M, Landry MR, Laws EA (1999) Iron-stimulated changes in 13C fractionation and export by equatorial Pacific phytoplankton. Paleoceanography 14(5):589–595

43. Boyd PW, Law CS, Wong CS, Nojiri Y et al (2004) The decline and fate of an iron-induced sub-arctic phytoplankton bloom. Nature 428:549–552
44. Boyd PW, Strzepek R, Takeda S et al (2005) The evolution and termination of an iron-induced mesoscale bloom in the northeast subarctic Pacific. Limnol Oceanogr 50: 1872–1886
45. Buesseler KO (1991) Do upper-ocean sediment traps provide an accurate record of particle flux? Nature 353:420–423
46. Buesseler KO, Michaels AF, Siegel DA, Knap AH (1994) A three dimensional time-dependent approach to calibrating sediment trap fluxes. Glob Biogeochem Cycles 8(2):179–193
47. de Baar HJW, Gerringa L, Laan P, Timmermans K (2008) Efficiency of carbon removal per added iron in ocean iron fertilization. Mar Ecol Prog Ser 364:269–282
48. Chever F, Sarthou G, Bucciarelli E, Blain S, Bowie AR (2010) An iron budget during the natural iron fertilisation experiment KEOPS (Kerguelen Islands, Southern Ocean). Biogeosciences 7:455–468
49. Wolff EW, Fischer H, Fundel F, Ruth U et al (2006) Southern Ocean sea-ice extent, productivity and iron flux over the past eight glacial cycles. Nature 440:491–496
50. Boyd PW (2009) Geopolitics of geoengineering in focus: carbon sequestration. Nat Geosci 2:812. doi:10.1038/ngeo710
51. Lenton TM, Vaughan NE (2009) The radiative forcing potential of different climate . . .. Discuss 9:2559–2608. doi:10.5194/acpd-9-2559-2009
52. Denman K (2008) Climate change, ocean processes, and iron fertilization. Mar Ecol Prog Ser 364:219–225
53. Gnanadesikan A, Sarmiento JL, Slater RD (2003) Effects of patchy ocean fertilization on atmospheric carbon dioxide and biological production. Glob Biogeochem Cycles 17:1050
54. Gnanadesikan A, Marinov I (2008) Export is not enough: nutrient cycling and carbon sequestration. Mar Ecol Prog Ser 364:289–294
55. Boyd PW (2008) Implications of large-scale iron fertilization of the oceans – introduction and synthesis. Mar Ecol Prog Ser 364:213–218
56. Markels M Jr, Barber RT (2001) Sequestration of carbon dioxide by ocean fertilization. Paper presented at the 1st Nat Conf on carbon sequestration, Natl Energy Technol Lab, Washington, DC, 14–17 May 2001
57. Lam PJ, Chisholm SW (2002) Iron fertilization of the oceans: reconciling commercial claims with published models. White Paper available at: http://web.mit.edu/chisholm/www/publications/fefert.pdf
58. Cullen JJ, Boyd PW (2008) Predicting and verifying the intended and unintended consequences of large-scale ocean iron fertilization. Mar Ecol Prog Ser 364:295–301
59. Sarmiento JL, Simeon J, Gnanadesikan A, Gruber N, Key RM, Schlitzer R (2007) Deep ocean biogeochemistry of silicic acid and nitrate. Glob Biogeochem Cycles 21:GB1S90. doi:10.1029/2006GB002720
60. Lao L, Caldeira K (2010) Can ocean iron fertilization mitigate ocean acidification. Clim Change 99:303–311
61. Stern N (2007) The economics of climate change. Cambridge University Press, Cambridge
62. Mignone BK, Socolow RH, Sarmiento JL, Oppenheimer M (2008) Atmospheric stabilization and the timing of carbon mitigation. Clim Change 88(3–4):251–265
63. Pacala S, Socolow R (2004) Stabilization wedges: solving the climate problem for the next 50 years with current technologies. Science 305:968–972
64. Fujii M, Yoshie N, Yamanaka Y, Chai F (2005) Simulated biogeochemical responses to iron enrichments in three high nutrient, low chlorophyll (HNLC) regions. Prog Oceanogr 64:307–324
65. Chisholm SW (2000) Stirring times in the Southern Ocean. Nature 407:685–687

Books and Reviews

Boyd PW (2008) MEPS thematic section. Implications of large-scale iron fertilization of the oceans. Mar Ecol Prog Ser 364:203–309

Buesseler KO, Doney SC, Karl DM, Boyd PW et al (2008) Ocean iron fertilization—moving forward in a sea of uncertainty. Science 319:162

Chisholm SW, Morel FMM (1991) What controls phytoplankton production in nutrient-rich areas of the open sea?. Limnol Oceanogr Preface Vol 36

Chisholm SW, Falkowski PG, Cullen JJ (2001) Dis-crediting ocean fertilization. Science 294:309–310

Glibert PM, Azanza R, Burford M, Furuya K et al (2008) Ocean urea fertilization for carbon credits poses high ecological risks. Mar Pollut Bull 56(6):1049–1056

IPCC (2001) Climate change 2001: the scientific basis. Contribution of working group I to the third assessment report of the Intergovernmental Panel on Climate Change. Cambridge University Press, Cambridge and New York

Johnson KS, Karl DM (2002) Is ocean fertilization credible and creditable? Science 296:467–468

Keith DW, Dowlatabadi H (1992) A serious look at geoengineering. Eos Trans AGU 73:289–293

Keith DW, Ha-Duong M, Stolaroff JK (2005) Climate strategy with CO2 capture from the air. Clim Change 74:17–45

Kintisch E (2007) Should we study geoengineering? A science magazine panel discussion. Science 318:1054–1055

London Convention (2007) Statement of concern regarding iron fertilization of the oceans to sequester CO2. LC-L P1(C): irc14, available at: http://www.imo.org/includes/blastData.asp/doc_id=8272/14.pdf. 13 July, 2007

Tortell PD (2005) Small-scale heterogeneity of dissolved gas concentrations in marine continental shelf waters. Geochem Geophys Geosyst 6:Q11M04

Walter S, Peeken I, Lochte K, Webb A, Bange HW (2005) Nitrous oxide measurements during EIFEX, the European Iron Fertilization Experiment in the subpolar South Atlantic Ocean. Geophys Res Lett 32:L23613

Zeebe RE, Archer D (2005) Feasibility of ocean fertilization and its impact on future atmospheric CO2 levels. Geophys Res Lett 32:L09703

Ocean Observatories and Information: Building a Global Ocean Observing Network

O. Schofield[1], S. M. Glenn[1], M. A. Moline[2], M. Oliver[3], A. Irwin[4], Y. Chao[5], M. Arrott[6]
[1]Coastal Ocean Observation Lab, Institute of Marine and Coastal Sciences, School of Environmental and Biological Sciences, Rutgers University, New Brunswick, NJ, USA
[2]Center for Marine and Coastal Sciences, California Polytechnic State University, San Luis Obispo, CA, USA
[3]School of Marine Science and Policy, College of Earth, Ocean and Environment, University of Delaware, Lewes, DE, USA
[4]Mount Allison University, Sackville, NB, Canada
[5]Jet Propulsion Laboratory, Pasadena, CA, USA
[6]Scripps Institution of Oceanography & Calit2, University of California at San Diego, La Jolla, CA, USA

Article Outline

Glossary
Definition of the Subject and Its Importance
Introduction
Future Directions
Bibliography

Glossary

Ocean observatory A collection of platforms that collect data over a range of spatial and temporal scales.

Definition of the Subject and Its Importance

Ocean observatories are collections of networks of sensors that are deployed to sample the ocean physics, chemistry, and biology. The goal of these networks is to overcome chronic undersampling of the oceans by providing sustained measurements in space and time. The data collected by these networks are used to address a range of basic and applied research questions, hindered by a lack of data. The ocean observatories represent collections of platforms capable of collecting data over a range of scales. The platforms include ships, satellites, radars, and a range of Lagrangian systems. Data from the individual platforms are aggregated by sophisticated cyberinfrastructure software systems, which when combined with global communications allow for two-way communication between the shoreside personnel and the networks that can be deployed anywhere in the world. This two-way communication allows the networks to be adaptively configured to improve sampling of specific processes. The maturation of these systems comes at a fortuitous time as the oceans are increasingly showing evidence of changes in the physics, chemistry, and biology over the last few decades. Understanding those changes will require the data collected by the ocean observatories.

Introduction

The Need for a Global Ocean Observing Network

The oceans cover the majority of Earth's surface, and despite centuries of human exploration, the oceans remain relatively unexplored. Oceanographers have historically collected data on the ocean and the seafloor from ships during cruises of limited duration. This expeditionary research approach has resulted in major advances that span understanding global ocean circulation, the energy associated with mesoscale circulation [1–4], plate tectonics (cf. [5]), global ocean productivity [6–8], and climate-ocean coupling [9–11]. These and many other successes have expanded our view of the role of ocean processes on Earth, and have demonstrated a need for sustained sampling spanning temporal and spatial scales that are not effectively carried out using ships. Filling these informational gaps will require the oceanographic community to develop new modes of sampling the oceans. Developing these new approaches is urgent, as data collected over the last few decades show that in many regions of the ocean the physics, chemistry, and biological properties are exhibiting significant change.

The observed changes in the oceans over the last few decades span from local scales (kilometers) to global effects operating over a wide range of spatial and temporal scales (Fig. 1). These changes reflect both natural cycles and increasingly reflect human activity, which now plays a significant role in structuring the world's oceans. Local changes include alterations in circulation, increased introduction of point source concentrations of macro- and micronutrients,

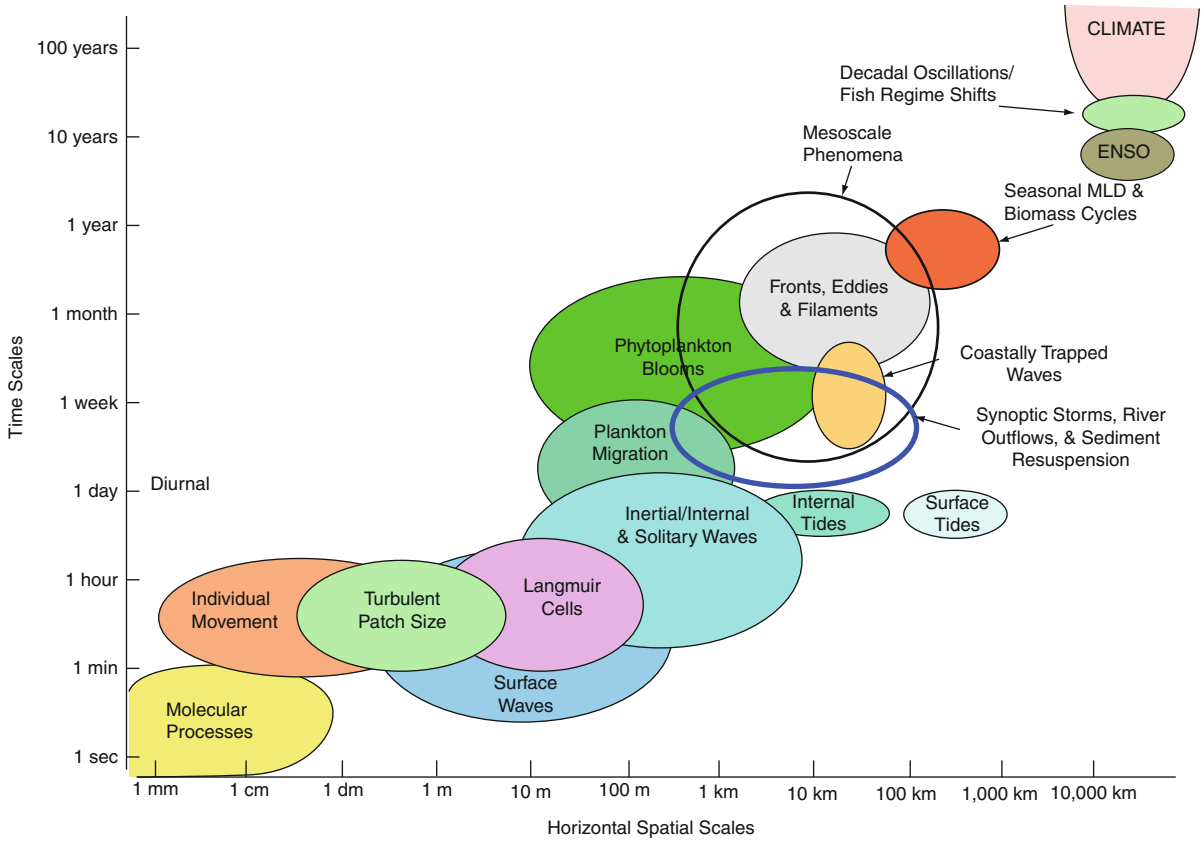

Ocean Observatories and Information: Building a Global Ocean Observing Network. Figure 1
A stommel diagram showing the range of spatial and temporal scales over which ocean processes operate. The figure was constructed by Tommy Dickey and is published with his permission

transport of pollutants to the sea, the introduction of invasive species, associated pressures of aquaculture efforts, and altered food web dynamics due to the overexploitation of commercially valuable species. These local features are embedded within regional and global scale changes. These large-scale changes include altered physical (temperature, salinity, sea level height), chemical (oxygen, pH, nutrients), and biological properties (fishing out of top predators).

Quantitatively understanding the relative role of natural and anthropogenic forcing of the ocean is a paramount challenge for oceanography. The urgency will only increase as in the next 20 years as anthropogenic environmental impacts associated with humans are expected to increase. This reflects the growth human populations [12] with current projections predicting the human population will reach ten billion by 2040. This will be especially prominent at the coastlines, which are predicted to show the largest population increases [13]. This will require a thorough understanding of ocean processes, which will be used to improve human health and safety, promote economic vitality, and provide the tools for sustainable environmental stewardship. These needs will require an improved fundamental understanding of the oceans.

Given the need for a quantitative understanding of the oceans, the ocean science community is fortunate to be poised to take advantage of many technical advances. These advances include a diverse set of new platforms capable of carrying sensors for sustained periods of time and the maturation of cyberinfrastructure tools that can link distributed individual observing networks to form a "system of systems." These components will provide the foundation for an international global ocean observing network. In this

entry, we will outline the developments and, where appropriate, provide specific examples of how the data will be used.

Design Considerations for Building an Ocean Observing Network

Ocean observing networks are designed to address a specific need, which is used to define the required sampling resolution in space and time. Defining the appropriate scales can be a difficult problem as many large-scale (thousands of kilometers), long period (annual-to-interannual) processes are determined by small-scale, short-period variations in atmospheric forcing, and small-scale, relatively short-lived, oceanic processes [14–18]. As highlighted by Munk [19], 95% of the oceanic kinetic energy is associated with meso-scale currents having time and space scales less than about 100 days and 100 km. Other forcing factors can operate over inertial or diurnal time scales [17]; therefore, a comprehensive understanding of the oceans will require nested sampling capable of resolving the feedbacks between processes operating over different scales. This generally requires a multiplatform strategy as each system samples a specific time and space domain (Fig. 2). Once the sampling requirements have been defined, it is possible to choose (1) the appropriate platforms, (2) the required measurements, (3) the data latency needs for a particular observatory, and (4) the funds available for construction. The costs generally increase with the flexibility of the system (Fig. 3). Increased power on a platform allows for greater flexibility in carrying a wider range of sensors.

As ocean infrastructure is expensive, most large infrastructure networks must often be able to address a range of basic research and applied science needs to justify the investment. Historically, basic and applied research efforts are often treated as separate enterprises; however, major issues confronting the ocean science communities reveal numerous commonalities that reflect the chronic undersampling of the oceans. Both applied and basic science require information on the physical hydrography, circulation, biological, and chemical properties; however, it is often the real-time availability of data that defines its utility for applied science where data are used to meet real-time needs such as weather forecasting, search and rescue, and national security. When available, however, real-time information has a great deal of utility as

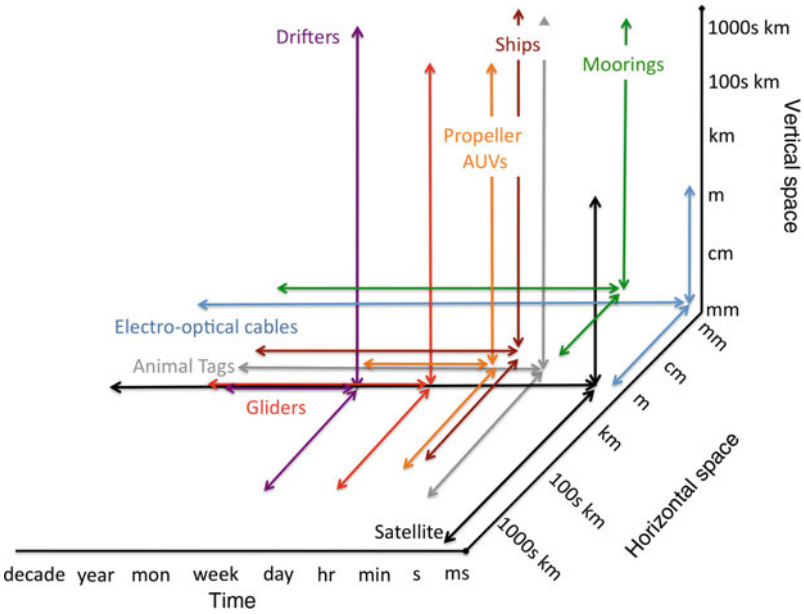

Ocean Observatories and Information: Building a Global Ocean Observing Network. Figure 2
The time and space sampling capabilities of different ocean platforms. The different colors represent different platforms

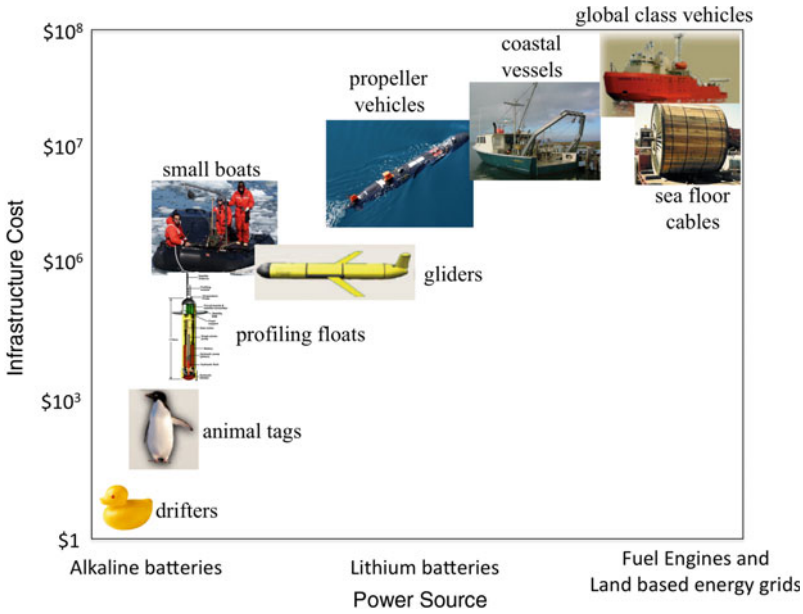

Ocean Observatories and Information: Building a Global Ocean Observing Network. Figure 3
The range of cost and power for a range of ocean sampling platforms

scientists use the information to optimize adaptive sampling techniques.

Platforms Available for Ocean Observing Networks

A range of platforms available for building ocean observing networks are described. Note that the list is not exhaustive, but reflects the major pieces of infrastructure widely used by the community today and form the observational backbone of the major ocean observing efforts. For this entry, we focus on physical systems that collect data about the ocean and do not discuss numerical models.

Ships. The primary tool for oceanographers for centuries has been ships and despite significant advances in new technologies (see below), ships will remain a central piece of infrastructure for the foreseeable future [18]. In the last decade, the range of ships available to the oceanographic community has grown with an expanding set of global class vessels being complemented with smaller, capable, coastal vessels. The increasing interdisciplinary needs have resulted in significant upgrades in the capabilities of the ships with improved capabilities in the dynamic positioning and station holding, multi-beam and side-scan sonar systems, and more complex sensors and instrumentation becoming routine tools when at sea.

Satellites. Satellites constitute the most important oceanographic technology innovation in modern times [19]. Satellite observations have resulted in numerous advances in our fundamental understanding of the oceans [20] by resolving both global features associated with the mesoscale circulation of physical and biological properties. It is the fundamental tool for understanding myriad ocean processes and land–air–sea interactions over decadal time scales. Satellite data are fundamental to weather and ocean state prediction. The data have revealed new phenomena over critical space and time scales that were previously inaccessible using only data from in situ observing systems. Physical parameters available from space-based sensors provide information on ocean surface temperature, wind speed and direction, sea surface height and topography, and sea ice distribution and thickness. Biogeochemical parameters are derived from ocean color radiometers (pigment concentration, phytoplankton functional groups, size distribution, particle concentration, colored dissolved organic material). A range of methods that include active scatterometry, microwave array spectrometers, microwave imagers, multi-beam

altimetric lidars, altimeters, and advanced gravity missions collect these observations. The coverage provided by a satellite is dependent on its orbit. Currently most environmental satellites are polar-orbiting, covering the whole globe over a period of days. These global maps can be complemented by geostationary satellites that can map the same area of the ocean several times a day, allowing one to resolve the temporal changes such as tidal effects or river plumes. These geostationary satellites are particularly important when monitoring episodic events required for many applied efforts such as monitoring hurricanes and/or oil spills.

The significant time required and high cost of deploying satellites has focused efforts on expanding the utility of existing platforms. These approaches include the development of new algorithms. These new algorithms have focused on objectively defining water masses ([21, 22], Fig. 4), deriving biological rate processes [23, 24], estimating nutrient concentrations [25], and mapping ocean salinity [26–28]. Algorithms are also being developed to allow the satellites to adaptively sample the ocean. This approach has been demonstrated with the scientists re-tasking the satellite to spotlight a region [29]. As flexibility in networks increases, these approaches are likely to become more common.

High Frequency Radar. High frequency radar is a technology for measuring ocean surface current velocities over hundreds of square miles simultaneously (Fig. 5). The systems can provide data on approximately hourly time scales and can collect data out to about 125 miles (200 km) from shore (Fig. 4). The HF radar systems can resolve spatial scales of about 1–10 km, unaffected by clouds, fog, or precipitation. This technology uses low-power transmitters and small stationary antennas that are relatively simple to deploy. Each site measures the radial components of the ocean surface velocity directed toward or away from the site [30–32] and the estimated velocity components allow surface currents (upper meter of water column) to be estimated [33]. These systems are cost-effective and currently much of the coastal zone is now sampled using this technology.

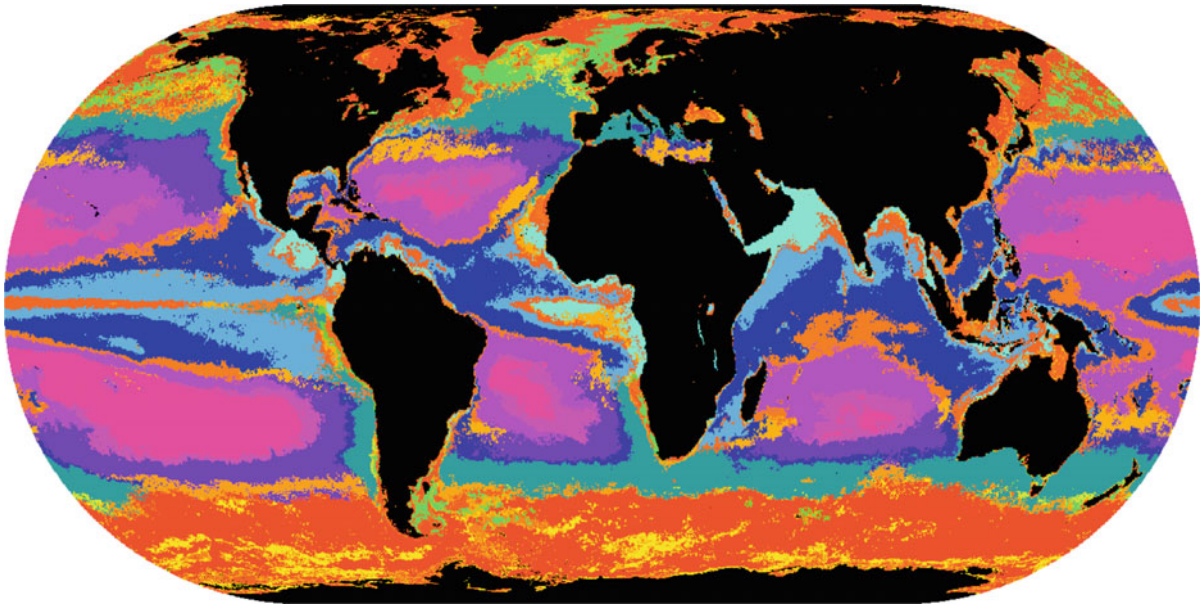

Ocean Observatories and Information: Building a Global Ocean Observing Network. Figure 4
A global map of the major ocean biomes as determined using an objective mapping algorithm [22]. The map was created by combining sea surface temperature maps with ocean color imagery, and provides a means to discriminate the major water masses by combining all available satellite remote sensing technologies. Each color represents a distinct water mass

HF radar provides a good example of a dual use technology. For example, HF Radar measures the movement of oceanic events like the winds in the atmosphere provide information about where and when weather systems occur (Fig. 5). The dynamic movements of the ocean and atmosphere are also used to determine where pollutants, man-made or natural, will travel. Modern weather now casts and forecasts generated by NOAA's National Weather Service depend on the thousands of critical wind measurements collected worldwide each hour, mostly from land and satellite-based sensors. In the coming decade, coastal managers will use HF radar data to measure the ocean current speed and direction to track plumes (rivers, pollution, oil), assist in coast guard search and rescue (SAR), assist in marine navigation, define shipping tracks and temporary anchorages offshore ports, and track the transport of harmful algal blooms. One specific example is the US Coast Guard, which currently ingests surface current data from high frequency radar sites into its SAR operations along the Mid-Atlantic coast, which has a mature HF radar network. It is estimated that if HF radar is deployed in all US coastal waters would save an additional 26–45 more lives annually and reduce the $30 M per year currently spent on rescue flights (http://ioos.gov/library/sarops_data_sources_uncert_nov2006.pdf).

Ocean Moorings. The modern ocean moorings grew out of the weather stations established in the 1940s. Since the 1960s modern buoys have enabled a wide range of studies addressing the ocean's role in climate, weather as well as providing insight into the biogeochemistry of the sea. Moorings provide the backbone to many of the global ocean networks studying ocean–atmosphere interactions and are the foundation for the global tsunami warning system network. They will continue to be a key element of ocean observing infrastructure that provides high frequency fixed location data to supplement the spatial data collected by ships, autonomous underwater vehicles, and satellite remote sensing by providing subsurface data.

Seafloor Cables. Scientists often require high bandwidth and power for sustained periods of time. Seafloor electro-optic cables offer potential means for providing the sustained presence in the ocean. There have been two general strategies when deploying seafloor cables. Cables have been deployed off the east and west coasts of the United States and Canada, Hawaii, Japan, and Europe. These cables have successfully been used to study a wide range of topics which include seafloor seismicity [34, 35], tsunamis [36], seafloor dynamics [37], coastal upwelling (Fig. 6, [38]), ecosystem productivity [39], hydrological optics [40], ocean turbulence [41], sediment resuspension [42, 43], gas hydrates [44], marine boundary layer dynamics [45], bioluminescence [46, 47], and animal swimming behavior [48].

Drifters and Floats. Passive, autonomous, Lagrangian platforms have become an indispensable tool in creating surface and subsurface maps of ocean properties. These platforms are relatively inexpensive and thus allow thousands of these platforms to be deployed. Surface maps of ocean currents and ocean properties (temperature) have been collected using surface drifters. Drifters have historically been a key tool for oceanography as evidenced by the important works of Benjamin Franklin [49] and Irving Langmuir [50]. Improved communications have allowed thousands of drifters to be deployed. The drifters have evolved to carry numerous sensors, which have allowed them to create global maps of surface circulation at a relatively low cost [51].

The first neutrally buoyant floats were designed to observe subsurface currents [52]. The subsurface floats were greatly enhanced in the early 1990s with communication capabilities [53] and now anchor the international ARGO program, which has over 3,000 floats deployed in the ocean (Fig. 7, http://www.argo.ucsd.edu/). The subsurface ARGO network has been a critical tool for oceanography [55] and to date has resulted in over 750 publications since 1998 (http://www.argo.ucsd.edu/Bibliography.html). Publications span from mapping global ocean hydrography, trended changes in ocean properties, and ocean biogeochemistry.

Gliders. Rudnick et al. [56] provided a detailed overview of glider systems for scientific uses. Gliders are a type of autonomous underwater vehicle that use small changes in buoyancy in conjunction with wings to convert vertical motion to horizontal motion, and thereby propel itself forward with very low-power consumption. These are similar in concept to profiling floats (see above) with the exception of the wings. Gliders follow a sawtooth path though the water,

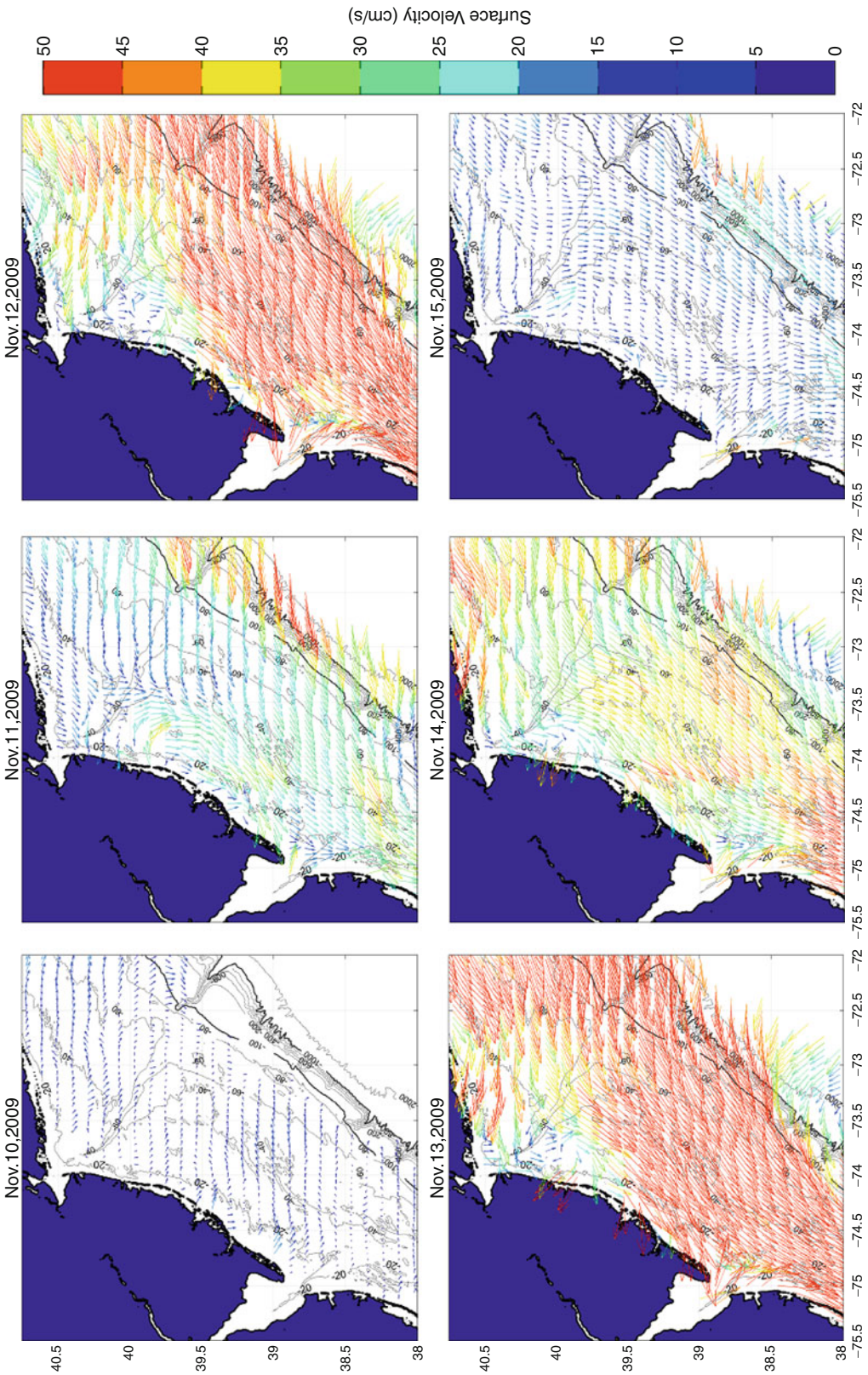

Ocean Observatories and Information: Building a Global Ocean Observing Network. Figure 5
The response of surface currents for the coastal waters offshore New Jersey (USA) due to the passage of a large coastal storm. The color of the surface current indicates the current velocity and the *arrows* indicate the direction of the current. The HF CODAR network was able to collect data throughout the storm when clouds interfered with remote sensing approaches and the violent waves would not allow for ship-based operations. Collecting data during such extreme events is of high importance to the ocean science community

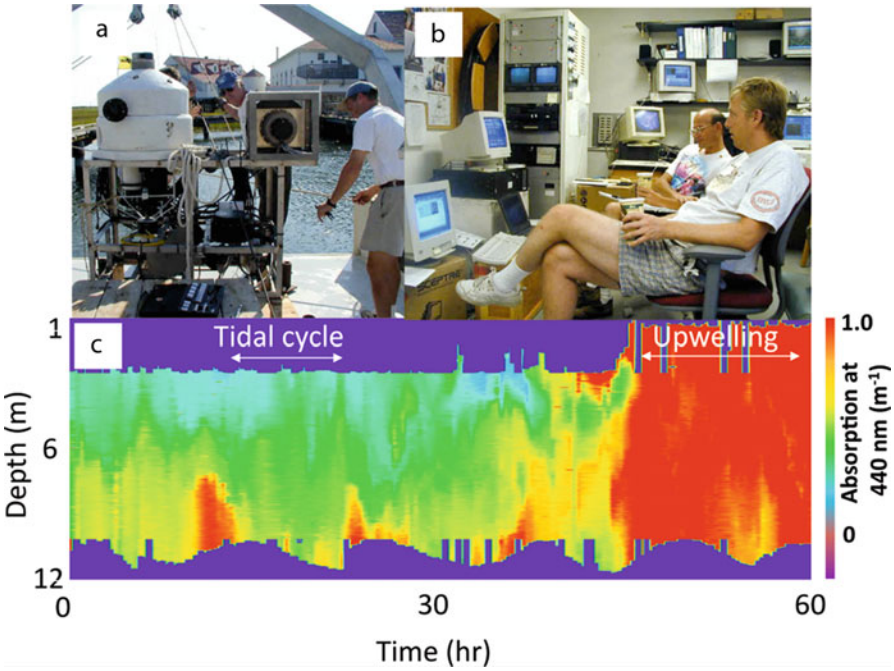

Ocean Observatories and Information: Building a Global Ocean Observing Network. Figure 6
Example of data collected by the Long term Ecosystem Observatory (LEO) which is located 5 km offshore the coast of New Jersey and is linked to shoreside laboratories via an electro-optical seafloor cable. (**a**) A profiling instrument node before being mounted to the LEO cable. (**b**) The shore side control center from where the profiler and instruments were controlled. The data was sent to shore in real time to scientists via the LEO cable. (**c**) Data collected during 60 h while continuously profiling the instrument package. The short time series represents over 600 vertical profiles. The data represents the absorption at 440 nm collected with a WetLabs absorption/attenuation meter. The high turbidity water (*red*) was associated with tidal outflows and with coastal upwelling

providing data on large temporal and spatial scales. They navigate with the help of periodic surface GPS fixes, pressure sensors, tilt sensors, and magnetic compasses. Using buoyancy-based propulsion, gliders have a significant range and duration, with missions lasting over half a year and over 3,500 km of range. There are currently three glider types [57–59] being used throughout the world's oceans (Fig. 8). Although the majority of gliders presently run on batteries, thermal-powered gliders, which take advantage of thermal gradients in the ocean, are being developed [59]. Gliders vary in the pressure, they are able to withstand but taken together, and they effectively sample waters depths from 10 to 3,300 m. The duration of the glider mission is variable and depends on (1) the type of battery used, (2) the number of sensors the gliders carry, and (3) the water column depths in which the glider is operating. Because these vehicles are designed for duration, they have limited power for sensors. The standard measurements currently on gliders include temperature, salinity, chlorophyll fluorescence, optical backscatter, bottom depth, and occasionally acoustic Doppler velocity and backscatter. By examining displacement between surface fixes, the vertically averaged absolute velocity can also be determined. The utility of gliders have demonstrated their value in collecting high resolution spatial datasets [60–67].

Propeller-driven AUVs are powered by batteries or fuel cells and can operate in water as deep as 6,000 m. AUVs can navigate by various means; inside a net of acoustic beacons, by position relative to a surface reference ship, or when operating completely autonomously, the AUV will surface and take its own GPS fix. Like gliders, AUVs relay data and mission information to shore via satellite. Between position fixes and for precise maneuvering, inertial navigation systems are

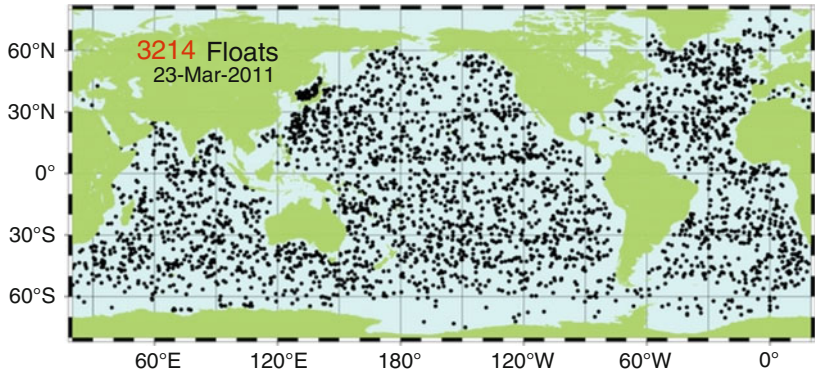

Ocean Observatories and Information: Building a Global Ocean Observing Network. Figure 7
The global distribution of ARGO profiling floats on March 23,2011. The floats are outfitted with sensors that measure temperature and salinity. A smaller number are outfitted with biogeochemical sensors [54]

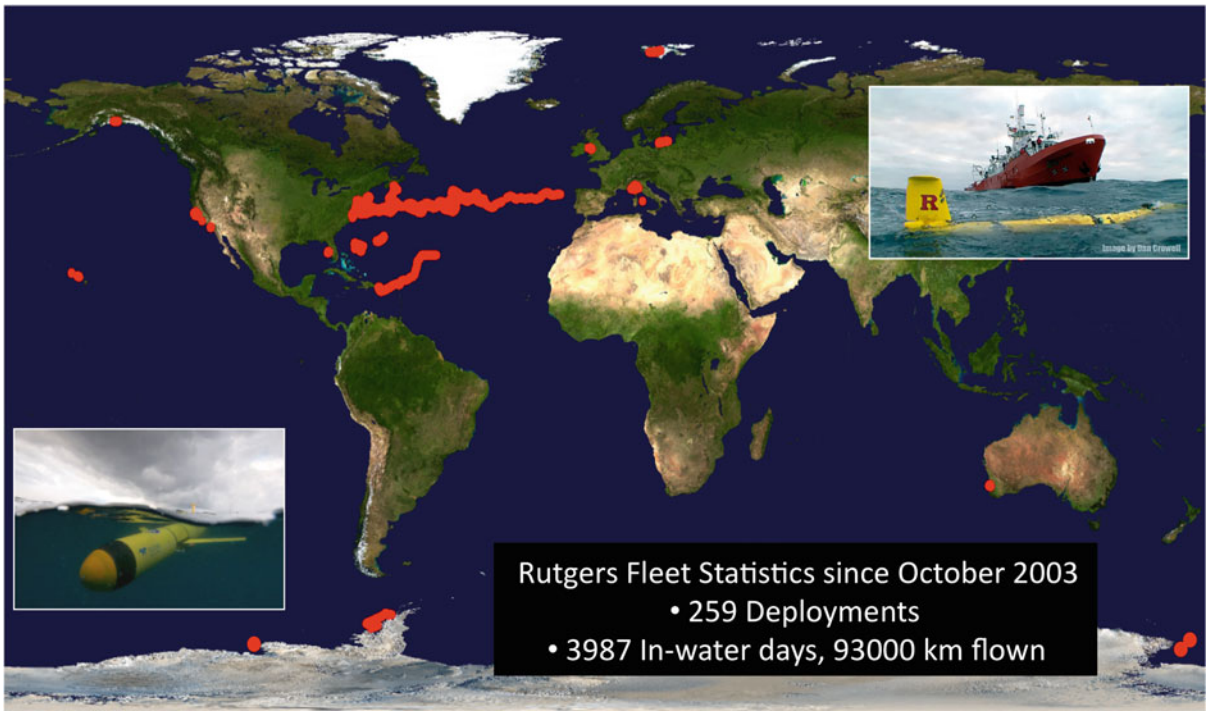

Ocean Observatories and Information: Building a Global Ocean Observing Network. Figure 8
Gliders are operated by individual laboratories and allow small groups to occupy a global presence at relatively low cost [29]. The figure shows the glider deployments conducted by Rutgers Coastal Ocean Observation Laboratory from October 2003 until February 2011. The missions represent almost 4,000 days at sea and the Rutgers glider fleet has flown 93,000 km underwater. Currently, there are over a dozen laboratories located throughout the world who maintain a similar sustained global glider presence at sea

often available onboard the AUV to measure the acceleration of the vehicle and, combined with Doppler velocity technology, is used to measure rate of travel. A pressure sensor measures the vertical position. AUVs, unlike gliders, can move against most currents nominally at 3–5 knots, and, therefore, can systematically and synoptically survey a particular line, area, and/or volume. This is particularly important for bottom surveys and operation near the coastline in areas hazardous to ships and small craft. The endurance of AUV systems depends on the size of the vehicle as well as the power consumption, but range from 6 to 40 h of operation under a single charge with ranges of 70–240 km over that period. The sensor payload is also dependent on the size of the vehicle (and battery capacity), with the standard array of sensors measuring, temperature, salinity, chlorophyll fluorescence, optical backscatter, bottom depth, and acoustic Doppler velocity and backscatter. Because of the additional power capacity of AUVs, numerous sensor suites have been integrated into AUVs and remain the primary autonomous platform for sensor development. Hundreds of different AUVs have been designed over the past 20 or so years. Blackwell et al. [68] provides an overview of the historical development of these vehicles.

Information Systems for Ocean Observatories

While the range of technologies available to oceanographers has been increasing over the last several decades, it is the availability of global communications and information technology that will allow these technologies to transform ocean sciences. Oceanographers have conducted experiments as either individuals or small groups within a single science focus at any given time; however, the broad scientific and civil demands for multidisciplinary and interdisciplinary research coupled with exponential growth in information technology are transforming oceanography. This history of working in small groups has resulted in the traditional data-centric cyberinfrastructure strategy, where typically a central data management system ingests data and serves them to users on a query basis. This approach is not sufficient to deal with the range of challenges that face ocean sciences.

Given this potential, the community is now dedicated to building the cyberinfrastructure that will be central to any global integrated ocean observing system. A modern cyberinfrastructure backbone will allow globally distributed scientists to operate as a community by aggregating data from individually deployed instruments for any experimental effort. If realized, this would allow anybody with access to the internet to utilize the global array of sensors to study any ocean process of interest.

Given the potential, ocean sciences are increasingly focused on building a system that will provide a comprehensive set of capabilities. Cyberinfrastructure systems must provide a comprehensive set of tools that include (1) end-to-end data preservation and access, (2) end-to-end, human-to-machine, and machine-to-machine control of how data are collected and analyzed, (3) direct, closed loop interaction of models with the data acquisition process, (4) virtual collaborations created on demand to drive data-model coupling and share ocean observatory resources (e.g., instruments, networks, computing, storage and workflows), (5) end-to-end preservation of the ocean observatory process and its outcomes, and (6) automation of the planning and prosecution of observational programs. Additionally the cyberinfrastructure systems must provide the required background messaging, governance, and service frameworks that facilitate interaction in a shared environment, similar to the role of the operating system on a computer. Such a system would provide a suite of tools capable of serving both basic and applied science simultaneously.

The potential of an interactive social network for the ocean sciences is in its infancy and the community is in the process of development and is conducting pilot experiments. One such example is the NSF Ocean Observatory Initiative (OOI), which has focused significant effort on developing a sophisticated cyberinfrastructure, that will link ocean observatories, computation, modeling, storage, and network infrastructure into a coherent system-of-systems. The software is also developing a web-based social network enabled by real-time visualization and access to model outputs to allow for adaptive sampling science.

One such example was a field experiment conducted in 2009, that allowed a distributed community of scientists to assess how well the software could aggregate data from ships, autonomous underwater vehicles (AUVs), shore-based radars, and satellites

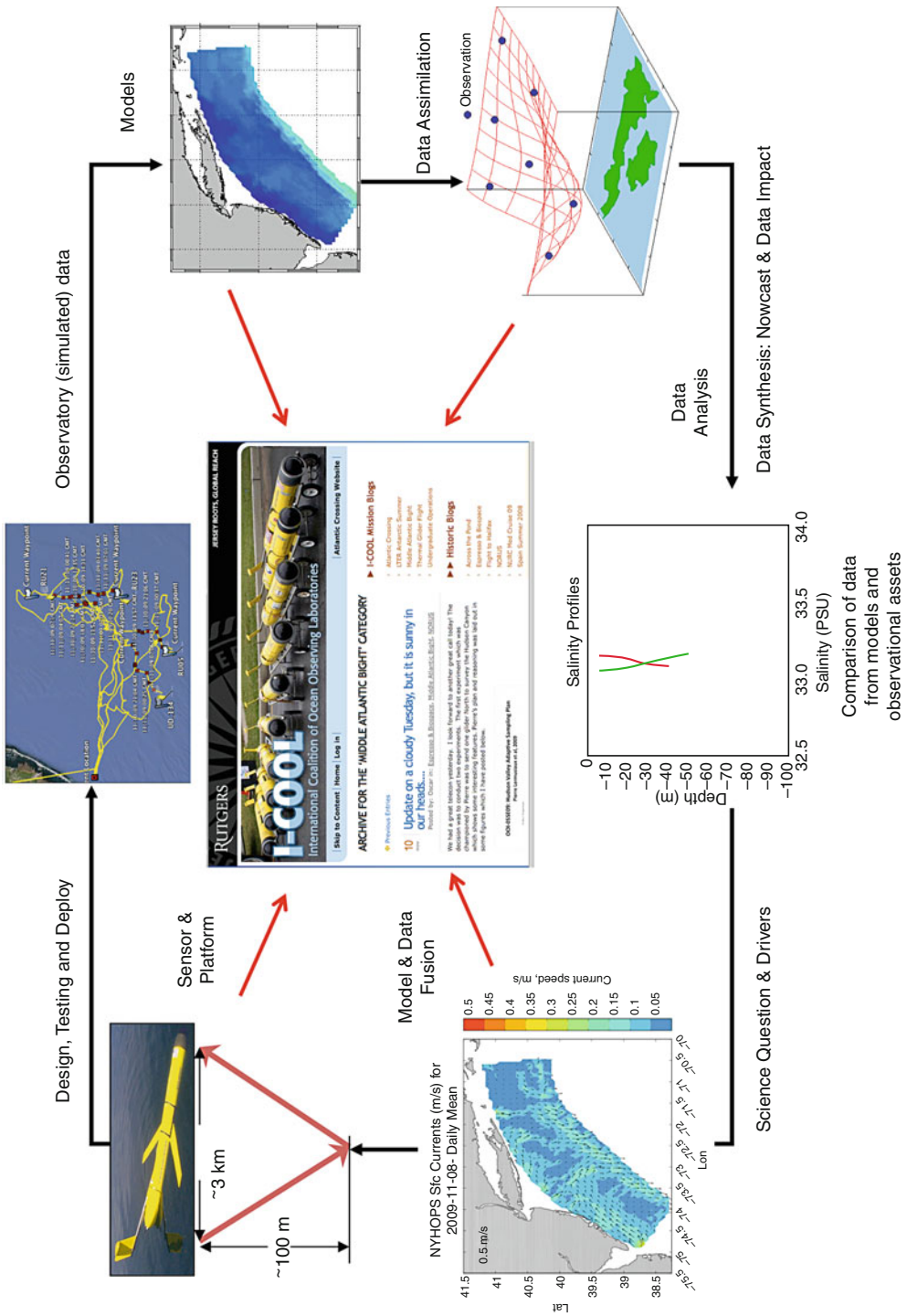

Ocean Observatories and Information: Building a Global Ocean Observing Network. Figure 9
The machine-to-machine data flow during the Ocean Observing Initiative's (OOI) Observation Simulation Experiment. A fleet of gliders were informed by model driven forecasts in order to optimize science sampling being conducted by a geographically distributed team of scientists. The observatory data was assimilated by an ensemble of numerical forecast models, which were used to optimize the glider sampling. Optimized glider data was also used to adjust the data collected by the Hyperion EO-1 satellite

and to make it available to ocean forecast models. Scientists used the model forecasts to guide future (next 24 h) glider missions which then were used to optimize data collection for model data assimilation, which demonstrated the feasibility of two-way interactivity between the sensor web and predictive models. The sensor web included the re-tasking of a satellite. The software allowed the distributed community to adaptively modify the in situ observation network throughout the experiment [29]. The net result was a science driven machine-to-machine interactive loop (Fig. 9). These machine networks will increasingly become standard tools for the ocean science community in the future.

As observatories consist of a series individual components that are linked to form a coherent sampling system, an often underemphasized, yet critical need is the ability to register to all components to a common time stamp. The time stamp functionality in the sensor network is necessary to compare the output of one sensor to another. This is not a trivial when sensors are dispersed geographically and the data from sensors need to be integrated with external datasets. The accuracy required is a function of the process being studied and the length of the time series to be collected. For example, seismic studies require time accuracy on the order of milliseconds, acoustic tomography of 1 μs and studies of phytoplankton growth rates require data on the time scale of hours. Additionally, avoiding drift for temporal time series will increasingly become critical as sustained time series become the norm for oceanography. Fortunately, the ability to register time accurately is increasingly improving. A dramatic example is the evolution of small low-power atomic clocks. Atomic clocks offer the frequency stability of one part in ten billion, which is equivalent to gaining or losing 1 s every 300 years. These technical developments are being powered by the evolution of Micro Electro Mechanical Systems (MEMS) chip technologies that can produce clocks with a volume of less than 0.1 cm^3 and consume power on the milli-watt scale. These advances will enable atomic clocks to be operated on batteries and could be integrated throughout the individual components of the ocean observatories.

The potential of cyberinfrastructure tools, such as described above, is dependent on the real-time availability of data; fortunately global communications have improved dramatically over the last few decades. In the early 1990s, the primary mode of communication from ship to shore was via satellite voice calls. This improved over the next decade as ship-based science was provided with limited email communication. Communications have continued to improve and now provide sufficient bandwidth to allow for video-transmission at hundreds of kilobits per second (http://hiseasnet.ucsd.edu/). These improvements are changing the type of science that ships conduct as real-time data allow scientists to adaptively sample the ocean. Additionally, the launch of low Earth orbit satellite communication systems have allowed for global communication and enabled rapidly evolving capabilities for communications to autonomous platforms. The communications have improved from one-way communications with data transmission limited to about 16,000 bits/day to global two-way communications at a rate of 2,400 bits/s.

Future Directions

The ocean science community will over the next decade construct a global ocean observing network by combining a diverse range of platforms. The multiplatform networks will allow scientists to sample over a wide range of time and space scales and the availability of real-time data transmission will allow for adaptive sampling. The development of a robust cyberinfrastructure will encourage distributed teams of scientists to conduct both applied and basic research. The research will allow the community to understand the present and future status of the oceans.

Bibliography

1. Crease J (1962) Velocity measurements in the deep water of the western North Atlantic. J Geophys Res 67:3173–3176
2. Ducet N, Le Traon PY, Reverdin G (2000) Global high-resolution mapping of ocean circulation from TOPEX/Poseidon and ERS-1 and -2. J Geophys Res 105:19477–19498
3. Schmitz WJ (1977) On the deep general circulation in the western North Atlantic. J Mar Res 35:21–28
4. Swallow JC (1971) The Aries current measurements in the western North Atlantic. Philos Trans R Soc Lond A270:451–460
5. Oreskes N (ed) (2003) Plate tectonics: an insider's history of the modern theory of the Earth. Westview Press Books, Boulder CO. 424 pp
6. Antoine D, Andre J, Morel A (1996) Oceanic pimary production 2. Estimation at global scale from satellite (coastal zone color scanner) chlorophyll. Global Biogeochem Cycles 10:57–69

7. Behrenfeld MJ, O'Malley RT, Siegel DA, McClain CR, Sarmiento JL, Feldman GC, Milligan AJ, Falkowski PG, Letelier RM, Boss ES (2006) Climate-driven trends in contemporary ocean productivity. Nature 444:752–755
8. Longhurst A, Sathyendranath S, Platt T, Caverhill C (1995) An estimate of global primary production in the ocean from satellite radiometer data. J Plankton Res 17:1245–1271
9. Graham NE (1994) Decadal-scale climate variability in the tropical and North Pacific during the 1970s and 1980s: observations and model. Climate Dynamics 10:135–162
10. Miller AJ, Schneider N (2000) Interdecadal climate regime dynamics in the North Pacific Ocean: theories, observation, and ecosystem, impacts. Prog Oceanogr 47:355–379
11. Rahmstorf S, Cazenave A, Church JA, Hansen JE, Keeling RF, Parker DE, Somerville RCJ (2007) Recent climate observations compared to projection. Science 316:709. doi:10.1126/science.1136843
12. De Souza R, Williamsn J, Meyerson FAB (2003) Critical links: population, health, and the environment. Popul Bull 58(3): 3–43
13. Vitousek PM, Mooney HA, Lubchenco J, Melillo JM (1997) Human domination of Earth's ecosystems. Science 277:494–499. doi:10.1126/science.277.5325.494
14. Large WG, Holland WR, Evans JC (1991) Quasi-geostrophic ocean response to real wind forcing: the effects of temporal smoothing. Am Meteorol Soc 21(7):998–1017
15. Milliff RF, Large WG, Holland WR, McWilliams JC (1996) The general circulation responses of high-resolution North Atlantic Ocean models to synthetic scatterometer winds. J Phys Oceanogr 26:1747–1768
16. Milliff RF, Large WG, Morzel J, Danabasoglu G, Chin TM (1999) Ocean general circulation model sensitivity to forcing from scatterometer winds. J Geophys Res 104: 11337–11358
17. Milliff RF, Morzel J (2001) The global distribution of the time-average wind stress curl from NSCAT. J Atmos Sci 58(2):109–131
18. National Research Council (2009) Science at sea: meeting future oceanographic goals with a Robust Academic Research Fleet. National Academy Press, Washington, DC
19. Munk W (2000) Oceanography before, and after, the advent of satellites. In: Halpern D (ed) Satellites oceanography and society. Elsevier Science, Amsterdam, pp 1–5
20. Halpern DA (2000) Satellites, oceanography and society. Elsevier Science, Amsterdam, 361 pp
21. Martin-Traykovski LV, Sosik HM (2003) Feature-based classification of optical water types in the Northwest Atlantic based on satellite ocean color data. J Geophys Res 108(C5):3150. doi:10.1029/2001JC001172
22. Oliver MJ, Kohut JT, Irwin AJ, Glenn SM, Schofield O, Moline MA, Bissett WP (2004) Bioinformatic approaches for objective detection of water masses. J Geophys Res 109: C07S04. doi:10.1029/2003JC002072
23. Beherenfeld MJ, Boss E, Siegel DA, Sutherland DM (2005) Carbon-based ocean productivity and phytoplankton physiology from space. Global Biogeochem Sci 19:GB1006. doi:10.1029/2004GB002299
24. Beherenfeld MJ, Falkowski PG (1997) A consumer's guide to phytoplankton primary productivity models. Limnol Oceanogr 42(7):1479–1491
25. Goes JI, Saino T, Oaku H, Jiang DL (1999) A method for estimation of sea surface nitrate concentrations from remotely sensed SST and chlorophyll a – a case study for the North Pacific Ocean using OCTS/ADEOS data. IEEE Trans Geosci Remote Sens 37:1633–1644
26. Swift CT, Mcintosh RE (1983) Considerations for microwave remote-sensing of ocean-surface salinity. IEEE Trans Geosci Remote Sens 21:480–491
27. Berger M, Camps A, Font J, Kerr Y, Miller J, Johannessen J, Boutin J, Drinkwater MR, Skou N, Floury N, Rast M, Rebhan H, Attema E (2002) Measuring ocean salinity with ESA's SMOS mission. ESA Bull 111:113f
28. Geiger EF, Grossi MD, Trembanis AC, Kohut JT, Oliver MJ (2011) Satellite-derived coastal ocean and estuarine salinity in the Mid-Atlantic. Cont Shelf Res (submitted)
29. Schofield O, Glenn S, Orcutt J, Arrott M, Brown W, Signell R, Moline MA, Chao Y, Chien S, Thompson D, Balasuriya A, Oliver M (2010) Automated sensor networks to advance ocean science. Trans Am Geophys Union 91(39):345–346. doi:10.1029/2010EO390001
30. Barrick DE (1972) First-order theory and analysis of mf/hf/vhf scatter from the sea. IEEE Trans Antennas Propag AP-20:2–10
31. Barrick DE, Evens MW, Weber BL (1977) Ocean surface currents mapped by radar. Science 198:138–144
32. Crombie DD (1955) Doppler spectrum of sea echo at 13.56 Mc/s. Nature 175:681–682
33. Stewart RH, Joy JW (1974) HF radio measurements of ocean surface currents. Deep Sea Res 21:1039–1049
34. Bromirski PD, Duennebier FK, Stephen RA (2005) Mid-ocean microseisms. Geochem Geophys Geosyst 6:Q04009. doi:10.1029/2004GC000768
35. Duennebier FK, Harris DW, Jolly J, Babinec J, Copson D, Stiffel K (2002) The Hawaii-2 observatory seismic system. IEEE J Oceanic Eng 27:212–217
36. Thomson DJ, Lanzerotti LJ, Maclennan CG, Medfor LV (1995) Ocean cable measurements of the tsunami signal from the 1992 Cape Mendocino earthquake. Pure Appl Geophys 144:427–440
37. Traykovski P, Hay A, Irish JD, Lynch JF (1999) Geometry, migration, and evolution of wave orbital ripples at LEO-15. J Geophys Res 104:1505–1524. doi:10.1029/1998JC900026
38. Schofield O, Bergmann T, Bissett WP, Grassle F, Haidvogel D, Kohut J, Moline M, Glenn S (2002) Linking regional coastal observatories to provide the foundation for a national ocean observation network. J Oceanic Eng 27(2): 146–154
39. Grundle DS, Timothy DA, Varela DE (2009) Variations of phytoplankton productivity and biomass over an annual cycle in Saanich inlet, a British Columbia fjord. Cont Shelf Res 29:2257–2269. doi:10.1016/j.csr.2009.08.013

40. Oliver MW, Schofield O, Bergmann T, Glenn SM, Moline MA, Orrico C (2004) In-situ optically derived phytoplankton absorption properties in coastal waters and its utility for estimating primary productivity rates. J Geophys Res 109:C07S11. doi:10.1029/2002JC001627
41. Kunze E, Dower JF, Beveridge I, Dewey R, Bartlett KP (2006) Observations of biologically generated turbulence in a coastal inlet. Science 313:1168–1170. doi:10.1126/science.1129378
42. Agrawal YC (2005) The optical volume scattering function: temporal and vertical variability in the water column off the New Jersey coast. Limnol Oceanogr 50:1787–1794
43. Gargett A, Wells J, Tejada-Martinez AE, Grosch CE (2004) Langmuir supercells: a mechanism for sediment resuspension and transport in shallow seas. Science 356:1925–1928
44. Edwards RN, Schwalenberg K, Wiloughby EC, Mir R, Scholl C (2010) Marine controlled source electromagnetics and the assessment of seafloor gas hydrate. In: Riedel M, Willoughby EC, Chopra S (eds) Geophysical characterization of gas hydrates, SEG monograph. Society of Exploration Geophysicists, Tulsa
45. Sullivan PP, Edson JB, Hristov T, Williams JC (2008) Large-eddy simulations and observations of atmospheric marine boundary layers above nonequilibrium surface waves. J Atmos Sci 65:1225–1245
46. Moline MA, Oliver MJ, Mobley CD, Sundman L, Blackwell SM, Bergmann T, Bissett WP, Case J, Raymond EH, Schofield O (2007) Bioluminescence in a complex coastal environment I: temporal dynamics of night-time water-leaving radiance. J Geophys Res 112. doi:10.1029/2007JC004138
47. Oliver MJ, Moline M, Mobley C, Sundman LK, Schofield O (2007) Bioluminescence in a complex coastal environment: 2. Prediction of bioluminescent source depth from spectral water-leaving radiance. J Geophys Res. doi:10.1029/2007JC004136
48. Rousseau S, Kunze E, Dewey R, Bartlett K, Dower J (2010) On the efficiency of turbulence production by swimming marine organisms in the open ocean and coastal waters. J Phys Oceanogr 40(9):2107–2121
49. Franklin B (1785) Sundry marine observations. Trans Am Philos Soc 1(2):294–329
50. Langmuir I (1938) Surface motion of water induced by wind. Science 87:119–123
51. Niiler PP, Maximenko NA, McWilliams JC (2003) Dynamically balanced absolute sea level of the global ocean derived from near-surface velocity observations. Geophys Res Lett 30(22):2164. doi:10.1029/2003GL018628
52. Swallow JC (1955) A neutral-buoyancy float for measuring deep currents. Deep Sea Res 3:74–81
53. Davis RE, Webb DC, Regier LA, Dufour J (1992) The autonomous lagrangian circulation explorer (ALACE). J Atmos Oceanic Technol 9:264–285
54. Johnson KS, Berelson WM, Boss ES, Chase Z, Claustre H, Emerson SR, Gruber N, Kortzinger A, Perry MJ, Riser SC (2009) Observing biogeochemical cycles at global scales with profiling floats and gliders: prospects for a global array. Oceanography 22(3):216–225
55. Gould J, Roemmich D, Wijffels SH, Freeland H, Ignaszewsky M, Jianping X, Pouliquen S, Desaubies Y, Send U, Radhakrishand K, Takeuchi K, Kim K, Danchenkov M, Sutton P, King B, Owens B, Riser S (2004) Argo profiling floats bring new era of in situ ocean observations. EOS 85(19):190–191. doi:10.1126/science.1136843
56. Rudnick DL, Davis RE, Eriksen CC, Fratantoni DM, Perry MJ (2004) Underwater gliders for ocean research. Mar Technol Soc J 38:73–84
57. Eriksen CC, Osse TJ, Light RD, Wen T, Lehman TW, Sabin PL, Ballard JW, Chiodi AM (2001) Seaglider: a long-range autonomous underwater vehicle for oceanographic research. IEEE J Oceanic Eng 26:424–436
58. Sherman J, Davis RE, Owens WB, Valdes J (2001) The autonomous underwater glider "Spray". IEEE J Oceanic Eng 26:437–446
59. Webb DC, Simonetti PJ, Jones CP (2001) SLOCUM: an underwater glider propelled by environmental energy. IEEE J Oceanic Eng 26:447–452
60. Castelao R, Glenn S, Schofield O, Chant R, Wilkin J, Kohut J (2008) Seasonal evolution of hydrographic fields in the central Middle Atlantic Bight from glider observations. Geophys Res Lett 35:L03617. doi:10.1029/2007GL032335
61. Chao Y, Zhijin L, Farrara JD, Moline MA, Schofield O, Majumdar SJ (2008) Synergistic applications of autonomous underwater vehicles and regional ocean modeling system in coastal ocean forecasting. Limnol Oceanogr 53(6): 2251–2263
62. Davis RE, Ohman MD, Rudnick DL, Sherman JT, Hodges B (2008) Glider surveillance of physics and biology in the southern California Current System. Limnol Oceanogr 53(5):2151–2168
63. Glenn SM, Jones C, Twardowski M, Bowers L, Kerfoot J, Webb D, Schofield O (2008) Studying resuspension processes in the Mid-Atlantic Bight using Webb slocum gliders. Limnol Oceanogr 53(6):2180–2196
64. Hjalmar H, Eriksen CC, Rhines PB (2007) Buoyant eddies entering the Labrador Sea observed with gliders and altimetry. J Phys Oceanogr 37:2838–2854
65. Hodges BA, Fratantoni DM (2009) A thin layer of phytoplankton observed in the Philippine Sea with a synthetic moored array of autonomous gliders. J Geophys Res 114:C10020. doi:10.1029/2009JC005317
66. Kahl A, Fraser W, Schofield O (2010) Autonomous gliders reveal water column features associated with Adélie penguin foraging. Integr Comp Biol. doi:10.1093/icb/icq098
67. Schofield O, Chant R, Cahill B, Castelao R, Gong D, Kahl A, Kohut J, Montes-Hugo M, Ramadurai R, Ramey P, Xu Y, Glenn SM (2008) Seasonal forcing of primary productivity on broad continental shelves. Oceanography 21(4):104–117
68. Blackwell SH, Moline MA, Schaffner A, Garrison T, Chang G (2008) Sub-kilometer length scales in coastal waters. Cont Shelf Res 28(2):215–226

Ocean Thermal Energy Conversion

Luis A. Vega
Hawaii Natural Energy Institute, School of Ocean And Earth Science And Technology, University of Hawaii at Manoa, Honolulu, HI, USA

Article Outline

Glossary
Definition of the Subject
Introduction
OTEC History
Ocean Thermal Resources
Technical Limitations and Challenges
Environmental Impact
Open-Cycle OTEC
The 210 kW OC-OTEC Experimental Apparatus
Closed-Cycle OTEC
State of the Art 10- MW CC-OTEC Pilot Plant
Site Selection Criteria for OTEC Plants
OTEC Economics
Future Directions: OTEC
Bibliography

Glossary

Baseload The minimum amount of power that a utility must make available to its customers.

Baseload plant An energy plant devoted to the production of baseload supply. Baseload plants typically run at all times through the year (24/7) except in the case of repairs or scheduled maintenance.

CWP Cold water pipe, the pipe used to transport deep ocean water to the OTEC condenser.

Draught (Draft) The depth of a ship's keel below the water surface.

Euphotic zone The upper layer of the ocean in which there is sufficient light for photosynthesis.

Externalities The costs generated by the production of electricity that are not included in the price charged to consumers. These costs manifest themselves through changes in the environment and other societal costs.

Gross power The electrical power generated by the turbine-generator.

Net power The electrical power available for export from the OTEC plant. The difference between gross power and in-plant power consumption needed to run all sweater and working fluid pumps.

Ocean thermal resource Defined by ΔT, the ocean temperature differences between water depths of 20 m (surface water) and 1,000 m.

OTEC Ocean Thermal Energy Conversion, the process of converting the ocean thermal energy into electricity.

OTEC transfer function The relationship between the thermal resource and the electricity generated.

Plantship A ship designed to house an OTEC power plant.

Re-entrainment The mixing of the water already used in the OTEC plant into the incoming warm (surface) water stream.

WOA05 World Ocean Atlas 2005 version.

Definition of the Subject

The vertical temperature distribution in the open ocean can be represented as two layers separated by an interface. The upper layer is warmed by the sun and mixed to depths of about 100 m by wave motion. The bottom layer consists of colder water formed at high latitudes. The interface or thermocline is sometimes marked by an abrupt change in temperature but more often the change is gradual. This implies that there are two reservoirs providing the heat source and the heat sink required for a heat engine. A practical application is found in a system designed to transform the thermal energy into electricity. This is referred to as OTEC for Ocean Thermal Energy Conversion.

At first, OTEC plantships providing electricity, via submarine power cables, to shore stations could be implemented. This would be followed, in 20 to 30 years, with OTEC factories deployed along equatorial waters producing energy-intensive products, like ammonia and hydrogen as the fuels that would support the post–fossil fuel era [2].

Apparently, there are sufficient petroleum resources (≈1400 billion barrels) to meet worldwide current demand (>30 billion barrels/year) for almost 50 years. Production, however, is peaking and humanity will face a steadily diminishing petroleum supply and higher demand due to emerging economies like China, India, and Brazil. Coal and natural gas resources

could meet current worldwide demand for 100 to 120 years, respectively.

It seems sensible toconsider OTEC as one of the renewable energy technologies of the future.

Introduction

It has been postulated that the ocean thermal resource, defined as the difference between surface water and water from about 1,000 m depth, could be used to generate most of the energy required by humanity [1]. What is pending, however, are realistic determinations of the costs and the potential global environmental impact of OTEC plants, and this can only be accomplished by deploying and subsequently monitoring operations with first-generation plants.

One might ask: is OTEC renewable energy? The simple answer is: *as long as the sun shines and, if and only if, deep-ocean cold water is provided by the thermohaline circulation, the ocean thermal resource is renewable.*

A pertinent question, however, is: what is the worldwide power resource that could be extracted with OTEC plants without affecting the thermohaline ocean circulation? The estimate is that the maximum steady-state OTEC exportable electrical power is at least 5 TW, e.g., 10,000x 500 MW OTEC plants [3]. This is about twice the amount projected for worldwide electricity consumption by 2025.

OTEC History

Captain Nemo, Jules Verne's alter ego in "Twenty Thousand Leagues Under the Sea" published in 1870, provides the first reference to the idea of producing electricity using the ocean thermal resource:

- "I was determined to seek from the sea alone the means of producing my electricity.". . . "From the sea?". . . "Yes, Professor, and I was at no loss to find these means. It would have been possible, by establishing a circuit between two wires plunged to different depths, to obtain electricity by the difference of temperature to which they would have been exposed. . .."

Although Nemo conceptualized a thermoelectric device, the seeds of the OTEC principle emanated from Verne's pen inspired by ongoing discussions in French academic circles.

Eleven years later, D'Arsonval documented a formal proposal to use the relatively warm (24–30°C) surface water of the tropical oceans to vaporize pressurized ammonia through a heat exchanger (i.e., evaporator) and use the resulting vapor to drive a turbine-generator. The cold ocean water transported (upwelled) to the surface from 800 m to 1,000 m depths, with temperatures ranging from 8°C to 4°C, would condense the ammonia vapor through another heat exchanger (i.e., condenser). D'Arsonaval concept is grounded in the thermodynamic Rankine cycle used to study steam (vapor) power plants. Because the ammonia circulates in a closed loop, this concept has been named closed-cycle OTEC (CC-OTEC).

D'Arsonval's concept was demonstrated in 1979 when the state of Hawaii and a consortium of U.S. companies produced more than 50 kW of gross power, with a net output of up to 18 kW from a small plant mounted on a barge off Hawaii [4]. Subsequently, a 100 kW gross power, land-based plant was operated in the island nation of Nauru by a consortium of Japanese companies. These plants were operated for a few months to demonstrate the concept. They were too small to be scaled to commercial-size systems. Since then, the US Department of Energy [5, 6] and researchers at Saga University in Japan have performed extensive testing of heat exchangers and have proposed the use of an ammonia-water mixture as the working fluid [7].

Forty years after D'Arsonval, Georges Claude, another French inventor, proposed to use the ocean water as the working fluid [8]. In Claude's cycle, the surface water is flash-evaporated in a vacuum chamber. The resulting low-pressure steam is used to drive a turbine-generator, and the relatively colder deep seawater is used to condense the steam after it has passed through the turbine. This cycle can, therefore, be configured to produce desalinated water as well as electricity. Claude's cycle is also referred to as open-cycle OTEC (OC-OTEC) because the working fluid flows once through the system. Claude demonstrated this cycle in Cuba (1930) with a small land-based plant making use of a direct contact condenser (DCC). Therefore, desalinated water was not a by-product. The plant failed to achieve net power production because of a poor site selection (e.g., thermal resource) and a mismatch of the power and seawater systems. However, the plant did operate for several weeks.

Claude, subsequently, designed a 2.2 MW floating plant for the production of up to 2,000 t of ice (this was prior to the wide availability of household refrigerators) for the city of Rio de Janeiro in Brazil. Claude housed his power plant in a ship (i.e., plantship), about 100 km offshore. Unfortunately, he failed in his numerous attempts to install the vertical long pipe required to transport the deep ocean water to the ship (the cold water pipe, CWP) and had to abandon his enterprise in 1935. His failure can be attributed to the absence of the offshore industry, and ocean engineering expertise presently available. His biggest technological challenge was the at-sea installation of a CWP. This situation is markedly different now that there is a proven record in the installation of several pipes during experimental operations [1].

The next step toward answering questions related to operation of OTEC plants was the installation of a small OC-OTEC land-based experimental facility in Hawaii (Fig. 1). The turbine-generator was designed for an output of 210 kW for 26°C warm surface water and a deep water temperature of 6°C. A small fraction (10%) of the steam produced was diverted to a surface condenser for the production of desalinated water. The experimental plant was successfully operated for 6 years (1993–1998). The highest production rates achieved were 255 kWe (gross) with a corresponding net power of 103 kW and 0.4 L/s of desalinated water. These are world records for OTEC [9, 10].

A two-stage OTEC hybrid cycle, wherein electricity is produced in a first-stage (closed cycle) followed by water production in a second-stage, has been proposed to maximize the use of the thermal resource available to produce water and electricity [1]. In the second-stage, the temperature difference available in the seawater effluents from an OTEC plant (e.g., 12°C) is used to produce desalinated water through a system consisting of a flash evaporator and a surface condenser (basically, an open cycle without a turbine-generator). In the case of an open cycle plant, the addition of a second-stage results in doubling water production.

The use of the cold deep water as the chiller fluid in air conditioning (AC) systems was proposed and implemented [11]. It has been demonstrated that these systems providing significant energy conservation independent of OTEC [12].

OTEC energy could be transported via chemical, thermal, and electrochemical carriers. The technical evaluation of nonelectrical carriers lead, for example, to the consideration of hydrogen produced using electricity and desalinated water generated with OTEC technology. The product would be transported from

Ocean Thermal Energy Conversion. Figure 1
210 kW OC-OTEC experimental apparatus (1993–1998)

the OTEC plantship located at distances of about 1,500 km (selected to represent the nominal distance from the tropical oceans to major industrialized centers throughout the world) to the port facility in liquid form to be primarily used as a transportation fuel. A 100 MW-net plantship can be configured to yield (by electrolysis) 1,300 kg/h of liquid hydrogen [13]. Unfortunately, the production cost of liquid hydrogen delivered to the harbor would be equivalent to at least $300 barrel-of-crude-oil (approximately four times present cost). The situation is similar for the other energy carriers considered (e.g., anhydrous ammonia). Presently, the only energy carrier that is cost-effective for OTEC energy is the submarine power cable. This situation would be different in future decades in the post fossil-fuels era.

A number of possible configurations for OTEC plants have been proposed. These range from floating plants to land-based plants, including shelf-mounted towers and other offshore structures. The primary candidate for commercial size plants appears to be the floating plant, positioned close to land, transmitting power to shore via a submarine power cable [1, 2].

Over a decade ago, the detailed evaluation of economic feasibility and financial viability of OTEC revealed that, in general, plants would have to be sized at about 50–100 MW to produce cost-competitive baseload electricity. Smaller plants could be cost effective in some niche markets. It was also concluded that, although experimental work with relatively small plants had unambiguously demonstrated continuous production of electricity [4, 9, 10] and desalinated water [9, 10], it would be necessary to build a pre-commercial plant sized around 5–10 MW to establish the operational record required to secure financing for the commercial size plants [12]. The pre-commercial plant would produce relatively high-cost electricity and desalinated water such that support funding was required from the federal and state governments. Unfortunately, development did not proceed beyond experimental plants sized at less than 0.25 MW [1].

In the mid 1990s, an engineering team in Hawaii designed a 5 MW pre-commercial plant and made the information available in the public domain [14]. However, because the price of petroleum fuels was relatively low and fossil fuels were considered to be abundantly available, government funding for the pre-commercial plant could not be obtained.

Direct extrapolation from the experimental plants to commercial sizes, bypassing the pre-commercial stage, would have required a leap of faith with high technical and economic risks that no financial institution was willing to take. Important lessons learned can be summarized as follows:

- All components must be considered in technical and economic assessments: *OTEC plants consist of several components or subsystems that must be integrated into a system.*
- The entire life cycle must be incorporated into design process.
- Equipment must be manufactured using commercially available practices in existing factories.
- Embellishment leads to negative consequences creating credibility barriers for others and unrealistic expectations from the public.

Ocean Thermal Resources

The vast size of the ocean thermal resource and the baseload capability of OTEC systems remain very promising aspects of the technology for many island and coastal communities across tropical latitudes. For example, OTEC plants could supply all the electricity and potable water consumed in the State of Hawaii throughout the year and at all times of the day. This is an indigenous renewable energy resource that can provide a high degree of energy security and minimize green house gas emissions. This statement is also applicable to all US Insular Territories (e.g., American Samoa, Guam, Northern Mariana Islands, Virgin Islands, and Puerto Rico). With the development of electric vehicles, OTEC could also supply all electricity required to support land transportation. The resource is plentiful enough to meet additional electricity demand equivalent to several times present consumption. Please see section "Site Selection Criteria for OTEC Plants" for further information.

Thermal resource characteristics are used along with the specific OTEC system transfer function to determine electricity production. Ocean thermal resources are defined by ΔT, the ocean temperature differences between water depths of 20 and 1,000 m.

ΔT characterizes extractable OTEC power as long as the local thermal structure is preserved.

The current resource evaluation benefits from high-resolution ocean models. The HYCOM + NCODA (1/12°) model is used by Prof. Gerard Nihous of the University of Hawaii to track changes on a daily basis over a wide area around different locations [15].

The optimized turbine-generator output P_{gross} varies with the square of ΔT so that for typical values of 20°C, a change of 1°C in ΔT will produce relative fluctuations of about 10% in P_{gross} [3]. Measurements performed during the operation of the *210 kW OC-OTEC Experimental Apparatus* confirmed this point [9, 10]. From a net power perspective, matters are even more sensitive since the in-plant power consumption needed to run all pumps represents about 30% of the reference value of P_{gross}; hence, changes of the order of 10% in P_{gross} approximately translate in 15% variations in net power output, which is the true basis for the determination of electricity production costs [3].

In the following discussion, the ocean thermal resource off the Hawaiian Islands is considered to illustrate the methodology that can be applied to any region of interest. The most recent, 2005 version of the World Ocean Atlas (WOA05) compiled by the National Ocean Data Center (NODC) represents an extremely valuable source of objectively analyzed statistical fields, including ocean temperature [16]. The data includes long-term historical averages of variables that have been determined from all available oceanographic measurements. Monthly averages also are available. The data is provided with a resolution of one-quarter degree latitude by one-quarter degree longitude.

Figure 2 shows a map of the average OTEC thermal resource ΔT from the WOA05 data base plotted with the Ocean Data View software (http://odv.awi.de).

As can be seen in Fig. 2, the Hawaiian Archipelago is very well located from a thermal resource perspective. The volcanic islands have a steep bathymetry that affords good access to deep water. Their isolation and nearly complete dependence on fossil fuels today make any local baseload power-production technology particularly attractive. Additional factors that would hamper other renewable energy technologies in Hawaii, such as limited land availability, pristine reefs, and valuable surf resources, would hardly affect OTEC.

Regarding OTEC thermal resources around the main Hawaiian Islands, a closer look at the WOA05 data in Fig. 2 suggests that such resources are not

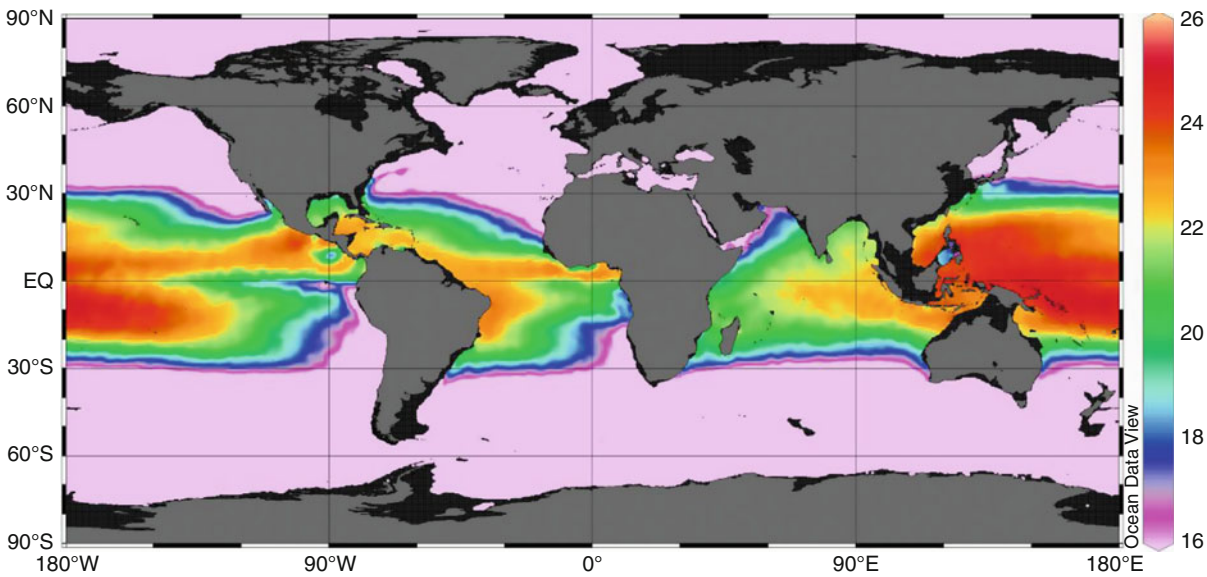

Ocean Thermal Energy Conversion. Figure 2
Average ocean temperature differences (between 20 and 1,000 m water depths) from WOA05 data with color palette from 16°C to 26°C (From [15])

enhanced from North to South, as would be intuitive, but roughly from Northeast to Southwest. Recently available predictive tools afford a much more detailed analysis. An ocean model called HYCOM (HYbrid Coordinate Ocean Model), subject to routine data assimilation via the Naval Research Laboratory (NRL)'s Coupled Ocean Data Assimilation (NCODA) protocol, allows daily assessments of ocean variables at a spatial resolution of 1/12° latitude by 1/12° longitude across the water column [17]. NCODA assimilates all available operational sources of ocean observations. The model output essentially should be interpreted as daily averages [15]. This data can be downloaded via public-domain servers such as http://ferret.pmel.noaa.gov/LAS.

Figure 3 shows the average available OTEC thermal resource ΔT over a period of 3 years, from July 1, 2007 through June 30, 2010. Areas that are shallower than 1,000 m are displayed in white to indicate that ΔT is not defined there. Although overall geographic variations in the selected area covering 7° of latitude and 9° of longitude are within 2°C, a prominent wedge can be seen; its apex roughly lies at the eastern tip of the Big Island, and the feature is somewhat symmetric across the latitude of that point; from the apex, a line running along the northeast (windward) coasts of the islands defines the angular overture of the wedge. The emergence of such a feature is likely to be the result of the strong influence the islands exert on large-scale ocean currents [18]. The westward-flowing North Equatorial Current (NEC) forks at the Big Island and gives rise to a branch that follows a northwesterly direction (North Hawaiian Ridge Current). West of the islands, the vorticity of the wind-stress curl associated with the wake of the islands causes a clockwise circulation centered at 19°N and a counter-clockwise circulation centered at 20°30′N, with the narrow Hawaiian Lee Counter Current (HLCC) extending between them from 170°W (or from as far as the Dateline) to 158°W. The eastward-flowing HLCC is responsible for the advection of warm water toward the lee of the Hawaiian archipelago [15, 18].

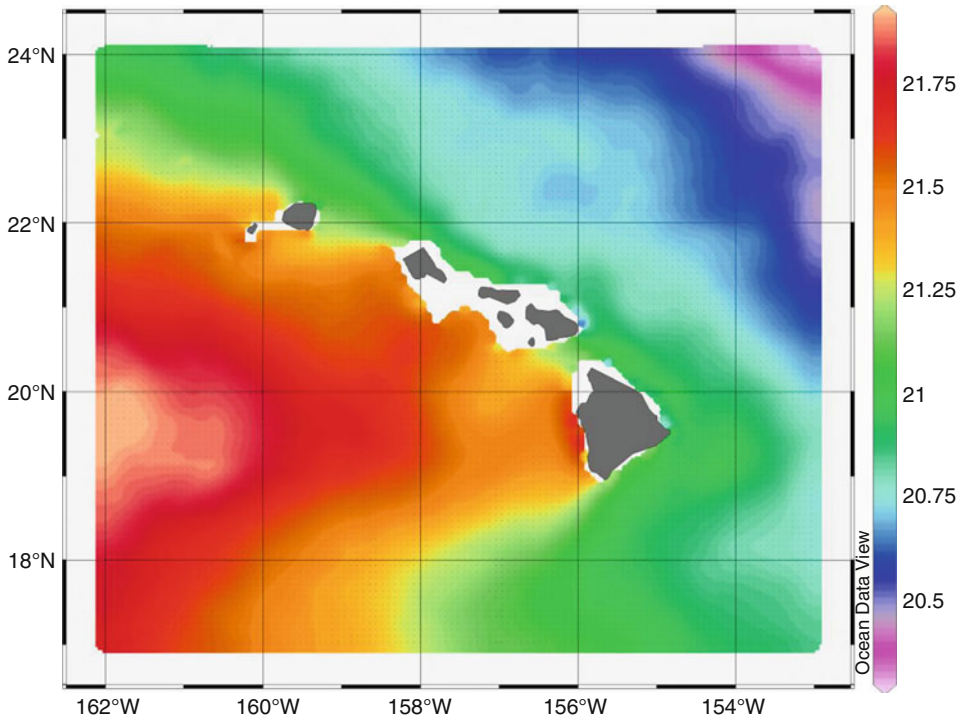

Ocean Thermal Energy Conversion. Figure 3
Average ocean temperature differences (between 20 and 1,000 m water depths) around the main Hawaiian Islands from HYCOM + NCODA (1/12°) data for the period July 1, 2007, through June 30, 2010 (From [15])

Technical Limitations and Challenges

The performance of OTEC cycles is assessed with the same thermodynamics concepts used for conventional steam power plants. The major difference arises from the large quantities of warm and cold seawater required for heat transfer processes, resulting in the consumption of a portion of the power generated by the turbine-generator in the operation of pumps. The power required to pump seawater is determined accounting for the pipe-fluid frictional losses and in the case of the cold seawater for the density head, i.e., gravitational energy due to the differences in density between the heavier (colder) water inside the pipe and the surrounding water column. The seawater temperature rise, due to frictional losses, is negligible for practical designs [1].

The ideal energy conversion for 26°C and 4°C warm and cold seawaters is 8%. An actual OTEC plant will transfer heat irreversibly at various points in the cycle yielding an energy conversion of 3–4%. These values are small compared to efficiencies obtained for conventional power plants; however, OTEC uses a resource that is constantly renewed by the sun.

The thermal performance of CC-OTEC and OC-OTEC is comparable. Approximately 5 m^3/s of warm seawater and 2.5 m^3/s of cold seawater, with a nominal temperature difference of 20°C, are required per MW of exportable or net electricity [1]. To keep the water pumping losses at about 30% of the gross power, an average speed of about 2 m/s is considered for the seawater flowing through the pipes transporting the seawater resource to the OTEC power block. Therefore, a 100 MW-net plant would use about 500 m^3/s of 26 C water flowing through a 17 m inside diameter pipe extending to a depth of 20 m, and 250 m^3/s of 4°C water flowing through a 12 m diameter pipe extending to depths of 1,000 m. Using similar arguments, a 22 m diameter pipe is required for the mixed water return. To minimize the environmental impact due to the return of the processed water to the ocean (mostly changes in temperature), a discharge depth of 60 m is sufficient for most sites considered feasible, resulting in a pipe extending to depths of 60 m.

The design and installation of a cost-effective pipe to transport large quantities of cold water to the surface (i.e., cold water pipe, CWP) presented an engineering challenge of significant magnitude complicated by a lack of evolutionary experience. This challenge was met in the USA with a program relying on computer-aided analytical studies integrated with laboratory and at-sea tests. The greatest outcome achieved has been the design, fabrication, transportation, deployment, and test at sea of an instrumented 2.4 m diameter, 120 m long, fiberglass-reinforced-plastic (FRP) sandwich construction pipe attached to a barge [19]. The data obtained was used to validate the design technology developed for pipes suspended from floating OTEC plants. This type of pipe is recommended for floating OTEC plants.

For land-based plants, there is a validated design for high-density polyethylene pipes of diameter less than about 2 m [20]. In the case of larger diameter pipes offshore techniques used to deploy large segmented pipes made of steel, concrete or FRP are applicable. Pressurized pipes made of reinforced elastomeric fabrics (e.g., soft pipes), with pumps located at the cold-water intake, seem to offer the most innovative alternative to conventional concepts. However, the operability of pumps in 800–1,000 m water depths over extended periods must be verified and the inspection, maintenance and repair (IM&R) constraints established before soft pipes can be used in practical designs.

Other components for OTEC floating plants that present engineering challenges are the position keeping system and the attachment of the submarine power cable to the floating plant. Deep ocean-mooring systems, designed for water depths of more than 1,000 m, or dynamic positioning thrusters developed by the offshore industry can be used for position keeping. The warm-water intake and the mixed return water also provide the momentum necessary to position the surface vessel. The offshore industry also provides the engineering and technological backgrounds required to design and install the riser for the submarine power cable.

The design of OTEC CWPs, mooring systems, and the submarine power cable must take into consideration survivability loads as well as fatigue-induced loads. The first kind is based on extreme environmental phenomena, with a relatively long return period, that might result in ultimate strength failure, while the second kind might result in fatigue-induced failure through normal operations.

OTEC systems are in the pre-commercial phase with several experimental projects having already demonstrated that the technology works but lacking the operational records required to proceeding into commercialization. Adequately sized pilot projects must be implemented to obtain these records. The largest OTEC experimental system was sized at 0.25 MW; however, our analysis indicates that a pilot plant sized at about 5–10 MW is required [2].

Major challenges to OTEC commercialization can be summarized as follows:

- How to overcome the lack of consistent government funding that is required for industry to proceed from concept design to the required OTEC pre-commercial demonstration phase.
- How to streamline the process of obtaining licenses and permits, including the necessary Environmental Impact Statement (EIS). The process is project specific, expensive, and estimated to require at least 2 years for commercial projects in the USA.
- How to evolve into a situation represented by a one-stop-shop (as envisioned in the USA 1980 OTEC Act), where industry can process all documentation stipulated for licensing and permitting under federal, state, city, and county regulations avoiding duplicity, contradictory requirements, and interdepartmental jurisdictional disputes.

In the USA, the proposed location determines the various federal, state, and county agencies and regulations that apply. In addition to the licenses and permits that must be secured from different agencies, the project must comply with several other applicable laws. The 1980 OTEC Act (OTECA) gives the National Oceanic and Atmospheric Administration (NOAA) of the Department of Commerce the authority for licensing the construction and operation of commercial OTEC plants. After the promulgation of OTECA in 1981, licensing regulations were developed by NOAA but, in 1996, NOAA rescinded these regulations and eliminated its OTEC office because no applications had been received. NOAA is currently in the process of developing new licensing regulations. Under OTECA, NOAA is required to coordinate with Coastal States and the US Coast Guard as well, as other Federal Agencies. An EIS would be required for each license. It is expected that the majority if not all federal, state, and local requirements would be handled through the NOAA licensing process.

The original Act gave the Secretary of Energy the authority to exempt Test Plants from NOAA's licensing requirements. A Test Plant was defined as "a test platform which will not operate as an OTEC facility or plantship after conclusion of the testing period." An EIS would be required if "there are other permits to be obtained that are considered a major federal action."

Perhaps a lesson can be learned from the successful commercialization of wind energy that was due to consistent government funding of pilot or pre-commercial projects that led to appropriate and realistic determination of technical requirements and operational costs in Germany, Denmark, and Spain. In this context, by commercialization we mean that equipment can be financed under terms that yield cost competitive electricity. This of course depends on specific conditions at each site.

Environmental Impact

While it is certain that physical, chemical, and biological impacts would occur during the construction and operation of an OTEC facility, the precise magnitude and extent of these impacts are not known. The cumulative or secondary impacts are largely undeterminable without long-term monitoring [21].

These impacts must be evaluated, and all licensing and permitting requirements must be fulfilled. However, it is of extreme importance to understand that the only process that differentiates OTEC from other well-established human activities and industries is the use of ocean water drawn from ~1,000 m depths and its return to the ocean below the photic zone. Given the intricate and dynamic nature of the ocean, it is nearly impossible to determine with a high degree of certainty what would be the effect of such process through basic research or the development of ecological theory. The only way to evaluate the OTEC environmental differentiator is to obtain field data with a pilot plant operating with flow rates corresponding to at least a 5 MW plant. Such plant must be operated and monitored through ongoing and adaptive experience for one to two continuous years, i.e., an adaptive management process.

To better understand the risks that these impacts pose, an environmental baseline is required prior to

installation. This site-specific baseline should include monitoring for presence and abundance of large and small biota, as well as the physical and chemical seawater characteristics. For certain impacts, a longer baseline may be desired to capture multi-year variability. Monitoring for changes to the baseline should occur during the installation and operation phase and would provide information on how the facility is impacting the local environment. Physical, chemical, and biological criteria should be monitored, including temperature; salinity; dissolved oxygen; pH; trace metals; and abundance, diversity, mortality, and behavioral changes in plankton, fish, marine mammals, turtles, and other biota [21].

The energy that could be provided by OTEC must be balanced with the impact to the marine environment that would be caused by OTEC plants. The return water from a 100 MW plant would be equivalent to the nominal flow of the Colorado River into the Pacific Ocean. Although river runoff composition is considerably different, providing a significant amount of power to the world with OTEC might have an impact on the environment below the oceanic mixed layer and, therefore, could have long-term significance in the marine environment. However, numerous countries throughout the world could use OTEC as a component of their energy equation with relatively minimal environmental impact. Tropical and subtropical island sites could be made independent of conventional fuels for the production of electricity and desalinated water.

OTEC offers one of the most benign power-production technologies, since the handling of hazardous substances is limited to the working fluid (e.g., ammonia) and no noxious by-products are generated. The carbon dioxide outgassing from the seawater used for the operation of an OC-OTEC plant is less than 1% of the approximately 700 g per kWh amount released by fuel oil plants. The value is even lower in the case of a CC-OTEC plant [1].

A sustained flow of cold, nutrient-rich, bacteria-free deep ocean water could cause sea surface temperature anomalies and biostimulation if resident times in the mixed layer and the euphotic zone respectively are long enough (i.e., upwelling). The euphotic zone is the upper layer of the ocean in which there is sufficient light for photosynthesis. This has been taken to mean the 1%-light-penetration depth (e.g., 120 m in Hawaiian waters). This is unduly conservative because most biological activity requires radiation levels of at least 10% of the sea surface value. Since light intensity decreases exponentially with depth, the critical 10%-light-penetration depth corresponds to, for example, 60 m in Hawaiian waters. The analyses of specific OTEC designs indicate that mixed seawater returned at depths of 60 m results in a dilution coefficient of 4 (i.e., 1 part OTEC effluent is mixed with 3 parts of the ambient seawater) and equilibrium (neutral buoyancy) depths below the mixed layer throughout the year [22]. This water return depth also provides the vertical separation, from the warm-water intake at about 20 m, required to avoid reingestion into the plant. This value will vary as a function of ocean current conditions. It follows that the marine food web should be minimally affected and that persistent sea surface temperature anomalies should not be induced. These conclusions need to be confirmed with actual field measurements that could be performed with pilot plants [21].

To have effective heat transfer, it is necessary to protect the heat exchangers from biofouling. It has been determined that, with proper design, biofouling only occurs in OTEC heat exchangers exposed to surface seawater [5]. Therefore, it is only necessary to protect the CC-OTEC evaporators by, for example, intermittent chlorination (50–100 parts per billion chlorine for 1 h/day). This amount, for example, is well below what is allowed under current US regulations.

Other potentially significant concerns are related to the construction phase. These are similar to those associated with the construction of any power plant, shipbuilding, and the construction of offshore platforms. What is unique to OTEC is the movement of seawater streams and the effect of passing such streams through the OTEC components before returning them to the ocean [23, 24]. The use of biocides and ammonia are similar to other human activities. If occupational health and safety regulations like those in effect in the USA are followed, working fluid and biocide emissions from a plant should be too low to detect outside the plant sites. Ammonia is used as a fertilizer and in ice skating–rink refrigeration systems. Chlorine is used in municipal water treatment plants and in steam power plants.

OTEC plant construction and operation may affect commercial and recreational fishing. Fish will be attracted to the plant, potentially increasing fishing in

the area. However, the losses of inshore fish eggs and larvae, as well as juvenile fish, due to impingement and entrainment and to the discharge of biocides may reduce fish populations. The net effect of OTEC operation on aquatic life would depend on the balance achieved between these two effects. Through adequate planning and coordination with the local community, recreational assets near an OTEC site may be enhanced.

It is essential that all potentially significant concerns be examined and assessed for each site and design to assure that OTEC is an environmentally benign and safe alternative to conventional power generation. The consensus among researchers is that the potentially detrimental effects of OTEC plants on the environment can be avoided or mitigated by proper design and that their impact is less than that of conventional power technologies.

Open-Cycle OTEC

The open cycle consists of the following steps: (1) flash evaporation of a fraction of the warm seawater by reduction of pressure below the saturation value corresponding to its temperature; (2) expansion of the vapor through a turbine to generate power; (3) heat transfer to the cold seawater thermal sink, resulting in condensation of the working fluid; and (4) compression of the noncondensable gases (air released from the seawater streams at the low operating pressure) to pressures required to discharge them from the system. These steps are depicted in Fig. 4. In the case of a surface condenser, the condensate (desalinated water) must be compressed to pressures required to discharge it from the power generating system. The evaporator, turbine, and condenser operate in partial vacuum ranging from 3% to 1% atmospheric pressure. This poses a number of practical concerns that must be addressed. First, the system must be carefully sealed to prevent in-leakage of atmospheric air that can severely degrade or shut down operation. Second, the specific volume of the low-pressure steam is very large compared to that of the pressurized working fluid used in closed cycle OTEC. This means that components must have large flow areas to ensure that steam velocities do not attain excessively high values. Finally, gases such as oxygen, nitrogen, and carbon dioxide that are dissolved

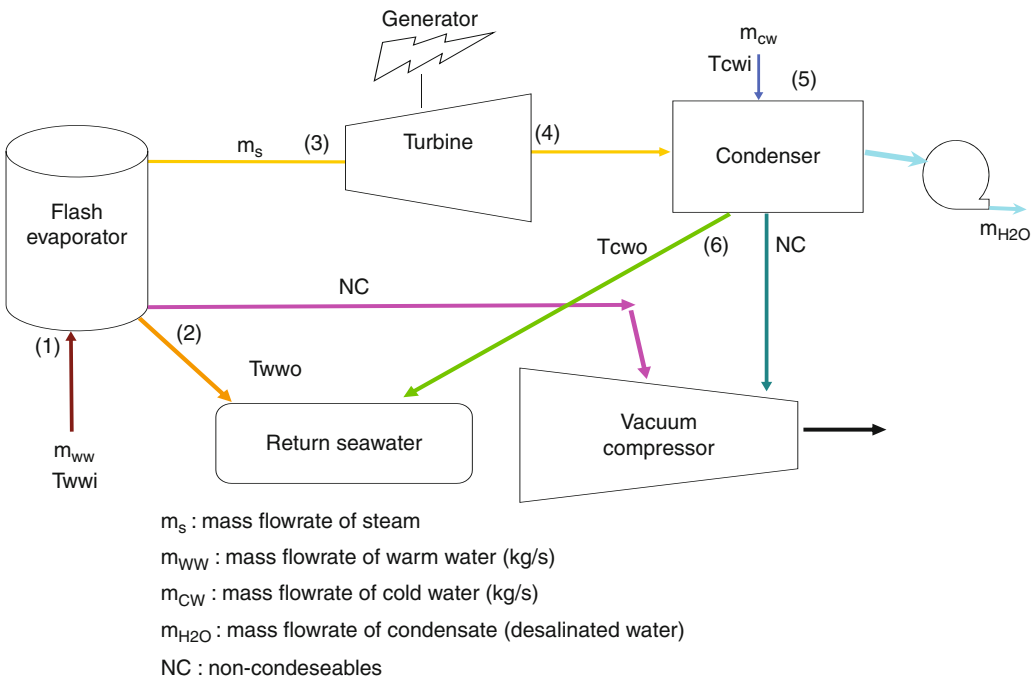

Ocean Thermal Energy Conversion. Figure 4
Open-cycle OTEC process flow diagram

in seawater (essentially air) come out of solution in a vacuum. These gases are not condensable and must be exhausted from the system.

In spite of the aforementioned engineering challenges, the Claude cycle enjoys certain benefits from the selection of water as the working fluid. Water, unlike ammonia, is nontoxic and environmentally benign. Moreover, since the evaporator produces desalinated steam, the condenser can be designed to yield fresh water. In many potential sites in the tropics, potable water is a highly desired commodity that can be marketed to offset the price of OTEC-generated electricity.

Flash evaporation is a distinguishing feature of open cycle OTEC. Flash evaporation involves complex heat and mass transfer processes. In the configuration tested with the *210 kW OC-OTEC Experimental Apparatus* [9, 10] warm seawater was pumped into a chamber through spouts designed to maximize the heat-and-mass-transfer surface area by producing a spray of the liquid. The pressure in the chamber (2.6% of atmospheric) was less than the saturation pressure of the warm seawater. Exposed to this low-pressure environment, water in the spray began to boil. As in thermal desalination plants, the vapor produced was relatively pure steam. As steam is generated, it carries away with it its heat of vaporization. This energy comes from the liquid phase and results in a lowering of the liquid temperature and the cessation of boiling. Thus, as mentioned above, flash evaporation may be seen as a transfer of thermal energy from the bulk of the warm seawater to the small fraction of mass that is vaporized to become the working fluid. Approximately 0.5% of the mass of warm seawater entering the evaporator is converted into steam.

A large turbine is required to accommodate the relatively large volumetric flow rates of low-pressure steam needed to generate any practical amount of electrical power. Although the last stages of turbines used in conventional steam power plants can be adapted to OC-OTEC operating conditions, existing technology limits the power that can be generated by a single turbine module, comprising a pair of rotors, to about 2.5 MW. Condensation of the low-pressure working fluid leaving the turbine occurs by heat transfer to the cold seawater. This heat transfer may occur in a Direct-Contact-Condenser (DCC), in which the seawater is sprayed directly over the vapor, or in a Surface Condenser (SC) that does not allow contact between the coolant and the condensate. DCCs are relatively inexpensive and have good heat transfer characteristics due to the lack of a solid thermal boundary between the warm and cool fluids. Although SCs for OTEC applications are relatively expensive to fabricate, they permit the production of desalinated water. Desalinated water production with a DCC requires the use of fresh water as the coolant. In such an arrangement, the cold seawater sink is used to chill the fresh-water coolant supply using a liquid-to-liquid heat exchanger.

Effluent from the low-pressure condenser must be returned to the environment. Liquid can be pressurized to ambient conditions at the point of discharge by means of a pump or, if the elevation of the condenser is suitably high, it can be compressed hydrostatically. Noncondensable gases, which include any residual water vapor, dissolved gases that have come out of solution, and air that may have leaked into the system, must be pressurized with a compressor. Although the primary role of the compressor is to discharge exhaust gases, it usually is perceived as the means to reduce pressure in the system below atmospheric. For a system that includes both the OC-OTEC heat engine and its environment, the cycle is closed and parallels the Rankine cycle. Here, the condensate discharge pump and the noncondensable gas compressor assume the role of the Rankine cycle pump.

The analysis of the cycle yields (Fig. 4):

Heat (added) absorbed from seawater (J/s)	$q_w = \dot{m}_{ww} Cp\,(T_{wwi} - T_{wwo})$
Steam generation rate (kg/s)	$\dot{m}_s = q_w/hfg$
Turbine work (J/s)	$w_T = \dot{m}_s(h_3 - h_4)$ $= \dot{m}_s\,\eta_T\,(h_3 - h_{4s})$
Heat (rejected) into seawater (J/s)	$q_c = \dot{m}_{cw} Cp\,(T_{cwo} - T_{cwi})$

where

$\dot{m}_{ww}$ is the mass flow rate of warm water; Cp the specific heat; T_{wwi} and T_{wwo} the seawater temperature at the inlet and outlet of the heat exchanger; hfg the heat of evaporation; and the enthalpies at the indicated points are given by h, with the subscript s referring to constant entropy. The turbine isentropic efficiency is given by η_T. The subscript cw refers to the cold water.

The 210 kW OC-OTEC Experimental Apparatus

The *210 kW OC-OTEC Experimental Apparatus* was conceived to answer questions related to operation of OTEC plants (Fig. 1). The apparatus was operated for 6 years (1993–1998), providing valuable data and pointing the way for future modifications and improvements in the OC-OTEC process. The turbine-generator was designed for an output is 210 kW for 26°C warm surface water and a deep water temperature of 6°C. A small fraction (10%) of the steam produced was diverted to a surface condenser for the production of desalinated water. The highest production rates achieved were 255 kW (gross) with a corresponding net power of 103 kW and 0.4 l/s of desalinated water. It must be noted that the net power was not optimized because pumping losses were relatively high due to the use of a seawater system that was already available. It is expected that for a commercial size plant the ratio of net to gross power will be about 0.7 [9, 10].

The relationships between power production and the system control parameters were established experimentally. From the perspective of the overall system, the control parameters are the flow rate of warm water; the flow rate of cold water; and the compressor subsystem setting as given, for example, by the inlet pressure. The other control parameters are set by seasonal variations of seawater temperature and cannot be set by the operator.

Figure 5 depicts the effect in gross power output as the cold-water temperature varies. The power increases as the temperature decreases with all other control parameters constant. The somewhat unexpected oscillation in cold-water temperature depicted in the figure is induced by internal waves of periods in the order of 1 h (with corresponding wave lengths of approximately 3,500 m) and 50 m height. These internal waves were present in the majority of the time history records.

The power output as a function of warm-water temperature, with all other control parameters constant is shown in Fig. 6. The relationship depicted in Fig. 6 is obvious. It is interesting to note that the temperature variations shown, by means of the 1 min averages of surface water temperature (20 m depth) sampled once per second, are apparently caused by a warmer water mass intrusion that could have been driven by an ocean gyre of the kind observed in coastal regions close to channels (in this case the Alenuihaha Channel between Maui and the Big Island of Hawaii).

Data records like these were used to establish that the variation of power output with seawater temperature is approximately 34 kW/°C at power levels of about 200 kW. It was also determined that the variation

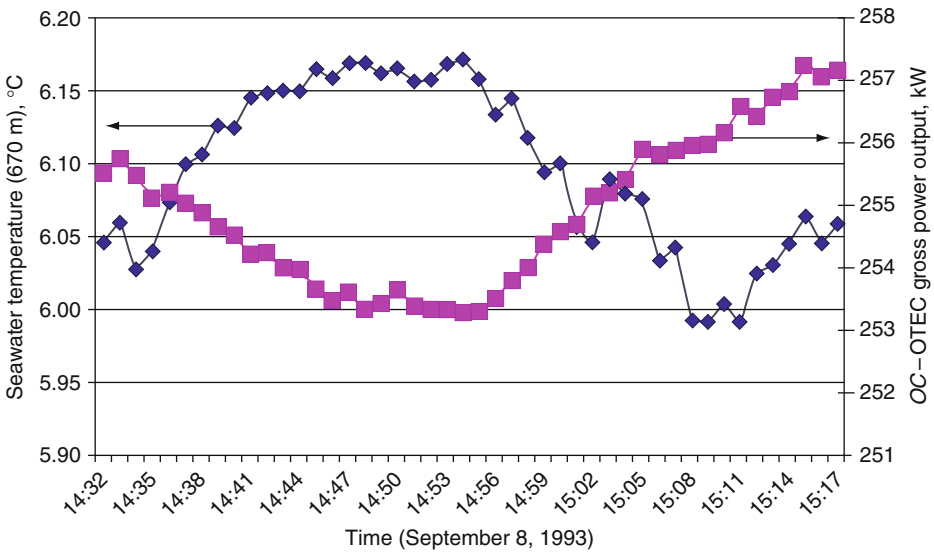

Ocean Thermal Energy Conversion. Figure 5

210 kW OC-OTEC experimental apparatus: Power output variation as a function cold-water temperature

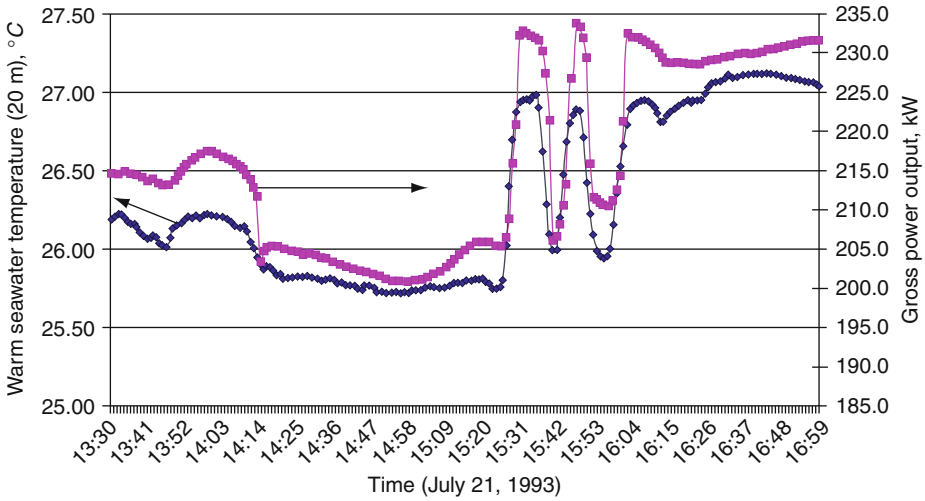

Ocean Thermal Energy Conversion. Figure 6
210 kW OC-OTEC experimental apparatus: Power output variation as a function warm-water temperature

of power with vacuum pumps inlet pressure, with all other control parameters kept constant, is given by 0.2 kW/Pa such that for an inlet pressure lowering of 5 Pa, an extra 1 kW of power is realized. The minimal inlet pressure achievable is dictated by the pumps' capability. This type of information is used to design of the controls for OTEC systems.

The data and experience obtained demonstrated that the OC-OTEC process is technically feasible for the production of base load electricity and desalinated water. This has been used as the basis for the design of a 50 MW OC-OTEC plant housed in a ship-shaped platform [25].

The most significant and exciting lessons learned were those which were fundamental new insights into the OC-OTEC process. The two main discoveries were the unstable synchronous generator output, and the violent outgassing of seawater in the heat exchangers. The most annoying problem was the frequent failures of the grease-lubricated bearings of the centrifugal pumps used for the vacuum and exhaust system. In retrospect, this was due to a major design oversight. Equipment operating at speeds higher than approximately 27,000 rpm should, in general, not use grease-lubricated bearings. It was concluded that high-speed centrifugal pumps with, for example, magnetic bearings can be used in future OC-OTEC systems to achieve extended life cycles, relatively low power consumption and, therefore, optimum net power.

Other significant lessons learned (or relearned) and observations from the perspective of an operator of the OTEC experimental or pilot plant facility were:

- Specifications should be written to emphasize the particulars of the job excluding "boiler plate" information.
- Make the plant "user friendly" from the standpoint of troubleshooting, maintenance, repair and modification.
- Include technical field support from suppliers of major equipment but be prepared to solve most problems on your own.
- Select equipment with excess capacity. It was appropriate to optimize design point performance, but there will always be off-design operations requiring additional capacity.
- Mechanical equipment specifically designed for OTEC must be instrumented to measure temperatures and pressures in as many locations as possible. For example, measurements performed with sensors installed, in the field, to estimate temperatures around the bearings of the high-speed centrifugal pumps revealed that they were failing because of two main causes: (1) deterioration of the bearing's lubricant grease due to high temperatures and/or (2) differential expansion of the outer and inner rings, resulting in squeezing of the ball bearings.

- If equipment has moving parts evaluate the bearing system and ask potential supplier to provide references of successful application of their design before purchase.
- Consider the corrosive saltwater, condensate, and the typically harsh environment of OTEC sites when making design decisions, especially material selection and placement of mechanical and electrical equipment.
- Concrete was an excellent material for the vacuum structures required for OC-OTEC.
- Avoid metal components, but if unavoidable, use the hot-dip-galvanized process from a factory with proven quality control procedures.
- Fresh Water, instead of seawater, should be used as the Coolant for the intercoolers used with the vacuum compressors.

The *210 kW OC-OTEC Experimental Apparatus* was also used to demonstrate that frequency control in the island mode is achieved with either a load-diversion-governor (LDG) or with the vacuum compression system. OTEC plants installed in isolated tropical locations would require some means of controlling turbine-generator speed to maintain 60 Hz (or 50 Hz) under varying conditions of power production and load demand. They would not have the line frequency, from an established electrical grid, to fix their turbine-generator speed. Such a stand-alone power plant is referred to as operating in an island mode or being islanded.

Alternating current (AC) power is produced by either a synchronous or induction generator. The 60 Hz AC comes from a two pole synchronous generator turning at 3,600 rpm or a four pole synchronous generator turning at 1,800 rpm, like the one used with the *210 kW OC-OTEC Experimental Apparatus*. A synchronous generator produces its own magnetic field through self-excitation and so can operate islanded without grid connection. An induction motor becomes an induction generator when driven slightly faster than synchronous speed (1,800 or 3,600 rpm) but requires VAR's (volt-amp-reactive) from the utility to produce its magnetic field. Therefore, an induction generator can never operate islanded.

Either type of generator connected to an infinitely stiff grid (very large power capacity compared to the generator size) is slaved to the grid frequency and must follow any variations in it. Because a synchronous generator operating islanded cannot depend on the grid for frequency regulation, a method of speed control is required. Without it, generator speed and AC frequency will remain constant only when its power output exactly matches that required by the load. If there is the slightest mismatch, the generator will slow down when the load increases or speed up when it decreases and thus the frequency will change.

Frequency control is referred to as governing and is accomplished with a device called a governor. Diesel generators, for example, have mechanical or electronic governors that regulate fuel flow. Likewise, steam or gas turbines have governors that control steam or fuel flow. A CC-OTEC ammonia turbine can be governed by adjusting the turbine inlet nozzles as was done in 1979 aboard the Mini-OTEC barge islanded offshore [4]. For OC-OTEC plants flow control, as done in conventional steam and ammonia turbines, is difficult due to the relatively large volumes of low density cold steam.

Large hydroelectric plants can be governed similarly to CC-OTEC. Small plants, however, are commonly allowed to run at full power and an electronic device called a load diversion governor (LDG) diverts (shunts) excess power to resistive water-heating elements to maintain 60 Hz frequency. A LDG was installed on the *210 kW OC-OTEC Experimental Apparatus*, and this control method was found to give appropriate frequency regulation. Gross control of power output is possible by regulating water flows, but this does not provide the precise frequency regulation required. This leaves process control via the vacuum compressor system as the only other alternative. Frequency control using modulation of the vacuum compressor system (i.e., varying the vacuum pumps speed to vary the condenser outlet pressure and, therefore, the power output) was also demonstrated to work.

Any islanded OC-OTEC plant would probably consist of multiple modules for purposes of redundancy and reliability, and because of limitations on the maximum size of a single module. Thus, it would be possible to bring online or drop offline modules as load demand varies. It might be possible to design the plant such that some modules could be operated as base load units without precise frequency control but slaved to units controlling the frequency.

Frequency control could be a combination of gross regulation via water flows, tuning of the process via modulation of the vacuum system, and precise control with a LDG. Being an electronic device, the LDG might present problems of reliability. Furthermore, it seems likely that the LDG would be sized to shunt only a small portion of the total power output for purposes of trimming the total load for precise frequency control. From the standpoint of plant wear and tear, it seems unlikely that a control module would be run at full capacity all the time with a large LDG wasting excess power, as with a small hydroelectric plant.

OC-OTEC Control Parameters

The OC-OTEC control parameters are: (1) mass flow rate of warm water, (2) mass flow rate of cold water, (3) vacuum compressor inlet pressure, (4) warm-water temperature, and (5) cold-water temperature. The gross power output from an OC-OTEC power plant can be controlled only with the first three parameters, while the water temperatures are dictated by natural processes. During operations with the *210 kW OC-OTEC Experimental Apparatus*, gross power output was controlled by varying the water stream flow rates with the water pumps and the inlet pressure with the vacuum pumps [9].

Closed-Cycle OTEC

The operation of a closed-cycle OTEC plant, using anhydrous ammonia as the working fluid, is modeled with the saturated Rankine cycle. Figure 7 shows the process flow diagram of the CC-OTEC cycle. The analysis of the cycle is straightforward. Based on a unit mass flow rate of ammonia vapor (kg/s) in the saturated cycle

Heat Added (J/kg)	$q_A = h_6 - h_5$
Turbine Work (J/kg)	$w_T = h_6 - h_7$
Heat Rejected (J/kg)	$q_R = h_8 - h_9$
Pump Work (J/kg)	$W_P = h_5 - h_9$
Cycle Net Work (J/kg)	$\Delta W_{net} = (h_6 - h_7) - (h_5 - h_9)$
Thermal Efficiency	$\eta th = \Delta W_{net}/q_A$

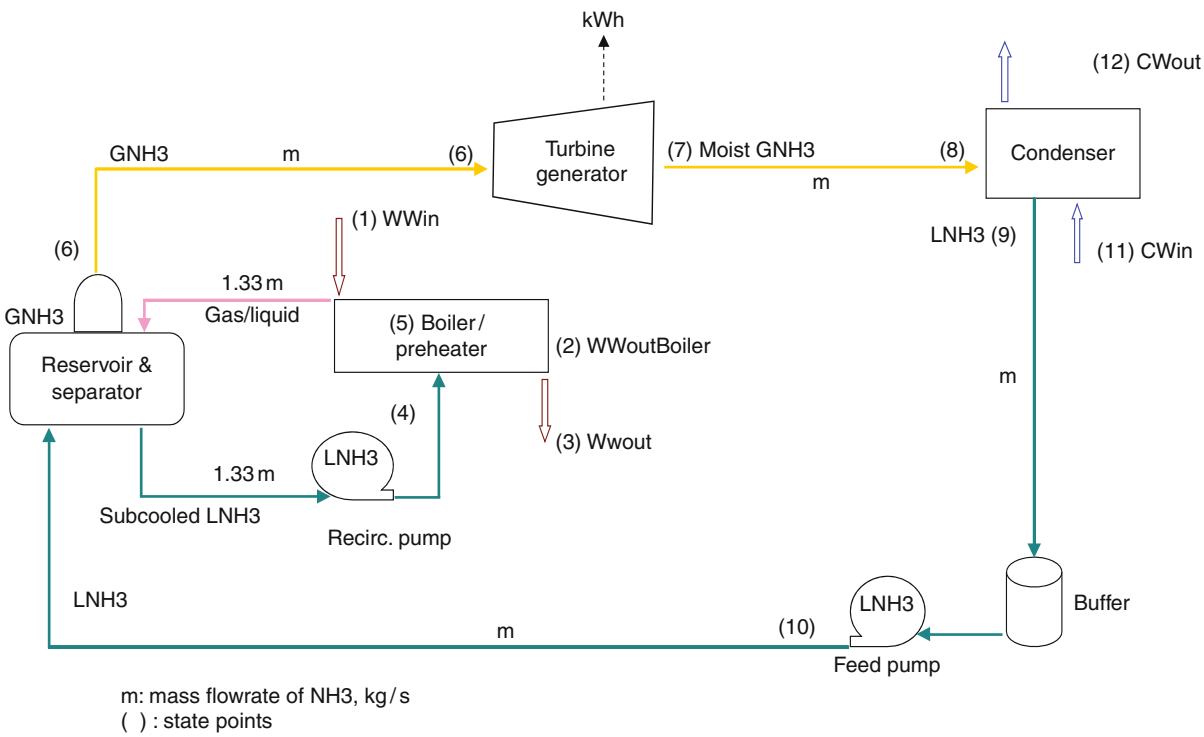

Ocean Thermal Energy Conversion. Figure 7
Closed-cycle OTEC flow diagram

where, h is the enthalpy at the indicated state point. It follows that the heat-added plus the pump-work is equal to the heat-rejected plus the turbine-work. Please see section "State of the Art 10 MW CC-OTEC Pilot Plant" for further information.

Evaporator Performance (CC-OTEC)

Relatively cold liquid ammonia (LNH_3) is fed to the evaporator system (encompasses the preheater and boiler) from the separator/reservoir tank with the recirculating pump. The preheater warms the LNH_3 to a temperature approaching the saturation temperature corresponding to the boiler's pressure. This is followed by the actual "boiling" of the ammonia into a wet vapor.

Conservation of energy, considering a control volume enclosing the entire evaporator system and neglecting the relatively small enthalpy difference between the liquid ammonia at the inlet and outlet, yields:

$$Cp\ dMww/dt\ \Delta\ Tww\ =\ hfg\ dMGNH_3/dt$$

where

Cp, the specific heat of seawater at constant pressure is 4 kJ/kg-°C under OTEC conditions
dMww/dt, the mass flow rate of warm seawater (kg/s)
ΔTww, the seawater temperature drop across the evaporator (°C)
hfg, is the latent heat of vaporization at the evaporator exit (kJ/kg)
$dMGNH_3/dt$, the mass flow rate of the ammonia gas at the evaporator exit (kg/s)

The water-side heat duty is given by the left-hand side of the equation and the ammonia-side heat duty by the right-hand side.

The overall heat transfer coefficient Uo (kW/m^2 K) can be estimated by equating the heat duty to [Uo A LMTD], where A is the effective heat transfer area and the log-mean-temperature-difference (LMTD) is defined such that:

$$UoA\ =\ Cp\ dMww/dt\ Ln\ [(Twwin - Tsat)/(Twwout - Tsat)]$$

where, Ln is the natural logarithm and Tsat is the saturation pressure at Pevpout. It must be noted that taking Tsat as the saturation temperature corresponding to the average ammonia pressure in the Evaporator increases the UoA estimate by a factor of approximately 1.35. This must be taken into consideration when comparing different types of evaporators.

Another parameter of importance in the evaluation of performance is the quality (χ) of the ammonia vapor leaving the evaporator. Quality is the ratio of the gas-mass flow rate to the total mass flow rate. That is, the ratio of the mass of ammonia flowing into the turbine to the mass flow rate into the boiler. This is estimated by the ratio of the flow rate measured downstream of the feed pump to the flow rate measured in the recirculating flow loop.

For optimum performance, the ammonia vapor at the exit of the evaporator must be relatively wet. As shown in Fig. 7, a closed-cycle OTEC system needs a device between the evaporator and the turbine to separate the gas from the liquid (i.e., a separator).

Condenser Performance (CC-OTEC)

Relatively dry ($\chi > 98\%$) ammonia vapor, exiting the turbine, flows into the condenser system. The relatively warm ammonia vapor flowing inside the condenser panels is cooled by cold seawater, flowing between the panels, and begins to condense. The heat released by the ammonia during the condensation process is absorbed by the cold seawater.

Conservation of energy, considering a control volume enclosing the entire condenser system and neglecting the relatively small enthalpy difference between the liquid ammonia at the inlet and outlet, yields:

$$Cp\ dMcw/dt\ \Delta Tcw = hfg\ \chi\ dMGNH_3/dt$$

where

Cp, the specific heat of seawater at constant pressure is 4 kJ/kg under OTEC conditions
dMcw/dt, the mass flow rate of cold seawater (kg/s)
ΔTcw, the seawater temperature drop across the condenser (°C)
hfg, is the latent heat of condensation at the condenser inlet pressure (kJ/kg)
$dMGNH_3/dt$, the mass flow rate of the ammonia gas at the evaporator exit (kg/s)
χ is the quality of the ammonia vapor at the inlet.

The left-hand side of the equation gives the water-side heat duty and the right-hand side the ammonia-side heat duty.

The overall heat transfer coefficient Uo (kW/m^2 K) can be estimated by equating the heat duty to [Uo A LMTD], where A is the effective heat transfer area and the log-mean-temperature-difference (LMTD) is defined such that:

$$UoA = Cp\ dMcw/dt\ Ln\ [(Tsat - Tcwin)/(Tsat - Tcwo)]$$

where, Ln is the natural logarithm and Tsat is the saturation pressure at Pcndin. It must be noted that taking Tsat as the saturation temperature corresponding to the average ammonia pressure in the condenser increases the UoA estimate by a factor of approximately 1.28. This must be taken into consideration when comparing different types of condensers.

CC-OTEC Control Parameters

The CC-OTEC control parameters are: (1) mass flow rate of warm water, (2) mass flow rate of cold water, (3) working fluid (e.g., NH3) mass flow rate and recirculating to feed flow ratios, (4) warm-water temperature, and (5) cold-water temperature. The gross power output from a CC-OTEC power plant can be controlled only with the first three parameters while the water temperatures are dictated by natural processes.

State of the Art 10- MW CC-OTEC Pilot Plant

The concept presented in this Section is based on state-of-the-art manufacturing and practices and could be designed, purchased, and installed to represent a complete scaled version of a commercial-size OTEC plant.

An optimized plant with flow rates of 27.7 m^3/s (28,450 kg/s), 4.5°C cold water drawn from a depth of 1,000 m; and, 52.8 m^3/s (54,000 kg/s) 26°C warm water drawn from a depth of about 20 m, would yield 16 MW at the generator terminals (P_{gross}) with 5.3 MW (P_{loss}) required to pump seawater and the working fluid (e.g., anhydrous ammonia) through the plant. The net output (P_{net}) would be 10.7 MW. To keep pumping losses at ~30% of P_{gross}, an average speed of less than 2 m/s is considered for the seawater flowing through the pipes transporting the seawater resource to the OTEC power block.

OTEC design parameters can be generalized as follows:

- In-house or parasitic electrical loads P_{loss} represent about 30% of P_{gross}, such that the exportable power (P_{net}) is about 70% of P_{gross};
- A cold-water flow rate (Q_{cw}) of 2.6 m^3/s is required per MW_{net};
- The optimal warm-water flow rate (Q_{ww}) is about $1.9 \times Q_{cw}$.

P_{gross} is proportional to the square of the temperature differential (ΔT) and the seawater flow rate, such that:

$$P_{net} = P_{gross} - P_{loss} = \beta Q_{cw}(\Delta T)^2 - P_{loss}$$

where β and P_{loss} are system specific. Considering nominal values, it can be shown that a 1°C change in ΔT leads to a change of approximately 15% in P_{net}. This generalization compares favorably with the site-specific heat and mass balance presented below.

A number of configurations for OTEC plants have been proposed. These include moored plants, grazing plants, land-based plants, shelf-mounted towers, guyed-tower, and tension leg plant concepts. Large and small waterplane platforms have been considered. In general, the former (ship shape) is considered cost effective in most commercial application studies. Moored OTEC configurations transmit electrical power to shore via a submarine power cable. The grazing plant operates as a self-contained factory ship on which an energy-intensive product like ammonia or hydrogen is produced. The main advantage of this design is that the plant, with its mobility, can cruise or graze around the tropical waters and is essentially decoupled from land [1].

The plant presented in this section would be housed in a 26,000 t deep draft ship moored 10–20 km offshore. The 1,000- m long 3.9 m i.d. fiber-reinforced-plastic (FRP) sandwich construction CWP is attached to a gimbal at midship. The mooring system consists of a single-point mooring system, including a power (electrical) swivel. The Aluminum plate-fin heat exchangers can be manufactured in existing factories.

The electricity is transmitted to shore via a commercially available submarine power cable (~10 cm diameter).

Major subsystem	10 MW pilot plant
Floating platform	Ship shaped: 90 m (LBP) × 32 m (beam) × 16 m (Height) with operational draft at 9 m
Mooring positioning and control	Single Point Moor (e.g., FPSO platforms) with dynamic positioning thrusters and power (electrical) swivel
Heat exchangers	Compact Al plate/fin installed below main deck
NH_3 turbine-generators	Installed on main deck
CWP	FRP Sandwich manufactured on-shore; horizontal tow and upended
Submarine power cable	34.5 kV, AC ethylene-propylene rubber insulation

The final design will have to integrate the following:

- Platform hull and structures
- Propulsion and positioning
- Land support system
- Seawater pipes and pumps
- Pipe/hull connection
- Deployment and attachment of seawater pipes to the platform
- The power block consisting of the evaporator, turbine-generator, and condenser along with the ammonia system and instrumentation and controls
- The electrical transmission system consisting of the submarine power cable and the power swivel connection

Design Environment

The design-oriented analysis of an OTEC system must consider both survivability design loads and operational/fatigue loads. The first kind are based on extreme environmental phenomena, with a long return period, that might result in ultimate strength failure, while the second kind result in fatigue-induced failure through normal operations. The meteorological, sea surface, water column, and sea floor description required to determine both kinds of loading for each major subsystem are established by considering the design processes.

Environmental loading conditions corresponding to a generic and somewhat extreme (e.g., relatively high surface current) site are considered as applicable until the specific site is identified (Table 1). Seafloor conditions are not considered at this stage of the design.

The operational environment for the pilot plant is given by up to 3.7 m (12′) significant wave height (7.5 s period) and surface currents below 1.5 m/s. The conditions used to determine survivability design loads are given by: 20 m/s winds, 1.5 m/s surface currents, 6.1 m (20′) significant wave height (9.6 s period) head seas. For environmental conditions exceeding these values, the vessel would release the CWP and the single-point mooring (with submarine power cable) and move away from the storm track. The CWP and single-point mooring attachment sequences must be designed to be reversible.

Power Cycle

A simplified block diagram of the power cycle is shown in Fig. 7. Given a surface water temperature range of 24–28°C and a 1,000 m deep ocean water temperature ranging from 4°C to 5°C, the design values were selected as 26°C and 4.5°C. Output would be ≈15,900 kW at the generator terminals with a corresponding net production of ≈10,600 kW.

Ocean Thermal Energy Conversion. Table 1 Baseline design environment for the 10 MW pilot plant

Ocean surface temperature:	26°C (Annual average) 24–28°C range
Ocean temperature at 1,000 m depth:	4.5°C (Annual average) 4–5°C range
Operational limit waves:	3.7 m significant wave height/ 7.5 s period
Survival conditions:	6.1 m significant wave height/ 9.6 s period 20 m/s wind (~40 knots) 1.5 m/s ocean current (~3 knots)

For the temperature range considered, the gross power output varies as a function of surface water temperature by ≈1,600 kW/°C such that for temperatures of 28°C and 4.5°C, a gross power output of ≈19,100 kW is sufficient to produce 13,800 kW-net with an in-plant consumption of 5,300 kW. In the case of the lower surface temperature, the net output would be 7,400 kW.

The facility would employ 550 kg/s of anhydrous ammonia (NH_3) as the working fluid with the power extracted through a commercially available turbine-generator and aluminum heat exchangers for the evaporator and condenser units. The design seawater flow rates are:

- 52.8 m^3/s (54,050 kg/s) of warm water
- 27.7 m^3/s (28,450 kg/s) of cold water

The flow rates of warm and cold seawater are optimization to maximize net power in the electricity production mode under the baseline conditions.

The process illustrated in Fig. 7 can be further described as follows. Warm seawater is drawn in from sumps by submersible pumps into the evaporator. The evaporator is designed to withstand extended exposure to seawater and ammonia. Pressurized liquid ammonia is fed into the evaporator through a system of pumps and valves. The evaporator includes a "preheater" to provide liquid ammonia to the "boiler" at the saturation temperature. Energy transferred from the warm seawater evaporates the ammonia, and the vapor that is produced rises up through a low-pressure-drop mist eliminator. The mist eliminator is included in the flow path of the wet vapor to separate the liquid ammonia and to ensure minimal carry-over of entrained liquid ammonia into the turbine. The separated liquid ammonia flows by gravity to the recirculation pump shown in Fig. 7.

The ammonia vapor exiting the evaporator flows past a series of stop and control valves before expanding through a single-flow axial turbine coupled to a synchronous electrical generator. A short diffuser downstream of the turbine stage is employed to recover some kinetic energy. The exiting vapor passes down into a second heat exchanger (condenser), where it is condensed using cold seawater brought up from a depth of 1,000 m. Several submersible pumps are used to draw the cold water from a sump connected to the CWP.

The pressure of the ammonia condensate is increased, and the liquid is transferred to the evaporator by means of a feed pump before beginning the cycle again. The ammonia power system flow loop is connected to an on-site ammonia storage and purification system. The purification system removes any water or solids which may have entered the working fluid.

Ammonia is used extensively in industry, and relevant codes, standards, and practices have been established (e.g., in the USA) for the construction and operation of ammonia systems. Temperatures and pressures encountered in the present application fall well within the ranges of practical experience. It is not anticipated that any significant safety risk will be entailed during normal operation of this facility if standard procedures are followed.

A chlorination unit will be included to minimize biofouling of the evaporator passages. It has been determined that biofouling from cold seawater is negligible and that evaporator fouling can be controlled effectively by intermittent chlorination (50–100 parts per billion chlorine for 1 h/day). Monitoring of the effluent water for elevated concentrations of ammonia or chlorine would be performed on a regular basis.

The volumetric space requirements for the heat exchangers and the turbine-generators are summarized in Table 2. It is understood that considerable design work would be required to develop the detailed engineering design. However, these global volumetric dimensions can be used to size the plantship.

Turbine-generator (TG) units required for the 10 MW-net plant are commercially available. It is understood that the maximum size available *off-the-shelve* is rated at about 15 MW-gross. Herein, it is assumed that 4 × 4 MW-gross units would be used. The overall dimensions of a 4 MW unit are 17 m (length) × 4 m (width) × 4 m (height), including the lube-oil-skid.

All seawater effluents are mixed together and returned to the ocean at a depth of 60 m by means of two 5.5 m inside diameter FRP pipes (or alternative one a 7.8 m i.d. pipe). This return depth meets the most stringent environmental standards.

Ocean Thermal Energy Conversion. Table 2 Power cycle heat exchangers and TG: Global volumetric space requirements

Unit	Core dimensions	4 MW-gross assembly w/flanges	Global volumetric space per 4 MW assembly, including seawater and NH_3 piping
NH_3/ seawater evaporator (Plate-fin)	6.1 m (L) 1.0 m (W) 4.6 m (H)	6.1 m (L) 4.0 m (W) 7.0 m (H)	Lower decks: 14 m (L) 10 m (W) 14 m (H)
NH_3/ seawater condenser (Plate-fin)	6.1 m (L) 1.0 m (W) 4.6 m (H)	6.1 m (L) 4.0 m (W) 7.0 m (H)	Lower decks: 14 m (L) 10 m (W) 14 m (H)
NH_3 turbines with lube oil skid	Not applicable	17 m (L) 4 m (W) 4 m (H)	Main deck: 17 m (L) 4 m (W) 4 m (H)

Electrical Interface

It is expected that the OTEC pilot plant would be operated in parallel with the local utility system. The plant will be equipped with the required protective devices (relays, circuit breaker, etc.), metering equipment, and synchronizing equipment called for in the interconnect agreement. A synchronous generator unit would be used which includes the required voltage and frequency relays to trip the tie breaker or generator breaker in the event of a fault. Supervised synchronizing would be employed.

Plantship, Mooring, Propulsion, and Position Control

The objectives for the ship-shaped baseline platform (i.e., plantship) for the pilot plant are:

- Develop a floating platform of sufficient size, and with adequate structural arrangements to support large OTEC components and seawater piping systems for normal operations, as well as for maintenance and repair procedures.
- The platform shall meet international regulatory body requirements for stability and damage subdivision and be reasonably sea-kindly for the safety and comfort of personnel in severe open sea conditions.
- Ensure that OTEC components are located for ease of accessibility rather that optimum power production and system efficiency.
- The platform construction shall be cost effective and based on "state-of-the-art" tanker construction procedures.
- In addition, the mooring, propulsion, and position control systems must:
  - Maintain platform position within a predetermined watch circle with acceptable loading on the seawater pipes and the power transmission cable while exposed to the operational environment.
  - Maintain vessel deck motions within allowable values for the operation of power cycle components.
  - Provide adequate propulsive power to depart site after CWP detachment, prior to extreme environment occurrence.

The platform for the OTEC pilot plant consists of a straight-walled 26,000 ton barge fitted with semicircular ends, 90 m long, and 32 m beam with an operating draught of 9 m and 16 m height. A 1,000- m-long pipe would be suspended from the vessel via a double gimbal joint, which effectively decouples the two structures in roll and pitch. The electricity produced would be transmitted to shore via a submarine power cable through a power (electrical) swivel.

The overall plantship dimensions given in Table 3 provide the space required for the heat exchangers (HXs), turbine-generators (TGs), and pumps with associated sumps. The HXs are located below the main deck with the TGs on the main deck. Figures 8 and 9 provide the side view and top view of the pilot plantship.

The conceptual position control system consists of two subsystems: a single-point moor to maintain position, within a given watch circle, during OTEC operations (~99% of the time) and up to the site departure condition; and four propulsion and position control thrusters to assist in directional positioning

Ocean Thermal Energy Conversion. Table 3 OTEC plantship baseline dimensions

Mode	LBP (m)	B beam (m)	D ops draught (m)	H height (m)	Displacement (t)
CC-OTEC 10 MW pilot plant	90	32	9	16	26,000
100 MW OTEC H_2 plantship [13]	250	60	20	28	285,000
"Typical" double-hull tanker	180	32.2	11.2	19.2	≈63,000
"Typical" double-hull container	205 LOA: 217	32.2	10.5	20.3	≈68,000
Panamax limits	≤294.1 (LOA)	≤32.3	≤12		

Displacement: LBP × B × D × ρ × Cb; *LBP* length-between-perpendiculars
ρ, density seawater 1,022 kg/m^3; Cb, block coefficient ≈0.95

(weather vaning) during operations and to provide the propulsive power required to depart the site. The baseline single-point mooring subsystem is commercially available. The four propulsion thrusters are rated at ≈2,500 kW each and would be used minimally during operations.

The position control requirements during operations are equivalent to having an annual thruster power of less than 1,500 kW. Thruster requirements are dominated by the current loading on the OTEC pipes under this somewhat extreme conditions with surface currents as high as 1.5 m/s. The actual schedule for thruster usage would be developed during the final design phase.

The SOA mooring system includes a power swivel linked to the OTEC plant at a turntable. This system provides a minimal-thruster-power-consumption means of holding the OTEC platform in position. The system provides mooring cable riser tension sufficient to limit the platform watch circle radius to about 25% of water depth; the attachment decouples the power transmission cable from the platform motions; and the power cable experiences minimum movement across the sea floor.

Auxiliary power diesel generators would be available to operate the thrusters during transit and departure, as well as in situ when OTEC power is not available.

Seawater Components

The OTEC seawater system consists of the pipes and pumps required to supply warm and cold seawater streams to the OTEC HXs and allow for the return of effluents to the ocean. Baseline parameters are summarized in Table 4. The concept considered for the cold water pipe (CWP) is a 3.9 m i.d. glass-fiber-reinforced plastic (FRP) sandwich pipe suspended from the OTEC platform to a depth of 1,000 m. Warm seawater would be drawn in through two 4.6 m i.d. pipes from a depth of about 20 m. The mixed effluent would be returned through two 5.5 m i.d. FRP pipe at a depth of 60 m. This return depth has been selected to minimize the environmental impact.

There is one 6-m-diameter cold-water sump and two 7-m-diameter sumps each for warm water and mixed effluent return water with appropriate distribution piping and pumps. Each of the five sumps has sufficient volume to sustain the head necessary for pumping during start-up and normal operations. The warm- and cold-water sumps house the submersible pumps envisioned for the pilot plant.

The CWP is attached to the platform with a gimbal located on the platform's inner bottom structure. Cold water in the sump is free to flood to the 9 m operating waterline of the platform. The deep-well pumping system located on centerline draws water up through the well and into a manifold that distributes cold water.

This pumping system supplies power for the flow of cold water from the pipe inlet to its discharge through the mixed effluent return pipes. The mixed effluent return from all of the condensers and evaporators is discharged from the mixed effluent sumps through two 5.5 m diameter by 50-m-long pipes. The return water pipes are attached to the inner bottom structure of the platform via a spherical head and inner bottom ring socket.

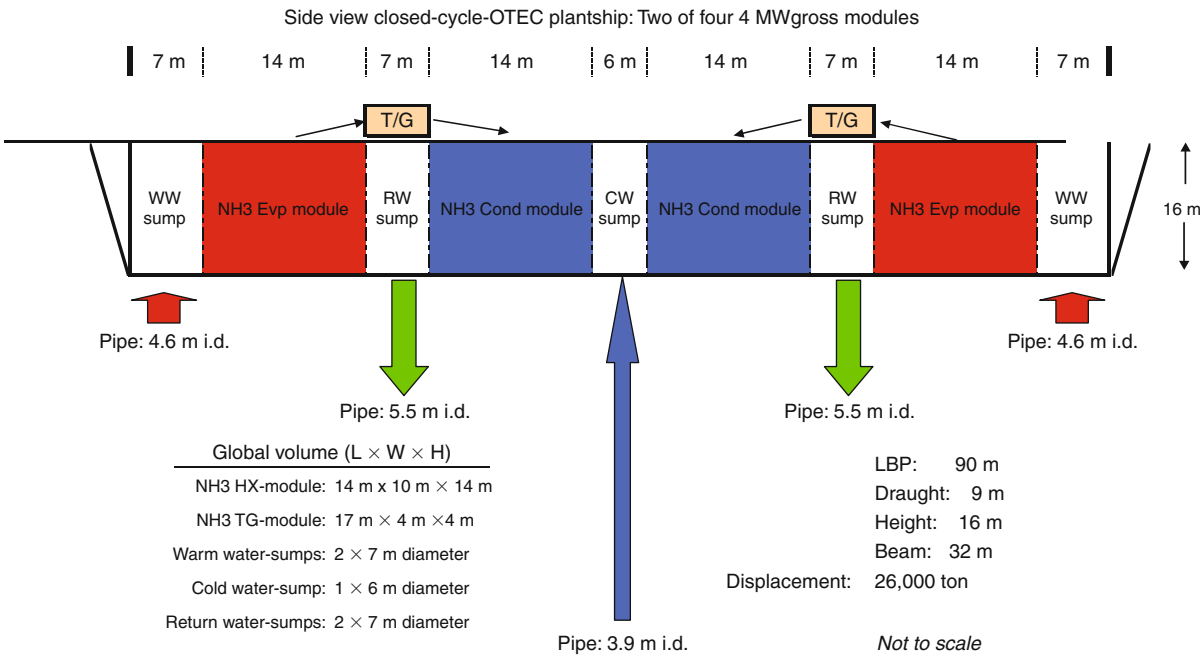

Ocean Thermal Energy Conversion. Figure 8

10 MW-net OTEC pilot plantship: *Side view*. *Broken lines* indicate space overlap

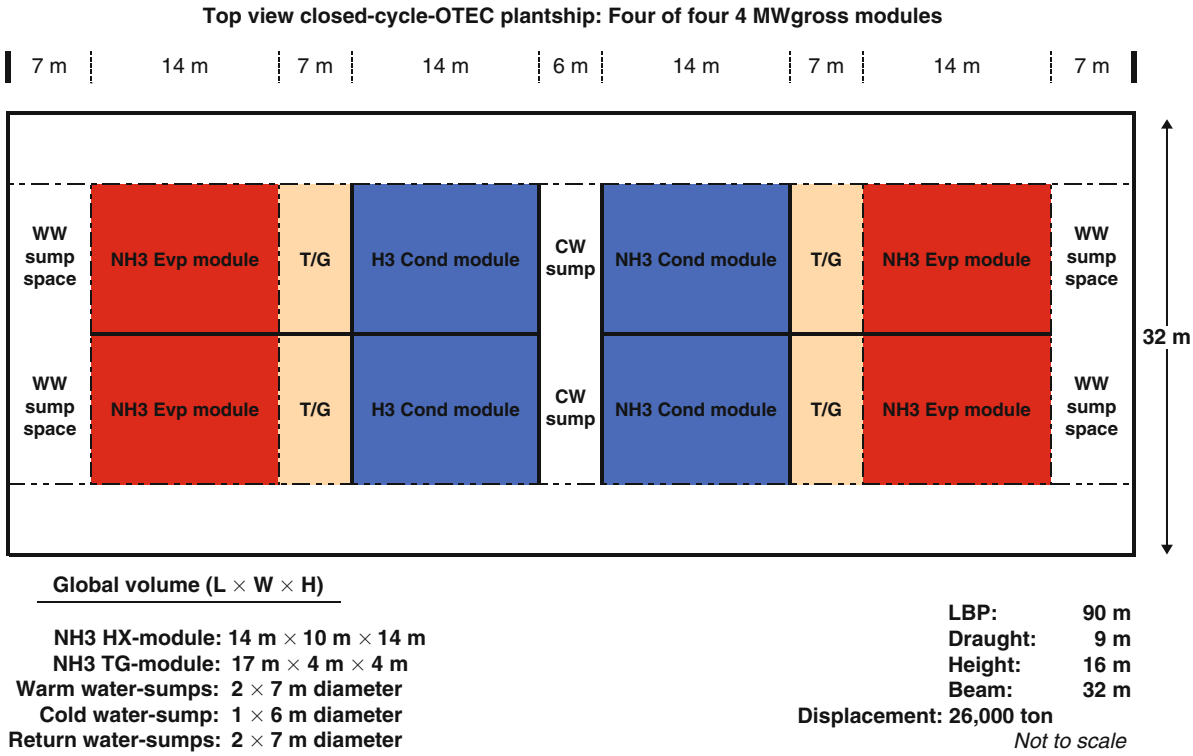

Ocean Thermal Energy Conversion. Figure 9

10 MW-net OTEC pilot plantship: *Top view*. *Broken lines* indicate space overlap

Ocean Thermal Energy Conversion. Table 4 Seawater system baseline parameters

Water system		
Cold water to condenser:	439,100	gpm
Cold-water volumetric rate:	27.7	m^3/s
Cold-water density:	1.0269	kg/l
Cold-water mass rate:	28,445	kg/s
Cold-water temperature:	4.5	°C
Cold-water pipe i.d.	3.9	m
Cold-water average speed:	2.3	m/s
Cold-water pump efficiency:	0.72	
Warm water to evaporator:	837,600	gpm
Warm-water volumetric rate:	52.8	m^3/s
Warm-water density:	1.0229	kg/L
Warm-water mass rate:	54,049	kg/s
Warm-water temperature:	26	°C
Warm-water pipes i.d.	2 × 4.6	m
Warm-water average speed:	1.6	m/s
Warm-water pump efficiency:	0.72	
Warm-to-cold-water ratio	1.9	
Combined return pipes i.d.	2 × 5.5	m

Cold Water Pipe

The cold water pipe (CWP) structural properties are summarized in Table 5. The selected CWP walls consist of a sandwich construction, with two 14 mm thick cross-plied unwoven FRP facesheets separated by a 50 mm syntactic foam layer (thus, the outer diameter of the CWP is 4.06 m). The load-bearing FRP provides structural strength, whereas the foam filler allows for the adjustment of wet weight and flexural bending stiffness, as well as for load transmission. The syntactic foam uses glass microspheres and milled fiber to achieve a density of 670 kg/m^3 for buoyancy control. The facesheets are helically wound using 450 yield strand interspersed with 20 oz unidirectional roving and a minor amount of chopped strand. The wind angle is 60° for the helical layers. The pipe is wound in a rotating mandrel. A vinylester resin is used.

The strength of the FRP facesheets is almost comparable to that of steel, with a modulus of elasticity

Ocean Thermal Energy Conversion. Table 5 Cold-water pipe structural properties

Parameter	Value
Inside diameter	3.9 m
Laminate (facesheet) thickness	14 mm
Core (syntactic foam) thickness	50 mm
Laminate density	1,714 kg/m^3
Outside diameter	4.056 m
Core density	670 kg/m^3
Dry (air) weight	1,010 kg/m
Wet (submerged) weight	33 kg/m
Flexural rigidity, EI	1.7×10^{10} N m^2 (4.2×10^{10} lb-ft^2)
Laminate modulus of elasticity	20,600 MPa (3×10^6 psi)
Core modulus of elasticity	2,360 MPa (0.34×10^6 psi)

E equal to 20,600 MPa (3×10^6 psi). The longitudinal bending stiffness EI is about 1.7×10^{10} N m^2. Eighty 12.5-m-long CWP segments would be fabricated to facilitate land transportation and butt-connected via splice joints near the launching site (harbor). The 150-mm-deep FRP ring stiffeners, located every 6 m, would provide enhanced lateral buckling capability to resist differential (suction) loads across the CWP walls. It is expected that pipe construction would require about 12–14 months.

Several different types of CWP/Hull platform attachment (gimbal) have been proposed. This is required to decouple the pipe from the roll and pitch of the platform and minimize bending moments at their interface. The attachment system must provide a water seal at the cold-water sump to insure the quality of the cold-water resource. The gimbal should provide ease of attachment of the CWP to the platform at sea. The gimbal system selected is based on the OTEC 1 design tested in Hawaii [13, 14].

CWP deployment procedures suggested for the various configurations proposed in different suspended CWP designs have been of two generic types: (1) horizontal tow of a full-length pipe with

subsequent upending at the deployment site or (2) vertical deployment, by sections, through the OTEC platform or an adjacent work platform. Most designs have proposed transporting the pipe to the deployment site independently of the platform because combined movement may result in excessive loads and untenable vessel handling problems. The deployment method selected is basically a function of material selection and CWP buoyancy characteristics. In general, configurations which are buoyant or neutrally buoyant would employ the upending technique, while designs that are fabricated from materials that are considerably denser than seawater would utilize the vertical, sectional approach, in which the CWP is actually assembled during the deployment process. A successful deployment scenario must ensure a minimum exposure time at sea, define weather windows clearly and be somewhat reversible [14]. This is especially important for the attachment of the CWP to the barge since detachment must be allowed before extreme events (e.g., hurricanes).

For the concept selected herein, the former procedure applies with the CWP transported awash (filled with water). Towing of the pipeline awash would be acceptable if the confidence of the deployment team in keeping the CWP reasonably well aligned with the dominant wave direction, or in short-term (≈48 h) weather forecasts, is high. Alternatively, submerging the CWP about one diameter deeper would theoretically provide a significant safety factor in reducing bending stresses through less favorable marine environmental conditions.

The conceptual CWP proposed herein will have to be reevaluated after the specific site in selected. Experience indicates bending stresses induced by platform motions as the most critical operational loads. Other concerns are fatigue failure and transportation (towing) bending stresses. A shell analysis of the CWP to quantify hoop stresses and confirm the pipe lateral buckling capability and load evaluation during CWP handling and attachment to the platform is left for the final design.

Submarine Power Cable

A submarine power cable is required to transmit the electricity produced by the 10 MW-net OTEC plant from the floating platform to shore. The baseline is a commercially available AC configuration with an ethylene- propylene rubber (EPR) insulation operating at a voltage of 34.5 kV. This voltage makes EPR insulation a prime choice since other types of insulation, which may be competitive for land-based applications, usually require the addition of a watertight metallic sheath in the marine environment. EPR insulation lends itself to the use of three-core power cables.

The submarine power cable would have an outside diameter of ≈10 cm. and it would be attached to the single point mooring system described above.

Inspection, Maintenance, and Repair (IM&R)

From the perspective of inspection, maintenance, and repair (IM&R), three general areas may be identified throughout the OTEC Platform:

- The components onboard the plantship, such as heat exchangers, turbine-generators, and pumps
- The platform hull and appendages
- The deep water components, such as CWP, submarine power cable, and mooring devices

Onboard the plantship, with adequate layout of the OTEC components, IM&R requirements should be comparable to those stipulated for onshore power plants. IM&R tasks are naturally more cumbersome for the platform itself because of the presence of seawater, and of possibly disturbing platform motions during rough weather. Diver operations and instrumentation/tool deployment from the platform decks should remain relatively easy most of the time. Moreover, the OTEC platform is not fundamentally different from other seagoing structures.

IM&R is challenging for the deep water components of the floating OTEC plant because the depths at stake place those components out of divers' reach. A failure of the mooring system could break the power cable, although thrusters are believed to provide excess redundancy in positioning the platform if the single-point moor fails.

Strict quality control procedures must be applied at the fabrication, shipping, and assembly stages before the structures are finally deployed at sea.

Site Selection Criteria for OTEC Plants

The search for renewable energy resources has resulted in OTEC's second revival. As it is well known, the

concept utilizes the differences in temperature, ΔT, between the warm tropical surface waters, and the cold deep ocean waters available at depths of about 1,000 m, as the source of the thermal energy required.

The historical monthly averages of ΔT for February and August are depicted in Figs. 10 and 11, respectively. Values are color coded as indicated in the right-hand side of the figures. The values were obtained from the National Ocean Data Center's World Ocean Atlas [16]. Deep seawater flows from the Polar Regions. These polar water, which represents up to 60% of all seawater, originates mainly from the Arctic for the Atlantic and North Pacific Oceans, and from the Antarctic (Weddell Sea) for all other major oceans. Therefore, T_{cw} at a given depth, approximately below 500 m, does not vary much throughout all regions of interest for OTEC. It is also a weak function of depth, with a typical gradient of 1°C per 150 m between 500 and 1,000 m. These considerations may lead to regard T_{cw} as nearly constant, with a value of 4–5°C at 1,000 m [3].

A desirable OTEC thermal resource of about 20°C requires typical values of T_{ww} of the order of 25°C. Globally speaking, regions between latitudes 20°N and 20°S are adequate. Some definite exceptions exist due to strong cold currents: along the West Coast of South America and to a lesser extent for the West Coast of Southern Africa. Moreover, T_{ww} varies throughout the year and, sometimes, exhibits a significant seasonal drop due to the upwelling of deeper water induced by the action of the wind: such are the cases of the West Coast of Northern Africa in the southern hemisphere winter (Fig. 11).

The following summarizes the availability of the OTEC thermal resource throughout the World:

- Equatorial waters, defined as lying between 10°N and 10°S, are adequate, except for the West Coasts of South America and Southern Africa.
- Tropical waters, defined as extending from the equatorial region boundary to, respectively, 20°N and 20°S, are adequate, except for the West Coasts of South America and of Southern Africa; moreover, seasonal upwelling phenomena would require significant temperature enhancement for the West Coast of Northern Africa, the Horn of Africa, and off the Arabian Peninsula.

The accessibility of deep cold seawater represents the most important physical criterion for OTEC site selection once the existence of an adequate thermal resource has been established. In the case of a floating plant, the issue of cold seawater accessibility is only relevant inasmuch as submarine power cables, and,

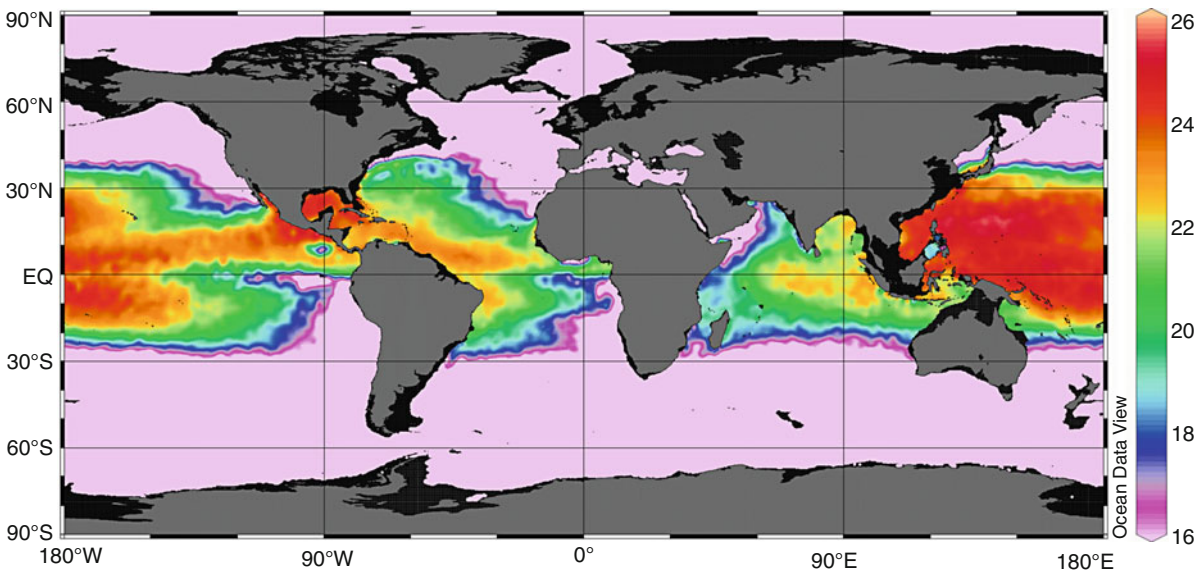

Ocean Thermal Energy Conversion. Figure 10
Historical monthly average of ΔT during February from WOA05 (From [15])

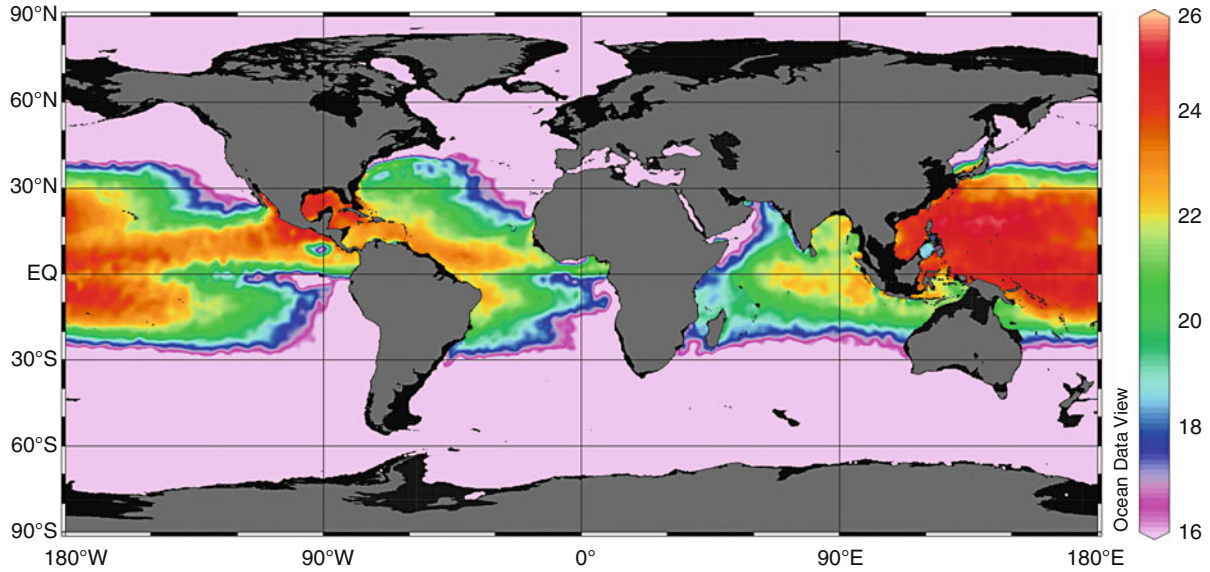

Ocean Thermal Energy Conversion. Figure 11
Historical monthly average of ΔT during August from WOA05 (From [15])

maybe, a desalinated water hose is needed to transfer the OTEC products to shore. For the grazing plantship, with energy intensive products like hydrogen or ammonia as the product, the distance is important from the perspective of the transit time for the vessels that would transport the product to shore.

Many other points must be considered when evaluating potential OTEC sites, from logistics to socioeconomic and political factors. One argument in favor of OTEC lies in its renewable character: it may be seen as a means to provide remote and isolated communities with some degree of energy independence and to offer them a potential for safe economic development. Such operational advantages, however, are often accompanied by serious logistical problems during the plant construction and installation phases: if an island is under development, it is likely to lack the infrastructure desirable for this type of project, including harbors, airports, good roads, and communication systems. Moreover, the population base should be compatible with the OTEC plant size: adequate manpower must be supplied to operate the plant, and the electricity and fresh-water plant outputs should match local consumption in orders of magnitude.

Another important point to consider is the preservation of the environment in the area of the selected site, inasmuch as preservation of the environment anywhere is bound to have positive effects elsewhere. As outlined in the section "Environmental Impact", OTEC is one of the most benign power-production technology since the handling of hazardous substances is limited to the working fluid (e.g., ammonia), and no noxious by-products are generated; OTEC merely requires the pumping and return of various seawater masses, which, according to preliminary studies, can be accomplished with virtually no adverse impact. This argument should be very attractive for pristine island ecosystems as well as for already polluted and overburdened environments. For example, the amount of CO_2 released from electricity-producing plants (expressed in gram of CO_2 per kWh) ranges from 1,000, for coal-fired plants, to 700, for fuel-oil plants, while for OC-OTEC plants it is at most ~1% of the amount released by fuel oil plants. The value is much lower in the case of a CC-OTEC plant.

Ninety-eight nations and territories with access to the OTEC thermal resource within their 200 nautical mile exclusive economic zone (EEZ) were identified in the 1980s. A partial list is provided in Table 6. For the majority of these locations, the OTEC resource is applicable only to floating plants. Unfortunately, now as then, there is no OTEC plant with an operational record available. This still remains the impediment to OTEC commercialization.

Ocean Thermal Energy Conversion. Table 6 List of nations with appropriate ocean thermal resource within their 200 nautical miles exclusive economic zone. From [12]

Geographical area	Mainland		Island	
Americas	Mexico	Guyana	Cuba	Guadeloupe
	Brazil	Suriname	Haiti	Martinique
	Colombia	French Guiana	Dominican	Rep. Barbados
	Costa Rica	Nicaragua	Jamaica	Dominica
	Guatemala	El Salvador	Virgin Is.	St. Lucia
	Honduras	Belize	Grenada	St. Kitts
	Panama	USA	St. Vincent	Barbuda
	Venezuela		Grand Cayman	Montserrat
			Antigua	The Grenadines
			Puerto Rico	Curacao
			Trinidad & Tobago	Aruba
			Bahamas	
Africa	Nigeria	Gabon	Sao Tome & Principe	
	Ghana	Benin	Ascension	
	Ivory Coast	Zaire	Comoros	
	Kenya	Angola	Aldabra	
	Tanzania	Cameroon	Madagascar	
	Congo	Mozambique		
	Guinea	Eq. Guinea		
	Sierra Leone	Togo		
	Liberia	Somalia		
Indian/Pacific Ocean	India	Australia	Indonesia	American Samoa
	Burma	Japan	Philippines	Northern Marianas
	China	Thailand	Sri Lanka	Guam
	Vietnam	Hong Kong	Papua New Guinea	Kiribati
	Bangladesh	Brunei	Taiwan	French Polynesia
	Malaysia		Fiji	New Caledonia
			Nauru	Diego Garcia
			Seychelles	Tuvalu
			Maldives	Wake Is.
			Vanuatu	Solomon Is.
			Samoa	Mauritius
			Tonga	Okinawa
			Cook Is.	Hawaii
			Wallis & Futuna Is.	

OTEC Economics

An analytical model is available to assess scenarios under which OTEC might be competitive with conventional technologies [12]. First, the capital cost for OTEC plants, expressed in $/kW-net, is estimated. Subsequently, the relative cost of producing electricity ($/kWh) with OTEC, offset by the desalinated water production revenue, is equated to the fuel cost of electricity produced with conventional techniques to determine the scenarios (i.e., *fuel cost and cost of fresh-water production*) under which OTEC could be competitive. For each scenario, the cost of desalinated water produced from seawater via reverse osmosis (RO) is estimated to set the upper limit of the OTEC water production credit. No attempt is made at speculating about the future cost of fossil fuels. It is simply stated that if a location is represented by one of the scenarios, OTEC could be competitive.

Two distinct markets were previously identified: (1) industrialized nations and (2) small island developing states (SIDS) with modest needs for power and fresh water. OC-OTEC plants could be sized at 1–10 MW, and 450,000 to 9.2 million gallons of fresh water per day (1,700–35,000 m^3/day) to meet the needs of developing communities with populations ranging from 4,500 to 100,000 residents. This range encompasses the majority of SIDS throughout the world [12].

Floating plants of at least 50 MW capacity would be required for the industrialized nations. These would be moored or dynamically positioned a few kilometers from land, transmitting the electricity to shore via submarine power cables. The moored vessel could also house an OC-OTEC plant and transport the desalinated water produced via flexible pipes.

It was also established that OTEC-based mariculture operations and air-conditioning systems could only make use of a small amount of the seawater available; and therefore, could only impact small plants. The use of energy carriers (e.g., Hydrogen, Ammonia) to transport OTEC energy generated in floating plants, drifting in tropical waters away from land, was determined to be technically feasible but requiring increases in the cost of fossil fuels of at least an order of magnitude to be cost effective.

Presently, the external costs of energy production and consumption are not included in the determination of the charges to the consumer. Considering all stages of generation, from initial fuel extraction to plant decommissioning, it has been determined that no energy technology is completely environmentally benign. The net social costs of the different methods of energy production continue to be a topic under study. Estimates of costs due to: corrosion, health impacts, crop losses, radioactive waste, military expenditures, employment loss, subsidies (tax credits and research funding for present technologies) are found in the literature. The range of all estimates is equivalent to adding from $80/barrel to over $400/barrel. Accounting for these externalities might eventually help the development and expand the applicability of OTEC but, in the interim, the scenarios that were identified in the original report should be considered again [12].

Industry did not take advantage of the information because in the 1990s, the prices of oil fuels and coal were such that conventional power plants produced cost-effective electricity (excluding externalities). Moreover, the power industry could only invest in power plants whose designs were based on similar plants with an operational record. It was concluded that before OTEC could be commercialized,

Ocean Thermal Energy Conversion. Table 7 First-generation OTEC plant capital cost estimates: (1) extrapolated archival estimates (1–50 MW) and current estimates (10–100 MW) in $/kW-net

Nominal plant size (MW-net)	Installed capital cost ($/kW)	Land/ floater	Source (extrapolated)
1.4	41,562	L	[12]
5	22,812	L	[26]
5.3	35,237	F	[14]
10	24,071	L	[12]
10	18,600	F	[26]
35	12,000	F	[26]
50	11,072	F	[12]
53.5	8,430	F	[26]
100	7,900	F	[26]

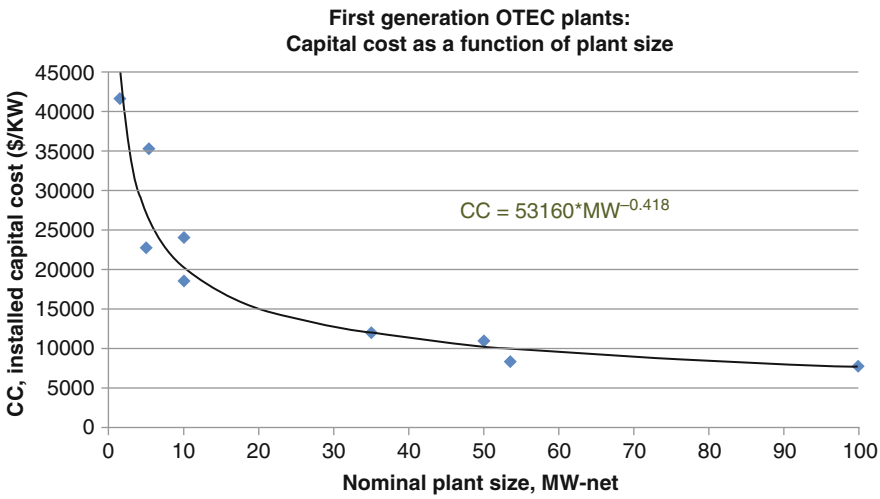

Ocean Thermal Energy Conversion. Figure 12
Capital cost estimated for first-generation OTEC plants

Ocean Thermal Energy Conversion. Table 8 Levelized COE (US-cents/kWh) for CC-OTEC plants with capital costs (CC) amortized through an 8%/15 year loan and annual inflation at 3%, considering US labor rates (O&M) and first-year repair and replacement cost (R&R) as indicated. First two entries are Land Based with lower O&M

Identifier nominal size (MW)	Capital cost ($/kW)	O&M ($M/year)	R&R ($M/year)	COEcc (c/kWh)	$COE_{OMR\&R}$ (c/kWh)	COE C/kWh
1.35	41,562	2.0	1.0	60	33.7	94.0
5	22,812	2.0	3.5	33	17	50.0
10	18,600	3.4	7.7	26.9	16.8	44.0
53.5	8,430	3.4	20.1	12.2	6.7	19.0
100	7,900	3.4	36.5	11.4	6	18.0
						8% 15 years

a prototypical plant must be built and operated to obtain the information required to design commercial systems and to gain the confidence of the financial community. Conventional power plants pollute the environment more than an OTEC plant would, and the fuel for OTEC is vast and free, as long as the sun heats the oceans; however, it is futile to use these arguments to convince the financial community to invest in an OTEC plant without operational records.

OTEC Capital Costs

OTEC archival information can be converted to present day costs using the USA 20-year average for equipment price-index inflation. Current technical specifications for 10, 50, and 100 MW OTEC plants have been used to solicit budgetary quotes [26]. All estimates are summarized in Table 7 and in Fig. 12.

These estimates are applicable for equipment purchased in the USA, Europe, or Japan and with installation by US firms. Deployment and installation costs are included. One might speculate, based on the implementation of similar technologies, that later-generation designs might reach cost reductions of as much as 30%. However, the premise herein is to indicate that first-generation plants can be cost effective

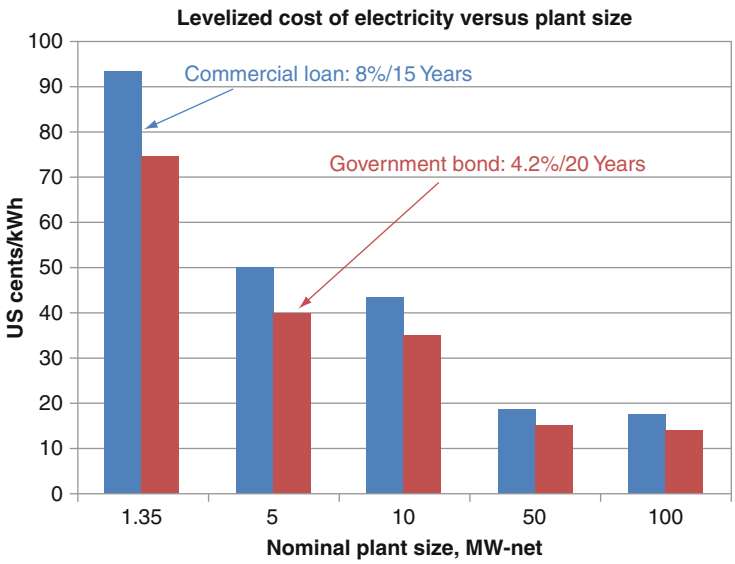

Ocean Thermal Energy Conversion. Figure 13
Cost of electricity (*Capital Cost Amortization + OMR&R Levelized Cost*) production for first-generation OTEC plants as a function of plant size with loan terms (*interest and term*) as parameter. Annual inflation assumed constant at 3%

under certain scenarios if the cost estimates presented here are met.

Figure 12 illustrates that OTEC capital cost ($/kW) is a strong function of plant size (MW). For convenience and future reference, a least-squares curve fit is provided:

$$\mathrm{CC}(\$/\mathrm{kW}) = 53,000 \times \mathrm{MW}^{-0.42}$$

A 100 MW OTEC plant, for example, could be housed in a floating platform stationed less than 10 km offshore and would have the capability of delivering 800 million kilowatt hour to the electrical grid every year. Budgetary quotes from potential equipment suppliers indicate that the installed cost would be $790 million using state-of-the-art components (Table 7).

The annual costs for operations and maintenance are estimated at $40 million (Table 8) such that under realistic financing terms (15 year loan at 8% annual interest and 3% average annual inflation), electricity could be produced at a levelized cost of less than 0.18 $/kWh such that a realistic power-purchase-agreement from the utility at around 0.20 $/kWh would include ample return on investment. It is interesting to note that if the plant could be funded via government bonds at a realistic rate of 4.2% over 20 years, the COE would be 0.14 $/kWh (Fig. 13).

Future Directions: OTEC

The major conclusion continues to be: *there is a market for OTEC plants that produce electricity and desalinated water*; however, operational data must be obtained by building and operating demonstration plants scaled down from sizes identified as potentially cost effective. OTEC systems are in the pre-commercial phase with several experimental projects having already demonstrated that the technology works but lacking the operational records required to proceeding into commercialization. Adequately sized pilot projects must be operated in situ and for at least one continuous year to obtain these records. A pilot (or pre-commercial demonstration) plant sized at about 10 MW must be operated prior implementation of 50–100 MW commercial plants.

Accounting for externalities in the production and consumption of electricity and desalinated water might eventually help the development and expand the applicability of OTEC. Unfortunately, it is futile

to use these arguments to convince the financial community to invest in OTEC plants without an operational record.

The major challenge continues to be the requirement to finance relatively high capital investments that must be balanced by the expected but yet to be demonstrated low operational costs. Perhaps, a lesson can be learned from the successful commercialization of wind energy due to consistent government funding of pilot or pre-commercial projects that led to appropriate and realistic determination of technical requirements and operational costs in Germany, Denmark, and Spain. In this context, by commercialization, we mean that equipment can be financed under terms that yield cost competitive electricity. This of course depends on specific conditions at each site.

In discussing OTEC's potential, it is important to remember that implementation of the first plant would take about 5-years after order is placed. This is illustrated with the baseline schedule shown in Table 9. Completion of the engineering design with specifications and shop drawings would take 1-year. Presently, it is estimated that the licensing and permitting process through NOAA (in accordance with the OTEC Act) would take at least 1 year for commercial plants with the provision of exemptions from the licensing process for plants considered to be *test plants* because of the limited duration of the operational phase.

A survey of factories that can supply the required equipment indicates that no technical breakthroughs are required but that some components would require as long as 3-years to be delivered after the order is placed. The solicitation of equipment quotes based on technical specifications indicates that long-lead items would require from 18 months to 36 months to be delivered. Based on experience with offshore projects of similar size, it is expected that 1 year would be required to complete the deployment with a second year set aside for commissioning.

As stated above, there are sufficient petroleum resources (≈1,400 billion barrels) to meet worldwide current demand (>30 billion barrels/year) for almost 50 years. Production, however, is peaking, and humanity will face a steadily diminishing petroleum supply and higher demand due to emerging economies like China, India, and Brazil. Coal and natural gas resources could meet current worldwide demand for 100–120 years, respectively.

Given that it takes decades for new energy technologies to reach maturity, it seems sensible to consider the ocean thermal resource as a renewable fuel for the future. At first, OTEC plantships providing electricity, via submarine power cables, to shore stations would be

Ocean Thermal Energy Conversion. Table 9 First-generation OTEC plantship implementation schedule

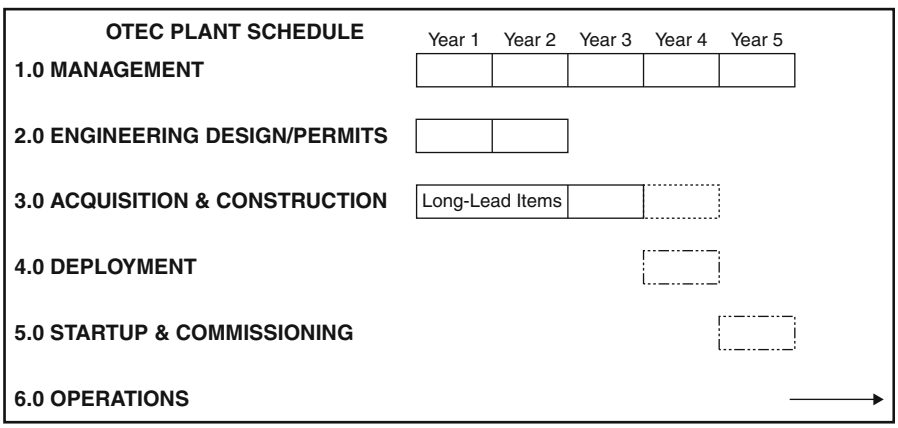

Ocean Thermal Energy Conversion. Table 10 OTEC implementation program required in preparation for the post–fossil fuel age

USA OTEC DEVELOPMENT		←	YEARS	→		
	1 to 5	6 to 10	11 to 15	16 to 20	21 to 25	26 to ∞
Pre-Commercial Plant (> 5 MW)		Ops				
Electricity (Desal Water) Plants in Hawaii and USA Territories: ~20 × 100 MW Plants	Prelim Design	Ops		Ops	→	→
NH3/H2 Plantships Supplying all States				Prelim Design	Ops	→

implemented. This would be followed, in 20–30 years, with OTEC factories deployed along equatorial waters producing energy intensive products, like ammonia and hydrogen as the fuels that would support the post-fossil fuels era.

The following Development Schedule (Table 10) can be used as an outline of the activities required to implement ocean thermal resources as a major source of energy for our post-fossil-fuels future. A pre-commercial plant would be implemented with government funding. The plant would be operational (supplying electricity to the distribution grid) within 5 years and would be operated for a few years to gather technical, as well as environmental impact information. Some of the valid questions regarding potential environmental impacts to the marine environment can only be answered by operating plants that are large enough to represent the commercial-size plants of the future.

The design of the first commercial plant sized at 50–100 MW would be completed and optimized after the first year of operations with the pre-commercial plant. This would be followed, for example, with the installation of numerous plants in Hawai'i and US Insular Territories for a cumulative total of about 2,000 MW over 15-years. As indicated in Table 10, the design of the grazing factory plantships that would produce the fuels of the future (e.g., hydrogen and ammonia) could be initiated as early as 15-years after the development program is implemented.

Bibliography

1. Vega L (2003) Ocean thermal energy conversion primer. Mar Technol Soc J 6(4):25–35
2. Coastal Response Research Center (2010) National oceanic and atmospheric administration (NOAA) technical readiness of ocean thermal energy conversion (OTEC). University of New Hampshire, Durham, NH 27 pp and appendices
3. Nihous GC (2007) A preliminary assessment of ocean thermal energy conversion resources. Trans ASME 29:10–17
4. Steinbach RB (1982) Mini-OTEC: a hardware perspective. In: Society of naval architects and marine engineers spring meeting, Honolulu, pp 289–306
5. Thomas A, Hillis DL (1989) Biofouling and corrosion research for marine heat exchangers, prepared by Argonne national Laboratory, Energy and Environmental Systems Division for US. Department of Energy, Wind/Ocean Technologies Division. Presented at Oceans'89, Seattle, Washington, DC
6. Kinelski EH (1985) Ocean thermal energy conversion heat exchangers: a review of research and development. Mar Technol J 22(1):64–73
7. Uehara H et al (1999) The experimental research on ocean thermal energy conversion using the Uehara cycle. In: Proceedings of the international OTEC/DOWA conference'99, Imari, pp 132–141
8. Claude G (1930) Power from the tropical seas. Mech Eng 52(12/19):1039–1044
9. Vega LA, Evans DE (1994) Operation of a small open-cycle OTEC experimental facility. In: Proceedings of Oceanology international 94, vol 5, Brighton
10. Vega LA (1995) The 210 kW apparatus: status report. In: Oceans'95 conference, San Diego
11. Syed MA, Nihous GC, Vega LA (1991) Use of cold seawater for air conditioning. In: Oceans'91, Honolulu

12. Vega LA (1992) Economics of ocean thermal energy conversion (OTEC). In: Seymour RJ (ed) Ocean energy recovery: the state of the art. American Society of Civil Engineers, New York
13. Nihous GC, Vega LA (1993) Design of a 100 MW OTEC-hydrogen plantship. Mar struct 6(2–3):207–221 (Published by Elsevier, England)
14. Vega LA, Nihous GC (1994) Design of a 5 MWe OTEC pre-commercial plant. In: Proceedings Oceanology international'94 conference, Brighton
15. Nihous GC (2010) Professor University of Hawaii (nihous@hawaii.edu). Personal Communication: Information about Global Ocean Thermal Energy Resources
16. Locarnini RA, Mishonov AV, Antonov JI, Boyer TP, Garcia HE (2006) NOAA atlas NESDIS 61. In: Levitus S (ed) World ocean atlas 2005: temperature, vol 1. U.S. Government Printing Office, Washington, DC, 182 pp
17. Chassignet EP, Hurlburt HE, Metzger EJ, Smedstad OM, Cummings JA, Halliwell GR, Bleck R, Baraille R, Wallcraft AJ, Lozano C, Tolman HL, Srinivasan A, Hankin S, Cornillon P, Weisberg R, Barth A, He R, Werner F, Wilkin J (2009) US GODAE: global ocean prediction with the HYbrid Coordinate Ocean Model (HYCOM). Oceanography 22(2):65–75
18. Flament P, Kennan S, Lumpkin R, Sawyer M, Stroup ED (1996) Ocean atlas of Hawaii. http://www.soest.hawaii.edu/hioos/oceanatlas/index.htm
19. Vega LA, Nihous GC (1988) At-sea test of the structural response of a large diameter pipe attached to a surface vessel. Paper #5798, Offshore Technology Conference, Houston
20. Nihous GC, Syed MA, Vega LA (1989) Conceptual design of a small open–cycle OTEC plant for the production of electricity and fresh water in a pacific island. In: Proceedings of the international conference on ocean energy recovery, Honolulu (Published by the American Society of Civil Engineers)
21. Coastal Response Research Center (2010) National oceanic and atmospheric administration (NOAA) ocean thermal energy conversion: assessing potential physical, chemical and biological impacts and risks. University of New Hampshire, Durham, NH, 39 pp and appendices
22. Nihous GC, Vega LA (1991) A review of some semi-empirical OTEC effluent discharge models. In: Oceans'91, Honolulu
23. Quinby-Hunt MS, Wilde P, Dengler AT (1986) Potential environmental impacts of open-cycle ocean thermal energy conversion. Environ Impact Assess Rev 6:77–93 (Elsevier, New York)
24. Quinby-Hunt MS, Sloan D, Wilde P (1987) Potential environmental impacts of closed-cycle ocean thermal energy conversion. Environ Impact Assess Rev 7:169–198 (Elsevier, New York)
25. Vega LA, Michaelis D (2010) First generation 50 MW OTEC plantship for the production of electricity and desalinated water. In: Offshore technology conference (OTC 20957), Houston
26. Vega LA (2010) Economics of ocean thermal energy conversion (OTEC): an update. In: Offshore technology conference (OTC 21016), Houston

Oceanic Fate and Transport of Chemicals

Robert P. Mason
Department of Marine Sciences & Chemistry, University of Connecticut, Groton, CT, USA

Article Outline

Glossary
Definition of the Subject and Its Importance
Introduction
The Transport of Chemicals to the Open Ocean
Ocean Cycling of Chemicals
Detailed Description of the Cycling of Important Elements and Chemicals
Future Directions
Bibliography

Glossary

Anthropogenic Produced by or derived from human-related activities.

Biogeochemical cycling The overall transport of chemicals through the ocean waters as modified by chemical, physical, and biological processes.

Chemical inputs The external sources of chemicals to the ocean from the atmosphere or from deep ocean environments or from rivers and other terrestrial sources.

Chemical sinks All elements and compounds can be removed from the ocean by various processes. The relative ratio of their input to their removal provides an indication of how they are distributed in the ocean, and whether human activity has increased their ocean concentration.

Major ions and nutrients Those chemicals present in the ocean at high concentrations and the major nutrients (nitrogen, phosphorous, and silica).

Metalloid An element in the periodic table that acts both as a metal and a nonmetal, depending on the chemical environment.

Micronutrients and trace elements Those chemicals present in the ocean at low concentrations but which still have an important impact of ocean biological productivity, either because they are

essential nutrients (e.g., iron and zinc) or toxic compounds (e.g., lead and mercury).

Organic chemicals In the context of this chapter these are chemicals manufactured purposely (e.g., PCBs, pesticides) or inadvertently (e.g., dioxins) by humans, and also released to the environment by human activity (petroleum compounds).

Persistent organic pollutants (POPs) Organic compounds that are stable in the environmental and not rapidly degraded and which are also bioaccumulative through the food chain and potentially toxic to organisms.

Definition of the Subject and Its Importance

or their consumers, are nonessential elements or compounds, or are major components with essentially uniform concentration across the ocean system. Given that there are over 100 elements on Earth, and a finite but very large number of organic chemicals, derived either from an original biochemical source or manufactured by humans, it would be impossible to deal with all these compounds and elements in any detail. Therefore, while this chapter contains a description of the cycling of compounds through the marine environment and identifies the main pathways of movement and the major sources and sinks for compounds, in both the solid and dissolved phases, the focus of the discussion is a smaller list of/or their consumers, are nonessential elements or compounds, or are major components with essentially uniform concentration across the ocean system. Given that there are over 100 elements on Earth, and a finite but very large number of organic chemicals, derived either from an original biochemical source or manufactured by humans, it would be impossible to deal with all these compounds and elements in any detail. Therefore, while this chapter contains a description of the cycling of compounds through the marine environment and identifies the main pathways of movement and the major sources and sinks for compounds, in both the solid and dissolved phases, the focus of the discussion is a smaller list of compounds whose inputs to the ocean and whose fate and transport have important consequences for oceanic life and the environmental health of the ocean and the biosphere in general. The four main groups of elements/compounds and their fate and transport, and how these have changed in the recent and geological past, and the consequences of these changes on the ocean are described.

The four main classes of compounds are: (1) nutrients, including both the major nutrients (nitrogen (N), phosphorous (P), silica (Si)), and the minor nutrients, which are constituents of important enzymes and biochemicals (e.g., iron (Fe), zinc (Zn) and other transition metals); (2) toxic metals and metalloids, such as mercury (Hg), lead (Pb), arsenic (As) and silver (Ag); (3) organic compounds, primarily those manufactured or extracted from the Earth by humans (petroleum-derived compounds, pesticides and fungicides, pharmaceutical products and related chemicals); and (4) radioactive compounds and other environmental pollutants not covered in the other classes. While the addition of carbon dioxide (CO_2), released by fossil fuel burning and other human activities, to the ocean has and will have a large and currently uncertain impact on the basic ocean chemistry through its exacerbation of ocean acidification, and will impact, for example, the ability of calcifying organisms to precipitate their external shells, this will not be covered in this chapter.

Much of the discussion focuses on chemicals whose concentration in the ocean has been exacerbated by human activities. It concentrates on their dominant sources to the ocean, the factors that control their overall distribution and fate, with a brief discussion of the mechanisms for their accumulation into the marine food chain. Human health and environmental health impacts of chemicals assimilated into marine biota will not be directly discussed but this is clearly the most important concern of the increased ocean concentrations of many compounds. Historically, it was thought that the "solution to pollution was dilution" and that the ocean was a large and limitless reservoir that could not be severely impacted by the input of human wastes and other chemicals into the environment. This notion was prevalent in the early part of the twentieth Century, and before, but it has become increasing clear that this idea is a fallacy and that human activity has markedly impacted the ocean, as it has the other reservoirs of the biosphere.

Therefore, there has been a resultant change in attitude that has resulted in numerous conventions and international activities to mitigate past anthropogenic

impacts and to ensure a sustainable future for marine resources. The debate however continues about the degree to which the ocean can be used as a "waste disposal site." Some scientists and ecosystem managers focus on the "precautionary principle" while many others think that the inputs can be effectively managed and assessed through the quantification of loading and an understanding of the level of the chemical in a particular environment that can be tolerated. These two approaches require different levels of understanding and knowledge. Therefore, there is the need to further examine and ascertain the degree to which the ocean can buffer ongoing inputs of chemicals. However, many such debates lack an appreciation for the complexity of the ocean system and how the inputs of chemicals in one location can impact the ocean more generally, and how chemicals are transported from one location to the other, and how long they actually reside in the ocean water column before being removed. This chapter attempts to provide the background and insights necessary to make such informed decisions.

Introduction

All the elements are found in the ocean, but their concentrations differ by many orders of magnitude in total concentration. The concentration of many elements and compounds has not changed substantially for thousands of years while those chemicals that have a strong anthropogenic component to their emissions to the atmosphere and to coastal waters have changed substantially in the last 100 years. The overall processes important in the cycling of chemicals in the ocean and across the important interfaces between the ocean and the rest of the biosphere are shown in Fig. 1. Exchange of chemicals occurs across the air–sea interface due to deposition of gases and particulate, as both wet and dry deposition. For gases, the direction of exchange – from the water to air or vice versa – depends on the relative concentrations of the compounds in each phase, and the relative solubility or volatility of the compound. Inputs of chemicals from the terrestrial environment are also important via riverine discharge as well as subsurface inputs from groundwater. Removal of chemicals from the surface ocean is due to mixing of ocean currents and internal cycling as well as the transport of chemicals through the sinking of particulate material to the deep ocean. For most chemicals that reach the deep ocean, the ultimate sink is removal to the sediment, and the relative rate of sedimentation to input from the surface ocean determines the net difference in surface and deep ocean concentrations. This is discussed further in the remainder of the chapter.

The major ions are sodium (Na) and chloride (Cl), both which are present at around 0.5 M concentration, with the other major ions (Calcium (Ca), magnesium (Mg), potassium (K), sulfate, and bicarbonate) being present at concentrations of 5–20 times less (Table 1) [77, 100]. In contrast, the major nutrients are present around 10^{-6} M or lower (often more than a thousand times less), the major transition metals are present at 10^{-8}–10^{-10} M and some of the more rare metal elements are present at $<10^{-12}$ M (a trillion times less) (Table 1). Total organic matter ranges from 10^{-3} to 10^{-5} M (on a carbon basis). Concentrations of many trace species are highest in coastal waters compared to the deep ocean and for elements and chemicals that interact and bind strongly with suspended particulate matter in the water, their total concentration is determined to a large degree by the suspended solids (TSS) levels, which vary from >100 mg/L for some rivers and estuaries to <1 mg/L in open ocean waters [100].

In terms of organic compounds, the focus of the discussion is contaminant and toxic compounds rather than the large suite of biochemicals and their degradation products found in seawater. The most important from an environmental health point of view are the so-called "persistent organic pollutants" (POPs), as defined by the Stockholm Convention. The POP designation includes a series of pesticides and other compounds initially termed the "dirty dozen" in earlier classifications of toxic and bioaccumulative organic compounds (aldrin, chlordane, dieldrin, endrin, heptachlor, DDT, and its breakdown products (designated here as ∑DDT), hexachlorobenzene, mirex, polychlorinated biphenyls (PCBs), polychlorinated dibenzo-*p*-dioxins (referred to as dioxins in this chapter), polychlorinated dibenzofurans, and toxaphene). Since then, polycyclic aromatic hydrocarbons (PAHs) and certain brominated flame-retardants (e.g., polychlorinated diphenyl ethers (PBDEs)), as well as some organometallic compounds such as tributyltin (TBT) and related

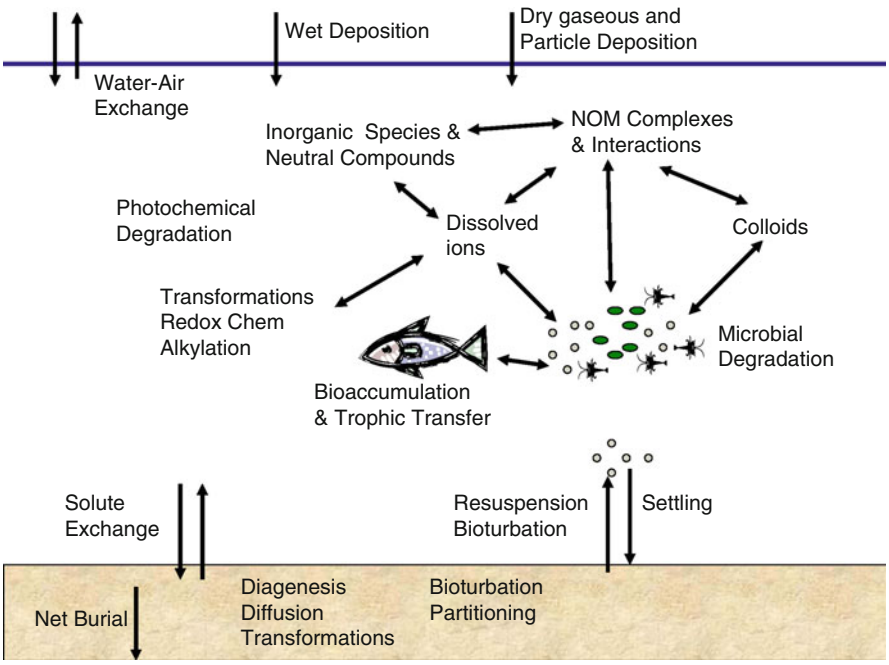

Oceanic Fate and Transport of Chemicals. Figure 1
Diagram showing the major sources and sinks for chemicals in the ocean and the major processes that are involved in determining their horizontal and vertical distributions and concentration

products (referred to here as alkylated tin compounds) have been added [57, 64].

While not specifically on the POP list, other organic chemicals that are of concern will be mentioned throughout the chapter. Concentrations of the classes of organic compounds are given in Table 1 and are typically low (pg/L range) [58, 64]. Given the range in compounds in each class of organic chemicals in the Table, and discussed in the chapter, concentrations are given on a mass basis.

As noted above, this chapter cannot cover all aspects of chemicals in the ocean. Important topics of marine environmental pollution that will not be dealt with in detail include the transport of sediments themselves to coastal waters due to enhanced erosion and human activities within the watershed, such as deforestation, agriculture, or due to activities in coastal waters, such as dredging and bottom trawling, and the impact of the resultant excessive sediment on the ecosystem health of coastal waters [12, 45]. Excessive turbidity and sedimentation in such waters will impact the growth and survival of bottom-dwelling (benthic) plants (sea grasses and other plants) and animals (e.g., bivalves), either as a result of light limitation for plants, or due to smothering of benthic organisms and habitat degradation. Excessive sediment input is an important environmental concern. Additionally, sediment transport is an important vehicle for contaminants and other chemicals [100], and this aspect will be considered in detail.

The chapter will also not directly consider the complex mixture termed "natural" organic matter (OM), either particulate or dissolved (POM or DOM) that is primarily derived from natural sources and biochemical processes, either those occurring in situ in the ocean or being derived from terrestrial inputs. Some of the OM comes from human activities such as sewage releases and dumping, and enhanced inputs to coastal waters have helped to drive water column oxygen depletion, although the major culprits are excessive amounts of nutrients. So, for this reason, OM will not be discussed directly although it has an impact on the cycling of the other chemicals to be discussed, and this will be included in the discussion.

As the chapter is focused on chemicals, there will be no discussion of the fate and transport of bacteria and

Oceanic Fate and Transport of Chemicals. Table 1 Estimated range and average concentrations for open ocean waters for major ions, trace elements and organic chemicals, and for the elements, the estimated residence time of each metal in the global ocean, and the major dissolved inorganic species in solution. The data for the organic chemicals are for the early 1990s. Taken from the literature ([17, 18, 21, 64, 111])

Element	Ocean Conc. Range (nM)	Average Conc. (nM, except where indicated)	Residence time ($\times 10^3$ year)	Major dissolved inorganic species for elements
Major ions	Na^+, Cl^-	0.49, 0,55 M	$>10^5$	Free ions
	K^+, Ca^{2+}, Mg^{2+}	9.7, 8.3, 4.4 mM		
	SO_4^{2-}, HCO_3^-	13, 1.8 mM		
Nitrate	<100–100,000	–	–	Free ions, acid–base pairs
Phosphate	<100–5,000	–		
Silicate	1,000–150,000	–		
Al	0.3–40	20	0.6	$Al(OH)_x^{3-x}$, x = 3, 4
Cr	3–5	4	8.2	CrO_4^{2-}
Mn	0.08–5	0.3	1.3	Mn^{2+}
Fe	0.01–2	0.5	0.05	$Fe(OH)_x^{3-x}$, x = 2, 3
Co	<0.01–0.3	0.02	0.34	Co^{2+}
Ni	2–12	8	8.2	Ni^{2+}
Cu	0.5–4.5	4	0.97	$CuCO_3^0$
Zn	0.05–9	5	0.51	Zn^{2+}
As	20–25	23	39	$HAsO_4^{2-}$
Mo	–	105	820	MoO_4^{2-}
Ag	<0.01–0.04	0.02	0.35	$AgCl_x^{1-x}$, x = 1–4
Cd	<0.01–1	0.5	–	$CdCl_x^{2-x}$, x = 1–4
Hg	<0.01	0.002	0.56	$HgCl_x^{2-x}$, x = 1–4
Pb	<0.01–0.15	0.1	0.81	$PbCO_3^0$
Se	0.5–2.3	1.7	26	SeO_4^{2-}
Total PCBs	1–50 pg/L	15 pg/L	NA	–
∑DDT	0.2–10 pg/L	2 pg/L	NA	–
∑Chlordanes	2–20 pg/L	5 pg/L	NA	–
∑HCH	0.05–2.1 ng/L	0.2 ng/L	NA	–

related organisms, and their potential impact on human health [12, 45]. The most common and well-known contamination of this kind is from *Escherichia coli* bacteria, a mammalian intestinal bacteria, and the number of such bacteria in a water sample is often used as a pollution indicator as they do not survive for long periods in seawater. Shellfish can also accumulate these and other toxic bacteria and their chemical products, and therefore cause toxicity onto their consumers. Additionally, there is the potential for the harmful algal blooms (HAB) in marine waters as a result of the rapid growth of dinoflagellates and other organisms, which again can result in human health impacts and disease. Overall, infections as a result of contaminated seafood can be viral, parasitic, or bacterial.

Finally, marine litter and debris is an ever-increasing ocean problem, especially in terms of small plastic materials and other smaller products that are more easily ingested by marine organisms. Many ships dump garbage and wastes while at sea, which is not biodegradable and accumulates on the ocean surface. Additionally, gear is lost from ships while at sea, and beach litter and other material are washed to sea during storms. Sewage inputs and storm-water overflow into coastal waters can be a source of household, medical, and other wastes. Plastic particles can be large or small (<1 mm in size) [110]. Given ocean circulation patterns, there are now regions of the ocean where there is an ever-growing accumulation of marine debris that is extensive in size, with densities of >10,000 particles per square kilometer. The main impact of large plastics is on marine animals, such as turtles, and birds. Recent action has lead to regulations banning dumping plastics and other non-degradable products at sea. Additionally, it is now being recognized that the smaller plastic particles can accumulate hydrophobic organic compounds [44] and therefore could have a role in the bioaccumulation of these compounds through their ingestion by benthic organisms and filter feeders. Further discussion on this topic can be found in a number of publications ([110]; etc.) and the important problem of ocean debris will not be further considered in this chapter.

The Transport of Chemicals to the Open Ocean

The three important sources of chemicals to the ocean are: (1) inputs from the atmosphere of chemicals in the gas phase and attached to particles (termed dry deposition) and inputs of chemicals with precipitation (wet deposition); (2) inputs from the terrestrial environment (watershed inputs, surface runoff, and point and nonpoint discharges and groundwater inputs); and (3) inputs from the deep ocean via release from sediments and/or from hydrothermal vents and other natural point source inputs (Fig. 1). Additionally, some chemicals present in seawater as a dissolved gas can build up in ocean surface waters to supersaturated concentrations and thereafter can be lost to the atmosphere via gas exchange processes; this gas exchange can be thought of as negative dry deposition. The relative importance of each source for the elements and organic chemicals is collated in Table 2.

Atmospheric Inputs

The information collected on the input of elements and chemicals to the ocean surface from the atmosphere (Table 2) is difficult to summarize for two reasons. One, sampling has occurred over a span of nearly 30 years and during these times there have been large changes in their deposition rates due to changes in anthropogenic inputs and loadings, and changes in human activity globally. For example, data from Bermuda suggest that the concentration of Pb in deposition has decreased by about 90% between 1982/93 and 1996/97 (Fig. 2c) [15, 106] and a similar decrease in ocean surface water concentrations has been found over the same period (Fig. 2a, b; ~60% decrease). Similarly, cadmium (Cd) has decreased by 80%, Zn by about 55%, copper (Cu) and nickel (Ni) by about 60%, and the decreases for the coastal east coast USA is of the same order [60].

This is also true for the POPs. The data for organic chemicals given below are from papers published in the early 1990s [33, 47, 111] and as many of these chemicals are now banned, these values have changed substantially as well. For example, emissions of α-HCH (lindane) has decreased by more than 90% since the early 1980s; emissions of PCBs more than 90% since their peak emissions in the 1970s; and DDT emissions have decreased by 50% in the last decade [57]. Overall, the data also suggest that the rate and timing of the changes are not all similar, reflecting the different anthropogenic sources to the atmosphere, changes in usage at different times and the differences in locations of emissions over time (e.g., for many chemicals, currently decreasing for North America and Europe; increasing for Asia, or in Africa).

Secondly, compiling data is difficult as it is often reported in different units and not all the same metals have been the focus of the various investigations. Thus, for some metals, there is a relatively large number of datasets to work from, while for other metals, data limitation is a problem [33, 34]. Also, for the crustal elements, the concentrations vary depending on the relative importance of dust input and therefore there are large ranges in the reported concentrations. For example, studies on Bermuda have shown that there are large seasonal differences in the concentration of metals in rain and in aerosols [60] and this reflects the

Oceanic Fate and Transport of Chemicals. Table 2 Estimated inputs of some elements and chemicals to the ocean from the atmosphere, coastal/riverine inputs and from hydrothermal vents. The atmospheric inputs include both wet and dry (gaseous and particulate) net deposition. The relative importance of each source is indicated for each metal. Data taken from the literature. Fluxes are in Gmol year^{-1} for the elements and in Mg year^{-1} for the organic compounds. Taken from the literature as noted in the text

Element	Fluvial flux	Pluvial flux	Hydro-therm.	%Pluvial[a]
N	1.5–5	3.5–10	–	~70
Al	5,445	2,156	0.4	28
Mn	35	11	25	16
Fe	1345	469	75	25
Co	0.65	0.23	0.070	24
Ni	3.0	1.5	–	34
Cu	3.4	0.65	0.75	14
Zn	6.7	1.3	2.0	13
As	5.0	0.08	–	2
Ag	0.60	0.050	0.001	8
Cd	0.042	0.04	0.007	45
Hg	0.003	0.017	0.001	81
Pb	0.78	1.3	0.001	62
∑PCB	~60	~230	NA	~80
∑DDT	~4	~170	NA	~98
∑HCH	~60	~4700	NA	~99
HCB	~4	~80	NA	~95
Dieldrin	~4	~40	NA	~91
Chlordane	~4	~22	NA	~85

NA not applicable
[a]Estimates of percentage are the fraction of the total flux

dominance of inputs from the east, with a relatively high dust component in summer, and inputs from the west, off the North American continent, being more dominant in fall-winter. Additionally, seasonal differences in rainfall amounts are obviously also important.

In addition to the total inputs, differences in the extent of input are also present given the dominance of anthropogenic sources near cities, and the locations of many large urban environments in coastal locations. This is illustrated by the compilation of data for the metals and the metalloids (Table 3) [21, 34]. An examination of the data indicates firstly that for the open ocean, wet deposition is the more important source, especially for the "anthropogenic metals" (Pb, Zn, As, Hg) and this reflects the typically low aerosol concentrations found over the open ocean. Thus, the dry deposition component is relatively small, and scavenging of the particles from the atmosphere by precipitation is the main mechanism of their removal. For the crustal metals (Al, Fe, Mn), the wet deposition is of somewhat lesser importance but still the dominant atmospheric flux, while for the other metals, the wet

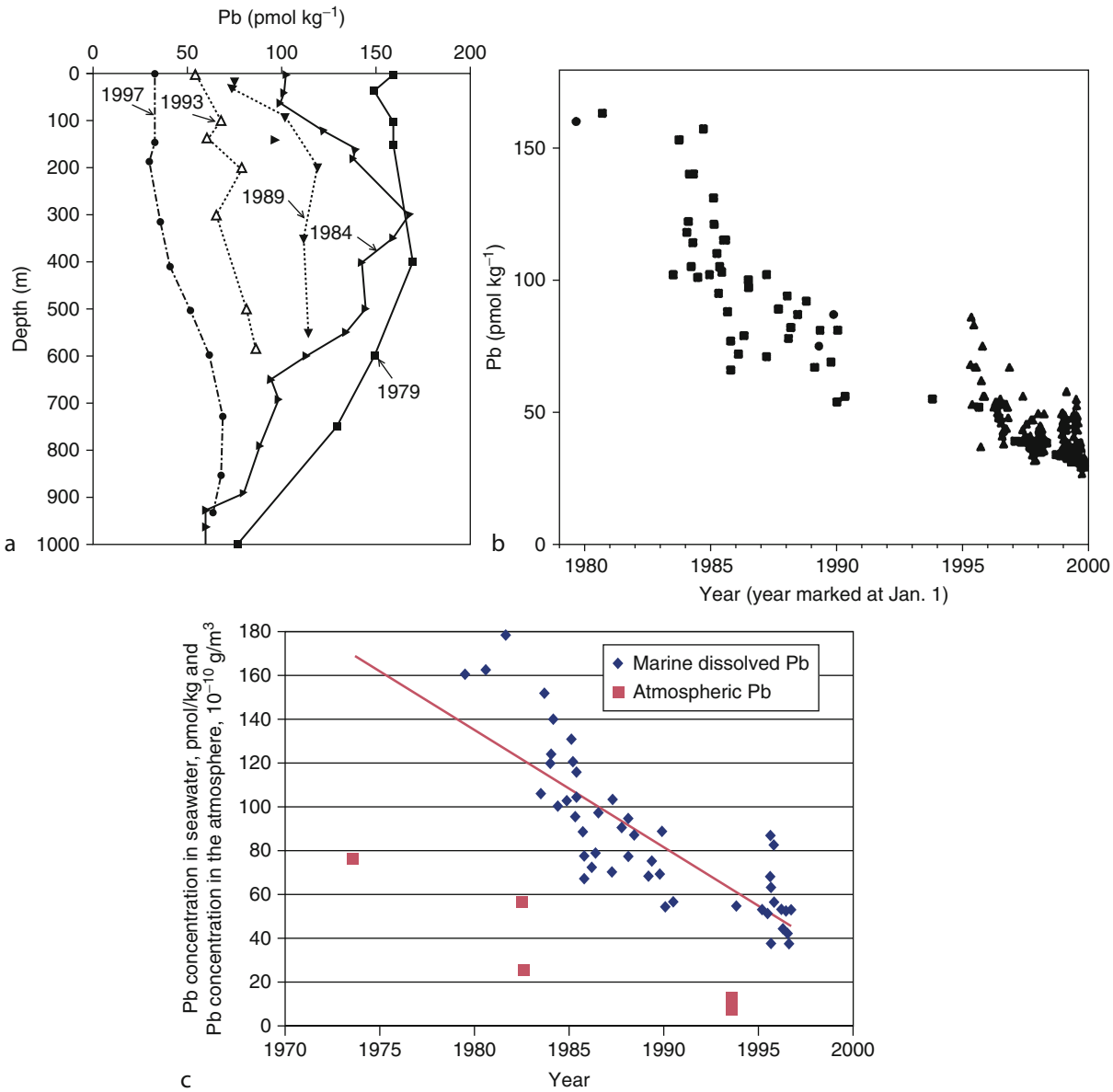

Oceanic Fate and Transport of Chemicals. Figure 2

(**a**) Vertical concentration profiles for lead in the North Atlantic at a location close to Bermuda over time; (**b**) A plot of the data from surface samples collections at the same location over time; and (**c**) A compilation of data for both the surface ocean and the atmosphere (atmospheric particle concentrations) from the same location. The first two figures are reprinted from "Anthropogenic Trace metals in the Ocean," a chapter by E.A. Boyle, pp. 273–280, with permission from Elsevier, and the third figure from "Atmospheric Input of Pollutants," a chapter by R.A. Duce, pp. 281–290, with permission from Elsevie, both chapters were published in *Marine Chemistry and Geochemistry*, Steele, J.H., Thorpe, S.A. and Turekian, K.K. (Eds), a derivative of the *Encyclopedia of Ocean Sciences*, 2nd Ed., Elsevier, Amsterdam, copyright (2010). Data are taken from various publications as indicated in the original figures

Oceanic Fate and Transport of Chemicals. Table 3 Range in the flux of metals from the atmosphere to the ocean surface. All values are given in μmol m^{-2} $year^{-1}$. Data taken from the literature and converted as necessary ([3–6, 21, 34, 60 74, 87, 95, 121, 123])

Element	Open ocean			Coastal/seas
	Wet	Dry	Total	Total[a]
Al	40–555	7–110	100–2,000	590–10^4
Cr	1.2		1.7–3.3	1.7–40
Mn	0.55–1.6	0.11	0.73–10.4	10–70
Fe	5.0–100	3.0	132–600	220–4570
Co	0.003–0.017	0.001	0.042–0.46	0.60–6.6
Ni			1.4–5.1	6.3–66
Cu	0.32–1.1	0.55	0.63–16	5.0–205
Zn	0.31–10	0.30–0.15	0.37–21	50–1,370
Cd	0.036		0.21–0.80	0.20–38
Pb	0.97–4.1	0.005	0.068–7.0	1.0–130
Hg	0.001–0.048	<0.001	0.001–0.048	0.05–0.15
Ag	0.28	0.009	0.18–0.32	0.28–0.83
As	0.13–0.4	0.09	0.36–0.4	1.3–38
Se	0.051–0.51	0.13	0.13–1.8	2.8–6.1

is typically greater than 70% of the total deposition. Total deposition fluxes vary most for the main crustal elements, while the variability appears to be lower for metals such as Cr, V, Ni, and Co, which have both a crustal source and an anthropogenic source. Metals such as Pb, Cu, and Cd show a large range in their values and this reflects the changes in their inputs over time, as noted above. For the crustal metals, changes on a decadal basis have been relatively small in the last 30 years.

There is a strong contrast between the fluxes for the open ocean and those for the coastal areas, and marginal seas (Table 3) (see references in Table legend). This is true both for the crustal metals and for the anthropogenically derived metals, and is likely also true for the organic chemicals. The increased flux for the crustal metals is primarily due to the higher aerosol concentrations in the coastal environments, while the higher fluxes for the other metals are mostly a consequence of their proximity to anthropogenic sources. Dust fluxes decrease exponentially offshore and most of the open ocean has inputs that are two orders of magnitude lower that the surrounding coastal environments, except for regions of high dust input (to the North Pacific from Asia; to the tropical Atlantic from Saharan Africa). Additionally, for those chemicals with a dominant anthropogenic signal (Pb, Hg, organic chemicals), inputs are highest in the Northern Hemisphere and have historically been higher into the North Atlantic, although this is changing depending on the specific chemical or element. Overall, the remote Atlantic, being a smaller ocean, has higher inputs, and there is clearly a strong gradient between the Northern and Southern Hemispheres.

Additionally, many cities are located in coastal areas or close to the coast, and therefore contribute substantially to the coastal fluxes, which are highest within a local radius of 50–100 km. For the anthropogenically dominated elements and organic chemicals, it has been shown that the fluxes measured in the urban environment are substantially greater than those representing the regional average value. In addition, continents with high urbanization and which typically have offshore air mass flow for all or part of the year (Asia and North

America in the Northern Hemisphere, in particular) result in a substantial input of contaminants to the coastal waters. The much higher fluxes for the coastal regions of Asia is a result of the current rapid urbanization in the region, as well as the substantial input of dust, particularly during the spring "dust period" (March–May) when a large fraction of the annual dust input occurs. In the case of Europe, it has been shown that due to meteorological conditions, there are periods where there is substantial transport from the continent to the Arctic region, and also clear evidence of contamination of the North Atlantic coastal waters and the Mediterranean, due to anthropogenic inputs [1, 33, 34, 48, 90]. Overall, there is much uncertainty in the flux estimates as a result of the sporadic nature of the measurements and the lack of consistency in the metals that are quantified in specific studies, and due to the relatively short duration of many studies.

For organic chemicals, their interaction between the atmosphere and the surface ocean is complex and this is particularly so for the chemicals where the fluxes are dominated by gas exchange as these chemicals are volatile enough to be reemitted to the atmosphere after deposition. Scientists therefore discuss the environmental fate of organic chemicals in terms of their overall mode of long-range transport. Based on their chemical properties, organic chemicals are classified as "fliers," "multi- hoppers," "single hoppers," and "swimmers" ([57, 64, 105]) and this designation was developed mostly to distinguish the ability of a chemical to be transported and deposited in the Arctic region. Most lower molecular weight organics that are volatile are "multi-hoppers" as after they are deposited to the ocean and land surfaces they can be efficiently reemitted on short timescales and this enhances their overall lifetime in the biosphere and the extent of their long-range transport. Such multiple exchanges are mostly driven by seasonal and spatial temperature differences. Less volatile chemicals are "single hoppers" as they tend to associate with particles and are not reemitted for the most part after deposition, except if the particles to which they are attached are resuspended. "Swimmers" are those chemicals that are relatively soluble and therefore are transported spatially mostly through movement of ocean currents while "fliers" are those compounds that do not have substantial air-sea exchange and their transport and fate is mostly within the atmosphere.

Deposition of N to the ocean is related to the distribution of its sources (urban areas and agriculture) as the primary sources of N are from release of nitrogen compounds (collectively termed NO_x) from coal and other fuel combustion, and from the use of N-containing fertilizers, as well as other sources related to human activity [34, 48]. It is estimated that 30–50% of the N input to the ocean is from anthropogenic sources [33]. Nitrogen fixation in the ocean provides an input that is about 50% of the external sources. Currently, inputs of N are changing from being dominated by inputs from North America and Europe to having a larger Asian signal, as is found for many other compounds which have an anthropogenic component. Given the importance of agriculture as a source, inputs from Africa are also expected to rise in the future [33].

Inputs from the Terrestrial Environment

The export of material from rivers to the coastal zone is not evenly distributed globally because of the dominance of export from large rivers such as the Amazon, and the large Asian rivers, and also as a result of spatial differences in terrain [42, 75]. In addition, material export is relatively higher for rivers draining steep topography compared to those rivers draining regions with a large coastal plain, especially for chemicals associated with particulate material. The export of particulate material from rivers to the ocean has been estimated by various groups. The three regions of high particulate discharge are: (1) the Amazon River region (~14% of the total input); (2) southern Asia (34%), and (3) eastern Asia (36%). These regions all have large rivers and periods of high rainfall that drive the high particulate discharge. Much of the particulate material is however removed in estuaries and at the coastal boundaries due to the mixing of fresh and saline waters, changes in water flow rate and coagulation processes [21, 75]. The difference in ionic strength, pH, and the concentrations of dissolved solids, causes a general coagulation and removal of organic material in the mixing zone. The continents with the widest coastal plain therefore tend to be locations where particulate removal in the estuary is enhanced.

The estimates in Table 2 are for the net transport of elements and chemicals from the coastal zone to the open ocean.

While it is most likely that many particle-reactive chemicals will be removed from the water column during estuarine mixing, it is possible for them to pass through without their concentration changing dramatically (so-called conservative elements) or they may even be added to the water column as a result of estuarine processing. If there is a linear change in concentration of a particular element or chemical relative to salinity through the estuary, then it is assumed that the concentration is the result of dilution of the riverine signal with seawater. In estuaries, salinity changes are not spatially linear with most of the salinity change occurring in a small mixing zone where the freshwater and saline waters meet. This region is also a region of high turbidity and particle settling.

For some elements and chemicals, the estuarine mixing of freshwater and seawater and the resultant chemical interactions that occur result in the elements being added or removed from the water column by precipitation, adsorption to suspended matter and resultant sinking to the sediment, or from release from particles with increasing salinity. Many metals and hydrophobic organic chemicals are highly particle reactive and are strongly retained in estuaries as most (~95%) of the suspended matter entering from rivers is not exported out of the coastal zone [21]. The role of other factors, such as biological productivity in surface waters and microbial degradation at depth also needs to be considered. While many of the redox processes that occur in estuaries can occur abiotically, it is now known that many of these processes are biotically mediated. Phytoplankton productivity plays an important role in estuarine processing of elements and chemicals. Phytoplankton productivity is driven by the supply of nutrients, which are typically in higher concentration in river waters than in coastal waters, and thus the input of freshwater and the estuarine mixing regime determines to a large degree the location where maximum productivity occurs, but it is often below the region of maximum turbidity, where light levels are low. Many elements and chemicals are actively accumulated by algae in this region, or bind strongly to the plankton, detrital material, and other particles. All these processes lead to the removal of chemicals in the high turbidity zone and in the maximum region of primary production, therefore potentially decreasing the dissolved concentration in surface waters. Their ultimate fate is sinking into the deeper waters and accumulation at the sediment–water interface. Thus, there are multiple mechanisms for the removal of dissolved constituents in the low salinity mixing regime of estuaries.

Chemical Inputs from Hydrothermal Vents, Ocean Seeps, and Sediments

The discovery of the presence of hydrothermal vents on the deep ocean floor, near the mid-ocean ridges and spreading centers in the late 1970s, and demonstration of the input of high temperature fluids from these systems changed our understanding of the sources and sinks of major and minor elements to the ocean [43, 104]. The percolation of seawater through the ocean crust leads to its heating followed by the addition or subtraction of chemicals due to reactions of the heated water with the crustal material. Temperatures can be as high as 350–400°C. The water becomes less dense and rises back to the surface where it is emitted and mixed with the surrounding cold seawater. Such processes are very important in the overall oceanic chemistry and fate of the major ions. Detailed chapters on hydrothermal vents and their importance to ocean geochemistry have been recently published and these provide much more information than can be detailed here [43, 54].

Magnesium and, to a lesser degree, Na and K, are removed during hydrothermal activity, while Ca, Fe, Mn (both in reduced forms), and other metals are added to the fluids. Sulfate is converted to sulfide in the low oxygen environment and bicarbonate (HCO_3^-) is converted into methane. The low pH (<4) leads to the conversion of dissolved carbonate species (primarily HCO_3^-) into CO_2 [43, 100]. The enriched elements in hot hydrothermal fluids are subsequently precipitated as the fluids cool or as these sulfidic, hot solutions are emitted into the oxygenated bottom ocean waters. Sulfides of Fe and other metals are precipitated, forming precipitate chimneys through which the fluids vent. Any remaining Fe and Mn will subsequently be oxidized and precipitate as their (hydr)oxides. Given the low solubility of many metal sulfides and/or their propensity to bind to and be scavenged by Fe-sulfide minerals and metal oxides precipitates, it is likely that

most trace metals in hydrothermal solutions are removed to the solid phase close to the emission source.

It has been difficult to accurately estimate the importance of these sources for trace metals to ocean waters (Table 2). The situation is further complicated by the fact that there is still limited measurement of the concentrations of trace metals in such plumes, and the measurements that have been made have found a large variation in concentration, reflecting the heterogeneous nature of this overall process. Average values for the concentration of trace metals in hydrothermal fluids are given in Table 2. Overall, it is apparent that the concentrations of some metals, such as Fe, Mn, Al can be enriched by many orders of magnitude over their concentration in seawater [43]. Most transition metals, and heavy metals such as Ag, Tl, Pb, and Hg, and the metalloids (As, Se, and Sb), are also enriched in vent fluids. Overall, however, it is concluded that few of the first row transitions metals and the heavy metals (Ag, Cd, Sn) have a strong net hydrothermal source (Table 2).

Inputs to the deep ocean from the sediment through changes in chemical form for elements due to diagenesis within the sediment are thought to be small compared to the other sources discussed. As discussed above, the mobility of some elements is a function of their oxidation state and many can be released into solution in low oxygen environments. However, as discussed above for hydrothermal systems, these elements are rapidly removed from solution to the particulate phase on encountering oxygenated waters above the sediment and therefore, even if released from the sediment, are not more than a local source. However, in contrast to metals and most elements, there are important natural sources of organic petroleum chemicals in some ocean regions, specifically natural petroleum hydrocarbon seeps. These are found in the Gulf of Mexico and off the coast of California, for example. The amount of oil that is released from these seeps (~15% of total inputs; [46]) is difficult to estimate accurately but is not trivial compared to other sources releasing petroleum products into the environment.

Comparison of Sources

Generally, for the ocean, based on the estimates in Table 2, an overall estimation of the importance of atmospheric versus riverine inputs can be made. For the human-derived chemicals, hydrothermal inputs are not considered. In making these estimates, different values in the literature needed to be reconciled (e.g., [7, 9, 10, 13, 20, 21, 33, 34, 36, 37, 41, 43, 55, 57, 58, 70, 74, 82, 86, 95, 100]). Additionally, in making these calculations, it was assumed that 90% of the riverine suspended material was trapped in estuaries and did not get transported to the open ocean, and it was assumed that if there was no data available for hydrothermal inputs for a particular element, it was not significant. Clearly, this assumption may not be valid. Also, there is little information on the potential importance of groundwater inputs or the release of metals from coastal sediments and their transport offshore, which has recently been suggested to be an important source of open ocean Fe. Overall, the estimated values and relative contributions give an idea of the important sources to the ocean and allow a comparison of the relative sources and the biogeochemical reasons for these differences.

It is evident from Table 2 that riverine inputs are the dominant source for most trace metals to the ocean. Based on these values, Hg has the highest relative atmospheric input from the atmosphere at 85% of the total flux. The input from riverine sources is higher than the hydrothermal input, but this flux is not well known. For Pb, the atmosphere is also the dominant source, with the estimate being 63% of the total (Table 2). Again, the global cycle of Pb has been substantially perturbed by human emissions of Pb to the atmosphere and this is likely the reason for the importance of the atmosphere as a source [36]. In addition, Pb is highly particle reactive and is therefore removed to a high degree during transport through the estuary. Cadmium is another metal with a relatively high atmospheric signal, which is also a relatively volatile metal with important anthropogenic sources. Hydrothermal sources are also relatively important for Cd. Additionally, hydrothermal sources are somewhat important sources for Co, Cu, and Zn, but they are the dominant input for Mn, accounting for about 40% of the total inputs, almost as much as is entering the ocean from riverine sources. The atmospheric source is not important for Mn, or any of the other crustal metals, especially Al, Fe, and Co.

For the organic chemicals, the data in Table 2, even though they are from an early compilation of data by Duce et al. [34], confirm that the atmosphere is the

dominant source for these chemicals to the ocean. Therefore, these compounds are determined to a substantial degree by long-range transport from their source regions to the locations of their deposition. The extent of their global versus regional deposition is a function of their residence time in the atmosphere. For petroleum-derived products, the inputs to the ocean come both from long-range transport (atmospheric and terrestrial inputs) and from local and regional inputs that are significant, and often highly variable [46]. Total inputs per year are in the region of 2–3 million tons. These include the inputs from marine accidents, discharges associated with offshore drilling, marine storage facilities and operations, and discharges from tankers and other ships.

For most metals and organic chemicals, removal to deep ocean sediments is the major and dominant sink for any of the compound transported into the deep ocean from the surface [21, 57, 64, 105]. However, this observation is only really true for those chemicals that are present in the dissolved phase as ionic species, or those that do not have a significant vapor pressure. This is true for most elements except those that have compounds that are volatile (e.g., Hg, Se) and the organic compounds. For Hg, which can exist in surface waters as a dissolved gas (elemental Hg), and many organic compounds loss to the atmosphere via gas exchange is the dominant loss term for the ocean [74]. For the majority of the organic chemicals, this is also true and the surface ocean concentration of these chemicals is mostly driven by the partitioning between the atmosphere and the surface waters. As discussed further below, the ocean can therefore be a source or sink of these compounds via gas exchange depending on the relative concentrations in each phase. As many of these chemicals have changed in atmospheric concentration rapidly compared to the mixing time of the upper ocean (years to decades, depending on location), many oceans are now a source of organic chemicals to the atmosphere where previously they may have been a net sink.

Ocean Cycling of Chemicals

The concentration and distribution of an element or chemical in the ocean is not directly related to its crustal abundance or its concentration in the surface soils, or its rate of release into the biosphere, but is rather determined by the complex interaction between its solubility, and its volatility, its ability to bind to or be incorporated into other phases, such particulate and dissolved organic matter (POM & DOM) or TSS (POM is a fraction of the TSS), and its potential to be present as colloidal material [17]. Scientists mostly measure the "dissolved" fraction of a chemical in seawater by filtration through membranes with openings of 0.2–0.8 μm, and therefore the filtered fraction can contain some colloidal material. Much of the DOM is likely in colloidal suspension and many insoluble metals such as Fe are potentially present as colloidal material as well in ocean waters.

A chemical's rate of biotic and abiotic transformation is also important and there are many microbial processes that can degrade organic chemicals or transform them into a different, and perhaps more toxic or mobile state. Microbial processes can also transform the toxicity of metals (e.g., methylation of Hg into methylmercury (CH_3Hg) produces a more toxic and bioaccumulative compound while methylation of As appears to reduce its toxicity). Intracellular transformations of organic compounds by Cytochrome P450 and other cellular degradation pathways can lead to more or less toxic products. The fate of some elements is also determined by the system oxidation state as their solubility is a strong function of this (Fe is more soluble when present as reduced Fe^{II}, chromium (Cr) is more soluble when oxidized as hexavalent Cr).

Besides the impact of biogeochemistry, particles, and organisms on the chemical distributions, there is also the impact of ocean circulation [17]. Ocean waters mix in a complex manner and this has a large impact of the fate and transport of chemicals. Therefore, a brief description of ocean circulation is required to understand the ocean distribution of chemicals. Vertically, the ocean is divided into: (1) the mixed layer (a few hundred meters deep), which is efficiently mixed by winds and currents, and where most of ocean photosynthesis occurs, and where most organisms reside; (2) the thermocline region, where there is a rapid change in temperature from the warmer upper waters to the colder deeper waters, and where there is strong density stratification and limited vertical mixing; and (3) the deep ocean. Below the thermocline, around 1,000 m in many oceans, is a region of oxygen depleted

waters where much of the remineralization of organic particles transported vertically from the surface ocean occurs. In the deep ocean, waters are cold and relatively uniform in characteristics. The complexities of the ocean circulation can be dived up into two classes – "wind-driven" and "thermohaline" circulation [85]. Surface currents are mostly driven by heating and wind-related forcing, as the passage of the wind over the ocean surface will move the upper water with it. For many ocean regions, winds are consistently in one direction (e.g., the trade winds) and this has set up an overall surface ocean large-scale circulation, which also results from the fact that the water is being moved on a the Earth spinning on its axis, and therefore the water movement is also influenced by the "Coriolis effect." This results in the water moving to the right of the wind direction in the Northern Hemisphere, and vice versa. In addition to this direct effect, when there is movement of water away from a coast or other barrier, conservation of mass will require the transport of water from depth to the surface to replace this water. Such "upwelling" of deeper water is an important part of the upper ocean circulation. Additionally, upwelling can occur at the equator as water masses are moving away from the equator due to the Coriolis force (there is a water mass divergence at the equator). Similarly, at higher latitudes, convergence and sinking upper air masses results in divergent air flow over the ocean surface, which forces convergence of ocean waters, and sinking of water masses which feed the intermediate waters of the main ocean basins. These sinking intermediate waters travel laterally toward the equatorial regions.

Such wind-driven circulation is enhanced and complemented by the thermohaline circulation that is driven by density differences in water masses, which is primarily a function of temperature but also related to salinity. As surface waters move away from the Equator they are heated and net evaporation increases salinity. When these water masses reach the mid-latitudes in winter, their cooling increases their density so that they become more dense that the waters below and sink. These sinking waters then travel in the main thermocline region (500–100 m) back toward the equator forming a cyclonic circulation that feeds upwelling at the equator. In the high North Atlantic and around the Antarctic Peninsula, surface waters become dense enough to sink to the deep ocean as formation of polar ice additionally increases the salinity of the surface waters, and cooling is greater. These sinking waters reach the deep ocean (>2,000 m) and supply and drive the deep water circulation of the ocean, and transport chemicals on a journey that takes 1,000 years on average. Overall, sinking water in the North Atlantic is transported south into the South Atlantic, skirting the Southern Ocean and passing through the Indian Ocean, and finally moving northward from the South to the North Pacific. To complete the water mass cycle, waters are generally transported upward (net upwelling) in the North Pacific Ocean to the surface, completing the water cycle.

The distribution of the major important characteristics of ocean waters that results from this circulation is illustrated by the data in Fig. 3 [93]. The salinity distribution along this Atlantic Ocean transect shows the presence of the intermediate water that has sunk from the surface in the South Atlantic and is moving north toward the equator. A similar process occurs in the North Atlantic and is also shown by the difference in salinity although the distribution is more diffuse. Sinking water in the Southern Ocean near Antarctica can be seen as deep water in the Southern Hemisphere. Similarly, water sinks in the North Atlantic around Iceland but this signal is not as evident in the salinity, but is shown in the phosphate distribution. The phosphate distribution also shows very clearly that its concentration has been depleted in the surface waters and is higher at depth. It also shows the two sinking water masses from the southern ocean regions which have higher phosphate concentrations than their surrounding waters. The oxygen distribution clearly shows the very low concentrations in the intermediate waters around the equator – due to oxygen consumption during organic matter remineralization. The south flowing deeper waters, that forms through water sinking in the North Atlantic Ocean, show a decreasing oxygen concentration as they progress south, further illustrating the consumption of oxygen in these deep waters due to organic matter degradation.

The movement of the water masses in the deep ocean can be tracked using the major chemical and nutrient distributions, as discussed in reference to Fig. 3, but there are also many other ways to track and age these water masses. The so-called "tracers"

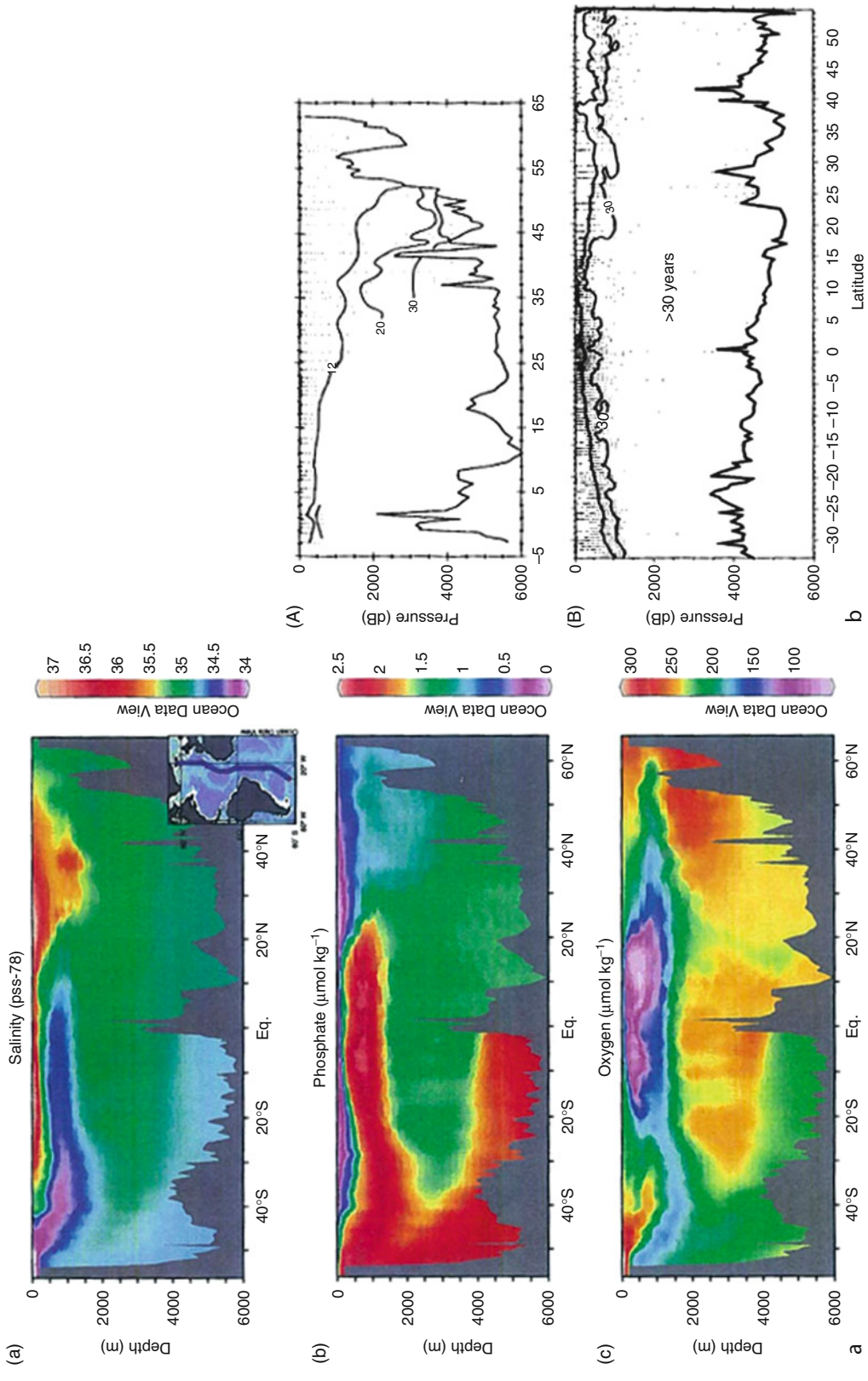

Oceanic Fate and Transport of Chemicals. Figure 3 (Continued)

are generally of two types: (1) radioactive chemicals whose concentration will change over time due to radioactive decay [61, 78, 112] and (2) chemicals whose input to the ocean is well known and transient [38]. The radioactive elements can be used as "clocks" as their rate of decay is first order and well known and therefore the ratio of the source ("parent") and product ("daughter") can give information on the time since the element was added to the ocean. Also, as many of the parent-daughter components have different reactivity or solubility, their relative concentrations can tell something about ocean processes. One example is the decay of uranium (U) that is very soluble to thorium (Th), which is very particle reactive and removed from the ocean by sinking particles [2, 19]. The resultant deficit in the ratio compared to that expected based on their decay rates can be used as a measure of the rate of particle removal from the ocean [22].

Some human-produced chemicals are also useful tracers. An example of this is the chlorofluorocarbons (CFSs), which were widely used for a number of industrial applications but which are now banned. Their extent of use and release to the environment is well known and so these compounds can be used to trace ocean water mass movement. An example is shown in Fig. 3, which shows the distribution of the ratio of CFC-11 and CFC-12, and the estimated age of the water in years based on this ratio [38]. This shows that the waters of the deep North Atlantic are relatively "young" as they are formed by sinking of surface ocean waters within the last 50 years. In contrast, in the Pacific, only the upper water masses show the presence of these chemicals and the deep waters show little evidence. Again, these distributions concur with the understanding of deep ocean circulation.

Other important tracers of ocean circulation are the radioactive elements released due to above ground atomic weapon testing (^{137}Cs, ^{14}C, ^{3}H) and the radioisotopes derived from the decay of U and Th (their specific isotopes and those of radium (Ra) (multiple radioisotopes), radon (^{222}Rn), ^{210}Pb and others) [112], and cosmogenic radioisotopes (^{14}C, ^{3}H, beryllium (Be) isotopes and many others) [113, 114].

Factors Controlling Ocean Chemical Distributions

The distribution of an element or chemical in the ocean has a characteristic distribution that relates to its solubility, degree of reaction, its requirement as a nutrient, and other factors (Fig. 4). Additionally, as discussed further below, many elements and chemicals are converted between different forms due to photochemical processes in the surface ocean, due to redox changes in the low oxygen intermediate waters, or due to their association with DOM. For many metals, complexation to dissolved ligands plays an important role in defining their concentration and distributions. The importance of mixing and other physical transport processes must also be considered, as detailed above. The overall range and average concentrations for a number of important elements or compounds are given in Table 1. For the elements, their major form and state in seawater is also given. A compilation of distributions for all the elements in the periodic table for the North Pacific has been compiled by Nozaki [81] (Fig. 5).

The major ions are found at a constant concentration across all the major ocean basins, and their distribution in the ocean has been termed a "conservative" distribution (Fig. 4) [17, 21]. Except for rare and

Oceanic Fate and Transport of Chemicals. Figure 3

(**a**) Meridional sections along the WOCE section A16 in the Atlantic Ocean for salinity, phosphate, and oxygen, with the cruise taken shown in the insert, indicating the vertical and horizontal distributions in the ocean, which result from ocean circulation, biological activity, and particulate remineralization; (**b**) Sections in the eastern Atlantic Ocean of the ratio of two chlorofluorocarbons (CFC-11 to CFC-12) along 20°W from 65°N to 5°S in summer 1998 and along 135°W in the eastern Pacific ocean from 54°N to 32°S in summer 1991. The first figure set is reprinted from "Inverse Modeling of Tracers and Nutrients," a chapter by R. Schlitzer, pp. 188–199, and the second figure set from "CFCs in the Ocean," a chapter by R.A. fine, pp.155–163, both published in *Marine Chemistry and Geochemistry*, Steele, J.H., Thorpe, S.A. and Turekian, K.K. (Eds), a derivative of the *Encyclopedia of Ocean Sciences*, 2nd Ed., Elsevier, Amsterdam, copyright (2010). Data are taken from various publications as indicated in the original figures

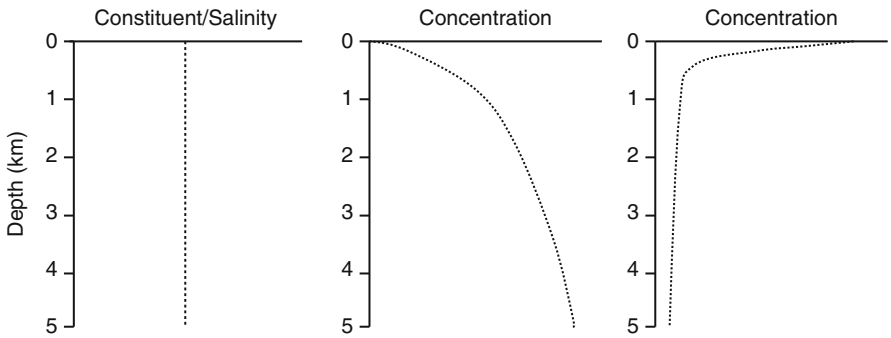

Oceanic Fate and Transport of Chemicals. Figure 4
Diagrammatic depiction of the distribution of a chemical that has (**a**) a conservative; (**b**) a nutrient-like; and (**c**) a scavenged profile in the ocean

specific circumstances in specific locations, all the major ions have this type of distribution. To exhibit such a distribution, their residence time of the element or compounds must be much longer than the mixing time of the ocean (which is around 1,000 years) so that they can become well mixed throughout the ocean basins, and most conservative elements have residence times of $>10^6$ years [17]. Most conservative elements are found at relatively high concentrations compared to their crustal abundance and this is because of their slow rate of removal from the ocean.

Elements or chemicals with a "nutrient"-type distribution are those whose concentration is depleted in the surface ocean due to their uptake into biomass, especially into photosynthetic microorganisms, and their removal from the upper waters by the sinking of particulate material (dead cells and organisms, fecal pellets). Decomposition of this material in deeper waters leads to a rapid increase in concentrations at mid-depth in the ocean and higher and relative uniform concentrations in the deep ocean, and this decomposition depletes the oxygen in these mid-depth regions. Furthermore, if these compounds and elements persist in the deeper waters and are not effectively removed by deep ocean particle scavenging, their concentration in the deep Pacific Ocean will be greater than that of the deep North Atlantic given the increased input of these chemicals over time from above as the water masses move through the ocean basins. Both nitrate and phosphate show such a distribution, as do other micronutrients [21].

A correlation between the concentrations of Zn and Si, and cadmium (Cd) and P, in the ocean was noted in the early 1980s (Fig. 6), suggesting that similar mechanisms control their ocean distribution and this has since been attributed to their "nutrient-like" behavior [21, 32]. Zinc has multiple roles in cellular metabolism and, most importantly, it is part of an important enzyme, carbonic anhydrase in marine phytoplankton, which is required to interconvert CO_2 and HCO_3^- within cells [76]. Thus, Zn is actively accumulated into plankton in surface waters and is released back into the water at depths when the organic matter decomposes, and has a similar profile with depth to the nutrient, Si. Deep water concentrations of both Si and Zn are higher in the Pacific Ocean compared to the Atlantic Ocean (Fig. 6) and this reflects the continued buildup of these elements during the "deep conveyor belt" circulation [17]. The correlation of Cd and P profiles was initially puzzling as Cd was thought of as a toxic metal but it has been subsequently demonstrated that Cd can actually substitute for Zn and other transition metals in carbonic anhydrase and therefore has a biological role in the ocean environment [76]. Given this fact, the correlation with P is explained.

Iron and Copper (Cu) are other micronutrient elements required for enzymes and other biochemicals but they have a more complex vertical profile as their relatively high particle reactivity and the insolubility of Fe results in their scavenging from deep ocean waters by particles. This results in a lack of increase in concentration in the North Pacific relative to the North Atlantic [18, 76]. Additionally, for Fe, its redox chemistry can result in changes in redox state in the low oxygen waters that can further complicate its ocean distribution. Finally, Fe, Cu, and other metals are released into the

Oceanic Fate and Transport of Chemicals. Figure 5
A depiction of the vertical distributions of the elements in the North Pacific Ocean. Originally published in EOS supplementary material in 1997, for an article by Y. Nozaki "A fresh look at element distributions in the North Pacific", copyright 1997, American Geophysical Union. Reprinted with permission from the American Geophysical Union

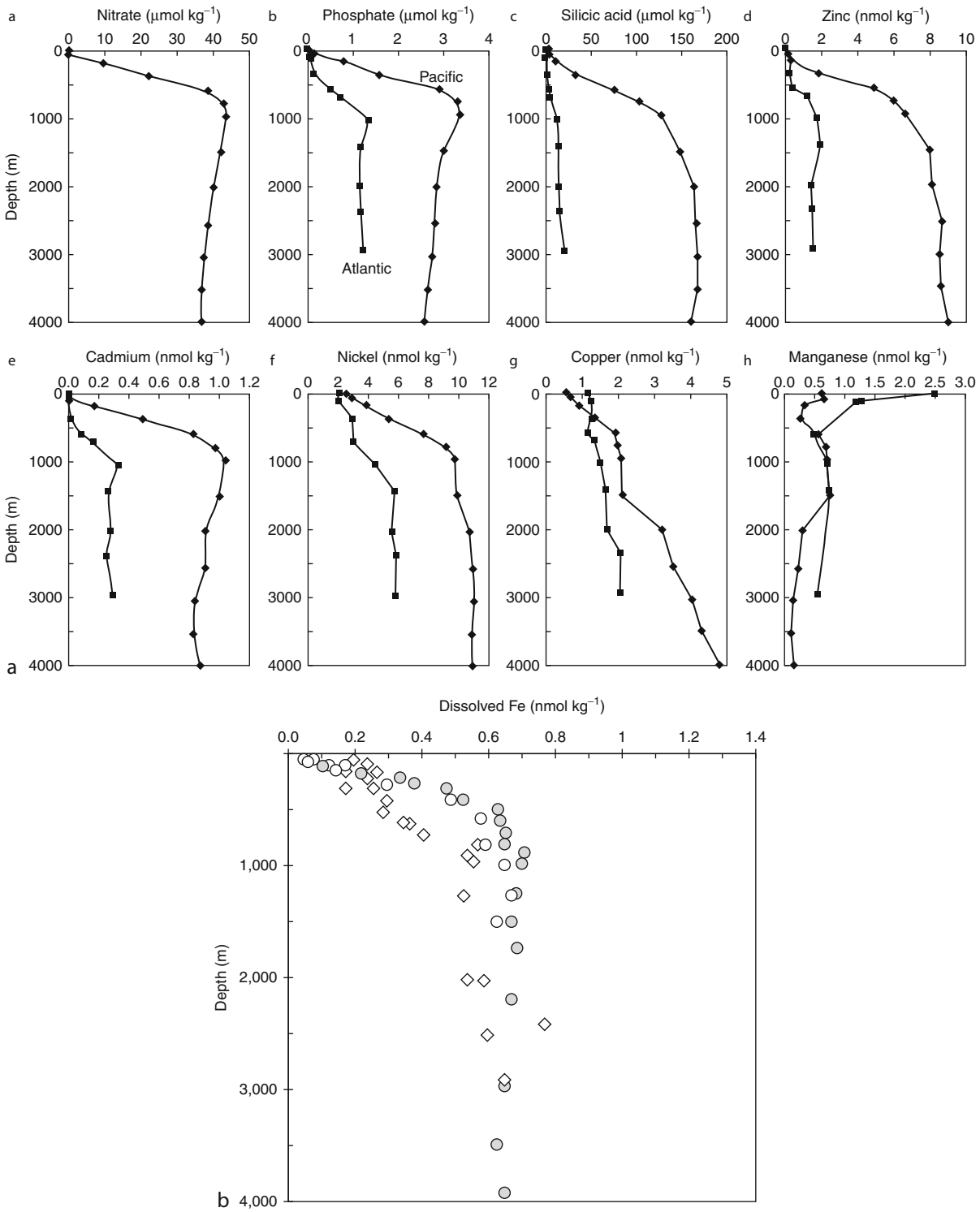

Oceanic Fate and Transport of Chemicals. Figure 6
(Continued)

deep ocean by hydrothermal activity and this can also influence the ocean distribution of these metals. Finally, in a similar manner to Cd, Cu is both an essential element and a potential toxic element and therefore there is a fine balance between its concentration needed to support growth and that which can hinder organisms. Other elements in this category are Se, and to a lesser degree As.

Another oceanic distribution is characterized by elements or chemicals that are particle reactive and/or relatively insoluble, and especially those metals or organic compounds that also have the majority of their input from the atmosphere (Fig. 4). These are referred to as "scavenged elements" and they have deep water concentrations that tend to decrease along deep water flow paths between the Atlantic and Pacific. Hence, their distributional features are often dominated by their point of entry and removal in the ocean. These elements and compounds have short residence times ($<10^3$ years). For example, surface water concentrations of Hg and Pb are typically elevated compared to deep waters [14, 40, 92], reflecting their dominant atmospheric input pathway to the ocean. Such metals are scavenged and removed from the surface ocean via particle transport, released back into the water column during the dissolution of the biological particles, but are often re-scavenged from deep ocean waters and therefore do not have a continuing increasing concentration with depth, and their concentration is depleted in deep ocean waters, or does not increase with depth, or with time.

Organic chemicals are added to the ocean via a variety of processes. Human-made chemicals such as pesticides, polychlorinated biphenyls (PCBs) and other industrial chemicals are typically added to the ocean from both direct runoff and atmospheric deposition. Some compounds, such as petroleum-derived compounds, are naturally formed in the deep Earth but are pollutants when added to the ocean in high concentrations. Most of these compounds are highly insoluble in water and have a high tendency to associate with particles (POM) and are taken up into microorganisms, and therefore are effectively removed from the surface ocean by particle sinking. Such chemicals are also likely strongly removed from solution in estuaries and coastal waters and therefore their input to the ocean is dominated by atmospheric inputs. These compounds likely have a scavenged distribution in the ocean water column. Other pharmaceuticals and organic chemicals are manufactured to be highly soluble in water but typically have a relatively short half-life before they are degraded by photochemical processes and microbes, and as many of these compounds have only been recently (on a ocean mixing timescale) added to the ocean, their distribution and fate are poorly known. Many of these compounds are accidentally added to the ocean or are released from coastal sources, such as treatment plant effluents and stormwater outflows.

In terms of the nutrients, it is often their excessive addition to the ocean as a result of anthropogenic inputs and human activity that have been the focus of study and environmental management. For example, excessive amounts of nitrogen, in particular, in coastal waters has lead to an increase in extent, duration, and severity of oxygen depletion in deep waters, and the persistence of hypoxic (oxygen content <4 mg/L) and anoxic waters (undetectable oxygen/presence of sulfide), which have been termed "dead zones" in many instances in the media and elsewhere. Oxygen depletion in coastal waters has important consequences and while the formation of such zones did occur in the

Oceanic Fate and Transport of Chemicals. Figure 6
(**a**) The vertical distributions of nutrients (N. P, Si) and metals (Zn, Cd, Cu, Ni, Mn) in the North Pacific and North Atlantic Oceans; (**b**) A similar plot for Fe for both oceans. The first figure set is reprinted from "Trace Metal Nutrients," a chapter by W.G. Sunda, pp. 17–28, published in *Marine Chemistry and Geochemistry*, Steele, J.H., Thorpe, S.A. and Turekian, K.K. (Eds), a derivative of the *Encyclopedia of Ocean Sciences*, 2nd Ed., Elsevier, Amsterdam, copyright (2010), with permission from Elsevier. The iron figure is from K. Bruland and M.C. Lohan "Controls of trace metals in seawater", pp. 23–47, a chapter in *The Oceans and Marine Geochemistry*, H. Elderfield (Ed), volume 6 in Holland, HD and Turekian, KK (Exec Eds), *Treatise on Geochemistry*, Amsterdam, Elsevier. Copyright (2004). Data are taken from various publications as indicated in the original figures

historic past, human activity has definitely increased the problem [115]. However, it is also important to understand the role of nutrient limitation in ocean chemistry and environmental health. Nutrient limitation is an important concern for open ocean ecosystems, and this is mainly due to the limitation of Fe input to the ocean. Such limitation has been little impacted by human activities in the last century and has its origins in the geological evolution of the Earth in the very distant past. In contrast to Fe, Si limitation is also important in some ocean locations and this can be linked to human activity as one important source of Si to the ocean is riverine inputs. While not all microorganisms require silica, it is an important nutrient for one class of phytoplankton (diatoms) and for other organisms that construct silicate shells, and therefore its limitation can have an important impact on coastal and ocean primary productivity. Construction of reservoirs on many rivers around the world has decreased the Si input to the ocean and therefore could be an important factor in determining the extent of this limitation [11, 23].

Detailed Description of the Cycling of Important Elements and Chemicals

Iron, Manganese, and Aluminum Cycling in Open Ocean Waters

Atmospheric and riverine inputs are the main sources of Fe, Mn, and Al (all crustally abundant) to the oceans (Table 1) and much of this input is in the particulate or colloidal fraction. While Fe is primarily present as Fe^{III} complexes and solids in oxic seawater, Mn can be found in its more reduced +2 oxidation state, and the reason for the persistency of the reduced Mn forms is its relatively slow oxidation rate compared to Fe [63, 65, 66]. Aluminum (Al) ranges widely in concentration and is elevated in regions of enhanced atmospheric input, such as the equatorial zones where rainfall is high, and is very low in polar surface waters. It is present as Al^{III} ($Al(OH)_4^-$, $Al(OH)_3$) [84]. Concentrations are higher in the North Atlantic (8–30 nM) than the North Pacific (<2 nM) due to its depletion via particle scavenging. It has high concentrations in the surface Mediterranean (>100 nM) due to the enhanced atmospheric (dust) inputs in that region. Aluminum is the element with the largest ocean variation.

While riverine inputs are important, most of it is removed in estuarine and coastal waters as all these metals are highly particle reactive. Given their increased insolubility with pH, these elements have low ocean concentrations even though they are some of the most abundant elements on the surface of earth. The relative insolubility of both Fe^{III} and Mn^{IV} leads to the rapid removal of these metals from the surface ocean. While both Mn and Fe have a role in the biochemistry of marine organisms [76], the concentration of Mn is relatively high in ocean waters compared to its nutrient requirement, and depletion of its surface concentration due to biological activity is not often found. In contrast, as noted above, dissolved Fe can show surface ocean depletion in regions of high primary productivity.

Representative profile for Fe in the major ocean basins are shown in Fig. 6c. In seawater, the concentration of dissolved Fe is higher than would be predicted based on its primary solubility in terms of Fe (hyd)oxides due to the presence of Fe-binding ligands in solution [18, 76]. In the absence of these ligands, the predicted concentration in equilibrium with $Fe(OH)_3$ (s) is around 0.1 pM, even considering that it is strongly hydrolyzed in seawater with the dominant inorganic complexes being $Fe(OH)_4^{2-}$, $Fe(OH)_3$ and $Fe(OH)_2$. The average measured concentration is 0.5 nM, three orders of magnitude higher (Fig. 6c). This is consistent with the electrochemical measurements which estimate that 99% or more of the Fe in surface ocean waters is complexed to organic ligands. Additionally, given that the measured values are for filtered waters, it is likely that this value reflects the presence of both organic and inorganic Fe-containing colloidal phases. In contrast, Mn forms only weak associations with both inorganic and organic ligands, and its dissolved concentration is much lower than the concentration expected from precipitation of Mn^{IV} hydroxide or carbonate phases.

The distributions of Fe and Mn in the water column are modified in the regions of low oxygen or anoxic waters. In some ocean locations, oxygen concentrations are sufficiently low that both Fe and Mn can be reduced, either through biologically mediated pathways or abiotically, and this has been observed, for example, in the oxygen minimum zone of the equatorial Pacific Ocean [21]. In addition to these sub-oxic environments, the distributions of Fe and Mn are

highly modified in anoxic environments with elevated levels of the reduced forms of the metals being present. However, the distributions are complex for Fe because, while in low oxygen environments Fe(II) is formed with an increase in solubility as sulfide levels increase, Fe(II) is precipitated as Fe-sulfide phases (FeS and FeS_2) and this leads to a maximum in dissolved Fe in low oxygen, but low sulfide environments.

In permanently or seasonally stratified systems, the redox cycling of metals can lead to a large gradient in their concentration, as well as for metals and other constituents that are strongly associated with the oxic particulate phases of Fe and Mn. The concentration of particulate Fe and Mn, and associated metals, are enriched above the interface due to the diffusion of dissolved, reduced Fe and Mn from below, and their subsequent oxidation and precipitation in the higher oxygen waters. Sinking of these particulate materials and their dissolution below the interface leads to a peak in dissolved species below the interface. This cycling across the interface has been termed the "ferrous wheel" in analogy to the amusement park ride.

Another location where increased concentrations of dissolved Mn and Fe can be found is in association with hydrothermal vents, especially for Mn given the slower rate of Mn^{II} oxidation. Elevated concentrations have been found to persist in the vicinity of hydrothermal vents, in plumes that are enriched in other tracers of such activity (^3He) [21, 43]. While hydrothermal vents are sources of many metals as discussed above, the removal of metals with the precipitation of Fe and Mn oxides after emission and oxidation of fluids from hydrothermal systems results in the local scavenging and removal, and decreases the importance of hydrothermal sources as input to the global ocean. These processes are important in the formation of oxide deposits and also in the formation of metal-rich nodules.

The Cycling of the Other First Row Transition Metals, Zinc, and Cadmium

The distribution of Zn in open ocean waters appears to be strongly controlled by biogeochemical processes, and its distribution is that of a "classic" nutrient metal. The release of Zn from decomposing organic material in the sub-thermocline waters results in higher concentrations in deeper waters and the relationship between the concentration of Zn and that of Si [116]. As the main source of Zn to the ocean is riverine and terrestrial input (Table 1), and the atmospheric input is a relatively small component, depletion of surface waters is more likely. Zn is relatively soluble in seawater in the presence of inorganic ligands and has an average concentration of 5 nM (Table 1), greater than that of Fe and Mn, which are much more abundant elements in the terrestrial environment and in riverine inputs. Additionally, there is no important redox chemistry for Zn in ocean waters, and Zn forms weak complexes with inorganic ligands. Complexation of Zn by dissolved organic ligands likely also stabilizes its dissolved concentration and it is suspected that these ligands are directly or indirectly produced by microbial organisms, even if they may not be produced specifically for Zn complexation. Even given its direct biological role, Zn has a relatively long residence time compared to the other first row transition metals that exist in solution predominantly as cations.

As Zn is present in the absence of organic ligands mostly as the free ion in seawater (Table 1), it is relatively easily acquired by organisms and therefore complexation with specific organic ligands to enhance uptake is likely not needed. Therefore, complexation of Zn by organic matter does not appear to provide a unique advantage to its uptake in contrast to Fe, which is a demonstrated limiting nutrient and therefore is acquired actively through organic complexation by some microbes, and Cu, which can be toxic to some organisms at higher ocean concentrations, and complexation can result in a reduction in toxicity.

In a similar fashion to Zn, the distribution of Cd, which is from the same group in the Periodic Table, in open ocean waters is strikingly similar to that of phosphate (Fig. 6b). As with some other elements, Cd can be both a toxic metal at high concentration and have a beneficial role at low concentration because of its ability to be incorporated into and act as an active metal center in enzymes. Therefore, Cd is considered a nutrient metal and there is evidence of its depletion from surface waters in many ocean regions. Similarl to Zn, Cd inputs to the ocean are not dominated by the atmosphere, but in contrast to Zn, the inorganic chemistry of Cd in the ocean is dominated by chloride complexation and the relative fraction of Cd as the

free metal ion is a few percent. It is also apparent that Cd is complexed to organic ligands in the ocean but the relative degree of complexation is lower than that of Zn [21] Overall, the major difference in speciation in seawater is likely not due to differences in the relative binding capacities to organic matter, but the differences in the binding to Cl. The concentration of Cd in the ocean is relatively low compared to other transition metals. Its residence time in the ocean is not well characterized as there is little information on its distribution through all the ocean basins. Given its sources and biogeochemical cycling, it is probable that it has a similar residence time to Zn and other relatively soluble transition metals.

Cobalt has received recent attention due to the potential importance of Co as a cofactor in cobalamin and other enzymes. The uptake of Co by microbes, especially in surface waters, could lead to differences in the distributions of Co and Ni, another transition metal with similar chemistry and sources. Copper is also a required nutrient metal and shows a distribution that is a mixture of that expected for a nutrient element, modified because of the tendency of Cu to complex with organic matter which enhances its solubility and residence time in deep waters.

Many studies have demonstrated the importance of organic complexation for Cu [21, 31]. It has been speculated that these ligands are biologically derived by certain microorganisms, such as cyanobacteria which are susceptible to Cu toxicity. This has been demonstrated in a few instances (e.g., [35]). Inorganically complexed Cu is a very small fraction of the total in deeper waters. As noted in Table 1, inorganic Cu is primarily present as the neutral $CuCO_3$ complex in seawater.

In contrast, both Ni and Co form much weaker complexes with inorganic ligands and are present predominantly as free metal ions in seawater. These differences in speciation likely impact the mechanisms of accumulation of these metals into microorganisms. Most transition metals have been shown to have a biochemical role, with Cu being incorporated into many enzymes, while the involvement of Ni is relatively small. The concentration of Ni ($\sim$8 nM) is higher than that of Cu, while the concentration of Co is sub-nM. While both Ni and Co are found organically bound, the relative fraction is smaller than for the other transition metals discussed, being 30–50%, or greater, in various open ocean locations.

The presence of cobalamin in surface ocean waters has been recently demonstrated although it is present at low pM concentrations [83]. It is possible that most of the organically complexed Co in seawater has a biological origin. The identification of specific biochemicals containing metals raises the possibility that some of the metal, identified as complexed to organic ligands, has been released into the environment as a result of cell leakage, purposeful cellular export (e.g., metals bound to metallothioniens and phytochelatins), cell death, from the release due to grazing or even from fecal material. Alternatively, these ligands could be purposely released into solution to aid in metal assimilation, as occurs for Fe (e.g., release of siderophores), or to reduce metal toxicity, as discussed for Cu above. Another example is the presence and assimilation of heme (Fe-containing) compounds as it has been shown that microbes can assimilate heme in laboratory cultures [56].

Anthropogenic Metals: Lead, Silver, and Mercury

The three most important heavy metals in the marine environment are Pb, Hg, and Ag. Studies of Pb reflect its known input to the atmosphere from Pb compounds in leaded gasoline, as well as its presence in other anthropogenic sources. The examination of Hg is driven by human and wildlife health concerns from the toxicity and bioaccumulation of CH_3Hg in marine food chains. Silver is also known to be toxic to organisms but its levels in the open ocean are generally low ($<$1 nM) [88]. Historically, elevated Ag in the coastal environment was considered an indicator of sewage and anthropogenic-related inputs [91], because of its extensive use in the photographic industry. This is now less the case due to changes in photographic technology (i.e., the emergence of digital cameras).

All these metals bind strongly to particles and are emitted to the atmosphere from anthropogenic sources although both Pb and Ag will be removed to a degree from stacks by particulate emission control devices. Of these elements, Hg has the highest relative natural source as it can be emitted from various terrestrial environments in its gaseous elemental form. For the open ocean, atmospheric inputs are important but

additionally coastal inputs also contribute both Hg and Pb from terrestrial runoff and point source inputs. Mercury is different as is can be present as a dissolved gas (Hg^0) in seawater and therefore air-sea exchange involves both deposition and gas evasion.

Concentrations of Ag in the ocean vary from low pM values typically found in the surface ocean to 100 pM or more in deep waters, and concentrations vary substantially between ocean basins [79, 89, 108, 109] (Fig. 7). Silver typically has a nutrient-type profile and it has been shown that its vertical distribution mimics that of Si, suggesting its incorporation into the more recalcitrant tissues of microbes and other organisms in the surface ocean and its relatively slow release from sinking particulate material [89, 109]. In the deep ocean, there is continual net increase as Ag is being continuously released from settling particulate matter but is not being scavenged in deep waters in a similar fashion to other metals, making the distribution of Ag similar to that of Al. Additionally, both elements are supplied to the ocean mainly from river and coastal sources, with atmospheric deposition being a secondary source [49, 88]. Concentrations are increasing over time in the oceans. A comparison of intermediate waters in the North Pacific Ocean suggests that Ag concentrations have increased in the last 20 years, reflecting increased anthropogenic inputs [89]. In contrast, a similar comparison for Hg concluded that there had not been a substantial increase in concentration over that time period [63], although more recent evidence suggests that concentrations have increased more recently [101].

A number of ongoing and detailed studies have documented the overall contamination of the ocean by anthropogenic Pb and have demonstrated the resultant decrease in ocean Pb as a result of the phasing out of Pb additives for gasoline [107] (Figs. 2 and 8). However, there is still Pb input to the atmosphere from other anthropogenic sources and current studies are evaluating the extent of this input. One unique aspect of examining Pb geochemistry is the fact that it has numerous isotopes, and these isotopes are daughters of the uranium-thorium (U–Th) decay series: ^{206}Pb is the stable product of the ^{238}U decay series, ^{207}Pb the stable product of the ^{235}U decay series, and ^{208}Pb is the stable product of the ^{232}Th decay series. Thus, the isotopic ratio of Pb in the environment is altered due to the presence of either U or Th in the medium. It has been demonstrated that Pb from different locations has ratios which are different enough to track the sources of the Pb in the ocean and other environments as the different isotope ratios allow for more resolution of the source signals (Fig. 8b). Data for the South and equatorial Atlantic Ocean collected in 1996 is plotted against the various potential source signals and demonstrates a range of potential sources, including inputs from North America, large rivers, and coastal sources. In contrast, the data for the deep waters of the North Pacific, which represent the "oldest" marine water masses, shows a Pb signal reflective of inputs via particle settling and from the anthropogenic enrichment of atmospheric deposition.

Most of the input of Pb to the ocean is atmospheric (Table 1) and the distribution of Pb in the ocean typically has a maximum concentration in the surface ocean and lower concentrations at depth (Fig. 8) [107], as well as higher concentrations in the Atlantic Ocean compared to the Pacific. The concentrations in the upper waters of the North Atlantic in the vicinity of Bermuda have been decreasing in the last 30 years (see Fig. 2) [106] from values above 150 pM in the late 1970s to concentrations around 50 pM today. It can be concluded that while the surface waters near Bermuda have decreased in concentration they are still substantially elevated above background and reflect the continual input of Pb from combustion and other industrial sources.

For Hg, both box and numerical models of the global cycle support the notion that anthropogenic releases of mercury (Hg) to the environment have impacted the biosphere substantially, enhancing deposition by a factor of 3–5, and influencing ocean concentrations ([39, 74, 70, 96, 102]). Besides atmospheric inputs, local and regional-scale contamination of the coastal zone by Hg has occurred due to runoff from the terrestrial environment and from point source inputs [103, 117]. Mercury distributions in surface waters reflect the magnitude of the atmospheric deposition source and the strength of local removal process (scavenging and gas evasion) superimposed on water circulation [63, 101, 102]. In some regions, concentrations change seasonally depending on the variability of atmospheric deposition, evasion, and removal of Hg by particulate sinking. Recent model output shows the

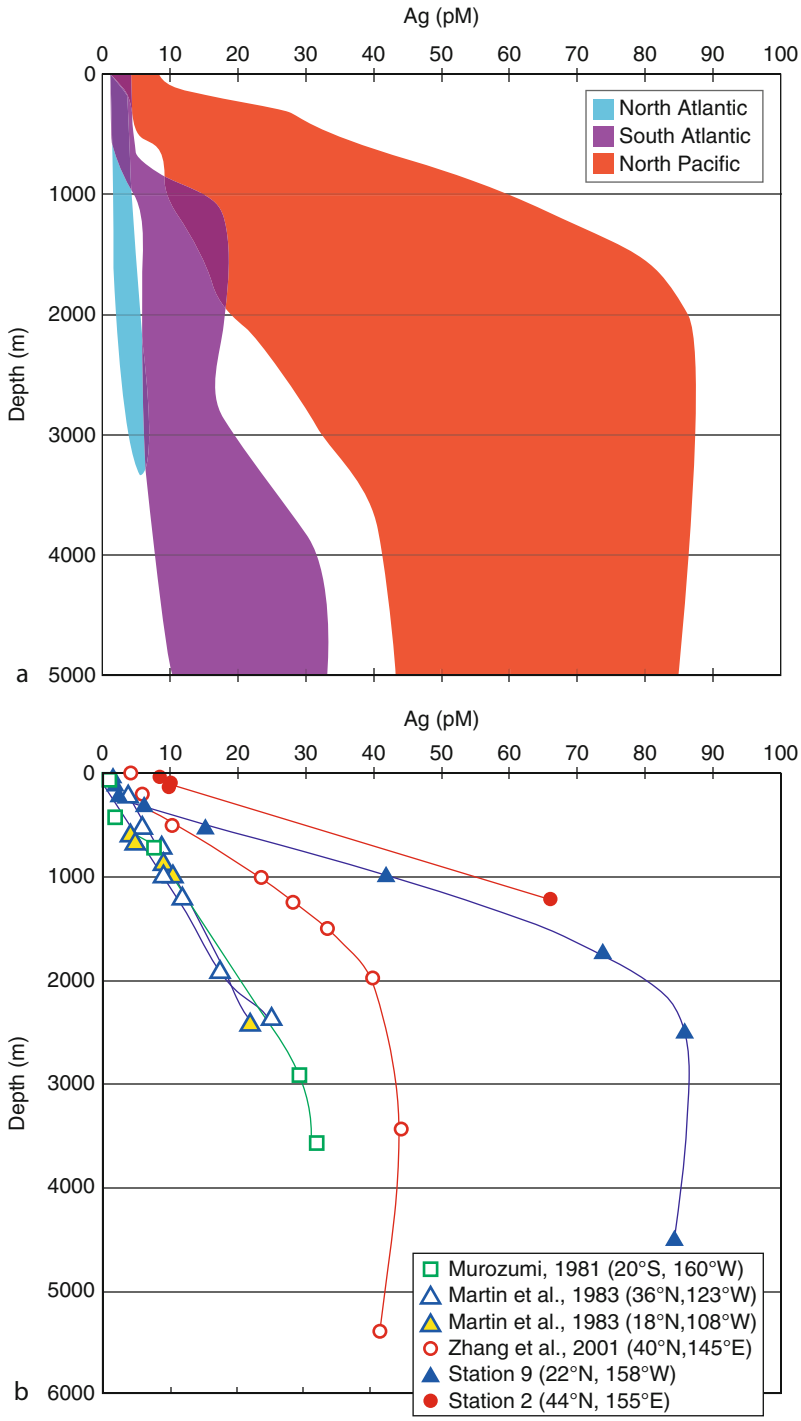

Oceanic Fate and Transport of Chemicals. Figure 7

(**a**) Distributions of silver in the various ocean basins and (**b**) Changes in the concentrations within the water column in the North Pacific over time. Taken from M.A. Ranville and A. R. Flegal "Silver in the North Pacific Ocean", published in *Geochemistry Geophysics Geosystems* volume 6, Art. No. Q03M01. Copyright (2005), American Geophysical Union. Reprinted with permission as stated by American Geophysical Union

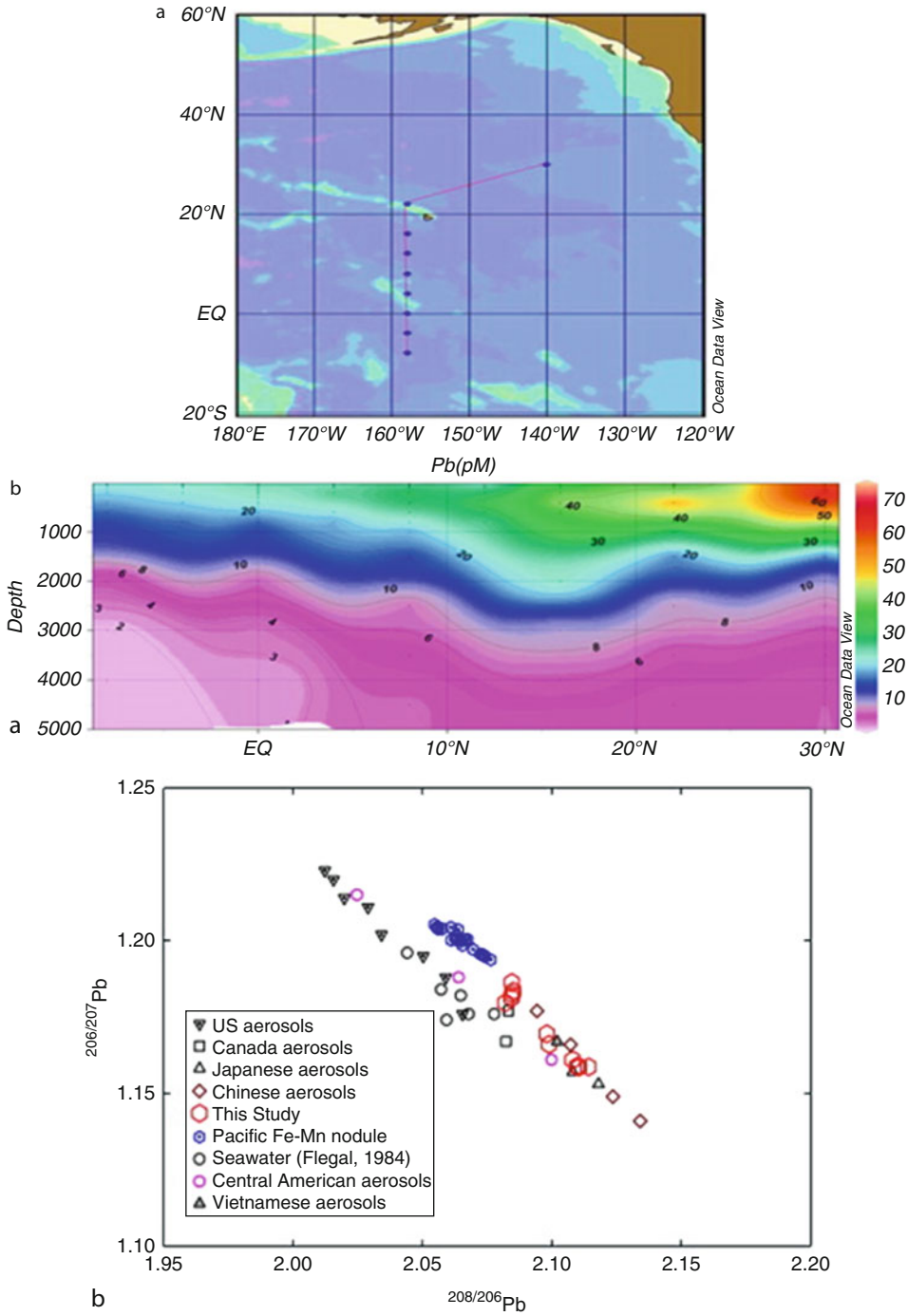

Oceanic Fate and Transport of Chemicals. Figure 8

(**a**) Cruise track and horizontal and vertical distributions of Pb collected during the cruise; (**b**) Relationship between the various isotope ratios of Pb for the samples collected during the cruise with comparison to other materials for which isotopes have been measured, and which could be sources for Pb in this region. Taken from J.F. Wu, R. Rember et al. "Isotopic evidence for the source of lead in the North Pacific abyssal water" published in *Geochimica et Cosmochimica Acta* volume 74(16), pages 4629–4638. Copyright (2010), and published with permission from Elsevier

potential variability that could exist for various Hg species in the ocean (Fig. 9a shows modeled inorganic Hg distributions). Concentrations vary between ocean basins due to differences in the relative impact of anthropogenic Hg in deposition (Fig. 9a), and these are changing over time – recently, more anthropogenic inputs from Asia and less from North America and Europe. Surface water concentrations are higher in the Atlantic Ocean and Mediterranean Sea than in the Pacific Ocean [25–27, 68, 69, 71, 73, 101, 118], and there is evidence for recent decreases in concentration in the North Atlantic and the Mediterranean Sea and these are consistent with model predictions [97, 98, 102].

The upper ocean Hg concentration can be transient, changing on short timescales due to changes in atmospheric inputs and seasonal water mixing [63]. For example, the input of Hg from the atmosphere was demonstrated through an increase in the concentration of Hg in the waters of the North Pacific Ocean seasonal mixed layer during the summer. However, this signal is eliminated as a result of deep water mixing in the fall. Seasonal mixing and latitudinal transport of sinking surface water within the permanent thermocline is a mechanism for the transport of Hg deposited at higher latitudes, which may have been deposited to the ocean a decade or more previously [85] to tropical and other regions ([72, 102]). The higher concentrations in the more recent data suggest the input of Hg to these mid-depth waters, and this coincides with an increasing anthropogenic signal from Asia, and such changes are not evident in the deep ocean waters [63, 101]. Such upper ocean cycling confounds the understanding of how the Hg concentration in ocean surface waters has changed as a result of increased anthropogenic inputs, and model predictions suggest that the response time of the ocean to changes in atmospheric Hg concentrations is decadal or longer [97].

The distribution of Hg in ocean waters reflects the sources and cycling as well as the internal cycling of mercury, methylation, demethylation, oxidation, and reduction. The biological production and destruction of methylated Hg species, primarily CH_3Hg and $(CH_3)_2Hg$ in the ocean, is important as the methylated forms are more toxic. In numerous profiles there appears to be an enhancement in the concentration of methylated Hg (CH_3Hg and $(CH_3)_2Hg$) at mid-depth [52, 101, 119, 122] (Fig. 9b). The analysis of the data and the relationships to environmental parameters suggest that the profiles can be best explained in terms of production of methylated Hg during the decomposition and remineralization of organic matter [52, 101]. The more recent studies examining the production of methylated Hg suggests that the presence of methylated Hg in low oxygen waters is more due to the same factors that cause the oxygen depletion – heightened bacterial activity, and slow vertical mixing, lack of water ventilation, and particulate scavenging – than to the activity of particular microorganisms [67, 101]. In freshwater and coastal environments and sediments, sulfate and iron-reducing bacteria have been demonstrated to be the most important methylating organisms [8, 120]. While little is known about the microorganisms or processes whereby Hg is methylated in the ocean, the fact that methylation has been demonstrated in relatively oxygenated waters, and the dominance in many instances of $(CH_3)_2Hg$, suggests that the pathways may be very different from those for freshwater and coastal environments, and in sediments. The net concentration of methylated Hg reflects the complex interactions that occur throughout the water column: production and destruction of methylated Hg by microbial processes and abiotic mechanisms; scavenging and release from particles; and uptake into the food chain.

Overall, there are strong similarities between the three major heavy metals in terms of their strong association with organic matter and the particulate phase. Mercury and Ag have similarities in that they are both Class B metals and form strong associations with reduced sulfide, and exist in seawater as chloride complexes in the absence of NOM. Lead can also be associated with sulfides and forms strong complexes, but to a lesser degree. Also, Pb does not form strong chloride complexes and is found as the neutral $PbCO_3$ complex in the absence of NOM (Table 1). Atmospheric sources are all important for these metals to the open ocean, and this is primarily related to the fact that their global cycles have been substantially impacted by anthropogenic sources. Besides Hg, the accumulation and fate of these elements in ocean microorganisms and in the oceanic food chain has been little examined and this could be an important area for future research.

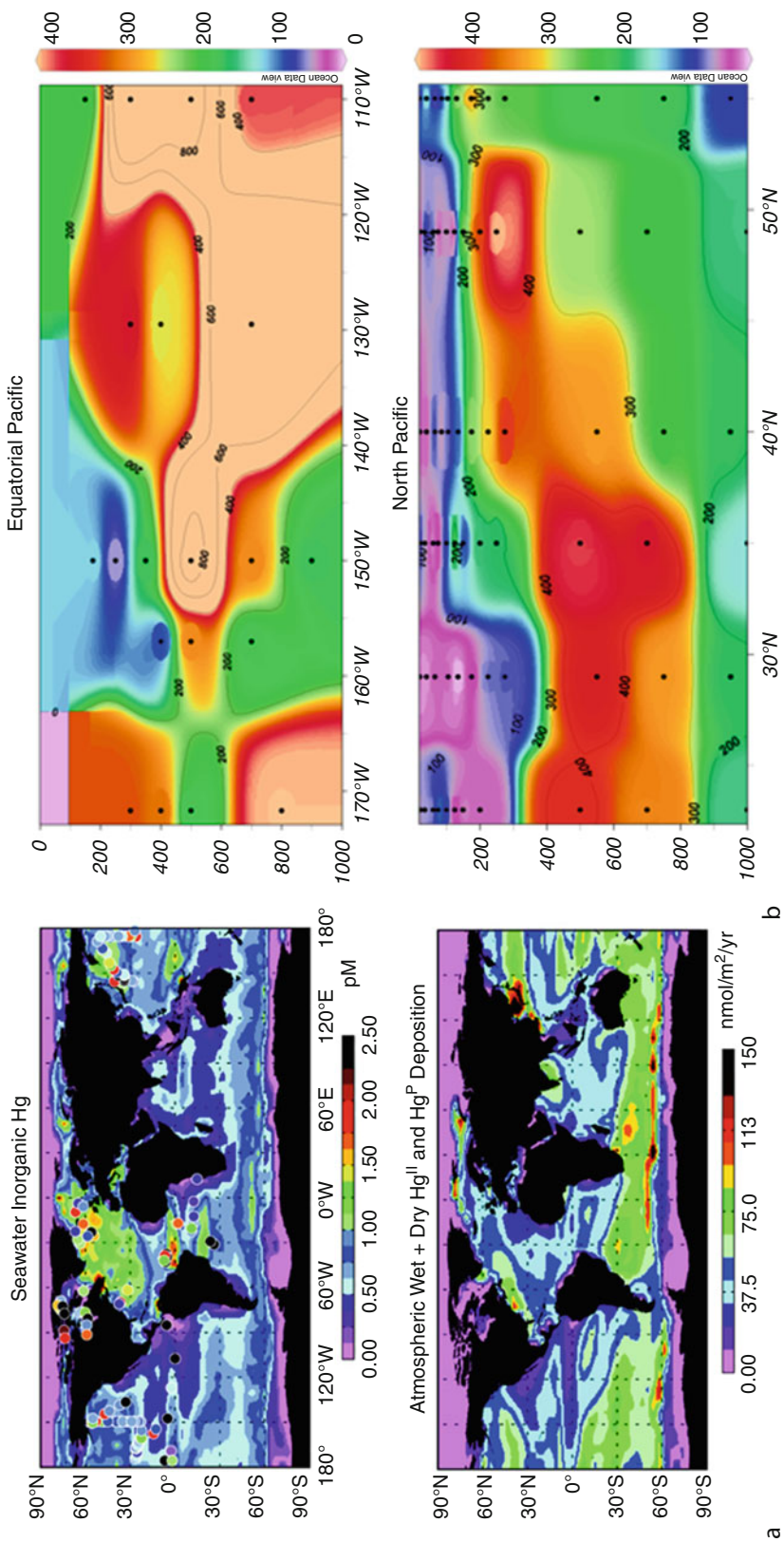

Oceanic Fate and Transport of Chemicals. Figure 9
(**a**) Modeled concentrations of inorganic Hg and of wet and dry deposition to the ocean surface for the global oceans, using the GEOS-Chem model framework. Circles in the figures represent the location and concentrations obtained during field campaigns; (**b**) Data for the concentrations of methylated species (both monomethylmercury and dimethylmercury) in the equatorial and North Pacific Ocean upper waters. The first figure was derived from A.L. Soerensen, E. M. Sunderland, et al. "An improved global model for air-sea exchange of mercury: High concentrations over the North Atlantic" published in *Environmental Science & Technology* volume 44(22), pp. 8574–8580. Copyright (2010) and reprinted with permission from the American Chemical Society. The second figure was compiled by Elsie Sunderland of Harvard University using information in Mason and Fitzgerald [68] and Sunderland et al. [101]

Metalloids and Other Important Elements

The main metalloids of interest in marine systems (e.g., As, Se) exist as oxyanions, and in a number of oxidation states (Table 1), although they are also found as methylated compounds, or even as larger metalloid-containing species, such as arsenobetaine and selenoproteins. These organic species and their formation mechanisms are not detailed here but their biochemical formation is relatively well known. Arsenic can be found as either As^{III} or As^{V} and as mono-, di-, and tri-methyl arsenic in marine waters, and similar forms and speciation are found for Se and the other metalloids (Sb, Ge). It is thought that the methylation of As is a detoxification and elimination mechanism for As from phytoplankton as As^{V} can be taken up inadvertently by microorganisms in low phosphate waters (both exist as polyprotic acids with similar pKa's). Methylation involves pre-reduction of the As^{V} to As^{III} before being methylated. This is a different mechanism to Hg methylation by sulfate-reducing bacteria. There is also often As^{III} present in conjunction with phytoplankton in surface waters due to this reduction pathway, which is contrary to what is expected based on thermodynamic equilibrium calculations. However, As^{III} is a small fraction of the total, as are the methylated species [28, 29]. In estuarine environments and freshwaters, As^{III} and the methylated forms can be a larger fraction of the total dissolved As [53, 80].

The two main inorganic redox states of Se appear to cover a similar range in concentration, with deep waters having a ratio of Se^{IV}/Se^{VI} of >0.5, but <1. Both inorganic species appear to be depleted in the surface waters, likely due to their uptake and incorporation into biota. Selenium is an essential element although it is only required at low concentrations. Most of the bioorganic Se compounds are proteins and are therefore being continually produced through microbial processes.

Overall, there has been little recent study of the inorganic and organic speciation of the metalloids in the ocean water column. It is probable that new insights and understanding could be gained from the examination of the various fractions in more detail, especially the "organic fraction." It is not clear whether these compounds are derived directly from microorganisms and other biota, or are primarily produced during organic matter remineralization. It has however been shown that microorganisms contain small and large molecular weight metalloid-containing molecules.

Cycling of Organic Chemicals in the Ocean

There have been few detailed studies of the ocean distribution of organic chemicals and this relates both to their difficulty of measurement and the lack of research focus. However, the cycling and fate of other organic chemicals can be estimated based on the knowledge of these chemicals if their general chemical characteristics are known. The physiochemical parameters needed to predict their fate and transport include: (1) their solubility and volatility; (2) their Henry's Law Constant (K_H), which defines their relative solubility in water versus air; (3) their dissolved-particulate partition coefficient, typically normalized to particulate organic content (K_{OM}); and (4) their octanol-water partition coefficient (K_{OW}) which is a measure of the hydrophobicity of the compounds.

The solubility of organic compounds ranges widely but most compounds of environmental interest are relatively insoluble in seawater. Additionally, their environmental concentrations do not approach their saturated solubilities (from 10^{-2} M for small chain compounds to 10^{-11} M for some PCB congeners; [94]). Solubility is a strong function of the composition of the organic chemical as compounds that can be ionized in water due to the presence of acidic or basic groups (e.g., carboxylic acids, amine, and other N-containing groups, phenols and alcohols and thiols) will be more soluble that a similar compound without an ionizable group. The pH of seawater is around 8.2, it has high ionic strength and water molecules are polar and therefore ionizable compounds will tend to dissociate or be protonated to some degree as a result. Nonpolar compounds are the most hydrophobic as there is little interaction between the compounds and water.

Related to solubility is the air-water partition coefficient (K_H = partial pressure (P_i)/dissolved water concentration (C_W)), which for environmental science can be considered as a measure of the potential for a compound to be lost from solution via gas exchange. Compounds with high values are volatile, but the degree to which a compound would be lost from water to the air is a function of K_H and the relative

concentration of the compound in each phase. Aliphatic hydrocarbons have relatively high K_H (~10^2–10^4 atm/M), PCBs intermediate (~0.01–1 atm/M), and PAHs lower values (~0.001–0.1 atm/M) [94].

The degree to which organic chemicals will remain dissolved in an environmental solution or partition into particulate phases, or become associated with high molecular weight dissolved organic material, such as humic substances, is a function of their hydrophobicity which is related to their solubility and is related to K_{OW}, which is the ratio of the concentration at equilibrium in water compared to octanol. The dissolved-POM partition coefficient is related to these parameters (Fig. 10a) [94]. Octanol is used as the comparative phase as it is thought to be a reasonable representative medium for the cell membrane and also likely provides a reasonable proxy for POM in seawater. Again, the values for organic chemicals range over a wide scale. The more soluble the compound, the smaller is the K_{OW} and K_{OM}.

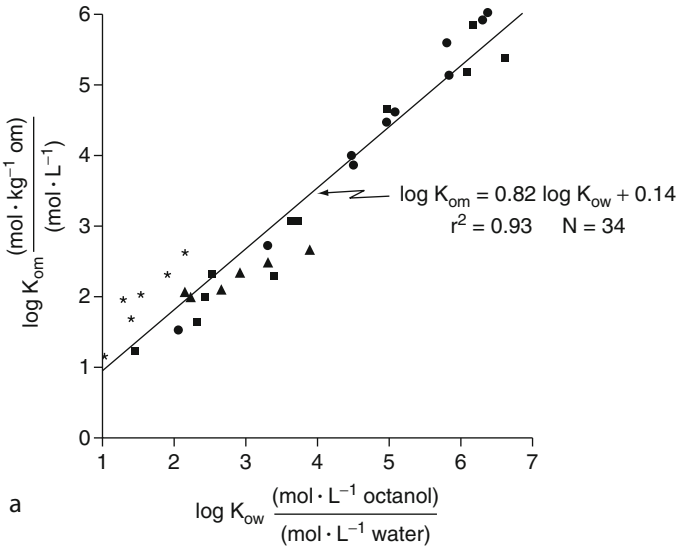

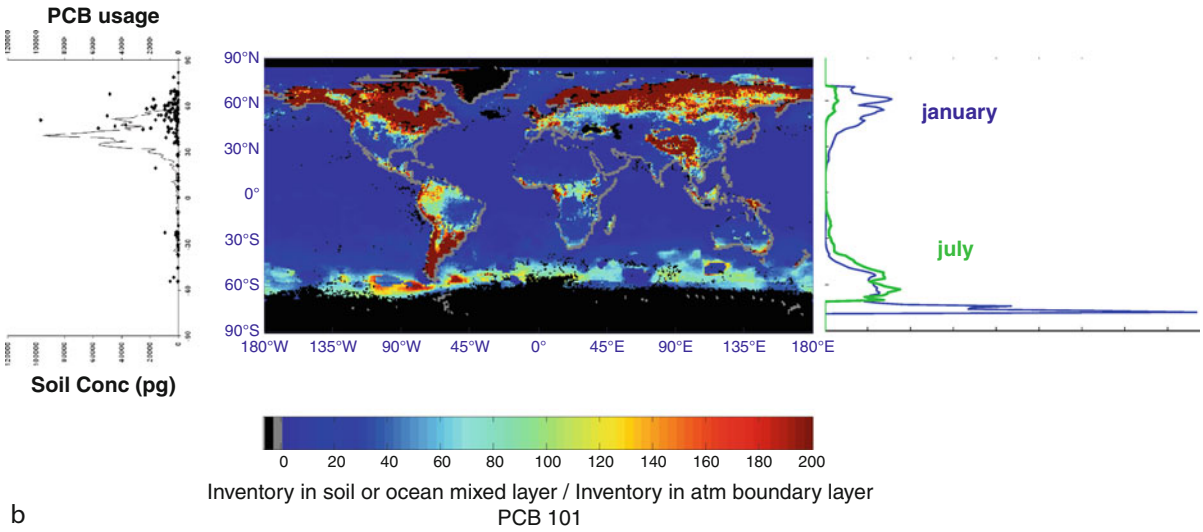

Oceanic Fate and Transport of Chemicals. Figure 10 (Continued)

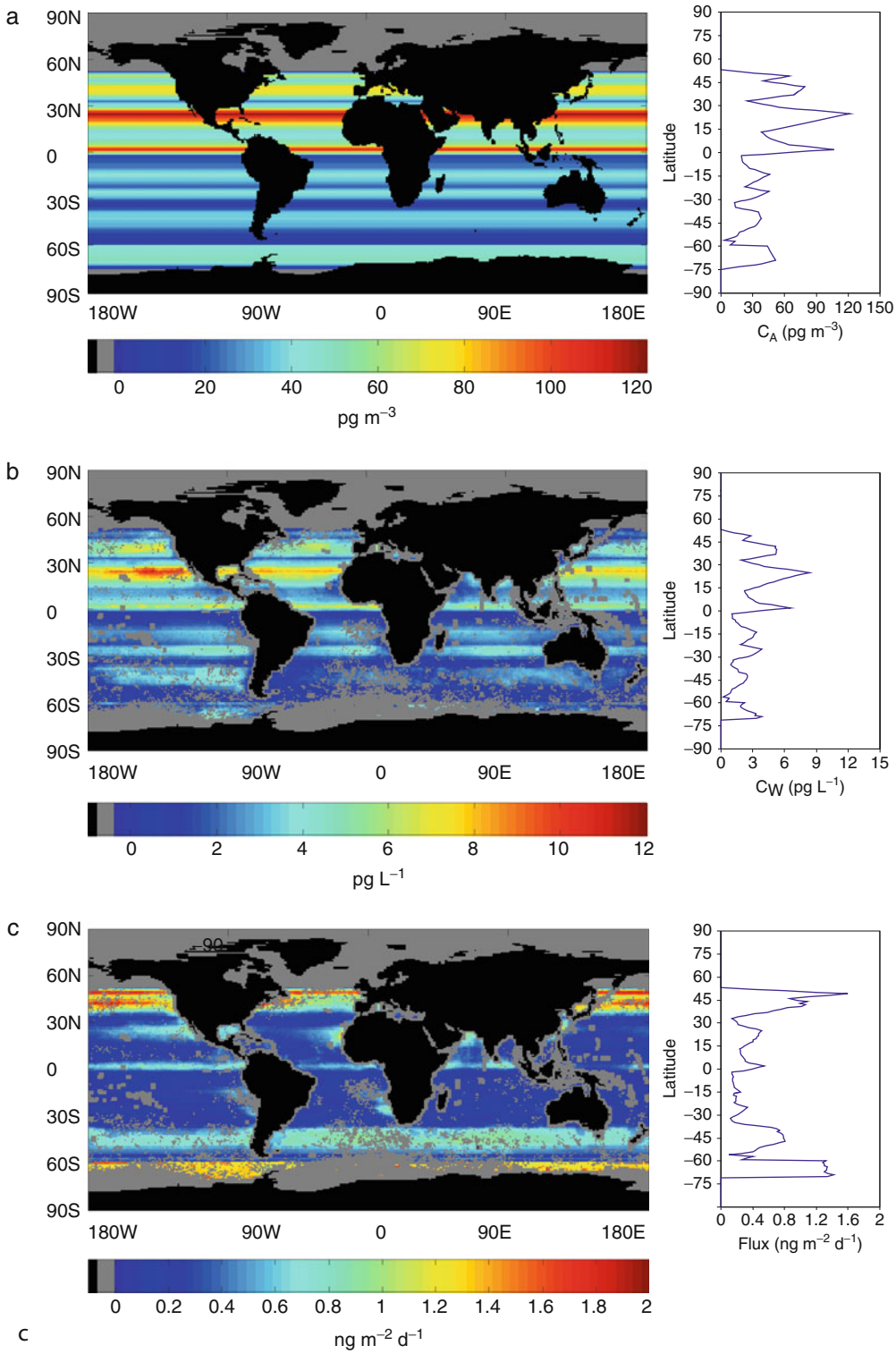

Oceanic Fate and Transport of Chemicals. Figure 10
(Continued)

As POPs are hydrophobic, they also attach to particles in the water, and the degree of association is a function of the particulate organic content, and therefore can be removed from the surface to deep ocean via sinking particles, especially in regions of high primary productivity. Thus, the factors controlling the overall distribution and fate of the more volatile POPs are similar to that of Hg. The degree to which the deep ocean is being enriched in these compounds is related to the rate of additional from above compared to their rate of removal to the deep sediment. As most of the organic matter sinking into the deeper ocean is remineralized, it is likely that the degree of incorporation of POPs into deep ocean sediments is less than that for metals and other compounds that form relatively strong associations with mineral phases.

The oceans play an important role in controlling the environmental transport, fate, and sinks of many POPs at regional and global scales [50, 58]. While the atmosphere is the most important global transport mechanism for many POPs, transport via ocean currents is important for some compounds. Deep ocean waters are usually considered the final sink for POPs, although an evaluation of the importance of their role in their environmental fate is uncertain, and modeling of their fate in the deep ocean has not been considered in a detailed fashion. POPs bound to sinking POM are exported from the mixed layer and will either accumulate in the deep ocean waters, as do the nutrients and some elements (Ag, Al), or will be finally removed to deep sediments. Marine sediments, and potentially the continental shelf could represent an important reservoir for POPs [59]. Gustafsson et al. [51] examined the settling fluxes of PCBs in the coastal and offshore North Atlantic Ocean by measuring their concentrations on particles and using ^{234}Th to estimate particle settling velocity. As may be suspected, the ratio of the flux to the sediment surface compared to that of the export flux from the mixed layer decreased with increasing water depth, and with the aqueous solubility of the PCB congeners, suggesting overall release from the dissolution of particles with increasing depth. Depending on the individual congener, the flux rates ranged from <1 to 10 pmol m^{-2} day^{-1} at the offshore stations to almost 100 pmol m^{-2} day^{-1} at the nearshore locations. Such fluxes are comparable to estimates by others. These authors inferred from the PCB distributions that atmospheric input was dominant source to the open ocean locations, and that particle scavenging and removal from the mixed layer was a more important sink for these compounds than photochemical decomposition in the marine boundary layer. Given the larger surface area of the open ocean environment, the flux in this region was a bigger fraction of the total input to deeper waters than the more nearshore waters, even though the fluxes in the shallow regions were higher [51].

Deep ocean sediments are likely important for many POPs. The relative importance of removal to the deep ocean and sediments versus reemission to the atmosphere will be different for different chemicals. Records of POP concentrations in deep ocean

Oceanic Fate and Transport of Chemicals. Figure 10
(**a**) Relationship between the octanol-water partition coefficient and the dissolved-solid partition coefficient (normalized to organic content) for a variety of organic chemicals. Taken from R.P. Schwarzenbach, P. M. Gschwend, et al. "Environmental Organic Chemistry" published by John Wiley and Sons. Copyright (1993) and reproduced with permission; (**b**) the distribution of PCB in various reservoirs of the biosphere: the historical usage and soil concentrations are shown in the left panel; the model predictions of the maximum reservoir capacity in the center figure, with the right figure showing the particular distribution for the Atlantic Ocean. Taken from R. Lohmann, K. Breivik, J. Dachs and D. Muir "Global fate of POPs: Current and future research directions" published in Environmental Pollution, volume 150, pp. 150–165. Copyright (2007) and published with permission from Elsevier; (**c**) the global spatial variability for PCB 52 in the atmosphere (gas phase) (*top*), dissolved surface ocean (*middle*) and predicted air-sea and sinking fluxes (*bottom*). Taken from J. Dachs, R. Lohmann, W.A. Ockenden, L. Mejanelle, S.J. Eisenreich and K.C. Jones "Oceanic biogeochemical controls on global dynamics of persistent organic pollutants" published in Environmental Science and Technology, volume 36, pp. 4229–4237. Copyright (2002) and reprinted with permission from the American Chemical Society

sediments are sparse and therefore it is difficult to evaluate for many compounds their degree of removal to the deep sediment. Estimates for ∑DDT are that 4–6% of these compounds have been removed to the deep ocean sediments and that most of the amount added to the ocean during their use is either still resident in the ocean or returned to the atmosphere.

Water column distributions and knowledge of the inter-basin variability in concentration of organic contaminants is much less well known that that of nutrients and metals but there are some similarities in the chemistry and partitioning that allows inferences to be made concerning their fate and transport in the ocean and the main processes controlling their internal cycling. Many of the POPs are sufficiently volatile and insoluble that air-sea gas exchange is an important part of their global cycle and determines to a large degree the extent of their accumulation and persistence in the ocean. For compounds that are relatively volatile, their upper ocean concentration is determined by the rate of input relative to the rate of re-emission to the atmosphere. For example, for PCBs, their upper ocean concentration is determined primarily by the gas exchange component with wet deposition and dry deposition of PCBs being relatively minor components [30]. The impact of the historical extent of emissions and atmospheric concentration on the ocean distribution of PCBs is illustrated with the model data shown in Fig. 10b. This further illustrates the importance of gas exchange on controlling concentrations as for the open ocean atmospheric particulate concentrations are low and these aerosols are dominated by large sea salt particles which are not effective is trapping POPs given their low organic content. It has been estimated that approximately 10% of the global releases of PCBs resides in the upper ocean [16], and similarly the upper ocean is a major reservoir for other compounds such as ∑DDT [99] and PFOS and their precursors.

Modeling studies suggest that the ocean, particularly in the Northern Hemisphere, was a net sink for ∑DDT during the period of its heightened use but that it is now a source as the banning and limited use of DDT has lead to a decrease in the atmospheric burden and as a result a degassing of ∑DDT from the ocean surface to the atmosphere [99]. The change from sink to source was slowest for the Northern Hemisphere as the air concentration in the region was buffered to a larger degree by re-emission of these chemicals from the terrestrial environment. This is because of both the relatively higher inputs of these chemicals in the Northern Hemisphere as well as the higher relative land mass in the north. The model results suggest that the ocean surface in the Southern Hemisphere became a source to the atmosphere in the late 1980s/early 1990s while the situation was delayed for about a decade in the Northern Hemisphere. The ocean gyre regions became a source more rapidly that regions of higher atmospheric inputs due to enhanced wet deposition, or regions with higher productivity as the enhanced removal of these compounds from the surface ocean to deep in association with particulate sinking delayed the buildup in surface concentrations relative to those in the atmosphere and resulted in a longer persistence of ocean uptake. This example again illustrates the importance of ocean circulation and primary productivity as factors that have a large influence over the overall fate and cycling of POPs.

Given the lack of data for many chemicals in the ocean, there have been several efforts over the years to model the systems to understand the fate and transport of these chemicals. Wania and Mackay [105] developed a zonal climatically differentiated nonequilibrium fugacity mass balance model for POPs including air, fresh and ocean water, and sediments/soils with advective connections to examine the main processes involved in the portioning and distribution of these chemicals across environmental media. Not surprisingly, temperature and chemical reactivity were highly important variables, as were the transport rates and the chemical composition, such as the media organic content and other physicochemical properties (e.g., solubility, K_{OW}, vapor pressure). Dachs et al. [30] further examined the biogeochemical controls over the cycling of POPs in the ocean and demonstrated the importance of air-sea exchange, and as a result, temperature in the cycling of the volatile components across this interface. Additionally, given the importance of particulate removal in the cycling of POPs in the upper ocean as a sink, and air-sea exchange as a potential source or sink, they determined that influx of gaseous POPs to the ocean was actually higher in productive regions as the particulate removal depleted the surface layers and resulted in net deposition of gaseous species from the atmosphere. This is shown in Fig. 10c, which shows the

model estimated parameters for gaseous concentrations over the ocean, predicted dissolved surface ocean concentrations, and the extent of air-sea exchange for a particular PCB congener. These results show that fluxes are into the ocean overall and are driven by the atmospheric concentration.

Overall, the results of the limited studies of POPs in the ocean indicate that their cycling is controlled by their degree to which gas exchange at the sea surface is important in their geochemical cycling. The more soluble compounds will be less impacted by gas exchange and the more hydrophobic compounds will attach to particles and be removed from the surface ocean more efficiently, driving further gas exchange input. Overall, while many of these chemicals have been banned in many parts of the world, or have now more restricted usage, there is a strong legacy remaining in the biosphere because of their buildup in the terrestrial soils, and because of their overall volatility, they can be reemitted to the atmosphere and continually contribute to the contamination of the ocean. Finally, it is clear that there are many similarities in the cycling and ocean biogeochemistry of elements and organic chemicals and that productivity and carbon export from the surface ocean are main drivers on upper ocean concentrations and the extent to which the ocean is a net sink. For many chemicals, buildup is occurring in the deep ocean as a result of human activity and this legacy will remain for an extended period given the slow deep cycling of the ocean waters.

Future Directions

The above discussions on the cycling of pollutant elements and chemicals in the ocean indicates that there has been both an increased awareness of the impact of human activities on the ocean and on its environmental health, as well as on that of the organisms that reside in the ocean, and on the consumers of ocean seafood, including and particularly humans. There has been a notable increase in the amount of study and regulation globally concerning the ocean and many nations are involved currently in assessments that will lead to further understanding and regulation. One such activity is the international GEOTRACERS program which is designed to measure the concentrations and distributions of a whole suite of metals and isotopes in all the major ocean basins, and this activity in its initial few years has produced many interesting and exciting results that are mentioned above. Additionally, there is a continual improvement in the analytical and sampling technology, and the development of continuous or in situ samplers for a variety of chemicals that are increasing enormously the amount of information gathered on chemicals in the ocean. Previously, ship time and resources have been a serious limiting factor but the developments of these new technologies are increasing the databases on chemicals in an exponential fashion, and there is now a need to develop extensive methods to compare and contrast and validate the measurements being made by a suite of countries around the globe.

The increasing information and knowledge that is occurring in terms of the elements is not happening to the same extent for the organic chemicals. This is the result of the fact that current analytical techniques are still time consuming and their detection limits are often comparable to the concentrations that are being measured. Further improvement in analytical methods is needed to further enhance the databases on these chemicals, which is still very sparse, especially for open ocean and deep waters. Furthermore, there is a constant development of new chemicals by industry and therefore while the understanding of past chemicals and their fate and transport are becoming better understood, there is little information on the newer chemicals released into the environment. To be able to keep pace with such developments and changes, it is necessary to develop an understanding of the underlying fundamental processes that control organic chemical fate and transport and transformation in the ocean. Only with such understanding can reliable predictions be made; currently most understanding is developed in an empirical fashion.

Model development and application can provide insights where there is a lack of data but the models themselves are only as good as their extent of validation, and so while it is possible to a degree to use models to fill gaps in data and knowledge, there is also a need to collect data and to constantly improve the models through validation and comparison with the data. Only through such interactions can our understanding of the complex cycling of chemicals in the ocean be further improved.

Bibliography

Primary Literature

1. Akeredolu FA et al (1994) The flux of anthropogenic trace-metals into the arctic from the mid-latitudes in 1979/80. Atmos Environ 28:1557–1572
2. Anderson RF (2004) Chemical tracers of particle transport. In: Enderfield H (ed) The oceans and marine geochemistry, vol 6. Elsevier, Amsterdam, pp 247–273
3. Arimoto R et al (1995) Trace-elements in the atmosphere over the North Atlantic. J Geophys Res Atmos 100(D1): 1199–1213
4. Arimoto R, Duce RA, Ray BJ, Tomza U (2003) Dry deposition of trace elements to the western North Atlantic. Global Biogeochem Cycles 17(1)
5. Arimoto R, Gao Y, Zhou M-Y, Soo D, Chen L, Gu D, Wang Z, Zhang X (1997) Atmospheric deposition of trace elements to the western Pacific Basin. In: Baker J (ed) Atmospheric deposition of contaminants to the great lakes and to coastal waters. SETAC Press, Pensacola, pp 195–208
6. Baker J, Poster DL, Clark CA, Church TM, Scudlark JR, Ondov JM, Dickhut RM, Cutter G (1997) Loadings of atmospheric trace elements and organic contaminants to the Chesapeake Bay. In: Baker J (ed) Atmospheric deposition of contaminants to the great lakes and coastal waters. SETAC Press, Pensacola, pp 171–194
7. Barbante C et al (2004) Historical record of European emissions of heavy metals to the atmosphere since the 1650s from alpine snow/ice cores drilled near Monte Rosa. Environ Sci Technol 38(15):4085–4090
8. Benoit JM, Gilmour CC et al (2003) Geochemical and biological controls over methylmercury production and degradation in aquatic ecosystems. Biogeochem Environ Important Trace Elem 835:262–297
9. Berg T, Steinnes E (2005) Atmospheric transport of metals. In: Sigel A, Sigel H, Sigel RKO (eds) Biogeochemistry, availability and transport of metals in the environment, vol 44, Metal ions in biological systems. Taylor & Francis, Boca Raton
10. Bergan T, Gallardo L, Rodhe H (1999) Mercury in the global troposphere: a three-dimensional model study. Atmos Environ 33(10):1575–1585
11. Billen G, Garnier J (2007) River basin nutrient delivery to the coastal sea: assessing its potential to sustain new production of non-siliceous algae. Mar Chem 106(1–2): 148–160
12. Boesch DF, Burroughs RH, Baker JE, Mason RP, Rowe CL, Siefert RL (2001) Marine pollution in the United States. Pew Oceans Commission Report, Washington, DC
13. Boutron C et al (2004) Anthropogenic lead in polar snow and ice archives. C R Geosci 336(10):847–867
14. Boyle EA, Sherrell RM et al (1994) Lead variability in the western North Atlantic Ocean and central Greenland ice – implications for the search for decadal trends in anthropogenic emissions. Geochim Cosmochim Acta 58(15):3227–3238
15. Boyle EA (2010) In: Steele JH, Thorpe SA, Turekian KK (eds) Marine chemistry and geochemistry. Elsevier, Amsterdam, pp 273–280
16. Breivik K, Wania F (2002) Mass budgets, pathways, and equilibrium states of two hexachlorocyclohexanes in the Baltic Sea environment. Environ Sci Technol 36(5):1024–1032
17. Broecker WS, Peng T-H (1982) Tracers in the sea. Eldigio Press, New York
18. Bruland K, Lohan MC (2004) Controls of trace metals in seawater. In: Elderfield H (ed), Holland HD, Turekian KK (Exec eds) The oceans and marine geochemistry, vol 6. Amsterdam, Elsevier, pp 23–47
19. Bruland KW, Coale KH (1986) Surface water 234Th/238U disequilibria: spatial and temporal variations of scavenging rates within the Pacific Ocean. In: Burton JD, Brewer PG, Chester R (eds) Dynamic processes in the chemistry of the upper ocean. Plenum Press, New York, pp 159–172
20. Callender E (2005) Heavy metals in the environment – historical trends. In: Lollar B, Holland HD, Turekian KK (eds) Environmental geochemistry, vol 5, Treatise on geochemistry. Elsevier, Amsterdam, pp 67–105
21. Chester R (2003) Marine geochemistry. Blackwell, Malden
22. Clegg S, Whitfield M (1990) A generalized model for the scavenging of trace metals in the open ocean–I. Particle cycling. Deep Sea Res 37:809–832
23. Conley DJ, Schelske CL et al (1993) Modification of the biogeochemical cycle of silica with eutrophication. Mar Ecol Prog Ser 81:121–128
24. Cossa D, Averty B et al (2009) The origin of methylmercury in open Mediterranean waters. Limnol Oceanogr 54(3): 837–844
25. Cossa D, Cotte-Krief MH et al (2004) Total mercury in the water column near the shelf edge of the European continental margin. Mar Chem 90(1–4):21–29
26. Cossa D, Martin J-M, Takayanagi K, Sanjuan J (1997) The distribution and cycling of mercury species in the western Mediterranean. Deep Sea Res 44:721–740
27. Cossa D, Michel P et al (1992) Vertical mercury profile in relation to arsenic, cadmium and copper at the eastern North Atlantic ICES reference station. Oceanol Acta 15: 603–608
28. Cutter GA (2010) Metalloids and oxyanions. In: Steele JH, Thorpe SA, Turekian KK (eds) Marine chemistry and geochemistry. Elsevier, Amsterdam, pp 64–71
29. Cutter GA, Cutter LS (2006) The biogeochemistry of arsenic and antimony in the North Pacific Ocean. Geochem Geophys Geosyst 7, doi:10.1029/2005GC001159
30. Dachs J, Lohmann R, Ockenden WA, Mejanelle L, Eisenreich SJ, Jones KC (2002) Oceanic biogeochemical controls on global dynamics of persistent organic pollutants. Environ Sci Technol 36:4229–4237
31. Donat J, Dryden C (2010) Transition metals and heavy metal speciation. In: Steele JH, Thorpe SA, Turekian KK (eds) Marine chemistry and geochemistry. Elsevier, Amsterdam, pp 72–80

32. Donat JR, Bruland KW (1995) Trace elements in the ocean. In: Salbu B, Steinnes E (eds) Trace metals in natural waters. CRC Press, Boca Raton, pp 247–281
33. Duce RA (2010) In: Steele JH, Thorpe SA, Turekian KK (eds) Marine chemistry and geochemistry. Elsevier, Amsterdam, pp 281–290
34. Duce R, Liss PS, Merrill JT et al (1991) The atmospheric input of trace species to the world ocean. Global Biogeochem Cycles 5:193–259
35. Dupont CL, Nelson RK, Bashir S, Moffett JW, Ahner BA (2004) Novel copper-binding and nitrogen-rich thiols produced and exuded by *Emiliania huxleyi*. Limnol Oceanogr 49:1754–1762
36. Erel Y, Patterson CC (1994) Leakage of industrial lead into the hydrocycle. Geochim Cosmochim Acta 58(15):3289–3296
37. Farrington JW (2010) Chlorinated hydrocarbons. In: Steele JH, Thorpe SA, Turekian KK (eds) Marine chemistry and geochemistry. Elsevier, Amsterdam, pp 163–174
38. Fine RA (2010) CFCs in the ocean. In: Steele JH, Thorpe SA, Turekian KK (eds) Marine chemistry and geochemistry. Elsevier, Amsterdam, pp 155–162
39. Fitzgerald WF, Lamborg CH, Hammerschmidt CR (2007) Marine biogeochemical cycling of mercury. Chem Rev 107:641–662
40. Fitzgerald WF, Mason RP (1996) The global mercury cycle: oceanic and anthropogenic aspects. In: Baeyens W et al (eds) Global and regional mercury cycles: sources, fluxes and mass balances. Academic, Netherlands, pp 85–108
41. Gabrielli P et al (2005) Variations in atmospheric trace elements in Dome C (East Antarctica) ice over the last two climatic cycles. Atmos Environ 39(34):6420–6429
42. Gaillardet J, Viers J, Dupre B (2004) Trace elements in river waters. In: Holland H, Turekian KK (eds) Treatise on geochemistry, vol 5. Elsevier, Amsterdam, pp 225–272
43. German CA, Von Damm KL (2004) Hydrothermal processes. In: Elderfield H (ed) The oceans and marine geochemistry, vol 6, Treatise on geochemistry. Elsevier, Amsterdam, pp 181–222
44. GESAMP, Bowmer T, Kershaw PT (eds) (2010) Proceedings of the GESAMP international workshop on microplastic particles as a vector in transporting persistent, bioaccumualtive and toxic substances in the ocean, Paris. GESAMP Report # 82, 68pp
45. GESAMP (2001) A sea of troubles. GESAMP, The Hague. GESAMP Report # 70, 40pp
46. GESAMP (1993) Impact of oil and related chemicals on the marine environment. GESAMP, London. GESAMP Report # 50, 180pp
47. GESAMP (1990) Review of potential harmful substances – choosing priority organochlorines for marine hazard assessment. Food and Agriculture Organization of the United Nations, Rome. GESAMP Report # 42, 24pp
48. GESAMP (1989) The atmospheric input of trace species to the World's ocean. World Meteorological Organization, Geneva. GESAMP Report # 38, 124pp
49. Gioia R et al (2008a) Polychlorinated biphenyls in air and water of the North Atlantic and Arctic Ocean. J Geophys Res 113(D19302). D19302 doi:10.1029/2007JD009750
50. Gioia R et al (2008) Polychlorinated biphenyls (PCBs) in air and seawater of the Atlantic Ocean: sources, trends and processes. Environ Sci Technol 42:1416–1422
51. Gustafsson O, Gschwend PM, Buesseler KO (1997) Settling removal rates of PCBs into the northwestern Atlantic derived from ^{238}U–^{234}Th disequilibria. Environ Sci Technol 31:3544–3550
52. Heimburger LE, Cossa D et al (2010) Methyl mercury distributions in relation to the presence of nano- and picophytoplankton in an oceanic water column (Ligurian Sea, North-western Mediterranean). Geochim Cosmochim Acta 74(19):5549–5559
53. Hellweger FL (2005) Dynamics of arsenic speciation in surface waters: As(III) production by algae. Appl Organomet Chem 19(6):727–735
54. Herzig PM, Hannington MD (2000) Input from the deep: hot vents and cold seeps. In: Schultz H, Zabel M (eds) Marine geochemistry. Springer, Heidelberg, pp 397–416
55. Hong SM, Candelone JP, Soutif M, Boutron CF (1996) A reconstruction of changes in copper production and copper emissions to the atmosphere during the past 7000 years. Sci Total Environ 188(2–3):183–193
56. Hopkinson BM, Roe KL et al (2008) Heme uptake by *Microscilla marina* and evidence for heme uptake systems in the genomes of diverse marine bacteria. Appl Environ Microbiol 74(20):6263–6270
57. HTAP, Dutchak S, Zuber A (eds) (2010) Hemispheric transport of air pollutants part c: persistent organic pollutants. ECE, Geneva. Air Pollution Studies #19
58. Iwata H et al (1994) Geographical distribution of persistent organochlorines in air, water and sediments from Asia and Oceania, and their implications for global redistribution from lower latitudes. Environ Pollut 85(1):15–33
59. Jonsson A, Gustafsson O, Axelman J, Sunberg H (2003) Global accounting of PCBs in the continental shelf sediments. Environ Sci Technol 37:245–255
60. Kim G, Alleman LY, Church TM (1999) Atmospheric depositional fluxes of trace elements, Pb-210, and Be-7 to the Sargasso Sea. Global Biogeochem Cycles 13(4):1183–1192
61. Krishnaswami S (2005) Uranium-thorium series isotopes in ocean profiles. In: Steele JH, Thorpe SA, Turekian KK (eds) Marine chemistry and geochemistry. Elsevier, Amsterdam, pp 214–224
62. Landing W, Bruland KH (1987) The contrasting biogeochemistry of iron and manganese in the Pacific Ocean. Geochim Cosmochim Acta 51:29–43
63. Laurier FJG, Mason RP et al (2004) Mercury distributions in the North Pacific Ocean – 20 years of observations. Mar Chem 90(1–4):3–19
64. Lohmann R, Breivik K, Dachs J, Muir D (2007) Global fate of POPs: current and future research directions. Environ Pollut 150:150–165
65. Luther GW (2005) Manganese(II) oxidation and Mn(IV) reduction in the environment – two one-electron transfer steps versus a single two-electron step. Geomicrobiol J 22(3–4):195–203

66. Luther GW (2010) The role of one- and two-electron transfer reactions in forming thermodynamically unstable intermediates as barriers in multi-electron redox reactions. Aquat Geochem 16(3):395–420
67. Malcolm EG, Schaefer JK et al (2010) Mercury methylation in oxygen deficient zones of the oceans: no evidence for the predominance of anaerobes. Mar Chem 122:11–19
68. Mason RP, Fitzgerald WF (1993) The distribution and biogeochemical cycling of mercury in the equatorial Pacific Ocean. Deep Sea Res 40(9):1897–1924
69. Mason RP, Fitzgerald WF (1996) Sources, sinks and biogeochemical cycling of mercury in the ocean. In: Baeyens W et al (eds) Global and regional mercury cycles: sources, fluxes and mass balances. Academic, Netherlands, pp 249–272
70. Mason RP, Fitzgerald WF et al (1994) The biogeochemical cycling of elemental mercury: anthropogenic influences. Geochim Cosmochim Acta 58(15):3191–3198
71. Mason RP, Lawson NM et al (2001) Mercury in the Atlantic Ocean: factors controlling air-sea exchange of mercury and its distribution in the upper waters. Deep Sea Res II 48:2829–2853
72. Mason RP, O'Donnell J et al (1994) Elemental mercury cycling within the mixed layer of the equatorial Pacific Ocean. In: Watras CJ, Huckabee JW (eds) Mercury as a global pollutant: towards integration and synthesis. Lewis, Boca Raton, pp 83–97
73. Mason RP, Sullivan KA (1999) The distribution and speciation of mercury in the south and equatorial Atlantic. Deep Sea Res Part II 46(5):937–956
74. Mason RP, Sheu GR (2002) Role of the ocean in the global mercury cycle. Global Biogeochem Cycles 16(4): Art. No. 1093
75. Maybeck M (2004) Global occurence of major elements in rivers. In: Drever JI (ed) Surface and ground water, weathering and soils, treatise on geochemistry, vol 5. Elesevier, Amsterdam, pp 207–223
76. Morel F, Milligan AJ, Saito MA (2004) Marine bioinorganic chemistry: the role of trace metals in the oceanic cycles of major nutrients. In: Elderfield H (ed) The oceans and marine geochemistry. In: Holland HD, Turekian KK (Exec eds) Treatise on geochemistry, vol 6. Elsevier/Pergamon, Amsterdam
77. Morel FMM, Hering JG (1993) Principals and applications of aquatic chemistry. Wiley, New York
78. Murnane R, Sarmiento J et al (1990) Thorium isotopes, particle cycling models, and inverse calculations of model rate constants. J Geophys Res 95:16,195–16,206
79. Ndung'u K, Thomas MA et al (2001) Silver in the western equatorial and South Atlantic Ocean. Deep Sea Res Part II 48(13):2933–2945
80. Nice AJ, Lung WS et al (2008) Modeling arsenic in the Patuxent estuary. Environ Sci Technol 42(13):4804–4810
81. Nozaki Y (1997) A fresh look at element distributions in the North Pacific. http://www.agu.org/eos_elec/97025e.html
82. Nriagu J (1978) Properties and the biogeochemical cycle of lead. In: Nriagu J (ed) The biogeochemistry of lead in the environment. Elsevier, Amsterdam, pp 1–14
83. Okbamichael M, Sanudo-Wilhelmy SA (2005) Direct determination of vitamin B-1 in seawater by solid-phase extraction and high-performance liquid chromatography quantification. Limnol Oceanogr Methods 3:241–246
84. Orians KJ, Merrin CL (2010) Refractory metals. In: Steele JH, Thorpe SA, Turekian KK (eds) Marine chemistry and geochemistry. Elsevier, Amsterdam, pp 52–63
85. Pickard GL, Emery WJ (1982) Descriptive physical oceanography. Pergamon Press, Oxford, 249pp
86. Pirrone N, Costa P, Pacyna JM, Ferrara R (2001) Mercury emissions to the atmosphere from natural and anthropogenic sources in the Mediterranean region. Atmos Environ 35(17):2997–3006
87. Pohl C, Loffler A, Schmidt M, Seifert T (2006) A trace metal (Pb, Cd, Zn, Cu) balance for surface waters in the eastern Gotland Basin, Baltic Sea. J Mar Syst 60(3–4):381–395
88. Ranville MA, Cutter GA et al (2010) Aeloian contamination of Se and Ag in the North Pacific Ocean from Asian fossil fuel combustion. Environ Sci Technol 44:1587–1593
89. Ranville MA, Flegal AR (2005) Silver in the North Pacific Ocean. Geochem Geophys Geosyst 6: Art. No. Q03M01
90. Ryaboshapko II, Gusev A, Afinogenova O, Berg T, Hjellbrekke A-G (1999) Monitoring and modeling of lead, cadmium and mercury transboundary transport in the atmosphere of Europe. EMEP, Meteorological Synthesizing Centre – East, Moscow
91. Sanudo-Wilhelmy SA, Flegal AR (1992) Anthropogenic silver in the southern California bight – a new tracer of sewage in coastal waters. Environ Sci Technol 26:2147–2151
92. Schaule B, Patterson CC (1983) Perturbations of the natural lead depth profile in the Sargasso Sea by industrial lead. In: Wong C, Boyle E, Bruland KW, Burton JD, Goldberg ED (eds) Trace metals in seawater. Plenum Press, New York, pp 487–503
93. Schlitzer R (2010) Inverse modeling of tracers and nutrients. In: Steele JH, Thorpe SA, Turekian KK (eds) Marine chemistry and geochemistry. Elsevier, Amsterdam, pp 188–199
94. Schwarzenbach RP, Gschwend PM et al (1993) Environmental organic chemistry. Wiley, New York
95. Scudlark J, Church TM (1997) Atmospheric deposition of trace metals to the mid-Atlantic bight. In: Baker J (ed) Atmospheric deposition of contaminants to the great lakes and coastal waters. SETAC Press, Pensacola, pp 195–208
96. Selin NE, Jacob DJ et al (2008) Global 3-D land-ocean–atmosphere model for mercury: present-day vs. preindustrial cycles and anthropogenic enhancement factors for deposition. Global Biogeochem Cycles (Accepted)
97. Selin NE, Sunderland EM et al (2010) Sources of mercury exposure for US seafood consumers: implications for policy. Environ Health Perspect 118(1):137–143
98. Soerensen AL, Sunderland EM et al (2010) An improved global model for air–sea exchange of mercury: high concentrations over the north Atlantic. Environ Sci Technol 44(22): 8574–8580

99. Stemmler I, Lammel G (2009) Cycling of DDT in the global oceans 1950–2002: world ocean returns the pollutant. Geophys Res Lett 36(L24602)
100. Stumm W, Morgan JJ (1996) Aquatic chemistry. Wiley, New York
101. Sunderland EM, Krabbenhoft DP et al (2009) Mercury sources, distribution, and bioavailability in the North Pacific Ocean: Insights from data and models. Global Biogeochem Cycles 23
102. Sunderland EM, Mason RP (2007) Human impacts on open ocean mercury concentrations. Global Biogeochem Cycles 21:GB4022. doi:10.1029/2006GB002876
103. USEPA (1997) The incidence and severity of sediment contamination in surface water of the United States. Office of Science and Technology, U.S. Environmental Protection Agency, Washington, DC, (Three volumes) http://water.epa.gov/polwaster/sediments/cs/upload/nsqszed-complete.pdf
104. Von Damm KL (2010) Hydrothermal vent fluids, chemistry of. In: Steele JH, Thorpe SA, Turekian KK (eds) Marine chemistry and geochemistry. Elsevier, Amsterdam, pp 81–88
105. Wania F, Mackay D (1995) A global distribution model for persistent organic chemicals. Sci Total Environ 160/161: 211–232
106. Wu JF, Boyle EA (1997) Lead in the western North Atlantic Ocean: completed response to leaded gasoline phaseout. Geochim Cosmochim Acta 61(15):3279–3283
107. Wu JF, Rember R et al (2010) Isotopic evidence for the source of lead in the North Pacific abyssal water. Geochim Cosmochim Acta 74(16):4629–4638
108. Zhang Y, Amakawa H et al (2001) Oceanic profiles of dissolved silver: precise measurements in the basins of the western North Pacific, Sea of Okhotsk and the Japan Sea. Mar Chem 75:151–163
109. Zhang Y, Obata H et al (2004) Silver in the Pacific Ocean and the Bering Sea. Geochem J 38:623–633
110. Libes S (1992) Introduction to marine biogeochemistry. Elsevier, San Diego, 909 pp
111. Iwata H, Tanabe S, Sakal N, Tatsukawa R (1993) Distribution of persistent organochlorines in the oceanic air and surface seawater and the role of ocean on their global transport and fate. Environ Sci Technol 27:1080–1098
112. van der Loeff MMR (2010) Uranium-thorium decay series in the ocean: overview, Chapter 23. In: Steele JH, Thorpe SA, Turekian KK (eds) Marine chemistry and geochemistry. Elsevier, Amsterdam, pp 203–213
113. Lal D (2010) Cosmogenic isotopes, Chapter 25. In: Steele JH, Thorpe SA, Turekian KK (eds) Marine chemistry and geochemistry. Elsevier, Amsterdam, pp 225–234
114. Key RM (2010) Radiocarbon, Chapter 26. In: Steele JH, Thorpe SA, Turekian KK (eds) Marine chemistry and geochemistry. Elsevier, Amsterdam, pp 235–250
115. Rabalais NN (2010) Hypoxia, Chapter 34. In: Steele JH, Thorpe SA, Turekian KK (eds) Marine chemistry and geochemistry. Elsevier, Amsterdam, pp 306–314
116. Sunda WG (2010) Trace metal nutrients, Chapter 4. In: Steele JH, Thorpe SA, Turekian KK (eds) Marine chemistry and geochemistry. Elsevier, Amsterdam, pp 17–28
117. Balcom PH et al (2004) Mercury sources and cycling in the Connecticut River and Long Island Sound. Marine Chem 90 (1–4):53–74
118. Gill GA, Fitzgerald WF (1988) Vertical mercury distributions in the oceans. Geochim Cosmochim Acta 52:1719–1728
119. Cossa D et al (2011) Mercury in the Southern Ocean. Geochim Cosmochim Acta 75(14):4037–4052
120. Hollweg T, Gilmour C, Mason R (2009) Factors controlling the methylation of mercury in sediments of the Chesapeake Bay and mid-Atlantic continental shelf. Marine Chem
121. Mason RP (2005) Air-sea exchange and marine boundary layer atmospheric transformations of mercury and their importance in the global mercury cycle. In: Pirrone N, Mahaffey KR (eds) Dynamics of mercury pollution on regional and global scales. Springer, New York, pp 213–239
122. Mason RP, Fitzgerald WF (1990) Mercury speciation in the equatorial Pacific Ocean. EOS 71(43):1413
123. Cutter GA (1993) Metalloids in wet deposition on Bermuda – concentrations, sources and fluxes. JGR-Atmos 98(D9): 16777–16786

Oceanic General Circulation Models

Jin-Ho Yoon, Po-Lun Ma
Atmospheric Science and Global Change Division, Pacific Northwest National Laboratory, Richland, WA, USA

O

Article Outline

Glossary
Definition of the Subject
Introduction
Equations of Motion
Horizontal and Vertical Grid System
Sub-grid Scale Parameterization
Simple Conceptual Models
Biogeochemical Cycle Modeling
Future Directions
Bibliography

Glossary

Bathymetry The depth of ocean floor. Bathymetric map represents the terrain of the seafloor.

Biogeochemical cycle A pathway that is described by the physical, biological, and chemical processes that

control the evolution of elements found in the Earth system.

Boussinesq approximation In Boussinesq approximation, a fluid parcel is assumed to maintain the same volume or density during its transport because of near incompressibility. This approximation was named after French physicist and mathematician, Joseph Valentin Boussinesq. By adopting this approximation, sound waves that propagate through a density change can be eliminated in numerical model.

Diapycnal mixing Mixing of a fluid across different density surfaces. To be contrasted with isopycnal mixing which occurs along the same density surfaces.

El Niño-Southern Oscillation (ENSO) A quasi-periodic change of the ocean and atmospheric conditions along the equatorial Pacific Ocean. The change in the sea surface temperature (SST) can be as large as $\pm 2°C$ during its extreme phases: anomalously warm over the tropical Pacific (El Niño) and cold (La Niña). Surface air pressures measured at both ends of the tropical Pacific basin vary closely with the change of SST.

Geostrophic approximation The angular momentum is balanced by the Coriolis force and the horizontal pressure gradient force. It is generally true when the spatial and temporal scales are large, roughly over 100 km and a few days in the deep ocean.

Hydrostatic approximation The equation describing vertical motion of the ocean column is simplified to assume that the vertical pressure at any level is due to the weight of the air and water above it. Variation of density is considered only in vertical direction when gravitational acceleration term (g) exists. This is valid when the vertical scale of a feature is small compared to the horizontal scale for both the atmosphere and ocean.

Isopycnal coordinate Vertical coordinate that follows a constant density surface.

Meridional overturning circulation (MOC) This has often been assumed to be the same as the thermohaline circulation. However, the MOC explicitly describes the ocean circulation system with the upwelling/downwelling and associates the northward/southward transport.

Ocean gyre A large-scale rotating circulation in the ocean primarily forced by the atmospheric wind and the Coriolis force. These include the North Atlantic Gyre, South Atlantic Gyre, Indian Ocean Gyre, North Pacific Gyre, and South Pacific which tend to be more elongated in the east-west direction. There are also other types of Gyre forced by different mechanisms such as baroclinicity.

(Oceanic) Mesoscale eddy A vigorous rotational circulation or vortex at spatial scales roughly 100 km and smaller, existing for weeks to months.

Rossby radius (of deformation) The horizontal scale at which rotational effect becomes as important as buoyancy or gravity wave effects. Mathematically, this can be computed in terms of potential temperature, temperature, wind speed, or the depth of the boundary layer. This radius is important in determining the phase speed and wavelength of Rossby waves.

Salinity Dissolved content of the salt in the ocean. Traditionally, salinity is represented in the unit of either g/Kg or PSU (Practical Salinity Unit).

Shallowness approximation This approximation can be applied when the vertical-to-horizontal aspect ratio is very small.

Structured (regular)/unstructured (irregular) grid A structured (unstructured) grid has regular (irregular) connectivity with neighboring points. In structured (unstructured) grid, its connectivity can (cannot) be easily represented with a two- or three-dimensional array.

Thermocline A distinct ocean layer where the temperature changes greatly with its depth compared to the layers above and below. It is often thought of as a boundary separating the well-mixed upper ocean and the deep ocean.

Thermohaline circulation The global oceanic circulation driven by the density gradients, primarily determined by salinity and temperature.

(Atmospheric) Wind stress The horizontal force exerted by the atmospheric wind on the ocean surface. This can also be interpreted as the vertical transfer of horizontal momentum from the atmosphere to the ocean surface. Wind stress is a function of the square of the wind speed.

Definition of the Subject

The purpose of this text is to provide an introduction to aspects of oceanic general circulation

models (OGCMs), an important component of Climate System or Earth System Model (ESM). The emerging need for understanding the Earth's climate system and especially projecting its future evolution has encouraged scientists to explore the dynamical, physical, and biogeochemical processes in the ocean. Understanding the role of these processes in the climate system is an interesting and challenging scientific subject. For example, a research question exploring how much extra heat or CO_2 generated by anthropogenic activities can be stored in the deep ocean is not only of scientific interest but also important in projecting future climate of the Earth. Thus, OGCMs have been developed and applied to investigate the various oceanic processes and their role in the climate system.

Coupled climate models incorporating some representation of ocean circulations have been used since the pioneering work of Manabe and Bryan [38]. Because of computational limits at that time, an extremely simplified Earth geography – composed of only one continent and ocean basin (Fig. 1) – was used. Despite its simplicity, this was the first numerical model to include reasonably complex formulations for the atmosphere, land, ocean, and more importantly feedbacks among these components. Later it was demonstrated that deep ocean circulation in this simplified coupled model was not at an equilibrium even after a century-long integration [64]. Like this case, processes that control the adjustment of deep ocean circulation toward an equilibrium remain an important issue in contemporary climate models. It took another 6 years for Manabe and Bryan to produce a coupled climate model with more realistic geography of the Earth [39]. Now contemporary OGCMs can resolve complex regional flows in a much more realistic way. However, there are still many issues to be solved and large room for improvement [48].

The goal in this text is to outline the basics of Ocean General Circulation modeling, reviewing the mathematical representation of the ocean circulation (section Equations of Motion), and the discretization method with horizontal and vertical coordinate systems (section Horizontal and Vertical Grid System). A brief discussion is provided on how the sub-grid scale processes are represented in relatively coarse-resolution OGCMs (section Sub-grid Scale Parameterization). Then, using a couple of relatively simple examples, the coupling between the ocean and other climate components, especially the atmosphere by various physical processes will be explained (section Simple Conceptual Models). Also, how the ocean is coupled in terms of biogeochemical cycle will be illustrated in the section Biogeochemical Cycle Modeling. The entry concludes with a brief description of contemporary OGCMs and its future development (section Future Directions).

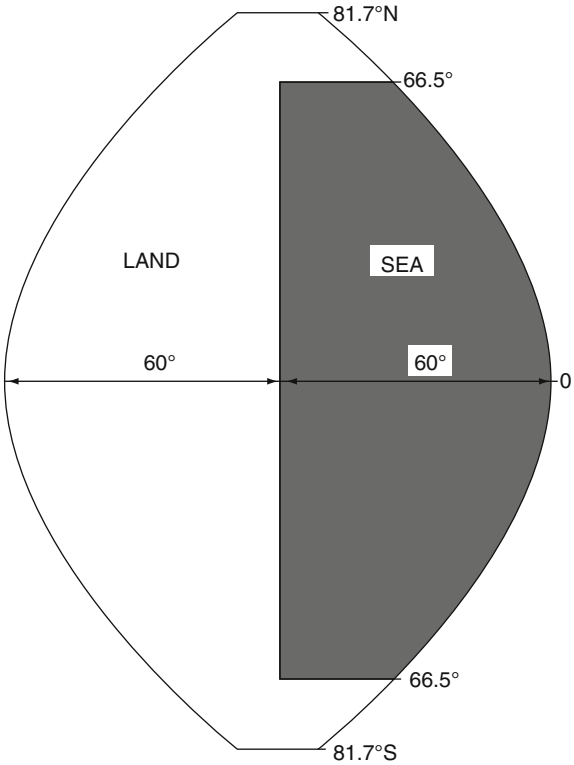

Oceanic General Circulation Models. Figure 1 Land-ocean configuration of the first coupled climate model of [38] (From Manabe and Bryan, J. Atmospheric Sciences 26 (1969): 786–789. © American Meteorological Society. Reprinted with permission)

Introduction

An oceanic general circulation model (OGCM) is used to simulate the physical and dynamical features of the global ocean using equations representing the conservation of momentum, energy, and mass for water and salt. These equations are usually called the equations of motion, and they describe how the temperature, salinity, and currents evolve with time in the ocean. OGCMs

also need appropriate boundary and initial conditions that describe how the ocean interacts with the atmosphere, land and sea ice and the state of the ocean when the model is started. An OGCM has a great similarity with its atmospheric counterpart in the entry ► Atmospheric General Circulation Modeling. However, there are important and non-negligible differences. First of all, the ocean is primarily forced at its surface boundaries by both thermal and mechanical forcings, while the atmosphere is forced throughout its entire volume mainly by thermal forcing. The global ocean is more strongly constrained by its complex terrain which results in oceanic gyres confined by lateral boundaries (continents and shelves), while the atmosphere is relatively less restricted. Also, very narrow boundary layers exist on almost every ocean surface and within its interior. Finally, observing the ocean is much more difficult than its atmospheric counterpart. The amount of ocean observation data is far less available than in the atmosphere. Thus, boundary and initial conditions are difficult to determine and the lack of long term and uniform observation imposes a challenge in validating the OGCMs' performance. Although a great deal of additional measurements has become available since satellite and buoys which have been deployed in the 1980s, it is estimated that data available to oceanic scientist in the 1990s is still an order of magnitude fewer than in the atmosphere [21].

The role played by the ocean in the global climate system is relatively well understood. For example, the ocean regulates the Earth surface heat budget through its large heat capacity and heat transport by the oceanic circulation from tropics to high latitudes. Large portions of this heat transport is carried out by both strong western boundary currents and oceanic mesoscale eddies (a dominant dynamical feature of the global ocean circulation at spatial scales from roughly 100 km and smaller with time scales of weeks to months). One example of a mesoscale eddy can be seen near the Atlantic coast of the USA in Fig. 2. The figure shows satellite-retrieved sea surface temperature from the NASA Aqua/MODIS mission over the western Atlantic where gray areas represent the land and color indicates temperature over the ocean surface. One can observe that generally warmer (colder) water exists in the south (north). Along the boundary that warm and cold waters are interwined, small-scale meanders and eddies are evident. These eddies are generated by strong shear instabilities in ocean currents, occurring particularly from currents along western boundaries and by horizontal density gradients. Oceanic kinetic energy is largely redistributed and transported by these eddies, and they are very important in the poleward transport of energy in the Earth's climate system.

In order for OGCMs to properly simulate these mesoscale eddies, they must operate at a high spatial resolution, resolving features that can be a few tens of kilometers and smaller. OGCMs divide the ocean up into small "cells" where temperature, salinity, and water velocity are calculated (discussed in more detail later). Ocean models that are designed to reproduce the behavior of eddies accurately (called Eddy-Permitting models) contain many cells and are extremely expensive in terms of computation. As of 2007, only a couple of the coupled climate models with eddy-permitting resolution (around 1/6° to 1/3°) successfully simulated these features explicitly [48].

OGCMs have historically been run at a much lower resolution to reduce the high computational burden. But since these lower resolution models are not able to explicitly represent these eddies, they must use other ways to represent the eddy effects. These effects are frequently treated through "parameterization" (more information on parameterization is provided below Sub-grid Scale Parameterization).

Recently ocean models now include representations of other important ocean components such as nutrient transports, ocean chemistry, and ecosystem evolution in order to calculate the evolution of biogeochemical cycles of the planet, including CO_2. The ocean regulates the amount of CO_2 stored through both biological and physical processes, which in general are similar to their terrestrial counterpart. The ocean absorbed about half of the CO_2 released in the last few centuries (e.g., [31]). And it becomes more important to understand how much of extra carbon can the ocean absorb in the near future.

This document has outlined the basis of the dynamical and physical properties of the ocean. More information on ocean processes can be found in various textbooks or other review articles (e.g., [24, 29]). In the next section, more emphasis will be given on the numerical formulation, and discretization of these processes will be provided, along with some information

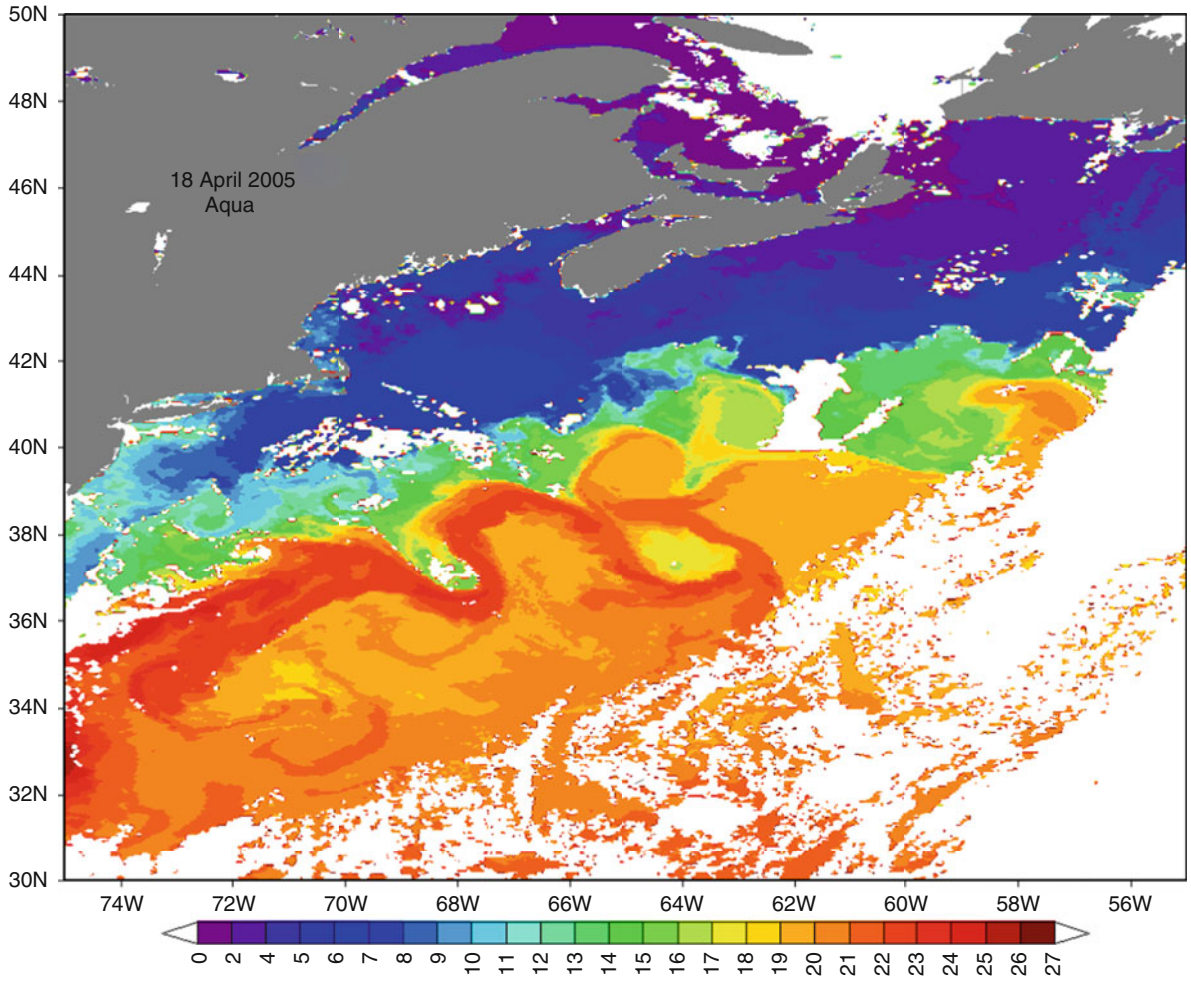

Oceanic General Circulation Models. Figure 2
Sea surface temperature at 18 April 2005 retrieved from Aqua MODIS [63]. Level 3 mapped data of MODIS SST was obtained from NASA JPL

on the coupling between atmosphere and the ocean in a numerical form.

Equations of Motion

Ocean models solve the equations governing oceanic flow using computational fluid dynamics (CFD) methods with specific assumptions and approximations appropriate to the ocean. The equations for global ocean models are, like atmospheric models, based on Newtonian mechanics and irreversible thermodynamics applied to a particular fluid. Conservation of momentum, heat, and mass of constituents comprise the equations used for an OGCM. However, a wide range of mathematical formulation has been used to represent the numerous oceanic processes and phenomena occurring at various spatial and temporal scales, in the ocean. Only the primitive equations of motion that are the core of OGCM numerical formulations are described. A more complete derivation can be found in Griffies [24] and Vernois [62].

Hydrostatic Primitive Equations

A number of approximations are used in simplifying the fluid equations when used to represent ocean circulations, namely, the hydrostatic, shallowness, Boussinesq, and rigid lid approximations.

The hydrostatic approximation assumes that the vertical momentum equation can be simplified by neglecting all terms except those resulting in the vertical pressure gradient being balanced by the gravitational acceleration (equivalently that the vertical pressure at any level is due to the weight of the air and water above it). The shallowness approximation assumes the ocean is thin compared to the Earth's radius. The Boussinesq approximation neglects variations in density except where density appears multiplied with gravity. The advantage of the Boussinesq approximation is to eliminate acoustic waves [7]. Although this approximation has been applied in many OGCMs, a couple of limitations seem to be found. One of the most noticeable limitations is that it cannot account for steric effect, i.e., thermal expansion and salinity-density compensation of sea water. Thus, sea-level change due to global warming cannot be properly predicted by this kind of model. Finally, the surface elevation of the global ocean is assumed static in the rigid lid approximation. With these approximations, the temporal and spatial variations of density are small compared to its mean value. Thus, it can be described in the following form:

$$\rho_{\text{tot}} = \bar{\rho} + \rho(x, y, z, t), \tag{1}$$

where $\bar{\rho}$ represents the mean density of the ocean and $\bar{\rho} \gg |\rho|$ is true and ρ can be replaced by $\bar{\rho}$ except the buoyancy term, ρg and in the thermodynamic density conservation equation.

With these approximations, the hydrostatic primitive equation in Cartesian coordinates is described in the following format:

$$\frac{du}{dt} = fv - \frac{1}{\bar{\rho}}\frac{\partial p}{\partial x} \tag{2}$$

$$\frac{dv}{dt} = -fu - \frac{1}{\bar{\rho}}\frac{\partial p}{\partial y} \tag{3}$$

$$\frac{\partial p}{\partial z} = -\rho g \tag{4}$$

$$\frac{dT}{dt} = 0 \tag{5}$$

$$\frac{dS}{dt} = 0 \tag{6}$$

and

$$\frac{\partial u}{\partial x} + \frac{\partial v}{\partial y} + \frac{\partial w}{\partial z} = 0, \tag{7}$$

where (x, y, z) represents Cartesian coordinates and (u, v, w) as current in the direction of x, y, and z, respectively. $\bar{\rho}$ is the mean density of the ocean as in Eq. 1, f is the Coriolis frequency, and T and S are temperature and salinity of the ocean. And the total derivative and local derivatives are related in the following way:

$$\frac{d}{dt} = \frac{\partial}{\partial t} + u\frac{\partial}{\partial x} + v\frac{\partial}{\partial y} + w\frac{\partial}{\partial z} \tag{8}$$

To close the set of equations (Eqs. 2–6), an equation of state, another equation of state to link density to ocean temperature, salinity, and pressure is added:

$$\rho = \rho(T, S, p) \tag{9}$$

It is also noted here that these sets of equation are written for spherical geometry in a global ocean model. Details can be found in Haidvogel and Bryan [29] or Bryan [5].

The above sets of equation are derived from the fluid dynamics with the help of approximations or assumptions. Some of the approximations, like Boussinesq approximation, have been still used in OGCM. Others, like the rigid lid approximation are not used any longer. There is a trend toward more explicitly representing the ocean status and processes. More realistic simulation of the ocean with better computational efficiency is now being achieved in contemporary OGCMs (see [27]).

Boundary Conditions

To solve the equations of motions, boundary conditions are needed. Upper boundary conditions are governed by interactions with the atmosphere or sea ice. The surface boundary condition on momentum below an ice-free atmosphere is governed by the wind stress:

$$\tau_x = \bar{\rho}\nu_x \frac{\partial u}{\partial z}\bigg|_{z=0}, \tag{10}$$

$$\tau_y = \bar{\rho}\nu_y \frac{\partial v}{\partial z}\bigg|_{z=0}, \tag{11}$$

where ν_x and ν_y are the turbulent eddy viscosity coefficients. The wind stress is sometimes provided by

observational estimates (from a measurement climatology) and other times is provided by an atmospheric model. More discussion will be given later in Atmospheric forcing section.

The boundary condition for temperature is also treated in a variety of ways. When ocean models are coupled with a climate model, they calculate turbulent fluxes of heat and radiative fluxes based upon the state of the atmosphere and ocean. When ocean models are driven with observations, other choices are possible. Sometimes sea surface temperature (SST) is specified. In other situations surface fluxes are calculated in a similar fashion to the way they are done when coupled to an atmospheric model.

Salinity boundary condition depends upon evaporation, and the freshwater flux from precipitation, river runoff, and sea ice melt. In simple models where feedback between salinity and its forcing is not considered, one can use the prescribed surface salinity flux. However, it is found that there is important feedback between salinity and its forcing even in the case when ocean models are not coupled to atmosphere and sea ice models (e.g., [6]).

The Surface Mixed Layer

In the ocean, the heating term can be neglected generally except in the regions where solar radiation can play a role and heat exchange with the overlaying atmosphere is active, which is called the surface mixed layer. Both vigorous mixing and surface heating play important roles. Therefore, the surface heating term has to be included in the temperature equation:

$$\frac{\partial T}{\partial t} = -\frac{\partial}{\partial z}(Tw) + \frac{1}{\bar{\rho} c_p} Q(z, t), \tag{12}$$

where the first term in the right hand side represents the heat exchange due to vertical mixing, the second term is the solar heating absorbed at depth in the water column, and c_p is the specific heat of water. Although the equation looks simple, complication arises how to close. Two general approaches are taken: differential and bulk models [33]. The Mellor Yamada level-2 model is an example of the former [43], in which the stress terms now include both eddy coefficients for both within and below the mixed layer. On the other hand, the Niler model [41] uses a bulk model in which the mixed layer is treated as a well-defined homogeneous layer.

Horizontal and Vertical Grid System

To solve the governing equations of the oceanic general circulation, these equations have to be discretized with appropriate horizontal and vertical grid systems. Various methodologies have been developed and applied in the different OGCMs. In this section, both horizontal and vertical grid systems will be reviewed.

Horizontal Grid System

OGCMs have widely adopted the finite volume and finite elements methods. These methods will be discussed here for brevity, but a few distinguishing characteristics be mentioned. Discretized governing equations are applied in flux form so scalars such as temperature, density, salinity, etc., are updated through fluxes at the boundaries of each grid, and therefore, these quantities are conserved. Structured meshes with regular distributions of neighboring grids throughout the entire domain and unstructured meshes where the number of neighboring grids varies throughout the domain are both utilized with finite volumes and finite element discretizations. Successful model implementations include orthogonal meshes (e.g., [58]), cubed sphere meshes (e.g., [1]), icosahedral meshes (e.g., [47, 51, 52]), and unstructured triangular meshes (e.g., [10, 12]). Figure 3 shows an example of a structured and unstructured grid.

Structured grids are computationally efficient, accurate, and convenient. However, the major shortcoming with structured grids is that the grid-spacing is not uniform. Lack of flexibility to increase resolution in coastal regions or regions with complex topography make the computation expensive if the resolution of the entire domain has to be increased at the same time. An irregular gridding system that can increase resolution near the coast while keeping lower resolution over the open ocean coarse provides better computational efficiency more easily. In addition, because the unstructured grid can better represent the coastal area, it is advantageous over structured grid in simulating coastal currents and eddies.

To avoid a singular point at the North Pole, where grid lines converge, the ocean models either rotate the global gridding system, or create a tripolar grid with poles located over Canada, Russia, and Antarctica, such that the singular points of the grids are positioned over land instead of ocean.

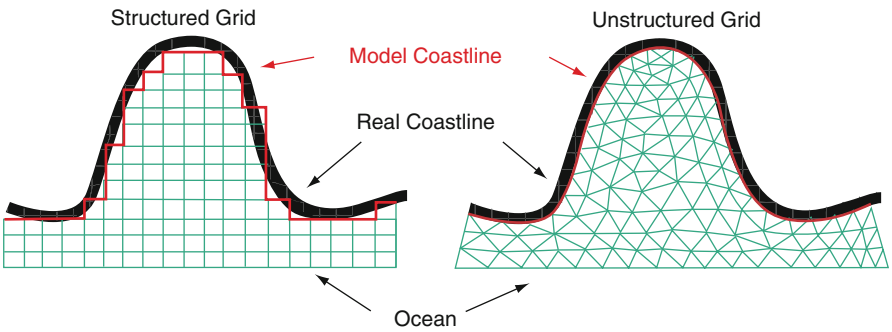

Oceanic General Circulation Models. Figure 3
An example of fitting a structured grid (*left*) and an unstructured grid (*right*) to a simple coastal embayment. The true coastline is shown in *black*, the model coastline in *red*. Note how the unstructured triangular grid can be adjusted so that the model coastline follows the true coastline, while the structured grid coastline is jagged – which can result in unrealistic flow disturbance close to the coast (Figure taken from Fig. 1 in Chen et al. [13] in *Oceanography*, reproduced with permission)

An unresolved issue is the resolution–dependent physics in ocean models. Parameterizations of sub-grid scale processes inevitably produce some "free" (undefined) parameters (hence the name) and need to be in accordance with observations. These parameters are at varying horizontal grid sizes to capture the effects of processes from eddies with different sizes. The diffusion and viscosity terms will need to be adjusted accordingly.

Vertical Coordinate

Ocean models have developed several different vertical coordinate systems: (1) geopotential coordinate (or *z*-coordinate), (2) terrain-following coordinate, and (3) isopycnal coordinate, as shown in Fig. 4. Also, there is hybrid coordinate which combines various coordinate systems. Each one has its own advantages and disadvantages.

The most popular coordinate system is the geopotential coordinate [42]. For example, the first coupled climate model also utilized this vertical coordinate system with the hydrostatic and Boussinesq approximations [26, 38]. The geopotential coordinate adopts a straightforward concept that the ocean water body is divided into regular boxes which are invariant with time. The vertical coordinate is based on the geopotential or depth of the ocean. Governing equations using lower-order finite difference methods are frequently used. In ocean models that adopt the geopotential coordinate (e.g., [35, 56]), the vertical resolution decreases as a function of depth (i.e., higher vertical resolution in the upper ocean and lower vertical resolution in the deep ocean) in order to better resolve processes around the thermocline. However, some studies have shown that the geopotential

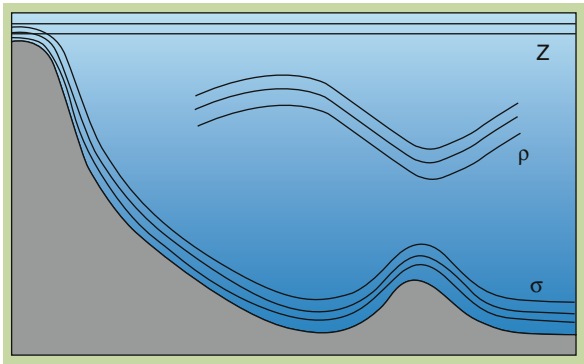

Oceanic General Circulation Models. Figure 4
A schematic diagram of an ocean basin illustrating the three regimes of the ocean germane to the considerations of an appropriate vertical coordinate. The surface mixed layer is naturally represented using fixed-depth *z* (or pressure *p*) coordinates, the interior is naturally represented using isopycnic ρ (density tracking) coordinates, and the bottom boundary is naturally represented using terrain-following σ coordinates (after [25]) (Figure taken from Box 1 in Chassignet et al. [11] in *Oceanography*, reproduced with permission)

coordinate models have problems simulating the topographical effects on the ocean circulation because of their "stepwise" representation of the topography. They also have mesoscale eddy-induced vertical diffusion much greater than the observations.

The discontinued representation of the bathymetry and sidewall geometry in the geopotential coordinate system has been related to spurious topographic effects on the ocean circulation. Terrain-following (or sigma) coordinate models have been developed to handle complex lateral and bottom boundaries and avoid some of these problems. The sigma coordinate system is based on a fractional depth scaled from 0 to 1, with 0 being the surface and 1 being the bottom of the ocean. However, because the pressure gradient term is projected to be along the sigma surfaces, the horizontal pressure gradient produces considerable errors as a function of topographical slope and the stratification near the sea floor [2, 16, 32, 57]. Due to this problem, studies have shown that models that adopt the terrain-following coordinate are not suitable for global-scale simulations, unless the horizontal resolution is very high (the order of 10 km).

The isopycnal coordinate system uses isopycnal surfaces to be the vertical levels. Its advantage is due to the fact that the ocean currents and the transport of tracers generally proceed along isopycnal surfaces, so that the model that adopts this coordinate can ease the treatment of advection. The diapycnal mixing due to eddies can be added to the model as a parameterization. Furthermore, since isopycnal surfaces evolve over time, the isopycnal coordinate is, by nature, an adaptive system. It can better resolve the frontal region and thermocline where sharp vertical gradients of density exist [4]. However, for areas with a low-density gradient such as the well-mixed shelf area or deepwater formation areas, the model has a lower resolution than it would with other vertical coordinate choices. Because it avoids some of the shortcomings of the two other coordinate systems, isopycnal models, or "hybrid" models using a combination of these coordinate systems have a great potential in becoming more and more viable for global climate simulations in the future. Examples of models that use hybrid coordinates include the Global Navy Coastal Ocean Model that uses sigma-z coordinate, and the experimental Hybrid Coordinate Ocean Model that uses the z- (or sigma) coordinate in the upper ocean and the isopycnal coordinate in the stratified ocean.

Sub-grid Scale Parameterization

With spatial discretization, one can solve the governing equation discussed in the section Equations of Motion. But, representing continuous fluid with limited number of grid points imposes some new challenges. For example, the global OGCM with horizontal grid scale of 200 km cannot explicitly simulate oceanic mesoscale eddies (Fig. 2). To overcome this, spatial resolution of the OGCM has been increasing greatly. Indeed, increasing the ocean resolution in the coupled climate model has resulted in many improvements in the simulation of ocean circulation features. However, the impact of higher ocean resolution on the atmospheric simulation in coupled models has been found to be relatively small and localized unless the resolution of the atmosphere is also changed [30]. Further it has been shown that increasing spatial resolution plays a secondary role in simulating ENSO properly [28]. To achieve realistic representation of the ocean circulation and physical status requires not only increasing resolution but also physical parameterization. In this section, these parameterizations are discussed.

There are many processes occurring in the ocean that are not expressed explicitly in the equations of motion, or that take place at time and space scales that are too small to be treated explicitly in a global ocean model. No OGCM can simulate process in the ocean explicitly due to computational constraints or lack of knowledge about these processes. However, these can be very important in influencing oceanic circulations. Sub-grid processes such as vertical mixing and eddies with a scale smaller than the grid that cannot be resolved are "parameterized" based on theoretical considerations, observational data, and/or results from finer-resolution models. In "non-eddy" resolving (or permitting) OGCMs, the effects of mesoscale eddies are represented by parameterizations called neutral diffusion [49, 59] and eddy-induced advection [19, 20]. Maltrud and McClean [37] have suggested that a horizontal grid-spacing of 50 km in mid-latitudes and 10 km in high latitudes is sufficient to resolve eddies. Higher resolution models are believed to be able to resolve these processes.

Turbulent mixing at the upper ocean surface must also be represented (e.g., [18, 34, 45]). The stirring and mixing at the ocean surface can penetrate to the interior of the ocean and trigger further vertical mixing. These waves can be reflected, scattered, or transformed by the seafloor at the bottom and lateral boundary of the ocean. The diapycnal mixing takes place as a result of baroclinic instability, and is brought to balance by geostrophic adjustment via radiation of gravity waves. These processes interact with the topography and the mean flow. Depending on the stability of the ocean, the diapycnal mixing can affect the general circulation or dissipate without having any effect.

Many sub-grid scale processes are recognized to be important but remain poorly understood. The lack of the four-dimensional observational data of ocean flows as well as the state variables of the ocean in the oceanic interior make validation of the parameterizations against observations difficult, so validations are usually performed by evaluating their bulk effect against a high-resolution model. Recently satellite measurements of sea surface height, sea surface temperature, winds, etc. that cover a large scale of domain with a reasonable resolution have proved very helpful for understanding the features of mesoscale eddies but more in situ measurements are necessary to validate the model and to calibrate satellite observations. With the coordinated efforts from both modeling and measurement communities, parameterizations in ocean models can be scientifically evaluated and improved accordingly.

Simple Conceptual Models

Continuing atmospheric-ocean coupling process, a brief review is provided in this section on two simple ocean models which describe two important oceanic phenomena that have a large impact on the entire climate system: (1) the El Niño Southern Oscillation and (2) the thermohaline circulation. The former feature produces the largest signal in interannual climate variability in the Earth system, and the latter is a feature that is very important in longer-term climate variability.

These features are most easily described using simple models based on the full sets of mathematical equations but with their complexity reduced to make it easier to describe the basic features of particular phenomena. For example, idealized geometries with simplified boundary conditions may be applied or several approximations can be made for some regions, which are not uniformly applicable to the global ocean. However, these simple models provide very useful insight on how a specific physical process is maintained and respond to individual forcing. For example, the ocean thermocline and wind-stress effects on El Niño Southern Oscillation can be easily understood and modeled in a Cane–Zebiak model. In this subsection, a couple of simple models will be reviewed. One is this Cane–Zebiak model and the other describes the oceanic thermohaline circulation [15].

Cane–Zebiak Model

El Niño Southern Oscillation (ENSO) is a climate pattern found in nature. The pattern is centered in the tropical pacific, but its signal can be detected globally. It is frequently described through an index measuring surface pressure differences between Tahiti and Darwin, or ocean surface temperature over the eastern Pacific but its signatures can be found in precipitation changes over tropics as well as mid-latitudes and in many other components of the Earth climate system. The feature has a very large interannual variability. On average there is an event every 3–6 years but it occurs irregularly. Various degrees of simple conceptual models have been proposed to explain and model ENSO. All these efforts can be summarized by the Bjerknes–Wyrtki model [3, 65], in which it was suggested that ENSO is an internal mode of oscillation of the coupled atmosphere-ocean system, driven by a continuous imbalance between the tightly coupled surface winds and temperatures on the one hand, and the more sluggish subsurface heat reservoir on the other. In the early 1980s, several highly idealized coupled models were developed based on the Bjerknes–Wyrtki model. The first one was that of Cane and Zebiak [9] and Zebiak and Cane [67]. Both the atmosphere and the ocean are highly simplified. These components are outlined in the next subsection.

The Atmosphere Model Tropical atmosphere exhibits a couple of unique characteristics. One is that the wind is driven by latent heat release due to

convection, and the other is a reversed polarity in the vertical structure, for example, low-level convergence with upper-level divergence in the divergent circulation. Therefore, linear dynamics with a single degree of freedom in the vertical coordinate has proven surprisingly accurate in reproducing the atmospheric circulation, classified as a Gill-type model [22, 44]. In ZC model, steady-state, linear shallow-water equation on an equatorial beta plane is used, just like a Gill-type model as follows:

$$\frac{\partial u}{\partial t} - \beta y v = -\frac{\partial \Phi}{\partial x} \tag{13}$$

$$\frac{\partial v}{\partial t} - \beta y u = -\frac{\partial \Phi}{\partial y} \tag{14}$$

$$\frac{\partial \phi}{\partial t} + c_a^2 \nabla \cdot \vec{V} = \frac{J}{C_p} \tag{15}$$

where $\vec{V} = (u, v)$ are the surface wind vector, ϕ is the geopotential, $\beta = df/dy$, with f being the Coriolis parameter, and c_a is a constant related to momentum and mass in the form of Newtonian cooling. Earlier, Matsuno [8] solved this equation for free tropics diabatic heating, and later Gill [22] found the steady solution for both the forced and damped versions. Lindzen and Nigam [36] introduced an alternative view on how surface wind was forced. They proposed the surface temperature gradient causes overlaying atmospheric pressure gradient and in turn surface wind anomalies.

The atmospheric heating anomaly Q is contributed by local evaporation (Q_S) and low-level moisture convergence (Q_L). It has been shown that the atmospheric moisture convergence is important for tropical heat budget and to maintain divergent circulation (e.g., [14]).

The Ocean Model The ZC model represents the ocean as a single basin, the tropical Pacific, consisting of two vertical layers with a simplification of the ocean dynamics called a linear reduced gravity model. Vertically, the change of the thermocline needs to be considered, which is assumed motionless and linear. The set of equations is as follows:

$$\frac{\partial u}{\partial t} - \beta y v = -\frac{\Delta\rho}{\rho}\frac{\partial h}{\partial x} + \frac{\tau_{S_x}}{\rho \bar{h}} - ru\,, \tag{16}$$

$$\beta y u = -\frac{\Delta\rho}{\rho}\frac{\partial h}{\partial y} + \frac{\tau_{S_y}}{\rho \bar{h}} - rv\,, \tag{17}$$

$$\frac{\partial h}{\partial t} + h\nabla \cdot \vec{V} = -rh\,, \tag{18}$$

$$\frac{\partial T}{\partial t} = -\vec{V} \cdot \nabla T - M w_s \frac{\partial T}{\partial z} - \alpha_S T\,, \tag{19}$$

where (u,v) is the horizontal velocity in the layer, h is the derivation of the layer thickness from its mean value H, r is a Rayleigh friction parameter, τ_S is the surface wind stress, and $\Delta\rho$ a characteristic density difference between the layers. The upwelling is represented as follows:

$$w_S = H_1 \nabla \cdot \vec{V}_1. \tag{20}$$

The function M accounts for the fact that surface temperature is affected by upwelling. The anomalous temperature gradient, $\partial T/\partial z$, is defined by

$$\frac{\partial T}{\partial x} = \frac{(T - T_e)}{H_1}, \tag{21}$$

$$T_e = (1-\gamma)T + \gamma T_d, \tag{22}$$

where H_1 is the surface layer depth, T_e measures temperature entrained into the surface layer, with γ as a mixing parameter (= 0.5), and T_d relates the subsurface temperature anomaly to the mean and anomalous thermocline depths.

In summary, the ocean model is essentially a reduced gravity model with one and half layer of ocean which includes the surface mixed layer and the layer below as one layer. Thus, the surface temperature is affected by both the atmospheric wind stress at the surface and the temperature entrained into the surface layer from the deep layer.

With reasonable choice of parameters, this coupled model has produced anomalous SST pattern and wind that resembles the observed ENSO anomalies (Fig. 5). El Niño occurs every 3–4 years, followed by the La Niña events. A well-known deficiency of this model is that ENSO occurs too regularly with the fixed period around 2 years.

Although it is an idealized and theoretical model, this model included both the atmosphere and the ocean dynamics and was shown to have a reasonable

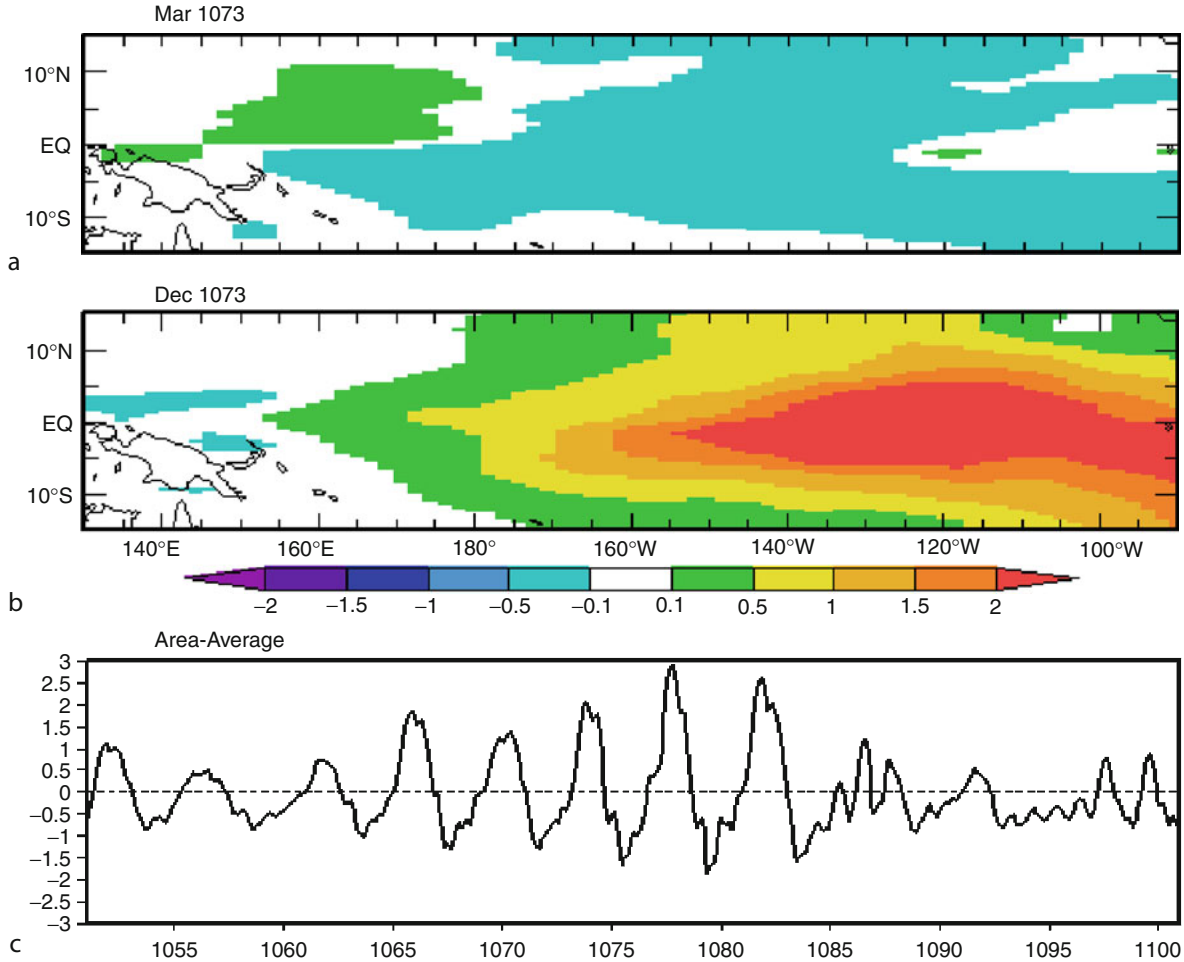

Oceanic General Circulation Models. Figure 5

An example of El Nino simulated by ZC model. (**a**) SST anomalies at March 1073, (**b**) same as (**a**) except December 1073, and (**c**) area averaged over the eastern equatorial Pacific (90° W to 150° W, 5° S to 5° N). The entire simulation was for the period of 1001–1200

evolution and life cycle of the ENSO compared to what was observed. Essentially, a Gill-type atmosphere with heating mainly tied to SST anomaly and convergence feedback term is coupled with a reduced gravity ocean model. In the mid-1980s, slightly different models were examined: one by Philander et al. [46], in which the SST anomaly was assumed proportional to both thermocline displacement and its anomaly; the other by Gill [68] in which the tendency of SST was assumed to be a function of advection of mean temperature by anomalous zonal current and atmospheric heating was determined by the SST anomaly. The former resulted a Kelvin wave response, while the latter a westward growing coupled mode.

These model variants, although far simpler than an OGCM, were constructed with careful thought on the processes influencing SST changes that are essential in producing the coupled ENSO phenomena. Simulating realistic ENSO remains a challenge for developers of climate models. Because ENSO is a dominant feature in interannual variability, and El Niño (La Niña) induces anomalous wet (dry) conditions all over the worlds, it is critical to simulate right. Understanding ENSO, and how it might change in an era of the global warming is

an important research topic. For example, a recent study using the IPCC's AR4 model projections showed the El Niño with its center over the central Pacific may dominate in the future [66].

A Box Model for Thermohaline Circulation

The ZC model is primarily forced by surface wind stress and buoyancy plays a minor role. However, in climate application, ocean circulation can be driven by salinity and density gradients, which contributes much longer-term variability than ENSO which is predominately in interannual timescales. Although state-of-the-art OGCMs can now simulate the thermohaline circulation relatively well, it has been one of the long-standing challenges for modelers. Therefore, different types of simple conceptual models have been developed and used. Difference between the ZC model and the thermohaline models are not limited to the physical forcing mechanisms, but also through the introduction of nonlinearity in the thermohaline circulation and different mathematical treatment associated with the vertical stratification of buoyancy.

Therefore, an alternative to the formal mathematical derivation of simplified models from the full equations of motion is used to pose a conceptual model or simple physical analog for the ocean system. In this entry, an idealized model by Marotzke [40] will be briefly described. Two boxes which represent tropical and polar regions of the ocean are considered. Several assumptions are made: (1) ocean temperature is very close to atmospheric temperature in each box, and (2) salinity is forced by a flux of moisture through the atmosphere from the low-latitude to the high-latitude box. Salinity forcing is used to make the low-latitude box saltier and denser, and the high-latitude box fresher and less dense (Fig. 6). The governing equation of salt can be described as follows following Haidvogel and Bryan [29]:

$$V\frac{dS_1}{dt} = -FS_0 + |q|(S_2 - S_1), \tag{23}$$

$$V\frac{dS_2}{dt} = -FS_0 + |q|(S_1 - S_2), \tag{24}$$

where V is the volume of the boxes which is assumed to be equal, S_0 is a constant reference salinity, and q is the rate of volume exchanged in the pipes which connect

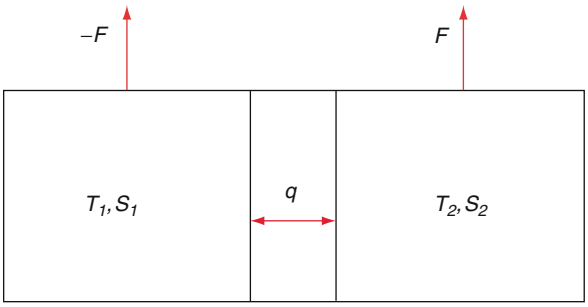

Oceanic General Circulation Models. Figure 6
A schematic diagram of the two-box model of the thermohaline circulation (modified from [29])

the low-latitude and polar boxes. Pressure differences between the two boxes drive the system, which can be modeled using resistivity k^{-1}:

$$q = -\frac{k}{\rho_0}(\rho_2 - \rho_1)\,. \tag{25}$$

These are completed using a linear equation of state:

$$\rho = \rho_0\,(1 - \alpha T + \beta S)\,, \tag{26}$$

where α is the thermal expansion coefficient and β is the haline contraction coefficient.

As mentioned above, the state-of-the-art climate models now can simulate decent thermohaline circulation. However, it is still difficult to observe this circulation and bias exists in its location and intensity simulated by OGCM.

Biogeochemical Cycle Modeling

The oceans play a role in not only through physical quantities, such as wind stress and surface energy exchange, but also through chemical species, especially greenhouse gases, such as CO_2 and N_2O. Also, sea salt from the ocean surface is an important source of natural aerosols which have impacts on climate through aerosol–climate interaction. In this section, a few aspects on modeling of the biogeochemical cycle in the OGCM are briefly reviewed.

Currently, approximately 6 Gt/year of carbon is released in the atmosphere due to anthropogenic activity. Only about half of carbon remains in the atmosphere and the rest is stored either in the vegetation and soil, or in biota and dissolved trace species in the ocean. This stored carbon is typically identified as terrestrial

and ocean carbon pools. These fluxes and reservoirs for carbon are summarized in Fig. 7. The size of the terrestrial and atmospheric carbon pools are about 2,200 and 750 Gt, while the Ocean carbon pool is estimated to hold about 40,000 Gt, the largest carbon pool except sediments and rocks.

The first generation of the Ocean Carbon model to treat the exchange process between atmosphere and ocean was developed more than 50 years ago by Revelle and Suess [50], which used two boxes of oceanic carbon pools with exchange processes between atmosphere and ocean. The rationale of this simple box model has been employed consistently through later generations of the ocean carbon model (e.g., [31]). Research questions about how much of the extra CO_2 released by human activity in the atmosphere can be stored in the ocean carbon pools resides at the core of climate change science, and how these large carbon pools will respond to global warming is also critical to understand.

The conservation equation for any trace constituent (like CO_2) in the ocean or atmosphere can be written as follows:

$$\frac{\partial C}{\partial t} = -\vec{V} \cdot \nabla C - C\nabla \cdot \vec{V} + C_{\text{Source}} - C_{\text{Sink}}, \quad (27)$$

where C is a mixing ratio of any trace constituent (units mass of trace constituent to mass of sea water).

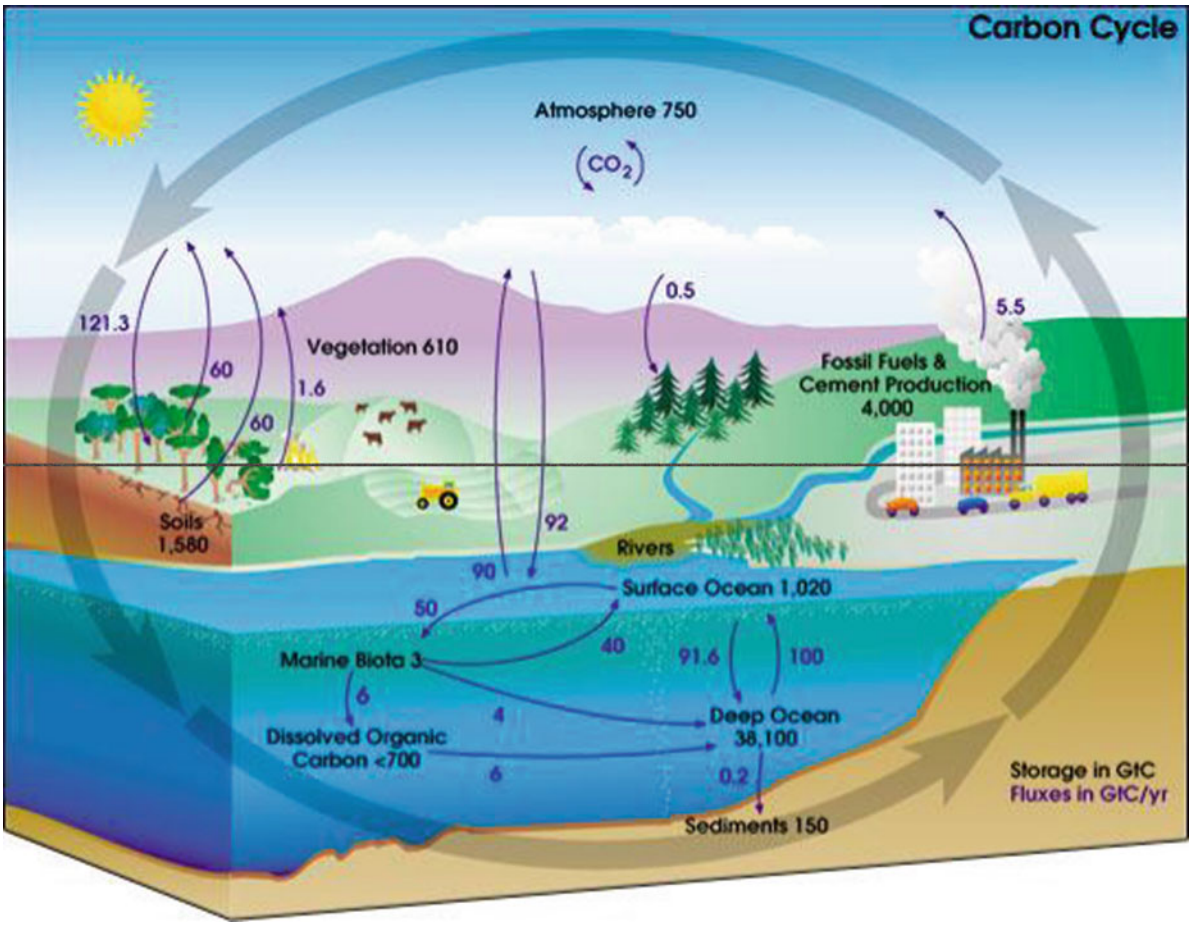

Oceanic General Circulation Models. Figure 7
A schematic diagram of the global carbon cycle, obtained from http://earthobservatory.nasa.gov/Features/CarbonCycle/carbon_cycle4.php

There exist two important source and sink processes for carbon in the ocean, that are typically labeled as the biological and solubility pumps. The biological pump refers to the transport of carbon from the oceanic surface to its interior in the form of carbon bound to other elements and labeled organic or inorganic carbon, according to whether the carbon resides in chemical compound that arises primarily through biological activity (organic) or other chemical reactions (inorganic). Various routes for the transport of carbon from the atmosphere into different parts of the ocean have been discovered and are treated in modern climate models treating biogeochemistry. The strength of this biological pump is measured by the so-called f-ratio, a fraction of total primary production fueled by nitrate [17].

Second, the solubility pump is a transport process that takes place through physical-chemical interactions. Both temperature in the ocean layers and the aforementioned thermohaline circulation are two important players in determining the strength of the solubility pump. The most of the climate models in the IPCC 4th Assessment Report (AR4) does not have representation of carbon cycle. However, the next generation of OGCMs to be used in the IPCC 5th Assessment Report (AR5) has some degree of numerical representation of these two pumps.

Future Directions

The simulations of the oceans by contemporary OGCM in coupled climate model still exhibit various degrees of biases compared to observations despite improvements. Further reduction of these biases is required. Some dynamical, physical, and even biological processes are poorly represented, and others are entirely missing. Thus, much emphasis has been weighted on developing more comprehensive and computationally efficient ocean climate model at the same time. As a first step, increasing spatial resolution has been pursued as a way forward by many modeling groups in the world and reduces the need for some subgrid scale processes which must currently be parameterized. Also, better numerical algorithm suitable for extreme computing environment has been sought at the same time.

In summary, several key aspects in the development of the next generation of the OGCM are as follows:

1. Multi-decadal natural variability-Atlantic Meridional Overturning Circulation (AMOC): This phenomenon is important for climate not only in the pan-Atlantic regions, but also for other regions in longer-term climate variability [60]. With limited availability of observational data, the OGCM has been playing an important role in understanding many processes involved with the AMOC and in simulating its historical evolution as well as current status. For example, most of climate simulations produce a weakening of the AMOC under the global warming due to increasing temperature [23, 55]. However, a role played by the fresh water budget on the AMOC has large uncertainty [61]. Many regional and international efforts have been made to collect more data and to improve model simulation of the AMOC [53].
2. Sea-level change in the warming world: Sea-level change in the global ocean is not only a function of temperature increase, but also many regional processes. As reviewed earlier, the OGCM with the Boussinesq approximation has its limitation in suitably simulating this sea-level change. Also, the ice sheet and sea ice variability and change have to be simulated and incorporated into the OGCM.
3. Simulation of marine ecosystem in the OGCM: The OGCM was typically for description of ocean circulation and physical properties. However, as our planet changes due to the anthropogenic activities, there are increasing demands on what would be the impact of climate change on marine ecosystem in a very regional scale (such as the coastal region of the Gulf of Mexico). On the other hand, proper simulation of marine ecosystem benefits better representation of the biological pump in the ocean biogeochemical cycle.

This entry introduces some of the basic concepts and examples of the OGCM. More details on each subject can be found in the following articles or textbooks. For example, general introductory and review on the contemporary OGCM can be found in Randall et al. [48], Griffies et al. [27], and Haidvogel and

Bryan [29]; numerical formulation can be found in Griffies [24], Griffies et al. [26], and Bryan [5]; and biogeochemistry in the OGCM can be described in much more detail in Sarmiento [54].

Bibliography

1. Adcroft A, Campin J-M, Hill C, Marshall J (2004) Implementation of an atmosphere–ocean general circulation model on the expanded spherical cube. Mon Weather Rev 132:2845–2863
2. Beckmann A, Haidvogel D (1993) Numerical simulation of flow around a tall isolated seamount. Part I: Problem formulation and model accuracy. J Phys Oceanogr 23:1736–1753
3. Bjerknes J (1969) Atmospheric teleconnections from the equatorial Pacific. Mon Weather Rev 97:163–172
4. Bleck R (1998) Ocean modeling in isopycnic coordinates. In: Chassignet EP, Verron J (eds) Ocean modeling and parameterization. Kluwer, Dordrecht, pp 423–448
5. Bryan K (1989) The design of numerical model of the ocean circulation. In: Anderson DLT, Willebrand J (eds) Oceanic circulation models: combining data and dynamics. Kluwer, Dordrecht, pp 465–500
6. Breugem W.-P, Chang P, Jang CJ, Mignot J, Hazeleger W (2008) Barrier layers and tropical Atlantic SST biases in coupled GCMs. Tellus A 60:885–897. doi: 10.1111/j.1600-0870.2008.00343.x
7. Gill AE (1982) Atmosphere-ocean dynamics. Academic Press, 662 pp
8. Matsuno T (1966) Quasi-geostrophic motions in the equatorial area. J Meteorol Soc Jpn 44:25–43
9. Cane MA, Zebiak S (1985) A theory for El Niño and the southern oscillation. Science 228:1085–1087
10. Casulli V, Walters RA (2000) An unstructured grid, three-dimensional model based on the shallow water equations. Int J Numer Methods Fluids 32:331–346
11. Chassignet EP, Hurlburt HE, Smedstad OM, Halliwell GR, Wallcraft AJ, Metzger EJ, Blanton BO, Lozano C, Rao DB, Hogan PJ, Srinivasan A (2006) Generalized vertical coordinates for eddy resolving global and coastal ocean forecasts. Oceanography 19(1):118–129
12. Chen C, Liu H, Beardsley RC (2003) An unstructured grid, finite-volume, three-dimensional, primitive equations ocean model: applications to coastal ocean and estuaries. J Atmos Ocean Technol 20:159–186
13. Chen C, Beardsley RC, Cowles G (2006) An unstructured-grid finite-volume coastal ocean model (FVCOM) system. Oceanography 19(1):78–89
14. Cornejo-Garrido AG, Stone PH (1977) On the heat balance of the Walker circulation. J Atmos Sci 34:1155–1162
15. Cox MD (1989) An idealized model of he world ocean. Part I: The global-scale water masses. J Phys Oceanogr 19:1730–1752
16. Deleersnijder E, Beckers J-M (1992) On the use of the σ-coordinate system in regions of large bathymetric variations. J Mar Syst 3:381–390
17. Eppley RW, Peterson BJ (1979) Particulate organic matter flux and planktonic new production in the deep ocean. Nature 282:677–680
18. Gaspar P, Gregoris Y, Lefevre J (1990) A simple eddy kinetic energy model for simulations of the oceanic vertical mixing: Tests at station Papa and long-term upper ocean study site. J Geophys Res 95:16179–16193
19. Gent PR, McWilliams JC (1990) Isopycnal mixing in ocean circulation models. J Phys Oceanogr 20:150–155
20. Gent PR, Willebrand J, McDougall TJ, McWilliams JC (1995) Parameterizing eddy induced tracer transports in ocean circulation models. J Phys Oceanogr 25:463–474
21. Ghil M, Malanotte-Rizzoli P (1991) Data assimilation in meteorology and oceanography. Adv Geophys 33:141–266
22. Gill AE (1980) Some simple solutions for heat induced tropical circulation. Q J R Meteorol Soc 106:447–462
23. Gregory JM et al (2005) A model intercomparison of changes in the Atlantic thermohaline circulation in response to increasing atmospheric CO_2 concentration. Geophys Res Lett 32: L12703. doi:10.1029/2005GL023209
24. Griffies SM (2004) Fundamentals of ocean climate models. Princeton University Press, Princeton, 518 pp
25. Griffies SM et al (2000) Developments in ocean climate modeling. Ocean Model 2:123–192
26. Griffies SM, Ganadesikan A, Dixon KW, Dunne JP, Gerdes R, Harrison MJ, Rosati A, Russell JL, Samuels BL, Spelman MJ, Winton M, Zhang R (2005) Formulation of an ocean model for global climate simulations. Ocean Sci 1:45–79
27. Griffies SM, Adcroft AJ, Banks H, Böning CW, Chassignet EP, Danabasoglu G, Danilov S, Deleersnijder E, Drange H, England M, Fox-Kemper B, Gerdes R, Gnanadesikan A, Greatbatch RJ, Hallberg RW, Hanert E, Harrison MJ, Legg S, Little CM, Madec G, Marsland SJ, Nikurashin M, Pirani A, Simmons HL, Schröter J, Samuels BL, Treguier A-M, Toggweiler JR, Tsujino H, Valllis GK, White L (2009) Problems and prospects in large-scale ocean circulation models. Community White Paper for OceanObs09. https://abstracts.congrex.com/scripts/jmevent/abstracts/FCXNL-09A02a-1672431-1-cwp2a07.pdf
28. Guilyardi E et al (2004) Representing El Niño in coupled ocean-atmosphere GCMs: the dominant role of the atmospheric component. J Climate 17:4623–4629
29. Haidvogel DB, Bryan FO (1992) Ocean general circulation modeling. In: Trenberth KE (ed) Climate system modeling. Cambridge University Press, New York, pp 371–412
30. Roberts MBH, Gedney N, Gregory J, Hill R, Mullerworth S, Pardaens A, Rickard G, Thorpe R, Wood R (2004) Impact of an eddy-permitting ocean resolution on control and climate change simulations with a global coupled GCM. J Clim 17:3–20
31. Sarmiento JL, Gruber N (2002) Sinks for anthropogenic carbon. Physics Today 55(8):30–36
32. Haney RL (1991) On the pressure gradient force over steep topography in sigma-coordinate ocean models. J Phys Oceanogr 21:610–619

33. Henderson-Sellers B, Davies AM (1989) Thermal stratification modeling for oceans and lakes. Annu Rev Numer Fluid Mech Heat Transfer 2:86–156
34. Jackson L, Hallberg R, Legg S (2008) A parameterization of shear-driven turbulence for ocean climate models. J Phys Oceanogr 38:1033–1053
35. Lehmann A (1995) A three-dimensional baroclinic eddy-resolving model of the Baltic Sea. Tellus 47A:1013–1031
36. Lindzen RS, Nigam S (1987) On the role of sea surface temperature gradients in forcing low level winds and convergence in the tropics. J Atmos Sci 44:2418
37. Maltrud M, McClean J (2005) An eddy resolving global 1/10° ocean simulation. Ocean Model 8:31–54
38. Manabe S, Bryan K (1969) Climate calculations with a combined ocean-atmosphere model. J Atmos Sci 26:786–789
39. Manabe S, Bryan K, Spelman MJ (1975) A global ocean-atmosphere climate model. Part I. The atmospheric circulation. J Phys Oceanogr 5:3–29
40. Marotzke J (1989) Instabilities and multiple steady states of the thermohaline circulation. In: Anderson DLT, Willebrand J (eds) Oceanic circulation models: combining data and dynamics. Kluwer, Dordrecht, pp 501–511
41. Martin PJ (1985) Simulation of the mixed layer at OWS November and Papa with several models. J Geophys Res 90:903–916
42. Meehl G et al (2007) The WRCP CMIP3 Multimodel Dataset: A new era in climate change research. Bull Am Meteorol Soc 88:1383–1394
43. Mellor GL, Yamada T (1982) Development of a turbulence closure model for geophysical fluid problems. Rev Geophys Space Phys 20:851–875
44. Neelin JD (1989) On the interpretation of the Gill model. J Atmos Sci 46:2466–2468
45. Noh Y, Kim H-J (1999) Simulations of temperature and turbulence structure of the oceanic boundary layer with the improved near-surface process. J Geophys Res 104:15621–15634
46. Philander SGH, Yamagata T, Pacanowski RC (1984) Unstable air-sea interaction in the tropics. J Atmos Sci 41:604–613
47. Randall D, Ringler T, Heikes R, Jones P, Baumgardner J (2002) Climate modeling with spherical geodesic grids. Comput Sci Eng 4:32–41
48. Randall DA, Wood RA, Bony S, Colman R, Fichefet T, Fyfe J, Kattsov V, Pitman A, Shukla J, Srinivasan J, Stouffer RJ, Sumi A, Taylor KE (2007) Climate models and their evaluation. In: Solomon S, Qin D, Manning M, Chen Z, Marquis M, Averyt KB, Tignor M, Miller HL (eds) Climate Change 2007: The Physical Science Basis. Contribution of Working Group I to the Fourth Assessment Report of the Intergovernmental Panel on Climate Change. Cambridge University Press, Cambridge, UK
49. Redi MH (1982) Oceanic isopycnal mixing by coordinate rotation. J Phys Oceanogr 12:1154–1158
50. Revelle R, Suess HE (1957) Carbon dioxide exchange between atmosphere and ocean and the question of increasing of atmospheric CO_2 during the past decades. Tellus 9:18–27
51. Ringler T, Ju L, Gunzburger M (2008) A multiresolution method for climate system modeling: application of spherical centroidal voronoi tessellations. Ocean Dyn 58:475–498
52. Sadourny R, Arakawa A, Mintz Y (1968) Integration of the non-divergent barotropic vorticity equation with an icosahedral-hexagonal grid for the sphere. Mon Weather Rev 96:351–356
53. Sanford TB, Kelly KA, Former DM (2011) Sensing the ocean. Phys Today 64(2):24–28
54. Sarmiento JL (1992) Biogeochemical ocean models. In: Trenberth KE (ed) Climate system modeling. Cambridge University Press, New York, pp 519–551
55. Schmittner A, Latif M, Schneider B (2005) Model projections of the North Atlantic thermohaline circulation for the 21st century assessed by observations. Geophys Res Lett 32:L32710. doi:10.1029/2005GL024368
56. Semtner AJ, Chervin RM (1992) Ocean general circulation from a global eddy-resolving model. J Geophys Res 97:5493–5550
57. Shchepetkin A, McWilliams J (2002) A method for computing horizontal pressure-gradient force in an ocean model with a non-aligned vertical coordinate. J Geophys Res 108:35.1–35.34
58. Smith R, Gent P (2004) Reference Manual for the Parallel Ocean Program (POP)—ocean component of the community climate system model. Los Alamos National Laboratory, LAUR-02-2484
59. Solomon H (1971) On the representation of isentropic mixing in ocean models. J Phys Oceanogr 1:233–234
60. Sutton RT, Hodson LR (2005) Atlantic forcing of North American and European summer climate. Science 309:115–118
61. Swingedouw D, Braconnot P, Marti O (2006) Sensitivity of the Atlantic Meridional overturning circulation to the melting from northern glaciers in climate change experiments. Geophys Res Lett 33:L07711. doi:10.1029/2006GL025765
62. Vernois G (1973) Large scale ocean circulation. In: Yih C-S (ed) Advances in applied mathematics, vol 13. Academic, New York, pp 1–92
63. Walton CC, Pichel WG, Sapper JF (1998) The development and operational application of nonlinear algorithms for the measurement of sea surface temperatures with the NOAA polar-orbiting environmental satellites. J Geophys Res 103(C12): 27999–28012
64. Weart SR (2008) The discovery of global warming: revised and expanded edition. Harvard University Press, Cambridge, MA. 240 p. ISBN: 978–0674031890
65. Wyrtki K (1975) El Niño – The dynamic response of the equatorial Pacific Ocean to atmospheric forcing. J Phys Oceanogr 4:91–103
66. Yeh S-W, Kug J-S, Dewtte B, Kwon M-H, Kirtman B, Jin F-F (2009) El Niño in a changing climate. Nature 461:511–514
67. Zebiak S, Cane MA (1987) A model El Niño-southern oscillation. Mon Weather Rev 115:2262–2278
68. Gill AE (1985) Elements of coupled ocean-atmosphere models for the tropics. In: Nihoul JCJ (ed) Coupled ocean-atmosphere models, vol 40. Elsevier Oceanogr. Ser., Amsterdam, pp 303–327

Oceans and Human Health, Introduction

Darrell Jay Grimes
Department of Coastal Sciences, The University of Southern Mississippi, Ocean Springs, MS, USA

Oceans and Human Health (OHH) is an emerging "metadiscipline" that involves oceanography, waterborne and seafood-borne diseases, harmful algal blooms, epidemiology, comparative animal physiology and pathology, natural products and synthetic organic chemistry, pharmacology, toxicology, social sciences, engineering, and other ocean-related areas. In large part, it evolved from the realization that the relationship between the oceans and human health is a "two-way street." Scientists, educators, and policymakers and enforcers have long focused on the things done by humankind that degrade the oceans and the marine organisms dependent upon them. More recently, new emphasis has been given to the useful and healthful products that derive from the oceans (e.g., η-3 fatty acids), and the concept of "One Health" (Fig. 1) is now being applied to the oceans (see http://onehealthinitiative.com/).

Oceans and Human Health, Introduction. Figure 1 The principles of one health applied to the ocean ecosystem

This *Encyclopedia of Sustainability Science and Technology* section is focused on the several disciplines that comprise OHH, with the exceptions of climate change, toxicology, and radioisotopes. These three disciplines are covered in other sections, and readers are encouraged to peruse these sections for relevant information (the section on "Environmental Radioactivity and Ecotoxicology of Radioactive Substances" by Dr. Glen Bird, the section on "Environmental Toxicology" by Dr. Ed Laws, "Climate Change Mitigation" for which the section editors are Dr. Tim Lenton and Dr. Nem Vaughan, and the section on "Climate Change Modeling Methodology" by Dr. Philip Rasch).

OHH had an interesting origin, and it is not the intent of this introduction to tell that story – instead, it will be told by three of the several creators of the OHH concept, Paul Sandifer, Tracy Collier, and Juli Trtanj, in Chapter "► Coastal Ecosystems, Sustainable Management." Three of the documents that had a heavy influence on the origin of OHH are a paper in *Science* by [1], the National Research Council, Ocean Studies Board report "From Monsoons to Microbes" [2], and a report authorized by the US Congress "An Ocean Blueprint for the 21st Century" [3]. These influential references and other topics relevant to the development of OHH will be discussed in Chapter "► Coastal Ecosystems, Sustainable Management."

Chapter "► Remote Sensing Applications to Ocean and Human Health" by Frank Muller-Karger discusses the history and current applications of remote sensing as a set of tools to better understand and predict ocean events that relate to OHH. Both Muller-Karger and Sandifer were USCOP commissioners [3].

Chapters "► Human Bacterial Diseases from Ocean" and "► Waterborne Diseases of the Ocean, Enteric Viruses" are focused on waterborne (seawater) and seafood-borne diseases. Grimes, Lisa Plano, and

Okechukwu Ekenna cover human bacterial diseases and intoxications from the ocean in "Human Bacterial Diseases from the Ocean," and Jackie Woods discusses human viral diseases that are conveyed by seawater and seafood in ► Waterborne Diseases of the Ocean, Enteric Viruses.

Human parasitic diseases that are contracted from seawater and seafood are discussed by Robin Overstreet in Chapter "► Waterborne Parasitic Diseases in Ocean." In Chapter "► Marine and Freshwater Fecal Indicators and Source Identification," Sandra McLellan, Alexandria Boehm, and Orin Shanks discuss fecal indicators and their sources; both of these topics relate to some of the diseases discussed in these chapters.

"► Harmful Algal Blooms" is the title of the chapter by Timothy McLean and Geoffrey Sinclair. Chapter "► Sentinel Species in Oceans and Human Health" is devoted to emerging tools – the use of sentinel species and habitats to better understand and predict how ocean changes impact human health; this chapter has been written by Lori Schwacke, Frances Gulland, and Susan White.

Chapter "► Drug Discovery in Ocean" has been written by the chief of the NIH/National Cancer Institute's Natural Products Branch that oversees the NCI effort in marine natural products, David Newman, along with his fellow workers Gordon Cragg and Paul Grothaus. Chapter "► Oceans and Human Health, Social and Economic Impacts" is coauthored by Jay Grimes, Mark Hamann, Jeffrey Lotz, Timothy McLean, Thomas McIlwain, and Catherine Price. The final chapter, "► Living Ocean, An Evolving Oxymoron," by Alonso Aguirre and Scott Weber is an educational and outreach piece.

Bibliography

1. Harvell CD, Kim K, Burkholder JM, Colwell RR, Epstein PR, Grimes DJ, Hoffmann EE, Lipp EK, Osterhaus ADME, Overstreet RM, Porter JW, Smith GW, Vasta GR (1999) Emerging marine diseases – climate links and anthropogenic factors. Science 285:1505–1510
2. NRC (1999) From monsoons to microbes. Understanding the ocean's role in human health. National Academy Press, Washington, DC
3. USCOP (2004) An ocean blueprint for the 21st century, final report. U.S. Commission on Ocean Policy, Washington, DC, (ISBN#0-9759462-0-X)

Oceans and Human Health, Social and Economic Impacts

Darrell Jay Grimes[1], Mark T. Hamann[2,3], Jeffrey M. Lotz[4], Timothy I. McLean[5], Thomas McIlwain[6], Catherine H. Price[7]

[1]Department of Coastal Sciences, The University of Southern Mississippi, Ocean Springs, MS, USA
[2]Pharmacognosy, Pharmacology, Chemistry & Biochemistry, The University of Mississippi, University, MS, USA
[3]Institute of Marine and Environmental Technology, University of Maryland Center for Environmental Science, Baltimore, MD, USA
[4]Department of Coastal Sciences, Ecology and Epidemiology of Parasites and Pathog, Gulf Coast Research Laboratory, The University of Southern Mississippi, Ocean Springs, MS, USA
[5]Department of Biological Sciences, University of Southern Mississippi, Hattiesburg, MS, USA
[6]Gulf Coast Research Laboratory, The University of Southern Mississippi, Ocean Springs, MS, USA
[7]Department of Casino, Hospitality, Tourism Management, College of Business, The University of Southern Mississippi, Hattiesburg, MS, USA

O

Article Outline

Glossary
Introduction
Definition of the Subject and Its Importance
Human Disease
Marine Natural Products
Marine Aquaculture
Algal Blooms
Fisheries
Tourism
Bibliography

Glossary

Epidemic The incidence of disease above the normal or endemic incidence.

Exclusive economic zone In general, the EEZ of a nation extends seaward 200 nautical miles from its shoreline.

Food intoxication Illness caused by the ingestion of food that contains a toxic substance.

Foodborne disease A disease that is caused by the ingestion of pathogens conveyed by food including seafood.

Marine aquaculture Aquaculture is the raising of aquatic animals and plants for commercial purposes. Marine aquaculture is the rearing of marine and estuarine animals. Marine aquaculture is sometimes referred to as mariculture.

Pandemic An epidemic of worldwide proportions.

Pathogenesis The production or development of a disease, specifically the cellular reactions and other pathologic mechanisms occurring in the progression of the disease.

Waterborne disease A disease that is transmitted by water.

Introduction

The social and economic impacts of the oceans on humankind are enormous. There are both positive and negative impacts, and they include both impacts from the oceans on humankind and anthropogenic impacts on the oceans. Further, these impacts range from the tangible and quantifiable (e.g., fish catch data and coastal tourism expenditures) to the intangible and not easily quantifiable or perhaps not quantifiable (e.g., lost work days due to gastroenteritis acquired from seafood).

Definition of the Subject and Its Importance

America's oceans and coasts are big business! The US has jurisdiction over 3.4 million square nautical miles of ocean territory in its exclusive economic zone (EEZ). In 2000, the ocean economy contributed more than $117 billion to American prosperity and over two million jobs. This contribution is 1.5 times greater than agricultural employment, and the economic output was 2.5 times that of the farm sector [1]. In 2010, the US Census Bureau reported that 309 million people live in the US [2]. In an earlier report, they stated that in 2008 87 million people lived on the coastline [3]. In addition, the number one tourist destination in the US is the coastline [1], and similar statistics are available for other countries in the world, a fact illustrated in Fig. 1, which was taken from the USCOP report [1]. Clearly, the oceans are of prime importance to humankind.

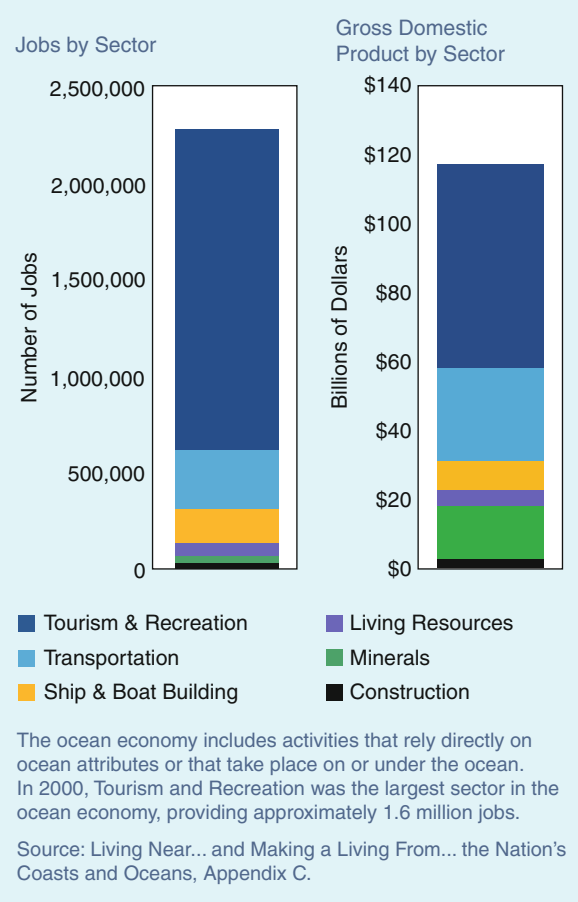

Oceans and Human Health, Social and Economic Impacts. Figure 1
The value of the oceans [1]

This chapter will focus on the social and economic impacts that derive from six major areas connecting the oceans to human health: human disease, marine natural products, marine aquaculture, algal blooms, fisheries, and tourism. Not covered is toxicology (both legacy chemicals and emerging environmental contaminants), radiation, input of pharmaceuticals to the coastal ocean, the use of marine animals as models of human health, and the human consumption of marine plants and animals including the application to traditional medicine (e.g., nori).

Human Disease

There are both measureable and intangible impacts to humans that result from waterborne and seafood-borne diseases. Clearly, the most dramatic and tragic

impact is the loss of a loved one through death; aside from the cost of medical aid and the funeral, this kind of loss is immeasurable. However, death caused by viruses, bacteria, and parasites has occurred since humans evolved and it will of course continue, to wit, the current cholera epidemic in Haiti. What follows here is a discussion of the measurable impacts.

In a recent presentation, the CDC reported that the cost of waterborne diseases in the USA probably exceeds $500 million annually. They used 2004–2007 data from an insurance claims database on three common waterborne diseases: Legionnaires' disease, cryptosporidiosis, and giardiasis [see http://www.cdc.gov/media/pressrel/2010/r100714.htm?s_cid=mediarel_r100714]. Although these diseases are not acquired from seawater or seafood, they illustrate the financial burden of waterborne diseases. The CDC estimated that Legionnaires' disease costs the US $101–321 million annually and that inpatient costs averaged $34,000 per patient. Costs for the other two waterborne diseases were slightly less.

The World Bank released a study in December 2010 showing that inadequate sanitation in India cost that nation US $53.8 billion in 2006 (6.4% of their GDP). In the report, it was noted that more than three-fourths of the mortalities in children under 5 years old are linked to GI infections, and dysentery costing an estimated $18 billion (US $) each year. [see http://web.worldbank.org/WBSITE/EXTERNAL/NEWS/0,,contentMDK:22794090~pagePK:64257043~piPK:437376~theSitePK:4607,00.html?cid=3001_7].

In December 2010, the Pan American Health Organization released a report that it was recommending the use of a cholera vaccine in Haiti. They estimated that the two companies producing the vaccine could supply two to three million doses per year and that the vaccine program could begin in March or April 2011. The cost is approximately US $1 per dose and three doses are required [see http://uk.reuters.com/article/2010/12/18/us-haiti-cholera-idUKTRE6BH04X20101218].

In a 2009 report on cholera, the World Health Organization estimated that the annual incidence of cholera worldwide is three to five million cases with 100,000–300,000 deaths; in recent years, most of these cases have occurred in Africa. Noting that there is little data available on the economic costs of cholera, either at the macro or micro level, the WHO provided some illustrative focused data. Mozambique reported that it spends approximately $145 million per year to fight cholera. In 1998, the European Union banned importation of fish from four African countries (Kenya, Uganda, Tanzania, and Mozambique) because of cholera outbreaks in those countries; this restriction resulted in a loss of trade estimated to be over $1 billion for the years 1998–2002 [http://www.who.int/immunization/sage/1_Background_Paper_Cholera_Vaccines_FINALdraft_13_oct_v2.pdf].

Finally, in 2004, an outbreak of Norovirus occurred in a tertiary care hospital in Maryland, affecting 355 individuals (90 patients and 265 health care workers). The report included a cost analysis that broke down the various costs associated with this nosocomial outbreak. The total lost revenue to the hospital for this 5-month outbreak was $418,370. Additional losses were cleaning ($96,961), replacement of supplies ($53,075), and sick leave and overtime ($89,239) for a total loss of $657,644 [4].

In conclusion, there are no good data on the overall impacts of human disease that arises from the ocean. However, the above focused reports do shed light on the magnitude of this problem. Without doubt, waterborne disease accounts for billions and probably trillions of dollars annually.

Marine Natural Products

The genesis of marine natural products resides largely with the discovery and development of modified nucleosides from sponges [5]. The discovery of marine nucleosides which differed from common nucleosides by the inversion of configuration of just a single stereogenic center paved the way to further exploration of both marine natural products and nucleosides as potential drug leads. The exploration of modified nucleosides through both synthesis and natural products discovery grew into an active field and, in 1982, the journal "*Nucleosides and Nucleotides*" began publishing research dedicated to the chemistry and biology of nucleosides. Arguably, no group of molecules has had such a significant impact on the control of HIV as the field of nucleoside chemistry. During the same period of time, the plant-derived natural product Taxol™ was generating tremendous interest as a potential candidate for the control of cancer and it also went on to become one of the most successful forms of cancer

chemotherapy available. These historic milestones along with the unprecedented chemistry associated marine natural product discoveries have established the field as an indispensable resource for the discovery of new natural product prototypes.

So what is it about the oceans that make them such a unique resource for natural products discovery? There are three distinct physical/chemical factors that distinguishes the oceans as a uniquely suited environment for complex secondary metabolism relative to their terrestrial counterparts. First is the magnitude and diversity of life supporting conditions found in the marine biosphere. It is well known that nearly 3/4 of the planet is covered by the ocean; however, the three-dimensional nature of the environment means that closer to 90% of the global biosphere is found in marine environments. A second unique aspect of this aqueous environment is that it provides for essentially limitless molecular weight and polarity involved in chemical communication and defense. As a result, low molecular weight, volatile, and fragrant molecules are relatively rare when compared to the variety utilized by plant species. A final unique aspect is the elemental composition of the marine environment which provides for the incorporation of elements, like bromine, which are extremely rare in terrestrial natural products. These unique characteristics of the marine environment provide for a seemingly limitless opportunity for the discovery of new and unique chemistry with potential utility in the control of human disease. Many times, the same molecules that plague the marine environment in regard to fish kills and harmful algal blooms (HABs) offer unique opportunities for drug discovery and development [6].

The broad molecular weight spectrum and unique elemental composition of marine natural products have introduced challenges and significant motivation to further expand the analytical tools and methodologies required to characterize highly complex marine molecules. The spectroscopic and mass spectrometric tools utilized to characterize marine natural products have helped drive significant expansion in sensitivity and resolution. The successful structural assignment and synthesis of many marine natural products represent significant milestones in human scientific achievement. The scientific challenges associated with the characterization and supply of marine natural products have also created significant hurdles in the successful translation of these discoveries into pharmaceutical products and better treatment for human disease.

Despite the challenges, the field of marine natural products continues to see consistent growth in regard to the number of leads entering the clinic. There have been a significant number of reviews published detailing the chemistry and biology of marine natural product drug leads at various stages of development including Mayer et al. [7] and Waters et al. [8].

Where will marine natural products go from here? The utility of marine natural products in regard to providing new and unique prototypes for the control of human illness is certain to withstand even the most dramatic changes and innovation the future has to offer. Some unique and timely opportunities include using this resource for the control of depression and post-traumatic stress disorder (PTSD) [9]. The more we learn regarding the structure of proteins, the greater the demand for unique ligands to interact and bind to reactive sites, validating structure and function of disease targets. Some of the significant opportunities that remain include exploiting nature's tools for drug delivery and biosynthesis of nanostructures. Just as intriguing as the natural products chemistry of small molecules is the mechanism by which marine species have evolved to successfully deliver these toxins to prey and predators. Harnessing the tools of marine microbial communities is certain to lead to revolutionary new approaches to killing cancer cells, drug-resistant bacteria, fungi, parasites, and viruses.

Marine Aquaculture

Seafood, of which marine and estuarine species constitute 70% of the world's supply, contributes to the world's human health and food security by providing a nutritionally valuable component with not only high-quality protein but also a range of essential micronutrients, fatty acids, and minerals. If there is a single food that could be used to address all of the different aspects of world malnutrition, it might be fish [10].

Seafood provides only about 3% of the world's food supply [11]; however, it supplies 16% of all consumed animal protein [12]. Although, presently, a small piece of the global food supply, seafood is increasing its share

and per capita consumption is rapidly increasing, having more than doubled from 17 lb in 1950 to 38 lb in 2009 [12]. Seafood derives from two sources, capture fisheries and aquaculture.

Capture fisheries have been stable over the past decade [12] and therefore are providing a decreasing share of the seafood supply. On the other hand, aquaculture is providing an increasing share of the world's seafood. In fact, aquaculture is the fastest growing food producing sector of agriculture, with per capita supply growing from 1.5 lb in 1970 to 17.2 lb in 2008. Aquaculture now provides nearly half of the world's seafood [12].

This rapid growth is due in large part to technical developments in aquaculture. For example, Duarte et al. [13] have argued that the rapid domestication of marine species compared to terrestrially farmed species has fueled that growth. Marine shrimp farming has expanded to become the most valuable aquaculture commodity in the world, largely through technological advances [14]. In particular development of domesticated, selectively bred, specific-pathogen-free *Litopenaeus vannamei* has contributed to the success of shrimp farming [15].

Much of the expansion in marine aquaculture over the last 30 years has been for high-value species like salmon and shrimp. Despite the focus on high-value crops, the promise of the "blue revolution" to help alleviate poverty and food shortages in some of the world's poorest countries still exists [16]. Low-income food deficit countries (LIFDCs) are defined by the food and agriculture organization (FAO) as nations that are (1) poor (annual net per capita income below the eligibility for International Development Association assistance) and (2) net importers of food. In many cases, these countries cannot produce enough food to meet their needs and lack sufficient national income to purchase food on the international market. Although these countries have deficits in food production, aquaculture in LIFDCs is growing faster than their populations. Therefore, aquaculture may be part of the answer to food deficits.

Small-scale marine aquaculture may be one of the few options for economic improvement for the poor in coastal communities. In Southeast Asia, culture of bivalves and seaweed is common at a small scale, particularly in Indonesia and the Philippines. Small-scale shrimp culture in India and the Philippines maintains sustainable livelihoods to family farms [17]. Backyard hatcheries in Thailand are small, often family-run operations that produce the post-larval (seed) shrimp that are used to stock production ponds. They are the backbone of Thai shrimp culture and provide income to small, poor family farmers [18].

Marine aquaculture can provide livelihoods for the poor, not only through small-scale farms but also through larger-scale operations. These larger enterprises can contribute to poverty reduction and hunger elimination by generating employment and stimulating the economy. The challenge is to expand sustainable marine aquaculture to achieve enhanced food security and economic development for the world's poor [19].

Adequate supply of food is a necessity for food security. However, other factors are also at play. In particular, the affordability and the availability of food are concerns. Increasing the supply of seafood through aquaculture will often reduce the price, making seafood more affordable. Further, by providing farmers with revenues obtained through the sale of their product and by creating employment, aquaculture enhances the poor's ability to purchase food. The supply not only must be adequate and affordable but it must also be easily transported. To that end, governments must provide networks of roads, rails, and waterway for transport of food from producers to consumers [20].

In the developed world where food insecurity as defined by the FAO is less of a problem, concerns over terrorism have caused governments to consider threats to the safety of their food supplies. For example, the US Department of Homeland Security, the Department of Agriculture, and the Food and Drug Administration work closely to ensure America's food supply is safe and unadulterated. One of the weak links in the USA attempt to ensure the safety of its food supply is the extent of foreign imports of seafood. The US imports about 15% of its total food supply [21] but over 80% of its seafood. In 2009, imports made up 84% of the seafood eaten in the USA [28]. In 2008, the USDA estimated that the USA had a 35 billion dollar trade surplus in agricultural products [22]. In 2010, the USA had a 10.7 billion dollar trade deficit in seafood. Despite the fact that US seafood consumption is increasing largely through imported seafood [23], the USA lags behind other developed countries in the

development of marine aquaculture. According to the Fishery and Aquaculture Country Profiles on the FAO website, http://www.fao.org/fishery/countryprofiles/search/en, the percent of total national seafood production from aquaculture is 22% in Japan, 20% in Australia, and between 20% and 30% for countries of the European Union. For the USA, the percentage is only 10%. The development of a domestic marine aquaculture industry can contribute to the food safety of the USA.

Algal Blooms

Primarily, a grouping of dozens of species of microalgae but also inclusive of some species of macroalgae and cyanobacteria, harmful algae can accumulate and/or grow to high density under certain environmental conditions. These "blooms" can be visible (often referred to as "red tides") or non-visible and result in extensive negative environmental impacts to affected areas (see Chapter "► Harmful Algal Blooms"). For example, a bloom can block sunlight to submerged aquatic vegetation, or when a bloom terminates, the remaining algal biomass may be degraded by aerobically respiring bacteria leading to the creation of large hypoxic or anoxic zones. Many harmful species also produce phycotoxins that can lead to massive mortalities of fish, marine mammals, birds, and other marine organisms. Human consumption of filter-feeding shellfish and higher-trophic level finfish that have bioaccumulated different phycotoxins in their tissues can lead to a variety of poisoning syndromes whose symptoms range from gastrointestinal sickness to death. As a consequence of these effects (and others), harmful algal blooms (HABs) have economic impacts to a variety of industries and sectors of society (see Table 1 for representative examples of such impacts). In addition to economic losses that blooms have on various industries, attention and resources are being focused on devising and implementing methods to detect and monitor harmful algae and their associated toxins and to understand the natural and/or anthropogenic factors that influence bloom dynamics. Though HABs are a natural phenomenon, the observations that HABs are occurring more frequently and evermore toxic species are being identified and found in more widespread locations raises the worry that HABs will increasingly continue to be an issue of concern in the future [25, 26, 29, 38].

Given the extent and variety of consequences of any particular HAB, it is of interest to assess more precisely, in monetary terms, the effects of a bloom, or all blooms, to all sectors of society at a variety of levels. Until recently, the economic impacts of HABs, as exemplified by the reports listed in Table 1, have been described in terms of lost direct revenues or decreased expenditures. The reason for this bias is that impact values are relatively easy to calculate. Unfortunately, these types of analyses do not measure true changes in value. Value, as defined in economics, is a surplus and can be calculated separately for consumers and producers. To calculate a surplus is difficult, if not impossible, particularly since the calculations require an understanding of relevant, local established markets and obtaining or finding relevant data with regard to how a HAB influences or changes that market. Compounding this lack of local knowledge may be the facts that HABs may occur at low frequency in a particular area or the HAB event may be small or localized in scale and hence not be adequately reported.

Using the results from many individual studies, such as those in Table 1, as well as numerous communications with local and national experts, preliminary national aggregate analyses of the economic impacts of HABs have been published [24, 32]. The most recently updated analysis of impacts based on data from 1987 to 2000 [31] concluded that HABs in the USA have an average annualized impact of $82 million (2005 dollars). A similar estimate, although using slightly different methodology, to calculate estimates of impacts in the European Union (EU) from a similar time span (1989–1998) equaled $813 million (2005 dollars) [31].

The totals were summed from figures derived from four broad sectors:

1. Public health costs resulting from shellfish and finfish poisonings included lost productivity of sick/dead workers, medical treatment, transportation, and investigations into the causes of sickness/death. USA = $37 million: EU = $11 million.
2. Commercial fisheries losses were derived from the closure of fisheries or aquaculture operations, prohibition of sales from recreational fisheries, real or perceived untapped fisheries resources, and "halo

Oceans and Human Health, Social and Economic Impacts. Table 1 Representative examples of economic impacts due to harmful algal blooms[a]

	Estimate[b]	Reference
Public health		
Capitalized costs of illnesses in Sarasota County, FL resulting from breathing aerosolized toxins generated during a bloom of *Karenia brevis*	0.525–4.2	[39]
Commercial fisheries		
Karenia brevis bloom in 1996 halted oyster harvests in LA waters	>5.7	[34]
Decline in seafood sales in local markets following a *Pfiesteria* spp. bloom in MD in 1997	57.45	[36]
Blooms of *Alexandrium fundyense* closed shellfish beds to harvesting in MA (2 months) and ME (5 months)	21.2	[33]
Local economies (recreation/tourism/residential)		
Decline in recreational fishing expenditures following a *Pfiesteria* spp. bloom in MD in 1997	5.75	[36]
Macroalgal blooms along Kihei coast of the Hawaiian island of Maui resulted in reduced property values, loss of rental incomes, and large-scale clean-up efforts	>24.5	[27]
Theoretical seasonal closure of recreational razor clam fishery in WA due to *Pseudo-nitzschia* spp. bloom	21.4	[30]

[a]These examples reflect direct output impacts, not changes in economic value such as lost consumer surplus or lost producer surplus
[b]In millions of dollars of expenditures and/or lost sales/reduced expenditures (in 2011 dollars)

effects" of decreased seafood demand due to HABs. USA = $38 million: EU = $147 million.

3. Recreation/tourism losses were calculated from theoretical lost revenues at coastal hotels and restaurants and from decreased recreational activities, including recreational fishing. USA = $4 million: EU = $637 million.
4. Monitoring/management costs include expenditures to detect HAB species/toxins and prevention or mitigation efforts of HABs, but they do not include government-sponsored HAB-related research. USA = $3 million: EU = $18 million.

The public health and monitoring/management costs between the USA and EU are directly comparable. The higher costs in the USA for public health are related to high numbers of a particular poisoning event (ciguatera fish poisoning) prevalent in tropical locations, and the lower costs for monitoring are likely a result of a lack of information from various state governments about current, if any, monitoring efforts. The EU figures for commercial fishing and recreation are true determinations of changes in value, i.e., surpluses, versus the crude impact estimates for the USA, and hence, are probably more accurate estimates over the conservative estimates of US impacts. These US estimates should be considered conservative due to a number of factors, namely: (1) only large, well-documented events that occurred during the years studied were included in the analysis, (2) only direct measures of lost gross revenues and/or expenditures could be calculated, i.e., the lack of detailed knowledge of local market structures and market interactions prohibited the inclusion of economic multipliers, and (3) many non-market costs were not included.

Economic impact studies are not suitable instruments upon which to base management decisions in response to HAB events. These studies, however, do have benefits. They determine a sense of scale toward developing appropriate levels of responses for prevention, mitigation, and control of HABs. Employing "welfare economics" in which the estimated benefits of employing mitigating actions are juxtaposed to the estimated damages of HAB, the appropriate level of response can be calculated to minimize the *total cost* of a HAB event [31]. Secondly, these types of analyses can identify relevant markets and locations where economic losses could occur when potential events

happen. Lastly, the analyses clearly point to needs for more careful and standardized documentation of HAB events. Such information as the duration of a bloom, the size of affected areas (either in terms of acreage or shoreline length), toxicity level(s), and the value of affected resources and consequential or lost expenditures need to be evaluated on a per-event basis at local and regional levels to allow for more comprehensive and accurate assessments [24]. Two recent studies, as examples, have been published that examined the effects of "red tides" on beachfront restaurants and hotels in particular areas of Florida (FL). When red tide conditions were present, three restaurants in southwestern FL experienced a 13.7–15.3% reduction in daily sales [37], and two small communities in northwestern FL recorded a 29–35% loss in restaurant and lodging revenues [35]. Much more research is warranted to tease apart true lost expenditures from redirected expenditures (e.g., absolute cancelations of dinners or vacations at the beach versus ones at alternate locations). It will also be important to determine and compare different impacts at the local versus state versus regional levels. Additionally, HABs can have effects to society that may or may not have direct economic components, e.g., worries over seafood safety could lead to decreased confidence in consuming seafood products that will affect relevant markets and public health, coastlines populated with dead fish or rotting seaweed could change the ways and places in which people recreate, and the closure of fisheries could lead to an erosion of community identities that are based on oceanic or coastal ways of life, particularly among native cultures that rely on these resources for subsistence and traditional communal harvesting.

Fisheries

World fisheries play an important role in the diet and thus the human health of the world population. A significant portion of the protein in the diet of the world population comes from the fishery products harvested from the world's oceans which cover approximately 70% of the earth's surface. Currently, the harvest has stabilized at approximately 100 million metric tons. Approximately 9% of the world's fisheries are under exploited, 44% are fully exploited, 16% are overexploited, 6% are depleted, and approximately 3% are recovering. It is recognized that there is an overcapacity to harvest these fishery products primarily because of the increased use of more powerful vessels and the use of electronics used to locate fisheries products. Most of the fishery products are harvested on the continental shelf of the continents. In an effort to meet the world demand for protein and increase fishery production aquaculture is developing and now produces an additional 40 million metric tons of product. Because these products are produced and harvested in close proximity to the world's population centers, they are affected by the activities conducted on land. These include run off which is responsible for large dead zones each year such as the dead zone which occurs in the Gulf of Mexico annually and can encompass approximately 7,000 square miles of the Gulf which impacts the health of the fisheries of the Gulf. The runoff is not only responsible for the large dead zones, run off also carries bacterial contaminates and organic contaminates such as antibiotics and emerging environmental contaminants which can be introduced into the human food chain via fishery products. Other impacts caused by humankind activity include the red tides which impact fisheries and human health and the occurrence of such things as methyl mercury in fish populations due to accumulation in higher order fisheries which are consumed by humans. A new threat is the possible accumulation of radiation in fishery products due to the escapement of radioactive seawater from the damaged power plants on the coast of Japan.

Tourism

Tourism is loosely defined as personal or business travel of 100 miles or more and staying away from your home a minimum of one night and maximum of 100 nights. When one looks at the tourism network, it is a complex system of different industry groups that are symbiotically connected socially, culturally, and economically. Tourism exists in large sophisticated cities and small underdeveloped countries. Tourism has specialized markets that are defined by special interests of travelers that include heritage, adventure, medical to extremes of dark tourism to sites associated with suffering and death to sex tourism. It is at the same time called the world's largest industry and the world's largest service sector industry. Because of the overlapping nature of

tourism expenditures from various modes of travel, shopping across sectors, lodging accommodations, exchange rates, currency fluctuations, the data from one source can rarely be replicated. But there is no doubt that tourism is pervasive globally and growing each year. It has both positive and negative impacts socially, culturally, environmentally, and economically.

Of all tourist attractions those connected to the oceans, seas, and coastal shorelines are the most rapidly growing destinations in international tourism (1998 Year of the Ocean, Coastal Tourism and Recreation). The nature of many such destinations is disproportionate seasonal increases in population in relatively small geographic areas resulting in overcrowding, infrastructure overloads unable to handle capacity from highways, and traffic to a variety of forms of pollution with the most critical being waste management. Water pollution negatively impacts those swimming, diving, boating and eating seafood, and other products exposed to the polluted water. Human health concerns include gastrointestinal diseases and respiratory problems; however, the sea life is also subject to health impacts from toxins, habitat changes, noise, entanglements, and so on. The types of destinations included in this category are traditional beaches, diving, recreational fishing, and natural habitats such as dunes to an entirely anthropogenic cruise industry. Over the past 5 years, the cruise industry has been the fastest growing sector of the tourism industry. The growth is not only in demand from travelers but also an increasing number of destinations that want to be included on the cruise itinerary.

The economic impact of tourism is great for many destinations, as has been expressed in earlier chapters, but the concept of tourism as a "clean" industry is being eroded as the beaches, coral reefs, dunes, and other attractive features of water-based destinations are being worn down and damaged. Just as natural landscapes and fauna are negatively impacted, the local culture, also a part of the destination's attractiveness, is being lost or diluted by a high influx of visitors and seasonal workers, a new economy, new cultural mores and lifestyle and health influences. The sustainability of coastal and other water-based destinations is increasingly a concern for local hosts, the marine industry, and environmentalist.

Tourism must be viewed not only in the context of negative impacts but also the positive impacts that come from contributing over half of the economic value of the ocean economy. This supports employment, research, and maintenance of the ocean as a viable industry.

Recommendations – Three Ps

Partnerships: While there is a tendency to continually grow destinations, sustainability of the environment from the ocean floor to land-based coastal developments, communities must carefully plan for new developments with sustainability of the natural environment at the forefront. Often sustainability practices come from oversight by public agencies which, incidentally, have not yet emerged for tourism. Increasingly, there are calls for integration of plans among impacted groups forming partnerships with tourism planning boards and ocean/coastal specialists such as marine biologists.

Public awareness: There have been public awareness campaigns on environmental issues such as littering, recycling, green practices and isolated media coverage on the plight of the nesting loggerhead turtles, the environmental impacts of oil spills, and health issues related to cruise ships, but there is not a broad-based understanding of responsible human behaviors in marine and coastal environments and the interactions between economic and ecological systems. Coral reefs provide an excellent example of a natural resource that is a major destination attraction and is being destroyed by irresponsible swimmers, divers, and boaters. Increase public awareness of easily corrected malpractices can add years to this natural treasure.

Policies: It is necessary to provide policies and procedures for human interaction with natural resources to achieve sustainability. Policies require management and enforcement to be effective. Certain practices, behaviors, and activities have been passed down through generations of abusers who were not aware of the negative environmental, economic, and social impacts they were causing. Today, action groups from a variety of arenas, such as the green movement, have increased awareness of harmful practices and the scope of their impacts. Accordingly, the tourism industry has

directly experienced both negative impacts of ignorance and/or ignoring and the positive benefits of environmental responsibility.

As the tourism industry continues to grow and natural attractions grow in their appeal, all tourism destinations must inventory their tourism assets and be proactive in protecting them while maximizing the benefits to the local population.

Bibliography

1. USCOP (2004) An ocean blueprint for the 21st century: Final report. U.S. Commission on Ocean Policy, Washington, DC. ISBN #0-9759462-0-X
2. U.S. Census Bureau (2010) Preliminary vintage 2010 population estimates and 2010 census counts. http://www.census.gov/popest/eval-estimates/eval-est2010.html
3. Wilson SG, Fischette TR (2010) Coastline population trends in the United States: 1960 to 2008. US Census Bureau, Washington, DC, pp 25–1139
4. Johnston CP, Qiu H, Ticehurst JR, Dickson C, Rosenbaum P, Lawson P, Stokes AB, Lowenstein CJ, Kaminsky M, Cosgrove SE, Green KY, Perl TM (2007) Outbreak management and implications of a nosocomial Norovirus outbreak. Clin Infect Dis 45:534–540
5. Bergmann W, Feeney RJ (1950) The isolation of a new thymine pentoside from sponges. J Am Chem Soc 72:2809–2810
6. Meujo DAF, Hamann MT (2012) Science, policy, and risk management: the case of seafood safety. In: Mayers RA (ed) Environmental toxicology. Encyclopedia of sustainability science and technology. Springer, ISBN 978-1-4419-0851-3
7. Mayer AMS, Rodriguez AD, Berlink RGS, Hamann MT (2009) Marine pharmacology in 2005–2006: marine compounds with anthelmintic, antibacterial, anticoagulant, antifungal, anti-inflammatory, antimalarial, antiplatelet, antiprotozoal, antituberculosis, and antiviral activities; affecting the cardiovascular, immune and nervous systems, and other miscellaneous mechanisms of action. Biochim Biophys Acta 1790:283–308
8. Waters AL, Hill RT, Place AR, Hamann MT (2010) The expanding role of marine microbes in pharmaceutical development. Curr Opin Biotechnol 21(6):780–786
9. Kochanowska-Karamyan AJ, Hamann MT (2010) Marine indole alkaloids: potential new drug leads for depression and anxiety. Chem Rev 110:4489–4497
10. FAO (2005–2011) World inventory of fisheries. Contribution of aquaculture to food security. Issues fact sheets. Text by Rohana Subasinghe. FAO Fisheries and Aquaculture Department [online], Rome. Updated 27 May 2005. [Cited 17 May 2011]
11. Badgley C, Moghtader J, Quintero E, Zakem E, Chappell MJ, Aviles-Vazquez K, Samulon A, Perfecto I (2007) Organic agriculture and the global food supply. Renew Agri Food Syst 22:86–108
12. FAO (Food & Agriculture Organization of the United Nations) (2010) The state of world fisheries and aquaculture (SOFIA). FAO, Rome
13. Duarte CM, Marbá N, Holmer M (2007) Rapid domestication of marine species. Science 316:382–383
14. Chamberlain GW (2010) History of shrimp farming. In: Alday-Sanz V (ed) The shrimp book. Nottingham University Press, Nottingham, pp 1–34
15. Wyban J (2009) World shrimp farming revolution: industry impact of domestication, breeding and widespread use of specific pathogen free *Penaeus vannamei*. In: Browdy CL, Jory DE (eds) The rising tide, proceedings of the special session on sustainable shrimp farming, World Aquaculture 2009. The World Aquaculture Society, Baton Rouge, pp 12–21
16. Sachs JD (2007) The promise of the blue revolution. Sci Am 297:37–38
17. Jolly CM, Umali-Maceina G, Hishamunda N (2009) Small-scale aquaculture: a fantasy or economic opportunity. In: Bondad-Reantaso MG, Prein M (eds) Measuring the contribution of small-scale aquaculture: an assessment. FAO Fisheries and Aquaculture Technical Paper No. 534. FAO, Rome, pp 73–86
18. Kongkeo H, Davy FB (2009) Backyard hatcheries and small scale shrimp and prawn farming in Thailand. In: De Silva SS, Davy FB (eds) Success stories in Asian aquaculture. Springer, London, pp 67–83
19. Wattage P (2009) Millenium development goals and aquaculture: indicators to evaluate the conservation of the resource base for poverty reduction. In: Bondad-Reantaso MG, Prein M (eds) Measuring the contribution of small-scale aquaculture: an assessment. FAO Fisheries and Aquaculture Technical Paper No. 534. FAO, Rome, pp 59–72
20. Subasinghe R, Soto D, Jia J (2009) Global aquaculture and its role in sustainable development. Rev Aquac 1:2–9
21. Jerardo A (2004) The U.S. Ag trade balance. . . more than just a number. Amber Waves 2:36–41
22. Agricultural Statistics (2010) Chapter XV. United States Department of Agriculture National Agricultural Statistics Service. United States Government Printing Office, Washington
23. Current Fisheries Statistics (2011) NO. 2010–2 Imports and exports of fishery products annual summary, 2010. Fishery Statistics Division. NOAA Fisheries Office of Science & Technology, Silver Spring
24. Anderson DM, Hoagland P, Kaoru Y, White AW (2000) Estimated annual economic impacts from harmful algal blooms (HABs) in the United States. WHOI-2000–11. Department of Biology, Woods Hole Oceanographic Institution, Woods Hole. http://www.whoi.edu/fileserver.do?id=24159&pt=10&p=19132
25. Hallegraeff GM (1993) A review of harmful algal blooms and their apparent global increase. Phycologia 32:79–99

26. Anderson DM (1989) Toxic algal blooms and red tides: a global perspective. In: Okaichi T, Anderson D, Nemoto T (eds) Red tides: biology, environmental science, and toxicology. Elsevier, New York, pp 11–16
27. Cesar H, van Beukering P, Pintz S, Dierking J (2002) Economic valuation of the coral reefs of Hawaii: final report. Hawaii Coral Reef Initiative Research Program. University of Hawaii, Honolulu
28. Fishwatch – US Seafood Facts (2010) National oceanic and atmospheric administration, national marine fisheries service [Cited 22 May 2011]. http://www.nmfs.noaa.gov/fishwatch/trade_and_aquaculture.htm
29. Anderson DM, Glibert PM, Burkholder JM (2002) Harmful algal blooms and eutrophication: nutrient sources, composition, and consequences. Estuaries 25(4): 704–726
30. Dyson K, Huppert DD (2010) Regional economic impacts of razor clam beach closures due to harmful algal blooms (HABs) on the Pacific coast of Washington. Harmful Algae 9(3):264–271
31. Hoagland P, Scatasta S (2006) The economic effects of harmful algal blooms. In: Graneli E, Turner J (eds) Ecology of harmful algae. Springer, Dordrecht, pp 391–401
32. Hoagland P, Anderson DM, Kaoru Y, White AW (2002) The economic effects of harmful algal blooms in the United States: estimates, assessment issues, and information needs. Estuaries 25(4b):819–837
33. Jin D, Thunberg E, Hoagland P (2008) Economic impacts of the 2005 red tide event on commercial shellfisheries in New England. Ocean Coast Manag 51(5):420–429
34. Lavergne DR (1997) Estimated economic impact to the Louisiana oyster harvester due to red tide. Mimeo. Louisiana Department of Wildlife and Fisheries, Baton Rouge
35. Larkin SL, Adams CM (2007) Harmful algal blooms and coastal business: economic consequences in Florida. Soc Nat Resour 20(9):849–859
36. Lipton DW (1999) *Pfiesteria*'s economic impact on seafood industry and recreational fishing. In: Proceedings of the conference "economics of policy options for nutrient management and *Pfiesteria*." Center for Agricultural and Natural Resource Policy, University of Maryland, College Park, pp 35–38, 16 Nov 1998
37. Morgan KL, Larkin SL, Adams CM (2009) Firm-level economic effects of HABS: a tool for business loss assessment. Harmful Algae 8(2):212–218
38. Smayda TJ (1990) Novel and nuisance phytoplankton blooms in the sea: evidence for a global epidemic. In: Graneli E et al (eds) Toxic marine phytoplankton. Elsevier, New York, pp 213–228
39. Hoagland P, Jin D, Polansky LY, Kirkpatrick B, Kirkpatrick G, Fleming LE, Reich A, Watkins SM, Ullmann SG, Backer LC (2009) The costs of respiratory illnesses arising from Florida gulf coast *Karenia brevis* blooms. Environ Health Perspect 117(8):1239–1243

Offshore Wind Energy Technology Trends, Challenges, and Risks

James F. Manwell
Department of Mechanical and Industrial Engineering, University of Massachusetts, Amherst, MA, USA

Article Outline

Glossary
Definition of the Subject and Its Importance
Introduction
Offshore Wind Resource
External Design Conditions
Wind Turbine Aerodynamics
Wind Turbine Mechanics and Dynamics
Components of Offshore Wind Turbines
Offshore Wind Plant Electrical System
Design of Offshore Wind Plants
Installation
Environmental Aspects and Permitting
Economics
Future Directions
Bibliography

Glossary

Blade The part of a wind turbine rotor which produces mechanical forces through the action of the wind.

Cut-in wind speed Lowest wind speed at hub height at which the wind turbine starts to produce power.

Cut-out wind speed Highest wind speed at hub height at which the wind turbine is designed to produce power.

External conditions Factors affecting the design and operation of an offshore wind turbine, including the environmental conditions, other climatic factors, and the electrical network conditions.

Foundation The part of an offshore wind turbine support structure which transfers the loads acting on the structure into the seabed.

Gearbox The part of a wind turbine which converts rotational mechanical power at one speed to comparable power at a higher speed.

Nacelle The housing which contains the drive-train and other elements on top of a horizontal axis wind turbine tower.

Offshore wind turbine A wind turbine whose support structure is subject to hydrodynamic loading.

Rated wind speed Minimum wind speed at hub height at which a wind turbine's rated power is achieved.

Rotor The part of a wind turbine which converts the kinetic energy of the wind into rotational mechanical energy.

Rotor–nacelle assembly (RNA) The part of the offshore wind turbine that includes the rotor and the nacelle.

Sea state Condition of the sea in which its statistics remain stationary.

Seabed Soil below the seafloor in which a support structure is founded.

Sub-structure The part of an offshore wind turbine support structure which extends upward from the seabed and connects the foundation to the tower.

Support structure The part of an offshore wind turbine which consists of the tower, sub-structure, and foundation.

Tower The part of an offshore wind turbine support structure which connects the sub-structure to the rotor–nacelle assembly.

Wind turbine A device for converting the kinetic energy in the wind into a mechanically useful form, normally electricity.

Definition of the Subject and Its Importance

Offshore wind energy is one of the newest large-scale, renewable energy technologies. It also appears to hold significant potential for increasingly greater use. As compared to onshore utility-scale wind farm development, offshore wind energy has the following promising attributes:

- Generally higher wind speeds compared to onshore sites.
- Lower intrinsic turbulence intensities.
- Lower wind shear.
- Ability to utilize larger turbine designs.
- Greater area available for siting large projects.
- Proximity to cities and load centers.
- Potential for lower environmental impacts.

At the same time this technology faces some significant engineering challenges, namely:

- Higher project costs due to specialized installation and service vessels and equipment and more expensive support structures.
- More difficult environmental and working conditions.
- More difficult and expensive installation procedures.
- Decreased availability due to limited accessibility for maintenance.
- Necessity for special corrosion prevention measures.

Offshore wind energy consists of the use of offshore wind turbines, deployed in groups or "wind farms," which convert the energy in the winds offshore shore to electricity. That electricity is transmitted to shore via submarine cables where the electricity is introduced into conventional transmission systems for delivery to land-based end users. The accepted formal definition of an offshore wind turbine [1] is "a wind turbine with a support structure which is subject to hydrodynamic loading." A typical offshore wind turbine is illustrated in Fig. 1.

The main components of an offshore wind turbine are the following:

- Rotor–nacelle assembly (RNA) – This is the part of a wind turbine which is carried by the support structure. It includes:
  - Rotor, which is part of a wind turbine consisting of the blades and hub.
  - Nacelle assembly, which consists of all the components above the tower that are not part of the rotor. These include the drive train (shafts, couplings, gearbox, generator(s), and brakes), bed plate, yaw system, and the nacelle enclosure.
- Support structure – This consists of the tower, sub-structure, and foundation:
  - Tower – This is the part of the support structure which connects the sub-structure to the rotor–nacelle assembly.
  - Sub-structure – This part of the support structure extends upward from the seabed and connects the foundation to the tower (typically at a transition piece).
  - Foundation – This is the part of the support structure which transfers the loads acting on the structure into the seabed.

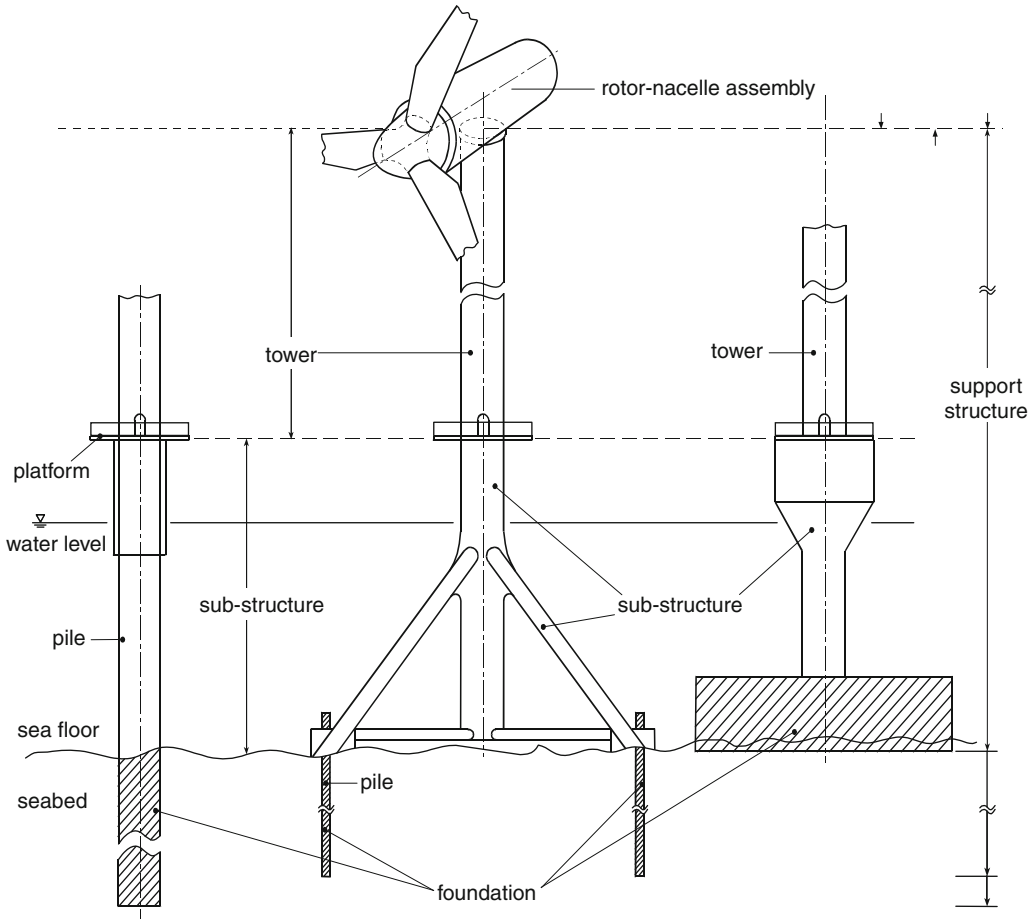

Offshore Wind Energy Technology Trends, Challenges, and Risks. Figure 1
Components of an offshore wind turbine (Reproduced by permission of Germanischer Lloyd [2])

As of the present time all commercial offshore wind turbines are supported by the seabed. There are some floating offshore wind turbine concepts which are being investigated, and it is anticipated that in the foreseeable future a number of commercial floating offshore wind turbines will be used. A floating offshore wind turbine may be defined as an offshore wind turbine whose sub-structure is vertically supported by the buoyancy of the structure itself and for which the horizontal forces induced by the wind, waves, and current are resisted by mooring lines and anchors.

Introduction

Although offshore wind energy for bulk supply of electricity is a relatively new technology, the historical precedents for it go back a long way. As will become apparent, offshore wind energy has resulted fundamentally from a marriage of modern wind turbines with offshore structures, particularly the technology developed by the offshore oil and gas industry.

Modern wind turbines have a particularly long history. They are descendents of mechanical windmills which first appeared in Persia as early as the seventh century [3] and then re-appeared in northern Europe in the Middle Ages. They were considerably developed during the eighteenth and nineteenth centuries and then formed the basis for the first electricity-generating wind turbine in the late nineteenth century. Development continued sporadically through the mid-twentieth century, with modern turbines beginning to emerge in the 1970s. It was the introduction of

other technologies, such as electronics, computers, control theory, composite materials, and computer-based simulation capability, that led to the successful development of the large-scale, autonomously operating wind turbines that have become so widely deployed on land over the past 20 years.

As wind turbine generators were evolving, the idea of using the wind turbines in the water was also developing. As early as 1893, Fridtjof Nansen employed a wind turbine on his ship *Fram* in his attempt to reach the North Pole [4]. In the 1930s, Hermann Honnef [5] in Germany proposed an anchored offshore pontoon platform supporting a wind turbine using two rotors (Fig. 2). In the 1950s, Ulrich Hütter, also of Germany, installed a relatively small turbine on an offshore platform [6]. The vision for large-scale offshore wind farms is credited to William Heronemus from the University of Massachusetts [7] who in the early 1970s proposed large arrays of floating wind turbines (see Fig. 3). In his case, the idea was to produce electricity but then utilize that electricity to electrolyze water into hydrogen for use as a fuel.

Ocean engineering has a long history as well. It originally arose from the need to provide ports, harbors, light houses, and similar structures for use by ships. The building of such structures began well before the era of ancient Rome [8]. What is thought of today as ocean engineering is much more recent, however, and it developed in parallel with the widespread use of petroleum [9]. The first offshore oil platform was built in 1887 off the coast of California in a few meters of water. In 1910, an oil well was drilled in Ferry Lake, Louisiana, and in 1929, the first international oil well was drilled in Lake Maricaibo, Venezuela. By 1959, the industry developed enough to install a 30-m deep platform in Grand Isle, Louisiana. This platform was installed by Shell. Offshore oil explorations in the Persian Gulf and the North Sea started in 1960, and by the 1970s, the technology began to develop rapidly, with structures in much deeper waters. As of the early 1970s, the deepest water in which structures were built was approximately 100 m. By 1993, a structure had been installed in water more than 870 m deep. The types of structures developed for these applications – jackets, spars, tension leg platforms – are among those that are being utilized or considered for use offshore wind turbines in deeper water.

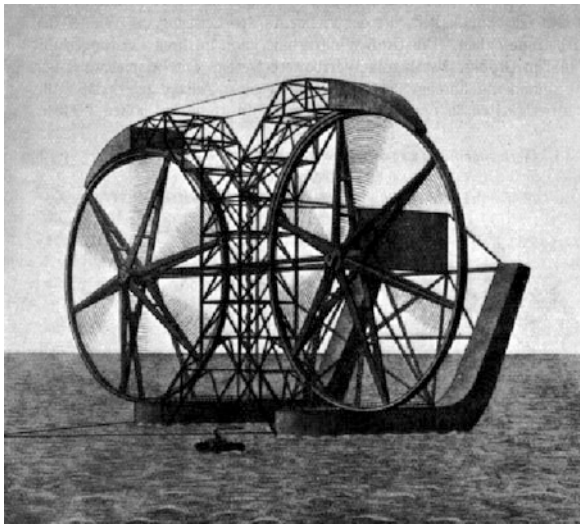

Offshore Wind Energy Technology Trends, Challenges, and Risks. Figure 2
W. Honnef's concept of an offshore wind turbine, 1932

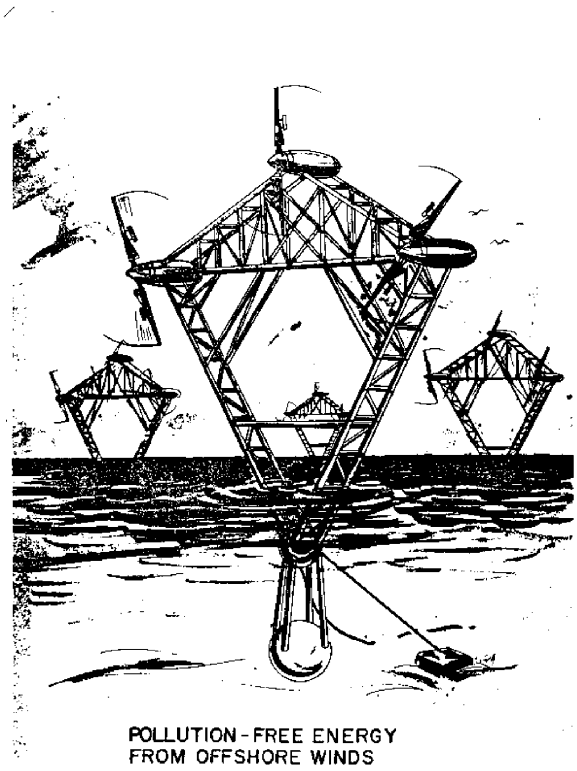

Offshore Wind Energy Technology Trends, Challenges, and Risks. Figure 3
W. Heronemus' concept for offshore wind turbines, 1973

In spite of the early visions of offshore wind turbines for generating electricity for use on land, none of them were actually built until the 1990s. The fundamental reason for this is that wind turbines of sufficient generating capacity and reliability were not yet available. By the early 1990s, that situation had changed. The first offshore wind farm was built in 1991 in relatively shallow water (2–5 m) off the coast of Denmark at Vindeby. This offshore wind farm, which is still operating, consists of eleven 450-kW machines approximately 3 km from the shore. In 2002 and 2003, the initial utility-scale (capacities exceeding 100 MW) offshore wind farms were being installed in Denmark with the first large projects at Horns Rev and Nysted. As of 2009, there were over 2,000 MW of offshore wind turbines installed in Europe (where the majority of offshore turbines are located). The European Union has also set a goal to have installed 150,000 MW offshore wind–generating capacity by 2030. This amount of generation would provide approximately 15% of Europe's electricity [10].

Offshore Wind Resource

The wind is the most important external factor in offshore wind energy. It can be thought of as the "fuel" of the wind turbine, even though it is not consumed in the process. The wind determines the amount of energy that is produced and is, therefore, referred to as the resource. One of the most significant characteristics of winds offshore is that they are generally significantly higher on average than are the winds on land. Average wind speeds generally increase with distance from shore as well. A typical situation is illustrated in Fig. 4. Additional maps showing the offshore wind resource in the United States may be found in [10].

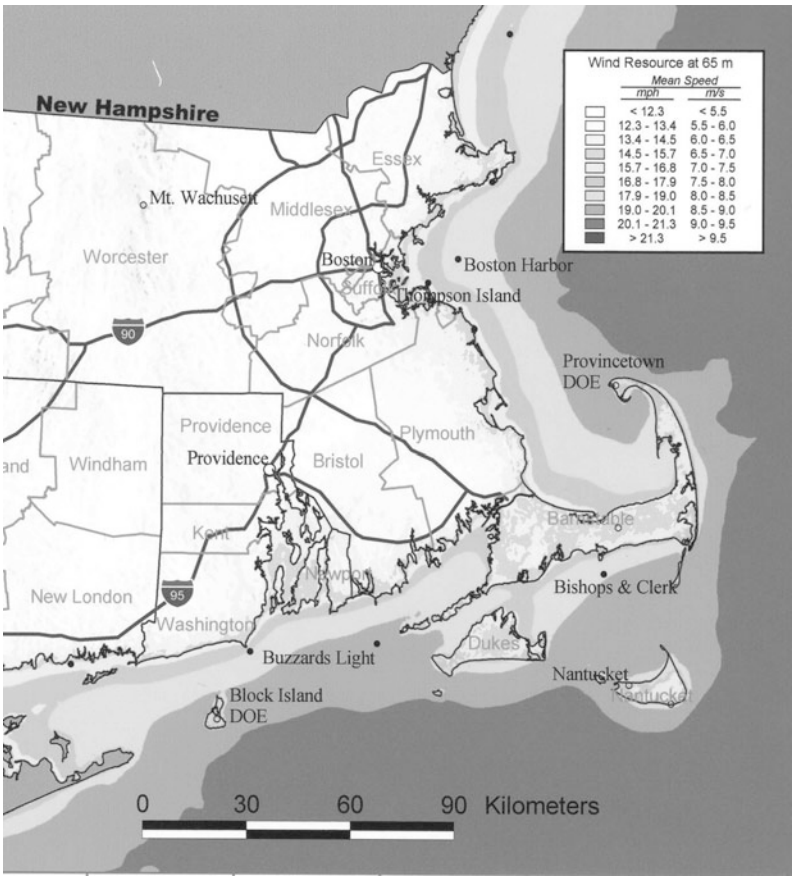

Offshore Wind Energy Technology Trends, Challenges, and Risks. Figure 4
Wind resource off the coast of Massachusetts (Massachusetts Technology Collaborative)

This section summarizes the basic characteristics of the wind in so far as they relate to wind turbine power production. Much more detail on this topic is provided in [11]. The wind will also affect the design of the wind turbines, and for this purpose it is referred to as an "external design condition." This aspect of the wind is discussed in more detail in a later section.

Origin of the Wind

The wind originates from sunlight due to the differential heating of various parts of the earth. This differential heating produces zones of high and low pressure, resulting in air movement. The motion of the air is also affected by earth's rotation. Considerations regarding the wind insofar as it relates to offshore wind turbine operation include the following: (1) the winds aloft (geostrophic wind), (2) atmospheric boundary layer meteorology, (3) the variation of wind speed with height, (4) surface roughness, and (5) turbulence.

The geostrophic wind is the wind in the upper atmosphere which results from the combined effects of the pressure gradient and the earth's rotation (via the Coriolis force). The gradient wind can be thought of as an extension of the geostrophic wind, the difference in this case being that centrifugal effects are included. These result from curved isobars (lines of constant pressure) in the atmosphere. It is these upper atmosphere winds that are the source of most of the energy that eventually impinges on wind turbines. The energy in the upper atmosphere is transferred down closer to the surface via a variety of mechanisms, most notably turbulence, which is generated mechanically (via surface roughness) and thermally (via the rising of warm air and falling of cooler air).

Although driven by higher-altitude winds, the wind near the surface is affected by the surrounding topography and surface conditions. For offshore locations, the topography in the immediate vicinity is usually flat or nearly flat. Nonetheless, the presence of complex terrain (such as mountain ranges) on land, even if at some distance, can have an effect on the wind. Regardless of the effect of topography, surface roughness can also significantly affect the wind. Most obviously, the sea surface will change due to wind-generated waves. In addition, different surface roughness on nearby land can affect the wind over the water, especially when it blows from that direction.

Variability of the Wind

One of the singular characteristics of the wind is its variability, both temporal and spatial. The temporal variability includes: (1) short term (gusts and turbulence), (2) moderately short term (e.g., hour to hour means), (3) diurnal (variations over a day), (4) seasonal, and (5) inter-annual (year to year). The wind may vary spatially as well, both from one location to another or with height above the ground.

Figure 5 illustrates the variability of the hourly average wind speeds for 1 year for an offshore location.

As can be seen, the wind in this example varies significantly over the year, ranging from zero to nearly 30 m/s.

Figure 6 illustrates wind speed at an offshore location recorded twice per second over a 23-h period. There is significant variability here as well. Much of this variability in this figure is associated with short-term fluctuations, or turbulence. Turbulence has some effect on power generation, but has a more significant effect on the design of wind turbines, due to the material fatigue that it tends to engender. Turbulence is discussed in more detail in a later section.

In spite of the variability in the wind time series, summary characteristics have much less variability. For example, the annual mean wind speed at a given location is generally within +/− 10% of the long-term mean at that site. Furthermore, the distribution of wind speeds, that is to say the frequency of occurrence of winds in various wind speed ranges, also tends to be similar from year. The general shape of such distributions is also similar from one location to another, even if the means are different. In fact, statistical models such as the Weibull distribution can be used to model the occurrences of various wind speeds in most locations on the earth. For example, the number of occurrences of wind speed in various ranges from the data set illustrated in Fig. 5 are shown in Fig. 7, together with those occurrences as modeled by the Weibull distribution.

The Weibull distribution's probability density function is given by:

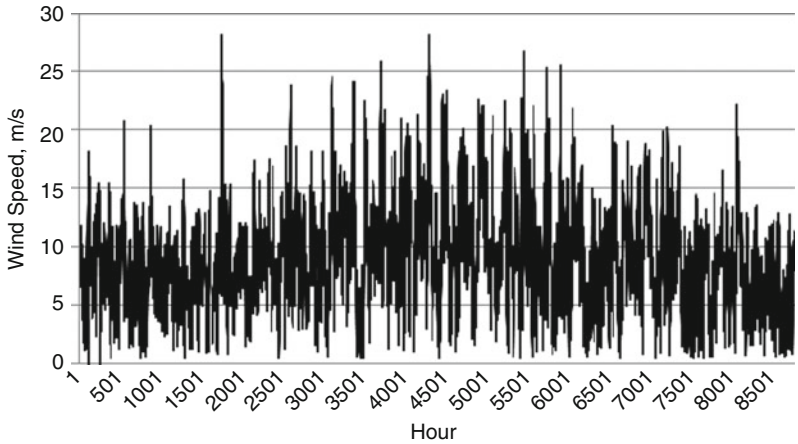

Offshore Wind Energy Technology Trends, Challenges, and Risks. Figure 5
Typical hourly wind speeds over a year

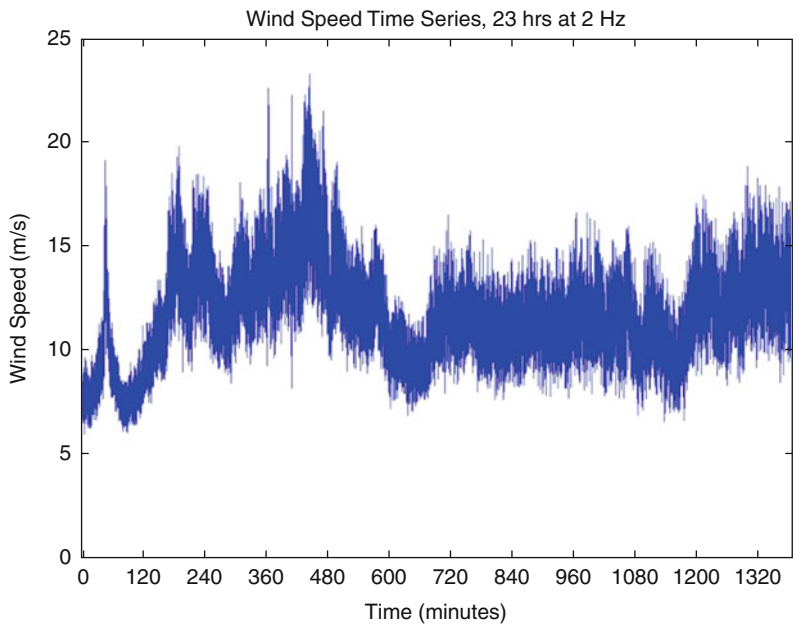

Offshore Wind Energy Technology Trends, Challenges, and Risks. Figure 6
Typical offshore wind data, sampled at 2 Hz for a 23-h period

$$p(U) = \left(\frac{k}{c}\right)\left(\frac{U}{c}\right)^{k-1} \exp\left[-\left(\frac{U}{c}\right)^{k}\right]$$

where c = Weibull scale factor and k = Weibull shape factor.

For the purposes of modeling the occurrences of wind speeds, the scale and shape factors may be approximated as follows:

$$k \approx \left(\frac{\sigma_U}{\bar{U}}\right)^{-1.086}$$

$$c \approx \bar{U}(0.568 + 0.433/k)^{-(1/k)}$$

where $\bar{U}$ is the long-term mean wind speed (based on 10-min or hourly averages) and σ_U is the standard

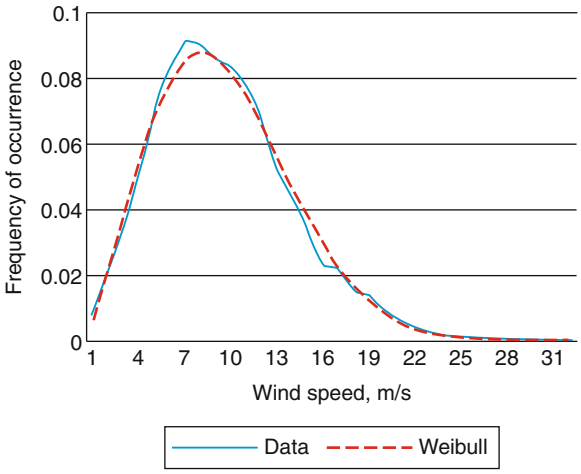

Offshore Wind Energy Technology Trends, Challenges, and Risks. Figure 7
Typical frequency of occurrence of wind speeds, based on data and statistical model

deviation of the wind speed, based on the same 10-min or hourly averages.

Power in the Wind

The power available in the wind can be predicted from the fundamental principles of fluid mechanics. First of all, the energy per unit mass of a particle of air is given simply by one half times the square of the velocity, U (m/s). The mass flow rate of the air through a given area, A (m^2), perpendicular to the direction of the wind is $\dot{m} = \rho AU$ where ρ is the density of the air (kg/m^3). The power in the wind per unit area, P/A, (W/m^2) is then:

$$P/A = (\dot{m}/A)\frac{1}{2}U^2 = \frac{1}{2}\rho U^3$$

Wind Shear

Wind shear is the variation of wind speed with height. Wind shear has relevance both to power generation and to turbine design. The variation of wind speed with height offshore is typically modeled with a log law as follows:

$$U_2 = U_1\left[\frac{\ln(h_2/z_0)}{\ln(h_1/z_0)}\right]$$

where U_1 = speed at reference height h_1, U_2 is the wind speed to be estimated at height h_2, and z_0 is the roughness length. Roughness lengths offshore range from approximately 0.2 mm for a flat sea to 0.5 mm or more when the waves are present. Methods have been developed to estimate surface roughness, given significant wave height and wave length, but they are outside the scope of this essay.

Wind shear can also be affected by the stability of the atmosphere. Equations have been developed which allow the incorporation of stability parameters in the analysis, but these too are outside the scope of this essay.

Land/Sea Breezes

Land and sea breezes can sometimes be significant contributors to the offshore wind resource at certain locations. These breezes arise as a result of the different heat capacities and thermal conductivities of land and water. During the day, solar heating of the ground results in warm air rising. Cooler air over the ocean flows in, resulting in an onshore breeze. At night, the ground cools off more quickly than the sea. Warmer air above the sea rises, and air from the land flows out, resulting in an offshore breeze.

Offshore Wind Data Collection

Wind data is gathered offshore by a variety of methods [12]. Some data are already available from National Oceanographic and Atmospheric Administration (NOAA) buoys, the voluntary observation ship program (VOS), the Comprehensive Ocean Atmospheric Data Set (COADS), and hindcast estimates from a variety of sources. These data sets may have limited utility, and on-site measurements are always preferable. The approach that is presently preferred for wind energy applications is to install an offshore platform and tower and then to place conventional anemometry on the tower at multiple heights. Such structures are quite expensive, however, and remote sensing instrumentation such as SODAR and LIDAR are being actively developed to serve as alternatives to tower mounted anemometry.

External Design Conditions

There are many phenomena in the external environment which need to be considered in the design of an offshore wind turbine. These are called "external design

conditions." The most important of these are the wind itself, ocean waves, and sub-sea soil properties. In addition, currents, floating ice, and salinity among others, may also be significant to the design.

Wind as Design Condition

As discussed previously, the wind is of particular interest in offshore wind turbine applications since it is the source of the energy. It is also the source of significant structural loads which the turbine must be able to withstand. Some of these loads occur when the turbine is operating; others occur when it is stopped. Extreme winds, for example, are likely to affect a turbine when it is stopped. High winds with sudden directional change during operation can also induce high loads. Turbulence during normal operation results in fatigue. Wind and waves when occurring together can have significant combined effects. The following is a summary of the key aspects of the wind which affect the design of wind turbines. More details may be found in [11].

Offshore Turbulence Turbulence in the wind can have significant effect on the structure of a wind turbine as well as its operation, and so it must be considered in the design process. Turbulence refers to the short-term variations in the speed and direction of the wind. It manifests itself as apparently random fluctuations superimposed upon a relatively steady mean flow. Turbulence is not actually random, however. It has some very distinct characteristics, at least in a statistical sense.

Turbulence is characterized by a number of measures. These include: (1) turbulence intensity, (2) turbulence probability density functions (pdf), (3) autocorrelations, (4) integral time scales and length scales, and (5) power spectral density functions.

The turbulence intensity of a turbulent (sampled) wind speed time series u_i is given by:

$$TI = \frac{\sigma_u}{U}$$

where σ_u is the standard deviation, which is given by:

$$\sigma_U = \sqrt{\frac{1}{N_s - 1}\sum_{i=1}^{N_s}(u_i - U)^2}$$

and where U is the mean wind speed, as averaged over a 10-min or 1-h period.

The normal probability density function (pdf) is commonly used for turbulence:

$$p(u) = \frac{1}{\sigma_u\sqrt{2\pi}}\exp\left[-\frac{(u-U)^2}{2\sigma_u^2}\right]$$

where u is a continuous random variable corresponding to the wind speed.

The autocorrelation function of a wind speed time series is found from the following:

$$R(r\,\delta t) = \frac{1}{\sigma_u^2(N-r)}\sum_{i=1}^{N-r}(u_i - U)(u_{i+r} - U)$$

where r = lag number and δt = sample interval between points. The autocorrelation of a turbulent time series normally crosses the x-axis at a lag corresponding to a few minutes and then goes back and forth indefinitely.

The integral time scale, Ti, gives an indication of a characteristic time period associated with the turbulence. It is estimated from the area under the autocorrelation function between a lag of zero and the first zero crossing.

The integral length scale, L, indicates the characteristic size of the turbulent eddies. It is found by multiplying the integral time scale by the mean velocity:

$$L = (Ti)U$$

A number of power spectral density functions are used to model the turbulent wind. One of them is the von Karman spectrum, which is given by:

$$S(f) = \frac{\sigma_u^2\,4\,(L/U)}{\left[1 + 70.8\,(f\,L/U)^2\right]^{5/6}}$$

where $S(f)$ is the psd ((m/s)^2/Hz) and f is frequency (Hz) (note that $L/U = Ti$).

An illustration of the von Karman spectrum and a spectrum based on actual data is shown in Fig. 8.

The intrinsic turbulence offshore is actually relatively low compared to that on shore. However, within large arrays of wind turbines, which are likely to become ever more common offshore, the turbulence level can become quite high.

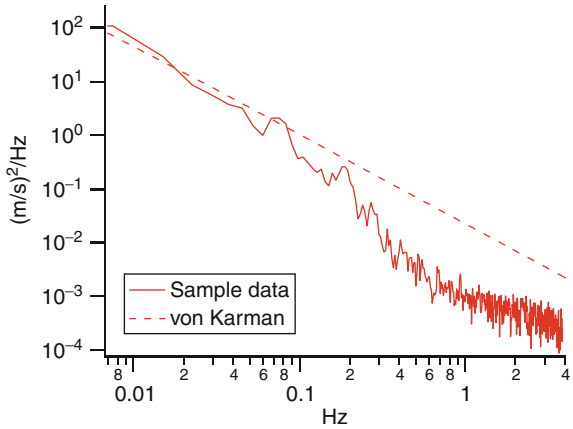

Offshore Wind Energy Technology Trends, Challenges, and Risks. Figure 8
Spectrum of turbulent wind, from data and von Karman equation

Gusts A gust is discrete increase and then decrease in wind speed, possibly associated with a change in wind direction, which can be of significance to the design of a wind turbine. Gusts are typically associated with turbulence.

Extreme Winds Extreme winds need to be considered for the design of a wind turbine. Extreme winds are normally associated with storms. They occur relatively rarely but often enough that the possibility of their occurring cannot be ignored. Statistical models, such as the Gumbel distribution [13], are used to predict the likelihood of such winds occurring at least once every 50 or 100 years. Such intervals are called return periods.

Cyclones/Hurricanes Certain types of weather phenomena can be of particular significance for offshore wind turbines. Among these are cyclones and hurricanes, which can include very high winds as well as waves. In locations where they may occur, their severity and likelihood need to be considered.

Waves

Waves can have significant effect on the design on an offshore wind turbine. The section below provides a summary of ocean waves in so far as they affect wind turbines. More details on waves may be found in [9, 14, 15].

Waves occur in the ocean due primarily to the action of the wind. The higher the wind speed, the longer it blows, and the greater the distance over the sea upon which it acts (fetch), the higher the waves become. As the waves become higher, they begin to break, and at some point a quasi-stable equilibrium is reached. At this point the power imparted from the wind is equal to power dissipated in the breaking waves. Some terminology is helpful at this point. "Sea" describes situation in which waves are being formed. "Sea state" refers to characteristics of the sea in terms of wave height, period, and direction. A "fully developed sea state" is one in which the power in from wind equals the power being dissipated in breaking waves.

Waves can be classified as follows: regular waves, irregular waves, random waves, extreme waves, solitons, and tsunamis. The first four of these will be discussed briefly below. Solitons are large waves that occur in relative isolation, usually in the open ocean. Tsunamis arise from earthquakes. Both of these types of waves are outside the scope of this essay. Some of the various types of waves are illustrated in Fig. 9.

Regular waves are also known as first-order, small-amplitude, or Airy waves. They were first described mathematically by Airy [16]. Airy's model is most applicable to deep water swell, but it forms a useful and elegant starting point for discussion of more complex wave behavior. According to the Airy model (see Fig. 10), a wave can be modeled as a sinusoid.

The Airy wave profile is defined by

$$\zeta = \hat{\zeta}_a \cos(kx - \omega t)$$

where $\hat{\zeta}_a$ is the amplitude of the waves.

The height of the wave, H, is $2\hat{\zeta}_a$

The wave number is given by $k = 2\pi/L$, where L = wave length (m).

The angular frequency is $\omega = 2\pi/T$, where T = wave period (s).

The water particles travel in circular orbits with radius $= \hat{\zeta}\, e^{kz}$, where z is the distance up from mean water level.

The wave crest advances with celerity (speed), c.

The Airy model embodies a number of assumptions. These include:

- Water is a homogeneous and incompressible fluid.
- Surface tension is neglected.

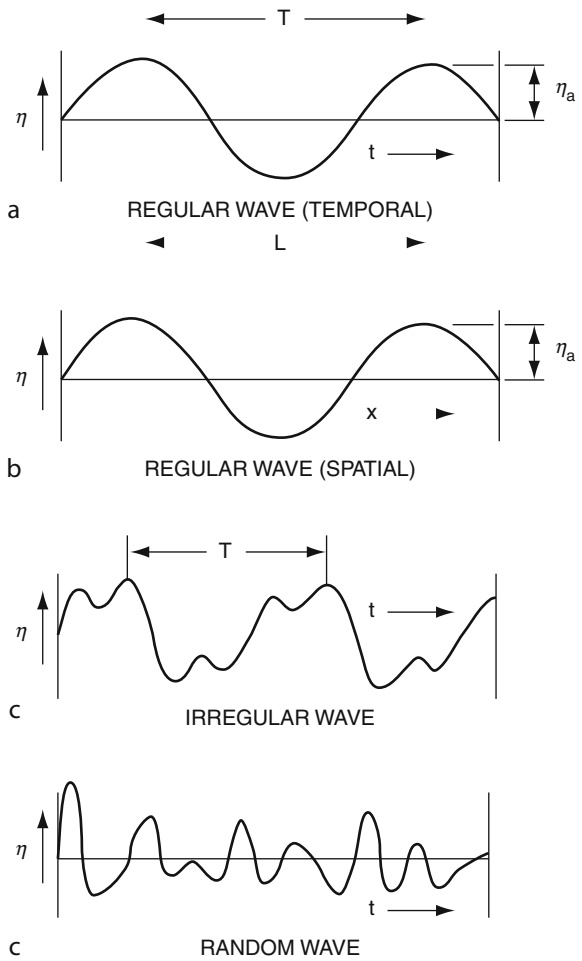

Offshore Wind Energy Technology Trends, Challenges, and Risks. Figure 9
Various types of waves [15]

- Coriolis effects are neglected.
- The pressure at the free surface (air/water interface) is constant.
- Viscosity is neglected.
- Waves do not interact with other water motions.
- The motion is irrotational.
- The velocity at the seabed is zero.
- The wave amplitude is small, and the waveform is invariant in time and space.
- The wave is long-crested (i.e., it is two-dimensional).

The wavelength is related to the wave period and the water depth, d, by the following implicit equation:

$$L = \frac{gT^2}{2\pi}\tanh\left(\frac{2\pi d}{L}\right)$$

The celerity of the wave is defined by $c = L/T$.

Random Waves Irregular waves differ from Airy waves in that there is a mixture of waves of varying heights and varying wave lengths. Non-repeating irregular waves are called "random waves." Random waves are the result of multiple regular or irregular waves from different directions, distances, and sources which all combine. The formation process of random waves is illustrated in Fig. 11. A typical wave train (series of waves) is shown in Fig. 12.

Random waves are characterized by a significant wave height, H_s; a peak period, T_p; or mean period, T_z; and a spectrum. The significant wave height is approximately equal to the average height of the highest one third of the waves, but it is also defined more precisely in terms of the standard deviation or the spectrum (see below). The spectrum, $S(f)$, analogous to that of turbulent wind, provides a measure of the amount of power in waves of varying frequency. In terms of the standard deviation or the spectrum, the significant wave height is given by:

$$H_s = 4\sigma_H = 4\sqrt{\int_0^{H_{\max}} S(f)\,df}$$

where $H_{\max}$ is the highest wave encountered and σ_H is standard deviation of the water height relative to the still water level.

The spectrum most commonly used to model wave heights is known as the Pierson–Moskowitz (PM). It is given by:

$$S_{\mathrm{PM}}(f) = 0.3125 \cdot H_s^2 \cdot f_p^4 \cdot f^{-5} \cdot \exp\left(-1.25\left(\frac{f_p}{f}\right)^4\right)$$

where f_p is the peak frequency and is given by $f_p = 1/T_P$. Note that the peak period may be similar to the mean period, but it is not necessarily equal to it. It is best determined by a spectral analysis of the data. A typical Pierson–Moskowitz spectrum is illustrated in Fig. 13. In this illustration, H_s is equal to 2.25 m and T_p is equal to 7 s.

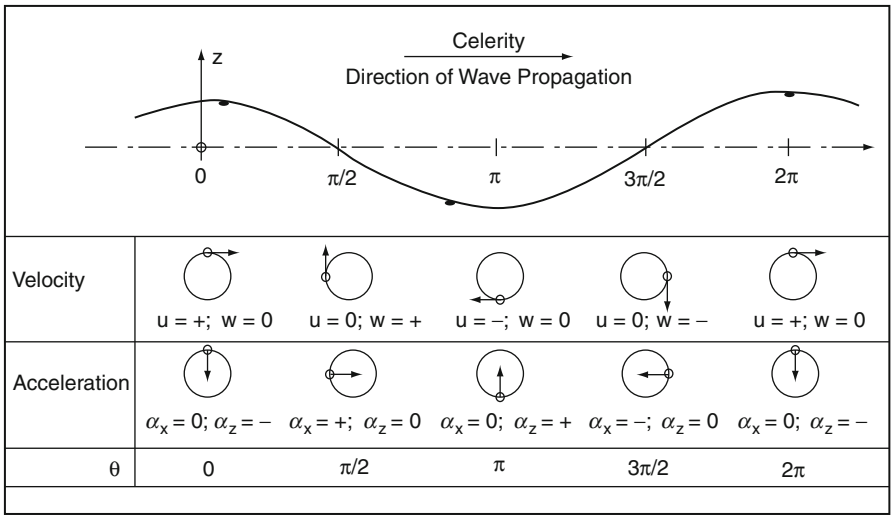

Offshore Wind Energy Technology Trends, Challenges, and Risks. Figure 10
Particle motion in airy waves [15]

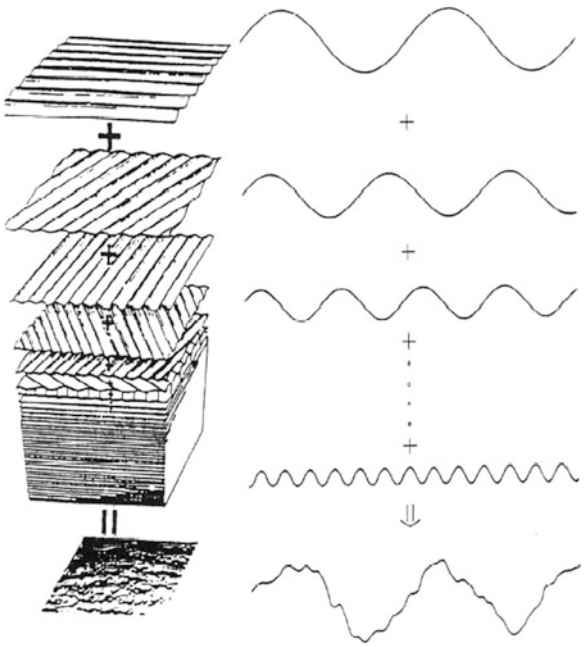

Offshore Wind Energy Technology Trends, Challenges, and Risks. Figure 11
Formation of random waves [15]

Another spectrum used to model the waves is the JONSWAP spectrum. It includes a "peak factor" and a "normalizing factor" and can be adjusted to fit a range of depths and fetches.

Breaking Waves A wave is said to break when its crest collapses rather than continuing to move forward. Breaking waves can originate in a variety of ways. They are more common in shallow water, but occur in deep water as well. Regardless of their origin, breaking waves can be significant for the design of offshore wind turbines because they can impart higher forces than would non-breaking waves of similar characteristics.

Extreme Waves Extreme waves are the highest waves that occur over some relatively long period of time. Within a sea state, one can estimate the extreme wave by considering the total number of waves (based on the mean wave period) and then applying Rayleigh distribution (which is actually the same as the Weibull distribution with the Weibull $k = 2$). To estimate extreme waves over a long period, such as 50 or 100 years, one may gather actual highest annual wave heights for a number of years and then apply the Gumbel distribution.

Wind/Wave Correlations

It is well known that high waves generally accompany high winds. However, the correlation is not perfect. For the proper design of a turbine, it is necessary to have a measure of the joint probability of occurrence of wind and waves. Figure 14 illustrates typical occurrences of wind waves from an offshore buoy.

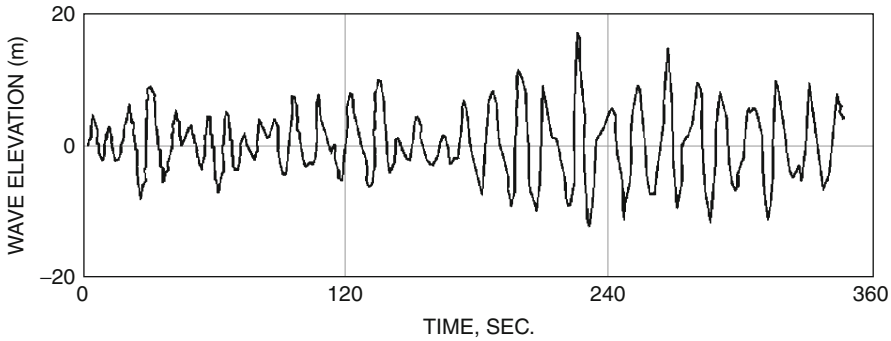

Offshore Wind Energy Technology Trends, Challenges, and Risks. Figure 12
Typical wave train [15]

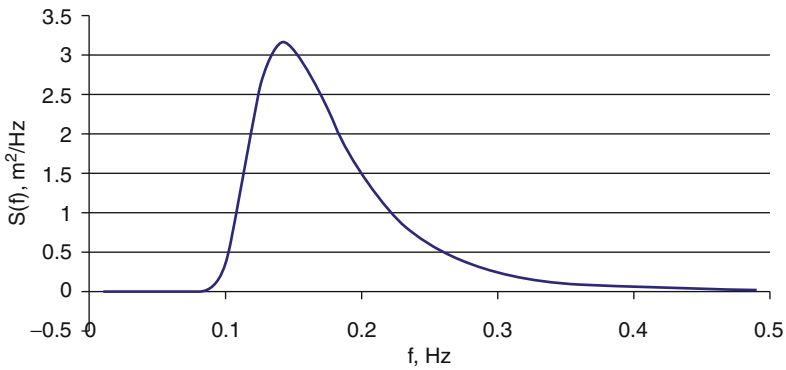

Offshore Wind Energy Technology Trends, Challenges, and Risks. Figure 13
Typical Pierson–Moskowitz spectrum

Wave Height H_s (m)	NOAA Buoy #44013 1984-2004						
	Wind Speed (m/s)						
	0-5	5-10	10-15	15-20	20-25	>25	sum
0-1	53235	48019	5518	92	1	0	106865
1-2	7041	13319	8063	660	9	0	29092
2-3	815	2502	2446	310	4	0	6077
3-4	69	413	1058	240	5	0	1785
4-5	13	55	302	206	9	0	585
5-6	1	10	74	144	16	1	246
6-7	0	0	11	62	17	0	90
7-8	0	0	0	20	6	0	26
8-9	0	0	0	1	1	0	2
>9	0	0	0	0	1	0	1
sum	61174	64318	17472	1735	69	1	144769

Offshore Wind Energy Technology Trends, Challenges, and Risks. Figure 14
Occurrences of significant wave heights and mean wind speed at NOAA buoy 44013

Currents

Currents may occur in the ocean, particularly as a result of tidal flows. These can be significant as a cause of erosion, or scour, around the base of the foundation of the offshore wind turbine and must be considered in the design.

Wave Forces

Hydrodynamic forces due to waves must be considered in the design of offshore wind turbines. There are two main types of forces due to the waves: (1) drag forces (associated with the velocity of the water, u) and (2) inertial forces (associated with the acceleration of the water, $\mathrm{d}u/\mathrm{d}t$). The simplest equation characterizing the forces on a structure due to waves is the Morison equation. For example, force per unit length on cylinder of diameter D is as follows:

$$\tilde{F} = C_M \rho_w A_c \frac{du}{dt} + C_D \rho_w \frac{D}{2} |u| u$$

where C_M is an inertial coefficient, C_D is a drag coefficient, and ρ_w is the density of the water. Drag coefficients are typically between 0.5 and 1.5; inertial coefficients are on the order of 2.0 [17].

It is worth noting that Morison's equation can be used together with the Airy model to find closed form expressions for the total inertial and drag forces, F_I and F_D, from waves on a cylinder (such as a monopile) of diameter D in water of depth d. They are:

$$F_I = \rho_w g \frac{C_m \pi D^2}{4} \hat{\zeta}_a \tanh(kd)$$

$$F_D = \rho_w g \frac{C_d D}{2} \hat{\zeta}_a^2 \left[\frac{1}{2} + \frac{kd}{\sinh(2kd)}\right]$$

Similarly, closed form expressions for bending moments at the seabed, M_I and M_D, may also be found:

$$M_I = \rho_w g \frac{C_m \pi D^2}{4} \hat{\zeta}_a d \left[\tanh(kd) + \frac{1}{kd}\left(\frac{1}{\cosh(kd)} - 1\right)\right]$$

$$M_D = \rho_w g \frac{C_d D}{2} \hat{\zeta}_a^2 \left[\frac{d}{2} + \frac{2(kd)^2 + 1 - \cosh(2kd)}{4k\sinh(2kd)}\right]$$

The above equations can be useful for approximate results or for illustration, but in practice hydrodynamic forces are usually calculated using numerical models.

Offshore Wave and Current Data Collection Offshore wave and current data is obtained by a variety of methods [12]. As with the wind, some data are already available from NOAA buoys, the voluntary observation ship (VOS) program, the Comprehensive Ocean Atmospheric Data Set (COADS), and hindcast estimates. On-site wave data is gathered by buoys or the use of devices such as acoustic Doppler profilers (ADPs). ADPs may also be used to measure currents.

Soils

Soils are also important for the design of an offshore wind project. They affect the design of: offshore wind turbine foundations, anchoring of floating offshore wind turbines, and the placement of electrical cables. The situation is actually more complex with offshore wind turbines than with many other civil structures due to time-varying loading which the operating turbine will impose upon the soil. The following section will focus on the more conventional ways to consider soils in foundations, but the reader should be aware of the particular characteristics of wind turbines which a foundation designer would need to take into account. See Westgate and De Jong [18] and Byrne and Houlsby [19] for more discussion of soils and offshore wind turbine foundations.

In the big picture, the soils are closely related to the geology of a given area. General characteristics of soils may therefore often be inferred based on the location. For actual design, however, a geotechnical site investigation would be required. This would include a detailed study of the target area soil including variation with depth or from one area within the wind farm to another. A geotechnical investigation would include soil coring and sampling for material, identification and characterization of the material, and subsequent laboratory testing. Properties of interest include: (1) macroscopic (e.g., historical and regional characteristics), (2) mechanical (e.g., strength and in situ stress conditions), (3) microscopic (e.g., particle size, roundness, and shape), (4) chemical (e.g., molecular structure), and (5) water content properties.

Soil effects of interest include: (1) bearing capacity, especially for gravity foundations; (2) movement of soil under load, especially for piled foundations; (3) resistance to movement of anchors; and (4) resistance to trenching for submarine cables.

In general, soil can be divided into the following categories, based on the size of the particles: (1) rock, (2) boulders, (3) cobbles, (4) gravel, (5) sand, (6) silt, and (7) clay. The particle size in these categories range from more than 20 cm (boulders) to less than 2 μm (clay).

Various methods may be employed to determine soil properties. These include: (1) the standard penetration test (SPT), the cone penetration test (CPT), acoustic sub-bottom profiling, vibracoring, soil sampling, and laboratory tests. The standard penetration test involves counting the number of hammer blows it takes to drive a specified sampling device a certain distance into the ground. The cone penetration test consists of pushing an instrumented cone, with the tip facing down, into the ground at a controlled rate (usually 2 cm/s) and recording the amount of force required. This method provides more continuous data than the SPT. In acoustic sub-bottom profiling, sound is produced by "boomer" which is towed behind a boat. The sound penetrates soil to various depths, and some of that sound is returned. The return signal is analyzed to provide information about the soil. This method is used to identify discontinuities in soil characteristics below the ocean floor and is ordinarily performed preliminary to soil borings. Figure 15 illustrates the results of typical acoustic sub-bottom profiling test. Vibracoring is a method of retrieving undisturbed core samples of sub-bottom sediment. With this method, samples are taken from relatively close to the seabed. Vibracoring is often used to study possible electrical cable paths. Sub-bottom soil borings involve the use of an offshore drilling rig. Soil samples from sub-bottom borings are used in conjunction with the design of the wind turbine support structures and their foundations. Borings often go through 25 m or more of soil and into the underlying rock (when it exists).

Some of the soil properties which are obtained during the course of these investigations include: undrained shear strength, S_u (kPa); specific weight, γ (kN/m^3); angle of internal friction, φ (degrees); compressive strength (MPa); and shear modulus, G (MPa). By way of illustration, undrained shear strength of clay can range from a low of 0 kPa (very soft clay) to more than 400 kPa (very hard clay).

An important consideration in the design of gravity-based support structures (see the section below on substructures) is the bearing capacity of the soil. This refers to the ability of the underlying soil to support the foundation loads without shear failure. For conventional foundations, bearing capacity factors are used in a bearing capacity equation. The bearing capacity factors are empirically derived factors and typically are correlated with the angle of internal friction. One widely used method is the Terzaghi ultimate bearing capacity theory. This method takes into account soil cohesion, foundation depth, and foundation dimension.

For the design of piles, the p-y method is commonly used. This is a method of analyzing the ability of deep foundations (e.g., piles) to resist loads applied in the lateral direction. It uses a finite element method and p-y graphs to find a solution. The p-y graphs relate the force (p) applied to the soil to the lateral deflection (y)

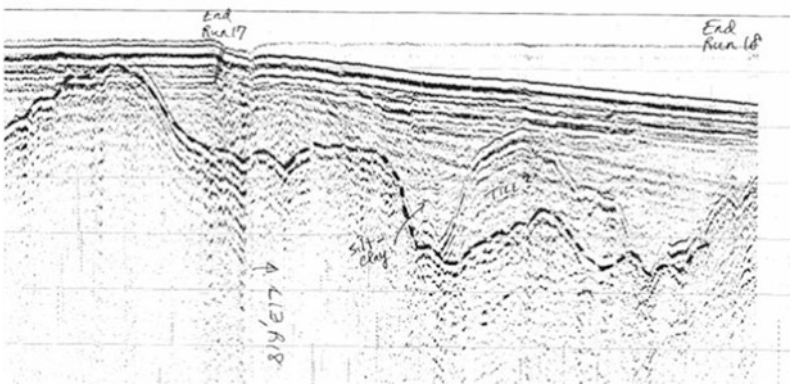

Offshore Wind Energy Technology Trends, Challenges, and Risks. Figure 15
Typical results from acoustic sub-bottom profiling

of the soil. The *p-y* relations are used to model the soil as a series of non-linear springs which are attached to the foundation in place of the soil. Equations of the form $p = k\ y$ are used. Here, k is the non-linear spring stiffness defined by the *p-y* curve, y is the deflection of the spring, and p is the force applied to the spring.

Wind Turbine Aerodynamics

The heart of any wind turbine is the rotor. This is the device which extracts the kinetic energy from the wind and converts it into a mechanical form. Below is a summary of wind turbine rotor aerodynamics. More details may be found in [11].

A wind turbine rotor is comprised of blades that are attached to a hub. The hub is in turn attached to a shaft (the main shaft) which transfers the energy through the remainder of the drive train to the generator where is it converted to electricity. The maximum power that a rotor can extract from the wind is first of all limited by the power in the wind which passes through an area defined by the passage of the rotor. All offshore wind turbines at the present time utilize a rotor with a horizontal axis. That is, the axis of rotation is (nominally) parallel to the earth's surface. Accordingly, the area that is swept out by the rotor is circular. Assuming a rotor radius of R (m), the maximum power P (W) available in the wind is

$$P = \frac{1}{2}\rho\pi R^2 U^3$$

Early in the twentieth century, it was shown by Betz (among others, see van Kuik [20]) that the maximum power that could be extracted was less than the power in the wind; in fact, it was 16/27 times that value. Betz' work led to the definition of a power coefficient, C_p, which expresses the ratio of the actual power extracted by a rotor to the power in the wind. When considering efficiencies of other components in the drive train, as expressed by the η, the total power out a wind turbine, P_{WT}, would be given by:

$$P_{\mathrm{WT}} = C_p \eta \frac{1}{2}\rho\pi R^2 U^3$$

The maximum value of the power coefficient, known as the Betz limit, is thus 16/27.

Betz' original analysis was based on the fundamental principles of fluid mechanics including linear momentum theory. It also included the following assumptions: (1) homogenous, incompressible, steady state fluid flow; (2) no frictional drag; (3) a rotor with an infinite number of (very small) blades; (4) uniform thrust over the rotor area; (5) a non-rotating wake; and (6) the static pressure far upstream and far downstream of the rotor is equal to the undisturbed ambient static pressure.

A real rotor operating on a horizontal axis will result in a rotating wake. Some of the energy in the wind will go into that rotation and will not be available for conversion into mechanical power. The result is that the maximum power coefficient will actually be less than the Betz limit. The derivation of the maximum power coefficient for the rotating wake case uses a number of terms: (1) the rotational speed of the turbine rotor, Ω, in radians/s; (2) tip speed ratio, $\lambda = \Omega R/U$; (3) local speed ratio, $\lambda_r = \lambda\ r/R$; (4) rotational speed of wake, ω; (5) an axial induction factor, a, which relates the free-stream wind speed to the wind speed at the rotor and the wind speed in the far wake ($U_{\mathrm{rotor}} = (1-a)\ U_{\mathrm{free\,stream}}$ and $U_{\mathrm{wake}} = (1-2a)\ U_{\mathrm{free\,stream}}$); and (6) an angular induction factor, $a' = \omega/2\,\Omega$. According to this analysis, the maximum possible power coefficient is given by:

$$C_{P,\max} = \frac{8}{\lambda^2}\int_0^{\lambda} a'\,(1-a)\,\lambda_r^3\,d\,\lambda_r$$

The maximum power coefficient for a rotor with a rotating wake and the Betz limit are illustrated in Fig. 16.

Neither of the analyses summarized above gives any indication as to what the blades of the rotor actually look like. For this purpose, a method called blade element momentum (BEM) theory was developed. This approach assumes that the blades incorporate an airfoil cross section. Figure 17 shows a typical airfoil, including some of the nomenclature.

The BEM method equates the forces on the blades associated with air flowing over the airfoil with forces associated with the change in momentum of the air passing through the rotor. The starting point for this analysis is the assessment of the lift force on an airfoil. Lift is a force perpendicular to the flow. It is given by:

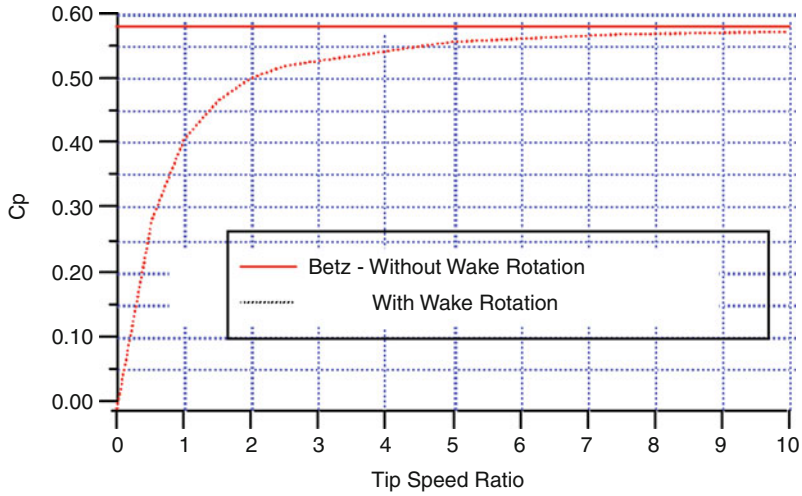

Offshore Wind Energy Technology Trends, Challenges, and Risks. Figure 16
Maximum theoretical power coefficients for rotating and non-rotating wakes

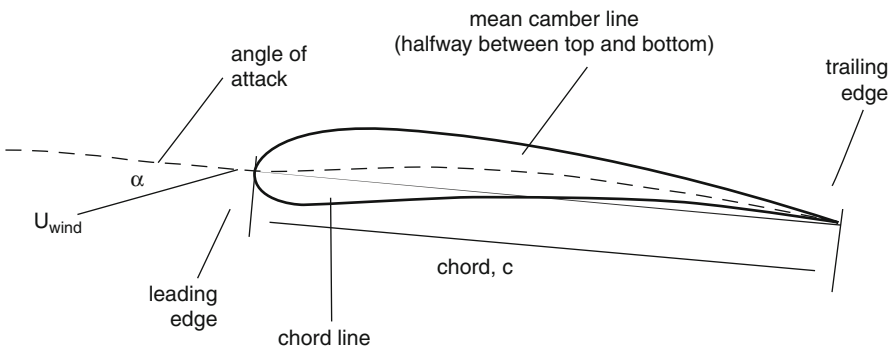

Offshore Wind Energy Technology Trends, Challenges, and Risks. Figure 17
Airfoil nomenclature

$$\tilde{F}_L = C_L \frac{1}{2} \rho \, c U^2$$

where:

$\tilde{F}_L$ = force per unit length, N/m.
C_L = lift coefficient.
c = chord length (distance from leading edge to trailing edge of airfoil, m).

Thin airfoil theory predicts that for a very thin, ideal airfoil, the lift coefficient is given by

$$C_L = 2\pi \sin \alpha$$

where α is the angle of attack, which is the angle between the flow and the chord line of the airfoil.

The lift coefficient for real airfoils typically includes a constant term, but the slope, at least for low angles of attack, is similar to that for an ideal airfoil. For greater angles of attack (above 10°–15°), the lift coefficient begins to decrease, eventually approaching zero. This is known as stall. A typical lift coefficient versus angle of attack curve is illustrated in Fig. 18.

There is always some drag force associated with fluid flow. This force is in line with the flow. Drag force (per unit length) is given by:

$$\tilde{F}_D = C_D \frac{1}{2} \rho \, c U^2$$

where C_D = drag coefficient.

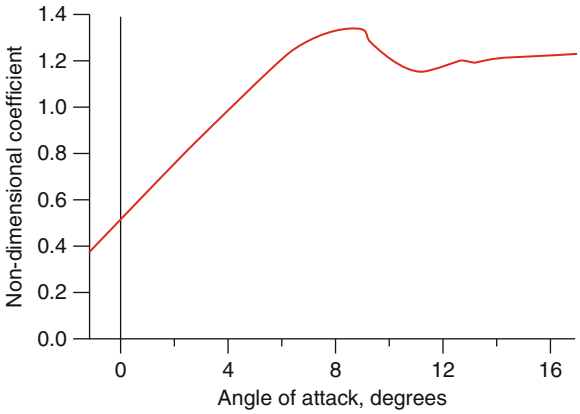

Offshore Wind Energy Technology Trends, Challenges, and Risks. Figure 18
Typical airfoil lift versus angle of attack

When designing blades for a wind turbine, it is generally desired to minimize the drag to lift ratio at the design point. This generally results in a lift coefficient in the vicinity of 1.0 and a drag coefficient of approximately 0.006, although these values can differ depending on the airfoil.

Blade element momentum theory, as noted above, relates the blade shape to its performance. The following approach is used. The blade is divided into elements and the rotor is divided into annuli. Two simultaneous equations are developed: One expresses the lift and drag coefficient (and thus forces) on the blade elements as a function of airfoil data and the wind's angle of attack. The other expresses forces on the annuli as a function of the wind through the rotor, rotor characteristics, and changes in momentum. Some of the key assumptions are: (1) the forces on blade elements are determined solely by lift/drag characteristics of the airfoil, (2) there is no spanwise flow, (3) lift and drag force are perpendicular and parallel respectively to a "relative wind," and (4) forces are resolved into components perpendicular to the rotor ("thrust") and tangential to it ("torque").

Using BEM theory, it may be shown for an ideal rotor that the angle of relative wind, φ, as a function of tip speed ratio and radial position on the blade is given by:

$$\varphi = \left(\frac{2}{3}\right)\tan^{-1}(1/\lambda_r)$$

Similarly, the chord length is given by:

$$c = \frac{8\pi r}{BC_L}(1 - \cos\varphi)$$

where B = the number of blades.

There are some useful observations to be drawn out of the above equations. First of all, in the ideal case, the blade will be twisted. In fact, the twist angle will differ from the angle of relative wind by the angle of attack and a reference pitch angle θ_p as follows:

$$\theta_T = \varphi - \alpha - \theta_p$$

It may also be noted that the twist angle will at first increase slowly when moving from the tip inward and then increase more rapidly. Second, the chord of the blade will also increase upon moving from the tip inward, at first slowly and then more rapidly. In the ideal case then, a wind turbine blade is both significantly twisted and tapered. Real blades, however, are designed with a less than optimal shape for a variety of practical reasons.

Another important observation has to do with the total area of the blades in comparison to the swept area. The ratio of the projected blade area is known as the solidity, σ. For a given angle of attack, the solidity will decrease with increasing tip speed ratio. For example, assuming a lift coefficient C_L of 1.0, the solidity of an optimum rotor designed to operate at a tip speed ratio of 2.0 is 0.43, whereas an optimum rotor designed to operate at a tip speed ratio of 6.0 would have a solidity of 0.088. It is therefore apparent that in order to keep blade material (and thus cost) to a minimum, it is desirable to design for a tip speed ratio as high as possible.

There are other considerations in selecting a design tip speed ratio for a turbine other than the solidity, however. On the one hand, higher tip speed ratios will result in gearboxes with a lower speed up ratios for a given turbine. On the other hand, the effect of drag and surface roughness of the blade surface may become more significant for a higher tip speed ratio rotor. This effect could result in decreased performance. Another concern is material strength. The total forces on the rotor are nearly the same on the rotor regardless of the solidity. Thus, the stresses would be higher. A final consideration is noise. Higher tip speed ratios generally result in more noise produced by the blades. This is more likely to be of concern on land than

offshore, so offshore turbines generally are designed to operate at higher tip speed ratios than are those for use on land.

There are numerous other considerations regarding the design of a wind turbine rotor, including tip losses, type of airfoil to be used, ease of manufacturing and transport, type of control used, selection of materials, etc. These are all outside the scope of this essay, however.

Real wind turbine rotors are designed taking into account many factors, including, but not only, their aerodynamic performance. In addition, the rotor must be controlled so as to generate electricity most effectively and so as to withstand continuously fluctuating forces during normal operation and extreme loads during storms. Accordingly, a wind turbine rotor does not in general operate at its own maximum power coefficient at all wind speeds. Because of this, the power output of a wind turbine is generally described by curve, known as a power curve, rather than an equation such as the one for P_{WT} which is given earlier. Figure 19 illustrates a typical power curve. As shown there, below the cut-in speed (3 m/s in the example), no power is produced. Between cut-in and rated wind speed (14.5 m/s in the example), the power increases significantly with wind speed. Above the rated speed, the power produced is constant, regardless of the wind speed, and above the cut-out speed (25 m/s in the example), the turbine is shut down.

Wind Turbine Mechanics and Dynamics

The Wind Turbine Aerodynamics section discussed the aerodynamic aspects of a wind turbine, and how they are related to its design, performance, and appearance. The next major consideration has to do with the turbine's survivability. This topic includes its ability to withstand the forces to which the turbine will be subjected, deflections of various components, and vibrations that may result during operations.

Issues that need to be considered include: (1) ultimate strength; (2) relative motion of components; (3) vibrations; (4) loads; (5) responses; (6) stresses; (7) unsteady motion, resulting in fatigue; and (8) material properties (see section "Offshore Wind Plant Electrical System").

The types of loads that a turbine may be subjected to are as follows: static (non-rotating), steady (rotating), cyclic, transient, impulsive, stochastic, and resonance-induced. Sources of loads may include aerodynamics, gravity, dynamic interactions, or mechanical control. To understand the various loads that a wind turbine may experience, the reader may wish to review the fundamentals of statics (no motion), dynamics (motion), Newton's second law, the various rotational relations (kinematics), strength of materials (including Hooke's law and finding stresses from moments and geometry), gyroscopic forces/moments, and vibrations. Among other topics, the cantilevered beam is particularly important since rotor blades as well as towers have similar characteristics.

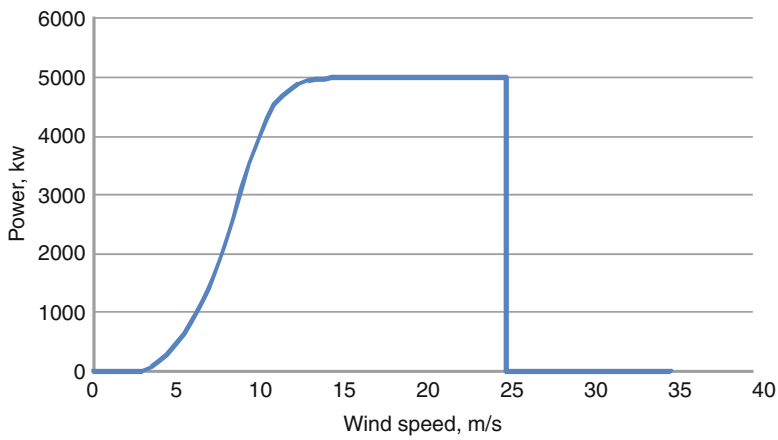

Offshore Wind Energy Technology Trends, Challenges, and Risks. Figure 19
Typical offshore wind turbine power curve

Wind turbines are frequently both the source of and are subject to vibrations. Although the topic can become quite complicated, it is worthwhile to recall that the natural frequency of simple oscillating mass, m, and spring, with spring constant, k, is given by:

$$\omega = \sqrt{\frac{k}{m}}$$

Similarly, rotational natural frequency about an axis of rotation is given by:

$$\omega = \sqrt{\frac{k_\theta}{J}}$$

where k_θ is the rotational spring constant and J is the mass moment of inertia.

A continuous body, such as a wind turbine blade, will actually have an infinite number of natural frequencies (although only the first few are important), and associated with each natural frequency will be a mode shape which characterizes its deflection. The vibration of a uniform cantilevered beam can be described relatively simply through the use of Euler's equation [11]. Non-uniform elements require more complex methods for their analysis.

Rotor Motions

There is a variety of motions that occur in the rotor that can be significant to the design or operation of the turbine. These include those in the flapwise, edgewise, and torsional directions.

Flapwise motions are those that are perpendicular to plane of the rotor and are considered positive in the direction of the thrust. Flapwise forces are the source of the highest aerodynamic bending moments and accordingly the most significant stresses.

Lead-lag, or edgewise, motions are in the plane of the rotor and are considered positive when in the direction of the torque. Fluctuating motions in this direction are reflected in the power.

Torsion refers to the twisting of blade about its long axis. Torsional moments in the blades must be accounted for in the design of pitch control mechanisms.

The most important rotor load is the thrust. This is the total force on the rotor in the direction of the wind (flapwise). It is associated with the conversion of the kinetic energy of the wind to mechanical energy. The thrust, T, (N) is given by:

$$T = C_T \, \frac{1}{2} \, \rho \, \pi \, R^2 \, U^2$$

where C_T is the thrust coefficient. For the ideal rotor in which the axial induction factor, a, is equal to 1/3 (corresponding to the Betz limit), it is easy to show that the thrust coefficient is equal to 8/9. For the same rotor, the thrust coefficient may be as high as 1.0, but this would not occur at $C_p = C_{p,\mathrm{Betz}}$.

This thrust gives rise to flapwise bending moments at the root of the blade. For example, for the ideal rotor when $a = 1/3$, and assuming a very small hub, it may be shown that the flapwise bending moment M_β at the root of the blade would be given by:

$$M_\beta = \frac{T}{B}\frac{2}{3}R$$

where B = number of blades.

From the bending moment, it is straightforward to find the maximum bending stress in the blade. For example, suppose that a blade is $2t$ m thick at the root, has a symmetrical airfoil, and that the thrust force is perpendicular to the chord line. Then the bending stress would be:

$$\sigma_{\beta,\max} = \frac{M_\beta \, t}{I_b}$$

(Note that for a real blade, the asymmetry and the angles would complicate the calculation, but the principle is the same.)

Another important load is torque, Q (Nm). Torque is given by:

$$Q = C_Q \, \frac{1}{2} \, \rho \, \pi \, R^2 \, U^2$$

where C_Q = the torque coefficient, which is also equal to C_p/λ.

Note that torque is also given by:

$$Q = P/\Omega$$

where P = power (W).

The dynamics of a wind turbine rotor are quite complicated and do not lend themselves to simple illustrations. There is one approach, however, due to Stoddard [21] and summarized by Manwell et al. [11]

which is relatively tractable, but will not be discussed here. In general, the dynamic response of wind turbine rotors must be simulated by numerical models, such as the FAST code [22] developed by the National Renewable Energy Laboratory.

Fatigue

Fatigue is an important phenomenon in all wind turbines. The term refers to the degradation of materials due to fluctuating stresses. Such stresses occur constantly in wind turbines due to the inherent variability of the wind, the rotation of the rotor, and the yawing of the rotor–nacelle assembly (RNA) to follow the wind as its direction changes. Fatigue results in shortened life of many materials and must be accounted for in the design. Figure 20 illustrates a typical time history of bending moment which would give rise to fluctuating stresses of similar appearance.

The ability of a material to withstand stress fluctuations of various magnitudes is typically illustrated in an S–N curve. In such curves, the stress level is shown on the *y* axis and is plotted against the number of cycles to failure. As is apparent from the figure above, stress fluctuations of a variety of magnitudes are likely. The effect of a number of cycles of different ranges is accounted for by the damage due to each cycle using Miner's rule. In this case, an amount of damage, *d*, due to *n* cycles, where the stress is such that *N* cycles will result in damage, is found as follows:

$$d = \frac{n}{N}$$

Miner's rule states that the sum of all the damage, *D*, from cycles of all magnitudes must be less than 1.0, or failure is to be expected imminently:

$$D = \sum n_i / N_i \leq 1$$

Miner's rule works best when the cycling is relatively simple. When cycles of varying amplitude follow each other, an algorithm called "rainflow cycle counting" [23] is used.

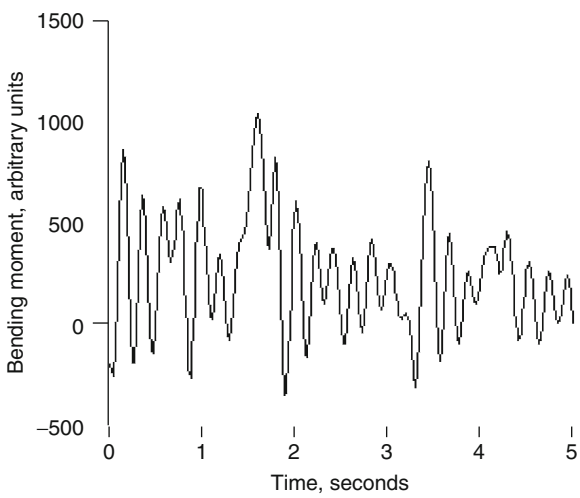

Offshore Wind Energy Technology Trends, Challenges, and Risks. Figure 20
Typical wind turbine blade bending moment

Components of Offshore Wind Turbines

Offshore wind turbines consist of two main subsystems, the rotor–nacelle assembly and the support structure, and each of these is comprised of many components. The following provides some more description of these subsystems. More details, particularly on the rotor–nacelle assembly, may be found in [11].

Rotor–Nacelle Assembly

The rotor–nacelle assembly (RNA) includes the majority of the components associated with the conversion of the kinetic energy of the wind into electrical energy. There are two major component groupings in the RNA as well as a number of ancillary components. The main groupings are the rotor and the drive train. The rotor includes the blades, the hub, and the pitch control components. The drive train includes shafts, bearings, gearbox (if any), couplings, mechanical brake, and generator. Other components include the bedplate, yaw bearing and yaw drive, oil cooling system, climate control, other electrical components, and parts of the control system.

Rotor The primary components of the rotor are the blades. Most offshore wind turbines at the present time have three blades, and they are oriented so as to operate upwind of the tower. It is to be expected that in the future, some offshore wind turbines will have two blades and will be oriented downwind of the tower, however. The general shape of the blades is chosen in

accordance with the principles discussed in the section on aerodynamics. The other major factor is the required strength of the blades. For this reason, it is often the case that thicker airfoils are used nearer the root than are used closer to the tip. Blades for offshore wind turbines are constructed of composites. The laminates are primarily fiberglass with some carbon fiber for additional strength. The binders are polyester or epoxy.

At the root of the blades, the composite material is attached to a steel root, which can then be subsequently bolted to the hub. Most offshore wind turbines at present include blade pitch control, so there is a mechanism present at the interface of the hub and the blades that will both secure the blades and facilitate their rotation about their long axis.

The hub of the wind turbine rotor is constructed from steel. It is designed so as to attach to the main shaft of the drive train as well as to connect with the blades.

Drivetrain

Shafts The main shaft of the drive train is designed to transmit the torque from the rotor to the gearbox (if there is one) or directly to the generator if there is no gearbox. This shaft may also be required to carry some or all of the weight of the rotor. The applied torque will vary with the amount of power being produced, but in general it is given by the power divided by the rotational speed. As discussed in the aerodynamics section, a primary consideration in the aerodynamic design of a wind turbine rotor is the tip speed ratio. A typical design tip speed ratio is seven. Consider an offshore wind turbine with a diameter of 126 m, designed for most efficient operation at a wind speed 10 m/s. The rotational speed of the main shaft under these conditions would be 10.6 rpm.

Gearbox Offshore wind turbines are intended to generate electricity, but most conventional generators are designed to turn at higher speeds than do wind turbine rotors (see below). Therefore, a gearbox is commonly used to increase the speed of the shaft that drives the generator relative to that of the main shaft. Gearboxes consist of a housing, gears, bearings, multiple shafts, seals, and lubricants. Gearboxes for wind turbines are typically either of the parallel shaft or planetary type. Frequently, a gearbox incorporates multiple stages since the maximum allowed ratio per stage is usually well under 10:1. There are trade-offs in the selection of gearbox. Parallel shaft gearboxes are generally less expensive than planetary, but they are also heavier. Gearboxes are generally quite efficient. Thus, the power out is very nearly equal to the power in. The torque in the shafts is then equal to the power divided by the speed of the shaft.

Brake Nearly all wind turbines incorporate a mechanical brake somewhere on the drive train. This brake is normally designed to stop the rotor under all foreseeable conditions, although in some cases it might only serve as a parking brake for the rotor. Mechanical brakes on offshore wind turbines are mostly of the caliper/disk type, although other types are possible. Brakes may be placed on either the low-speed or the high-speed side of the gearbox. The advantage of placing it on the high-speed side is that less braking torque is required to stop the rotor. On the other hand, the braking torque must then pass through the gearbox, possibly leading to premature failure of the gearbox. In either case, the brake must be designed to absorb all of the rotational energy in the rotor, which is converted into heat as the rotor stops.

Generator Electrical generators operate via the rotation of a coil in a magnetic field. The magnetic field is created by one or more pairs of magnetic poles situated opposite each other across the axis of rotation. The magnetic field may be created either by electromagnets (as in conventional synchronous generators), by induction in the rotor (as in induction generators), or with permanent magnets. In alternating current systems, the number of pairs of poles and the grid frequency determine the nominal operating speed of the generator. For example, in a 60-Hz AC system, such as the United States, a generator with two pairs of poles would have a nominal operating speed of 1,800 rpm. In most AC generators, the field rotates and the current is generated in a stationary armature (the stator).

The majority of offshore wind turbines today use wound rotor induction generators (WRIG). This type of generator can function over a relatively wide range of speeds (on the order of 2:1). Wound rotor induction generators are employed together with a power electronic converter in the rotor circuit. In such an

arrangement, approximately two third of the power is produced on the stator in the usual way. The other third of the power is produced on the rotor and converted to AC of the correct frequency by the power electronic converter. In this configuration, the WRIG is often referred to as a doubly fed induction generator (DFIG).

A number of offshore wind turbines use permanent magnet generators. Such generators often have multiple pole pairs as well. This can allow the generator to have the same nominal speed as the wind turbine rotor, so the main shaft can be connected directly to the generator without the use of a gearbox. Most permanent magnet generators are designed to operate together with power electronic converters. These converters facilitate variable speed operation of the turbine while ensuring that the electricity that is produced is of constant frequency and compatible with the electrical grid to which the turbine is connected.

Bedplate The bedplate is a steel frame to which components of the drive train and other components of the RNA are attached. It ensures that all the components are properly aligned.

Yaw System All offshore wind turbines today include a yaw system. This system facilitates orienting the RNA into the wind as the wind direction changes. First of all, there is a slewing bearing which connects the top of the tower to the RNA, allowing the latter to rotate with respect to the former. Also attached to the top of the tower, and often to the outside perimeter of the slewing bearing, is a large-diameter bull gear. A yaw motor connected to a smaller gear is attached to the bedplate. When the yaw motor is energized, the small gear engages the bull gear, causing the RNA to move relative to the tower. A yaw controller ensures that the motion is in the proper direction and that it continues until the RNA is aligned with the wind. A yaw brake holds the RNA fixed in position until the yaw controller commands a new orientation.

Control System An offshore wind turbine will have a control system which ensures the proper operation of the turbine at all times. The control system has two main functions: supervisory control and dynamic control. The supervisory control continuously monitors the external conditions and the operating parameters of the turbine and starts it up or shuts it down as necessary. The dynamic control system ensures smooth operation of various controllable components, such as the pitch of the blades or the electrical torque of the generator. The control system may also be integrated with or at least be in communication with a condition monitoring system which watches over the condition of various key components.

Ancillary Components Offshore wind turbines typically include a number of other components which are worth noting. A nacelle cover provides a housing to protect the components within from the weather. Climate control in the nacelle maintains the air at relatively low humidity so as to minimize corrosion. A flexible power cable carries the generated electricity from the RNA to the base of the turbine. A crane within the nacelle can be used to lift heavy items for servicing. A platform on the top of the nacelle can allow access to the turbine from a helicopter.

Support Structure

The support structure of an offshore turbine is any part of the turbine which is below the yaw bearing. The support structure may be conceptually divided into three main parts: the tower, the substructure, and the foundation.

Tower The tower of an offshore wind turbine is normally constructed of tapered steel tubes. The tubes are bolted together on-site or in the port to form a single structure of the desired height. The tower of an offshore wind turbine is usually considered to end at a transition piece which is well above water level.

Substructure: Bottom Mounted The substructure is the rest of the support structure below the tower. There are three main options for the substructure in water depths of 50 m or less. They are the monopile, the gravity structure, and the multi-member structure. The choice depends primarily on the water depth and soil conditions. In water depths of roughly 20 m or less, the least expensive option is usually a monopile. The monopile is a steel cylinder of relatively large wall thickness. The diameter of the monopile is at least as

large as the diameter of the bottom of the tower. For example, the diameter of the monopiles for a farm of 2-MW offshore turbines installed in water depth of 20–25 m was 4 m. The diameters of monopiles for larger turbines would be correspondingly larger. The embedded length of the monopile is determined in accordance with the soil conditions and the size of the turbine. In firmer soils, the monopile will not be as long as in weaker soils. Typically, embedded lengths of monopiles are between 20 and 50 m.

When the soil conditions allow for it, monopiles are driven into the seabed with a large hammer. The impact of the hammering is one of the considerations in the choice of the wall thickness. In certain types of soils, driving a pile may not be possible. In those cases, a large-diameter drill may be used to bore a socket into which the monopile is inserted.

The hammering on the top of the monopile will tend to distort it. A transition piece is therefore affixed to the top of the monopile, leveled and grouted into place. The tower is then bolted to the transition piece.

By way of example, in one conceptual design [24], a 5-MW turbine was to be installed on a monopile. The rotor was 126 m in diameter and the RNA had a mass of 350 metric tons. The tower, which was 77.6 m high, had a top diameter of 3.87 m and base diameter of 6 m. The tower had a thickness varied from 0.19 m at the top to 0.03 m at the base. The transition piece was 10 m above the sea surface. The water depth was 15 m. The soil was assumed to be clay. For this situation, a monopile with a diameter of 6 m, total length of 75 m, and wall thickness of 0.06 m was selected as the most suitable. The total mass of the monopile, assuming an effective density of the steel of 8,500 kg/m^3, would have been 740 t.

As larger turbines are designed and built, the use of monopiles for the support structures becomes more problematic. This is because of the difficulty of finding seagoing hammers large enough to drive in the very large monopiles that would be required.

Gravity Structures Another support structure option is the gravity base. These are used in relatively shallow water where the soil is firm. Gravity base structures are also attractive alternatives to the monopile when driving the monopile would present difficulties. Gravity structures rest on a prepared area of the sea bottom. They must be heavy enough to withstand the overturning moment from the wind turbine under any foreseeable conditions. These structures have relatively large-diameter bases so as to limit the stresses applied to the soil to acceptable levels. Gravity base structures are precast on shore or in a dry dock, taken to the wind turbine site by ship or barge and lowered into place by a large crane. The weight of the structures is large enough that finding vessels to transport and install them can be a challenge. To the extent possible, therefore, the structures are built so as to accommodate additional ballast once installed. This keeps the weight of the structure to a minimum while still allowing for the total required weight of the completed installation. Due to the high weight of gravity base structures and the difficulty of finding suitable vessels, some companies are now investigating the possibility of constructing the structures so that they can be floated out to the installation site and then sunk into place without the need for large vessels or cranes.

Multi-member Support Structure A third type of support structure is the multi-member structure. These actually come in a variety of configurations, depending on the application. Two of the most promising configurations are the tripod and the jacket. Multi-member structures are likely to be used in deeper water and for larger turbines. They require a relatively small amount of steel for their fabrication, but considerable effort is involved in the fabrication process. Tripods, as the name implies, have three legs. The legs are connected to a central tube which projects above the water level. The tower is bolted to the top of the central tube. Jacket structures have four main legs, connected together with smaller-diameter bracing. Jackets used for offshore wind turbines are based on designs adapted from the offshore oil and gas industry. The first use of jackets for supporting offshore wind turbines was at the Beatrice project off the coast of Scotland. The water depth here was approximately 45 m. The jackets were fabricated on shore, brought to the site, and lowered into place. They were secured to the seabed by relatively small piles at each of the legs.

Substructure: Floating The idea of floating offshore wind turbines (FOWTs) is quite attractive and has been so for some time. This is the case because most of the ocean is too deep for bottom-mounted wind turbines

and the area potentially available for energy production would be greatly expanded if FOWTs were realistic options. At the present time, however, there are no commercially available floating offshore wind turbines. In spite of the lack of existing FOWTs, there are a few options that look plausible and are being seriously investigated. In all cases, the RNA and the tower would be comparable to what we have discussed previously. The main difference would be in the support structures. The most promising floating support structure options are the spar buoy, the barge, and the tension leg platform (TLP). These concepts are illustrated in Fig. 21. The FOWT on the far left in the figure is mounted on a barge. The next FOWT from the left and the one on the far right are on spars. The other two are TLPs.

Spar Buoy In the case of the spar buoy, the wind turbine is supported by hollow steel spar floating vertically in the water. The spar would be heavily ballasted so as to remain upright. In one conceptual design [25], the same 5-MW turbine as considered in the monopile example was to be supported by spar buoy. For this case, the steel spar had a diameter of 9.4 m, was 120 m long, had a wall thickness of 0.03 m, and had a total mass of 900 t. In order to maintain stability, 6,600 t of ballast was required to be placed in the bottom of the spar. The displaced volume of the spar was sufficient for the entire structure to float at a reasonable depth. The length and ballasted weight of the spar kept the heeling of the spar within an acceptable range during operation.

Barge Another type of support structure for a floating offshore wind turbine is a barge. In a barge, the center of mass is higher than the center of buoyancy. Stability is achieved through the lateral movement of the center of buoyancy as the barge begins to heel. To maintain stability, the water plane area of the barge must be quite large. For example, a conceptual barge which would support the 5-MW turbine of the previous examples has been developed [26]. For this case, the barge would be circular in shape with diameter of 36 m and a height of 9 m. The total mass of the barge, including ballast, would be 4,500 t.

Tension Leg Platform The third type of floating structure being considered to support offshore wind turbines is the tension leg platform (TLP). In this arrangement, the turbine is mounted on a hull. The hull is attached to tendons which are in turn secured to anchors on the ocean floor. When installation is complete, the tendons are under tension. The tension in the tendons keeps the hull in place and serves to counteract the overturning moment. Further discussion of TLPs is outside the scope of this essay.

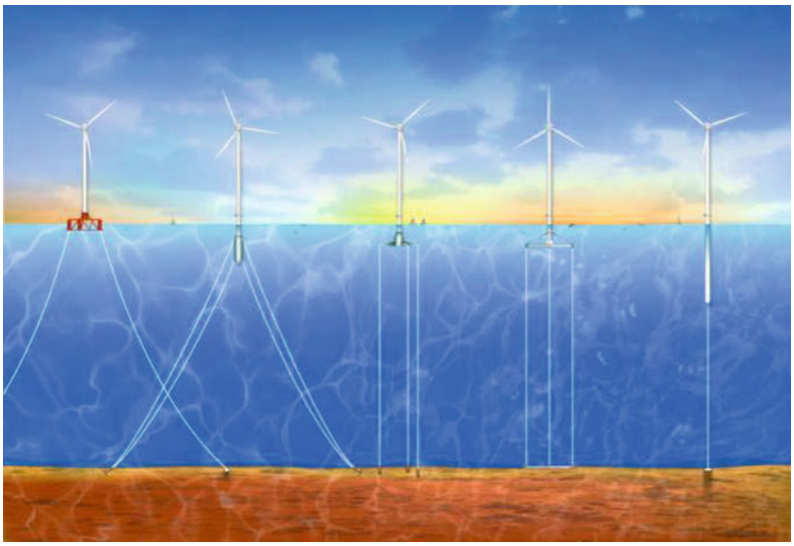

Offshore Wind Energy Technology Trends, Challenges, and Risks. Figure 21
Some support structure options for floating offshore wind turbines (Musial 2010)

Mooring Systems Regardless of the type of support structure which may be used with a floating offshore wind turbine, lateral movement of the structure must be prevented. This is accomplished by station-keeping facilities. These consist of anchors and mooring lines or tendons for the three types of floating structures discussed above.

Foundation The foundation of an offshore wind turbine is, strictly speaking, the part of the support structure which is in contact with the seabed. In the bottom-mounted structures discussed so far, the foundation is actually the lower part of the sub-structure. In some cases, distinct types of foundations might be used. One of these is the suction bucket. The suction bucket is like an inverted can placed on the ocean floor. Air is pumped from the bucket, and water pressure forces it down into the seabed. Once in place, it is very difficult to remove the bucket unless air is pumped back into it. Suction buckets have not been widely used with offshore wind turbines so far, but it is expected that they will become more common in the future. They may also have an application as part of the mooring system for floating offshore wind turbines.

Materials for Offshore Wind Turbines

The primary types of materials used in the various components of offshore wind turbines are steel, copper, composites, and concrete. Offshore conditions, especially in salt water, can result in much more rapid degradation of materials than would be experienced on land. Understanding the behavior of materials in the offshore environment and the proper selection of materials for offshore wind turbines are crucial.

There are three main forms of interaction with the marine environment which can affect the behavior of materials. These are: (1) forces, (2) physical and chemical interaction, and (3) thermal fluxes. The forces include dynamic and static loads on the fixed and moving parts, caused by both wind and waves. The physical-chemical interactions include corrosion, erosion, and oxidation. Thermal fluxes are due to temperature differences between the turbine components and the water and atmospheric environments – as affected by parts having different thermal properties (e.g., blades and hub). There may also be synergistic interactions between physical loads and physical-chemical processes. These interactions can modify the behavior of metals by increasing and accelerating the effects of fatigue loads. For example, cracking due to stress corrosion and corrosion fatigue will occur more rapidly in a saline environment. When combined with fluctuating stresses, such as in a wind turbine, the resulting lifetime of the material may be much less than normal.

Location is also an important factor in the response of a material. For example, steel in the splash zone may deteriorate much more rapidly than that which is always submerged or that which is well above the splash zone.

The adverse effects of corrosion may be minimized by selecting the right material for the situation, by coating the material, or by controlling the environment, depending on the situation. Sometimes cathodic protection is used to reduce the rate of corrosion of steel.

Offshore Wind Plant Electrical System

The electricity generated by offshore wind turbines must be transmitted to shore. This is accomplished via the use of an offshore electrical transmission system. A summary of such systems is provided below. More details may be found in [27].

For a large offshore wind farm, the transmission system will consist of the following: (1) submarine cables within the wind farm, (2) an offshore substation with transformer, (3) a submarine transmission cable to shore, (4) an onshore substation, and (5) connection to the onshore grid. Generally speaking, the cables within the wind farm are of relatively low voltage (for example, 24 or 33 kV), whereas the transmission cable to shore operates at a higher voltage (for example, 115 or 150 kV). A schematic of a typical offshore wind farm electrical system is shown in Fig. 22.

A typical three-phase submarine cable is illustrated in Fig. 23. The primary components of a submarine cable are the conductors. The electrical power that is generated in and transmitted from an offshore wind farm has so far always been three-phase AC. Accordingly, a submarine cable normally includes three conductors, one for each of the phases. The three conductors are built up of copper strands. Each conductor

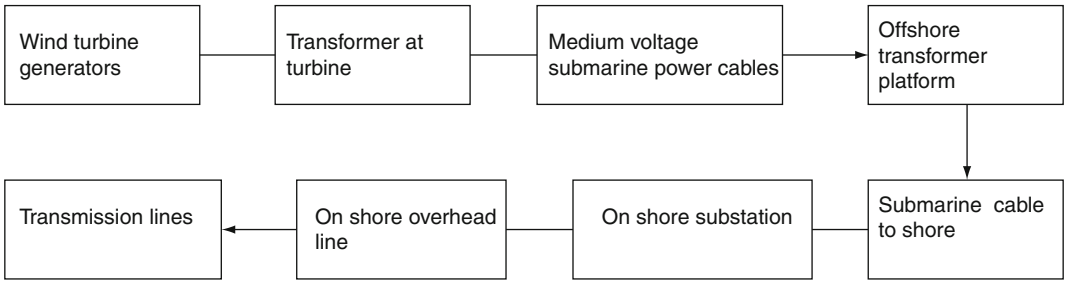

Offshore Wind Energy Technology Trends, Challenges, and Risks. Figure 22
Typical offshore wind farm electrical system

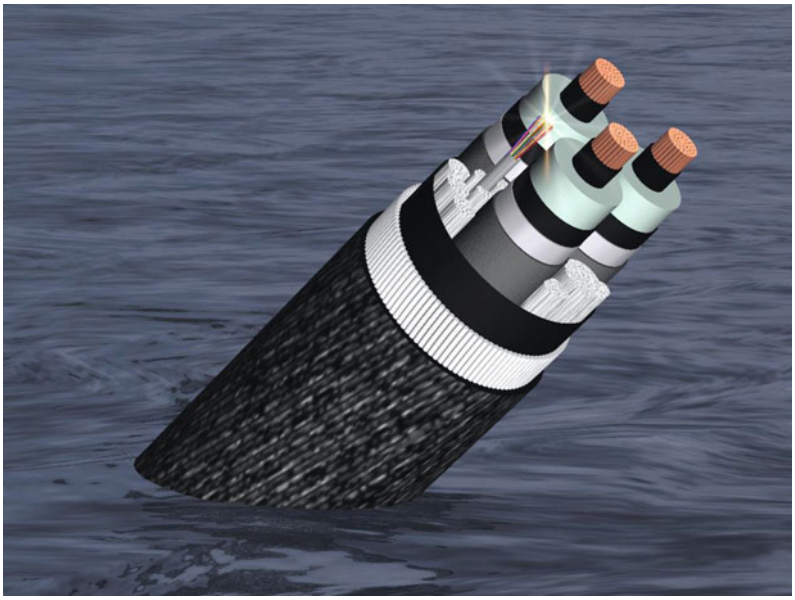

Offshore Wind Energy Technology Trends, Challenges, and Risks. Figure 23
Typical submarine cable. Source: http://www.nexans.com/Corporate/2009/Nexans_HV_submarine_3cores_cable.jpg

is first insulated individually. Then the entire assembly is surrounded by more insulation and protection against damage from the environment. Cross-linked polyethylene (XLPE) is commonly used for the insulation. Surrounding all the conductors is a metallic sheathing. This helps to ground the cable as a whole and will carry fault current if the cable is damaged. It will also serve as a moisture barrier. An overall jacket and then armoring may be used on the outside of the cable. Armoring protects cables against damage from surroundings, e.g., stray ship anchors. It should also be noted that fiber optic lines for communications and control are often bundled into the cables.

Submarine cables may be laid directly on the ocean floor, but most often they are buried approximately 2 m below the seabed. Burying the cables helps to protect them from damage. Laying the cable requires a special-purpose cable-laying vessel. Burying the cables is carried out with the use of underwater trenching machines.

Two factors that must be considered in the design of the offshore electrical system are losses in the cables and the ampacity of the cables. Losses arise due to the resistance of the conductors. The resistance of a cable depends on the resistivity of the material (copper) and the length of the cable. It is also inversely proportional to the cross-sectional area of the cable. The power loss

in cables is given by the square of the current times the resistance. Larger-diameter cables result in lower losses, but they require more copper and thus are more costly. There are also pros and cons regarding the voltage rating of a cable. Therefore, a trade-off analysis has to be done as part of selecting the cable.

The ampacity of a cable is the maximum amount of current that the cable can safely carry. It is based on the allowable temperature rise in the cable, which is in turn a function of the current, the thermal properties of the cable, and the seabed and the temperature of the surroundings. See Neher and McGrath [28] for the original model of this calculation.

Submarine cables tend to be quite heavy, due primarily to density of the conductor material and the required dimension of the conductors for a given amount of current. Typical unit weights of submarine cables are in the range of 40–90 kg/m. Various accessories may be used in conjunction with cable installations. These include: attachment devices, sea–land power transition joints, clamps, disconnecting link boxes, sea–land optical transition joints, and a "J tube" at the base of the offshore wind turbine itself.

Although all offshore wind farms to date have used AC cables, high-voltage direct current (HVDC) is likely to be used for some future installations. The advantages of HVDC include: (1) fewer cables are required, (2) there are no reactive power issues to contend with, (3) the losses are lower, and (4) transmission with minimal losses over large distances is possible. There are disadvantages with HVDC, however. First of all, there is a need to have power converters on each end of the line, and such converters are expensive. In addition, there are significant issues providing for circuit breakers in HVDC circuits. HVDC is likely to be most attractive for use in very large wind farms and where the required transmission line length is relatively long.

Design of Offshore Wind Plants

The design of an offshore wind plant involves two major topics: (1) the design of the turbines themselves and (2) the design of the wind farm itself. The design of the turbines is undertaken by applying the principles summarized previously. The process begins with a detailed assessment of the external design conditions at the site of interest. The next step is the development of preliminary designs for the turbines and their support structures. The design process is facilitated by the use of detailed structural dynamic computer models, such as FAST, which was mentioned earlier. These are used to predict forces, moments, and stresses throughout the turbine and help to ensure that suitable materials of the proper dimensions are employed. The recommended process for the design of offshore turbines is described in detail by a standard developed by the International Electrotechnical Commission, 61400-3 [1].

The layout of the wind turbines within a wind farm involves numerous considerations. For example, the wind speed, and hence energy production, from wind turbines usually increases with distance from shore. However, the water depth is also usually greater at greater distances, and so the installed costs tend to be greater. The closer the turbines can be placed to each other, the lower will be the cost of the cables within the wind farm. However, increased turbulence and energy losses associated with the turbine wakes can result in reduced energy production and higher maintenance cost. Thus, the layout of an offshore wind farm involves an optimization process. An example of such an optimization process is provided by Elkinton [29].

Installation

Installation of offshore wind turbines is a significant undertaking. It involves pre-assembly of the components on shore, delivering them to the offshore location, and placing them in their final position. Major components that need to be installed include the support structures, the rotor–nacelle assemblies, the electrical cables, and offshore platforms. Port facilities of sufficient staging area and channel depth are needed. A variety of vessels may be required. These may include jack-up barges, floating cranes, and dynamically positioned vessels. Special-purpose vessels designed specifically for transporting and installing offshore wind turbines are becoming more common. A typical example of one of these is illustrated in Fig. 24. Limitations in access due to adverse weather must also be planned for.

Environmental Aspects and Permitting

Offshore wind energy facilities invariably require consideration of their anticipated environmental

Offshore Wind Energy Technology Trends, Challenges, and Risks. Figure 24
Offshore wind turbine installation vessel, A2Sea's Sea Energy (http://www.marine-marchande.net/Collection%20Le%20Mens/LeMens13/A2sea.htm)

impact as part of the permitting process prior to their installation. There are two major aspects of these topics: the positive and the negative. On the one hand, the use of offshore wind energy instead of conventional energy sources can result in significant environmental benefits. Offshore wind turbines do not emit any greenhouse gases or other pollutants during operation and are responsible for the production of only minimal pollution during their construction. On the other hand, the presence of an offshore wind farm in a location where there was not one previously can result in changes to the environment. Overall, there also is the question of what are the relative risks of doing something (such as installing offshore wind turbines) versus doing nothing (and continuing with the status quo). See Ram [30] for more discussion of these issues.

Regardless of the positive aspects of offshore wind energy in general, in any actual project, a number of topics may need to be investigated. This could include (but not be limited to) the following: visual impact and public acceptance, noise impact, impact on radar and radio signals, impact on seabirds, impact on fish, impact on marine mammals, impact on benthic communities, effect of electromagnetic fields on marine organisms, and the possibility of ship collisions. The question of alternate uses of the sea needs to be considered, such as shipping routes, as well as marine archeological sites.

Within any country or state, a regulatory process is generally in place which sets the requirements for obtaining a permit to install an offshore wind project. This typically involves the preparation of a study listing the possible impacts of a proposed project. The regulatory body in charge will review this initial study and issue requirements regarding any additional studies that might be needed.

In this essay, two areas of potential impact will be briefly summarized, that on birds and that on fish. More detailed discussion is outside the scope of this essay.

Regarding birds, the following are possible: (1) collision risk, (2) short-term habitat loss during construction phase, (3) long-term habitat loss due to disturbance from wind turbines after installation and from ship traffic during maintenance, (4) barriers to movement in migration routes, and (5) separation from others of the same species. For example, consider the first of these potential impacts. Quantitative risk estimates for collision are difficult to obtain: collisions are highly site dependent, inadequate data exist on bird migration routes and flight behavior, measurements address only bird corpses that are found, and results to date are often contradictory between studies.

In effort to help address this situation, there are two major research areas at the present time: (1) development of remote technologies for bird collision measurements and (2) development of collision prediction models.

Regarding fish, the following could be significant and may need to be investigated: (1) loss of habitat, (2) possible injury to or dislocation of fish due to turbidity during the construction phase, (3) injury to or dislocation of fish due to vibrations and noise during construction and operation of the wind farm, (4) barrier effects within or outside the wind farm due to electromagnetic fields, and (5) warming of the seafloor and the water in the near vicinity of cables.

Economics

Offshore wind energy economics is an important and multi-faceted area. The following is an overview of the main topics. See Ozkan [31] for an in-depth examination of offshore wind energy economics.

Assessment of the economics involves consideration of a number of topics, including the capital cost of the offshore wind energy projects, energy production, operation and maintenance, market value of the energy produced, and the monetization of the environmental benefits. A cost breakdown for typical offshore wind energy projects is shown in Fig. 25.

First of all, the capital costs of offshore wind energy projects at the present time are relatively high, especially compared to onshore wind projects. The primary reason for this is that the support structures are considerably more expensive offshore. Installation cost of the turbines and support structures is also high due to the need for specialized and expensive vessels. Laying submarine cables is also expensive compared to installing power lines on land.

On the positive side, energy production per square meter of swept area from offshore turbines is generally considerably higher offshore than on land. This is due to the excellent wind resource which is generally available offshore.

Operation and maintenance, however, is generally much more expensive offshore than it is on land. Again, this is due primarily to the difficulties of access. When considered on a per MWh basis, O&M may be

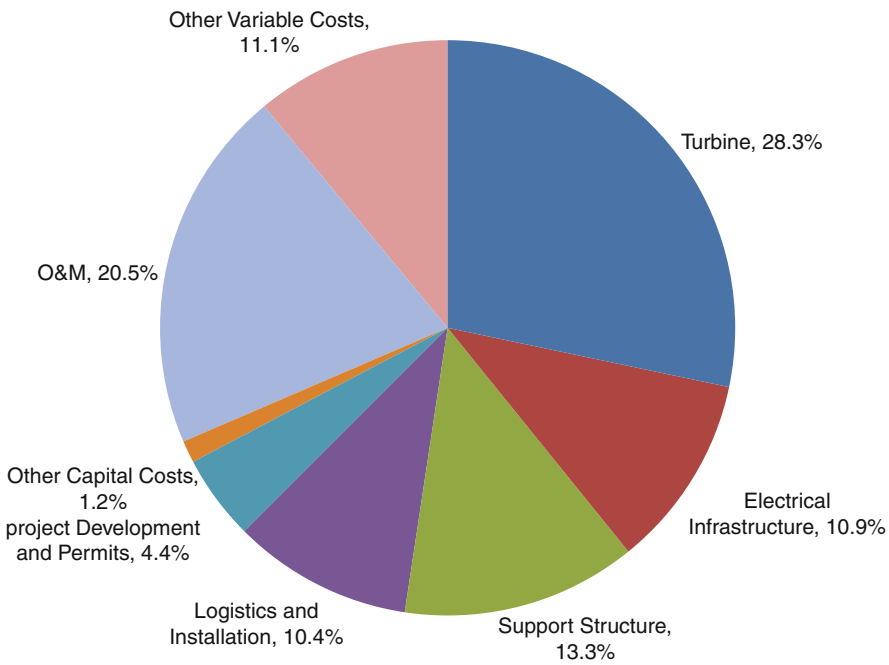

Offshore Wind Energy Technology Trends, Challenges, and Risks. Figure 25
Estimated life-cycle cost breakdown for a typical baseline offshore wind project (Musial 2010)

one of the most significant contributors to the overall cost of energy.

The average cost ($/MWh) to produce electricity from an offshore wind plant may be determined by conventional cash flow methods, taking into account the various fixed and variable costs, interest rate on the loan, discount rate, projected inflation rates, energy production, lifetime of the project, etc., in the usual way. A simplified approach is the fixed charge rate method. This method assumes that charges that occur on an annual basis (the most important of which is the loan interest and repayment) can be combined to a single multiplier, the fixed charge rate (FCR), which is used in the following equation:

$$\mathrm{COE} = \frac{\mathrm{CC} \times \mathrm{FCR} + \mathrm{O\&M}}{\mathrm{AEP}}$$

where

COE = cost of energy, $/MWh.
CC = capital cost, $.
O&M = annual operation and maintenance cost.
AEP = annual energy production, MWh/year.

The annual energy production is in turn found from the rated power, the numbers of hour in a year (8,760), and the capacity factor (either known or estimated, or from the power curve of the turbine, applied to the hourly average wind speed for every hour of a representative year).

By way of example, suppose that an offshore wind energy project has a rated capacity of 500 MW, that the unit cost of the project is $4,000,000/MW, that it will operate with a capacity factor (average power divided by rated power) of 0.4, that the operation and maintenance cost is 2% of the original capital cost/year, and that the fixed charge rate is 0.10. The cost of energy from the project would therefore be:

$$\begin{aligned}\mathrm{COE} &= \frac{\mathrm{CC} \times \mathrm{FCR} + \mathrm{O\&M}}{\mathrm{AEP}} \\ &= \frac{(500)(4{,}000{,}000)(0.1) + (500)(4{,}000{,}000)(0.02)}{(500)(8{,}760)(0.4)} \\ &= \$137/\mathrm{MWh}\end{aligned}$$

In order for the project to be viable, the total revenues must at least match the total costs. The primary source of revenue is derived from the sale of the electricity on the wholesale market. This rate may vary with the price of fossil fuels, but normally a developer would secure a long-term power purchase agreement from a utility before commencing construction. At the present time, however, the cost of energy from an offshore wind energy project normally exceeds the rate that would be offered in a standard power purchase agreement. Some other mechanism is needed to make up the difference. In much of the world, governments set guaranteed rates to facilitate the development of renewable energy projects, including offshore wind facilities. These are known as "feed-in" tariffs. The difference between the feed-in tariffs is, in effect, a subsidy and can be viewed as a monetization of the environmental benefits associated with the project. In some other countries, or in some states of the United States, another mechanism is used. This is the "renewable portfolio standard" (RPS). In this case, a utility (or equivalent entity) is responsible for supplying a certain fraction of their electricity from renewable energy sources. This mechanism is mediated through the use of renewable energy certificates (RECs) which may take on varying values depending on the supply and demand. Where an RPS is in place, the project developer will normally seek a purchase agreement for the RECs as well as one for the power. Regardless of the mechanism, subsidies for offshore wind energy projects are likely to be required for some time, at least until the capital and operating costs are reduced through technology improvements and increased experience.

Future Directions

The use offshore wind energy is expected to continue expanding significantly in the future. This expansion is likely to be accompanied by continuing development of the technology, particularly regarding deep water support structures, large rotors, infrastructure, and operations and maintenance. There will likely be extensive use of remote sensing, structural condition monitoring, and system-wide control. Robotic inspection and maintenance are plausible. Special-purpose vessels will become more prevalent. Turbines which can be assembled in port and towed to the site of installation will also be investigated. There will be a continuing effort to increase the amount of

generation associated with each support structure. Toward this end, increasingly larger rotors will be developed, probably at least 10 MW in capacity. Two-bladed, downwind rotors will be developed for use offshore. There will be efforts to pursue other innovative concepts in rotor configurations as well.

The issues associated with integrating large amounts of offshore wind in to the overall energy supply will need to be addressed. Part of the solution is expected to include electrical load management, smart grid technology, and system-wide energy storage. In order to bring large amounts of power onshore, dedicated offshore electrical transmission "backbones" will be needed. In addition, the onshore electrical transmission system will need to be upgraded, particularly the connections between the main high-voltage lines and the shore. As the contribution of offshore wind energy increases even more, efforts will be made to use the electricity for fuel production, for example hydrogen, ammonia, or synthetic hydrocarbons.

Bibliography

Primary Literature

1. IEC (2009) Wind turbines, Part 3: design requirements for offshore wind turbines, IEC 61400-3. International Electrotechnical Commission, Geneva
2. GL (2005) Guidelines for the certification of offshore wind turbines. Germanischer Lloyd, Hamburg
3. Vowles HP (1932) Early evolution of power engineering. Isis 17(2):412–420
4. Nansen F (1897) Farthest north. MacMillan, London
5. Honnef H (1932) Windkraftwerke. Friedrich Vieweg & Sohn, Braunschweig
6. Dörner H (2002) Drei Welten – ein Leben. Prof. Dr. Ulrich Hütter. Hochschullehrer – Konstrukteur – Künstler, 2nd edn, Heilbronn, Germany
7. Heronemus WE (1972) Pollution-free energy from offshore winds. In: Proceedings of 8th annual conference and exposition Marine Technology Society, Washington, DC, 1972
8. Casson L (1959) The ancient mariners. Victor Gollancz, London
9. Randall RE (1997) Elements of ocean engineering. The Society of Naval Architects and Marine Engineers, Jersey City
10. Musial W, Ram B (2010) Large-scale offshore wind power in the United States assessment of opportunities and barriers. NREL/TP-500-40745. National Renewable Energy Laboratory, Golden CO
11. Manwell JF, McGowan JG, Rogers AL (2009) Wind energy explained: theory, design and application, 2nd edn. Wiley, Chichester
12. Manwell JF, Elkinton C, Rogers AL, McGowan JG (2007) Review of design conditions applicable to offshore wind energy in the United States. Renewable Sustain Energy Rev 11(2):183–364
13. Gumbel EJ (1958) Statistics of extremes. Columbia University Press, New York
14. Ochi MK (1998) Ocean waves – the stochastic approach. Cambridge University Press, Cambridge
15. USACE (2002) Coastal engineering manual. CEM M 1110-2-1100. US Army Corps of Engineers (USACE), Washington, DC
16. Airy GB (1845) On tides and waves. In: Encyclopedia Metropolitana, vol 5, pp 241–396, J. J. Griffin, London
17. Yuan Z, Huang Z (2010) An experimental study of inertia and drag coefficients for a truncated circular cylinder in regular waves. In: 9th international conference on hydrodynamics, Shanghai, 2010
18. Westgate ZJ, De Jong JT (2005) Geotechnical considerations for offshore wind turbines. Technical Report, Dept. of Civil Engineering, University of Massachusetts, Amherst. http://www.usowc.org/pdfs/GeotechOffshoreFoundations-MTC-OWC.pdf. Accessed 24 Aug 2011
19. Byrne BW, Houlsby GT (2003) Foundations for offshore wind turbines. Philos Trans R Soc Lond A 361:2909–2930
20. van Kuik GAM (2007) The Lanchester–Betz–Joukowsky limit. Wind Energ 10:289–291
21. Eggleston DM, Stoddard FS (1987) Wind turbine engineering design. Van Nostrand Reinhold, New York
22. Jonkman J (2005) FAST user's guide. NREL/EL-500-38230. National Renewable Energy Laboratory, Golden
23. Downing SD, Socie DF (1982) Simple rainflow counting algorithms. Int J Fatigue 4(1):31–40
24. Anon (2010) Comparative Study of OWTG Standards. MMI Project MMW 528. MMI Engineering, Oakland
25. Jonkman J (2010) Definition of the floating system for phase IV of OC3. NREL/TP-500-47535. National Renewable Energy Laboratory, Golden
26. Jonkman J (2007) Dynamics modeling and loads analysis of an offshore floating wind turbine. NREL/TP-500-41958. National Renewable Energy Laboratory, Golden
27. Wright SD, Rogers AL, Manwell JF, Ellis A (2002) Transmission options for offshore wind farms in the United States. In: Proceedings of AWEA annual conference, Portland, 2002
28. Neher H, McGrath MH (1957) The calculation of the temperature rise and load capability of cable systems. AIEE Trans Part III 76:752–772
29. Elkinton CN (2007) Offshore wind farm layout optimization. PhD dissertation, University of Massachusetts, Amherst
30. Ram B (2009) An integrated risk framework for gigawatt-scale deployments of renewable energy: the U.S. wind energy case. NREL/SR-500-47129. National Renewable Energy Laboratory, Golden
31. Ozkan D (2010) Financial analysis and cost optimization of offshore wind energy under uncertainty and in deregulated markets. PhD dissertation, George Washington University, Washington, DC

Books and Reviews

Barltrop NDP, Adams AJ (1991) Dynamics of fixed marine structures. Butterworth Heinemann, Oxford

Barthelmie RJ, Courtney MS, Højstrup J, Larsen SE (1996) Meteorological aspects of offshore wind energy: observations from the Vindeby wind farm. J Wind Eng Industrial Aerodynamics 62(2–3):191–211

Burton T, Sharpe D, Jenkins N, Bossanyi E (2011) Wind energy handbook. Wiley, Chichester

Cheng PW (2002) A reliability based design methodology for extreme responses of offshore wind turbines. PhD dissertation, Delft University of Technology, Delft

Dicorato M, Forte G, Pisani M, Trovato M (2011) Guidelines for assessment of investment cost for offshore wind generation. Renew Energ 36:2043–2051

Elkinton CN, Manwell JF, McGowan JG (2008) Optimizing the layout of offshore wind energy systems. J Marine Technol Soc 42(2):19–27

Gardner P, Craig LM, Smith GJ (1998) Electrical systems for offshore wind farms. Proceedings of 1998 British wind energy association conference, Bakersfield. Professional Engineering Publishing Limited, UK

Gerdes G, Tiedemann A, Zeelenberg S (2010) Case study: European offshore wind farms – a survey for the analysis of the experiences and lessons learnt by developers of offshore wind farms. Deutsche WindGuard GmbH, Deutsche Energie-Agentur GmbH (dena), University of Groningen. http://www.offshore-wind.de/page/fileadmin/offshore/documents/Case_Study_European_Offshore_Wind_Farms.pdf. Accessed 24 Aug 2011

Hsu SA (2003) Estimating overwater friction velocity and exponent of power-law wind profile from gust factor during storms. J Water Port Coastal Ocean Eng 129(4): 174–177

Kühn M (2001) Dynamics and design optimisation of offshore wind energy conversion systems. PhD dissertation, Delft University of Technology, Delft

Lange B, Højstrup J (1999) The influence of waves on the offshore wind resource. In: Proceedings of the 1991 European wind energy conference, Nice, 1999

Musial W (2007) Offshore wind electricity: a viable energy option for the coastal United States. Marine Technol Soc J 41(3):32–43

Twidell J, Gaudiosi G (2009) Offshore wind power. Multi-Science, Brentwood

Van der Tempel J (2006) Design of support structures for offshore wind turbines. PhD dissertation, Delft University of Technology, Delft

Veldkamp D (2006) Chances in wind energy: a probabilistic approach to wind turbine fatigue design. PhD dissertation, Delft University of Technology, Delft

Westinghouse Electric Corp (1979) Design study and economic assessment of multi-unit offshore wind energy conversion systems application. DOE WASH-2830-78/4

Offshore Wind Power

Göran Dalén
WPD Scandinavia AB, Stockholm, Sweden

Article Outline

Glossary
Definition of the Subject and Its Importance
Introduction
External Conditions
Environmental Impact
Technology
Installation
Operation and Maintenance
Economy
Future Directions
Bibliography

Glossary

Environmental conditions Characteristics of the environment (wind, waves, sea currents, water level, sea ice, marine growth, scour, overall seabed movement, etc.) which may affect the wind turbine behavior.

External conditions (wind turbines) Factors affecting operation of an offshore wind turbine, including the environmental conditions, the electrical network conditions, and other climatic factors (temperature, snow, ice, etc.).

Fetch Distance over which the wind blows constantly over the sea with approximately constant wind speed and direction.

Power collection system (wind turbines) Electric system that collects the power from one or more wind turbines. It includes all electrical equipment connected between the wind turbine terminals and the network connection point. For offshore wind farms, the power collection system may include the connection to shore.

Scour Removal of seabed soils by currents and waves or caused by structural elements interrupting the natural flow regime above the sea floor.

Significant wave height Statistical measure of the height of waves in a sea state, defined as $4^{*}\sigma\eta$

where $\sigma\eta$ is the standard deviation of the sea surface elevation. In sea states with only a narrow band of wave frequencies, the significant wave height is approximately equal to the mean height of the highest third of the zero up-crossing waves.

Splash zone External region of support structure that is frequently wetted due to waves and tidal variations. This shall be defined as the zone between the highest still water level with a recurrence period of 1 year increased by the crest height of a wave with height equal to the significant wave height with a return period of 1 year, and the lowest still water level with a 20 recurrence period of 1 year reduced by the trough depth of a wave with height equal to the significant wave height with a return period of 1 year.

Wind shear Variation of wind speed across a plane perpendicular to the wind direction.

Definition of the Subject and Its Importance

Offshore wind power is defined as construction of wind farms, located in the water, generating electricity from wind.

Land-based wind power will remain dominant in the immediate future but installations at sea will become increasingly important.

Compared to onshore wind, offshore wind is more complex and costly to install and maintain but also has a number of key advantages. Winds are typically stronger and more stable at sea than on land, resulting in significantly higher production per unit installed. At sea, wind turbines can be bigger than on land because of the logistical difficulties of transporting very large turbine components from the place of manufacturing by road to installation sites on land. Wind farms at sea also have less potential to cause concern among neighboring citizens and other stakeholders unless they interfere with competing maritime activities or impact negatively on important marine environmental interests. In fact, wind farms at sea may be advantageous to protect marine ecosystems and may generate synergies with other emerging uses of the sea such as offshore aquaculture, which can benefit from the substructures of wind farms.

The large-scale development of offshore wind power must overcome the bottlenecks in the existing electricity grid since the grid is not adapted to the changes in the generation infrastructure.

Offshore wind power has been developed during the last 20 years. The total installed capacity in Europe in 2010 was 2,946 MW and the predicted installed capacity of offshore wind energy in Europe alone in 2030 is 150 GW [1].

Three clear tendencies can be distinguished looking back at the first 10 years of development:

1. The size of wind turbines is steadily growing.
2. The water depths are increasing.
3. The distance to the shore is getting bigger.

These trends are clearly demonstrated in Figs. 1–3 below.

Introduction

The first offshore wind power plant was installed in the Baltic Sea in 1991 and consisted of a 220 kW demonstration unit, located 250 m outside the harbor of Nogersund in Sweden in 6 m water depth (Fig. 4).

The turbine, named "Svante" was mounted on a tripod construction welded in Corten steel and the

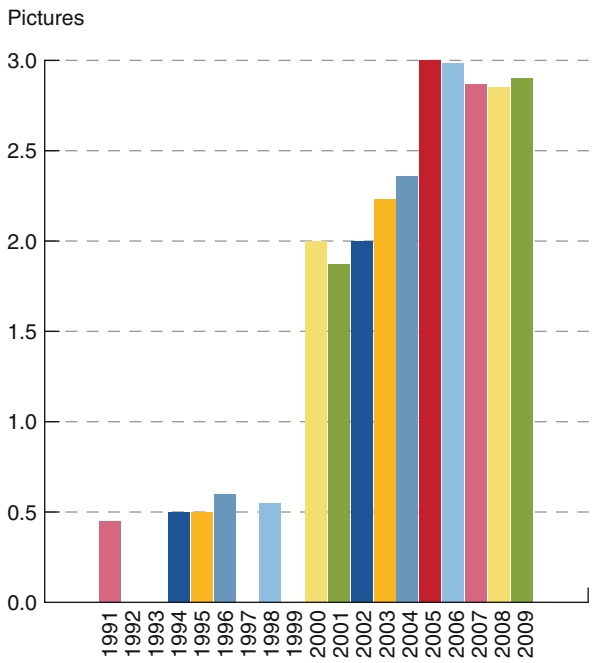

Offshore Wind Power. Figure 1
Increasing size of wind turbines in MW (EWEA)

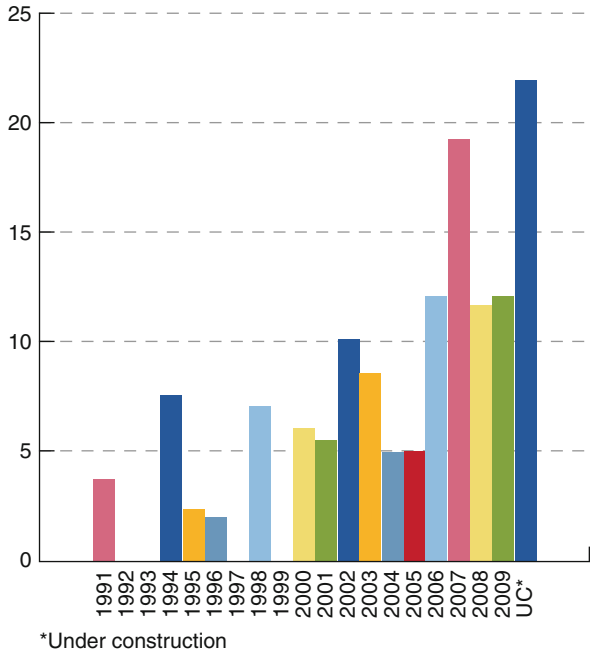

Offshore Wind Power. Figure 2
Increased water depths in meter (EWEA)

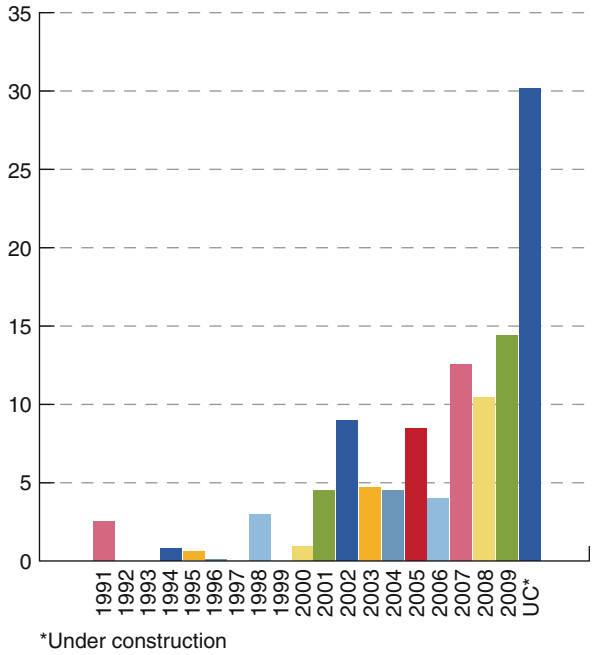

Offshore Wind Power. Figure 3
Increased distance to the shore in km (EWEA)

design was aimed to be economical for future large offshore wind turbines. Today, German company Bard Engineering is using essentially the same design for its 5 MW turbines, to be installed in 2011 in the German sector of the North Sea.

It was early recognized that the energy potential from wind power is very big offshore but also that it is very different conditions with a harsh environment requiring new technology to be developed.

The energy output from wind power equals to the wind speed to the power of three and it is easy to recognize that windy offshore sites are of big interest.

Offshore wind power is still a young technology with a huge future potential. It is natural that the development starts in sheltered waters, near the shore, and in modest water depths.

- The average offshore wind farm size in 2010 was 155 MW [2].
- The average water depth of offshore wind farms installed in 2010 was 17 m [2].
- The average distance to shore of offshore wind farms installed during 2010 was 27 km [2].

Projects are however under development of completely different magnitudes; 1,000 MW wind farms, located 100 km offshore in 40 m water depth (Fig. 5).

The wind characteristics are different offshore with more laminar air flow compared with onshore. This has an impact on both the energy production as well as on the loads on the individual wind turbines, something that must be taken into consideration during the development phase. One consequence is that the distance between the wind turbines must be bigger offshore compared with onshore since the turbulence behind a wind turbine stays intact for a longer distance (minimum distance offshore is 6–8 rotor diameters). The picture below is a good example of the wake effects from the offshore project Horns Rev in Denmark (Fig. 6).

It is important to develop international standards that can be used during the introduction of a new technology. Laws and safety regulations are based on domestic requirements but IEC 61400-3 "Design requirements for offshore wind turbines" defines all major design requirements for offshore wind turbines plants to be taken into consideration.

Offshore Wind Power. Figure 4
First offshore wind turbine in the world; Svante. (EWEA)

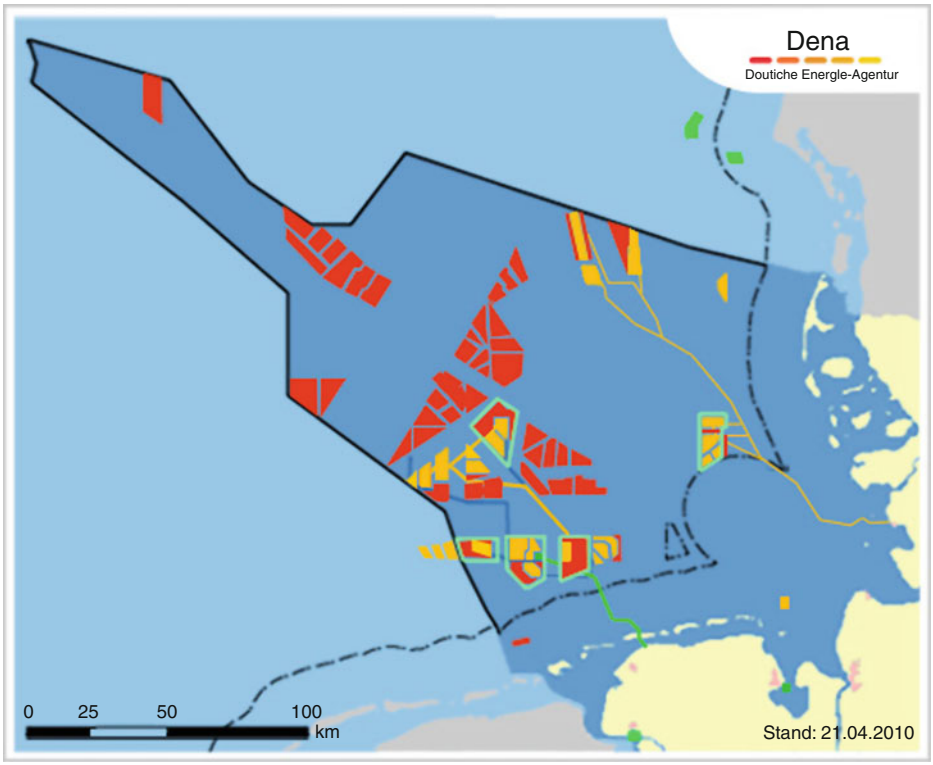

Offshore Wind Power. Figure 5
German offshore wind projects in the North Sea (Dena)

Offshore Wind Power. Figure 6
Wake effects at Horns Reef (EWEA)

External Conditions

The design of an offshore wind power plant depends very much of the external conditions. Compared with onshore wind power, a big number of external conditions must be considered for the design of the offshore wind power plant as well as for the connection to the shore and the overall strategy of the operation and maintenance of the plant.

The harsh environment will reduce the lifetime of the wind power plant if particular requirements are not taken into consideration regarding humid atmosphere, high salt content, and corrosion.

Figure 7 illustrates the different external conditions that an offshore wind turbine including foundation must be designed for.

Soil Conditions

Choice of foundations depend on the kind of soil conditions found at the site but also floating structures must be secured to the seabed and the connection to the shore with electric cables, etc. must be well secured and protected.

Different techniques are used to provide information about the seabed. Bathymetric investigations are carried out to provide detailed information about the water depth. Side scanning sonar is used to give information about obstacles on the seabed. Magnetometric investigations give information about any magnetic object on the seabed as well as magnetic object buried under the top layer of the seabed. This is important information since ammunition and grenades unfortunately are common in shallow waters outside, for instance, the European coastline. Seismic investigations are carried out to give soil profiles in the upper 20 m or so.

Soil data is also needed deeper down to establish the design parameters needed for the design of the foundations. The most common techniques are CPT (Cone Penetration Test) which is an "in situ" technique that provides data about soil resistance, pore pressure, and friction angle by pushing down a cone into the soil. Samples from the sea bottom are collected and analyzed in laboratories to establish all required soil parameters. The shear strength of the different soil layers can be determined together with long-term dynamic load tests. The samples can be collected by various techniques of which core drilling is the most common and also the most expensive technique.

It is also important to find out if there is any risk of liquefaction at certain layers.

The original strength can vanish completely if there is access to additional water ingress in combination with vibrations that can develop during, for instance, piling operations.

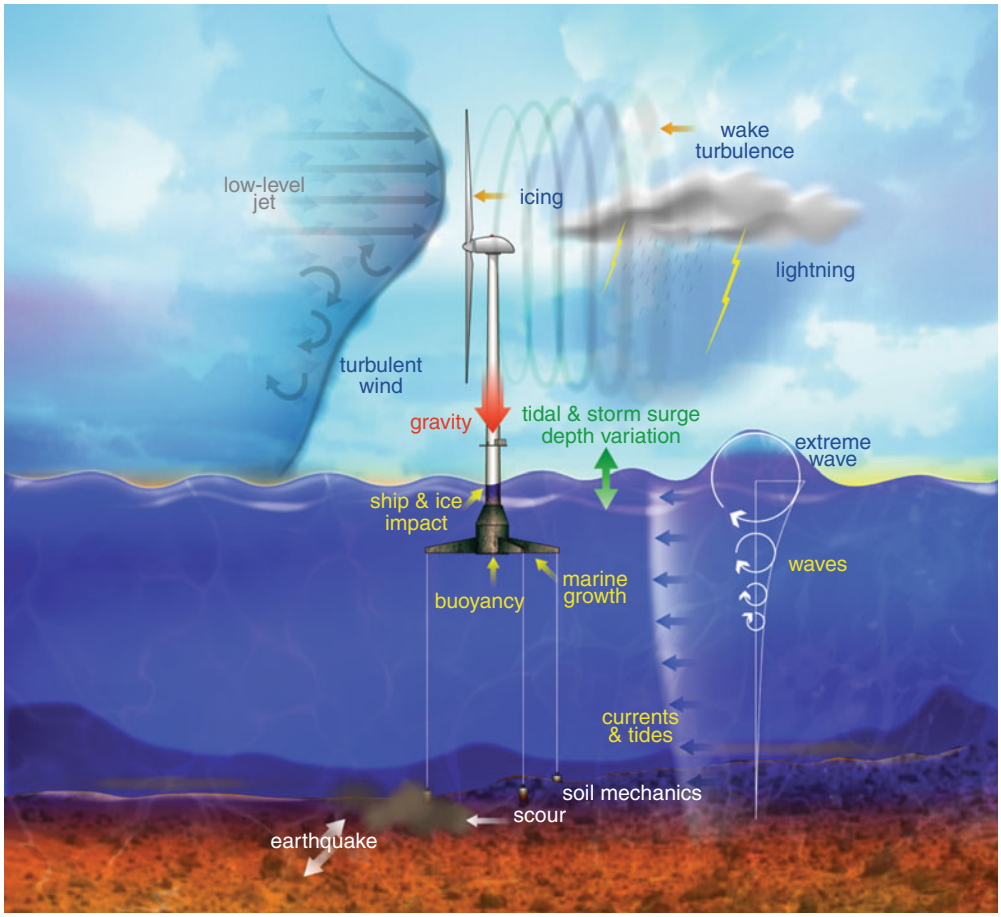

Offshore Wind Power. Figure 7
Loads on offshore wind turbine including foundation (NREL)

New techniques are developed to get a three-dimensional information of the soil properties without physically collecting samples. These techniques using acoustic corers will not replace the drilling campaigns but they will add valuable information and thereby result in more cost-effective foundations.

Figure 8 shows a system using two acoustic sensors (transponders and receivers) mounted on a boom that rotates 180°. The sensors travel in increments toward the center and the result is a three-dimensional picture of the soil which can detect objects like boulders, shipwrecks, etc.

Wind Conditions

The wind conditions offshore are in general better than onshore. The average wind speed is higher and the turbulence is less providing that the wind power plant is located some distance from the coastline. Higher average wind speed is of course a big advantage since the captured energy is the wind speed up to the power of three. The fact that the turbulence is less is in general an advantage but the distance between the wind turbines must be bigger offshore compared with onshore due to the increased wake effect offshore.

Water Depths

The water depths vary very much. The average water depth on the earth is over 3,700 m. But offshore wind power plants are located in shallow waters less than 50 m and close to the coast to bring the total cost down. The average water depth for offshore installations carried out in 2009 was 12 m. Many projects under

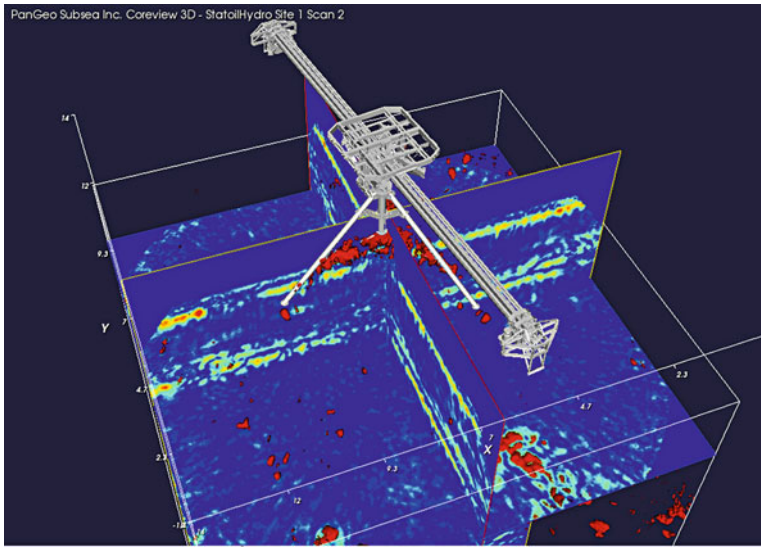

Offshore Wind Power. Figure 8
Acoustic coring (PanGeo)

development are however located in deeper waters and one example that has been built is the DOWNVInD/Beatrice R&D project where two 5 MW wind turbines were installed in 44 m water depth outside Scotland in 2007. Future development of floating structures will possibly change this but shallow water areas are common within the continental shelf and provide a huge energy resource ready to be harvested before the deeper areas are developed.

Waves

Waves are wind-driven but in open seas there is always a combination of swell ("old waves") and actual wind-driven waves. These waves can be of different directions. The wave conditions depend on the water depth and the fetch (the distance in the wind direction to nearest shore). The most important design parameters are the significant wave height and the wave period. The definition of the significant wave height is the average wave height (thrust to crest) of the one third highest waves during a certain time period. The shape of the waves (longer waves in open seas and shorter steeper waves in more shallow waters) will also have an impact on the loads.

The interaction between wind and wave directions must also be taken into consideration in the design work. It is in general conservative to assume that the biggest wave always interacts with the strongest wind. But this cannot be taken for granted and the interaction based on statistical information about wind directions and wave directions must be considered individually for each project.

Current and Tidal Effects

Currents are either wind-driven or tidal currents. Wind-driven currents are normally not a design driver but can result in scour problems around foundations.

Tidal currents can be very strong and cause serious problems if not considered in a proper way. Tidal current will add big loads but also make the installation and maintenance work more complicated and costly. Tidal charts are however available for the most areas that are of interest for offshore wind power.

Ice

Sea ice can be a severe design driver for offshore wind power. The static loads can be very big and the dynamic effects introducing coupled vibrations with the total system (foundation, tower, and wind turbine) must be avoided. Ice charts are available and specific design requirements are available.

Marine Spatial Planning

Marine spatial planning is a tool that brings together multiple users of the ocean – including energy,

industry, government, conservation, and recreation – to make informed and coordinated decisions about how to use marine resources. It uses maps to create a more comprehensive picture of a marine area – identifying where and how an ocean area is being used and what natural resources and habitat exist [2].

Environmental Impact

Noise

Airborne noise from wind turbines in operation is in general a smaller problem offshore compared with onshore since the wind turbines are located further away from where people live. It should be recognized, however, that noise travels a longer distance offshore and local effects with atmospheric layers with different density can result in extremely poor damping of the noise.

Underwater noise is also an issue that must be taken into consideration. Noise travels five times faster in water compared with air and noise can propagate to the water through the foundation.

Noise generated during the installation of the wind turbine plant must also be considered. The installation period is short but technologies such as under water piling can be very noisy. Special preventive measures must be taken to ensure that noise-sensitive animals are kept out of the area. This can be done by "soft starting" of the piling operation or the usage of pingers.

Barriers of Water Flow

Offshore wind power plants act as barriers of the natural water flow. This is a common effect for bridges and shall also be considered when the wind power plant is located in straits or other areas where the water flow is of importance for the water balance. It is however not considered to be a big problem for offshore wind power.

Visual Impact

Visual impact offshore is less than onshore since the wind turbines normally are located at a greater distance from where people live. It should however be pointed out that the impact still can be big since a free horizon will be affected by offshore wind turbines if the distance is less than approximately 20 km. Requirements to have different kind of aviation warning lights can be a problem for nearshore projects (less than 20 km from the shore). Synchronization of the warning lights and also implementation of different sensors that will control the intensity of the light in correlation with the weather conditions are getting normal building standards and will decrease the visual impact during the night.

Birds and Bats

Wind turbines will act as obstacles for migrating birds but research has so far not revealed any big impact; the migrating birds tend to seek alternative routes to avoid the barrier created by the wind turbines [3].

Stationary birds are mainly affected during the installation phase (noise from installation and disturbance by installation vessels) and there is also an impact during the operation due to the service vessels running in and out to the wind turbines. New sediment structure can also have an impact on the normal food chain with negative and positive effects; the old food chain may be changed but the new developed hard surfaces created by the foundations may lead to increased supply of algae and nutrition.

Benthic Fauna and Flora

The change in sediment structure will have an impact. During the installation, an increased turbidity will occur, especially if the preparations include dredging. These are however of a temporary nature and no long-term effects are foreseen.

The effect from placing hard structures on the seabed will to some extent result in "artificial reefs" that attracts mussels and other microhabitats. Studies in cold waters verify an increased diversity of benthic fauna and flora in the near vicinity of offshore wind turbines [4].

Fish

All kinds of man-made objects change the habitat for fish, not necessarily in a negative way. Wind turbine foundations act as artificial reefs and create a new habitat for fish. But it will also change the "natural" composition of different species. In some situations will also the wind turbine foundations work as refuge for fish since it is prohibited to use trawlers inside the wind power parks [4].

The impact of electromagnetic fields from the cables can also have a local impact on fish.

The biggest impact is during the installation when the seabed can be drastically changed and alter the "natural" habitat for a long time. Also the noise can disturb the fish and even destroy the sensitive hearing organs.

Sea Mammals

Mammals like seals, dolphins, and porpoise are curious animals that often are attracted by construction activities. It is therefore important to prepare means to scare them away from the construction site during installation in order not to damage their sensitive organs. Research has showed that the mammals return to the area within a couple of months after the installation has been completed [5].

Technology

Offshore Wind Turbines

Wind turbines used offshore are exposed to a harsh environment. Until now "marinised" onshore wind turbines have been used which is logic since it is important to use a reliable design offshore. Several factors do however indicate that special offshore wind turbines will be developed in the near future. The market is expanding rapidly and there is a big need of new technology. The investments are however very big and it will take some time before the market feels confident in investing in new technology.

Onshore wind turbines "marinised" for offshore use can be characterized as well proven technology, modified for offshore use. Better corrosion protection, dehumidifiers, and additional cranes in nacelle are examples of some of these modifications (Fig. 9).

Offshore wind turbines based on onshore technology can be characterized as well-proven technology with integrated solutions developed for offshore. Automatic lubrication systems, integrated backup systems for redundancy, and monitoring systems are examples of these solutions.

Next generation of big wind turbines are entering the market with sizes up to 10 MW and a rotor diameter of 150 m (Fig. 10).

Advanced offshore wind turbines are under development and a big variety of future trends can be identified; Fig. 11 is an example of a new design with a downwind located two-bladed rotor, direct-driven generator, and where the foundation continues all the way up to the nacelle. It will result in a low-weight wind turbine, which also is easier and therefore cheaper to install.

The future development is toward

Offshore Wind Power. Figure 9
Siemens 2.3 MW (Siemens)

Offshore Wind Power. Figure 10
Clipper 10 MW (Clipper)

Offshore Wind Power. Figure 11
2-B Energy 6 MW (2-B Energy)

- Bigger wind farms. One advantage offshore is the available space. The cost of installation and operation is bigger offshore than onshore so the bigger the wind farms are the more cost effective will the final production of electricity be.
- Bigger wind turbines. Each wind turbine needs an expensive foundation and also the service cost offshore is big so the fewer the number of turbines the better it is. Of course assuming that each wind turbine will have a high reliability.

- Simpler wind turbines. It is better to make each wind turbine simple to bring the cost down and the reliability up. The quality of the electricity can be arranged onshore before feeding it into the grid.
- Permanent magnet generators. They are heavier but the disadvantage in regard to transport and installation is less offshore. The advantage by eliminating the gearbox is big.
- Modular design will make it easier to repair/replace components.
- Integration of the wind turbine with the foundation will also be of interest to bring the total weight and cost down.

Foundations

Most of the offshore wind projects built today use monopiles or gravity-based foundations designed for shallow waters down to 20 m. Future sites will however require new concepts designed for deeper waters. Floating foundation structures are also under development but it is still not competitive for the big majority of recognized sites.

The design of the offshore foundations is more complicated than onshore. The foundation and the wind turbine tower act as one structure and the total eigen frequency must stay within a frequency window, prescribed by the wind turbine manufacturer to guarantee a safe operation. The loads are a combination of wind, waves, current, ice plus normal and extreme operation loads. Individual calculations must be carried out for different water depths and soil conditions. The design process is normally carried out as a couple of iterations until a final design can be established that fulfills the requirements (Fig. 12).

Gravity-based foundations are used in shallow waters and have proven to be very cost effective. The seabed must be capable to support the weight of the foundation. The structure has a large flat base to resist overturning moments imposed by the rotor. The size is depending on the water depth and the wave conditions. An ice-breaking cone is normally used in

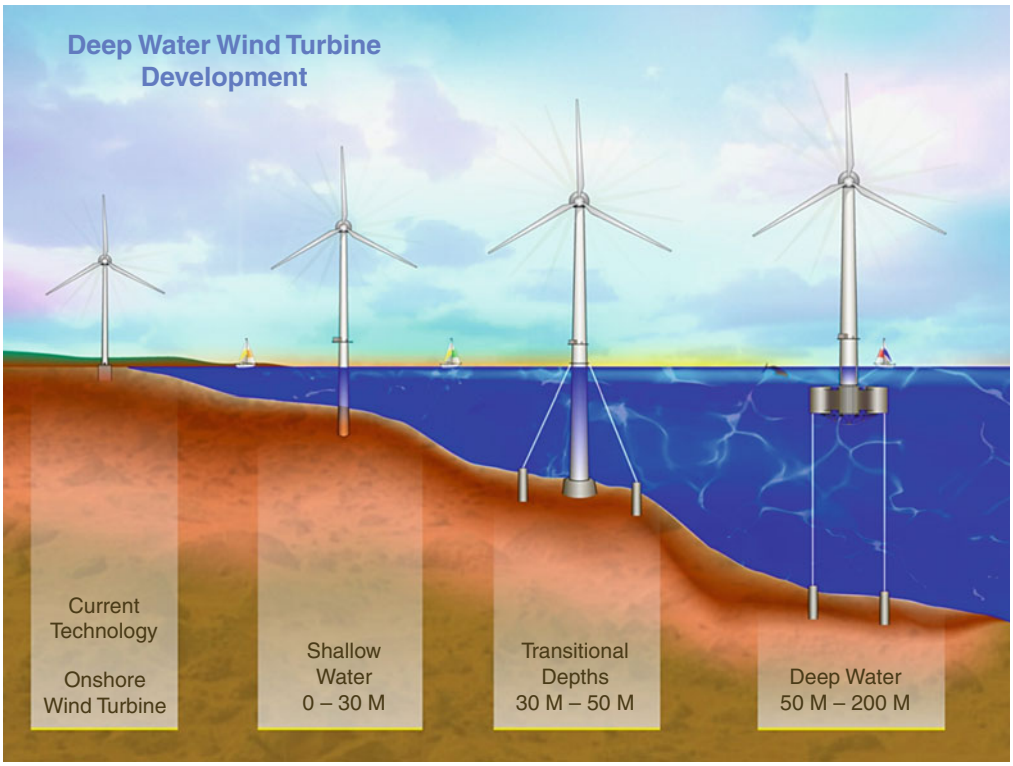

Offshore Wind Power. Figure 12
Foundations (NREL)

icy waters and the ice-cone can also be used as an access platform. This is specifically suitable in areas without tidal changes which is the case in the Baltic Sea. The gravity-based foundation can be prefabricated on shore and towed out to the location, either loaded onboard a barge or floating. When correctly positioned, the foundation is lowered down to the seabed which has been prepared in advance. Ballast material consisting of stones or other suitable material is then filled inside the foundation to ensure final stability (Fig. 13).

Monopile foundations are quite common and used in water depths between 15 and 40 m. A monopile consists of two major parts; one pile and one transition piece, both made by high-grade steel.

The pile is a cylindrical tube that is hammered down into the soil using a hydraulic hammer. Suitable soil conditions for monopiles are sand and silt layers. Hard rock and areas with big amount of boulders makes the installation of the piles more complicated and expensive since it also requires predrilling.

The transition piece is the top part on which the tower is bolted. The transition piece is fully equipped with boat landing system, platforms, davit crane, navigation lights, etc. It is also possible to locate some of the switchgear equipment inside the transition piece.

The transition piece is connected to the pile with a grouting system that also is capable to compensate any misalignment caused during the installation phase. The grouting system is a concrete-based material, with or without fibers that is able to cure in relatively low temperatures, normally 5°C. The grouting process requires stable weather conditions during the hardening period to ensure that the desired tolerances are kept.

The advantages with monopiles are that they can be produced rather cheap and all necessary secondary steel such as boat landing systems can be preinstalled onshore. The slender design also minimizes the wave and ice loads on the structure.

The disadvantages are that the size of the monopiles increases drastically with bigger wind turbines which results in more weight and fewer production facilities that can roll and weld the structures. Installation is also getting difficult when the diameter of the monopile increases since there are no hydraulic hammers available on the market. Underwater noise during the piling operation is also an issue that needs careful consideration (Fig. 14).

Jacket structures have been used successfully within the offshore oil and gas industry for many years. They are characterized by low weight and suitable in water

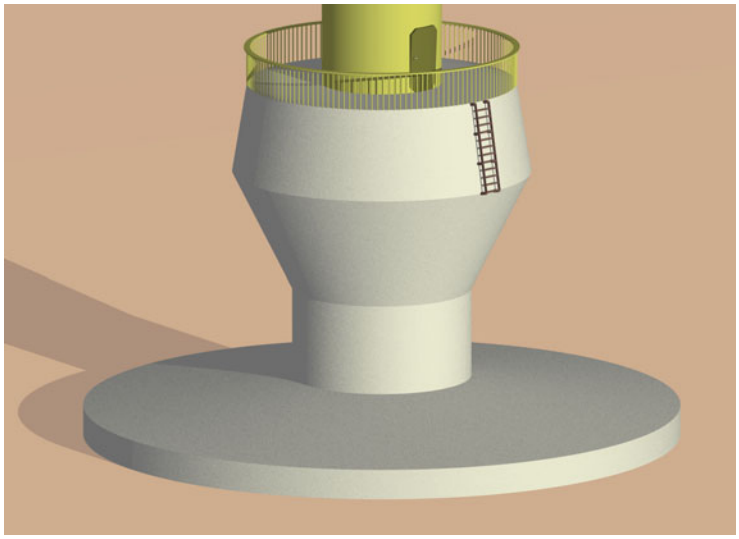

Offshore Wind Power. Figure 13
Gravity-based foundation (Garrad Hassan & Partners)

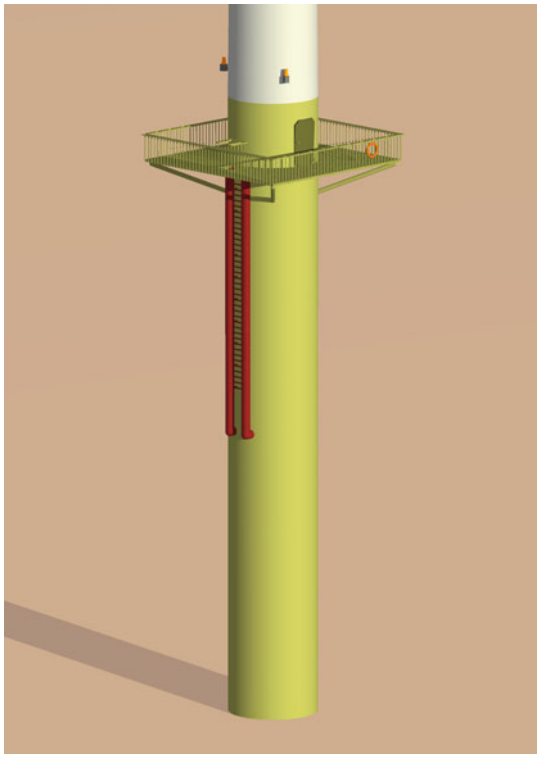

Offshore Wind Power. Figure 14
Monopile foundation (Garrad Hassan & Partners)

depths over 20 m. The most common type is a four-sided but also three-sided jackets are available.

The jacket is secured to the seabed by piles, located in each corner. The piles are driven into the seabed by a hydraulic hammer to suitable depth. Bedrock and big boulders can be a problem.

The piles can be preinstalled using a template or installed through the jacket sleeves. The connection between the piles and the jacket can be by grouted or swedged. Grouting is cheaper but requires a longer period of stable weather. A swedged connection is done by inserting a hydraulic tool inside the jacket pile, expanding the tool and thereby causing a permanent deformation between the jacket sleeve and the mono pile. Swedging is a fast but expensive method.

The advantages with jackets are that they are stiff constructions that can be used in deeper waters without increasing the steel weight drastically. It is also possible to use standardized dimensions of pipes, connections, etc., which will keep the costs down when building big number of foundations.

The disadvantage is that it is more complicated to arrange with secondary steel such as boat landing systems, etc., and the installation procedure is also more complicated and expensive (Fig. 15).

Tripod foundations are being considered for deeper waters but the optimum solution is not yet certain and may well be a concept currently being brought into the field by offshore and coastal engineering specialists. There has already actually been one offshore wind turbine constructed on a tripod, the first wind turbine built at Nogersund in Sweden; however this was a small turbine located in shallow water for demonstration purposes (Fig. 16).

Floating foundations are more expensive than bottom-mounted foundations and suitable for deeper waters. The potential for floating foundations is going to depend whether the current cost disadvantages can be overcome by the development of innovative solutions to constructions and installation. Countries in North Europe are fortunate in that many have significant stretches of shallow water near to their shore and these will be the first to be developed. But the energy potential is however enormous if deeper waters can be utilized and interesting concepts are under development (Fig. 17).

Internal Electricity Grid or Offshore Collector System

The wind turbines are connected to an offshore substation (OSS) unless the distance to shore is very small (<8 km), making it possible to bring the electricity direct to shore from the individual wind turbines.

All wind turbines today produce AC power. It is possible that this may change in the future but today they all have a small AC transformer on each wind turbine (in the nacelle or in the bottom of the tower), transforming the voltage to a suitable voltage, depending on the distance to the OSS or to the shore.

The internal electricity grid consists normally of medium voltage AC cables (33 kV is a common voltage used for the internal grid). The cables are designed with three core cables made of copper or aluminum, often integrated with fiber optics and protected by a rigid armor layer.

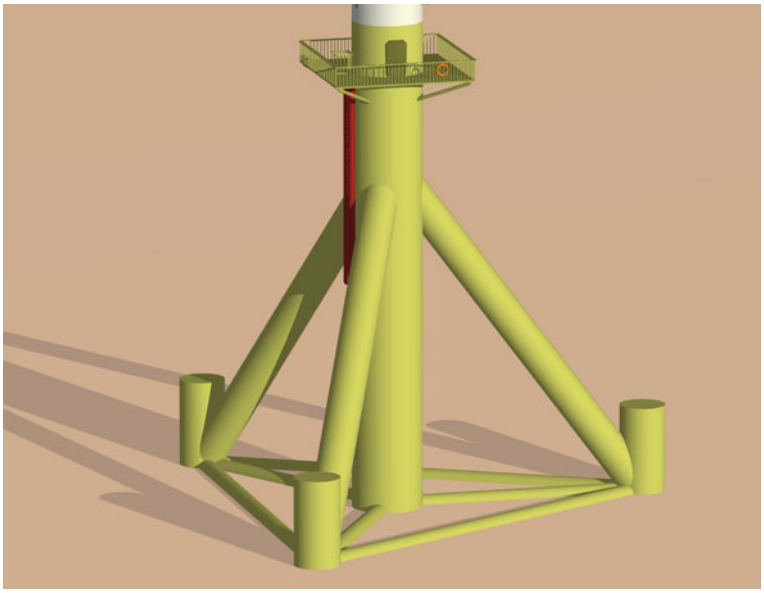

Offshore Wind Power. Figure 15
Tripod foundation (Garrad Hassan & Partners)

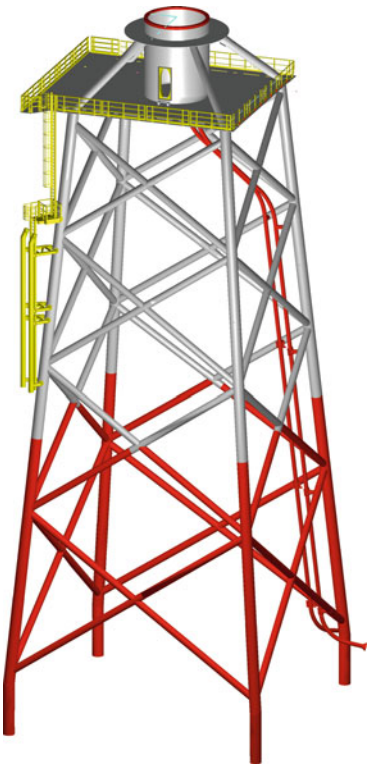

Offshore Wind Power. Figure 16
Jacket foundation (OWEC Tower AS)

Offshore Wind Power. Figure 17
Hywind (StatoilHydro)

The layout of the internal grid is based on radial feeders or ring feeders or a mixture of the two. Radial feeders are cheaper but the disadvantage is that a single fault on the cable can cut out a complete string of wind turbines.

The installation of the cables must be carried out with great care to avoid any damages. The installation of the wind turbines and the foundations are often carried out by jack-up vessels which means that the foot print of the jack-up vessel must penetrate the sea bottom without damaging the cables. Installation of the electric cables is normally carried out after the installation of the foundation but before the wind turbines since the wind turbines needs to be energized as soon as possible after the installation to prevent any damage on gear boxes, bearings, etc.

The internal sea cables are normally buried in the seabed to protect the cables from damages by erosion from current, local fishing, anchoring, etc.

Connection to Shore and Offshore Substation

An offshore substation is located within the internal grid so that the layout of the internal grid can be optimized in regard to cable losses and installation costs. The OSS accommodates switch gear for the low voltage (used for the internal grid) and for the high-voltage system (used for the connection to the shore) together with a suitable transformer. The OSS can also accommodate accommodation facilities together with a helicopter pad and other required control equipment (Fig. 18).

The deployment of offshore wind power requires a dedicated offshore electricity system. Europe's offshore grid should be built to integrate the expected 40 GW of offshore wind power by 2020, and the expected 150 GW of offshore wind power by 2030. Both AC and DC systems will be used. AC systems are generally cheaper but has the disadvantage of bigger cable losses and requires reactive compensation if the distance is too big. DC systems, on the other hand must have an AC/DC converter station offshore and a DC/AC converter station onshore. These converter stations also suffer from considerable losses even if the expectations are that the losses will drop significantly in the future when new materials like silicon carbide can be commercially used. Exactly where the limit is regarding maximum distance for AC cables must be determined for each individual project (Fig. 19) [6].

The utilization of HVDC (high voltage direct current) technology is attractive due to lower losses and because it offers the controllability needed for implementation of big amounts of offshore wind power.

Conventional HVDC (also called line commuted converter) has been used for a long time for transmission of electricity and more than 60 GW has been installed worldwide.

Offshore Wind Power. Figure 18
Subsea station Alpha Ventus (Vattenfall)

Offshore Wind Power. Figure 19
Medium voltage cable ABB cable XLPE 10–220 kV AC (ABB)

Offshore Wind Power. Figure 20
HVDC-light cable ABB 50–150 kV (ABB)

Voltage source converter (VSC)-based HVDC technology is a possible alternative that has big advantages since it does not require a strong offshore or onshore AC network and it is also possible to control the active and reactive power supply independent of each other (Fig. 20).

Until now, almost offshore wind power farms operate with AC systems. The first DC systems werer introduced in 2010, connecting the Bard 1 offshore wind park located 100 km from the shore to the German mainland.

Installation

Offshore wind parks are getting bigger and bigger. Projects with a total installed capacity of 1,000 MW are in the planning process now. Common size of offshore wind Turbines today is between 2.3 and 5 MW. This means that a 1,000 MW offshore wind power plant, using 5 MW turbines, consists of 200 wind turbines, a huge internal grid, a couple of offshore substructures to carry the transformers and other electric equipment and finally several export cables to connect the offshore wind power plant to the onshore grid (Fig. 21).

Offshore wind power is for obvious reasons located where there are good wind conditions meaning hash environmental conditions. Northern Europe, where the majority of the development takes place, is also characterized by big seasonal variations; it is much preferred to carry out installation work during spring and summer.

What can be done onshore must be carried out onshore. Everything is more complicated, more dangerous, more time consuming, and more expensive offshore (Fig. 22).

Bigger wind turbines and deeper waters also call for bigger installation vessels. They exist in the oil and gas sector but they are not designed to install hundreds of structures of the same kind.

Considering the different aspects pointed out above, it is very obvious that logistics is the keyword for installation of offshore wind power plants (Fig 23).

There will always be an element of risk when installing an offshore wind farm. Risk assessment tools exist that will help the developer to anticipate the risk and decide on the best way to manage the risk.

Offshore Wind Power. Figure 21
Bard foundation (Jens Maier)

Offshore Wind Power. Figure 22
Installation vessel Svanen (Ballast Nedam)

Operation and Maintenance

Reliability

As offshore wind turbines are located at remote sites and operate under harsh environmental conditions, the demand for high reliability and low operational costs becomes higher compared with onshore wind turbines.

Many systems have full redundancy by using backup systems for lubricating systems, hydraulic motors, etc. Conditioning monitoring systems of the drive train is used to detect component errors at an early stage.

Calendar-based maintenance is as far as possible replaced by condition-based maintenance.

Availability

The availability of a wind farm is defined as the percentage of time it is able to produce electricity. It is a function of reliability, maintainability, and serviceability of the wind farm. And the accessibility is an important factor for offshore wind energy.

The availability is in general lower for offshore wind power plants compared with onshore. The environment is tougher but the main reason is that it takes longer time to get out to the wind turbines and severe failures are more difficult to repair. The reliability of the

Offshore Wind Power. Figure 23
Installation of Beatrice Jacket foundation (Talisman UK Ltd)

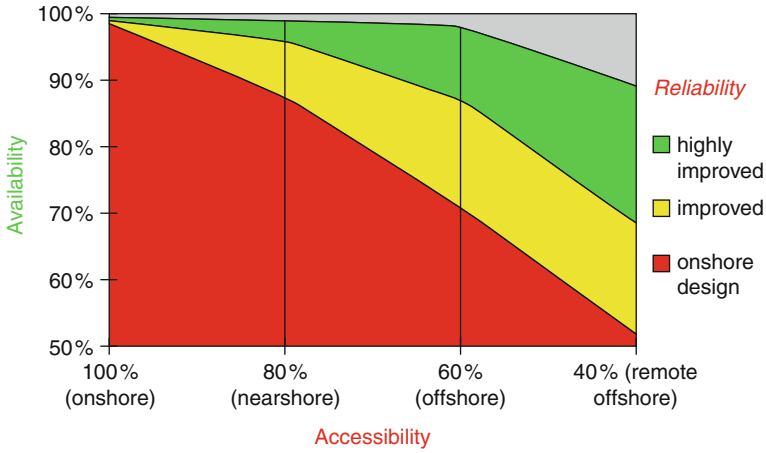

Offshore Wind Power. Figure 24
Availability (Delft University)

offshore wind power plant has been described above and it is a necessity to increase the reliability if the availability can be improved. Figure 24 shows in theory the impact on availability if the distance to the shore increases and if onshore technology is used offshore without modifications.

The other important factor is to improve the access to offshore wind farms. The general rule is to "keep it simple and robust" and "don't compromise with safety."

For access to offshore wind turbines, every site is different. Key factors influencing the design of the access system are distance from harbor, wind direction, wave fetch, wave height, tide levels, current, safety regulations, and possibly ice and of course the type of foundation used.

The environmental conditions can be described as "normal conditions" and "extreme conditions." "Normal conditions" describe the time the wind power plant is operating as planned and when the sea

Offshore Wind Power. Figure 25
Swath (Abeking & Rasmussen)

Offshore Wind Power. Figure 26
Ampelmann access system (Ampelmann Operations)

conditions are acceptable for transport and access. This time corresponds to 70–80% of the time in European waters. "Extreme conditions" are characterized by high waves, extreme wind speeds, and ice. This time corresponds to about 20–30% of the time in European waters.

The access system must be able to work during "normal conditions" but to what content it shall be able to work in "extreme conditions" is an optimization that has to be done for each project. A combination of different systems like combining "normal" crew vessels with helicopters can also be the optimal solution.

There are a big number of different vessels available on the market today and specially designed systems are currently under development. Mono hull vessels are most common but catamarans have an advantage being more stable and faster although the cost for the vessels is higher. Specially developed vessels like SWATH will further improve the capability in high

seas. It is also possible to use helicopters, but only for winching down one person at the time onto the nacelle roof [6].

Figure 25 shows a design called SWATH that is characterized by small water plane displacement and submerged hull pontoons that results in high transfer speed and very good stability during docking.

Different methods exist on how to dock the vessel to the structure:

1. Pushing the vessel against the structure with propeller thrust
2. Tying the vessel to the structure
3. Keeping the vessel at a short distance from the structure

Methods 1 and 2 above are most common but method 3 is getting more interesting when using more sophisticated systems like the Ampelmann system which is based on a computer-controlled platform that is located on the vessel and compensates for all motions up to 2.5 m significant wave height (Fig. 26).

Economy

Offshore projects require initially higher investments than onshore due to turbine support structures and grid connection. The cost of grid connection to the shore is typically around 25%, which is a much higher fraction than for connection of onshore projects. Other sources of additional cost include foundations (up to 30%), operation and maintenance (with expected lower availability), and marinisation of turbines. Figure 27 shows a possible distribution of the capital investment costs; however, the water depth and distance to shore can have a significant impact on redistributing the costs. Note that the O&M costs are excluded and these will typically amount to around a quarter of the levelized production costs (LPC). The similar magnitudes of cost for several different components (wind turbine, support structure, power collection and transmission, and O&M) emphasizes the importance of an integrated approach to the design of the whole wind farm development.

Future Directions

Offshore wind power will grow significantly during the next decade. The major development is expected to be in European waters and the reason is that there are good wind conditions, need of renewable energy, and highly populated areas in Europe. It is still a young technology with very big potential for further development in order to get the costs down.

Large-scale wind turbines in the size of 10–20 MW especially designed for offshore applications will be developed together with integrated designs of innovative floating and bottom-mounted substructures. The manufacturing of the substructures will also be more automated so that big number of similar structures can be fabricated in a cost-effective way.

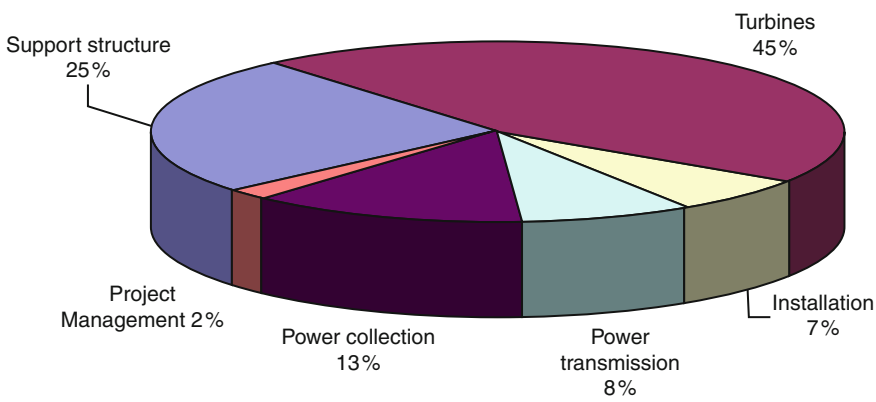

Offshore Wind Power. Figure 27
Typical distribution of cost from an offshore wind farm (Delft University)

Offshore Wind Power. Figure 28
New installation vessels (Beluga Hochtief)

Development of innovative logistics including transport and installation techniques are also foreseen together with the development of new design tools and improved offshore wind energy standards (Fig. 28).

Development of grid integration techniques for large penetration of offshore wind energy is necessary including:

- Grid connection and power transmission
- Secure and stable system dynamics
- Balancing and market operation

Finally, the offshore wind power sector needs continuous technology transfer from the oil and gas sector and a well-planned education and training program so that the increasing market for offshore wind power does not get hampered due to lack of experienced engineers and technicians.

Bibliography

Primary Literature

1. EWEA (2009) The European Off-shore wind industry – key trends and statistics
2. EWEA Oceans of Opportunity. www.ewea.org
3. Hüpopp O, Dierschke J, Exo K-M, Fredrich E, Hill R (2006) Bird migration and off-shore wind turbines. In: Köller J, Köppel J, Peters W (eds) Off-shore wind energy: research on environmental impacts. Springer, Berlin/Heidelberg
4. Aspects of off-shore renewable energy and the alterations of marine habitats (2009) Dan Wilhelmsson doctoral thesis in anomal ecology at Stockholm University, Sweden, ISBN 9789171559708
5. Summary on seal monitoring 1999–2005 around Nysted and Horns Rev Off-shore Wind Farms (2006) Technical report to Energi E2 A/S and Vattenfall Ministry of the Environment Denmark
6. Off-shore Wind Power, John Twidell and Geatano Gaudiosi, Multi-Science Publishing Co. Ltd, ISBN 9780906522639

Books and Reviews

Design and operation of power systems with large amount of wind power, ISBN 978-95138-66334

DNV off-shore wind turbine guideline DNV-OS-J101

European Wind Integration Study (EWIS) Final report 2007-01-15

EWEA Pure Power wind energy targets for 2020 and 2030. www.ewea.org

Guidelines for the certification of off-shore wind turbines, Germanisher Lloyd IV Industrial Services

IEC 61400–1 Design requirements for Wind Turbines

IEC 61400–3 "Design requirements for Off-shore wind turbines"

Initial conceptual designs for off-shore electrical collector system, Graham Ault, doc no EC/DOWNVIND/TR/2005-001, University of Strathclyde in Glasgow

Off-shore Windenergie wab. www.windenergie-agentur.de

Overview of transmission solutions for the connection of large off-shore wind farms to the on-shore power system, Thomas Ackermann, Report from Royal Institute of Technology, Department of Electrical Engineering

Strategic Research Agenda TPWind secretariat European wind energy technology platform

Submarine Power Cables Thomas Worzyk Springer Verlag ISBN 9783642012693

Oil and Natural Gas: Global Resources

Peter J. McCabe
School of Earth, Environmental and Biological Sciences, Queensland University of Technology, Brisbane, QLD, Australia

Article Outline

Glossary
Definition of the Subject
Introduction
Oil and Gas in Conventional Fields
Tight Gas
Oil Sands
Coal Bed Methane
Oil Shale and Shale Oil
Shale Gas
Gas Hydrates
Estimated Volumes of Remaining Oil and Gas Resources
Future Directions
Bibliography

Glossary

Coal bed methane (CBM) Natural gas (methane) that can be extracted from coal beds. Synonymous with coal bed gas and coal seam gas (CSG).

Conventional oil and gas Oil and natural gas that occur in the subsurface and that can be produced using conventional methods of well drilling.

Gas hydrates Accumulations of natural gas that are trapped in ice-like crystalline solids consisting of gas molecules surrounded by cages of water molecules. Hydrates are stable at certain temperatures and pressures within some sea-floor sediments and within permafrost in polar regions. Synonymous with gas clathrates.

Oil sands Sandstones that are naturally impregnated with bitumen, a highly viscous form of petroleum. Synonymous with bituminous sands and tar sands.

Oil shale A rock that contains significant amounts of solid organic chemical compounds (kerogen) that can generate oil when heated.

Reserves The discovered, but not yet produced, amounts of oil or gas that could be extracted profitably with existing technology under present economic conditions.

Resources The amounts of oil and gas that have been discovered plus the estimated amount that remains to be discovered.

Shale gas Natural gas that is produced from shale.

Tight gas Natural gas that is extracted from rocks with very low porosity and permeability and which is, therefore, relatively difficult to produce.

Unconventional oil and gas Oil and natural gas accumulations that require extraction techniques that allow easier flow of oil and gas to a well (for example, hydraulic fracturing to open pathways or in situ heating to reduce viscosity) or by processing after mining.

Definition of the Subject

Crude oil and natural gas (mostly methane but including some longer-chain hydrocarbons) have been used by humans for thousands of years for a variety of purposes including lighting, heating, and medicinal uses. However, use was limited by access to natural seeps of oil and gas and the available technologies to extract and store the products. The earliest known oil wells were drilled in China in the fourth century using bamboo. It was not, however, until the mid-nineteenth century that large-scale production began, when metal piping allowed deeper drilling into hard rock. Early commercial production began in Poland and Romania and this was followed rapidly by drilling successes in the Russian Empire, in what is now Azerbaijan, and in the United States. Development of the process of fractional distillation at this time fuelled the demand for crude oil, which could now be economically refined into kerosene for use in oil lamps. The development of the internal combustion engine also created a demand for oil and this greatly expanded with Karl Benz's invention of the gasoline-powered automobile, patented in 1886. The transport sector became the dominant user of oil and currently accounts for 61.4% of oil consumption [1]. Other major uses include lubrication, chemical feedstock, and domestic heating. Production has risen dramatically over the last century (Fig. 1) and production of crude oil today is approximately 73 million barrels per day (a "barrel" is 42 US gallons).

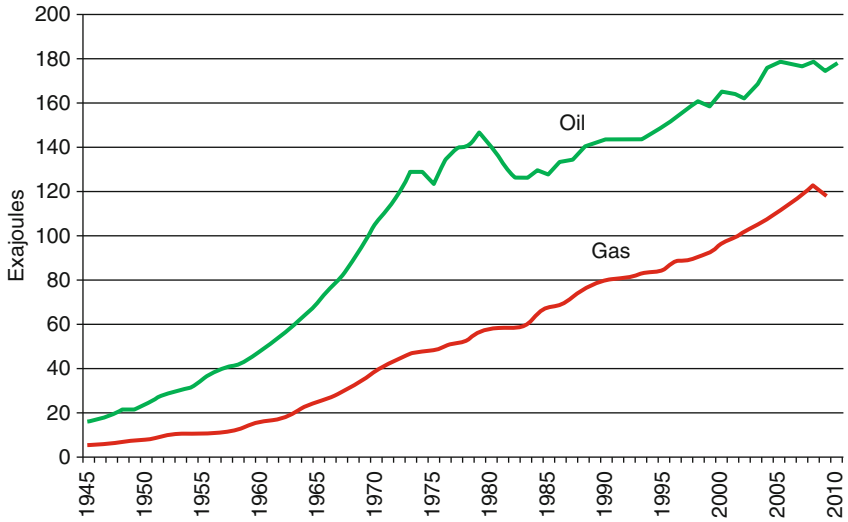

Oil and Natural Gas: Global Resources. Figure 1
World production of crude oil and natural gas since World War II expressed in units of energy for comparative purposes. Based on EIA data [2]

The United States dominated world oil production for the first half of the twentieth century, accounting for over 50% of the world's annual production until 1960. After World War II demand for oil increased at a rapid rate and production increased fivefold between 1950 and 1972. As the world economy rapidly grew, international trade in oil was facilitated by the development of supertankers. The dominance of the United States decreased as several other regions increased their share of production, particularly the Middle East and the Soviet Union. The Organization of the Petroleum Exporting Countries (OPEC) was formed in 1960 and by 1972 was responsible for over 50% of the world's oil production. The cartel restricted the supply of oil during the 1970s, resulting in a fivefold increase in prices. The resulting fall in demand and oversupply led to a price collapse in the early 1980s. OPEC has subsequently never exceeded 42% of world production [2] but the rapid economic expansion of many countries in the first decade of the twenty-first century resulted in relatively high prices again as demand increased substantially. Today 60% of the world's oil production is from six countries, of which five belong to OPEC (Table 1).

Oil and Natural Gas: Global Resources. Table 1 Major producers of crude oil. From [1]

Country	% of world total
Russia	12.9
Saudi Arabia	11.8
USA	8.3
Iran	5.4
China	5.0
Canada	4.0
Mexico	3.8
Venezuela	3.3
Kuwait	3.2
U.A.E.	3.1
Rest of world	39.2

Although natural gas had long been used in limited amounts for illumination, much of the natural gas that was originally discovered in association with oil was vented or flared because there was no way of commercializing the gas. Reliable pipelines to transport gas were not developed until after World War II. Natural gas is now used primarily for electrical generation in power plants, domestic heating, manufacturing fertilizers, and for other industrial purposes. World production of natural gas grew steadily in the 30 years after World War II, though at a slower rate

than oil production. Production was dominated by the United States, which produced over 50% of the world's annual production until 1973. Since the early 1970s world gas production has risen at a similar rate to oil production (Fig. 1). While the market for natural gas was once limited to the reach of pipelines, natural gas can now be transported globally using liquefied natural gas (LNG) tankers. This requires removal of impurities and cooling of the gas to approximately −160°C. LNG now accounts for 6% of the global market. Today ten countries produce 65% of the world's natural gas (Table 2).

Together oil and natural gas currently comprise 54.3% of the world's total annual consumption of energy and, as such, are a major foundation of the global economy. In particular, the transportation of food, raw materials, and goods to market, as well as public and private transport systems, are all heavily dependent on oil and natural gas: they fuel over 96% of the transport sector. On the negative side they are a major source of CO_2 emissions, though cleaner than coal per unit of power generated. The successful development of cleaner and economically viable alternative fuels is essential in the long run but the world's economy today is heavily dependent on the supply of oil and natural gas. This raises the question as to how much oil and natural gas remain in the ground. How long will oil and gas resources be available for mankind?

Oil and Natural Gas: Global Resources. Table 2 Major producers of natural gas. From [1]

Country	% of world total
USA	19.2
Russia	19.0
Canada	5.1
Iran	4.6
Norway	3.4
China	2.9
Qatar	2.9
Algeria	2.6
Netherlands	2.5
Indonesia	2.5
Rest of world	35.3

Introduction

Predictions of future shortages of oil began shortly after commercial production started in the late nineteenth century. In the first half of the twentieth century, there was national concern about imminent and irreversible shortages of oil on at least six occasions [3]. In the 1950s M. King Hubbert, a geophysicist at Shell Development Company in Houston, developed a model of a cycle of production of finite nonrenewable resources that aimed to predict future production from analysis of production-to-date and estimates of the amount of remaining resource in the ground [4, 5]. In a series of publications Hubbert predicted that US oil production would peak by 1975 at the latest: actual peak production was in 1970. The peak in US production gave credence to Hubbert's methodology, which is now commonly referred to as the "Hubbert curve" [6].

Fears arose of global depletion of fossil energy resources. In 1972 a report for the Club of Rome, a global think tank, examined known reserves of oil and gas and predicted the time of total depletion under various scenarios [7]. Assuming exponential growth in consumption, the report predicted depletion of known reserves of oil by 1992 and natural gas by 1994. Even under what was considered an optimistic scenario wherein reserves could be increased fivefold by new exploration, oil was predicted to be totally depleted by 2022 and gas by 2021. These predictions, though influential at the time, proved unfounded largely because consumption did not increase at an exponential rate.

In 1962 Hubbert predicted that world oil production would peak in 2000 and, again, in 1969 predicted the peak would be between 1990 and 2000 [5]. As the turning point of the millennium approached predictions of "peak oil" increased. Most of the predictions suggested a peak in the first years of the twenty-first century. For example, in 1988 Campbell, using the Hubbert curve analysis, predicted a peak between 2000 and 2005 [8]. Actual production between 2006 and 2010 has been 4.7% higher than in the previous 5 years (Fig. 1). However, predictions of imminent "peak oil" persist and proponents point

out that production has been relatively level for the last 6 years (to 2010). Others point to global political and economic reasons for the recent relatively flat production rate.

The basic problem with the Hubbert curve analysis is that estimates of remaining resources change through time. The amount of oil and gas on the planet is undoubtedly finite. The amount is large but much of it would be prohibitively expensive to produce using present-day technologies. Resource estimates therefore tend to focus on oil and gas accumulations that are anticipated to be economically viable for production, either at present or within the foreseeable future. Advances in technology, however, may make accumulations technically accessible at lower costs over time, thus increasing the size of estimated remaining resources. In addition, advances in geologic concepts and subsurface imaging through geophysical techniques have shown oil and gas resources to be substantially more extensive than was at one time thought. As a result, many predictions using the Hubbert curve analysis have been far less successful than Hubbert's prediction of US peak production. Hubbert [5] in 1962, for example, predicted US natural gas production would peak in 1975 but production in 2010 was at an all time high. Another example is Campbell's 1988 prediction [8] that underestimated US oil production in 2010 by 70%.

The following sections describe the various types of geologic occurrence of oil and gas and how scientific and technological advances have changed the perception of the size and economic viability of the resources over the last few decades. Oil and gas resources are often divided into conventional or unconventional resources. The definition of what is conventional varies between authors but generally refers to those resources that can be produced using long-established methods of well-drilling where the oil and gas can be brought to the surface under its own pressure or by pumping without significant stimulation such as in situ fracturing of the host rock. Unconventional resources, by contrast, require more complex methods of extraction of the resource from the host rock. They include tight gas, oil sands, coal bed methane (CBM), shale gas, shale oil, and gas hydrates.

Oil and Gas in Conventional Fields

Oil and gas is generated from organic-rich rocks by thermogenic or biogenic processes. When such "source rocks" are exposed over periods of geologic time to high temperatures the organic material breaks down releasing oil and gas that then migrate toward the surface due to buoyancy. The temperature required for thermal maturation of a source rock varies depending on the type of organic material but the minimum temperature for oil generation is approximately 50°C and for gas generation is 100°C. Most thermogenic oil and gas are generated at depths of 2–6 km. Methane may also be produced from source rocks by the biogenic breakdown of organic material in source rocks. Such biogenic gas is produced at lower temperatures and at shallower depths. Whether of thermogenic or biogenic origin, oil and gas can be trapped by buoyancy in "reservoirs" in porous rocks beneath an impermeable layer of rock typically at depths of over 1 km. The permeable nature of the host rock, high pressures related to depth of burial, and the concentration of oil and gas in discrete reservoirs allow relatively easy extraction of oil and gas by drilling wells. Until the 1990s almost all the world's oil and gas production was produced from such "conventional" fields. Natural gas in conventional fields may occur with ("associated gas") or without ("nonassociated gas") oil. In either case the gas may contain compounds that can be separated at the surface as liquids. Natural gas liquids (NGLs) such as propane, butane, and pentane are sometimes included in reporting oil production but are not insignificant: they comprise, for example, 3.5% of the total energy production of the United States.

Estimates of the world's original endowment of conventional oil and gas resources have tended to increase because of the advances in technology over time [9]. Advances in geologic concepts, drilling technologies, seismic imaging, and computer modeling using large datasets have progressively revolutionized the search for oil and gas over the last century. Likewise, advances in production technologies, pipeline construction, and tankers have all made resources available that at one time would have been considered economically unviable. Advances in science and technology allow more oil and gas to be found in old fields, within existing petroleum provinces, and in new frontier regions.

Existing oil and gas fields that have already been in production for years may, at first blush, seem unusual sites to look for further reserves. However, the US Geological Survey (USGS) in 2000 estimated that 48% of the oil and 41% of the natural gas that remains to be added to reserves in the future lie within existing fields [10]. Increases in successive estimates of the estimated recoverable oil and gas are known as "reserve growth." On average, only 22% of the oil is currently recovered from fields worldwide [11]. There are many reasons for such a low percentage. Much of the oil within a reservoir rock will not easily move toward wells. Enhanced recovery methods such as gas reinjection, water-flooding, and flushing with polymers and surfactants can free up more of the oil. While such secondary and tertiary recovery methods are commonly used in mature oil fields in developed countries, they are not yet widely used in many other regions. Another reason for reserve growth is that there is rarely a single reservoir within an oil or gas field as most are split into numerous compartments, each containing amounts of oil/gas in varying amounts. Advances in seismic imaging over the last 20 years have allowed not only good visualization of these compartments but also the fluids within the compartments. At the same time, technological advances allow drilling with much greater precision permitting access to much smaller subsurface targets over time. While it will never be possible to economically drain all the oil and gas out of a field, recovery rates of over 70% may eventually be feasible in many areas [12].

Much oil and natural gas also remains to be found in undiscovered fields within existing petroleum provinces. The largest fields tend to be discovered early in the exploration history of a basin and progressively smaller ones are found over time. The infrastructure that is built to develop the larger fields allows fields to be developed that would otherwise be too small to justify the construction of pipelines, platforms, ports, and processing facilities. By analogy estimates can be made of the number and size of remaining undiscovered fields from the discovery history of a petroleum province. This methodology may underestimate the total resource if more than one type of oil and gas accumulation is present. For example, the discovery of giant oil and gas fields in the subsalt regions in offshore regions of the Gulf of Mexico added a new "play" in what was thought to be a mature oil province.

There is a strong possibility that further major accumulations of conventional oil and gas will also be found in frontier basins where little or no exploration has taken place. Most of the potential areas are in regions of deepwater or harsh climates. Over time technological advances have made exploration feasible in areas once thought inaccessible. This has been particularly true in the ability to drill to deeper depths. In 1960 any drilling in water depths over 20 m was regarded as "deepwater" but by 1980 oil fields had been found in over 300 m water depth, by 1990 in over 850 m water depth, and by 2010 in over 2,400 m water depth [13]. Total drilling depths also increased dramatically with a record set in 2009 with the discovery of the giant Tiber oil field in the Gulf of Mexico which is at 1,200 m water depth, with a total drilling depth of 10,680 m. In the last decade giant oil fields have been found in ultra-deepwater areas not only in the Gulf of Mexico but also offshore West Africa and Brazil. The giant Brazilian Tupi field lies not only in deepwater (>2,000 m) but also below a 2,000 m thick layer of salt. It is only recently that seismic technology has allowed an understanding of the structures below thick salts and drilling technologies have permitted drilling through such strata.

As in the past, technological advances will permit exploration for oil and gas in frontier regions currently regarded as inaccessible. Future exploration in deepwater will likely lead to more significant discoveries. Outside the Atlantic realm other regions with potential for deepwater exploration include offshore East Africa, the Great Australian Bight, and offshore New Zealand. There is a growing interest in the potential of the Arctic region where geologists believe there are substantial oil and gas resources but where the severe climate, ice floes, and icebergs all make exploration and development hazardous and in many areas either prohibitively expensive or impossible using currently available technologies [14].

Tight Gas

In conventional fields gas moves easily through the permeable host rock and naturally moves toward wells and up to the surface because of pressure

differences. By contrast, sandstones that have very low permeability require considerably more effort to produce the gas. These sandstones are generally thinner than those in conventional fields and have been buried to great depth. The pores in the sandstone, in which the gas is trapped, have been reduced in size by compaction and cementation during burial. These "tight sands" typically occur near the center of sedimentary basins and are sometimes referred to as "basin-centered gas" accumulations. Production of gas from tight sands requires extensive and complex drilling. Because each well produces relatively small volumes of natural gas, many wells must be drilled. Hydraulic fracturing of the host rock can increase the rate of flow of gas to a well.

Although basin-centered gas accumulations can occur over very wide geographic areas, production is generally from limited regions of a basin. The geologic nature of these so-called "sweet spots" is debated as to whether they are regions with enhanced permeability created by natural fractures in the rock or are buoyancy traps similar to conventional gas fields [15]. Resource estimates of basin-centered gas are typically very large but in some cases may be reevaluated as geologists develop a better understanding of the nature of sweet spots. Nevertheless, tight gas is undoubtedly a major resource and, historically, it has been the most important component of unconventional gas production in North America but relatively few tight gas fields have yet been developed outside of North America. Production has risen from 10% of total natural gas production in the United States in 1990 to 28% in 2009 [2, 16]. Given the magnitude and widespread nature of these accumulations in North America it seems likely that tight gas resources occur in many sedimentary basins worldwide. Exploration and development of such resources must compete with conventional gas resources that are much cheaper to produce, and which in many cases may lie at shallower depths within the same sedimentary basin. However, it is probably only a matter of time before tight gas resources are developed in many regions of the world.

Oil Sands

Oil sands are rocks that consist predominantly of sandstones which contain bitumen within the pore spaces that has been produced by the biodegradation of oils in the subsurface. Most oil reservoirs are sufficiently hot that biogenic activity is curtailed or absent. However, oil that migrates into shallow reservoir rocks may be altered completely to bitumen that is very viscous. Although found close to the surface, production of oil from oil sands is expensive. The bitumen must be heated before it will flow and commercial extraction requires large amounts of energy. Once extracted the bitumen must also be upgraded by purification and hydrogenation before it can be refined like conventional crude oil.

Although oil sands have long been recognized and used in limited ways, it is only within the last 40 years that commercial production has grown. Canadian oil sands production began in 1967 and production has grown steadily. By 2009 production from oil sands was equivalent to over 550 million barrels of oil, accounting for 49% of Canada's oil production in 2009 [17]. Though production was initially subsidized, production costs have fallen with technological advances and is now economically viable at $50/barrel and production is forecast to more than triple by 2025 [18]. Venezuela also has substantial oil sand deposits [19] and smaller accumulations are known in Russia and the Middle East.

Coal Bed Methane

The presence of methane in coal beds had long been a hazard for underground coal mining and it is only recently that this gas has been seen as an economic resource. Modern mining techniques aimed at mitigating the potential for lethal build-up of methane in mines extracts the gas during or before mining as coal mine methane (CMM), which in some cases is used for power generation. More significant from an energy resource perspective is the natural gas extracted from coal beds by wells in regions where no mining is planned: this is known as coal bed methane (CBM) or coal seam gas (CSG).

Commercial production of CBM began in the United States in 1989 and annual production had grown to almost 2 trillion cubic feet (TCF) in 2009, which was 8% of total US gas production [2]. Early production was predominantly from bituminous coals in the San Juan and Raton Basins of New Mexico and Colorado. Production from these areas still accounts

for almost 50% of US production. In 2000 production began from the lower-rank subbituminous and lignite coals of the Powder River Basin in Wyoming which by 2010 comprised 28% of US CBM production. Over the last decade, the technology and knowhow for CBM extraction has spread from the United States to other major coal-bearing regions, particularly Canada, Australia, China, and parts of Europe. Australia plans to export CBM gas as LNG [20].

CBM occurs at much shallower depths than most conventional gas fields: generally less than 900 m. Extraction of CBM, however, requires many closely spaced wells: over 20,000 wells had been drilled in the Powder River Basin [21] and over 17,000 in Alberta [22]. The gas is adsorbed onto the pore space in coals and must be released by depressurization, allowing the gas to flow toward the well along natural fractures known as "cleats" or by pathways produced by artificial hydraulic fracturing.

Oil Shale and Shale Oil

Oil can be produced from some organic-rich fine-grained rocks that are normally referred to as "shales" even if the host rock is not strictly a shale by a geologic definition. Production from such sources has a long history. Production of oil from shales for illumination preceded the discovery of conventional petroleum resources in the mid-nineteenth century but for most of the twentieth century production of such oil was a very minor component of global petroleum production. However, in the first decade of the twenty-first century there has been a resurgence of interest in these resources because of advances in technology and rising energy prices.

"Oil shales" are rocks that contain significant amounts of solid organic chemical compounds (kerogen) that have not been buried deeply enough to allow for oil maturation. Production is generally done by mining the rock and heating it in a retort in a processing plant close to the mine where the oil and associated gases can be captured. The oil may also be extracted using in situ methods which require heating the subsurface rock by injection of hot fluids, gases, or steam, or by the use of heating elements. As the oil is expelled from the kerogen it can then be induced to flow toward conventional oil wells for extraction.

The leading producer of oil shale in the world is Estonia, where 90% of the power is generated from that source. By far the largest accumulations of oil shale, however, are in the United States, particularly in the Green River Formation of Colorado, Utah, and Wyoming, that were deposited within ancient saline lake systems some 40–50 million years ago. There are also major accumulations in Devonian–Mississippian black shales in the eastern United States that were deposited in marine environments over 350 million years ago. With the high oil prices of the late 1970s a number of pilot projects produced oil from the Green River Formation in Colorado but plans for major commercial exploitation were abandoned when prices fell in the early 1980s. Interest in the potential for production has been rekindled with the high oil prices in recent years. Other countries with significant oil shale accumulations include Australia, Brazil, the Democratic Republic of the Congo, and Russia [23].

"Shale oil" is oil that is trapped within a fine-grained rock. Extraction of the oil does not require heating but the low permeability of the rocks requires that the rock be artificially fractured in situ to allow flow toward a well. Once regarded only of scientific interest, recent advances in hydraulic fracturing have made shale oil economically viable in some areas. The best known shale oil accumulation is the Bakken Formation of the Williston Basin of Montana and North Dakota and adjoining parts of Canada [24]. From a geologic perspective, the Bakken is a petroleum source rock that reached maturation but, unlike most mature source rocks, the oil was never expelled to migrate to conventional traps.

Shale Gas

Natural gas is present in some organic-rich mudrocks. Shale gas has been produced in small quantities for well over a century but recent advances in technology allow much higher rates of production. Shale beds are relatively thin and vertical wells provide access to a very limited volume of rock. It is now possible to drill at any angle and to deviate wells at depth to follow individual shale beds over great distances, allowing access to large volumes of gas-bearing shale. While production used to be primarily from naturally fractured shales, much recent production from

shales is aided by hydraulic fracturing technologies. The fractures provide avenues for gas migration toward the wells.

The new technologies for shale gas production have revolutionized US gas production. Shale gas production was approximately 1% of total US production in 2000 but had risen to 14% of total production in 2009 and is forecast to be 45% of production by 2035 [2]. The potential of shale gas has been questioned by some [25]. Like tight gas, production is from sweet spots whose nature and lateral extent remains to be better defined. The dramatic rise in US production has, however, spurred interest in shale gas in many other parts of the world, especially in Canada, Central Europe, China, India, and Australia.

Gas Hydrates

Gas hydrates (also called clathrates) are solid ice-like substances consisting of rigid cages of water molecules that enclose molecules of gas – mainly methane. Hydrates are stable in a restricted range of temperatures and pressures and occur in two regions: in polar regions, where they are associated with permafrost, and at shallow depths in sediment on the outer continental shelves, in water depths over 300 m [26]. Hydrates can pose an environmental problem because natural breakdown of accumulations can result in slumping of the seabed and outgassing of methane to the atmosphere. On the other hand, if appropriate technologies are developed, hydrates may be a future source of natural gas. Current technologies allow production only at costs substantially above the market prices that have prevailed over the last decade [27]. Production would require depressurization, thermal stimulation, or injection of inhibitors to destabilize the hydrate lattices, releasing the methane to flow toward wells.

Estimated Volumes of Remaining Oil and Gas Resources

Proved reserves are the volume of known oil and gas accumulations that can be produced at a profit under existing economic and operating conditions. Estimates of world-proved reserves of oil and gas are compiled using best available information by several organizations including the International Energy Agency, IHS Energy, and BP. Proved reserves of oil and gas are not routinely reported in many countries. In fact, some of the largest producers consider reserves as state secrets. This lack of transparent reporting has led some to question the size of global reserves giving credence to predictions of imminent production declines [28]. However, though differing in detail the reserves estimated by different agencies are similar in estimated overall size. As of the end of 2009, BP [29] estimated globally proved reserves of 1,333 billion barrels of oil (BBO), equivalent to over 45 years of production at 2009 rates. With the exception of 237 billion barrels of oil in the Canadian oil sands, these reserves are entirely of conventional oil. BP also estimated globally proved reserves of natural gas at 6,621 trillion cubic feet (TCF), equivalent to 63 years of production. These reserves are predominantly conventional gas.

In addition to proved reserves, there are undiscovered resources and "contingent resources" that are currently noncommercial but could probably be produced under different economic conditions. The most recent comprehensive global estimate of undiscovered oil and gas resources was published by the USGS in 2000 [10]. This was a geologically based study of 128 geologic provinces that included the producing basins that accounted for more than 95% of the world's known oil and gas outside of the United States. The study also examined the discovery history of each province up to 1996. The report included probabilistic estimates of the volumes of conventional oil, gas, and natural gas liquids that might be added to proved reserves from new field discoveries in the studied provinces from the 1996 baseline. The assessment estimated that there was a 95% chance of discovering another 334 BBO of conventional oil and a 5% chance of discovering 1,107 BBO. The median estimate, the 50% chance, was that 607 BBO of oil might yet be found in the studied provinces. For conventional natural gas, the assessment estimated that there was a 95% chance of discovering another 2,299 TCF and a 5% chance of discovering 8,174 TCF. The median estimate was that 4,333 of natural gas might be found in the studied provinces.

More recent estimates by the USGS that have concentrated on specific regions of the world suggest that

on balance their 2000 estimates are probably reasonable estimates of the global picture though there is need for revision in some areas. A 2010 study [30] estimates 17% less undiscovered oil and 20% less undiscovered natural gas than in the 2000 assessment in eight basins in Southeast Asia; however, there had been at least 10 years of discoveries between the two assessments. Furthermore, the 2010 assessment examined a number of additional basins in Southeast Asia resulting in an overall increase in estimated undiscovered oil of 71% and natural gas by 66%. The 2008 USGS assessment of the Arctic revised down the estimate of undiscovered oil by 48%, largely because of a reappraisal of the West Siberian Basin, but increased the estimate of natural gas by 21% by including a number of basins not in the 2000 assessment [14].

The USGS 2000 assessment [10] also estimated the amount of reserve growth that could be anticipated to 2025 for fields that had been discovered prior to 1996. The median estimate for reserve growth for conventional oil was 612 BBO and for conventional natural gas 3,305 trillion cubic feet. At the time of writing, the midpoint of the time interval has been reached over which reserve growth was predicted and a substantial amount of the predicted reserve growth has already occurred [31]. It seems unreasonable, however, to assume that reserve growth will cease in 2025 and interestingly King [32], using a different methodology and separate data from that used by the USGS, estimated future reserve growth of oil at between 200 to 1,000 BBO – almost exactly the same range that the USGS predicted would occur from 1996.

Table 3 provides an estimate of remaining oil resources at the end of 2007. The proved reserve numbers are from BP [29] and are slightly lower than those of EIA [2]. The estimated volume of oil in undiscovered fields is revised down from the median estimate in the USGS 2000 assessment because 16.5% of that volume had been discovered by 2007 [31]. However, it should be noted that this may be conservative as the 2000 assessment did not include the United States and many geologic basins that have relatively small volumes of discovered oil or where there has been little or no exploration. The reserve growth numbers are based on King [31] for crude oil, as discussed above, and 50% of the USGS 2000 estimated median reserve growth for NGL that was predicted to occur between 1996 and 2025. The oil sand reserve and resource estimates are for Canada [33] and Venezuela [19] only though there are smaller oil sand accumulations in several other countries. The shale oil estimate is from Dyni [23]. The estimated remaining conventional oil is equivalent to 79 years of annual production at 2009 rates. The estimated unconventional oil adds up to the equivalent of 125 years of annual production.

Oil and Natural Gas: Global Resources. Table 3 Estimate of remaining oil resources including NGL (billion barrels). Sources and rationale for estimates are given in text. For comparison, annual production of oil was approximately 29.2 billion barrels in 2009

Conventional	
Proved reserves	1,236
Reserve growth	600
Undiscovered fields	600
Total conventional	2,436
Unconventional	
Oil sands proved reserves	237
Oil sands resources (incl. reserves)	820
Oil shale resources	2,826
Total unconventional	3,141

Global reserves of natural gas in 2010 were estimated at a little over 6,600 TCF by BP [29] and EIA [2]. Taking into account discoveries since 1996 [31] and revising down the median estimate of gas in undiscovered fields from the USGS 2000 assessment, and also assuming 50% of the estimated reserve growth has taken place, the remaining conventional natural gas resources are estimated at approximately 11,850 TCF, equivalent to about 87 years of annual production at 2009 rates. Estimating global abundance of unconventional gas resources is difficult because development of these resources is largely in its infancy, especially outside of North America. Recently published estimates of recoverable shale gas resources in the United States and Canada vary between 50 and 1,000 TCF [34]. Estimates for the rest of the world would likely have an even larger range. It is particularly important to discriminate

between "in-place resources" and those that are economically recoverable. The USGS [35] estimated that the United States has 700 TCF of CBM gas in place but only 100 TCF that would be economically recoverable. As 20.5 TCF was produced over the following 13 years under a major drilling effort, 100 TCF may be an optimistic estimate of ultimate recovery. The USGS [35] also suggested that global in-place CBM gas resources may be as high as 7,500 TCF but recoverable resources may well be an order of magnitude lower. Australia, for example, has 9% of the world's coal resources [2] and an estimated 153 TCF of recoverable CBM gas, of which 90% is currently sub-economic or not yet proven by drilling [20]. While extraordinarily large estimates of unconventional gas resources (particularly for hydrates) should be regarded with some scepticism from an economic perspective, there is ample evidence that unconventional gas resources are abundant. In the United States, which has a wide variety of geologic basins, 50% of the gas produced in 2010 was unconventional and it is not unreasonable to suppose that globally the abundance of unconventional gas resources is of a similar scale to conventional gas resources.

Future Directions

A strong case could be made that the estimates of remaining oil and gas presented above are on the low side because, as in the past, unanticipated technological advances may make additional oil and gas accumulations economically viable. Forty years ago large-scale economic extraction of oil from oil sands, gas from gas shales, gas from coal beds, and gas from tight sandstones all seemed improbable, but all are now a significant part of world production. However, even if the estimates are somewhat optimistic, it is clear that there is a large volume of remaining recoverable oil and gas resources. How much of that resource will eventually be extracted remains to be seen.

There are clearly environmental costs to oil and gas extraction. Pursuing hard-to-get resources raises the risk of disasters such as the BP Deepwater Horizon spill in 2010 [13] that can profoundly influence public opinion. Ecosystems are impacted by large-scale mining of oil sands and oil shales and some in situ extraction of unconventional oil and gas has the potential to influence groundwater supplies. Large volumes of water can be produced during CBM development. The biggest concern, however, is in the consumption of oil and gas with associated rising levels of greenhouse gases in the atmosphere and predictions of global climate change. On the other hand, substitution of natural gas for coal in power plants, more efficient vehicles, and carbon capture and storage could also make substantial reductions in global greenhouse gas emissions.

How much of the remaining oil and gas resources will be produced will depend on competition over time from other energy sources, especially renewables and nuclear. It is sometimes assumed that the depletion of global oil resources will inevitably lead to high oil prices that will allow more expensive energy sources to become competitive. However, historically substitution of one energy source by another has taken place primarily by reduction in costs of the substituting energy source [9]. Rather than a result of long-term depletion of the resource, the high oil prices of the first decade of the twenty-first century arguably reflect more restrictions of supply related to conflicts and political problems coinciding with a rapid rise in demand, especially from developing countries. Oil and natural gas may lose global market share in the future either because technological advances permit cheaper production of alternate energy sources or because of political influence on the market, including restrictions on supplies of oil and natural gas or incentives against their consumption, such as carbon taxes. Nevertheless, given the rising global demand for energy, it seems likely that oil and gas will be a major part of the energy mix for most, if not all, of the twenty-first century.

Bibliography

Primary Literature

1. International Energy Agency (2010) Key world energy statistics. OECD/IEA, Paris
2. Energy Information Agency (2011) http://www.eia.doe.gov/. Accessed April 2011
3. Fanning LM (1950) A case history of oil-shortage scares. In: Fanning LM (ed) Our oil resources. McGraw-Hill, New York, pp 306–406

4. Hubbert MK (1956) Nuclear energy and the fossil fuels, Shell Development Company Publication 95. Shell Development Company, Houston, 40 p
5. Hubbert MK (1962) Energy resources: a report to the Committee on Natural Resources, National Academy of Sciences-National Research Council Publication 1000-D. National Academy of Sciences-National Research Council, Washington, 141 p
6. Deffeyes KS (2001) Hubbert's peak: the impending world oil shortage. Princeton University Press, Princeton, 208 p
7. Meadows DH, Meadows DL, Randers J, Behrens WW III (1972) The limits to growth. Universe Books, New York, 205 p
8. Campbell CJ (1988) The coming oil crisis. MultiScience, Brentwood, 210 p
9. McCabe PJ (1998) Energy resources – cornucopia or empty barrel? AAPG Bull 82:2110–2134
10. United States Geological Survey (2000) World petroleum assessment 2000 – description and results, U.S. Geological Survey Digital Data Series DDS-60. U.S. Geological Survey, Denver. http://pubs.usgs.gov/dds/dds-060/
11. Sandrea I, Sandrea R (2007) Global oil reserves-1: recovery factors leave vast target for EOR technologies. Oil Gas J 105(Nov 5):44–47
12. Sandrea I, Sandrea R (2007) Global oil reserves-2: recovery factors leave EOR plenty of room for growth. Oil Gas J 105(Nov 12):39–42
13. National Commission on the BP Deepwater Horizon Oil Spill and Offshore Drilling (2011) Deep water: the Gulf oil disaster and the future of offshore drilling. 380 p, https://s3.amazonaws.com/pdf_final/DEEPWATER_ReporttothePresident_FINAL.pdf
14. Gautier DL, Bird KJ, Charpentier RC, Grantz A, Houseknecht DW, Klett TR, Moore TE, Pitman JK, Schenk CJ, Schuenemeyer JH, Sørensen K, Tennyson ME, Valin ZC, Wandrey CJ (2009) Assessment of undiscovered oil and gas in the Arctic. Science 324:1175–1179
15. Shanley KW, Cluff RM, Robinson JW (2004) Factors controlling prolific gas production from low-permeability sandstone reservoirs: implications for resource assessment, prospect development, and risk analysis. AAPG Bull 88: 1083–1121
16. Nehring R (2008) Growing and indispensable: the contribution of production from tight-gas sands to U.S. gas production. In: Cumella SP, Shanley KW, Camp WK (eds) Understanding, exploring, and developing tight-gas sands – 2005 Vail Hedberg conference, AAPG Hedberg Series, No. 3. American Association of Petroleum Geologists, Tulsa, pp 5–12
17. Canadian Association of Petroleum Producers (2011) Statistical handbook for Canada's upstream petroleum industry. Canadian Association of Petroleum Producers, 2011–9999, Calgary, 211 p
18. The Economist (2011) Muck and brass. Economist 398(8717):77–80
19. United States Geological Survey (2009) An estimate of recoverable heavy oil resources of the Orinoco oil belt, Venezuela, U.S. Geological Survey Fact Sheet 2009–3028. U.S. Geological Survey, Reston, 4 p
20. Australian Government (2010) Australian energy resource assessment. Department of Resources, Energy and Tourism, Canberra, 358 p
21. Swindell GS (2007) Powder River Basin coalbed methane wells – reserves and rates. Society of Petroleum Engineers Report SPE 107308
22. Energy Resources Conservation Board (2010) ST109: Alberta coalbed methane well locations. Energy Resources Conservation Board, Calgary, 426 p
23. Dyni JR (2006) Geology and resources of some world oil-shale deposits, U.S. Geological Survey Scientific Investigations Report 2005–5294. U.S. Geological Survey, Reston, 42 p
24. U.S. Geological Survey (2008) Assessment of undiscovered oil resources in the Devonian-Mississippian Bakken Formation, Williston Basin province, Montana and North Dakota, U.S Geological Survey Fact Sheet 2008–3021. U.S. Geological Survey, Reston
25. Klump E, Polson J (2009) Shale-gas skeptic's supply doubts draw wrath of Devon (update 2). http://www.bloomberg.com/apps/news?pid=newsarchive&sid=asEUlpJcuZB4. Accessed April 2011
26. Kvenvolden KA (1993) A primer on gas hydrates. In: Howell DG et al (eds) The future of energy gases, US Geological Survey Professional Paper 1570. U.S. G.P.O, Washington, DC, pp 279–291
27. Walsh MR, Hancock SH, Wilson SJ, Patil SL, Moridis GJ, Boswell R, Collett TS, Koh CA, Sloan ED (2009) Preliminary report on the commercial viability of gas production from natural gas hydrates. Energy Econ 31:815–823
28. Simmons MW (2005) Twilight in the desert. Wiley, Hoboken, 422 p
29. BP (2010) BP Statistical review of world energy, June 2010. http://bp.com/statisticalreview. Accessed April 2011
30. United States Geological Survey (2010) Assessment of undiscovered oil and gas resources of Southeast Asia, USGS Fact Sheet 2010–3015. U.S. Geological Survey, Reston
31. Gautier DL, McCabe PJ, Ogden J, Demayo TN (2010) Resources, reserves, and consumption of energy. In: Graedel TE, van der Voet E (eds) Linkages of sustainability, Strüngmann Forum Report. MIT, Cambridge, MA, pp 323–340
32. King KC (2007) Growth; are we underestimating recent discoveries?: abstracts, annual meeting. AAPG 2007:77
33. Government of Canada (2010) Oil sands – a strategic resource for Canada, North America and the world. Natural Resources Canada, Ottawa, http://www.nrcan-rncan.gc.ca/eneene/pdf/os-sb-eng.pdf
34. Mohr SH, Evans GM (2010) Shale gas changes N. American gas production projections. Oil Gas J 108(July 26):60–64
35. U.S. Geological Survey (1997) Coalbed methane – an untapped energy resource and an environmental concern, USGS Fact Sheet FS-019-97. U.S. Geological Survey, Denver, http://energy.usgs.gov/factsheets/Coalbed/coalmeth.html

Oil Shale Processing, Chemistry and Technology

Vahur Oja[1], Eric M. Suuberg[2]
[1]Department of Chemical Engineering, Tallinn University of Technology, Tallinn, Estonia
[2]Division of Engineering, Brown University, Providence, RI, USA

Article Outline

Glossary
Definition of the Subject
Introduction
General Characteristics of Oil Shale
Oil Shale Conversion Processes: An Overview
Shale Oil Production
Technological Aspects of Shale Oil Recovery
Final Considerations and Future Directions
Bibliography

Glossary

Bitumen Organic solvent-soluble portion of oil shale organic matter.

Direct retorting Retorting in which the process heat requirement is accomplished by combustion of a portion of the oil shale within the retort.

Ex situ retorting Oil shale retorting performed aboveground (requiring mining of the oil shale).

Indirect retorting Retorting in which the process heat requirement is provided by heated gaseous or solid heat carriers produced outside the retort, and then brought into contact with the retort contents.

In situ retorting Heating of oil shale underground in order to release shale oil (also called underground retorting). Confinement of the shale is provided by the surrounding earth, in this case.

Kerogen Macromolecular and organic solvent-insoluble organic matter of oil shale, but more broadly applied to these sorts of organic components of sedimentary rocks.

Oil shale Oil shale has a wide range of definitions. A general definition that encompasses most is that it consists of a sedimentary rock containing various amounts of solid organic material bound dispersedly in a mineral matrix and yielding principally a shale oil upon pyrolysis.

Pyrolysis A thermochemical decomposition process of organic matter, effected by heating the material in the absence of oxygen.

Retort gas Noncondensable combustible gas, a mixture of gases from an oil shale retort that remains after particulate matter and condensed liquids have been removed.

Retort water Water collected during oil shale retorting from offgas stream together with oil.

Retorting In shale oil recovery technologies, retorting is a pyrolytic process designed to produce oil. Generally, this process is performed by placing oil shale in a sealed vessel heated in order to promote pyrolysis; this reactor is called a retort.

Retorting residue or spent shale Solid waste material remaining after retorting. This material contains most of the mineral matter of the original shale (possibly partially decomposed) and a carbon-rich (char) residue from the organic fraction (which may sometimes be referred to as a semicoke).

Shale oil Room temperature liquid phase organic material, oil product, recoverable from the thermal decomposition of kerogen or separated from the offgas stream of an oil shale retort.

Thermobitumen A bitumen not contained in the original oil shale, but produced by the action of heat on the shale; a thermal degradation (pyrolysis) product of kerogen.

Definition of the Subject

Oil shale is a complex mixture of organic and inorganic phases, in which the organic phase is normally that of the greater economic and practical value. In nature there exists a wide range of materials that include these same components, and not all of these materials are candidates for actual use; in some instances, the organic content is simply too low to make processing of the oil shale of any economic interest. Thus, one of the first things that needs to be answered in asking what oil shales it makes sense to study is the question of what sorts of oil shale should be considered as the subject of practical use. This summary begins with a consideration of this fundamental question, and is guided by what has historically been accepted as

definitions of oil shales of practical interest. It is recognized that these definitions come from different locations and time periods, with differing demands for the energy or raw materials that the oil shale could provide. This, in turn, means that these definitions can change with time and place, but here they offer a framework for the discussion that follows.

Because in oil shale the organic and inorganic phases form such an intimate mixture, it is critical to consider how this might influence the practical conversion processes to which the oil shale is ultimately subjected. At the same time, it is essential to recognize how the experimental research used to develop these practical processes can be influenced by decisions on how to prepare the oil shale for testing. Isolation of the kerogen material from the oil shale offers advantages in terms of simplifying or enabling certain types of organic fraction analysis, or the evaluation of proposed processing steps in the laboratory. In many instances, this might make good scientific sense, but in other cases, it is important to note that there might be inadvertent changes induced in the material, and in its potential conversion chemistry, by the separation. This summary will only provide a brief overview of some of the aspects of research performed on the different phases present in the oil shale, and offer only this general warning to be cautious regarding the possibility of artifacts induced by separations of the raw material.

The main focus of this entry is on the chemistry of oil shale conversion. Virtually all oil shale conversion processes begin with a thermal degradation of the organic macromolecular structure. The organic fraction of oil shale is largely unrecoverable in any useful form without such a thermal degradation, since the extractable bitumen content in unheated oil shale is normally but a few percent at most. The thermal degradation is critical whether the oil shale is processed to recover oil or burned directly to generate heat, and from that, electricity. In the case of combustion, the thermal degradation is what releases the small organic molecular fragments that can burn in the vapor phase. The less that remains in a solid semicoke phase after the initial heating in a boiler, the more quickly and smoothly the combustion of the shale can take place, and the more efficiently used will be the organic fraction for its heating value content. Most shale oil combustion processes do operate at very high degrees of burnout of the organic matter.

In the case of oil recovery from the oil shale, there is a much-studied set of conditions used to maximize the recovery of oil. There is a balance between the need to achieve sufficient breakdown of the macromolecular structure of the organic phase, which will permit fragments to escape as oil, and the further pyrolysis of the organic phase to release light gases and leave behind a hydrogen-depleted semicoke that has much lower value than oil (and that is embedded in the remaining mineral matrix, making it difficult to utilize). This entry summarizes several aspects of what is known regarding the chemistry of thermal conversion and its kinetics, and offers an overview of some practical technologies in which the thermal conversion of the material takes place.

Introduction

This entry focuses on the chemical nature of oil shale, and some key aspects of its conversion to oil. One of the first difficulties encountered in this field is deciding what starting materials qualify as "oil shale." A brief review of various practical definitions is first offered. Different practical definitions arise from the different applications of the material. Next, the chemical structure of the shale is considered, including both the inorganic and organic phases contained therein. In this section, there is also consideration of how the organic phase can be analyzed, including how it may be separated from the whole shale.

In section "Definition of the Subject", the chemical processes that result in the practical conversion processes of oil shale are introduced in general terms. In this section it is noted that not all oil shale is necessarily used to produce an oil product. In some instances, the oil shale may be directly burned in devices similar to those used for combustion of coal. In Sect. 3, attention is turned toward retorting to produce oil products. Except for recent decades in Estonia, where direct firing of oil shale for producing electrical power and heat has been practiced, retorting for oil has been the main driver for worldwide interest in oil shale. This section reviews the parameters that influence the results of retorting, as well as providing an overview of some chemical aspects of the process. This review closes in

Sect. 4 with a brief consideration of different classes of technology developed for carrying out the retorting process.

It is important to recognize that there is a much more voluminous literature on oil shale chemistry and conversion than has been discussed here. The authors maintain that the present selection does, however, provide a reasonably comprehensive overview of the topic, while emphasizing some of the newer contributions to the literature.

General Characteristics of Oil Shale

Oil Shale Classification

Oil shale can be defined as a sedimentary rock containing various amounts of solid organic material dispersedly bound in a mineral matrix. Oil shales from different deposits vary in their mineral contents and types, chemical composition of organic matter, geological period of deposition, depositional condition, etc. [22, 31]. Therefore, there are a number of definitions of oil shale based upon application, operational, or scientific point of view [55]. Similarly there are various oil shale classification schemes [32, 54, 55, 76]. Moreover, the term "oil shale" is itself somewhat misleading as the organic matter is not oil-like and the mineral matter is not always classifiable as shale [141].

Following are some selected definitions of oil shale, proposed by several authors in the connection with its energy production or other technological utilization:

1. Gavin [43] defined oil shale as a "compact laminated rock of sedimentary origin, yielding over 33% of ash and containing organic matter that yields oil when distilled, but not appreciably when extracted with ordinary solvents for petroleum."
2. Ozerov and Polozov have described oil shale as "a hard foliated combustible rock formed by joint accumulation of pelagic plants and animals and mineral mass which had been transformed by the action of geographic conditions and chemical, biochemical and hydro-chemical processes" [90].
3. Schlatter has characterized oil shale as "a heterogeneous mixture of organic and mineral matter. It is a fine-grained, tight rock with essentially no permeability or porosity" [114].

It is important to note that in defining oil shale for energy-technological purposes, the following oil shale characteristics have been emphasized:

- A high mineral matter content, which may be about two to five times higher than the organic matter content (generally significantly higher in comparison to coals, which contain mineral matter, by definition, of less than 40%).
- The major portion of oil shale organic matter is insoluble in organic solvents (this in contrast to tar sands).
- The organic matter has hydrogen/carbon atomic ratios typically in the range 1.2–1.6 (which is significantly enriched in hydrogen compared with coals, but hydrogen deficient relative to crude oil).
- The capacity of oil shales to ignite and burn without separation of the organic matter from the mineral matter.
- They undergo thermal decomposition that results in production of a significant amount of liquid organic product or shale oil (higher grade oil shales can yield 100 L or more per ton of dry oil shale).
- They have a moisture content of less than 10–13%.
- They exhibit a low permeability of the rock to gases, vapors, and oils.

The organic matter (often termed kerogen; see below) content of oil shale varies widely, ranging typically from 10% to 40%. As the organic matter of oil shale is the source of energy and/or synthetic fuels value, there have been several attempts to classify oil shale by minimum and maximum organic matter content. The upper limit of organic matter content has been proposed to be about 50% [2, 76], or even higher [141]. The lower organic matter limit is usually defined in relation to the minimum energy requirement of oil shale as an industrial raw material. For example, a lower limit of 5% of organic matter has been proposed to define "commercial deposits." This is because the organic matter content of an oil shale should be at least roughly about 2.5 wt% for the latter to provide the calorific requirements necessary to heat the rock to 500°C [38, 82].

Oil shale grade or energy potential is currently classified or characterized for commercial purposes on either a heating value or an average oil yield basis.

1. The heating value is used to evaluate the quality of an oil shale in the context of direct firing of oil shale in a power plant to produce heat, commonly used to raise steam for electricity generation. The heating value of typical oil shale kerogen is about 40 MJ/kg. For example, the heating value of an Estonian kukersite oil shale kerogen has been reported to be 37.3 MJ/kg [2], while for US Green River formation kerogen the value is around 41.1 MJ/kg and for eastern US Devonian kerogen around 37.5 MJ/kg [99]. This is, of course, not the same as the heating value of the oil shale as would be determined for the whole rock, using a standard calorimeter (in which the dilution effect of the zero, or negative, heating value mineral matter is important). A combustion grade oil shale is defined as that having a minimum upper caloric value (for the whole oil shale rock) of 3.1 MJ/kg (dry basis) [38], though a heating value limit of not less than about 4.2–6.3 MJ/kg has been suggested for practical purposes [50, 141].
2. Average oil yield, or oil production potential, is determined using a "modified" Fischer assay method (the most widely used standardized technique, ASTM D-3904-80) or an equivalent analytical technique in which the shale is subjected to heating in order to liberate oil from the kerogen. The oil yield depends mostly on kerogen per mass of oil shale, but may also depend upon the fraction of kerogen convertible to oil (there are differences between different kerogens). On the basis of this assay, an "oil shale" is a shale that yields at least 42 L/t of dry shale (or 10 US gal/t, the basis used by the US Geological Survey) [99], though a limit as low as 25 L/t has also been suggested. Similarly, a crude dividing line between lower and higher grade shale has been defined at about 100 L of oil/t of shale (with those yielding below 90 L/t considered "low grade," 90–150 L/t "moderate grade," and those above 150 L/t "high grade" [2, 38]). Commercial grade oil shales range from about 100–200 L/t of shale. However, the Fischer assay does not actually indicate the maximum oil yield that can be actually produced by a given oil shale. Yields greater than Fischer assay have been obtained by hydropyrolysis, donor solvents, and rapid heating, especially for lower oil yield, non-softening oil shales [23, 106].

More than 600 oil shale deposits have been discovered around the world [2]. Oil shales are found in many countries around the world, with nearly 100 major deposits in 27 countries [128]. There exist many surveys/reviews on history of oil shale development throughout the world [98, 128, 129].

Oil shale resources are typically expressed in either of two different ways: (1) as tons of oil shale, and (2) as crude-shale-oil equivalents contained in the oil shale. Global deposits have been estimated to be about 411 metric gigatons or to range from 2.8 to 3.3 trillion barrels (4.5×10^{11} to 5.2×10^{11} m^3) of recoverable oil equivalent [155].

When talking about known oil shale deposits, there is a need to distinguish between two terms – "resources" and "reserves." Resources typically refer to estimates of all deposits of oil shales, while reserves refer only to those from which oil extraction can be economically profitable with the use of existing technologies. It should be noted that these technologies are constantly developing, and because of that, estimates of reserves will not necessarily remain constant over time, irrespective of use or discovery of new resources.

Oil Shale Composition

Oil shale is composed of mineral and organic matter whose proportions vary with the grade of oil shale.

Mineral Matter Oil shale mineral matter contains several classes of minerals such as carbonates (calcite and dolomite), silicates, sulfides, and others. The inorganic composition of oil shales varies widely. The oil shale mineral composition can change from mostly calcareous to mostly aluminosilicate. For example, a typical mineral composition (in weight percent of the mineral matter alone) of carbonate-rich Kukersite oil shale from Estonia [100] is dolomite 3%, calcite 65%, quartz 8%, illite 15%, orthoclase 5%, chlorite 1%, and pyrite 3%. For the carbonate-rich Mahogany-zone US Green River formation oil shale [99], the composition is somewhat different: dolomite 32%, calcite 16%, quartz 15%, illite 19%, albite 10%, microcline 6%, pyrite 1%, and analcite 1%. In the case of siliceous Eastern US Devonian oil shale [99], a typical mineral composition is quartz 28%, illite 40%, feldspar 12%, pyrite 14%, and other minerals 6%.

Quite often, mineral matter composition is represented by the chemical composition of oil shale ash, in which the mineral components have been converted to their oxides during combustion. This is illustrated in Table 1. It is, however, very important to keep in mind that the minerals are fundamentally altered by the combustion process, and the ash composition is only an approximate guide to what minerals existed in the raw oil shale.

In addition to the main minerals, oil shales contain a large number of trace elements (also referred to as minor elements). The content of the trace elements is typically in the parts per million (ppm) range. Trace element data for several deposits are available in the literature [92, 117, 141].

Organic Matter Oil shale organic matter is composed of solvent-soluble and insoluble organic materials. The organic matter in oil shales is mostly in the form of solvent insoluble cross-linked macromolecular structure or kerogen. However, the term "kerogen" is often used for whole organic matter of oil shale, including a small solvent-extractable fraction of the oil shale (termed bitumen).

Because organic matter is not easily extractable from the whole oil shale, there is an issue of how to quantify it. One simple way is to assume that it is the fraction that can be burned in air. Of course any loss of mineral components during burning (as by dehydration or decarbonylation reactions) can lead to an overestimate of the organic matter.

The organic matter content is thus often expressed on a dry shale basis as "conditional organic matter," $Org_{cond}{}^{d} = 100 - A^{d} - (CO_2)_M{}^{d}$, in which A^{d} is ash yield upon combustion, $(CO_2)_M{}^{d}$ is carbonate-derived CO_2 released by the mineral matter at high temperatures, and a dry basis is indicated by the superscript d [141]. Basically, this formula embodies the concept that what is not left after combustion as ash, or released by carbonate decomposition, must have been organic matter. Both the ash and decomposable carbonate are available from separate analyses. In reality, the actual organic matter content can be somewhat different than that obtainable from the formula above since, for example, the formation of $SO_4{}^{-2}$ ion from combustible sulfur can contribute to the mass of ash, even if the sulfur originated in the organic matter. Also, any other volatilization of mineral components, beyond decomposition of the carbonates, would also lead to errors in estimates of organic matter.

Therefore for specific oil shales more detailed equations have been developed. For example, for Kukersite oil shale, which has a true organic matter content somewhat lower than that typically calculated from the "conditional organic matter," the following formula has been proposed: $Org^{d} = 100 - 1.028A^{d} - 0.964(CO_2)_M{}^{d} + 0.637(SO_4{}^{-2} - 0.07)$, where $SO_4{}^{-2}$ is the sulfate content [104]. For Dictyonema shale, with a true organic matter content somewhat higher than the calculated "conditional organic matter," the following equation has been recommended: $Org^{d} = 100 - A^{d} + 0.125FeO - (H_2O)_M - 0.625S_{pyr} - (CO_2)_M{}^{d}$, where FeO is iron oxide content in ash, $(H_2O)_M$ is the content of mineral water of hydration, and S_{pyr} is the pyritic sulfur content [72]. The difference between true organic matter and "conditional organic matter" is generally not greater than 1–3%.

It is clear that for most technological uses of oil shale, there will be a need to go beyond simple estimates of organic weight fraction in characterizing the material.

Kerogen Kerogen is the major fraction of oil shale organic matter, and it is insoluble in organic solvents. It has a solid cross-linked macromolecular structure,

Oil Shale Processing, Chemistry and Technology.
Table 1 Mineral matter composition in some oil shales presented as oxides in ash, wt%

Compound	Green River [USA] [99]	Kukersite [Estonia] [88]	El-lajjun [Jordan] [88]	Dictyonema [Estonia] [88]
SiO_2	40–60	28.25	28.86	63.72
Al_2O_3	10–15	9.84	7.43	16.43
Fe_2O_3	5–10	5.44	3.70	8.80
CaO	10–25	41.02	52.79	0.85
MgO	5–10	5.05	1.30	0.50
K_2O		3.60		8.72
Na_2O			0.3	
SO_3		6.07	1.30	0.70
P_2O_5			5.9	

and in this respect is somewhat similar to coal. Accordingly, kerogen is swellable, but not soluble, in organic solvents. The term "kerogen" was introduced by Professor Crum Brown to describe the insoluble organic matter in oil shales that gives shale oil on heating and decomposition [158]. Nowadays the term kerogen is used to characterize solid organic matter in all sedimentary rocks [56].

There are several excellent publications on kerogens available in the literature [32, 110, 144, 145]. Oil shale kerogens possess relatively high atomic hydrogen to carbon atomic ratios (typically 1.2–1.6), at least in comparison to coals, for which this ratio is typically less than unity. It is the high hydrogen to carbon ratio (combined with low oxygen to carbon ratio) that makes oil shale kerogens of interest as a potential source of liquid fuels. Heating values of kerogens have been shown to be in the range of 24–40 MJ/kg, though as noted above the typical values are around 35–40 MJ/kg [90, 99].

The macromolecular structure of oil shale kerogens is complex – kerogen is not a "homopolymer." Instead of being built of repeating regular structural units as are synthetic polymers or natural materials such as cellulose, it is composed of highly variable structural units, both in terms of size and chemical character. The exact chemical structure of an oil shale kerogen is difficult to describe, therefore studies of "kerogen structure" can provide data only on average structural parameters. This is the same situation as exists for such natural materials as coals or lignins.

Due to kerogen's insolubility in organic solvents, it was historically somewhat difficult to characterize with respect to its chemical structure. Attempts to liberate it from the oil shale rock would necessarily involve risk of chemical degradation. Even if the approach involves dissolving away the mineral matter (see below), there are concerns regarding whether the kerogen has been altered, and of course, there remains the problem of reliable characterization of the chemical structure of a solid organic macromolecular substance once it is isolated. This latter point is similar to the situation in the field of coal chemistry, where decades of effort have been expended in establishing structures on which there is now reasonably general, though not yet total, agreement. Aspects of kerogen structure have in recent decades also yielded to more sophisticated characterization methods, though again, one can do little more than characterize average structures or structural elements.

As a result of the intractability of the raw kerogen structure, much has been done using its elemental composition as the simplest indicator of properties or predictor of behavior. The composition of kerogens is typically presented based on carbon (C), hydrogen (H), sulfur (S), nitrogen (N), and oxygen (O) content, since these are by far and away the major elements of interest. For more precise compositional characterization of Kukersite oil shale kerogen, chlorine (Cl) is also included [164]. Table 2 presents some sample kerogen (or organic matter) elemental compositions of oil shales from major deposits.

Kerogens can be classified in different ways on the basis of elemental composition. One of the most common is based on the Van Krevelen diagram originally developed for classifying coals (Fig. 1). Kerogens fall into certain groups on the basis of the atomic ratios of hydrogen to carbon and oxygen to carbon. Kerogens can be grouped as Type I, II, III, or IV with further

Oil Shale Processing, Chemistry and Technology. Table 2 Examples of kerogen [141] (or organic matter,* [99]) elemental compositions

Oil shale	C	H	S	N	O	H/C	O/C
Kukersite (Estonia)	77.3	9.8	1.7	0.4	10.8	1.52	0.105
Green River (USA)	78.3	9.9	1.6	2.1	8.1	1.52	0.078
Dictyonema (Estonia)	70.5	7.4	4.2	2.5	15.4	1.26	0.164
Kasphir (Russia)	67.1	8.0	10.2	1.2	13.5	1.43	0.151
Timahdit (Morocco)	68.9	8.5	7.0	3.0	12.6	1.48	0.137
Eastern USA Devonian*	82.0	7.4	2.3	2.0	6.3	1.08	0.058

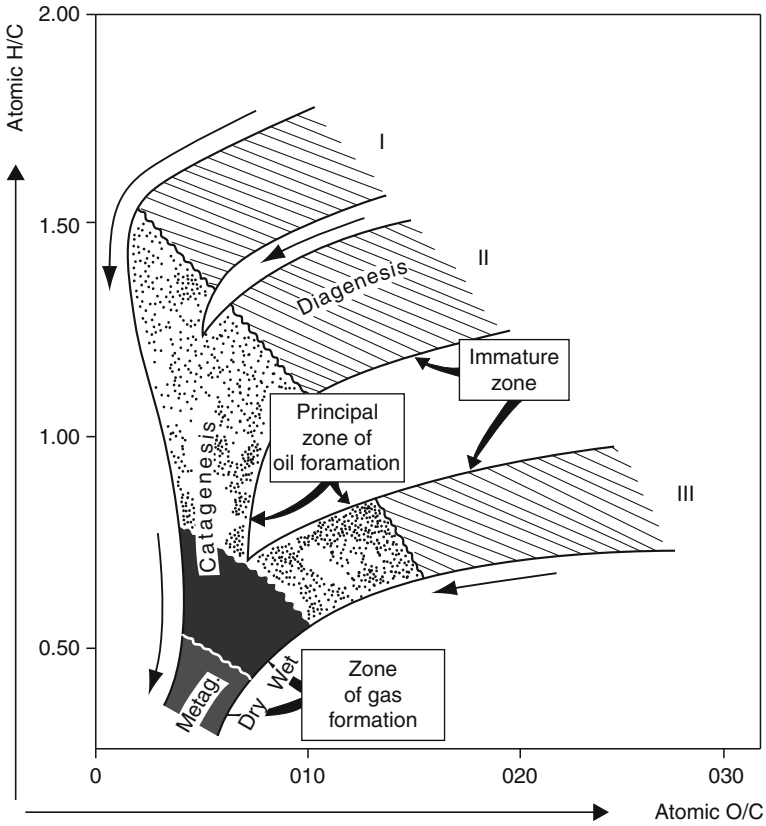

Oil Shale Processing, Chemistry and Technology. Figure 1
The van Krevelen diagram, showing the approximate locations of different kerogen types, based upon atomic ratios (from [145], with permission)

subgrouping according to sulfur content. Oil shale kerogens are predominantly Type I (Green River Oil Shale from Uinta Basin is a typical kerogen of this group) and II (Torcian Oil Shale from the Paris Basin is an example from this group). The less common coaly shales belong to Type III (Upper Cretaceous sedimentary rock from the Doula Basin, as one example) [33, 145]. The following numerical H/C and O/C ratio ranges have been suggested: for Type I H/C > 1.25 and O/C < 0.15, for Type II H/C < 1.25 and 0.03 < O/C < 0.18, and for Type III H/C < 1.0 and 0.03 < O/C < 0.3 [145]. Somewhat different H/C and O/C, and also O/S, ratios are found for kerogens at the end of diagenesis, but the above are the values for the materials of practical importance.

Kerogen Isolation An important tool in the field of kerogen study is that of kerogen isolation (or concentration) from the oil shale matrix. This involves the removal of solvent solubles (bitumen) and mineral matter, leaving behind the kerogen. Several reviews are available on isolation or concentration procedures (for information readers are referred to [6, 34, 108, 128, 145]).

Solvent solubles are removable by ordinary solvent extraction. Since all unextracted organics report as kerogen, the efficacy of extraction is important in establishing actual kerogen content. The amount of extractable obtained, and its properties, may vary considerably depending upon the solvent used for extraction. The amount of the extracted matter also increases with an increase in extraction process temperature and with the polarity and chemical activity of the extractant [159]. Typical extraction yields are low, representing only a few percent of organic matter, but varying significantly from shale to shale see (Table 3, for examples).

Oil Shale Processing, Chemistry and Technology.

Table 3 Yield of bitumen per conditional organic matter. Atomic H/C ratios of some oil shale kerogens and bitumens are shown for comparison [141]

Oil shale	Yields per conditional organic matter (%) (solvents used)	H/C bitumen	H/C kerogen
Kukersite (Estonia)	0.71 (benzene: methanol (1:1))	1.75	1.52
Kultak-Zevardy (Uzbekistan)	12.01 (benzene: methanol (3:1))	1.42	1.2
Uktha (Russia, Komyi)	21.42 (benzene: methanol (3:1))	1.58	1.21
Green River (USA)	5.4 (chloroform)		
Dictyonema (Estonia)	3.36 (benzene: methanol (3:1))		

A number of physical separation methods used to separate kerogen from the mineral part of oil shale are described in the literature [42, 107, 135]. These methods involve primarily such physicochemical processes as flotation and centrifugation. Combination techniques, involving such processes as ultrasonication or electrostatic and magnetic separations are also physical methods used in kerogen enrichment [159]. It is worthwhile to note that for certain oil shales, some physical methods are of value, since particle size reduction is accompanied by an increase in particle organic matter concentration.

The most widely used laboratory techniques for kerogen isolation from inorganic matter are based on chemical methods. In this regard, oil shale minerals can be grouped as carbonates (which are soluble in dilute acids), silicates (soluble in HF), and sulfides (which can be removed by oxidizing and reducing agents). Mineral composition determines the reagents (and the efficiency of reagents) to be used for demineralization [108]. For oil shale demineralization with chemical methods readers are referred to [108].

Kerogen Degradative Analysis Although elemental analysis offers valuable information for classification, other destructive and nondestructive techniques have been used to obtain information on functional groups and on structural functionalities of different oil shales [46, 110]. Earlier quantitative characterizations of kerogen functionalities were based on destructive techniques [146]. The destructive techniques include thermal degradation (pyrolysis, hydrogenolysis, supercritical extraction) and chemical degradation with different chemical reagents based on the specificity of the reagents (for more information concerning this topic see [128, 146]). Destructive analysis techniques are based on obtaining smaller identifiable compounds that have a structural relationship to the kerogen [146].

To describe the pyrolytic behavior of kerogen, detailed knowledge of kerogen structure is critical since the structural properties and functionalities of kerogen strongly influence its pyrolytic behavior. It has been shown in coal pyrolysis studies that devolatilization rates and product compositions can be correlated with coal organic matter chemical structure [123, 127]. So while certain types of functional groups may be directly related to their pyrolytic products, use of this fairly nonspecific method is of limited value.

The analysis of kerogen thermal degradation product molecular weight distributions has provided some insights into the size of the systems being examined. There was a recent study of kukersite (Type I) and dictyonema (Type II) oil shale samples involving Field Ionization Mass Spectrometry (FIMS) pyrolysis under high vacuum. This investigation indicated number-average molecular weight values of 408 and 383 Da with standard deviation values of 141 and 128 for kukersite and dictyonema oil shale pyrolysis products, respectively (estimated using a three-parameter Gaussian distribution function to describe the results) [111].

Earlier studies have, however, pointed to the possibility of higher molecular weights for the decomposition products. Suuberg and Sherman [131] studied pyrolysis of Green River oil shale under vacuum conditions, and obtained a weight-average molecular weight of around 800 Da, using a gel permeation liquid chromatographic technique. This compared favorably with a weight-average molecular weight of around 850 Da obtained for the same Green River shale, using the FIMS pyrolysis method [125]. The latter studies showed the importance of pressure on molecular weight distributions. Oils obtained using a Fischer

assay method showed a much narrower molecular weight distribution, shifted to much lower molecular weights. Hence, it is dangerous to compare the molecular weight distributions from different studies unless the mass transport conditions are known to be identical. In any event, all of the above studies point to the typical characteristics of a macromolecular system being thermally degraded to provide fragments exhibiting a distribution of molecular weights (which are all, of course, lower than the original matrix molecular weight).

Nondestructive Analysis of Kerogen Structure During the last 3 decades there have been a number of qualitative and quantitative studies aimed at characterizing the structure of oil shale kerogens using nondestructive techniques such as solid-state nuclear magnetic resonance (NMR) techniques (cross polarization, magic-angle spinning), Electron Spin Resonance (ESR), Fourier Transform Infrared Spectroscopy, and X-ray photoelectron spectroscopy [66, 82, 115, 120].

One recent comprehensive study on the structure of kerogens was carried out using both X-ray photoelectron spectroscopy and solid-state ^{13}C nuclear magnetic resonance techniques [66]. This study determined the average chemical compositions of 18 oil shale kerogens (hydrogen-carbon skeleton, oxygen functionalities, nitrogen functionalities, sulfur functionalities). The data of this study revealed that the average carbon-hydrogen skeletal units of immature Type I and Type II oil shale kerogens (according to H/C and O/C ratios) are generally composed of two to three ring-hydroaromatic/aromatic clusters with a significant number of short attachments and long, roughly linear, alkyl chains. These data also indicated that the number-average molecular weight of the "average repeating structural unit" of oil shale kerogens might be around 400 amu. These values compare favorably with the molecular weight distributions from the actual degradation studies cited above.

Several other studies have been concerned with characterization of kerogen macromolecular structures using solvent swelling in different solvents or solvent mixtures [74, 75, 111, 112]. These studies were performed to evaluate at least semiquantitatively the number-average molecular weight between cross-links (or cross-link density), a fundamental property of a cross-linked macromolecular network. These studies indicate that oil shale kerogen solvent swelling ratios are lower (therefore cross-link density higher and molecular weight between cross-links smaller) than those seen in bituminous coals [76].

Extensive structural data are available for a few oil shale kerogens, especially for oil shales of major deposits. For several kerogens the structural information has been the basis for detailed molecular models of a portion of the structures (e.g., for Rundle Ramsay Crossing [120], Green River [120], and Kukersite [164] (see also [128]). Reviews of the history of development of hypothetical structural models of the Green River Formation kerogen can be found in the literature [128, 158]. For illustrative purposes, a recent two-dimensional model of kukersite oil shale kerogen chemical structure is shown in Fig. 2a [164] and another model of Green River Shale in Fig. 2b [120]. Again, it needs to be emphasized that what is shown are "averaged" structures that accurately depict elemental ratios and to some extent functional groups, but which cannot be held out as necessarily representing the actual linkages between different groups, and which certainly do not represent the different molecular weight distributions present in the kerogens. It should also be emphasized that kukersite oil shale kerogen is a somewhat unique Type I kerogen due to its high hydroxyl (phenolic) group content [146]. This is apparent in comparing Fig. 2a and b. Hence, care should be exercised in using any published model of kerogen structure in trying to understand the chemical behavior of any other type of kerogen. Due to its high oxygen content, kukersite kerogen is also sometimes categorized as straddling Type I and Type II, since the lines between the different kerogen types is not necessarily as hard and fast as might be inferred from Fig. 1.

Bitumen or Bitumoid Bitumen (bitumoid) is a minor fraction of oil shale organic matter that is soluble in common organic solvents (representing up to 20% of organic material [159]) and is therefore recoverable by solvent extraction. Some authors define the bitumen as a benzene-soluble matter, while others define this material as soluble in petroleum-based solvents, yet others define it more broadly as material soluble in any organic solvents, and finally, some define it as material entirely soluble in CS_2. According to [144]

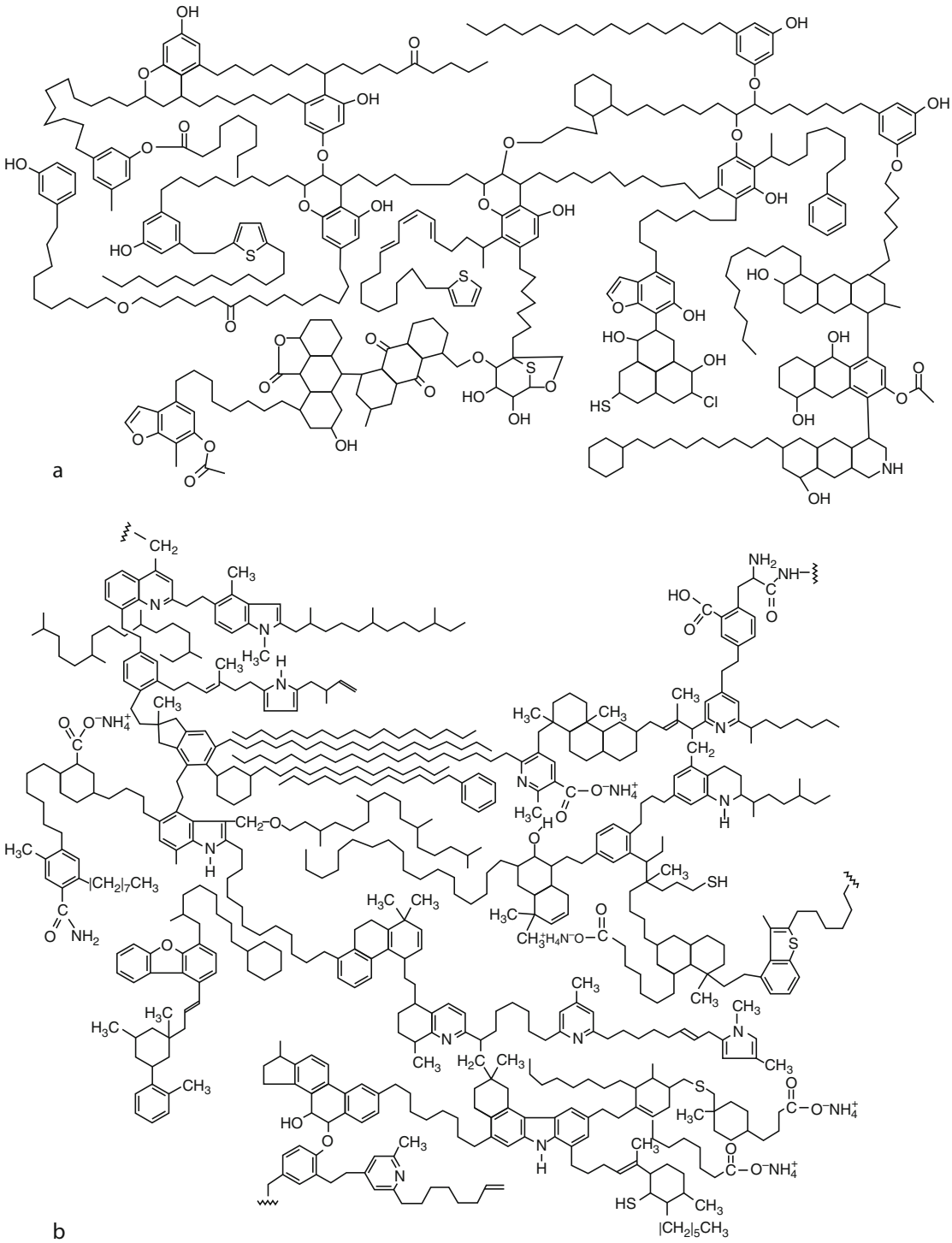

Oil Shale Processing, Chemistry and Technology. Figure 2

Two-dimensional models of kerogen chemical structure. (**a**) Model of Estonian kukersite kerogen with molecular mass 6,581 Da and empirical formula $C_{421}H_{638}O_{44}S_4NCl$ (from [164], with permission). (**b**) Model of Colorado Green River kerogen (from [120], with permission)

there are no standard protocols for extraction procedures, either in terms of the solvent polarity, sample grinding, temperature, duration of extraction, or stirring efficiency. Perhaps the main reason why there has not been greater emphasis on this point is that from a practical point of view, the amounts involved typically represent only a few percent by mass of the organic matter.

These extractables, bitumen, contain biomarkers or organic compounds whose structures are related to the chemical structures of the biological material from which the organic matter was derived [45, 143]. The atomic H/C ratio of bitumen has been shown to be somewhat higher than of corresponding kerogen see (Table 3).

Oil Shale Conversion Processes: An Overview

Oil shale resources are abundant and widespread throughout the world and oil shale has been used for energy-technological purposes for hundreds of years (e.g., there is a shale oil extraction patent dating from 1694, granted by the British Crown, [103]). Despite this, currently only few countries (Estonia, China, Brazil, Germany, and Israel) exploit oil shale on a commercial scale. The main reason for this is that oil shale is a low-grade solid fuel. It cannot compete with coal as a solid fuel, since the latter is available in richer (lower ash content) easily accessible deposits. Oil shale is a potential source of liquid fuels, but suffers there from the fact that the world oil market situation has historically been economically unfavorable in terms of fostering development of upgrading technologies. Generally, there has been need of government subsidies in order to consider development of an industry based upon this resource, and the energy market itself (influenced mainly by crude oil price range and electricity cost) has made oil shale upgrading truly economical only in the few countries mentioned. Moreover, the economic feasibility of oil shale development is certain to be strongly affected by further strengthening environmental regulations (air, water, and land use), socioeconomic issues, and market and investment risks. Taken purely on the basis of greenhouse gas emission per unit of energy, oil shale is unattractive in much the same way as is any other solid fossil fuel, such as coal. Therefore oil shale development in recent decades has been quite chaotic and episodic, and there have been many processes/technologies proposed and many have been abandoned due to economic reasons.

Just as is coal, oil shale is also a multiuse organic-mineral raw material whose economic value has sometimes extended beyond its fuel value. From some oil shales, uranium and other minerals and rare elements can be extracted. As an example, in 1946–1952, a marine type of Dictyonema shale [81] was used for uranium production in Sillamäe, Estonia, and in 1950–1989 alum shale was used in Sweden for the same purpose [36].

Integrated retorting techniques (both ex situ and in situ) have been under consideration to recover shale oil together with nahcolite, alumina, and soda ash from some oil shale deposits [77]. However, the major emphasis in oil shale upgrading has remained on kerogen thermochemical conversion methods (processes using heat to liberate oil). There have also been a few studies (laboratory research) on the use microbial activities to break up kerogen in its mineral matrix [16, 159].

In principle the general thermochemical upgrading processes that have been developed and utilized for coals (combustion, gasification, liquefaction, and pyrolysis) can also be used for oil shale upgrading. The goal is, broadly speaking, to transform the chemical energy locked within oil shale into more concentrated and conveniently useable forms. However, due to oil shale's thermal behavior and character, some types of processes are more favorable than others. It is important to note that the hydrogen/carbon ratio of oil shale organic matter (typically 1.2–1.6) is more favorable to production of liquids than that found in coal (typically 0.7–1), and this reduces the pressure to increase H/C ratio, which has economically been one of the major stumbling blocks of coal to liquid conversion processes. On the other hand, with mineral content of between 70% and 90%, considerably higher than that of commercial coal deposits, oil shale presents the problem of processing a solid with a high mineral rock content, whose handling and heating in any thermal process is economically quite unattractive.

Direct Combustion

Oil shale can be utilized as a fuel for thermal power plants, where it is burned directly as is coal. Currently

there are several countries that utilize oil shale as fuel for power plant fuel: Estonia, Israel, Germany, and China [14, 102]. Some countries have closed their oil shale-fueled power plants (Romania) or turned to other fuels (Russia). Other countries are planning to build such plants (Jordan and Egypt), or burn oil shale together with coal (Canada and Turkey) [14, 51].

There are three commercial technologies in use for oil shale combustion [3]: (1) pulverized combustion or pulverized firing (PF), as is used in the older units in Estonia; (2) fluidized bed combustion (FBC), used by Rohrbach Zement in Dotternhausen, Germany; and (3) circulating fluidized bed combustion (CFBC), used in two new units at the Narva Power Plant in Estonia, Huadian Power Plant in China, and PAMA power plant at Mishor Rotem in Israel. Generally speaking, PF technology is no longer in favor, because it operates at such a high temperature that there can be no sulfur capture by the carbonates present in the mineral matter, and therefore it is environmentally much more problematic. The thermal efficiency of the new Estonian CFBC units has been reported to be in the neighborhood of about 36%, which is typical of this sort of fluidized bed combustion system. The older PF units operated at only about 30% thermal efficiency to electricity [52].

An exceptionally extensive study of the correlation between the heating value and various compositional parameters of Estonian kukersite has been presented by [7]. While the quantitative results of that study are applicable only to this particular oil shale, the methodology may well be generalizable. That study suggested that a good working formula for estimation of the higher heating value of the organic part of oil shale is

$$Q_H = 0.3566C + 1.0623H - 0.1339O + 0.0658S + 0.0106N - 0.0280Cl$$

in which the heating value is in MJ/kg and the element symbols represent the mass percentages of the respective elements in the organic fraction of the oil shale. As part of the same original study by Saar, the lower heating value of the typical dried whole Estonian shale is (see [89])

$$Q_L = 34.45 - 0.302A - 0.4369(CO_2)_c$$

in which A is the dry oil shale ash content and $(CO_2)_c$ represents the content of carbonate mineral CO_2 in the dry oil shale.

Since direct combustion of oil shale is not the main focus of this review, the reader is referred to the comprehensive volume recently published by Ots on this topic [89].

Low-Temperature Pyrolysis

Low-temperature pyrolysis up to at about 500°C (also referred as retorting or semicoking or low-temperature carbonization) has been historically the most favored thermochemical conversion process for high-grade oil shales. In this pyrolysis or retorting process, the organic matter is converted to oil (termed retort oil, shale oil, shale crude oil), gas (typically called retort gas), and solid residue (typically termed semicoke in the oil shale industry). The processes can be carried out either by mining the oil shale and then producing oil by heating it in aboveground retorting facilities (termed ex situ processing), or by heating the oil shale underground without mining it and bringing it to the surface (termed in situ processing). Limiting the processing temperature to below 500°C is desirable, in terms of maximizing oil yield.

Oil shales are commonly retorted in commercial ex situ retorts without beneficiation (organic matter is not concentrated). Commercial ex situ shale oil production facilities are in operation in Estonia, Brazil, and China. Commercially produced shale oils are presently used as heating fuels or as feedstocks for producing chemicals [85]. Due to their broad boiling point distributions, high pour points, high viscosities, and high heteroatom contents (nitrogen, sulfur, and oxygen), raw shale oils need to be upgraded to be considered for higher value uses. Retorts could be included within a petroleum refinery. There have been a number of investigations on the use the shale oils as refinery feedstocks for manufacture of motor fuels [87].

High-Temperature Pyrolysis and Gasification

High-temperature pyrolysis (or gasification) under self-generated atmospheres was historically used to produce town gas (e.g., commercial-scale chamber ovens used in Estonia, [30]). Just as in the case of town gas produced from coal feedstocks, gas production from oil shale was abandoned due to economic reasons, largely having to do with the low cost of production of natural gas.

Modern gasification technologies, applied to conversion of coals or biomass, use partial oxidation (steam, oxygen) or hydrogen environments. In these gasification processes, the solid feed material is converted to synthetic gases (composed mainly of hydrogen and carbon monoxide) that can be further used as combustion fuel in, for example, Integrated Gasification Combined Cycle (IGCC) plants designed to produce electrical power, or further catalytically converted (via Fischer–Tropsch reactions) to produce chemicals, including liquid fuels. However, existing commercial gasification technologies that would lend themselves to integration with upgrading plants are not economically/technically suitable for oil shale feed materials, unless the mineral matter is reduced before gasification. There have been no demonstrations of large-scale oil shale beneficiation technologies for concentrating oil shale organic matter (to reduce mineral matter) to levels suitable for proven gasification technologies. Although in principle, oil shale gasification could be more attractive than shale oil extraction via retorting, especially for low oil yield oil shales, this thermochemical conversion process has not been a subject of commercial interest. Over the course of time a number of laboratory-scale to pilot-scale studies have been carried out on this topic [8, 10, 37, 57, 113].

Other Thermochemical-Based Conversion Technologies

Thermal dissolution or heating in presence of solvent has been considered as an alternative to "dry" thermochemical conversion such as classical retorting. These attempts have included those in subcritical and supercritical fluids, reactive and nonreactive fluids, and of special interest have been hydrogen-donor solvents that can provide hydrogen in the conversion process. In the latter case, gaseous molecular H_2 can also be introduced. Again, there is strong analogy to methods that have been suggested for direct liquefaction or solvent refining of coals. Examples include processes such as Solvent-Refined Coal processes (SRC-I and the improved version, SRC-II), the Exxon Donor Solvent (EDS) process, and the H-Coal process [8, 94, 99]. A brief review on recent advances in direct coal liquefaction and a list of major direct coal liquefaction processes is given by Shui et al. [118].

The thermal dissolution processes generally involve heating the oil shale to temperatures below those characterized by active devolatilization, as there is a desire to maximize oil yields and minimize gas production. The temperature range of active devolatilization depends somewhat upon gas pressure applied to the system.

The thermal dissolution of oil shales has been mainly of academic or research interest as the H/C ratio of oil shale organic matter is already much more favorable than of coal. For more information on oil shale thermal dissolution, there are recent brief reviews covering the topic [48, 136] and, separately, supercritical extraction [67, 139]. One step toward commercial development is the proposed 1 ton/h so-called Rendall process demonstration plant under construction in Australia by Blue Ensign Technologies Limited. This process is designed to use oil shale from the Julia Creek deposit in Queensland and to hydrotreat it in a two-stage process using a petroleum-based solvent. Again, this proposal is only at a laboratory stage.

A considerable amount of work (up to process-development unit scale) has been published on hydropyrolysis or pyrolysis under high hydrogen pressures, including catalytic hydropyrolysis and hydrogasification [8, 109]. Indeed, this technology was already explored in Estonia in the 1930s [68].

Shale Oil Production

General Considerations Regarding Process Temperatures

Technologies to recover oil from oil shale are based on thermal breakup of kerogen, the cross-linked macromolecular organic matter of oil shale. All present technological approaches require heat to take kerogen to temperatures at which thermochemical conversion processes are sufficiently fast to be of interest from a practical point of view. As noted above, depending on process conditions the thermochemical conversion results in three general classes of products with different quantities and varying qualities. These products are the oil (more generally non-polymeric organic compounds with a wide molecular weight distribution), a carbon-rich solid residue, and gas (including water vapor).

Kerogen decomposition rates increase with temperature, subject to the Arrhenius rate law. The rates will

be quantitatively explored in a later section. Kerogen decomposition is slow at low temperatures and occurs on a time scale of days to years below 350°C, which is why practical processes are generally carried out at higher temperatures. The decomposition becomes fast enough for practical purposes at temperatures of 400°C and above. Cummins and coworkers [25] studied Green River oil shale low-temperature isothermal pyrolysis from 150°C to 350°C. They showed that 2% of kerogen was converted to benzene solubles in 90 days at 150°C and in 360 days 7.7% of kerogen was converted. At 200°C in 90 days 3% was converted, and in 360 days 8.9%. When the temperature was raised to 300°C in 0.5 days 3.3% was converted and in 4 days 12.8% yield was obtained. Finally, at 350°C in 0.5 days 27.6% and in 4 days 65.1% of kerogen was converted into benzene solubles.

The above demonstrates that there is actually no lower temperature limit for kerogen decomposition, consistent with what would be concluded from Arrhenius kinetics; rather, the question lies in establishing the time scale needed at any particular temperature. It is the fact that practical ex situ (i.e., in retort) conversion processes must be carried out on the timescale of minutes or hours, at most, that sets the commonly cited "lower temperature limit" for decomposition. These limits may be extended for in situ techniques, where confinement volume in an aboveground retort is no longer a consideration, but there is still a lower limit at which the process would simply take too long to be practical.

Real processes can be run under conditions varying from slow heating rate and long residence time to fast heating rate and short residence time. For example, in aboveground (ex situ) retorting equipment, heating rates, and residence times can vary from the order of 1°C/min and hours to of order of 1,000°C/min and seconds, respectively. The former is encountered, for example, in moving bed coal gasifier type retorting equipment, which utilizes particles with size on order of 100 mm (e.g., 10–125 mm for the Kiviter process, [101]). The latter high heating rate conditions are encountered in fluidized bed reactors, which use small particles with sizes below a few millimeters. In all these retorting processes (which take place in an inert gas environment or under self-generated gas environment with very low oxygen content, or in a reactive, non-oxygen environment), the oil shale is heated up to the active pyrolytic reaction region from 450°C to 550°C, where oils and gases evaporate and hydrogen-deficient organic matter or semicoke is left in the solid phase.

In situ processes generally involve heating rates below 1°C/min, because of the impracticality of rapid heating in an in situ environment. The relatively low-temperature range of 340–370°C, with time scales of years, is utilized by Shell in its in situ (underground) conversion process (Shell Oil Shale Test project) [77]. The above-cited timescales for kerogen conversion show that it is not the kinetics of conversion alone that determine these long times; rather, they are also influenced by the time needed to heat the large volumes of rock and to allow the released oil to flow out of the shale.

Other Processes Taking Place During Retorting

Destruction of kerogen by heating is accompanied by processes in other oil shale constituents, that is, in bitumen and mineral matter. These processes include:

- Solvent-extractable organic matter or bitumen (non-covalently linked non-polymeric compounds) can vaporize or decompose, depending on their thermal stability. Depending on the oil shale, the bitumen content can constitute up to 20% of organic matter [159], though as noted above it is generally much less than this. If able to quickly escape the hot oil shale and be cooled, these compounds should be captured in a relatively minimally altered form.
- Mineral matter present in oil shale can have catalytic effect on thermochemical conversion processes of kerogen [41, 116]. Also, the minerals themselves can decompose at temperatures of thermochemical conversion of kerogen. Some minerals can partly or fully decompose even under typical retorting conditions (e.g., nahcolite, dawsonite, analcite, smectite, kaolinite, siderite, and pyrite) [76, 89, 92]. These decomposition reactions are generally endothermic. At temperatures around 450°C magnesium carbonate starts to decompose [76]. The interaction of a mineral with organic matter or other minerals present in the oil shale can cause altered thermal behavior, relative to the pure

mineral [103]. Rajeshwar and coworkers have summarized thermal characteristics/behavior of minerals (17 minerals) commonly found in oil shale deposits [103]. Thermochemical properties and mineral reactions of oil shale minerals have been reviewed by many authors (e.g., [76, 77, 88, 92, 103]).

- Trace elements of oil shale can distribute between retorting gas, oil, solid residue, and retort water [93]. For example, there may be the presence of trace elements of environmental concern (arsenic, selenium, mercury) in retort oil, gas, or water [8, 92], or trace elements in oil (vanadium, iron, nickel, arsenic) can poison refinery catalysts [92, 93]. Actual concentration values depend on the retorting process and, of course, the trace element composition of specific oil shale. Most of the trace elements are retained in the solid spent shale itself [8].

Thermal Effects During Retorting

Large quantities of heat are required to manufacture a usable fuel (liquid or gaseous) from oil shale. Heat requirements include (1) heating the mineral and organic matter to reaction temperature; (2) providing the heat of reaction related to organic matter decomposition and heat effects covering chemical changes in mineral matter; (3) providing the heat of vaporization of volatiles (oil and water). The thermal management of processes must also include provision for cooling the products of the process back to ambient temperatures. The major amount of process heat is consumed with heating mineral matter. The total heat requirement for heating oil shale to 500°C, including allowing for vaporizing volatiles, is observed to be about 650–750 kJ/kg of oil shale [99]. The heat of the pyrolysis reactions is by itself relatively small [8, 99]. A review of some recent applications of differential scanning calorimetry (DSC), mainly aimed at providing kinetic information, also provides reference to some recent work on thermal effects of pyrolysis [70].

Assay Methods: Determining Potential Oil Yield and Its Relationship to Other Properties

Procedures for determining oil production potentials are known as assay methods. Assay methods generally involve laboratory scale slow heating rate (order of 10°C/min) batch pyrolysis systems or so-called carbonization tests. The procedures were developed to provide a simple and reproducible basis for fossil fuel (coal, lignite, oil shale) characterization and comparison, as opposed to providing scientific insights into the material.

The modified Fischer assay method has been widely used (since 1946) to evaluate the approximate oil potential of oil shale deposits and compare different oil shales. The term "modified" denotes that the original Franz Fischer method [161], used in Germany to characterize coals was taken over to characterize oil shales and has gone through improvement in this process. The technique has been standardized as the American Society for Testing and Materials Method (ASTM method) D-3904-80, D3904-85, and D3904-90 or as the International Organization of Standardization (ISO) standard ISO 647-74 or as the GOST 3168-93 (the GOST is the former Soviet Union Standard).

The standardized modified Fischer assay method (ISO 647-74; GOST 3168-93) consists of heating a 50-g dried and crushed oil shale (90% particles passing through a 1-mm mesh, with not more than 50% particles passing through a 0.2-mm mesh) in a specially designed cast aluminum retort (made of 99.5% aluminum) to 520°C in 70 min with decreasing heating rate, followed by holding the sample at that temperature for 10 min. The process is performed in a self-generated atmosphere. The distilled vapors of oil, gas, and water are passed through a condenser cooled with ice water, and collected into a graduated centrifuge tube. The oil and water are then separated by centrifuging. The quantities reported are the weight percentages of shale oil (and its specific gravity), water, shale residue, and "gas plus loss" by difference.

The above procedures were developed to provide a reproducible basis for oil shale characterization/comparison. Estimated errors are not expected to be greater than 5% (relative) under the standardized conditions used [55]. However, the Fischer assay is a static assay under self-generated "inert" atmosphere and factors such as cracking of volatiles due to long residence time in a hot zone, and char forming reactions [38] can limit the oil yield. Therefore, for example, use of an inert gas sweep [38] provides greater oil yields than from Fischer assay under a self-generated atmosphere.

It is not uncommon to encounter laboratory retorting results in which oil yields exceed Fischer Assay results.

Other assays, developed for carbonization tests of fossil fuels, have also been applied to characterizing oil shales, and include the Heinze retort [24], the Gray and King method (developed in England) [152, 161], the original Franz Fischer method [161], the Bureau of Mines oil shale method [161], the Tosco material balance assay (with collection of gaseous products) [8], and the "material balance" Fischer assay method (modification for collection of gaseous products) [47]. Also, results based upon various TGA analyses have been used by many investigators, and are not necessarily directly comparable to the results from Fischer assay methods.

One widely applied oil shale rapid characterization and screening method is Rock-Eval analysis [9, 73]. Rock-Eval pyrolysis has been used to evaluate the maturity of the rock, as well as its richness (organic carbon content) and quality (oil and gas potential) [95]. The technique is based on temperature-programmed heating of a small sample (under 100 mg) in an inert atmosphere (helium or nitrogen) up to 600°C (to 800°C using version Rock-Eval 6). Evolution of hydrocarbon volatiles is monitored by a flame ionization detector, and carbon dioxide (CO_2) by other means, such as an infrared analyzer or a thermal conductivity detector, for example. The basic method was designed to measure the amount of free hydrocarbons in the sample (S_1), the evolution peak temperature (T_{max}) and the amount of hydrocarbons generated through thermal cracking of nonvolatile organic matter (S_2), and the amount of CO_2 produced during pyrolysis of kerogen (S_3). Based on these, the Hydrogen Index (HI) as mg S_2 per gram of total organic carbon, Oxygen Index (OI) as mg S_3 per gram of total organic carbon, and Productivity Index (PI) as $S_1/(S_1 + S_2)$ can be calculated. Rock-Eval pyrolysis temperature T_{max} and HI are used to evaluate maturity of oil shales. HI and OI have been used to construct a modified van Krevelen diagram.

Thus the approximate grade of oil shale (average oil yield) has been determined historically in laboratory batch retorts such as the "modified" Fischer assay method or the Rock-Eval technique. There are high and low oil yield kerogens based on modified Fischer assay results. Tables 4–6 are compiled to show how the composition of kerogen affects the product yield and product composition. Table 4 also confirms a general observation that the amount volatiles generated during thermochemical conversion under an inert environment up to about 500°C decreases from kerogen Type I to Type II, and gas to oil ratio and semicoke to oil ratio increase from Type I to Type II [128]. It should be noted that a Van Krevelen diagram-based classification of oil shale behavior (based upon H/C and O/C ratios) provides only a rough prediction of behavior, and better correlations between pyrolysis yields and organic matter types might need additional indicators or different classification approaches [166].

As the modified Fischer assay has been a standardized method for evaluating oil yields of different oil shales, the chemical and physical properties of different oil shale deposits have been correlated with

Oil Shale Processing, Chemistry and Technology. Table 4 Fischer assay yields, dry organic matter basis, of some selected Type I and II oil shales. Parent organic matter H/C and O/C ratios are also shown

	Green River (Utah, USA) [141]	El-lajjun [88]	Kukersite [141]	Eastern USA Devonian (Antrim) [141]	Dictyonema [141]
H/C ratio of organic matter	1.52	1.42	1.51		1.14
O/C ratio of organic matter	0.08	0.05	0.11		0.23
Kerogen type	I	I	I/II	II	II
Oil yield, wt%	59.3	61.9	60.0	22.2	19.8
Gas yield, wt%	22.7	20.9	21.5	25.1	16.5
Semicoke yield, wt%	11.8	10.8	9.1	42.5	45.4
Retorting water	6.2	6.4	9.4	10.2	18.3

Oil Shale Processing, Chemistry and Technology. Table 5 Fischer assay gas compositions of the selected Type I and II oil shales shown in Table 4

Gas composition, vol%	Green River (Utah, USA) [141]	El-lajjun [88]	Kukersite [141]	Eastern USA Devonian (Antrim) [141]	Dictyonema [141]
CO_2	30.3	14.5	25.0	9.7	13.6
H_2S	3.3	25.2	8.8	29.1	20.3
C_mH_n	2.0	9.3	16.1	2.6	7.5
CO	16.8	1.0	7.9	14.3	5.7
H_2	24.2	21.6	8.2	22.4	27.1
C_nH_{2n+2}	21.2	28.4	34.0	19.2	25.8

Oil Shale Processing, Chemistry and Technology. Table 6 Fischer assay oil elemental compositions of the some selected Type I and II oil shales shown in Table 4 [141]

	Green River (Utah, USA)	Kukersite	Eastern USA Devonian (Antrim)	Dictyonema
C	84.7	83.0	83.8	83.3
H	12.0	9.9	10.6	9.3
S	0.6	1.1	1.8	2.6
N	2.1	0.1	0.7	1.0
O (by difference)	0.6	5.9	3.1	3.8
H/C	1.7	1.43	1.52	1.34
O/C	0.005	0.05	0.03	0.03

Fischer assay results. Properties that are successfully correlated include, for example, density, thermal conductivity, organic carbon, total hydrogen, aliphatic/aromatic carbon, and unpaired electron concentration [82]. In general, each specific deposit exhibits its own correlations and these correlations need to be derived for the specific deposit, as the relationships are mostly empirical.

Thermochemical conversion of oil shale kerogen to oil produces changes in oil chemical composition relative to the original oil shale organic matter. Analysis of data on hundreds of oil shales (compiled by Urov and Sumberg [141]) indicates that the Fischer assay oil H/C ratio can be either lower or higher than that of the parent organic matter. This is consistent with an observation that shale oil aromaticity can be greater or lower than that of the parent kerogen [82].

There are a number of papers [90, 141] concerned with characterization of Fischer assay oils, examining, for example, elemental composition, molecular weight (varying from 190 to 310 Da), density (or specific gravity varying from 0.8 to 1.04, with only a few exceptions <1), heating value (39–44 MJ/kg), viscosity, boiling range (30–70% boiling over up to 350°C), and chemical groups (nonaromatic hydrocarbons, aromatic hydrocarbons, heteroatomic compounds, etc.).

It was already noted that the Fischer assay is a standard method and it does not provide either the maximum or minimum oil yield that can be produced from a given oil shale. Changes in parameters such as reactor configuration, particle size, heating rate, pressure, or pyrolysis environment also can affect product yields and compositions [8, 23, 157]. In real processes these factors are not always independent, as, for example, high heating rates require fine particles or hydrogen environment is used with high pressure.

Heating Rate Effects on Retorting Oil Yields

Fluidized bed retorting, where heating rates reach 1,000°C/min and particle sizes below a few millimeters are used, produce higher oil yields than obtainable from Fischer assay. For example, yields about 110% relative to Fischer assay have been reported in the case of Green River oil shale and about 150% of Fischer assay for eastern US Devonian shale [23]. Fluidized

bed pyrolysis shows, in addition to increased oil yield and decreased gas yield, different oil properties such as higher aromaticity, molecular weight, density, and viscosity [23], as compared to Fischer Assay oils. It should also be noted that laboratory-scale fluidized bed retorting experiments usually resulted in higher oil yield than commercial-scale design retorts [23].

In large-scale retorting systems, high heating rates require high heat-transfer rates, and thus, a finely ground feed. Therefore differences in products from low and high heating rate thermochemical conversion processes are influenced also by the effect of particle size. The larger the particle, the slower the mass transfer rate of volatiles to the outer surface of particle, and thus, the more opportunity for the products to undergo secondary reactions that would alter their nature. Hence, it is difficult in most cases to separate the effects of heating rate and particle size.

Pressure Effects on Retorting Yields

The mass transfer of oil out of pyrolyzing particles is affected by the pressure difference between the particle interior, where the products are produced, and the surrounding atmosphere. Delayed escape of the volatiles can result in secondary cracking reactions of higher molecular weight products, resulting in lower oil yields and increase gas and char yields.

With an increase in pressure under an inert environment (or self-generated environment) the oil yield decreases, the gas yield increases, the char yield increases, and oil specific gravity and viscosity decrease. Also, the amount of lighter distillate oil fraction increases [8]. All of these phenomena are consistent with a process of cracking of higher molecular weight oils to lighter oils (with deposition of coke). Different results can be seen when reactive pyrolysis atmospheres (such as hydrogen or steam) are used. On the other hand, these conclusions are not necessarily general, as in high heating rate (1,000 K/s), small particle pyrolysis, oil yields were observed to be quite similar, decreasing only a small amount with increasing pressure above a temperature range of 800–900 K [131]. The oil loss at higher pressures was associated with the occurrence of cracking reactions. The molecular weight distributions of the shale oil were relatively insensitive to pressure, though at higher temperatures, higher pressures tended to slightly favor lower molecular weights. The results of this work also showed clearly that there was an evaporative equilibrium responsible for determining the molecular weight distribution in the oil, as the average molecular weights in the oil were significantly below those of the extractable thermobitumen left in the shale. Hence the effects of pressure are associated with evaporative processes, though these effects are not as significant as they are in determining the yields of tars from coal pyrolysis [127, 132].

Effect of Gas Atmosphere on Retorting

An inert gas sweep of a retort provides greater oil yields than obtained from the Fischer assay procedure under self-generated atmospheres [38]. Pyrolysis in a steam atmosphere has been shown to have favorable effect on products by improving yield and quality of shale oil [38] relative to Fischer assay. In fluidized bed experiments, steam has been studied as one possible fluidization medium [23, 38]. However, the beneficial effect of steam relative to nitrogen is the subject of dispute among different researchers [38].

Pyrolysis under high hydrogen pressure (hydroretorting, hydropyrolysis) is shown to be a potential way to upgrade low-oil grade oil shales to oil. Hydroretorting results in increased oil yield and more aromatic oil with lower heteroatom content and lower molecular weight distribution [106]. Hydrogen pressures of ca 5–10 MPa were sufficient to have an effect [106]. In some studies, higher pressures, 15 MPa, have been used [24]. A hydroretorting assay unit has been developed along with a standardized procedure for its use [106]. In this unit (538°C and hydrogen pressure 6.9 MPa) for low oil yield oil shales (Type II kerogens), oil yields can be increased several times relative to Fischer assay, even 400% over Fischer assay yield [106].

Chemical Aspects of Oil Recovery by Retorting

Shale Pyrolysis in Comparison to Coal Pyrolysis The process of recovering shale oil is concerned with decomposition of kerogen, the major portion of oil shale organic matter. Kerogen is a cross-linked macromolecular structure whose thermal behavior depends upon the severity of heating, yielding either mostly hydrogen-rich solvent soluble material or light

volatiles (oil, gas) and a carbon-rich solid residue. The overall pyrolysis process is extremely complex with a variety of physical-chemical mechanisms. The composition and yields of pyrolysis products depend on the type and characteristics of oil shale (primarily of kerogen), and as noted above, the particle size, final temperature, heating rate, residence time of vaporizing products in hot zone, pressure, and pyrolysis atmosphere. The possibly important role of secondary reactions has been noted in several places above.

In the period from 1970 to 1990, there were extensive theoretical and experimental studies on coal pyrolysis, and relatively fewer such studies on oil shale. The aim of both research communities was to improve the fundamental understanding of pyrolysis chemistry with an ultimate objective of developing realistic simulation models. The examination of coal pyrolysis tended to place great emphasis on the importance of the interplay between chemical and physical processes encountered in pyrolysis, something that received less attention in the shale pyrolysis work.

Coal pyrolysis is an important phenomenon inasmuch as it is an initial step in all major coal thermochemical conversion processes such as combustion, gasification, carbonization, and liquefaction. The past 4 decades resulted remarkable advances in the modeling of coal pyrolysis. There was a shift away from simple, empirical kinetic models to use of more complex "network" devolatilization models. Those models provide detailed predictions of pyrolytic behavior for a wide variety of coals under variable temperature, pressure, and heating rate conditions. There are many extensive reviews and books published on coal pyrolysis [76, 127], covering the chemistry of pyrolysis, mass transfer effects, comparison of experimental data and models, etc.

In some ways oil shale is similar to coal as the organic matter is mostly a macromolecular three-dimensional structure, however, with different organic compositions and hydrogen-carbon skeletons. Therefore, oil shale pyrolysis is characterized by different product characteristics and by different rates and extents of pyrolytic process events (cross-linking, swelling, softening, resolidification, and devolatilization). The pyrolytic devolatilization processes of oil shales occur at somewhat lower temperatures than do the same sorts of processes in coals. The active devolatilization starts at about 350–400°C with a maximum in the range of 400–500°C and completes at about 500–550°C. The oily pyrolysis products are more volatile (with higher hydrogen/carbon ratio and lower molecular weight distribution) than the coal tarry products. Oja has demonstrated that the kukersite oil shale primary tar (oil) produced during moderate rate pyrolysis (~5°C/s) under a nitrogen sweep in a tubular furnace is easily volatile below the temperatures of active devolatilization [86]. This is not generally the case for coal liquid (tar) pyrolysis products.

It can be assumed that the general principles used to model the mechanisms of coal pyrolysis could also be used to describe oil shale kerogen pyrolysis. For coal, the following pyrolysis event sequence was proposed [127]: disruption of hydrogen bonds; vaporization and transport of non-covalently bonded "guest" molecules; low-temperature cross-linking (in low rank coals) that is accompanied with CO_2 and H_2O evolution; bridge breaking and fragmentation of the macromolecular network (depolymerization); hydrogen utilization to stabilize free radicals; vaporization and gas phase transport of light fragments; moderate temperature cross-linking reactions to resolidify the macromolecular network; decomposition of functional groups to produce light species or gases; and high-temperature condensation of the macromolecular network involving hydrogen elimination. In most respects, the same processes must take place in oil shale pyrolysis.

The importance of the extent and timing of cross-linking in the pyrolytic processes of coals has been emphasized in coal pyrolysis models. A number of studies have been performed on swelling of thermally pretreated coals indicating loosening and/or tightening of coal structures in the temperature region prior to tar evolution or active pyrolysis. This phenomenon was found to depend on coal rank: changes in lower rank coals indicate low-temperature cross-linking whereas trends in higher rank coals vary from no observable changes to structural relaxation. It was observed that the extent of low-temperature cross-linking was associated with decomposition of carboxyl groups and possibly hydroxyl groups as formation of new cross-links before devolatilization happened together with CO_2 and water release. It has been concluded that low-temperature cross-linking results in low tar yield and can be a reason for the non-softening pyrolytic

behavior seen in low rank coals. The importance of such processes in oil shale pyrolysis will be considered below.

General Observations of Oil Shale Pyrolysis Phenomena A large number of studies (including reviews) on pyrolysis of oil shales have been conducted and reported over the course of history. The pyrolytic behavior of oil shales have been investigated generally based on individual oil shales or in some cases generalized to oil shale kerogen types (Type I, II, or III in accordance of Van Krevelen diagram) [35, 46, 121]. Although kerogen types (similar to coal ranks) have been shown to be useful for generalizing oil shale kerogen (organic matter) behavior, it should be kept in mind that differences between kerogens make a large difference in behavior, and the trends with kerogen type have not been firmly established.

There have been a number of studies of the changes in kerogen structure (in the solid organic residue) during pyrolysis/heating. These changes involve elemental composition, functional group losses and other structural modifications, as well as changes in the number of free radicals. Techniques employed for tracking the changes include, for example, elemental analysis, Fourier transform infrared spectroscopy, solid-state nuclear magnetic resonance (NMR) spectroscopy, electron microscope or electron spin resonance [28, 119]. There are of course also a great number of studies on volatile product evolution during pyrolysis. This includes evolution of volatile products correlated with kerogen functional group decomposition. Techniques used have included Fourier transform infrared spectroscopy, mass spectrometry, or gas chromatography [105].

For properties of crude shale oils readers are referred to [8, 85, 99, 142].

Observations Regarding Changes in the Macromolecular Structure of Oil Shale Kerogens During Pyrolysis In relation to the different oil yields observed in the case of pyrolysis of Type I and Type II kerogens (see Tables 4–6), solvent swelling experiments on thermally pretreated oil shales have indicated that high oil yield kukersite kerogen (Type I), which exhibits softening pyrolysis behavior during pyrolysis, shows a tendency toward structural relaxation in the low-temperature pre-pyrolysis region [111]. This observation is qualitatively comparable to that seen in high tar-yield softening coals. On the other hand, low oil yield Dictyonema kerogen (Type II), which exhibits non-softening pyrolysis behavior, shows a tendency for pre-pyrolysis cross-linking or structural tightening [163], similar to what happens in low rank non-softening coals [126].

Mechanisms and Kinetics of Kerogen Decomposition Mechanisms of kerogen decomposition have been the subject of numerous studies, including many different experimental techniques, and have involved both isothermal and non-isothermal procedures. Techniques used have included thermogravimetry, differential scanning calorimetry, differential thermal analysis, Rock-Eval, and various other types of reactors. These studies tracked changes in at least one pyrolyzing kerogen-related component (parent material or product) as a function of time and temperature. In many such studies, complex materials, such as pyrolysis oil, are considered as single pseudo-components. There are many papers that consider the mechanisms and kinetics of kerogen decomposition, and only a sampling of these is offered here [4, 5, 13, 18, 26, 27, 29, 39, 53, 58, 61, 63, 69, 76, 103, 121, 130, 134, 136, 138, 148, 150, 153, 154, 156]. Despite the existence of a relatively extensive literature on oil shale pyrolytic behavior, very few analyses and reviews are available that offer comparison between the available information or comparison to coal and biomass research results.

Different mechanisms, with various degrees of complexity, have been proposed to describe oil shale pyrolytic behavior. Generally, these are based on tracking intermediate, primary, and secondary pyrolysis products, often without a clear identification of all of the products in any of the classes being tracked. Kinetic parameters have been calculated by fitting experimental data to an assumed semi-empirical model of the pyrolysis process. There is, thus, not surprisingly a large variation in reported kinetic parameters (activation energies and frequency factors). Consequently, the results are often of limited generality, applicable to the particular experimental conditions studied, often potentially influenced by heat and mass transfer limitations on observed kinetics.

A sampling of kinetic results is shown in Fig. 3. These results have been taken from studies in which both activation energies and pre-exponential factors have been reported. Except as noted, they are based upon a model of pyrolysis that is first order in kerogen, and normally the rate data are those either for total mass loss or the production of oil. Hence, the "model" can be simply represented as:

$$dX/dt = -A\exp(-E/RT)X$$

in which X is a conversion parameter, expressed in terms of remaining unconverted fraction. In many of

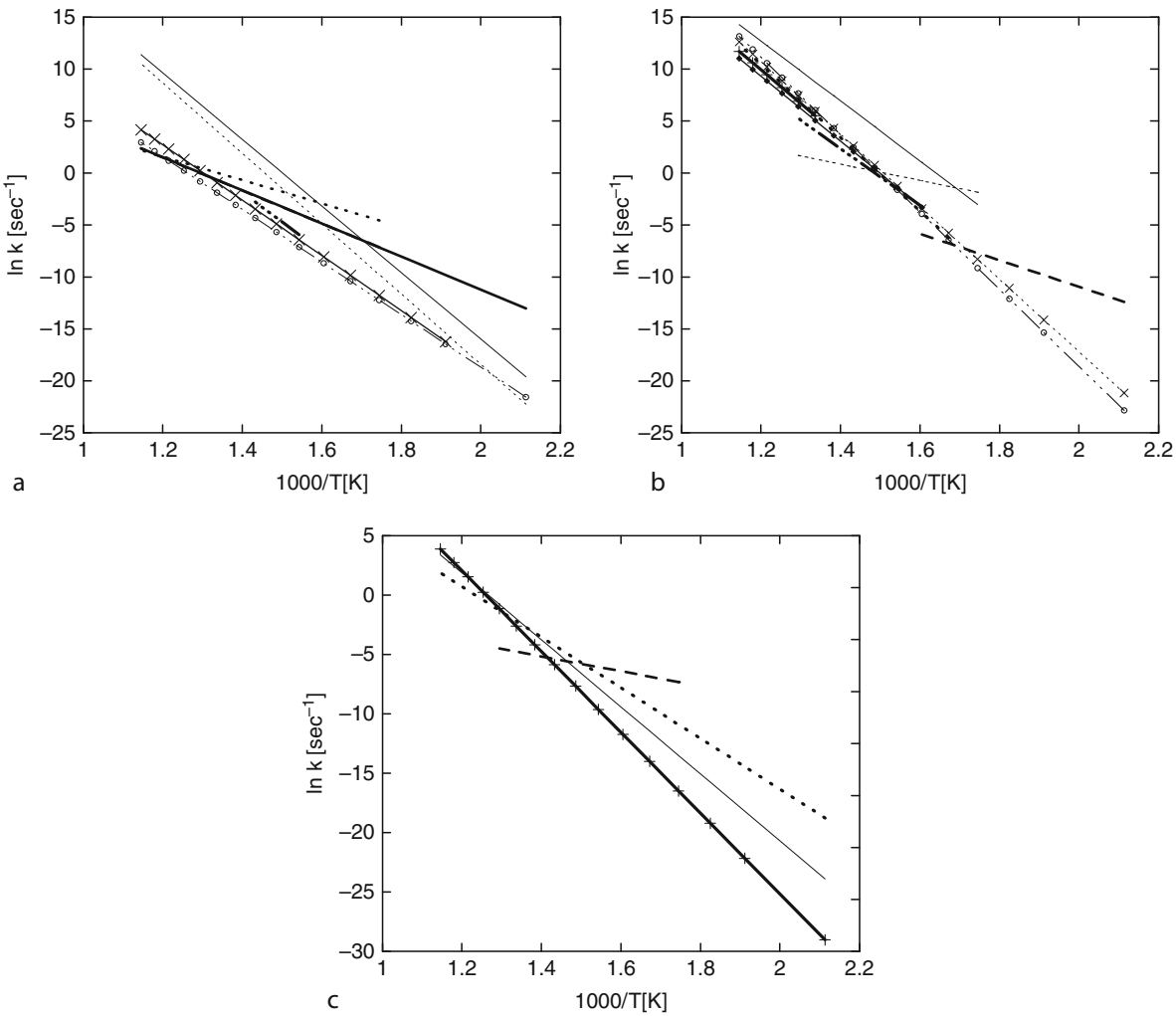

Oil Shale Processing, Chemistry and Technology. Figure 3
Comparisons of kinetics of kerogen pyrolysis. (**a**) A comparison of rates on Estonian kukersite kerogens. Thick lines [59, 60, 62]; thin lines from Oja (unpublished results); lines with crosses [96]; line with small circles, [160]. (**b**) A comparison of rates obtained on Colorado Green River Oil Shale. Dark line with crosses [12]; thin solid line [78]; heavy dashed line [25]; heavy dotted line [21]; heavy dashed-dotted line [149]; thin line with small black points [124]; thin dotted line with crosses [96]; thin dashed-dotted line with circles [19]; thin dashed line [84]. (**c**) A comparison of rates obtained on kerogens from Rundle Australian Oil Shale. Heavy line with crosses, [147]; thin line [96]; heavy dashed line [84]; dotted line [91]

these studies, a variety of different fitting techniques were employed (e.g., Friedman, Coates-Redfern, and simple Arrhenius). The point here is not to evaluate the different methods or studies one against the other, but to provide a rough sense of how much agreement there is in the literature on pyrolysis kinetics.

It is immediately apparent that despite the clustering of results on the graphs, the actual rates in the temperature regions of most interest can diverge from one another by significant amounts. In the case of the kukersite samples of Fig. 3a, the difference near 400°C (1,000/T[K] = 1.49) is about two orders of magnitude. The spread in reported values for Green River oil shale is not as great near 400°C see (Fig. 3b, which shows an order of magnitude spread), but there are still significant differences in reported activation energies that lead to differences of even greater magnitude near temperatures of interest. Likewise, there is a significant disparity in the results reported for Rundle Australian oil shale kerogen in Fig. 3c. Also, these results point out that there can be significant differences between the kerogens from different samples. The kerogen from kukersite shows typically higher reactivity than is shown by the Green River or Rundle samples. Hence, there is not surprisingly a dependence of kinetics on the origin of the shale.

This comparison of kinetics is not offered to evaluate the relative merits of any one study over another. It is to point out that there remain significant unresolved differences in reported kinetics, and that this is an issue that will seemingly require further work to resolve.

The Nature and Role of Thermobitumen At many pyrolysis conditions, thermobitumen (also referred as pyrolytic bitumen or "metaplast" in coal chemistry) is an important intermediate of oil shale pyrolysis. The formation of the thermobitumen has historically caused technological problems in retort design and development due its sticky and plugging character. The thermobitumen can be defined as an intermediate organic substance, which is organic solvent-soluble but nonvolatile at its formation temperatures. Several researchers define the bitumen more specifically as a benzene soluble pyrolysis intermediate [165]. The nonvolatile thermobitumen is used in models as a single pseudo-component that precedes oil generation. In contrast to the thermobitumen, the oil is defined as a volatile organic product of the pyrolysis process. The kinetics of thermobitumen formation have been described in several papers, for Green River oil shale in [18, 165] and for Kukersite oil shale [62, 64, 136].

The observation of thermobitumen formation has been incorporated into a number of mechanisms [8, 76, 83]. Generally pseudo-first-order formation reactions are assumed. For example, a qualitative thermal degradation mechanism proposed by [1], and now fairly widely accepted in general form by many other researchers, is shown in Fig. 4. It embodies the well-established feature that there is a breakdown of kerogen to extractable bitumen that precedes a significant amount of oil release. The thermobitumen formation, its composition, and yield, are related to the time–temperature history of the process and to the oil shale kerogen structure. It is now more generally believed that it is the second stage of volatiles formation (from the thermobitumen) that gives rise to most of the oil product. Light gases may be released in both volatiles' release periods.

Figure 5 shows the time and temperature dependence of thermobitumen yields for western US high oil yield Colorado oil shales (Type I kerogens) and eastern US low oil yield Kentucky New Albany oil shale (Type II kerogens). Figure 5 indicates that low oil yield non-softening oil shales cannot form considerable amounts of intermediate pyrolytic bitumen. This has been explained by cross-linking behavior of these oil shale kerogens and direct kerogen conversion to residue, but also by autocatalytic reactions between bitumen and kerogen [165].

There are few studies on thermobitumen characterization, but generally its chemical, physical, and thermodynamic properties have been little studied. The properties and composition (elemental composition, molecular weight distribution) of thermobitumen is

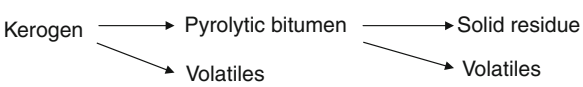

Oil Shale Processing, Chemistry and Technology.
Figure 4
A generally accepted mechanistic scheme for pyrolysis of kerogen

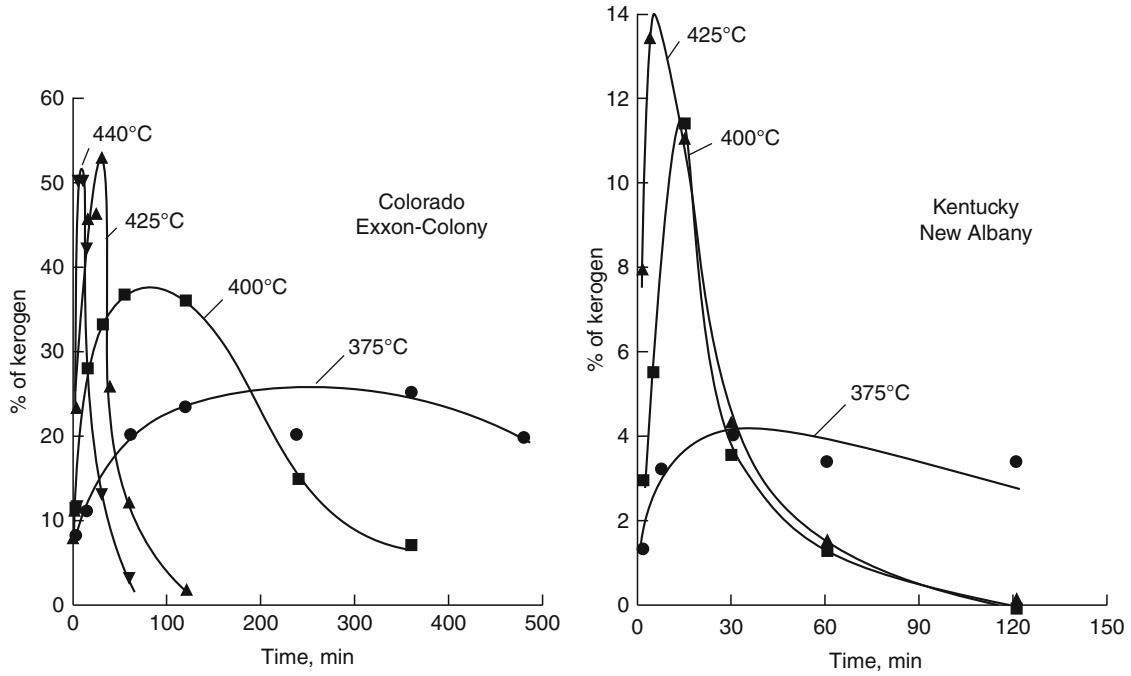

Oil Shale Processing, Chemistry and Technology. Figure 5
Time and temperature dependence of pyrolytic bitumen for Colorado and Kentucky oil shales ([165], with permission)

temperature and time dependent. Figure 6 shows the average molecular weights of oil and bitumen as a function of time and temperature for western US Colorado (Exxon-Colony) and eastern US Kentucky (New Albany) oil shales, and Table 7 presents thermobitumen characteristics of Estonian kukersite oil shale. The results of Table 7 show the expected decrease in bitumen molecular weight as conversion progresses to greater extents at higher temperatures.

These and other available studies [136, 137] indicate that the thermobitumen relative to oil produced at same temperature has lower H/C atomic ratio (and higher aromaticity) and higher number-average molecular weight (depending on oil shale and temperature-time history, the thermobitumen can exceed a value of 1,500 Da). It was noted by Miknis and Turner [165] that atomic H/C and number-average molecular weights of the thermobitumen produced were strongly time and temperature dependent, while oil showed remarkably constant values at all times and temperatures. These results on bitumen are in general agreement with the results of [131] on Colorado oil shale, which showed that this fraction had a very high molecular weight (a significant fraction >1,000 Da). In this latter study, the oil itself had a higher number-average molecular weight than observed by Miknis and Turner [165], presumably due to the difference in pyrolysis conditions, which favored evaporation of higher molecular weight fractions.

In addition to direct pyrolysis (retorting) other technological solutions, such as supercritical gas extraction, hydropyrolysis, or thermal dissolution with solvents, take advantage of the chemical processes that occur at thermobitumen formation stage.

Competitive Reaction Processes and Hydrogen An important concept in coal thermochemical decomposition is formation of volatile and nonvolatile reactive radical components as a result of bond breaking in the macromolecular structure. Reactions between radical components can lead to char formation, if the radical species involved are located on large fragments of the network structure. Stabilization of radicals by hydrogen can result in volatiles (or potential volatiles), if the hydrogen capping of the structures prevents their incorporation into a new network structure.

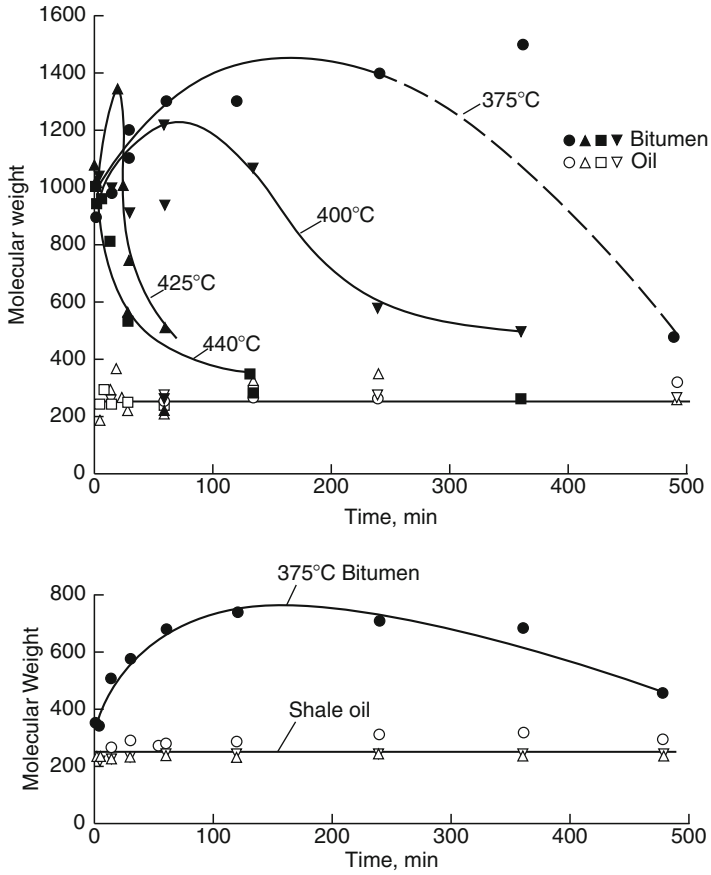

Oil Shale Processing, Chemistry and Technology. Figure 6
Molecular weights of oil and bitumen versus time and temperature for (**a**) Colorado (Exxon-Colony) and (**b**) Kentucky (New Albany) oil shale ([165], with permission)

On the other hand, the formed volatiles can undergo secondary reactions prior to escaping the reacting particles. This may happen in contact with solid material or in the vapor phase. Such secondary reactions are promoted by long residence times in high-temperature zones within a particle or a reactor. Thermochemical conversion in the presence of hydrogen can result in an increase in non-polymeric volatile hydrocarbons, if a radical secondary reaction pathway can be intercepted by hydrogen capping of a radical. In addition to helping reduce the macromolecular structure to smaller species by the above routes, hydrogen is also consumed in reducing sulfur, nitrogen, and oxygen that exist in the kerogen structure [99]. Hydrogen can be introduced into these roles either directly from the gas phase or from a hydrogen-donor solvent [99]. There are effects of temperature, pressure, and catalysts on these hydrogen reaction pathways [99, 107].

Technological Aspects of Shale Oil Recovery

The fundamental chemical and heat and mass transfer processes in oil shale retorting have been described to a limited degree in comparison to similar coal and biomass processes. By comparison, there is a rich literature on practical oil shale retorting technologies (including flow sheets, process descriptions, and product characterizations) [8, 30, 99]. There are also reviews/reports covering processes from laboratory scale through process-development unit scale to commercial scale: [15, 20, 85, 97, 101, 122, 140, 142]. The above books and reviews also cover a number of other

Oil Shale Processing, Chemistry and Technology. Table 7 Thermobitumen characteristics of Kukersite oil shale (elemental composition of organic matter C 82.1%, H 10.63%, S 0.75%, O + N 6.5% and atomic H/C 1.55) from thermochemical conversion in a Fischer retort [65, 162]

Process conditions (temperature, time)	Yield, % thermobitumen per organic matter	Elemental composition, %				H/C	Mol. weight
		C	H	S	O + N		
275°C, 456 h	17.9	83.0	10.1	0.50	6.7	1.46	710
300°C, 387 h	69.8	85.1	8.77	0.32	5.8	1.24	1,300
340°C, 12 h	59.8	83.8	9.78	0.52	5.9	1.40	1,240
360°C, 4 h	63.8	83.6	9.56	0.50	6.3	1.37	790
380°C, 4 h	35.6	85.3	8.85	0.53	5.3	1.25	651

important topics associated with oil shale processing, such as availability of oil shale reserves [77, 85, 142], oil shale mining [8, 85], research and development needs [77, 85], socioeconomical problems [85], environmental impact [77, 85, 142], oil shale upgrading economics and shale oil cost components [38], shale oil refining [85, 129] and future perspectives [129, 142].

Over hundreds of years of oil shale development, hundreds of retorts (retorting processes) have been invented [85]. Through the long history of oil shale utilization, ex situ (above the ground or surface) retorting technologies have been practically the only commercial technology for oil production from oil shale. In ex situ processing, the oil shale must be mined (using surface mining or underground mining), crushed, and transported to the processing plant for retorting. By comparison, in situ processes cause less land surface disturbance associated with mining. This may involve limited excavation to access oil shale sources or to create permeability by fracturing or drilling heater holes or production wells. Because the oil shale is retorted in the ground, in situ processing requires that the produced oil be extracted through an oil well in the same way as is conventional crude oil [20]. Therefore, commonly cited advantages of in situ process are limited mining and solids' (oil shale and spent shale) handling, and no expense associated with aboveground retorting equipment. The disadvantage of in situ processing involves the complexity in controlling process parameters. There are also concerns raised regarding the ability to capture all of the oil produced underground.

In addition to the issues of technical viability (including process controllability) and capital cost, the choice to use ex situ as opposed to in situ processes depends on factors such as richness of the oil shale, the depth or thickness of the shale bed, the accessibility to deposits, and environmental considerations (associated with escape of oil into groundwater or extraction of materials from spent shale, e.g.,). Again, ex situ processes are often also regarded as environmentally problematic beyond their mining impacts, due to problems of solid residue disposal and potential for groundwater pollution from that source.

Besides the simple ex situ and in situ classifications, there are many other retorting classification schemes used in the literature as technologies can differ in various aspects such as process principle. These include process modes such as batch, semi-batch, or continuous, as well as process flows including cocurrent, counter-current, or crosscurrent. An important classification is based upon heat-transfer mechanism to the shale (direct or indirect, and what the carrier is in direct) as well as heat generation method. In addition, retort style, complexity of technology or by-product processing can be bases of classification.

A vitally important design consideration is always thermal management, both in terms of heat generation and heat transfer to the shale to be retorted. Heat can be transferred to oil shale by different means:

1. *By conduction through a retort wall.* To this group belonged ex situ technologies such as the vertical Pumpherston retort (Bryson retort) [79] or Davidson horizontal rotary retort [80]. In these

types of ex situ technologies, heat is transferred through the retort wall. Due to the slow conduction that characterizes such retorts, many such processes are mainly of historical interest as their throughputs per unit of vessel volume are low. Development phase processes of this genre are the Oil-Tech electrically heated vertical retort process (Ambre Energy Limited) [140] and the A.F.S.K. Hom Tov co-pyrolysis process (Mishor Rotem).

The principle of wall conduction can also be applied to in situ technologies. In that case, it involves placing heating elements or heating pipes into the oil shale deposit. Representative of this approach is the Shell In Situ Conversion Process (ICP) technology (Shell Mahogany Project) [140], which uses electric-resistance heaters combined with a surrounding "freeze wall" to confine the retorting products. Another example is the EGL Oil Shale process [140] in which heat is transferred by superheated steam (in a closed system) through a series of pipes serving as heat exchangers below the oil shale bed. The Geothermic Fuel Cell™ approach (GFL™) developed by Independent Energy Partners, Inc. (IEP) uses a high-temperature fuel cell stack [140].

2. *By gases from shale combustion in the retort* (referred to as the directly heated retorts approach). These technologies utilize heat that originates from burning materials (char and oil shale gas) inside the retort and is therefore also called internal combustion retorting. The heat is transferred through the retort by gases generated in the combustion process. In combustion retorts the retorting gas is diluted and has low calorific value (for syngas classification depending on the heating values, see [77]). A currently used commercial ex situ retorting technology of this type is the Fushun process [101] in China. Other examples of thoroughly investigated ex situ technologies based upon this approach are the Kiviter process (early versions), Nevada-Texas-Utah (NTU), Paraho Direct, Union "A" and Superior Multimineral processes [8, 77]. In situ retorting also utilized this principle in technologies that burned oil shale underground. An example of this was the Occidental Petroleum Corporation Oxy process [85] (modified in situ combustion retorting process).
3. *By gaseous heat carrier heated outside retort* (referred as indirectly heated retorts). In this case, heat is transferred by hot gases heated in an outside furnace and then injected into the retort (or retorting bed). Again, in these systems the retorting gas is diluted and has low calorific value. Currently used commercial ex situ technologies of this group are the current Kiviter process in Estonia and Petrosix process in Brazil [8]. Other main ex situ technology examples are Union "B," Paraho Indirect, Superior Indirect processes [8], and fluidized bed-based processes. Similarly, in situ technologies can utilize gases that are heated aboveground (such as by combustion), which are then injected into the oil shale formation as heat carriers. Examples of such hot-gas injecting methods are the Chevron CRUSH process and the Petro Probe process and the in situ gas extraction technology (IGE) of Mountain West Energy [140].
4. *By solid heat carrier heated outside the retort* (referred indirectly as heated retort). In this instance, heat is transferred by mixing hot solid particles (heated outside the retort) with the oil shale. Reactive heat carriers, such as oil shale ash, or nonreactive, such as sand or ceramic balls, have been used. In these processes retort gases with high calorific value are produced. These are ex situ processes that typically take place in rotating kiln-type retorts. Currently used commercial ex situ technology of this type includes the Galoter process [44] in Estonia, which utilizes hot shale ash as the heat-carrying medium. Other main technologies of this type include the Alberta Taciuk Process (ATP), TOSCO II (developed by The Oil Shale Corporation, utilizing externally heated ceramic balls 15 mm in diameter as heat carrier) Lurgi-Ruhrgas (retorting is accomplished by mixing with spent shale/sand) [77], the Shell SPHER Process (Shell Pellet Heat Exchange Retorting) [49], and the LLNR HRS (Lawrence Livermore National Laboratory Hot Recycled Solid) process [20].
5. *By other means* such as radio frequency [15], microwave [11], solar [17] or nuclear explosion (e.g., Project Bronco) [8], etc. A number of recent shale oil in situ recovery schemes (e.g., Raytheon/Schumberger; PyroPhase) have been proposed based on volumetric heating by means such as

radio frequency or microwave heating [140]. These have thus far been mostly of interest on the research and development level [15].

6. *By combinations of the above.* For example, a combination of solid and gaseous heat carriers is utilized in hot recycle solids fluidized bed retorting systems (e.g., KENTORT II, [23, 133]). Since gas density is about 1,000 times lower than that of oil shale, assuming that roughly same mass heat carrier must be contact the shale, then a large volume of gas is needed to heat the oil shale [18]. The KENTORT II [23, 133] uses recirculating hot spent shale from a gasification section.

The above-mentioned Shell SPHER process and LLNR HRS process could arguably also be included in this class of processes.

An example of an in situ combined heat-transfer mode process could be Electrofrac™ (Exxon Mobil Corporation) [140], which combines wall conduction and volumetric heating through electrically conductive material (used to fill fractures).

There are a large number of different retorting solutions. Generally, the performance of retorts (in situ or ex situ reactors) are typically evaluated or compared based on the percentage of Fischer assay yield achieved and an overall thermal efficiency (as energy efficiency). Typical commercial-scale retorts, with the exception of fluidized bed retorts, have lower oil yields than obtainable from Fischer assay. For example, for modified in situ internal combustion retorting, it is around 60% [99] of Fischer assay. For a Fushun generator type of retort, this value is 65% [101] and for the Kiviter type of retort 70% [101]. Higher values are obtained with Petrosix retorting 85–90% [101], Galoter retorting 85–90% [101], and for Taciuk retorting 82% [101].

The thermal efficiency is defined as heat of desired product divided by the total heat of the process [99]. For example, some comparisons may involve using the equation

$$\text{Thermal efficiency} = \frac{\text{Gross Galorific value of (oil + gas)}}{\text{Gross Galorific value of shale + heat of retorting}}$$

which can be found in Probstein and Hicks [99].

More detailed evaluation of processes comes down to desired product yields (oil and gas) and energy consumption per unit of desired product produced, including additional energy requirement such as for gas purification, spent shale disposal, or water treatment.

References offering insights regarding the construction details and operational principles of the retorting equipment referred to above, including product characteristics, are found in Tables 8 and 9. As there are hundreds of retorting options that have been considered, this is far from being a complete list of possibilities. Nonetheless, it offers some insight into some significant processes. The next sections offer a few more details on selected ex situ and in situ processes.

Ex Situ Technologies: An Example and Some Further Considerations

There are many ex situ retorting technologies that differ by reactor types (fluidized bed, moving packed bed, solid mixers), by operating conditions (temperature, residence time), technical details such as drying of feed, feed distributor, discharge of spent shale, oil and gas separation (oil and gas separation from offgas), heat recovery or by-product utilization. Therefore in addition to the pyrolysis reactor, the heart of retorting process, a particular retorting technology includes various other components (unit operations) in the plant.

Figure 7 shows a principal schematic diagram of the Galoter process [44]. The principle of the Galoter process is heating fine-grained oil shale (particles with size below 25 mm) in a horizontal rotary kiln-type retort, with contact of hot oil shale ash obtained from solid retorting residue combustion outside of the retort. The process operates in continuous mode with oil shale and ash in cocurrent flows. The properties of the shale oil produced (specific gravity, H/C ratio, viscosity, boiling range, and hydrocarbon types) depend upon retorting temperature and residence time, of course, but can also depend on other factors such as condenser construction and temperature of recovery and separation of shale oil and the reactive properties of the hot shale residue heat carrier.

A heat-transfer medium (the heat carrier) can generally be reactive or nonreactive. Examples of reactive heat carriers include the gaseous heat carriers such as hydrogen or solid heat carriers such as oil shale ash. Oil shale ash from carbonate oil shales has chemisorptive properties, due to its alkaline nature, and can reduce

Oil Shale Processing, Chemistry and Technology.
Table 8 Some selected ex situ retorting technologies

Process/retort	References
Fushun retort	[101]
Brazilian Petrosix	[77, 85]
The Nevada-Texas-Utah retort or NTU (also known as the Dundas-Howes retort)	[8, 85]
The Paraho direct/indirect process	[85, 99]
The Union Oil retort "A" (Union Oil Company)	[8, 76, 77, 159]
The Union Oil retort "B" indirectly heated retort (Union Oil Company)	[8, 76, 77, 85, 159]
The Union Oil Steam Gas Recirculation (RSG) retorting process (Union Oil Company)	[8]
The Superior Oil process	[8, 85]
TOSCO II (Tosco corporation)	[77, 85, 99]
The Lurgi-Ruhrgas process	[8, 76, 77, 85, 142]
Kiviter process	[8, 101, 159]
Galoter process	[8, 44, 101, 159]
Aostra Taciuk Process (ATP)	[8, 101, 142]
Chamber oven (similar to coke batteries)	[159]
HYTORT (Institute of Gas Technology, IGT)	[38, 106]
Chattanooga process (pressurized fluid bed reactor)	[140]
Gas combustion retort, US Bureau of Mines	[8, 76, 77, 142, 159]
Oil-Tech vertical surface retort technology (Millenium Synfuels, LLC)	[140]
KENTOR II	[133]
Shell SPHER processes (Shell Pellet Heat Exchange Retorting)	[49]

Oil Shale Processing, Chemistry and Technology.
Table 9 Some selected in situ retorting processes and technologies

Process/retort	References
Occidental Petroleum "Oxy"	[8, 77, 85]
Sinclair oil and gas company process	[76, 77]
Equity Oil company process	[76, 77]
Shell Oil's thermally conductive in situ conversion process	[77, 140, 142]
Osborne's in situ process	[77]
Dow Chemical Co.'s process	[8, 77]
Equity Oil company process	[8]
Chevron's Technology for the Recovery and Upgrading of Oil from Shale (CRUSH) process	[140]
EGL oil shale process	[140]
Electrically enhanced oil production (EEOP) (Electro-Petroleum, Inc.)	[140]
PetroProbe process (Petro Probe, Inc.)	[140]
Electrofrac™ (Exxon Mobil Incorporation)	[140]
Geothermic Fuel Cell™ technology (GFL™)	[140]
In situ gas extraction technology (IGE), Mountain West Energy	[140]
Radio frequency/critical fluid oil extraction technology (Ryethon and CF technology)	[140]
EchoShale in-capsule process (Red Leaf Resources, Inc.)	[140]
PyroPhase	[140]
American Shale Oil Company (AMSO) process: Conduction, Convection, Reflux (CCR) process (former EGL Resources process)	[140]

the concentration of H_2S in the product gas as well as phenolic compounds in the oil [88]. Also the iron oxide in ash shows potential to reduce H_2S in the gas, but has little effect on phenolic compounds [88]. It should, however, be emphasized that heat carrier ash used in solid heat carrier retorts does not affect significantly the sulfur concentration in oils (i.e., organic sulfur) [40, 88].

It needs to be emphasized again that an important parameter in ex situ retorting design is the heat up time of the retorted shale. This determines overall process time and therefore reactor volume and thus retorting process cost [18], but also impacts retort oil quality. The time to transfer heat to shale depends on the feed oil shale particle size. Often, operational details require

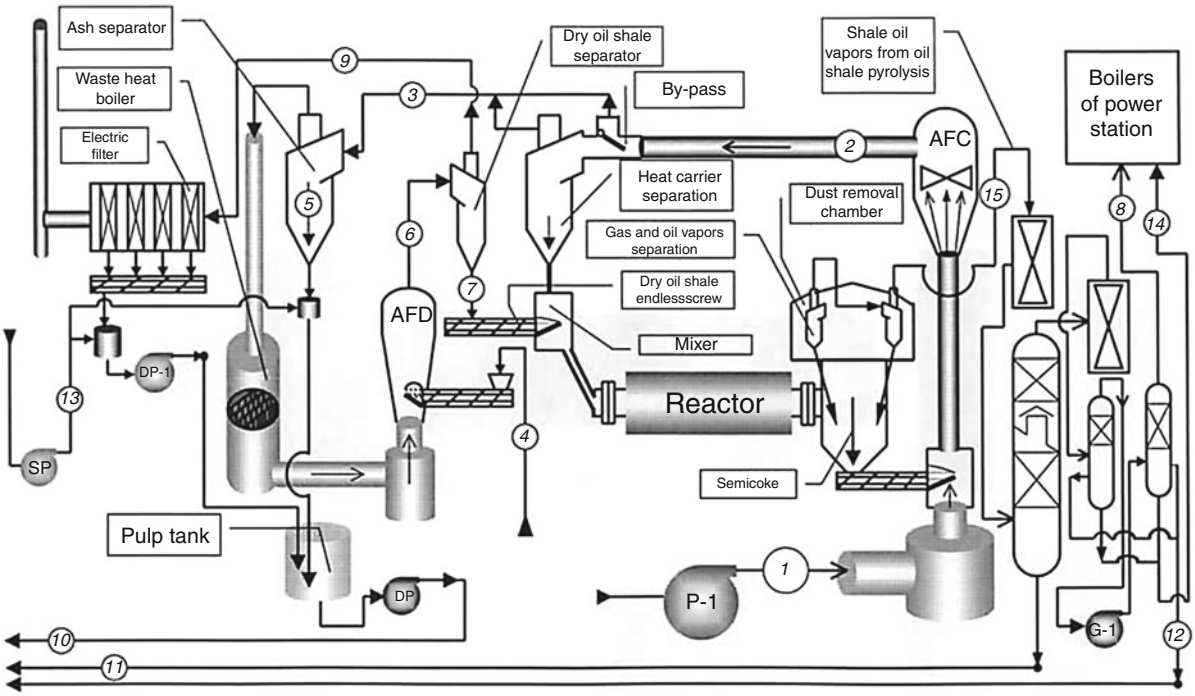

Oil Shale Processing, Chemistry and Technology. Figure 7
Galoter Retorting Process ([44], with permission). The key features of this process are the "Reactor" – the drum reactor in which oil shale pyrolysis takes place, after mixing of raw and hot spent shale; "AFC" – aerofountain combustor for spent shale (semicoke) burnout; "AFD" – aerofountain dryer for raw shale; P-1 – centrifugal air blower; DP – dredger pump; DP-1 – small dredger pump of electric filters; SP – pump for settled recycle water; G-1 – centrifugal gas blower; 1 – compressed air given to the retort; 2 – solid heat carrier mixture with stack gas after combustion of semicoke in the AFC; 3 – mixture of ash and stack gas after separation of solid heat carrier required for oil shale pyrolysis process; 4 – raw oil shale feed; 5 – ash separated by first, second, and third stage ash cyclones; 6 – dried oil shale mixture with stack gas after AFD; 7 – dried oil shale separated by first, second, and third stage cyclones prior to entering the system of dry oil shale screw conveyers; 8 – retort gas for firing in power station boilers; 9 – stack gas to ESP for final purification; 10 – ash slurry for storage/disposal; 11 – shale oils to storage; 12 – light oil or gasoline fraction (separated from water) to storage; 13 – recycle water to ash hydroremoval system; 14 – phenolic water to incineration in power station boilers; 15 – oil vapors from retort, after cyclone separators, to condensation system

specific particle size ranges [8]. It has been indicated that [18] the heat up time of the oil shale particles larger than 1 cm scales roughly as diameter squared and thus a heat up time of 2.5 min can be estimated for 10-mm particles and 4 h for 100-mm particles. Accordingly, the ex situ technologies have been divided in three groups, based upon particle size:

1. Processes with large feed particle sizes (so-called lump oil shale). These processes take place over the longest time scale; the shale residence time in retorts is measured in hours. For example, the industrial Kiviter process [8] uses a feed size of 10–125 mm and the Fushun process of 10–75 mm [2].
2. Processes that use coarsely ground particles. The shale residence time scale is of minutes. For example, the industrial Galoter process [8] uses a feed size of 0–25 mm [2].
3. Processes fed with pulverized oil shale with size below 5 mm. The residence time is shortest, with the time scale of seconds. This is used in fluidized bed retorting units [151]. The fluidized bed retorting systems are less developed than the two former types and no commercial units are yet in use.

In Situ Technologies: Further Considerations

The common principle of in situ processes is heating the oil shale deposit underground. Different versions use different methods of heat transfer, as already described. With in situ technologies there is an opportunity to utilize poorer and deeper oil shale deposits than can be used for conventional aboveground processing [71]. Although a number of field-scale experiments have been conducted over the last decades in several countries [15, 77, 85, 97] no in situ technology-based commercial plant has been placed in operation to date. However, several of the latest innovative technological approaches involve in situ processes [140].

There are different possible ways of classifying in situ technologies (see [77]). The most common is classification into true in situ processes and modified in situ processes. Some define the true in situ processes as involving minimal disturbance of the oil shale ore bed, and the modified in situ as processes as any that use rubblizing either through blasting or partial mining. Therefore the distinction between true and modified in situ processes is a matter of degree of the bed disturbance.

True in situ processes thus do not generally require significant mining. This category of in situ processes uses natural rock permeability or permeability created by artificial fracturing (by explosives or hydrostatic pressure) in place. The true in situ processes follow a general sequence involving dewatering and establishing measures to minimize contact between groundwater and the reaction zone; fracturing or rubblizing to create permeability (if natural permeability is not sufficient); heating the oil shale by ignition, hot fluids, or other means; recovering oil and gas through wells [85].

The modified in situ processes involve partial mining under the oil shale deposit to create void space followed by rubblizing the rest into the created void. To create voids about 10–25% of overall space is mined out [77].

Final Considerations and Future Directions

This review was intended to capture many aspects of the current state of knowledge and basic research directions in the field of oil shale research. It did so in the context provided by currently and historically explored technologies for oil shale conversion. Generally speaking, there is more new development interest in oil production processes, but the direct combustion processes will remain in use in particular instances (such as in Estonia). While the pyrolytic phenomena that shale undergoes are common to both oil production and combustion processes, there has not been as much emphasis on fundamental exploration of these phenomena from the combustion side, and in that case there are other technologically important issues that have captured more basic research interest (e.g., the behavior of ash in the boilers, the high-temperature corrosion of boilers, the problems of ash handling and disposal, the problems of sulfur capture). For the combustion community, the behavior of the organic portion of the ash has been somewhat secondary, and even the final phases of organic materials' burnout, which has captured the attention of many researchers in the coal combustion community, has been of less interest, because of the inherently higher reactivity of oil shale chars as compared to coal chars.

From the perspective of those who seek to produce oil, the major problems have been those of thermal management and the handling of large amounts of solids, as well as dealing with a range of environmental problems associated with the processing (whether aboveground or in situ). What can be economically done with oil shale in light of the above has dictated the nature of the processes more than consideration of the chemical aspects. Nonetheless, it has been observed that there can be factors whose importance may be sometimes overlooked. Issues of mass transport can materially impact both yields and quality of the product oils, and may be sensitive to factors such as pressure, particle size, heating rate, temperature, and residence time in a hot environment and gaseous environment. All of these factors have been studied, but the general impression is that more work is needed to better establish general trends. Likewise, there have been an enormous number of studies performed on elucidating the kinetics of pyrolysis, but rarely has there been a critical examination of results obtained on the same material examined by different means in different laboratories. As a result, there is a crude understanding of rate processes, but one that for predictive purposes cannot be claimed to be better than an order of magnitude. Despite large numbers of carefully performed studies, there has not yet been closure on the overall nature and rates of the many processes that determine behavior in practical processes.

Bibliography

Primary Literature

1. Aarna AY (1954) Isothermal destruction of Baltic oil shale. Trans Tallinn Polytech Inst A 57:32–34 (in Russian)
2. EASAC (European Academies Science Advisory Council) (2007) A study on the EU oil shale industry – viewed in the light of the Estonian experience. European Academies Science Advisory Council
3. Alali J, Abdelfattah AS, Suha MY, Al-Omari W (2006) Oil shale. In: Sahawneh J, Madanat M (eds), Natural Resources Authority of Jordan
4. Al-Ayed OS, Matouq M, Anbar Z, Khaleel AM, Abu-Nameh E (2010) Shale pyrolysis kinetics and variable activation energy principle. Appl Energy 87:1269–1272
5. Allred VD (1966) Kinetics of oil shale pyrolysis. Chem Eng Prog 62:55–60
6. Arbiter N (1983) Concentration of oil shale. Miner Process Technol Rev 1:207–248
7. Arro H, Prikk A, Pihu T (2003) Calculation of qualitative and quantitative composition of Estonian oil shale and its combustion products. Fuel 82:2179–2195, 2197–2204
8. Baughman GL (1978) Synthetic fuels data handbook, 2nd edn. Cameron Engineering, Denver
9. Behar F, Beaumont V, Penteado HL (2001) Rock-Eval 6 technology: performances and developments. Oil Gas Sci Technol – Rev IFP 56:111–134
10. Bjerle I, Ecklund H, Svensson O (1980) Gasification of Swedish Black Shale in the fluidized bed. Reactivity in steam and carbon dioxide atmosphere. Ind Eng Chem Process Des Dev 19:345–351
11. Bradhurst DH, Worner HK (1996) Evaluation of oil production from the microwave retorting of Australian shales. Fuel 75:285–288
12. Braun RL, Burnham AK (1986) Kinetics of Colorado oil shale pyrolysis in a fluidized bed reactor. Fuel 65:218–225
13. Braun RL, Rothman AJ (1975) Oil shale pyrolysis: kinetics and mechanism of oil production. Fuel 54:129–131
14. Brendow K (2003) Global oil shale issues and perspectives. Oil Shale 20:81–92
15. Bridges JE (2007) Wind power energy storage for in situ shale oil recovery with minimal CO_2 emission. IEEE Trans Energy Convers 22:103–109
16. Bryant RS, Bailey SA, Stepp AK, Evans DB, Parli JA, Kolhatkar AR (1998) Biotechnology for heavy oil recovery. No. 1998.110
17. Burnham AK (1989) On solar thermal processing and retorting of oil shale. Energy 14:667–674
18. Burnham AK (1995) Chemical kinetics and oil shale processing design. In: Snape C (ed) Composition, geochemistry and conversion of oil shales. NATO ASI Series. Kluwer, The Netherland
19. Burnham AK, Braun RL, Coburn TT, Sandvik EI, Curry DJ, Schmidt BJ, Noble RA (1996) An appropriate kinetic model for well-preserved algal kerogens. Energy Fuels 10:49–59
20. Burnham AK, McConaghy JR (2006) Comparison of the acceptability of various oil shale processes. In: Twenty-sixth oil shale symposium, Golden, 16–18 Oct 2006. UCRL-CONF-226717
21. Campbell JH, Koskinas GH, Stout ND (1978) Kinetics of oil generation from Colorado oil shale. Fuel 57:372–376
22. Cane RF (1976) The origin and formation of oil shale. In: Yen TF, Chilingarian GV (eds) Oil shale. Elsevier, Amsterdam
23. Carter SD, Graham UM, Rubel AM, Robl TL (1995) Fluidized bed retorting of oil shale. In: Snape C (ed) Geochemistry and conversion of oil shales. NATO ASI Series. Kluwer, London
24. Citiroglu M, Türkay S, Cepni ZI, Snape CE (1996) Fixed bed pyrolysis and hydropyrolysis of an immature Type I Turkish oil shale. Turk J Chem 20:175–185
25. Cummins JJ, Robinson WE (1972) Thermal degradation of Green River Kerogen at 150°C to 350°C. U.S. Bureau of Mines Report of Investigations 7620
26. Degirmenci L, Durusoy T (2002) Effect of heating rate on pyrolysis kinetics of Gönyük oil shale. Energy Sources 34:931–936
27. Degirmenci L, Durusoy T (2005) Effect of heating rate and particle size on the pyrolysis of Gönyük oil shale. Energy Sources 27:787–795
28. Derenne S, Largeau C, Casadevall E, Damste JSS, Tegelaar EW, Leeuw JW (1989) Characterization of Estonian Kukersite by spectroscopy and pyrolysis: evidence for abundant alkyl phenolic moieties in an Ordovician, marine, type II/I kerogen. Org Chem 16:873–888
29. Dieckmann V, Schenk HJ, Horsfield B, Welte DH (1998) Kinetics of petroleum generation and cracking by programmed-temperature closed-system pyrolysis of Toarcian Shales. Fuel 77:23–31
30. Dinneen GU (1976) Retorting technologies of oil shales. In: Yen TF, Chilingarian GV (eds) Oil shale. Elsevier, Amsterdam
31. Duncan DC (1976) Geologic settings of oil shale deposits and world prospects. In: Yen TF, Chilingarian GV (eds) Oil shale. Elsevier, Amsterdam
32. Durand B (1980) Kerogen. Insoluble organic matter from sedimentary rocks. Technip, Paris
33. Durand B, Monin JC (1980) Elemental analysis of kerogens (C, H, O, N, S, Fe). In: Durand B (ed) Kerogen. Insoluble organic matter from sedimentary rocks. Technip, Paris
34. Durand B, Nicaise C (1980) Procedures of kerogen isolation. In: Durand B (ed) Kerogen. Insoluble organic matter from sedimentary rocks. Technip, Paris
35. Durand-Souron C (1980) Thermogravimetric analysis and associated techniques applied to kerogens. In: Durand B (ed) Kerogen. Insoluble organic matter from sedimentary rocks. Technip, Paris
36. Dyni JR (2006) Geology and resources of some world oil shale deposits. Scientific Investigations Report 2005–5294. United States Department of the Interior, United States Geological Survey
37. Ecklund H, Svensson O (1983) Reactor model for the gasification of Black Shale in the fluidized bed. Comparison with the pilot plant data. Ind Eng Chem Process Des Dev 22:396–401

38. Ekinci E, Yürüm Y (1995) Steam and coprocessing of oil shales. In: Snape C (ed) Composition, geochemistry and conversion of oil shales. NATO ASI Series. Kluwer, The Netherland
39. Ekstrom A, Callaghan G (1987) The pyrolysis kinetics of some Australian oil shales. Fuel 66:331–337
40. Elenurm A, Oja V, Elenurm A, Tali E, Tearo E, Yanchilin A (2008) Thermal processing of dictyonema argillite and kukersite oil shale: transformation and distribution of sulfur compounds in pilot-scale Galoter process. Oil Shale 25:328–334
41. Espitalie J, Madec M, Tissot B (1980) Role of mineral matrix in kerogen pyrolysis: influence on petroleum generation and migration. AAPG Bull 64:59–66
42. Forsman JP (1963) Geochemistry of kerogen. In: Breger IA (ed) Organic geochemistry. Pergamon, Oxford, pp 148–182
43. Gavin JM (1924) Oil shale. U.S. Government Printing Office, Washington, DC
44. Golubev N (2003) Solid oil shale heat carrier technology for oil shale retorting. Oil Shale 20:324–332
45. Gonzalez-Vila FJ (1995) Alkane biomarkers. Geochemical significance and application in oil shale geochemistry. In: Snape C (ed) Geochemistry and conversion of oil shales. NATO ASI Series. Kluwer, London
46. Gonzalez-Vila FJ, Ambles A, del Rio JC, Grasset L (2001) Characterization and differentiation of kerogens by pyrolytic and chemical degradation techniques. J Anal Appl Pyrol 58–59:315–328
47. Goodfellow L, Haberman CE, Atwood MT (1968) Modified Fischer assay equipment, procedures and product balance determinations. In: Joint symposium on oil shale, tar sand, and related materials. American Chemical Society, San Francisco National Meeting, 2–5 April 1968.
48. Gorlov EG (2007) Thermal dissolution of solid fossil fuels. Solid Fuel Chem 41:290–298
49. Gwyn JE, Roberts SC, Hardesty DE, Johnson GL, Hinds GP (1980) Shell pellet heat exchange retorting: the SPHER energy-efficient process for retorting oil shale. American Chemical Society, San Francisco, pp 59–69
50. Hamarneh YM (1984) Oil shale deposits in Jordan. Symposium on characterization and chemistry of oil shales. Am Chem Soc 29(3):41–50
51. Hamarneh Y (2006) Oil shale resources development in Jordan. Natural Resources Authority of Jordan, Amman, 1998. Revised and Updated by Dr. Jamal Alali, Amman
52. Hotta A, Parkkonen R, Hiltunen M, Arro H, Loosaar J, Parve T, Pihu T, Prikk A, Tiikma T (2005) Experience of Estonian oil shale combustion based on CFB technology at Narva Power Plants. Oil Shale 22:381–397
53. Huss EB, Burnham AK (1982) Gas evolution during pyrolysis of various Colorado oil shales. Fuel 66:1188–1196
54. Hutton AC (1987) Petrographic classification of oil shales. Int J Coal Geol 8:203–231
55. Hutton AC (1995) Organic petrography of oil shales. In: Snape C (ed) Geochemistry and conversion of oil shales. NATO ASI Series. Kluwer, The Netherland
56. Hutton A, Bharati S, Robl T (1994) Chemical and petrographic classification of kerogen/macerals. Energy Fuels 8:1478–1488
57. Jaber JO (2000) Gasification potential of Ellajjun oil shale. Energy Convers Manage 41:1615–1624
58. Johannes I, Zaidentsal A (2008) Kinetics of low-temperature retorting of kukersite oil shale. Oil Shale 25:412–425
59. Johannes I, Kruusment K, Veski R (2007) Evaluation of oil potential and pyrolysis kinetics of renewable fuel and shale samples by Rock-Eval analyzer. J Anal Appl Pyrol 79:183–190
60. Johannes I, Kruusment K, Veski R, Bojesen-Koefoed JA (2006) Characterisation of pyrolysis kinetics by Rock-Eval basic data. Oil Shale 23:249–257
61. Johannes I, Tiikma L (2004) Kinetics of oil shale pyrolysis in an autoclave under non-linear increase of temperature. Oil Shale 21:273–288
62. Johannes I, Tiikma L, Zaidenstal A (2010) Comparison of the thermobituminization kinetics of Baltic oil shales in open retorts and autoclaves. Oil Shale 27:17–25
63. Johannes I, Tiikma L, Zaidenstal A, Luik L (2009) Kinetics of kukersite low-temperature pyrolysis in autoclaves. J Anal Appl Pyrol 85:508–513
64. Johannes I, Zaidenstal A (2008) Kinetics of low-temperature retorting of kukersite oil shale. Oil Shale 25:412–425
65. Kask KA (1955) About bituminization of kerogen of oil shale kukersite. Report I. Trans Tallinn Polytech Inst A 63:51–64 (in Russian)
66. Kelemen SR, Afeworki M, Gorbaty ML, Sansone M, Kwiatek PJ, Walters CC, Freund H, Siskin M, Bence AE, Curry DJ, Solum M, Pugmire RJ, Vandenbroucke M, Leblond M, Behar F (2007) Direct characterization of kerogen by x-ray and solid-state ^{13}C nuclear magnetic resonance methods. Energy Fuels 21:1548–1561
67. Koel M, Ljovin S, Hollis K, Rubin J (2001) Using neoteric solvents in oil shale studies. Pure Appl Chem 73:153–159
68. Kogerman PN, Kopwillem JJ (1932) Hydrogenation of Estonian oil shale and shale oil. J Inst Petrol Technol 18:833–845
69. Kök MV (2002) Oil shale: pyrolysis, combustion, and environment: a review. Energy Sources 24:135–143
70. Kök MV (2008) Recent developments in the application of thermal analysis techniques in fossil fuels. J Therm Anal Calorim 91:763–773
71. Kök MV, Guner G, Bağci AS (2008) Application of EOR techniques for oil shale fields (in-situ combustion approach). Oil Shale 25:217–225
72. Krym YS (1932) About laboratory methods for determination the tendency of selfignition for coals. Khim Tverd Topl 2–3:7–22 (in Russian)
73. Lafargue E, Marquis F, Pillot D (1998) Rock-Eval 6 applications in hydrocarbon exploration, production and soils contamination studies. Oil Gas Sci Technol 53:421–437
74. Larsen JW, Li S (1994) Solvent swelling studies of Green River Kerogen. Energy Fuels 8:932–936
75. Larsen WJ, Parikh H, Michels R (2002) Changes in the cross-linking density of Paris Basin Toarcian kerogen during maturation. Org Geochem 33:1143–1152

76. Lee S (1991) Oil shale technology. CRC, Boca Raton
77. Lee S, Speight JG, Loyalka SK (2007) Handbook of alternative fuel technology. CRC, Boca Raton
78. Li S, Yue C (2003) Study of pyrolysis kinetics of oil shale. Fuel 82:337–342
79. Louw SJ, Addison J (1985) Studies of the Scottish oil shale industry, vol 1: History of the industry, working conditions, and mineralogy of Scottish and Green River formation shales. Final Report on US Department of Energy. Institute of Occupational Medicine
80. Luts K (1944) Estonian oil shale kukersite, its chemistry, technology and analysis. Revalen Buchverlag, Reval (in German)
81. Maalmann I (2003) Historical survey of nuclear non-proliferation in Estonia 1946–1995. Estonian Radiation Protection Centre
82. Miknis FP (1995) Solid state ^{13}C NMR in oil shale research: an introduction with selected applications. In: Snape C (ed) Composition, geochemistry and conversion of oil shales. NATO ASI Series. Kluwer, The Netherland
83. Miknis FP, Turner TF, Berdan GL, Conn PJ (1987) Formation of soluble products from thermal decomposition of Colorado and Kentucky oil shales. Energy Fuels 1:477–483
84. Nutall HE, Guo TM, Schrader S, Thakur DS (1983) Pyrolysis kinetics of several key world oil shales. ACS symposium series, vol 230, pp 269–300
85. Office of Technology Assessment (1980) An assessment of oil shale technology. Congress of the United States, Office of Technology Assessment, Washington, DC
86. Oja V (2005) Characterization of tars from Estonian Kukersite oil shale based on their volatility. J Anal Appl Pyrol 74:55–60
87. Oja V (2006) A brief overview of motor fuels from shale oil of kukersite. Oil Shale 23:160–163
88. Oja V, Elenurm A, Rohtla I, Tali E, Tearo E, Yanchilin A (2007) Comparison of oil shales from different deposits: oil shale pyrolysis and copyrolysis with ash. Oil Shale 24:101–108
89. Ots A (2006) Oil shale fuel combustion. Tallinn Book Printers, Tallinn
90. Ozerov IM, Polozov VI (1968) Principles of oil shale commercial classification. In: United Nations symposium on the development and utilization of oil shale resources, Tallinn
91. Parks TJ, Lynch LJ, Webster DS (1987) Pyrolysis model of rundle oil shale from in-situ ^{1}H NMR data. Fuel 66:338–344
92. Patterson HJ (1994) A review of the effects of minerals in processing of Australian oil shales. Fuel 73:321–327
93. Patterson JH, Dale LS, Chapman JF (1988) Partitioning of trace elements during the retorting of Australian oil shales. Fuel 67:1353–1356
94. Perry RH, Green DW (1997) Perry's chemical engineering handbook, 7th edn. McGraw-Hill, USA
95. Peters KE (1986) Guidelines for evaluating petroleum source rock using programmed pyrolysis. AAPG Bull 70:318–329
96. Petersen HI, Bojesen-Koefoed JA, Mathiesen A (2010) Variations in composition, petroleum potential and kinetics of Ordovician-Miocene Type I and Type I–II source rocks (oil shales): implications for hydrocarbon generation characteristics. J Petrol Geol 33:19–42
97. Prien CH (1951) Pyrolysis of coal and oil shale. Ind Eng Chem 43:2006–2015
98. Prien CH (1976) Survey of oil shale research in the last three decades. In: Yen TF, Chilingarian GV (eds) Oil shale. Elsevier, Amsterdam
99. Probstein RF, Hicks RE (2006) Synthetic fuels. Dover, New York
100. Puura E (1999) Technogenic minerals in the waste rock heaps of Estonian oil shale mines and their use to predict the environmental impact of the waste. Oil Shale 16:99–107
101. Qian J, Wang J (2006) World oil shale retorting technologies. In: International conference on oil shale: recent trends in oil shale, 7–9 Nov 2006, Jordan
102. Qian J, Wang J, Li S (2003) Oil shale development in China. Oil Shale 20:356–359
103. Rajeshwar K, Nottenburg R, Dubow J (1979) Thermophysical properties of oil shales. J Mater Sci 14:2025–2052 (Review)
104. Raudsepp H (1953) About the method for determining of organic mass in Baltic oil shales. Proc Tallinn Polytech Inst A 46:3–22 (in Russian)
105. Reynolds JG, Crawford RW, Burnham AK (1991) Analysis of oil shale and petroleum source rock pyrolysis by triple quadrupole mass spectrometry: comparisons of gas evolution at the heating rate of 10°C/min. Energy Fuels 5:507–523
106. Roberts MJ, Snape CE, Mitchell SC (1995) Hydropyrolysis: fundamentals, two-stage processing and PDU operations. In: Snape C (ed) Geochemistry and conversion of oil shales. NATO ASI Series. Kluwer, The Netherland
107. Robinson WE (1969) Isolation procedures for kerogens and associated soluble organic materials. In: Eglinton G, Murphy MTJ (eds) Organic geochemistry. Springer, Berlin, pp 181–195
108. Robl TL, Taulbee DN (1995) Demineralization and kerogen macerals separation and chemistry. In: Snape C (ed) Geochemistry and conversion of oil shales. NATO ASI Series. Kluwer, London
109. Rocha JD, Brown SD, Love GD, Snape CE (1997) Hydropyrolysis: a versatile technique for solid fuel liquefaction, sulphur specification and biomarker release. J Anal Appl Pyrol 40–41:91–103
110. Rullkötter J, Michaelis W (1990) The structure of kerogen and related materials. A review of recent progress and future trends. Org Geochem 16:829–852
111. Savest N, Hruljova J, Oja V (2009) Characterization of thermally pretreated kukersite oil shale using the solvent-swelling technique. Energ Fuel 23:5972–5977
112. Savest N, Oja V, Kaevand T, Lille Ü (2007) Interaction of Estonian kukersite with organic solvents: a volumetric swelling and molecular simulation study. Fuel 86:17–21
113. Schachter Y (1979) Gasification of oil shale. Isr J Technol 17:51–57
114. Schlatter LE (1968) Definition, formation and classification of oil shales. In: United Nations symposium on the development and utilization of oil shale resources, Tallinn
115. Schmitt KD, Sheppard EW (1984) Determination of carbon center types in solid fuel by CP/MAS NMR. Fuel 63:1241–1244

116. Sert M, Ballice L, Yüksel M, Saglam M (2009) Effect of mineral matter on product yield and composition at isothermal pyrolysis of Turkish oil shales. Oil Shale 26:463–474
117. Shpirt MYa, Punanova SA, Strizhakova YuA (2007) Trace elements in black and oil shales. Solid Fuel Chem 41:119–127
118. Shui H, Cai Z, Xu C (2010) Recent advances in direct coal liquefaction. Energies 3:155–170
119. Silbernagel BG, Gebhard LA, Siskin M, Brons G (1987) ESR study of kerogen conversion in shale pyrolysis. Energy Fuels 1:501–506
120. Siskin M, Scouten CG, Rose KD, Aczel T, Colgrove SG, Pabst RE Jr (1995) Detailed structural characterization of the organic material in Rundle Ramsay Crossing and Green River oil shales. In: Snape C (ed) Composition, geochemistry and conversion of oil shales. NATO ASI Series. Kluwer, The Netherland
121. Skala D, Korica S, Vitorovic D, Neumann H-J (1997) Determination of kerogen type by using DSC and TG analysis. J Therm Anal 49:745–753
122. Smith MW, Shadle LJ, Hill DL (2007) Oil shale development from the perspective of NETL's unconventional oil resource repository. DOE/NETL-IR-2007-022
123. Smith LK, Smoot LD, Fletcher TH, Pugmire RJ (1994) The structure and reaction processes of coal. The Plenum chemical engineering series. Plenum, New York
124. Sohn HY, Yang HS (1985) Effect of reduced pressure on oil shale retorting. 1. Kinetics of oil generation. Ind Eng Chem Process Des Dev 24:265–270
125. Solomon PR, Carangelo RM, Horn E (1986) The effects of pyrolysis conditions on Israeli oil shale properties. Fuel 65:650–662
126. Solomon PR, Serio MA, Despande GV, Kroo E (1990) Cross-linking reactions during coal conversion. Energy Fuels 4:42–54
127. Solomon PR, Serio MA, Suuberg EM (1992) Coal pyrolysis: experiments, kinetic rates and mechanism. Prog Energy Combust Sci 18:133–220
128. Speight JG (2007) The chemistry and technology of petroleum, 4th edn. CRC, Boca Raton
129. Speight JG (2008) Synthetic fuels handbook. Properties, processes and performance. McGraw-Hill, USA
130. Strizhakova YuA, Usova TV (2008) Current trends in the pyrolysis of oil shale: a review. Solid Fuel Chem 24:197–201
131. Suuberg EM, Sherman J, Lilly WD (1987) Product evolution during rapid pyrolysis of Green River Formation oil shale. Fuel 66:1176–1184
132. Suuberg EM, Unger PE, Lilly WD (1985) Experimental study on mass transfer from pyrolyzing coal particles. Fuel 64:956–962
133. Taulbee DN, Carter SD (1992) Investigation of product coking by hot recycle solids in the KENTORT II fluidized bed retort. American Chemical Society, San Francisco, pp 800–809
134. Thankur DS, Nutall HE (1987) Kinetics of pyrolysis of Moroccan oil shale by thermogravimetry. Ind Eng Chem Res 26:1351–1356
135. Thomas RD, Lorentz PB (1970) Use of centrifugal separation to investigate how kerogen is bound to the minerals in oil shale. U. S. Bur. Mines, Rep. Invest., 7378
136. Tiikma L, Johannes I, Luik H, Zaidentsal A, Vink N (2009) Thermal dissolution of Estonian oil shale. J Anal Appl Pyrol 85:502–507
137. Tiikma L, Zaidentsal A, Tensorer M (2007) Formation of thermobitumen from oil shale by low-temperature pyrolysis in an autoclave. Oil Shale 24:535–546
138. Torrente MC, Galán MA (2001) Kinetics of the thermal decomposition of oil shale from Puertollano (Spain). Fuel 80:327–334
139. Tucker JD, Masri B, Lee S (2000) A comparison of retorting and supercritical extraction techniques on El-Lajjun oil shale. Energy Sources 22:453–463
140. U.S. Department of Energy (2007) Secure fuels from domestic resources. The continuing evolution of American's oil shale and tar sands industries
141. Urov K, Sumberg A (1999) Characteristics of oil shales and shale like rocks of known deposits and outcrops. Oil Shale 16:1–64
142. US DOE (March 2004) Strategic significance of America's oil shale resources, vol II: Oil shale resources, technology, and economics. U.S. Department of Energy
143. Vandenbroucke M (1980) Structure of kerogens as seen by investigations on soluble extracts. In: Durand B (ed) Kerogen. Insoluble organic matter from sedimentary rocks. Technip, Paris
144. Vandenbroucke M (2003) Kerogen: from types to models of chemical structure. Oil Gas Sci Technol – Rev IFP 58:243–269
145. Vandenbroucke M, Largeau C (2007) Kerogen origin, evolution and structure. Org Geochem 38:719–833
146. Vitorovic D (1980) Structure elucidation of kerogen by chemical methods. In: Durand B (ed) Kerogen. Insoluble organic matter from sedimentary rocks. Technip, Paris
147. Wall GC, Smith SJC (1987) Kinetics of production of individual products from the isothermal pyrolysis of seven Australian oil shales. Fuel 66:345–350
148. Wang Q, Liu H, Sun B, Li S (2009) Study on pyrolysis characteristics of Huadian oil shale with isoconversional method. Oil Shale 26:148–162
149. Wang CC, Noble RD (1983) Composition and kinetics of oil generation from non-isothermal oil shale retorting. Fuel 62:529–533
150. Wang Q, Sun B, Hu A, Bai J, Li S (2007) Pyrolysis characteristics of Huadian oil shales. Oil Shale 24:147–157
151. Wang WD, Zhou CY (2009) Retorting of pulverized oil shale in fluidized-bed pilot plant. Oil Shale 26:108–113
152. Watson NC (1984) A modified Gray-King assay method for small oil shale samples. Fuel 63:1455–1458
153. Williams PT, Ahmad N (2000) Investigation of oil shale pyrolysis processing conditions using thermogravimetric analysis. Appl Energy 66:113–133
154. Wiser WH, Anderson LL (1975) Transformation of solids to liquid fuels. Annu Rev Phys Chem 26:339–357
155. World Energy Council (2007) Survey of energy resources 2007. World Energy Council 2007, United Kingdom
156. Xue HQ, Li SY, Wang HY, Zheng DW, Fang CH (2010) Pyrolysis kinetics of oil shale from Northern Songliao Basin in China. Oil Shale 27:5–16

157. Yang HS, Shon HY (1985) Effect of reduced pressure on oil shale retorting. Ind Eng Chem Proc DD 24:271–273
158. Yen TF (1976) Structural aspects of organic components in oil shales. In: Yen TF, Chilingarian GV (eds) Oil shale. Elsevier, Amsterdam
159. Yen TF, Chilingarian GV (1976) Introduction to oil shales. In: Yen TF, Chilingarian GV (eds) Oil shale. Elsevier, Amsterdam
160. Burnham AK, Braun RL (1999) Global kinetic analysis of complex materials. Energy Fuels 13:1–22
161. Davis JD, Galloway AE (1928) Low-temperature carbonization of lignites and sub-bituminous coals. Ind Eng Chem 20:612–617
162. Kask KA (1956) About bituminizing of kerogen of oil shale-kukersite. Report II. Trans Tallinn Polythec Inst A 73:23–40 (in Russian)
163. Kilk K, Savest N, Yanchilin A, Kellogg DS, Oja V (2010) Solvent swelling of Dictyonema oil shale: low temperature heat-treatment caused changes in swelling extent. J Anal Appl Pyrol 89:261–264
164. Lille Ü, Heinmaa I, Pehk T (2003) Molecular model of Estonian kukersite kerogen evaluated by ^{13}C MAS NMR spectra. Fuel 82:799–804
165. Miknis FP, Turner TF (1995) The bitumen intermediate in isothermal and nonisothermal decomposition of oil shales. In: Snape C (ed) Composition, geochemistry and conversion of oil shales. NATO ASI Series. Kluwer, The Netherland
166. Rahman M, Kinghorn RF, Gibson PJ (1994) The organic matter in oil shales from the lowmead basin, Qeensland, Australia. Journ Petrol Geol 17:317–326

Books and Reviews

Ogunsola OI, Hartstein AM, Ogunsola O (2010) Oil shale: a solution to the liquid fuel dilemma. Oxford University Press, USA
Qian J (2010) Oil shale – petroleum alternative. China Petrochemical Press, Beijing
Yen TF, Chilingarian GV (1976) Oil shale. Elsevier Scientific, Amsterdam

Oil Spill Remote Sensing

Mervin Fingas[1], Carl Brown[2]
[1]Spill Science, Edmonton, AB, Canada
[2]Emergencies Science and Technology Section, Environment Canada, Ottawa, ON, Canada

Article Outline

Glossary
Definition of the Subject and Its Importance
Introduction
Atmospheric Properties
Oil Interaction with Light and Electronic Waves
Visible Indications of Oil
Optical Sensors
Laser Fluorosensors
Microwave Sensors
Slick Thickness Determination
Integrated Airborne Sensor Systems
Satellite Remote Sensing
Oil Under Ice Detection
Underwater Detection and Tracking
Small Remote-Controlled Aircraft
Real-Time Displays and Printers
Routine Surveillance
Future Directions
Bibliography

Glossary

Laser fluorosensor A specific substance detection systems that employ a laser to excite a substance which then gives off radiation at another wavelength. This wavelength is typically unique to the substance being detected.

Microwave sensor Devices which detect radiation in the microwave region of the electromagnetic spectrum. Some devices, such as radar, also emit waves in the microwave spectrum to analyze the reflectivity of the fields of view.

Optical sensor Sensors which analyze the field-of-view in the electromagnetic spectrum from the infrared to the ultraviolet region. Typically the focus is the visible region.

Passive microwave sensor A sensor which analyzes the natural microwave radiation in a field-of-view.

Radarsat One of two radar satellites that are often used to detect and track oil spills.

Radiometer Any device that measures electromagnetic radiation typically the abundance of radiation in a given spectral range is measured.

Scatterometer A device that measures the scattering of a particular spectral range of radiation.

Ship discharge An oil spill resulting from a discharge (usually illegal) from a ship. Ships may discharge lubrication oil, oil from washing, or other waste oils.

Thickness sensor Any oil spill sensor that specifically measures oil slick thickness.

Definition of the Subject and Its Importance

Remote-sensing for oil spills is reviewed. The technical aspects of sensors are reviewed and the benefits and limitations of each sensor are given. Oil spill response often requires that remote sensing is used to detect and map the spill of interest. A wide variety of technologies had been tried.

A common and economical sensor is an infrared camera or an IR/UV system. This sensor class has limited utility but has the lowest cost of any sensor. The inherent weaknesses include the inability to discriminate oil on beaches, among weeds or debris and under certain lighting conditions, oil is not detected. Furthermore, water-in-oil emulsions are often not detected in the infrared. The laser fluorosensor is a most-useful instrument because of its unique capability to identify oil on backgrounds that include water, soil, weeds, ice, and snow. It is the only sensor that can positively discriminate oil on most backgrounds.

Radar offers the only potential for large area searches, day/night and foul weather remote sensing. Radar is costly, requires a dedicated aircraft, and is prone to many interferences. False targets can be as high as 95%. Satellite-borne radar sensors are useful, however, their frequency of overpass and lesser spatial resolution render them useful for mapping large spills or assisting in ship and platform discharge monitoring. Much effort is currently underway to remove oil look-alikes such as low wind areas, biogenic slicks, oceanographic fronts, etc., from the imagery.

Equipment that measures relative slick thickness is still under development. Passive microwave has been studied for several years, but instruments lack sufficient spatial resolution to be practical, operational instruments. A laser-acoustic instrument, which provides the only technology to measure absolute oil thickness, has been tested.

Equipment operating in the visible spectrum, such as cameras and scanners, is useful for documentation or providing a basis for the overlay of other data. It is not useful beyond this because oil shows no spectral characteristics in the visible region. Less use is being made of visible equipment in recent years.

Sensors for measuring oil thickness and detecting oil in ice are briefly reviewed. These technologies are relatively new, although there are some promising concepts that require further research.

Introduction

Spills of oil and related petroleum products in the marine environment may have serious environmental impacts [1]. Remote sensing is playing an increasingly important role in oil spill response efforts. Public and media scrutiny is usually intense following a spill, with demands that the location and extent of the oil spill be determined. Cleanup crews require location information on at least a daily basis. Through the use of modern remote sensing instrumentation, oil can be monitored on the open ocean on a 24-h basis [2]. Another role for remote sensing has been the strong interest in detection of illegal discharges, especially in view of the large seabird mortality associated with such discharges [3].

Even though sensor design and electronics are becoming increasingly sophisticated and much less expensive, the operational use of remote sensing equipment lags behind the technology. In remote sensing, a sensor, other than the eye or conventional photography, is used to detect the target of interest at a distance. The most common forms of oil spill surveillance and mapping are still sometimes carried out with simple still or video photography. Remote sensing from an aircraft is a common form of oil spill tracking. Remote sensing from satellites using radar sensors is now becoming a common technique.

It is important to divide the uses of remote sensing into the end use or objective as the utility of the sensor or sensor system is best defined that way. Oil spill remote sensing systems used for routine surveillance certainly differ from those used to detect oil on shorelines or land. One tool does not serve all functions. For a given function, many types of systems may, in fact, be needed. Further it is necessary to consider the end use of the data. The end use of the data, be it location of the spill, enforcement or support to cleanup, may also dictate the resolution or character of the data needed.

There are several broad uses of oil spill remote sensing:

1. Enforcement of ship discharge laws
2. Surveillance and general slick detection
3. Provision of evidence for prosecution
4. Mapping of spills for various reasons
5. Direction of oil spill countermeasures
6. Determination of slick trajectories

Several general reviews of oil spill remote sensing have been prepared [4–9]. These reviews show that there is progress in oil spill remote sensing; however, that progress is not necessarily moving at the speed that one might hope. These reviews show that specialized sensors offer advantages compared to off-the-shelf sensors.

Atmospheric Properties

The atmosphere has certain windows that affect the way that one can carry out remote sensing. Figure 1 shows the atmospheric attenuation at different electromagnetic wavelengths. This figure shows that the commonly used wavelengths in the visible, long-wave infrared, and radar bands are relatively free of atmospheric adsorption. One must consider rain, fog, and snow which limit operations in both the visible and the infrared regions. This leaves radar as the only all-weather and day and night sensor. Radar, as noted below, has many limitations in that it does not actually detect oil but only detects the dampening of sea capillary waves at a certain range of wind speeds.

Oil Interaction with Light and Electronic Waves

Oil interacts with light and electromagnetic waves in certain specific ways, and this can yield detectability of oil.

Krol et al. measured the optical properties of fresh and weathered crude oils and a water-in-oil emulsion [10]. Weathering of oil increases the light absorption of the oil along with an increase in light scattering. An emulsion also absorbs more light and attenuates the light in the water column. Evdokimov and Losev studied the UV and visible absorption of oils for analytical purposes, noting that crude oils were opaque and thus had to be diluted. The implication for remote sensing is that UV and visible signatures of oil are insufficient for characterization [11]. Otremba and co-workers studied the light reflectance of crude oils floating on water. If the oils are opaque, the reflectance is relatively free of spectral information [12–14].

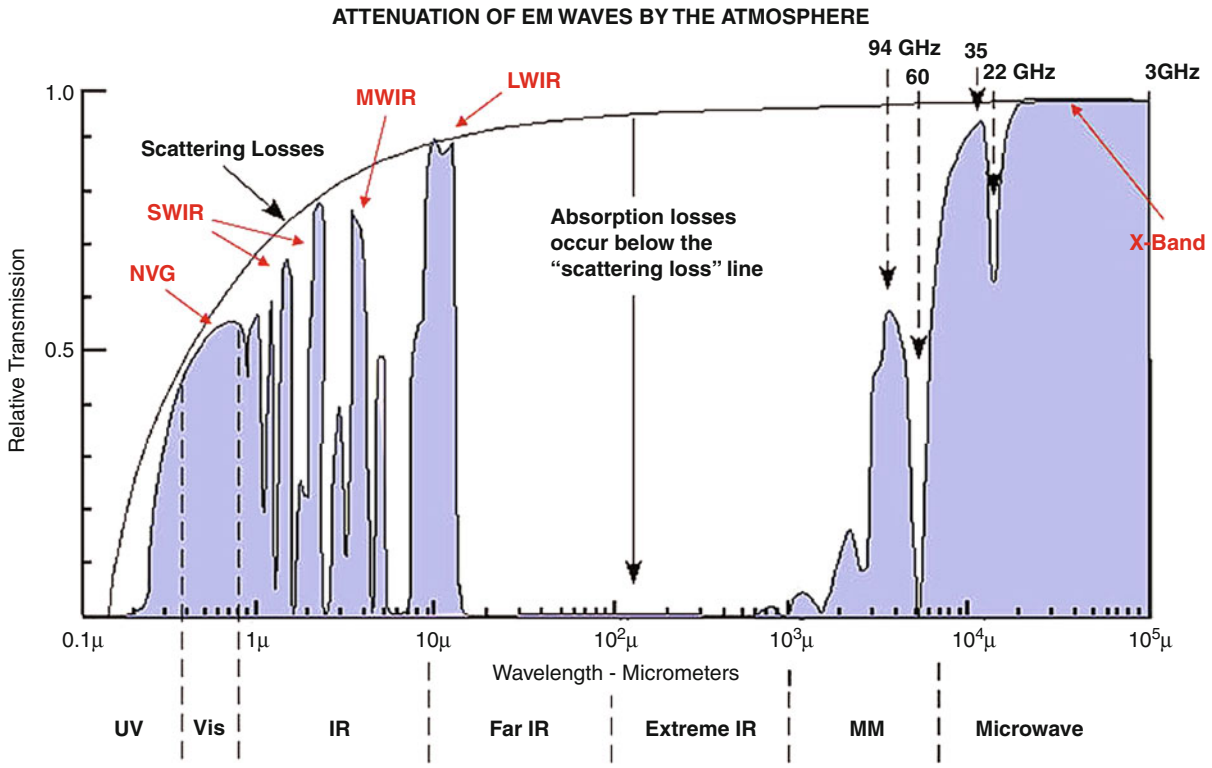

Oil Spill Remote Sensing. Figure 1
The attenuation of the electromagnetic spectrum by the atmosphere

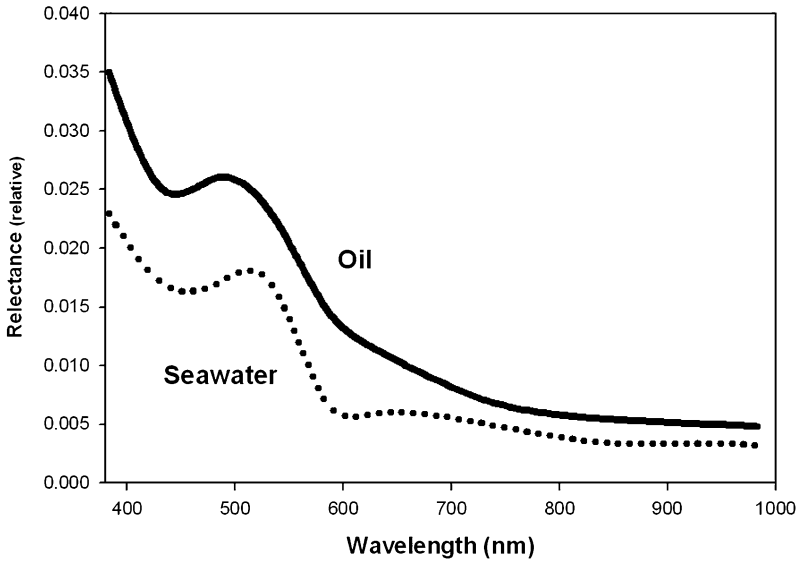

Oil Spill Remote Sensing. Figure 2
The differential reflection of water and oil

Hong and Shin suggest that infrared images could be used to detect oil spills at sea at night [15]. Instead of using the IR image, they suggest that the images be used to calculate the difference in refractive indices. Seawater has a refractive index of 1.227 and oil 1.53 at IR wavelength of 10 μm. The refractive index can be calculated from the IR data (in this case MODIS), thus possibly enabling the discrimination of surface oil or water.

The reflectance of oil is greater than seawater and increases with decreasing wavelength, that is, is greater in the blue-green region. Figure 2 shows typical reflectance curves between oil and water. Several researchers have tried to use this reflectance difference to discriminate oils, however, the best that it can do is use it as an indicator of oil on the surface. Ma et al. noted that the spectral bands between 400 and 500 nm were particularly useful for visible detection of oil from the MODIS satellite [16].

In summary, there are few very distinct characteristics that oil has in the visible, IR, or smaller wavelengths. One depends on secondary effects for oil detection and mapping.

Visible Indications of Oil

Under many circumstances oil is not visible on the surface to the eye [8]. Other than the obvious situations of nighttime and fog, there exist many situations where oil cannot be seen. A very common situation is that of thin oil such as from ship discharges or the presence of materials such as sea weed, ice, and debris that mask oil presence. Often there are conditions on the sea that may appear like oil, when indeed there is no oil. These include wind shadows from land forms, surface wind patterns on the sea, surface dampening by submerged objects or weed beds, natural oils or biogenic material and oceanic fronts. In the case of large spills, the area may be too great to be mapped visually. Several of these cases are illustrated in Figs. 3–5. All these factors dictate that remote sensing systems be used to assist in the task of mapping and identifying oil. In many cases, aerial observation and remote sensing are necessary to direct cleanup crews to slick locations. Figure 6 shows a case where no aerial direction was given and a skimmer crew is missing the slick by about half kilometers.

Optical Sensors

Visible

The use of human vision alone is not considered remote sensing, however, still forms the most common technique for oil-spill surveillance. In the past, major campaigns using only human vision were mounted with varying degrees of success [4]. Optical techniques,

Oil Spill Remote Sensing. Figure 3
A view of an oceanic front. The darker material is river water flowing into the ocean. There is no oil in this photograph

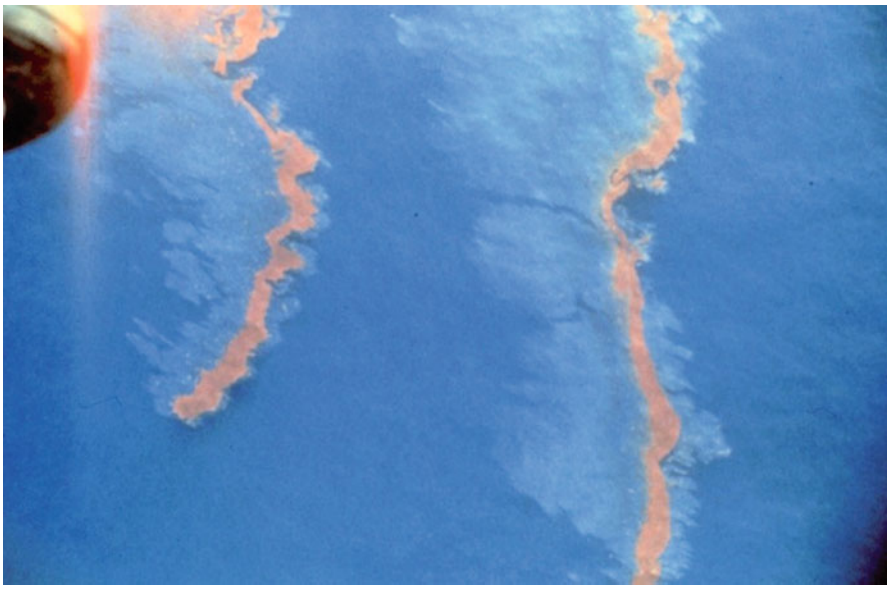

Oil Spill Remote Sensing. Figure 4
A view of a slick that is very clear and contrasts with the background. The emulsified oil with its red color provides good contrast

using the same range of the visible spectrum detection, are the most common means of remote sensing. Cameras, both still and video, are common because of their low price and commercial availability. Systems are now available to directly map remote sensing data onto base maps [4].

In the visible region of the electromagnetic spectrum (approximately 400–700 nm), oil has a higher

Oil Spill Remote Sensing. Figure 5
A slick that is barely visible. The rainbow sheen became visible here only after the photographer adjusted the angle with respect to the sun

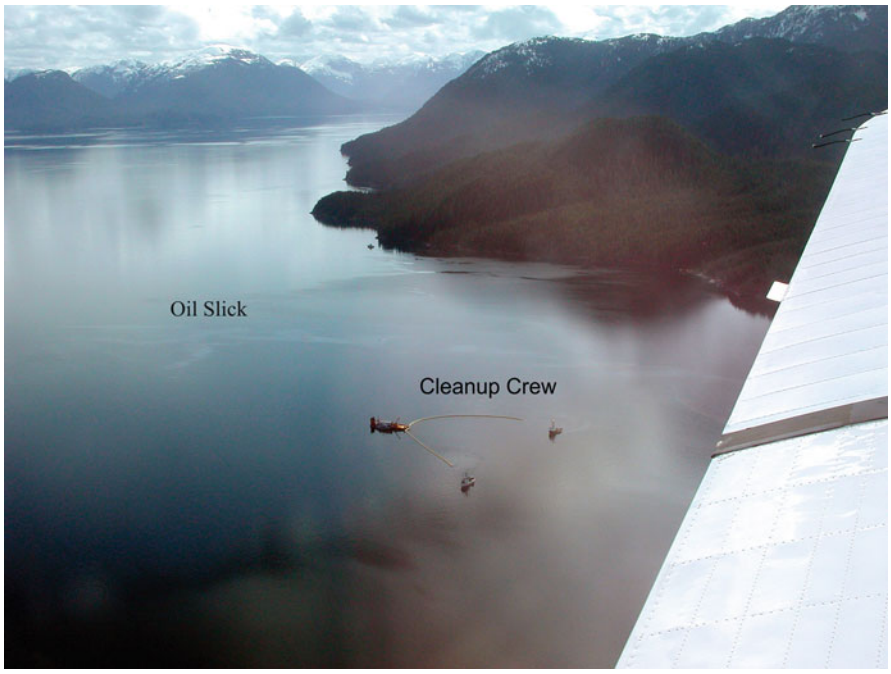

Oil Spill Remote Sensing. Figure 6
A cleanup crew missing the slick by a wide margin as no aerial direction was given

surface reflectance than water, but shows limited nonspecific absorption tendencies. Oil generally manifests throughout the entire visible spectrum. Sheen shows up silvery and reflects light over a wide spectral region down to the blue. As there is no strong information in the 500–600-nm region, this region is often filtered out to improve contrast [17]. Overall, however, oil has no specific characteristics that distinguish it from the background [18]. Taylor studied oil spectra in the laboratory and the field and observed flat spectra with no usable features distinguishing it from the background [19]. Therefore, techniques that separate specific spectral regions do not increase detection capability. Some researchers noted that while the oil spectra are flat, the presence of oil may slightly alter water spectra [20]. It has been suggested that the water peaks are raised slightly at 570–590, 780–710, and 810–710 nm. At the same time there are depressions or troughs at 650–680 nm and 740–760 nm. It has been found that high contrast in visible imagery can be achieved by setting the camera at the Brewster angle (53° from vertical) and using a horizontally aligned polarizing filter which passes only that light reflected from the water surface [21]. This is the component that contains the information on surface oil [17]. It has been reported that this technique increases contrast by up to 100%. Filters with band-pass below 450 nm can be used to improve contrast. View angle is important and some researchers have noted that the thickness changes the optimal view angle [22].

On land, hyperspectral data (use of multiple bands, typically 10–100) has been used to delineate the extent of an oil well blowout [23]. The technique used was spectral reflectance in the various channels as well as the usual black appearance of oil.

Video cameras are often used in conjunction with filters to improve the contrast in a manner similar to that noted for still cameras. This technique has had limited success for oil spill remote sensing because of poor contrast and lack of positive discrimination [24]. With new light-enhancement technology (low lux), video cameras can be operated even in darkness. Tests of a generation III night vision camera shows that this technology is capable of providing imagery in very dark night conditions [25, 26].

Scanners were used in the past as sensors in the visible region of the spectrum. A rotating mirror or prism sweeps the field-of-view (FOV) and directs the light toward a detector. Before the advent of CCD (charge-coupled device) detectors, this sensor provided much more sensitivity and selectivity than video cameras. Another advantage of scanners was that signals were digitized and processed before display. In the current era, newer technology has evolved and similar digitization can be achieved without scanning by using a CCD imager and continually recording all elements, each of which is directed to a different field-of-view on the ground. This type of sensor, known as a push-broom scanner, has many advantages over the older scanning types. It can overcome several types of aberrations and errors, and all data are collected simultaneously for a given line perpendicular to the direction of the aircraft's flight. Several types of scanners were developed. In Canada, the MEIS (Multi-detector Electro-optical Imaging Scanner) and the CASI (Compact Airborne Spectrographic Imager) have been developed, and in the Netherlands, the Caesar system was developed [17, 27, 28]. In China, the MAMS and AISA systems have been developed [29].

Digital photography has enabled the combination of photographs and the processing of images. Locke et al. used digital photography from vertical images to form a mosaic of an area impacted by an oil spill [30]. It was then possible to form a singular image and to classify oiling areas by color within the image. Video cameras are often used in conjunction with filters to improve the contrast in a manner similar to that noted for still cameras. This technique has had limited success for oil spill remote sensing because of poor contrast and lack of positive discrimination.

The detection or measurement of oil-in-water has never been successfully accomplished using remote visible technology. There may be potential for light scattering technology. Stelmaszewski and co-workers measured the light scattering of crude oil-in-water emulsions and noted that scattering increase with wavelength in the UV range and decreases slightly with the wavelength of visible light [31].

The use of visible techniques in oil spill remote sensing is largely restricted to documentation of the spill because there is no mechanism for positive oil detection. Furthermore, there are many interferences or false alarms. Sun glint and wind sheens can

be mistaken for oil sheens. Biogenic material such as surface seaweeds or sunken kelp beds can be mistaken for oil. Oil on shorelines is difficult to identify positively because seaweeds look similar to oil and oil cannot be detected on darker shorelines. In summary, the usefulness of the visible spectrum for oil detection is limited. It is an economical way to document spills and provide baseline data on shorelines or relative positions.

Infrared

Oil, which is optically thick, absorbs solar radiation and re-emits a portion of this radiation as thermal energy, primarily in the 8–14-μm region. In infrared (IR) images, thick oil appears hot, intermediate thicknesses of oil appear cool, and thin oil or sheens are not detected. The thicknesses at which these transitions occur are poorly understood, but evidence indicates that the transition between the hot and cold layer lies between 50 and 150 μm and the minimum detectable layer is between 10 and 70 μm [32–35]. The reason for the appearance of the "cool" slick is also not fully understood. A plausible theory is that a moderately thin layer of oil on the water surface causes destructive interference of the thermal radiation waves emitted by the water, thereby reducing the amount of thermal radiation emitted by the water [8]. This is analogous to the appearance of the rainbow sheen which is explained in section "Visual Thickness Indications" below. The cool slick would correspond to the thicknesses as observed above, because the minimum destructive thickness would be about two times the wavelength which is between 8 and 10 μm. This would yield a destructive onset of about 16–20 μm to about four wavelengths or about 32–40 μm. The destructive area is usually only seen with test slicks, which might be explained by the fact that the more rapidly spreading oil is more transparent than the remaining oil and also by the fact that only a recently spilled test slick actually has such intermediate thicknesses. The onset of the hot thermal layer would in theory then be at thicknesses greater than this or at about 50 μm.

Infrared devices cannot detect emulsions (water-in-oil emulsions) under most circumstances [36]. This is probably a result of the high thermal conductivity as emulsions typically contain 70% water and thus do not show temperature differences from water.

Infrared cameras are now very common and commercial units are available from several manufacturers. In recent times, uncooled detectors are commonplace and have entirely replaced the older, cooled detectors.

Most infrared sensing of oil spills takes place in the thermal infrared at wavelengths of 8–14 μm. Specific studies in the thermal infrared (8–14 μm) show that there is no spectral structure in this region [37]. Tests of a number of infrared systems show that spatial resolution is extremely important when the oil is distributed in windrows and patches, emulsions are not always visible in the IR, and cameras operating in the 3–5-μm range are only marginally useful [38, 39]. Nighttime tests of IR sensors show that there is detection of oil (oil appears cold on a warmer ocean), however, the contrast is not as good as during daytime [40].

The relative thickness information in the thermal infrared can be used to direct skimmers and other countermeasures equipment to thicker portions of the slick. Figures 7–9 illustrate the utility of infrared oil imaging compared to that of visible imaging. Oil detection in the infrared is not positive, however, as several false targets can interfere, including seaweeds, shoreline, and oceanic fronts [41]. Infrared sensors are reasonably inexpensive, and are currently a common tool used by the spill response community.

Near-Infrared

Clark et al. and Leifer et al. proposed that color composite images assembled from both visible and near-IR wavelengths can be used to make images of thick oil, but such images also show strong reflections from clouds and the glint from the ocean surface [42, 43]. Clark et al. proposed that spectroscopic analysis of the reflectance spectra within remote-sensing imagery could resolve the absorptions due to the organic compounds in oil and can better discriminate the spectral shape of oil [42]. A method to analyze absorptions due to specific materials is called absorption-band-depth mapping Clark and others showed that simple three-point band-depth mapping will show the location of absorption features but cannot identify specific compositions of compounds

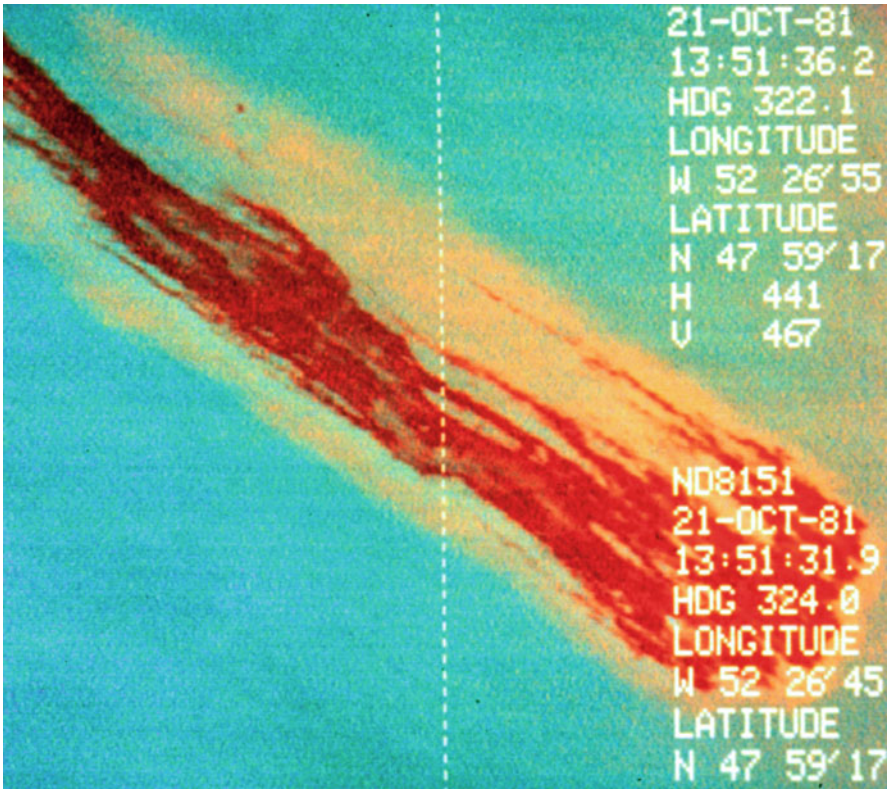

Oil Spill Remote Sensing. Figure 7
A slick highlighted in the infrared

causing these features when multiple compounds have absorptions near the same wavelength [42]. In the case of open ocean images, comprised of pixels containing water, oil/water mixtures, and clouds, the organic compounds in the oil and oil/water mixtures have absorption features that are distinct from those from water and clouds. These spectral differences allow one to map qualitative variations in oil abundance. The researchers used the NASA Airborne Visible/Infrared Imaging Spectrometer (AVIRIS). AVIRIS provides data on the spectrum of the surface at each pixel from 0.35 to 2.5 μm (the visible spectrum is: blue: 0.4 μm, green 0.53 μm, deep red 0.7 μm) in 224 channels. AVIRIS data from oil overflights are used to produce a three-point band-depth map, indicating potential locations of thick oil, by the following methods: (1) Radiance data are converted to surface reflectance using a two-step process [42]. (2) Three-point band-depth images are computed using continuum-removed reflectance spectra using the equation, [42]

$$D = 1 - 2Rb/(Rl + Rr) \quad (1)$$

where Rb is the reflectance around the absorption maximum (minimum reflectance)

Rl = the reflectance of the left continuum end point

Rr = the reflectance of the right continuum end point

The proposed adsorption scheme is shown in Fig. 10 (from Leifer et al. [43]).

For AVIRIS, the following wavelength intervals were used in three-point band-depth computations [42]:

1.2-μm feature:

Rb = average of the channels in the interval from 1.197 to 1.216 μm

Rl = average of the channels in the interval from 1.073 to 1.102 μm

Rr = average of the channels in the interval from 1.273 to 1.293 μm

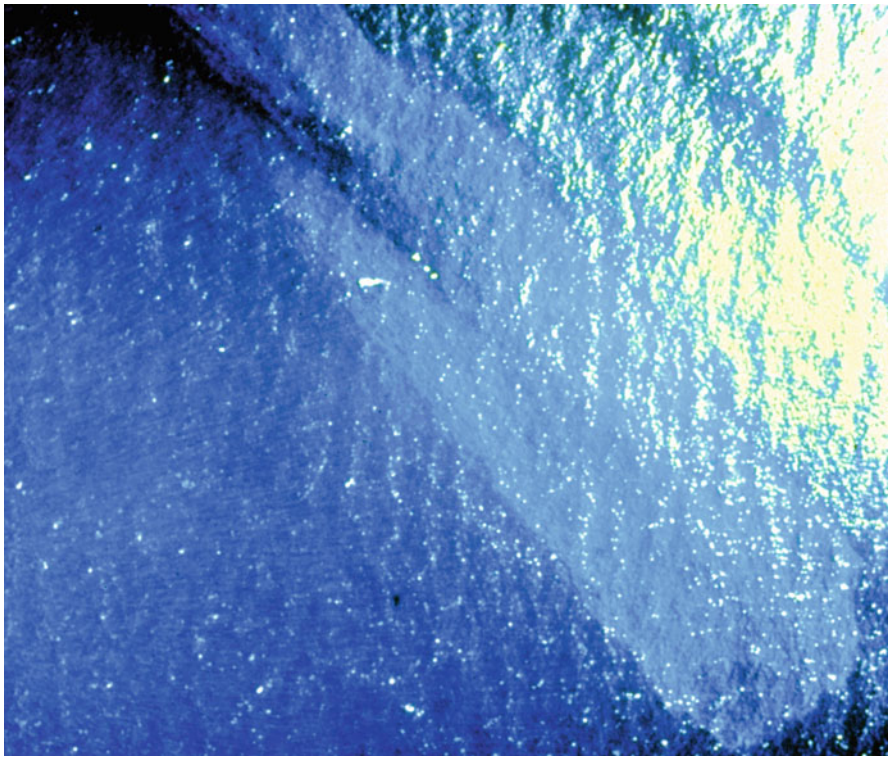

Oil Spill Remote Sensing. Figure 8
The same slick as shown in Fig. 7 but in the visible. The contrast between the oil and sun glint is poor in the visible

1.7-μm feature:

Rb = average of the channels in the interval from 1.712 to 1.732 μm

Rl = average of the channels in the interval from 1.622 to 1.642 μm

Rr = average of the channels in the interval from 1.782 to 1.802 μm

2.3-μm feature:

Rb = average of the channels in the interval from 2.287 to 2.327 μm

Rl = average of the channels in the interval from 2.198 to 2.238 μm

Rr = average of the channels in the interval from 2.407 to 2.447 μm

The band-depth images produced from these three calculations are combined into a color composite image as follows: the 2.3-μm feature in the red channel, the 1.73-μm feature in the green channel, and the 1.2-μm feature in the blue channel. The thicker oil then shows up in the green-blue regions of the image.

The Gulf oil spill was mapped using the AVIRUS sensor in the ER aircraft and thickness maps were plotted [42]. This method appears to work for the Gulf oil spill, however, confirmation of this technique on other spills awaits.

Ultraviolet

Ultraviolet sensors can be used to map sheens of oil since oil slicks display high reflectivity of ultraviolet (UV) radiation even at thin layers (<0.1 μm). The utility of mapping out sheen areas, which in fact contain very little oil has been questioned by many. However, overlaid ultraviolet and infrared images are often used to produce a relative thickness map of oil spills. This is illustrated in Fig. 9. Ultraviolet cameras, although inexpensive, are not often used in this process, however, as it is difficult to overlay camera images [44]. Data from infrared scanners and that derived from push-broom scanners can be easily superimposed to produce these IR/UV overlay maps. Ultraviolet data are also subject to many interferences

Oil Spill Remote Sensing. Figure 9
A test slick highlighted using overlaid infrared and visible imagery. This results in a very relative "thickness map" of this particular slick. This technique is not particularly useful for most slicks as they do not show this gradient, which is only typical for small, recently spilled slicks

or false images such as wind slicks, sun glints, and biogenic material. Since these interferences are often different than those for infrared sensing, combining IR and UV can provide a more positive indication of oil than using either technique alone.

Laser Fluorosensors

Laser fluorosensors are sensors that utilize the fact that aromatic compounds in petroleum oils absorb ultraviolet light and become electronically excited. This excitation is rapidly removed through the process of fluorescence emission, primarily in the visible region of the spectrum. Since very few other compounds show this tendency, fluorescence is a strong indication of the presence of oil. Natural fluorescing substances, such as chlorophyll, fluoresce at sufficiently different wavelengths than oil to avoid confusion. As different types of oil yield slightly different fluorescent intensities and spectral signatures, it is possible to differentiate between classes of oil under ideal conditions [45–54].

Laser fluorosensors used for oil spill detection employ a laser operating in the ultraviolet region of 308–355 nm [45, 55, 56]. With this wavelength of activation, there exists a broad range of fluorescent response for organic matter, centered at 420 nm. This is referred to as Gelbstoff or yellow matter, which can be easily annulled. Chlorophyll yields a sharp peak at 685 nm. The fluorescent response of crude oil ranges from 400 nm to 650 nm with peak centers in the 480-nm region. The use of laser fluorosensors for chlorophyll and other applications has also been well documented [45].

Another phenomenon, known as Raman scattering, involves energy transfer between the incident light and the water molecules. When the incident ultraviolet

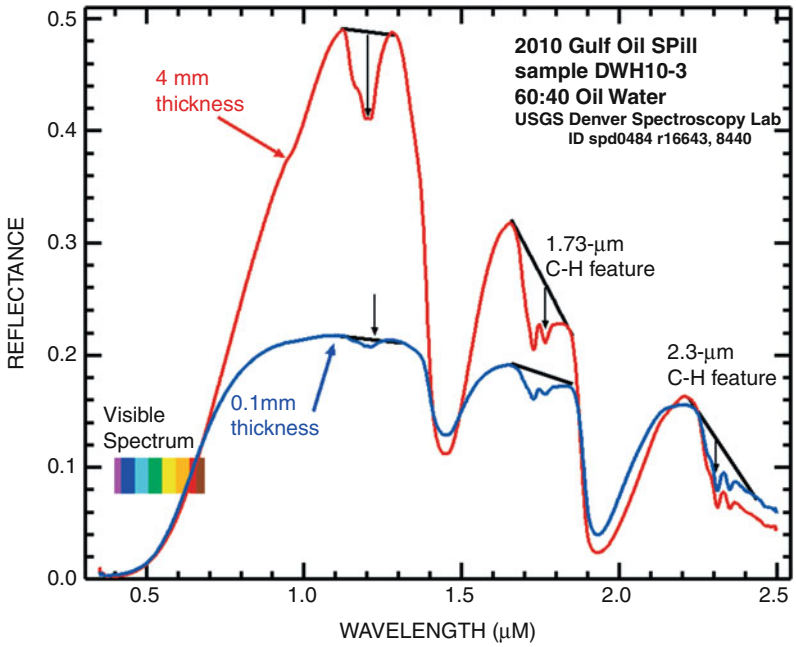

Oil Spill Remote Sensing. Figure 10
Wavelength versus reflectance in the near infrared. This shows the wavelength proposed by Clark et al. to map slick thicknesses [43]

light interacts with the water molecules, Raman scattering occurs. This involves an energy transfer between the incident light and the water molecules. The water molecules absorb some of the energy as rotational-vibrational energy and scatter light at a wavelength which is the difference between the incident radiation and the vibration-rotational energy of the molecule. The Raman signal for water occurs at 344 nm when the incident wavelength is 308 nm (XeCl laser). The water Raman signal is useful for maintaining wavelength calibration of the fluorosensor in operation, but has also been used in a limited way to estimate oil thickness, because the strong absorption by oil on the surface will suppress the water Raman signal in proportion to thickness [57, 58]. This thickness is limited and is true for only very thin slicks. The point at which the Raman signal is entirely suppressed depends on the type of oil, since each oil has a different absorption coefficient. The Raman signal suppression has led to estimates of sensors detection limits of about 0.05–0.1 µm [59].

Laser fluorosensors have shown high utility in practice and are now becoming an essential sensor in many remote sensing packages. The information in the output is unique and the technique provides a unique method of oil identification. Figure 11 shows an operator display of a laser fluorosensor.

Laser fluorosensors have significant potential as they may be the only means to discriminate between oiled and unoiled seaweeds and to detect oil on different types of beaches. Tests on shorelines show that this technique has been very successful [60]. Algorithms for the detection of oil on shorelines have been developed [61]. Work has been conducted on detecting oil in the water column such as occurs with the heavy, emulsified oil product, Orimulsion [62–66]. The fluorosensor is also the only reliable means of detecting oil in certain ice and snow situations. Operational use shows that the laser fluorosensor is a powerful tool for oil spill remote sensing [45]. Currently, one company makes two commercial models of the instrument.

Microwave Sensors

Radiometers

Microwave radiometers detect the presence of an oil film on water by measuring an interference pattern

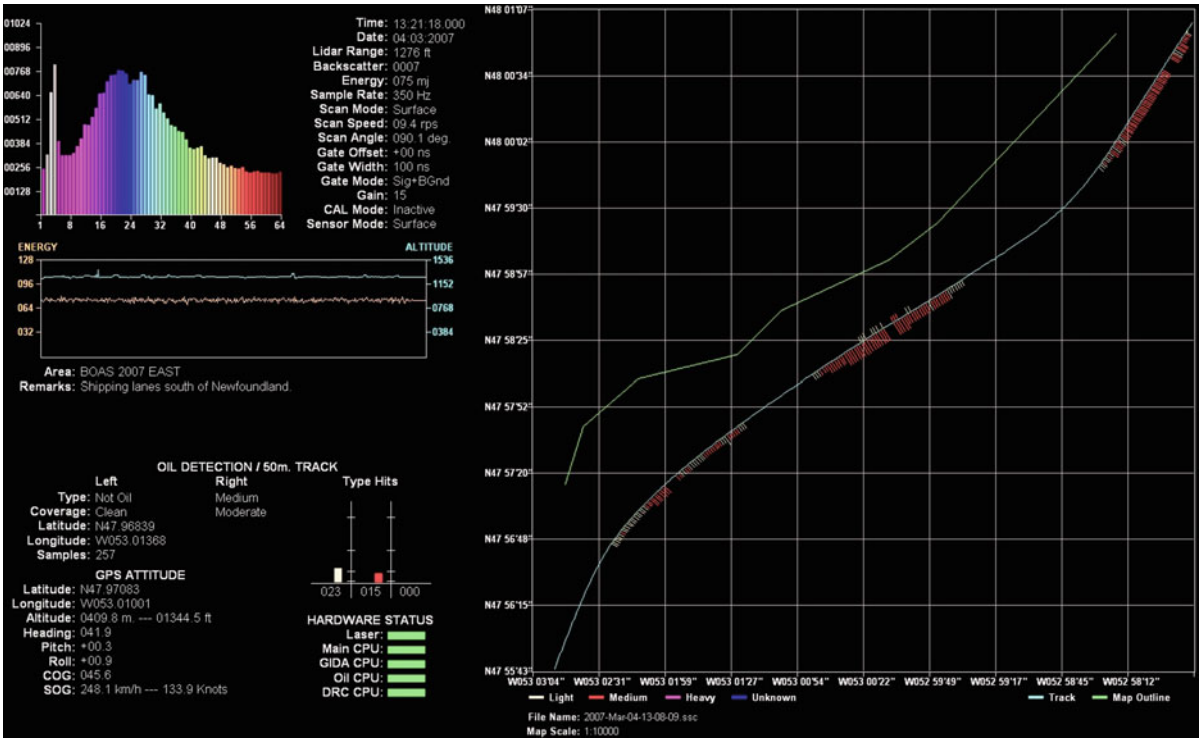

Oil Spill Remote Sensing. Figure 11

An illustration of a fluorosensor display. On the *left* instrument and detection criteria are given. On the *right*, the flight track is annotated with oil detection "hits" shown as bars

excited by the radiation from free space. The apparent emissivity factor of water is 0.4 compared to 0.8 for oil [67]. A passive microwave radiometer can detect this difference in emissivity and could therefore be used to detect oil. In addition, as the signal changes with thickness, in theory, the device could be used to measure thickness. This detection method has not been very successful in the field, however, as several environmental and oil-specific parameters must be known. In addition, the signal return is dependent on oil thickness but in a cyclical fashion. A given signal strength can imply any one of two or three signal film thicknesses within a given slick. One way to overcome this is to use more than one wavelength of microwave. Microwave energy emission is greatest when the effective thickness of the oil equals an odd multiple of one quarter of the wavelength of the observed energy. Biogenic materials also interfere and the signal-to-noise ratio is low. In addition, it is difficult to achieve high spatial resolution (might need resolution in meters rather than the typical tens of meters for a radiometer) [68].

The Swedish Space agency has carried out work with different systems, including a dual band, 22.4- and 31-GHz device, and a single band 37-GHz device [69]. Skou, Sorensen, and Poulson describe a 2-channel device operating at 37.5 and 10.7 GHz [70]. Mussetto and co-workers at TRW described the tests of 44-94-GHz and 94-154-GHz, 2-channel devices over oil slicks [71]. They showed that correlation with slick thickness is poor and suggests that factors other than thickness also change surface brightness. They suggest that a single-channel device might be useful as an all-weather, relative-thickness instrument. Tests of single-channel devices over oil slicks have also been described in the literature, specifically a 36-GHz and a 90-GHz device [72, 73]. A novel method of microwave radiometry has been developed in which the polarization contrasts at two orthogonal polarizations are measured in an attempt to measure oil slick

thickness [74, 75]. A series of frequency-scanning radiometers have been built and appear to have overcome the difficulties with the cyclical behavior [76, 77].

In summary, passive microwave radiometers may have potential as all-weather oil sensors. Their potential as a reliable device for measuring slick thickness, however, is uncertain at this time.

Radar

Capillary waves on the ocean reflect radar energy, producing a "bright" image known as sea clutter. Since oil on the sea surface dampens capillary waves, the presence of an oil slick can be detected as a "dark" sea or one with an absence of this sea clutter [78]. Unfortunately, oil slicks are not the only phenomena that are detected in this way. There are many interferences or false targets, including freshwater slicks, wind slicks (calms), wave shadows behind land or structures, seaweed beds that calm the water just above them, glacial flour, biogenic oils, and whale and fish sperm [79–83]. As a result, radar can be ineffective in locations such as Prince William Sound, Alaska where dozens of islands, freshwater inflows, ice, and other features produce hundreds of such false targets. Figures 12–15 illustrate some of the many slick look-alikes which appear in radar displays. Despite these limitations, radar is an important tool for oil spill remote sensing because it is the only sensor that can be used for searches of large areas and it is one of the few sensors that can detect anomalies at night and through clouds or fog.

The two basic types of imaging radar that can be used to detect oil spills and for environmental remote

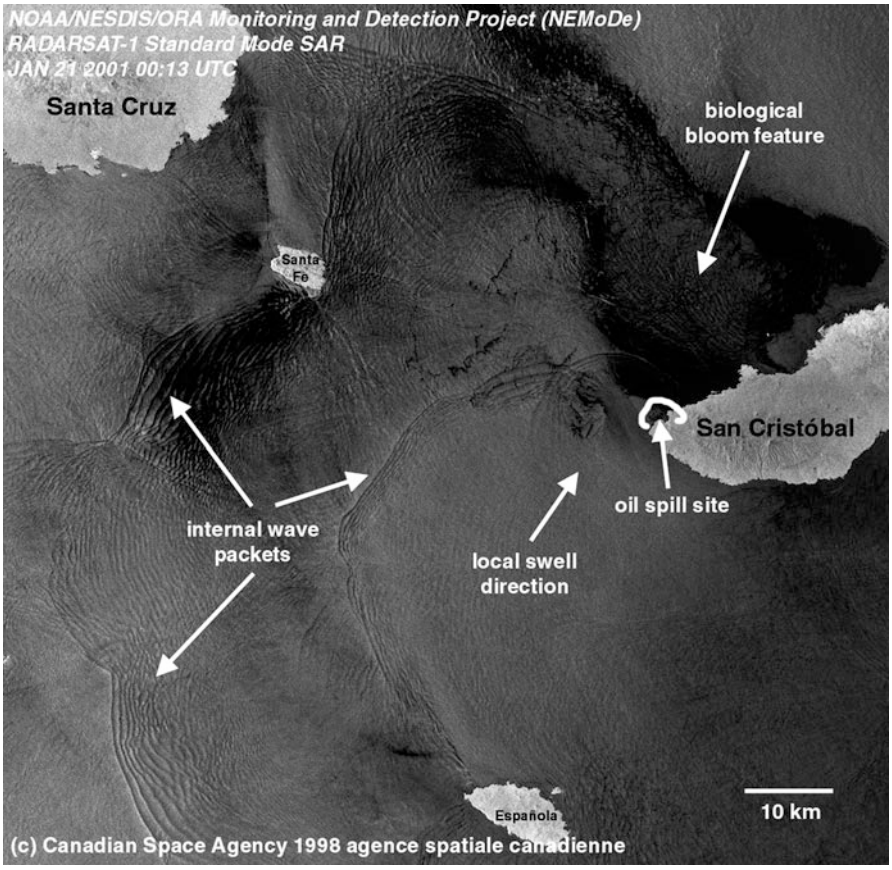

Oil Spill Remote Sensing. Figure 12
A Radarsat I image of a spill area in the Galapagos Islands. There are so many features that dampen waves in this area that is doubtful if much oil is shown in this image

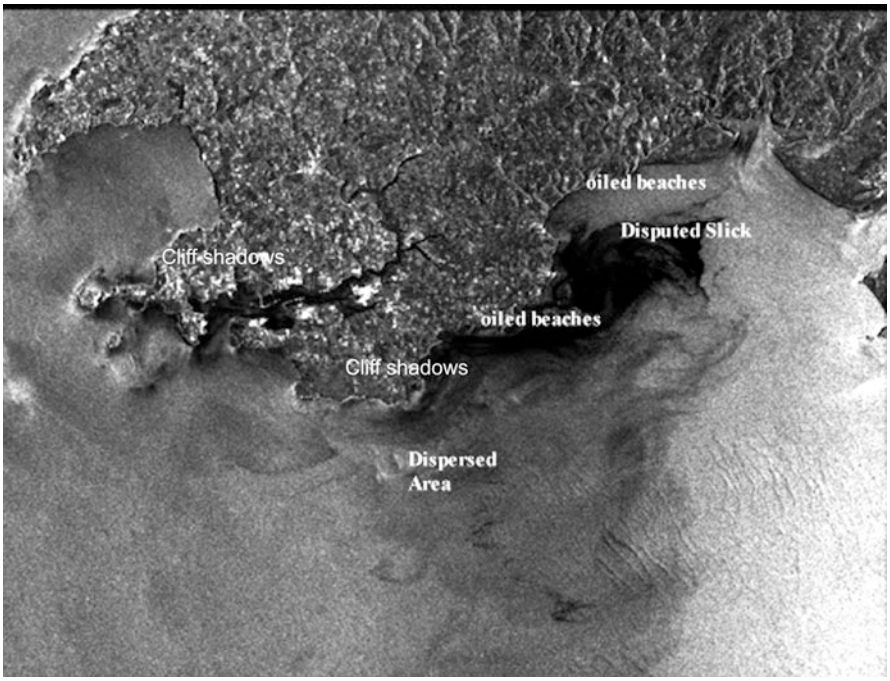

Oil Spill Remote Sensing. Figure 13
A Radarsat I image of a spill area off the coast of Wales. The *black* areas near the shore are cliff shadows and appear also in areas where there was no oiling. The annotation shows that some of the slick were found in areas where there was not thought to be slicks

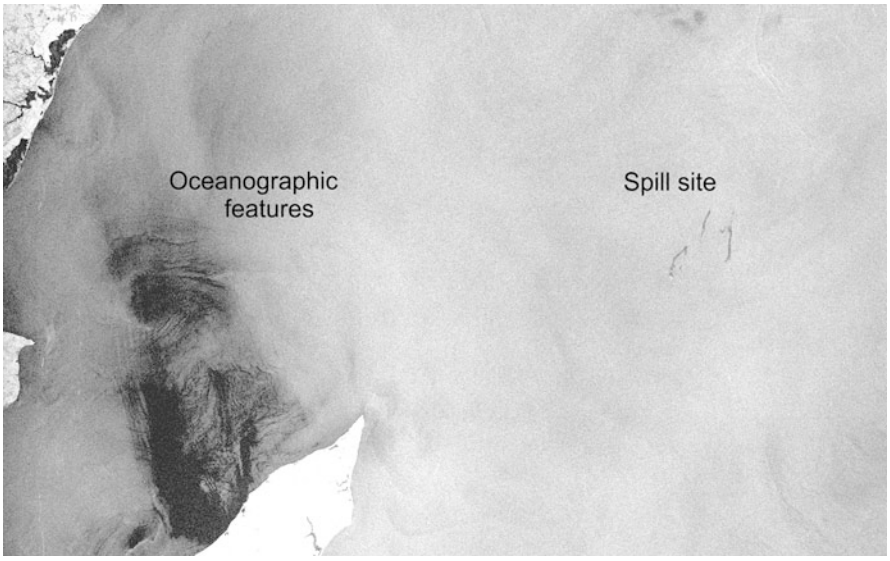

Oil Spill Remote Sensing. Figure 14
A Radarsat I image of an area north of Prince Edward Island. Most of the image area is taken up with oceanographic features. A known spill is noted in a small area of the image

Oil Spill Remote Sensing. Figure 15
An ERS II image off the coast of Belgium. There are many features that might appear to be oil, however, there is no oil present. The long thin object is a vessel track, there are many oceanographic features and areas near the coast that show suppressed capillary waves

sensing in general are Synthetic Aperture Radar (SAR) and Side-Looking Airborne Radar (SLAR). The latter is an older, but less expensive technology, which uses a long antenna to achieve spatial resolution. Synthetic aperture radar uses the forward motion of the aircraft to synthesize a very long antenna, thereby achieving very good spatial resolution, independent of range, with the disadvantage of requiring sophisticated electronic processing. While inherently more expensive, the SAR has greater range and resolution than the SLAR. In fact, comparative tests show that SAR is vastly superior [84–86]. Search radar systems, such as those frequently used by the military, cannot be used for oil spills as they usually remove the clutter signal, which is the primary signal of interest for oil spill detection. Furthermore, the signal processing of this type of radar is optimized to pinpoint small, hard objects, such as periscopes. This signal processing is very detrimental to oil spill detection.

SLAR has predominated airborne oil spill remote sensing, primarily because of the lower price [87, 88]. There is some recognition among the operators that SLAR is very subject to false hits, but solutions are not offered. Experimental work on oil spills has shown that X-band radar yields better data than L- or C-band radar [89, 90].

Several different polarizations exist based on vertical (V) and horizontal (H). Typically transmission and reception are in the same polarity, that is, VV or HH. But, there are actually four poles available: HH, VV, HV, and VH. Use of all four of these is designated as quadrapole. It has also been shown that vertical

antenna polarizations for both transmission and reception (VV) yield better results than other configurations [84, 91–93]. Additionally, phase differences can be used to detect oil. Migliaccio et al. calculated that the co-polarized phase difference (CPD) would yield a larger signal for oil compared to that for the sea [94].

The ability of radar to detect oil is also limited by sea state. Sea states that are too low will not produce enough sea clutter in the surrounding sea in contrast to the oil and very high seas will scatter radar sufficiently to block detection inside the troughs. Indications are that minimum wind speeds of 1.5 m/s (∼3 knots) are required to allow detectability and a maximum wind speed of 6 m/s (∼12 knots) will again remove the effect [95–97]. The most accepted limits are 1.5 m/s (∼3 knots) to 10 m/s (∼20 knots). This limits the environmental window of application of radar for detecting oil slicks. Gade et al. studied the difference between extensive systems from a spaceborne mission and a helicopter-borne system [98]. They found that at high winds, it was not possible to discriminate biogenic slicks from oil. At low wind speeds, it was found that images in the L-band showed discrimination. Under these conditions the biogenic material showed greater damping behavior in the L-band. Okamoto et al. studied the use of ERS-1 using an artificial oil (oleyl alcohol) and found that an image was detected at a wind speed of 11 m/s, but not at 13.7 m/s [99].

SAR can be polarimetric that is horizontal-horizontal (HH), vertical-vertical (VV), and cross combinations of these. Several researchers have shown that VV is best for oil spill detection and discrimination [94, 100–102]. Migliaccio et al. showed that the co-polarized phase difference – for example, the difference between the HH and VV phases, can be used to discriminate oil slicks from biogenic slicks. [100]. A larger standard deviation for the slick compared to the sea typically indicates that it is oil. Figures 16 and 17 show the differences between VV and HH polarization.

Radar has also been used to measure currents and predict oil spill movements by observing frontal movements [103]. Work has shown that frontal currents and other features can be detected by SAR [104].

Shipborne radar has similar limitations and the additional handicap of low altitude, which restricts its range to between 8 and 30 km, depending on the height of the antenna. Ship radars can be adjusted to reduce the effect of sea clutter de-enhancement. Shipborne radar successfully detected many slicks and commercial systems are now available. During the *Prestige* spill, a Netherlands vessel successfully used this technique to guide a recovery vessel into slicks [105]. The technique is, however, very limited by sea state and in all cases where it was used, the presence and location of the slick were already known or suspected. Recently researchers have carried out work on improving the imaging of slicks from shipborne radars [105]. Today, there are some commercial products to enhance the images from shipborne radar to enable some oil imaging.

Gangeskar has proposed an automatic system that could be mounted on oil drilling platforms [106]. This system would use standard X-band ship navigation units and would provide an alert if an oil spill is present. The system includes an extensive post-processing system to provide both a user-friendly GUI and an automatic detection and alert system. The system has not been fully tested to date.

In summary, radar optimized for oil spills is useful in oil spill remote sensing, particularly for searches of large areas and for nighttime or foul weather work. The technique is highly prone to false targets, however, and is limited to a narrow range of wind speeds. Because of the all-weather and day-night capability, radar is now a common means of remote sensing oil spills.

Radar Processing Because radar detection of oil spills is so highly susceptible to false images, much work has taken place on means to differentiate oil slicks and false targets, often called look-alikes. These look-alikes include low wind areas, areas sheltered by land, rain cells, organic films, grease ice, wind fronts, up-welling zones, oceanic fronts, algae blooms, current shear zones, etc. [107]. The discussion in this subsection is relevant to both satellite and airborne SAR systems.

Several "automatic" systems have been designed for slick detection in the past [108, 109]. Limited testing with actual satellite output has shown that many false signals are present in most locations [110, 111]. Extensive effort on data processing appears to improve

Oil Spill Remote Sensing. Figure 16
A HH (horizontal-horizontal) polarized view of the sea surface

the chances of oil detection [112]. In recent years, automatic systems have given way to systems involving smart algorithms and manipulated by operators [113–115].

The most common way to eliminate wind-origin, look-alikes is to map the wind fields in the same coordinates as the radar data [112, 116]. The most common slick look-alike is low wind areas. One group of researchers used radar wind data calibrated to wind data from an ocean buoy to map oil seeps in the southern Gulf of Mexico [116].

Most researchers used some form of neural networks or fuzzy logic to assist in the discrimination of look-alikes and the intended targets [118–120]. Others used various forms of models such as range dependence models [121].

Topouzelis and co-workers developed several series of mathematical networks for differentiating slicks from look-alikes [122–126]. The basis of these networks is generally that oil slicks are imaged through a complex series of processes and conditions. Thus imaging is not a simple statistical manipulation. The same group developed a fuzzy classification to differentiate look-alikes from oil spills. The methodology involved four procedures. The first is the segmentation of the image into large image segments with different statistical values. In the second procedure, a detailed scale segmentation is carried out and statistical values

Oil Spill Remote Sensing. Figure 17
A VV polarized view of the same area of sea surface. Note that this polarization yields a slightly clearer image of sea surface details than that shown in Fig. 16

of each segment compared to the threshold of the large segment it came from. Third, the dark portions are classified according to the properties of the surrounding areas. Finally, the dark areas are classified using knowledge bases. The group also examined the use of forward feed neural networks to discriminate slicks from look-alikes [122, 126]. Several topologies of forward feed neural networks were examined and none were better than others. The networks yielded classification accuracies as high as 91.3–93.6% for the given example. A recent work by Topouzelis used the inputs of shape texture, asymmetry, mean difference to neighbors, and power to the mean images in a neural network [107]. The workers used forward feed neural networks. It was found that the classification accuracy was 99.4% for the MLP network in the test case. Later, Topouzelis and coworkers used a method similar to that mentioned above to test a data set of 69 oil spills and 90 look-alikes [124]. They found that a combination of ten features out of a possible 25 features were most useful for discrimination. The ten features found to be best for discrimination are: perimeter, shape factor II, object mean value, ratio of the power to mean ratios, local area contrast ratio, mean border gradient, maximum border gradient, standard deviation border gradient, maximum border

gradient, mean difference to neighbors and spectral texture. Use of these factors resulted in classification accuracies if 85.3% for oil spills and 84.4% for look-alikes.

A similar approach is to use a classification scheme that incorporates some of the same input parameters. Karantzalos and Argialas proposed a classification scheme involving processes and then a classification scheme. The first processing step involves filtering and levels [127]. The second step is segmentation of the images to include all suspected slicks. The final step is to classify the potential slicks according to area, perimeter, shape complexity eccentricity, orientation, segment mean border gradient, inside segment standard deviation, and outside segment standard deviation.

Several researchers have used GIS databases to assist in the interpretation of SAR imagery [128–134]. The technique divides the area of interest into segments and notes data such as currents, proximity to land, wind, sea lanes, etc. These parameters are then correlated to the SAR images. For example, oil spills are much more likely under the correct wind conditions, in sea lanes and far from land. Tahvonen used data sets including wind speed and direction, sea surface temperature, heavy rain, and location of algae blooms to assist in the discrimination [128]. Muellenhoff proposed a dataset consisting of: wind information, sea surface temperature, chlorophyll-a-concentration, geostrophic currents, wave information, contextual background information, and existing oil spill databases [131]. The assigned influences were: wind speed – 30%, wind direction – 12%, Sea surface temperature – 14%, Chlorophyll-a-concentration – 10%, oil ports – 10%, and main traffic lines – 20%. Wave and current direction only accounted for 2% each.

Shu et al. used the density (concentration of the number of similar intensity points) to discriminate between oil and water [135]. A detection window is passed over all the pixels of the target image and thresholds are assigned to various spots. Then the pixels are assigned to either background or oil categories if there is a sufficient number of them (density) in the proximity. It should be noted that to be successful, this technique requires that the oil images are much larger than any oil look-alikes.

Migliaccio and group studied the processing of SAR images from an aircraft-based sensor [134, 136, 137]. It was noted that the main obstacle to analysis was speckle in the images. Speckle is caused by stray reflectances such as from rough seas. Speckle is also caused by random constructive and destructive interference. Since speckle is temporary, multi-look imaging is one way to decrease speckle by a large amount. Further processing can then be achieved by combining multi-look data with wind data, best obtained from satellite scatterometers. The technique proposed for multi-look data, is to divide the SAR imagery into sub-bands and then generating lower-resolution imagery. Then the images are averaged. This results in reduction of speckle. To process single-look data with high speckle content, filters are used. First speckle is removed and the ROA (ratio of average) filter is used. In both techniques, edge detection is used to find the actual limits of the slicks or look-alikes.

Marghany and co-workers used a fractal method to analyze SAR data [97, 138]. The images are broken into fractals and these fractals have dimensions which are different for oil spills and look-alikes. A further study under different wind speeds showed that there were differences only in the wide beam mode for low wind zones and current shear features between real oil slicks [138]. Further work showed that the fractal dimensions for the W1 (wide) mode of Radarsat I are about 1.7 for oil spills, 2.5 for low wind areas, 2.7 for look-alikes, 3.2 for sea surface roughness, and 3.7 for ships. These are similar but different for the narrow mode, S2. A similar approach was utilized by Danisi et al. [139].

Another method employed by researchers to separate oil slicks from look-alikes is to use textural analysis [140, 141]. Direct statistical methods are also employed. Tello et al. noted that an algorithm characterizing the border between oil spill candidates and the surrounding sea allows for good classification [141]. Lounis et al. used a measure of similarity between the local probability density function of clean water and of the dark area to be examined [142]. Comparing the two values is said to result in discrimination between oil and look-alikes. Pelizzari employed a similar technique using graph cuts to estimate a smoothness factor [143].

Ferraro et al. describe the development of an operational system for the Mediterranean Sea and show a procedure for the identification of oil spills as:

(1) isolation and contouring of all dark signatures, (2) extraction of shape and backscattering contrast signatures, (3) test of these values against standard values, and (4) calculation of the probabilities of each patch [144, 145, 146].

Another series of techniques involves the use of two streams of information. Several researchers used both SAR and visible information from the MODIS (Moderate Resolution Imaging Spectroradiometer) satellites to discriminate between look-alikes and oil slicks [147]. The visible imagery is subject to false images, but not the same ones as SAR and thus discrimination can be achieved to a degree. Similarly, Sipelgas used visible imagery from the MODIS satellite to assist in discrimination of false images from oil slicks in the Gulf of Finland [148]. Adamo et al. used three streams for information: SAR data, MODIS, and MERIS data to discriminate look-alikes from actual spills [147].

Microwave Scatterometers

A microwave scatterometer is a device that measures the scattering of radar energy by a target. One radar scatterometer was flown over several oil slicks and used a low-power transmitter operating in the Ku band (13.3 GHz) [17]. The scatterometer detected the oil, but discrimination was poor. The "Heliscat," a device with five frequencies has been used to investigate capillary wave damping [95]. The advantage of a microwave scatterometer is that it has an aerial coverage similar to optical sensors and it can look at several incident angles. The main disadvantages include the lack of discrimination for oil and the lack of imaging capability.

Surface Wave Radars

It is possible to send radio waves along the sea using high frequency. The conductivity of the sea acts as a form of wave guide. These radars can be used to detect ships as far out as 500 km [149]. Since these are surface wave phenomena only targets above the surface are detected, thus slicks may not be detected by this technique [150]. Modeling of the technique does not show whether there is potential for this method or not [151].

Interferometric Radar

Radars can be used to measure height, currents, and other surface elevation phenomena using interferometric techniques. Some radar systems on aircraft are fitted for this application such as the Government of Canada Convair 580. This can also be carried out in space using two satellites traveling in tandem. One research group employed the tandem satellite pairs of ERS-2 and ENVISAT to carry out such work but there are no reports on the use on oil spills [152].

Slick Thickness Determination

There has long been a need to measure oil slick thickness; this need has been expressed both within the oil spill response community and among academics in the field. There are presently no reliable methods, either in the laboratory or the field, for accurately measuring oil-on-water slick thickness. The ability to do so would significantly increase understanding of the dynamics of oil spreading and behavior. Knowledge of slick thickness would make it possible to determine the effectiveness of certain oil spill countermeasures including dispersant application and in situ burning. Indeed, the effectiveness of individual dispersants could be determined quantitatively if the oil remaining on the water surface following dispersant application could be accurately measured [153, 154, 155].

Visual Thickness Indications

A very important tool for working with oil spills has been the relationship between appearance and thickness. Careful study of the literature on this and comparing this to field experience shows that there is limited potential to scale thicknesses to visual appearance [8]. The only physical-based appearance that occurs are thicknesses of about 0.7–2.5 μm at which the rainbow colors appear as a result of multiple constructive and destructive interferences by light. Table 1 shows summation of the best knowledge on this phenomenon. Rainbow sheens are the only color appearance that has a physical slick thickness associated with it.

Lehr argues that the visual indications of slick thickness are so poor as to not allow for any slick thickness estimation [156]. In particular he notes that the Bonn agreement thickness code provides insufficient proof for greater thicknesses as it purports

Oil Spill Remote Sensing. Table 1 Relationship of thickness to appearance

	Visibility thresholds (μm)				
	Minimum/silvery	Rainbow	Darkening colors	Dull colors	Dark
Typical thickness	0.1	0.6[a]	0.9	2.7	8.5

[a]This is the only physical-based appearance phenomenon

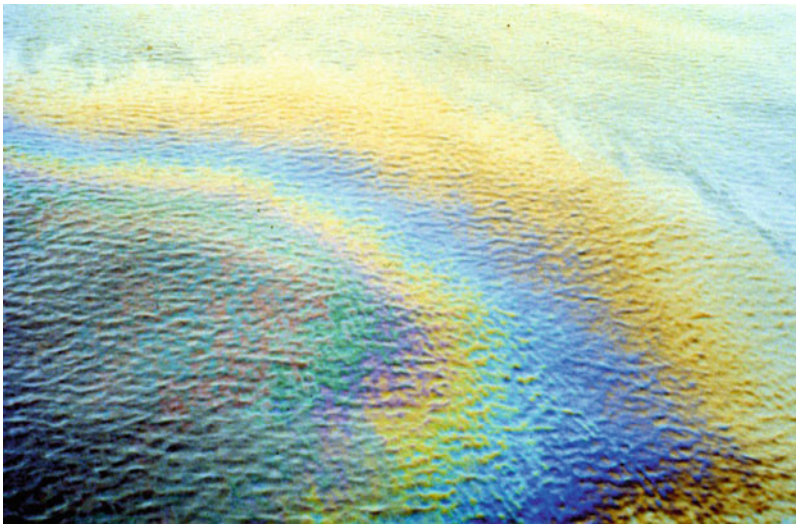

Oil Spill Remote Sensing. Figure 18
A picture of a rainbow sheen. This is the only spill thickness that has a physical explanation

to. Lehr suggests that the solution to this is simply to use two thickness regimes, sheen and thicker oil and not to estimate slick volumes from this (Fig. 18).

Slick Thickness Relationships in Remote Sensors

A number of investigators tried to correlate slick thickness with appearance in various remote sensing instruments. Hollinger and Mennella conducted a series of eight controlled oil spills off Virginia to investigate the use of microwave radiometry to delineate oil spills [157]. They used 19.4 and 69.8 GHz radiometers on the spills. Measurements using sorbents were used to calibrate the radiometer. It was noted that the sheens typically had a thickness of 2–4 μm (considered today to be very thick). It was found that 90% of the oil was in 10% of the slick area and that the microwave threshold was about 0.1 mm (100 μm).

A series of experiments was carried out in 1979 to evaluate infrared (IR) and side-looking airborne radar (SLAR) for oil spill detection [158]. The imagery was correlated against visual and sorbent measurements, which were used to derive a thickness estimate. It was concluded that the infrared threshold was between 25 and 50 μm and for SLAR 100 nm. Further, manipulation of data showed that a mass balance could be achieved if the thickness at which the infrared showed oil to be colder at the sea occurred at 100 μm and for the heated portion of the oil at 1,000 μm.

The United Kingdom conducted Isowake Experiments in 1982 [159, 160]. On the basis of estimations and calculations it was concluded that the lowest detectable slick thickness for IR was between 10 and 50 μm, whereas hot spots in the IR image could be as much as 1,000 μm.

MacDonald used photography from the space shuttle to define up to 124 slicks in an area of the Gulf of Mexico, offshore Louisiana [161]. Similarly, a thematic image from Landsat showed at least 66 slicks

in one large area. Some of the thickness relationships were based on unpublished experimental data from Duckworth.

Brown et al. conducted experiments to measure the visibility of oil slicks. The observers and an ultraviolet (UV) and visible camera were mounted in a crane basket 30 m over the slick [162]. It was found that the detection ability decreased by over 50% for most oils and for the cameras when the angle was changed from 90° to 55° from the horizontal (equivalent incidence angle of 0° to 35°). Detectability degraded to 70% and sometimes to nil as the viewing angle was decreased past 55° through 35°. Brown et al. conducted several experiments to ascertain the relationship between thickness of slicks and the density (or intensity) of the infrared image [41]. The thicknesses of oil varied between 1 and 10 mm and thicknesses were measured using an acoustic system from under water. No relationship between slick thickness and infrared brightness was found.

Specific Thickness Sensors

The suppression of the water Raman peak in laser fluorosensor data has not been fully exploited or tested. This technique may work for very thin slicks, but not necessarily for thick ones, at least not with a single excitation frequency. Attempts have been made to calibrate the thickness appearance of infrared imagery, but also without success. It is suspected that the temperatures of the slick as seen in the IR are highly dependent on oil type, sun angle, and weather conditions. It may not be possible to use IR as a calibrated tool for measuring thickness. As accurate ground-truth methods do not exist, it is very difficult to calibrate existing equipment [163, 164]. The use of sorbent techniques to measure surface thickness yields highly variable results [153]. As noted in the section on microwave radiometers, the signal strength measured by these instruments can imply one of several thicknesses. This methodology does not appear to have potential, other than for measuring relative oil thickness.

A variety of electrical, optical, and acoustic techniques for measuring oil thickness has been investigated [163, 164]. Two promising techniques were pursued in a series of laboratory measurements. In the first technique, known as "thermal mapping," a laser is used to heat a region of oil and the resultant temperature profiles created over a small region near this heating are examined using an infrared camera [164]. The temperature profiles created are dependent on the oil thickness. A more promising technique involves laser acoustics [165–167]. The Laser Ultrasonic Remote Sensing of Oil Thickness (LURSOT) sensor consists of three lasers, one of which is coupled to an interferometer to accurately measure oil thickness [167–172]. The sensing process is initiated with a thermal pulse created in the oil layer by the absorption of a powerful CO_2 laser pulse. Rapid thermal expansion of the oil occurs near the surface where the laser beam was absorbed, which causes a step-like rise of the sample surface as well as an acoustic pulse of high frequency and large bandwidth (~15 MHz for oil). The acoustic pulse travels down through the oil until it reaches the oil–water interface where it is partially transmitted and partially reflected back towards the oil-air interface, where it slightly displaces the oil's surface. The time required for the acoustic pulse to travel through the oil and back to the surface again is a function of the thickness and the acoustic velocity of the oil. The displacement of the surface is measured by a second laser probe beam aimed at the surface. Motion of the surface induces a phase or frequency shift (Doppler shift) in the reflected probe beam. This phase or frequency modulation of the probe beam can then be demodulated with an interferometer [172]. The thickness can be determined from the time of propagation of the acoustic wave between the upper and lower surfaces of the oil slick. This is a very reliable means of studying oil thickness and has great potential. Laboratory tests have confirmed the viability of the method and a test unit has been flown to confirm its operability [163]. Figure 19 shows the first airborne absolute measurement of slick thickness.

Several attempts have been made to measure thickness by using visible spectral imaging. As there is no visual indications other than the rainbow sheen area around 0.8 μm, these efforts are wasted [173]. Similarly, several workers have tried to use the assumption that the oil layer is transparent, therefore the differences in reflection from the water surface and the top of the oil layer could yield a thickness measurement [174, 175].

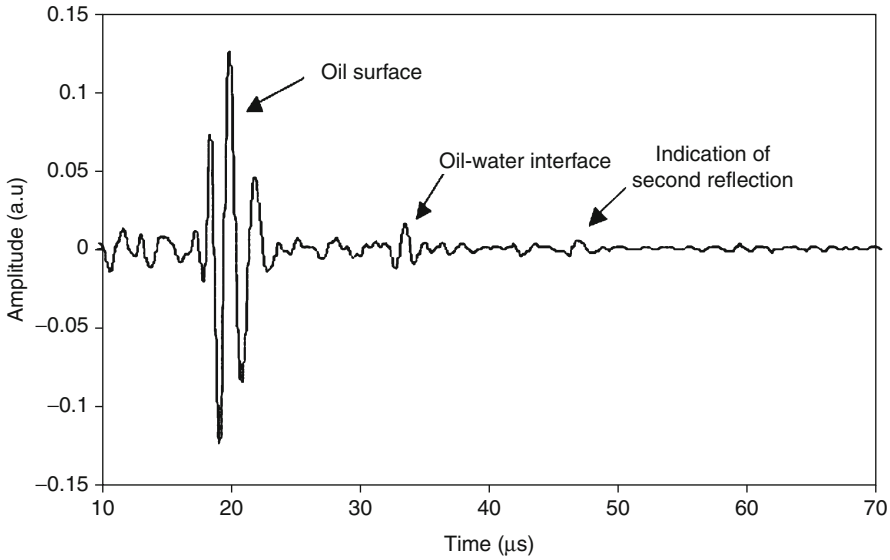

Oil Spill Remote Sensing. Figure 19
The signal from a three-laser thickness sensor. The time corresponds to a thickness of about 6 mm. This was measured by a prototype sensor mounted in an aircraft and flying over containers with various thicknesses of oil on water

Unfortunately, this oil is not transparent in the visible ranges, therefore such methods do not work.

Integrated Airborne Sensor Systems

Increasingly, a number of different types of airborne oil spill remote sensors are being consolidated into sensor systems. The reason for this integration is to take advantage of the different information provided by each of the specific sensors and combine the information to provide a more complete and comprehensive information product. Although each of the individual sensors has specific inherent weaknesses such as false detections, these false detections are often different for each sensor type, hence a consolidation of information can help resolve and remove some of the uncertainties that exist from a single data source. Furthermore, additional information such as the relative thickness of the oil slick can be deduced from the overlaying of imagery from several sensor types. Although the absolute thickness of an oil slick remains the subject of continued research and scientific opinion, the ability to locate the thicker portions of the slick is essential in terms of operational spill cleanup and response. In addition to the integration of a number of remote sensors into a sensor system, information from other sources such as marine vessel traffic surveillance systems (i.e., automatic identification system, AIS) can be integrated and can play an essential role in identifying the source of the marine pollution.

Two commercially available airborne marine oil spill remote sensing systems are the MEDUSA and the MSS 6000 [176, 177]. MEDUSA incorporates a number of sensor technologies such as laser fluorosensors, infrared/ultraviolet line scanners, forward-looking infrared sensors, microwave radiometers, side-looking airborne radar systems and camera systems, as well processing software into a flexible real-time data acquisition and processing system. The data from the various sensors are geo-referenced and fused with information from AIS and marine surveillance radars into a GIS-based display output format. The processing software is known as the Oil Spill Scene Analysis System (OSSAS) and allows for the extraction of features such as the area of oil coverage including areas of intermediate and thicker portions of the slick. The MSS 6000 Maritime Surveillance System is comprised of a flexible suite of sensors such as side-looking airborne radar systems, infrared/ultraviolet line scanners, forward-looking infrared sensors,

microwave radiometers, and camera systems, along with data processing and mission management software in order to perform the oil spill remote sensing surveillance task. The MSS 6000 also focuses on sensor integration and includes navigation and marine search radar inputs. All sensor data, imagery, slick targets, vessels etc. are annotated using navigation data from a single source to form an integrated part of a Geographic Information System (GIS). Both the MEDUSA and MSS 6000 can distribute their data in near-real time via direct downlink or satellite communications to vessels or shore-based communications centers. A large number of maritime nations are now employing integrated airborne sensor systems [178, 179].

Satellite Remote Sensing

The use of optical satellite remote sensing for oil spills has been attempted several times. The slick from the IXTOC I well blowout in Mexico was detected using GOES (Geostationary Operational Environmental Satellite) and by the AVHRR (Advanced Very High Resolution Radiometer) on the LANDSAT satellite [18]. A blowout in the Persian Gulf was subsequently detected. The large EXXON VALDEZ slick was detected on SPOT (Satellite Pour l'Observation de la Terre) satellite data [180]. Oiled ice in Gabarus Bay resulting from the KURDISTAN spill was detected using LANDSAT data [181, 182]. Several workers were able to detect the Arabian Gulf War Spill in 1991 [183–186]. The HAVEN spill near Italy was also monitored by satellite [187]. A spill in the Barents Sea was tracked using an IR band on NOAA 10 [188]. It is significant to note that, in all these cases, the position of the oil was known and data had to be processed to actually see the oil, which usually took several weeks. Newer findings show that the ability to detect oil may be a complex function of conditions, oil types and view angles [189–191].

There are several problems associated with relying on satellites operating in optical ranges, for oil spill remote sensing. The first is the timing and frequency of overpasses and the absolute need for clear skies to perform optical work [192]. The chances of the overpass and the clear skies occurring at the same time give a very low probability of seeing a spill on a satellite image. This point is well illustrated in the case of the EXXON VALDEZ spill [193]. Although the spill covered vast amounts of ocean for over a month, there was only one clear day that coincided with a satellite overpass, and that was on April 7, 1989. Another disadvantage of satellite remote sensing is the difficulty in developing algorithms to highlight the oil slicks and the long time required to do so. For the EXXON VALDEZ spill, it took over 2 months before the first group managed to "see" the oil slick in the satellite imagery, although its location was precisely known. Recently several workers have attempted to use MODIS visible data to detect oil spills [194, 195]. These techniques generally rely on ancillary data such as suspected position or other satellite data, to be successful. However, Srivastava and Singh used only MODIS to detect known oil spills in Lake Maracaibo, Venezuela [196]. First, the use of L1B data visually did show oil, however, uncorrected features at 469, 555 and 645 nm showed significant indications of oil. Further study showed that the ratio of the difference and sum at 645 and 555 nm, normalized by 469 nm provided the best results. More recently, several workers used MODIS and other satellite data to detect the oil during the Macondo spill in the U.S. Gulf of Mexico [197].

Li et al. (highlighted the differences between optical and radar satellites [198]. This research group studied the Montara spill in the Timor Sea using the ALOS PALSAR (L-band radar), the Envisat ASAR (C-band radar) and the MODIS (AQUA – color visible) satellite data. The ALOS PALSAR did function, but as expected from L-band radar was not clear. The Envirsat ASAR data was the clearest and provide useful imagery always. The visible data from MODIS function well only during completely clear skies, but most of the time did not yield useful images. Cloud interference in the latter was cited as a reason, but the lack of specific oil coloration should have also been noted.

There is some information on slicks available from sensor angular orientation. For example, Chust and Sagarminaga used the Multi-angle Imaging SpectroRadiometer (MISR) sensors aboard a satellite to detect oil spills on Lake Maracaibo, Venezuela [199]. This sensor uses nine push-broom cameras at fixed angles from nadir to 70.5° to examine particular surfaces. A comparison of this angular sensor shows that better contrast was obtained than a simple nadir camera on

another satellite. Data analysis showed that oil spills appear in greater contrast in those view angles affected by sun glitter because of the presence of oil.

IR data from satellite has been used to map the land oil pollution in Kuwait [200]. It was found that the old hydrocarbon-contaminated areas showed as much as 10°C difference from the surrounding land. Ground-truthing was used extensively in compiling the data. Casciello also made an attempt to use IR imagery from the thermal infrared region of the AVHRR satellite to locate known oil spills [201].

Radar satellites, including ERS-1 and -2, Radarsat-1 and 2, and ENVISAT, have usefulness for detecting large offshore spills and for spotting anomalies [86, 202–204]. Radarsat has been used for detecting oil seeps and smaller spills resulting from an oil barge [205, 206]. The relative location of these smaller slicks was known before the detection. A novel application of Radarsat has been the study of oil lakes in the deserts of Kuwait [207]. Radar satellites are now used routinely by a number of nations to provide imagery for larger spills and to give indications of ship discharges. ERS-1 and 2 have been used for mapping of oil spills in the Caspian Sea [208]. Fortuny describes the use of ERS-2 and ENVISAT to provide imagery during the Prestige incident off Spain [209]. Torres Palenzuela and co-workers used two ASAR (Advanced SAR) images from the Envisat satellite to study the same Prestige spill off Spain [210]. Using several techniques that were readily-available such as filtering and comparison to GIS data of the areas, several slicks were identified. These slicks were confirmed by recorded sightings from helicopters and ships.

Several countries have instituted satellite monitoring systems for oil pollution [211–213]. Many of these use processing methods as described above. Extensive programs are in place in the Baltic Sea, North Sea and English Channel [145]. There are now programs in the Black, Caspian and Azov Seas [213, 214]. Canada has had a program in place for several years [215]. The Mediterranean Sea has had such a program for a long time [144, 145]. A constellation of monitoring satellites is proposed for the Mediterranean Sea.

In recent years there have been a number of new satellite-borne SAR sensors launched, see Table 2. While one of these sensors, RADARSAT-2, operates in the traditional C-band, TerraSAR-X and Cosmos Skymed operate in the X-band, and the PALSAR sensor on ALOS operates in the L-band. As noted above, X-band is the preferred band for oil spill remote sensing in terms of Bragg scattering. All four of these new SAR satellites have polarimetric imaging modes (some are experimental vs operational modes) and much higher spatial resolution (down to 3 m) which may have application for oil spill remote sensing. RADARSAT-2, like its predecessor is an operational commercial satellite that can be tasked to respond to emergency situations like major oil spills. The time required to task RADARSAT-2 in emergency mode

Oil Spill Remote Sensing. Table 2 Current and future satellite-borne SAR sensors

Satellite	Launch date	Owner/ operator	Band
ERS-1	1991 (end 2000)	European Space Agency	C
ERS-2	1995	European Space Agency	C
RADARSAT-1	1995	Canadian Space Agency	C
RADARSAT-2	2007	Canadian Space Agency	C
ENVISAT (ASAR)	2002	European Space Agency	C
ALOS (PALSAR)	2006 (end 2011)	Japan Aerospace Exploration Agency	L
TerraSAR-X	2007	German Aerospace Center	X
Tandem-X	TBD (was scheduled for 2009)	German Aerospace Center	X
Cosmos Skymed-1/2	2007	Italian Space Agency	X
TecSAR	2008	Israel Aerospace Industries	X
Sentinel-1	2012	European Space Agency	C
RADARSAT-Constellation (3-satellites)	2014	Canadian Space Agency	C

is now 4 h, which is a large improvement from the 12 h required to task its predecessor. As noted above VV polarization provides a superior clutter to noise ratio (CNR) over HH polarization for oil spill detection [212]. RADARSAT-2 is fully polarimetric and there is interest in investigating whether a dual polarization ScanSAR mode utilizing VV/VH polarizations will work for oil and ship detection respectively as part of the Integrated Satellite Tracking of Pollution (ISTOP) program [215]. The increased number of SAR satellites plus the plans to operate constellations of small satellites like Cosmos (Constellation of Small Satellites for Mediterranean basin Observation) will provide increased temporal coverage with revisit times down to a few hours in some circumstances. The opportunity for increased frequency of image collection should prove useful to the oil spill response community. Figures 12–15 show the use of radar satellites and the look-alikes to oil that sometimes appear in the images.

Oil Under Ice Detection

The difficulties in detecting oil in or under ice are numerous. Ice is never a homogeneous material but rather incorporates air, sediment, salt, and water, many of which may present false oil-in-ice signals to the detection mechanisms. In addition, snow on top of the ice or even incorporated into the ice adds complications. During freeze-up and thaw in the spring, there may not be distinct layers of water and ice. There are many different types of ice and different ice crystalline orientations. This is a separate field and readers may consult the literature [216].

Underwater Detection and Tracking

Many different techniques have been tried for underwater oil detection. First, the division should be made between oil in the water column or floating on a pycnocline, and oil on the bottom. Quite different physics and conditions can apply to these different situations.

Several parties have tried to use standard sonars to detect submerged oil on the bottom. Oil on the bottom can appear as a softer surface than ordinary bottom sediment. The problem arises in that vegetation on the bottom also appears similar and thus many false positives arise. In the water column, sonar can be useful as it can locate intermediate oil on pycnoclines; however, there is no unique signature and there are often weeds and other debris on pycnoclines. Wendelboe et al. report on tests using a 200 and 400 kHz (dual-frequency) multi-beam system [217]. The contributing signal is the lower acoustic reflectivity of the oil than typical bottom geological formation or the better reflection than weed beds. Wendelboe et al. used the back scatter signals from several tests to develop algorithms for oil detection. This was tested in a tank with a 90% success rate and a 23% false detection rate [218]. Hansen reviewed various systems noting that the narrow-scan sonar systems showed promise [219].

Oil on the bottom has successfully been mapped by underwater cameras, often mounted on sleds [220–222]. The problems with this technique are the bottom visibility – often insufficient to discriminate, and the difficulty in towing the camera vehicle as slow as 1 knot, the necessary speed. Pfeifer et al. were successful in employing mosaics of photographs to determine the aerial extent of oil on the sea floor [221, 222].

A low-technology approach had been historically employed. Heavy oil, such as would sink, often adheres to oil snares or pom-poms, which are polypropylene strips mounted as a cheerleaders' pom-pom. These can be mounted on a beam and towed over the bottom and then raised periodically to see if oil has adhered [220]. Alternatively they can be mounted on an anchor with a marker buoy. These are then raised periodically to check if the subsurface oil has contacted them.

Camilli et al. have successfully applied mass spectrometry to the detection of sunken heavy oil (Fuel Oil #6) [223]. Using the small and enclosed mass spectrometer, TETHYS, the low molecular weight hydrocarbons coming from sunken oil masses are monitored. The mass spectrometer is mounted in a submersible which is driven over the sea floor. The exact position of the submersible is monitored closely using an acoustic positioning system on the surface. Signals then can be correlated closely to the position on the seafloor. Three ion peaks of m/z 43, 41, 27 are monitored to establish hydrocarbon presence. Tests show that the ion peaks provide sensitivity as low as 0.4 ppb. This is fully sufficient to monitor sunken oil. Tests were conducted in a test tank and latter over actual spills in the Gulf of Mexico. The technique was able to find concentrations of sunken oil and place the locations within 1 m. The tests in the Gulf of Mexico

were conducted at depths of 200 m and confirmed by using cameras on the submersible.

Small Remote-Controlled Aircraft

Several parties have suggested remote-controlled aircraft to provide more economical solutions for response personnel [224–226]. In fact, remote-controlled aircraft have been used by a number of parties for monitoring a variety of pollutants since the 1970s [226].

Belgium employs a UAV of the B-Hunter class to routinely monitor its portion of the North Sea [225]. This is a large UAV which has visible and IR camera systems aboard. The unit has a 10-h endurance over the targets.

A variety of commercial platforms are now available which can provide carriage for small sensors such as visible and IR cameras. Further, automatic navigation technology has now made these units, especially helicopters, very much easier to fly than in previous years.

Real-Time Displays and Printers

A very important aspect of remote sensing is the production of data so that operations people can quickly and directly use it. Real-time displays are important so that remote sensor operators can adjust instruments directly in flight and provide information quickly on the location or state of the spill. A major concern of the client is that data be rapidly available [227]. An additional concern is that the data from various sensors be available in a combined or fused form [87]. Further there is a need to correct this data for aircraft motion and to annotate the data with time and position. At this time, existing hardware and software must be adapted as commercial off-the-shelf equipment for directly outputting and printing sensor data is not yet available.

One means to overcome some of these problems is the development of entire packages for oil spill remote sensing. Robbe and Hengsterman describe the MEDUSA system which consists of an integrated system with IR, UV, SLAR, Microwave Radiometer, laser fluorosensor, and navigation systems [2].

Routine Surveillance

One of the applications of oil spill remote sensing equipment is to detect and map slicks resulting from illegal discharges of oil from ships and offshore platforms. Historically this has always been performed using visual techniques, but in the past decade has been increasingly turned over to aircraft with some instrumentation. Typical instrumentation includes a SLAR, IR/UV scanner, and cameras. This sensor package is economical compared to more ideal packages and greatly improves capability beyond just visual observation. Limitations include limited ability to "look into" ship wakes, limited night operations, and inability to positively identify oil slicks. Recent additions such as improved SLAR systems, better display systems, and nighttime cameras have added to the capability, but do not overcome these limitations.

There are many efforts to perform surveillance of illegal discharges. Most existing operative remote systems are dedicated to this function. These are estimated to be around 35, most of these around Europe [2, 179, 228]. There are intensive programs in some areas, for example, in the North Sea. Carpenter reports on the 18-year program of surveillance in the North Sea [229]. Some interesting statistics are noted. In 2004, 418 unidentified slicks were found, 65 slicks from oil rigs and 57 slicks from ships. In 2004, 3,314 h were flown in daylight and 594 in darkness. In the same year, 91 slicks were found in the darkness and 449 in daylight.

Ferraro et al. describe a routine surveillance program using satellite and aircraft data for the Mediterranean Sea [145]. Future work in the Mediterranean Sea proposes a cluster of radar satellites to constantly monitor oil pollution [230].

A word about aircraft is suitable here. A variety of aircraft are deployed as remote sensing aircraft. Typically different types are deployed for routine surveillance and for remote sensing research. The latter requires flexibility in mounting sensors and in access to the outside of the aircraft.

Future Directions

Advances in sensor technology will continue to drive the use of remote sensors as operational oil spill response tools in the future. Cameras and thermal infrared cameras that offer high sensitivity are cheap and plentiful. This improvement not only reduces the size and complexity of the sensor, but also the cost. In the next decade, advances in laser technology, in

particular diode-pumped solid-state and possibly excimer lasers, will greatly reduce the size and energy consumption of laser-based remote sensors. This will promote the use of these sensors in smaller, more economical aircraft within the budget of many more regulatory agencies and maritime countries. Rapidly improving computer capabilities will allow for true real-time processing. At the present time and for the foreseeable future, there is no single "Magic Bullet" sensor that will provide all the information required to detect, classify, and quantify oil in the marine and coastal environment. An example of the improvement in recent years is that of the night vision camera. It is now possible to use this sensor to visualize oil at night.

It will require the combined advances in sensor technologies and computer capabilities noted above to gather, integrate, and merge several sources of data into a real-time format, usable by response crews in the field. If this type of information can be made available to response crews in a short enough time frame following a spill incident, then it can be used to lessen the potentially disastrous effects of a major oil spill on the marine ecosystem.

As technology in remote-controlled systems evolve, it is possible to employ such technology in oil spill remote sensing. First efforts in the deployment of remote-controlled sensing aircraft have posted success and will, no doubt, be expanded in the future [231].

Recommendations are based on the above considerations and include economy as a major factor. Table 3 shows the considerations related to the development state, cost, and use of the sensor. The laser fluorosensor offers the only potential for discriminating between oiled and unoiled weeds or shoreline, and for positively identifying oil pollution on ice, among ice and in a variety of other situations. This instrument, however, is large and expensive. A cheap sensor recommended for oil spill work is an infrared camera. This is the cheapest but undiscriminating device. This is the only piece of equipment that can be purchased off-the-shelf. All other sensors require special order and, often, development. Radar, although low in priority for purchase, offers the only potential for large area searches and foul weather remote sensing. Most other sensors are experimental or do not offer good potential for oil detection or mapping. Any sensor package should include a real-time printer and display, and a downlink.

Oil Spill Remote Sensing. Table 3 Attributes for airborne sensor selection

Sensor	State of development	Amount of experience in use	Specific to oil	Immunity to false targets	Typical coverage (km)	Acquisition cost range k$	Aircraft physical requirements
Still Camera	High	High	Poor	Poor	0.25–2	1–5	No
Video	High	High	Poor	Poor	0.25–5	1–10	No
Night Vision Camera	Medium	Medium	Poor	Poor	0.25–2	5–20	No
IR Camera (8–14 μm)	High	Medium	Medium	Medium	0.25–2	20–50	No
UV Camera	Medium	Medium	Poor	Poor	0.25–2	4–20	No
Multispectral Scanner	Medium	Medium	Poor	Poor	0.25–2	100–200	Some
Radar	High	High	Medium	Poor	5–50	1,200–8,000	Yes-Dedicated
Microwave Radiometer	Medium	Low	Medium	Medium	1–5	400–1,000	Yes-Dedicated
Laser Fluorosensor	Medium	Low	Good	Excellent	0.01–2	300–1,000	Yes-Dedicated

In order to respond effectively to major marine oil spills, it is recommended that one employs a combination of airborne and satellite-borne sensor systems. Improvements in the resolution of satellite-based systems, particularly SAR systems combined with the increased number of such systems and the ability to steer them to image the area of the oil spill will lead to their increased use in a tactical role. Being capable of imaging vast areas of the open ocean will ensure that satellite-borne sensors will also continue to be used in a strategic manner. There are a number of commercially available airborne sensor systems which provide near-real-time information on oil slick location and indications of thicker areas of the pollution in an easily interpretable graphical manner. These airborne sensor systems are currently being employed by a large number of maritime nations in conjunction with satellite-based sensor systems.

There are an increasing number of satellite-borne SAR and optical sensors, some of which currently or soon will operate in constellations to provide increased coverage of the Earth's surface. These enhanced capabilities will allow for the possible use of these sensors in a tactical mode of operation. In spite of these increased capabilities, there remains an essential role for airborne oil spill remote sensing platforms. The ability to collect and deliver real-time oil slick location information will ensure the continued use of airborne systems in spite of their high operational costs.

If this type of real-time oil spill remote sensing information can be made available to response crews in a short enough timeframe following a spill incident, the information can be used to mitigate the potentially disastrous effects of a major oil spill on the marine ecosystem.

Bibliography

1. NAS (2003) Oil in the sea. National Academy of Sciences, Washington, DC
2. Robbe N, Hengstermann T (2006) Remote sensing of marine oil spills from airborne platforms using multi-sensor systems. In: Brebbia CA, Antunes do Carmo JS (eds) Water pollution VIII: modelling, monitoring and management. WIT Press, Southampton, p 347
3. Serra-Sogas N, O'Hara PD, Canessa R, Keller P, Pelot R (2008) Visualization of spatial patterns and temporal trends for aerial surveillance of illegal oil discharges in western Canadian marine waters. Mar Pollut Bull 56:815
4. Fingas M, Brown CE (2011) Oil spill remote sensing: a review. In: Fingas M (ed) Oil spill science and technology. Gulf, New York, pp 111–169 (Chap 6)
5. Fingas M, Brown CE (2005) Review of oil spill remote sensing. In: Proceedings of the 8th international conference on remote sensing for marine and coastal environments, Altarum
6. Hengstermann T, Robbe N (2008) Airborne oil spill remote sensing. Hydro Int 10:2008
7. Jha MN, Levy J, Gao Y (2008) Advances in remote sensing for oil spill disaster management: state-of-the-art sensors technology for oil spill surveillance. Sensors 8:236
8. Fingas MF, Brown CE, Gamble L (1999) The visibility and detectability of oil slicks and oil discharges on water. Arctic Mar Oilspill Progr Tech Sem 2:865
9. Brown CE, Fingas MF (2009) The latest developments in remote sensing technology for oil spill detection. In: Proceedings of the Interspill 2009, Marseille
10. Krol T, Stelmaszewski A, Freda W (2006) Variability in the optical properties of a crude oil-seawater emulsion. Oceanologia 48:203
11. Evdokimov IN, Losev AP (2007) Potential of UV-visible absorption spectroscopy for characterizing crude petroleum oils. Oil Gas Bus 1
12. Otremba Z, Piskozub J, Król T (2003) Modelling the reflectance of sea areas polluted with oil emulsion. Fresenius Environ Bull 12(9):1109–1113
13. Otremba Z, Piskozub J (2001) Modelling of the optical contrast of an oil film on a sea surface. Opt Express 9(8):411–416
14. Otremba Z, Piskozub J (2000) The modification of light flux leaving a wind-roughened, oil covered sea surface example of computations for shallow seas. Oceanol Stud 29(1):117–133
15. Hong SI, Shin I (2010) Nightime detection of oil spills on the sea surface using spaceborne infrared images. Korea Meteorological Administration
16. Ma L, Li Y, Liu Y (2009) Oil Spill monitoring based on its spectral characteristics. Environ Forensic 10:317
17. O'Neil RA, Neville R, Thompson V (1983) The arctic marine oilspill program (AMOP) remote sensing study. Environment Canada Report EPS 4-EC-83-3, Ottawa
18. Brown HM, Bittner JP, Goodman RH (1996) The limits of visibility of spilled oil sheens. In: Proceedings of the second thematic international airborne remote sensing conference and exhibition, ERIM conferences, San Francisco, vol III, p 327
19. Taylor S (1992) 0.45 to 1.1 μm spectra of Prudhoe crude oil and of beach materials in Prince William Sound, Alaska. CRREL Special Report No. 92–5. Cold Regions Research and Engineering Laboratory, Hanover
20. Huang M, Yu Y, Zhang SJ, Qi X (2008) Analysis of water spectral features of petroleum pollution and estimate models from remote sensing data. SPIE 7123:712312
21. Ahmed S, Gilerson A, Oo M, Zhou J, Chowhardy J et al (2006) The polarization properties of reflectance from coastal waters and the ocean–atmosphere system. SPIE 6360:636003
22. Carnesecchi F, Byfield V, Cipollini P, Corsini G, Diani M (2008) An optical model for the interpretation of remotely sensed multispectral images of oil. SPIE 7105:710504

23. Bianchi R, Cavalli RM, Marino CM, Pignatti S, Poscolieri M (1995) Use of airborne hyperspectral images to assess the spatial distribution of oil spilled during the Trecate blow-out (Northern Italy). SPIE 2585:352
24. Bagheri S, Stein M, Zetlin C (1995) Utility of airborne videography as an oil spill-response monitoring system. In: Cheremisinoff PN (ed) Encyclopedia of environmental control technology. Gulf, Houston, p 367
25. Brown CE, Fingas MF, Marois R (2004) Oil spill remote sensing: laser fluorosensor demonstration flights off the east coast of Canada. Arctic Mar Oilspill Progr Tech Sem 317
26. Brown CE, Fingas MF, Marois R (2005) Oil spill remote sensing flights in the coastal waters around Newfoundland. In: Proceedings of the eighth international conference on remote sensing for marine and coastal environments, Altarum
27. Palmer D, Borstad GA, Boxall SR (1994) Airborne multi spectral remote sensing of the January 1993 Shetlands oil spill. In: Proceedings of the second thematic conference on remote sensing for marine and coastal environments: needs, solutions and applications. ERIM, Ann Arbor, vol II, p 546
28. Wadsworth A, Looyen WJ, Reuter R, Petit M (1992) Aircraft experiments with visible and infrared sensors. Int J Remote Sens 13:1175
29. Wang D, Gong F, Pan D, Hao Z, Zhu Q (2010) Introduction to the airborne marine surveillance platform and its application to water quality monitoring in China. Oceanol Sin 29:33
30. Locke C, White M, Michel J, Henry C, Sellars JD, Aslaksen ML (2008) Use of vertical digital photography at the Bayou Perot, LA, spill for oil mapping and volume estimation. In: Proceedings of the IOSC 2008, Savannah, p 127
31. Stelmaszewski A, Krol T, Toczek H (2009) Light scattering in Baltic crude oil – seawater emulsion. Oceanologia 51:405
32. Hurford N (1989) Review of remote sensing technology. In: Lodge AE (ed) The remote sensing of oil slicks. Wiley, Chichester, p 7
33. Goodman RH (1989) Application of the technology in North America. In: Lodge AE (ed) The remote sensing of oil slicks. Wiley, Chichester, p 39
34. Belore RC (1982) A device for measuring oil slick thickness. Spill Tech News 7:44
35. Neville RA, Thompson V, Dagg K, O'Neil RA (1979) An analysis of multispectral line scanner imagery from two test spills. In: Proceedings of first workshop sponsored by working group I of the pilot study on the use of remote sensing for the control of marine pollution, NATO challenges of modern society, p 201
36. Bolus RL (1996) Airborne testing of a suite of remote sensors for oil spill detecting on water. In: Proceedings of the second thematic international airborne remote sensing conference and exhibition. ERIM, Ann Arbor, vol III, p 743
37. Salisbury JW, D'Aria DM, Sabins FF (1993) Thermal infrared remote sensing of crude oil slicks. Remote Sens Environ 45:225
38. Hover G (1994) Testing of infrared sensors for U.S. Coast Guard oil spill response applications. In: Proceedings of the second thematic conference on remote sensing for marine and coastal environments: needs, solutions and applications. ERIM, Ann Arbor, vol I, p 47
39. Grierson IT (1998) Use of airborne thermal imagery to detect and monitor inshore oil spill residues during darkness hours. Environ Manage 22:905
40. Shih W-C, Andrews AB (2008) Infrared contrast of crude-oil-covered water surfaces. Opt Lett 33:3019
41. Brown HM, Baschuk JJ, Goodman RH (1998) The limits of visibility of spilled oil sheens. Arctic Mar Oilspill Progr Tech Sem:805
42. Clark RN, Swayze GA, Leifer I, Livo KE, Lundeem S et al (2010) A method for qualitative mapping of thick oil using imaging spectroscopy. United States Geological Survey. http://pubs.usgs.gov/of/2010/1101/
43. Leifer IR, Clark RN, Swayse G, Roberts D, Kokaly R et al (2011) Imaging spectroscopy of the deepwater horizon spill: a 21st century oil spill response (in press)
44. Goodman RH (1988) Simple remote sensing system for the detection of oil on water. Environmental Studies Research Fund Report Number 98, Ottawa
45. Brown CE (2011) Laser fluorosensors. In: Fingas MF (ed) Oil spill science and technology. Gulf, Oxford, pp 171–184
46. Brown CE, Fingas MF, An J (2001) Laser fluorosensors: a survey of applications and developments of a versatile sensor. Arctic Mar Oilspill Progr Tech Sem 1:485
47. Brown CE, Nelson R, Fingas MF, Mullin JV (1997) Airborne laser fluorosensing: overflights during lift operations of a sunken oil barge. In: Proceedings of the fourth thematic conference on remote sensing for marine and coastal environments. ERIM, Seattle, vol I, p 23
48. Brown CE, Marois R, Fingas MF, Choquet M, Monchalin J-P, Mullin J, Goodman R (2001) Airborne oil spill sensor testing: progress and recent developments. IOSC 2001, Tampa, p 917
49. Brown CE, Fingas MF (2003) Review of the development of laser fluorosensors for oil spill application. Mar Pollut Bull 47:477
50. Hengstermann T, Reuter R (1990) Lidar fluorosensing of mineral oil spills on the sea surface. Appl Opt 29:3218
51. Balick L, DiBenedetto JA, Lutz SS (1997) Fluorescence emission spectral measurements for the detection of oil on shore. In: Proceedings of the fourth thematic conference on remote sensing for marine and coastal environments. ERIM, Ann Arbor, vol I, p 13
52. Sarma AK, Ryder AG (2006) Comparison of the fluorescence behaviour of a biocrude oil and crude petroleum oil. Energy Fuels 20:783
53. Samberg A (2007) The state-of-the-art of airborne laser systems for oil mapping. Can J Rem Sens 53:143
54. Jha MN, Gao Y (2008) Oil spill contingency planning using laser fluorosensors and web-based GIS. In: Proceedings Oceans Marine Technology Society, Quebec City
55. Diebel D (1989) Laser fluorosensing of mineral oil spirits. In: Lodge AE (ed) The remote sensing of oil slicks. Wiley, Chichester, p 127

56. Geraci AL, Landolina F, Pantani L, Cecchi G (1993) Laser and infrared techniques for water pollution control. IOSC, 525
57. Hoge FE, Swift RN (1980) Oil film thickness measurement using airborne laser-induced water Raman backscatter. Appl Opt 19:3269
58. Piskozub J, Drozdowska V, Varlamov V (1997) A lidar system for remote measurement of oil film thickness on sea surface. In: Proceedings of the fourth thematic conference on remote sensing for marine and coastal environments. ERIM, Ann Arbor, vol I, p 386
59. Goodman R, Brown CE (2005) Oil detection limits for a number of remote sensing systems. In: Proceedings of the eighth international conference on remote sensing for marine and coastal environments, Halifax, Alterum conferences
60. Dick R, Fruhwirth M, Brown C (1992) Laser fluorosensor work in Canada. In: Proceedings of the first thematic conference on remote sensing for marine and coastal environments. ERIM, p 223
61. James RTB, Dick R (1996) Design of algorithms for the real-time airborne detection of littoral oil-spills by laser-induced fluorescence. Arctic Mar Oilspill Progr Tech Sem 2:1599
62. Brown CE, Fingas MF, Gamble RL, Myslicki GE (2002) The remote detection of submerged oil. In: Proceedings of the third R&D forum on high-density oil spill response, Brest France. IMO, pp 46–54
63. Brown CE, Marois R, Myslicki G, Fingas MF (2002) Initial studies on the remote detection of submerged orimulsion with a range-gated laser fluorosensor. AMOP, Environment Canada, Ottawa, p 773
64. Brown CE, Marois R, Myslicki G, Fingas MF, MacKay R (2003) Remote detection of submerged orimulsion with a range-gated laser fluorosensor. In: Proceedings of the IOSC 2003, Vancouver, p 779
65. Brown CE, Marois R, Gamble RL, Fingas MF (2003) Further studies on the remote detection of submerged orimulsion with a range-gated laser fluorosensor. Arctic Mar Oilspill Progr Tech Sem 1:279
66. Brown CE, Fingas M, Marois R, Fieldhouse B, Gamble RL (2004) Remote sensing of water-in-oil emulsions: initial laser fluorosensor studies. Arctic Mar Oilspill Progr Tech Sem 1:295
67. Ulaby FT, Moore RK, Fung AK (1989) Microwave remote sensing: active and passive. Artech House, Norwood, 1466
68. Goodman RH (1994) Remote sensing resolution and oil slick inhomogeneities. In: Proceedings of the second thematic conference on remote sensing for marine and coastal environments: needs, solutions and applications. ERIM, Ann Arbor, p I-1-17
69. Fäst O (1986) Remote sensing of oil on water – air and space-borne systems. In: Proceedings of the DOOS seminar, Trondheim
70. Skou N, Sorensen BM, Poulson A (1994) A new airborne dual frequency microwave radiometer for mapping and quantifying mineral oil on the sea surface. In: Proceedings of the second thematic conference on remote sensing for marine and coastal environments. ERIM, Ann Arbor, p 559
71. Mussetto MS, Yujiri L, Dixon DP, Hauss BI, Eberhard CD (1994) Passive millimeter wave radiometric sensing of oil spills. In: Proceedings of the second thematic conference on remote sensing for marine and coastal environments: needs, solutions and applications. ERIM, Ann Arbor, vol I, p 35
72. Zhifu S, Wiesbeck W (1988) A study of passive microwave remote sensing. In: Proceedings of the 1988 international geoscience and remote sensing symposium, Edinburgh, p 1091
73. Süss H, Grüner K, Wilson WJ (1989) Passive millimeter wave imaging: a tool for remote sensing. Alta Freq LVIII:457
74. Pelyushenko SA (1995) Microwave radiometer system for the detection of oil slicks. Spill Sci Technol Bull 2:249
75. Pelyushenko SA (1997) The use of microwave radiometer scanning system for detecting and identification of oil spills. In: Proceedings of the fourth thematic conference on remote sensing for marine and coastal environments. ERIM, Ann Arbor, vol I, p 381
76. McMahon OB, Brown ER, Daniels GD, Murphy TJ, Hover GL (1995) Oil thickness detection using wideband radiometry. In: Proceedings of the IOSC 1995, Long Beach, CA, p 15
77. McMahon OB, Murphy TJ, Brown ER (1997) Remote measurement of oil spill thickness. In: Proceedings of the fourth thematic conference on remote sensing for marine and coastal environments. ERIM, Ann Arbor, vol I, p353
78. Nunziata F, Migliaccio M, Sobieski P (2008) A BPM two-scale contrast model. In: Proceedings of the IGARSS, Boston, vol IV, p 593
79. Frysinger GS, Asher WE, Korenowski GM, Barger WR, Klusty MA, Frew NM, Nelson RK (1992) Study of ocean slicks by nonlinear laser processes in second-harmonic generation. J Geophys Res 97:5253
80. Alpers W, Hühnerfuss H (1987) Radar signatures of oil films floating on the sea surface. In: Proceedings of the IGARSS, Ann Arbor, p 741
81. Poitevin J, Khaif C (1992) A numerical study of the backscattered radar power in presence of oil slicks on the sea surface. In: Proceedings of the first thematic conference on remote sensing for marine and coastal environments. ERIM, Ann Arbor, p 171
82. Hühnerfuss H, Alpers W, Witte F (1989) Layers of different thicknesses in mineral oil spills detected by grey level textures of real aperture radar images. Int J Remote Sens 10:1093
83. Gens R (2008) Oceanographic applications of SAR remote sensing. GISci Remote Sens 45:275
84. Bartsch N, Grüner K, Keydel W, Witte F (1987) Contribution to oil spill detection and analysis with radar and microwave radiometer: results of the Archimedes II campaign. IEEE Trans Geosci Remote GE.25:677
85. Mastin G, Mason JJ, Bradley JD, Axline RM, Hover GL (1994) A comparative evaluation of SAR and SLAR. In: Proceedings of the second thematic conference on remote sensing for marine and coastal environments: needs, solutions and applications. ERIM, Ann Arbor, vol I, p 7

86. Brown CE, Fingas MF (2003) Synthetic aperture radar sensors: viable for marine oil spill response? Arctic Mar Oilspill Progr Tech Sem 1:299
87. Zielinski O, Robbe N (2004) Past and future of airborne pollution control. In: Proceedings of the Interspill 2004, Trondheim
88. Dyring A, Fäst O (2004) MSS puts the aircraft in the oil spill tracking network. In: Proceedings of the Interspill 2004, Trondheim
89. Intera Technologies (1984) Radar surveillance in support of the 1983 COATTF oil spill trials. Environment Canada Report EE-51
90. C-CORE (Centre for Cold Ocean Resources Engineering) (1981) Microwave systems for detecting oil slicks in ice-infested waters: phase I – literature review and feasibility study. Environment Canada Report EPS 3-EC-81-3
91. Macklin JT (1992) The imaging of oil slicks by synthetic aperture radar. GEC J Res 10:19
92. Kozu TT, Umehara T, Ojima T, Suitsu T, Masuyko H, Inomata H (1987) Observation of oil slicks on the ocean by X-band SLAR. In: Proceedings of the IGARSS 1987, Ann Arbor, p 735
93. Madsen S, Skou N, Sorensen BM (1994) Comparison of VV and HH polarized SLAR for detection of oil on the sea surface. In: Proceedings of the second thematic conference on remote sensing for marine and coastal environments: needs, solutions and applications. ERIM, Ann Arbor, vol I, p 498
94. Migliaccio M, Nunziata F, Gambardella A (2009) On the co-polarized phase difference for oil spill observation. Int J Remote Sens 30:1587
95. Hühnerfuss H, Alpers W, Dannhauer H, Gade M, Lange PA, Neumann V, Wismann V (1996) Natural and man-made sea slicks in the North Sea investigated by a helicopter-borne 5-frequency radar scatterometer. Int J Remote Sens 17:1567
96. Hielm JH (1989) NIFO comparative trials. In: Lodge AE (ed) The remote sensing of oil slicks. Wiley, Chichester, p 67
97. Marghany M, Cracknell AP, Hasim M (2009) Modification of fractal algorithm for oil spill detection from RADARSAT-1 SAR data. Int J Appl Earth Observ Geoinform 11:96
98. Gade M, Alpers W, Huehnerfuss H, Wismann V (1996) Radar signatures of different oceanic surface films measured during the SIR-C-X-SAR missions. In: Proceedings of the remote sensing 1996. Balkema, Rotterdam, p 233
99. Okamoto K, Kobayashi T, Masuko H, Ochiai S, Horie H, Kumagai H, Nakamua K, Shimada M (1996) Results of experiments using synthetic aperture radar onboard the European remote sensing satellite 1–4. Artificial oil pollution detection. J Commun Res Lab 43:327
100. Migliaccio M, Gambardella A, Tranfaglia A (2007) SAR polarimetry to observe oil spills. IEEE Trans Geosci Remote 45:506
101. Gambardella A, M. Migliaccio M, De Grandi G (2007) Wavelet polarimetric SAR signature analysis of sea oil spills and look-alike features. In: Proceedings of the IGARSS 2007, Barcelona, p 983
102. Nunziata F, Gambardella A, Migliaccio M (2008) On the use of dual-polarized SAR data for oil spill observation. In: Proceedings of the IGARSS 2008, Boston, vol II, p 225
103. Forget P, Brochu P (1996) Slicks, waves and fronts observed in sea coastal area by an X-band airborne synthetic aperture radar. Remote Sens Environ 57:1
104. Marmorino GO, Thompson DR, Graber HC, Trump CL (1997) Correlation of oceanographic signatures appearing in synthetic aperature radar and interferometric synthetic aperture radar imagery with in-situ measurements. J Geophys Res 18:723
105. Nøst E, Egset CN (2006) Oil spill detection system – results from field trials. In: Proceedings oceans marine technology society
106. Gangeskar R (2004) Automatic oil-spill detection by marine X-band radars. Sea Technol 45:40–45
107. Topouzelis K, Karanthanassi V, Pavlakis VP, Rokos D (2009) Potentiality of feed-forward neural networks for classifying dark formation to oil spills and look-alikes. Geocarto Int 24:179
108. Solberg R, Theophilopoulos N (1997) ENVISYS – a solution for automatic oil spill detection in the Mediterranean. In: Proceedings of the fourth thematic conference on remote sensing for marine and coastal environments. ERIM, Ann Arbor, vol I, p 3
109. Ferraro G, Baschek B, de Montpellier G, Njoten O, Perkovic M, Vespe M (2010) On the SAR derived alert in the detection of oil spills according to the analysis of the EGEMP. Mar Pollut Bull 60:91
110. Wahl T, Eldhuset K, Skøelv Å (1993) Ship traffic monitoring and oil spill detection using ERS-1. In: Proceedings of the international symposium "operationalization of remote sensing", ITC, Enschede, p 97
111. Bern T-I, Wahl T, Anderssen T, Olsen R (1993) Oil spill detection using satellite based SAR: experience from a field experiment. Photogramm Eng Remote Sens 59:423
112. Yan X-H, Clemente-Colon P (1997) The maximum similarity share matching (MSSM) method applied to oil spill feature tracking observed in SAR imagery. In: Proceedings of the fourth thematic conference on remote sensing for marine and coastal environments. ERIM, Ann Arbor, vol I, p 43
113. Bentz CM, Politano AT, Ebecken NFF (2007) Automatic recognition of coastal and oceanic environmental events with orbital radars. In: Proceedings of the IGARSS 2007, Barcelona, p 914
114. Trivero P, Biamino W, Nirchio F (2007) High resolution COSMO-SkyMed SAR images for oil spills automatic detection. In: Proceedings of the IGARSS 2007, Barcelona, p 2
115. Tian W, Shao Y, Wang S (2008) A system for automatic identification of oil spill in ENVISAT ASAR. In: Proceedings of the IGARSS 2008, Boston, vol III, p 1394
116. Shao Y, Tian W, Wang S, Zhang F (2008) Oil spill monitoring using multi-temporal SAR and microwave scatterometer data. In: Proceedings of the IGARSS 2008, Boston, vol III, p 1378
117. Rodriguez MH, Bannerman K, Caceres RG, Pellon de Miranda F, Pedroso EC (2007) Cantarell natural seep modelling using SAR derived ocean surface wind and meteo-oceanographic buoy data. In: Proceedings of the IGARSS 2007, Barcelona, p 3257

118. Robson M, Secker J, Vachon PW (2006) Evaluation of eCognition for assisted target detection and recognition in SAR imagery. In: Proceedings of the IGARSS 2006, Denver, p 145
119. Garcia-Pineda O, MacDonald I, Zimmer B (2008) Synthetic aperture radar image processing using the supervised textural-neural network classification algorithms. In: Proceedings of the IGARSS, Boston, vol IV, p 1265
120. Morales DJ, Moctezuma M, Parmiggiani F (2008) Detection of oil slicks in SAR images using hierarchial MRF. In: Proceedings of the IGARSS, Boston, vol III, p 1390
121. Bertacca M (2006) A FEXP model short range dependence analysis for improving oil slicks and low-wind areas discrimination in SAR imagery. In: Proceedings of the IGARSS, Denver, p 959
122. Topouzelis KN (2008) Oil spill detection by SAR images: dark formation detection, feature extraction and classification algorithms. Sensors 8:6642
123. Topouzelis K, Karanthanassi V, Pavlakis P, Rokos D (2008) Dark formation detection using neural networks. Int J Remote Sens 29:4705
124. Topouzelis K, Stathakis D, Karanthanassi V (2009) Investigation of genetic contribution to feature selection for oil spill detection. Int J Remote Sens 30:179
125. Karathanassi V, Topouzelis K, Pavlakis P, Rokos D (2006) An object-oriented methodology to detect oil spills. Int J Remote Sens 27:5235
126. Topouzelis K, Karanthanassi V, Pavlakis P, Rokos D (2007) Detection and discrimination between oil spills and look-alike phenomena through neural networks. ISPRS J Photogramm Remote Sens 62:264
127. Karantzalos K, Argialas D (2008) Automatic detection and tracking of oil spills in SAR imagery with level set segmentation. Int J Remote Sens 29:6281
128. Tahvonen K, Pyhaelahti T (2006) The use of environmental data in reliability: assessment of oil spill detection by SAR imagery. In: Proceedings of the IGARSS 2006, Denver, p 3671
129. Karvonen J, Heiler I, Similae M, Tahvonen K (2006) Oil spill detection with RADARSAT-1 in the Baltic Sea. In: Proceedings of the IGARSS 2006, Denver, p 4075
130. Shi L, Ivanov AY, He M, Zhao C (2008) Oil spill mapping in the western part of the East China Sea using synthetic aperture radar imagery. Int J Remote Sens 29:6315
131. Muellenhoff O, Bulgarelli B, Ferraro G, Topouzelis K (2008) The use of ancillary metocean data for the oil spill probability assessment in SAR images. Fresenius Environ Bull 17:1382
132. Muellenhoff O, Bulgarelli B, Ferraro G, Perkovic M, Topouzelis K, Sammarini V (2008) Geospatial modelling of metocean and environmental ancillary data for the oil probability assessment in SAR images. Proc SPIE 7110:71100R
133. Assilzadeh H, Gao Y (2008) Oil spill emergency response mapping for coastal area using SAR imagery and GIS. In: Proceedings oceans marine technology society
134. Migliaccio M (2005) A physical approach for the observation of oil spills in SAR images. IEEE J Oceanic Eng 30:496
135. Shu Y, Li J, Yousef H, Gomes G (2010) Dark-spot detection from SAR intensity imagery with spatial density thresholding for oil-spill monitoring. Remote Sens Environ 114:2026
136. Migliaccio M, Ferrara G, Gambardella A, Nunziata F, Sorrentino A (2007) A physically consistent stochastic model to observe oil spills and strong scatterers on SLC SAR images. In: Proceedings of the IGARSS 2007, Barcelona, p 1322
137. Gambardella A, Giacinto G, Migliaccio M (2008) On the mathematical formulation of the SAR oil-spill observation problem. In: Proceedings of the IGARSS 2008, Boston, vol III, p 1382
138. Marghany M, Cracknell AP, Hasim M (2009) Comparison between RADARSAT-1 SAR different data modes for oil spill detection by a fractal box counting algorithm. Int J Dig Earth 2:237
139. Danisi A, Di Martino G, Iodice A, Riccio D, Ruello G et al (2007) SAR simulation of ocean scenes covered by oil slicks with arbitrary shapes. In: Proceedings of the IGARSS 2007, Barcelona, p 1314
140. Zhang F, Shao Y, Tian W, Wang S (2008) Oil spill identification based on textural information of SAR images. In: Proceedings of the IGARSS 2008, Boston, vol IV, p 1308
141. Tello M, Bonastre R, Lopez-Martinez C, Mallorqui JJ, Danisi A (2007) Characterization of local regularity in SAR imagery by means of multiscale techniques: application to oil spill detection. In: Proceedings of the IGARSS 2007, Barcelona, p 5228
142. Lounis B, Mercier G, Belhadj-Aissa A (2008) Statistical similarity measure for oil slick detection in SAR images. In: Proceedings of the IGARSS 2008, Boston, vol I, p 233
143. Pelizzari S, Bioucas-Dias J (2007) Oil spill segmentation of SAR images via graph cuts. In: Proceedings of the IGARSS 2007, Barcelona, p 1318
144. Ferraro G, Bernardini A, David M, Meyer-Roux S, Muellenhoff O et al (2007) Towards an operational use of space imagery for oil pollution monitoring in the Mediterranean basin: a demonstration in the Adriatic Sea. Mar Pollut Bull 54:403
145. Ferraro G, Meyer-Roux S, Muellenhoff O, Pavilha M, Svetak J, Tarchi D, Topouzelis K (2009) Long-term monitoring of oil spills in European seas. Int J Remote Sens 30:627
146. Ferraro G, Baschek B, De Monpellier G, Njoten O, Perkovic M (2010) On the SAR derived alert in the detection of oil spills according to the analysis of the EGEMP. Mar Pollut Bull 60:91–102
147. Adamo M, De Carolis G, De Pasquale V, Pasquariello G (2006) On the combined use of sun glint MODIS and MERIS signatures and SAR data to detect oil slicks. Proc SPIE 6360:63600G
148. Sipelgas L, Uiboupin R (2007) Elimination of oil spill like structures from radar image using MODIS data. In: Proceedings of the IGARSS 2007, Barcelona, p 429
149. Vesecky JF, Laws K, Paduan JD (2008) Monitoring of coastal vessels using surface wave HF radars: Multiple frequency, multiple site and multiple antenna considerations. In: Proceedings of the IGARSS 2008, Boston, vol I, p 405

150. Pinel N, Bourlier C (2008) Forward propagation of thick oil spills on sea surface for a coastal coherent radar. In: Proceedings of the IGARSS 2008, Boston, vol IV, p 1125
151. Demarty Y, Gobin V, Thirion L, Guinvarc'h R, Lesturgie M (2007) Exact electromagnetic modeling of the scattering of realistic sea surfaces for HFSWR applications. In: Proceedings of the IGARSS 2007, Barcelona, p 1004
152. Schultz-Stellenfleth J, Lehner S, Koenig T, Reppucci A, Brusch S (2007) Use of tandem pairs of ERS-2 and ENVIRSAT SAR data for the analysis of oceanographic and atmospheric processes. IGARSS 2007, Barcelona, p 3265
153. Goodman RH, Fingas MF (1988) The use of remote sensing for the determination of dispersant effectiveness. Arctic Mar Oilspill Progr Tech Sem 1:377
154. Jensen HV, Andersen JHS, Daling PS, Noest E (2008) Recent experience from multiple remote sensing and monitoring to improve oil spill response operations. In: Proceedings of the IOSC 2008, Savannah, p 407
155. Hollinger JP, Mennella RA (1973) Oil spills: measurements of their distributions and volumes by multifrequency microwave radiometry. Science 181:54
156. Lehr WJ (2010) Visual observations and the Bonn agreement. Arctic Mar Oilspill Progr Tech Sem 2:669
157. Horstein B (1973) The visibility of oil–water discharges. In: Proceedings of the IOSC 1973, Washington, DC, pp 91–99
158. Parker HD, Cormack D (1979) Evaluation of infrared line scan (IRLS) and side-looking airborne radar (SLAR) over controlled oil spills in the North Sea. Warren Spring Laboratory Report, Stevenage
159. Hurford N, Martinelli FN (1982) Use of an infrared line scanner and a side-looking airborne radar to detect oil discharges from ships. Warren Spring Laboratory Report, Stevenage
160. Hurford N, Martinelli FN (1984) Use of an infrared line scanner and a side-looking airborne radar to detect oil discharges from ships. In: Massin JM (ed) Remote sensing for the control of marine pollution. Plenum Press, New York, p 405
161. MacDonald IR, Guinasso NL Jr, Ackleson SG, Amos JF, Duckworth R, Sassen R, Brooks JM (1993) Natural oil slicks in the Gulf of Mexico visible from space. J Geophys Res 16:351
162. Brown HM, Bittner JP, Goodman RH (1995) Visibility limits of spilled oil sheens. Imperial Oil Internal Report, Calgary
163. Brown CE, Fingas MF, Monchalin J-P, Neron C, Padioleau C (2006) Airborne measurement of oil slick thickness. Arctic Mar Oilspill Progr Tech Sem 1:911
164. Reimer ER, Rossiter JR (1987) Measurement of oil thickness on water from aircraft; A: Active microwave spectroscopy; B: Electromagnetic thermoelastic emission. Environmental Studies Revolving Fund Report Number 078
165. Goodman R, Brown H, Bittner J (1997) The measurement of thickness of oil on water. In: Proceedings of the fourth thematic conference on remote sensing for marine and coastal environments, ERIM, Ann Arbor, vol I, p 31
166. Aussel JD, Monchalin J-P (1989) Laser-ultrasonic measurement of oil thickness on water from aircraft, feasibility study. Industrial Materials Research Institute Report, Québec
167. Krapez JC, Cielo P (1992) Optothermal evaluation of oil film thickness. J Appl Phys 72:1255
168. Choquet M, Héon R, Vaudreuil G, Monchalin J-P, Padioleau C, Goodman RH (1993) Remote thickness measurement of oil slicks on water by laser ultrasonics. IOSC, Boucherville
169. Brown CE, Fingas MF, Choquet M, Blouin A, Drolet D, Monchalin J-P, Hardwick CD (1997) The LURSOT sensor: providing absolute measurements of oil slick thickness. In: Proceedings of the fourth thematic conference on remote sensing for marine and coastal environments. ERIM, Ann Arbor, vol I, p 393
170. Brown CE, Fingas MF (2003) Development of airborne oil thickness measurements. Mar Pollut Bull 47:485
171. Brown CE, Fingas MF, Monchalin J-P, Neron C, Padioleau C (2005) Airborne oil slick thickness measurements: realization of a dream. In: Proceedings of the eighth international conference on remote sensing for marine and coastal environments, Altarum
172. Monchalin JP (1986) Optical detection of ultrasound. IEEE Trans Ultrason Ferroelectr Freq Control 33:485
173. Svejkovsky J, Muskat J, Mullin J (2008) Mapping oil spill thickness with a portable multispectral aerial imager. In: Proceedings of the IOSC 2008, Savannah, p 131
174. Lue L, Ge B, Yao W, Zhang Y (2011) A method for measuring the thickness of transparent oil film on water surface using laser trigonometry. Opt Lasers Eng 49:13
175. Lu Y-C, Tian Q-J, Li Z (2011) The remote sensing inversion theory of offshore oil slick thickness based on a two-beam interference model. Sci China Earth Sci 54:4154
176. Optimare (2011) http://www.optimare.de/cms/en/divisions/fek.html. Accessed June 2011
177. Swedish Space Corporation (2011) http://www.ssc.se/?id=5772. Accessed June 2011
178. Armstrong L, Fäst O, Schneider HA, Abrahamsson AH (2008) Integration of airborne AIS brings a new dimension to the detection of illegal discharge of oil spills. In: Proceedings of the IOSC 2008, Savannah, p 179
179. Brown CE, Fingas MF (2005) A review of current global oil spill surveillance, monitoring and remote sensing capabilities. Arctic Mar Oilspill Progr Tech Sem 2:789
180. Dean KG, Stringer WJ, Groves JE, Ahlinas K, Royer TC (1990) The EXXON VALDEZ oil spill: satellite analyses. In: Spaulding ML, Reed M (eds) Oil spills: management and legislative implications. ASCE, New York, p 492
181. Dawe BR, Parashar SK, Ryan TP, Worsfold RO (1981) The use of satellite imagery for tracking the KURDISTAN oil spill. Environment Canada Report EPS 4-EC-81-6, Ottawa
182. Alfoldi TT, Prout NA (1982) The use of satellite data for monitoring oil spills in Canada. Environment Canada Report EPS 3-EC-82-5, Ottawa

183. Cross A (1992) Monitoring marine oil pollution using AVHRR data: observations off the coast of Kuwait and Saudi Arabia during January 1991. Int J Remote Sens 13:781
184. Rand RS, Davis DA, Satterwhite MB, Anderson JE (1992) Methods of monitoring the Persian Gulf oil spill using digital and hardcopy multiband data. U.S. Army Corps of Engineers Report, TEC-0014
185. Al-Ghunaim I, Abuzar M, Al-Qurnas FS (1992) Delineation and monitoring of oil spill in the Arabian Gulf using landsat thematic mapper (TM) data. In: Proceedings of the Proceedings of the first thematic conference on remote sensing for marine and coastal environments. ERIM, Ann Arbor, p 1151
186. Al-Hinai KG, Khan MA, Dabbagh AE, Bader TA (1993) Analysis of landsat thematic mapper data for mapping oil slick concentrations – Arabian Gulf oil spill 1991. Arabian J Sci Eng 18:85
187. Cecamore P, Ciappa A, Perusini V (1992) Monitoring the oil spill following the wreck of the tanker HAVEN in the Gulf of Genoa through satellite remote sensing techniques. In: Proceedings of the first thematic conference on remote sensing for marine and coastal environments. ERIM, Ann Arbor, p 183
188. Voloshina IP, Sochnev OY (1992) Observations of surface contamination of the region of the Kol'shii Gulf from IR measurements. Sov J Remote Sens 9:996
189. Li Y, Yu S, Ma L, Liu M, Li Q (2008) Satellite image processing and analyzing for marine oil spills. Proc SPIE 7145:712311
190. Alawadi F, Amos C, Byfield V, Petrov P (2008) The application of hyperspectral image techniques on Modis data for the detection of oil spills in the RSA. Proc SPIE 7110:71100Q
191. Lotliker A, Mupparthy R, Kumer S, Nayak S (2008) Evaluation of hi-resolution MODIS-Aqua data for oil spill monitoring. Proc SPIE 7150:71500S
192. Clark CD (1989) Satellite remote sensing for marine pollution investigations. Mar Pollut Bull 20:92
193. Noerager JA, Goodman RH (1991) Oil tracking, containment and recovery during the EXXON VALDEZ response. In: Proceedings of the IOSC, Washington, DC, p 193
194. Li Y, Liu Y, Ma L, Li X (2007) Oil spill monitoring using MODIS data. Proc SPIE 6795:67955G
195. Li Y, Ma L, Yu S, Li C, Li Q (2008) Remote sensing of marine oil spills and its applications. SPIE :71450 C712311
196. Shrivastava H, Singh TP (2010) Assessment and development of algorithms to detection of oil spills using MODIS data. J Indian Soc Remote Sens 38:161
197. Leifer I, Lehr B, Simecek-Beatty D, Bradley E, Clark R, Dennison P, Hu Y, Matheson S, Jones C, Holt B, Roberts D, Svejkovsky J, Swayse G (2011) State of the art satellite and airborne oil spill remote sensing: application to the BP deepwater horizon oil spill. Remote Sens Environ (submitted)
198. Li X, Ge L, Hu Z, Chang H-C (2010) The 2009 Montara oil spill in the Timor sea as observed by earth observation satellites. University of New South Wales, Australia
199. Chust G, Sagarminaga Y (2007) The multi-angle view of MISR detects oil slicks under sun glitter conditions. Remote Sens Environ 107:232
200. ud Din S, Al Dousari A, Literathy P (2008) Evidence of hydrocarbon contamination from the Burgan oil field, Kuwait – interpretations from thermal remote sensing data. J Environ Manage 86:605
201. Casciello D, Lacava T, Pergola N, Tramutoli V (2007) Robust satellite techniques (RST) for oil spill detection and monitoring. In: Proceedings of the MultiTemp 2007–2007 international workshop on the analysis of multi-temporal remote sensing images, Leuven
202. Brown CE, Fingas MF (2001) New space-borne sensors for oil spill response. In: Proceedings of the IOSC 2001, Tampa, p 911
203. Brown CE, Fingas MF (2001) Upcoming satellites: potential applicability to oil spill remote sensing. Arctic Mar Oilspill Progr Tech Sem 2:495
204. Brown CE, Fingas MF, Lukowski TJ (2002) Airborne and space-borne synergies: the old dog teaches tricks to a new bird. In: Proceedings of the fifth international airborne remote sensing conference and exhibition, Veridien
205. Biegert EK, Baker RN, Berry JL, Mott S, Scantland S (1997) Gulf offshore satellite applications project detects oil slicks using RADARSAT. In: International symposium: geomatics in the era of RADARSAT, Ottawa
206. Werle D, Tittley B, Theriault E, Whitehouse B (1997) Using RADARSAT-1 SAR imagery to monitor the recovery of the Irving Whale oil barge. In: Proceedings of international symposium: geomatics in the era of RADARSAT, Ottawa
207. Kwarteng AY, Singhroy V, Saint-Jean R, Al-Ajmi D (1997) RADARSAT SAR data assessment of the oil lakes in the greater Burgan oil field, Kuwait. In: Proceedings of international symposium: geomatics in the era of RADARSAT, Ottawa
208. Ivanov AY, Ermoshkin IS (2004) Mapping of oil spills in the Caspian Sea using the ERS-1.ERS-2 SAR image quick-looks and GIS. In: Proceedings of the Interspill 2004, Trondheim
209. Fortuny J, Tarchi D, Ferraro G, Sieber A (2004) The use of satellite radar imagery in the Prestige accident. Interspill 2004, Trondheim
210. Torres Palenzuela JM, Vilas LG, Cuadrado MS (2006) Use of ASAR images to study the evolution of the Prestige oil spill off the Galician coast. Int J Remote Sens 27:1931
211. Gauthier M-F, Weir L, Ou Z, Arkett M, De Abreu R (2007) Integrated satellite tracking of pollution: a new operational program. In: Proceedings of the IGARSS 2007, Barcelona, p 967
212. Brekke C, Solberg AHS (2005) Oil spill detection by satellite remote sensing. Remote Sens Environ 95:1
213. Olga L, Marina M, Tatiana B, Andrey K, Vladimir K (2008) Multisensor approach to operational oil pollution monitoring in coastal zones. In: Proceedings of the IGARSS 2008, Boston, vol III, p 1386
214. Kostianoy A, Lavrova O, Mityagina M, Bocharova T, Litovchenko K et al (2007) Complex monitoring of oil pollution in the Baltic, Black and Caspian Seas. In: Proceedings of the Envisat symposium, Montreux, p 23

215. DeAbreu R, Gauthier M-F, Wychen W (2006) SAR-based oil pollution surveillance in Canada: operational implementation and research priorities. In: Proceedings OceanSAR 2006 – third workshop on coastal and marine applications of SAR, St. John's
216. Fingas MF, Brown CE (2002) Detection of oil in and under ice. Arctic Mar Oilspill Progr Tech Sem 2:199–214
217. Redman R, Pfeifer C, Brzozowski E, Markian R (2008) A comparison of methods for locating, tracking and quantifying submerged oil used during the T/B DBL 152 incident. In: Proceedings of the IOSC 2008, Savannah, p 255
218. Wendelboe G, Fonseca ELM, Hvidbak F, Mutschler M (2009) Detection of heavy oil on the seabed by application of a 400 kHz multibeam echo sounder. Arctic Mar Oilspill Progr Tech Sem 2:791
219. Hansen KA (2010) Research efforts for detection and recovery of submerged oil. Arctic Mar Oilspill Progr Tech Sem 2:1055
220. Michel J (2008) Spills of nonfloating oil: evaluation of response technologies. In: Proceedings of the IOSC 2008, Savannah, p 261
221. Pfeifer C, Brzozowski E, Markian R, Redman R (2008) Quantifying percent cover of submerged oil using underwater video imagery. In: Proceedings of the IOSC 2008, Savannah, p 269
222. Pfeifer C, Brzozowski E, Markian R, Redman R (2008) Long-Term monitoring of submerged oil in the Gulf of Mexico following the T/B DBL 152 incident. In: Proceedings of the IOSC 2008, Savannah, p 275
223. Camilli R, Bingham B, Reddy CM, Nelson RK, Duryea AN (2009) Method for rapid localization of seafloor petroleum contamination using concurrent mass spectrometry and acoustic positioning. Mar Pollut Bull 58:1505
224. Lehr WJ (2008) The potential use of small UAS in spill response. In: Proceedings of the IOSC 2008, Savannah, p 431
225. Donnay E (2009) Use of unmanned aerial vehicle (UAV) for the detection and surveillance of marine oil spills in the Belgian part of the North Sea. Arctic Mar Oilspill Progr Tech Sem 2:771
226. Li K, Fingas MF, Paré JRP, Boileau P, Beaudry, P Dainty E (1994) The use of remote-controlled helicopters for air sampling in an emergency response situation. Arctic Mar Oilspill Progr Tech Sem 2:139
227. Goodman RH (1994) Overview and future trends in oil spill remote sensing. Spill Sci Technol 1:11
228. Huisman J (2006) Use of surveillance technology to support response decision making and impact assessment. In: Proceedings of the Interspill 2006, London
229. Carpenter A (2007) The Bonn agreement aerial surveillance programme: trends in North Sea oil pollution: 1986–2004. Mar Pollut Bull 54:149
230. De Dominicis M, Pinardi N, Coppini G, Tonani M, Guarnieri A et al (2009) Interspill
231. Allen J, Walsh B (2008) Enhanced oil spill surveillance, detection and monitoring through the applied technology of unmanned air systems. In: Proceedings of the IOSC 2008, Savannah, p 113

Olivine Phosphate Cathode Materials, Reactivity and Reaction Mechanisms

Atsuo Yamada
Department of Chemical System Engineering, The University of Tokyo, Tokyo, Japan

Article Outline

Glossary
Definition of the Subject and Its Importance
Introduction
Binary Phase Diagram
Size Effect Versus Surface Effect
Air Poisoning
Careful Verification of Phase Diagram
Experimental Verification of Lithium Diffusion in Li_xFePO_4
Summary and Future Directions
Bibliography

Glossary

Cathode Oxidizing agent in Battery.

Diffusion Spontaneous movement of some species (ions in the present case).

$LiFePO_4$ A promising low-cost and safe cathode materials for LIB.

Lithium-ion battery (LIB) A rechargeable battery with highest energy density.

Miscibility gap A compositional region where two species cannot mix.

Olivine A name of mineral Mg_2SiO_4 with identical structure of $LiFePO_4$.

Phase diagram Stable phase map as a function of composition, temperature.

Definition of the Subject and Its Importance

Crystalline size has tremendous effect to the thermodynamics and kinetics in intercalation compounds. This includes diffusion/transport length, effective surface area for exchange current, surface energy, and interphase energy. The focus now is on Li_xFePO_4, where the phase changes by simple two-phase separation but with controllable miscible character by raising

temperature and/or reducing crystalline size, thereby provides simple model system to rationalize thermodynamics and electrochemistry in electrode reaction. Systematic experimental results on this issue are reviewed and summarized. Negative aspects of nanoparticle including surface poisoning by air contact and its diagnosis will be also demonstrated. As an atomic-scale phenomenon, experimental verification of one-dimensional lithium diffusion in Li_xFePO_4 will be also demonstrated.

Introduction

The crystal chemistry of phospho-olivine Li_xFePO_4 ($0 < x < 1$) has received much attention ever since it was introduced as an alternative cathode material for new generation lithium-ion batteries. The material provides several advantages over the conventional cathodes; lower cost, much safer performance, lower toxicity, and extremely flat charge-discharge profile at reasonably high potential of ca. 3.4 V versus Li/Li^+ [1, 2]. Nevertheless, at an early stage of the development, its poor intrinsic electronic conductivity, on the order of 10^{-9} $S{\cdot}m^{-1}$, and small tap density had been addressed as major problems to be solved before it can be deployed on a commercial scale [3–5]. Now, at least the first problem has been overcome by using small particle of <100 nm and the efficient formation of composites with conductive phase, typically carbon. Surprisingly high specification for the power density of more than 5 kW/kg is reported on the commercial cells with $LiFePO_4$ cathode.

One of the essential reasons for the very low conductivity measured for the stoichiometric $LiFePO_4$ seems to be in the pre-factor rather than in the activation energy. In addition, a key feature of the Li_xFePO_4 cathode is its extremely flat charge-discharge profile, typical of two-phase reaction systems. Conventional belief based on the Gibbs phase rule was that the reaction proceeds in a topotactic manner, varying the $FePO_4/LiFePO_4$ ratio throughout the range of x in Li_xFePO_4 [1]. However, carrier (mobile electron or hole) densities in the monovalent stoichiometric end members should be negligible, and this evidently accounts for the very low electronic conductivity of $<10^{-9}$ S/cm in $LiFePO_4$, despite its relatively small binding energy for polaron localization of 390–500 meV.

It is true that within the polaronic conduction mechanism and the conventional $FePO_4/LiFePO_4$ two-phase model, the number of charge carriers in monovalent systems such as $LiFePO_4$ or $FePO_4$ is determined extrinsically by impurities. Defect chemistry studies of related $Li_{1-3x}Fe_xNiPO_4$ phases suggest that cation vacancies can be accommodated in the olivine structure [6]. However, without any external doping in $LiFePO_4$, a rapid electrochemical response as well as a good rate capability has been achieved in the lab with an optimized electrode composite of pure $LiFePO_4$. These motivated a closer look at the phase change of Li_xFePO_4 at room temperature to determine if the creation of charge career is spontaneous in non-doped Li_xFePO_4 during the electrochemical charge/discharge process (i.e., does lithium or lithium defect function as a carrier-doping impurity).

Once the mechanisms of charge carrier formation are understood, the next important information is the geometry of the charge movement. Successful visualization of lithium diffusion path in olivine Li_xFePO_4 will be demonstrated together with its methodology by combination of neutron diffraction and maximum entropy method. This is a first experimental visualization of ion motion in any battery electrode.

Binary Phase Diagram

As in many binary systems, thermodynamics suggests there are two solid-solution regions outside the miscibility gap at finite temperatures. Generally, these two solid-solution regions grow as a function of temperature finalized by the continuous solid solution over the whole composition between the two end members as there is an increasing contribution of entropy to the total free energy at elevated temperatures. This is typically seen in spinodal decomposition in binary liquid systems with an inverse-parabolic phase boundary in the temperature-composition diagram. For intercalation solid electrode materials, this behavior was intensively studied in the 1980s using a lattice gas model based on mean field theory, where the attractive interaction between lithium ions is essential to induce phase separation. Onset temperature of the miscibility gap varies from ca. 270 K for metallic Sheverel $Li_xMo_6Se_8$ ($0 < x < 1$) [7, 8] to ca. 1,200 K for insulating NASICON-type $Na_{1+x}Ti_2(PO_4)_3$ ($0 < x < 2$) [9].

Analogous to these compounds, the intermediate phase in the Li_xFePO_4 cathode at room temperature may be dominated by the mixture of the $Li_\alpha FePO_4$ and $Li_{1-\beta}FePO_4$ phases with the narrow monophase regions, $0 < x < \alpha$ and $1-\beta < x < 1$, close to the stoichiometric end members of $LiFePO_4$ and $FePO_4$ at each end of the region.

This was first proved by the refinement of x-ray diffraction profiles measured for Li_xFePO_4 ($0 \leq x \leq 1$) phases at room temperature [10]. In the bi-phase reaction of Li_xFePO_4 at room temperature, the orthorhombic lattice constants in each phase slightly deviate from those of the stoichiometric end components of $LiFePO_4$ and $FePO_4$. The deviation can be explained by assuming a model in which a most of the intermediate phase in the Li_xFePO_4 cathode is dominated by the mixture of $Li_\alpha FePO_4$ and $Li_{1-\beta}FePO_4$ phases (Fig. 1).

Size Effect Versus Surface Effect

Meethong et al. have suggested that the miscibility gap shrinks systematically with decreasing particle size and increasing temperature [11]. Such a size-dependent miscibility gap is a general phenomena observed in other two-phase intercalation reactions such as Li_xTiO_2 or MgH_x systems [12, 13]. Thermodynamically, the dependence can be explained by the increasing contribution of the elastic energy induced along coherent two-phase interphase in the smaller particles by a factor of $r \sim A(x)/V(x)$, where r is the particle radius, $A(x)$ is the interface area, and $V(x)$ is the particle volume. The coexistence of two crystallographic phases within one particle leads to a domain wall related energy penalty, which is determined by the strain mainly due to a difference in lattice parameters. Such a strain-induced energy penalty can destabilize the two-phase coexistence in smaller particles. As a result, the energy gain due to phase separation, represented by the free energy of mixing ΔG_{mix}, will decrease for smaller particle sizes. This will gradually close the miscibility gap for decreasing particle size, which explains the enhanced solubility of Li in the smaller particles. More recently, Gibot et al. reported the inherent

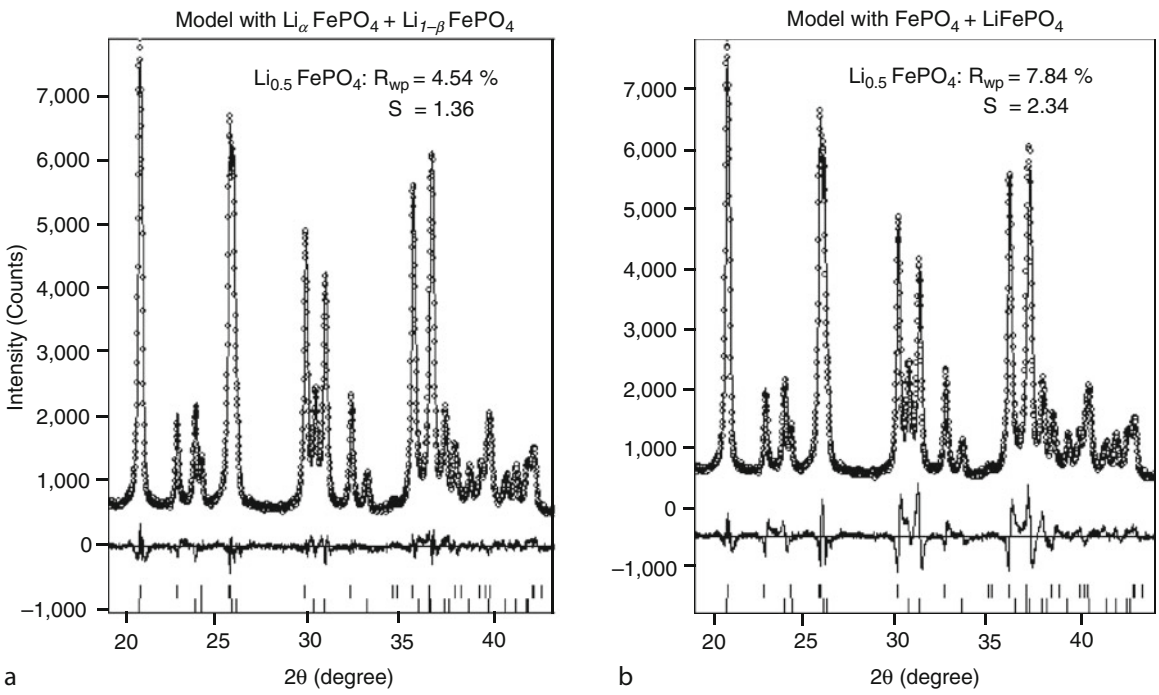

Olivine Phosphate Cathode Materials, Reactivity and Reaction Mechanisms. Figure 1
Difference in the goodness of fit in the Reitveld refinement of $Li_{0.5}FePO_4$ under the model with (**a**) a mixture of the stoichiometric $FePO_4$ and $LiFePO_4$, and (**b**) a mixture of the nonstoichiometric $Li_\alpha FePO_4$ and $Li_{1-\beta}FePO_4$ (α = ca. 0.030, β = ca. 0.036) phases

crystalline disorder coupled with nano-crystallization below 40 nm leads to the peculiar situation, where solid solution dominates most of the lithium compositional region in Li_xFePO_4 even at room temperature [14]. Such a thermodynamic concept have been verified in detail by Wagemaker et al. [15], including the effect of particle shape. Meethong et al. [16] related this intriguing findings to the kinetics of phase-boundary movement, where the reduction in lattice strain caused by the reduction in lattice mismatches in smaller particles was claimed to be suitable to form coherent interface between $Li_\alpha FePO_4$ and $Li_{1-\beta}FePO_4$ so as to enhance the cooperative phase-boundary movement upon electrochemical reaction with minimum formation of dislocation or clacks. This logic was regarded to give comprehensive understanding of the enhanced electrochemical activity of the nano-sized $LiFePO_4$ particle as compared to the other slower two-phase electrode system with larger mismatch.

However, attention should be paid that the surface portion of the particle abruptly increases when the size is smaller than 100 nm. A simple estimation based on the sphere particle gives the surface (one unit cell) portions to be ca. 4%, 7% and 17% for the particles with 100 nm, 50 nm, and 20 nm diameters, respectively. In such nanoscale regime, there is an increasing possibility to observe the simultaneous effects both from bulk crystal and from particle surface, which may lead to some confusion. For example, surface redox potential was calculated to be dependent on the crystallographic plane and was shown a wide dispersion over the range of 2.95–3.84 V [17]. Both of the surface impurities and the redox on the specific crystallographic facet plane would be important as the perturbation that may cause parasitic capacity above or below the bulk two-phase equilibrium potential in the voltage curve. The capacity outside the two-phase region for Li_xFePO_4 have been used as one of the indicator of the bulk solubility limit of lithium and lithium defect in $Li_\alpha FePO_4$ and $Li_{1-\beta}FePO_4$ and, then, may need careful reinvestigation.

More importantly, the side reaction upon ambient exposure is known to be pronounced for smaller particle, leading to a spontaneous lithium extraction and surface oxidation [18, 19]. Before going to any further discussions, such a side reaction should be removed; then, this phenomenon is explained in the next section.

Air Poisoning

XRD has been carried out to investigate the effect of different atmosphere exposure conditions. Table 1 summarizes the lattice dimensions. In all cases, the diffractograms display a single phase with an ordered olivine structure indexed to the orthorhombic Pnmb space group. The Rietveld refinement permits to approximate the olivine crystallites size to 75 nm, which is verified on the SEM image of the powder presented.

Olivine Phosphate Cathode Materials, Reactivity and Reaction Mechanisms. Table 1 Parameters and cell volumes of $LiFePO_4$ calculated from XRD refinement after different atmosphere exposure conditions

Stage condition		a(Å)	b(Å)	c(Å)	V(Å3)	*x*
Dry air standard	Room temperature	10.3308(2)	6.00813(11)	4.69444(10)	291.378(6)	0
Ambient air	Room temperature,1 h	10.3275(2)	6.00656(13)	4.69271(12)	291.1040(12)	0.007
	Room temperature,1 day	10.3254(2)	6000573(11)	4.69329(11)	291.037(10)	0.011
	Room temperature, 21 days	10.3227(2)	6.00428(15)	4.69346(14)	290.903(14)	0.017
	120°C, 1 day	10.3188(2)	6.00303(15)	4.69451(14)	290.79(4)	0.023
Dry air (N_2/O_2)	Room temperature,1 day	10.3294(4)	6.0072(2)	4.6932(2)	291.22(2)	0.004
	120°C, 1 day	10.3254(3)	6.0054(2)	4.69373(19)	291.048(19)	0.012
Dry CO_2	Room temperature,1 h	10.3302(4)	6.0078(2)	4.6936(2)	291.29(2)	0.001
	120°C, 1 day	10.3290(3)	6.00716(18)	4.696361(17)	291.231(16)	0.004

Systematic decrease of the cell volume upon atmosphere exposure was clearly observed together with the corresponding changes in lattice parameters. It begins to be visible even after a short time (1 h) of ambient air exposure at room temperature and become more evident after longer time (10 days) or higher temperature (120°C) exposure. Water and oxygen should be included in this side reaction as the effect is significantly suppressed by using dry O_2 20%/N_2 80% and become negligible by using dry CO_2. These volume changes can be linked to the solid-solution compositional domain in $Li_{1-x}FePO_4$ ($x < \beta$) [10, 11, 19, 20], in which olivine can accommodate the corresponding lithium defect without first-order phase transformation.

Figure 2 demonstrates the linear relative dependence of the *a* and *b* lattice constants following the Vegard's law in the hypothesis of a solid solution between $LiFePO_4$ prepared with no contact with air and $FePO_4$. These results show that some lithium is certainly extracted when $LiFePO_4$ is put in contact with atmosphere. The Vegard's law gives 2.3% of missing lithium after ambient air exposure for 24 h at 120°C. It has to be noted that the lattice constants obtained by avoiding air contact are very close to the ones reported for pure, much larger particles [21], which present less possibilities of reactivity with air due to smaller solid-solution domain and smaller exposed surface. It tends to prove that the sample has been well protected during the experiment and that possible air pollution during storage in glove box has been minimized.

For a subsequent study of size-dependent phase diagram, effort was taken to eliminate such fluctuant factor in the pristine samples because it would degrade the quality of any crystallographic and/or electrochemical data and, hence, mislead the subsequent quantitative discussions. The controlled pristine $LiFePO_4$ samples used in this study are free from such poisoning by air exposure, and the particle size is the only varied parameter. The samples used in this study are free from any disorder as the lattice dimensions are almost

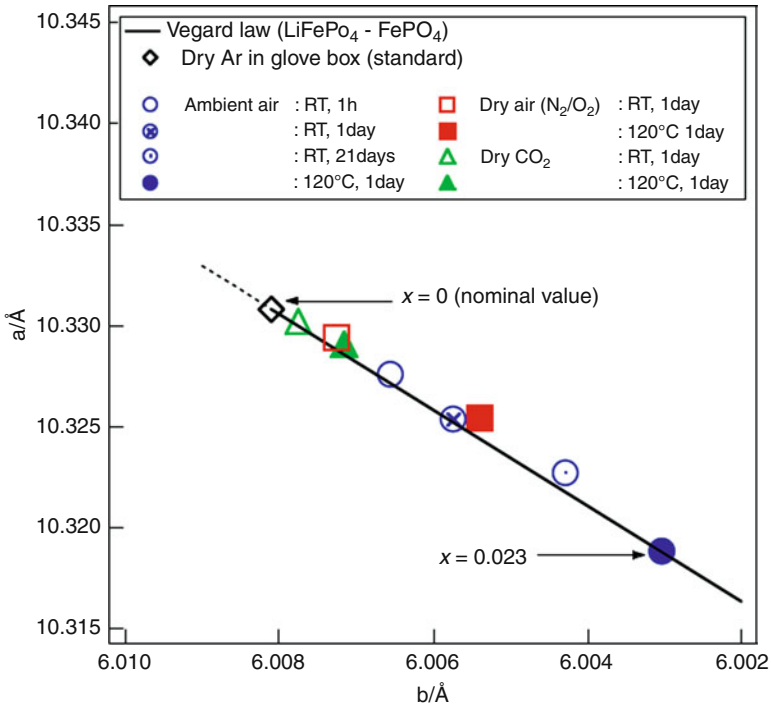

Olivine Phosphate Cathode Materials, Reactivity and Reaction Mechanisms. Figure 2
Lattice constants change for $Li_{1-x}FePO_4$ after the different air contact experiments compared to Vegard's law (*arrow*). The values for *x* are calculated using Vegard's law and $FePO_4$ cell parameters (a = 9.8142 Å and b = 5.7893 Å)

identical to the single crystal values (a = 10.332(4) Å, b = 6.010(5) Å, c = 4.692(2) Å, V = 291.4(3) Å^3) [21] and showed negligible dependence on the particles size, while air-exposed samples suffered from significant volume contraction particularly on smaller particles as in Table 2. With the same trend in variations of the lattice dimensions, Mössbauer spectra for the controlled pristine samples were analyzed by single Fe^{2+} doublet inherent to $LiFePO_4$, while parasitic Fe^{3+} subsignal was always observed for the air-exposed samples increasing its intensity for smaller particles, as shown in Fig. 3.

Careful Verification of Phase Diagram

Electrochemical Approach

The first step for the analysis is the accurate determination of the open-circuit voltage (OCV) profile versus lithium composition x for three samples with different particle sizes of 40 nm, 80 nm and 200 nm. Initially, the cell was charged galvanostatically at C/20 rate at 25°C followed by maintenance at 4.5 V for 24 h forming $FePO_4$. Capacity close to the theoretical capacity of 170 mAh/g was confirmed for all samples. Then, it was discharged under a rate of C/20 for 12 min, which

Olivine Phosphate Cathode Materials, Reactivity and Reaction Mechanisms. Table 2 Lattice dimensions of pristine and air-exposed $LiFePO_4$ with various particle sizes

No air exposure				
Particle size (nm)	a(Å)	b(Å)	c(Å)	V(Å^3)
200	10.33046(13)	6.00846(7)	4.69238(7)	291.257(7)
80	10.3303(2)	6.00764(12)	4.69313(11)	291.259(11)
40	10.3301(5)	6.0052(3)	4.6947(3)	291.23(2)
Air exposure: Room temperature, 1 day				
Particle size (nm)	a(Å)	b(Å)	c(Å)	V(Å^3)
200	10.32839(15)	6.00767(8)	4.69228(8)	291.157(8)
80	10.3253(2)	6.00590(12)	4.69335(11)	291.047(11)
40	10.3223(5)	6.0015(3)	4.6955(3)	290.88(2)

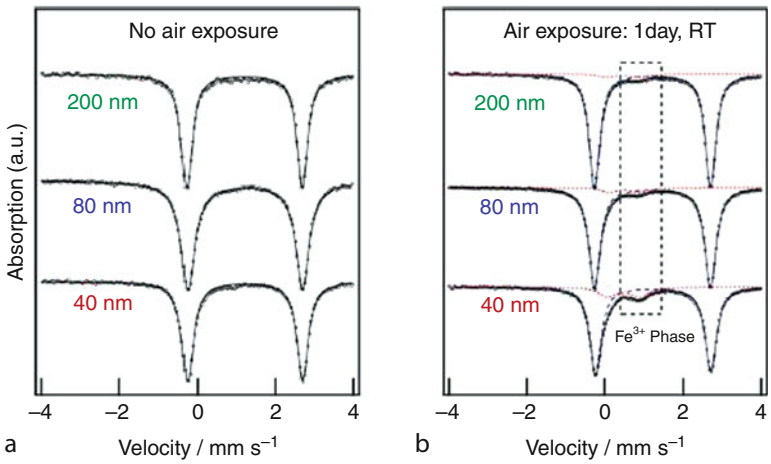

Olivine Phosphate Cathode Materials, Reactivity and Reaction Mechanisms. Figure 3 Mössbauer spectra measured for pristine (**a**) and air-exposed (**b**) $LiFePO_4$ with various particle sizes of 40, 80, and 200 nm

corresponds to ca. 1% of the theoretical capacity. The open-circuit voltage at 25°C was measured after 24 h. Again, the cell was discharged under a rate of C/20 for 12 min. These procedures were repeated several times until the open-circuit voltage at 25°C become constant at ca. 3.42 V in the biphasic region. A similar experiment was performed starting from $LiFePO_4$ toward the anodic direction and confirmed the identical OCV values at same lithium compositions. Size-dependent OCV curves for Li_xFePO_4 are given in Fig. 4, where the capacity observed below or above the two-phase equilibrium potential becomes larger as particle size decreases.

Structural Approach

Two target lithium compositions of x in Li_xFePO_4 ($x = 0.6$, $x = 0.93$) were chosen and were adjusted by the chemical way, allowing more homogeneous Li^+ incorporation over electrochemical reactions. Based on the room temperature phase diagram reported previously [10, 19, 20], the composition near an end member, $Li_{0.93}FePO_4$, was selected as an experimental criterion phase since it would be around the phase transition zone between the two-phase region and the single-phase region in the $FePO_4$ – $LiFePO_4$ binary phase diagram, where the two-phase (larger particle) to single-phase (smaller particle) transformation is expected as a function of the particle size. The composition $x = 0.6$, $Li_{0.60}FePO_4$, was selected as a reference phase because it should be composed of a mixture of two intermediate phases, analysis of which should lead to the definitive positions of the solid solubility limits, α and β, in $Li_\alpha FePO_4$ and $Li_{1-\beta}FePO_4$. In order to set the lithium composition in Li_xFePO_4 to $x = 0.6$ or $x = 0.93$, all of the lithium in pristine $LiFePO_4$ was first removed to form isostructural $FePO_4$ using a strong oxidizing agent NO_2BF_4 in acetonitrile. Then, $FePO_4$ was reacted with the specific amount of mild reducing agent LiI in acetonitrile to form Li_xFePO_4 with $x = 0.6$ or $x = 0.93$. The chemical treatment was performed for each pristine $LiFePO_4$ sample with three different particle sizes of 40, 80, and 200 nm for the subsequent high-resolution synchrotron x-ray diffraction.

In order to overview the change in the room-temperature phase diagram with decreasing particle size, the lattice parameters refined for $Li_{0.6}FePO_4$ (two-phase mixture of $Li_\alpha FePO_4$ and $Li_{1-\beta}FePO_4$) were analyzed. For all particle sizes, $Li_{0.6}FePO_4$ is evidently in two-phase state as typically seen in the two diffraction peaks clearly observed at around 13.5° and 14.5°, corresponding to the (200) reflection of $Li_{1-\beta}FePO_4$ and the (200) reflection of $Li_\alpha FePO_4$, respectively. All of the lattice parameters refined for the two separated phases in $Li_{0.6}FePO_4$ deviates from those of stoichiometric $FePO_4$ and $LiFePO_4$, and can be explained by assuming partial lithium occupancy α to $FePO_4$ and partial lithium deficiency β from $LiFePO_4$, as well as Vegard's low along $FePO_4$–$LiFePO_4$ solid solution.

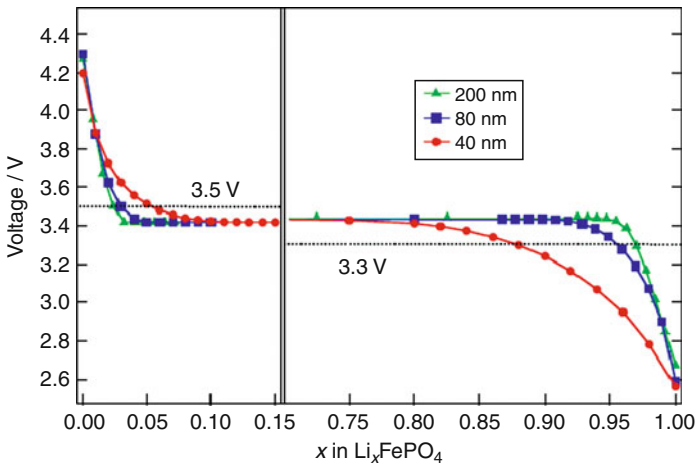

Olivine Phosphate Cathode Materials, Reactivity and Reaction Mechanisms. Figure 4
Open-circuit voltage (OCV) curves measured for Li_xFePO_4 with various mean particle sizes of 200, 80, and 40 nm

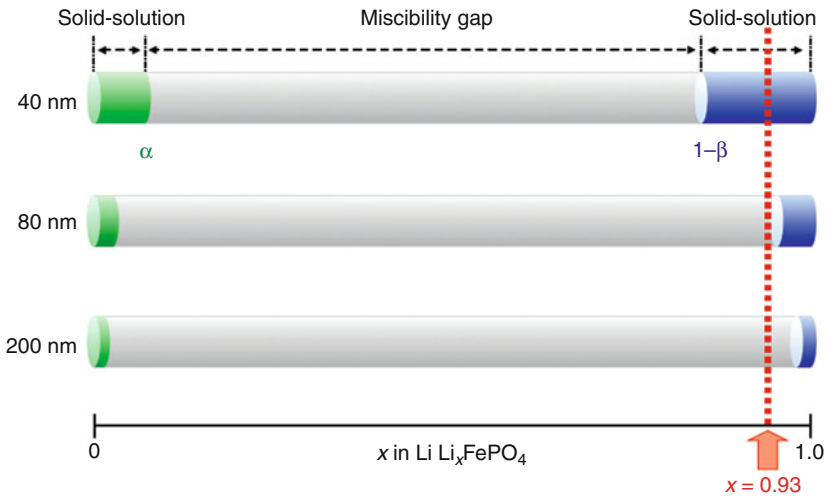

Olivine Phosphate Cathode Materials, Reactivity and Reaction Mechanisms. Figure 5
Schematic derivation of the size-dependent $FePO_4$–$LiFePO_4$ binary phase diagram using the XRD data for $Li_{0.6}FePO_4$

Schematic derivation of the size-dependent $FePO_4$–$LiFePO_4$ binary phase diagram using the XRD data for $Li_{0.6}FePO_4$ is illustrated in Fig. 5, which highlights the fact that the solid solubility limits α, β, in $Li_{\alpha}FePO_4$, and $Li_{1-\beta}FePO_4$ systematically increases along with the reduction in particle size. Most probably, these systematic variations originate from the elastic thermodynamic effects on the miscibility gap as discussed in the various other binary systems. The solid–solid phase transitions are thermodynamically first order and involve a change in enthalpy (ΔH), which is highly related to the particle size as depicted by $\Delta H = \Delta H_{intinsic} + \Delta H_D$, where ΔH_D represents the particle size contribution of opposite sign [15]. If the particle size decreases, the Gibbs free energy (ΔG) of mixing would be decreased by the increasing contribution of the penalty in elastic energy at the two-phase boundary, resulting in extension of the single-phase regions near the end members on the composition phase diagram.

The extended solid solution has been claimed to be beneficial both for the charge movement and the subsequent cooperative phase-boundary movement because the diffusion/hopping pre-factor along the one-dimensional diffusion path is increased while the lattice mismatch along the two-phase boundary is reduced. However, experimental evidences given so far for the existence of the small solid-solution compositional domain are not direct ones and led some controversy whether they really originate from the bulk effect or from the artifact by the enhanced surface effect in nanoregime [17]. Then, isolation of the solid-solution phase would give more definitive and straightforward experimental evidence for the size-dependent miscibility gap model.

Toward this end, the focus is on the sample with $x = 0.93$, which is around the phase transition compositional zone between the two-phase region and the single-phase region in the $FePO_4$–$LiFePO_4$ binary phase diagram (see Fig. 5). At the composition of $x = 0.93$, the two-phase (larger particle) to single-phase (smaller particle) transformation is expected as a function of the particle size as easily speculated from the phase behavior along the vertical compositional line at $x = 0.93$ in Fig. 5. The changes in the lattice parameter a are summarized in Fig. 6 together with the low-angle peaks of $Li_{0.93}FePO_4$ indexed as $(200)_T$ (lithium-rich triphylite phase) and $(200)_H$ (lithium-poor heterosite phase) at different particle sizes. The intensity of $(200)_H$ is gradually decreased when the particle size is reduced and finally disappeared for the 40 nm particle. More importantly, the deviation of the lattice constant a at $x = 0.93$ from those of the phase-separated $Li_{0.6}FePO_4$ was observed only for 40 nm particle. Furthermore, it is noteworthy that the lattice constant a at $x = 0.93$ for 40 nm particle positions strictly on the line of Vegard's low assuming the complete solid-solution of $FePO_4$ and $LiFePO_4$. The same behavior was identified also for the b-, c-axes.

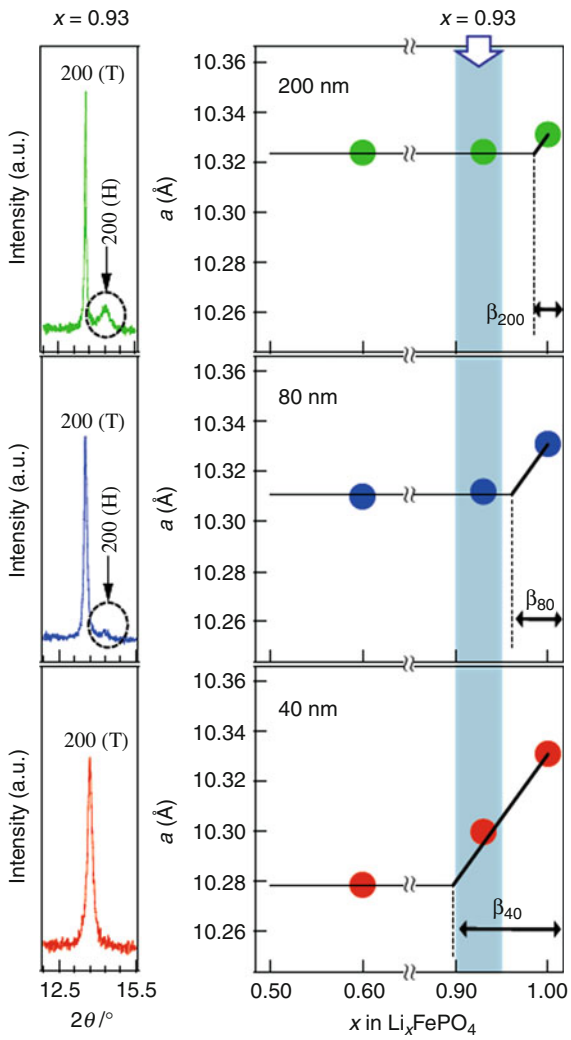

Olivine Phosphate Cathode Materials, Reactivity and Reaction Mechanisms. Figure 6
Left: magnified view of the 200 peak measured for $Li_{0.93}FePO_4$ with different particle sizes of 200, 80, and 40 nm at room temperature. *Right*: derivation of changes in *a*-axis lattice parameter as a function of lithium composition *x* for different particle sizes

Clearly, the immiscible–miscible transition is induced by the particle size reduction at the identical lithium composition $x = 0.93$, and the solid-solution in Li_xFePO_4 is isolated at $x = 0.93$ in the 40 nm particle, details of which are described below.

As for the 200 nm particle at $x = 0.93$, two independent peaks were clearly observed as indexed $(200)_T$ and $(200)_H$, respectively, which indicates that the $Li_{0.93}FePO_4$ phase consists of two intermediate phases, $Li_\alpha FePO_4$ and $Li_{1-\beta}FePO_4$. This is a reasonable result because the lithium composition for the immiscible–miscible transition was estimated to be $1 - \beta_{200} = 0.98$, which is much larger than the present lithium composition, $x = 0.93$. The lattice parameters are almost identical with those of $Li_{0.6}FePO_4$, which also reveal that the $Li_{0.93}FePO_4$ with a particle size of 200 nm is inside the miscibility gap at room temperature.

When the particle size is reduced to 80 nm, the phase at $x = 0.93$ is still in the two-phase separation, but the intensity of the $(200)_H$ peak has significantly decreased in the synchrotron XRD profile, which can be explained by the reduction of the $Li_\alpha FePO_4$ phase fraction in the two phase mixture of $Li_\alpha FePO_4$ and $Li_{1-\beta}FePO_4$, following the size-dependent miscibility gap model [11]. The estimated lithium composition for the immiscible-miscible transition, $1-\beta_{80}$, has now decreased to 0.96 and becomes closer to the present lithium composition, $x = 0.93$. The $Li_{0.93}FePO_4$ phase with an average particle size of 80 nm is in close to the transition zone from immiscible to miscible state and contains smaller amount of $Li_\alpha FePO_4$ at room temperature. The lattice constants are still identical with those of bi-phased $Li_{0.6}FePO_4$; the $Li_{0.93}FePO_4$ with a particle size of 80 nm is still inside the miscibility gap at room temperature but in closer access to the immiscible–miscible transition zone.

At the 40 nm particle size with $x = 0.93$, the $(200)_H$ peak has disappeared, and the discrepancies in the lattice parameters from the two-phase values are prominent. Instead, the lattice constants are exactly on the line of Vegard's low assuming the complete solid solution between $FePO_4$ and $LiFePO_4$. This behavior proves that the $Li_{0.93}FePO_4$ phase with 40 nm size is in the single-phase solid-solution range and allows to conclude that a solid solution of Li_xFePO_4 could be isolated as a single phase with the solid solubility of $\beta_{40} > 0.1$.

For a direct comparison between the stoichiometric $LiFePO_4$ and the isolated solid solution of $Li_{0.93}FePO_4$ with an identical particle size of 40 nm, synchrotron x-ray diffraction profiles of the two samples are shown in Fig. 7 with some magnified presentations of the typical peaks. Peak shifts are visually evident and large enough to confirm the wide lithium compositional range of at least 7% for solid solution. The shift

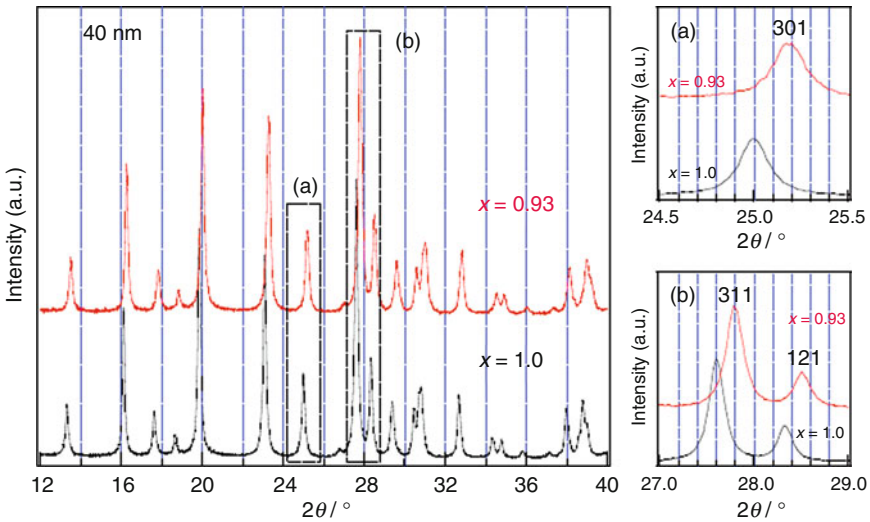

Olivine Phosphate Cathode Materials, Reactivity and Reaction Mechanisms. Figure 7
Comparison of the synchrotron x-ray diffraction profiles measured for stoichiometric $LiFePO_4$ and the isolated solid solution of $Li_{0.93}FePO_4$ with an identical particle size of 40 nm with magnified presentations of 301, 311, and 121 as the typical peaks

observations without appearing of any second phase further support the room-temperature isolation of solid solution in Li_xFePO_4.

Consistency Between Electrochemical and Structural Data

For a further confirmation of the inverse relationship between the solid solubility and particle size, the composition x has been electrochemically controlled by galvanostatically charging the cells in a potential range of 2.0–4.5 V and then potentiostatically discharging them at a constant potential below the equilibrium potential at 3.30 V, which corresponds to $Li_{0.98}FePO_4$ (200 nm), $Li_{0.96}FePO_4$ (80 nm), and $Li_{0.88}FePO_4$ (40 nm) in OCV curves in Fig. 4. Similar experiment was performed with higher constant potential above equilibrium potential at 3.50 V, which corresponds to $Li_{0.02}FePO_4$ (200 nm), $Li_{0.03}FePO_4$ (80 nm), and $Li_{0.06}FePO_4$ (40 nm) in OCV curves in Fig. 4. The cell was dismantled in an Ar glove box, and then the cathode electrode was washed in dimethyl carbonate (DMC) for subsequent XRD measurements.

Size-dependent peak shift is clear both for samples in equilibrium at 3.30 V and at 3.50 V as shown in Fig. 8. The lattice parameters were refined for all samples by Rietveld analyses and are summarized in Table 3. The extent of lithium nonstoichiometry x in Li_xFePO_4 were calculated for each samples assuming the Vegard's low between $FePO_4$ and $LiFePO_4$, showing excellent agreement with the electrochemical estimation of x, i.e., x (Vegard's low) = x (OCV), for all of the six cases with three different particle sizes (40, 80, 200 nm) and two different OCV (3.30, 3.50 V). This provides firm experimental evidence that the capacity observed below or above the two-phase equilibrium potential is not caused by some impurities or the potential distribution dependent on the crystalline surface but largely due to the bulk lithium nonstoichiometry at least for particle sizes larger than 40 nm.

Further inspections on the solid-solution compositional domain were performed for the electrochemically adjusted Li_xFePO_4 with a particle size of 40 nm, which allow largest miscibility in the present study. The potential was set to 3.8, 3.6, 3.5, 3.3, 3.2, 3.1, 3.0, and 2.8 V versus Li^+/Li. They correspond to the lithium composition of 0.02, 0.04, 0.06, 0.88, 0.91, 0.93, 0.95, and 0.95, respectively, with an eye to the OCV data shown in Fig. 9 and are inside the solid-solution domains. All the samples were subjected to the X-ray diffraction experiments with the subsequent Rietveld analysis, and the plots of lattice parameters versus lithium compositions are given in Fig. 9. All the

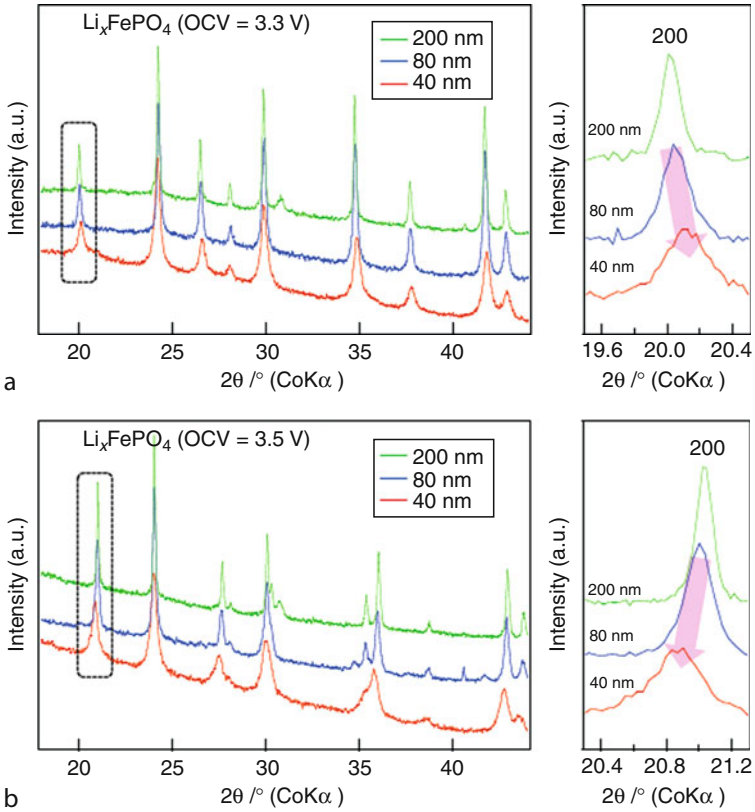

Olivine Phosphate Cathode Materials, Reactivity and Reaction Mechanisms. Figure 8
X-ray diffraction profiles for Li_xFePO_4 electrode with various mean particle sizes of 200, 80, and 40 nm, equilibrated at 3.3 V (**a**) and 3.5 V (**b**), with magnified presentation of the 200 diffraction peaks

Olivine Phosphate Cathode Materials, Reactivity and Reaction Mechanisms. Table 3 Lattice dimensions of Li_xFePO_4 electrode with various mean particle sizes of 200, 80, and 40 nm, equilibrated at 3.3 V (a) and 3.5 V (b). Lithium nonstoichiometry from $x = 1$ and $x = 0$ estimated by two different method, Vegard's law and OCV curves, show excellent agreement. The extent of the lithium nonstoichiomery is enhanced as mean particle size decreases

Li-rich (Triphylite, OCV = 3.3 V)						
Particle size (nm)	*a*(Å)	*b*(Å)	*c*(Å)	V(Å^3)	*x* (Vegard's law)	*x* (OCV)
200	10.3224(4)	6.0039(2)	4.6909(2)	290.67(2)	0.975	0.98
80	10.3184(7)	6.0016(4)	4.6904(4)	490.46(3)	0.965	0.96
40	10.2790(13)	5.9525(6)	4.7054(7)	289.35(6)	0.891	0.88
Li-poor (Heterosite phase, OCV = 3.5 V)						
Particle size (nm)	*a*(Å)	*b*(Å)	*c*(Å)	V(Å^3)	*x* (Vegard's law)	*x* (OCV)
200	9.8159(9)	5.7891(4)	4.7814(4)	271.70(4)	–	0.022
80	9.8292(19)	5.7994(5)	4.7792(11)	272.43(5)	0.030	0.029
40	9.8486(13)	5.8138(6)	4.7831(7)	273.90(6)	0.074	0.056

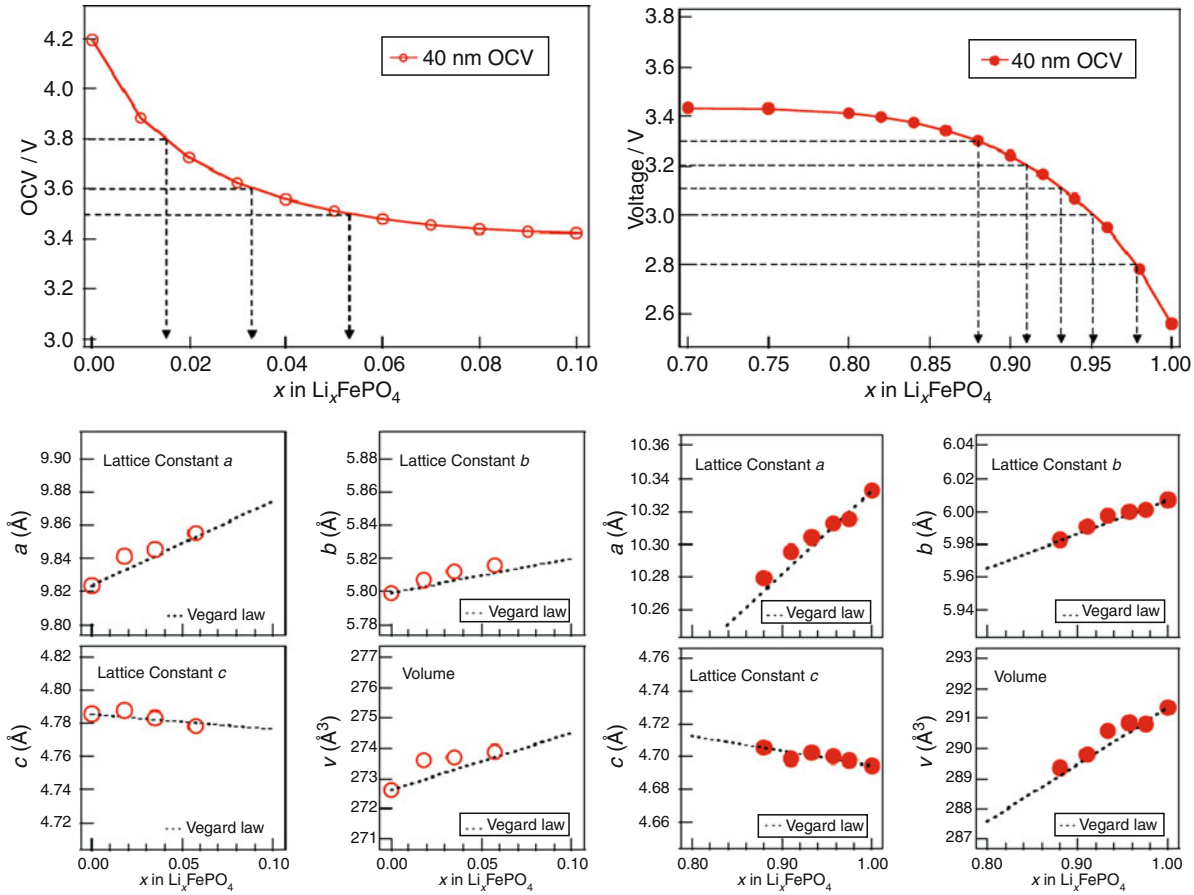

Olivine Phosphate Cathode Materials, Reactivity and Reaction Mechanisms. Figure 9
Open-circuit voltage curve and change in lattice dimensions above (**a**) and below (**b**) the two-phase equilibrium potential. Lithium composition was adjusted potentiostatically (equilibrium condition: <0.1 μA) and estimated by the OCV curves as indicated by dashed lines. The linear lines along the plot of lattice constants show the Vegard's law between $FePO_4$ and $LiFePO_4$

data are on the line of Vegard's Law of $FePO_4$–$LiFePO_4$ solid solution without any systematic deviation and further support the two main conclusions of this paper with no ambiguity: (1) Validity of the size-dependent miscibility gap model in Li_xFePO_4, and (2) Bulk miscibility dominates the electrochemical behavior of Li_xFePO_4 at least for particle sizes larger than 40 nm.

Thermodynamic Approach

The thermodynamic experimental evidences for the solid solution outside of the miscibility gap are addressed now [20]. Microcalorimetry can directly measure entropy changes versus x at fixed temperature T during the electrochemical reaction. Observed heat flow P is related to entropy change ΔS by $P = -IT\Delta S/nF$, where I is the input current and F is the Faraday constant. The classical entropy of mixing $S_{cf}(x)$ can be calculated for a fully disordered lattice of lithium atoms and vacant sites, and heat flow varies linearly with $\Delta S_{cf}(x) = k_B \ln[1/x]$, where lithium atom–vacancy disorder when $0 < x < 1$. Although this expression is singular at $x = 0$ and $x = 1$, an important overall trend demonstrates that the heat flow changes symmetrically from negative at initial composition $x = 0$ to positive at final composition $x = 1$. Typical anomalies can be clearly seen at the very beginning of charging $LiFePO_4$, as shown in Fig. 10. However, the

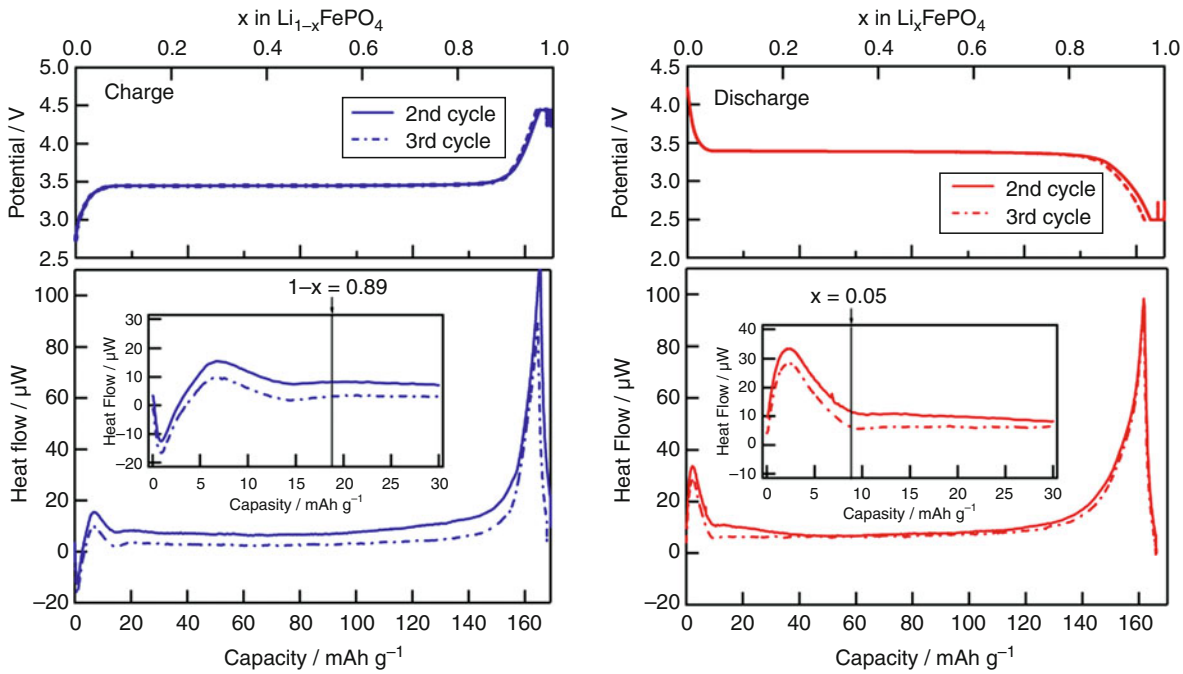

Olivine Phosphate Cathode Materials, Reactivity and Reaction Mechanisms. Figure 10
Calorimetric measurements for a 2032 type coin cell for charging and discharging processes of Li_xFePO_4. A clear anomaly typical for disordered region exists at the beginning of both charge and discharge. Vertical lines are the monophase/biphase boundary estimated from the Li site occupancy number shown in Table 1. Except for these two monophase regions, heat flow exhibited almost constant exothermic behavior with no significant anomalies, explained by a simple two-phase reaction scheme with a continuous phase-boundary movement without any structural or electronic phase transition. Abrupt increase of the exothermic heat flow at the end of charge/discharge processes in Li_xFePO_4 is due to the increasing polarization and hinders the thermal anomaly for one of the two monophase regions

endothermic region is narrow compared to the subsequent anomalous exothermic region. Similar anomalies were also detected at the very beginning of $FePO_4$ discharge, but again with a much narrower, negligible endothermic region. Such strong asymmetries for endothermic/exothermic behavior may be due to the dynamic character of calorimetric measurements. These two thermally anomalous compositional regions close to $LiFePO_4$ and $FePO_4$ in Li_xFePO_4 show good agreement with the values of α and $1 - \beta$ in $Li_\alpha FePO_4$ and $Li_{1-\beta}FePO_4$ obtained by structural data also with the region in which the deviation of open-circuit voltage from the constant value of $V_{oc} = 3.42$ V is evident (see Fig. 4). Furthermore, these initial anomalies in entropy upon charge/discharge were not observed when measurement was initiated at any point inside the miscibility gap. Therefore, it is likely they represent the change in configurational entropy in solid solution outside the miscibility gap in Li_xFePO_4.

Experimental Verification of Lithium Diffusion in Li_xFePO_4

Intuitive expectations based on the polyhedral network in the structure provide two possible continuous lithium pathways as shown in Fig. 11: Case (1) a chain of octahedral lithium ion 4a sites – face-shared vacant tetrahedral sites – face-shared nearest neighbor octahedral 4a sites along the [010] direction; and Case (2) a chain of octahedral lithium ion 4a sites – face-shared vacant octahedral sites – face-shared second nearest neighbor octahedral 4a sites along the [001] direction (see Fig. 1c, d). The ab initio study of Morgan et al. using the nudged elastic band (NEB) method

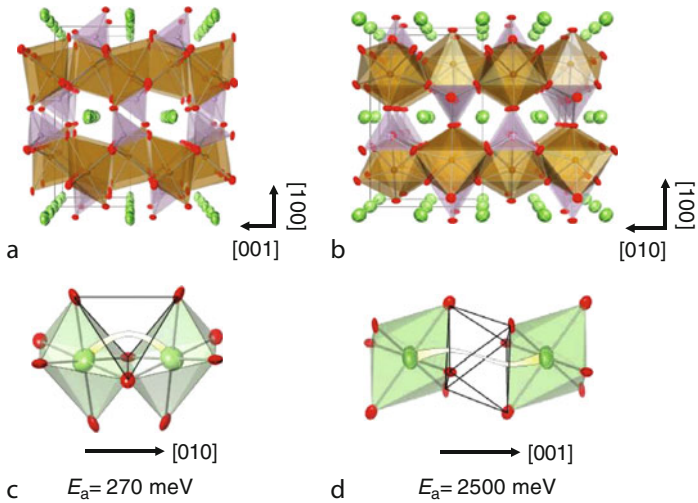

Olivine Phosphate Cathode Materials, Reactivity and Reaction Mechanisms. Figure 11
The crystal structure of $LiFePO_4$ projected along the (**a**) [010] and (**b**) [001] directions; (**c**) and (**d**) Possible Li diffusion pathways are parallel to these directions. The structure can be described as a distorted hexagonal close-packed (hcp) oxygen sub-array, in which Li, Fe, and P atoms occupy interstitial sites to form (1) corner-sharing FeO_6 octahedra that are nearly coplanar to form a distorted two-dimensional square lattice perpendicular to the *a* axis, (2) edge-sharing LiO_6 octahedra aligned in parallel chains along the *b* axis, and (3) tetrahedral PO_4 groups connecting neighboring planes or arrays. The green, brown, purple, and red ellipsoids indicate Li, Fe, P, and O atoms, respectively. Intuition leads to two possible lithium migration paths: (**c**) along the [010] direction through face-shared vacant tetrahedral sites; and (**d**) along the [001] direction through face-shared octahedral sites. One-dimensional diffusion along the [010] direction (**c**) was predicted by the computational method [22, 23]

indicated that while Li^+ mobility is high in the tunnels along the [010] direction (Case 1, Fig. 1c), Li^+ hopping between tunnels (Case 2, Fig. 1d) is very unlikely [22]. Similar conclusions were reached by Islam et al. using empirical potential models [23]. However, no experimental report based on direct observation of lithium motion in the atomic scale has been reported.

Neutron diffraction profiles include useful information on lithium because the scattering ability of the lithium nucleus (amplitude of coherent scattering length) is relatively large and independent of scattering vector $Q = 4\pi\sin\theta/\lambda$. This nature is amenable for detailed analysis of the thermal motion of the lithium nucleus in contrast to the negligible X-ray scattering ability of lithium or lithium ions with only two or three electrons. To enhance this advantage $^7LiFePO_4$ was prepared using ^{7}Li-enriched Li_2CO_3 as the raw material. This greatly improved data quality since the natural existence of 7.5% ^{6}Li causes: (1) ca. 2×10^5 larger absorption, (2) ca. 15% decrease of coherent scattering length, and, hence, (3) larger incoherent scattering.

Figure 12a demonstrates the Rietveld refinement pattern for time-of-flight (TOF) neutron diffraction data measured at room temperature for $^7LiFePO_4$. Fitting was satisfactory (R_{wp} = 2.66%, R_f = 0.46%, S = 1.34) with accurately refined atomic positions as well as anisotropic atomic displacement parameters for all atoms under the classical harmonic oscillation model.

Important information is included in the anisotropic atomic displacement parameters for lithium, which determine the overall anisotropy of the thermal vibration by the shape of ellipsoid. Green ellipsoids shown in Figs. 11a, c and 13 represent the refined lithium vibration. The preferable direction of thermal displacement is toward the face-shared vacant tetrahedra. The expected curved one-dimensional continuous chain of lithium atoms is drawn in Fig. 13 and is consistent with the computational prediction

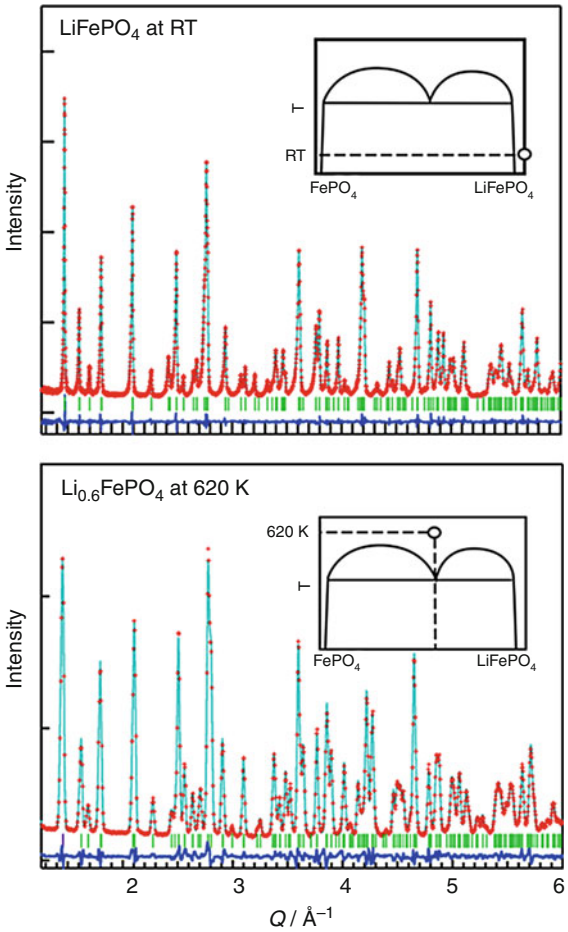

Olivine Phosphate Cathode Materials, Reactivity and Reaction Mechanisms. Figure 12
Rietveld refinement patterns for: (**a**) the time-of-flight neutron diffraction profile measured for $LiFePO_4$ at room temperature; and (**b**) angle dispersive neutron diffraction profile measured for $Li_{0.6}FePO_4$ at 620 K. Two different neutron diffractometers were used for different target information for each measurement as explained in the experimental section. The data points are plotted using the common scale $Q = 4\pi\sin\theta/\lambda$ and the common Q range for VEGA and HERMES for comparison. Specific points of measured composition and temperature are given in the inset phase diagram reported by Delacourt [24] and Dodd [25]. Observed intensity $Y_{obs.}$ and calculated intensity $Y_{calc.}$ are represented by red plus signs and the green solid line, respectively. The blue curve at the bottom represents the residual difference, Y_{obs}–Y_{calc}. No impurity phase was identified, and the crystal structure was successfully refined with the space group *Pnma*

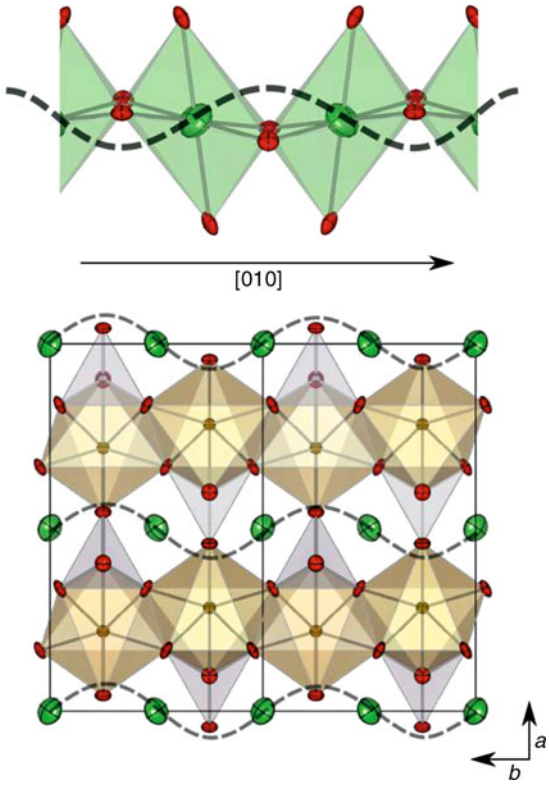

Olivine Phosphate Cathode Materials, Reactivity and Reaction Mechanisms. Figure 13
Anisotropic harmonic lithium vibration shown as the green thermal ellipsoids with 95% probability refined by Rietveld analysis for room-temperature neutron diffraction data measured for $LiFePO_4$. Expected curved one-dimensional continuous chains of lithium motion were drawn by the dashed lines to show how the motions of Li atoms evolve from vibrations to diffusion

by Morgan et al. [22] and Islam et al. [23]. Such anisotropic thermal vibrations of lithium were further supported by the Fourier synthesis of the model-independent nuclear distribution of lithium (see Fig. 14).

The subsequent experimental direction was significant enhancement of lithium motion by introducing a large number of lithium defects at elevated temperatures to show how the motions of Li atoms evolve from vibrations to diffusion. This was possible with respect to the phase diagram of Li_xFePO_4 reported in the literature, which is shown in the inset of Fig. 12. Delacourt et al. [24] and Dodd et al. [25] confirmed the small

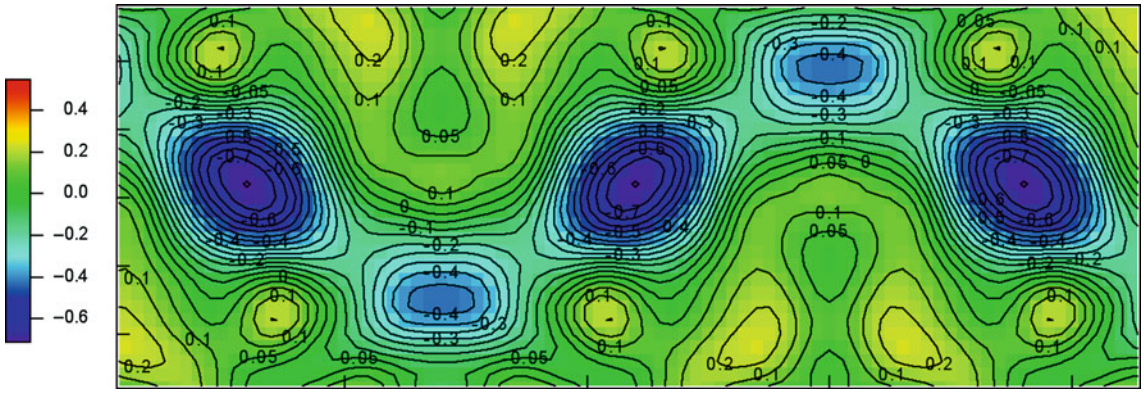

Olivine Phosphate Cathode Materials, Reactivity and Reaction Mechanisms. Figure 14
The 010 plane slice of difference Fourier scattering length density plot of $^{7}LiFePO_4$ with contours in 0.05 fm Å^{-3} steps. The map was calculated by $F_o(Li) = F_o(^{7}LiFePO_4) - F_{calc.}(Li_0FePO_4)$, where F_o and $F_{calc.}$ are the observed and calculated structure factors, respectively, and Li_0FePO_4 expresses the $FePO_4$ framework having identical structural parameters with $LiFePO_4$. The nuclear density distribution of lithium itself is anisotropic with the same direction as the refined thermal vibration

miscibility at low temperatures [10, 20], but also reported an unusual eutectoid point at ca. 500 K where the solid-solution phase emerges at approximately $x = 0.6$. At temperatures higher than 570 K, solid solution dominates all compositions [24, 25]. Rapid hopping and delocalization of lithium ions coupled with small polarons were confirmed by motional narrowing of Mössbauer spectra in the solid-solution phases formed at elevated temperatures [26, 27].

Based on the above binary phase diagram and corresponding lithium dynamics, the composition and temperature of the choice for further neutron diffraction study was $x = 0.6$ and $T = 620$ K, as shown in Fig. 12b. A solid-solution phase of $^{7}Li_{0.6}FePO_4$ was formed simply by mixing the end members, $^{7}LiFePO_4$ and $FePO_4$, in a 6:4 ratio and heating to 620 K in vacuum. Significant difference of the neutron diffraction pattern with that measured at room temperature (0.6 $LiFePO_4$ + 0.4 $FePO_4$) is shown in supplemental Fig. 15. Temperature-dependent X-ray diffraction profiles were measured in a helium-sealed cell prior to the neutron diffraction experiment and confirm the formation of a single phase of compositionally homogeneous $Li_{0.6}FePO_4$ solid solution only in the very narrow temperature range of 600–630 K, as shown in supplemental Fig. 16.

The first analysis performed for the $Li_{0.6}FePO_4$ solid-solution phase at 620 K was the Rietveld refinement for the neutron diffraction profile and the resultant pattern is summarized in Fig. 12b. To evaluate the dynamic disorder of lithium, maximum entropy method (MEM) was applied to estimate the neutron scattering length density distribution, which corresponds to the nuclear density distribution. MEM is a model-free method used to calculate precise nuclear densities in solids, including some disorder and/or anharmonic vibrations using experimentally obtained structure factors as an initial input. The MEM is primarily an information-theory-based technique that was first developed by Gull and Daniel [28] in the field of radioastronomy to enhance the information from noisy data. Afterward, Collins et al. [29] applied its methodology to crystallography for electron density enhancement from X-ray diffraction. In the theory of this methodology, information entropy, which deals with the most probable distribution of numerical quantities over the ensemble of pixels, is considered. Successful MEM enhancement makes it possible to evaluate not only the missing and heavily overlapped reflections but also any type of complicated electron or nuclear distribution, which is hard to describe with classical structure model. By applying this method, possible bias imposed by the empirical static structural model is reduced, allowing any type of complicated nuclear distribution as long as it satisfies the symmetry requirements. The validity of such methodology has

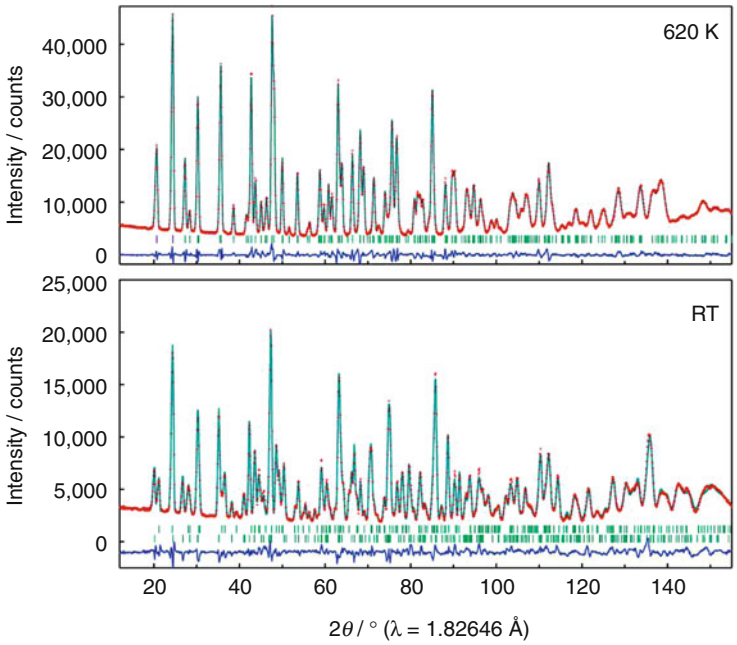

Olivine Phosphate Cathode Materials, Reactivity and Reaction Mechanisms. Figure 15
Comparative powder neutron diffraction pattern measured for $Li_{0.6}FePO_4$ measured at 620 K (solid-solution) and at room temperature (two-phase mixture of $LiFePO_4$ and $FePO_4$) using the same diffractometer HERMES

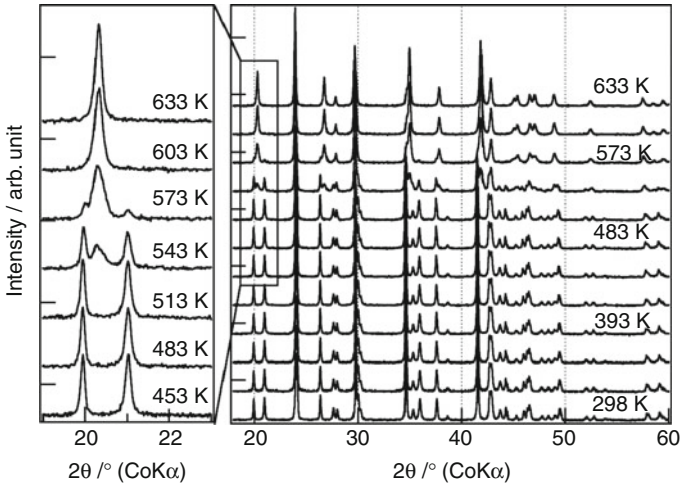

Olivine Phosphate Cathode Materials, Reactivity and Reaction Mechanisms. Figure 16
X-ray diffraction patterns of a mixture of 0.6 $LiFePO_4$ and 0.4 $FePO_4$ recorded at 30 K steps from 298 to 633 K with magnification of 200 reflections. Bruker AXS D8 ADVANCE powder diffractometer was used with Co-Kα radiation and linear position-sensitive detector Vantec-1. Measurement ranges were from 15° to 120°. The measurements were conducted under a high-purity He atmosphere in an Anton Paar HTK 450 temperature-controlled chamber

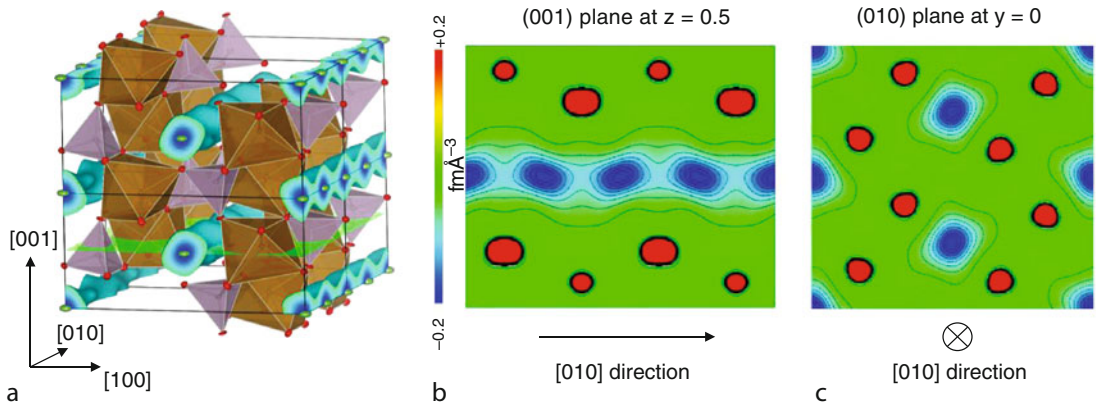

Olivine Phosphate Cathode Materials, Reactivity and Reaction Mechanisms. Figure 17
Nuclear distribution of lithium calculated by maximum entropy method (MEM) using neutron powder diffraction data measured for $Li_{0.6}FePO_4$ at 620 K. The classic static atom models with harmonic vibration were no longer appropriate to describe the dynamic disorder of lithium ion $Li_{0.6}FePO_4$ at 620 K; the MEM nuclear density distribution provided much information on the time and spatially averaged complicated dynamic disorder upon lithium diffusion. (**a**) Three-dimensional Li nuclear density data shown as blue contours (equi-value 0.15 fm $Å^{-3}$ of the negative portion of the coherent nuclear scattering density distribution). The brown octahedra represent FeO_6 and the purple tetrahedra represent PO_4 units. (**b**) Two-dimensional contour map sliced on the (001) plane at $z = 0.5$; lithium delocalizes along the curved one-dimensional chain along the [010] direction, while Fe, P, and O remain near their original positions. (**c**) Two-dimensional contour map sliced on the (010) plane at $y = 0$; all atoms remain near their original positions

been well established for various ionic conductors [30–32].

A three-dimensional contour surface (0.15 fm $Å^{-3}$) of nuclear distribution of lithium atoms is shown in Fig. 17. The probability density of lithium nuclei strictly distributes into the continuous curved one-dimensional chain along the [010] direction, which is consistent with the computational predictions by Morgan et al. [22] and Islam et al. [23]. Other atoms, Fe, P, and O remained to be localized at the initial positions even after MEM analysis. Given the two possible diffusion paths in Fig. 11, the microscopic reason of the diffusion anisotropy can be the difference in the electrostatic repulsion, which should be much pronounced if there are face-sheared polyhedra. Along the [010] direction, whatever the site occupied by the lithium ion during the diffusion process (octahedral 4a site–intermediate tetrahedral vacant site–octahedral 4a site), there is no face sharing with other occupied polyhedra. On the contrary, when the diffusion occurs along the [001] direction, the intermediate octahedral site shares two faces with PO_4 tetrahedra; therefore, the presence of lithium in this octahedral site is very unlikely, leading to a high activation energy. Recall that lithium ions are localized on the initial 4a sites in stoichiometric $LiFePO_4$ at room temperature, but they possess small thermal vibrations along the continuous one-dimensional distribution as shown in Fig. 13. In $Li_{0.6}FePO_4$ at temperatures as high as 620 K, a large number of lithium defects as lithium acceptor are thermodynamically stabilized, and enough kinetic motional energy is given to each lithium ion to overcome the hopping barrier of the excitonic Li^+–e^- pair.

Summary and Future Directions

These systematic findings on nano-size effects for the phase diagram of important electrode material of Li_xFePO_4 redefine guidelines for understanding the polaronic transport, cooperative phase-boundary movement, and its thermodynamics in biphasic intercalation processes. Polaronic insulators of the transition-metal polyanion family show a wide variety of

framework structure and accommodate various transition metals and guest atoms. Recent advances in carbon coating technology have been applied to many of these compounds to shed light on their potential application as intercalation battery cathodes. There is, therefore, still plenty of scope for further investigations on this issue. The long-awaited experimental evidence of strong dimensional restriction of lithium motion in Li_xFePO_4 was provided. Beyond Li_xFePO_4, this is, to our knowledge, the first visual demonstration of the ion diffusion path in a battery electrode. Delocalization of mobile ions at elevated temperatures is a universal phenomena occurring in any intercalation electrode material, and can be utilized to shed light on the ion dynamics. Particularly, such temperature-driven motional enhancement should be more significant in the electron/hole localized system, which recently has been recognized to form an important emerging materials group that may yield new electrode materials. Therefore, high-temperature neutron diffraction coupled with the maximum entropy method is a powerful tool for future battery electrode research.

Bibliography

1. Padhi AK, Nanjundaswamy KS, Goodenough JB (1997) Phospho-olivines as positive-electrode materials for rechargeable lithium batteries. J Electrochem Soc 144:1188
2. Yamada A, Chung SC, Hinokuma K (2001) Optimized $LiFePO_4$ for lithium battery cathodes. J Electrochem Soc 148:A224
3. Huang H, Yin S-C, Nazar LF (2001) Approaching theoretical capacity of $LiFePO_4$ at room temperature at high rates. Electrochem Solid State Lett 4:A170
4. Chung SY, Bloking JT, Chiang YM (2002) Electronically conductive phospho-olivines as lithium storage electrodes. Nat Mater 1:123–128
5. Chen Z, Dahn JR (2002) J Electrochem Soc 149:A1184
6. Goňi A, Lezama L, Arriortua MI, Barberis GE, Rojo T (2000) J Mater Chem 10:423
7. Dahn JR, McKinnon WR (1985) Phys Rev B32:3003
8. Dahn JR, McKinnon WR, Murray JJ, Haering RR, McMillan RS, Rivers-Bowerman AH (1985) Phys Rev B32:3316
9. Delmas C, Nadiri A, Soubeyroux JL (1988) Solid State Ionics 28–30:419
10. Yamada A, Koizumi H, Sonoyama N, Kanno R (2005) Phase change in Li_xFePO_4. Electrochem Solid State Lett 8:A409
11. Meethong N, Huang H-YS, Carter WC, Chiang Y-M (2007) Size-dependent lithium miscibility gap in nanoscale $Li_{1-x}FePO_4$. Electrochem Solid State Lett 10:A134
12. Wagemaker M, Borghols WJH, Mulder FM (2007) J Am Chem Soc 129:4323
13. Schimmel HG, Huot J, Chapon LC, Tichelaar FD, Mulder FM (2005) J Am Chem Soc 127:14348
14. Gibot P, Casa-Cabanas M, Laffont L, Levasseur S, Carlach P, Hamelet S, Tarascon JM, Masquelier C (2008) Nat Mater 7:741
15. Wagemaker M, Mulder FM, Van der Ven A (2009) Adv Mater 25:2703
16. Meethong N, Huang H-YS, Speakman SA, Carter WC, Chiang Y-M (2007) Strain accommodation during phase transformations in olivine-based cathodes as a materials selection criterion for high-power rechargeable batteries. Adv Func Mater 17:1115
17. Wang L, Zhou F, Meng YS, Ceder G (2007) Phys Rev B 76:165435
18. Martin JF, Yamada A, Kobayashi G, Nishimura S, Kanno R, Guyomard D, Dupre N (2008) Electrochem Solid State Lett 11:A12
19. Kobayashi G, Nishimura S, Park M-S, Kanno R, Yashima M, Ida T, Yamada A (2009) Adv Func Mater 19:395
20. Yamada A, Koizumi H, Nishimura S, Sonoyama N, Kanno R, Yonemura M, Nakamura T, Kobayashi Y (2006) Room-temperature miscibility gap in Li_xFePO_4. Nat Mater 5:357
21. Streltsov VA, Belokoneva EL, Tsirelson VG, Hansen NK (1993) Acta Crystallogr B49:147
22. Morgan D, Van der Ven A, Ceder G (2004) Li conductivity in Li_xMPO_4 (M = Mn, Fe, Co, Ni) olivine materials. Electrochem Solid State Lett 7:A30
23. Islam M, Driscoll D, Fisher C, Slater P (2005) Atomic-scale investigation of defects, dopants, and lithium transport in the $LiFePO_4$ olivine-type battery material. Chem Mater 17:5085
24. Delacourt C, Poizot P, Tarascon JM, Masquelier C (2005) The existence of a temperature-driven solid solution in Li_xFePO_4 for $0<x<1$. Nat Mater 4:254
25. Dodd J, Yazami R, Fultz B (2006) Phase diagram of Li_xFePO_4. Electrochem Solid State Lett 9:A151
26. Ellis B, Perry LK, Ryan DH, Nazar LF (2006) Small polaron hopping in Li_xFePO_4 solid solutions: coupled lithium-ion and electron mobility. J Am Chem Soc 128:11416
27. Dodd J, Halevy I, Fultz B (2007) Valence fluctuations of ^{57}Fe in disordered $Li_{0.6}FePO_4$. J Phys Chem C 111:1563
28. Gull SF, Daniel GJ (1978) Image reconstruction from incomplete and noisy data. Nature 272:686
29. Collins DM (1982) Electron density images from imperfect data by iterative entropy maximization. Nature 298:49
30. Shikanai F (2006) Neutron powder diffraction study on the high-temperature phase of $K_3H(SeO_4)_2$. Physica B 385–386:156
31. Yashima M, Itoh M, Inaguma Y, Morii Y (2005) Crystal structure and diffusion path in the fast lithium-ion conductor $La_{0.62}Li_{0.16}TiO_3$. J Am Chem Soc 127:3491
32. Yashima M (2003) Conduction path and disorder in the fast oxide-ion conductor $(La_{0.8}Sr_{0.2})(Ga_{0.8}Mg_{0.15}Co_{0.05})O_{2.8}$. Chem Phys Lett 380:391
33. Nishimura S, Kobayashi G, Ohoyama K, Kanno R, Yashima M, Yamada A (2008) Experimental visualization of lithium diffusion in Li_xFePO_4. Nat Mater 7(9):707–711

Organic Batteries

Hiroyuki Nishide, Kenichi Oyaizu
Department of Applied Chemistry, Waseda University, Tokyo, Japan

Article Outline

Glossary
Definition of the Subject
Introduction
Conjugated Polymers and Redox Polymers for Electrode-Active Materials
Organic Radical Polymers as Electrode-Active Materials
Performance of Organic Radical Batteries
Future Directions
Bibliography

Glossary

C Rate 1C (or 1 I_t) Discharging corresponds to the constant-current discharging of rated capacity at 1 h. For example, the 1 C discharging of a lead acid battery with a rated capacity of 12 Ah corresponds to the discharging at 12 A, and 2 C corresponds to the discharging at 24 A. The C rate is also used to show the charging current.

Capacity The quantity of electricity (Ah) that can be obtained by discharging until the cell reaches the end of life. Electricity for 1 mol of e^- = 1 Faraday (F) = 96,485 C = 26.8 Ah.

Cyclability Capability of charging/discharging cycles without loss of capacity for secondary batteries. A commercial cell must be capable of completely discharging and then fully recharging for >300 times and not losing >20% of its capacity, which requires a robust system and reversible electrode reactions. There should be no side reactions that result in the loss of the active materials during the cycle. High cyclability secondary batteries reduce their environmental load.

Electrode-active material The material that generates electrical current by means of a chemical reaction within the battery. The *anode*- and *cathode*-active materials are used in the negative and positive electrodes associated with oxidative and reductive chemical reactions that release and gain electrons through the external circuit during discharging, respectively. Organic batteries use organic redox-active molecules, which are typically polymers, for the electrode-active materials.

Electrolyte Salt solution (or ionic liquid) capable of electric conduction by ionic transport. The electrolyte layer in batteries serve as a simple buffer for ionic flow between the electrodes as in Li-ion and Ni-Cd cells, or it participates in the electrochemical reaction as in Pb-acid cells. For battery sustainability and safety, the low flammability and leakage are required so that (semi)solid electrolyte is often employed such as those with poly(ethylene glycol).

Electromotive force (emf) A difference in potential that tends to give rise to electric current. For a cell with a configuration of

$$\text{Anode}|\text{Ox}_2, \text{Red}_2|\text{Electrolyte}|\text{Ox}_1, \text{Red}_1|\text{Cathode},$$

the overall reaction is $n_2\text{Ox}_1 + n_1\text{Red}_2 \rightleftarrows n_2\text{Red}_1 + n_1\text{Ox}_2$ and the emf is given by

$$E = E_1 - E_2 = \Delta E^\circ - RT/(n_1 n_2 F) \ln\{(a_{\text{Red}_1}{}^{n_2} a_{\text{Ox}_2}{}^{n_1})/(a_{\text{Ox}_1}{}^{n_2} a_{\text{Red}_2}{}^{n_1})\}.$$

The cell voltage is $V = E - IR$ where R is the resistance of the cell. The power is P (W) = current I (A) × cell voltage V (V). Thus, large emf is advantageous to produce large power, although special attention has to be paid to the safety of the battery.

Faraday efficiency (Coulomb efficiency) Efficiency of active mass = (actual capacity)/(theoretical capacity).

Rechargeable (secondary) battery An electrochemical cell for the generation of electrical energy in which the cell, after being discharged, is restored to its original charged condition reversibly by an electric current flowing in the direction opposite to the flow of current when the cell was discharged. The reusability lowers the price and the environmental load per supplied electrical power.

Self-discharge The loss of performance when a battery is not in use, which is related to the loss of energy accompanied by the energy storage with the battery.

Li − MnO_2 primary cells will deliver 90% of their energy even after 8 years on the shelf; that is, their self-discharge is low. Rechargeable batteries generally have more rapid loss of capacity on storage. The rechargeable Ni − MH cell, for instance, will lose up to 30% of its capacity in a month. In organic batteries, immobilization of the organic electrode-active materials is crucial to prevent or suppress the self-discharge. Cross-linking is often applied to the polymeric materials to avoid dissolution into electrolyte solutions.

Separator A substance, such as microporous polyethylene, that separates the anode and the cathode. An organic shutdown separator, which is molecularly designed to shut down the battery on over-temperature or overcharging and discharging, is desired for the safety concerns, especially in the case of Li-ion batteries.

Specific capacity (in mAh/g or Ah/kg) 1,000/(electrochemical equivalent × 3,600), where electrochemical equivalent is the mass of element or molecule (in g) transported by 1 C of electricity. Examples: Li (6.941 g/mol), $Li \rightarrow Li^+ + e^-$, electrochemical equivalent = 6.941/96,485 = 7.19×10^{-5} g, specific capacity = 1,000/($7.19 \times 10^{-5} \times 3{,}600$) = 3,863 mAh/g. PTMA (240.3 g/mol unit), electrochemical equivalent = 2.49×10^{-3} g, specific capacity = 112 mAh/g.

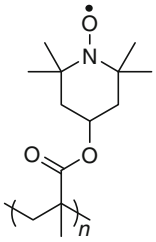

PTMA

Sustainable battery Energy devices designed to store and supply electric power, characterized by clean and reduced CO_2 emission, effective utilization of alternative fuels, low environmental load, and safety, for a sustainable society. Organic batteries are inherently sustainable, owing to the environmentally benign fabrication and disposing processes, low toxicity and safety, based on the use of organic, resource-unlimited, and heavy metal-free materials.

Definition of the Subject

Batteries are composed of cathode- and anode-active materials, a separator to separate the two electrode-active materials, an electrolyte layer, and current collectors. The cathode- and anode-active materials of conventional primary and secondary batteries are usually metal oxides, such as manganese, silver, lead, nickel, and vanadium oxides, and metals, such as zinc, lead, cadmium, and lithium. All the electrodes of conventional batteries are composed of metals and metal oxides (except oxygen and carbon that are used for the air battery cathode and the lithium battery anode, respectively), many of which come from limited resources.

Recent development of organic batteries aiming at increasing the energy density has made them promising candidates of energy-storage devices to complement the conventional inorganic-based batteries. Definition of organic battery in this entry is based on the use of organic materials designed for the electrode-active materials. (Note that those using organic materials for electrolyte layers have often been called likewise.) Organic materials for the electrode-active materials are π-conjugated polymers using their doping/de-doping behaviors, and redox polymers, either conjugated or nonconjugated, involving polyaniline-based disulfides and other organic redox sites such as tetracyanoquinodimethane. The most typical and recently developed organic battery includes a radical battery, using organic radical polymers which are a class of aliphatic or nonconjugated redox polymers with organic robust radical pendant groups as the redox site. The advantage of organic battery in terms of sustainability also comes from the excellent recyclability and safety as the inherent virtue of the organic materials.

Introduction

Development of sustainable processes for energy storage and supply is one of the most important worldwide concerns today. Primary batteries, such as alkaline manganese and silver oxide batteries, produce electric current by a one-way chemical reaction and are not rechargeable and hence useless for reversible electricity storage. Portable electronic equipments, electric vehicles, and robots require rechargeable secondary

batteries. Li-ion, lead acid, and nickel-metal hydride batteries are generally used at the present to power them. Solar cells and wind-power generators expect a parallel use of rechargeable batteries for leveling and preserving their generated electricity. Ubiquitous electronic devices such as integrated circuit smart cards and active radio-frequency identification tags need rechargeable batteries that are bendable or flexible and environmentally benign for durability in daily use. Designing of soft portable electronic equipments, such as roll-up displays and wearable devices, also require the development of flexible batteries. It is essential to find new, low-cost, and environmentally benign electroactive materials based on less-limited resource for electric energy storage and supply [1]. Reversible storage materials of electric energy or charge that are currently under use in electrodes of rechargeable batteries are entirely inorganic materials, such as Li-ion-containing cobalt oxide, lead acid, and nickel-metal hydride.

Among the secondary batteries, Li-ion batteries are becoming the most popular [2, 3]. Almost eight billion batteries which are worth US$9.5 billion were produced worldwide in 2009 [4]. Typical Li-ion battery is configurated with the cathode composed of Li-ion-containing metal oxides, such as lithium cobalt oxide, and the anode of graphite carbon [5]. During the charging process, Li ions are eliminated from the lattice of the metal oxide cathode and intercalated into the carbon anode. During the discharging process, the cobalt oxide is regenerated by the elimination of the Li ions. Li is one of the smallest elements to yield large specific capacity ($Li_6C \rightarrow 6Li^+ + 6e^- + C$: 372 mAh/g) and the very large electromotive force generated by the Li ion ($0.5C_6Li + Li_{0.5}CoO_2 \rightleftarrows 3\ C + LiCoO_2$: 3.6 V), which result in a significantly high energy density and the highest given voltage of the battery. Another feature of the Li-ion battery is the rocking-chair-type intercalation reactions of the Li ion between the cathode- and the anode-active materials [3, 5]. The intercalation of Li ions into the electrodes suppresses metallic Li (dendrite) formation by separating and immobilizing each Li ion in the lattice and the layered structure. However, the intercalating diffusion of Li ions accompanied by transformation of the lattice and the layer structure during the electrode reactions results in slow kinetics and heat generation in the charging and discharging processes, often producing overheating and occasional ignition. Indeed, battery makers often issued recalls of their million-scale Li-ion batteries for mobile phones and laptop computers, due to overheating accidents.

Tedious waste processing of used batteries is difficult and crucial issue of the metal- and metal oxide-based conventional batteries. Used batteries are, in these days of environmental concern, being collected and recycled. Among the recycling of used batteries, the Li-ion batteries are highly valued for their excellent collection yield (e.g., 60% in Japan [6, 7]) from personal computers and mobile phones. The typical recycle processing of used Li-ion batteries includes several steps of calcination, sieving, dissolving in acid, and solvent extraction, and is reasonably working at least in Japan [6, 7]. However, the collection yields of used Li-ion batteries are somewhat decreasing because the batteries are being equipped in many varieties of small devices. Additionally, other used batteries are often found in landfill disposal or simply stand at the level at 60 kt/year even in Japan. The conventional metal-based batteries involve several inherent unsolved issues from the standpoint of sustainable technology.

Organic functional polymers have been developed as alternatives of inorganic functional materials because of their lightweight, flexibility, thin film–forming ability, processability, metal-free and benign environmental aspects, and fewer limitations of organic resources. A new trend in materials research is emerging recently, focusing on the fabrication of organic electrodes or electrodes composed of electrode-active organic compounds, characterized by the redox (oxidative/reductive or electron-releasing/gaining reaction) activity and/or electric conduction of organic molecules that typically consist of redox polymers and/or conducting polymers. The exploration of properties of such organic materials leads to new technological perspectives of various totally organic electrochemical devices, not only batteries and hybrid capacitors but sensors and displays as well. The organic batteries and devices are free from using (heavy) metals and limited resources, and are potentially involved in the carbon cycle. In this entry, the concept and outline of organic electrodes for use in rechargeable batteries is reviewed, emphasizing the material science of the organic polymers for charge

transport and storage for the development of sustainable science and engineering.

Conjugated Polymers and Redox Polymers for Electrode-Active Materials

Research on organic electrode-active materials was prompted by the discovery of the electric conductivity of doped polyacetylene, which led to explore organic batteries by employing the redox capability of polyacetylene based on the reversible *p*-type and *n*-type doping/de-doping processes for the cathode and the anode, respectively, as the principal electrode reactions [8]. Electrically conducting polymers with π-conjugated skeleton structures, such as polyaniline, polypyrrole, polythiophene, and their related derivatives (Scheme 1a), have been similarly examined as electrode-active materials, based on their reversible electrochemical doping behaviors [9]. The polymers are conveniently placed on the surface of a current collector by a solution-based wet process such as spin-coating and electropolymerization methods. The limitations of the π-conjugated polymers as the electrode-active materials are based on their insufficient doping levels, the resulting low redox capacities, and fluctuation of the cell voltage through the doping/de-doping process. Chemical instability of the doped states of the π-conjugated polymers is the fatal flaw to practical application because it frequently leads to the self-discharge and degradation of the rechargeable properties of the resulting batteries.

A pair of p- and n-type redox-active organic π-conjugated compounds, such as indigo derivatives bearing two sulfonic acid groups, was incorporated as dopants into polypyrrole [10]. The doped polypyrrole held the redox-active dopants through electrostatic interaction and worked as the electroconductive cathode and anode for a rechargeable battery. However, amount of the loadable redox-active dopants was limited by the doping degree and the battery lacked in stability to elute the dopant through the discharging process.

Organodisulfide compounds such as those derived from [1,3,4]thiadiazole-2,5-dithiol (362 mAh/g) (Scheme 1b) act as a cathode-active material with a high charge capacity through their two-electron redox reaction according to

$$n\,{}^{\ominus}\mathrm{S{-}R{-}S}^{\ominus} \underset{+2ne^-}{\overset{-2ne^-}{\rightleftharpoons}} \left(\mathrm{S{-}R{-}S}\right)_n$$

Emf of the redox reaction versus Li is 2.7–3.0 V to give significantly high energy density [11]. However, the redox reaction involves the formation of the disulfide polymers (Scheme 1) with the formation and cleavage of the chemical bond or the formation and the scission of the polymer chain, which renders the rate performance of the cathode low. Blending of the organothiolate with polyaniline as a conducting polymer has been examined to improve the rate performance, where the polyaniline served as a conducting pathway for the redox reaction of the disulfide. Nasty odor of the sulfur compounds was still a problematic issue. The test battery in conjunction with the lithium anode performed the output voltage of ca 3.5 V with discharging capacity of ca. 150 Ah/kg.

Organodisulfide residue has been intramolecularly combined in the repeating unit of polyaniline [12], as represented in Scheme 1. Cyclability in the redox reactivity and the smelly problem were much improved, while there still remained limitation of slow kinetics in the charging/discharging processes.

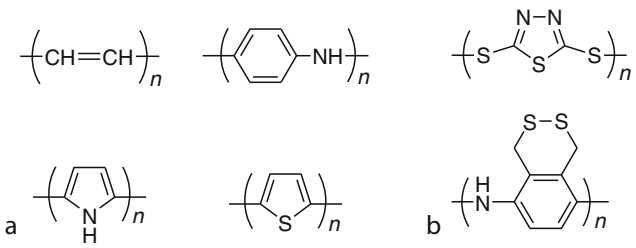

Organic Batteries. Scheme 1
Chemical structures of the (**a**) π-conjugated polymers and (**b**) the dithiol/disulfide-based electrode-active materials

Organic Radical Polymers as Electrode-Active Materials

Another avenue toward the organic electrode-active materials is based on the sufficiently large redox capacity of aliphatic radical polymers, that is, organic polymers densely populated with pendant redox-isolated sites. The principal finding to permit the use of the nonconjugated radical polymers is the capability of organic robust radicals, or open-shell molecules, to allow fully reversible one-electron redox reactions featuring fast electrode kinetics and reactant cyclability [13]. Organic radicals are stabilized thermodynamically by effective delocalization of the unpaired electron and/or kinetically by bulky substituents to employ as the redox sites. The nitroxide radicals such as 2,2,6,6-tetramethylpiperidine-1-oxyl (TEMPO) derivatives and nitronyl nitroxides, the nitrogen radicals such as triarylaminium cation radicals, diphenylpicrylhydrazyl derivatives and verdazyls, and the oxygen radicals such as phenoxyls and galvinoxyls are typically examined as the pendant group of the radical polymers (Scheme 2). These radicals are persistent at ambient temperatures under air and characterized by a rapid and reversible $1e^-$ electrode reactions, typically with heterogeneous electron-transfer rate constants in the order of $k_0 = 10^{-1}$ cm/s [14, 15].

Nitroxide radicals are oxidized to oxoammonium cations near 1 V and reduced to aminoxy anions near −0.5 V by $1e^-$ transfer processes. The negative charging of the neutral radicals usually takes place at more negative potentials than those for the positive charging. Attempts have been made to use these reactions for the electrode-active materials. The most typically used radicals for the cathode and the anode are TEMPO and phenoxyl (or galvinozyl), respectively, which give the corresponding oxoammonium cation and the phenolate (or galvinolate) anion upon the electrochemically reversible $1e^-$ reactions (Scheme 3).

A variety of polymer backbones have been employed to bind the radicals, such as poly(meth)acrylates, polystyrene derivatives, poly(vinyl ether)s, polyethers, and polynorbornenes. The radical sites must be bound to polymer chains because of the need to immobilize them at current collectors for exclusion of elution into electrolyte solutions that lead to discharging, to accomplish appropriate mobility of the counterions, to make the electrode-active materual amorphous and plasticized to accommodate deformation without heat generation, and to allow wet fabrication processes. Unpaired electron density of the polymers, determined by SQUID measurements, has revealed the presence of the radicals

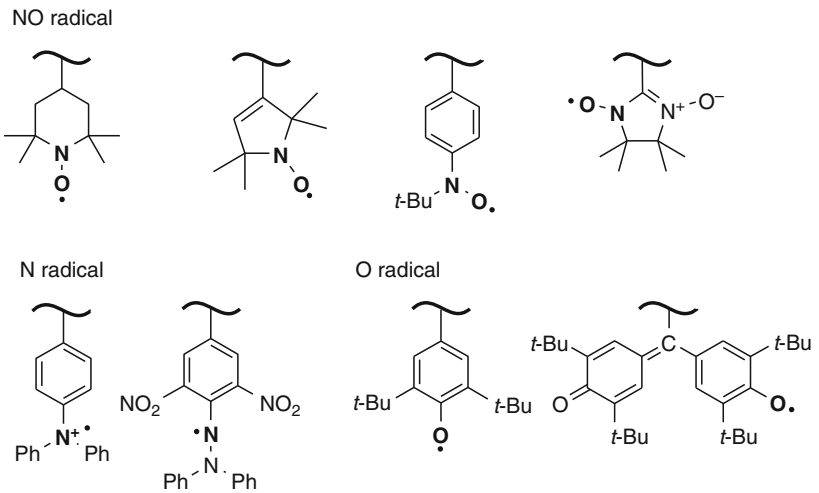

Organic Batteries. Scheme 2
Chemical structures of organic robust radicals in the radical polymers as the electrode-active materials in organic batteries

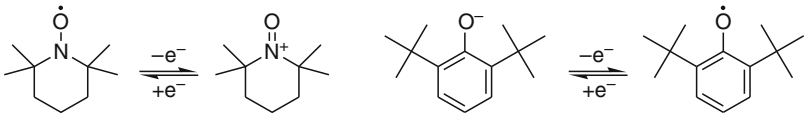

Organic Batteries. Scheme 3
Redox couples of TEMPO and phenoxyl

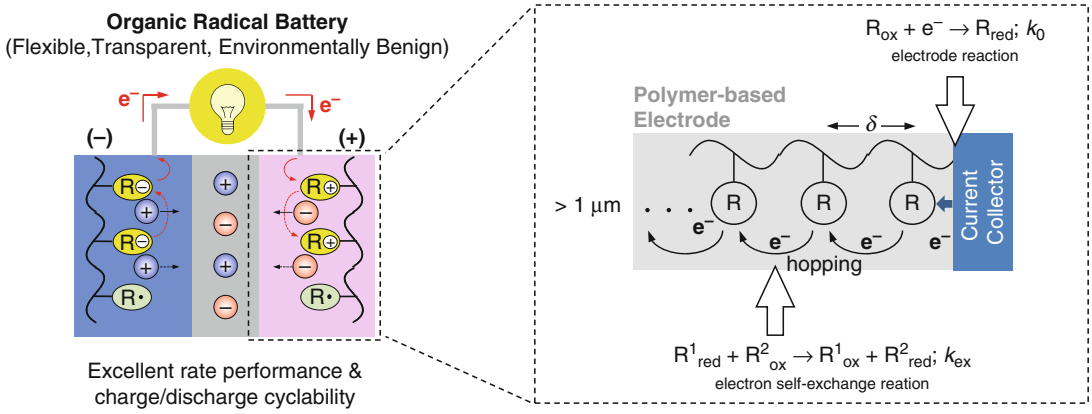

Organic Batteries. Figure 1
Discharging processes of the totally organic radical battery, showing the redox gradient-driven charge transport in the radical polymer layer at the current collector surface. Charge propagation is accomplished within redox polymer layers, swollen in electrolyte solutions, by an electron self-exchange (hopping) mechanism. R represents the redox site in the polymer

substantially per repeating unit. Specific capacities based on the formula weight of the repeating unit are in the range of 50–150 mAh/g.

The unpaired electron density of the radical polymers amount to several molars in the bulk of the swollen polymer equilibrated in electrolyte solutions. Under these conditions, charge propagation within the polymer layer is sufficiently fast leading to high-density charge storage, because the redox sites are so populated that electron self-exchange reaction goes to completion within a finite distance of the polymer layer. The concentration gradient-driven charge propagation is accomplished by the electron self-exchange reaction. The exchange reaction is sufficiently fast for the diffusion-limited outer-sphere redox reactions, resulting in the efficient transfer of charge produced at the surface of the current collector (Fig. 1). Combination of the fast electrode process ($k_0 \sim 10^{-1}$ cm/s) and self-exchange reaction ($k_{ex} \sim 10^{6-8}$ $M^{-1}s^{-1}$) lead to the high rate performance of the radical-based organic battery.

The radical polymers act as both cathode- and anode-active materials, depending on the redox potential. A couple of polymers, different in redox potentials, are used as the electroactive materials in the organic radical battery (Fig. 1). The charging process corresponds to the oxidation of the radical to the cation at the cathode, and the reduction of the radical to the anion at the anode. The electromotive force is close to the potential gap between the two redox couples, which typically amounts to 0.5–1.5 V. The radical polymers are reversibly converted to the corresponding polyelectrolytes during the charging process. The rapid electrode reaction of the radicals and the efficient charge propagation within the polymer layer lead to a high rate performance, allowing rapid charging and large discharge currents without substantial loss of output voltages.

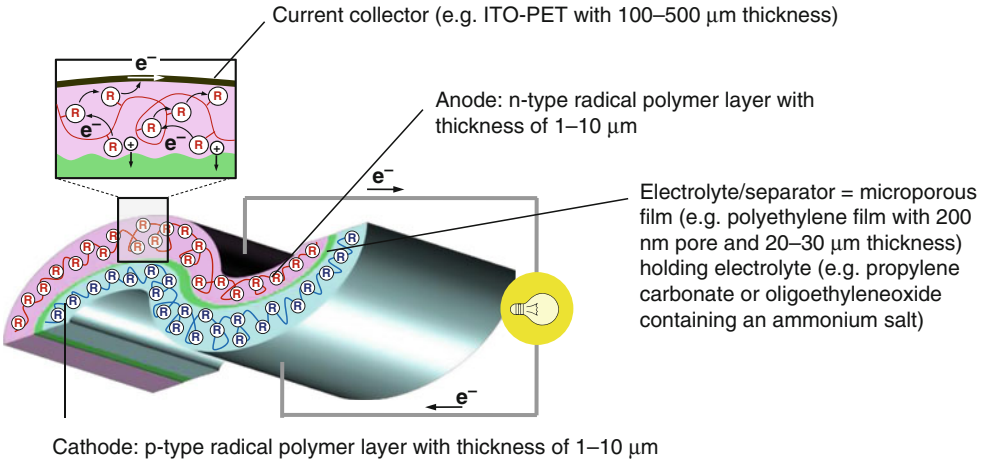

Organic Batteries. Figure 2
Charge-storage configuration of a flexible organic radical battery

Performance of Organic Radical Batteries

The amorphous radical polymers allow fabrication of flexible thin-film devices (Fig. 2) [16]. A curious feature of the radical battery is the excellent rate performance to produce burst power (50 mA/cm^2 and >95% capacity at 60 C discharging), which also allow instant full charging (i.e., in a few seconds). Optimization of the battery has allowed retention of >90% capacity even after 1,000 charging/discharging cycles. The maximum energy and power densities are 120 Wh/kg and 20 kW/kg, respectively. The resulting radical battery has allowed the rated performance of the power density of 5 kW/L for more than 10^4 times pulse charging/discharging at 100 mA, and 1 A discharging and 2 W power from only <1 mm-thick flexible battery, that is suitable for IC cards, electronic papers, and active Radio Frequency Identification (RFID) [17, 18].

Radical batteries have proved to be a new class of organic rechargeable devices, which are characterized by the excellent rate performance and the moderate energy density as illustrated by the Ragone plots (Fig. 3). The mass-specific energy density is placed between those of polyacetylene- and disulfide-based organic batteries, but the power density is much larger and comparable to those of supercapacitors. Efforts have been directed toward further increasing the theoretical energy density of the radical batteries. For this purpose, radical polymers with even smaller formula weights per repeating unit are designed.

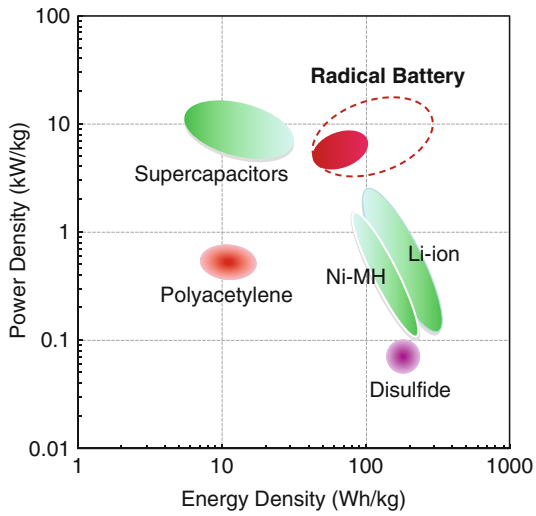

Organic Batteries. Figure 3
Energy versus power density plots for batteries and supercapacitors

Future Directions

The organic batteries have several advantages over the Li-ion batteries, such as higher safety, adoptability to wet fabrication processes, easy disposability, and capability of fabrication from less-limited resources. While

organic batteries have intrinsically lower volumetric energy density, this limitation can be overcome in the near future so that they can be designed to be compatible with and installable in various electronic equipments.

Bibliography

1. Service RF (2006) New 'Supercapacitor' promises to pack more electrical punch. Science 313:902
2. Pistoia G (2005) Batteries for portable devices. Elsevier, Amsterdam
3. Scrosati B, Schalkwijk WAV (2002) Advances in lithium-ion batteries. Plenum, New York
4. Report of Battery Association of Japan. http://www.baj.or.jp/statistics/01.html. Accessed 19 March 2011
5. Balakrishnan PG, Ramesh R, Kumar TP (2006) Safety mechanisms in lithium-ion batteries. J Power Sources 155: 401–414
6. Report from Ministry of Economy, Trade and Industry, Japan. Year-book of Machinery Statistics (2008)
7. Report from Japan Portable Rechargeable Battery Recycling Centor. http://www.jbrc.net/hp/contents/recycle/index.html. Accessed 19 March 2011
8. Nigrey PJ, MacDiarmid AG, Heeger AJ (1979) Electrochemistry of polyacetylene, $(CH)_x$: electrochemical doping of $(CH)_x$ films to the metallic state. J Chem Soc Chem Commun (14):594–595
9. Roncali J (1997) Synthetic principles for bandgap control in linear π-conjugated systems. Chem Rev 97:173–205
10. Song HK, Palmore GTR (2006) Redox-active polypyrrole: toward polymer-based batteries. Adv Mater 18:1764–1768
11. Oyama N, Tatsuma T, Sato T, Sotomura T (1995) Dimercaptan −polyaniline composite electrodes for lithium batteries with high energy density. Nature 373:598–600
12. Takemura I, Iwasaki T, Takeoka S, Nishide H (2004) 3-Dithiolthione-substituted polythiophene and its redox activities. Chem Lett 33:1482–1483
13. Oyaizu K, Nishide H (2009) Radical polymers for organic electronic devices: a radical departure from conjugated polymers? Adv Mater 21:2339–2344
14. Yonekuta Y, Oyaizu K, Nishide H (2007) Structural implication of oxoammonium cations for reversible organic one-electron redox reaction to nitroxide radicals. Chem Lett 36:866–867
15. Suga Y, Pu YJ, Oyaizu K, Nishide H (2004) Electron-transfer kinetics of nitroxide radicals as an electrode-active material. Bull Chem Soc Jpn 77:2203–2204
16. Nishide H, Oyaizu K (2008) Toward flexible batteries. Science 319:737–738
17. http://www.nec.co.jp/press/ja/0512/0702.html. Accessed 19 March 2011
18. http://www.nec.co.jp/press/ja/0902/1302.html. Accessed 19 March 2011

Organic Solar Cells

Eric Daniel Głowacki[1], Niyazi Serdar Sariciftci[1], Ching W. Tang[2]

[1]Linz Institute for Organic Solar Cells (LIOS), Johannes Kepler University, Linz, Austria

[2]Department of Chemical Engineering, University of Rochester, Rochester, NY, USA

Article Outline

Glossary
Definition of the Subject
Introduction
Operating Principles
Building an Organic Solar Cell: Materials, Fabrication, Optimization
Future Directions
Conclusions
Bibliography

Glossary

Bulk heterojunction A mixture of interpenetrating electron-donor and electron-acceptor conjugated molecules that allows absorption of light, generation of excitons, splitting of excitons at the donor-acceptor interface, and efficient transport of positive and negative charges to opposite electrodes.

Conjugated molecule An organic (carbon-based) molecule with delocalized electrons moving through π bonding orbitals. Conjugated molecules strongly absorb certain wavelengths of light due to excitation of π electrons from bonding π-orbitals to higher energy orbitals. As a result of delocalization of electrons, conjugated molecules also conduct charge. All organic semiconductors belong to this family of compounds.

Electron acceptor A molecule that can accept electrons, thereby becoming reduced. The measure of electron acceptor strength is electron affinity, which also corresponds to work function in metals and semiconductors.

Electron donor A molecule that donates electrons to another compound, thereby becoming oxidized. Following excitation with light, excited electrons can be donated to an acceptor molecule with

a lower electron energy level. How easily a molecule gives up an electron depends on its ionization potential.

Exciton A quasiparticle that forms in insulators and semiconductors following absorption of a photon. Consisting of a Coulombically bound electron and positive hole pair, it can be split due to interaction with a neighboring electron-accepting conjugated molecule into free positive and negative charges. Its binding energy depends on the dielectric constant of the material in which it forms.

P3HT poly(3-hexyl thiophene) A polythiophene with a pendant 6-carbon side-chain which provides high solubility in organic solvents. P3HT is a good electron donor material that effectively transports positive holes. When blended together with PCBM, 5% efficiency solution-processed solar cells can be achieved.

PCBM ([6,6]-phenyl C_{61}-butyric acid methyl ester) A soluble derivative of buckminsterfullerene (C_{60}) that is one of the most successful electron acceptor materials used in solution-processed organic solar cells. It effectively transports electrons from molecule to molecule as well.

Phthalocyanines A family of macrocyclic pigments with strong absorption in the red part of the visible spectrum, good electron-donor properties, high stability, and effective hole transport. They can be sublimed in vacuum to form thin films used in vacuum-evaporated organic solar cells.

Definition of the Subject

Organic photovoltaics (OPVs) are devices made of organic (carbon-based) semiconducting small molecules or polymers for converting incident sunlight into electrical power. They differ significantly from inorganic photovoltaic (PV) devices in the physical principles of their operation, as well as in their methods of production. OPVs are based on organic thin films of tens to a few hundreds of nanometers and can be fabricated using printing, vacuum evaporation, and roll-to-roll coating techniques, and thus offer the potential for ultra low-cost mass-producible photovoltaic devices. This is in contrast with the costly and energy-intensive fabrication of traditional crystalline silicon-based photovoltaics. OPV can be easily integrated into consumer electronics devices, even textiles and other mechanically flexible structural elements due to their production methods. An intrinsic advantage that organic semiconductors offer is that through molecular engineering, organic materials with custom-tailored optical, electrical, and mechanical properties can be synthesized. Since the late 1980s, organic solar cell efficiencies have consistently risen from <1% to around 8% as of the end of 2010. The continued improvement of efficiency has been driven by deeper understanding of the physics governing the operation of OPVs, development of new molecular architectures for more efficient solar energy conversion, and optimization of nanostructure and processing. With continued performance improvements and successful demonstrations of high-volume production, OPV is now being accepted by many as a serious contender in future PV energy solutions. Figure 1 shows a simple diagram of the structure of an OPV, as well as a photo of a laboratory example.

Introduction

Photovoltaic devices (PVs) harvest energy from the sun and convert it into usable electrical power. The mechanism behind the action of all types of PV devices is grounded in quantum theory of light. Light, or more strictly an electromagnetic wave, is described as discrete packets of energy called photons. The energy of a photon is solely dependent on the frequency, or color, of the light. In semiconductors, the energy of photons of the visible spectrum is sufficient to excite electrons from valence band to conduction band across the forbidden energy gap. Typically, following excitation by a photon, the excited electrons will quickly (lifetime of around nanoseconds) relax back to their ground state. However, what all photovoltaics have in common is some sort of built-in asymmetry which pulls the excited electrons and holes away into an external circuit before they can recombine. Thus, electrons and their positively charged vacancies in the material, called holes, are collected at electrodes and generate an electrical potential which can be used to do work.

Due to their ability to directly convert sunlight into electricity, various photovoltaic technologies are poised to play an important part in the future energy mix.

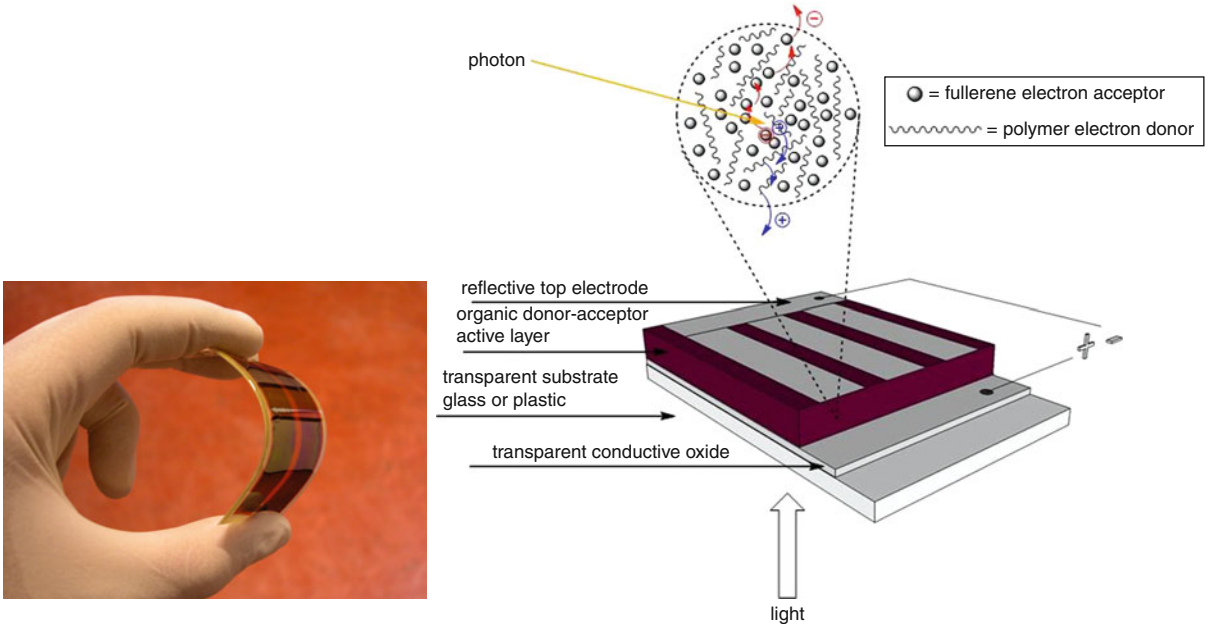

Organic Solar Cells. Figure 1
A laboratory example of a polymer-fullerene organic solar cell fabricated on a flexible plastic substrate is shown on the *left*. A cross-sectional schematic drawing of this type of device is shown on the *right*. The *inset* shows that the active layer is composed of a percolating network of electron donor and acceptor components

The foreseeable shortage of fossil fuels as well as the necessity of limiting CO_2 emissions are the urgent motivations for harvesting renewable and sustainable energy sources. The widespread adaptation of PV based on traditional inorganic semiconductors, such as crystalline silicon, is hampered by relatively high cost as well as an energy-intensive production process that severely subtracts from the overall "clean" energy yield over the device's lifecycle.

The idea of organic solar cells began as early as the 1950s [1, 2]. The inspiration of using organic molecules as light absorbing materials comes from the simple observation that photosynthetic systems in plant life on earth use molecular systems to harvest light and convert it into useful chemical energy. The notion of exploiting organic dyes mimicking those used in the photosynthetic process is thus a natural logical step. Early experiments, starting in 1958, focused on sandwiching bio-inspired organic dyes such as porphyrins, phthalocyanines [1], merocyanines [2] or chlorophylls [3, 4] between two metals with a large work function offset. These early cells did not exceed efficiencies of <1%. A significant breakthrough came in 1986, when Ching W. Tang published a 2-layer design demonstrating a power conversion efficiency of about 1% [5]. The photovoltaic properties of his device were determined by the interface between two thermally evaporated organic materials, one absorbing light and generating an excited state as electron donor, and the other acting as an acceptor, pulling away the photoexcited electron. This donor-acceptor photoinduced charge transfer principle is the fundamental mechanism that all subsequent organic solar cell designs rely on. The next important development in the OPV story came in 1992, when Sariciftci et al. discovered the highly efficient photoinduced charge transfer between a semiconducting polymer and Buckminsterfullerene (C_{60}) [6]. This paved the way for high-volume solution-processable (i.e., roll-to-roll) organic solar cells. These two milestones also represent seminal demonstrations of the two distinct types of OPV technologies that are most successful today: Vacuum-processed evaporated organic solar cells and solution-processed polymer-fullerene organic solar cells.

OPV represents a potentially cheap and sustainable large-scale PV technology. The field has been a very

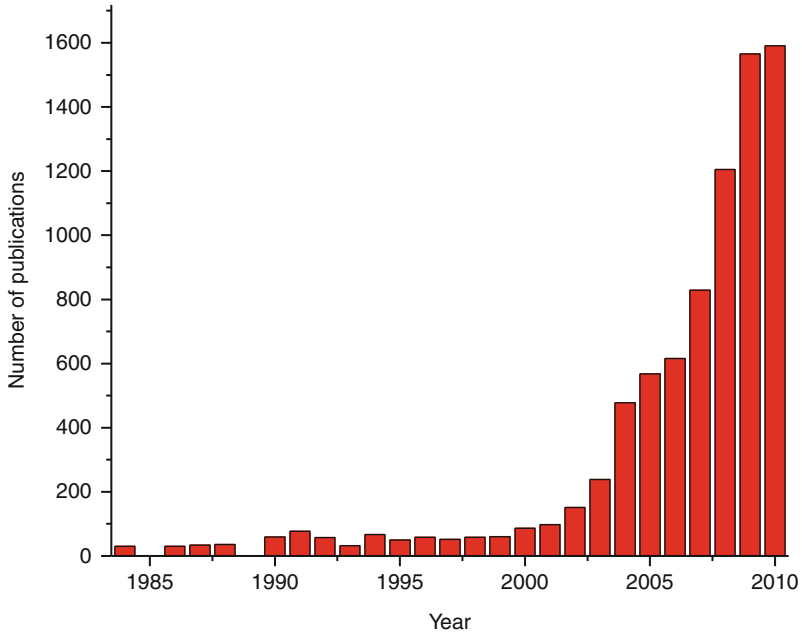

Organic Solar Cells. Figure 2
The number of academic publications on "Organic Solar Cells" from 1984 through 2010. Accessed through the ISI Web of Science, December 2010

active and continually growing area of research. Figure 2 shows the impressive growth in the number of academic publications on OPV over the past 25 years. Several companies worldwide have, in the past decade, begun the process of commercialization of OPVs, both vacuum-processed and solution-processed architectures, and have demonstrated successful mass production ability. With the top efficiencies for both types of OPV cells now in the 7–8% range, it has been estimated that OPV will make a significant market breakthrough [7] when efficiencies reach 10%. The growing economic success of organic light-emitting diodes in display applications in recent years foreshadows that OPV technology will follow a similar path. The factors determining the commercial success of OPV are depicted in Fig. 3.

Operating Principles

Light Absorption in Organic Semiconductors

The band gap for an organic molecule originates from the molecular orbitals that make up a conjugated π-bonding system. For an organic molecule or polymer to be a candidate for use in an OPV device, it must have a conjugated π electron system. Conjugated molecules exhibit an alternating single-bond double-bond structure of sp^2-hybridized carbon atoms. The electrons in the p_Z-orbitals of each sp^2-hybridized carbon atom form collectively the π-band of the conjugated polymer. Due to the isomeric effects, these π-electrons are delocalized, resulting in high electronic polarizability – this is known as the resonance effect. The existence of a band gap in a one-dimensional system of conjugated chains was predicted by Rudolf Peierls in the 1950s. The phenomenon of Peierls instability splits the originally half-filled p_Z-molecular orbital into two: the π- and π^*-bands. In the lower energy ground state, the outermost, or valence electrons, will occupy the π orbital, known as the bonding orbital. Since the valence electrons occupy this energy level it is called the "highest occupied molecular orbital," HOMO. Upon absorption of a photon of sufficient energy, electrons will be excited from the bonding π- into the anti-bonding π^*-band. This absorption corresponds to the first optical excitation from the highest occupied molecular orbital (HOMO) to the lowest unoccupied molecular orbital (LUMO) [8]. The common value of this HOMO-LUMO band gap of conjugated molecules is

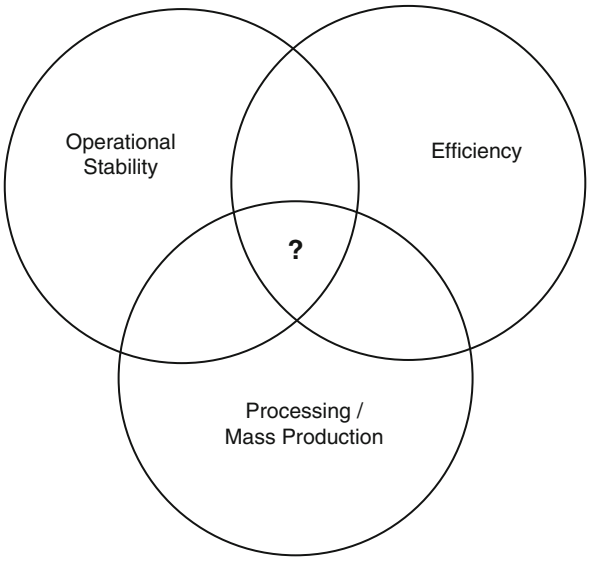

Organic Solar Cells. Figure 3
A Venn diagram representing the challenges for OPV. Of the necessary requirements for wide-scale commercialization of OPV, devices satisfying two out of three of the necessary conditions have been demonstrated. Additionally, ultimate success of OPV also includes environmental sustainability of the raw materials used to make them

in the range of 1.5–3 eV, and can be systematically changed through synthetic modification of the molecule [9]. An example of structure to band gap relation is shown in Fig. 4.

In Fig. 5, the absorption coefficients of thin films from two common conjugated polymers poly (2-methoxy-5-(3',7'-dimethyl-octyloxy))-p-phenylene vinylene (MDMO-PPV), poly(3-hexyl thiophene) (P3HT) and Zinc Phthalocyanine, (ZnPc), a common vacuum-deposited donor material, are shown. Also the acceptor material [6,6]-phenyl C_{61}-butyric acid methyl ester (PCBM) is shown. The air-mass (AM 1.5) standard solar spectrum is overlaid in this figure as well. It is easy to see that a major drawback of current OPV materials is that a large amount of photons in the >700 nm region are not absorbed. In comparison, the silicon band gap and onset of optical absorption spectrum is around 1.1 eV (ca. 1,100 nm). An advantage of organic materials is that their absorption coefficients are comparatively high ($\approx 10^5$ cm^{-1}) relative to inorganic materials. This allows for efficient absorption in very thin active layers on the order of tens to hundreds of nanometers. Conventional crystalline silicon solar cells, in contrast, are typically more than a 100-μm thick [10].

Photoinduced Charge Transfer Photogeneration of charges in organic semiconductors involves excitons. Light absorption by an organic semiconductor first leads to the creation of excitons, which are bound electron-hole pairs with typically a binding energy of a few tenths of an electron volt and a lifetime of ~1 ns at room temperature [11, 12]. These excitons can diffuse from molecule to molecule during their lifetime with a diffusion length generally limited to about 5–20 nm [13–15] and subsequently either decay by recombination or dissociate to form free electrons and holes. Because of their large binding energy, these excitons can only dissociate in the presence of an electric field or at a donor-acceptor interface where the dissociation is driven by charge transfers between the donors and acceptors [11, 16, 17]. In early single-layer organic solar cells, exciton dissociation in the bulk was usually achieved using a metal/organic/metal architecture where the electric field on the organic semiconductor is derived from using electrodes of sufficiently different work functions. However, the exciton dissociation efficiency proved relatively low because of the limited built-in electric field strength. A major breakthrough came with the discovery of the donor/acceptor bilayer cell, where efficient exciton dissociation takes place at the

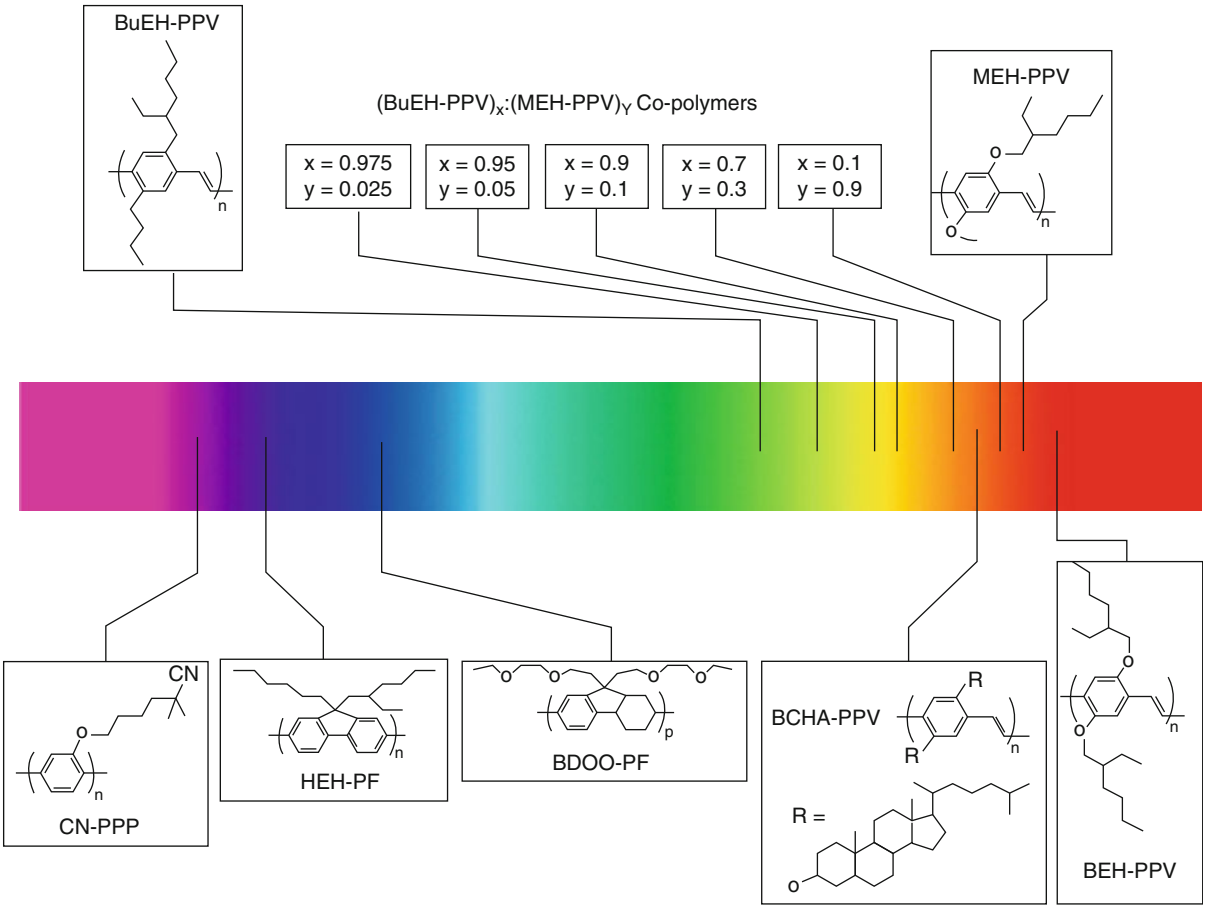

Organic Solar Cells. Figure 4

The modification of chemical structure in organic semiconductors results in changes of the band gap, that is, absorption edge of the solar cells and/or emission color of the light emitting devices

donor/acceptor interface [5, 92]. In this process, electron transfer from the donor to acceptor requires that the LUMO of the donor is above that of the acceptor, and hole transfer from the acceptor to donor requires that the HOMO of the donor is above that of the acceptor.

$$I_p(\text{Donor}) - E_A(\text{Acceptor}) - U_p < 0$$

Where I_p is the ionization potential, E_A the electron affinity, U_p all Coulomb effects including the polarization effects.

This process is illustrated in Fig. 6.

Photoinduced charge transfer processes are of fundamental interest for understanding photoconduction in organic solids. Important technologies based on organic photoconductors have been developed. Starting in the 1950s, photoinduced processes in organic thin films were extensively studied for xerography applications, and by the 1970s nearly all printers and copiers were based on the action of organic charge-generation layers and organic photoconductors [18]. This is a powerful inspiration for organic solar cells, as the printing and xerography industries have demonstrated the efficacy of low-cost high-volume production of robust organic-based products.

A basic description of the photoinduced charge transfer between a donor molecule D and an acceptor molecule A can be described as follows:

Step 1: $D + A \rightarrow D^* + A$ (photoexcitation of D – generation of exciton)

Step 2: $D^* + A \rightarrow (D{-}A)^*$ (exciton delocalization between D and A)

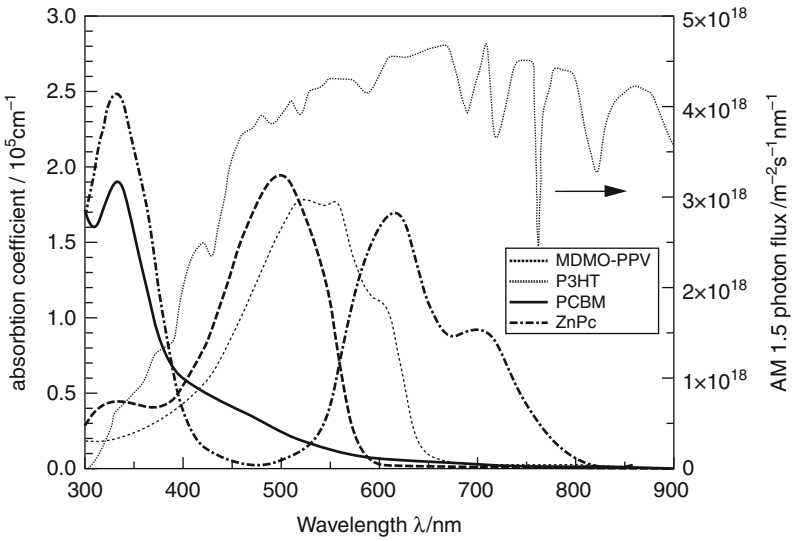

Organic Solar Cells. Figure 5
The solar spectrum, with units on the right axis, plotted against the absorption coefficients of three donor materials, MDMO-PPV, P3HT, and ZnPc and acceptor materials, PCBM

Step 3: $(D{-}A)^* \rightarrow (D^{\delta+}{-}A^{\delta-})^*$ (polarization of excitation: partial charge transfer)

Step 4: $(D^{\delta+}{-}A^{\delta-})^* \rightarrow (D^{\bullet+}{-}A^{\bullet-})$ (radical anion-cation pair formed)

Step 5: $(D^{\bullet+}{-}A^{\bullet-}) \rightarrow D^{\bullet+} + A^{\bullet-}$ (complete charge separation)

The example given here is for electron transfer from excited donor onto the acceptor. Alternatively, a positive hole transfer from an excited acceptor onto a donor can be written equivalently. A and D have to be either covalently bound (intramolecular charge transfer) or spatially very close (intermolecular charge transfer) for success of this process. To initiate step 2 in the above scheme, the electronic wavefunctions of A and D must have a significant overlap, so the distance between the molecules must be small [19, 20]. In this process, the orientation and symmetry between the participating molecules is often of great importance [21].

In order for step 4 to occur, the energy levels of the participating molecules must be properly aligned. Only if the offset between the LUMOs (for electron transfer) or the HOMOs (for hole transfer) of donor and acceptor is large enough to overcome the Coulombic attraction holding together the exciton, charge separation will be possible. The theories developed by Marcus and Jortner describe the energetics and kinetics of the photoinduced charge transfer taking into account the orientation and the distance between the donor and acceptor chromophore [22, 23].

If all requirements are met, charge transfer can be very efficient with transfer rates as high as $k_T = 10^{12}s^{-1}$ [14, 24]. The charge transfer state can be metastable due to a fast delocalization of the charge carriers on one or both of the molecules and nanophases [25]. Since charge transfer happens on a faster timescale than radiative decay in most organic chromophores, such as conjugated polymers, successful photoinduced charge transfer can be experimentally verified by measuring the quenching of the luminescence and decrease of luminescence lifetime for both compounds when they are brought in close contact with each other.

The most prominent electron acceptor used in OPVs is fullerene. C_{60} fullerene can be readily thermally evaporated for vacuum-processed cells. For solution processing, C_{60} must be derivatized due to its limited solubility. The most popular such derivative is PCBM ([6,6]-phenyl C_{61}-butyric acid methyl ester). Many organic materials undergo photoinduced electron transfer to fullerenes, such as conjugated polymers [14], metal phthalocyanine [26] or porphyrin molecules [27]. A great advantage of using fullerenes as

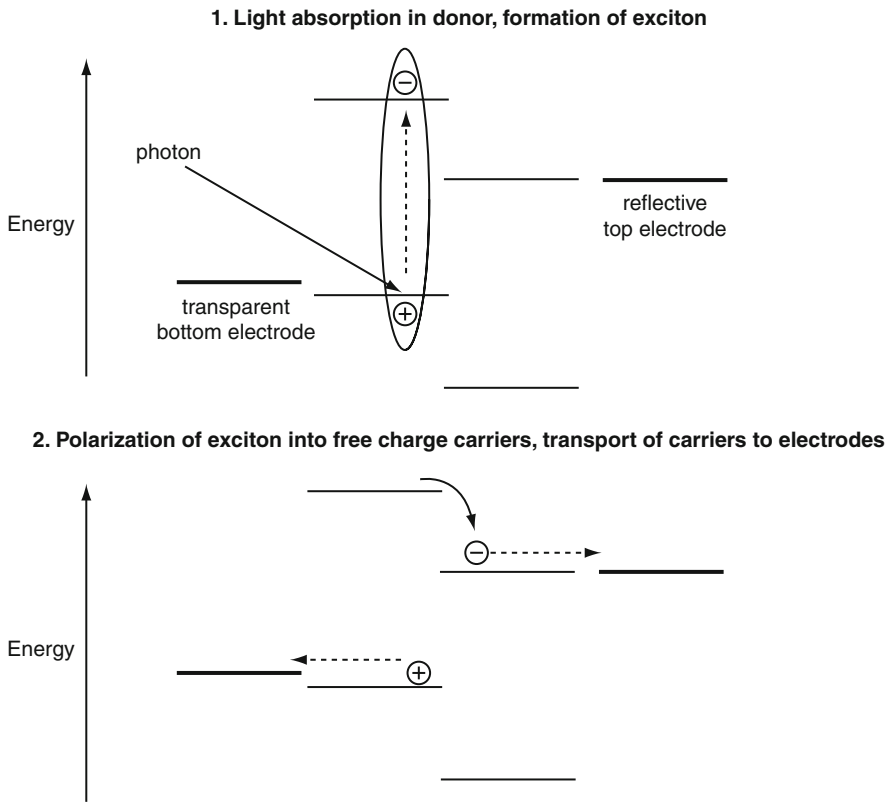

Organic Solar Cells. Figure 6
Depiction of the absorption of light in the donor and formation of a Coulombically bound excited state, the exciton. This excited state is polarized by the electron acceptor, creating separated charges. These charges, in step two, are transported to the electrodes due to internal electrical field-induced drift and/or charge carrier concentration-induced diffusion

photoinduced charge transfer acceptors for other molecules is their high symmetry that leads to a good contact with the neighboring molecules, almost independent on the fullerene orientation. One of the most striking aspects of the photoinduced charge transfer between organic donor molecules, especially conjugated polymers and fullerenes, is the long lifetime of the charge-separated state. Under favorable conditions, the photoinduced charge transfer is ultrafast with rates above 10^{12} s^{-1} while the back transfer is almost ten orders of magnitude slower at room temperature. This phenomenon is at the heart of the operating principles of an OPV device.

Charge Carrier Transport Charge separation is necessary, but not sufficient, for the eventual conversion of light to electricity. In the next step, the separated charges must be transported to and collected by the opposite electrodes. Positive holes will move along donor molecules due to diffusion (electrochemical gradient-driven) and/or drift (driven by built-in electric field) toward the cathode, while electrons will move along electron acceptor molecules in a direction opposite to the holes, toward the anode. The mechanism for charge transport in organic thin films is a subject of intensive research interest, and of course its efficiency is of paramount importance to the overall organic solar cell efficiency. The following equations for charge carrier velocity, v, and current density, j, describe the charge-transport occurring within an OPV device.

$$v = \mu \cdot E$$

$$j = j_{\text{drift}} + j_{\text{diffusion}}$$

$$j_{\text{drift}} = e \cdot n \cdot \mu \cdot E$$

$$J_{\text{diffusion}} = D\frac{\partial n}{dx} = \mu\frac{kT}{e} \cdot \frac{\partial n}{dx}$$

Charge transport issues are related to carrier mobility, μ, which is defined as the velocity of the charge carrier (electron or hole) per unit electric field, and n, the number of carriers. The total current density, j, in a solar cell is the sum of the drift currents driven by electric field (j_{drift}) and by diffusion current ($j_{\text{diffusion}}$) driven by the concentration gradient, ($\frac{\partial n}{dx}$), of the carriers. In inorganic materials, charge transport is relatively straightforward. The periodic crystal lattice creates extended conduction and valence bands in which charge carriers can move with very high mobilities. Long-range order and strongly coupled covalently bound atoms result in delocalized energy bands that allow free carrier transport. Transport velocity is limited by scattering events, that is, mobile electrons can collide with an atomic displacement (phonon scattering) or some impurity in the crystal lattice (impurity scattering). In organic thin films, however, molecules do not arrange with long-range (i.e., single crystalline) ordering, but rather form a disordered (amorphous) solid with no long-range ordering and no translational symmetry. This is the result of weak intermolecular interactions (van der Waals forces), as opposed to the strong covalent bonding in silicon crystals. Thus, positive and negative charges, once formed following the dissociation of an exciton, must travel from molecule to molecule. The nature of charge transport in organic films is a complex problem and explaining these models is beyond the scope of this chapter. The interested reader is referred to several reviews of the subject [28–30]. Basically, charge transport in organic films can be efficient within the conjugated π system of a molecule; however, carriers must hop from one delocalized π system of one molecule to that of an adjacent molecule. This is known as the hopping transport, a mechanism that limits the overall mobility in most organic thin films. Mobilities in OPV films are many orders of magnitude lower than in inorganic single-crystalline materials. One important concept is the density of energetic states. A single π-conjugated molecule in a vacuum would have a HOMO, LUMO, and a discreet forbidden energy gap between. However, once in the solid state, many molecules are placed adjacent to one another, interacting with each other through weak van der Waals forces; there is an inevitable dispersion of HOMO and LUMO levels from molecule to molecule. When statistically added up, the energy levels will have a statistical distribution (commonly Gausssian). This is known as the density of states (DOS). This concept is illustrated in Fig. 7. The profile of DOS and the density of photogenerated electrons will have a profound influence on charge mobility (Fig. 8).

Experiments with single-crystalline organic solids and single polymer chains have demonstrated mobilities greater than 1 $cm^2\ v^{-1}\ s^{-1}$ orders of magnitude higher than the typical mobilities found in amorphous organic films. Thus, if ideally crystalline organic films with separate donor and acceptor domains can be produced to form OPV devices, theoretically high mobilities can also be obtained. Experimental observations show that the charge mobilities in high-efficiency OPV devices are not high, but the carrier lifetimes are [31]. When holes and electrons are separately transported within spatially separated domains, the probability for charge recombination is reduced considerably leading to long charge carrier lifetimes. The recombination of charge carriers is much less efficient in P3HT-PCBM solar cells as compared to the expected Langevin recombination rate, and the origin of this discrepancy is still under debate. The carrier drift length, or the distance that a charge carrier can travel without recombination, is shown in the following relation:

$$d = \mu \cdot \tau \cdot E$$

Thus, work in the OPV field focuses on controlling the microscopic morphology of donor-acceptor domains in such a way as to maximize charge carrier lifetime in these domains where the carrier mobilities are intrinsically low. Charge carrier mobilities in organic solar cells are around 10^{-4}–10^{-2} $cm^2\ v^{-1}\ s^{-1}$, however carrier lifetimes can be as high as milliseconds, though typically tens of microseconds. This allows for effective charge transport to electrodes. Indeed, in many organic solar cell systems, absorbed photon-to-electron conversion efficiencies are ≈90% [7, 31].

As mentioned before, the charge carrier extraction is driven by internal electric fields across the photoactive layer caused by the different work function

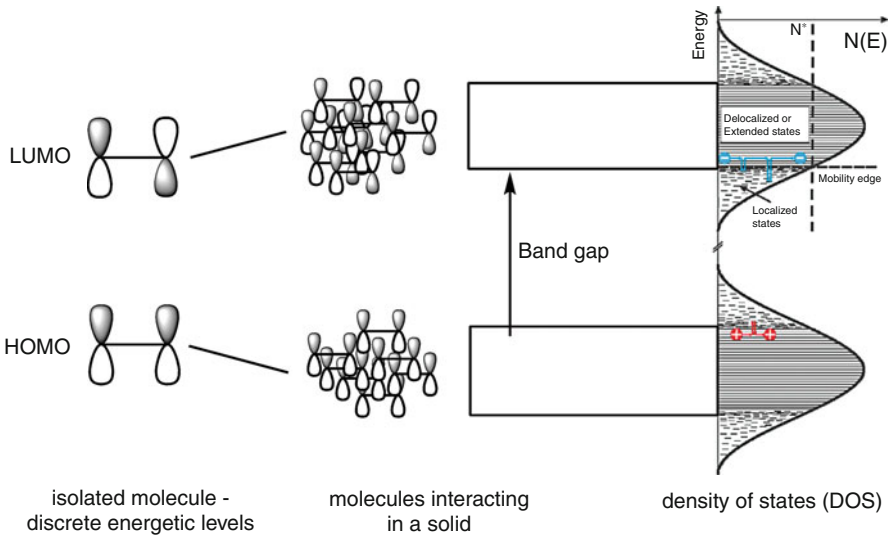

Organic Solar Cells. Figure 7
Diagram showing an ensemble of conjugated π molecules interacting in the solid state to create a density of available electronic states

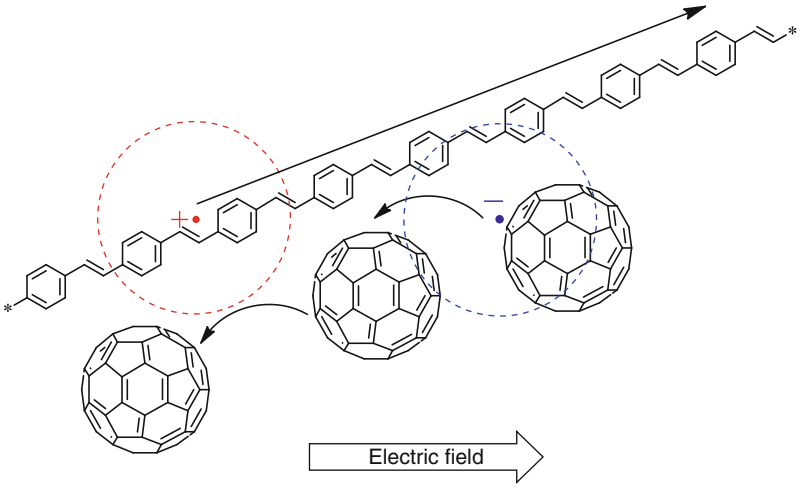

Organic Solar Cells. Figure 8
Charge transport in a polymer-fullerene solar cell. Positive holes will be transported down the polymer π conjugated chain. Transport along one polymer chain is very rapid, hopping from chain to chain is the "slow" process. Electrons will move along acceptor fullerenes. Electron mobility in fullerenes is typically high enough to allow nearly 100% efficient extraction of electrons to the anode

electrodes for holes and electrons, as well as by diffusion. The internal electric field E that drives this drift current under photovoltaic operation is generally originating from the difference in the electrodes' work functions. For example, in an OPV device with 90 nm thick active layer, with gold as the hole-accepting (work function, $\varphi = 5.2$ eV) and aluminum being the electron accepting electrode ($\varphi = 4.3$ eV), an internal electric field of 10^5 V/cm is present at short-circuit conditions under the assumption of a metal-insulator-metal

picture [32]. Assuming charge carrier mobilities of 10^{-4} cm^2 v^{-1} s^{-1}, and charge carrier lifetimes of 1 μs, a drift length d = 100 nm at short circuit conditions is calculated. This means that theoretically under these conditions 100% of carriers should be successfully collected at the electrodes. Without a detailed analysis, one can generally assume that thin film organic devices (≈100 nm) are mostly field drift dominated. This calculation of electric field across the device assumed the metal-insulator-metal (MIM) model. This is only valid when the organic semiconductors are treated as insulators and as long as there is no significant space charge built up during operation, which would result from an unbalanced electron and hole transport. Charge injection into and charge extraction from the molecular HOMO or LUMO levels produce diode-like rectifying behavior in an organic photovoltaic cell [7, 33]. The cell working under different electrical bias, using a MIM model, is shown in Fig. 9.

The different working regimes of a photovoltaic device are shown in Fig. 9 and can be correlated with current-voltage curve in Fig. 10. Point (a) corresponds to the short circuit photocurrent I_{SC}, where the diode is operating under a maximum built-in electric field; (b) the diode is in flat band condition with no current, producing a maximum photovoltage or open circuit voltage V_{OC}; at point (c), the diode is reversed bias, increasing the internal electric, and (d), the diode is forward biased, increasing the dark current flow as the internal field is reversed and charge injection is increased. OPV devices operate in the forward bias region for power generation, but the photocurrent is opposed to the dark forward bias current and produced under a reduced internal field as compared to regions (a) and (c). Because most OPV devices are based on low-mobility semiconductors, the maximum power that can be extracted from an OPV device is highly dependent on their transport properties, which in turn can limit the light absorption due to the necessary use of a very thin film as the absorber.

The power conversion efficiency, (η) of a solar cell is defined as follows:

$$\eta = \frac{P_{out}}{P_{in}} = \frac{I_{mpp} \cdot V_{mpp}}{P_{in}} = \frac{FF \cdot I_{sc} V_{oc}}{P_{in}}$$

P_{mpp} is the maximum power output point for a given optical power, P_{in}, incident on the solar cell. As shown in Fig. 10, P_{mpp} is a product where the ratio

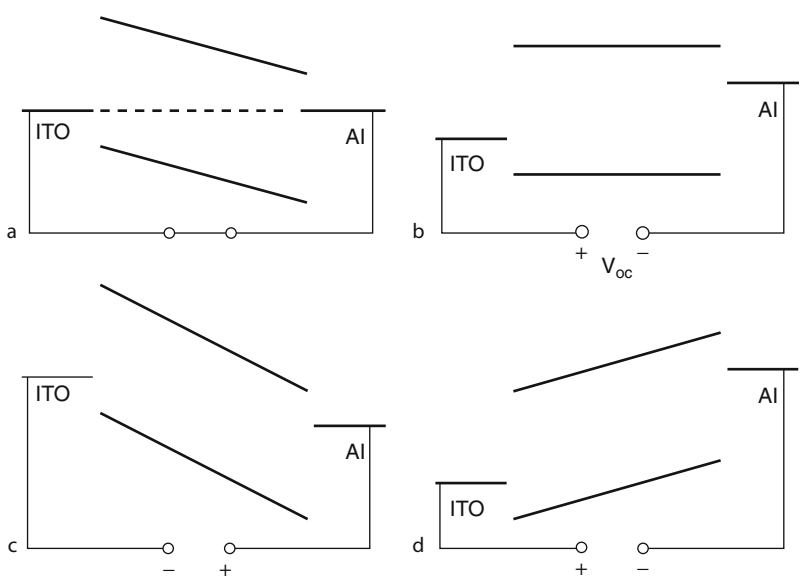

Organic Solar Cells. Figure 9

Metal-Insulator-Metal Model – Electric Potential for organic semiconducting layers sandwiched between two commonly used metallic electrodes: (**a**) short circuit condition, (**b**) flat band condition, (**c**) reverse bias, and (**d**) forward bias. Band bending effects at the contacts are neglected. *ITO* = Indium-doped Tin Oxide, a transparent conductive oxide

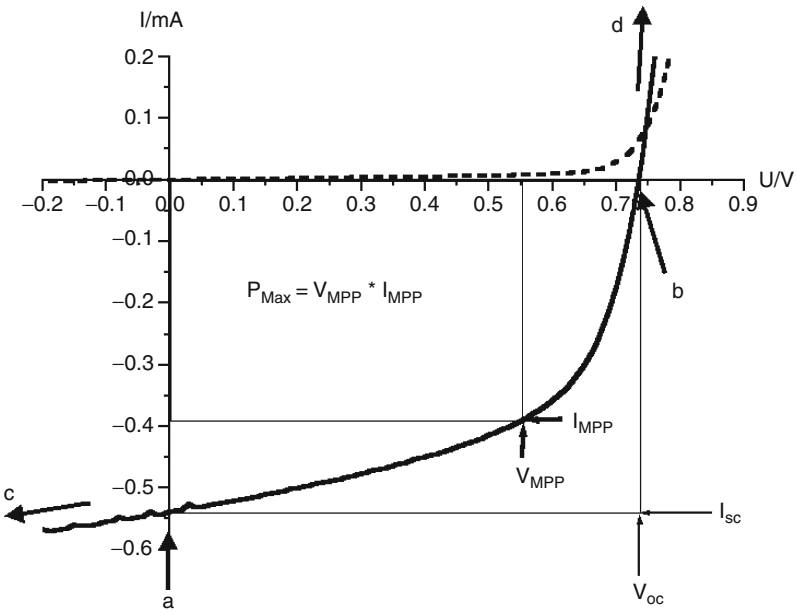

Organic Solar Cells. Figure 10
Current-voltage (I-V) characteristics of an organic solar cell under illumination (*solid line*) and in the dark (*dashed line*)

of $I_{mpp} \cdot V_{mpp}/V_{oc} \cdot I_{sc}$ is maximum. This ratio is commonly known as the fill factor, FF, and the P_{mpp} can be expressed in terms of three key photovoltaic parameters: $P_{mpp} = V_{oc} \cdot I_{sc} \cdot FF$. In general, the fill factor is a reflection of the field-dependent charge generation and transport characteristics of an OPV.

Optimizing an OPV features requires simultaneously maximizing short circuit photocurrent (I_{sc}), open circuit voltage (V_{oc}), and fill factor (FF). The short circuit current is proportional to the amount of light absorbed in the active layer. Thus to optimize I_{sc}, the organic semiconductors forming the absorber layer should have a wide absorption spectrum that matches the solar radiation in the visible and near-IR range. Although it is desirable to use a thick absorber layer to capture as much light as possible in an OPV, in practice, the thickness of this layer is limited to usually no more than a few hundred nanometers due to the high resistivity and field-dependent transport characteristics of most organic semiconductors. The open circuit voltage, V_{oc}, is related to the built-in potential, which is primarily determined by the relative energy gap between the HOMO of the donor and the LUMO of the acceptor (Fig. 11). Experimentally, V_{oc} is found to be linearly dependent on this energy gap to the following relation [39], where delta (δ) is the additional energy loss term associated with possible polarization:

$$V_{oc} \propto (1/e)\left(|E_{donor}\mathrm{HOMO}| - |E_{acceptor}\mathrm{LUMO}|\right) - \delta(\mathrm{losses})$$

The total photovoltage is ideally equal to the band gap value of the light absorbing semiconductor. However, due to the high exciton-binding energy in organic materials, donor-acceptor cells are utilized with a LUMO-LUMO offset needed to polarize the exciton. This energy difference directly subtracts from total photovoltage. The goal for V_{oc} should be that V_{oc} approach the magnitude of the band gap; that is, the LUMO offset (donor relative to acceptor) should be just large enough to obtain the charge transfer. The factors governing the origin and optimization of open circuit voltage in OPVs have been extensively studied [34–39].

Building an Organic Solar Cell: Materials, Fabrication, Optimization

The Substrate

The fabrication of an OPV device uses glass or plastic substrates. In OPV research, the most frequently employed substrate is glass, due to its low cost, stability,

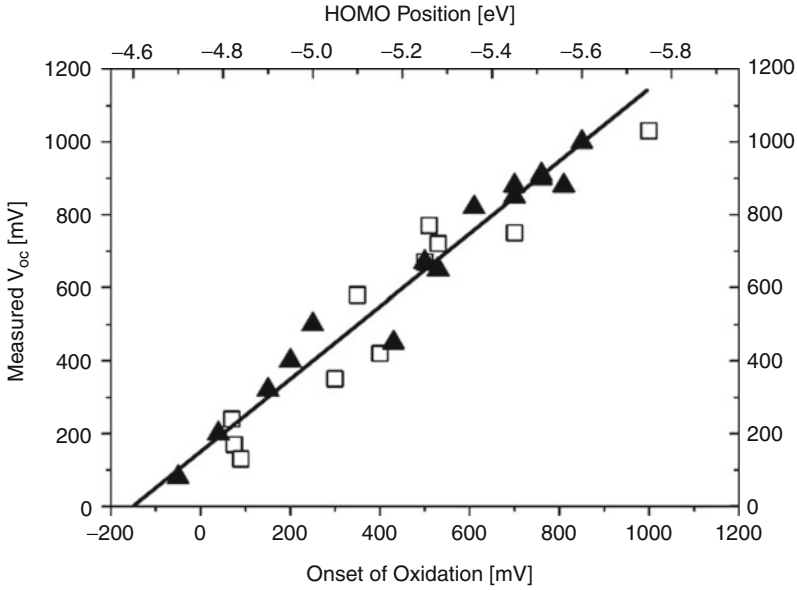

Organic Solar Cells. Figure 11
The experimentally determined linear relationship between the HOMO levels of many different conjugated polymers (determined electrochemically against an Ag/AgCl reference electrode) and the V_{oc} of devices of the polymer/PCBM device (From [39])

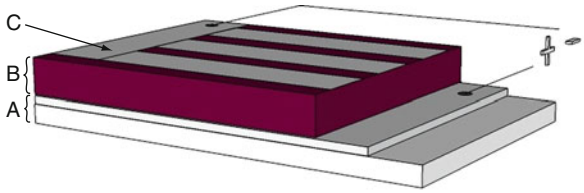

Organic Solar Cells. Figure 12
Schematic view of an organic solar cell covered in this section

and extremely effective barrier properties. However, in the laboratory, OPVs have been demonstrated on flexible plastic substrates such as poly (ethylene terephthalate) (PET), poly (ether sulfonate) (PES), and polycarbonate [40]. High-volume production of solution-processed OPVs has also been demonstrated on flexible plastic substrates using roll-to-roll methods [40–42] (Fig. 12).

Suitable substrates for organic PV devices should fulfill several requirements: (1) low-cost, (2) chemical and thermal compatibility/stability with subsequent processing steps, (3) mechanical and environmental stability, with good barrier properties to oxygen and water, and (4) high optical transparency.

Currently, OPV devices use a transparent conductive oxide (TCO), typically deposited on the substrate, as one of the electrodes. The most commonly utilized TCO is indium-doped tin oxide (ITO), which demonstrates a good balance between transparency and conductivity. The work function of ITO can be varied over a wide range, between about 3.7 and 5.1 eV, by controlling the oxygen stoichiometry through preparation technique and surface treatment/cleaning. Carbon-containing residues present on the surface are known to lower the work function, whereas treatments with oxidizing agents such as oxygen plasma are effective in raising the work function [43–45]. The natural abundance of elemental indium is a concern for the widespread use of ITO, which has spurred the development of ITO substitutes, such as zinc oxide-based as well as carbon-based (nanotubes and graphenes) TCOs [46, 47].

In solution-processed OPVs, the ITO electrode is typically coated with an additional layer of conductive polymer as a contact buffer for the organic semiconductor layer. The most commonly used conductive polymer is PEDOT:PSS, a polyethylenedioxythiophene doped with poly(styrene sulfonate).

PEDOT:PSS, deposited from an aqueous solution, serves to reduce the ITO surface roughness and provide a surface with a more defined work function [48, 49]. However, it is known that PEDOT:PSS has degradation issues, which are related to its affinity for moisture and acidic nature [50–52]. In vacuum-processed OPVs, the ITO electrode is often supplanted with a transition metal oxide, such as MoO_x and NiO_x, for raising the work function and forming an Ohmic contact for holes to p-type organic semiconductors such as the phthalocyanines [53, 54].

The Active Layer

In this section, the active layers for both solution-processable and vaccum-depositied OPVs will be discussed with focus on materials and fabrication processes. Solution-processed OPVs rely on the bulk heterojunction (BHJ) as the active layer, which typically comprises a mixture of conjugated polymer and a small-molecule component, such as the prototypical P3HT:PCBM. The BHJ is an interpenetrating network of donor and acceptor domains created by casting a thin film on a substrate (such as ITO glass) from a common solution of the donor and acceptor. By controlling the donor and acceptor concentrations in the solution, the type of solvent, and the coating conditions such as casting speed, drying duration, and post-deposition annealing, the BHJ can be fine-tuned to produce the desired phase segregation between the donor and acceptor for charge generation while maintaining a continuous path in each phase for the transport of electrons and holes [7, 55]. In a bulk heterojunction, this interpenetrating network creates a high density of donor/acceptor interfaces on the nanoscale of 10–20 nm and ensures excitons produced by light absorption anywhere in the BHJ will reach the donor/acceptor interface to be dissociated, and the separated charge pairs will be transported through the network without significant loss through recombination and collected by the electrodes.

Early work on solution-processed OPVs rely on BHJs, comprising derivatives of PPV poly(phenylene

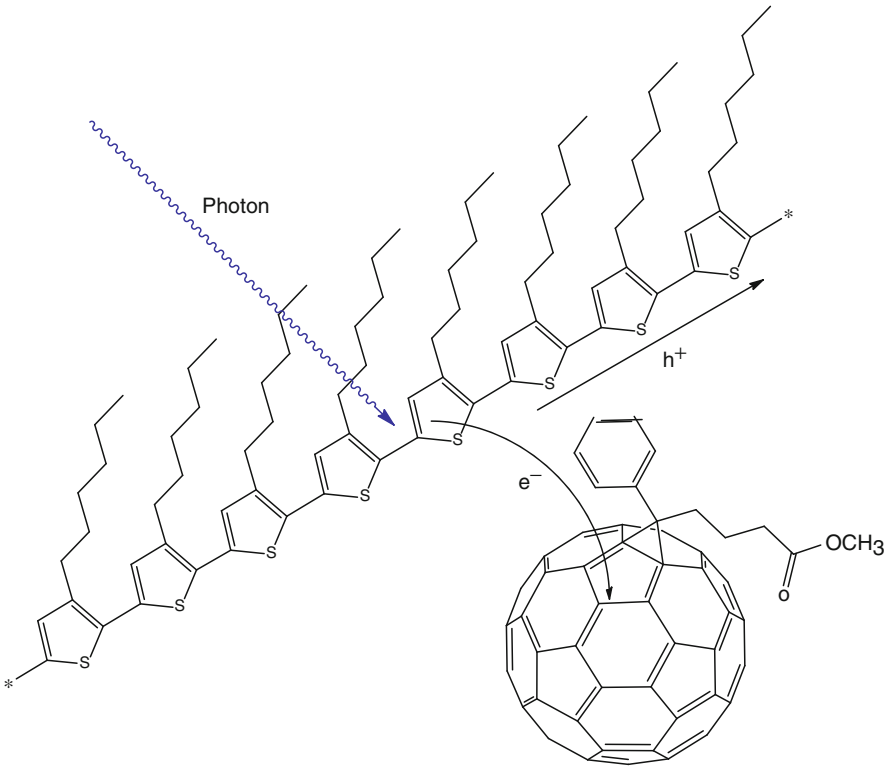

Organic Solar Cells. Figure 13
A model system – the P3HT – PCBM bulk heterojunction solar cell

vinylene) as the polymeric donor and PCBM as the molecular acceptor. Although these PPV-based OPVs were able to demonstrate efficiencies up to 2% in the early 2000s [56, 57], they quickly fell out of favor due to low mobility and chemical instability issues, [58–60] and were superceded by the polythiophene family of polymers. The prototypical system is the P3HT/PCBM, (Fig. 13), which has been extensively studied with respect to OPV device performance and its correlation with material composition and fabrication processes [61, 62]. Table 1 lists the efficiency of P3HT/PCBM OPVs achieved during the last decade.

Polythiophenes can be synthesized in several different ways. The first method, historically, is a transition metal-catalyzed coupling between dibrominated thiophenes. The second most often employed method is oxidative polymerization with ferric chloride, $FeCl_3$, as an oxidizer, or electrochemical polymerization where the polymerized thiophene is deposited on an anode. Polymerization induced with $FeCl_3$ is used on an industrial scale for the production of poly(2,3-ethylene dioxy thiophene), PEDOT [63, 64]. A very significant development was made in 1993 with a metal-catalyzed method that yielded regioregular polythiophenes [65]. Most polythiophenes are substituted with alkyl groups in the 3 position of the thiophene ring in order to allow high solubility in organic solvents. There are four permutations of coupling patterns available for thiophenes substituted with alkyl groups in the 3 position, shown in Fig. 14.

Polymerization with controlled regioregularity selectively produces polymers with repetition of one pattern only and leads to considerably higher charge carrier mobilities. The structure of the alkyl chain has a large effect on morphology of the active layer film, and thus on the mobility [66, 67].

Spontaneous phase separation in BHJ blends occurs since there is no entropy of mixing for high molecular weight polymers (the entropy of mixing goes to zero as the polymerization index approaches infinity). Thus, even though the donor and acceptor components are each soluble in the solvent used for processing, the BHJ networks will spontaneously phase separate as the solvent evaporates. The interfacial energy can be controlled using additives such as amphiphilic molecules for optimizing nanoscale phase separation. The length scale of such phase-separated domains must be comparable to exciton diffusion length, approximately 10–20 nm [70, 90].

The morphology of the BHJ blend can be fine-tuned by controlling the phase separation during the film formation (during evaporation) or by subsequent treatment of the solid film. The following parameters have been identified for their influence on the nanoscale morphology of the BHJ blends:

(a) Casting solvent: viscosity, boiling point, interaction with substrate
(b) Donor:Acceptor ratio
(c) Chemical additives

Organic Solar Cells. Table 1 A nonexhaustive summary of P3HT/PCBM optimization history

Year	Weight ratio to PCBM	Active layer thickness (nm)	Solvent	Max EQE%	V_{oc} (mV)	FF	J_{sc} (mA·cm^{-2})	PCE %	Light intensity (mW cm^{-2})	Refs.
2002	1:3	350	–	76	580	0.55	8.7	2.8	100	[68]
2003	–	110	Dichlorobenzene	70	550	0.60	8.5	3.5	80	[69]
2005	1:1	–	Chlorobenzene	58	610	0.53	9.4	3.0	100	[74]
2005	1:1	63	Dichlorobenzene	–	610	0.62	10.6	4.0	100	[84]
2005	1:1	≈220	Dichlorobenzene	63	610	0.67	10.6	4.4	100	[71]
2005	1:0.8	–	Chlorobenzene	–	630	0.68	9.5	5.0	80	[60]
2006	1:1	175	Chlorobenzene	70	600	0.52	12	4.4	85	[87]
2008	1:1	≈220	Dichlorobenzene	87	640	0.69	11.3	**5.2**	100	[54]

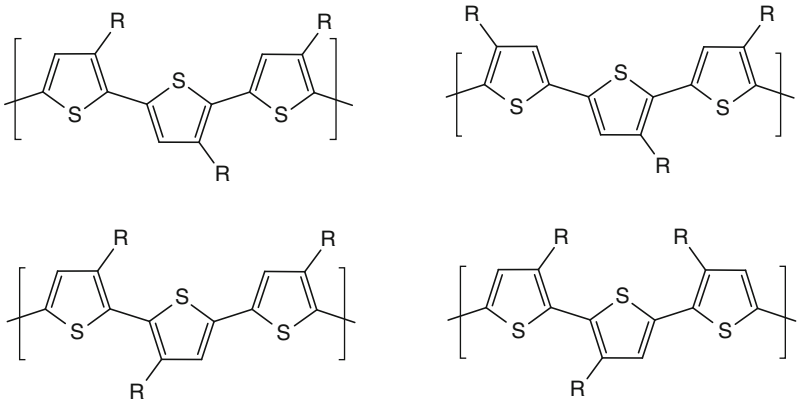

Organic Solar Cells. Figure 14
Examples of regioregular poly(3-alkyl thiophene)

(d) Concentration of Donor:Acceptor in the solution
(e) Control of phase separation by thermal and/or solvent annealing
(f) Molecular structure of the materials and their mutual miscibilities

The molecular structures of the donor and acceptor materials determine their solubility in organic solvents and their miscibility with each other. The solvent volatility dictates the drying time during film formation. Thermal and/or solvent vapor annealing induce diffusion and nanoscale crystallization of one or both components in the BHJ blend [71]. These process steps, taken individually or together, can lead to various degree of phase separation and, ideally, the formation of continuous crystalline domains. Post-fabrication thermal annealing has been extensively explored to achieve high efficiency in the P3HT:PCBM solar cell material system. As shown in Fig. 15, transmission electron microscopy (TEM) images of the P3HT/PCBM films reveal that the film (a) prior to annealing has an ultrafine grain structure with no apparent phase segregation between the donor and acceptor domains. After thermal annealing (10 min at 150°C), an interpenetrating network of donor and acceptor is beginning to develop as can be seen in film (b), which becomes more pronounced with prolonged annealing (2 h), film (c). The observable morphological feature has a scale of ~10–20 nm and appears to be somewhat elongated [72].

Annealing at high temperatures increases the crystallinity within the phase-separated networks, causing enhanced charge transport to the electrodes and thus increased efficiency. Stable solar cell performance is observed for P3HT:PCBM even after annealing at 150°C. This remarkable thermal stability of the nanoscale interpenetrating donor-acceptor networks suggests the possibility of long lifetimes with BHJ solar cells. These changes in the morphology are accompanied by changes in the optical absorption (Fig. 16) strongly suggesting improvements in the local structural order. Importantly, these changes induced by thermal annealing are permanent; they remain after cooling the films to room temperature [73].

A hypothesis that vertical phase segregation, perpendicular to the electrodes, between P3HT and PCBM results from the thermal annealing was advanced by Kim et al. [74]. The orientation is such that the hole are transport toward the PEDOT:PSS electrode and electron transport to the top-aluminum electrode are facilitated. Yang et al. reported phase-contrast TEM and electron diffraction results of P3HT:PCBM blends [75], showing an increase in crystallinity for both P3HT and PCBM phases as well as a fibrillar P3HT morphology with extended length following thermal annealing. Phase contrast TEM provides an enhanced method for spatially imaging the donor and acceptor regions of an active layer. They concluded that the expanded crystalline domains are responsible for the improved device performance. Figure 17 shows the TEM images together with the electron diffraction images for the untreated and the annealed P3HT:PCBM blend.

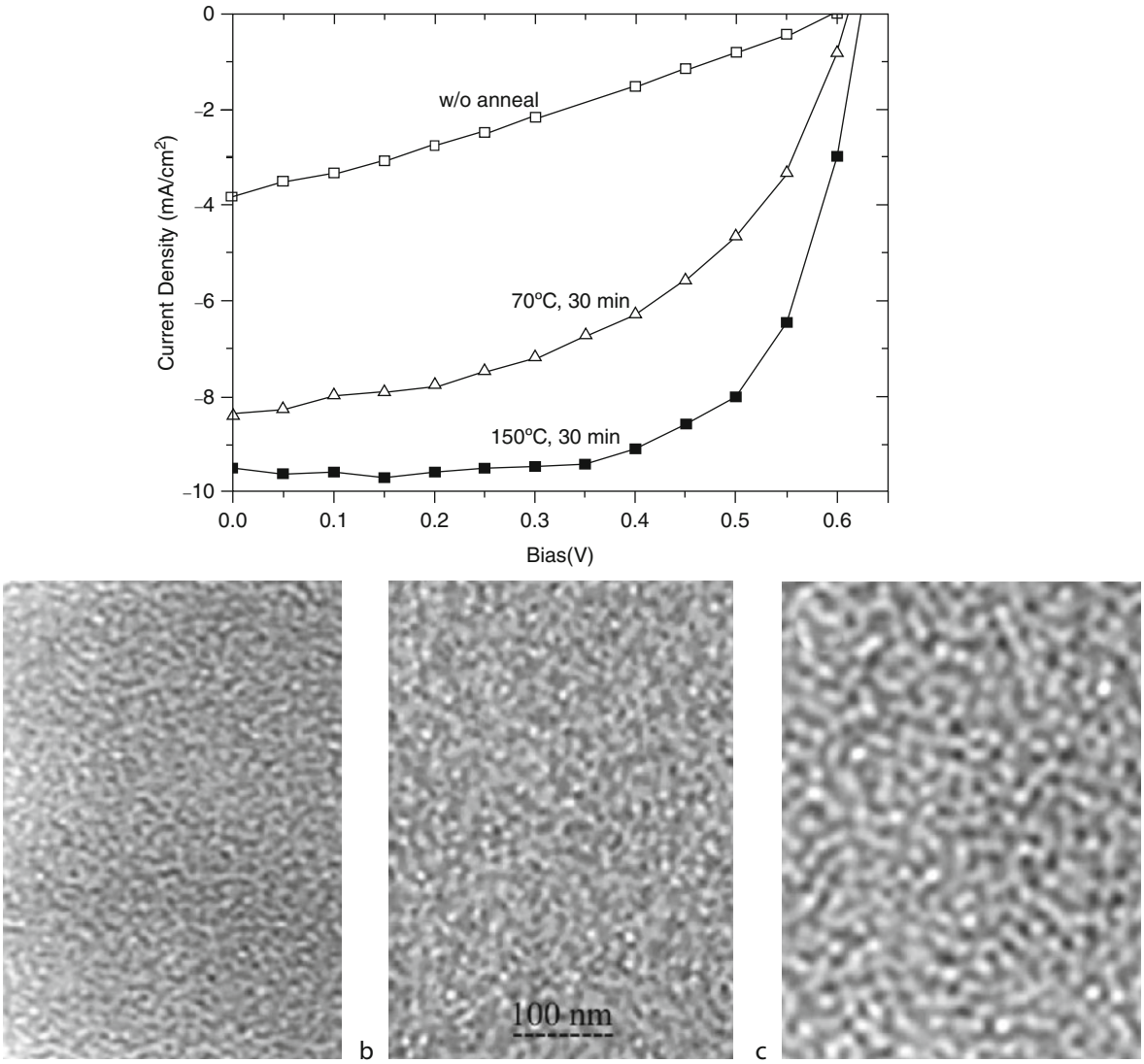

Organic Solar Cells. Figure 15

(*Top*) Current-voltage characteristics for P3HT:PCBM measured before and after thermal annealing. (*Bottom*) Phase contrast TEM images of P3HT:PCBM film. The scale bar on the center bottom is 100 nm for all the images; (**a**) Prior to annealing; (**b**) annealed at 150°C for 10 min; (**c**) annealed at 150°C for 2 h (From [72])

Here, the P3HT backbone is oriented vertical to the P3HT-fibrils, with the π-π stacking direction parallel to the fibril axis of the P3HT crystal [66]. Hence, there are better charge carrier mobilities resulting along the π-π stacking direction (long axis of fibrils).

Erb et al. further investigated the crystalline structure of P3HT:PCBM bulk heterojunctions by grazing incidence X-ray diffraction (GID-XRD) [76], showing that upon annealing P3HT crystallites with dimensions of about 10 nm are grown. The polymer backbone orientation within these crystallites was found to be parallel to the substrate, with the side chains oriented perpendicular to the substrate. The XRD signals before and after thermal annealing of P3HT:PCBM composites are shown in Figs. 18 and 19.

It has been shown by electron diffraction that PCBM is capable of self-organizing into crystalline order in pristine PCBM films [78]. In a study on

MDMO-PPV:PCBM blends, Yang et al. detected diffraction fringes in the blend films of varying composition and concluded that PCBM phase is consisted of nanocrystallites. Furthermore, upon annealing, the PCBM tends to form larger crystals and thereby destroys the original blend morphology. The conclusion of morphological instability at elevated temperatures was drawn for poly(phenylene vinylene)/fullerene systems [79]. In contrast, Yang et al. found that P3HT:PCBM blends are considerably more stable than the PPV:PCBM blends. Apparently, the morphology of the P3HT:PCBM blends is stable with annealing for over 1,000 h at an elevated temperature of 70°C [75]. Hence, they suggested that the ability of P3HT to crystallize has a stabilizing effect on the blend morphology. Schuller et al. reported similar results for annealing at an even higher temperature of 85°C and under simultaneous illumination [80]. Drees et al. demonstrated that, by introducing a reactive epoxy group into PCBM, the fullerenes could be polymerized by using a catalyst along with annealing [81]. Unlike conventional P3HT:PCBM blends, morphological stabilization could be achieved using cross-linked epoxy-modified C_{61}-butyric acid glycidol ester (PCBG). Figure 20 shows tapping-mode AFM images obtained on P3HT:PCBM and P3HT:PCBG blend films, both untreated and after thermal annealing. Clearly the phase separation inside the P3HT:PCBG blend is stopped before larger fullerene crystallites (c) can be developed due to cross-linking.

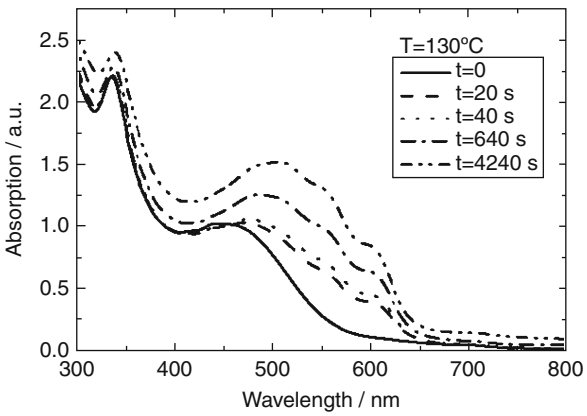

Organic Solar Cells. Figure 16
Absorption spectra of a P3HT:PCBM composite film as cast (*solid curve*) and after four successive thermal annealing steps. The PCBM concentration is 67 wt% (From [72])

Another method to control the nanoscale morphology in PCBM:P3HT blends was demonstrated by Sivula et al. Amphiphilic (surfactant) diblock copolymers were used as the stabilizing agent [82]. Reducing the PCBM concentration in PCBM:P3HT blends can also lead to high morphological stability. Ma et al. confirmed that using blends with 45% or less PCBM, PCBM aggregation is suppressed and the film is stable

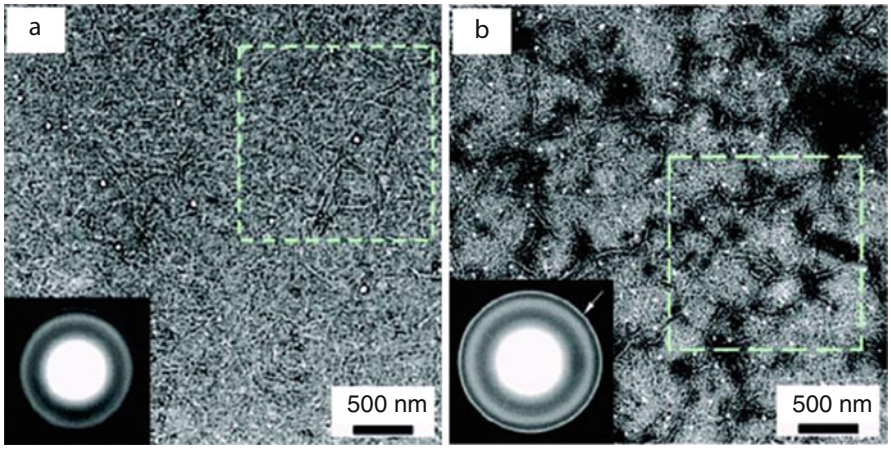

Organic Solar Cells. Figure 17
TEM images with insets of electron diffraction patterns of untreated (**a**) and thermally annealed (**b**) P3HT:PCBM blend films. *Black areas* indicate PCBM-rich domains, while the *white areas* are P3HT. The growth of larger continuous PCBM domains and longer fibrillar P3HT regions due to annealing is apparent after annealing (From [75])

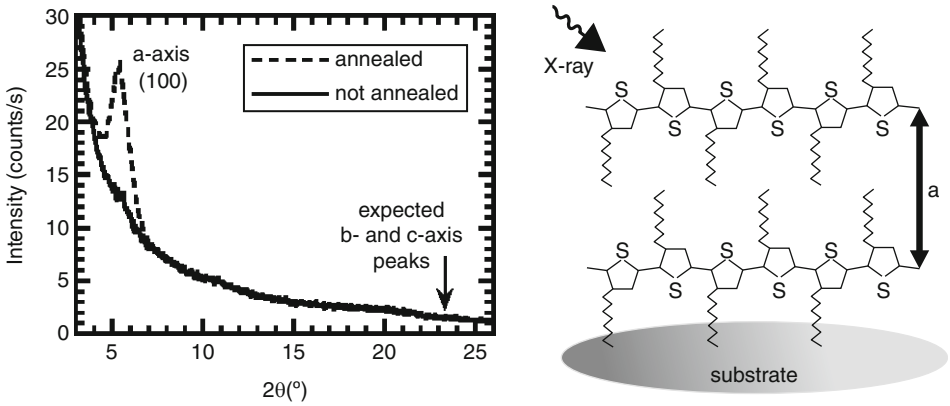

Organic Solar Cells. Figure 18
X-Ray diffraction plot of nontreated and annealed P3HT:PCBM blend films deposited on glass/ITO/PEDOT:PSS substrates (*left*). The corresponding a-axis orientation of the crystals is shown in the *right* (From [76])

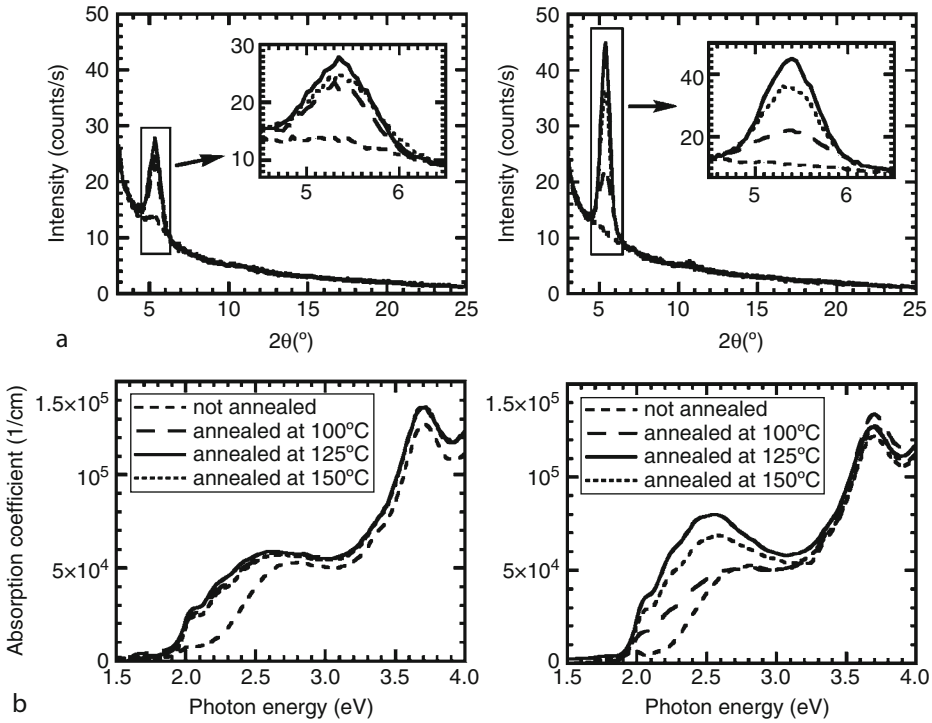

Organic Solar Cells. Figure 19
XRD crystallinity (**a**) and absorption coefficient (**b**) of P3HT:PCBM blends spin cast from either chlorobenzene (*left*) or chloroform (*right*) for various annealing temperatures. Interestingly, the increase in crystallinity is accompanied by a quantitatively correlated increase in optical absorption in the 2.0–2.5 eV region (From [77])

at annealing temperature as high as 150°C. These results suggest that solution processed OPVs with polymer-fullerene BHJs can possess high thermal stability.

A parameter critical to the OPV performance is charge mobility in the BHJ. To improve both electron and hole mobilities in the BHJ, it is necessary to understand their dependence on the BHJ

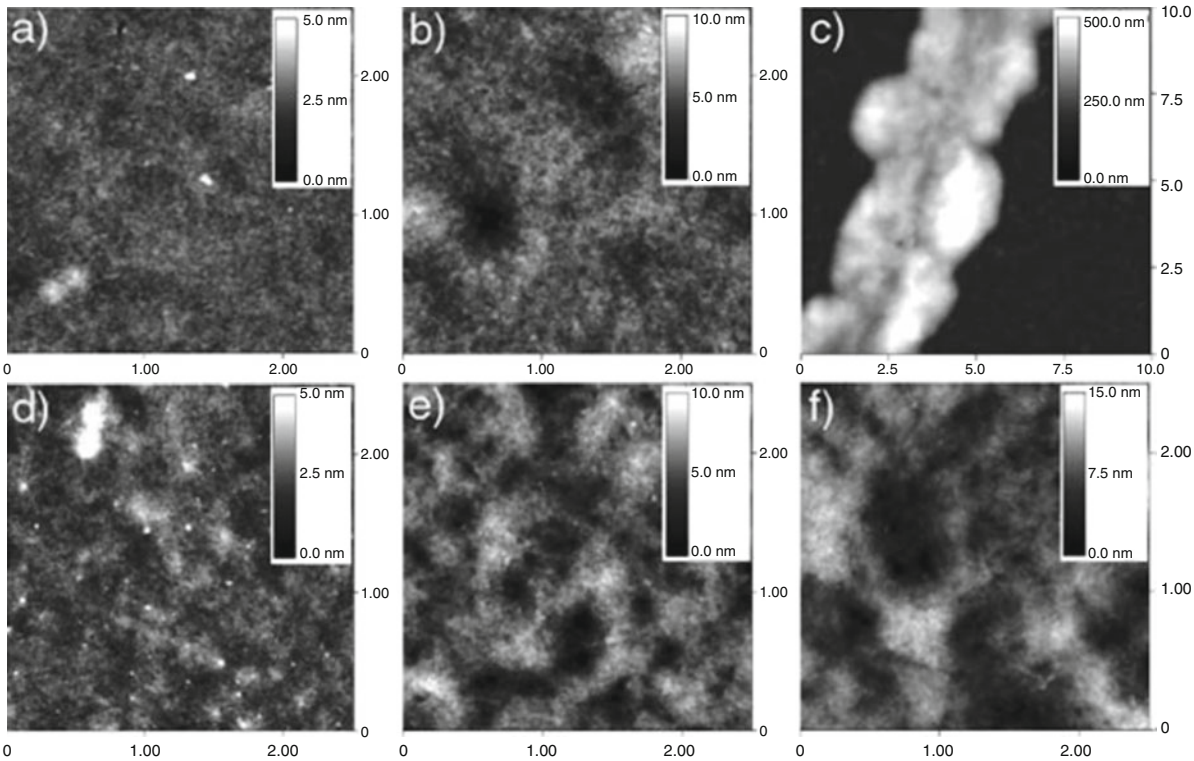

Organic Solar Cells. Figure 20

AFM images of P3HT–PCBM (**a**–**c**) and P3HT–PCBG (**d**–**f**) blend films spin cast on glass. The images show unheated films (**a** and **d**), films annealed for 4 min at 140°C (**b** and **e**), and films annealed for 1 h at 140°C (**c** and **f**) (From [81])

composition and nanomorphology induced by various processing steps. Using time-of-flight (ToF) technique, Huang et al. showed that the optimal weight ratio between P3HT and PCBM is around 1:1 to obtain a balanced charge transport in the OPV [83] (Fig. 21).

Li et al. have shown that optimal power conversion can be achieved with very thin BHJs. Using P3HT:PCBM as the BHJ with a thickness of only 63 nm, OPVs of 4% efficiency were demonstrated. With thicker films, >100 nm, the photocurrent is reduced due to transport limitations and possibly optical interference [84]. With thinner films, <100 nm, photocurrent was found to increase with increasing thickness as more light is absorbed leading to more charge carriers. As the thickness continues to increase, the effect of optical inference set in, producing maxima and minima periodically as a function of interference effects from interaction of light reflected from the back contact and the complex multilayered structure comprising an OPV device [85]. This effect is shown in Fig. 22.

Finally, the polymer molecular weight and/or polydispersity influence on the power conversion efficiencies: Schilinsky et al. found that higher weight fractions, collected from the same P3HT batch, show better performances than the lower weight fractions [86]. This observation is in agreement with measurements on field effect transistors that showed higher mobilities for larger molecular weights of P3HT. In addition to high molecular weight, highly regioregular polythiophene accounts for significant increase in performance, as shown in Fig. 23.

Active Layers in Vacuum-Processed OPVs

In vacuum-processed OPVs, the layer architecture is fabricated by vapor deposition in a vacuum chamber. ($1 \times 10^{-6} - 1 \times 10^{-10}$ mbar). At sufficiently low pressure ($\sim 1 \times 10^{-6}$ mbar), the mean free path

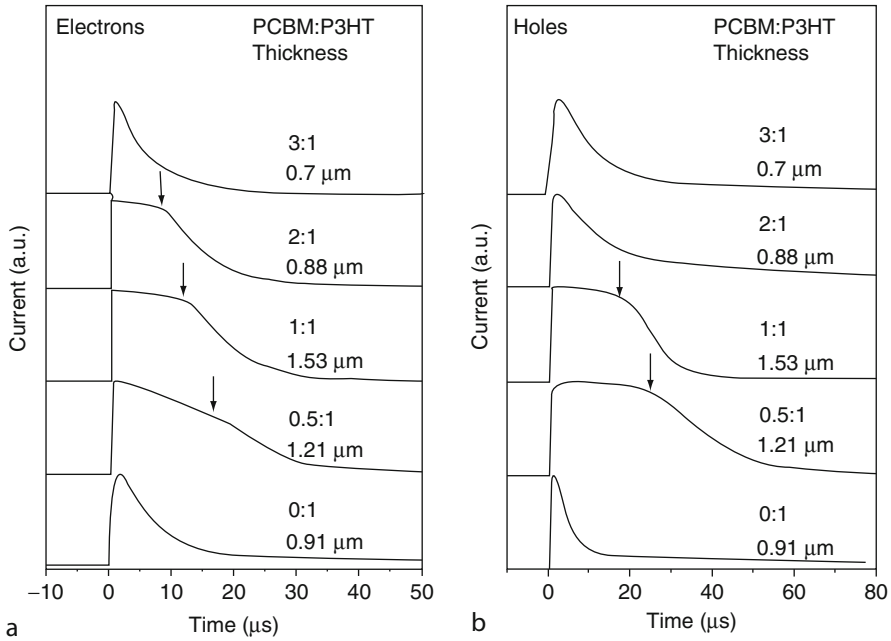

Organic Solar Cells. Figure 21

Time-of-flight (ToF) transients for P3HT:PCBM blend films of various compositions. It can be clearly seen that the blending ratio of 1:1 yields nondispersive charge transport and similar mobilities (transition times) for both the electrons and the holes (From [83])

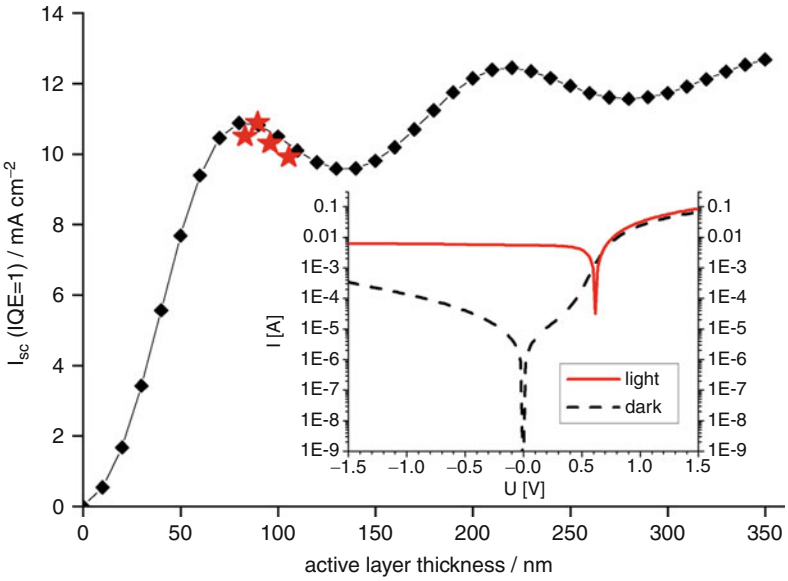

Organic Solar Cells. Figure 22

Photocurrent as a function active layer thickness (P3HT:PCBM). The effects of interference are clearly visible at thicknesses >100 nm. The inset shows the typical I-V characteristics for a 100 nm cell (From [85])

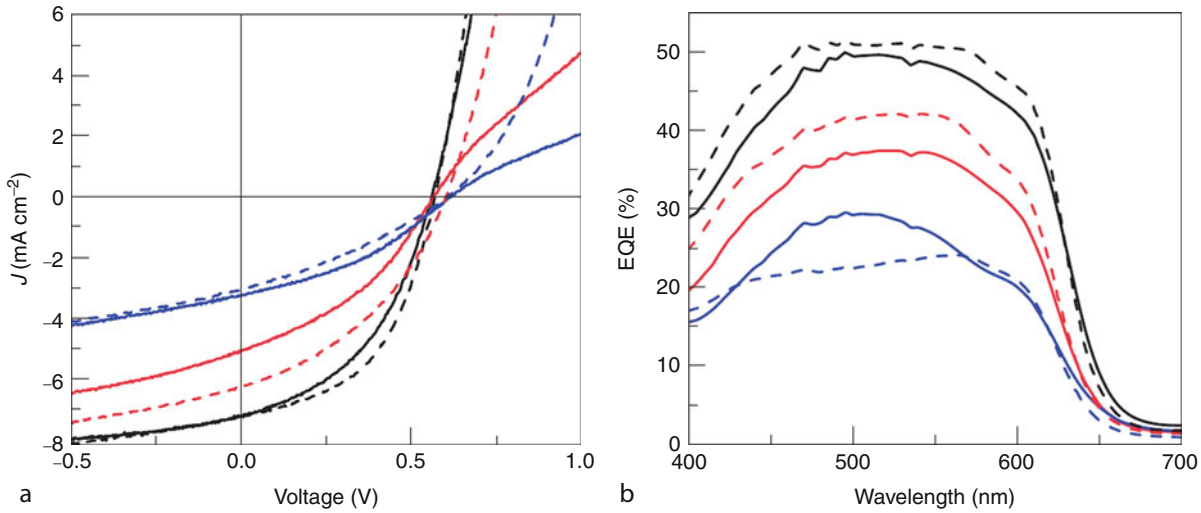

Organic Solar Cells. Figure 23

Influence of regioregularity of P3HT in blends with PCBM on IV-characteristics and external quantum efficiency (EQE). *Full lines* represent devices before, *broken lines* after thermal annealing at °C. It is evident that larger regioregularity (*black*, 95.2%; *red*, 93%; and *blue* 90.7%) lead to larger photovoltaic performances (From [87])

between molecular collisions is long enough such that the evaporant from a heated source will travel unimpeded to condense at an intended substrate to form a film. Using multiple evaporant sources, multilayer films and uniformly mixed films equivalent to BHJs can be readily obtained by vapor deposition. The main advantage of the vapor deposition method is that the entire OPV device can be made with precise control of the individual layer thickness and composition, all in a vacuum environment free of contaminants [88].

The first vacuum-processed OPV based on a donor/acceptor bilayer structure was reported by C.W. Tang in 1986 [5]. The donor and acceptor materials were evaporable organic dyes, Copper Phthalocyanine, CuPc, and a perylenediimide derivative, PTCDI, respectively (Fig. 24). These materials were used extensively as photoconductors in electrophotography and known to be exceptionally stable thermally and photochemically [89]. Although an efficiency as high as 1% was demonstrated, it was almost immediately recognized that the efficiency was largely limited by the absorption of the thin donor and acceptor layers. Short exciton diffusion length and the planar configuration of the donor/acceptor heterojunction were the key issues limiting the utility of this simple device [2, 90, 91].

An extension of the bilayer OPV structure was the p-i-n structure reported by Hiramoto et al. [92]. The middle layer *i* was an intermixed layer of donor and acceptor, sandwiched between the donor and acceptor layers, – the n and p layers, respectively. These terms refer simply to p being hole conducting and n being electron conducting. The p-i-n design led to improvement in photocurrent generation due to enhanced interfacial donor-acceptor area. Historically, the next improvement came with the realization that organic layers that were thin enough would allow some excitons to diffuse all the way to a single metal electrode, thereby discharging without leading to photocurrent. This problem was overcome with adding a so-called exciton-blocking layer (EBL) that has a potential barrier to accepting the exciton but would still function as a good conductor for charge [93, 94]. Furthermore, it was recognized that in vacuum systems co-deposition could easily be adapted to "dope" organic transport layers with materials that would slightly ionize the layers, thereby leading to a decrease in their electrical resistance. Suitable dopants are species that introduce charges into the transporting layers by either oxidizing

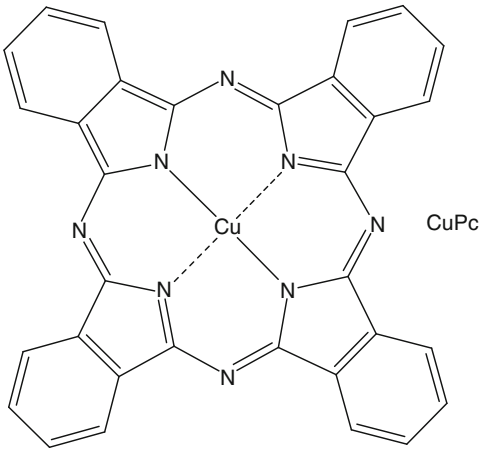

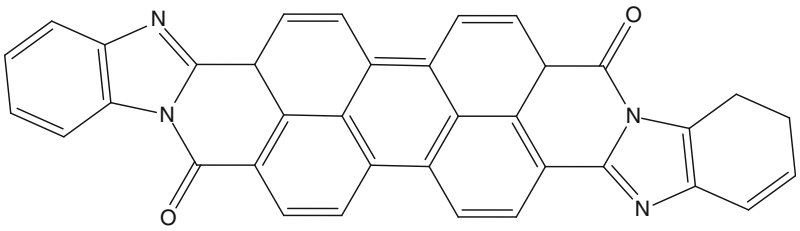

Organic Solar Cells. Figure 24
Donor material Copper Phthalocyanine (CuPc) and acceptor PTCDI, a perylene diimide derivative. These two components made up the first bilayer solar cell

or reducing the molecules that constitute the transporting layers. This leads to an increase in their conductivity analogous to the way that bringing dopants into inorganic crystalline semiconductors reduce their resistance. Unlike in inorganic semiconductors, these dopants are not immobile by virtue of being incorporated into the lattice; therefore, care must be taken to prevent unwanted diffusion of dopant species throughout the device. This is usually achieved by choosing dopants that are sufficiently bulky or that strongly interact with the doped species [95, 96]. This allows essentially Ohmic contacts to be formed between the electrodes and the charge transport layers. Doped transport layers up to 100 nm can be fabricated without incurring significant Ohmic losses; therefore, thicknesses can be adjusted to optimize the optical properties of the device [97]. This is based on positioning the absorbing heterojunction layer in the stack with respect to the absorption in the optical interference pattern forming due to the reflecting back contact. These four structural designs, planer heterojunction, p-i-n cell, planer heterojunction with EBL, and p-i-n with doped transport layers are shown in Fig. 25.

The ability to make relatively complex multilayer heterojunctions in a controlled way is an intrinsic advantage of vapor deposition. It follows that vacuum-processed OPVs, with tandem architecture, can be readily produced. A tandem cell, consisting of multiple series-connected subcells with different band gaps, allows theoretical efficiency to surpass the Shockley-Queisser limitation of a single cell [98]. The maximum efficiency of a single cell under nonconcentrated sunlight is about 30%. With a tandem cell, the maximum efficiency can rise above 40% for a 2-subcell structure, and to nearly 50% for a 3-subcell structure by selecting materials with matching band gaps for the subcells [99]. A tandem design can help overcome the inherent limitation of insufficient light collection in OPVs due to : (1) low carrier mobility which limits absorber layer thickness and (2) narrow absorption bandwidth which

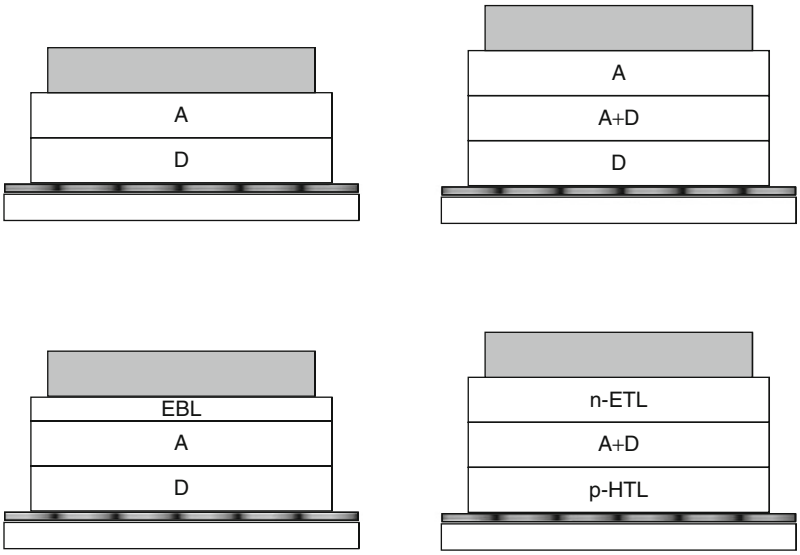

Organic Solar Cells. Figure 25
Four structural elements utilized in organic vacuum-processed cells. *Upper-left*: Planer bilayer heterojunction between donor and acceptor. *Upper-right*: Donor and Acceptor co-deposited bulk heterojunction between donor and acceptor layers. *Lower-left*: Bilayer with a high-band gap exciton blocking layer. *Lower-right*: Donor-Acceptor bulk heterojunction between two doped transport layers

is characteristic of almost all organic materials. In a typical OPV tandem design, subcells, each with a p-i-n structure, are simply stacked on top of each other with an interlayer connecting the adjacent subcells. The interlayer acts as a recombination layer to maintain charge neutrality. The series connection imposes the condition that the total photocurrent flowing through the tandem cell is controlled by the subcell that generates the smallest photocurrent, whereas the total photovoltage is the sum of voltages generated by the subcells. Therefore, it is important that a tandem cell should be constructed with subcells that are well matched with respect to band gaps in order to maximize light absorption and thus photocurrent generation. A simple example of a stacked device is shown in Fig. 26.

In general, a tandem cell designed with subcells absorbing various parts of the solar spectrum requires the placement of the subcells in the order such that the subcell with a higher band gap is positioned before the subcell of a lower band gap with respect to the incoming light [100, 101]. A record efficiency of 8.3% has recently been demonstrated for a fully vacuum-processed tandem cell [102].

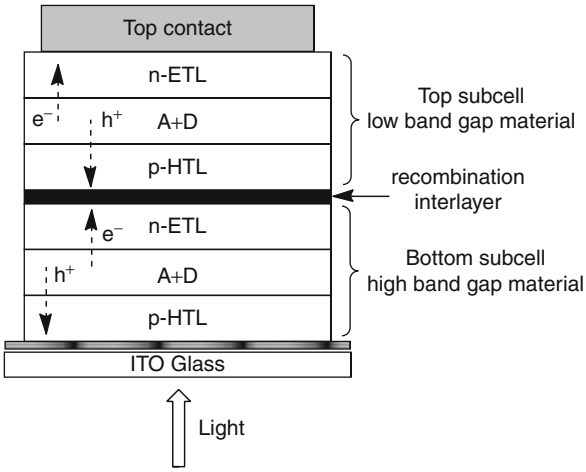

Organic Solar Cells. Figure 26
A tandem cell of two PIN cells with different absorptions. Photocurrent is limited by the subcell producing less photocurrent; however, photovoltage of the two subcells is added

The Top Contact The final step for OPV fabrication involves the deposition of a top metal contact. In most cases, the top electrode is applied using vacuum deposition. In some instances, it has demonstrated that it is

possible to laminate the top electrode onto the active layer of the OPV using a plastic foil precoated a metallic film [103, 104] or a layer conductive nanotubes [105, 106]. In general, the top contact metal is selected based on its work function to achieve Ohmic contact with the underlying active organic layer, which is typically an n-type material. This has been a challenge as a low work-function metal, such as calcium or magnesium, is required. These materials are reactive and liable to environmental degradation [107–109]. Unfortunately, the reactivity of metals is inversely proportional to their work function. Hence, more stable metals, such as aluminum, often form blocking contacts because of their higher work function. Adapted from OLED technology [110], a top contact based on LiF/Al, where LiF is an ultrathin interlayer (~1 nm) between the organic active layer and the Al electrode, has become an effective top contact for OPVs. Essentially, LiF/Al resembles a low work function contact due to the formation of charge-transferred species involving the Li^+ cation and the organic material during Al deposition [111, 112]. In the case of polymer-fullerene OPVs, an Ohmic contact with the fullerene can be formed with vacuum-evaporated aluminum alone [113, 114].

Operational Stability and Degradation

The lifetime of photovoltaic devices is vital to their economic success. Lifetime optimization remains one of the biggest challenges in developing organic solar cells. Organic materials are susceptible to degradation due to exposure to moisture and oxygen, and detrimental reactivity is often aggravated by sustained illumination. An example is the photooxidation of polymers, where the photogenerated excited state of the polymer will transfer energy to oxygen, forming highly reactive superoxides or hydrogen peroxides that attack the polymer. The extent of this degradative pathway is highly dependent on the structure of the polymer and can be mitigated by appropriate molecular design. It was shown in the earlier section that proper nanomorphology is crucial for high-performance organic devices. Over time, components of a donor-acceptor blend can "de-mix" and lower

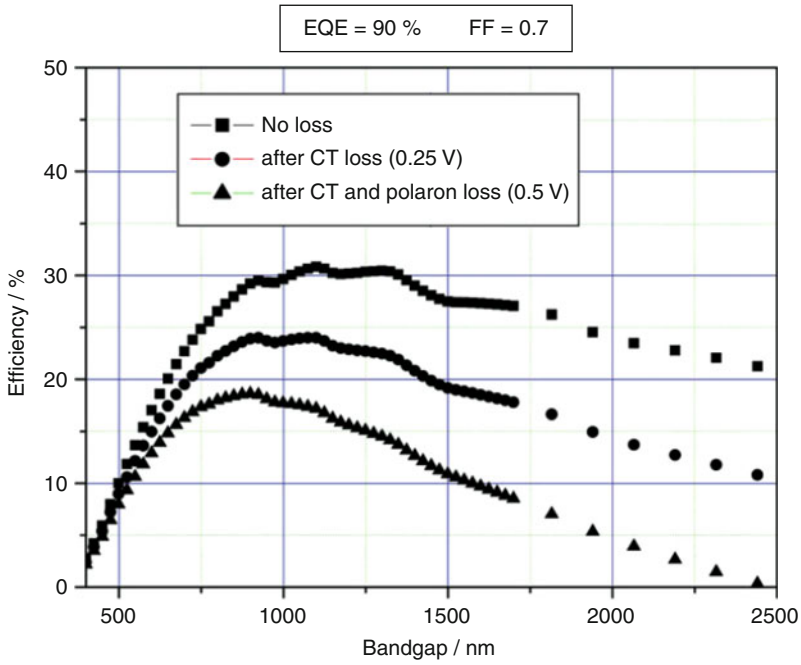

Organic Solar Cells. Figure 27
Practical maximum efficiency versus band gap for BHJ solar cells with reasonable assumption of FF = 0.7 and EQE = 90%. With lower band gap donor materials, 10+ percent efficiency cells with optimized morphology and contacts should be readily accessible. (From [7])

efficiencies. To prevent this, materials with good thermal stability must be chosen, which in the case of polymers means selecting polymers with the highest possible glass transition temperature [60]. In practicality, successful OPV devices are based on relatively stable organic materials combined with some encapsulation technology in the form of a plastic with good barrier properties. In rooftop studies, plastic-encapsulated solar cells were shown to have lifetimes of at least 3–5 years, with manufacturers reporting even longer lifetimes [41, 60].

Future Directions

In order to evaluate the potential of OPVs for practical solar cell applications, it is necessary to have a realistic estimate of the limits of OPVs. The achievable efficiency, based on a single cell structure, has been proposed by Dennler, Sharber, and Brabec and is summarized here [7]. The model assumes: (1) All photons of the band gap value or higher will be absorbed and contribute to photocurrent. (2) The air mass AMG 1.5 standard for solar irradiance will be used. (3) The fill factor value will be fixed instead of being calculated as a function of the band gap. First the balance of loss from the total possible photovoltage from the photoinduced charge transfer loss and polaron loss must be estimated. From experimental data, from bulk heterojunction devices, a LUMO-LUMO offset from donor to acceptor of 0.1–0.25 eV is needed to polarize the exciton. For the polaron, a loss of 0.25 eV will be assumed. Both of these values depend on material properties as well as morphology issues; however, assuming the "worst case," the total loss will be 0.5 eV. Figure 27 shows the efficiency versus donor band gap calculation assuming an external quantum efficiency of 90% (which is the highest end for reported solar cells) and a fill factor of 0.7.

It is clear from the estimation that OPV devices with efficiencies greater than 10% can be achieved

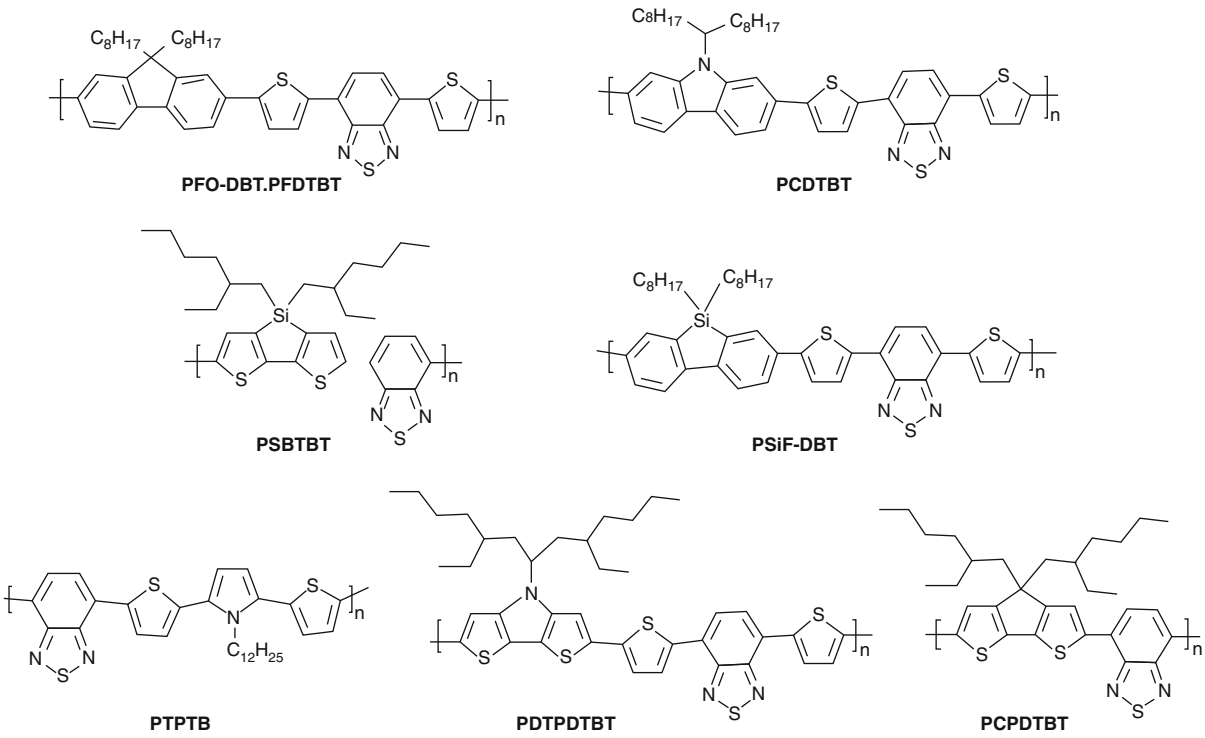

Organic Solar Cells. Figure 28
The electron-acceptor benzothiadiazole copolymerized with various electron-donating components. This class of polymers is one of the successful examples in next generation low-band gap polymers for OPV (From [9])

even with losses due to charge transfer and polaron effects provided that organic materials with lower band gap can be used.

Design of Low Band Gap Polymers

Many factors influence the band gap value of a conjugated polymer. The π conjugation length is the most important. Increase in conjugation length lowers the band gap as can be understood in quantum mechanical particle-in-the-box model. A second factor is aromaticity; aromatic molecules are π conjugated systems that have 4n + 2 number of π electrons, where n is an integer. They are considerably more stable, and by designing molecules with enhanced aromaticity in the excited states, the band gap energy can be lowered as well [115]. Another strategy to decrease the band gap of a conjugated polymer is to incorporate electron-rich π conjugated elements with electron-deficient units in alternation into a single polymer chain (push pull backbone) [116]. The substituents on the donor and acceptor units can also affect the band gap. The energy level of the HOMO of the donor can be increased by attaching electron-donating groups (EDG), such as thiophene and pyrrole. Similarly, the energy level of the LUMO of the acceptor is lowered when electron withdrawing groups (EWG), such as nitrile, thiadiazole, and pyrazine, are attached. The benzothiadiazole electron-poor element is one of the most popular building blocks for low band gap polymers. Fluorene and carbazole are typical electron-donating elements. Such hybrid copolymers can have band gaps approaching 1.2 eV. Several copolymers (Fig. 28) when mixed with fullerene acceptors, demonstrate power conversion efficiencies on the 5–6% range.

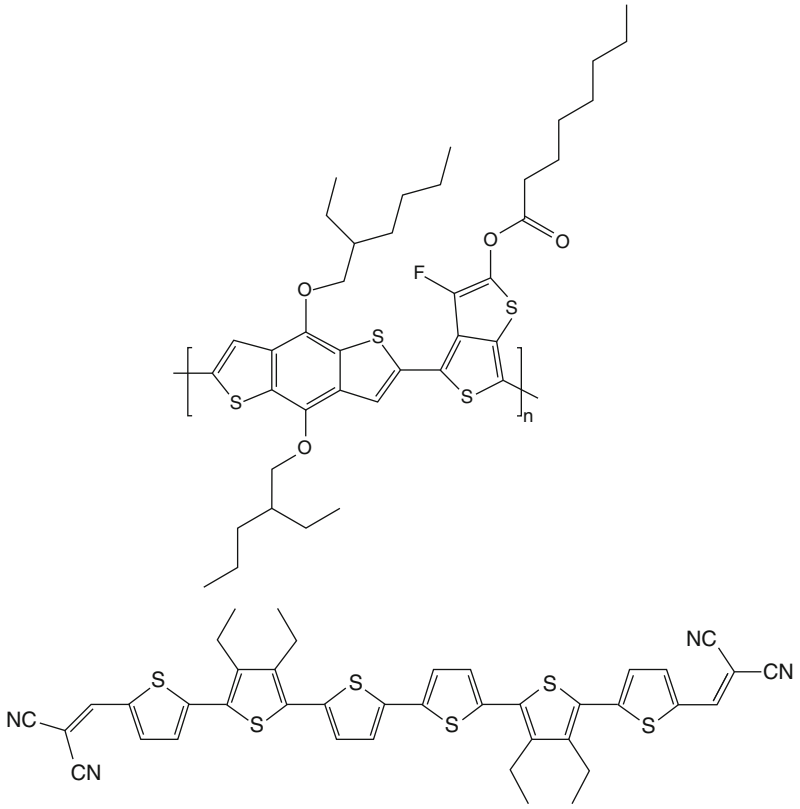

Organic Solar Cells. Figure 29

Top: PBDTTT-derivative polymer demonstrating low band gap (1.6 eV) and 7.7% efficiency when blended with a fullerene acceptor [117] *Bottom*: One of the family of sublimable dicyanovinyl oligothiophene donor materials used with fullerene in top (>7% efficiency) vacuum-processed tandem cells by Heliatek [118]

An illustrative example of optimization in polymer engineering is provided in a recent report by Yang and Wu [117]. The authors demonstrated high V_{oc} in OPVs with an electron-rich/electron-poor copolymer having a broad optical absorption stretching to 770 nm. This polymer, poly[4,8-bis-substituted-benzo[1,2-b:4,5-b'] dithiophene-2,6-diyl-alt-4-substituted-thieno-[3,4-b] thiophene-2,6-diyl (PBDTTT), when mixed with fullerene - $PC_{71}BM$, demonstrated a power conversion efficiency of 7.7% (Fig. 29).

Conclusions

With increasing the need for developing low-cost photovoltaic power generation, organic solar cells have emerged as one of the most promising photovoltaic technologies on the horizon. Based on synthetic materials of abundant elements and thin-film device configurations that are adaptable for high-speed mass production, organic solar cells present an attractive alternative to the inorganic solar cells which are expensive to process, such as silicon solar cells, or constrained by the elemental abundance, such as the thin-film CdTe and CIGS solar cells. With widespread academic interest as well as commercial incentives, the recent years have seen dramatic improvements in the performance of organic photovoltaic cells. The major improvements are in the efficiencies – nearly unity photon-to-electron quantum efficiency already demonstrated and the power conversion efficiency rapidly approaching the 10% benchmark, which are achieved through systematic design and optimization of the donor-acceptor bulk heterojunction structures and new material compositions. Both polymeric and small-molecule photovoltaic cells are being pursued actively and further advances can be expected with major efforts on increasing the overall absorption with low band gap materials to match the solar spectrum and achieving a large built-in potential through optimization of the energy levels of the donor and acceptor pair. Furthermore, efficiencies much greater than 10% can be expected from tandem organic solar cells, which in contrast to the inorganic tandem cells are intrinsically easier to construct and therefore likely to be more economical to produce. Even though these overall efficiencies are lower than incumbent inorganic technologies, such as silicon, the substantially lower module cost can make OPV a much more attractive technology. Additionally, continued development of flexible, lightweight, and high-volume OPVs would make installation and integration into structural elements and mobile devices very facile. The lifetime of organic photovoltaic cells has been significantly improved, although it remains to be a critical issue for long-term use. Useful lifetime on the order of several years are being demonstrated in the laboratory and current commercial organic solar cells, and further improvements can be expected with more robust materials and device encapsulation. From the point of view of cost and versatility, organic photovoltaic technology stands to be a significant player in the future renewable energy balance.

Bibliography

Primary Literature

1. Kearns D, Calvin M (1958) Photovoltaic effect and photoconductivity in laminated organic systems. J Chem Phys 29: 950–951
2. Morel DL, Stogryn EL, Ghosh AK, Feng T, Purwin PE, Shaw RF, Fishman C, Bird DR, Piechowski AP (1984) Organic photovoltaic cells. Correlations between cell performance and molecular structure. J Phys Chem 88:923–933
3. Tang CW, Albrecht AC (1975) Photovoltaic effects of metal–chlorophyll-a–metal sandwich cells. J Chem Phys 62:2139
4. Corker GA, Lundstrom I (1978) Trapped-electron doping of photovoltaic sandwich cells containing microcrystalline chlorophyll a. J Appl Phys 49:686–700
5. Tang CW (1986) Two-layer organic photovoltaic cell. Appl Phys Lett 48:183–185
6. Sariciftci NS, Smilowitz L, Heeger AJ, Wudl F (1992) Photoinduced electron transfer from a conducting polymer to buckminsterfullerene. Science 258:1474–1476
7. Dennler G, Scharber MC, Brabec CJ (2009) Polymer-fullerene bulk-heterojunction solar cells. Adv Func Mat 21:1323–1338
8. Atkins P, de Paula J (2001) Physical chemistry. Oxford University Press, New York
9. Brunetti FG, Kumar R, Wudl F (2010) Organic electronics from perylene to organic photovoltaics: painting a brief history with a broad brush. J Mater Chem 20:2934–2948
10. Nelson J (2003) Physics of solar cells. Imperial College Press, London
11. Sariciftci NS (ed) (1999) Primary photoexcitations in conjugated polymers: molecular exciton versus semiconductor band model. World Scientific, Singapore
12. Pope M, Swenberg CE (1999) Electronic processes in organic crystals and polymers, 2nd edn. Oxford University Press, New York
13. Tang CW, VanSlyke SA, Chen CH (1989) Electroluminescence of doped organic thin films. J Appl Phys 65:3610

14. Halls JJM, Pichler K, Friend RH, Moratti SC, Holmes AB (1996) Exciton diffusion and dissociation in a poly(p-phenylenevinylene)/C60 heterojunction photovoltaic cell. Appl Phys Lett 68:3120
15. Haugeneder A, Neges M, Kallinger C, Spirkl W, Lemmer U, Feldmann J, Scherf U, Harth E, Gügel A, Müllen K (1999) Exciton diffusion and dissociation in conjugated polymer/fullerene blends and heterostructures. Phys Rev B 59:15346
16. Lungenschmied C, Dennler G, Neugebauer H, Sariciftci NS, Ehrenfreund E (2006) Internal electric field in organic-semiconductor-based photovoltaic devices. Appl Phys Lett 89:223519–223521
17. Zhu X-Y, Yang Q, Muntwiler M (2009) Charge-transfer excitons at organic semiconductor surfaces and interfaces. Acc Chem Res 42:1779–1787
18. Weiss DS, Abkowitz M (2010) Advanced in organic photoconductor technology. Chem Rev 110:479–526
19. Rice MJ, Gartstein YN (1996) Theory of photoinduced charge transfer in a molecularly doped conjugated polymer. Phys Rev B 53:10764–10770
20. Wu MW, Conwell EM (1998) Theory of photoinduced charge transfer in weakly coupled donor-acceptor conjugated polymers: application to an MEH-PPV:CN-PPV pair. Chem Phys 227:11–17
21. Beckers EHA, Meskers SCJ, Schenning APHJ, Chen ZJ, Wurthner F, Marsal P, Beljonne D, Cornil J, Janssen RAJ (2006) Influence of intermolecular orientation on the photoinduced charge transfer kinetics in self-assembled aggregates of donor-acceptor arrays. J Am Chem Soc 128:649–657
22. Paddon-Row MN (1994) Investigating long-range electron-transfer processes with rigid, covalently linked donor-(norbornylogous bridge)-acceptor systems. Acc Chem Res 27:18–25
23. Guldi DM (2002) Fullerene-porphyrin architectures; photosynthetic antenna and reaction center models. Chem Soc Rev 31:22–36
24. Kraabel B, Hummelen JC, Vacar D, Moses D, Sariciftci NS, Heeger AJ, Wudl F (1996) Subpicosecond photoinduced electron transfer from conjugated polymers to functionalized fullerenes. J Chem Phys 104:4267–4273
25. Müller JG, Lupton JM, Feldmann J, Lemmer U, Scharber MC, Sariciftci NS, Brabec CJ, Scherf U (2005) Ultrafast dynamics of charge carrier photogeneration and geminate recombination in conjugated polymer:fullerene solar cells. Phys Rev B 72:195208
26. Tsuzuki T, Shirota Y, Rostalski J, Meissner D (2000) The effect of fullerene doping on photoelectric conversion using titanyl phthalocyanine and a perylene pigment. Sol Energ Mat Sol C 61:1–8
27. Hwang KC, Mauzerall D (1993) Photoinduced electron transport across a lipid bilayer mediated by C_{70}. Nature 361:138–140
28. Karl N (2003) Charge carrier transport in organic semiconductors. Synth Met 133–134:649–657
29. Jaiswal M, Menon R (2006) Polymer electronic materials: a review of charge transport. Polym Int 55:1371–1384
30. Kline RJ, McGehee MD (2006) Morphology and charge transport in conjugated polymers. J Macromol Sci 46:27–45
31. Pivrikas A, Sariciftci NS, Juska G, Österbacka R (2007) Review of charge transport and recombination in polymer/fullerene organic solar cells. Prog Photovoltaics: Res Appl 15:677–696
32. Sze SM, Kwok NK (2006) Physics of semiconductor devices, 3rd edn. Wiley-Interscience, Hoboken
33. Parker ID (1994) Carrier tunneling and device characteristics in polymer light-emitting diodes. J Appl Phys 75:1656
34. Zhang M, Wang H, Tang CW (2010) Effect of the highest occupied molecular orbital energy level offset on organic heterojunction photovoltaic cells. Appl Phys Lett 97:143503–143506
35. Brabec CJ, Cravino A, Meissner D, Sariciftci NS, Fromherz T, Rispens MT, Sanchez L, Hummelen JC (2001) Origin of the open circuit voltage of plastic solar cells. Adv Funct Mater 11:374
36. Kooistra FB, Knol J, Kastenberg F, Popescu LM, Verhees WJH, Kroon JM, Hummelen JC (2007) Increasing the open circuit voltage of bulk-heterojunction solar cells by raising the LUMO level of the acceptor. Org Lett 9:551
37. Kim H, Jin S-H, Suh H, Lee K (2004) Origin of the open circuit voltage in conjugated polymer–fullerene photovoltaic cells. In: Kafafi ZH, Lane PA (eds) Organic photovoltaics IV. SPIE Proc 5215:111
38. Gadisa A, Svensson M, Andersson MR, Inganäs O (2004) Correlation between oxidation potential and open-circuit voltage of composite solar cells based on blends of polythiophenes/fullerene derivative. Appl Phys Lett 84:1609
39. Scharber MC, Mühlbacher D, Koppe M, Denk P, Waldauf C, Heeger AJ, Brabec CJ (2006) Design rules for donors in bulk-heterojunction solar cells – towards 10% energy-conversion efficiency. Adv Mater 18:789
40. Krebs FC (2009) Fabrication and processing of polymer solar cells: a review of printing and coating techniques. Sol Energ Mat Sol C 93:394–412
41. Konarka Website (http://www.konarka.com/). Accessed 10 Dec 2010
42. Pagliaro M, Ciriminna R, Palmisano G (2008) Flexible solar cells. Wiley-VCH, Weinheim
43. Brumbach M, Veneman F, Saneeha M, Schulmeyer T, Simmonds A, Xia W, Lee P, Armstrong NR (2007) Surface compositions and electrical and electrochemical properties of freshly deposited and acid-etched indium Tin oxide electrodes. Langmuir 23:11089–11099
44. Forrest S, Xue J (2004) Carrier transport in multilayer organic photodetectors: II effects of anode preparation. J Appl Phys 95:1869–1877
45. Armstrong NR, Veneman PA, Ratcliff E, Placencia D, Brumbach M (2009) Oxide contacts in organic photovoltaics: characterization and control of near-surface composition in indium – Tin oxide (ITO) electrodes. Acc Chem Res 42:1748–1757
46. Kyaw AKK, Sun XW, Jiang CY, Lo GQ, Zhao DW, Kwong DL (2008) An inverted organic solar cell employing a sol-gel derived ZnO electron selective layer and thermal evaporated MoO_3 hole selective layer. Appl Phys Lett 93:221107–221110

47. Murdoch GB, Hinds S, Sargent EH, Tsang SW, Mordoukhovski L, Lu ZH (2009) Aluminum doped zinc oxide for organic photovoltaics. Appl Phys Lett 94:213301–213303
48. Aernouts T, Vanlaeke P, Geens W, Poortmans J, Heremans P, Borghs S, Mertens R, Andriessen R, Leenders L (2004) Printable anodes for flexible organic solar cell modules. Thin Solid Films 22–25:451–452
49. Dietrich M, Heinze J, Heywang G, Jonas F (1994) Electrochemical and spectroscopic characterization of polyalkylenedioxythiophenes. J Electroanal Chem 369:87–92
50. Vitoratos E, Sakkopoulos S, Dalas E, Paliatsas N, Karageorgopoulos D, Petraki F, Kennou S, Choulis SA (2009) Thermal degradation mechanisms of PEDOT:PSS. Org Electron 10: 61–66
51. Nardes AM, Kemerink M, de Kok MM, Vinken E, Maturova K, Janssen RAJ (2008) Conductivity, work function, and environmental stability of PEDOT:PSS thin films treated with sorbitol. Org Electron 9:727–734
52. Norrman K, Madsen MV, Gevorgyan SA, Krebs FC (2010) Degradation patterns in water and oxygen of an inverted polymer solar cell. J Amer Chem Soc 132:16883–16892
53. Zhang M, Irfan DH, Gao Y, Tang CW (2010) Organic Schottky barrier photovoltaic cells based on MoO_x/C_{60}. Appl Phys Lett 96:183301–183303
54. Irwin MD, Buchholz DB, Hains AW, Chang RPH, Marks TJ (2008) p-Type semiconducting nickel oxide as an efficiency-enhancing anode interfacial layer in polymer bulk-heterojunction solar cells. PNAS 105:2783–2787
55. Moulé AJ, Meerholz K (2009) Morphology control in solution-processed bulk-heterojunction solar cell mixtures. Adv FuncMat 19:3028–3036
56. Brabec CJ, Sariciftci NS, Hummelen JC (2001) Plastic solar cells. Adv Func Mat 11:15–26
57. Wienk MM, Kroon JM, Verhees WJH, Knol J, Hummelen JC, van Hal PA, Janssen RAJ (2003) Efficient methano[70]fullerene/MDMO-PPV bulk heterojunction photovoltaic cells. Angewandte Chemie 115:3493–3497
58. Melzer C, Koop EJ, Mihailetchi VD, Blom PWM (2004) Hole transport in poly(phenylene vinylene)/methanofullerene bulk-heterojunction solar cells. Adv Funct Mater 14:865–870
59. Cumpston BH, Jensen KF (1998) Photooxidative stability of substituted poly(phenylene vinylene) (PPV) and poly (phenylene acetylene) (PPA). J Appl Polym Sci 69:2451–2458
60. Jorgensen M, Norrman K, Krebs FC (2008) Stability/degradation of polymer solar cells. Sol Energ Mat Sol C 92:686–714
61. Ma W, Yang C, Gong X, Lee K, Heeger A (2005) Thermally stable, efficient polymer solar cells with nanoscale control of the interpenetrating network morphology. Adv Func Mat 15:1617–1622
62. Brabec CJ, Gowrisanker S, Halls JJM, Laird D, Jia S, Williams SP (2010) Polymer–fullerene bulk-heterojunction solar cells. Adv Mat 22:3839–3856
63. McCullough RD (1998) The chemistry of conducting polythiophenes. Adv Mat 10:93–116
64. Roncali J (1997) Synthetic principles for bandgap control in linear π-conjugated systems. Chem Rev 97:173–206
65. McCullough RD, Lowe RD (1992) Enhanced electrical conductivity in regioselectively synthesized poly(3-alkylthiophenes). J Chem Soc, Chem Comm 1:70–72
66. McCullough RD, Tristram-Nagle S, Williams SP, Lowe RD, Jayaraman M (1993) Self-orienting head-to-tail poly(3-alkylthiophenes): new insights on structure-property relationships in conducting polymers. J Am Chem Soc 115:4910–4911
67. Roncali J (1992) Conjugated poly(thiophenes): synthesis, functionalization, and applications. Chem Rev 92:711–738
68. Schilinsky P, Waldauf C, Brabec CJ (2002) Recombination and loss analysis in polythiophene based bulk heterojunction photodetectors. Appl Phys Lett 81:3885–3887
69. Padinger F, Rittberger R, Sariciftci NS (2003) Effects of post-production treatment on plastic solar cells. Adv Func Mat 13:85–88
70. Moon Ji Sun, Takacs CJ, Cho S, Coffin RC, Kim H, Bazan GC, Heeger AJ (2010) Effect of processing additive on the nanomorphology of a bulk heterojunction material. Nano Lett 10:4005–4008
71. Li G, Shrotriya V, Huang J, Yao Y, Moriarty T, Emery K, Yang Y (2005) High-efficiency solution processable polymer photovoltaic cells by self-organization of polymer blends. Nat Mater 4:864–868
72. Ma W, Yang C, Gong X, Lee K, Heeger A (2005) Thermally stable, efficient polymer solar cells with nanoscale control of the interpenetrating network morphology. Adv Func Mat 15:1617–1622
73. Chirvase D, Parisi J, Hummelen JC, Dyakonov V (2004) Influence of nanomorphology on the photovoltaic action of polymer–fullerene composites. Nanotechnology 15:1317–1323
74. Kim Y, Choulis SA, Nelson J, Bradley DDC, Cook S, Durrant JR (2005) Device annealing effect in organic solar cells with blends of regioregular poly(3-hexylthiophene) and soluble fullerene. Appl Phys Lett 86:63502–63505
75. Yang X, Loos J, Veenstra SC, Verhees VJH, Wienk MM, Kroon JM, Michels MAJ, Janssen RAJ (2005) Nanoscale morphology of high-performance polymer solar cells. Nano Lett 5:579–583
76. Erb T, Zhokhavets U, Gobsch G, Raleva S, Stühn B, Schilinsky P, Waldauf C, Brabec CJ (2005) Correlation between structural and optical properties of composite polymer films for organic solar cells. Adv Func Mater 15:1193–1196
77. Erb T, Zhokhavets U, Gobsch G, Al-Ibrahim M, Ambacher O (2006) Relation between absorption and crystallinity of poly(3-hexylthiophene)/fullerene films for plastic solar cells. Chem Phys Lett 418:347–350
78. Yang X, van Duren JKJ, Rispens MT, Hummelen JC, Janssen RAJ, Michels MAJ, Loos J (2004) Crystalline organization of a methanofullerene as used for plastic solar-cell applications. Adv Mater 16:802–806
79. Yang X van Duren JKJ, Janssen RAJ, Michels MAJ, Loos J (2004) Morphology and thermal stability of the active layer in poly(p-phenylenevinylene)/methanofullerene plastic photovoltaic devices. Macromolecules 37:2151–2158

80. Schuller S, Schilinsky P, Hauch J, Brabec CJ (2004) Determination of the degradation constant of bulk heterojunction solar cells by accelerated lifetime measurements. Appl Phys A 79:37–40
81. Drees M, Hoppe H, Winder C, Neugebauer H, Sariciftci NS, Schwinger W, Schäffler F, Topf C, Scharber MC, Zhu Z, Gaudiana R (2005) Stabilization of the nanomorphology of polymer/fullerene "bulk heterojunction" blends using a novel polymerizable fullerene derivative. J Mater Chem 15:5158–5163
82. Sivula K, Ball ZT, Watanabe N, Fréchet JMJ (2006) Amphiphilic diblock copolymer compatibilizers and their effect on the morphology and performance of polythiophene:fullerene solar cells. Adv Mater 18:206–210
83. Huang J, Li G, Yang Y (2005) Influence of composition and heat-treatment on the charge transport properties of poly(3-hexylthiophene) and [6,6]-phenyl C_{61}-butyric acid methyl ester blends. Appl Phys Lett 87:112105–112107
84. Li G, Shrotriya V, Yao Y, Yang Y (2005) Investigation of annealing effects and film thickness dependence of polymer solar cells based on poly(3-hexylthiophene). J Appl Phys 98:43704–43708
85. Hoppe H, Shokhovets S, Gobsch G (2007) Inverse relation between photocurrent and absorption layer thickness in polymer solar cells. Phys Stat Sol 1:R40
86. Schilinsky P, Asawapirom U, Scherf U, Biele M, Brabec CJ (2005) Influence of the molecular weight of poly(3-hexylthiophene) on the performance of bulk heterojunction solar cells. Chem Mater 17:2175–2180
87. Kim Y, Cook S, Tuladhar SM, Choulis SA, Nelson J, Durrant JR, Bradley DDC, Giles M, McCulloch I, Ha C-S, Ree M (2006) A strong regioregularity effect in self-organizing conjugated polymer films and high-efficiency polythiophene:fullerene solar cells. Nat Mater 5:197–203
88. Forrest SR (1997) Ultrathin organic films grown by organic molecular beam deposition and related techniques. Chem Rev 97:1793–1896
89. Diamond AS, Weiss DS (eds) (2002) Handbook of imaging materials. Marcel Dekker, New York
90. Tang CW, VanSlyke SA, Chen CH (1989) Electroluminescence of doped organic thin films. J Appl Phys 65:3610–3616
91. Peumans P, Yakimov A, Forrest SR (2003) Small molecular weight organic thin-film photodetectors and solar cells. J Appl Phys 93:3693–3723
92. Hiramoto M, Fujiwara H, Yokoyama M (1991) 3-layered organic solar-cell with a photoactive interlayer of codeposited pigments. Appl Phys Lett 58:1062–1064
93. Peumans P, Bulovic V, Forrest SR (2000) Efficient photon harvesting at high optical intensities in ultra thin organic double-heterostructure photovoltaic diodes. Appl Phys Lett 76:2650–2652
94. Vogel M, Doka S, Breyer C, Lux-Steiner M, Cand Fostiropoulos K (2006) On the function of a bathocuproine buffer layer in organic photovoltaic cells. Appl Phys Lett 89: 163501–163503
95. Drechsel J, Maennig B, Gebeyehu D, Pfeiffer M, Leo K, Hoppe H (2004) MIP-type organic solar cells incorporating phthalocyanine/fullerene mixed layers and doped wide-gap transport layers. Org Electron 5:175–186
96. Falkenberg C, Uhrich C, Olthof S, Maennig B, Riede M, Leo K (2008) Efficient p–i–n type organic solar cells incorporating 1,4,5,8-napthalenetetracarboxylic dianhydride as transparent electron transport material. J Appl Phys 104:34506
97. Walzer K, Maennig B, Pfeiffer M, Leo K (2007) Highly efficient organic devices based on electrically doped transport layers. Chem Rev 107:1233–1271
98. Shockley S, Queisser HJ (1961) Detailed balance limit of p-n junction solar cells. J Appl Phys 32:510–519
99. De Vos A (1980) Detailed balance limit of the efficiency of tandem solar cells. J Phys D 13:839–846
100. Schueppel R, Timmreck R, Allinger N, Mueller T, Furno M, Uhrich C, Leo K, Riede M (2010) Controlled current matching in small molecule organic tandem solar cells using doped spacer layers. J Appl Phys 107:044503–044508
101. Timmreck R, Olthof S, Leo K, Riede M (2010) Highly doped layers as efficient electron–hole recombination contacts for tandem organic solar cells. J Appl Phys 108:33108–33113
102. Heliatek and IAPP achieve production-relevant efficiency record for organic photovoltaic cells. http://www.heliatek.com/news. Accessed on Dec 2010
103. Kim JB, Lee S, Toney MF, Chen Z, Facchetti A, Kim YS, Loo Y-L (2010) Reversible soft-contact lamination and delamination for non-invasive fabrication and characterization of bulk-heterojunction and bilayer organic solar cells. Chem Mater 22:4931–4938
104. Kim J, Khang D-Y, Kim J-H, Lee HH (2008) The surface engineering of top electrode in inverted polymer bulk-heterojunction solar cells. Appl Phys Lett 92:133307–133309
105. Lee J-Y, Connor ST, Cui Y, Peumans P (2010) Semitransparent organic photovoltaic cells with laminated top electrode. Nano Lett 10:1276–1279
106. Gaynor W, Lee J-Y, Peumans P (2010) Fully solution-processed inverted polymer solar cells with laminated nanowire electrodes. ACS Nano 4:30–34
107. Choong V-E, Mason MG, Tang CW, Gao Y (1998) Investigation of the interface formation between calcium and tris-(8-hydroxy quinoline) aluminum. Appl Phys Lett 72:2689–2691
108. Park Y, Choong V-E, Hsieh BR, Tang CW, Wehrmeister T, Mullen K, Gao Y (1997) Electron spectroscopy studies of interface formation between metal electrodes and luminescent organic materials. J Vac Sci Technol A 15:2574–2578
109. Park Y, Choong V-E, Hsieh BR, Gao Y, Wehrmeister T, Mullen K, Tang CW (1997) Effects of Al, Ag, and Ca on luminescence of organic materials. J Vac Sci Technol A 15: 1745–1749
110. Hung LS, Mason MG, Tang CW (1997) Enhanced electron injection in organic electroluminescence devices using an Al/LiF electrode. J Appl Phys Lett 70:152–154
111. Shaheen SE, Jabbour GE, Morrell MM, Kawabe Y, Kippelen B, Peyghambarian N, Nabor M-F, Schlaf R, Mash EA,

Armstrong NR (2009) Bright blue organic light-emitting diode with improved color purity using a LiF/Al cathode. J Appl Phys 84:2324–2327

112. Glowacki ED, Marshall KL, Tang CW, Sariciftci NS (2011) Doping of organic semiconductors induced by lithium fluoride/aluminum electrodes studied by electron spin resonance and infrared reflection-absorption spectroscopy. Appl Phys Lett 99:043305–043307
113. Mihailetchi VD, Koster LJA, Blom PWM (2004) Effect of metal electrodes on the performance of polymer:fullerene bulk heterojunction solar cells. Appl Phys Lett 85:970–973
114. Frohne H, Shaheen SE, Brabec CJ, Müller DC, Sariciftci NS, Meerholz K (2002) Influence of the anodic work function on the performance of organic solar cells. Chemphyschem 3:795–799
115. Brunetti F, Gong X, Tong M, Heeger A, Wudl F (2010) Strain and Hückel aromaticity: driving forces for a promising new generation of electron acceptors in organic electronics. Angew Chem 122:542–546
116. Mammo W, Admassie S, Gadisa A, Zhang F, Inganas O, Andersson MR (2007) New low band gap alternating polyfluorene copolymer-based photovoltaic cells. Sol Energ Mat Sol C 91:1010–1018
117. Liang Y, Wu Y, Feng D, Tsai S-T, Son H-J, Li G, Yu L (2009) Development of new semiconducting polymers for high performance solar cells. J Am Chem Soc 131:56–57
118. Wynands D, Levichkova M, Riede M, Pfeiffer M, Baeuerle P, Rentenberger R, Denner P, Leo K (2010) Correlation between morphology and performance of low bandgap oligothiophene:C_{60} mixed heterojunctions in organic solar cells. J Appl Phys 107:014517–014523

Books and Reviews

Andre Moliton A (2006) Optoelectronics of molecules and polymers. Springer, Berlin

Brabec C, Dyakonov V, Parisi V, Sariciftci NS (eds) (2003) Organic photovoltaics. Springer, Berlin

Brabec C, Dyakonov V, Scherf U (eds) (2008) Organic photovoltaics. Wiley VCH, Weinheim

Dennler G, Sariciftci NS, Brabec CJ (2007) Conjugated polymer based organic solar cells. In: Hadziioannou G, Mallarias GG (eds) Semiconducing polymers, 2nd edn. Wiley-VCH, Weinheim

Mozer AJ, Sariciftci NS (2007) Conjugated polymer-based photovoltaic devices. In: Skotheim T, Reynolds JR (eds) Handbook of conducting polymers, 3rd edn. CRC Press/Taylor and Francis Group, Boca Raton, Florida

Nalwa HS (ed) (1997) Handbook of organic and conductive molecules and polymers. Wiley, Chichester, UK

Sun SS, Dalton L (eds) (2008) Introduction to organic electronic and optoelectronic materials and devices. Taylor and Francis, Boca Raton

Sun SS, Sariciftci NS (eds) (2005) Organic photovoltaics: mechanisms materials and devices. Taylor and Francis, Boca Raton

Würfel P (2005) Physics of solar cells. Wiley VCH, Weinheim

Oxidation Catalysts for Green Chemistry

Colin P. Horwitz
GreenOx Catalysts, Inc, Pittsburgh, PA, USA

Article Outline

Glossary
Definition of the Subject and Its Importance
Introduction
Oxidation Chemistry
Industrial Catalysts
Specialty Chemical Catalysts
Catalysts for the Environment
Energy
Future Directions
Bibliography

Glossary

Catalyst A substance that initiates or increases the rate of a chemical reaction by reducing the activation energy for the reaction without itself undergoing any permanent chemical change.

Commodity chemicals Chemicals that are produced on the millions of tons per year scale that are used as building blocks for more sophisticated chemicals.

Green chemistry The design of chemical products and processes that reduce or eliminate the use and generation of hazardous substances.

Oxidation The loss of electrons or the increase in oxidation state of a molecule, atom, or ion.

Self-oxidation A situation where the active oxidation catalyst oxidizes itself, usually resulting in degradation and loss of activity.

Speciality chemicals Chemicals that are produced on a relatively small scale often for a particular application.

Definition of the Subject and Its Importance

Green Oxidation Catalysts

The term "green catalyst" has no single definition. Currently, it is most commonly associated with catalysts that are recoverable or prepared from readily available starting materials. A truer definition, although circular, is that a green oxidation catalyst, or any catalyst for that matter, is one that conforms to green chemistry and green engineering principles. Creating a green oxidation catalyst *a priori* is a complex task because every aspect of the catalyst needs examination and to be of practical value it must provide a cost benefit to the end-user. Here, some general guidelines for what a green oxidation catalyst might be are presented. One of the foremost factors is the catalyst's elemental composition. The chart in Fig. 1 shows the relative abundance of chemical elements in the earth's crust. The vast majority of man-made and nature's catalysts contain metals from the middle of the periodic table. While not a hard and fast rule, organisms have evolved to effectively utilize metals at high-ambient concentrations, while those at lower concentrations tend to be toxic; exposure to iron (Fe) is likely to be much less of a concern than ruthenium (Ru) or osmium (Os), its family members in Group 8 of the periodic table [1, 2]. Catalysts containing metals with known toxicity issues like mercury or lead cannot be considered as green because the potential hazards associated with the elements unintentionally getting into the environment outweigh the benefits of the reaction. Currently, the USEPA is developing a *Framework for Metals Toxicity* that is intended to provide guidance regarding various properties of metals, such as environmental chemistry, bioavailability, and bioaccumulation [3]. Next, it has to be ascertained where and how the metal was sourced. For example, new and exciting developments are occurring using gold catalysts [4], but this needs to be tempered with the cost to humans and the environment that has long been associated with mining gold. Mining is always a hazard minimization operation. If organic molecules are used as the catalyst or as an integral part of the catalyst, it is needed to at least ask how were they synthesized, where were the raw materials sourced, and what is being done with the waste generated during their production. Others factors to include in assessing a green oxidation catalyst are determining whether the catalyst is a general or specific one (can one catalyst handle multiple steps, or do intermediates need to be isolated), the impact of the choice of oxidizing agent (e.g., potential chlorinated by-products if hypochlorite is used), the energy metrics of the process, and the potential for nonproductive use of the oxidizing

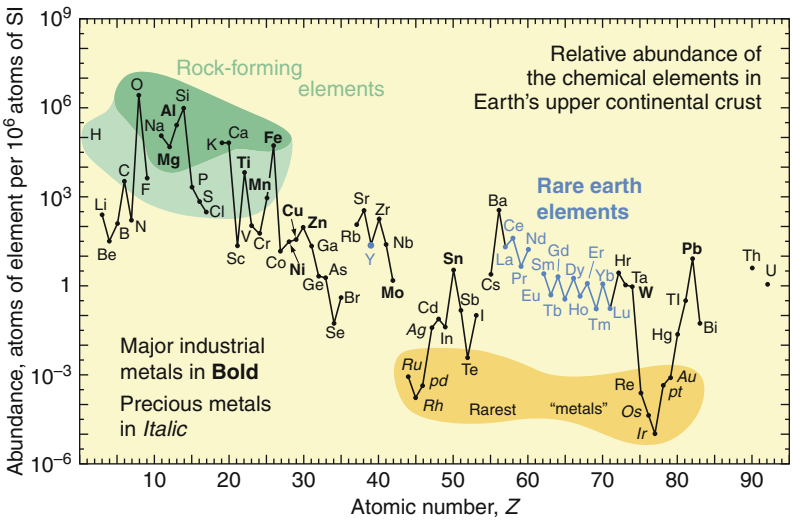

Oxidation Catalysts for Green Chemistry. Figure 1
Abundance of the chemical elements in Earth's upper continental crust as a function of atomic number (Figure courtesy of the U.S. Geological Survey)

agent. It is essential that these questions and others become a part of the culture of catalyst design. This is basically a restatement of a life cycle assessment (LCA) approach but focused on the catalyst itself. For now, less than ideal catalysts must be used to achieve desired goals as the means to make and implement these designs and then test them are still being developed. The challenge will be to find ways to rapidly adapt and adopt new technologies that bring us closer to the ideals.

Introduction

Catalysis -> Green Chemistry/Engineering -> Sustainable development These three concepts and practices are inexorably connected. *Catalysis* is the process whereby materials and energy are saved in a chemical transformation. *Green Chemistry and Green Engineering* are the pursuit of products and processes that reduce or eliminate hazard (physical, toxicological, ecotoxicological, and others) [5, 6]. *Sustainable development* is development that "meets the needs of the present without compromising the ability of future generations to meet their own needs" [7].

The imperative of sustainable development is leading to a wholesale rethinking of the way that humankind needs to approach its continued existence on earth. The green chemistry movement is bringing guidance as to how chemistry should be practiced now and in the future [8]. Over the last nearly two decades, there has been the gradual development and increasing acceptance of green chemistry both in academia and industry. In 2005, the Nobel Prize was awarded to Dr. Yves Chauvin, Professor Richard Schrock, and Professor Robert Grubbs for their work on the olefin metathesis reaction with the Nobel committee clearly stating that their work was a "*great step forward for "green chemistry," reducing potentially hazardous waste through smarter production.*" The general concepts that define green chemistry are that the entire life-cycle of a chemical should do no harm and that all aspects of the chemistry should be sustainable. These concepts are embodied in the 12 principles of green chemistry that were first put forward by Professor Paul Anastas and Dr. John Warner in their landmark 1998 book "Green Chemistry: Theory and Practice" [9]. These principles are augmented by the green engineering principles espoused in 2003 by Professor Anastas and Professor Julie Zimmerman [6]. When current and future chemical products and processes incorporate these principles, then chemistry will flourish for the foreseeable future.

Catalysis is at the heart of Green Chemistry as it is the means to increase efficiency and efficacy of chemical and energy resources while promoting environmental friendliness and intensifying time and cost savings in chemical synthesis [10]. A catalyst's function

simply is to provide a pathway for chemicals (reactants) to combine in a more effective manner than in its absence. This is generally depicted as a reaction coordinate diagram like the one shown in Fig. 2. In the absence of a catalyst, heat is usually the way to overcome the energy barrier, but this increases energy consumption and often results in unwanted side reactions. A catalyst cannot make an energetically unfavorable reaction occur or change the chemical equilibrium of a reaction because the catalyzed rate of both the forward and the reverse reactions are equally affected.

The concept of catalysis traces its birth to the 1830s when Jöns Jacob Berzelius [11] rationalized the results of other investigators into the concept of "catalytic power" and coined the word catalysis [12]. Interestingly, it was Sir Humphry Davy in 1817 who first noted the catalytic properties of a metal when he described the reaction of coal gas and oxygen over platinum and palladium wires. In that report, he noted that the reaction did not proceed in the presence of copper, silver, gold, and iron. Roberts proposes in his brief history of catalysis [13] that this may have been the earliest recorded pattern of selectivity in catalysis.

Oxidation Chemistry

Oxidation chemistry – what is it and what is it good for? Oxidation is defined as the loss of electrons or the increase in oxidation state of a molecule, atom, or ion.

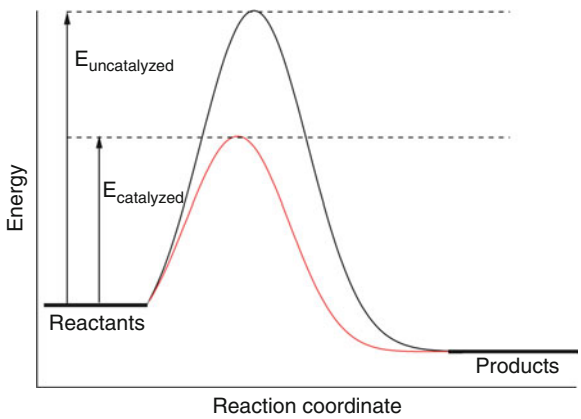

Oxidation Catalysts for Green Chemistry. Figure 2 Reaction coordinate diagram showing the different activation energies for catalyzed and uncatalyzed reactions. The catalyst opens a lower-energy pathway to the desired products

Combustion of organic matter like coal, natural gas, or gasoline is a familiar oxidation reaction. This is a destructive or nonselective form of oxidation chemistry. Here, a "reduced" form of carbon is being taken and combined with oxygen and then oxidized to CO_2 with water as the other product. In the constructive or selective regime of oxidation chemistry, the one practiced by most chemists, the organic matter is transformed either using oxygen or some other electron acceptor into a new chemical that is of higher value. Oxidation chemistry is probably the largest branch of chemistry pursued by industry, human activity and diverse natural systems.

- Oxidation chemistry is being used when doing laundry, where bleach (sodium hypochlorite) or hydrogen peroxide is the oxidizing agent that destroys or degrades the molecules responsible for the stains on clothes.
- The society benefits from the application of oxidation chemistry at the wastewater treatment plant that treats sewage and the drinking water treatment plant that provides clean drinking water. When the chlorination of drinking water was developed, many of the water-borne pathogens that caused so much suffering and misery were removed and human health took a great leap forward. However, it has been known for many years that some of the by-products from water chlorination, which are referred to as disinfection by-products (DBPs), are human health hazards. In order to avoid DBPs, alternative oxidants such as chloramine and ozone are being implemented, but these too have some negative consequences associated with their application.
- The catalytic converter on automobiles might be considered one of the most successful and detrimental oxidation catalysts from the perspective of human health and the environment. The modern 3-way catalytic converter oxidizes carbon monoxide and unburnt hydrocarbons to carbon dioxide and water while reducing nitrogen oxides to nitrogen gas and water. This catalyst system has made the environment vastly better by reducing smog causing chemicals and eliminating the use of leaded gasoline. Among its negatives are the production of carbon dioxide that contributes to global climate change, expansion of the automobile industry

because smog producing chemicals are less prevalent in automobile exhaust, loss of land as a result of road building, and the catalyst materials are precious metals (platinum, palladium, and rhodium) that are obtained by mining.

- Oxidation reactions are constantly occurring in biological systems. The cytochrome P450 enzyme in the liver detoxifies chemicals that are ingested by oxidizing them to less toxic substances. Cytochrome P450 is an exquisitely designed oxidation catalyst system that uses oxygen in a precise and controlled manner to destroy the toxin. Chemists and biologists have been fascinated by the cytochrome P450s, resulting in hundreds if not thousands of research publications describing their chemical, physical, and biological properties.
- In the environment, many different kinds of organisms are essential for the degradation of natural and unnatural substances that constantly enter soils and waterways. For example, a decaying tree in the forest might be under attack from the enzymes lignin peroxidase and manganese peroxidase in white rot fungi that utilize hydrogen peroxide to degrade the lignin. In this case, the degraded material ends up as new fertilizer for the forest floor. Interestingly, lignin peroxidase also has been found to degrade some recalcitrant, man-made pollutants.

These examples of oxidation chemistry only scratch the surface of the field. Oxidation processes are used for odor control, bleaching of pulp for paper production, wastewater treatment, disinfection, bulk and specialty chemical production, aquatics and pools, food and beverage processing, cooling towers, agriculture/farming, and many others. It is often noted in reviews about oxidation chemistry that catalysts would make the field substantially more efficient. In fact, there are a great many oxidation reactions that are catalytically driven. A search of the Chemical Abstracts Services database using *chemical oxidation catalyst* as the search criteria and limiting results to patents and journal article returned more than 500 entries for the year 2009, likewise the Royal Society of Chemistry's RSC Catalysis and Catalysed Reactions database resulted in more than 100 entries using *Reaction type – oxidation*, and a search of patent application titles at the US Patent and Trademark Office with *oxidation* and *catalyst* in the title yielded 230 entries since 2001 – undoubtedly, there were many more.

Oxidation reactions whether they be catalytic or not remain an enormous undertaking from the laboratory scale to industrial production. An oxidation reaction might be contemplated on a molecule that already has one or more functional groups that might be affected by the oxidation process. Thus, a successful oxidation process involves a deep understanding of inherent chemical and physical properties of the target molecule and how these might be impacted by the choice of oxidation catalyst, the oxidant, and the reaction medium [14].

The definition of oxidation gives wide latitude to what is desired from an oxidation catalyst. Indeed, one of the great challenges in oxidation chemistry is the breadth of the field. The most recent edition of *March's Advanced Organic Chemistry: Reactions, Mechanisms, and Structure, 6th Edition*, a standard reference source for the organic chemist lists six groups of oxidations that comprise 32 different types of oxidation reactions [15]. Entire libraries of catalysts have been developed to achieve a single type of oxidation process. For example, 2001 Nobel Prize winner Professor K. Barry Sharpless developed a catalytic system for the enantioselective epoxidation of allylic alcohols, Fig. 3 [16]. However versatile these catalysts might be within their class of oxidations, they are not generally applicable to the epoxidation of other olefin containing compounds.

Catalytic oxidation processes are used in the production of some extremely large volume industrial chemicals. For example, a cobalt/manganese catalyst with a bromine promoter is used to oxidize *p*-xylene to terephthalic acid, Fig. 4 [17], a roughly 44 million ton/year chemical. The terephthalic acid ultimately is used for polyethylene terephthalate, the polymer used in many drinking bottles. Large-scale chemical manufacturers know that they have to adapt their processes as feedstock resources become more limited and that they will have to comply with ever more stringent environmental guidelines [18].

Finally, oxidation catalysts can play a crucial function cleaning organic pollutants from the environment. There are roughly 30,000 chemicals used on a regular basis throughout commerce, approximately 84,000 are registered with the USEPA under the Toxic Substances Control Act. Some of these ultimately find their way

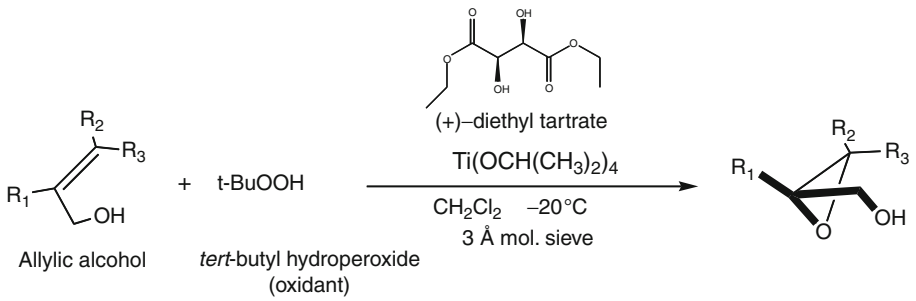

Oxidation Catalysts for Green Chemistry. Figure 3
Typical Sharpless epoxidation conditions. Substitution of the nonnatural (-)-diethyl tartrate results in oxygen addition on the upper face of the allylic alcohol

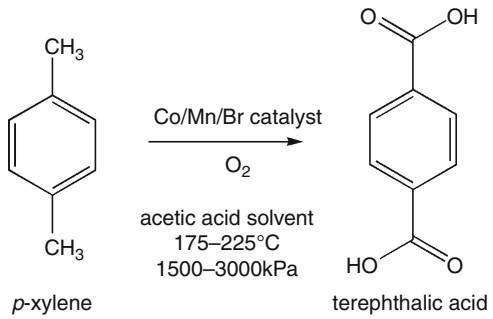

Oxidation Catalysts for Green Chemistry. Figure 4
The Amoco industrial synthesis of terephthalic acid

into the water that sustains life. The effects of many of these chemicals on human health are not well known although the President's Cancer Panel recently suggested that the role of environmental toxins (pollutants) as cancer causing agents is substantially underestimated. Fortunately, there are many technologies to remove toxic compounds from water. Oxidation catalysts can play a pivotal role in breaking down the recalcitrant compounds that are not degradable by biological means. A number of different oxidation technologies are being investigated, but only a few employ catalysts [19]. Fenton's reagent, an iron-based catalytic process that utilizes H_2O_2, is a popular option; photocatalytic processes using titanium dioxide is another approach; catalytic wet-air oxidations for waste streams containing high concentrations of organic materials is a powerful methodology, and an emerging technology is based on using oxidatively robust small molecule catalysts. The real test is determining which catalysts are green and getting them adopted as widely as possible by moving them from the chemical literature to commercial ventures.

Industrial Catalysts

Industrial, bulk, or commodity chemicals are those chemicals that are produced on a vast scale (millions of tons per year, Mt a^{-1}), often as building blocks for more sophisticated chemicals. As such, they generally cost less than \$0.50/lb. In the industrial chemical sector, there is tremendous pressure to make chemicals as inexpensively as possible – economics drives production of large-volume chemicals and the application of green chemistry principles enhances the bottom line. Catalysis plays a vital role in providing pathways to these chemicals. Table 1 provides examples of some bulk chemicals produced by catalytic oxidation processes on the Mt a^{-1} scale.

Many, if not most, of the organic bulk chemicals in Table 1 are produced from nonrenewable resources such as petroleum or natural gas so their use and preparation violate Green Chemistry principles. It is often proposed that careful stewardship of the nonrenewable resources is what is needed to sustain the chemical industry. However, if the chemical industry truly needs to continue supplying these chemicals, renewable resources will have to be used and transformations of these natural materials based on Green Chemistry principles developed [20]. This is clearly as exciting a goal for current and future chemists and biologists as the one that led prior generations to the current portfolio of chemicals [21]. It is heartening to know that substantial advances are taking place to

Oxidation Catalysts for Green Chemistry. Table 1 Examples of bulk chemicals produced by catalytic oxidation processes

Chemical	Chemical precursor	Production (Mt a^{-1})	Example end uses
Terephthalic acid	*p*-Xylene	44	Polyethylene terephthalate (PET) drink bottles
Formaldehyde	Methanol	19	Resin component
Ethylene oxide	Ethylene	18	Polyester fiber, automotive engine antifreeze, production of polyethylene terephthalate
Propylene oxide	Propylene	8	Polyurethane systems
Cyclohexanone	Cyclohexane	6	Nylon 6,6
Phthalic anhydride	*o*-Xylene	5	Plasticizers
Maleic anhydride	Butane	2	Polyester and alkyd resins, lacquers, plasticizers, copolymers, and lubricants

include renewable resources among these feedstocks [22, 23]. Still, the vast scale of production of "bulk" chemicals means that it will be decades before renewable resource-derived products and the associated processes can replace current practices on the industrial scale. Until such time, catalytic oxidation of petroleum and natural gas-derived feedstocks will prevail.

The vast majority of catalysts for bulk chemicals is heterogeneous and are either of the supported or bulk type. Ease of separating the catalyst from reactants and products, thermal stability, and recyclability of the catalyst are among the most important reasons for using heterogeneous systems. Virtually, all of the heterogeneous catalysts contain transition metals from the middle of the periodic chart as the catalyst or as additives that promote the catalytic reaction. Chemists have done an amazing job over the years in understanding how these metals function and how to manipulate their activity and reactivity. However, some are also well known for their toxicity [24] and for the environmental [25] and societal damage that extracting them from the earth causes. Nevertheless, for the foreseeable future, metal-containing catalysts will remain the first choice for the chemical industry. Fortunately, there are many catalyst recycling businesses, most of which claim to recover the metals in an environmentally friendly manner.

Challenges in Industrial Oxidation Catalysis

There have been many recent advances in catalysts and catalytic reactions for some of the chemicals listed in Table 1. Excellent recent reviews cover selected "dream" reactions for oxidative catalysis that are currently under investigation or have become commercial processes [22, 26]. The incredible volume of activity in the industrial oxidation area makes it impossible to assess the greenness of each catalyst here. To provide illustrative examples, two of these processes, oxidation of propene to propylene oxide and adipic acid synthesis, will be examined in some detail with respect to how the catalysts being evaluated conform to Green Chemistry/Engineering principles.

As already mentioned, the chemicals in Table 1 must be produced with an eye to economics. This leads to the use of oxygen (or air) as the primary oxidant. Oxygen is certainly a green reagent; however, there is risk of explosion and fire, so risk management in terms of oxygen concentration and equipment construction always must be considered. Hydrogen peroxide is the next best oxidant as its by-product is water. However, its cost can be prohibitive especially when the reaction consumes multiple equivalents of hydrogen peroxide. Hydrogen peroxide is also inherently a water-based process, so the chemistry must be compatible with this type of environment.

Propene to Propylene Oxide The first reaction described is conversion of propene to propylene oxide, which is becoming recognized as a green process. Propylene oxide is 6 Mt a^{-1} bulk chemical used primarily for the production of polyether polyols, polyurethane precursors, as well as for propylene glycol and glycol ethers. The ideal reaction is direct epoxidation of

propene with oxygen, but when allylic hydrogen atoms are present, as they are in propene, selectivity becomes a factor as over-oxidation occurs. The chlorohydrin process for propylene oxide production uses chlorine gas in the reaction, Fig. 5, and it is this process that is targeted for replacement. In addition to using the highly toxic and dangerous gas chlorine, the chlorohydrin process requires for each ton of propylene oxide, 1.4 t of chlorine, and 1.0 t of calcium hydroxide. In terms of waste, approximately 2.0 t of $CaCl_2$ are obtained and a large volume of salt-containing wastewater is generated [18].

Catalytic oxidations of propylene to propylene oxide using H_2O_2 or cumyl hydroperoxide are recent commercial successes. Work began in the early 1990s on catalytic oxidation of propylene using H_2O_2 and a titanium silicalite (TS-1) as the catalyst [27–29]. The generalized reaction is shown in Fig. 6. The practical potential for this chemistry is enormous since it is direct conversion to product, only one equivalent of H_2O_2 is needed, and the waste product is water. This chemistry has evolved into the so-called HPPO process (Hydrogen Peroxide Propylene Oxide), where propylene is oxidized to propylene oxide under mild reaction conditions. It is run at $<60°C$ in aqueous methanol as solvent and a propylene pressure of ca. 4 bar (3.95 atm or 58 psi). The methanol is recycled. Selectivity to product is $>90\%$ and can be as high as 97% based on hydrogen peroxide [30].

An Evonik–Uhde partnership has licensed the TS-1/H_2O_2 technology to the Korean firm SKC of Seoul that commissioned a 100,000 t/year propylene to propylene oxide plant in 2008. This plant also uses a platinum/palladium-based catalyst technology developed by Headwaters Technology Innovation that makes H_2O_2 directly from H_2 and O_2. The catalyst, NxCat™ lowers energy use, uses renewable resources and generates no toxic waste during the H_2O_2 production. This technology was the recipient of a 2007 USEPA Presidential Green Chemistry Challenge Award. A BASF – Dow Chemical partnership recently commissioned a 300,000 Mt a^{-1} propylene to propylene oxide plant using a titanium silicate oxidation catalyst for H_2O_2 activation. According to BASF/Dow, wastewater is reduced by 70–80%, and energy usage by 35%, compared with existing PO technologies. The BASF-Dow Chemical process received a 2010 USEPA Presidential Green Chemistry Challenge Award.

Sumitomo has commercialized a process that also utilizes a proprietary titanium-silicate catalyst. The Sumitomo method is interesting as it couples the non-catalytic oxidation of cumene to cumene hydroperoxide with the catalytic oxidation of propylene to propylene oxide, Fig. 7. This oxidation route is viable in part because of the high stability of cumyl hydroperoxide that results in high recyclability of cumene.

TS-1 is a crystalline zeolite type material containing tetrahedral TiO_4 and SiO_4 units with a three-dimensional system of channels. It is particularly good at activating H_2O_2, and it has been a significant addition to the industrial catalysis field where many reactions now use it alone or in modified form [31]. TS-1 contains less than 2% titanium, and these appear to be the catalytic sites as the Ti-free material does not show a comparable activity.

Current technologies to prepare TS-1 and many other mesoporous materials can be categorized as being modestly green. TS-1 is synthesized by controlled hydrolysis of a synthesis gel comprised of a

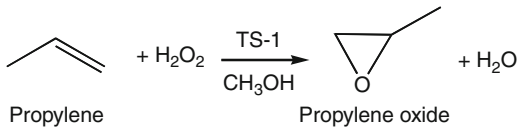

Oxidation Catalysts for Green Chemistry. Figure 6
Direct oxidation of propylene to propylene oxide using a catalyzed HPPO process

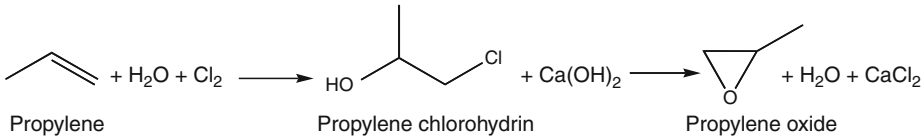

Oxidation Catalysts for Green Chemistry. Figure 5
Chlorohydrin process for producing propylene oxide

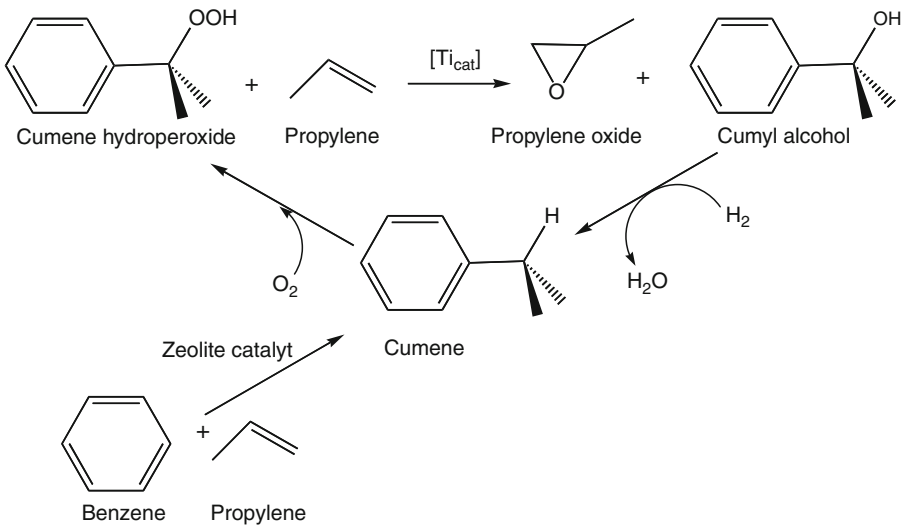

Oxidation Catalysts for Green Chemistry. Figure 7
Sumitomo catalytic oxidation of propylene to propylene oxide using a proprietary titanium-based catalyst Ti_{cat}

tetraalkyltitanate, tetraalkylsilicate, and a tetrapropylammonium hydroxide [32]. An excellent recent review that tackles many of the green issues associated with sol-gel methods for preparing silicates is available [33]. For TS-1, the proportions of the different reagents are important for controlling catalyst activity. From a green catalyst perspective, the mass yield of catalyst is relatively low. In 1992, Professor Roger Sheldon [34–37] codified the *E*-factor (*E* = *E*nvironmental) which takes into account the actual amount of waste produced in a given process and includes reagents, solvent losses, process aids and fuel. In simplest terms, it is the ratio of kilograms of by-product/kilograms product [38]. The TS-1 synthesis from a 2005 Degussa patent US 6,841,144 states:

"This synthesis method resulted in a consumption of *tetra-n*-propyl ammonium hydroxide (40% solution) of 1.6 kg per kg TS-1, a yield of 110 g TS-1 per kg synthesis gel . . .."

This results in an *E*-factor for TS-1 of at least 8 - (*E*-factor = (1.0 kg synthesis gel – 0.110 kg TS-1)/(0.110 kg TS-1), and it could be higher if purification methods are needed. During the hydrolysis process, the alcohol formed must be distilled and then either recycled or removed as waste. Finally, tetraalkyltitanates and tetraalkylsilicates are flammable and thus require careful handling. Attention is being given in many laboratories that prepare these materials to find alternative, efficient synthesis methods [39].

Adipic Acid Synthesis There are significant efforts underway to change adipic acid production to a catalytic process using what appear to be mostly green catalysts. Adipic acid is used in the synthesis of nylon 6-6. An overview of the current practice for adipic acid synthesis is given in Fig. 8. It is essentially a two-step process, where cyclohexane is first oxidized to a mixture of cyclohexanol and cyclohexanol (KA oil) [40], and then this mixture is oxidized with nitric acid, HNO_3, to adipic acid. The oxidation is catalyzed with a homogeneous catalyst containing Cu^{II} nitrate and ammonium metavanadate [18]. The objective is to remove HNO_3 as the oxidant because it is a serious hazard from a chemical safety point of view, and its reduction product N_2O is a powerful greenhouse gas (300 kg of N_2O are produced per ton of adipic acid). Most adipic acid producers have means to decompose, trap, reuse, or recycle the N_2O.

Depicted in Fig. 9 are some of the catalytic routes and catalysts being contemplated. An excellent recent review detailing efforts ongoing in this area is available [19]. Among the limitations of the catalysts are poor conversion levels, moderate to low selectivity, challenging processability, and some demand a specific

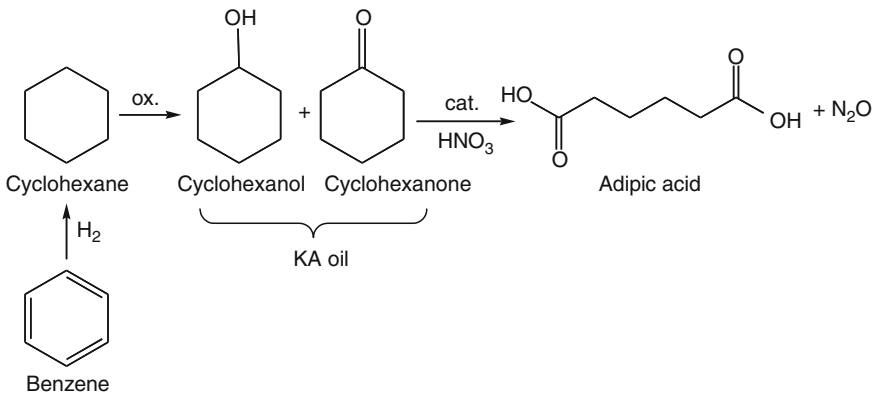

Oxidation Catalysts for Green Chemistry. Figure 8
Adipic acid synthesis from benzene. Nitric acid (HNO_3) is the oxidant and generates N_2O a greenhouse gas. The catalyst (cat.) is homogeneous, containing Cu^{II} salts and an ammonium metavanadate

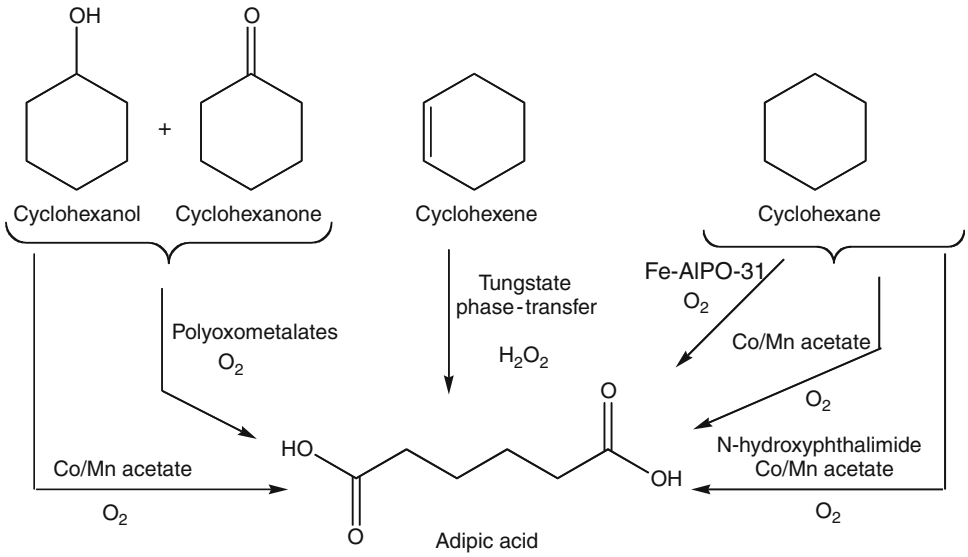

Oxidation Catalysts for Green Chemistry. Figure 9
Potential new catalytic routes to adipic acid. Information for figure adapted from Cavani [18]

oxidizing agent. From a pure materials perspective, the Fe^{III}AlPO-31 catalyst is the most green. It is based on aluminophosphate molecular sieve, where Fe^{III} substitutes some of the Al^{III} in the framework. Interestingly, other aluminophosphate structures are not as selective as AlPO-31. It is suggested that AlPO-31 has narrow pores which easily absorb cyclohexane, but intermediate oxidation products are less easily desorbed than adipic acid [41]. Benzene, a petroleum product, is the precursor to the cyclohexane derivatives used in each synthesis. Ultimately, it will be necessary to replace or sustainably produce the benzene or preferably the KA oil. There are efforts particularly in the biocatalysis field to produce adidpic acid free of a benzene source [42].

Economic viability will be the ultimate driving force for adopting new adipic acid technologies. For example, cyclohexene oxidation with the tungstate catalyst Na_2WO_4 in Fig. 8 is elegant chemistry that currently is not cost competitive with other technologies [43]. Na_2WO_4 might be considered a green catalyst as it has low toxicity toward fish [44], but speciation toward the metatungstate ($3Na_2WO_4{\cdot}9WO_3$) increases toxicity

[45]. The cyclohexene is catalytically oxidized with aqueous 30% H_2O_2 to adipic acid in a one-step process in the presence of the catalyst and the phase-transfer agent $CH_3(n\text{-}C_{18}H_{17}N)_3HSO_4$, there are no added solvents. Na_2WO_4 has good water solubility, but cyclohexene does not, so the phase-transfer agent is used to introduce the catalyst and cyclohexene into the same phase. Reaction temperatures are mild 75–90°C, the cyclohexene is converted directly to analytically pure, crystalline adipic acid in almost quantitative yield, and H_2O_2 consumption is nearly ideal (theoretical consumption is 4.0 mol of H_2O_2 per mol of cyclohexene and actual is 4.4 mol H_2O_2). Nevertheless, at current H_2O_2 prices, the process is not economically viable because of the relatively large amount of H_2O_2 needed [46, 47]. This example raises the point that a catalyst cannot change the stoichiometry of a reaction, so the fundamental chemical economics of a process can be determined without consideration of the catalyst. An integrated process as in polypropylene oxidation, where H_2O_2 cost is controlled, or one in which the cyclohexene cost is much less than the other starting materials might overcome economic issues, and then the issue will be changing from an entrenched multi-Mt a^{-1} process to a new one.

Long-term Industrial Challenges

Synthesis gas, which is carbon monoxide and hydrogen gas, is the current economically viable route for converting methane into commercially useful fuels, gasoline and diesel, and chemicals, principally methanol. The methanol is subsequently converted to olefins as building blocks for other chemicals [48]. The methane can come from natural gas deposits but, from a sustainability perspective, the methane produced from the decay or fermentation of organic material, biogas is the more desirable source. Steam reforming of methane, Eq. 1, currently is the large-scale process for natural-gas conversion to synthesis gas. This is an energy intensive process because the reaction is energetically uphill by a substantial amount ($\Delta H_{298\ K}$ = +206 kJ/mol). Temperatures in the range 700–1,000°C and steam under 3–25 bar pressure are used. The problem could be solved by oxidation, Eq. 2, as this is an energetically favorable process ($H_{298\ K} = -36$ kJ/mol). Oxidation catalysts for synthesis gas production are receiving substantial research efforts in industry and academia. The main stumbling block at this time is further oxidation (over-oxidation) of the CO to CO_2 [49].

$$\text{Steam reforming } CH_4 + H_2O(+\text{heat}) \rightarrow CO + 3H_2 \quad (1)$$

$$\text{Partial Oxidation } CH_4 + {}^1\!/_2O_2 \rightarrow CO + 2H_2\ (+\text{heat}) \quad (2)$$

Selective catalytic oxidation of hydrocarbons to oxygen-containing chemicals like alcohols, aldehydes, and carboxylic acids are also targets [50]. This would allow the direct conversion of light hydrocarbons from refinery operations to useful chemicals or precursors to more complex products. Hydrocarbons generally are unreactive, except in the presence of metal catalysts at high temperatures and pressures or in the presence of specifically designed reaction media [51]. With clear economic and energy metrics for direct conversion to oxygenates, intense research efforts are underway to make better homogeneous and heterogeneous catalysts. The use of fossil fuel-based products is not a sustainable approach to chemical manufacturing, but the energy and resource savings make this direct conversion an acceptable interim measure until renewable resources take their place.

The oxidative dehydrogenation (ODH) of alkanes to alkenes is another oxidation reaction that continues to receive considerable attention, Eq. 3 [52]. Ethylene is the largest production chemical at about 95 million tons/year. It is used directly in polymers like polyethylene, chlorinated for polyvinyl-chloride production, combined with benzene to produce ethylbenzene, the precursor of polystyrene, and oxidized to other smaller volume chemicals [53]. Currently, ethylene is manufactured by steam cracking of napthas from petroleum feedstocks. Like the synthesis gas reaction, this is energy intensive because the thermodynamics of the process are unfavorable, and so high temperatures, 800–850°C, are used to overcome the barrier. The high temperatures can result in cracking of the hydrocarbons to smaller fragments and reduction to coke [54].

$$2CH_4 + O_2 \rightarrow C_2H_4 + 2H_2O \quad (3)$$

In an ODH process, reaction temperatures can be substantially lowered because the added O_2 reacts with the hydrogen from the alkane producing water that

provides the thermodynamic driving force for the reaction [53, 55]. If the technology could be developed for production of butadiene from butane, for example, this would have high commercial value since butadiene is used in the manufacture of automobile tires, synthetic rubbers, specialty polymers, and chemicals [54]. Despite the extensive literature describing the oxidative dehydrogenation of alkanes, information about the individual reaction steps comprising alkene formation is somewhat limited. Catalyst composition focuses around a few transition metals, nickel, vanadium, and molybdenum, with different additives or promoters such as potassium and calcium, and a host of different support materials each of which can influence the chemistry. Cerium oxide-based materials are showing significant promise in ODH chemistry, and these can be considered as green catalysts as long as no inherently toxic metals are used [52]. However, like many other catalyst systems and catalyst reactions, there is still much work to be done to understand how catalyst composition and structure relate to activity and selectivity [50].

Specialty Chemical Catalysts

The birth of the synthetic chemical industry can be traced to 1856 when William Henry Perkin oxidized aniline to mauveine. Under the direction of August Wilhelm Hofmann at the Royal College of Chemistry in Oxford Street, London, Perkin had been studying the reactions of various constituents in coal tars. Hofmann's research focused on manipulating the organic chemicals present in coal tars, a by-product of the gas-manufacturing plants that were lighting the streets of London. Perkin was directed to synthesize the antimalarial drug quinine from coal-tar components. In Perkin's home laboratory, he attempted a synthesis of quinine by oxidizing allyltoluidine with potassium dichromate. He expected a colorless product but rather obtained a dark reddish-brown solid. A repeat of this experiment using aniline rather than allyltoluidine resulted again in a dark black solid. Perkin, as any well-trained synthetic chemist would do, dug into this complex mixture and isolated a purple component, which he quickly found made an excellent fabric dye. After testing the dye in various dyehouses and achieving outstanding results, Perkin applied for and ultimately received a patent in for the synthesis of dyes. His procedure for preparing the dye powder is described in the patent as follows:

- I take a cold solution of sulphate of aniline, or a cold solution of sulphate of toluidine or a cold solution of xylidine, or a mixture of any one of such solutions with any others of other of them, and as much of a cold solution of a soluble bichromate as contains base enough to convert the sulphuric acid in any of the above-mentioned solutions into a neutral sulphate. I then mix the solutions and allow them to stand for ten or twelve hours, when the mixture will consist of a black powder and a solution of a neutral sulphate. I then throw this mixture upon a fine filter and wash it with water till free from the neutral sulphate. I then dry the substance thus obtained at a temperature of 100 degrees centigrade, or 212 degrees Fahrenheit and digest it repeatedly with coal-tar naphtha until it is free from a brown substance which is extracted by the naphtha. I then free the residue from the naphtha by evaporation and digest it with methylated spirit or any other liquid in which the colouring matter is soluble, which dissolves out the new colouring matter. I then separate the methylated spirit from the colouring matter by distillation, at a temperature of 100 or 212°F.

Buoyed by successful trials at various dyehouses, in 1857 Perkin, his father and brother established the company Perkin and Sons at Greenford Green, near Harrow, to manufacture and supply the dye. The success of the scale-up and subsequent commercialization process for Perkin and Sons is well described in many accounts of Perkin's life and career as a chemist.

Interestingly, it was not until 1994 that the structural components that comprised mauveine were conclusively identified [56, 57]. These are shown in Fig. 10. The components are a combination of aniline and o-toluidine and p-toluidine. Thus, the aniline that was supplied to Perkin contained toluidine impurities. Performing reproducible synthetic reactions on aniline that had varying amounts of impurities must have been challenging, especially with the crude apparatus available at the time. This makes Perkin's achievements even more remarkable.

With no disrespect to Perkin, a review of the aniline oxidation reaction in terms of green chemistry principles, reveals that very little of it would be described as "green." Aniline itself is still produced by "nongreen"

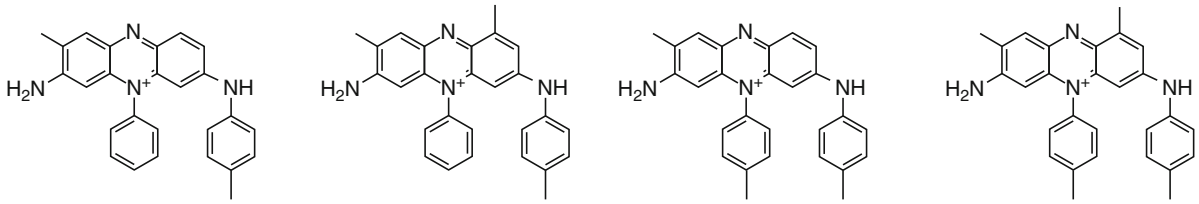

Oxidation Catalysts for Green Chemistry. Figure 10
Major components of the dye produced by Perkin upon oxidation of aniline, *o*-toluidine and *p*-toluidine

methods and from nonrenewable resources, although there are ongoing efforts to green its preparation [58, 59]. Furthermore, mauveine is synthesized by the stoichiometric addition of the oxidant potassium dichromate to an impure solution of aniline in acidic water. Here, the potassium dichromate oxidizes the aniline, and its reduced form becomes a by-product of the reaction that must be separated and disposed of safely (at least in modern times). Today, there are green catalytic oxidation alternatives to stoichiometric reagents like dichromate, so it is possible that mauveine can be prepared catalytically. In fact, there is a suggestion of such possibility in a 1935 publication when a peroxidase enzyme is used with H_2O_2 to oxidize aniline, and it is proposed that mauveine is one of the products [60].

Specialty Chemicals

The development of synthetic organic chemistry began well before Perkin's time and has resulted in an enormous body of work. Today, there are numerous compendia that the chemist can turn to for insights into how to perform their particular reaction. Chemists are very skilled at devising new target molecules on paper and then mounting what frequently becomes a complex synthetic campaign covering many reaction steps and several years to make them. In fact, it can be stated with reasonable certainty that if a molecule can be envisioned, then there is a synthetic pathway that will successfully lead to its preparation. The reaction sequence often has steps with high *E*-factors and others having low ones. During the preparation, the chemist could be considering aspects of chemoselectivity (conversion of one functional group in the presence of another), regioselectivity (preference of reaction at one of two or more possible reaction sites), or stereoselectivity (the production of one stereoisomer of the product in preference to the other). This synthetic complexity accounts for the vast array of catalysts that have been reported and the libraries of catalysts developed to achieve a subset of reactions within a larger class. Catalysts used for bulk chemical production often employ more forcing conditions with respect to temperature and pressure than are available in many synthetic laboratories, and they tend not to have the kinds of selectivities desired by the specialty chemical producer.

In the specialty chemical area, many oxidation catalysts are based on transition metals surrounded by more or less complicated organic structures which are referred to as ligands [61]. The design of the ligands is a difficult endeavor because once reaction is initiated, then all species in solution, including the catalyst, are targets for oxidation. In an ideal scenario, the oxidation process is selective toward the target of interest. However, it is more often the case that the ligand is oxidized at nearly the same rate as the target molecule. This has lead to the development of complex protection schemes for ligands (and associated reaction pathways to make them) or alternatively the use of low catalyst to substrate ratios (higher than desirable quantities of catalyst). While both means ultimately lead to the desired oxidation product, neither exemplifies Green Chemistry principles. Nevertheless, a large amount of valuable information and useful oxidation reactions have been achieved with these systems. The most ideal approach then is to design ligands that are inherently stable under oxidizing conditions. This should result in the use of less catalyst and bring the overall process closer to Green Chemistry principles [62].

Oxidation Catalysts Inspired by Biology

One of the most logical starting points to begin the design of green oxidation catalysts is to look at how

nature handles the oxidation problem. Biology has had billions of years of practice perfecting its repetitive oxidation reactions, but chemists began systematically exploring the diverse field of oxidation chemistry only little more than two centuries ago. Many biological oxidation processes are catalytic and are arranged such that a single catalyst reaction center, or a combination of reaction centers, reacts with many, many target molecules before returning to their resting state until called upon to do the reaction again. Repair and replacement mechanisms for these catalysts are an important part of the biological process, so the catalytic reaction center does not need to be robust. The chemist generally does not have the luxury of mid-process catalyst repair, and replacement means adding more of the often precious catalyst to keep the reaction proceeding.

Biocatalysis Although enzyme systems have been intensively studied for many years, over the past decade chemists, biologists, and chemical and pharmaceutical companies have begun to aggressively embrace enzymes as new engines, *biocatalysts*, for making some of the products that are used every day [63]. The beauty of enzymes is that they are generally nontoxic, they can be grown rather than synthesized in the laboratory, they have high selectivity, their turnover frequencies are often high (10–10,000 s^{-1}), and their waste products should not be an environmental burden. These attributes clearly place biocatalysts at the top level in terms of green oxidation catalysts. The discoveries and applications of biocatalysis are still in their relative infancy, but bulk chemicals, pharmaceutical and agrochemical intermediates, active pharmaceuticals, and food ingredients are being made using biocatalysts [64]. As directed enzyme evolution, genomics, and the exploration of new biological sources evolve, biocatalysis is likely to play an increasing role in the chemical enterprise [65]. Still, it will be many years before biocatalysts replace some of the traditional chemical processes because they must provide a clear cost benefit over the current process, and it is likely that there will remain some or even many chemicals that cannot be made by biocatalytic means.

There are a plethora of interesting biocatalytic oxidations involving the oxidation of racemic alcohols, C–H bonds, Baeyer–Villager oxidations, and many others, and the details of these studies are best left to the reader to explore [66]. One clever example of a biocatalytic sulfur oxidation is provided by Professor Roger Sheldon, a leader and pioneer in the green chemistry community and movement. His group combined a heme-dependent chloroperoxidase enzyme with in situ H_2O_2 formation produced *via* the glucose/glucose oxidase reaction to enantioselectively oxidize thioanisole to the corresponding sulfoxide, Fig. 11. The key element in Sheldon's study was to co-immobilize the chloroperoxidase enzyme and glucose oxidase in a polyurethane foam [67]. Immobilization of the chloroperoxidase enzyme vastly improved its stability toward oxidative degradation, and in situ generation of H_2O_2 meant that supplying an external source of the oxidant (a hazard) was avoided. In a broader sense, this work brings together 11 of the 12 green chemistry principles – the only one not embodied is real-time analysis for pollution prevention.

Biocatalysis has had to overcome many obstacles during its relatively brief development time. Among the concerns voiced regarding its viability are: (a) limited substrate specificity, (b) availability of enzymes, (c) enzyme stability, and (d) the need for cofactors to regenerate the active enzyme. All of these have been addressed successfully by creative and insightful

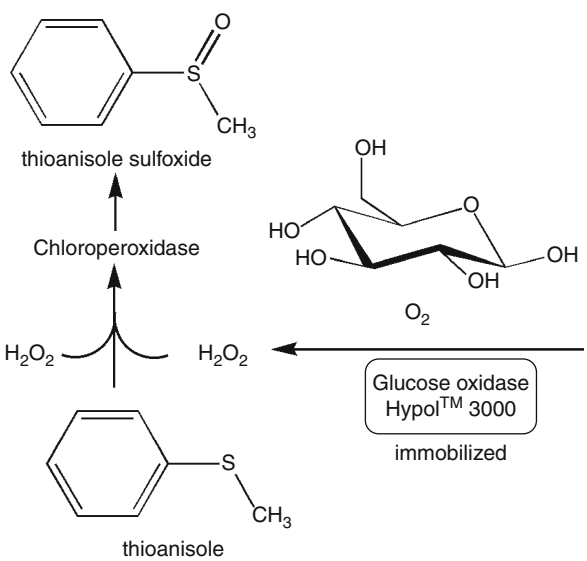

Oxidation Catalysts for Green Chemistry. Figure 11 Oxidation of thioanisole using chloroperoxidase and glucose oxidase co-immobilized in the urethane polymer derived from Hypol™ 3000

scientific approaches. One of the remaining obstacles in biocatalysis remains water demand for production of the enzyme and its use. In one recent example, an analysis of the oxidation of styrene to enantiopure (S)-styrene oxide styrene using three chemical and one biocatalytic approach revealed that the biocatalytic route required from twofold to nearly 40-fold more demand in water [68].

Biomimicry The area of biomimicry is the examination of all aspects of nature, including its systems, processes, and elements, in order to solve human problems sustainably. A bit more narrow focus for the discussion here is biomimetics, which uses nature to inspire the creation of materials and products by reverse engineering. A biomimetic catalyst is a catalyst that carries out a reaction in a mode of action that resembles a natural enzyme. A generalized scheme for biomimetic reactions is shown in Fig. 12. Biomimetic oxidation reactions, especially those catalyzed by transition metal complexes, have provided a vast amount of scientific information with regard to structure, function, thermodynamics, kinetics, mechanism, synthesis, and enhanced or new analytical and spectroscopic methods [69, 70].

The biomimetic chemist has the advantage in the design of a green catalyst as nature mostly limits its metals choices to those that are readily available in the geosphere and also those that are nontoxic. Manganese, iron, and copper probably are the dominant metals involved in biological oxidation processes, although vanadium and others play prominent roles as well. As can be seen in Fig. 1, these are generally abundant metals. In addition, they are able to readily cycle through the electron-transfer steps that are needed for the oxidation process. Excellent reviews, books, and multivolume sets exist around the topic of biomimetic chemistry, so this subject will not be discussed in detail.

Nature's oxidations generally employ transition metals held in place by organic ligands. As mentioned earlier, one of the main problems with the design of oxidation catalysts is to avoid oxidative degradation of the ligand structure. Nature avoids the ligand degradation by elaborate design around the catalytic center to control access to it for only those chemicals that need to be oxidized, careful timing of the process, turning on and off the oxidation as needed, and living systems can rapidly repair and replace damaged catalytic centers. With few exceptions, the issue of ligand oxidation has hampered the development of highly successful commercial biomimetic oxidation catalysts. Nevertheless, even these less-than-ideal catalysts can be considered as green catalysts because they use nature's elements, and they can be useful under certain circumstances.

Cytochrome P450 The modeling of the enzyme system known as cytochrome P450 is vast both in terms of structural models and kinetic and mechanistic studies. Cytochrome P450 is a family of heme–iron enzymes, more than 2,000 are known, that activate molecular oxygen to catalyze the oxidation of organic substances incorporating one of the oxygen atoms in the substrate and the other oxygen is reduced to water, Eq. 4. Figure 13 shows the prosthetic group (prosthetic group is the tightly bound, nonprotein portion of an enzyme) that is conserved between the cytochrome P450's and the chemistry associated with its function. The heme-iron makes an ideal green oxidation catalyst as iron is the central metal and the heme ligand is relatively simple. In their natural environment, the

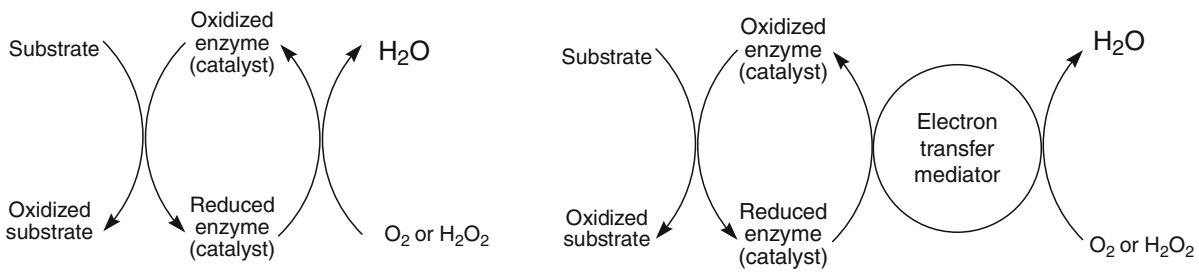

Oxidation Catalysts for Green Chemistry. Figure 12
Biomimetic catalysis based on (*left*) direct reoxidation of the enzyme (catalyst) or (*right*) electron-transfer mediator reoxidation of the enzyme (catalyst) by O_2 or H_2O_2 [71]

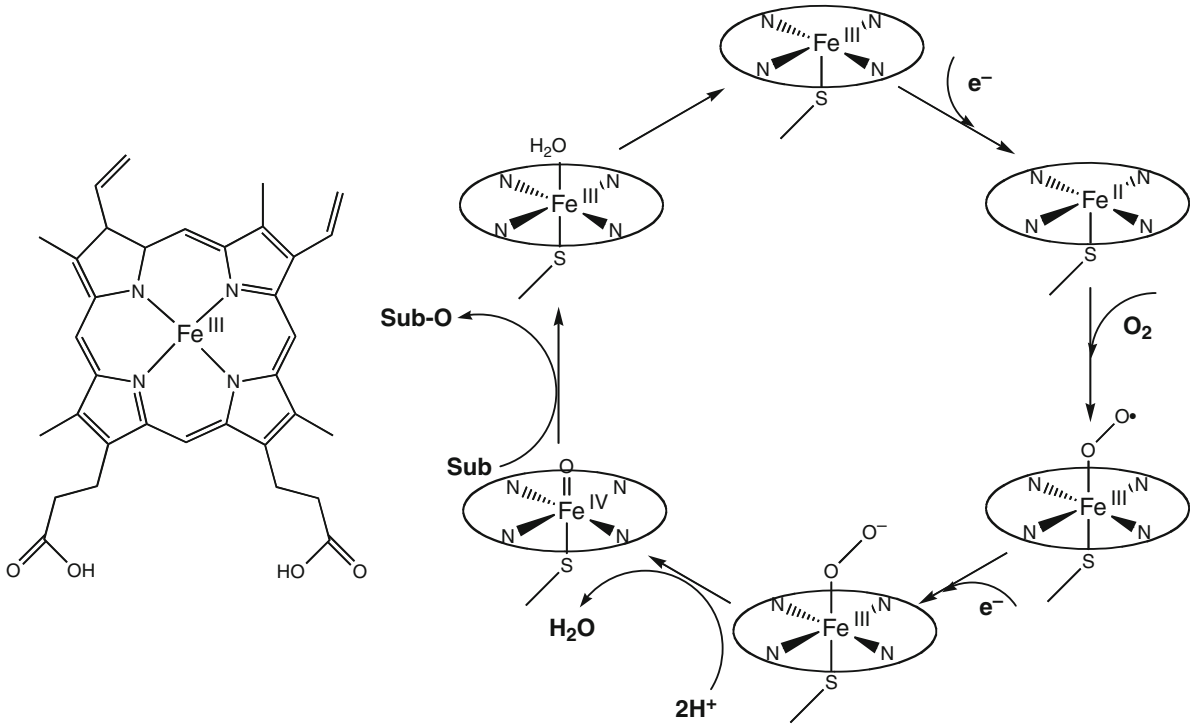

Oxidation Catalysts for Green Chemistry. Figure 13
Prosthetic heme-b group of the cytochrome P450 enzyme family and the catalytic cycle of the enzyme (Sub is the Substrate)

P450 enzymes oxidize a large array of endogenous and exogenous compounds and most can oxidize multiple substrates. They are known to catalyze hydroxylations, epoxidations, various dealkylations, nitrogen oxidations, sulfur oxidations, and dehalogenations. Cytochrome P450 is the line of defense in the liver that metabolizes drugs, toxic compounds, and other metabolic products.

$$\text{Substrate} + O_2 + 2e^- + 2H^+ \xrightarrow{\text{cytochrome P450}} \text{Substrate} - O + H_2O \quad (4)$$

Even though they are exquisite in their content and fascinating in their scientific design, the kinetic and mechanistic details regarding the modeling of cytochrome P450 are beyond the scope of this contribution [72, 73]. The key elements of the mechanism are the binding of O_2 to the iron(II) center of the prosthetic group, which is then followed by breaking of the O-O bond and formation of the active oxidant an iron-oxo species. It is this iron-oxo species that has particularly fascinated chemists and biologists for years and many attempts have been made to characterize it. Some of the issues that make its characterization difficult are its rapid reactivity and ligand decay by oxidation.

The first reports related toward mimicking P450-type catalysis were done with 5,10,15,20-tetraphenylporphyrin [(TPP)FeCl]. This catalyst suffered from rapid self-oxidation and, as a result, low efficiency [74]. Since then, considerable efforts have been invested in preparing synthetic porphyrin ligands for use as oxidation catalysts. Bulky substituents and electron withdrawing groups have been appended onto the porphyrin ligand to inhibit formation of unreactive oxo-bridged dimers and decrease the rate of self-oxidation. These approaches are somewhat successful but often rely on using functional groups like chlorine or fluorine, which severely lower the relative greenness of the catalysts as [75] many chlorinated compounds are toxic and fluorinated ones are environmentally persistent. The approach of supporting the catalysts on solids, resins, and polymers provides the catalyst more resistance toward intermolecular oxidations, but they cannot lessen the rate of intramolecular oxidation. Furthermore, many of the reactions are too slow to be

of practical value [76]. Overall, synthetic porphyrins cannot be considered as ideal green oxidation catalysts because their synthesis is relatively complex, yields tend to be low, and despite the many attempts to increase their functioning lifetimes, they still remain low. Nevertheless, they may have a role to play if they are the best or only current means for oxidizing a substrate of particular value or importance [77–79].

Other Biomimetic Catalysts

An entire branch of biomimetic oxidations has developed using transition metals such as palladium, ruthenium, osmium, and others as the catalyst [71, 80]. In many cases, the catalysts are relatively simple salts of the transition metal because the problem of ligand oxidation has not been solved. Acetoxylation of cycloalkenes, oxidative carbocyclization of allene-substituted olefins, aerobic oxidation of primary and secondary alcohols, dihydroxylation of alkenes, and others are among the wide array of reactions that have been achieved using these precious metal catalysts.

A classic example using nonbiological metals is the Wacker process, Fig. 14, which was reported in the 1950s. This is a very well studied reaction that uses palladium to oxidize the organic substrate and copper to reoxidize the palladium. Since palladium metal is oxidized with great difficulty by O_2, this gives rise to the need for the copper portion of the catalytic cycle. The Wacker oxidation is an important industrial process and the details of its mechanism still fascinate chemists.

Oxidations based on these precious metals are only biomimetic in terms of mechanism as nature does not choose these metals in its chemistry. In the strictest sense then, they cannot be considered as green catalysts because they use metals that are rare, osmium is less than 0.05 ppb in the continental crust, they are toxic [81], and they are derived from mining operations that severely impact the environment. The "problem" is that these are important reactions that are an integral portion of the synthetic chemists' arsenal for the preparation of often valuable molecules. Replacement of some of these catalysts by green alternatives provides a great and exciting objective and the potential for significant economic benefits.

Polyoxometalate (POM) Catalysts

Heteropolyacids (HPAs) and the closely related polyoxometalate (POM) compounds have become valuable tools in the collection of the synthetic chemist for catalytic oxidation processes [82]. These compounds are derived from virtually any transition metal ion, oxygen, and main group elements like aluminum, phosphorous, and silicon. They are prime candidates for oxidation catalysts as they are stable toward self-oxidation because they contain no organic ligands and the transition metal and main-group elements are usually in their highest oxidation state. POMs generally have dozens of atoms arranged in well-defined structures. Examples of some classes of POMs are given in Fig. 15; their nomenclature is well developed [83].

A significant advantage of the POMs over many other potential oxidation catalysts is that they can self-assemble from simple, individual components by pH control. Complex molecules are thus prepared in only one synthetic step, which from a green chemistry perspective is ideal. However, in order to maintain the

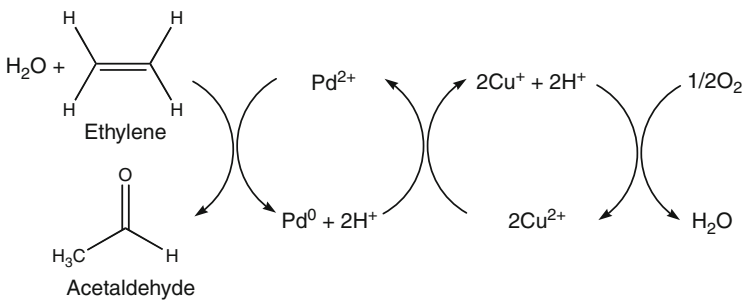

Oxidation Catalysts for Green Chemistry. Figure 14
The Wacker process for olefin oxidation using palladium as the oxidation catalyst for the olefin and copper as the co-catalyst to reoxidize the palladium

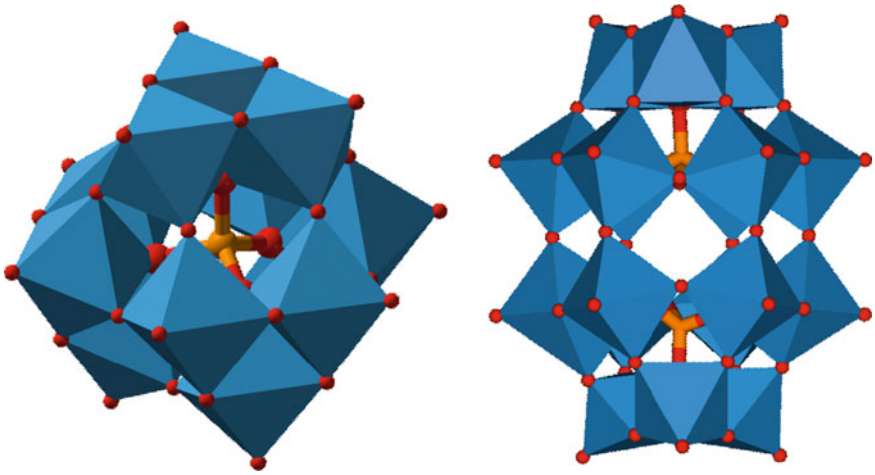

Oxidation Catalysts for Green Chemistry. Figure 15
Two polyoxometalate structures. The left is the Keggin type and the right is the Dawson. The general formula for the Keggin type is $XM_{12}O_{40}n^-$ and the Dawson type is $X_2M_{18}O_{62}n^-$, where X is typically S or P and M is Mo or W

$$\text{Oxidation: } SubH_2 + [PV^{V}{}_2Mo_{10}O_{40}]^{-5} \rightarrow Sub_{ox} + 2H^+ + [PV^{IV}{}_2Mo_{10}O_{40}]^{-7}$$

$$\text{POM Regeneration: } [PV^{IV}{}_2Mo_{10}O_{40}]^{-7} + 2H^+ + \tfrac{1}{2}O_2 \rightarrow H_2O + [PV^{V}{}_2Mo_{10}O_{40}]^{-5}$$

Oxidation Catalysts for Green Chemistry. Scheme 1
Catalytic cycle for substrate oxidation by a polyoxometalate. The polyoxometalate catalyst is regenerated by a proton coupled two-electron transfer.

discrete structure during the oxidation reaction, careful pH control throughout the application might be necessary [84]. Professor Craig L. Hill has pioneered the use of POMs as oxidation catalysts. POMs have versatility well beyond oxidation chemistry and good reviews can be found on their synthesis, properties, and applications [85, 86].

POMs can oxidize target molecules either as electron-transfer oxidants or direct oxygen atom transfer oxidants [87]. The electron-transfer pathway depicted in Scheme 1 using the compound $H_5PV_2Mo_{10}O_{40}$ as an example is the more common [88]. In the first step, the substrate, $SubH_2$, transfers two electrons to the polyoxometalate to yield an oxidized product, Sub_{ox}, a reduced polyoxometalate ($[PV_2Mo_{10}O_{40}]^{-7}$), and two protons. In the second step, $[PV_2Mo_{10}O_{40}]^{-7}$ is oxidized by O_2. The reduced O_2 product reacts with the protons generated in the first step producing water. Here, the molecular oxygen functions as a two-electron/two-proton acceptor and the chemistry type is referred to as oxidase pathway. This mode of oxidation means that the POM must have sufficient oxidizing power such that it can remove one or two electrons from the substrate. It is often the case that organic molecules are hard to oxidize by electron-transfer pathways, so POMs must have high oxidation potentials.

Catalysis with POMs can be considered as green in the sense that they can use O_2 (or H_2O_2) for the oxidation of alcohols, amines, and phenols, and sulfur-containing compounds. In addition, their solubility can be manipulated so that they can be soluble in a variety of "green" solvents [88]. Examples are available for catalysis in aqueous biphasic reaction media, the nontoxic- and nonvolatile-solvent polyethylene glycol, supercritical CO_2 [89], and perfluorinated solvents [90]. Fluorous solvents have many positive attributes, but they are environmentally persistent which limits their greenness [91].

A principle drawback to POM-based catalysts is that they are not efficient reservoirs of oxidizing equivalents. Most POMs have molecular weights far in excess of 1,000 amu (the cation component is often "ignored"

when discussing a POM, but it should not be as it can add substantially to the overall molecular weight of the catalyst), and they contain many metal centers in high oxidation states, yet each POM only will participate in a 1 or 2 electron transfer with the substrate [92]. The POM in Scheme 1 has 12 transition metal ions, but only the two vanadium ions take part in the electron-transfer process. Even though in many cases high substrate to POM molar ratios are used in the catalytic process and impressive turnover numbers and lifetimes have been reported [93], the Mass Intensity (MI) index (MI = the total mass involved during the reaction/the mass of the final product) is low [94]. On the laboratory or preparative scale, the MI is not a significant issue, but it can become a problem as the synthetic process is scaled. Still, POMs are an excellent choice for many applications because they are oxidatively robust and often easily recovered.

Epoxidation Catalysts

Epoxides are key synthetic intermediates for a large number of specialty chemicals and pharmaceuticals and a catalytic method for generating them with high enantioselectivity opens doors for many more synthetic manipulations. A search of the Royal Society of Chemistry database using the term *epoxidation* and limited to the journal *Green Chemistry*, returned more than 120 different entries (1999–2010). Most are catalytic processes, utilize H_2O_2 as the oxidant, and they cover a wide range of types of materials and methods. Each report generally focuses on the epoxidation of a narrow set of compounds, and it is not clear how widely applicable they will become. Nevertheless, the choices in catalysts fall clearly on the green side. A non-exhaustive list includes titanium on silica, enzymes, polyoxometalates, and supported transition metal complexes. In this contribution, two of the most well-known epoxidation catalysts are examined.

Sharpless Epoxidation

A discussion of oxidation catalysts is not complete without describing one of the most important breakthroughs in stereoselective synthesis. In 1997, Professor K. Barry Sharpless won the Nobel Prize in Chemistry for stereoselective oxidation reactions (Sharpless epoxidation, asymmetric dihydroxylation, and oxyamination) [16].

The Sharpless approach is given in Fig. 3. It is an excellent example of a synthetically powerful reaction for a focused oxidation, namely conversion of allylic alcohols to epoxides. Its tolerance, which can be interpreted as being unreactive, toward other oxidizable groups in the molecule like acetals, alkynes, alcohols, aldehydes, amides, esters, ethers, olefins, pyridines, sulfones, and others is a testament to the reason why there are so many specialized oxidation catalysts. The catalyst is comprised of a titanium alkoxide and a chiral dialkyl tartrate to direct the point of attack by the oxidant on the allylic alcohol. The catalyst has one of the same building blocks found in TS-1, a titanium alkoxide, which places a boundary on its greenness. From a green process perspective, the solvent for the Sharpless epoxidation needs to be nonaqueous, CH_2Cl_2 is generally the best, the reaction is very sensitive to water so it is typically run in the presence of molecular sieves, and temperatures below room temperature are used. Nevertheless the utility of the catalyst is outstanding since high enantioselectivities (>90%) and yields (>80%) are obtained for a range of substituted allylic alcohols. From an economic perspective, all of the starting chemicals for the catalyst are commercially available and reasonably priced, and other than the solvent, there should not be issues with disposal of the spent catalyst [95]. There does not appear to have been concerted efforts to enhance the greenness of the reaction [96], but its power for certain segments of the specialty chemical market is so high that it is likely to receive attention at some point.

Schiff-Base Epoxidation Catalysis

One of the most successful catalytic oxidation systems for pharmaceutical and specialty chemical applications is the so-called Jacobsen-catalyst. In 1990, Professor Eric Jacobsen [97] and Professor Tsutomu Katsuki [98, 99] reported that chiral manganese(III) Schiff-base complexes like those shown in Fig. 16 could epoxidize olefins with high enantioselectivity. The foundations for this chemistry were laid out in studies designed around iron porphyrin complexes and achiral manganese(III) Schiff-base compounds as models for the cytochrome P-450 enzyme system and the oxygen evolving complex (OEC) of photosystem II (see below) [74, 100–102], These catalyst now are commercially available from a variety of sources.

Hugo Schiff reported the Schiff-base ligands in 1864. They coordinate virtually every transition metal ion, and they bind some main-group metals as well. In general, Schiff-base complexes are simple to prepare from readily available starting materials, yields are high, and the ability exists to manipulate structural and electronic properties in straightforward and predictable manner. Synthesis of the Jacobsen catalyst as described in Fig. 16 is typical for Schiff-base complexes where diamine and benzaldehyde derivatives are combined to make the ligand under mild conditions and then the metal is inserted using a simple salt. Manganese is an essential element for biological function, and according to the USEPA, it is one of the less toxic transition metals. Thus, manganese Schiff-base complexes fit reasonably well into the criteria for being green catalysts. However, as the structure of the Schiff-base ligand becomes more complicated, the number of synthetic steps toward precursors increases which can have a significant negative impact on the overall green nature of the catalyst.

The Jacobsen-type epoxidation catalysts initially were used in nonaqueous solvents with oxidants such as iodosylbenzene rather than the favored green ones, O_2 or H_2O_2. However, over time, they have evolved tremendously to the point where they are commercially available, recoverable by their attachment to surfaces and polymers [103–105], reasonably stable during the oxidation, usable in aqueous environments, and capable of activating H_2O_2 and O_2 [106, 107]. They have achieved an impressive record for catalytic oxidations.

It was recognized early on in the epoxidation chemistry that O_2 was the oxidant of choice rather than the activated oxidants. In general, manganese(III) complexes do not react with O_2, but manganese(II) compounds readily activate oxygen. However, olefin epoxidation could be effected electrocatalytically by both manganese porphyrins [108] and achiral Schiff-base complexes [109] through the oxygen activation scheme shown in Fig. 17. Catalyst lifetimes for both systems were not long. A turnover number of only 2.4 was determined for the Schiff-base complex. Once again, oxidative degradation of the ligand was a factor in catalyst deactivation pathway and inactive oxo-bridged dimers also were observed. Nevertheless, these studies were extended to the use of the Jacobsen-type

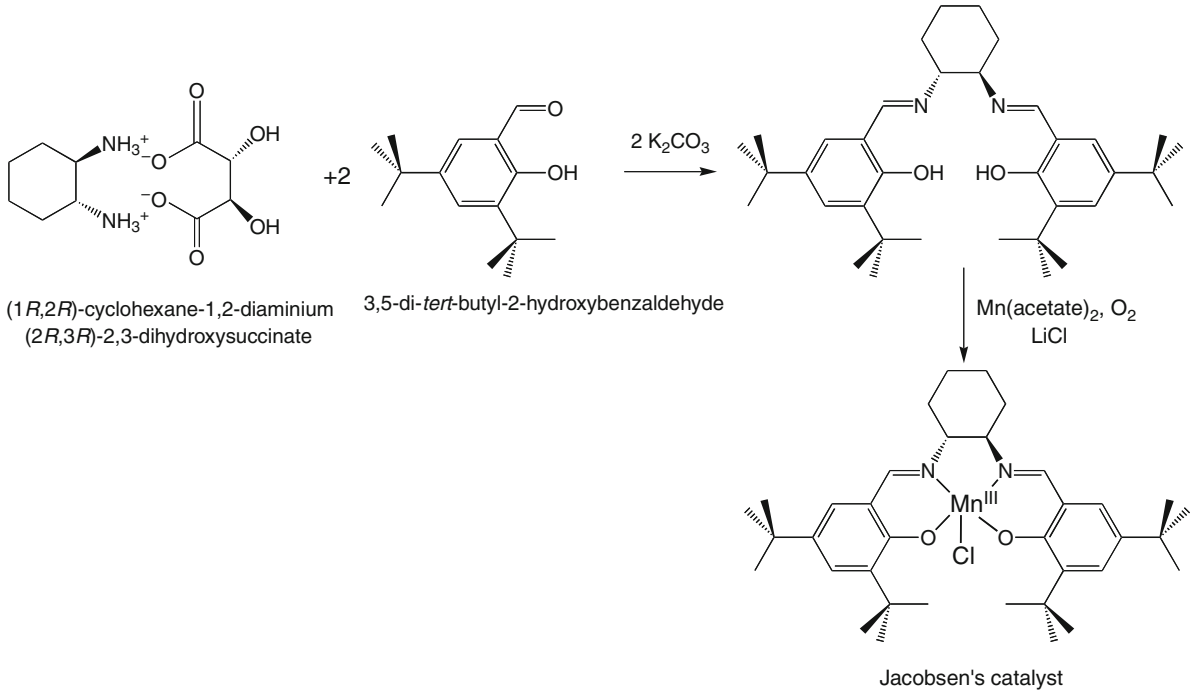

Oxidation Catalysts for Green Chemistry. Figure 16
The chiral Jacobsen's Schiff-base catalyst used for epoxidation of chiral olefins

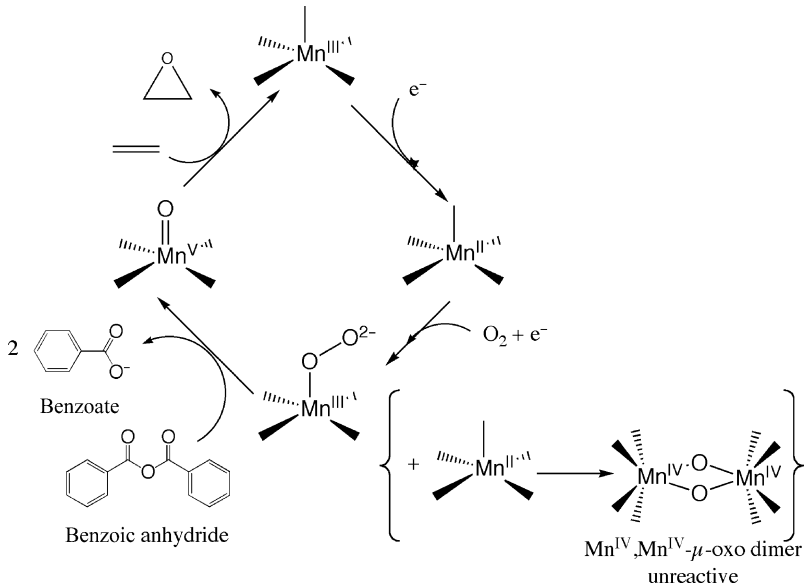

Oxidation Catalysts for Green Chemistry. Figure 17
Proposed pathway for electrocatalytic epoxidation reactions. The manganese is either in porphyrin or Schiff-base ligands. Ligand degradation and Mn^{IV},Mn^{IV}-μ-oxo dimer formation are deactivation pathways in this chemistry

complexes for enantioselective electrocatalytic epoxidation of olefins [110]. Immobilization of the catalyst onto an electrode surface was a significant advancement as turnover numbers approaching 1,250 and an enantiomeric excess greater than 75% were achieved using this immobilized catalyst [111]. The turnover number is still modest, but the result clearly shows the advantage of limiting dimer formation, but self-oxidation is probably the limiting factor.

The electrocatalytic approach suffers from the need to use a sacrificial reagent (benzoic anhydride in Fig. 17) to remove one oxygen atom in order to generate the epoxidation catalyst. The sacrificial reagent significantly reduces the overall efficiency of the process and negatively impacts its *E*-factor. However, it is possible that with judicious choice of sacrificial reagent two useful products could be derived using the electrocatalytic concept. This enhanced efficiency combined with chemically modified electrodes could lead to the development of a useful and important green epoxidation catalyst.

Organonocatalysis

The previous discussion centered largely on the use of transition metal-containing compounds as oxidation catalysts for making new chemicals. The subject now shifts to organocatalysis which is "*catalysis with small organic molecules, where an inorganic element is not part of the active principle*" [112]. Professor David MacMillan in a Commentary in the journal *Nature* noted that the use of organic molecules as catalysts was mentioned "sporadically" prior to the late 1990s. Now it is recognized as a new field of research and development in organic synthesis [113]. Since the naming of the field in 2000, there have been well in excess of 2,000 publications relating to organocatalysis. This is clearly a testament to the versatility of the field, the recognition of its diversity of synthesis, and the great potential that it has to the pharmaceutical, specialty chemical and bulk chemical markets.

The use of metal-free small organic molecules to catalyze organic transformations is thought to have broad savings in terms of reaction cost, time, and energy. Among the perceived advantages of organocatalysis over the more traditional metal-based systems are the general insensitivity of organic molecules to oxygen and moisture, the variety of organic molecules available from simple synthetic or natural sources as single enantiomers and, especially, that molecules derived from natural sources are more likely to

be nontoxic and environmentally friendly. Thus, organocatalysts have many of the attributes that need to be incorporated in green oxidation catalysts. As the pace of organocatalysis accelerates, the toxicity and ecotoxicity of these chemical systems must be evaluated prior to their large-scale adoption. These new chemicals may be discharged in wastewater streams in the course of their application, and their treatment as wastes needs careful evaluation.

The strength of organocatalysis appears to be in enantioselective syntheses. It has broad utility in forming asymmetric carbon–carbon and carbon–heteroatom bonds. It was noted in a 2008 review of the subject that organocatalysts have been used across a broad spectrum of reactions, including epoxidation, aldol condensation, amination of aldehydes, Diels–Alder, and 1,3-dipolar cycloadditions, Mannich and Michael reactions, hydride transfer, nitroalkane addition to enones, and α-halogenation [114].

The use of organocatalysts for oxidation reactions was reviewed recently, and the details of the catalysts and their reactions are best left for the interested reader to pursue [115]. Here, an example illustrating the evolution of an organocatalytic reaction from a nongreen process into one that is relatively green is described. This transformation was achieved by attending to some aspects of the reaction that did not conform to green chemistry principles in addition to focusing on product output. There is still room for improvement in the chemistry, but it can serve as a model for other catalytic reactions.

In 1996, Professor Yian Shi reported that a fructose-derived ketone was an effective enantioselective catalyst for the epoxidation of *trans*- and trisubstituted olefins [116]. Compound **1**, in Fig. 18 is readily synthesized by a two-step process from naturally occurring D-fructose and readily available and inexpensive reagents and solvents. Thus, according to one of the common usages of the term green catalyst, which is a catalyst derived from "readily available starting materials," then compound **1** is a green catalyst. However, the catalyst synthesis method is illustrative of the balance that is made between the value of the catalytic reaction and the synthetic route used to prepare the catalyst. In the first step, 70% perchloric acid is used. There is always the potential for an explosion when perchloric acid and organic materials are combined. Often it is impurities that are the problem. Then, in the second step, a stoichiometric oxidant, pyridinium chlorochromate, rather than a catalytic one, is used to oxidize the alcohol to the ketone. Chromium wastes need to be handled with care, and the mass of the spent chromium reagent is significant, so this reaction has a low *E*-factor.

In the 1996 report by Shi, olefins were oxidized to the corresponding epoxide in high yield, generally >75%, and with high enantioselectivities, typically >85%. However, the reaction conditions would not be considered green. First, Oxone® ($2KHSO_5 \cdot KHSO_4 \cdot K_2SO_4$) was the oxidant. Oxone is considered to be environmentally friendly compared to Caro's acid, the traditional source of the oxidant [HSO_5], but only 5% of the mass of Oxone is the active oxidant. The mass intensity and *E*-factors are low. Second, buffers were needed to carefully control solution pH. Third, Na_2·EDTA was used to chelate any metal ions in the solution that might cause rapid Oxone

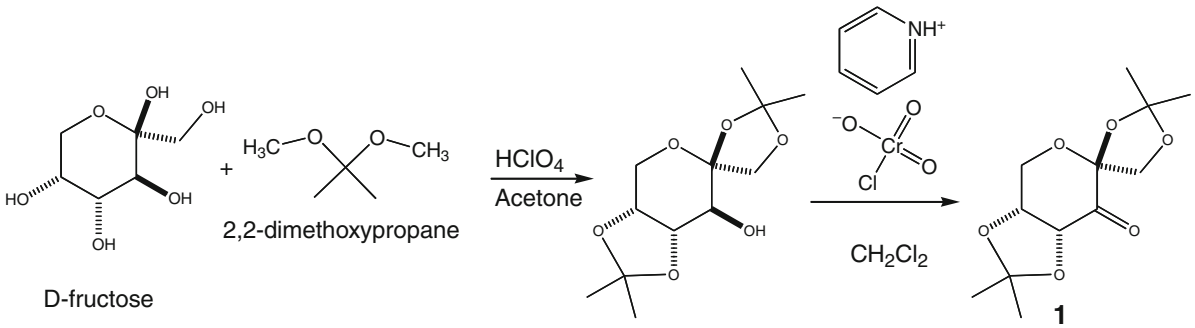

Oxidation Catalysts for Green Chemistry. Figure 18
Synthesis of a highly enantioselective epoxidation catalyst

decomposition. Clearly, hydrogen peroxide is the desired substitute for Oxone because of its higher active oxygen content and its reduction product is water. Subsequent studies with compound **1** showed that indeed H_2O_2 could be used as the oxidant [117]. Replacement of Oxone with H_2O_2 had additional benefits such as the quantities of solvent and salts were reduced substantially (buffer and EDTA were still used) and oxidant addition was streamlined. Most importantly, epoxidation results, yield and enantioselectivity, are comparable to those using Oxone [115].

TEMPO

TEMPO and its derivatives occupy a unique position among the oxidation organocatalysts because they have received widespread academic and industrial acceptance. TEMPO was first reported 50 years ago [118]. It is one of a class of stable radicals referred to nonconjugated nitroxyl radicals. Their stability as radicals arises from delocalization of the unpaired electron over the nitrogen-oxygen bond as shown in Fig. 19, and their robustness as catalysts is due to the lack of a hydrogen atom on the carbon adjacent to the nitrogen, the α-hydrogen atom [119]. The synthesis of TEMPO is challenging and costly, but there are green methods for its preparation under development [120].

Over the years, TEMPO and its derivatives have been applied as spin labels in biology, free-radical scavengers, stoichiometric oxidants, and organocatalysts. Among the most compelling suggestions that TEMPO might be a green oxidation catalyst was the application in 1996 for a USEPA Presidential Green Chemistry Challenge Award by Pharmacia and Upjohn. The collaboration resulted in a new, "green" synthesis for bisnoraldehyde (BNA), a precursor for corticosteroids

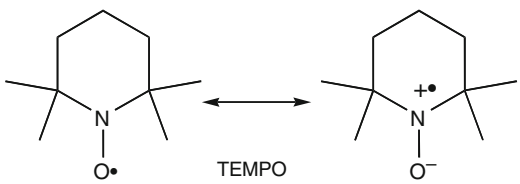

Oxidation Catalysts for Green Chemistry. Figure 19 The stable organic radical TEMPO showing the delocalization of the unpaired electron over the nitrogen-oxygen bond

and progesterone. Pharmacia and Upjohn state in their application:

- This new synthetic route to progesterone is founded on both the development of a new fermentation process which improves the utilization of a renewable, naturally derived feedstock from 15 to 100 percent, and the development of a chemical oxidation process that offers high selectivity and reduced waste streams. The fermentation employs a genetically modified bacterium to convert soya sterols directly to a new synthetic intermediate, bisnoralcohol. The new chemical process oxidizes bisnoralcohol (BA) to bisnoraldehyde {4-hydroxy-TEMPO as the catalyst to activate sodium hypochlorite (bleach)}, a key intermediate for the registered, commercial manufacture of progesterone.

Elimination of the carcinogenic organohalogen-solvent ethylene dichloride and production of the same amount of product as the previous route with 89% less nonrecoverable organic solvent waste and 79% less aqueous waste are additional green benefits of the new process. Industrially, organohalogen solvents like ethylene dichloride have been a favorite because they have many perceived beneficial properties such as robustness, recyclability, solvating ability, and others. However, they are highly regulated because of their health and safety issues and replacements are being sought.

Specialty chemical and pharmaceutical companies have described a number of commercially viable catalytic oxidations using TEMPO, TEMPO derivatives, and other nitroxyl radical organocatalysts [118, 121]. Along with adopting the TEMPO processes, these companies have replaced hypochlorite by oxidants generated electrochemically, used O_2 along with active metal catalysts (Ru^{2+}, Mn^{2+}/Co^{2+} and Cu^{+}) as the oxidant source, and reduced TEMPO cost by making immobilized systems. This is a clear indication that these industries and the ones that support them with new discoveries of TEMPO applications continue their rapid alignment with green chemistry principles. The enlightened outlook of these companies needs to be translated throughout the synthetic organic chemistry community where green synthesis development needs to gain a stronger foothold.

Catalysts for the Environment

The vast majority of oxidation catalysts have been designed for use in the specialty chemical or pharmaceutical areas. However, catalysts for the oxidative degradation of organic pollutants are equally significant, but they have received less attention, especially from chemists. The disposal and treatment of waterborne organic pollutants in an environmentally sound manner and at a reasonable cost is of great importance. These pollutants are from many different sources. They may be waste products from the process that makes a good that is used every day to the actual good itself once it has served its useful life. Or, they can be chemicals or products that were thought at the time to be harmless but ultimately are found to damage the environment (PCBs and CFCs are excellent examples). The environmental movement got its start with the realization by Rachel Carson that some pesticides, in particular DDT, were doing far more harm than good, and that these chemicals needed to be banned and removed from the environment. Her book *Silent Spring*, published in 1962 [122], has been named by Discover Magazine as one of the 25 greatest science books of all time.

It has often been stated that water is the only true green solvent. However, upon performing any reaction with organic chemicals in water or even contacting water with an organic substance a treatment option must be considered before discharging the water. Removal of organic (and inorganic) chemicals, now pollutants, from process waste streams is the business of hundreds of companies around the world worth multiple billions of dollars, each applying technologies that try to remove these pollutants so that the water can be safely returned to the environment possibly to be used downstream as drinking water. Thus, water is only a green solvent if it can be treated in a biological treatment plant alone [123].

Most water treatment scenarios use a biological process as the first-line attempt to remove organic pollutants from wastewaters. However, since many organic pollutants are nonbiodegradable or toxic to bacteria a more technically advanced solution needs to be applied. Physical methods like adsorption or filtration are often used but these do not solve the problem but rather shift it. For example, carbon filters remove a host of organic and inorganic pollutants by absorption or adsorption processes. Once the binding capacity of the carbon is reached, the carbon must be disposed of responsibly or regenerated which is often a thermal treatment. In contrast, a chemical oxidation may be the better choice for decontaminating the biologically recalcitrant compound because the oxidation process potentially can convert it to CO_2 and H_2O in a process referred to as mineralization or it might convert it into benign products [124]. The benign oxidation products may then undergo a subsequent biological treatment. It is important that the application of any such treatment results in cleaned water that may be directly discharged to a receiving stream or to a municipal wastewater-treatment facility without having any negative impact. The most common oxidation treatments applied to cleaning water are Fenton's reagent, wet-air oxidations (WAOs), catalytic wet-air oxidations (CWAOs), and non-Fenton processes.

Advanced Oxidation Processes (AOPs)

Fenton Chemistry When discussing an AOP it is often assumed that the hydroxyl radical ($HO^{\bullet}$) is formed during the process. The hydroxyl radical is considered to be one of the most powerful oxidizing agents. It functions primarily by abstracting a hydrogen atom from a target organic molecule to make water (the driving force for the reaction) and a carbon centered radical. Carbon-centered radicals typically are not stable and the molecule literally disintegrates, of course helped along by more hydroxyl radical chemistry. Other more controlled reactions can be observed for the hydroxyl radical such as addition to C = C bonds or aromatic rings [125] and electron-transfer reactions [126]. Among the oldest and most thoroughly studied AOP is the so-called Fenton's reagent. More than a century ago, Henry J. H. Fenton described the oxidation of tartaric acid in the presence of iron salts and H_2O_2 [127]. The abstract reads:

- Experiments were made with standard solutions of tartaric acid, ferrous sulfate, and hydrogen peroxide to study the nature of the oxidation of tartaric acid in the presence of iron. Measured volumes of these solutions were mixed in the order named, made alkaline with soda, diluted to the same volume in tall glasses,

and the depths of violet color compared. With equal quantities of tartaric acid and a fixed proportion of iron, it was observed that the depth of color increased with increasing quantities of hydrogen peroxide up to a certain limit, beyond which the color diminished as the peroxide increased, and beyond a certain limit disappeared together. From these results, it seems that the action of iron is "catalytic", a very small quantity of iron being sufficient to determine the oxidation in this direction of an almost unlimited amount of tartaric acid.

This article has been cited more than 500 times. Fenton's contribution, which appeared roughly 50 years after Perkin's, might be considered the disclosure of one of the first green oxidation catalysts as it uses the nontoxic element iron to activate the environmentally benign oxidant H_2O_2. Fenton-based technologies generally are viewed as economical and convenient but only after biological and physical treatment options are exhausted. There are excellent reviews of what is commonly referred to as "Fenton chemistry" and only some of the highlights are discussed here as they relate to the green or nongreen aspects of the chemistry [128].

Fenton chemistry is broadly applied. One can find it used in the remediation of contaminated soils [129] removal of colored effluents from the dye industry, oxidative degradation of hazardous chemicals like 2,4,6-trinitrotoluene and chlorinated organics [19]. It is often the first line of defense against a wastewater containing recalcitrant organic chemicals [130].

$$H_2O_2 + Fe^{2+} \longrightarrow Fe^{3+} + HO^{\bullet} + OH^{-}$$

$$H_2O_2 + Fe^{3+} \longrightarrow Fe^{2+} + HO_2^{\bullet} + H^{+}$$

$$HO^{\bullet} + H_2O_2 \longrightarrow HO_2^{\bullet} + H_2O$$

$$HO^{\bullet} + Fe^{2+} \longrightarrow Fe^{3+} + OH^{-}$$

$$Fe^{3+} + HO_2^{\bullet} \longrightarrow Fe^{2+} + O_2 + H^{+}$$

$$Fe^{2+} + HO_2^{\bullet} + H^{+} \longrightarrow Fe^{3+} + H_2O_2$$

$$HO_2^{\bullet} + HO_2^{\bullet} \longrightarrow H_2O_2 + O_2$$

Oxidation Catalysts for Green Chemistry. Scheme 2 Reactions of iron, hydrogen peroxide, and hydrogen peroxide derived species in the Fenton reaction

Fenton's reagent is catalytic with respect to iron according to Eqs. 5 and 6.

$$Fe^{2+} + H_2O_2 \rightarrow Fe^{3+} + OH^{\bullet} + OH^{-} \quad (5)$$

$$Fe^{3+} + H_2O_2 \rightarrow Fe^{2+} + OOH^{\bullet} + H^{+} \quad (6)$$

It can be seen that hydrogen peroxide acts to oxidize Fe^{2+} to Fe^{3+} and form the highly reactive hydroxyl radical ($OH^{\bullet}$), but it also reduces Fe^{3+} to Fe^{2+} forming the hydroperoxyl radical ($OOH^{\bullet}$) which is only a slow oxidizing agent in solution [131]. At a maximum, 50% of the H_2O_2 is used in productive oxidation reactions.

The chemistry is actually far more complicated than shown above and a more accurate set of reactions is given in Scheme 2. The significance of Scheme 2 is that the Fenton process is an inefficient one in terms of hydrogen peroxide consumption.

In addition to inefficient use of the oxidant, Fenton-based processes have other drawbacks such as the need to do reactions under acidic conditions (pH 3) and the formation of iron sludges that must be removed. The pH is an issue because at near neutral pH precipitation of the iron as $Fe_2O_3 \bullet nH_2O$, rust, occurs which inhibits the Fe(III)/Fe(II) cycle [132]. This has been addressed to some extent by adding chelating ligands like aminopolycarboxylates, polyhydroxy aromatics, N-heterocyclic carboxylates, and others to try to prevent formation of the sludge. While some lifetime increase is observed, these ligands are themselves oxidized and thus of limited value [133–135]. Despite these drawbacks, Fenton's reagent remains an important "green" oxidation catalyst for removing pollutants.

Catalytic Wet Air Oxidation (CWAO) Catalytic wet-air oxidation is a process in which molecular oxygen and a catalyst are used at relatively high temperatures and pressures to oxidize organic pollutants present in water [136]. The goal of a CWAO process is to convert all of the pollutant into CO_2 and H_2O or to degrade the pollutant to a level that it can be treated biologically. Lenntech, a supplier of CWAO equipment states: "The effect of the catalyst is to provide a higher degree of COD removal than is obtained by WAO at comparable conditions (over 99% removal can be achieved), or to reduce the residence time." This is a nearly perfect statement of the function of a catalyst. Faster reactions and deeper oxidations reduce risk while allowing

greater throughput, which should result in a more economic process.

CWAO processes are applied to water-containing high concentrations of organic pollutants – chemical oxygen demand (COD) levels greater that 10,000 mg/L, in part because the quantity of alternative oxidants like H_2O_2 is too high and the waste is too recalcitrant for standard physical, biological, or chemical treatments. The majority of catalysts used in CWAO processes are oxides of Cu, Co, Mn, Cr, V, Ti, Bi, and Zn, and supported precious metals [136]. A drawback to CWAO treatments is leaching of the metal from the oxide or support into the water being treated. The metal must then be removed from the water before it can be discharged. This adds cost to the process and can make it uneconomical. There clearly are some metals in the list, particularly chromium, that have more potential for harm than others should they be discharged into our waterways. Thus judicious choice of metal can make these materials green oxidation catalysts. The benefits of using such catalysts to treat recalcitrant organic pollutants appear to be clear since in all likelihood these pollutants would have entered our water system.

Non-Fenton AOP

In 1999, Professor Terrence Collins received the Presidential Green Chemistry Challenge Award for the development and potential for wide applicability of TAML® catalysts. Collins focused on using nontoxic elements and oxidatively robust organic building blocks to surround a catalytically active iron center [137]. An iterative design strategy was developed that centered on finding and replacing weak or oxidatively sensitive points in each earlier version of the catalyst [62]. This catalyst development strategy involved the four-step process depicted in Fig. 20 and also resulted in a set of design parameters that define oxidatively stable catalysts. Another critical feature during the design phase of the catalysts was toxicity screening. In all instances, the catalysts were found to have toxicity well below their application level so that they could be safely discharged to the environment. The ligand design strategy of using nontoxic elements and testing for catalyst and oxidation product toxicity provide a model pathway for the development of green oxidation catalysts.

The design process produced an expanding family of iron-based TAML® catalysts. Structures of first and second generation TAML catalysts are shown in Fig. 21 [138]. The catalysts are extremely active, achieving many thousands of reactions before being deactivated. They do this at quantities measured in the single parts per million levels or lower, which is a testament to the high stability and high catalytic activity of these molecules. Unlike most other oxidation catalysts, the TAML catalysts function in water over a pH range from acidic to highly basic (pH >14). All of these factors allow for manipulating catalyst and/or reaction conditions to achieve desired selectivities and reaction rates. Excellent recent reviews that detail kinetic and mechanistic details of the catalysts are available [139, 140].

The first generation TAML catalysts are noteworthy for the ability to manage their reactivities and lifetimes by manipulating the X and R substituents on the

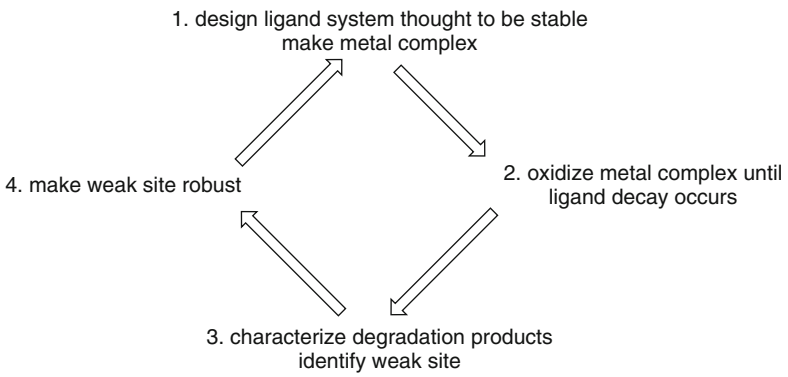

Oxidation Catalysts for Green Chemistry. Figure 20
Ligand design strategy to secure oxidatively robust catalysts

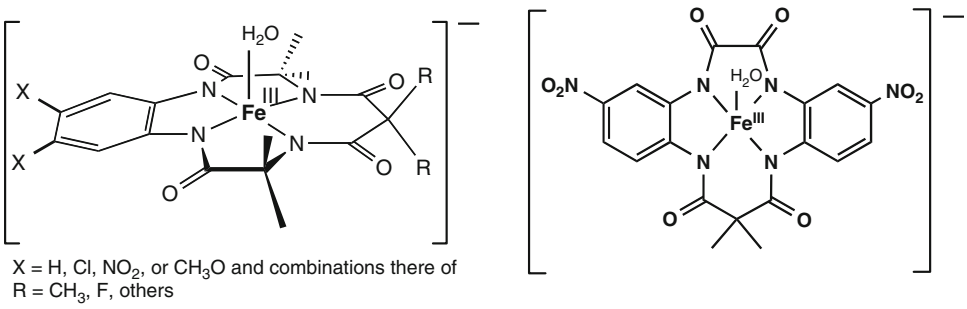

Oxidation Catalysts for Green Chemistry. Figure 21
First- (*left*) and second- (*right*) generation TAML catalysts

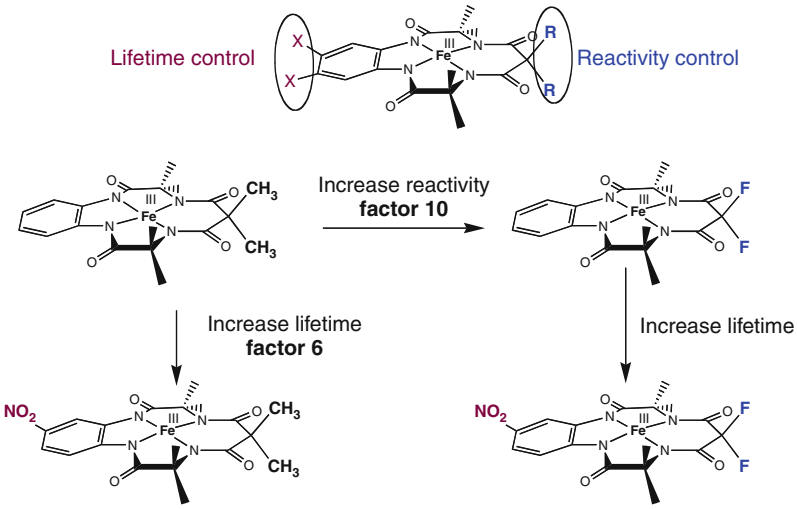

Oxidation Catalysts for Green Chemistry. Figure 22
Representation of the relationship between lifetime control and reactivity control for first-generation TAML catalysts. Note that all the catalysts have one negative charge and, in water, have two water molecules attached to the iron. These are omitted for clarity

macrocycle. Shown in Fig. 22 is a summary of the deep understanding surrounding the catalysts [141]. Controlling catalyst lifetime is a particularly significant attribute as an oxidation catalyst that is intended for environmental work should not be persistent nor constantly active in the environment [142].

The TAML catalysts forte is the oxidative degradation of organic pollutants in water. The degradation does not appear to occur via a hydroxyl radical pathway [143]. Wastewater treatment has become one of the many interesting potential application areas for the TAML catalysts as they degrade chlorinated pollutants [144], phenols, dyes [145, 146], pulp-mill effluent [147], pesticides [148], pharmaceuticals, bacterial spores, [149] and endocrine disrupting compounds (EDCs) like the active ingredient in the birth-control pill – ethinylestradiol [150]. Furthermore, the oxidation products using H_2O_2 have proven to be less toxic than the target pollutant.

GreenOx Catalysts, Inc. is commercially developing TAML catalysts. They are being applied in a number of different application areas. Recombinant Innovation uses a TAML®/H_2O_2 AOP as a tankside add to completely degrade chlorinated biocides in spent metal working fluids (MWFs) in order to lower disposal costs. Approximately, 75–100 million liters per year of MWFs contain the biocide. Until development of the TAML®/H_2O_2 AOP, no simple, cost-effective

technology existed for a tankside biocide removal. VeruTEK Technologies has developed an AOP using TAML® catalysts with their VeruSOL® technology for *in situ* remediation of contaminated soils. The TAML® catalysts substantially speed up treatment times thereby decreasing cost and risk and they provide a more complete contaminant destruction process. This combination of green chemistry and green engineering provides an excellent opportunity for demonstrating how real-world problems can be solved by green technology approaches. Catalyst concentrations in these fields of use are less than 10 ppm and can be as low as 1 ppm. These examples attest to the power of TAML®-based AOPs.

Energy

Supplying mankinds voracious and increasing appetite for energy in a sustainable manner is arguably the most important scientific and technical challenge. All fossil fuel–based technologies eventually will need replacement. The splitting of water to oxygen and hydrogen by photochemical means (artificial photosynthesis) has far-reaching potential for sustainability as it is the basis of the solar fuel-cell technology shown schematically in Fig. 23. The oxidation of water to O_2 is a complex four-electron process that also requires the release of four protons [151, 152]. Photosynthetic organisms like plants and algae, as well as certain cyanobacteria oxidize water by means of a gorgeous chemical process carried out in the oxygen-evolving complex (OEC) of photosystem II (PSII) [153, 154]. The O_2 is a by-product of splitting water into the electrons and protons that are ultimately used to store energy and reduce CO_2 to carbohydrates. Remarkably, only a single class of oxygen-evolving enzymes is found in all photosynthetic organisms, and they all have an inorganic core with the formula $Mn_4Ca_1O_xCl_{1-2}(HCO_3)_y$.

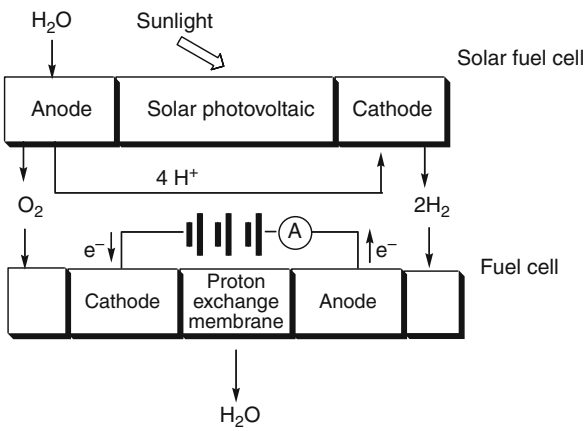

Oxidation Catalysts for Green Chemistry. Figure 23 The solar fuel cell uses sunlight to oxidize water to O_2 at the anode and reduce the released protons at the cathode to hydrogen. In the fuel cell, the hydrogen and oxygen are recombined across a membrane, which generates a flow of electrons producing electrical energy

While the oxidation of water to O_2 now is a simple reaction in nature, it is a difficult problem physically and chemically to replicate in the laboratory. Practically, the oxidation catalyst must function efficiently for long periods of time (years), integrate with the other components of the entire charge-separating network, and be comprised of materials that are as green as possible. Efficiency means that the catalyst must remove the four electrons from two water molecules at or near the thermodynamic potential of 1.23 V. Any increase in voltage above the thermodynamic potential, which is referred to as the overvoltage, means a loss of the energy derived from the sun.

Significant advances in approaches toward development of water oxidation catalysts have occurred over the last few years. Professor Daniel Nocera has reported that nickel or cobalt ions in the presence of a variety of buffer systems produce oxygen-evolving catalyst films that operate at near 100% current efficiency [155, 156]. The catalysts are robust and are likely to integrate with other systems of the cell. From a green catalyst perspective, nickel is the better choice as it has lower toxicity [157] and is more abundant than cobalt. Furthermore, cobalt is a relatively diffuse element in the earth's crust and its main sources are mines in the Democratic Republic of the Congo and Zambia.

Professor Royce Murray is using iridium oxide nanoparticles electro-flocculated onto electrode surfaces as the electrocatalysts [158]. These electrocatalysts are very efficient for O_2 evolution. The mesoporous nature of the films encourages facile water and ion permeation. In addition, the number of active iridium sites is high, the oxidations are relatively fast one electron/one proton steps, and the overpotential is only about 0.25 V. This is an excellent conceptual approach but it is based on iridium, which is one of nature's rarest elements. Furthermore, there are ongoing

debates regarding nanoparticle materials in the environmental as their toxicity is still unresolved issue.

Finally, Professor Craig Hill has expanded his research efforts around polyoxometalates as oxidation catalysts for organic molecules to the water splitting problem [159]. Hill has found that cobalt containing polyoxometalates are excellent homogeneous water-oxidation catalysts. The catalysts themselves are comprised of cobalt, tungsten, phosphorous, and oxygen. The reliance on cobalt has the same issues as the solid state form described by Professor Nocera. In addition, polyoxometalates have very high molecular weights so the substrate to catalyst mass ratio is very low. With water as the substrate, low substrate to catalyst mass ratios will inevitably be the case.

Future Directions

Outlook for Green Oxidation Catalysts

The future for green oxidation catalysis is bright. Catalysis has traditionally been in the hands of "catalysis experts" and they have provided a tremendous foundation upon which to build. Now, creative thinkers are meshing the information that has been gathered over the decades about catalyzed and uncatalyzed reactions into new paradigms.

- Rapid growth is happening in interdisciplinary approaches to solving complicated syntheses with catalysis as a major contributor to the process. One example is coupling organocatalysts with biocatalysts into clever reaction schemes that produce compounds that are particularly difficult to synthesize [160]. Both organocatalysis [113] and biocatalysis [161] are relatively new fields themselves having blossomed in the last decade. The rapid adoption of these technologies is a clear indication that interdisciplinary approaches are playing an increasing role in the field of catalysis, which only bodes well for making even more rapid and significant contributions.
- The elimination of even a single isolation step in a multistep synthesis saves on time, materials, and cost. Cascade and tandem catalysis are powerful methodologies, where one or more catalyst is combined with multiple reactants to assemble complex molecules without recovering intermediate products [162, 163]. These single reaction vessel reactions are challenging ones to design because all reagents in the mixture must be compatible, but the potential benefits are great.
- Organic–inorganic hybrid catalysts are the marriage of solid catalysts, which have the advantage of generally straightforward recovery and recyclability with soluble catalysts, which have a greater breadth in the variety of reactions that they can catalyze. Many different approaches, some well established and others new, are being taken to the preparation of these materials. These include adsorbing the soluble catalyst in pores of the support, assembling the soluble catalyst within a cavity of the solid catalyst so that it cannot escape (analogous to a "ship-in-bottle"), making a covalent bond between the solid material and the soluble catalyst, and finally directly synthesizing the hybrid material [164–166]. For example, the power of the oxidation organocatalyst TEMPO is great, but a drawback is its cost. Current efforts are to covalently link it to a silica substrate like MCM-41. MCM-41 has a large surface area and a regular mesoporous structure which allows for designing a well-defined hybrid material. Preparation of the TEMPO/MCM-41 material is a relatively complicated synthetic process itself and illustrates one of the issues that must be considered in deciding whether the catalyst itself is green [167].
- Process and Green Engineering issues are also making rapid advancements in catalysis. Environmentally benign or green solvents for all types of chemical reactions, including catalysis are an intense research topic [168]. Solvents play a number of roles in catalytic processes including dissolving one or more reactant, controlling reaction temperature, isolating the desired chemical by extraction, distillation, or crystallization and other functions. They are typically used in much larger volumes than the reactants themselves and therefore pose challenges such as disposal (cost and methodology), volatilization into the atmosphere, CO_2 generation as a result of energy needed to heat and cool, and others. Solvents of the future [169] include water, ionic liquids [170], fluorous liquids [171], supercritical fluids, gas-expanded liquids [172], liquid polymers, and switchable surfactants [173]. The breadth of application space for each one of these solvents systems is still in its early stages and

new solvents are likely to be developed in the coming years. It should be emphasized that fluorous solvents have many positive attributes, but they tend to be persistent in the environment (nonbiodegradable) which makes them nongreen [91]. Bi-phasic solvent systems, phase-transfer catalysis, and even solvent-free processes are considered as making major contributions to advances in green solvent systems.

- Computer-aided molecular design of environmentally benign catalysts is an expanding research area. Computer modeling of existing molecules is a highly refined process. In the case of catalyst design, the methodology is still in its early stages, but it holds the promise of greatly decreasing the time and effort required to design catalysts and to improve catalyst properties [174]. The catalysts are essentially broken into pieces with each piece evaluated for its role in the catalytic process and also its potential for environmental effects. By eliminating "negative" pathways in the catalyst design, more fruitful outcomes will result [138, 142, 175].
- High-throughput experimentation (HTE) is a tool that has been applied to catalysis during the past decade [176]. HTE utilizes an array of microreactions in which parameter space around a catalytic reaction is probed essentially simultaneously. These microreactions, which generally are robot controlled, produce a vast amount of experimental data that needs to be carefully sorted. As with any other investigation mode into a process that is ultimately destined for commercial application, it is important to investigate those parameters that are critical for scaling to laboratory, pilot-plant and commercial plant. A number of companies have been born that provide HTE services.

Clearly, this is a remarkable time to be involved in catalysis research as the field reinvents itself from one heavily focused on converting petroleum-based feedstreams for commodity chemicals into one that looks at the entire picture of the products and processes that are used for our short- and long-term needs [20, 177, 178]. It also brings into focus a "new" feedstock, renewable resources, for chemists to manipulate into value-added chemicals [20, 177]. However, the chemical knowledge base for manipulating renewable resources into high-value chemicals is limited and catalytic processes are even less well developed [179]. This knowledge gap exists because unlike petroleum-based feedstocks, those derived from renewable resources are highly functionalized molecules and thus require new methods for their manipulation. Of course, all of this must be done economically [178]. Nevertheless, the rapid increase in global demand for raw materials in all sectors of society means that better and more intelligent uses of alternative and sustainable resources are needed. Green oxidation catalysts will play a vital role in the challenge to convert these complicated feedstocks [180] into tomorrow's products.

Bibliography

1. Walker JD, Enache M, Dearden JD (2006) Quantitative cationic activity relationships for predicting toxicity of metal ions from physicochemical properties and natural occurrence levels. QSAR Comb Sci 26:522–527
2. Walker JD, Enache M, Dearden JC (2003) Quantitative cationic-activity relationships for predicting toxicity of metals. Environ toxicology chemistry SETAC 22:1916–1935
3. USEPA (2007) Framework for Metals Risk Assessment. http://www.epa.gov/raf/metalsframework/pdfs/metals-risk-assessment-final.pdf. Accessed 17 May 2010
4. Min BK, Friend CM (2007) Heterogeneous gold-based catalysis for green chemistry: low-temperature CO oxidation and propene oxidation. Chem Rev 107:2709–2724
5. Anastas PT, Kirchhoff MM, Williamson TC (2001) Catalysis as a foundational pillar of green chemistry. Appl Catal A Gen 221:3–13
6. Anastas PT, Zimmerman JB (2003) Peer reviewed: design through the 12 principles of green engineering. Environ Sci Technol 37:94–101
7. World Commission on Environment and Development (1987) Our common future. Oxford University Press, Oxford
8. Anastas PT, Williamson TC (1996) Green chemistry: an overview. ACS Symp Ser 626:1–17
9. Anastas PT, Warner JC (1998) Green: chemistry theory and practice. Oxford University Press, Oxford
10. Centi G, Perathoner S (2003) Catalysis and sustainable (green) chemistry. Catal Today 77:287–297
11. Wsniak J (2000) Jöns Jacob Berzelius a guide to the perplexed chemist. Chem Educ 5:343–350
12. Berzelius JJ (1836) Jahres-Bericht über die Fortschritte der Physichen Wissenschaften. 15:237–245 H. Laupp, Tübingen
13. Roberts M (2000) Birth of the catalytic concept (1800–1900). Catal Lett 67:1–4
14. Brégeault J-M (2003) Transition-metal complexes for liquid-phase catalytic oxidation: some aspects of industrial reactions and of emerging technologies. J Chem Soc Dalton Trans 17:3289–3302

15. Smith MB, March J (2007) March's advanced organic chemistry: reactions, mechanisms, and structure, 6th edn. Wiley, Hoboken
16. Katsuki T, Sharpless KB (1980) The first practical method for asymmetric epoxidation. J Am Chem Soc 102:5974–5976
17. Sheehan RJ (2005) Terephthalic acid, dimethyl terephthalate, and isophthalic acid. In: Book ullmann's encyclopedia of industrial chemistry. Wiley, Weinheim, pp 1–13
18. Cavani F, Teles JH (2009) Sustainability in catalytic oxidation: an alternative approach or a structural evolution? ChemSusChem 2:508–534
19. Gogate P, Pandit AB (2004) A review of imperative technologies for wastewater treatment I: oxidation technologies at ambient conditions. Adv Enviro Res 8:501–551
20. van Haveren J, Scott EL, Sanders J (2008) Bulk chemicals from biomass. Biofuels Bioprod Biorefin 2:41–57
21. Werpy T, Holladay J, White J, Peterson G, Bozell JJ, Aden A, Manheim A (2004) Top value added chemicals from biomass, vol 1.), Results of screening for potential candidates from sugars and synthetic gas U.S. Department of Energy, NREL/TP-510-35523
22. Cavani F, Ballarini N, Luciani S (2009) Catalysis for society: towards improved process efficiency in catalytic selective oxidations. Top Catal 52:935–947
23. Cavani F, Ballarini N (2009) Recent achievements and challenges for a greener chemical industry. In: Mizuno N (ed) Modern heterogenous oxidation catalysis: design, reactions and characterization. Wiley, Weinheim, pp 289–331
24. Valko M, Morris H, Cronin MTD (2005) Metals, toxicity and oxidative stress. Curr Med Chem 12:1161–1208
25. Teng Y, Jiao x, Wang J, Xu W, Yang J (2009) Environmentally geochemical characteristics of vanadium in the topsoil in the Panzhihua mining area, Sichuan Province. China Chin J Geochem 28:105–111
26. Hermans I, Spier ES, Neuenschwander U, Turrá N, Baiker A (2009) Selective oxidation catalysis: opportunities and challenges. Top Catal 52:1162–1174
27. Clerici MG, Bellussi G, Romano U (1991) Synthesis of propylene oxide from propylene and hydrogen peroxide catalyzed by titanium silicalite. J Catal 129:159–167
28. Clerici MG (2009) Titanium silicalite-1. In: Jackson SD, Hargreaves JSJ (eds) Metal oxide catalysis, vol 2. Wiley, Weinheim, pp 705–754
29. Nijhuis TA, Makkee M, Moulijn JA, Weckhuysen, BM (2006) The production of propene oxide: A catalytic processes and recent developments. Ind Eng Chem Res 45:3447–3459
30. Nijhuis TA, Huizinga BJ, Makkee M, Moulijn JA (1999) Direct epoxidation of propene using gold dispersed on TS-1 and other titanium-containing supports. Ind Eng Chem Res 38(3):884
31. Stare J, Henson NJ, Eckert J (2009) Mechanistic aspects of propene epoxidation by hydrogen peroxide. Catalytic role of water molecules, external electric field, and zeolite framework of TS-1. J Chem Info Mod 49:833–846
32. Li YG, Lee YM, Porter JF (2002) The synthesis and characterization of titanium silicalite-1. J Mater Sci 37:1959–1965
33. Baccile N, Babonneau F, Thomas B, Coradin T (2009) Introducing ecodesign in silica solìgel materials. J Mater Chem 19:8537–8559
34. Sheldon RA (1992) Organic synthesis – past, present and future. Chem Ind Lond 23:903–906
35. Sheldon RA (1997) Catalysis: the key to waste minimization. J Chem Technol Biotechnol 68:381–388
36. Sheldon RA (2007) The E factor: fifteen years on. Green Chem 9:1273–1283
37. Calvo-Flores FG (2009) Sustainable chemistry metrics. ChemSusChem 2:905–919
38. Eckelman MJ, Zimmerman JB, Anastas PT (2008) Toward green nano: e-factor analysis of several nanomaterial syntheses. J Ind Ecol 12:316–328
39. Dahl JeA, Maddux BLS, Hutchison JE (2007) Toward greener nanosynthesis. Chem Rev 107:2228–2269
40. Hermans I, Peeters J, Jacobs PA (2008) Autoxidation chemistry: bridging the gap between homogeneous radical chemistry and (heterogeneous) catalysis. Top Catal 48:41–48
41. Thomas JM, Raja R (2006) The advantages and future potential of single-site heterogeneous catalysts. Top Catal 40:3–17
42. Niu W, Draths KM, Frost JW (2002) Benzene-free synthesis of adipic acid. Biotechnol Progr 18:201–211
43. Sato K, Aoki M, Noyori R (1998) A "Green" route to adipic acid: direct oxidation of cyclohexenes with 30 percent hydrogen peroxide. Science 281:1646–1647
44. Strigul N, Koutsospyros A, Christodoulatos C (2010) Tungsten speciation and toxicity: acute toxicity of mono – and polytungstates to fish. Ecotoxicol Environ Saf 73:164–171
45. Smith BJ, Patrick VA (2000) Quantitative determination of sodium metatungstate speciation by 183W NMR spectroscopy. Aust J Chem 53:965–970
46. Deng Y, Ma Z, Wang K, Chen J (1999) Clean synthesis of adipic acid by direct oxidation of cyclohexene with H_2O_2 over peroxytungstate-organic complex catalysts. Green Chem 1:275–276
47. Buonomenna MG, Golemme G, De Santo MP, Drioli E (2010) Direct oxidation of cyclohexene with inert polymeric membrane reactor. Org Proc Res Dev 14:252–258
48. York APE, Xiao T, Green MLH (2003) Brief overview of the partial oxidation of methane to synthesis gas. Top Catal 22:345–358
49. Enger BC, Lødeng R, Holmen A (2008) A review of catalytic partial oxidation of methane to synthesis gas with emphasis on reaction mechanisms over transition metal catalysts. Appl Catal A Gen 346:1–27
50. Arakawa H, Aresta M, Armor JN, Barteau MA, Beckman EJ, Bell AT, Bercaw JE, Creutz C, Dinjus E, Dixon DA, Domen K, DuBois DL, Eckert J, Fujita E, Gibson DH, Goddard WA, Goodman DW, Keller J, Kubas GJ, Kung HH, Lyons JE, Manzer LE, Marks TJ, Morokuma K, Nicholas KM, Periana R, Que L, Rostrup-Nielson J, Sachtler WMH, Schmidt LD, Sen A, Somorjai GA, Stair PC, Stults BR, Tumas W (2001) Catalysis research of relevance to carbon management: progress, challenges, and opportunities. Chem Rev 101:953–996

51. Kirillova MV, Kozlov YN, Shul'pina LS, Lyakin OY, Kirillov AM, Talsi EP, Pombeiro AJL, Shul'pin GB (2009) Remarkably fast oxidation of alkanes by hydrogen peroxide catalyzed by a tetracopper(II) triethanolaminate complex: promoting effects of acid co-catalysts and water, kinetic and mechanistic features. J Catal 268:26–38
52. Beckers J, Rothenberg G (2010) Sustainable selective oxidations using ceria-based materials. Green Chem 12:939
53. Czuprat O, Werth S, Schirrmeister S, Schiestel T, Caro J (2009) Olefin production by a multistep oxidative dehydrogenation in a perovskite hollow-fiber membrane reactor. ChemCatChem 1:401–405
54. Madeira LM, Portela MF (2002) Catalytic oxidative dehydrogenation of n-butane. Catal Rev 44:247–286
55. Grabowski R (2006) Kinetics of oxidative dehydrogenation of C_2-C_3 alkanes on oxide catalysts. Catal Rev 48:199–268
56. Meth-Cohn O, Smith M (1994) What did W. H. Perkin actually make when he oxidized aniline to obtain mauveine? Perkin Trans 1:5–7
57. Sousa MM, Melo MJ, Parola AJ, Morris PJT, Rzepa HS, de Melo JSS (2008) A study in mauve: unveiling Perkin's dye in historic samples. Chem Euro J 14:8507–8513
58. He L, Wang L-C, Sun H, Ni J, Cao Y, He H-Y, Fan K-N (2009) Efficient and selective room-temperature gold-catalyzed reduction of nitro compounds with CO and H_2O as the hydrogen source. Angew Chem Int Ed 48:9538–9541
59. Li S-C, Diebold U (2010) Reactivity of TiO_2 rutile and anatase surfaces toward nitroaromatics. J Am Chem Soc 132:64–66
60. Mann PJG, Saunders BC (1935) Peroxidase action. I. The oxidation of aniline. Proc R Soc Lond B Biol Sci 119:47–60
61. Sheldon RA, Kochi JK (1981) Metal-catalyzed oxidations of organic compounds. Academic, New York
62. Collins TJ (1994) Designing ligands for oxidizing complexes. Acc Chem Res 27:279–285
63. Schmid A, Dordick J, Hauer B, Kiener A, Wubbolts M, Witholt B (2001) Industrial biocatalysis today and tomorrow. Nature 409:258
64. Schoemaker HE, Mink D, Wubbolts MG (2003) Dispelling the myths – biocatalysis in industrial synthesis. Science 299:1694–1697
65. Yuryev R, Liese A (2010) Biocatalysis: the outcast. ChemCatChem 2:103–107
66. Matsuda T, Yamanaka R, Nakamura K (2009) Recent progress in biocatalysis for asymmetric oxidation and reduction. Tetrahedron Asymmetr 20:513–557
67. van de Velde F, Lourenço ND, Bakker M, van Rantwijk F, Sheldon RA (2000) Improved operational stability of peroxidases by coimmobilization with glucose oxidase. Biotechnol Bioeng 69:286–291
68. Kuhn D, Kholiq MA, Heinzle E, Bühler B, Schmid A (2010) Intensification and economic and ecological assessment of a biocatalytic oxyfunctionalization process. Green Chem 12:815–827
69. Que L Jr, Tolman WB (2008) Biologically inspired oxidation catalysis. Nature 455:333–340
70. Costas M, Chen K, Que L Jr (2000) Biomimetic nonheme iron catalysts for alkane hydroxylation. Coord Chem Rev 200–202:517–544
71. Piera J, Bäckvall J-E (2008) Catalytic oxidation of organic substrates by molecular oxygen and hydrogen peroxide by multistep electron transfer – a biomimetic approach. Angew Chem Int Ed 47:3506–3523
72. Meunier B, de Visser SP, Shaik S (2004) Mechanism of oxidation reactions catalyzed by cytochrome P450 enzymes. Chem Rev 104:3947–3980
73. McLain JL, Lee J, Groves JT (2000) Biomimetic oxygenations related to cytochrome P450: metal-oxo and metal-peroxo intermediates. In: Meunier B (ed) Biomimetic oxidations catalyzed by transition metal complexes. Imperial College Press, London, pp 91–169
74. Groves JT, Nemo TE, Myers RS (1979) Hydroxylation and epoxidation catalyzed by iron-porphine complexes. oxygen transfer from iodosylbenzene. J Am Chem Soc 101:1032–1033
75. Leroy J, Bondon A (2007) β-Fluorinated porphyrins and related compounds: an overview. Eur J Org Chem 2008:417–433
76. Cai Y, Liu Y, Lu Y, Gao G, He M (2008) Ionic manganese porphyrins with S-containing counter anions: mimicking cytochrome P450 activity for alkene epoxidation. Catal Lett 124:334–339
77. Nagarajan S, Nagarajan R, Bruno F, Samuelson LA, Kumar J (2009) A stable biomimetic redox catalyst obtained by the enzyme catalyzed amidation of iron porphyrin. Green Chem 11:334–338
78. Liu Y, Zhang H-J, Lu Y, Cai Y-Q, Liu X-L (2007) Mild oxidation of styrene and its derivatives catalyzed by ionic manganese porphyrin embedded in a similar structured ionic liquid. Green Chem 9:1114–1119
79. Lente G, Espenson JH (2005) Oxidation of 2, 4, 6-trichlorophenol by hydrogen peroxide Comparison of different iron-based catalysts. Green Chem 7:28–34
80. Stahl SS (2004) Palladium oxidase catalysis: selective oxidation of organic chemicals by direct dioxygen-coupled turnover. Angew Chem Int Ed 43:3400–3420
81. Allardyce CS, Dyson PJ (2001) Ruthenium in medicine: current clinical uses and future prospects. Platinum Met Rev 45:62–69
82. Pope MT, Muller A (2002) Polyoxometalate chemistry from topology via self assembly to applications. Kluwer, New York
83. Jeannin YP (1998) The nomenclature of polyoxometalates: how to connect a name and a structure. Chem Rev 98:51–76
84. Hill CL, Delannoy L, Duncan DC, Weinstock IA, Renneke RF, Reiner RS, Atalla RH, Han JW, Hillesheim DA, Cao R, Anderson TM, Okun NM, Musaev DG, Geletii YV (2007) Complex catalysts from self-repairing ensembles to highly reactive air-based oxidation systems. Comptes rendus Chim 10:305–312
85. Kozhevnikov IV (1998) Catalysis by heteropoly acids and multicomponent polyoxometalates in liquid-phase reactions. Chem Rev 98:171–198
86. Long D-L, Burkholder E, Cronin L (2007) Polyoxometalate clusters, nanostructures and materials: from self assembly to designer materials and devices. Chem Soc Rev 36:105–121

87. Trubitsyna T, Kholdeeva O (2008) Kinetics and mechanism of the oxidation of 2, 3, 6-trimethylphenol with hydrogen peroxide in the presence of Ti-monosubstituted polyoxometalates. Kinet Catal 49:371–378
88. Neumann R (2010) Activation of molecular oxygen, polyoxometalates, and liquid-phase catalytic oxidation. Inorg Chem 49:3594–3601
89. Maayan G, Ganchegui B, Leitner W, Neumann R (2006) Selective aerobic oxidation in supercritical carbon dioxide catalyzed by the $H_5PV_2Mo_{10}O_{40}$ polyoxometalate. Chem Commun 21:2230–2232
90. Vazylyev M, Sloboda-Rozner D, Haimov A, Maayan G, Neumann R (2005) Strategies for oxidation catalyzed by polyoxometalates at the interface of homogeneous and heterogeneous catalysis. Top Catal 34:93–99
91. Clark JH, Tavener SJ (2007) Alternative solvents: shades of green. Org Proc Res Dev 11:149–155
92. Collins TJ (2001) Papermaking: green chemistry through the mill. Nature 414:161–162
93. Weiner H, Finke RG (1999) An all-inorganic, polyoxometalate-based catechol dioxygenase that exhibits >100 000 catalytic turnovers. J Am Chem Soc 121:9831–9842
94. Curzons AD, Constable DJ, Mortimer DN, Cunningham VL (2001) So you think your process is green, how do you know? Using principles of sustainability to determine what is green – a corporate perspective. Green Chem 3:1–6
95. Höft E (1993) Enantioselective epoxidation with peroxidic oxygen. Top Curr Chem 164:63–77
96. Canali L, Karjalainen JK, Sherrington DC, Hormi O (1997) Efficient polymer-supported sharpless alkene epoxidation catalyst. Chem Commun 1997:123–124
97. Zhang W, Loebach JL, Wilson SR, Jacobsen EN (1990) Enantioselective epoxidation of unfunctionalized olefins catalyzed by (Salen)manganese complexes. J Am Chem Soc 112:2801–2803
98. Irie R, Noda K, Ito Y, Matsumoto N, Katsuki T (1990) Catalytic asymmetric epoxidation of unfunctionalized olefins. Tetrahedron Lett 31:7345–7348
99. Katsuki T (1995) Catalytic asymmetric oxidations using optically-active (salen)manganese(III) complexes as catalysts. Coord Chem Rev 140:189–214
100. Srinivasan K, Michaud P, Kochi JK (1986) Epoxidation of olefins with cationic (salen)Mn^{III} complexes. The modulation of catalytic activity by substituents. J Am Chem Soc 108: 2309–2320
101. Groves JT, Myers RS (1983) Catalytic asymmetric epoxidations with chiral iron porphyrins. J Am Chem Soc 105:5791–5796
102. Limburg J, Brudvig GW, Crabtree RH (2000) Modeling the oxygen-evolving complex in photosystem II. In: Meunier B (ed) Biomimetic oxidations catalyzed by transition metal complexes. Imperial College Press, London, pp 509–541
103. Zou X, Fu X, Li Y, Tu X, Fu S, Luo Y, Wu X (2010) Highly enantioselective epoxidation of unfunctionalized olefins catalyzed by chiral Jacobsen's catalyst immobilized on phenoxy-modified zirconium poly(styrene-phenylvinylphosphonate)phosphate. Adv Synth Catal 352:163–170
104. Das P, Silva AR, Carvalho AP, Pires J, Freire C (2009) Enantioselective epoxidation of alkenes by Jacobsen catalyst anchored onto aminopropyl-functionalised laponite, MCM-41 and FSM-16. Catal Lett 129:367–375
105. Fraile JM, García JI, Mayoral JA (2009) Noncovalent immobilization of enantioselective catalysts. Chem Rev 109:360–417
106. Grigoropoulou G, Clark JH, Elings JA (2003) Recent developments on the epoxidation of alkenes using hydrogen peroxide as an oxidant. Green Chem 5:1–7
107. Bhattacharjee S, Anderson JA (2004) Epoxidation by layered double hydroxide-hosted catalysts. Catalyst synthesis and use in the epoxidation of R-(+)-Limonene and (-)-α-Pinene using molecular oxygen. Catal Lett 95:119–125
108. Creager SE, Raybuck SA, Murray RW (1986) An efficient electrocatalytic model cytochrome P-450 epoxidation cycle. J Am Chem Soc 108:4225–4227
109. Horwitz CP, Creager SE, Murray RW (1990) Electrocatalytic olefin epoxidation using manganese Schiff-base complexes and dioxygen. Inorg Chem 29:1006–1011
110. Guo P, Wong K-Y (1999) Enantioselective electrocatalytic epoxidation of olefins by chiral manganese Schiff-base complexes. Electrochem Commun 1:559–563
111. Fatibello-Filho O, Dockal ER, Marcolino-Junior LH, Teixeira MFS (2007) Electrochemical modified electrodes based on metal-salen complexes. Anal Lett 40:1825–1852
112. List B (2007) Introduction: organocatalysis. Chem Rev 107:5413–5415
113. MacMillan DWC (2008) The advent and development of organocatalysis. Nature 455:304–308
114. Dondoni A, Massi A (2008) Asymmetric organocatalysis: from infancy to adolescence. Angew Chem Int Ed 47: 4638–4661
115. Wong OA, Shi Y (2008) Organocatalytic oxidation. Asymmetric epoxidation of olefins catalyzed by chiral ketones and iminium salts. Chem Rev 108:3958–3987
116. Tu Y, Wang Z-X, Shi Y (1996) An efficient asymmetric epoxidation method for trans-olefins mediated by a fructose-derived ketone. J Am Chem Soc 118:9806–9807
117. Shu L, Shi Y (1999) Asymmetric epoxidation using hydrogen peroxide (H_2O_2) as primary oxidant. Tetrahedron Lett 40:8721–8724
118. Sheldon RA, Arends IWCE (2004) Organocatalytic oxidations mediated by nitroxyl radicals. Adv Synth Catal 346:1051–1071
119. Bowman DF, Gillan T, Ingold KU (1971) Kinetic applications of electron paramagnetic resonance spectroscopy. III. Self-reactions of dialkyl nitroxide radicals. J Am Chem Soc 93:6555–6561
120. Phukan P, Khisti RS, Sudalai A (2006) Green protocol for the synthesis of N-oxides from secondary amines using vanadium silicate molecular sieve catalyst. J Mol Catal A Chem 248:109–112

121. Ciriminna R, Pagliaro M (2010) Industrial oxidations with organocatalyst TEMPO and its derivatives. Org Proc Res Dev 14:245–251
122. Carson R (1962) Silent spring. Houghton Mifflin, Boston
123. Blackmond DG, Armstrong A, Coombe V, Wells A (2007) Water in organocatalytic processes: debunking the myths. Angew Chem Int Ed 46:3798–3800
124. Mantzavinos D, Psillakis E (2004) Enhancement of biodegradability of industrial wastewaters by chemical oxidation pretreatment. J Chem Tech Biotech 79:431–454
125. Walling C (1975) Fenton's reagent revisited. Acc Chem Res 8:125–131
126. Richter HW, Waddell WH (1983) Mechanism of the oxidation of dopamine by the hydroxyl radical in aqueous solution. J Am Chem Soc 105:5434–5440
127. Fenton HJH (1894) Oxidation of tartaric acid in presence of iron. J chem Soc Trans 65:899–910
128. Masarwa A, Rachmilovich-Calis S, Meyerstein N, Meyerstein D (2005) Oxidation of organic substrates in aerated aqueous solutions by the fenton reagent. Coord Chem Rev 249: 1937–1943
129. Watts RJ, Teel AL (2005) Chemistry of modified fenton's reagent (catalyzed H_2O_2 propagations-CHP) for in situ soil and groundwater remediation. J Enviro Eng 131:612–622
130. Millioli VS, Freire DDC, Cammarota MC (2002) Testing the efficiency of Fenton's reagent in treatment of petroleum-contaminated sand. Engenharia Térmica, Edição Especial 44–47
131. Nadtochenko V, Kiwi J (1998) Photoinduced mineralization of xylidine by the Fenton reagent. 2. Implications of the precursors formed in the dark. Environ Sci Technol 32:3282–3285
132. Yu R-F, Chen H-W, Liu K-Y, Cheng W-P, Hsieh P-H (2010) Control of the fenton process for textile wastewater treatment using artificial neural networks. J Chem Technol Biotechnol 85:267–278
133. Sun Y, Pignatello JJ (1992) Chemical treatment of pesticide wastes. Evaluation of Fe(III) chelates for catalytic hydrogen peroxide oxidation of 2, 4-D at circumeutral pH. J Agric Food Chem 40:322–327
134. Sun Y, Pignatello JJ (1993) Activation of hydrogen peroxide by iron(III) chelates for abiotic degradation of herbicides and insecticides in water. J Agric Food Chem 41:308–312
135. Lewis S, Lynch A, Bachas L, Hampson S, Ormsbee L, Bhattacharyya D (2009) Chelate-modified fenton reaction for the degradation of trichloroethylene in aqueous and two-phase systems. Enviro Eng Sci 26:849–859
136. Cybulski A (2007) Catalytic wet air oxidation: are monolithic catalysts and reactors feasible? Ind Engr Chem Res 46:4007–4033
137. Collins TJ, Gordon-Wylie SW, Bartos MJ, Horwitz CP, Woomer CG, Williams SA, Patterson RE, Vuocolo LD, Paterno SA, Strazisar SA, Peraino DK and Dudash CA (1998) The design of green oxidants. In: Anastas P, Warner JC (eds) Greem Chemistry, pp. 46–71
138. Ellis WC, Tran CT, Denardo MA, Fischer A, Ryabov AD, Collins TJ (2009) Design of more powerful iron-TAML peroxidase enzyme mimics. J Am Chem Soc 131:18052–18053
139. Collins TJ, Khetan SK, Ryabov AD (2009) Chemistry and applications of iron-TAML catalysts in green oxidation processes based on hydrogen peroxide. In: Anastas PT, Crabtree R (eds) Handbook of green chemistry, vol 1. Wiley, Weinheim, pp 39–77
140. Ryabov AD, Collins TJ (2009) Mechanistic considerations on the reactivity of green FeIII-TAML activators of peroxides. Adv Inorg Chem 61:471–521
141. Chanda A, Ryabov AD, Mondal S, Alexandrova L, Ghosh A, Hangun-Balkir Y, Horwitz CP, Collins TJ (2006) Activity-stability parameterization of homogeneous green oxidation catalysts. Chem Euro J 12:9336–9345
142. Polshin V, Popescu D-L, Fischer A, Chanda A, Horner DC, Beach ES, Henry J, Qian Y-L, Horwitz CP, Lente G, Fabian I, Muenck E, Bominaar EL, Ryabov AD, Collins TJ (2008) Attaining control by design over the hydrolytic stability of Fe-TAML oxidation catalysts. J Am Chem Soc 130: 4497–4506
143. Georgi A, Schierz A, Trommler U, Horwitz CP, Collins TJ, Kopinke F (2007) Humic acid modified Fenton reagent for enhancement of the working pH range. Appl Catal B Enviro 72:26–36
144. Gupta SS, Stadler M, Noser CA, Ghosh A, Steinhoff B, Lenoir D, Horwitz CP, Schramm K-W, Collins TJ (2002) Rapid total destruction of chlorophenols by activated hydrogen peroxide. Science 296:326–328
145. Horwitz CP, Fooksman DR, Vuocolo LD, Gordon-Wylie SW, Cox NJ, Collins TJ (1998) Ligand design approach for securing robust oxidation catalysts. J Am Chem Soc 120:4867–4868
146. Chahbane N, Popescu D-L, Mitchell DA, Chanda A, Lenoir D, Ryabov AD, Schramm K-W, Collins TJ (2007) Fe^{III}-TAML-catalyzed green oxidative degradation of the azo dye Orange II by H_2O_2 and organic peroxides: products, toxicity, kinetics, and mechanisms. Green Chem 9:49–57
147. Horwitz CP, Collins TJ, Spatz J, Smith HJ, Wright LJ, Stuthridge TR, Wingate KG, McGrouther K (2006) Iron-TAML catalysts in the pulp and paper industry. ACS Symp Ser 921:156–169
148. Chanda A, Khetan SK, Banerjee D, Ghosh A, Collins TJ (2006) Total degradation of fenitrothion and other organophosphorus pesticides by catalytic oxidation employing Fe-TAML peroxide activators. J Am Chem Soc 128: 12058–12059
149. Banerjee D, Markley AL, Yano T, Ghosh A, Berget PB, Minkley E Jr, Khetan SK, Collins TJ (2006) "Green" oxidation catalysis for rapid deactivation of bacterial spores. Angew Chem Int Ed 45:3974–3977
150. Shappell NW, Vrabel MA, Madsen PJ, Harrington G, Billey LO, Hakk H, Larson GL, Beach E, Horwitz CP, Ro K, Hunt PG, Collins TJ (2008) Destruction of estrogens using

Fe-TAML/peroxide catalysis. Environ Sci Technol 42: 1296–1300
151. Lewis NS, Nocera DG (2006) Powering the planet: chemical challenges in solar energy utilization. Proc Nat Acad Sci 103:15729–15735
152. Nocera DG (2009) Chemistry of personalized solar energy. Inorg Chem 48:10001–10017
153. Dismukes GC, van Willigen RT (2006) Manganese: the oxygen-evolving complex & models. Encyclopedia of Inorganic Chemistry 5:1–15
154. Raymond J, Blankenship RE (2008) The origin of the oxygen-evolving complex. Coord Chem Rev 252:377–383
155. Dincă M, Surendranath Y, Nocera DG (2010) Nickel-borate oxygen-evolving catalyst that functions under benign conditions. Proc Nat Acad Sci 107:10337–10341
156. Surendranath Y, Dinca M, Nocera DG (2009) Electrolyte-dependent electrosynthesis and activity of cobalt-based water oxidation catalysts. J Am Chem Soc 131:2615–2620
157. Cross DP, Ramachandran G, Wattenberg EV (2001) Mixtures of nickel and cobalt chlorides induce synergistic cytotoxic effects: implications for inhalation exposure modeling. Ann Occup Hyg 45:409–418
158. Nakagawa T, Beasley CA, Murray RW (2009) Efficient electro-oxidation of water near its reversible potential by a Mesoporous IrOx Nanoparticle Film. J Phys Chem C 113:12958–12961
159. Yin Q, Tan JM, Besson C, Geletii YV, Musaev DG, Kuznetsov AE, Luo Z, Hardcastle KI, Hill CL (2010) A fast soluble carbon-free molecular water oxidation catalyst based on abundant metals. Science 328:342–345
160. Baer K, Kraußr M, Burda E, Hummel W, Berkessel A, Gröger H (2009) Sequential and modular synthesis of chiral 1, 3-diols with two stereogenic centers: access to all four stereoisomers by combination of organo- and biocatalysis. Angew Chem Int Ed 48:9355–9358
161. Turner NJ (2009) Directed evolution drives the next generation of biocatalysts. Nat Chem Biol 5:567–573
162. Fogg DE, dos Santos EN (2004) Tandem catalysis: a taxonomy and illustrative review. Coord Chem Rev 248:2365–2379
163. Nicolaou KC, Chen JS (2009) The art of total synthesis through cascade reactions. Chem Soc Rev 38:2993–3009
164. Forster PM, Cheetham AK (2003) Hybrid inorganic-organic solids: an emerging class of nanoporous catalysts. Top Catal 24:79–86
165. Kaneda K, Mizugaki T (2009) Development of concerto metal catalysts using apatite compounds for green organic syntheses. Energy Enviro Sci 2:655–673
166. Wight AP, Davis ME (2002) Design and preparation of organic-inorganic hybrid catalysts. Chem Rev 102:3589–3614
167. Brunel D, Fajula F, Nagy JB, Deroide B, Verhoef MJ, Veum L, Peters JA, van Bekkum H (2001) Comparison of two MCM-41 grafted TEMPO catalysts in selective alcohol oxidation. Appl Catal A Gen 213:73–82
168. Capello C, Fischer U, Hungerbühler K (2007) What is a green solvent? a comprehensive framework for the environmental assessment of solvents. Green Chem 9:927–934
169. Olivier-Bourbigou H, Magna L, Morvan D (2009) Ionic liquids and catalysis: recent progress from knowledge to applications. Appl Catal A Gen 373:1–56
170. Deetlefs M, Seddon KR (2010) Assessing the greenness of some typical laboratory ionic liquid preparations. Green Chem 12:17–30
171. Zhang W (2009) Green chemistry aspects of fluorous techniques-opportunities and challenges for small-scale organic synthesis. Green Chem 11:911–920
172. Akien GR, Poliakoff M (2009) A critical look at reactions in class I and II gas-expanded liquids using CO_2 and other gases. Green Chem 11:1083–1100
173. Liu Y, Jessop PG, Cunningham M, Eckert CA, Liotta CL (2006) Switchable surfactants. Science 313:958–960
174. Chavali S, Lin B, Miller DC, Camarda KV (2004) Environmentally-benign transition metal catalyst design using optimization techniques. Comput Chem Eng 28:605–611
175. Guidoni L, Spiegel K, Zumstein M, Röthlisberger U (2004) Green oxidation catalysts: computational design of high-efficiency models of galactose oxidase. Angew Chem Int Ed 43:3286–3289
176. Schüth F, Busch O, Hoffmann C, Johann T, Kiener C, Demuth D, Klein J, Schunk S, Strehlau W, Zech T (2002) High-throughput experimentation in oxidation catalysis. Top Catal 21:55–66
177. Corma A, Iborra S, Velty A (2007) Chemical routes for the transformation of biomass into chemicals. Chem Rev 107:2411–2502
178. Christensen CH, Rass-Hansen J, Marsden CC, Taarning E, Egeblad K (2008) The renewable chemicals industry. ChemSusChem 1:283–289
179. Bozell JJ, Petersen GR (2010) Technology development for the production of biobased products from biorefinery carbohydrates – the US Department of Energy's "Top 10" revisited. Green Chem 12:539–554
180. Scott EL, Sanders JPM, Steinbüchel A (2010) Perspectives on Chemicals from Renewable Resources. In: Sustainable biotechnology, pp 195–210

P

Parabolic Trough Solar Technology

Eckhard Lüpfert
DLR Deutsches Zentrum für Luft- und Raumfahrt German Aerospace Center, Institute of Technical Thermodynamics, Solarforschung, Koeln/Cologne, Germany

Article Outline

Glossary
Definition of the Subject and Its Importance
Introduction
Technology Description
Future Directions
Bibliography

Glossary

Collector loop (PTC) Unit of several PTC connected in series to heat the fluid from inlet to outlet header temperature.

Direct normal irradiance, beam irradiance Direct part of the sunlight, coming from within the sun disk as almost parallel light onto a surface, measured as power density in kW/m^2.

Drive (PTC) Unit consisting of motor and gear or hydraulic drive with valves and cylinders, and the controller to turn the PTC into the correct operational tracking angle.

Efficiency Ratio of useful energy and total energy input.

Efficiency (PTC) Ratio of thermal energy output from the PTC and total solar radiation received on the aperture area.

Heat transfer fluid ("HTF") Fluid receiving the thermal energy in the receivers and transporting it to the heat exchangers, etc., of the power block. HTF for PTC is mostly synthetic oil or water/steam. Some installations also use molten salt or pressurized CO_2.

Intercept factor Relative amount of rays hitting the absorber tube as fraction of the total number of reflected rays from the mirror area.

Mirror, mirror panel (PTC) Reflecting panel, made of silvered glass or other reflecting sheet material, curved to reflect sunlight onto the absorber.

Module (PTC) Parabolic trough collector section between pylons, including structure, mirrors, and receivers.

Parabolic trough collector ("PTC") Concentrating solar collector with mirrors, absorber, and tracking system for providing solar energy at temperatures of 100–600°C.

Pylon (PTC) Support post of the PTC modules.

Receiver (PTC) Component of a concentrating collector system, especially PTC, consisting of absorber tube, with additional elements such as glass tube and expansion bellow.

Solar field Unit of parallel connected collector loops, typically also including connection piping, sensors and controls, land area, and heat transfer fluid of the collector installation of a solar plant.

Sun sensor Sensor for feedback of the tracking to the drive.

Tracking (PTC) Action of adjusting the collector angle to the sun position during the operation.

Definition of the Subject and Its Importance

Parabolic trough (solar) collectors (PTCs) are technical devices to collect the energy in form of solar radiation and convert it typically into thermal energy at temperature ranges of 150–500°C at industrial scale. The cylindrical trough shape of the reflecting surface with parabolic section of the mirror shape has the ability to concentrate the incident sunlight onto an absorber tube

Robert A. Meyers (ed.), *Encyclopedia of Sustainability Science and Technology*, DOI 10.1007/978-1-4419-0851-3,
© Springer Science+Business Media, LLC 2012

in the focal line of the collectors. Typical width of such PTC is 0.5–10 m. Main use of PTC is in solar power generation. In large-scale concentrating solar power applications, the PTC is the most successful type of concentrating collector design. The first troughs are reported at the end of the nineteenth and beginning of the twentieth century for industrial-scale steam generation. The wide expansion of coal, oil, and gas for heat and power generation left solar energy technology behind until oil price shocks initiated a development step in the 1980s, leading to the successful commercial start of the parabolic trough solar power plants SEGS I–IX in California until 1990. Larger scale capacities have been installed in Spain since 2007, and from there and since then spreading out worldwide.

PTCs are the main technology for large-scale concentrating solar power (CSP) solar fields. The increasing application in CSP is due to the high conversion efficiency in combination with a standardized modular design with relevant economic advantages over other CSP variants.

Introduction

PTCs feature a concentrator shell with parabolic sections in a cylindrical configuration. The focus of the cylinder parabola is a straight line. The aperture width is typically about three to four times longer than the focal distance of the parabola between vertex and absorber tube (Figs. 1 and 8).

A PTC consists of modules; these are the units supported between pylons.

Main components of a PTC module are the curved mirror and the absorber tube. Its support structure holds the components in place and connects the modules between each other.

PTCs are among the most efficient available concentrating solar collectors, only superseded by the paraboloidal dish concentrators (reference to Article). The advantage of the PTC increases in larger installations, where the collection of the heat from a solar field with many collectors to a central conversion system is needed with a wide system of heat transfer pipes.

Parabolic trough collectors are tracking reflector systems. There is no reasonable chance to avoid the continuous rotation of the collector to always point with the optical axis (symmetry axis) plane to the sun. The tracking accuracy must be typically in the range of 0.1°. This order of magnitude applies to all orientations of any of the components of the concentrating collector.

The sun is the energy source for PTC. The sun apparently moves daily over the sky, due to a rotation speed of the earth axis of 15°/h. The sun changes its path over the sky throughout the year due to the tilt of the earth's rotation axis of +/−23° from the rotation plane around the sun. Nevertheless, PTCs require only one horizontal rotation axis for the tracking. The tracking axis is typically oriented north–south for commercial application, as this results in the best output over the year in the typical latitudes of PTC application.

Typical dimensions of a PTC are given in Table 1 and illustrated in Fig. 1.

Parabolic Trough Solar Technology. Table 1 PTC dimensions of a typical CSP plant, e.g., EuroTrough

Collector width	5.78 m
Collector length	150 m
Focal distance	1.71 m
Module length	12.3 m
Number of modules per collector	12
Effective aperture per collector	818 m^2
Absorber tube diameter	70 mm
Ideal concentration factor	82×
Geometric concentration factor	26×
Absorber tube length	4.06 m
Glass tube diameter	120 mm
Number of panels per section	4
Mirror panel size	1.64 × 1.7 m^2
Mirror thickness	3.8 mm
Solar weighted reflectance of mirror	>94%
Curvature accuracy of collector module	<3 mrad
Specific weight without foundations	<30 kg/m^2
Operational wind speed	<15 m/s
Max wind speed (survival position), typical	38 m/s

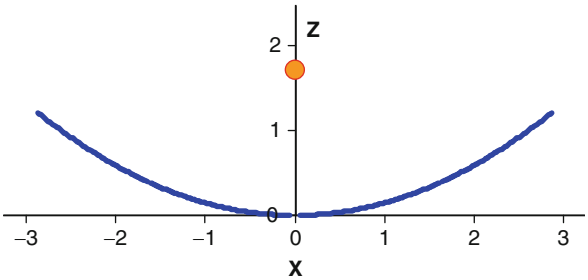

Parabolic Trough Solar Technology. Figure 1
PTC section – dimensions of EuroTrough, LS-3, and other designs, in meters

Technology Description

Main components of a parabolic trough collector module are the curved mirror and the absorber tube. Its support structure holds the components in place and connects the modules between each other.

PTC Mirror

Mirrors are required to directionally reflect the incoming sunlight onto the absorber tube. Relevant properties of the mirrors are thus:

1. High direct (specular) reflectance (evaluated for the solar spectrum, e.g., ASTM G-173 direct+circumsolar). Typical benchmark values are >92% of solar-weighted direct reflectance.
2. Shape fidelity of the parabolic shape. Deviations produce an inaccurate focus and can lead to "spillage." Goal is an intercept factor of >95% over the majority of the annual operating conditions.
3. Shape stiffness under dead load and wind load. Deformations are allowed for high wind speed, as they occur only in a limited number of operating hours of the collector.
4. Durability in terms of surface quality (hard coat, not scratched) and in terms of reflector quality. The preferred reflecting material is silver due to its good optical properties for reflecting the solar spectrum. Aluminum and multilayer coatings are under development. Metallic coatings are sensitive to corrosion and require appropriate long-life protection.

Typical CSP mirrors are made from float glass of 3–4 mm thickness with low iron content to avoid absorption in the glass, with a silvered backside, protected by a multilayer protection coating from the backside (copper, protection paints, and final lacquer). Options from aluminum and polymers typically suffer from lower optical, mechanical, and durability properties.

Absorber (Receiver)

The absorber of a PTC usually is a dark-coated metal tube to absorb the incoming solar radiation. It absorbs the concentrated radiation reflected from the mirror, and also the global radiation hitting from top. The absorber tube optical properties are preferably selective, with absorptance of 95% and more in the solar spectrum range (300–2,500 nm) and low emittance for the infrared radiation (beyond 2 μm) to reduce the thermal losses in operation. This is achieved with sputtered Cermet coatings consisting of several layers of metallic and ceramic coatings. Also, galvanic black-nickel and black-chrome coatings are applied but have less temperature resistance and higher emissivity.

The absorber tube must be protected by a glass tube to reduce convective heat losses and to protect the sensitive absorber surface from soiling and mechanical damage. For temperatures above 250°C, it is useful to have the gap between absorber and glass tube evacuated. This reduces oxidation degradation of the surface and eliminates convective heat losses. However, such design requires sophisticated geometries to compensate the thermal expansion of the absorber tube and keep a long-life vacuum stable. Critical elements are the bellow and joint between glass and metal tubes, to avoid thermal tensions that lead to glass damage. Careful design and extensive tests are required. Additional stabilizer for the vacuum conditions is a so-called getter from reactive metal such as barium. An indicator color change to white identifies vacuum loss.

Most widespread geometry is the receiver, originally developed by Luz Industries, with 70-mm absorber tube diameter and 4,060-mm length at ambient temperature (Table 2).

The length of the receiver tube between supports is limited by the bending of the absorber tube under dead weight of tube and contained fluid (Fig. 2). A bending of about 2–5% of the absorber tube diameter can be accepted. More bending would lead to losses in intercept factor. Resulting distance between supports

Parabolic Trough Solar Technology. Table 2 PTC receiver typical properties (UVAC, PTR70, HEMS, and others)

	Typical	Range
Absorber tube diameter	70 mm	10–110 mm
Absorber tube wall thickness	2 mm (2–6 mm)	2 mm (1–10 mm)
Receiver length (cold/hot)	4.06/4.08 m	2–6 m
Glass tube outer diameter	115–125 mm	
Effective useful absorber length (hot)	96.5%	94–97%
Glass transmittance	96%	>90%
Absorptance	96%	>94%
Overall optical efficiency	88%	80–90%
Heat loss at 350°C	180 W/m	
	0.9 kW/m^2	
Insulation	Vacuum	
Expected lifetime	>25 years	

strongly depends on the area inertia of the tube, in particular, on the tube diameter, and is typically of 3–5 m maximum.

Performance Properties of Receivers for PTC The optical performance of receivers is determined by the properties of the absorber coating and of the surrounding glass tube. Absorptance of the absorber coating is determined by measuring spectral reflectance and calculating the solar spectrum weighted value. Typical range at current state of the art is 95–96%. New coatings are under development to further increase the properties. However, the requirement of low emittance in the infrared range sets limits in the range of overlap between solar spectrum (gains) and thermal radiation (loss) in the range of 1.5–2.5 μm. Very low reflectance is desired at shorter wavelengths (sunlight), and very high reflectance at longer wavelengths (infrared). These properties are, however, difficult to measure on an intact receiver. For measuring the performance characteristics of such receivers, DLR has developed laboratory tests for receivers for the heat loss properties and their optical efficiency [14, 15] and applies them in

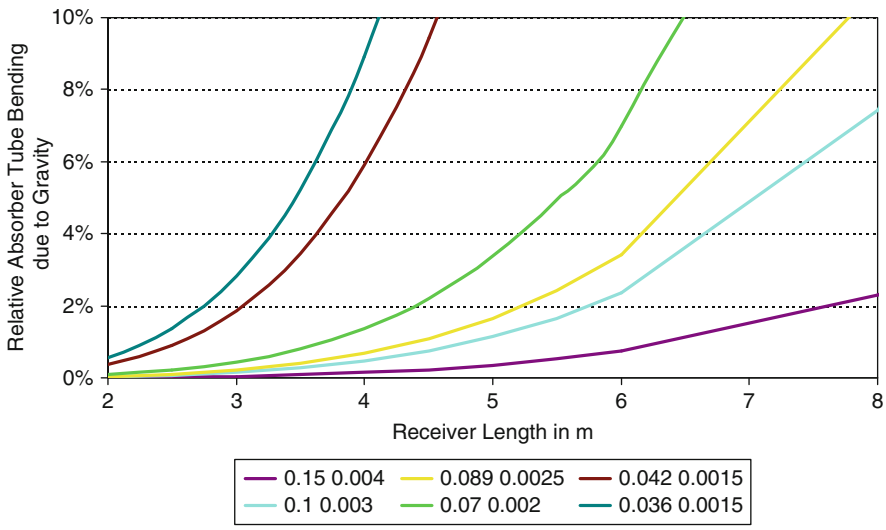

Parabolic Trough Solar Technology. Figure 2
Absorber tube bending relative to absorber diameter for stainless steel tubes for 40 bars, welded ends, filled with oil, at operating temperature, for receiver geometry layout

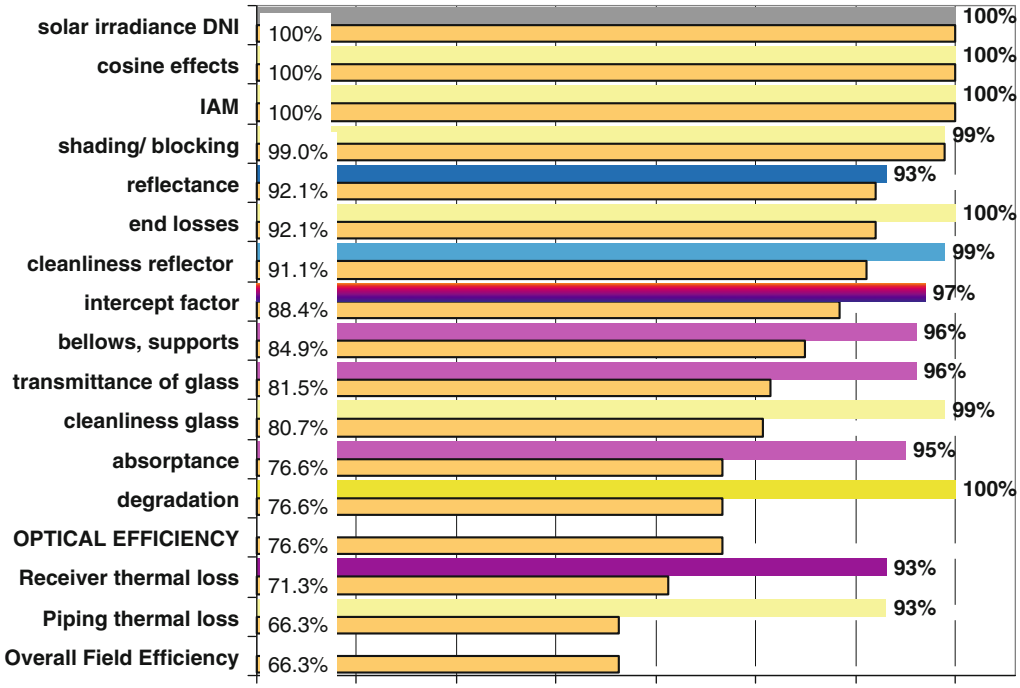

Parabolic Trough Solar Technology. Figure 3
Efficiency diagram for high performance trough collector field

Parabolic Trough Solar Technology. Figure 4
Parabolic trough collector (EuroTrough) solar field installation

Parabolic Trough Solar Technology. Figure 5
Parabolic trough collector (EuroTrough) solar field installation

Parabolic Trough Solar Technology. Figure 6
Andasol-1 solar power plant in Granada (Spain)

its QUARZ Center, with other test labs preparing similar tests and test standards.

Optical efficiency is the product of area factor × transmittance × absorptance. It may depend on incidence angle and absorber temperature. Heat loss depends on absorber temperature and is tested for constant homogeneous absorber temperature. The test result is a heat loss curve over absorber temperature and specific values in W/m or kW/m^2 for standard temperatures of 350°C, 400°C, etc.

Parabolic Trough Solar Technology. Figure 7
Parabolic trough solar field, La Florida (Extremadura), Spain

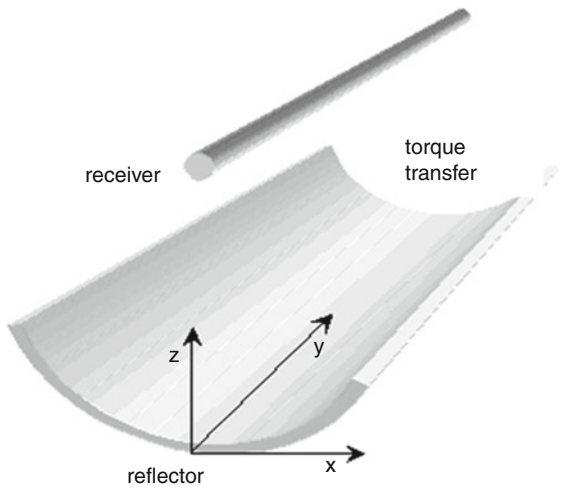

Parabolic Trough Solar Technology. Figure 8
Main elements of parabolic trough collector

Support Structure

The PTC support structure carries the key components of the collector module and is responsible for their accurate alignment in any operating conditions and over an operation period of several decades. Main criteria beside geometric accuracy and cost effectiveness are thus mechanical stiffness and corrosion resistance. The loads affecting the structure include dead load, weight of the components, loads of the receivers, and wind loads (bending and torque).

The structure needs to be designed in a modular way to ease the assembly of the collectors and proper alignment in the solar field.

Tracking3 and Drive Mechanism

The concentrating properties of the collector require tracking of the PTC to the apparent movement of the sun over the sky. The PTC as on-axis concentrator

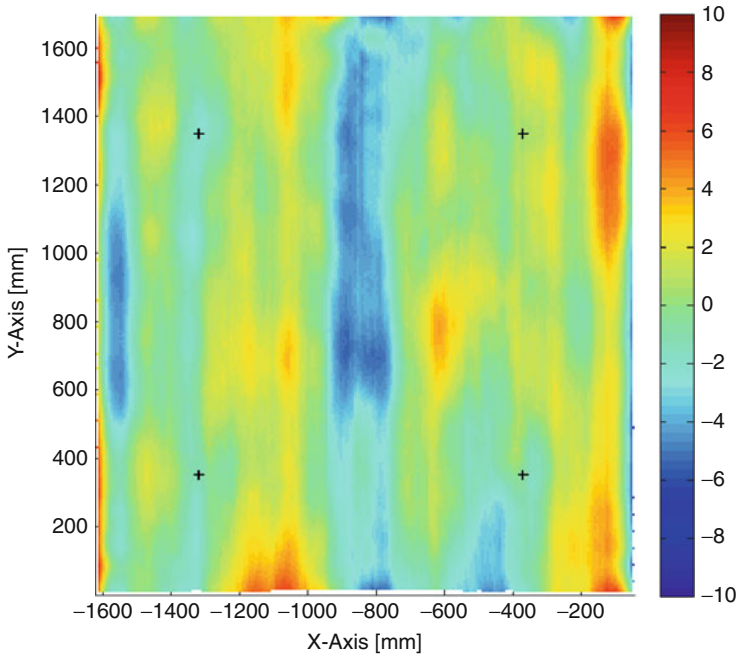

Parabolic Trough Solar Technology. Figure 9
Mirror shape measurement result from QDec system, slope deviation SDx in mrad

Parabolic Trough Solar Technology. Figure 10
Parabolic trough test platform at Plataforma Solar de Almería, Spain

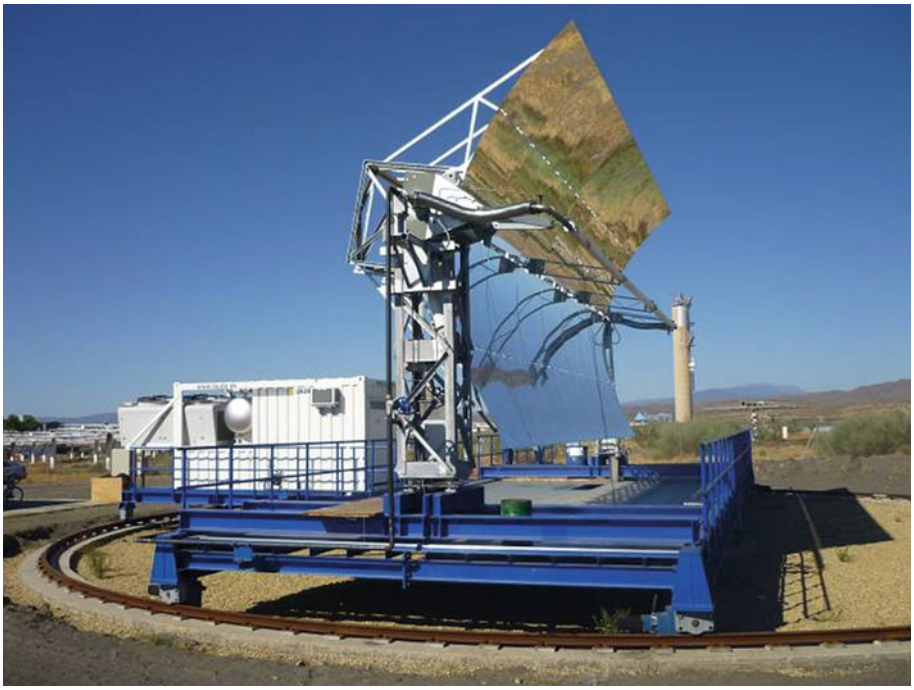

Parabolic Trough Solar Technology. Figure 11
Parabolic trough test platform at PSA, Almería, Spain

Parabolic Trough Solar Technology. Figure 12
EuroTrough support structure

Parabolic Trough Solar Technology. Figure 13
Solar field layout configuration, as seen from space (SEGS XIII and SEGS IX, California, Source: GoogleEarth)

geometry requires that the sun is on the plane spanned by the optical axis and absorber axis. The angle between normal on the aperture area of the tracked collector and the sun beam is called incident angle. Good accuracy of the tracking is required to obtain high intercept factor. The required accuracy is about 1 mrad (0.02°). The tracking controller is usually connected to a central control system linking the field control and the power block control.

The most widely used drive mechanism for PTC is based on hydraulic systems. They provide high force, slow speed, no backlash, and long-term reliability under outdoor conditions in a solar field.

The angular encoder accuracy must be below 0.05°. Also, differential solar sensors are used to enhance the accuracy of the tracking for reaching the tracking accuracy.

Foundation and Pylons

Foundations, usually concrete blocks or piles, are fixing the collectors in the ground. The concrete base carries the pylons with the bearings on which the collector turns with the tracking movement. Preferred orientation of the collectors is with the horizontal rotation axis in north–south direction. Although it is common to level the field, it is not required to have a leveled collector axis. Slopes of up to 3% toward north or south have been demonstrated with the EuroTrough collector and other similar variants. Loads to be taken into account are dead load and wind load. The foundation and pylons need to be designed for local wind load standards. Typical assumptions for wind load are for the range of 34–41 m/s as maximum design wind speed. The maximum load case should be assumed for a 30-year or 50-year wind gust, according to the local codes that are also used in other construction works in the region. Wind-tunnel testing is recommended to get additional information for optimization of the design.

The effect of wind on the collector field can be reduced drastically by turning the collectors in stow toward horizon or slightly below, to prevent the wind from passing below the collectors as well as by installing a fence or hedge or other wind protection device around the collector field, in particular, toward the main wind direction.

Heat Transfer Fluid

Proven heat transfer fluids (HTF) for parabolic trough collectors are synthetic oil and water/steam. Typical HTF is a biphenyl/diphenyl oxide fluid with temperature stability up to 400°C. Its use at elevated temperature requires elevated pressure in the solar field and

heat transfer system. Lifetime of the HTF should not be limited, but recovery techniques are usually required to maintain fluid properties constant. The HTF transports the thermal energy from the solar field to the heat-exchanger steam generator systems providing the superheated steam for the turbine of typically 370–380°C. The flow rates through the receivers must be high enough to ensure appropriate heat removal from the absorber walls and low enough to keep pumping power for the fluid reasonably low. The loop length of a PTC field depends on heat transfer fluid properties and preheater outlet temperatures.

Lower temperatures up to 320°C allow the use of mineral oils with lower vapor pressure.

Water as heat transport fluid in the receivers can be used to produce steam at temperatures above 400°C. Extended pilot scale testing at Plataforma Solar de Almeria has shown the feasibility of the evaporation and superheating of steam in PTC loops successfully. First commercial installations are also using water and steam for the heat transport from the PTC field. They demonstrate that the control aspects of the direct solar steam generation are solvable at large scale, resulting in cost savings and better environmental evaluation of the technology.

Future Directions

New developments, size, materials, fluids, field design, and standards.

Bibliography

1. http://www.solarpaces.org/Tasks/Task3/reflectance_guideline.htm
2. www.helioscsp.com and www.protermosolar.com
3. www.dlr.de/sf and www.dlr.de/energie (news, downloads, . . .)
4. www.dlr.de/tt (Trans-CSP and Med-CSP reports)
5. www.estelasolar.eu (European association)
6. www.solarpaces.org (International Energy Agency, CSP implementing agr)
7. www.nrel.gov/csp/troughnet (excellent technical info base)
8. www.psa.es (Plataforma Solar de Almería)
9. www.desertec.org (news, link to 10'000 Solar Gigawatts)
10. ec.europa.eu/research/energy/nn/nn_rt/nn_rt_cs/article_1114_en.htm
11. www.powerfromthesun.net (B. Stine, Solar Technology)
12. www.stadtwerke-juelich.de (1.5 MW solar tower in Germany)
13. www.solarmillennium.de (developer, technical info, news)
14. Lüpfert E, Riffelmann K-J, Price H, Moss T (2006) Experimental analysis of overall thermal properties of parabolic trough receivers. SolarPaces Sevilla (Poster, A2-P4 Parabolic-Trough Collector Technology (2), ISBN 84-7834-519-1, and J Sol Energy Eng 130, 2008
15. Pernpeintner J, Schiricke B, Lüpfert E, Lichtenthäler N, Macke A, Wiesemeyer K (2009) Combined measurement of thermal and optical properties of receivers for parabolic trough collectors: In: Solarpaces conference, Berlin

Passive House (Passivhaus)

Katrin Klingenberg
Passive House Institute US, Urbana, IL, USA

Article Outline

Glossary
Definition of Subject
Introduction
The Early Developments in North America Inspired Europe
Recent Developments in the USA and Canada
Climate-Changing Opportunity
Principles of Passive House Design
Future Directions of Passive House in the USA, Canada, and Internationally
For More Information

Glossary

Airtight construction A method of construction for building envelopes that is aimed at the lowest possible result close to zero infiltration when tested for air leakage.

Balanced mechanical ventilation with heat recovery Highly energy efficient mechanical equipment for airtight homes to provide equal amounts of fresh air at all times to the inhabitants as well as to exhaust the same amount of air to remove moisture, stale air, and indoor pollutants while recovering the energy at the highest possible level, which is useful to maintain thermal comfort in the building.

Passive house building A building achieving close to thermal stasis by optimizing heat loss and gain through the building shell (primarily by limiting transmission losses through climate-specific insulation levels of its components and appropriate

window specifications) so that thermal comfort in winter and summer can be maintained mostly without energy input and during the peak temperature periods with only very small amounts of energy input of roughly 1 W/sqft.

Superinsulation Adequate, climate-specific amount of insulation to balance heat gains and losses in a cost-effective manner.

Thermal Bridge free A building component, for example, a stud in a wall, is considered to be thermal bridge free when it has a lower conductivity than 0.006 BTU/(ft°F).

Definition of Subject

Performance based energy metrics and Passive Design Standards, history, development, methods and tools, current state of implementation, and future outlook.

Introduction

The Passive House Building Energy Standard is the most ambitious energy standard in the world. Buildings account for 40–50% of the total US carbon emissions – depending on how the sector is defined – stemming from buildings. The Passive House design and construction approach proposes to slash space conditioning energy consumption of buildings by up to an amazing 90–95% and overall energy use of space conditioning and household electricity by 70–80%, depending on which reference baseline home or energy code is used for comparison. Thousands of homes as well as educational and commercial buildings have been built or remodeled to meet the Passive House standard in Europe. Widespread application of Passive House design principles and construction methods in the USA – to both new construction and retrofit scenarios – would dramatically reduce the country's energy use and reduce carbon and other harmful admissions. And, structures built to the Passive House Building Energy Standard have a high quality, long lasting envelope, and in practice provide superior comfort and indoor air quality.

The Passive House Building Energy Standard actually evolved from the superinsulated buildings of the 1970s, many of which were built and pioneered in North America. The Small Homes Council of the University of Illinois (now known as the Building Research Council), developed the Low-Cal house in the late 1970s, and Wayne Schick, a member of the architectural faculty then, is credited with coining the term "superinsulation." A second group of early designs incorporated passive solar heating strategies instead of superinsulation primarily.

The Canadian National Research Council and Minnesota's Housing Finance Agency were instrumental in supporting the construction of very low-energy prototypes and in launching of low energy programs like R2000. The history and list of early adopters and realized projects in Canada as well as in the USA is extensive as also the accompanying research, and would warrant a book in itself. By the end of 1986, an estimated 10,000 very low-energy homes had been built in North America. Many of these early prototypes are still around today and provide excellent long-term experience with this construction type. They are, to this day, comfortable, energy-efficient homes with very good indoor air quality (IAQ) and long-lasting, high-quality envelopes.

However, it was in Europe – in the early 1990s – that pioneering concepts like superinsulation and passive solar approaches were further refined into a comprehensive approach called Passivhaus in Germany. It was a quantum leap triggered by the passage of an ambitious, rigorous energy standard in 1988 for new buildings in Sweden. Other European countries later followed suit in tightening their energy codes significantly. In response to the new Swedish standard, Swedish professor Bo Adamson and German physicist Wolfgang Feist envisioned a building that could meet and even exceed this standard – the Passive House. Construction on the first prototype, a four-unit row house structure, started in 1989 in Darmstadt, Germany. It was completed in 1991. Then as now, the primary components of a Passive House were thick insulation, few or no thermal bridges, an airtight envelope, excellent insulated glazing, and balanced heat recovery ventilation.

The Early Developments in North America Inspired Europe

The term "Passive House" seems to have originated in Canada and the USA. In the 1970s and 1980s, the term "Passive Housing" was a well-known scientific term

describing a combined approach of superinsulation and measured passive solar strategies minimizing space conditioning to extremely low loads. The term was translated into *Passivhaus* in German and was kept as the design principles were optimized by Feist and Adamson. They understood the term to be appropriate to describe a holistic design strategy. Tailored to the moderately cold, heating-dominated Central European climate, it aimed at requiring so little energy to heat to comfortable conditions that a conventional heating system could be eliminated. Instead, a single 1,000-W post-heating element in a balanced supply ventilation stream provided all the heating requirements for a home of approximately1,000 ft or 100 m. The annual total heating demand could be minimized by making careful use of existing internal heat sources – people, lights, and appliances; and optimized (not maximized) solar energy admitted by the windows. A fresh-air heating supply would be pre-warmed by highly efficient heat recovery from the exhaust air, and also in the earlier Passive House projects in Europe by an earth tube, which is a passive geothermal heating-and-cooling system (also intended to prevent the heat exchange core of the ventilation system from freezing).

Early prototypes were designed so that the maximum heat load in the German winter was to be less than 10 Watt per square meter (W/m^2), or 0.9 watts per square foot (W/ft^2), of floor area. Under these circumstances, the heat load could be comfortably supplied using fresh-air ventilation – eliminating the need for a separate means of heat distribution. On the active solar and renewable side, cost-optimized solar thermal systems for hot water production were specified but there was no necessity or emphasis on any active-solar contribution such as photovoltaic. It was recognized early on that the additional investment cost for Passive House measures to conserve energy were far less and more cost-effective than active photovoltaic systems to reduce energy consumption. Passive House as a conservation baseline has since been recognized in the European Union to be the most cost-effective way to achieve near zero or zero energy buildings. Supported by research grants from the German state of Hessen, Dr. Feist created detailed computerized simulations modeling the energy behaviors of wall and window assemblies and other construction elements. Then he systematically varied these elements to arrive at the best possible construction packages, based on energy efficiency, installation expense, and sustainability.

In 1995, Amory Lovins – himself an American energy pioneer and founder of the Rocky Mountain Institute – visited the optimized Passive House prototype at Darmstadt and was deeply impressed. Lovins had implemented Passive House principles in his own home, and saw in Feist's work more than a concept. He encouraged Feist to use the project as a basis for a practical way to meet energy needs for a broad range of implementation. All that was needed was to redesign some details to reduce construction costs.

In 1996, Dr. Feist founded the Passivhaus Institut (PHI) in Darmstadt. The PHI has flourished under his leadership, designing, testing, calculating, certifying, and analyzing data on buildings constructed to the Passive House standard, and their components. The Passive House Planning Package (PHPP) is the Institut's energy-modeling program. The methodology used in this program is profoundly thorough and balanced for interdependencies, and it has been used to design thousands of projects of all building types across Europe. The measured energy performance of the homes has been shown to closely match the modeled performance predicted. The PHPP modeling tool is the most accurate and simple-to-use design software available today to predict the energy consumption of extremely low load homes. Its granularity has been calibrated to see the smallest design effects on the energy performance of a building. Some of those effects are precise calculation of transmission losses through all components of the thermal envelope, solar gains, shading, thermal bridging effects, the influence of thermal mass, ventilation losses, systems efficiencies, and ventilation system design for minimized fresh air conditioning.

The Passive House Building Energy Standard defines the lowest energy metric and standard worldwide. It requires that a building use no more than 15 kilowatt-hours per square meter (kWh/m^2) per year in heating and cooling energy, which is equivalent to 1.35 kWh/ft^2 or 4.75 thousand British thermal units per square foot ($kBtu/ft^2$) annually. It further requires that the building's total primary energy consumption – that is, source energy used for space

conditioning, hot water, and electricity – not exceed 120 kWh/m^2 (10.8 kWh/ft^2 or 38 kBtu/ft^2) per year.

The energy metric is in reference to the interior treated floor area minus circulation spaces and discounted storage and mechanical spaces. Passive Houses also tend to have thicker exterior envelopes than typical construction, and the energy calculation is more accurate if they are excluded. It is important to note that most modeling tools in the USA use the exterior dimensions of a building to determine the per-square-foot energy metric of a building. This has led to some confusion in comparing the Passive House energy metrics to commonly used energy intensity units in the USA. Typically, if put in relation to the exterior building dimensions – as is customary in US energy modeling, the Passive House metric is approximately 20–30% lower than the certification requirements mentioned above, depending on size and design of the building. Using exterior building dimensions, the Passive House metric would result in roughly 3.4 kBtu/ft^2 annually for the total space heating and cooling demand and in roughly 28 kBtu/ft^2 annually for the source energy requirement.

Structures built to the Passive House Building Energy Standard – and the techniques and products developed for them – were further popularized in Europe through the European Union-sponsored Cost Efficient Passive Houses as European Standards (CEPHEUS) project, which validated that the Passive House concept worked in five European countries over the winter of 2000–2001. Thousands of Passive Houses have been built across Europe, as interest in the benefits that they provide has skyrocketed. Many provinces and cities there are now mandating that all new construction built with public monies be built to the Passive House Building Energy Standard. The European Union has proposed to adopt the Passive House Building Energy Standard Europe-wide to meet their action plan, which calls for near zero energy buildings by 2020 for all new construction.

Recent Developments in the USA and Canada

In the spring of 2002, German-born architect Katrin Klingenberg traveled from the USA, where she has lived since 1994, to Germany to tour Passive Houses with Manfred Brausem, a leading architect and Passive House pioneer there. An ardent advocate of sustainable architecture, Klingenberg was powerfully affected by what she saw. She returned to the USA and began designing her own Passive House, the Smith House, which broke ground that October in Urbana, Illinois. In 2003, Klingenberg attended the Seventh International Passive House Conference, in Hamburg, where she met Dr. Feist. She returned to finish the Smith House, which became the first Passive House in North America that used the Passive House Planning Package software as a design tool. Monitoring devices installed at the Smith House after its completion confirmed the predictions:

- The house uses only 11 kWh/m^2 (1 kWh/ft^2 or 3.5 kBtu/ft^2) per year in heating energy (in reference to the Passive House interior treated floor area).
- The highest monthly energy use ever for space and water heating, appliances, and lighting – in short, for all purposes – was 599 kWh.
- With an average electrical base load of 265 kWh, the highest monthly energy use for space heating has been 334 kWh.

The construction of the Smith House was successful in more than just one way. It confirmed the applicability and accuracy of the European-developed design tool for this North American location, as well as cost-effectiveness and relative ease of transfer to local construction techniques.

In 2005, Stephan Tanner, a Swiss-born architect started working on the first American school Passive House building, the BioHaus in Bemidji, Minnesota – located in an even more challenging climate. Designed as a learning facility for the German-language Concordia Village, the BioHaus succeeded in meeting the Passive House Building Energy Standard and was certified in 2006. In October 2006, Klingenberg and Tanner teamed up to organize the first North American Passive House conference at the BioHaus in Minnesota. Interest was piqued; new projects were started.

Climate-Changing Opportunity

In April 2007, Klingenberg and Passive House builder Mike Kernagis cofounded the Passive House Institute United States (PHIUS) to disseminate information

about, and promote the construction of, Passive Houses and Buildings in North America. They steadily promoted the Passive House standard at symposia, workshops, and conferences from coast to coast. Passive House projects have been built in the full range of North American climates since, from Fairbanks, Alaska to Lafayette Louisiana. Although most Passive House construction to date consists of new buildings, a few retrofit projects have been started as well. By mid-2011, there were a total of 22 certified Passive House projects in the USA, with two in Canada registered. More than 100 others from the USA and Canada have applied for pre-certification and are in progress. More than 500 professionals have taken the certification training to become a Certified Passive House Consultant; the number who have taken and passed the final rigorous exam has surpassed 200.

Passive House design and construction methods and the overall approach to homebuilding best meet today's energy and environmental needs worldwide. The Passive House concept is a timely and powerful solution that is now quickly gaining traction in the USA and Canada. Many Passive House projects in this country are so new that empirical data on their energy performance are limited, but extensive data on the energy performance of Passive Houses in Europe are available, through the CEPHEUS project at www.cepheus.de/eng/index.html. According to Guenter Lang, the former executive director of the IGPassivhaus Austria, a member-based interest group, Austria would reach a projected 25% market penetration of Passive House Buildings for new construction by the end of 2010. In the USA, various Building America teams are involved in monitoring the early Passive House projects and many have completed their first year of data collection. Soon there will be publications available on measured Passive House performances in the USA and Canada.

Early indications from that data suggest strongly that adoption of the Passive House Building Energy Standard will continue to accelerate in North America. The PHIUS, the existing North American Passive House community – active consultants organized as the National Passive House Alliance a membership organization – and future Passive House adopters together face a terrific opportunity and an enormous challenge. For the Passive House Building Energy Standard to become the prevalent energy performance standard, it is critical that:

- Training and continuing education opportunities grow to meet the need.
- Experiences in North America's diverse climate regions are measured and shared with the building community. That experience must drive continual refinement of Passive House design principles, construction techniques, component design, and manufacture to meet the special requirements of each climate zone.
- To maintain integrity in the marketplace, rigorous project and professional certification programs must be maintained and subscribed to.

Principles of Passive House Design

The Passive House concept is a comprehensive approach to cost-effective, high quality, healthy, and sustainable construction. It seeks to achieve two goals: minimizing energy losses and maximizing passive energy gains. A Passive House requires *up to* 95% less energy for space heating and cooling than a conventionally constructed house. To attain such outstanding energy savings, Passive House consultants and builders work together to systematically implement the following seven principles:

- Superinsulation (depending on climate).
- Eliminating thermal bridges.
- Airtight construction.
- Heat or energy recovery ventilation (depending on climate).
- High-performance windows and doors (depending on climate).
- Optimization of passive-solar and internal heat gains (depending on climate).
- Calculating the energy balance.

Superinsulation

The insulation applied to a house works in much the same way as the insulation in a thermos bottle. In both cases, the insulating outer shell or envelope blocks or slows heat transmission and maintains the contents at a relatively constant temperature. Warm contents stay warm, cool contents stay cool, even when the

temperature on the outside hits one extreme or another. In a building constructed to the Passive House standard, the entire envelope of the building – walls, roof, and floor or basement – is well insulated.

How well insulated? That depends, of course, on the climate. To achieve the Passive House standard, a home in Sonoma, California, required only 6 in. of blown-in cellulose insulation to meet the standard, while a home in the far colder climate of Urbana, Illinois, needed 16 in. – almost three times as much. Often, the first feature of a Passive House to catch a visitor's attention is the unusual thickness of the walls. This thickness is needed to accommodate the required level of insulation.

The Comfort Principle Thermal comfort in summer and winter is the focus for determining the required thickness of the insulation based on climate. Human thermal comfort in a building depends on many factors, but most commonly and directly perceived according to air temperature in the space and air movement. If the mean radiant surface temperature of a building's exterior wall components is way below the surface temperature of the interior walls, then there is convection induced. If there are convective currents from warm to cold then the consequence is stratification: different temperatures near the floor of a room compared to the ceiling, or significant differences in first floor temperatures and second floor temperatures. In addition, if exterior walls are cold, then the human body starts to lose heat to the colder exterior surfaces by radiation, which leads to discomfort and feeling cold in winter. In summer, the hot exterior surfaces radiate to the interior.

There is an easy solution to this problem: maintaining the exterior surface temperature uniformly at a level so that convection is nearly eliminated. By determining the set points for the interior room temperature for summer and winter comfort, and looking at the summer and winter design temperatures in any given climate, the R-value can be calculated so that the exterior wall temperature even during the coldest design day in winter or warmest in summer will remain within the acceptable range. In a Passive House, the difference in temperature of exterior and internal wall surfaces should not exceed 4°F to always maintain human thermal comfort.

Insulation Materials Choices Even with this insulation requirement, Passive House designers have a wide range of choices for the materials used to create superinsulated building envelopes for various climates. Wall assemblies can be built using conventional lumber or masonry construction, double-stud construction, structural insulated panels (SIPs), insulated concrete forms (ICFs), truss joist I-beams (TJIs), steel or concrete frame, or straw bale construction.

Similarly, designers can choose from a number of different types of insulation. These include cellulose, high-density blown-in fiberglass, polystyrene, spray foam, and again straw bale. Although spray foams have a high R-value and are easy to apply, many builders prefer not to use them because they are petroleum-based products, have high embodied energy, and because the currently market dominant expansion agents can contribute significantly to global warming. Manufacturers are seeking to develop spray foams that do not have these disadvantages. Vacuum insulated panels (VIPs) are a relatively new, and still pricey, option with an exceptionally high R-value per inch. Using VIPs allows designers and builders to greatly decrease the thickness of the walls in homes where that is a consideration. Still higher-tech insulations are in development such as aero gels.

No matter which type of insulation gets chosen, Passive House builders need to make sure that the product is installed correctly. It is important to assure and measure the proper density on site before insulation is blown in if loose fill insulation such as cellulose or high density fiberglass is being used to prevent any settling. In any case, with or without having measured the installed density during the insulation process, the application and performance of insulation can be directly measured using thermographic imaging. All objects emit infrared (IR) radiation, and the amount of radiation emitted increases with the temperature of the object. Variations in IR radiation, and therefore in temperature, can be observed using a thermographic, or IR, camera – a useful tool for testing buildings during the quality assurance process. Since these cameras can readily detect heat loss, they can usually identify areas where insulation is insufficient, incomplete, damaged, or settled. Technicians who read thermal

images of properly constructed Passive Houses have jokingly called them boring, as they often reveal little substantive heat loss.

Eliminating Thermal Bridges

Heat loss follows the path of least resistance: Heat will pass very quickly through an element that has a higher thermal conductivity than the surrounding material, forming what is known as a thermal bridge. Thermal bridges can significantly increase heat losses, which can create areas in or on the walls that are cooler than their surroundings. In the worst-case scenario, this can cause moisture problems: when warm, moist air condenses on a cooler surface.

Thermal bridges occur at edges, corners, connections, and penetrations. A bridge can be as simple as a single lintel that has a higher thermal conductivity than the surrounding wall or several steel wall ties that pass through an envelope. A cantilevering balcony slab that is not insulated from, and thus thermally isolated from, an interior concrete floor can be a potent thermal bridge. An effective thermal isolation is called a thermal break. Without a thermal break, the balcony will act as a very large cooling fin – in the wintertime!

In a Passive House, there are few or no thermal bridges. When the thermal bridge coefficient, which is an indicator of the extra heat loss caused by a thermal bridge, is less than 0.01 watts per meter per Kelvin (W/mK) or 0.006 British Thermal Units per hour foot and degree Fahrenheit (BTU/h ft °F) , the detail or wall assembly is said to be thermal bridge free. Additional heat loss through this detail is negligible, and interior temperatures are sufficiently stabilized to eliminate moisture problems and to meet the comfort criteria. It is critical for the Passive House designer and builder to plan for reducing or eliminating thermal breaks by limiting penetrations, and by using heat transfer-resistant, thermally broken materials. Here also, thermographic imaging during the quality control visits can be used to determine how effective the efforts to eliminate thermal bridges have been.

Airtight Construction

Airtight construction helps the performance of a building by reducing or eliminating drafts – whether hot or cold – thereby reducing the need for space conditioning to maintain comfort. Airtightness also helps to prevent warm, moist air from penetrating the structure, condensing inside the wall, and causing structural damage.

Airtight construction is achieved by wrapping an intact, continuous layer of airtight materials around the entire building envelope. Special care must be taken to ensure continuity of this layer around windows, doors, penetrations, and all joints between the roof, walls, and floors. Insulation materials are generally not airtight and that includes spray foams. The materials used to create an intact airtight layer include various membranes, tapes, plasters, glues, shields, and gaskets. These materials are durable, adherent, easy to apply, and environmentally sound, which in turn makes it easier for a builder to meet the stringent airtightness requirement of the Passive House standard.

Airtightness of a House: A Measurable Dimension of the Quality of Construction Testing airtightness requires the use of a blower door, which is essentially a large fan used in conjunction with sensitive measuring instruments. The blower door can be used to either depressurize or pressurize a house to a designated pressure. With the fan set to maintain this designated pressure, a technician can assess how much air is infiltrating the building through all its gaps and cracks. Specific leaks can be detected during the test either by hand, by employing tracer smoke, or by looking at thermographic images if there is a temperature difference between inside and outside. It is best to conduct the blower door test at a point in construction when the airtight layer can still be easily accessed, and any leaks can be readily addressed.

Passive Houses are extremely tight. At a standard test pressure of 50 Pa, a building that meets the Passive House standard must allow no more that 0.6 ACH *(Air Changes per Hour)* in order to achieve certification. Projects that have successfully met the Passive House standard have been built from timber, masonry, prefabricated elements, and steel or concrete frame buildings with superinsulated curtain walls.

The tightness standard of 0.6 ACH50 is not an arbitrary measure. As walls get superinsulated and airtightened, they become more prone to moisture damage. The typical vapor profile and drying potential

changes, sometimes significantly. Consequently, 0.6ACH50 has been determined to be the safe limit for superinsulated walls even in very cold climates to avoid moisture damage through infiltration and diffusion.

Airtightness does not mean that one cannot open the windows. Passive House building have fully operable windows, and most are designed to take full advantage of natural ventilation to help maintain comfortable temperatures in the spring, fall, and even the summer, depending on the local climate.

Heat or Energy Recovery Ventilation

Perhaps the most common misperception regarding Passive Houses concerns air flow. "A house needs to breathe," builders might say disapprovingly, when first presented with the idea of building very tight homes. Buildings that meet the Passive House standard do breathe – exceptionally well. However, rather than breathing unknown volumes of air through uncontrolled leaks, Passive Houses breathe controlled volumes of air by mechanical ventilation. Mechanical ventilation continuously circulates measured amounts of fresh air through the house and exhausts known quantities of stale air from the house. This makes for excellent IAQ. The amount of air exchanged is strictly based on the exchange necessary to assure that all pollutants get sufficiently removed. Only the air needed for excellent IAQ is exchanged. The health and comfort of the occupants come first for the Passive House designer, and excellent IAQ is indispensable for occupant health.

A Passive House building is ventilated using a balanced mechanical ventilation system. Needless to say, this ventilation system must be extremely energy efficient. To that end, Passive House designers specify energy recovery ventilators (ERVs) or heat recovery ventilators (HRVs) in cold, dry, and marine climates. These machines incorporate an air-to-air energy recovery system, which conserves most of the energy in the exhaust air and transfers it to the incoming fresh air. This significantly reduces the energy needed to heat that incoming air.

State-of-the-art ventilation systems have measured and verified heat recovery rates of 7,592%. The energy consumed by the motor of the ventilator is also considered. To avoid a total net loss of input energy versus heat recovery effectiveness, the efficiency of the motor needs to be extremely high. The energy efficiency limit for Passive House ventilation system motors should meet 0.45 watt hours per cubic meter (Wh/m^3) of air or 0.76 watts per cubic foot and minute (W/cfm) of air.

The ventilation system generally exhausts air from the rooms that produce moisture and unwanted odors, such as the kitchen and bathrooms. The flow rate is set to a low level. For a typical single family home, the base airflow rate is approximately 90–120 cfm total. Timed overrides are typically installed in the exhaust rooms to allow the user a short period of time to increase the ventilation flow rate if moisture or odor levels are elevated. The exhaust air gets drawn through the ventilator on its way out of the building. There it passes through a heat exchanger that transfers the reusable heat energy to the incoming fresh air. It is important to note that the exhaust air is not mixed with the incoming air; only its heat is transferred. Acceptable contamination of the two air steams is limited to 3% max. While return air is circulated back to the furnace in a forced air system, no air is recirculated with a mechanical ventilation system. All supply air is fresh air.

When operating, the ventilator constantly provides a steady supply of fresh air. At the same time, it removes excess moisture, CO_2, other pollutants like VOCs from furniture, unwanted odors and even radon. The incoming air is filtered and balanced. Filtration is important for indoor hygiene as well as for a long-lasting ventilation system. Passive Houses have a requirement of a minimum filter quality of F7 (Europe) or MERV 11. The air is distributed at the low flow rate through small, unobtrusive, but highly effective, diffusers. The system is generally very quiet and draft-free. Dust circulation is minimized. The PHPP recommends an ACH of 0.3–0.4 times the volume of the building, and a guideline ACH of 30 cubic meters (m^3) per person.

The main difference between an HRV and an ERV is that the HRV conserves heat and cooling energy, while the ERV does both and transfers humidity as well. In summer, an ERV helps keep the humidity outside; in winter, it helps prevent indoor air from becoming too dry. For in-between seasons, when no conditioning is needed, a bypass can be installed for either system to

avoid heating the incoming air. Alternatively, the ventilation system can be turned off altogether, and windows can be thrown open to bring in fresh air.

Either system's efficiency can be increased by pre-warming or pre-cooling the incoming air. This is done by passing the incoming air through earth tubes. Since the ground maintains a more consistent temperature throughout the year than the outdoors, passing the air through tubes buried in the earth either pre-heats or pre-cools the air, depending on the season. Pre-heating and pre-cooling can also be accomplished indirectly, by circulating water in an underground pipe and using it to heat or cool the air with a water-to-air heat exchanger integrated with the intake air stream between the ventilator and the envelope. This way, potential condensate in humid climates can drain in a controlled location rather than occurring in the earth tube.

High-Performance Windows and Doors

In modeling the energy balance of a building, the designers of Passive House buildings choose windows and doors based largely on their insulating value. At one time it was hard to find doors and windows that had the exceptional insulating properties required by the Passive House comfort and the few that existed were very expensive.

That is no longer the case. There have been extraordinary advances in window quality over the past 30 years, and thermal losses from windows have dropped dramatically even for North American products. Many brands of windows and doors are now being made tighter, reducing losses through infiltration and exfiltration. Doors have been provided with appropriate thermal breaks and double gaskets. Overall, high-performance windows and doors are proving to be cost-effective in Passive House applications.

One development that has significantly affected the heat conductivity of window glazing is the introduction of low-emissivity (low-e) coatings. These are microscopically thin, transparent layers of metal or metallic oxide deposited on the surface of the glass. The coated side of the glass faces into the gap between two panes of a glazed assembly. The gap is filled with low-conductivity argon or krypton gas rather than air, greatly reducing the window's radiant heat transfer. Different low-e coatings have been designed to allow for high, moderate, or low solar gain. This provides a range of options for houses in all climates, from heating dominated to cooling dominated. Today, builders can choose to install triple-pane low-e-coated, argon-filled windows with special low-conductivity spacers and insulated, thermally broken frames. These windows eliminate any perceptible cold radiation or convective cold air flow, even in periods of heavy frost. For the moderate cool climate (climate zone 4) and the central European climate a U-value of 0.85 (W/m^2K) or 0.15 BTU/h ft^2 °F is recommended for the entire installed assembly accounting for frame values, glass values, spacer and installation thermal bridge effects.

Optimization of Passive-Solar and Internal Heat Gain

Not only must designers of Passive House buildings minimize energy loss, they must also carefully manage a home's energy gains. The first step in designing a Passive House is to consider how the orientation of a building – and its various parts – will affect its energy losses and gains. There are many issues to be considered. Where should the glazing be to allow for maximum sunlight when sunlight is wanted, and minimal heat gain when heat gain is unwanted? The more direct natural lighting there is, the less energy will be needed to provide light. Designers can enhance residents' enjoyment of available sunlight by orienting bedrooms and living rooms to the south, and putting utility rooms, closets, and circulating spaces, where sunlight is not needed, to the north.

However, it is not always possible to site a house in this ideal way. There may be buildings, trees, or landforms that cast shadows during short winter days, blocking out much of the low sunlight. Or the designer may need to accommodate the homeowner's demand for a certain view – a view that would not be available in an ideal orientation.

Windows are designed, oriented, and installed to take advantage of the outstanding passive solar energy that can be gained through them. But the goal is not simply to allow for as much solar gain as possible. Some early superinsulated buildings suffered from overheating because not enough consideration was given to the amount of solar gain that the house

would experience. A good design should balance solar gain within the home's overall conditioning needs – and within the glazing budget. Even very efficient windows can lose more heat over a year than they gain, depending on their location, and large windows are expensive. In the northern hemisphere, in climates with cold winters, windows on the north allow for no direct solar heat gain, while those on the south allow for a great deal of it. In summertime, and in primarily cooling climates, it is very important to prevent excess solar heat gain. This can be done by shading the windows. Roof eaves of the proper length can effectively shade south-facing windows when the sun is higher in the summer, and still allow for maximum solar heat gain in the winter, when the sun is lower and the days are colder. Deciduous trees or vines on a trellis can also block out sunlight in the summer and admit it in the winter. In climates that have a significant cooling load, the designer should consider limiting unshaded east- and west-facing windows, and specifying only windows that have low-solar-gain, low-e coatings. During the morning and late afternoon, low-angle sunlight can generate a great deal of heat in such windows. A guiding value for Passive House solar gain optimization in colder climates is the recommendation of a solar heat gain coefficient of approximately 50% or slightly higher, in cooling climates it should be below 30%.

Another, perhaps less obvious, source of heat gain is internal. Given the exceptionally low levels of heat loss in a Passive House, heat from internal sources can make quite a difference. Household appliances, electronic equipment, artificial lighting, candles, people – all can have a significant effect on the heat gain in a Passive House. While designers may not be choosing how many or which appliances will be installed in a house, designers often select lighting sources, and must take into account these heat gains when calculating the overall internal energy gains.

Energy Balancing – Modeling with PHPP (Passive House Planning Package)

There are many elements of Passive House design that need to be integrated with one another. They include wall thickness, R- or U-values, thermal bridges, airtightness, ventilation sizing, windows, solar orientation, climate, and energy gains, and losses. Modeling software for Passive Houses needs to facilitate accurate energy use prediction helping a designer to integrate each of these components into the design so that the final design will meet Passive House requirements and the projected performance. One starts with considering the whole building as one zone for the energy calculation. The designer considers all of the house's basic characteristics, including orientation, size, window location, insulation levels, and so on. One then computes the energy balance of the design and calculates the equivalent "miles per gallon" energy consumption for the house. If needed, the designer can change a house's components – window location or size for example – and model the impact of those changes on the overall energy balance.

Out of all energy balancing models out there, the PHPP, Passive House Planning Package, developed by the Passivhaus Institut in Germany, is a very responsive what-if tool, allowing designers to readily shift the variables of design to reach these goals. It also effectively models such things as solar water heating for combined space heating and domestic hot water, natural ventilation such as night cooling, and the efficiency of heat/energy recovery ventilation. The PHPP incorporates an impressive depth and level of detail when considering the variables that create a building's unique energy balance. Other modeling tools on the market are starting to incorporate similar strategies increasing their calculation granularity to calculate the energy balance of extremely low energy buildings accurately and could be used to calculate Passive Houses as well.

A Word on Cooling and Dehumidification The Passive House Building Energy Standard was developed primarily in Central Europe, which has a relatively mild, primarily heating-oriented climate. Implementation of designs that meet the Passive House standard is more challenging in climates of more extreme cold, heat, or humidity. Already, many Passive Houses have been built in extremely cold climates, a few Passive Houses have been completed in hotter climates and more are being submitted for certification review.

In cooling load (as in heating load) situations, the space conditioning load must be minimized. This takes careful planning. As explained earlier, the high levels of insulation in a Passive House help to keep indoor

temperatures cool. In addition to the standard measures for preventing excess solar gain, convective venting behind siding and roofing and night cooling will often help to maintain indoor comfort. In humid climates, an additional cooling load may stem from the need to remove latent moisture from the air. A very small and efficient air-to-air heat pump – also known as a mini-split – can remove this moisture and provide adequate cooling. In extremely humid climates, such as in Louisiana, additional dehumidification might be necessary.

Economic Sustainability Passive House design focuses on balancing energy gains and losses in order to attain a level of energy efficiency that is far beyond the norm. But the norm is changing, and many people now recognize that energy efficiency is profoundly important, both economically and environmentally. It has been called a low-hanging fruit, an innovation that can, and should, be readily attained.

This focus on energy efficiency makes Passive Houses more expensive to build. Construction costs generally run 10–15% higher for single family homes than the costs for conventional houses. The additional upfront costs for more insulation, better windows and doors, and more labor for higher quality installations are partially offset by the lower cost of the heating and cooling systems. Because Passive Houses have such small heating and cooling requirements, conventional heating and cooling systems can be replaced with miniaturized components and efficient mechanical ventilation. This is one example of how the integrated planning required to build a Passive House helps builders to "tunnel through the cost barrier," in the words of Amory Lovins. The additional construction cost is readily recovered in savings on the homeowner's energy bill. These savings will continue throughout the life of the house. And – perhaps most important in the long run – the Passive House will generate a carbon footprint that is a fraction of the size of that of a conventional house. On-site renewable energy resources can be added to create a true zero-energy, or even plus-energy, house – one that produces more power than it consumes.

In the past, most homes were built with scant attention paid to their long-term energy consumption. This approach needs to change. It is important to use our limited natural resources wisely and to build our homes with quality and durability in mind. The costs of energy consumption are high, and they are going higher. The savings to be realized over the life of a Passive House are remarkable, both economically and environmentally.

Future Directions of Passive House in the USA, Canada, and Internationally

The Passive House Institute US was the first outpost in North America that made it its mission as a nonprofit organization in 2007 to increase the number of ultra energy efficient buildings in the USA by promoting the adoption rate of the Passive House Building Energy Standard. The organization has worked diligently with limited capacities to provide services such as Certification, Design, Training, Education, and Research nationwide. The National Passive House Alliance, a nationwide membership organization focuses on educating its members and the general public on the topic, improving the recognition of Passive House construction and principles in various legislative programs, and providing continuing education opportunities to its members. Since 2008, the number of Certified Passive House Consultants in the USA and Canada has been exponentially growing. The demand is expected to increase significantly over the next years. Passive House buildings in the certification process in the USA are now representing commercial and residential buildings in almost all NA climate zones. This number also continues to grow rapidly. Now, also other organizations and the government have become interested, such as the USGBC as well as federal and state legislators, to include Passive House as a Low/Net Zero Energy alternative into their programs.

The success and fast uptake over the past 4 years of a performance-based energy metric clearly defining the level of conservation that should be reached was surprising. It has made it clear that there is the need in the market to increase capacity to train professionals as well as students in the field of Passive House design and construction. This not only helps Passive House to meet environmental needs but it is also a way to reclaim many jobs in the construction industry that were lost in the housing melt down.

While the initial success in North America is hopeful it is also a reason to be cautious. There is an

increased need for the output of quality publications and design guidelines documenting especially the experiences of Passive House designs in North American climates to date and to increase monitoring programs of larger developments in various climates that will serve as proof of concept. In conclusion, it can be said that the Passivhaus standard, as it is known today in central Europe, was developed in a relatively easy and homogenous climate, a climate most closely resembling the climate in the North West of the USA. The recent Passive House iterations of the USA and Canadian projects have shown that still a lot of research and transfer is needed to assure an equally successful and widespread dissemination of the concept, especially in the very cold and humid, mixed humid, and hot humid climates of the USA where the energy savings potentials from conservation are extremely high. It is to be expected that there will be variations on the theme from the central Europe so successful core Passive House metric developed in Germany. Here, in North America, the movement is just beginning its way to Main Street.

Internationally, the implementation of the principles in different countries poses new challenges altogether. Existing building culture, exiting building components in the market, and cultural acceptance of the Passive Design standards will play a big role in how far the concept can continue to grow internationally also. Many initial groups have formed from New Zealand to China and Russia disseminating the knowledge similarly to what PHIUS has done in the USA over the past 6 years. The International Energy Agency, headquartered in Paris, France, has invested a lot into research on how to guide and make recommendations to governments with regard to the implementation of highly efficient building codes aiming at envisioning cost-effective zero energy buildings by 2030 as an international goal. The successful strategy will most likely be a coordinated guided code implementation approach coupled with a grass roots effort from organizations and individuals working from the bottom up.

For More Information

The Passive House Institute United States (PHIUS) is a nonprofit certifying, consulting, and research firm working to further the implementation of Passive House Building Energy Standards nationwide. For information about the institute, go to www.passivehouse.us.

Passive Solar Heating in Built Environment

Robert Hastings
AEU Ltd. Architecture, Energy & Enviornment, Wallisellen, Switzerland

Article Outline

Glossary
Definition and Importance of Passive Solar Heating
Introduction
History
Principles, Applications, and Integration
Direct Gain
Indirect Gain
Isolated Gain/Hybrid
Future Directions
Acknowledgments
Bibliography

Glossary

Solar architecture The deliberate use of solar energy by means of the building architecture, thereby reducing purchased energy dependence while enhancing the quality of enclosed space.

Passive Not requiring actions to achieve a desired goal. In the case of passive solar energy use, solar energy is captured and distributed in a building without machinery by using the physics of conduction, free convection, and radiation.

Direct gain The direct gain of heat within a building by sunlight entering through glazed openings in the enclosure, which then traps and stores the heat.

Indirect gain Solar energy absorbed in some fashion on or in walls or roofs and converted to heat. This heat either remains entrapped in the building envelope to reduce building heat losses, or it is transferred into the building by conduction or convection. There may be a delay between the

time when sunlight is absorbed and when heat penetrates into the enclosed volume.

Isolated gain Solar energy absorbed outside the insulated building envelope and then transported by free convection to the enclosed volume.

Solar air system Type of isolated gain system where heat from the collector transported to the point of use or storage by air (verses water in active thermal systems).

Hybrid solar system A passive system assisted by a small fan to increase system efficiency, possibly PV-powered. The energy ratio of heat output to electrical input can easily exceed 20:1.

Definition and Importance of Passive Solar Heating

Passive solar heating is the use of solar energy to heat a building without mechanical or electrical energy. The architecture and construction capture, store, and distribute the sun's energy. Every building with windows exposed to the sun is passively heated, but heat losses may exceed the solar gains. Accordingly, if the passive heat gain is to reduce heating costs, the system heat losses must be minimized. Ideally, the concept includes mass to store daytime solar heat for nights, increasing the usability of the gains. Finally, the heating system must shut off when solar heating achieves the desired room temperature. Two constraints on passive solar use are glare control and shading during non-heating months.

Maximizing usable passive solar gains is an important design aspect, but often designers focus only on minimizing heat losses. Taking the finance world as an analogy, no one will accumulate wealth through savings alone, income must be maximized and wisely invested. So, not only reducing heat loss is essential to low energy architecture, maximizing solar gains is important, as it has been over the history of building.

An often cited early example of solar design awareness is the "Megaron House" described by Socrates in the year 400 B.C. Numerous other examples can be found, i.e., the New England "salt box" of the seventeenth century or Swiss farm houses of the eighteenth century. In the twentieth century, the term "solar house" became popular and following the first oil shock of 1973, the term "passive solar buildings" was coined. In all these examples, the basic principles are the same; maximize the south exposure of a building to capture as much solar heat as possible and insulate the enclosure well to keep the heat in.

Passive solar building design is an important means for slowing climate change by reducing the burning of fossil fuels. It is not, however, a least first-cost way to build. Larger, better insulating windows or opaque collector constructions cost more than conventional constructions. Three arguments justifying this investment are:

- Long-term (>10 years) good return on the investment
- Economy and security as future fossil fuel prices increase and supply subject to interruptions
- Living qualities of passive solar buildings flooded with light and natural warmth (Fig. 1)

Passive Solar Heating in Built Environment. Figure 1 A living room flooded with sunlight from large south-facing windows (photo source: robert.hastings@aeu.ch)

Introduction

Concepts

Buildings that consume less fossil fuel are "nice to have" today, but will be essential in the future. Since buildings are long-term investments, they must be built or rebuilt looking to the future.

Heating is a major use of energy in buildings and dependence on fossil fuels for heating can be dramatically reduced through two strategies: reducing heat loses and increasing the use of solar heat. Logically, a combination of these two strategies is desirable.

Solar energy can be used by passive or active means:

- *Passive solar use* does not rely on mechanical components to capture, store, and distribute the heat, the building construction fulfills these functions.
- *Active solar use* typically involves a remote solar collector and a pump or fan to transfer the heat to storage and from storage to point of use.

A low energy building must lose as little heat as possible, hence the importance given to insulation, air tightness, and heat recovery. An example design standard promoting extreme energy conservation is the "Passive House Standard" [1]. To meet this standard in Europe, three requirements must be fulfilled:

- The annual heating requirement must be less than 15 kWh/(m^2a) or maximum heating power 10 W/m^2a based on the net heated floor area.
- The combined primary energy consumption for heating, hot water and household electricity may not exceed 120 kWh/(m^2a).
- The air leakage of the enclosure tested under a pressured difference of 50 Pa (n_{50}) may not exceed 0.6 house air volumes per hour.

A passive solar building is not defined to this extent; it simply describes a structure in which the designer deliberately maximized using solar energy passively. So, in fact, a passive house can also be a passive solar house and indeed, in the planning recommendation for a passive house, using passive solar energy is encouraged and credited.

Three passive solar heating concepts were defined after the first oil shock of 1973 and are still useful today:

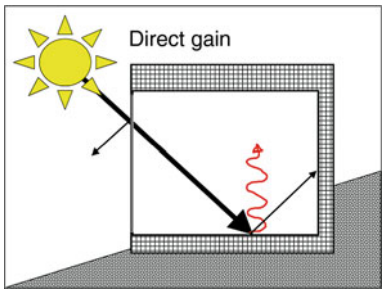

Direct gain: Windows capture the sun in a well-insulated building; interior construction mass stores the potentially excess daytime gains into the night; and some form of shading provides comfort during non-heating seasons. Direct gain is the oldest and still most cost-effective concept, given its potential to also enhancing the quality of life in buildings.

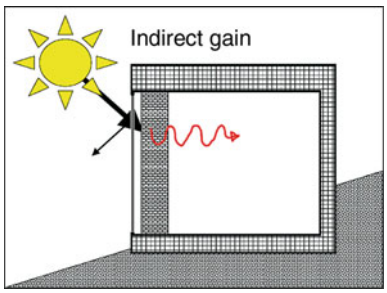

Indirect gain: The building envelope captures solar heat, which is then conducted and/or convected to the building interior, possibly with a time delay of up to 8 h. Alternatively, the goal may be simply to capture enough solar heat in the envelope construction to eliminate heat losses from the building much of the time, i.e., a dynamic *U*-value over the heating season approaching zero. Indirect gain systems nicely compliment direct gain systems.

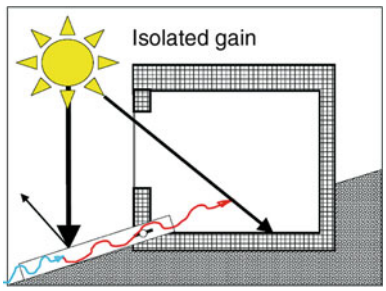

Isolated gain passive: Solar energy is converted to heat outside the insulated building envelope and then

deliverd to the building interior or storage. This can be by gravity-driven convection, or with the help of a small fan (a "hybrid" system). While not purely passive, hybrid systems are reported here because the proportion of delivered heat to electrical energy is so small.

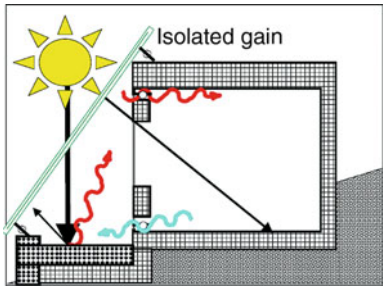

A sunspace or attached greenhouse with controlled opening to the building is also an isolated gain system. Isolated gain systems are the most complex and expensive, but offer the most control of when and how much solar heat is delivered into the building.

It can be useful to consider passive solar heating opportunities by building types and climates. Note, that in this section, locations north of the equator are assumed. South of the equator, north orientations have priority.

Building Types

Buildings where heating loads dominate over cooling loads are the obvious candidates for passive solar design, i.e., residential buildings and small commercial or institutional buildings. Three factors are decisive here:

- As the ratio of enclosing surface to enclosed volume increases, heat loss increases, so a solar heating can be more beneficial.
- As the density of heat production from people or appliances increases, the usefulness of solar heat decreases.
- Direct solar gains in the form of heat and light are a combined asset, i.e., for hospitals, old age homes, and schools as well as residences. (Examples and Design insights for passive solar use in commercial and institutional buildings were researched and documented in an IEA project [2].

The energy optimization of a building must balance passive solar and daylight benefits against mechanical cooling and electric lighting energy demands, both of which have very high primary energy factors.

Climates

Northern climates such as Scandinavia would seem to pose a problem for passive solar use. Winter days are short, the sun is weak, and the sun path is at a very low angle. This means, however, that windows or vertical collection surfaces intercept the sun at a more direct angle. Furthermore, the heating season is very long, extending from early autumn to late spring. Before 21 September or after 21 March, heating is still needed, when days are longer than in southern latitudes. Passive solar concepts must maximize the usefulness of spring and autumn solar heating, while minimizing mid-winter heat losses.

Temperate climates are the ideal situation for passive solar buildings. Not just sunny temperate, but also overcast temperate climates. This has become possible with the development of very high-performance glass (U-value < 1.0 W/m^{2}K). Consider the example of diffuse solar radiation at only 100 W/m^2 for 6 h and an ambient temperature of 5°C. The solar gains through a glass with a g-value of 0.5 (admitting 50% of the solar radiation) will offset the 24 h heat losses of a glass with a U_{glass} of 0.8 W/m^{2}K. If the sun shines with more intensity or more hours, it is a passive solar winner. Because temperate climates often have hot summers, the concept must also include shading.

Mild climates offer a challenge: to achieve zero-heating energy buildings by combining passive solar design and conservation without degrading summer comfort. This is at least as challenging as achieving net-zero-energy buildings. The latter achieve a net zero balance by taking a credit from the summer electrical output of a large PV-roof (multiplied by a high primary energy factor) against the energy deficit in winter, which must somehow be met. Passive solar heating of a highly insulated building can answer part of the "somehow" question.

Strengths and Weaknesses

+	Living quality: daylight and naturally warmth from the sun's warmth.
+	Security: in the event of energy supply interruptions.
+	Costs: only the marginal costs of added aperture area, be it collector or window area and mass, must be amortized by energy savings.
+	Return on investment: As energy prices rise, return on the investment in passive solar measures increasingly attractive.
+	Low maintenance: There are no maintenance costs for pumps or fans.
+	All of these factors can positively affect resale value of the property.
–	Operation: often passive solar use requires active occupants adjusting sun-shading or opening windows or vents.
–	Poorly designed or incorrectly used passive solar buildings may use more energy than conventional buildings. Informed design, strict quality control, and intelligent operation are essential.

Road Map to This Section

A historic review of passive solar design shows how this approach has developed in parallel with technological developments of building components. It is instructive to examine which concepts came into existence, evolved, flourished, or died out. This may save reinventing a broken wheel, or ideas might arise for new variations or concepts.

Principles and applications review different approaches to passively capturing, storing, and using solar energy to heat buildings.

Direct, indirect, and isolated gain concepts are reported in detail.

Finally, the past, present, and future of passive solar heating are discussed in the context of expected energy supply developments, demographics, and increasingly well-insulated and automated buildings.

History

Concepts for passive solar heating date back millennia. Materials and components were very primitive by today's standards, but comfort expectations were also much lower. A net solar gain is possible even with single glazing if the required room temperature is only 16°C. The twentieth century saw dramatic developments in material science and production techniques, e.g., in glass production. The evolution in the last century has been equally spectacular. Single glazing at the beginning of the twentieth century ($U = 5.8$ W/m^{2}K), evolved to fused double glazing in the 1950s ($U = 2.8$ W/m^{2}K). Insulating glazing ($U = 1.2$ W/m^{2}K) in the 1990s is now available in triple glazing ($U = 0.5$ W/m^{2}K), or more than a factor 10 better than window glazing a century ago.

As a result, some concepts, which earlier proved ineffective for a given climate or building type, may indeed be effective today and should be "rediscovered." Following is a short-time journey through the evolution of passive solar heating.

Ancient times

The most often cited example of awareness of passive solar use is a concept house, the "Megaron House" (Fig. 2) described by Socrates (469–397 B.C.). He expressed the following thoughts: "Doesn't the sun shine into houses facing south in winter, whereas in summer the sun wanders over us and the roof so that we have shade? Because this is comfortable, then

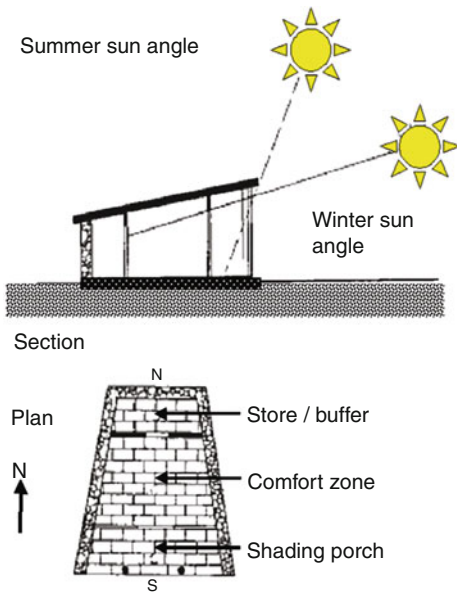

Passive Solar Heating in Built Environment. Figure 2 The Megaron House concept described by Socrates

south-oriented rooms should be built higher in order not to shut out the sun, whereas the north rooms should be lower because of the cold north wind." This was the logic for this funnel-shaped house concept, opening in plan and section to the south. A roofed porch admitted sunlight into the main room in winter but shaded it in summer. A room to the north served as both storage and as a buffer from the north exposure.

1600–1900

New England Salt Box: A classic passive solar house form appeared between 1650 and 1830 in New England, the "Salt Box" (Fig. 3). Its name is derived from the shape of boxes used to store salt at that time. Initially, the house form came about when an addition was made to the rear and the roof slope carried down from the two-story main house. Typically, the addition incorporated a kitchen with its own fireplace, a pantry, and a room for child birth or nursing the ill [3]. The main chimney rose inside the house to keep its heat inside. Also, very practical are the double-hung windows. The sashes were hung on ropes with counterweights of iron or bricks in a cavity of the window frame. The upper sash could be lowered and/or the lower sash raised independently. The height difference between the upper and lower openings induced air circulation.

Swiss Appenzell House: The Swiss Appenzell houses from the eighteenth to early nineteenth century had facades with many window bands protected by a projecting roof at each storey (Fig. 4). This afforded summer shading and weather protection for the windows. The curved white under surfaces captured and deflected additional daylight down to the windows.

1900–1950s

In The year 1927 saw a breakthrough in glass production. Using the Penn vernon Drawing Machine, glass was pulled through rollers in a new process implemented by PPG Industries. For the first time,

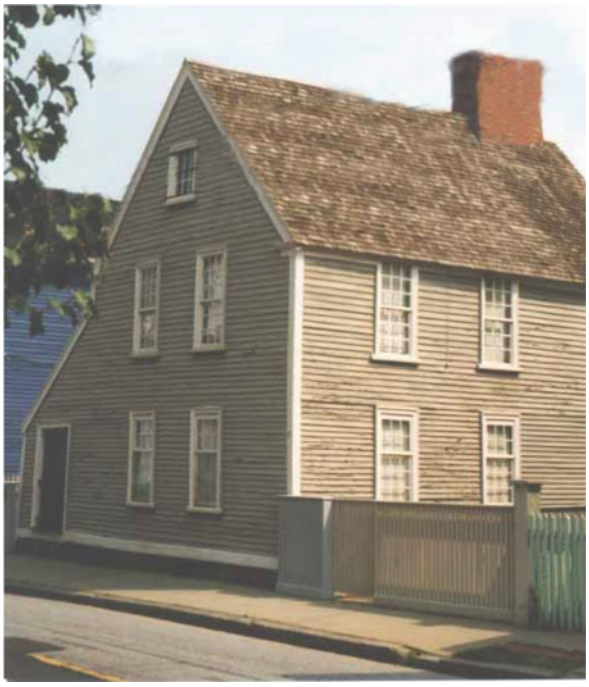

Passive Solar Heating in Built Environment. Figure 3
A New England "salt box" house with large south façade and long protecting roof to the north (photo source: robert.hastings@aeu.ch)

Passive Solar Heating in Built Environment. Figure 4
An Appenzell house with large window area protected by multiple roof projections (photo: robert.hastings@aeu.ch)

large sheets of glass could be produced. This opened exciting new architectural possibilities, but with large heat losses and comfort problems. With the introduction of insulating glass by LOF, it was possible to have large window areas and net solar heat gains. Architects played with the design opportunities this new technology offered. Researchers quantified how long a room could be kept warm by what outside conditions. The press publicized what was then possible with new solar houses. Solar buildings were a mainstream topic. An example of such architecture is the work of the Architect George Fred Keck. Figure 5 shows the living room with a stone floor and fireplace to absorb the sunlight flooding in from the full southwest front of windows [4]. This house, built for Dr. and Mrs. Hugh Duncan of Flossmore, IL, United States, was monitored by two researchers. The performance was surprisingly good. One winter day in 1941, when the ambient temperature was −20°C, the heating system shut off by 08:30 h and stayed off until 20:30 h [5].

1960s

Oil was plentiful and cheap, everyone was happy, renewable energy was not a topic of any popular importance and very little happened.

1970–1980s

In 1973, an oil embargo imposed on the United States led to a crisis of historic proportions. Americans can react astonishingly effectively and quickly to a crisis and this was the case then: "overnight," a national program to reduce foreign oil dependency was initiated. The Energy Research and Development Administration (ERDA) was activated on 19 January 1975 and the Solar Energy Research Institute (SERI) in Golden CO was founded. The department of Housing and Urban Development (HUD) held a national competition with grants for building the solar houses. Many built projects were monitored by national laboratories and published [6], as, for example, the Balcomb house shown in Fig. 6. In 1977, the first National Passive Solar conference was held [7] and in subsequent years, each conference drew over a 1,000 enthusiasts.

Passive solar use was a major topic of the American Solar Energy Society (ASES), a national organization linked with the International Solar Energy Society (ISES). These were the boom years for passive solar buildings. Research and demonstration projects were well funded at the federal and state levels. Atomic physicists "saw the light" and became solar building physicists at renowned national laboratories, including Los Alamos, Lawrence Berkeley, Brookhaven, and the National Bureau of Standards. Exemplary demonstration projects were sponsored by the Tennessee Valley Authority (TVA), an enormous interstate electrical utility. Regional solar energy centers oversaw the evaluation and publicizing of countless solar buildings.

To help energy consultants, researchers, and academics analyze concepts, complex computer models were developed. These could quantify the dynamics of solar and heating input, heat storage, and building heat

Passive Solar Heating in Built Environment. Figure 5 Direct gain maximized in the Duncan House (picture by permission of Pilkington, North America, Inc.)

Passive Solar Heating in Built Environment. Figure 6 The Balcomb house in New Mexico (photo source: robert.hastings@aeu.ch)

losses. Auxiliary heat demand and comfort performance were reported on an hourly basis. These tools were, however, difficult to use. Input was cumbersome and errors easily made. Computers in the 1970s still had to be "spoken to" via punched cards. The input was in rows of numbers, separated by spaces or commas punched into cards. Examples of programs include DEROB, NBSLD and BLAST, and later, DOE2. To provide design consultants (designers couldn't compute) with calculation tools, two approaches were followed:

- Gigantic data bases were computed using research computer models for all thinkable design variations, and then clever nomographs generated. The Passive Solar Handbook by Doug Balcomb and R. Jones is a classic example [8].
- Simplified calculation tools were programmed, such as SERIRES (later called SUNREL) and CALPAS. These were small enough to run on the first versions of portable computers ("mini" or "midi" computers).

The goal was to learn how sensitive performance was to a given parameter. To demonstrate how terrific a design was, it was useful to compare it to a conventional builder house of the time. For this purpose three reference houses were defined, based on statistics from the national home builders association (NHBA). The reference designs were published by the National Bureau of Standards (NBS, today NIST) [9].

To be sure, the computer models were telling the truth, measurement data from components and even whole buildings were essential. Test cabins for monitoring systems became a common sight at many national research facilities. Figure 7 shows a test house with an interchangeable modular south façade and clerestory windows sun lighting the north rooms.

Meanwhile at universities, architecture schools continued to teach Le Corbusier as the model for good design. Energy and solar use were not significant design issues, with the exceptions of a small but growing number of architecture and engineering professors. They were the authors of some superb text books, which clearly presented passive solar design principles. Some examples are a passive solar textbook for architects [10], a guide for adapting solar concepts to regional climates and constructions across the whole continent [11], and guidelines for window design strategies to conserve energy [12].

Passive Solar Heating in Built Environment. Figure 7 NBS (NIST) test house 1980, Gaithersburg, MD (architect and photo source: robert.hastings@aeu.ch)

Passive Solar Heating in Built Environment. Figure 8 The Michel–Trombe wall house in Odello, FR (photo: robert.hastings@aeu.ch)

During this period, there were a few good examples of passive solar innovation in Europe as well. The Michelle–Trombe Wall concept was a notable example (Fig. 8). The original pilot building was constructed at

the Centre National de la Rescherche Scientifique (CNRS) in 1967 in the south of France and further developed with a vented version of the wall in 1974 [13].

1990s

Europeans began to take interest in the American passive solar movement. Many architects and building researchers travelled to the United States to personally visit passive solar houses. Passive houses began to appear across Europe, from Scandinavia to Italy. National research programs investigated how to optimize passive solar concepts to local European climates and constructions. This was essential. Several passive solar buildings did not function as hoped. Europe gets less sun than New Mexico!

During this time, windows were still mostly double glazed or at best triple glazed (U_{glass}=3.0 or 2.2 W/m^{2}K). Glazing with selective coatings and noble gas fillings were just beginning to enter the market. Accordingly, only windows facing south achieved a net passive solar gain. In northern climates, night insulation of windows was needed for the long dark winters. Several innovative, but expensive roll-down insulating blankets were developed for windows. These largely disappeared from the market as high-performance glazings appeared.

By the end of the 1990s, the growing pains of adapting passive solar architecture to European climates and constructions were over and countless exemplary projects had been built and published. An IEA SHC program searched out and documented exemplary projects [14].

2000

During this period, many conventional passive solar-heated houses were built across Europe. Sunspaces were a favored architectural element. Many houses included active solar systems to heat domestic hot water, with Austria leading in the number of such houses. European architects often succeeded in adapting passive solar house designs into good architecture. An example project from 1992 by a Norwegian architect practicing in Austria, Sture Larsen is shown in Fig. 9 [15]. The exterior of the house is in light, wooden framing, the interior is in massive construction. Solar heated air is circulated through the walls and floors to radiate into the rooms. A sunspace also helps heat the house.

Passive Solar Heating in Built Environment. Figure 9 An Austrian passive solar house with solar air radiant heating and a sunspace in Nüziders, Vorarlberg (architect and photo source: Sture Larsen, www.solarsen.com)

By the year 2000, a new concept, The Passivhaus (Passive House) had become well established and on the way to becoming the new mark of excellence in low-energy design. It came out of the PHD work of Wolfgang Feist under his Professor, Bo Adamson in Sweden. To reach this standard requires a highly insulated, thermal bridge-free, and airtight building enclosure. Mechanical ventilation is needed to assure good air quality by such tight construction. Heat from exhaust air is then recovered to preheat incoming air. The ventilation air can be used to deliver the small amount of heating needed (maximum 15 kWh/m^2 heated floor area). Obviously, passive solar heating of such houses is also desired, but challenging to dimension because of the small heating load and short heating season.

2010

Today, in the second decade of the new millennium, the term "passive solar heating" is less common. This is paradoxical because with new window frame and glazing systems, highly insulated building envelopes, and sophisticated heating control systems, passive solar gains can cover all heating needs for an extended part of the year in temperate climates. However, the interaction between passive solar gains, internal gains and envelope heat loss needs to be carefully studied to assure comfort and the hope for energy savings.

The former research computer models to study passive solar building concepts, requiring several hours on a main frame computer, today can run in seconds on a laptop. However, today's tools do not consider many of the phenomena the former models did, such as when mass is directly sunlit or only indirectly warmed by room air, or how passive solar heat in south rooms convects to other rooms. This can strongly affect passive solar usability and comfort.

Principles, Applications, and Integration

Principles

Passive solar heating requires glass, frames, seasonal sun shading, mass, and extra planning effort. The economics are clear: energy won is more expensive than the energy saved by adding insulation or eliminating air leakage up to a certain point. However, as the insulation thickness is increased, the marginal energy and economic benefits of the next increment decrease. Further, when conventional thicknesses are exceeded, the costs of anchoring the insulation and detailing jump. In contrast to this, the cost of a larger window is not proportional to the window area increase. Larger windows loose less heat per unit area. There is less perimeter for the glass area, so edge losses are smaller. Also, there are increased benefits such as more daylight, the view outside and sense of well being from being sun-warmed (especially for cats). The challenging questions are therefore, which passive solar heating concept is most effective for a given building type and climate, and how big should the system be?

Applications by Building Types

Well-Suited Building Types *Residences* are the most common passive solar application. Detached single-family houses with four outside walls, a roof, and earth contact can best benefit from passive solar gains. Row houses and apartment buildings have many units with only two exposures. If they face east and west, passive solar heating is difficult. One idea would be to install an indirect gain system on the south-facing end walls to compliment morning and afternoon direct gains.

Large buildings suitable for passive solar indirect heating include warehouses, gyms (American), or athletic halls (i.e., tennis halls) [2]. Because a lower air temperature is acceptable or even desired, passive solar gains can make a greater contribution to meeting the heating demand. Heat losses of glazed areas decrease proportionately with less inside to outside temperature difference. Lower required space temperatures increase system efficiency and number of hours when useful passive solar heat can be delivered.

Swimming pool halls are a potentially good building type for passive solar heating because a high air temperature is needed, so there is a very long heating season, well into long day spring and fall seasons. Also, there is a great appeal for the space being sunlit. Direct gain, indirect gain for radiant comfort, and isolated solar air systems for humidity control are possibilities.

Limited Cases *School* class rooms have high internal gains and high ventilation requirements. The benefit of passive solar heating occurs primarily during heating season weekends and holidays. At that time, typically there is a temperature set back and temperature swings are tolerated, maximizing the usability of passive solar gains. The obvious choice is direct gain with daylighting within the constraints of glare control, thermal comfort near the windows, and the view out being more interesting than the view to the front. Isolated passive solar heating is another alternative. Figure 10 shows a Swiss school with glazed-in balconies off the classrooms.

Passive Solar Heating in Built Environment. Figure 10 A Swiss school in Gumpenwiese ZH with sunspaces tied into the ventilation concept [16] (photo: robert.hastings@aeu.ch)

Sunspace heated air preheats incoming ventilation air over a heat exchanger for the classrooms [16].

Old-age homes, nursing homes, and hospitals can benefit especially from direct gain with daylighting. Indirect gains systems to supply heat at night or isolated gain systems to preheat ventilation supply air are further possibilities. The occupancy tends to be "24/7" and demand somewhat higher room temperatures, extending the heating season.

Hotels have a transient occupancy. Guest rooms may be vacant with no internal loads for heating, but must be kept at room temperature or, if the thermostat is set back, very quickly warmed up. Accordingly, passive solar gains to maintain a minimal room temperature can be very useful, but mass can slow the heat-up. Daylight and view out may be assets, but overheating is totally unacceptable. Hotels in cities often may have to be isolated from traffic or airport noise. This can be solved with acoustical glazing or by using an indirect or isolated passive solar concept.

Passive Solar Heating in Built Environment. Figure 11 Renovation with solar and conservation, 60 examples of projects across Europe and Canada [17]

New Construction Verses Renovation *New construction* should have very low energy demand as a result of very good insulation, mechanical ventilation with heat recovery. They likely will have a sophisticated heat production, delivery, and control system. Therefore, internal heat from occupancy and appliances will maintain the desired room temperature later in autumn and earlier in spring. The design of passive solar heating must consider this shorter heating season. Storing solar heat is very important because the gains can quickly exceed demand and result in overheating. Ideally, the thermal mass should be sunlit directly. Indirect passive solar systems can contribute to helping shorten the heating season.

Renovation is an excellent opportunity to increase passive solar heating. Older buildings have a greater and longer heating demand than well-done new structures. The subject of renovating existing housing was studied in a 4 year project of the Solar Heating and Cooling Program (SHC) of the International Energy Agency (IEA). As part of this work, 60 exemplary projects and an overview with insights were documented in brochures and are available on the Internet (Fig. 11) [17]. Included are apartment buildings, row houses, and single-family houses as well as the special case of historic buildings. The examples come from 10 countries: AT, BE, CA, CH, DE, DK, I, NL, NO, and SE.

Inappropriate Building Types Since the sun shines during the daytime, all buildings that do not need heat during the day are not good candidates. Large office buildings, shopping centers, airport terminals are examples of inappropriate building types. Such buildings must cope with energy-intensive cooling problems.

Applications by Climate

The best climates for passive solar heating buildings are climates that are sunny (so there is energy available) and cold (so there is heat demand). Buildings located at high elevations often have both sun and long heating seasons, which is ideal for passive solar heating. Not surprisingly, there are many good examples of buildings in alpine regions in Europe or the Rocky Mountains in the United States. The absolute best climate for passive solar heating is the southwest of the United States, which is why the passive solar renaissance after the oil shock began there. A very good tool for generating climate data to analyze systems is Meteonorm [18].

Cold climates in northern regions have short days in mid-winter. This disadvantage is somewhat offset by the heating season beginning before the autumn equinox and extending past the spring equinox. At those times, days are longer than in more southern latitudes. A further help is that, due to the low sun path, windows or wall collectors intercept sunrays more directly.

Temperate climates are well suited for all types of passive solar heating, as is evidenced by the many examples in temperate regions of North America and Europe. In overcast, temperate climates, direct gains systems can profit from even diffuse solar gains, given the highly insulating glass available today.

Mild climates pose the challenge to achieve zero heating energy performance through conservation and passive solar measures. Paradoxically, people in mild and sunny climates have the least interest in passive solar design. This is perhaps due to priority being given to passive cooling.

Dry climates generally have very good solar availability and large day–night temperature swings. Passive solar heating with mass for storage can be very effective.

Humid climates are a problem for both passive solar heating and natural cooling. Humidity reduces solar intensity, day–night ambient temperature swings and blocks night sky radiation for natural cooling. Humid climates are difficult.

Architectural Integration

Direct gain, indirect gain, and isolated gain are simple concepts; the challenge is to translate a diagram into architecture. The aesthetics of solar design is interesting to observe historically.

Before the twentieth century, building glass was expensive. In some cities, windows were even taxed. Because of their value, they were carefully and artistically integrated into a façade design. Baroque facades are a beautiful example of the celebration of windows, in contrast to the austere holes punched in "contemporary" buildings, as can be seen in a street photo taken in Pilsen CR (Fig. 12).

Early twentieth century architects could play with large glass formats for the first time, but the resulting architecture, while making history books, often resulted in buildings that were an energy disaster.

Passive Solar Heating in Built Environment. Figure 12 Classical and "modern" fenestration of facades, two contrasting buildings in Pilsen CR (photo source: robert.hastings@aeu.ch)

After the oil shock of 1973 passive solar design (post oil shock), an epoch of innovation and experimentation, both technically and also aesthetically, began. The aesthetics varied greatly, from "California hippy" and New Mexico oil drum to developer Colonial Style. Inventors developed movable reflectors to concentrate sunlight on passive solar elements and movable shading systems for overheat protection. Also, thermal mass became a design opportunity, with glass blocks filled with colored water, glazing filled with phase change material, and rock bins as standing wall elements. Many components were used before they were technically mature. As a result, some components disappeared as quickly as they had appeared, and a design aesthetic never really matured.

By the end of the twentieth century, only technically and economically viable passive solar heating concepts remained. In Europe, the aesthetics of passive solar architecture profited from the attention given to detailing and superb craftsmanship. Design also suffered, however, from the box form architecture which became a craze and results in sterile, boring cubes. Name architects began to apply such concepts, wanting to profit from the growing environmental awareness. North American architects shifted to green architecture, with an emphasis on use of natural material and renewable

energy in environmentally benign designs. The best examples are corporate offices and local institutional buildings from schools to park headquarters.

In the twenty-first century, the focus is on conservation. Manufacturers have responded to demand from Passive House planners, so there are now very good components on the market. An example is the windows, now available with a combined *U*-value (frame and glazing) of 0.8 W/m^{2}K.

The aesthetic integration of passive solar, active solar, and photovoltaic (PV) systems is still evolving. Too often, the engineering may be excellent but the resulting appearance not, or vice versa. First semester architectural design principles are also valid for solar systems integration. The resulting "design" should please laymen and not just editors of high-end architecture journals. These concerns were discussed in a session of the Passivhaus conference in Krems AT [19].

Following is a presentation of the three passive solar heating concepts and their variations with example built projects, hopefully which appeal also as "designs."

Direct Gain

Principles

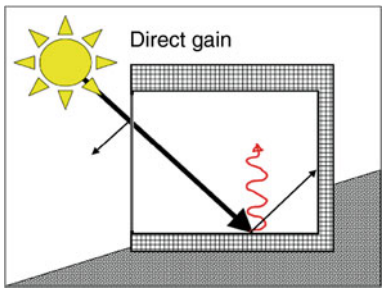

Windows transmit sunlight into the building interior where it is absorbed, and becomes heat. The windows trap the heat in the room and interior construction mass stores some of the heat for the night.

How well the glass transmits solar energy is characterized by its g_{value}. A value of 100% would mean all the solar energy gets through the window, i.e., when the window is open. Otherwise, the glass absorbs some of the radiation and is warmed. The warmth is radiated to the ambient and into the room. Since the ambient in winter is colder than the room, it receives more of that heat. Still, some of the heat absorbed in the glass is radiated into the room. That heat plus solar energy transmitted through the glass comprise the total solar gain. This sum divided by the amount of solar radiation striking the window is the *g*-value. Multiple pane glazing systems with selective coating drastically reduce heat loss, but also let less solar radiation into the room. However, the benefit of the lesser heat loss overweighs the reduced solar transmission.

The usefulness of passive solar gains depends strongly on the match or mismatch of solar intensity, occupancy heat gains, and heating demand over the course of a day. Table 1 summarizes characteristics of different window orientations.

Advantages and disadvantages of direct gain:

+	Simplicity	Window construction is highly developed with a long history of passive solar heating experience.
+	Efficiency	Mid-winter solar usability can approach 100%.
+	Economy	People need daylight; buildings need windows, so only marginal cost for better, larger windows must be amortized by energy savings.
+	Aesthetics	Light and warmth from the sun are assets. Fenestration strongly defines the "personality" of a building, hopefully linked to functionality.
–	Overheating	Risk greater than a windowless, mechanically cooled, and ventilated insulated cube. This risk, however, can be calculated and minimized and such a cube is no alternative for providing living quality.
–	Glare	Sunlight on a work surface, computer screen, or poster from Klimt is highly detrimental. Variable, occupant-adjusted shading is essential.

Components

Glazing: Table 2 compares daylight transmission (*t*-value), solar transmission (*g*-value), and heat loss (*U*-values) for a sample of glazings [20]. Exact values are readily available from glass manufacturers' catalogs. The first three glass types are seldom used today and serve here a reference for comparing modern glass.

Passive Solar Heating in Built Environment. Table 1
Window orientations and characteristics

Orientation	Characteristic
South	Maximum usable winter solar gains. Easiest summer shading
West	Poor solar usability (solar gains follow all day occupancy gains). Overheating risk in summer. Shading more difficult (adjustable vertical elements)
East	Limited solar gains in winter, especially by morning fog. Good solar usability (solar gains after night set-back). Less overheating risk (no direct sunlight after mid-morning)
North	Least solar gains. Greater heat loss (colder microclimate of north side of bld.). Best, daylight orientation, least glare problem Ideal for offices, school class rooms. Good insulation glass required for comfort near windows
Tilted	Construction complicated, expensive. More difficult to keep weather and water-tight. Greater summer overheating risk (except tilted north). Mounting movable shading elements more difficult
Roof	Maximal daylight by overcast skies. Highest overheating risk (max. solar gains in summer). Difficult to shade. Greatest heat losses in winter accentuated by clear night sky radiation, minimal solar gains on flat roofs

Passive Solar Heating in Built Environment. Table 2
Glass properties

Glass type	*t*-Value%	*g*-Value%	*U*-Value W/m^{2}K
Single 3 mm	90	85	5.8
Double	82	75	2.9
Triple	73	65	2.2
Double, low e, Argon	80	60	1.1
Triple, low e, noble gas	76	56	0.6
Double, low e, vacuum	68	50	1.2

Vacuum glazing: In multiple pane glazings, heat is transported by radiation between the panes and convection of the gas in the cavity between the glass panes. To improve performance, coatings are applied to the cavity side of the glass. The coating selectively lets more solar radiation through than heat back out. To reduce the convection heat loss, a noble gas, like Argon or Krypton, can be used. Their higher viscosity slows the convection loop. If there is no gas in the cavity, there can be no convection heat transfer. The only problems are to keep the atmospheric pressure from collapse, the glass panes together, and to maintain the vacuum. Small plastic pillars spaced evenly across the glazing area can keep the panes separated. Maintaining the vacuum is addressed in several patented edge sealing technologies. An important benefit of vacuum glazing is its slimness, with a total thickness of 6.5–11 mm depending on the needed glass strength. The gap for the vacuum is only about 0.25 mm. A vacuum between 4 and 10 Torr is used (a pressure unit equal to 1/760 of an atmosphere). This is a relatively weak vacuum; a thermos bottle has 6–10 Torr [21].

Glazing spacers in multiple-pane glazing are thermal bridges. Earlier insulating glazing used aluminum spacers. Unfortunately, aluminum is a good heat conductor, so edge losses were high. A next generation used stainless steel spacers, with a lower conductivity. Modern insulating glass units use spacers with a plastic thermal break. The improvement is substantial. Aluminum spacers have linear heat loss (Ψ) of 0.07–0.8 W/mK. The Ψ of a thermally separated spacer (i.e., stainless steel separated with plastic) can be as low as 0.04 W/mK. Table 3 illustrates how strongly the linear thermal bridging of the edge spacer affects the overall *U*-value of the glazing, depending on glass area [22].

Assumptions	U_{frame} = 1.6 W/(m^{2}K)
	U_{glass} = 1.1 W/(m^{2}K)
	Ψ = 0.070 W/(mK)

Window frames are the weak thermal component of windows with highly insulating glass. The frame has a worse *U*-value and of course it blocks the sunlight. So, frames with a small profile are desirable. Frames with some form of thermal break to interrupt the heat path

Passive Solar Heating in Built Environment. Table 3 U_{window} value of different windows sizes, including the effect of the edge spacer

w × h (mm × mm)	A_{window} (m^2)	Perimeter (m)	A_{window}/Perimeter	U_w (W/(m^2 K)
400 × 800	0.32	2,400	0.133	1.8
1,300 × 1,300	1.69	5,200	0.023	1.5
1,230 × 1,480	1.82	5,420	0.024	1.4
2,750 × 2,500	6.88	10,500	0.014	1.3

are desirable. Even the *U*-value of a solid wooden window must today be judged as optimal for very low energy buildings, as can be compared in Table 4. Note that, with the exception of the aluminum frames, good *U*-values can be obtained for all materials. Exact *U*-values should be obtained from manufacturers because the values given here can vary relative to specific products. Also, of course, insulation value is only one selection criteria among many, i.e., strength to resist wind forces, life span, and maintenance costs.

Fixed shading by roof overhangs is promoted as a solution for south facades. This must be questioned for climates with overcast winters. By an overcast sky, the most daylight comes from the zenith. Therefore, fixed overhangs block daylight during long gray periods when daylight is most desired. For such climates, moveable shading is superior.

To estimate the adequacy of a south-facing overhang, the highest and lowest noon sun angles (21st June and December) are calculated as follows:

21 June	90° – latitude + 23.45°
21 December	90° – latitude – 23.45°

Taking Zurich (latitude approx. 47°N) as an example, the highest and lowest sun angles are 66.45° and 19.55°, respectively.

While this is a good first estimation for designing a shading geometry, the problem is that the sun has a lower angle before and after solar noon. An overhang should extend horizontally beyond either side of the window to give diagonal shading as the sun rises, falls, and moves laterally before and after noon.

Passive Solar Heating in Built Environment. Table 4 Example window frame constructions and thermal properties

Frame construction	U_f frame (W/m^{2}K)
Solid wood[1]	1.3
Wood-aluminum[1]	1.2
Wood with air cavities[2]	1.1
Plastic[1]	1.1
Aluminum[3]	2.2
Aluminum with break[3]	0.9

[1]EgoKiefer, CH-9450 Altstätten SG, www.swiss-topwindows.ch
[2]Tischlerei Sigg GmbH, AT-6912 Hörbranz, www.passivhausfenster.at
[3]Schüco/Jansen AG, CH-9463 Oberriet, www.jansen.com

East- and west-facing windows need vertical shading since at sunrise and sunset the sun will get under any overhang. Vertical shading elements that can be rotated away from the lateral movement of the sun are best, to allow shading and some view concurrently.

Mass increases the effectiveness of passive solar gains and is especially effective if directly sunlit (primary mass). It is up 150% more effective than secondary mass heated indirectly by the room air [10]. A recommendation for middle European-like climates is to provide 2,800 kg of mass per m^2 of window area [23]. Another recommendation is that for each m^2 of south-facing glass above 7% of the floor area, there should be between 6 and 8 m^2 of exposed thermal mass. An example would be a 200 m^2 house with 20 m^2 of south facing glazing. 6 m^2 of that glazing will require 36–48 m^2 of solar-exposed thermal mass [24].

Passive Solar Heating in Built Environment. Table 5 Heat storage properties of common construction materials [25]

Material	Density ρ (kg/m^3)	Conductivity λ (W/mK)	Thermal capacity *c* (Wh/kgK)	Volumetric heat capacity Wh/m^3
Metamorphic stone	2,800	3.5	0.26	728
Sedimentary stone	2,600	2.3	0.22	572
Clay	1,700	0.9	0.24	408
Sand, gravel	1,800–2,000	0.7	0.22	418
Concrete reinforced	2,400	1.8	0.3	720
Concrete aerated	1,000	0.3–1.0	0.3	300
Interior plaster	1,400	0.7	0.26	364
Gypsum board	900	0.21	0.22	198
Wood (pine, fir)	450–500	0.14	0.55–0.66	287
Wood (oak)	700–800	0.21	0.55–0.66	454
Wood (fiber board)	800	0.17	0.7	560

Also, note for day–night heat storage, thickness greater than approximately 10 cm will not increase the sola usability.

If the primary mass, i.e., a stone floor or brick wall, is a dark color, it will absorb the solar radiation better, but the impact on daylight distribution must be considered. Light-colored sunlit surfaces, especially floors or side walls, are essential to diffuse daylight deeper into a room. Such surfaces should have a mat color to avoid glare.

How well a materials stores heat is indicated by its capacity. Table 5 gives the physical properties of some construction materials to compare their effectiveness as thermal storage [25].

An Example Building: A very impressive example of passive solar heating with windows is a single family house built at 900 m above sea level in Trin, CH. It has no auxiliary heating, not even a wood stove. The architect, Andrea G. Ruedi, matched a very large, south-facing window area (46 m^2), very plentiful mass inside the insulated envelope (Fig. 13). The envelope is wooden frame construction to simplify achieving a high insulation value (0.14 W/m^{2}K); the interior incorporates limestone bricks and concrete (see Table 6). The room temperatures were measured in a research project over the heating season, with no auxiliary heating. They varied between 18 and 23°C. Only very rarely did the temperature fall below 19°C. The theoretical annual heating energy, were 20°C maintained, was calculated to be less than 30 L of heating oil equivalent (1.1 kWh/m^{2}a) [26].

Passive Solar Heating in Built Environment. Figure 13 Extreme example of a direct-gain house in Trin/CH with no auxiliary heating (architect Andrea Ruedi, CH-7000 Chur)

Passive Solar Heating in Built Environment. Table 6
Properties of the solar House in Trin CH

Properties	Trin solar house	A reference house
South window area	48 m^2, (8% frame)	28 m^2, (20% frame)
South-facing window to façade proportion	56%	33%
Interior storage mass	277 t	190 t
Wall construction	Exterior: insulated wooden frame, Interior: limestone masonry	15 cm limestone
		30 cm cellulose insulation

Design Advice

Maximize solar gains

- Orient direct-gain window gains between ±45° from south
- South window to façade ratio: 30–50%, not more
- Large, uninterrupted glass areas (to minimize frame and glass edge losses)
- Window $U_{window} < 1.0$ W/m^2K (including frame) and a good *g*-value (>50%)
- Account for winter sun blockage by neighboring buildings, trees, terrain

Maximize usefulness of passive solar gains

- Interior construction with adequate sunlit (primary) mass
- Room interior finishes light color to maximize light distribution
- Open floor plan. Largest rooms on south-side (small rooms overheat faster)
- Auxiliary heat control responsive to passive solar gains
- Shading elements: horizontal for south, vertical for east/west
- Adjustable shading to allow concurrent view and ventilation
- Exterior sun shading to keep absorbed heat outside
- Generous operable window area with max. height difference to induce natural ventilation (diurnal cooling where possible)

Indirect Gain

Principles

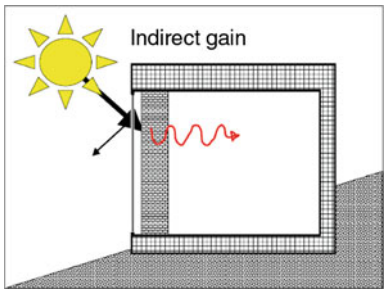

Sun warms building walls and roofs but normally the heat is radiated and convected back to the ambient. By protecting the surface behind glass, heat can be trapped within the construction, stored or transported into the building to reduce auxiliary heating demand.

Several variations of this concept have been built including: the mass wall, mass roofs, transparent insulation, and solar insulation. Of the many innovative concepts, only a few have survived into the present, but with rising energy prices and availability of new high-performance components, these concepts can be promising.

How much passive solar heat gains can reduce purchased heat demand depends on the intensity and timing of the sunlight, occupancy heat gains, and room temperatures desired. Table 7 summarizes characteristics of different window orientations.

Advantages and Disadvantages:

+	Simplicity	The concept is simple, some variations do not have any moving parts.
+	Aesthetics	Most systems include large glass areas, which can be integrated with window areas into an attractive transparent façade concept.
−	Inefficiency	Heat losses from the solar energy captured in the collector are radiated both to the inside and the ambient, reducing system efficiency.

+	Natural cooling	The chimney effect of an indirect gain system can draw cooler air from a ground channel or the north facade through the building for summer comfort.
–	Complexity	Many systems need seasonal shading to avoid summer overheating. Some require dampers to regulate and direct air flows.
–	Cost-benefit	Complex systems proved, in most cases, to be too expensive for the energy benefit.

Following are four variations of indirect gain systems, mass walls, mass roofs, transparent insulation, and solar insulation.

Mass Walls

A stone, concrete, brick, or adobe wall will absorb and store solar heat, but the heat is rapidly radiated and convected back to the ambient with little or no benefit to the heated building space. If the wall is protected behind glass, the heat is better retained. With a time delay, much of the heat can then penetrate and be radiated and convected to the room behind the wall (Fig. 14). This is the principle of the solar wall, patented in 1881 by Edward Morse, an American Botanist. In 1964, a French engineer, Felix Trombe and architect Jacques Michel built such a wall to demonstrate this principle. Since then, the mass wall or Michell–Trombe Wall has become popularly known as the Trombe Wall [27].

The wall has been built in two variations. In the unvented version, the wall delivers heat to the room only by conduction and then radiation from the wall surface, with up to an 8–10 h time delay, depending on how massive the wall is. In the vented version (Fig. 14), the vents open when the air in the cavity is sun-warmed. The air circulates into the room at the top of the wall and returns to the cavity through slots at the bottom. This variation delivers heat sooner so is better for east-facing walls, and would not be good for a west-facing wall. To prevent back circulation of cold air in the gap into the room at night, dampers are needed. One solution was a Mylar film damper, which simply flapped open or was pressed closed against a wire mesh by the air pressure. In summer, dampers could be opened at the top and bottom of the air gap to vent it to the outside. Alternatively, only the top damper could be opened and a north window of the house opened. The chimney effect of the mass wall draws cooler air from the north side of the house, across the room and exhausts it out the top of the mass wall to the ambient.

Passive Solar Heating in Built Environment. Table 7
Indirect gain system orientations and characteristics

Orientation	Characteristic
South	Maximum usable winter solar gains. Fixed overhang possible
West	Less solar gains compared to south-facing facades. Heat delivered to space at time of day when least needed, so storage important. Greatest risk of summer discomfort
East	Limited solar gains compared to south-facing facade. Less overheating risk (no direct sunlight after mid-morning). If storage included, heat delivered at mid-day when least needed
North	Least solar gains, questionable cost-benefit
Roof	Maximal night-sky cooling in summer, least benefit in winter. Steeper roofs intercept winter sun better

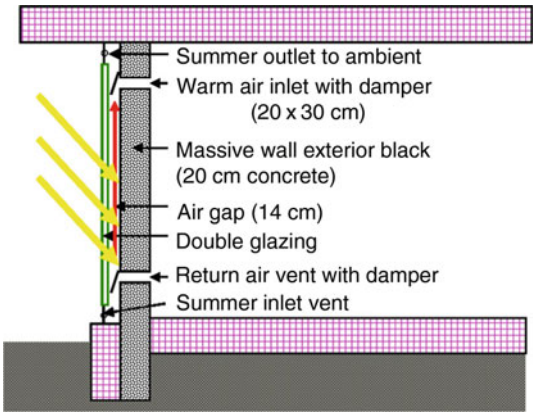

Passive Solar Heating in Built Environment. Figure 14
Concept of the Michel–Trombe mass wall

Passive Solar Heating in Built Environment. Figure 15 The prototype Michel–Trombe wall house in Odeillo, FR (source: Robert.hastings@aeu.ch)

Passive Solar Heating in Built Environment. Figure 16 A mass roof: the Skytherm house in Atascadero California by Harold Hay (photo source: Evelyn and Harold Hay Fund at Cal Poly, San Luis Obispo, USA)

The first project in Odeillo France (Fig. 15) was subsequently copied at Los Alamos, NM, United States, where it was instrumented and a computer model of its physics calibrated. Versions were then built in the 1980s in middle Europe. The performance during long, overcast winter periods was disappointing, while in summer the rooms behind the wall were too warm. Another solution was needed for this climate.

Mass Roof

An innovative alternative to a solar mass wall is a solar mass roof. It can provide both winter heating and summer cooling. One innovative concept uses a series of roof water bags (like a water bed) and moveable insulation panels. During the winter days, the insulation is slid back on its tracks, so that the water is sun-warmed. Nights, the insulation is rolled back over the water bags, which then conduct heat through the steel deck ceiling to be radiated down to the rooms beneath. In summer, the process is reversed. Nights the cover is removed and the water is cooled by radiation to the sky, days the insulation is slid in place and the rooms below are cooled by the cold water bags.

A prototype house was built in 1973 by the inventor of the concept, Harold R. Hay (Fig. 16). The three-bedroom, two-bath structure in Atascadero California was constructed and monitored with funding from the US department of HUD. It was the first documented 100% passive solar heated and cooled building and the only instrumented passive solar house in operation during the 1973 energy crisis. To engineer the system, the then new generation of computer simulation tools was used (simulations for this project done by Phil Niles) [28]. It could be worthwhile to reexamine this concept, given the materials and insulation systems available today.

Transparent Insulation

The transparent insulation wall (TWD) improved the performance of the mass wall concept by addressing one of its weaknesses. In the cavity, the air warmed by the black surface of the solar wall rises, while cooler air against the surface of the glass falls. The resulting circulation loop transports heat from the wall to the glass where it is then lost by conduction to the ambient. In the transparent insulation system, the air gap is filled with some form of transparent cellular structure, inhibiting the convective loop (Fig. 17). The infill material is typically a cylindrical, rectangular, or honeycomb geometry, which directs the light in multiple reflections to the mass wall at the back. A small vertical gap between the TWD and glass should be maintained, to allow moisture to diffuse and prevent the TWD from being in direct contact with the hot absorber surface.

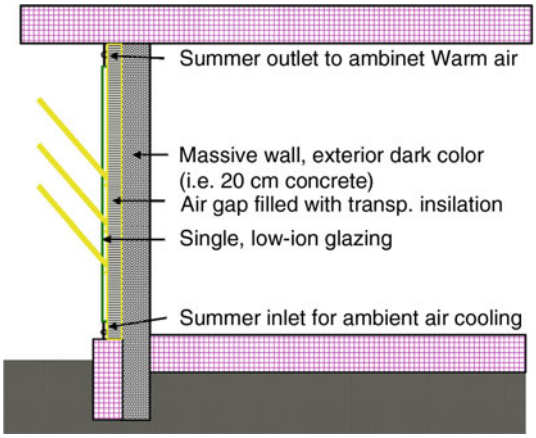

Passive Solar Heating in Built Environment. Figure 17 Transparent insulated wall concept

Passive Solar Heating in Built Environment. Figure 18 Swiss TWD house at Hundwiler Höhe (architect and photo source: P. Dransfeld, www.dransfeld.ch)

In non-heating months, vents to the ambient can be opened at the top and bottom to the ambient to cool the wall. These proved to be difficult to keep air tight in winter and added cost. Some form of shading for the wall was needed. Window roller blinds are effective, but make the whole system prohibitively expensive. An innovative solution was to use fixed, metal micro louvers with the fins set at an angle to block high summer sun angles. They, unfortunately, also reduced winter solar performance and were expensive. A third variation uses fused transparent spheres 2–3 mm in diameter as the glazing, applied like transparent stucco. These let less solar energy through, but with the benefit of much better summer comfort behind the wall. The area of the glazing patches is for physical reasons limited [29].

Several transparent materials and geometries have been used to fill the air gap, including extruded PMMA-Capillaries or Polymethlymethacrylat (Plexiglas), extruded PC Polycarbonate (Makrolon) capillaries or honeycomb forms, and extruded polycarbonate multi-cell panels. Critical for the selection are the upper temperature tolerance and UV-stability. Some materials are stable up to 120°C, other to only 90°C. A good overview of products and properties is available from the association of TWD manufacturers [29].

A well-publicized example of a TWD-building under extreme conditions is a Swiss alpine hostel at Hundwiler Höhe at an elevation of 1′306 m above sea level (Fig. 18). It was built in 1995 and 42 m^2 of prefab TWD-Modules $130 \times 90 \times 18.5$ cm ($h \times w \times d$) were used. No summer solar protection was needed at this altitude. The 185 cm thick TWD wall construction (outside to inside) is as follows: 8 mm framing projection beyond the glass, 4 mm glass, 30 mm gap, 120 mm transparent insulation, 8 mm absorber, 15 mm air gap between the absorber and wall. This air gap was needed to provide the needed tolerance for mounting the prefab TWD modules. The gap was estimated to cause a 10% reduction in efficiency, which was considered acceptable. Simulations indicated that the temperature in the TWD construction should not exceed 80–90°C, well within the 110°C tolerance of the TWD material used [30].

Solar Insulation

The solar wall concept is the simplest of the indirect gain systems and perhaps, therefore, most economical.

The goal of this concept is to provide dynamic wall insulation. During the day, air chambers in the cavity protected by glass are warmed by the sun. Nights, the cavity slowly cools down. The air chambers together with the glazing to the outside and insulation to the inside help reduce heat loss from the building.

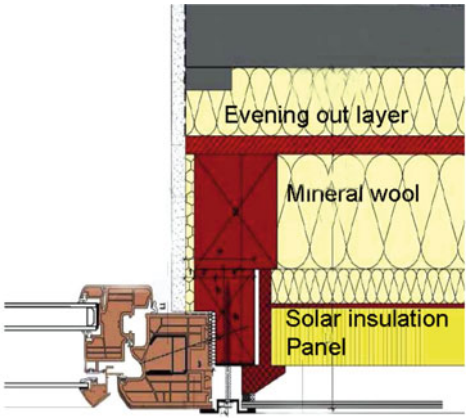

Passive Solar Heating in Built Environment. Figure 19 Wall section of a cellulose solar wall insulation system (Redrawn based on a figure in the report: Domenig-Meisinger et al. [31])

Passive Solar Heating in Built Environment. Figure 20 Apartment building with the GAP solar insulation on Makartstraße, Linz AT (photo source: S. Grünewald and S. Rottensteiner)

Two construction variations exist for creating the insulating air chambers: a type of treated, corrugated cardboard and wood routed with horizontal slits.

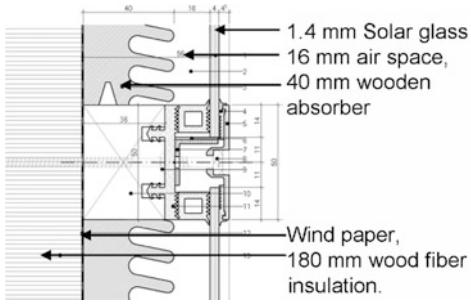

Passive Solar Heating in Built Environment. Figure 21 A solar insulated wall detail of the routed wooden Lucido system (source: Lucido Solar AG Solares Bauen, www.lucido-solar.com)

The cellulose system (GAP), shown in Fig. 19, achieves on south facades a dynamic *U*-value of 0.08 W/mK in middle Europe [31].

A well-publicized example project using this concept is an Austrian Apartment building on Makartstraße, Linz (Fig. 20). To minimize disturbing the tenants, prefabricated wall panels including the solar walls, windows, sun-shading systems, and ventilation channels were mounted. The south facades achieve a dynamic *U*-value of 0.08 W/mK averaged over the heating season. As a result of a combination of this wall system and other measures, the heating demand could be reduced by 92% to 13.4 kWh/m^{2}K [31] and [32].

The routed wooden system (Lucido) entraps air in inward-sloping slots (Fig. 21). Important in this and also the cellulose board system is that the wall behind the solar wall be well insulated. A benefit of the wooden absorber is that, being weather protected, it can be left natural and hence conveys the character of a wooden façade.

Design Advice

Following is design advice for temperate climates. In mild climates, these systems might make it possible to reduce auxiliary heating demand to zero, but summer comfort strategies must be well done. In a humid, hot climate, this system make no sense, nor is performance likely to be good in northern, very cold and weak-sun winter climates. Many

projects were built in temperate climates but a market breakthrough has not yet occurred. The energy they save for the investment is high compared to energy from cheap fossil fuel.

- Because indirect solar gain is less efficient than direct gain, a large collection area is needed. South-facing orientations are most sensible. Depending on the desired timing of heat release, east- or west-facing solar mass walls are possible, but the absolute amount of delivered heat will be smaller.
- Overheating is a risk in mass wall systems, so summer sun shading and venting are important. The solar insulation concept has the comfort advantage of having an insulated wall separating it from the building interior.
- Durability was a problem for early prototypes, including untight vent dampers and degradation of sun-exposed wooden framing. A typical greenhouse construction with a metal cap to protect exterior wood is one solution. Transparent insulation can deform at high temperatures, so the right material must be chosen for the design, or reliable shading provided. Freeze protection UV-durable materials are obvious requirement for the roof-mass system using water.
- The thickness and density of a mass wall and hourly solar radiation should be calculated to dimension a mass wall to deliver its heat to the room when desired.
- System performance might be improved by very good insulating glass. This is a trade-off of *g*-value and *U*-value in the context of the economics. Single glazing in low-iron glass could still be the best solution (maximizing the *g*-value).
- The mass roof system is only plausible in clear-sky climates with both a heating and cooling demand.
- The room side of the mass wall or transparent insulation wall should not be blocked by furniture. For the solar insulation system, this is not an issue. The room surface of all the wall concepts can be any color desired.
- Prefabrication can provide cost savings for a second project, not necessarily the first project. The benefits are shorter on-site erection time, less disturbance of occupants, and better quality control, which can lead to better durability.
- Indirect gain systems are well suited for building renovations.
- These systems have gone through development pains; valuable experience is available from the project designers, research institutes, and the manufacturers of system solutions. Homework to assure a new project starts from the state-of-the-art is essential!

Isolated Gain/Hybrid

Principles

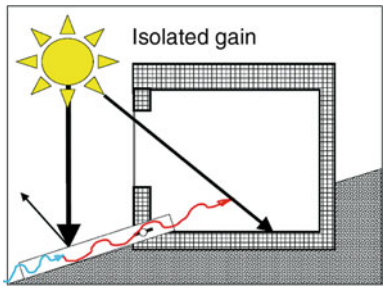

Solar energy is collected outside the insulated envelope of the building, then transported as heat by convection into the building or into storage. Two variations are considered here: solar air systems (with or without mass) and sunspaces.

The orientation of a sunspace, like any room, depends on view and when sunlight is wanted. For solar air systems, design issues are similar to those of indirect gain systems. Buildings uninhabited and kept at a minimum temperature much of the year (i.e., vacation homes) are an ideal application.

Advantages and disadvantages:

+	Simplicity	These systems are simple and reliable.
+	Dependability	The gravity-driven solar air systems work without moving parts. However, a small fan would improve the efficiency and can easily be PV-powered, making the system immune to grid power interruptions.
+	Economy	Reduced purchased energy costs and reduced wear from less running time of the auxiliary heating system, extending its lifetime.

+	Function	Sunspaces are built for the space they provide, energy savings are only a fringe benefit, so in effect a bonus.
+	Overheating	Isolated solar gains systems, because they are outside the insulated building, are advantageous regarding summer comfort. Sunspaces need large, low, and high ventilation openings, and effective shading and glare protection.
+	Natural cooling	The chimney effect of an isolated solar collector or sunspace can draw cooler air from a ground channel or the north facade through the building.

Solar Air Systems

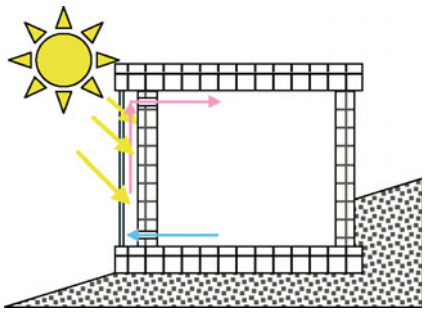

A solar air system is in effect a sunspace with the depth reduced to a few centimeters. The principle is the same as an active solar water system, except that heat is transported from the collector to the point of need or storage by air. Two variations are reviewed here: systems that are directly coupled to the building and systems in which the sun-warmed air passes through mass before entering the building. All together, six system types were researched in a project of the International Energy Agency. Out of this work, a design handbook for solar air systems [33] and a book of example built projects [34] were published. The other four system types typically require an electrical fan, dampers, and more complex control systems to function, so are not included here under passive systems.

No-Mass Solar Air Systems

These systems operate on the principle that sun-warmed air in a vertical or upward sloped volume behind glass will rise. This warm air can then be channeled through the insulated wall of a building to provide solar heating (Fig. 22). Two variations are possible for the air supply at the bottom of the collector:

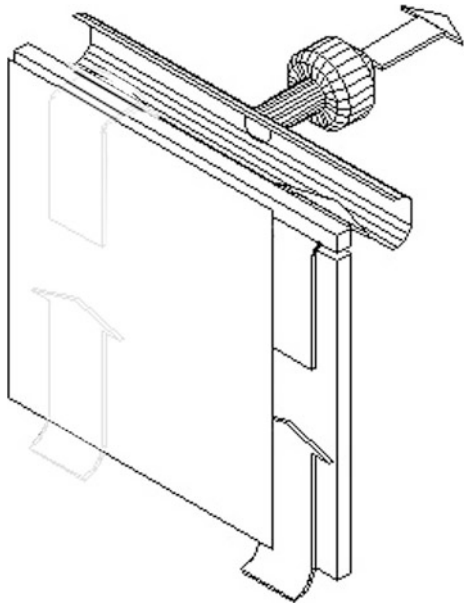

Passive Solar Heating in Built Environment. Figure 22 Diagram of a free convecting façade solar air collector

- If the opening is to the ambient, the collector can deliver sun-warmed fresh air to the building.
- If the opening is to the building, the collector delivers recirculated, higher temperature air than the first variation. In either configuration, in summer an outlet at the top can be opened to the ambient to exhaust the hot air.

Example: Figure 23 shows a solar air system to keep a vacation home in Koroni GR heated to a low level, ventilated and dry during periods of vacancy. Two collectors, each 6 m^2, circulate up to 200 m^3/h of fresh air into the house. A small PV panel (50 wp) integrated into a corner of the air collector powers a small fan to increase the efficiency of the system, which has been in operation since 2004.

Mass Solar Air Systems

This concept is like the no-mass solar air system described above, except that the solar-heated air

Passive Solar Heating in Built Environment. Figure 23
A solar air heater for a vacation home on a Greek island (photo and system information: www.grammer-solar-bau.de)

Passive Solar Heating in Built Environment. Figure 25
Solar apartment buildings in Marostica by Barra Costantini (photo: Gianni Scudo)

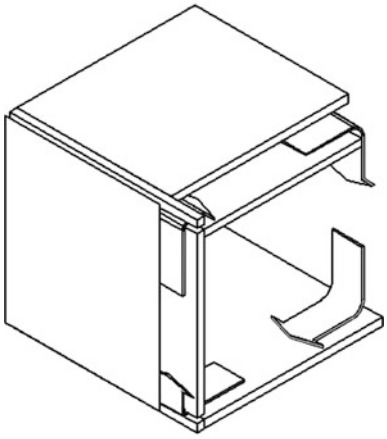

Passive Solar Heating in Built Environment. Figure 24
A solar air collector linked to air channels in the building structure

circulates through the building structural mass before entering the room (Fig. 24). In this way, the air enters the room at not as high a temperature, and the mass continues to radiate the stored heat after sunset. The mass may be a concrete ceiling or floor (hypocaust) or walls (murocaust) with air channels. The system can function with only free convection of air movement [33].

Example: Figure 25 shows an apartment building in Marostica, Italy (20 km from Vicenza) with a façade integrated passive solar air system. The sun-warmed air in the collector rises naturally and circulates though channels in the concrete ceiling/floor structure before entering the apartments in the north-facing rooms. The concept was developed by Barra-Costantini. Each 84 m^2apartment is heated by 16 m^2 of collector. Each m^2 of collector is estimated to contribute about 100 kWh/a [34].

Design Advice

- The collector can be mounted below floor level, i.e., in the case of a building with an above-grade basement. The height difference strengthens the free convection.
- No-mass solar air systems are well suited for buildings often vacant, which need to be tempered and supplied fresh air. In permanently occupied buildings, mass is essential to maximize the usefulness of the collector gains and avoid overheating.
- Dampers are essential to prevent reverse-flow and cooling of room air into the collector at night.
- A small fan can increase system efficiency. Commercial solar air systems with PV-powered fans are available.
- The collector and solar-heated air channeling require good engineering. Consult the literature to not have to reinvent the wheel [33, 34].

Sunspaces

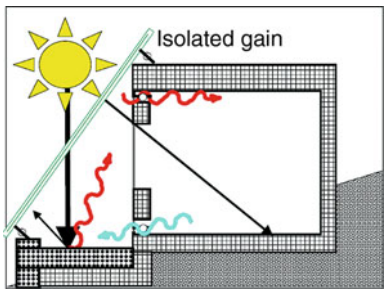

Sunspaces became popular element of passive solar architecture. They were designed as an architectural feature which, in addition, reduced purchased energy consumption in several ways:

- Passively by creating a warm buffer zone on the south side of the house, reducing wall and window heat losses.
- Passively by occupants simply opening house windows and doors into the sunspace when its temperature exceeded the house temperature. Alternatively, a small thermostat could open a damper and switch on a fan to automate this.
- Actively, when sunspace supplied sun-warmed air to a mechanically ventilated building. Alternatively, the sunspace air could be ducted to a heat exchanger to warm incoming ventilation air for the building.

Today, in highly insulated buildings, a sunspace's buffering effect is no longer a significant energy saving. In mechanically ventilated buildings with heat recovery, the benefit of heating the incoming air is also less significant, but still a benefit. Sunspace heated air can exceed room temperature, thus supplying useful heat. A sunspace can increase purchased energy consumption if occupants heat it to near room temperatures. Comfort expectations of a sunspace must be less than for rooms.

Example: The Wydacker row houses in Zollikofen (Bern) CH are earth sheltered to the north and protected behind a sunspace to the south (Fig. 26). This construction provides energy benefits and protection from nearby street noise.

Each house has a 108 m^2 sunspace with a 57 m^2 of insulated glass (U=2.9 W/m^2K) at a 60° slope oriented 20° west of south. Being slightly west of south is beneficial. Frequent morning fog reduces solar radiation mornings compared to afternoons. Sun shading is provided by a roller shade beneath the glazing. The concrete block wall of the house and concrete pavers over gravel provide thermal mass for the sunspace. The measured heating energy consumption of the houses was 37 kWh/m^2a, which for the year 1995 was excellent performance [35].

Passive Solar Heating in Built Environment. Figure 26 Attached sunspaces as part of the concept of low energy row housing in Bern (Architects, AARPLAN; Bern, CH)

Design Advice

- Insulating glazing for both the sunspace (minimize freeze risk for plants) Insulating glazing for the house to minimize heat loss to the sunspace.
- Sunspace frame out of laminated wood to be dimensionally stable and metal exterior cap to reduce weathering. Alternatively, aluminum framing with a thermal break.
- Two or more story sunspaces offer d more collection area for the enclosed volume. Comfort is better because stack effect ventilation improves with stack height).
- Large operable sash at base of the sunspace and at its top, ideally with rain sensor-activated closers. Rule of thumb: Minimum1/6 glass area operable.
- Sun shading on exterior most effective, on interior it is less subject to wind damage and weathering. Interior sunshade installed min. 10 cm below glass

so gap acts as thermal chimney between operable low inlet and high outlet sashes.
- As in direct gain systems, thermal mass helps reduce temperature swings (i.e., minimize hours below freezing.
- A freeze-protecting heater with thermostat activation when the sunspace temperature falls below 4°C can help protect plants. If the sunspace is designed, the purchased energy for this is well worth the plants.

Future Directions

The future directions to using passive solar energy can best be forecast by reviewing technical and political events in the past. In the early twentieth century, when production of glass in large formats became possible, architects began experimenting with large glazed areas. The resulting buildings were uncomfortable to occupy in winter and expensive to heat. First, with the introduction of insulating glass, a net passive solar heat gain in winter became possible. After World War II, oil became plentiful and cheap and interest in solar dwindled. Then, the oil crisis of 1973 renewed interest in finding alternatives to fossil fuels. New solar building concepts evolved under the collective term "passive solar heating." The first of annual "National Passive Solar Conference" was held in 1977 in Sante Fe, NM (United States) A US federal department (HUD) held a landmark national competition for innovative passive and active solar building concepts. Interest and built projects spread from the sunny southwestern United States across the entire continent. By the next decade, passive solar heating concepts were being applied by architects in Europe as well. Passive solar concepts, originating from inventive individuals, became a topic for national research institutions. Test cells and buildings were monitored, computer models developed, and engineering handbooks written.

Today, the term, "passive solar buildings" is less commonly heard. The similar sounding concept "Passive House" now enjoys international attention. The new, future-oriented trend is sustainable buildings [36, 37], net-zero-energy buildings, carbon neutral buildings, and even energy-plus buildings. Well-designed new buildings constructed to such high standards need very little heat, and so passive solar gains are less beneficial than before, but still an asset. Such solar gains help delay when the heating season finally begins and end the heating season earlier. Passive solar gains are also a major heat source when a building is unoccupied during the day or for extended periods. The daylighting aspect of direct solar gain concepts will continue in the future, being a major appealing factor.

Future buildings must address new requirements. There will be

- More elderly people (demographics) with greater comfort expectations.
- High energy prices, regardless whether the source is increasingly scarce fossil fuels, electricity, or renewable energy.
- Less disposable income because salary increases will not match the inflation of energy costs affecting prices of all goods and services.

New technological developments will offer new possibilities for meeting these requirements. Likely developments may include:

- Nanotechnology selective coatings for glazings to allow larger passive solar collection areas in winter and no overheating in summer. Similarly, material science will deliver high-performance coatings for absorber surfaces.
- Vacuum technologies for both window glazing and as very compact insulation for indirect or isolated gain systems.
- Intelligent, self-learning control systems for switchable property components, responding to solar intensity, ambient temperatures, and programmable occupant comfort profiles.
- Chemical thermal storage for heat or "cold" to provide very compact and high density, compact storage with no losses during storage.
- Building skins, which produce both electricity and low-temperature heat amplified by high-efficiency heat pumps for space and water heating.

Finally, in the future as in the past, political developments may result in supply interruptions. In any event, as the world-known reserves diminish, prices will not steadily and gradually increase. Large price swings amplified by speculation can be expected.

These changing occupant requirements, technical developments, and possible political and oil market events will change how new buildings are constructed

and existing buildings renovated. They will more effectively draw energy from the environment, providing heat, light, and "cool" with less external energy input. Buildings and climate will no longer be combatants, but allies working together. The needed investment and maintenance costs will have to be low, simply because there will be less disposable income. Passive solar heating was, is, and will be an important strategy for achieving low-energy buildings offering excellent living quality.

Acknowledgments

The author thanks in particular three institutions in his career, whose support made possible the personal experiences to write this section.

The Swiss Federal Office of Energy, Buildings Program (in particular, Gerhard Schriber).

The International Energy Agency, Solar Heating and Cooling Program and, in particular, all the researchers and architects who, with such dedication, worked together in research tasks over the decades and the founder of the Program, Fred Morse.

The Donau University-Krems, Department of Buildings and Environment (in particular: Peter Holzer, who convinced me to become a professor so people would believe my stories).

Bibliography

1. Feist W (2007) Certification as "Quality Approved Passive House" criteria for residential-use passive houses. www.passiv.de/07_eng/phpp/Criteria_Residential-Use.pdf
2. Hastings R (ed) (1994) Passive solar commercial and institutional buildings – a sourcebook of examples and design insights. Earthscan, London. www.earthscan.co.uk. ISBN 0-471-93943-9
3. Broadhurst T (ed) (2010) Saltbox, 1650–1830. http://www.oldhouseweb.com/forums/viewtopic.php?f=4&t=26402&p=234896&hilit=Saltbox#p234918
4. Simon MJ (1947) Your solar house. Simon and Schuster, New York in cooperation with Libbey-Owens-Ford Glass Co., (Pilkington, North America, Inc.)
5. Butti K, Perlin J (1980) A golden thread: 2500 years of solar architecture and technology. Cheshire Books, Palo Alto. ISBN 0-917352-07-6
6. Franklin Research Center (1979) The first passive solar home awards. US Dept. of Housing and Urban Development, Office of Policy Development and Research, available from US Government Printing Office, Washington, DC
7. ASES (1977) 1st National passive solar conference. American Solar Energy Society, Boulder. www.ases.org
8. Balcomb D, Jones R (1980) Passive solar design handbook: vol 1 – passive solar design concepts. Total Environment Action, Inc.; vol 2 – passive solar design analysis. Los Alamos Scientific Laboratory; vol 3 – passive solar design analysis. Los Alamos National Laboratory. Available from National Technical Information Service, Alexandria
9. Hastings SR (1977) Three proposed typical house designs for energy conservation research, NBSIR 77-1309. National Institute for Standards and Technology (NIST), Gaithersburg
10. Mazria E (1979) The passive solar energy book, Expanded professionalth edn. Rodale Press, Emmaus. ISBN 0-87857-238-4
11. Loftness V (1978) Regional guidelines for building passive energy conserving homes. US Department of Housing and Urban Development, Washington, DC, HUD-PDR-355
12. Hastings R, Crenshaw R (1977) NBS BSS 104 window design strategies. National Technical Information Service, Alexandria
13. Porteous Colin, MacGrego Kerr (2005) Solar architecture in cool climates. Earthscan, Longon. ISBN 10: 1-84407-281-1 and SIBN-13: 978-1-84407-281-1
14. Hestnes AG, Hastings R, Saxhof B (eds) (1997/2003) Solar energy houses – strategies, technologies and examples. Earthscan, London. ISBN 1-902916-43-3
15. Larsen S (2010) Built examples: house Frei, Architekturbüro Larsen, Erlachstrasse 25, AT-6912 Hörbranz. http://www.solarsen.com
16. SIA (1989) Demonstrationsprojekt Schulhaus Gumpenwiesen, Reihe "Planungsunterlagen zu Energie und Gebäude", SIA-Dokumentation; D035. SIA Schweizerischer Ingenieur- und Architekten-Verein, Zürich
17. Hastings R (ed) (2010) Lessons from exemplary housing renovations, IEA SHC 37B. www.iea-shc.org/task37/
18. METEOTEST (2010) Meteonorm 6.1. Fabrikstrasse 14, CH-3012 Bern. www.meteonorm.ch
19. Hastings R (2004) Passivhäuser und Lebensfreude. In: Eighth European Passivhaus Tagung und Messe, Krems, 16–17 Apr 2004. www.passivhaustagung.at
20. Troska Christoph (2009) Vom einfachglas zum vakuumisolierglas. Pilkington, Wikon
21. Rattner E (2008) Revolutionary vacuum glass. http://thefutureofthings.com/news/1167/revolutionary-vacuum-glass.html
22. Hermes M (2002) Aktuelles aus dem Regelwerk. In: Die neue wärmedämmtechnische Bewertung von Fenstern mit Einführung der EnEV 2002, Teil 1: Grundlagen. Integratio® – Forum. www.fensterberater.de/PagEnEV1.htm
23. ZIEGE (2010) Wärmespeicherung – planungsregeln. Verband Österreischer Ziegelwerke, Wien. www.ziegel.at
24. Chiras D (2002) The solar house: passive heating and cooling. Chelsea Green, White River Junction. ISBN 1931498121
25. SIA (1981) SIA 381/1 baustoff-kennwerte. Schweizerischer Ingenieur- und Architektenverein, Zürich also copyright 2000 SIA
26. Hässig W, Hardegger P (1996) Messprojekt direktgewinnhaus trin. Forschungsstelle für Solararchitektur, Zürich, Dokumente: 194637.pdf. www.bfe.admin.ch/dokumentation/energieforschung/

27. Gary (14 May 2006) Solar wall constructions. http://www.builditsolar.com/Projects/SpaceHeating/SolarWall/SolarWall.htm
28. Douglass E (10 Nov 2007) A pioneer refuses to fade away His passion for solar still burns – forty years ago, Harold Hay came up with a way to heat and cool homes using water and the sun. Los Angeles Times, Los Angeles
29. Fachverband Transparente Wärmedämmung e.V (2000) Bestimmung des solaren energiegewinns durch massivwände mit transparenter wärmedämmung. Fachverband Transparente Wärmedämmung e.V, Gundelfingen. www.umwelt-wand.de
30. Humm O (1998) Transparente wärmedämmung – mehr kollektor als wärmedämmung. Oerlikon Journalisten AG, Zürich
31. Domenig-Meisinger I, Willensdorfer A, Krauss B, Aschauer J, Lang G (2007) Erstes mehrfamilien-passivhaus im altbau passivhausstandard und -komfort in der altbausanierung am beispiel eines großvolumigen MFH in Linz. BMVIT, Vienna. http://www.nachhaltigwirtschaften.at
32. Domenig-Meisinger I, Grünewald S, Rottensteiner S (2010) Apartment building on Makartstraße, Linz AT, IEA SHC Task 37 Results. IEA, Linz. www.iea.shc.org
33. Hastings R, Morck O (eds) (2000) Solar air systems – a design handbook. Earthscan, London. ISBN 1-873936-86-9
34. Hastings R (ed) (2000) Solar air systems – built examples. Earthscan, London. ISBN 1-873936-85-0
35. Schoch R (1995) Reihenhäuser wydacker, zollikofen. Aarplan Architects/Matter+Ammann HVAC, Bern. www.energienetz.ch/solargebaeude/Text/SG/ATR/Zollikofen.pdf
36. Hastings R, Wall M (2007) Sustainable solar housing: vol 1, strategies and solutions. ISBN-13: 978-184407-325-2; vol 2, exemplary buildings and technologies. ISBN-13: 978-184407-326-9. Earthscan, London
37. Hanus C, Hastings R (2007) Bauen mit solarenergie. Vdf Hochschulverlag AG, Zürich. ISBN 978-3-7281-3085-3

Pathogen and Nutrient Transfer Through and Across Agricultural Soils

David M. Oliver[1,2], Louise A. Heathwaite[2]
[1]Biological & Environmental Sciences, School of Natural Sciences, University of Stirling, Stirling, UK
[2]Centre for Sustainable Water Management, Lancaster Environment Centre, Lancaster University, Lancaster, UK

Article Outline

Glossary
Definition of the Subject
Introduction
Agriculture, Livestock, Manures, and Contaminants
The Transfer of Pathogens and Nutrients Through and Across Soils
Future Directions
Bibliography

Glossary

Hydrological connectivity The linkage of spatial locations through different hydrological flow paths (surface and subsurface) within the catchment drainage network.

Farmyard manure Feces and urine mixed with bedding material (such as straw) used for housed livestock, and recycled back to land as an organic fertilizer.

Fecal indicator bacteria (FIB) Nonpathogenic microbial parameters that can be used as surrogate measures of infection risk to humans.

Leaching The movement and loss of soluble elements and colloids from soil via drainage water to both surface water and ground water environments.

Matrix flow The slow percolation of water through the soil pore system.

Mobilization Term used – in the context of this paper – to describe the initiation of contaminant transfer and the process by which those contaminants begin movement from soil.

Nonpoint source pollution Comprises contamination and pollution arising from many dispersed sources.

Pathogens Microorganisms capable of causing disease or illness in a host and used here to refer to bacteria and protozoa originating from fecal material.

Preferential flow Rapid movement of water and contaminants through the soil architecture. Much of the flow is focused in regions of enhanced flux, such as earthworm burrows or larger soil pores (macropore flow).

Slurry A liquid mix of feces and urine produced by housed livestock combined with water during management, and usually incorporating some bedding material to give dry matter content of 1–10%.

Surface runoff Flow generated from rainfall and other water sources that facilitates the transfer of

contaminants across the soil surface due to saturation excess or infiltration excess conditions.

Transfer A term used here to describe the movement of pollutants through soil-water systems.

Definition of the Subject

Human activity can place heavy stress on agricultural soils across the world. Soil systems are continually manipulated in order to support the increase in crop yields and accommodate more intensive livestock production and thus provide the planet's ever-growing population with a diverse array of ecosystem services, among which food production features highly. The recycling of livestock manures to land provides a sustainable solution to support the ecosystem services that soils provide and a host of benefits both in terms of improving soil structure and also soil fertility. However, livestock manures and feces may contain a high number of fecal microorganisms that pose a threat to human well-being and potentially large concentrations of nutrients harmful to the ecology of freshwater systems that the soils often buffer. To manage water quality in agricultural catchments value should be placed on adopting appropriate land, livestock, and manure management. To do this effectively requires a comprehensive understanding of the role of soil in facilitating contaminant transfer via a suite of hydrological pathways, and its ability to filter or absorb key pathogens or limiting nutrients during their passage through the soil network. Uncertainties in quantifying episodic transfers of contaminants through spatially and temporally dynamic pathways in soils at different scales ensures that multidisciplinary teams of scientists will not be short of challenges posed by soil complexity for decades to come.

Introduction

Soils are central to the functioning of agricultural systems and provide the planet's ever-growing population with a diverse array of ecosystem services, among which food production features highly. If managed effectively they can provide a host of benefits to society by, among other things, buffering flooding and hindering the transfer of numerous pollutants [1]. Conversely, if managed inappropriately the consequences can be far reaching, moving beyond the farm boundary to impact on local, regional and national health, livelihoods, food security, and downstream environmental quality. In terms of water quality, this can mean contamination of the ground and surface water supplies with the potential for chronic and acute impacts on human health [2, 3].

In the past nonpoint source pollution from agriculture has been synonymous with nutrient and sediment impacts on water quality. However, there is now a growing recognition that microbial pollution is a significant contributor to water quality impairment across the world [4]. Indeed, pathogen contamination of receiving waters has implications not only for water quality but also human health [5] with pathogens, or indicators of their presence, now topping the list of leading contaminants causing watercourse impairment across the USA [6]. Contamination of surface waters with microbial pollutants and nutrients is therefore potentially problematic both in an ecological and human health context. However, to put this in perspective, while the consequences of large-scale waterborne disease outbreaks linked to agriculture can be fatal, their occurrence is relatively rare. Nonetheless, coastal waters and often lakes and rivers too can be used for bathing, and their deterioration in water quality with fecally derived microbes from agricultural lands provides a key route of recreational exposure of potential pathogens to the human population. The reader is referred to ► Bioaccumulation/Biomagnifications in Food Chains for a substantial discussion surrounding further impacts of microbial transfer from land to water on food chain contamination. For nutrients, eutrophication is a clear consequence of overloading surface waters with supplies of nitrogen (N) and phosphorus (P). While being aesthetically displeasing, its toxic impacts on freshwater ecology include oxygen depletion leading to fish kills, and cyanobacterial blooms that can prove harmful to humans and animals (e.g., dogs and sheep) [7]. The degree to which eutrophication is considered a problem throughout the world depends on the place and people concerned, but it is an issue for a large number of water quality regulators across many nations.

Pathogen-contaminated groundwater has caused much waterborne disease worldwide [8]. Similarly, nitrate contamination of groundwater supplies is often linked to nonpoint source pollution in agricultural catchments, and it too can cause adverse effects on human health [9]. Waterborne outbreaks of any variety often have a large impact on society, but the actual disease burden attributed from such incidents in Europe is difficult to approximate and most likely underestimated [10]. An example of an outbreak of illness linked to microbial contamination of fresh water supplies is the Walkerton *Escherichia coli* O157: H7 Outbreak, Ontario, Canada in 2000 whereby over 2,500 people became ill through a drinking water well contaminated with farm runoff, and at least seven died directly as a result of drinking the contaminated water. The health implications (both anecdotal and case report data) of exposure to freshwater cyanobacteria are perhaps more contested and debated and have been reviewed recently by Stewart et al. [11]. Protection of surface and groundwater supplies from both nutrients and microbial contaminants thus requires a need to understand the differing transport behavior of these pollutants in agricultural systems, and critically this means understanding the role of soil in providing a potential buffer between agricultural activity and receiving waters. Thus, there is considerable value in appreciating that the quality of approaches to land management should be reflected in the quality of watercourses that drain catchments. This chapter considers the movement of pathogens through and across soil systems in agricultural settings and draws on nutrient studies to provide a comparative analysis of the differences in the importance of pathway functioning for different contaminant typologies, which ultimately is a key requirement for making measured assessments of the potential for pollution swapping linked to management shifts on-farm. The reader is referred to ► Microbial Risk Assessment of Pathogens in Water for a discussion of chemicals and pathogens in aquatic systems, and therefore this current chapter does not consider in-stream dynamics of nutrients or pathogens and their response to aquatic conditions when delivered into receiving waters. However, the movement of these biological and chemical contaminants through hillslopes and associated soil matrices is critical in linking on-farm activity to wider downstream impacts at both riverine and coastal environments, but also groundwater supplies too as identified in Fig. 1 (see ► Microbial Risk Assessment of Pathogens in Water).

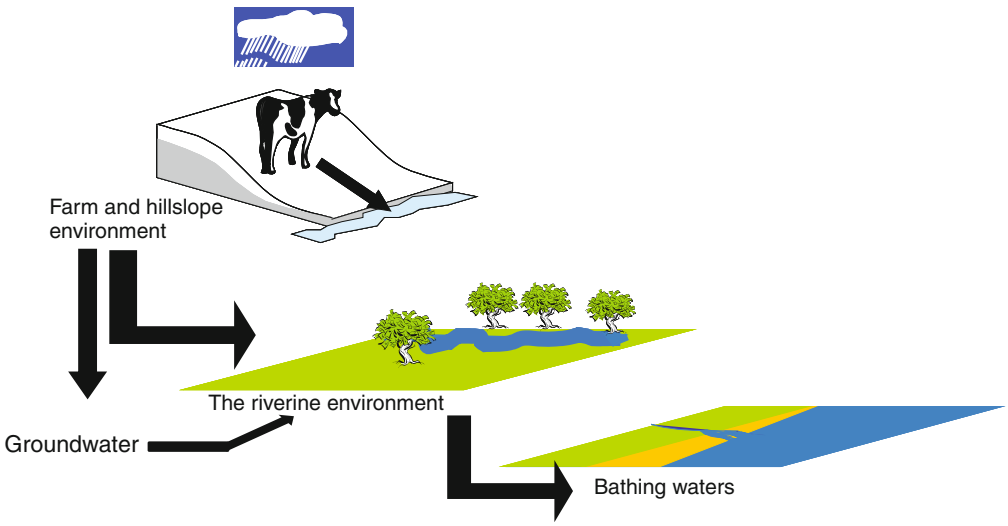

Pathogen and Nutrient Transfer Through and Across Agricultural Soils. Figure 1
"Farm gate to the bathing zone": diverse subsectors of catchments requiring investigation of nutrient and fecally derived microorganism fate and transfer

Agriculture, Livestock, Manures, and Contaminants

Pasture that receives manure, through either land application in varying forms (e.g., solid, liquid) or via direct deposition by livestock, will accommodate some degree of risk for contributing fecal microorganisms and nutrients to watercourses, as will arable soils (though direct defecation is not an important input for these systems). Many jurisdictions mandate how livestock wastes are managed to protect adjacent water quality from microbial and chemical contaminants that pose an environmental and human health challenge [12]. The likelihood of microbial or nutrient loss from land to water may vary in relative magnitude from negligible through to very high risk potential. This will depend on the combination of a number of site-specific source, transfer and connectivity drivers (see Fig. 2) thought to moderate the risk of contaminant loss from land to water. Landscape features and management practices help determine this risk potential [13]. In effect, catchment contaminant dynamics depend on a complex interaction between spatial patterns of land use and management, soils, antecedent conditions, and rainfall/event characteristics [14]. For example, different soil types can play a large role in determining the magnitude of transfer of fecal microbes, delivered to land via applied manures, through different soil hydrological pathways. In turn, the varied soil characteristics linked to different soil types can impact on the survivability and viability of microbes once within the soil habitat (either as freely suspended entities, or associated with soil or organic matter). Soils are also critical in facilitating, enhancing, or hindering the transfer of nutrients and fecal microorganisms through the pore architecture. Similar to microbial pollutants, nutrients too are input to land via organic wastes, but are additionally sourced from inorganic fertilizers. Background levels of nutrients

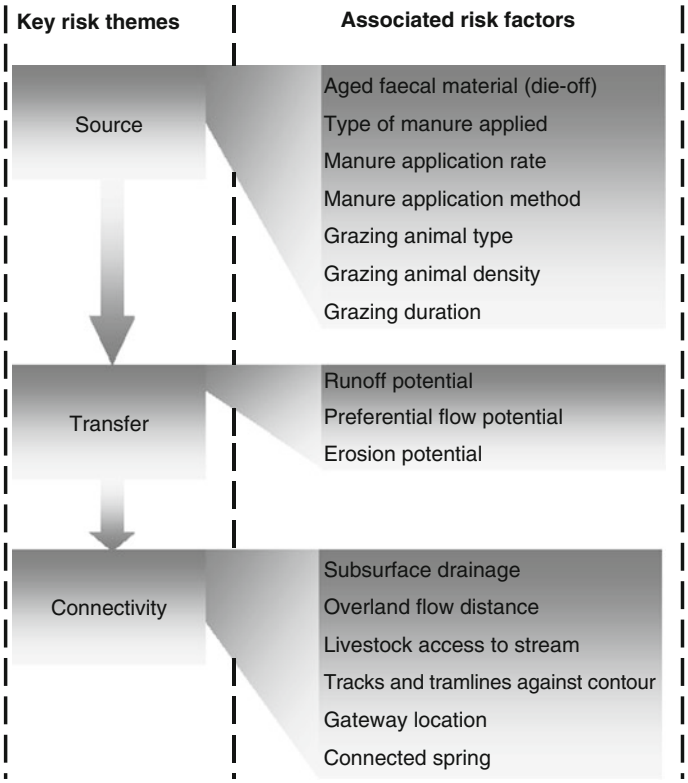

Pathogen and Nutrient Transfer Through and Across Agricultural Soils. Figure 2
Risk factors associated with source, transfer, and connectivity of pathogens and nutrients in the farm environment. The in-stream and in-river impacts are considered in ► Microbial Risk Assessment of Pathogens in Water

within soil reservoirs also provide a secondary source of nutrients that can be mobilized and transferred through the soil system, with a proportion ultimately delivered to receiving waters. Clearly, how land use patterns affect the transport, source, and relative longevity of pathogens (and nutrients) in the environment is a significant issue for policy formulation [15, 16].

Dangerous Microorganisms in Agricultural Systems

Livestock host a diversity of microbes within their rumen and digestive tract. A proportion of this microflora may comprise pathogenic microorganisms meaning that agricultural systems can harbor reservoirs of bacteria and protozoa potentially harmful to human beings. These reservoirs may be found both within animals but also their excreted fecal material. Thus, microorganisms such as *E. coli* O157, *Salmonella* spp., *Campylobacter jejuni*, *Listeria monocytogenes*, *Cryptosporidium parvum*, and *Giardia intestinalis* may contaminate pasture because of feces excreted during grazing regimes, and due to manures and slurries being applied to land via traditional farming practices. As a result, it is inevitable that the soil system will, at least periodically, harbor fecally derived microbes both at the soil surface and within the network pore structure [17]. Future emerging pathogens will likely arise from existing ones through adaptation and via unpredictable changes linked to biotic and abiotic mechanisms [18].

Fecal indicator bacteria (FIB) are bacteria that are indicative of fecal pollution and are present within all human and livestock feces. They do not pose a significant health hazard themselves; rather they suggest the potential for the presence of pathogenic microorganisms (whether bacterial, protozoan, or viral). The most commonly used FIB are *E. coli*. There are lively debates surrounding the validity of FIB as surrogates for bacterial, protozoan, and viral pathogens [19, 20], but currently FIB are used by many regulatory bodies across the world to monitor microbial water quality. In considering the transfer of microbial pollutants through and across soil there are a number of critical research questions that have driven the continued investigation of this research area. These are summarized in Fig. 3. Clearly there is a need to account not only for microbial transfer, but simultaneously appreciate their survivability when excreted into an environment outside of the animal gut. If survivability is so unlikely under the environmental conditions typical of agricultural settings then the likelihood for mobilization and delivery to watercourses and downstream impact is much reduced. That said, many microbial pathogens and associated indicators are able to survive for lengthy periods outside of the gut, meaning that there is a key need to understand how they transfer in addition to how their population profiles may change through time when associated with different environmental matrices. The entry ► Recreational Water Risk: Pathogens and Fecal Indicators provides a comprehensive overview of monitoring approaches used in the detection of pathogens and FIB in the environment.

The Nutrients of Concern

The primary nutrients of concern considered in this chapter with regard to movement through soils are phosphorus (P) and nitrogen (N), specifically nitrate (NO_3^-). Both P and N are key limiting nutrients in aquatic systems. Contamination of surface and groundwater with anthropogenic inputs of N and P following their passage through and across soils risks the quality of drinking water supplies and may lead to excessive harmful algal blooms [21]. Nutrients are introduced as a comparative contaminant within this Chapter to highlight differences in terms of their transfer dynamics in relation to microbial transfers. The FIB and pathogens discussed within this chapter generally range in size from 1 to 5 μm and can be classified as biological "particles." In contrast, phosphorus can be divided into a particulate and soluble fraction (soluble in this instance being based on an artificial laboratory subdivision of 0.45 μm), and NO_3^- is highly soluble. This intuitively leads to clear differences in modes of transfer linked to physical mobilization by water for particulate contaminant typologies, in contrast to dilution effects associated with increased discharge volume for soluble contaminants and therefore suggests that there are differences in transfer linked to contaminant functional type. Another important property of P that can impact on its transfer dynamics is related to its high capacity for sorption to soil relative to NO_3^- and its association as colloidal P. Indeed, in soils NO_3^- remains free in soil solution because the nitrate anion is not adsorbed onto soil surfaces due to soil

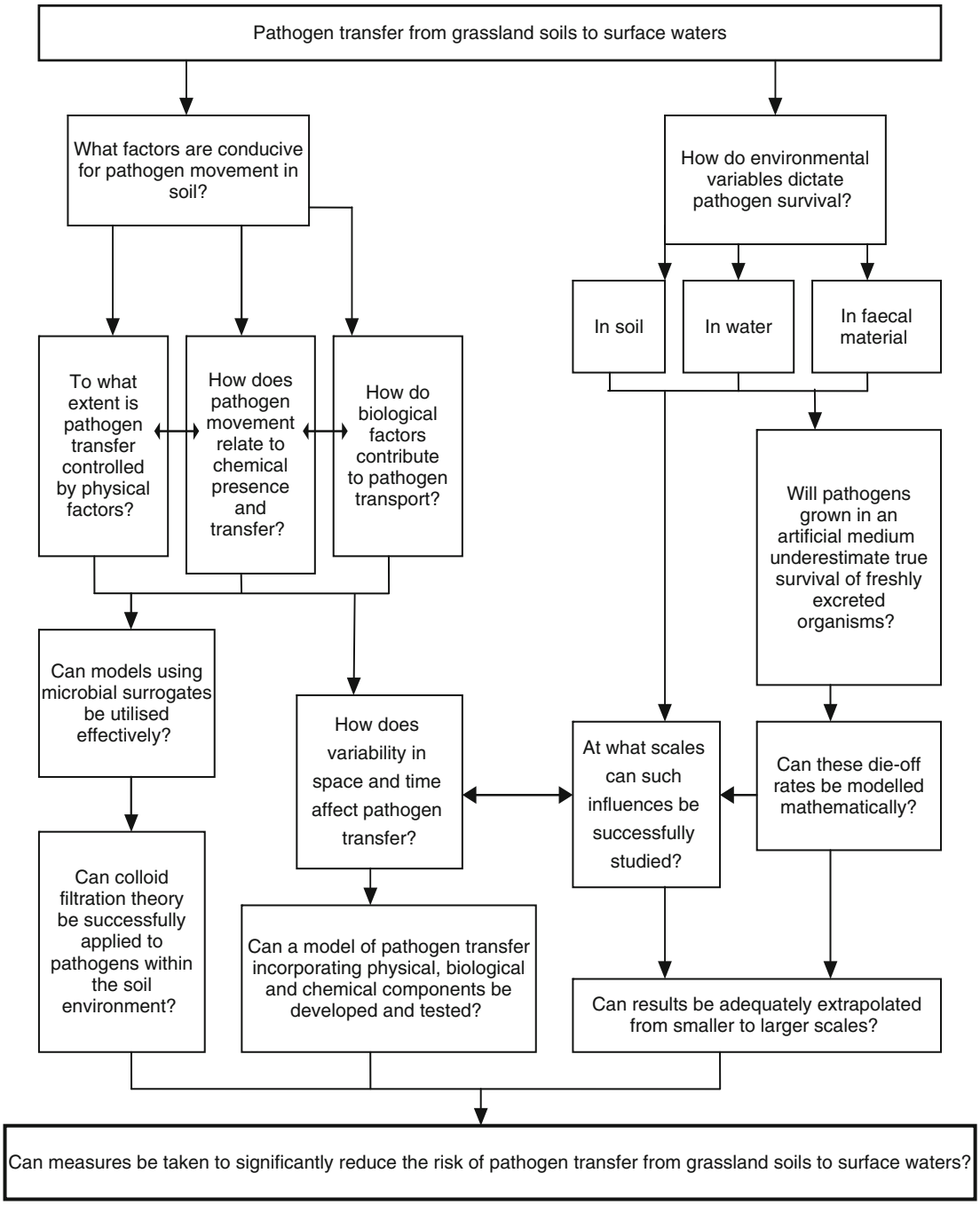

Pathogen and Nutrient Transfer Through and Across Agricultural Soils. Figure 3
A questioning framework of key research needs for pathogen transfer studies in the environment (Reproduced from Oliver et al. [17])

particles having a partial negative surface charge. As a result, NO_3^- is highly mobile in soils. In contrast, ammonium (NH_4^+) is positively charged and can therefore attach and associate with soil particles to be retained within the soil body. However, this chapter only provides an introduction to the differing properties of NO_3^- and P relative to microbial contaminants and much more comprehensive detail specifically on nutrient mobility in agricultural systems can be found within recent comprehensive reviews of Heathwaite [22], Edmeades [23], and Haygarth et al. [24].

Sources of Pathogens, Indicators, and Nutrients

The presence of pathogens, FIB and nutrients within the farm environment can be largely attributed to either point or nonpoint sources. Point sources are readily identifiable inputs that can be traced to a point of origin. They represent "end-of-pipe" locations and can include agricultural ditches, leaking septic tanks and manure stores, and farm hard standings. Nonpoint sources relate to inputs that occur over a large area and are attributed to land use. Nonpoint sources can include dung deposited to pasture by grazing animals [25, 26] and liquid and solid manures spread to land [27]. In addition, treated human wastes can be recycled back to land (biosolids) and still may contain a number of fecal microorganisms of concern. Untreated human waste (i.e., waste from septic tanks) may sometimes be spread back to land, though in the UK this is against regulatory policy. However, anecdotal evidence suggests this activity does take place, though published data on such practice are notably scarce. Wildlife can also serve as a source of microbial pollutants and indeed additional P and N inputs to land via their excretions. However, the significance and quantification of the wildlife source component is an often overlooked contributor to pasture-based budgets [28].

The soil matrix can sustain fecal microorganism survival, especially if microbes are incorporated in association with fecal material. Indeed some studies have detailed bacterial cell survival in excess of several months [29]. This can be due to protective microsites and protection from desiccation and UV radiation. Clearly then, it is not only fresh additions of manures to land that may be capable of impacting the microbial quality of watercourses, and aged fecal remnants can still contribute bacterial numbers to runoff following rainfall [30]. Slurries, solid manures, and feces all harbor different numbers of fecal microbes, and all impact on differential fecal microbe die-off patterns [31]. Furthermore, the consistency of each manure type (e.g., dry matter content) allows for differing degrees of mobility of fecal microbes accommodated within these manure source locations [32].

Nutrient sources in agricultural systems are somewhat different in that they do not depend on a fecal store to convey signal strength in receiving waters. For example, natural sources of N and P exist in the environment, and for N there are atmospheric sources too. The soil can therefore serve as a reservoir for N and P, meaning that even without continued anthropogenic inputs to land there will still be considerable losses of NO_3^- and P from land to water following rainfall events. This is a critical difference between the fecally derived bacterial and protozoan contaminant typologies and nutrient contaminant typologies. While microbial contaminants can persist for lengthy periods, there are not significant soil stores of fecal pathogens and their indicators *independent* of manure applications or livestock activity, though some studies report the potential for naturalized *E. coli* populations in the soil environment [33–35]. In contrast, liver fluke and intestinal worms and similar livestock pathogens do have significant soil stores that are important for their cycling, but they are not considered in this chapter under the definition of pathogens (e.g., fecal bacteria or fecal protozoa). Therefore, lag time between cessation of contaminant inputs to land and a measured reduction of pollutant losses at the edge-of-field scale varies by the pollutant type and depends strongly on the behavior of the pollution source [36]. Circumstances where farming practices have led to excessive soil P levels can be particularly problematic because even if nutrient management leads to a reduction of P inputs to levels below crop removal rates, the timescale needed to exhaust the P from the soil to the point where dissolved P in runoff is effectively reduced may well be years to decades [36]. Of course, soil with a high P index (high P content) does not always result in high P transport as this is dependent on the way that the P is "locked" into the soil and its likelihood for subsequent mobilization.

Manure and slurries are applied to land via a range of techniques and equipment. Broadcast-applied manures (i.e., those spread to land using a splash

plate and distributed onto the surface of blades of grass) are likely to be considered more risky in terms of contaminant loss than injected or plowed manures because of the opportunity for incidental contaminant losses from land to water [37]. However, broadcast applied slurry is likely to lead to a more rapid destruction of associated bacteria through UV radiation and desiccation [38]. Livestock grazing is equally, if not more important than manure applications in loading the landscape with fecal microbes [39]. The key difference between land applied manures and livestock excretions is the resulting spatial patterning of contaminants across the landscape. Similarly for nutrients, in this case NO_3^-, McGechan and Topp [40] have found higher levels of NO_3^- pollution in tile drains following grazing compared to fields receiving slurry and have suggested that high levels of NO_3^- pollution could be attributed to various factors, including the fact that cows tend to congregate in certain areas of a field at a localized stocking rate much higher than the overall stocking rate, and due to deposition of N at times when grass cannot utilize it as a plant nutrient. Animal type is a critical factor to consider with regard to the source strength of contaminants in farmed environments. This is because age and variety of livestock governs the number of organisms per gram of feces excreted onto pasture (e.g., lambs shed higher numbers of *E. coli* than beef cattle) but also dictates the daily excretion rates of feces (and therefore nutrients and microbes contained within) to farmed land and impacts on the differential release of FIB from various types of livestock feces at different times of the year. Logically, grazing density bears an impact on land-based loading of fecal microorganisms and nutrients too, and it has been shown that the concentration of FIB in streams in sub-catchments with high stocking densities can be four to eight times higher compared to sub-catchments accommodating low stocking densities [41], and grazing duration is potentially important for both nutrient and microbial contaminants based on the accumulating reservoirs of fecal excretion to land through time.

The Transfer of Pathogens and Nutrients Through and Across Soils

The transfer of water across and through the soil environment, and contaminants dissolved or entrained within, is subject to a series of spatial and temporal controls that dictate this potential for transfer and which vary both spatially and temporally [42]. Temporal controls on microbial and nutrient transfers include meteorological inputs that provide an energy source and driving force to initiate transfer processes. Additionally, hydrological pathways are susceptible to change through time, for example, pore networks can collapse, drain pathways can silt up, and extreme events can remove existing pathways and reconfigure hydrological conduits. The significance of a particular pathway in facilitating microbial and chemical transfers from land to receiving waters is controlled by properties of the pollutant of concern and also the form of the contaminant, for example, whether it be particulate, particle associated, or soluble (i.e., the contaminant functional type) [43]. Climate and weather too are key dictating factors controlling the magnitude of transferred loads. Whether considering individual storm events or interannual variability, these climatic drivers can have a significant effect on the magnitude of multiple pollutants over many timescales. Spatial factors impacting on transfer include the particular soil type that microbes or nutrients are negotiating their passage through or across. Soil types dictate hydrological pathways, some being more likely to hinder transfer via filtration, whereas others may be more likely to permit rapid transfers via large cracks or pores in the soil (macropore flow). Research has demonstrated the importance of water flow velocity and soil particle size distributions, for example, on *E. coli* transport through soil [44].

For transfers across the soil surface, it would appear logical to assume that slope gradient and slope shape can be useful indicators for transfer potential, and many models accommodate a slope term as a control over particle transfer, with increased transfer associated with increased slopes. However, some studies suggest the need for caution when dealing with what appears to be a relatively straightforward assumption. Such relationships tend to be based on data collected over a wide range of slopes and using relatively small soil flumes. Recent work by Armstrong and Quinton [45] used laboratory rainfall simulation on a large soil flume to investigate interrill soil erosion of a silt loam under a rainfall intensity of 47 mm h^{-1} on 3%, 6%, and 9% slopes. Results from replicate experiments showed wide

variations in runoff and sediment concentration that were explained by the complexities in interrill soil erosion processes. Critically, the data also demonstrated that at low slope (on arable soils) processes related to surface area connectivity, soil saturation, flow patterns, and water depth may dominate over those related to gravity, and Armstrong and Quinton [45] therefore query the validity of risk assessments and soil erosion models with a dominant slope term when assessing soil erosion from agricultural land at low slopes. However, it is important to acknowledge the scale at which this reported study was conducted, and caveats should be applied in upscaling such laboratory-based findings to field situations. For more topographically diverse landscapes, alternative approaches use landscape wetness as a metric of delivery potential by integrating the small-scale spatial variation in runoff generation and probability of hydrological connection linked to topography [46, 47].

Physical, geochemical, and biological processes can be used to classify the key transport mechanisms responsible for microorganism and nutrient movement within soils. The physical processes include advection, whereby pathogens or FIB and nutrients are carried in bulk water and move according to the water velocity, and dispersion, which can involve the spreading of microorganisms and nutrients as they move along the water path. Geochemical processes act to delay microbial and particulate transfer through the soil matrix and consist of filtration, sorption, and sedimentation mechanisms [48, 49]. Finally, biological processes, such as growth and chemotactic responses, may influence microbial transfer through the soil habitat, albeit to a lesser extent [50, 51]. This ability to self-propel through the soil system because of their biological attributes (e.g., pili, fimbriae) differentiates microbes from their nutrient counterparts. While at the pore scale this transfer mechanism is important, in the grander scheme of the catchment or hillslope, the role of biological transfer is likely to be minimal in contrast to the physical mobilization facilitated by rainfall and the resulting water flows.

The transfer of agriculturally sourced contaminants from soils to ground and surface waters is largely driven by rainfall and resulting surface and subsurface runoff. Conceptually, transfers can be classified as low energy or high energy. For example, slow flow microbial and nutrient transfers may operate between storm events and are thought to be associated with the steady percolation of precipitation inputs through the soil profile. This contrasts with overland flows and bypass flows resulting from high-energy precipitation (or storm) events, which enable the physical movement of soils, manures, and potential pathogens into streams, creating a more rapid and direct transfer route. However, it is interesting to draw attention to findings from Sharpley et al.'s [52] recent study that showed that small storms were more important than large storms in delivering P to watercourses over a 10-year research period. These two contrasting energy levels of transfer will be discussed in later sections of this chapter and are illustrated in Fig. 4. Nitrate (and some forms of P), being soluble, follow a different trend than that of microorganisms and particulate P, and instead can be diluted under heavy water flow [53]. Table 1 is provided as a point of reference to direct the reader to scale-appropriate studies of the transfer of a variety of agricultural contaminants through soil systems. Current understanding of the transfer capability of different hydrological pathways in space and time is growing for microbial pollutants, but this remains a complex and underexploited interdisciplinary research topic necessitating the collaboration of soil hydrologists and environmental microbiologists. While understanding the spatial and temporal intricacies of environmental transfer of fecal microorganisms lags some way behind current knowledge surrounding N and P dynamics in agricultural systems, that does not mean the knowledge of P and N dynamics is satisfactory. There remains for these nutrients need to further the understanding of the relative importance of different hydrological pathways in providing *delivery* (in quantifiable terms) from land to water [95]. Some have argued for the critical development of appropriate methods to quantify the delivery process and thus new monitoring tools capable of providing a framework for understanding contaminant transfer and delivery at a range of scales in agricultural catchments [88]. Deasy et al. [88] highlighted the dominant role of a field drain in transferring P from land to water and argued that overland flow inputs, despite being directly connected to the stream and containing higher P concentrations, contributed less to the stream P flux. Such data are key reminders that the obvious and visible routes of

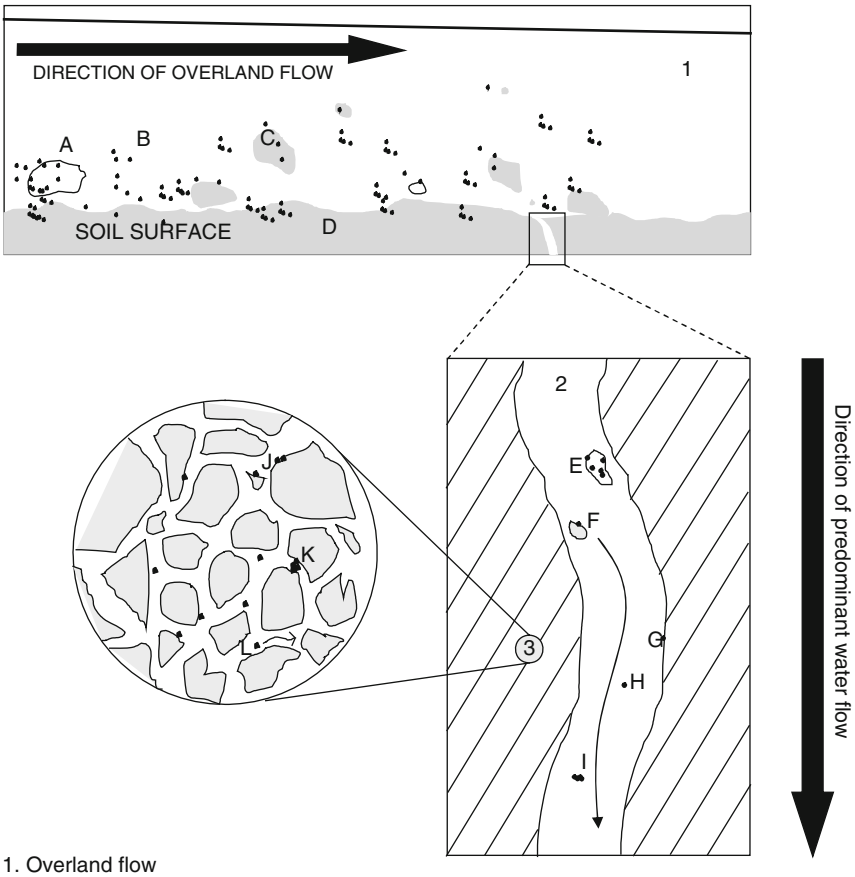

1. Overland flow
A: Microbial transfer within dislodged faecal material in direction of flow
B: Micro-organisms freely suspended in overland flow pathway (both isolated and consortia)
C: Soil-particle associated transfer
D: Retention on microbes in soil surface layers

2. Soil macropore
E: Microbial transfer within faecal particles
F: Soil-particle associated transfer
G: Microbial adsorption to macropore wall and consequent ripening effect with time
H: Microbial advection (movement of unattached microbes carried by water in direction of flow)
I: Transfer of microbial flocs via advection

3. Soil matrix
J: Microbial adsorption within matrix
K: Bio-clogging (blocking of pores through straining and filtering of cells)
L: Microbial dispersion (movement of microbes carried by water in direction other than that of flow)

Pathogen and Nutrient Transfer Through and Across Agricultural Soils. Figure 4
Natural transfer pathways available to fecally derived microorganisms applied to soil surfaces (Reproduced from Oliver et al. [17])

transfer do not always equate into dominant and critical flow pathways upon which mitigation efforts must be focused to protect our water resources. The P transfer continuum concept has been outlined by Haygarth et al. [96] as a framework within which the factors that contribute to nonpoint P fluxes from catchments can be operationally divided into *source*, *mobilization*, and *delivery*. These divisions are a convenient way of grouping processes that determine P behavior and accommodate transferability in terms of conceptualizing other contaminants in agricultural systems (cf. Fig. 2).

Pathogen and Nutrient Transfer Through and Across Agricultural Soils. Table 1 A "look-up" table of research studies investigating microbial and nutrient transfer through and across soils at a range of different scales

Scale of study	Contaminant type			
	Bacterial	Protozoan	P	N
Laboratory soil columns/boxes	Artz et al. [54] Donnison and Ross [58] Garbrecht et al. [44] Horswell et al. [64] Rosa et al. [65]	Mawdsley et al. [55] Boyer et al. [59] Harter et al. [62]	Matula [56] Tarkalson and Leytem [60] Brock et al. [63]	Entry et al. [57] Miller et al. [61]
Vertical Lysimeters	Bech et al. [66] Brennan et al. [34] Guzman et al. [69]		Turner and Haygarth [67]	Di et al. [68]
Soil plot : small	Muirhead et al. [70] Abu Ashour and Lee [72] Soupir et al. [75] Mishra et al. [77] Thiagarajan et al. [79] Oliver et al. [82] Kouznetsov et al. [84] Collins et al. [86]	Ferguson et al. [71] Ramirez et al. [80]	Preedy et al. [37] Tunney et al. [73] Quinton et al. [74] Withers et al. [76] Heathwaite et al. [78] Haygarth et al. [81]	Alfaro et al. [83] Olson et al. [85]
Hillslope Sub-catchment - Catchment	Kay et al., [87] Close et al. [90] Davies-Colley et al. [93] McKergow and Davies-Colley [14]	Keeley and Faulconer, [15]	Deasy et al. [42, 88] Heathwaite and Johnes [91] Rothwell et al. [94]	Botter et al. [89] Dougherty et al. [92] Heathwaite and Johnes [91]

Soil Characteristics Impacting on Transfer

Rainfall and resulting runoff and drainage from farmed land is critical for the transfer of agricultural pollutants such as phosphorus, NO_3^- and sediments from land to water (e.g., [37, 97]), and there are a series of key soil characteristics that impact on the transfer of pathogens and FIB through lysimeters, hillslopes, and catchments too. Soil water content, soil structure, and soil texture are among those that shall be discussed within this chapter. The physiochemical properties of soils and the resulting interactions with potential pollutants means that the navigation of pathogens and nutrients through the soil architecture is extremely complex, and particular attention will be given to these rapid versus slow transfers as dictated by soil properties in the following sections of the chapter. Particulate-type contaminants experience more rapid travel times in coarser textured soils with larger pore spaces as opposed to finer textured soils, with the soil matrix operating as a filtration system. In soils where matrix flow dominates it is therefore generally accepted that water-induced particle transport is strongly correlated with particle size.

In addition to the physical make-up of soil and the associated network of conduits, pores, and microhabitats, it is pertinent to appreciate the variability in sorption properties attributed to different soil types. This property of soil and associated colloidal material can have a marked influence on microbial and P transfer [98, 99]. The major soil components affecting sorption of bacteria and P are clay and organic matter, and particle and colloid facilitated TP delivery from soils to water via different hydrological pathways has been shown to be dominated by the transfer of TP associated with clay and colloidal fractions [81]. For *Cryptosporidium*, hydrophobicity and zeta potential have been highlighted to exert a significant influence in the adhesion mechanisms of the oocysts [100], and more recently the presence of manure in solution has been shown to enhance the extent of adhesion of these

protozoa to soil particles. However, the role of manure in facilitating attachment of *Cryptosporidium* to soil particles is complex, with indications that an optimal concentration of a "facilitating" component of the manure exists (at somewhere between 0% and 1.0%) [101]. Clearly, the sorption of microorganisms and nutrients to soil surfaces cannot be attributed to a single factor; instead it is important to appreciate an array of forces interacting to govern microbial retention. Table 2 provides a definition of the common mechanisms through which FIB and bacterial pathogens associate with soil particles.

From a conventional soil science perspective the concept of sorption is normally applied to chemical contaminants and the derivation of their associated adsorption isotherm. Elements of sorption theory can be considered transferable for the determination of bacterial association with soil. Adsorption is an important process that partly governs the aqueous concentration of contaminants in soil environments, and therefore their mobility. The common approach is to use a batch equilibration method to obtain adsorption coefficients. This is based on the assumption that partitioning of the contaminant is a thermodynamically motivated distribution between two readily separable, homogeneous phases [102]. Many other studies have investigated the adsorption of a broad range of potential contaminants, including heavy metals, pesticides, herbicides, and fertilizers.

The adsorption isotherms of nutrients such as P often fit models such as those described by the single and double Langmuir, Freundlich, and Tempkin equations whose profiles suggest that a maximum loading of P with the soil occurs, after which no more sorbate may be adsorbed. The linear isotherm is essentially a special case of the Freundlich isotherm, and this suggests that no point is reached whereby the solid fraction has had all its available sorption sites exhausted. Oliver [103] observed a linear isotherm when investigating the affinity of *E. coli* to soil particles suggesting that sites for cell interactions remain available. However, the linearity of the data may in fact reflect multilayer cellular associations with particles whereby cell consortia have associated with a contact point of the particle. Koopmans et al. [104] discuss isotherm linearity with respect to P adsorption and propose that a linear profile is often either: (1) a function of a narrow range of concentrations being tested; or (2) linked to the use of a wide soil to solution ratio. In the *E. coli* isotherm described by Oliver [103] neither of the two factors discussed by Koopmans et al. [104] were thought to apply to the data because the range of concentrations used was large in terms of a realistic minima and maxima, and an appropriate soil to water ratio was determined in one

Pathogen and Nutrient Transfer Through and Across Agricultural Soils. Table 2 Summary table of mechanisms of bacterial sorption/attachment to soil particles

Potential mechanism of sorption/attachment	Description
Van der Waal forces of attraction	Cells overcome electrostatic repulsion and are held at a finite distance from a particle surface
Charge attraction of opposite signs	Metal oxide coatings on soil particles confer a positive charge to the particle surface and this results in a much tighter adhesion of the cell to the surface
Hydrophobic forces	Hydrophobic bacteria have the tendency to adsorb to surfaces in water due to repulsion from the polar water molecule
Positive chemotaxis (cellular mobility)	Higher nutrient content of a particle surface may cause motile bacteria to move toward surface as a result of nutrient gradient
Irreversible anchoring via pili and fimbriae	Biological mechanism of attachment where contact is made between cell and surface via hair-like appendages. The presence of a localized positive charge at the tip of fimbriae can aid attachment to a negatively charged soil particle
Charge fluctuations	Heterogeneities in surface charge provide locally favorable regions for attachment

of the preliminary stages of designing the isotherm experiment. Of course, if the concentration of cells was increased further then the *E. coli* isotherm may reach a plateau at a potential retention maximum, but the applicability of such results to field situations is likely to be limited. While some studies have determined that over 99% of cells adsorb to soil [105], the numbers do not necessarily equate to real-world observations whereby a greater proportion than the remaining 1% of total applied cells loaded onto the soil surface via manure and feces may emerge via runoff and subsurface drainage. The reasons for this are numerous. For starters, hydrological factors play a role at larger scales and are unaccounted for in laboratory batch-scale experiments. Essentially, water flux may prevent cell interaction with the soil because preferential and rapid overland flow pathways can allow bacteria to bypass the soil matrix and those soil horizons that adsorb contaminants strongest. Additionally, bacteria entering the soil system under field conditions are not necessarily free-living cells as introduced to the soil-water system under experimental conditions. Fecal bacteria may already be associated with organic matter derived from excrement, and this may impact on soil–cell interactions. The extent to which laboratory findings can be extrapolated to the environment is, therefore, a little unclear. However, such comparative studies can provide a mechanistic understanding of an important process and as long as their limitations are acknowledged such experiments are important tools in the development of the understanding of soil-contaminant interactions.

Colloid and Particle Associated Transfer

In addition to retention of microbial and nutrient contaminants within the soil architecture there also exist the potential for these contaminants to associate with colloidal and particulate soil material, which may subsequently provide a vehicle for contaminant transfer through the pore network. There are two particularly important properties associated with colloids that enable them to function as important contaminant carriers. The first is that colloids have a very large specific surface area, in excess of 10 $m^2\ g^{-1}$ [106]. Second, these colloids remain stable in suspension for significant periods, and if bacteria attach or nutrients such as P adsorb to the large available surface area, their dispersal through the soil may be aided considerably. Those colloids that remain more in the center stream of the flow path are likely to remain uncaptured and thus migrate along these faster, more permeable flow paths.

The strong positive relationships between suspended sediments and P in drainage waters reported throughout the literature demonstrate the clear linkage between this nutrient and soil particles. Much work has considered colloidal P transfer through agricultural systems, and it is an accepted mechanism by which a significant fraction of P loss from agricultural land can occur. Colloidal material falling within the notional "dissolved" fraction (i.e., <0.45 μm) has thus been shown to serve as an important vehicle for the transfer of P from soils [78]. In fact, a whole range of particle and colloid size fractions have been shown to function as P carriers with linear regression highlighting strong significant relationships (r^2 = 0.86) between water extractable supernatant turbidity and colloidal P release across particle sizes ranging between 2 and 0.0003 μm for a suite of different soil types [78]. The association of P with these colloidal fractions allows for a relatively rapid transfer of sorbed material because of the exclusion of colloidal size fractions from soil micropores and restricts their passage to the more rapid flow routes via macropores.

Association of FIB with soil particles has been discussed too (e.g., [72, 107–109]), though there remains a large degree of uncertainty regarding "vehicles" for cell transfer under environmental settings and a clear need for continued research to consolidate understanding of processes governing cell partitioning with different sedimentary fractions and the importance of such interactions in freshwater systems [5]. Importantly, the size of *E. coli* itself is generally regarded as being approximately 2 μm in length and 0.5 μm wide. In one of the few studies examining the preferential attachment of *E. coli* to different particle size fractions of an agricultural grassland soil [108] it was shown that 35% of introduced *E. coli* cells were associated with soil particulates >2 μm diameter. Of this 35%, most of the *E. coli* (14%) were found to be associated with the size fraction 15–4 μm. This was attributed to the larger number of particles within this size range and its consequently greater surface area available for attachment. When results were *normalized* with respect to estimates of the surface area

available for bacterial cell attachment to each size fraction, it was found that *E. coli* preferentially attached to those soil particles within the size range 30–16 μm. For soil particles >2 μm, *E. coli* showed at least 3.9 times more preference to associate with the 30–16 μm than any other fraction apart, from the <2 μm grouping. Undoubtedly the range of methods used to arrive at estimates of bacterial attachment to suspended sediments can in many respects be responsible for the discrepancies observed in different studies [110]. Within emerging drainage water, a measure of turbidity should be correlated with FIB concentrations if the majority of cells are truly associated with suspended solids and, in addition, such association is unaffected by other water quality parameters. However, both strong and very weak relationships have been observed by various authors between *E. coli* concentrations and turbidity, and between *E. coli* concentrations and total suspended solids concentrations [110]. This is perhaps not too surprising given that the microbial consortia being measured reflect a combination of life-cycle stages. For example, turbid water can often be found draining pasture that has not been grazed for several months. The length of time between the removal of livestock and the collection of runoff water can mean that the majority of FIB may have perished as a result of UV radiation and desiccation and so the relationship between turbidity and FIB concentrations is weak. In contrast, a storm event that generates highly turbid runoff from pasture grazed by a large number of cattle will likely result in a strong relationship between the suspended particle concentration and FIB numbers because the population of FIB present are abundant within freshly deposited material. Tracking the actual emergence of FIB, pathogens, and turbidity peaks with storm hydrographs provides one interesting means of analyzing the strength of association of microbial contaminants with the soil fraction. Such observation as reported by Oliver et al. [103] identified a similar but delayed emergence pattern of *E. coli* and turbidity peaks in subsurface runoff via artificial drainage from grassland plots. Thus, the peaks for turbidity, flow, and *E. coli* concentration were not identical, but occurred in respective order as a function of increasing time. The results suggested that *E. coli* may have been associated with hydrologically energized soil particles of a particular size fraction.

Rapid Pathways of Contaminant Transfer

Intensity of water flow through soils is undisputedly one of the most critical factors responsible for driving the transfer of fecal microbes and nutrients from land to receiving waterbodies. However, when entering receiving waters that may have a high discharge there is the potential for high dilution capacity. Surface runoff processes that generate overland flow are often perceived to be the dominant transfer pathway for pathogens and microbial contaminants. The growing evidence base detailing pathogen and FIB transfers through agricultural systems is beginning to add weight to such hypotheses. If antecedent soil conditions are conducive to generate overland flow and heavy rains occur shortly after slurry application or an intensive grazing season, then there is potential for significant runoff of fecal microorganisms and particulate P following their entrainment into a variety of flow pathways. Overland flow that directly connects with a watercourse has been shown to deliver substantial loads of FIB to the stream network [86], though the numbers may be diluted if entering a receiving water with high discharge. It is likely that a greater *uninterrupted* overland flow distance and contributing area will enhance the potential for accumulated carriage and delivery of FIB to the watercourse. However, there is little proof that overland flow, once started, actually delivers contaminants to streams and primary water systems in a single event. It may instead provide a pulsing mechanism of transfer or be interrupted by buffers before having impact on receiving waters. Alternatively, particulate contaminants (e.g., cells or particulate P) that are transferred via the surface runoff pathway may be deposited and resuspended numerous times before being finally delivered to a watercourse. The role of high rainfall and storm events and the resulting flow signatures in dictating microbial transfer from soil to water has been documented by a growing number of studies. Recent examples include: McKergow and Davies-Colley [14], Sinclair et al. [111], Wilkes et al. [20], Davies-Colley et al. [93], and Oliver et al. [82]. Similarly for P and N a large amount of literature is available on the response of these nutrients to hydrological drivers (e.g., [53, 78, 89, 112]). Some recent studies on P delivery from land to water have however challenged prior assumptions of the

importance of large storm events [52, 113]. Sharlpley et al. [88] compared the surface runoff contributing area and stream flow and total P response for 248 storms over a 10-year period from 1997 through to 2006 and found that 93% of storm flows had a return period of <1 year and delivered 63% of the flow and 47% of the total P load. Similarly Jordan et al. [113] were able to demonstrate the importance of high resolution sampling frequency on detecting P delivery to water from diffuse sources independent of storm events and others have recognized the need to adopt appropriate time intervals and lengthy data records to observe useful diffuse pollution trends across scales [22].

Coarser textured soils tend to allow for rapid vertical transfer of NO_3^- relative to fine textured soils, though it must be acknowledged that rapid NO_3^- transfers can occur within finer textured soils via cracks or fissures, particularly if NO_3^- is heavily loaded onto the soil surface. Overall, NO_3^- losses via rapid overland flow pathways are relatively minor compared with NO_3^- lost via leaching and drainage. For a soluble contaminant such as NO_3^- it is interesting to observe response trends over both seasonal and storm-event timescales. For example, NO_3^- emergence generally reduces during the growing season and increases during the winter owing to uptake from plants during the summer. However, superimposed on this seasonal pattern of increasing and decreasing concentrations are dilution effects attributed to storm events whereby heavy rainfall effectively causes a reduction in concentration through increased water volume. Downscaling from seasonal timeframes to individual storm-events, the relationship between flow and NO_3^- concentration is in fact much more complex and not a straightforward dilution for every rain event.

For microbial transfer, Tyrrel and Quinton [114] summarize overland flow transport scenarios as (1) incorporation of free microbes into overland flow; (2) mobilization of soil or waste particles into overland flow carrying attached microbes; and (3) detachment of microbes from soil surfaces arising from shearing forces of raindrop or flow action. However, there remains much work to be done in quantifying the efficiency of overland flow in facilitating the wash-in of fecal material from pasture to stream. The complexity of predicting contaminant delivery to water courses cannot be understated, and while wash-in of fecal matter has long been recognized as a consequence of overland flows generated within the contributing areas of a catchment [115], within large and complex watersheds the bacteriological and chemical quality of a stream is the resultant effect of a variety of indistinguishable sources, and so determination of the loading capability of a particular transfer route is difficult. Poaching and pugging, which are terms used to refer to the compaction and breakup of soil due to trampling by livestock, can lead to a lower soil infiltration rate [116] and can enhance the initiation of overland flow. Poaching and pugging are therefore of critical importance in localized areas and hence may be more important at such scales within surface water dominated catchments compared to groundwater dominated catchments, where their effects are likely to be more hydrologically isolated [117]. Despite the apparent complexity in understanding contaminant transfers through soil systems at catchment scales some studies suggest that complex behavior patterns can be reduced to surprisingly low variability in model outputs [118].

Rapid routes of water transfer other than overland flow do exist and include macropores and artificial drainage systems, and a suite of rapid flow pathways are illustrated in Fig. 5. Such bypass routes within the soil matrix facilitate a rapid transfer of water and the soluble and particulate contaminants carried within. The significance of large pores and voids in facilitating the movement of water and colloidal material through the soil has long been acknowledged [119–121]. Macropores may be formed naturally or through soil fauna activity, plant root presence, or soil shrinkage. Preferential flow in soil has both environmental and human health implications since it favors contaminant transport to groundwater without interaction with the chemically and biologically reactive upper layer of soil [122]. The interconnected pore network therefore allows for a slow transfer of particulate-type contaminants via infiltration into the soil matrix coupled with a rapid transfer of microbes and particles (and solutes) within larger sized pores capable of increased soil water velocities. In the absence of macropores the distribution of microbes may be mostly confined to the uppermost zones of the soil profile [54]. However, for FIB, after a dry spell, the rapid entry of cells into soil following rainfall does not guarantee rapid downward

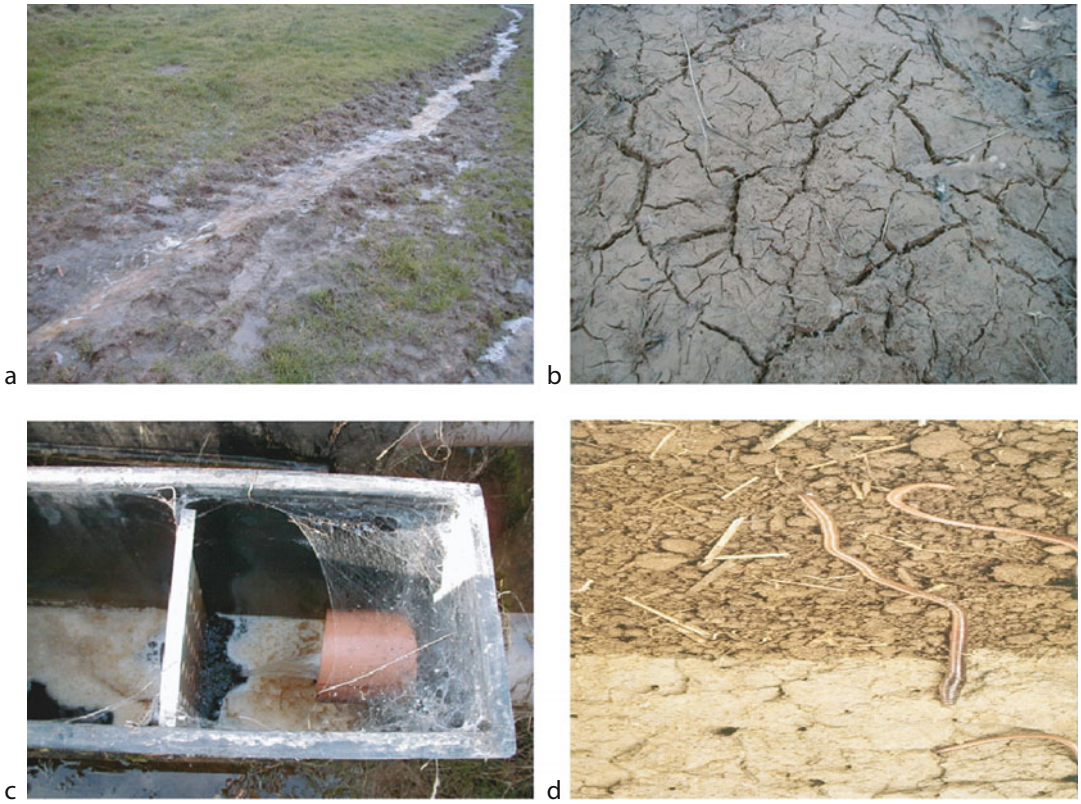

Pathogen and Nutrient Transfer Through and Across Agricultural Soils. Figure 5
Rapid transfer pathways across and through soils: (**a**) overland flow conduits across a clay loam soil; (**b**) soil cracking on exposed grassland soil surface for a clay loam; (**c**) drain flow exported from mole and tile drains on clay loam grassland plots; (**d**) creation of macropores within soil by earthworms

transport because of the potential for cellular retention in the upper dry topsoil aggregates [123]. Rather, as soils wet up over time the interaction with wet soil particles reduces and cells are able to transfer more freely. Thus, Guber et al. [123] showed that FIB were able to associate with dry soil aggregates in increased number compared to wet aggregates, leading the authors to propose an interesting interplay between soil water content prior to a rainfall event and the subsequent transfer of manure-borne bacteria with infiltrating rainfall. Similarly it has been shown that fecal bacteria sticking efficiency to quartz sand particles decreases with distance traveled [124].

Although macropores often make up only a small volume of the soil body they can serve as vertical and lateral routes of relatively rapid water flow and allow microorganisms, among other colloids and contaminants, to successfully bypass the sieving and constraining architecture of the soil matrix (see Fig. 4). Attempts have been made to develop relationships between soil type classes in New Zealand and breakthrough curves [125] and to therefore generate datasets of regionalized potential for microbial bypass flow based on soil classifications that become useful for larger scale modeling scenarios. The role of continuous macropores within silt loam and loam soils has been well documented by Abu-Ashour et al. [120]. Their experimental protocol was designed to create artificial macropores (vertical and straight) through sieved and packed soil. A comparison was made between columns (175 mm high x 89 mm diameter) accommodating artificial macropores (and columns without) in their ability to transfer a slug of cell suspension to depth. Irrigation was applied 24 h after inoculation at a rate of

60 mL h^{-1} for 2 h. For all packed soils without macropores no biotracer was ever detected in the effluent, regardless of initial water content, rainfall rate, or soil type. The study concluded that initial soil moisture appeared to have a notable effect on bacterial movement through soils especially in the presence of a macropore. The effect of the macropore was not substantial when the soil was dry. Aislabie et al. [126] compared four contrasting soil types for macroporous transfer of bacteria and showed the importance of macropore flow in breakthrough curves of clayey soils. This complements the studies of Paterson et al. [127] and Mawdsley et al. [65], who also demonstrated greater recoveries of introduced microbes in leachates from clay loam compared with loamy sand cores. The study of McLeod et al. [128] observed FIB numbers emerging from saturated intact columns (500 × 500 mm) of 2 contrasting soil types following dairy shed effluent application and simulated rainfall (5 mm h^{-1}). The patterns of microbial emergence were indicative of bypass flow and led the authors to stress the need to consider the nature of soil hydraulics in addition to conventional theory of direct entry into mole drains. Critically, studies reporting on the role of macropore flow have provided strong evidence to suggest that very different conclusions can be reached regarding the efficiency of soils as bacterial filters (or particulate filters in general) depending on whether soil cores used within experiments are disturbed or intact.

The action of disrupting macropore continuity can therefore prove effective in limiting contaminant transfer via these rapid flow conduits. For example, on arable soils there can be increased water transfer within no till soils relative to tilled soils. This is thought to be a direct influence of the increased macropore continuity within the no till soils. The action of tillage physically disrupts the soil structure and significantly reduces the extent of macropore connectivity within the soil system. Such a finding has been shown to hold true for reducing *Cryptosporidium* transfer to tile drains [80]. Tillage therefore represents a useful management approach for limiting rapid translocation of microbial pollutants (and particulate associated P) in arable soils and indicates that alternative methods of disrupting the soil structure on a no-till soil would be beneficial for reducing pathogen and FIB loss from land to water. This provides a useful management option for arable land, but for livestock systems and grazed grasslands such approaches are obviously not possible without destruction of pasture.

The presence of subsurface drains (e.g., mole and tile drains) effectively increases subsurface connectivity provided that the age and condition of the features is such that the pathway still functions efficiently as a hydrological conduit. Field drains have been reported to be a rapid route of nutrient export from agricultural land [129] and have also been shown to export *E. coli* from land to water during storm events at similar loads to that of undrained fields using replicated 1 ha plots [82]. The use of natural fluorescence as a tracer has also demonstrated the importance of drain flow in contributing toward nonpoint pollution impacts [130]. Figure 6 shows the relationship between *E. coli* load exported via a mole drain pathway on replicated 1 ha grassland plots (clay loam) in response to rainfall events following the removal of livestock (in this case four beef steers) at the end of a 6-month grazing season. So while the installation of mole and tile drains to lower the water table may be seen as advantageous in limiting the load of potential pollutants transferred rapidly by surface runoff or near surface flow pathways it must also be appreciated that contaminants may be re-routed via different subsurface pathways [82]. Figure 6 shows clearly that significant loads of *E. coli* can be exported from drained plots, even after livestock have been removed, and that these bacteria must have transferred through the soil profile, probably via fissures and cracks in the clay soil to reach drain pathways.

Slow Pathways of Contaminant Transfer

Much research has focused on the infiltration and vertical transfer of pathogens, FIB, and nutrients in soil leachate, and for particulate contaminants there has been considerable assessment of FIB and pathogen movement in relation to colloid filtration theory (e.g., [49, 67, 130]). Vertical displacement of microbes and nutrients through the soil profile has been demonstrated in a variety of soil column experiments (see Table 1). For bacterial transfer, the moisture content of the soil determines cell movement because continuous water films allow for transfer that is essentially limited to the aqueous phase and the solid-liquid

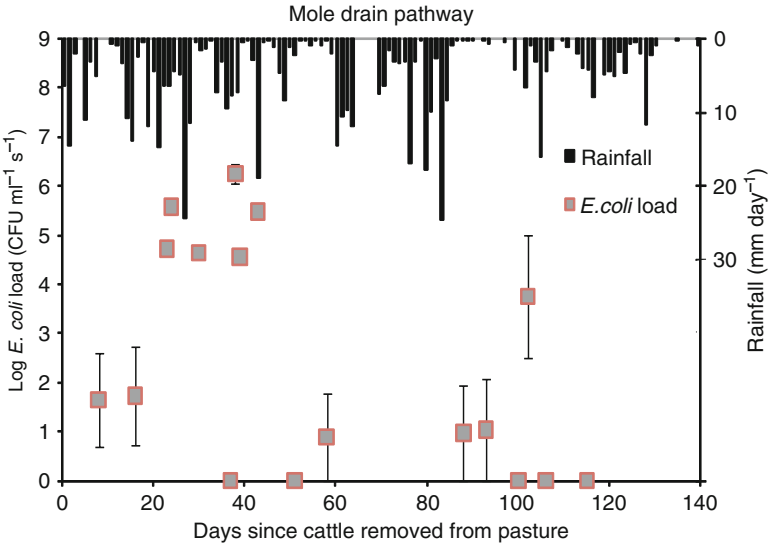

Pathogen and Nutrient Transfer Through and Across Agricultural Soils. Figure 6
Escherichia coli loads exported from mole and tile drains of grassland plots in relation to daily rainfall. X-axis represents day of sampling since cattle removed. Error bars represent 1 S.E. of logarithmic mean (Modified from Oliver et al. [82])

interface. Thus, it has been proposed that appreciable bacterial movement in soil can only occur if there are enough water filled pores of the required diameter to enable a continuous pathway [131]. Nitrate is undoubtedly the main form of N leached from agricultural systems, and greater concentrations will be detected in leachate from soils where N inputs on the land surface produce NO_3^- in excess of amounts required by plant uptake. The soluble and highly mobile nature of NO_3^- means that those soils in climatic zones typical of wet weather regimes will deliver potentially high concentrations of NO_3^-, though because of dilution the concentrations detected will be less.

Under conditions that promote water movement through soil pores, the carriage and translocation of microbes within the drainage water through the soil structure will depend on sieving effects imposed by pore openings. Under conditions of limited pore clogging, bacterial transfer is possible to considerable depths below the soil surface layers following the initial application of a surface applied manure source [132]. However, the transfer of microbes and particulates through the soil architecture can lead to pore clogging that may subsequently restrict such contaminant transfer by the physical blocking of a pore entrance. Bioclogging of the pore network is clearly a function of the particle size of the porous medium and the diameter of the microbial consortia that transfer through the soil system. Bacteria, protozoa, and particulate phosphorus suspended in flow can be effectively strained by the soil matrix and then accumulate within soil passages when pore openings are too small to permit their continued transfer. These pores then become immobile regions that may exist in the filter matrix in the form of ineffective micropores, resulting in the trapping of microbes and sediments in dead end pores. Recent work by Donnison and Ross [58] investigated the effect of soil type on transfer of zoonotic bacteria to rural streams using intact cores and turfs of a gley soil and a sandy loam. Farm dairy effluent, containing laboratory grown *E. coli* O157:H7 and *Campylobacter*, was added to cores and turfs that were stored at 10°C. It was found that the relative timing of application of zoonotic bacteria to soil and that of subsequent rainfall determine whether significant numbers of these bacteria are likely to reach streams. This timing varied for different soil types. For the sandy loam soil there was little transport of cells to drainage after 14 days but for the gley soil there was little change in the proportion of

surviving *E. coli* O157:H7 that was washed out over 35 days, and it was found that *E. coli* O157 could be mobilized relatively easily from this soil. Donnison and Ross [58] highlighted that although far fewer bacteria are washed out than are retained, even immediately after application, the actual numbers can be substantial and could contribute to waterborne disease.

Under conditions of low rainfall, the soil may act as a more efficient filter matrix; this is because the slow percolation of FIB, pathogens, and P into the soil associated with light rainfall will increase microbial and P exposure time to soil surfaces in contrast to rapid water flows, and allow for an increased potential of contact with soil. This does not follow for NO_3^-, which does not interact or associate with the surrounding soil. In well-structured soils N will be retained to a high degree when protected within the bulk of the soil and will therefore only transfer through the soil profile with the slow percolation of mobile water. For microbes and P, implications of forming a cell-particle or P-particle composite may have impact once delivered to surface waters. The significant proportion of *E. coli*, for example, that remains unattached or associated with particles ≤ 2 μm are likely to remain in the water column and cause potential contamination problems further downstream. In contrast, the proportion of *E. coli* associated with larger soil particles are more likely to sediment out into the stream bed and therefore pose a delayed threat to water quality upon their resuspension. Further affinity studies of FIB are required, using different soil types, to test for the effects of an array of environmental variables such as pH, soil mineralogy, and temperature on the affinity of *E. coli* for soil.

Interesting observations have been made regarding the effect of cattle manure and slurry application on the percolation of the pathogens *E. coli* O157:H7 and *S. enterica* serovar Typhimurium. In the study of Semenov et al. [133] a greater number of cells were found to percolate to greater soil depths after slurry application compared to cells applied via manure application. Such results suggest that surface application of solid manures rather than their liquid counterparts may decrease the risk of contamination of groundwater supplies. Phosphate sorption (and release) in soils has also been investigated in relation to fertilizer sources. Such sorption is affected by reactions that take place at the solution-soil surface interface and recent work has demonstrated that phosphate binding strength can be up to 50% less in manured soils than in soils fertilized with inorganic triple superphosphate [134]. Such findings imply manure applications to some soil types result in an increased net negative surface charge and therefore a reduced soil phosphate adsorption capacity leading to increased losses from the soil system. These slower vertical transfers may eventually allow for connection with groundwater supplies, which are covered in the next section of this chapter.

The Role of Groundwater

Microbial and nutrient transport to surface water can occur by deposition of manure directly in the water or by wash-off in surface and subsurface runoff. However, transport to groundwater is a somewhat lesser concern in that it requires that the contaminant of study move through soil and bedrock to reach the water table. Nevertheless, groundwater systems are the predominant reservoir and strategic reserve of global freshwater storage at ca. 30% of the global water total and 98% of freshwater in liquid form [22], and protection of the microbial and chemical quality of this precious freshwater resource is therefore essential to safeguard human health and maintain sustainable freshwater resources. While a number of contaminants may interact with groundwater supplies, it is generally accepted that the most widely studied contaminant of groundwater supplies is NO_3^-. However, it cannot be disputed that the groundwater pollutants that most concern human health are microbiological, causing disease and sometimes death [135].

Manure application to land is regarded as the primary source of bacterial groundwater contamination in agricultural settings [136]. However, most pathogens are suspected to have life cycles far shorter (i.e., high die-off or inactivation rates outside of the animal gut) than typical groundwater travel times, except in karstic aquifers because of their dual porosity or where the source is very close to the point of water abstraction. Even so, continued investigation on microbial persistence within a range of agricultural environments is needed, and published persistence profiles of robust

pathogens such as *C. parvum* propose that this pathogen can remain viable well in excess of hundreds of days [17], suggesting potential implications for groundwater quality upon emergence. The larger size of this protozoan relative to bacterial cells means it is more likely to be filtered by the overlying soil, but direct wash-in of such pathogens into private water supplies is not unheard of and can cause significant human illness. Of course, in addition to nitrates, bacteria, and protozoa, there remain other contaminants of groundwater, their presence dictated by their mobility and reactivity with the aquifer matrix and its overlying soil [135].

A recent case study of contamination of groundwater with microbial pollutants is illustrated by a small dryland watershed in central Chile [137]. This study suggested that concentrations of FIB were temporally dynamic with levels varying between seasons with higher concentrations in winter. As discussed in earlier sections of this chapter, causes of contamination could be linked to the easy access of domestic animals to the water source (i.e., wells in this case) and to the permeable well casing material. Local precipitation runoff would also have a direct influence on the bacterial concentrations found in such wells, with seasonality influencing runoff volumes and climatic characteristics important for driving transfer. Undoubtedly, the climatic conditions typical of winter can also favor survival of pathogens and FIB, with cooler temperatures often considered advantageous for lengthy persistence of these microbes. Studies of *Cryptosporidium* through undisturbed, macroporous karst soil have demonstrated that leaching is an important mechanism of oocyst transport in karst soils but have also provided evidence for the significant role played by macropores (detailed earlier in this chapter) in the soil physical structure. Thus oocysts leaching from soils into the epikarst could accumulate and remain viable for months until hydrological conditions are right for flushing the oocysts into the conduit flow system [59].

Studies have also shown that high concentrations of nitrate in groundwater samples do not relate well to concentrations of bacterial contaminants. A Vietnamese study took measurements of NO_3^- and FIB in groundwater samples taken from both dug wells and bores and found that a significant number (18%) of samples had NO_3^- concentrations in excess of the WHO Guideline value for drinking water of 50 mg L^{-1} (11.3 mg L^{-1} as nitrate-nitrogen). High concentrations of FIB were found in many of the dug wells and even in the deeper drilled bores, but there was no correlation between NO_3^- concentration and bacterial content [138], probably reflecting the different transfer pathways and mobilities of these contaminant typologies through and across the surrounding landscape. Attempts to curb groundwater contamination from nitrate and FIB include novel approaches to mitigation and management such as tree planting within agricultural systems to allow for a more efficient use of resources, since the rooting system of the trees captures nutrients that are not captured by crops, for example. In particular, intercropping systems have been shown to offer potential mitigating effects on *E coli* movement to the groundwater [92].

In contrast to NO_3^-, phosphate is mostly immobile in the subsurface, with the flux of P to groundwater being controlled by the degree of attenuation in soil. It has therefore generally been viewed as presenting minimal threat to groundwater quality. However, recent contrary views have been published contesting the long-held belief that adsorption and metal complex formation retain the majority of potentially mobile phosphorus. The relative contributions of potential sources for these elevated concentrations of P in groundwater are currently unclear but there is evidence to suggest that they are probably partly anthropogenic. Recent findings therefore suggest that groundwater P concentrations are such that they may be a more important contributor to surface water phosphorus, contrary to prior thinking [139]. Fracture flow is critically important because it allows turbulent flow to transport colloidal- and particulate-attached P to groundwater via a pathway where there is low rock–water interaction (see earlier discussion of macropore flow). Similar to concepts governing high levels of emergence of contaminants via macropore flow, the connectivity between fractures rather than fracture presence per se provide major controls on water residence time distribution from the surface system to the receiving surface water body.

Groundwater–surface water interactions are a final point to note for the upwelling of nutrient sources into

streams and rivers. Spatial and temporal distributions of NO_3^- can be observed along the upwelling flow path from groundwater to surface water along stream reaches. A UK study on a Cumbrian stream reach identified that upwelling flows dominated the exchange between groundwater and surface water throughout a period of investigation. In particular, for this stream reach, NO_3^- concentrations along upwelling flow paths appeared to follow two opposite trends, with both decreasing and increasing nitrate concentrations being observed at different points in the experimental reach. The magnitude of variation in NO_3^- concentration along the upwelling flow path to the streambed was thought to be governed by the sediment structure and characteristics in the two contrasting field sites [140]. Research studies detailing microbial pollution linked to groundwater–surface water interactions are scarce, though it is an interesting aspect for future consideration. Under baseflow conditions, the general assumption is that no resuspension of FIB occurs under steady state flow conditions, and only during storm event flows do stream sediments become resuspended in the overlying water column [141]. However, there may be potential for uncontaminated (FIB-free) groundwater to become contaminated as it travels through upwelling flow paths of the hyporheic zone and the sediment associated store of FIB, possibly adding to the baseflow load of FIB. This is clearly an underexplored research agenda for FIB at current time.

Future Directions

Continued research conducted across a range of scales to understand better the transfer of pathogens and chemicals through and over soils is paramount. Different scales of study investigating mechanistic processes through to catchment scale real-world responses of landscape systems all serve key roles in enhancing understanding of pollutant dynamics in the soil-water continuum. Ultimately, management of livestock and their manure must be undertaken with a view to ensure the sustainability of key ecosystem services, such as the provision of clean and safe recreational and drinking water [142] and targeting of mitigation options to protect watercourses needs to be grounded on sound science. The database of such scientific results continues to grow and provides an expanding (though this is immature for FIB and pathogens relative to P and N) body of empirical science that can form the "evidence base" for good regulatory practice [4]. A growing number of initiatives continue to emerge that advocate the drive for integrated catchment management and the need for greater stakeholder engagement to help reduce contaminant transfers. For successful mitigation of pollutant transfers through and across soil that reduce impact on water quality there is a clear need to tailor mitigation options to reap the most "bang for the buck," and therefore management interventions and changes must be considered in terms of both cost and efficiency [143]. Making informed decisions at the field scale is therefore crucial because agricultural land is heterogeneous, and inherent spatial variability in soils and hydrological flow pathways influences the loss of pollutants from land to water, often at subfield scales [144]. Clearly, land management options such as manure incorporation into soil and reduced application rates to pasture can help avoid scenarios likely to enhance transport and serve as viable approaches to minimize nonpoint-source contamination while ensuring the least public health risk [64]. However, mitigation strategies are often much more complex to implement in practice and accommodate site specific constraints. The lag time between implementation of management practices on the land and water quality response is an unfortunate reality in watershed management and adds an extra layer of complexity to matters [36].

While efforts continue in an attempt to limit contaminant transfers through and across soils, there are parallel challenges for the research and policy community. It is critical that soil and water scientists make progress on quantifying losses from (and delivery via) spatially and temporally dynamic pathways rather than only appreciating the existence of such pathways for facilitating pollutant transfers. In particular, quantifying exports of pathogens remains elusive at farm and catchment scales. However, future research agendas for pathogen transport through soil systems must accommodate the need to characterize microbial behavior across a broad range of environmentally relevant conditions. Critically, the transfer pathways of both pathogens and chemicals will be impacted by the likely

changes in climatic conditions [43], which may also impact indirectly on contaminant transfers because of changes to transport and movement of animals, intensity of livestock farming, and habitat change [145, 146]. Flooding too represents a transfer mechanism by which pathogens, FIB, and nutrients can be catastrophically exported from agricultural land in considerable numbers and result in much greater exposure of the human population to pollutants [3, 147]. Thus flooding represents an example of a very different route of transfer, which at present remains poorly understood [148] but which is sure to warrant much attention as an exposure pathway of increasing significance.

What this chapter has attempted to show, in part, is that various pollutant typologies (soluble, particulate, inert, biological etc.) behave and respond to environmental drivers and conditions in different ways. Pathways through and across the soil are used to a different extent by different pollutant types and are influenced by spatial and temporal characteristics of rainfall and soil types. The warning message for mitigation options implemented to reduce pollutant transfer through soil systems is that different strategies will impact on pollutants in different ways. A mitigation strategy designed to impede particulate transfer may, in fact, enhance the movement of soluble contaminants, or even impact on greenhouse gas emissions. The need for holistic understanding of multi-pollutants is now essential to reflect the potential for such "pollution swapping" risks [149, 150]. In turn, approaches for modeling agricultural systems and the flows and transfers of associated contaminants within the soil-water continuum now require frameworks that can explore the effectiveness of nonpoint pollutant mitigation options for multiple pollutants (including those designed for pathogens). Undoubtedly, such tools are high on the agenda for policy-makers who are required to identify which mitigation options are likely to reduce the target pollutant without increasing impact from others [151]. Indeed, integrated water and agricultural management is needed so that decision makers can recognize interdependencies in environmental systems and prioritize management responsibilities for optimal protection of environmental resources [152, 153].

Finally, new technologies continue to push forward the boundaries of science. Higher resolution and continuous sampling is highlighting trends in diffuse pollutants previously undetected and substantiating our knowledge of catchment response to environmental drivers. For detection of microbial pollutants and associated transfer routes through the environment, the future is likely to embrace molecular approaches. Studies are beginning to emerge that investigate molecular versus culture-based approaches for the detection of FIB, and such initiatives are key in examining relationships between quantitative PCR (qPCR) and culture-based FIB counts in an attempt to optimize and standardize methods for current indicators. However, currently, very few studies have attempted to quantify the uncertainty in quantitative qPCR data, though this is likely to be rectified over the coming years. Indeed, such tools are continuing to be investigated, developed, and tested on "end-point receptor" waters (e.g., coastal waters) (e.g., [154]). With continued evaluation of these approaches against standard culture-based techniques (for bacterial studies), there is much potential for these methods to be developed further to determine potential sources and pathways of pollution linked to both surface and groundwater contamination.

Bibliography

Primary Literature

1. Haygarth PM, Ritz K (2009) The future of soils and land use in the UK: soil systems for the provision of land-based ecosystem services. Land Use Policy 26S:S187–S197
2. Pepper IL, Gerba CP, Newby DT, Rice CW (2009) Soil: a public health threat or savior? Crit Rev Environ Sci Technol 39:416–432
3. Bridge JW, Oliver DM, Chadwick D, Godfray C, Heathwaite AL, Kay D, Maheswaran R, McGonigle D, Nichols G, Pickup R, Porter J, Wastling J, Banwart SA (under review). Minimising the waterborne disease burden in affluent nations: a key role for environmental sciences. Bull World Health Organ
4. Kay D, Crowther J, Fewtrell L, Francis CA, Hopkins M, Kay C, McDonald AT, Stapleton CM, Watkins J, Wyer MD (2008) Quantification and control of microbial pollution from agriculture: a new policy challenge? Environ Sci Policy 11:171–184
5. Kay D, Edwards AC, Ferrier RC, Francis C, Kay C, Rushby L, Watkins J, McDonald AT, Wyer M, Crowther J, Wilkinson J (2007) Catchment microbial dynamics: the emergence of a research agenda. Prog Phys Geogr 31:59–76
6. USEPA (2010) National summary of impaired waters and TMDL information. U.S. Environmental Protection Agency,

Washington. Available at: http://iaspub.epa.gov/waters10/attains_nation_cy.control?p_report_type=T. Accessed 4 Feb 2010
7. Hunter PR (1992) Cyanobacteria and human health. J Med Microbiol 36:301–302
8. Pang L, Nowostawska U, Ryan JN, Williamson WM, Walshe G, Hunter KA (2009) Modifying the surface charge of pathogen-sized microspheres for studying pathogen transport in groundwater. J Environ Qual 38:2210–2217
9. Infascelli R, Pelorosso R, Boccia L (2009) Spatial assessment of animal manure spreading and groundwater nitrate pollution. Geospat Health 4:27–38
10. Bartram J, Thyssen N, Gowers A, Pond K, Lack T (2002) Water and health in Europe. A joint report from the European Environment Agency and the WHO regional office foe Europe. WHO Regional Publications, Copenhagen
11. Stewart I, Webb PM, Schluter PJ, Shaw GR (2006) Recreational and occupational field exposure to freshwater cyanobacteria – a review of anecdotal and case reports, epidemiological studies and the challenges for epidemiologic assessment. Environ Health 5:6
12. Topp E, Scott A, Lapen DR, Lyautey AR, Duriez P (2009) Livestock waste treatment systems for reducing environmental exposure to hazardous enteric pathogens: some considerations. Bioresour Technol 100:5395–5398
13. Monaghan RM, Carey PL, Wilcock RJ, Drewry JJ, Houlbrooke DJ, Quinn JM, Thorrold BS (2009) Linkages between land management activities and stream water quality in a border dyke-irrigated pastoral catchment. Agric Ecosyst Environ 129:201–211
14. McKergow LA, Davies-Colley RJ (2009) Stormflow dynamics and loads of *Escherichia coli* in a large mixed land use catchment. Hydrol Process 24:276–289
15. Kay D, Anthony S, Crowther J, Chambers BJ, Nicholson FA, Chadwick D, Stapleton CM, Wyer MD (2010) Microbial water pollution: a screening tool for initial catchment-scale assessment and source apportionment. Sci Total Environ (in press)
16. Arinaminpathy N, McLean AR, Godfray HCJ (2009) Future UK land use policy and the risk of infectious disease in humans, livestock and wild animals. Land use Policy s6S:S124–S133
17. Oliver DM, Clegg CD, Haygarth PM, Heathwaite AL (2005a) Assessing the potential for pathogen transfer from grassland soils to surface waters. Adv Agron 85:125–180
18. Sobsey MD, Pillai SD (2009) Where future emerging pathogens will come from and what approaches can be used to find them, besides VFARs. J Water Health 7:S75–S93
19. St.-Pierre K, Levesque S, Frost E, Carrier N, Arbeit RD, Michaud S (2009) Thermotolerant coliforms are not a good surrogate for *Campylobacter* spp. In environmental waters. Appl Environ Microbiol 75:6736–6744
20. Wilkes G, Edge T, Gannon V, Jokinen C, Lyautey E, Medeiros D, Neumann N, Ruecker N, Topp E, Lapen D (2009) Seasonal relationships among indicator bacteria, pathogenic bacteria, *Cryptosporidium* oocysts, *Giardia* cysts and hydrological indices for surface waters within an agricultural landscape. Water Res 43:2209–2223
21. Conley DJ, Paerl HW, Howarth HW, Boesch DF, Seitzinger SP, Havens KE, Lancelot C, Likens GE (2009) Controlling eutrophication: nitrogen and phosphorus. Science 323:1014–1015
22. Heathwaite AL (2010) Multiple stressors on water availability at global to catchment scales: understanding human impact on nutrient cycles to protect water quality and water availability in the long term. Freshw Biol 55:241–257
23. Edmeades DC (2003) The long-term effects of manures and fertilizers on soil productivity and quality: a review. Nutr Cycl Agroecosyst 66:165–180
24. Haygarth PM, Heathwaite AL, Jarvis SC, Harrod TR (2000) Hydrological factors for phosphorus transfer from agricultural soils. Adv Agron 69:153–178
25. Muirhead RW (2009) Soil and fecal material reservoirs of *Escherichia coli* in a grazed pasture. NZ J Agric Res 52:1–8
26. Oliver DM, Page T, Heathwaite AL, Haygarth PM (2010a) Reshaping models of *E. coli* population dynamics in livestock feces: increased bacterial risk to humans? Environ Int 36:1–7
27. Chadwick DR, Fish RD, Oliver DM, Heathwaite AL, Hodgson CJ, Winter M (2008) Management of livestock and their manure to reduce the risk of microbial transfers to water – the case for an interdisciplinary approach. Trends Food Sci Technol 19:240–247
28. Oliver DM, Heathwaite AL, Fish RD, Chadwick DR, Hodgson CJ, Winter M, Butler AJ (2009) Scale appropriate modeling of diffuse microbial pollution from agriculture. Prog Phys Geogr 33:358–377
29. Unc A, Goss MJ (2006) Culturable *Escherichia coli* in soil mixed with two types of manure. Soil Sci Soc Am J 70:763–769
30. Oliver DM, Page T, Hodgson CJ, Heathwaite AL, Chadwick DR, Fish RD, Winter M (2010b) Development and testing of a risk indexing framework to determine fields-scale critical source areas of faecal bacteria on grassland. Environ Modell Softw 25:503–512
31. Oliver DM, Haygarth PM, Clegg CD, Heathwaite AL (2006) - Differential *E. coli* die off patterns associated with agricultural matrices. Environ Sci Technol 40:5710–5716
32. Hodgson CJ, Bulmer N, Chadwick DR, Oliver DM, Heathwaite AL, Fish RD, Winter M (2009) Establishing relative release kinetics of fecal indicator organisms from different fecal matrices. Lett Appl Microbiol 49:124–130
33. Brennan FP, O'Flaherty V, Kramers G, Grant J, Richards KG (2010) Long-term persistence and leaching of *E. coli* in temperate maritime soils. Appl Environ Microbiol 76(5):1449–1455
34. Lyautey E, Zexun L, Lapen DR, Wilkes G, Scott A, Berkers T, Edge TA, Topp E (2010) Distribution and diversity of *Escherichia coli* populations in the South Nation River Drainage Basin, Eastern Ontario, Canada. Appl Environ Microbiol 76(5):1486–1496
35. Nautiyal CS, Rehman A, Chauhan PS (2010) Environmental *Escherichia coli* occur as natural plant growth promoting soil bacterium. Arch Microbiol 192:185–193

36. Meals DW, Dressing SA, Davenport TE (2009) Lag time in water quality response to best management practices: a review. J Environ Qual 39:85–96
37. Preedy N, McTiernan K, Matthews R, Heathwaite AL, Haygarth PM (2001) Rapid incidental phosphorus transfers from grassland. J Environ Qual 30:2105–2122
38. Hutchison ML, Walters LD, Moore A, Crookes KM, Avery SM (2004) Effect of length of time before incorporation on survival of pathogenic bacteria present in livestock wastes applied to agricultural soil. Appl Environ Microbiol 70:5111–5118
39. Oliver DM, Heathwaite AL, Hodgson CJ, Chadwick DR (2007a) Mitigation and current management attempts to limit pathogen survival and movement within farmed grasslands. Adv Agron 93:95–152
40. McGechan MB, Topp CFE (2004) Modeling environmental impacts of deposition of excreted nitrogen by dairy cows. Agric Ecosyst Environ 103:149–164
41. Aitken MN (2003) Impact of agricultural practices and river catchment characteristics on river and bathing water quality. Water Sci Technol 48:217–224
42. Deasy C, Brazier RE, Heathwaite AL, Hodgkinson R (2009) Pathways of runoff and sediment transfer in small agricultural catchments. Hydrol Process 23:1349–1358
43. Boxall ABA, Hardy A, Beulke S, Boucard T, Burgin L, Falloon PD, Haygarth PM, Hutchinson T, Kovats RS, Leonardi G, Levy LS, Nichols G, Parsons SA, Potts L, Stone D, Topp E, Turley DB, Walsh K, Wellington EMH, Williams RJ (2009) Impacts of climate change on indirect human exposure to pathogens and chemicals from agriculture. Environ Health Perspect 117: 508–514
44. Garbrecht K, Fox GA, Guzman JA, Alexander D (2009) *E. coli* transport through soil columns: implications for bioretention cell removal efficiency. Trans ASABE 52:481–486
45. Armstrong A, Quinton JN (2010) Variability of interrill erosion at low slopes. Earth Surf Process Landforms
46. Lane SN, Brookes CJ, Kirkby AJ, Holden J (2004) A network-indexbased version of TOPMODEL for use with high-resolution digital topographic data. Hydrol Process 18:191–201
47. Reaney SM, Lane SN, Heathwaite AL, Dugdale LJ (2010) Risk-based modeling of diffuse land use impacts from rural landscapes upon salmonid fry abundance. Ecol Model (in press)
48. Yaron B, Dror I, Berkorwitz B (2010) Contaminant geochemistry – a new perspective. Naturwissenschaften 97:1–17
49. Bridge JW, Banwart SA, Heathwaite AL (2006) Noninvasive quantitative measurement of colloid transport in mesoscale porour media using time lapse fluorescence imaging. Environ Sci Technol 40:5930–5936
50. Zonia L, Bray D (2009) Swimming patterns and dynamics of simulated *Escherichia coli* bacteria. J R Soc Interface 6:1035–1046
51. Tu YH, Shimizu TS, Berg HC (2008) Modelling the chemotactic response of *Escherichia coli* to time-varying stimuli. Proc Natl Acad Sci USA 105:14855–14860
52. Sharpley AN, Kleinman PJA, Heathwaite AL, Bburek WJ, Folmar GJ, Schmidt JR (2008) Phosphorus loss from an agricultural watershed as a function of storm size. J Environ Qual 37:362–368
53. Granger SJ, Hawkins JMB, Bol R, White SM, nadan P, Old G, Bilotta GS, Brazier RE, Macleod CJA, Haygarth PM (2010) High temporal resolution monitoring of multiple pollutant responses in drainage from an intensively managed grassland catchment caused by a summer storm. Water Air Soil Pollut 205:377–393
54. Artz RRE, Townend J, Brown K, Towers W, Killham K (2005) Soil macropores and compaction control the leaching potential of *Escherichia coli* O157:H7. Environ Microbiol 7:241–248
55. Mawdsley JL, Brooks AE, Merry RJ (1996) Movement of the protozoan pathogen *Cryptosporidium parvum* through three contrasting soil types. Biol Fertil Soils 21:30–36
56. Matula J (2009) Possible phosphorus losses from the top layer of agricultural soils by rainfall simulations in relation to multi-nutrient soil tests. Plant Soil Environ 55:511–518
57. Entry JA, Sojka RE, Hicks BJ (2010) Matrix-based fertilizers reduce nutrient and bacterial leaching after manure application in a greenhouse column study. J Environ Qual 39:384–392
58. Donnison A, Ross C (2009) Survival and retention of *Escherichia coli* O157:H7 and *Campylobacter* in contrasting soils from the Toenepi catchment. NZ J Agric Res 52:133–144
59. Boyer DG, Kuczynska E, Fayer R (2009) Transport, fate, and infectivity of *Cryptosporidium parvum* oocysts released from manure and leached through macroporous soil. Environ Geol 58:1011–1019
60. Tarkalson DD, Leytem AB (2009) Phosphorus mobility in soil columns treated with dairy manures and commercial fertilizer. Soil Sci 174:73–80
61. Miller JJ, Beasley BW, Chanasyk DS, Larney FJ, Olson BM (2008) Short-term nitrogen leaching potential of fresh and composted beef cattle manure applied to disturbed soil cores. Compost Sci Util 16:12–19
62. Harter T, Atwill ER, Hou L, Karle BM, Tate KW (2008) Developing risk models of *Cryptosporidium* transport in soils from vegetated, tilted, soilbox experiments. J Environ Qual 37: 245–258
63. Brock EH, Ketterings QM, Kleinman PJA (2007) Measuring and predicting the phosphorus sorption capacity of manure-amended soils. Soil Sci 172:266–278
64. Horswell J, Hewitt J, Prosser J, Van Schaik A, Croucher D, Macdonald C, Burford P, Susarla P, Bickers P, Speir T (2010) Mobility and survival of *Salmonella Typhimurium* and human adenovirus from spiked sewage sludge applied to soil columns. J Appl Microbiol 108:104–114
65. Rosa BA, Yim MI, Burdenuk L, Kjartanson B, Leung KT (2010) The transport of *Escherichia coli* through freeze-fractured clay soil. Water Air Soil Pollut 210:243–254
66. Bech TB, Johnsen K, Dalsgaard A, Laegdsmand M, Jacobsen OH, Jacobsen CS (2010) Transport and distribution *of Salmonella enterica* serovar Typhimurium in loamy and sandy soil monoliths with applied liquid manure. Appl Environ Microbiol 76:710–714

67. Turner BL, Haygarth PM (2000) Phosphorus forms and concentrations in leachate under four grassland soil types. Soil Sci Soc Am J 64:1090–1099
68. Di HJ, Cameron KC, Shen JP, He JZ, Winefield JS (2009) A lysimeter study of nitrate leaching from grazed grassland as affected by a nitrification inhibitor, dicyandiamide, and relationships with ammonia oxidizing bacteria and archaea. Soil Use Manage 25:454–451
69. Guzman JA, Fox GA, Malone RW, Kanwar RS (2009) *Escherichia coli* transport from surface-applied manure to subsurface drains through artificial biopores. J Environ Qual 38: 2412–2421
70. Muirhead RW, Collins RP, Bremer PJ (2006) Interaction of *Escherichia coli* and soil particles in runoff. Appl Environ Microbiol 72:3406–3411
71. Ferguson CM, Davies CM, Kaucner C, Krogh M, Rodehutskors J, Deere DA, Ashbolt NJ (2007) Field scale quantification of microbial transport from bovine feces under simulated rainfall events. J Water Health 5:83–95
72. Abu-Ashour J, Lee H (2000) Transport of bacteria on sloping soil surfaces by runoff. Environ Toxicol 15:149–153
73. Tunney H, Kurz I, Bourke D, O'Reilly C (2007) RTDI programme 2000–2006 eutrophication from agricultural sources: the impact of the grazing animal on phosphorous loss from grazed pasture. Teagasc, Wexford
74. Quinton JN, Catt JA, Hess TM (2001) The selective removal of phosphorus from soil: is event size important? J Environ Qual 30:538–545
75. Soupir ML, Mostaghimi S, Yagow ER, Hagedorn C, Vaughan DH (2006) Transport of fecal bacteria from poultry litter and cattle manures applied to pastureland. Water Air Soil Pollut 169:125–136
76. Withers PJA, Hodgkinson RA, Bates A, Withers CL (2007) Soil cultivation effects on sediment and phosphorus mobilization in surface runoff from three contrasting soil types in England. Soil Tillage Res 93: 438–451
77. Mishra A, Benham BL, Mostaghimi S (2008) Bacterial transport from agricultural lands fertilized with animal manure. Water Air Soil Pollut 189:127–134
78. Heathwaite AL, Haygarth PM, Matthews R, Preedy N, Butler P (2005) Evaluating colloidal phosphorus delivery to surface waters from non-point agricultural sources. J Environ Qual 34:287–298
79. Thiagarajan A, Gordon R, Madani A, Stratton GW (2007) Discharge of *Escherichia coli* from agricultural surface and subsurface drainage water: tillage effects. Water Air Soil Pollut 182:3–12
80. Ramirez NE, Wang P, Lejeune J, Shipitalo MJ, Ward LA, Sreevatsan S, Dick WA (2009) Efffect of tillage and rainfall on transport of manure-applied *Cryptosporidium* parvum oocysts through soil. J Environ Qual 38:2394–2401
81. Haygarth PM, Hepworth L, Jarvis SC (1998) Forms of phosphorus transfer in hydrological pathways from soil under grazed grassland. Eur J Soil Sci 49:65–72
82. Oliver DM, Heathwaite AL, Haygarth PM, Clegg CD (2005) Transfer of *Escherichia coli* to water from drained and undrained grassland after grazing. J Environ Qual 34:918–925
83. Alfaro M, Salazar F, Iraira S, Teuber N, Villarroel D, Ramirez L (2008) Nitrogen, phosphorus and potassium losses in a grazing system with different stocking rates in a volcanic soil. Chil J Agric Res 68:146–155
84. Kouznetsov MY, Roodsari R, Pachepsky YA, Shelton DR, Sadeghi AM, Shirmohammadi A, Starr JL (2007) Modeling manure-borne bromide and fecal coliform transport with runoff and infiltration at a hillslope. J Environ Manage 84:336–346
85. Olson BM, Bennett DR, McKenzie RH, Ormann TD, Atkins RP (2009) Nitrate leaching in two irrigated soils with different rates of cattle manure. J Environ Qual 38:2218–2228
86. Collins R, Elliot S, Adams R (2005) Overland flow delivery of fecal bacteria to a headwater pastoral stream. J Appl Microbiol 99:126–132
87. Kay D, Aitken M, Crowther J, Dickinson I, Edwards AC, Francis C, Hopkins M, Jeffrey W, Kay C, McDonald AT, McDonald D, Stapleton CM, Watkins J, Wilkinson J, Wyer M (2007) Reducing fluxes of fecal indicator compliance parameters to bathing waters from non-point agricultural sources: the Brighouse Bay study. Scotland Environ Pollut 147:138–149
88. Deasy C, Heathwaite AL, brazier RE (2008) A field methodology for quantifying phosphorus transfer and delivery to streams in first order agricultural catchments. J Hydrol 350:329–338
89. Botter G, Milan E, Bertuzzo E, Zanardo S, Marani M, Rinaldo A (2009) Inferences from catchment-scale tracer circulation experiments. J Hydrol 369:368–380
90. Close M, Dann R, Ball A, Pirie R, Savill M, Smith Z (2008) Microbial groundwater quality and its health implications for a border-strip irrigated dairy farm catchment, South Island, New Zealand. J Water Health 6:83–98
91. Heathwaite AL, Johnes PJ (1996) Contribution of nitrogen species and phosphorus fractions to stream water quality in agricultural catchments. Hydrol Process 10:971–983
92. Dougherty MC, Thevathasan NV, Gordon AM, Lee H, Kort J (2009) Nitrate and *Escherichia coli* NAR analysis in tile drain effluent from a mixed tree intercrop and monocrop system. Agric Ecosyst Environ 131:77–84
93. Davies-Colley R, Lydiard E, Nagels J (2008) Stormflow-dominated loads of fecal pollution from an intensively dairy-farmed catchment. Water Sci Technol 57:1519–1523
94. Rothwell JJ, Dise NB, Taylor KG, Allott TEH, Scholefield P, Davies H, Neal C (2010) A spatial and seasonal assessment of river water chemistry across North West England. Sci Total Environ 408:841–855
95. Beven K, Heathwaite AL, Haygarth PM, Walling D, Brazier R, Withers P (2005) On the concept of delivery of sediment and nutrients to stream channels. Hydrol Process 19:551–556
96. Haygarth PM, Condron LM, Heathwaite AL, Turner BL, Harris GP (2005) The phosphorus transfer continuum: linking source to impact with an interdisciplinary and multi-scaled approach. Sci Total Environ 344:5–14

97. Armstrong A, Quinton JN (2009) Pumped rainfall simulators: the impact of rain pulses on sediment concentration and size. Earth Surf Process Land 34:1310–1314
98. Mankin KR, Wang L, Hutchinson SL, Marchin GL (2007) *Escherichia coli* sorption to sand and silt loam soil. Trans ASABE 50:1159–1165
99. Penn CJ, Mullins GL, Zelanzny LW (2005) Mineralogy in relation to phosphorus sorption and dissolved phorphorus losses in runoff. Soil Sci Soc Am J 69:1532–1540
100. Drozd C, Schwartzbrod J (1996) Hydrophobic and electrostatic cell surface properties of Cryptosporidium parvum. Appl Environ Microbiol 62:1227–1232
101. Kuczynska E, Shelton DR, Pachepsky Y (2005) Effect of bovine manure on *Cryptosporidium parvum* oocyst attachment to soil. Appl Environ Microbiol 71:6394–6397
102. Voice TC, Weber WJ (1985) Sorbent concentration effects in liquid/solid partitioning. Environ Sci Technol 19:789–796
103. Oliver DM (2005) Hydrological pathways and processes of *Escherichia coli* transfer from grassland soils to surface waters. Ph.D. thesis, University of Sheffield
104. Koopmans GF, McDowell RW, Chardon WJ, Oenema O, Dolfing J (2002) Soil phosphorus quantity-intensity relationships to predict increased soil phosphorus loss to overland and subsurface flow. Chemosphere 48:679–687
105. Ling TY, Achberger EC, Drapcho CM, Bengtson RL (2002) Quantifying adsorption of an indicator bacteria in a soil-water system. Trans ASAE 45:669–674
106. Kretzschmar R, Borkovec M, Grolimund D, Elimelech M (1999) Mobile subsurface colloids and their role in contaminant transport. Adv Agron 66:121–193
107. Soupir ML, Mostaghimi S, Dillaha T (2010) Attachment of *Escherichia coli* and Enterococci to particles in runoff from bare soils. J Environ Qual (in press)
108. Oliver DM, Clegg CD, Heathwaite AL, Haygarth PM (2007b) Preferential attachment of *Escherichia coli* to different particle size fractions of an agricultural grassland soil. Water Air Soil Pollut 185:369–375
109. Muirhead RW, Collins RP, Bremer PJ (2006) The association of *E. coli* and soil particles in overland flow. Water Sci Technol 54:153–159
110. Pachepsky YA, Shelton DR (2011) *Escherichia coli* and fecal coliforms in freshwater and estuarine sediments. Crit Rev Environ Sci Technol (in press)
111. Sinclair A, Hebb D, Jamieson R, Gordon R, Benedict K, Fuller K, Stratton GW, Madani A (2009) Growing season surface water loading of fecal indicator organisms within a rural watershed. Water Res 43:1199–1206
112. Haygarth PM, Wood FL, Heathwaite AL, Butler P (2005) Phosphorus dynamics observed through increasing scales in a nested headwater-to-river channel study. Sci Total Environ 344:83–106
113. Jordan P, Arnscheidt J, McGrogan H, McCormick S (2007) Characterising phosphorus transfers in rural catchments using a continuous bank-side analyser. Hydrol Earth Syst Sci 11:372–381
114. Tyrrel SF, Quinton JN (2003) Overland flow transport of pathogens from agricultural land receiving fecal wastes. J Appl Microbiol 94:87S–93S
115. McDonald A, Kay D (1981) Enteric bacterial concentrations in reservoir feeder streams – baseflow characteristics and response to hydrograph events. Water Res 15:961–968
116. Heathwaite AL, Burt TP, Trudgill ST (1990) The effect of land use on nitrogen, phosphorus and suspended sediment delivery to streams in a small catchment in southwest England. In: Boardman J, Foster LDL, Dearing JA (eds) Soil erosion on agricultural land. Wiley, Chichester/New York/Brisbane/Toronto/Singapore, pp 161–177
117. Page T (2008) Uncertainty assessment of phosphorus risk to surface waters. Environment Agency Science Report – SC050035
118. Kirchner JW, Feng XH, Neal C (2000) Fractal stream chemistry and its implications for contaminant transport in catchments. Nature 403:524–527
119. Beven K, Germann P (1982) Macropores and water-flow in soils. Water Resour Res 18:1311–1325
120. Abu-Ashour J, Joy DM, Lee H, Whiteley HR, Zelin S (1998) Movement of bacteria in unsaturated soil columns with macropores. Trans ASAE 41:1043–1050
121. Geohring LD, McHugh OV, Walter MT, Steenhuis TS, Akhtar MS (2001) Phosphorus transport into subsurface drains by macrpores after manure applications: implications for best manure management practices. Soil Sci 166:896–909
122. Allaire SE, Roulier S, Cessna AJ (2009) Quantifying preferential flow in soils: a review of different techniques. J Hydrol 378:179–204
123. Guber AK, Pachepsky YA, Shelton DR, Yu O (2009) Association of fecal coliforms with soil aggregates: effect of water content and bovine manure application. Soil Sci 174:543–548
124. Lutterodt G, Basnet M, Foppen JWA, Uhlenbrook S (2009) The effect of surface characteristics on the transport of multiple *Escherichia coli* isolates in large scale columns of quartz sand. Water Res 43:595–604
125. McLeod M, Aislabie J, Ryburn J, McGill A (2008) Regionalizing potential for microbial bypass flow through New Zealand soils. J Environ Qual 37:1959–1967
126. Aislabie J, Smith JJ, Fraser R, McLeod M (2001) Leaching of bacterial indicators of faecal contamination through four New Zealand soils. Aust J Soil Res 39:1397–1406
127. Paterson E, Kemp JS, Gammack SM, Fitzpatrick EA, Cresser MS, Mullins CE, Killham K (1993) Leaching of genetically-modified pseudomonas fluorescens through intact soil microcosms – influence of soil type. Biol Fertil Soils 15:308–314
128. McLeod M, Aislabie J, Ryburn J, McGilla A, taylor M (2003) Microbial and chemical tracer movement through two southland soils, New Zealand. Aust J Soil Res 41:1163–1169
129. Heathwaite AL, Burke SP, Bolton L (2006) Field drains as a route of rapid nutrient export from agricultural land receiving biosolids. Sci Total Environ 365:33–46

130. Mosaddeghi MR, Mahboubi AA, Zandsalimi S, Unc A (2009) Influence of organic waste type and soil structure on the bacterial filtration rates in unsaturated intact soil columns. J Environ Manage 90:730–739
131. Bowen GD, Rovira AD (1999) The rhizosphere and its management to improve plant growth. Adv Agron 66:1–102
132. Gagliardi JV, Karns JS (2000) Leaching of *Escherichia coli* O157:H7 in diverse soils under various agricultural management practices. Appl Environ Microbiol 66:877–883
133. Semenov AV, van Overbeek L, van Brugger AHC (2009) Percolation and survival of *Escherichia coli* O157:H7 and *Salmonella enterica* Serovar Typhimurium in soil amended with contaminated dairy or slurry. Appl Environ Microbiol 75:3206–3215
134. Jiao Y, Whalen JK, Hendershot WH (2007) Phosphate sorption and release in a sandy-loam soil as influenced by fertilizer sources. Soil Sci Soc Am J 71:118–124
135. Lerner D, Harris B (2009) The relationship between land use and groundwater resources and quality. Land Use Policy 26S: S265–S273
136. Pachepsky YA, Sadeghi AM, Bradford SA, Shelton DR, Guber AK, Dao T (2006) Transport and fate of manure-borne pathogens: modeling perspective. Agric Water Manage 86:81–92
137. Valenzuela M, Lagos B, Claret M, Mondaca MA, Perez C, Parra O (2009) Fecal contamination of groundwater in a small rural dryland watershed in rural Chile. Chil J Agric Res 69:235–243
138. Cam PD, Lan NTP, Smith GD, Verma N (2008) Nitrate and bacterial contamination in well waters in Vinh Phuc province, Vietnam. J Water Health 6:275–279
139. Holman IP, Whelan MJ, Howden NJK, Bellamy PH, Willby NJ, Rivas-Casado M, McConvey P (2008) Phosphorus in groundwater-an overlooked contributor to eutrophication? Hydrol Process 22:5121–5126
140. Krause S, Heathwaite L, Binley A, Keenan P (2009) Nitrate concentration changes at the groundwater-surface water interface of a small Cumbrian river. Hydrol Process 23:2195–2211
141. Rehmann CR, Soupir ML (2009) Importance of interactions between the water column and the sediment for microbial concentrations in streams. Water Res 43:4579–4589
142. Pretty J (2008) Agricultural sustainability: concepts, principles and evidence. Philos Trans R Soc B Biol Sci 363: 447–465
143. Haygarth PM, ApSimon H, Betson M, Harris D, Hodgkinson R, Withers PJA (2009) Mitigating non-point phosphorus transfer from agriculture according to cost and efficiency. J Environ Qual 38:2012–2022
144. Hewett CJM, Quinn PF, Whitehead PG, Heathwaite AL, Flynn NJ (2004) Towards a nutrient export risk matrix approach to managing agricultural pollution at source. Hydrol Earth Syst Sci 8:834–845
145. Gale P, Drew T, Phipps LP, David G, Wooldridge M (2009) The effect of climate change on the occurrence and prevalence of livestock diseases in Great Britain: a review. J Appl Microbiol 106:1409–1423
146. Semenza JC, Menne B (2009) Climate change and infectious diseases in Europe. Lancet Infect Dis 9:365–375
147. Nagels JW, Davies-Colley RJ, Donnison AM, Muirhead RW (2002) Faecal contamination over flood events in a pastoral agricultural stream in New Zealand. Water Sci Technol 12:45–52
148. Wheater H, Evans E (2009) Land use, water management and future flood risk. Land Use Policy 26S:S251–S264
149. Stevens CJ, Quinton JN (2009a) Policy implications of pollution swapping. Phys Chem Earth 34:589–594
150. Stevens CJ, Quinton JN (2009b) Non-point pollution swapping in arable agricultural systems. Crit Rev Environ Sci Technol 39:478–520
151. Cuttle SP, Macleod CJA, Chadwick DR, Scholefield D, Haygarth PM, Newell-Price P, Harris D, Shepherd MA, Chambers BJ, Humphrey R (2007) An inventory of methods to control non-point water pollution from agriculture (DWPA) user manual. Defra, London, Defra project code ES0203, 113p
152. Fish RD, Ioris AAR, Watson NM (2010) Integrating water and agricultural management: collaborative governance for a complex policy problem. Sci Total Environ (in press)
153. Macleod CJA, Scholefield D, Haygarth PM (2007) Integration for sustainable catchment management. Sci Total Environ 373:591–602
154. Fremaux B, Gritzfeld J, Boa T, Yost CK (2009) Evaluation of host specific bacteriodales 16S rRNA gene markers as complementary tool for detecting fecal pollution in a prairie watershed. Water Res 43:4838–4849
155. Naden PS, Old GH, Eliot-Laize C, Granger SJ, Hawkins JMB, Bol R, Haygarth P (2010) Assessment of natural fluorescence as a tracer of non-point agricultural pollution from slurry spreading on intensely-farmed grasslands. Water Res 44(6):1701–1712

Books and Reviews

Burton CH, Turner C (2003) Manure management: treatment strategies for sustainable agriculture, 2nd edn. Silsoe Research Institute, Bedford

Ferguson C, Husman AMD, Altavilla N, Deere DA, Ashbolt N (2003) Fate and transport of surface water pathogens in watersheds. Crit Rev Environ Sci Technol 33:299–361

Haygarth PM, Jarvis SC (2002) Agriculture, hydrology and water quality. CABI, Wallingford

McDowell RW, Houlbrooke DJ, Muirhead RW, Mueller K, Shepherd M, Cuttle SP (2008) Grazed pastures and surface water quality. Nova Science Publishers, Hauppauge, p 238

Unc A, Goss MJ (2004) Transport of bacteria from manure and protection of water resources. Appl Soil Ecol 25:1–18

Whitehead PG, Wilby RL, Batterbee RW, Kernan M, Wade AJ (2009) A review of the potential impacts of climate change on surface water quality. Hydrol Sci J 54:101–123

PEM Fuel Cell Materials: Costs, Performance and Durability

A. de Frank Bruijn[1,2], Gaby J. M. Janssen[1]
[1]Energy Research Centre of the Netherlands, Petten, The Netherlands
[2]Energy and Sustainability Research Institute Groningen, University of Groningen, The Netherlands

Article Outline

Glossary
Definition of the Subject and Its Importance
Introduction
PEMFC Component Costs and Performance: Targets, Status, and Developments
Operating Conditions Leading to Performance Loss and Shortening the PEMFC Lifetime
Materials Degradation and the Relation to Performance Loss and Shortening the PEMFC Lifetime
Future Directions
Bibliography

Glossary

Bipolar plate Forms the connection between MEAs in a fuel cell stack. The bipolar plate includes the gas flow channels and may also include cooling channels. Bipolar plates are also called flow plates.

Degradation The gradual loss of performance. Irreversible degradation is due to change of materials properties. Reversible degradation can be caused by non-optimal operating conditions. Quantitatively, the degradation can be expressed as a voltage decay rate.

Durability The capability of the fuel cell to operate in the operating window with limited loss of performance.

Lifetime The number of hours that a fuel cell can be operated in the operating window with a predefined performance loss relative to the initial performance.

MEA Membrane electrode assembly is the result of joining two electrodes and the electrolytic membrane together. Usually, the gas diffusion media are considered to be part of the MEA.

Operating window The range of conditions in which the PEMFC can be stably operated. Within this operating window, performance can still depend on the conditions, but irreversible performance loss is limited. The operating window includes the modes of operation, such as start/stop events and load cycling.

PEMFC Proton exchange membrane fuel cell. The operating temperature is around 80°C. Cold start, below 0°C, is possible. For transport applications, the PEMFC is the fuel cell of choice.

Robustness The capability of the fuel cell to operate outside the operating window without a significant irreversible loss of performance.

Definition of the Subject and Its Importance

The Proton Exchange Membrane Fuel Cell, PEMFC or PEFC, is in development for transport applications as well as for power generators ranging from a few Watts to tens of kilo Watts. Despite the fact that fuel cells have many advantages, such as a high conversion efficiency at partial load, clean exhaust gases, modular design and low noise production, their marketability will depend heavily on whether these fuel cells can compete with the incumbent technologies on performance, cost, and reliability in a specific application. For transport, the benchmark at present is the internal combustion engine, which has been mass-produced since 1908, and is characterized by high performance, high reliability, and relatively low cost.

Performance

The internal combustion engine can be cold started within seconds and can be operated worldwide under all climate conditions. It has become quite standard to have 100 kW of engine power under the hood, enabling highway and uphill driving without any concession. A fuel cell vehicle will have to meet the same standards with regard to a fast cold start, availability of power without compromising the available space for the user under all foreseeable conditions. The power density of the complete fuel cell system must be 650 W L^{-1} and

650 W kg^{-1}, which translates to 2,000 W L^{-1} and 2,000 W kg^{-1} for the fuel cell stack [1].

Lifetime and Reliability

Service intervals for passenger vehicles have dropped to once per 30,000 km or once per 2 years, and vehicles last 10–15 years without major revisions, running more than 250,000 km. Consumers are not used anymore to car breakdowns, especially not within the first 5 years of first ownership. Fuel cell vehicles will have to meet the expectations of today, rather than develop along the line of the internal combustion engine, that is, provide reliability comparable to that of the internal combustion engine of decades ago.

This means that at the time of mass-market introduction, their expected lifetime needs to be 5,000 h, with an end of life performance, which is at least 90% of the performance at the beginning of life. No external conditions, except for severe crashes, might lead to severe deterioration of the fuel cell performance. In practice, this means that the fuel cell system needs to operate between −40°C and +50°C ambient temperature, under all relative humidities.

Costs

For the PEMFC to become a viable option for transport, the cost of buying and operating a fuel cell system, which comprises all parts at present not part of a conventional vehicle, must be comparable to that of an internal combustion engine. A higher investment cost of a fuel cell system can be offset by a lower fuel cost, determined by the cost of hydrogen and the fuel economy of the fuel cell vehicle. Although consumers are increasingly eager to take fuel costs or reduced CO_2 emissions into account when making their buying decision, there will be limits to the additional price they will want to pay. A cost-neutral switch from the internal combustion engine to a fuel cell system leads to an allowable cost of US$30/kW for a complete PEMFC system and US$15/kW for a PEMFC stack, which will be operated on hydrogen [1]. These costs are a reflection of the costs of the components and the assembly of the PEMFC stack and system, with the implicit assumption that it will last for the whole lifetime of the vehicle.

The Role of Materials

The materials used in the PEMFC play a key role in the fuel cell systems performance, cost, and reliability. This article aims to present a comprehensive treatment of the performance, cost, and durability issues, especially but not exclusively, in light of their application in transport, as this provides so far the most challenging combination of these issues.

Introduction

As of 2010, fuel cells have matured considerably: Hundreds of fuel cell–driven passenger vehicles have been demonstrated, with an impressive improvement of systems performance. Major car companies such as Honda, Toyota, Daimler, General Motors, Ford, and Hyundai have recently produced a new generation of passenger vehicles that can meet consumer expectations with respect to driving speed, acceleration, and driving range. Furthermore, they can be operated under severe conditions, such as extreme ambient temperature or demanding driving conditions. This accomplishment is based on a combination of advances on both fuel cell components as well as on systems level. On the one hand, the properties of materials determine the real power density of the fuel cell and the volumetric power density of the fuel cell stack. On the other hand, the systems layout, balance of plant and control strategy determine which conditions the fuel cell materials actually experience.

A schematic presentation of cell and stack components is given in Fig. 1.

The electrolyte of the PEMFC consists of a proton exchange membrane. Besides conducting ions from one electrode to the other, the electrolyte serves as gas separator and electronic insulator. At either side of the membrane, a catalytically active electrode is intimately attached to the membrane, to form a so-called membrane electrode assembly, the MEA. At the anode, hydrogen is oxidized to protons. At the cathode, oxygen is reduced to water. The theoretical voltage at open circuit of a hydrogen–oxygen fuel cell is 1.23 V at 298 K. Under load conditions, the cell voltage is between 0.5 and 1 V, producing a current density up to 1.5 A cm^{-2}, depending on conditions.

The type of materials being used in PEM fuel cells has stayed the same since the early 1990s [2].

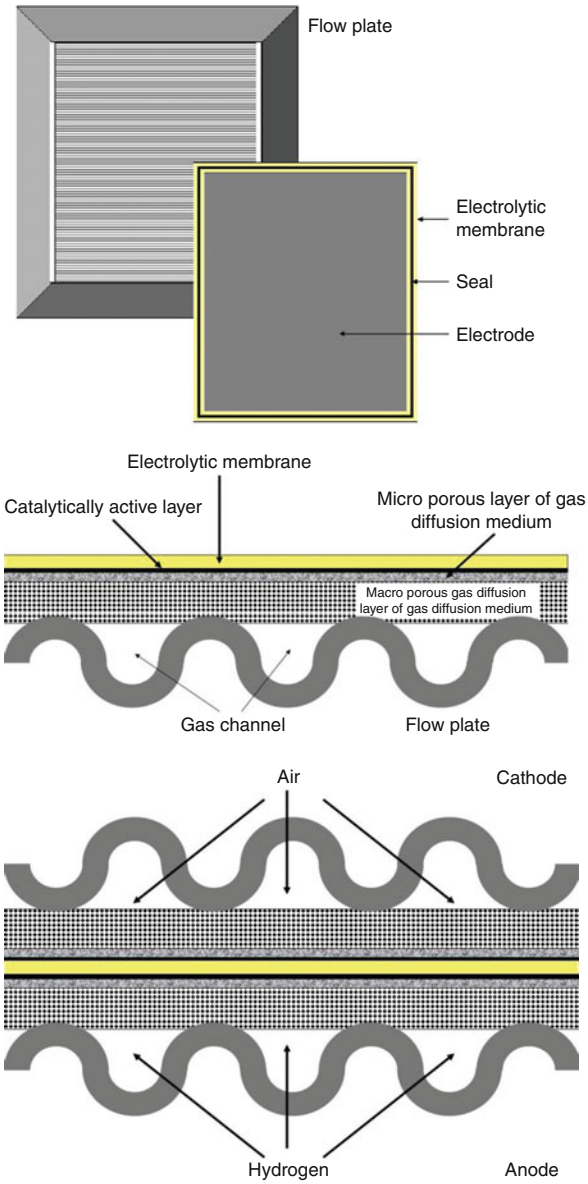

PEM Fuel Cell Materials: Costs, Performance and Durability. Figure 1
Cell and stack components. *Top*: top view of separator plate and MEA with seal; *middle*: cross-section view of one site of MEA on flow field; *bottom*: cross-section view of complete cell package

For the electrolyte, perfluorosulfonic acid/tetrafluoroethylene copolymer membranes (usually referred to as PFSA membranes) have been used for decades. Chemically, this polymer can be considered as a Teflon or polytetrafluoroethylene (PTFE) backbone, with Teflon-like side chains bearing a SO_3H (sulfonic acid) group. Dissociation of this sulfonic acid group leads to mobile protons. Produced as thin, flexible sheets that become conductive when containing water, these membranes enable high volume manufacturing of complete cells by coating the electrodes on these sheets. Originally developed for chlor-alkali electrolysers, the membranes provide a combination of properties that is unsurpassed: high proton conductivity and a high chemical stability. For optimal conductivity, the water content of the membrane needs to be such that the H_2O/SO_3H ratio λ is larger than 14 [3], which for state-of-the-art materials is only achieved at 100% RH. The latest developments on perfluorosulfonic acid/tetrafluoroethylene copolymer membranes that have been applied in fuel cells have been on even further improvement of their chemical stability and the development of ever thinner membranes down from 175 to 25 μm, among others by using reinforcements for maintaining strength.

For the electrodes, platinum on carbon catalysts have long been used in both anode and cathode for hydrogen/air fuel cells. Commercial electrodes contain around 0.2–0.4 mg cm^{-2} platinum, generating a power density of 0.5–0.7 W cm^{-2} [2]. Using a total loading of 0.6 mg cm^{-2} and a power output of 0.5 W cm^{-2}, the platinum usage amounts to 1.2 g kWe^{-1}. It has, however, been demonstrated that fuel cells with 0.4 g_{Pt} kWe^{-1} are achievable when using clean hydrogen and air [4]. The long-term stability of such cells is, however, not known yet, and the use of reformate prescribes higher loadings of Pt–Ru at the anode, 0.2 mg_{PtRu} cm^{-2} at minimum. The ultimate goal is to lower the platinum usage to less than 0.2 g_{Pt} kWe^{-1}.

The use of noble metals is an important factor in the cost of the fuel cell. Whereas the cost of many components drops when the scale of manufacturing increases, this is not the case for the noble metal catalysts. The concern of a real shortage of platinum in case of large-scale use of fuel cells in vehicles has been proven not to be substantiated [5], but this is based on a significant reduction of its use to 15 g/vehicle, corresponding to the 0.2 g_{Pt} kWe^{-1} mentioned before. The key issue is to minimize the amount

of platinum per kW fuel cell power, while maintaining the power density of the present state-of-the-art. It makes no sense to substitute platinum by another metal when this leads to a reduction of the power density.

The catalysts used as a base for electrode manufacturing consist of high loadings of noble metal on carbon, of 40 wt% or even higher. These high loadings are used to render a thin electrode with high enough amount of active sites, typically 10 μm thick. The platinum particle sizes are even at these high noble metal loadings in the range of 2–3 nm [6].

Even in electrodes with a high catalytic activity, the performance is heavily dependent on the electrode structure, as oxygen transport becomes crucial at practical current densities. Water removal plays a key role in this, as the diffusion constant of oxygen in water is a factor of 5,700 lower than that in air at 60°C. Gas Diffusion Media (GDM) play a decisive role in the water management of the fuel cells. Gas diffusion media, which consist of a macro porous gas diffusion layer (GDL) of 200–400 μm covered by a micro porous layer (MPL) of 30–50 μm, facilitate the transport of gas and electrons between the catalytically active layer and the flow plate. While the macroporous gas diffusion layer needs a certain thickness to distribute the gas in horizontal direction, the microporous layer facilitates the removal of liquid product water, preventing the so-called flooding of the electrode. Effective prevention of such flooding can extend the voltage current curve by around 0.5–1 A cm^{-2}.

The component that has the highest impact on the weight and volume of the fuel cell stack is the flow plate or bipolar plate. Whereas the flow plates used to be made from high-density graphite, nowadays the material of choice is a moldable graphite/polymer composite material. Although the latter has a somewhat lower conductivity than pure graphite, it enables the use of plates with lower thickness due to its higher mechanical strength and its higher flexibility. This directly leads to reduction of stack weight and volume. A major advantage of polymer/graphite plates is the fact that they can be manufactured by means of injection molding [7]. An alternative to graphite and polymer/graphite material plates is the metal plate. The main advantage of metal plates is the fact that very thin metal sheets can be used, and mass manufacturing techniques are available for forming flow patterns in these sheets [2].

Operating Window and Performance

As the area power density of a fuel cell is determining for the overall cost of the system, it is essential to optimize the operating window of the fuel cell stack. Of all conditions, the relative humidity has the largest influence on power density. This relative humidity is governed by the water content of the feed gases and their stoichiometry, the amount of product water, which is directly proportional to the current density, and the cell temperature.

The minimum requirement for water is set by the dependence of the proton conductivity of the PFSA membrane on its water content. In case this minimum requirement is not met, drying out of the membrane and the ionomer phase of the electrode leads to rapid decline of the power density. A maximum is clearly set by the transport of oxygen through the electrode, as liquid water is an effective barrier for the transport of gas to the reaction interface. In the catalytic layer of the cathode, these two factors determine an optimum: sufficient liquid water in the ionomer for proton conduction while simultaneously allowing gas phase transport of oxygen [8]. Figure 2 schematically draws the optimum situation as well as the situation of drying out and flooding.

The water accumulation at the cathode catalyst layer not only originates from product water but also from the electroosmotic drag, that is, protons migrating from anode to cathode also carry water with them. This electroosmotic drag is roughly proportional to the current density. Removal of this accumulated water can take place in two directions. First, water will be transported through the cathode gas diffusion medium to the air gas channel either as vapor or in the liquid form. Second, there will be back-transport of water through the membrane and the anode gas diffusion layer to the fuel gas channel. The respective rates at which these processes take place depend on the driving force for the water transport in either direction and the water permeability of the components [9].

The driving force is the difference in the chemical potential of water (determined by vapor pressure or

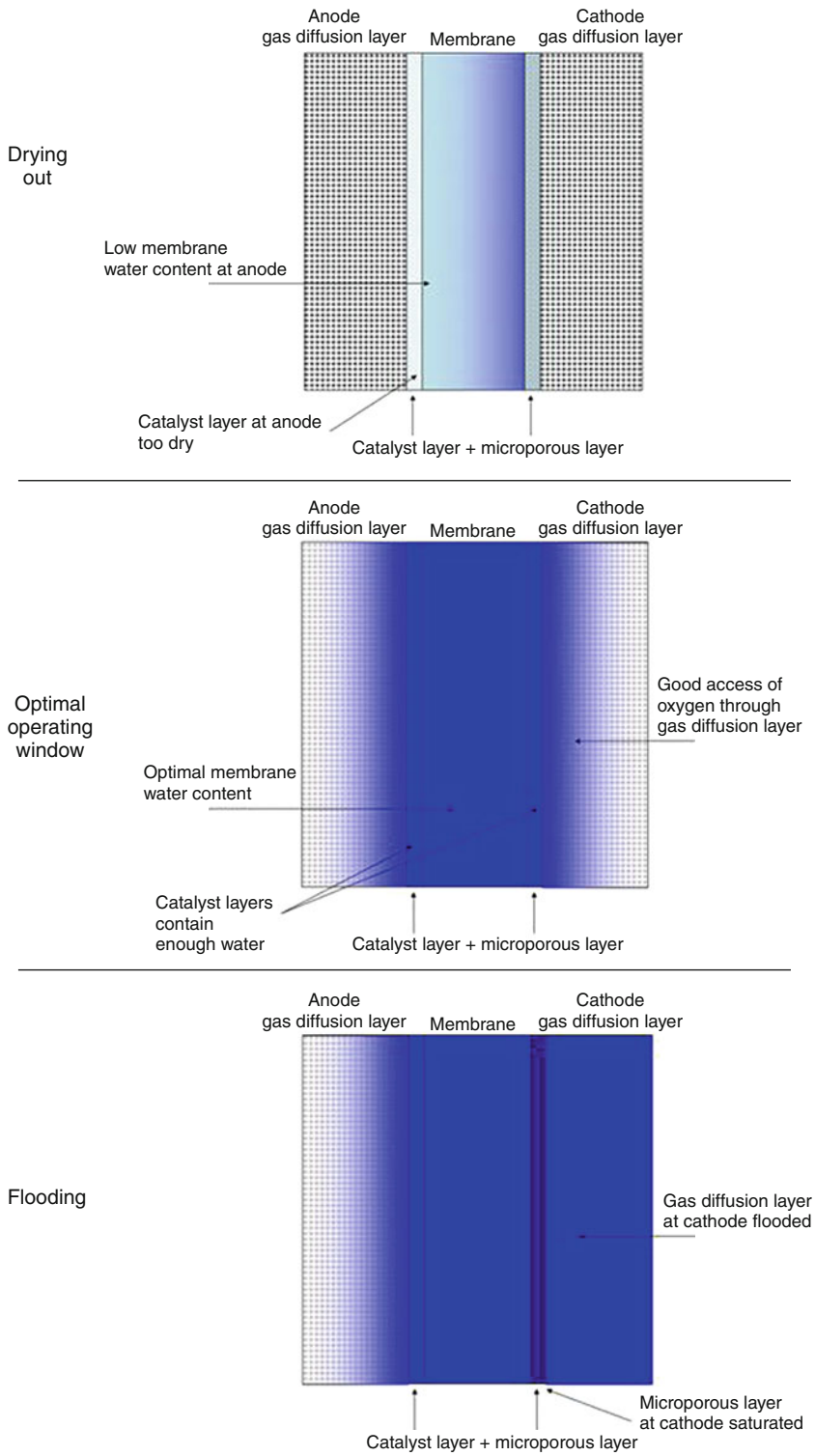

PEM Fuel Cell Materials: Costs, Performance and Durability. Figure 2
Water content of electrode parts and membrane in optimal operating window, as well as under too dry and too wet conditions

hydraulic pressure) in the catalyst layer and the gas channel. The first depends strongly on the current density, the second on the relative humidity of the gas channel, factors that can to some extent be controlled and matched.

The water permeability of the components is at least as important. Thin membranes allow for fast water transport to the anode, reducing flooding at the cathode. In thin membranes, the back-transport of water can often overcompensate the water transport that is associated with the electroosmotic drag, thus preventing drying out at the anode.

The state-of-the-art gas diffusion media are hydrophobized to such an extent that they allow transport of liquid water, an important mechanism at near-saturated conditions, as well as of water vapor and reactant gases. An important role is played by the micro porous layer (MPL). Because of the presence of small hydrophobic pores, a substantial liquid water capillary pressure can be built up, enabling a good gradient in the chemical potential of water to drier sections [10]. The optimization of gas diffusion media and the application of the MPL have led to significant improvement of the fuel cell performance at saturated conditions, showing their critical role.

The occurrence of flooding leads to an almost immediate drop in power output, which cannot be restored instantaneously. Proper design of the flow field, the cell characteristics, and knowledge of the operating window in which flooding as well as membrane drying can be avoided with the hardware used should lead to system control design avoiding these conditions. Sensors that measure the relative humidity continuously do exist [11] but seem to be too bulky and costly to be applied in a fuel cell system. In fact, the accurate measurement of the water content of gases is very complicated. Most systems therefore rely on the proper functioning of the humidifier, the cell temperature sensor, gas flow sensors, and the preservation of the water management properties of the gas diffusion media. If in the course of the cell lifetime, the water removal capability of the gas diffusion media declines, one could compensate for this by increasing the reactant stoichiometries at high current densities.

A more drastic prevention from flooding would be to work at drier conditions. In such a case, the conditions in the gas channel are such that the driving force for water removal is enhanced. In addition to the strategy of developing membranes and catalysts that do not require a high humidity, the water permeability of the gas diffusion media should be reduced. Whereas mere reduction of gas permeability may also deteriorate the access of especially oxygen, improved water management may come from optimized MPLs. The capability to work at drier conditions would also allow increase of the upper limit of the window of operating temperature.

In the following sections, the fuel cell components are discussed in detail: options and needs for further cost reduction, for operation at more desired conditions, and durability issues.

PEMFC Component Costs and Performance: Targets, Status and Developments

Cost and Performance Breakdown

Directly or indirectly, all R&D efforts on PEMFC materials and components can be brought down to cost reduction. The progress on cost reduction over the last decade has been impressive. Based on high volume numbers, 500,000 systems per year, the cost of a PEMFC system using the materials available in 2009 would be $61/kW coming from $275 in 2002 [12]. These costs are a reflection of the costs of the components and the assembly of the PEMFC stack and system, with the implicit assumption that it holds for the rest of the lifetime of the vehicle. The durability requirement of 5,000 h for a passenger vehicle is treated separately.

For commercial applications, operation and maintenance costs are considered as important as the initial investment costs. Durability becomes in that case a matter of maintenance costs, both from the point of replacing individual components, as well as taking into account the time needed to replace these components. An individual seal in a fuel cell stack might cost only 1 dollar, but when the complete stack has to be disassembled to replace that individual seal, it is obviously worthwhile to apply more robust seals that minimize the need for replacement. Similarly, accepting higher fuel costs, caused by a lower cell voltage needed to generate the same fuel cell power after a certain voltage decay has accumulated over time, may be preferred to replacing MEAs or even a complete stack.

The most consistent monitoring of the progress on cost reduction is probably done by the US Department of Energy (DoE). Cost targets are set for 2010 and 2015, where the 2015 target is meant to meet commercial requirements, and the 2010 target is meant as intermediate milestone. An annual production volume of 500,000 vehicles per year is used to take into account the beneficial effect of mass manufacturing, which does not imply that a learning factor is incorporated in the cost figures. The cost per kW follows from the cost of components used per m^2 cell area and the power density of such a cell under the specified conditions. The use of expensive components can thus lead to low costs per kW provided the power density of such a cell is high enough.

Figure 3 gives the progressive cost reduction of a PEMFC stack for the years for which enough details are present to make a deeper assessment of the cost breakdown.

It must be noted that the DoE analysis has some tentative aspects. New materials are taken into account in the cost figures without the guarantee that these will actually survive the operating conditions over the full lifetime of the fuel cell. On a cell level, these materials might have survived relevant accelerated tests, but that does not mean that in combination with stack and system hardware, and used under real-life conditions, these materials will qualify. It is at present the only publicly known assessment of fuel cell costs that is regularly updated, and that takes into account all fuel cell stack and system components on an equal basis.

According to the most updated report [13], the cost of an 80 kW PEMFC system, when produced in a quantity of 500,000 systems per year, would amount to \$60–\$80/kW_{net}. The contribution of the stack and systems components is illustrated in Fig. 4.

From Fig. 4, it becomes clear that the stack is the most expensive single component of the fuel cell system, and that on stack level, the catalyst is the most expensive single component. It is important to notice that all costs are expressed per kW system output. It can

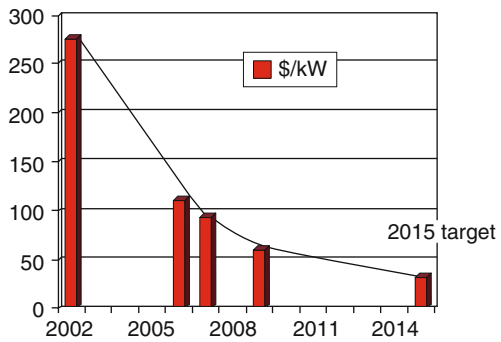

PEM Fuel Cell Materials: Costs, Performance and Durability. Figure 3
Cost progress for PEFMC stack, \$ per kW for an 80 kW stack, when manufactured at 500,000 pieces per year (Data from [12])

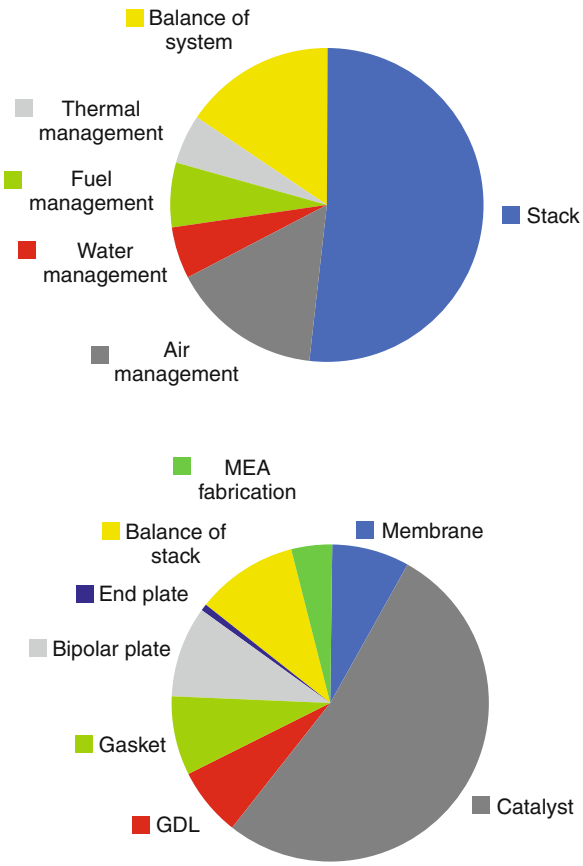

PEM Fuel Cell Materials: Costs, Performance and Durability. Figure 4
Contribution of components to total stack costs, taking the cost estimate from Tiax [13]. Top figure: cost breakdown of an 80 kW system; bottom figure: cost breakdown of an 86 kW PEMFC stack. Note that an additional 6 kW is necessary to power balance of system components

therefore be important to improve a component that has a big impact on fuel cell performance without being expensive itself. When a better performing membrane or gas diffusion layer leads to a doubling of the power density while the catalysts cost per square meter stays the same, its cost will halve per kW due to this membrane or GDL improvement. Vice versa: It is not helpful to decrease the loading of platinum per square meter, when this leads to a lower power density: All components' costs per kW will increase, possibly offsetting the cost gain of the lower platinum cost.

In PEMFC, the cost targets strongly determine the performance targets, which includes MEA performance as well as the allowable operating window. As a result, targets are more demanding for automotive than for stationary applications.

For automotive conditions, the DoE has set for 2015 a target rated cell power density of 1 W cm^{-2}, that is, 1.5 A cm^{-2} at 0.68 V corresponding to 55% LHV electrical efficiency. The requested efficiency at 25% power is 65%, which implies 0.8 V at 0.25 W cm^{-2} or 0.31 A cm^{-2}. Furthermore, the cost requirements demand that the total precious metal loading should not exceed 0.15 g kW^{-1}, which results in 0.2 mg cm^{-2} [1]. In automotive conditions, the peak power will be achieved at the higher end of the temperature window, in extreme situations near 120°C, which will mean that the relative humidity will be low, in the order of 25% maximum.

In stationary systems (including APU), the power density may be lower, with 0.6–0.7 W cm^{-2} at 0.7 V a typical target but with higher precious metal loadings in the order of 0.5 mg cm^{-2}. For reformate fed systems, there is the additional requirement of CO tolerance up to 50 ppm. The temperature and relative humidity can be kept closer to what are called the ideal PEMFC conditions, although increase of temperature up to 120°C, without increasing the dew point of the gases, would contribute to efficiency of the utilization of heat in μCHP systems. As automotive performance targets seem to encompass stationary targets with the exception of reformate tolerance, in the following, the emphasis will be on automotive targets.

Figure 5 shows a deconvolution of the total cell voltage compared to the voltage corresponding to the Lower Heating Value. Three different types of losses are usually identified, ohmic loss, activation loss and transport losses. The curves shown correspond to the target situation, that is, the overall ohmic resistance is 0.04 Ω cm^2, the total performance matches the efficiency requirements at rated power and 25% rated power, and the activation losses are limited to what may be expected if the catalysts satisfy the targets of the DoE, that is, a mass activity for the oxygen reduction reaction (ORR) of 0.44 A mg^{-1} (900 mV, H_2/O_2, 80°C, 100% RH, 150 kPa), and 0.15 mg_{Pt} cm^{-2} cathode loading [1]. At 0.05 mg_{Pt} cm^{-2} anode loading, anode losses are assumed to be negligible. The difference between the targeted curve and the curve representing activation and ohmic losses reflects the maximum acceptable transport losses.

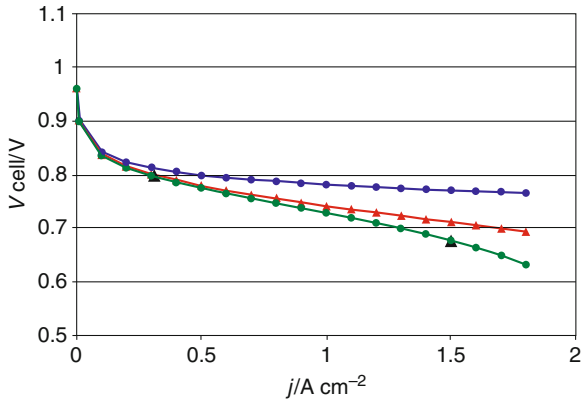

PEM Fuel Cell Materials: Costs, Performance and Durability. Figure 5
Deconvolution of the total cell voltage according to DoE targets. The blue line includes activation losses only, the red line includes ohmic losses as well, and the green line gives the overall performance in agreement with the DoE targets (▲)

The most significant contributions to the ohmic losses are due to the membrane, the bipolar/cooling plates and the electrodes (GDM + catalyst layer), including contact resistance between components. In a H_2/air-fed fuel cell, the activation losses are mainly at the cathode. The catalyst layer, the microporous layer (MPL), and the macroporous gas diffusion layer (GDL) of the gas diffusion medium (GDM) as well as the gas channel design (i.e., the bipolar plate) all contribute to transport losses of reactants.

The PEM fuel cell contains a number of components of which the performance varies with operating conditions. This relation can be either instantaneous or become apparent after longer exposure to such conditions. The components that are most sensitive for operating conditions are the proton exchange membrane and the electrodes for hydrogen oxidation and oxygen reduction.

The PEMFC based on perfluorinated sulfonic acid membranes can be operated from sub-freezing conditions to around 80°C, the upper limit depending on the operating pressure and relative humidity of the inlet gases. Although the PEMFC can be started subzero, systems will generally be controlled in such a way that the cell temperature is allowed to increase to the desired set-point between 60°C and 80°C, where power output is at its maximum while improving water management. At low pressures and low relative humidity, this set-point will be close to 60°C, while at high pressures and high relative humidity, the set-point will be close to 80°C.

It has been amply demonstrated that the membrane performance is at its maximum when fully wetted by water. The proton conductivity is in this case at its maximum. Under stationary conditions, using fully humidified gases and moderate temperatures not exceeding 70°C, the stability of the membrane was proven sufficient to sustain stable performance for 26,000 [14] – 36,000 [15].

For the fuel cell electrodes, the picture is more complex, partially because of the various electrode components and functions merged together. For proton conductivity, an ionomer similar to that used for the proton-conducting membrane is dispersed throughout the electrode. As for the membrane, it needs to be wet to provide sufficient proton conductivity. At the same time, an upper limit for wetting exists for the catalyst layer to prevent flooding. For the electrocatalyst, the electrode potential is the dominant factor determining activity and stability, provided that hydrogen and oxygen are sufficiently available at the reaction interface. For hydrogen oxidation, the activation losses are moderate, so that in practice the anode is between 10 and 50 mV versus RHE. For oxygen reduction, however, the activation losses are substantial; the cathode potential is, depending on the current density, between 500 and 800 mV versus RHE. There has always been a trade-off between efficiency and power output, which can be translated into a trade-off between fuel efficiency and fuel cell investment cost. The relation between cell current density and cell voltage, efficiency, and power density is illustrated in Fig. 6.

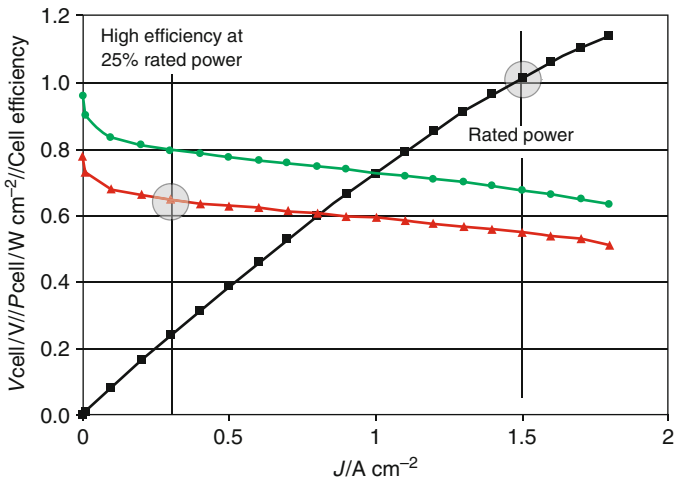

PEM Fuel Cell Materials: Costs, Performance and Durability. Figure 6
Cell voltage (*green*), power density (*black*), and efficiency (*red*) versus cell current density. The points of rated power and 25% rated power are indicated. Follow vertical lines to find the corresponding cell characteristics at these points

The fuel cell electrical efficiency is directly proportional to the fuel cell voltage ΔE_{cell}:

$$Eff_{FC,\ LHV} = \frac{\Delta E_{Cell}}{1.23\ V}, \quad or \quad Eff_{FC,\ HHV} = \frac{\Delta E_{Cell}}{1.48\ V}$$

for the lower heating efficiency (LHV) and the higher heating efficiency (HHV), respectively, at room temperature. In Fig. 6, the green line represents the relation between cell voltage and current density, which is the same as in Fig. 5; the red line represents the LHV cell efficiency versus current density, according to the equation above, while the black line represents the cell power density versus current density. For the fuel cell and conditions of Fig. 6, the point of rated power density, in this case 1 W cm^{-2}, lies at 0.68 V, at which the cell LHV efficiency amounts to 55%. At a cell LHV efficiency of 65%, the power density equals 0.25 W cm^{-2} at a cell voltage of 0.8 V. In practice, a system containing a cell with characteristics shown in Fig. 6 will be operated near the high efficiency point for most of its time, while at occasional times, when the rated power is needed, the cell is operated at lower cell voltage. Opposed to internal combustion engines, the operation at low power demands, for example, when idling, leads to higher efficiencies of the fuel cell. At systems level, this is partly offset by the energy consumption of balance of system components.

When developing new materials and components for reducing costs, their durability should be the starting point instead of the sanity check afterward. The durability standard is set by the components used in today's technology, and should only become better. Cheaper alternatives that would lead to lower durability are not welcome, as they would lead to the previously mentioned early replacement of complete stacks or disassembling of the stack to replace individual components.

Moreover, cheaper cell materials leading to lower power density will lead in most cases to higher stack costs at the end. Except for the catalyst, no single component constitutes more than 10% of overall stack costs. Using the overall cost numbers of the Tiax analysis [13], total cost per cell will be $4,80 including bipolar plates. The power of such a single cell is 196 W, that is, costs are $24.50 per kW. The membrane, generally regarded as an expensive component, will cost $0.43 per single cell. Suppose a cheap alternative membrane, costing only $0.10 per cell, would lead to a performance of 180 W per cell. In this case, a very substantial cost reduction of more than 75% for a particular component leads to a power output loss of less than 10%. Per kW, the cell with the low cost membrane is more expensive, $24.8 per kW than the cell with the expensive membrane. This simple example shows that improvement of the cell power density rather than mere component cost reduction should be driving materials R&D.

The complexity of the fuel cell system is for a considerable part caused by the large influence of the relative humidity in the cell on the performance of the MEA. The heat removal capacity of a fuel cell system operating at 70–80°C is limited, since it is directly proportional to the temperature difference between the cooling liquid temperature and the ambient temperature. Moreover, nearly all the heat produced in the fuel cell stack has to be rejected over the coolant/radiator/ambient air heat exchanger, while in the internal combustion engine, much heat is rejected through the tailpipe. Under certain conditions, that is, when delivering full power at a limited speed at high ambient temperature, this can easily lead to stack temperatures up to 120°C. Volkswagen has a test drive in Death Valley to test their cars on their capability to deal with this [16]. Although the occurrence of such events can be minimized by increasing, for example, the radiator size of the system, from a point of view of system robustness, it is preferred that the stack can operate at such conditions.

However, maintaining a constant high relative humidity at temperatures rising above 70–80°C is not feasible due to the large amount of water that would need to be circulated as well as the negative effect it would have on the oxygen partial pressure, Therefore, a large R&D effort is currently spent on developing MEAs that do not show a drop in power output at, increasing temperatures with concomitant reduction in relative humidity. Although such widening of tolerable relative humidity range could lead to some reduction in cost for thermal management and water management, see Fig. 4, the prime advantage is on increasing robustness of the system.

In the following sections, the individual cell and stack components are discussed in view of their performance and cost.

Costs and Performance Developments of Components

Membranes The targeted values for the membrane resistance are 0.02 Ω cm^2 [1]. The accepted commercial standard for membranes (Nafion, Flemion, Aciplex,) consists of a PTFE backbone with a perfluorovinylether side chain that ends with a sulfonic acid group. Variations in this side chain distinguish the different trade names. The commercial standard membranes have equivalent weights (EW) in the order of 1,100 g eq^{-1} (weight per mol sulfonic acid groups). At ideal conditions (i.e., 80°C, liquid water present), a conductivity of 0.1 S cm^{-1} is a standard value for commercial PFSA membranes. The resistance target therefore corresponds to a maximum thickness of 20 μm. Whereas this was a few years ago still at conflict with requirements on gas tightness and durability, the implementation of reinforced membranes has made this feasible as was shown by Gore, Dupont, and 3M [17–19]. Such a reinforcement is made of PTFE or a ultrahigh molecular weight polyethylene. The latter materials, however, are less suitable for operation near 120°C. These high EW PFSA membranes of 25–30-μm thick, either reinforced (DTI) or not (TIAX), form the basis of the membrane cost in the DoE analysis. These costs amount to $2.4(Tiax) or $3.3 (DTI) per kW [13].

The conductivity of high EW membranes, however, drops dramatically with relative humidity to less than 5 mS cm^{-1} at 25% RH, that is, by more than an order of magnitude [20]. Although conductivity values increase slightly with temperature, this implies that at 120°C, 25% RH these membranes do not meet the target. This fact has motivated considerable research into membranes that can operate at drier conditions, with already quite promising results.

Several routes have been and are to time still being explored, which include (1) low EW PFSA membranes, (2) hybrid inorganic/organic membranes where inorganic additives should take care of water retention and/or proton conductivity, and (3) membranes that enable intrinsically dry proton conduction, such as systems based on imidazole or phosphonic acid rather than water as a proton carrier or relying on phosphoric acid as the proton-conducting medium.

Low EW membranes have higher proton conductivity values at a given humidity. The equilibrium number of water molecules per acid group (λ) at a certain humidity value is not dependent on the EW, which results in an increased water uptake per volume or weight unit. In addition, the mobility of the protons tends to increase with decreasing EW, supposedly due to morphological changes associated with the higher water fraction [21]. The combination of higher concentration of protons and enhanced mobility results in conductivity values that at the same λ are higher for low EW polymers. At low EW, however, the degree of crystallinity of the membrane is reduced, which results in water-soluble membranes. Approaches to reduce the water solubility have included modification of the polymer, cross linking, and blending.

A modification of the polymer that has been adopted by various groups is to have shorter side chains as compared to Nafion. Short side chains increase the crystallinity of the PFSA, thus reducing the solubility. Solvay Solexis has developed Aquivion, a membrane based on Hyflon, which is a copolymer of Teflon and sulfonyl fluoride vinyl ether with low EW (790–870) and good crystallinity, with proton conductivity values in the order of 30 mS cm^{-1} at 120°C, 30% RH [22]. A similar approach is followed by 3M, who have shown 580 EW membranes approaching 100 mS cm^{-1} at 120°C and RH 50% [23]. Gore recently reported values >50 mS cm^{-1} at 30% RH and > 100 mS cm^{-1} 50% RH with a new, undisclosed ionomers [24]. DuPont recently presented results on MEAs with new ionomer that showed a much reduced dependence on the RH as compared to Nafion-based membranes [17].

Cross-linking can be achieved through the backbone, but also through the acidic groups. Dongyue Shenzhou New Materials uses sulfonimide links to this end [25]. Values of 200 mS cm^{-1} at 80°C and 95% RH to 12 mS cm^{-1} at 120°C and 25% RH have been reported with this material. Also 3M is considering introducing (aromatic) imide groups to the sulfonic end group either to attach cross-linkable groups or more acid groups per side chain [23]. So far, approaches involving blending of soluble and insoluble material do not seem to have been successful in stopping the dissolution of the soluble material. Reinforcements may also reduce the solubility of low EW materials.

The durability aspects, however, have not been fully established. These will be discussed in section

"Materials Degradation and the Relation to Performance Loss and Shortening the PEMFC Lifetime."

Also the addition of inorganic materials to enhance water retention and/or proton conductivity has had some success, for example, by adding zirconium phosphate. Such additions have also been successful in increasing the mechanical strength of materials [26, 27].

Hydrocarbon membranes, such as sulfonated PEEK or sulfon imides, usually show lower conductivity values and increased swelling, or water solubility. The proton conductive paths in these materials are not as effective as in PFSA membranes. Not unrelated, however, is the observation of much reduced gas cross-over rates in such membranes [25, 28]. While this may be unfavorable for the application of such materials as proton-conducting phase in the electrode, it has a positive impact on the durability of the membrane as will be discussed in section "Materials Degradation and the Relation to Performance Loss and Shortening the PEMFC Lifetime." This has recently given a new incentive to research in this area [29]. Sulfonated PEEK membranes are commercialized by Fumatech GmbH in Germany [30]. Low equivalent weight membranes (EW 675–850) with a conductivity ranging from 0.04 S cm^{-1} at 40°C to more than 0.08 S cm^{-1} at 80°C are offered.

The success of widening the operating temperature for water-based proton conduction system has so far not been matched in the field of intrinsically dry proton conductors. Although interesting developments were reported in the field of polymers having tethered imidazole groups [31–34], these and other approaches based on phosphonated polymers, either in their pure form or as acid–base copolymers or blends, show conductivity values, which are at least an order of magnitude too low [34–36].

The proton conduction based on the phosphoric acid is the basis of HT-PEMFC Celanese technology [37], mostly referred to as phosphoric acid-doped PBI (polybenzimidazole) This membrane enables operation at temperatures as high as 180°C, without the need for external humidification. Heat dissipation at this temperature is much easier than at the 70–80°C operating temperature of fuel cell systems using standard PFSA membranes. The CO tolerance at 180°C is such that even 1% CO leads to a minor loss of power density compared to that using the same membrane on pure hydrogen. The downside of this membrane is its low conductivity below 100°C, making a cold start impossible, as well as the lower power density at its optimal temperature.

At 23°C, the power density of a phosphoric acid–doped PBI-based MEA is quoted to amount to 8 mW cm^{-2} [38], while the best performing MEA at 160°C shows a power density of 0.28 W cm^{-2} at 0.7 V [39], less than half of the PFSA-based MEAs used for the DoE cost analysis. The only car manufacturer pursuing the use of phosphoric acid-doped PBI membranes has been Volkswagen. For stationary applications, it has been primarily PlugPower that has developed fuel cell systems based on phosphoric acid-doped PBI membranes.

Unassisted start-up at freezing conditions, another automotive requirement, does not seem to be compatible with systems not based on water. First, as already mentioned, their proton conductivity is too low at such temperatures. Secondly, they cannot play the role of water storage medium during start-up. By pre-drying PFSA membranes, the water content can be reduced so much that only non-freezable water remains. This results in a remaining conductivity in the order of 10 mS cm^{-1} that is sufficient for a start-up procedure. The low initial performance induces heat generation. In a previously dried system, product water can then be stored, keeping the gas channels in the active layers free from ice [40, 41]. This start-up procedure is not feasible for membranes unable to adsorb liquid water, such as PA-doped systems where water adsorption would lead to washing out of the acid.

In a cost comparison by Gebert et al. [42], it is concluded that sulfonated Polyether ether ketone (S-PEEK) and phosphoric acid-doped polybenzimidazole (H_3PO_4-PBI) could be a factor of five cheaper than Nafion. As discussed earlier, this cost advantage is only helpful when not offset by lower MEA power density.

Electrodes and Gas Diffusion Media As noted in the expert review of the two parallel cost estimates for the DoE program [13], the cost reduction realized in the past 3 years is almost entirely caused by the reduction in platinum loading to 0.25 mg cm^{-2} at an areal power density of 0.715 mW cm^{-2}. It takes into account

a prescribed platinum cost of $1,100 per troy ounce (= 31.1 g), to avoid a high volatility of fuel cell cost caused primarily by the volatility of the platinum price. At the same time, the high impact of the platinum price on the fuel cell cost is a serious problem: As the loading target is distilled from the platinum price and the allowable cost per kW, a successful reduction of the platinum loading can easily be offset by an increase in the platinum price. A further reduction of the platinum loading could alleviate this dependence.

The catalytic layer used for the DoE cost review [13] is based on a ternary PtCoMn alloy, either supported by carbon or by organic whiskers, as developed by 3M, with a platinum loading of 0.25 mg cm^{-2} cell area. The cost of the support and the ionomer is insignificant compared to the precious metal cost of the catalytic layer. Most R&D is devoted to decreasing the use of precious metal, primarily platinum, while at the same time preserving power density and durability.

The PtCoMn alloy as developed by 3M that was adopted for the cost review is so far the only catalyst for which the activity data set by the DoE have been met in MEA tests under relevant conditions, but long-term field data are absent for stacks or systems based on the PtCoMn alloy. The most applied cathode catalyst to date is Pt supported on carbon, while at the anode, either Pt or Pt alloyed with Ru and or Mo is used. At present, these catalysts do not meet yet the target activity.

Further electrode performance improvements, and thus reductions in use of platinum per kW, can either come from a further reduction of ohmic losses, activation losses, or from transport losses.

Ohmic losses: The ohmic losses associated with the electrodes are related to electron transport through the gas diffusion media and the catalyst layers. The proton transport in the catalyst layer is associated with transport losses, as its contribution is not ohmic but depends on current density [43]. In state-of-the-art components, carbon is the electron conductor.

The in-plane as well as the through-plane resistance of the GDM contributes to the ohmic resistance due to their function of evening out the current distribution. As most current GDM's are based upon non-isotropic materials such as paper or woven materials, these differ often by an order of magnitude. The through plane resistance of the material depends strongly upon the compression, a factor that has to be taken into account for application in a fuel cell. In general, the overall ohmic loss through the GDM is quite small, in the order of 2 mV at 1 A cm^{-2} [44].

The presence of a so-called microporous layer at the interface with the catalyst layer has a positive effect on the contact resistance. For carbon black–based catalyst layers, it is usually assumed that electron transport losses are negligible. This may not be the case when less well-conducting oxide or carbide supports are considered.

Activation losses: In an H_2/air-fed fuel cell, the activation losses are mainly at the cathode. The hydrogen oxidation rate is very fast on the standard Pt catalyst, indeed such that it is hard to measure it accurately. Estimates of the exchange current density are in the order of 0.24–0.60 A cm_{Pt}^{-2} [45]. There is substantial evidence that the anode Pt loading can be as low as 0.05 mg cm^{-2} with losses in the order of mV only [4]. Durability issues as well as the presence of CO may require a higher loading; this will be further discussed in the next chapters.

The research is therefore focused at the cathode. The state-of-the-art catalyst Pt/C shows only a low specific activity in the order of 0.2 mA cm^{-2} Pt at 900 mV (IR-free, at 1 bar 80°C) This is compensated by the large Electrochemically Active Surface Area values (ECSA) obtained with these catalysts, which can be in the order of 60–90 m^2 g^{-1}. The corresponding mass activities, which are the product of the ECSA and the specific activity, are between 0.12 and 0.18 A mg^{-1}, about a factor 3 lower than the target, resulting in a required Pt loading in the order of 0.4–0.6 mg cm^{-2} Pt [46].

A further increase of the ECSA does not seem useful; this would imply particles smaller than 2 nm, which are not very active. Specific activity decreases with particle size or specific surface area due to more low coordinated Pt atoms and longer Pt–Pt bond distances, which have a pronounced effect on the electronic structure. Ensuing strong OH adsorption blocks the sites for oxygen adsorption. Whereas 0.2 mA cm^{-2} seems a sort of maximum for Pt nanoparticles, the maximum specific activity for pure Pt with well-defined crystal faces is much higher, in the order of 2.2 and 1.9 mA cm^{-2} for Pt (110) and (111), respectively, measured in $HClO_4$, an electrolyte that due to its non-adsorbing anions

mimics PFSA best [47]. For Pt black and Pt polycrystalline disk, higher values for the specific activity are also found [46]. 3M showed with their so-called Pt Nano-Structured Thin Films (NSTF) a specific activity of up to 1.7 mA cm^{-2} Pt at 900 mV (IR-free, at 1 bar 80°C) with ECSA values in the order of 10–15 m^2 g^{-1} [48, 49]. The NSTF is a continuous layer of polycrystalline Pt deposited on non-conductive, inorganic whiskers [50], with a surface mostly showing Pt (111) facets [51].

Several ways to improve the mass activity are currently explored. In the concept of nanoparticles on carbon black, alloying Pt with other metals is intensively studied. It is well known that the specific activity of Pt can be improved by alloying. The effect is ascribed mostly to changes in the electronic structure, which bring the system nearer to the optimum where both O–O bond dissociation and OH formation take place [52, 53]. Very high specific activity values were recently reported for certain Pt_3M alloys (M = Ni, Co, Fe), where the activity of Pt_3Ni (111) was shown to be ten times that of Pt(111), that is, 19 mA cm_{Pt}^{-2} [53, 54]. These findings have motivated studies into supported Pt binary and ternary nano-sized catalysts as well as extended Pt alloy catalysts.

Nano-sized binary alloys of Pt with Cr, Co, Mn, Ti, Co have been widely studied indicating a 3–4 fold increase in specific activity, but also identifying serious stability problems [6, 46, 55, 56]. More recently, ternary systems including PtIrCo, PtIrCr, and PtMnCo are considered with the aim to improve durability. Mass activity values of some PtIrM catalysts come close or exceed the 0.44 A mg^{-1} target value [57]. Increased activity can also be achieved by Pt skin nanoparticles. Here the core of a particle is made of cheap transition metal with a skin of Pt. By carefully selecting the base material, the skin Pt atoms may be more active than the Pt on the outside of a pure Pt nanoparticle [58]. High mass activities have been reported for particles consisting of a Pt or PtIr monolayer on Pd_3Co cores (order 0.7 A mg^{-1}Pt) [59].

A relatively new class of catalysts are pre-leached alloys, e.g., Cu-Pt. It was found that after leaching of Cu from the outer layers of $Pt_{0.25}Cu_{0.75}$, the remaining $Pt_{1-x}Cu_x$ showed a Pt-rich surface with high activity, again most likely due to favorable Pt–Pt distances and related electronic effects [60, 61]. Also Pt-free precious metal alloys, such as Pd with a transition metal, are currently being investigated [62].

Changing the support material may also have an effect on the mass activity. In many cases, it was found that on low surface area carbon supports, which are expected to be more stable, the Pt cannot be so well dispersed resulting in lower specific surface area and mass activity. However, it may be envisaged that either through inducing a certain particle morphology or by an electronic interaction, the specific activity may increase in such a way that this outweighs the loss of surface area. Examples of this have recently been reported for Pt on nitrogen-modified carbon [63]. Other such effects have been reported for WC and VC supports. Other alternative supports include conducting oxides, which can also have an enhanced electronic effect [63, 64].

Non-supported catalysts seem a way not only to avoid durability issues related to the support (such as carbon corrosion), but also introduce extended surfaces and therefore the possibility of higher activity. The NSTF is an example, but also improved Pt black, Pt nano-wires or tubes, Pt-coated carbon nanotubes, or mesoporous Pt structures. Although such structures have been made, they have, with the exception of Pt black and NSTF, not yet been extensively tested in fuel cells. The high mass activity of NSTF Pt was already mentioned. By using extended alloys, that is, NSTF of PtCoMn, the DoE target has been exceeded for PtCoMn (>0.44 A mg^{-1}) [49].

The last class to mention are non-metal catalysts. The use of catalysts not using metallic catalysts at all has intrigued many researchers for long time. Inspiration has come from nature, where hemoglobin structures in mammals bind oxygen, while porphyrin structures do so in plants. The most promising class of non-metal catalysts are the composite catalysts derived from heteroatomic organic precursors (e.g., polyaniline, polypyrrole, cyanamide, etc.), transition metals (Co or Fe), and carbon [65, 66]. The mechanism has not been completely clarified, but it is becoming increasingly clear that four M–N bonds are required. An essential step in the preparation is heat treatment at 600–1,100°C and subsequent activation steps. A target here is a volume activity of 130 A cm^{-3} at 0.80 V-IR-free. This target is not so much derived from cost considerations but from the requirements on the

dimension of the electrode [46]. Still, here stability problems are reported as well as intrinsic mass transport losses [66, 67].

The effect of the humidity on activity has not been well explored due to a lack of suitable systems. It has been reported that activity drops when RH < 50%, due to reduced proton activity [68]. Key to a high mass activity is the utilization of the catalyst, which is determined by accessibility for reactants. Under well-humidified conditions, supports with small pores show good utilization due to the presence of liquid water, which transport protons. This becomes critical at low humidity although smaller pores dry out less easily than larger.

Transport losses: The catalyst layer, the MPL, the GDL and the gas channel design (i.e., the bipolar plate) all contribute to transport losses of reactants. In the catalyst layers, both proton transport as well as transport of reactants takes place. At the anode side, transport losses are usually negligible. Hydrogen transport is fast, and the reaction seems to take place close to the membrane interface. At the cathode, the problems can be considerable due to the lower partial pressure of oxygen in air and the water accumulation. This implies the reaction does not just take place at the interface, and therefore, proton transport also plays an important role. Transport losses increase with current density. The oxygen gain, which usually gives a fair indication of mass transport losses, can be as high as 150 mV at 1.5 A cm^{-2} [69].

The proton resistance of the catalyst layer can be reduced by adding more ionomer phase or low EW ionomer to the system, but this is outweighed by reduced oxygen transport. As gas phase diffusion is several orders of magnitude faster than diffusion through liquid water, it is essential to create a system that does not completely fill with liquid water, that is, contains fairly hydrophobic materials and not too small pore sizes. The state-of-the-art carbon blacks do not seem to meet this criterion. CNT or other more graphitic structures seem better suited. Also alternative supports should be selected with their potential for improved mass transport. Oxides may be less suitable in that respect but this certainly requires further investigations. At low RH, the requirements may be different, to some extent the structure needs to retain water for proton conductivity, as well as for proton activity. It has been observed that dry ionomers of the PFSA type are not very well permeable for gases. Reduced catalytic activity and more specifically increased transport losses are the reason why present state-of-the-art MEAs still have a poor performance at low RH and high T, in spite of acceptable ohmic resistance of the membrane. This requires improved ionomer to be used also in the electrode [70].

In general, thin catalyst layers will have the lower proton resistance. However, they may also fill up more easily with water as is, for example, the case with the very thin NSTF electrodes by 3M, which only seem to function well at non-saturated conditions. Also for start-up under freezing conditions, a thicker electrode, or at least a higher pore volume, seems to be an advantage as complete filling with ice is even more detrimental.

A certain amount of mass transport problems must be ascribed to the GDL and MPL. The presence of an MPL usually prevents the GDL from becoming saturated with water; in most state-of-the-art GDL's, the diffusion through the microporous layer is not limiting, although this may change upon aging. The MPL, although relatively dense, improves the transport by optimizing the water management [10]. When the fuel cell is to be operated at relatively dry conditions, water retention is more important than water removal. Also in this case, the GDM plays a critical role [71].

The cost of Gas Diffusion Media (MPL + GDL) [13] is quoted to be around \$10–\$15 per m^2, and is likely to be primarily determined by processing costs. Both carbon/graphite paper as woven structures are being used as substrate, which is made hydrophobic by, for example, a PTFE coating. The microporous layer mostly consists of carbon powder mixed with a PTFE emulsion, which is cured by a heat treatment. Clear directions for cost reduction have not been found. As the gas diffusion media play a critical role in the performance of the PEMFC, especially determining the maximum power output makes it worthwhile to focus on the GDM performance, rather than on the cost per m^2.

Bipolar Plates For bipolar plates, a total (bulk and contact) resistance value of 10 mΩ cm^2 is usually specified [72]. This would result in 0.02 Ω cm^2 (two plates, coolant between), which at 1.5 A cm^{-2} would result in 30 mV voltage loss. Bipolar plates are made of carbon,

carbon/polymer composite, or metal. Both the resistance and weight/volume aspects demand thin bipolar plates. This has to be combined with low H_2 permeability ($<2 \times 10^{-6}$ cm^3 cm^{-2} s^{-1}) and good mechanical integrity.

From a materials durability point of view, carbon/polymer composite materials are to be preferred. However, metal-based bipolar plates enable the use of very thin plates, thus leading to an increase in volumetric power density. Major car manufacturers such as Honda and Toyota are using metal-based bipolar plates in the fuel cell stacks that are used in their latest generation fuel cell vehicles. Power density of 1.9 kW L^{-1} by both Honda [73] and Nissan [74] is ascribed to the use of metal-based bipolar plates.

From the total costs for metal bipolar plates as stated in the DoE cost review report, the costs of the metal plates amount to \$20 m^{-2} active cell area, which will be at maximum 10% lower per m^2 metal area. For the metal-based bipolar plates, the materials costs are significantly higher than the processing costs. As metal, coated 316L stainless steel is selected.

The use of metal-based bipolar plates brings two concerns [2]. At the anode, corrosion leads to the release of metal ions that can exchange with protons in the ionomer in the electrode as well as in the membrane, resulting in increased resistance of the electrode and membrane. At the cathode, the major concern is an increase in contact resistance, caused by the buildup of an oxide layer that has lower bulk conductivity than the metal itself. The stack compression force has an important effect on the contact resistance; the lower the compression force, the higher the contact resistance [75].

Various approaches are therefore being followed. A material, such as a stainless steel with high corrosion resistance, and with a low tendency to form a high resistance oxide layer, could be applied as plate material. Stainless steels need the right amount of chromium, nickel, and nitrogen to form a thin corrosion resistant layer on the surface that does not have a too negative effect on the contact resistance Examples of stainless steels that have been qualified are 904L, and to a lesser extent 316L and 310S [76].

Recently, incorporation of nitrogen into the surface of especially nickel-based alloys by thermal nitration was shown feasible. In this way, the contact resistances are reduced and the corrosion resistance of the materials is increased, thus meeting the targets set by the DoE [77]. Nitration of cheaper Fe-based stainless steels is being considered.

Another approach is to select steels that qualify when coated with a coating [2], that either prevents direct contact with the electrolyte and is not oxidized at the cathode. In this respect, ceramic metal nitride coatings are considered (Cr, Ti, TiAl nitride) [78]. If the coating is perfectly dense and stable, any base material could be applied. Alternative base metals being considered are aluminum or titanium [79].

The coating may be applied before or after the flow pattern is stamped in the plate, depending on whether it is possible to avoid damaging the coating layer during the forming process. Some stack manufactures advocate the use of thin gold coating, which results in a well-conducting coating but needs to exceed a thickness of several nanometers to be sufficiently dense and hence may not meet the cost targets [13]. Conductive polymers have also been suggested as coatings, although their stability under the fuel cell conditions is a concern [80].

Graphite/polymer composite materials made of a graphite, and carbon combined with a polymeric resin, are less susceptible to corrosion, and have low contact resistance but higher bulk resistance than metals. Also the gas permeability is higher than in metals. This results in thicker plates, which may still be acceptable for stationary applications. Target values for the bulk conductivity are in the order of >10 S cm^{-1} [79].

Expanded graphite foil, as alternative to metal plates, would cost \$18 m^{-2} [13, 81]. With respect to plate thickness and processibility [82], expanded graphite foil is similar to metal plates, enabling a stack power density of 2.1 kW L^{-1} [81].

Note that the flow field design of the bipolar plate is a critical factor for reactant supply and water management of stack and individual cells. As will be discussed later, a suboptimal flow field and manifold design can lead to an uneven distribution of reactants, and by this to fuel and air starvation.

Seals and Edge Protection The seals or gaskets provide protection to leakage of gases and coolants outside their compartments. They also control the stack height

and compensate for tolerances in material thickness. These materials consist of several components, the amount and type of which determines the final properties. Usually a base rubber is selected, to which additional fillers for mechanical strength and a plasticizer for flexibility are added. The seals have to be thermally stable as well as stable against hydrogen, oxygen, acid media, and coolants, and be compatible with other stack parts such as the bipolar plate.

Base rubbers may be based on silicone, fluoropolymers, or hydrocarbons. Although silicone rubbers such as silicone S and G have been applied in stacks, it has become clear that they are not sufficiently stable [83–85]. Materials like ethylene-propylene-diene-monomer (EPDM), butyl rubber (IRR), or fluororubbers (FKM such as Viton®)seem better suited. Further research is carried out to optimize properties like hardness, tensile strength, and stress relaxation. Also the morphology is being considered, with apparently a preference for profiled over flat gaskets.

Seals can be provided as separate stack components, but preferentially they are integrated in the MEA or the bipolar plate. This of course puts demands to the processibility of the base materials and the manufacturing process, which may involve curing to achieve cross-linking of the polymeric materials.

Misalignments of the anode and cathode, compression forces from the GDM, fibers stretching out from the GDM may all put electrochemical, chemical, and mechanical stress on the membrane, which the thin, state-of-the-art membranes cannot withstand. Therefore, some manufactures advise the inclusion of edge-protection on the membrane, that is, a layer of gas-tight and non-conducting material covering the membrane not covered by catalyst and GDL, and protruding slightly onto the area between the GDL (or catalyst layer) and membrane at the edges of the GDL. Suggested materials include polyimide [86]. These materials are there to reduce degradation of the membrane, but add to the complexity of the MEA and introduce yet other materials. Another option would be to let the edges of the electrodes coincide with the MEA, but this puts larger demands on the seals as well introduces the risk of shortening [13].

From the DoE cost review [13], it can be concluded that sealing of the cells comprises a higher cost than the electrolytic membrane. Depending on the design, one needs one frame per MEA, or even three frames per MEA. The lack of literature on seals development is at least remarkable. Although sealing is a quite generic topic that plays a role in many devices where leakage of gases or liquids has to be prevented, the sealing in fuel cells is extra demanding, both due to the aggressive environment as well as due to the sensitivity of the PEMFC for contaminants.

Operating Conditions Leading to Performance Loss and Shortening the PEMFC Lifetime

Definitions and Targets

Besides cost reduction, durability is a key topic in the PEMFC R&D. The projected operational lifetime of a passenger vehicle is 5,000 h. While until recent years, PEM fuel cells R&D was especially focused on increasing the power density and decreasing the cost; attention during the last years has been shifted to durability issues. It has been recognized that during operation, the PEMFC cannot always be kept in its ideal window of operation, which has been found out to be steady operation at a constant voltage between 0.5 and 0.7 V, under fully humidified conditions and mild temperatures (70°C) using clean hydrogen and air [87]. Under these conditions, operating times far exceeding the required 5,000 h have been demonstrated with voltage decay rates of 1–2 $\mu V\ h^{-1}$, which would limit the total voltage loss during a life of 5,000 h to 10 mV, which translates into a loss of efficiency of only 1%.

The numerous lifetime and durability studies on PEMFC in situ as well as on individual components ex situ have identified the main sources for performance decay and the related materials issues. A gradual decay of performance is mainly ascribed to effects in the cathode, notably loss of catalyst activity and increase of mass transport losses. The loss of activity was shown to result from dissolution and coarsening of the catalyst nanoparticles. The increased mass transport losses were ascribed to a decrease of the hydrophobicity of both catalyst layer and gas diffusion layer. Other factors contributing to the gradual decay are similar processes occurring in the anode and degradation of the bipolar plates and the seals of the MEA. The cause of sudden failure of the PEMFC was identified as the membrane losing its integrity, as a result of chemical as well as

mechanical stresses. These principal degradation mechanisms were found to be strongly dependent on conditions, where deviations from ideal conditions (70°C, 100% RH, constant load) usually exacerbate the effects. These deviations also include the presence of contaminants, either as degradation products from the system itself (bipolar plates, seals, catalyst ions, membrane fragments) as well as contaminants in the fuel, (CO, H_2S, CH_4, NH_3) and in the air (SO_x, NO_x, NH_3).

The targets currently accepted for automotive application are 5,000 h operation under drive cycle conditions or 40,000 h for stationary conditions with less than 10% performance decay. Such requirements imply that the decrease of mass activity should be limited and that the membranes will have to be able to perform without failure during the envisaged lifetime. The increase of mass transport losses should be minimal, putting demands on the stability of the support.

In this section, operating conditions and modes that contribute to voltage decay or limit performance will be discussed. In section "Materials Degradation and the Relation to Performance Loss and Shortening the PEMFC Lifetime," the durability issues related to the different components of the fuel cell, that is, catalyst, the gas diffusion layers, membranes, bipolar plates, and seals will be presented in more detail.

Real-Life Conditions That Have an Impact on Fuel Cell Performance

PEM fuel cells are in development to be ultimately deployed in the real world. The real world can vary considerably, from indoor use in buildings or warehouses to outdoor use under arctic conditions. Load variations can vary from continuous idle with occasional periods at maximum power for backup power systems, to highly dynamic operation in transport applications or working at continuous power for Combined Heat and Power systems. The level of control over all relevant parameters can be limited in a fuel cell system, and malfunctioning of control hardware can lead to conditions that fall outside the intended operating window. When compared to testing an MEA in a fuel cell laboratory in test hardware that excludes all influences but those deliberately applied by the operator, a large number of imperfections can be listed:

- The cell voltage is not constant during operation; extremes can be caused by systems malfunctioning
- The temperature and humidity control in the cell are limited, and are not constant; extremes can be caused by systems malfunctioning
- The feed of anode and cathode feeds can be fully interrupted due to systems malfunctioning, or become sub-stoichiometric in individual cells
- The inlet air will contain contaminants
- The hydrogen will contain contaminants, and for many applications other than road transport, only be a part of the anode feed
- Wear of cell and systems components may generate contaminants that can diffuse to other cell components susceptible to these contaminants
- The system might be placed in climate conditions, which are much harsher than anticipated in the design phase

Cell Voltage Variations and Excursions

Especially in fuel cell vehicles, the load demand to the drive train is characterized by a very dynamic pattern. When viewed over the entire lifetime of the vehicle, it is most of the time shut off, in case of a passenger vehicle typically 95% of the time. During operation, the load demand to the drive train contains significant periods of idling, load cycles, and start-up/shut off periods. It has become apparent that especially those events leading to relatively high voltages, that is, low power demands, lead to durability problems.

In two recent papers by Nissan and Toyota [74, 88], degradation in fuel cells used in actual vehicles has been linked to the type of drive pattern and occurrence of non-steady state periods. In the paper by Nissan [74], it is shown that the correlation between performance loss on the one side and total vehicle operation hours and vehicle mileage on the other side is rather weak. It is especially the occurrence of start/stop cycles, idling and load cycling that contribute to the performance loss of the fuel cell stacks. Based on a model, verified with actual vehicle data, an estimate is made that 44% of performance loss can be attributed to start/stop cycles, 28% to idling, and 28% to load cycling. Vehicles used in Japan and the USA show different ratios, where start/stop cycles were occurring more frequently in Japan than in the USA, and the relative contribution of idling

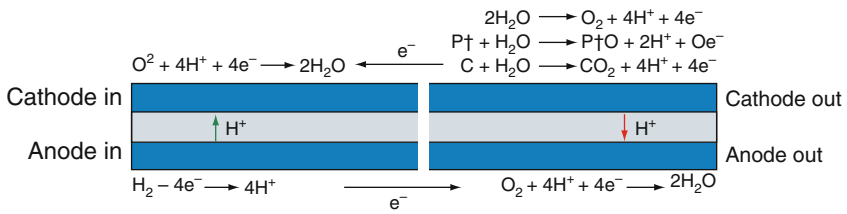

PEM Fuel Cell Materials: Costs, Performance and Durability. Figure 7
Electrochemical reactions take place when both hydrogen and air are present in the anode compartment (Figure previously published by the authors in Fuel Cells [87])

and load cycling is highly dependent on individual vehicle use.

During standstill, oxygen leaks in the anode compartment. In all cases where a hydrogen/air front arises, two horizontal fuel cell processes can take place as illustrated in Fig. 7. At open circuit, the electrons can only be exchanged horizontally in the same compartment, while protons will take the shortest distance in vertical direction through the membrane. In the bottom side, representing the anode, hydrogen is oxidized by oxygen. As the upper side, representing the cathode, lacks hydrogen, other oxidizable components can be oxidized, where the local potential is defined by the pull on electrons and protons by the oxygen reduction at both left and bottom of this cell section. This can lead to local potential values exceeding 1.5 V versus NHE. This mechanism has been previously described by Reiser [89]. The length of standstill appears to be an important factor as well: the longer the standstill period, the higher the oxygen concentration in the anode compartment becomes, and the more severe degradation becomes [74].

In the paper by Toyota [88], a marked difference is shown between performance loss and the type of simulated driving conditions. Whereas 20% performance loss is obtained after less than 100,000 km under low speed or congested conditions, it takes 350,000 km to reach this 20% performance loss under medium- to high-speed conditions. Analysis of the Japanese 10–15 drive cycle shows that 58% of the time the vehicle speed is zero or declining, that is, the fuel cell stack is operated at reduced power. Avoidance of high potentials leads to a sixfold decrease in the rate of performance loss: While operation between 0.65 V and OCV leads to 20% performance loss in less than 1,000 h, a lowering of 50 mV of the maximum potential (OCV being equal to 1.0 V) leads roughly to a doubling of this time to reach 20% performance loss. However, it is clearly shown in the Toyota paper that this lowering of the upper voltage is at the expense of system efficiency, that is, better materials need to be developed to enable the high cell voltage excursions at periods of low power demand.

Interruption of Anode and Cathode Feeds

Individual cells as well as complete stacks can be deprived of the fuel and air they need. In case of suboptimal stack design, the gas distribution over the individual cells becomes uneven, especially at high utilization. This can lead to individual cells running on sub-stoichiometric feeds, generally called fuel starvation when occurring at the anode, and air starvation when occurring on the cathode. When only individual cells are starved, these cells, placed in a series of hundreds of cells, are forced to generate the current that all other cells generate. When starved of fuel, other components present in the anode compartment are oxidized, starting those with the lowest Nernst potential and activation barrier. Carbon corrosion and platinum dissolution are two processes widely reported to take place under such conditions [90–92]. As water is relatively easy to oxidize as well, one of the mitigation strategies to protect the carbon and platinum is to include catalysts, such as iridium, that oxidize water at a lower potential than pure platinum. Knights et al. [90] have elegantly shown how the current generation requirement leads to a progressively increasing anode potential upon depleting the anode compartment of oxidizable species, up to the point that the anode potential surpasses that of the cathode, leading to cell reversal.

Air starvation is less well documented, and is believed to be less detrimental than fuel starvation. As the lack of oxygen needs to be replaced by other components to be reduced, this will generally lead to the reduction of protons to form hydrogen, which on itself leads to a negative cell voltage, as the proton reduction potential lies below the hydrogen oxidation potential [90].

One should be aware of the fact that fuel and air starvation lead to current-driven processes, with the resulting potential being an indication of the reaction taking over the normal fuel cell reaction. It is not an external potential imposed on the electrode that leads to an oxidation or reduction process.

Shortage of Water: Temperature Overshoots and Concomitant Reduction of Relative Humidity

Cell temperature can differ from the design temperature structurally because of improper stack design, as well as occasionally due to malfunctioning of temperature probes or failing cooling systems. Over the cell area, there is always a limited temperature variation due to a finite heat transfer from cell to cooling medium. In air-cooled stacks, the temperature variations are generally bigger than when using liquid cooling media. Continuous higher temperatures of a few degrees than the design temperature will lead to a higher voltage decay rate, as many degradation mechanisms show a positive relation between degradation rate and temperature [87].

More severe in the context of PEMFC is the strong dependence of the relative humidity on the temperature. The delicacy of the water balance in the PEMFC has been described in section "Introduction." The water vapor pressure required for 100% relative humidity increases strongly with temperature. Extreme temperature excursions caused by malfunctioning of thermo couples or the cooling circuit, most probably, leads to drying of the MEA, which is difficult to restore in the fuel cell stack.

Impact of Air Contaminants

In most fuel cell applications foreseen, a continuous flow of atmospheric air will be taken in while the system is in operation. This exposes the cathode, in the absence of air filters, directly to the substances present in the air, their concentrations possibly diminished as a result of air humidification.

For transport, air contaminants such as CO, volatile organic components, nitrogen oxides, and sulfur dioxide are likely to be encountered, their concentration varying with the local air quality. Especially in the first period of introduction, where the fraction of zero emission vehicles is close to zero, while heavily polluting diesel engines are abundant, the fuel cell vehicle is likely to inhale dirty air. The mean value of typical contaminant concentrations in European cities are: 42 μg m^{-3} for NO_2 and 12 μg m^{-3} SO_2 [93], 1 μg m^{-3} is approximately 1 ppb. However, especially in Asia, much higher levels are common. In Shanghai, China, SO_2 concentrations exceeding 150 μg m^{-3} and NO_2 concentrations exceeding 170 μg m^{-3} have been measured [94]. In the end report of the HyFleet Cute project [95], a fuel cell buses demonstration project in eight European cities as well as Perth, Australia and Beijing, China, it is specifically mentioned that air contaminants in Beijing caused performance problems of the fuel cell stacks. In volcanic regions in Japan, SO_2 concentrations as high as 20 ppm and H_2S concentrations as high as 4.5 ppm have been measured [96]. A drive cycle pattern developed by the Japanese FCCJ even includes a period for driving by a hot spring [97]. Some contaminants are very specific for certain applications of fuel cells, such as sulfur-containing combat gases as mustard gas for military use or salt-containing aerosols near the sea.

For rural areas, exposure to NH_3 is likely to occur near intensive livestock farming. Ammonia concentration of 10 ppm is not uncommon, and was shown to lead to rapid drop in performance of around 10% in 2–4 h [98], of which 5% proved to be irreversible.

The influence of those contaminants on the MEA level has been assessed in a number of studies [96, 99] as well as reviewed in [100]. A linear dependence of the voltage drop on the NO_x concentration was observed at a current density of 0.175 A cm^{-2}, the above quoted 42 μg m^{-3} would lead to a voltage drop of around 15 mV, while NO_2 concentrations exceeding 170 μg m^{-3} would lead to a voltage drop of 60 mV [99].

Narusawa et al. assessed the allowable concentrations of air contaminants on platinum cathodes [96]. While CO did not lead to any measurable poisoning at the cathode, presumably because the oxygen present

oxidizes CO at a high rate, NO_2 and SO_2 do lead to a loss in performance, albeit reversible. The allowable concentration of the air contaminants, defined as the concentration of a contaminant leading to a performance loss equal to 2 ppm of CO in the anode feed when using a Pt–Ru anode, is 257 ppm for CO, 2.6 ppm for NO_2, and 1.8 ppm for SO_2.

With respect to this reversibility, the data shown in [96] are not conclusive, as no graph demonstrates full recovery after exposure to NO_2 or SO_2 is stopped. In [98], exposure of a Pt cathode to 0.5 ppm SO_2 during consecutive periods of 2–4 h, leads during the first periods to a 5% decline in performance per period, without any intermediate recovery. Lower performance levels following next SO_2 periods were recoverable, but never to more than 90% of the original performance.

The simplest mitigation for air contaminants is the use of an air filter [101]. Activated carbon is widely applied as air filter for many applications requiring contaminant free air, as it has a quite generic adsorption capacity for both organic and inorganic contaminants. Although the application of an air filter comes at the cost of a pressure drop, which leads to extra compressor power, it is a relatively easy precaution that's worth considering. As the exposure to contaminants is unpredictable in the type and concentration of the contaminants, the breakthrough of the filter is unpredictable; frequent replacement of the air filter is probably the most practical and safe approach.

Mitigation of the influence of air contaminants by adapting the composition of the cathode catalyst is so far not applied.

Impact of Hydrogen Contaminants

Technically, the hydrogen can be made as pure as necessary. For laboratory purposes, hydrogen quality is quoted as the percentage of hydrogen present in the gas. Hydrogen 6.0 stands for a gas containing 99.9999% of hydrogen, that is, the maximum of all other contaminants totals 0.0001%. For fuel cells, this quality standard is not helpful, as the standard does not discriminate between inert components and those with a detrimental effect on fuel cell performance.

Components that poison the fuel cell anode or membrane might have an adverse effect at even lower concentrations than 0.0001% (=1 ppmv, parts per million by volume). Inert components can be tolerated toward a certain level, as their only effect is that of diluting the hydrogen. Although recycling hydrogen at the anode would lead to building up of such inert contaminants [102], it shouldn't lead to such strict purity requirements, as nitrogen cross-over from the cathode through the membrane takes place anyway. For the purpose of defining fuel cell grade hydrogen specifications, international actions are being pursued to identify the tolerable contaminants for PEM fuel cells [103]. Sixty components are suggested to have a potential harmful impact on fuel cell performance.

Much knowledge on the effect of poisons has been generated in connection to reformer-based PEMFC systems. Both for transport as well as for stationary applications, the presence of CO, CO_2, NH_3 has to be taken into account besides N_2 and H_2O [100]. For reformer-based systems that are operated dynamically, that is, including many cold starts and load variations, CO concentrations exceed the 10 ppm level frequently [104]. The effect of CO is studied most extensively. For unalloyed platinum electrodes, CO concentrations as low as 10 ppm lead to a performance loss of 100 mV [105] at 70°C. When reformer-based systems are fueled with logistic fuels, such as diesel and kerosene, other contaminants than CO and CO_2 are present in the reformate. Especially aromatics and unsaturated hydrocarbons can poison the fuel cell anode fast and irreversibly, even in concentrations so low that they are hardly detectable with state-of-the-art analytics.

Narusawa et al. assessed the allowable concentrations of hydrogen contaminants on platinum and platinum–ruthenium anodes [96]. Using the effect of 2 ppm CO on Pt–Ru anodes as benchmark, the allowable concentration of hydrogen contaminants is on Pt–Ru 0.33 ppm for HCHO (formaldehyde), 6.8 ppm for HCOOH (formic acid), 15 ppm for C_6H_6 (benzene), 3.3 ppb for H_2S (hydrogen sulfide), and 11 ppb for SO_2 (sulfur dioxide). On Pt anodes, these allowable concentrations are 0.05 ppm for CO, 0.56 ppm for HCHO, 17 ppm for HCOOH, 24 ppm for C_6H_6, 8.4 ppb for H_2S and 10 ppb for SO_2. Methane did not generate any effect at concentrations as high as 1,000 ppm.

The persistent issue of fuel cell poisoning in combination with fuel processor complexity has driven the vehicle manufacturers to pure hydrogen as the preferred fuel. For stationary and some off-road transport

applications, the use of gaseous and liquid carbon-based fuels is still preferred so that tolerance toward higher concentrations of species as CO is still pursued. The development of high temperature PEMFCs, such as phosphoric acid-doped PBI, that can be operated at 150–200°C, show a remarkable high tolerance toward CO. Concentrations as high as 3% CO can be tolerated at 200°C; at 125°C concentrations of 1,000 ppm, CO leads to only a minor voltage drop [106].

Wear of Cell and Systems Components

Due to the sensitivity of the MEA components to fouling, wear of stack and systems components can have a negative influence on MEA performance. Best described is probably the effect of corrosion products when metal-based bipolar plates are used in stacks [2]. In addition, metal ions can be formed in other parts of the fuel cell system, upon contact with demineralized water used for cooling or humidification. The metal ions can exchange with protons on the electrolytic membrane, as well exchange the ionomer in the electrodes. As the conductivity of metal ions is much less than that of protons, this exchange effectively leads to a higher cell resistance.

Metal deposition on the electrocatalysts active sites can take place as well. Although elements such as chromium are used to enhance the activity of cathode catalysts, it must be in the alloyed form for such enhancement, while in the case of corrosion of metal plates, it will form an adlayer on the catalytic surface, blocking platinum atoms becoming inactive for oxygen or hydrogen dissociation.

Components leaching from seals are a potential cause for loss of MEA performance as well, although no such examples have been found. In long-term tests, seals have been noted to deteriorate completely, probably leading to the release of components as softeners and polymer fragments [87]. The direct influence of such components has not widely been reported.

Freezing

Both transport systems, as well as outdoor installed stationary systems are exposed to climate conditions depending on their location. The vehicle DoE demonstration fleet, that is monitored by NREL, has been shown to be operated at ambient temperatures between −10°C and +50°C [107].

In most developed countries, freezing conditions occur during winter. The effect of freeze/thaw cycles has been studied to some extent. An immediate effect of freezing can occur during start-up. At −10°C, the conductivity of Nafion, around 0.025 S cm^{-1} [108], is enough to start the cell. As the water saturation pressure at this temperature is extremely low, liquid water will be formed and ice formation can easily occur, blocking the gas diffusion media pores, preventing start-up. It is among others for this reason that car manufactures have switched to metal bipolar plates, leading to a lower thermal mass of the fuel cell stack, and thus to a quick rise in temperature during start-up [109].

Without precautions, freeze/thaw cycles have a negative effect on cell performance, especially when liquid water in the MEA is still present under freezing conditions. Especially interfacial stresses can lead to delamination, while increasing ohmic resistances in membrane and electrode have been reported. The Daimler/EVO city buses demonstrated in the CUTE project were therefore always parked indoors overnight. In the latest systems, freezing of liquid water is avoided by water removal procedures when cooling down. Most passenger vehicles and buses of the major OEMs do not need indoor parking anymore.

Stationary PEMFC systems are even operated under arctic conditions, with a guaranteed lifetime of 4,000 h by Dantherm Power [110].

Materials Degradation and the Relation to Performance Loss and Shortening the PEMFC Lifetime

Catalyst Issues

Pt Coarsening/Dissolution Pt catalysts in PEMFCs gradually lose their activity, mostly as a result of loss of ECSA. With present materials, the loss of ECSA can be in the order of 60% over ten thousands hours of constant load operation, and is found to be accelerated by load variations [87]. It has been well established that the loss of ESCA is due to growth of Pt particles as well as to loss of Pt into the ionomer phase of the MEA [111–113]. In a review by Shao-Horn et al. [114], four mechanisms are distinguished: (1) an electrochemically induced Ostwald ripening (2) electrochemical dissolution and deposition in the ionomer phase (3) migration

of crystallites on the carbon support followed by coalescence, and (4) detachment from the carbon support.

The Ostwald ripening and electrochemical dissolution are strongly related. Although Pt is one of the most stable elements in the Periodic Table, thermodynamics predict electrochemical Pt dissolution in acid media at the potentials as encountered at the cathode [115], either directly according to the reaction:

$Pt \leftrightarrow Pt^{2+} + 2e^-$	E_0 = 1.188 V versus RHE

or indirectly through oxide formation

$Pt + H_2O \leftrightarrow PtO + 2H^+ + 2e^-$	E_0 = 0.980 V versus RHE
$PtO + 2H^+ \leftrightarrow Pt^{2+} + H_2O$	

Electrochemical studies on Pt thin films, Pt wires, and Pt nanoparticles on carbon have shown that at potentials <0.85 V, the dissolution process has a Nernstian potential dependence and that the equilibrium electrochemical potential of the Pt dissolution decreases with particle size [116]. Accordingly, higher equilibrium Pt^{2+} concentrations were measured for Pt/C than predicted for bulk Pt [111] at 80°C. According to mechanism 1, Pt^{2+} dissolved into the ionomer phase can redeposit on other (larger) particles in the cathode, due to the higher equilibrium potential of dissolution on these particles [117]. These particles need to be on the carbon support in order to allow for the exchange of electrons. The difference in dissolution potential is considered to be related to the surface tension. The above mechanism of dissolution and redeposition is an example of Ostwald ripening, that is, minimization of the surface energy is the driving force. The Pt^{2+} ions may also be reduced in the ionomer phase of electrode or in the membrane by H_2 crossing over from the anode side (mechanism 2).

At potentials above 0.85 V versus RHE, it has been observed that Pt dissolution does not show the strong Nernstian potential dependence, and even has a maximum around 1.15 V [111, 118, 119]. This is ascribed to formation of the oxide layer, which impedes further Pt dissolution. However, upon lowering the potential, these oxides are reduced accompanied by Pt dissolution. It is thought that oxide formation is related to the observation that potential cycling enhances the Pt dissolution. Kawahara et al. have studied the dissolution of Pt during cycling ex situ [120, 121]. It is known from literature of the early 1990s that fast cycling leads to oxides that are difficult to reduce, often called β-oxides [122, 123], and that the reduction of these β-oxides is accompanied by dissolution of platinum [124]. At potentials higher than 1.2 V, the formation of an oxygen skin was observed, with Pt atoms replacing oxygen atoms at even higher potentials leading to disintegration of the Pt surface [125].

Mechanism 3 and 4 are not electrochemical processes. For mechanism 3, Brownian motion is the assumed driving force, causing surface diffusion of particles with random collisions leading to coalescence [126]. Usually the fact that sintering does not occur significantly in catalysts in the gas phase at temperatures below 500°C is considered to be an indication that coalescence is not the prevailing mechanism [111, 127, 128]. Still, although both mechanisms 1 and 3 lead to an increase of the average particle size with an asymptotic particle size distribution (PSD), the coalescence mechanism has a log-normal distribution (tail at large sizes) and the Ostwald ripening has a tail at the smaller particle sizes but with a maximal particle size cut-off [129]. In many studies, a log-normal distribution of Pt particle sizes was found in virgin and used electrodes [111, 112, 127, 129, 130]. However, it must be noted that such analysis requires a good sampling also of small particles and results can be affected by the fact that several mechanisms are active at the same time [111, 127].

Accelerating factors are increasing temperature, potential cycling with the upper voltage limit being critical, and high relative humidity [130–132]. The effect of temperature on electrochemical dissolution is very strong, ex situ studies have shown an increase of orders of magnitude between 65°C and 80°C [118, 133]. It should be noted that reduction of the Pt loading, as required for cost reduction result, makes the system more sensitive for degradation to the extent that increased degradation rates were observed [132].

Non-nano-sized Pt is not immune for oxide formation or dissolution, but the equilibrium potential of oxide formation is higher compared to nano sized particles. Pt black and NSTF electrodes have either much larger Pt particles or even a continuous phase Pt. This results in lower specific surface area but more

stable activity as was convincingly demonstrated by the life-time studies carried out on NSTF electrodes by 3M [49].

Stability of Alloys Both at the anode and cathode, binary Pt–M alloys are proposed, either to enable operation on CO containing fuel or to increase the activity for the oxygen reduction reaction. The M–metal is usually a transition metal, that is, Co, Ni, Fe, Mn, Ir. These metals themselves are thermodynamically less stable than Pt. As regards the stability of the alloy, several factors play a role: the degree of alloying, the particle size, and the degree of ordering in the alloy.

When a Pt–M particle contains unalloyed M, this will easily dissolve at potentials of 0.6–0.9 V versus NHE. This has led to the use of pre-leached catalysts, some of which show improved stability even compared to pure Pt in this potential range [46]. However, recent work, which includes also cycling to potentials as low as 0 V versus NHE showed a strong decrease of activity. During this cycling, oxides that are formed at high potential and that have a passivating effect are reduced by cycling to low potential, followed by dissolution of the metal. On the other hand, the Pt seems to become less soluble [132].

The loss of the alloyed non-noble metal does not always lead to a decrease of activity. As already mentioned, in some cases, an increase of activity was found, ascribed to as surface roughening or electronic effects [61]. On the other hand, in other cases, the activity decreases because the beneficial effect on the electronic structure of Pt is lost. In any case, metal ions leaching from the catalyst will have a negative effect on the membrane and ionomer phase in the electrode.

Accelerating factors are similar to the factors accelerating the Pt coarsening and dissolution, that is, elevated temperature, potential cycling and high humidity, but for cathode catalysts, cycling to low potentials (i.e., 0 V vs NHE) seems to be an additional stressing factor [132].

Mitigating effects are also the same as the same as for Pt degradation. Large alloy particles are in general more stable than small particles [55], and at drier conditions, dissolution seems to be slower.

Contaminants for Catalysts Chemical species present in the fuel cell can further deactivate the catalyst, either through surface poising or by (electro)chemical reactions, which drastically modify the catalyst. Such chemical species are then called contaminants, they can have their source outside as well as inside the system.

At the anode: CO adsorbs strongly on Pt at the fuel cell operating temperatures. Even at 10 ppm, the cell voltage loss is in the order of 100 mV. The effects are reversible and mitigated by increased temperature. Some Pt alloys mitigate the CO poisoning, either because the adsorption is less strong or because they facilitate the CO oxidation at low potentials. Among these alloys, well-dispersed Pt–Ru supported on carbon is widely accepted as the standard catalyst for reformate feeds. Tolerance is improved to 100 ppm, with a loss $<$20 mV at 500 mA cm^{-2} at 80°C, using 0.5 mg cm^{-2} Pt–Ru at the anode. These loadings seem high, but reformate application is only considered for stationary applications where such loadings may be acceptable. There is some debate on the mechanism of CO tolerance of Pt–Ru. For well-alloyed material, the interaction with CO is less strong, and on both alloyed and non-alloyed material, OH adsorption followed by CO oxidation can take place at low potential. Both mechanisms are probably involved, which one dominates will depend on the composition and preparation of the catalyst. The hydrogen oxidation on Pt–Ru is still sufficiently fast, even when just a part of the surface area is available.

Other catalysts, such as PtMo, mainly favor the CO oxidation. This is effective only if sufficient CO is oxidized at low potential, which is not always the case. Bilayer electrodes have been proposed to separate the CO oxidation from the H_2 oxidation. In this concept, CO oxidation takes place in a layer adjacent to the GDL, catalyzed, for example, by PtMo, and hydrogen oxidation in Pt–Ru layer adjacent to the membrane. This improved the CO tolerance significantly compared to the tolerance obtained with monolayer system of either catalyst [134, 135].

Dissolution of Ru or Mo from Pt alloys in anodes and migration to the cathode have been reported, and seem enhanced at high anode potentials, such as occuring during fuel starvation and severe poisoning [136]. $PtWO_x$ is expected to be much more stable, but the activity relies on the capacity to form bronzes, for which H_2 needs to dissociate on Pt. As the Pt becomes poisoned, these materials lose their activity [137].

Mixing small amounts (2–4%) of air into the fuel, the so-called air bleeds, can also be effective. The CO is then chemically oxidized. Air bleeds can have detrimental effect on durability, both on the catalyst as the chemical oxidation induces heat effects, as well as on the membrane as detrimental radicals such as OH• can be formed.

Reduction of the CO content in reformate feeds below 10 ppm is usually not advantageous, since the resulting feed still contains high fractions (10–25%) of CO_2. On Pt in the potential range where adsorbed H is present, CO_2 reacts along the so-called reverse Water Gas Shift reaction:

$$2H_{ads} + CO_2 \leftrightarrow CO_{ads} + H_2O$$

The reaction product is adsorbed CO, poisoning the catalyst. Again this effect is mitigated on Pt–Ru due to the strong adsorption [138–140].

The tolerance for H_2S is usually <0.1 ppm. H_2S will decompose on the anode surface and poison the Pt, an effect, which can be irreversible at high potential or with high S concentration when Pt–S is formed (thermodynamically at very low potential already). H_2S can migrate to the cathode and form Pt–S there as well. The only way to remove Pt–S is to oxidize it at very high potential (1.2 V vs NHE). Pt-based catalysts promoting S oxidation at low temperature are not yet known [100].

A remarkable finding in the previously cited study by Narusawa [96] is that while alloying of platinum with ruthenium mitigates the poisoning of CO, it aggravates the poisoning of many other contaminants, such as HCHO (formaldehyde), HCOOH (formic acid), H_2S (hydrogen sulfide), and C_6H_6 (benzene). For all contaminants studied, the addition of an alloying metal does not make irreversible adsorption reversible, that is, the decrease of the potential at which oxygen and hydroxyl adsorption start is not high enough to shift the onset of the oxidation of adsorption to a useful potential range.

At the cathode: Contaminants with a strong interaction with the cathode catalyst might accumulate over time and lead to performance loss after reaching a certain threshold.

When a fuel cell is operated during 5,000 h at an air stoichiometry of 2, the accumulated number of contaminant molecules present in a concentration of 1 ppmv outnumbers the amount of platinum surface atoms by a factor of 300. Molecules that adsorb irreversibly on platinum will easily poison the platinum surface to such an extent that fuel cell performance is bound to approach zero in the course of 5,000 h. While the surface coverage of the contaminant slowly builds up, the available sites for oxygen reduction decrease. As two adjacent platinum sites are needed for oxygen desorption, the oxygen reduction activity at constant potential is proportional to $(1 - \theta_c)^2$, in which θ_c stands for the degree of coverage by the contaminant.

Except for ammonia, all air contaminants are believed to lead to poisoning of the catalytic sites. Ammonia is thought to lead to a loss of ionic conductivity in the ionomer in the cathode layer, as a result of an acid–base reaction between the basic ammonia and the acidic sulfonic acid group of the ionomer.

SO_2 in air can chemically adsorb on the catalyst, but also reduction of SO_2 on Pt leads also to Pt–S formation, with Pt–SO as intermediate product. Surface adsorption of NO on Pt has also been reported. The effect of NO_2, on the other hand, is not related to surface adsorption, rather NH_4^+ is formed by electrochemical reduction, which poisons the membrane conducting phase see below) [100, 141].

Internal sources: Some metal ions may deposit on the catalyst, that is, such as Ru on Pt cathode [136], which will deactivate them. Also Cl^-, which may be present as a result of the catalyst manufacturing is a strong poisoning for Pt catalysts [142].

Carbon Corrosion Both electrochemical oxidation and thermal degradation of carbon in humid air at temperatures <125°C have been reported, and it seems established that these corrosion mechanisms are accelerated by the presence of Pt. Carbon corrosion will first modify the surface of the support, which will become less hydrophobic. It has also been reported that carbon corrosion may enhance the mobility of Pt on the surface, accelerating the Pt sintering discussed above. Further carbon corrosion will degrade the electron-conducting network, rendering Pt particles inactive.

Thermodynamically carbon is less stable in acid media than, for example, Pt, but due to the slow reaction kinetics, carbon can still be used in fuel cell [143].

Carbon (graphite) can be electrochemically oxidized to CO_2 at quite low potentials:

$C + 2H_2O \leftrightarrow CO_2 + 4H^+ + 4e^-$	$E_0 = 0.207$ V versus RHE

Electrochemical ex situ studies [131, 144, 145] in the temperature range 25–80°C have shown that at a potential higher than 0.3 V versus RHE, CO_{surf} starts to form irreversibly on the carbon particle surface. One specific species is the quinone group that is electrochemically active with a redox peak at 0.55 V versus RHE that can be identified in cyclic voltammetry. The presence of Pt catalyzes the subsequent oxidation to CO_2. The carbon corrosion mechanism consists of the following steps:

$$C + H_2O \rightarrow CO_{surf} + 2H^+ + 2e^- \qquad E > 0.3\ V\ vs\ RHE$$

$$CO_{surf} + H_2O \xrightarrow{Pt} CO_2 + 2H^+ + 2e^- \qquad E = 0.8\ V\ vs\ RHE$$

In the absence of Pt, CO_2 emission was observed only at potentials above 1.1 V versus RHE. Carbon corrosion is often quantified in potential hold tests, where the catalyst is held at potentials >1.2 V [145, 146].

The thermal degradation of carbon and platinum-loaded carbon in air is not expected to take place below 100°C [147], although at higher temperatures, it was shown to be accelerated by the presence of Pt nanoparticles. However, the humidification of air substantially enhances the thermal corrosion rate of carbon, by providing an additional pathway for chemical carbon oxidation through a direct reaction with water [148, 149].

In most carbon corrosion studies, it is observed that the corrosion rate (in g h^{-1}) increases with the specific surface area (m^2 g^{-1}). High surface area carbons have more edge features and are therefore sensitive to oxidation centers [144]. An effective method to reduce the carbon corrosion is therefore to decrease the number of dangling bonds, that is, use a more graphitic carbon. Heat-treated carbon was shown to be more stable as were materials that by nature have a more graphitic surface such as carbon nanotubes, as well as some type of carbon nanofibers. Good stability has been shown in fuel cell accelerated stress tests but a drawback is the lower surface area of these materials, which results in larger metal particles or lower metal loading [150, 151].

Accelerating conditions for carbon corrosion include high potentials as during air/hydrogen fronts and fuel starvation. The role of humidity is still under some dispute. On the one hand, the carbon corrosion reactions require the presence of water; on the other hand, oxidation of water may proceed at higher rate than carbon corrosion. The recent research into water oxidation catalysts to mitigate carbon corrosion is based on this. However, it must be noted that the inclusion of such (metal-alloyed) catalysts has concomitant durability issues.

Gas Diffusion and Microporous Layers

The GDL and MPL experience conditions much similar to the catalyst layer, only there is no ionomer to provide protons, and there is no Pt catalyst to enhance reactions. The water phase is acidic due to the presence of degradation products from other components (CO_2, SO_3^-, F^-), resulting in a pH of about 4 [152]. The presence of fluorinated binders in MPL and GDL protects the carbon to some extent, but surface oxidation or even oxidation to CO or CO_2 can occur in the environment of liquid water, with O_2 present in the gas phase and dissolved in water. Schulze et al. present evidence for decomposition of PTFE on the basis of XPS data, but a mechanism has not been proposed [133].

The result of these degradation mechanisms is that that the GDL and the MPL both lose their hydrophobic character [133, 153, 154], and that the pore structure of the materials changes. The relation between microstructure and surface properties and mass transport properties has been the subject of several recent experimental studies [155, 156], which indicate that indeed mass transport can be seriously affected by the hydrophobicity of the GDL and MPL as well as by the pore size. This will contribute to the gradual decay of the performance, though it is hard to distinguish the effects of changes in the GDL/MPL to those of changes in the catalyst layer.

The decreased hydrophobicity can result in widening the window in which flooding can occur. Flooding itself is not regarded as a main cause for degradation.

Although in some overviews it is stated that flooding might lead to accelerated carbon corrosion and platinum dissolution, one should realize that the occurrence of both flooding and a high cathode potential is unlikely. The potentials needed to lead to significant platinum dissolution and carbon corrosion are 0.9 V and higher [87, 157], hardly a potential that occurs at the cathode during high power output.

An important function of the GDL is to even out the compression forces in the stack. These compression forces are also a source for degradation. Lee and Mérida concluded from ex situ experiments that the compressive strain increased with the applied pressure but even more strongly with temperature, and the GDL strain was influenced by the PTFE stability [158]. Properties such as in-plane electrical resistivity, surface contact angle, bending stiffness, and porosity were not affected. However, it was found that convective airflow through the GDL under strain can lead to loss of material. The GDL degradation can also contribute to sudden failure as GDL fibers can puncture the membrane, either when as a result of degradation they do not distribute the compression forces well any more or when they are even broken themselves.

Membranes

Chemical Stability Chemical instability of membranes has always been associated with the formation of peroxide in the PEMFC. Peroxide and related radicals can attack aliphatic groups, resulting in chemical degradation. Therefore, perfluorinated or highly aromatic polymers have been considered only, with perfluorinated materials now being the commercially available option. The removal of end-groups like carboxyl or H has resulted in a much enhanced stability. An important recent development has been the identification of the hydroxyl ($^{\bullet}OH$) radical as the detrimental species rather than peroxide [159]. For this radical to form from H_2O_2, the presence of oxidizable metal ions such as Fe^{2+} is required; hence, it was thought that contaminating ions were required to induce radical formation. Recently, however, it was reported [160, 161] that they can be formed under fuel cell operation in a direct reaction of H_2 and O_2. It is now assumed that H_2O_2, •OH, and •OOH are formed due to gas crossover reaction of H_2 and O_2 either chemically at electrodes and in the membrane or electrochemically at the anode, and that their concentrations are related through the equilibrium:

$$H_2O_2 + \bullet OH \leftrightarrow \bullet OOH + H_2O$$

The presence of these radicals would lead to the classical unzipping mechanisms induced by an attack on C–H and COOH groups, present in small quantities in the polymer after manufacturing. This mechanism would result in continuous HF release, no chain scission, and "ideal PFSA," not containing such reactive end-groups, would not be vulnerable [162].

Still, also improved PFSA materials suffer from chemical degradation as was established by increasing HF release, which indicates a chain scission process [159]. Further analysis showed that the •OH radical can react with H_2 to form H•, which can react with the tertiary fluorine atom, thus initiating a main chain scission process, as shown in Fig. 8.

A second mechanism involving •OH is exacerbated by dry conditions, when the deprotonation of the sulfon groups is incomplete. The proton on the sulfon group reacts with the •OH radical, leaving a sulfonyl radical, which has a weak bond to the carbon atom. This initiates another scission mechanism. This is illustrated in Fig. 9.

Recognition of these two mechanisms has led to the conclusion that •OH is the "killer species" [159]. A possible mitigation strategy is the addition of radical scavengers, such as Ce^{3+} or Mn^{3+}, which react with •OH

$$Ce^{3+} + \bullet OH + H^+ \rightarrow Ce^{4+} + H_2O$$

and which are recovered through reaction with H_2O_2, •OOH, H_2O, H_2

$$Ce^{4+} + H_2O_2 \rightarrow Ce^{3+} + \bullet OOH + H^+$$

$$Ce^{4+} + \bullet OOH \rightarrow Ce^{3+} + O_2 + H^+$$

Unlike Fe^{2+} ions, the mitigating ions should *not* reduce H^+/H_2O_2 as this would result in •OH formation, as is the basis of Fenton's test [87].

$$Fe^{2+} + H_2O_2 + H^+ \rightarrow Fe^{3+} + \bullet OH + H_2O$$

This requirement involves careful matching of reduction potentials and reaction rates but has led to much increased stability [163–165].

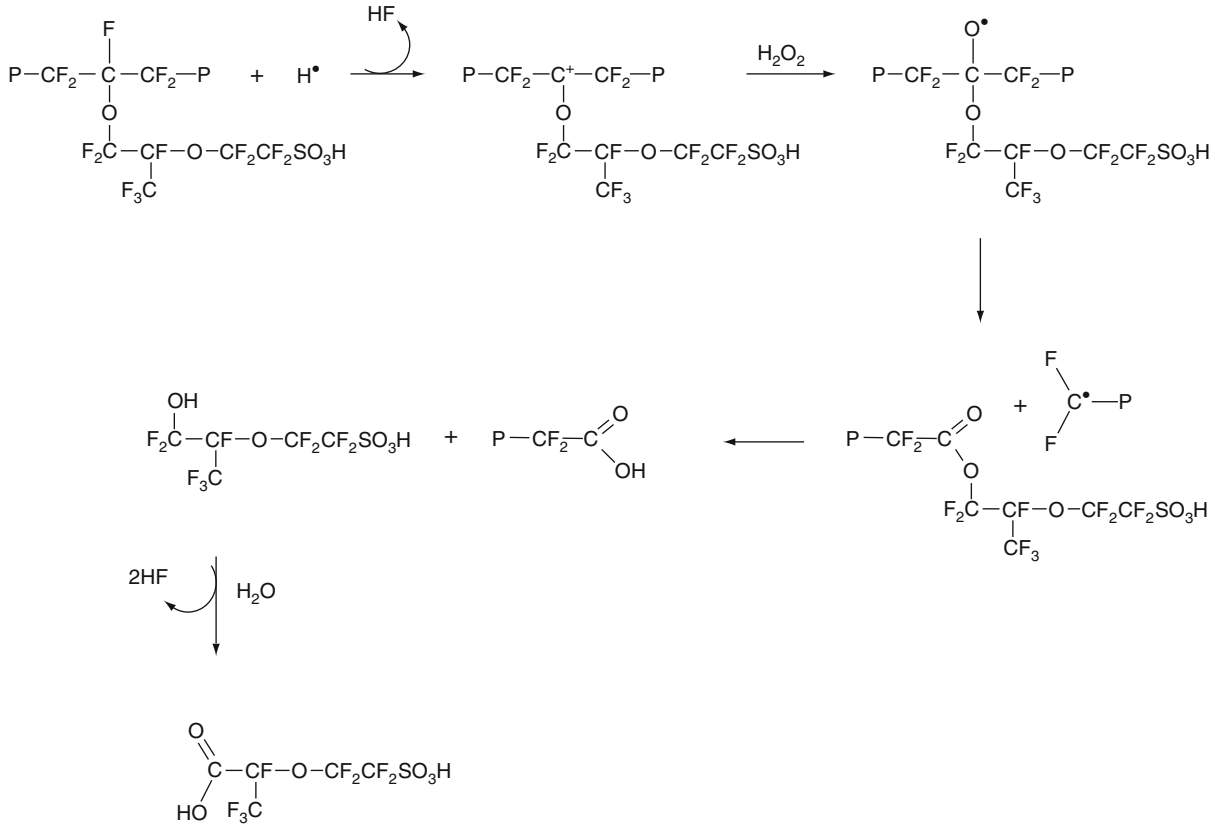

PEM Fuel Cell Materials: Costs, Performance and Durability. Figure 8
Scheme showing the degradation of "ideal" PFSA induced by the attack of a H• radical on a tertiary fluorine atom (After reference [159])

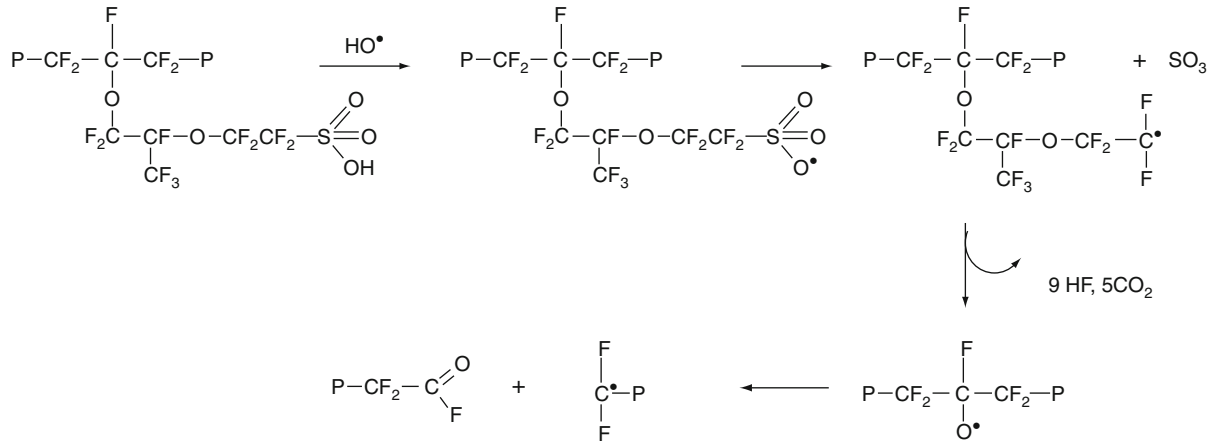

PEM Fuel Cell Materials: Costs, Performance and Durability. Figure 9
Scheme showing the degradation of PFSA in dry conditions initiated by an •OH radical (After reference [159])

The relation between the chemical degradation of the membrane and cross-over of the reactant gases has also shed new light on the stability of (aromatic) hydrocarbon-based membranes such as sulfonated PEEK. Although such materials perform dramatically bad in the Fenton's test, which shows that they are vulnerable for attack by •OOH and •OH, stable performance has been obtained for such membranes [28, 166]. This may be associated with the gas cross-over rates that are lower in hydrocarbon membranes than in PFSA membranes by a factor 5–40 [28, 167], thus reducing the rate of radical formation. However, depending on the degree of aromaticity of some non-fluorinated compounds such as PEEK are susceptible to the loss of the sulfonic acid group by hydrolysis at wet conditions [166], while others like polysulfones are much more stable [168].

Chemical degradation of PFSA membranes seems to be accelerated by elevated temperature, OCV conditions, low relative humidity, and elevated gas pressures. The main mitigation is the addition of radical scavengers and removal of non-perfluorinated groups. Note, that the amount of metal scavenger ions added to the membrane is limited and does not affect much the conductivity.

Mechanical Degradation Sulfonated membranes take up liquid water, which enables them to conduct protons, but which also results in swelling of the membrane. Hence, stresses occurring during temperature and humidity cycling [169, 170] can lead to mechanical failure of the membrane. Mechanical failure can also result from nonuniform contact pressure [171], high differential initial gas pressure over the membrane, and punctures as well as fatigue from stresses occurring.

Fig. 10 shows the effect of both temperature and hydration on the storage and loss modulus of Nafion NRE212, as measured by dynamic mechanical analysis [172]. While temperature has already a marked effect on the elasticity of Nafion, as expressed by the drop of the storage modulus, hydration leads to a decrease in the storage modulus over the whole temperature range.

Therefore, most commercial membranes are now reinforced, for example, by a porous polyethylene or PTFE [170, 173] material that enhances the dimensional stability and reduces the shrinkage stress in the membrane during drying. Reinforced membranes

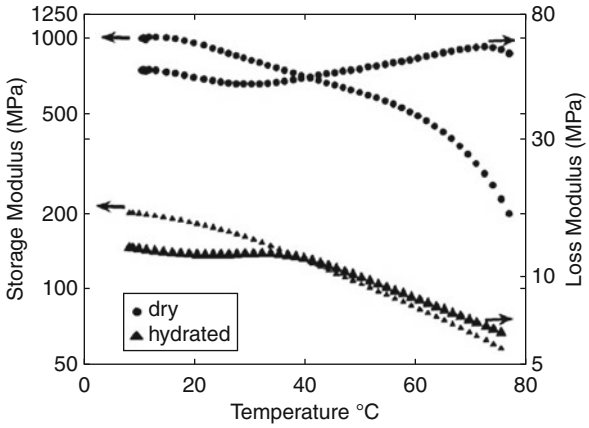

PEM Fuel Cell Materials: Costs, Performance and Durability. Figure 10
Storage modulus and loss factor as a function of temperature for dry and hydrated as-received Nafion NRE212 (Reprinted from [172]; with permission from Elsevier)

show a lower decrease of the OCV [169] and longer lifetime at elevated temperature and low humidity [173].

A successful way to achieve good proton conduction at low humidity has been though low EW PFSA. A durability problem is that these low EW materials suffer loss of crystallinity and therefore are also easily water soluble, resulting in a lack of mechanical integrity, which shows, for example, during humidity cycling. Several solutions have been suggested such as cross linking, either of the backbone or of the sulfonic groups, blending and changing the protogenic group as was discussed in section "PEMFC Component Costs and Performance: Targets, Status and Developments".

Freezing Conditions Freezing conditions result in a reduction of the conductivity of the PFSA membranes but do not seem to induce irreversible changes [174]. In a PFSA membrane, 90% of the water can freeze, but some water is non-freezable. The temperature at which freezing is observed varied with the water content. McDonalds et al. studied N112 membranes that underwent up to 385 F/T cycles between −40°C and +80°C. These materials were in a relatively dry state (only humidified by ambient conditions). These studies did not indicate any serious physical or chemical

damage. The toughness of membranes seemed to decrease somewhat, as well as the permeability of the membrane for oxygen. It was suggested that a rearrangement of the sulfonic acid groups in the ionomer might have occurred.

Contamination by Ionic Species Metal ions that originate from other parts of the system (electrode, bipolar plates, coolant, BOP) or from the fuel or air can be absorbed into the membrane. NH_3 present in the fuel or in air will migrate into the membrane to form NH_4^+. Another source of NH_4^+ is NO_2, that can be present in air and can be electrochemically reduced at the cathode [141]. The sulfonate sites have a stronger affinity to cations except Li^+, than for protons, leading to exchange of the protons by the metal ion when present. The direct effect is a reduction of the proton conductivity that is proportional to the decrease in proton concentration [171, 175]. An indirect effect is the lower hydrophilicity of metal ions in comparison to protons, which can result in partial drying out of membrane, thus also reducing the proton conductivity.

Bipolar Plates

Bipolar plates are made from graphite, graphite/polymer composite, or metal. A loss of mechanical integrity of the bipolar plate would result in mixing of the fuel or oxidant with the coolant, or even of mixing fuel with air, leading to severe degradation of performance or failure. Moreover, the electronic current is passed from one cell to the other by the polar plate, which means that any change in intrinsic resistance or contact resistance will affect the ohmic losses. The conditions experienced by the bipolar plates are similar to the ones experienced by the GDLs, with the addition of exposure to the coolant.

For graphite and graphite composite plates, corrosion and release of contaminants are under normal operation not an issue. At normal operating conditions, the cathode potential is not high enough for oxide formation on the surface, and the contact resistance remains constant during fuel cell operation [75, 176]. Especially under start/stop or fuel starvation conditions, electrodes can be exposed to higher potentials but the pH is about 4 [152], that is, much higher than the catalyst layer. However, chemical degradation is possible by oxidation of carbon in a reaction with H_2O_2, which may be formed due to O_2 gas crossing over to the anode during a stop period [177]. The polymer of the composite plate may be subject to similar degradation effects, which may in the end lead to embrittlement, leaching from the coolant or gas cross-over. A serious durability issue with graphite/composite plates is the prolonged exposure to temperatures in the order of 120°C, which may result in creep and deformation of some resins, or the brittleness of thermosetting resins.

The use of metal bipolar plates brings about serious durability issues, as was already discussed in section "Bipolar Plates" Most metals form a passive layer on the surface at the potential in which the cathode operates, which affects the contact resistance. As discussed, this requires either a dense, stable, and conductive coating or a surface modification that enhances contact resistances as well as improves stability. At the anode, the conditions are usually not such that oxide layers are formed, but during starvation, poisoning or start/stop oxidation is accelerated resulting in metal ions being directly released into the fuel cell. Similarly, low potentials occurring at the cathode may result in reduction of the passivating layer, thus releasing metal ions. Such ions will further contaminate membrane and catalysts.

Seals Degradation [87]

Fuel cell stacks contain seals on the MEA side as well as on the coolant side of the bipolar plate. Not only are they meant to prevent leakage of the gases and the coolants outside their containments, seals function as electrical insulation, stack height control, and variability control as well [178]. The degradation phenomena connected to seals do not only refer to the loss of the functionality of the seals themselves, but also to the leakage of seal components that could poison the MEA.

Degradation phenomena on seals are in general poorly understood, and only a very few number of papers have been published on seal degradation [84, 85, 178, 179]. Papers from Frisch [178] and Du [179] report on the selection of seals that meet fuel cell requirements. PlugPower used an ex situ method to test the seals resistance against a specific coolant as well as against acids that mimic the fuel cell

environment [179]. Weight change and the release of contaminants are used as indicators for the compatibility of the seals. Without giving hints to specific materials, the differences between various materials appeared to be huge.

Dow Corning [178] considered silicone elastomers as seals. The stability against coolant is not seen as a problem by Dow Corning for these silicone elastomers, while there is concern about the stability in the MEA compartment. Exposure of sealing materials to a mixture of various acids in a 1 M concentration at undefined temperature is used as ex situ aging test. General purpose silicone elastomers show cracks after 336 h in such a test, while special fuel cell grade silicone elastomers survive such a test for over a year without showing cracks.

In a study by Tan [85], the stability of various sealing materials has been tested in simulated environment at 60°C and 80°C. This simulated environment consisted of solutions containing HF and H_2SO_4, in two different concentrations. It was concluded that Silicone S and Silicone G are heavily degraded in the concentrated solutions as well as the diluted concentrations, although most of the data are collected in the concentrated solutions. Degradation reveals itself by weight loss, complete disintegration, as well as by leaching of Mg and Ca. The latter stem from magnesium oxide and calcium carbonate, which are used as fillers for obtaining the desired tensile strength, hardness, and resistance to compression. When these components are leached out, mechanical properties will be lost, and one might expect a negative influence on fuel cell performance as well, as these components can replace protons in the membrane as well as affect the properties of gas diffusion media and electrodes. An increase in temperature, as well as exposure to stress accelerates the degradation. The degradation mechanism is thought to involve de-crosslinking as well as backbone scission. Materials that much better survive the exposure to the solutions are ethylene-propylene-diene-monomer (EPDM) and fluoroelastomers.

Only in a couple of long-term experiments was seal degradation observed, and this might have been the consequence of an inappropriate materials selection. Silicone seals in direct contact with a perfluorosulfonic acid membrane suffer from degradation, at the anode as well as at the cathode [84]. The degradation is probably caused by acidic decomposition of the sealing material, leading to coloration of the membrane and detectable amounts of silicon on the electrodes. No fuel cell performance loss or increase in gas leakage along the seal has been observed. The same observation has been made by St. Pierre et al. after an 11,000 h test with a Ballard Mark 513 stack [180]. The seals were visibly oxidized, albeit more in the humidification section than in the active section. In the 26,000 h testing by Gore, complete degradation of the glass-reinforced silicone seal has been observed [14]. It forced them to increase the compression force to keep the cell gas tight. This might have had an impact on effective porosity of the gas diffusion media. The silicon of the seal could be detected throughout the MEA, especially on the gas diffusion media.

Future Directions

Fuel cell vehicles are being demonstrated worldwide, and have reached a maturity that allows daily driving in demonstration schemes while offering a performance that meets consumer expectations. The latest generation fuel cell vehicles combine the user characteristics of modern passenger cars, such as a maximum speed of around 160 km h^{-1}, a driving range of 400 km or more, with a low energy use. Refueling can be done in a couple of minutes. The progress in materials development from the past years has brought the cost, performance, and durability targets set for market introduction of road transport applications in sight. The *caveat* with respect to costs as presented in this contribution is that they are based on an annual production volume of 500,000 vehicles. The fuel cell systems in the first generation of commercially produced vehicles will certainly be more expensive than those projected for the 500,000 vehicles volume.

As cost reduction and durability improvement will not automatically go hand in hand, it is important to define priorities. For the acceptance of a new technology, robustness and performance are crucial, more than costs. With many alternative drive trains and energy carriers foreseen to be introduced in the coming decade, failures on robustness and performance will not be tolerated by consumers. If market stimulation packages by governments to stimulate the sales of clean vehicles are put in place, the last part of the cost

reduction can be postponed to next generation vehicles, when the technology already has been adopted. In any case, the options for further cost reduction should be present.

For cost reduction, the major contribution has to come from alternative electrodes, in which the mass activity of platinum is driven to its maximum, and transport limitations are driven to their minimum. A better control on catalyst layer and gas diffusion medium structures will be crucial in this respect, both on design and on maintaining the beginning-of-life properties. In this respect, the focus should be directed more than in the past on materials that are intrinsically stable under the harsh fuel cell conditions. Theoretically, the targets are achievable with presently known materials.

For robustness, it seems of key importance to use proton-conducting materials that can be used at higher temperatures and lower relative humidities than presently used materials. Application of such materials in the membrane as well as in the electrodes can lead to a considerably simpler and more robust fuel cell system. The combination of new components with other new or already existing components that need to be integrated in a new MEA is part of the development work that should not be underestimated. Given the benefits that fuel cells offer for clean and efficient transport, it will be worth the effort.

Bibliography

Primary Literature

1. US Department of Energy (2007) Multi-year research, development and demonstration plan, hydrogen, fuel cells & infrastructure technologies program, DOE/GO-102007-2430
2. de Bruijn FA, Makkus RC, Mallant RKAM, Janssen GJM (2007) Materials for state-of-the-art PEM fuel cells, and their suitability for operation above 100°C. In: Zhao T, Kreuer KD, Nguyen T (eds) Advances in fuel cells. Elsevier, The Netherlands
3. Zawodzinski TA Jr, Derouin C, Radzinski S, Sherman RJ, Smith VT, Springer TE, Gottesfeld S (1993) Water uptake by and transport through Nafion® 117 membranes. J Electrochem Soc 140:1041–1047
4. Gasteiger HA, Panels JE, Yan SG (2004) Dependence of PEM fuel cell performance on catalyst loading. J Power Sources 127:162–171
5. TIAX LLC (2003) Platinum availability and economics for PEMFC commercialization, DOE report number: DE-FC04-01AL67601
6. Ralph TR, Hogarth MP (2002) Catalysis for low temperature fuel cell Part I. The cathode challenges. Platinum Met Rev 46:3–14
7. Heinzel A, Mahlendorf F, Niemzig O, Kreuz C (2004) Injection moulded low cost bipolar plates for PEM fuel cells. J Power Sources 131:35–40
8. Stumper J, Stone C (2008) Recent advances in fuel cell technology at Ballard. J Power Sources 176:468–476
9. Janssen GJM (2001) A phenomenological model of water transport in a proton-exchange-membrane fuel cell. J Electrochem Soc 148:A1313–A1323
10. Weber AZ, Newman J (2005) Effects of microporous layers in polymer electrolyte fuel cells. J Electrochem Soc 152:A677–A688
11. Hurvitz N (2008) An in-situ, real-time gas humidity sensor for fuel cells, fuel cells durability and performance. The Knowledge Press, Brookline, pp 231–244
12. Satayapal S (2009) Overview of hydrogen and fuel cell activities, 27-10-2009 Fuel Cells & Hydrogen Joint Undertaking Stakeholders General Assembly, Brussels
13. Ernst WD, Stone C, Wheeler D (2009) Fuel cell system cost for transportation-2008 Cost Estimate, NREL/BK-6A1-45457
14. Cleghorn SJC, Mayfield DK, Moore DA, Moore JC, Rusch G, Sherman TW, Sisofo NT, Beuscher U (2006) A polymer electrolyte fuel cell life test: 3 years of continuous operation. J Power Sources 158:446–454
15. Yamazaki O, Oomori Y, Shintaku H, Tabata T (2005) Evaluation Study of PEFC Single Cell at Osaka Gas, 2005 Fuel Cell Seminar Abstracts. Courtesy Associates, Washington
16. Huth H (2008) Volkswagen's high temperature polymer electrolyte fuel cell, 4th annual international conference fuel cells durability and performance, Cambridge, 9-12-2008
17. Perti D (2009) DuPont next generation membrane and membrane electrode assembly development. In: FC Expo 2009, Tokyo
18. Johnson WB, Bazkowski C, Berta T, Crum M, Greene L, Kunitz B, Mao H, Priester S, Rudolph J, Ryan K, Seligura C (2011) MEA degradation issues opportunities and challenges using thin, reinforced polymer electrolyte membranes. In: 2nd international workshop on degradation issues on fuel cells, Greece, 21–23 Sept 2011
19. Hicks MT (2006) MEA and stack durability for PEM fuel cells. DOE hydrogen program FY 2006 annual progress report, pp 722–726
20. Sone Y, Ekdunge P, Simonsson D (1996) Proton conductivity of Nafion 117 as measured by a four-electrode AC impedance method. J Electrochem Soc 143:1254–1259
21. Maalouf M, Pyle B, Sun CN, Wu D, Paddison SJ, Schaberg M, Emery M, Lochhaas KH, Hamrock SJ, Ghassemi H, Zawodzinski TA (2009) Proton exchange membranes for high temperature fuel cells: equivalent weight and end group effects on conductivity. ECS Trans 25:1473–1481

22. Aquivion PFSA mebrane performance data. http://www.solvaysites.com/sites/solvayplastics/EN/specialty_polymers/Specialties/Pages/Aquivion_PFSA.aspx
23. Hamrock S (2009) Membranes and MEAs for dry, hot operating conditions. DOE hydrogen programme FY 2009 annual progress report, pp 1042–1047
24. Cleghorn S, Griffith M, Liu W, Pires J, Kolde J (2007) Gore's development path to a commercial automotive membrane electrode assembly. 2007 fuel cell seminar. Courtesy Associates, Washington
25. Zhang YM, Li L, Tang J, Bauer B, Zhang W, Gao HR, Taillades-Jacquin M, Jones DJ, Roziere J, Lebedeva N, Mallant R (2009) Development of covalently cross-linked and composite perfluorosulfonic acid membranes. ECS Trans 25:1469–1472
26. Jones DJ, Rozière J (2003) Inorganic/organic composite membranes. In: Vielstich W, Gasteiger HA, Lamm A (eds) Handbook of fuel cells-fundamentals, technology and applications, vol 3. John Wiley & Sons, Chichester, pp 447–455
27. Kerres J (2005) Blended and cross-linked Ionomer membranes for application in membrane fuel cells. Fuel Cells 5:230–240
28. Aoki M, Asano N, Miyatake K, Uchida H, Watanabe M (2006) Durability of sulfonated polyimide membrane evaluated by long-term polymer electrolyte fuel cell operation. J Electrochem Soc 153:A1154–A1158
29. de Araujo CC, Kreuer KD, Schuster M, Portale G, Mendil-Jakani H, Gebel G, Maier J (2009) Poly(p-phenylene sulfone)s with high ion exchange capacity: ionomers with unique microstructural and transport features. Phys Chem Chem Phys 11:3305–3312
30. FumaPem - High performance membranes for fuel cells, Products section of company website www.fumatech.com
31. Herz HG, Kreuer KD, Maier J, Scharfenberger G, Schuster MFH, Meyer WH (2003) New fully polymeric proton solvents with high proton mobility. Electrochim Acta 48:2165–2171
32. Scharfenberger G, Meyer WH, Wegner G, Schuster M, Kreuer KD, Maier J (2006) Anhydrous polymeric proton conductors based on imidazole functionalized polysiloxane. Fuel Cells 6:237–250
33. Schuster MFH, Meyer WH, Schuster M, Kreuer KD (2004) Toward a new type of anhydrous organic proton conductor based on immobilized imidazole. Chem Mater 16:329–337
34. Bozkurt A, Karadedeli B (2007) Copolymers of 4(5)-vinylimidazole and ethyleneglycol methacrylate phosphate: synthesis and proton conductivity properties. React Funct Polym 67:348–354
35. Steininger H, Schuster M, Kreuer KD, Maier J (2006) Intermediate temperature proton conductors based on phosphonic acid functionalized oligosiloxanes. Solid State Ionics 177:2457–2462
36. Bozkurt A, Meyer WH, Gutmann J, Wegner G (2003) Proton conducting copolymers on the basis of vinylphosphonic acid and 4-vinylimidazole. Solid State Ionics 164:169–176
37. Seel DC, Benicewicz BC, Xiao L, Schmidt TJ (2009) High-temperature polybenzimidazole-based membranes. In: Vielstich W, Yokokawa H, Gasteiger HA (eds) Handbook of Fuel Cells-Fundamentals, Technology and Applications, vol 5. John Wiley & Sons, Chichester, pp 300–312
38. PBI/H_3PO_4 fuel cell starts up at room temperature. Fuel Cells Bulletin November 2008, p 10
39. Li Q, Jensen JO, Savinell RF, Bjerrum NJ (2009) High temperature proton exchange membranes based on polybenzimidazoles for fuel cells. Prog Polym Sci 34:449–477
40. Ahluwalia RK, Wang X (2006) Rapid self-start of polymer electrolyte fuel cell stacks from subfreezing temperatures. J Power Sources 162:502–512
41. Oszcipok M, Hakenjos A, Riemann D, Hebling C (2007) Start up and freezing processes in PEM fuel cells. Fuel Cells 7:135–141
42. Gebert M, Hoehlein B, Stolten D (2004) Benchmark cost analysis of main PEFC ionomer membrane solutions. J Fuel Cell Sci Technol 1:56
43. Springer TE, Wilson MS, Gottesfeld S (1993) Modeling and experimental diagnostics in polymer electrolyte fuel cells. J Electrochem Soc 140:3513–3526
44. Mathias MF, Roth J, Fleming J, Lehnert W (2003) Diffusion media materials and characterisation. In: Vielstich W, Gasteiger HA, Lamm A (eds) Handbook of fuel cells – fundamentals, technology and applications, Vol. 3. John Wiley & Sons, Chichester, pp 515–537
45. Neyerlin KC, Gu W, Jorne J, Gasteiger HA (2007) Study of the exchange current density for the hydrogen oxidation and evolution reactions. J Electrochem Soc 154:B631–B635
46. Gasteiger HA, Kocha SS, Sompalli B, Wagner FT (2005) Activity benchmarks and requirements for Pt, Pt-alloy, and non-Pt oxygen reduction catalysts for PEMFCs. Appl Catal, B 56:9–35
47. Markovic NM, Ross PN (2002) Surface science studies of model fuel cell electrocatalysts. Surf Sci Rep 45:117–229
48. Bonakdarpour A, Stevens K, Vernstrom GD, Atanasoski R, Schmoeckel AK, Debe MK, Dahn JR (2007) Oxygen reduction activity of Pt and Pt-Mn-Co electrocatalysts sputtered on nanostructured thin film support. Electrochim Acta 53:688–694
49. Debe MK, Schmoeckel AK, Vernstrom GD, Atanasoski R (2006) High voltage stability of nanostructured thin film catalysts for PEM fuel cells. J Power Sources 161:1002–1011
50. Debe MK (2003) Novel catalysts, catalyst support and catalyst coated membrane methods. In: Vielstich W, Gasteiger HA, Lamm A (eds) Handbook of fuel cells-fundamentals, technology and applications, vol 3. John Wiley & Sons, Chichester, pp 576–590
51. Gancs L, Kobayashi T, Debe MK, Atanasoski R, Wieckowsk A (2008) Crystallographic characteristics of nanostructured thin-film fuel cell electrocatalysts: a HRTEM study. Chem Mater 20:2444–2454
52. Zhang JL, Vukmirovic MB, Xu Y, Mavrikakis M, Adzic RR (2005) Controlling the catalytic activity of platinum-monolayer electrocatalysts for oxygen reduction with different substrates. Angew Chem Int Ed 44:2132–2135
53. Stamenkovic VR, Mun BS, Mayrhofer KJJ, Ross PN, Markovic NM, Rosswmeisl J, Greeley J, Norskov JK (2006) Changing the activity of electrocatalysts for oxygen reduction by tuning the surface electronic structure. Angew Chem Int Ed 45:2897–2901

54. Stamenkovic VR, Fowler B, Mun BS, Wang G, Ross PN, Lucas CA, Markovic NM (2007) Improved oxygen reduction activity on $Pt_3Ni(111)$ via increased surface site availability. Science 315:493–497
55. Antolini E, Salgado JRC, Gonzalez ER (2006) The stability of Pt-M (M=first row transition metal) alloy catalysts and its effect on the activity in low temperature fuel cells. J Power Sources 160:957–968
56. Mukerjee S, Srinivasan S (1993) Enhanced electrocatalysis of oxygen reduction on platinum alloys in proton exchange membrane fuel cells. J Electroanal Chem 357:201–224
57. Murthi VS (2009) Highly dispersed alloy catalyst for durability. DOE hydrogen programme FY 2009 annual progress report, pp 1075–1080
58. Adzic RR, Zhang J, Sasaki K, Vukmirovic MB, Shao M, Wang JX, Nilekar AU, Mavrikakis M, Valerio JA, Uribe F (2007) Platinum monolayer fuel cell electrocatalysts. Top Catal 46:249–262
59. Ball SC, Burton SL, Fisher J, ÓMalley R, Tessier BC, Theobald B, Thompsett D, Zhou WP, Su D, Zhu Y, Adzic R (2009) Structure and activity of novel Pt core-shell catalysts for the oxygen reduction reaction. ECS Trans 25:1023–1036
60. Neyerlin KC, Srivastava R, Yu C, Strasser P (2009) Electrochemical activity and stability of dealloyed Pt-Cu and Pt-Cu-Co electrocatalysts for the oxygen reduction reaction (ORR). J Power Sources 186:261–267
61. Strasser P (2009) Dealloyed Pt bimetallic electrocatalysts for oxygen reduction. In: Vielstich W, Yokokawa H, Gasteiger HA (eds) Handbook of fuel cells-fundamentals, technology and applications, vol 5. John Wiley & Sons, Chichester, pp 30–47
62. Wang X, Kariuki N, Niyogi S, Smith MC, Myers DJ, Hofmann T, Zhang Y, Bar M, Heske C (2008) Bimetallic palladium-base metal nanoparticle oxygen reduction electrocatalysts. ECS Trans 16:109–119
63. Zhou Y, Holme T, Berry J, Ohno TR, Ginley D, ÓHayre R (2009) Dopant-induced electronic structure modification of HOPG surfaces: implications for high activity fuel cell catalysts. J Phys Chem C 114:506–515
64. Shao Y, Liu J, Wang Y, Lin Y (2009) Novel catalyst support materials for PEM fuel cells: current status and future prospects. J Mater Chem 19:46–59
65. Bashyam R, Zelenay P (2006) A class of non-precious metal composite catalysts for fuel cells. Nature 443:63–66
66. Lefevre M, Proietti E, Jaouen F, Dodelet JP (2009) Iron-based catalysts with improved oxygen reduction activity in polymer electrolyte fuel cells. Science 324:71–74, Washington
67. Wu G, Artyushkova K, Ferrandon M, Kropf AJ, Myers D, Zelenay P (2009) Performance durability of polyaniline-derived non-precious cathode catalysts. ECS Trans 25:1299–1311
68. Neyerlin KC, Gasteiger HA, Mittelsteadt CK, Jorne J, Gu W (2005) Effect of relative humidity on oxygen reduction kinetics in a PEMFC. J Electrochem Soc 152:A1073–A1080
69. Kocha SS (2003) Principles of MEA preparation. In: Vielstich W, Gasteiger HA, Lamm A (eds) Handbook of fuel cells-fundamentals, technology and applications, vol 3. John Wiley and Sons, Chichester, UK, pp 538–565
70. Xie Z, Zhao X, Gazzarri J, Wang Q, Navessin T, Holdcroft S (2009) Identification of dominant transport mechanisms in PEMFC cathode catalyst layers operated under low RH. ECS Trans 25:1187–1192
71. Quick C, Ritzinger D, Lehnert W, Hartnig C (2009) Characterization of water transport in gas diffusion media. J Power Sources 190:110–120
72. Hermann A, Chaudhuri T, Spagnol P (2005) Bipolar plates for PEM fuel cells: a review. Int J Hydrogen Energy 30:1297–1302
73. Morikawa H, Kikushi H, Saito N (2009) Development and advances of a V-flow FC stack for FCX clarity. SAE Int J Engines 2:955–959
74. Shimoi R, Aoyama T, Iiyama A (2009) Development of fuel cell stack durability based on actual vehicle test data: current status and future work. SAE Int J Engines 2:960–970
75. Makkus RC, Janssen AHH, de Bruijn FA, Mallant RKAM (2000) Use of stainless steel for cost competitive bipolar plates in the SPFC. J Power Sources 86:274–282
76. Suria OV, Bruno M, Bois P, Maggiore P, Cazzolato C (2009) Fuel size and weight reduction due to innovative metallic bipolar plates: Technical process details and improvements, SAE Technical Papers Series, pp 2009-01-1009
77. Brady MP, Yang B, Wang H, Turner JA, More KL, Wilson M, Garzon F (2006) The formation of protective nitride surfaces for PEM fuel cell metallic bipolar plates. JOM 58:50–57
78. Cho EA, Jeon US, Hong SA, Oh IH, Kang SG (2005) Performance of a 1-kW-class PEMFC stack using TiN-coated 316 stainless steel bipolar plates. J Power Sources 142:177–183
79. Mepsted GO, Moore JM (2003) Performance and durability of bipolar plate materials. In: Vielstich W, Gasteiger HA, Lamm A (eds) Handbook of fuel cells-fundamentals, technology and applications, vol 3. John Wiley & Sons, Chichester, pp 286–293
80. Joseph S, McClure JC, Sebastian PJ, Moreira J, Valenzuela E (2008) Polyaniline and polypyrrole coatings on aluminum for PEM fuel cell bipolar plates. J Power Sources 177: 161–166
81. Ahluwalia R, Wang X, Lasher S, Sinha J, Yang Y, Sriramulu S (2007) Performance of automotive fuel cell systems with nanostructured thin film catalysts, 2007 fuel cell seminar, 15-10-2007. Courtesy Associates, Washington
82. Dobrovol'skii YuA, Ukshe AE, Levchenko AE, Arkhangel'skii IV, Ionov SG, Avdeev VV, Aldoshin SM (2007) Materials for bipolar plates for proton-conducting membrane fuel cells. Russ J Gen Chem 77:752–765
83. Cleghorn SJC, Mayfield DK, Moore DA, Moore JC, Rusch G, Sherman TW, Sisofo N, Beuscher U (2006) A polymer electrolyte fuel cell life test: 3 years of continuous operation. J Power Sources 158:4–455
84. Schulze M, Knöri T, Schneider A, Gülzow E (2004) Degradation of sealings for PEFC test cells during fuel cell operation. J Power Sources 127:222–229
85. Tan J, Chao YJ, Van Zee JW, Lee WK (2007) Degradation of elastomeric gasket materials in PEM fuel cells. Mater Sci Eng A 445–446:669–675

86. Ralph TR, Barnwell DE, Bouwman PJ, Hodgkinson AJ, Petch MI, Pollington M (2008) Reinforced membrane durability in proton exchange membrane fuel cell stacks for automotive applications. J Electrochem Soc 155: B411–B422
87. de Bruijn FA, Dam VAT, Janssen GJM (2008) Review: durability and degradation issues of PEM fuel cell components. Fuel Cells 8:3–22
88. Noto H, Kondo M, Otake Y, Kato M (2009) Development of fuel cell hybrid vehicle by Toyota, SAE technical paper series, pp 2009-01-1002
89. Reiser CA, Bregoli L, Patterson TW, Yi JS, Yang JD, Perry ML, Jarvi TD (2005) A reverse-current decay mechanism for fuel cells. Electrochem Solid-State Lett 8:A273–A276
90. Knights SD, Colbow KM, St-Pierre J, Wilkinson DP (2004) Aging mechanisms and lifetime of PEFC and DMFC. J Power Sources 127:127–134
91. Ferreira-Aparicio P, Chaparro AM, Gallardo B, Folgado M, Daza L (2009) Anode degradation effects in PEMFC stacks by localized fuel starvation, 2009 fuel cell seminar. Courtesy Associates, Washington
92. Schmittinger W, Vahidi A (2008) A review of the main parameters influencing long-term performance and durability of PEM fuel cells. J Power Sources 180:1–14
93. Baldasano JM, Valera E, Jimenez P (2003) Air quality data from large cities. Sci Total Environ 307:141–165
94. Huang W, Tan J, Kan H, Zhao N, Song W, Song G, Chen G, Jiang L, Jiang C, Chen R, Chen B (2009) Visibility, air quality and daily mortality in Shanghai, China. Sci Total Environ 407:3295–3300
95. A Report on the achievements and learnings from the HyFleet: CUTE Project 2006 – 2009
96. Narusawa K, Myong K, MurookaK, Kamiya Y (2007) A study regarding effects of proton exchange membrane fuel cell poisoning due to impurities on fuel cell performance, SAE technical paper series, pp 2007-01-0698
97. Adjemian K, Iiyama A (2008) MEA development for automotive applications, fuel cells durability and performance, 3rd edn. The Knowledge Press, Inc., Brookline, pp 5–16
98. Veldhuis JBJ, de Bruijn FA, Mallant RKAM (1998) Fuel cell seminar abstracts, 16-11-1998 Courtesy Associates, Washington, pp 598
99. Knights SD, Jia N, Chuy C, Zhang J (2005) Fuel cell seminar abstracts, 14-11-2005 Courtesy associates, Washington
100. Cheng X, Shi Z, Glass N, Zhang L, Zhang J, Song D, Liu ZS, Wang H, Shen J (2007) A review of PEM hydrogen fuel cell contamination: Impacts, mechanisms, and mitigation. J Power Sources 165:739–756
101. Kennedy DM, Cahela DR, Zhu WH, Westrom KC, Nelms RM, Tatarchuk BJ (2007) Fuel cell cathode air filters: methodologies for design and optimization. J Power Sources 168:391–399
102. Matsuda Y (2009) Accumulation behavior of impurities in fuel cell hydrogen circulation system, 2009 fuel cell seminar, 16-11-2009 Courtesy associates, Washington
103. Papasavva S (2005) Developing hydrogen (H2) specification guidelines for proton exchange membrane (PEM) fuel cell vehicles, SAE technical series papers, pp 2005-01-0011
104. Recupero V, Pino L, Vita A, Cipiti F, Cordaro M, Lagana M (2005) Development of a LPG fuel processor for PEFC systems: Laboratory scale evaluation of autothermal reforming and preferential oxidation subunits. Int J Hydrogen Energy 30:963–971
105. de Bruijn FA, Rietveld G, van den Brink RW (2007) Hydrogen production and fuel cells as the bridging technologies towards a sustainable energy system. In: Centi G, Santen RA (eds) Catalysis for renewables. Wiley-VCH, Weinheim, pp 299–336
106. Li Q, He R, Gao J-A, Jensen JO, Bjerrum NJ (2003) The CO poisoning effect in polymer electrolyte fuel cells operational at temperatures up to 200°C. J Electrochem Soc 150:A1599–A1605
107. Wipke K, Sprik S, Kurtz J, Ramsden T (2009) Controlled hydrogen fleet and infrastructure demonstration and validation project, NRELNREL/TP-560–46679
108. Mallant RKAM, Lebedeva NP, Zhang YM, Li L, Tang JK, Bukhtiyarov VI, Romanenko AV, Voropaev I, Bauer B, Zhang W, Jones DJ, Rozière J, Gao HR (2009) Significant steps towards medium temperature/low RH PEMFC, 2009 fuel cell seminar. Courtesy Associates, Washington
109. Bono T, Kizaki M, Mizuno H, Nonobe Y, Takahashi T, Matsumoto T, Kobayashi N (2010) Development of new Toyota FCHV-adv fuel cell system. SAE Int J Engines 2:948–954
110. Power backup solutions for telecom and related networks. Dantherm Power Catalogue 2008
111. Ferreira PJ, la Ó GJ, Shao-Horn Y, Morgan D, Makharia R, Kocha S, Gasteiger HA (2005) Instability of Pt/C electrocatalysts in proton exchange membrane fuel cells. J Electrochem Soc 152:A2256–A2271
112. Xie J, Wood DL, More KL, Atanassov P, Borup RL (2005) Microstructural changes of membrane electrode assemblies during PEFC durability testing at high humidity conditions. J Electrochem Soc 152:A1011–A1020
113. Guilminot E, Corcella A, Charlot F, Maillard F, Chatenet M (2007) Detection of Pt[sup z+] Ions and Pt nanoparticles Inside the membrane of a used PEMFC. J Electrochem Soc 154:B96–B105
114. Shao-Horn Y, Sheng WC, Chen S, Ferreira PJ, Holby EF, Morgan D (2007) Instability of supported platinum nanoparticles in low-temperature fuel cells. Top Catal 46:285–305
115. Pourbaix M (1974) Atlas of electrochemical equilibria in aqueous solutions. National Association of Corrosion Engineers, New York
116. Darling RM, Meyers JP (2003) Kinetic model of platinum dissolution in PEMFCs. J Electrochem Soc 150:A1523–A1527
117. Virkar AN, Zhou Y (2007) Mechanism of catalyst degradation in proton exchange membrane fuel cells. J Electrochem Soc 154:B540–B547
118. Dam VAT, de Bruijn FA (2007) The stability of PEMFC electrodes. J Electrochem Soc 154:B494–B499

119. Wang X, Kumar R, Myers DJ (2006) Effect of voltage on platinum dissolution. Electrochem Solid-State Lett 9:A225–A227
120. Kawahara S, Mitsushima S, Ota K, Kamiya N (2006) Deterioration of Pt catalyst under potential cycling. ECS Trans 3:625–631
121. Kawahara S, Mitsushima S, Ota K, Kamiya N (2006) Comsumption of Pt catalyst under electrolysis and fuel cell operation. ECS Trans 1:85–100
122. Burke LD, Buckley DT (1994) Anomalous stability of acid-grown hydrous platinum oxide films in aqueous media. J Electroanal Chem 366:239–251
123. Burke LD, ÓDwyer KJ (1992) Multilayer oxide growth on Pt under potential cycling conditions. Electrochim Acta 37:43–50
124. Birss VI, Chang M, Segal J (1993) Platinum oxide film formation-reduction: an in-situ mass measurement study. J Electroanal Chem 355:181–191
125. Nagy Z, You H (2002) Applications of surface X-ray scattering to electrochemistry problems. Electrochim Acta 47:3037–3055
126. Kinoshita K (1992) Electrochemical oxygen technology. John Wiley & Sons, Inc., New York
127. Guilminot E, Corcella A, Chatenet M, Maillard F, Charlot F, Berthome G, Iojoiu C, Sanchez JY, Rossinot E, Claude E (2007) Membrane and active layer degradation upon PEMFC steady-state operation. J Electrochem Soc 154:B1106–B1114
128. Honji A, Mori T, Tamura K, Hishinuma M (1988) Agglomeration of platinum particles supported on carbon in phosphoric acid. J Electrochem Soc 135:355–359
129. Ascarelli P, Contini V, Giorgi R (2002) Formation process of nanocrystalline materials from x-ray diffraction profile analysis: application to platinum catalysts. J Appl Phys 91:4556–4561
130. Borup RL, Davey JR, Garzon FH, Wood DL, Inbody MA (2006) PEM fuel cell electrocatalyst durability measurements. J Power Sources 163:76–81
131. Mathias MF, Makharia R, Gasteiger HA, Conley JJ, Fuller TJ, Gittleman CJ, Kocha SS, Miller DP, Mittelsteadt CK, Xie T, Yan SG, Yu PT (2005) Two fuel cell cars in every garage. Electrochem Soc Interface 14(Fall):24–35
132. Haas HR, Davis MT (2009) Electrode and catalyst durability requirements in automotive PEM applications: technology status of a recent MEA design and next generation challenges. ECS Trans 25:1623–1631
133. Schulze M, Wagner N, Kaz T, Friedrich KA (2007) Combined electrochemical and surface analysis investigation of degradation processes in polymer electrolyte membrane fuel cells. Electrochim Acta 52:2328–2336
134. Janssen GJM, de Heer MP, Papageorgopoulos DC (2004) Bilayer anodes for improved reformate tolerance of PEM fuel cells. Fuel Cells 4:169–174
135. Yu H, Hou Z, Yi B, Lin Z (2002) Composite anode for CO tolerance proton exchange membrane fuel cells. J Power Sources 105:52–57
136. Piela P, Eickes C, Brosha E, Garzon F, Zelenay P (2004) Ruthenium crossover in direct methanol fuel cell with Pt-Ru black anode. J Electrochem Soc 151:A2053–A2059
137. Lebedeva NP, Rosca V, Janssen GJM (2010) CO oxidation and CO2 reduction on carbon supported PtWO3 catalyst. Electrochim Acta 55:7659–7668
138. de Bruijn FA, Papageorgopoulos DC, Sitters EF, Janssen GJM (2002) The influence of carbon dioxide on PEM fuel cells anodes. J Power Sources 110:117–124
139. Janssen GJM (2004) Modelling study of CO_2 poisoning on PEMFC anodes. J Power Sources 136:45–54
140. Ahluwalia RK, Wang X (2008) Effect of CO and CO_2 impurities on performance of direct hydrogen polymer-electrolyte fuel cells. J Power Sources 180:122–131
141. Mohtadi R, Lee W, Van Zee JW (2004) Assessing durability of cathodes exposed to common air impurities. J Power Sources 138:216–225
142. Paulus UA, Schmidt TJ, Gasteiger HA (2003) Poisons for the O_2 reduction reaction. In: Vielstich W, Gasteiger HA, Lamm A (eds) Handbook of fuel cells-fundamentals, technology and applications, vol 2. John Wiley & Sons, Chichester, pp 555–569
143. Kinoshita K (1988) Carbon. Electrochemical and physicochemical properties. John Wiley & Sons, Inc., New York
144. Giordano N, Antonucci PL, Passalacqua E, Pino L, Arico AS, Kinoshita K (1991) Relationship between physicochemical properties and electrooxidation behaviour of carbon materials. Electrochim Acta 36:1931–1935
145. Ball SC, Hudson SL, Thompsett D, Theobald B (2007) An investigation into factors affecting the stability of carbons and carbon supported platinum and platinum/cobalt alloy catalysts during 1.2 V potentiostatic hols regimes at a range of temperatures. J Power Sources 171:18–15
146. Garland N, Benjamin T, Kopasz J (2007) DOE fuel cell program: durability technical targets and testing protocols. ECS Trans 11:923–931
147. Stevens DA, Dahn JR (2005) Thermal degradation of the support in carbon-supported platinum electrocatalysts for PEM fuel cells. Carbon 43:179–188
148. Stevens DA, Hicks MT, Haugen GM, Dahn JR (2005) Ex situ and in situ stability studies of PEMFC catalysts12. J Electrochem Soc 152:A2309–A2315
149. Cai M, Ruthkosky MS, Merzougui B, Swathirajan S, Balogh MP, Oh SE (2006) Investigation of thermal and electrochemical degradation of fuel cell catalysts. J Power Sources 160:977–986
150. Shao Y, Yin G, Gao Y, Shi P (2006) Durability study of Pt/C and Pt/CNTs catalysts under simulated PEM fuel cell conditions. J Electrochem Soc 153:A1093–A1097
151. Tang Z, Ng HY, Lin J, Wee ATS, Chua DHC (2010) Pt/CNT-based electrodes with high electrochemical activity and stability for proton exchange membrane fuel cells. J Electrochem Soc 157:B245–B250
152. Healy J, Hayden C, Xie T, Olson K, Waldo R, Brundage M, Gasteiger H, Abbott J (2005) Aspects of the chemical degradation of PFSA ionomers used in PEM fuel cells. Fuel Cells 5:302–308
153. St-Pierre J, Wilkinson DP, Knights SD, Bos M (2000) Relationships between water management, contamination and

lifetime degradation in PEFC. J New Mater Electrochem Syst 3:99–106
154. Wood D, Davey J, Garzon F, Atanassov P, Borup R (2005) Mass-transport phenomena and long-term performance limitations in H_2-air PEMFC durability testing, 2005 fuel cell seminar abstracts, 14-11-2005 Courtesy Associates, Washington
155. Jordan LR, Shukla AK, Behrsing T, Avery NR, Muddle BC, Forsyth M (2000) Diffusion layer parameters influencing optimal fuel cell performance. J Power Sources 86:250–254
156. Williams MV, Begg E, Bonville L, Kunz HR, Fenton JM (2004) Characterization of gas diffusion layers for PEMFC. J Electrochem Soc 151:A1173–A1180
157. de Bruijn FA, Dam VAT, Janssen GJM, Makkus RC (2009) Electrode degradation in PEMFCs as studied in model systems and PEMFC testing. ECS Trans 25:1835–1847
158. Lee C, Merida W (2007) Gas diffusion layer durability under steady-state and freezing conditions. J Power Sources 164:141–153
159. Coms FD (2008) The chemistry of fuel cell membrane chemical degradation. ECS Trans 16:235–255
160. Liu H, Gasteiger HA, LaConti AB, Zhang J (2006) Factors impacting chemical degradation of perfluorinated sulfonic acid ionomers. ECS Trans 1:283–293
161. Mittal VO, Kunz HR, Fenton JM (2007) Membrane degradation mechanisms in PEMFCs. J Electrochem Soc 154:B652–B656
162. Curtin DE, Lousenberg RD, Henry TJ, Tangeman PC, Tisack ME (2004) Advanced materials for improved PEMFC performance and life20. J Power Sources 131:41–48
163. Coms FD, Liu H, Owejan JE (2008) Mitigation of perfluorosulfonic acid membrane chemical degradation using cerium and manganese ions. ECS Trans 16:1735–1747
164. Endoh E (2008) Development of highly durable PFSA membrane and MEA for PEMFC under high temperature and low humidity conditions. ECS Trans 16:1229–1240
165. Trogadas P, Parrondo J, Ramani V (2008) Degradation mitigation in polymer electrolyte membranes using free radical scavengers. ECS Trans 16:1725–1733
166. Rozière J, Jones DJ (2003) Non-fluorinated polymer materials for proton exchange membrane fuel cells. Annu Rev Mater Res 33:503–555
167. Zhang L, Ma CS, Mukerjee S (2003) Oxygen permeation studies on alternative proton exchange membranes designed for elevated temperature operation. Electrochim Acta 48:1845–1859
168. Schuster M, Kreuer KD, Andersen HT, Maier J (2007) Sulfonated poly(phenylene sulfone) polymers as hydrolytically and thermooxidatively stable proton conducting ionomers. Macromolecules 40:598–607
169. Escobedo G, Raiford K, Nagarajan GS, Schwiebert KE (2006) Strategies for mitigation of PFSA polymer degradation in PEM fuel cells. ECS Trans 1:303–311
170. Stone C, Calis GHM (2006) Improved composite membranes and related performance in commercial PEM fuel cells, 2006 fuel cell seminar abstracts. Courtesy Associates, Washington
171. LaConti AB, Hamdan M, McDonald RC (2003) Mechanisms of membrane degradation. In: Vielstich W, Lamm A, Gasteiger HA (eds) Handbook of fuel cells, 3. Wiley, Chichester, pp 647–663
172. Silberstein MN, Boyce MC (2010) Constitutive modeling of the rate, temperature, and hydration dependent deformation response of Nafion to monotonic and cyclic loading. J Power Sources 195:5692–5706
173. Liu W, Ruth K, Rusch G (2001) Membrane durability in PEM fuel cells. J New Mat Electrochem Syst 4:227–231
174. McDonald RC, Mittelsteadt CK, Thompson EL (2004) Effects of deep temperature cycling on Nafion® 112 membranes and membrane electrode assemblies. Fuel Cells 4:208–213
175. Okada T (2003) Ionic Contaminants. In: Vielstich W, Lamm A, Gasteiger HA (eds) Handbook of fuel cells, 3. Wiley, Chichester, pp 627–646
176. Davies DP, Adcock PL, Turpin M, Rowen SJ (2000) Bipolar plate materials for solid polymer fuel cells. J Appl Electrochem 30:101–105
177. Gallagher KG, Wong DT, Fuller TF (2008) The effect of transient potential exposure on the electrochemical oxidation of carbon black in low-temperature fuel cells. J Electrochem Soc 155:B488–B493
178. Frisch L (2001) PEM fuel cell stack sealing using silicone elastomers. Sealing Technol 2001:7–9
179. Du B, Guo R, Pollard R, Rodriguez D, Smith J, Elter J (2006) PEM fuel cells: status and challenges for commercial stationary power applications. JOM 8:45–49
180. St-Pierre J, Jia N (2002) Succesful demonstration of Ballard PEMFCs for space shuttle applications. J New Mater Electrochem Syst 5:263

Books and Reviews

Barbir F (2005) PEM fuel cells, theory and practice. Elsevier, Amsterdam

Büchi FN, Inaba M, Schmidt TJ (eds) (2009) Polymer electrolyte fuel cell durability. Springer, New York

Larminie J, Dicks A (2003) Fuel cell systems explained, 2nd edn. Wiley, Chichester

Scherer GG (ed) (2008) Fuel cells I, advances in polymer science, vol 215. Springer, New York

Scherer GG (ed) (2008) Fuel cells II, advances in polymer science, vol 216. Springer, New York

Vielstich W, Lamm A, Gasteiger HA (eds) (2003) Handbook of fuel cells, fundamental, technology and applications, 4th edn. Wiley, Chichester

Vielstich W, Yokokawa H, Gasteiger HA (eds) (2009) Handbook of fuel cells: advances in electrocatalysis, materials, diagnostics and durability, vol 5 & 6. Wiley, Chichester

Zhang J (ed) (2009) PEM fuel cell electrocatalysts and catalyst layers. Springer, New York

Zhao TS, Kreuer KD, Van Nguyen T (eds) (2007) Advances in fuel cells I. Elsevier, Amsterdam

PEM Fuel Cells and Platinum-Based Electrocatalysts

Junliang Zhang
Electrochemical Energy Research Laboratory, General Motors Global R&D, Honeoye Falls, NY, USA

Article Outline

Glossary
Definition of the Subject
Introduction
Electrocatalysis of the ORR at Platinum Surfaces
Pt-Alloy Electrocatalysts
Pt Monolayer Electrocatalysts
Pt and Pt-Alloy Nanowire and Nanotube Electrocatalysts
Facet- and Shape-Controlled Pt-Alloy Nanocrystal Electrocatalysts
Future Directions
Bibliography

Glossary

Anode An electrode where the electrochemical oxidation reaction(s) occurs, generating free electrons that flow through a polarized electrical device and enter the cathode. In a fuel cell, the fuel oxidation reaction happens at the anode.

Cathode An electrode where the electrochemical reduction reaction(s) occurs, by consuming the electrons originated from the anode. In a fuel cell, the oxygen reduction reaction happens at the cathode.

Electrocatalyst A material that is applied on the surface of an electrode to catalyze half-cell reactions.

Normal hydrogen electrode (NHE) Also known as the standard hydrogen electrode (SHE), it is a redox reference electrode which forms the basis of the thermodynamic scale of oxidation–reduction potentials. The potential of the NHE is defined as zero and based on equilibrium of the following redox half-cell reaction, typically on a Pt surface:$2H^+(aq) + 2e^- \rightarrow H_2(g)$ The activities of both the reduced form and the oxidized form are maintained at unity. That implies that the pressure of hydrogen gas is 1 atm and the concentration of hydrogen ions in the solution is 1 M.

Oxygen reduction reaction (ORR) An electrode reaction, in which oxygen gas is reduced at the cathode of an electrochemical cell. The product of the reaction can be water molecules, hydroxyl ions (OH^-), or sometimes hydrogen peroxide molecules. It is a very important and much-studied electrochemical reaction because it occurs at the cathode of practically all fuel cells.

Proton-exchange membrane fuel cells (PEMFC) Also known as polymer electrolyte membrane fuel cells, these are a type of fuel cells that use proton-conducting-ionomer membrane as the electrolyte to separate anode and cathode. Their distinguishing features include low operating temperature (~80°C), high power density, quick start-up, and quick match to shifting demands for power. They are being developed for transport applications as well as stationary and portable applications.

Pt mass activity The kinetic current of the oxygen reduction reaction normalized by the mass of Pt metal contained in the electrocatalyst.

Pt-specific activity The kinetic current of the oxygen reduction reaction normalized by the electrochemical surface area of the Pt metal contained in the electrocatalyst.

Reversible hydrogen electrode (RHE) This differs from the NHE by the fact that the hydrogen-ion concentration of RHE reaction is the same as that in the actual electrolyte solution used for the working electrode. The potential of RHE is therefore (−0.059* (pH of the electrolyte)) V.

Definition of the Subject

H_2/air-powered PEM fuel cells are a future substitute for combustion engines as the green power source for transport application. In PEM fuel cells, because of their low operating temperature and low pH, both anode and cathode reactions are catalyzed by Pt or Pt-based electrocatalysts. Pt is a precious and expensive noble metal, and therefore its loading requirement plays a major role in determining the cost of fuel cells in mass production. The anode hydrogen oxidation reaction on Pt is intrinsically fast and requires very little Pt, while the cathode oxygen reduction reaction (ORR)

is a very sluggish reaction that consumes about 90% of the total Pt content in PEM fuel cells. The current Pt loading in the most advanced fuel cell vehicles that use state-of-the-art Pt-based catalysts is about four- to eightfold higher than the target established for mass-produced fuel cell vehicles. Therefore, lowering the Pt loading at the cathode is the most critical mission for the PEM fuel cell development. To do that, significant depth of knowledge in understanding the ORR on Pt and Pt-based electrocatalysts' surfaces is required; and the search for novel Pt-based electrocatalysts with enhanced ORR activity is seemingly the most productive pathway.

Introduction

Ever since 1839, when Sir William Robert Grove introduced the first concept of fuel cells [1, 2], researchers have been continuously trying to apply fuel cells for stationary and mobile power sources [3, 4], because of their high energy efficiency and low environmental footprint. Fuel cells can be customarily classified according to the electrolyte employed, with different electrolytes operating at different temperature ranges. The operating temperature then dictates the types of fuels and electrode materials that can be used in a fuel cell. For example, aqueous electrolytes are limited to operating temperatures of about 200°C or lower because of their high water vapor pressure. At these temperatures the fuel is, in applications requiring high current density and low cost, restricted to hydrogen. To accommodate the slow kinetics of the electrochemical reactions at such low temperature in acid environments, platinum catalysts are required for both cathode and anode. In high temperature fuel cells, CO or even CH_4 can be used as the fuel, and the catalyst is not necessary to be noble metals, because of the inherently fast electrode reaction kinetics.

Among various types of fuel cells, proton exchange membrane fuel cells (PEMFCs) have attracted the most attention in recent years due to their low operating temperature (about 80°C), high power density, quick start-up, and quick match to shifting demands for power [3]. Hydrogen/air-powered PEMFCs make them the primary candidate for the power source of light-duty vehicles and buildings. In a recent study by Thomas [5], the author compared fuel cell and battery as the power sources for all-electric vehicles, and found that for any vehicle range greater than 160 km (100 miles), fuel cells are superior than batteries in terms of mass, volume, cost, initial greenhouse gas reductions, refueling time, well-to-wheel energy efficiency (using natural gas and biomass as the source) and life cycle costs. PEMFCs also allow direct use of methanol without a processor, called DMFC. DMFCs are the primary candidates for portable electronic applications; low power densities and high Pt requirements have precluded their use in vehicles to date.

One difficult challenge to make PEMFC vehicles cost-competitive with traditional combustion engine cars is the high platinum catalyst loading and poor catalyst durability of the fuel cells [6, 7]. In the mid- to late-1980s and in the early 1990s, the fuel cell team at Los Alamos National Laboratory (LANL) succeeded in demonstrating high performance H_2/air fuel cells with a platinum loading less than 0.5 mg Pt/cm^2 per electrode, which was one magnitude lower than its previous level [8–11]. In that effort, Raistrick [8] was the first one to cast ionomer into the electrocatalyst layer by impregnating a Pt/C electrode into the ionomer solution before hot-pressing it onto the membrane, and thus greatly increased the electrocatalyst–electrolyte interfacial contact area. Wilson et al. [9–11] improved that process by mixing the Pt/C powder catalyst with ionomer solution before coating the electrode. Those research achievements at LANL partly led to the renaissance in PEMFCs in the past 2 decades [4].

In a PEMFC, if pure hydrogen is used as fuel, the anode reaction is then the hydrogen oxidation reaction (HOR) at the surface of the anode platinum electrocatalyst. The hydrogen oxidation reaction (HOR) and hydrogen evolution reaction (HER) are by far the most thoroughly investigated electrochemical reaction system [12]. Due to the fast electrode kinetics of hydrogen oxidation at platinum surface [12–14], the anode platinum loading can be reduced down to 0.05 mg Pt/cm^2 without significant performance loss [15]. The cathode reaction in a PEM fuel cell is the oxygen reduction reaction (ORR) at platinum surface in an acidic electrolyte. In contrast to HOR at the anode, the cathode ORR is a highly irreversible reaction even at temperatures above 100°C at the best existing catalyst – the platinum surface [16–19]. Gasteiger et al. [20] found that 0.4 mg Pt/cm^2 was close to the optimal

platinum loading for the air electrode using the state-of-the-art Pt/C catalyst and an optimized electrode structure. Further reduction of the cathode platinum loading will result in cell voltage loss at low current densities that follows the ORR kinetic loss. The high platinum loading at the cathode originates from the slow kinetics of (ORR) at platinum surface. To make the fuel cell vehicles commercially viable on the market, the platinum loading on the cathode has to be reduced significantly. As shown in Fig. 1, when Pt loading requirement is translated from the target set for power-specific Pt consumption in g Pt/kW, a fourfold Pt mass activity (activity per unit platinum mass) improvement is required, if combined with a 50% reduction in mass transport-related voltage loss [21]. Recent increases in Pt prices suggest that one should be striving for at least an eightfold improvement.

There are two ways one might think of that could help to reach that goal: further increasing the platinum dispersion (defined as the ratio of surface metal atoms to total number of atoms) by making finer platinum particles, if there is no decrease of Pt-specific activity (activity per unit Pt surface area); or alternatively, increasing the Pt-specific activity. One could also seek a combination of these two approaches.

This selected brief review will be focused on the research and development progress on ORR kinetics. The origin of the problem related with the low ORR activity of platinum will be discussed, followed by a review of recent progress in making more active, more durable platinum-based ORR catalysts. These include platinum alloy catalysts, platinum monolayer catalysts, platinum nanowire and nanotube catalysts, and the more recent shape- and facet-controlled platinum-alloy nanocrystal catalysts. The progress in the mechanistic understanding on the correlation between the activity and the electronic and structural properties of surface platinum atoms will be reviewed as well. The future direction of the research on platinum-based catalysts for PEM fuel cell application will be proposed.

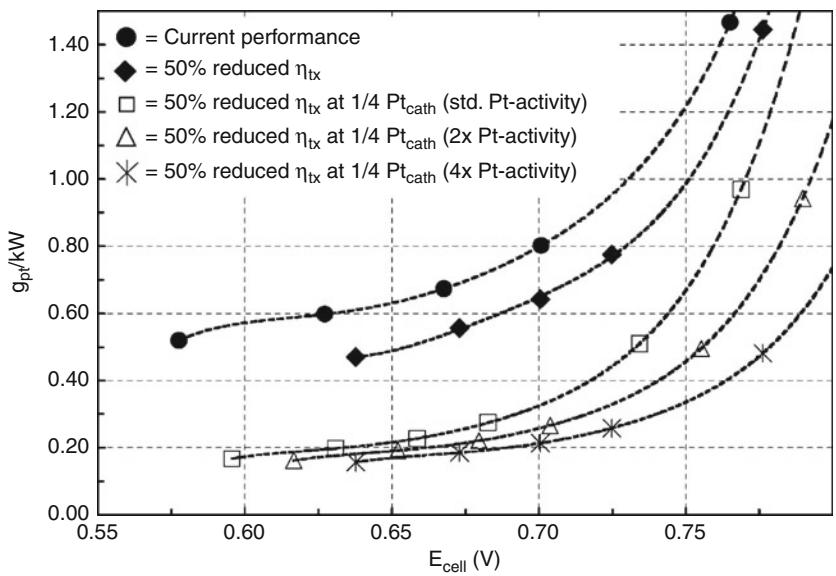

PEM Fuel Cells and Platinum-Based Electrocatalysts. Figure 1
Pt-mass-specific power density [g_{Pt}/kW] versus cell voltage, E_{cell} [V], based on a 50 cm^2 single-cell H_2/air performance. η_{tx} = cell-voltage loss caused by mass transport; Pt_{cath} = cathode-Pt loading. The cell was tested at T_{cell} = 80°C, 100% RH (relative humidity), at a total pressure of 150 kPa_{abs} and stoichiometric flows of s = 2.0/2.0. Catalyst-coated membrane (CCM) was based on a ca. 25 μm low-EW (equivalent weight = 900) membrane, and ca. 50 wt% Pt/carbon (0.4/0.4 mg Pt/cm^2 (anode/cathode)). It was assumed that the cell performance could be maintained at a reduced anode loading of 0.05 mg Pt/cm^2 (Reproduced from [21]. With permission)

Electrocatalysis of the ORR at Platinum Surfaces

It is widely accepted that the ORR on platinum surfaces is dominantly a multistep and four-electron reduction process with H_2O being the final product. However, the detailed mechanism of ORR still remains elusive [17]. The overall four electron reduction of O_2 in acid aqueous solutions is

$$O_2 + 4H^+ + 4e^- \rightarrow 2H_2O;$$
$$E_0 = 1.229\,\text{V Vs NHE at } 298\,\text{K}$$

Since the four-electron reduction of oxygen is highly irreversible, the experimental verification of the thermodynamic reversible potential of this reaction is very difficult. The irreversibility of ORR imposes serious voltage loss in fuel cells. In most instances, the current densities practical for kinetic studies are much larger than the exchange current density of ORR; therefore the information obtained from current-potential data are confined only to the rate-determining step (RDS). On the other hand, in the ORR kinetic potential region, the electrode surface structure and properties strongly depend on the applied potential and the time held at that potential, which makes the reaction more complicated. While the relationship between the overall kinetics and the surface electronic properties is not well understood, it is widely accepted that in the multistep reaction, the first electron transfer is the rate-determining step, which is accompanied by or followed by a fast proton transfer [16–18]. Two Tafel slopes are usually observed for ORR on Pt in RDE tests in perchloric acid, from −60 mV/decade at low current density, transitioning to −120 mV/decade at high current density. The lower Tafel slope of the ORR in perchloric acid at low current density has been attributed to the potential dependent Pt oxide/hydroxide coverage at high potentials [22–26].

Recently, by using Density Functional Theory (DFT), Norskov and coworkers [27] calculated the Gibbs free energy of ORR intermediates as a function of cathode potential based on a simple dissociative mechanism, i.e., with the adsorbed oxygen and hydroxide being the only intermediates. They found that oxygen or hydroxide is so strongly bound to the platinum surface at the thermodynamic equilibrium potential that proton and electron transfer become impossible. By lowering the potential, the stability of adsorbed oxygen decreases and the reaction may proceed. They suggested that these effects are the origin of the overpotential of the ORR on platinum surfaces.

By setting the reference zero potential to be NHE, the proton chemical potential in the electrolyte is related to the electrode potential. The authors made DFT calculations to get the bond energies of O^* and HO^* for a number of interesting metals. From this, they can evaluate the reaction free energies of the two basic steps: the hydrogenation of the two adsorbed intermediates O^* and HO^*. The larger one of the two reaction free energies was taken as the activation energy barrier of the rate-determining step (RDS) in ORR. By using a microkinetic model they constructed, the rate constant of the RDS, and therefore the ORR activity, can be evaluated based on the activation energy barrier. As shown in Fig. 2a, the model predicts a volcano-shaped relationship between the rate of the ORR and the oxygen adsorption energy, with platinum and palladium being among the best metals for electrocatalysis of ORR. Figure 2b shows that the bonding energy of OH is roughly linearly correlated to that of O, indicating both are nearly equivalent parameters in determining the ORR activity.

More recently, Wang et al. [28] derived an intrinsic kinetic equation for the four-electron ($4e^-$) oxygen reduction reaction (ORR) in acidic media, by using free energies of activation and adsorption as the kinetic parameters, which were obtained through fitting experimental ORR data from a Pt(111) rotating disk electrode (RDE). Their kinetic model consists of four essential elementary reactions: (1) a dissociative adsorption (DA); (2) a reductive adsorption (RA), which yields two reaction intermediates, O and OH; (3) a reductive transition (RT) from O to OH; and (4) a reductive desorption (RD) of OH, as shown below [28] (Reproduced with permission from [28]).

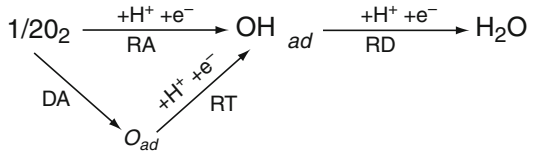

In contrast to a conventional ORR kinetic model, in this work there is no single particular RDS assumed, as the authors believe that a single RDS assumption may

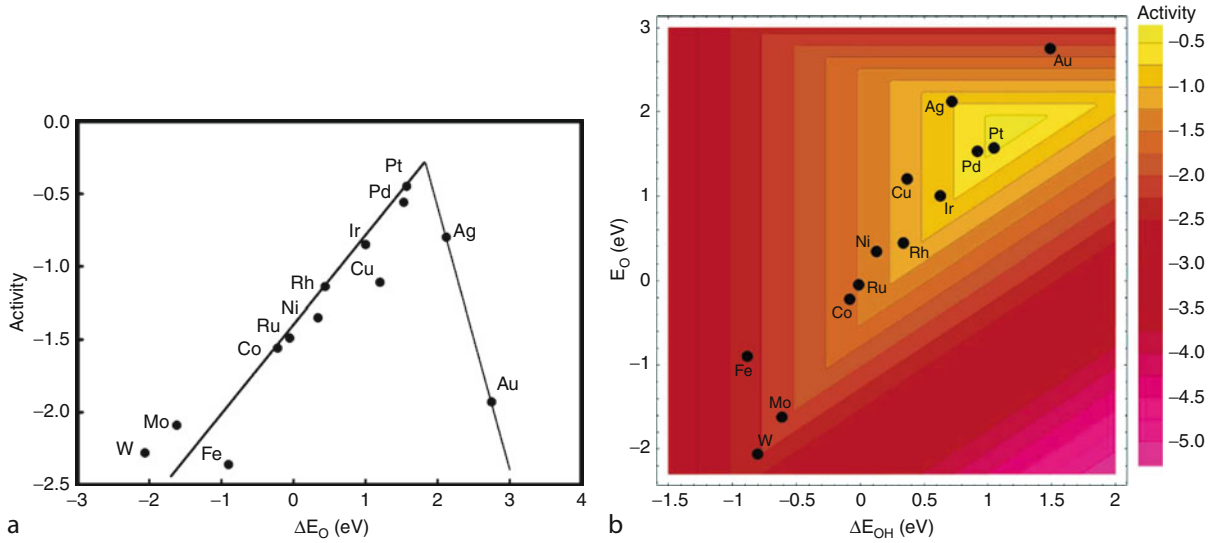

PEM Fuel Cells and Platinum-Based Electrocatalysts. Figure 2
(**a**) Trends in oxygen reduction activity plotted as a function of the O-binding energy. (**b**) Trends in oxygen reduction activity plotted as a function of both the O and the OH-binding energy (Reproduced from [27]. With permission)

not hold over a wide potential region since the reaction pathway may change with potential, or there may exist two RDSs with similarly high activation barriers. The results indicate that the first electron transfer in the RA reaction ($\Delta G^{*0}_{\mathrm{RA}} = 0.46$eV, where ΔG^{*0}_{i} is the activation energy of reaction i (at equilibrium potential)) is not the rate-determining step (RDS) for the ORR on Pt at high potentials, because dissociative adsorption ($\Delta G^{*0}_{\mathrm{DA}} = 0.26$ eV) provides a more active adsorption pathway. However, the reaction intermediates, O and OH, are strongly trapped on the Pt surface, requiring considerable overpotential to overcome the barriers for O to OH transition ($\Delta G^{*0}_{\mathrm{RT}} = 0.50$ eV) and OH reduction to water and desorption ($\Delta G^{*0}_{\mathrm{RD}} = 0.45$eV). Thus, the ORR on Pt is desorption-limited at high potentials, exhibiting a low apparent Tafel slope at those potentials. Wang et al. [29] further used this kinetic model to fit a typical IR-free polarization curve of a PEMFC, by adjusting the parameters to reflect the fuel cell-operating conditions at 80°C. The results showed that the transition of the Tafel slope occurs at about the same 0.77 V that is the equilibrium potential for the transition between adsorbed O and OH on a Pt surface with low adsorbed O coverage [27].

Neyerlin et al. [30–32] investigated the ORR kinetics on high-surface-area carbon-supported platinum catalyst Pt/C in an operating PEMFC. By assuming the transfer coefficient $\alpha = 1$ and using a single Tafel slope, i.e., −70 mV/decade at 80°C, three kinetic parameters could be extracted through fitting the kinetic model to the fuel cell data: the exchange current density or current density at a constant IR-free cell potential, the reaction order with respect to oxygen partial pressure, and the activation energy. One may need to note that the lower limit of the electrode potential after IR and transport correction in this work is about 0.77 V, so that this single-Tafel-slope treatment can still be consistent with Wang et al.'s [29] result. Neyerlin et al. [30] were concerned about the accuracy of the kinetic current extracted from low potentials in RDE tests, since at these low potentials the experimental measured current is more than ten times lower than the kinetic current derived from it. The transport correction used in RDE analysis assumes perfect first-order kinetics, which is not strictly true, and errors from this imperfect correction could become large at low potentials. The authors also studied the relative humidity (RH) effects on ORR kinetics in PEMFCs [32]. They found that when RH is above 50–60%, the kinetics are independent of the RH, but they observed significant ORR kinetic losses at lower RH. The reduction of ORR kinetics at low RH was interpreted as most likely

due to a lowering of the proton activity (therefore only indirectly related to the lowering of the water activity) via hydration of acidic groups and the sequestering of protons at low RH.

Another factor that plays an important role in determining the minimum loading of Pt catalyst required for PEMFCs is the Pt size effect on ORR, not only through altering the fraction of surface Pt atoms over the number of total Pt atoms, but also through changing the ORR kinetics per surface Pt atom (Pt specific activity). Earlier results by Blurton et al. [33] showed that in 20% H_2SO_4 at 70°C, the highly dispersed Pt (with size of about 1.4 nm) supported on conductive carbon prepared through ion exchange on resin followed by pyrolysis has a Pt-specific activity 20 times lower than that of crystalline Pt black (with size of about 10 nm), though it is not clear to what extend the lower activity could be caused by contamination of Pt and/or a "burying effect" during the catalyst preparation. Blurton et al. [33] correlated the decreased ORR specific activity with the decreased coordination number of surface Pt atoms on smaller Pt particles, causing more severe oxidation of the Pt surface. Peuckert et al. [34] later investigated a series of Pt-on-carbon catalysts with Pt weight percents from 5% to 30% prepared by an impregnation method, with corresponding fractions of metal atoms on the surface from 1.0 (Pt size < 1 nm) to 0.09 (Pt size $\sim$ 12 nm). The Pt-specific activity toward ORR in 0.5 M H_2SO_4 at 298 K on these catalysts was found to be constant for Pt particle sizes above 4 nm but to decrease by a factor of 20 as the particle size decreased from 3 to 1 nm. Taking into account the larger percentage of buried and these inactive Pt atoms in larger particles, this result suggested that the optimal Pt size for the maximum Pt mass activity is about 3 nm. Kinoshita [35] also reviewed and analyzed the particle size effect for ORR on Pt/C catalysts. Based on the literature data of ORR on Pt/C collected in H_3PO_4 [36–38] and H_2SO_4 [34] solutions, Kinoshita proposed the decrease of Pt-specific activity with decrease of Pt particle size is a consequence of the changing distribution of surface atoms at the (100) and (111) crystal faces. Recent literature data [18] in H_3PO_4 reported that when Pt particle size increases from 2.5 to 12 nm, there is about threefold of increase in Pt-specific activity and confirmed the optimal Pt particle size for maximum mass activity to be around 3 nm. Gasteiger et al. [21] investigated Pt/C and Pt black catalysts for ORR in $HClO_4$ solution at 60°C, with the Pt particle size ranging from 2 nm to over 10 nm, and found that the magnitude of activity improvement is comparable to that in literature data [39, 40], although the absolute values are about ten times higher than those reported in Ref. [40], due in part to the use of a less-strongly adsorbing electrolyte.

It is well established that ORR on Pt single crystals is structure-sensitive, depending on the electrolyte. In H_2SO_4, the order of activity of Pt(hkl) increases in the sequence (111) $<<$ (100) $<$ (110) [19, 41]. The variation in H_2SO_4 originates from highly structure-specific adsorption of sulfate/bisulfate anions in this electrolyte, which has a strongly inhibiting effect on the (111) surface. Given that the dominant Pt crystal facets of high-surface-area Pt/C catalysts are {111} and {100}, the Pt size effect on ORR activity in H_2SO_4 can be explained by the structure-sensitive adsorption. In perchloric acid, the variation in activity at is relatively small between the three low index faces, with activity increasing in the order (100) $<$ (111) (110)[42], owing to the structure sensitive inhibiting effect of OH_{ads}, i.e., a stronger inhibiting effect on (100) and smaller effects on (110) and (111)[41]. Norskov and other researchers [43–48], based on their DFT calculations, recently proposed using the concept of averaged d-band center energy to explain the reactivity of metal surface atoms, which was supported by numerous experimental data. According to them, when Pt particle size decreases, the average coordination number of surface Pt atoms decreases, causing the d-band center to move closer to the Fermi level and the reactivity of those atoms to increase. As a result of that, the Pt atoms bind oxygen–hydroxide stronger, and therefore, have a lower ORR activity. A stronger adsorption of OH species on Pt surface when the particle size is reduced to below 5 nm was reported in Ref. [49].

While the Pt particle-size effect on ORR suggests that a further increase of Pt dispersion by decreasing the particle size to much smaller than 3 nm will not improve Pt mass activity, it is worth noting that the Pt-size effect is not universally believed. Recently, Yano et al. [50] studied ORR on a series of carbon-supported Pt-nanoparticle electrocatalysts (Pt/C) with average diameters in the range of roughly 1–5 nm, combined with measurements on ^{195}Pt electrochemical

nuclear magnetic resonance (EC-NMR) spectroscopy. They observed that ORR rate constants and H_2O_2 yields evaluated from hydrodynamic voltammograms measurements did not show any particle size dependency. The apparent activation energy of 37 kJ mol^{-1}, obtained for the ORR rate constant, was found to be identical to that obtained for bulk platinum electrodes. This was consistent with the negligible difference in the surface electronic properties of these Pt/C catalysts, revealed from the practically no change of surface peak position of ^{195}Pt NMR spectra and the spin-lattice relaxation time of surface platinum atoms with the particle size variation.

Nevertheless, facilitating the ORR kinetics by augmenting the Pt specific activity is important for the future of fuel cells. A recent perspective in *Science* by Gasteiger and Markovic [51] showed some promising advances in this aspect.

Pt-Alloy Electrocatalysts

Pt-alloy catalysts, predominantly Pt binary and ternary alloys with 3D transition metals, have been the main focus of catalyst research for PEM fuel cells in the past decades, as they confer enhanced ORR activities over those available from pure Pt catalysts. Great progress has been made in past decades in developing more active and durable Pt alloy catalysts and in understanding the mechanism of their activity enhancements. Two- to threefold specific activity enhancements versus pure Pt were typically reported in literature [21, 40, 52–54], while exceptions existed from earlier results, claiming either no enhancement [55–57], or over an order of magnitude enhancement [58]. As far as which alloy and what alloy compositions confer the highest ORR activity, there seems to be lack of general agreement. This is probably because the measured activity depends highly on the catalyst surface and near-surface atomic composition and structure, on impurities on the surface, and on particle size and shape, all of which could be affected by the preparation method, heat treatment protocol, and testing conditions. For example, to achieve the optimal alloy structure for maximum activity, different Pt alloy particles may require different annealing-temperature protocols to accommodate the distinctions between metal melting points and particle sizes [59, 60]. In a number of earlier papers [61–63] it was showed that Pt-Cr is the most active ORR cathode catalyst in phosphoric acid fuel cells, while some recent results reported that in the PEMFC-oriented settings, the most active Pt alloy ORR catalyst could be Pt-Co [64], Pt-Fe [58, 65], Pt-Cr [52], Pt-Ni [66], or Pt-Cu [67] at specific atomic ratios of Pt to the alloying elements. Several representative mechanisms have been proposed in the literature to explain the enhanced activities observed on Pt alloy catalysts: (1) a surface roughening effect due to leaching of the alloy base metal [68, 69]; (2) decreased lattice spacing of Pt atoms due to alloying [52, 61, 70]; (3) electronic effects of the neighboring atoms on Pt, such as increased Pt d-band vacancy [52, 58, 65, 71] or depressed d-band center energy upon alloying [42, 64, 67, 72, 73]; and/or (4) decreased Pt oxide/hydroxide formation at high potential [52, 74–76]. The increased Pt surface roughness alone may help increase Pt mass activity but will not increase the Pt-specific activity. Other mechanisms are correlated with each other, for example, the decreased lattice spacing may affect the electronic structure of Pt atoms, which in turn may inhibit the Pt oxide/hydroxide formation. A more detailed discussion follows.

Jalan and Taloy [61] believed that the nearest-neighbor distance between Pt atoms plays an important role in the ORR, based on the reaction model proposed by Yeager et al. [16], i.e., the rate-determining step being the rupture of O–O bond via various dual site mechanisms. They proposed that the distance between nearest-neighbor atoms on the surface of pure Pt is not ideal for dual site adsorption of O_2 or "HO_2" and that the introduction of foreign atoms that reduce the Pt nearest-neighbor spacing would result in higher ORR activity. By testing a number of carbon-supported Pt-M alloy catalysts fabricated into gas diffusion electrodes, with various nearest-neighbor Pt atom distances determined from X-ray diffraction, a linear relationship was obtained between the activity and the distance, with Pt-Cr exhibiting highest ORR activity and smallest nearest-neighbor distance, as shown in Fig. 3. While the geometric distance between the neighboring Pt atoms is shorter in alloys, the surface electronic structure of Pt alloys is different from that of pure Pt as well, so it is difficult to separate the two factors. Yet other studies [55, 68, 69] claimed no activity enhancement was observed on Pt-Cr alloy over

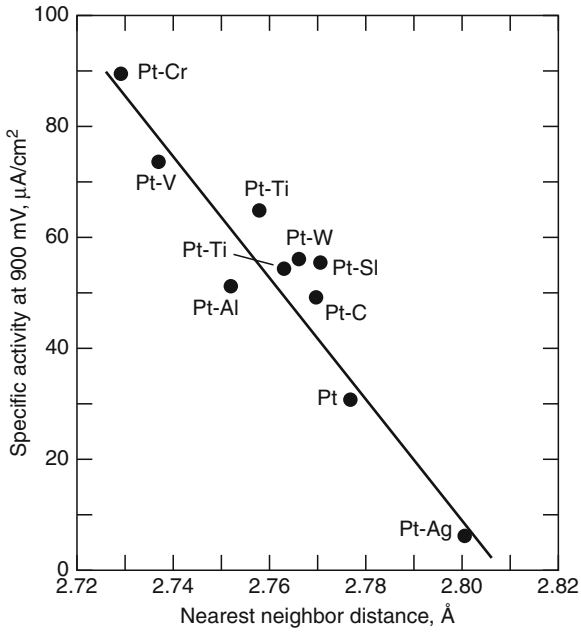

PEM Fuel Cells and Platinum-Based Electrocatalysts. Figure 3

Specific activity for the ORR versus electrocatalyst nearest-neighbor distance (Reproduced from [61]. With permission)

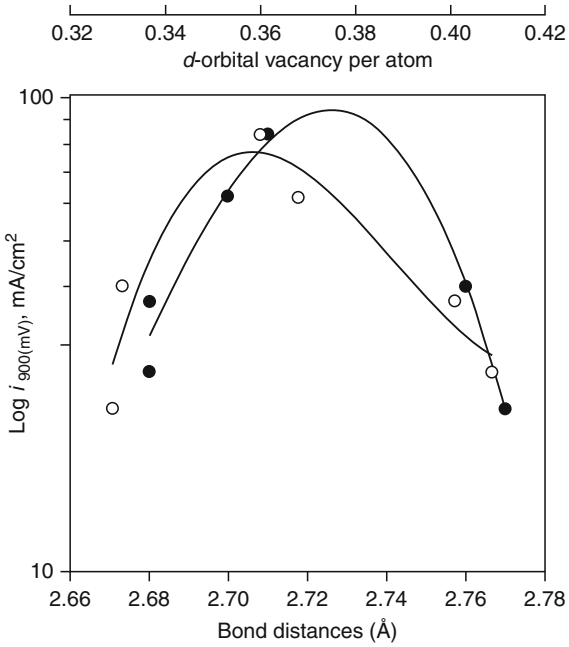

PEM Fuel Cells and Platinum-Based Electrocatalysts. Figure 4

Correlation of the ORR performance of Pt and Pt-alloy electrocatalysts in PEMFC with Pt–Pt bond distance (*solid circles*) and the d-band vacancy of Pt (*empty circles*) obtained from in situ XAS (Reproduced from [52]. With permission)

pure Pt, except for the increased surface roughness [68, 69], but this has not been supported by more recent literature [52, 70].

Mukerjee and coworkers did a series of studies [52, 74, 77, 78] on Pt binary alloys for ORR applying in situ X-ray absorption spectroscopy (XAS) to electrochemical systems. The spectra consist of two parts, the near-edge part XANES (X-ray absorption near-edge structure), which gives chemical information and EXAFS (extended X-ray absorption fine structure), which gives the structural information around the element of interest. In a related study, Mukerjee et al. [52] investigated five binary Pt alloys (PtCr/C, PtMn/C, PtFe/C, PtCo/C, and PtNi/C) supported on high-surface-area carbon for ORR in a proton exchange membrane fuel cell. The electrode kinetic studies on the Pt alloys showed a two- to threefold increase in ORR activity relative to a reference Pt/C electrocatalyst, with the PtCr/C alloy exhibiting the best performance. Contractions in the Pt–Pt bond distances were observed by both EXAFS and XRD. In addition, they found that in the double-layer potential region (0.54 V versus RHE), the alloys possess higher Pt d-band vacancies than Pt/C, while in the high potential region (0.84 V versus RHE), Pt/C shows higher d-band vacancy relative to alloys. This was interpreted by the adsorption of OH species at high potential on Pt/C but to a lesser extent on Pt alloys. Correlation of the electronic (Pt d-band vacancies) and geometric (Pt–Pt bond distance) with the electrochemical performance characteristics exhibits a volcano-type behavior with the PtCr/C alloy being at the top of the curve, shown in Fig. 4. They rationalized the enhanced activity on alloys on the basis of electronic and geometric effects, and of inhibition of OH adsorption. Similar observations were also reported from the ORR measurements in phosphoric acid [66], and in alkaline solution [79–81].

Surface segregation of Pt has been experimentally observed in a wide range of Pt-M binary alloys, such as Pt-Fe [82], Pt-Ni [83], Pt-Co [84], Pt-Ru [85], and has also been reported in theoretical calculations [86, 87]. Furthermore, it has been reported that the topmost layer is composed of pure Pt while the second layer is

enriched in the transition metal M for Pt-rich Fe, Co, and Ni alloys [72, 76, 88], produced by displacement of Pt and M atoms in the first two layers to minimize the surface free energy during annealing. Stamenkovic et al. [76] studied polycrystalline Pt_3Ni and Pt_3Co alloys for electrocatalysis of ORR in acid electrolytes using the rotating ring disk electrode (RRDE) method. Polycrystalline bulk alloys of Pt_3Ni and Pt_3Co were prepared in ultra-high vacuum (UHV) having two different surface compositions: one with 75% Pt (by sputtering) and the other with 100% Pt (by annealing). The latter was called a "Pt-skin" structure and is produced by an exchange of Pt and Co in the first two layers. Activities of Pt-alloys for the ORR were compared to those of polycrystalline Pt in 0.5 M H_2SO_4 and 0.1 M $HClO_4$ electrolytes. It was found that in H_2SO_4, the activity increased in the order $Pt_3Ni > Pt_3Co > Pt$; in $HClO_4$, however, the order of activities was "Pt-skin/Pt_3Co" > $Pt_3Co > Pt_3Ni > Pt$. The catalytic enhancement was greater in 0.1 M HClO4 than in 0.5 M H_2SO_4, with the maximum enhancement observed for the "Pt-skin" on Pt_3Co in 0.1 M $HClO_4$ being three to four times that for pure Pt. The activity enhancement was attributed to the inhibited Pt-OH_{ad} formation on an alloy, even one covered with pure Pt, relative to the surface of a pure-Pt electrode, and the ORR reaction mechanism (pathway) was found to be the same on alloys as on a pure-Pt electrode. In a more recent study, Stamenkovic et al. [64] investigated polycrystalline Pt_3M (M = Ni, Co, Fe, Ti, V) surfaces for ORR in 0.1 M $HClO_4$, for both "Pt-skin" and sputtered alloy surfaces. The activity was correlated to the d-band center energy obtained in UHV via ultraviolet photoemission spectroscopy (UPS). A "volcano behavior" was revealed with the Pt_3Co has the highest activity for both "Pt-skin" and sputtered surfaces. The "Pt-skin" surface was found to be more active than sputtered surface again for each Pt_3M. The electrochemical and post-electrochemical UHV (ultra-high vacuum) surface characterizations revealed that Pt-skin surfaces are stable during and after immersion to an electrolyte. In contrast, all sputtered surfaces formed Pt-skeleton outermost layers due to dissolution of transition metal atoms [89].

By using DFT calculations, Xu et al. [47] studied the adsorption of O and O_2 and the dissociation of O_2 on the (111) faces of ordered Pt_3Co and Pt_3Fe alloys and on monolayer Pt skins covering these two alloys. Results were compared with those calculated for two Pt(111) surfaces, one at the equilibrium lattice constant and the other laterally compressed by 2% to match the strain in the Pt alloys. The absolute magnitudes of the binding energies of O and O_2 follow the same order in the two alloy systems: Pt skin < compressed Pt(111) < Pt(111) < $Pt_3Co(111)$ or $Pt_3Fe(111)$. The reduced bonding strength of the compressed Pt(111) and Pt skins for oxygen was rationalized as being due to the shifting of the d-band center increasingly away from the Fermi level. They proposed that an alleviation of poisoning by O and enhanced rates for reactions involving O could be some of the reasons why Pt skins are more active for the ORR.

Chen et al. [88, 90] recently studied carbon supported Pt_3Co nanoparticles for ORR and correlated their activity with the chemical composition and structural information of individual particles. Conventional and aberration-corrected high-angle annular dark-field (HAADF), scanning transmission electron microscopy (STEM), and high resolution transmission electron microscopy (HRTEM) were used to obtain the particle compositional and structural information. For the acid treated Pt_3Co nanoparticles, they observed the formation of percolated Pt-rich and Pt poor regions within individual nanoparticles, analogous to the skeleton structure observed for sputtered polycrystalline Pt alloy surfaces after acid leaching [89]. The acid treated alloy nanoparticles yielded about two times the specific activity of pure-Pt nanoparticles. After annealing of the acid-treated particles, sandwich-segregation surfaces of ordered Pt_3Co nanoparticles were directly observed, with the topmost layer being pure Pt atoms. The specific activity of annealed nanoparticles was about four times that of pure Pt nanoparticles. The enhanced Pt-specific activity toward ORR was attributed to the reduced binding energy of oxygenated species, owing to combined two effects, i.e., the increased compressive strain in Pt atoms, and the ligand effect from underlying Co atoms.

Strasser et al. [59, 67, 91–94] recently applied a freeze-drying technique in the synthesis of Pt alloy nanoparticle catalysts with enhanced ORR activity. The Pt-Cu alloy catalyst after electrochemical dealloying was reported to have both mass and specific activities about four to six times those of a standard commercial Pt/C catalyst, in both RDE and MEA tests. The synthesis

involved an impregnation/freeze-drying route followed by annealing. Preparation started with impregnation and sonication of a commercial 30 wt% Pt/C catalyst with an aqueous solution of a copper nitrate, with Pt:Cu atomic ratio of 1:3, followed by freezing in liquid N_2. The frozen sample was subsequently freeze-dried under a moderate vacuum (0.055 mbar). Reduction and alloying of Pt and Cu on the carbon support was thermally driven under a reductive H_2 atmosphere in a tube furnace. Electrochemical etching (voltammetric dealloying) was employed to remove the surface Cu atoms from Cu-rich Pt-Cu alloy precursors. Bulk and surface structural and compositional characterization suggested that the dealloyed active catalyst phase consists of a core-shell structure in which a multilayer Pt rich shell is surrounding a Pt-poor alloy particle core. This work constitutes significant progress on initial activity, since a fourfold of increase of Pt mass activity is the performance target for commercially viable fuel cell cathode catalyst [21]. Figure 5a shows a schematic of the dealloying process, and Fig. 5b exhibits the Pt mass activities of Pt-Cu/C synthesized at different temperatures, compared with the Pt/C catalyst.

As to the mechanistic origin of the activity enhancement in dealloyed Pt-Cu catalyst, the authors believe geometric effects play a key role, because the low residual Cu near-surface concentrations make significant electronic interactions between Pt and Cu surface atoms unlikely. Therefore, they suspect that the dealloying creates favorable structural arrangements of Pt atoms at the particle surface, such as more active crystallographic facets or more favorable Pt–Pt interatomic distances for the electroreduction of oxygen, as predicted by DFT calculations [47]. A fourfold

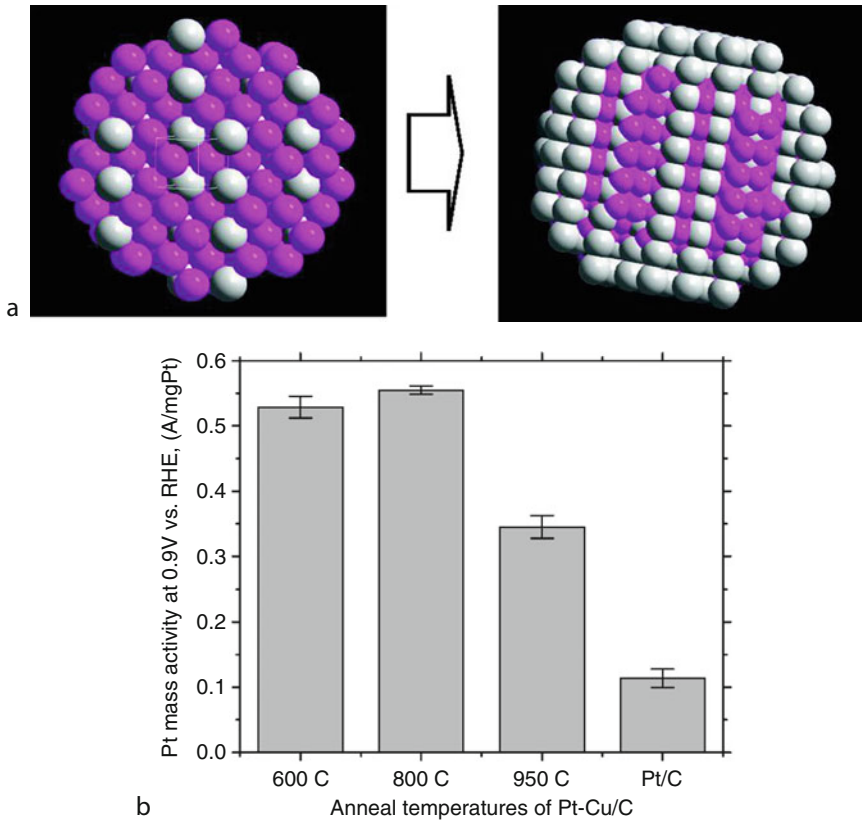

PEM Fuel Cells and Platinum-Based Electrocatalysts. Figure 5

(**a**) The schematic model of a Pt-Cu alloy particle before and after electrochemical dealloying of the near-surface Cu atoms (*pink balls* = Cu atoms; *gray balls* = Pt atoms); (**b**) Pt mass activities of Pt-Cu/C catalysts at various annealing temperatures compared to that of Pt/C catalyst (Reproduced from [67]. With permission)

enhancement in Pt mass activity on monodispersed Pt_3Co nanoparticles with particle size of 4.5 nm was also reported recently [95].

Watanabe and coworkers carried out a series of studies on the mechanism for the enhancement of ORR activity on Pt-Fe, Pt-Ni, and Pt-Co alloys [53, 58, 65, 71, 96, 97]. By using X-ray photoelectron spectroscopy combined with an electrochemical cell (EC-XPS) [96, 97], they identified quantitatively oxygen-containing species adsorbed on electrodes of a pure Pt and a Pt skin layer (generated by acid treatment, not annealing, and therefore equivalent to the "skeleton" layers described by Stamenkovic et al. [89]) formed on Pt-Fe and Pt-Co alloys' surface from N_2- and O_2-saturated 0.1 M HF solution. Four types of species were distinguished with binding energies at 529.6, 530.5, 531.1, and 532.6 eV; the first two were assigned to O_{ad} and OH_{ad}, while the latter two were assigned to the bilayer water molecules, $H_2O_{ad,1}$ and $H_2O_{ad,2}$. The XPS results showed that the Pt skin layer exhibited a higher affinity to O_{ad} but less to H_2O compared to pure Pt, particularly in the O_2-saturated solution. The enhanced ORR activity at the Pt skin/Pt-alloy electrode was ascribed to higher coverage of O_{ad} than that at pure Pt. They also found that such an enhancement is induced without changing the activation energy but the corresponding frequency factor value in the pre-exponential term from that of pure Pt. From the measurements in a flow channel with 0.1 M $HClO_4$, in the temperature range of 20–50°C, a two to fourfold of ORR-specific activity enhancement was reported for those Pt alloys [53].

Pt metal dissolution in fuel cells has been reported to play a key role in Pt surface area loss and cell performance loss [98]. While Pt-alloy catalysts with fourfold enhancement in both Pt mass activity and specific activity relative to standard Pt/C catalyst seem achievable, as has been shown above, the long-term durability of the alloy catalysts is still a concern, due to dissolution of the base metal from the alloys [21, 99]. For Pt-Cu alloy catalysts, an additional possible risk is that the dissolved Cu may migrate from cathode through membrane to anode and deposit on the anode Pt surface, causing a poisoning effect on anode hydrogen oxidation kinetics, as the Cu redox potential is higher than the anode hydrogen redox potential. Fortunately, the durability of the cathode catalyst can be compensated by careful system control, mainly through lowering the cathode upper potential limit and narrowing its operating potential window [100, 101].

Pt Monolayer Electrocatalysts

Pioneered by Adzic et al. [102, 103], the idea of a Pt monolayer electrocatalyst has been one of the key concepts in reducing the Pt loading of PEM fuel cells in recent years. Pt submonolayers deposited on Ru nanoparticles had been earlier demonstrated to give superior performance with ultra-low Pt loading compared to commercial Pt/C or Pt-Ru alloy catalysts for the anode CO-tolerant hydrogen oxidation reaction [103–107]. More recently, Adzic and coworkers applied this concept in making novel Pt monolayer catalysts for the cathode ORR, which will be the focus of the review in this section. In general, the new method of synthesizing Pt monolayer catalysts involves underpotential deposition (UPD), a technique well known to produce an ordered atomic monolayer to multilayer metal deposition onto a foreign metal substrate [108–110]. Specifically, the method consists of two steps [111, 112]: first, a monolayer of a sacrificial less-noble metal is deposited on a more noble metal substrate by UPD, such as Cu UPD on Au or Pd; second, the sacrificial metal is spontaneously and irreversibly oxidized and dissolved by a noble metal cation, such as a Pt cation, which is simultaneously reduced and deposited onto the foreign metal substrate. The whole procedure can be repeated in order to deposit multilayers of Pt (or another noble metal) on the foreign metal.

The advantages of Pt monolayer catalysts include (1) full utilization of the Pt atoms that are all on the surface, and (2) that the Pt activity and stability can be tailored by the selection of the substrate metals. For example [102], when a Pt monolayer is deposited onto different substrate metals, as shown in Fig. 6, due to the lattice mismatch between the metals, it can experience compressive or tensile stress, which is known to affect the Pt activity by adjusting its d-band center energy [43, 47] and consequently its ORR activity.

Pt monolayer deposits on Pd(111) single crystals (Pt/Pd(111)) and on Pd/C nanoparticles (Pt/Pd/C) have been studied for ORR [112], and improved activities compared to Pt(111) and commercial Pt/C, respectively, were reported. The ORR reaction mechanism of

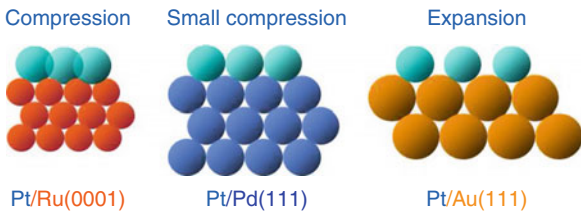

PEM Fuel Cells and Platinum-Based Electrocatalysts. Figure 6
Models of pseudomorphic monolayers of Pt on three different substrates inducing compressive strain (Ru(0001) and Pd(111)) and tensile strain (Au(111)). (Reproduced from [102]. With permission)

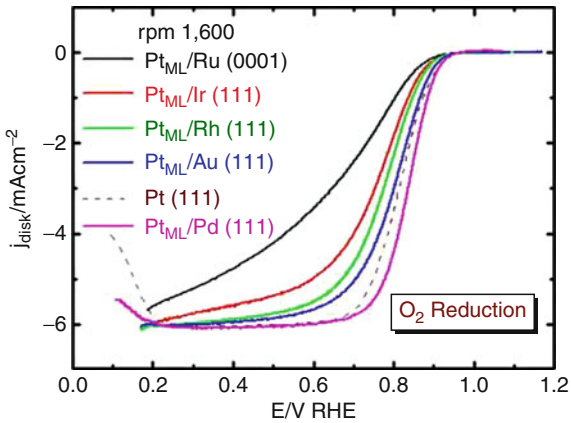

PEM Fuel Cells and Platinum-Based Electrocatalysts. Figure 7
Polarization curves for O_2 reduction on platinum monolayers in 0.1 M $HClO_4$ solution on a RDE. Rotation rate = 1,600 rpm (Reproduced from [114]. With permission)

the monolayer catalysts was found to be the same as that on pure Pt surface. Pt/Pd(111) was found to have a 20 mV improvement in half-wave potential versus Pt (111), and the Pt/Pd/C had a Pt-mass activity five- to eight-times higher than that of Pt/C catalyst. If the total noble metal amount (Pt + Pd) is counted, the mass activity is about 80% higher than that of Pt/C catalyst [112]. The enhanced ORR activity is attributed to the inhibited OH formation at high potential, as evidenced from XAS measurements. In a real fuel cell test, 0.47 g Pt/kW was demonstrated at 0.602 V [113].

In order to understand the mechanism for the enhanced activity of a Pt monolayer deposited on Pd metal, the ORR was investigated in O_2-saturated 0.1 M $HClO_4$ solution on platinum monolayers supported on Au(111), Ir(111), Pd(111), Rh(111), and Ru(0001) single-crystal RDE surfaces [114]. A comparison of the polarization curves at 1,600 rpm is shown as in Fig. 7. The trend of the ORR activities increase in the sequence Pt/Ru(0001) < Pt/Ir(111) < Pt/Rh(111) < Pt/Au(111) < Pt(111) < Pt/Pd(111).

The authors further correlated the kinetic activities of the "monolayers" with the Pt d-band center energies (not shown) and Pt-O binding energies, and found a "volcano" relationship, with the Pt/Pd(111) having the optimal d-band center, as well as Pt_{ML}-O-binding energy, for the maximum ORR activity. The "volcano" behavior was rationalized as being controlled by the two key steps in ORR, the O–O bond dissociation which is followed by the other step, the O–H bond formation. As shown in Fig. 8, the activation energies of the two steps both correlated linearly with the Pt_{ML}-O-binding energies (and with the

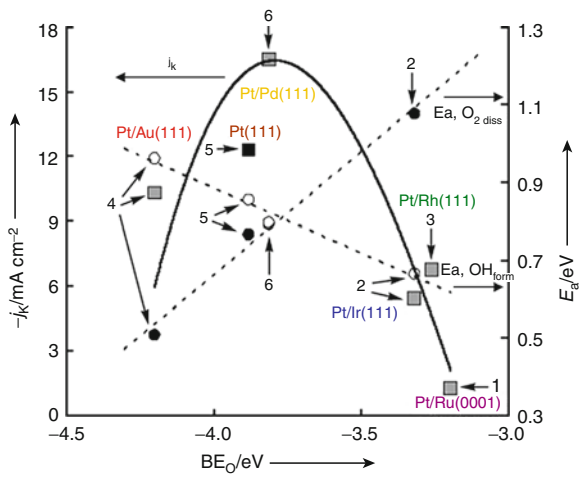

PEM Fuel Cells and Platinum-Based Electrocatalysts. Figure 8
Kinetic currents (j_K; *square symbols*) at 0.8 V (versus RHE) calculated from Fig. 7 for ORR and the activation energies for O_2 dissociation (*solid circles*) and for OH formation (*empty circles*) on Pt/Ru(0001) (1); Pt/Ir(111) (2), Pt/Rh(111) (3), Pt/Au(111) (4), Pt(111) (5) and Pt/Pd(111) (6), as functions of the calculated binding energy of atomic oxygen (BEO) (Reproduced from [114]. With permission)

d-band center energies, not shown), but in the opposite trend, indicating the Pt_{ML}-O binding can be neither too strong, nor too weak, for the best ORR activity.

For further fine-tuning of the monolayer Pt/Pd ORR activity, they further introduced mixed metal + Pt monolayer catalysts [115], which contained 0.2 monolayer of a foreign metal from selection of (Au, Pd, Rh, Ir, Ru, Os, and Re) combined with 0.8 monolayer of Pt co-deposited on Pd(111) or on Pd/C nanoparticles. The foreign metals have either a weaker M–OH bond (for the case of Au–OH), or a stronger M–OH bond (for the rest of the cases) than the Pt–OH bond. DFT calculations [115] showed that, in addition to altering the Pt d-band center energies, the $OH_{(-M)}-OH_{(-Pt)}$ (or $O_{(-M)}-OH_{(-Pt)}$) repulsion plays an important role in augmenting the ORR activity, as shown below in Fig. 9. Instead of adjusting the composition of the top-most Pt monolayer, replacing the substrate Pd(111) with $Pd_3Fe(111)$ to generate Pt/$Pd_3Fe(111)$ was recently reported to also have an enhanced ORR activity [116].

Another type of Pt monolayer catalyst showing improved ORR activities are Pt monolayers deposited on (noble metal)/(non-noble metal) core-shell nanoparticles [117]. The synthesis approach started with impregnation of high surface carbon into a mixed solution of noble metal precursor and non-noble metal precursor, followed by stir-drying in air. Core-shell metal substrates were formed by surface segregation of the noble metal at elevated temperature in a reductive atmosphere. A Pt monolayer was then deposited on the core/shell substrates by galvanic displacement of a Cu monolayer that was UPD-deposited onto the core-shell substrate particles. Three combinations were investigated: Pt/Au/Ni, Pt/Pd/Co, and Pt/Pt/Co. The enhancement of Pt mass activity of the best case (Pt/Au/Ni) was reported as being over an order of magnitude relative to the commercial Pt/C catalyst. The total noble metal mass activities were reported to be 2.5–4 times higher than that of Pt/C, with the Pt/Pt/Co having the highest number. The enhancement of activities was attributed to the geometric effect induced by the fine-tuning of the Pt lattice spacing with the substrate core-shell particles and to the inhibited PtOH formation because of lowering of the d-band center position relative to the Fermi level.

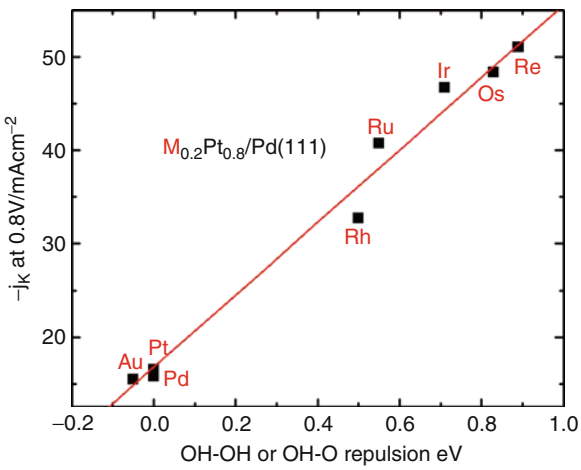

PEM Fuel Cells and Platinum-Based Electrocatalysts. Figure 9
Kinetic current at 0.80 V as a function of the calculated interaction energy between two OHs, or OH and O. Positive energies indicate more repulsive interaction compared to Pt/Pd(111) (Reproduced from [115]. With permission)

In a related study, Zhang et al. [118] investigated a partial monolayer of Au deposited on Pt(111) and on Pt/C nanoparticles for ORR. The catalysts were synthesized by Au displacement of a monolayer Cu that was deposited with UPD onto the Pt(111) or Pt/C substrates. Due to the valence–state difference between Au^{3+} and Cu^{2+}, two thirds of a monolayer of Au was deposited onto each of the Pt surfaces. The Au atoms appeared to form clusters on Pt surfaces. While the ORR activities of the Au/Pt(111) and Au/Pt/C catalysts were slightly lower than those of pure Pt(111) and Pt/C catalysts, respectively; the stability of the Au/Pt/C was superior compared to that of Pt/C catalyst. Potential cycling tests were performed on RDE in 0.1 M $HClO_4$ solution, with the potential cycling window between 0.6 and 1.1 V, for 30,000 cycles. The catalytic activity of Au/Pt/C, measured as half-wave potentials on the O_2 reduction polarization curves obtained before and after potential cycling, showed only a 5 mV degradation in over the cycling period. In contrast, the corresponding change for Pt/C amounted to a loss of 39 mV. In situ X-ray absorption near-edge spectroscopy (XANES) with respect to the potential applied on the catalyst surfaces revealed the oxidation of Pt nanoparticles covered by Au at high potentials was decreased in comparison with the oxidation of Pt nanoparticles lacking such coverage.

More recently, Wang et al. [119] investigated the ORR on well-defined Pt/Pd and Pt/PdCo core-shell nanoparticles for the effects of particle size, facet

orientation, and Pt shell thickness. The Pt shell was generated and the shell thickness was controlled by a novel method called the Cu-UPD-mediated electrodeposition method, in which repeated Cu-UPD/stripping, potential cycling, and Pt irreversible deposition occurred simultaneously in the same electrolyte, with the Pt deposition under diffusion control, until a desired thickness of Pt was achieved. Atomic level analysis using Z-contrast scanning transmission electron microscopy (STEM) coupled with element-sensitive electron energy loss spectroscopy (EELS) showed that well-controlled core-shell particles were obtained. ORR tests on RDE showed that Pt-monolayer catalysts on 4 nm Pd and 4.6 nm Pd_3Co cores exhibited 1.0 and 1.6 A/mg Pt mass activities at 0.9 V, respectively, about five- and ninefold enhancements over that of 3 nm Pt nanoparticles. Also, two- and threefold enhancements in specific activity were observed respectively, which were mainly attributed to the nanosize- and lattice-mismatch-induced contraction in (111) facets based on the DFT calculations using a nanoparticle model. Scale-up methods were developed for synthesis of the core-shell particles [120].

In summary, Pt monolayer catalysts show a promising pathway toward solving one of the major problems facing PEM fuel cells by enhancing the Pt-specific activity and the utilization of Pt atoms, and therefore reducing the cost of the cathode catalyst, although more fuel cell tests of durability are needed before the monolayer catalysts can be put in fuel cell vehicles. There is still a need for a reduction in the total noble metals in these catalysts.

Pt and Pt-Alloy Nanowire and Nanotube Electrocatalysts

As has been discussed in the introduction, low activity and limited durability are the two major issues related to the high-surface-area-carbon-dispersed Pt nanoparticle catalysts (Pt/C) in PEM fuel cells. Shao-Horn et al. [121] have given a comprehensive review on the instability considerations of Pt/C catalysts. Conventional PEM fuel cell catalysts typically consist of Pt nanoparticles in size of 2–3 nm that are supported on high-surface carbon with 20–50 nm primary carbon particles for electrical conductivity and high levels of catalyst activity. As it has been shown above, this kind of catalyst has already approached the maximum Pt mass activity as a pure Pt/C catalyst, as the Pt particle size is close to the optimal value. However, the 2–3 nm Pt nanoparticles are intrinsically not stable enough under PEM fuel cell operating conditions if no system-mitigation methods are applied. As an example, for a fuel cell short stack operating at steady-state open-circuit voltage (OCV, ~0.95 V versus RHE), with H_2/air flows (stoichiometric reactant flows of $s = 2/2$) at 80°C, fully humidified and 150 kPa_{abs} for 2,000 h, the Pt surface area decreased from ~70 m^2/g Pt to ~15 m^2/g Pt, corresponding to an almost 80% of Pt surface area loss [98]. If accompanied by a similar percentage loss of activity, this is not acceptable for commercialization of fuel cell vehicles. In addition, corrosion of carbon support makes the situation even more serious [122, 123]. One way to address this issue is to lower the upper voltage limit of the fuel cell through system mitigation [100, 101], or alternatively, to improve the intrinsic Pt stability through catalyst design, such as using Pt or Pt-alloy nanowire/nanotube catalysts. The local curvature of the nanowire/nanotube Pt or its alloy is expected to be small (in at least one direction), and it consequently has a lower surface free energy and higher stability. On the other hand, the Pt-specific activity of the nanowire/nanotube is expected to be higher than its nanoparticle counterpart, as it should bind OH/O less strongly.

The 3 M nanostructured thin film (NSTF) catalyst is such a non-conventional catalyst [124, 125]. The support particle is a crystalline organic pigment material, perylene red (PR), which is vacuum-deposited and converted to an oriented whisker phase by thermal annealing. The result is a uniquely structured thin film composed of highly oriented, densely packed crystalline organic whiskers [126]. A crystalline Pt coating can be vacuum-deposited on the whiskers. Figure 10 shows SEM images of the NSTF catalyst-coated whiskers prior to incorporation onto the surfaces of a PEM to form a catalyst-coated membrane [127]. The cross section of the whiskers is on the order of 50 nm, and the lengths of the whiskers are controllable by the thickness of the as-deposited PR film, typically in the range of 0.5–2 μm. For a practical loading of ~0.2 mg Pt/cm^2, the typical Pt crystallite size of the coated PR whiskers is 10–11 nm, and the specific surface areas of the NSTF-Pt catalysts are ~10 m^2/g Pt [124].

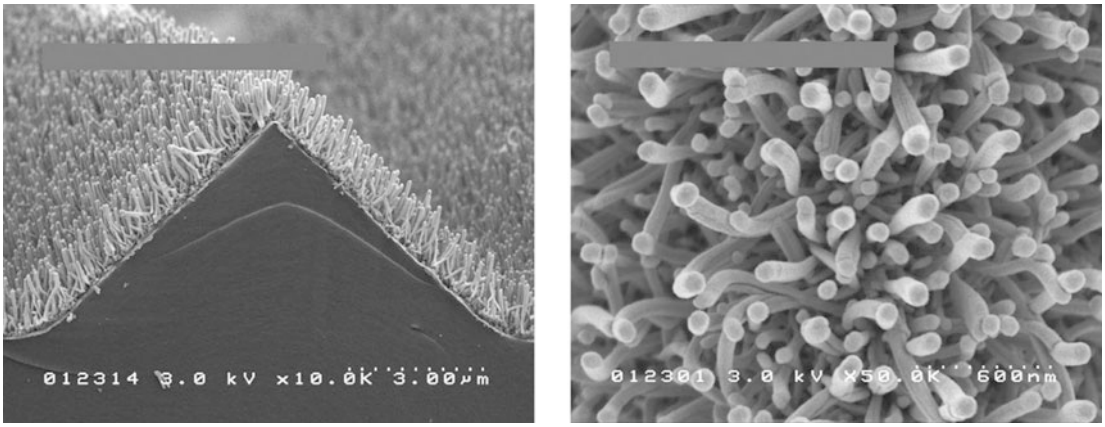

PEM Fuel Cells and Platinum-Based Electrocatalysts. Figure 10
Scanning electron micrographs of typical NSTF catalysts as fabricated on a microstructured catalyst transfer substrate, seen (*top*) in cross section with original magnification of ×10,000, and (*bottom*) in plain view with original magnification of ×50,000. The dotted scale bar is shown in each micrograph (Reproduced from [127]. With permission)

Bonakdarpour et al. [128] investigated Pt/NSTF and Pt–Co–Mn/NSTF for ORR by using the rotating ring disk electrode (RRDE). The nominal chemical composition of the ternary alloy was calculated to be $Pt_{0.68}Co_{0.3}Mn_{0.02}$. The catalyst-coated whiskers were carefully brushed off of the original substrate web and applied onto the glassy carbon disk of the RRDE. The measurements were done in O_2-saturated 0.1 M $HClO_4$ at room temperature. The Pt-specific activity of the Pt/NSTF was found to be close to that of a Pt polycrystalline disk. A twofold gain of Pt specific activity was observed on Pt–Co–Mn/NSTF versus Pt/NSTF. In PEMFC measurements for the same loading of 0.2 mg Pt/cm^2, using GM recommended conditions for measuring specific and mass activity at 80°C, saturated H_2/O_2 at 150 kPa_{abs}, at 900 mV, the NSTF Pt-Co-Mn catalyst-coated membrane (CCM) generated specific activities of 2.93 mA/cm^{2}Pt, and mass activities of 0.18 A/mg^1 Pt. The specific activity is ~12 times higher, and mass activity is about two times higher than those of TKK 47 wt% Pt/C.

To investigate the NSTF electrode stability under high voltage cycling, Debe et al. [129] tested a series of NSTF Pt and NSTF Pt-ternary catalysts along with Pt/C (Ketjen Black) and Pt/C (graphitic) types by scanning at 20 mV/s, between 0.6 and 1.2 V under saturated H_2/N_2 at 80°C. The MEA's contained the same 3 M-ionomer PEM having a 1,000 equivalent weight (EW), and the same 3 M-coated GDL. The NSTF electrodes had loadings of 0.1 mg/cm^2, while the carbon- and graphitic-carbon-supported catalysts had loadings of 0.4 mg/cm^2. Figure 11 compares the normalized surface area as a function of the number of CV cycles for all the samples. It is interesting to note that

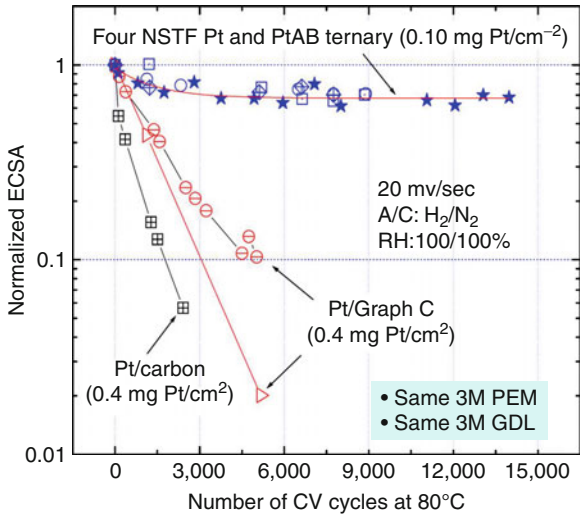

PEM Fuel Cells and Platinum-Based Electrocatalysts. Figure 11
Normalized surface area versus number of CV cycles from 0.6 to 1.2 V for four NSTF catalyst samples and three Pt/carbon catalysts at 80°C. All MEAs used the same 3 M ionomer PEM and GDL (gas diffusion layer) (Reproduced from [129]. With permission)

for the NSTF samples the Pt and ternary catalysts behave similarly and lose approximately 30% of the surface area out to 14,000 cycles. The Pt/C and Pt/graphitic carbon, on the other hand, lose substantially more surface area in significantly fewer cycles. The superior ability of the NSTF catalyst to withstand thousands of fast voltage scans over the potential range most critical for Pt dissolution and Pt agglomeration demonstrated a significant differentiating feature over carbon-supported catalysts [129].

Recently, Chen et al. [130] developed supportless Pt nanotubes (PtNTs) and Pt-alloy nanotubes (e.g., Pt-Pd alloy nanotubes (PtPdNTs)) as cathode catalysts for PEMFCs. PtNTs were synthesized by a galvanic replacement of silver nanowires (AgNWs) by following a similar method developed by Xia and coworkers [131, 132]. The AgNWs were synthesized using a polyol method [133] and were subsequently heated at reflux temperature with $Pt(CH_3COO)_2$ in an aqueous solution. For the preparation of PtPdNTs, mixed aqueous $Pt(CH_3COO)_2$ and $Pd(NO_3)_2$ solutions were used. The diameter (Fig. 12a, b) and length of AgNWs are about 40 nm and 10 μm, respectively. After Pt replacement, the diameter, wall thickness (Fig. 12c, d), and length of the PtNTs are about 40 nm, 6 nm, and 10 μm, respectively.

Chen et al. [130] tested the durability of these materials by cycling the electrode between 0 and 1.3 V versus RHE at a scan rate of 50 mV/s in argon-purged 0.5 M H_2SO_4 solution at 60°C. As shown in Fig. 13a, the electrochemical surface area (ECSA) of the PtNTs decreased by about 20% after 1,000 cycles, while the Pt-black and Pt/C catalysts lost about 51% and 90% of their platinum ECSA, respectively. Figure 13b shows the comparison of typical ORR polarization curves of the respective catalysts obtained at room temperature in O_2-saturated 0.5 M H_2SO_4 using a rotating disk electrode (RDE) at 1,600 rpm. At 0.85 V versus RHE, the mass activity of PtNTs was reported slightly higher than that of Pt/C, and 1.4 times higher than that of Pt-black catalysts. The specific activity of the PtNTs was 3.8 times and 1.8 times higher than those of Pt/C and Pt-black catalysts, respectively. For PtPdNTs, the mass activity was measured 1.4 times and 2.1 times higher

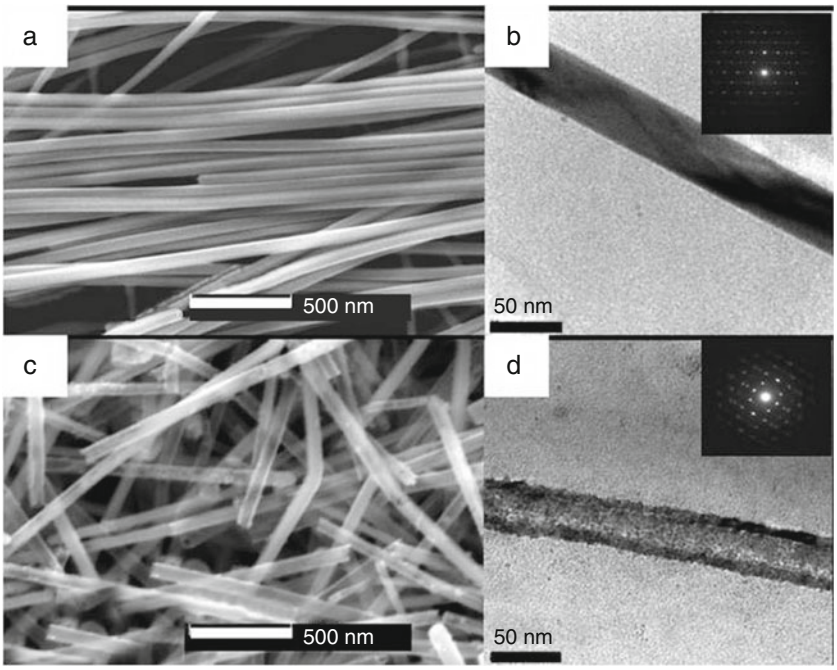

PEM Fuel Cells and Platinum-Based Electrocatalysts. Figure 12
(**a**) SEM image of AgNWs. (**b**) TEM image and electron diffraction pattern (inset) of AgNWs. (**c**) SEM image of PtNTs. (**d**) TEM image and electron diffraction pattern (inset) of PtNTs (Reproduced from [130]. With permission)

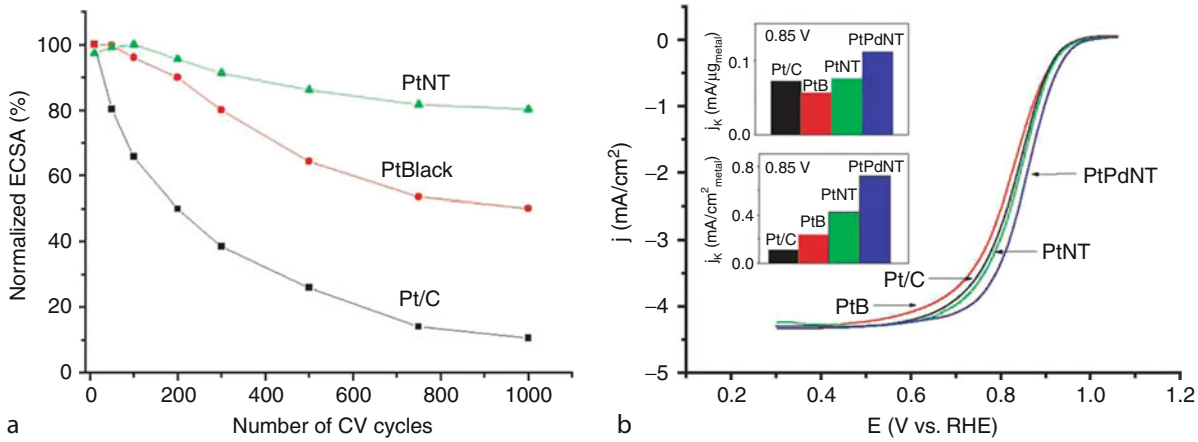

PEM Fuel Cells and Platinum-Based Electrocatalysts. Figure 13
(**a**) Loss of electrochemical surface area (ECSA) of Pt/C (E-TEK), platinum-black (PtB; E-TEK), and PtNT catalysts with number of potential cycles in Ar-purged 0.5 M H_2SO_4 solution at 60°C (0–1.3 V versus RHE, sweep rate 50 mV/s). (**b**) ORR curves (shown as current–voltage relations) of Pt/C, platinum black (PtB), PtNTs, and PdPtNTs in O_2-saturated 0.5 M H_2SO_4 solution at room temperature (1,600 rpm, sweep rate 5 mV/s). Inset: Mass activity (*top*) and specific activity (*bottom*) for the four catalysts at 0.85 V (Reproduced from [130]. With permission)

than those of Pt/C and Pt-black catalysts, while the specific activity was 5.8 times and 2.7 times higher than those of Pt/C and Pt-black catalysts, respectively.

The examples given above illustrate that it is possible to achieve both activity and durability goals of Pt-based catalysts through special morphology and structural design of the catalyst and electrode. There are many other important advancements not discussed here on nanostructured Pt and Pt-alloy catalysts/electrodes showing improvements in activity and/or durability for ORR, such as single-crystal-Pt nanowires grown on continuous carbon-layer-coated Sn-fiber 3D electrodes [134], Pt-Pd bimetallic nanodendrites [135, 136], faceted Pt nanocrystals [137], nanoporous Pt alloy electrodes [138–140].

Facet- and Shape-Controlled Pt-Alloy Nanocrystal Electrocatalysts

Stamenkovic and coworkers [42] demonstrated in $HClO_4$ that on RDE $Pt_3Ni(111)$ single-crystal surfaces of ~6 mm in diameter, the specific activity for ORR is about an order of magnitude higher than on the Pt (111) surface and is about 90 times higher than on Pt/C catalyst, while the other two low-index surfaces, [Pt_3Ni (100) and $Pt_3Ni(110)$] are much less active than $Pt_3Ni(111)$. This result is very intriguing in that it suggests that if one can make Pt_3Ni nanocrystals with all exposed surfaces having {111} orientations, one can hope to gain an enhancement of specific activity by up to two orders of magnitude relative to state-of-the-art Pt/C catalysts. Recently, two interesting papers [141, 142] have shown progress on synthesizing such Pt alloy nanocrystals.

Wu et al. [141] recently reported an approach to the preparation of truncated-octahedral Pt_3Ni (*t,o*-Pt_3Ni) catalysts that have dominant exposure of {111} facets. The shape-defined Pt-Ni nanoparticles were made from platinum acetylacetonate [$Pt(acac)_2$] and nickel acetylacetonate [$Ni(acac)_2$] in diphenyl ether (DPE) using a mixture of borane-tert-butylamine complex (TBAB) and hexadecanediol as the reducing agents. Long-alkane-chain amines were used as the main capping agents, and adamantanecarboxylic acid (ACA) or adamantaneacetic acid (AAA) was used to affect the reaction kinetics. The population of truncated octahedral crystals could be adjusted by the types and amounts of the reducing agents and capping agents. Three sets of Pt_3Ni nanocrystals were generated with various truncated-octahedral crystal populations; see Fig. 14.

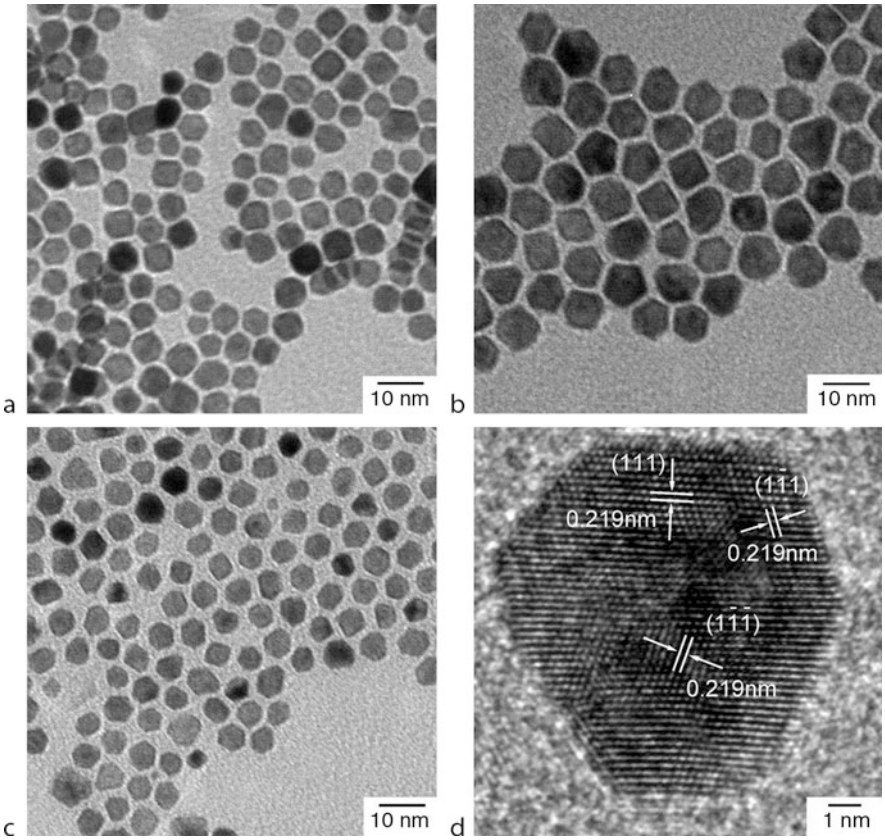

PEM Fuel Cells and Platinum-Based Electrocatalysts. Figure 14
TEM images of Pt_3Ni nanocrystals with truncated octahedron population of (**a**) 70%, (**b**) 90%, (**c**) 100%, and (**d**) HR-TEM image of a truncated octahedron showing the (111) lattice (Reproduced from [141]. With permission)

While Fig. 14a, b contain 30% and 10% of Pt_3Ni cubes (with the remaining particles being truncated-octahedrons), respectively, Fig. 14c contains only truncated-octahedrons. The particle size is on the order of 5 to 7 nm. Only two types of facets are exposed of all the nanocrystals, i.e., the {111} and {100}. The fractions of the {111} surface area over the total surface area could be calculated based on the geometries of the shapes and the population statistics. The ORR kinetics of the nanocrystals were studied on RDEs in O_2-saturated 0.1 M $HClO_4$, at room temperature, at 1,600 rpm, with a potential scan rate of 10 mV/s. Figure 15 shows comparison of polarization curves, cyclic-voltammetry curves, mass activities, and specific activities of the Pt3Ni nanocrystals to the standard TKK Pt/Vulcan carbon catalyst. As shown in Fig. 15d, almost-linear correlations were obtained for both mass activities and specific activities versus the fraction of the (111) surface area over the total surface area. A tabulated kinetic activity comparison is shown in Table 1. The mass activity and specific activity comparisons were made at 0.9 V versus RHE. Roughly 4× mass-activity and specific-activity enhancements were observed on the 100% truncated octahedral Pt_3Ni nanocrystals over the Pt/C catalyst. While the {111} facets of the nanocrystals showed much higher specific activity than the {100} facets, as indicated in Fig. 15d, in agreement with trend found on bulk Pt_3Ni single crystal disks, the absolute values of the specific activities of the nanocrystals are still far below those observed on bulk single-crystal surfaces [42].

Another interesting report is from Zhang et al. [142] on the synthesis and ORR activity of Pt_3Ni nano-octahedra and nanocubes, with the two shapes

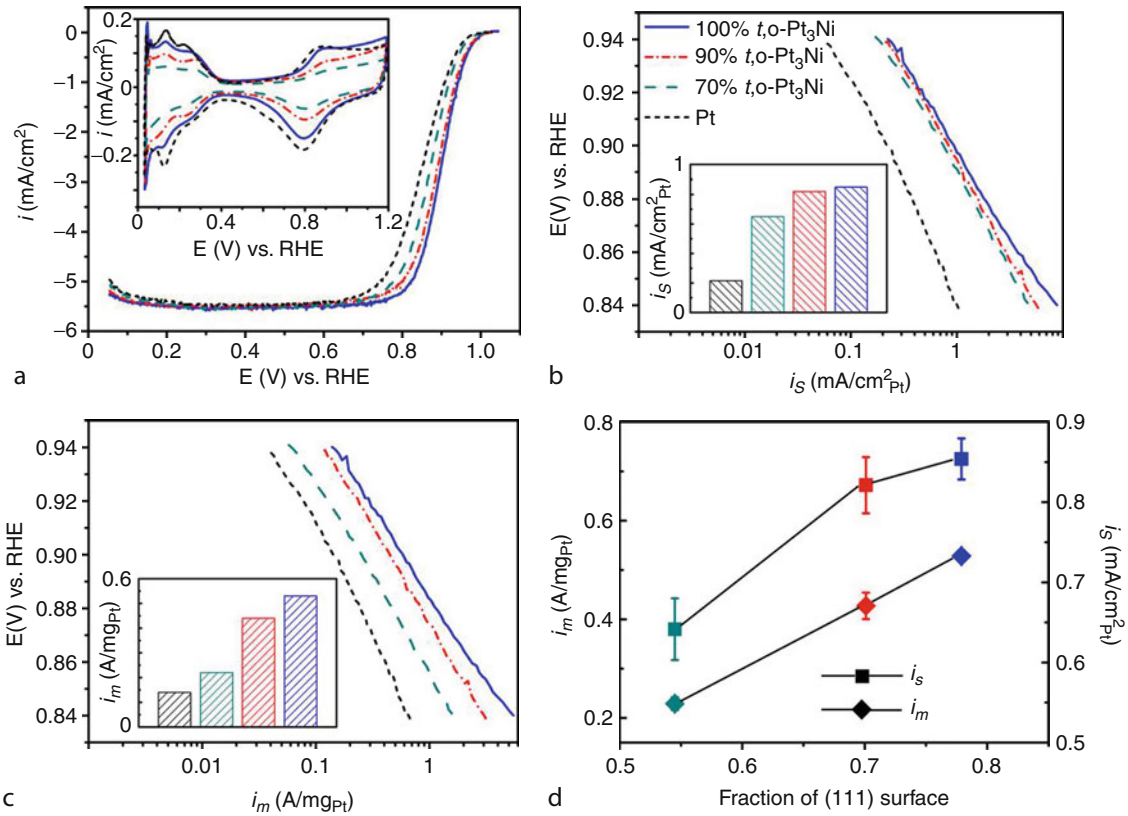

PEM Fuel Cells and Platinum-Based Electrocatalysts. Figure 15
(**a**) Polarization curves and CV curves (*inset*), (**b**) area (mA/cm^{2}Pt), (**c**) mass (A/mg Pt) specific ORR activity for the *t,o*-Pt_3Ni and reference Pt catalysts; and (**d**) the correlations between specific activities and fractions of (111) surfaces of these Pt_3Ni catalysts. The ORR polarization curves were collected at 1,600 rpm (Reproduced from [141]. With permission)

PEM Fuel Cells and Platinum-Based Electrocatalysts. Table 1 ECSA, mass- and area- specific ORR activities of Pt_3Ni and Pt/catalysts (at 0.9 V versus RHE) (Reproduced from [141]. With permission)

Sample name	Pt loading [$\mu g_{Pt}/cm_{disk}^2$]	ECSA [m^2/g_{Pt}]	Mass activity [A/mg_{Pt}]	Specific activity [mA/cm_{Pt}^2]
100% *t,o*-Pt_3Ni	9.3	62.4	0.53	0.85
90% *t,o*-Pt_3Ni	9.3	53.7	0.44	0.82
70% *t,o*-Pt_3Ni	9.3	33.8	0.22	0.65
Pt/C (TKK)	11	65	0.14	0.215

of nanocrystals having only {111} facets and {100} facets exposed, respectively. The monodispersed Pt_3Ni nano-octahedra and nanocubes were synthesized via a high-temperature organic solution chemistry approach, which involved using mixed oleylamine and oleic acid at elevated temperature as the reducing agent and capping agent, and tungsten hexacarbonyl W $(CO)_6$ as the shape controlling agent. Detailed procedures for synthesis of the nanocrystals can be found in Ref. [142]. Figure 16 shows the SEM and TEM images of those shape and size controlled nano-octahedral (a–e) and nanocube (f–j) crystals. The chemical

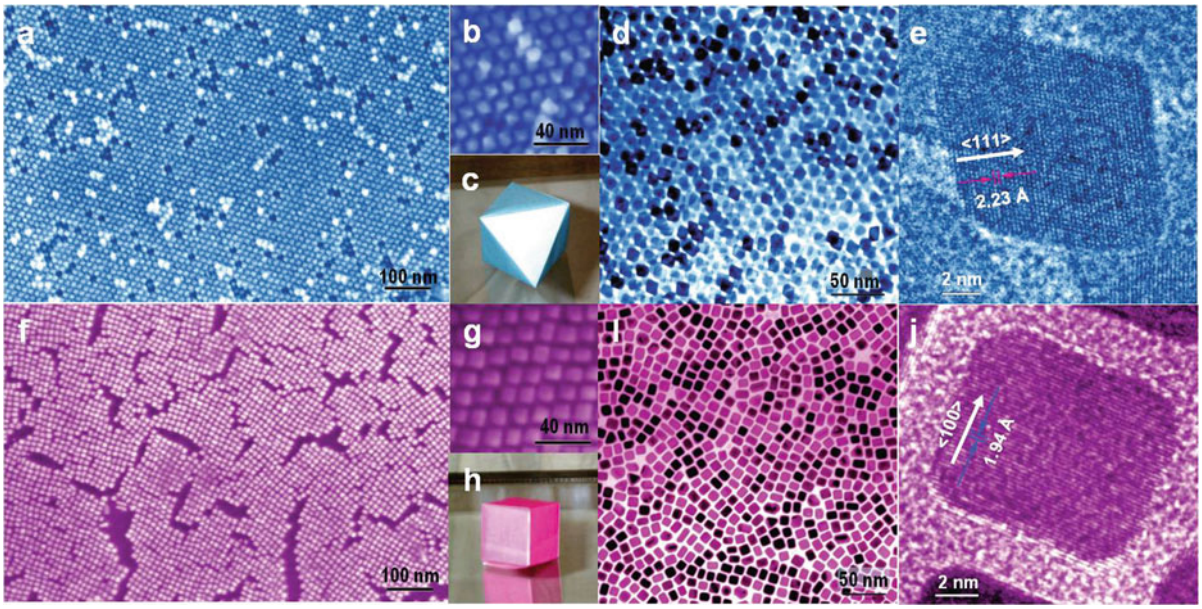

PEM Fuel Cells and Platinum-Based Electrocatalysts. Figure 16
(**a**–**e**) Images for Pt_3Ni nano-octahedra. (**f**–**j**) Images for Pt_3Ni nanocubes. (**a**, **f**) Field-emission SEM images. (**b**, **g**) High-resolution SEM images. (**c**) 3D model of an octahedron. (**d**, **i**) TEM images. (**e**, **j**) High-resolution TEM images of single nanocrystals. (**h**) 3D model of a cube (Reproduced from [142]. With permission)

compositions of the crystals were analyzed by using combined ICP-MS and EDS techniques (from both TEM and SEM), and the results suggested that the average molar ratio of Pt over Ni was 3:1.

Zhang et al. [142] further investigated ORR activities of the shape controlled nanocrystals by using RDE measurements. The ORR measurements were conducted in an O_2-saturated 0.1 M $HClO_4$ solution at 295 K. A characteristic set of polarization curves at 900 rpm for the ORR on Pt3Ni nano-octahedra, Pt3Ni nanocubes, and Pt nanocubes are displayed in Fig. 17a. After mass transport correction using Koutecky–Levich equation, and normalizing by the Pt surface area and mass, the kinetic activities (specific activity and mass activity) at 0.9 V were plotted in Fig. 17b. The Pt-specific activity of Pt_3Ni nano-octahedra were determined to be 5.1 times of that of the Pt_3Ni nanocubes and ~6.5 times that of the Pt nanocubes, while the Pt mass activity of the Pt_3Ni nano-octahedra was ~2.8 times of that of Pt_3Ni nanocubes and ~3.6 times of that of Pt nanocubes. The significant shape dependence of ORR activity agreed with the observation from the extended Pt_3Ni single crystal surfaces, although the absolute values of specific activities observed on Pt_3Ni nanocubes and nano-octahedra were about four- to sevenfold lower than those reported in Ref. [42], respectively. One apparent puzzle in these reported results is that the Pt surface area or ECSA of the nanocrystals derived from the specific activity and mass activity (ECSA per unit mass of Pt = mass activity/specific activity) is 5–10 times lower than one would expect from the size of particles revealed by SEM and TEM images. The discrepancy may come from the low utilization of the surface area because of impurities or from overlap of the nonsupported nanocrystals. Another set of data for the high surface carbon supported those nanocrystals was reported in the online supporting information of the paper, and this showed a better agreement between measured ECSA and diameter to TEM, suggesting that particle aggregation caused the low area observed for the unsupported catalysts.

In summary, the size- and shape-controlled synthesis of nanocrystal Pt-based electrocatalysts has shown a promising path to high Pt-specific activity, although the absolute number of the activity is still not comparable

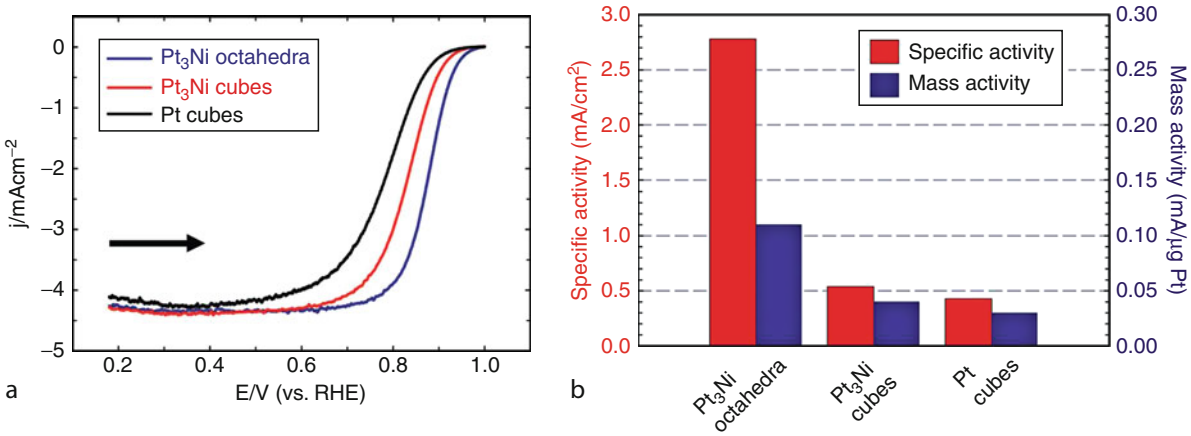

PEM Fuel Cells and Platinum-Based Electrocatalysts. Figure 17
(**a**) Polarization curves for ORR on Pt_3Ni nano-octahedra, Pt_3Ni nanocubes, and Pt nanocubes supported on a rotating glassy carbon disk electrode in O_2-saturated 0.1 M $HClO_4$ solution at 295 K; with scan rate = 20 mV/s; rotation rate = 900 rpm. Catalyst loading in terms of Pt mass: Pt_3Ni octahedra, 3.0 μg; Pt_3Ni cube, 2.0 μg; Pt cube, 1.1 μg. Current density was normalized to the glassy carbon geometric surface area (0.196 cm^2). The arrow indicates the potential scan direction. (**b**) Comparison of the ORR activities on the three types of catalysts. Specific activity and mass activity were all measured at 0.9 V versus RHE at 295 K (Reproduced from [142]. With permission)

to that observed on extended Pt alloy single-crystal surface, probably due to the size effect, residual impurities and defects in the nanocrystal surface, and incomplete formation of smooth, segregated Pt layers on the facet surfaces. The Pt mass activity achieved for the best case is already about four times higher than state-of-the-art Pt/C catalyst. If the core of the nanocrystals can be replaced with some corrosion-resistant material but keeping the surface of the Pt alloy shell still in {111} facets, one could expect a significant further reduction of the Pt loading required for the cathode catalyst. In addition, the size of the particles can be larger to gain the benefits of the particle size effect, as the Pt consumption is determined by the thickness of the shell. The durability of such nanocrystals could be expected to be high because of the lack of low-coordination atoms in their surfaces.

Future Directions

Low platinum loading, high activity, and more durable catalysts still remain as critical challenges for PEFCs for automotive applications. Further fundamental understanding of the correlations between activity, stability, and structural properties at the atomic level are most desired from both theoretical and experimental perspectives. Studies of the connections between the activities of controlled-facet-orientation nanoparticles and extended single-crystal surfaces would be helpful. Structure- and surface-controlled syntheses of catalysts (Pt monolayer catalysts, nanostructured catalysts and electrodes, size- and facet- controlled Pt alloy nanocrystals, combined with core-shell structure) should provide a practical viable path to achieving fuel cell catalyst loadings required for large-scale commercialization.

Bibliography

Primary Literature

1. Andujar JM, Segura F (2009) Fuel cells: history and updating. A walk along two centuries. Renew Sustain Energy Rev 13(9):2309–2322
2. Grimes PG (2000) Historical pathways for fuel cells – the new electric century. IEEE Aerosp Electron Syst Mag 15(12):7–10
3. Appleby AJ (1990) From Sir William Grove to today: fuel cells and the future. J Power Sources 29(1–2):3–11
4. Perry ML, Fuller TF (2002) A historical perspective of fuel cell technology in the 20th century. J Electrochem Soc 149(7): S59–S67
5. Thomas CE (2009) Fuel cell and battery electric vehicles compared. Int J Hydrogen Energy 34(15):6005–6020

6. Gottesfeld S (2007) Fuel cell techno-personal milestones 1984–2006. J Power Sources 171(1):37–45
7. Mathias MF, Makharia R, Gasteiger HA, Conley JJ, Fuller TJ, Gittleman CJ, Kocha SS, Miller DP, Mittelsteadt CK, Xie T, Yan SG, Yu PT (2005) Two fuel cell cars in every garage? Electrochem Soc Interface 14(3 Fall 2005):24–35
8. Raistrick ID (1986) In: Zee JWV, White RE, Kinoshita K, Burney HS (eds) Diaphragms, separators, and ion-exchange membranes, the electrochemical society proceedings series. The Electrochemical Society, Pennington, p 172
9. Wilson MS, Gottesfeld S (1992) Thin-film catalyst layers for polymer electrolyte fuel cell electrodes. J Appl Electrochem 22(1):1–7
10. Wilson MS, Gottesfeld S (1992) High performance catalyzed membranes of ultra-low Pt loadings for polymer electrolyte fuel cells. J Electrochem Soc 139(2):L28–L30
11. Wilson MS, Valerio JA, Gottesfeld S (1995) Low platinum loading electrodes for polymer electrolyte fuel-cells fabricated using thermoplastic ionomers. Electrochim Acta 40(3):355–363
12. Conway BE, Tilak BV (2002) Interfacial processes involving electrocatalytic evolution and oxidation of H-2, and the role of chemisorbed H. Electrochim Acta 47(22–23):3571–3594
13. Gasteiger HA, Markovic NM, Ross PN (1995) H_2 and CO electrooxidation on well-characterized Pt, Ru, and Pt-Ru.2. rotating disk electrode studies of CO/H_2 mixtures at 62-degrees C. J Phys Chem 99(45):16757–16767
14. Mukerjee S, McBreen J (1996) Hydrogen electrocatalysis by carbon supported Pt and Pt alloys – an in situ x-ray absorption study. J Electrochem Soc 143(7):2285–2294
15. Neyerlin KC, Gu WB, Jorne J, Gasteiger HA (2007) Study of the exchange current density for the hydrogen oxidation and evolution reactions. J Electrochem Soc 154(7):B631–B635
16. Tarasevich MR, Sadkowski A, Yeager E (1983) Oxygen electrochemistry. In: Conway BE, Bockris JO, Yeager E, Khan SUM, White RE (eds) Comprehensive treatise in electrochemistry. Plenum Press, New York, p 301
17. Adzic RR (1998) Recent advances in the kinetics of oxygen reduction. In: Lipkowski J, Ross PN (eds) Electrocatalysis. Wiley-VCH, New York, pp 197–241
18. Kinoshita K (1992) Electrochemical oxygen technology. Wiley, New York
19. Markovic NM, Gasteiger HA, Ross PN (1995) Oxygen reduction on platinum low-index single-crystal surfaces in sulfuric-acid-solution – rotating ring-Pt(Hkl) disk studies. J Phys Chem 99(11):3411–3415
20. Gasteiger HA, Panels JE, Yan SG (2004) Dependence of PEM fuel cell performance on catalyst loading. J Power Sources 127(1–2):162–171
21. Gasteiger HA, Kocha SS, Sompalli B, Wagner FT (2005) Activity benchmarks and requirements for Pt, Pt-alloy, and non-Pt oxygen reduction catalysts for PEMFCs. Appl Catal B Environ 56(1–2):9–35
22. Damjanovic A, Brusic V (1967) Electrode kinetics of oxygen reduction on oxide-free platinum electrodes. Electrochim Acta 12(6):615–628
23. Wang JX, Markovic NM, Adzic RR (2004) Kinetic analysis of oxygen reduction on Pt(111) in acid solutions: intrinsic kinetic parameters and anion adsorption effects. J Phys Chem B 108(13):4127–4133
24. Markovic NM, Gasteiger HA, Grgur BN, Ross PN (1999) Oxygen reduction reaction on Pt(111): effects of bromide. J Electroanal Chem 467(1):157–163
25. Adzic RR (1992) Surface morphology effects in oxygen electrochemistry. In: Scherson D, Tryk D, Xing X (eds) Proceedings of the workshop on structural effects in electrocatalysis and oxygen electrochemistry. The Electrochemical Society, Pennington, p 419
26. Uribe FA, Wilson MS, Springer TE, Gottesfeld S (1992) Oxygen reduction (ORR) at the Pt/recast ionomer interface and some general comments on the ORR at Pt/aqueous electrolyte interfaces. In: Scherson DD, Tryk D, Xing X (eds) Proceedings of the workshop on structural effects in electrocatalysis and oxygen electrochemistry. The Electrochemical Society, Pennington, p 494
27. Norskov JK, Rossmeisl J, Logadottir A, Lindqvist L, Kitchin JR, Bligaard T, Jonsson H (2004) Origin of the overpotential for oxygen reduction at a fuel-cell cathode. J Phys Chem B 108(46):17886–17892
28. Wang JX, Zhang JL, Adzic RR (2007) Double-trap kinetic equation for the oxygen reduction reaction on Pt(111) in acidic media. J Phys Chem A 111(49):12702–12710
29. Wang JX, Uribe FA, Springer TE, Zhang JL, Adzic RR (2008) Intrinsic kinetic equation for oxygen reduction reaction in acidic media: the double Tafel slope and fuel cell applications. Faraday Discuss 140:347–362
30. Neyerlin KC, Gu WB, Jorne J, Gasteiger HA (2006) Determination of catalyst unique parameters for the oxygen reduction reaction in a PEMFC. J Electrochem Soc 153(10):A1955–A1963
31. Neyerlin KC, Gu W, Jorne J, Clark A, Gasteiger HA (2007) Cathode catalyst utilization for the ORR in a PEMFC – analytical model and experimental validation. J Electrochem Soc 154(2): B279–B287
32. Neyerlin KC, Gasteiger HA, Mittelsteadt CK, Jorne J, Gu WB (2005) Effect of relative humidity on oxygen reduction kinetics in a PEMFC. J Electrochem Soc 152(6):A1073–A1080
33. Blurton KF, Greenberg P, Oswin HG, Rutt DR (1972) The electrochemical activity of dispersed platinum. J Electrochem Soc 119(5):559–564
34. Peuckert M, Yoneda T, Betta RAD, Boudart M (1986) Oxygen reduction on small supported platinum particles. J Electrochem Soc 133(5):944–947
35. Kinoshita K (1990) Particle size effects for oxygen reduction on highly dispersed platinum in acid electrolytes. J Electrochem Soc 137(3):845–848
36. Ross PN (1986) Structure-property relations in noble metal electrocatalysis. In: The Gordon conference on chemistry at interfaces, Lawrence Berkeley Laboratory, Berkeley/Meriden, July 21–25, 1986. p. LBL-21733
37. Ross PN (September 1980) Oxygen reduction on supported Pt alloys and intermetallic compounds in phosphoric acid, final

report prepared for the electric power research institute. Electric Power Research Institute, Palo Alto, September 1980
38. Sattler ML, Ross PN (1986) The surface structure of Pt crystallites supported on carbon black. Ultramicroscopy 20:21–28
39. Landsman DA, Luczak FJ (2003) Catalyst studies and coating technologies. In: Vielstich W, Gasteiger H, Lamm A (eds) Handbook of fuel cells. Wiley, Chichester, p 811
40. Thompsett D (2003) Pt alloys as oxygen reduction catalysts. In: Vielstich W, Gasteiger H, Lamm A (eds) Handbook of fuel cells – fundamentals, technology and applications. Wiley, Chichester, p 467
41. Markovic N, Gasteiger H, Ross PN (1997) Kinetics of oxygen reduction on Pt(hkl) electrodes: implications for the crystallite size effect with supported Pt electrocatalysts. J Electrochem Soc 144(5):1591–1597
42. Stamenkovic VR, Fowler B, Mun BS, Wang GF, Ross PN, Lucas CA, Markovic NM (2007) Improved oxygen reduction activity on Pt3Ni(111) via increased surface site availability. Science 315(5811):493–497
43. Hammer B, Norskov JK (2000) Theoretical surface science and catalysis – calculations and concepts. In: Gates BC, Knozinger H (eds) Advances in catalysis, vol 45. Academic, San Diego, pp 71–129
44. Norskov JK, Bligaard T, Logadottir A, Bahn S, Hansen LB, Bollinger M, Bengaard H, Hammer B, Sljivancanin Z, Mavrikakis M, Xu Y, Dahl S, Jacobsen CJH (2002) Universality in heterogeneous catalysis. J Catal 209(2):275–278
45. Lopez N, Janssens TVW, Clausen BS, Xu Y, Mavrikakis M, Bligaard T, Norskov JK (2004) On the origin of the catalytic activity of gold nanoparticles for low-temperature CO oxidation. J Catal 223(1):232–235
46. Xu Y, Mavrikakis M (2003) Adsorption and dissociation of O2 on gold surfaces: effect of steps and strain. J Phys Chem B 107(35):9298–9307
47. Xu Y, Ruban AV, Mavrikakis M (2004) Adsorption and dissociation of O2 on Pt-Co and Pt-Fe alloys. J Am Chem Soc 126(14):4717–4725
48. Greeley J, Rossmeisl J, Hellman A, Norskov JK (2007) Theoretical trends in particle size effects for the oxygen reduction reaction. Z Phys Chemie-Int J Res Phys Chem Chem Phys 221(9–10):1209–1220
49. Mukerjee S, McBreen J (1998) Effect of particle size on the electrocatalysis by carbon-supported Pt electrocatalysts: an in situ XAS investigation. J Electroanal Chem 448(2): 163–171
50. Yano H, Inukai J, Uchida H, Watanabe M, Babu PK, Kobayashi T, Chung JH, Oldfield E, Wieckowski A (2006) Particle-size effect of nanoscale platinum catalysts in oxygen reduction reaction: an electrochemical and Pt-195 EC-NMR study. Phys Chem Chem Phys 8(42):4932–4939
51. Gasteiger HA, Markovic NM (2009) Just a dream-or future reality? Science 324(5923):48–49
52. Mukerjee S, Srinivasan S, Soriaga MP, McBreen J (1995) Role of structural and electronic-properties of Pt and Pt alloys on electrocatalysis of oxygen reduction – an in-situ Xanes and Exafs investigation. J Electrochem Soc 142(5):1409–1422
53. Wakabayashi N, Takeichi M, Uchida H, Watanabe M (2005) Temperature dependence of oxygen reduction activity at Pt-Fe, Pt-Co, and Pt-Ni alloy electrodes. J Phys Chem B 109(12):5836–5841
54. Paulus UA, Wokaun A, Scherer GG, Schmidt TJ, Stamenkovic V, Markovic NM, Ross PN (2002) Oxygen reduction on high surface area Pt-based alloy catalysts in comparison to well defined smooth bulk alloy electrodes. Electrochim Acta 47(22–23):3787–3798
55. Glass JT, Cahen JGL, Stoner GE, Taylor EJ (1987) The effect of metallurgical variables on the electrocatalytic properties of PtCr alloys. J Electrochem Soc 134(1):58–65
56. Paffett MT, Daube KA, Gottesfeld S, Campbell CT (1987) Electrochemical and surface science investigations of PtCr alloy electrodes. J Electroanal Chem 220(2):269–285
57. Beard BC, Ross JPN (1990) The structure and activity of Pt-Co alloys as oxygen reduction electrocatalysts. J Electrochem Soc 137(11):3368–3374
58. Toda T, Igarashi H, Uchida H, Watanabe M (1999) Enhancement of the electroreduction of oxygen on Pt alloys with Fe, Ni, and Co. J Electrochem Soc 146(10):3750–3756
59. Koh S, Hahn N, Yu CF, Strasser P (2008) Effects of composition and annealing conditions on catalytic activities of dealloyed Pt-Cu nanoparticle electrocatalysts for PEMFC. J Electrochem Soc 155(12):B1281–B1288
60. Schulenburg H, Muller E, Khelashvili G, Roser T, Bonnemann H, Wokaun A, Scherer GG (2009) Heat-treated $PtCo_3$ nanoparticles as oxygen reduction catalysts. J Phys Chem C 113(10):4069–4077
61. Jalan V, Taylor EJ (1983) Importance of interatomic spacing in catalytic reduction of oxygen in phosphoric acid. J Electrochem Soc 130(11):2299–2302
62. Jalan V, Taylor EJ (1984) Importance of interatomic spacing in the catalytic reduction of oxygen in phosphoric acid. In: McIntyre JDE, Weaver MJ, Yeager EB (eds) The Electrochemical Society Softbound Proceedings Series. The Electrochemical Society, Pennington, p 546
63. Landsman DA, Luczak FJ (1982) Noble metal-chromium alloy catalysts and electrochemical cell. US Patent 4,316,944, United Technologies Corporation: US
64. Stamenkovic VR, Mun BS, Arenz M, Mayrhofer KJJ, Lucas CA, Wang GF, Ross PN, Markovic NM (2007) Trends in electrocatalysis on extended and nanoscale Pt-bimetallic alloy surfaces. Nat Mater 6(3):241–247
65. Toda T, Igarashi H, Watanabe M (1999) Enhancement of the electrocatalytic O2 reduction on Pt-Fe alloys. J Electroanal Chem 460(1–2):258–262
66. M-k M, Cho J, Cho K, Kim H (2000) Particle size and alloying effects of Pt-based alloy catalysts for fuel cell applications. Electrochim Acta 45(25–26):4211–4217
67. Koh S, Strasser P (2007) Electrocatalysis on bimetallic surfaces: modifying catalytic reactivity for oxygen reduction by voltammetric surface dealloying. J Am Chem Soc 129(42):12624

68. Gottesfeld S (1986) The ellipsometric characterization of Pt + Cr alloy surfaces in acid solutions. J Electroanal Chem 205(1–2):163–184
69. Paffett MT, Beery JG, Gottesfeld S (1988) Oxygen reduction at $Pt_{0.65}Cr_{0.35}$, $Pt_{0.2}Cr_{0.8}$ and roughened platinum. J Electrochem Soc 135(6):1431–1436
70. Mukerjee S, Srinivasan S (1993) Enhanced electrocatalysis of oxygen reduction on platinum alloys in proton exchange membrane fuel cells. J Electroanal Chem 357(1–2): 201–224
71. Toda T, Igarashi H, Watanabe M (1998) Role of electronic property of Pt and Pt alloys on electrocatalytic reduction of oxygen. J Electrochem Soc 145(12):4185–4188
72. Mun BS, Watanabe M, Rossi M, Stamenkovic V, Markovic NM, Ross PN (2005) A study of electronic structures of Pt3M (M = Ti, V, Cr, Fe, Co, Ni) polycrystalline alloys with valence-band photoemission spectroscopy. J Chem Phys 123(20):204717
73. Greeley J, Stephens IEL, Bondarenko AS, Johansson TP, Hansen HA, Jaramillo TF, Rossmeisl J, Chorkendorff I, Norskov JK (2009) Alloys of platinum and early transition metals as oxygen reduction electrocatalysts. Nat Chem 1(7):552–556
74. Mukerjee S, Srinivasan S, Soriaga MP, McBreen J (1995) Effect of preparation conditions of Pt Alloys on their electronic, structural, and electrocatalytic activities for oxygen reduction-XRD, XAS, and electrochemical studies. J Phys Chem 99(13):4577–4589
75. Uribe FA, Zawodzinski TA (2002) A study of polymer electrolyte fuel cell performance at high voltages. Dependence on cathode catalyst layer composition and on voltage conditioning. Electrochim Acta 47(22–23):3799–3806
76. Stamenkovic V, Schmidt TJ, Ross PN, Markovic NM (2002) Surface composition effects in electrocatalysis: kinetics of oxygen reduction on well-defined Pt3Ni and Pt3Co alloy surfaces. J Phys Chem B 106(46):11970–11979
77. Murthi VS, Urian RC, Mukerjee S (2004) Oxygen reduction kinetics in low and medium temperature acid environment: Correlation of water activation and surface properties in supported Pt and Pt alloy electrocatalysts. J Phys Chem B 108(30):11011–11023
78. Teliska M, Murthi VS, Mukerjee S, Ramaker DE (2005) Correlation of water activation, surface properties, and oxygen reduction reactivity of supported Pt-M/C bimetallic electrocatalysts using XAS. J Electrochem Soc 152(11):A2159–A2169
79. Lima FHB, Ticianelli EA (2004) Oxygen electrocatalysis on ultrathin porous coating rotating ring/disk platinum and platinum-cobalt electrodes in alkaline media. Electrochim Acta 49(24):4091–4099
80. Lima FHB, Giz MJ, Ticianelli EA (2005) Electrochemical performance of dispersed Pt-M (M = V, Cr and Co) nanoparticles for the oxygen reduction electrocatalysis. J Braz Chem Soc 16(3 A):328–336
81. Lima FHB, Salgado JRC, Gonzalez ER, Ticianelli EA (2007) Electrocatalytic properties of PtCoC and PtNiC alloys for the oxygen reduction reaction in alkaline solution. J Electrochem. So. 154(4)
82. Creemers C, Deurinck P (1997) Platinum segregation to the (111) surface of ordered $Pt_{80}Fe_{20}$: LEIS results and model simulations. Surf Interface Anal 25(3):177–189
83. Gauthier Y, Joly Y, Baudoing R, Rundgren J (1985) Surface-sandwich segregation on nondilute bimetallic alloys: Pt50Ni50 and Pt78Ni22 probed by low-energy electron diffraction. Phys Rev B 31(10):6216–6218
84. Gauthier Y, Baudoing-Savois R, Bugnard JM, Hebenstreit W, Schmid M, Varga P (2000) Segregation and chemical ordering in the surface layers of $Pt_{25}Co_{75}$(111): a LEED/STM study. Surf Sci 466(1–3):155–166
85. Gasteiger HA, Ross PN Jr, Cairns EJ (1993) LEIS and AES on sputtered and annealed polycrystalline Pt-Ru bulk alloys. Surf Sci 293(1–2):67–80
86. Ruban AV, Skriver HL, Norskov JK (1999) Surface segregation energies in transition-metal alloys. Phys Rev B 59(24):15990–16000
87. Ma Y, Balbuena PB (2008) Pt surface segregation in bimetallic Pt3M alloys: a density functional theory study. Surf Sci 602(1):107–113
88. Chen S, Ferreira PJ, Sheng WC, Yabuuchi N, Allard LF, Shao-Horn Y (2008) Enhanced activity for oxygen reduction reaction on "Pt3CO" nanoparticles: direct evidence of percolated and sandwich-segregation structures. J Am Chem Soc 130(42):13818–13819
89. Stamenkovic VR, Mun BS, Mayrhofer KJJ, Ross PN, Markovic NM (2006) Effect of surface composition on electronic structure, stability, and electrocatalytic properties of Pt-transition metal alloys: Pt-skin versus Pt-skeleton surfaces. J Am Chem Soc 128(27):8813–8819
90. Chen S, Sheng WC, Yabuuchi N, Ferreira PJ, Allard LF, Shao-Horn Y (2009) Origin of oxygen reduction reaction activity on "Pt3Co" nanoparticles: atomically resolved chemical compositions and structures. J Phys Chem C 113(3): 1109–1125
91. Koh S, Leisch J, Toney MF, Strasser P (2007) Structure-activity-stability relationships of Pt-Co alloy electrocatalysts in gas-diffusion electrode layers. J Phys Chem C 111(9): 3744–3752
92. Mani P, Srivastava R, Strasser P (2008) Dealloyed Pt-Cu core-shell nanoparticle electrocatalysts for use in PEM fuel cell cathodes. J Phys Chem C 112(7):2770–2778
93. Srivastava R, Mani P, Hahn N, Strasser P (2007) Efficient oxygen reduction fuel cell electrocatalysis on voltammetrically dealloyed Pt-Cu-Co nanoparticles. Angew Chem Int Ed Engl 46(47):8988–8991
94. Neyerlin KC, Srivastava R, Yu CF, Strasser P (2009) Electrochemical activity and stability of dealloyed Pt-Cu and Pt-Cu-Co electrocatalysts for the oxygen reduction reaction (ORR). J Power Sources 186(2):261–267
95. Wang C, Van Der Vliet D, Chang KC, You H, Strmcnik D, Schlueter JA, Markovic NM, Stamenkovic VR (2009) Monodisperse Pt3Co nanoparticles as a catalyst for the oxygen reduction reaction: size-dependent activity. J Phys Chem C 113(45):19365–19368

96. Watanabe M, Wakisaka M, Yano H, Uchida H (2008) Analyses of oxygen reduction reaction at Pt-based electrocatalysts. ECS Trans 16:199–206
97. Wakisaka M, Suzuki H, Mitsui S, Uchida H, Watanabe M (2008) Increased oxygen coverage at Pt-Fe alloy cathode for the enhanced oxygen reduction reaction studied by EC-XPS. J Phys Chem C 112(7):2750–2755
98. Ferreira PJ, la O GJ, Shao-Horn Y, Morgan D, Makharia R, Kocha S, Gasteiger HA (2005) Instability of Pt/C electrocatalysts in proton exchange membrane fuel cells – a mechanistic investigation. J Electrochem Soc 152(11): A2256–A2271
99. Colon-Mercado HR, Popov BN (2006) Stability of platinum based alloy cathode catalysts in PEM fuel cells. J Power Sources 155(2):253–263
100. Morita T, Kojima K (2008) Development of fuel cell hybrid vehicle in Toyota. ECS Trans 16:185–198
101. Uchimura M, Sugawara S, Suzuki Y, Zhang J, Kocha SS (2008) Electrocatalyst durability under simulated automotive drive cycles. ECS Trans 16(2):225–234
102. Adzic RR, Zhang J, Sasaki K, Vukmirovic MB, Shao M, Wang JX, Nilekar AU, Mavrikakis M, Valerio JA, Uribe F (2007) Platinum monolayer fuel cell electrocatalysts. Top Catal 46(3–4): 249–262
103. Brankovic SR, Wang JX, Adzic RR (2001) Pt submonolayers on Ru nanoparticles – a novel low Pt loading, high CO tolerance fuel cell electrocatalyst. Electrochem Solid State Lett 4(12): A217–A220
104. Sasaki K, Mo Y, Wang JX, Balasubramanian M, Uribe F, McBreen J, Adzic RR (2003) Pt submonolayers on metal nanoparticles – novel electrocatalysts for H2 oxidation and O2 reduction. Electrochim Acta 48(25–26):3841–3849
105. Wang JX, Brankovic SR, Zhu Y, Hanson JC, Adzic RR (2003) Kinetic characterization of PtRu fuel cell anode catalysts made by spontaneous Pt deposition on Ru nanoparticles. J Electrochem Soc 150(8):A1108–A1117
106. Brankovic SR, McBreen J, Adzic RR (2001) Spontaneous deposition of Pt on the Ru(0001) surface. J Electroanal Chem 503(1–2):99–104
107. Sasaki K, Wang JX, Balasubramanian M, McBreen J, Uribe F, Adzic RR (2004) Ultra-low platinum content fuel cell anode electrocatalyst with a long-term performance stability. Electrochim Acta 49(22–23 SPEC. ISS):3873–3877
108. Kolb DM, Przasnyski M, Gerischer H (1974) Underpotential deposition of metals and work function differences. J Electroanal Chem 54(1):25–38
109. Herrero E, Buller LJ, Abruna HD (2001) Underpotential deposition at single crystal surfaces of Au, Pt, Ag and other materials. Chem Rev 101(7):1897–1930
110. Aramata A (1997) Underpotential deposition on single-crystal metals. In: Bockris JO, White RE, Conway BE (eds) Modern aspects of electrochemistry. Plenum, New York
111. Brankovic SR, Wang JX, Adzic RR (2001) Metal monolayer deposition by replacement of metal adlayers on electrode surfaces. Surf Sci 474(1–3):L173–L179
112. Zhang J, Mo Y, Vukmirovic MB, Klie R, Sasaki K, Adzic RR (2004) Platinum monolayer electrocatalysts for O2 reduction: Pt monolayer on Pd(111) and on carbon-supported Pd nanoparticles. J Phys Chem B 108(30):10955–10964
113. Zhang J, Vukmirovic MB, Sasaki K, Uribe F, Adzic RR (2005) Platinum monolayer electro catalysts for oxygen reduction: effect of substrates, and long-term stability. J Serb Chem Soc 70(3):513–525
114. Zhang JL, Vukmirovic MB, Xu Y, Mavrikakis M, Adzic RR (2005) Controlling the catalytic activity of platinum-monolayer electrocatalysts for oxygen reduction with different substrates. Angew Chem Int Ed Engl 44(14):2132–2135
115. Zhang JL, Vukmirovic MB, Sasaki K, Nilekar AU, Mavrikakis M, Adzic RR (2005) Mixed-metal Pt monolayer electrocatalysts for enhanced oxygen reduction kinetics. J Am Chem Soc 127(36):12480–12481
116. Zhou WP, Yang XF, Vukmirovic MB, Koel BE, Jiao J, Peng GW, Mavrikakis M, Adzic RR (2009) Improving electrocatalysts for O-2 reduction by fine-tuning the Pt-support interaction: Pt monolayer on the surfaces of a Pd3Fe(111) single-crystal alloy. J Am Chem Soc 131(35):12755–12762
117. Zhang J, Lima FHB, Shao MH, Sasaki K, Wang JX, Hanson J, Adzic RR (2005) Platinum monolayer on nonnoble metal-noble metal core-shell nanoparticle electrocatalysts for O2 reduction. J Phys Chem B 109(48):22701–22704
118. Zhang J, Sasaki K, Sutter E, Adzic RR (2007) Stabilization of platinum oxygen-reduction electrocatalysts using gold clusters. Science 315(5809):220–222
119. Wang JX, Inada H, Wu LJ, Zhu YM, Choi YM, Liu P, Zhou WP, Adzic RR (2009) Oxygen reduction on well-defined core-shell nanocatalysts: particle size, facet, and pt shell thickness effects. J Am Chem Soc 131(47):17298–17302
120. Sasaki K, Wang JX, Naohara H, Marinkovic N, More K, Inada H, Adzic RR (2010) Recent advances in platinum monolayer electrocatalysts for oxygen reduction reaction: scale-up synthesis, structure and activity of Pt shells on Pd cores. Electrochim Acta 55(8):2645–2652
121. Shao-Horn Y, Sheng WC, Chen S, Ferreira PJ, Holby EF, Morgan D (2007) Instability of supported platinum nanoparticles in low-temperature fuel cells. Top Catal 46(3–4):285–305
122. Yu PT, Gu W, Makharia R, Wagner FT, Gasteiger HA (2006) The impact of carbon stability on PEM fuel cell startup and shutdown voltage degradation. ECS Trans 3:797–809
123. Yu PT, Kocha S, Paine L, Gu W, Wagner FT (2004) The effects of air purge on the degradation of PEM fuel cells during startup and shutdown procedures. In: 2004 AIChE spring national meeting, conference proceedings, New Orleans, pp 521–527
124. Debe MK (2003) Novel catalyst, catalyst support and catalyst coated membrane methods. In: Vielstich W, Gasteiger HA, Lamm A (eds) Handbook of fuel cells – fundamentals technology and applications. Wiley, Chichester
125. Gancs L, Kobayashi T, Debe MK, Atanasoski R, Wieckowski A (2008) Crystallographic characteristics of nanostructured thin-film fuel cell electrocatalysts: a HRTEM study. Chem Mater 20(7):2444–2454

126. Debe MK, Drube AR (1995) Structural characteristics of a uniquely nanostructured organic thin film. J Vac Sci Technol B Microelectron Nanometer Struct 13(3):1236–1241
127. Debe MK, Schmoeckel AK, Vernstrorn GD, Atanasoski R (2006) High voltage stability of nanostructured thin film catalysts for PEM fuel cells. J Power Sources 161(2):1002–1011
128. Bonakdarpour A, Stevens K, Vernstrom GD, Atanasoski R, Schmoeckel AK, Debe MK, Dahn JR (2007) Oxygen reduction activity of Pt and Pt-Mn-Co electrocatalysts sputtered on nano-structured thin film support. Electrochim Acta 53(2):688–694
129. Debe MK, Schmoeckel AK, Hendricks SM, Vernstrom GD, Haugen GM, Atanasoski RT (2005) Durability aspects of nanostructured thin film catalysts for PEM fuel cells. ECS Trans 1:51–66
130. Chen ZW, Waje M, Li WZ, Yan YS (2007) Supportless Pt and PtPd nanotubes as electrocatalysts for oxygen-reduction reactions. Angew Chem Int Edit Engl 46(22):4060–4063
131. Mayers B, Jiang X, Sunderland D, Cattle B, Xia Y (2003) Hollow nanostructures of platinum with controllable dimensions can be synthesized by templating against selenium nanowires and colloids. J Am Chem Soc 125(44):13364–13365
132. Sun Y, Tao Z, Chen J, Herricks T, Xia Y (2004) Ag nanowires coated with Ag/Pd alloy sheaths and their use as substrates for reversible absorption and desorption of hydrogen. J Am Chem Soc 126(19):5940–5941
133. Sun Y, Yin Y, Mayers BT, Herricks T, Xia Y (2002) Uniform silver nanowires synthesis by reducing $AgNO_3$ with ethylene glycol in the presence of seeds and poly(vinyl pyrrolidone). Chem Mater 14(11):4736–4745
134. Sun SH, Zhang GX, Geng DS, Chen YG, Banis MN, Li RY, Cai M, Sun XL (2010) Direct growth of single-crystal Pt nanowires on Sn@CNT nanocable: 3D electrodes for highly active electrocatalysts. Chem Eur J 16(3):829–835
135. Peng ZM, Yang H (2009) Synthesis and oxygen reduction electrocatalytic property of Pt-on-Pd bimetallic heteronanostructures. J Am Chem Soc 131(22):7542
136. Lim B, Jiang M, Camargo PHC, Cho EC, Tao J, Lu X, Zhu Y, Xia Y (2009) Pd-Pt bimetallic nanodendrites with high activity for oxygen reduction. Science 324(5932):1302–1305
137. Lim BW, Lu XM, Jiang MJ, Camargo PHC, Cho EC, Lee EP, Xia YN (2008) Facile synthesis of highly faceted multioctahedral Pt nanocrystals through controlled overgrowth. Nano Lett 8(11):4043–4047
138. Erlebacher J, Snyder J (2009) Dealloyed nanoporous metals for PEM fuel cell catalysis. ECS Trans 25:603–612
139. Zeis R, Mathur A, Fritz G, Lee J, Erlebacher J (2007) Platinum-plated nanoporous gold: An efficient, low Pt loading electrocatalyst for PEM fuel cells. J Power Sources 165(1):65–72
140. Erlebacher J (2009) Materials science of hydrogen/oxygen fuel cell catalysis. In: Ehrenreich H, Spaepen F (eds) Solid state physics – advances in research and applications. Academic, New York, pp 77–141
141. Wu J, Zhang J, Peng Z, Yang S, Wagner FT, Yang H (2010) Truncated octahedral Pt_3Ni oxygen reduction reaction electrocatalysts. J Am Chem Soc 132(14):4984–4985
142. Zhang J, Yang H, Fang J, Zou S (2010) Synthesis and oxygen reduction activity of shape-controlled Pt3Ni nanopolyhedra. Nano Lett 10(2):638–644

Books and Reviews

Bard AJ, Faulkner LR (2001) Electrochemical methods, fundamentals and applications, 2nd edn. Wiley, New York
Lipkowski J, Ross P (eds) (1998) Electrocatalysis (frontiers in electrochemistry). Wiley-VCH, Danvers
Markovic NM, Ross PN Jr (2002) Surface science studies of model fuel cell electrocatalysts. Surf Sci Rep 45(4–6):117–229
Newman J, Thomas-Alyea KE (2004) Electrochemical system, 3rd edn. Wiley, Hoboken
Vielstich W, Gasteiger H, Lamm A (eds) (2003) Handbook of fuel cells: fundamentals, technology, applications. Wiley, Chichester
Vielstich W, Gasteiger H, Lamm A (eds) (2009) Handbook of fuel cells: advances in electrocatalysis, materials, diagnostics and durability, vol 5 and 6. Wiley, New York
Wieckowski A, Savinova ER, Vayenas CG (eds) (2003) Catalysis and electrocatalysis at nanoparticle surfaces, 1st edn. CRC Press, Boca Raton
Zhang J (ed) (2008) PEM fuel cell electrocatalysts and catalyst layers: fundamentals and applications, 1st edn. Springer, London

PEM Fuel Cells, Materials and Design Development Challenges

Stephen J. Paddison[1], Hubert A. Gasteiger[2]
[1]Department of Chemical & Biomolecular Engineering, University of Tennessee, Knoxville, TN, USA
[2]Department of Chemistry, Technische Universität München, Munich, Germany

Article Outline

Glossary
Definition of the Subject and Its Importance
Introduction
Processes in an MEA and Voltage-Loss Terms
Ion and Water Transport in Ionomers
Degradation of Pt-Based Catalysts

Carbon-Support Corrosion
Membrane Development Needs and Approaches
Temperature Targets
Proton Conductivity
Reactant Gas Permeability
Morphology
Choice of the Protogenic Group
Future Directions
Bibliography

Glossary

Hydrogen oxidation reaction (HOR) The electrochemical oxidation of molecular hydrogen occurring at the anode of a fuel cell.

Membrane electrode assembly (MEA) The assembly consisting of the electrolyte membrane sandwiched between the anode and cathode.

Oxygen reduction reaction (ORR) The electrochemical reduction of molecular oxygen through a four electron transfer at the cathode of a fuel cell.

Perfluorosulfonic acid (PFSA) The CF_2SO_3H group is the protogenic group on ionomers and membranes utilized in catalyst layer and electrolyte in a fuel cell.

Proton exchange membrane (PEM) A solid polymer thin film that is proton conducting and functions as the central component of a fuel cell.

Definition of the Subject and Its Importance

Substantial resources have been devoted over the past decade to the development of proton exchange membrane (PEM) fuel cells that use hydrogen fuel and oxygen from the air to produce electricity for applications including automotive propulsion. Remaining challenges include the design of inexpensive and stable robust catalysts for the electrochemical reaction at the cathode (i.e., the reduction of oxygen) of the fuel cell and the synthesis of robust (i.e., chemical and mechanical stable) electrolyte membranes exhibiting high proton conductivity under hot and dry conditions.

Introduction

The development of commercially viable proton exchange membrane (PEM) fuel cell systems powered by hydrogen or hydrogen-rich reformate faces a significant number of materials and MEA (membrane electrode assembly) design-related performance and durability challenges, which need to be addressed via:

1. Improvement of current platinum-based catalysts for the oxygen reduction reaction (ORR) and the hydrogen oxidation reaction (HOR) or substitution by platinum-group metal (PGM) free catalysts in order to meet the platinum cost and design constraints for commercial applications [1].
2. Development of more durable ORR and HOR catalysts, which are resistant to the voltage-cycles occurring during the transient operation of fuel cell vehicles (owing to the variable power demand during typical vehicle drive cycles) [2, 3].
3. Substitution of currently used perfluorosulfonic acid (PFSA) ionomers and ionomer membranes (e.g., Nafion®) by novel materials with substantially improved proton conductivity at low relative humidity (RH), which would eliminate the need for fully humidified reactants and thereby significantly simplify fuel cell system design [2, 4, 5].
4. Modification/development of ionomers and ionomeric membranes to obtain enhanced chemical durability under low-RH conditions [6, 7] as well as increased mechanical stability during RH-cycles, both of which are frequently occurring conditions under automotive fuel cell operation [2, 8].
5. Replacement of current high-surface area carbon supports (e.g., Ketjen blacks) with more corrosion-resistant materials (e.g., fully graphitized carbon supports or noncarbon-based supports) in order to minimize the damage caused by local hydrogen starvation [9, 10] and during fuel cell start/stop processes [11, 12], so that more complex system-design based mitigation strategies can be avoided [13].
6. Design of HOR catalysts which have no activity for the ORR [14] and their integration into anode electrodes, which is an alternative approach to mitigating degradation caused by start/stop.
7. Mitigation of possible cell-voltage reversal caused by temporary hydrogen under-supply during fast transients, which can be achieved by incorporation of efficient oxygen evolution catalysts into the anode electrode [15] or by corrosion-resistant

anode catalyst supports (e.g., whisker electrodes developed by 3M [16]).

8. Optimization of electrode and MEA performance with new electrode materials (catalysts, catalyst supports, and ionomers [2]), particularly for high-current density operation with low platinum loadings.
9. Design of high-performing gas-diffusion media (DM) and microporous layer (MPL) coatings which are resistant to contamination [17] and aging caused by fuel cell system transients (i.e., extensive voltage-cycling, start/stop [18]).
10. Development of *ab initio* catalyst models, particularly for the ORR catalysis [19] as well as rigorous MEA performance models [20, 21] and in situ diagnostic methods [22–24] in order to provide effective analytical methods required for the screening and implementation of improved electrode materials and MEA designs.

Despite this impressively long list of technical hurdles, the development of fuel cell vehicles has advanced significantly in the past 10 years, and hydrogen fuel cell vehicle fleet tests are now demonstrating drive-cycle efficiencies of 52–58% (lower heating value), real-world vehicle operating life ranging from 700 to 1,900 h, and refueling times on the order of 5 min [25], with the capability of starting from temperatures as low as −20°C [26]. Nevertheless, in order to meet the automotive cost targets (<50 US$ per kW system power), the platinum supply constraints (<10 g platinum per vehicle), and the required durability targets (6,000 operating hours), the above listed challenges remain and the cutting-edge research on these topics is being presented in the subsequent entries of this book.

In the following, we will provide only a very brief overview of some of the basic materials and MEA design concepts and the interested reader is referred to the very detailed articles in the remainder of this encyclopedia or to the cited literature.

Processes in an MEA and Voltage-Loss Terms

In order to define the limiting factors in fuel cell performance, it is helpful to review the various reactions and transport processes occurring in a PEM fuel cell, which are illustrated in Fig. 1. The HOR and ORR reactions catalyzed by the anode and cathode catalysts, respectively, require facile proton transport through the ionomeric membrane and also throughout the porous electrodes which are typically composed of carbon-supported catalysts and proton-conducting ionomer (exceptions are nanostructured electrodes, for example, those developed by 3M [16]). At the same time, hydrogen and oxygen supplied via flow-field channels in the bipolar plates (BP, see Fig. 1) need to be supplied via gas-phase diffusion through

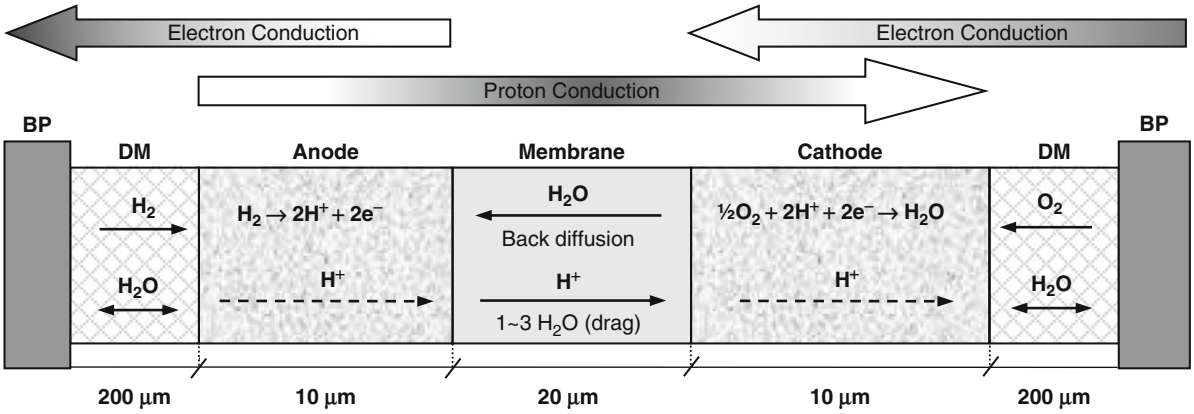

PEM Fuel Cells, Materials and Design Development Challenges. Figure 1
Schematic of a PEMFC repeating unit showing the electrode reactions, H_2 and O_2 gas transport, water transport, as well as proton and electron charge transfer. Typical values of component thickness are shown (not drawn to scale) (Reproduced from W. Gu et al. [20] by permission from Wiley)

the porous gas-diffusion layers [27] and throughout the electrodes. At the design point for automotive operating conditions, that is, at an average humidity of the exiting gas-streams of <100% [20], reactant diffusion can be described by a simple effective diffusion coefficient [28]. However, under conditions where the relative humidity of the exiting gas-streams exceeds 100% (e.g., at fuel cell temperatures below 50°C), the quantitative description of gas transport is more complex due to the presence of liquid water inside the porous layers [29].

The local relative humidity also determines the proton conductivity of the ionomeric membrane [30] and of the electrodes [31], leading to major voltage losses below 50% RH. An additional voltage loss, particularly at high-current densities and low relative humidity, arises from the dry-out of the anode-side of the membrane, which is due to the electro-osmotic drag of water caused by protons flowing from the anode to the cathode (vide infra). Owing to the drastically increasing proton conduction resistance at low RH [30], the associated voltage loss can be substantial, unless membranes are very thin in order to allow for fast water back-transport from the cathode to the anode; for this reason, membranes in state-of-the-art PEMFCs are typically not thicker than 15–20 μm.

In addition to the voltage losses caused by the overpotentials of the HOR, η_{HOR} , and the ORR, η_{ORR}, as well as by the proton- and gas-transport resistances, substantial voltage losses can arise from purely electronic resistances from the bipolar plate all the way throughout the electrode, $R_{electronic}$. However, the bulk resistances of carbon-black based electrodes, carbon-fiber based diffusion media, and stainless steel or carbon-composite based bipolar plates are generally negligible compared to the electronic contact resistances between electrodes/DMs and DMs/BPs [20], so that the measured electronic resistances are mostly due to contact resistances. The largest contribution here comes from the strongly compression-dependent contact resistance between the bipolar plate and carbon-fiber based diffusion media [27].

The above described voltage losses can be summarized by a conceptually simple equation, describing the fuel cell voltage, E_{cell}, as a function of current density, i:

$$E_{cell} = E_{rev.} - i \times (R_{electronic} + R_{membrane}) - \eta_{HOR} - \eta_{ORR} - i \times R_{H+,eff.} - \eta_{tx,gas(dry)} - \eta_{tx,gas(wet)} \quad (1)$$

where $E_{rev.}$ is the reversible thermodynamic potential depending on temperature and gas partial pressure. The proton conduction resistances of the membrane, $R_{membrane}$, and the electrodes, $R_{H+,eff.}$, are strongly dependent on the local relative humidity and, in contrast to $R_{electronic}$, do also depend on current density and on the local temperature which again is mostly determined by thermal conductivity resistances between the electrode/DM and the DM/bipolar plate interfaces [20, 31, 32]. For fuel cells fed with pure hydrogen and air, the gas-diffusion overpotential, $\eta_{tx,gas(dry)}$, is primarily due to the diffusion of oxygen in air through the diffusion medium and the cathode electrode in the absence of liquid water, that is, at operating conditions where the RH of the exiting reactants is <100%; the additional gas-diffusion overpotential losses caused by the presence of liquid water in the diffusion media and the electrodes are here described as $\eta_{tx,gas(wet)}$ and become significant at wet operating conditions (i.e., at >100% RH of the exiting reactants).

The various voltage losses under typical automotive operating conditions are shown in Fig. 2. At the highest current density of 1.5 A cm^{-2}, the voltage loss caused by the slow ORR kinetics amounts to approximately 70% of the overall voltage loss, while the voltage loss for the HOR is negligibly small under these conditions (<<5 mV [33]). At the maximum power density of 0.93 W cm^{-2} (0.62 V at 1.5 A cm^{-2}) and the total platinum loading of 0.5 g_{Pt} cm^{-2} shown in Fig. 2, the platinum specific power density is 0.54 g_{Pt} kW^{-1}, implying that 54 g_{Pt} would be required for a typical 100 kW automotive fuel cell. Even though the fast HOR kinetics allow for a lowering of the anode catalyst loading to 0.05 mg_{Pt} cm^{-2} without notable performance loss [33], the thus obtained platinum specific power density of 0.38 g_{Pt} kW^{-1} is still too high for commercially viable fuel cells. Therefore, major foci in current fuel cell R&D is the development of either more active platinum-based ORR catalysts or of PGM-free ORR catalysts [1, 34, 35] as well as the development of suitable electrode structures for these novel catalysts. The other voltage loss terms shown in Fig. 2 are

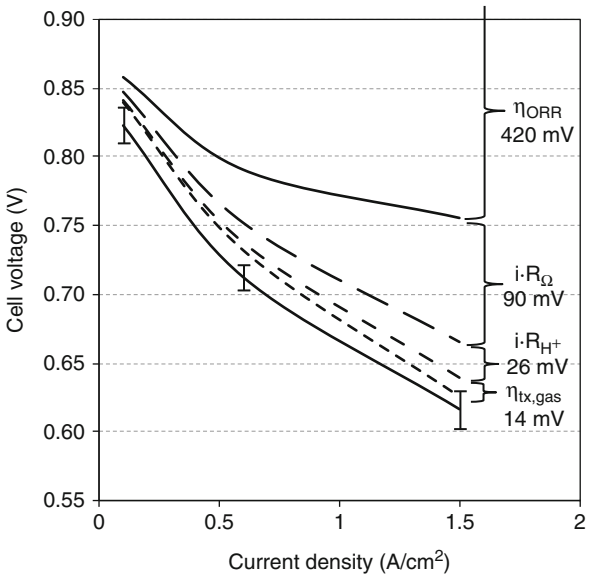

PEM Fuel Cells, Materials and Design Development Challenges. Figure 2
Voltage loss terms in state-of-the-art H_2/air PEMFCs operated under representative automotive conditions. *MEAs:* 0.2/0.3 mg_{Pt} cm^{-2} (anode/cathode) coated on an 18 μm thick composite membrane and sandwiched between ≈200 μm thick DMs (SGL 25BC). *Operating conditions:* H_2 and air stoichiometric flows of 2 and 1.8–5.5, respectively, stack pressure of 110–176 kPa_{abs}, gas inlet humidities of 30–60% RH, and stack temperature of 70–80°C. For details see [20] (Reproduced from W. Gu et al. [20] by permission from Wiley)

significantly smaller and dominated by the ohmic resistances, R_Ω, which represent $R_{membrane}$ and $R_{electronic}$ (s. Eq. 1), whereby 60 of the 90 mV losses at 1.5 A cm^{-2} are mostly due to the electronic contact resistance between the DMs and the bipolar plates.

From a systems point of view, it would also be desirable to develop ionomers and ionomeric membranes with increased conductivity at low RH, since this would enable the design of fuel cell systems operating with either dry gas-feeds and/or at higher fuel cell temperature [5]. The latter would reduce the vehicle radiator requirements, which are quite demanding for fuel cell vehicles due to the large heat load which has to be dissipated via the radiator [4], contrary to internal combustion engine-based vehicles where a large fraction of the produced heat is discharged via the latent heat of the engine exhaust gases. A brief discussion on the membrane development toward this goal is given below.

Ion and Water Transport in Ionomers

The central component of a PEM fuel cell is a thin film polymer that is an ionomer or ion-containing polymer that critically functions as the separator of gases and electrodes but also as a proton conductor completing the internal circuit. Typically, a proton conductivity of 0.1 S cm^{-1} is required for efficient function of the fuel cell. PEMs for automotive applications require that the ionomer function both at high temperature (>90°C) to dissipate waste heat and low pressures (<170 kPa_{abs}) to minimize pumping parasitics [2]. This necessitates operation at low relative humidities but currently utilized PFSA-based PEMs require water to facilitate the dissociation and long range transport of protons [36]. Although there are a large number of materials and systems that conduct protons (as shown in Fig. 3), those exhibiting sufficient proton conductivity in the target temperature range (for fuel cell operation) are almost nonexistent. It is also interesting to note that while the majority of the materials substances display an increase in conductivity with increasing temperature, the benchmark PFSA ionomer Nafion® exhibits just the opposite if the water vapor pressure remains constant (note: this means that the relative humidity decreases with increasing temperature). This is, of course, due to the dehydration of the membrane as the temperature approaches and then exceeds the boiling point of water (at a water pressure of 1 atm.). All PFSA ionomers show a sharp decrease in proton conductivity as the water content falls (see the entry on "► Proton Exchange Membrane Fuel Cells: High-Temperature, Low-Humidity Operation" by Hamrock and Herring). Several different approaches have been used to improve the proton conductivity of PEMs including changes in the backbone and/or side chain chemistry and are described in detail in the entry "► Membrane Electrolytes, from Perfluoro Sulfonic Acid (PFSA) to Hydrocarbon Ionomers" by Miyatake.

Several approaches have been devised to reduce the resistance of the membrane at low RH, including increasing the density of the acidic groups and making the membrane thinner. There is, of course, a limit to the

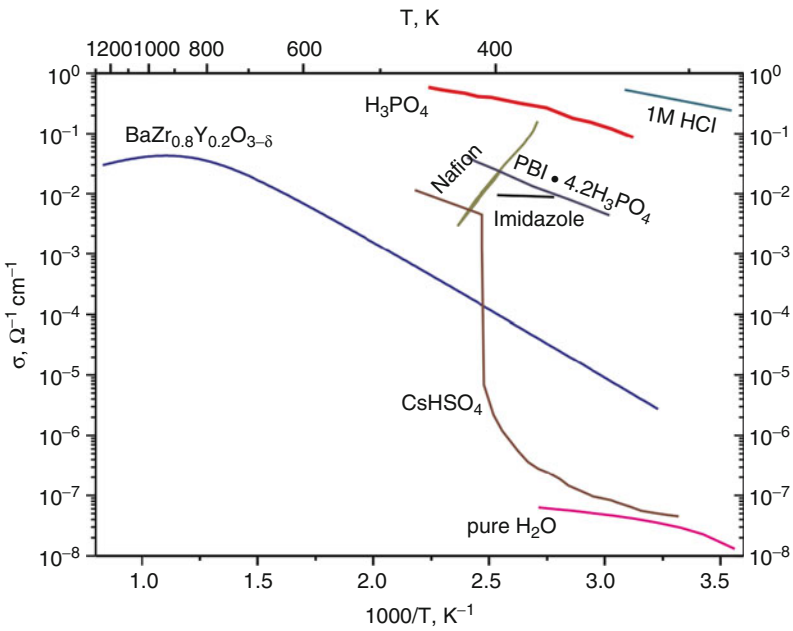

PEM Fuel Cells, Materials and Design Development Challenges. Figure 3
Measured proton conductivity for various materials as a function of temperature. In the temperature regime of interest (80–120°C) for PEM fuel cells, the only presently available conductors are the hydrated ionomers (Nafion®, etc.) and display a significant decrease in conductivity as the temperature is increased (due to a decrease in water content)

extent to which the acid content may be increased, and the membrane thickness decreased. Membranes with a very high ion exchange capacity suffer mechanical robustness as the low degree of crystallinity and high amounts of water result in materials that dissolve and/or fall apart. Very thin membranes are also prone to mechanical failure and are no longer impermeable to gases which results in both loss of performance and membrane degradation due to the crossover of the reactant gases. Further details of these issues are provided in the entry on "▶ High Temperature, Low Humidity Operation of Proton Exchange Membrane Fuel Cells."

Degradation of Pt-Based Catalysts

A significant part of the performance degradation of fuel cells with current platinum-based catalysts derives from the dissolution and sintering of platinum. This is due to the relatively high solubility of platinum in the strongly acidic electrolyte [37], whereby the dissolution rate is enhanced by voltage-cycling of the cathode electrode during the dynamic load-following required by the fuel cell in automotive drive cycles [2, 37]. The enhanced Pt dissolution rate is caused by the transition between mostly metallic platinum at high-current density (viz., at high cathode overpotential) and an oxidized platinum surface at low current density or open circuit potential (viz., at low cathode overpotential) [38, 39]. As illustrated in Fig. 4, dissolved platinum species either redeposit on other platinum particles via an Ostwald ripening process or diffuse in the electrolyte phase toward the membrane, where they precipitate inside the ionomer phase by reaction with hydrogen which is permeating through the membrane from the anode side. Within the ionomer phase, precipitated platinum crystallites form a clearly defined platinum band (see Fig. 4b), the location of which can be predicted by the partial pressure of hydrogen and oxygen in the anode and cathode feed-gases, respectively [40].

Since several hundred thousand large voltage-cycles would be encountered during the lifetime of an automotive fuel cell [2], the associated significant loss of active platinum surface area must be mitigated either by more dissolution-resistant cathode catalysts or by

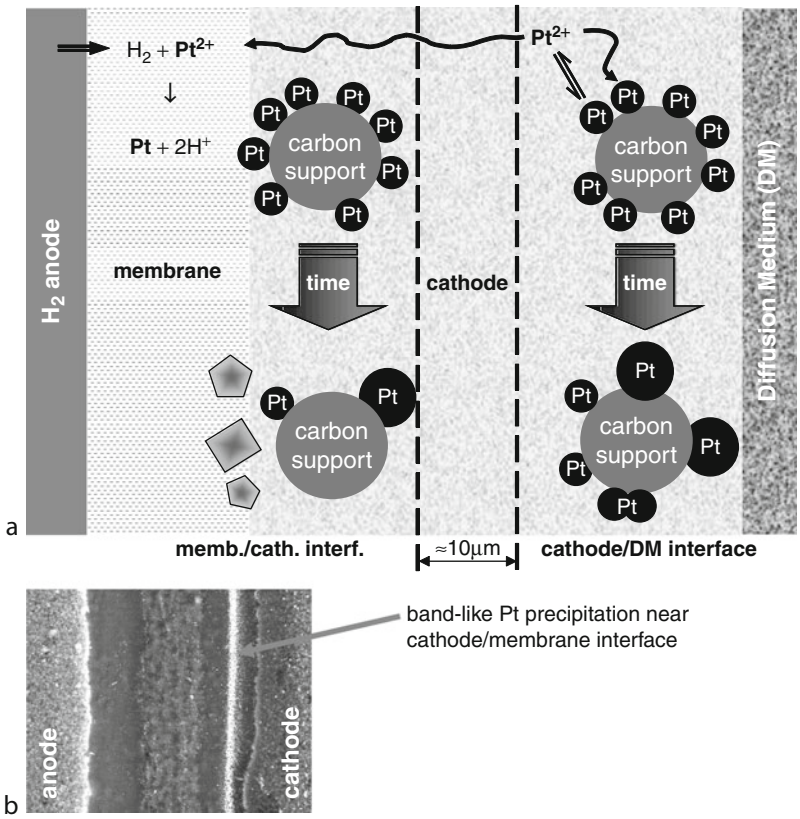

PEM Fuel Cells, Materials and Design Development Challenges. Figure 4
(**a**) Schematic representing platinum surface area loss on (i) the nanometer scale, where platinum particles grow on the carbon support via Ostwald ripening and (ii) the micrometer scale, where dissolved platinum species diffuse toward the membrane, become reduced by hydrogen permeating from the anode through the membrane, and precipitate as platinum particles in the membrane. (**b**) SEM cross section of a short-stack MEA operating at open circuit voltage for 2,000 h, where the bright band in the image indicates platinum deposited in the membrane near the membrane/cathode interface (Reproduced from P. J. Ferreira et al. [37] by permission from The Electrochemical Society)

hybridizing a fuel cell system with a large propulsion battery (tens of kW battery power), by which the number of large voltage-cycles can be substantially reduced. In many instances, it was observed that platinum-alloy catalysts displayed an increased resistance to platinum dissolution [2, 3, 41], but much of the effect is due to the larger particle size of platinum-alloys which favorably affects the platinum dissolution rate via the Gibbs-Thomson effect [42]. Indeed, more recent data demonstrated that voltage-cycling of platinum-alloy cathode catalysts leads to core/shell structures, with platinum-shells forming around a platinum-alloy core, so that the initially higher specific activity of platinum-alloys slowly approaches that of pure platinum in the course of extensive voltage-cycling [43]. This phenomenon is illustrated in Fig. 5.

In summary, while fuel cell/battery hybrid systems reduce the degradation from platinum surface area loss from voltage-cycling to an acceptable level, novel cathode catalysts with increased stability toward voltage-cycling would bring significant benefits and are therefore a very active field of research.

Carbon-Support Corrosion

The excellent gas-transport properties of fuel cell electrodes are due to their high porosity, with void volume fractions of ≈60% for the typical ionomer/carbon weight ratios of 1/1 (volume fractions of

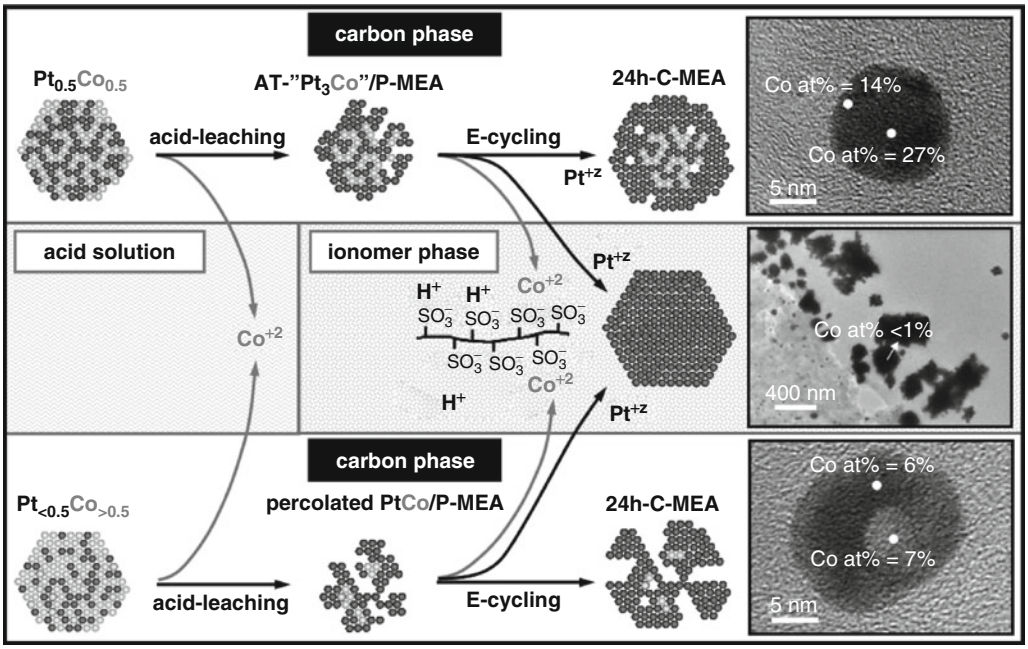

PEM Fuel Cells, Materials and Design Development Challenges. Figure 5
Schematic of the evolution in morphology and composition of a $Pt_{0.5}Co_{0.5}$ cathode catalyst caused by acid leaching and voltage-cycling. The *upper panel* represents particles attached to the carbon-support ("carbon phase"), with *skeleton* Pt_xCo particles obtained after acid leaching, and transforming via Ostwald ripening into *core/shell* particles. The *center panel* represents both the liquid acid phase during pre-leaching and the "ionomer phase" both in the membrane and the electrodes, with large single-crystalline Pt (agglomerates) forming in the membrane and Co^{2+} ion-exchanging into the ionomer phase. The *lower panel* is a proposed mechanism for the formation of *percolated* Pt_xCo alloy particles deriving from precursors with higher than average Co content ("$Pt_{<0.5}Co_{>0.5}$") and resulting in Pt-rich *spongy particles*. TEM bright-field images and spot-resolved EDS compositions (analysis area of 2.5 nm in diameter) of the various types of aged nanoparticles in the 24 h-C-MEA are shown on the right-hand-side (Reproduced from S. Chen et al. [43] by permission from The Electrochemical Society)

ionomer and carbon being ≈20% each) [20]. This high void volume fraction is due to the use of highly structured carbon blacks (e.g., Vulcan XC72 or Ketjen black), which have an intrinsically low packing density which is maintained up to compressions of ≈100 MPa (in comparison, MEAs in fuel cell stacks are compressed at ≈1 MPa). However, at sufficiently high potentials, viz., above ≈1 V versus the reversible hydrogen electrode (RHE) potential, the electrochemical oxidation of carbon by water ($C + 2H_2O \rightarrow CO_2 + 4H^+ + 4e^-$) is substantial, and after the oxidation of approximately 5–10 wt% of the carbon support, the carbon structure collapses [44], resulting in a rapid decrease of the fuel cell performance, as is shown in Fig. 6.

Under normal fuel cell operating conditions, the highest oxidative potentials in the cathode range between ≈0.6 V (vs. RHE) at high-current density and ≈0.95 V (vs. RHE) at open circuit (the anode potential remains always near 0 V vs. RHE), so that carbon-support corrosion is negligible. However, under start/stop conditions or in the case of localized hydrogen starvation, the cathode potential significantly exceeds 1 V versus RHE and the associated rapid carbon-support corrosion leads to a loss of electrode void volume which experimentally is observed as a so-called cathode thinning. This is illustrated by the SEM cross section shown in Fig. 7 for a cathode electrode, where 8 wt%. of the carbon support had been oxidized by applying a cathodic potential (the extent

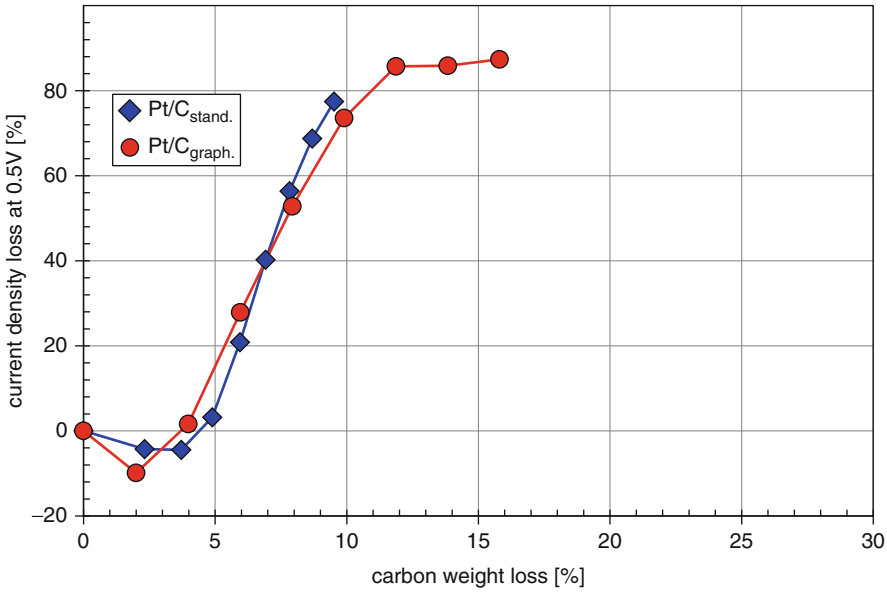

PEM Fuel Cells, Materials and Design Development Challenges. Figure 6
Fuel cell performance loss as a function of the extent of carbon-support corrosion. Conditions: H_2/air (s = 2/2) performance at 80°C, 100%RH, 150 kPa_{abs} (Reproduced from H.A. Gasteiger et al. [3] by permission from Springer)

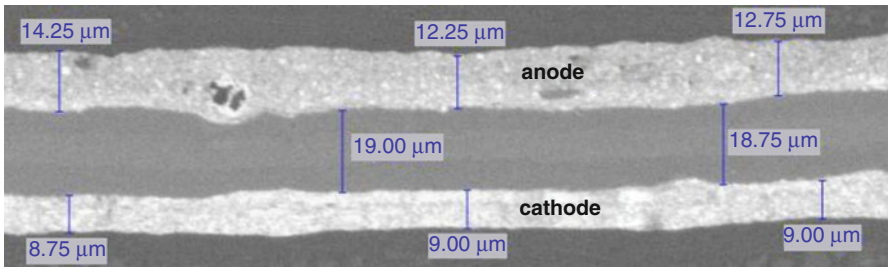

PEM Fuel Cells, Materials and Design Development Challenges. Figure 7
Scanning electron microscopy (SEM) cross section of an MEA of which 8% wt. of the cathode carbon-support had been corroded (see also Fig. 6). The initial cathode electrode thickness was identical to the anode electrode thickness shown in the picture (Reproduced from H.A. Gasteiger et al. [3] by permission from Springer)

of carbon support-corrosion was measured by on-line monitoring of the CO_2 formation rate).

As shown in Fig. 7, the extent of cathode thinning can be monitored by cross section measurements via SEM or optical microscopy [23]. It is accompanied by a loss of electrode void volume as is illustrated in Fig. 8, showing high-resolution SEM cross sections of a nondegraded cathode electrode (left-hand-side) and of a degraded cathode (right-hand-side).

The fundamental start/stop mechanism was first reported by Reiser et al. [11], and occurs when one part of the anode flow-field is partially filled with hydrogen and another part is filled with air, a situation which occurs during the start-up of a fuel cell (hydrogen displacing air in the anode flow-field) or during shutdown (air diffusing into a hydrogen filled anode flow-field after the hydrogen supply is shut off). Detailed explanations of the processes which lead to very high voltages on the cathode electrode (>>1 V vs.

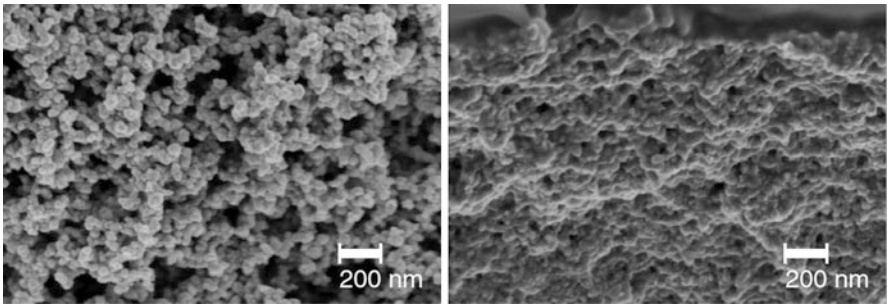

PEM Fuel Cells, Materials and Design Development Challenges. Figure 8
SEM micrographs of freeze fractured sections of the cathode electrodes of MEAs. *Left:* nondegraded MEA; *right:* MEA aged by localized hydrogen starvation. SEM analysis was done without mounting of the MEAs in epoxy (Reproduced from R.N. Carter et al. [23] by permission from John Wiley & Sons)

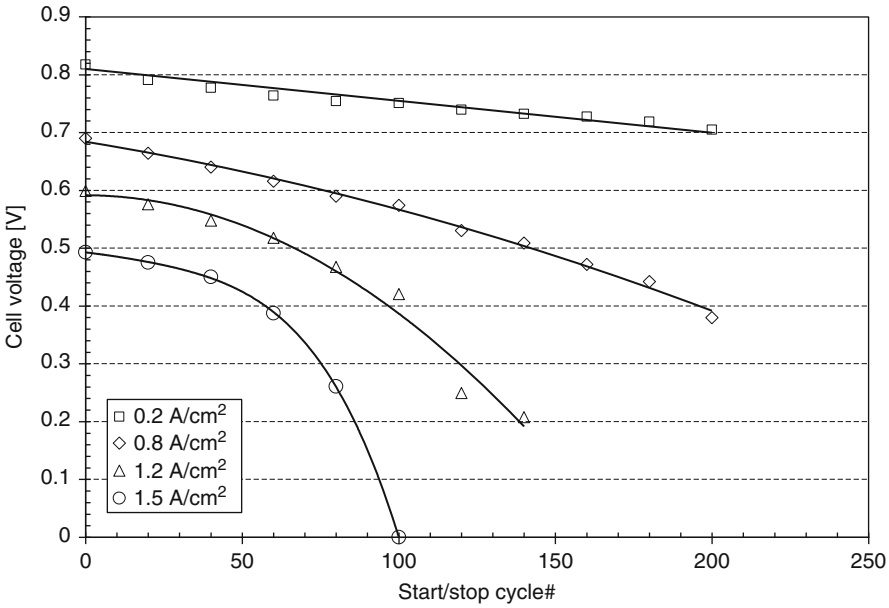

PEM Fuel Cells, Materials and Design Development Challenges. Figure 9
Cell-voltage decays for different current densities as a function of start/stop cycles for an MEA with a platinum catalyst supported on a conventional carbon-support. Conditions: H_2/air (66% inlet RH) at 150 kPa_{abs} and 80°C, aged at a H_2/air-front residence time of 1.3 s (Reproduced from P. T. Yu et al. [12] by permission from The Electrochemical Society)

RHE) have been given elsewhere [11, 34] and the interested reader is referred to these references. The voltage degradation rates produced by start/stop can be simulated conveniently by sending H_2/air fronts through the anode flow-field of a fuel cell (single cell or stack), whereby the voltage degradation rates are proportional to the residence time of the H_2/air front and increase with increasing current density [12], as would be expected for gas-transport induced voltage losses. Such an experiment is shown in Fig. 9, whereby the H_2/air-front residence time of 1.3 s is roughly 10 times longer than that which can be achieved during the start-up of a fuel cell stack (residence times much shorter than 0.1 s are typically not achievable due to engineering constraints). Under these conditions, the cell voltage at 1.5 A cm^{-2} decreases to 0 V within only

100 cycles! Under normal start-up conditions, the residence time would be roughly 10 time shorter, so that a maximum of 1,000 start-up cycles could be performed, which is far short from the automotive target of ≈40,000 starts during the life time of a vehicle.

Therefore, mitigation strategies had to be devised and implemented. Currently, most mitigation strategies are based on system design (short residence times, stack storage under hydrogen, cell shorting, etc. [13]), but on the long-term, additional materials-based mitigation strategies are required. These include implementation of graphitized carbon-supports [12, 44, 45] or of more corrosion-resistant alternative support materials, lowering of the anode catalyst loading which reduces the ORR activity of the anode electrode or development of anode catalysts with low ORR activity [14], or the incorporation of highly active oxygen evolution catalysts in the cathode electrode. Again, the reader is referred to the literature for a detailed discussion [12, 44, 45].

A mechanism very closely related to the start/stop degradation is the so-called localized hydrogen starvation. It was first discussed by Patterson and Darling [9], and occurs when large sections of the anode flow-field are not being supplied with hydrogen due to blockage of the flow-field channel or of the diffusion medium by liquid water. In that case, oxygen permeating through the membrane from the anode to the cathode side creates an analogous situation to that produced by a H_2/air front, viz., the simultaneous presence of hydrogen and oxygen in the anode. Consequently, cathode thinning is observed also in the case of localized hydrogen starvation [10, 23], albeit at a slower rate. While the systems mitigation strategies are different from those used in the case of start/stop, the materials mitigation strategies are identical, with one additional materials mitigation approach: since the maximum carbon corrosion rate is limited by the oxygen permeation rate through the membrane, ionomeric membranes with reduced oxygen permeability (typical for most hydrocarbon-based ionomers) would lower the damage by localized H_2 starvation [10].

Membrane Development Needs and Approaches

As indicated earlier, water is needed in the membrane to dissociate protons (i.e., making the material proton conducting) from the acid functionality or protogenic groups and then secondly to establish a continuous pathway for long range proton transport. The water content of a PEM decreases with decreasing water activity. It has been observed [30] that the water uptake in sulfonic acid ($-SO_3H$)-based PEMs is essentially identical when plotted as function of the water content when the latter is expressed in terms of, λ, the number of water molecules per acid group (i.e., $\lambda = H_2O/SO_3H$) as seen in Fig. 10. It is also clear from this data that the isotherms of the various PEM are essentially identical to that of sulfuric acid at relatively low levels of hydration (i.e., $\lambda < 6$), suggesting that it is the enthalpy of hydration of the $-SO_3H$ group which is driving water uptake in the low-RH region.

This experimental isotherm has been shown to fit either the Brunauer-Emmett-Teller model [46] or a simple empirical polynomial fit at a given temperature [47]. Finally, above $\lambda \approx 6$ (i.e., >80% RH) the isotherms diverge, indicating that properties including polymer structure and morphology, charge density, cross-linking, etc., impact the absorption of water at high water content.

Temperature Targets

For automotive application, it has been determined that a reasonable target for high temperature membrane operation is between 110°C and 120°C for H_2 fueled fuel cell vehicles [5]. Heat rejection at this temperature with conventional packaging becomes feasible and the purity requirement for onboard H_2 is reduced as the tolerance for CO improves to approximately 50 ppmv CO without air bleed at low anode catalyst loading (0.1–0.2 $mg_{noble\text{-}metal}\ cm^{-2}$) [48]. Operation of stationary systems at 140–160°C with hydrocarbon-based H_2 reformate would result in an increase in CO tolerance to about 0.1–0.5% allowing for a simpler or possibly no preferential oxidation (PROX) reactor. Although there is a small improvements in the oxygen reduction reaction kinetics if the system were operated at 160°C, this would be offset with a loss of about 70 mV in equilibrium voltage [49]. Furthermore, the strong specific adsorption of phosphate ions on platinum catalysts leads to a reduced ORR activity in the presence of phosphoric acid electrolyte if compared to sulfonic acid-based ionomers

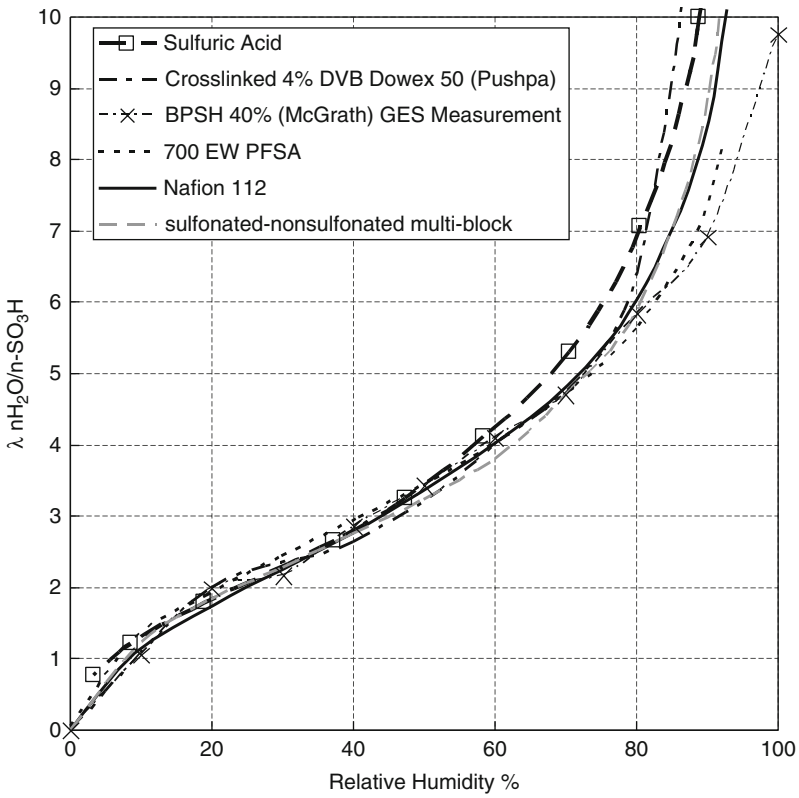

PEM Fuel Cells, Materials and Design Development Challenges. Figure 10
Water uptake isotherms of various ionomers and sulfuric acid at 80°C. Dowex 50 is an ion-exchange resin made of 4% cross-linked polystyrene divinyl benzene; BPSH 40 is a 2-mil 40% randomly sulfonated biphenol sulfone; 700 EW PFSA is a 1-mil membrane with a structure similar to Nafion®; Nafion 112® is a 2-mil extruded membrane; and, PAEK triblock is a 1-mil triblock polyaryl ether ketone with a sulfonated middle block (Reproduced from C.K. Mittelsteadt and H. Liu. [30] by permission from John Wiley & Sons)

(see Table 4 and Fig. 20 in [50]). At temperatures >160°C, the stability of the carbon-support material is compromised [51].

Proton Conductivity

Figure 11 displays the results of a seemingly rather subtle change in the length of the side chain in PFSA membranes: the Dow ionomers have a shorter perfluoroether side chain ($-OCF_2CF_2SO_3H$) than Nafion ($-OCF_2CF(CF_3)OCF_2CF_2SO_3H$). This plot clearly indicates that the density of the sulfonic acid groups as realized through alteration of the equivalent weight (EW, the grams of polymer per mole of acid) may bring about a fairly large change in the proton conductivity across the majority of the hydration isotherm. The proton conductivity of both ionomers, however, drops precipitously at water contents below 5 H_2O/SO_3H.

The dependence of proton conductivity on RH for 1100 EW Nafion at 80°C and 120°C is shown in Fig. 12 and indicates that although the conductivity falls from about 0.10 to 0.01 S cm^{-1} as the relative humidity is decreased from 100% to ≈30% it is essentially independent of temperature [5]. This is in stark contrast to polybenzimidazole (PBI) and phosphoric acid-doped PBI (also plotted in Fig. 12) which although exhibiting the typical fall in proton conductivity as the hydration level is decreased, show significantly higher conductivity at elevated temperatures [54]. Although the PBI

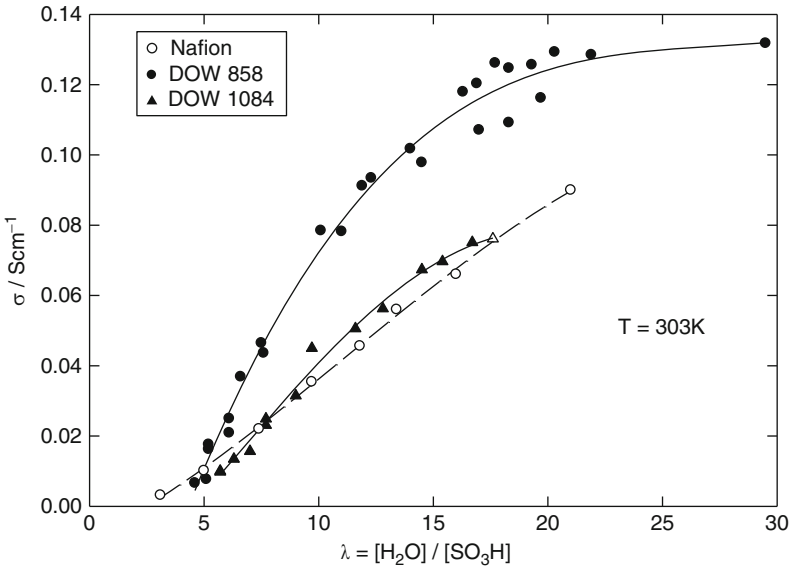

PEM Fuel Cells, Materials and Design Development Challenges. Figure 11
Room temperature proton conductivity of the short side chain (SSC) PFSA ionomer at 2 different (i.e., Dow 858 and Dow 1084 $g_{ionomer}$ per mol_{H+}) equivalent weights (EW) and Nafion as a function of water content expressed as $\lambda = [H_2O]/[-SO_3H]$. The data clearly shows the significant effect the equivalent weight has on proton conductivity with the Dow 858 exhibiting conductivity twice that of the higher EW PFSAs (Reproduced from K. D. Kreuer et al. [52] by Elsevier Science)

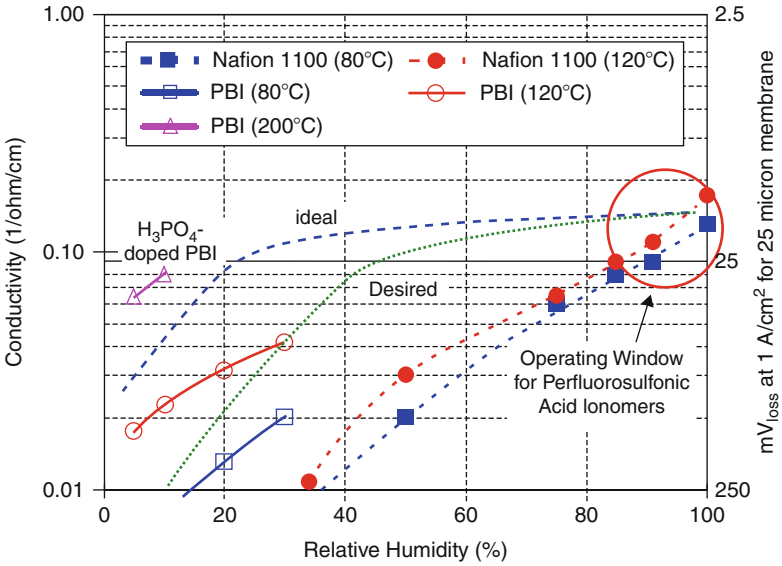

PEM Fuel Cells, Materials and Design Development Challenges. Figure 12
Relationship between proton conductivity and adjoining gas stream humidity at various temperatures for Nafion (1100 EW) [5] and phosphoric acid-doped polybenzimidazole (PBI) [54]. The data clearly demonstrate that the increase in temperature from 80°C to 120°C has little effect on the conductivity of Nafion but a significant effect on the PBI systems. A curve is also shown for a material exhibiting the desired conductivity as a function of the relative humidity that would be ideal for system simplification (The figure is reproduced from Gasteiger and Mathias [5] with permission from The Electrochemical Society)

systems appear to offer the promise of high temperature fuel cell operation, they suffer from other issues including adsorption on the surfaces of platinum-based catalysts and the leaching of phosphoric acid from the electrolyte. Although a significant body of research has focused on determining the hydrated morphology of PFSA membranes, the connections between the structure and morphology with the transport properties are not fully understood. The microstructure of the PFSA polymer not only affects the proton conductivity but also other properties including methanol permeability (i.e., for direct methanol fuel cells), water diffusion, and electro-osmotic drag.

Reactant Gas Permeability

Other important properties of the ionomer include the permeability to both H_2 and O_2 gas. The PEM must not be too permeable to the reactive gases, as excessive gas crossover through the membrane would result in fuel efficiency loses. However, the ionomer in the electrodes must possess sufficient permeability to allow transport of the reactant without imposing any significant concentration gradients and/or mass transfer losses.

The rate of the permeation of gases in PFSA membranes is proportional to the product of the permeability coefficient and the partial pressure (i.e., the driving force) and inversely proportional to the membrane thickness. The permeation leads to a fuel cell crossover efficiency loss due to two components: hydrogen consumption at the anode from O_2 crossover and hydrogen loss to the cathode and subsequent reaction with oxygen. A relatively straightforward analysis [5] based on fuel cell operation with instantaneously varying loads of 0.05 A cm^{-2} at 60°C and 2 A cm^{-2} at 120°C has estimated both upper and lower limits for the permeability of H_2 and O_2 which are shown as a function of temperature in Figs. 13 and 14, respectively. The permeability window for both reactant gases is approximately 3–4 orders of magnitude. Hence, the permeability coefficient, k, for H_2 transport must fall within the range: $1 \times 10^{-17} < k_{H_2} < 1 \times 10^{-12}$ mol cm

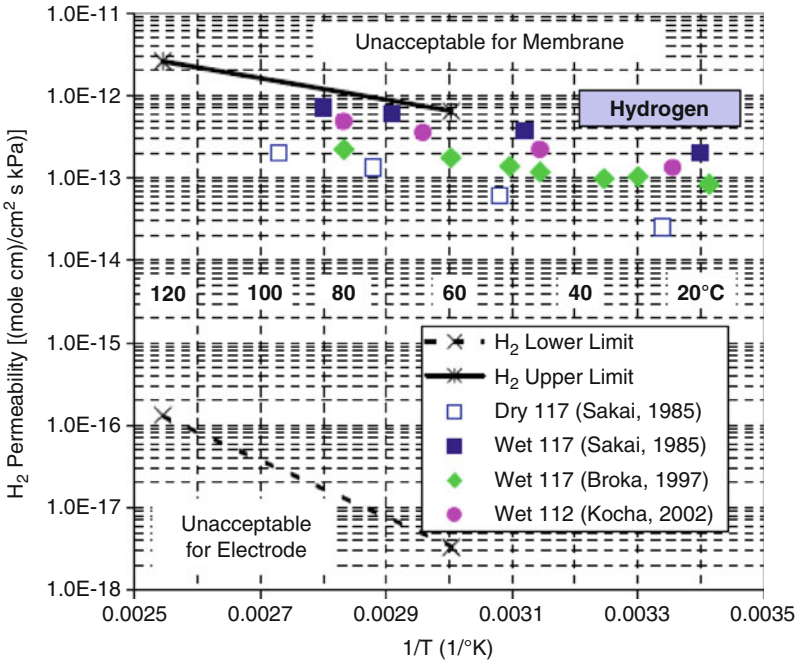

PEM Fuel Cells, Materials and Design Development Challenges. Figure 13
Hydrogen gas permeability as a function of both temperature and relative humidity. Upper limit (*solid line*) defined by crossover losses (assuming no contribution from O_2 crossover), lower limit (*dotted line*) defined by the transport requirements of the ionomer in the electrode. Data for both dry and wet Nafion 1100 EW membranes taken from Refs. [55–57] (Reproduced from H.A. Gasteiger and M.F. Mathias [5] with permission from The Electrochemical Society)

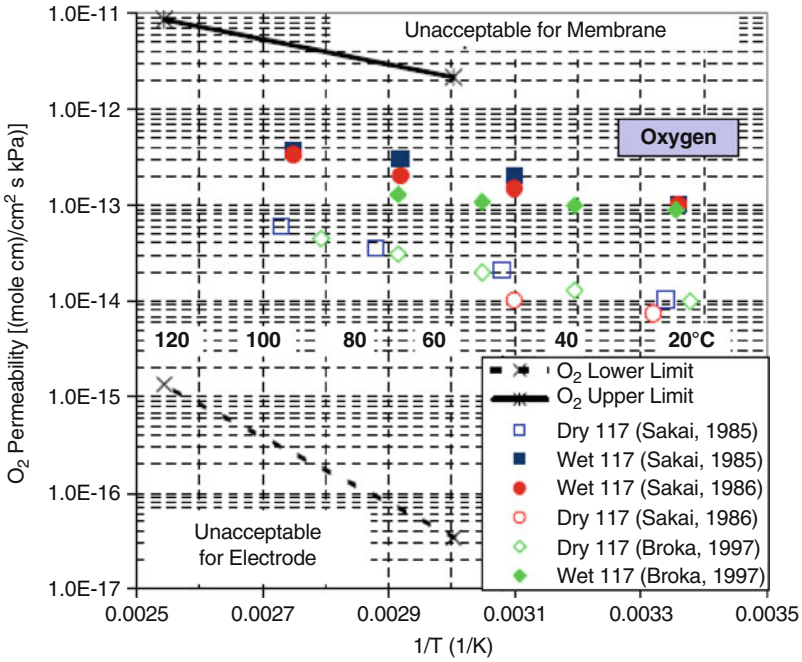

PEM Fuel Cells, Materials and Design Development Challenges. Figure 14
Oxygen gas permeability as a function of both temperature and relative humidity. Upper limit (*solid line*) defined by crossover losses (assuming no contribution from H_2 crossover), lower limit (*dotted line*) defined by the transport requirements of the ionomer in the electrode. Data for both dry and wet Nafion 1100 EW membranes taken from Refs. [55–57] (Reproduced from H.A. Gasteiger and M.F. Mathias [5] with permission from The Electrochemical Society)

$cm^{-2}\,s^{-1}\,kPa^{-1}$, and for O_2 transport within the range: $1 \times 10^{-16} < k_{H_2} < 3 \times 10^{-12}$ mol cm $cm^{-2}\,s^{-1}\,kPa^{-1}$, where the lower limits are dictated by the ionomer in the electrodes and the upper limits by the ionomer in the membrane.

Morphology

As indicated earlier, all presently available PEMs must be humidified in order to exhibit sufficient proton conductivity to function effectively as the electrolyte in a fuel cell. When humidified, the PEMs swell with the absorbed water resulting in a hydrated morphology where the aqueous phase is confined within the polymer to domains that are typically only a few nanometers in dimensions [56–62]. This morphology and the interactions driving their formation are key to the understanding of the morphological stability of the ionomer and transport properties [63, 64]. Both are of paramount importance for the application of such materials in PEM fuel cells: morphological stability under operating conditions is not only important for keeping the integrity of the ionomer membrane but also for a stable microstructure of the active electrode layers usually containing a high volume fraction of ionomer. Proton transport is actually a very complex phenomenon [36, 63, 65] comprising different species (protonic charge carriers, water, and gases dissolved therein) and different transport modes (diffusional, hydrodynamic), but the key process here remains the proton conductivity.

The microstructure is usually the consequence of a constrained hydrophobic/hydrophilic separation, and this can be controlled by adjusting the concentration of protogenic groups (ion-exchange capacity IEC). A high IEC corresponds to a high charge carrier concentration and generally leads to a high uptake of water, both being favorable for high proton conductivity. However, the high IEC leads to severe swelling which goes along with a loss of morphological instability and

eventually leads to a complete dissolution of the ionomer. Therefore, the optimum IEC is essentially a tradeoff between these two properties.

Interestingly, this is different for different types of ionomers which is because of the differences in the backbone/backbone interactions and hydrated morphology. Such morphological details are usually obtained from small angle X-ray (SAXS) diffraction experiments (see Fig. 15). A recent interpretation of the SAXS spectra of fully swollen Nafion has attracted considerable attention [62]. The authors claim the existence of parallel cylindrical micelles bearing the water and the dissociated protons. Such a morphology could easily explain the relatively high conductivity of PFSA membranes at low water contents corresponding to a low IEC and low degree of hydration (low RH): cylindrical structures provide high connectivity within the water structure even for low water volume fractions and a high local proton mobility because of their relatively large width compared to water structures of higher dimensionality (a cylinder width of 2.4 nm is suggested which is large compared to about 1 nm suggested by other models). But it should be noted that other groups have raised serious doubts about this model [67, 68]. It has recently been proposed that the morphology resembles two dimensional water structures, and that it is essentially the tortuosity of locally flat water structures which determines percolation and therefore proton conductivity in such materials.

In any case, there is a clear difference in the morphology of PFSA and hydrocarbon membranes which was first pointed out in a comparative SAXS study [60]. While proton conductivity at high levels of hydration is mainly dependent on the IEC only, the decrease in proton conductivity with decreasing water content is more severe in hydrocarbon membranes. The reason for this characteristic difference is suggested to be the more pronounced hydrophobic/hydrophilic separation of PFSA ionomers which leads to a better connectivity within the aqueous domain and locally to more bulk-like properties of the water of hydration. But there are

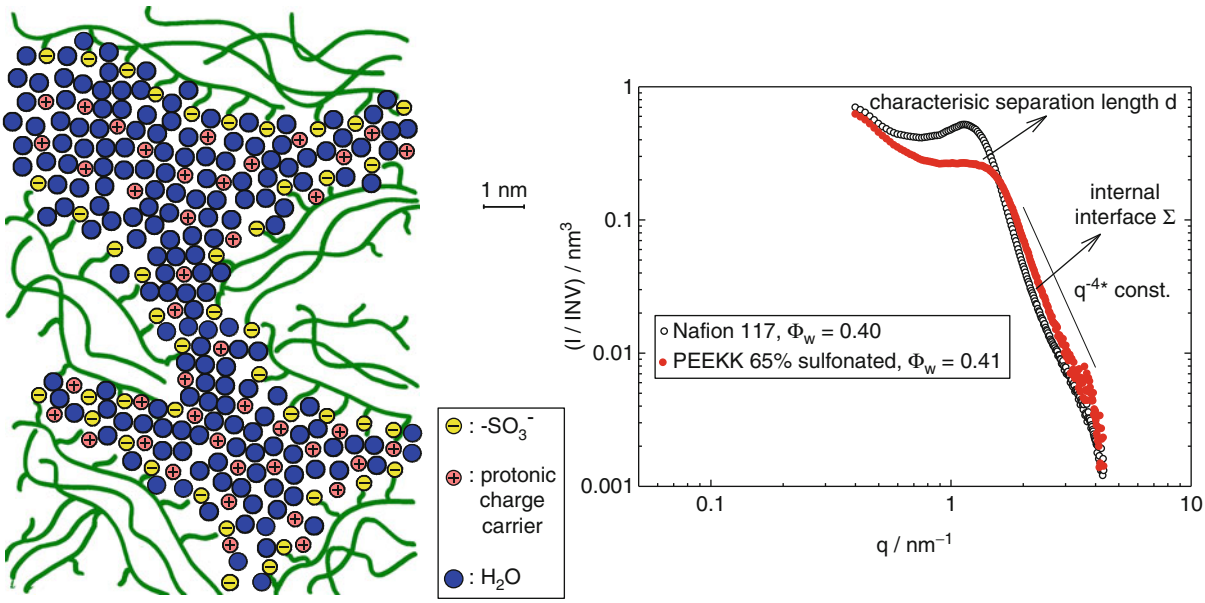

PEM Fuel Cells, Materials and Design Development Challenges. Figure 15
Left: A schematic representation of the fully hydrated morphology of a PFSA ionomer (e.g., Nafion) under the assumptions of a cubic lattice model which fitted data from small angle X-ray scattering (SAXS) experiments. *Right*: SAXS spectra of hydrated Nafion and a hydrated sulfonated polyetherketone. The characteristic hydrophobic/hydrophilic separation lengths are obtained from the position of the ionomer peaks while the internal hydrophobic/hydrophilic interfaces are obtained from the intensities in the Porod regime. First reported in Ref. [66]

also characteristic disadvantages of PFSA membranes: (1) because of the bulk-like properties of the hydration water, the transport of water has a large hydrodynamic component which shows up as large electro-osmotic water drag and high water/gas permeation coefficients and (2) the viscoelastic properties are severely decaying with temperature. At this stage, it should be noted that so-called short side chain ionomers show a slightly weaker hydrophobic/hydrophilic separation which actually reduces the conductivity for a given IEC. But the significantly higher morphological stability especially at higher temperature (higher T_g) allows for significantly higher IECs without significantly compromising the elastic properties (storage modulus). PFSA membranes with shorter side chains (e.g., Dow, 3 M, Aquivion) seem to be a real improvement over the traditional long side chain PFSA membrane Nafion [52].

Despite the disadvantageous conductivity behavior at low levels of hydration, the other alternatives are hydrocarbon membranes. They usually do not show softening in the temperature range of fuel cell operation and the higher dispersion of the hydration water (smaller width of the water domain) leads to significantly lower hydrodynamic water transport. The lower conductivity can actually be increased by introducing another heterogeneity with respect to the degree of sulfonation (IEC) on the 10–100 nm scale. This can lead to a significant increase of proton conductivity provided that bi-continuous morphologies are formed. The reason is the highly nonlinear increase of proton conductivity with increasing IEC. An interesting approach toward such morphologies is the formation of multiblock copolymers consisting of an alternating sequence of highly sulfonated hydrocarbon segments and unsulfonated segments [69]. When cast from solutions, such polymers undergo a constrained microphase separation. The hydrophilic sulfonated phase then still provides a sufficiently high conductivity while the nonsulfonated phase can give the material morphological stability and reduces swelling to an acceptable level (see also the entry in this encyclopedia: "► Membrane Electrolytes: from Perfluoro Sulfonic Acid to Hydrocarbon Ionomers" by Miyatake).

Optimizing and controlling the microstructure of such materials is one of the major materials design issues. Here, the main challenges are to maximize the local concentration of sulfonic acid functions within the hydrophilic phase and to obtain morphological stability with relatively small volume fractions of unsulfonated phase. A recent study on the model system of aqueous methylsulfonic acid ($CH_3SO_3H(aq)$) clearly demonstrates that there is still a huge potential for increasing proton conductivity at low relative humidity [70].

Choice of the Protogenic Group

The source of the protons in current state-of-the-art PEM fuel cells is the highly acidic sulfonic acid functional group. As pointed out above, hydration is required to dissociate the protons of these groups and to mobilize the protonic charge carriers through solvation (hydration). Since the hydration requirement is one of the issues limiting the operation temperature of sulfonic acid-based electrolytes, there has been an extensive search for other protogenic groups which may enable high proton conductivity at lower water activities [71, 72]. One of the most interesting approaches is to use functional groups which are amphoteric in the sense that they may act both as a proton donor and as a proton acceptor. Conceptually, they can combine the role of the proton source and the proton solvent in one functional group: high self-dissociation may lead to a sufficiently high charge carrier concentration and structural diffusion (i.e., proton hopping or shuttling) within a dynamically disordered hydrogen bond network and thereby provide high charge carrier mobility. The concept has been proven for imidazole [73] and phosphonic functionalized model compounds [74]. A comparative study, however, of sulfonic acid, phosphonic acid, and imidazole as protogenic groups suggests that only phosphonic acid has some potential to substitute for the sulfonic acid functional group [75, 76]. Experimentally determined proton conductivities of functionalized heptanes examined in this study [75] and corresponding computed proton transfer barriers are shown in Fig. 16. This study actually investigated not only transport but also stability issues and the participation of these groups in the electrochemical reactions. Apart from the fact that the imidazole functionalized oligomer showed the lowest proton conductivity, reaction with oxygen was observed and the platinum catalyst was

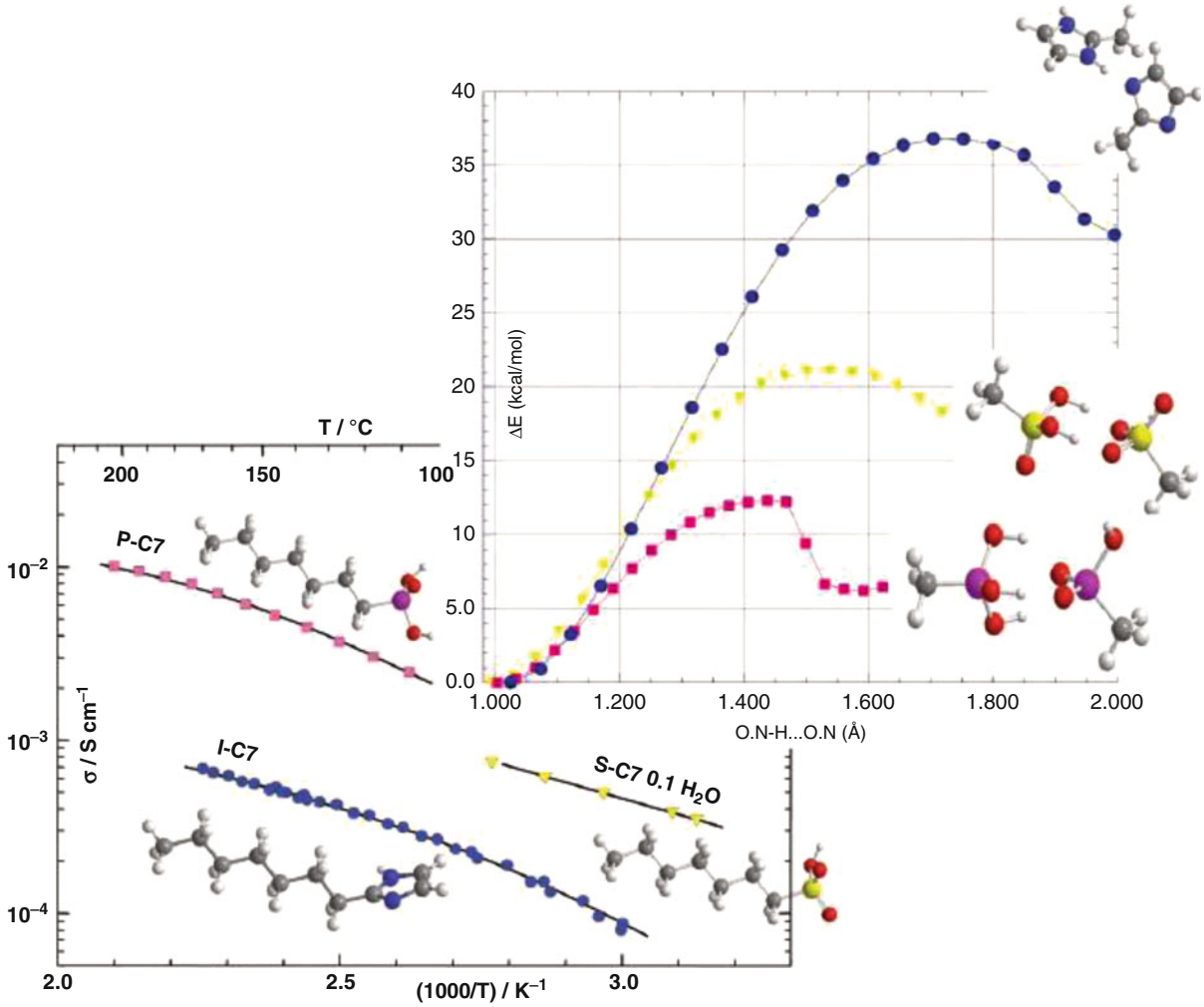

PEM Fuel Cells, Materials and Design Development Challenges. Figure 16
A compound figure consisting of both experimental [75] and theoretical results [76]. *Lower Left:* Measured proton conductivities under dry conditions versus temperature of three monofunctionalized heptanes: 1-heptylphosphonic acid (P-C7), *magenta squares*; 1-heptylsulfonic acid (S-C7), *yellow triangles*; and 2-heptylimidazole (I-C7), *blue circles*. *Upper Right:* Computed energetic barriers for neat (i.e., acid to acid) proton transfer for methylphosphonic acid, *magenta squares*; methylsulfonic acid, *yellow triangles*; and methylimidazole, *blue circles*. The combined results suggest that proton conductivity is at least partially a function of the barrier for proton transfer: the experimental proton conductivities are inversely related to the computed proton transfer barrier

blocked at high potentials where oxygen reduction takes place. The phosphonic acid-based system showed a clear signature of proton conductivity in the "water free" state, but some water activity was essential to prevent condensation reactions which immediately suppress proton conductivity. It appears that the condensation issue is more severe for systems with immobilized phosphonic acid groups compared to pure liquid phosphonic and phosphoric acid, and it remains a challenge to immobilize phosphonic acid functional groups without increasing the susceptibility for condensation [77].

Future Directions

Despite the significant and substantial progress in PEM fuel cell technology achieved during the past couple of decades, the large-scale market introduction of this technology into applications such as vehicular power will require overcoming the high costs associated with the components of the fuel cell stack (i.e., the anode and cathode catalysts, the ionomeric membrane, bipolar plates, etc.). The platinum or platinum-alloy based electrodes in current state-of-the-art fuel cells will constitute a significant fraction of the overall cost of a PEMFC stack if produced at large number. The precious metal catalysts are the only component in the fuel cell stack that will not benefit from an economies of scale, and hence the research and development of nonprecious metal catalysts is an important challenge that must be overcome.

Although it would be best if the platinum catalysts were replaced at both electrodes, the reduction of oxygen (at the cathode) requires much more Pt and hence the development of nonnoble metal catalysts with sufficient and durable ORR activity is a major focus of current and ongoing research [78–80]. Significant effort and progress has recently been achieved toward the development of catalysts with nitrogen coordinated with either iron or cobalt in a carbon matrix or support (i.e., Fe/N/C or Co/N/C). These systems are showing great promise with turnover frequencies comparable to that of current Pt/C catalysts. A major challenge (and still largely unexplored) is the stability and durability of these catalysts in the hostile electrochemical environment of an operating fuel cell [81].

Although substantial progress has been made on the development of advanced high performance PEMs, there are currently no ionomers that exhibit sufficiently high proton conductivity and durability under hot (i.e., $>100°C$) and "dry" ($<30\%$ RH) conditions. However, there are several potentially promising routes that may ultimately lead to electrolytes exhibiting both high chemical and thermal stability and not requiring humidification. Increasing the density of sulfonic acid groups (i.e., by lowering the IEC) in PFSA ionomers through shortening the side chain and/or having tethering more than one protogenic group per side chain warrants further research. The development of the highly sulfonated polysulfones also seems to offer some promise as these materials demonstrate that with interpenetrating aqueous domains of very small diameters the proton conductivity is still very high. This class of materials, however, must be made with lower water solubility in water and with resistance to breakage through elongation.

Bibliography

1. Gasteiger HA, Marković NM (2009) Just a dream – or future reality? Advances in catalyst development offer hope for commercially viable hydrogen fuel cells. Science 324:48–49
2. Mathias MF, Makharia R, Gasteiger HA, Conley JJ, Fuller T, Gittleman C, Kocha SS, Miller D, Mittelsteadt C, Xie T, Yan SG, Yu PT (2005) Two fuel cell cars in every garage? Electrochem Soc Interface 14(2):24–35, Pennington
3. Gasteiger HA, Gu W, Litteer B, Makharia R, Brady B, Budinski M, Thompson E, Wagner FT, Yan SG, Yu PT (2007) Catalyst degradation mechanisms in PEM and direct methanol fuel cells. In: Kakac S, Pramuanjaroenkij A, Vasiliev L (eds) Proceedings of the conference of the NATO-Advanced-study-institute on mini-micro fuel cells – fundamentals and applications, Cesme Izmir, 22 July–03 Aug. Springer, Dordrecht, pp 225–233
4. Masten DA, Bosco AD (2003) System design for vehicle applications – GM/Opel. In: Vielstich W, Lamm A, Gasteiger HA (eds) Handbook of fuel cells – fundamentals, technology and applications, vol 4. Wiley, Chichester, pp 714–724
5. Gasteiger HA, Mathias MF (2005) Fundamental research and development challenges in polymer electrolyte fuel cell technology. In: Murthy M, Fuller TF, Van Zee JW (eds) Proceedings of the symposium on proton conducting membrane fuel cells III, 202nd ECS Meeting, held in Salt Lake City, Utah in the year 2002, vol PV 2002–31. The Electrochemical Society, Pennington, pp 1–24
6. Endoh E (2009) Highly durable PFSA membranes. In: Vielstich W, Gasteiger HA, Yokokawa H (eds) Handbook of fuel cells – advances in electrocatalysis, materials, diagnostics, and durability, vol 5. Wiley, Chichester, pp 361–374
7. Liu H, Coms FD, Zhang J, Gasteiger HA, LaConti AB (2009) Chemical degradation: correlations between electrolyzer and fuel cell findings. In: Büchi FN, Inaba M, Schmidt TJ (eds) Polymer electrolyte fuel cell durability. Springer, New York, pp 71–118
8. Lai YH, Dillard DA (2009) Mechanical durability characterization and modeling of ionomeric membranes. In: Vielstich W, Gasteiger HA, Yokokawa H (eds) Handbook of fuel cells – advances in electrocatalysis, materials, diagnostics, and durability, vol 5. Wiley, Chichester, pp 403–419
9. Patterson TW, Darling RM (2006) Damage to the cathode catalyst of a PEM fuel cell caused by localized fuel starvation. Electrochem. Solid-State Lett. 9:A183–A185
10. Gu W, Yu PT, Carter RN, Makharia R, Gasteiger HA (2010) Modeling of membrane-electrode assembly degradation in proton-exchange-membrane fuel cells – local H_2

starvation and start-stop induced carbon-support corrosion. In: Pasaogullari U, Wang C-Y (eds) Modeling and diagnostics of polymer electrolyte fuel cells, vol 49, Modern aspects of electrochemistry. Springer, New York, pp 45–85
11. Reiser CA, Bregoli L, Patterson TW, Yi JS, Yang JDL, Perry ML, Jarvi TD (2005) A reverse current decay mechanism for fuel cells. Electrochem. Solid-State Lett. 8:A273–A276
12. Yu P, Gu W, Makharia R, Wagner FT, Gasteiger HA (2006) The impact of carbon stability on PEM fuel cell startup and shutdown voltage degradation. ECS Trans 3:797–809
13. Perry ML, Patterson TW, Reiser C (2006) System strategies to mitigate carbon corrosion in fuel cells. ECS Trans 3: 783–795
14. Genorio B, Subbaraman R, Strmcnik D, Tripkovic D, Stamenkovic VR, Marković NM (2011) Tailoring the selectivity and stability of chemically modified platinum nanocatalysts to design highly durable anodes for PEM fuel cells. Angew Chem Int Ed 50:1–6
15. Ralph TR, Hudson S, Wilkinson DP (2006) Electrocatalyst stability in PEMFCs and the role of fuel starvation and cell reversal tolerant anodes. ECS Trans 1:67–84
16. Debe MK, Schmoeckel AK, Vernstrom GD, Atanasoski R (2006) High voltage stability of nanostructured thin film catalysts for PEM fuel cells. J Power Sources 161:1002–1011
17. Carter RN, Greszler TA, Baker DR (2009) Technique for measuring gas transport resistance in application-scale aged fuel cell gas diffusion media. ECS Trans 25:225–231
18. Perry ML, Patterson T, Madden T (2010) GDL degradation in PEFC. ECS Trans 33:1081–1087
19. Stephens IEL, Bondarenko AS, Perez-Alonso FJ, Calle-Vallejo F, Bech L, Johansson TP, Jepsen AK, Frydendal R, Knudsen BP, Rossmeisl J, Chorkendorff I (2011) Tuning the activity of Pt (111) for oxygen electroreduction by subsurface alloying. J Am Chem Soc 133:5485–5491
20. Gu W, Baker DR, Liu Y, Gasteiger HA (2009) Proton exchange membrane fuel cell (PEMFC) down-the-channel performance model. In: Vielstich W, Gasteiger HA, Yokokawa H (eds) Handbook of fuel cells – advances in electrocatalysis, materials, diagnostics, and durability, vol 5. Wiley, Chichester, pp 631–657
21. Pasaogullari U (2009) Heat and water transport models for polymer electrolyte fuel cells. In: Vielstich W, Gasteiger HA, Yokokawa H (eds) Handbook of fuel cells – advances in electrocatalysis, materials, diagnostics, and durability, vol 5. Wiley, Chichester, pp 616–630
22. Freunberger SA, Reum M, Büchi FN (2009) Design approaches for determining local current and membrane resistance in polymer electrolyte fuel cells (PEFCs). In: Vielstich W, Gasteiger HA, Yokokawa H (eds) Handbook of fuel cells – advances in electrocatalysis, materials, diagnostics, and durability, vol 5. Wiley, Chichester, pp 603–615
23. Carter RN, Gu W, Brady B, Yu PT, Subramanian K, Gasteiger HA (2009) Membrane electrode assembly (MEA) degradation mechanism studies by current distribution measurements. In: Vielstich W, Gasteiger HA, Yokokawa H (eds) Handbook of fuel cells – advances in electrocatalysis, materials, diagnostics, and durability, vol 5. Wiley, Chichester, pp 829–843
24. Trabold TA, Owejan JP, Gagliardo JJ, Jacobson DL, Hussey DS, Arif M (2009) Use of neutron imaging for proton exchange membrane fuel cell (PEMFC) performance analysis and design. In: Vielstich W, Gasteiger HA, Yokokawa H (eds) Handbook of fuel cells – advances in electrocatalysis, materials, diagnostics, and durability, vol 5. Wiley, Chichester, pp 658–672
25. Wipke K, Sprik S, Kurtz J, Garbak J (2009) Field experience with fuel cell vehicles. In: Vielstich W, Gasteiger HA, Yokokawa H (eds) Handbook of fuel cells – advances in electrocatalysis, materials, diagnostics, and durability, vol 6. Wiley, Chichester, pp 893–904
26. Thompson EL, Gu W, Gasteiger HA (2009) Performance during start-up of proton exchange membrane (PEM) fuel cells at subfreezing conditions. In: Vielstich W, Gasteiger HA, Yokokawa H (eds) Handbook of fuel cells – advances in electrocatalysis, materials, diagnostics, and durability, vol 5. Wiley, Chichester, pp 699–717
27. Mathias M, Roth J, Fleming J, Lehnert W (2003) Diffusion media materials and characterization. In: Vielstich W, Lamm A, Gasteiger HA (eds) Handbook of fuel cells – fundamentals, technology and applications, vol 3. Wiley, Chichester, pp 517–537
28. Baker DR, Caulk DA, Neyerlin KC, Murphy MW (2009) Measurement of oxygen transport resistance in PEM fuel cells by limiting current methods. J Electrochem Soc 156: B991–B1003
29. Caulk DA, Baker DR (2011) Modeling two-phase water transport in hydrophobic diffusion media for PEM fuel cells. J Electrochem Soc 158:B384–B393
30. Mittelsteadt CK, Liu H (2009) Conductivity, permeability, and ohmic shorting of ionomeric membranes. In: Vielstich W, Gasteiger HA, Yokokawa H (eds) Handbook of fuel cells – advances in electrocatalysis, materials, diagnostics, and durability, vol 5. Wiley, Chichester, pp 345–359
31. Liu Y, Ji C, Gu W, Jorne J, Gasteiger HA (2011) Effects of catalyst carbon support on proton conduction and cathode performance in PEM fuel cells. J Electrochem Soc 158: B614–B621
32. Neyerlin KC, Gu W, Jorne J, Clark A, Gasteiger HA (2007) Cathode catalyst utilization for the ORR in a PEMFC – analytical model and experimental validation. J Electrochem Soc 154: B279–B287
33. Neyerlin KC, Gu W, Jorne J, Gasteiger HA (2007) Study of the exchange current density for the hydrogen oxidation and evolution reactions. J Electrochem Soc 154:B631–B635
34. Gasteiger HA, Baker DR, Carter RN, Gu W, Liu Y, Wagner FT, Yu PT (2010) Electrocatalysis and catalyst degradation challenges in proton exchange membrane fuel cells. In: Stolten D (ed) Hydrogen and fuel cells. fundamentals, technologies, and applications. Wiley-VCH, Weinheim, pp 3–16
35. Jaouen F, Proietti E, Lefèvre M, Chenitz R, Dodelet J-P, Wu G, Chung HT, Johnston CM, Zelenay P (2011) Recent advances in

non-precious metal catalysis for oxygen reduction reaction in polymer electrolyte fuel cells. Energy Environ Sci 4:114–130
36. Paddison SJ (2003) Proton conduction mechanisms at low degrees of hydration in sulfonic acid-based polymer electrolyte membranes. Annu Rev Mater Res 33:289–319
37. Ferreira PJ, la O' GJ, Shao-Horn Y, Morgan D, Makharia R, Kocha SS, Gasteiger HA (2005) Instability of Pt/C electrocatalysts in proton exchange membrane fuel cells: a mechanistic investigation. J Electrochem Soc 152:A2256–A2271
38. Kinoshita K, Lundquist JT, Stonehart P (1973) Potential cycling effects on platinum electrocatalyst surfaces. J Electroanal Chem 48:157–166
39. Kawahara S, Mitsushima S, Ota K-I, Kamiya N (2006) Deterioration of Pt catalyst under potential cycling. ECS Trans 3(1): 625–631
40. Zhang J, Litteer BA, Gu W, Liu H, Gasteiger HA (2007) Effect of hydrogen and oxygen partial pressure on Pt precipitation within the membrane of PEMFCs. J Electrochem Soc 154: B1006–B1011
41. Wagner FT, Yan SG, Yu PT (2009) Catalyst and catalyst-support durability. In: Vielstich W, Gasteiger HA, Yokokawa H (eds) Handbook of fuel cells – advances in electrocatalysis, materials, diagnostics, and durability, vol 5. Wiley, Chichester, pp 250–263
42. Shao-Horn Y, Sheng WC, Chen S, Ferreira PJ, Holby EF, Morgan D (2007) Instability of supported platinum nanoparticles in low-temperature fuel cells. Top Catal 46:285–305
43. Chen S, Gasteiger HA, Hayakawa K, Tada T, Shao-Horn Y (2010) Platinum-Alloy catalyst degradation in proton exchange membrane fuel cells: nanometer-scale compositional and morphological changes. J Electrochem Soc 157:A82–A97
44. Yu PT, Gu W, Zhang J, Makharia R, Wagner FT, Gasteiger HA (2009) Carbon-support requirements for highly durable fuel cell operation. In: Büchi FN, Inaba M, Schmidt TJ (eds) Polymer electrolyte fuel cell durability. Springer, New York, pp 29–53
45. Gallagher KG, Darling RM, Fuller TF (2009) Carbon-support corrosion mechanisms and models. In: Vielstich W, Gasteiger HA, Yokokawa H (eds) Handbook of fuel cells – advances in electrocatalysis, materials, diagnostics, and durability, vol 5. Wiley, Chichester, pp 819–828
46. Thampan T, Malhorta S, Tang H, Datta R (2000) Modeling of conductive transport in proton-exchange membranes for fuel cells. J Electrochem Soc 147:3242–3250
47. Springer TE, Zawodzinski T, Gottesfeld S (1991) Polymer electrolyte fuel cell model. J Electrochem Soc 138:2334–2342
48. Springer T, Zawodzinski T, Gottesfeld S (1997) In: McBreen J, Mukerjee S, Srinivasan S (eds) Electrode materials and processes for energy conversion and storage, Proceedings series, vol PV 97–13. The Electrochemical Society, Pennington, pp 15–24
49. Bernardi DM, Verbrugge MW (1992) A mathematical model of the solid-polymer-electrolyte fuel-cell. J Electrochem Soc 139:2477–2491
50. Gasteiger HA, Garche J (2008) Fuel cells. In: Ertl G, Knözinger H, Schüth F, Weitkamp J (eds) Handbook of heterogeneous catalysis, 2nd edn. Wiley-VCH, Weinheim, pp 3081–3121
51. Breault RD (2003) PAFC stack materials and stack design. In: Vielstich W, Lamm A, Gasteiger HA (eds) Handbook of fuel cells: fundamentals, technology, and applications, vol 3. Wiley, Chichester
52. Kreuer KD, Schuster M, Obliers B, Diat O, Traub U, Fuchs A, Klock U, Paddison SJ, Maier J (2008) Short-side-chain proton conducting perfluorosulfonic acid ionomers: why they perform better in PEM fuel cells. J Power Sources 178: 499–509
53. Alberti G, Casciola M, Massinelli L, Bauer B (2001) Polymeric proton conducting membranes for medium temperature fuel cells (110–160°C). J Membrane Sci 185:73–81
54. Wainwright JS, Litt MH, Savinell RF (2003) High-temperature membranes. In: Vielstich W, Lamm A, Gasteiger HA (eds) Handbook of fuel cells – fundamentals, technology and applications, vol 3. Wiley, Chichester, pp 436–446
55. Sakai T, Takenaka H, Wakabayashi N, Kawami Y, Torikai E (1985) Gas permeation properties of solid polymer electrolyte (SPE) membranes. J Electrochem Soc 132:1328–1332
56. Broka K, Ekdunge P (1997) Oxygen and hydrogen permeation properties and water uptake of Nafion(R) 117 membrane and recast film for PEM fuel cell. J Appl Electrochem 27:281–289
57. Kocha SS (2003) Principles of MEA preparation. In: Vielstich W, Lamm A, Gasteiger HA (eds) Handbook of fuel cells – fundamentals, technology and applications, vol 3. Wiley, Chichester, p 538
58. Hsu WY, Gierke TD (1982) Elastic theory for ionic clustering in perfluorinated ionomers. Macromolecules 15:101–105
59. Gebel G (2000) Structural evolution of water swollen perfluorosulfonated ionomers from dry membrane to solution. Polymer 41:5829–5838
60. Kreuer KD (2001) On the development of proton conducting polymer membranes for hydrogen and methanol fuel cells. J Membrane Sci 185:29–39
61. Rubatat L, Gebel G, Diat O (2004) Fibrillar structure of Nafion: matching fourier and real space studies of corresponding films and solutions. Macromolecules 37:7772–7783
62. Schmidt-Rohr K, Chen Q (2008) Parallel cylindrical water nanochannels in Nafion fuel-cell membranes. Nat Mater 7:75–83
63. Kreuer KD, Paddison SJ, Spohr E, Schuster M (2004) Transport in proton conductors for fuel-cell applications: simulations, elementary reactions, and phenomenology. Chem Rev 104:4637–4678
64. Elliott JA, Paddison SJ (2007) Modelling of morphology and proton transport in PFSA membranes. Phys Chem Chem Phys 9:2602–2618
65. Kreuer KD (2000) On the complexity of proton conduction phenomena. Solid State Ionics 136:149–160
66. Ise M (2000) Polymer Elektrolyt Membranen: Untersuchungen zur Mikrostruktur und zu den Transporteigenschaften für Protonen und Wasser, PhD thesis, University of Stuttgart
67. Kreuer KD (2011) Advances in materials for proton exchange membrane fuel cells systems 2011. Asilomar, Pacific Grove, 20–23 Feb 2011

68. Gebel G (2011) Advances in materials for proton exchange membrane fuel cells systems 2011. Asilomar, Pacific Grove, 20–23 Feb 2011
69. Hickner MA, Ghassemi H, Kim YS, Einsla BR, McGrath JE (2004) Alternative polymer systems for proton exchange membranes (PEMs). Chem Rev 104:4587–4612
70. Telfah A, Majer G, Kreuer KD, Schuster M, Maier J (2010) Formation and mobility of protonic charge carriers in methyl sulfonic acid–water mixtures: a model for sulfonic acid based ionomers at low degree of hydration. Solid State Ionics 181:461–465
71. Desmarteau DD (1995) Novel perfluorinated ionomers and ionenes. J Fluorine Chem 72:203–208
72. Schaberg MS, Abulu JE, Haugen GM, Emery MA, O'Conner SJ, Xiong PN, Hamrock SJ (2010) New multi acid side-chain Ionomers for proton exchange membrane fuel cells. ECS Trans 33(1):609–627
73. Herz HG, Kreuer KD, Maier J, Scharfenberger G, Schuster MFH, Meyer WH (2003) New fully polymeric proton solvents with high proton mobility. Electrochim Acta 48: 2165–2171
74. Steininger H, Schuster M, Kreuer KD, Maier J (2006) Intermediate temperature proton conductors based on phosphonic acid functionalized oligosiloxanes. Solid State Ionics 177:2457–2462
75. Schuster M, Rager T, Noda A, Kreuer KD, Maier J (2005) About the choice of the protogenic group in PEM separator materials for intermediate temperature, low humidity operation: a critical comparison of sulfonic acid, phosphonic acid and imidazole functionalized model compounds. Fuel Cells 5: 355–365
76. Paddison SJ, Kreuer KD, Maier J (2006) About the choice of the protogenic group in polymer electrolyte membranes: ab initio modelling of sulfonic acid, phosphonic acid, and imidazole functionalized alkanes. Phys Chem Chem Phys 8: 4530–4542
77. Steininger H, Schuster M, Kreuer KD, Kaltbeitzel A, Bingöl B, Meyer WH, Schauff S, Brunklaus G, Maier J, Spiess HW (2007) Intermediate temperature proton conductors for PEM fuel cells based on phosphonic acid as protogenic group: a progress report. Phys Chem Chem Phys 9: 1764–1773
78. Bashyam R, Zelenay P (2006) A class of non-precious metal composite catalysts for fuel cells. Nature 443:63–66
79. Lefèvre M, Proietti E, Jaouen F, Dodelet JP (2009) Iron-based catalysts with improved oxygen reduction activity in polymer electrolyte fuel cells. Science 324:71–74
80. Wu G, More KL, Johnston CM, Zelenay P (2011) High-performance electrocatalysts for oxygen reduction derived from polyaniline, iron, and cobalt. Science 332:443–447
81. Proietti E, Jaouen F, Lefèvre M, Larouche N, Tian J, Herranz J, Dodelet JP (2011) Iron-based cathode catalyst with enhanced power density in polymer electrolyte membrane fuel cells. Nature Comm 2: doi:10.1038/ncomms1427

Personal Rapid Transit and Its Development

Shannon S. McDonald
Southern Illinois University, Carbondale, IL, USA

Article Outline

Glossary
Definition of the Subject
Introduction
The Development of PRT: Personal Rapid Transit System
Key Sustainable/Energy and Planning/Architectural
Future Directions
Bibliography

Glossary

AGT Automated Guideway Transit – Updating the original AGT definition (US Congress, Office of Technology Assessment, 1975), Automated Guideway Transit (AGT) is defined as a class of transportation systems in which fully automated vehicles operate along dedicated guideways.

APM Automated People Movers – According to the General Accounting Office (1980), Automated People Movers are driverless vehicles operating on a fixed guideway. Vehicle capacities range up to 100 passengers and may be operated as single units or as trains up to 30 miles/h.

ATRA Advanced Transit Association

Dual-mode A transportation system where in one mode the vehicle operates under its own power and control, usually on existing streets and in the second mode it operates under automated control and/or external power.

FRT Freight Rapid Transit – Characteristics of PRT but the vehicles are designed to handle freight only.

GRT Group Rapid Transit – which is similar to personal rapid transit but with higher occupancy vehicles and grouping of passengers with potentially different origin–destination pairs. As noted in an early study (US Congress, 1975), the starting capacity for GRT is six passengers per car while the upper limit is around 16 or 18; there are no clear

distinctions between GRP and APM in terms of vehicle capacities.

Network system Interconnecting links that form the layout of transit routes and stops that constitute the total system – as opposed to a loop or corridor system

Off-line stations A station design where the vehicle is removed from the main line for loading or unloading allowing other vehicles to continuously flow on the main line.

Point-to-point The vehicle is on demand and takes the rider from his or her starting point directly to rider's destination point with no stops in between – a nonstop journey bypassing intermediate stations that relies on the use of offline stations in a network.

PRT Personal Rapid Transit – The definition of PRT can be a subcategory of AGT systems that offer on-demand, non-stop transportation, offline stations using small, automated vehicles on a network of dedicated guideways.

Definition of the Subject

Personal Rapid Transit (PRT) is in the class under Automated Guideway Transit (AGT) that includes Automated People Movers, sometimes identified as a subset of APM [1, 2]. Personal Rapid Transit is a driverless automated transit technology that has a unique movement pattern for the transit rider. A rider who uses PRT will travel point to point – similar to a cab – in comparison to a "typical" transit system where the rider stays on the system through many "unnecessary" stops until reaching their final destination. PRT is a fixed system, it is transit, with predetermined stops but how you travel from Stop A to Stop B is one of the key paradigm changes for this emerging transit technology as it is not designed in its fullest implementation as a loop or corridor system. The on-demand and point-to-point approach will provide much faster travel time and more destination choices; and along with its smaller size (two to four people vehicles), operating system, and offline stations, it can attract more riders to transit due to a higher level of service.

PRT was originally designed beginning in the 1950s for the lower-density transit environments that more commonly exist in the United States. The Morgantown system at the West Virginia University became the first driverless system placed in operation, 1972/6, and has been in continuous operation, since its opening. It is technically considered a GRT, group rapid transit system, due to the fact that the transit vehicles holds 20 people rather than the two to four people in a "true" PRT. The offline stations allow the point-to-point movement pattern to function along with computer control systems; however due to the larger vehicle, many other design possibilities of "pure" PRT did not occur [3].

Currently, a "pure" PRT system, with small vehicles is opening at Heathrow airport connecting a long-term parking lot with a parking garage linking directly to Terminal 5. To park in this lot will be more expensive due to the direct and quick access to the airport. The computerized control systems have dramatically improved since the Morgantown system allowing the initial vision of PRT to finally be constructed and operated. The system is designed to be expanded to 50 stations, 350 vehicles, and 30 km of track connecting many different airports and local associated functions [4].

PRT not only changes the way transit functions for the user, but as well can redefine how we design our built environment, allowing for more frequent smaller transit stops encouraging walkable design and more compact development. Mazdar City, a new planned city in Abu Dhabi will rely on PRT as a major part of its transportation system. Requiring a much smaller right-of-way and lighter tracks, the infrastructure for the system is much less expensive and less visually obtrusive. Its smaller size not only reduces impact on the built environment but can also allow for alternative energy sources to power the system; such as solar and electric [5].

This system is also the perfect connector system between other forms of movement: transit, car, airplane, bus, bicycle, and walking, and for major activity centers such as downtowns, hospitals, universities, and airports, where the more traditional automated people mover system has been implemented over the years.

The reason why the PRT vision has never died and many continue to advocate for its use today is due to its potential to change our living patterns for the betterment of our society. This technology has the ability to allow for more options and flexibility of movement

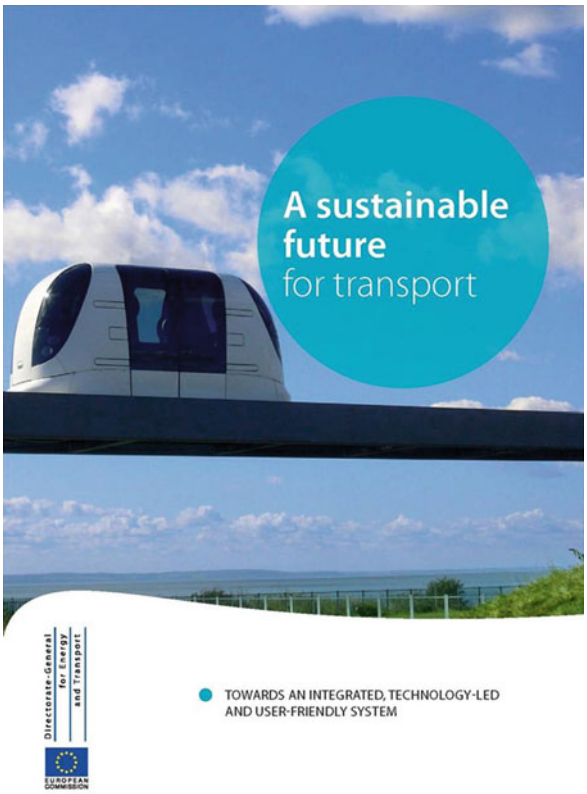

Personal Rapid Transit and Its Development. Figure 1
ULTra: PRT sustainable transport (Martin Lowsen of ULTra)

for all people while improving the living environment. It has been named one of the twenty-first century top 20 proven ways to save the earth by the London Times and the Sustainable Transportation Solution by the Directorate-General of Energy and Transport for the European Commission (Fig. 1).

Introduction

The history of PRT is a confluence of new communication technology, planning visions allowing for automated control technology and transit to merge spurring innovative ideas and solutions to urban transportation providing totally new paradigms for movement and urban design. The seeds of the system started in the late 1800s and it sustained itself as an idea well into the beginning of the computer age. The early innovators and adaptors understood the power of the computer to provide new ways to manage and control these innovative transit vehicles and in turn our movement patterns within the lower density environments of the United States.

Several individuals and companies were at the forefront of creating PRT systems. Edward O. Haltom (a contractor) Donn Fichter (a city transportation planner who believed that automated transit was the right solution for medium- to low-density populations), Monocab, TTI, Inc., Alden StaRRcar, Uniflo, Jet Rail, M.I.T, Bartells, and Dr. Jarold Kieffer each created and worked with early PRT ideas in the United States. The Urban Mass Transportation Act of 1964 and Housing and Urban Development Studies furthered the study and advanced the reality of the Morgantown system based upon the Alden StaRRcar. Numerous other innovators were involved in the early explorations, including General Motors, Raytheon, General Research Corporation, IBM, MITRE Corporation, Parsons Company, LTV Aerospace Corporation, Honeywell, Renault Engineering, Bendix, Ford Motor Company, and Otis Elevator Company along with Johns Hopkins, Ohio State, University of Minnesota, San Diego State, Battelle Columbus Laboratories, Aerospace Corporation, Jet Propulsion Lab, and Booz-Allen Applied Research [6, 7].

A series of 17 studies sponsored by Housing and Urban Development spurred the research and development of PRT. The HUD studies were summarized in a report, *Tomorrow's Transportation* by Leon Monroe Cole [8]. The two most influential studies were one by the Stanford Research Institute and the other by the General Research Corporation of Santa Barbara. The Stanford research paper was on various new concepts from moving sidewalks to PRT to dual-mode that estimated their economic benefits. The GRC study modeled alternative systems in several actual cities to compare alternative transport systems to conventional systems [9, 10].

Activity in other countries was also occurring at this time. Ed Anderson concluded that the stimulus for these explorations came from the US inventors and/or the HUD studies. The following foreign companies/countries/municipalities also advanced the work in this area: Cabtrack, CVS, Cabinentaxi, Aramis, Gothenburg, Sweden and Canada. From 1968 to 1971 the not-for-profit Aerospace Corporation proved the feasibility of operating large PRT networks appropriate for urban application. The newly formed Department of Transportation led by Secretary John A. Volpe

wanted a system in operation before 1972, so a large team was put into place and the system barely opened by 1972 – a very ambitious goal for this fledgling technology; however, the Morgantown system is still functioning today. The final cost of the system was four times as planned due to many issues related to design as a result of creating a larger GRT system along with many other issues related to this. This and other early system studies are thoroughly covered in a book written by Catherine G. Burke titled: *Innovation and Public Policy: The Case of Personal Rapid Transit* [11].

However, although Morgantown, WVA, was the only system built for the public and due to its cost overruns slowed other PRT systems from being developed in the public domain; the work with and about PRT continued as the system provides so many benefits. Several test facilities built around the world proving various aspects of the concept continued and now we are seeing the benefits of this advancing technology. This concept for transit innovation has never died, and numerous attempts have been made to implement the original PRT vision of small automated point-to-point vehicles, offline stations on a dedicated network. Gayle Franzen, Chairman of the Northeastern Illinois Regional Transportation Authority initiated a new PRT program in 1990 that did not proceed.

Morgantown, WVA, is the most important historical example with the Heathrow airport system by ULTra coming into operation for the public late in 2010 leading the way into the future. Currently, several other systems and several test tracks, one in Uppsala, Sweden, a joint venture between the South Koreans and the Swedes for the Vectus system, are on line to move forward. Larry Fabian, ATRA, identifies more than 100 applications along the various spectrums of AGT technologies around the world including shuttles or circulators, major activity center circulation, and public transit, and now we can add a true PRT application to the mix [12, 13].

This article will trace the beginning PRT explorations all the way to the first implementation for public use of the complete paradigm change for transit – PRT. This has involved a complex interrelationship between innovative thinking in technology, communication systems, hardware, architecture, transportation, and urban design/planning spanning the globe.

The Development of PRT: Personal Rapid Transit System

History/Overview/Development of Systems in the United States

The evolution of the PRT transit "idea" to its first real-world application at Heathrow airport, 2010, is to understand how a paradigm change in transit can occur, when the idea has merit, no matter how methodical and complex the route. Sending a man to the moon was easier! Only through the tenacity, belief, and hard work of many people from multiple disciplines over decades has this "vision" now occurred, so that the benefits can be "proven" – that an automated network of small personal point-to-point vehicles with offline stations can improve the built environment and as well improve transit for all people. Several papers and books have been written about this evolution; one specifically titled: Some *Early History of PRT* by Edward J. Anderson, University of Minnesota, much of the following history is a synopsis of this report [7].

A group of "transit" technologies currently known as Automated People Movers now understood as a subset of Automated Guided Transit that most of us have experienced mainly in airports around the world has been the home for the development of a true PRT system. These systems have a worldwide presence and according to Larry Fabain they are currently distributed as in Fig. 2.

In 1953, PRT was born simultaneously out of practicality and urban vision by two people who may not

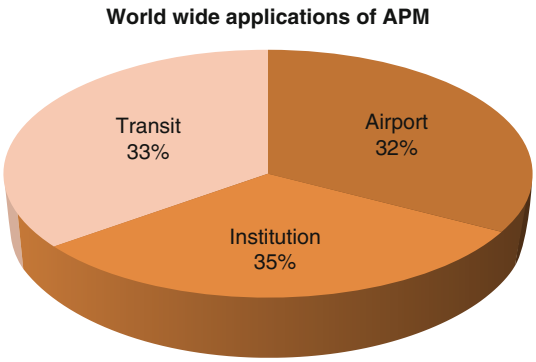

Personal Rapid Transit and Its Development. Figure 2 Distributions of APM applications (Based on data by Fabian 2010 [1])

have initially known each other; Donn Fichter and Edward O. Haltom. Donn Fichter, a transportation graduate student in Chicago, IL, and Edward O. Haltom, a Dallas, TX, contractor who was working on a monorail system. Mr. Fichter sketched a system called Veyar and gradually developed a systems concept integrated into a city with the essential PRT ideas, although he was not a technician. He published a book in 1964 titled *Individualized Automated Transit and the City* [6]. Mr. Haltom saw a way to "improve" the monorail system that he was working on (that has been in existence since the first monorail constructed in St. Paul, Minnesota in the 1880s) by thinking of smaller guideways and smaller vehicles and invented the monocab. This system eventually became a full-scale test track in California with a totally new switching system owned by Rohr Corporation where linear induction propulsion was added to the system. The patents were purchased by Boeing and the transit system continued to be developed by UMTA (Urban Mass Transportation Administration) Advanced Group Rapid Transit until the mid-1980s.

General Motors Research Laboratories had been working for the military in the late 1950s and created a system that could become public transit, called Hovair. They formed a corporation called TTI, Inc, Transportation Technology Incorporated. A full-scale testing occurred in Detroit in 1969 and the company was eventually owned by Otis Elevator. A second test track was built in Denver. The system was a combination of air-suspension and the linear induction motor and was implemented at Duke University Medical Center. Otis also constructed several cable-drawn versions of this system.

William Alden, a graduate of the Harvard Business School invented, built, and drove a small electric vehicle that could be driven on public roads and then link to a guideway. He called it the staRRcar and it is considered the first dual-mode-system and had an on-board switching mechanism. A test track was built in Bedford, Massachusetts in 1968, the Morgantown system was based on this prototype; however a team of professionals was formed to implement the concept at Morgantown, WVA (Fig. 3).

Honeywell also in its military division through the efforts of Lloyd Berggran wanted to create urban transportation that could be competitive with the automobile. He also concluded the same set of PRT characteristics. However, due to his background he created an independent "pod" with all the active power and controlling systems as part of the track. His system was called Uniflo and was designed to be in an enclosed tube. A full-scale test track was constructed by Rosemont Engineering.

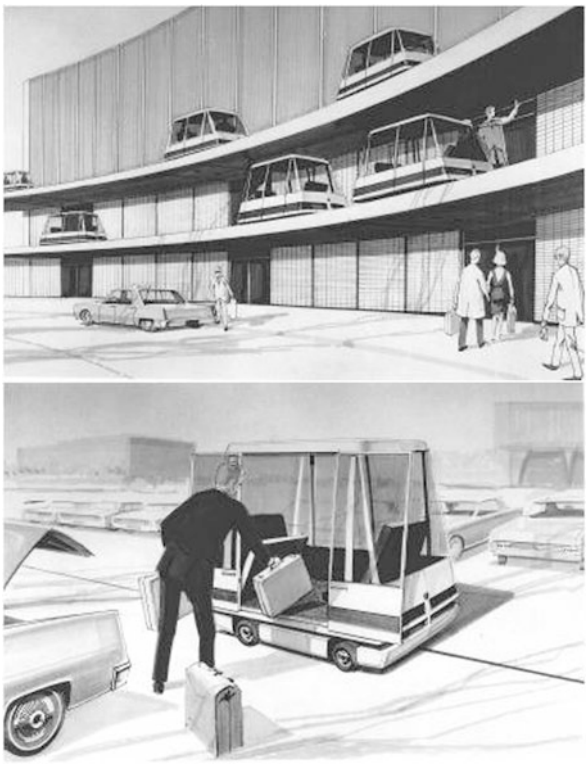

Personal Rapid Transit and Its Development. Figure 3 William Alden StaRRcar – dual-mode vehicle (William Alden)

Jet Rail was designed by George Adams. He designed, built, and operated a system for Braniff Airlines at Love Field in Dallas that was less expensive but similar to Monocab and proved that a lightweight guideway could be successfully constructed. Cornell Aeronautic Laboratories in the early 1960s designed Urbmobile, it was never built but the automatic control technologists were able to show that short headways could provide adequate capacity – safely. MIT in the mid-1960s produced a report call Project Metran that included the PRT ideas and influenced its continued development.

A planning director, Robert J. Bartells, and a public affairs head of a university, Dr. Jarold Kieffer, both seeking to solve real needs of transit movement for large numbers of people, independently came to the same conclusion of the PRT paradigm. Robert J. Bartells was the director of Planning for the City of Hartford, CT imagined the PRT concepts and ideas and explained and supported them as an important planning director. Dr. Jarold Kieffer, as Head of the School of Public Affairs at the University of Oregon while on a vacation at a sky resort also understood the basic concepts of PRT and has been a continual advocate for the development of the technology.

US Government Participation

It was only through the actions of the Federal Government that the first public system was put into place both technically advancing and greatly hindering the PRT vision. Not fully understanding how totally new public-use transit paradigms need to develop if they are to have long-term success, many boasted and believed that a system could be put into place within 2 years – as we had won the race to the moon! Public-transit is a much more complex and integrated effort of many governmental agencies, organizations, and professionals.

Henry S. Reuss of Milwaukee, Wisconsin in the 1960s urged political support for the development of new transit concepts. He participated in the development of the Urban Mass Transportation Act of 1964 where a Section 6 was added focusing on research, development, and demonstration of new systems for people and goods that stated:

- The secretary shall undertake a study and prepare a program of research, development and demonstration of new systems of urban transportation that will carry people and goods within metropolitan areas speedily, safely without polluting the air, and in a manner that will contribute to sound city planning. The Program shall (1) concern itself with all aspects of new systems of urban transportation for metropolitan areas of various sizes, including technological, financial, economic, governmental and social aspects; (2) take into account the most advanced available technologies and materials; and (3) provide national leadership to efforts of states, localities, private industry, universities and foundations [12].

At this time, the US Department of Transportation did not exist; however, the Urban Mass Transportation Act established the Urban Mass Transportation Administration as a unit of the Department of Housing and Urban Development. Seventeen studies were authorized and these became known as the HUD studies and were summarized in a report titled: *Tomorrow's Transportation*. Two studies were very influential: A study by Stanford Research Institute and the General Research Corporation (GRC) of Santa Barbara. Stanford focused on new concepts from moving sidewalks to PRT to dual mode and their economic benefits while the main focus of GRC was to computer-model "advanced" systems in real cities and compares them to conventional transit.

There was a team of 17 specialists from various fields that contributed to this study identifying Boston, Houston, Hartford, and Tucson. This study strongly favored new systems due to population growth and increased use of automobiles traditional transit could not continue to meet the demand. This work published in an article, in 1969, by Scientific American titled Systems Analysis of Urban Transportation, became a classic for the technology and brought a national commitment to develop new technologies through the voice of Ben Alexander, the chairman of GRC [8–10].

Once the HUD reports had been released The Aerospace Corporation, a not-for-profit corporation created by the United States Air Force, wanted to use aerospace technology to solve urban problems. Dr. Jack H. Irving concluded that working on high capacity PRT was a good focus for their skilled engineers. They invented new devices such as: powering the vehicles with a pair of linear pulsed direct current motors in interaction with permanent magnets in the track. Except at the switching points they used electromagnets resulting in a no-moving parts switch. The motor could be controlled by solid-state circuitry and was very efficient. They also believed that the guideway should have minimal visual impact so the vehicle was supported by two wheels in tandem. They tested this on a scale model. They were able to develop the system to a very advanced state and used computer simulations proving the feasibility of complex short headway networks. They performed analysis for Los Angeles and Tucson and released their work in

a book titled: *Fundamentals of Personal Rapid Transit, 1978* [3] (Fig. 4).

The Morgantown system was awarded and built during a very complex time for the newly formed Urban Mass Transportation Administration. Most importantly a presidential change took place bringing all new people into a process that they had no history or detailed understanding of. They wanted immediate results along with preventing the collapse of existing transit systems – two competing goals; and of course they were understaffed.

The Development of the Morgantown GRT

The West Virginia University is located in the hilly, snowy mountain valley town of Morgantown in the Monongahela Valley of West Virginia, and its campus is spread between three different sections of the city. Buses transported students through the center of the city along with all other traffic, creating at that time extreme traffic issues. Professor Samy Elias, Head of the Industrial Engineering Department, became aware of PRT and the PRT test tracks and studies. He believed that this could be a solution for Morgantown. Due to

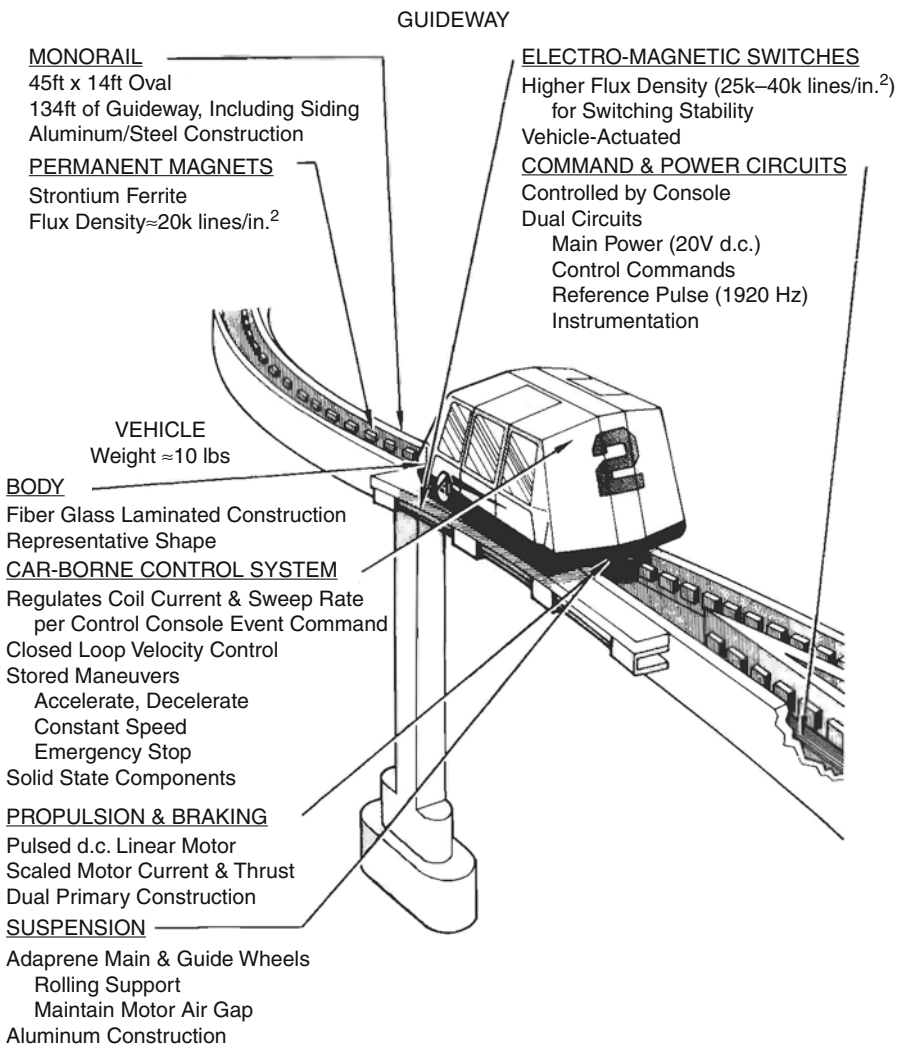

Personal Rapid Transit and Its Development. Figure 4
Aerospace Corporation (Reproduced from [11]. With permission)

the support of the city, the University and the West Virginia congressional delegation money was obtained for a grant to study three systems. The Alden staRRcar was chosen as the appropriate solution for Morgantown. Due to political connections and pressures, this project was taken very seriously. So, with the 1972 presidential election in mind, the new Head of the Department of Transportation, John A. Volpe, stated that by October 1972 the president should be able to ride the system and therefore this became a federal demonstration project and a team needed to be formed. A contract was signed in December 1970 with the Jet Propulsion Laboratory in Pasadena, California, Boeing, Seattle, WA was the vehicle manufacture, Bendix, Ann Arbor, MI the control system supplier and F.R. Harris Engineering Company of Stanford, CT for the design and construction of the guideway. None of these groups had been working on PRT and there was no time for analysis or a learning curve. This of course led to a complicated and difficult outcome costing four times the original estimate as all of their expertise did not fit with the paradigm changing technology. Recently WVU was awarded a Federal Transit Authority grant that will be a part of the funds to upgrade the existing system (Fig. 5).

Personal Rapid Transit and Its Development. Figure 5 Heathrow PRT system (Stan Young, Kansas DOT, University of Maryland, Center for Advanced Transportation Technology)

Expositions and International Conferences

In 1972, UMTA sponsored an international exposition of four different PRT systems called Transpo72. Millions of federal dollars were set aside for the four systems to be constructed and money to be matched by their respective companies after being chosen. The companies were TTI, Monocab, Dashaveyor, and Ford. Each was to exhibit a minimum piece of guideway and one station in hopes to produce requests for capital grants. However, again due to a short time frame, work to improve the technologies took precedence and those attending the Expo did not understand how these systems could provide a better service and successfully integrate into and improve the built environment. While no city was ready to put its own funds into the development of PRT, many cities did want 100% federally funded programs to integrate the new technology. However the UMTA saw their role as one to encourage private investment [14].

In the years 1972, 1973, and 1975, three major international conferences were held by the American Society of Civil Engineers (ASCE) People Mover Committee and a volume of published proceedings were produced. However, by 1973, attendance had peaked and the organizing committee worked to develop a permanent organization. In 1976 the ATRA, Advanced Transit Association was formed. ATRA held its own conference in 1978 and more research was added to the body of knowledge. In 1988, ATRA published a broadly based technical committee report to further the importance of the PRT concept. ATRA and the ASCE – People Movers Committees – have continued their work producing published proceedings and a journal [15, 16].

Planners' and Architects' Visions

While the visual impact of an overhead track had been identified from the beginning as an important factor in the acceptance of a PRT system, more emphasis was placed on the engineering aspects than exploring the many approaches that could support visual acceptance. Now, due to advanced technology, the first true PRT system is partially on grade and partially on elevated tracks, only where necessary within an airport, while the Mazdar City PRT system in Abu Dhabi, UAE, will be completely under the city with the vehicles on

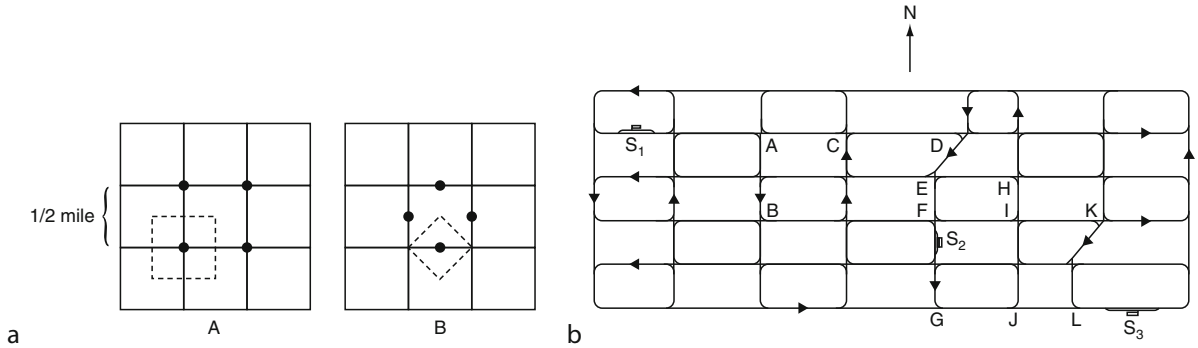

Personal Rapid Transit and Its Development. Figure 6
Aerospace Corporation Station placement and walking distance studies (Reproduced from [11]. With permission of Aerospace Corporation)

grade – while many lovely integrative solutions can still be explored! Some architects and architectural studies appeared during the 1970s and 1980s such as in the work of Victor Gruen, Paul Rudolph, and Ulrich Franzen.

Paul Rudolph and Ulrich Franzen were sponsored by the Ford Foundation and the American Federation of Arts producing a book in 1974 titled *Evolving City – Urban Design Proposals* [17] (Fig. 7). This publication contained amazing drawings and models for New York City including POD vehicle types and drawings that incorporated PRT into an urban setting. Victor Gruen, known as the shopping center architect, in his Fort Worth Central Business District project in 1950, envisioned "small electric vehicles" under the city to allow full access for all people to the city center. He also created the first pedestrian-only street in Kalamazoo, MI, that still exists today. The two concepts of PRT and walking environments have been connected by architects and planners since the beginning of PRT research, due to the ability of PRT to have smaller stations closer together providing a faster, more accessible, and greater choice in destination [3] (Fig. 6). PRT was also understood as a transit system of choice when connecting other forms of transportation such as automobiles and existing longer-haul transit systems (Fig. 7).

In Great Britain, a steering group for the 1963 UK Department of Transport produced with Colin Buchanan as the key author *Traffic in Towns* [18] that also became known as the Buchanan Report. He was an influential planner and this report discussed how

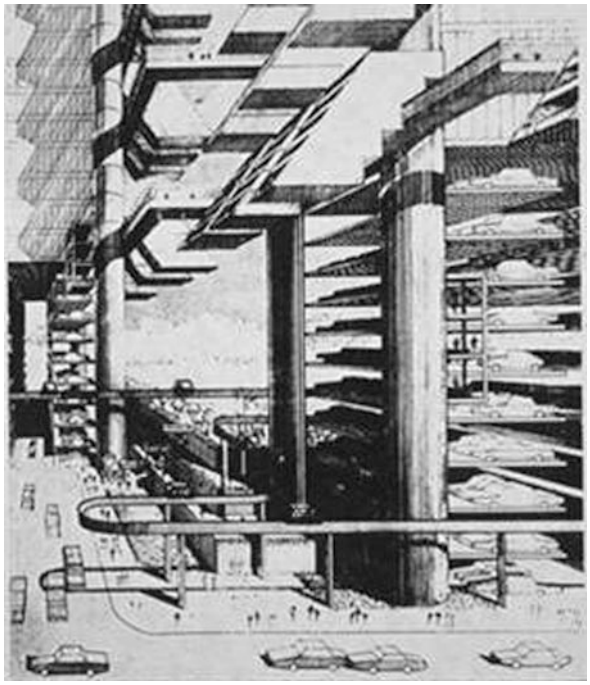

Personal Rapid Transit and Its Development. Figure 7
Paul Rudolph and Ulrich Franzen, Evolving City [17]

a balance must be found as increasing automobile ownership was going to challenge the urban environment. Four key points were identified, two being: Towns should be created as environmental areas with quality of living coming first and creating a transit system that could offer an acceptable alternative. This balanced, classic, and seminal report is still referred to

today in transportation planning and it is this firm, headed by his son Malcolm Buchanan, that has led the PRT initiative at Heathrow Airport.

History/Overview of Systems in Other Countries

In the early years of PRT, the HUD reports generated the interest in understanding and developing PRT systems around the world. Great Britain, Japan, Germany, France, Sweden, and Canada all became involved to some degree in studying and designing PRT systems.

L. R. Blake wrote an article of his own synthesis of what he saw occurring with PRT development in American and designed Autotaxi with the British-built environment in mind [19]. The company was started as a private venture, sold to Brush Electric and then was funded by the British National Research and Development Board now being called Cabtrack, a true PRT system. The system was being studied in a systematic and complete way through a step-by-step process including a contract to a large British architectural firm to integrate the system into a section of London as reported in the Architects Journal of May 1971. However, after a new election in Great Britain, the Cabtrack program was stopped. The results and reports of this process are of great value and may have contributed to the success of the Heathrow project.

The Japanese had a full-scale test facility operating in 1972 outside of Tokyo with 4.8 km of guideway and 60 vehicles. Operating with a 1-s headway and a four-passenger vehicle, a 1,000-vehicle network was simulated. Although many planning and costing studies were evaluated including one for the City of Baltimore, MD, in the United States, several design issues had not been fully considered such as the guideway, station design, and cold weather conditions.

In Germany, two companies inspired by the HUD reports were independently working on PRT concepts. They pooled their resources and thoroughly analyzed many alternatives creating a three-passenger cab supported both above and below a track. They used linear induction motors, one on each side of the vehicle and asynchronous control that was more flexible in the real world. A full-scale test facility was in operation by 1973 and was advertised in 1974 as a successful project. Called Cabintaxi, it was studied to be implemented in Freiberg and Hagen, Germany, and was marketed in the United States. The central business district of Indianapolis tested the system. A program to build a demonstration of a 12-passenger version in Hamburg was underway, as well it was a leading competitor for the Downtown People Movers Program in Detroit, MI, sponsored by UMTA, when the economic crisis of 1980 occurred and the German government withdrew its support. Information can be found about this system as some believe its potential still exists today [20].

The French PRT system called Aramis began with Gerard Bardet in 1967 whose patents were bought by Engins Matra, and in 1970 Matra received a contract. Orly International Airport became the place for a full-scale testing, in 1974, the first phase for proof testing was complete and a contract was awarded for a public demonstration in a suburb of Paris. However the system was based on a platoon concept of grouping vehicles and was designed as a ring system around Paris so vehicle size was increased and the project eventually failed; however, the work with berthing vehicles at stations provided the facts to show that loading and unloading at stations did not slow capacity for the entire system. This project was discussed in a book titled: *Aramis or the Love of Technology* [21] (Fig. 8).

The Swedish City of Gothenburg, since their city was built on solid rock, were facing a problem of how to deal with expanding mass transportation. Excited by the British efforts they did a great deal of research on PRT systems around the world and decided that the

Personal Rapid Transit and Its Development. Figure 8 Aramis vehicle, France (Reproduced from [11]. With permission)

technology was not ready for public deployment, but continued to be interested in the technology as it was continued to be developed. PRT studies have continued to this day in Sweden as they now move closer to an urban application.

Canada also did a comparative study of PRT, conventional highway and transit technology; however they were interested in freight as well as people movement and called PRT "Programmed Modules." In 1973 in Ontario, the Urban Transportation Development Corporation developed a system; however due to other influences, the vehicle was designed for 40 passengers with all that that implied and met with minimal success in reference to the concept of pure PRT.

After Morgantown

In the late 1970s money was appropriated for a study of automated transit including PRT for Indianapolis using the Cabintaxi system developed in Germany. Several different-sized passenger vehicles were tested in this comprehensive study with the result that the smallest vehicle providing the lowest total cost per passenger mile. This system had the support of business, government, and civic organizations. When this project did not proceed into a real-life application, Raymond MacDonald and J. Edward Anderson began a development program in 1981 at the University of Minnesota that was to take into account all prior research and work to develop the "perfect" PRT system, although they concluded that the aerospace PRT system was the "closest to being right" [22].

A company was formed with the assistance of the University of Minnesota and a Chicago company funded the work until 1986, when Dr. Anderson moved to Boston University. Raytheon and local Boston engineers intrigued by the Chicago-Area Regional Transportation Authority (RTA) were seeking a new approach. Two teams were organized developing designs for one to be chosen for an application. This beginning culminated in the RTA selecting the Taxi 2000 system with Raytheon to design, build, and operate the test PRT system in Rosemount, IL. In 1999, Raytheon terminated its work on PRT 2000; TAXI 2000 Corporation bought back its rights and has continued to develop its concept, now called Skyweb Express.

The PRT concept continued with 2getthere in the Netherlands implementing several successful projects, all on grade: three considered GRT and one PRT. The ParkShuttle technology was applied in the Business Park Riviam, the Airport Schiphol, and the Antibes Demonstration. The CyberCab project, a true PRT system, was tested at a public Flower Show – Floriade at Hoofddorph, Netherlands in 2002. Developed by 2getthere, all of these projects were successfully operated and Riviam continues today as a public form of transit. 2gethere is now designing the PRT system being installed as part of the new carbon neutral Masdar City further discussed below [23].

Ford appeared on the PRT scene briefly with a study of a dual-mode system called PRISM that actually is a Program for Individual Sustainable Mobility [24]. This concept had some similarities to the NEV (Neighborhood Electric Vehicle) initiative. It included very lightweight small vehicles that are on a controlled system. It is an all-electric program that would start small in a few cities eventually growing into a national network linking to high-speed rail. The reason for this program was traffic congestion and the data collected by The Texas Transportation Institute of 68 US urban areas. They understood a system like this could increase fuel efficiency, reduce emissions, and be safer as less driver error would occur.

The South Koreans had been working since 1990 on a PRT system called Vectus and in 2005 began collaborating with the Swedish to construct a test-track in Uppsala, Sweden, that is designed for winter weather application. The test facility passed safety requirements in 2007, had public access to the system in 2008 and now several studies for real projects in both Sweden and South Korea are underway. The test-track layout has an outer loop of 300 m, allowing speeds up to 12.5 m/s, and a station track of 100 m with a two-berth station. The station track is designed be long enough to allow merge operations at full speed [25].

The British Company ULTra moved forward with its demonstration project in 2002, followed by a feasibility study in 2004, for implementing PRT at Heathrow airport and is now our first "pure" PRT system in operation. A more detailed discussion follows [26].

Personal Rapid Transit versus Existing Transportation

In understanding the paradigm-changing value of the modern pure PRT to the transportation field, a comparison of PRT to existing systems is crucial. This chart initially from Wikipedia has been adapted for this entry [27]:

Personal Rapid Transit versus Existing Transportation

Similar to automobiles	• Vehicles are small – typically two to six passengers • Vehicles are individually used, like taxis, and shared only with the passengers of one's choosing • On-demand, around-the-clock availability • Travel is point to point, with no intermediate stops or transfers
Similar to trams, buses, and monorails	• A public amenity (although not necessarily publicly owned) shared by multiple users • Passengers embark and disembark at discrete and fixed stations • Can be elevated or use air rights over existing highways – reducing land usage and congestion
Similar to automated people movers	• Fully automated, including vehicle control, routing, and collection of fares
Distinct features	• Vehicle movements are coordinated, unlike the autonomous human control of automobiles and bikes • Reduced local pollution (alternative energy sources such as electric power and solar) • Small vehicle size allows transit infrastructure to be smaller than other transit modes • Vehicles travel along a network of guideways where interconnection and multiple station options are standard

Current Systems in Operation or Under Construction

Currently, two GRT networks are operational, one PRT system is operational, one PRT in testing, one full-PRT network is under construction, and several more are in various stages of upgrade, planning, and design. Again the chart is adapted and updated from Wikipedia [27].

In the United States many cities, towns, and activity centers are in various stages of planning with San Jose, CA, and Ithaca, NY, currently leading the way. San Jose is working through a municipal process while Ithaca, NY is studying PRT through a NYSERDA research grant. Alameda Point, CA, Mountain View, CA, Santa Cruz, CA, that is attempting a solar powered system and Fresno, CA, November 2006, the citizens voted to spend $36 million to establish a fund to begin a PRT effort in their downtown and is currently in the study phase, the others are in various stages of the process. Tysons Corner, VA, and Amber Glen, OR, are all also looking at PRT. In England, Bath, Cardiff, and Corby have been studied for PRT implementation. While in the United Arab Emirates, capital city Dubai, Lulu Island, Abu Dhabi, and Bawadi, Dubai, all are considering PRT systems. Several studies are beginning in India and other European countries. The technology is now being understood for its benefits to people around the world [28].

Heathrow Airport PRT

Heathrow Airport ULTra PRT will be the first "true" PRT project for public use. It has already won a prestigious UK award for transit technology advancement and has been called one of the 20 proven ways to save the earth by the UK Times and also a Sustainable Form of Transport by the Directorate General for Energy and Transport of the European Union.

Heathrow is the main international airport in the UK and one of the busiest in the world. The airport is committed to PRT as the solution to provide connectivity within a very complicated airport system. The initial application and the pilot program connected Terminal 5 with a businessman's parking lot. A higher

Location	Status	System	Date	Guideway	Stations/ vehicles	Notes
Morgantown, West Virginia, USA	Operational	WVU PRT	1975	13.2 km	5/73	Up to 20 passengers per vehicle, some rides not point to point during low usage periods
Schiphol Airport Amsterdam, Netherlands	Temporarily operational	Park Shuttle	1997–2004	2,000 m 2 loop network	10/4	Connection from parking to airport 24/7 operation
Rivium Business Park	Operational	Park Shuttle II	1999-today	18,000+ m	8/6	Public Transportation to Business Park and City Functions 20 passengers
Hoofddorp, Netherlands	Temporarily operational	CyberCab 2GetThere	2002	700 m	2/25	Four passengers, transport to view a flower show from a hill peak 40 m high
London Heathrow Airport, UK	Construction completed, open to public	ULTra	2010	3.8 km	3/18	Will be the world's first true commercial PRT system, initially connecting Terminal 5 with a long-term car park. If successful, BAA plans to extend it throughout the airport
Hospital Rovisco Pais, Portugal	Construction completed, under testing	Critical Move	2010			The Hospital Rovisco Pais, a center for physical rehabilitation, uses the Move between the several buildings of the hospital
Masdar City, Abu Dhabi, UAE	Under construction	2getthere	2011	Magnets in pavement, automated driving	83/2,500	Automobiles will be banned, the only powered transport will be PRT and intercity light rail
Suncheon, Republic of Korea	In planning	Vectus	2013	5 km (3.1 miles)	?/40	Will connect Suncheon to the future site of the International Gardening Festival

cost to park can be applied to the businessman as the dramatically reduced time for them from car to terminal is well worth it (Fig. 9).

The initial system is a 3.9 km (2.4 mile) single guideway connecting three stations. Having 21 vehicles to travel between the stations takes about 5 min. The system had to be constructed over a very complex site that included two rivers, seven roads, green-belt land as well as complex airport conditions. If this initial application is successful then it will be extended to include a full network of 350 vehicles, 50 stations, and 30 km of track linking all airport private and public functions [29].

The ULTra pods can hold four adults and two children and can easily accommodate wheelchairs, bicycles and safely carry those who are physically challenged. The pods are battery controlled by a system on the pod. They will save 70% of energy compared to cars

and consume less than 50% of traditional buses [30]. The cost in comparison to light rail and transitional automatic people moves is quite less, while a traditional bus could be less expensive, the level of service and benefits provided to the community cannot be compared (Figs. 10–12).

Personal Rapid Transit and Its Development. Figure 9
Heathrow Airport PRT Phase One (Martin Lowsen of ULTra)

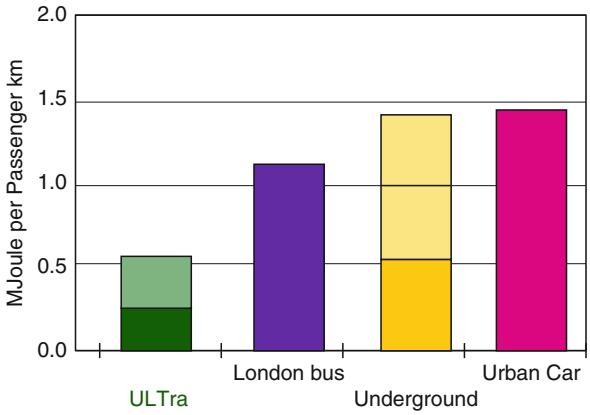

a

	$m/mile
Automatic People Movers ("APM")	30–100
Light Rail	20–40
ULTra	10–15

b

Personal Rapid Transit and Its Development. Figure 10
ULTra: PRT sustainable transport (Martin Lowsen of ULTra)

Personal Rapid Transit and Its Development. Figure 11
Two Heathrow Station Design (Martin Lowsen of ULTra)

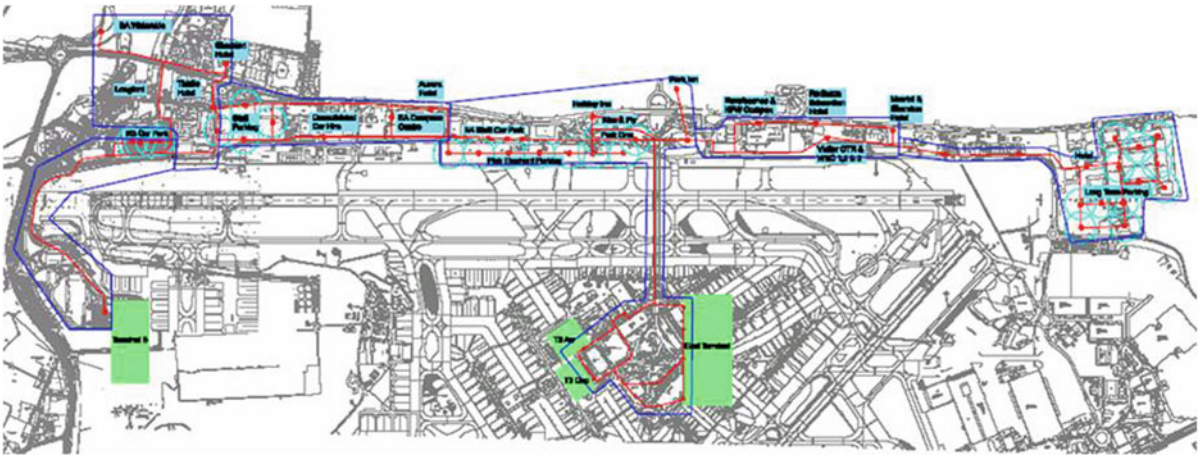

Personal Rapid Transit and Its Development. Figure 12
Heathrow expansion (Martin Lowsen of ULTra)

Hospital Rovisco Pais, Portugal

This is a PRT system for a hospital setting so that all within the complex have equal access to full mobility – PRT is perfect for this. It is a fully automated electric vehicle, on demand and point to point within a dedicated right-of-way. The user can have communication with the system operator while in the vehicle and can also control the position where the vehicle stops. The vehicle can accommodate eight passengers.

Key Sustainable/Energy and Planning/ Architectural

Being able to synergize transportation, energy, planning, and architecture to meet sustainable goals is a rare confluence of technology/people interconnections. PRT has always been understood for its benefits in minimizing energy usage, while also providing the opportunity for the system to be designed connected to other sources of energy, new planning strategies and architectural design. Peter Calthrope, a Yale-educated architect and sustainability advocate from the 1976 calls it "The ideal transit technology: (a) stations right where you are, within walking distance, (b) no waiting." He has been the supporter of the Alameda Point Project since 2008 especially with the discussion of an additional 60,000 housing units to the area. He advocated ULTra PRT as it would enhance carpooling and other forms of transit by allowing all of them to interconnect. PRT can also extend bicycle commutes and enhance walkable community design. At Alameda Point, PRT can assist with interconnections along

the Red and Orange lines between Fruitvale BART, Downtown/Park Street shopping, Marina Village jobs, College of Alameda and Rapid Bus transfer, Alameda Point 53-acre Sports Complex, Alameda Point National Wildlife Refuge, Bridgeside Shopping Center, Alameda Point cafes and parks, and Fruitvale Shopping Center.

Suncheon, Republic of Korea

Vectus, a company founded in South Korea that teamed with the South Koreans to construct a test track in Uppsula, Sweden, is now in the planning and design phases for a project in Suncheon, S Korea. The PRT system was chosen to be constructed at the famous Suncheon Coastal Wetlands Park. It marks the first time that the governmental agency has chosen PRT over conventional transit and the environmental reasons could not be more appropriate. Including all of the characteristics that have been mentioned throughout this paper, the South Koreans chose it because it was less costly to build, takes less than half of the construction time and emits no pollutants including CO_2 [31].

The first phase of the system will connect the parking lot to the entrance of the wetlands and will contain 40 vehicles on a 5 km system. Mr. Dong Hee Lee, President and Chief Investment Officer of POSCO stated: "POSCO is on the forefront of the global efforts to protect the environment while improving the quality of life". The City will host the International Garden Expo in 2013 and there are hopes that the initial system may even be expanded by this time to connect with the Central Train Station and the city's downtown.

Masdar City, Abu Dhabi, UAE

Masdar City has been under development as the world's first zero-carbon city. This entire 6^2 km city is completely new and has been totally designed from scratch so that every decision is based upon creating a living place that interacts with its local environment without adversely changing it while also improving the lives of the people who live there. Recently – at the 2009 World Future Energy Summit – the cyber taxi by 2getthere was acknowledged as one of the key features in creating such an environment. They have anticipated 3,000 electric cars with 90 stops connecting light rail, parking, and linking to strategic walking points to the city above. They will operate 24 h a day. The vehicles can travel at 40 kmph and are guided by magnets imbedded in the streets that interact with an onboard navigation system.

It is anticipated that the longest trip by PRT around the city will take no more than 10 min. The city is raised on a podium with all of the vehicles running below the pedestrian-friendly city. The PRT system is anticipated to eventually have 3,000 vehicles serving 130,000 trips/day. The PRT system will also operate freight delivery to the whole city – FRT (Freight Rapid Transit). The FRT is designed for 5,000 trips a day. Renewable energy in the form of lithium phosphate batteries allow the vehicles to be charged at the stations and will only require a 1.5 h charge for 60 km of use.

Masdar City and *2getthere* have the exclusive rights to apply the FROG-technology, the supervisory planning and control system TOMS, as well as unique proprietary subsystems and components (such as the FrogBox and Magnet Ruler – MMS) and a number of related patents for Automated People Mover Systems. These are the technologies that allow this system to run on grade and they have a track record of 22+ years [32].

- The FROG (Free Ranging On Grid) technology creates intelligent vehicles that can operate in any environment. The on board FROG-box® controls the vehicle based on electronic maps (route planning). While driving, the vehicles measure distance and direction traveled by counting the number of wheel revolutions and measuring the steering angle (odometry). External reference points (magnets embedded in the road surface) are used to correct possible small inaccuracies in reference to the planned route (calibration). The reliability of the navigation system has been proven in all previous applications realized and tested successfully by TNO during the FMECA safety-procedure for the ParkShuttle Rivium application that has been operating since 1999.

San Jose Airport, San Jose, CA

The City of San Jose has identified the area around the Sam Maneta airport as a place where the PRT concept can assist with linking all of the existing movement systems such as Caltrain, BART, and VTA Light Rail as well as potentially connecting to other places not directly related to the airport such as North San Jose, as

well as to new growth. They have earmarked $4 million to conduct two simultaneous studies, one technical and the other with a focis on transportation and urban planning. Laura Stuchinksy, a sustainability officer for the San Jose Department of Transportation and many other city officials see PRT as a complement to all of these systems and one that will allow all of them to function as a complete transportation system for the airport and local area – a circulator system interconnecting all the systems. This was noted in a paper by Young, Miller, and McDonald. In September 2008, they issued the initial request that is now in the final contract negotiation phase. They expect to have an operational system by the end of 2015 (Fig. 13).

The following is an excerpt from the City of San Jose:

- It will start with a limited demonstration project and proceed in three phases:
  - Phase 1: Preliminary Design – A determination of feasibility as described above.
  - Phase 2: Final Design – Selection of system design and construction contractor(s); completion and verification of detailed design.
  - Phase 3: Construction, Integration and Testing – Physical construction of the system on-site culminating in operational certification.

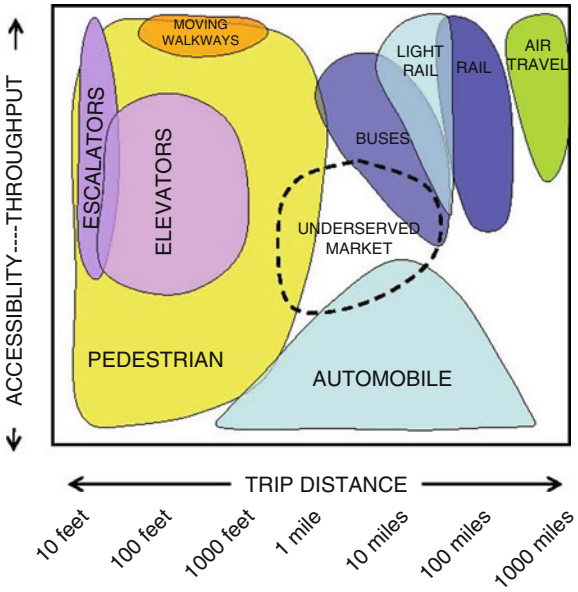

Personal Rapid Transit and Its Development. Figure 13 Conceptual comparison of modes in the accessibility – throughput spectrum from Young, Miller, McDonald. Keys to innovative transport development. Presented at the 87 Annual Meeting of the Transportation Research Board, Washington, DC, 2007

All typical analysis for transportation infrastructure such as ridership forecasts, routing determinations, architectural development, civil engineering design, environmental impact assessments, and community outreach will be a part of the process. While nonconventional aspects of this project include new usage and operational models, completely new civil architectures and their integration with the as-built environment, along with new elements of the technical system – innovative designs for propulsion, control, vehicles, guideways, and vehicle management systems, for example, that may be selected, are specified and arranged in various ways to provide varying degrees of utility and capability.

New approaches and guidelines/standards may need to be developed, as will ridership forecasting and performance evaluation models. A thorough review of technical capabilities and maturity level relative to the resulting performance requirements is required as is an assessment regarding the ability of the still-small vendor base to deliver such systems.

The CITY has selected two consultants as project advisors, The Aerospace Corporation (SYSTEMS CONSULTANT) and Arup North America Limited (TRANSPORTATION CONSULTANT). In general, TRANSPORTATION CONSULTANT will address all conventional transportation infrastructure issues. SYSTEMS CONSULTANT and TRANSPORTATION CONSULTANT will together address the unconventional project issues; the TRANSPORTATION CONSULTANT focusing on the civil infrastructure-related items and the SYSTEMS CONSULTANT focusing on the technical system, as described generally above.

General Approach The two consultants will work collaboratively as part of an Integrated Project Team (PROJECT TEAM) led by the CITY. They will share information and provide input necessary to each

System	Location	Active	Status	Seating Capacity (per vehicle)
Morgantown PRT (Boeing)	West Virginia	Yes	In service	8 seated plus 12 standing
ULTra (ATS Ltd)	UK	Yes	In testing for final commissioning	4
Critical Move	Portugal	Yes	In on-site testing	4
2getthere PRT	Netherlands	Yes	10 vehicles produced for Masdar City	6
Vectus PRT (POSCO)	South Korea	Yes	Full prototype, Sweden; Suncheon, Korea	4
Cabinentaxi [24]	Germany	No	Completed system: 1980s approval for federal transit programs in Germany and US	3,12,18
PRT2000 (Raytheon)	USA	No	Full prototype	4
Skyweb Express (Taxi2000)	Minnesota	Yes	Partial prototype	3
MISTER	Poland	Yes	Partial prototype	5
JPods	USA	Yes	Mockup	4
SkyTaxi	Russia	Yes	Concept	1,2,4
Launchpoint Technologies SPM Maglev [25]	USA	Yes	Concept	?
Skycab AB Skycab	Sweden	Yes	Concept	?
SkyTran Unimodal	USA	Yes	Full scale prototype	3

other's work and project deliverables, integrating their workflows to achieve the CITY's project objectives [33].

The Basics of Several PRT Systems

Future Directions

High-Tech/Low-Tech Connections: Man and Machine

As PRT becomes more available for public use, the positive connections between technology, the environment, our communities, and ourselves – the low-tech/High-tech connection will be better understood and allowed to flourish. What are the high technologies of the future and how are they transforming the ways that we travel through space, place, and time. The test is how many lives can be transformed for the better, for greater accessibility and the long-term sustainability of our planet – these technologies should be explored, developed, and expanded.

PRT with automated transit technologies will continue to evolve to become a greater part of our future built world. They have the ability to transform the way that we design and build our places for living, just as positively as the car did over 100 years ago. Following that technological innovation many peoples lives were changed and for the betterment of all. Since the late nineteenth century, world's fairs have offered futuristic visions of how people could and would live. Automated People Movers are among the visions that have become reality from them. Although most people connect monorails with world's fairs and amusement parks, there is no reason to limit advanced transit technology to such environments. For many land uses – such as airports, medical centers, and colleges – automated people movers have tremendous potential to address congestion, increase connectivity, mitigate parking shortages, and provide links to parking and PRT has the most potential within this category to really transform our lives.

Because of its human scale, PRT allows the pedestrian experience to be preserved – minus the traffic and congestion. It can also provide a more flexible link between man and machine: because it so small, quiet, and light (compared with conventional transit), PRT can be adapted to a wider array of environments. Although PRT does not eliminate the need for parking in many situations, it does offer opportunities to change the parking paradigm. In an automated parking facility, for example, PRT vehicles could easily change direction or move between levels within a small space [34].

PRT systems can provide excellent transit coverage for urban or suburban areas; such a system would be ideal, for example, in locations such as Destiny USA – the environmentally sensitive entertainment, shopping, and technology project in Syracuse, New York. PRT would be equally appropriate in more traditional urban locations, particularly as a link between parking and other land uses. As part of a larger effort to explore the transformation of office parks into transit villages, Cities21, a nonprofit research organization based in Palo Alto, California, is completing an EPA-funded study of the environmental benefits of a PRT system within the Hacienda Business Park [35].

In the 1960s, William Alden designed the StarrCar, a vehicle that could function independently, on the road, or on dedicated tracks, as part of a transit system. At the time, technology had not yet caught up to Alden's vision, although part of Alden's concept was the basis for the Morgantown PRT system. Today, however, with advanced automotive technology, Alden's vision is almost within reach. Within a system that allowed vehicles to be taken off the tracks as needed, for example, PRT vehicles may be used to pick up drivers at their parking spots and take them to their next destination. The parking facility could both provide space for traditional vehicles, and become an active participant in new approaches to transit and movement! (As automotive technologies advance, moving in the direction of "cars that drive themselves," it may be possible to drop off a car at a garage and have the car park itself as you connect to the PRT system. As PRT, automated vehicles, and other high-tech transportation options become integrated into the overall transportation system, they will affect parking garage design in ways that cannot yet be imagined [36]).

Beauty, technology, function, engineering, and civic purpose: the pieces are all in place. But determining the solutions of the future – whether urban, suburban, or rural – will mean connecting, at a deeper level, to the ways in which people relate to the world around them. It will be through these deeper connections that new solutions emerge. Horst Bredekamp, in an exploration of the phenomenon of the Kunstkammer – the cabinets of art and curiosities that were the precursors to modern museums – notes that

> No one wants to return to the deliberate chaos of the Kustkammer as museums. But the boundaries between art, technology, and science are beginning to break down in a similar manner as has been demonstrated by the Kunstkammer. In view of this fact, their lessons of visual association and thought processes which precede language systems take on a significance which might even surpass their original status. Highly technological societies are experiencing a phase of Copernican change from the dominance of language to the hegemony of images [36].

In looking toward the future of PRT, advances in new transit technology have been hindered by a lack of focus on research and development in this area. However, in fits and starts, and often with private money and due to the perseverance of innovators and visionaries, PRT is just starting on its path to its full potential, finding its way into our world of public transit linking with all existing forms of movement.

One of key area of future advancement is the control software that allows for flexibility and openness so that the complex and time-consuming tasks that will allow a large fully operational city PRT system to function safely and quickly can be applied to public transit. Systems of this type are being implemented in Automated Guided vehicles for warehouses and manufactures as well as being used successfully in airport luggage systems and emerging PRT systems.

The motivation behind PRT is to provide not just an advanced commuter transit experience but to provide a type and level of service that meets the needs of those who cannot or do not have access to the automobile, a truly new way to move and live in our modern world. It is a transit system that attempts to put people and cities first through technology while making an improvement to the quality of urban life.

The theory and reality of PRT shows this technology to be the transit technology of the future. From 2002 to 2005 the EDICT project funded by the European Union and involving 12 research organizations concluded that PRT [37]:

- Would provide future cities "a highly accessible, user-responsive, environmentally friendly transport system which offers a sustainable and economic solution"
- Could "cover its operating costs, and provide a return which could pay for most, if not all, of its capital costs"
- Would provide "a level of service which is superior to that available from conventional public transport"
- Would be "well received by the public, both public transport and car users"

The risks of being the first to implement the system are being removed and so we should see the technology move forward and provide the level of service to all users of transit that has been envisioned since its beginnings. A review of all of the literature shows many detailed specific studies about networks, walkabilty, systems concepts, human affect, and proposals that indicate all that is claimed about PRT is real so now according to Rachel Liu [1] all that is required are:

- multiple business models so that its many applications can find funding. As concluded in a recent PRT study (Carnegie and Hoffman 2007), AGT possesses the virtue of sustainability due to its small footprint, lower cost and lower impact on the environment. On the other hand, its small size and low-key profile have fostered a large number of applications worldwide without garnering any major headlines, which may, however, suppress its potential as a unique solution to urban circulation and congestion problems.

  Along with:

  on-going PRT studies reveals that the specifications of technology and assessment of costs may be relatively straightforward, but quantifying benefits associated with the implementation of a transportation project and evaluating the market conditions are complex. There are a number of analytical tools to assign a dollar value to benefits; however, some impacts such as congestion relief, safety improvements, or air quality improvements are often difficult to quantify financially. Other qualities, such as aesthetic appearance, may not even be quantifiable. Environmental and societal impacts are often referred to as "external" effects of transportation activities since they are not directly reflected in monetary costs and benefits of project implementation. By externalizing these factors, benefit/cost analyses often do not capture the full value of beneficial impacts. However, the significance of all impacts, both positive and negative, needs to be considered in the decision-making process.

Bibliography

Primary Literature

1. Liu R (Rachel) (2010) Spectrum of automated guideway transit (AGT) technology and its applications. In: Kutz M (ed) Handbook of transportation engineering. McGraw-Hill, New York
2. Committee of Automated People Mover Standards (2006) Automated people mover standards, Part 3. American Society of Civil Engineers, Reston
3. Irving J (ed) (1978) Fundamentals of personal rapid tansit. DC Heath, Lexington
4. Morgantown PRT: http://transportation.wvu.edu/prt
5. Gunter M (7 Mar 2008) Building the world's cleanest city. Fortune Magazine
6. Fichter D (1964) Individualized automated transit and the city. BH Sikes, Providence, RI
7. Anderson JE (1996) Some lessons from the history of personal rapid transit. Paper presented at the international conference on personal rapid rransit (PRT) and other emerging transportation systems, Minneapolis, Minnesota, 18–20 Nov 1996. http://advancedtransit.org/doc.aspx?id=1025
8. Cole LM, Merritt HW (eds) (1968) Tomorrow's transportation: new systems for the urban future, US Department of Housing and Urban Development, Office of Metropolitan Development Chapters available online: "Summary," pp. 1–5; "Recommended Future Systems," pp. 58–77. http://faculty.washington.edu/jbs/itrans/tomtran.htm.
9. Henderson C et al (1968) Future urban transportation systems: descriptions, evaluations and programs, Final report, Volumes 1 and 2. Prepared for the US Department of Housing and Urban Development by the Stanford Research Institute
10. Systems Analysis of Urban Transportation Systems (1969) Scientific American 221:19–27
11. Burke C (1979) Innovation and public policy: the case of personal rapid transit. Lexington Books, D.C. Heath
12. Andreasson I (2000) Innovative transit systems, VINNOVA: Swedish Agency of Innovation Systems. http://vinnova.se/publ/list_vr.htm#03 as well as Vectus web site http://www.vectusprt.com/
13. Lowson M ULTra Urban Light Transport, Advanced Transport Systems. http://www.atsltd.co.uk/
14. United States Congress, Office of Technology Assessment (June 1975) Automated guideway transit: an assessment

PRT and other new systems. US Government Printing Office, Washington, DC
15. Merritt HW (1993) Reflections on the New Systems Study Project, pp 35–59 in Automated People Movers IV: Proceedings of the 4th international conference on automated people movers, American Society of Civil Engineers, Irving, Texas, 18–20 Mar 1993. http://faculty.washington.edu/jbs/itrans/reflec2.htm
16. US Congress, Office of Technology Assessment (June 1975) Automated guideway transit: an assessment of PRT and other new systems. Prepared for the Senate Committee on Appropriations, Transportation Subcommittee. http://ntl.bts.gov/data/OTA/7503/7503.htm
17. Wolf P (1975) Evolving city. American Federation for the Arts, New York
18. Reports of the Steering Group (1963) Traffic in towns. H.M. Stationery Office, London and reprint Penguin Books in association with HMSO
19. Blake LR (1966) A public transport system using four-passenger, self-routing cars, Inst. Mech. Eng. convention on guided land tTransport, vol 181, Pt. 3 G
20. Tadi R, Utpal D (1997) Detroit downtown people mover: ten years after. paper presented at the 6th international conference on automated people movers, Las Vegas, NV
21. Latour B (1996) Aramis or the love of technology. Harvard University Press, Harvard
22. MacDonald R, Anderson JE (1978) Transit systems theory. Lexington Books, D.C. Heath. 21st century personal rapid transit, Self-publish
23. 2getthere: http://www.2getthere.eu/
24. Proposal for Independent Sustainable Mobility (PRISM) (pdf). Ford Advanced Research Division (2003) http://faculty.washington.edu/jbs/itrans/PRISMGPCPaper.pdf. Accessed 3 Aug 2010
25. http://www.vectusprt.com/
26. Heathrow airport web site: http://www.heathrowairport.com/portal/controller/dispatcher.jsp?CiID=e993760079e1d110VgnVCM10000036821c0a____&ChID=10b35109350d3110VgnVCM10000036821c0a____&Ct=B2C_CT_PRESS_RELEASE&CtID=a22889d8759a0010VgnVCM200000357e120a____&ChPath=Home%5EHeathrow%5EHeathrow+press+releases
27. http://en.wikipedia.org/wiki/Personal_rapid_transit
28. Multiple website concerning PRT http://www.princeton.edu/~alaink/Orf467F04/NJ%20PRT%20Final%20Small.pdf
29. Lowson M (2004) (doc) A new approach to sustainable transport systems. 13th World Clean Air and Environmental Protection Congress London, 22–27 Aug 2004. http://www.ultraprt.com/media/papers/
30. Rodgers L (2007) Are driverlss pods the future. http://news.bbc.co.uk/2/hi/uk_news/7148731.stm. Accessed Aug 2010
31. http://www.vectusprt.com/center/news_view.php
32. Masdar: http://www.masdar.ae/en/home/index.aspx
33. San Jose: http://www.sanjoseca.gov/transportation/SupportFiles/admin/RFI_Auto mated_transit_networkQA.pdf
34. Cities21: http://www.cities21.org/cms/
35. McDonald S (2007) The parking garage: design and evolution of a modern urban form. Urban Land Institute, Washington, DC
36. Bredekamp H (1995) The lure of antiquity and the cult of the machine: the Kunstkammer and the evolution of nature, art, and technology. M. Wiener Publishers, Princeton, pp 113
37. EDICT: EDICT Final Report (pdf) from cardiff.gov.uk

Books and Reviews

Advanced Transit Association (1988) Personal rapid transit: another option for urban transit? J Adv Transport 2(38):192–314

Anderson JE (July 2009). An intelligent transportation network system: rationale, attributes, status, economics, benefits, and courses of study for engineers and planners. PRT International, LLC

Anderson J, Romig S (1974) Personal rapid transit II. Audio-Visual Extension, University of Minnesota, Minneapolis, MN

Carnegie JA, Hoffman PS (2007) Viability of personal rapid transit in New Jersey. New Jersey Department of Transportation, New Jersey, 141p

Institute for Transportation in Cooperation with the Advanced Transit Association (1966–present) Advanced Transport Quarterly, Wiley-Blackwell

Muller P (2007) A personal rapid Transit/Airport Automated People Mover Comparison" Proceedings of the 29th international air transport conference. American Society of Civil Engineers. http://www.prtconsulting.com/

Richards B (2001) Future transport in cities. Spon Press, London

Schneider JB (2011) Innovative Transportation Systems. This web site offers a wealth of information, including summaries and excerpts from many other sources of information. http://faculty.washington.edu/jbs/itrans/

Warren R (1998) The urban oasis: Guideways and greenways in the human environment. McGraw-Hill, New York

Petroleum and Oil Sands Exploration and Production

James G. Speight
CD&W Inc., Laramie, WY, USA

Article Outline

Glossary
Definition of the Subject
Introduction
Petroleum Exploration and Production

P

Oil Sand Exploration and Production
Future Directions
Bibliography

Glossary

Bitumen A semisolid to solid hydrocarbonaceous material found filling pores and crevices of sandstone, limestone, or argillaceous sediments such as tar sand.

Exploration The search for petroleum using a variety of physical and spectrographic methods.

Hot-water process The recovery of bitumen from tar sand by use of hot water whereby the bitumen floats and the sand sinks.

In situ conversion Partial or complete conversion of heavy oil or tar sand bitumen in the reservoir or deposit as part of the recovery process.

Oil mining The recovery of petroleum using a mining method whereby an underground chamber is produced by mining and the oil is allowed or encouraged to drain into the chamber.

Recovery Recovery of petroleum at the surface using primary, secondary, and tertiary recovery methods.

Tar sand mining Recovery of tar sand by mining (digging) tar sand from the formations at or close to the surface.

Definition of the Subject

Exploration for petroleum is an essential part of petroleum technology. Depletion of reserves is continuing at a noticeable rate and other sources of hydrocarbons are required – these include heavy oil (a type of petroleum) and tar sand bitumen.

Introduction

Petroleum occurs in the microscopic pores of sedimentary rocks that form a reservoir – typically, reservoir rock consists of sand, sandstone, limestone, or dolomite. However, not all of the pores in a rock will contain petroleum – some will be filled with water or brine that is saturated with minerals.

Both oil and gas have a low specific gravity relative to water and will thus float through the more porous sections of reservoir rock from their source area to the surface unless restrained by a trap. A trap is a reservoir that is overlain and underlain by dense impermeable cap rock or a zone of very low or no porosity that restrains migrating hydrocarbon. Reservoirs vary from being quite small to covering several thousands of acres, and range in thickness from a few inches to hundreds of feet or more.

In general, petroleum is extracted by drilling wells from an appropriate surface configuration into the hydrocarbon-bearing reservoir or reservoirs. Wells are designed to contain and control all fluid flow at all times throughout drilling and producing operations. The number of wells required is dependent on a combination of technical and economic factors used to determine the most likely range of recoverable reserves relative to a range of potential investment alternatives.

There are three phases for recovering oil from reservoirs (Fig. 1):

1. *Primary recovery* occurs as wells produce because of natural energy from expansion of gas and water within the producing formation, pushing fluids into the well bore and lifting the fluids to the surface.
2. *Secondary recovery* requires energy to be applied to lift fluids to surface – this may be accomplished by injecting gas down a hole to lift fluids to the surface,

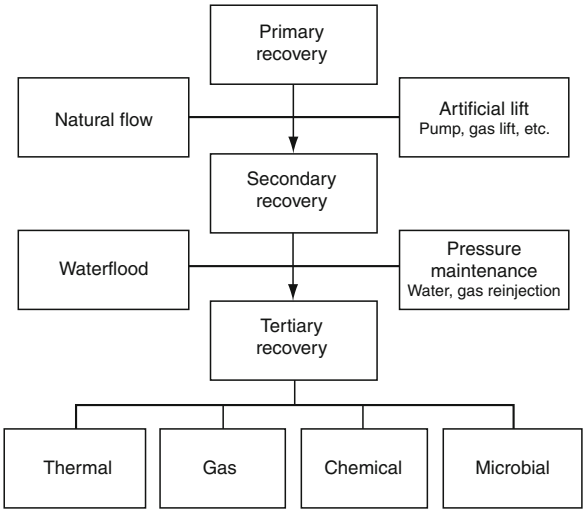

Petroleum and Oil Sands Exploration and Production. Figure 1
Methods for oil recovery

installation of a subsurface pump, or injecting gas or water into the formation itself.

3. *Tertiary recovery* occurs when a means is required to increase fluid mobility within the reservoir – this may be accomplished by introducing additional heat into the formation to lower the viscosity (thin the oil) and improve its ability to flow to the well bore. Heat may be introduced by either (1) injecting chemicals with water (*chemical flood*, *surfactant flood*), (2) injecting steam (*steam flood*), or (3) injecting oxygen to enable the ignition and combustion of oil within the reservoir (*fire flood*).

Production rates from reservoirs depend on a number of factors, such as reservoir geometry (primarily formation thickness and reservoir continuity), reservoir pressure, reservoir depth, rock type and permeability, fluid saturations and properties, extent of fracturing, number of wells and their locations, and the ratio of the permeability of the formation to the viscosity of the oil [1, 2].

The geological variability of reservoirs means that production profiles differ from field to field. Heavy oil reservoirs can be developed to significant levels of production and maintained for a period of time by supplementing natural drive force, while gas reservoirs normally decline more rapidly.

Petroleum Exploration and Production

Exploration

Exploration for petroleum originated in the latter part of the nineteenth century when geologists began to map land features that were favorable for the collection of oil in a reservoir. Of particular interest to geologists were outcrops that provided evidence of alternating layers of porous and impermeable rock. The porous rock (typically a sandstone, limestone, or dolomite) provides the reservoir for the petroleum while the impermeable rock (typically clay or shale) prevents migration of the petroleum from the reservoir.

By the early part of the twentieth century, most of the areas where surface structural characteristics offered the promise of oil had been investigated and the era of subsurface exploration for oil began in the early 1920s. New geological and geophysical techniques were developed for areas where the strata were not sufficiently exposed to permit surface mapping of the subsurface characteristics. In the 1960s, the development of geophysics provided methods for exploring below the surface of the earth.

The principles used are basically *magnetism* (*magnetometer*), *gravity* (*gravimeter*), and *sound waves* (*seismograph*). These techniques are based on the physical properties of materials that can be utilized for measurements and include those that are responsive to the methods of applied geophysics. Furthermore, the methods can be subdivided into those that focus on *gravitational properties*, *magnetic properties*, *seismic properties*, *electrical properties*, *electromagnetic properties*, *properties*, and *radioactive properties*. These geophysical methods can be subdivided into two principal groups: (1) those methods without depth control and (2) those methods having depth control.

In the first group of the measurements (those without depth control), the methods incorporate effects from both local and distant sources. For example, gravity measurements are affected by the variation in the radius of the earth with latitude. They are also affected by the elevation of the site relative to sea level, the thickness of the earth's crust, and the configuration and density of the underlying rocks, as well as by any abnormal mass variation that might be associated with a mineral deposit.

In the second group of measurements (those with depth control), seismic or electric energy is introduced into the ground and variations in transmissibility with distance are observed and interpreted in terms of geological quantities. Depths to geological horizons having marked differences in transmissibility can be computed on a quantitative basis and the physical nature of these horizons deduced.

However, geophysical exploration techniques cannot be applied indiscriminately. Knowledge of the geological parameters likely to be associated with the mineral or subsurface condition being studied is essential both in choosing the method to be applied and in interpreting the results obtained. Furthermore, not all the techniques described here may be suitable for petroleum exploration.

In petroleum exploration, terms as *geophysical borehole logging* can imply the use of one or more of the geophysical exploration techniques. This procedure involves drilling a well and using instruments to log

or make measurements at various levels in the hole by such means as *gravity* (*density*), *electrical resistivity*, or *radioactivity*.

A basic rule of thumb in the upstream (or producing) sector of the oil and gas industry has been (and maybe still is in some circles of exploration technology) that the best place to find new crude oil or natural gas is near formations where it has already been found. The financial risk of doing so is far lower than that associated with drilling a rank wildcat hole in a prospective, but previously unproductive, area. On the other hand, there is a definite tradeoff between rewards for risk. The returns on drilling investment become ever leaner as more wells are drilled in a particular area because the natural distribution of oil and gas field volumes tends to be approximately log-geometric – there are only a few large fields, whereas there are a great many small ones [3].

Drilling does not end when production commences and continues after a field enters production. Extension wells must be drilled to define the boundaries of the crude oil pool. In-field wells are necessary to increase recovery rates, and service wells are used to reopen wells that have become clogged. Additionally, wells are often drilled at the same location but to different depths, to test other geological structures for the presence of crude oil.

Finally, the drilling job is complete when the drill bit penetrates the reservoir and the reservoir is evaluated to see whether the well represents the discovery of a *prospect* or whether it is a dry hole. If the hole is dry, it is plugged and abandoned.

At the stage when the prospect has been identified, reservoir evaluation is usually initiated by examining the cuttings from the well bore for evidence of hydrocarbons while the drill bit passes through a reservoir trap. The evaluation of these cuttings helps pinpoint the possible producing intervals in the well bore. At this time, a wire-line is lowered into the hole and an electric log is run to help define possible producing intervals, presence of hydrocarbons, and detailed information about the different formations throughout the well bore. Further tests (such as pressure tests, formation fluid recovery, and sidewall core analysis) can also be run on individual formations within the well bore.

If hydrocarbons are detected, the prospect becomes a *live prospect* and once the final depth has been reached, the well is completed to allow oil to flow into the casing in a controlled manner. First, a *perforating gun* is lowered into the well to the production depth. The gun has explosive charges to create holes in the casing through which oil can flow. After the casing has been perforated, a small-diameter pipe (*tubing*) is run into the hole as a conduit for oil and gas to flow up the well and a *packer* is run down the outside of the tubing. When the packer is set at the production level, it is expanded to form a seal around the outside of the tubing. Finally, a multivalve structure (the *Christmas tree*; Fig. 2) is installed at the top of the tubing and cemented to the top of the casing. The Christmas tree allows them to control the flow of oil from the well.

Finally, the development of an onshore shallow gas reservoir located among other established fields may be expected to incur relatively high cost and be nominally complex. A deep oil or gas reservoir located in more than 1 mile of water depth located miles away from other existing producing fields will push the limits of emerging technology at extreme costs.

Onshore developments may permit the phasing of facility investments as wells are drilled and production established to minimize economic risk. However, offshore projects may require 65% or more of the total planned investments to be made before production start-up, and impose significant economic risk.

As might be expected, the type of exploration technique employed depends upon the nature of the site. In other words, and as for many environmental operations, the recovery techniques applied to a specific site are dictated by the nature of the site and are, in fact, *site specific*. For example, in areas where little is known about the subsurface, preliminary reconnaissance techniques are necessary to identify potential reservoir systems that warrant further investigation. Techniques for reconnaissance that have been employed to make inferences about the subsurface structure include *satellite and high-altitude imagery* and *magnetic and gravity surveys*.

Production

Recovery, as applied in the petroleum industry, is the production of oil from a reservoir. There are several methods by which this can be achieved that range from recovery due to reservoir energy (i.e., the oil flows from

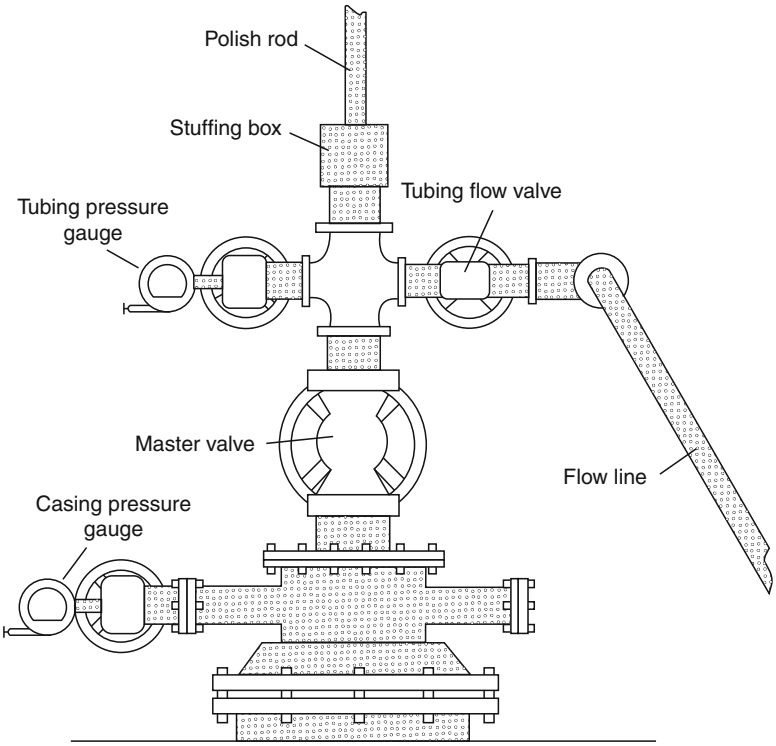

Petroleum and Oil Sands Exploration and Production. Figure 2
The Christmas tree

the well hole without assistance) to enhanced recovery methods in which considerable energy must be added to the reservoir to produce the oil. However, the effect of the method on the oil and on the reservoir must be considered before application.

Generally, crude oil reservoirs sometimes exist with an overlying *gas cap*, in communication with aquifers, or both. The oil resides together with water and free gas in very small holes (pore spaces) and fractures. The size, shape, and degree of interconnection of the pores vary considerably from place to place in an individual reservoir. Below the oil layer, the sandstone is usually saturated with salt water. The oil is released from this formation by drilling a well and puncturing the limestone layer on either side of the limestone dome or fold. If the peak of the formation is tapped, only the gas is obtained. If the penetration is made too far from the center, only salt water is obtained.

Therefore, in designing a recovery project, it is a general practice to locate injection and producing wells in a regular geometric pattern so that a symmetrical and interconnected network is formed and production can be maximized. However, the relative location of injectors and producers depends on: (1) reservoir geometry, (2) lithology, (3) reservoir depth, (4) porosity, (5) permeability, (6) continuity of reservoir rock properties, (7) magnitude and distribution of fluid saturations, and last, but certainly not least (8) fluid, i.e., oil, properties. Overall, the goal is to increase the mobility of the oil.

Once production begins, the performance of each well and reservoir is monitored and a variety of engineering techniques are used to progressively refine reserve recovery estimates over the producing life of the field. The total recoverable reserves are not known with complete certainty until the field has produced to depletion or its economic limit and abandonment.

Generally, the first stage in the extraction of crude oil is to drill a well into the underground reservoir. Often many wells (*multilateral wells*) will be drilled into the same reservoir, to ensure that the extraction rate will be economically viable. Also, some wells (*secondary wells*) may be used to pump water, steam, acids, or various gas mixtures into the reservoir to raise

or maintain the reservoir pressure, and so maintain an economic extraction rate.

Directional drilling is also used to reach formations and targets not directly below the penetration point or drilling from shore to locations under water [4]. A controlled deviation may also be used from a selected depth in an existing hole to attain economy in drilling costs. Various types of tools are used in directional drilling along with instruments to help orient their position and measure the degree and direction of deviation; two such tools are the *whipstock* and the *knuckle joint*. The whipstock is a gradually tapered wedge with a chisel-shaped base that prevents rotation after it has been forced into the bottom of an open hole. As the bit moves down, it is deflected by the taper about 5° from the alignment of the existing hole.

If the underground pressure in the oil reservoir is sufficient, the oil will be forced to the surface under this pressure (*primary recovery*). Natural gas (*associated natural gas*) is often present, which also supplies needed underground pressure (*primary recovery*). In this situation, it is sufficient to place an arrangement of valves (the *Christmas tree*; Fig. 2) on the well head to connect the well to a pipeline network for storage and processing.

For limestone reservoir rock, acid is pumped down the well and out the perforations. The acid dissolves channels in the limestone that lead oil into the well. For sandstone reservoir rock, a specially blended fluid containing *proppants* (sand, walnut shells, aluminum pellets) is pumped down the well and out the perforations. The pressure from this fluid makes small fractures in the sandstone that allow oil to flow into the well, while the proppants hold these fractures open. Once the oil is flowing, production equipment is set up to extract the oil from the well.

A well is always carefully controlled in its flush stage of production to prevent the potentially dangerous and wasteful *gusher*. This is actually dangerous condition, and is (hopefully) prevented by the blowout preventer and the pressure of the drilling mud. In most wells, acidizing or fracturing the well starts the oil flow.

Whatever the nature of the reservoir rock (sandstone or limestone), over the lifetime of the well the pressure will fall, and at some point, there will be insufficient underground pressure to force the oil to the surface. *Secondary oil recovery* uses various techniques to aid in recovering oil from depleted or low-pressure reservoirs. Sometimes pumps, such as beam pumps (*horsehead pumps*) and electrical submersible pumps, are used to bring the oil to the surface. Other secondary recovery techniques increase the reservoir's pressure by water injection, natural gas reinjection, and gas lift, which injects air, carbon dioxide, or some other gas into the reservoir.

Reservoir heterogeneity, such as fractures and faults, can cause reservoirs to drain inefficiently by conventional methods. Also, highly cemented or shale zones can produce barriers to the flow of fluids in reservoirs and lead to high residual oil saturation. Reservoirs containing crude oils with low API gravity often cannot be produced efficiently without application of *enhanced oil recovery* (EOR) methods because of the high viscosity of the crude oil.

Conventional primary and secondary recovery processes are ultimately expected to produce about one third of the original oil-in-place (OOIP), although recoveries from individual reservoirs can range from less than 5% to as high as 80% v/v of the original oil-in-place. This broad range of recovery efficiency is a result of variations in the properties of the specific rock and fluids involved from reservoir to reservoir as well as the kind and level of energy that drives the oil to producing wells, where it is captured.

Conventional oil production methods may be unsuccessful because the management of the reservoir was poor or because reservoir heterogeneity has prevented the recovery of crude oil in an economical manner. In some cases, the reservoir pressure may have been depleted prematurely by poor reservoir management practices to create reservoirs with low energy and high oil saturation.

Crude oil is also produced from offshore fields, usually from steel drilling platforms set on the ocean floor. In shallow, calm waters, these may be little more than a wellhead and workspace but the larger ocean rigs include the well equipment and processing equipment as well as crew quarters. Such platforms include the *floating tension leg platform* that is secured to the sea floor by giant cables and drill ships. Such platforms can hold a steady position above a sea floor well using constant, computer-controlled adjustments. In Arctic

areas, islands may be built from dredged gravel and sand to provide platforms capable of resisting drifting ice fields.

Primary Recovery Methods Petroleum recovery usually starts with a formation pressure high enough to force crude oil into the well and sometimes to the surface through the tubing [5]. In this situation, it is sufficient to place the Christmas tree (Fig. 2) on the wellhead to connect the well to a pipeline network for storage and processing.

For a newly opened formation and under ideal conditions, the proportions of gas may be so high that the oil is, in fact, a solution of liquid in gas that leaves the reservoir rock so efficiently that a core sample will not show any obvious oil content. A general rough indication of this situation is a high ratio of gas to oil produced. This ratio may be zero for fields in which the rock pressure has been dissipated. The oil must be pumped out to as much as 50,000 ft^3 or more of gas per barrel of oil in the so-called condensate reservoirs, in which a very light crude oil (0.80 specific gravity or lighter) exists as vapor at high pressure and elevated temperature.

Crude oil moves out of the reservoir into the well by one or more of three processes. These processes are: *dissolved gas drive*, *gas cap drive*, and *water drive*. Early recognition of the type of drive involved is essential to the efficient development of an oil field.

In *dissolved gas drive* (*solution gas drive*) [2, 4], the propulsive force is the gas in solution in the oil, which tends to come out of solution because of the pressure release at the point of penetration of a well. Dissolved gas drive is the least efficient type of natural drive as it is difficult to control the gas-oil ratio and the bottom-hole pressure drops rapidly.

If gas overlies the oil beneath the top of the trap, it is compressed and can be utilized (*gas cap drive*) to drive the oil into wells situated at the bottom of the oil-bearing zone [2, 4]. By producing oil only from below the gas cap, it is possible to maintain a high gas-oil ratio in the reservoir until almost the very end of the life of the pool. If, however, the oil deposit is not systematically developed so that bypassing of the gas occurs, an undue proportion of oil is left behind.

Usually the gas in a gas cap (*associated natural gas*) contains methane and other hydrocarbons that may be separated out by compressing the gas. A well-known example is *natural gasoline* that was formerly referred to as *casinghead gasoline* or *natural gas gasoline*. However at high pressures, such as those existing in the deeper fields, the density of the gas increases and the density of the oil decreases until they form a single phase in the reservoir. These are the so-called retrograde condensate pools because a decrease (instead of an increase) in pressure brings about condensation of the liquid hydrocarbons. When this reservoir fluid is brought to the surface and the condensate is removed, a large volume of residual gas remains. In many cases, this gas is recycled by compression and injection back into the reservoir, thus maintaining adequate pressure within the gas cap, and condensation in the reservoir is prevented.

The most efficient propulsive force in driving oil into a well is natural *water drive*, in which the pressure of the water forces the lighter recoverable oil out of the reservoir into the producing wells [2, 4]. In anticlinal accumulations, the structurally lowest wells around the flanks of the dome are the first to come into water. Then the oil–water contact plane moves upward until only the wells at the top of the anticline are still producing oil; eventually these also must be abandoned as the water displaces the oil. The force behind the water drive may be hydrostatic pressure, the expansion of the reservoir water, or a combination of both. Water drive is also used in certain submarine fields.

Gravity drive is an important factor when oil columns of several thousands of feet exist. Furthermore, the last bit of recoverable oil is produced in many pools by gravity drainage of the reservoir. Another source of energy during the early stages of withdrawal from a reservoir containing undersaturated oil is the expansion of that oil as the pressure reduction brings the oil to the bubble point (the pressure and temperature at which the gas starts to come out of solution).

The recovery efficiency for primary production is generally low when liquid expansion and solution gas evolution are the driving mechanisms. Much higher recoveries are associated with reservoirs with water and gas cap drives and with reservoirs in which gravity effectively promotes drainage of the oil from the rock pores. The overall recovery efficiency is related to how the reservoir is delineated by production wells.

For primary recovery operations, no pumping equipment is required. If the reservoir energy is not

sufficient to force the oil to the surface, then the well must be pumped. In either case, nothing is added to the reservoir to increase or maintain the reservoir energy or to sweep the oil toward the well. The rate of production from a flowing well tends to decline as the natural reservoir energy is expended. When a flowing well is no longer producing at an efficient rate, a pump is installed.

Two processes used to improve formation characteristics are *acidizing* and *fracturing*. *Acidizing* involves injecting an acid into a soluble formation, such as a carbonate, where it dissolves rock. This process enlarges the existing voids and increases permeability. *Hydraulic fracturing* (*fracking*) involves injecting a fluid into the formation under significant pressure that makes existing small fractures larger and creates new fractures.

Heavy oil and Tar sands (*oil sands*) have a shorter history of production and generally heavy oil reservoirs and tar sand deposits have only been subject to only one recovery technology. In the case of tar sands, primary and secondary recovery technologies, as defined for conventional oil, are not applicable because tar sand bitumen is not mobile at reservoir conditions [2, 4]. Therefore, tar sands developments generally start with a thermal recovery technology which would be considered a tertiary method or enhanced recovery method for conventional oil. However, as the development of heavy oil and tar sand technology matures, the concept of applying more than one recovery technology in a specific order is likely to also be applied to heavy oil reservoirs and tar sand deposits. In particular, in the Lloydminster area (Alberta, Canada), producers have already been investigating for several years the concept of follow-up recovery technologies once primary production is no longer economic.

Secondary Recovery Petroleum production is invariably accompanied by a decline in reservoir pressure and *primary recovery* comes to an end as the reservoir energy is reduced. At this stage, secondary recovery methods are applied to replace produce reservoir fluids and maintain (or increase) reservoir pressure.

Secondary oil recovery methods use various techniques to aid in recovering oil from depleted or low-pressure reservoirs. Sometimes pumps on the surface or submerged (electrical submersible pumps, ESPs) are used to bring the oil to the surface. Other secondary recovery techniques increase the reservoir's pressure by water injection and gas injection, which injects air or some other gas into the reservoir. In fact, the first method recommended for improving the recovery of oil was a pressure maintenance project which involved the reinjection of natural gas, and there are indications that gas injection was utilized for this purpose before 1900 [6, 7].

The most common follow-up, or *secondary recovery*, operations usually involve the application of pumping operations or of injection of materials into a well to encourage movement and recovery of the remaining petroleum. The pump, generally known as the *horsehead pump* (*pump jack*, *nodding donkey*, or *sucker rod pump*), provides mechanical lift to the fluids in the reservoir.

The up-and-down movement of the sucker rods forces the oil up the tubing to the surface. A walking beam powered by a nearby engine may supply this vertical movement, or it may be brought about through the use of a pump jack, which is connected to a central power source by means of pull rods. Depending on the size of the pump, it generally produces up to one third of a barrel of an oil–water emulsion at each stroke. The size of the pump is also determined by the depth and weight of the oil to be removed, with deeper extraction requiring more power to move the heavier lengths of polish rod.

There are also *secondary oil recovery* operations that involve the injection of water or gas into the reservoir. When water is used, the process is called a *waterflood*; when gas is used, it is called a *gas flood*. Separate wells are usually used for injection and production. The injected fluids maintain reservoir pressure or re-pressure the reservoir after primary depletion and displace a portion of the remaining crude oil to production wells.

During the withdrawal of fluids from a well, it is usual practice to maintain pressures in the reservoir at or near the original levels by pumping either gas or water into the reservoir as the hydrocarbons are withdrawn. This practice has the advantage of retarding the decline in the production of individual wells and considerably increasing the ultimate yield. It also may bring about the conservation of gas that otherwise would be wasted, and the disposal of brines that

otherwise might pollute surface and near-surface potable waters.

In the *waterflooding process*, water is injected into a reservoir to obtain additional oil recovery through movement of reservoir oil to a producing well. Generally, the selection of an appropriate flooding pattern for the reservoir depends on the quantity and location of accessible wells. Frequently, producing wells can be converted to injection wells whereas in other circumstances, it may be necessary or advantageous to drill new injection wells.

The mobility of oil is the effective permeability of the rock to the oil divided by the viscosity of the oil.

$$\lambda = k/\mu$$

where λ is the mobility, mD/cP, k is the effective permeability of reservoir rock to a given fluid, mD, and μ is the fluid viscosity, cP. Thus, the mobility ratio (M) is the mobility of the water divided by the mobility of oil:

$$M = K_{rw}\mu_o/K_{ro}\mu_w$$

where K_{rw} is the relative permeability to water, K_{ro} is the relative permeability to oil, μ_o is the viscosity of the oil, and μ_w is the viscosity of water.

The mobility ratio (M) refers that K_o is the mobility of oil ahead of the front (measured at S_{wc}) while K_w is the mobility of water at average water saturation in the water-contacted portion of the reservoir.

The mobility ratio of a waterflood will remain constant before breakthrough, but will increase after water breakthrough corresponding to the increase in water saturation and relative permeability to water in the water-contacted portion of the reservoir. Furthermore, the mobility ratio at water breakthrough is the term that is of significance in describing relative mobility ratio, i.e., $M < 1$ indicates a favorable displacement as oil moves faster than water and $M = 1$ indicates a favorable displacement as both oil and water move at equal speed whereas $M > 1$ indicates an unfavorable displacement as water moves faster than oil.

Generally, the choice of pattern (Table 1) for waterflooding must be consistent with the existing wells. The objective is to select the proper pattern that will provide the injection fluid with the maximum possible contact with the crude oil to minimize bypassing by the water.

Petroleum and Oil Sands Exploration and Production.

Table 1 The ratio of injectors to producers for various well patterns

Pattern	Ratio of producing wells to injection wells	Drilling pattern required
Four spot	2	Equilateral triangle
Five spot	1	Square
Seven spot	1/2	Equilateral triangle
Inverted seven spot	2	Equilateral triangle
Nine spot	1/3	Square
Inverted nine spot	3	Square
Direct line drive	1	Rectangle
Staggered line drive	1	Offset lines of wells

In a *four-spot pattern*, the distance between all like wells is constant. Any three injection wells form an equilateral triangle with a production well at the center. The four spot may be used when the injectivity is high or the heterogeneity is minimal.

In a *five-spot pattern*, the distance between all like wells is constant. Four injection wells form a square with a production well at the center. If existing wells were drilled on square patterns, five-spot patterns (as well as nine-spot patterns) are most commonly used since they allow easy conversion to a five-spot waterflood.

In the *seven-spot pattern*, the injection wells are located at the corner of a hexagon with a production well at its center. If the reservoir characteristics yield lower than preferred injection rates, either a seven-spot (or a nine-spot) pattern should be considered because there are more injection wells per pattern than producing wells.

In the *nine-spot pattern*, the arrangement is similar to that of the five spot but with an extra injection well drilled at the middle of each side of the square. The pattern essentially contains eight injectors surrounding one producer. If existing wells were drilled on square patterns, nine-spot patterns (as well as

five-spot patterns) are most commonly used. If the reservoir characteristics yield lower injection rates than those desired, one should consider using either a nine-spot pattern (or a seven-spot pattern) where there are more injection wells per pattern than producing wells.

In the *inverted seven-spot pattern*, the arrangement is similar to the normal seven-spot pattern except where the position of the producer well was in the normal seven-spot pattern there is now an injector well. Likewise where the injector wells were in the normal seven-spot pattern, there are now producer wells. The inverted seven-spot pattern may be used when the injectivity is high or the heterogeneity is minimal.

In the *inverted nine-spot pattern*, the arrangement of the wells is similar to the normal nine-spot pattern except the position of the producer well in the normal nine-spot pattern is occupied by an injector well. Likewise where the positions of the injector wells were in the normal nine-spot, there are now producer wells. If the reservoir is fairly homogenous and the mobility ratio is unfavorable, the inverted nine-spot pattern may be promising.

In the *direct line-drive pattern*, the lines of injection and production are directly opposite to each other. If the injectivity is low or the heterogeneity is large, direct line drive is a good option. Anisotropic permeability, permeability trends, or oriented fracture systems favor line drive patterns.

In the *staggered line-drive pattern*, the wells are in lines as in the direct line, but the injectors and producers are no longer directly opposed but laterally displaced by a distance by a specified that is dependent upon the distance between wells of the same type and the distance between the lines of injector wells and producer wells. The staggered line-drive pattern is also effective for reservoirs there is anisotropic permeability or where permeability trends or oriented fracture systems.

Reservoir uniformities (and heterogeneity) also dictate the choice of pattern and mobility ratio has an important influence on pattern selection. If the ratio is unfavorable, the injectivity of an injector will exceed the productivity of a producer and water injection will supersede oil production. Hence, to balance the production with the water injection, more producers than injectors are required. On the other hand, if the mobility ratio is favorable, the injectivity is impaired, and the pattern should have more injectors than producers.

Enhanced Oil Recovery Traditional primary and secondary recovery methods typically recover less than half (sometimes less than one third) of the oil only one third of the original oil-in-place. It is at some point before secondary recovery ceases to remain feasible that enhanced oil recovery methods must be applied if further oil is to be recovered.

Enhanced oil recovery (*tertiary oil recovery*) is the incremental ultimate oil that can be recovered from a petroleum reservoir over oil that can be obtained by primary and secondary recovery methods [2, 4, 8, 9]. Enhanced oil recovery methods offer prospects for ultimately producing 30–60%, or more, of the reservoir's original oil-in-place.

Enhanced oil recovery processes use *thermal*, *chemical*, or *fluid phase behavior* effects to reduce or eliminate the capillary forces that trap oil within pores, to thin the oil or otherwise improve its mobility or to alter the mobility of the displacing fluids. In some cases, the effects of gravity forces, which ordinarily cause vertical segregation of fluids of different densities, can be minimized or even used to advantage. The various processes differ considerably in complexity, the physical mechanisms responsible for oil recovery, and the amount of experience that has been derived from field application. The degree to which the enhanced oil recovery methods are applicable in the future will depend on development of improved process technology. It will also depend on improved understanding of fluid chemistry, phase behavior, and physical properties, and also on the accuracy of geology and reservoir engineering in characterizing the physical nature of individual reservoirs [10].

For taxation purposes, the Internal Revenue Service of the United States has listed the projects that qualify as enhanced oil recovery projects [11] and are therefore available for a tax credit and these projects are:

1. *Thermal recovery methods*:

   Thermal methods of recovery reduce the viscosity of the crude oil by heat so that it flows more easily into the production well.

(a) *Steam drive injection* – the continuous injection of steam into one set of wells (injection wells) or other injection source to effect oil displacement toward and production from a second set of wells (production wells).
(b) *Cyclic steam injection* – the alternating injection of steam and production of oil with condensed steam from the same well or wells.
(c) *In situ combustion* – the combustion of oil or fuel in the reservoir sustained by injection of air, oxygen-enriched air, oxygen, or supplemental fuel supplied from the surface to displace unburned oil toward producing wells. This process may include the concurrent, alternating, or subsequent injection of water.

Steam-based methods are the most advanced of all enhanced oil recovery methods in terms of field experience and thus have the least uncertainty in estimating performance, provided that a good reservoir description is available. Steam processes are most often applied in reservoirs containing heavy crude oil, usually in place of rather than following secondary or primary methods. Commercial application of steam processes has been underway since the early 1960s.

2. *Gas flood recovery methods*:
(a) *Miscible fluid displacement* – the injection of gas (e.g., natural gas, enriched natural gas, a liquefied petroleum slug driven by natural gas, carbon dioxide, nitrogen, or flue gas) or alcohol into the reservoir at pressure levels such that the gas or alcohol and reservoir oil are miscible.
(b) *Carbon dioxide–augmented waterflooding* – the injection of carbonated water, or water and carbon dioxide, to increase waterflood efficiency.
(c) *Immiscible carbon dioxide displacement* – the injection of carbon dioxide into an oil reservoir to effect oil displacement under conditions in which miscibility with reservoir oil is not obtained; this process may include the concurrent, alternating, or subsequent injection of water.
(d) *Immiscible nonhydrocarbon gas displacement* – the injection of nonhydrocarbon gas (e.g., nitrogen) into an oil reservoir, under conditions in which miscibility with reservoir oil is not obtained, to obtain a chemical or physical reaction (other than pressure) between the oil and the injected gas or between the oil and other reservoir fluids; this process may include the concurrent, alternating, or subsequent injection of water.

3. *Chemical flood recovery methods*:

Three enhanced oil recovery processes involve the use of chemicals – surfactant/polymer, polymer, and alkaline flooding [12]. However, each reservoir has unique fluid and rock properties, and specific chemical systems must be designed for each individual application. The chemicals used, their concentrations in the slugs, and the slug sizes depend upon the specific properties of the fluids and the rocks involved and upon economic considerations.
(a) *Surfactant flooding* is a multiple-slug process involving the addition of surface-active chemicals to water [13]. These chemicals reduce the capillary forces that trap the oil in the pores of the rock. The surfactant slug displaces the majority of the oil from the reservoir volume contacted, forming a flowing oil–water bank that is propagated ahead of the surfactant slug. The principal factors that influence the surfactant slug design are interfacial properties, slug mobility in relation to the mobility of the oil–water bank, the persistence of acceptable slug properties and slug integrity in the reservoir, and cost.
(b) *Microemulsion flooding* also known as *surfactant-polymer flooding* involves injection of a surfactant system (e.g., a surfactant, hydrocarbon, cosurfactant, electrolyte, and water) to enhance the displacement of oil toward producing wells; and [2] *caustic flooding* – the injection of water that has been made chemically basic by the addition of alkali metal hydroxides, silicates, or other chemicals.
(c) *Polymer-augmented waterflooding* – the injection of polymeric additives with water to improve the areal and vertical sweep efficiency of the reservoir by increasing the viscosity and decreasing the mobility of the water injected; polymer-augmented waterflooding does not include the injection of polymers for the

purpose of modifying the injection profile of the wellbore or the relative permeability of various layers of the reservoir, rather than modifying the water-oil mobility ratio.

Certain types of reservoirs, such as those with very viscous crude oils and some low-permeability carbonate (limestone, dolomite, or chert) reservoirs, respond poorly to conventional secondary recovery techniques. The viscosity (or the API gravity) of petroleum is an important factor that must be taken into account when heavy oil is recovered from a reservoir.

In these reservoirs, it is desirable to initiate *enhanced oil recovery* operations as early as possible. This may mean considerably abbreviating conventional secondary recovery operations or bypassing them altogether.

Thermal methods for oil recovery have found most use when the oil in the reservoir has a high viscosity. For example, heavy oil is usually highly viscous (hence the use of the adjective *heavy*), with a viscosity ranging from approximately 100 cP to several million centipoises at the reservoir conditions. In addition, oil viscosity is also a function of temperature and API gravity [2, 14]. Thus, for heavy crude oil samples with API gravity ranging from 4 to 21°API (1.04–0.928 kg/m^3):

$$\log \log(\mu\sigma + \alpha) = A - B\log(T + 460)$$

In this equation, $\mu\sigma$ is oil viscosity in cP, T is temperature in °F, A and B are constants, and α is an empirical factor used to achieve a straight-line correlation at low viscosity. This equation is usually used to correlate kinematic viscosity in centistokes, in which case an α of 0.6–0.8 is suggested (dynamic viscosity in cP equals kinematic viscosity in cSt times density in g/mL).

An alternative equation for correlating viscosity data (where a and b are constants, and T^* is the absolute temperature) is:

$$\mu = ae^{b/T^*}$$

Thermal-enhanced oil recovery processes add heat to the reservoir to reduce oil viscosity and/or to vaporize the oil. In both instances, the oil is made more mobile so that it can be more effectively driven to producing wells. In addition to adding heat, these processes provide a driving force (pressure) to move oil to producing wells.

Steam drive injection (*steam injection*) has been commercially applied since the early 1960s. The process occurs in two steps: (1) steam stimulation of production wells, that is, direct steam stimulation and (2) steam drive by steam injection to increase production from other wells (indirect steam stimulation).

When there is some natural reservoir energy, steam stimulation normally precedes steam drive. In steam stimulation, heat is applied to the reservoir by the injection of high-quality steam into the production well. This cyclic process, also called *huff and puff* or *steam soak*, uses the same well for both injection and production. The period of steam injection is followed by production of reduced viscosity oil and condensed steam (water). One mechanism that aids production of the oil is the flashing of hot water (originally condensed from steam injected under high pressure) back to steam as pressure is lowered when a well is put back on production.

Cyclic steam injection is the alternating injection of steam and production of oil with condensed steam from the same well or wells. Thus, steam generated at surface is injected in a well and the same well is subsequently put back on production.

A cyclic steam injection process includes three stages. The first stage is injection, during which a measured amount of steam is introduced into the reservoir. The second stage (*the soak period*) requires that the well be shut in for a period of time (usually several days) to allow uniform heat distribution to reduce the viscosity of the oil (alternatively, to raise the reservoir temperature above the pour point of the oil). Finally, during the third stage, the now-mobile oil is produced through the same well. The cycle is repeated until the flow of oil diminishes to a point of no returns.

The high gas mobility may limit recovery through its adverse effect on the sweep efficiency of the burning front. Because of the density contrast between air and reservoir liquids, the burning front tends to override the reservoir liquids. To date, combustion has been most effective for the recovery of viscous oils in moderately thick reservoirs in which reservoir dip and continuity provide effective gravity drainage or operational factors permit close well spacing.

Using combustion to stimulate oil production is regarded as attractive for deep reservoirs [15] and, in contrast to steam injection, usually involves no loss of heat. The duration of the combustion may be short (<30 days) or more prolonged (approximately 90 days), depending upon requirements. In addition, backflow of the oil through the hot zone must be prevented or coking occurs.

Both forward and reverse combustion methods have been used with some degree of success when applied to tar sand deposits. The forward-combustion process has been applied to the Orinoco deposits [16] and in the Kentucky sands [15]. The reverse combustion process has been applied to the Orinoco deposit [17] and the Athabasca [2, 4]. In tests such as these, it is essential to control the airflow and to mitigate the potential for spontaneous ignition [17]. A modified combustion approach has been applied to the Athabasca deposit [2, 4]. The technique involved a heat-up phase and a production (or blowdown phase) followed by a displacement phase using a fireflood-waterflood (COFCAW) process.

Oil Sand Exploration and Production

Heavy oil and bitumen (the component of interest in tar sand) are often defined (loosely and incorrectly) in terms of API gravity. A more appropriate definition of bitumen, which sets it aside from heavy oil and conventional petroleum, is based on the definition offered by the US government as the *extremely viscous hydrocarbon which is not recoverable in its natural state by conventional oil well production methods including currently used enhanced recovery techniques* [2, 4].

By inference, conventional petroleum and heavy oil (recoverable by *conventional oil well production methods including currently used enhanced recovery techniques*) are different to tar sand bitumen. Be that as it may, in some stage of production, conventional petroleum (in the later stages of recovery) and heavy oil (in the earlier stages of recovery) may require the application of enhanced oil recovery methods for recovery.

Oil Mining

Oil mining includes recovery of oil and/or heavy oil by drainage from reservoir beds to mine shafts or other openings driven into the rock or by drainage from the reservoir rock into mine openings driven outside the reservoir but connected with it by boreholes or mine wells.

Oil mining methods should be applied in reservoirs that have significant residual oil saturation and have reservoir or fluid properties that make production by conventional methods inefficient or impossible. The high well density in improved oil mining usually compensates for the inefficient production caused by reservoir heterogeneity.

However, close well spacing can also magnify the deleterious effects of reservoir heterogeneity. If a high-permeability streak exists with a lateral extent that is less than the inter-well spacing of conventional wells but is comparable to that of improved oil mining, the channeling is more unfavorable for the improved oil mining method.

Tar Sand Mining

The bitumen occurring in tar sand deposits poses a major recovery problem. The material is notoriously immobile at formation temperatures and must therefore require some stimulation (usually by thermal means) in order to ensure recovery. Alternately, proposals have been noted which advocate bitumen recovery by solvent flooding or by the use of emulsifiers. There is no doubt that with time, one or more of these functions may come to fruition, but for the present, the two commercial operations rely on the mining technique.

The alternative to in situ processing is to mine tar sand, transport the mined material to a processing plant, extract the bitumen, and dispose of the waste sand. Such a procedure is often referred to as *oil mining*. This is the term applied to the surface or subsurface excavation of petroleum-bearing formations for subsequent removal of the heavy oil or bitumen by washing, flotation, or retorting treatments.

The tar sand mining method of recovery has received considerable attention since it was chosen as the technique of preference for the only two commercial bitumen recovery plants in operation in North America. In situ processes have been tested many times in the United States, Canada, and other parts of the world and are ready for commercialization. There are also conceptual schemes that are a combination of

both mining (aboveground recovery) and in situ (non-mining recovery) methods.

Engineering a successful oil mining project must address a number of items because there must be sufficient recoverable resources, the project must be conducted safely, and the project should be engineered to maximize recovery within economic limits. The use of a reliable screening technique is necessary to locate viable candidates. Once the candidate is defined, this should be followed by an exhaustive literature search covering the local geology, drilling, production, completion, and secondary and tertiary recovery operations.

The reservoir properties, which can affect the efficiency of heavy oil or bitumen production by mining technology, can be grouped into three classes:

1. *Primary properties*, i.e., those properties that have an influence on the fluid flow and fluid storage properties and include rock and fluid properties, such as porosity, permeability, wettability, crude oil viscosity, and pour point
2. *Secondary properties*, i.e., those properties that significantly influence the primary properties, including pore size distribution, clay type, and content
3. *Tertiary properties*, i.e., those other properties that mainly influence oil production operation (fracture breakdown pressure, hardness, and thermal properties) and the mining operations (e.g., temperature, subsidence potential, and fault distribution)

There are also important rock mechanical parameters of the formation in which a tunnel is to be mined and from where all oil mining operations will be conducted. These properties are mostly related to the mining aspects of the operations, and not all are of equal importance in their influence on the mining technology. Their relative importance also depends on the individual reservoir.

Surface mining is the mining method that is currently being used by Suncor Energy and Syncrude Canada Limited to recover tar sand from the ground. Surface mining can be used in mineable tar sand areas which lie under 250 ft or less of overburden material. Less than 10% of the Athabasca Oil Sands deposit can be mined using the surface mining technique, as the other 90% of the deposit has more than 250 ft of overburden. This other 90% will have to be mined using different mining techniques.

There are two methods of mining currently in use in the Athabasca Oil Sands. Suncor Energy uses the truck and shovel method of mining whereas Syncrude uses the truck and shovel method of mining, as well as draglines and bucket-wheel reclaimers. These enormous draglines and bucket-wheels are being phased out and soon will be completely replaced with large trucks and shovels. The shovel scoops up the tar sand and dumps it into a heavy hauler truck. The heavy hauler truck takes the tar sand to a conveyor belt that transports the tar sand from the mine to the extraction plant. Presently, there are extensive conveyor belt systems that transport the mined tar sand from the recovery site to the extraction plant. With the development of new technologies, these conveyors are being phased out and replaced with hydrotransport technology.

Hydrotransport is a combination of ore transport and preliminary extraction. After the bituminous sands have been recovered using the truck and shovel method, it is mixed with water and caustic soda to form a slurry and is pumped along a pipeline to the extraction plant. The extraction process thus begins with the mixing of the water and agitation needed to initiate bitumen separation from the sand and clay.

Mine spoils need to be disposed of in a manner that assures physical stabilization. This means appropriate slope stability for the pile against not only gravity but also earthquake forces. Since return of the spoils to the mine excavations is seldom economical, the spoil pile must be designed as a permanent structure whose outline blends into the landscape. Straight, even lines in the pile must be avoided.

Underground mining options have also been proposed but for the moment have not been developed because of the fear of collapse of the formation onto any operation/equipment. This particular option should not, however, be rejected out-of-hand because a novel aspect or the requirements of the developer (which remove the accompanying dangers) may make such an option acceptable.

The tar sand recovered by mining is sent to the processing plant for separation of the bitumen from the sand prior to upgrading.

The Hot-Water Process

The *hot-water process* is, to date, the only successful commercial process to be applied to bitumen recovery from mined tar sands in North America [18–22]. Many process options have been tested with varying degrees of success, and one of these options may even supersede the hot-water process.

The process utilizes (1) the film of water coats most of the mineral matter, which permits extraction by the *hot-water process*, (2) the linear and the nonlinear variation of bitumen density and water density, respectively, with temperature so that the bitumen that is heavier than water at room temperature becomes lighter than water at 80°C (180°F), and (3) natural surface-active materials (surfactants) in the tar sand which also contribute to freeing the bitumen from the sand.

In the process, the tar sand is introduced into a *conditioning* drum where the sand is heated and mixed with water to encourage agglomeration of the oil particles. Conditioning is carried out in a slowly rotating drum that contains a steam-sparging system for temperature control as well as mixing devices to assist in lump size reduction and a size ejector at the outlet end. The tar sand lumps are reduced in size by ablation and mixing action. The conditioned *pulp* has the following characteristics: (1) solids 60–85% and (2) pH 7.5–8.5.

Lumps of as-mined tar sand are reduced in size by ablation, and the conditioned pulp is screened through a double-layer vibrating screen. Water is then added to the screened material (to achieve more beneficial pumping conditions), and the pulp enters the separation cell through a central feed well and distributor. The bulk of the sand settles in the cell and is removed from the bottom as tailing, but the majority of the bitumen floats to the surface and is removed as froth. A middlings stream (mostly water with suspended fines and some bitumen) is withdrawn from approximately midway up the side of the cell wall. Part of the middlings is recycled to dilute the conditioning-drum effluent for pumping. Clays do not settle readily and generally accumulate in the middlings layer. High concentrations of clays increase the viscosity and can prevent normal operation in the separation cell.

The separation cell acts like two settlers – one on top of the other – and in the lower settler, the sand settles down, whereas in the upper settler, the bitumen floats. The bulk of the sand in the feed is removed from the bottom of the separation cell as tailings. A large portion of the feed bitumen floats to the surface of the separation cell and is removed as bituminous froth. A middlings stream consists mostly of water with some suspended fine minerals and bitumen particles, and a portion of the middlings may be returned for mixing with the conditioning-drum effluent in order to dilute the separation-cell feed for pumping. The remainder of the middlings is withdrawn from the separation cell to be rejected after processing in the scavenger cells.

The combined froth from the separation cell and scavenging operation contains an average of about 10% by weight mineral material and up to 40% by weight water. The dewatering and demineralizing is accomplished in two stages of centrifuging; in the first stage, the coarser mineral material is removed but much of the water remains. The feed then passes through a filter to remove any additional large-size mineral matter that would plug up the nozzles of the second stage centrifuges.

In the scavenging cell, froth flotation with air is usually employed to recover more bitumen. The scavenger froth is combined with the separation-cell froth to be further treated and upgraded to synthetic crude oil. Tailings from the scavenger cell join the separation-cell tailings stream and go to waste.

The bituminous froth from the hot-water process may be mixed with a hydrocarbon diluent, e.g., coker naphtha, and centrifuged. The Suncor process employs a two-stage centrifuging operation, and each stage consists of multiple centrifuges of conventional design installed in parallel. The bitumen product contains 1% by weight to 2% by weight mineral (dry bitumen basis) and 5% by weight to 15% by weight water (wet diluted basis). Syncrude also utilizes a centrifuge system with naphtha diluent.

One of the major problems that arises from the hot-water process is the disposal and control of the tailings. The fact is that each ton of tar sand in place has a volume of about 16 ft^3, which will generate about 22 ft^3 of tailings giving a volume gain on the order of 40%. If the mine produces about 200,000 t of tar sand per day, the volume expansion represents a considerable solids disposal problem. Tailings from

the process consist of about 49–50% by weight of sand, 1% by weight of bitumen, and about 50% by weight of water. The average particle size of the sand is about 200 mm, and it is a suitable material for dike building. Accordingly, Suncor used this material to build the sand dike, but for fine sand, the sand must be well compacted.

Environmental regulations in Canada or the United States will not allow the discharge of tailings streams into (1) the river; (2) on to the surface; or (3) on to any area where contamination of groundwater domains or the river may be contaminated. The tailings streams is essentially high in clays and contains some bitumen, hence the current need for tailings ponds, where some settling of the clay occurs. In addition, an approach to acceptable reclamation of the tailings ponds will have to be accommodated at the time of site abandonment.

The structure of the dike may be stabilized on the upstream side by beaching. This gives a shallow slope but consumes sand during the season when it is impossible to build the dike. In remote areas such as the Fort McMurray (Alberta) site, the dike can only be built in above-freezing weather because (1) frozen water in the pores of the dike will create an unstable layer and (2) the vapor emanating from the water creates a fog, which can create a work hazard. The slope of the tailings dike is about 2.5:1 depending on the amount of fines in the material. It may be possible to build with 2:1 slopes with coarser material, but steeper slopes must be stabilized quickly by beaching. After discharge from the hot-water separation system, it is preferable that attempts be made to separate the sand, sludge, and water, hence, the tailings pond. The sand is used to build dikes and the runoff that contains the silt, clay, and water collects in the pond. Silt and some clay settle out to form sludge, and some of the water is recycled to the plant.

In summary, the hot-water separation process involves extremely complicated surface chemistry with interfaces among various combinations of solids (including both silica sand and aluminosilicate clays), water, bitumen, and air. The control of pH is critical with the preferred range being 8.0–8.5, which is achievable by use of any of the monovalent bases. Polyvalent cations must be excluded because they tend to flocculate the clays and thus raise the viscosity of the middlings in the separation cell.

Other Processes

The issues arising from bitumen mining and bitumen recovery may be alleviated somewhat by the development of process options that require considerably less water in the sand/bitumen separation step. Such an option would allow a more gradual removal of the tailings ponds.

A *cold-water process* for bitumen separation from mined tar sand has also been recommended [23, 24]. The process uses a combination of cold water and solvent, and the first step usually involves disintegration of the tar sand charge that is mixed with water, diluent, and reagents. The diluent may be a petroleum distillate fraction such as aromatic naphtha or kerosene and is added in approximately a 1:1 weight ratio to the bitumen in the feed. The pH is maintained at 9–9.5 by the addition of wetting agents and approximately 0.77 kg of soda ash per ton of tar sand. The effluent is mixed with more water, and in a raked classifier, the sand is settled from the bulk of the remaining mixture. The water and oil overflow the classifier and are passed to thickeners where the oil is concentrated. Clay in the tar sand feed has a distinct effect on the process; it forms emulsions that are hard to break and are wasted with the underflow from the thickeners.

The *sand-reduction process* is a cold-water process without solvent. In the first step, the tar sand feedstock is mixed with water at approximately 20°C (68°F) in a screw conveyor in a ratio of 0.75–3 t per ton of tar sand (the lower range is preferred). The mixed pulp from the screw conveyor is discharged into a rotary-drum screen, which is submerged in a water-filled settling vessel. The bitumen forms agglomerates that are retained by an 840-μm (20-mesh) screen. These agglomerates settle and are withdrawn as oil product. The sand readily passes through the 840 μm (20 mesh) screen and is withdrawn as waste stream. The process is called sand reduction because its objective is the removal of sand from the tar sand to provide a feed suitable for a fluid coking process; ca 80% of sand is removed. Nominal composition of the oil product is 58% by weight (bitumen), 27% by weight mineral matter, and 15% by weight water.

The *spherical agglomeration process* resembles the sand-reduction process. Water is added to tar sands and the mixture is ball-milled. The bitumen forms

dense agglomerates of 75% by weight to 87% by weight bitumen, 12% by weight to 25% by weight sand, and 1% by weight to 5% by weight water.

An *oleophilic sieve process* [25, 26] offers the potential for reducing tailings pond size because of a reduction in the water requirements. The process is based on the concept that when a mixture of an oil phase and an aqueous phase is passed through a sieve made from oleophilic materials, the aqueous phase and any hydrophilic solids pass through the sieve but the oil adheres to the sieve surface on contact. The sieve is in the form of a moving conveyor, the oil is captured in a recovery zone, and recovery efficiency is high.

An anhydrous *solvent extraction process* for bitumen recovery has been attempted and usually involves the use of a low-boiling hydrocarbon. The process generally involves up to four steps. In the mixer step, fresh tar sand is mixed with recycle solvent that contains some bitumen and small amounts of water and mineral and the solvent-to-bitumen weight ratio is adjusted to approximately 0.5. The drain step consists of a three-stage countercurrent wash. Settling and draining time is approximately 30 min for each stage. After each extraction step, a bed of sand is formed and the extract is drained through the bed until the interstitial pore volume of the bed is emptied. The last two steps of the process are devoted to solvent recovery solvent recovery from the bitumen and from the solids, which holds the key to the economic success the process.

Another aboveground method of separating bitumen from mined tar sand involves *direct heating of the tar sand* without previous separation of the bitumen [27]. Thus, the bitumen is not recovered as such but is an upgraded overhead product. In the process, the sand is crushed and introduced into a vessel, where it is contacted with either hot (spent) sand or with hot product gases that furnish part of the heat required for cracking and volatilization. The volatile products are passed out of the vessel and are separated into gases and (condensed) liquids. The coke that is formed as a result of the thermal decomposition of the bitumen remains on the sand, which is then transferred to a vessel for coke removal by burning in air. The hot flue gases can be used either to heat incoming tar sand or as refinery fuel. As expected, processes of this type yield an upgraded product but require various arrangements of pneumatic and mechanical equipment for solids movement around the refinery.

In *improved mining*, directional (horizontal or slant) wells are drilled into the reservoir from a mine in an underlying formation to drain oil by pressured depletion and gravity drainage. In the process of gravity drainage extraction of liquid crude oil, the wells are completed so that only the forces acting within the reservoir are used. A large number of closely spaced wells can be drilled into a reservoir from an underlying tunnel more economically than the same number of wells from the surface. In addition, only one pumping system is required in underground drainage, whereas at the surface, each well must have a pumping system. The objective of using a large number of wells is to produce each well slowly so that the gas–oil and water–oil interfaces move toward each other efficiently. By maintaining the reservoir pressures because of forces acting on the reservoir, it is then assured that the oil production is provided by the internal forces due to gravity (the buoyancy effect) and capillary effects.

Large vertical shafts sunk from the surface are generally the means through which underground openings can be excavated. These shafts are one means of access to offer an outlet for removal of excavated rock, provide sufficient opening for equipment, provide ventilation, and allow the removal of oil and gas products during later production. These requirements plus geological conditions and oil reservoir dimensions determine the shaft size. It is expected that an access shaft will range from 8 to 20 ft in diameter.

Non-mining Methods

Whereas conventional crude oils may have a viscosity of several poise (at 40°C, 105°F), the tar sand bitumen has a viscosity of the order of 50,000–1,000,000 cP or more at formation temperatures (approximately 0–10°C, 32–50°F depending upon the season). This offers a formidable (but not insurmountable) obstacle to bitumen recovery.

In principle, the *non-mining recovery of bitumen from tar sand deposits* is an enhanced recovery technique and requires the injection of a fluid into the formation through an injection wall. This leads to the in situ displacement of the bitumen from the sand

followed by bitumen production at the surface through an egress well (production well).

In tar sand deposits, it is often desirable to initiate *enhanced oil recovery* (EOR) operations as early as possible, which mean considerably abbreviating conventional secondary recovery operations or bypassing them altogether. Thermal floods using steam and controlled in situ combustion methods are also used. Thermal methods of recovery reduce the viscosity of the crude oil by heat so that it flows more easily into the production well [28].

The technologies applied to oil recovery involve different concepts, some of which can cause changes to the oil during production. Technologies such as alkaline flooding, microemulsion (micellar/emulsion) flooding, polymer-augmented waterflooding, and carbon dioxide miscible/immiscible flooding do not require or cause any change to the oil. The steaming technologies may cause some steam distillation that can augment the process when the steam-distilled material moves with the steam front and acts as a solvent for oil ahead of the steam front. Again, there is no change to the oil although there may be favorable compositional changes to the oil insofar as lighter fractions are recovered and heavier materials remain in the reservoir.

The technology where changes do occur involves combustion of the oil in situ. The concept of any combustion technology requires that the oil be partially combusted and that thermal decomposition occur to other parts of the oil. This is sufficient to cause irreversible chemical and physical changes to the oil to the extent that the product is markedly different to the oil-in-place, indicating upgrading of the bitumen during the process. Recognition of this phenomenon is essential before combustion technologies are applied to oil recovery.

Thermal recovery methods (Fig. 1) have found most use when heavy oil or bitumen has an extremely high viscosity under reservoir conditions [2, 4]. For example, bitumen is highly viscous, with a viscosity ranging up to a million centipoises or more at the reservoir conditions.

Thermal-enhanced oil recovery processes (i.e., cyclic steam injection, steam flooding, and in situ combustion) add heat to the reservoir to reduce oil viscosity and/or to vaporize the oil. In both instances, the oil is made more mobile so that it can be more effectively driven to producing wells. In addition to adding heat, these processes provide a driving force (pressure) to move oil to producing wells.

In the *modified* in situ *extraction* processes, combinations of in situ and mining techniques are used to access the reservoir. A portion of the reservoir rock must be removed to enable application of the in situ extraction technology. The most common method is to enter the reservoir through a large-diameter vertical shaft, excavate horizontal drifts from the bottom of the shaft, and drill injection and production wells horizontally from the drifts. Thermal extraction processes are then applied through the wells. When the horizontal wells are drilled at or near the base of the tar sand reservoir, the injected heat rises from the injection wells through the reservoir, and drainage of produced fluids to the production wells is assisted by gravity.

There are, however, several serious constraints that are particularly important and relate to bulk properties of the tar sand and the bitumen. In fact, both must be considered in the context of bitumen recovery by non-mining techniques. For example, the Canadian deposits are unconsolidated sands with a porosity ranging up to about 45% whereas other deposits may range from predominantly low-porosity, low-permeability consolidated sand to, in a few instances, unconsolidated sands. In addition, the bitumen properties are not conducive to fluid flow under deposit conditions. Nevertheless, where the general nature of the deposits prohibits the application of a mining technique, a non-mining method may be the only feasible bitumen recovery option.

Another general constraint to bitumen recovery by non-mining methods is the relatively low injectivity of tar sand formations. Thus, it is usually necessary to inject displacement or recovery finds at a pressure such that fracturing (parting) is achieved. Such a technique therefore changes the reservoir profile and introduces a series of channels through which fluids can flow from the injection well to the production well. On the other hand, the technique may be disadvantageous insofar as the fracture occurs along the path of least resistance, giving undesirable (i.e., inefficient) flow characteristics within the reservoir between the injection and production wells, leaving

a large part of the reservoir relatively untouched by the displacement or recovery fluids.

Another general constraint to bitumen recovery by non-mining methods is the relatively low injectivity of tar sand formations. It is usually necessary to inject displacement/recovery fluids at a pressure such that fracturing (parting) is achieved. Such a technique, therefore, changes the reservoir profile and introduces a series of channels through which fluids can flow from the injection well to the production well. On the other hand, the technique may be disadvantageous insofar as the fracture occurs along the path of least resistance giving undesirable (i.e., inefficient) flow characteristics within the reservoir between the injection and production wells which leave a part of the reservoir relatively untouched by the displacement or recovery fluids.

Steam-Based Processes Steam-based processes are the most advanced of all enhanced oil recovery methods in terms of field experience and thus have the least uncertainty in estimating performance, provided that a good reservoir description is available. Steam processes are most often applied in reservoirs containing heavy oil, which is mobile at reservoir temperature. Commercial application of steam processes has been underway since the early 1960s.

Steam drive injection (*steam injection*) has been commercially applied since the early 1960s. The process occurs in two steps: (1) steam stimulation of production wells, that is, direct steam stimulation, and (2) steam drive by steam injection to increase production from other wells (i.e., indirect steam stimulation). Steam drive requires sufficient effective permeability (with the immobile bitumen in place) to allow injection of the steam at rates sufficient to raise the reservoir temperature to mobilize the bitumen and drive it to the production well.

Cyclic steam injection (also called *huff and puff* or *steam soak*) is the alternating injection of steam and production of oil with condensed steam from the same well or wells. This process is predominantly a vertical well process, with each well alternately injecting steam and producing heavy oil and steam condensate. In practice, steam is injected into the formation at greater than fracturing pressure followed by a *soak* period after which production is commenced. The heat injected warms the heavy oil and lowers its viscosity. A heated zone is created through which the warmed heavy oil can flow back into the well. This is a well-developed process; the major limitation is that less than 30% (usually less than 20%) of the initial oil-in-place can be recovered.

Combustion Processes In situ *combustion* (*fireflood*) is normally applied to reservoirs containing low-gravity oil but has been tested over perhaps the widest spectrum of conditions of any enhanced oil recovery process. In the process, heat is generated within the reservoir by injecting air and burning part of the crude oil. This reduces the oil viscosity and partially vaporizes the oil-in-place, and the oil is driven out of the reservoir by a combination of steam, hot water, and gas drive. Forward combustion involves movement of the hot front in the same direction as the injected air; reverse combustion involves movement of the hot front opposite to the direction of the injected air.

During the process, energy is generated in the formation by igniting bitumen in the formation and sustaining it in a state of combustion or partial combustion. The high temperatures generated decrease the viscosity of the oil and make it more mobile. Some cracking of the bitumen also occurs, and an upgraded product rather than bitumen itself is the fluid recovered from the production wells.

The relatively small portion of the oil that remains after the displacement mechanisms have acted becomes the fuel for the in situ combustion process. Production is obtained from wells offsetting the injection locations. In some applications, the efficiency of the total in situ combustion operation can be improved by alternating water and air injection. The injected water tends to improve the utilization of heat by transferring heat from the rock behind the combustion zone to the rock immediately ahead of the combustion zone.

The use of combustion to stimulate oil production is regarded as attractive for deep reservoirs. In contrast to steam injection, it usually involves no loss of heat. The duration of the combustion may be less than 30 days or much as 90 days depending on requirements. In addition, backflow of the oil through the hot zone must be prevented or coking will occur.

Forward combustion involves movement of the hot front in the same direction as the injected air while reverse combustion involves movement of the hot front

opposite to the direction of the injected air. In forward combustion, the hydrocarbon products released from the zone of combustion move into a relatively cold portion of the formation. Thus, there is a definite upper limit of the viscosity of the liquids that can be recovered by a forward-combustion process. On the other hand, since the air passes through the hot formation before reaching the combustion zone, burning is complete; the formation is left completely cleaned of hydrocarbons.

Reverse combustion is particularly applicable to reservoirs with lower effective permeability (in contrast with forward combustion). It is more effective because the lower permeability would cause the reservoir to be plugged by the mobilized fluids ahead of a forward-combustion front. In the reverse combustion process, the vaporized and mobilized fluids move through the heated portion of the reservoir behind the combustion front. The reverse combustion partially cracks the bitumen, consumes a portion of the bitumen as fuel, and deposits residual coke on the sand grains. In the process, part of the bitumen will be consumed as fuel and part will be deposited on the sand grains as coke leaving 40–60% recoverable. This coke deposition serves as a cementing material, reducing movement and production of sand.

The addition of water or steam to an in situ combustion process can result in a significant increase in the overall efficiency of that process. Two major benefits may be derived. Heat transfer in the reservoir is improved because the steam and condensate have greater heat-carrying capacity than combustion gases and gaseous hydrocarbons. Sweep efficiency may also be improved because of the more favorable mobility ratio of steam-bitumen compared with gas-bitumen.

Applying a preheating phase before the bitumen recovery phase may significantly enhance the steam or combustion extraction processes. Preheating can be particularly beneficial if the saturation of highly viscous bitumen is sufficiently great as to lower the effective permeability to the point of production being precluded by reservoir plugging. Preheating partially mobilizes the bitumen by raising its temperature and lowering its viscosity. The result is a lower required pressure to inject steam or air and move the bitumen.

In the *fracture-assisted steam technology* (FAST) process, steam is injected rapidly into an induced horizontal fracture near the bottom of the reservoir to preheat the reservoir. This process has been applied successfully in three pilot projects in southwest Texas. Shell has accomplished the same preheating goal by injecting steam into a high-permeability bottom water zone in the Peace River (Alberta) field. Electrical heating of the reservoir by radio-frequency waves may also be an effective method.

In situ combustion has been field tested under a wide variety of reservoir conditions, but few projects have proven economical and advanced to commercial scale and the concept has been abandoned by many recovery operators. However, in situ combustion may make a comeback with a new concept. THAI (toe-to-heel air injection) (Fig. 3) is based on the geometry of horizontal wells that may solve the problems that have plagued conventional in situ combustion. The well geometry enforces a short flow path so that any instability issues associated with conventional combustion are reduced or even eliminated [2, 4].

In situ conversion, or underground refining, is a promising new technology to tap the extensive reservoirs of heavy oil and deposits of bitumen. The new technology [29, 30] features the injection of high-temperature, high-quality steam, and hot hydrogen into a formation containing heavy hydrocarbons to initiate conversion of the heavy hydrocarbons into lighter hydrocarbons. In effect, the heavy hydrocarbons undergo partial underground refining that converts them into a synthetic crude oil (or *syncrude*). The heavier portion of the syncrude is treated to provide the fuel and hydrogen required by the process, and the lighter portion is marketed as a conventional crude oil.

Thus, below ground, superheated steam and hot hydrogen are injected into a heavy oil or bitumen formation, which simultaneously produces the heavy oil or bitumen and converts it in situ (i.e., within the formation) into syncrude. Above ground, the heavier fraction of the syncrude is separated and treated on-site to produce the fuel and hydrogen required by the process, while the lighter fraction is sent to a conventional refinery to be made into petroleum products (United States Patent 6,016,867; United States Patent 6,016,868).

The potential advantages of an in situ process for bitumen and heavy oil include (1) leaving the

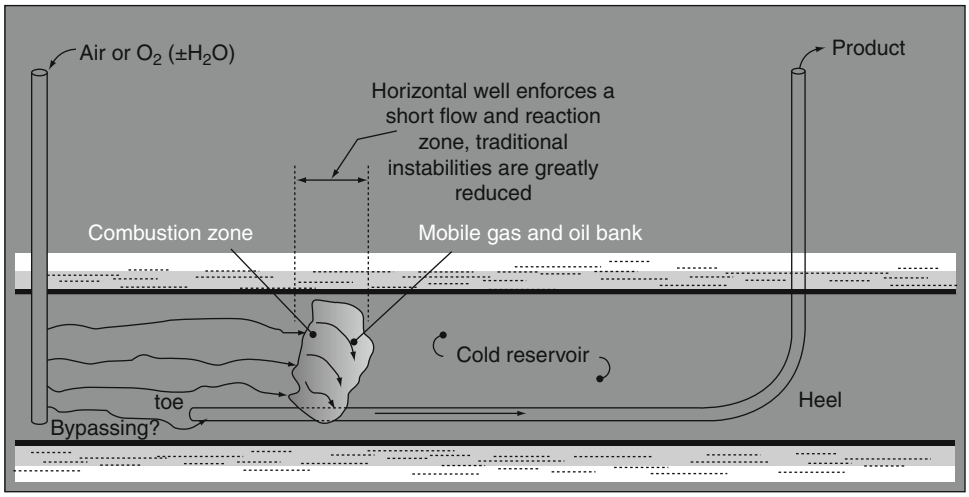

Petroleum and Oil Sands Exploration and Production. Figure 3
The THAI process

carbon-forming precursors in the ground, (2) leaving the heavy metals in the ground, (3) reducing sand handling, and (4) bringing a partially upgraded product to the surface. The extent of the upgrading can, hopefully, be adjusted by adjusting the exposure of the bitumen of heavy oil to the underground thermal effects.

Finally, by all definitions, the quality of the bitumen from tar sand deposits is poor when considered as a refinery feedstock. As in any field in which primary recovery operations are followed by secondary or enhanced recovery operations and there is a change in product quality, such is also the case for tar sand recovery operations. Thus, product oils recovered by the thermal stimulation of tar sand deposits show some improvement in properties over those of the bitumen in-place.

In situ recovery processes (although less efficient in terms of bitumen recovery relative to mining operations) may have the added benefit of *leaving* some of the more obnoxious constituents (from the processing objective) in the ground.

Other Processes Many innovative concepts in heavy oil production have been developed in the last 10 years [2, 4]. However, there are varying degrees of success and all are dependent on the properties of the deposit. There is no panacea for bitumen recovery that can be applied on a worldwide basis.

Long *horizontal wells* with several multilateral branches have been used widely in the development of the heavy oils of Venezuela, where production rates as high as 2,000–2,500 bbl/day in some wells have been achieved through the use of aggregate horizontal lengths as large as 10,000 m in oil of 1,200–5,000 cP viscosity. Unfortunately, this technology can only achieve 8–15% v/v recovery of the oil and only from the best high-permeability zones.

Inert gas injection (IGI) is a technology for conventional oils in reservoirs where good vertical permeability exists, or where it can be created through propped hydraulic fracturing. It is generally viewed as a *top-down* process with nitrogen or methane injection through vertical wells at the top of the reservoirs, creating a gas–oil interface that is slowly displaced toward long horizontal production wells [2, 4]. As with all gravity drainage processes, it is essential to balance the injection and production volumes precisely so that the system does not become pressure driven, but remains in the gravity-dominated flow regime.

SAGD (steam-assisted gravity drainage) (Fig. 4) was developed first in Canada for reservoirs where the immobile bitumen occurs [31]. This process uses paired horizontal wells. Low-pressure steam continuously injected through the upper well creates a steam chamber along the walls of which the heated bitumen flows and is produced in the lower well.

In the process, a pair of horizontal wells that are separated vertically by about 15–20 ft are drilled at the bottom of a thick unconsolidated sandstone reservoir.

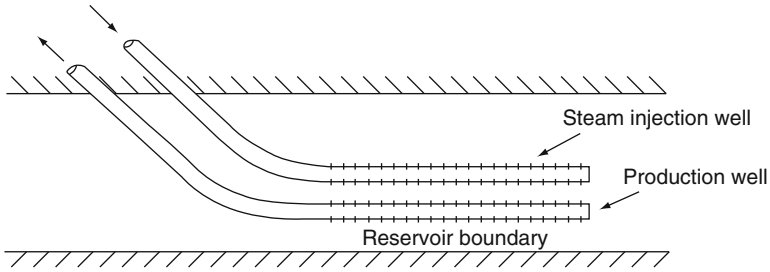

Petroleum and Oil Sands Exploration and Production. Figure 4
The SAGD process

Steam, perhaps along with a mixture of hydrocarbons that dissolve into the oil and help reduce its viscosity, is injected into the upper well. The heat reduces the oil viscosity to values as low as 1–10 cP (depending on temperature and initial conditions) and develops a *steam chamber* that grows vertically and laterally. The steam and gases rise because of their low density, and the oil and condensed water are removed through the lower well. The gases produced during SAGD tend to be methane with some carbon dioxide and traces of hydrogen sulfide.

The SAGD process, as for all gravity-driven processes, is extremely stable because the process zone grows only by gravity segregation, and there are no pressure-driven instabilities such as channeling, coning, and fracturing. SAGD seems to be relatively insensitive to shale streaks and similar horizontal barriers, even up to several meters thick (3–6 ft), that otherwise would restrict vertical flow rates. The combined processes of gravity segregation and shale thermal fracturing make SAGD so efficient that recovery ratios of 60–70% are claimed. Nevertheless, the process is not universally applicable to all reservoirs and deposits.

Cold heavy oil production with sand (CHOPS) is also used as a production approach in unconsolidated sandstones. The process results in the development of high-permeability channels (*wormholes*) in the adjacent low cohesive strength sands, facilitating the flow of oil foam that is caused by solution gas drive. Instead of blocking sand ingress by screens or gravel packs, sand is encouraged to enter the wellbore by aggressive perforation and swabbing strategies. Vertical or slightly inclined wells (vertical to 45°) are operated with rotary progressive cavity pumps (rather than reciprocating pumps) and old fields are converting to higher-capacity progressive cavity pumps, giving production boosts to old wells. Because massive sand production creates a large disturbed zone, the reservoir may be positively affected for later implementation of thermal processes.

Typically, a well placed on CHOPS production will initially produce a high percentage of sand, greater than 20% by volume of liquids. However, this generally drops after some weeks or months. The huge volumes of sand are disposed of by slurry fracture injection or salt cavern placement or by sand placement in a landfill in an environmentally acceptable manner. Obviously, the production of excessive amounts of sand is a cause for mechanical and environmental concern.

Pressure pulsing technologies (PPT) involves a radically new aspect of porous media mechanics discovered and developed into a production enhancement method in the period 1997–2003. The mechanism by which PPT works is to generate a porosity dilation wave (a fluid displacement wave similar to a tsunami); this generates pore-scale dilation and contraction so that oil and water flow into and out of pores, leading to periodic fluid accelerations in the pore throats. As the porosity dilation wave moves through the porous medium at a velocity of about 50–100 ft/s (40–80 m/s), the small expansion and contraction of the pores with the passage of each packet of wave energy helps unblock pore throats, increase the velocity of liquid flow, overcome part of the effects of capillary blockage, and reduce some of the negative effects of instability due to viscous fingering, coning, and permeability streak channeling.

PPT promises to be a major adjunct to a number of oil production processes, particularly all pressure-driven processes, where it will both accelerate flow

rates as well as increasing oil recovery factors. It is also now used in environmental applications to help purge shallow aquifers of nonmiscible phases such as oil. The basis for its use in tar sand deposits is largely unknown and unproven.

Vapor-assisted petroleum extraction (VAPEX) is a new process in which the physics of the process are essentially the same as for SAGD and the configuration of wells is generally similar. The process involves the injection of vaporized solvents such as ethane or propane to create a vapor-chamber through which the oil flows due to gravity drainage [32–35]. The process can be applied in paired horizontal wells, single horizontal wells, or a combination of vertical and horizontal wells. The key benefits are significantly lower energy costs, potential for in situ upgrading, and application to thin reservoirs, with bottom water or reactive mineralogy.

Because of the slow diffusion of gases and liquids into viscous oils, this approach, used alone, perhaps will be suited only for less viscous oils although preliminary tests indicate that there are micromechanisms that act so that the VAPEX dilution process is not diffusion rate limited and the process may be suitable for the highly viscous tar sand bitumen [36, 37].

Nevertheless, VAPEX can undoubtedly be used in conjunction with SAGD methods. As with SAGD and IGI, a key factor is the generation of a three-phase system with a continuous gas phase so that as much of the oil as possible can be contacted by the gaseous phases, generating the thin oil film drainage mechanism. As with IGI, vertical permeability barriers are a problem, and must be overcome through hydraulic fracturing to create vertical permeable channels, or undercut by the lateral growth of the chamber beyond the lateral extent of the limited barrier, or "baffle." As with any solvent process, the loss of solvents in geological formations (such as by adsorption on clay and other minerals) drastically affects process economics and raises many serious environmental issues.

Hybrid approaches that involve the simultaneous use of several technologies are evolving and will see greater applications in the future. In addition to hybrid approaches, the new production technologies, along with older, pressure-driven technologies, will be used in successive phases to extract more oil from reservoirs, even from reservoirs that have been abandoned after primary exploitation. These hybrid approaches hold (on paper at least) the promise of significantly increasing recoverable reserves worldwide, not just in heavy oil cases.

Microbial-enhanced oil recovery (MEOR) processes involve use of reservoir microorganisms or specially selected natural bacterial to produce specific metabolic events that lead to enhanced oil recovery.

In microbial-enhanced oil recovery processes, microbial technology is exploited in oil reservoirs to improve recovery [38–40]. From a microbiologist's perspective, microbial-enhanced oil recovery processes are somewhat akin to in situ bioremediation processes. Injected nutrients, together with indigenous or added microbes, promote in situ microbial growth and/or generation of products which mobilize additional oil and move it to producing wells through reservoir repressurization, interfacial tension/oil viscosity reduction, and selective plugging of the most permeable zones [41, 42].

This technology requires consideration of the physicochemical properties of the reservoir in terms of salinity, pH, temperature, pressure, and nutrient availability [43, 44].

The microbial-enhanced oil recovery process may modify the immediate reservoir environment in a number of ways that could also damage the production hardware or the formation itself. Certain sulfate reducers can produce H_2S, which can corrode pipeline and other components of the recovery equipment, and considerable uncertainty still remains regarding process performance. In addition, conditions vary from reservoir to reservoir, which calls for reservoir-specific customization of the microbial-enhanced oil recovery process, and this alone has the potential to undermine microbial process economic viability. Even though microbes produce the necessary chemical reactions in situ, there is need for caution and astute observation of the effects of the microorganisms on the reservoir chemistry.

Finally, recent developments in *upgrading* of heavy oil and bitumen [2, 4] indicate that the near future could see a reduction of the differential cost of upgrading heavy oil. These processes are based on a better understanding of the issues of asphaltene solubility effects at high temperatures, incorporation of

a catalyst that is chemically precipitated internally during the upgrading, and improving hydrogen addition or carbon rejection.

Future Directions

With the current energy problems, the motivation for recovering as much as possible of the in-place reserves is greater than ever. There is a potentially uncomfortable and politically disastrous situation where the gap between energy requirements and available energy supplies is widening quickly.

Consequently, the search for new domestic supplies has shifted in large measure to increasingly hostile environments such as the Alaskan North Slope and the offshore waters along the outer continental shelves of the United States. These changes in production operations (not to mention the associated environmental disasters that often accompany such venture) have meant both significantly higher costs of production operations and fewer and fewer new commercial discoveries.

The importance of improving the rate of recovery from domestic petroleum reservoirs is underscored by the increasing difficulty of finding significant new reserves to meet the increasing demand for energy. One solution lies in greater emphasis on a multidisciplinary approach – on an intracompany basis and on a cooperative intercompany basis within the industry.

In the near term, a more immediate solution lies in improved application of existing technology as regards selection and quality control of materials, rigorous application of procedures, and the training and supervision of personnel. Part of the answer to the shortage, at least for the short term, has been to import more crude oil, but this is a less than ideal solution for a number of economic and political reasons.

In terms of petroleum recovery, steam-based processes will remain the processes of choice for the recovery of much of the oil in the ground over the next 2 or 3 decades. In some instances, fire flooding will be rejuvenated as the need to recovery of bitumen and residual oil becomes more important.

With the preponderance of heavier oils and tars and bitumen, it is likely that efforts will be made to emphasize partial (or full) upgrading in situ as an integral part of the recovery process. Any type of upgrading during recovery will enhance the quality of the recovered oil, leaving some of the undesirable constituents in the ground as thermal products. Enhancement of the quality of the recovered oil will facilitate upgrading of the oil in the refinery.

Biotechnology will play a more significant role in enhancing crude oil recovery from the depleted oil reservoirs to solve stagnant petroleum production. Such enhanced oil recovery processes (microbial-enhanced oil recovery, MEOR) involve stimulating indigenous reservoir microbes or injecting specially selected consortia of natural bacteria into the reservoir to produce specific metabolic events that lead to improved oil recovery. This also involves flooding with oil recovery agents produced ex situ by industrial or pilot scale fermentation. However, like all recovery processes, a complete evaluation and assessment of microbial from a scientific and engineering standpoint must be performed and must be based on economics, applicability, and the performance standards required to further improve the process efficiency.

Above all, there is the need to manage recovery operations in such a manner that environmental issues do not become issues!

Bibliography

Primary Literature

1. Taber JJ, Martin FD (1983) Technical screening guides for the enhanced recovery of oil. In: Proceedings of the 58th SPE annual technical conference and exhibition, San Francisco, 5–8 Oct 1983 (SPE 12069)
2. Speight JG (2009) Enhanced recovery methods for heavy oil and tar sands. Gulf Publishing, Houston
3. Drew LJ (1997) Undiscovered mineral and petroleum deposits: assessment & controversy. Plenum, New York (Chap. 3)
4. Speight JG (2007) The chemistry and technology of petroleum, 4th edn. CRC Press/Taylor and Francis, Boca Raton
5. Lake LW, Walsh MP (2004) Primary hydrocarbon recovery. Elsevier, Amsterdam
6. Craft BC, Hawkins MF (1959) Applied petroleum reservoir engineering. Prentice-Hall, Englewood Cliffs
7. Frick TC (1962) Petroleum production handbook, vol II. McGraw-Hill, New York
8. Lake LW (1989) Enhanced oil recovery. Prentice-Hall, Englewood Cliffs
9. Arnarnath A (1999) Enhanced oil recovery scoping study. Report No. TR-113836, Electric Power Research Institute, Palo Alto

10. Borchardt JK, Yen TF (1989) Oil field chemistry, Symposium series No. 396. American Chemical Society, Washington, DC
11. CFR 1.43-2 (2004) Internal revenue service, Department of the Treasury, Government of the United States, Washington, DC
12. OTA (1978) Enhanced oil recovery potential in the United States. Office of Technology Assessment, Washington, DC. NTIS order #PB-276594
13. Reed RL, Healy RN (1977) Some physicochemical aspects of microemulsion flooding: a review. In: Shah DO, Schechter RS (eds) Improved oil recovery by surfactant and polymer flooding. Academic, New York
14. Speight JG (2000) Desulfurization of heavy oils and residua, 2nd edn. Marcel Dekker, New York
15. Terwilliger PL (1975) Paper 5568. In: Proceedings of 50th annual fall meeting of the Society of Petroleum Engineers, Dallas. American Institute of Mechanical Engineers, Dallas
16. Terwilliger PL, Clay RR, Wilson LA, Gonzalez-Gerth E (1975) J Petrol Technol 27:9
17. Burger J (1978) Developments in petroleum science. In: Chilingarian GV, Yen TF (eds) Bitumens, asphalts and tar sands, vol 7. Elsevier, New York, p 191
18. Clark KA (1944) Hot-water separation of Alberta bituminous sand. Trans Can Inst Min Met 47:257
19. Carrigy MA (1963) Bulletin No. 14. Alberta Research Council, Edmonton
20. Carrigy MA (1963) The oil sands of Alberta. Information Series No. 45. Alberta Research Council, Edmonton
21. Fear JVD, Innes, ED (1967) In: Proceedings seventh world petroleum congress, Mexico, vol 3, p 549
22. Speight JG, Moschopedis SE (1978) Fuel Process Technol 1:261
23. Miller JC, Misra M (1982) Fuel Process Technol 6:27
24. Misra M, Aguilar R, Miller JD (1981) Sep Sci Technol 16(10):1523
25. Kruyer J (1982) In: Proceedings of the second international conference on heavy crude and tar sands, Caracas, 7–17 Feb 1982
26. Kruyer J (1983) Preprint No. 3d. Summer national meeting of the American Institute of Chemical Engineers, Denver, 28–31 Aug 1983
27. Gishler PE (1949) Can J Res 27:104
28. Pratts M (1986) Thermal recovery. Society of Petroleum Engineers, New York
29. Gregoli AA, Rimmer DP, Graue DJ (2000) Upgrading and recovery of heavy crude oils and natural bitumen by in situ hydrovisbreaking. US Patent 6,016,867, 25 Jan 2000
30. Gregoli AA, Rimmer DP (2000) Production of synthetic crude oil from heavy hydrocarbons recovered by in situ hydrovisbreaking. US Patent 6,016,868, 25 Jan 2000
31. Dusseault MB, Geilikman MB, Spanos TJT (1998) J Petrol Technol 50(9):92–94
32. Butler RM, Mokrys IJ (1991) J Can Pet Technol 30(1):97–106
33. Butler RM, Mokrys IJ (1995) Process and apparatus for the recovery of hydrocarbons from a hydrocarbon deposit. US Patent 5,407,009, 18 Apr 1995
34. Butler RM, Mokrys IJ (1995) Process and apparatus for the recovery of hydrocarbons from a hydrocarbon deposit. US Patent 5,607,016, 4 Mar 1995
35. Butler RM, Jiang Q (2000) J Can Pet Technol 39:48–56
36. Yang C, Gu Y (2005a) A novel experimental technique for studying solvent mass transfer and oil swelling effect in a vapor extraction (VAPEX) process. Paper No. 2005–099. In: Proceedings of the 56th annual technical meeting. The Canadian international petroleum conference, Calgary, 7–9 Jun 2005
37. Yang C, Gu Y (2005b) Effects of solvent-heavy oil interfacial tension on gravity drainage in the VAPEX process. Paper No. SPE 97906. In: Society of petroleum engineers international thermal operations and heavy oil symposium, Calgary, 1–3 Nov 2005
38. Banat IM (1995) Biosurfactant production and possible uses in microbial enhanced oil recovery and oil pollution remediation. Bioresour Technol 51:1–12
39. Clark JB, Munnecke DM, Jenneman GE (1981) In situ microbial enhancement of oil production. Dev Ind Microbiol 15:695–701
40. Stosur GJ (1991) Unconventional EOR concepts. Crit Rep Appl Chem 33:341–373
41. Bryant RS, Lindsey RP (1996) World-wide applications of microbial technology for improving oil recovery. In: Proceedings of the SPE symposium on improved oil recovery of the society of petroleum engineers, Richardson, pp 27–134
42. Bryant RS, Donaldson EC, Yen TF, Chilingarian GV (1989) Microbial enhanced oil recovery. In: Donaldson EC, Chilingarian GV, Yen TF (eds) Enhanced oil recovery II: processes and operations. Elsevier, Amsterdam, pp 423–450
43. Khire JM, Khan MI (1994) Microbially enhanced oil recovery (MEOR). Part 1. Importance and mechanisms of microbial enhanced oil recovery. Enzyme Microb Technol 16: 170–172
44. Khire JM, Khan MI (1994) Microbially enhanced oil recovery (MEOR). Part 2. Microbes and the subsurface environment for microbial enhanced oil recovery. Enzyme Microb Technol 16:258–259

Books and Reviews

Ancheyta J, Speight JG (2007) Hydroprocessing of heavy oils and residua. CRC Press/Taylor & Francis, Boca Raton

Bower T (2009) Oil: money, politics, and power in the 21st century. Grand Central Publishing, Hachette Book Group, New York

Gudmestad OT, Zolotukhin AB, Jarlsby ET (2010) Petroleum resources, with emphasis on offshore fields. WIT Press, Billerica

Nersesian RL (2010) Energy for the 21st century: a comprehensive guide to conventional and alternative sources, 2nd edn. M.E. Sharpe, Armonk

Speight JG (2008) Synthetic fuels handbook: properties, processes, and performance. McGraw-Hill, New York

Wihbet PM (2009) The rise of the new oil order. Academy & Finance, Geneva

Petroleum Refining and Environmental Control and Environmental Effects

James G. Speight
CD&W Inc, Laramie, WY, USA

Article Outline

Glossary
Definition of the Subject
Introduction
Definitions
Environmental Regulations
Processes and Process Wastes
Future Directions
Bibliography

Glossary

Emissions Gaseous, liquid, or solid by-products introduced into the environment as a result of refining processes.

Environmental control The use of various technologies to control and even prevent refinery emissions from entering the environment.

Environmental effects The effects of refinery emissions on the flora and fauna in the various ecosystems.

Refining The processes by which petroleum is distilled and/or converted by application of physical and chemical processes to form a variety of products.

Regulations The laws by which environmental emissions are controlled.

Definition of the Subject

The work summarizes the various process emissions that occur during petroleum refining. There are also general descriptions of the various pollution, health, and environmental problems especially specific to the petroleum industry and places in perspective the government regulations as well as industry efforts to adhere to these regulations. The objective is to indicate the types of emissions and the laws that regulate these emissions.

Introduction

Petroleum as an energy source use is a necessary part of the modern world and will be a primary source of energy for the next several decades, hence the need for control over the amounts and types of emissions from the use of petroleum and its products. Furthermore, the capacity of the environment to absorb the effluents and other impacts of process technologies is not unlimited and the environment should be considered to be an extremely limited resource, and discharge of chemicals into it should be subject to severe constraints – as a result, it is necessary to understand the nature and magnitude of the problems involved [1].

Both the production and processing of crude oil involve the use of a variety of substances [2], some toxic, including lubricants in oil wells and catalysts and other chemicals in refining (Fig. 1). The amounts used tend to be relatively easy to control, and the spillage of crude oil is more detrimental to the environment.

The purpose of this work is to summarize and generalize the various pollution, health, and environmental problems especially specific to the petroleum industry and to place in perspective government laws and regulations as well as industry efforts to control these problems [3–6]. The objective is to indicate the types of emissions and the laws that regulate these emissions.

Definitions

Briefly, petroleum production and petroleum refining produce *chemical waste* [6]. If this *chemical waste* is not processed in a timely manner, it can become a *pollutant*. Under some circumstances, chemical waste is reclassified as *hazardous waste*.

Hazardous waste is any gaseous, liquid, or solid waste material that, if improperly managed or disposed of, may pose hazards to human health and the environment. In some cases, the term "*chemical waste*" is used interchangeably (often incorrectly) with the term "*hazardous waste*," but chemical waste is always hazardous and the correct use of the terms must be used.

A *pollutant* is a substance present in a particular location (*ecosystem*) – usually it is not indigenous to the location or is present in a concentration greater than the concentration that occurs naturally. The substance

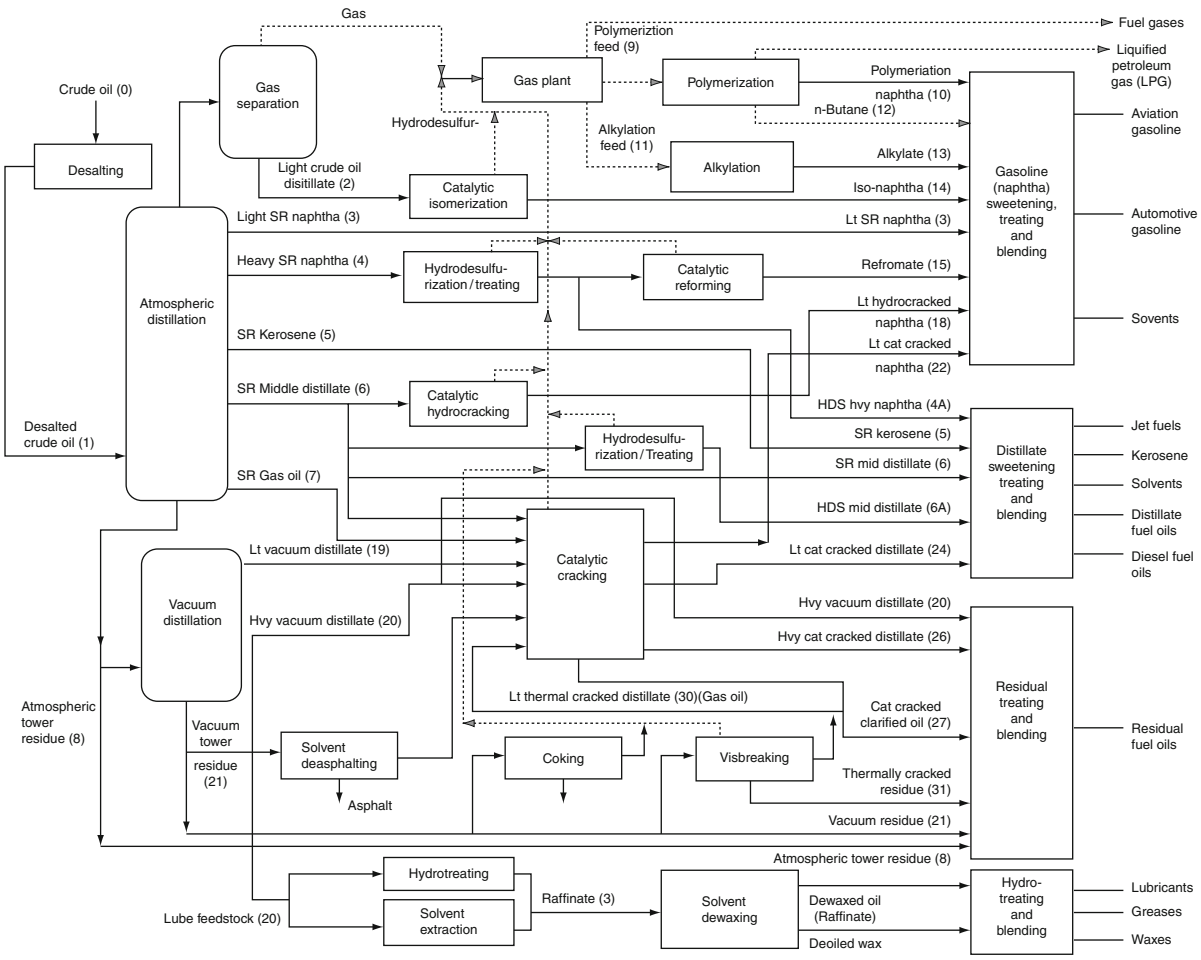

Petroleum Refining and Environmental Control and Environmental Effects. Figure 1
Schematic overview of a refinery (OSHA technical Manual, Section IV, Chapter 2: Petroleum Refining Processes, http://www.osha.gov/dts/osta/otm/otm_iv/otm_iv_2.html)

is often the product of human activity and has a detrimental effect on the environment, in part or in toto. Pollutants can also be subdivided into two classes: primary and secondary.

$$\text{Source} \rightarrow \text{Primary pollutant} \rightarrow \text{Secondary pollutant}$$

A *primary pollutant* is a pollutant that is emitted directly from the source. In terms of atmospheric pollutants from petroleum, examples are carbon oxides, sulfur dioxide, and nitrogen oxides from fuel combustion operations:

$$2[\mathrm{C}]_{\text{petroleum}} + \mathrm{O_2} \rightarrow 2\mathrm{CO}$$

$$[\mathrm{C}]_{\text{petroleum}} + \mathrm{O_2} \rightarrow \mathrm{CO_2}$$

$$2[\mathrm{N}]_{\text{petroleum}} + \mathrm{O_2} \rightarrow 2\mathrm{NO}$$

$$[\mathrm{N}]_{\text{petroleum}} + \mathrm{O_2} \rightarrow \mathrm{NO_2}$$

$$[\mathrm{S}]_{\text{petroleum}} + \mathrm{O_2} \rightarrow \mathrm{SO_2}$$

Hydrogen sulfide and ammonia are produced from processing sulfur-containing and nitrogen-containing feedstocks:

$$[\mathrm{S}]_{\text{petroleum}} + \mathrm{H_2} \rightarrow \mathrm{H_2S} + \text{hydrocarbons}$$

$$2[\mathrm{N}]_{\text{petroleum}} + 3\mathrm{H_2} \rightarrow 2\mathrm{NH_3} + \text{hydrocarbons}$$

A *secondary pollutant* is a pollutant that is produced by the interaction of a primary pollutant with another chemical. A *secondary pollutant* may also be produced

by dissociation of a primary pollutant, or other effects within a particular ecosystem. Again, using the atmosphere as an example, the formation of the constituents of acid rain is an example of the formation of secondary pollutants:

$$SO_2 + H_2O \rightarrow H_2SO_3 \text{ (sulfurous acid)}$$

$$2SO_2 + O_2 \rightarrow 2SO_3$$

$$SO_3 + H_2O \rightarrow H_2SO_4 \text{ (sulfuric acid)}$$

$$NO + H_2O \rightarrow HNO_2 \text{ (nitrous acid)}$$

$$3NO_2 + 2H_2O \rightarrow HNO_3 \text{ (nitric acid)}$$

In many cases, these secondary pollutants can have significant environmental effects, such as participation in the formation of acid rain and smog [5].

An *environmental regulation* is a legal mechanism that determines how the policy directives of an environmental law are to be carried out. An *environmental policy* is a requirement that specifies operating procedures that must be followed. An *environmental guidance* is a document developed by a governmental agency that outlines a position on a topic or which gives instructions on how a procedure must be carried out. It explains how to do something and provides governmental interpretations on a governmental act or policy.

Environmental Regulations

Environmental issues range from the effects of pollutants on the population at large to effects on the lives of workers in various occupations where sickness or doisability can result from exposure to chemical agents [5, 7, 8].

There are a variety of regulations (Table 1) that apply to petroleum refining [6]. The most *popular* is

Petroleum Refining and Environmental Control and Environmental Effects. Table 1 Environmental regulations that apply to energy production

	First enacted	Amended
Clean Air Act	1970	1977 1990
Clean Water Act (Water Pollution Control Act)	1948	1965[a] 1972[b] 1977 1987[c]
Comprehensive Environmental Response, Compensation and Liability Act	1980	1986[d]
Hazardous Material Transportation Act	1974	1990
Occupational Safety and Health Act	1970	1987[e]
Oil Pollution Act	1924	1990[f]
Resource Conservation and Recovery Act	1976	1980[g]
Safe Drinking Water Act	1974	1986[h]
Superfund Amendments and Reauthorization Act (SARA)	1986	
Toxic Substances Control Act	1976	1984[i]

[a]Water Quality Act
[b]Water Pollution Control Act
[c]Water Quality Act
[d]SARA Amendments
[e]Several amendments during the 1980s
[f]Interactive with various water pollution acts
[g]Federal cancer policy initiated
[h]Several amendments during the 1970s and 1980s
[i]Import rule enacted

the series of regulations known as the Clean Air Act that first was introduced in 1967 and was subsequently amended in 1970 and most recently in 1990. The most recent amendments provide stricter regulations for the establishment and enforcement of national ambient air quality standards for, as an example, sulfur dioxide. These standards do not stand alone, and there are many national standards for sulfur emissions.

The laws of relevance to the petroleum industry are:

The Clean Air Act Amendments

The first *Clean Air Act* of 1970 and the 1977 Amendments consisted of three titles. *Title I* dealt with stationary air emission sources, *Title II* with mobile air emission sources, and *Title III* with definitions of appropriate terms as well as applicable standards for judicial review.

The *Clean Air Act Amendments of 1990* contain extensive provisions for control of the accidental release of toxic substances from storage or transportation as well as the formation of acid rain (acid deposition). In addition, the requirement that the standards be technology based removes much of the emotional perception that all chemicals are hazardous as well as the guesswork from legal enforcement of the legislation. The requirement also dictates environmental and health protection with an ample margin of safety.

The Water Pollution Control Act (The Clean Water Act)

There are several acts that relate to the protection of the waterways in the United States but of particular interest to the petroleum industry in the present context is the *Water Pollution Control Act* (*Clean Water Act*). The objective of the Act is to restore and maintain the chemical, physical, and biological integrity of water systems.

The original Water Pollution Control Act of 1948 and The Water Quality Act of 1965 were generally limited to control of pollution of interstate waters and the adoption of water-quality standards by the states for interstate water within their borders. The first comprehensive water-quality legislation in the United States came into being in 1972 as the Water Pollution Control Act, which was amended in 1977 and retitled to become the Clean Water Act. Further amendments in 1978 were enacted to deal more effectively with spills of crude oil, with other amendments following in 1987 under the new name of the Water Quality Act.

Section 311 of the Clean Water Act includes elaborate provisions for regulating intentional or accidental discharges of petroleum and of hazardous substances. Included are response actions required for oil spills and the release or discharge of toxic and hazardous substances. As an example, the person in charge of a vessel or an onshore or offshore facility from which any chemical substance is discharged, in quantities equal to or exceeding its reportable quantity, must notify the appropriate federal agency as soon as such knowledge is obtained. The *Exxon Valdez* disaster and the recent spillage of oil into the Gulf of Mexico by BP are well-known examples of such a discharge of chemicals – the chemical being oil.

The Safe Drinking Water Act

The Safe Drinking Water Act, first enacted in 1974, was amended several times in the 1970s and 1980s to set national drinking water standards. The Act calls for regulations that (1) apply to public water systems, (2) specify contaminants that may have any adverse effect on the health of persons, and (3) specify contaminant levels. Statutory provisions are included to cover underground injection control systems. The Act also requires maximum levels at which a contaminant must have no known or anticipated adverse effects on human health, thereby providing an *adequate margin of safety*.

The Superfund Amendments and Reauthorization Act (SARA) set the same standards for groundwater as for drinking water in terms of necessary cleanup and remediation of an inactive site that might be a former petroleum refinery. Under the Act, all underground injection activities must comply with the drinking water standards as well as meet specific permit conditions that are in unison with the provisions of the Clean Water Act.

The Resource Conservation and Recovery Act

Since its initial enactment in 1976, the Resource Conservation and Recovery Act (RCRA) continues to promote safer waste management programs. Besides the regulatory requirements for waste management, the

Act specifies the mandatory obligations of generators, transporters, and disposers of waste as well as those of owners and/or operators of waste treatment, storage, or disposal facilities. The waste might be garbage, refuse, and sludge from a treatment plant or from a water supply treatment plant or air pollution control facility and other discarded material, including solid, liquid, semisolid, or contained gaseous material resulting from industrial, commercial, mining, and agricultural operations and from community activities.

The Act also states that solid waste does not include solid, or dissolved, materials in domestic sewage, or solid or dissolved materials in irrigation return flows or industrial discharges. A solid waste becomes a hazardous waste if it exhibits any one of four specific characteristics: (1) ignitability, (2) reactivity, (3) corrosivity, or (4) toxicity. Certain types of solid wastes (e.g., household waste) are not considered to be hazardous, irrespective of their characteristics.

The Toxic Substances Control Act

The Toxic Substances Control Act was first enacted in 1976 and was designed to provide controls for those chemicals that may threaten human health or the environment. Particularly hazardous are the cyclic nitrogen species and that often occur in high-boiling petroleum fractions, distillation residua, and cracked residua.

The Act specifies a *premanufacture notification* requirement by which any manufacturer must notify the Environmental Protection Agency at least 90 days prior to the production of a new chemical substance. Notification is also required even if there is a new use for the chemical that can increase the risk to the environment. No notification is required for chemicals that are manufactured in small quantities solely for scientific research and experimentation.

A *new chemical substance* is a chemical that is not listed in the Environmental Protection Agency Inventory of Chemical Substances or is an unlisted reaction product of two or more chemicals. In addition, the term "*chemical substance*" means any organic or inorganic substance of a particular molecular identity, including any combination of such substances occurring in whole or in part as a result of a chemical reaction or occurring in nature, and any element or uncombined radical. The term "*mixture*" means any combination of two or more chemical substances if the combination does not occur in nature and is not, in whole or in part, the result of a chemical reaction.

The Comprehensive Environmental Response, Compensation, and Liability Act

The Comprehensive Environmental Response, Compensation, and Liability Act (CERCLA), generally known as *Superfund*, was first signed into law in 1980. The purpose of this Act is to provide a response mechanism for cleanup of any hazardous substance released, such as an accidental spill, or of a threatened release of a chemical.

Under this Act, a hazardous substance is any substance requiring (1) special consideration due to its toxic nature under the Clean Air Act, the Clean Water Act, or the Toxic Substances Control Act and (2) any waste that is hazardous waste under RCRA. Additionally, a pollutant or contaminant can be any other substance not necessarily designated by or listed in the Act but that *will or may reasonably* be anticipated to cause any adverse effect in organisms and/or their offspring.

The Occupational Safety and Health Act

The *Occupational Safety and Health Administration* (*OSHA*) came into being in 1970 and is responsible for administering the Occupational Safety and Health Act. Occupational health hazards are those factors arising in or from the occupational environment that adversely impact health.

The goal of the Act is to ensure that employees do not suffer material impairment of health or functional capacity due to a lifetime occupational exposure to chemicals. The Act is also responsible for the means by which chemicals are contained.

The Oil Pollution Act

The Oil Pollution Act of 1990 deals with pollution of waterways by crude oil. The Act specifically deals with petroleum vessels and onshore and offshore facilities and imposes strict liability for oil spills on their owners and operators.

The Hazardous Materials Transportation Act

The Hazardous Materials Transportation Act authorizes the establishment and enforcement of hazardous material regulations for all modes of transportation by highway, water, and rail. The purpose of the Act is to ensure safe transportation of hazardous materials. The Act prevents any person from offering or accepting for transportation a hazardous material (any substance or material, including a hazardous substance and hazardous waste, which is capable of posing an unreasonable risk to health, safety, and property) for transportation anywhere within the United States.

The Act also imposes restrictions on the packaging, handling, and shipping of hazardous materials in which the appropriate documentation, markings, labels, and safety precautions are required.

Processes and Process Wastes

Enhanced oil recovery (EOR) processes rely upon the use of chemical or thermal energy to recover crude oil that is trapped in pores of reservoir rock after primary and secondary (waterflood) crude oil production has ceased [2, 9].

Chemicals used for enhanced oil recovery include surfactants to reduce the interfacial tension between oil and water, and oil and rock interfaces. Many microorganisms produce biosurfactants and perform this activity by fermentation of inexpensive raw materials such as molasses. Several biosurfactants are being evaluated for use in enhanced oil recovery.

A major issue in enhanced oil recovery processes is the variation of permeability in petroleum reservoirs. When water is injected to displace oil, the water will preferentially flow through areas of highest permeability, and bypass much of the oil. When chemicals are injected, they may also flow preferentially into high-permeability zones with the water, but then will grow and block those zones. When high-permeability zones are blocked, sweep efficiency is improved, and thus oil recovery.

Transportation

In addition to the conventional meaning of the term *process*, the *recovery* and *transportation* of petroleum also needs to be considered here.

Oil spills during petroleum *transportation* have been the most visible problem. There have also been instances of oil wells at sea "blowing out," or flowing uncontrollably, although the amounts from blowouts tend to be smaller than from tanker accidents.

Tanker accidents typically have a severe impact on ecosystems because of the rapid release of hundreds of thousands of barrels of crude oil (or crude oil products) into a small area.

While oil is at least theoretically biodegradable, large-scale spills can overwhelm the ability of the ecosystem to break the oil down. Over time, the lighter portions of crude oil evaporate, leaving the nonvolatile portion. Oil itself breaks down the protective waxes and oils in the feathers and fur of birds and animals. Some crude oils contain toxic metals as well. The impact of any given oil spill is determined by the size of the spill, the degree of dispersal, and the chemistry of the oil. Spills at sea are thought to have a less detrimental effect than spills in shallow waters.

Refining

Petroleum *refining* is a complex sequence of chemical events that result in the production of a variety of products (Fig. 1). In fact, petroleum refining might be considered as a collection of individual, yet related processes that are each capable of producing effluent streams [2, 6].

Petroleum refining, as it is currently known, will continue at least for the next 3 decades. In spite of the various political differences that have caused fluctuations in petroleum imports, it is reality that imports of petroleum and petroleum products into the United States are on the order of 67% of the total requirements [2].

Petroleum, like any other raw material, is capable of producing chemical waste. By 1960, the petroleum refining industry had become well established throughout the world. Effluent water, atmospheric emissions, and combustion products also became a focus of increased technical attention [4, 5, 10–13].

Refineries produce a wide variety of products from petroleum feedstocks and feedstock blends [2, 14]. During petroleum refining, refineries use and generate an enormous amount of chemicals, some of which are present in air emissions, wastewater, or solid wastes (Table 2) [2, 6]. Emissions are also created through

Petroleum Refining and Environmental Control and Environmental Effects. Table 2 Emissions and waste from refinery processes

Process	Air emissions	Residual wastes generated
Crude oil desalting	Heater stack gas (CO, SO_x, NO_x, hydrocarbons, and particulates), fugitive emissions (hydrocarbons)	Crude oil/desalter sludge (iron rust, clay, sand, water, emulsified oil and wax, metals)
Atmospheric distillation Vacuum distillation	Heater stack gas (CO, SO_x, NO_x, hydrocarbons and particulates), vents and fugitive emissions (hydrocarbons), steam ejector emissions (hydrocarbons), heater stack gas (CO, SO_x, NO_x, hydrocarbons, and particulates), vents and fugitive emissions (hydrocarbons)	Typically, little or no residual waste generated
Thermal cracking/ visbreaking	Heater stack gas (CO, SO_x, NO_x, hydrocarbons, and particulates), vents and fugitive emissions (hydrocarbons)	Typically, little or no residual waste generated
Coking	Heater stack gas (CO, SO_x, NO_x, hydrocarbons, and particulates), vents and fugitive emissions (hydrocarbons), and decoking emissions (hydrocarbons and particulates)	Coke dust (carbon particles and hydrocarbons)
Catalytic cracking	Heater stack gas (CO, SO_x, NO_x, hydrocarbons, and particulates), fugitive emissions (hydrocarbons), and catalyst regeneration (CO, NO_x, SO_x, and particulates)	Spent catalysts (metals from crude oil and hydrocarbons), spent catalyst fines from electrostatic precipitators (aluminum silicate and metals)
Catalytic hydrocracking	Heater stack gas (CO, SO_x, NO_x, hydrocarbons, and particulates), fugitive emissions (hydrocarbons), and catalyst regeneration (CO, NO_x, SO_x, and catalyst dust)	Spent catalysts fines
Hydrotreating/ hydroprocessing	Heater stack gas (CO, SO_x, NO_x, hydrocarbons, and particulates), vents and fugitive emissions (hydrocarbons), and catalyst regeneration (CO, NO_x, SO_x)	Spent catalyst fines (aluminum silicate and metals)
Alkylation	Heater stack gas (CO, SO_x, NO_x, hydrocarbons, and particulates), vents and fugitive emissions (hydrocarbons)	Neutralized alkylation sludge (sulfuric acid or calcium fluoride, hydrocarbons)
Isomerization	Heater stack gas (CO, SO_x, NO_x, hydrocarbons, and particulates), HCl (potentially in light ends), vents and fugitive emissions (hydrocarbons)	Calcium chloride sludge from neutralized HCl gas
Polymerization	H_2S from caustic washing	Spent catalyst containing phosphoric acid
Catalytic reforming	Heater stack gas (CO, SO_x, NO_x, hydrocarbons, and particulates), fugitive emissions (hydrocarbons), and catalyst regeneration (CO, NO_x, SO_x)	Spent catalyst fines from electrostatic precipitators (alumina silicate and metals)
Solvent extraction	Fugitive solvents	Little or no residual wastes generated
Dewaxing	Fugitive solvents, heaters	Little or no residual wastes generated
Propane deasphalting	Heater stack gas (CO, SO_x, NO_x, hydrocarbons and particulates), fugitive propane	Little or no residual wastes generated
Wastewater treatment	Fugitive emissions (H_2S, NH_3, and hydrocarbons)	API separator sludge (phenols, metals and oil), chemical precipitation sludge (chemical coagulants, oil), DAF floats, biological sludge (metals, oil, suspended solids), spent lime

the combustion of fuels, and as by-products of chemical reactions occurring when petroleum fractions are upgraded. A large source of air emissions is, generally, the process heaters and boilers that produce carbon monoxide, sulfur oxides, and nitrogen oxides, leading to pollution and the formation of acid rain.

$$CO_2 + H_2O \rightarrow H_2CO_3 \text{ (carbonic acid)}$$

$$SO_2 + H_2O \rightarrow H_2SO_3 \text{ (sulfurous acid)}$$

$$2SO_2 + O_2 \rightarrow 2SO_3$$

$$SO_3 + H_2O \rightarrow H_2SO_4 \text{ (sulfuric acid)}$$

$$NO + H_2O \rightarrow HNO_2 \text{(nitrousacid)}$$

$$2NO + O_2 \rightarrow NO_2$$

$$NO_2 + H_2O \rightarrow HNO_3 \text{ (nitric acid)}$$

Hence, there is the need for gas-cleaning operations on a refinery site so that such gases are cleaned from the gas stream prior to entry into the atmosphere.

Fugitive emissions of volatile hydrocarbons arise from leaks in valves, pumps, flanges, and other similar sources where crude and its fractions flow through the system. While individual leaks may be minor, the combination of fugitive emissions from various sources can be substantial. These emissions are controlled primarily through leak detection and repair programs and occasionally through the use of special leak-resistant equipment.

In terms of individual processes, the potential for waste generation and, hence, leakage of emissions is as follows.

Desalting Petroleum often contains water, inorganic salts, suspended solids, and water-soluble trace metals. As a first step in the refining process, to reduce corrosion, plugging, and fouling of equipment and to prevent poisoning the catalysts in processing units, these contaminants must be removed by desalting (dehydration) [2].

The two most typical methods of petroleum desalting are (1) chemical separation and (2) electrostatic separation. In chemical desalting, water and chemical surfactant (demulsifiers) are added to the petroleum, heated so that salts and other impurities dissolve into the water or attach to the water, and then held in a tank where they settle out. Electrical desalting is the application of high-voltage electrostatic charges to concentrate suspended water globules in the bottom of the settling tank. Surfactants are added only when the crude has a large amount of suspended solids. A third and less-common process involves filtering heated petroleum using diatomaceous earth.

In the desalting process, the feedstock crude oil is heated to between 65°C and 177°C (150°F and 350°F) to reduce viscosity and surface tension for easier mixing and separation of the water, but the temperature is limited by the vapor pressure of the petroleum constituents. In both methods, other chemicals may be added – ammonia is often used to reduce corrosion and caustic or acid may be added to adjust the pH of the water wash. Wastewater and contaminants are discharged from the bottom of the settling tank to the wastewater treatment facility while the desalted crude is continuously drawn from the top of the settling tanks and sent to the crude distillation tower.

Desalting (Fig. 2) creates an oily desalter sludge that may be a hazardous waste and a high temperature salt wastewater stream (treated along with other refinery wastewaters). The primary polluting constituents in desalter wastewater include hydrogen sulfide, ammonia, phenol, high levels of suspended solids, and dissolved solids, with a high biochemical oxygen demand (BOD). In some cases, it is possible to recycle the desalter effluent water back into the desalting process, depending upon the type of crude being processed.

Distillation Atmospheric and vacuum distillation units (Figs. 3 and 4) are closed processes and exposures are expected to be minimal.

Both atmospheric distillation units and vacuum distillation units produce refinery fuel gas streams containing a mixture of light hydrocarbons, hydrogen sulfide, and ammonia. These streams are processed through gas treatment and sulfur recovery units to recover fuel gas and sulfur. Sulfur recovery creates emissions of ammonia, hydrogen sulfide, sulfur oxides, and nitrogen oxides.

When sour (high-sulfur) petroleum is processed, there is potential for exposure to hydrogen sulfide in the preheat exchanger and furnace, tower flash zone

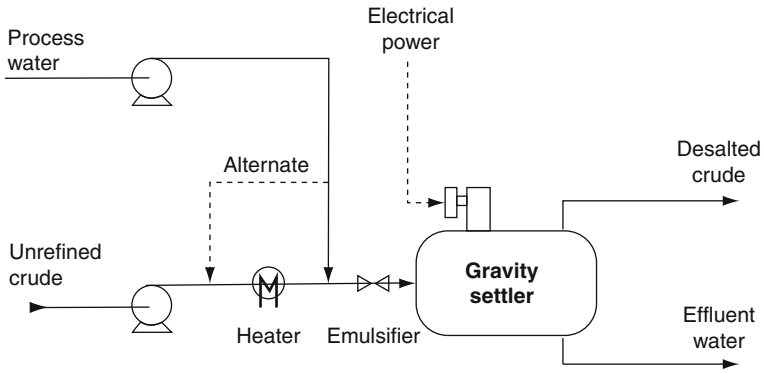

Petroleum Refining and Environmental Control and Environmental Effects. Figure 2
Schematic of an electrostatic desalting unit (OSHA technical manual, Section IV, Chapter 2: Petroleum Refining Processes, http://www.osha.gov/dts/osta/otm/otm_iv/otm_iv_2.html)

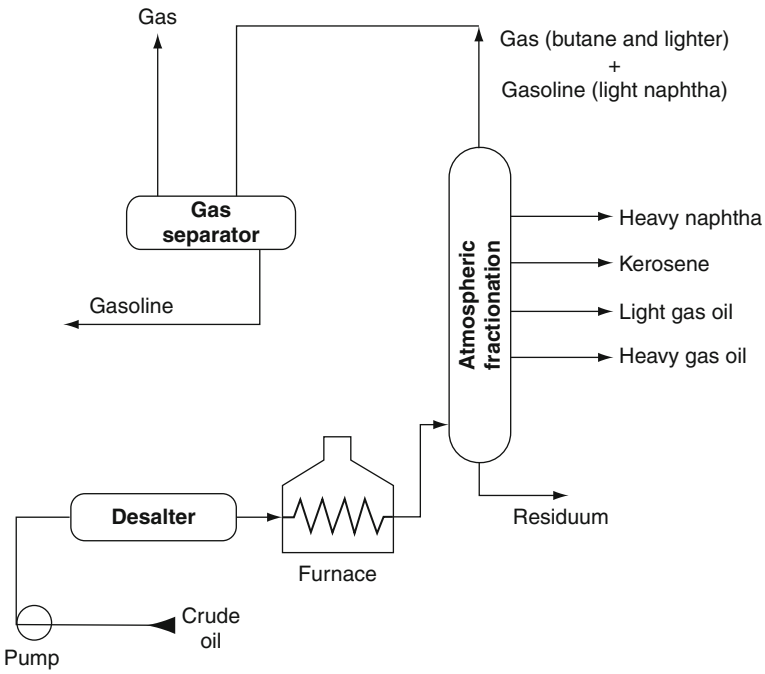

Petroleum Refining and Environmental Control and Environmental Effects. Figure 3
An atmospheric distillation unit (OSHA technical manual, Section IV, Chapter 2: Petroleum Refining Processes, http://www.osha.gov/dts/osta/otm/otm_iv/otm_iv_2.html)

and overhead system, vacuum furnace and tower, and bottoms exchanger. Hydrogen chloride may be present in the preheat exchanger, tower top zones, and overheads. Wastewater may contain water-soluble sulfides in high concentrations and other water-soluble compounds such as ammonia, chlorides, phenol, mercaptans, etc., depending upon the crude feedstock and the treatment chemicals. Safe work practices and/or the use of appropriate personal protective equipment may be needed for exposures to chemicals and other hazards such as heat and noise, and during sampling, inspection, maintenance, and turnaround activities.

The primary source of emissions is combustion of fuels in the crude preheat furnace and in boilers that

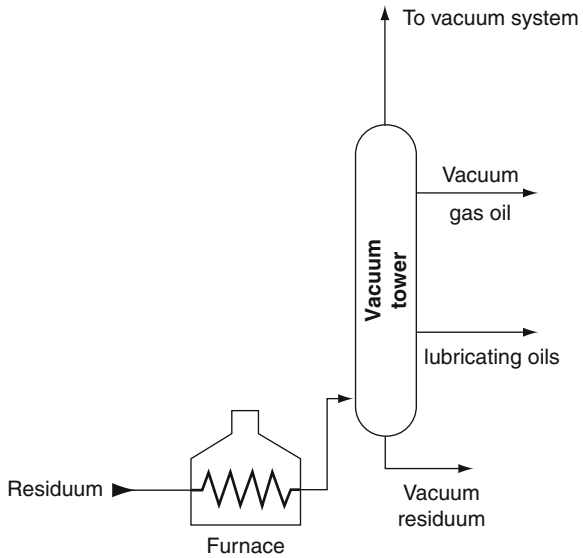

Petroleum Refining and Environmental Control and Environmental Effects. Figure 4
A vacuum distillation unit (OSHA technical manual, Section IV, Chapter 2: Petroleum Refining Processes, http://www.osha.gov/dts/osta/otm/otm_iv/otm_iv_2.html)

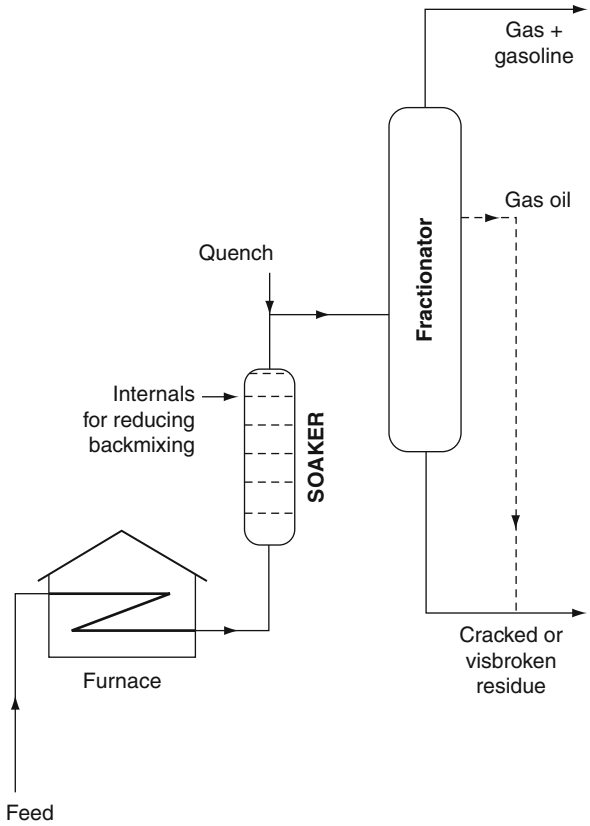

Petroleum Refining and Environmental Control and Environmental Effects. Figure 5
A soaker visbreaking unit (OSHA technical manual, Section IV, Chapter 2: Petroleum Refining Processes, http://www.osha.gov/dts/osta/otm/otm_iv/otm_iv_2.html)

produce steam for process heat and stripping. When operating in an optimum condition and burning cleaner fuels (e.g., natural gas, refinery gas), these heating units create relatively low emissions of sulfur oxides, (SO_x), nitrogen oxides (NO_x), carbon monoxide (CO), hydrogen sulfide (H_2S), particulate matter, and volatile hydrocarbons. If fired with lower grade fuels (e.g., refinery fuel pitch, coke) or operated inefficiently (incomplete combustion), heaters can be a significant source of emissions.

Petroleum distillation units generate considerable wastewater – often an oily sour wastewater and the constituents of sour wastewater streams include hydrogen sulfide, ammonia, suspended solids, chlorides, mercaptans, and phenol, characterized by a high pH.

Visbreaking and Coking *Visbreaking* (Fig. 5), like many thermal cracking processes, tends to produce a relatively small amount of fugitive emissions and sour wastewater [2, 6]. Usually some wastewater is produced from steam strippers and the fractionator. Wastewater is also generated during unit cleanup and cooling operations and from the steam injection process to remove organic deposits from the soaker or from the coil. Combined wastewater flows from thermal cracking and coking processes are about 3.0 gal per barrel of process feed.

Delayed coking is the oldest, most widely used process and has changed very little in the 5 or more decades in which it has been on stream in refineries [2]. *Fluid coking* is a continuous fluidized solids process that cracks feed thermally over heated coke particles in a reactor vessel to gas, liquid products, and coke [2]. Heat for the process is supplied by partial combustion of the coke, with the remaining coke being drawn as product. The new coke is deposited in a thin fresh layer on the outside surface of the circulating coke particle.

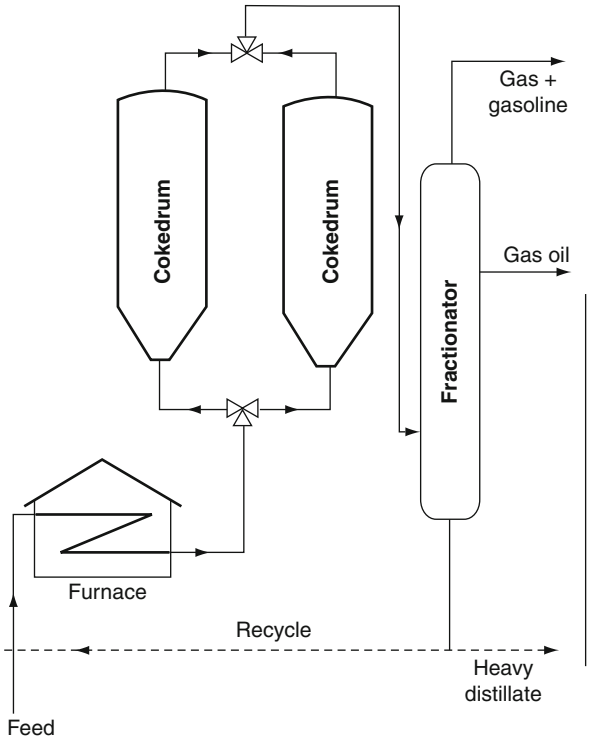

Petroleum Refining and Environmental Control and Environmental Effects. Figure 6
A delayed coking unit (OSHA technical manual, Section IV, Chapter 2: Petroleum Refining Processes, http://www.osha.gov/dts/osta/otm/otm_iv/otm_iv_2.html)

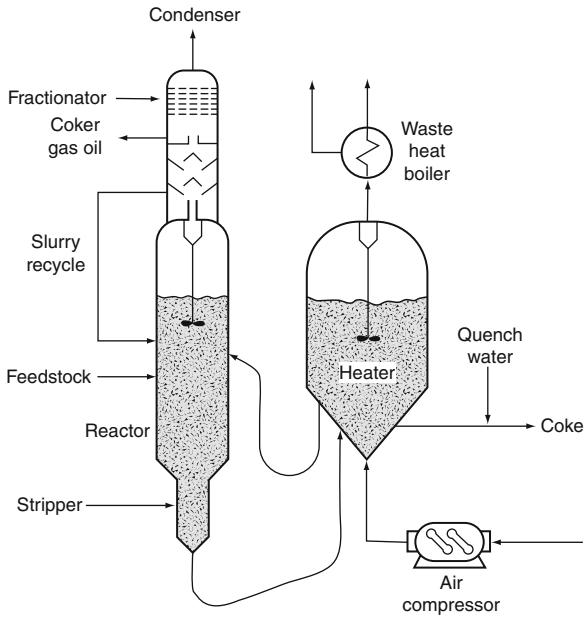

Petroleum Refining and Environmental Control and Environmental Effects. Figure 7
A fluid coking unit [12]

Coking processes (Figs. 6 and 7) produce a relatively small amount of sour wastewater from steam strippers and fractionators. Wastewater is generated during coke removal and cooling operations and from the steam injection process to cut coke from the coke drums. Combined wastewater flows from thermal cracking and coking processes are about 3.0 gal per barrel of process feed.

Particulate emissions from decoking can also be considerable. Coke-laden water from decoking operations in delayed cokers (hydrogen sulfide, ammonia, suspended solids), coke dust (carbon particles and hydrocarbons) occur.

Fluid Catalytic Cracking Fluid catalytic cracking (Fig. 8) is one of the largest sources of air emission in refineries [2, 6]. Air emissions are released in process heater flue gas, as fugitive emissions from leaking valves and pipes, and during regeneration of the cracking catalyst. If not controlled, catalytic cracking is one of the most substantial sources of carbon monoxide and particulate emissions in the refinery. In non-attainment areas where carbon monoxide and particulates are above acceptable levels, carbon monoxide waste heat boilers (CO boiler) and particulate controls are employed. Carbon monoxide produced during regeneration of the catalyst is converted to carbon dioxide either in the regenerator or further downstream in a carbon monoxide waste heat boiler (CO boiler). Catalytic crackers are also significant sources of sulfur oxides and nitrogen oxides. The nitrogen oxides produced by catalytic crackers is expected to be a major target of emissions reduction in the future.

Catalytic cracking units, like coking units, usually include some form of fractionation or steam stripping as part of the process configuration. These units all produce sour waters and sour gases containing some hydrogen sulfide and ammonia. Like crude oil distillation, some of the toxic releases reported by the refining

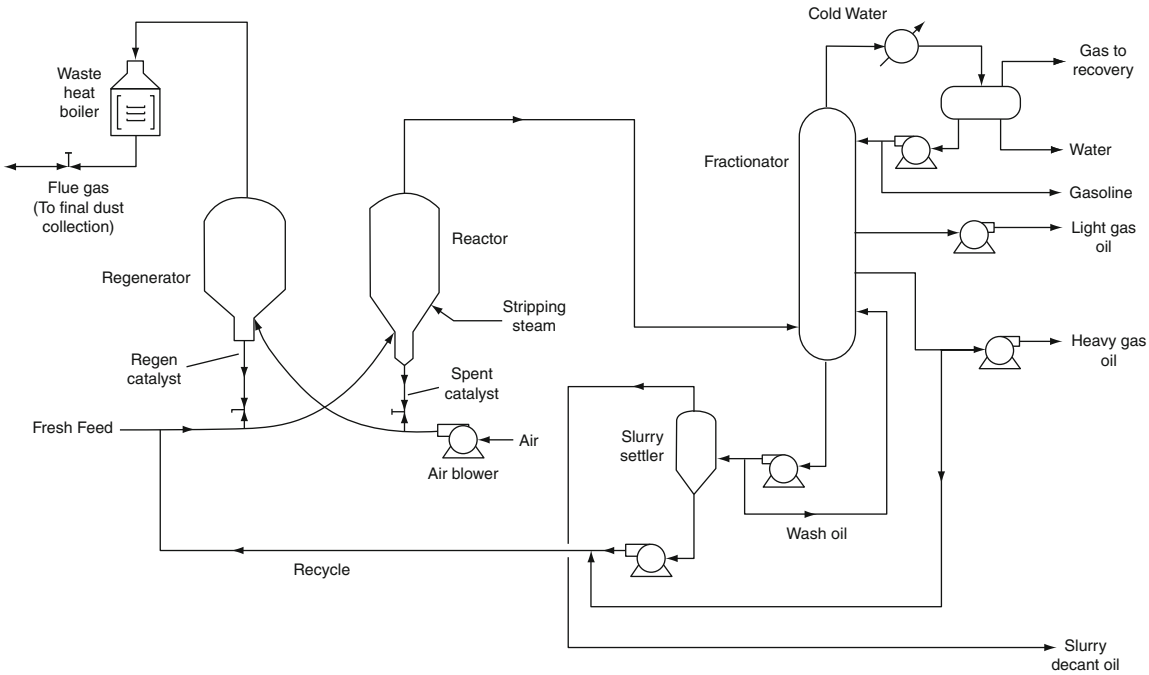

Petroleum Refining and Environmental Control and Environmental Effects. Figure 8
Schematic of a fluid catalytic cracking unit [12]

industry are generated through sour water and gases, notably ammonia. Gaseous ammonia often leaves fractionating and treating processes in the sour gas along with hydrogen sulfide and fuel gases [6].

Catalytic cracking (primarily fluid catalytic cracking) generates considerable sour wastewater from fractionators used for product separation, from steam strippers used to strip oil from catalysts, and in some cases from scrubber water. The steam stripping process used to purge and regenerate the catalysts can contain metal impurities from the feed in addition to oil and other contaminants. Sour wastewater from the fractionator/gas concentration units and steam strippers contains oil, suspended solids, phenols, cyanides, hydrogen sulfide, ammonia, spent catalysts, metals from crude oil, and hydrocarbons.

Catalytic cracking generates significant quantities of spent process catalysts (containing metals from crude oils and hydrocarbons) that are often sent off-site for disposal or recovery or recycling. Management options can include land filling, treatment, or separation and recovery of the metals. Metals deposited on catalysts are often recovered by third-party recovery facilities. Spent catalyst fines (containing aluminum silicate and metals) from electrostatic precipitators are also sent off-site for disposal and/or recovery options.

Catalytic crackers also produce a significant amount of fine catalyst dust that results from the constant movement of catalyst grains against each other. This dust contains primarily alumina (Al_2O_3) and small amounts of nickel (Ni) and vanadium (V), and is generally carried along with the carbon monoxide stream to the carbon monoxide waste heat boiler. The dust is separated from the carbon dioxide stream exiting the boiler through the use of cyclones, flue gas scrubbing, or electrostatic precipitators.

Hydrocracking and Hydrotreating *Hydrocracking* (Fig. 9) generates air emissions through process heater flue gas, vents, and fugitive emissions [2, 6]. Unlike fluid catalytic cracking catalysts, hydrocracking catalysts are usually regenerated off-site after months or years of operations, and little or no emissions or dust is

generated. However, the use of heavy oil as feedstock to the unit can change this balance.

Hydrocracking produces less sour wastewater than catalytic cracking. Hydrocracking, like catalytic cracking, produces sour wastewater at the fractionator. These processes include processing in a separator (API separator, corrugated plate interceptor) that creates sludge [2, 6]. Physical or chemical methods are then used to separate the remaining emulsified oils from the wastewater. Treated wastewater may be discharged to public wastewater treatment, to a refinery secondary treatment plant for ultimate discharge to public wastewater treatment, or may be recycled and used as process water. The separation process permits recovery of usable oil, and also creates a sludge that may be recycled or treated as a hazardous waste.

Like catalytic cracking, hydrocracking processes generate toxic metal compounds, many of which are present in spent catalyst sludge and catalyst fines generated from catalytic cracking and hydrocracking. These include metals such as nickel (Ni), cobalt (Co), and molybdenum (Mo).

Hydrotreating is the less severe removal of heteroatomic species by treatment of a feedstock or product in the presence of hydrogen [2, 6]. The process (Fig. 10) generates air emissions through process heater flue gas, vents, and fugitive emissions [6]. Unlike fluid catalytic cracking catalysts, hydrotreating catalysts are usually regenerated off-site after months or years of

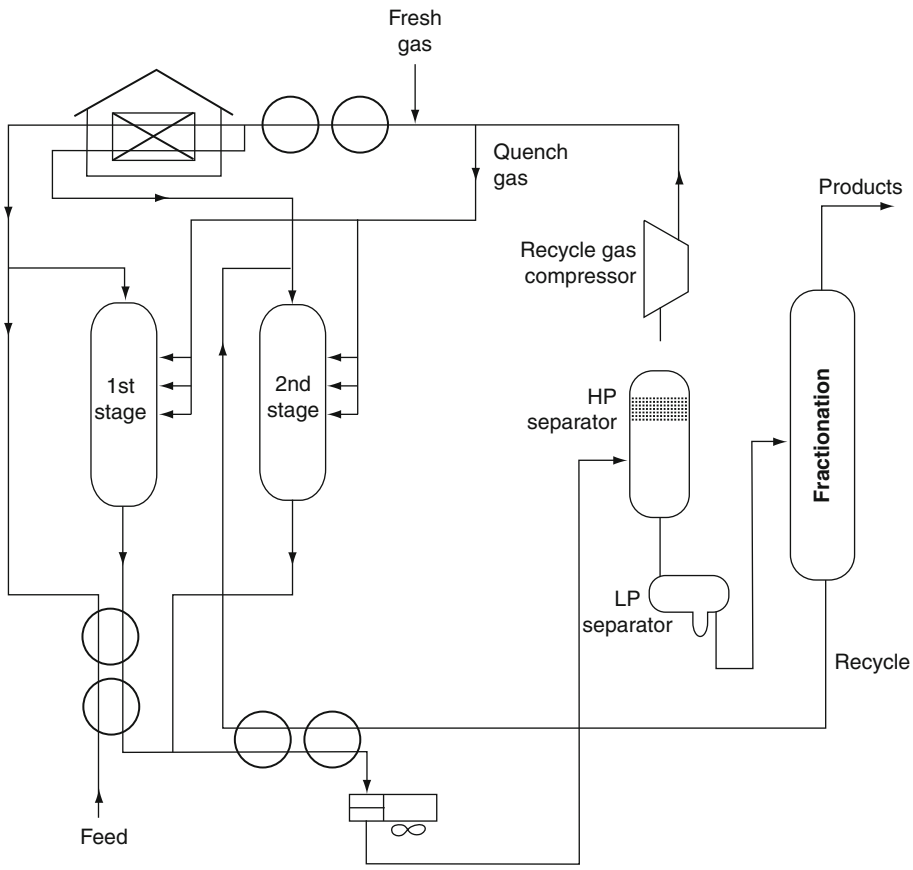

Petroleum Refining and Environmental Control and Environmental Effects. Figure 9
A two-stage hydrocracking unit (OSHA technical manual, Section IV, Chapter 2: Petroleum Refining Processes, http://www.osha.gov/dts/osta/otm/otm_iv/otm_iv_2.html)

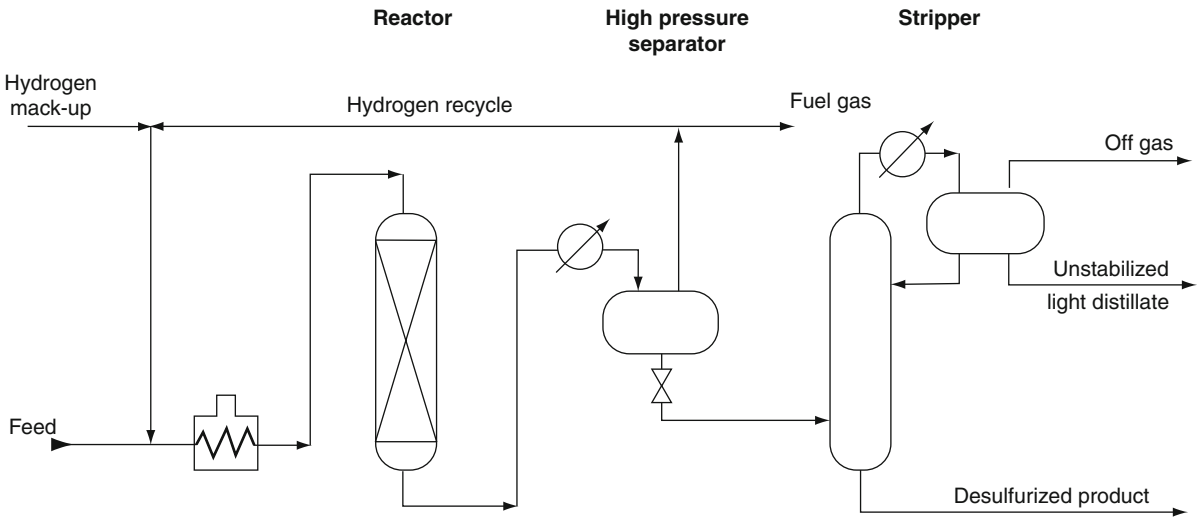

Petroleum Refining and Environmental Control and Environmental Effects. Figure 10
A distillate hydrotreating unit (OSHA technical manual, Section IV, Chapter 2: Petroleum Refining Processes, http://www.osha.gov/dts/osta/otm/otm_iv/otm_iv_2.html)

operations, and little or no emissions or dust is generated from the catalyst regeneration process at the refinery. Air emissions factors for emissions from process heaters and boilers used throughout the refinery can be calculated (Emissions Factors & AP 42, *Compilation of Air Pollutant Emission Factors*).

Fugitive air emissions of volatile components released during hydrotreating may also be toxic components. These include toluene, benzene, xylenes, and other volatiles that are reported as toxic chemical releases under the EPA Toxics Release Inventory.

Hydrotreating generates sour wastewater from fractionators used for product separation. Like most separation processes in the refinery, the process water used in fractionators often comes in direct contact with oil, and can be highly contaminated. It also contains hydrogen sulfide and ammonia and must be treated along with other refinery sour waters.

Oily sludge from the wastewater treatment facility that result from treating oily and/or sour wastewaters from hydrotreating and other refinery processes may be hazardous wastes, depending on how they are managed. These include API separator sludge, primary treatment sludge, sludge from various gravitational separation units, and float from dissolved air flotation units.

Hydrotreating also produces some residuals in the form of spent catalyst fines, usually consisting of aluminum silicate and some metals (e.g., cobalt, molybdenum, nickel, tungsten). Spent hydrotreating catalyst is now listed as a hazardous waste (K171) (except for most support material). Hazardous constituents of this waste include benzene and arsenia (arsenic oxide, As_2O_3). The support material for these catalysts is usually an inert ceramic (e.g., alumina, Al_2O_3).

Alkylation and Polymerization Alkylation (Fig. 11) combines low-molecular-weight olefins (primarily a mixture of propylene and butylene) with isobutene in the presence of a catalyst, either sulfuric acid or hydrofluoric acid [2]. The product is called alkylate and is composed of a mixture of high-octane, branched-chain paraffinic hydrocarbons. Alkylate is a premium blending stock because it has exceptional antiknock properties and is clean burning. The octane number of alkylate depends mainly upon the kind of olefins used and upon operating conditions.

Emissions from alkylation processes (Figs. 11 and 12) and polymerization processes (Fig. 13) include fugitive emissions of volatile constituents in the feed, and

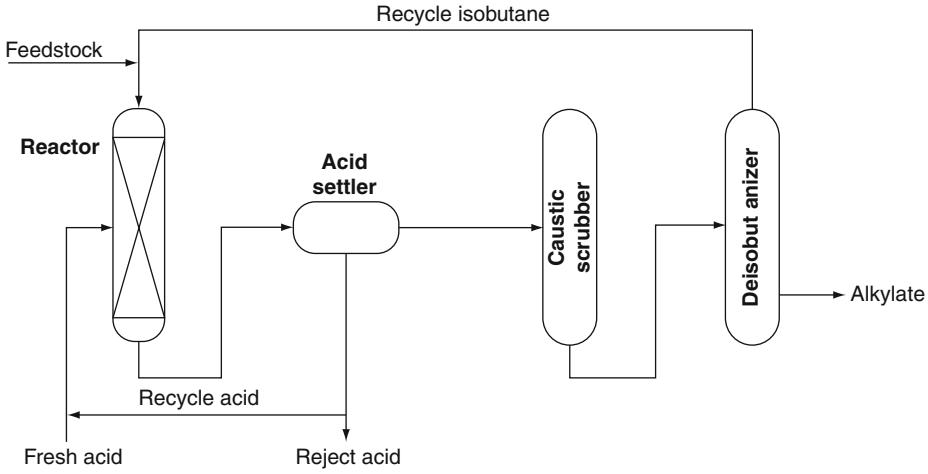

Petroleum Refining and Environmental Control and Environmental Effects. Figure 11
An alkylation unit (sulfuric acid catalyst) (OSHA technical manual, Section IV, Chapter 2: Petroleum Refining Processes, http://www.osha.gov/dts/osta/otm/otm_iv/otm_iv_2.html)

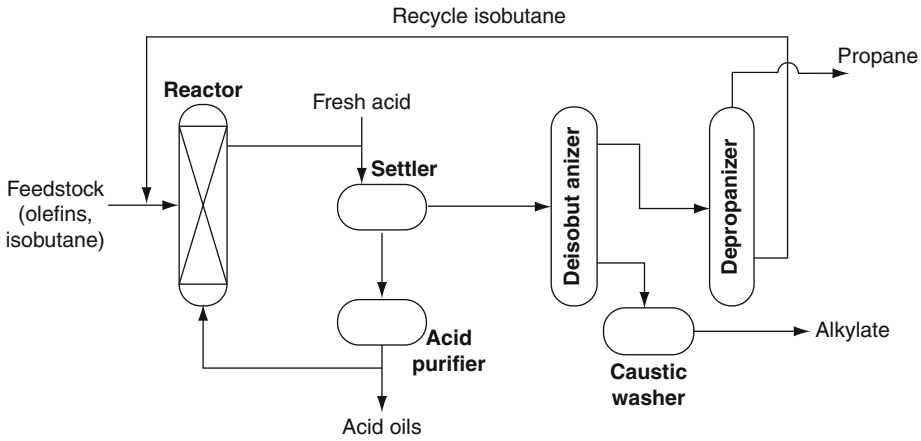

Petroleum Refining and Environmental Control and Environmental Effects. Figure 12
An alkylation unit (hydrogen fluoride catalyst) (OSHA technical manual, Section IV, Chapter 2: Petroleum Refining Processes, http://www.osha.gov/dts/osta/otm/otm_iv/otm_iv_2.html)

emissions that arise from process vents during processing. These can take the form of acidic hydrocarbon gases, nonacidic hydrocarbon gases, and fumes that may have a strong odor (from sulfonated organic compounds and organic acids, even at low concentrations). To prevent releases of hydrofluoric acid, refineries install a variety of mitigation and control technologies (e.g., acid inventory reduction, hydrogen fluoride detection systems, isolation valves, rapid acid transfer systems, and water spray systems).

In hydrofluoric acid alkylation processes, acidic hydrocarbon gases can originate anywhere hydrogen fluoride is present (e.g., during a unit upset, unit shutdown, or maintenance) [2, 6]. Hydrofluoric acid alkylation units are designed to pipe these gases from acid vents and valves to a separate closed-relief system where the acid is neutralized.

Another source of emissions is combustion of fuels in process boilers to produce steam for strippers. As with all process heaters in the refinery, these boilers

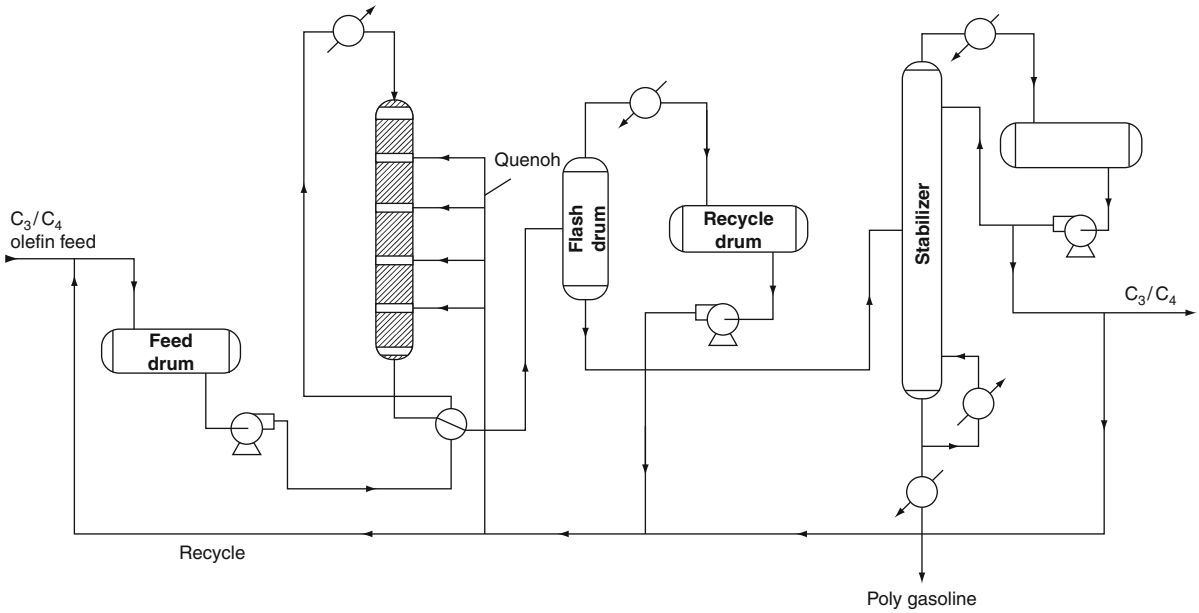

Petroleum Refining and Environmental Control and Environmental Effects. Figure 13
A polymerization process (OSHA technical manual, Section IV, Chapter 2: Petroleum Refining Processes, http://www.osha.gov/dts/osta/otm/otm_iv/otm_iv_2.html)

produce significant emissions of sulfur oxides, nitrogen oxides, carbon monoxide, particulate matter, and volatile hydrocarbons.

Alkylation generates relatively low volumes of wastewater, primarily from water washing of the liquid reactor products. Wastewater is also generated from steam strippers, depropanizers, and debutanizers, and can be contaminated with oil and other impurities. Liquid process waters (hydrocarbons and acid) originate from minor undesirable side reactions and from feed contaminants, and usually exit as a bottoms stream from the acid regeneration column. The bottom layer is an acid–water mixture that is sent to the neutralizing drum. The acid in this liquid eventually ends up as insoluble calcium fluoride.

Sulfuric acid alkylation generates considerable quantities of spent acid that must be removed and regenerated. Nearly all the spent acid generated at refineries is regenerated and recycled and, although technology for on-site regeneration of spent sulfuric acid is available, the supplier of the acid may perform this task off-site. If sulfuric acid production capacity is limited, acid regeneration is often done on-site. The development of internal acid regeneration for hydrofluoric acid units has virtually eliminated the need for external regeneration, although most operations retain one for start-ups or during periods of high feed contamination.

Both sulfuric acid and hydrofluoric acid alkylation units generate neutralization sludge from treatment of acid-laden streams with caustic solutions in neutralization or wash systems. Sludge from hydrofluoric acid alkylation neutralization systems consists largely of calcium fluoride and unreacted lime, and is usually disposed of in a landfill. It can also be directed to steel manufacturing facilities, where the calcium fluoride can be used as a neutral flux to lower the slag-melting temperature and improve slag fluidity. Calcium fluoride can also be routed back to a hydrofluoric acid manufacturer.

A basic step in hydrofluoric acid manufacture is the reaction of sulfuric acid with fluorspar (calcium fluoride) to produce hydrogen fluoride and calcium sulfate. Spent alumina is also generated by the defluorination of some hydrofluoric acid alkylation products over alumina. It is disposed of or sent to the alumina supplier for recovery. Other solid residuals from hydrofluoric acid alkylation include any porous materials that may have come in contact with the hydrofluoric acid.

Catalytic Reforming Catalytic reforming (Fig. 14) converts alkanes to cycloalkanes and to aromatics and emissions from catalytic reforming include fugitive emissions of volatile constituents in the feed, and emissions from process heaters and boilers [2, 6]. As with all process heaters in the refinery, combustion of fossil fuels produces emissions of sulfur oxides, nitrogen oxides, carbon monoxide, particulate matter, and volatile hydrocarbons.

Benzene, toluene, and the xylene isomers are toxic aromatic chemicals that are produced during the catalytic reforming process and used as feedstocks in chemical manufacturing. Due to their highly volatile nature, fugitive emissions of these chemicals are a source of their release to the environment during the reforming process. Point air sources may also arise during the process of separating these chemicals.

In a continuous reformer, some particulate and dust matter can be generated as the catalyst moves from reactor to reactor, and is subject to attrition. However, due to catalyst design, little attrition occurs, and the only outlet to the atmosphere is the regeneration vent, which is most often scrubbed with a caustic to prevent emission of hydrochloric acid (this also removes particulate matter). Emissions of carbon monoxide and hydrogen sulfide may occur during regeneration of catalyst.

Isomerization Isomerization (Fig. 15) converts n-butane, n-pentane, and n-hexane into their respective iso-paraffins of substantially higher octane number [2]. The straight-chain paraffins are converted to their branched-chain counterparts whose component atoms are the same but are arranged in a different geometric structure. Isomerization is important for the conversion of n-butane into iso-butane, to provide additional feedstock for alkylation units,

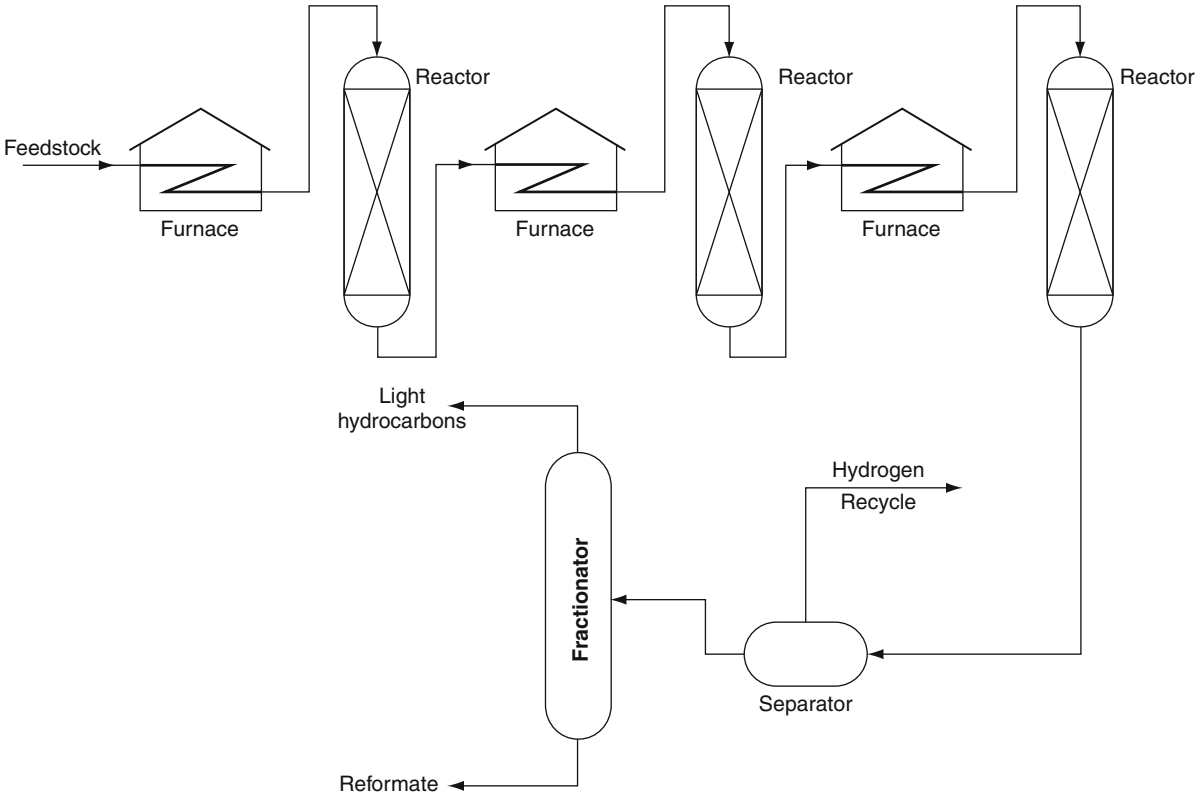

Petroleum Refining and Environmental Control and Environmental Effects. Figure 14
A catalytic reforming unit (OSHA technical manual, Section IV, Chapter 2: Petroleum Refining Processes, http://www.osha.gov/dts/osta/otm/otm_iv/otm_iv_2.html)

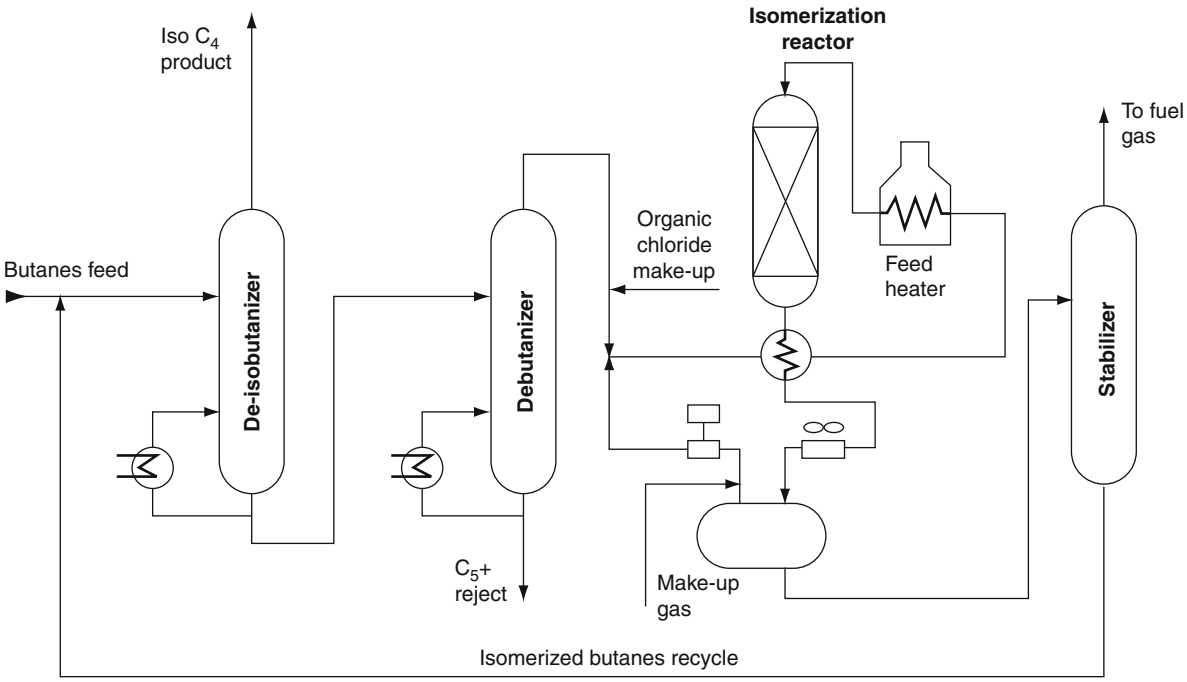

Petroleum Refining and Environmental Control and Environmental Effects. Figure 15
A butane isomerization unit (OSHA technical manual, Section IV, Chapter 2: Petroleum Refining Processes, http://www.osha.gov/dts/osta/otm/otm_iv/otm_iv_2.html)

and the conversion of normal pentanes and hexanes into higher branched isomers for gasoline blending.

Isomerization processes produce sour water and caustic wastewater. The ether manufacturing process utilizes a water wash to extract methanol or ethanol from the reactor effluent stream. After the alcohol is separated, this water is recycled back to the system and is not released. In those cases where chloride catalyst activation agents are added, a caustic wash is used to neutralize any entrained hydrogen chloride. This process generates caustic wash water that must be treated before being released.

Deasphalting and Dewaxing Propane deasphalting (Fig. 16) produces lubricating oil base stocks by extracting asphaltenes and resins from vacuum distillation residua [2]. Propane is the usual solvent of choice due to its unique solvent properties. At lower temperatures (38–60°C, 100–140°F), paraffins are very soluble in propane, and at higher temperatures, (approximately 93°C, 200°F) hydrocarbons are almost insoluble in propane. The propane deasphalting process is similar to solvent extraction in that a packed or baffled extraction tower or rotating disk contactor is used to mix the oil feed stocks with the solvent.

Air emissions may arise from fugitive propane emissions and process vents. These include heater stack gas (carbon monoxide, sulfur oxides, nitrogen oxides, and particulate matter) as well as hydrocarbon emission such as fugitive propane and fugitive solvents. Steam stripping wastewater (oil and solvents) and solvent recovery wastewater (oil and propane) are also produced.

Dewaxing (Fig. 17) processes also produce heater stack gas (carbon monoxide, sulfur oxides, nitrogen oxides, and particulate matter) as well as hydrocarbon emission such as fugitive propane and fugitive solvents [2, 6]. Steam stripping wastewater (oil and solvents) and solvent recovery wastewater (oil and propane) are also produced. The fugitive solvent emissions may be toxic (toluene, methyl ethyl ketone, methyl isobutyl ketone).

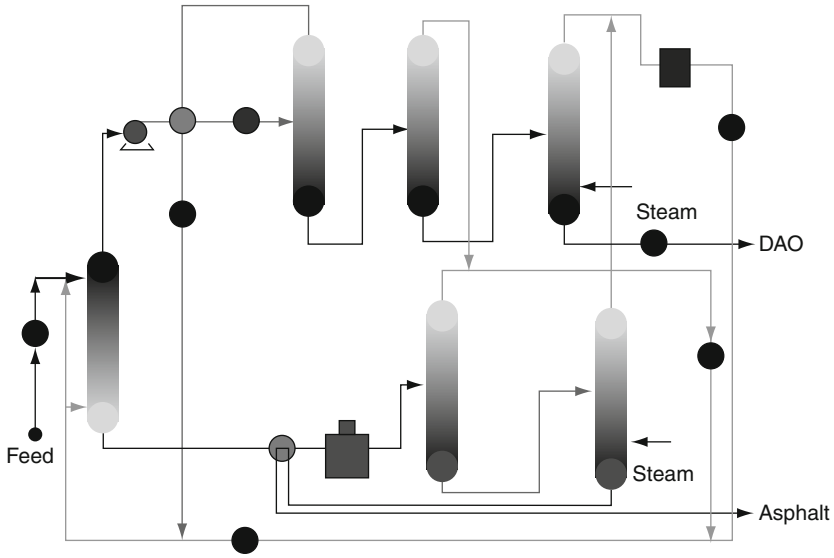

Petroleum Refining and Environmental Control and Environmental Effects. Figure 16
A deasphalting unit

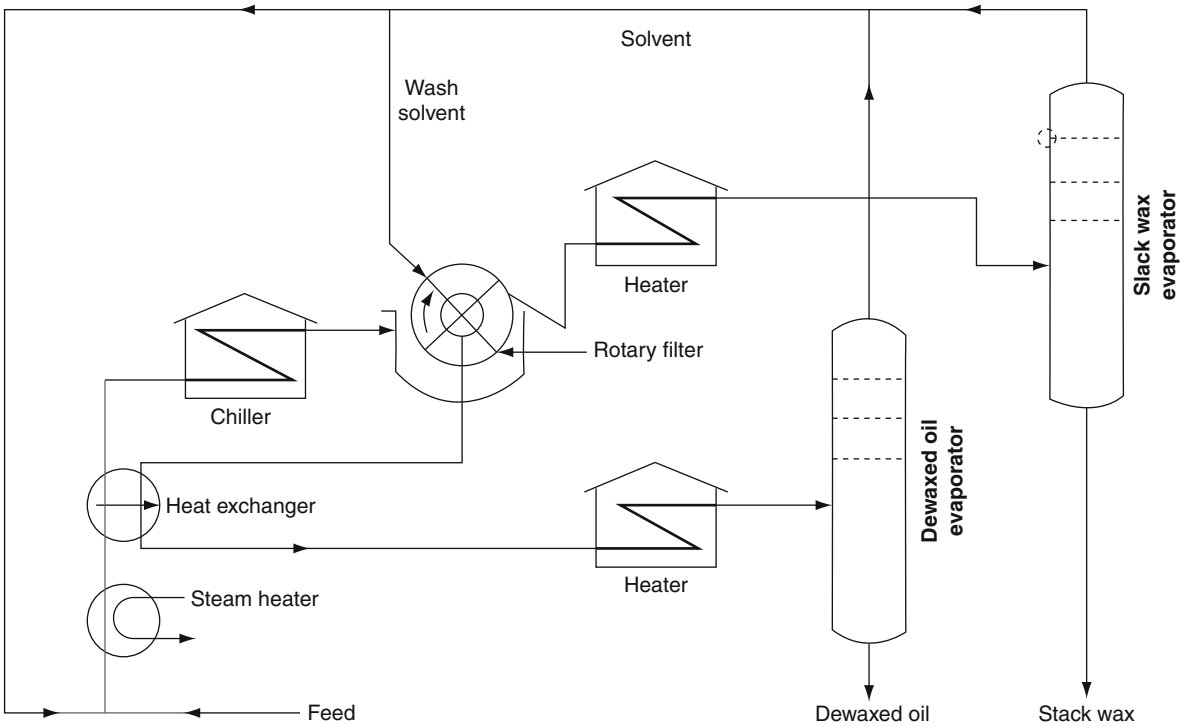

Petroleum Refining and Environmental Control and Environmental Effects. Figure 17
A solvent dewaxing unit (OSHA technical manual, Section IV, Chapter 2: Petroleum Refining Processes, http://www.osha.gov/dts/osta/otm/otm_iv/otm_iv_2.html)

Gaseous Emissions

Gaseous emissions from petroleum refining create a number of environmental problems [2, 6]. During combustion, the combination of hydrocarbons, nitrogen oxide, and sunlight results in localized low levels of ozone, or smog. This is particularly evident in large urban areas and especially when air does not circulate well. Petroleum use in automobiles also contributes to the problem in many areas. The primary effects are on the health of those exposed to the ozone, but plant life has been observed to suffer as well.

Refinery and natural gas streams may contain large amounts of acid gases, such as hydrogen sulfide (H_2S) and carbon dioxide (CO_2) [4, 5]. Hydrogen chloride (HCl), although not usually considered to be a major pollutant in petroleum refineries, can arise during processing from the presence of brine in petroleum that is incompletely dried. It can also be produced from mineral matter and other inorganic contaminants, gaining increasing recognition as a pollutant which needs serious attention.

Acid gases corrode refining equipment, harm catalysts, pollute the atmosphere, and prevent the use of hydrocarbon components in petrochemical manufacture. When the amount of hydrogen sulfide is large, it may be removed from a gas stream and converted to sulfur or sulfuric acid. Some natural gases contain sufficient carbon dioxide to warrant recovery as *dry ice*, i.e., solid carbon dioxide. And there is now a conscientious effort to mitigate the emission of pollutants from hydrotreating process by careful selection of process parameters and catalysts [2, 6, 15].

The terms "*refinery gas*" and "*process gas*" are also often used to include all of the gaseous products and by-products that emanate from a variety of refinery processes [5, 6]. There are also components of the gaseous products that must be removed prior to release of the gases to the atmosphere or prior to use of the gas in another part of the refinery, i.e., as a fuel gas or as a process feedstock.

Petroleum refining produces gas streams that often contain substantial amounts of acid gases such as hydrogen sulfide and carbon dioxide. More particularly hydrogen sulfide arises from the hydrodesulfurization of feedstocks that contain organic sulfur:

$$[S]_{feedstock} + H_2 \rightarrow H_2S + \text{hydrocarbons}$$

Petroleum refining involves, with the exception of some of the more viscous crude oils, a primary distillation of the hydrogen mixture, which results in its separation into fractions differing in carbon number, volatility, specific gravity, and other characteristics [2, 6]. The most volatile fraction, that contains most of the gases which are generally dissolved in the crude, is referred to as *pipe still gas* or *pipe still light ends* and consists essentially of hydrocarbon gases ranging from methane to butane(s), or sometimes pentane(s).

The gas varies in composition and volume, depending on crude origin and on any additions to the crude made at the loading point. It is not uncommon to re-inject light hydrocarbons such as propane and butane into the crude before dispatch by tanker or pipeline. This results in a higher vapor pressure of the crude, but it allows one to increase the quantity of light products obtained at the refinery. Since light ends in most petroleum markets command a premium, while in the oil field itself propane and butane may have to be re-injected or flared, the practice of *spiking* crude oil with liquefied petroleum gas is becoming fairly common.

In addition to the gases obtained by distillation of petroleum, more highly volatile products result from the subsequent processing of naphtha and middle distillate to produce gasoline. Hydrogen sulfide is produced in the desulfurization processes involving hydrogen treatment of naphtha, distillate, and residual fuel, and from the coking or similar thermal treatments of vacuum gas oils and residual fuels. The most common processing step in the production of gasoline is the catalytic reforming of hydrocarbon fractions in the heptane (C_7) to decane (C_{10}) range.

In a series of processes commercialized under the generic name *reforming*, paraffin and naphthene (cyclic non-aromatic) hydrocarbons are altered structurally in the presence of hydrogen and a catalyst into aromatics, or isomerized to more highly branched hydrocarbons. Catalytic reforming processes thus not only result in the formation of a liquid product of higher octane

number, but also produce substantial quantities of gases. The latter are rich in hydrogen, but also contain hydrocarbons from methane to butanes, with a preponderance of propane ($CH_3CH_2CH_3$), *n*-butane ($CH_3CH_2CH_2CH_3$), and *iso*-butane [$(CH_3)_3CH$].

A second group of refining operations that contributes to gas production is that of the *catalytic cracking* processes [2, 6]. These consist of fluid-bed catalytic cracking in which heavy gas oils are converted into gas, liquefied petroleum gas, catalytic naphtha, fuel oil, and coke by contacting the heavy hydrocarbon with the hot catalyst. Both catalytic and thermal cracking processes, the latter being now largely used for the production of chemical raw materials, result in the formation of unsaturated hydrocarbons, particularly ethylene ($CH_2{=}CH_2$), but also propylene (propene, $CH_3.CH{=}CH_2$), *iso*-butylene [*iso*-butene, $(CH_3)_2C{=}CH_2$], and the *n*-butenes ($CH_3CH_2CH{=}CH_2$, and $CH_3CH{=}CHCH_3$) in addition to hydrogen (H_2), methane (CH_4) and smaller quantities of ethane (CH_3CH_3), propane ($CH_3CH_2CH_3$), and butanes [$CH_3CH_2CH_2CH_3$, $(CH_3)_3CH$]. Diolefins such as butadiene ($CH_2{=}CH.CH{=}CH_2$) are also present.

Additional gases are produced in refineries with visbreaking and/or coking facilities that are used to process the heaviest crude fractions. In the visbreaking process, fuel oil is passed through externally fired tubes and undergoes liquid phase cracking reactions, which result in the formation of lighter fuel oil components. Oil viscosity is thereby reduced, and some gases, mainly hydrogen, methane, and ethane, are formed. Substantial quantities of both gas and carbon are also formed in coking (both delayed coking and fluid coking) in addition to the middle distillate and naphtha. When coking a residual fuel oil or heavy gas oil, the feedstock is preheated and contacted with hot carbon (coke) which causes extensive cracking of the feedstock constituents of higher molecular weight to produce lower molecular weight products ranging from methane, via liquefied petroleum gas and naphtha, to gas oil and heating oil. Products from coking processes tend to be unsaturated, and olefin components predominate in the tail gases from coking processes.

A further source of refinery gas is hydrocracking, a catalytic high-pressure pyrolysis process in the presence of fresh and recycled hydrogen. The feedstock is again heavy gas oil or residual fuel oil, and the process is directed mainly at the production of additional middle distillates and gasoline. Since hydrogen is to be recycled, the gases produced in this process again have to be separated into lighter and heavier streams; any surplus recycle gas and the liquefied petroleum gas from the hydrocracking process are both saturated.

Both hydrocracker gases and catalytic reformer gases are commonly used in catalytic desulfurization processes. In the latter, feedstocks ranging from light to vacuum gas oils are passed at pressures of 500–1,000 psi with hydrogen over a hydrofining catalyst. This results mainly in the conversion of organic sulfur compounds to hydrogen sulfide,

$$[S]_{\text{feedstock}} + H_2 \rightarrow H_2S + \text{hydrocarbons}$$

The reaction also produces some light hydrocarbons by hydrocracking.

Thus refinery streams, while ostensibly being hydrocarbon in nature, may contain large amounts of acid gases such as hydrogen sulfide and carbon dioxide. Most commercial plants employ hydrogenation to convert organic sulfur compounds into hydrogen sulfide. Hydrogenation is effected by means of recycled hydrogen-containing gases or external hydrogen over a nickel molybdate or cobalt molybdate catalyst.

In summary, refinery process gas, in addition to hydrocarbons, may contain other contaminants, such as carbon oxides (CO_x, where $x = 1$ and/or 2), sulfur oxides (SO_x, where $x = 2$ and/or 3), as well as ammonia (NH_3), mercaptans (R-SH), and carbonyl sulfide (COS).

The presence of these impurities may eliminate some of the sweetening processes, since some processes remove large amounts of acid gas but not to a sufficiently low concentration. On the other hand, there are those processes not designed to remove (or incapable of removing) large amounts of acid gases whereas they are capable of removing the acid gas impurities to very low levels when the acid gases are present only in low-to-medium concentration in the gas.

From an environmental viewpoint, not only are the means by which these gases can be utilized important but also equally important are the effects of these gases on the environment when they are introduced into the atmosphere.

In addition to the corrosion of equipment of acid gases, the escape into the atmosphere of sulfur-containing gases can eventually lead to the formation of the constituents of acid rain, i.e., the oxides of sulfur (SO_2 and SO_3). Similarly, the nitrogen-containing gases can also lead to nitrous and nitric acids (through the formation of the oxides NO_x, where $x = 1$ or 2) which are the other major contributors to acid rain. The release of carbon dioxide and hydrocarbons as constituents of refinery effluents can also influence the behavior and integrity of the ozone layer.

Hydrogen chloride, if produced during refining, quickly picks up moisture in the atmosphere to form droplets of hydrochloric acid and, like sulfur dioxide, is a contributor to acid rain [6]. However, hydrogen chloride may exert severe local effects because, unlike sulfur dioxide, it does not need to participate in any further chemical reaction to become an acid. Under atmospheric conditions that favor a buildup of stack emissions in the area of a large industrial complex or power plant, the amount of hydrochloric acid in rainwater could be quite high.

Natural gas is also capable of producing emissions that are detrimental to the environment. While the major constituent of natural gas is methane, there are components such as carbon dioxide (CO), hydrogen sulfide (H_2S), and mercaptans (thiols; R-SH), as well as trace amounts of sundry other emissions. The fact that methane has a foreseen and valuable end-use makes it a desirable product, but in several other situations, it is considered a pollutant, having been identified a greenhouse gas.

A sulfur removal process must be very precise, since natural gas contains only a small quantity of sulfur-containing compounds that must be reduced several orders of magnitude. Most consumers of natural gas require less than 4 ppm in the gas.

A characteristic feature of natural gas that contains hydrogen sulfide is the presence of carbon dioxide (generally in the range of 1–4% v/v). In cases where the natural gas does not contain hydrogen sulfide, there may also be a relative lack of carbon dioxide.

Acid rain occurs when the oxides of nitrogen and sulfur that are released to the atmosphere during the combustion of fossil fuels are deposited (as soluble acids) with rainfall, usually at some location remote from the source of the emissions.

It is generally believed (the chemical thermodynamics are favorable) that acidic compounds are formed when sulfur dioxide and nitrogen oxide emissions are released from tall industrial stacks. Gases such as sulfur oxides (usually sulfur dioxide, SO_2) as well as the nitrogen oxides (NO_x) react with the water in the atmosphere to form acids:

$$SO_2 + H_2O \rightarrow H_2SO_3$$

$$2SO_2 + O_2 \rightarrow 2SO_3$$

$$SO_3 + H_2O \rightarrow H_2SO_4$$

$$2NO + H_2O \rightarrow 2HNO_2$$

$$2NO + O_2 \rightarrow 2NO_2$$

$$NO_2 + H_2O \rightarrow HNO_3$$

Acid rain has a pH less than 5.0 and predominantly consists of sulfuric acid (H_2SO_4) and nitric acid (HNO_3). As a point of reference, in the absence of anthropogenic pollution sources, the average pH of rain is 6.0 (slightly acidic; neutral pH = 7.0). In summary, the sulfur dioxide that is produced during a variety of processes will react with oxygen and water in the atmosphere to yield environmentally detrimental sulfuric acid. Similarly, nitrogen oxides will also react to produce nitric acid.

Another acid gas, hydrogen chloride (HCl), although not usually considered to be a major emission, is produced from mineral matter and the brines that often accompany petroleum during production and is gaining increasing recognition as a contributor to acid rain. However, hydrogen chloride may exert severe local effects because it does not need to participate in any further chemical reaction to become an acid. Under atmospheric conditions that favor a buildup of stack emissions in the areas where hydrogen chloride is produced, the amount of hydrochloric acid in rainwater could be quite high.

In addition to hydrogen sulfide and carbon dioxide, gas may contain other contaminants, such as mercaptans (R-SH) and carbonyl sulfide (COS). The presence of these impurities may eliminate some of the sweetening processes since some processes remove large amounts of acid gas but not to a sufficiently low concentration. On the other hand, there are those processes that are not designed to remove (or are incapable

of removing) large amounts of acid gases. However, these processes are also capable of removing the acid gas impurities to very low levels when the acid gases are there in low-to-medium concentrations in the gas.

On a regional level, the emission of sulfur oxides (SO_x) and nitrogen oxides (NO_x) can also cause the formation of acid species at high altitudes, which eventually precipitate in the form of *acid rain*, damaging plants, wildlife, and property. Most petroleum products are low in sulfur or are desulfurized, and while natural gas sometimes includes sulfur as a contaminant, it is typically removed at the production site.

At the global level, there is concern that the increased use of hydrocarbon-based fuels will ultimately raise the temperature of the planet (*global warming*), as carbon dioxide reflects the infrared or thermal emissions from the earth, preventing them from escaping into space (*greenhouse effect*). Whether or not the potential for global warming becomes real will depend upon how emissions into the atmosphere are handled. There is considerable discussion about the merits and demerits of the global warming theory [16] and the discussion is likely to continue for some time. Be that as it may, the atmosphere can only tolerate pollutants up to a limiting value. And that value needs to be determined. In the meantime, efforts must be made to curtail the use of noxious and foreign (non-indigenous) materials into the air.

In summary, and from an environmental viewpoint, petroleum and natural gas processing can result in similar, if not the same, gaseous emissions as coal [2, 4, 6]. It is a question of degree insofar as the composition of the gaseous emissions may vary from coal to petroleum but the constituents are, in the majority of cases, the same.

There are a variety of processes which are designed for sulfur dioxide removal from gas streams [2], but scrubbing process utilizing limestone ($CaCO_3$) or lime [$Ca(OH)_2$] slurries have received more attention than other gas scrubbing processes.

The majority of the gas scrubbing processes are designed to remove sulfur dioxide from the gas streams; some processes show the potential for removal of nitrogen oxide(s).

Liquid Effluents

It is convenient to divide the hydrocarbon components of petroleum into the following three classes:

- *Paraffins*: saturated hydrocarbons with straight or branched chains
- *Naphthenes* (*alicyclic hydrocarbons*): saturated hydrocarbons containing one or more rings, each of which may have one or more paraffin side chains
- *Aromatic compounds*: hydrocarbons containing one or more aromatic nuclei (for example, benzene, naphthalene, and phenanthrene) which may be co-joined with (substituted) naphthene rings and/or paraffin side chains

Thermal processing can significantly increase the concentration of polynuclear aromatic hydrocarbons in the product liquid because the low-pressure hydrogen-deficient conditions favor aromatization of naphthene constituents and condensation of aromatics to form larger ring systems. To the extent that more compounds like benzo(a)pyrene are produced, the liquids from thermal processes will be more carcinogenic than asphalt.

The sludge produced on acid treatment of petroleum distillates [2, 6], even gasoline and kerosene, is complex in nature. Esters and alcohols are present from reactions with olefins; sulfonation products from reactions with aromatic compounds, naphthene compounds, and phenols; and salts from reactions with nitrogen bases. To these constituents must be added the various products of oxidation–reduction reactions: coagulated resins, soluble hydrocarbons, water, and free acid.

The disposal of the sludge is a comparatively simple process for the sludge resulting from treating gasoline and kerosene, the so-called light oils. The insoluble oil phase separates out as a mobile tar, which can be mixed and burned without too much difficulty.

In all cases, careful separation of reaction products is important to the recovery of well-refined materials. This may not be easy if the temperature has risen as a consequence of chemical reaction. This will result in a persistent dark color traceable to reaction products that are redistributed as colloids. Separation may also be difficult at low temperature because of high viscosity of the stock, but this problem can be overcome by dilution with light naphtha or with propane.

In addition, delayed coking also requires the use of large volumes of water for hydraulic cleaning of the coke drum. However, the process water can be recycled if the oil is removed by skimming and suspended coke particles are removed by filtration. If this water is used in a closed cycle, the impact of delayed coking on water treatment facilities and the environment is minimized. The flexicoking process offers one alternative to direct combustion of coke for process fuel. The gasification section is used to process excess coke to mixture of carbon monoxide (CO), carbon dioxide (CO_2), hydrogen (H_2), and hydrogen sulfide (H_2S) followed by treatment to remove the hydrogen sulfide. Currently, maximum residue conversion with minimum coke production is favored over gasification of coke.

Solid Effluents

Catalyst disposal is a major concern in all refineries. In many cases, the catalysts are regenerated at the refinery for repeated use. Disposal of spent catalysts is usually part of an agreement with the catalysts manufacturer whereby the spent catalyst is returned for treatment and re-manufacture.

The formation of considerable quantities of coke in the *coking* processes is a cause for concern since it not only reduces the yield of liquid products but also initiates the necessity for disposal of the coke. Stockpiling to coke may be a partial answer unless the coke contains leachable materials that will endanger the ecosystem as a result of rain or snow melt.

In addition, the generation and emission of sulfur oxides (particularly sulfur dioxide) originates from the combustion of sulfur-containing coke as plant fuel. Sulfur dioxide (SO_2) has a wide range of effects on health and on the environment. These effects vary from bronchial irritation upon short-term exposure to contributing to the acidification of lakes. Emissions of sulfur dioxide, therefore, are regulated in many countries.

Future Directions

The petroleum refining industry includes integrated process operations that are engaged in refining crude petroleum into refined petroleum products, especially liquid fuels such as gasoline and diesel as well as processes that produce raw materials for the petrochemical industry.

Over the past 4 decades, the refining industry has experienced significant changes in oil market dynamics, resource availability, and technological advancements. Advancements made in exploration, production, and refining technologies allow utilization of resources such as heavy oil and tar sand bitumen that were considered economically and technically unsuitable in the middle decades of the past century. Along with the many challenges, it is imperative for refiners to raise their operations to new levels of performance. Merely extending today's performance incrementally will fail to meet most company's performance goals.

Petroleum refining in the twenty-first century will continue to be shaped by the factors such as consolidation of oil companies, dramatic changes in market demand, customization of products, and a decrease in the API gravity and sulfur content of the petroleum feedstocks. In fact, in addition to a (hopeful but unlikely) plentiful supply of petroleum, the future of the refining industry will base on the following factors such as (1) increased operating costs or investments due to stringent environmental requirements for facilities and products, (2) accelerating globalization resulting in stronger international petroleum price scenarios. The effect of these factors is likely to reduce refinery profit margins further, and petroleum companies worldwide will need to make significant changes in their operation and structure to be competitive on global basis.

As global petroleum consumption increases and resources are depleted, the production of fuels and petrochemicals from residua, heavy oil, and tar sand bitumen will increase significantly. In fact, over the next decade, refineries will need to adapt to receiving heavier oils as well as a range of bio-feedstocks. It is conceivable that current refineries could not handle such a diverse slate of feedstocks without experiencing shutdowns and related problems.

As feedstocks to refineries change, there must be an accompanying change in refinery technology as petroleum feedstocks are becoming highly variable. At the same time, more stringent anti-pollution regulations are forcing greater restrictions on fuel specifications. There are fundamental limitations on how far current

processes can go in achieving proper control over feedstock behavior. This means a movement from conventional means of refining heavy feedstocks by using (typically) a coking process to more development and use of more innovative processes that will produce the maximum yields of liquid fuels (or other desired products) fuels from the feedstock.

Thus, the need for the development of upgrading processes continues in order to fulfill the product market demand as well as to satisfy environmental regulations. One area in particular, the need for residuum conversion, technology has emerged as result of declining residual fuel oil market and the necessity to upgrade crude oil residua beyond the capabilities of the visbreaking, coking, and low-severity hydrodesulfurization processes.

Technological advances are on the horizon for alternate sources of transportation fuels. For example, gas-to-liquids and biomass-to-liquids are just two of the concepts currently under development. However, the state of many of these technologies coupled with the associated infrastructure required to implement them leaves traditional refining of petroleum hydrocarbons for transportation fuels as the *modus operandi* for the foreseeable future, which for the purposes of this text is seen to be 50 years. The near future challenge for refiners will be how to harness new technologies to remain alive in a changing global marketplace.

It is imperative for refiners to raise their operations to new levels of performance. Merely extending current process performance incrementally will fail to meet most future performance goals. To do this, it will be necessary to reshape refining technology to be more adaptive to changing feedstocks and product demand and to explore the means by which the technology and methodology of refinery operations can be translated not only into increased profitability but also into survivability.

Furthermore, environmental regulations could either preclude unconventional production or, more likely, raise the cost significantly. If future US laws limited and/or taxed greenhouse gas emissions, these laws will lead to substantial increase in the costs of production of fuels from unconventional sources. In addition to increases in the volumes of carbon dioxide, restrictions on access to water also could prove costly, especially in the arid or semiarid western States. In addition, environmental restrictions on land use could preclude unconventional oil production in some areas of the United States.

The general prognosis for reduction of emissions or emission cleanup is optimistic. It is considered likely that most of their environmental impact of petroleum refining can be substantially abated. A considerable investment in retrofitting or replacing existing facilities and equipment will be needed although a conscious goal must be to improve the efficiency with which petroleum is transformed and consumed.

Bibliography

Primary Literature

1. Ray DL, Guzzo L (1990) Trashing the planet: how science can help us deal with acid rain, depletion of the ozone, and nuclear waste (among other things). Regnery Gateway, Washington, DC
2. Speight JG (2007) The chemistry and technology of petroleum, 4th edn. CRC Press/Taylor & Francis, Boca Raton
3. Majumdar SB (1993) Regulatory requirements for hazardous materials. McGraw-Hill, New York
4. Speight JG (1993) Gas processing: environmental aspects and methods. Butterworth Heinemann, Oxford
5. Speight JG (1996) Environmental technology handbook. Taylor & Francis, Washington, DC
6. Speight JG (2005) Environmental analysis and technology for the refining industry. Wiley, Hoboken
7. Lipton S, Lynch J (1994) Handbook of health hazard control in the chemical process industry. Wiley, New York
8. Boyce A (1997) Introduction to environmental technology. Van Nostrand Reinhold, New York
9. Speight JG (2009) Enhanced recovery methods for heavy oil and tar sands. Gulf, Houston
10. Carson PA, Mumford CJ (1995) The safe handling of chemicals in industry. Wiley, New York
11. Renzoni A, Fossi MC, Lari L, Mattei N (1994) Contaminants in the environment: a multidisciplinary assessment of risks to man and other organisms. CRC Press, Boca Raton
12. Edwards JD (1995) Industrial wastewater treatment: a guidebook. CRC Press, Boca Raton
13. Thibodeaux LJ (1995) Environmental chemodynamics. Wiley, New York
14. Meyers RA (1997) Handbook of petroleum refiing processes, 2nd edn. McGraw-Hill, New York
15. Occelli ML, Chianelli R (1996) Hydrotreating technology for pollution control. Marcel Dekker, New York
16. Hileman B (1996) Environmental hormone disruptors focus of major research intitatives. Chem Eng News 74(34):33

Books and Reviews

Abraham H (1945) Asphalts and allied substances, vol I. Van Nostrand, New York
Forbes RJ (1958) A history of technology, vol V. Oxford University Press, Oxford
Gary JH, Handwerk GE (2001) Petroleum refining: technology and economics, 4th edn. Marcel Dekker, New York
Hoiberg AJ (1960) Bituminous materials: asphalts, tars and pitches, vol I & II. Interscience, New York
Hsu CS, Robinson PR (2006) Practical advances in petroleum processing, vol 1 and 2. Springer, New York
Khan MR, Patmore DJ (1997) Heavy oil upgrading processes. In: Speight JG (ed) Petroleum chemistry and refining. Taylor & Francis, Washington, DC. Chapter 6
McKetta JJ (ed) (1992) Petroleum processing handbook. Marcel Dekker, New York
Shih SS, Oballa MC (eds) (1991) Tar sand upgrading technology. Symposium series No. 282. American Institute for Chemical Engineers, New York
Speight JG (2000) The desulfurization of heavy oils and residua, 2nd edn. Marcel Dekker, New York
Speight JG, Ozum B (2002) Petroleum refining processes. Marcel Dekker, New York
Speight JG (2008) Handbook of synthetic fuels: properties, processes, and performance. McGraw-Hill, New York

PHEVs and BEVs in Coupled Power and Transportation Systems

Mladen Kezunovic[1], S. Travis Waller[2]
[1]Department of Electrical and Computer Engineering, Texas A&M University, College Station, TX, USA
[2]Department of Civil Engineering, The University of Texas at Austin, Austin, USA

Article Outline

Glossary
Definition
Introduction
Policy Issues
Modeling of Complex Systems
Benefits
Conclusions and Future Research
Acknowledgments
Bibliography

Glossary

BEV Battery electric vehicle.
DSM Demand side Management; utility-sponsored programs to influence the time of use and amount of energy use by select customers.
G2V Grid-to-vehicle; using the electrical grid to charge the battery of a vehicle.
HEV Hybrid electric vehicle.
OM Outage management; set of manual and/or automated procedures used by operators of electric distribution systems to assist in restoration of power.
PHEV Plug-in hybrid electric vehicle.
V2B Vehicle-to-building; exporting electrical power from a vehicle battery into a building.
V2G Vehicle-to-grid; exporting electrical power from a vehicle battery to the electrical grid.

Definition

With the price of oil peaking in the recent past close to the once unimaginable $150 per barrel and the threat of global climate change increasingly acknowledged, the transportation sector is employing a number of new technologies that will enhance energy security by reducing the current dependency on oil-based fuels. Should the gasoline cost increase in the future, Plug-in Hybrid Electric Vehicles (PHEVs) and Battery Electric Vehicles (BEVs) will become the economical choice for transportation. Widespread adoption of PHEVs/BEVs will also improve air quality and carbon footprint, since point source pollution is easier to control than mobile source pollution. This level of control is essential for effective implementation of carbon cap-and-trade markets, which should spur further innovation. In USA, sales of Hybrid Electric Vehicles (HEVs) have grown 80% each year since 2000, proving that PHEVs/BEVs are likely an eventual reality that must be dealt with [1]. The implications of this reality will be highly dependent on the policies in place to use PHEVs/BEVs to the benefit of the transportation and power systems, as well as the drivers, industry, and public at large.

Beyond fuel costs and sustainability, the primary concern of the transportation sector is congestion. In 2005, congestion was estimated to cost the US economy $78.2 billion in wasted time and fuel [2]. If PHEV/BEV drivers are given appropriate incentives

(e.g., strategically placed energy exchange stations), traveler behavior (e.g., choice of routing, departure time, and destination) impacting congestion may be affected.

In addition, the power industry is currently challenged to maintain reliability of operation while expanding the grid to meet growing demand. Large blackout such as the northeastern one in 2003 may create loses in billions of dollars [3]. Introducing the renewable resources to meet growing demand requires energy storage to deal with interfacing [4]. If proper policy is in place PHEVs/BEVs can provide a promising solution acting as mobile decentralized storage (MDS) of electrical energy. In this capacity, PHEVs/BEVs can serve in two modes: grid-to-vehicle (G2V) and vehicle-to-grid (V2G), each providing benefits to the power system operation. The G2V mode can be used to charge PHEVs/BEVs at reduced cost when the power system load is reduced and generation capacity is abundant, such as during night time. The V2G mode may be used when demand is high or supply is accidentally lost since the stored electric energy can be released from PHEVs/BEVs in an aggregated way, which will offer major contributions to regulation service and spinning reserves, as well as load-shedding prevention. The mobility of the energy storage in PHEVs/BEVs allows for strategic placement of the distributed generation source to optimize power system needs.

Figure 1 illustrates the spatial and temporal coupling of the power and transportation systems through showing an example of a PHEV/BEV driver's route, highlighting destinations where the driver could potentially engage in G2V or V2G activity. Options for meeting selected criteria for electricity and transportation networks simultaneously are numerous. Developing policy strategy requires understanding of trade-offs involved in pursuing certain solutions at the expense of others. The all-encompassing theoretical framework for such studies to the best of our knowledge is not available.

Traditionally, scientists have adopted a divide and conquer approach to understanding complex phenomena. Unfortunately, systems with emergent dynamics that are dominated by contextual interactions are not well suited to this classical approach (e.g., [5–7]). In such cases, directly addressing the couplings of system components may actually hasten progress. While this linkage presents new opportunities to improve the functioning and capacity utilization of each system, it also raises the spectrum of increasing dynamic complexity and cascading failures across systems.

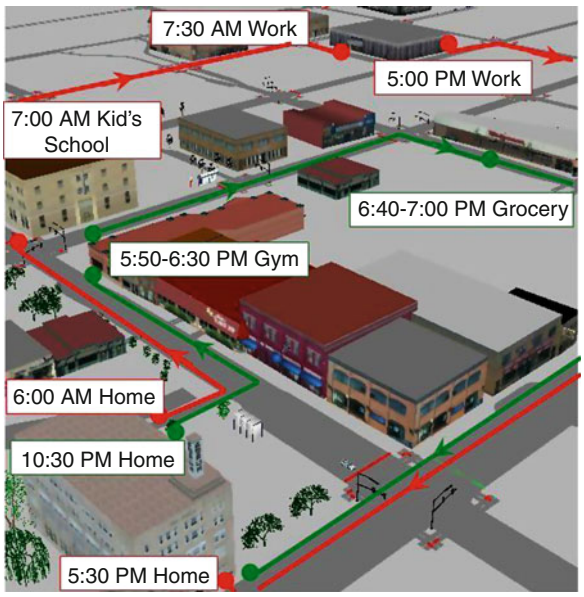

PHEVs and BEVs in Coupled Power and Transportation Systems. Figure 1
Temporal and spatial dimensions of plug-in opportunities

In this entry, several open policies and research goals will be discussed, which facilitate optimizing the integration of the transportation systems and the behavior of its travelers with the electricity systems and behavior of its end-customers. PHEVs/BEVs based demand side management (DSM) and outage management (OM) are also presented as an application of PHEVs/BEVs using in the coupled power and transport system.

Introduction

The impacts PHEVs/BEVs will have on transportation systems, power systems, and air quality are very complex. Studies conducted to date on this topic make many assumptions to simplify the problem. As stated in the definition, the problem space must be treated as one large complex system in order to capture emergent behavior.

The complexity of the issues involved in studying PHEVs/BEVs and their interaction with electricity and transportation networks is shown in Fig. 2, where

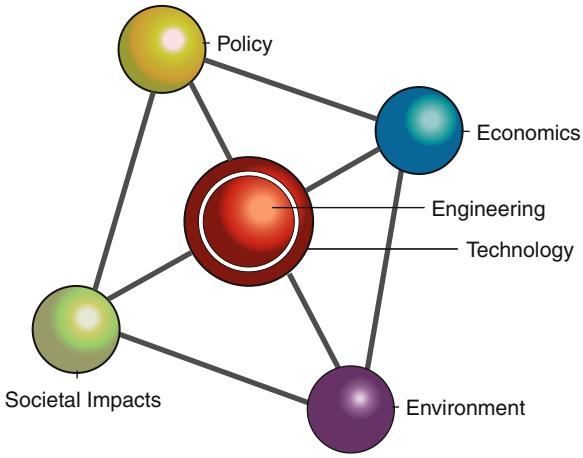

PHEVs and BEVs in Coupled Power and Transportation Systems. Figure 2
Illustration of multidisciplinary nature of problem

several disciplines that need to be involved in researching this multidisciplinary problem are shown.

Recent analyses confirm the feasibility of the grid-to-vehicle (G2V) and vehicle-to-grid (V2G) concepts [8–13]. The Electric Power Research Institute speculates that V2G could reduce the requirement for global, central-station generation capacity by up to 20% by the year 2050 [14]. Several studies omit any consideration of vehicle locations and desired activity patterns and assume a percentage of vehicles are plugged in and available when estimating the benefits to the grid and to drivers [8, 10, 11].

Many researchers have investigated the various potential benefits and implementation issues of the V2G concept. Kempton and Tomić studied the fundamentals of using PHEVs/BEVs for load leveling, regulation, reserve, and other purposes [15, 16]. Hadley and Tsvetkova analyzed the potential impacts of PHEVs on electricity demand, supply, generation, structure, prices, and associated emission levels in 2020 and 2030 in 13 regions specified by the North American Electric Reliability Corporation (NERC) [17]. Meliopoulos et al. considered the impacts of PHEVs/BEVs on electric power network components [18]. Anderson et al. performed the case studies of PHEVs/BEVs as regulating power providers in Sweden and Germany [19]. Guille and Gross presented a proposed framework to effectively integrate the aggregated battery electric vehicles into the grid as distributed energy resources [20]. The combined impact PHEVs/BEVs make on both electric power system and transportation network has not been explored as much. When considering the role of PHEVs/BEVs as dynamically configurable (mobile) energy storage, the potential impacts on both electricity and transportation networks may become quite diverse. The flow of traffic is an important factor in deciding the flow of electric power that could be utilized from PHEVs/BEVs. Correlating the movement of people to the movement of the power load offers new opportunities in the smart grid.

One of the major advantages of PHEVs/BEVs is their usefulness as an MDS. MDS is a revolutionary concept because currently the power grid has no storage except for 2.2% of its capacity in pumped storage [11]. Without significant and reliable storage of energy, maintaining grid stability and reliability under the growing electricity demand is a complex problem. Utilities may contract with others to provide power in any one of the four types of markets: base-load power, peak power, spinning reserves, and regulation services. Several studies have shown that PHEVs/BEVs can provide ancillary services (spinning and regulation) at a profit [8, 10, 11]. Spinning reserves receive payment for providing continuous capacity regardless of whether energy is provided, and receive further payment if called on to feed energy into the grid. Regulation services feed a nominal amount of energy into the grid, and receive payment for reducing or increasing their energy consumption as needed. In the case of PHEVs/BEVs, being plugged-in in a predictable way means that capacity is available to feed into the system if called upon. PHEVs/BEVs are particularly well suited for regulation services since the impact on vehicle's energy resources may be zero.

The pricing of V2G and G2V services is expected to cause a fundamental shift in the behavior of PHEVs/BEVs drivers. Further research is needed to investigate the exact nature of this shift; however, if the pricing schemes are developed with both the power system and transportation system in mind, then PHEVs/BEVs could help solve problems plaguing the traffic network, particularly congestion. The pricing scheme should also consider air quality impacts caused by charging at different times in the day. As mentioned earlier, MDS will allow for renewable energy to be used more

efficiently. There will however remain times of the day more dominated by "dirty" fuels than others.

As observed, the body of research literature related to the multidimensional impact of PHEVs/BEVs is quite small. The remainder of this section will focus separately on the dual problems of improving the stability and reliability of the electrical grid and improving the efficiency of the roadway network.

Stability and Reliability of the Electric Grid

Stability and reliability of the US electric grid have become issues of increasing concern since the occurrence of several blackouts in the 1990s (Western Interconnect in 1994 and 1996, and the Eastern Interconnect in 1999) and system deregulation. The devastating impact of the northeast blackout from August 14, 2003 reminded that the situation with the grid is only worsening and not improving. Here, a stable system is defined as one in which the phase and frequency of power generation units are constant. Ability of the system to maintain the state of equilibrium during normal and abnormal conditions is a measure of stability. Reliability is defined as the ability of the system to meet unexpected demand and respond to failures. Ability of the system to deliver electricity to customers within the accepted standards, which may be affected by the failure rate, repair rate, or duration of loss, is a measure of reliability. Figure 3 illustrates the worsening stability problem. Order 888 in Fig. 3 relates to the Open Access to Transmission issued by Federal Regulatory Commission in 1996, which is the result of an authorization passed by the Congress as a part of the Energy Policy Act of 1992.

A major challenge in achieving these goals (stability and reliability) is the lack of energy storage. Figure 4 depicts the peaking structure of an example power load over the course of 1 day. In this example, demand grows rapidly starting at 6 a.m. and begins to decline after hitting a peak around 3 p.m. This peaking phenomenon is especially important to consider given that different energy sources are available at different times of day. For example, wind energy is most widely available at night when the demand for power is the lowest. While it may seem intuitive that a flat demand curve is the ideal, this is not necessarily true. More research is required to determine if parts of the system (e.g., transformers) require time to cool down. The large scale use

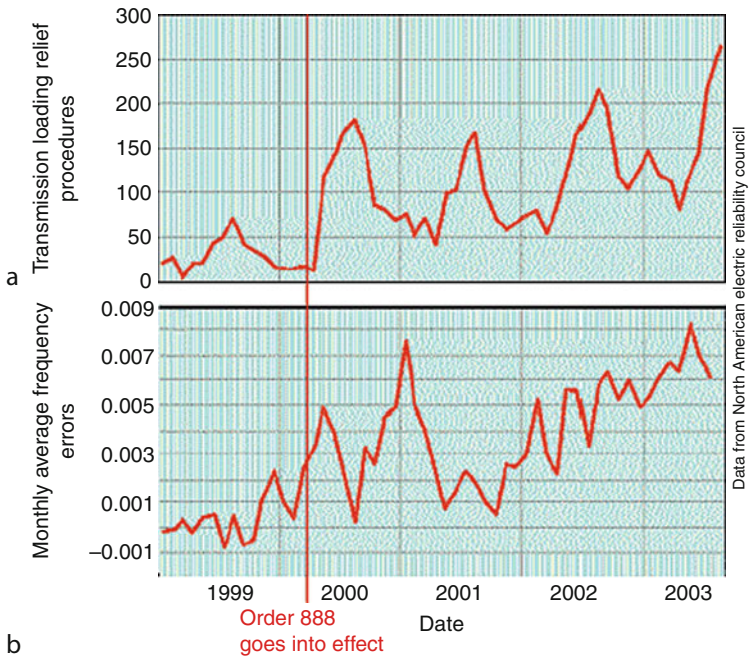

PHEVs and BEVs in Coupled Power and Transportation Systems. Figure 3
Illustration of multidisciplinary nature of problem [21]

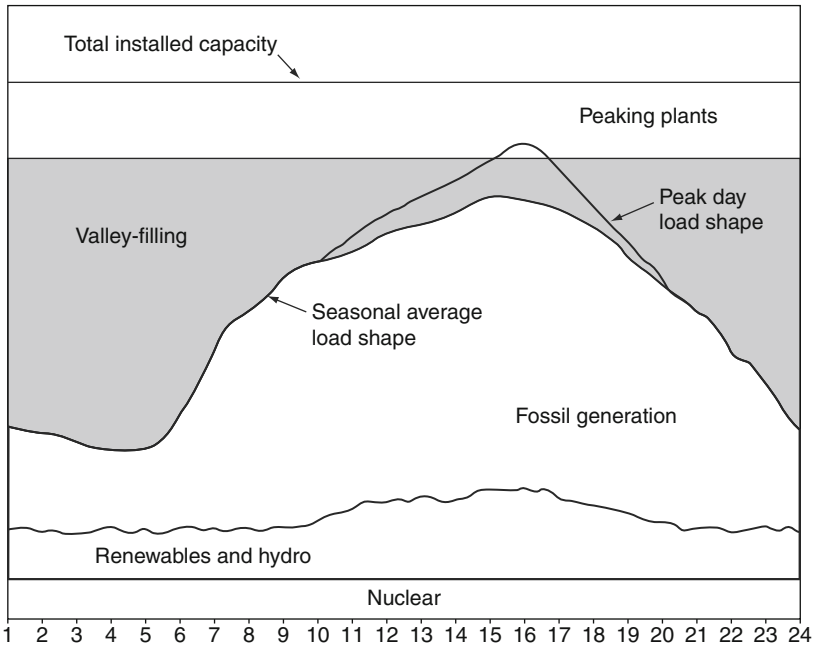

PHEVs and BEVs in Coupled Power and Transportation Systems. Figure 4
Illustrative peaking of electricity load [12]

of energy storage would significantly help meeting the stability and reliability needs, including managing the load variations shown in Fig. 4.

Efficiency of the Roadway Network

Congestion is a problem not only in the electricity grid network, but also in the roadway network. Vehicle miles traveled (VMT) has risen consistently since the advent of the automobile, with dips when gasoline prices rise quickly (See Fig. 5 for the VMT trend since 1992). If the transportation sector is shifted to an alternative fuel source (i.e., electricity) with greater price stability, and especially if the source of the fuel is renewable, then VMT is expected to continue to increase into the foreseeable future. While mobility is an indicator of economic success, the expansion of a roadway system is limited by available space and finances. Roadway network efficiency is further constrained by the individual autonomy of drivers who act in their self-interest instead of the interest of the system (see [22] for a theoretical description of traveler behavior).

Extensive research has been conducted on improving the efficiency of the transportation system via methods such as pricing and technology, but few solutions proposed offer a case even close to being as comprehensive as PHEVs/BEVs.

Policy Issues

The policy issues presented here are centered on incentives to help industry develop and bring new value to end users of electricity and transportation networks, and society at large, while encouraging competition and development of new business opportunities.

Improve Electric Grid Performance

Widespread deployment of PHEVs/BEVs will allow for increased energy storage, and improved reliability and stability of the electric grid. Linking the transportation and power systems through PHEVs/BEVs will allow for electrical energy storage on a scale much larger than is currently feasible. The additional energy capacity will be directly proportional to the penetration of PHEVs/BEVs into the automobile market, and modeling (see the modeling section) is needed to determine the exact increase in capacity across the space and time dimensions.

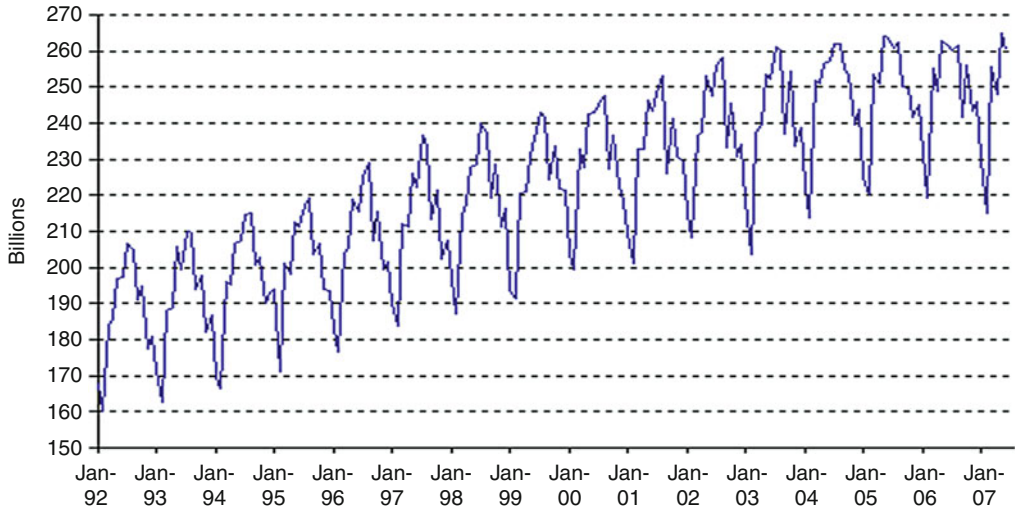

PHEVs and BEVs in Coupled Power and Transportation Systems. Figure 5
US highway VMT [23]

The new mobile storage can only benefit the electric grid if it is available at the right time and place to service the grid when needed. To determine PHEVs/BEVs' demand for electric energy across space and time, travel patterns must be considered. Figure 1 shows an example of such a pattern, highlighting several destinations where a driver could potentially engage in G2V or V2G.

Stability and reliability issues were mentioned earlier. V2G is poised to greatly aid the grid in becoming more reliable and stable because vehicles are only in use for a small portion of each day (average daily travel time person in 2001 was 82.3 min [24]). During the remainder of the day, the vehicles can be plugged in and provide services (e.g., ancillary or regulatory).

This approach requires a policy shift to allow use of the MDS for energy to maintain stability and reliability. Also, policy that encourages utilities to cooperate with the PHEV/BEV owners or aggregators and provide tariff incentives for their participation in programs aimed at demand and distributed generation management and optimization is missing at the moment.

Enhance Penetration of Renewable Energy Sources to Improve Energy Security

Increasing energy capacity by using PHEVs/BEVs as MDS will allow for increased investment in renewable energies by alleviating concerns related to the temporarily highly variable nature of solar (daytime) and wind (primarily nighttime). Using renewable energy has benefits not only for the environment and air quality, but also for energy security by reducing reliance on the supply from oil producing countries.

This approach requires a policy shift to allow and encourage large scale use of the MDS for energy to support interfacing of renewable generation.

Reduce and Redistribute Pollution in the Electric Grid and Transportation Network

By shifting the source of pollution away from vehicles, PHEVs/BEVs will change the transportation-based air pollution problem from a mobile source issue to a point source issue. This redistribution of pollution will likely have the effect of reducing pollution because point sources are much easier to control and some already have emission caps in place. Hadley [25] conducted initial research into the potential air quality impacts of PHEVs/BEVs, describing the impacts of G2V charging on air quality, and considering the types of power generation that are typically used at different times of day (e.g., coal-fired generation is prevalent at night in some regions).

Some policies are already in place to ensure that the redistribution of pollution that will occur with widespread deployment of PHEVs/BEVs will actually lead to a reduction in pollution. Further policy analysis is needed to ensure that V2G and G2V services are incentivized to occur at times when it will result in the maximum improvement in air quality.

Create New Markets and Further Deregulate Existing Markets

PHEVs/BEVs are poised to open new markets and increase opportunities in existing ones. Carbon-trade markets should be aided because they facilitate the change of the transportation-based air pollution problem from a mobile source issue to a point source issue (as described earlier). While point sources of pollution are much easier to control, if they are nonrenewable, they will likely need to trade carbon credits to counter the increased emissions.

PHEVs/BEVs will also create new modes for participation in the electricity markets. There will be opportunities for businesses to act as Qualified Scheduling Entities (QSE) to the electric utility by facilitating V2G/G2V interactions. Such a QSE that aggregates across vehicles is necessary because any one vehicle's contribution will be too small to allow it to participate directly in the market. PHEVs/BEVs will likely function akin to small generators as a distributed energy resource.

Policy that enhances market development and deregulation allowing a new type of QSE to bid in a variety of markets is needed to facilitate the aggregated use of PHEVs/BEVs in "transportation-energy" markets.

Plan and Develop Energy Exchange Stations

Energy exchange stations (for G2V and V2G) could take one of at least two forms. The first, the way considered by most electric vehicle research to date, assumes that individual drivers plug in and charge their vehicle over a period of several hours. Some examples of potential charging station locations are shopping malls, recreational areas, schools, and of course homes.

Further, rather than requiring drivers to plug into the grid and wait several hours to charge their batteries, battery exchange locations could be as ubiquitous as gas stations and automatically exchange discharged batteries with fully charged batteries. Charging PHEVs in this way has benefits for drivers because the process takes only a few minutes as opposed to several hours. Also, this system would require a leasing system for batteries similar to the system in place for leasing cell phones, alleviating driver concerns about battery life. The benefit for utilities is that control over charging and servicing the grid is centralized.

In reality, charging (G2V) and discharging (V2G) services will likely be based on a hybrid of the two methods mentioned above (individual drivers plugging into the grid and stations designed to exchange batteries). Depending on the pricing structure in place, it may make sense for drivers to exchange batteries during long drives and plug in to a household plug at night. Incentive structures will need to be developed that consider the different players – energy exchange stations and individual drivers.

The temporal and spatial aspects of the activity patterns travelers choose (see, e.g., Fig. 1) adds a layer of complexity to the problem of locating charging stations to link the transportation and energy systems. This requires both micro (neighborhood, city, and metropolitan area) and macro (region, state, and nation) driver behavioral dynamics to be studied in detail. If appropriate incentives are developed, drivers could be encouraged not only to act in a way that best serves the grid, but also to act in a way that best serves the transportation system. The incentives could be passive such as pricing electricity for planned contribution at the location of charging facilities (either stations or induction charging embedded in the roadway), or active such as pricing electricity based on congestion in both the power grid and local transportation system. Cognitive and behavioral research is needed to determine the appropriate incentives.

Policy that addresses the planning requirements for charging stations and regulates emerging energy exchange markets is needed. Comprehensive policy that develops joint electricity and transportation programs for incentivizing drivers to participate in the transportation and electricity grid optimization are not yet proposed or even clearly defined.

Modeling of Complex Systems

To develop policy strategies that allow for faster and more significant penetration of PHEVs/BEVs, research is needed to model the interactive performance of two complex systems, power and transportation, linked through the behavior of individual vehicle operators, where this linkage is determined by the location of interface infrastructure. The behavior of travelers defines the required inputs into power modeling since time-dependent PHEVs/BEVs locations are critical. Every aspect of this meta-system enterprise (power, transport, consumer choice, and infrastructure development) is interlinked, therefore fully understanding policy issues is quite challenging. This section explores each aspect of the modeling approach beginning with transportation modeling, and then power systems modeling, then modeling the role of human agents, and finally determining economic feasibility (see Fig. 2 for illustration).

Transportation Modeling

Travel models typically contain demand and supply components. While most demand models used in practice are static and consider each leg of a trip separately, activity-based models are gaining momentum. Lemoine et al. [1] illustrate the problems that PHEVs/BEVs could pose if proper incentives are not given to ensure that energy exchange occurs at times beneficial to the grid. Activity-based travel models are better suited for PHEVs/BEVs modeling because they recognize that travel arises from a fundamental need to participate in activities, and thus the models capture trip-chaining behavior (e.g., home to work to grocery to home). Other benefits of activity-based models are the incorporation of intra-household interactions, interpersonal and intrapersonal consistency measures, consideration of space-time constraints on activities and travel, and emphasis on individual level travel patterns (as opposed to monitoring aggregate travel demands). A number of micro-simulation platforms that employ the activity-based paradigm of transportation demand forecasting have been developed in the last 5 years (e.g., [26–28]).

On the supply side, conventional techniques of trip assignment are static in nature, and consider vehicle flows aggregated over one or several hour time periods. The limitations of the static assignment procedures and the increase in computing capacity have allowed the field to move toward more behaviorally realistic dynamic traffic assignment (DTA) models. DTA techniques offer a number of advantages including capturing the spatial and temporal evolution of traffic dynamics across the transportation network, superior capability to capture traffic congestion buildup and dissipation, and explicitly representing the route-choice effect of external dynamic prices and other costs and incentives. A number of simulation-based DTA modules have been developed in recent years [29–32]. The above mentioned features of DTA make it an ideal choice for modeling the network congestion patterns induced by PHEVs/BEVs usage and their impact on other vehicles.

Travel models produce numerous outputs, metrics, and system properties. Of critical importance for connecting the transportation and energy models are predictions regarding time-dependent vehicle locations. This inference directly relates to the number of PHEVs/BEVs present at a specific power grid node, which will be related to the node's self-admittance described in the next subsection on power systems modeling. Consideration of multiple classes of travelers, PHEVs/BEVs and non-PHEVs/BEVs, will be critical until PHEVs/BEVs reach high percentage penetration.

It has been long understood that through pricing-based incentives, the system-level performance of transportation networks can be greatly improved. The entire field of congestion pricing (e.g., [33, 34]) addresses this fact. For instance, PHEVs/BEVs provide a novel opportunity to achieve gains in controlling and managing congestion in transportation systems through an incentive based approach that persuades users to act in an altruistic manner. Further, such incentives provide a unique opportunity (and complexity) in that dual objectives must be balanced: improving the efficiency of the transportation as well as that of the power system. For the transportation system, incentives influence route, departure, as well as destination choice. Incentives change the fundamental costs traveler's associate with their choices and a new general cost dynamic equilibrium emerges (for normal operating states). This requires a further broadening of the previously mentioned integrated modeling

approach to include generalized costs as well as heterogeneous values of time.

Clearly, there will be significant uncertainty in the model inputs that must be built-in to ensure that the policy recommendations work well for a wide range of potential future outcomes. A vast amount of research has already been performed on stochastic transportation modeling both on the demand and supply side [35–40].

Power Systems Modeling

The planning, design, and operation of modern power systems call for extensive and detailed simulation. Models used to simulate power system behavior depend on the purpose and uses. When considering the need of studying PHEVs/BEVs impact on power system, different levels of modeling are required.

At the macro level, the power system planning related to the uses of PHEVs/BEVs requires understanding of the generation, storage, and load characteristics, as well as power flow projections impacted by the anticipated use of PHEVs/BEVs. A stochastic nature of PHEV/BEV use in the multiple possible roles will require advanced probabilistic methods for power flow analysis, as well as stochastic optimization related to operation and investment planning of dispersed generation [41, 42]. Enhanced modeling techniques must be developed for PHEV/BEV behavior as a load to assess dynamic stability of the power system operating in G2V mode [43]. Hadley [25] used the Oak Ridge Competitive Electricity Dispatch (ORCED) model to simulate PHEV/BEV electricity demand. It did not directly include transmission and distribution impacts, but discussed the issues of increased continuous transmission. Also, power system contingency analysis must be improved to account for the dynamic nature of both temporal and spatial properties of PHEVs/BEVs. In the V2G mode, PHEVs/BEVs may impact power grid operation in many different roles, both as energy storage used to improve performance of renewable energies such as wind and solar [44], as well as a market participant through aggregated distributed generation [10, 11, 45]. While it has been recognized that PHEVs/BEVs can be used for regulation services [10, 11], some studies also suggested the PHEVs/BEVs use for peak power "shaving" services [46]. A customized modeling tool that allows examining the potential impacts of large scale deployment of PHEVs/BEVs on a given electricity system, such as the "PHEV-load" tool developed by the National Renewable Energy Laboratory (NREL) may be needed [47].

At the micro level, the PHEV/BEV powertrain system itself, which is a very complex dynamic electromechanical system, may be studied. Specialized modeling and simulation tools, such as Argon National Laboratory's (ANL's) Powertrain System Analysis Toolkit (PSAT) are well suited for such an analysis [48]. This toolkit allows detailed modeling of charging and discharging dynamics of PHEVs/BEVs, which is crucial when defining properties of PHEVs/BEVs as loads, energy storage, or generation, as discussed above, Other ANL's tools such as GCtool, GREET, and AirCred may also be needed to asses other impacts [48].

The impact of PHEVs/BEVs ranges from the macro to micro scales, both in size and time. Different power system states (steady state, dynamic, and transient) may need to be represented in a framework using different types of mathematical formulations (waveforms, phasor, and algebraic). This leads to a new requirement for developing a method for linking different modeling techniques for accurate and efficient simulation when representing large scale penetration of PHEVs/BEVs as generators, storage elements, or loads [49].

Human Behavior Modeling

The widespread adoption of PHEVs/BEVs will place human vehicle operators at the intersection of power and transportation systems. Thus, it is critical to understand human decision making in the context of PHEV/BEV usage and how behavior can be shaped by incentive structures and training interventions. The large disparate group of decision makers includes not only drivers, but also utilities, battery exchange location coordinators, and fleet managers. Cognitive research will be critical to not only to understand and optimize human decision making involving PHEVs/BEVs, but to also increase the rate of PHEV/BEV adoption.

Route planning for any type of vehicle is an example of a dynamic decision task [50]. Choosing a route

requires a series of interrelated decisions that occur in a changing and uncertain environment. PHEVs/BEVs introduce a number of additional decision elements, such as whether to draw energy from the grid or deliver energy to the grid at destinations with facilities allowing such interfaces. Complicating this decision process, G2V costs and V2G credits vary through time and are not perfectly predictable from the driver's perspective.

One successful framework for modeling human performance in dynamic decision making tasks is reinforcement learning (RL) [51, 52]. The theory of RL comprises an array of techniques for learning temporally extended tasks in dynamic environments. An agent is assumed to be immersed in its environment, with some number of actions available to be taken at any given time. The chosen action has an effect, depending on the current state of the environment, the immediate reward (or punishment) the agent receives, and the future state of the environment. Thus actions can influence situations and rewards arbitrarily far into the future, and successful performance hinges on effective planning and coordination of extended sequences of actions [53].

Previous research demonstrates that RL agents and humans are more likely to discover the underlying structure of a task when state cues are present that allow for generalization [54]. A state cue in the context of PHEV/BEV decision making would include observable properties – such as time of day, weather conditions, and congestion – that enable prediction of G2V credits and V2G costs. State cues play a critical role in shaping learning and it has been shown that variability in state predictors disrupts performance more than equivalent variability in the reward structure [55]. Further research is needed to examine how variability in state cues and reward structure affects PHEV/BEV route selection. Establishing how PHEV/BEV driver performance (with respect to improving conditions on the grid and transportation system) declines with variability in state cues is important because transient changes in incentives could have negative, unintended consequences, making it difficult for people to acquire the basic pricing contingencies. Research is also needed to find the best methods for PHEV/BEV operators or aggregators to learn about incentive structures. Various types of feedback are available (e.g., Reward Only, First Error), and the optimal approach should be determined via experiment.

Determining Economic Feasibility

To take advantage of the proposed "transportation-energy" markets, interface infrastructure – the facilities that will bridge the two systems and serve as energy transfer points – must be developed and planned. While prevalence of PHEVs/BEVs in the future is unknown, their ultimate value can only come if the interfaces are in place. This leads to a situation where the demand for PHEVs/BEVs depends on the infrastructure supply, which in turn is defined by the demand. The traditional project valuation models fall short of accounting for this feedback loop.

Developing interface infrastructure is a uniquely challenging problem because the equipment must not only adjust energy flow over time, but the location of transfer points must be determined to maximize long-term value and minimize risks. Technology adoption, incentives, and system interdependencies all play a role.

To maximize the value of developing interface infrastructure in a particular location, two aspects of the problem must be considered: (1) the value created to the grid by using PHEVs/BEVs for regulation services, and (2) the value of the activity-based travel patterns that could include a visit to the interface infrastructure. The former value can be explicitly determined, but unless the latter is considered and travelers are enticed to use the new infrastructure, the value to the grid will not be achieved. Typically, the traveling public selects route and activity patterns without considering energy exchange opportunities. New methodologies and modeling techniques must be developed for valuing interface infrastructure given its dependence on traveler behavior.

Unlike most past research into making investment decisions for infrastructure projects that focus on a single system (e.g., [56, 57]), the problem posed here must consider the interdependencies between several systems as well as the rate of technology adoption (availability of PHEVs/BEVs to use this facility and generate value). In fact, this problem exhibits both spatial network effects and strategic "bandwagon"

network externalities (see seminal contributions in this area by Rohlfs [58], Farrell and Saloner [59], and David and Greenstein [60]).

It is clear that in the face of this bandwagon effect, the value of deferral flexibility is marginal. Hence, the project developer action space should consider actions that promote early adoption without fully committing to irreversible capital expenditures. Stochastic modeling approaches could be useful here to consider that the outcome and uncertainty space of the valuation problem is decision dependent (see, e.g., [61]).

Benefits

This section aims at demonstrating the potential benefits of PHEVs/BEVs that may be used to feed power back to home or office building, which is known as "Vehicle-to-Building" (V2B) operation. The new parking facility called "smart garage" is introduced and its eclectic power capacity is discussed. Based on the availability analysis of smart garages, a strategy to adopting PHEV/BEV uses in the V2B mode under peak load and outage condition is proposed. V2B approach considers PHEVs/BEVs as a generation resource for the buildings at certain periods of time via bidirectional power transfers, which could increase the flexibility of the electrical distribution system operation. It is expected that V2B operation will improve the reliability of the distribution system, provide extra economic benefits to the vehicle owners, and reduce the home or building electricity purchase cost based on the demand side management and outage management programs with customer incentives.

Demand Side Management (DSM)

For electric utility, DSM is defined as "Utility-sponsored programs to influence the time of use and amount of energy use by select customers," which includes peak clipping, valley filling, load shifting, strategic conservation, strategic load growth, and flexible load shape [62]. However, for utility end-user (customer), DSM is often understood to include two components: energy efficiency (EE) and demand response (DR). EE is designed to reduce electricity consumption during all hours of the year; DR is designed to change on-site demand for energy in intervals and associated timing of electric demand by transmitting changes in prices, load control signals, or other incentives to end users to reflect existing production and delivery costs [63]. By cooperative activities between the utility and its customers to utilize DSM, it will provide the benefits to the customer, utility, and society as a whole, which is summarized in Table 1 [64].

PHEVs and BEVs in Coupled Power and Transportation Systems. Table 1 DSM benefits to customer, utility, and society [64]

Customer benefits	Societal benefits	Utility benefits
Satisfy electricity demands	Reduce environmental impacts	Lower cost of service
Reduce/stabilize costs	Conserve resources	Improved operating efficiency
Improve value of service	Protect global environment	Flexibility of operation
Maintain/improve lifestyle	Maximize customer welfare	Reduced capital needs

In the V2B option, the owners will plug in their vehicles during the day at their final destination for a given time frame. As an example, this may be either at their workplace (central business district) or at the place of their study (university). The destinations, either parking lots or parking garages next to the buildings, are assumed to be equipped with a bidirectional charger and controller. The parking facility should allow either charge or discharge mode for the car batteries when necessary. The idea is that the parking facility can offer an aggregation service for charging the batteries when the building demand is lower than its peak load and discharge the batteries to partially supply the building to reduce the peak demand during a high demand. This mode will be considered as DSM by V2B. Considering the electricity rate when the vehicle batteries were charged is lower than when the batteries are discharged, the battery storage may be used to offset high cost during the peak demand.

Outage Management (OM)

Another important benefit of V2B is using the battery energy storage in PHEVs/BEVs as an emergency backup power for the commercial facility/building, which increases the reliability of the power supply for that load.

An outage is typically caused by several unplanned events, and a timely detection and mitigation of such situations is a real concern for the utility. Outage management system helps the operators to locate an outage, repair the damage, and restore the service. Outage management must be performed very quickly to reduce outage time. Recently completed project proposes an optimal fault location scheme which will help the operator to find the faulted section very quickly [65]. In this entry, the restoration strategy under an outage will be mainly discussed.

The following types of outages and studies about the impact of PHEVs/BEVs adoption are considered:

(a) *Outage beyond the distribution system*: These may be caused by generator failure, fault in transmission line, or substation busbar. Usually spinning reserves are kept for these circumstances. From the previous studies it is concluded that PHEVs/BEVs can be a candidate solution for spinning reserves (as the traditional fastest acting spinning reserve generators are highly costly while PHEVs/BEVs qualify for fast response with lesser cost). One may consider using a real-time security constrained optimal power flow under the contingencies to calculate the amount of PHEV/BEV battery capacity required for a certain location at a specific instance.

(b) *Outage in distribution system*: These may be caused by fault inside the distribution system and can be mitigated by precise spatial adjustment of PHEV/BEV battery generation that may be used to feed electricity locally during and after outage.

To propose the restoration strategy where PHEV/BEV batteries are used to mitigate an outage condition, the information about events (where the fault is located and how the impact will propagate) and the location of the battery storage need to be correlated. Thus, a spatial as well as temporal analysis should be performed.

The restoration strategy can be executed in the following steps:

1. Detect a fault.
2. Estimate the location of the fault.
3. Analyze the amount of battery generation required and the availability of PHEVs/BEVs that can provide an alternative generation support in the vicinity of the faulted area until the faulted section is repaired. This will also consider the generation duration requirement (i.e., time to repair the faulted section).
4. Schedule the aggregated PHEVs/BEVs generation optimally. This is a multi-objective optimization problem which can be formulated to minimize the distance between location of the fault and available PHEVs/BEVs battery generation locations as well as minimize the operating cost under system operation and security constraints.

Garage Location and Charging/Discharging Infrastructure

Commercial and public parking garages in a central business district (CBD) provide thousands of parking spaces for commuters and visitors. After penetrating the conventional vehicle market, owners of PHEVs/BEVs will be using these parking garages, which may

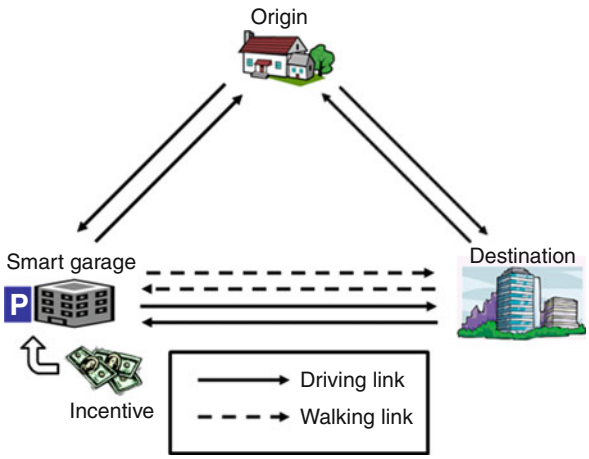

PHEVs and BEVs in Coupled Power and Transportation Systems. Figure 6
Simple transportation network with smart garage

provide an aggregated service to act as an electric power source or storage.

Figure 6 shows a simple transportation network with smart garage building. As a smart garage is constructed, PHEV/BEV drivers have two options: proceed to final destination directly or park at the smart garage and walk to the destination along walking links. Drivers in transportation network select parking garage based on the location and financial incentives (less parking fee), which can be modeled as traffic assignment problem. Demand of smart garage (number of parked PHEVs/BEVs) calculated from the traffic assignment problem would vary by the location and incentive of the smart garage.

Electric power capacity of smart garage is estimated based on demand of smart garage. Demand of smart garage building is not constant. Generally, the demand of smart garage building during the day would be higher than during the night, similar to the demand structure for a conventional garage as shown in Fig. 7. Due to the versatility, electric power capacity needs to be defined in two parts: for periodic service and for continuous service as in Fig. 7. The available electric power estimated based on the demand of smart garage can be used for determining the support service that can be provided during outage management and demand side management in vehicle-to-building (V2B) mode.

Case Study

Test cases for two scenarios are studied: demand side management using V2B mode during peak power demand and outage management using V2B mode during faults.

Demand Side Management During Peak Power Demand In this case, a large commercial building is analyzed to demonstrate the potential savings using demand side management based on V2B operation. Itron, Inc. prepared a technical survey for the California Energy Commission (CEC), which modeled difference commercial sectors, including large office building [66]. The load shapes include typical day, hot day, cold day, and weekend for each of four seasons. According to the definition used in this report, large office buildings are defined as premises with total floor area equal or larger than 30,000 sq ft. The largest electric end-uses in this building type are interior lighting, cooling, office equipment, and ventilation [66].

The summer typical load shape for a large office building is selected for our case study. The single building demand is obtained from the results reported in the literature [66]. The following assumptions are taken:

- The studied building is 450,000 sq ft.
- There are up to 80 PHEVs/BEVs that arrive at 8 a.m. and are available for the entire day.

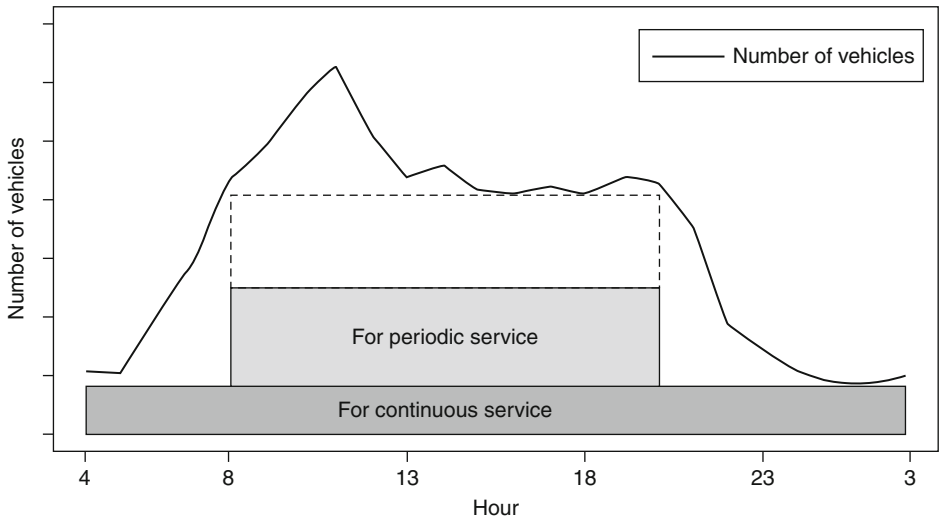

PHEVs and BEVs in Coupled Power and Transportation Systems. Figure 7
Demand of smart garage for a day

- Maximum capacity of each vehicle is 10 kWh (very conservative for BEVs).
- The batteries in PHEVs/BEVs are drained by an average of 4.0 kWh by the driving cycle used.

When PHEVs/BEVs are on site, the building can charge the batteries during the morning hours (lower electricity price) and drain the batteries by an equal amount during afternoon hours (higher electricity price). Thus the owner of PHEV/BEV will have the required energy in his/her battery to make sure the driving cycle to return home can be met. Figure 8 shows the impacts of charging PHEVs by faster charging methods (AC Level 3 or DC charging). It will elevate the peak demand to 1.86 MW of the office building since the faster charging method will cause a large load in a short period (10–15 min), which is not recommend for either utilities or customers.

Figure 9 shows the change in the load shape for the typical summer day by using the AC Level 1 charging method defined by the Society for Automotive Engineers (SAE) J1772 [67]. The load curve was changed by shifting the afternoon peak load to the morning off-peak load when charging and discharging PHEVs/BEVs. Considering the rate structures for peak and off-peak load in commercial buildings, peak load shifting using V2B mode may provide the electricity bill saving. Further study could be conducted to show the total saving expressed in dollars.

Outage Management During Faults The proposed restoration scheme was tested on a small distribution system (IEEE 37 node radial test feeder [68]).

This is an actual feeder located in California, which consists of several unbalanced spot loads. The nominal voltage is 4.8 kV.

Figure 10 shows the test feeder with smart garages at some nodes.

The following assumptions are taken:

- Three nodes are specified as smart garages (nodes 718, 735, and 740).
- Maximum capacity of each vehicle is 10 kWh.
- Discharge vehicles with state of charge (soc >70%.
- PHEV/BEV tariff for charging is 5 c/kWh and for discharging is (15–40) c/kWh (depending on different garages). Discharging tariff for node 718 is 40 c/kWh, for node 735 is 30 c/kWh, and for node 740 is 25 c/kWh.

Under normal operating condition, node no. 799 acts as an infinite bus and all the loads are fed through it. Two different outage cases are studied:

1. Case 1: Fault on or beyond node 799: PHEVs/BEVs at nodes 718, 735, and 740 were scheduled to satisfy all the loads on the feeder. Table 2 shows the case results.
2. Case 2: Fault on line segment 703–730: Node 799 will supply all the loads beyond this line segment.

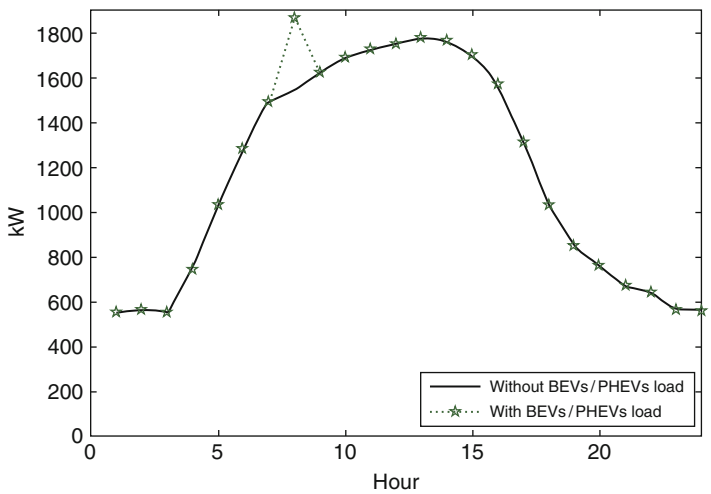

PHEVs and BEVs in Coupled Power and Transportation Systems. Figure 8
Impacts of faster charging PHEVs/BEVs on load demand

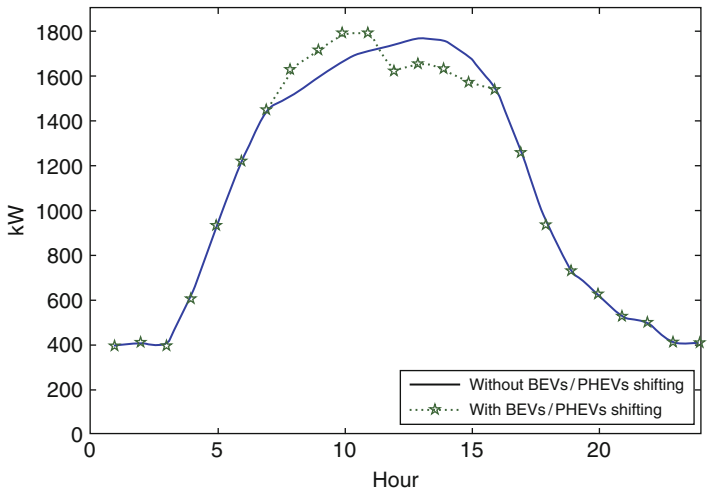

PHEVs and BEVs in Coupled Power and Transportation Systems. Figure 9
Peak load shifting with PHEVs/BEVs for a typical summer daily load

PHEVs/EBVs at nodes 735 and 740 will be scheduled to satisfy the island created by a fault on line 703–730. Table 3 shows the case results.

Conclusions and Future Research

The policy implications of widespread PHEV/BEV deployment in the energy and transportation systems are explored. Previous research has approached the problem from selected angles, making many simplifying assumptions. Some thoughts on how the problem may be approached from a non-myopic perspective are provided.

In summary, numerous policy shifts are needed to realize the full potential of PHEVs/BEVs, and the cooperation of the transportation and energy sectors is vital. If policies such as the ones outlined in this paper are adopted, PHEVs/BEVs can provide many benefits to the electric grid in terms of reliability and stability by acting as mobile decentralized storage and allowing for vehicle-to-grid and grid-to-vehicle services. PHEVs/BEVs will also allow for enhanced penetration of renewable energy resources such as wind and solar, which will also aid with energy security by reducing dependence on foreign sources of oil. Important benefits can be made to air quality through transferring pollution from numerous mobile sources to fewer point sources that are easier to control and may participate in cap-and-trade markets. In addition to the carbon market, new markets will be created in power systems due to the potential for PHEVs/BEVs (or aggregators of PHEVs/BEVs) to participate, particularly with ancillary and regulation services. Lastly, charging stations must be planned and developed carefully to allow for flexibility in driver options and optimal performance of the transportation and electricity networks.

The proposed multi-layered modeling framework considers the spatial and temporal nature of the system interactions. PHEV/BEV time-dependent travel patterns are outputs of a transportation model and inputs to power systems model. The framework also includes cognitive behavior modeling for the purposes of developing appropriate incentives to encourage drivers to behave in a way that improves the efficiency of the transportation and energy systems.

The potential benefits of using PHEVs/BEVs as dynamically configurable dispersed energy storage that can serve as load or generation in a power system as needed is discussed. If serving in G2V as well as V2B mode and if aggregated, PHEVs/BEVs may play a major role in both the electricity and the transportation networks. Selecting garage location and charging/discharging infrastructure needs special attention from the transportation system demand point of view. For demand side management in electricity networks, the

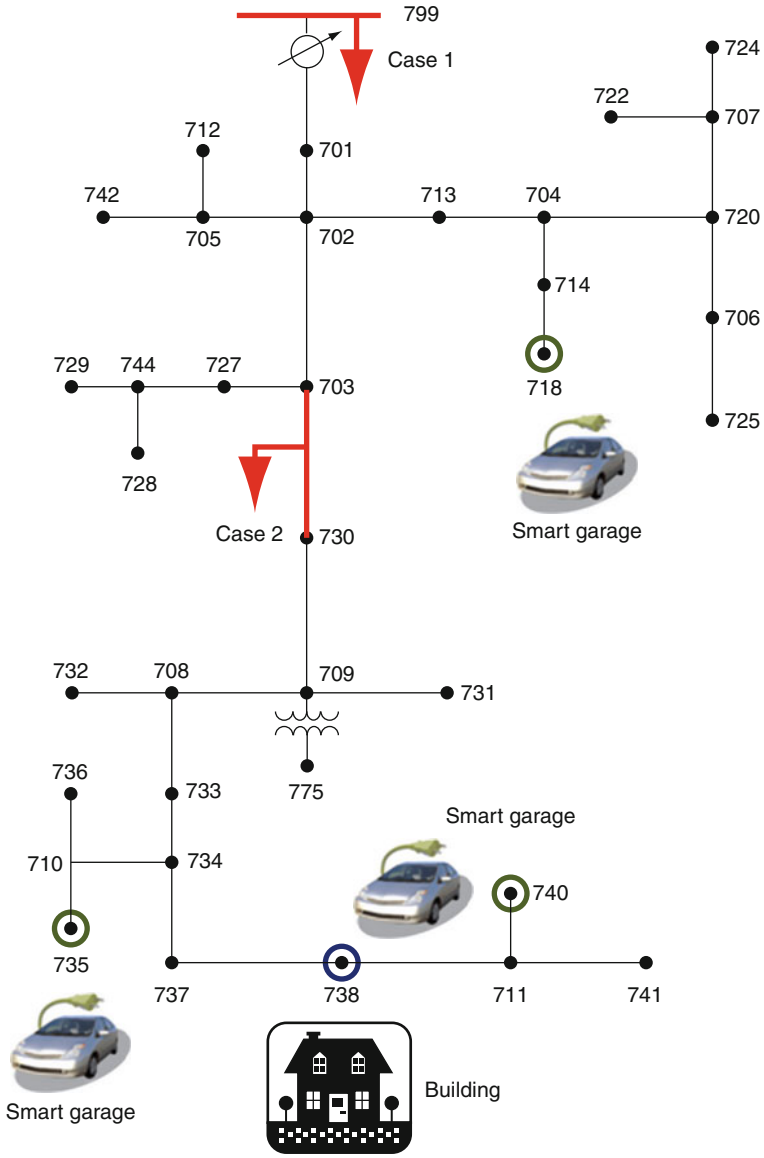

PHEVs and BEVs in Coupled Power and Transportation Systems. Fig. 10
Diagram of test feeder with smart garages

PHEVs and BEVs in Coupled Power and Transportation Systems. Table 2 Case study 1: results for PHEV/BEV generation scheduling

Node 718			Node 735			Node 740		
Ph-1 (kW)	Ph-2 (kW)	Ph-3 (kW)	Ph-1 (kW)	Ph-2 (kW)	Ph-3 (kW)	Ph-1 (kW)	Ph-2 (kW)	Ph-3 (kW)
0	0	411	300	300	300	427	339	380

Total cost for three phases is $733.2/h

PHEVs and BEVs in Coupled Power and Transportation Systems. Table 3 Case study 2: results for PHEV/BEV generation scheduling

Node 735			Node 740		
Ph-1 (kW)	Ph-2 (kW)	Ph-3 (kW)	Ph-1 (kW)	Ph-2 (kW)	Ph-3 (kW)
300	127	300	51	0	81

Total cost for three phases is $221.35/h

use of PHEVs/BEVs to create a peak load shifting strategy can reduce the electricity purchase cost for the customer and vehicle owner. For outage management in electricity networks, the use of PHEVs/BEVs to generate power during outage restoration stage is envisioned by solving a multi-objective optimization problem of merit-order scheduling of PHEVs/BEVs under operating constraints.

In recent years, Smart Grid revolution has begun with the sponsorship and involvement from government, businesses, utilities, and other stakeholders, especially with the development and integration of renewable energy resources. Envisioning the longer-term impact, if there is enough aggregated PHEV/BEV vehicles, such as a fleet, they can serve as backup generation and storage for renewable energy in smart grid applications. Many other functions of the future electricity network may be affected when PHEVs/BEVs act as dynamically configurable energy storage, which may have profound impact on the transportation networks as well. Better understanding of the role of PHEVs/BEVs in coupled power and transportation systems will be beneficial to transform existing power grid into the Smart Grid, a power system that is more efficient, reliable, resilient, and responsive.

Acknowledgments

The author wishes to acknowledge numerous colleagues and graduate students who contributed to the findings of this entry: Dr. Bradley Love, and Dr. Jennifer Duthie from The University of Texas at Austin, as well as Dr. Ivan Damnjanovic, and graduate students Mr. Chengzong Pang, Ms. Papiya Dutta, and Mr. Seok Kim from Texas A&M University. Funding for this study came from the National Science Foundation through I/UCRC grant for the Center for "PHEVs/BEVs: Transportation and Electricity Convergence," and another NSF I/UCRC grant for the "Power Systems Engineering Research Center."

Bibliography

Primary Literature

1. Lemoine DM, Kammen DM, Farrell AE (2008) An innovation and policy agenda for commercially competitive plug-in hybrid electric vehicles. Environ Res Lett 3(1):014003
2. Schrank D, Lomax T (2007) The 2007 urban mobility report. Texas Transportation Institute
3. U.S.-Canada Power System Outage Task Force (2004) Final report on the August 14, 2003 Blackout in the United States and Canada: causes and recommendations. http://www.nerc.com
4. Burges K, Twele J (2005) Power systems operation with high penetration of renewable energy – the German case. In: 2005 international conference on future power systems, Amsterdam, pp 1–5
5. Kelso JAS (1995) Dynamic patterns: the self-organization of brain and behavior. MIT Press, Cambridge, MA
6. Turvey MT, Moreno M (2006) Physical metaphors for the mental lexicon. Ment Lexicon 1:7–33
7. Van Orden GC, Holden JG, Turvey MT (2003) Self-organization of cognitive performance. J Expr Psychol Gen 132:331–350
8. Brooks AN (2002) Vehicle-to-grid demonstration project: grid regulation ancillary service with a battery electric vehicle. AC Propulsion, California
9. Duncan R, Osborne MJ (2005) Report on transportation convergence, Austin energy
10. Kempton W, Tomic J, Letendre S, Brooks A, Lipman T (2001) Vehicle-to-grid power: battery, hybrid, and fuel cell vehicles as resources for distributed electric power in California. Report # UCD-ITS-RR-01-03, Electric transportation program
11. Kempton W, Tomic J (2005) Vehicle to grid implementation: from stabilizing the grid to supporting large-scale renewable energy. Power Sources 144(1):280–294
12. Kintner-Meyer M, Schneider K, Pratt R (2007) Impacts assessment of plug-in hybrid vehicles on electric utilities and regional U.S. power grids, part 1: technical analysis
13. Solomon J, Vincent R (2003) Development and evaluation of a plug-in HEV with vehicle-to-grid power flow. Final report, A.C. Propulsion
14. Letendre S, Perez R, Herig C (2002) Battery-powered, electric-drive vehicles providing buffer storage for PV capacity value. In: Proceedings of the 2002 American solar energy society annual conference, Boulder
15. Kempton W, Tomić J (2005) Vehicle-to-grid power fundamentals: calculating capacity and net revenue. J Power Source 144(1):268–279

16. Kempton W, Tomić J (2005) Vehicle-to-grid implementation: from stabilizing the grid to supporting large-scale renewable energy. J Power Source 144(1):280–294
17. Hadley SW, Tsvetkova A (2008) Potential impacts of plug-in hybrid electric vehicles on regional power generation. Oak Ridge National Laboratory, Oak Ridge, TN, ORNL/TM-2007/150. http://apps.ornl.gov/~pts/prod/pubs/ldoc7922_regional_phev_analysis.pdf
18. Meliopoulos S, Meisel J, Cokkinides G, Overbye T (2009) Power system level impacts of plug-in hybrid vehicles, PSerc project T34 final report #09-12. http://www.pserc.wisc.edu/documents/publications/reports/2009_reports/
19. Andersson SL, Elofsson AK, Galus MD, Goransson L, Karlsson S, Johnsson F, Andersson G (2010) Plug-in hybrid electric vehicles as regulating power providers: case studies of Sweden and Germany. Energy Policy 38(6): 2751–2762
20. Guille C, Gross G (2009) A conceptual framework for the vehicle-to-grid (V2G) implementation. Energy Policy 37(11):4379–4390
21. Lerner EJ (2003) What's wrong with the electric grid? The industrial Physicist, Oct/Nov 2003
22. Wardrop JG (1952) Some theoretical aspects of road traffic research. Proc Inst Civil Eng 1(2):325–378
23. U.S. Department of Transportation, Federal Highway Administration, Office of Highway Policy Information (2007) Traffic volume trends. http://www.fhwa.dot.gov
24. Toole-Holt L, Polzin SE, Pendyala RM (2005) Two minutes per person per day each year: exploration of growth in travel time expenditures. Transp Res Rec 1917:45–53
25. Hadley SW (2006) Impact of plug-in hybrid vehicles on the electric grid. Oak Ridge National Laboratory, for the U.S. department of energy, ORNL/TM-2006/554
26. Bhat CR, Guo JY, Srinivasan S, Sivakumar A (2004) A comprehensive econometric microsimulator for daily activity-travel patterns. Transp Res Rec 1894:57–66
27. Vovsha P, Petersen E, Donnelly R (2004) Impact of intra-household interactions on individual daily activity-travel patterns. In: Proceedings of the 83rd annual meeting of the transportation research board, Washington, DC
28. Bowman JL, Bradley MA (2005) Activity-based travel forecasting model for SACOG, technical memos numbers 11–11. http://jbowman.net
29. Waller ST, Ziliaskopoulos AK (1998) A visual interactive system for transportation algorithms. In: Proceedings of the 78th annual meeting of the transportation research board, Washington, DC
30. Taylor NB (1990) CONTRAM 5: an enhanced traffic assignment model. TRLL research report 249
31. Ben Akiva M, Bierlaire M, Koutsopoulos H, Mishalini R, DynaMIT (1998) A simulation-based system for traffic prediction and guidance generation. Presented at TRISTAN III, Delft, The Netherlands
32. Mahmassani HS, Hu TY, Jayakrishnan R (1992) Dynamic traffic assignment and simulation for advanced network informatics (DYNASMART). In: Proceedings of the second international capri seminar on urban traffic networks, Italy
33. Arnott R, Small K (1994) The economics of traffic congestion. Am Scientists 20:123–127
34. Hearn DW, Ramana MV (1998) Solving congestion toll pricing models. In: Marcotte P, Nguyen S (eds) Equilibrium and advanced transportation modeling. Kluwer, Boston, pp 109–124
35. Morrison SA (1986) A survey of road pricing. Transp Res 20A (2):87–97
36. Waller ST, Schofer JL, Ziliaskopoulos AK (2001) Evaluation with traffic assignment under demand uncertainty. Transp Res Rec 1771:69–75
37. Karoonsoontawong A, Waller ST (2006) Dynamic continuous network design problem: linear bi-level programming and metaheuristic approaches. Transp Res Rec 1964:104–117
38. Ukkusuri S, Tom VM, Waller ST (2007) Robust network design problem under demand uncertainty. Comput-Aided Civ Infrastruct Eng 22:6–18
39. Waller ST, Ziliaskopoulos AK (2006) A chance-constrained based stochastic dynamic traffic assignment model: analysis, formulation and solution algorithms. Transp Res C: Emerg Technol 14(6):418–427
40. Duthie J, Unnikrishnan A, Waller ST (2006) Network evaluation with uncertain and correlated long-term demand. In: Proceedings of 85th transportation research board meeting, Washington, DC
41. Stefopoulos G, Meliopoulos APS, Cokkinides G (2005) Probabilistic power flow with non-conforming electric loads. Int J Electr Power Energy Syst 27(9–10):627–634
42. Gollmer R, Neise U, Schultz R (2007) Risk modeling via stochastic dominance in power systems with dispersed generation. Technical report, Department of mathematics, University of Duisburg, Germany
43. Choi BK, Chiang HD, Li YH (2006) Measurement-based dynamic load models: derivation, comparison, and validation. IEEE Trans Power Syst 21:1689–1697
44. Short W, Denholm P (2006) A preliminary assessment of plug-in hybrid electric vehicles on wind generation markets. Technical report, NREL/TP-620-39729
45. Tomic J, Kempton W (2007) Using fleets of electric drive vehicles for grid support. J Power Sources 168(2):459–468
46. Kempton W, Kubo T (2000) Electric-drive vehicles for peak power in Japan. Energy Policy 28:9–18
47. Denholm P, Short W (2006) An evaluation of utility system impacts and benefits of optimally dispatched plug-in hybrid electric vehicles. Technical report, NREL/TP-620-40293
48. Argon National Laboratory Tools. http://www.transportation.anl.gov/software/PSAT/index.html
49. Kasztenny B, Kezunovic M (2000) A method for linking different modeling techniques for accurate and efficient simulation. IEEE Trans Power Syst 15(1):65–72

50. Busemeyer JR (2002) Dynamic decision making. In: Smelser NJ, Baltes PB (eds) International encyclopedia of the social and behavioral sciences, vol 6. Elsevier, Oxford, pp 3903–3908
51. Fu WT, Anderson JR (2006) From recurrent choice to skill learning: a reinforcement-learning model. J Exp Psychol Gen 135:184–206
52. Gray WD, Sims CR, Fu W-T, Schoelles MJ (2006) The soft constraints hypothesis: a rational analysis approach to resource allocation for interactive behavior. Psychol Rev 113:461–482
53. Sutton RS, Barto AG (1998) Reinforcement learning: an introduction. MIT Press, Cambridge, MA
54. Gureckis TM, Love BC (2009) Short term gains, long term pains: reinforcement learning in dynamic environments. Cognition 113:293–313
55. Gureckis TM, Love BC (2009) Learning in noise: dynamic decision-making in an uncertain environment. J Math Psychol 53:180–193
56. Zhao T, Fu CC (2006) Infrastructure development and expansion under uncertainty: a risk-preference-based lattice approach. ASCE J Constr Eng Manag 132(6):620–625
57. Zhang Z, Damnjanovic I (2006) Quantification of risk cost associated with short-term warranty-based specifications for pavements. Transp Res Rec 1946:3–11
58. Rohlfs JH (1974) A theory of interdependent demand for a communication service. Bell J Econ Manag Sci 5(1):16–74
59. Farrell J, Saloner G (1985) Standardization, compatibility and innovation. Rand J Econ 16:70–82
60. David PA, Greenstein S (1990) The economics of compatibility standards: an introduction to recent research. Econ Innovat New Tech 1:3–41
61. Jonsbraten TW, Wets RJB, Woodruff DL (1998) A class of stochastic programs with decision dependent random elements. Ann Oper Res 82:83–106
62. Gellings CW (1985) The concept of demand-side management for electric utilities. Proc IEEE 73(10):1468–1470
63. NERC (2007) Data collection for demand-side management for quantifying its influence on reliability: results and recommendations. In: North American electric Reliability Corporation, Princeton. http://www.nerc.com/docs/pc/drdtf/NERC_DSMTF_Report_040308.pdf
64. IIEC (2006) Demand side management best practices guidebook or pacific island power utilities. International Institute for Energy Conservation, Washington, DC. www.sidsnet.org/docshare/other/20070110DSMBestpractices.pdf
65. Kezunovic M, Ward J et al (2009) Integration of asset and outage management tasks for distribution systems. PSerc project T36 final report #09-11. http://www.pserc.wisc.edu/documents/publications/reports/2009_reports/
66. Itron, Inc. (2006) California commercial end-use survey: consultant report. CEC-400-2006-005, California Energy Commission. http://www.energy.ca.gov/2006publications/CEC-400-2006-005/CEC-400-2006-005.PDF
67. SAE (2010) Recommended practice for electric vehicle and plug in hybrid electric vehicle conductive charger coupler, SAE standard J1772, Jan 2010
68. Radial Test Feeders – IEEE distribution system analysis subcommittee. http://ewh.ieee.org/soc/pes/dsacom/testfeeders.html

Books and Reviews

Dowds J, Hines P et al (2010) Plug-in hybrid electric vehicle research project: phase two report. Burlington, VT, Transportation research center. UVM TRC report #:10–001. http://www.uvm.edu/~trans. . .reports/UVM-TRC-10-001.pdf

Galus MD, Andersson G (2008) Demand management of grid connected plug-in hybrid electric vehicles (PHEV). In: Energy 2030 conference, ENERGY 2008. IEEE, 17–18 Nov 2008, pp 1–8

Galus MD, Andersson G (2009) Integration of plug-in hybrid electric vehicles into energy networks. PowerTech, 2009 IEEE bucharest. June 28–July 2 2009, pp 1–8

Galus MD, Andersson G (2009) Power system considerations of plug-in hybrid electric vehicles based on a multi energy carrier model. In: Power & energy society general meeting, PES '09. IEEE. 26–30 July 2009, pp 1–8

Kempton W, Udo V et al (2008) A test of vehicle-to-grid (V2G) for energy storage and frequency regulation in the PJM system. University of Delaware, Pepco Holdings, Inc, PJM interconnect, and Green Mountain College. http://www.magicconsortium.org/_Media/test-v2g-in-pjm-jan09.pdf

Markel T, Simpson A (2005) Energy storage systems considerations for grid-charged hybrid electric vehicles. In: Vehicle power and propulsion, 2005 IEEE conference. 7–9 Sept 2005. http://www.nrel.gov/vehiclesandfuels/vsa/pdfs/38538.pdf

Morrow K, Karner D et al (2008) Plug-in hybrid electric vehicle charging infrastructure review, Idaho National Laboratory. Report #: INL/EXT-08-15058. http://avt.inel.gov/pdf/phev/phevInfrastructureReport08.pdf

ORNL (2010) Plug-in hybrid value proposition study final report, Oak Ridge National Laboratory (ORNL). Report #: ORNL/TM-2010/46. http://www.sentech.org/phev/pdfs/PHEV%20Value%20Proposition%20Study%20Final%20Report%20Draft.pdf

Sullivan JL, Salmeen IT et al (2009) PHEV marketplace penetration: an agent based simulation. University of Michigan, Ann Arbor, Transportation Research Institute. Report #: UMTRI-2009-32. http://deepblue.lib.umich.edu/bitstream/2027.42/63507/1/102307.pdf

Turton H, Moura F (2008) Vehicle-to-grid systems for sustainable development: an integrated energy analysis. Technol Forecasting Soc Change 75(8):1091–1108

Wynne J (2009) Impact of plug-in hybrid electric vehicles on California's electricity grid. Masters of environmental management degree, Duke University

Phosphoric Acid Fuel Cells for Stationary Applications

Sridhar V. Kanuri, Sathya Motupally
UTC Power, South Windsor, CT, USA

Article Outline

Glossary
Definition of the Subject
Introduction
Market Requirements
Phosphoric Acid Fuel Cells
Cell Stack Assembly Components
Cell Stack Assembly Life
PAFC Applications
Future Directions
Acknowledgments
Bibliography

Glossary

ADG Anaerobic digester gas.
BOP Balance of plant. Involves components other than fuel cell stacks in a power plant.
Bubble pressure Ability of a component filled with acid to withstand a given pressure of gas.
Carbonization This process involves heating resin-impregnated material to ~1,000°C to carbonize.
CH_4 Methane.
CHP Combined heat and power. Equipment that generates both electrical and thermal energy.
Cloud tower Equipment to deposit catalyst onto GDL.
ECA Electrochemical area, ideally the Pt surface area available for oxygen reduction or Hydrogen oxidation reaction.
Efficiency Energy output/Energy input.
ETU Electrolyte take-up: Quantity of electrolyte (H_3PO_4) taken up by a unit weight of carbon.
FEP Fluorinated ethylene propylene.
Floc Mixture of carbon-coated catalyst and PTFE®.
GDL Gas diffusion layers.
GDL Gas diffusion layers or substrates.
Graphitization This process involves in heating carbon material to temperatures of 2,500–3,000°C to improve thermal conductivity and corrosion resistance.
H_2 Hydrogen.
H_3PO_4 Phosphoric acid.
HT-PEM High-temperature polymer electrolyte membrane fuel cell.
Ionic resistance Resistance for the flow of H^+ through the electrolyte matrix.
kW Kilo watts.
NG Natural gas.
O_2 Oxygen.
PAFC Phosphoric acid fuel cell.
PAN Polyacrylonitrile.
Performance decay Loss of fuel cell performance due to kinetic, ionic, or mass transport losses.
PTFE® Polytetrafluoroethylene.
SiC Silicon Carbide.

Definition of the Subject

Fuel cells generate power by electrochemically combining fuel such as hydrogen and oxidant such as oxygen in air to produce electrical and thermal energy. Fuel cells generally consist of an anode electrode where fuel is oxidized and cathode electrode where oxygen in air is reduced. The electrolyte which is usually placed between the two electrodes acts as a medium to transport charge carriers (e.g., H^+, CO^-). Fuel cells are particularly interesting as energy generating devices because they consume reactants without combustion, thus providing higher efficiencies and avoiding the issue of pollution. A fuel cell reaction typically produces water as a by-product which is usually removed from the cell by reactant exhaust.

There are various types of fuel cells that are under development. The most noticeable ones are polymer electrolyte membrane (PEM) fuel cells, phosphoric acid fuel cells (PAFC), molten carbonate fuel cells (MCFC), and solid oxide fuel cells (SOFC). PEM fuel cells are mainly being targeted toward transportation needs due to their ability to provide high power densities at reasonable operating temperatures (~100°C). PAFCs and MCFCs are being developed primarily for stationary applications since their power densities are lower than PEM. SOFCs are currently being developed for both stationary applications and transportation applications but high-temperature material development is needed before they become commercially viable.

Introduction

Medium-temperature fuel cells can be classified as those operating between 120°C and 250°C. Two main categories of fuel cells fall in this category. One is phosphoric acid fuel cell and the other is high-temperature polymer electrolyte membrane fuel cells (HT-PEMFC). While PAFC is the only fuel cell technology that has demonstrated over 70,000 h of field operation it has cost challenges that have to be overcome for commercialization. On the other hand, significant amount of government and private funding is being devoted to the development of HT-PEMFC for automotive and stationary applications [47]. So far HT-PEM has shown little progress in lab-scale evaluation and has a long road to full-scale demonstration.

This temperature range is particularly interesting because it allows the fuel cell to run on reformed fuel and have tolerance to CO which is the main fuel cell poison generated in the reforming reaction. Most importantly, these temperatures allow for combined heat and power (CHP) capability that can be used in most commercial buildings for either space heating, hot water generation, cooling applications, etc. Today, commercial CHP is the best application for fuel cells in the stationary space due to price of electricity, price of gas, the opportunity for customer energy savings, and the impact of such savings on world energy consumption. Fuel cells in CHP applications need to be efficient (80–90% efficiency), cost effective (less than $2,000/kW installed), have useable heat (temperatures in the neighborhood of 150–250°C), and long life times (10 years) to provide the required value proposition to customers. PAFCs fit very well with the above requirements except for cost which is being addressed currently by both industry and government.

Market Requirements

Stationary fuel cell applications include commercial buildings such as supermarkets, data centers, schools, hotels, and hospitals, and industrial users such as chemical plants and refineries and distribution utilities. The primary driver for acceptance of any energy application is the payback period associated. For reference purposes, the payback period in the energy industry is usually on the 3–5 year time scale. In addition to payback period, strategic factors such as grid congestion and unreliability, rising energy costs, urbanization, global warming, ability to use waste heat, and avoidance of peak load constraints are also factoring more and more into the decision making of customers evaluating fuel cells for stationary applications.

Payback period is usually a function of initial cost of the system and the life cycle costs associated with the system. Initial cost of a PAFC system involves the cost of fuel cell stacks and balance of plant components, cost of integration and assembly of these components and factory acceptance test. Life cycle costs are primarily a function of the efficiency of the system, cost of fuel and maintenance costs. Efficiency in the case of CHP applications involves both electrical and thermal efficiency.

PAFCs have a payback period of 3–5 years (with various government incentives) when the customers use waste heat generated by the fuel cell. These systems have an initial electrical efficiency greater than 40% and an average lifetime electrical efficiency of 38%. Utilization of all of the waste heat generated by the system allows the customer to achieve 90% overall utilization.

Phosphoric Acid Fuel Cells

PAFCs are the first fuel cells to be commercially available. The major manufacturers of these fuel cells are UTC Power, Toshiba Corporation, HydroGen Corporation, Fuji Electric Corporation and Mitsubishi Electric Corporation. UTC Power introduced for sale a 200 kW PAFC system in 1991, and over 260 units were delivered to various customers worldwide. The design operational lifetime for these units was 40,000 h and most of the fielded units have met or exceeded this requirement. A number of these units are still operational today with fleet leader at Mohegun Sun in Uncasville, Connecticut, USA, accumulating more than 76,000 h [48]. Fuji's phosphoric acid fuel cell power plants, launched in 1998 have also demonstrated 40,000 h of life in field and some units after overhaul have exceeded 77,000 h of operational lifetime [1].

Phosphoric acid fuel cells usually operate on natural gas but they can operate on other fuels such as H_2 exhaust from chemical plants and anaerobic digester gas (ADG) from waste treatment plants. UTC Power's

phosphoric acid fuel cell system is usually designed to operate in water balance, i.e., it does not consume water from the site nor produce excess water at the site. These power plants operate at ambient pressures and have the capability to transition between grid connect and grid independent model. This capability allows the customer to draw electricity when required from grid and export excess electricity generated by the fuel cell power plant when the customer loads are lower than the power generated by fuel cell. Basic description of an ambient pressure natural gas operating UTC Power's PAFC system is shown in Fig. 1.

Natural gas is fed to the fuel processor where CH_4 in natural gas is converted to H_2-rich fuel using steam reforming. H_2-rich fuel from reformer is fed to the cell stack where it is electrochemically combined with O_2 in air to generate DC power and thermal energy. DC power is sent to power conditioning system where it is converted to AC power. Makeup water is used only during the start-up of power plant to fill the thermal management system or in situations where the power plant is operated outside its design specifications for extended period of time.

The cell stack assembly is the heart of the power plant which produces both electrical and thermal energy by electrochemically combining H_2 in fuel and O_2 in air. The basic description of a phosphoric acid fuel cell is shown in Fig. 2.

PAFCs operate at temperatures between 150°C and 225°C. H_2 from fuel is split into protons and electrons at the anode electrode. The protons travel through the electrolyte (H_3PO_4) and reach the cathode catalyst layer where they combine with O_2 in air producing DC power, water, and waste heat. The electrolyte is usually held in a refractory nonconducting matrix like silicon carbide. Water generated in the fuel cell is removed by cathode exhaust. Cathode exhaust is sent to the condenser where generated water is condensed. This condensed water is sent back to the water treatment system where it is purified to minimize the conductivity and sent to the thermal management system. Coolant exhaust from cell stack is sent to steam separator where steam required for fuel processor is separated and the remaining hot coolant water is sent through multiple heat exchangers to supply thermal energy to customers.

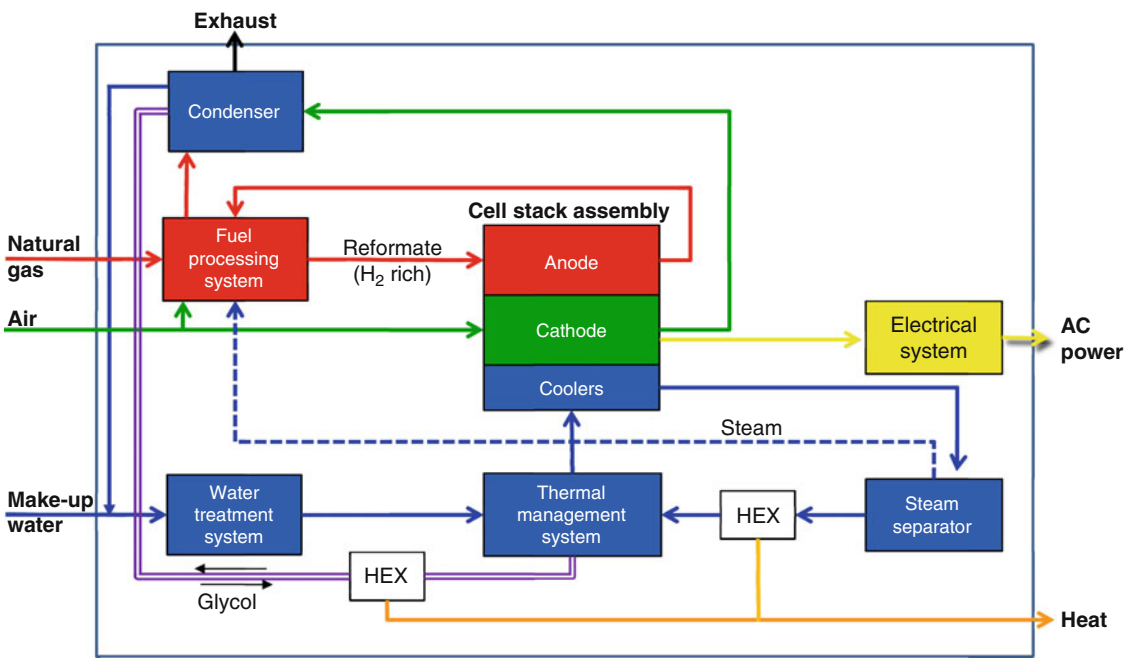

Phosphoric Acid Fuel Cells for Stationary Applications. Figure 1
Description of an ambient pressure operating PAFC system

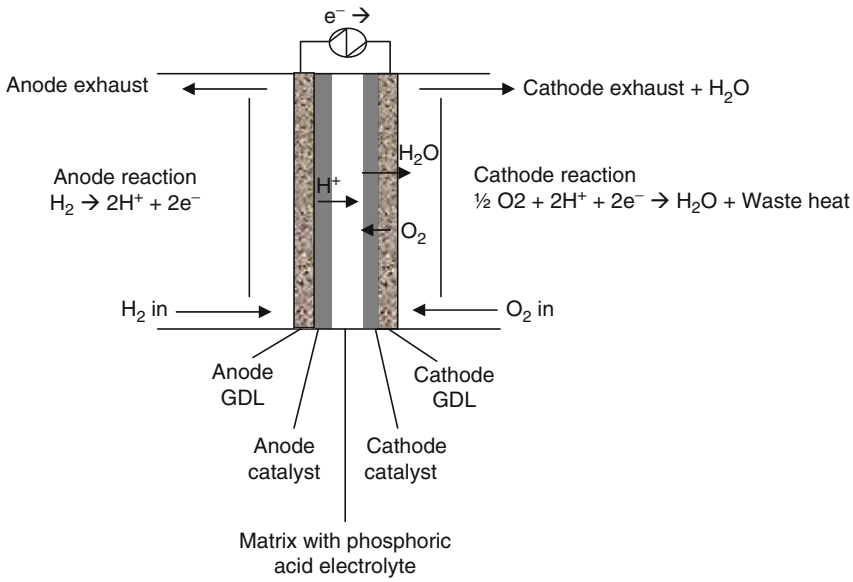

Phosphoric Acid Fuel Cells for Stationary Applications. Figure 2
Phosphoric acid fuel cell

Cell Stack Assembly Components

The main components of a PAFC are bipolar plates, gas diffusion layers, catalyst layers, and matrix layer [3]. Typical cell designs include a sandwich of these layers as arranged in Fig. 2 between coolers. Multiple cells per cooler designs are generally employed to improve power density and this unit is called a sub stack. A cell stack assembly consists of multiple sub stacks held between two pressure plates under compression to minimize reactant leakage and contact resistance losses.

Gas diffusion layers (GDLs): As the name suggests, GDL allows for gas to diffuse from the bulk flow in channels to the catalyst layer; provides mechanical support to the catalyst layer; allows for water management, i.e., removal of product water to the bulk flow in channels and heat transfer from the catalyst layer to the coolers. GDLs are made by turning polyacrylonitrile (PAN)-based carbon fiber into carbon paper. Carbon paper is then impregnated with a phenolic resin by a prepreg process, hot laminated to cure the resin in place and to achieve the desired thickness. It is then heat treated at ~1,000°C to turn the phenolic resin into carbon and then graphitized at ~2,500°C in an inert atmosphere [4, 5]. Graphitization helps impart better thermal and electrical conductivity to the GDL.

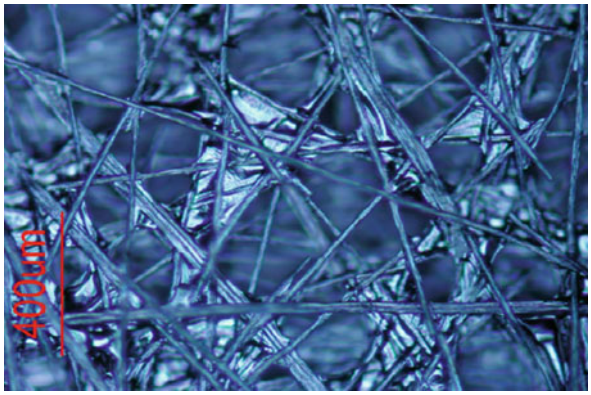

Phosphoric Acid Fuel Cells for Stationary Applications. Figure 3
Graphitized carbon fibers in PAFC GDL

A finished substrate is approximately 70% porous with a mean pore size of 25–30 μm. These finished substrates as shown in Fig. 3 are usually hydrophobic and hence they are impregnated with a wettability coating (e.g., Vulcan or Black Pearl Carbon) to facilitate water and acid management.

Electrolyte matrix: Matrix in PAFC holds H_3PO_4 electrolyte and hence facilitates the movement of protons from anode to cathode. The matrix layer should be

wettable, sufficiently porous to hold H_3PO_4 electrolyte, should have minimal reactivity with H_3PO_4 during operating temperatures, have sufficient electrical isolation to prevent shorting in cells and finally have sufficient bubble pressure (~35 kPa) to minimize reactant crossover. Materials such as wettable PTFE, papers formed using organic polymers and silicon carbide have been evaluated as matrix layers by various fuel cell manufacturers. Wettable PTFE layers failed because they lost their wettable properties over the course of operation leading to expulsion of acid from the matrix layer and hence cell failure due to reactant crossover. Organic polymers such as polyetherketones (PEK) and polybenzimidazoles (PBI) have acceptable beginning-of-life properties but seem to lose desirable properties over the course of time. Silicon carbide matrix layer has been used in UTC Power's PAFC and it has retained its material properties over long life operation. This matrix layer is formed by spraying 5 μm particle size SiC with 5% PTFE as binder onto the catalyst layer and then heating the coated electrode to ~300°C to evaporate the solvent and form the layer. These layers are typically 25–50 μm to minimize ionic losses, 50% porous, have a bubble pressure of ~70 kPa and an effective ionic resistivity of 6–7 Ωcm [6, 7]. They have worked pretty well in UTC Power's PureCell® Model 200 for greater than 70,000 h.

Cathode catalyst layer: Cathode catalyst layers in PAFCs are made using a mixture of PTFE and catalyst-coated graphitized carbon. These layers are around 100–125 μm thick and are approximately 70% porous. Catalyst is usually Pt or an alloy of Pt. Graphitized carbon is used on cathode to ensure minimal carbon corrosion during long life operation. Oxidizing environment on cathode can cause significant corrosion issues during steady state operation and starting/stopping of the power plant. Thus, to minimize carbon corrosion for long life (10–20 years), it is essential to use corrosion-resistant graphitic carbon [8, 9]. PTFE is used in the mixture to produce an optimum balance between hydrophilic and hydrophobic pores in the catalyst layer. Hydrophilic pores take up acid and allow for proton transport while hydrophobic pores allow for reactant air or fuel to reach catalyst sites. It is very critical to achieve this balance to have an optimum electrolyte fill in the catalyst layer while providing enough path ways for gas to reach the catalyst. If the catalyst layers are underfilled or have low electrolyte take-up, it results in the cell having high IR losses; if the catalyst layers are overfilled or have high electrolyte take-up, it results in low cell performance due to flooding or mass transport losses. Hence it is very critical to achieve optimum fill level and remain at that fill level during the course of operation. UTC's catalyst layers have demonstrated the ability to retain this pore structure over the course of field operation. UTC's cathode catalyst layer is manufactured in batch process [10–13]. Graphitized carbon coated with Pt alloy is mixed with PTFE particles to form floc using various wet mixing techniques. This floc is then dewatered and dried to form floc pellets. Floc pellets are then finely ground and deposited onto the GDL using a cloud tower. These electrodes then go through a sintering oven where the PTFE flows over the graphitized carbon to form hydrophilic and hydrophobic pores. SEM image of a typical PAFC electrode where catalyst-coated carbon particles are further coated with PTFE is shown in Fig. 4.

Anode catalyst layer: Anode catalyst layers are manufactured using the same process described above but these catalyst layers use carbon instead of graphitized carbon. Since anode electrode is mostly in H_2 environment, there is very little to no corrosion of the anode electrode and hence the use of carbon instead of graphitized carbon [9]. Regular carbon has a higher surface area than graphitized carbon thus allowing for better Pt loading characteristics and thus improved

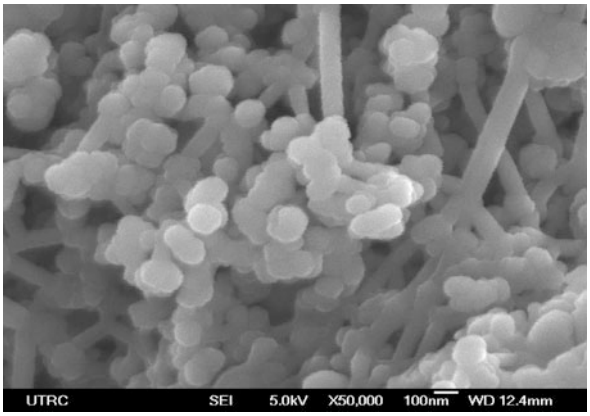

Phosphoric Acid Fuel Cells for Stationary Applications. Figure 4
PAFC catalyst particles coated with PTFE

H_2 oxidation reaction kinetics. Anode catalyst layers are made slightly more hydrophilic than cathode catalyst layers since H_2 kinetics are fast and thus mass transport losses set in at much higher current densities than operating current densities.

Bipolar plates: The main function of bipolar plates is to transport reactants to the catalyst layers, prevent reactant crossover from one cell to another, prevent acid migration from one cell to another, provide good electrical properties to minimize IR loss through the plate and provide good thermal properties to transport heat generated in the cell to the coolers. UTC Power's bipolar plates are usually made of mixture of flaky graphite and FEP. FEP is limited to less than 20% to minimize the impact of IR loss and thermal conductivity loss in the plate. This mixture of FEP and graphite is placed in mold and compacted at high pressures (500–1,000 psi) to make molded performs. The bipolar plates in PAFCs should have very low porosity to reduce electrolyte take-up. Reducing the electrolyte take-up prevents the formation of a continuous electrolyte pathway through the thickness of the plate thereby mitigating electrolyte pumping as discussed in electrolyte management section. In order to achieve this low porosity, two preforms are laminated on either side of a highly nonporous separator plate to form the integral separator plate as shown in Fig. 5. After lamination of molded preforms to the separator plate, channels are either machined or molded in the plate. Separator plate is manufactured by impregnating carbon paper with a phenolic resin. After resin impregnation, multiple layers of paper are laminated and carbonized in a slow carbonization process at 1,000°C. The carbonization process has to be slow to prevent the formation of pores in the structure. After carbonization, the plate is graphitized at ~2,500°C to improve corrosion resistance, thermal and electrical properties. UTC Power's bipolar plates have <5% porosity with very high tortuosity and have performed robustly in the field in mitigating acid transfer through plane in the plate. Channels in these plates are coated with wettable carbon to allow for acid management during fuel cell operation [14]. The perimeter of the plate also needs to be hydrophobic to prevent electrolyte being pumped on the edge of the plate. This hydrophobic break is achieved by placing PTFE flaps around the perimeter [15–22].

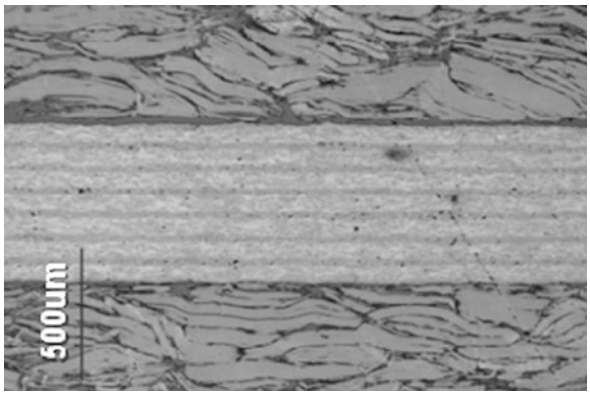

Phosphoric Acid Fuel Cells for Stationary Applications. Figure 5
UTC's phosphoric acid fuel cell bipolar plate

Edge seals: UTC Power's cell stack design uses external manifolds to transport reactants in and out of the cell stack. As a result, the edge of the anode GDL in air manifold and similarly cathode GDL in fuel manifold need to be sealed against reactant mixing in these locations. The obvious method of sealing is to fill the perimeter of the GDL with fuel cell–compatible filler material to minimize porosity. UTC Power's design fills the perimeter with a wettable carbon. Some of the previous designs also accomplished edge sealing using silicon carbide. The particle size of this filler material is usually around 5 μm and thus when impregnated into the GDL it forms pores that are much smaller than the pores in the GDL. Edge seals are made by forming a viscous ink of these particles and using a screen printing process to apply the ink to the GDL. Subsequent drying of the electrode removes the volatiles used in the ink leaving carbon in the GDL. When these GDLs are filled with acid during the assembly process, the edge seals take up acid due to capillary action and thus form wet seals which prevent gas from leaking into manifolds [23–26].

Coolers: Coolers in UTC Power's PAFCs are made of stainless steel tubes embedded in molded material (mixture of FEP and Graphite) as shown in Fig. 6. These coolers use the same manufacturing process as that of the bipolar plates. A serpentine cooler tube is placed between two molded preforms and laminated together at high pressures and temperatures. The ends of the tubes coming out of the molded material are

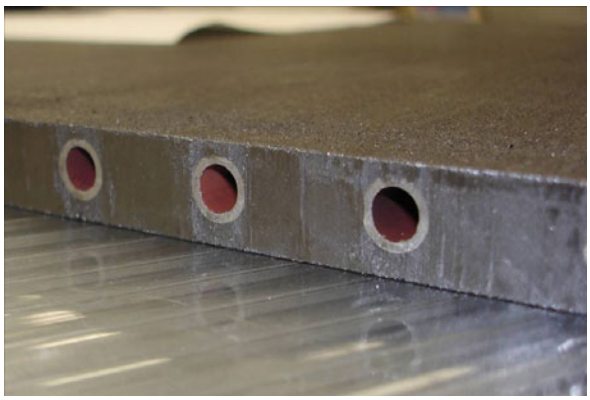

Phosphoric Acid Fuel Cells for Stationary Applications. Figure 6
UTC Power's PAFC cooler

wrapped in PTFE film or coating to prevent attack of stainless steel tubes by phosphoric acid. In UTC Power's PAFC system, water is used as coolant. This coolant enters the cell stack as liquid water and exists as a mixture of steam and liquid water between 150°C and 180°C. As a result, the coolant temperature rises as the water is heating up in single phase and once it reaches the saturated pressure, it stays at the same temperature but starts generating steam inside the coolers. The steam from coolant exit is used in the reforming reaction and the remaining hot water is used to supply thermal energy to customers. Due to the two-phase cooling, it is very essential to ensure that the liquid pressure drop is sufficiently greater than the two-phase pressure drop. If not, the variability in performance between cells can cause the system to run into thermal imbalance and as a result some cells would be operating much hotter than other cells, decreasing their life substantially. Increase in liquid pressure drop is obtained by inserting orifices or some other kind of flow restrictors at the coolant inlet to the cell stack. Orifice design has to ensure that there is no potential for clogging of coolant inlet to the cell stack. Thus, in order to mitigate issues associated with clogging, increase in pressure drop is accomplished by using a long tube coiled in front of each cooler [27–30].

Non-repeat components: The components described in the previous section are usually referred to as repeat components since every cell has those components with multiple cells present in a cell stack. Non-repeat components are those that are used only once in a cell stack. The main non-repeat components in a cell stack assembly are pressure plates, coolant inlet and outlet manifolds, reactant inlet and outlet manifolds, and manifold seals. Multiple cells placed between coolers are stacked between two stainless steel pressure plates and loaded axially to around 60 psi with the help of tie rods that run the entire length of the cell stack. Reactant manifolds are then assembled onto the cell stack with manifold seals placed between the cell stack and the manifold. These reactant manifolds are made of stainless steel and coated with PTFE coating to prevent phosphoric acid attack of the manifolds. It is very essential to ensure that there are no pin holes in the PTFE coating for the same reason mentioned above. In phosphoric acid fuel cells, manifold seals made with high fluorine content fluoroelastomers. Fluoroelastomers are very resistant to hot phosphoric acid environment and hence they have lifetimes greater than 10 years. It is very essential that these seals have very low porosity. Seals with high porosity take up acid and due to the potential difference between the top and bottom of the cell stack, acid pumps to the top of the stack thus causing the bottom of the stack to fail due to loss of acid and top of the stack to fail due to flooding by acid. In addition, these seals need to conform to the variations in the layup of cells along the height of the stack. UTC Power uses a seal mechanism where a cured fluoroelastomer is placed adjacent to the manifold and uncured fluoroelastomer placed adjacent to the cell stack. During the heat-up of the cell stack to operating temperature, the uncured manifold seal melts, flows, and cures in place to seal the skyline that is formed due to the variations in the layup of cells.

Cell Stack Assembly Life

Phosphoric acid fuel cells life is primarily a function of catalyst decay and acid management.

Catalyst decay: Catalyst decay occurs due to steady state operation and start-stops. Steady state decay occurs due to agglomeration of Pt particles in the catalyst layer. Pt deposited onto the carbon support in PAFC catalyst has a particle size of approximately 4–5 nm. Due to the high temperature of operation and high operating lifetimes (~80,000 – 100,000 h), these Pt particles tend to agglomerate and loose surface area. Smaller the particle size, higher the surface area and

more sites for O_2 reduction or H_2 oxidation, but these particles are much more unstable and tend to agglomerate quickly. Even though these Pt catalysts tend to have high performance at beginning of life, their performance drops quickly due to Pt particle agglomeration. UTC Power's PAFCs use a Pt alloy, Pt–Cr–Co on cathode and Pt on anode. The use of alloy on cathode allows for improving the surface area while reducing the agglomeration of catalyst. On anode pure Pt is used with approximately one third loading of that of the cathode. Low loadings are used on anode since H2 kinetics are fast. These Pt particles are approximately 2–3 nm in size and tend to agglomerate faster than the cathode. As a result, anode catalyst electrochemical area decreases much faster than cathode.

UTC Power has deployed more than 260 Purecell® model 200 power plants and their performance decay was as expected in field. This model power plant operated at 200 kW and Fig. 7 shows the operational experience of this model.

Teardown analysis has been performed on some of these units that have returned from field after their design operational lifetime of 40,000 h. The catalyst in these power plants has degraded as mentioned above. The average ECA of a new catalyst sample is 50 m^2/g while catalyst that has aged in field for 43,000 h has an average ECA of 6.5 m^2/g. Field operation increased the particle size from 4–5 nm to 20–25 nm. Figure 8 shows how catalyst ages with operational time.

Based on Model 200 experience, UTC Power has developed model 400 which has a design life of 85,000 h or 10 years. To meet 10 year performance requirements, cell operating conditions have been changed in addition to modification of catalyst properties during manufacture.

In addition to improving the catalyst, system strategies such as using a mixture of H_2/N_2 as purge gas during shutdown and use of voltage clipping are being deployed to mitigate start/stop losses in model 400. Figure 9 shows performance data of model 400 catalyst vs. design requirements.

Electrolyte management: Phosphoric acid has a finite vapor pressure and a low contact angle with all of the components used in fuel cells except for catalyst layers. As a result, managing evaporation and migration of acid is very critical to maintaining the life of the fuel cell. Evaporation of acid from a cell is controlled by the reactant exhaust temperature. If the reactant exhaust temperature is high, the acid lost in vapor phase increases. Acid loss due to temperature is

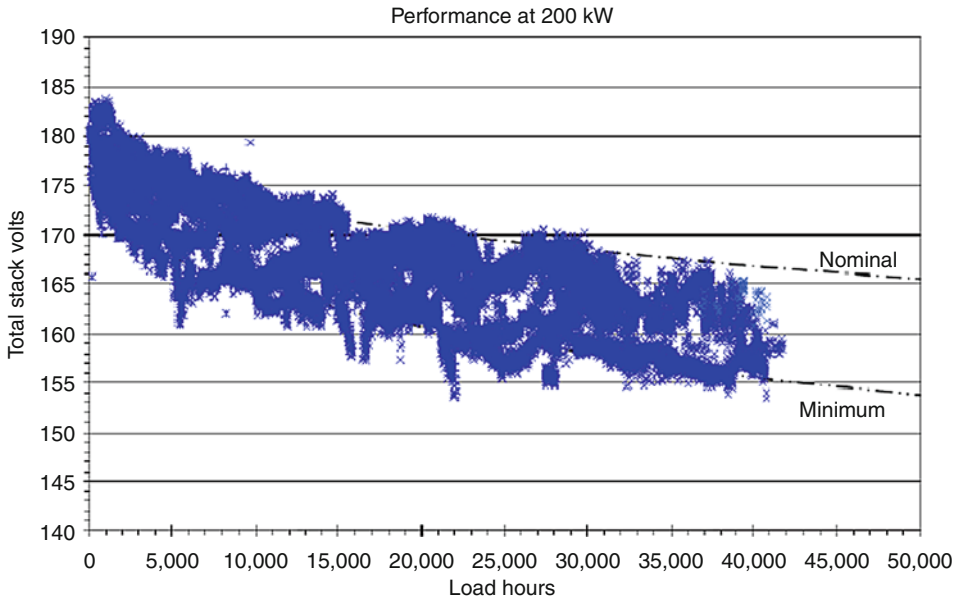

Phosphoric Acid Fuel Cells for Stationary Applications. Figure 7
Purecell® model 200 operational performance

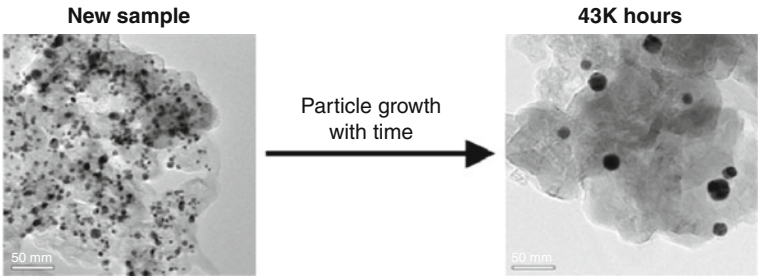

Phosphoric Acid Fuel Cells for Stationary Applications. Figure 8
PAFC catalyst on carbon

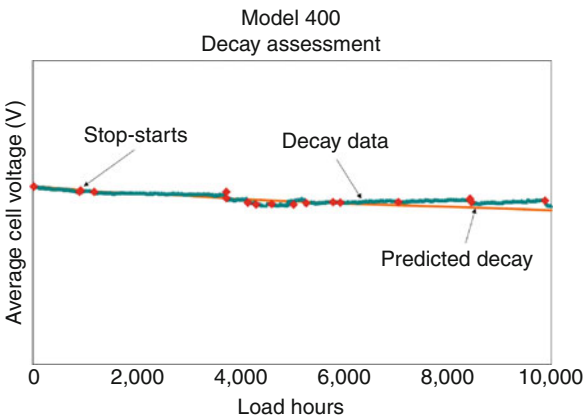

Phosphoric Acid Fuel Cells for Stationary Applications. Figure 9
PureCell® model 400 performance verification

exponential in the region of operation of phosphoric acid fuel cells. In addition, reactant flow has a linear relationship to acid loss. Hence, if the reactant utilization in a cell is low, the loss of acid is high due to higher exit flow. PAFC cell designs need to balance the loss of acid due to exit temperature and flow. UTC's cell designs operate such that the cell is hot enough to ensure maximum performance with high reactant utilization while the reactant exhaust is cold enough to ensure long life operation [31–33]. This is accomplished by placing coolant inlet to the cell near the reactant exhaust. The cell adjacent to the cooler is the coldest cell and the cell equidistant to coolers on either side is the hottest. Cold cell acid loss is less than hot cell acid loss, and thus hot cell is the life limiter due to evaporation. Water management is not an issue in phosphoric acid fuel cells. Design features such as incorporating a nonactive condensation zone near the exit location of the reactant stream, having an electrolyte reservoir in the cell, etc., are also used in addition to managing the thermal profile of the cell. UTC Power's phosphoric acid fuel cells operate at ambient pressures and between temperatures of 150°C and 225°C. As a result, water generated in the fuel cell is in vapor phase and leaves with the reactant exhaust. A PAFC cell is generally in water balance. These cells operate between 95% and 105% acid concentration depending on cell operating conditions. If the reactant flow is high, the acid in the cell is more concentrated and more water vapor leaves the cell and vice verse if the flow is low [3].

The movement of acid within the cell is managed using capillary action between various layers. The GDLs have the biggest pore size followed by matrix layer and finally the catalyst layers. During operation, acid is lost due to evaporation from the GDLs as they have the lowest capillary pressure of all the components. Once GDLs reach ~2–3% fill level, the pores in the matrix layer start emptying. Void spots in the matrix layer cause gas crossover between anode and cathode resulting in cell failure.

Acid movement within a cell is a complex phenomenon. During the build of a phosphoric acid fuel cell, acid is deposited onto the porous components [34, 35]. When load is applied to the cell, protons start moving from anode to cathode. Since phosphoric acid is a weak acid, it dissociates and is in the form of H^+ and $H_2PO_4^-$ in the cell. Thus, in order to maintain charge balance, these phosphate ions start moving from cathode to anode. This flow of acid from cathode to anode is balanced by the liquid pressure difference between anode and cathode. Once acid starts accumulating in

the anode, liquid pressure in the anode GDL increases and starts balancing the flow of acid due to charge imbalance. Thus, at steady state, approximately 75% of the acid deposited into the cathode GDL during build moves into the anode GDL. Evaporation over the course of life results in depleting anode and cathode GDL fill levels, and at end of life, matrix layer starts emptying of acid resulting in reactant crossover.

Acid can also move between cells if appropriate hydrophobic breaks are not inserted between cells [16, 17]. Bipolar plates have very low porosity but they are easily wetted by acid. As a result, the edge of the bipolar plate gets wetted by acid easily and forms a liquid connection between two adjacent cells (referred to as cell 1 and cell 2) across the bipolar plate. In a typical cell one side of the bipolar plate is in reducing environment (H_2 flow channels) and the other side of the plate is in an oxidizing environment (air flow channels). In a simple explanation, electrolyte in cathode GDL of cell 1 is near the cathode potential of the cell 1. The electrolyte potential across this bipolar plate between cell 1 and cell 2 is close to the hydrogen reference potential. As a result, the potential difference across the bipolar plate is equal to that of one cell's voltage. This potential difference can drive a very small shunt current through the acid film that has formed on the edge of the plate thus moving protons from cell 2 to cell 1. Due to movement of protons from cell 2 to cell 1, phosphate ions start moving from cell 1 to cell 2. Over the course of short time intervals, this shunt current can drive enough acid such that cell 1 fails due to dry out and cell 2 fails due to flooding by acid. UTC's cell design includes a hydrophobic break or PTFE flap between cells to mitigate the formation of a continuous film between cells thus mitigating movement of acid due to shunt currents [16, 17].

Teardown of UTC's Purecell® Model 200 units from field and measuring the acid content in these cells indicates that the PTFE flap between cells has worked very effectively in mitigating shunt migration of acid between cells. In addition, the loss of acid due to evaporation is very close to model predictions [36] as shown in Fig. 10.

PAFC Applications

PAFC fuel cells are a natural fit for combined heat and power applications. The use of CHP fuel cell systems in commercial buildings such as supermarkets, office towers, schools, data centers, industrial buildings, etc., improves overall efficiency by displacing low efficiency electricity provided by grid while providing enough thermal energy to displace fuel required for space heating and/or domestic hot water.

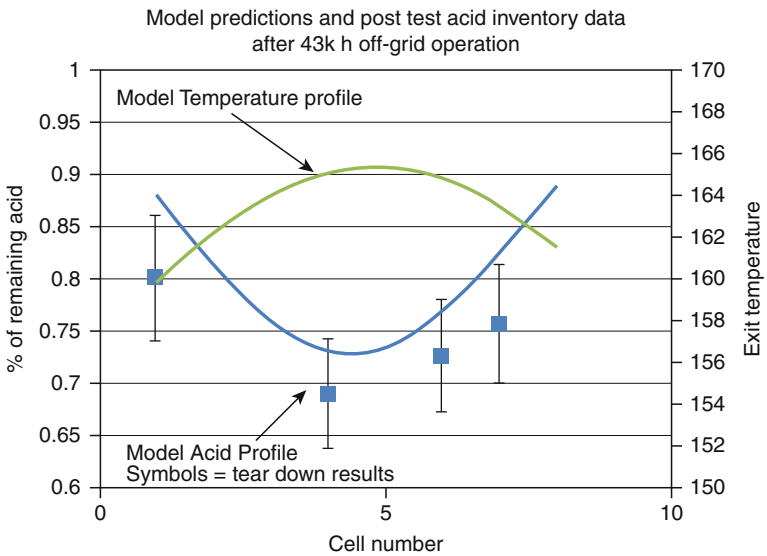

Phosphoric Acid Fuel Cells for Stationary Applications. Figure 10
Acid loss as a function of cell temperature

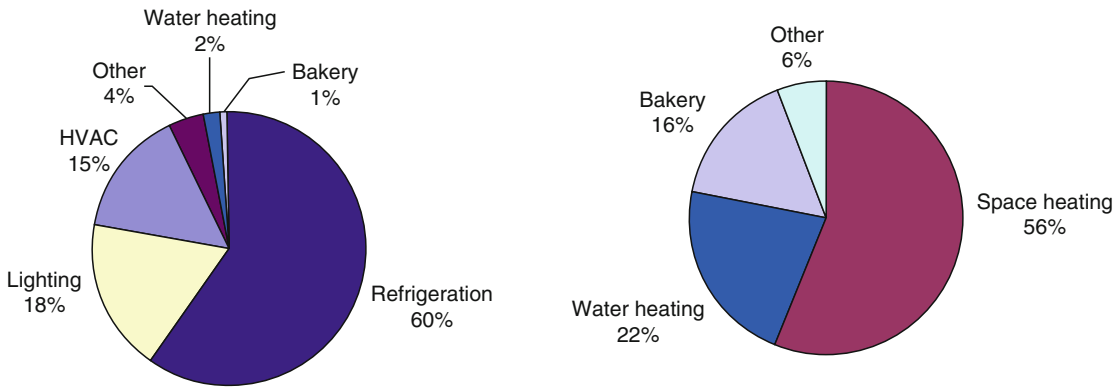

Phosphoric Acid Fuel Cells for Stationary Applications. Figure 11
Supermarket energy consumption [37, 38]

UTC's PAFC system has been used in a wide variety of applications and given below is an example of how this application can be used in supermarkets. A typical supermarket's energy needs are met 80% by electricity and remaining by natural gas. For a typical supermarket it has been estimated that a 10% reduction in energy costs is equivalent to increasing net profit margins by 16%. In other words, $1 in energy savings is equivalent to increasing sales by $59 [37, 38]. Hence energy-efficient methods of operating stores are a top priority for supermarkets. Supermarket's energy usage is primarily a function of the square footage of the store and its operating hours. Electricity in a supermarket is used mostly for refrigeration while natural gas is used mostly for space heating as shown in Fig. 11.

Supermarkets need reliable and low-cost energy to maintain freshness of produce and to improve their margins. Using a fuel cell application with CHP capabilities can improve their efficiencies significantly thereby reducing energy costs. UTC Power's PAFC system is being currently evaluated by various supermarkets to achieve high efficiency and hence reduced energy costs. Shown in Fig. 12 is a Model 400 application which supplies the store with 324 kW of electricity, 63 kW of high-grade heat which is used for space heating and refrigeration using absorption chilling and 92 kW of low-grade heat for domestic hot water. Absorption chilling is driven by heat energy rather than mechanical energy [38, 39]. The power plant uses 750 kW (LHV) of natural gas to generate above the energy required by the store thus achieving overall efficiency of 65%. As energy costs continue to increase, CHP applications provide the value proposition required by customers to improve their margins.

Another example of UTC's Purecell® model 200 fuel cell system being used for commercial application is the installation at Mohegun Sun Casino in Uncasville, Connecticut, USA. This facility uses both high-grade and low-grade heat from the fuel cell along with electric power (Fig. 13). Customer needs heating all year long and effective integration allowed for achievement of ~85% efficiency with this unit [38, 39].

Future Directions

Cost must be reduced aggressively to enable commercialization of combined heat and power (CHP) fuel cells. A significant portion of the fuel cell system cost is the cost of cell stack materials and manufacturing processes including labor. Cost of fuel cell components is roughly split half and half between materials and manufacturing costs. Significant R&D investments to enable continuous efficiency improvements along with operational excellence are essential to drive down manufacturing costs. Development of high-volume manufacturing techniques along with high-speed quality control process will enable reduction of a significant portion of this cost [40].

Unique processes used in the manufacture of PAFC components result in increased part cost. Current processes for manufacturing GDLs, electrodes, bipolar plates, etc., employ batch processes and require

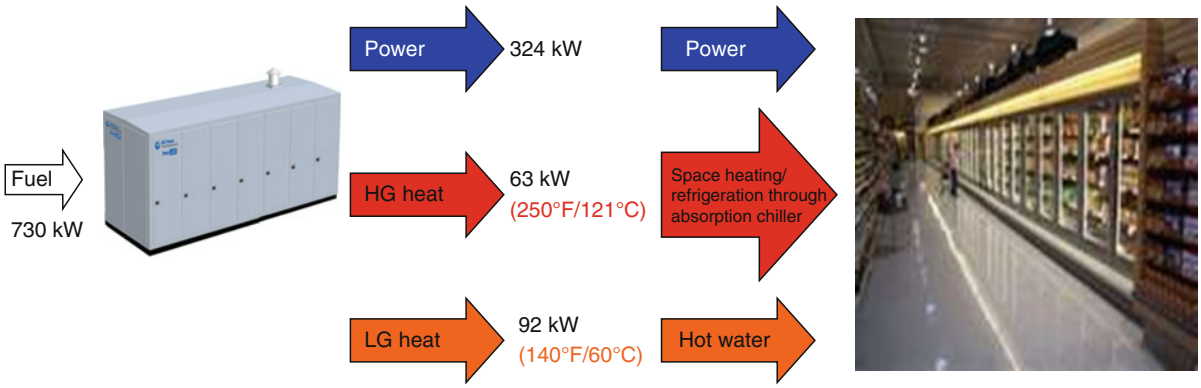

Phosphoric Acid Fuel Cells for Stationary Applications. Figure 12
Use of a PAFC system for supermarket application

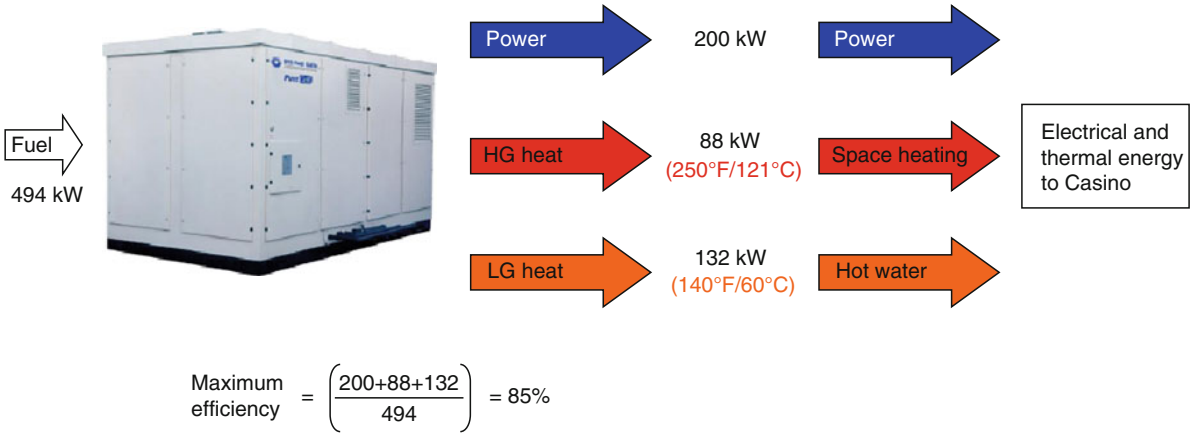

Phosphoric Acid Fuel Cells for Stationary Applications. Figure 13
Use of a PAFC system for commercial building application

continuous manufacturing processes to reduce cost and also to meet projected high volumes.

GDL manufacturing for high-temperature CHP fuel cells currently involves a lot of batch processes such as turning the fiber into resin-impregnated felt, carbonization, graphitization (for tolerance to high-temperature operation), etc., before electrodes are deposited onto the part. Continuous manufacturing processes for making GDLs can be enabled by use of double belt press, but this requires process development. Double belt press process integrates all of the various steps involved in making GDLs wherein fiber can be fed from one end of the press with finished substrate emerging from the other end of the press. Similarly, bipolar plates used in PAFCs are currently manufactured using unconfined compression molding followed by machining, wet treatment of bipolar plate and incorporation of hydrophobic edges to prevent acid migration from cell to cell. Continuous manufacturing processes such as net-shaped molding can enable integrating these operations into one operation thus enabling high-volume manufacturing and significantly reducing the cost of component. Finally, fuel cell industry needs to move toward manufacturing

that can help bring the processes to the part rather than parts moving through the process to reduce factory footprint costs, handling costs, and energy costs, and thus reduce cost of manufacturing. Fuel cell industry currently adopts processes that have been developed in other industries. For example, Gravure coating which is used to coat thin layers at high speeds is being used to coat thick layers of electrolyte matrix at low speeds. The fuel cell industry needs the development of new manufacturing processes for fuel cells that are tailored toward optimum manufacture of a part keeping its fundamental requirements in consideration.

Since every component used in a cell (GDL, catalyst layer, bipolar plate, matrix layer, etc.) is critical for the operation of the cell stack, these components have to be within a very tight specification and meet defined key product characteristics. This requires the implementation of a robust quality control system. For example, substrates in PAFCs have to be checked for porosity, IR, thermal conductivity, thickness, density, compressive strength, flex strength, etc. All of these quality checks impart cost to the substrate. Ability to integrate these measurements into one tool will enable help high-volume manufacturing. Similarly high-speed measurement techniques (e.g., ultrasonic crack detection methods) that can detect defects/cracks in electrode layers and bipolar plates in a few seconds are required for high-volume manufacturing of these components. In addition, improving manufacturing processes to achieve high level of robustness will reduce the number of cell stack rebuilds and/or infant mortalities thus reducing cost. Finally, all of the proposed high-volume manufacturing techniques need to yield product at a very minimal scrap rate to reduce part cost.

Another approach for reducing cost is to improve the efficiency of the power plant. Since cell stack has the lowest efficiency of all the components, improving its efficiency provides maximum benefit but at the same time cell efficiency improvements are not easy to achieve. Improved efficiency can be capitalized by removing cells out of the cell stack to generate the same power at baseline efficiency or it can be used to provide cheaper power to the customer. Phosphate ions poison cathode catalyst, i.e., they occupy valuable sites on Pt catalyst thus reducing the number of sites available for oxygen reduction reaction. This leads to lower cell performance (typically < 0.25 W/cm^2 of electrode) and hence more number of cells making the stack cost challenging. The only way to eliminate phosphate poisoning is to use a new electrolyte instead of H_3PO_4. New liquid electrolytes which do not have phosphate poisoning effect can lead to significantly improved electrical efficiency. Truls Norby's paper on "Solid state protonic conductors: Principles, properties, progress and prospects" [41] discusses properties of potential materials that can be used as electrolytes in the temperature ranges discussed. Another way of improving efficiency could be by improving the O_2 solubility/diffusion in H_3PO_4. Literature shows that additives to H_3PO_4 can improve O_2 solubility in H_3PO_4 and hence improved efficiencies. Additives such as silicon oils, C4 and C6 compounds, Pyrroles, protonated polyamine, etc., evaluated by various researchers have shown performance improvements but further research is needed to determine if these performance improvements are sustainable [42].

Conditioning and qualification of cell stack after it is assembled and final qualification of power plant after integrating cell stacks with balance of plant (BOP) takes significant time increasing product cost. Conditioning of cell stacks involves processes that cure seals and set them in place and enable electrolyte movement into the catalyst layers making them functional. After conditioning, acceptance testing is performed on cell stacks where diagnostics are done to ensure that flow to the cells is appropriate, seals are set in place, catalyst layers are functional, and that the product meets design performance requirements. Ability to assemble hundreds of cells in a power plant in the same manner every time will enable the industry to go to a limited sampling technique rather than testing every power plant thus reducing costs. Developing methods to perform conditioning and acceptance testing on modules of cells rather than on fully assembled cell stack will enable removal of problem parts early in the build and prevent costly teardowns. Further understanding of the electrode manufacturing process at a fundamental level could enable integrating conditioning procedures into manufacturing process thus eliminating post component manufacture conditioning and acceptance testing. R&D aspects that can reduce or eliminate conditioning

and acceptance testing of CHP fuel cells should be developed.

Balance of plant (BOP) in fuel cell power plants also adds significant cost to the power plant. The ability to deliver contaminant-free fuel to the cell stacks, ability to provide reactants very quickly as the load changes, etc., add significant cost to the power plant. The fuel processing system (FPS) is one of the most expensive subsystems in the fuel cell power plant BOP, at 20% of total power plant cost. The catalytic steam reformer (CSR) is the single most expensive component (18%) within the FPS. The CSR is effectively a catalyst-augmented heat exchanger. As such its cost can be significantly reduced by manufacturing designs and techniques to improve heat transfer such as direct application of catalyst to reformer walls (catalyzed walls improve heat transfer by eliminate film losses, thus enabling reduction heat transfer area), improve catalysts to reduce poisons to the stack (such as and sulfur and ammonia which accelerate stack decay and increase stack costs), improve high-volume manufacturing techniques such as spin casting to lower tube costs, and advanced casting techniques to form the reformer burner which is presently made by welding many smaller sheet metal pieces. Automated welding processes are also critical to obtaining repeatable high-quality welds at high volume and low cost. A significant but overlooked BOP cost is piping. Cost reductions can be realized by replacing complex pipe runs requiring threaded or welded assembly with pipe or tube bending. Improved pipe bending capability can reduce manufacturing and assembly time and expense, especially at high volumes.

Heat exchangers are essential in fuel cell power plants to control temperatures for the major components (stack, reformer, shift converter), provide valuable cogeneration energy to customers, and reject waste heat. Brazed plate heat exchangers offer the most cost-effective heat transfer in many applications, but are often limited by poor thermal cycle durability which effects transient capability, especially in CHP power plants where load following and variable customer heat usage cause numerous thermal cycles. Manufacturing development to improve the durability of the brazed plate–type heat exchangers would significantly reduce overall BOP costs by enabling their use in more applications within the CHP fuel cell power plants.

Another critical area of the BOP components is the power conversion system as this system is the customer interface to the fuel cell and contains much of the key product performance characteristics necessary to achieve the customers' needs. Significant cost reduction could be achieved by developing a modular high-frequency power conversion system. A modular approach would enable use of the same design across the entire product line offered to various customers. Using this same design would allow for improvements in manufacturing volumes as the manufacturing of all current power conversion designs could be consolidated instead of the current mix of various designs in low volume. This would also drive down the cost of the power conversion system by increasing the volume of similar components that would be sourced for the power conversion of the various products offered. Having a modular design would also reduce test time in manufacturing as this would enable improved testing techniques in the supply base (i.e., automated testing) and reduce the mix of power conversion systems encountered at the final assembly.

Development of markets at lower volumes of 50–100 units/year needs to be facilitated so that design-driven cost reduction can be learned out. Demonstration programs where state or federal commercial buildings are converted to using power from fuel cell power plants should be encouraged. Finally, cost reduction as a key aspect of demonstration programs should be emphasized.

Acknowledgments

The authors would like to acknowledge Tom Jarvi for his valuable input into framing the outline for the entry.

Bibliography

1. www.fujielectric.com
2. http://www1.eere.energy.gov/hydrogenandfuelcells/fuelcells/fc_types.html
3. Breault RD (2003) Stack materials and stack design. In: Vielstich W, Lamm A, Gasteiger HA (eds) Handbook of fuel cells: fundamentals, technology and applications, vol 4, Part 4. Wiley, Chichester, pp 797–810. ISBN: 0-471-49926-9

4. Miwa K, Shimizu K, Fukui H (1989) Electrode substrate for fuel cell and process for producing same. US Patent 4,851,304, 25 July 1989
5. Breault R (2006) Electrode substrate for electrochemical cell from Carbon and cross-linkable resin fibers. PCT No: PCT/US2006/041494. 23 Oct 2006
6. Spearin W (1989) Process for forming a fuelcell matrix. European Patent 0,344,089 A1, 29 Nov 1989
7. Breault R (1977) Silicon carbide electrolyte retaining matrix for fuel cells. US Patent 4,017,664, 12 Apr 1977
8. Breault R, Mientek A, Sawyer R (1993) Minimized corrosion fuel cell device and method of making same. US Patent 5,270,132, 14 Dec 1993
9. Breault R, Fredley R, Scheffler G (1998) Corrosion resistant fuel cell assembly. US Patent 5,837,395, 17 Nov 1998
10. Reiser C, Landau M (1980) Method for reducing cell output voltage to permit low power operation. US Patent 4,202,933, 13 May 1980
11. Breault R, Harding R, Kemp F (1977) Method of fabricating a fuel cell electrode. US Patent 4,043,933, 23 Aug 1977
12. Goller G, Salonia J (1981) Dry floc method for making an electrochemical cell electrode. US Patent 4,287,232, 1 Sept 1981
13. Goller G, Salonia J (1982) Dry method for making an electrochemical cell electrode. US Patent 4,313,972, 2 Feb 1982
14. Dufner B (2008) Wettability ink, process and carbon composite articles made therewith. PCT No: PCT/US2007/007045, 25 Sept 2008
15. Breault R, Luoma W, Roche R (2008) Fuel cell separator plate assembly. US Patent 20,080,057,373, PCT No: PCT/US04/44007, 06 Mar 2008
16. Roche R (1993) Extruded fuel cell stack shunt current prevention arrangement. US Patent 5,178,968, 12 Jan 1993
17. Breault R (1983) Method for reducing electrolyte loss from an electrochemical cell. US Patent 4,414,291, 8 Nov 1983
18. Breault R, Martin R, Roche R, Kline R (1996) Cathode reactant flow field for a fuel cell stack. US Patent 5,558,955, 23 Sept 1996
19. Breault R (1980) Fuel cell electrolyte reservoir layer and method for making. US Patent 4,185,145, 22 Jan 1980
20. Breault R, Gorman M (1994) Laminated electrolyte reservoir plate. US Patent 5,366,825, 22 Nov 1994
21. Uemura T, Murakami S (1988) Method for producing a carbon sheet and a fuel cell separator. US Patent 4,737,421, 12 Apr 1988
22. Emanuelson R, Luoma W, Taylor W (1981) Separator plate for electrochemical cells. US Patent 4,301,222, 17 Nov 1981
23. Trocciola J, Schroll C, Elmore D (1975) Wet seal for liquid electrolyte fuel cells. US Patent 3,867,206, 18 Feb 1975
24. Schroll C (1974) Liquid electrolyte fuel cell with gas seal. US Patent 3,855,002, 17 Dec 1974
25. DeCasperis T, Roethlein R, Breault R (1981) Method of forming edge seals for fuel cell components. US Patent 4,269,642, 26 May 1981
26. Singelyn J, Gelting R, Mientek A (1988) Expanded high-temperature stable chemical resistant seal material. US Patent 4,774,154, 27 Sept 1988
27. Grevstad P (1976) Fuel cell cooling system with shunt current protection. US Patent 3,964,929, 22 June 1976
28. Breault R, Sawyer R, DeMarche T (1986) Cooling system for electrochemical fuel cell. US Patent 4,574,112, 4 Mar 1986
29. Breault R, Martin R, Roche R, Scheffler G, O'Brien J (2000) Coolant plate assembly for a fuel cell stack. US Patent 6,050,331, 18 Apr 2000
30. Grasso A, Martin R, Roche R (2000) Composite article. US Patent 6,039,823, 21 Mar 2000
31. Breault R, Fredley R (2007) Fuel cell with electrolyte condensation zone. US Patent Pub. No: US 2007/0224476 A1, 27 Sept 2007
32. Breault R, Rohrbach C (2007) Fuel cell assembly with operating temperatures for extended life. US Patent Pub. No: US 2007/0292725 A1, 20 Dec 2007
33. Breault R, Fredley R (2008) Fuel cell assembly having long life characteristics. US Patent Pub. No: US 2008/0118789 A1, 22 May 2008
34. Congdon J, English J (1986) Method and apparatus for adding electrolyte to a fuel cell stack. US Patent 4,596,749, 24 June 1986
35. Grevstad P (1986) Process for adding electrolyte to a fuel cell stack. US Patent 4,612,262, 16 Sept 1986
36. Ferro J (2009) PAFC history and successes. In: MCFC & PAFC R&D workshop, 2009 Fuel cell seminar, 16 Nov 2009
37. Facility type: Supermarkets and grocery stores. In: Energy star® building manual, chap 11. http://www.energystar.gov/ia/business/EPA_BUM_CH11_Supermarkets.pdf
38. Supermarkets: An overview of energy use and energy efficiency opportunities, Energy star®
39. Jarvi T, Kanuri S (2010) Progress in phosphoric acid fuel cells. FC Expo, Tokyo, 5 Mar 2010
40. Gang X et al (1993) Electrolyte additives for phosphoric acid fuel cells. J Electrochem Soc 140(4):896–902
41. Jarvi T (2009) Fuel cells for combined heat and power applications. University of Pennsylvania, 26 Sept 2009
42. Norby T (1999) Solid-state protonic conductors: principles, properties, progress and prospects. Solid State Ionics 125:1–11
43. Grevstad P, Gelting R (1976) Fuel cell cooling system using a non-dielectric coolant. US Patent 3,969,145, 13 July 1976
44. Kanuri S (2009) PAFC cost challenges. In: MCFC & PAFC R&D workshop, 2009 Fuel cell seminar, 16 Nov 2009
45. Kanuri S UTC Power response to DOE Request for Information DE-FOA-0000225
46. Goller G, Salonia J, Petraglia V (1979) Dry mix method for making an electrochemical cell electrode. US Patent 4,175,055, 20 Nov 1979
47. http://www.fuelcells.org/InternationalH2-FCpolicyfunding.pdf
48. Kanuri S, Motupally S (2011) Engineering and application of phosphoric acid fuel cell system. ICEPAG, Costa Mesa, CA

Photo-catalytic Hydrogen Production

Jiefang Zhu
Department of Materials Chemistry, Ångström Laboratory, Uppsala University, Uppsala, Sweden

Article Outline

Glossary
Definition of the Subject
Introduction
Principle of Photocatalytic H_2 Production
Evaluation of Photocatalytic H_2 Production
Experimental Setup for Photocatalytic H_2 Production
Photocatalysts for H_2 Production
Development and Modification of H_2 Production Photocatalysts
Future Directions
Bibliography

Glossary

Band gap In solid-state physics, a band gap, also called an energy gap, is an energy range in a solid where no electron states can exist. In graphs of the electronic band structure of solids, the band gap generally refers to the energy difference (in electron volts) between the top of the valence band and the bottom of the conduction band in insulators and semiconductors. This is equivalent to the energy required to free an outer shell electron from its orbit about the nucleus to become a mobile charge carrier, able to move freely within the solid material.

Conduction band In the solid-state physics field of semiconductors and insulators, the conduction band is the range of electron energies, higher than that of the valence band, sufficient to free an electron from binding with its individual atom and allow it to move freely within the atomic lattice of the material. Electrons within the conduction band are mobile charge carriers in solids, responsible for conduction of electric currents in metals and other good electrical conductors.

Dopant A dopant, also called a doping agent, is a trace impurity element that is inserted into a substance (in very low concentrations) in order to alter the electrical properties or the optical properties of the substance. In the case of crystalline substances, the atoms of the dopant very commonly take the place of elements that were in the crystal lattice of the material.

Doping In semiconductor production, doping is the process of intentionally introducing impurities into an extremely pure (also referred to as intrinsic) semiconductor to change its electrical properties.

Dye sensitization The process in which the dye absorbs light to yield an excited state, which in turn transfers an electron (or energy) onto the semiconductor.

Hydrogen The chemical element with atomic number 1. It is represented by the symbol H. At standard temperature and pressure, hydrogen is a colorless, odorless, nonmetallic, tasteless, highly combustible diatomic gas with the molecular formula H_2.

Hydrogen production The industrial method for generating hydrogen.

Photocatalysis In chemistry, photocatalysis is the acceleration of a photoreaction in the presence of a catalyst (called photocatalyst). In catalyzed photolysis, light is absorbed by an adsorbed substrate (called photocatalyst). In photogenerated catalysis, the photocatalytic activity depends on the ability of the catalyst (called photocatalyst) to create electron–hole pairs, leading to secondary reactions.

Photocatalyst A substance that is able to promote, by absorption of light quanta, chemical transformations of the reaction participants, repeatedly participating in intermediate chemical interactions and regenerating its chemical composition after each cycle of such interactions.

Photocatalytic water splitting The production of hydrogen (H_2) and oxygen (O_2) from water by directly utilizing the energy from light. Photocatalytic water splitting has the advantage of the simplicity of using powder or film photocatalysts in solution and (sun)light to produce H_2 and O_2 from water.

Semiconductor A material that has an electrical conductivity due to flowing electrons (as opposed to ionic conductivity) which is intermediate in magnitude between that of a conductor and an

insulator. This means roughly in the range 10^{-8}–10^{3} S/cm. In semiconductors, current is often schematized as being carried either by the flow of electrons or by the flow of positively charged "holes" in the electron structure of the material. Actually, however, in both cases only electron movements are involved.

Valence band In solids, the valence band is the highest range of electron energies where electrons are normally present at absolute zero temperature. The valence electrons are bound to individual atoms, as opposed to conduction electrons, which can move freely within the atomic lattice of the material. On a graph of the electronic band structure of a material, the valence band is located below the conduction band, separated from it in insulators and semiconductors by a band gap. In metals, the conduction band has no energy gap separating it from the valence band.

Definition of the Subject

Increasing environmental concerns from using non-sustainable fossil fuels and a growing energy demand are forcing human beings to pursue clean and sustainable sources of energy. Hydrogen exists as a light, diatomic gas with high energy content by weight, but small energy content by volume. Hydrogen can react cleanly with oxygen in a highly exothermic reaction, with pure water as the only product. The energy stored in the chemical bond of hydrogen can be released by simply burning it in a combustion engine, or more efficiently by oxidizing it in a fuel cell. Based on the above properties, hydrogen is often considered an attractive alternative to the current, fossil fuel-based energy carrier. However, the currently most widely used methods to produce hydrogen are based on the conversion of fossil fuel resources and thus deviate completely from the environmentally friendly intention of using hydrogen.

Photocatalysis is a technique to convert light (ideally sunlight) energy to chemical energy or electrical power. Photocatalytic H_2 production is a technique utilizing the energy from (sun)light to produce H_2 from water (or other hydrogen resources). Photocatalytic H_2 production from water has been accepted as one of the most promising ways to realize a hydrogen economy for three reasons: (1) this technology is based on photon (or solar) energy, which is a clean, perpetual source of energy, and mainly water, which is a renewable resource; (2) it is an environmentally safe technology without undesirable by-products and pollutants; and (3) the photochemical conversion of solar energy into a storable form of energy, i.e., hydrogen, allows one to deal with the intermittent character and seasonal variation of the solar influx [1].

Photocatalytic water splitting has the advantage of simply using powder or film photocatalysts, and in this entry, it excludes the contents on photoelectrochemical (PEC) water splitting, which is described in another entry of this encyclopedia. The redox mechanism of photocatalytic H_2 production is similar to that of PEC H_2 generation. The main difference between the two approaches lies in the location of the redox reactions, as illustrated in Fig. 1. In the photocatalytic process, both oxidation and reduction reactions occur on the surface of a photocatalyst (powder or film), and as a result, a mixture of H_2 and O_2 is evolved together (the left-hand side of Fig. 1). In the photoelectrochemical process, oxidation and reduction take place at spatially separated photoanode and cathode, respectively, resulting in H_2 and O_2 being evolved separately (the right-hand side of Fig. 1). It should be noted that the efficiency of photocatalysts is normally lower than that of photoanodes in H_2 generation, since hydrogen and oxygen have a tendency to react back to water if they are evolved at the same location. However, compared to photoanodes, photocatalysts do not need a conductive substrate for charge collection, so that a much broader selection of synthetic methods, such as solid-state high temperature synthesis, can be adopted. This allows photocatalysts to be prepared with relative ease and at a competitive cost. In a photocatalytic system, cocatalysts can be easily introduced by firing and mixing. Furthermore, research on photocatalysts may provide a convenient screening approach for the selection of suitable photoanodes.

Introduction

Photocatalytic H_2 production has been developing for 40 years. The increasing number of scientific publications constitutes clear bibliographical evidence for the

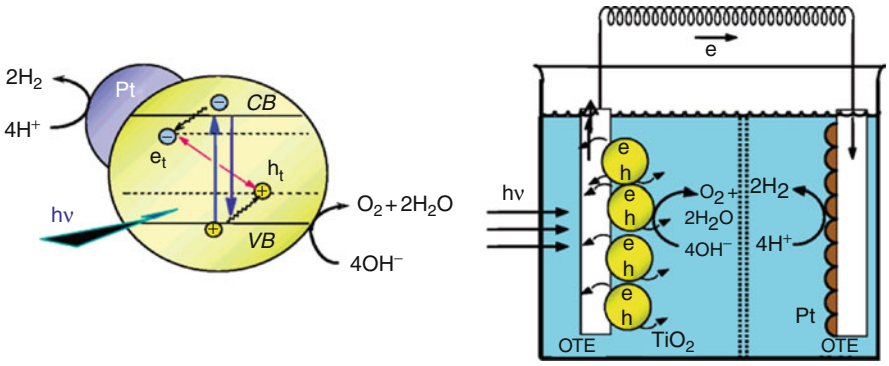

Photo-catalytic Hydrogen Production. Figure 1
Photocatalytic splitting of water following the band gap excitation of the semiconductor nanoparticle (*left-hand side*) and a photoelectrolysis cell based on a nanostructured semiconductor film electrode (*right-hand side*) (Reprinted with permission from [2]. Copyright 2007 American Chemical Society)

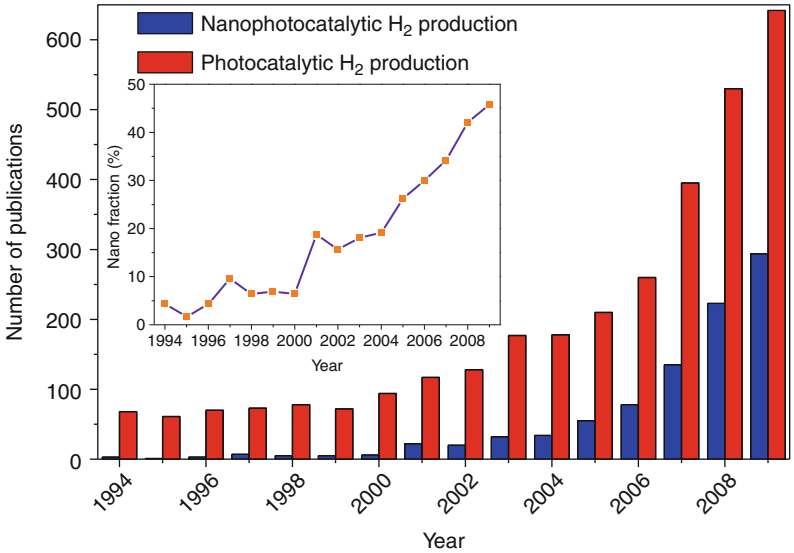

Photo-catalytic Hydrogen Production. Figure 2
The number of publications on (nano)photocatalytic H_2 production sorted by year. The inset shows the fraction of publications on photocatalytic H_2 production that deal with nano-aspects (Data were collected from the "Web of Science," and entries until October 14, 2010, have been considered)

significance of this hot field, as shown in Fig. 2. Recently, nanoscience and nanotechnology opened a new vista in this field. Since 2004, the number of publications on nanophotocatalytic H_2 production has increased by a factor of about 1.5 times every year. Many papers recently studied the impact of different nanostructures and nanomaterials on the performance of photocatalysts, since it was found that the total energy conversion efficiency is largely determined by nanoscale properties of photocatalysts. Although progress has been made in many fields concerning photocatalytic H_2 production during these years, such as photocatalytic reactor design, product separation and detection, and light harvesting, the key factor determining its practical application is the materials, i.e., photocatalysts.

In 1972, the initial work of Fujishima and Honda indicated that PEC water splitting could be performed by using a TiO_2 photoanode [3]. The setup in that work is similar to that shown on the right-hand side of Fig. 1. Photogenerated electrons and holes are formed in TiO_2 when it is irradiated by UV light. The photogenerated electrons flow to a Pt counter electrode to reduce water to H_2, while water is oxidized to O_2 by photogenerated holes on the TiO_2 side. Following this exciting finding, H_2 production by semiconductor photocatalysis and electrolysis has been attracting more and more attention. During the 1970s and the first half of the 1980s, the photocatalysts used for H_2 production from water splitting mainly focused on TiO_2, $SrTiO_3$ [4, 5], and ZnO. Compared to TiO_2, $SrTiO_3$ can split water without an external bias due to its higher conduction band level. In the middle of the 1980s, Pt/CdS [6–8] and ZnS [9] were identified as highly active photocatalysts for H_2 evolution under visible-light irradiation in the presence of sacrificial reagents. In the second half of the 1980s, new photocatalysts, such as $K_4Nb_6O_{17}$ [10–13], $Na_2Ti_3O_7$ [14], $K_2Ti_2O_5$ [14], and $K_2Ti_4O_9$ [14], were used for water splitting. Many tantalate [15–19], tungstate [20, 21], and molybdate [20] photocatalysts have shown high activity for H_2 production from an aqueous solution containing a sacrificial reagent since the second half of the 1990s. After coming into the new century, the database of photocatalysts for water splitting has become more plentiful. Many oxide photocatalysts consisting of the metal cations Ga^{3+}, In^{3+}, Ge^{4+}, Sn^{4+}, and Sb^{5+}, with d^{10} configuration (i.e., metal cations having fully filled (with ten electrons) outermost d orbitals), and assisted with RuO_2 as a cocatalyst have recently been reported [22–26]. Non-oxide Ge_3N_4 with a RuO_2 cocatalyst was also found to be a photocatalyst for H_2 production [27]. Oxynitrides [28–31] and oxysulfides [32, 33] have been widely developed in research led by K. Domen for H_2 and O_2 evolution under visible-light irradiation in the presence of sacrificial reagents. Cr-Rh oxide/GaN:ZnO is a solid solution of GaN and ZnO, which is also active for overall water splitting [34]. The solid solution of ZnO and $ZnGeN_2$, $(Zn_{1+x}Ge)(N_2O_x)$ was recently discovered as another active d^{10} metal oxynitride photocatalyst for pure water splitting under visible light [35]. A Z-scheme photocatalytic water splitting system, which involved two-step photoexcitation under visible-light irradiation, was recently developed by mimicking the natural photosynthesis of green plants [36, 37].

Principle of Photocatalytic H_2 Production

As mentioned above, H_2 is an energy carrier, and the combustion of it produces only water and traces other pollutants with a large amount of heat releasing (Eq. 1). Moreover, H_2 is also an important raw material in chemical industries, e.g., industrial ammonia synthesis. However, a large fraction of hydrogen production is currently based on fossil fuel resources. The processes involved in the conversion of fossil fuels, such as the reforming of natural gas (Eq. 2), coal gasification (Eq. 3)/liquefaction, and coal electrolysis, require large amounts of energy, either in the form of heat or electricity, and all these processes are accompanied with the release of vast amounts of carbon dioxide. In order to actualize the hydrogen economy, there is a demand for other carbon-neutral feedstocks from which hydrogen can be produced with the energy provided by a sustainable source. Alternative feedstocks under consideration include wood, other biomass, organic waste, and water, where the former options are not necessarily carbon neutral, however. The latter option constitutes an entirely sustainable energy system, where hydrogen is produced from water (Eq. 4) and later on recovered back into water in a combustion engine or a fuel cell. This entry therefore focuses on hydrogen production from water.

In principle, water can be split into H_2 and O_2 by several different pathways and utilizing various energy sources. The commonly used method is to dissociate water in an electrolysis cell. However, electrolysis is a two-step process, and the potential of achieving a highly efficient, simple, and cost-effective conversion is limited. A better idea is to directly split water in a single device into its component gases, without the production of electricity in advance. Photocatalysis can directly utilize photon energy to decompose water into H_2 and O_2.

$$2H_{2(g)} + O_{2(g)} = 2H_2O_{(g)}; \quad \Delta H = -484\,\mathrm{kJ}\cdot\mathrm{mol}^{-1} \tag{1}$$

$$CH_{4(g)} + H_2O_{(g)} = CO_{(g)} + 3H_{2(g)}; \quad \Delta H = +216\text{kJ} \cdot \text{mol}^{-1} \tag{2}$$

$$C_{(s)} + H_2O_{(g)} = CO_{(g)} + H_{2(g)}; \quad \Delta H = +135\text{kJ} \cdot \text{mol}^{-1} \tag{3}$$

$$2H_2O_{(l)} = 2H_{2(g)} + O_{2(g)}; \quad \Delta H = +504\text{kJ} \cdot \text{mol}^{-1} \tag{4}$$

Photocatalytic H_2 production (or water splitting) occurs on the surface of semiconductor materials, as shown in Fig. 3. Figure 3 shows three basic steps in photocatalytic H_2 production. The first step is the absorption of photons. A semiconductor has a valence band (VB) and a conduction band (CB), which are separated from one another by a band gap (E_g), as shown in Fig. 3c. In the ground state, all electrons exist in the VB. Under irradiation by photons with energy equivalent to or larger than E_g, some of the electrons are excited from the VB to the CB, leaving empty states, so-called holes, in the VB. The second step is the charge separation and migration, as shown in Fig. 3b. The photogenerated electrons and holes from the first step may recombine in the bulk or on the surface of the semiconductor on a time scale which is slower than the time required for their generation (Fig. 3b, c). Some electrons and holes that travel to the surface of the semiconductor without recombination can cause reduction (H_2 formation) and oxidation (O_2 formation) reactions, respectively, in the last step called surface chemical reactions. The important parameters in photocatalysts are the width of the band gap and the levels of the conduction and valence bands. From Fig. 3c, the theoretical minimum band gap (or photon energy) for water splitting is 1.23 eV, corresponding to a wavelength of 1,008 nm, according to the formula E_g (eV) equal to 1,240/λ (nm).

However, if taking into account thermodynamic losses at various steps in the photocatalytic process, overpotential is necessary to ensure a reasonable reaction rate, and effective photocatalysts exhibit band gaps larger than 2 eV, corresponding to a wavelength below 620 nm. If the sunlight is to be used for water splitting, visible-light-responsive photocatalysts should have band gaps between 2 and 3.1 eV, since the intensity of sunlight is small in the UV region, i.e., for wavelengths below 400 nm (3.1 eV). Apart from the band gap requirement, for H_2 production to take place, the CB bottom edge should be more negative than the reduction potential of H^+/H_2 ($E_{H^+/H_2} = 0$V vs NHE at pH 0), while the VB top edge should be more positive than the oxidation potential of O_2/H_2O ($E_{O_2/H_2O} = 1.23$V vs NHE at pH 0) for O_2 evolution from water to occur, as shown in Fig. 3c. Figure 4 lists the band edge positions for

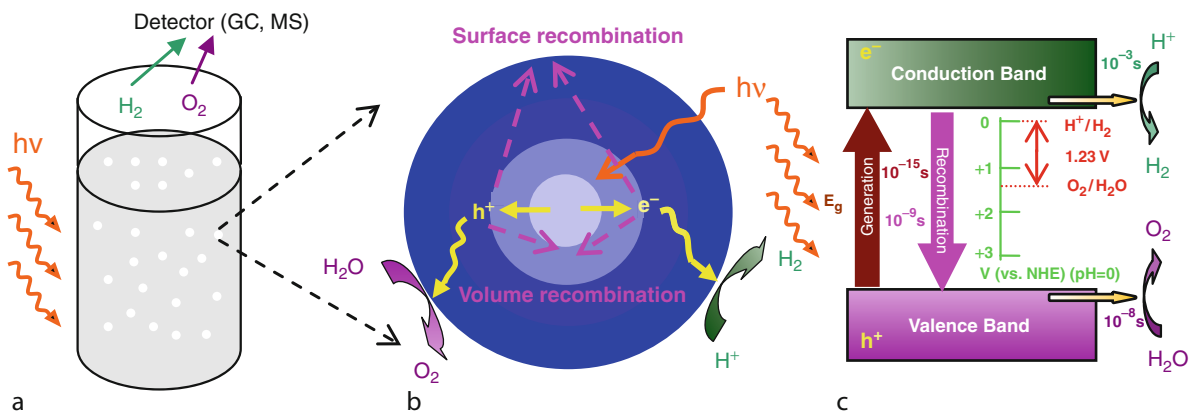

Photo-catalytic Hydrogen Production. Figure 3

(**a**) A suspension of photocatalyst powders in water under irradiation. (**b**) The processes involved in water splitting by a photocatalyst particle are photon absorption, electron–hole generation (and recombination), charge transport, and oxidation/reduction reactions on the semiconductor surface. (**c**) The principle and energy diagram for photocatalytic water splitting on a semiconductor (Reprinted from [1], Copyright (2009), with permission from Elsevier)

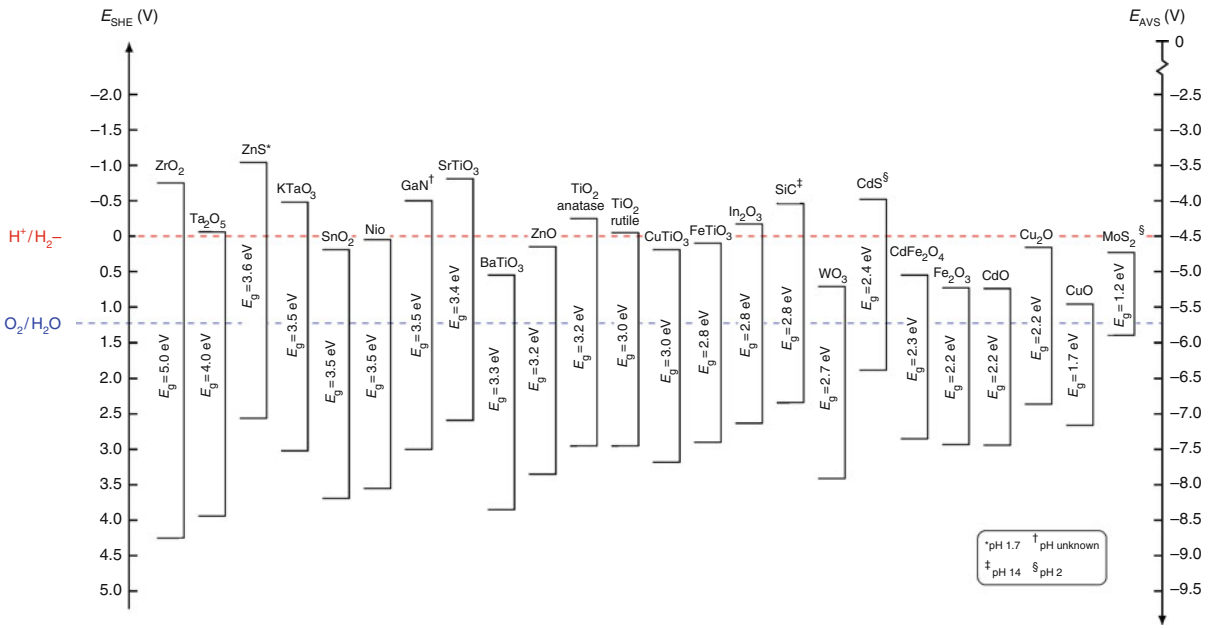

Photo-catalytic Hydrogen Production. Figure 4
Valence and conduction band edge positions of various semiconductors with respect to the standard hydrogen electrode (*SHE*) scale and the vacuum reference energy scale E_{AVS}. All values were reported being tested at pH 1, unless otherwise noted

commonly used semiconductors. It can be seen that there are not many semiconductors meeting the requirements of band gap and band levels for ideal photocatalysts for water splitting. Besides thermodynamic requirements, an ideal photocatalyst should also have kinetic advantages, e.g., high photocatalytic activity for H_2 and O_2 production. There are a few non-oxide semiconductors that meet requirements mentioned above. However, they are unstable and/or easily corroded (e.g., CdS). It has proven difficult to find a simple and cost-effective photocatalyst meeting all the requirements [1].

Evaluation of Photocatalytic H_2 Production

There is no perfect standard for comparing H_2 productivity of different photocatalysts in different photocatalytic systems. Therefore, researchers normally compare their homemade photocatalysts in their setups with some references, e.g., commercial TiO_2 photocatalysts, which are well known for their high activity, like P25 (a product of Evonik Degussa GmbH), Hombikat UV-100 (a product of Sachtleben Chemie GmbH), and ST-01 (a product of Ishihara Sangyo Kaisha, Ltd.). However, there are some terms that are commonly used to describe photocatalytic activity, and these are discussed below.

Turnover Quantities

The quantitative measurements of photocatalytic activity of a solid photocatalyst are normally derived from process kinetics to express a rate referenced to the number of photocatalytic sites to infer how many times a catalytic cycle turnovers. Traditionally, these parameters are the turnover number (TON), turnover rate (TOR), and turnover frequency (TOF). In H_2 production, turnover rate (TOR) is considered as the number of H_2 molecules produced per active site per unit time (units: molecules site^{-1} time^{-1}) (Eq. 5); turnover frequency (TOF) as the number of H_2 molecules produced per unit time (units: molecules time^{-1}) (Eq. 6); and turnover number (TON) as a quantity that describes how many times a H_2 evolution reaction or process turnovers at active sites integrated over time (units: molecules site^{-1}) (Eq. 7).

$$\mathrm{TOR} = \frac{\text{Number of } H_2 \text{ molecules produced}}{\text{Number of activesites} \cdot \text{Reaction time}} \quad (5)$$

$$\mathrm{TOF} = \frac{\text{Number of } H_2 \text{ molecules produced}}{\text{Reaction time}} \quad (6)$$

$$\mathrm{TON} = \frac{\text{Number of } H_2 \text{ molecules produced}}{\text{Number of activesites}} \quad (7)$$

Using these turnover quantities, it can be judged whether a given process is truly photocatalytic, as TON of a real photocatalytic reaction is much higher than 1. In addition, these turnover quantities are also supposed to be useful in assessing new materials as photocatalysts, and reproducible or comparable across various laboratories. Normally, it is difficult to determine the number of active sites for a photocatalyst, and the active sites and non-active sites can switch during photocatalytic process. Therefore, the number of atoms in a photocatalyst or on the surface of a photocatalyst, instead of the number of active sites, is often employed in Eqs. 5 and 7. However, the irradiated surface area is not equal to the total surface area of the photocatalyst, and the active sites can only lie in the irradiated surface area. Thus, the practical determination of turnover quantities remains very complex, and cannot be accurate.

Quantum Yield and Photonic Efficiency

Quantum yield (Φ) is defined as the number of defined events that occur per photon absorbed by the system, or as the amount (mol) of reactant consumed or product (H_2) formed per amount of photons (mol or Einstein) absorbed (Eq. 8). The definition of quantum yield makes it difficult to describe photocatalytic efficiency in real heterogeneous media, particularly for complex reactor geometries. In suspension systems, the sum of reflection, scattering, and transmission should be measured precisely, in order to determine the amount of photons absorbed by the photocatalyst.

$$\Phi = \frac{\text{Number of } H_2 \text{ molecules produced}}{\text{Number of photons absorbed by photocatalyst}} \quad (8)$$

A simple alternative method of comparing process efficiencies for equal absorption of photons has been proposed by N. Serpone for heterogeneous photocatalysis: (relative) photonic efficiency [38]. Photonic efficiency (ξ) describes the number (or mols) of reactant molecules transformed or product (H_2) molecules formed divided by the number or Einsteins of photons at a given wavelength incident on the reactor cell (Eq. 9). Alternatively, the photonic efficiency can also be described by the ratio of the initial rate of the event to the rate of incident photons reaching the reactor as obtained by actinometry (Eq. 10).

$$\xi = \frac{\text{Number of } H_2 \text{ molecules produced}}{\text{Number of incident photons on reactor}} \quad (9)$$

$$\xi = \frac{\text{The rate of } H_2 \text{ production}}{\text{The rate of photons impinging on reactor}} \quad (10)$$

To avoid unnecessary errors and the effects from reactor geometry and light source, together with the properties (e.g., size, surface area) of the photocatalyst material used, another kind of efficiency has been defined so that it could be used to compare experiments within the same laboratory or even with other laboratories, and it would be reactor independent: the relative photonic efficiency (ξr). It is related to an acceptable standard process, a standard photocatalyst material, or a standard "secondary actinometer" in photocatalytic processes (Eq. 11). For example, the determination of the total incident photon in the wavelength regions by chemical actinometry ferrioxalate has been performed in the same reactor, in order to avoid the corrections for any influence of light reflection, beam position, and reactor geometry. In the experimental description of a relative photonic efficiency, reactor geometry, light source, and photocatalyst properties should be constant in assessing ξr. To be really useful and comparable, ξr values should not depend on light irradiance and reactor geometry, or even on other parameters such as pH, photocatalyst loading, substrate concentration, and temperature [38], which is not easy in practice.

$$\xi r = \frac{\text{The rate of } H_2 \text{ production}}{\text{The rate of standard process under identical conditions}} \quad (11)$$

Experimental Setup for Photocatalytic H_2 Production

There are several kinds of setups for photocatalytic H_2 production and/or water splitting. Generally speaking,

these setups consist of four parts. The first part is a light source. A high-pressure mercury lamp is often used with quartz apparatuses for broad band gap semiconductors, since UV-light irradiation is needed. A xenon lamp is used for visible-light irradiation, when a cut-off filter is employed to avoid infrared heating. A solar simulator (AM1.5) with its radiance of 100 mW·cm^{-2} is ideal for solar hydrogen production study. Alternatively, a xenon lamp and several filters can be assembled for a solar simulator. In this case, the emission spectrum should be measured to make sure of its identity to solar spectrum, and the intensity should be calibrated by a thermopile or Si photodiode. The second part is a reaction cell. There are different shapes and sizes of reactors for photocatalytic H_2 production and/or water splitting. They should be transparent enough for light irradiation, and they are connected to the third part, a gas line. Vacuum pump, pressure gauge, and carrier gas are normally connected to the gas line. The last part is gas detection and/or collection part, which draws in the produced gases (H_2 and O_2) from gas line. Gas chromatography and mass spectrometry are employed for microanalysis, while volumetric measurement is suitable for a large amount of gas evolution. The whole system (including reactor, gas line, gas detector, and collector) should stay gas tight during operation.

Photocatalysts for H_2 Production

Most photocatalysts are composed of both metal and nonmetal ions. Metal cations show their highest oxidative states with d^0 (red area in Fig. 5) or d^{10} (green area) electronic configuration, while O, S, and N (blue area) exist as their most negative states. The conduction band bottom consists of the d and sp orbitals of the metal cations, while the valence band top in metal oxides is composed of O 2p orbitals, which is normally located at ca. +3 V (vs SHE) or higher. The valence bands of metal oxysulfides and oxynitrides are formed by S 3p and O 2p, and N 2p and O 2p, respectively. In some compounds, alkali (Li, Na, K, Rb, and Cs), alkaline earth (Mg, Ca, Sr, and Ba), and transition metal (Y, La, and Gd) ions can constitute the crystal structures of these compounds, rather than make any contribution to the energy structures. In this section, the commonly used materials for photocatalytic H_2 production will be introduced.

TiO_2 has been one of the most important photocatalysts for H_2 production, due to its availability, low price, nontoxicity, high photoactivity, and stability. The biggest disadvantage of TiO_2 is the low utilization of visible light, as a consequence of its wide band gaps, which are 3.2 eV (corresponding to an absorption edge of 380 nm) and 3.0 eV (400 nm) for

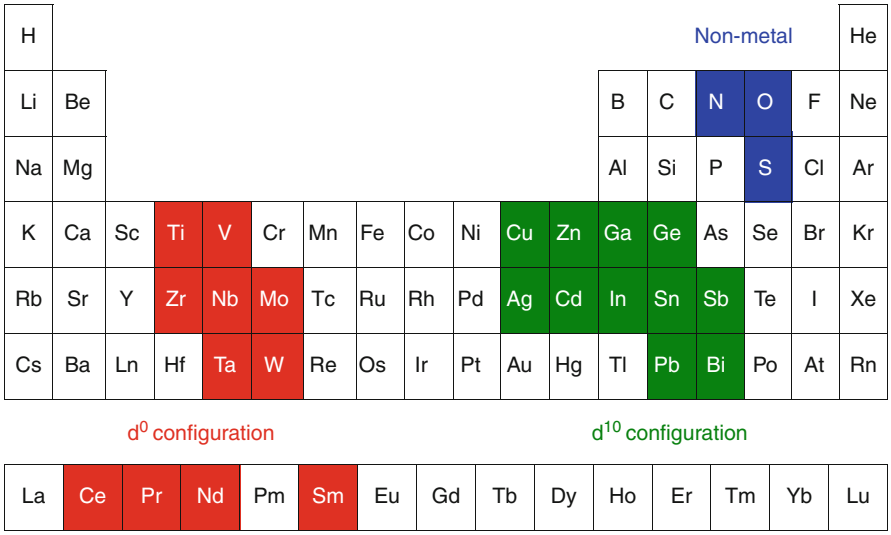

Photo-catalytic Hydrogen Production. Figure 5
Elements constructing photocatalysts (Reprinted from [1], Copyright (2009). With permission from Elsevier)

anatase and rutile, respectively. At any rate, TiO_2 is a good reference and starting material for research. ZnO has the similar advantages (including availability, low price, nontoxicity, high photoactivity, and enough potential for both H_2 and O_2 evolution) with TiO_2 and single-crystalline ZnO even has fast electron mobility. However, it is unstable in strong acids (Eq. 12) and alkalis (Eq. 13), and after long-time irradiation, ZnO suffers from photo-corrosion, due to the oxidation of O^{2-} in ZnO by photogenerated holes (Eq. 14). WO_3 has a relatively narrow band gap of 2.7 eV, but enables it to utilize part of the visible light. WO_3 is a successful photocatalyst for O_2 evolution from water, while its conduction band is not negative enough to reduce H^+ to H_2. In practice, WO_3 is applied to water splitting by coupling to another semiconductor or by doping. α-Fe_2O_3 has several advantages of narrow band gap of 2.2 eV, good photo stability, chemical inertness, and low cost. However, it has the same problem as WO_3 with respect to its positive conduction band level. Furthermore, it suffers from fast e^--h^+ recombination and poor charge transportation.

$$ZnO + 2H^+{}_{(aq)} \rightarrow Zn^{2+}{}_{(aq)} + H_2O \quad (12)$$

$$ZnO + H_2O \rightarrow Zn(OH)_2 \quad (13)$$

$$2ZnO + 4h_{VB}{}^+ \rightarrow 2Zn^{2+}{}_{(aq)} + O_{2(g)} \quad (14)$$

When TiO_2 is fused with other metal oxides (SrO, BaO, Ln_2O_3 (Ln = lanthanide)), metal titanates with perovskite structure are formed. Perovskites have the general formula ABX_3, and several hundred oxides own this structure. Among them, $SrTiO_3$ and $BaTiO_3$ both with a band gap of 3.3 eV have been widely studied as semiconductors for photocatalytic water splitting. Alkaline metal hexatitanates ($M_2Ti_6O_{13}$; M = Na, K, Rb) are normally used in powder form in suspensions, together with a cocatalyst. There are more complex perovskites containing two different cations, and many of these have a layered structure. Two main classes of such oxides, which have been studied in water splitting, are the Dion–Jacobson series ($AM_{n-1}B_nO_{3n+1}$, e.g., $KCa_2Ti_3O_{10}$), and the Ruddlesden–Popper series ($A_2M_{n-1}B_nO_{3n+1}$, e.g., $K_2La_2Ti_3O_{10}$). Another type of layered perovskites has the generic composition $A_nB_nO_{3n+2}$ (n = 4, 5; A = Ca, Sr, La; B = Nb, Ti). Among them, $La_2Ti_2O_7$ (i.e., $La_4Ti_4O_{14}$) and $La_4CaTi_5O_{17}$ are representative titanates. The band gaps of $La_2Ti_2O_7$ and $La_4CaTi_5O_{17}$ are 3.2 and 3.8 eV, and when loaded with nickel they showed a quantum yield of 12% (<360 nm) and 20% (<320 nm) for water splitting, respectively [39].

Tantalates and niobate oxides with corner-sharing octahedral MO_6 (M = Ta, Nb) structures have shown high photocatalytic activity for the cleavage of water, since the photogenerated electron–hole pairs can easily migrate and separate through the corner-shared MO_6 units. Tantalates, $MTaO_3$ (M = Li, Na, K) were reported as effective photocatalysts for water splitting under UV irradiation. These oxides own perovskite structure, and their band gaps are 4.7 eV (Li), 4.0 eV (Na), and 3.7 eV (K), respectively [40]. Some layered oxides (e.g., $K_4Nb_6O_{17}$) have two kinds of interlayers, which exist alternately. H_2 is evolved from one interlayer, where cocatalysts are selectively introduced. In $K_4Nb_6O_{17}$ case, H_2 and O_2 evolutions are separated by the photocatalytic niobate sheet, which will be described later.

Generally speaking, oxides containing d^0 transition metal cations, like Ti^{4+}, Nb^{5+}, or Ta^{5+}, have wide band gaps (>3.0 eV). Thus, these materials can only be excited under UV irradiation. Interestingly, $K_4Ce_2M_{10}O_{30}$ (M = Ta, Nb) and their solid solutions $K_4Ce_2Ta_{10-x}Nb_xO_{30}$ (x = 0–10) were found to have band gaps of ca. 1.8–2.3 eV (corresponding to absorption edges of 540–690 nm), and they performed well under visible-light irradiation. This may be ascribed to the hybrid construction of their valence bands [41].

Many metal sulfide photocatalysts are active under visible-light irradiation. The valence bands of metal sulfides consist of S 3p orbitals, which make the valence band potential more negative and thus narrows the band gap, compared to the valence bands composed of O 2p orbitals in corresponding metal oxides. CdS with wurtzite structure is the most studied metal sulfide photocatalyst. It has a narrow band gap (2.4 eV), which makes it absorb visible-light below a wavelength of 510 nm. Although the valence and conduction bands of CdS are perfectly suitable for O_2 and H_2 evolution, CdS is apt to be photo-corroded (Eq. 15), which is common for most metal sulfides. In order to avoid photo-corrosion, scavengers (electron donors, such as cysteines, EDTA, sulfide, or sulfite species) are often

used to consume photogenerated holes during the photocatalytic water splitting by CdS.

$$2h_{VB}{}^{+} + CdS = Cd^{2+}{}_{(aq)} + S_{(s)} \quad (15)$$

Enlightened by the N doping effect, Ta_3N_5 was prepared by nitriding Ta_2O_5 in an NH_3 atmosphere. Reasonably, the band gap shrinks from ~4.0 eV for Ta_2O_5 to ~2.1 eV for Ta_3N_5. The narrower band gap results from a higher-lying valence band derived from N 2p orbitals in Ta_3N_5 other than O 2p orbitals in Ta_2O_5. This material photocatalytically produced H_2 and O_2 under visible irradiation (<600 nm) [42]. Nitrides with d^{10} electronic configuration, such as Ge_3N_4 and GaN, also performed the cleavage of water under UV-light irradiation. In these d^{10} electronic configuration nitrides, the conduction band formed by broad hybridized sp orbitals makes it easy to transfer the photogenerated electrons to cocatalysts, e.g., RuO_2 [27, 43].

Oxynitrides and oxysulfides were recently designed to split water under visible-light irradiation. For oxynitrides and oxysulfides with d^0 electronic configuration metal ions, such as TaON and $Sm_2Ti_2S_2O_5$, the valence band mainly consists of hybridized N 2p (or S 3p) and O 2p orbitals, while the conduction band is still composed of the empty d orbitals of the corresponding metal. In such compounds, photogenerated holes can move smoothly in the broad valence band, which benefits to the oxidation of water. Oxynitride photocatalysts consisting of d^0 configuration metal cations such as Ti^{4+}, Nb^{5+}, and Ta^{5+} are active for H_2 or O_2 evolution in the presence of sacrificial reagents. TaON prepared by partial nitridation of Ta_2O_5 showed high activity under visible-light irradiation (420 nm $\leq \lambda \leq$ 500 nm). The band gap of TaON was estimated to be 2.5 eV. Photocatalytic H_2 production by TaON was performed in an aqueous methanol solution and with a Ru cocatalyst [28, 30]. As mentioned above, compared to photocatalysts containing d^0 metal ions, the photocatalysts composed of d^{10} metal ions (such as Ge and Ga) have the conduction band bottom made up of hybridized sp orbitals of d^{10} metal ions. These hybridized sp orbitals increase the mobility of photogenerated electrons in the conduction band and high photocatalytic activity for reduction of water. The solid solutions $(Ga_{1-x}Zn_x)(N_{1-x}O_x)$ [34] and $(Zn_{1+x}Ge)(N_2O_x)$ [35] are two examples of these d^{10} metal oxynitrides.

P-type III–V semiconductors have several attractive features, such as a high charge carrier mobility, an ideal band gap, and high photoelectrochemical stability, which make them suitable photocatalytic materials for reducing water to H_2. P-InP photocathodes are capable of producing H_2 from HCl or $HClO_4$ electrolytes with high efficiency [44]. Photocathodes of p-$GaInP_2$ (a solid solution of GaP and InP) have also evolved H_2 efficiently by using a GaAs p-n junction bias [45].

Development and Modification of H_2 Production Photocatalysts

Whether photocatalytic H_2 production can have practical application depends largely on the development of photocatalytic materials. That is why material research is the focus of this topic. Both the development of existing photocatalysts and the exploitation of new photocatalysts are necessary. The progress of related fields in materials science, chemistry, and physics also add new vigor to the field of photocatalytic H_2 production.

Nanosize Effect

With the development of advanced fabrication and characterization, nanosized photocatalysts have become the main object of material study. When a photocatalyst becomes smaller, it has a larger surface area, which provides more active sites for reactant adsorption and decomposition, and light harvest. In photocatalysts, photogenerated electrons and holes transfer to the surface to have effect. Small particles provide a short distance for the charge carrier transfer, largely avoiding the bulk recombination. When a particle is smaller than some critical size (normally in the nanosize range), the energy levels within the filled (valence band) and empty (conduction band) states become discrete, and simultaneously the band gap increases, compared to its bulk counterpart. This leads to a blue shift in the absorption spectra for nanosized particles. Different materials have different critical sizes. With the broadening of the band gap, electrons at the bottom edge of the conduction band and holes at the top edge of the valence band acquire more negative and positive potentials, respectively, which means that they have stronger redox powers in such nanoparticles.

Porous Structures

Porous materials have high surface area and good adsorption ability, and can concentrate reactants around active sites. Selective photocatalysis can be achieved by adjusting the pore size. Recently, advanced fabrication techniques have been developed to prepare porous photocatalysts with high surface area and suitable pore size. It has been reported that hydrothermally synthesized TiO_2 nanoparticles without calcination had a large specific surface area (438 m^2/g) and small crystallites (2.3 nm) dispersed among amorphous mesoporous domains, and exhibited much better photocatalytic activity for H_2 production compared with samples calcined at various temperatures, and also the commercial photocatalyst P25 [46].

A novel synthesis was carried out by using KCl electrolyte to control the electrostatic repulsive force between TiO_2 nanoparticles toward the formation of a mesoporous structure, which showed the highest photocatalytic activity for H_2 production, compared to nonporous colloidal TiO_2, and commercial Degussa P25 and Hombikat UV-100 (HBK) samples [47]. Cocatalysts can also be easily deposited and dispersed onto these porous photocatalysts. The photocatalytic reduction of metal cations (M = Ni^{2+}, Co^{2+}, Cu^{2+}, Cd^{2+}, Zn^{2+}, Fe^{2+}, Ag^{+}, Pb^{2+}) on the surface of mesoporous TiO_2 (specific surface area 130–140 m^2/g, pore diameter 5–9 nm, and anatase content 70–90%) resulted in the formation of nanostructured metal–semiconductor composites (TiO_2/M). These metal–TiO_2 nanostructures showed a remarkable photocatalytic activity for hydrogen production from water–alcohol solutions, and the efficiency was 50–60% greater than that of the metal-containing nanocomposites based on Degussa P25. The anatase content and pore size proved to be the main parameters determining the photoreaction rate [48].

Porous materials are often used as supports for catalysts and photocatalysts. Highly dispersed and coordinated metal species on microporous zeolite and mesoporous silica materials have shown very high photocatalytic activity, and were referred to as "single-site photocatalysts." Photocatalytic H_2 production by CdS has been improved by its porous supports, such as aluminum-substituted mesoporous silica molecular sieve (Al-HMS) [49], microporous and mesoporous silicas [50], porous polyethylene terephthalate fibers (PET) [51], and ETS-4 zeolite [52].

Low-Dimensional Nanostructure

One-dimensional (1D) nanostructures (nanowires, nanorods, nanotubes, and nanofibers) have shown their outstanding properties in photocatalytic H_2 production. Compared to aspheric nanoparticles with the same volume or weight, 1D nanomaterials have higher surface areas. They can normally provide fast charge transportation, especially for those single-crystalline 1D nanostructures. Anders et al. found that photoelectrodes with nanorods oriented perpendicular to the conductive substrate can shorten the transport distance for electrons to the back contact (electron collector) and avoid recombination losses at grain boundaries between nanoparticles, compared to photoelectrodes with nanoparticle deposits [53]. Disorder, order, and different orientations of the 1D units also affect the photoelectrochemical properties. In the same research [53], the reported photon-to-current efficiency is lower for the Fe_2O_3 electrode with the nanorods parallel to the substrate, compared to nanorods perpendicular to the substrate. The electrons have a more straightforward pathway to the back contact with nanorods perpendicular to the substrate, which leads to the elimination of recombination losses at nanorod boundaries and higher incident photon-to-electron conversion efficiency (IPCE) values.

As mentioned above in the section Photocatalysts for H_2 Production, the poor charge transportation (mainly due to low mobility of holes) of α-Fe_2O_3 largely limits its application in photoelectrochemical and photocatalytic H_2 production. One way to solve this problem is to use 1D α-Fe_2O_3 with high aspect ratios. It was demonstrated that the transportation distance for photogenerated holes to the α-Fe_2O_3/solution interface was largely shortened in α-Fe_2O_3 nanowires [54]. The limitation from hole transportation can be reasonably overcome, if the α-Fe_2O_3 nanowire radius is shorter than the hole diffusion length. 1D nanostructured photocatalysts, e.g., TiO_2 nanotubes [55–58], nanocolumns [59], nanowires [60] and nanofibers [61], and CdS nanorods [62] and

nanowires [63], have been playing a very important role in photocatalytic H_2 production.

Two-dimensional (2D) structured materials (nanosheets, nanoscrolls, and nanolayers) have attracted special interest in catalysis and photocatalysis. They can have a high surface area, expose a certain facet with high photocatalytic activity, and provide fast charge transfer. Pt/TiO_2 nanosheets with exposed (001) facets showed high photocatalytic activity for H_2 production [64]. High surface energy of (001) facets is effective for dissociative adsorption of reactant molecules, and water molecules can chemically dissociate on the (001) surface. So the authors believed that the exposed (001) facets contributed to the high photocatalytic activity in H_2 production [64], which had been also suggested by Amano [65] and Lu et al. [66].

The following example shows the fast charge transfer of nanosheets and nanoscrolls. In a dye-sensitized semiconductor photocatalytic H_2 production system, the semiconductor transfers electrons from the photoexited dye to the hydrogen evolution catalyst (typically Pt or Rh). Niobate nanoscrolls and nanosheets acted as good electron transfer mediators between a phosphonated $[Ru(bpy)_3]^{2+}$ derivative and Pt, as shown in Fig. 6. An external quantum yield (incident photo-to-current yield) of 20–25% was observed for hydrogen evolution in this system [67].

Layered structures have been widely used in photocatalytic H_2 production. $K_4Nb_6O_{17}$ has a structure with two types of interlayers. H_2 is produced from one interlayer, in which cocatalysts are introduced by ion exchange or interlayer reaction, while O_2 is evolved in the other interlayer, as shown in Fig. 7. In this way, the sites for H_2 and O_2 evolution are separated by the photocatalytic niobate sheet [68].

Dye-Sensitized Semiconductor

Some wide band semiconductors (such as TiO_2, $SrTiO_3$, and ZnO) show very high photocatalytic activity in H_2 production under UV illumination, but cannot absorb visible light, which limits their application in solar energy conversion. One way to extend their light response to visible range is to use a dye, which can absorb visible light. This system is called a dye-sensitized semiconductor system. In this system, the dye absorbs the visible light, becomes excited, and its excited state injects electrons into the semiconductor conduction band, on which H_2 is produced usually in the presence of a metal cocatalyst. In order to regenerate dyes, electron donors, such as I_3^-/I^- pair and EDTA, are added into the solution to supply the dyes with electrons and sustain the reaction cycle. The excitation, electron injection, and dye regeneration can be expressed as in the following Eqs. 15–17. The steps

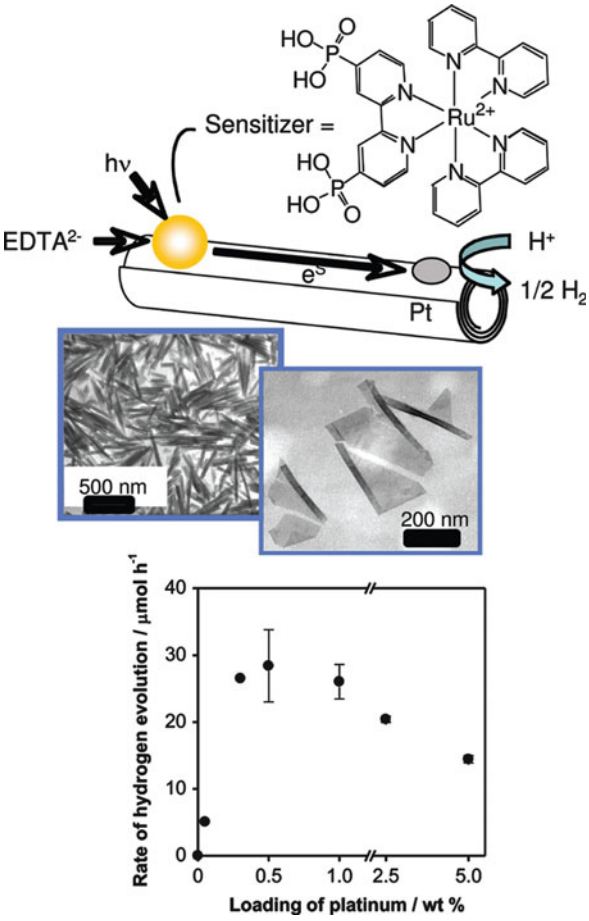

Photo-catalytic Hydrogen Production. Figure 6 (*Top*) Schematic representation of photoinduced electron transfer from a phosphonated $[Ru(bpy)_3]^{2+}$ sensitizer to Pt catalyst particles, mediated by $H_4Nb_6O_{17}$ nanoscrolls. (*Center*) TEM images of individual nanosheets (*right*) and of nanoscrolls precipitated from a suspension of exfoliated $H_4Nb_6O_{17}$ (*left*). (*Bottom*) The dependence of hydrogen evolution rate on Pt loading (Reprinted with permission from [67]. Copyright 2009 American Chemical Society)

involved are illustrated in Fig. 8. Porphyrins, $[Ru(bipy)_3]^{2+}$, $[Fe(CN)_6]^{4-}$, carboxylic (c-RuL_3) compounds, phosphonic (p-RuL_3) compounds, diamine and dithiolate complexes of Pt^{IV}, eosin, Cu phthalocyanine, and dipyridyl complexes of Ru, and complex of Zn with cytochrome C are commonly used as dye sensitizers. It is not easy to find a stable dye without any degradation by sensitized photocatalyst after long time irradiation. The dye should also have a strong absorption in visible light and a suitable energy level of its excited state (more negative than the conduction band of the sensitized semiconductor).

$$\text{dye} + h\nu \rightarrow \text{dye}* \tag{15}$$

$$\text{dye}* + \text{semiconductor} \rightarrow \text{dye}^+ + e_{cb}^- \tag{16}$$

$$\text{dye}^+ + D \rightarrow \text{dye} + D^+ \tag{17}$$

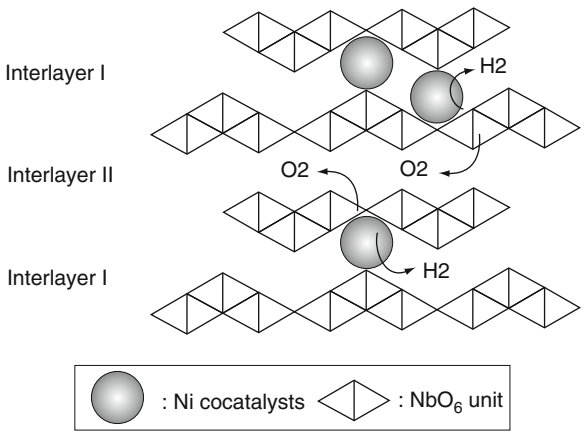

Photo-catalytic Hydrogen Production. Figure 7
Water splitting over $K_4Nb_6O_{17}$ photocatalyst with layered structure (From [68]. Reproduced by permission of The Royal Society of Chemistry)

Cocatalyst Deposited Semiconductor

Cocatalysts, typically noble metal nanoparticles, are normally needed in photocatalytic systems for H_2 production. Apart from noble metals, cocatalyst chemistries also include RuO_2, Ni and its oxide, the mixed oxides of Rh and Cr, tungsten carbide, MoS_2, and so on. The promoting mechanism by cocatalysts is illustrated in Fig. 1. When a semiconductor is excited by light irradiation with enough energy, photogenerated electrons are transited from the valence band to the conduction band of the semiconductor, raising the Fermi level of the semiconductor. The Fermi level difference between the semiconductor and the deposited noble metal drives the photogenerated electrons to the noble metal, and this increases the Fermi level of the noble metal, which drives the electrons from the noble metal to an electron acceptor in the solution (H^+ for H_2 production). From this process, the cocatalyst improves photocatalytic H_2 production by acting as (1) an electron sink to separate electrons and holes, reducing their recombination, and (2) an electron

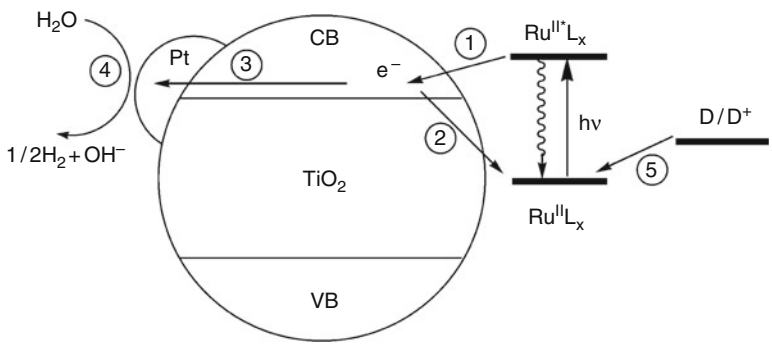

Photo-catalytic Hydrogen Production. Figure 8
Illustration of visible light–induced H_2 production on a ruthenium complex-sensitized TiO_2 particle in water. The number represents the major electron pathways: 1, electron injection from the excited sensitizer to CB; 2, back electron transfer to the oxidized sensitizer ($Ru^{III}L_x$); 3, electron migration and trapping in Pt deposits; 4, interfacial electron transfer to H_2O (or H^+) on Pt; 5, sensitizer regeneration by an electron donor (D) (Reproduced with permission from [69]. Copyright 2007 Society of Photo Optical Instrumentation Engineers)

transfer to shuttle photogenerated electrons from the semiconductor to an acceptor, reducing the activation energy for the reduction of water. Both the species and size of the noble metal affect the energetics and the electron transfer between the semiconductor and noble metal. From the practical viewpoint, it is economical to exploit and develop cheap noble metal species for deposition modification.

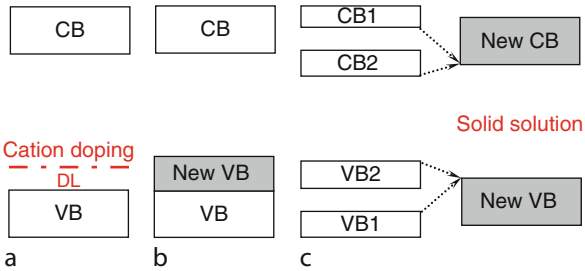

Photo-catalytic Hydrogen Production. Figure 9 Existing band engineering approaches: (**a**) cation doping, which creates a discrete impurity energy level (*DL*) within the forbidden band gap; (**b**) valence band modification, which forms a new valence band with higher top; and (**c**) solid solution formation, producing a new couple of valence and conduct bands, whose band gap is between those of the component semiconductors (Reprinted from [1], Copyright (2009). With permission from Elsevier)

Doped Semiconductor

Doping has been widely used to extend the optical response of wide band gap semiconductors to visible range. Transition metal doped TiO_2 was systemically investigated [70]. The photoreactivity of doped TiO_2 appears to be a complex function of the dopant concentration, the energy level of dopants within the TiO_2 lattice, their d electronic configuration, the distribution of dopants, the electron donor concentration, and the light intensity. It is important to tune the species, content, depth, and distribution of dopants inside the structure of host photocatalysts. Sometimes, cation-doping-induced visible-light absorption cannot become a substantial condition for photocatalytic activity in the visible range, since the absorption of doped semiconductors results from several absorption transitions of different origins. The doping of wide band gap semiconductors with transition metal ions creates discrete new energy levels within the forbidden band. Visible-light absorption and photoactivity are induced by the interband, as shown in Fig. 9a. This induced visible-light photoactivity is normally low, due to the limited amount of dopants that can be incorporated, as indicated by a small shoulder in the visible-light region, instead of a total red shift of the absorption edge. Increasing the dopant concentration in the semiconductor matrix can, to some extent, improve visible-light absorption, but excessive doping can easily disturb the original structure, or form separate impurity phases. Sometimes, doping can extend the lifetime of photogenerated charge carriers by transient and shallow charge carrier trapping. In most cases, dopants can also act as recombination centers for photogenerated electrons and holes and decrease photocatalytic activity.

Anion doping to improve photocatalytic H_2 production under visible-light irradiation is a quite new field, compared to transition metal cation doping. Although there has been some work on anion doping, the state of anion dopants, and the origin of visible-light absorption and photoactivity are still in the debate. Among all the anion dopants (N, F, C, S, and P), N-doped TiO_2 has been mostly investigated as a representative, since N has the similar atomic radius and chemical state with O, which makes it easy to substitute O in metal oxide lattice. N-doped TiO_2 and its visible-light response were first reported by Asahi et al. in 2001 [71], and this work has been followed by various theoretical and experimental studies. Asahi et al. suggested that the N 2p level (above the O 2p level in TiO_2) could mix with the valence band of TiO_2 composed of O 2p orbits, which forms a new valence band and narrows the band gap (Fig. 9b). The conduction band of N-doped TiO_2 remains unchanged and higher than the H_2 reduction potential, while the valence band is shifted up, but still enough for water oxidation. However, this mechanism was challenged by arguing that a low level of doping ($\leq$2 at.%) can only form midgap state above the valence band of TiO_2, like cation doping, and cannot shift up the valence band unless a high level of doping ($\geq$20%) is carried out. In practice, high-level doping may form oxynitrides (or oxysulfides) or even nitrides (or sulfides). It was also argued that the visible-light response is due to the

advent of color centers (e.g., F, F^+, F^{++}, and Ti^{3+}), and the formation of midgap energy level and oxygen vacancies induced by doping [72, 73].

Solid Solution Semiconductor (Semiconductor Alloy)

Another approach to adjust the band gap and band positions is to form a solid solution semiconductor (or a semiconductor alloy) between wide and narrow band gap semiconductors (Fig. 9c). If two (or more) semiconductors have similar crystal lattice structures, solid solution is likely formed by them. The band gap of solid solution can be tuned, to some extent, by varying the composition of the solid solution. The reported solid solutions include GaN-ZnO, ZnS-CdS, ZnS-$AgInS_2$, ZnS-$AgInS_2$-$CuInS_2$, CdS-CdSe, ZnO-$ZnGeN_2$, GaP-InP, and others. Interestingly, despite the large band gaps of pure GaN and ZnO (>3 eV), GaN-ZnO solid solutions have visible absorption with band gaps of 2.4–2.8 eV, and can decompose water under visible light. Density functional theory (DFT) calculations indicated that the conduction band bottom of GaN-ZnO was mainly composed of 4s and 4p orbitals of Ga, while the valence band top consisted of N 2p orbitals, followed by Zn 3d orbitals. The presence of Zn 3d and N 2p electrons in the upper valence band might provide p-d repulsion for extending the valence band, narrowing the band gap [34].

Semiconductor Composites

Photogenerated charge carrier recombination can be minimized by coupling two semiconductors, if their band positions are crossed, as illustrated in Fig. 10. Photogenerated holes tend to accumulate in the semiconductor with the less positive valence band (semiconductor 1 in Fig. 10), while photogenerated electrons are collected by the semiconductor with the less negative conduction band (semiconductor 2 in Fig. 10). This efficient charge separation largely enhances the photocatalytic efficiency. It is very useful to choose a narrow band gap semiconductor as one coupling semiconductor in order to utilize visible light. Semiconductors, such as CdS, PbS, Bi_2S_3, CdSe, InP, and n-Si, that can absorb visible light serve as inorganic sensitizers in semiconductor/semiconductor composites. Photocatalytic H_2 production by semiconductor composites can be successfully achieved if the following conditions are met: (1) the band levels of two semiconductors should be matched well, leading to wide charge carrier separation, (2) the less negative conduction band of the composite should still be more negative than the water reduction potential, and (3) there should be good contact between the two semiconductors, which ensures fast and efficient charge carrier injection between them.

Multiphotonic System (Z-Scheme) for H_2 Production

By mimicking the natural photosynthesis by green plants, a Z-scheme photocatalytic water splitting

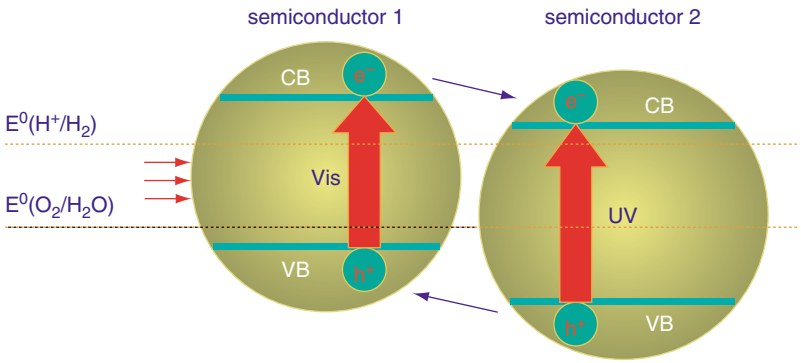

Photo-catalytic Hydrogen Production. Figure 10
Band structure of a composite photocatalyst with an enhanced visible-light response, prepared by a mixture of wide and narrow band gap photocatalysts (Reproduced with permission from [74]. Copyright 2009 Wiley-VCH Verlag GmbH & Co. KGaA)

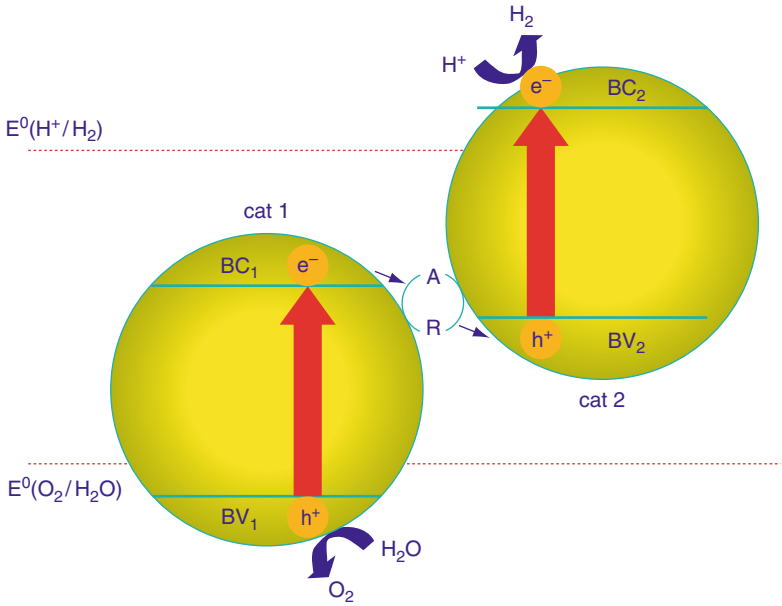

Photo-catalytic Hydrogen Production. Figure 11
Diagram of a dual photocatalyst system employing a redox shuttle (A/R) (Reproduced with permission from [74]. Copyright 2009 Wiley-VCH Verlag GmbH & Co. KGaA)

system was developed [36]. This system involved two-photon-excitation under visible light. The Z-scheme system consisted of a H_2-evolution photocatalyst (Cat 2 in Fig. 11), an O_2-evolution photocatalyst (Cat 1 in Fig. 11), and a reversible redox mediator (Ox/Red) that acted separately as the electron donor (R in Fig. 11) and acceptor (A in Fig. 11) for the respective half reactions. Protons are reduced to hydrogen molecules by the conduction band electrons of the photocatalyst with the more negative conduction band level, and R scavenges its valence band holes. Water is oxidized to oxygen by the photocatalyst with the more positive valence band level, and A reacts with its conduction band electrons. Photocatalysts, which only work in half reactions in water splitting, combine with each other to run the whole water splitting in this system. These photocatalysts are partly free of the strict energy limitations for the band structure of a single water splitting photocatalyst. They can have narrow band gaps with only one band (conduction or valence band) level enough for water reduction or oxidation. $SrTiO_3$, TaON, $CaTaO_2N$, and $BaTaO_2N$ can work as H_2 evolution photocatalysts, while WO_3, $BiVO_4$, and Bi_2MoO_6 can act as O_2 evolution photocatalysts. The IO_3^-/I^-, Fe^{3+}/Fe^{2+}, and Ce^{4+}/Ce^{3+}redox couples normally act as reversible electron shuttles. The key factors for designing a good Z-scheme system are to find a pair of photocatalysts for separate H_2 and O_2 production with high efficiency, and an efficient reversible electron mediator, the redox potential of which can meet the energy requirements of being electron donor and acceptor in the respective half reactions.

Dissolved Additives for H_2 Production Improvement

Photocatalytic H_2 or O_2 production is often carried out in the presence of electron donors including low aliphatic alcohols (methanol, ethanol, isopropanol), sulfides (H_2S, Na_2S), sulfites (Na_2SO_3), hydrazine, aliphatic amines (triethylamine, triethanolamine), carboxylic acids (formic acid, EDTA), carbohydrates and other organic compounds, or electron acceptors including persulfate, Ag^+, and Fe^{3+}. The mechanism of photocatalytic reaction using these sacrificial reagents is illustrated in Fig. 12.

Taking photocatalytic H_2 production for example, after the excitation of the photocatalyst by light with enough energy, the photogenerated electrons in the conduction band reduce absorbed water molecules

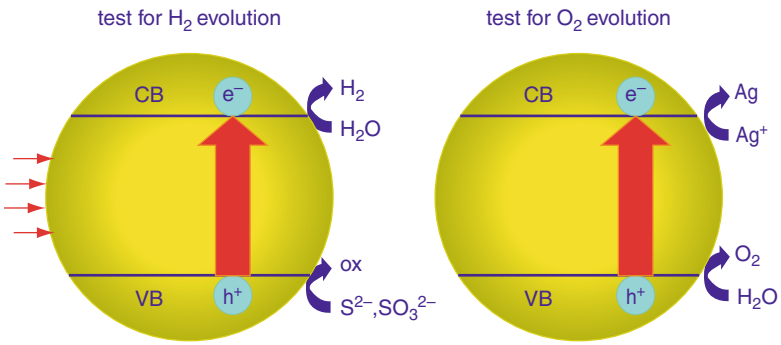

Photo-catalytic Hydrogen Production. Figure 12
Half reactions of water splitting for H_2 and O_2 evolution reactions in the presence of sacrificial reagents (Reproduced with permission from [74]. Copyright 2009 Wiley-VCH Verlag GmbH & Co. KGaA)

to H_2, while a hole in the valence band is filled with an electron from a sacrificial reagent (S^{2-}, SO_3^{2-} in Fig. 12). The thermodynamic requirement for the occurrence of such a process is the potential of the conduction band more negative than the water reduction potential, and the potential of the valence band more positive than the oxidation potential of the electron donor, rather than water. This requirement sometimes does not need strong oxidation ability of photocatalyst, depending on the reducing reagent used.

Although these half reactions are not overall water splitting reaction, they are very useful to test a given semiconductor's kinetic and thermodynamic performance for H_2 or O_2 evolution. Scavengers, e.g., S^{2-}/SO_3^{2-}, are commonly used when hydrogen production is performed by metal sulfides. When metal sulfides are used for photocatalytic hydrogen production, photo-corrosion occurs due to the S^{2-} in metal sulfides being oxidized by photogenerated holes in the valence band. As a sacrificial reagent, S^{2-} can easily react with two holes to form S. Then, the added SO_3^{2-} can dissolve S into $S_2O_3^{2-}$, preventing any detrimental deposition of S on CdS. Therefore, photo-corrosion of CdS is avoided. Interestingly, a process of simultaneous hydrogen production and H_2S removal was performed by a composite photocatalyst made of bulk CdS decorated with TiO_2 nanoparticles, i.e., CdS (bulk)/TiO_2, under visible light. Hydrogen originated from both H_2S and H_2O when H_2S was dissolved in alkaline water [75].

Since electron donors are sacrificially consumed during photocatalytic H_2 production, continuous addition of electron donors is normally necessary for sustaining H_2 production. The effect from different hydrocarbon electron donors was qualitatively investigated. It was found that the decomposition of these hydrocarbons could also contribute to a higher H_2 yield, since H_2 is one of their decomposition products [76]. The integration of clean H_2 fuel production and pollutant decomposition is promising and significant in practical application, since some pollutants (oxalic acid, formic acid, and formaldehyde) can act as electron donors [77].

Addition of carbonate salts was found to enhance H_2 and O_2 production stoichiometrically [78]. Several carbonate species were formed through the following reactions (Eqs. 18–21). Photogenerated holes were consumed by reacting with HCO_3^- to form carbonate radicals ($HCO_3\cdot$, $CO_3^-\cdot$) (Eqs. 19, 20), which is beneficial for photogenerated charge carrier separation. Peroxycarbonates ($C_2O_6^{2-}$) could be easily decomposed by holes into O_2 and CO_2 (Eq. 22). The evolution of CO_2 promoted the desorption of O_2 from the photocatalyst surface, and thus minimized the back reaction between H_2 and O_2. Then desorbed CO_2 could be dissolved and converted into HCO_3^- again.

$$CO_3^{2-} + H^+ \rightleftarrows HCO_3^- \quad (18)$$

$$HCO_3^- + h^+ \rightarrow HCO_3\cdot \quad (19)$$

$$HCO_3\cdot \rightleftarrows H^+ + CO_3^-\cdot \quad (20)$$

$$2CO_3^-\cdot \rightarrow C_2O_6^{2-} \quad (21)$$

$$C_2O_6^{2-} + 2h^+ \rightarrow O_2 + 2CO_2 \quad (22)$$

Addition of iodide was also found to promote hydrogen production [79]. Iodide anion (I^-) in a suspension can be adsorbed preferentially onto cocatalyst surface, forming an iodine layer. The iodine layer can suppress backward reaction between H_2 and O_2, which enhanced the production of hydrogen and oxygen significantly. However, adding too much carbonate salts or iodide anions could make these species excessively enriched on the photocatalyst surface, decreasing light harvesting.

Future Directions

Worldwide energy consumption and man-made global warming result from humans excessively using limited fossil fuel on the earth, so it is time for society to pursue sustainable, clean energy systems. It is likely that the topic of this entry (photocatalytic H_2 production) will contribute greatly to a sustainable, clean energy system, but with uncertain timing for deployment. Although the efficiency of photocatalytic H_2 production is lower than that of photoelectrochemical (PEC) water splitting, the former technology provides a simple and convenient manipulation platform and valuable information for the development of the latter. There are also other promising technologies for sustainable, clean energy systems, which should also be paid attention to, and can be studied together with photocatalytic and PEC water splitting. Photocatalytic fuel generation from CO_2 is one of them. It converts CO_2 and H_2O to chemical fuels (e.g., methanol) by using solar energy, which decreases global emission of CO_2 and keeps global neutral carbon cycle. It allows, to some extent, human beings to keep using fossil fuel. This technology has many similarities with photocatalytic H_2 production, e.g., water oxidation is also evolved in its process. The research outcomes from photocatalytic H_2 production may well be applicable to the rising technology of photocatalytic CO_2 fixation.

Although photocatalytic water splitting (H_2 production) has been studied for almost 40 years, a further understanding of this process has dropped behind the reported phenomena. Although this field has seen some achievements, the total solar-to-hydrogen conversion efficiency is still much lower (about 1%) than the expected (about 10%) for practical application. Fundamental research on scientific details is necessary. For instance, is the charge carrier recombination so fast that too few reductive and oxidative sites can be reached by water? Where are the surface-active sites? What is their nature? Does desorption of products mainly determine the low efficiency? Besides studying the mechanism, the criteria for evaluation of photocatalytic H_2 production should be established, which makes the comparison of results from different labs much easier. This kind of criteria has already been set up in the solar cell field. Material development can strongly promote the breakthroughs in this technology. Some traditional semiconductors (metal oxides, metal sulfides) should be modified, rather than discarded, since they have their potential advantages in practical application. Of course, the study of their modification is always important.

Simultaneously, there is an increasing opportunity to exploit novel photocatalysts for H_2 production with the accumulation of theoretical and experimental knowledge. The focus should still be on stable, low-cost photocatalysts that can be manufactured on a large scale. Since using sunlight for H_2 production is a trend or target, the sensitization of photocatalysts and multiphotonic systems are expected topics in this field. Nanoscience and nanotechnology will continue to play an important role in many aspects, including the preparation and characterization of photocatalysts, the modification of optical and electronic structures of photocatalysts, and the design for light harvesting and management. Nanoreactors and well-controlled model systems are expected to be very useful for better understanding of the basic physics and chemistry involved in photocatalytic H_2 production. Further down the road, there will be a significant engineering challenge to integrate individual components into a fully functional device, the scalability and sustainability of which should also be achieved.

Bibliography

Primary Literature

1. Zhu J, Zäch M (2009) Nanostructured materials for photocatalytic hydrogen production. Curr Opin Colloid Interface Sci 14:260–269
2. Kamat PV (2007) Meeting the clean energy demand: nanostructure architectures for solar energy conversion. J Phys Chem C 111:2834–2860

3. Fujishima A, Honda K (1972) Electrochemical photolysis of water at a semiconductor electrode. Nature 238:37–38
4. Domen K, Naito S, Onishi T, Tamaru T, Soma M (1982) Study of the photocatalytic decomposition of water vapor over a nickel (II) oxide-strontium titanate ($SrTiO_3$) catalyst. J Phys Chem 86:3657–3661
5. Domen K, Kudo A, Onishi T, Kosugi N, Kuroda H (1986) Photocatalytic decomposition of water into hydrogen and oxygen over nickel (II) oxide-strontium titanate ($SrTiO_3$) powder. 1. Structure of the catalysts. J Phys Chem 90:292–295
6. Matsumura M, Saho Y, Tsubomura H (1983) Photocatalytic hydrogen production from solutions of sulfite using platinized cadmium sulfide powder. J Phys Chem 87:3807–3808
7. Kakuta N, Park KH, Finlayson MF, Ueno A, Bard AJ, Campion A, Fox MA, Webber SE, White JM (1985) Photoassisted hydrogen production using visible light and coprecipitated ZnS·CdS without a noble metal. J Phys Chem 89:732–734
8. Reber JF, Rusek M (1986) Photochemical hydrogen production with platinized suspensions of cadmium sulfide and cadmium zinc sulfide modified by silver sulfide. J Phys Chem 90:824–834
9. Reber JF, Meier K (1984) Photochemical production of hydrogen with zinc sulfide suspensions. J Phys Chem 88:5903–5913
10. Kudo A, Tanaka A, Domen K, Maruya K, Aika K, Onishi T (1988) Photocatalytic decomposition of water over NiO–$K_4Nb_6O_{17}$ catalyst. J Catal 111:67–76
11. Kudo A, Sayama K, Tanaka A, Asakura K, Domen K, Maruya K, Onishi T (1989) Nickel-loaded $K_4Nb_6O_{17}$ photocatalyst in the decomposition of H_2O into H_2 and O_2: structure and reaction mechanism. J Catal 120:337–352
12. Domen K, Kudo A, Tanaka A, Onishi T (1990) Overall photodecomposition of water on a layered niobiate catalyst. Catal Today 8:77–84
13. Yoshimura J, Kudo A, Tanaka A, Domen K, Maruya K, Onishi T (1988) H_2 evolution caused by electron transfer between different semiconductors under visible light irradiation. Chem Phys Lett 147:401–404
14. Shibata M, Kudo A, Tanaka A, Domen K, Maruya K, Onishi T (1985) Photocatalytic activities of layered titanium compounds and their derivatives for H_2 evolution from aqueous methanol solution. Chem Lett 16:1017–1018
15. Kato H, Kudo A (1998) New tantalate photocatalysts for water decomposition into H_2 and O_2. Chem Phys Lett 295:487–492
16. Mitsui C, Nishiguchi H, Fukamachi K, Ishihara T, Takita Y (1999) Photocatalytic decomposition of pure water over NiO supported on KTa(M)O_3 (M = Ti^{4+}, Hf^{4+}, Zr^{4+}) perovskite oxide. Chem Lett 28:1327–1328
17. Ishihara T, Nishiguchi H, Fukamachi K, Takita Y (1999) Effects of acceptor doping to $KTaO_3$ on photocatalytic decomposition of pure H_2O. J Phys Chem B 103:1–3
18. Kato H, Kudo A (1999) Photocatalytic decomposition of pure water into H_2 and O_2 over $SrTa_2O_6$ prepared by a flux method. Chem Lett 28:1207–1208
19. Machida M, Yabunaka J, Kijima T (1999) Efficient photocatalytic decomposition of water with the novel layered tantalate $RbNdTa_2O_7$. Chem Commun 1999:1939–1940
20. Kudo A, Hijii S (1999) H_2 or O_2 evolution from aqueous solutions on layered oxide photocatalysts consisting of Bi^{3+} with 6 s^2 configuration and d^0 transition metal ions. Chem Lett 28:1103–1104
21. Kudo A, Kato H (1997) Photocatalytic activities of $Na_2W_4O_{13}$ with layered structure. Chem Lett 26:421–422
22. Sato J, Saito S, Nishiyama H, Inoue Y (2001) New photocatalyst group for water decomposition of RuO_2-loaded p-block metal (In, Sn, and Sb) oxides with d^{10} configuration. J Phys Chem B 105:6061–6063
23. Ikarashi K, Sato J, Kobayashi H, Saito S, Nishiyama H, Inoue Y (2002) Photocatalysis for water decomposition by RuO_2-dispersed $ZnGa_2O_4$ with d^{10} configuration. J Phys Chem B 106:9048–9053
24. Sato J, Saito S, Nishiyama H, Inoue Y (2003) Photocatalytic activity for water decomposition of indates with octahedrally coordinated d^{10} configuration. I. Influences of preparation conditions on activity. J Phys Chem B 107:7965–7969
25. Sato J, Kobayashi H, Inoue Y (2003) Photocatalytic activity for water decomposition of indates with octahedrally coordinated d^{10} configuration. II. Roles of geometric and electronic structures. J Phys Chem B 107:7970–7975
26. Sato J, Kobayashi H, Ikarashi K, Saito S, Nishiyama H, Inoue Y (2004) Photocatalytic activity for water decomposition of RuO_2-dispersed Zn_2GeO_4 with d^{10} configuration. J Phys Chem B 108:4369–4375
27. Sato J, Saito N, Yamada Y, Maeda K, Takata T, Kondo JN, Hara M, Kobayashi H, Domen K, Inoue Y (2005) RuO_2-loaded β-Ge_3N_4 as a non-oxide photocatalyst for overall water splitting. J Am Chem Soc 127:4150–4151
28. Hara M, Takata T, Kondo JN, Domen K (2004) Photocatalytic reduction of water by TaON under visible light irradiation. Catal Today 90:313–317
29. Yamasita D, Takata T, Hara M, Kondo JN, Domen K (2004) Recent progress of visible-light-driven heterogeneous photocatalysts for overall water splitting. Solid State Ionics 172:591–595
30. Kasahara A, Nukumizu K, Takata T, Kondo JN, Hara M, Kobayashi H, Domen K (2003) $LaTiO_2N$ as a visible-light ($\leq$600 nm)-driven photocatalyst (2). J Phys Chem B 107:791–797
31. Liu M, You W, Lei Z, Zhou G, Yang J, Wu G, Ma G, Luan G, Takata T, Hara M, Domen K, Li C (2004) Water reduction and oxidation on Pt–Ru/$Y_2Ta_2O_5N_2$ catalyst under visible light irradiation. Chem Commun 2004:2192–2193
32. Ishikawa A, Takata T, Kondo JN, Hara M, Kobayashi H, Domen K (2002) Oxysulfide $Sm_2Ti_2S_2O_5$ as a stable photocatalyst for water oxidation and reduction under visible light irradiation ($\lambda \leq 650$ nm). J Am Chem Soc 124:13547–13553
33. Ishikawa A, Takata T, Matsumura T, Kondo JN, Hara M, Kobayashi H, Domen K (2004) Oxysulfides $Ln_2Ti_2S_2O5$ as stable photocatalysts for water oxidation and reduction under visible-light irradiation. J Phys Chem B 108:2637–2642
34. Maeda K, Teramura K, Lu DL, Takata T, Saito N, Inoue Y, Domen K (2006) Photocatalyst releasing hydrogen from water-Enhancing catalytic performance holds promise for

hydrogen production by water splitting in sunlight. Nature 440:295
35. Lee Y, Terashima H, Shimodaira Y, Teramura K, Hara M, Kobayashi H, Domen K, Yashima M (2007) Zinc Germanium Oxynitride as a photocatalyst for overall water splitting under visible light. J Phys Chem C 111:1042–1048
36. Sayama K, Mukasa K, Abe R, Abe Y, Arakawa H (2002) A new photocatalytic water splitting system under visible light irradiation mimicking a Z-scheme mechanism in photosynthesis. J Photochem Photobiol A Chem 148:71–77
37. Tada H, Mitsui T, Kiyonaga T, Akita T, Tanaka K (2006) All-solid-state Z-scheme in CdS–Au–TiO2 three-component nanojunction system. Nat Mater 5:782–786
38. Parmon V, Emeline AV, Serpone N (2002) Glossary of terms in photocatalysis and radiocatalysis. Int J Photoenergy 4:91–131
39. Kim HG, Hwang DW, Kim J, Kim YG, Lee JS (1999) Highly donor-doped (110) layered perovskite materials as novel photocatalysts for overall water splitting. Chem Commun 1999:1077–1078
40. Kato H, Kudo A (2001) Water splitting into H_2 and O_2 on alkali tantalate photocatalysts $ATaO_3$ (A = Li, Na, and K). J Phys Chem B 105:4285–4292
41. Shangguan WF (2007) Hydrogen evolution from water splitting on nanocomposite photocatalysts. Sci Tech Adv Mater 8:76–81
42. Hitoki G, Ishikawa A, Takata T, Kondo JN, Hara M, Domen K (2002) Ta_3N_5 as a novel visible light-driven photocatalyst ($\lambda < 600$ nm). Chem Lett 31:736–737
43. Kida T, Minami Y, Guan G, Nagano M, Akiyama M, Yoshida A (2006) Photocatalytic activity of gallium nitride for producing hydrogen from water under light irradiation. J Mater Sci 41:3527–3534
44. Heller A (1984) Hydrogen-evolving solar cells. Science 223:1141–1148
45. Khaselev O, Turner JA (1998) A monolithic photovoltaic-photoelectrochemical device for hydrogen production via water splitting. Science 280:425–427
46. Yi H, Peng T, Ke D, Ke D, Zan L, Yan C (2008) Photocatalytic H_2 production from methanol aqueous solution over titania nanoparticles with mesostructures. Int J Hydrogen Energ 33:672–678
47. Lakshminarasimhan N, Bae E, Choi W (2007) Enhanced photocatalytic production of H_2 on mesoporous TiO2 prepared by template-free method: role of interparticle charge transfer. J Phys Chem C 111:15244–15250
48. Korzhak AV, Ermokhina NI, Stroyuk AL, Bukhtiyarov VK, Raevskaya AE, Litvin VI, Kuchmiy SY, Ilyin VG, Manorik PA (2008) Photocatalytic hydrogen evolution over mesoporous TiO2/metal nanocomposites. J Photochem Photobiol A Chem 198:126–134
49. Zhang YJ, Zhang L (2008) Synthesis of composite material CdS/Al-HMS and hydrogen production by photocatalytic pollutant degradation under visible light irradiation. J Inorg Mater 23:66–70
50. Ryu SY, Balcerski W, Lee TK, Hoffmann MR (2007) Photocatalytic production of hydrogen from water with visible light using hybrid catalysts of CdS attached to microporous and mesoporous silicas. J Phys Chem C 111:18195–18203
51. Lunawat PS, Senapati S, Kumar R, Gupta NM (2007) Visible light-induced splitting of water using CdS nanocrystallites immobilized over water-repellant polymeric surface. Int J Hydrogen Energ 32:2784–2790
52. Guan GQ, Kida T, Kusakabe K, Kimura K, Fang XM, Ma TL, Abe E, Yoshida A (2004) Photocatalytic H_2 evolution under visible light irradiation on CdS/ETS-4 composite. Chem Phys Lett 385:319–322
53. Beermann N, Vayssieres L, Lindquist S-E, Hagfeldt A (2000) Photoeletrochemical studies of oriented nanorod thin films of hematite. J Electrochem Soc 147:2456–2461
54. van de Krol R, Liang Y, Schoonman J (2008) Solar hydrogen production with nanostructured metal oxides. J Mater Chem 18:2311–2320
55. Lin CH, Lee CH, Chao JH, Kuo CY, Cheng YC, Huang WN, Chang HW, Huang YM, Shih MK (2004) Photocatalytic generation of H_2 gas from neat ethanol over Pt/TiO_2 nanotube catalysts. Catal Lett 98:61–66
56. Nam W, Han GY (2007) Preparation and characterization of anodized Pt-TiO_2 nanotube arrays for water splitting. J Chem Eng Jpn 40:266–269
57. Khan MA, Akhtar MS, Woo SI, Yang OB (2008) Enhanced photoresponse under visible light in Pt ionized TiO_2 nanotube for the photocatalytic splitting of water. Catal Commun 10:1–5
58. Kuo HL, Kuo CY, Liu CH, Chao JH, Lin CH (2007) A highly active bi-crystalline photocatalyst consisting of TiO_2 (B) nanotube and anatase particle for producing H_2 gas from neat ethanol. Catal Lett 113:7–12
59. Thimsen E, Rastgar N, Biswas P (2008) Nanostructured TiO_2 films with controlled morphology synthesized in a single step process: performance of dye-sensitized solar cells and photo watersplitting. J Phys Chem C 112:4134–4140
60. Jitputti J, Suzuki Y, Yoshikawa S (2008) Synthesis of TiO_2 nanowires and their photocatalytic activity for hydrogen evolution. Catal Commun 9:1265–1271
61. Lin CH, Chao JH, Liu CH, Chang JC, Wang FC (2008) Effect of calcination temperature on the structure of a Pt/TiO_2 (B) nanofiber and its photocatalytic activity in generating H_2. Langmuir 24:9907–9915
62. Janet CM, Viswanath RP (2006) Large scale synthesis of CdS nanorods and its utilization in photo-catalytic H_2 production. Nanotechnology 17:5271–5277
63. Jang JS, Joshi UA, Lee JS (2007) Solvothermal synthesis of CdS nanowires for photocatalytic hydrogen and electricity production. J Phys Chem C 111:13280–13287
64. Yu JG, Qi LF, Jaroniec M (2010) Hydrogen production by photocatalytic water splitting over Pt/TiO_2 nanosheets with exposed (001) facets. J Phys Chem C 114:13118–13125

65. Amano F, Prieto-Mahaney OO, Terada Y, Yasumoto T, Shibayama T, Ohtani B (2009) Decahedral single-crystalline particles of anatase titanium(IV) oxide with high photocatalytic activity. Chem Mater 21:2601–2603
66. Liu G, Yang HG, Wang XW, Cheng L, Lu H, Wang L, Lu GQ, Cheng HM (2009) Enhanced photoactivity of oxygen-deficient anatase TiO_2 sheets with dominant 001 facets. J Phys Chem C 113:21784–21788
67. Youngblood WJ, Lee SHA, Maeda K, Mallouk TE (2009) Visible light water splitting using dye-sensitized oxide semiconductors. Acc Chem Res 42:1966–1973
68. Kudo A, Miseki Y (2009) Heterogeneous photocatalyst materials for water splitting. Chem Soc Rev 38:253–278
69. Choi W (2007) Photocatalytic hydrogen production using surface modified titania nanoparticles. In: Guo J (ed) Solar hydrogen and nanotechnology II. Proc SPIE 6650:66500L
70. Choi W, Termin A, Hoffmann MR (1994) The role of metal-ion dopants in quantum-sized TiO_2: correlation between photoreactivity and charge-carrier recombination dynamics. J Phys Chem 98:13669–13679
71. Asahi R, Morikawa T, Ohwaki T, Aoki K, Taga Y (2001) Visible-light photocatalysis in nitrogen-doped titanium oxides. Science 293:269–271
72. Serpone N (2006) Is the band gap of pristine TiO_2 narrowed by anion- and cation-doping of titanium dioxide in second-generation photocatalysts? J Phys Chem B 110:24287–24293
73. Fujishima A, Zhang X, Tryk DA (2008) TiO_2 photocatalysis and related surface phenomena. Surf Sci Rep 63:515–582
74. Yerga RMN, Galván MCÁ, del Valle F, de la Mano JAV, Fierro JLG (2009) Water splitting on semiconductor catalysts under visible-light irradiation. ChemSusChem 2:471–485
75. Jang JS, Kim HG, Borse PH, Lee JS (2007) Simultaneous hydrogen production and decomposition of H_2S dissolved in alkaline water over CdS-TiO_2 composite photocatalysts under visible light irradiation. Int J Hydrogen Energ 32: 4786–4791
76. Nada AA, Barakat MH, Hamed HA, Mohamed NR, Veziroglu TN (2005) Studies on the photocatalytic hydrogen production using suspended modified TiO_2 photocatalysts. Int J Hydrogen Energ 30:687–691
77. Li YX, Lu GX, Li SB (2003) Photocatalytic production of hydrogen in single component and mixture systems of electron donors and monitoring adsorption of donors by in situ infrared spectroscopy. Chemosphere 52:843–850
78. Sayama K, Arakawa H (1992) Significant effect of carbonate addition on stoichiometric photodecomposition of liquid water into hydrogen and oxygen from platinum-titanium (IV) oxide suspension. J Chem Soc Chem Commun 2:150–152
79. Abe R, Sayama K, Arakawa H (2003) Significant effect of iodide addition on water splitting into H_2 and O_2 over Pt-loaded TiO_2 photocatalyst: suppression of backward reaction. Chem Phys Lett 371:360–364

Books and Reviews

Ashokkumar M (1998) An overview on semiconductor particle systems for photoproduction of hydrogen. Int J Hydrogen Energ 23:427–438

Best JP, Dunstan DE (2009) Nanotechnology for photolytic hydrogen production: colloidal anodic oxidation. Int J Hydrogen Energ 34:7562–7578

Fujishima A, Zhang X, Tryk DA (2007) Heterogeneous photocatalysis: from water photolysis to applications in environmental cleanup. Int J Hydrogen Energ 32: 2664–2672

Getoff N (1990) Photoelectrochemical and photocatalytic methods of hydrogen production: a short review. Int J Hydrogen Energ 15:407–417

Kaneko M, Okura I (2002) Photocatalysis: science and technology. Kodansha/Springer, Tokyo/Berlin

Kitano M, Hara M (2009) Heterogeneous photocatalytic cleavage of water. J Mater Chem 20:627–641

Kudo A (2007) Photocatalysis and solar hydrogen production. Pure Appl Chem 79:1917–1927

Kudo A (2007) Recent progress in the development of visible light-driven powdered photocatalysts for water splitting. Int J Hydrogen Energ 32:2673–2678

Kudo A, Kato H, Tsuji I (2007) Strategies for the development of visible-light-driven photocatalysts for water splitting. Chem Lett 33:1534–1539

Maeda K, Domen K (2007) New non-oxide photocatalysts designed for overall water splitting under visible light. J Phys Chem C 111:7851–7861

Moon SC, Matsumura Y, Kitano M, Matsuoka M, Anpo M (2003) Hydrogen production using semiconducting oxide photocatalysts. Res Chem Intermed 29:233–256

Navarro RM, Sánchez-Sánchez MC, Alvarez-Galvan MC, del Valle F, Fierro JLG (2009) Hydrogen production from renewable sources: biomass and photocatalytic opportunities. Energy Environ Sci 2:35–54

Osterloh FE (2008) Inorganic materials as catalysts for photochemical splitting of water. Chem Mater 20:35–54

Paleocrassas S (1974) Photocatalytic hydrogen production: a solar energy conversion alternative? Sol Energy 16:45–51

Rajeshwar K, McConnell R, Licht S (2008) Solar hydrogen generation. Springer, New York

Stroyuk AL, Kryukov AI, Kuchmii SY, Pokhodenko VD (2009) Semiconductor photocatalytic systems for the production of hydrogen by the action of visible light. Theor Exp Chem 45:209–233

Zhang H, Chen G, Bahnemann DW (2009) Photoelectrocatalytic materials for environmental applications. J Mater Chem 19:5089–5121

Zäch M, Hägglund C, Chakarov D, Kasemo B (2006) Nanoscience and nanotechnology for advanced energy systems. Curr Opin Solid State Mater 10:132–143

Photosynthetically Active Radiation: Measurement and Modeling

Matti Mõttus[1], Madis Sulev[2], Frédéric Baret[3], Raoul Lopez-Lozano[3], Anu Reinart[2]
[1]Department of Geosciences and Geography, University of Helsinki, Helsinki, Finland
[2]Tartu Observatory, Tõravere, Tartumaa, Estonia
[3]INRA, UMR Environnement Méditerranéen et Modélisation des Agro-Hydrosystèmes, EMMAH, Avignon, France

Article Outline

Glossary
Definition of the Subject
Introduction
Techniques for Measuring PAR
PAR in Various Environments
PAR in Vegetation Canopies
Future Directions
Bibliography

Glossary

Photosynthetically active radiation (PAR) The part of electromagnetic radiation that can be used as the source of energy for photosynthesis by green plants, measured as PAR irradiance or PPFD.

PAR waveband Spectral region for electromagnetic radiation defined by the wavelength limits of 400–700 nm.

PAR irradiance Radiant flux density, or the radiative energy received by unit surface area in unit time, carried by photons in the PAR waveband.

Photosynthetic photon flux density (PPFD) The number of photons with wavelengths in the PAR waveband passing through unit surface area in unit time; synonymous to PAR quantum flux.

Photosynthetic action spectrum The spectral dependence of photosynthetic productivity per unit absorbed energy, usually plotted in relative units.

IPAR Intercepted PAR, or the amount of incident PAR not directly transmitted to the ground by a vegetation canopy.

APAR Absorbed PAR, the amount of incident PAR absorbed by a vegetation canopy.

fIPAR The fraction of incident PAR not directly transmitted to the ground by a vegetation canopy.

fAPAR The fraction of incident PAR absorbed by a vegetation canopy.

Global PAR The sum of diffuse and direct PAR: total PAR falling on a horizontal surface.

Ideal PAR energy sensor PAR sensor with output proportional to PAR irradiance.

Ideal PAR quantum sensor PAR sensor with output proportional to PPFD.

Spectral error Broadband radiation measurement errors arising from the deviation of the predicted radiation spectrum from the actual one.

Radiative transfer theory (RTT) The mathematical framework for describing the radiation field in an absorbing, scattering, and emitting medium based on radiation beams traveling in straight lines.

Definition of the Subject

In the broad sense, photosynthetically active radiation (PAR) is the part of electromagnetic radiation that can be used as the source of energy for photosynthesis by green plants. Technically, it is defined as radiation in the spectral range from 400 to 700 nm [1, 2]. It is expressed either in terms of photosynthetic photon flux density (PPFD, μmol photons m^{-2} s^{-1}), since photosynthesis is a quantum process, or in terms of photosynthetic radiant flux density (PAR irradiance, W m^{-2}), more suitable for energy balance studies. A fundamental term in the quantification of light used by plants in the photosynthesis process is the fraction of absorbed photosynthetically active radiation (fAPAR) calculated as the ratio of absorbed to total incident PAR in a vegetation canopy. This variable is widely used in vegetation functioning models at a range of spatial scales from the plant to the globe as an indicator of the amount of energy available for photosynthesis [3].

Introduction

Defining PAR

Photosynthetically active radiation (PAR) is commonly defined as electromagnetic radiation in the waveband

between 400 and 700 nm, or 0.400–0.700 μm [1, 2, 4, 5]. The modern definition of PAR arises from the understanding that the measurement system should be based on a single, generalized spectral response curve based on measured data and usable with sufficient accuracy for all practical purposes [6]. This response curve is commonly known as the action spectrum of photosynthetic radiation and is defined as the photosynthetic productivity (measured as CO_2 uptake or production of O_2) of a leaf plotted against the wavelength λ of the incident spectral irradiance I_λ.

In addition to the action spectrum, the efficiency of photosynthesis is often presented as quantum yield: photosynthetic productivity divided by the amount of absorbed photons. Both quantities are plotted in relative units in Fig. 1: the maximum value of the action spectrum and the relative spectral quantum yield are normalized to unity. The action spectrum and relative spectral quantum yield differ (1) in the units used to measure radiation (amount of photons or amount of radiative energy), and (2) whether the incident or absorbed radiation flux is used. Radiation units for monochromatic radiation can be easily converted: the number of photons with wavelength λ and the corresponding spectral irradiance I_λ are connected via the Planck law (see section "Quantifying PAR"). Absorbed radiative energy (or, equivalently, the number of photons) for each wavelength can be obtained from incident energy by multiplying it by the leaf spectral absorptance.

The shape of photosynthetic action spectrum is almost universal [1, 7]. Small variations are due to between-species differences (e.g., differences in the blue and ultraviolet spectral regions have been noted for arboreous and herbaceous plants [7]), differences in development phase, place of growth, water supply, mineral nutrition, incident irradiance, and other locally varying conditions. This is due to all plants containing the same photochemical apparatus based on the same radiation-absorbing pigments like chlorophyll-A, chlorophyll-B, and carotenoids. These pigments also govern the leaf spectral absorption in the PAR waveband. Only at blue wavelengths, a considerable absorption by non-photosynthetic pigments can be observed [7].

The photosynthetic action spectrum does not decrease to zero at the limits of the PAR waveband

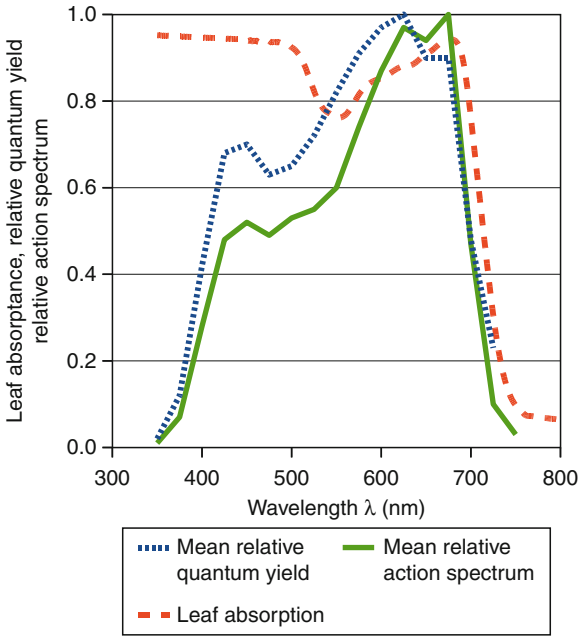

Photosynthetically Active Radiation: Measurement and Modeling. Figure 1
The mean spectral absorption of green leaves (average of measurements in Estonia for common local broad-leaf tree species in 2006) together with the action spectrum of PAR and the relative spectral quantum yield of photosynthesis for field-grown plants (Tables IV and VI in [1])

since the change in photosynthetic potential at 400 and 700 nm is fast but not abrupt. Thus, to exactly measure the true photosynthetic potential of incident radiation, one would need to calculate the incident photon flux density weighed by the relative photosynthetic action spectrum for all wavelengths where the action spectrum is not zero, between 360 and 760 nm. The quantity thus obtained is known as the yield photon flux (YPF) [8].

However, to simplify calculations and measurements, the limits of the PAR waveband have been set to 400 and 700 nm by convention, ignoring the relatively small photosynthetic contribution of photons with wavelengths below 400 nm or above 700 nm. Additionally, the true action spectrum and the spectral composition of incident radiation are generally not used, except for most detailed calculations. Instead, an integral value known as PPFD (section "Quantifying PAR")

is applied (both as a measured value and a theoretical driving force behind photosynthesis in mathematical models) as an adequate descriptor of the photosynthesis-inducing capability of incident radiation under most illumination conditions [2]. The small improvement achievable by using the detailed curve in Fig. 1 does not outweigh the increase in technical and computational complexities.

The radiation incident on a plant canopy arrives as direct and diffuse fluxes. The direct flux is formed by photons having passed through the atmosphere unscattered, whereas the diffuse flux consists of photons scattered by air molecules, aerosol particles, or clouds. As the two fluxes penetrate a vegetation canopy, photons hitting the leaves and other plant elements are intercepted, that is, removed from the incident fluxes. This photon flux hitting plant elements is known as the intercepted PAR flux and denoted with IPAR. Only the intercepted fraction of radiation, or IPAR, constitutes a potential energy source for photosynthesis. However, not all of this potential is realized: a fraction of radiation is always reflected or transmitted by the intercepting element. After being transmitted or reflected, photons may eventually escape the vegetation canopy without any contribution to photosynthesis.

Only photons actually absorbed by the canopy constitute the absorbed PAR (APAR) flux and may be used for photosynthesis. It usually holds that APAR < IPAR and a constant coefficient, APAR = 0.85 IPAR, has been proposed for radiation use efficiency calculations [9] based on the work presented in [10]. Both IPAR and APAR are often expressed in relative units as fractional IPAR (fIPAR) and fractional APAR (fAPAR), respectively, by dividing the relevant quantity by the incident PAR flux. These fractional quantities are expressed as numbers between 0 (no interception or no absorption) and 1 (total interception or total absorption). More details on calculating and measuring APAR, fAPAR, and fIPAR are given in section "PAR in Vegetation Canopies".

Quantifying PAR

The radiometric quantity for measuring the amount of radiation falling on unit area of a surface (e.g., plant leaf) is irradiance, also known as radiant flux density. The SI (International System of Units) unit for irradiance is watts per square meter (W m^{-2}): thus, electromagnetic radiation is described in terms of the energy it carries. Generally, the term "irradiance" is used to denote the energy carried by photons regardless of their wavelength. When dealing with photons in the PAR waveband, the term "PAR irradiance" should be used to denote the irradiance contributed by photons with wavelengths between 400 and 700 nm:

$$I_{\mathrm{PAR}} = \int_{400}^{700} I_{\lambda}(\lambda)\mathrm{d}\lambda, \tag{1}$$

where I_{λ} is spectral irradiance.

PAR measurement in plant sciences has aimed at quantitatively describing radiation as the driving force behind photosynthesis. The intensity of photosynthesis is better predicted by the number of absorbed photons than by the radiant energy received by a leaf [2, 6]. This is illustrated by the flatter, more rectangular shape of the quantum yield curve in Fig. 1 compared with that of the action spectrum. For this reason, PAR is often measured as a flux of photons, the quanta of electromagnetic radiation. As we are dealing with the PAR waveband, the particle flux is most commonly termed "photosynthetic photon flux density" or PPFD. Mathematically, PPFD is defined as the number of photons with wavelengths in the PAR waveband crossing a small surface element in unit time divided by the area of the element.

There is no official SI unit for photon flux or PPFD. A unit defined after the famous physicist, Einstein, is used to designate one mole or Avogadro's number ($N_A = 6.022 \times 10^{23}$) of photons. To describe the PPFD under natural illumination conditions, a suitable unit is thus μE m^{-2} s^{-1} (microeinsteins per square meter per second). In modern practice, however, μmol m^{-2} s^{-1} (micromoles of photons per square meter per second) is the most extensively used unit for PPFD. The increased popularity of micromoles compared with microeinsteins is explained by the common requirement of scientific publishers to use SI units whenever possible. The base unit for amount of substance of the international system of units is the mole. Although the (micro) einstein is based on the mole, it is not on the list of SI-derived units. At the same time, μmol m^{-2} s^{-1} is a combination of SI units and thus explicitly compatible with it. Use of μmol m^{-2} s^{-1} for

measuring PAR is also suggested by the International Commission on Illumination [5].

For a monochromatic beam of radiation, the flux of photons is proportional to the flux of energy. The coefficient of proportionality results from Planck law: the energy of a photon is related to its wavelength λ as $E = hc/\lambda$, where h is the Planck constant (6.34×10^{-34} J s) and c is the speed of light in vacuum ($c = 3.00 \times 10^{8}$ m s^{-1}). Thus, we may write the mathematical definition of PPFD as

$$Q_{\mathrm{PAR}} = \int_{400}^{700} \frac{I_\lambda(\lambda)}{hcN_A} \lambda \, \mathrm{d}\lambda \tag{2}$$

and define the broadband conversion factor

$$\frac{Q_{\mathrm{PAR}}}{I_{\mathrm{PAR}}} = \frac{1}{hcN_{\mathrm{A}}} \frac{\int_{400}^{700} I_\lambda(\lambda)\lambda \, \mathrm{d}\lambda}{\int_{400}^{700} I_\lambda(\lambda) \mathrm{d}\lambda}. \tag{3}$$

For a waveband such as that of PAR containing many wavelengths, the conversion factor $Q_{\mathrm{PAR}}/I_{\mathrm{PAR}}$ depends on the actual spectral composition of radiation, that is, on irradiance conditions [11]. The technical aspects of the problem are further discussed in section "Calibration and Spectral Corrections", and experimental values for PPFD to irradiance conversion are given in section "PAR Below the Atmosphere".

There have been several attempts to define PAR in the history of photosynthesis research. Currently, there is very little ambiguity in the term PAR with regard to the wavelength interval. However, other intervals have also been used [12–14], most notably the interval between 380 and 710 nm (e.g., in the Soviet Union, [15]). Thus, historical PAR measurement data may not be compatible with modern data sets despite similar measurement units: careful evaluation and recalibration is required when dealing with long time series.

PAR waveband coincides almost exactly with the visible part of the solar spectrum. The similarity of the wavelength ranges of PAR and visible light may be useful in solving scientific problems. For example, the directional distribution of diffuse sky brightness has been parametrized for different sky conditions [16] and using the high correlation between PAR and visible light, these distributions may be useful in modeling directional distribution of incident PAR. Similarly, an expression such as "availability of light" is reasonable in everyday use. In scientific literature, however, the less ambiguous term "radiation" should always be preferred to "light." Ambiguity may emerge as the science of visible light, photometry, has long traditions in quantitative measurements: a standardized luminosity function is used to describe the brightness of radiation as perceived by the human eye. The luminosity function is analogous to the action spectrum of PAR in defining the response of a biological system (the average human eye) to incident radiation. Photometric units have a strong user base with a wide field of applications. The modern unit for measuring visible light incident on a surface (illuminance), lux, was widely used in photosynthesis research half a century ago. However, despite the similarity of the luminosity function and the action spectrum, human vision is not related to the photobiology of photosynthesis, and the use of photometric units and terminology in treatment of PAR is strongly discouraged.

Fundamentals of Radiation Transfer Theory

The physical laws and concepts used in describing the complex interactions of electromagnetic waves with matter can be readily applied to describe the processes related to PAR. However, trying to follow this path would ultimately lead to tracking every wave or particle using quantum electrodynamics. While accurate laws are used, for example, to describe the scattering of radiation (including PAR) by molecules, aerosols, and cloud particles in the atmosphere, it is impractical to apply the fundamental theory to plants, vegetation canopies, or the whole planet. The common formulation used for accurate computations of PAR, called the radiative transfer theory (RTT), is a simplification based on ray optics: radiation is described in terms of photon bundles traveling in straight lines with infinite velocity.

In principle, RTT is a mathematical formulation of the law of conservation of radiative energy. Using given sources of radiation and the absorptive, scattering, and emissive properties of the medium, it predicts the detailed angular and spatial distribution of radiation. RTT describes radiation in terms of the energy it carries. However, since it is defined for monochromatic radiation, the particle and energy flows are proportional. RTT is a special case of the more general transfer theory dealing with particles (e.g., neutrons or

electrons) in a scattering, absorbing, and generating medium.

Radiative transfer theory is exactly applicable to monochromatic radiation (i.e., radiation consisting of a single wavelength). Solutions for the entire PAR waveband may be obtained by dividing the waveband into narrow spectral intervals, solving the radiative transfer equation for each wavelength, and then adding the contributions of the wavelength intervals. Thus, RTT deals with spectral radiance as the most detailed descriptor of the radiation field. (Spectral) radiance $R(\vec{\Omega})$, sometimes erroneously termed radiation intensity, is defined as the radiative energy arriving from a given direction crossing a small (imaginary) surface element per unit solid angle per unit surface area. The SI unit of radiance is W m^{-2} sr^{-1} (Watts per square meter per steradian). Evidently, $R(\vec{\Omega})$ is a function of the direction $\vec{\Omega}$, and thus describes the angular distribution of the radiation field. When dealing with the spectral characteristics of radiation, spectral radiance, or radiance per unit wavelength interval, is used. Similarly, when describing PAR, the PAR radiance $R_{\mathrm{PAR}}(\vec{\Omega})$ is used, or radiance carried by photons with wavelengths in the PAR waveband. The mathematical formulation of the theory does not depend on the wavelength interval and is the same for $R(\vec{\Omega})$ and $R_{\mathrm{PAR}}(\vec{\Omega})$. Similarly, the units of PAR radiance are those of the radiance $R(\vec{\Omega})$.

Integrating radiance over the hemisphere (corresponding to a solid angle of 2π) using cosine as the weighing function yields irradiance:

$$I\left(\vec{\Omega}\right) = \int_{2\pi} R\left(\vec{\Omega}'\right) \cos\left(\widehat{\vec{\Omega}', \vec{\Omega}}\right) \mathrm{d}\Omega', \tag{4}$$

where $\widehat{\vec{\Omega}', \vec{\Omega}}$ is the angle between the directions $\vec{\Omega}$ and $\vec{\Omega}'$. Irradiance I equals the amount of radiative energy carried through a unit area of the surface. A similar equation may be written to relate the PAR radiance R_{PAR} and the PAR irradiance I_{PAR}. From Eq. 4, it is evident that the irradiance I_{PAR} is a function of a directional variable $\vec{\Omega}$ describing the normal of the surface: for any given surface, the amount of radiative energy it receives depends on its orientation. Commonly, irradiance is measured on a horizontal surface. When measuring downward-directed flux arriving from the upper hemisphere (i.e., incident flux), $\vec{\Omega}$ points downward; when measuring reflected radiation, $\vec{\Omega}$ points upward.

Radiation flux, or the amount of radiation crossing a surface in unit time, is calculated by dividing the surface into small surface elements, finding the flux density (i.e., irradiance) for each element, and finally adding the contributions of the surface elements. In mathematical terms, the summation is performed as an integration. In this way, a quantitative measure of radiation flow can be obtained through any (possibly imaginary) surface regardless of its shape and orientation. When measuring PAR flux for estimating photosynthesis (in either quantum or energy units), the surface should be that of a plant leaf. To find PPFD on an arbitrarily inclined leaf surface, the angular distribution of the radiation field quantified by the radiance $R_{\mathrm{PAR}}(\vec{\Omega})$ has to be known. However, it is impractical, if not impossible, to measure the angular variation of radiance for each point inside a complex vegetation canopy. Under natural conditions, PAR arrives from the upper hemisphere only and to estimate the energy received, intercepted, and absorbed by a canopy, it is sufficient to measure fluxes on horizontal surfaces. This is in good accordance with the common practice of using the terms "irradiance" or "PPFD": unless specified otherwise, fluxes are measured using a horizontal (and leveled) sensor. However, for the sake of clarity, it is advisable to always specify the directionality of the radiation receiving surface when describing flux measurements.

Techniques for Measuring PAR

Sensors Used for PAR Measurements

The actual sensors used to measure PAR vary in construction and the principle behind the radiation-to-voltage conversion. Two broad classes may be defined, corresponding roughly to instruments for measuring the two quantities defined in the previous section, PPFD and PAR irradiance. Accordingly, two ideal PAR sensors may be defined: the ideal PAR quantum sensor, designed to measure PPFD, and the ideal PAR energy sensor, to measure PAR irradiance. The definition of an ideal sensor is not based on its construction quality or working principle, but on its spectral response function $\varepsilon(\lambda)$. This function, similar to the

photosynthetic action spectrum, describes the output of the instrument when illuminated by a monochromatic radiation source with wavelength λ. To obtain the response of the sensor to any natural radiation source, the spectral response function has to be integrated over the spectral sensor's sensitivity range:

$$M_{\mathrm{PAR}} = \int_{\lambda_{\min}}^{\lambda_{\max}} \varepsilon(\lambda) I_{\lambda}(\lambda) \mathrm{d}\lambda, \tag{5}$$

where M_{PAR} is the sensor reading, $\lambda_{\min}$ and $\lambda_{\max}$ define the spectral interval where the sensitivity function is nonzero, and I_{λ} is the spectral irradiance. The sensor reading M_{PAR} is usually obtained in electric units: voltage or current produced by the sensor. While M_{PAR} is not directly usable for characterization of the radiation field, it is assumed to be proportional to the radiometric quantity of interest. The coefficient of proportionality, or calibration coefficient, is discussed in the next section.

The spectral sensitivity function for an ideal PAR energy sensor is constant with wavelength, $\varepsilon_I(\lambda) = \mathrm{const}$ inside the PAR waveband. The ideal PAR quantum sensor measures the number of incident photons independent of their wavelengths. To achieve this, Planck's law prescribes that the spectral sensitivity function of an ideal PAR quantum sensor has to be proportional to wavelength, $\varepsilon_Q(\lambda) \sim \lambda$, in the spectral interval of 400–700 nm. Outside the PAR waveband, $\varepsilon_Q \equiv \varepsilon_I \equiv 0$. The spectral sensitivity functions of the two ideal sensors are presented in Fig. 2 together with the response functions of two commercially available sensors.

Real PAR quantum sensors are usually photovoltaic sensors based on the photoelectric effect. Use of the photoelectric effect makes the response to the number of photons, regardless of their wavelengths, almost linear. This also makes PAR quantum sensors very responsive: they respond to changes in PPFD almost instantly and the upper limit on temporal sampling frequency is determined by the timescale of natural PAR changes, not the technical capabilities of the sensor.

Common photovoltaic sensors are, in principle, photodiodes working in photo-galvanic regime. A complete hemispheric field of view is achieved by

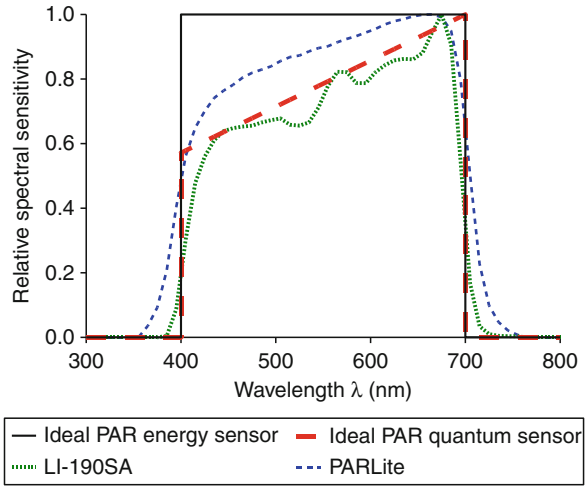

Photosynthetically Active Radiation: Measurement and Modeling. Figure 2
The relative spectral sensitivity functions (normalized so that the maximum value of each curve equals unity) of two ideal sensors for measuring PAR irradiance (Ideal PAR energy sensor) and PPFD (Ideal PAR quantum sensor) together with the curves for two real sensors (LI-COR LI-190SA and Kipp and Zonen PARLite)

placing a diffuser, a carefully shaped piece of diffusely transparent material, in front of the receiving element (the diode). The spectrally nonselective nature of the diffuser material in the PAR waveband makes the receiving surface look white. A suitable filter blocks out wavelengths outside the PAR region. Choice of the filter, along with the physical design of the instrument, brings the spectral response curve closer to that of an ideal sensor. The most widely used quantum sensor is the LI-190SA by LI-COR, Inc. [17, 18] which consists of a silicon photodiode covered by a visible band-pass interference filter and a colored glass filter. Since its introduction, use of quantum sensors to measure PAR has been expanding rapidly [19–24]. Currently, PAR sensors with silicon photodiodes are manufactured by several companies (e.g., PARLite by Kipp and Zonen, E90 Quantum sensor of Jauntering International Corp, SAT-LANTIC PAR sensor for underwater measurements) and form the most commonly used PAR sensor class.

Recently, GaAsP photodiodes have become available for use in PAR sensors (e.g., QSP-2100 by

Biospherical Instruments Inc., JYP 1000 by SDEC France). These sensors are inexpensive because the spectral sensitivity curve of a GaAsP photodiode is close to that of an ideal PAR quantum sensor. Wavelengths below 400 nm may be cut off by choosing a suitable material for the diffuser (usually polyacrylite), and special correction filters are not needed [25].

The second broad class of PAR sensors, PAR energy sensors, includes mostly thermoelectric instruments. These instruments are designed to measure PAR irradiance with a constant sensitivity function using a black receiving surface which is heated by incident radiation. Using a calibration coefficient, the temperature reading of the receiving surface is converted into irradiance. The receiving surface is covered by a glass filter to block photons with wavelengths outside the PAR waveband. Compared with quantum sensors, thermoelectric instruments are technically more complicated and expensive. However, such instruments can be constructed with the same bodies as standard shortwave solar radiation measurement devices, pyranometers and pyrheliometers, making the measurements robust and repeatable. The first hemispheric measurements of global, diffuse, and reflected PAR were made using pyranometers covered with hemispherical glass filters [14, 26–33] and measurements of direct solar PAR with pyrheliometers covered with flat glass filters [34–36]. A thermoelectric device for measuring submarine PAR was also constructed from a thermopile coated with Parsons' black lacquer and covered by a glass filter [37]. Compared to quantum receivers, thermoelectric instruments exhibit large inertia: changes in the temperature of the receiving surface follow the changes in irradiance after a substantial time delay. The time constant (the time it takes for the output signal to decrease by $e \simeq 2.72$ times after incident radiation is completely blocked) of common thermoelectric instruments is about 10 s. Although such timescales are reasonable when measuring incident PAR in the open (affected mainly by solar elevation and atmospheric transmission), variations in radiation fluxes inside a plant canopy happen on much shorter timescales.

An interesting novel idea is to use light emitting diodes (LEDs) in photo-galvanic regime as radiation sensors. A combination of blue and red LEDs provides an acceptable approximation of the PAR spectral curve. An inexpensive sensor consisting of blue SiC and red GaP or AlGaAs LEDs exhibited good correlation with the LI-COR LI-190SA quantum sensor when measuring global PAR [38].

The most complete way to describe radiation in the PAR waveband is to measure its spectral composition. Unfortunately, the instruments for spectral radiation measurements, spectroradiometers (more commonly called just spectrometers), have been expensive and not well suited for field measurement or long-time automatic monitoring. In recent years, developments in affordable photodiode array technology have made the construction of spectroradiometers with few or no moving parts possible. These lightweight field instruments typically measure radiation between 350 and 1,050 nm with a sampling interval of a few nanometers. However, judging from the relatively small number of published results, the simplicity, robustness, and low price of quantum sensors outweigh the increased amount of data and the higher price tag produced by a spectroradiometer. In many common applications in agriculture, horticulture, or monitoring of photosynthetic productivity, monitoring of the amount of available PAR, rather than its spectral composition, is sufficient. Nevertheless, advances in technology indicate that in the decades to come, radiometry will be shifting from broadband sensors toward spectral instruments.

Most sensors described above are intended to measure global PAR: they have been designed to integrate the radiation arriving from all directions in a hemisphere and output radiation flux density. Such sensors are also called cosine receivers after the weighing function used in the mathematical formulation of the integration formula (Eq. 4). Thus, the field of view (FOV) of a cosine receiver is 2π, the solid angle corresponding to a hemisphere. Sometimes, the FOV of an instrument is restricted to receive photons coming from a single direction, for example, the sun. Alternatively, to measure only diffuse sky radiation, sensors may be equipped with a shadow band blocking the diurnal path of the sun in the sky, or a tracking shade disc (i.e., a small disc mounted on an arm activated by a mechanical device used to keep scientific instruments directed toward the sun). To measure the direct solar

component of PAR, that is, the flux density of PAR not scattered by the atmosphere, a pyrheliometer may be equipped with glass filters; alternatively, a common hemispheric PAR sensor may be fitted with a view-limiting tube analogous to that of a pyrheliometer [39]. Unfortunately, no PAR quantum sensors specially designed to measure direct radiation are commercially available. A narrow FOV is also used to study the directional properties of radiation field: directional reflectance or directional distribution of incident radiation [40, 41]. Additionally, instruments to measure radiation arriving from all directions (corresponding to a solid angle of 4π) have been designed. Such instruments measure a quantity called radiation fluence rate and they are more commonly used in aquatic environments (see section "Description of PAR in Water").

To quantify the enormous variability of the radiation field inside and below a plant canopy, single sensors do not suffice. Elaborate systems can be combined with consumer equipment to obtain the best results. The measurement systems used in plant canopies are briefly discussed in section "Instruments for Measuring fAPAR". Although only a few of these devices include the PAR sensors described above, the implicit physical principles of radiometry in these instruments, and thus also the inherent limitations and potential errors, are exactly the same.

Calibration and Spectral Corrections

Direct comparison of two PAR sensors is not a simple task. The reading of a PAR sensor can be predicted from the reading of another sensor if the spectral sensitivity functions of both sensors are known as well as the spectral composition of incident radiation. Although most producers of PAR sensors provide the spectral response functions for their instruments, the spectral composition of incident radiation is generally unknown: the relatively stable spectral composition of extraterrestrial solar PAR is heavily altered when passing through the atmosphere. Inside a plant canopy, the spectral composition of PAR is further distorted by the removal of photons at blue and red wavelengths, where the absorptance of plant leaves is the highest. Thus, care must be taken when comparing the numerical outputs of different sensors in radiation absorption measurements as well as during calibration.

To calibrate a PAR sensor, one needs to measure its output in a controlled experimental situation (e.g., using a calibration lamp) where the value of the measured quantity is known. A calibration coefficient is the ratio of the actual value of the measurable quantity (e.g., I_{PAR}) to the instrument reading (M_{PAR}):

$$\mu_I = \frac{I_{\mathrm{PAR}}}{M_{\mathrm{PAR}}} = \frac{\int_{400}^{700} I_{\lambda,\mathrm{LAMP}}(\lambda)\mathrm{d}\lambda}{\int_{\lambda_{\min}}^{\lambda_{\max}} \varepsilon(\lambda) I_{\lambda\,\mathrm{LAMP}}(\lambda)\mathrm{d}\lambda}. \tag{6}$$

Two calibration coefficients are usually provided for PAR sensors: one to convert the sensor's reading into energy units (W m^{-2}) defined by Eq. 6 and one for quantum units (μmol m^{-2} s^{-1}). The coefficient for quantum units is defined similarly to that for energy units, $\mu_Q = Q_{\mathrm{PAR}}/M_{\mathrm{PAR}}$.

Most manufacturers calibrate the sensors in laboratory using standard lamps, which is indicated by using the subscript LAMP for the spectral irradiance in Eq. 6, $I_{\lambda,\mathrm{LAMP}}$. Thus, the manufacturers can control (within a given measurement uncertainty of a few percent determined by the calibration of the lamp) both the energy content and the spectral composition of incident radiation. If the spectral sensitivity of the actual sensor being calibrated deviates from that of the perfect sensor, as it invariably does, the calibration coefficient depends on the spectral composition of incident radiation. Therefore, the laboratory-derived calibration is only directly valid for irradiation by a calibration lamp and does not hold exactly under field conditions.

The errors arising from the mismatch of the predicted and actual field conditions are usually called spectral errors. Spectral errors depend on the spectral sensitivity of the sensor, the spectral composition of incident irradiance, and the spectral composition of radiation used to calibrate the sensor. Mathematically, the spectral error in PAR irradiance measurements can be written as

$$\beta_I = \frac{\mu_I \int_{\lambda_{\min}}^{\lambda_{\max}} \varepsilon(\lambda) I_\lambda(\lambda)\mathrm{d}\lambda}{\int_{400}^{700} I_\lambda(\lambda)\mathrm{d}\lambda}. \tag{7}$$

After substituting the expression for μ_I from Eq. 6 into Eq. 7, it becomes clear that spectral errors

disappear if (1) the sensor has a response function identical to that of the ideal sensor, $\varepsilon(\lambda) \equiv \varepsilon_I(\lambda)$, or (2) the irradiance conditions match the calibration lamp spectrum, $I_\lambda(\lambda) \equiv I_{\lambda,\mathrm{LAMP}}(\lambda)$ in the spectral interval from $\lambda_{\min}$ to $\lambda_{\max}$. The magnitude of the actual spectral error varies with sensor type. While it is reasonably small for the LI-190SA sensor, usually less than 1% for natural irradiance conditions, many other sensor exhibit considerably larger errors, especially under artificial illumination [11].

If the spectral composition of incident radiation or, more specifically, the difference between the spectral composition of radiation occurring during field measurements and during calibration, spectral error can be eliminated by using a spectral correction. It is evident that in the presence of the spectral error, multiplying the measurement result by the inverse of β_I (Eq. 7) would compensate completely for the differences in the spectra of incident radiation. Thus, if the actual spectral irradiance $I_\lambda(\lambda)$ is known, a spectral correction can be easily calculated. However, since $I_\lambda(\lambda)$ is usually not available, a general value characterizing the illumination conditions (clear or cloudy sky, different artificial light sources), $I_{\lambda,\mathrm{EST}}(\lambda)$, is used instead. Thus, the spectral correction factor is calculated as the reciprocal of β_I after replacing $I_\lambda(\lambda)$ by $I_{\lambda,\mathrm{EST}}(\lambda)$ in Eq. 7.

Therefore, when taking a measurement, the instrument reading is first multiplied by the calibration coefficient (μ_I or μ_Q, calculated individually for each sensor) and, optionally, by a spectral correction (calculated for a whole instrument class or model). As only the average spectral irradiance distribution for typical conditions is known, it is often preferable to ignore spectral corrections.

Another possibility to calibrate the sensors is to compare them with a reference sensor (or a spectroradiometer) with a reliable calibration by the manufacturer. When performing calibration under irradiance conditions reasonably close to those occurring under true measurement situations, spectral corrections are not required. For example, field calibrations of radiation measuring instruments are standard for the Baseline Surface Radiation Network (BSRN, [42]), an international network for global measurements of solar and atmospheric radiation at the highest available accuracy. Additionally, all PAR sensors continuously exposed to outdoor conditions should be checked regularly against well-maintained reference instruments. The sensitivity of sensors is apt to change due the aging of the diffuser and filters. Such aging is usually also documented in the instrument manual. When a frequently and reliably calibrated instrument is not available, it is strongly recommended to have a reference instrument stored under controlled conditions for periodical comparisons with the operating sensors.

Measurement Errors

As with all measurements, errors are inevitable and arise from (1) the impossibility of controlling all the physical processes that determine the measurement result, (2) the non-perfect construction of the measuring apparatus, and (3) the spectral composition of incident radiation. Since the last error source (spectral errors) was covered in section "Calibration and Spectral Corrections", only the first two categories are briefly discussed here.

Measurement errors can be reduced by carefully following the instructions for performing the measurements (usually provided by the manufacturer), using proper installment and maintenance procedures (e.g., checking for the directionality and leveling of the instrument), checking the performance of the instrument regularly, and accounting for material degradation and changes in operating environment (ambient temperature, irradiance conditions, humidity, etc.). Flux measurements with a hemispherically integrating sensor suffer from directionality effects: the sensor is not equally sensitive to radiation arriving from different directions. While manufacturing imperfections or physical damage may cause an instrument to have random sensitivity fluctuations with the azimuth angle of an incident beam, sensitivity to polar angle (or zenith angle for a leveled sensor looking upward) of the radiation source is usually more systematic. The dependence of sensitivity with the polar angle is called the cosine response of the sensor and the corresponding correction a cosine correction. The cosine response characteristics of several sensors designed for irradiance measurements, including two LI-COR 190 PAR sensors, are given in [43]. Cosine effects, together with leveling inaccuracies, are especially influential when a strong directional radiation

source is present, such as the direct solar radiation beam on a clear day. All these errors, some systematic and some random, can add to the spectral errors affecting instruments designed for measuring radiation in a spectral waveband as discussed in the previous section.

The official relative uncertainty of PAR instruments claimed by manufacturers, about 5%, can only be achieved under optimal conditions. During routine measurements, even if performed by trained specialists, the uncertainty can be considerably larger. For example, [44] gives an estimate of 10% uncertainty for PAR measurements in the FLUXNET network; a comparison performed by BSRN found significant systematic differences between different PAR sensor models and up to 20% spread within the group of 11 tested LI-190SA sensors [45].

PAR in Various Environments

PAR Below the Atmosphere

Without the influence of the atmosphere, the PAR irradiance would be determined by the solar spectrum and geometric conditions like the slightly varying distance from the earth to the sun, local solar elevation, and topographic shadowing. The spectral composition of radiation would be constant to the accuracy of the multiple scattering contribution of non-flat topography (illuminated slopes of mountains and valleys). Such direct topographic effects, although significant in shadow areas, are usually small when direct solar radiation is present and will be ignored hereafter. Under natural conditions, the amount and spectral composition of radiation in the PAR spectral band, in addition to the distance from the sun to the earth and solar elevation angle, is mainly determined by the presence of clouds, the amount and optical properties of aerosols, and, to a lesser extent, the chemical composition of the atmosphere.

Due to its universal nature, radiative transfer theory (RTT, section "Fundamentals of Radiation Transfer Theory") can be (and also has been) applied to predict the irradiation conditions under all possible atmospheric conditions. The actual precision of prediction is limited by the availability of input data and computer power. Models based on RTT can be used to calculate accurately the spectral irradiance for the different wavelengths comprising PAR, with subsequent integration to obtain I_{PAR}. For many practical purposes, however, simpler models applicable to longer timescales (hours, days, growing seasons) are sought and thus different broad-band models or physically based parametrizations are often used. For clear skies, the accuracy of the best broadband models is comparable to that of routine irradiance measurements in existing networks [46].

Models developed for predicting the behavior of sunlight in the atmosphere deal not only with PAR but with the whole shortwave spectral region. The shortwave spectral region is loosely defined as the range of wavelengths containing the bulk of the solar spectrum (magnitude wise), usually between 300 and 4,000 nm. The simplest case, global shortwave irradiance under a cloudless atmosphere, can be very accurately predicted when the following parameters are known (REST2 model, [46]): solar zenith angle, Ångström turbidity coefficient (i.e., aerosol optical depth at 1,000 nm), Ångström wavelength exponents, aerosol single-scattering albedo, air pressure, amounts of precipitable water and ozone, and ground albedo. These parameters allow to calculate the irradiance in two separate wavebands, PAR and short-wave infrared. To predict only PAR irradiance, a few parameters less are required, since ozone and water vapor have little influence on PAR.

Because not all of the listed atmospheric parameters are readily available, models based on easily measurable radiation field characteristics have also been developed [24, 47, 48]. Usually, parametrizations are based on approximately four parameters. While one parameter is always solar elevation, others describe the state of the atmosphere and can be either obtained from radiation measurements (e.g., ratio of diffuse to direct shortwave irradiance) [49] or routine meteorological data (e.g., dew point temperature). The variables explaining the majority of variance in PAR availability and the spectral quality of PAR (Q_{PAR}/I_{PAR} ratio) include solar elevation and a parameter to describe the turbidity of the atmosphere (e.g., a sky clearness parameter or the Ångström turbidity coefficient) [39, 47, 48, 50, 51].

Two downwelling PAR field components can be distinguished under a clear sky: the quasi-parallel direct beam arriving from the direction of the sun (with PAR irradiance on a horizontal surface $I_{PAR,dir}$) and the diffuse sky radiation arriving from all upward directions not blocked by topography ($I_{PAR,diff}$).

The sum of the two components is called global PAR, $I_{PAR} = I_{PAR,dir} + I_{PAR,diff}$. Depending on aerosol load and solar elevation, the ratio of diffuse PAR to global PAR irradiance on a horizontal surface ranges between 20% and 40% [52]. The presence of clouds decreases the global PAR irradiance usually by up to 80% [41] and the contribution of diffuse PAR irradiance may take any value between that corresponding to a clear sky and 100%. If the cloud cover is broken, the existence of the direct beam depends on the locations of gaps between clouds. Thus, two temporally and spatially variable phenomena have great influence on the amount of diffuse PAR: aerosol loading and clouds. Although the effect of aerosols may be dominating in places with low average cloud cover, it is expected that the contribution of clouds as the source of variations in diffuse PAR is larger for most locations.

The fraction of PAR in global shortwave irradiation I_{PAR}/I_{SW} varies little and is usually between 40% and 50% [53, 54]; values above 50% occur under very low sun, thick cloud cover, or rain [14]. As an example, measurements at Tõravere actinometric station (Estonia) are presented in Fig. 3 for variable cloud conditions during June 2009. The global PAR irradiance can be relatively reliably predicted from global shortwave irradiance, $I_{PAR} = 0.43\ I_{SW}$. The contribution of diffuse PAR irradiance $I_{PAR,diff}$ to global shortwave irradiance, on the other hand, was more variable (Fig. 3). Under completely overcast skies, the diffuse PAR irradiance $I_{PAR,diff}$ equals the global PAR irradiance I_{PAR}, which, as usual, contributed about 43% of global shortwave irradiance. Under clear skies, $I_{PAR,diff}$ is significantly smaller than I_{PAR}: in Fig. 3 the data points corresponding to clear sky form the lower cluster. Broken cloud cover conditions are represented by $I_{PAR,diff}$ values between the two extremes when plotted against I_{SW}.

Some variation in I_{PAR}/I_{SW} with elevation above sea level is expected, but this variation is difficult to detect [52]. However, using measurement sites at 550, 900, and 1,500 m above sea level, an increasing trend was noted with altitude, of 3.6% per km for hourly values of Q_{PAR}/I_{SW} under clear skies [55]. An inverse trend was found for hourly Q_{PAR}/I_{SW} under cloudy weather conditions: Q_{PAR}/I_{SW} decreased at a rate of 1.8% per km.

The spectral composition of global PAR is relatively stable [56]. It is reflected in the near-constant value of

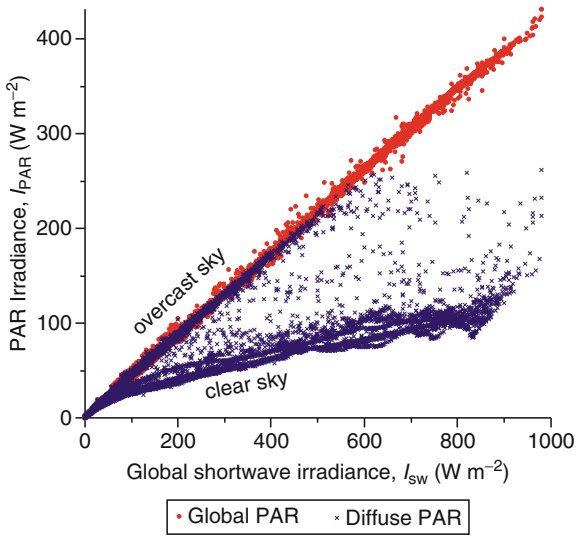

Photosynthetically Active Radiation: Measurement and Modeling. Figure 3
Global and diffuse PAR irradiance as functions of global shortwave irradiance in Tõravere, Estonia, in June 2009. Sky condition varied from clear to completely overcast. The labels "clear sky" and "overcast sky" indicate the characteristic values of diffuse PAR irradiance for the two atmospheric conditions

the ratio of PPFD to PAR irradiance, Q_{PAR}/I_{PAR} (Eq. 3). The classical value of $Q_{PAR}/I_{PAR} = 4.57\ \mu mol\ s^{-1}\ W^{-1}$ for global PAR proposed by McCree [2] has been verified by several later studies. For example, [57] reported that while 1-min average of Q_{PAR}/I_{PAR} varied from 4.23 to 4.68 $\mu mol\ s^{-1}\ W^{-1}$, 1-h averages were relatively insensitive to atmospheric composition with $Q_{PAR}/I_{PAR} = 4.56\ \mu mol\ s^{-1}\ W^{-1}$ for global PAR.

For the diffuse radiation field component, the ratio depends on atmospheric conditions. Under a blue sky, an average value of $Q_{PAR,diff}/I_{PAR,diff} = 4.28\ \mu mol\ s^{-1}\ W^{-1}$ was reported [52] along with the observation that the ratio increases with aerosol load. In the presence of clouds, $Q_{PAR,diff}/I_{PAR,diff}$ increases with increasing cloud cover from 4.24 $\mu mol\ s^{-1}\ W^{-1}$ (a value characteristic of blue sky) to the constant value for global radiation, $Q_{PAR}/I_{PAR} = 4.57\ \mu mol\ s^{-1}\ W^{-1}$ under an overcast sky [57]. The value of Q_{PAR}/I_{PAR} (or $Q_{PAR,diff}/I_{PAR,diff}$) describes the color of light: the smaller the ratio, the bluer the light looks to the human eye.

The angular distribution of PAR radiance can be approximated using models applicable to visible

light [16]. Additionally, several approximations exist for predicting the angular distribution of shortwave radiation. These models have been parametrized for use in the PAR waveband [40, 41] for different atmospheric conditions ranging from completely clear to overcast sky. The angular models describe sky radiance relative to the nadir direction and cannot be generally used to describe global PAR irradiance or PPFD.

A final remark on the spectral quality of PAR at the bottom of the atmosphere can be made based on the spectral composition of extraterrestrial solar radiation. The I_{PAR}/I_{SW} ratio outside the atmosphere based on the solar constant of $I_{SW} = 1367\ \mathrm{W\,m^{-2}}$ equals 38.8% [51]. Using $Q_{PAR} = 2426\ \mu\mathrm{mol\ s^{-1}\ m^{-2}}$ for the extraterrestrial irradiance on a surface perpendicular to sunrays [48], we obtain that the Q_{PAR}/I_{PAR} ratio outside the atmosphere equals 4.57 $\mu\mathrm{mol\ s^{-1}\ W^{-1}}$ – exactly that proposed by McCree [2]. While it may be concluded that the atmosphere has little effect on the spectral quality of PAR, the exact coincidence is most likely due to chance: an accuracy of two decimals is clearly beyond the uncertainties inherent in radiation measurements.

Description of PAR in Water

The waveband of radiation allowing phytoplankton to carry out photosynthesis (i.e., PAR) corresponds approximately to the same spectral band of electromagnetic radiation that penetrates into water. Pure water absorbs strongly in the ultraviolet ($\lambda < 400$ nm) and near-infrared ($\lambda > 700$ nm) spectral regions [58]. Otherwise, the underwater light field is determined by the incident irradiance (see section "PAR Below the Atmosphere"), the state and composition of the water body, and the optical properties of its bottom.

The spectrum of solar radiation penetrating a water body changes drastically as its irradiance diminishes with depth. While the scattering of radiation is commonly rather insensitive to wavelength in the PAR waveband, absorption by different components has a very strong spectral effect. The components having an optical effect are dissolved organic substances (also known as yellow substance), different species of phytoplankton, and inert particulate matter (Fig. 4). Since the concentration of these is highly variable, the spectral distribution of underwater irradiance in the PAR waveband can change rapidly.

In a vertically homogeneous water body, the value of the downwelling spectral irradiance I_λ diminishes approximately exponentially with depth z, that is, Beer's law holds (see also Eq. 8):

$$I_\lambda(z) = I_\lambda(0)\exp\left[-\int_0^z K_{\mathrm{diff}}(\lambda, z')\mathrm{d}z'\right]$$

where $K_{\mathrm{diff}}(\lambda,z)$ is the diffuse attenuation coefficient, a parameter often used to describe the optical properties of natural water bodies [62–64].

In addition to the spectral PAR irradiance I_λ and PPFD, a quantity called spectral fluence rate, or spectral spherical irradiance, is sometimes used to describe the amount of radiation in water. It is defined as the total amount of photons incident in unit time interval from all directions on a small sphere, divided by the

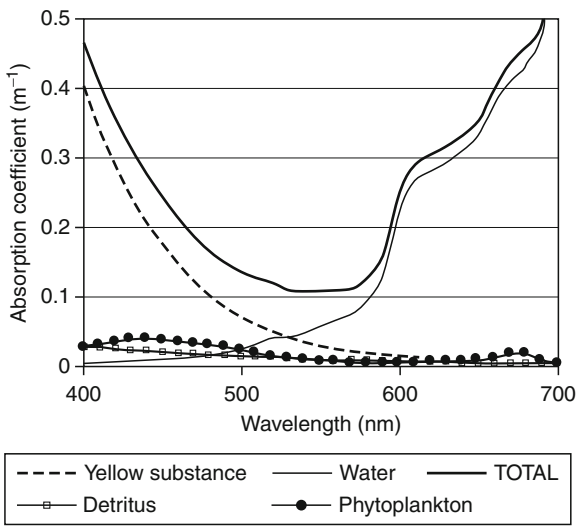

Photosynthetically Active Radiation: Measurement and Modeling. Figure 4
Decomposing the absorption spectrum of a water sample. Spectra of the absorption coefficients corresponding to pure fresh water [59]; 1.0×10^{-3} mg m^{-3} yellow substance (specific absorption coefficient at 380 nm 0.565 L mg^{-1} nm^{-1}); 1.0 mg m^{-3} chlorophyll-a (phytoplankton, [60]); and detritus (from the measured data of [61]). The total absorption of the water sample is plotted with a bold line

cross-sectional area of the sphere. Analogously to the PAR irradiance I_{PAR}, the PAR fluence rate may be defined by integrating over the PAR waveband. As both fluence rate and irradiance describe the amount of PAR in water, Beer's law can (with a different attenuation coefficient) also be applied to describe the change in spectral fluence rate with depth.

Beer's law is valid only for the spectral irradiance $I(\lambda)$, that is, the irradiance in a narrow spectral interval around wavelength λ. Many authors have shown that the exponential law fails when a single value of K_{diff} is applied over the whole PAR waveband. The reason for this failure lies in the change of spectral composition of PAR with depth. This can be illustrated using the wavelength corresponding to maximum penetration, λ^*, and the Q_{PAR}/I_{PAR} ratio. In clear oceanic waters, λ^* corresponds to the maximum in the extraterrestrial solar spectrum (~460 nm). When increasing the amount of optically active substances in water, λ^* is shifted toward larger values, as shown in Table 1, and can be even larger than 700 nm in brownish boreal lakes [65].

Photosynthesis in water takes place mainly in the so-called euphotic layer near the surface. At the bottom of the euphotic layer, the downward PAR irradiance has decreased to 1% of its value just below the surface [66]. In clear oceanic waters, the thickness of the euphotic layer can be of the order of a hundred meters. As a contrast, in turbid lakes, the layer may be only half a meter thick. Ice cover, and especially ice covered with snow, may substantially decrease the amount of PAR in water to a level not sufficient for even the minimum amount of photosynthetic activity, thus creating anoxic conditions [67].

Similarly to other environments, the PAR irradiance in water can be given in energy units (I_{PAR}, W m^{-2}) or quantum units (Q_{PAR}, μmol s^{-1} m^{-2}). The quanta-to-energy ratio Q_{PAR}/I_{PAR} (μmol s^{-1} W^{-1}) changes with the variation of the spectral distribution of irradiance. Above water, Q_{PAR}/I_{PAR} is practically constant with an average value Q_{PAR}/I_{PAR} = 4.57 μmol s^{-1} W^{-1} over a wide range of conditions (see section "PAR Below the Atmosphere"). In clear oceanic water, Q_{PAR}/I_{PAR} decreases with depth. As a contrast, in turbid coastal waters and lakes, it increases with depth and approaches an asymptotic value. Thus, sufficiently deep below the surface of turbid waters, the spectral distribution of PAR, but not the value of PAR irradiance, can be considered almost constant. The average value of Q_{PAR}/I_{PAR} there has been estimated at 4.15 ± 0.40 μmol s^{-1} W^{-1} [68]; a value of Q_{PAR}/I_{PAR} = 4.45 ± 0.48 μmol s^{-1} W^{-1} has been suggested for Norwegian coastal waters [69]. In lakes, Q_{PAR}/I_{PAR} varies from 4.72 to 5.86 μmol s^{-1} W^{-1} [65]. Additionally, there is a strong linear correlation between Q_{PAR}/I_{PAR} and K_{diff} (r = 0.95) and, in deeper waters, Q_{PAR}/I_{PAR} can be estimated using K_{diff} measurements in the surface layer [65].

Measurement Stations and Networks

Unfortunately, no international network to measuring PAR currently exists. As can be seen from their documentation, large international radiation measurement networks like the Baseline Surface Radiation Network (BSRN http://www.gewex.org/bsrn.html) [70] have discussed the subject of PAR measurements, but standardized measurements have not started. The PAR irradiance (and also APAR) is recorded as a by-product in some networks specialized in other measurements. For example, the FLUXNET project (http://daac.ornl.gov/FLUXNET/) [71, 72], which is aimed at

Photosynthetically Active Radiation: Measurement and Modeling. Table 1 Wavelength of maximum penetration λ^*, ratio Q_{PAR}/I_{PAR}, and relative difference D of Q_{PAR}/I_{PAR} from its value above the surface for different water types as classified by [62]

Water type	I	II	III	1	3	5	7	9
λ^* (nm)	465	480	505	530	540	547	565	582
Q_{PAR}/I_{PAR} (μmol s^{-1} W^{-1})	3.9	4.0	4.2	4.4	4.5	4.5	4.7	4.9
D (%)	16	14	9	4	2	2	2	6

quantifying the exchanges of carbon dioxide, water vapor, and energy between the biosphere and atmosphere, has PAR data available for many sites. The solar radiation budget network SURFRAD (http://www.srrb.noaa.gov/surfrad/) [73] measures, among other variables, the incident PAR irradiance. A promising start is SolRad-Net (http://solrad-net.gsfc.nasa.gov/), a companion to the successful global AERONET aerosol network. However, the number of SolRad-Net sites where PAR is measured today is still very small. Routine monitoring of PAR and APAR as key factors in global photosynthetic productivity [74] has been proposed several times. Currently, the only global data sets available are those based on remote sensing data (see section "APAR and fAPAR from Satellite Observations"). Although remote sensing can provide excellent spatial coverage unachievable in any ground-based network, indirect remote retrievals should still be validated against direct measurements of the variable under investigation.

PAR in Vegetation Canopies

PAR Absorption by Leaves

PAR Absorption by Leaf Pigments Electromagnetic radiation in the PAR spectral domain is mainly absorbed by photosynthetic pigments in the leaf. Among these, chlorophylls a and b are the most important. They are found across a wide range of species, from algae to higher plants, and they participate in transforming radiation into energy, which is later stored as chemical bonds of carbohydrates. Chlorophylls are characterized by two absorption peaks at 450 and 670 nm corresponding to the blue and red color, respectively, explaining the green color of leaves (Fig. 5). Besides chlorophylls, green leaves contain also other pigments. Pigments such as carotenes and xanthophylls belonging to the carotenoid family associated with chlorophylls are known to improve radiation harvesting. They mainly absorb in the blue region with absorption peaks at 450 and 470 nm making them look orange or yellow. Additionally, carotenoids prevent oxidation of the photosynthetic system in case of excess incident radiation. Other pigments like anthocyans absorb radiation in the PAR waveband with maximum absorption between 450 and 600 nm [77]. They protect the leaf against UV radiation by preventing formation of free radicals and are responsible for the reddish colors of some leaves during the autumn. The rest of the biochemical leaf constituents responsible for the brown color (such as polyphenols, which develop during leaf senescence), although absorbing in the PAR waveband (Fig. 5), have no direct role in photosynthetic processes.

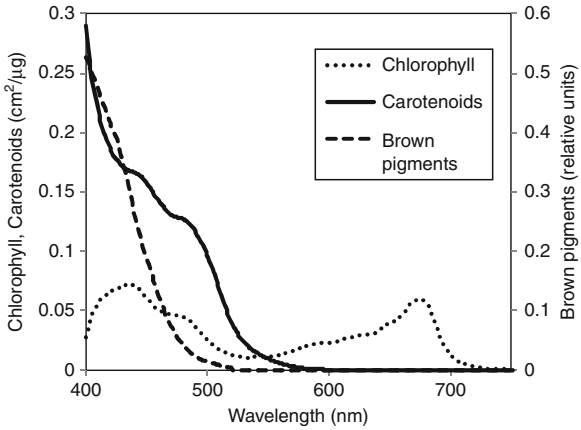

Photosynthetically Active Radiation: Measurement and Modeling. Figure 5
Specific absorption coefficients of chlorophyll (a + b), carotenoids and brown pigments from the PROSPECT model [75, 76]

The Role of Leaf Structure The efficiency with which a leaf absorbs visible radiation depends not only on chlorophyll content per unit leaf area, but also on the specific mechanisms plants have developed to utilize radiation. Chlorophylls are concentrated in chloroplasts, mainly located in the palisade mesophyll consisting of tightly packed elongated cells just under the upper epidermis (Fig. 6). The tubular shape of palisade cells enhances the forward propagation of PAR, thus directing photons to the chloroplasts located at the bottom of the palisade. In a number of species, the epidermis cells act as lens focusing radiation on the chloroplasts thus increasing radiation absorption by the photosynthetic pigments [78]. The spongy mesophyll of higher plants contains little PAR-absorbing pigments. Instead, the numerous voids in this layer act as a mirror to scatter back a large fraction of the radiation transmitted through the palisade mesophyll, further improving absorption of radiation by chloroplasts.

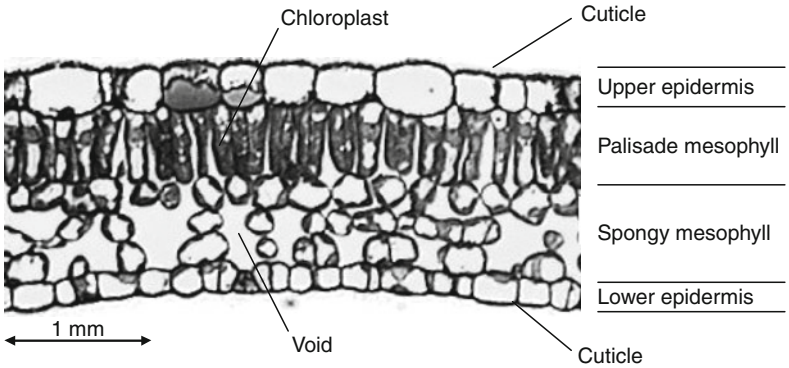

Photosynthetically Active Radiation: Measurement and Modeling. Figure 6
Structure of a typical dicotyledon leaf (young maple)

When the capacity of the leaf to use the available PAR is exhausted by drought or nutrient stress, plants may use different strategies to minimize absorbed radiation. Besides changing the orientation of a leaf away from direct sunlight, adaptations have been developed at the upper epidermis level. The cuticle may turn to crystalline and the amount of hair on the leaf surface may increase, thus also increasing the leaf reflectivity and directing radiation away from chloroplasts.

The Fate of Absorbed PAR in the Leaf The energy carried by photons absorbed by the leaf is transformed into several types of energy. The dominant type is heat, accounting for more than 75% of the absorbed PAR energy. Therefore, only a maximum of 25% of APAR is left for photosynthesis. When photosynthesis is limited by temperature, water, or nutrient availability, the radiation use efficiency of a leaf decreases even further. Additionally, a part of the excess PAR energy absorbed by the pigments may be dissipated as fluorescence, that is, reradiated as photons with different, longer wavelengths.

Under optimal water, temperature, and nutrient conditions, the efficiency of photosynthesis at the leaf level is determined both by the absorbed PPFD and the CO_2 concentration in the leaf [79]. Figure 7 shows that the photosynthetic rate increases almost linearly with incident PPFD up to some threshold value. After the threshold is reached, the rate of photosynthesis becomes constant, limited by the CO_2 concentration in the leaf. This concentration in the leaf, in turn, is driven by the CO_2 concentration in the atmosphere and the stomatal conductance of the leaf, itself determined by the hydraulic status of the leaf and the plant as a whole [80]. The maximum photosynthetic rate, achieved at large PPFD values, also strongly depends on the fraction of the incident PAR absorbed by the leaf [81], which is determined mostly by leaf chlorophyll content.

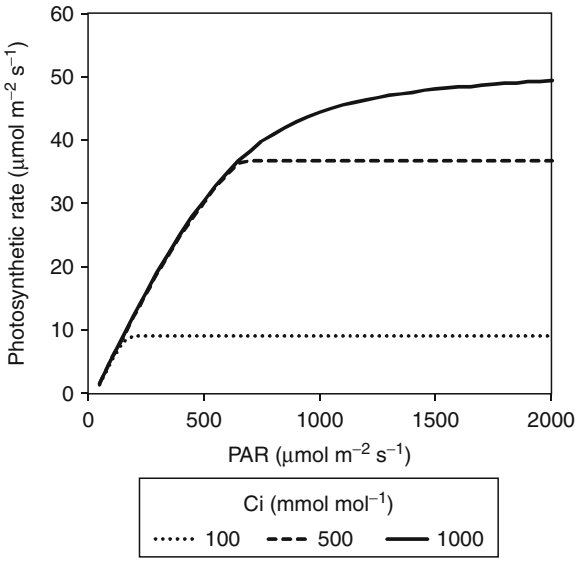

Photosynthetically Active Radiation: Measurement and Modeling. Figure 7
Relation between incident PAR photon flux density and photosynthesis rate at different intercellular concentration of CO_2 (C_i), simulated using model of C3 photosynthesis [79]

Since chlorophyll absorbs the majority of incident PAR and uses only a small fraction of it for photosynthesis, the excess energy must be dissipated in a way that keeps the photosynthetic apparatus functional. For this purpose, plants have developed several photoprotection mechanisms. One of such mechanisms is based on xanthophyll pigments: the conversion of violaxanthin into zeaxanthin can remove the excess energy from chlorophyll and dissipate it as heat. When conditions become more favorable, this conversion is reversed, and zeaxanthin is changed back to violaxanthin. The status of the xanthophyll cycle may be used to evaluate the various stresses experienced by plants, since it affects the leaf optical properties, or leaf reflectance spectrum, in the 500–600 nm spectral region [82].

The second pathway for dissipating excess energy absorbed by photosynthetic pigments is fluorescence. When photosynthesis is limited by stress factors or when a leaf is exposed to too high irradiance, a small but measurable fraction of the excess energy is reemitted at a longer wavelength than that of absorption. The peak of chlorophyll fluorescence emission is in the blue-green (455 nm), red (685 nm), and far-red (735 nm) spectral regions [83]. The energy lost in this process amounts to a few percent of the total PAR energy absorbed by the leaf [84].

Quantitative Description of PAR in Vegetation Canopies

Radiative Transfer in Plant Canopies When dealing with PAR in vegetation canopies [85, 86], it is assumed that the only scatterers are plant leaves (or needles, shoots, etc.), that radiation originates from the sun only, and that thermal emission can be ignored. Thermal emission in the PAR waveband is indeed negligible (nonexistent for all practical purposes) at temperatures suitable for photosynthesis. The existence of fluorescence by green leaves, an emission source concurrent with photosynthesis, assumes the presence of incident PAR. The energy contribution of fluorescence is small compared to that of scattered PAR, and is generally masked by scattered radiation [87].

When using RTT, the optical thickness of a canopy is often described by its leaf area index (LAI): one-sided leaf area (or half of the total leaf area for plants with non-flat leaves) per unit ground area. Quite commonly, the downward cumulative LAI, $L(z)$, calculated as LAI above height z, is used instead of the geometric vertical coordinate z. At the top of the canopy, $L(z_{\text{top}})$ equals 0, then increases with depth inside the canopy. Finally, below the plant layer, $L(0) = \text{LAI}$.

Radiation Interception When RTT is applied to describe the attenuation of radiation in vegetation, a well-known result is obtained. In an environment where the scattering elements fill a volume uniformly and randomly, and are infinitesimally small, the radiance decreases exponentially:

$$R_{\text{PAR}} = R_{\text{PAR}}(z_{\text{top}})\, e^{-kx}, \tag{8}$$

where $R_{PAR}(z_{top})$ is the radiance before entering the scattering medium, k is the attenuation coefficient, and x is the distance from the point where radiation enters the medium (depth inside the canopy). The exponential decay described by Eq. 8 is commonly known as Beer's law, sometimes called Beer–Lambert's or Beer–Lambert–Bouguer's law. The terms attenuation and interception are used interchangeably: interception of radiation attenuates the unscattered radiation field.

The tradition of using Beer law for radiation transmission in vegetation canopies consisting of flat leaves started with the classic work by Monsi and Saeki [88, 89]. They plotted the logarithms of light transmittance of vegetation canopies during overcast days against the LAI of the canopy, and obtained straight lines (Fig. 8). They explained the variations in the slopes of the lines (i.e., attenuation coefficients) theoretically, using leaf inclination angles. Since then, Beer's law has been routinely applied to approximate PAR availability in plant canopies [90, 91].

Generally, Beer's law is exactly valid for monochromatic radiation only and is not directly applicable to radiation arriving from the whole hemisphere (i.e., irradiance I_{PAR}). To obtain non-intercepted PAR irradiance on a horizontal surface below a plant canopy, Beer's law (Eq. 8) has to be integrated over the upper hemisphere:

$$I_{\text{PAR}} = \int_0^{\pi/2} \int_0^{2\pi} R_{\text{PAR}}(z_{\text{top}}, \vartheta, \phi) \mathrm{e}^{-k(\vartheta,\phi)x(\vartheta,\phi)} \times \cos\vartheta \sin\vartheta \, \mathrm{d}\theta \mathrm{d}\phi, \tag{9}$$

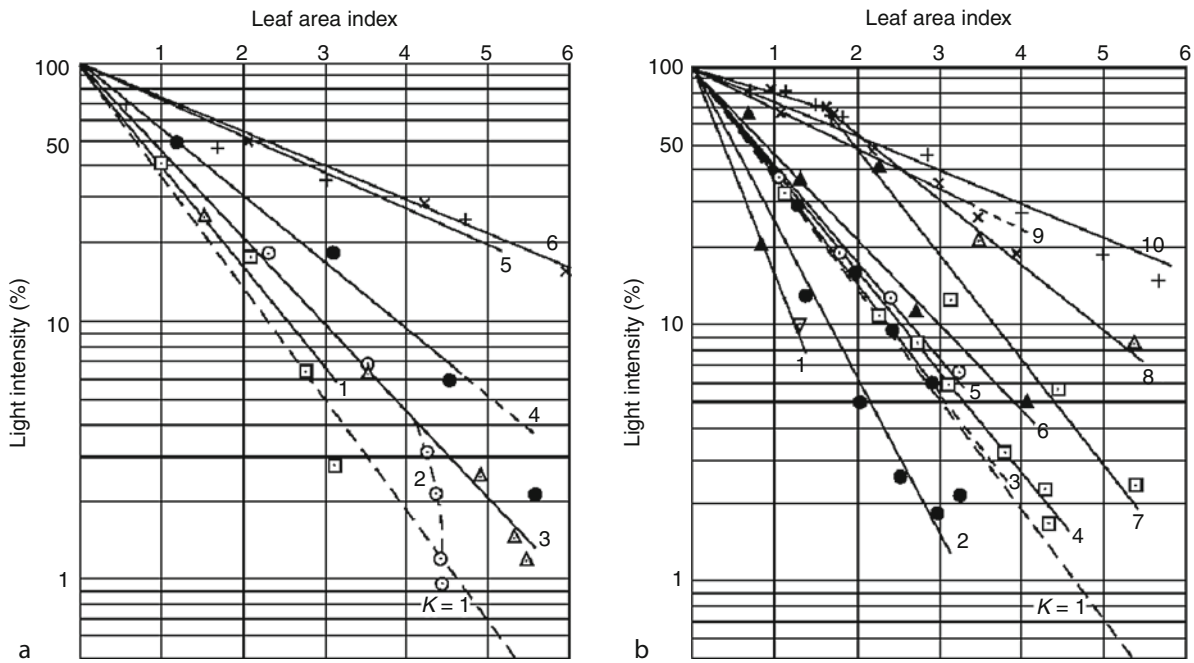

Photosynthetically Active Radiation: Measurement and Modeling. Figure 8
Light intensity–leaf area index curves of some plant communities measured under mostly overcast conditions on different days (Reprinted from [89]). (**a**) The communities of the Kirigamine montane meadow; (**b**) the communities of the Tazima meadow and in the vicinity of Tokyo. Light intensity, a good proxy for PAR irradiance, decreases near-exponentially (See the original article for more details. Published with permission from Oxford University Press)

where ϑ and ϕ are the zenith and azimuth coordinates describing a direction in the upper hemisphere, respectively. The distance from the bottom to the top of the canopy in the direction (ϑ,ϕ) depends mostly on the zenith angle ϑ. For a canopy layer of uniform thickness, $x(\vartheta,\phi) = 1/\cos\vartheta$. Equation 9 is identical to the equation relating irradiance and radiance, Eq. 4. The former can be obtained from the latter by expressing radiance as a function of canopy transmittance (which is Beer's law for vegetation canopies, Eq. 8) and considering that the differential of a solid angle can be expressed in polar coordinates as $d\Omega = \sin\vartheta\, d\theta d\phi$. Computations involving numerical integrations of canopy interceptance over the upper hemisphere similar to Eq. 9 are common in optical estimations of LAI [92, 93].

In most applications of RTT, the probability of a scattering event, and thus the extinction coefficient k, does not depend on the direction (ϑ,ϕ) of photon travel. However, this does not generally hold in a vegetation canopy of flat leaves. For example, in a canopy consisting of mainly horizontal leaves, the probability of hitting a leaf is much larger for a photon traveling in the vertical direction than for one traveling in the horizontal direction. Thus, the Ross–Nilson G-function (a function returning a value between zero and one for every direction) is used to describe the effect of foliage orientation: it equals the ratio of leaf area projected in a given direction (ϑ,ϕ) to the total leaf area [85].

The distribution of foliage inside a natural canopy is not uniform and the assumptions of Beer's law are not fulfilled. To accurately describe the attenuation of radiation (including PAR) inside vegetation, more complex methods have to be used, and one must take into account the structure of the vegetation layer. In addition to the above-mentioned angular distribution of foliage, additional variables describing the geometric properties of plants at various levels (shoot, branch, crown, etc.) have to be used. Introduction of larger-scale structures decreases interception at the top of the canopy and increases it in middle canopy layers [94, 95].

Scattering Inside the Canopy The small fraction of photons in the PAR waveband not absorbed when hitting a leaf give rise to a phenomenon commonly known as beam enrichment. After one or two scatterings in the canopy (very few photons in the PAR waveband survive more), photons may be inserted back into the beam traveling in the direction of the receiver. In other words, as plant leaves are not black (completely absorbing), the downward flux of radiation is "enriched" by scattered photons. Naturally, the amplitude of this effect depends on the scattering properties of the scattering elements, leaves, and needles.

To describe the reflectance and transmittance properties of plant leaves, they are usually assumed to be Lambertian surfaces – the angular distribution of reflected (or transmitted) radiance does not depend on the direction of scattering. Actual leaves deviate from Lambertian surfaces, mainly due to the specular (mirror-like) reflectance from the wax coating. However, for practical purposes, there is no information that the assumption of Lambertian scattering would lead to considerable errors [96]. Therefore, the scattering properties of flat leaves are generally described by up to three numbers: the two leaf reflectance values for the abaxial and adaxial leaf sides, and one leaf transmittance (the general reciprocity relations require for the two sides of a Lambertian surface to have identical transmittance [95]). However, quite often reflectances are not available separately for the two leaf sides and the reflectances of the adaxial and abaxial sides are taken equal.

The reflectance properties of leaves depend somewhat on species, growing conditions, and leaf status. Some approximate values are given in the literature. In his seminal book, Ross used the values 0.06 and 0.09 for leaf reflectance and transmittance in the PAR region, respectively [85]. Relatively little between-species variability in leaf optical properties, compared to within-species variability, was found during an extensive study in Texas, USA [97], indicating that the leaf optical properties in this spectral region are dynamically stable along a pronounced climate gradient. For trees and shrubs, a leaf reflectance of 0.09 (standard deviation 0.01) and a leaf transmittance of 0.06 ($\pm$0.03) was proposed; for grasses the resulting numbers were 0.12 ($\pm$0.01) for reflectance and 0.06 ($\pm$0.02) for transmittance [97]. Although the measurements were performed in the spectral interval of channel 1 of the AVHRR satellite sensor (550–700 nm) which corresponds to the green–red part of PAR, they can also be used to approximate the leaf optical properties in the whole PAR waveband with reasonably small errors.

Radiation Field Inside a Vegetation Canopy Canopy photosynthesis depends not only on the amount of available PAR, but also on how the irradiance is distributed: high and low PAR irradiance levels have different photosynthetic potentials. Without going into further details, it is possible to divide the locations inside a plant canopy into three groups.

1. Full sunlight. In areas inside the canopy where the sun is completely visible, or "sunflecks," the radiation field is strongly dominated by the direct solar radiation beam. Under natural conditions, one can safely ignore the contribution of scattered PAR and assume that the spectral distribution of radiation is identical to that above the canopy.
2. Penumbra. Due to the nonzero diameter of the solar disc, shadows cast by sunrays do not have sharp edges. Full sunlight and complete shadow are always separated by a narrow strip with smoothly varying irradiance. If the angular dimensions of the shadowing object are smaller than the apparent diameter of the solar disc, for example, the object is far from the receiver, no complete shadowing can occur. Depending on the fraction of the solar disc visible, the PAR flux and spectrum in penumbra may be close to what they would be under either direct sunlight or complete shadow.
3. Shadow (umbra). Behind large objects or sufficiently deep down into the canopy, the direct solar irradiance can be considered zero. Thus, the radiation conditions in umbra are determined by the possible presence of diffuse sky radiation, radiation scattered by plant elements, and radiation reflected by the underlying soil. The spectral composition of radiation depends on skylight conditions, the amount of visible sky, and the spectral properties of canopy elements. On an overcast day, the whole canopy is effectively in a shadow cast by clouds.

The division as given above is just one of the possible approaches to categorizing the radiation field. No standard practice has emerged yet in the scientific literature: the word "sunfleck" is the general term used to

describe areas with increased irradiance, whereas the penumbra is often ignored. Depending on application, the penumbra may be treated as either an area where the sun is obstructed (i.e., shadow) or, in contrast, an area where the irradiance is above the threshold determined by the reading below a dense canopy (i.e., sunfleck).

Due to the dynamic nature of sunflecks, the radiation field inside a canopy can be highly variable, both spatially and temporally [98]. Variations in the diffuse field are generally much smaller, and thus global irradiance in umbra is much easier to measure. For this reason, canopy transmittance measurements made on a cloudy day are much more representative. For example, 412 radiometers would be required to estimate the instantaneous downward radiation flux in a pine stand with a maximum error of 10% in the midday flux above the canopy, whereas just one instrument is needed for a full-day average in a hardwood canopy [99]. When averaged over the path, the sun follows on a day or a growing season, the mean transmittance of direct radiation can be approximated by a single measurement of transmittance of diffuse sky radiation. However, due to natural limitations in the solar elevation and azimuth angles which are specific to each geographic location, systematic errors may occur [90].

Even if one has sufficient data to quantify the average PAR irradiance inside and below a vegetation canopy, this will not suffice for photosynthesis modeling purposes. It has been known for a long time that the photosynthetic response of a leaf is not linear with PAR irradiance (see section "PAR in Vegetation Canopies"). Thus, the radiation field is commonly described as composed of two fluxes, direct and diffuse PAR, and PPFD values at leaf surfaces are calculated separately for the two fluxes [100]. Beside atmospheric conditions, the availability of direct solar radiation depends only on canopy structure. In contrast, diffuse radiation is generated via more numerous mechanisms.

The first source of what can be called diffuse radiation, or radiation of diminished radiance compared with direct solar radiance above the vegetation canopy, is penumbra. Penumbral effects are purely geometric and are most evident in a tall canopy of small scatterers, for example, in a needle-leaf boreal forest. At high latitudes, low sun angles further increase the pathlength of direct solar beam in the canopy, thus making the penumbra dominate the radiation field on a clear day. In a canopy consisting of shoots, the penumbral effect alters the irradiance distribution, but also vertically redistributes the photosynthetic potential inside the canopy [101]. Coupling the nonzero angular diameter of the sun and the three-dimensional structure of the vegetation canopy can lead (at least in model calculations) to an increase in canopy photosynthetic capacity by tens of percent [102, 103]. Such computations are rare in the scientific literature since the correct prediction of penumbral irradiation assumes nonzero scatterer sizes, which is beyond the scope of traditional RTT.

The second source of diffuse radiation, multiple scattering inside vegetation, depends on the canopy structure and cannot be easily predicted without a radiative transfer model. However, whereas modeling penumbra requires special consideration for both the spatial distribution and the dimensions of canopy elements, the dimensions of leaves are usually ignored when calculating multiple scattered radiation fluxes. Assuming infinitesimally small leaves makes it possible to apply the traditional methods for solving RTT [85, 86].

The third component of the diffuse PAR field inside a vegetation canopy is contributed by diffuse sky radiation: some of the photons scattered by the atmosphere can penetrate the vegetation layer without being intercepted by canopy elements. Depending on cloudiness and other atmospheric conditions, the diffuse sky irradiance can vary within large limits. The complications related to calculating this PAR component originate in the difficulties of correctly estimating the variability of above-canopy diffuse radiance. In contrast, the canopy transmittance can be modeled from simple structural assumptions or measured from hemispheric photography.

The diffuse sky PAR irradiance is usually less than one-third of the global PAR irradiance (section "PAR Below the Atmosphere"). Considering that not all of the sky is visible inside the canopy, the diffuse PAR irradiance (on a horizontal surface) is at least one order of magnitude smaller than the direct PAR irradiance in a sunfleck. The adaptation of leaves in deeper canopy layers (where sunflecks are rare) to low irradiances makes diffuse sky radiation more effective in inducing photosynthesis than direct PAR [104]. In other words, the light use efficiency is generally larger

for diffuse radiation than for direct irradiance: this effect is sometimes termed diffuse-radiation fertilization. Thus, an increase in diffuse PAR can lead to increased carbon assimilation. This mechanism has been proposed as the explanation of the decrease in global CO_2 concentration after Mt. Pinatubo's eruption in 1991. Volcanic eruptions are known to increase the amount of atmospheric aerosol for several years thus enhancing diffuse sky radiation [105, 106] and global carbon assimilation. The adverse effect of decreasing the amount of anthropogenic sulfate aerosol could similarly lead to a decrease or fall in global photosynthesis [107].

The spectral distribution of PAR above and below a vegetation canopy is shown in Fig. 9. Four spectral distributions are shown, corresponding to global and diffuse radiation above and below a closed alder canopy (LAI = 2). The distributions are normalized so that their maximum value in the PAR waveband equals unity. Whereas changes in the spectral distribution of global PAR are relatively small, alteration of the spectral distribution for the diffuse field is quite significant. Above the canopy, the diffuse radiation spectrum peaks at blue wavelengths. The diffuse PAR field below a canopy reaches its maximum at about 550 nm, which corresponds to green light. Further, in the near-infrared (NIR) region, at wavelengths immediately above 700 nm, the diffuse spectral irradiance below the canopy increases to levels much higher than those in the PAR waveband. Such an increase emphasizes the requirement to consider spectral errors with care: if the sensor sensitivity cutoff at 700 nm is not sharp enough, measurements of diffuse PAR inside a vegetation canopy are contaminated by the high NIR irradiance. Also, the differing spectral composition of diffuse radiation between the higher and lower canopy layers must be taken into account when calculating the contribution of diffuse radiation to canopy photosynthesis.

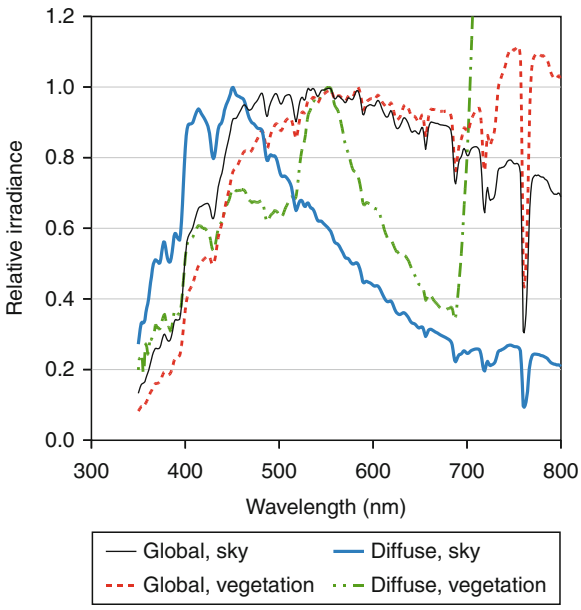

Photosynthetically Active Radiation: Measurement and Modeling. Figure 9
Spectral distribution of radiation on a clear day above and below a vegetation canopy. Measurements were made inside and next to a gray alder (*Alnus incana*) plantation (leaf area index L = 2.1) in Tõravere, Estonia

Explicit treatment of the total PAR available for photosynthesis is thus a complex task [98]. Exact computations require that many factors are taken into account: dimensions of the solar disc and the scattering elements, detailed structure of the vegetation canopy, spectral properties of leaves, nongreen canopy elements and soil, spectral and angular distributions of incident radiation, etc. Due to the large spatial and temporal variability of PAR inside a plant canopy, its measurement and empirical analysis are also extremely complicated and only a few examples are presented in the literature [20, 108].

Measurement of PAR Absorbed by Canopies

Direct Measurement of APAR The PAR flux absorbed by plant canopies (APAR) may be either measured directly using PAR sensors or estimated indirectly, based on canopy gap fraction measurements. Leaf area index (LAI) measurements may also be used to estimate the PAR absorbed by the canopy. First, a description of direct PAR measurements is given.

The PAR absorbed by vegetation equals the total amount of radiative energy absorbed by all plant surfaces and can thus be measured in either quantum or energy units. The formulation of the problem is identical for the two representations. Here, the quantum APAR (Q^4_{PAR}) is used as an example. Due to the different spectral compositions of PAR that is incident or reflected and transmitted by a vegetation canopy,

converting between Q^A_{PAR} and its companion quantity in energy units, I^A_{PAR}, is not a straightforward task. Thus, estimates of fAPAR from quantum measurements are not directly comparable with fAPAR values calculated in energy units. However, considering the measurement uncertainties and the errors related to retrieval of fAPAR from remote sensing measurements, the differences are ignored here.

Q^A_{PAR} is computed from the energy conservation law in the canopy using hemispherical fluxes:

$$Q^A_{\mathrm{PAR}} = Q^{\downarrow}_{\mathrm{PAR}}(z_{\mathrm{top}}) - Q^{\uparrow}_{\mathrm{PAR}}(z_{\mathrm{top}}) - Q^{\downarrow}_{\mathrm{PAR}}(0) + Q^{\uparrow}_{\mathrm{PAR}}(0). \tag{10}$$

where $Q^*_{\mathrm{PAR}}(z)$ represents downward $Q^{\downarrow}_{\mathrm{PAR}}(z)$ or upward $Q^{\uparrow}_{\mathrm{PAR}}(z)$ hemispherical PAR fluxes at the bottom ($z = 0$) or top ($z = z_{top}$) of the canopy. Therefore, the hemispherical PAR sensors should be precisely located to obtain representative measurements of the several terms in the PAR balance:

- $Q^{\downarrow}_{\mathrm{PAR}}(z_{\mathrm{top}})$, the incident PAR at the top of the canopy is measured using upward-looking sensors at the top of the canopy
- $Q^{\uparrow}_{\mathrm{PAR}}(z_{\mathrm{top}})$, the reflected PAR is measured using downward-looking sensors at the top of the canopy
- $Q^{\downarrow}_{\mathrm{PAR}}(0)$, the transmitted PAR is measured by upward-looking sensors placed at the bottom of the canopy
- $Q^{\uparrow}_{\mathrm{PAR}}(0)$, the PAR reflected by the soil is measured using downward-looking sensors at the bottom of the canopy

The number of sensors used to measure the several terms in a representative way depends mainly on the heterogeneity of the canopy and on the typical footprint of the sensor. About half of the flux collected by a hemispherical sensor comes from inside a circle whose radius equals the distance of the sensor from the object it is looking at [109]; about 96% of the signal originates from inside a circle with a radius of five times the distance. Therefore, many sensors (between 5 and 50) are required to properly measure all the terms in Eq. 10 at the bottom of the canopy: the distance from the sensor to the bottom of the canopy (when measuring $Q^{\downarrow}_{\mathrm{PAR}}(0)$) or the soil (when measuring $Q^{\uparrow}_{\mathrm{PAR}}(0)$) is generally limited. Conversely, just one sensor is required for the incoming PAR, $Q^{\downarrow}_{\mathrm{PAR}}(z_{\mathrm{top}})$, and only a few for the reflected PAR, $Q^{\uparrow}_{\mathrm{PAR}}(z_{\mathrm{top}})$, depending on the distance between the sensor and the top of the canopy (Fig. 10).

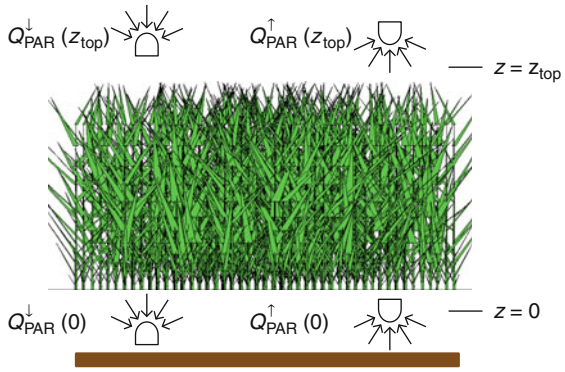

Photosynthetically Active Radiation: Measurement and Modeling. Figure 10
Configuration of PAR sensors to measure APAR and fAPAR. Sensor A measures the incident PAR $\left(Q^{\downarrow}_{\mathrm{PAR}}(z_{\mathrm{top}})\right)$, sensor B measures the reflected PAR $\left(Q^{\uparrow}_{\mathrm{PAR}}(z_{\mathrm{top}})\right)$, sensor C measures the transmitted PAR $\left(Q^{\downarrow}_{\mathrm{PAR}}(0)\right)$, and sensor D (usually omitted) measures the soil reflectance $\left(Q^{\uparrow}_{\mathrm{PAR}}(0)\right)$

The fraction of absorbed PAR $\left(\mathrm{fAPAR}, F^A_{\mathrm{PAR}}\right)$, may be derived from Eq. 10 by dividing all the terms by the incident PAR:

$$F^A_{\mathrm{PAR}} = 1 - r_{\mathrm{CAN}} - t_{\mathrm{CAN}}(1 - r_{\mathrm{SOIL}}), \tag{11}$$

where r_{CAN} is the reflectance of the canopy, t_{CAN} is the transmittance of the canopy, and r_{SOIL} is the soil reflectance. As mentioned above, F^A_{PAR} is used here to denote the quantum fAPAR, or the absorbed fraction of incident photons in the PAR waveband. Note that all these variables are bihemispherical quantities [110, 111], although the directional integration of incident radiation requires, as a minimum, weighing the direct and diffuse components of canopy transmittance. According to Eq. 11, fAPAR is a very convenient quantity: it is independent on the magnitude of the incident irradiance. However, fAPAR is somewhat sensitive to the irradiance geometry: the attenuation of the direct component of the incident radiation field varies strongly with the direction of the sun as well as canopy characteristics.

If the soil reflectance r_{SOIL} is assumed to be known, the PAR balance may be approximated by using measurement data for the three first terms only, that is, the incident $\left(Q^{\downarrow}_{PAR}(z_{top})\right)$, reflected $\left(Q^{\uparrow}_{PAR}(z_{top})\right)$, and transmitted $\left(Q^{\downarrow}_{PAR}(0)\right)$ radiation. Equation 11 may further be simplified as in the PAR domain, where very little multiple scattering is expected,

$$F^{A}_{PAR} \simeq (1 - t_{CAN})(1 - r_{\infty}), \tag{12}$$

where r_{∞} is the asymptotic value of canopy reflectance when the leaf area index, L, tends toward infinity. Values of r_{∞} are generally small in the PAR domain (around 0.06 [112]) since most photons are absorbed by the green leaves. In these conditions, the PAR balance, Eq. 10, may be approximated by measuring only the incident $\left(Q^{\downarrow}_{PAR}(z_{top})\right)$ and the transmitted $\left(Q^{\downarrow}_{PAR}(0)\right)$ terms. It is thus possible to avoid problems in measuring the soil reflectance r_{SOIL}: as highlighted earlier, many sensors are required due to the small distance between soil and sensor and the possible effect of the sensor shadow in its footprint. It also avoids problems related to the dependence of r_{SOIL} on the directionality of incident radiation.

Because the PAR balance and thus fAPAR both depend on the varying illumination geometry, continuous measurements are required. Furthermore, fAPAR measurements are generally used in light-use efficiency models [3, 113] which require daily and even seasonally integrated fAPAR values. The PAR radiance measurement system thus needs to be set in place from several days up to several months. In practice, this calls for weatherproof systems with sufficient autonomy both in terms of energy and memory. Affordable systems meeting these requirements and able to replicate individual observations for improved spatial sampling have been developed only recently. However, instantaneous measurements using several view directions may be achieved by different existing systems, allowing the reconstruction of fAPAR values for any (possibly modeled) illumination geometry.

In all situations, the approach based on radiation balance assesses the value of PAR absorbed by the canopy, independently of the nature of the radiation intercepting elements. As a consequence, when non-photosynthetic material (such as trunks, branches, or senescent leaves) constitutes a significant fraction of canopy, the true fAPAR, or PAR absorbed by the green photosynthetically active elements, is overestimated.

Estimation of fAPAR from fIPAR Green leaves generally absorb a very large fraction of light in the PAR domain, that is, they appear almost black from a pure radiative standpoint. Considering this, the fraction of absorbed PAR may be approximated by the fraction of intercepted PAR $\left(\text{fIPAR}, F^{I}_{PAR}\right)$:

$$F^{A}_{PAR} = 1 - t_{CAN}. \tag{13}$$

Combining Eqs. 12 and 13 provides a relation between the fraction of absorbed PAR and the intercepted fraction:

$$F^{A}_{PAR} = F^{I}_{PAR}(1 - r_{\infty}).$$

The validity of this approximation has been extensively investigated and found to hold with reasonable accuracy [114–117].

Instruments for Measuring fAPAR

Directional and Flux Measurements Based on the directionality of measurements, fAPAR sensors can be divided into two subgroups. The first group contains instruments that disregard the directional distribution of incident PAR (either by integrating over the upper hemisphere or looking into only one particular direction); the second group consists of instruments measuring with a field of view divided between different directions (multidirectional devices). Generally, the lack of directional sampling by instruments in the first group must be compensated by increased spatial sampling.

Ceptometers are devices consisting of an array of hemispherical sensors aligned on a single support, allowing for spatial representativeness. They are particularly well suited for crops: a ceptometer covering a transect representative of a forest canopy would be too long to be moved easily between the measurement locations. While a ceptometer is used to measure radiation below the canopy, the incident PAR can be simultaneously recorded with an additional PAR sensor. Examples of such sensor arrays are AccuPAR (Decagon, USA), SunScan (Delta-T, UK), and PAR/LE (Solems, France).

Other specialized multipoint radiation measurement systems have been developed (for mainly in-house use) on various scales. For example, spatial distributions of the radiation field (with focus on PAR) affecting a conifer shoot have been measured using optical fibers and a CCD matrix [118]. At the other end of the scale are systems capable of characterizing tree-level heterogeneity using hundreds of sensors attached to 5-m-long booms [119]. PAR @METER [120] is a recently developed device capable of continuously monitoring the transmitted PAR at different points inside and above a vegetation canopy. Incident and transmitted PAR are simultaneously recorded and stored in a network of sensors placed according to a predefined spatial sampling scheme using wireless computer connections.

Directional devices are generally less common than the hemispherical instruments listed above. Examples of directional, below-canopy radiation measuring devices are TRAC (Natural Resources, Canada) and DEMON (CSIRO, Australia). They measure direct sunlight and use different approximations to characterize the plant architecture. TRAC inverts the light transmittance profiles obtained on a transect based on a model of canopy gap size distribution [121]. It accounts for the nonhomogeneous distribution of foliage in certain canopies (also called clumping effect [122]) by inverting the measured sunfleck length distribution. DEMON makes use of Beer's law and a special zenith angle at which canopy transmittance does not depend on leaf orientation [123] to retrieve LAI from incident and transmitted PAR measurements.

The instruments mentioned above are designed for measurements of transmitted PAR. However, by adding canopy reflectance measurements, the complete PAR balance can be obtained (Fig. 10). From such balance measurements, it is also possible to calculate the fraction of absorbed PAR, fAPAR.

Multidirectional Transmission Instruments The incoming PAR may be decomposed into the direct component coming from the sun and the diffuse component due to light scattering in the atmosphere. For each of those components, a fAPAR value can be associated. The total fAPAR can then be written as:

$$F^A_{PAR} = \left(1 - f_{diff}\right) F^A_{PAR}(\Omega_S) + f_{diff} F^A_{PAR}(2\pi^+), \quad (14)$$

where f_{diff} is the diffuse fraction of radiation in global irradiance, Ω_S is the direction of the sun, and $2\pi^+$ is used to denote the upper hemisphere; $F^A_{\mathrm{PAR}}(\Omega_S)$ and $F^A_{\mathrm{PAR}}(2\pi^+)$ are thus the fAPAR values for direct-only or diffuse-only incidence, respectively. Sometimes, $F^A_{\mathrm{PAR}}(\Omega_S)$ is called the black-sky fAPAR and correspondingly, $F^A_{\mathrm{PAR}}(2\pi^+)$ the white-sky fAPAR. To apply Eq. 14 to the calculation of F^A_{PAR} for all sky conditions, the directional characteristics of t_{CAN} (Ω) have to be known.

Directional devices provide measurements of canopy transmittance, t_{CAN} (Ω), in a number of directions $\Omega = (\vartheta,\phi)$. Two types of devices are mainly used: the LAI-2000 instrument [124] and digital hemispherical cameras (DHC) [125, 126]. Lidar systems may also access the directional variation of light transmittance, although the technique might be better suited for other applications related to detailed characterization of canopy architecture. The LAI-2000 instrument measures light transmitted in the blue wavelengths to the bottom of the canopy in five concentric rings of 15° in the range $0 < \vartheta < 70°$. For each ring, all azimuths directions are accounted for. Measurements are generally taken under diffuse conditions to prevent an unwanted sensitivity to the specific sun direction, while minimizing any possible sun glint on the leaves. The blue spectral region is used since, at these wavelengths, leaves appear almost black and diffuse sky scattering is at its peak. The view azimuth angle can be modified using a series of view-limiting caps to block out a part of the sky or focus the measurements toward specific directions of interest.

Hemispherical cameras provide estimates of the gap fraction over the whole hemisphere. If the angular distribution of incident radiation is known, the gap fraction may be converted into canopy non-interceptance. Again, assuming that leaves are black at the visible wavelengths used by cameras, the canopy interceptance is converted into canopy absorptance. DHC usually involves a high-resolution digital camera and an attached fisheye lens. This fisheye lens projects the whole upper hemisphere onto the digital array of the camera, producing circular images. However, historical data recorded on black-and-white film may still be encountered and, in some cases, photographs made using ordinary lens are used (i.e., any lens not covering the whole hemisphere). The a posteriori processing of digital images provides the fraction of the upper

hemisphere covered by vegetation. This is done by classifying each pixel as sky or non-sky, that is, applying a threshold to divide the pixels constituting the image into two classes [126].

Furthermore, the variations in vegetation canopy transmittance with zenith (and sometimes also azimuth) angle may be used to reconstruct the diurnal variation of fAPAR. Note that, similarly to sensors measuring the transmitted PAR, no distinction is made between green photosynthetically active elements and the non-photosynthetic material. This may lead to an overestimation of the actual value of the true fAPAR. However, when using hemispherical photographs taken from above canopies, it may be possible to distinguish between green and nongreen elements. Unfortunately, downward looking photography is limited to relatively short canopies for obvious practical reasons. DHC techniques are very efficient by allowing instantaneous measurements that can be replicated multiple times to improve the spatial sampling while accessing the diurnal variation of fAPAR. However, such measurements are only representative of the current canopy architecture, and measurements should be repeated along the growing season to match the canopy architecture dynamics.

A novel approach consists in using digital cameras as hemispherical radiation receivers [127, 128]. Similarly to the traditional DHC approach, a fish-eye lens projects the whole hemisphere onto the sensor array. However, instead of just applying a threshold to identify the gaps in the canopy, the new "calibrated camera" method treats the receiving surface of the camera as a two-dimensional array of miniature quantum receivers. Each array element receives radiation from a single direction in the upper hemisphere. The spectral sensitivity functions of the array elements have maxima in the optical region of electromagnetic radiation, that is, in the PAR waveband. Therefore, after proper laboratory calibration, a raw digital image stored in the camera can be treated as a (PAR) radiance measurement result. However, these measurements must be treated with care because modern consumer cameras are complex optical systems designed for producing visually good-looking images, not recording spectral radiance values.

Relationships Between fAPAR and LAI The devices described above are often used (or even designed) for measuring canopy leaf area index (LAI) [92, 93]. Generally, all techniques to estimate LAI from PAR transmittance measurements rely on Beer's law (Eq. 8). The directional instruments allow for a more accurate integration over the hemisphere required for the accurate application of Beer's law. However, a direct use of it, without spectral integration, is still quite common when relating PAR irradiance and LAI [129]. The opposite link is also often made: if the canopy LAI is known, fAPAR can be modeled using the known optical properties of the elements constituting the vegetation canopy and some basic knowledge of canopy structure. All these calculations are based on the Beer's law specially formulated for vegetation canopies, as described in section "Quantitative Description of PAR in Vegetation Canopies".

APAR and fAPAR from Satellite Observations

The fraction of absorbed photosynthetically active radiation, fAPAR was probably the first biophysical variable to be estimated from remote sensing observations from NDVI, the normalized difference vegetation index computed as $\mathrm{NDVI} = \frac{r_{\mathrm{NIR}} - r_{\mathrm{RED}}}{r_{\mathrm{NIR}} + r_{\mathrm{RED}}}$, where r_{NIR} and r_{RED} are the top-of-canopy reflectance in the near-infrared (NIR) and red (RED) bands, respectively [130]. The early empirical relationships were later explained by investigating the radiative transfer in canopies [112, 131]. Compared to other biophysical variables (such as LAI), fAPAR appears to be retrievable much more accurately and robustly [132, 133]. The optimal configuration for retrieving fAPAR includes four spectral bands: red, near-infrared, green, and red edge. Simple observations in the red and near-infrared in view directions close to nadir were found to lead to slightly degraded performance.

The optimal view angle for a satellite instrument is not directly down (nadir), but in the principal solar plane close to the hot spot (the direction of the sun, corresponding to backward scattering), and in the perpendicular solar plane at zenith angles close that of the sun [132, 133]. Alternatively, directions around 60° from nadir in the backscattering direction or in the perpendicular plane were also shown to be close to optimal [134]. However, as these optimal configurations are not generally available, most algorithms for fAPAR retrieval focus on the minimization of

directional effects by simply making use of whatever remote sensing data can be obtained.

In addition to NDVI, indices have been developed to correct for the contribution of soil to the measured reflectance, or to use the more readily available top-of-atmosphere reflectance instead of the top-of-canopy value [116, 134]. Further, look-up tables have been used to derive fAPAR from MODIS top-of-canopy reflectance observations after calibration with radiative transfer model simulations [135]. However, when the physically based algorithm (known as the main algorithm) fails, a backup algorithm is triggered using relationships between fAPAR and MODIS NDVI. Neural networks have also been used [120, 136] to operationally retrieve fAPAR from satellite-measured radiances.

The main fAPAR products derived from satellite observations (Table 2) thus demonstrate a wide range of either empirical or physically based approaches. To obtain these fAPAR products, the needed inputs are either top-of-canopy or top-of-atmosphere reflectance values observed in 2–13 reflectance bands. Some

Photosynthetically Active Radiation: Measurement and Modeling. Table 2 Examples of fAPAR values derived from satellite-based reflectance measurements

Product name	Approach	Sensor	Reference
NDVI	Empirical linear regression	AVHRR	[130, 137, 140]
NDVI	Linear regression of RT simulations	AVHRR	[112, 141]
RDVI	Linear regression of RT simulations	POLDER	[134]
JRC-FAPAR	VI calibrated using RT simulations	PARASOL, SEVIRI	[116]
TOC-VEG	NN calibrated using RT simulations	MERIS	[136]
TOA-VEG	NN calibrated using RT simulations	MERIS	[142]
MODIS	LUT from RT simulations	MODIS	[135]
CYCLOPES	NN calibrated using RT simulations	Vegetation	[120]
GLOBCARBON	Derived from LAI product	Vegetation, MERIS, AATSR	[143]
GEOLAND2	NN calibrated using other products	Vegetation	[144]

VI vegetation index, *RT* radiative transfer, *NN* neural network, *LUT* look-up table

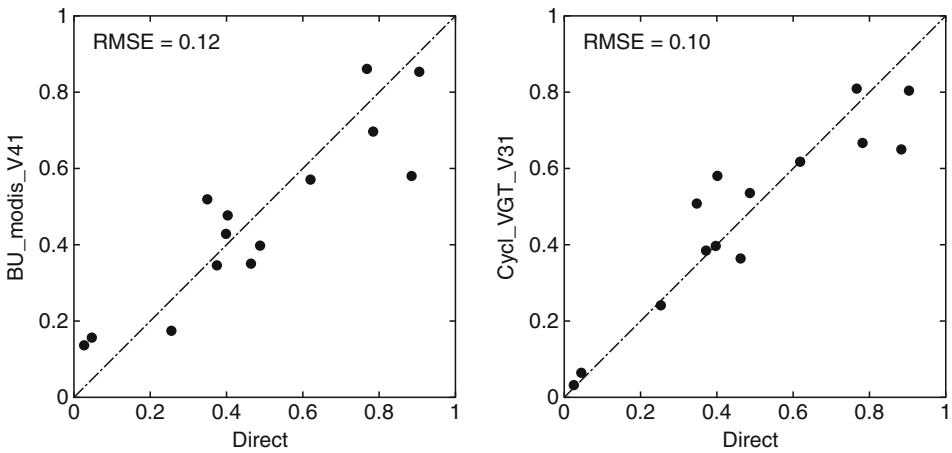

Photosynthetically Active Radiation: Measurement and Modeling. Figure 11
Comparison of ground-measured (horizontal axis) and satellite (vertical axis) estimates (MODIS: left, CYCLOPES: right) of fAPAR

algorithms use a priori information on vegetation type or rely on a land cover map. Most of the algorithms provide an instantaneous black-sky fAPAR value at the time of satellite overpass, while a few others use multidirectional observations, to provide a daily integrated black-sky value. Note that most of the polar orbiting sensors considered here are on satellites in sun-synchronous orbits with equatorial crossing time close to 10:00 local time. Under these conditions, the instantaneous black-sky fAPAR value is a good approximation of the daily integrated fAPAR value.

Individual validation exercises have been reported by several authors [116, 137–139]. They generally show a reasonable agreement between ground-measured fAPAR and satellite estimates, with RMSE values around 0.10–0.15 (in fAPAR units) (Fig. 11). Considering the complex interactions between radiation and vegetation canopies described above, fAPAR also has a most desirable feature: it is almost independent of scale. Values of fAPAR derived from algorithms applied at higher spatial resolution and integrated over a coarser spatial domain provide similar values to those derived using the same algorithm applied directly to the coarser spatial resolution [133]. Unfortunately, the same cannot be said of any other vegetation parameter derived from remote sensing data.

Future Directions

The current research related to PAR measurement (and, inevitably, modeling) is aimed at utilizing the technological advances in (remote) sensing technology to better characterize the environment we live in. Photosynthesis is the energy source for all life on earth. The raw energy for life is originally dispersed in the form of electromagnetic radiation arriving from our closest star. Although the importance of photosynthesis, and the role of shortwave radiation in it, has always been acknowledged, there are still large gaps in our understanding.

From a more technical point of view, the most evident and surprising gap is a lack of comprehensive ground-based measurement network. Fortunately, this lack of basic monitoring does not result in severe ignorance of global PAR availability. This is evidenced by the ongoing satellite measurements and the simultaneous model developments – to convert satellite sensor readings into radiation fluxes absorbed by vegetation hundreds of kilometers below. The progress is also witnessed by the large number of scientific articles with keywords such as fAPAR, satellite remote sensing, and global productivity. The ultimate goal of this research, however, is not only to give a detailed quantitative measure of the health of our planet, but also to provide the physical basis for describing and understanding the very fundamental links between the physical and biological environments.

Bibliography

1. McCree KJ (1972) The action spectrum, absorptance and quantum yield of photosynthesis in crop plants. Agric Meteorol 9(3–4):191–216
2. McCree KJ (1972) Test of current definitions of photosynthetically active radiation against leaf photosynthesis data. Agric Meteorol 10(6):443–453
3. Monteith JL (1977) Climate and efficiency of crop production in Britain. Philos Trans R Soc Lond B Biol Sci 281(980):277–294
4. Shibles R (1976) Terminology pertaining to photosynthesis. Crop Sci 16(3):437–439
5. CIE (1993) Terminology for photosynthetically active radiation for plants. CIE Collect Photobiol Photochem 106(6):42–46, ISBN 3900734461
6. McCree KJ (1965) Light measurements in plant growth investigations. Nature 206(4983):527–528
7. Inada K (1976) Action spectra for photosynthesis in higher-plants. Plant Cell Physiol 17(2):355–365
8. Barnes C, Tibbitts T, Sager J, Deitzer G, Bubenheim D, Koerner G, Bugbee B (1993) Accuracy of quantum sensors measuring yield photon flux and photosynthetic photon flux. Hortscience 28(12):1197–1200
9. Bonhomme R (2000) Beware of comparing RUE values calculated from PAR vs solar radiation or absorbed vs intercepted radiation. Field Crops Res 68(3):247–252, cited By (since 1996) 16
10. Sinclair TR, Muchow RC (1999) Radiation use efficiency. Adv Agron 65:215–265
11. Ross J, Sulev M (2000) Sources of errors in measurements of PAR. Agric For Meteorol 100(2–3):103–125
12. Gaastra P (1959) Photosynthesis of crop plants as influenced by light, carbon dioxide, temperature, and stomatal diffusion resistance. Mededel Landbouwhogeschool Wageningen 59:1–68
13. Nichiporovich A (1960) Conference on measurement of visible radiation in plant physiology. Sov Plant Physiol 7:744–747
14. McCree K (1966) A solarimeter for measuring photosynthetically active radiation. Agric Meteorol 3(5–6):353–366, cited By (since 1996) 20
15. Ross J (1975) Radiative transfer in plant communities. In: Monteith JL (ed) Vegetation and the atmosphere, vol 1. Academic, London/New York, pp 13–55

16. ISO (2004) Spatial distribution of daylight. CIE standard general sky. ISO 15469:2004/CIE 011:2003. ISO, 2004
17. LI-COR (1986) LI-COR radiation sensors. instruction manual. Publ. no 8609-56. Lincoln, Nebraska
18. LI-COR (1991) LI-COR radiation measurement instruments. Lincoln, Nebraska
19. Pearcy R (1989) Radiation and light measurements. In: Pearcy R, Ehleringer J, Mooney H, Rundel P (eds) Plant physiological ecology. Chapman & Hall, New York, pp 97–116, ch. 6
20. Ross J, Sulev M, Saarelaid P (1998) Statistical treatment of the PAR variability and its application to willow coppice. Agric For Meteorol 91(1–2):1–21
21. Norman JM, Tanner CB, Thurtell GW (1969) Photosynthetic light sensor for measurements in plant canopies. Agron J 61(6):840–843
22. Britton CM, Dodd JD (1976) Relationships of photosynthetically active radiation and shortwave irradiance. Agric Meteorol 17(1):1–7
23. Howell TA, Meek DW, Hatfield JL (1983) Relationship of photosynthetically active radiation to shortwave radiation in the San-Joaquin Valley. Agric Meteorol 28(2):157–175
24. Alados I, FoyoMoreno I, Alados-Arboledas L (1996) Photosynthetically active radiation: Measurements and modelling. Agric For Meteorol 78(1–2):121–131
25. Fielder P, Comeau P (2000) Construction and testing of an inexpensive PAR sensor. Ministry of Forests Research, British Columbia, Working Paper 53/2000
26. Rodskjer N, Kornher A (1971) Über die bestimmung der strahlungsenergie im wellen-längenbereich von 0, 3–0, 7 [mu] in pflanzenbeständen. Agric Meteorol 8:139–150
27. Slomka J, Slomka K (1986) Participation of photosynthetically active radiation in global radiation. In: Publications of the Institute of Geophysics, Polish Academy of Sciences, p 197
28. Stanhill G, Fuchs M (1977) Relative flux-density of photosynthetically active radiation. J Appl Ecol 14(1):317–322
29. Stigter CJ, Musabilha VMM (1982) The conservative ratio of photosynthetically active to total radiation in the tropics. J Appl Ecol 19(3):853–858
30. Blackburn WJ, Proctor JTA (1983) Estimating photosynthetically active radiation from measured solar irradiance. Sol Energy 31(2):233–234
31. Hansen V (1984) Spectral distribution of solar-radiation on clear days - a comparison between measurements and model estimates. J Climate Appl Meteorol 23(5):772–780
32. Rao CRN (1984) Photosynthetically active components of global solar-radiation – measurements and model computations. Arch Meteorol Geophys Bioclimatol B Theor Appl Climatol 34(4):353–364
33. Spitters CJT, Toussaint HAJM, Goudriaan J (1986) Separating the diffuse and direct component of global radiation and its implications for modeling canopy photosynthesis. 1. components of incoming radiation. Agric For Meteorol 38(1–3):217–229
34. Tooming H, Niilisk H (1967) Transition coefficients from integrated radiation to photosynthetic active radiation (PAR) under field conditions. In: Phytoactinometrical investigations of plant canopy (in Russian). Valgus Publishers, Tallinn, pp 140–149
35. Karalis JD (1989) Characteristics of direct photosynthetically active radiation. Agric For Meteorol 48(3–4):225–234
36. Jacovides CP, Kallos GB, Steven MD (1993) Spectral band resolution of solar-radiation in Athens, Greece. Int J Climatol 13(6):689–697
37. Stephens K, Strickland JDH (1962) Use of a thermopile radiometer for measuring the attenuation of photosynthetically active radiation in the sea. Limnol Oceanogr 7(4):485–487
38. Mims FM (2003) A 5-year study of a new kind of photosynthetically active radiation sensor. Photochem Photobiol 77(1):30–33
39. Mõttus M, Ross J, Sulev M (2001) Experimental study of ratio of PAR to direct integral solar radiation under cloudless conditions. Agric For Meteorol 109(3):161–170
40. Grant RH, Heisler GM, Gao W (1996) Photosynthetically-active radiation: Sky radiance distributions under clear and overcast conditions. Agric For Meteorol 82(1–4):267–292
41. Grant R, Heisler G (1997) Obscured overcast sky radiance distributions for ultraviolet and photosynthetically active radiation. J Appl Meteorol 36(10):1336–1345
42. McArthur LJB (2004) Baseline Surface Radiation Network (BSRN) operations manual, version 2.1. Technical Report WMO/TD-No. 879, World Climate Research Programme Baseline Surface Radiation Network. http://www.bsrn.awi.de/fileadmin/user_upload/Home/Publications/McArthur.pdf
43. Michalsky JJ, Harrison LC, Berkheiser WE (1995) Cosine response characteristics of some radiometric and photometric sensors. Sol Energy 54(6):397–402
44. Su WY, Charlock TP, Rose FG, Rutan D (2007) Photosynthetically active radiation from Clouds and the Earth's Radiant Energy System (CERES) products. J Geophys Res Biogeosci 112(G2):G02022
45. BSRN (2005) UV and PAR measurement. Report of the eighth session of the Baseline Surface Radiation Network (BSRN) workshop and scientific review meeting (Exeter, UK, 26–30 July 2004), vol 4/2005, pp 14–16. World Climate Research Programme, Informal Report 4/2005, 2005
46. Gueymard CA (2008) REST2: High-performance solar radiation model for cloudless-sky irradiance, illuminance, and photosynthetically active radiation – validation with a benchmark dataset. Sol Energy 82(3):272–285
47. Alados I, Alados-Arboledas L (Jan 1999) Direct and diffuse photosynthetically active radiation: measurements and modelling. Agric For Meteorol 93:27–38
48. Bosch JL, Lopez G, Batlles FJ (Jan 2009) Global and direct photosynthetically active radiation parameterizations for clear-sky conditions. Agric For Meteorol 149:146–158
49. Perez R, Ineichen P, Seals R, Michalsky J, Stewart R (1990) Modeling daylight availability and irradiance components from direct and global irradiance. Sol Energy 44(5):271–289
50. Alados I, Olmo FJ, Foyo-Moreno I, Alados-Arboledas L (Apr 2000) Estimation of photosynthetically active radiation under cloudy conditions. Agric For Meteorol 102:39–50

51. Alados-Arboledas L, Olmo FJ, Alados I, Perez M (2000) Parametric models to estimate photosynthetically active radiation in Spain. Agric For Meteorol 101(2–3):187–201
52. Jacovides CP, Timbios F, Asimakopoulos DN, Steven MD (1997) Urban aerosol and clear skies spectra for global and diffuse photosynthetically active radiation. Agric For Meteorol 87(2–3):91–104
53. Papaioannou G, Papanikolaou N, Retalis D (1993) Relationships of photosynthetically active radiation and shortwave irradiance. Theor Appl Climatol 48(1):23–27
54. Jacovides CP, Tymvios FS, Asimakopoulos DN, Theofilou KM, Pashiardes S (2003) Global photosynthetically active radiation and its relationship with global solar radiation in the Eastern Mediterranean basin. Theor Appl Climatol 74(3–4):227–233
55. Wang Q, Kakubari Y, Kubota M, Tenhunen J (Jan 2007) Variation on PAR to global solar radiation ratio along altitude gradient in Naeba Mountain. Theor Appl Climatol 87:239–253
56. McCree K (1981) Photosynthetically active radiation. In: Pirson A, Zimmermann M (eds) Encyclopedia of plant physiology, vol 12A. Springer, Berlin, Heidelberg, pp 41–55
57. Dye DG (2004) Spectral composition and quanta-to-energy ratio of diffuse photosynthetically active radiation under diverse cloud conditions. J Geophys Res Atmos 109(D10): D10203
58. Kirk JTO (1994) Light and photosynthesis in aquatic ecosystems, 2nd edn. Cambridge University Press, Cambridge/England
59. Buiteveld H, Hakvoort JH, Donze M (Oct 1994) Optical properties of pure water. In: Jaffe JS (ed) Society of Photo-Optical Instrumentation Engineers (SPIE) conference series, vol 2258 of Society of Photo-Optical Instrumentation Engineers (SPIE) Conference Series, pp 174–183
60. Bricaud A, Babin M, Morel A, Claustre H (1995) Variability in the chlorophyll-specific absorption-coefficients of natural phytoplankton - analysis and parameterization. J Geophys Res Oceans 100(C7):13321–13332
61. Bricaud A, Stramski D (1990) Spectral absorption-coefficients of living phytoplankton and nonalgal biogenous matter - a comparison between the Peru upwelling area and the Sargasso sea. Limnol Oceanogr 35(3):562–582
62. Jerlov NG (1976) Marine optics. Elsevier, Amsterdam/New York
63. Austin RW, Petzold TJ (1986) Spectral dependence of the diffuse attenuation coefficient of light in ocean waters. Opt Eng 25(3):471–479
64. Reinart A, Herlevi A (1999) Diffuse attenuation coefficient in some Estonian and Finnish lakes. Proc Estonian Acad Sci Biol Ecol 48(4):267–283
65. Reinart A, Arst H, Blanco-Sequeiros A, Herlevi A (1998) Relation between underwater irradiance and quantum irradiance in dependence on water transparency at different depths in the water bodies. J Geophys Res Oceans 103(C4):7749–7752
66. Dera J (1992) Marine physics. Elsevier, Amsterdam
67. Ehn J, Granskog MA, Reinart A, Erm A (2004) Optical properties of melting land-fast sea ice and underlying seawater in Santala Bay, Gulf of Finland. J Geophys Res Oceans 109(C9):C09003
68. Morel A, Smith RC (1974) Relation between total quanta and total energy for aquatic photosynthesis. Limnol Oceanogr 19(4):591–600
69. Aas E (1971) Natural history of Hardangerfjord. 9. Irradiance in Hardangerfjorden 1967. Sarsia 46:59–78
70. Ohmura A, Dutton EG, Forgan B, Frohlich C, Gilgen H, Hegner H, Heimo A, Konig-Langlo G, McArthur B, Muller G, Philipona R, Pinker R, Whitlock CH, Dehne K, Wild M (1998) Baseline surface radiation network (BSRN/WCRP): New precision radiometry for climate research. Bull Am Meteorol Soc 79(10):2115–2136
71. Baldocchi D, Falge E, Gu LH, Olson R, Hollinger D, Running S, Anthoni P, Bernhofer C, Davis K, Evans R, Fuentes J, Goldstein A, Katul G, Law B, Lee XH, Malhi Y, Meyers T, Munger W, Oechel W, Paw KT, Pilegaard K, Schmid HP, Valentini R, Verma S, Vesala T, Wilson K, Wofsy S (2001) FLUXNET: A new tool to study the temporal and spatial variability of ecosystem-scale carbon dioxide, water vapor, and energy flux densities. Bull Am Meteorol Soc 82(11):2415–2434
72. Friend AD, Arneth A, Kiang NY, Lomas M, Ogee J, Rodenbeckk C, Running SW, Santaren JD, Sitch S, Viovy N, Woodward FI, Zaehle S (2007) FLUXNET and modelling the global carbon cycle. Glob Change Biol 13(3):610–633
73. Augustine JA, DeLuisi JJ, Long CN (2000) SURFRAD - a national surface radiation budget network for atmospheric research. Bull Am Meteorol Soc 81(10):2341–2357
74. Hari P, Andreae MO, Kabat P, Kulmala M (2009) A comprehensive network of measuring stations to monitor climate change. Boreal Environ Res 14(4):442–446
75. Jacquemoud S, Baret F (1990) Prospect - a model of leaf optical-properties spectra. Remote Sens Environ 34(2):75–91
76. Feret JB, Francois C, Asner GP, Gitelson AA, Martin RE, Bidel LPR, Ustin SL, le Maire G, Jacquemoud S (2008) PROSPECT-4 and 5: Advances in the leaf optical properties model separating photosynthetic pigments. Remote Sens Environ 112(6):3030–3043
77. Sims DA, Gamon JA (2002) Relationships between leaf pigment content and spectral reflectance across a wide range of species, leaf structures and developmental stages. Remote Sens Environ 81(2–3):337–354
78. Martin G, Josserand SA, Bornman JF, Vogelmann TC (1989) Epidermal focusing and the light microenvironment within leaves of medicago-sativa. Physiol Plant 76(4):485–492
79. Farquhar GD, Caemmerer SV, Berry JA (1980) A biochemical-model of photosynthetic CO2 assimilation in leaves of C-3 species. Planta 149(1):78–90
80. Tardieu F, Simonneau T (1998) Variability among species of stomatal control under fluctuating soil water status and evaporative demand: modelling isohydric and anisohydric behaviours. J Exp Bot 49:419–432
81. Emerson R (1929) The relation between maximum rate of photosynthesis and concentration of chlorophyll. J Gen Physiol 12(5):609–622
82. Peñuelas J, Baret F, Filella I (1995) Semiempirical indexes to assess carotenoids chlorophyll-a ratio from leaf spectral reflectance. Photosynthetica 31(2):221–230

83. Moya I, Camenen L, Evain S, Goulas Y, Cerovic ZG, Latouche G, Flexas J, Ounis A (2004) A new instrument for passive remote sensing 1, measurements of sunlight-induced chlorophyll fluorescence. Remote Sens Environ 91(2):186–197
84. Maxwell K, Johnson GN (2000) Chlorophyll fluorescence - a practical guide. J Exp Bot 51(345):659–668
85. Ross J (1981) The radiation regime and architecture of plant stands. Dr. W. Junk Publishers, The Hague
86. Myneni R, Ross JE (1991) Photon-vegetation interactions. Springer, Berlin, Heidelberg
87. Malenovsky Z, Mishra KB, Zemek F, Rascher U, Nedbal L (2009) Scientific and technical challenges in remote sensing of plant canopy reflectance and fluorescence. J Exp Bot 60(11): 2987–3004
88. Monsi M, Saeki T (1953) Über den lichtfaktor in den pflanzengesellschaften und seine bedeutung für die stoffproduktion. Jpn J Bot 14:22–52
89. Monsi M, Saeki T (2005) On the factor light in plant communities and its importance for matter production. Ann Bot 95(3):549–567
90. Lieffers V, Messier C, Stadt K, Gendron F, Comeau P (1999) Predicting and managing light in the understory of boreal forests. Can J For Res 29(6):796–811
91. Campbell GS, Norman JM (1998) Introduction to environmental biophysics, 2nd edn. Springer, New York
92. Breda NJJ (Nov 2003) Ground-based measurements of leaf area index: a review of methods, instruments and current controversies. J Exp Bot 54:2403–2417
93. Jonckheere I, Fleck S, Nackaerts K, Muys B, Coppin P, Weiss M, Baret F (Jan 2004) Review of methods for in situ leaf area index determination - Part I theories, sensors and hemispherical photography. Agric For Meteorol 121:19–35
94. Ni WG, Li XW, Woodcock CE, Roujean JL, Davis RE (Dec 1997) Transmission of solar radiation in boreal conifer forests: Measurements and models. J Geophys Res Atmos 102:29555–29566
95. Mõttus M, Sulev M (2006) Radiation fluxes and canopy transmittance: Models and measurements inside a willow canopy. J Geophys Res Atmos 111(D2):D02109
96. Chelle M (2006) Could plant leaves be treated as Lambertian surfaces in dense crop canopies to estimate light absorption? Ecol Modell 198(1–2):219–228
97. Asner GP, Wessman CA, Schimel DS, Archer S (Mar 1998) Variability in leaf and litter optical properties: Implications for BRDF model inversions using AVHRR, MODIS, and MISR. Remote Sens Environ 63:243–257
98. Baldocchi D, Collineau S (1994) The physical nature of solar radiation in heterogeneous canopies: spatial and temporal attributes. In: Exploitation of environmental heterogeneity by plants: ecophysiological processes above- and below ground. Academic, San Diego, pp 21–71
99. Reifsnyder W, Furnival G, Horowitz J (1971–1972) Spatial and temporal distribution of solar radiation beneath forest canopies. Agric Meteorol 9:21–37
100. DePury DGG, Farquhar GD (May 1997) Simple scaling of photosynthesis from leaves to canopies without the errors of big-leaf models. Plant Cell Environ 20:537–557
101. Oker-Blom P (1985) Photosynthesis of a Scots pine shoot – simulation of the irradiance distribution and photosynthesis of a shoot in different radiation-fields. Agric For Meteorol 34(1):31–40
102. Myneni RB, Asrar G, Wall GW, Kanemasu ET, Impens I (1986) Canopy architecture, irradiance distribution on leaf surfaces and consequent photosynthetic efficiencies in heterogeneous plant canopies. 2 results and discussion. Agric For Meteorol 37(3):205–218
103. Stenberg P (1998) Implications of shoot structure on the rate of photosynthesis at different levels in a coniferous canopy using a model incorporating grouping and penumbra. Funct Ecol 12(1):82–91
104. Gu LH, Baldocchi D, Verma SB, Black TA, Vesala T, Falge EM, Dowty PR (2002) Advantages of diffuse radiation for terrestrial ecosystem productivity. J Geophys Res Atmos 107(D5–6):4050
105. Roderick ML, Farquhar GD, Berry SL, Noble IR (Sept 2001) On the direct effect of clouds and atmospheric particles on the productivity and structure of vegetation. Oecologia 129:21–30
106. Gu LH, Baldocchi DD, Wofsy SC, Munger JW, Michalsky JJ, Urbanski SP, Boden TA (2003) Response of a deciduous forest to the Mount Pinatubo eruption: Enhanced photosynthesis. Science 299(5615):2035–2038
107. Mercado LM, Bellouin N, Sitch S, Boucher O, Huntingford C, Wild M, Cox PM (Apr 2009) Impact of changes in diffuse radiation on the global land carbon sink. Nature 458:1014–1017
108. Vesala T, Markkanen T, Palva L, Siivola E, Palmroth S, Hari P (Feb. 2000) Effect of variations of PAR on CO2 exchange estimation for Scots pine. Agric For Meteorol 100:337–347
109. Schmid HP (1997) Experimental design for flux measurements: matching scales of observations and fluxes. Agric For Meteorol 87(2–3):179–200
110. Schaepman-Strub G, Schaepman ME, Painter TH, Dangel S, Martonchik JV (2006) Reflectance quantities in optical remote sensing-definitions and case studies. Remote Sens Environ 103(1):27–42
111. Nicodemus FE (1970) Reflectance nomenclature and directional reflectance and emissivity. Appl Opt 9(6):1474–1475
112. Baret F, Guyot G (1991) Potentials and limits of vegetation indexes for LAI and APAR assessment. Remote Sens Environ 35(2–3):161–173
113. McCallum I, Wagner W, Schmullius C, Shvidenko A, Obersteiner M, Fritz S, Nilsson S (2010) Comparison of four global FAPAR datasets over Northern Eurasia for the year 2000. Remote Sens Environ 114(5):941–949
114. Asrar G (1989) Theory and applications of optical remote sensing. Wiley, New York
115. Begue A, Desprat JF, Imbernon J, Baret F (1991) Radiation use efficiency of pearl-millet in the Sahelian zone. Agric For Meteorol 56(1–2):93–110
116. Gobron N, Pinty B, Aussedat O, Chen JM, Cohen WB, Fensholt R, Gond V, Huemmrich KF, Lavergne T, Melin F,

Privette JL, Sandholt I, Taberner M, Turner DP, Verstraete MM, Widlowski JL (2006) Evaluation of fraction of absorbed photosynthetically active radiation products for different canopy radiation transfer regimes: methodology and results using joint research center products derived from SeaWiFS against ground-based estimations. J Geophys Res Atmos 111(D13110):1–15

117. Russel G, Jarvis P, Monteith J (1989) Absorption of radiation by canopies and stand growth. In: Russel G, Marshall B, Jarvis PG (eds) Plant canopies: their growth, form and function. Cambridge University Press, New York, pp 21–39
118. Palva L, Garam E, Manoochehri F, Sepponen R, Hari P, Rajala K, Ruotoistenmaki H, Seppala I (1998) A novel multipoint measuring system of photosynthetically active radiation. Agric For Meteorol 89(2):141–147
119. Palva L, Markkanen T, Siivola E, Garam E, Linnavuo M, Nevas S, Manoochehri F, Palmroth S, Rajala K, Ruotoistenmaki H, Vuorivirta T, Seppala I, Vesala T, Hari P, Sepponen R (2001) Tree scale distributed multipoint measuring system of photosynthetically active radiation. Agric For Meteorol 106(1):71–80
120. Baret F, Hagolle O, Geiger B, Bicheron P, Miras B, Huc M, Berthelot B, Nino F, Weiss M, Samain O, Roujean JL, Leroy M (2007) LAI, fAPAR and fCover CYCLOPES global products derived from VEGETATION - part 1: Principles of the algorithm. Remote Sens Environ 110(3):275–286
121. Chen JM (1996) Optically-based methods for measuring seasonal variation of leaf area index in boreal conifer stands. Agric For Meteorol 80(2–4):135–163
122. Nilson T (1971) Theoretical analysis of frequency of gaps in plant stands. Agric Meteorol 8(1):25–38
123. Lang ARG (1986) Leaf-area and average leaf angle from transmission of direct sunlight. Aust J Bot 34(3):349–355
124. Welles JM, Norman JM (1991) Instrument for indirect measurement of canopy architecture. Agron J 83:818–825
125. Baret F, Andrieu B, Folmer J, Hanocq J, Sarrouy C (1993) Gap fraction measurement from hemispherical infrared photography and its use to evaluate PAR interception efficiency. In: Crop structure and microclimate: characterization and applications, INRA edn. Paris, pp 359–372
126. Leblanc SG, Chen JM, Fernandes R, Deering DW, Conley A (2005) Methodology comparison for canopy structure parameters extraction from digital hemispherical photography in boreal forests. Agric For Meteorol 129:187–207
127. Cescatti A (2007) Indirect estimates of canopy gap fraction based on the linear conversion of hemispherical photographs: Methodology and comparison with standard thresholding techniques. Agric For Meteorol 143:1–12
128. Lang M, Kuusk A, Mõttus M, Rautiainen M, Nilson T (2010) Canopy gap fraction estimation from digital hemispherical images using sky radiance models and a linear conversion method. Agric For Meteorol 150(1):20–29
129. Campbell GS (1986) Extinction coefficients for radiation in plant canopies calculated using an ellipsoidal inclination angle distribution. Agric For Meteorol 36(4):317–321
130. Asrar G, Fuchs M, Kanemasu ET, Hatfield JL (1984) Estimating absorbed photosynthetic radiation and leaf-area index from spectral reflectance in wheat. Agron J 76(2):300–306
131. Myneni RB, Williams DL (1994) On the relationship between fAPAR and NDVI. Remote Sens Environ 49(3):200–211
132. Weiss M, Baret F (1999) Evaluation of canopy biophysical variable retrieval performances from the accumulation of large swath satellite data. Remote Sens Environ 70(3):293–306
133. Weiss M, Baret F, Myneni RB, Pragnere A, Knyazikhin Y (2000) Investigation of a model inversion technique to estimate canopy biophysical variables from spectral and directional reflectance data. Agronomie 20(1):3–22
134. Roujean JL, Breon FM (1995) Estimating PAR absorbed by vegetation from bidirectional reflectance measurements. Remote Sens Environ 51(3):375–384
135. Myneni RB, Hoffman S, Knyazikhin Y, Privette JL, Glassy J, Tian Y, Wang Y, Song X, Zhang Y, Smith GR, Lotsch A, Friedl M, Morisette JT, Votava P, Nemani RR, Running SW (2002) Global products of vegetation leaf area and fraction absorbed PAR from year one of MODIS data. Remote Sens Environ 83(1–2):214–231
136. Bacour C, Baret F, Beal D, Weiss M, Pavageau K (2006) Neural network estimation of LAI, fAPAR, fCover and LAIxC(ab), from top of canopy MERIS reflectance data: Principles and validation. Remote Sens Environ 105(4):313–325
137. Fensholt R, Sandholt I, Rasmussen MS (2004) Evaluation of MODIS LAI, fAPAR and the relation between fAPAR and NDVI in a semi-arid environment using in situ measurements. Remote Sens Environ 91(3–4):490–507
138. Morisette JT, Baret F, Privette JL, Myneni RB, Nickeson JE, Garrigues S, Shabanov NV, Weiss M, Fernandes RA, Leblanc SG, Kalacska M, Sanchez-Azofeifa GA, Chubey M, Rivard B, Stenberg P, Rautiainen M, Voipio P, Manninen T, Pilant AN, Lewis TE, Iiames JS, Colombo R, Meroni M, Busetto L, Cohen WB, Turner DP, Warner ED, Petersen GW, Seufert G, Cook R (2006) Validation of global moderate-resolution LAI products: A framework proposed within the CEOS Land Product Validation subgroup. IEEE Trans Geosci Remote Sens 44(7):1804–1817
139. Weiss M, Baret F, Garrigues S, Lacaze R (2007) LAI and fAPAR CYCLOPES global products derived from VEGETATION, part 2: validation and comparison with MODIS collection 4 products. Remote Sens Environ 110(3):317–331
140. Wiegand CL, Maas SJ, Aase JK, Hatfield JL, Pinter PJ, Jackson RD, Kanemasu ET, Lapitan RL (1992) Multisite analyses of spectral-biophysical data for wheat. Remote Sens Environ 42(1):1–21
141. Sellers PJ (1985) Canopy reflectance, photosynthesis and transpiration. Int J Remote Sens 6(8):1335–1372
142. Baret F, Pavageau K, Béal D, Weiss M, Berthelot B, Regner P (2006) Algorithm theoretical basis document for MERIS top of atmosphere land products (TOA_VEG). INRA-CSE, 2006
143. Deng F, Chen JM, Plummer S, Chen MZ, Pisek J (2006) Algorithm for global leaf area index retrieval using satellite imagery. IEEE Trans Geosci Remote Sens 44(8):2219–2229

144. Baret F, Weiss M, Lacaze R, Camacho F, Pacholcyzk P, Makhmara H, Smets B (2010) Consistent and accurate LAI, FAPAR and FCOVER global products: principles and evaluation of GEOV1 products. In Sobrino (ed) Proceedings of the third international symposium on recent advances in quantitative remote sensing, Valencia (Spain), pp 208–213

Photovoltaic Energy, Introduction

Daniel Lincot
Institute of Research and Development of Photovoltaic Energy, Chatou, Cedex, France

Article Outline

Glossary

Glossary

III-V Solar cells Solar cells based on compound combining elements from the Ga and As columns (III and V).

Cadmium telluride (CdTe) solar cells Solar cells based on this compound, used in the form of thin films.

Chalcopyrite solar cells Solar cells based on the compound $Cu(In,Ga)Se_2$, also noted CIGS, in the form of thin films.

Dye sensitized solar cells (DSSC) Solar cells based on mesoscopic tintanium oxide thin film sensitized with dye photoactive molecules and impregnated by an electrolyte.

Hot carrier solar cell New high efficiency concept allowing to convert high energy photons in electrical charges in the external circuit without thermal losses.

Life cycle analysis (LCA) To quantify all the steps from mining, utilization to recycling in terms of energy consumption, material utilization, environmental and health impacts.

Multijunction solar cell High efficiency solar cell based on the association of several elementary solar cells made of sing junctions.

Organic solar cells Solar cells based on organic components like carbon fullerenes and polymers, blended in the form of thin films.

Pay back time Time needed by a solar cell under operation to reimburse the total energy used for its fabrication.

Photovoltaics Conversion of photon energy to electricity.

Siicon solar cells Solar cells based on silicon element, either in crystalline or amorphous forms.

Solar cells Device allowing to absorb photon energy and convert it to electricity in an external circuit.

Up, down conversion New high efficiency concept using optical processes allowing to convert low (resp. high) energy photons to medium visible energy photons for maxium conversion efficiency.

Photovoltaics is the direct conversion of solar energy into electricity. It results from the fundamental mechanism of absorption of photons in matter, with the excitation of electrons from their equilibrium lower energy state to a nonequilibrium excited state of higher energy. That means that electrons are being transferred to more negative electrical potential. Then, they usually return to equilibrium by giving back the initial photon energy in form of thermal energy (with the interactions with phonons), light with the emission of new photons via luminescence processes or chemical species via electrochemical oxydo reduction processes in the case of photosynthesis. The uniqueness and beauty of photovoltaics is to "plug" on the initial step when electrons are just excited to a lower potential, and to have them directly transferred in an external circuit where the energy can be used directly in the electrical form. The device to do it is just a solar cell. However, to have it efficient imposes to be able to compete with the naturally occurring spontaneous processes! This was not easy and from the discovery of the photovoltaic effect in 1839 by Edmond Becquerel to the first efficient silicon solar cell in 1954 it took more than one century and then 50 years more to reach the years 2000s to assist to the large scale industrial endeavor of photovoltaic conversion of solar energy, bringing for the first time in the human history this new renewable energy technology as an alternative to fossil fuels and nuclear utilizations. While laboratory record efficiency for any photovoltaic cells is reaching the incredible value of 43%, approaching the 50% level, more than 20 GW of photovoltaic peak power sources have been produced by the industry in 2010. This is the

reason why this section of the encyclopedia on photovoltaics is timely.

It aims to give the most advanced analyses of the context of photovoltaic deployment in the present days and the frontiers of key solar cell technologies and concepts in their booming research environment. These entries will be authored by upmost specialists in each field, who have been or are still directly active in key advances.

► PV Policies and Markets, authored by Dr. Wolfgang Palz, former European Union Official in charge of photovoltaic R&D programs for long time, and presently President of the World Council on Renewable Energies, will present an insight analysis of photovoltaic policy and markets, discuss specific questions associated with fast changes of players and fast decrease of prices and presents his views on challenges for the future.

► Photovoltaics, status of presents an extensive review of the status of photovoltaics, starting with an overview of the existing and emerging technologies, followed by the analysis of research and developments issues and presenting then the state of the art of the photovoltaic industry. In the second part of the entry, it is presented the photovoltaic market with specific focuses on the European Union, the Asia and Pacific region, and then North America. This broad view entry is authored by Dr Arnaulf Jaeger Waldau, from the Joint Research Center of the European Commission. Dr Arnulf Jaeger Waldau is the author of the famous series of yearly edited PV Status reports.

Life cycle analysis (LCA) is a key concern in the photovoltaic domain in order to assess and quantify their benefit for contributing to creating a fully sustainable society. Life cycle analysis is thus a very important emerging domain also in all other area of the human activity, considering for a given product all its aspects from mining, processing, use, and recycling steps. Prof. Vasilis Fthenakis, from the Brookhaven National Laboratory, is a pioneer and one of the most eminent researcher on LCA in the field of photovoltaics. He authored this specific area in entry ► Solar Cells: Energy Payback Times and Environmental Issues by considering two aspects, one is the energy payback time of solar cells, that means the time needed for the device to reimburse by its own production the energy which has been used for its production, the other one concerns environmental issues. The analysis and discussion will cover the different photovoltaic technologies at their present state of the art and give detailed information for the reader.

After these three supplementary entries, devoted to economical and environmental aspects of photovoltaics, the next entries will focus on each photovoltaic technology, ranging of established crystalline silicon technologies and emerging thin film technologies to very high efficiency devices and new concepts. Organic and hybrid photovoltaic devices will complete the panorama of actual and future photovoltaic technologies.

The entry on crystalline wafer-based silicon technologies, ► Silicon Solar Cells, Crystalline, which is by far, the majoritary technology (87% of the market in 2010) is authored by a group of researchers specialists of these technologies under the lead of Prof. Santo Martinuzzi from the University of Marseille, a pioneer of silicon photovoltaics, well-known for his contributions to the characterization and understanding of electrical defects and passivation effects in silicon material. The entry will recall some historical aspects of the crystalline silicon technology and fundamental processes used for silicon production, purification, and device elaboration. It will present very important phenomena associated to defect characterization and passivation which control the cell efficiencies. It will be concluded by presenting the remarkable developments in new solar cell architectures which pave the way of future generations of crystalline silicon solar cells.

► Silicon Solar Cells, Thin-film is authored by Prof. Christopher Wronsky, from Pennsylvania State University and Prof. Nicolas Wyrsch from the Ecole Polytechnique Fédérale de Lausanne (EPFL) and devoted to thin film silicon solar cells, based on long standing amorphous to newly introduced microcrystalline materials, and representing 5% of the market in 2010. C.W. is a pioneer of amorphous silicon solar cells, which is the historical thin film solar cell technology, and specialist of their fundamental properties. He discovered key physical phenomenon known as the Straebler-Wronski effect. N.W. is highly involved in the unique R&D experience in microcrystalline solar cells alone or combined with amorphous solar cells known as the micromorph concept. The entry will go in depth along the whole sequences of thin film Si solar

cells, from the growth to devices physics and properties. It contains unique descriptions of physicochemical properties of layers controlling the device efficiencies and properties. Future directions in this promising technology are addressed at the last section of the entry.

► CdTe Solar Cells deals with another thin film technology based on cadmium telluride devices which has experienced an exceptional development since 2005, moving from a secondary industrial position to the first one in 2009, only in 5 years. It represents 5% of the market in 2010. CdTe technology is now the leading thin film technology and was capable to demonstrate in practice for the first time the cost reduction breakthrough expected for thin film technologies. The entry is written by Prof. Ayodya Tiwari and S. Buecheler,L. Kranz, J. Perrenoud from his group. Prof. Tiwari is a leading researcher in the field of CdTe solar cells. The entry will bring the reader from the description of state of the art of CdTe solar cells to in depth presentation and analysis of key processing steps and properties of layers and devices. Environmental and material resource aspects which are real concerns for this technology will be also considered, together with future directions.

► Solar Cells, Chalcopyrite-based Thin Film will continue this travel within thin film solar cell technologies with an another exceptional nonsilicon material based on the ternary compound $CuInSe_2$ noted CIS and its alloys with Ga, Al, S (mainly with Ga noted CIGS). CIS technologies are just starting their industrial endeavor (1.6%) while cell record efficiencies at the laboratory level now overpasses 20%, similar to that obtained with wafer-based polycrystalline silicon solar cells. This opens a new direction for thin film solar cells in competing also in the field of high efficiency devices. Prof. Hans Schock for Helmholz Zentrum Berlin (HZB), a pioneer and main actor of the CIGS adventure, recipient of the famous Becquerel price, has authored this entry with insights in key aspects of growth and properties of CIGS layers, junction formation, and device properties, from fundamental to process oriented focus. He will discuss present bottlenecks and future challenges of this technology.

The two next entries are devoted to the field of emerging technologies based on organic solar cells. This represents a new avenue for photovoltaics which was historically based on inorganic materials like silicon and compound semiconductors. The idea is that using organic materials may allow new cost reduction breakdowns and the use of low temperature processing compatible with plastic substrates. Up to the 90s, the use of organic photoactive layers was hampered by limited performances in charge separation and electronic transport required for efficient devices. A revolutionary concept was demonstrated in 91 in the case of hybrid solar cells is that of interpenetrated networks junctions, and then also introduced in the field of full organic junctions, and named bulk heterojunction concept. Since this time, organic-based solar cells are associated to a booming R&D activity.

► Mesoscopic Solar Cells presents the advent of hybrid nanostructured solar cells, based on the sensitization of nanoporous oxide layers, mostly titanium oxide, with dye molecules, followed by the impregnation by a liquid electrolyte containing an energetically suite redox couple (mostly iode-iodide). These cells, also named Dye Sensitized Solar Cells (DSSC) which are photoelectrochemical cells, reach impressive performances, up to 12% record cells and start to be industrially produced for niche markets. The author of the entry "► Mesoscopic Solar Cells" is Prof. Michael Graetzel, from the Ecole Polytechnique Fédérale de Lausanne. He is the inventor of DSSCs in 91 and since this time leads with his group key advances in the field related to the optimization of the electrode, the dye molecules, and also the replacement of the liquid electrolyte by a solid state one. His entry will present key aspects of this technology and future challenges.

► Organic Solar Cells is devoted to the field of full organic solar cells, based on carbon fullerenes, polymers, and small organic molecules. Will these "plastic solar cells," as their sister devices of organic electroluminescence devices (OLED), bring a new revolution in photovoltaics, together with Dye cells? This is clearly an open avenue which can be anticipated from the constant progress in performances and stability during the last period, with record cell efficiencies increasing from a few per cent in 2000 to about 10% now. Even if the module efficiencies are still about a few per cent and time stability is a concern, niche markets are already open. This status is the result of key researchers in the field as Prof. Saricifti of the Linz

Institute for Organic Solar Cells and Prof. Ching Tang from the University of Rochester who are authoring with Dr Daniel Glowacki this entry on organic solar cells. From operating principles to actual state and future directions, key aspects of this booming field will be presented and analyzed in great detail.

► Solar Cells, High-Efficiency opens the magic box of photovoltaics with the graal of obtaining ultra high Efficiency devices. While the efficiency of standard single junctions is theoretically limited to around 32%, according to the Schockley Queisser (S-Q) theory, and being approached by record silicon devices (25%) and even closer recently with GaAs devices (28%), theoretical studies predict that the efficiency could be as high as around 85%. Increasing the efficiency of solar cells beyond the S-Q limit is thus a key challenge for photovoltaic research, with achieving for instance 50% efficiencies as a practical achievable goal. In fact devices based on multijunctions, which exist for long time, are already able to escape the S-Q limit. A fascinating race is engaged between different laboratories using triple junctions based on gallium arsenide (GaAs) and it allows with P and Al operating under concentration, and recent record is now 43.5%. With about 30 layers deposited epitaxially, these devices are the cathedrals of photovoltaic technology which may gain 1 or to levels to reach 50%. Beyond the multijunction concept, new revolutionary concepts base on simpler device architectures have been proposed in the last decade, based on changing the wavelengths of the photons by up and down conversion optical processes (photon conversion concept), or by introducing additional levels in the band gap of single junctions (intermediate gap), or by collecting the generated charges just after their formation before partial relaxation (hot carrier concept). This entry will be authored by Dr Jean François Guillemoles from IRDEP and Dr Alex Freundlich from the University of Houston who are eminent specialists in these fields.

The entry will thus give a detailed view of the state of the art of photovoltaics with a specific focus on solar cell technologies which are the active component, the engine, in energy transformation, and a booming domain. Other aspects, which have not been treated yet in the section, but which are also very important are photovoltaic systems and PV integration in architecture or in solar farms.

Photovoltaics, Status of

Arnulf Jäger-Waldau
European Commission, DG Joint Research Centre, Institute for Energy and Transport;
Renewable Energy Unit, Ispra (VA), Italy

Article Outline

Glossary
Definition of the Subject
Introduction
Technology Overview
Research and Development in Photovoltaics
The Photovoltaic Industry
The Photovoltaic Market
Conclusions
Future Directions
Exchange Rates
Bibliography

Glossary

Photovoltaics (PV) PV is a method of generating electrical power by converting solar radiation into direct current electricity using semiconductors that exhibit the photovoltaic effect and are called solar cells.

Photovoltaic capacity The capacity of PV systems is given in Wp (watt peak). This characterizes the maximum DC (direct current) output of a solar module under standard test conditions, that is, at a solar radiation of 1,000 W/m^2 and at a temperature of 25°C.

Photovoltaic electricity generation The actual electricity generation potential of a photovoltaic electricity system depends on the solar radiation and the system performance, which depends on the BOS component losses. For a solar radiation between 600 and 2,200 kWh/m^2/year an average PV system can produce between 450 and 1,650 kWh of AC electricity.

Photovoltaic module and photovoltaic system A number of solar cells form a solar "Module" or "Panel," which can then be combined to solar systems, ranging from a few Watts of electricity output to multimegawatt power stations.

Photovoltaic (PV) energy system A PV system is composed of three subsystems:

- On the power generation side, a subsystem of PV devices (cells, modules, arrays) converts sunlight to direct current (DC) electricity.
- On the power use side, the subsystem consists mainly of the load, which is the application of the PV electricity.
- Between these two, we need a third subsystem that enables the PV-generated electricity to be properly applied to the load. This third subsystem is often called the "balance of system" or BOS.

Polisilicon or polycrystalline silicon Polisilicon or Polycrystalline silicon is a material consisting of small silicon crystals.

EC framework program This is the main instrument of the European Union for funding research.

Feed-in tariff A feed-in tariff is a policy mechanism which obliges regional or national electric grid utilities to buy renewable electricity (electricity generated from renewable sources, such as solar power, wind power, wave and tidal power, biomass, hydropower, and geothermal power) from all eligible participants at a fixed price over a fixed period of time.

Power purchase agreement (PPA) A PPA is a legal contract between an electricity generator (provider) and a power purchaser (host).

Solar cell production capacities

- In the case of wafer silicon–based solar cells, only the cells
- In the case of thin films, the complete integrated module
- Only those companies which actually produce the active circuit (solar cell) are counted
- Companies which purchase these circuits and make cells are not counted.

Definition of the Subject

Solar energy is the most abundant of all energy resources, and the rate at which solar energy is intercepted by the Earth is about 10,000 times greater than the rate at which all energy is used on this planet.

Solar energy can be used by a family of technologies capable of being integrated amongst themselves, as well as with other renewable energy technologies. The solar technologies can deliver heat, cooling, electricity, lighting, and fuels for a host of applications.

The conversion of solar energy into electricity, the photovoltaic effect, was discovered by Alexandre-Edmond Becquerel in 1839. However, it took more than a 100 years, until in 1954 scientists at the Bell Laboratories unveiled the first modern solar cell, using a silicon semiconductor to convert light into electricity.

With the oil crisis of the 1970s, many countries in the world started solar energy research and development (R&D) programs, but it took another 20 years until the first market implementation programs for grid-connected solar photovoltaic electricity generation systems started in the 1990s and began to prepare the basis for the development of a photovoltaics industry.

Introduction

For more than 10 years, photovoltaics has been one of the fastest growing industries with growth rates well beyond 40% per annum. This growth is driven not only by the progress in materials and processing technology, but by market introduction programs in many countries around the world and the increased volatility and mounting fossil energy prices. Despite the negative impacts of the economic crisis which started in 2008, photovoltaics is still growing at an extraordinary pace.

Reported production data for the global cell production in 2010 vary between 18 and 27 GW. The significant uncertainty in the data for 2010 is due to the highly competitive market environment, as well as the fact that some companies report shipment figures, others report sales and again others report production figures. In addition, the difficult economic conditions and increased competition led to a decreased willingness to report confidential company data. The data presented, collected from various companies and colleagues were compared to various data sources and thus led to an estimate of 24 GW (Fig. 1), representing a doubling of production compared to 2009.

Since 2000, total PV production increased almost by two orders of magnitude, with annual growth rates

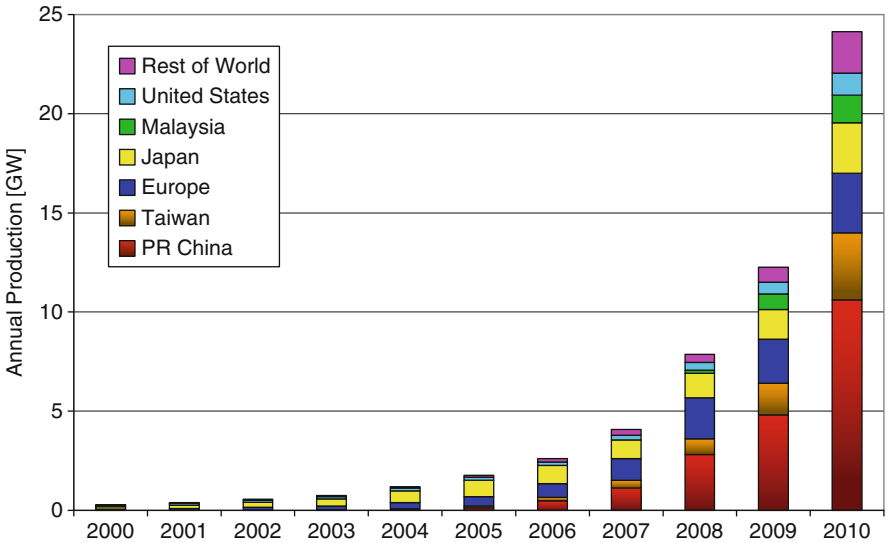

Photovoltaics, Status of. Figure 1
Worldwide PV Production from 2000 to 2010 (Data Source: Navigant Consulting [1, 2], PV News [3], Photon International [4], and own analysis)

between 40% and 90%. The most rapid growth in annual production over the last 5 years could be observed in Asia, where China and Taiwan together now account for almost 60% of worldwide production.

Public-traded companies manufacturing solar products, or offering related services, have attracted a growing number of private and institutional investors. In 2010, worldwide new investments into the renewable energy and energy efficiency sectors increased to a new record of $243 billion (€ 187 billion), up 30% from 2009 and for the third year in a row solar power attracted, behind wind, the second largest amount of new investments into renewable energies [5]. Europe was still the leading region in terms of renewable energy investments, totaling $94.4 billion (€ 72.6 billion), followed by Asia/Oceania with $82.8 billion (€ 63.7 billion) and the Americas with $65.8 billion (€ 50.6 billion) [6].

The number of consulting companies and financial institutions offering market studies and investment opportunities has considerably increased in the last years, and business analysts are very confident that despite the current economic turmoil, the Photovoltaics sector is in a healthy long-term condition. Following the stock market decline, as a result of the financial turmoil, the PPVX (Photon Pholtovoltaic stock index) declined to 2,095 points at the end of 2008. At the beginning of July 2011, the index stood at 2,107 points and the market capitalization of the 30-PPVX companies was € 36.4 billion.

The PPVX is a noncommercial financial index published by the solar magazine "Photon" and "Öko-Invest." The index started on August 1, 2001 with 1,000 points and 11 companies and is calculated weekly using the Euro as reference currency. Only companies which made more than 50% of their sales in the previous year with PV products or services are included [7]. Please note that the composition of the index changes as new companies are added and others have to leave the index.

At the end of 2010, about 48% or $94.8 billion (€ 72.9 billion) of the $194.3 billion (€149.5 billion) global "green stimulus" money from governments aimed to help relieve the effect of the recession, had reached the markets [5]. For 2011 another $68 billion (€52.3 billion) are expected.

Market predictions for the 2011 PV market vary between 17.3 GW by the Navigant Consulting conservative scenario [2], 22 GW by IMS Research [8], and 24.9 GW by iSuppli [9], with a consensus value in the 20 GW range. Massive capacity increases are underway or announced and if all of them are realized, the

worldwide production capacity for solar cells would exceed 80 GW at the end of 2012. This indicates that even with the optimistic market growth expectations, the planned capacity increases are way above the market growth. The consequence would be the continuation of the low utilization rates and therefore a continued price pressure in an over-supplied market. Such a development will accelerate the consolidation of the photovoltaics industry and spur more mergers and acquisitions.

The current solar cell technologies are well established and provide a reliable product, with sufficient efficiency and energy output for at least 25 years of lifetime. This reliability, the increasing potential of electricity interruption from grid overloads, as well as the rise of electricity prices from conventional energy sources, add to the attractiveness of Photovoltaic systems.

About 80% of the current production uses wafer-based crystalline silicon technology. A major advantage of this technology is that complete production lines can be bought, installed, and be up and producing within a relatively short time frame. This predictable production start-up scenario constitutes a low-risk placement with calculable return on investments. However, the temporary shortage in silicon feedstock and the market entry of companies offering turn-key production lines for thin-film solar cells led to a massive expansion of investments into thin-film capacities between 2005 and 2009. More than 200 companies are involved in the thin-film solar cell production process ranging from R&D activities to major manufacturing plants.

Projected silicon production capacities available for solar in 2012 vary between 140,000 t from established polysilicon producers, up to 185,000 t including the new producers [10] and 250,000 t [11]. The possible solar cell production will in addition depend on the material use per Wp. Material consumption could decrease from the current 8 g/Wp to 7 g/Wp or even 6 g/Wp, but this might not be achieved by all manufacturers.

Similar to other technology areas, new products will enter the market, enabling further cost reduction. Concentrating Photovoltaics (CPV) is an emerging market with approximately 30–40 MW cumulative installed capacity at the end of 2010. In addition, Dye-cells are getting ready to enter the market as well. The growth of these technologies is accelerated by the positive development of the PV market as a whole.

Further photovoltaic system cost reductions will depend not only on the technology improvements and scale-up benefits in solar cell and module production, but also on the ability to decrease the system component costs as well as the whole installation, projecting, operation, and financing costs.

Technology Overview

In order to give an overview of the technologies discussed, this entry will list the different technologies under investigation and in production with general descriptions rather than techno-scientific details, which are better championed by respective specialists. For categorization reasons, the solar cell technologies are divided into two categories of "*existing PV technologies*" and "*emerging technologies*."

Existing PV Technologies

These technologies include wafer-based crystalline silicon PV as well as the thin-film technologies *copper-indium/gallium-disulfide/diselenide* (CIGS), *cadmium telluride* (CdTe), and thin-film silicon PV (amorphous and microcrystalline). Mono- and poly(multi)crystalline silicon PV (including ribbon technologies) are the dominant technologies on the PV market, with a 2010 market share of about 80%.

Crystalline silicon modules are typically produced in a processing sequence along a value chain that starts with purified silicon, which is melted and solidified using different techniques to produce ingots or ribbons with variable degrees of crystal perfection. The ingots are then shaped into bricks and sliced into thin wafers by wire-sawing. In the case of ribbons, wafers are cut from the sheet typically using a laser. Cut wafers and ribbons are processed into solar cells and interconnected in weatherproof packages designed to last for at least 25 years.

In the laboratory, the externally verified record cell conversion efficiency is 25.0% for *monocrystalline silicon* and 20.4% for *multicrystalline cells* [12–14] under standard reporting conditions (i.e., 1,000 W/m^2, AM1.5, 25°C). The theoretical Shockley-Queisser limit of a single-junction Si solar cell is 31% conversion efficiency [15] while the specific maximum

efficiency for crystalline silicon has been calculated to be 29% [16].

Several variations for higher efficiency have been developed, for example, *heterojunction solar cells* and *interdigitated back contact solar cells*. These solar cells consist of a crystalline silicon wafer base with a (deposited) amorphous silicon emitter. The highest efficiency of heterojunction solar cells is 23% for a 100-cm^2 cell [17]. In an interdigitated back contact solar cell both the base and the emitter are contacted at the back of the cell, with as one of the advantages the avoidance of shading of the front of the cell by a top electrode. The highest efficiency of such a monocrystalline silicon back contact cell reported is 23.4% [18].

Wafers have decreased in thickness from 400 μm in 1990 to less than 200 μm in 2009 and have increased in area from 100 cm^2 to over 200 cm^2. Modules have increased in efficiency from about 10% in 1990 to typically 13–15% today, with the best performers above 17%. In addition, manufacturing facilities have increased from the typical 1–5 MWp annual outputs in 1990 to hundreds of MWp for today's largest factories. The processes in the value chain have progressed significantly during recent years, but they still have potential for further large improvements. Commercial module efficiencies for wafer-based silicon PV range from 12% to 20%.

Commercial thin-film technologies include a range of material systems, from silicon-based cells to the chalcopyrite material family like cadmium telluride (CdTe) or copper indium gallium diselenide disulfide (CIGSS). These solar cells have a base material of a few micrometer thickness deposited on glass, metal, or plastic substrates with sizes up to 5.7 m^2.

The *amorphous silicon* (a-Si) solar cell, introduced in 1976 [19] with initial efficiencies of 1–2%, has been the first commercially successful thin-film solar cell technology. Amorphous Si is a quasi-direct-bandgap material and hence has a high light absorption coefficient; therefore, the thickness of an a-Si cell can be 1,000 times thinner than that of a crystalline Si (c-Si) cell. Developing better efficiencies for a-Si has been limited by inherent material quality and by light-induced degradation – the Staebler–Wronski effect [20]. However, research efforts have successfully lowered the impact of the Staebler–Wronski effect to around 10% or less by controlling the microstructure of the film. The highest stabilized efficiency reported is 10.1% [21].

Higher efficiency has been achieved by using multijunction technologies with alloy materials, for example, germanium and carbon to form semiconductors with lower or higher bandgaps, respectively, to cover a wider range of the solar spectrum [22]. Another approach to increase the efficiency of thin-film silicon devices is through a tandem consisting of a microcrystalline silicon bottom cell with an amorphous silicon top cell [23, 24]. Stabilized efficiencies of 12–13% have been measured for various laboratory devices [12].

CdTe solar cells using a heterojunction with CdS have shown significant promise, because CdTe has a suitable energy bandgap of 1.45 electron-volts (eV) with a high coefficient of light absorption. The best efficiency of this cell is 16.5% [25], and commercially available modules have an efficiency of around 10%. Goncalves et al. predicted that the maximum efficiency will be 17.6%, and future improvements will focus on how to further reduce manufacturing costs, which are already the lowest in the industry [26]. The toxicity of metallic cadmium and the relative scarcity of tellurium are issues commonly associated with this technology. CdTe itself is a semiconductor and only limited toxicological data are available. Therefore, the evaluation of potential health risks is so far based on other forms of cadmium [27]. The currently known toxic health effects described on a typical material safety data sheet are limited to dust inhalation and ingestion. Recent investigations by Zayed et al. on the acute oral and inhalation toxicity in rats show that the toxicity potential is much lower than that of cadmium [28]. But this potential hazard is mitigated by using a glass-sandwiched module design and by recycling the entire module, as well as industrial waste [27]. Contrary to the commonly associated scarcity of tellurium, Wadia et al. found that the currently known economic tellurium reserves would allow the installation of approximately 10 TW of CdTe solar cells [29].

The *copper indium gallium sulfur selenide* material family is the base for the highest efficiency thin-film solar cells so far. The $CuInSe_2$/CdS solar cell was invented in the early 1970s at Bell Labs [30]. Incorporating Ga and/or S to produce $CuInGa(Se,S)_2$ (CIGSS)

results in the benefit of a widened bandgap depending on the composition [31]. CIGS-based solar cells yield a maximum efficiency of 20.3% [32], using a double graded layer of Ga in the absorption layer to realize both high current density and high open-circuit voltage. Due to higher efficiencies and lower manufacturing energy consumptions, CIGSS cells are currently in the industrialization phase with best commercial module efficiencies of up to 13.1% [33] for $CuInGaSe_2$ and 8.6% for $CuInS_2$ [34]. Contrary to the commonly associated scarcity of indium, Wadia et al. found that the currently known economic indium reserves would allow the installation of more than 10 TW of CIGSS based photovoltaic systems [29].

High-efficiency solar cells based on GaAs and InGaP (i.e., III-V semiconductors) have superior efficiencies but are also expensive, devices. Double- and triple-junction devices are currently being commercialized. An economically feasible application is the use of these cells in concentrator PV systems [35]. The most commonly used cell is a three-junction device based on GaInP/GaAs/Ge, with a record efficiency of 41.6% [36] under 364× concentrated light. Concentrator application requires a high fraction of direct (vs diffuse) irradiation, and is thus only suited for the sunbelt regions, that is, using the optical systems available so far.

Emerging Technologies

These are technologies that are still under development and in laboratory or (pre-) pilot stage, but could become commercially viable within the next decade. These are based on very low-cost materials and/or processes and include technologies such as dye-sensitized solar cells, organic solar cells and low-cost (printed) versions of existing inorganic thin-film technologies.

Electricity generation by *dye-sensitized solar cells* (DSSCs) is based on light absorption in dye molecules (the "sensitizers") attached to the very large surface area of a nanoporous oxide semiconductor electrode (e.g., TiO_2), followed by injection of excited electrons from the dye into the oxide. The dye/oxide interface thus serves as the separator of negative and positive charges, like the p-n junction in other devices. The injected electrons are then replenished by electrons supplied through a liquid electrolyte which penetrates the pores and which provides the electrical path from the counter electrode [37]. State-of-the-art DSSCs have achieved a top conversion efficiency of 10.9% [12]. Despite the gradual improvements since its discovery in 1991 [38], long-term stability, in combination with a reasonable efficiency (depending on the application) is a key issue in commercializing these PV cells.

Organic PV (OPV) cells use stacked solid organic semiconductors, either polymers or small organic molecules. A typical structure of a small molecule OPV cell consists of a stack of p-type and n-type organic semiconductors forming a planar heterojunction. The short-lived nature of the excited states (excitons) formed upon light absorption limits the thickness of the semiconductor layers that can be used and therefore the efficiency of such devices. Note that excitons need to move to the interface where positive and negative charges can be separated before they de-excite. If the travel distance is short, the "active" thickness of the material is small and not all light can be absorbed within that thickness. The efficiency that can be achieved with single-junction OPV cells is about 5% [39]. To decouple exciton transport distances from optical thickness (light absorption), so-called bulk-heterojunction devices have been developed. In these devices, the absorption layer is made of a nanoscale mixture of p- and n-type materials (respectively polymers such as P3HT and fullerenes) to allow the excitons to reach the interface within their lifetime, while also enabling a sufficient macroscopic layer thickness. This bulk-heterojunction structure plays a key role in improving the efficiency, to a record value of 8.3% [12]. The developments in cost and processing [40, 41] of materials have caused OPV research to advance further. Also here the main development challenge is the achievement of a sufficiently high stability in combination with a reasonable efficiency.

Novel technologies are potentially disruptive (high-risk, high-potential) approaches based on new materials, devices, and conversion concepts. Generally, their practically achievable conversion efficiencies and cost structure are still unclear. Examples of

these approaches include intermediate band semiconductors, hot carrier devices, spectrum converters, plasmonic solar cells, and various applications of quantum dots. Whereas the emerging technologies described in the previous section primarily aim at very low cost, while achieving a sufficiently high efficiency and stability, many (not all) novel technologies aim at reaching very high efficiencies, by making better use of the entire solar spectrum from infrared to ultraviolet. Generally, their *practically* achievable conversion efficiencies and cost structure are still unclear.

Photovoltaic System

A *photovoltaic system* is composed of the PV module, as well as the balance of system, which includes storage, system utilization, and the energy network. The system must be reliable, cost-effective, attractive, and match with the electric grid in the future. Detailed information can be found in various studies and roadmaps from organizations around the world (U.S. Photovoltaic Industry Roadmap [42]; Navigant Consulting Inc. [43]; EU PV European Photovoltaic Technology Platform [44]; Kroposki [45]; NEDO [46].

At the component level, a major objective of balance-of-system (BOS) development is to extend the lifetime of BOS components for grid-connected applications to that of the modules, typically 20–30 years, in addition to further reducing the cost of components and of installation. The highest priority is given to developing inverters, storage devices, and new designs for specific applications such as building-integrated PV. For systems installed in isolated, off-grid areas, component lifetime should be increased to around 10 years, and components for these systems need to be designed so that they require little or no maintenance. Storage devices are necessary for off-grid PV systems and will require innovative approaches to the short-term storage of small amounts of electricity (1–10 kWh); in addition, approaches are needed for integrating the storage component into the module, thus providing a single streamlined product that is easy to use in off-grid and remote applications. Moreover, devices for storing large amounts of electricity (over 1 MWh) will be adapted to large PV systems in the new energy network. As new module technologies emerge in the future, some of the ideas relating to BOS may need to be revised. Furthermore, the quality of the system needs to be assured and adequately maintained according to defined standards, guidelines, and procedures. To assure system quality, assessing performance is important, including online analysis (e.g., early fault detection) and off-line analysis of PV systems. The knowledge gathered can help to validate software for predicting the energy yield of future module and system technology designs.

To increasingly penetrate the energy network, PV systems must use technology that is compatible with the electric grid and energy supply and demand. System designs and operation technologies must also be developed in response to demand patterns by developing technology to forecast power generation volume and to optimize the storage function. Moreover, inverters must improve the quality of grid electricity by controlling reactive power or filtering harmonics with communication in a new energy network such as the Smart Grid.

Research and Development in Photovoltaics

With the oil crisis of the 1970s, many countries in the world started solar energy research and development (R&D) programs. A vast amount of the research efforts was and is still concentrated on improving the solar cell and module efficiencies, but research efforts in photovoltaic system components, reliability and manufacturing technologies is of equal importance to drive down costs. A new field of research is emerging, which is not only crucial to photovoltaic generated electricity but all fluctuating renewable energy sources – the integration into existing infrastructures or the design of new smart grid structures. In this entry, the main research issues are shortly described as well as the research activities in some world regions.

Research Issues

PV modules are the basic building blocks of flat-plate PV systems. Further technological efforts should lead to cost reduction, performance enhancement, and an

improved environmental profile. It is useful to distinguish between technology categories that require specific R&D approaches.

1. Wafer-based crystalline silicon.
2. Existing thin-film technologies.
3. Emerging and novel technologies (including "boosters" to technologies in 1 and 2).

   For these three technology categories, the following paragraphs list the R&D topics of highest importance. More details can be found in the different PV roadmaps, for example, Strategic Research Agenda for Photovoltaic Solar Energy Technology [44], U.S. Photovoltaic Industry Roadmap [42], and Japanese PV Roadmap [46, 47].

   - *Efficiency, energy yield, stability, and lifetime*

     Research often aims at optimization rather that maximization of these parameters, which means that additional costs and gains are critically compared. Since research is primarily aimed at reducing the cost of electricity generation it is important not to focus on initial costs (€/Wp) only, but also on lifecycle gains, that is, actual energy yield (kWh/Wp over the economic or technical lifetime).
   - *High productivity manufacturing, including in-process monitoring and control*

     Throughput and yield are important parameters in low-cost manufacturing and essential to achieve the cost targets. In-process monitoring and control are crucial tools to increase product quality and yield. Dedicated developments are needed to bring PV manufacturing to maturity.
   - *Environmental sustainability*

     The energy and materials requirements in manufacturing as well as the possibilities for recycling are important parameters in the overall environmental quality of the product. Further shortening of the energy pay-back time, design for recycling and, ideally, avoiding of the use of critical materials are the most important issues to be addressed here.
   - *Applicability*

     As discussed in more detail in the paragraphs on BOS and systems, standardization and harmonization are important to bring down the costs of PV. Some of the related aspects have to be addressed on a module level. In addition, improved ease of installation is partially related to module features. Finally, aesthetic quality of modules (and systems) is an important aspect for large-scale use in the built environment.
4. Concentrator systems are a separate category, because the R&D issues are fundamentally different compared to flat-plate technologies.

   It is noted, however, that some of the concepts discussed under "Emerging and novel technologies" might in the end be especially suited for use in concentrator systems.

   Concentrated Photovoltaics (CPV) offers a variety of technical solutions and these solutions are given on system level. The research issues can be divided into the following activities:

   - Concentrator solar cell manufacturing
   - Optical system
   - Module assembly and fabrication method of concentrator modules and systems
   - System aspects – tracking, inverter, and installation issues

   However, it has to be stated once more clearly: CPV is a system approach! Only if all the interconnections between the components are considered the whole system is optimized. This means that the optimized component is not necessarily the best choice for the optimum CPV system. This requires strong interactions between different research groups.
5. Balance-of-System (BoS) components and systems.

   It is at the system level that the user meets PV technology and their interest is in a reliable, cost-effective and attractive solution to their energy supply needs. This research agenda concentrates on topics that will achieve one or more of the following:

   - Reduce costs at the component and/or system level
   - Increase the overall performance of the system, including aspects of increased and harmonized component lifetimes, reduction of performance losses and maintenance of performance levels throughout system life
   - Improve the functionality of and the services provided by the system, so adding value to the electricity produced

6. Standards, quality assurance, safety, and environmental aspects.

   National and especially local authorities and utilities require that PV systems meet agreed standards (like building standards, including e.g., fire safety requirements and electrical safety standards). In a number of cases, either existing standards or differences in local standards (inverter requirements/settings) or the lack of standards (e.g., PV modules/PV elements not being certified as a building element because of the lack of an appropriate standard) hinder the development of the PV market. Standards and/or guidelines are required for the whole value chain. The development of new and adapted standards and guidelines implies in many cases that dedicated research and development is required.

   Quality assurance is an important tool assuring the effective functioning of both individual components in a PV system and of the PV system as a whole. Standards and guidelines are an important basis for quality assurance. In-line production control procedures and guidelines also need to be developed. At the system level, monitoring techniques need to be developed for early fault detection.

   Recycling is an important building block to ensure a sustainable PV industry. So far most attention has been paid to recycling of crystalline silicon solar modules. Methods for recycling of thin-film modules and BoS components (in the case where no recycling procedures exist) need to be addressed in the future. LCA studies have become an important tool to evaluate the environmental profile of the various renewable energy sources. In order to assure the position of PV with respect to other sources, reliable LCA data are required. From these data properties like the CO_2 emission per kWh of electricity produced and the energy payback time can be calculated. In addition, the results of LCA data can be used in the design phase of new processes and equipment for cell and module production lines.

Research Activities

China In the National Outlines for Medium and Long-term Planning for Scientific and Technological Development (2006–2020) [48], solar energy is listed as a priority theme: *New and renewable energy technologies*: to develop low-cost, large-scale renewable energy development and utilization technologies, large-scale wind power generation equipment; to develop technology of Photovoltaic cells with high cost-effect ratio and its utilization; to develop solar power generation technology and study integration of solar powered buildings; to develop technologies of fuel cells, hydropower, biomass energy, hydrogen energy, geothermal energy, ocean energy, biogas, etc.

Also the National Medium-and-Long Term Renewable Energy Development Plan [49] has listed solar Photovoltaic power generation as an important developing point. Within the National Basic Research Programme of China, the so-called 973 Programme, there is an additional topic on "Basic research of mass hydrogen production using solar energy." In January 2010, China's Ministry of Science and Technology announced the approval of the first two *PV State Key Laboratories* to foster and accelerate the development of PV technologies.

European Union In addition to the 27 national programs for market implementation, research and development, the European Union has been funding research (DG RTD) and demonstration projects (DG ENER, formerly DG TREN) with the Research Framework Programmes since 1980. Compared to the combined national budgets, the EU budget is rather small, but it plays an important role in creating a European Photovoltaic Research Area. This is of particular interest and importance, as research for Photovoltaics in a number of Member States is closely linked to EU funds. A large number of research institutions from small University groups to large research centers, covering everything from basic material research to industry process optimization, are involved and contribute to the progress of Photovoltaics.

The European Commission's Research and Development activities are organized in multi-annual Framework Programmes (FP). In addition to the technology-oriented research projects, there are Marie Curie Fellow-ships and the "Intelligent Energy - Europe" (EIE) Programme. The current 7th EC Framework Programme for Research, Technological Development has a duration of 7 years and runs from 2007 to 2013. The Commission expects the following impacts from the research activities: *Through*

technological improvements and economies of scale, the cost of grid-connected PV electricity in Europe is expected to be lowered to a figure in the range of 0.10–0.25 €/kWh by 2020. Research and development should lead to reduced material consumption, higher efficiencies and improved manufacturing processes, based on environmentally sound processes and cycles.

In 2007, the European Commission initiated the European Strategic Energy Technology Plan (SET-PLAN) [50]. The aim of the SET-Plan is to focus, strengthen, and give coherence to the overall effort in Europe with the objective of accelerating innovation in cutting edge European low carbon technologies. In doing so, it will facilitate the achievement of the 2020 targets and the 2050 vision of the Energy Policy for Europe. The Communication on the SET-Plan states:

- Europe needs to act now, together, to deliver sustainable, secure and competitive energy. The inter-related challenges of climate change, security of energy supply and competitiveness are multifaceted and require a coordinated response. We are piecing together a far-reaching jigsaw of policies and measures: binding targets for 2020 to reduce greenhouse gas emissions by 20% and ensure 20% of renewable energy sources in the EU energy mix; a plan to reduce EU global primary energy use by 20% by 2020; carbon pricing through the Emissions Trading Scheme and energy taxation; a competitive Internal Energy Market; an international energy policy. And now, we need a dedicated policy to accelerate the development and deployment of cost-effective low carbon technologies.

Within the SET-Plan, Photovoltaics was identified as one of the key technologies and the SET-Plan calls for six different European industry initiatives, one of them being solar. The *Solar Europe Industry Initiative* will focus on large-scale demonstration for Photovoltaics and concentrated solar power and is launched in June 2010.

India In 2008, Prime Minister Manmohan Singh announced India's first National Action Plan on Climate Change. To cope with the challenges of Climate Change, India identified eight National Missions aimed to develop and use new technologies. The use of solar energy with Photovoltaics and Concentrating Solar Power (CSP) is described in the National Solar Mission (NSM). The objective of the National Solar Mission is to establish India as a global leader in solar energy, by creating the policy conditions for its diffusion across the country as quickly as possible [51]. The actions for Photovoltaics in the National Solar Mission call for R&D collaboration, technology transfer, and capacity building.

R&D projects are supported by the Ministry of Non-Conventional Energy Sources (MNRE) for more than three decades. The range of topics includes the development of poly silicon and other materials, development of device fabrication processes and improvements in crystalline silicon solar cell/module technology, development of thin- film solar cell technology (based on amorphous silicon films, cadmium telluride (CdTe) films and copper indium diselenide (CIS) thin films, organic, dye sensitized, and carbon nanotubes). MNRE is also supporting development of photovoltaic systems and components used in manufacture of such systems. For the 11th plan period (2008 – 2012), the Ministry has identified so-called *Thrust Areas of R&D in Solar Photovoltaic Technology* with the aim to reduce module costs to INR 120/Wp (€ 2.00) [52].

The identified key areas of R&D and technology development are focused on the development of:

1. Poly silicon and other materials
2. Efficient silicon solar cells
3. Thin films materials and solar cell modules
4. Concentrating PV systems
5. PV system design, with the objective of significantly reducing the ratio of capital cost to conversion efficiency

Japan In Japan, the Independent Governmental Entity New Energy Development Organisation (NEDO) is responsible for the Research Programme for Renewable Energies. The current program for Photovoltaics in the frame of Energy and Environment Technologies Development Projects has three main pillars [53]:

- New Energy Technology Development
- Introduction and Dissemination of New Energy and Energy Conservation
- International Projects

One of the dominant priorities, besides the future increase in PV production, is obviously the cost reduction of solar cells and PV systems. In addition to these activities, there are programs on future technology (in and outside NEDO) where participation of Japanese institutes or companies occurs by invitation only. For the participation of non-Japanese partners, there are "future development projects" and the NEDO Joint Research Programme, mainly dealing with non-applied research topics.

Within the *New Energy Technology Development* Programme there are projects on Photovoltaic technology specific issues, problems of grid-connected systems, as well as public solicitation.

The *Introduction and Dissemination of New Energy and Energy Conservation Programme* consists of various promotional and awareness campaign projects.

The *International Projects* mainly focus on neighboring Asian developing countries to promote technological development.

Korea Korea's National PV programs have been based on the second 10-year basic plan for New and Renewable Energy (NRE) RD&D established to enhance the level of self-sufficiency in energy supply, to meet the challenging of climate change and to consolidate infrastructure of NRE industry.

The government budget in 2009 for PV R&D was KRW 70.6 billion (€ 48.7 million), a 25% increase from the previous year. The 32 new and 25 continued projects have been initiated under the five R&D subprograms categorized into

- Strategic R&D
- Basic and Innovative R&D
- Core Technologies Development
- Demonstration
- International Joint Research

The R&D budget for the 32 new projects is KRW 31.2 billion (€ 21.5 million). The representative "Strategic R&D" projects funded newly in 2009 are "Development of commercialization technologies of flexible $CuInGaSe_2$ thin-film solar cells using metal foil substrates" and "Development of large area dye-sensitized solar cells with high reliability." The second phase R&D support has been continued in the projects initiated in 2008. This includes "Development of mass production facilities for c-Si solar cells," "Development of commercialization technologies of large area silicon and CIGS thin-film modules," and "High efficiency a-Si/c-Si hetero-junction solar cells."

Taiwan In 2009, the Taiwanese National Energy Programme started with a four year budget of NTD 30 billons for 4 years. Solar PV is one of the energy technologies amongst the 8 different ones which are supported via this program.

The Industrial Technology Research Institute (ITRI), a Government-backed research organization, has drawn up an R&D Strategy for Taiwan with the aim to lower module costs to around 1 US$/Wp (0.77 €/Wp) between 2015 and 2020. The research topics identified range from efficiency increase in the various wafer-based and thin-film solar cells to concentrator concepts and novel devices. Despite the fact that the national R&D budget should be doubled within the next 4 years from NTD 5 billion (€ 125 million) per year to NTD 10 billion (€ 250 million) per year, it is visible that the main focus is on the industry support to increase production capacities and improved manufacturing technologies.

United States The research activities for solar photovoltaics are a part of the US Solar Energy Technologies Programme (SETP or Solar Programme), which aims to develop cost-competitive solar energy systems for America. The current multi-annual work-program runs from 2008 to 2012 [54]. More than $ 170 million (€ 130.8 million) are spent each year for research and development on the two solar electric technologies which are considered to have the greatest potential to reach cost competitiveness by 2015: photovoltaics and concentrating solar power. The program names as the greatest R&D challenges the reduction of costs, improvement of system performance, and the search for new ways to generate and store energy captured from the sun.

The goal of the Solar Technology Research Plan is to help overcoming the challenges and barriers to massive manufacturing, sales, and installation of PV technology. Multiple technologies are being pursued that are at differing stages of maturity. With an effective combination of the talents in industry, university, and national laboratories, the needed cost, performance,

and reliability goals should be achieved. Specific PV R&D efforts toward achieving these goals include:

1. PV Systems and Module Development
2. PV Materials and Cell Technologies
3. Testing and Evaluation
4. Grid/Building Integration

The Photovoltaic Industry

In 2010, the photovoltaic world market doubled in terms of *production* to 24 GW. The market for installed systems doubled again and values between 16 and 18 GW were reported by various consultancies and institutions. This mainly represents the grid-connected photovoltaic market. To what extent the off-grid and consumer-product markets are included is unclear. The difference of roughly 6–7 GW has therefore to be explained as a combination of unaccounted off-grid installations (approx. 1–200 MW off-grid rural, approx. 1–200 MW communication/signals, approx. 100 MW off-grid commercial), consumer products (ca. 1–200 MW), and cells/modules in stock.

In addition, the fact that some companies report shipment figures whereas others report production figures adds to the uncertainty. The difficult economic conditions contributed to the decreased willingness to report confidential company data. Nevertheless, the figures show a significant growth of the production, as well as an increasing silicon supply situation.

The announced production capacities, based on a survey of more than 350 companies worldwide, increased, even with difficult economic conditions. Despite the fact that a number of players announced a scale back or cancelation of their expansion plans for the time being, the number of new entrants into the field, notably large semiconductor or energy-related companies overcompensated this. At least on paper the expected production capacities are increasing. Only published announcements of the respective companies and no third source info were used. The cut-off date of the info used was August 2011.

It is important to note that production capacities are often announced, taking into account different operation models such as number of shifts, operating hours per year, etc. In addition, the announcements of the increase in production capacity do not always specify when the capacity will be fully ramped up and operational. This method has of course the setback that a) not all companies announce their capacity increases in advance and b) that in times of financial tightening, the announcements of the scale back of expansion plans are often delayed in order not to upset financial markets. Therefore, the capacity figures just give a trend, but do not represent final numbers.

If all these ambitious plans can be realized by 2015, China will each have about 67% of the worldwide production capacity of 104 GW followed by Taiwan (15%), Europe (9%), and Japan (7%) (Fig. 2) [55, 56].

All these ambitious plans to increase production capacities, at such a rapid pace, depend on the expectations that markets will grow accordingly. This, however, is the biggest uncertainty, as the market estimates for 2011 vary between 17 and 24 GW, with a consensus value in the 20 GW range. In addition, most markets are still dependent on public support in the form of feed-in tariffs, investment subsidies, or tax-breaks.

Technology Mix

Wafer-based silicon solar cells is still the main technology and had around 85% market shares in 2010. Polycrystalline solar cells still dominate the market (45–50%) even if the market shares are decreasing since 2003. Commercial module efficiencies are within a wide range between 12% and 22%, with monocrystalline modules between 14% and 22% and polycrystalline modules between 12% and 18%. The massive capacity increases for both technologies are followed by the necessary capacity expansions for polysilicon raw material.

More than 200 companies are involved in thin-film solar cell activities, ranging from basic R&D activities to major manufacturing activities and over 120 of them have announced the start or increase of production. In 2005, production of Thin-Film solar modules reached for the first time more than 100 MW per annum. The first 100 MW thin-film factories became operational in 2007, followed by the first 1 GW factory in 2010. If all expansion plans are realized in time, thin-film production capacity could be 17 GW, or 21% of the total 82 GW in 2012 and 27 GW, or 26%, in 2015 of a total of 104 GW (Fig. 3).

One should bear in mind that only one third of the over 120 companies, with announced production

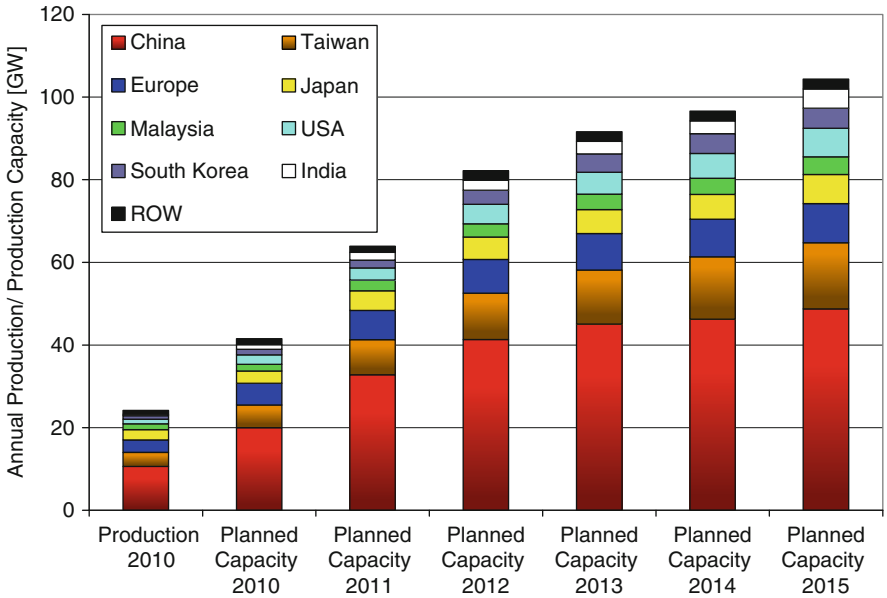

Photovoltaics, Status of. Figure 2
Worldwide PV Production 2010 with future planned production capacity increases

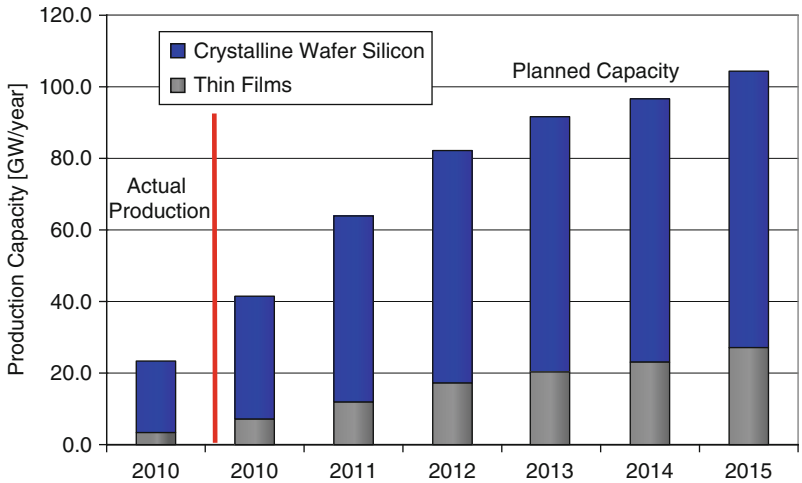

Photovoltaics, Status of. Figure 3
Annual PV production capacities of thin-film and crystalline silicon-based solar modules

plans, have produced thin-film modules of 10 MW or more in 2010 (Fig. 4).

More than 70 companies are silicon-based and use either amorphous silicon or an amorphous/microcrystalline silicon structure. Thirty-six companies announced using Cu (In,Ga) $(Se,S)_2$ as absorber material for their thin-film solar modules, whereas nine companies use CdTe and eight companies go for dye and other materials.

Concentrating Photovoltaics (CPV) is an emerging market with approximately 17 MW cumulative installed capacity at the end of 2008. There are two main tracks – either high concentration >300 suns (HCPV) or low to medium concentration with

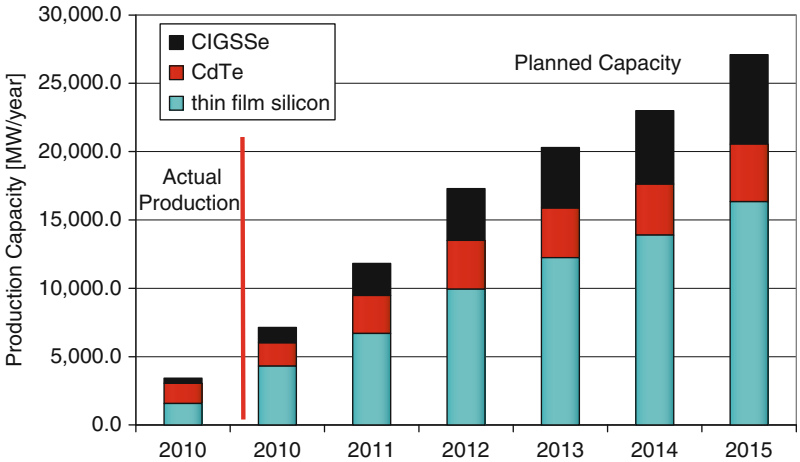

Photovoltaics, Status of. Figure 4
Annual thin-film PV production capacities of thin-film and crystalline silicon-based solar modules

a concentration factor of 2 to approximately 300. In order to maximize the benefits of CPV, the technology requires high Direct Normal Irradiation (DNI) and these areas have a limited geographical range – the "Sun Belt" of the Earth. The market share of CPV is still small, but an increasing number of companies are focusing on CPV. In 2008, about 10 MW of CPV were produced, market estimates for 2009 are in the 20–30 MW range and for 2010 about 100 MW are expected.

Price Trends

The costs for PV systems and their components have decreased by more than a factor of 10 over the last 30 years. However, if we look at prices, these depend not only on technology development and market size, but also on the global or local competition in the respective market segment. Support schemes, permitting rules, and grid access regulations have a significant influence on prices as well.

The average global PV module factory prices dropped from more than 23 $/W (2010 $) in 1980 to about 1.5 $/W (2010 $) in 2010 [57]. The majority of studies about learning curve experience in photovoltaics focus on PV modules because they represent the single-largest cost item of a PV system [58]. For the PV modules a range between 11% and 26% is given for the learning experience [59–62] with a median progress ratio of 80%. This leads to a learning rate (price experience factor) of 20%, which means that the price is reduced by 20% for each doubling of cumulative sales [63, 64]. Figure 5 shows the price developments for crystalline silicon modules over the last 35 years. The huge growth of demand after 2003 led to an increase of prices due to the supply-constrained market, which then changed into a demand-driven market leading to a significant price reduction due to module overcapacities in the market [65].

BOS components are responsible for the second largest technical-related cost part of a PV system. Within the BOS components, the single-largest item is the inverter. While the overall BOS experience curve was between 78% and 81%, or a 19–22% learning rate, quite similar to the module rates learning rates for inverters were just in the range of 10% [67]. A similar trend was found in the USA for cost reduction for labor costs attributed to installed PV systems [68].

The average cost of installed PV systems has also decreased significantly over the past couple of decades and is projected to continue decreasing rapidly as the PV technology and markets mature. However, as already pointed out earlier, the system price decrease varies significantly from region to region and depends strongly on the implemented support schemes and maturity of markets [69]. This study found that the capacity-weighted average costs of PV systems installed in the USA declined from 10.8 $/W (2010 $) in 1998 to 7.5 $/W (2010 $) in 2009. This decline was attributed primarily to a drop in non-module (BOS) costs.

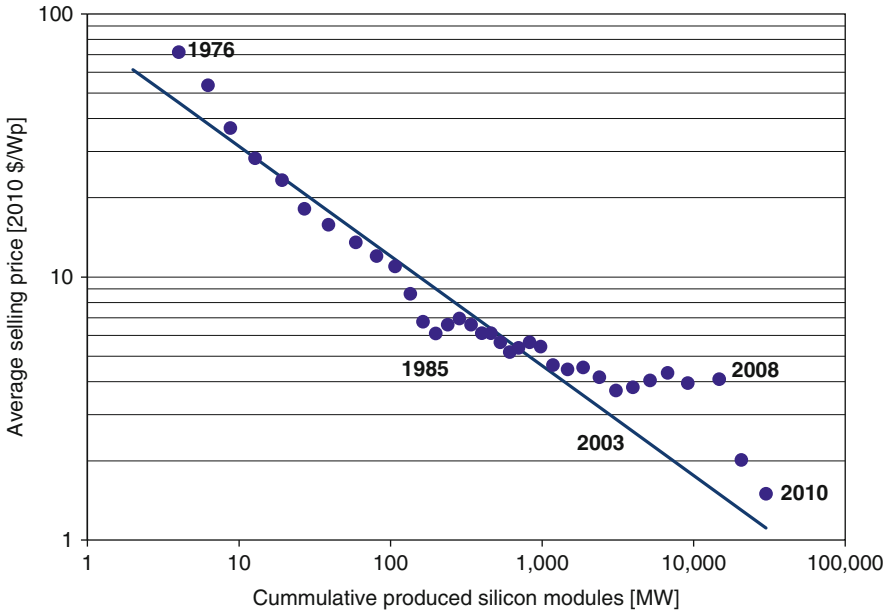

Photovoltaics, Status of. Figure 5

Price experience or learning curve for silicon PV modules. The *straight line* on this log-log plot represents a learning rate of 25% and the actual data follow the supply and demand fluctuations [57, 66]

Figure 6 shows the system price developments in Europe, Japan, and the USA.

Since the second half of 2008, PV system prices have decreased considerably due to the increased competition between PV companies because of huge increases in production capacity and production overcapacities. Already now, electricity production from photovoltaic solar systems has shown that it can be cheaper than peak prices in the electricity exchange.

Average US prices in the first quarter of 2011 were given as: residential systems 6.41 ± 2.0 $/W (4.93 ± 1.54 €/W), nonresidential systems 5.35 ± 1.65 $/W (4.12 ± 1.27 €/W), and utility scale systems 3.85 ± 1.15 $/W (2.96 ± 1.04 5/W) [74]. In the second quarter of 2011, the German average price index, for rooftop systems up to 100 kWp, was given with € 2,422/kWp without tax or half the price of 5 years ago [75]. With such investment costs, the electricity generation costs are already at the level of residential electricity prices in some countries, depending on the actual electricity price, and the local solar radiation level.

But only if markets and competition continue to grow, prices of the photovoltaic systems will continue to decrease and make electricity from PV systems for consumers even cheaper than from conventional sources. In order to achieve the price reductions and reach grid parity for electricity generated from photovoltaic systems, public support, especially on regulatory measures, will be necessary for the next decade.

Solar Cell Production Companies

Worldwide, more than 350 companies produce solar cells. The following subsections give a short description of the 20 largest companies, in terms of actual production/shipments in 2010. More information about solar cell companies and details can be found in various market studies or in the annual *PV Status Report* published by the European Commission's Joint Research Centre [76]. The capacity, production, or shipment data are from the annual reports or financial statements of the respective companies or the cited references.

Suntech Power Co. Ltd. (PRC) Suntech Power Co. Ltd. (www.suntech-power.com) is located in Wuxi. It was founded in January 2001 by Dr. Zhengrong Shi and went public in December 2005. Suntech specializes in the design, development, manufacturing, and sale of

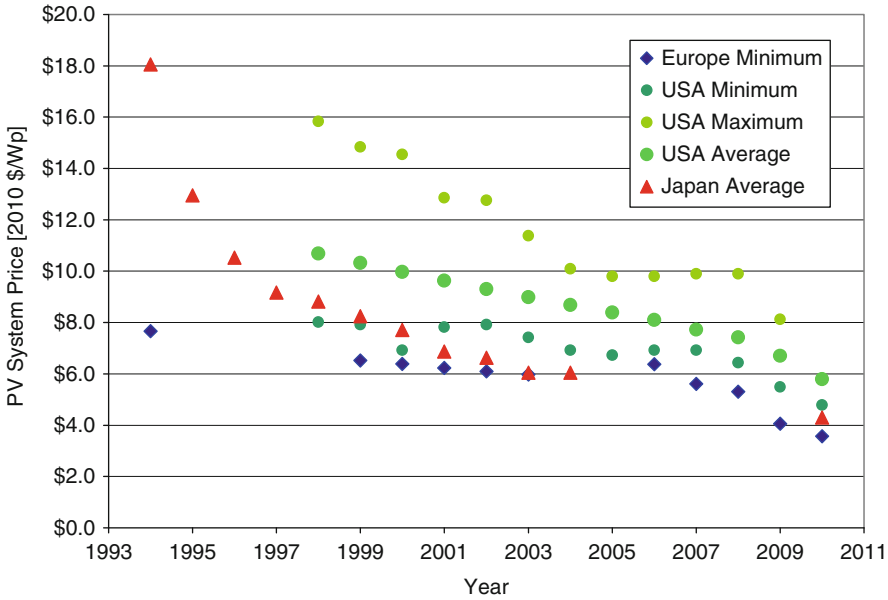

Photovoltaics, Status of. Figure 6
Installed cost of PV systems smaller 100 kW_p in Europe, Japan, and the USA (Data Sources: [69–73])

photovoltaic cells, modules, and systems. For 2010, Suntech reported shipments of 1507 MW, taking the top rank amongst the solar cell manufacturers. The annual production capacity of Suntech Power was increased to 1.8 GW by the end of 2010, and the company plans to expand its capacity to 2.4 GW in 2011.

JA Solar Holding Co. Ltd. (PRC) JingAo Solar Co. Ltd. (http://www.jasolar.com) was established in May 2005 by the Hebei Jinglong Industry and Commerce Group Co. Ltd., the Australia Solar Energy Development Pty. Ltd. and Australia PV Science and Engineering Company. Commercial operation started in April 2006 and the company went public on February 7, 2007. According to the company, the production capacity should increase from 1.9 GW at the end of 2010 to 2.5 GW in 2011. For 2010, shipments of 1,460 MW are reported.

First Solar LLC (USA/Germany/Malaysia) First Solar LLC (http://www.firstsolar.com) is one of the few companies worldwide to produce CdTe-thin-film modules. The company has currently three manufacturing sites in Perrysburg (USA), Frankfurt/Oder (Germany), and in Kulim (Malaysia), which had a combined capacity of 1.5 GW at the end of 2010. The second Frankfurt/Oder plant, doubling the capacity there to 512 MW, became operational in May 2011 and the expansion in Kulim is on track to increase the production capacity to 2.3 GW at the end of 2011. Further expansions are under way in Meze (AZ), USA, and Dong Nam Industrial Park, Vietnam, to increase the production capacity to 2.9 GW at the end of 2012. The new factory planned in the framework of a joint venture with EdF Nuovelles in France is currently on hold. In 2010, the company produced 1.4 GW and currently sets the production cost benchmark with 0.75 $/Wp (0.58 €/Wp) in the first quarter of 2011.

Sharp Corporation (Japan/Italy) Sharp (www.sharp-world.com) started to develop solar cells in 1959 and commercial production got under way in 1963. Since its products were mounted on "Ume," Japan's first commercial-use artificial satellite, in 1974, Sharp has been the only Japanese maker to produce silicon solar cells for use in space. Another milestone was achieved in 1980, with the release of electronic calculators, equipped with single-crystal solar cells.

In 2010, Sharp had a production capacity of 1,070 MWp/year, and shipments of 1.17 GW were reported [79]. Sharp has two solar cell factories in Japan,

Katsuragi, Nara Prefecture (550 MW c-Si and 160 MW a-Si their triple-junction thin-film solar cell), and Osaka (200 MW c-Si and 160 MW a-Si), one together with Enel Green Power and STMicroelectronics in Catania, Italy (initial capacity 160 MW at the end of 2011), six module factories and the Toyama factory to recycle and produce silicon. Three of the module factories are outside Japan, one in Memphis, Tennessee, USA with 100 MW capacity, one in Wrexham, UK, with 500 MW capacity and one in Nakornpathom, Thailand.

Trina Solar Ltd., PRC (PRC) Trina Solar (http://www.trinasolar.com/) was founded in 1997 and went public in December 2006. The company has integrated product lines, from ingots to wafers and modules. In December 2005, a 30 MW monocrystalline silicon wafer product line went into operation. According to the company, the production capacity was 750 MW for ingots and wafers and 1.2 GW for cells and modules at the end of 2010. For 2011, it is planned to expand the capacities to 1.2 GW for ingots and wafers and to 1.9 GW for cells and modules. For 2010, shipments of 1.06 GW were reported.

In January 2010, the company was selected by the Chinese Ministry of Science and Technology to establish a State Key Laboratory to develop PV technologies within the Changzhou Trina PV Industrial Park. The laboratory is established as a national platform for driving PV technologies in China. Its mandate includes research into PV-related materials, cell and module technologies, and system-level performance. It will also serve as a platform to bring together technical capabilities from the company's strategic partners, including customers and key PV component suppliers, as well as universities and research institutions.

Yingli Green Energy Holding Company Ltd. (PRC) Yingli Green Energy (http://www.yinglisolar.com/) went public on June 8, 2007. The main operating subsidiary, Baoding Tianwei Yingli New Energy Resources Co. Ltd., is located in the Baoding National High-New Tech Industrial Development Zone. The company deals with the whole set, from solar wafers, cell manufacturing, and module production. According to the company, production capacity reached 1 GW in July 2010. A further expansion project to 1.7 GW is ongoing and should be operational at the end of 2011. The financial statement for 2010 gave shipments of 1.06 GW.

In January 2009, Yingli acquired Cyber Power Group Limited, a development stage enterprise designed to produce polysilicon. Through its principle operating subsidiary, Fine Silicon, the company started trial production of solar-grade polysilicon in late 2009 and is expected to reach its full production capacity of 3,000 t per year by the end of 2011.

In January 2010, the Ministry of Science and Technology of China approved the application to establish a national-level key laboratory in the field of PV technology development, the State Key Laboratory of PV Technology at Yingli Green Energy's manufacturing base in Baoding.

Q-Cells AG (Germany/Malaysia) Q-Cells SE (http://www.qcells.de) was founded at the end of 1999 and is based in Thalheim, Sachsen-Anhalt, Germany. Solar cell production started in mid 2001, with a 12 MWp production line. In the 2010 Annual Report, the company stated that the nominal capacity was 1.1 GW by the end of 2010, 500 MW in Germany and 600 MW in Malaysia. In 2010, production was 936 MW, 479 MW in Germany, and 457 MW in Malaysia.

In the first half of the last decade, Q-Cells broadened and diversified its product portfolio by investing in various other companies, or forming joint ventures. Since the first half of 2009, Q-Cells has sold most of these holdings and now has one fully owned solar cell manufacturing subsidiary, Solibro (CIGS) with a 2010 production of 75 MW.

Motech Solar (Taiwan/PRC) Motech Solar (http://www.motech.com.tw) is a wholly owned subsidiary of Motech Industries Inc., located in the Tainan Science Industrial Park. The company started its mass production of polycrystalline solar cells at the end of 2000, with an annual production capacity of 3.5 MW. The production increased from 3.5 MW in 2001 to 850 MW in 2010. In 2009, Motech started the construction of a factory in China which should reach its nameplate capacity of 500 MW in 2011. Production capacity at the end of 2010 was given as 1.2 GW (860 MW in Taiwan and 340 MW in China).

In 2007, Motech Solar's Research and Development Department was upgraded to Research and

Development Centre (R&D Centre), with the aim not only to improve the present production processes for wafer and cell production, but to develop next generation solar cell technologies.

At the end of 2009, the company announced that it acquired the module manufacturing facilities of GE in Delaware, USA.

Gintech Energy Corporation (Taiwan) Gintech (http://www.gintech.com.tw/) was established in August 2005 and went public in December 2006. Production at Factory Site A, Hsinchu Science Park, began in 2007 with an initial production capacity of 260 MW and increased to 930 MW at the end of 2010. The company plans to expand capacity to 1.5 GW in 2011. In 2010, the company had a production of 827 MW [3].

Kyocera Corporation (Japan) In 1975, Kyocera (http://global.kyocera.com/prdct/solar/) began with research on solar cells. The Shiga Yohkaichi Factory was established in 1980 and R&D and manufacturing of solar cells and products started with mass production of multicrystalline silicon solar cells in 1982. In 1993, Kyocera started as the first Japanese company to sell home PV generation systems.

Besides the solar cell manufacturing plants in Japan, Kyocera has module manufacturing plants in China (joint venture with the Tianjin Yiqing Group (10% share) in Tianjin since 2003), Tijuana, Mexico (since 2004), and in Kadan, Czech Republic (since 2005).

In 2010, Kyocera had a production of 650 MW and is also marketing systems that both generate electricity through solar cells and exploit heat from the sun for other purposes, such as heating water. The Sakura Factory, Chiba Prefecture, is involved in everything from R&D and system planning to construction and servicing and the Shiga Factory, Shiga Prefecture, is active in R&D, as well as the manufacturing of solar cells, modules, equipment parts, and devices, which exploit heat. Like solar companies, Kyocera is planning to increase its current capacity of 650 MW in 2010 to 800 MW in 2011 and 1 GW in 2012.

SunPower Corporation (USA/Philippines/Malaysia) SunPower (http://us.sunpowercorp.com/) was founded in 1988 by Richard Swanson and Robert Lorenzini to commercialize proprietary high-efficiency silicon solar cell technology. The company went public in November 2005. SunPower designs and manufactures high-performance silicon solar cells based on an interdigitated rear-contact design for commercial use. The initial products, introduced in 1992, were high-concentration solar cells with an efficiency of 26%. SunPower also manufactures a 22% efficient solar cell, called Pegasus, that is designed for non-concentrating applications.

SunPower conducts its main R&D activity in Sunnyvale, California, and has its cell manufacturing plant outside of Manila in the Philippines, with 590 MW capacity (Fab. No 1 and No 2). Fab. No. 3, a joint venture with AU Optronics Corporation (AUO), with a planned capacity of 1.4 GW, is currently under construction in Malaysia. Production in 2010 was reported at 584 MW.

Canadian Solar Inc. (PRC) Canadian Solar Inc. was founded in Canada in 2001 and was listed on NASDAQ in November 2006. CSI has established six wholly owned manufacturing subsidiaries in China, manufacturing ingot/wafer, solar cells, and solar modules. According to the company, it had 200 MW of ingot and wafer capacity, 800 MW cell capacity and 1.3 GW module manufacturing capacity in 2010. The company reports that it is on track to expand their solar cell capacity to 1.3 GW and the module manufacturing capacity to 2 GW, including 200 MW in Ontario, Canada, in 2011. For 2010, the company reported production of 522 MW solar cells and sales of 803 MW of modules.

Hanwah Solar One (PRC/South Korea) Hanwah Solar One (http://www.hanwha-solarone.com) was established in 2004 as Solarfun Power Holdings, by the electricity meter manufacturer, Lingyang Electronics, the largest Chinese manufacturer of electric power meters. In 2010, the Korean company, Hanwha Chemical, acquired 49.99% of the shares and a name change was performed in January 2011. The company produces silicon ingots, wafers, solar cells, and solar modules. The first production line was completed at the end of 2004 and commercial production started in November 2005. The company went public in December 2006 and reported the completion of its production

capacity expansion to 360 MW in the second quarter of 2008.

As of April 30, 2011, the company reported the following capacities: 1 GW PV module production capacity, 700 MW of cell production capacity, 415 MW of ingot production capacity, and 500 MW of wire-sawing capacity. It is planned to expand the module production capacity to 1.5 GW, cell production capacity to 1.3 GW and ingot and wafer production capacity to 1 GW by the end of 2011.

The 2010 annual production was reported with 360 MW ingots, 387 MW wafers, 502 MW solar cells, and 759 modules.

Neo Solar Power Corporation (Taiwan) Neo Solar Power (http://www.neosolarpower.com/) was founded in 2005 by PowerChip Semiconductor, Taiwan's largest DRAM company, and went public in October 2007. The company manufactures mono- and multicrystalline silicon solar cells and offers their SUPERCELL multicrystalline solar cell brand with 16.8% efficiency. Production capacity of silicon solar cells at the end of 2010 was 820 MW and the expansion to more than 1.3 GW is planned for 2011. In 2010, the company had shipments of about 500 MW.

Renewable Energy Corporation as (Norway/Singapore) REC's (http://www.recgroup.com/) vision is to become the most cost-efficient solar energy company in the world, with a presence throughout the whole value chain. REC is presently pursuing an aggressive strategy to this end. Through its various group companies, REC is already involved in all major aspects of the PV value chain. The company located in Høvik, Norway, has five business activities, ranging from silicon feedstock to solar system installations.

REC ScanCell is located in Narvik, producing solar cells. From the start-up in 2003, the factory has been continuously expanding. In 2010, production of solar cells was 452 MW, with a capacity at year end of 180 MWp in Norway, and 550 MW in Singapore.

Solar World AG (Germany/USA) Since its founding in 1998, Solar World (http://www.solarworld.de/) has changed from a solar system and components dealer to a company covering the whole PV value chain, from wafer production to system installations. The company now has manufacturing operations for silicon wafers, cells and modules in Freiberg, Germany, and Hillsoboro (OR), USA. Additional solar module production facilities exist in Camarillo (CA), USA, and since 2008 with a joint venture between Solarworld and SolarPark Engineering Co. Ltd. in Jeonju, South Korea.

For 2010, solar cell production capacities in Germany were reported at 250 MW and 500 MW in the USA. Total cell production in 2010 was 451 MW, with 200 MW coming from Germany and 251 MW form the USA.

In 2003, the Solar World Group was the first company worldwide to implement silicon solar cell recycling. The Solar World subsidiary, Deutsche Solar AG, commissioned a pilot plant for the reprocessing of crystalline cells and modules.

Sun Earth Solar Power Co. Ltd. (PRC) Sun Earth Solar Power (http://www.nbsolar.com/), or NbSolar, has been part of China's PuTian Group since 2003. The company has four main facilities for silicon production, ingot manufacturing, system integration, and solar system production. According to company information, Sun Earth has imported solar cell and module producing and assembling lines from America and Japan.

In 2007, Sun Earth Solar Power relocated to the Ningbo high-tech zone, with the global headquarters of Sun Earth Solar Power. There the company produces wafers, solar cells, and solar modules. The second phase of production capacity expansion to 350 MW was completed in 2009. Further expansion is planned from 450 MW in 2010, 700 MW in 2011, and 1 GW in 2012. For 2010, shipments of 421 MW were reported [3].

E-TON Solartech Co. Ltd. (Taiwan) E-Ton Solartech (http://www.e-tonsolar.com) was founded in 2001 by the E-Ton Group; a multinational conglomerate dedicated to producing sustainable technology and energy solutions and was listed on the Taiwan OTC stock exchange in 2006.

At the end of 2010, the production capacity was 560 MW per annum and a capacity increase to 820 MW is foreseen for 2011. Shipments of solar cells were reported at 420 MW for 2010.

SANYO Electric Company (Japan) Sanyo (http://sanyo.com/solar/) commenced R&D for a-Si solar cells in 1975. In 1980 marked the beginning of Sanyo's a-Si solar cell mass productions for consumer applications. Ten years later in 1990, research on the HIT (Heterojunction with Intrinsic Thin Layer) structure was started. In 1992, Dr. Kuwano (former president of SANYO) installed the first residential PV system at his private home. Amorphous Silicon modules for power use became available from SANYO in 1993 and in 1997 the mass production of HIT solar cells started. In 2010, Sanyo produced 405 MW solar cells [3]. The company announced increasing its 2009 production capacity of 500 MW HIT cells to 650 MW by 2011.

At the end of 2002, Sanyo announced the start of module production outside Japan. The company now has a HIT PV module production at SANYO Energy S.A. de C.V.'s Monterrey, Mexico, and it joined Sharp and Kyocera to set up module manufacturing plants in Europe. In 2005, it opened its module manufacturing plant in Dorog, Hungary.

Sanyo has set a world record for the efficiency of the HIT solar cell, with 23% under laboratory conditions [17]. The HIT structure offers the possibility to produce double-sided solar cells, which has the advantage of collecting scattered light on the rear side of the solar cell and can therefore increase the performance by up to 30%, compared to one-sided HIT modules in the case of vertical installation.

China Sunergy China Sunergy was established as CEEG Nanjing PV-Tech Co. (NJPV), a joint venture between the Chinese Electrical Equipment Group in Jiangsu and the Australian Photovoltaic Research Centre in 2004. China Sunergy went public in May 2007. At the end of 2008, the Company had five selective emitter (SE) cell lines, four HP lines, three capable of using multicrystalline and monocrystalline wafers, and one normal P-type line for multicrystalline cells, with a total nameplate capacity of 320 MW. At the end of 2010, the company had a cell capacity of 400 MW and a module capacity of 480 MW. For 2011, a capacity increase to 750 MW cells and 1.2 GW of modules is foreseen. For 2010, a production of 347 MW was reported vThin Film Solar Cell Production Companies.

Thin Film Solar Cell Production Companies

Worldwide, about 40 companies have produced thin-film modules of 10 MW or more in 2010. The following subsections give a short description of the ten largest companies not yet mentioned in section "Solar Cell Production Companies" (First Solar, Sharp, Solibro as part of Q-Cells), in terms of actual production/shipments in 2010. More information about solar cell companies and details can be found in various market studies or in the annual *PV Status Report* published by the European Commission's Joint Research Centre [76]. The capacity, production, or shipment data are from the annual reports or financial statements of the respective companies or the cited references.

Trony Solar Holdings Company Ltd Trony Solar is located in Shenzhen, Guangdong Province, and manufactures thin-film silicon solar cells and modules for BIPV and consumer applications. According to the company, the capacity was 205 MW at the end of 2010. In May 2010, Trony Technology's "1,000 MW Thin-Film Solar Cell Industrial Base" was recognized as one of the "Top 500 Modern Industrial Projects" of Guangdong Province. For 2010, a production of 145 MW is reported [4].

United Solar Systems United Solar Systems Corp. is a subsidiary of Energy Conversion Devices, Inc. (ECD). The first 25 MW manufacturing facility of the flexible a-Si triple-junction solar cell is located in Auburn Hills (MI) and was inaugurated in 2002.

According to the company, production capacity was foreseen to expand to 320 MW by 2010 and 720 MW in 2011. In 2008, financing deals were closed which would allow an expansion to 1 GW in 2012 [Ecd 2008]. The current nameplate capacity in Auburn Hills is quoted with 58 MW and in Greenville, Michigan, 120 MW. A joint venture United Solar Ovonic Jinneng Limited was set up with Tianjin Jinneng Investment Company (TJIC) to operate a 30 MW module plant in Tianjin. In April 2011, the company announce to build another module manufacturing plant with an initial capacity of 15 MW in Ontario. Production in 2010 is reported with 120 MW [3].

Solar Frontier Solar Frontier is a 100% subsidiary of Showa Shell Sekiyu K.K. In 1986, Showa Shell Sekiyuki

started to import small modules for traffic signals, and started module production in Japan, cooperatively with Siemens (now Solar World). The company developed CIS solar cells and completed the construction of the first factory with 20 MW capacity in October 2006. Commercial production started in FY 2007. In August 2007, the company announced the construction of a second factory with a production capacity of 60 MW to be fully operational in 2009. In July 2008, the company announced they would open a research center "to strengthen research on CIS solar powered cell technology, and to start collaborative research on mass production technology of the solar modules with Ulvac, Inc." The aim of this project is to start a new plant in 2011 with a capacity of 900 MW. The ramp up started in February 2011. In 2010, the company changed its name to Solar Frontier and production is reported with 74 MW [3].

Kaneka Solartech Kaneka has been involved in the development of amorphous solar cells for over 25 years. Initially, this was aimed at the consumer electronics market, but overall R&D, as well as business strategy, changed in 1993 when Kaneka decided to move into the power module market for residential and industrial applications.

Currently Kaneka produces a-Si and amorphous/microcrystalline silicon modules for rooftop application and built-in roofing types for the Japanese, as well as export markets. The built-in roofing types were developed for the Japanese housing market in cooperation with Quarter-House and Kubota and are either shingle type modules or larger roofing elements. In 2006, the company opened a module factory in Olomouc, Czech Republic, where the capacity was increased to 30 MW in 2008. In FY 2010, the total production capacity was expanded to 150 MWp/year. A further expansion to 350 MW in 2011 and to 1 GW in 2015 was announced by the company. In FY 2010, production was 58 MW [3].

Mitsubishi Heavy Industries Mitsubishi Heavy Industries (MHI) started their pilot plant production in 2001, because solar energy has attracted increasing attention as an environment-friendly form of energy. In 2010, MHI produced 50 MW of amorphous silicon solar cells [4] and had a production capacity of 118 MW.

The plasma CVD deposition, used by MHI, allows rapid deposition on large size glass and flexible substrates (roll-to-roll). MHI has stabilized the a-Si single-junction efficiency at 8%, starting with 10% initial efficiency. The degradation process lasts for approximately 3–4 months, before the stabilized efficiency is reached. Long-time outdoor exposure tests performed at JQA showed that the stabilized efficiency does not change and that the lifetime expectancy can be rated at 20–25 years. Mitsubishi is currently working on improving the efficiency to 12% by using a microcrystalline/a-Si structure in the future. Another feature of the Mitsubishi modules is their high voltage. The modules are produced with either 50 V or 100 V and power ratings between 24 and 100 Wp.

Schott Solar AG (Germany) Schott Solar AG has been a fully owned subsidiary of Schott AG, Mainz, since 2005, when Schott took over the former joint venture RWE-Schott Solar, except for the Space Solar Cells Division in Heilbronn. Schott Solar's portfolio comprises crystalline wafers, cells, modules and systems for grid-connected power and stand-alone applications, as well as a wide range of ASI® thin-film solar cells and modules. In 2010, the company had a production capacity of 350 MW and an actual production of 320 MW [3].

Development of amorphous silicon solar cells started at MBB in 1980. Phototronics (PST) was founded in 1988. In 1991, one of the world's first large-area pilot production facilities for amorphous silicon was built. In January 2008, the company started shipments of modules from its new 33 MW manufacturing facility for amorphous silicon thin-film solar modules in Jena, Germany.

Sunwell Solar Corporation Sunwell Solar is a subsidiary of CMC Magnetics Corporation, Taiwan's top compact disk maker, contracted a 45 MW thin-film PV production plant with Oerlikon Solar. The plant started production at the beginning of September 2008. For 2010, a production of 45 MW is reported [4].

Auria Solar Co Auria was founded in October 2007 as a joint venture between E-Ton Solar, Lite-On Technology Corp, Hermes-Epitek Corp. and the MiTAC-SYNNEX Group to manufacture thin-film solar cells. The company has chosen Oerlikon as equipment supplier and plans to produce amorphous/micromorph silicon thin-films. The first factory, with a capacity of 60 MW, began pilot production at the end of 2008 and ramped up to full capacity in 2019. In March 2011, the company announced a cooperation agreement with Mitsubishi Heavy Industries (Japan) for their next expansion to 200 MW in 2012. For 2010, a production of 40 MW is reported [4].

Baoding TianWei SolarFilms Co., Ltd Baoding TianWei Solar Films was set up in 2008. It is a subsidiary of the Baoding TianWei Group Co., Ltd., a leading company in the China power transformer industry. Phase I of the production was set up with a capacity of 50 MW and the start of commercial operation was in the second half of 2009. The company plans to reach a capacity of 500 MW in 2015. For 2010, a production of 40 MW is reported [4].

Moser Baer Moser Baer Photovoltaic Limited (MBPV) and PV Technologies India Limited (PVTIL) are subsidiaries of Moser Baer India Limited. They were launched between 2005 and 2007 with the primary objective of providing reliable solar power as a competitive nonsubsidized source of energy.

At the end of 2010, the production capacity was given by the company with 90 MW crystalline cells, 100 MW crystalline modules, and 50 MW thin-films with expansion plans in place.

Polysilicon Supply

The rapid growth of the PV industry since 2000 led to the situation where, between 2004 and early 2008, the demand for *polysilicon* outstripped the supply from the semiconductor industry. Prices for purified silicon started to rise sharply in 2007 and in 2008 prices for polysilicon peaked around 500 $/kg and consequently resulted in higher prices for PV modules. This extreme price hike triggered a massive capacity expansion, not only of established companies, but many new entrants as well. In 2009, more than 90% of total polysilicon, for the semiconductor and photovoltaic industry, was supplied by seven companies: Hemlock, Wacker Chemie, REC, Tokuyama, MEMC, Mitsubishi, and Sumitomo. However, it is estimated that now about seventy producers are present in the market.

The massive production expansions, as well as the difficult economic situation, led to a price decrease throughout 2009, reaching about 50–55 $/kg at the end of 2009, with a slight upward tendency throughout 2010 and early 2011.

For 2010, about 140,000 t of solar-grade silicon production were reported, sufficient for around 20 GW, under the assumption of an average materials need of 7 g/Wp [77]. China produced about 45,000 t, or 32%, capable of supplying about 75% of the domestic demand [78]. According to the Semi PV Group Roadmap, the Chinese production capacity rose to 85,000 t of polysilicon in 2010.

In January 2011, the Chinese Ministry of Industry and Information Technology tightened the rules for polysilicon factories. New factories must be able to produce more than 3,000 t of polysilicon a year and meet certain efficiency, environmental, and financing standards. The maximum electricity use is 80 kWh/kg of polysilicon produced a year, and that number will drop to 60 kWh at the end of 2011. Existing plants that consume more than 200 kWh/kg of polysilicon produced at the end of 2011 will be shut down.

Projected silicon production capacities available for solar in 2012 vary between 250,000 t [11] and 410,665 t [79]. The possible solar cell production will in addition depend on the material use per Wp. Material consumption could decrease from the current 7–8 g/Wp down to 5– 6 g/Wp, but this might not be achieved by all manufacturers.

Silicon Production Processes The high growth rates of the photovoltaic industry and the market dynamics forced the high-purity silicon companies to explore process improvements mainly for two chemical vapor deposition (CVD) approaches – an established production approach known as the Siemens process, and a manufacturing scheme based on fluidized bed (FB) reactors. Improved versions of these two types of processes will very probably be the workhorses of the polysilicon production industry for the near future.

Siemens process: In the late 1950s, the Siemens reactor was developed and has been the dominant production route since. About 80% of total polysilicon manufactured worldwide was made with a Siemens-type process in 2009. The Siemens process involves deposition of silicon from a mixture of purified silane or trichlorosilane gas with an excess of hydrogen onto high-purity polysilicon filaments. The silicon growth then occurs inside an insulated reaction chamber or "bell jar," which contains the gases. The filaments are assembled as electric circuits in series and are heated to the vapor deposition temperature by an external direct current. The silicon filaments are heated to very high temperatures between 1,100°C and 1,175°C at which trichlorsilane with the help of the hydrogen decomposes to elemental silicon and deposits as a thin-layer film onto the filaments. Hydrogen Chloride (HCl) is formed as a by-product.

The most critical process parameter is temperature control. The temperature of the gas and filaments must be high enough for the silicon from the gas to deposit onto the solid surface of the filament, but well below the melting point of 1,414°C that the filament do not start to melt. Second, the deposition rate must be well controlled and not too fast because otherwise the silicon will not deposit in a uniform, polycrystalline manner, making the material unsuitable for semiconductor and solar applications.

Fluidized bed process: A number of companies develop polysilicon production processes based on fluidized bed (FB) reactors. The motivation to use the FB approach is the potentially lower energy consumption and a continuous production compared to the Siemens batch process. In this process, tetrahydrosilane or trichlorosilane and hydrogen gases are continuously introduced to the bottom of the FB reactor at moderately elevated temperatures and pressures. At a continuous rate high-purity silicon seeds are inserted from the top and are suspended by the upward flow of gases. At the operating temperatures of 750°C, the silane gas is reduced to elemental silicon and deposits on the surface of the silicon seeds. The growing seed crystals fall to the bottom of the reactor where they are continuously removed.

MEMC Electronic Materials, a silicon wafer manufacturer, has been producing granular silicon from silane feedstock using a fluidized bed approach for over a decade. Several new facilities will also feature variations of the FB. Several major players in the polysilicon industry, including Wacker Chemie and Hemlock, are developing FB processes, while at the same time continuing to produce silicon using the Siemens process as well.

Upgraded metallurgical grade (UMG) silicon was seen as one option to produce cheaper solar-grade silicon with 5- or 6-nines purity, but the support for this technology is waning in an environment where higher-purity methods are cost competitive. A number of companies delayed or suspended their UMG-silicon operations as a result of low prices and lack of demand for UMG material for solar cells.

Polysilicon Manufacturers

Worldwide more than 100 companies produce or start-up polysilicon production. The following subsections give a short description of the ten largest companies in terms of production capacity in 2010. More information about polisilicon companies and details can be found in various market studies or in the annual *PV Status Report* published by the European Commission's Joint Research Centre [49].

Hemlock Semiconductor Corporation (USA) Hemlock Semiconductor Corporation (http://www.hscpoly.com) is based in Hemlock, Michigan. The corporation is a joint venture of Dow Corning Corporation (63.25%) and two Japanese firms, Shin-Etsu Handotai Company, Ltd. (24.5%) and Mitsubishi Materials Corporation (12.25%). The company is the leading provider of polycrystalline silicon and other silicon-based products used in the semiconductor and solar industry.

In 2007, the company had an annual production capacity of 10,000 t of polycrystalline silicon and production at the expanded Hemlock site (19,000 t) started in June 2008. A further expansion at the Hemlock site, as well as a new factory in Clarksville, Tennessee, was started in 2008 and brought total production capacity to 36,000 t in 2010. A further expansion to 40,000 t in 2011 and 50,000 t in 2012 is planned [79].

Wacker Polysilicon (Germany) Wacker Polysilicon AG (http://www.wacker.com) is one of the world's

leading manufacturers of hyper-pure polysilicon for the semiconductor and photovoltaic industry, chlorosilanes, and fumed silica. In 2010, Wacker increased its capacity to over 30,000 t and produced 30,500 t of polysilicon. The next 10,000 t expansion in Nünchritz (Saxony), Germany, started production in 2011. In 2010, the company decided to build a polysilicon plant in Tennessee with 15,000 t capacity. The groundbreaking of the new factory was in April 2011 and the construction should be finished at the end of 2013.

OCI Company (South Korea) OCI Company Ltd. (formerly DC Chemical) (http://www.oci.co.kr/) is a global chemical company with a product portfolio spanning the fields of inorganic chemicals, petro and coal chemicals, fine chemicals, and renewable energy materials. In 2006, the company started its polysilicon business and successfully completed its 6,500 metric ton P1 plant in December 2007. The 10,500 metric ton P2 expansion was completed in July 2009 and P3 with another 10,000 t brought the total capacity to 27,000 t at the end of 2010. The debottlenecking of P3, foreseen in 2011, should then increase the capacity to 42,000 t at the end of the year. Further capacity expansions P4 (20,000 t by 2012) and P5 (24,000 t by 2013) have already started (P4) or will commence in the second half of this year (P5).

GCL-Poly Energy Holdings Limited (PRC) GCL-Poly (http://www.gcl-poly.com.hk) was founded in March 2006 and started the construction of their Xuzhou polysilicon plant (Jiangsu Zhongneng Polysilicon Technology Development Co. Ltd.) in July 2006. Phase I has a designated annual production capacity of 1,500 t and the first shipments were made in October 2007. Full capacity was reached in March 2008. At the end of 2010, polysilicon production capacity had reached 21,000 t and further expansions to 46,000 t in 2011 and 65,000 t in 2012 are underway. For 2010, the company reported a production 17,850 t of polysilicon.

In August 2008, a joint venture, Taixing Zhongneng (Far East) Silicon Co. Ltd., started pilot production of trichlorsilane. Phase I will be 20,000 t, to be expanded to 60,000 t in the future.

MEMC Electronic Materials Inc. (USA) MEMC Electronic Materials Inc. (http://www.memc.com/) has its headquarters in St. Peters, Missouri. It started operations in 1959 and the company's products are semiconductor-grade wafers, granular polysilicon, ultra-high purity silane, trichlorosilane (TCS), silicon tetraflouride (SiF4), and sodium aluminum tetraflouride (SAF). MEMC's production capacity in 2008 was increased to 8,000 t and 9,000 t in 2009 [79].

Renewable Energy Corporation as (Norway) REC's (http://www.recgroup.com/) vision is to become the most cost-efficient solar energy company in the world, with a presence throughout the whole value chain. REC is presently pursuing an aggressive strategy to this end. Through its various group companies, REC is already involved in all major aspects of the PV value chain. The company located in Høvik, Norway has five business activities, ranging from silicon feedstock to solar system installations.

In 2005, Renewable Energy Corporation AS ("REC") took over Komatsu's US subsidiary, Advanced Silicon Materials LLC ("ASiMI"), and announced the formation of its silicon division business area, "REC Silicon Division," comprising the operations of REC Advanced Silicon Materials LLC (ASiMI) and REC Solar-Grade Silicon LLC (SGS). Production capacity at the end of 2010 was around 17,000 t [79] and according to the company, 11,460 t electronic grade silicon was produced in 2010.

LDK Solar Co. Ltd. (PRC) LDK (http://www.ldksolar.com/) was set up by the Liouxin Group, a company which manufactures personal protective equipment, power tools, and elevators. With the formation of LDK Solar, the company is diversifying into solar energy products. LDK Solar went public in May 2007. In 2008, the company announced the completion of the construction and the start of polysilicon production in its 1,000 t polysilicon plant. According to the company, the total capacity was 12,000 t at the end of 2010 which will be increased to 25,000 t in 2011. In 2010, polysilicon production was reported at 5,050 t.

Tokuyama Corporation (Japan) Tokuyama (http://www.tokuyama.co.jp/) is a chemical company involved in the manufacturing of solar-grade silicon, the base

material for solar cells. The company is one of the world's leading polysilicon manufacturers and produces roughly 16% of the global supply of electronics and solar-grade silicon. According to the company, Tokuyama had an annual production capacity of 5,200 t in 2008 and has expanded this to 9,200 t in 2010. In February 2011, the company broke ground for a new 20,000 ton facility in Malaysia. The first phase with 6,200 t should be finished in 2013.

A verification plant for the vapor to liquid-deposition process (VLD method) of polycrystalline silicon for solar cells has been completed in December 2005. According to the company, steady progress has been made with the verification tests of this process, which allows a more effective manufacturing of polycrystalline silicon for solar cells.

Tokuyama has decided to form a joint venture with Mitsui Chemicals, a leading supplier of silane gas. The reason for this is the increased demand for silane gas, due to the rapid expansion of amorphous/microcrystalline thin-film solar cell manufacturing capacities.

Kumgang Korea Chemical Company (South Korea) Kumgang Korea Chemical Company (KCC) (http://www.kccworld.co.kr/english/) was established by a merger of Kumgang and the Korea Chemical Co. in 2000. In February 2008, KCC announced its investment in the polysilicon industry and began to manufacture high-purity polysilicon with its own technology at the pilot plant of the Daejuk factory in July of the same year. In February 2010, KCC started to mass-produce polysilicon, with an annual capacity of 6,000 t.

Mitsubishi Materials Corporation (Japan) Mitsubishi Materials (http://www.mmc.co.jp) was created through the merger Mitsubishi Metal and Mitsubishi Mining and Cement in 1990. Polysilicon production is one of the activities in their Electronic Materials and Components business unit. The company has two production sites for polysilicon, one in Japan and one in the USA (Mitsubishi Polycrystalline Silicon America Corporation) and is a shareholder (12.25%) in Hemlock Semiconductor Corporation. With the expansion of the Yokkachi, Mie, Japan, polysilicon plant, by 1,000 t in 2010, total production capacity was increased to 4,300 t.

The Photovoltaic Market

In 2010, the worldwide photovoltaic market more than doubled, driven by major increases in Europe. For 2010, the market volume of newly installed solar photovoltaic electricity systems varies between 17 and 19 GW, depending on the reporting consultancies (Fig. 7). This represents mostly the grid-connected photovoltaic market. To what extent the off-grid and consumer

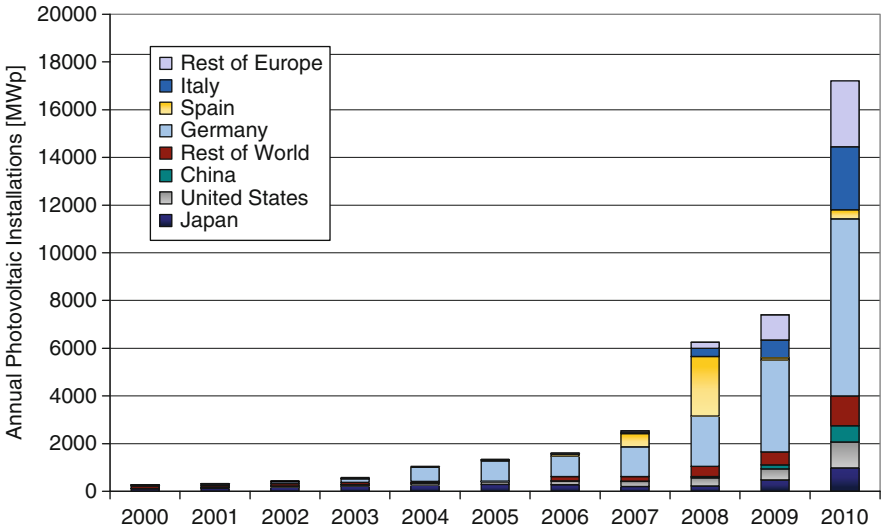

Photovoltaics, Status of. Figure 7
Annual photovoltaic installations from 2000 to 2010 (Data Source: EPIA [80], Eurobserver [81] and own analysis)

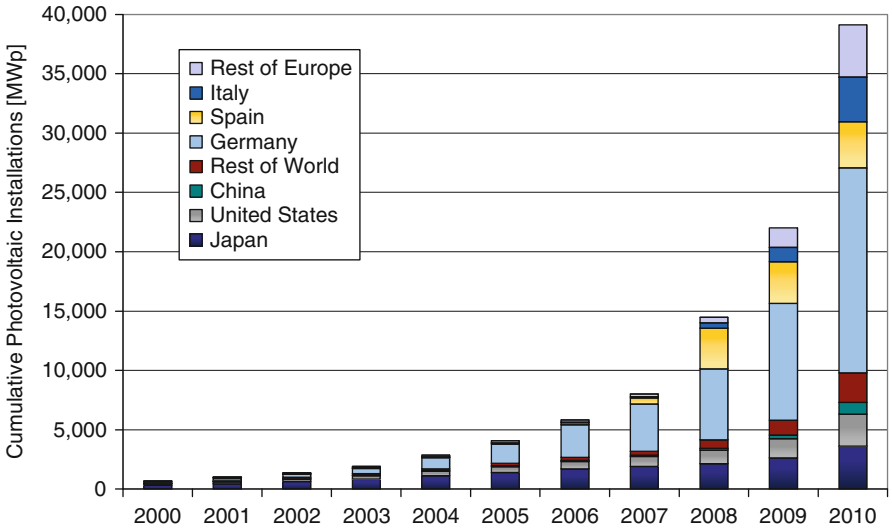

Photovoltaics, Status of. Figure 8
Cumulative photovoltaic installations from 2000 to 2010 (Data Source: EPIA [80], Eurobserver [81] and own analysis)

product markets are included is not clear, but it is believed that a substantial part of these markets are not accounted for, as it is very difficult to track them. A conservative estimate is that they account for approximately 400–800 MW (approx. 1–200 MW off-grid rural, approx. 1–200 MW communication/signals, approx. 100 MW off-grid commercial and approx. 1–200 MW consumer products).

With a cumulative installed capacity of over 29 GW, the European Union is leading in PV installations with a little more than 70% of the total worldwide 39 GW of solar photovoltaic electricity generation capacity at the end of 2010 (Fig. 8).

European Union and Turkey

Market conditions for photovoltaics differ substantially from country to country. This is due to different energy policies and public support programs for renewable energies and especially photovoltaics, as well as the varying grades of liberalization of domestic electricity markets. Within one decade, the solar photovoltaic electricity generation capacity has increased 160 times from 185 MW in 2000 to 29.5 GW in 2010 [80–83].

A total of about 58.8 GW of new power capacity was constructed in the EU last year and 2.5 GW were decommissioned, resulting in 56.3 GW of new net capacity (Fig. 9) [81, 84]. Gas-fired power stations accounted for 28.3 GW, or 48% of the newly installed capacity. However, in the recent years about 30 GW of additional gas-fired power station projects were suspended or canceled according to Platts [85]. Solar photovoltaic systems moved to the second place with 13.5 GW (23%), followed by 9.4 GW (16%) wind power; 4.1 GW (7%) MW coal-fired power stations; 570 MW (>1%) biomass; 450 MW (>1%) CSP, 210 MW (>1%) hydro, 230 MW (>1%) peat, and 150 MW (>1%) waste. The net installation capacity for oil-fired and nuclear power plants was negative, with a decrease of 245 MW and 390 MW respectively. The renewable share of new power installations was 40% in 2010.

Belgium Belgium showed another strong market performance year in 2010, with new photovoltaic system installations of 420 MW bringing the cumulative installed capacity to 790 MW. However, most of the installations were done in Flanders, where since January 1, 2006 Green Certificates exist with 0.45 €/kWh for 20 years. In Brussels and Wallonia, the Green Certificates have a guaranteed minimum price between 0.15 and 0.65 €/kWh, depending on the size of the systems and region (Brussels 10 years, Wallonia 15 years).

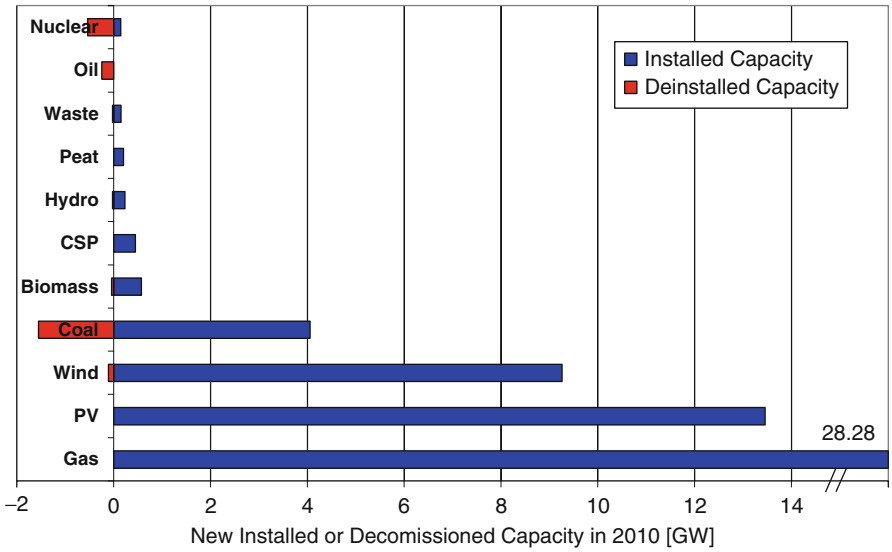

Photovoltaics, Status of. Figure 9
New installed or decommissioned electricity generation capacity in Europe in 2010 [81, 84]

Czech Republic In the Czech Republic, photovoltaic systems with about 1.5 GW capacity, were installed in 2010, bringing the cumulative nominal capacity to 1.95 GW exceeding their own target of 1.65 GW set in the National Renewable Action Plan for 2020. The Law on the Promotion of Production of Electricity from Renewable Energy Sources went into effect on August 1, 2005 and guarantees a feed-in tariff for 20 years. The annual prices are set by the Energy Regulator. The electricity producers can choose from two support schemes, either fixed feed-in tariffs or market price + Green Bonus. The 2010 feed-in rate in the Czech Republic was CZK 12.25 per kilowatt hour (0.48 €/kWh).

On February 3, 2010, the Czech transmission system operator, EPS, requested all main distribution system operators (EZ, E-ON, PRE) to stop permitting new renewable energy power plants, due to a virtual risk of instability of the electricity grid caused by intermittent renewable sources, especially photovoltaic and wind. Distribution System Operators (DSO) met the requirement on February 16, 2011. The moratorium still exists and SRES (Czech Association of Regulated Energy Companies) announced that the moratorium will continue until at least September.

A number of legislative changes took place in the second half of the year, which resulted in a lower feed-in tariff for systems larger than 30 kW (5.5 CZK/kWh or 0.216 €/kWh), the phase-out of ground-mounted PV systems from March 1, 2011 onward and the introduction of a retroactive tax on benefits generated by PV installations.

France In 2010, 720 MW of PV systems were connected to the grid in France, including about 100 MW which were already installed in 2009. This led to an increase of the cumulative installed capacity to 1.05 GW. However, this positive development came to a sudden stop when the French Prime Minister declared a three-month moratorium on new PV installations above 3 kW and a suspension of projects waiting for grid connection in December 2010.

This rapid growth led to a revision of the feed-in scheme in February 2011, setting a cap of 500 MW for 2011 and 800 MW for 2012 [86]. The new tariff levels only apply to rooftop systems up to 100 kW in size. In addition, those installations are divided into three different categories: residential; education or health; and other buildings with different feed-in tariffs, depending on the size and type of installation. The tariffs for these installations range between 0.2883 €/kWh and 0.46 €/kWh. All other installations up to 12 MW are just eligible for a tariff of 0.12 €/kWh.

Germany Germany had the biggest market with 7.4 GW [82]. The German market growth is directly correlated to the introduction of the Renewable Energy Sources Act or "*Erneuerbare Energien Gesetz*" (EEG) in 2000 [87]. This Law introduced a guaranteed feed-in tariff for electricity generated from solar photovoltaic systems for 20 years and already had a fixed built in annual decrease, which was adjusted over time to reflect the rapid growth of the market and the corresponding price reductions. Due to the fact that until 2008 only estimates of the installed capacity existed, a plant registrar was introduced from January 1, 2009 on.

The German market showed two installation peaks during 2010. The first one was in June, when more than 2.1 GW were connected to the grid prior to the 13% feed-in cut which took effect on July 1, 2010. The second peak was in December with almost 1.2 GW just before the scheduled tariff reduction of another 13% on January 1, 2011. Compared to 2009, the feed-in tariff has been reduced by 33–36% depending on the system size and classification. In June 2011, the Bundesnetzagentur (German Federal Network Agency) announced the results of the PV system installation projection required under the Renewable Energy Sources Act (EEG) in order to determine the degression rates for the feed-in tariffs [88]. According to the Agency approximately 700 MW of PV systems were commissioned between March and May 2011 resulting in a projected annual growth of 2.8 GW, which is below the 3.5 GW threshold set for an additional reduction of the tariffs starting July 2011.

Greece Greece introduced a new feed-in tariff scheme on January 15, 2009. The tariffs remained unchanged until August 2010 and are guaranteed for 20 years. However, if a grid-connection agreement was signed before that date, the unchanged FIT was applied if the system is finalized within the next 18 months. For small rooftop PV systems, an additional program was introduced in Greece on June 4, 2009. This program covers rooftop PV systems up to 10 kWp (both for residential users and small companies). In 2011, the tariffs decreased by 6.8–8.5%, depending on the size and location of the installation. In 2010, about 150 MW of new installations were carried out, bringing the total capacity to about 205 MW.

Italy Italy again took the second place, with respect to new installations and added a capacity of about 2.5 GW, bringing cumulative installed capacity to 3.7 GW at the end of 2010 [83]. In the middle of August 2011, the total connected PV capacity has surpassed 9.4 GW [89]. The *Quarto Conto Energia* (Fourth Energy Bill) was approved by the Italian Council of Ministers on May 5, 2011 [Gaz 2011]. The Bill introduced monthly reductions of the tariffs, starting from June 2011 until January 2012 and then another one in July 2012. In addition, the new Bill limits the feed-in tariffs for new systems up until the end of 2016, or until a cap of 23 GW is reached. In addition, separate caps for large systems are set for the second half of 2011 (1.35 GW) and 2012 (1.75 GW).

Spain Spain is second regarding the total cumulative installed capacity with 3.9 GW. Most of this capacity was installed in 2008 when the country was the biggest market, with close to 2.7 GW in 2008 [80]. This was more than twice the expected capacity and was due to an exceptional race to install systems before the Spanish Government introduced a cap of 500 MW on the yearly installations in the autumn of 2008. A revised Decree (Royal Decree 1758/2008) set considerably lower feed-in tariffs for new systems and limited the annual market to 500 MW, with the provision that two thirds are rooftop mounted and no longer free-field systems. These changes resulted in a new installed capacity of about 100 MW and about 380 MW in 2010.

In 2010, the Spanish Government passed the Royal Decrees 1565/10 [90] and RD-L 14/10 [91]. The first one limits the validity of the feed-in tariffs to 28 years, while the latter reduces the tariffs by 10–30% for existing projects until 2014. Both Bills are "retroactive" and the Spanish Solar Industry Association (ASIF) [92] has already announced taking legal actions against them.

United Kingdom The United Kingdom introduced of a new feed-in tariff scheme in 2010, which led to the installation of approximately 55 MW, bringing the cumulative installed capacity to about 85 MW. However, in March 2011, the UK Government proposed significant reductions of the tariffs, especially for systems larger than 50 kW.

Other European Countries and Turkey Despite high solar radiation, solar photovoltaic system installation in *Portugal* has only grown very slowly and reached a cumulative capacity of 130 MW at the end of 2010.

The market in *Slovakia* showed an unexpected growth from less than 1 MW installed at the end of 2009 to about 144 MW at the end of 2010. In December 2010, the Slovak Parliament adopted an Amendment to the Renewable Energy Sources (RES) Promotion Act, decreasing the feed-in tariffs and from February 1, 2011 on only solar rooftop facilities or solar facilities on the exterior wall of buildings, with capacity not exceeding 100 kW, are eligible for the feed-in tariff. As a result, larger new solar projects in Slovakia are on hold.

In *Turkey* in March 2010, the Energy Ministry unveiled its 2010–2014 Strategic Energy Plan. One of Government's priorities is to increase the ratio of renewable energy resources to 30% of total energy generation by 2023. At the beginning of 2011, the Turkish Parliament passed a Renewable Energy Legislation which defines new guidelines for feed-in tariffs. The feed-in tariff is 0.133 $/kWh (0.10 €/kWh) for owners commissioning a PV system before the end of 2015. If components "*Made in Turkey*" are used, the tariff will increase by up to $0.067 (€ 0.052), depending on the material mix. Feed-in tariffs apply to all types of PV installations, but large PV power plants will receive subsidies up to a maximum size of 600 MWp.

Asia and Pacific Region

The Asia and Pacific Region shows an increasing trend in photovoltaic electricity system installations. There are a number of reasons for this development, ranging from declining system prices, heightened awareness, favorable policies, and the sustained use of solar power for rural electrification projects. Countries such as Australia, China, India, Indonesia, Japan, Malaysia, South Korea, Taiwan, Thailand, The Philippines and Vietnam show a very positive upward trend, thanks to increasing governmental commitment toward the promotion of solar energy and the creation of sustainable cities.

The introduction or expansion of feed-in-tariffs is expected to be an additional big stimulant for on-grid solar PV system installations for both distributed and centralized solar power plants in countries such as Australia, Japan, Malaysia, Thailand, Taiwan, and South Korea.

The Asian Development Bank (ADB) launched an Asian Solar Energy Initiative (ASEI) in 2010, which should lead to the installation of 3 GW of solar power by 2012 [93]. In their report, ADB states: *Overall, ASEI aims to create a virtuous cycle of solar energy investments in the region, toward achieving grid parity, so that ADB developing member countries optimally benefit from this clean, inexhaustible energy resource.*

Australia In 2010, 383 MW of new solar photovoltaic electricity systems were installed in Australia, bringing the cumulative installed capacity of grid-connected PV systems to 571 MW [94]. The 2010 market was dominated by the increase of grid-connected distributed systems, which increased from 67 MW in 2009 to 378 MW in 2010. The newly installed PV electricity generation capacity in Australia accounted for 20% of the new electricity generation capacity in 2010.

Most installations took advantage of the incentives under the Australian Government's Solar Homes and Communities Plan (SHCP), Renewable Energy Target (RET) mechanisms and feed-in tariffs in some States or Territories. At the beginning of 2010, eight out of the eleven Australian Federal States and Territories had introduced some kind of feed-in tariff scheme for systems smaller than 10 kWp. All of these schemes have built-in caps which were partly reached that year so that in 2011 only five State schemes are still available for new installations and additional changes are expected in the course of this year.

India For 2010, market estimates for solar PV systems vary between 50 and 100 MW, but most of these capacities are for off-grid applications. The Indian National Solar Mission was launched in January 2010, and it was hoped that it would give impetus to the grid-connected market, but only a few MW were actually installed in 2010. The majority of the projects announced will come online from 2011 onward.

The National Solar Mission aims to make India a global leader in solar energy and envisages an installed solar generation capacity of 20 GW by 2020, 100 GW by 2030, and 200 GW by 2050. The short-term outlook up

until 2013 was improved as well when the original 50 MW grid-connected PV system target in 2012 was changed to 1,000 MW for 2013.

Japan In 2010, the Japanese market experienced a high growth, doubling its volume to 990 MW, bringing the cumulative installed PV capacity to 3.6 GW. In 2009, a new investment incentive of ¥ 70,000/kW for systems smaller than 10 kW, and a new surplus power purchase scheme, with a purchase price of ¥ 48/kWh for systems smaller than 10 kW, was introduced and the start of the discussion about a wider feed-in tariff.

In April 2011, METI (Ministry for Economy, Trade and Industry) announced a change in the feed-in tariffs and increased the tariff for commercial installations from ¥ 20 to 40/kWh and decreased the tariff for residential installations to ¥ 42/kWh.

As a consequence of the accident at the Fukujima Daiichi Nuclear Power Plant, Prime Minister Naoto Kan announced an overall review of the country's Basic Energy Plan. At the G8 Summit held in Deauville, France, on May 26, 2011, he announced that Japan plans to increase the share of renewable energy in total electricity supply to over 20% in the 2020s. One measure to achieve this goal is to install a PV system on some 10 million houses suitable for it.

People's Republic of China The 2010 Chinese PV market estimates are between 530 and 690 MW, bringing the cumulative installed capacity to about 1 GW. This is a significant increase from the 160 MW in 2009, but still only 5–7% of the total photovoltaic production. This situation will change because of the revision of the PV targets for 2015 and 2020. According to press reports, the National Energy Administration doubled its capacity target for installed photovoltaic electricity systems to 10 GW in 2015 and further up to 50 GW in 2020 [95].

According to the 12th Five-Year Plan, which was adopted on March 14, 2011, China intends to cut its carbon footprint and be more energy efficient. The targets are 17% less carbon dioxide emissions and 16% less energy consumption unit of GDP. The total investment in the power sector under the 12th Five-Year Plan is expected to reach $803 billion (€ 618 billion), divided into $416 billion (€ 320 billion), or 52%, for power generation, and $386 billion (€ 298 billion) to construct new transmission lines and other improvements to China's electrical grid.

Renewable, clean, and nuclear energy are expected to contribute to 52% of the increase and it is planned to increase power generation capacity from nonfossil fuels to 474 GW by 2015.

The investment figures necessary are in-line with a World Bank report stating that China needs an additional investment of $64 billion (€ 49.2 billion) annually over the next 2 decades to implement an "energy-smart" growth strategy [96]. However, the reductions in fuel costs through energy savings could largely pay for the additional investment costs according to the report. At a discount rate of 10%, the annual net present value (NPV) of the fuel cost savings from 2010 to 2030 would amount to $145 billion (€ 111.5 billion), which is about $70 billion (€ 53.8 billion) more than the annual NPV of the additional investment costs required.

South Korea In 2010, about 180 MW of new PV systems were installed in South Korea, about the same as the year before, bringing the cumulative capacity to a total of 705 MW. The Korean PV industry expects a moderate increase for 2011, due to the fact that the feed-in tariff scheme is in its final year and the Korean Government continues its "One Million Green Homes" Project, as well as other energy projects in the provinces. The implementation of the Renewable Portfolio Standard in 2012 has additional consequences, as systems will need to be installed by the end of 2011 to generate electricity.

In January 2009, the Korean Government had announced the Third National Renewable Energy Plan, under which renewable energy sources will steadily increase their share of the energy mix between now and 2030. The Plan covers such areas as investment, infrastructure, technology development, and programs to promote renewable energy. The new Plan calls for a renewable energies share of 4.3% in 2015, 6.1% in 2020, and 11% in 2030.

Taiwan In June 2009, the Taiwan Legislative Yuan gave its final approval to the Renewable Energy Development Act, a move that is expected to bolster the development of Taiwan's green energy industry. The new law authorizes the Government to enhance

incentives for the development of renewable energy via a variety of methods, including the acquisition mechanism, incentives for demonstration projects, and the loosening of regulatory restrictions. The goal is to increase Taiwan's renewable energy generation capacity by 6.5 GW to a total of 10 GW within 20 years. In January 2011, the Ministry of Economic Affairs (MOEA) announced the revised feed-in tariffs for 2011. In 2011, the price paid by the state-owned monopoly utility, Taiwan Power, will fall 30% from 11.12 NT$/kWh (0.264 €/kWh) to 7.33 NT$/kWh per kWh (0.175 €/kWh) for solar installations, with an exception for rooftop installations which will be eligible for rates of 10.32 NT$/kWh (0.246 €/kWh).

Despite the favorable feed-in tariff, the total installed capacity at the end of 2010 was only between 19 and 20 MW and the annual installation of about 7–8 MW was far less than 1% of the 3.2 GW solar cell production in Taiwan that year.

Thailand Thailand enacted a 15-year Renewable Energy Development Plan (REDP) in early 2009, setting the target to increase the Renewable Energy share to 20% of final energy consumption of the country in 2022. Besides a range of tax incentives, solar photovoltaic electricity systems are eligible for a feed-in premium or "Adder" for a period of 10 years. However, there is a cap of 500 MW eligible for the original 8 THB/kWh (0.182 €/kWh) "Adder" (facilities in the three Southern provinces and those replacing diesel systems are eligible for an additional 1.5 THB/kWh (0.034 €/kWh)), which was reduced to 6.5 THB/kWh (0.148 €/kWh) for those projects not approved before June 28, 2010.

As of October 2010, applications for 1.6 GW, under the *Very Small Power Producer Programme* (VSPP), and 477 MW, under the *Small Power Producer Programme* (SPP), were submitted. In 2010, it is estimated that between 20 and 30 MW were actually added, increasing the total cumulative installed capacity to 60–70 MW.

Emerging Markets

- *Bangladesh*: In 1997, the Government of Bangladesh established the Infrastructure Development Company Limited (IDCOL) to promote economic development in Bangladesh. In 2003, IDCOL started its Solar Energy Programme to promote the dissemination of solar home systems (SHS) in the remote rural areas of Bangladesh, with the financial support from the World Bank, the Global Environment Facility (GEF), the German Kreditanstalt für Wiederaufbau (KfW), the German Technical Cooperation (GTZ), the Asian Development Bank, and the Islamic Development Bank. Since the start of the program, more than 950,000 SHS, with an estimated capacity of 39 MW, have been installed in Bangladesh by May 2011.

  According to a press report, the Government plans to implement a mega project of setting up 500 MW of PV electrical power generation and the Asian Development Bank (ADB) has, in principal, agreed to provide financial support to Bangladesh for implementing the project within the framework of the Asian Solar Energy Initiative [97, 98].
- *Indonesia*: The development of renewable energy is regulated in the context of the national energy policy by Presidential Regulation No.5/2006 [99]. The decree states that 11% of the national primary energy mix in 2025 should come from renewable energy sources. The target for solar PV is 870 MW by 2024. At the end of 2010, about 20 MW of solar PV systems were installed, mainly for rural electrification purposes.
- *Malaysia*: The Malaysia Building Integrated Photovoltaic (BIPV) Technology Application Project was initiated in 2000 and at the end of 2009 a cumulative capacity of about 1 MW of grid-connected PV systems has been installed.

  The Malaysian Government officially launched their GREEN Technology Policy in July 2009 to encourage and promote the use of renewable energy for Malaysia's future sustainable development. By 2015, about 1 GW must come from Renewable Energy Sources according to the Ministry of Energy, Green Technology and Water (KETHHA). The Malaysian Photovoltaic Industry Association (MPIA) proposed a five-year program to increase the share of electricity generated by photovoltaic systems to 1.5% of the national demand by 2015. This would translate into 200 MW grid-connected and 22 MW of grid systems. In the long-term beyond 2030, MPIA is calling for a 20% PV

share. Pusat Tenaga Malaysia (PTM), and its IEA international consultant, estimated that 6,500 MW power can be generated by using 40% of the nation's house rooftops (2.5 million houses) and 5% of commercial buildings alone. To realize such targets, a feed-in tariff is still under discussion and it is hoped to be under way in the second half of 2011.

First Solar (USA), Q Cells (Germany), and Sunpower (USA) have started to set up manufacturing plants in Malaysia, with a total investment of RM 12 billion and more than 2 GW of production capacities. Once fully operational, these plants will provide 11,000 jobs and Malaysia will be the world's sixth largest producer of solar cells and modules.

- *The Philippines:* The Renewable Energy Law was passed in December 2008 [100]. Under the Law, the Philippines has to double the energy derived from Renewable Energy Sources within 10 years. On June 14, 2011, Energy Secretary, Rene Almendras unveiled the new Renewable Energy Roadmap, which aims to increase the share of renewables to 50% by 2030. The program will endeavor to boost renewable energy capacity from the current 5.4 GW to 15.4 GW by 2030.

  Early 2011, the country's Energy Regulator National Renewable Energy Board (NREB) has recommended a target of 100 MW of solar installations that will be constructed in the country over the next 3 years. A feed-in tariff of 17 PHP/kWh (0.283 €/kWh) was suggested, to be paid from January 2012 on. The initial period of the program is scheduled to end on December 31, 2014.

  At the end of 2010, about 10 MW of PV systems were installed, mainly off-grid. SunPower has two cell manufacturing plants outside of Manila. Fab. No 1 has a nameplate capacity of 108 MW and Fab. No 2 adds another nameplate capacity of 466 MW.
- *Vietnam*: In December 2007, the National Energy Development Strategy of Vietnam was approved. It gives priority to the development of renewable energy and includes the following targets: increase the share of renewable energies from negligible to about 3% (58.6 GJ) of the total commercial primary energy in 2010, to 5% in 2020, 8% (376.8 GJ) in 2025, and 11% (1.5 TJ) in 2050.

  The Indochinese Energy Company (IC Energy) broke ground for the construction of a thin-film solar panel factory with an initial capacity of 30 MW and a final capacity of 120 MW in the central coastal Province of Quang Nam on May 14, 2011.

  In March 2011, First Solar broke ground on its four-line photovoltaic module manufacturing plant (250 MW) in the Dong Nam Industrial Park near Ho Chi Minh City.

North America

Canada In 2010, Canada more than tripled its cumulative installed PV capacity to about 420 MW, with 300 MW new installed systems. This development was driven by the introduction of a feed-in tariff in the Province of Ontario, enabled by the *"Bill 150, Green Energy and Green Economy Act, 2009."* On the Federal level, only an accelerated capital cost allowance exists under the Income Tax Regulations. On a Province level, nine Canadian Provinces have *Net Metering Rules*, with solar photovoltaic electricity as one of the eligible technologies, *Sales Tax Exemptions* and *Renewable Energy Funds* exist in two Provinces and *Micro Grid Regulations* and *Minimum Purchase Prices* each exist in one Province.

The Ontario feed-in tariffs were set in 2009 and depend on the system size and type, as follows:

Rooftop or ground-mounted $\leq$ 10 kW	80.2 ¢/kWh (0.59 €/kWh)
Rooftop $>$ 10 kW $\leq$ 250 kW	71.3 ¢/kWh (0.53 €/kWh)
Rooftop $>$ 250 kW $\leq$ 500 kW	63.5 ¢/kWh (0.47 €/kWh)
Rooftop $>$ 500 kW	53.9 ¢/kWh (0.40 €/kWh)
Ground-mounted*$>$10 kW $\leq$ 10 MW	44.3 ¢/kWh (0.33 €/kWh)

*Eligible for Aboriginal or community adder

The feed-in tariff scheme has a number of special rules, ranging from eligibility criteria, which limit

the installation of ground-mounted PV systems on high-yield agricultural land to domestic content requirements and *additional "price adders" for Aboriginal and community-based projects*. Details can be found in the Feed-in Tariff Program of the Ontario Power Authority [101].

United States With close to 900 MW of new installed PV capacity, the USA reached a cumulative PV capacity of 2.5 GW at the end of 2010. Utility PV installations more than tripled compared to 2009 and reached 242 MW in 2010. The top ten states – California, New Jersey, Nevada, Arizona, Colorado, Pennsylvania, New Mexico, Florida, North Carolina, and Texas accounted for 85% of the US grid-connected PV market [74].

PV projects with Power Purchase Agreements (PPAs), with a total capacity of 6.1 GW, are already under contract and to be completed by 2014 [102]. If one adds those 10.5 GW of projects which are already publicly announced, but PPAs have yet to be signed, this make the total "pipeline" more than 16.6 GW.

After years of political deadlock and negotiations concerning the support of renewable energies in the USA, things started to move in 2005. The main breakthrough was reached, when the 2005 Energy Bill was passed by the Senate on July 29, 2005 and signed by President Bush on August 8, 2005. The next milestone was the final approval of the Californian "Million Solar Roofs Plan" or Senate Bill 1 (SB1) in 2006. The *"Energy Improvement and Extension Act of 2008"* as part of H.R. 1424, the *"Emergency Economic Stabilization Act of 2008"* and the *"American Reinvestment and Recovery Act of 2009"* were the next steps to support the implementation of renewable energies and solar photovoltaic electricity generation.

There is no single market for PV in the USA, but a conglomeration of regional markets and special applications for which PV offers the most cost-effective solution. In 2005, the cumulative installed capacity of grid-connected PV systems surpassed that of off-grid systems. Since 2002, the grid-connected market has been growing much faster, thanks to a wide range of "buy-down" programs, sponsored either by States or utilities.

Many State and Federal policies and programs have been adopted to encourage the development of markets for PV and other renewable technologies. These consist of direct legislative mandates (such as renewable content requirements) and financial incentives (such as tax credits). DOE has defined a financial incentive as one that: (1) transfers economic resources by the Government to the buyer or seller of goods or a service that has the effect of reducing the price paid or increasing the price received; (2) reduces the cost of producing the goods or service; and/or (3) creates or expands a market for producers [103]. Financial incentives typically involve appropriations or other public funding, whereas direct mandates typically do not. In both cases, these programs provide important market development support for PV. The types of incentives are described below. Amongst them, investment rebates, loans, and grants are the most commonly used – 42 States, the District of Columbia and the Virgin Islands – have such programs in place. Most common mechanisms are:

- Personal tax exemptions (Federal Government, 24 States + Puerto Rico)
- Corporate tax exemptions (Federal Government and 25 States)
- Sales tax exemptions for renewable investments (28 States + Puerto Rico)
- Property tax exemptions (34 States + Puerto Rico, 15 local)
- Buy-down programs (23 States + District of Columbia, Puerto Rico, Virgin Islands, 398 utilities, 17 local)
- Loan programs and grants (Federal Gov., 42 States + District of Columbia, Virgin Islands; 72 utilities, 22 local, 13 private)
- Industry support (Federal Government, 21 States + Puerto Rico, 1 local)

One of the most comprehensive databases about the different support schemes in the USA is maintained by the Solar Centre of the State University of North Carolina. The Database of State Incentives for Renewable Energy (DSIRE) is a comprehensive source of information on State, local, utility, and selected federal incentives that promote renewable energy. All different support schemes are described there and it is highly recommended to visit the DSIRE web-site http://www.dsireusa.org/ and the corresponding interactive tables and maps for more details.

Conclusions

The increase of conventional energy prices has increased the investment attention for renewable energies and in particular photovoltaics significantly. Despite the difficult economic conditions the worldwide production continued to increase with growth rates above 40%. There is a dynamic growth rate in system installation, but due to the tremendous capacity increase production surplus will continue to exist at least for the next 2–3 years. This development is connected to an increasing industry consolidation, which presents a risk and an opportunity at the same time. If the new large solar cell companies use their cost advantages to offer lower-priced products, customers will buy more solar systems and it is expected that the PV market will show an accelerated growth rate. However, this development will influence the competitiveness of small and medium companies as well. To survive the price pressure of the big and financial strong companies, they have to specialize in niche markets with high value added in their products. The other possibility is to offer technologically more advanced and cheaper solar cell concepts.

Even with the current economic difficulties, the increasing number of market implementation programs worldwide, as well as the overall rising energy prices and the pressure to stabilize the climate, will continue to keep the demand for solar systems high. In the long-term, growth rates for Photovoltaics will continue to be high, even if the economic frame conditions vary and can lead to a short-term slowdown. This view is shared by an increasing number of financial institutions, which are turning toward renewables as a sustainable and lucrative long-term investment. Increasing demand for energy is pushing the prices for fossil energy resources higher and higher. Already in 2007, a number of analysts predicted that oil prices could well hit 100 $/bbl by the end of 2007 or early 2008 [104]. After the spike of oil prices in July 2008, with close to 150$/bbl, prices have decreased due to the worldwide financial crisis and hit a low around 37 $/bbl in December 2008. However, the oil price has rebounced and is back in the 80 $/bbl range in the first half of 2010. It is obvious that the fundamental trend of increasing demand for oil will drive the oil price higher again. In an interview at the beginning of March 2009, the IEA Executive Director Nobuo Tanaka warned that the next oil crisis with oil prices at around 200 $/bbl due to a supply crunch, could be as close as 2013 because of lack of investments in new oil production.

Already for a few years, we have now observed a continuous rise of oil and energy prices, which highlights the vulnerability of our current dependence on fossil energy sources and increases the burden developing countries are facing in their struggle for future development. On the other hand, we see a continuous decrease in production costs for renewable energy technologies as a result of steep learning curves. Due to the fact that external energy costs, subsidies in conventional energies and price volatility risks are generally not taken into consideration, renewable energies and Photovoltaics are still perceived as more expensive in the market than conventional energy sources. Nevertheless, electricity production from Photovoltaic solar systems have already shown now that it can be cheaper than peak prices in the electricity exchange in a wide range of countries and if market growth continues at the current pace, electricity generation cost with Photovoltaic systems will have reached grid parity in most of Europe by 2020. In addition, solar photovoltaic generated electricity offers, contrary to conventional energy sources, a reduction of prices rather than an increase in the future.

Future Directions

The progress of photovoltaics will depend on a parallel development of markets and progress in research. A number of science areas can make a big impact in the future.

Material Science: Fundamental material research and the systematic screening, synthetization, and characterization of potential solar cell materials can play an important role to find and identify new solar cell materials or substitute certain rare materials in the current family of solar cells. In the field of solar photovoltaics, the range of used materials is limited to few elements like silicon (wafer based and thin film), GaAs and its derivatives, CdTe, a few chalcopyrites ($CuInGa(SSe)_2$) and some dye and organic compounds. Already in the first half of the 1950s I-II-VI_2 components were researched and the first II-IV-V_2 compounds were synthesized. The invention of the $CuInSe_2$/CdS solar cell in

the early 1970s at Bell Labs spurred an increased research activity to use compound semiconductors as base material for solar cells. Fundamental theoretical bandstructure calculations were performed and identified a wide range of compound materials as possible candidates for solar cells in the 1970s. However, the systematic synthetization and investigation and characterization of these potential materials has been not done so far, but offer a chance for new material compositions and or efficiency increases.

Microelectronics: The further large-scale implementation of PV modules and systems will require *intelligent modules* in order minimize losses attributed to partial shading or power fluctuations. To realize this smarter control strategies and alternative power electronics topologies that dynamically optimize the yearly production of these modules have to be developed. There is a need to control (e.g., the conversion factor of DC/DC converters) and monitor (e.g., distributed temperature sensing) various parameters in real time to enable the plant-level controller to optimize the energy yield. Ultimately, he might be able to make trade-offs between lifetime and maximizing power here and now. From a technological point of view, this implies that additional power electronic circuits and sensors need to be placed in and around the module.

Storage Technologies: Future grid-connected PV systems will be subject to more stringent regulatory requirements for the delivery of "ancillary services" to support the electricity grid when reserve and reactive power injection (for voltage support) has to be delivered. As the electricity grid has to deal with positive as well as negative balances, this involves the "shaving" of peak production and temporarily boosting power output. Lowering the output is easily achieved by moving away from the MPP, but when storage is at hand, the energy conversion can be kept at maximum level and the output difference is stored for later recovery.

Such storage functions may be centralized or distributed – a possibly micro-storage for short-term needs could be introduced at the module level in close conjunction to DC/DC converters. These storage components could consist of improved supercapacitors with low leakage and innovative thin-film battery approaches.

To realize such innovative approaches needs the further development of the respective power components and storage technologies as solar modules increase in temperature during operation which is not favorable for the lifetime of current power electronics and storage technologies.

Exchange Rates

1 € = 1.35 CAD
1 € = 25.52 CZK
1 € = 9.5 RMB
1 € = 60 INR
1 € = 1,450 KRW
1 € = 42 NT$
1 € = 60 PHP
1 € = 44 THB
1 € = 1.30 US$

Bibliography

1. Paula Mints (2010) Manufacturer shipments, capacity and competitive analysis 2009/2010. Navigant Consulting Photovoltaic Service Program, Palo Alto
2. Paula Mints, Global PV demand 2011 and beyond, Webinar: vote solar, 12 Jan 2011
3. PV News, published by Greentech Media (2011) ISSN 0739–4829
4. Photon International, March 2011
5. World Economic Forum (2011) Green investing 2011 – reducing the cost of financing, Ref. 200311, April 2011
6. The PEW Charitable Trusts (2011) Who's winning the clean energy race? 2010 edition. www.pewtrusts.org
7. Photon Photovoltaic Stock Index PPVX, http://www.photon-international.com/news/news_01-08-01_eu_ppvx.htm
8. IMS Research, Press release, 31 May 2011
9. iSupply, PV perspectives, Feb 2011
10. Homan G, Presentation at intersolar 2009
11. Bernreuther J, Haugwitz F (2010) The who's who of silicon production. Bernreuter Reserach, Würzburg, Germany
12. Green M, Emery K, Hishikawa Y, Warta W, Dunlop EE (2011) Solar cell efficiency tables (version 38). Prog Photovolt: Res Appl 19:565–572
13. Zhao J, Wang A, Green MA, Ferrazza F (1998) Novel 19.8% efficient "honeycomb" textured multicrystalline and 24.4% monocrystalline silicon solar cells. Appl Phys Lett 73:1991–1993
14. Schultz O, Glunz SW, Willeke GP (2004) Multicrystalline silicon solar cells exceeding 20% efficiency. Prog Photovolt: Res Appl 12:553–558
15. Shockley W, Queisser HJ (1961) Detailed balance limit of efficiency of p-n junction solar cells. J Appl Phys 32(3):510–519
16. Swanson RM (2005) Approaching the 29% limit efficiency of silicon solar cells. In: Proceedings of the 20th European photovoltaic solar energy conference, Dresden, 584–589 pp. ISBN 3-936338-25-6

17. Taguchi M, Tsunomura Y, Inoue H, Taira S, Nakashima T, Baba T, Sakata H, Maruyama E, (2009) High-efficiency HIT solar cell on thin (<100 μm) silicon wafer. In: Proceedings of the 24th European photovoltaic solar energy conference, Hamburg, 1690–1693 pp. ISBN 3-936338-25-6
18. Swanson R (2008) The SunPower story: The path from R&D concentrator cells to a high volume PV panel and system manufacturer. In: Proceedings of the 33 rd IEEE photovoltaic specialists conference, San Diego
19. Carlson DE, Wronski CR (1976) Amorphous silicon solar-cell. Appl Phys Lett 28(11):671–673
20. Staebler DL, Wronski CR (1977) Reversible conductivity changes in discharge-produced amorphous Si. Appl Phys Lett 31(4):292–294
21. Benagli S, Borrello D, Vallat-Sauvain E, Meier J, Kroll U, Hoetzel J, Bailat J, Steinhauser J, Marmelo M, Monteduro M, Castens L (2009) High-efficiency amorphous silicon devices on LPCVD-ZnO-TCO prepared in industrial KaiTM-M R&D reactor. In: Proceedings of the 24th European photovoltaic solar energy conference, Hamburg, 2293–2298 pp. ISBN 3-936338-25-6
22. Yang J, Guha S (1992) Double-junction amorphous silicon-based solar-cells with 11-percent stable efficiency. Appl Phys Lett 61(24):2917–2919
23. Yamamoto K, Nakashima A, Suzuki T, Yoshimi M, Nishio H, Izumina M (1994) Thin-film polycrystalline Si solar cell on glass substrate fabricated by a novel Low temperature process. Jpn J Appl Phys 33:L1751–L1754
24. Meier J, Dubail S, Platz R, Torres P, Kroll U, Selvan JA, Pellaton Vaucher N, Hof C, Fischer D, Keppner H, Flückiger R, Shah A, Shklover S, Ufert K-D (1997) Towards high-efficiency thin-film silicon solar cells with the "micromorph" concept. Sol Energ Mat Sol C 49(1–4):35–44
25. Wu X, Keane JC, Dhere RG, DeHart C, Albin DS, Duda A, Gessert TA, Asher S, Levi DH, Sheldon P (2001) In: Proceedings of the 17th European photovoltaic solar energy conference 2001. ISBN 3-936338-08-6, p 995
26. Goncalves LM, Bermudez VD, Ribeiro HA, Mendes AM (2008) Dye-sensitized solar cells: a safe bet for the future. Energ Environ Sci 1(6):655–667
27. Sinha P, Kriegner ChJ, Schew WA, Kaczmar SW, Traister M, Wilson DJ (2008) Regulatory policy governing cadmium-telluride photovoltaics: a case study contrasting life cycle management with the precautionary principle. Energ Policy 36:381–387
28. Zayed J, Philippe S (2009) Acute oral and inhalation toxicities in rats with cadmium telluride. Int J Toxicol 28(4):259–265
29. Wadia C, Alivisatos AP, Kammen DM (2009) Materials availability expands the opportunity for large-scale photovoltaic deployment. Environ Sci Technol 43(6):2072–2077
30. Wagner S, Shay JL, Migliorato P, Kasper HM (1974) $CuInSe_2$/CdS heterojunction photovoltaic detectors. Appl Phys Lett 25:434
31. Dimmler B, Schock HW (1996) Scaling-up of CIS technology for thin-film solar modules. Prog Photovolt: Res Appl 4(6):425–433
32. Jackson P, Hariskos D, Lotter E, Paetel S, Wuerz R, Menner R, Wischmann W, Powalla M (2011) New world Record efficiency for Cu(In,GA)Se2 thin-film solar cells beyond 20%. Prog Photovolt: Res Appl. doi: 10.1002/pip.1078
33. Kushiya K (2009) Key near-term R&D issues for continuous improvement in CIS-based thin-film PV modules. Sol Energ Mat Sol C 93:1037–1041
34. Meeder A, Neisser A, Rühle U, Mayer N (2007) Manufacturing the first MW of large-area CuInS2-based solar modules – recent experiences and progress. In: Proceedings of the 22nd European photovoltaic solar energy conference, Milan, p 2115. ISBN 3-936338-22-1
35. Bosi M, Pelosi C (2007) The potential of III-V semiconductors as terrestrial photovoltaic devices. Prog Photovolt: Res Appl 15(1):51–68
36. King RR, Boca A, Hong W, Liu X-Q, Bhusari D, Larrabee D, Edmondson KM, Law DC, Fetzer CM, Mesropian S, Karam NH (2009) Band-gap-engineered architectures for high-efficiency multijunction concentrator solar cells. In: Proceedings of the 24th European photovoltaic solar energy conference, Hamburg. ISBN 3-936338-25-6
37. Gratzel M (2001) Photoelectrochemical cells. Nature 414(6861):338–344
38. O'Regan B, Gratzel M (1991) A Low-cost, high-efficiencyh solar-cell based on dye-sensitized colloidal TiO2 films. Nature 353(6346):737–740
39. Li G, Shrotriya V, Huang JS, Yao Y, Moriarty T, Emery K, Yang Y (2005) High-efficiency solution processable polymer photovoltaic cells by self-organization of polymer blends. Nat Mater 4(11):864–868
40. Brabec CJ (2004) Organic photovoltaics: technology and market. Sol Energ Mat Sol C 83(2–3):273–292
41. Krebs FC (2005) Alternative PV: large scale organic photovoltaics. REfocus 6(3):38–39
42. U.S. Photovoltaic Industry Roadmap Steering Committee (2001) Solar-electric power: the U.S. photovoltaic industry roadmap, 36 p. Solar Electricity Industry Association, Washington, DC, USA
43. Navigant Consulting Inc (2006) A review of PV inverter technology cost and performance projections. National Renewable Energy Laboratory, Golden, 100 pp
44. EU PV European Photovoltaic Technology Platform (2007) A strategic research agenda for photovoltaic solar energy technology. European Communities. Sixth European Framework Programme for research and technological development, Luxembourg, 76 p. ISBN 978-92-79-05523-2
45. Kroposki B, Margolis R, Kuswa G, Torres J, Bower W, Key T, Ton D (2008) Renewable systems interconnection. National Renewable Energy Laboratory, Golden, Colorado, 23 p
46. NEDO (2009) The roadmap PV2030+; new energy and industrial technology organization (NEDO), Kawasaki, Japan
47. Kurokawa K, Aratani F (2004) Perceived technical issues accompanying large PV development and Japanese

"PV2030". In: Proceedings of the 19th European photovoltaic solar energy conference and exhibition, Paris. ISBN 3-936338-14-0
48. Government of China (2006) Medium and long-term planning for scientific and technological development (2006–2020), Feb 2006
49. National Development and Reform Commission (2007) Medium and long-term development plan for renewable energy in China, Sep 2007
50. Communication from the Commission to the Council, the European Parliament, the European Economic and Social Committee and the Committee of the Regions A European Strategic Energy Technology Plan (SET-Plan) – Towards a low carbon future; 22 November 2007; COM(2007) 723 final, {SEC (2007) 1508}; {SEC(2007) 1509}; {SEC(2007) 1510}; {SEC(2007) 1511}
51. Ministry of New & Renewable Energy, Government of India Solar mission document (2009) http://mnre.gov.in/pdf/mission-document-JNNSM.pdf
52. Indian Ministry of New & Renewable Energy Thrust Areas of R & D in solar photovoltaic technology (2008) http://www.mnre.gov.in/spv-thrust.htm
53. NEDO Brochure, Energy and Environment Technologies, December 2007. http://www.nedo.go.jp/kankobutsu/pamphlets/kouhou/2007gaiyo_e/87_140.pdf
54. U.S. Department of Energy (2008) Solar energy technologies programme (solar programme): 2008–2012 multi-year programme plan, Apr 2008
55. Company Web-sites and Press Releases
56. Data received from Companies during personal visits
57. Bloomberg (2010) Bloomberg new energy finance – renewable energy data. http://bnef.com/
58. Yang CJ (2010) Reconsidering solar grid parity. Energ Policy 38:3270–3273
59. Maycock PD (2002) The world photovoltaic market – report (January). PV Energy Systems, Warrenton
60. Parente V, Goldemberg J, Zilles R (2002) Comments on experience curves for PV modules. Prog Photovolt: Res Appl 10:571–574
61. Neij L (2008) Cost development of future technologies for power generation–a study based on experience curves and complementary bottom-up assessments. Energ Policy 36:2200–2211
62. International Energy Agency (2010) Technology roadmap. Solar Photovoltaic Energy. International Energy Agency, Paris, France
63. Hoffmann W (2009) The role of PV solar electricity to power the 21st century's global prime energy demand. IOP Conf Ser: Earth Environ Sci 8:012007
64. Hoffmann W, Wieder S, Pellkofer T (2009) Differentiated price experience curves as evaluation tool for judging the further development of crystalline silicon and thin film PV solar electricity products. In: 24th European photovoltaic solar energy conference, Hamburg, Germany, 21–25 Sep 2009
65. Jäger-Waldau A (2010) Status and perspectives of thin film photovoltaics. In: Thin film solar cells: current status and future trends. Nova Publishers, New York
66. Maycock P (1976–2003) PV News. PV Energy Systems
67. Schaeffer GJ, Seebregts AJ, Beurskens LWM, Moor HHC, Alsema EA, Sark W, Durstewicz M, Perrin M, Boulanger P, Laukamp H, Zuccaro C (2004) Learning from the sun: analysis of the use of experience curves for energy policy purposes – the case of photovoltaic power. Final Report of the Photex Project, DEGO: ECN-C-04-035
68. Hoff TE, Pasquier BJ, Peterson JM (2010) Market transformation benefits of a PV incentive program. In: SOLAR 2010 conference proceedings, American Solar Energy Society, Phoenix, Arizona, 17–22 May 2010
69. Barbose G, Darghouth N, Wiser R (2010) Tracking the Sun III: the installed cost of photovoltaics in the U.S. from 1998–2009. Lawrence Berkeley National Laboratory, Berkeley
70. Urbschat C, Barban F, Baumgartner B, Beste M, Herr M, Schmid-Kieninger A, Rossani F, Stry-Hipp G, Welke M (2002) Sunrise 2002 – the solar thermal and photovoltaic markets in Europe, Berlin
71. Jäger-Waldau A (2005) Photovoltaics status report 2005: research, solar cell production and market implementation of photovoltaics. Office for Official Publications of the European Communities, EUR 21836 EN. ISBN 92-79-00174-4
72. Bundesverband Solarwirtschaft e.V (2010) Statistische Zahlen der deutschen Solarstrombranche (photovoltaik). Bundesverband Solarwirtschaft e.V. (BSW Solar), Berlin, Germany, 4 pp
73. Solar Energy Industry Association (SEIA) (2010) U.S. solar market insight, 2nd Quarter 2010, executive summary
74. Solar Energy Industry Association (SEIA) (2011) U.S. solar market insight, 1st Quarter 2011, executive summary
75. Bundesverband Solarwirtschaft e.V (2011) Statistische Zahlen der deutschen Solarstrombranche (photovoltaik). Bundesverband Solarwirtschaft e.V. (BSW Solar), Berlin, Germany, 4 pp
76. Jäger-Waldau A PV status report 2011, Office for Official Publications of the European Union, EUR 24807 EN. ISBN 978-92-79-20171-4
77. ICIS news, Asia polysilicon prices to firm in 2011 on solar demand, 13 Jan 2011
78. Semi PV Group, Semi China Advisory Committee and China PVIndustry Alliance (CPIA) (2011) China's solar future – a recommended China PV policy roadmap 2.0, April 2011. Semiconductor Industry Association, San Jose, USA
79. Ikki O (2011) PV activities in Japan. PV status report, vol 17, no. 5, May 2011
80. European Photovoltaic Industry Association (2011) Global market outlook for photovoltaics until 2015. European Photovoltaic Industry Association, Brussels, Belgium
81. Photovoltaic Energy Barometer (2011) Systèmes Solaires, le journal du photovoltaique n° 5 – 2011, April 2011, ISSN 0295–5873
82. German Federal Network Agency (Bundesnetzagentur), Press release 21 Mar 2011

83. Gestore Servici Energetici, Press release, 15 Feb 2011
84. European Wind Energy Association (2011) Wind in power – 2010 European statistics, Feb 2011
85. Platts (2011) Power in Europe, Jan 2011. www.platts.com
86. Ministère de l'Économie, de l'industrie et de l'emploi, Press release, 24 Feb 2011
87. Gesetz über den Vorrang Erneuerbaren Energien (Erneuerbare-Energien-Gesetz – EEG), Bundesgestzblatt Jahrgang 2000 Teil I, Nr. 13, p 305 (29.03.2000)
88. German Federal Network Agency (Bundesnetzagentur), Press release 16 June 2011
89. Gestore Servici Energetici, Aggiornamento, 16 Aug 2011
90. Royal Decree 1565/10, published on 23 Nov 2010. http://www.boe.es/boe/dias/2010/11/23/pdfs/BOE-A-2010-17976.pdf
91. Royal Decree RD-L 14/10, published on 24 Dec 2010. http://www.boe.es/boe/dias/2010/12/24/pdfs/BOE-A-2010-19757.pdf
92. Asociación de la Industria Fotovoltaica (ASIF). http://www.asif.org/principal.php?idseccion=565
93. Asian Development Bank (2011) Asia solar energy initiative: a primer. ISBN 978-92-9092-314-5, April 2011. Asian Development Bank, Manila, Philippines
94. Watt M, Passey R, Johnston W (2011) PV in Australia 2010 – Australian PV survey report 2010, Australian PV Association, May 2011
95. Reuters (2011) China doubles solar power target to 10 GW by 2015, 6 May 2011. http://www.reuters.com/article/2011/05/06/china-solar-idUKL3E7G554620110506
96. The World Bank (2010) Winds of change – East Asia's sustainable energy future, May 2010
97. The Daily Star, Target 500 MW solar project, 15 May 2011. http://www.thedailystar.net/newDesign/news-details.php?nid=185717
98. UNB connect, ADB assures fund for 500 MW solar system, 4 June 2011. http://www.unbconnect.com/component/news/task-show/id-49440
99. Presidential Regulation 5/2006, National Energy Policy, published 25 Jan 2006
100. Republic of the Philippines, Congress of the Philippines, Republic Act No. 9513 December 16, 2008, AN ACT PROMOTING THE DEVELOPMENT, UTILIZATION AND COMMERCIALIZATION OF RENEWABLE ENERGY RESOURCES AND FOR OTHER PURPOSES
101. Ontario Power Authority, Feed-In Tariff Programme, 30 September 2009. http://fit.powerauthority.on.ca/Storage/97/10759_FIT-Program-Overview_v1.1.pdf
102. Greentech Media Inc., Enfinity America Corporation (2011) The US PV Market in 2011 – Whitepaper
103. Gielecki M, Mayes F, Prete L EIA, Renewable energy 2000: issues and trends, section on Incentives, mandates, and government programs for promoting renewable energy, DOE/Energy Information Administration, DOE/EIA-0628
104. International Herald Tribune, 24 July 2007. http://www.iht.com/articles/2007/07/24/bloomberg/bxoil.php

Suggested Readings and Internet Sites

European Commission, DG JRC, Annual PV Status Report (since 2002) http://re.jrc.ec.europa.eu/refsys/

European Photovoltaic Industry Association, (various publications) www.epia.org

European Renewable Energy Council, www.erec.org

Intergovernmental Panel on Climate Change (IPCC), www.ipcc.ch. Special report on renewable energy sources and climate change mitigation (SRREN), http://srren.ipcc-wg3.de/report

International Energy Agency, photovoltaic implementation agreement http://www.iea-pvps.org/

Renewable energy policy network for the 21st century, www.ren21.net

Solar Energy Industry Association (SEIA), http://www.seia.org/

United Nations Environment Programme & Bloomberg New Energy Finance, Global Trends in renewable Energy Investment (series), www.unep.org; www.bnef.com

Pig Breeding for Increased Sustainability

Pieter W. Knap
PIC International Group, Schleswig, Germany

Article Outline

Glossary
Definition of the Subject
Introduction
Biodiversity
Pollution
Animal Welfare
Future Directions
Acknowledgments
Bibliography

Glossary

Allele Allele is one of the several possible forms of the DNA sequence at a particular locus.

BLUP (best linear unbiased prediction) BLUP is a method to estimate breeding values by taking account of the pedigree relationships among the individuals instead of assuming uncorrelated residuals as in ordinary least squares methodology.

Corticosteroids Corticosteroids are steroid hormones such as cortisol, produced in the adrenal cortex. They are involved in energy metabolism, immune response, stress response, and many other functions.

Cryoconservation Cryoconservation is the conservation of living material by freezing.

Effective population size Effective population size is a measure of the genetic variability of a population. It is defined as the number of breeding individuals in a stable population with a 1:1 sex ratio, no overlapping generations, and random mating and reproduction, that would lead to the same rate of inbreeding as what occurs in the population under study.

Fitness constraint Fitness constraint is a reduction of the health and strength of an individual.

Microsatellite Microsatellite is a repeating sequence of a few DNA base pairs, highly variable and therefore used as molecular markers in genetic analyses. Typically neutral, i.e., not associated with functional genes. The alleles differ in terms of the number of repeats, so there can be many.

SNP (single nucleotide polymorphism) SNP is a mutation of a single DNA base pair at a specific locus, possibly in a functional gene. SNPs are used as molecular markers in genetic analyses. They usually carry two alleles.

Stereotypy Stereotypy is a repetitive, apparently purposeless, behavior such as pacing, rocking, chewing, and licking during psychological distress. This behavior is seen in captive animals, often caused by the lack of options to exercise *other* instinctive behavior patterns because their required substrate (e.g., space or companions) is not available.

Definition of the Subject

The sustainability of farm animal production depends largely on strategies for animal management, health care, and nutrition, and on strategies for processing and marketing the products (e.g., meat, eggs, milk, and manure). Strategies for animal *breeding* exploit genetic and reproductive technology to better match the next generation of production animals to what the market requires. Breeding creates gradual changes in the animal species, providing a way to support sustainable development: better match the next generation of production animals to what enhanced sustainability requires. The technological challenge is to consider the balance among the various sustainability elements (profitability, human nutrition, environmental load, resource management, animal welfare), and to design genetic strategies to support that balance.

Introduction

Gamborg and Sandøe [1, 2] write about "applying the notion of sustainability" in animal breeding. They first explain why this is relevant at all: "animal breeding [. . .] is a largely unnoticed, yet economically vital part of the agriculture and food sector. But despite remarkable advances in productivity [it has] negative impacts: for example, on animal health and welfare, and on genetic diversity. This raises the question of what limits to acceptable practice we should set in this area." This is about societal regulation of industry practice: about a *license to breed*.

These authors notice that "discussions of sustainability may open up dialogue on ethical issues and [may] help to set an agenda," and describe projects where "breeders were required [. . .] to develop a definition of sustainable farm animal breeding [. . .]. They were asked to identify their key concerns and priorities, to characterize any resulting dilemmas, and to suggest ways towards a meaningful operationalization.

The [. . .] breeders [could describe and clarify] the concerns they considered relevant [. . .]. But they found it harder to identify the concerns they had chosen to *exclude* [. . .] Most difficult [. . .] was the prioritization of potentially conflicting concerns. Roughly speaking, there are two ways to overcome conflict here:

1. technological solutions, in which relevant conflict is resolved through technological changes in breeding practice
2. increased transparency, in which clear statements about the relative priorities [. . .] are essential."

The rest of the above text focuses on point (2).

By contrast, the present chapter deals mainly with point (1), focusing on pig breeding while borrowing from poultry and cattle breeding where relevant.

Prioritization of the relevant, and potentially conflicting, concerns is indeed difficult, but essential in any concrete case. Such a prioritization cannot be attempted here, as it will always depend on that concrete case.

The classical "triple bottom line" of Elkington [3] is extended here with a fourth element, leading to the sustainability targets

People – Pigs – Planet – Profit

The possible contribution of the technology of pig breeding and genetics to two of these targets is discussed here: *Pigs* is about animal welfare, *Planet* deals with biodiversity and pollution.

People is about social justice, with little connection to pig breeding technology. A possible case would be biopiracy which is more a political and economic issue than a technological one, and more relevant in the plant breeding sector – but see [4] for a case study of the immigration of Meishan into western pig populations, a commercial failure due to unforeseen technological developments. Influencing *Profit* by pig breeding has been covered intensely since selection indexes were designed – there is no need to repeat that here.

It must be borne in mind throughout that "sustainability will always be a matter of more or less: it can never be an absolute goal" [2].

Biodiversity

FAO's *State of the world's animal genetic resources for food and agriculture* [5] mentions 140 known extinct and 599 non-extinct pig breeds. Of the 599, 90% are *local breeds* (LB, occurring in one country only) and 6% are *international transboundary breeds* (ITB). Of these 599 breeds, 22% are "at risk" based on population size: roughly, populations with less than 1,000 breeding females or 20 breeding males are considered to be at risk, genetic survival being endangered. The risk status of 38% of the breeds is unknown, 40% are "not at risk."

Livestock breeds become endangered in many ways. FAO [5] gives three categories: (1) emergencies: drought, flooding, earthquakes, famine, war; (2) epidemics and zoonosis eradication campaigns; (3) most important: livestock sector trends, described earlier [6–8] in terms of displacement by other breeds, indiscriminate crossbreeding with exotic germplasm, overfocus on a single trait, no sustained breeding program, changes in production systems or producer preferences, and technology development. To this can be added the reduction of demand for the breed's products – for pigs, since about 1950, such a product would typically be fat. Most pig breeds have evolved as an intrinsic part of a production system, catering for demands for particular products. When the production system (or the demand for its products) disappears, its associated breeds (e.g., lard-type pigs) will disappear with it – unless they find an alternative niche.

Extinction of a livestock breed can be undesirable for several reasons. A pressing one is (A) when it contributes to "maintaining the identity of human communities" [9], e.g., pigs in the South Pacific, or even more when the livelihood of a human group depends on it; this typically involves ruminant breeds. Simianer [10] gives two other categories: (B) "the insurance argument": "genetic diversity can be seen as an insurance against future changes, [with] the objective [...] to maintain sufficient genetic diversity to be able to adapt to the challenges that are ahead" – bearing in mind that those challenges are increasingly unpredictable in times of global climatic change and intensifying global trade; and (C) cultural arguments: "farm animal breeds must be seen as a man-made good with a long history, often parallel with [human] cultural development [...] and therefore similar arguments for conservation apply as for other cultural assets [such as historical] buildings or artwork".

All these arguments call for genetic conservation, most pressingly with regard to category (A). With regard to category (C), the question is how to objectivize the cultural *value* of a livestock breed [11], which will be necessary when the costs of its conservation are being budgeted.

With regard to category (B), the main question is what kind of future challenges might require the breeding sector to exploit genetic material that previously has been unsatisfactory enough to become endangered; why [12] "preserve animals that farmers have abandoned"? The interest must then be in traits that were not important in mainstream breeding, e.g., meat quality traits (covering unexpected changes in consumer preferences) or robustness traits that facilitate

adaptation to previously uncommon conditions, covering unexpected changes in options for health or climate control, or nutrition.

There is serious doubt among geneticists whether this insurance argument for breed conservation is realistic at all. To quote [13, 14], rearranged for consistency: "little use is made of conserved populations in mainstream commercial production of livestock; modern populations [...] are so far ahead of conserved strains in production traits, that adaptation of [the modern populations] offers far more opportunity than crossing back to far out of date stocks; even in countries where highly adapted breeds have evolved, typically these breeds are not perceived as having sufficient immediate utility to make them commercially viable; there are no present-day commercial animal-improvement companies or organizations that feel the need to invest in conservation as an insurance; the main perceived insurance benefit [...] is the conservation of adapted [sets of] alleles that are confined to one or a few breeds; there is [...] no reason to assume that there is [...] little variation in fitness associated traits in livestock populations simply due to selection; another important justification for conservation [...] is the value [...] for the increasingly powerful genomics analyses that have the potential to shed much light on the basic biology of adaptive traits; with moves towards genomic selection [...] the emphasis moves more towards best utilization of the large amounts of variation present in [...] commercial populations." Much earlier, Dempfle [15] wrote "only in very exceptional cases would a geneticist interested in improving [a leading] breed consider going to another breed to exploit interbreed variation, since most likely this would result in lowering of the mean. This is not likely to change very much, even with future technology."

Despite such skeptical points of view, endangered breed conservation is a current political commitment and an actively promoted reality, so it is valid to consider its technical issues.

Category (B) above centers around disappearance of (possibly) useful alleles – emphasizing within-species genetic diversity rather than particular breeds. From a technological point of view, in vitro cryoconservation would be adequate. So, allowing for the 38% "unknown" risk status breeds mentioned above, the technological challenge is to conserve the useful alleles carried by 130–360 pig breeds. Most of these are LBs.

Conservation of animal genetic resources is expensive, logistically complicated, and its worldwide funding is limited and fragmentary. Conservation of all genetic diversity is therefore not feasible and choices will have to be made with regard to funding the conservation of particular breeds, and not other ones: *global genetic resource management*. FAO [5] presents criteria (the breed's status, value, and potential for improvement) to support decision-making around conservation and genetic improvement actions, see Fig. 1. It holds several items where animal breeding and genetics technology can usefully contribute: (1) genetic distinctiveness; (2) population size and structure; (3) utility for food and agriculture, including adaptive traits. On a higher level, the balance between distinctiveness, risk status, and utility: (4) the ultimate priority level of the breed. Further elements are (5) target traits for genetic improvement and (6) genetic improvement programs. Sections "Genetic Distinctiveness" to "Genetic Improvement Programs" deal with these items in this order.

Genetic Distinctiveness

Megens et al. [16] describe the genetic diversity among 46 Chinese and 51 European pig breeds. Microsatellite marker genotypes were converted to genetic distance estimates among breeds, which can be worked into phylogenetic trees (dendrograms) and other cluster representations; see [17] for background information about various techniques. The results of this analysis are in Fig. 2, which shows genetic distance estimates among these breeds through three-dimensional scaling. This reveals a marked difference between the Chinese breeds (strongly diverse in all three dimensions, falling apart into five geographic clusters) versus the European breeds which form a separate cluster, much tighter when compared on the same scale. The European dendrogram (not shown here) gives more detail, suggesting distinct groups of English and south-European LBs. The authors relate their results in beautiful detail to the domestication history of the breeds.

An earlier study of roughly these same European DNA samples [18, 19] measured the *allelic richness* of these breeds, in terms of the mean effective number of

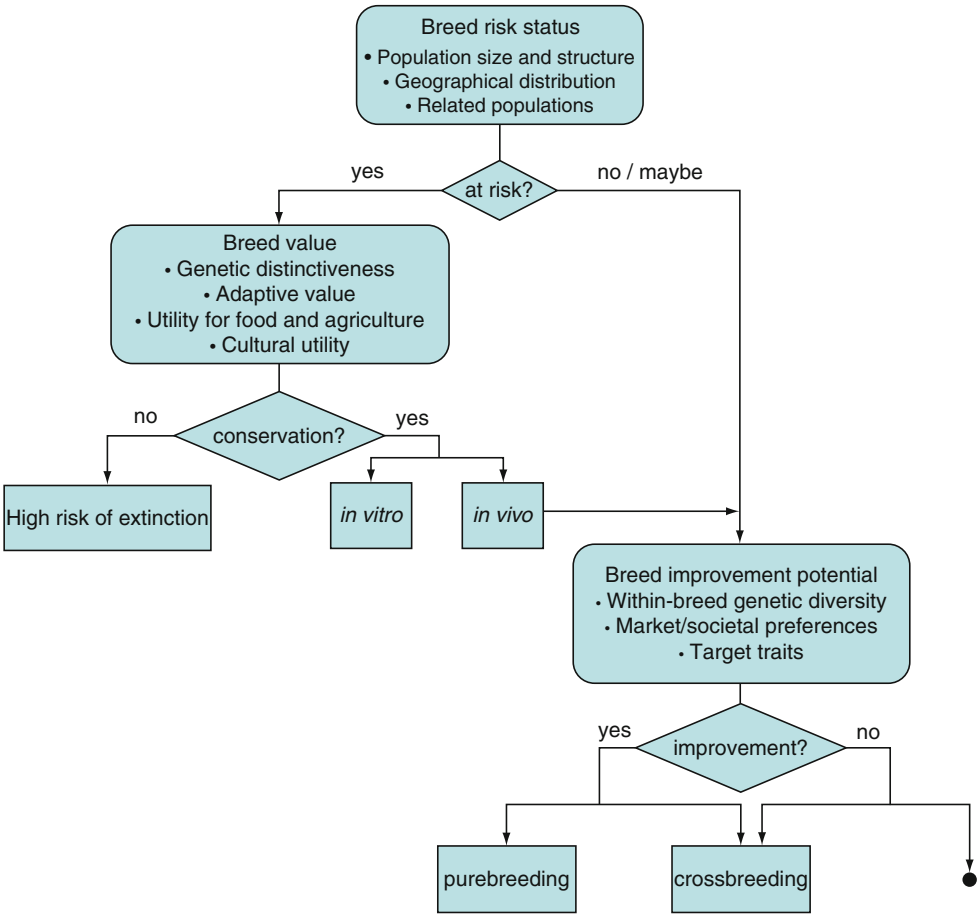

Pig Breeding for Increased Sustainability. Figure 1
Information required to design strategies for global genetic resource management (Modified from [5])

alleles per marker (2.3–3.5 in the ITBs, 1.9–4.0 in the LBs, for microsatellites), and the number of *private alleles* (found in one breed only) – zero to five, with an outlier at 15.

Many similar analyses have been reported since 1995 ([20]; four Belgian breeds). Recent ones involve three Brazilian LBs, one ITB and an industrial synthetic [21], and twelve North and South American LBs, three ITBs, and three wild varieties [22].

Obviously, the accuracy of such analyses depends on the number of markers per breed. Alves et al. [23] show a diminishing-returns pattern for the accuracy of clustering six pig breeds and wild boar, as a function of numbers of microsatellites analyzed – with ∼24 markers required for 95% overall clustering accuracy, and ∼35 to cluster the "less divergent populations." The accuracy of clustering parameter estimates is commonly quantified by bootstrapping. Felsenstein [24] notices that such resampling techniques are particularly valuable when the function to be estimated (e.g., a dendrogram) is algebraically complicated so that its variance cannot be derived analytically. An example of analytical derivation is in [25] where the standard error of the genetic distance estimate was obtained from observed allele frequencies. Contrary to data-specific procedures such as the bootstrap, analytical forms allow for algebraic rearrangement of terms so that data volume and structure required for a particular accuracy level can be obtained – as done empirically in [23].

To support the decision-making process of Fig. 1, quantification of genetic distinctiveness of a breed must consider within-breed and between-breeds diversity. The breed's (possibly unique) alleles will be of

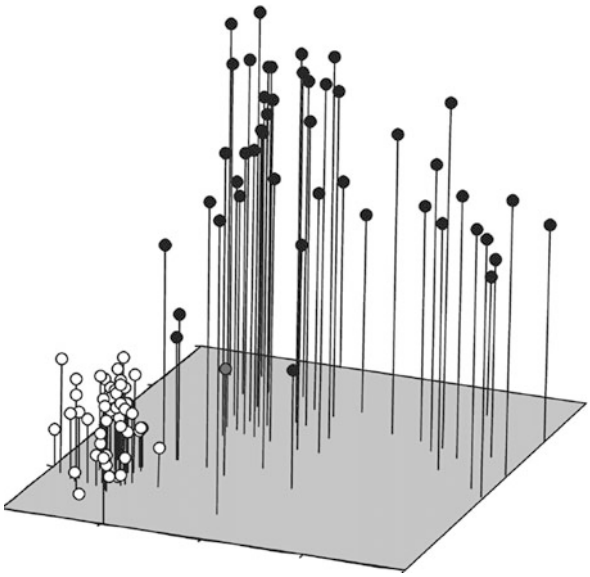

Pig Breeding for Increased Sustainability. Figure 2 Estimated genetic distances among 46 Chinese (*black circles*) and 51 European (*white circles*) pig breeds, and one Sino-European synthetic (*gray circle*). The genetic distance between two breeds is quantified here by the physical distance between their two circles (From [16])

future interest more likely (1) when it shows a clear genetic distance to other breeds in the between-breeds diversity as in Fig. 2, and (2) when it shows a larger within-breed diversity (carries a larger number of different alleles). Also, a successful breeding program will be easier to implement for breeds with larger within-breed diversity, see the section on "Genetic Improvement Programs". Therefore a breed's genetic distinctiveness should be quantified by some combination of (1) genetic distance to other breeds and (2) within-breed genetic variability. Their relative weighting will depend on the value of parameters such as the proportion of total diversity due to diversity between breeds (Wright's F_{ST}, estimated at <0.3 in the above studies, naturally dependent on the sample's breed composition); the "standard" approach [26] is to weight item (1) by F_{ST} and (2) by $(1 - F_{ST})$. It will also depend on strategic issues like the breed's intended purpose. For example, the between-breeds component would count more if the breed must play a role in a terminal crossbreeding program [27] and less if the breed must be merged into a synthetic for subsequent genetic improvement. Approaches are described, discussed, and/or illustrated by [28–31] and sources referenced therein. A practical suggestion [32] is "to consider how much diversity the breed adds to a core set constituted by commercial lines or breeds that are already subject to successful conservation."

All the above presumes a random approach: no specific traits are targeted and genetic diversity is valued as a neutral entity. Neutral markers like microsatellites are appropriate if future needs are indeed unknown: "since we need to maintain the genetic capacity to cope with challenges not even known today, this can be best accomplished by maintaining neutral genetic diversity" [10].

Nevertheless, some studies have deliberately used markers associated with specific traits. Ciobanu et al. [33] argue that "the relationship between variability at neutral marker loci [. . .] and adaptation or individual fitness is still unclear" and "to characterize a breed not only in terms of genetic distance [. . .] but also in terms of variation at interesting loci associated with phenotypes, [. . .] will give more opportunity to elaborate an efficient strategy for conservation of breeds, maintaining their 'useful' genetic diversity and providing important resources for possible new unique traits." Likewise, half of the markers typed by Iannuccelli et al. [34] were SNPs "chosen for their position close to interesting QTLs." They mention that in addition to comparisons between breeds, they have "focused on the diversity within genomic regions containing genes that influence economically important traits, the variability of which is supposed to have evolved under the influence of artificial selection. [This has] allowed us to reveal regions where artificial selection favored certain alleles. For some SNPs where both alleles were found in all breeds, the frequencies were very different between breeds, suggesting different selection histories" (translated). A method to combine neutral diversity and diversity due to selection into a single criterion is presented in [35].

Population Size and Structure

There are three ways to estimate effective population size (N_e). Two make use of quantitative genetics theory [36].

First, from census counts of breeding males and females (N_m, N_f), typically through approximations developed for scenarios without selection, such as $N_e \approx 4\times(N_m\times N_f)/(N_m+N_f)$, possibly expanded with information on variation in family structures. This method has been applied to Romanian, Japanese, and Croatian pig breeds [37–39]. The European Farm Animal Biodiversity Information System (EFABIS; http://efabis.tzv.fal.de) holds data on livestock breeds, including N_e derived this way. Figure 3 shows its estimated N_e values for 111 pig breeds, in relation to their N_f values. These datapoints are not on a straight line because of variation in the (N_f/N_m) ratio; the reference lines indicate where N_f equals 5 (*top*), 10, or 100 (*bottom*) times N_m. Therefore, datapoints above the two highest reference lines represent situations with less than five (or ten) recorded breeding females per recorded breeding male – not very feasible scenarios in pig breeding, certainly at N_f values above 100. This only illustrates the difficulty of obtaining consistent census counts, and the limitations to deriving credible N_e estimates from them.

Second, through the rate of inbreeding (ΔF) as calculated from pedigree analysis, exploring the fact that $N_e = 1/(2\,\Delta F)$ under random mating. The main resource required here is a complete pedigree. This method has been applied to Japanese, American, German, and Finnish pig breeds [38, 40–42]. The approach can be taken an important step further by focusing on its across-breeds distribution characteristics [43].

A third approach makes use of molecular genetics technology, with various ways of analyzing marker data – for an overview see [44]. Álvarez et al. [45] analyzed the full pedigree of a small fragmented sheep population and genotyped microsatellites. They conclude that co-ancestry coefficients as estimated from pedigree data and from molecular data become rapidly correlated when pedigree depth increases, so that the expense of recording "molecular information in well established conservation programs may not be justified"; on the other hand, for small populations with a shallow pedigree "neither [pedigree] nor molecular information by themselves are sufficient [...]; each available parameter offers partial information."

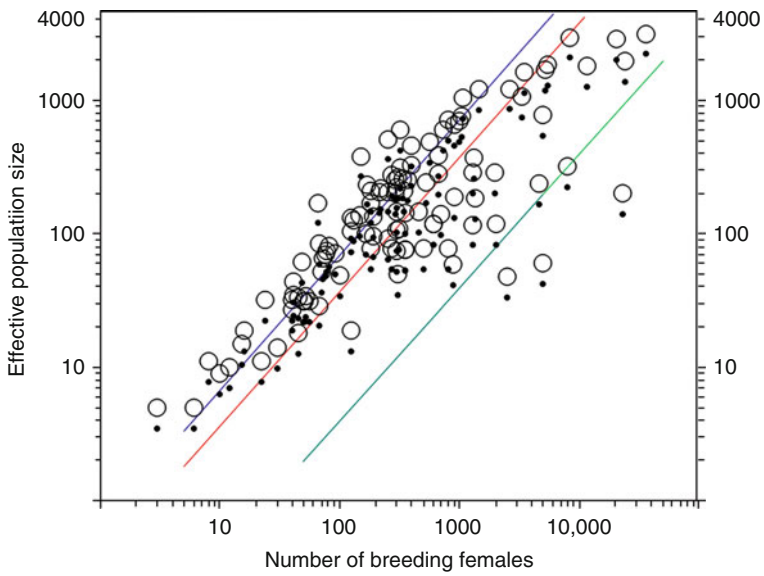

Pig Breeding for Increased Sustainability. Figure 3
Reported numbers of breeding females (N_f) in 111 European pig breeds, and the associated N_e values from $4\times(N_m\times N_f)/(N_m+N_f)$; N_m is the number of breeding males. The reference lines indicate where N_f equals 5 (*top*), 10, or 100 (*bottom*) times N_m. Open circles, raw data; small dots, multiplied by 0.7 in an attempt to adjust for the effects of selection (Data from EFABIS, December 2009)

For the correlation between pedigree-based and molecular measures of diversity "to be substantial, a considerable number of loci is required and, more importantly, a high variance of the [pedigree-based] inbreeding values should be present; [...] it should be preferable to use pedigree information whenever available, and limiting the use of markers to verify, correct, complete or even implement pedigree recording" [32].

Of course, in livestock breeds, deep and complete pedigrees are almost as scarce as dense DNA marker data, so "markers could be most useful in cases where little information on population history is available" [46]. Toro et al. [47] give a beautiful example of two LB varieties with complete 20-generation pedigree data, but these were maintained on an experimental farm – not a common situation.

Therefore, the molecular approach is widely seen as potentially more powerful than classical quantitative methods. Aspi et al. [48] write: "Owing to variation in family size and overlapping generations [...] N_e is [...] difficult to estimate from demographic field surveys. [...] Genetic methods may provide more effective ways for estimating N_e." They genotyped microsatellites and estimated N_e at ~40. Moreover, from those same data "large genetic variation was found in the population despite a recent demographic bottleneck. No spatial population subdivision was found, even though a significant negative relationship between genetic relatedness and geographic distance suggested isolation by distance." This is about a wolf population; similar quantification of N_e, demography, and subdivision would be very useful in livestock genetic resource management.

An effective population size of 40 would be regarded as dangerously low. Meuwissen [49] mentions a "critical effective size" (below which fitness steadily decreases) of 50–100, at least in populations not selected for traits negatively correlated to fitness. Ollivier et al. [50] transform N_e into the *extinction probability* P_{ext}, operationally defined as the expected level of inbreeding (accumulating deleterious mutations, which eventually leads to extinction) after 50 generations: $P_{ext} = 1 - e^{-50/(2N_e)}$. With a pig generation interval of 1 year, this goes back to [51] where risk of extinction is based on cumulative inbreeding over 50 years. The above $N_e = 40$ works out as a dangerous 46% probability that the population will not survive 50 generations. A slightly different approach is the *degree of endangerment* described by [52]. The relationships among P_{ext}, N_e, and ΔF are described in more detail in [53–55], at different levels of complication. The latter source also considers the estimate's accuracy, which will be useful once such estimates are to be used in practice.

Effective population size influences the extent of genetic drift, which affects the development of linkage disequilibrium (LD), i.e., the correlation between genotypes at different loci. Loci that are closer together are less often separated by recombination – so they are more strongly correlated, with higher LD values. In terms of data analysis of biallelic loci, the relevant relationships can be generalized [56] in terms of what is actually happening (due to N_e) and of what can be observed (due to sample size) as

$$E(r^2) \approx \frac{1}{\alpha + kcN_e} + \frac{1}{n} \quad (1)$$

$E(r^2)$ is the expectation of the square of the abovementioned correlation, a common parameter to quantify LD. Parameter α equals 1 in the absence of mutation, and 2 if mutation is accounted for; k equals 4 for autosomes, and 2 for the X chromosome; c is the recombination rate between the markers being analyzed (their genetic distance from each other, in Morgan); n is sample size.

For an analysis of many autosomal markers, ignoring mutation, this works out as

$$N_e \approx \frac{1 - r^2}{4cr^2} + \frac{1}{4cr^2(nr^2 - 1)} \quad (2)$$

Hayes et al. [57] introduced *chromosome segment homozygosity* (CSH), an alternative parameter to r^2 for quantifying LD. CSH has a smaller sampling variance than r^2, but the same approximate expectation (Eq. 1). When population size changes linearly over time, the effective population size of 1/(2 c) generations ago can be approximated as (1 – CSH)/(4 c CSH), the same form as Eq. 2 when n is large.

Accordingly, when many individuals are genotyped for many biallelec DNA markers varying widely in their mutual distance c, then the (supposedly linear) history of N_e can be traced by plotting $\frac{1-CSH}{4cCSH}$ against $\frac{1}{2c}$.

Amaral et al. [58] estimated LD decay (reduction of r^2 with increasing c) on SNP markers in ten European

and ten Chinese pig breeds (subsets of the breeds in Fig. 1). Figure 4 shows those data reworked into Hayes's relationship, using r^2 instead of CSH, for the European breeds ($N_e \geq 10{,}000$ for the Chinese breeds). Comparable data on commercial pig lines [59, 60, 226] has been added.

Figure 4 illustrates that this method can reveal interesting information about a population's demography. Such information would be most relevant to livestock genetic resource management when it covers recent generations, as [59, 60, 226] do. This requires large c values: from the equation above, the situation of two and five generations ago is represented by LD among markers 0.25 and 0.10 Morgan apart. The maximum distance between Amaral's markers was 0.03 Morgan.

This methodology is statistically demanding. England et al. [61] report on "simulations to show that [the most widely used LD] estimator is strongly biased when sample size is small [...] and below true N_e. This is probably due to [LD] generated by the sampling process itself." They also proposed "a way to determine whether a given sample size exceeds population N_e and can therefore be used for computation of an unbiased estimate." Waples [62] confirmed this by describing how Eq. 1 above is inappropriate for low values of n and N_e, particularly when $n < N_e$.

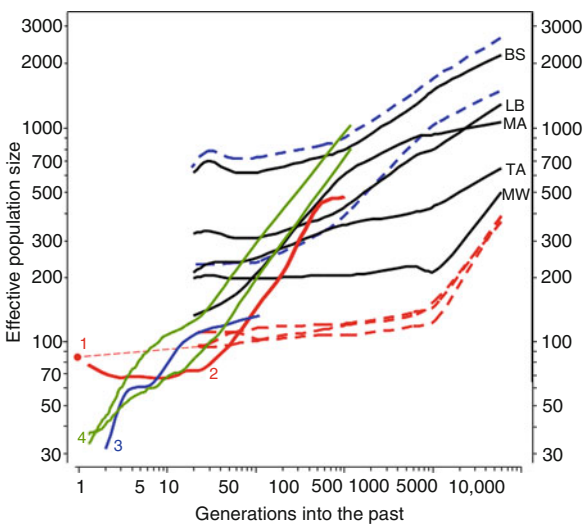

Pig Breeding for Increased Sustainability. Figure 4 Time trends in effective population size for 14 European pig breeds, estimated from linkage disequilibrium decay patterns according to [57]. Blue dashed line, transboundary breeds; black solid line, local breeds (British Saddleback, Large Black, Tamworth, Middle White, Mangalica); Others, commercial lines: "1" from [67]; "2" from [59]; "3" from [60]; "4" from [226] (All other data from [58])

The accuracy of the N_e estimator of Eq. 2 depends not only on the numbers of individuals and markers involved, but also on N_e and c. Based on [44], for a system with n individuals genotyped for m pairs of markers, each with a within-pair distance of c Morgan, an approximation of the standard error of estimated N_e is

$$\mathrm{stderr}(N_e) \approx \left(N_e + \frac{2c(2-c)}{(1-c)^2 + c^2} \times \frac{N_e^2}{n} \right) \times \sqrt{\frac{2}{m}} \quad (3)$$

From this equation, estimates of $N_e = 100$ or $N_e = 200$ for five generations into the past (c = 0.1 Morgan) would require n = 100 individuals genotyped for m = 400 or m = 750 marker pairs to achieve a standard error of 10% of the estimate (i.e., 100 ± 10 or 200 ± 20). Similar accuracies for one generation into the past (c = 0.5 Morgan) would require m = 3,000 or m = 10,000 marker pairs. N_e estimates for more recent situations require more data for a given proportional accuracy. However, high accuracies (low standard errors) are easier achieved for lower N_e levels – often the more interesting ones from a resource management point of view.

Other molecular approaches to estimate N_e trace changes in allele frequencies over time (the *temporal* method), or derive (small) population size from (large) sampling errors of observed heterozygote proportions deviated from Hardy–Weinberg proportions (the *heterozygote excess* method). Schwartz et al. [63] give a review; further developments are described in [64–66]. The latter paper introduces the immigration rate into the equation – a useful issue in livestock scenarios with their common introgression of extraneous germplasm. Abdallah et al. [67] also take immigration into account when analyzing 12 of the breeds of Fig. 2. One of these was also analyzed by Amaral [58]; Fig. 4 gives Abdallah's estimate as the end point of the Hayes approach to Amaral's data.

Relative Utility

Comparisons of pig lines are difficult to organize and expensive to run: (semi)-governmental versions of such tests have run for several decades as *commercial product evaluation* in western Europe, focusing on growth and carcass traits. Reproductive traits are sometimes included by across-farm analysis of routine field data, with its inevitable and unpredictable bias. Robustness traits are very rarely included, not surprisingly given the demanding nature of categorical trait analysis. Such a test was designed [68] for growth and carcass traits to detect differences between genotypes of 0.25 trait standard deviations at 95% significance, with a statistical power of 75%; this led to a scheme with, on average, 67 sires per genotype, 2.6 litters per sire, and 1.8 tested pigs per litter. Subsequent tests also covered reproduction and longevity traits; these schemes specify 65 sires, 3 litters per sire, and 2.7 tested daughters per litter [69]. The statistical significance of breed differences must be tested against the variation among sires within breed, which requires inconvenient sampling schemes.

Gibson et al. [70] (condensed here) discuss characterization for production and robustness traits: this can only be genetically meaningful when the production environment is properly accounted for; environmental factors are so complex that records from different locations or times cannot be validly compared; valid breed comparisons are possible, first, when breeds are recorded simultaneously at the same location under identical management [as in the previous paragraph]; second, through meta-analyses linking records from different locations or times through overlapping breeds, statistically adjusting for environmental effects; such meta-analyses are powerful, but only valid when genotype×environment interactions are negligible (as in controlled confinement conditions); it will remain problematic that lifetime productivity traits are extremely difficult to record.

These authors stress that the functionality of information systems "must be greatly increased to allow extraction and customized analysis of phenotype and molecular genetic data within and between data sources; [...] breed information can be linked to [...] environment and production system mapping, allowing [...] disease resistance and adaptation traits to be predicted from past and current breed distribution and use." They conclude that "these are substantial but fully achievable functions."

Tixier-Boichard et al. [46] emphasize characterization for robustness: "local breeds survive in harsh environments and this needs to be better understood; epidemics are major threats for all animal genetic resources across the world; climatic change is likely to increase the spread of tropical diseases to temperate areas. [Scientific evidence] that local breeds are adapted and resistant [...] has been obtained in several instances [...], well documented for parasitic diseases [...], with local breeds maintaining a better performance in the presence of parasites and/or exhibiting lower levels of parasite infestation [tolerance]". These authors take a utilitarian position: "data on production systems, phenotypes and molecular markers should be used altogether in an integrated approach to characterization. [...] Decisions regarding conservation should incorporate all descriptors. Conserving without documenting would be useless."

In summary, a livestock breed's direct-use utility value should be assessed in terms of production traits and robustness traits like disease resistance/tolerance, adaptation to unfavorable conditions, and lifetime productivity. This assessment must use any available phenotypic and molecular data (the latter element comes back to the work of Ciobanu [33] and Iannuccelli [34], section "Genetic Distinctiveness"). All this will require extensive information systems, difficult to achieve but not impossible. Without such functionality, utility-directed breed conservation is not feasible.

Of course, phenotypic and molecular characterization can only focus on known characteristics. The main drawback is that the traits of true future interest (covering unexpected changes in consumer preferences, or in options for health or climate control or nutrition) cannot, by definition, be defined or measured. This makes it difficult to combine the utility issue with the insurance argument for conservation: it calls for option values. Viral diseases (e.g., PRRS, PMWS, influenza) are expected to break out on a wide scale every few years [71, 72], and any breed that happens to carry full resistance would suddenly have a very high utility value. This would require fast and widespread testing, and challenging logistics to distribute the relevant alleles throughout the worldwide pig industry – which

may well become feasible with further development of genomics and reproductive technologies. But that particular breed's utility is likely to drop dramatically again, as soon as the next outbreak (of a different virus) occurs.

Urgency, Importance, and Feasibility: Priority Level of the Breed

To quote Wikipedia, Covey et al. [73] introduced "a framework for prioritizing work that is aimed at long-term goals, at the expense of tasks that appear to be urgent but are in fact less important." This is about time management, but the same is relevant in global genetic resource management. Sections "Genetic Distinctiveness" to "Relative Utility" describe different features that might make a livestock breed a candidate for conservation – but limited funding requires prioritization. Obviously, highest conservation priority should be given to breeds that (1) have a great utility, (2) are strongly distinct from other breeds with much within-breed variation, and (3) are strongly endangered due to inadequate population size or structure. Items (1) and (2) are about *importance*; item (3) is about *urgency*. This requires integration of these issues, preferably quantitatively so that priority levels can be ranked and funding allocated. Another element to include is then (4) the cost of conservation – introducing the issue of *feasibility*: "identified benefits could be quantified so that society has some sense of how much the conservation is worth. Society can then determine how much they would want to spend on a conservation effort" [74].

A comprehensive way to deal with the above elements [75] defines the genetic distinctiveness of a breed (calculated with the relevant emphasis on between-breeds and within-breed diversity) as D, its utility value (for all relevant purposes) as U, recalls its extinction probability P_{ext} (based on its N_e and possibly on additional parameters) and defines the cost of reducing it (through any relevant conservation action) by ΔP_{ext} units as C. Then the priority ranking R for such a conservation action would simply be

$$R = \frac{(D + U) \times \Delta P_{ext}}{C} \quad (4)$$

This would be calculated for every breed in the conservation portfolio, assuming that all their D, U, P_{ext}, and C values can be directly compared – which requires D and U to be expressed in the same unit, and everything to be calculated using the same algorithm and parameter definitions across breeds. Breeds with higher R values get a higher priority for conservation – because their conservation is more important (D, U), more urgent (P_{ext}), and/or more feasible (C). The probability P_{ext} takes values from 0 to 1, and ΔP_{ext} from 0 to P_{ext}: reducing the extinction probability by its full value (i.e., $\Delta P_{ext} = P_{ext}$) comes down to safeguarding the breed entirely.

These authors notice that the costs of the most complicated in vivo, in situ conservation schemes would likely be proportional to conservation effort, i.e., $\Delta P_{ext}/C$ is roughly constant and ranking is based on D and U. By contrast, the costs of the simplest in vitro cryoconservation schemes might vary only little, i.e., C is roughly constant and ranking for complete safeguarding is based on the *cryoconservation potential* $(D+U) \times P_{ext}$. Real-life conservation programs would fall between these extremes.

Simianer et al. [76] compared three forms of the actual relationship between C and ΔP_{ext}, applied these to a set of breeds characterized in terms of genetic distances and extinction probabilities, and found that "conservation funds should be spent on only three to nine of the 23 breeds, depending on the model used." This approach was further formalized [77] into a comparison of *maximum-risk*, *maximum-diversity*, and *maximum-utility* strategies to determine the optimum set of breeds to conserve, which favors the latter strategy which combines diversity and utility – although it obviously requires the quantification of U, which makes it difficult to implement in practice. The latter two approaches quantify the *expected conserved diversity* or the *expected conserved utility* of possible sets of breeds that may be successfully conserved at some point in the future, and then calculate the *marginal diversity* or *marginal utility* of each breed by differentiating with respect to the breed's P_{ext}. These are then multiplied by P_{ext} to obtain the breed's conservation potential, similar to the term $(D+U) \times P_{ext}$ of Eq. 4.

As argued at the end of the section on "Relative Utility," utility is the weakest element here: conservation aims at the future, and future utility cannot be predicted. All the other elements can in principle be dealt with by a complete pedigree and/or dense DNA

samples from ~100 individuals. One of the options would be to drop U from the equation and rank conservation priorities on D only (the *maximum-diversity* option of above). This reasoning is taken to its logical extreme by suggesting to "devote the majority of present conservation budgets to freezing [...] samples from existing breeds [...] concentrate on ova and sperm from abattoir material, and somatic cells, e.g., ear clips (the latter in anticipation of the increasing effectiveness of somatic cloning)," because future "genomic tools will open up completely novel means of exploiting genetic resources" [14]. In line with this, the USA has "invested in the establishment of an in vitro conservation program and a genebank [covering 18 local pig breeds and one ITB at the time of reporting]. Collections are being built up very quickly, in close collaboration with the industry. Breeding companies use the genebank as a backup of their breeding work. In Canada, a program for in vitro conservation [...] will be implemented in the near future" [5], as later documented by www.ushrl.saa.ars.usda.gov/SP2UserFiles/Place/54020500/documents/update%208-10-02.pdf and dsp-psd.pwgsc.gc.ca/collection_2008/agr/A52-88-2008E.pdf.

Target Traits for Genetic Improvement

Livestock breed improvement requires a breeding goal and a selection strategy best suited to the needs of the production system and the market that it supplies – this is one of the elements of *population-level genetic resource management*. Animal breeding technology has a long tradition in this field, but improvement of an endangered breed may require substantially different goals and strategies than in mainstream industry breeding programs. FAO [5] write: "the most appropriate strategies for managing these breeds may involve only limited genetic change [...] to maintain adaptation to the local environment and disease challenges, and [...] to maintain the level of a production trait [...] if this is currently [near] an optimum level." Of course, the insurance argument for breed conservation assumes that the breed may, at some time, support a different production system than its original one, because it happens to carry alleles (likely adaptive ones) of large utility, then and there. This adaptive utility must be balanced with production utility, which will likely be much lower than in commercial lines. The actual uptake of the breed as a source of adaptive alleles will be much easier when the production-related lag is limited. So for the insurance argument, genetic improvement of production traits is desirable – but not at the expense of adaptive quality: possible genetic antagonisms between production traits and anything else require specific attention. "The genetic basis of population differentiation for fitness traits will be non-additive, with different adaptive gene complexes evolved in each breed. Genetic improvement programs therefore should start with an adapted population, with selection then for production traits" [78].

Another argument in favor of improvement of production traits is that many endangered breeds are endangered precisely because they lag behind other breeds in terms of production traits. The common idea that improvement of production traits inevitably leads to a reduction of robustness is false – it just requires a sensible breeding program, see the section on "Robustness."

Genetic Improvement Programs

As argued above, any livestock breed with a future must support an agricultural production system. Rege [79] writes: "the most rational and sustainable way to conserve animal genetic resources is to ensure that indigenous breeds remain functional parts of production systems, that is, *conservation through use*. This is possible only if economically important attributes of indigenous breeds are identified, studied and incorporated in breed improvement programmes." Genetic improvement will always be required – unless the production system is completely static, without any interactions with the world around it. A useful concrete example is from [80]: "during the past few years the Limousin pig, endangered and neglected during the 1970s and 1980s in favor of the better-performing large breeds, has become popular with consumers looking for quality. Today it is victim to its own success with supply being lower than demand, so that it has become necessary to develop its productivity" (translated).

This requires a breeding goal and a selection strategy best suited to the needs of the production system and the market that it supplies, as discussed in the

Section on "Target Traits for Genetic Improvement." A checklist of items that play a role here, from definition of the product and the market to evaluation of the breeding program's profitability, is in [81].

The breed also has to be *maintained* – preserving as much of its genetic variation as is feasible. And its qualities must be *exploited* in an optimal way, making efficient use of other resources.

Livestock breed *maintenance* requires strategies and tools to keep N_e sufficiently high. This comes down to keeping inbreeding under control, usually by minimizing co-ancestry in the breeding population. There is a possible antagonism with the previous point: selection in a population reduces N_e, so a balance will have to be found and maintained. There are many rules-of-thumb to delay inbreeding (e.g., *keep one son from every sire* or *maximize generation intervals*); an example of implementation in commercial lines is in [82]. Many of these rules perform well on the short term but have unexpected long-term effects, and they usually reduce genetic improvement unpredictably, leading to uncertain genetic resource management. N_e can be affected by age at first breeding and culling policy in quite counterintuitive ways [83], so that "the general tendency is contrary to the expectation that [N_e] would increase with increasing [longevity]." High longevity increases generation length but reduces genetic drift; the combined effect favors a short productive lifetime, so that N_e can actually be increased by early culling.

A better solution is to apply co-ancestry management and mate selection based on optimum contribution theory or similar frameworks. The principles are covered in detail in [49, 84, 85]. The latter source's *mate selection index* (MSI) is an optimized criterion, based on an objective function such as [86]:

$$\mathrm{MSI} = \mathrm{EBV} - \lambda_1 \, x' \, Ax - \lambda_2 \overline{F} \qquad (5)$$

Here, (1) EBV holds estimated breeding values; (2) $x' \, Ax$ represents average co-ancestry in the system: A holds the additive relationships among all animals, weighted by their contributions x (numbers of progeny) to the next generation; (3) $\overline{F}$ is their average inbreeding coefficient, calculated from A; λ_1 and λ_2 are positive weighting factors. This is a cost-benefit equation, with element (1) representing the benefit and (2) and (3) representing the (genetic) cost: EBV, A, and $\overline{F}$ are known, so the system can be solved to deliver the contributions x that give the best (genetic) cost-benefit for particular values of λ_1 and λ_2. The result of this is a list, based on x, with animals to select and animals to mate to each other (the optimum selections and optimum matings that lead to optimum contributions).

Proper genetic resource management can lift populations much smaller than the FAO threshold of 1,000 breeding females to the "not at risk" level. Many industrial pig lines are maintained at far less than that population size (e.g., see Fig. 4) with a secure genetic future. Careful immigration and admixture is regular practice in the breeding industry, but it is often avoided by breed societies and similar structures for chauvinistic reasons.

For example, Fig. 5 shows an intensive network of historical genetic connections among the European black-belted and saddled pig breeds, with a genetically useful loop with Hampshire (an ITB). Many of these populations have a herd size far lower than 1,000 sows, and most of those focus on the same set of characteristics (meat quality and robustness, and of course coat color) when describing their distinctiveness in the associated Web sites. This would suggest a clear case for the quantification of the various elements of Eq. 4 above, followed by regular and careful genetic exchange to make resource management easier.

Exploitation: A common negative term in the literature on genetic resource management is *indiscriminate crossbreeding*. For example, "very often, crossbreeding has been indiscriminate and the local breeds that underpin the crossbreeding program have been lost because of a lack of understanding [...] that these pure breeds must be maintained to support the system" [87]. This is clearly a management issue. On the other hand, these authors mention systems where crossbreeding is "used for gradual breed replacement with [...] the controlled [...] formation of composites [...] for specific production systems," as "a rapid method of introducing desirable traits into local well-adapted breeds," and "as a way out of a narrowed genetic base in commercial breeds." The logical way of making use of exotic germplasm without any risk of endangering the LBs is "structured cross-breeding systems, such as 'terminal crossing' where [F_1] animals are slaughtered or where specialized crossbred dam lines are used."

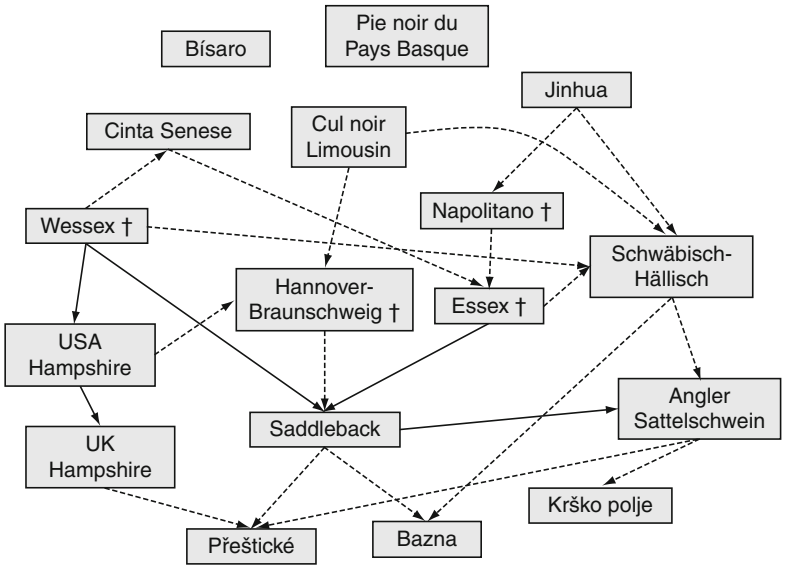

Pig Breeding for Increased Sustainability. Figure 5
Genetic connections from ~1,770 (Jinhua) to present, among black-belted and saddled pig breeds. Consecutive series of arrows do not imply any chronological development. Solid arrows represent the main source of a breed; dashed arrows imply the existence of other sources not included here. (Data from [16, 37, 222–225]; Lenoir H, 2010, IFIP Institute du Porc, Le Rheu, France, Personal communication; www.elbarn.org; www.besh.de; efabis.tzv.fal.de; dad-training.fao.org/cgi-bin/EfabisWeb.cgi; www.thepigsite.com/info/swinebreeds.php)

Pig examples are from Germany where Angler Sattelschwein, Schwäbisch-Hällisch, and Bunte Bentheimer are crossed with Pietrain; and from Spain where various Iberico strains are crossed with Duroc, all to optimize meat quality versus meat quantity in the terminal F_1 product.

This chapter is about science and technology. But "logistics, not science, is the underpinning of a successful breeding policy. Without a system for handling the details of livestock identification, classification and movement, the science is of little avail" [88]. This certainly holds for endangered populations, typically managed by fragmented groups of independent-thinking people. Nimbkar et al. [87] stress the importance of "structures to organize the keepers of animals and help motivate communal efforts [...] allowing livestock keepers better access to information, [...] extension services, facilitating the organization of training, and improving [...] marketing. In Europe, there are strong farmer cooperatives and breeding organizations that go back a century." Indeed, successful breeding programs were founded on equally fragmented conditions in many European countries and also in Canada, starting out with breeds with similar production performance as the ones from that same area that are now endangered or extinct. Apart from the clear need for incentive and for institutional backing, there are two prerequisites for such development. First, technically: an efficient system for ensuring genetic connections among farms, e.g., through regular exchange of males or across-farm AI – everything else of a technical nature will have to build upon that. Second, organizationally [89]: employment of professional genetic expertise by the breeders' organization – so that the system does not have to rely on fragmented and unstable governmental service, and can arrange for effective feedback between breeders' objectives and technological options.

Pollution

FAO's *Livestock's long shadow: environmental issues and options* report [90] gives an overview of the amount of nitrous oxide (N_2O) released from livestock manure and urine, worldwide, in 2004. Of the total emission of 3.69×10^9 kg, 12% was due to pigs – just over half of

that from Asia. N_2O is an effective greenhouse gas (GHG), also involved in the depletion of the ozone layer. Other nitrogen compounds that enter the environment from livestock excreta are ammonia (NH_3) and nitrogen oxides (NO and NO_2), involved in acidification or, indirectly, in global warming.

Technology

The FAO report [90] devotes much text to options for reduction of nitrogen emission, most of which involve manure management and improved animal nutrition. For example (p. 122): "An important mitigation pathway lies in raising the low animal nitrogen assimilation efficiency [...] through more balanced feeding (i.e., by optimizing proteins or amino acids to match the exact requirements of individual animals or animal groups). Improved feeding practices also include [...] improving the feed conversion ratio [FCR] by tailoring feed to physiological requirements. However, even when good management practices are used to minimize nitrogen excretion, large quantities still remain in the manure." This is quantified in another table in the report (p. 137) with typical values for nitrogen intake, retention, and excretion in cattle, pigs, and poultry. According to these numbers (which go back to [91]), across these species, only about 19% of nitrogen ingested in "less productive situations" is retained in meat, eggs, and/or milk – in "highly productive situations," this goes up to 30%. Likewise nitrogen retention rates (N_{ret}) of about 34% for pigs were reported for the 1995 "highly productive situations" of France, Denmark, and the Netherlands [92].

These retention rates are indeed low, but the difference between the above productivity levels is considerable, suggesting scope for increase by "improved feeding practices". Dourmad et al. [93] state that "the ultimate reduction of N excretion can be reached when multi-phase feeding is combined with a perfect balance of essential amino acids and [...] optimization of the supply of non-essential amino acids" – ideally on a daily basis. They refer to a 1995 experiment [94] where the use of a single diet over a growing period from 26 to 101 kg body weight was compared to such an optimized multiphase feeding strategy, and where N_{ret} values at 34% (single diet) and 50% (optimized regime) of the ingested nitrogen were found.

Later studies in laboratory conditions have achieved higher retention rates. De Lange et al. [95] studied the effect of dietary amino acid levels on protein deposition rate in pigs from 39 to 77 kg liveweight, and present results that lead to N_{ret} = 61% at complete amino acid availability – "at a more typical protein digestibility, this would become 56%" (cf. de Lange, personal communication, 2010). Similarly, Buraczewska et al. [96] measured N_{ret} of up to 57% in 35-kg and 45-kg pigs of a "high lean gain potential" genotype, after optimization of the dietary amino acid composition. In more practical conditions, Pomar et al. [97] fed pigs from 25 to 105 kg liveweight according to a "traditional three-phase feeding program" or with "individually tailored diets," obtaining N_{ret} = 37% and 48%, respectively.

Curiously, the FAO report [90] pays no attention to a logical alternative to "improving [FCR] by tailoring feed to physiological requirements," i.e., improving it by tailoring these physiological requirements themselves, through animal breeding [98]. When nitrogen excretion data of growing (Landrace × Large White) and (Hampshire × Duroc) pigs were adjusted for body weight and feed intake, significantly different values were obtained between the genotypes – which reveals genetic variation so that "genetic selection may be an effective method for altering nutrient utilization and output" [98]. Heritabilities for laying-hen excretion traits such as dry excreta weight, excreta humidity rate, and the ratios of dry excreta and nitrogen excreta to feed intake (0.25–0.46) and for dairy cow methane production (0.12) were reported in [99, 100].

Improvement of traits like litter size, sow feed intake, growth rate, and FCR reduces nitrogen excretion (N_{excr}) from sows and growing pigs [101]. The 1988–2007 genetic trends for growth rate (+8.5 g/day/year), FCR (−0.02 kg/kg/year), and litter size (0.16 pigs/litter/year) in the UK pig sector were estimated to cause 0.8% annual reduction of the associated global warming potential of GHG emission [102]. In that study, the genetic reduction of FCR explains about 70% of the reduction in N_2O emission; the genetic increase of growth rate explains about 70% of the reduction in NH_3 and methane emission. The genetic increase of litter size (which reduces the sow herd with its emission, for a fixed number of slaughter pigs) explains about 20% of all three elements. The future

scope for emission reduction is underestimated in that study, for two reasons. First: genetic trend of lean content (which was substantial in the UK during this period, probably about 0.5%/year) was not taken into account. Second: future trends in all these traits may be expected to be stronger than the historic values, due to further development of genetic technology and of the "uptake rate of improved genetics by the commercial level" [102].

The reduction of N_{excr} due to genetic improvement of production traits is quantified by the simulation results in Fig. 6, obtained with the model of [103]. The time trends of model parameters such as maximum protein deposition rate (PD_{max}) that were described for six pig sire lines [104] can be used to model N_{ret} and N_{excr} at the nucleus level throughout the 1969–2004 period. The simulations involve these six progressively advanced genotypes, grown from 20 to 120 kg body weight. Each of these genotypes was fed ad libitum on each of seven three-phase (20–50, 50–80, and 80–120 kg) diet specifications, targeting overall lean tissue growth rates (LTGR) from 275 to 425 g/day in steps of 25 g/day [105]. This involves diets with a fixed digestible energy content (DE = 14.2 MJ/kg) and varying levels of crude protein (e.g., from 12.2% to 15.5% in phase 3) and essential amino acids (e.g., lysine from 0.525 to 0.765% in the diet, ditto).

The older genotypes in this simulation do not have the potential to achieve the higher LTGR targets, with the consequence of low N_{ret} and high N_{excr} levels. Low LTGR targets obviously lead to low N_{ret} as well, more so in the older genotypes. Figure 6 shows clear optimum trajectories across genotypes and feeding strategies, for both N_{ret} and N_{excr}. It also shows that these optimum trajectories follow different paths for both characteristics, particularly in the more advanced genotypes.

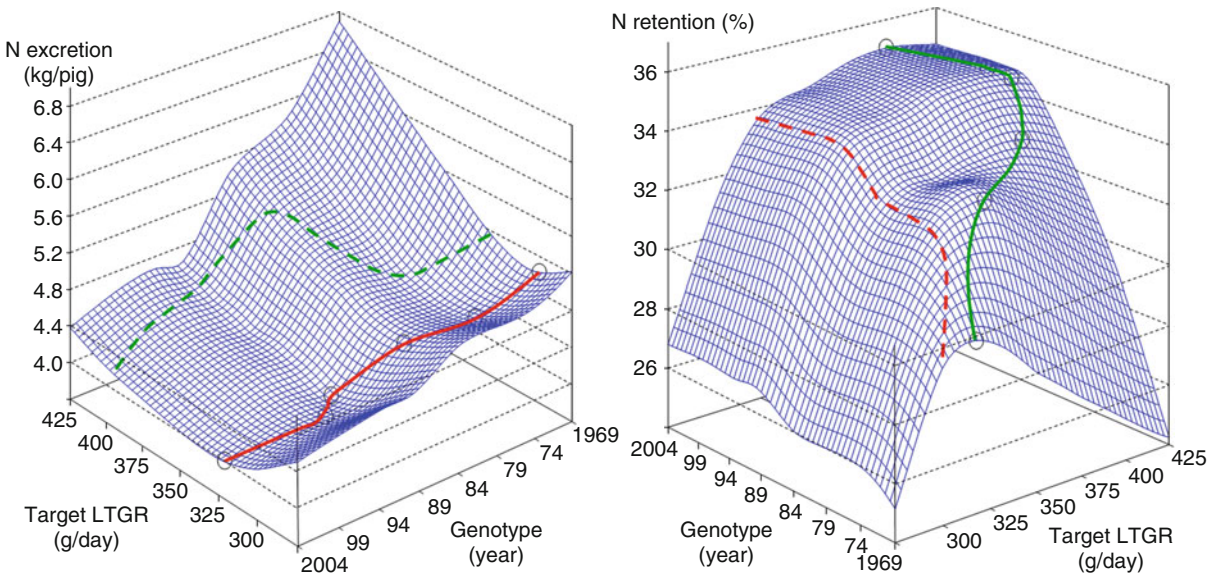

Pig Breeding for Increased Sustainability. Figure 6

Nitrogen excretion (*left*) and retention rate (*right*) in simulated growing pigs of six genotypes (representing sire lines from 1969, 1976, 1984, 1990, 1993, and 2004; From [104]). Each genotype was fed from 20 to 120 kg liveweight on three-phase diet specifications targeting [275, 300,. . .,400, 425] g/day lean tissue growth rate (LTGR), according to [105] – the higher LTGR targets are beyond the potential of the older genotypes, and the more advanced genotypes do not realize their potential due to inadequate nutrient supply. The blue response surfaces are spline interpolation plots through the 6×7=42 simulated datapoints. The red and green trend lines represent minimum excretion and maximum retention, respectively, for each genotype. Each broken trend line mirrors the solid one of the same color (with its datapoints as black circles) in the other graph, approximately

Along these optimum trajectories (i.e., when fed to achieve maximum N_{ret}, or minimum N_{excr}, within the limits of the three-phase feeding program) the 2004 genotype shows a proportionally 19% higher N_{ret} or, alternatively, a 20% lower N_{excr} than the 1969 genotype. Deviations from these optimum diet composition settings have much stronger effects in the older genotypes than in the more advanced ones.

The more advanced genotypes in this simulation show a clear diminishing-returns pattern for N_{ret} with a very flat asymptote around N_{ret} = 35%. But the simulated PD_{max} levels (i.e., genetic potential for N_{ret}) increase progressively throughout the 1969–2004 period covered here – so the expression of that potential must be constrained by the three-phase fixed-diet program employed here. This comes back to the real-life results of Pomar et al. ([97]; above) who obtained N_{ret} = 37% with a three-phase fixed-diet program and N_{ret} = 48% with "individually tailored diets." The latter strategy involved a daily analysis of the performance-to-date of each pig, to predict today's individual body weight, growth rate, nutrient requirements, and ad libitum feed intake. Each pig was then fed a mixture of basic rations via automated feeders to match these predictions.

It follows that the more advanced genotypes require more advanced feeding strategies to bring their more sustainable performance potential to expression.

This was further explored by Morel and Wood [106], who used simulation modeling to quantify nitrogen flux in growing pigs of low, medium, and high LTGR genotypes, on a variety of dietary regimes. Their simulated high LTGR genotype achieved N_{ret} = 57% when fed daily individually tailored diets (similar to Pomar et al.'s [97] diets mentioned above) with a strong focus on the minimization of N_{excr}. By contrast, the simulated low LTGR genotype achieved N_{ret} = 29% on a three-phase fixed-diet program with all focus on gross margin (i.e., carcass return minus feed costs). So the various N_{ret} results of these simulations (see Fig. 7) span the relevant range of commercial and high-tech conditions described above.

These authors conclude that although "a reduction in nitrogen excretion is mainly achieved through a reduction in nitrogen intake" (as in Fig. 6), "genotypes with a high lean growth potential can be more profitable [in terms of gross margin] *and* have improved nitrogen excretion." A simple ANOVA of their results of gross margin and N_{ret} across the simulated scenarios (supplementary data from Morel PCH, 2010, personal communication) quantifies this. The low versus high LTGR genotypes show least-square means for simulated gross margin at 102.0 versus 150.0 CHF per pig, and for N_{ret} at 34.1% versus 46.8%, respectively. Their "three-phase fixed-diet" versus "individually tailored" feeding regimes show least-square means for gross margin at 116.3 versus 138.6 CHF, and for N_{ret} at 36.7% versus 45.0%, respectively. So Morel's genetic scenarios [106] are *more* effective (because further apart) than his feeding regimes, for improving both gross margin and N_{ret}. With some generalization, this can be put into perspective as follows.

With the 1969–2004 trend of PD_{max} in pig sire lines from [104] (above), the PD_{max} input values of Morel's simulated genotypes (120, 160, and 200 g/day) can be

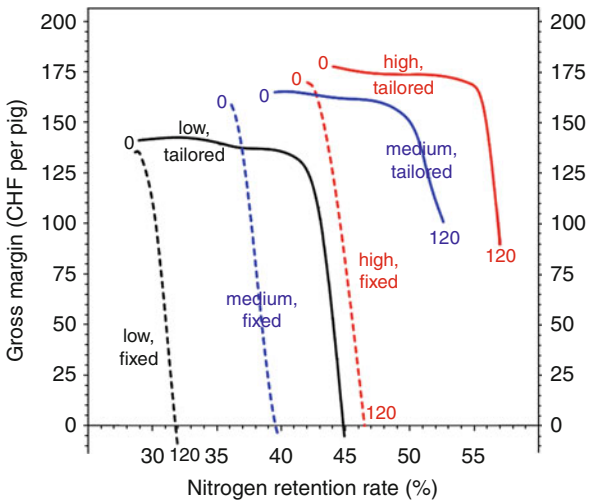

Pig Breeding for Increased Sustainability. Figure 7 Gross margin (from growth rate, backfat depth, and feed intake) in relation to nitrogen retention rate (N_{ret}) in simulated growing pigs of three genotypes (low, medium, and high lean tissue growth rate), fed three-phase fixed diets or individually tailored rations. The labels "0" and "120" indicate the extremes of a range of weighting [N_{ret}: margin] from [0:1] to [120:1] in the objective function for diet optimization. CHF: Swiss Francs (Data from [106] and Morel PCH, 2010, personal communication)

located in time at 1970, 1987, and 1997, respectively – so his low and high LTGR genotypes are 27 years of sire line genetic improvement apart. The simulated gross margin of those genotypes (three-phase fixed-diet, full focus on gross margin) differs by 35.7 CHF (i.e., about 23 EUR).

Time trends of growth and carcass traits in commercially available slaughter pig genotypes [107] can be converted to gross margin trends as in Fig. 8. The average range for a contemporary comparison of seven genotypes (the most common configuration in this data, and also a fair representation of practical local availability of genotypes) is 10 EUR per pig.

This provides an (under)estimate of the range in gross margin among the various slaughter pig genotypes that are commercially available at any point in time (an underestimate, because these CPE trials do not include *all* available genotypes, particularly not the less advanced ones). This number is equivalent to 10/23 = 43% of the difference between Morel's [106] low and high LTGR genotypes. Combined with the above surmise that "Morel's genetic scenarios are more effective [...] than his feeding regimes are, both for improving gross margin and for improving N_{ret}," it follows that a well-informed choice of the most appropriate slaughter pig genotype *available at any point in time* will have almost half of the influence on N_{ret} (and on margin) that full implementation of individually tailored diet optimization will have.

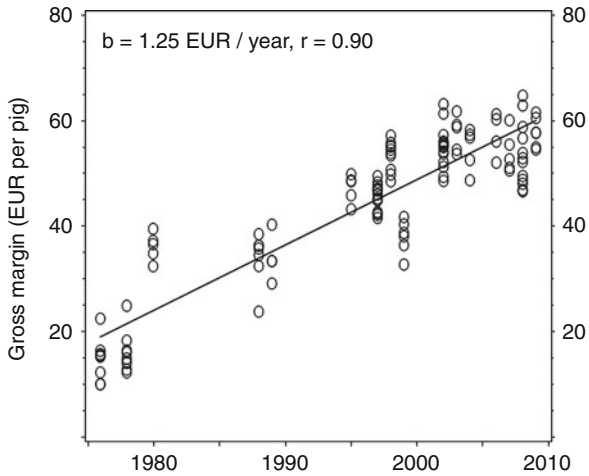

Pig Breeding for Increased Sustainability. Figure 8 Gross margin (from growth rate, estimated lean content, and feed intake) in slaughter pigs of commercially available genotypes, as recorded 1976–2009 in public Commercial Product Evaluation trials. The trend line is the linear regression. EUR: European Euros (Data from [107])

Strategies

The above section shows that pig breeding in general makes a considerable contribution to the reduction of nitrogen emission from growing pigs. Up to now, these effects have not been incorporated into formal breeding goals, so they are not under control and cannot be credited, as such. Many governments have an increasingly active policy of pollution reduction, and the global warming potential of the excreta from livestock production is under increasing scrutiny. This has led to a series of economic studies into the effectiveness of taxation of nitrogen (and other chemicals) emission on the farm level, focusing on countries as politically (and productively) different as Italy, Switzerland, and the Netherlands [108–110].

A central element in the associated econometric approaches is the *shadow price* of nitrogen emission. Paul et al. [111] describe the "shadow values for the bad outputs" of an agricultural production system as "the marginal amount that producers [...] would be willing to pay for unrestricted use of the environment" to dispose of those bad outputs – e.g., for the right to increase their bad outputs in a situation where legislation attempts to reduce these.

Operationally, shadow prices are estimated as the partial derivative of the producer's profit equation with respect to the bad output factor – equivalent to marginal economic values for production traits in animal breeding. These are demanding statistics. Key et al. [112] studied the productivity of the USA slaughter pig sector, and note that estimating the "shadow price of manure [...] with the data available would require making a set of assumptions that would likely introduce substantial error [...], an accounting of hog farm output that includes manure is left for future research."

The shadow price of nitrogen emission from growing pigs, sows, and dairy cows in the Netherlands was estimated at 2.7, 10.8, and 6.5 NLG/kg, respectively [110, 113].

The UK government has included the shadow price of GHGs as a structural element of its cost-benefit evaluation of any policy that it funds or supports, using values based on [114] where a shadow price of CO_2 is derived that can be converted to a shadow price of nitrogen (as a component of N_2O) at 9.25 GBP/kg.

Obviously, such shadow prices depend on practically every feature of the production system and its surrounding conditions. Using again Paul et al.'s [111] description above, the amount that producers would be willing to pay for the right to increase their bad outputs in a situation where legislation attempts to reduce these, would depend on (1) how strongly this legislation attempts to enforce the reduction, and (2) the impact of such a reduction on the remaining elements of the producer's profitability. Point (1) is largely a political factor; the UK government was criticized by environmental NGOs for the supposedly artificially low value of its abovementioned shadow price of CO_2. Point (2) may well lead the producer to decide to *not* reduce his bad outputs, because that is still more profitable – as was the case in Paul's study which focused on pesticide usage: her shadow price estimates were negative.

Wall et al. [115] notice the equivalence of the shadow price of a bad output and the marginal economic value of a production trait, in the sense that both can be used to weight their characteristic into a breeding goal. They refer to the EU-ETS Emissions Trading Scheme that was set up to support the EU to meet its commitments to the Kyoto Protocol (ec.europa.eu/environment/climat/emission/index_en.htm), which will effectively determine the shadow price of GHG emission in the EU. They write "suppose [...] that agriculture is forced into an [ETS] and that farmers must hold valuable permits either through initial allocation or by purchasing in the ETS. [This] will immediately move GHG mitigation traits from a public to a private breeding objective [...]; the prevailing emissions price becomes the relevant economic weight that should be incorporated in any breeding index that includes mitigation potential." The demand for "breeding indexes that include mitigation potential" will become very concrete, once pig producers have to deal with such a scheme – in line with this, the total costs of 2007 environmental government policy in the Netherlands were estimated at "around 0.11 EUR per kg [carcass] weight, of which 0.08 EUR was for manure disposal. In 2013, these costs will be 0.02 EUR higher as a result of the ammonia emission reduction policy" [116].

Figures 6 and 7 show that such a pig breeding policy is technically feasible: Nitrogen retention rate is favorably correlated with the conventional production traits and can easily be included into breeding goals and selection strategies.

Animal Welfare

In 1976, the member states of the European Community ratified the *European convention for the protection of animals kept for farming purposes*, regulating that livestock must be properly housed, fed, and cared for. In 1992, the following text was added (condensed here for clarity): "Breeding procedures which may cause suffering or injury to animals shall not be practiced. No animal shall be kept unless it can be expected, on the basis of its phenotype or genotype, that it can be kept without detrimental effects on its health or welfare." Five years later again, the EC's Scientific Veterinary Committee recommended that "no selection should occur without reference to the effects of that selection on welfare of [pigs]. The continuation of new genetic lines in which the welfare of the animals is, on average, worse than that of existing lines should not be permitted" [117].

Such statements leave the impression that animal breeding may be bad for the animals involved. This goes back to the late 1970s when animal breeding technology became much more powerful than before, due to improved data recording and processing (BLUP and, above all, computing power), and improved reproductive technology. Simultaneously, animal production in the western world experienced strong intensification connected to a long period of low, volatile, and unpredictable farm profitability [118]. The production sector therefore developed a strong and focused demand for animals with improved production performance.

This led to a strong and effective focus on production traits in livestock breeding in that period, with less attention for animal robustness traits. This lack of balance has caused fitness constraints in pigs, particularly in environmental conditions inadequate to

support the improved production potential, and particularly before this problem was being dealt with in modern pig breeding.

Intensification of animal production has also led to housing and management conditions that shelter the pig from climatic, nutritional, parasitic, and predatory challenges – but compromise much of the expression of its instinctive behavioral repertoire. This deprivation leads to frustration, with welfare problems for the affected individual and for its penmates.

Fitness constraints and deprivation are among the "criteria for determining the ethical limit for genetic selection" [119]. A third issue is formed by the routine invasive treatments that have been common, worldwide, since the onset of animal domestication – in pigs mainly tail docking and castration. These aim at a pragmatic (but unrefined and reoccurring) reduction of undesirable features that can also be dealt with through animal breeding – more complicated, but permanent and less physically invasive.

While worldwide demand for pig meat increases, it will become more and more relevant to resolve problems with pig welfare in intensive production systems. It is unlikely that this increasing demand will be met by any other production system than intensive ones, particularly in Latin America, Russia, and Asia. In accordance with FAWC's [120] plea for "a greater emphasis in breeding programs on traits associated with good welfare," animal breeding and genetics technology can then contribute in three areas: (1) robustness, (2) deprivation, and (3) avoidance of invasive treatments. In practice, each of these areas raises (4) ethical arguments, sometimes intense enough to dominate the issue – so although this chapter is about technology, these will be addressed as well. Sections "Robustness" to "Ethical Aspects" deal with these areas in this order.

Robustness

When animals of high-performance genotypes are kept in production systems that are inadequate to provide the resources they need to express their potential, the animals commonly show disturbed resource allocation [121] and functional disorders of the skeletal and cardiovascular systems, muscle physiology, the reproductive system, or immunocompetence [122]. For pigs, obvious indicators of reduced animal welfare in this respect are (1) increased mortality rates and reduced sow longevity, (2) disease (morbidity), and (3) lameness.

The issue here is one of environmental sensitivity. There are two ways to deal with the problem: make the environment more resource providing or make the genotype less sensitive. There are two strategies for the latter: (1) direct selection for robustness traits and (2) selection against environmental sensitivity as measured through reaction norms.

Selection for Robustness Traits Livestock robustness can be defined as "the ability to combine a high production potential with resilience to stressors, allowing for unproblematic expression of a high production potential in a wide variety of environmental conditions" [123]. The classical problem with this ability is in genetic antagonisms between production traits and resilience [121] – natural selection is not powerful enough to maintain (or improve) animal robustness in intensive production systems; it must be supported by artificial selection. Genetic antagonisms can be neutralized by using adequate selection criteria to select for an adequate breeding goal. Earlier breeding goals were inadequate in this respect, as they did not include robustness traits [124]. Following Gjedrem [125], a breeding goal should include all heritable traits that have an impact on profitability – and mortality, morbidity, and lameness certainly do. Knol et al. [126] discuss this in detail and stress that "simplicity and straightforwardness of the breeding goal has to be weighted against completeness and complexity." Such traits can be included in the profit equation for pig production [127]; this provides marginal economic values, required for inclusion in the breeding goal.

The various strategies for genetic improvement of piglet vitality and survival, leg weakness and longevity, stress sensitivity, and disease resistance are summarized in [128]. These are hard-to-measure traits, mostly categorical with low incidences and relatively low heritabilities, so that large data volumes from adverse environments are required for meaningful breeding value estimation [129]. Their genetic improvement has benefited considerably from BLUP and will benefit just as much from MAS [130, 131]. Figures 9–11 show

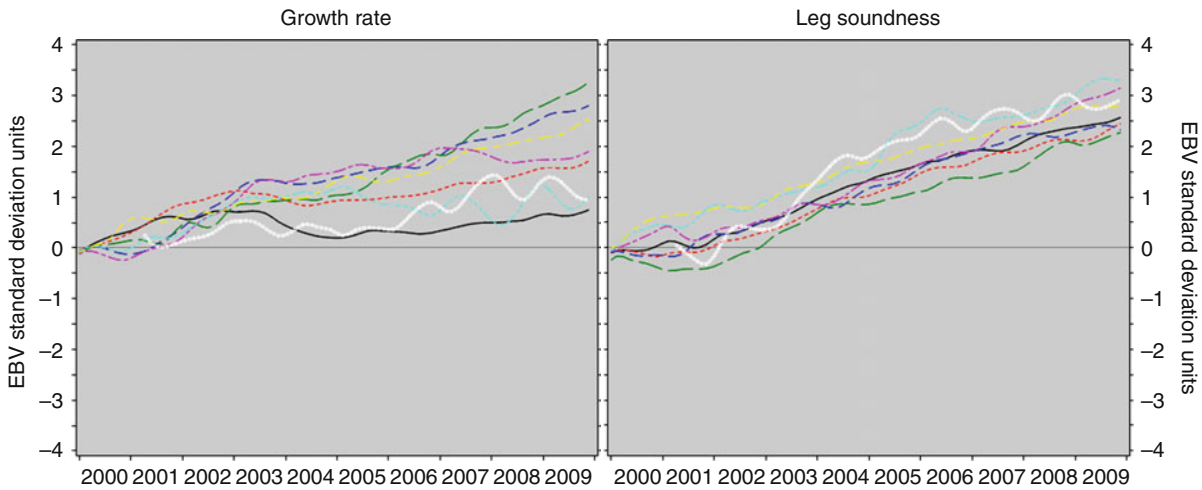

Pig Breeding for Increased Sustainability. Figure 9
Simultaneous genetic trends of growth rate and leg soundness in eight pig lines. Each trait was scaled by the standard deviation of its estimated breeding values; all trend lines for each trait were forced through the same origin in 2000 to make the trends comparable across lines

realized genetic improvement of leg soundness and mortality traits, coinciding with improvement of production performance, in eight pig lines.

SVC [117] write: "The criterion for selecting animals for use in breeding has been an increase in economic performance and this has often not coincided with improved animal welfare. Hence the term *genetic improvement* is misleading since, in some cases, the changes are not improvements for the animal but may make the life of the animal more difficult." The genetic trends of Figs. 9–11 show that this can be overcome: antagonistic correlations do exist, but genetic improvement can be achieved in production traits and robustness traits simultaneously – neutralizing genetic antagonisms by adequate selection. This effect will depend on the emphasis given to each trait in the breeding goal of each line.

Reaction Norms When progeny of specific sires are (1) identified as such, (2) spread across a wide environmental range (usually through artificial insemination), and (3) recorded for a production trait, their production performance can be regressed on a descriptor of the environment (e.g., a herd-year-season effect). This produces a positive slope overall: better environments lead to better production. When the regression is performed separately for sire progeny groups, and if there is genetic variation in environmental sensitivity of the trait's production potential, regression lines are produced ("reaction norms" in population genetics) with different intercepts and slopes for different sires. The intercepts are equivalent to the conventional estimated breeding values for the trait. The slopes quantify an animal's requirements for environmental support of its genetic potential; they detect robustness as defined above.

Environmental sensitivity in pigs was analyzed this way in [132, 133]. Friggens and Van der Waaij [134] discuss how selection for increased production levels (i.e., for high reaction norm intercepts) will cause a gradual increase of environmental sensitivity (i.e., of the slopes). This was confirmed [133] in terms of a strongly positive genetic correlation between intercept and slope of their reaction norms for litter size. The slopes have a very low heritability in that data, so the increase of environmental sensitivity would be very slow. This presents another example of genetic antagonisms, which can be neutralized by including both the intercept and the slope of the reaction norm of each production trait in the breeding goal and in the

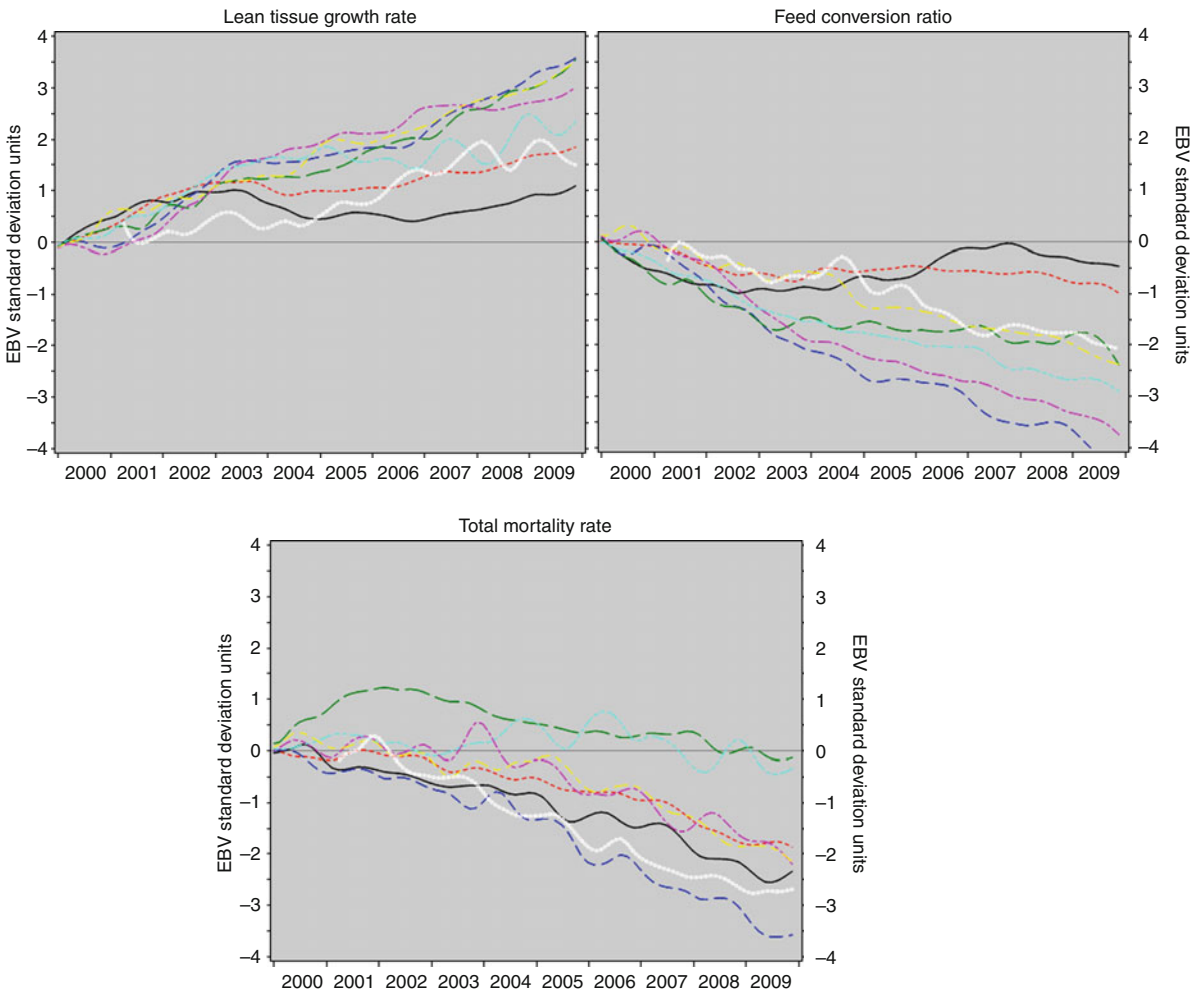

Pig Breeding for Increased Sustainability. Figure 10

Simultaneous genetic trends of lean tissue growth rate, feed conversion ratio, and total mortality from birth to slaughter in eight pig lines (same formatting as in Fig. 9)

selection criterion. A way to calculate their marginal economic values is in [123].

These are demanding statistics. Knap and Su [133] analyzed their data in three consecutively larger subsets. The medium subset held more than 50,000 sows – comparable to the largest litter size datasets in the scientific literature. Still, its parameter estimates for the reaction norm slopes differed considerably from those from the largest dataset with more than 120,000 sows, and the accuracy of its slope estimates was too low to be useful in practical breeding. The smallest subset held more than 30,000 sows, but its parameter estimates were clearly unrealistic and not significantly different from zero. Similar issues hold for the required environmental range in the data.

A single trait's reaction norm is equivalent to "a single-trait definition of robustness" and, as such, not a simple and foolproof recipe that can be applied without proper care for the system as a whole. An animal "that maintains [. . .] production in the face of decreasing [environmental support] is deemed to be robust, but [it] must be diverting nutrients away from other life functions. [. . .] When robustness can be understood as the ability to cope with environmental

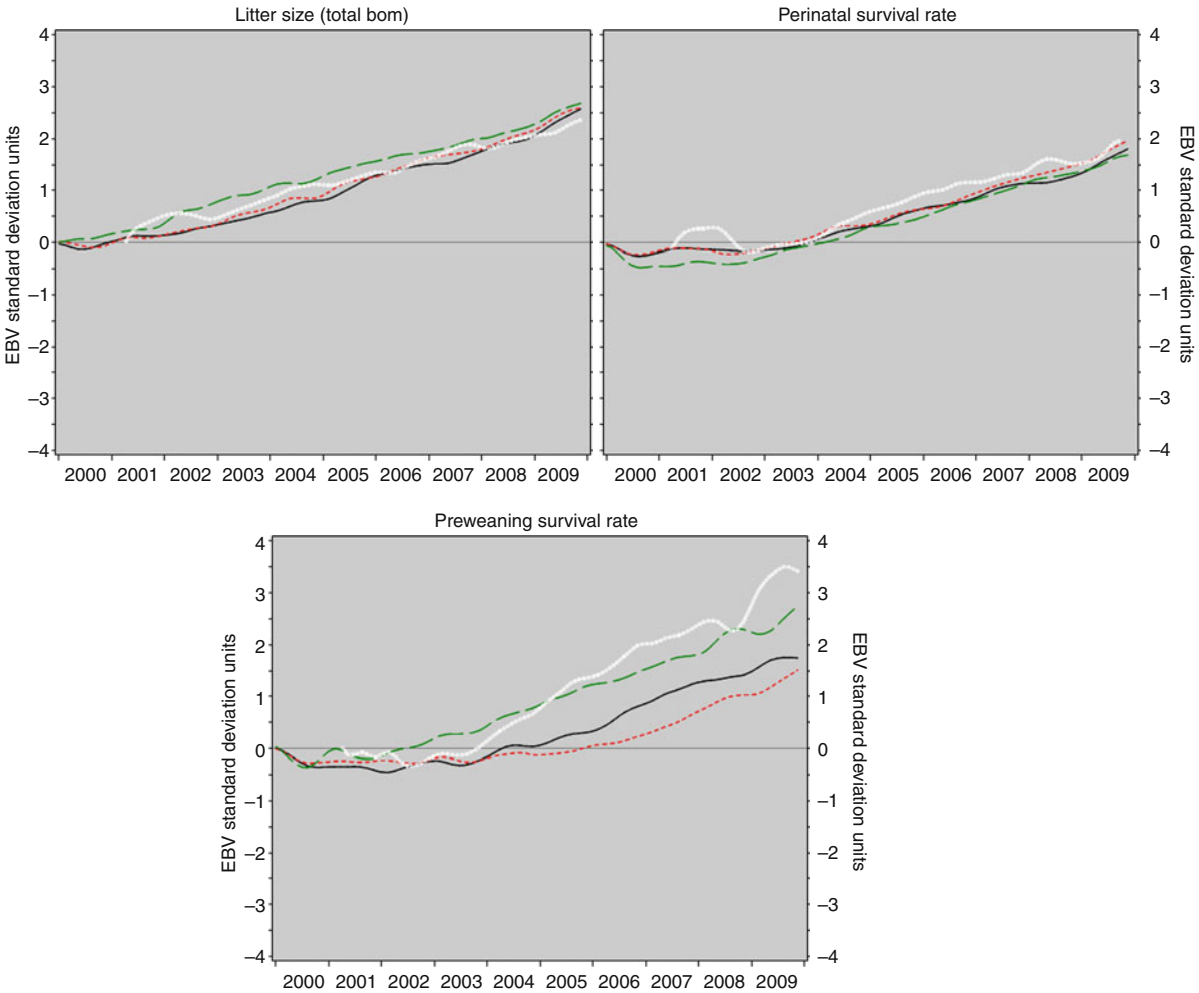

Pig Breeding for Increased Sustainability. Figure 11
Simultaneous genetic trends of litter size, perinatal survival rate, and preweaning survival rate in four pig damlines (same formatting as in Fig. 9)

challenges [. . .] an animal that maintains milk production by suppressing its immune function is clearly less robust than an animal that maintains milk production by reducing growth rate" [134]. Which means that (1) it becomes interesting how the environmental sensitivity rates are correlated among traits, and (2) breeding goals must be designed and monitored with care, as argued above.

Deprivation

Intensive housing and management systems tend to compromise the expression of instinctive behavior patterns ("motivations" [135]) of the pig: foraging, rooting, and exploring in all age classes [117], and nest-building in sows [136] – because intensive housing environments do not provide the required space or substrates. Something similar holds for deprivation of social contact in individually housed sows [137], where the "required substrate" is other pigs. For more detail see [138]. This results in frustration, leading to apparently irrationally redirected behavioral outlet functions: stereotypies or apathy occur when the animal is severely or chronically frustrated [139–141]. Mason and Bateson [142] describe this situation as "internal

states of deprivation [...] leading to sustained high motivations that the [animal] cannot reduce: it cannot perform the activity that would result in negative feedback." Another outlet function is wide-sense agonistic behavior such as tail biting [143, 144]; see the section on "Harmful Social Behavior."

In sentient species, such frustration leads to suffering. A sentient animal has been described [145] as an animal that has the capacity to suffer when it learns that it is unable to cope with stress: "it may fail to cope, either because the stress is too [intense], or because [the animal] is constrained in such a way that it is prevented from doing what it feels necessary to relieve the stress." This leads to anxiety or depression. Figure 12 illustrates the interdependence of the various components.

Held et al. [138] write: "pigs used today for pork production seem to have retained many of the faculties of their wild ancestors, and may therefore be behaviourally, cognitively and emotionally at odds with the husbanded environment [...]. Understanding the cognitive abilities, behavioural priorities and emotions of commercial pigs therefore lies at the very heart of improving their welfare." Jensen [146] describes those "faculties of the wild ancestors" as "subtle [behavioural] differences between domestic and wild animals [...] attributed to modified stimulus thresholds, causing some behaviour patterns to become more common and others to be rarer during domestication." Such changes in pig behavior are described in detail in [147, 148].

One of the options for resolving such cognitive and emotional conflicts in an intensive environment would be to further reduce those faculties of the wild boar, further modifying those stimulus thresholds and simplifying what the animal feels necessary to relieve its stress. Kruska [149] sees changes in behavior and brain size as "adaptations to the special ecological niche of domestication." "Modern housing systems [have a] short history compared to the history of the pig as a domestic animal, and it is likely that adaptation has not kept pace with the intensification of pig

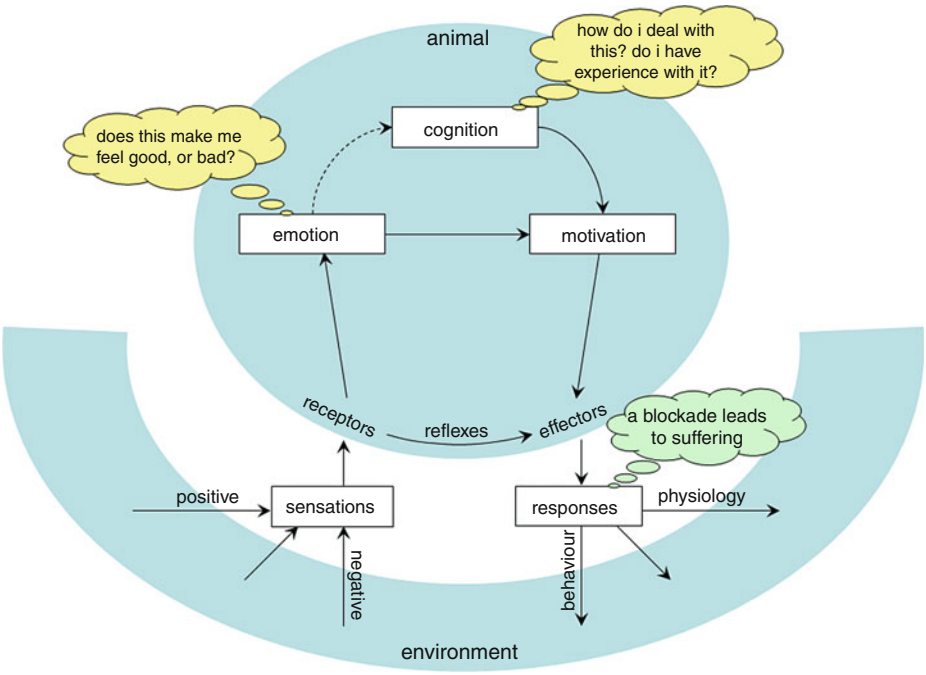

Pig Breeding for Increased Sustainability. Figure 12
Relationships between emotional, cognitive, and motivational information processing in sentient animals (Modified from [145] and [139])

husbandry" [150]; also, of course, because most housing systems were not designed to match behavioral needs.

Neuroendocrinology The neuroendocrinological aspects of *coping with stress* (as above) are studied in relation to human conditions such as mental depression [151]. This is a novel area for animal breeding, with legible summaries of the state of the art from [139, 152–154]. Chronic stress affects the hypothalamus-pituitary-adrenal (HPA) axis; it can cause a persistent overproduction of corticosteroids, which can disturb neurotransmitter systems by causing a chronic downregulation and/or an imbalanced activation of the various types of corticosteroid receptors in the brain. Probably independent of the HPA axis (but interacting with its corticosteroids) is the mediation of stress-induced stereotypic behavior by the mesolimbic pathway. Figure 13 presents a simplified model of these systems.

The sympathetic nervous system also influences corticosteroid production, and its interaction with the HPA axis leads to *active* versus *passive* coping strategies. These terms represent the extremes of a continuous distribution of animal-intrinsic behavioral flexibility. This has been described [154–157] as follows: active copers rely on stable conditions, show poor adaptation to changing conditions, and attempt to deal with any challenge through routines and behavior patterns that were successful previously, trying to remove the stressor or move themselves away from it. Passive copers show higher cognitive performance, thrive better in changing conditions, and face challenges by modifying their behavior to deal with a new stressor in its own way, aiming at reduction of the emotional impact of the stress.

This approach has been criticized as an attempt to fit a multidimensional system (reactivity to external factors) into a single (coping) dimension. Ramos and Mormède [158] mention three such dimensions (activity, emotionality, and aggressiveness), and present studies in rodents that quantify these through Principal Components Analysis and similar techniques. Obviously, control of the system through animal breeding would benefit from a detailed focus, so that the various dimensions can be brought under control independently from each other.

These traits are heritable (both coping strategies have natural selective advantages), and rodent populations have been successfully selected into either direction, using various selection criteria [159–161]. Veenema [154] found a higher stress susceptibility in passively coping than in actively coping mice. Her surmise is that this is due to differences in (1) perception of the stressor during acute stress, and (2) coping or habituation during chronic or repeated stress. Under changing conditions, passively coping mice may perform better in terms of dealing with the stressor. But exposure to chronic psychosocial stressors (i.e., living together with a dominant aggressive penmate) induced long-lasting increased activity of the HPA system in Veenema's passively coping animals, which may cause mood disorders like anxiety and depression.

Karman [153] measured the effects of chronic stress (caused by 5 months of individual housing) in gilts that had previously been scored for coping strategy. She characterizes the two strategies in terms of differences in the regulation by the hypothalamus of the pituitary's ACTH production: via CRH in passive copers, and via vasopressin in active copers. In both cases, ACTH levels and corticosteroid production are increased – which comes back to the disturbed neurotransmitter systems of above. Karman concludes that "individual housing is detrimental for the welfare of pigs, independent of coping strategy. Selection of coping strategy [...] will therefore not benefit the welfare of the animals."

If Karman's findings hold, the generic effects of chronic stress in pigs will not be resolved by breeding for an active coping strategy, which would seem to be the obvious approach with Veenema's [154] mice.

This would shift the focus upstream in Fig. 13, aiming at a resolution, through animal breeding, of the effects of chronic stress on the limbic system areas (amygdala, hippocampus) that regulate the hypothalamus. De Kloet [156] makes a distinction between "(1) the core of the HPA axis with emphasis on dysregulations in the [hypothalamus] and (2) dysregulations in [...] stress inputs to the [hypothalamus] (e.g., from medial prefrontal cortex, hippocampus, amygdala, and brain stem) that are also targets for the stress hormones."

Morris [162] notices that during chronic stress "the hippocampus may become impeded in its role in 'shutting off' HPA axis stress activity. This results in increased secretion of [corticosteroids] and, in

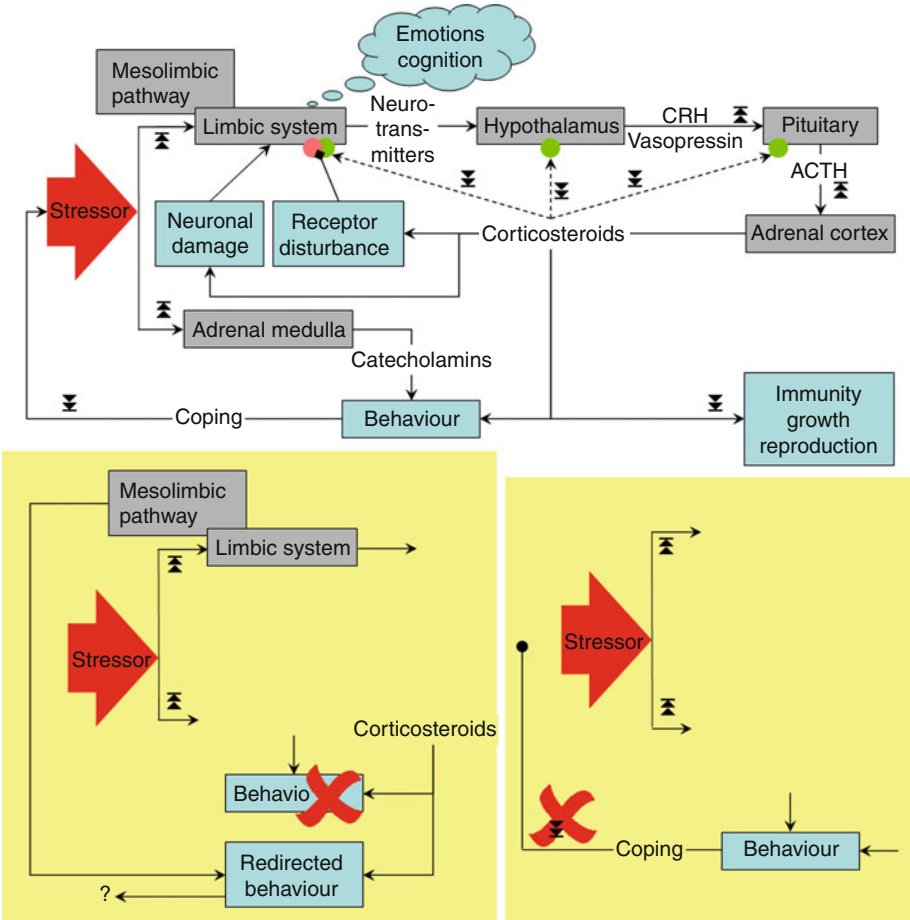

Pig Breeding for Increased Sustainability. Figure 13
A simplified model of the neuroendocrine aspects of unsuccessful coping with stress in mammals. *Top*: the full system with its negative-feedback loops that keep the levels of circulating corticosteroids under control. The flow starts with the occurrence of a stressor (*red arrow*). The ⏭ symbol pointing up or down represents upregulation or downregulation, respectively, of the downstream activity. Green and pink circles represent different types of corticosteroid receptors; in the limbic system, these can be disturbed by persistently high corticosteroid levels, obstructing the negative feedback loop. The stressor is neutralized by coping behavior, which terminates its triggering of corticosteroid and catecholamine production. *Bottom*: two options for obstruction of this system. *Left*: an external factor prevents the expression of the required behavior, which leads to redirected behavior (e.g., stereotypies, agonistic behavior) as an outlet function with uncertain consequences. *Right*: an external factor keeps the stressor in place in spite of coping behavior, effectively blocking the stressor's downregulation that would normally follow from coping. In both cases, the stressor is not neutralized and the levels of circulating corticosteroids are out of control; this can result in a reduction of immunity, growth, and reproduction traits, and in damage to the limbic system which brings the system further out of control

a positive feedback cycle with negative consequences, ends up in damaging the hippocampus itself, thereby further reducing [its] ability to regulate the HPA axis. [...] This brain structure is both [i] centrally involved in the neural reaction to aspects of prolonged stress and [ii] itself a target of chronic stress." Loijens [152] reports such findings in tethered sows.

The significant issue here is that the limbic system also regulates emotional and cognitive functions (Fig. 13) – which provides the conceptual connection

to Fig. 12. "Sustained activation of [corticosteroid] receptors in the hippocampus [...] may lead to an impairment of declarative (rule-) learning during high levels of chronic stress. [...] The amygdala [...] has been demonstrated to [influence] hippocampal plasticity and hence may be the central link between stress and declarative learning [...]. In farm animals this type of learning occurs during adaptation to [housing] facilities, milking regimes etc." [139].

Selection Objectives "An array of stress-responsive genes has been identified," including genes "related to structural differences in hippocampus of [passively and actively coping] mice. [...] These altered gene patterns can be postulated as markers for *predisposition* for stress-related disorders" [156]. Such gene patterns are being studied in pigs as well, exploring changes of gene expression in the hippocampus, amygdala, and/or frontal cortex due to early weaning and/or social isolation of piglets [163, 164].

"The evidence for a significant genetic contribution to stress responsiveness in vertebrates is overwhelming. [...] Given the complexity of the issues, there is no firm consensus as to whether modification of stress responsiveness can benefit an animal within an intensive rearing environment" [165].

In line with this, the main conclusion from the section on "Deprivation" would be that straightforward selection against specific behavior patterns such as stereotypies and apathy (which would not be difficult to record in intensively housed sows) may be counterproductive. In terms of Fig. 13, such selection might just remove the "redirected behavior" pathway that serves as an outlet for frustrated motivations, and as such forms the animal's final way to deal with the load of the stressor. This would create a system under stress (with its negative consequences for homeostatis and production) without any security valve. D'Eath et al. [166] refer to such animals as *stoics* "because outward signs of suffering appear to be reduced" while the "root cause of the stereotypy" is not changed.

A second conclusion is that the active and passive coping strategies do not seem to offer a useful criterion for pig breeding.

It seems much more useful to look for the abovementioned "adaptations to the special ecological niche of domestication" [149] in terms of changes of the predisposition for stress-related disorders and of perception of the stressor, rather than a change of coping patterns. This would have to target the limbic system, which makes the task much more challenging.

From a very different point of view, Morris [162] quotes Sapolsky: "the body simply has not evolved the capacity or tendency to not secrete [corticosteroids] during a crisis," and adds to this "in effect, evolution has only gotten so far." Clearly, evolution could be moved on (into a more convenient direction) by a much focused targeting of the system that regulates the HPA axis, i.e., the limbic system again.

This amounts to a strategy to modify instinctive patterns so that the motivation for behavior that cannot be supported by the production system is reduced. This would "change the intensity of a behavioral response," which is equivalent to domestication [119]; antipredator responses would be an obvious example. Adaptation of behavior through selection is then effectively an extension of 9,000 years of pig domestication: a process of reducing the animal's drives for exploration, aggression, etc.

Such characteristics form the ultimate example of *hard-to-measure traits* in animal breeding. Genetic improvement will therefore logically focus on marker-assisted selection; phenotypic records will still be required in large volume for marker effect estimation, but recording can be scheduled on a project basis, and on other animals than selection candidates. As with every trait of livestock species studied up to now, very large numbers of genes are likely to be involved, which makes the candidate gene approach and its search for major genes not very promising – also because of the currently "limited basic knowledge about psychobiological dimensions underlying behavioral trait variability, and the availability of reliable and meaningful measures of these [...] free from environmental influences" [167]. The *quantomics* approach that was put forward at www.quantomics.eu seems to offer more power to bring such a system under control: it should "provide the tools to identify rapidly the causative DNA variation underpinning sustainability in livestock, and [...] exploit high-density genomic

information." Essentially, making use of large numbers of anonymous markers (as in genomic selection) to identify functional elements and their connection to the phenotype (as in QTL studies).

Dominance Aggression Another issue of intensive production systems is avoidance of dominance aggression, particularly when pigs are being mixed into new groups [168, 169] – confinement does not allow for escape from aggressors. Such behavior has significant genetic components [170], possibly but not very clearly connected to coping strategies. The main factor that would complicate selection against such behavior is the difficulty of data recording, which makes marker-assisted selection an interesting option again. QTL associated with such behavior are in the process of being discovered [171, 172].

The ethical aspects of all this are considered in the section on "Ethical Aspects."

Avoidance of Invasive Treatments

There is much societal drive to reduce painful treatments like castration and tail docking of piglets. The relevant issues are then the genetic options to reduce (1) boar taint and (2) tail biting – these form the reasons why those treatments are performed.

Boar Taint Piglet castration needs to be carried out under anesthesia in Norway and Switzerland. The German pig production sector has been recommending castration with analgesia since 2009, and aims at castration-free production on the longer term. The Dutch pig sector aims at castration-free production by 2015; leading Dutch retailers have decided to stop the sales of meat from castrated pigs starting 2011. A logical extrapolation is that by 2020 the European pig production sector will leave most of its male pigs uncastrated. While this provides progress in animal welfare (apart from aggression among entire male penmates), and an advance in gross profitability because entire males grow more efficiently than castrates [173, 174], it causes logistical and technical challenges because of boar taint.

Boar taint is an unpleasant odor of pig meat (occurring in roughly 3–10% of entire males) caused by several chemical components, most importantly androstenone (a sex hormone) and skatole (a metabolite of the gut microflora). The tissue concentrations of both components are variable, line specific, and heritable [175–177], and the genes that influence them are gradually being identified [178, 179] so that it is feasible to select pigs for reduced boar taint levels. Such genetic improvement is a crucial element of the sustainability of sector-wide non-castration: although it is largely uncertain how consumers will react to increased amounts of meat from entire male pigs appearing on the market, boar taint incidence will have to be reduced to manageably low levels to avoid situations where consumer demand for pig meat collapses, or where the processing industry shifts to imported meat from castrates.

Because androstenone is a sex hormone, attempts to reduce its circulating levels may affect similar hormones such as testosterone and the estrogens, with a negative impact on male and female fertility, respectively. This must be counteracted through "balanced breeding" [177], i.e., by simultaneous selection for the relevant fertility traits.

Harmful Social Behavior SVC [117] write about "tail injury caused by biting. Although the motivation of the pig which bites the tail is likely to be investigation, manipulation and perhaps feeding rather than aggression, the consequence for the bitten pig is serious. Bitten tails may attract further biting so that the injury is to the abdomen at the base of the tail after the tail itself has been bitten off." Tail biting is a form of "harmful social behaviour" [180] (HSB; "social" because it involves other pigs) in intensive animal production [181, 182], possibly a form of redirected outlet behavior (as in the section on "Deprivation") in the absence of rooting substrate such as straw [183]. Other forms are vulva biting in group-housed sows [184], piglet savaging by sows [185], and feather pecking in poultry. Feather pecking and subsequent cannibalistic actions form a major problem in poultry production [186]. In practice, this vice is prevented by beak trimming of the potential actor, whereas tail biting in pigs is prevented by tail docking of the potential recipient; both at a very young age. Both treatments compromise animal welfare, but not performing them may do so too – a circular lose–lose situation to be broken.

Su et al. [187] selected laying hens for increased or reduced feather pecking incidence. Figure 14 shows the genetic trends in their first five generations. The selection trait was the number of pecking bouts delivered by a bird during 3 h, recorded by examining video footage of 250 birds each generation. Behavioral traits are notoriously time intensive to record and therefore a prime candidate for marker-assisted selection (phenotypic records will still be required in large volume for marker effect estimation, but recording can be scheduled on a project basis and on other animals than selection candidates). Motivated by this, "a major dominant allele affecting the [feather pecking] behavior" was identified in the eighth generation of the high-incidence line [188]. More genes with significant associations to feather pecking were found in similar selection lines [189]. Likewise, Quilter et al. [190] report on a search for QTL associated with piglet savaging behavior in sows.

Social behavior traits involve a recipient and an actor; genetic evaluation should take both into account. Ellen et al. [191] notice that "cannibalism [...] differs from conventional breeding traits because it depends on social interactions [...]. Selection strategies [...] should consider both the direct effect of an individual on its own survival and the social effect of the individual on the survival of its group members (the so-called associative effect)."

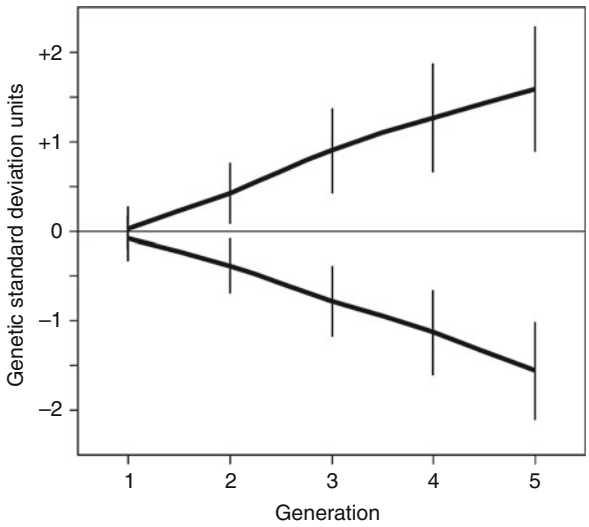

Pig Breeding for Increased Sustainability. Figure 14 Genetic trends of feather pecking incidence in divergent laying-hen selection lines (Data from [187]). The data for each line have been scaled by the within-line genetic standard deviation. Vertical bars represent one standard error each side of the mean value

In group housing, an individual's phenotype for any trait (growth rate, mortality, etc.) is influenced by its own direct breeding value for the trait and the associative breeding values of its penmates, positive or negative. Hence, if associative effects are significant for the trait, they should be part of the analysis in breeding value estimation – to effectively equip the social environment with a pedigree structure and capture it in more statistical detail. This principle has been worked out in detail for growth rate and feed intake in growing pigs [192, 193]; associative effects contributed the majority of heritable variance in these traits. Intuitively, the same would hold for mortality rates due to cannibalistic HSB.

Muir and Craig [194] discuss *group selection* in laying hens, where "hens of each sire family were housed as a group in a multiple-bird cage and selected as a group" for egg production and survival rate. These hens were housed intensively and were not subjected to beak trimming, allowing for unconstrained expression of HSB. After seven generations of selection, in group housing, the group selection line showed a 20% mortality rate at 58 weeks, compared to 54% in an unselected control line and 89% in a related commercial line (which was selected for egg production and survival rate in individual housing; Muir WM, personal communication, 2010). Plumage scores revealed significantly less HSB in the group selection line. Egg production in group housing was highest in the group selection line.

These authors conclude that this approach "is effective in improving [welfare] of layers in a relatively short period of time without sacrificing productivity. The way for commercial breeders to develop birds that do not need beak trimming is clear." A study of the endocrine and immune system traits in these lines [195] concluded that "group selection altered the chickens' physiological homeostasis which is reflected in the

line's unique coping ability with intensified domestic environments." But the physiological effects of this selection approach are cell-specific [196].

Gunsett [197] describes an application of group selection in pig breeding. He mentions advantages in terms of profitability (improved image of intensive production, increased stocking density, reduced abattoir penalties for damaged carcasses) and animal welfare: (1) reduced incidence of damaged carcasses, i.e., of pigs injured due to HSB, (2) reduced mortality rates, and (3) more docile behavior. He also mentions practical difficulties with the implementation of the method, due to reduced selection intensity and increased rate of inbreeding. Hence the program was changed to a system where the direct and associative breeding values were estimated in an extended BLUP approach [198], which was formally worked out by Bijma [199]. Group selection is then not required anymore. These principles were applied to HSB and its resulting mortality rates in laying hens, leading to the conclusion that "including associative effects in the model will give substantially higher heritable variation than when using the conventional direct effects model [...]; prospects for reduction of mortality using the direct-associative effects model are good [...]; selection targeting both direct and associative effects is expected to substantially reduce one of the major welfare problems in egg production" [191].

The extension to tail biting in pigs is obvious: Breuer et al. [180] estimated heritabilities of tail biting in two populations (both with an actor incidence of about 3%) at 0.00 and 0.05 on the observed scale, and bravely conclude that "it would be possible to develop a selection index to reduce [...] tail-biting behavior through selective breeding" – but any statistical method that delivers substantially higher heritable variation would be very useful here.

Muir and Craig [194] conclude from their selection results that "because group selection is shown to improve well-being in multiple-bird cages, alternatives such as redesigning cage environments, or housing such as floor pens or free ranges, may not be needed." Likewise, Conington et al. [200] write "breeding animals to adapt to their environment, rather than focus on changing environments to match new genotypes (such as altering housing and cubicle design) can minimize the mismatch between them" [200]. Such statements are under debate, following the argument that it would be preferable to adapt the production system to the animal, rather than vice versa, which goes back to Faure [201]. This is in clear conflict with domestication in general, which has always attempted to adapt animals to captivity systems, sometimes by considerable force. The ethical aspects are dealt with in the next section.

Ethical Aspects

Farm animals are there to produce food that people need and want. With an increasing human population and its worldwide purchasing power, there is an equally increasing demand (what people want) for animal products. One of the options of dealing with this increasing demand is to disapprove of it, arguing that the world's carrying capacity does not allow for it [202] and that everyone (particularly in the developed world) should eat less animal products. This raises one of the many arguments in an ethical discussion: to what extent it can be justified to deny people (particularly in the developing world) what they clearly want.

Another (nonexclusive) option is to look for technological solutions. Without doubt, intensive systems will be the norm in worldwide pig and poultry production of the 2020s: in USA, Brazil, the Middle East, Russia, and China – where the enforcement of extraneous norms and regulations is difficult and arguably ethically unjustified. Sections "Robustness" to "Avoidance of Invasive Treatments" show that pig breeding can produce genotypes that are better equipped to fare well in such systems. This would also enhance profitability in such systems (due to lower mortality and morbidity rates), leading to increased worldwide sustainability. The pragmatic approach would then be to accept this and aim at adapting the pig species to such conditions. There is much debate about this proposition.

Hörning [203] writes: "In general it seems ethically dubious when behavioral problems of intensive production must be reduced by breeding, rather than by

changing the management-related causes. On the other hand, selection for certain behavior patterns in extensive production conditions has been recommended by some livestock ethologists: [...] maternal behavior of sows in loose housing systems [...] or against feather pecking in laying hens in alternative housing systems" (translated).

In line with this, the genetic adaptation of goats, sheep, and beef cattle to marginal (mountainous, wetland, arid) extensive conditions is much explored [204, 205]. Those conditions often lead to severe and persistent violation of the freedom from thirst, hunger, thermal discomfort, parasites, and disease – the breeding of animals that withstand such harsh low-input conditions evokes Kojak's maxim *to survive is a lousy way to live*. The justification of such adaptation strategies is commonly phrased in terms of the economical and/or cultural importance of livestock for such marginal areas (see the section on "Biodiversity," and more specifically pp. 405–419 of [5]), which entirely overlooks animal welfare.

By contrast, animal welfare problems in intensive production systems center around robustness and behavioral deprivation. Strategies to reduce deprivation problems by animal breeding (as outlined in the section on "Deprivation") meet with criticism of an ethical nature, as from Hörning [203], above.

The issue is if *genetic adaptation of livestock species to* the violation of their welfare by thirst, hunger, thermal discomfort, parasites, and disease in extensive conditions (for economic and cultural reasons) would be ethically justified, whereas genetic adaptation to behavioral deprivation in intensive systems (for economic reasons) would be wrong. If it is justified to select poultry against feather pecking in alternative housing systems, the question is valid why such selection in battery cages would be wrong.

There are two elements here: (1) the production system as such and (2) the process of adapting animal species to it through artificial selection. These are difficult to separate, because the argumentation is partly circular.

"Since biology appears to impose few limitations on what is possible, changing the animal to suit the environment raises the question of the ethical acceptability of the environment" [166]. The underlying notion here is that the environment may be intrinsically wrong. Nevertheless, *successful* adaptation of an animal species to any production system would make that system acceptable from the point of view of animal welfare – for that particular species, in that particular system. For anyone who finds such systems unacceptable a priori, such adaptation is therefore undesirable: the circular argument appears here. A housing system that is deemed unacceptable a priori, without taking animal welfare into account, can only make sense from a human perspective.

Artificial Selection Domestication through artificial selection is a human activity, and therefore subject to ethics. By contrast, natural selection just happens.

Natural selection has adapted species to previously hostile conditions: freezing (Antarctic icefish, *Dissostichus mawsoni*), molten sulfur (western Pacific tonguefish, *Symphurus thermophilus)*, cobra venom (mongoose, *Herpestes ichneumon*), high CO_2 and low oxygen levels (naked molerat, *Heterocephalus glaber*), compression (sperm whale, *Physeter macrocephalus*), drought (Arabian camel, *Camelus dromedarius*) and crowding (Mexican free-tailed bat, *Tadarida brasiliensis*), among many others. Natural selection is also adapting *Sus scrofa domesticus* to intensive housing conditions – this is happening now, but so slowly that it is very difficult to notice. Artificial selection can do the same, much faster.

Like natural selection, domestication used to be a slow process – its resulting changes were hardly noticeable with a normal human time horizon. These changes have accelerated considerably since the 1980s, to the extent that they are now measurable within, say, a decade (as in Figs. 9–11) – and many people feel uncomfortable with this. Despite education and popularization of science, the notion of evolution (i.e., genetic change) as a process that is actually taking place today is not widely appreciated. Judeo-Christian

culture regards species as fixed entities, which makes people resist a noticeable change of a species' instinctive repertoire because it is experienced as "unnatural" (which is exactly what it is: domestication, like every other aspect of civilization, is a deliberate move away from nature). This resistance is toward genetic change of the pig *as we know it*. Nine thousand years of domestication have reduced the cephalization ratio (brain size as a proportion of body size) of the domestic pig by 30–40% as compared to the wild boar, the same as the dog-wolf comparison [149, 206]; significantly, the limbic system is most affected, see the section on "Selection Objectives." There is no reason to think that this process has stopped – nor will any dog owner argue that the current situation is wrong. What many people resist is to notice such a process of change actually taking place, if it would be accelerated by more effective artificial selection procedures as in Belyaev's famous fox selection lines [207]. The pig *as we know it* represents one particular stage of an evolutionary continuum, much of which lies in the future. Because this stage is familiar, now, it is experienced as the "natural" one – which it is not: by definition there is no such thing as a natural domestic animal. Accordingly, FAWC [120] stress the distinction between "natural" and "normal" behavior in farm animals.

A common argument is that such further adaptations to the niche of domestication would reduce the animal to a means to an agricultural end, to a commodity – which "embodies an excessively instrumental view on living creatures" [208]; they would violate the animal's *integrity*, "making it in some way less complete than it was previously" [181].

Integrity "Would it be right to produce [...] a pig unable to feel pain and unresponsive to other pigs? [...] such a pig would not be able to suffer, and its use might lead to significant productivity gains. Someone arguing that [this] would be wrong, would not be able to argue thus on the grounds of animal suffering" [120]. Rather, such argumentation is typically phrased in terms of *integrity*. It is useful to distinguish between two integration levels here: the individual animal, and the species as such.

One view is that violation of an individual animal's integrity is wrong; this is about production systems that keep animals in persistent pain, frustration, or fear – and [209] about breeding that predisposes animals to such conditions.

Quite another view is that it is wrong to breed animals that experience less pain, frustration, or fear in such production systems [210]. This is about species integrity: although the individual pig's integrity is less violated, it would be *less of a pig*, which sounds uncomfortable. Conversely, it can be argued that such a pig would be *less of a wild boar* (*Sus scrofa scrofa*) and therefore *more of a pig* (*Sus scrofa domesticus*) on the evolutionary continuum mentioned above. Importantly, the argument is not about animal welfare but about human values.

Appleby and Sandøe [211] analyze the various schools of philosophical thought on this issue "so that scientists may be more aware of the strengths and weaknesses of their own ideas about animal welfare." Thompson [212] gives an overview of the same; one approach holds that it is important for animals to express their instinctive behavior motivations (see the section on "Deprivation"), as far as "they actually have these [...], but whether or not a given animal does or does not have these drives is immaterial. Or put differently, one cannot harm an animal by frustrating a [motivation] that it does not have. Because this view revolves around the [motivations] that individual animals actually have, it does not see anything problematic about producing animals that have different motivations." This goes back to Rollin [213].

An opposing view is that such animals (1) "can be said to have been harmed, even if there is no corresponding adverse affect in terms of animal bodies or animal minds"; this (2) "would regard the use of genetic strategies to address welfare problems as morally problematic" [212]. Gavrell Ortiz [214] disagrees with point (1) but defends point (2) on the grounds of violated animal *dignity*, "even if the modification would improve the animal's welfare."

All this reduces animal welfare to "a subset of human welfare, the animals' preferences and [welfare] having relevance only to the extent that they are important to *us*" [215]. This was extended by Würbel [216]: "it is [...] important to distinguish between our intention to protect animals (which may be partly selfish) and true animal protection. Animal protection is *ethically* justified by our own human values. What animals need for their protection, however, needs to be justified *biologically* by values that apply to the animals. Only by acknowledging this distinction will we arrive at an ethical and legal framework that satisfies our ethical claims as well as doing justice to the animals" (our emphasis).

The conclusion from this section on "Animal Welfare" is simple and uncomfortable. Intensive pig production systems will expand considerably, particularly in the developing world. Adapting the species to such conditions is technically challenging but feasible; it will improve animal welfare. Argumentation against this serves human moral values, and not animal welfare.

Future Directions

To repeat from the end of the Introduction: *Sustainability will always be a matter of more or less: it can never be an absolute goal.* This can now be made more concrete in terms of conflicting concerns about the various targets of sustainable production (people, pigs, planet, profit), as follows.

De Boer and Cornelissen [217] evaluated three laying-hen housing systems for the sustainability indicators economic performance, ammonia emission, energy use, animal welfare, farmer welfare, and egg quality. These authors notice conflicts such as "improvement of farmer welfare is difficult to achieve in animal-friendly [systems], because unfavorable thoracic dust concentrations [...] are a direct result of the presence of litter." With equal weighting to each indicator, the battery cage ranked considerably better for overall sustainability than deep-litter and aviary systems.

Likewise, three scenarios for enhanced sustainability of pig production were studied [218, 219] focusing on (1) animal welfare, (2) pollution, or (3) product quality and safety. Among the reported conflicts are a higher contribution to acidification, a higher greenhouse gas emission, and higher production costs in (1) the animal welfare scenario than in (2) the pollution scenario. "Ranking between the different aspects of sustainability may [...] differ between different people and over time. How to evaluate [them] is mainly a political question, and legislation and political decisions can easily change the ranking of the scenarios." This is about production systems, differing in animal management, housing, and feed production strategies. The breeding goals specified in that study were not dramatically different among the scenarios: (1) lean tissue growth rate (LTGR), feed intake, mothering ability, and longevity; (2) LTGR and feed efficiency; and (3) LTGR and meat quality – sets that occur alongside each other in any transnational breeding program, see Figs. 9–11 in the section on "Selection for Robustness Traits," and also Fig. 5 in [107].

However, the inclusion in breeding programs of specific sustainability targets (biodiversity, pollution, animal welfare) will create conflicts that need careful prioritization, as illustrated in Fig. 15. Priorities can be based on economic approaches such as shadow prices (as illustrated for nitrogen excretion in the Pollution section), or benefit functions for animal welfare traits [220]. But the outcome must be a political compromise, and as such will change over time.

A recurring theme of this chapter is: *this technology is statistically demanding*. It follows that sustainable animal breeding equals high-tech animal breeding – just as sustainable animal production must involve precision farming [221] to overcome its inherent conflicts. Earlier breeding programs delivered at lower sustainability levels not only because of incomplete breeding goals (focusing on narrow-sense profitability) but also because the required data recording and processing methodology was not available.

Future directions will have to be set by the production sector and the society that it is part of. The commercial pig breeding sector does not have its own agenda: breeding goals are set based on what the market for breeding stock demands, and those demands are influenced by society – e.g., through legislation, or market regulation, around pollution and animal welfare. This chapter shows that the genetic technology to meet such demands is available, and can be exploited.

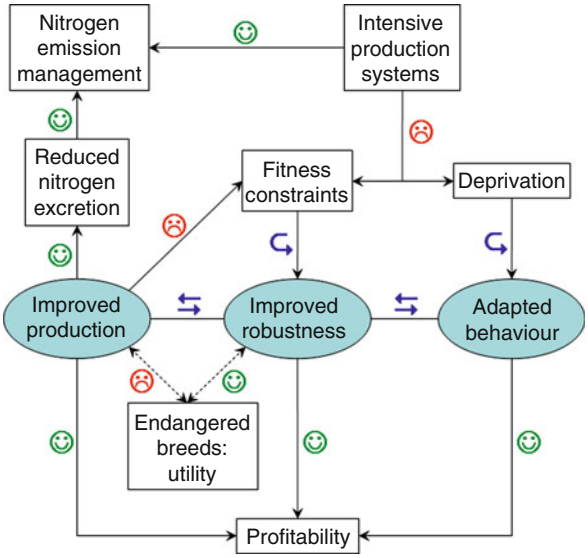

Pig Breeding for Increased Sustainability. Figure 15 Elements of pig breeding goals (blue ovals) and their relationships with sustainability issues. The symbols ☹ and ☺ indicate (un-)favorable influences on the downstream element; ↳ indicates that solution of the upstream issue requires the downstream element; ⇆ indicates that a balance must be established. Dotted arrows characterize the sustainability issue in terms of breeding goal elements

Acknowledgments

Thanks are due to Gé Backus, Andrea Doeschl-Wilson, Eildert Groeneveld, Irene Hoffmann, Robert Hoste, Bas Kemp, Cees de Lange, Herveline Lenoir, Asko Mäki-Tanila, Elżbieta Martyniuk, Dave McLaren, Marnie Mellencamp, Patrick Morel, Bill Muir, Candido Pomar, Rainer Roehe, Lotta Rydhmer, Montse Torremorell, Simon Turner, Eldon Wilson, and Hanno Würbel.

Bibliography

1. Gamborg C, Sandøe P (2003) Breeding and biotechnology in farm animals: ethical issues. In: Levinson R, Reiss MJ (eds) Key issues in bioethics: a guide for teachers. RoutledgeFalmer, London, pp 133–141
2. Gamborg C, Sandøe P (2005) Applying the notion of sustainability – dilemmas and the need for dialogue. In: Gunning J, Holm S (eds) Ethics, law and society. Asghate, Aldershot, pp 123–130
3. Elkington J (1999) Cannibals with forks – the triple bottom line of 21st century business. Capstone, Oxford
4. Knap PW, Neeteson-Van Nieuwenhoven AM (2006) Private and public roles in conservation. In: Options and strategies for the conservation of farm animal genetic resources: report of an international workshop and presented papers (CD-ROM). CGIAR Biodiversity International, Rome, pp 62–67
5. FAO (2007) In: Rischkowsky B, Pilling D (eds) The state of the world's animal genetic resources for food and agriculture. Food and Agriculture Organization, Rome. ISBN 978-92-5-105762-9
6. Rege JEO (1999b) The state of African cattle genetic resources. 1: Classification framework and identification of threatened and extinct breeds. Anim Genet Res Info 25:1–25
7. Rege JEO, Gibson JP (2003) Animal genetic resources and economic development: issues in relation to economic valuation. Ecol Econ 45:319–330
8. Tisdell C (2003) Socioeconomic causes of loss of animal genetic diversity: analysis and assessment. Ecol Econ 45: 365–376
9. Gandini GC, Oldenbroek JK (2007) Strategies for moving from conservation to utilisation. In: Oldenbroek JK (ed) Utilisation and conservation of farm animal genetic resources. Wageningen Academic Publishers, Wageningen, pp 29–54
10. Simianer H (2005) Decision making in livestock conservation. Ecol Econ 53:559–572
11. Gandini GC, Villa E (2003) Analysis of the cultural value of local livestock breeds: a methodology. J Anim Breed Genet 120:1–11
12. Ollivier L (2005) Economic relevance of animal diversity conservation. In: Rosati A, Tewolde A, Mosconi C (eds) Animal production and animal science worldwide. Wageningen Academic Publishers, Wageningen, pp 271–279
13. Hill WG, Zhang XS (2009) Maintaining genetic variation in fitness. In: Van der Werf JHJ, Graser HU, Frankham R, Gondro C (eds) Adaptation and fitness in animal populations. Springer, Berlin, pp 59–82
14. Nicholas FW (2009) Discussion. In: Van der Werf JHJ, Graser HU, Frankham R, Gondro C (eds) Adaptation and fitness in animal populations. Springer, Berlin, pp 233–234
15. Dempfle L (1990) Conservation, creation, and utilization of genetic variation. J Dairy Sci 73:2593–2600
16. Megens HJ, Crooijmans RPMA, SanCristobal M, Hui X, Li N, Groenen MAM (2008) Biodiversity of pig breeds from China and Europe estimated from pooled DNA samples: differences in microsatellite variation between two areas of domestication. Genet Sel Evol 40:103–128
17. Eding H, Bennewitz J (2007) Measuring genetic diversity in farm animals. In: Oldenbroek JK (ed) Utilisation and conservation of farm animal genetic resources. Wageningen Academic Publishers, Wageningen, pp 103–130
18. San Cristobal M, Chevalet C, Haley CS, Joosten R, Rattink AP, Harlizius B, Groenen MAM, Amigues Y, Boscher M-Y, Russell G, Law A, Davoli R, Russo V, Désautés C, Alderson L, Fimland E, Bagga M, Delgado JV, Vega-Pla JL, Martinez AM, Ramos M, Glodek P, Meyer JN, Gandini GC, Matassino D, Plastow GS, Siggens KW, Laval G, Archibald AL, Milan D, Hammond K, Cardellino R (2006a) Genetic diversity within and between

European pig breeds using microsatellite markers. Anim Genet 37:189–198
19. SanCristobal M, Chevalet C, Peleman J, Heuven H, Brugmans B, Van Schriek M, Joosten B, Rattink AP, Harlizius B, Groenen MAM, Amigues Y, Boscher MY, Russell G, Law A, Davoli R, Russo V, Dèsautés C, Alderson L, Fimland E, Bagga M, Delgado JV, Vega-Pla JL, Martinez AM, Ramos M, Glodek P, Meyer JN, Gandini G, Matassino D, Siggens K, Laval G, Archibald A, Milan D, Hammond K, Cardellino R, Haley C, Plastow G (2006b) Genetic diversity in European pigs utilizing amplified fragment length polymorphism markers. Anim Genet 37:232–238
20. Van Zeveren A, Peelman L, Van de Weghe A, Bouquet Y (1995) A genetic study of Belgian pig populations by means of seven microsatellites. J Anim Breed Genet 112:191–204
21. Sollero BP, Paiva SR, Faria DA, Guimarães EF, Castro STR, Egito AA, Albuquerque MSM, Piovezan U, Bertani GR, Da San Mariante A (2009) Genetic diversity of Brazilian pig breeds evidenced by microsatellite markers. Livest Sci 123:8–15
22. Souza CA, Ramayo Y, Megens HJ, Rodríguez MC, Loarca A, Caal E, Soto H, Melo M, Revidatti MA, De la Rosa SA, Shemereteva IN, Okumura N, Cho IC, Delgado JV, Paiva SR, Crooijmans RPMA, Schook LB, Groenen MAM, Ramos-Onsins SE, Pérez-Enciso M (2010) Porcine colonization of the Americas: a 60k SNP story. In: 9th WCGALP, Leipzig, Germany (Communication 0510)
23. Alves E, Barragán C, Fernández AI, Rodríguez C, Silió L (2006) Success rate of genetic clustering of domestic and wild pigs as a function of the number of markers. In: 8th WCGALP, Belo Horizonte, Brazil (Communication 33–24)
24. Felsenstein J (1985) Confidence limits on phylogenies: an approach using the bootstrap. Evolution 39:783–791
25. Flury C, Weigend S, Ding X, Täubert H, Simianer H (2007) Haplotype kinship for three populations of the Goettingen minipig. Genet Sel Evol 39:159–179
26. Petit RJ, El Mousadik A, Pons O (1998) Identifying populations for conservation on the basis of genetic markers. Conserv Biol 12:844–855
27. Toro MA, Mäki-Tanila A (2007) Genomics reveals domestication history and facilitates breed development. In: Oldenbroek JK (ed) Utilisation and conservation of farm animal genetic resources. Wageningen Academic Publishers, Wageningen, pp 75–102
28. Eding H, Crooijmans RPMA, Groenen MAM, Meuwissen THE (2002) Assessing the contribution of breeds to genetic diversity in conservation schemes. Genet Sel Evol 34:613–633
29. Fabuel E, Barragán C, Silió L, Rodríguez MC, Toro MA (2004) Analysis of genetic diversity and conservation priorities in Iberian pigs based on microsatellite markers. Heredity 93:104–113
30. Bennewitz J, Meuwissen THE (2005) A novel method for the estimation of the relative importance of breeds in order to conserve the total genetic variance. Genet Sel Evol 37:315–337
31. Ollivier L, Foulley JL (2005) Aggregate diversity: new approach combining within- and between-breed genetic diversity. Livest Prod Sci 95:247–254
32. Toro MA, Fernández J, Caballero A (2009) Molecular characterization of breeds and its use in conservation. Livest Sci 120:174–195
33. Ciobanu DC, Day AE, Nagy A, Wales R, Rothschild MF, Plastow GS (2001) Genetic variation in two conserved local Romanian pig breeds using type 1 DNA markers. Genet Sel Evol 33: 417–432
34. Iannuccelli N, Riquet J, Mercat MJ, Legros H, SanCristobal M, Lacoste A, Bidanel JP, Milan D (2006) Diversité génétique des populations porcines françaises dans les régions chromosomiques soumises à la sélection: projet DIVQTL. Les Actes du BRG 6:111–128
35. Bonin A, Nicole F, Pompanon F, Miaud C, Taberlet P (2007) Population adaptive index: a new method to help measure intraspecific genetic diversity and prioritize populations for conservation. Conserv Biol 21:697–708
36. Falconer DS, Mackay TFC (1996) Introduction to quantitative genetics, 4th edn. Longman, Harlow
37. Draganescu C, Ghita E, Nagy A (2008) Note on the genetic history of the Romanian Saddleback (Bazna) pig breed conservation nucleus. Archiva Zootechnica 11:65–69
38. Nomura T, Ieiri S, Yamashita J (2008) Effective size and inbreeding in closed breeding herds of pig. 1: Pedigree analysis. Jpn J Swine Sci 45:149–155
39. Dikić M, Salajpal K, Karolyi D (2009) Biological characteristics of Turopolje pig breed as factors in renewing and preservation of population. DAGENE annual meeting, Zagreb, Croatia, http://www.dagene.eu/annual zagreb 2009/Dikic et al_DAGENE 2009.pdf
40. Welsh CS, Blackburn HD, Schwab C (2009) Population status of major US swine breeds. J Anim Sci 87(Suppl 3):160
41. Tholen E, Staack J, Müller P, Ingwersen J (2010) Degree of endangerment of different German pig herdbook populations. In: 9th WCGALP, Leipzig, Germany (Communication 0264)
42. Uimari P, Sevón-Aimonen ML, Strandén I (2010) Pedigree analysis of Finnish Landrace and Yorkshire pig populations. In: 9th WCGALP, Leipzig, Germany (Communication 0090)
43. Villanueva B, Sawalha RM, Roughsedge T, Rius-Vilarrasa E, Woolliams JA (2010) Development of a genetic indicator of biodiversity for farm animals. Livest Sci 129:200–207
44. Wang J (2005) Estimation of effective population sizes from data on genetic markers. Philos Trans R Soc Lond B Biol Sci 360:1395–1409
45. Álvarez I, Royo LJ, Gutiérrez JP, Fernández I, Arranz JJ, Goyache F (2008) Relationship between genealogical and microsatellite information characterizing losses of genetic

variability: empirical evidence from the rare Xalda sheep breed. Livest Sci 115:80–88
46. Tixier-Boichard M, Ayalew W, Jianlin H (2008) Inventory, characterization and monitoring. Anim Genet Res Info 42:29–44, Food and Agriculture Organization, Roma, Italy
47. Toro MA, Rodriganez J, Silio L, Rodriguez C (2000) Genealogical analysis of a closed herd of black hairless Iberian pigs. Conserv Biol 14:1843–1851
48. Aspi J, Roininen E, Ruokonen M, Kojola I, Vilà C (2006) Genetic diversity, population structure, effective population size and demographic history of the Finnish wolf population. Mol Ecol 15:1561–1576
49. Meuwissen THE (2007) Operation of conservation schemes. In: Oldenbroek JK (ed) Utilisation and conservation of farm animal genetic resources. Wageningen Academic Publishers, Wageningen, pp 167–194
50. Ollivier L, Alderson L, Gandini GC, Foulley JL, Haley CS, Joosten R, Rattink AP, Harlizius B, Groenen MAM, Amigues Y, Boscher MY, Russell G, Law A, Davoli R, Russo V, Matassino D, Désautés C, Fimland E, Bagga M, Delgado JV, Vega-Pla JL, Martinez AM, Ramos AM, Glodek P, Meyer JN, Plastow GS, Siggens KW, Archibald AL, Milan D, SanCristobal M, Laval G, Hammond K, Cardellino R, Chevalet C (2005) An assessment of European pig diversity using molecular markers: partitioning of diversity among breeds. Conserv Genet 6:729–741
51. Simon DL, Buchenauer D (1993) Genetic diversity of European livestock breeds. EAAP publication 66, Wageningen Pers, Wageningen, Netherlands
52. Gandini GC, Ollivier L, Danell B, Distl O, Georgoudis A, Groeneveld E, Martyniuk E, Van Arendonk JAM, Woolliams JA (2004) Criteria to assess the degree of endangerment of livestock breeds in Europe. Livest Prod Sci 91:173–182
53. Lynch M, Conery J, Burger R (1995) Mutation accumulation and the extinction of small populations. Am Nat 146:489–518
54. Theodorou K, Couvet D (2006) On the expected relationship between inbreeding, fitness, and extinction. Genet Sel Evol 38:371–387
55. Bennewitz J, Meuwissen THE (2005) Estimation of extinction probabilities of five German cattle breeds by population viability analysis. J Dairy Sci 88:2949–2961
56. Tenesa A, Navarro P, Hayes BJ, Duffy DL, Clarke GM, Goddard ME, Visscher PM (2007) Recent human effective population size estimated from linkage disequilibrium. Genome Res 17(4):520–526
57. Hayes BJ, Visscher PM, McPartlan HC, Goddard ME (2003) Novel multilocus measure of linkage disequilibrium to estimate past effective population size. Genome Res 13:635–643
58. Amaral AJ, Megens HJ, Crooijmans RPMA, Heuven HCM, Groenen MAM (2008) Linkage disequilibrium decay and haplotype block structure in the pig. Genetics 179:569–579
59. Du FX, Clutter AC, Lohuis MM (2007) Characterizing linkage disequilibrium in pig populations. Int J Biol Sci 3:166–178
60. Harmegnies N, Farnir F, Davin F, Buys N, Georges M, Coppieters W (2006) Measuring the extent of linkage disequilibrium in commercial pig populations. Anim Genet 37:225–231
61. England PR, Cornuet JM, Berthier P, Tallmon DA, Luikart G (2006) Estimating effective population size from linkage disequilibrium: severe bias in small samples. Conserv Genet 7:303–308
62. Waples RS (2006) A bias correction for estimates of effective population size based on linkage disequilibrium at unlinked gene loci. Conserv Genet 7:167–184
63. Schwartz MK, Tallmon DA, Luikart G (1998) Review of DNA-based census and effective population size estimators. Anim Conserv 1:293–299
64. Wang J (2009) A new method for estimating effective population sizes from a single sample of multilocus genotypes. Mol Ecol 18:2148–2164
65. Meuwissen THE, Goddard ME (2007) Multipoint identity-by-descent prediction using dense markers to map quantitative trait loci and estimate effective population size. Genetics 176:2551–2560
66. Vitalis R, Couvet D (2001) Estimation of effective population size and migration rate from one- and two-locus identity measures. Genetics 157:911–925
67. Abdallah JM, SanCristobal M, Chevalet C (2006) Estimation of effective size and migration rates in twelve European pig populations using non equilibrium model. In: 8th WCGALP, Belo Horizonte, Brazil (Communication 33–19)
68. Baas TJ, Goodwin RN, Christian LL, Johnson RK, Robison OW, Mabry JW, Clark K, Tokach M, Henry S, Berger PJ (2003) Design and standards for genetic evaluation of swine seedstock populations. J Anim Sci 81:2409–2418
69. Moeller SJ, Goodwin RN, Johnson RK, Mabry JW, Baas TJ, Robison OW (2004) The National Pork Producers Council maternal line national genetic evaluation program: a comparison of six maternal genetic lines for female productivity measures over four parities. J Anim Sci 82:41–53
70. Gibson JP, Ayalew W, Hanotte O (2007) Measures of diversity as inputs for decisions in conservation of livestock genetic resources. In: Jarvis DI, Padoch C, Cooper HD (eds) Managing biodiversity in agricultural ecosystems. Columbia University Press, New York, pp 117–140. ISBN 978-0231136488
71. Nichol ST, Arikawa J, Kawaoka Y (2000) Emerging viral diseases. Proc Natl Acad Sci USA 97:12411–12412
72. Pybus OG, Rambaut A (2009) Evolutionary analysis of the dynamics of viral infectious disease. Nat Rev Genet 10:540–550
73. Covey S, Merrill AR, Merrill RR (1994) First things first. Simon and Schuster, New York. ISBN 0-684-80203-1
74. Mendelsohn R (2003) The challenge of conserving indigenous domesticated animals. Ecol Econ 45:501–510
75. Ollivier L, Foulley JL (2009) Managing genetic diversity, fitness and adaptation. In: Van der Werf JHJ, Graser HU, Frankham R,

Gondro C (eds) Adaptation and fitness in animal populations. Springer, Berlin, pp 201–228
76. Simianer H, Reist-Marti SB, Gibson J, Hanotte O, Rege JEO (2003) An approach to the optimal allocation of conservation funds to minimize loss of genetic diversity between livestock breeds. Ecol Econ 45:377–392
77. Bennewitz J, Eding H, Ruane J, Simianer H (2007) Selection of breeds for conservation. In: Oldenbroek JK (ed) Utilisation and conservation of farm animal genetic resources. Wageningen Academic Publishers, Wageningen, pp 131–146
78. Barker JSF (2001) Conservation and management of genetic diversity: a domestic animal perspective. Can J For Res 31: 588–595
79. Rege JEO (1999a) Characterisation and conservation of animal genetic resources: What is it about? In: Rege JEO (ed) Economic valuation of animal genetic resources. In: Proceedings of an FAO/ILRI workshop. International Livestock Research Institute, Nairobi, Kenya pp 22–24
80. Delanotte M (2007) Un avenir en rose pour une race qui a parfois broyé du noir. L'Union Agricole 21 December 2007. limousin.synagri.com/ca1/PJ.nsf/TECHPJPARCLEF/08102
81. Woolliams JA, Berg P, Mäki-Tanila A, Meuwissen THE, Fimland E (2005) Sustainable management of animal genetic resources. Nordic Gene Bank Farm Animals, Ås, Norway
82. Rathje TA (2000) Strategies to manage inbreeding accumulation in swine breeding company nucleus herds: some case studies. J Anim Sci 79(Suppl 1):1–8
83. Ollivier L, James JW (2004) Predicting the annual effective size of livestock populations. Genet Res 84:41–46
84. Woolliams JA (2007) Genetic contributions and inbreeding. In: Oldenbroek JK (ed) Utilisation and conservation of farm animal genetic resources. Wageningen Academic Publishers, Wageningen, pp 147–165
85. Kinghorn BP, Banks R, Gondro C, Kremer VD, Meszaros SA, Newman S, Shepherd RK, Vagg RD, Van der Werf JHJ (2009) Strategies to exploit genetic variation while maintaining diversity. In: Van der Werf JHJ, Graser HU, Frankham R, Gondro C (eds) Adaptation and fitness in animal populations. Springer, Berlin, pp 191–200
86. Kremer VD, Newman SN, Kinghorn BP, Knap PW, Wilson ER (2009) Strategic management of pig genetics. In: EAAP, Barcelona, Spain (Communication 13–25)
87. Nimbkar C, Gibson J, Okeyo M, Boettcher P, Soelkner J (2007) Sustainable use and genetic improvement. In: Report of the scientific forum on animal genetic resources held during the international technical conference on animal genetic resources for food and agriculture, Interlaken, Switzerland. Food and Agriculture Organization, Rome, Italy, pp 49–64
88. Whittemore CT (2006) Development and improvement of pigs by genetic selection. In: Kyriazakis I, Whittemore CT (eds) Whittemore's science and practice of pig production, 3rd edn. Blackwell, Oxford, pp 184–262
89. Knap PW (1990) The herdbook society/breed association. In: 4th WCGALP, Edinburgh, UK, 15:439–442
90. Steinfeld H, Gerber P, Wassenaar T, Castel V, Rosales M, De Haan C (2006) Livestock's long shadow: environmental issues and options. Food and Agriculture Organization, Rome
91. Brandjes PJ, De Wit J, Van der Meer HG, Van Keulen H (1995) Environmental impact of animal manure management. International Agricultural Centre, Wageningen
92. Dourmad JY, Sève B, Latimier P, Boisen S, Fernández J, Van der Peet-Schwering C, Jongbloed AW (1999a) Nitrogen consumption, utilisation and losses in pig production in France, the Netherlands and Denmark. Livest Prod Sci 58:261–264
93. Dourmad JY, Guingand N, Latimier P, Sève B (1999b) Nitrogen and phosphorus consumption, utilisation and losses in pig production: France. Livest Prod Sci 58:199–211
94. Bourdon D, Dourmad JY, Henry Y (1995) Réduction des rejets azotés chez les porcs en croissance par la mise en oeuvre de l'alimentation multiphase, associée a l'abaissement du taux azoté. Journées de la Recherche Porcine en France 27:269–278
95. De Lange CF, Gillis AM, Simpson GJ (2001) Influence of threonine intake on whole-body protein deposition and threonine utilization in growing pigs fed purified diets. J Anim Sci 79:3087–3095
96. Buraczewska L, Święch E, Le Bellego L (2006) Nitrogen retention and growth performance of 25 to 50 kg pigs fed diets of two protein levels and different ratios of digestible threonine to lysine. J Anim Feed Sci 15:25–36
97. Pomar C, Hauschild L, Zhang GH, Pomar J, Lovatto PA (2010) Precision feeding can significantly reduce feeding cost and nutrient excretion in growing animals. In: Sauvant D, Van Milgen J, Faverdin P, Friggens N (eds) Modelling nutrient digestion and utilisation in farm animals. Wageningen Academic Publishers, pp 327–334
98. Crocker AW, Robison OW (2002) Genetic and nutritional effects on swine excreta. J Anim Sci 80:2809–2816
99. De Verdal H, Narcy A, Le Bihan-Duval E, Chapuis H, Bastianelli D, Même N, Mignon-Grasteau S (2010) Selection for excretion traits in chicken. In: 9th WCGALP, Leipzig, Germany (Communication 0123)
100. Cassandro M, Cecchinato A, Battagin M, Penasa M (2010) Genetic parameters of methane production in Holstein Friesian cows. In: 9th WCGALP, Leipzig, Germany (Communication 0837)
101. Van der Peet-Schwering CMC, Jongbloed AW, Aarnink AJA (1999) Nitrogen and phosphorus consumption, utilisation and losses in pig production: the Netherlands. Livest Prod Sci 58:213–224
102. Jones H, Warkup C, Williams A, Audsley E (2008) The effect of genetic improvement on emissions from livestock systems. In: 59th EAAP, Vilnius, Lithuania (Contribution 05-6)

103. Knap PW (1999) Simulation of growth in pigs: evaluation of a model to relate thermoregulation to body protein and lipid content and deposition. Anim Sci 68:655–679
104. Knap PW, Rauw WM (2008) Selection for high productivity in pigs. In: Rauw WM (ed) Resource allocation theory applied to farm animal production. CABI, Wallingford, pp 288–301
105. NRC (1998) Nutrient requirements of swine, 10th revised edn. National Academy Press, Washington, DC
106. Morel PCH, Wood GR (2005) Optimisation of nutrient use to maximise profitability and minimise nitrogen excretion in pig meat production systems. Acta Horticulturae (ISHS) 674: 269–275
107. Knap PW (2009) Voluntary feed intake and pig breeding. In: Torrallardona D, Roura E (eds) Voluntary feed intake in pigs. Wageningen Academic Publishers, Wageningen, pp 11–33
108. Teizzi S (1999) External effects of agricultural production in Italy and environmental accounting. Environ Resour Econ 13:459–472
109. Hartmann M, Hediger W, Peter S (2008) Reducing nitrogen losses from agricultural systems – an integrated economic assessment. Schriften der Gesellschaft für Wirtschafts- und Sozialwissenschaften des Landbaus (Landwirtschaftsverlag, Münster, Germany) 43:335–344
110. Fontein PF, Thijssen GJ, Magnus JR, Dijk J (1994) On levies to reduce the nitrogen surplus: the case of Dutch pig farms. Environ Resour Econ 4:455–478
111. Paul CJM, Ball VE, Felthoven RG, Grube A, Nehring RF (2002) Effective costs and chemical use in United States agricultural production: using the environment as a "free" input. Am J Agr Econ 84:902–915
112. Key N, McBride W, Mosheim R (2008) Decomposition of total factor productivity change in the US hog industry. J Agr Appl Econ 40:137–149
113. Fontein PF, Thijssen GJ, Magnus JR, Dijk J (1999) Optimal taxation for the reduction of nitrogen surplus Dutch dairy farms, 1975–1989. In: Mahendrarajah S, Jakeman AJ, McAleer M (eds) Modelling change in integrated economic and environmental systems. Wiley, Chichester, pp 273–296
114. Price R, Thornton S, Nelson S (2007) The social cost of carbon and the shadow price of carbon: what they are, and how to use them in economic appraisal in the UK. Department for Environment, Food and Rural Affairs, London
115. Wall E, Simm G, Moran D (2010) Developing breeding schemes to assist mitigation of greenhouse gas emissions. Animal 4:366–376
116. Hoste R, Puister L (2009) Productiekosten van varkens: een internationale vergelijking. LEI Wageningen UR, Den Haag, Netherlands. Report 2008-082
117. SVC (1997) The welfare of intensively kept pigs. Scientific Veterinary Committee of the European Commission, Brussels, Belgium. Report XXIV/B3/ScVC/0005/1997
118. Fraser D (2005) Animal welfare and the intensification of animal production. An alternative interpretation. Food and Agriculture Organization, Rome
119. Grandin T, Deesing MJ (1998) Genetics and behavior during handling, restraint and herding. In: Grandin T (ed) Genetics and the behavior of domestic animals. Academic, San Diego, CA, pp 113–144
120. FAWC (2009) Farm animal welfare in Great Britain: past, present, future. Farm Animal welfare Council, London
121. Rauw WM, Kanis E, Noordhuizen-Stassen EN, Grommers FJ (1998) Undesirable side effects of selection for high production efficiency in farm animals: a review. Livest Prod Sci 56:15–33
122. Knap PW, Rauw WM (2009) Selection for high production in pigs. In: Rauw WM (ed) Resource allocation theory applied to farm animal production. CAB International, Wallingford, pp 210–229
123. Knap PW (2005) Breeding robust pigs. Aust J Exp Agric 45:763–774
124. Goddard M (2009) Fitness traits in animal breeding programs. In: Van der Werf JHJ, Graser HU, Frankham R, Gondro C (eds) Adaptation and fitness in animal populations. Springer, Berlin, pp 41–52
125. Gjedrem T (1972) A study on the definition of the aggregate genotype in a selection index. Acta Agric Scand 22:11–16
126. Knol EF, Duijvesteijn N, Leenhouwers JI, Merks JWM (2010) New phenotypes for new breeding goals in pigs. In: EAAP Heraklion, Greece (Communication 02-2)
127. Knap PW (2009a) Robustness. In: Rauw WM (ed) Resource allocation theory applied to farm animal production. CAB International, Wallingford, pp 288–301
128. Rydhmer L, Lundeheim N (2008) Breeding pigs for improved welfare. In: Faucitano L, Schaefer AL (eds) Welfare of pigs from birth to slaughter. Wageningen Academic Publishers, Wageningen, pp 243–270
129. Newman S, Wang L, Anderson J, Casey D (2010) Utilizing crossbred records to increase accuracy of breeding values in pigs. In: 9th WCGALP, Leipzig, Germany (Communication 0632)
130. Henryon M, Sørensen AC, Berg P, Nielsen B (2010) Breeding pigs for resistance to disease is difficult even with genomic selection. In: 9th WCGALP, Leipzig, Germany (Communication 0854)
131. Onteru SK, Fan B, Garrick DJ, Stalder KJ, Rothschild MF (2010) Whole-genome association analyses for sow lifetime production, reproduction and structural soundness traits using the PorcineSNP60 beadchip. In: 9th WCGALP, Leipzig, Germany (Communication 0273)
132. Hermesch S, Huisman AE, Luxford BG, Graser HU (2006) Analysis of genotype by feeding level interaction in pigs applying reaction norm models. In: 8th WCGALP, Belo Horizonte, Brazil (Contribution 06-03)

133. Knap PW, Su G (2008) Genotype by environment interaction for litter size in pigs as quantified by reaction norms analysis. Animal 2:1742–1747
134. Friggens N, Van der Waaij L (2008) Modelling of resource allocation patterns. In: Rauw WM (ed) Resource allocation theory applied to farm animal production. CAB International, Wallingford, pp 302–320
135. Hughes BO, Duncan IJH (1988) The notion of ethological 'need', models of motivation and animal welfare. Anim Behav 36:1696–1707
136. Damm BI, Lisborg L, Vestergaard KS, Vanicek J (2003) Nest-building, behavioural disturbances and heart rate in farrowing sows kept in crates and Schmid pens. Livest Prod Sci 80:175–187
137. Ruis MAW, Te Brake JHA, Engel B, Buist WG, Blokhuis HJ, Koolhaas JM (2001) Adaptation to social isolation Acute and long-term stress responses of growing gilts with different coping characteristics. Physiol Behav 73:541–551
138. Held S, Cooper JJ, Mendl MT (2009) Advances in the study of cognition, behavioural priorities and emotions. In: Marchant-Forde JN (ed) The welfare of pigs. Springer, Berlin, pp 47–94
139. Manteuffel G (2002) Central nervous regulation of the hypothalamic-pituitary-adrenal axis and its impact on fertility, immunity, metabolism and animal welfare – a review. Archive für Tierzucht 45:575–595
140. Tuyttens F (2007) Stereotypies. In: Velarde A, Geers R (eds) On farm monitoring of pig welfare. WAP, Wageningen, pp 41–46
141. Wemelsfelder F (2007) Apathy. In: Velarde A, Geers R (eds) On farm monitoring of pig welfare. WAP, Wageningen, pp 47–52
142. Mason G, Bateson M (2009) Motivation and the organization of behaviour. In: Jensen P (ed) The ethology of domestic animals, 2nd edn. CABI, Wallingford, pp 38–56
143. Beattie VE, Walker N, Sneddon IA (1995) Effects of environmental enrichment on behaviour and productivity of growing pigs. Anim Welfare 4:207–220
144. Beattie VE, O'Connell NE, Moss BW (1999) The influence of environmental enrichment on behaviour, performance and meat quality of domestic pigs. In: BSAS conference, Scarborough (Communication 192)
145. Webster J (2006) Ideals and realities: what do we owe to farm animals? In: Turner J, D'Silva J (eds) Animals, ethics and trade. Earthscan, London, pp 149–158
146. Jensen P (2009) Behaviour genetics, evolution and domestication. In: Jensen P (ed) The ethology of domestic animals, 2nd edn. CABI, Wallingford, pp 10–24
147. Jensen P (2002) Behaviour of pigs. In: Jensen P (ed) The ethology of domestic animals, 1st edn. CABI, Wallingford, pp 159–172
148. Stolba A, Wood-Gush DGM (1989) The behaviour of pigs in a semi-natural environment. Anim Prod 48:419–425
149. Kruska DCT (2005) On the evolutionary significance of encephalization in some eutherian mammals: effects of adaptive radiation, domestication, and feralization. Brain Behav Evol 65:73–108
150. Bolhuis JE (2004) Personalities in pigs: individual characteristics and coping with environmental challenges. Ph.D. thesis, Wageningen University, The Netherlands
151. Carroll BJ (2009) The neuroendocrinology of mood disorders. In: Pfaff DW, Arnold AP, Fahrbach SE, Etgen AM, Rubin RT (eds) Hormones, brain and behavior, vol 5, 2nd edn. Academic, San Diego, CA, pp 2899–2926
152. Loijens LWS (2002) Stress, endogenous opioids and stereotypies in tethered pigs. Ph.D. thesis, Wageningen University, The Netherlands
153. Karman AG (2003) Neuroendocrine adaptation to stress in pigs. Ph.D. thesis, Wageningen University, The Netherlands
154. Veenema AH (2003) Coping style and stressor susceptibility: neuroendocrine and neurochemical studies with genetically selected mouse lines. Ph.D. thesis, University of Groningen, The Netherlands
155. Benus RF, Bohus B, Koolhaas JM, Van Oortmerssen GA (1991) Heritable variation for aggression as a reflection of individual coping strategies. Cell Mol Life Sci 47:1008–1019
156. De Kloet ER (2004) Hormones and the stressed brain. Ann NY Acad Sci 1018:1–15
157. Keeling L, Jensen P (2009) Abnormal behaviour, stress and welfare. In: Jensen P (ed) The ethology of domestic animals, 2nd edn. CABI, Wallingford, pp 85–101
158. Ramos A, Mormède P (1998) Stress and emotionality: a multidimensional and genetic approach. Neurosci Biobehav Rev 22:33–57
159. Van Oortmerssen GA, Bakker TC (1981) Artificial selection for short and long attack latencies in wild Mus musculus domesticus. Behav Genet 11:115–126
160. Cools AR, Brachten R, Heeren D, Willemen A, Ellenbroek B (1990) Search after neurobiological profile of individual-specific features of Wistar rats. Brain Res Bull 24:49–69
161. Touma C, Bunck M, Stein H, Zeh R, Landgraf R (2006) Mice selected for high or low stress reactivity: a new animal model for affective disorders. Front Neuroendocrinol 27:56
162. Morris R (2006) Stress and the hippocampus. In: Andersen P (ed) The hippocampus book. Oxford University Press, New York, pp 751–768
163. Poletto R, Steibel JP, Siegford JM, Zanella AJ (2005) Effects of early weaning and social isolation on the expression of glucocorticoid and mineralocorticoid receptor and 11β-hydroxysteroid dehydrogenase 1 and 2 mRNAs in the frontal cortex and hippocampus of piglets. Brain Res 1067:36–42
164. Kanitz E, Puppe B, Tuchscherer M, Heberer M, Viergutz T, Tuchscherer A (2009) A single exposure to social isolation in domestic piglets activates behavioural arousal, neuroendocrine stress hormones, and stress-related gene expression in the brain. Physiol Behav 98:176–185
165. Pottinger TG (2000) Genetic selection to reduce stress in animals. In: Moberg GP, Mench JA (eds) The biology of animal

stress: basic principles and implications for animal welfare. CABI, Wallingford, pp 291–308
166. D'Eath RB, Conington J, Lawrence AB, Olsson IAS, Sandøe P (2010) Breeding for behavioural change in farm animals: practical, economic and ethical considerations. Anim Welfare 19(Suppl 1):17–27
167. Mormède P (2005) Molecular genetics of behaviour: research strategies and perspectives for animal production. Livest Prod Sci 93:15–21
168. Jensen P (1994) Fighting between unacquainted pigs. Effects of age and of individual reaction pattern. Appl Anim Behav Sci 41:37–52
169. Couret D, Otten W, Puppe B, Prunier A, Merlot E (2009) Behavioural, endocrine and immune responses to repeated social stress in pregnant gilts. Animal 3:118–127
170. Turner SP, Roehe R, D'Eath RB, Ison SH, Farish M, Jack MC, Lundeheim N, Rydhmer L, Lawrence AB (2009) Genetic validation of post-mixing skin injuries in pigs as an indicator of aggressiveness and the relationship with injuries under more stable social conditions. J Anim Sci 87:3076–3082
171. Murani E, D'Eath RB, Turner SP, Evans G, Foury A, Kurt E, Thölking L, Klont R, Ponsuksili S, Mormède P, Wimmers K (2009) Identification of genes involved in the genetic control of aggressiveness, stress responsiveness, pork quality and their interactions. In: EAAP Barcelona, Spain (Communication 26-7)
172. Terenina E, Bazovkina D, Rousseau S, Salin F, Monllor S, Kulikov A, Turner SP, D'Eath RB, Mormede P (2010) Association between aggressive behavior and candidate gene polymorphisms: study of the brain serotonergic system in pigs. In: 9th WCGALP, Leipzig, Germany (Communication 0864)
173. Pauly C, Ampuero S, Bee G (2010) Expected effects on carcass and pork quality when surgical castration is omitted: results of a meta-analysis study. In: EAAP Heraklion, Greece (Communication 17-6)
174. PigCas (2008) Attitudes, practices and state of the art regarding piglet castration in Europe. University of Newcastle, UK. http://w3.rennes.inra.fr/pigcas/Public reports/D3 3 Final report evaluation.pdf
175. Squires EJ (2006) Possibilities for selection against boar taint. Acta Vet Scand 48(Suppl 1):S8
176. Tajet H, Andresen Ø, Meuwissen THE (2006) Estimation of genetic parameters of boar taint; skatole and androstenone and their correlations with sexual maturation. Acta Vet Scand 48(Suppl 1):S9
177. Merks JWM, Bergsma R, Bloemhof S, Roelofs-Prins DT, Knol EF (2010) Quantitative genetic opportunities to ban castration. In: EAAP Heraklion, Greece (Communication 17-7)
178. Moe M, Lien S, Aasmundstad T, Meuwissen THE, Hansen MHS, Bendixen C, Grindflek E (2009) Association between SNPs within candidate genes and compounds related to boar taint and reproduction. BMC Genet 10:32
179. Schenkel FS, Squires EJ (2010) Reducing boar taint in pigs using SNP markers. In: 9th WCGALP, Leipzig, Germany (Communication 0674)
180. Breuer K, Sutcliffe MEM, Mercer JT, Rance KA, O'Connell NE, Sneddon IA, Edwards SA (2005) Heritability of clinical tail-biting and its relation to performance traits. Livest Prod Sci 93:87–94
181. Turner SP, Roehe R, Lawrence AB (2010) Social behaviour in pigs. In: 9th WCGALP, Leipzig, Germany (Communication 0060)
182. Taylor NR, Main DCJ, Mendl M, Edwards SA (2009) Tail-biting: a new perspective. Vet J 186(2):137–147
183. Bolhuis JE, Schouten WGP, Schrama JW, Wiegant VM (2006) Effects of rearing and housing environment on behaviour and performance of pigs with different coping characteristics. Appl Anim Behav Sci 101:68–85
184. Bracke MBM (2007) Vulva biting. In: Velarde A, Geers R (eds) On farm monitoring of pig welfare. Wageningen Academic Publishers, Wageningen, pp 65–70
185. Harris MJ, Li YZ, Gonyou HW (2003) Savaging behaviour in gilts and sows. Can J Anim Sci 83:819–821
186. Kjaer JB, Mench JA (2003) Behaviour problems associated with selection for increased production. In: Muir WM, Aggrey SE (eds) Poultry genetics, breeding and technology. CAB International, Wallingford, pp 67–82
187. Su G, Kjaer JB, Sørensen P (2005) Variance components and selection response for feather-pecking behavior in laying hens. Poult Sci 84:14–21
188. Labouriau R, Kjaer JB, Abreu GCG, Hedegaard J, Buitenhuis AJ (2009) Analysis of severe feather pecking behavior in a high feather pecking selection line. Poult Sci 88:2052–2062
189. Wysocki M, Stratz P, Preuss S, Bennewitz J (2010) Functional investigation of candidate genes affecting feather pecking in chickens. In: 9th WCGALP, Leipzig, Germany (Communication 0254)
190. Quilter CR, Gilbert CL, Oliver GL, Jafer O, Furlong RA, Blott SC, Wilson AE, Sargent CA, Mileham A, Affara NA (2008) Gene expression profiling in porcine maternal infanticide: a model for puerperal psychosis. Am J Med Genet B Neuropsychiatr Genet 147B:1126–1137
191. Ellen ED, Visscher J, Van Arendonk JAM, Bijma P (2008) Survival of laying hens: genetic parameters for direct and associative effects in three purebred layer lines. Poult Sci 87:233–239
192. Bergsma R, Kanis E, Knol EF, Bijma P (2008) The contribution of social effects to heritable variation in finishing traits of domestic pigs (Sus scrofa). Genetics 178:1559–1570
193. Chen CY, Kachman SD, Johnson RK, Newman S, Van Vleck LD (2008) Estimation of genetic parameters for average daily gain using models with competition effects. J Anim Sci 86:2525–2530
194. Muir WM, Craig JV (1998) Improving animal well-being through genetic selection. Poult Sci 77:1781–1788

195. Cheng H, Muir WM (2005) The effects of genetic selection for survivability and productivity on chicken physiological homeostasis. Worlds Poult Sci J 61:383–397
196. Cheng HW, Eicher SD, Chen Y, Singleton P, Muir WM (2001) Effect of genetic selection for group productivity and longevity on immunological and hematological parameters of chickens. Poultry Sci 80:1079–1086
197. Gunsett F (2005) Group selection in swine – a case study. National Swine Improvement Federation Conference, Ottawa, Canada. www.nsif.com/Conferences/2005/pdf/GroupSelectionSwine.pdf
198. Muir WM, Schinckel AP (2002). Incorporation of competitive effects in breeding pro-grams to improve productivity and animal well being. In: 7th WCGALP, Montpellier, France (Communication 14-07)
199. Bijma P (2009) Maintaining fitness by within breed selection. In: Van der Werf JHJ, Graser HU, Frankham R, Gondro C (eds) Adaptation and fitness in animal populations. Springer, Berlin, pp 103–124
200. Conington J, Gibbons J, Haskell MJ, Bünger L (2010) The use of breeding to improve animal welfare. In: 9th WCGALP, Leipzig, Germany (Communication 0057)
201. Faure JM (1980) To adapt the environment to the bird or the bird to the environment? In: Moss R (ed) The laying hen and its environment. Nijhoff, Den Haag, pp 19–42
202. Garnett T (2009) Livestock-related greenhouse gas emissions: impacts and options for policy makers. Environ Sci Policy 12:491–503
203. Hörning B (2008) Auswirkungen der Zucht auf das Verhalten von Nutztieren. Tierzuchtfonds für artgemässe Tierzucht, Kassel University Press, Kassel, Germany
204. Lee DHK (2006) Problems in the environmental adaptation of domestic animals. Ann NY Acad Sci 91:608–616
205. François D, Boissy A, Jacquiet P, Allain D, Bibé B, Rupp R, Moreno CR, Bodin L, Hazard D, Bouix J (2010) Genetics of adaptation traits for harsh environment in sheep. In: 9th WCGALP, Leipzig, Germany (Communication 0453)
206. Herre W, Röhrs M (1990) Haustiere – zoologisch gesehen, 2nd edn. Fischer Verlag, Stuttgart
207. Belyaev DK, Trut LN (1975) Some genetic and endocrine effects of selection for domestication in silver foxes. In: Fox MW (ed) The wild canids. Van Nostrand Reinhold, New York, pp 416–426
208. Reiss MJ, Straughan R (1996) Improving nature? The science and ethics of genetic engineering. Cambridge University Press, Cambridge
209. Webster J (2005) Ideals and realities: what do we owe to farm animals? In: From Darwin to Dawkins: the science and implications of animal sentience (DVD). Compassion in World Farming Trust, Petersfield
210. FAWC (2004) Report on the welfare implications of animal breeding and breeding technologies in commercial agriculture. Farm Animal Welfare Council, London
211. Appleby MC, Sandøe PT (2002) Philosophical debate on the nature of well-being: implications for animal welfare. Anim Welfare 11:283–294
212. Thompson PB (2010) Why using genetics to address welfare may not be a good idea. Poult Sci 89:814–821
213. Rollin BE (2003) Ethics and species integrity. Am J Bioeth 3:15–17
214. Gavrell Ortiz SE (2004) Beyond welfare: animal integrity, animal dignity, and genetic engineering. Ethics Environ 9:94–120
215. McInerney J (2004) Animal welfare, economics and policy. Defra, London. www.defra.gov.uk/evidence/economics/foodfarm/reports/documents/animalwelfare.pdf
216. Würbel H (2009) Ethology applied to animal ethics. Appl Anim Behav Sci 118:118–127
217. De Boer IJM, Cornelissen AMG (2002) A method using sustainability indicators to compare conventional and animal-friendly egg production systems. Poult Sci 81: 173–181
218. Cederberg C, Flysjö A (2004) Environmental assessment of future pig farming systems: quantifications of three scenarios from the FOOD21 synthesis work. Swedish Institute for Food and Biotechnology, Göteborg, Sweden, SIK-report 723. chaos.bibul.slu.se/sll/institutet_livsm_bioteknik/sik-rapport/SIK723/SIK723.pdf
219. Stern S, Sonesson U, Gunnarsson S, Kumm KI, Öborn I, Nybrant T (2005) Sustainable pig production in the future: development and evaluation of different scenarios. Swedish University of Agricultural Sciences, Uppsala, Sweden, Report FOOD21-5/2005. citeseerx.ist.psu.edu/viewdoc/download?doi=10.1.1.121.7315&rep=rep1&type=pdf
220. Stott AW, Gunn GJ (2008) Use of a benefit function to assess the relative investment potential of alternative farm animal disease prevention strategies. Prev Vet Med 84:179–193
221. Lokhorst C, Groot Koerkamp PWG (2009) Precision livestock farming '09. Wageningen Academic Publishers, Wageningen
222. Krüger L (1961) Geschichtliche Entwicklung der Rassen in der europäischen Tierzucht. In: Hammond J, Johansson I, Haring F (eds) Handbuch der Tierzüchtung 3-1: Rassenkunde. Parey, Hamburg, pp 25–53
223. Mason IL (1969) A world dictionary of livestock breeds, types and varieties, 4th edn. CAB International, Wallingford
224. Porter V (1993) Pigs. A handbook to the breeds of the world. Helm Information, Mountfield, Robertsbridge
225. Falkenberg H, Hammer H (2007) Zur Geschichte und Kultur der Schweinezucht und -haltung. 3: Schweinezucht und -haltung in Deutschland von 1650 bis 1900. Züchtungskunde 79:92–110
226. Huisman A, Cherel P, Van Haandel B (2010) Linkage disequilibrium and signatures of selection on chromosome 1 in a commercial sire and dam line. In: 9th WCGALP, Leipzig, Germany (Communication 0840)

Plant Breeding Under a Changing Climate

M. Fernanda Dreccer[1], David Bonnett[2], Tanguy Lafarge[3,4]
[1]CSIRO Plant Industry Cooper Laboratory, Gatton, QLD, Australia
[2]CIMMYT Int, Mexico D.F, Mexico
[3]CIRAD, UMR AGAP, Montpellier, France
[4]IRRI, CESD, Los Baños, Philippines

Article Outline

Glossary
Definition of the Subject
Introduction
Breeding in a Changing Environment
A Combination of Breeding Approaches Needed to Advance Yield in a Changing Climate
A Niche for Indirect Selection for Yield Using Physiological Parameters
Identification of Variation for Physiological Traits from Exotic Germplasm Sources
Conclusions and Future Directions
Acknowledgments
Bibliography

Glossary

Phenotyping The activity of measuring the physiological, morphological, developmental, and chemical characteristics of plants.

Trait A measurable phenotypic character or attribute, for example, plant height.

Definition of the Subject

The next generation of crops, capable of being productive in an increasingly variable and changing climate, will rely on genetic interventions based on process understanding, selection of target traits in managed environments, and high-throughput phenotyping and genotyping more than ever before. This entry discusses examples from wheat and rice, recent advances in plant breeding for high yield potential environments, and also those where abiotic stress is a major limitation to productivity. The methodologies and lessons learnt are discussed in the context of breeding in the face of climate change.

Introduction

The effects of climate change on agricultural production and food security are already taking place, creating new challenges for plant breeders to act quickly. The consequences of climate change on agricultural systems across the globe will be heterogeneous [35]. The projections for 2050 indicate that the increase in temperature (1–3°C) and CO_2 together with rainfall changes may benefit crops in the mid- to high latitudes, as temperatures will be closer to optimal for growth and the growing season longer. Over the same period, a decline in agricultural productivity is projected for low-latitude agricultural systems due to detrimental thermal conditions and more frequent extreme weather–related events. In the longer term, if the effects of climate change are not counteracted, productivity could decline both in low and mid- and high latitudes, primarily due to detrimental impacts of high temperatures and water stress [35, 66]. Rising temperatures will lower production by limiting the length of the growing season, exerting direct negative effects on resource capture and processes underpinning growth and yield. Another consequence of rising global temperatures over the next few decades is likely to be the increase in evaporation and acceleration of the global hydrological cycle, which could potentially dry subtropical areas and increase precipitation at higher latitudes. Ongoing challenges to food security will result from these changes, as most developing countries are situated at low latitudes in regions that are already warm and semi-arid [66]. To illustrate this point, two thirds of the undernourished people in the world live in just seven countries (Bangladesh, China, the Democratic Republic of the Congo, Ethiopia, India, Indonesia, and Pakistan) and over 40% live in China and India alone [23].

While general trends are described above, changes can already be observed. In Australia, average temperatures have increased 0.9°C since 1950, with significant regional variation, while the frequency of hot days and nights has increased and that of cold days and nights has declined (www.climatechangeinaustralia.com.au). In parallel, since 1950, most of Eastern and Western Australia has experienced substantial rainfall decline,

while North-West Australia has become wetter. In this context, new crops and crop varieties represent a technical adaptation with the potential to be instrumental in at least reducing climate-related vulnerability at the farm level [33]. For Australia's wheat crops, it has been estimated that, in the absence of adaptive measures, a 1.5–2°C increase in temperature would cancel out the grain yield increase derived from a CO_2 doubling, assuming no change in varietal adaptation ([33] and references therein).

It is important to consider that plant breeding takes time. The objective of a plant breeding program is to create new genetic variation and select gene combinations to create genotypes with superior performance in the target population of environments (TPE) [16]. Combining a range of methods, from traditional plant breeding to molecular tools, it is estimated that it takes 7–12 years to release a wheat cultivar (David Bonnett, pers. comm.) and 5–10 years to release a rice cultivar [9]. Increased climate variability in terms of rainfall patterns and the trends in the evolution of major weather variables such as temperature will lead to longer-term changes in the TPE. Under increased weather variability, a higher genotype x environment interaction (GEI) is expected. An increase in GEI, observed through altered genotypic rankings, makes it harder for breeders to make sustained genetic gains, as already documented for drought [65]. The paradox is that at a time when farmers' needs for new varieties as an adaptation tool intensify, breeding progress may become slower.

In this context, three of the main challenges plant breeding faces in relation to adaptation to climate change are (1) identifying the new target population of environments (TPE), (2) translating this knowledge into practical selection methods to uncover new genetic variation, including large mass phenotyping of potential parental lines, progeny, and wild genetic resources, and (3) integrating complex genotypic information with the large volume of data from high-throughput phenotyping systems. This entry looks at some of the recent advances in plant breeding for high yield potential environments and also those where abiotic stress is a major limitation to productivity. The methodologies and lessons learnt could become useful when breeding in the face of climate change. Examples are given for rice and wheat, because of their important contribution in volume and value to the world economy [24].

Breeding in a Changing Environment

Yield is a complex trait underpinned by many different processes and, as such, highly influenced by environmental conditions. Breeding programs utilize multi-environment trials as a way of sampling the target population of environments (TPE). However, the conditions (weather, soil, agronomy) in those trials are not always a good representation of the TPE that the lines will grow in during their commercial life ([13] and references therein). This gap, between the "selection" TPE and the "commercial life TPE" may increase as a result of increased climate variability. Predicting which type of environments breeders will be targeting and their frequency of occurrence may become a key piece of information in designing the best targeting of selection schemes.

Some lessons can be learnt from experience in breeding for drought-prone environments that could be adopted more widely and potentially extended to selecting for adaptation to high temperatures. In drought-prone areas, an important proportion of the GEI has been attributed to the timing of drought stress with respect to the crop stage. Not surprisingly, different outcomes in yield progress can be expected when selection takes place under different drought patterns [13]. An attempt to describe "types of environment" for a particular region has been conducted for sorghum [13] and wheat [15] in Northern Australia utilizing historic weather data, soil characteristics, and current and virtual crop characteristics (e.g., sorghum: [14]) using the crop simulation model APSIM [38]. This could be expanded to a larger regional scale using synthetic weather data ("future climates") aiming at different outcomes. Although climate projections have their own uncertainty, there is consensus in some of the predicted global trends [32]. At a large scale, describing "types of environments" using synthetic weather data could be a tool to identify shifts in the cultivated area and regions that are likely to experience increased frequency of events that will lead to yield loss [42], for example, high temperature or drought during pollen meiosis in wheat [37] or high temperatures at anthesis in rice [36]. This information can be used to design the layout of multi-environment trials or create managed environment facilities that reliably "reproduce" these conditions, for example, irrigation in the desert (such

as CIMMYT's Obregon facility), rain-out shelters, temperature gradient tunnels, etc., that, depending on their scale, could be used for particular stages of the breeding program. Ultimately, this information could be used to set selection criteria prioritizing particular traits (e.g., [67]) and devise the appropriate tests and technologies to screen for them (Fig. 1).

A Combination of Breeding Approaches Needed to Advance Yield in a Changing Climate

A modern wheat variety carries an elite combination of alleles for productivity, grain quality, and resistance or tolerance to a suite of the most important biotic and abiotic stresses in the environments in which they are grown. In a breeding program targeting development of new varieties for production by farmers, it is usually necessary to make crosses between parents with a high co-ancestry and many attributes in common while differing for a small number of traits important to farmers and end users. Often they will be current varieties or advanced breeding lines. With this approach, the gains made in one breeding cycle are built on in subsequent cycles and progress is incremental. However, in spite of this relative conservatism, most crosses still fail to produce their desired outcome, and breeders

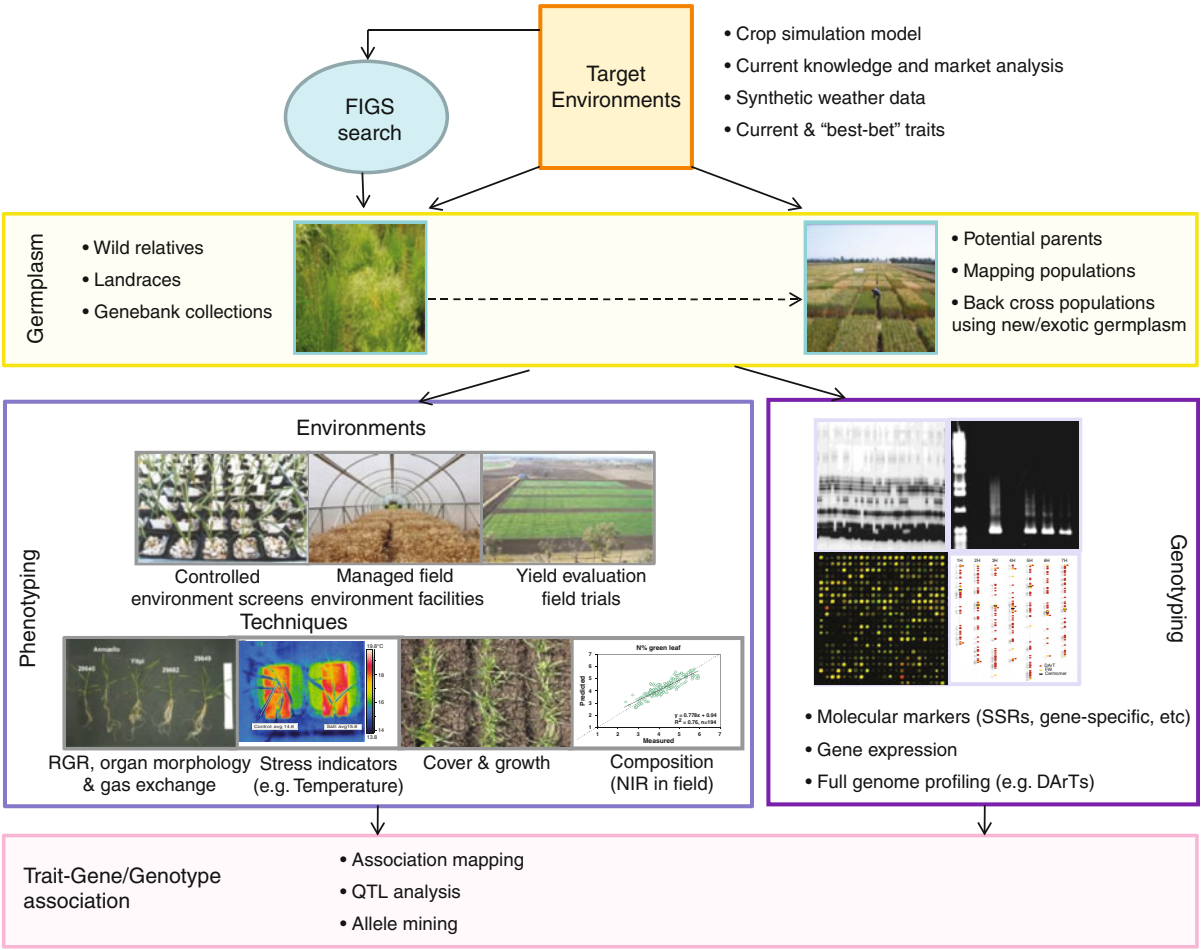

Plant Breeding Under a Changing Climate. Figure 1
Example of how to target traits to introduce in a breeding program for a changing climate. Defining target environments can help direct a FIGS search for exotic germplasm and set up specific populations. Phenotyping will be necessary both in the exotic germplasm and the breeding populations. Genotyping information combined with phenotypic data is the basis for trait–gene association

must make multiple crosses to spread risk. In drier environments subject to greater GEI, progress for yield is usually slower than in more favorable environments. In spite of these constraints, breeding programs have successfully improved water-limited yields over an extended period and new approaches must offer tangible benefits if they are to be adopted [46, 52, 75].

The already commonplace and increasing use of molecular markers in wheat breeding is a good example of the adoption of a technology that successfully supplements conventional approaches. Most markers implemented so far have been for genes of large effect associated with disease resistance, grain quality, or, more recently, the major genes controlling plant phenology. Few if any "yield," "drought tolerance" or "heat tolerance" quantitative trait loci (QTL) have been used in wheat breeding to date. Nonetheless, the major gene markers are useful in allowing more effective selection in earlier generations for a greater range of traits, while still leaving sufficient variation to allow selection of superior individuals for quantitative traits in later generations through conventional phenotypic selection (e.g., [77]). Removal of inferior individuals and alleles earlier in the breeding process means that fewer individuals entering the expensive later stages of yield and quality evaluation will be discarded because they lack some key major genes.

The identification of robust, yield-related QTL markers should allow early generation enrichment of the frequencies of these alleles in much the same way as for major genes. These QTL can be identified through a number of approaches. Initially, biparental mapping populations were used but these have two key problems. First, the population sizes and number of test environments required to accurately identify QTL for yield are large, even in the absence of GEI. Usually, suboptimal population sizes and numbers of test environments were used, leading to some QTL not being identified and the effects of others being overestimated [5]. Other problems with this approach are that only two parents are sampled per population and identified QTL are often population- or environment-specific (e.g., [60]). Further, parents commonly differed for major genes controlling height or phenology and these had by far the largest effects on the quantitative trait being measured making it difficult to identify previously unknown sources of variation in the face of further-reduced effective population sizes [54].

Association mapping and whole genome prediction models (e.g., based on full genome profiling techniques such as DArTs [39]) have been proposed as alternative methods to identify and combine useful variation for a range of traits [10, 30, 31, 43]. The advantages of this approach are that alleles from a greater range of parents can be examined which may have greater relevance to breeding populations if the set is appropriately formulated. In the context of a breeding program aiming to make progress for yield, the most appropriate lines are likely to be breeding lines, and the phenotyping will comprise the routine yield evaluation trials. A key advantage is that the resources allocated to phenotyping are likely to be much greater than is available to any stand-alone QTL mapping project and the associations identified are more likely to be relevant to breeding populations as they were developed in breeding populations. Given the likelihood that the effects of QTLs for complex traits will change over time through fixation of important regions and differing interactions with new alleles at other loci, a continual reassessment of the value of QTLs in breeding populations may be needed in parallel with their use in selection [57]. This requires integration of good multi-environment yield data and efficient whole genome fingerprinting techniques that can be applied to the large numbers of lines making up the yield trials of commercial breeding programs. This approach depends on large amounts of resource for phenotyping, genotyping, and information management that are currently not available within the public sector. Further, association mapping approaches may not give good clues to the underlying mechanisms responsible for the yield effects of QTLs, but given that conventional breeding has achieved yield gains despite ignorance of contributory mechanism(s), this need not be an impediment to their use. Given that there is not a perfect correlation between any one physiological parameter and yield and interrelationships between physiological characters and their effects on yield are often not well understood, widespread mapping and use of QTL for physiological characters are not likely in the public or private sectors in the near future.

A Niche for Indirect Selection for Yield Using Physiological Parameters

Given that all increases in yield must have a physiological basis, it should in theory be possible to identify and select for this variation. "Physiological" or "trait-based" breeding has a niche value as complementary to more conventional crossing and selection methods [63, 73]. For selection of physiological characters to be viable in a breeding program a demonstrated genetic correlation with yield is a prerequisite as is development of a cheap, high-throughput selection tool. The ultimate outcome of selection for yield-related physiological characters must be greater genetic gain per breeding cycle or per unit of investment. The fact that physiological measurements do not depend on knowledge of the number and location of QTLs segregating in any given population means they can be used across a greater number of populations. This also means they can be used to screen exotic germplasm, such as wild relatives, sources for variation that may be based on novel alleles and could be introgressed into breeding populations. High order or composite traits evaluated in the field have been particularly successful as targets of this approach, compared to traits evaluated at the cellular level, which are more prone to be subject to upscaling problems [72]. This is also of value given that agronomically important complex traits have not been particularly amenable to improvement using marker-assisted selection [31].

An analytic physiological approach is also likely to be useful to improve candidate traits for which genetic variation is not readily available, as could be the case in the response to high temperatures, and a targeted search and introduction strategy is needed. To illustrate the possibilities, an example of the use of physiological traits–based breeding to cope with limited water in wheat and improve yield under favorable conditions in rice is presented below.

Packaging Traits to Cope with Limited Water in Wheat and Links with Breeding for High Temperatures

A number of relationships between yield and physiological parameters have been identified in wheat and indirect selection methods for yield subsequently implemented. A good example resulted from the discovery of a positive relationship between irrigated yields and stomatal conductance in a historical series of CIMMYT wheats [25]. Subsequent research showed that selection for higher stomatal conductance could be used in indirect selection for increased yield in irrigated conditions [17]. Selection for high stomatal conductance using canopy temperature as a surrogate is now a routine procedure in the rainfed wheat program at CIMMYT (Manes, personal communication 2010).

Discovery of the relationship between C^{12}/C^{13} carbon isotope discrimination (CID) and yield under drought is another example that grew from postulation of a relationship based on theoretical considerations, subsequent identification of variation in wheat germplasm, demonstrating a relationship with yield, development of a selection tool and germplasm, and ultimately in release of improved varieties Drysdale and Rees [55, 56, 65].

Later genetic dissection identified QTL for CID in several mapping populations that had not been specifically developed for mapping CID and in which the parents were mainly commercial varieties [60]. Although the parents of these populations did not have the most extreme CID levels, the populations showed the genetic complexity of the trait, that diversity for CID alleles was present in current varieties and that it was possible to recover transgressive segregants for CID from these populations as extreme as any identified in previous germplasm surveys. Therefore, with knowledge of the relationship between CID and yield under drought, availability of an appropriate selection screen should allow breeders to indirectly select for higher yield in drought-prone environments. Although use of mass spectrometry to determine carbon isotope composition is a relatively expensive procedure and has not been applied routinely by commercially focused breeding programs, it was successfully applied in germplasm development efforts at CSIRO that led to the release of varieties Drysdale and Rees in collaboration with varietal breeding programs [55, 56]. Development of cheaper techniques to screen for the increased WUE that result in the CID differences may be applicable on a more routine basis in breeding programs.

QTL mapping of water soluble carbohydrate (WSC) contents in stem [60] and coleoptile length [59]

reveal similarly widespread and potentially useful variation for these traits in elite germplasm. In cereals, water soluble carbohydrates (WSC) stored in stems have been acknowledged as contributing to maintenance of grain filling rate when photosynthesis declines due to various stresses, for example, drought ([6, 47 81], heat stress [7], and possibly disease [8]. Increased coleoptiles length can be a useful option for systems utilizing moisture-seeking strategies, such as sowing in deep furrows. This is likely to be a useful combination of traits for climate change in Australia, with the projected temperature increase and the decrease in average annual and winter rainfall (fewer and drier sowing opportunities) in the southern areas of the wheatbelt toward 2030 [32]. Progress for these traits could be made by selecting variation already present in breeders' populations if an efficient selection screen were available.

As mentioned before some of the traits targeted for drought stress are potentially useful under heat stress, which is particularly the case for those related to transpirational cooling [54]. Increased root growth in a soil profile with water available at depth can increase the transpirational cooling of the crop, uncoupling it from air temperature and helping keep tissues in a "safer" temperature window. Epicuticular waxiness is another trait with a dual function, reducing heat load and transpiration. Waxiness can be scored visually in the field, but, despite the theoretical impact there have been no comprehensive studies of its impact in crops [64]. Flowering time has been exploited under terminal drought as a simple way of manipulating the water balance, early flowering leaving more water available to be used during grain filling. Early flowering can also be used to avoid high temperatures during grain filling. In both cases, advancing flowering can carry the penalty of lower biomass at flowering and increased probability of frost damage.

Some processes are directly affected by high temperatures, among them respiration, inflorescence fertility, and starch composition, and hence grain quality ([2, 4, 78, 82]). Night respiration and photorespiration are processes directly affected by temperature; however, the lack of an easy way to phenotype large number of lines and study its effects at the crop level makes it inaccessible as a target for breeders at this point in time. Susceptibility of pollen to high temperatures and traits contributing to heat tolerance (biochemical mechanisms) and avoidance (e.g., anther dehiscence early in the day) is a topic much researched in rice (see [78] and references therein). Pollen sterility induced by drought and genetic variation for it has been confirmed in wheat [37] and could also be potentially triggered by high temperatures. This is likely to be a trait to be screened for in controlled environment facilities or using molecular markers, given how unpredictable high temperatures can be at a particular crop stage in the field. For the purpose of marker development or QTL identification it will be important to "detangle" the phenotype appropriately as, for instance, reduced pollen sterility under high temperature could occur due to lower tissue temperature in a line that has high transpirational cooling due to higher stomatal conductance.

Physiological Traits to Raise Yield Potential in Rice: Different Targets for Temperate Versus Tropical Regions

As highlighted earlier, an increase in the length of the growing season as well as improved growing seasonal conditions are forecasted for high latitudes under climate change. This section illustrates the experience in rice in breeding for increased yield potential. Yield potential is defined as grain yield only limited by incoming radiation and temperature at a given site. Most of rice production is derived from tropical and subtropical areas, where it is grown with irrigation water from the monsoon [79]. The yield potential of rice in the tropics has been stable at 9–10 t ha^{-1} for the last 20 years [51]. However, the arable land for rice is continuously decreasing as a consequence of increasing urbanization, in parallel with the increase in the population of rice consumers. An increase in yield potential of rice of 10–15% is now necessary to cope with this raising demand [69]. Among the main limitations to rice yield potential in the tropics are (1) the limited amount of incoming radiation (combination of short days and cloudiness), (2) high relative humidity underlying high resistance to transpiration, and (3) a trend toward a short crop cycle to allow the growth of two to three crops per year. Indeed, the highest rice yield potential today is slightly higher or similar to that of IR64, that is, comparable to introgression lines of IR64

background [29], a benchmark inbred line which was developed by IRRI breeders in the middle of the 1980s. Most of the increases in rice yield in the field have been achieved with hybrid rice [50]. In contrast, the main gain in crop productivity in the last 20 years has been observed undernutrient or water limitation [34]. Grain quality has also been a great focus of the last 20 years and has diversified significantly to meet the variable expectations of consumers from different regions [27].

The International Rice Research Institute was a pioneer in using physiological concepts in breeding for an ideotype, as illustrated by the so-called "new plant type" which reached limited success [51]. These guiding principles are still utilized in current efforts to improve yield potential in rice focusing in increasing biomass and harvest index as discussed below. One challenging option is to develop a rice plant with the C_4 photosynthesis pathway: the radiation use efficiency would be increased considerably and so the yield potential up to by 30–50% [44, 68, 80]. It is taking an integrated program involving molecular biologists, geneticists, biotechnologists, and physiologists working together for a considerable number of years. The search for genetic variation in different aspects of the C_4 pathway, such as leaf anatomical and cellular specialization and variation in mechanisms underlying the CO_2 compensation point is already presenting a considerable phenotyping challenge [83, 84]. Another option, still challenging but perhaps more realistic in a shorter timeframe, is to improve the current plant types for high yield. In the tropics, both improved biomass accumulation and partitioning underpin the superiority of hybrid rice versus rice elite inbred lines, with margins between 10% and 20% from wet to dry seasons [11, 40, 49, 50]. It is possible to assume that breeding programs for yield potential could gain much by incorporating traits relevant to hybrid rice superiority into improved inbred lines and lead to a substantial yield gain [41].

Work conducted at the International Rice Research Institute has extensively examined the basis for yield differences between hybrid rice and elite inbred lines of similar crop duration [11, 12, 40]. With an initial focus in the tropics, these authors confirmed, under a range of contrasting conditions, that superior biomass production in the succeeding phenological phases and improved partitioning play a significant role in the higher yields of the hybrids. Hybrids are characterized by (1) higher crop growth rate during each phenological phase leading to overall higher plant biomass at maturity, (2) earlier cessation of tiller production (associated with earlier biomass partitioning to culm and earlier accumulation of reserves) with similar tiller production rate, (3) larger pool of reserves in the culm at anthesis (estimated through a lower value of specific culm length, SCL), (4) larger remobilization of the accumulated reserves from the culm to the panicle during grain filling (associated with quicker grain filling and higher SCL at maturity), and (5) lighter unfilled spikelets indicating that grain filling was more efficient with less partially filled spikelets (associated with larger number of filled grains) [40, 41]. It is clear that it is worth looking for genetic variation in storage of soluble sugars in the stem as well as remobilization capacity, in line with results in wheat [81] and in view of identifying the driving force of the dynamics of soluble sugars. Bueno et al. [12] speculated that improved partitioning, more than source supply, is the key component driving crop performance of high-yielding genotypes in the tropics where variability in biomass accumulation among genotypes is poorly expressed due to low evaporative demand. The sink strength index, as an improved harvest index taking into account the culm vigor [12, 41], can be used as an integrated trait for screening genotypes with high or low partitioning efficiency. It cannot, however, be considered as a "foundation" trait for high yield potential, unlike the traits cited earlier, and seems rather to be the integrated expression at maturity, as sink size at anthesis, of the cumulated higher efficiency of more simple traits. Some other important considerations concern remobilizing assimilates from senescing to productive tillers, avoiding lodging and delaying root senescence during grain filling. Maintaining functional roots throughout grain filling, and maintaining nitrogen uptake, should help delaying leaf senescence; however, leaf senescence has to be fast toward the end of grain filling to maximize remobilization.

Identification of Variation for Physiological Traits from Exotic Germplasm Sources

While the wheat example cited above indicates considerable variation for several yield-related physiological

traits already existing in varieties and advanced breeding lines adapted to drier environments, for some traits, key genetic variation is lacking in existing breeding material. An example of this problem is the difficulty of recovering long coleoptile semidwarfs in wheats carrying the semidwarf alleles *Rht-B1b* and *Rht-D1b* [1, 76]. These alleles are virtually ubiquitous in modern semidwarf genes but have negative pleiotropic effects on coleoptile length. In order to develop semidwarf wheats with substantially longer coleoptiles the introduction of novel dwarfing genes that do not affect coleoptile length is necessary [22, 58]. For other traits such as root depth, likely to be related to yield under drought or heat stress, variation has been found in landraces and wild or synthetic hexaploid material that is greater or absent in existing wheat germplasm available to breeders [61, 62]. The introduction and exploitation of variation from synthetic hexaploid wheats in the CIMMYT wheat program is an example of the potential gains that can be made from exotic germplasm sources. These synthetic wheats were produced by re-synthesizing bread wheat from progenitor species the tetraploid durum wheat and the diploid wild grass *Triticum tauschii* [70, 71]. Derivatives of crosses between synthetic hexaploids and bread wheat now comprise around 30% of the breeding populations in CIMMYTs rainfed wheat program and the best lines have superior yield under drought stressed and more favorable environments than the best conventional wheats [18]. While this demonstrates the possibility of gains from exotic germplasm sources, a more targeted approach in which exotic sources are prescreened for traits related to yield under drought or high temperatures may produce even greater gains. A possible pathway of integration is shown in Fig. 1. In many cases novel yield-related variation in exotic germplasm sources would be difficult or impossible to identify simply by screening directly for yield because it is present in agronomically poor backgrounds. In such instances, screening for physiological traits likely to be related to yield may be a useful precursor to crossing to introduce new variation [62].

A number of other approaches may allow selection of better initial material even prior to screening for physiological traits. Molecular diversity studies have shown, for example, that genetic diversity of emmer wheat is greater than that in durum wheat [19] and studies of synthetic wheats produced by crossing emmers with *A. tauschii* have shown greater yield under drought stress in Mexico, Pakistan, and Eastern India than synthetics produced by durum wheat x *A. tauschii* crosses [71]. Given the distribution of emmer wheats in drought-prone Mediterranean environments the useful variation present in this material may have been predictable. Better predictions based on a greater array of climatic, soil, and location data as exemplified by the focused identification of germplasm strategy or FIGS (e.g., [20, 21]) should further improve the quality of germplasm selected to screen for variation in phenotypic traits (Fig. 1).

Robust and time-efficient phenotyping is also critical for trait-based selection of potential parents for crossing blocks and evaluation of the progeny, such as needed to underpin physiological breeding [63]. Non-invasive technologies, such as those based on spectral reflectance and thermal sensing have a role in the identification and selection of traits in a breeding context, by allowing several crop characteristics to be surveyed in a single measurement at the crop scale [45] (Fig. 1). For example, spectral reflectance has been used to simultaneously survey canopy cover, nitrogen, and water status of the crop [25, 48], while canopy temperature has been used as an indicator of leaf conductance and water use [85]. Potential for continuous developments for high throughput include introducing changes in platforms (wireless systems, unmanned aerial vehicles, etc.) to allow more frequent data capture and greater area coverage. While glasshouse or lab-based screens have been indicated as an option for some traits (e.g., [28, 74]), in most cases, there is a low correlation between this level of evaluation and field-based rankings. The interactions involved not only in upscaling to the crop/canopy level but with the changing environment itself get in the way (examples in [72]). Instead, field canopy scale measurements have more potential since selection can take place at the crop level, which avoids scaling up issues (e.g., [62]). For instance, reflectance-based indices have proved very useful as indirect selection criteria to increase the efficiency of selection in wheat growing in a reasonably stable environment where the terminal drought is managed [3], while indicators of canopy cover and canopy temperature were a good proxy for performance or QTL detection in a hot environment [54].

Conclusions and Future Directions

Improved crop varieties will be a vital component of adaptation to climate change. Plant breeding will have to operate at a higher level of efficiency to make the necessary genetic progress to address current and projected food needs. In this context, the three main challenges plant breeding faces in relation to climate change are (1) identifying the new target population of environments, (2) translating this knowledge into practical selection methods to uncover new genetic variation, including mass phenotyping of potential parental lines, progeny, and wild genetic resources, and (3) linking genetic and phenotypic information. How to link and interpret the new and comprehensive information on genotypic characteristics and the large volume of data generated by high-throughput phenotyping platforms will be a critical step toward selecting the next generation of traits fit to less predictable environments.

Acknowledgments

The authors thank Lynne McIntyre (CSIRO) and Andrzej Kilian (DArTs Pty Ltd) for contributing illustrations on genotyping. FD acknowledges the financial support of the Department of Agriculture, Fisheries and Forestry, CSIRO and the Climate Adaptation Flagship.

Bibliography

Primary Literature

1. Allan RE (1989) Agronomic comparisons between Rht1 and Rht2 semi-dwarf genes in winter wheat. Crop Sci 29:1103–1108
2. Atkin OK, Tjoelker MG (2003) Thermal acclimation and the dynamic response of plant respiration to temperature. Trends Plant Sci 8:343–351
3. Babar MA, van Ginkel M, Reynolds MP, Prasad B, Klatt AR (2007) Heritability, correlated response, and indirect selection involving spectral reflectance indices and grain yield in wheat. Aust J Agric Res 58:432–442
4. Barnabas B, Jager K, Feher A (2008) The effect of drought and heat stress on reproductive processes in cereals. Plant Cell Environ 31:11–38
5. Beavis WD (1998) QTL analyses: power, precision, and accuracy. In: Patterson AH (ed) Molecular dissection of complex traits. CRC Press, Boca Raton, pp 145–162
6. Bidinger F, Musgrave RB, Fischer RA (1977) Contribution of stored pre-anthesis assimilates to grain yield in wheat and barley. Nature 270:431–433
7. Blum A, Sinmena B, Mayer J, Golan G, Shpiler L (1994) Stem reserve mobilisation supports wheat-grain filling under heat stress. Aust J Plant Physiol 21:771–781
8. Blum A (1998) Improving wheat grain filling under stress by stem reserve mobilisation. Euphytica 100:77–83
9. Brar D, Virk P (2010) How a modern rice variety is bred. Rice Today 9(Jan–March):11–12
10. Breseghello F, Sorrells ME (2006) Association mapping of kernel size and milling quality in wheat (Triticum aestivum L.) cultivars. Genetics 161(2):1165–1177
11. Bueno CS, Lafarge T (2009) Higher crop performance of rice hybrids than elite inbreds in the tropics. 1. Hybrids accumulate more biomass during each phenological phase. Field Crops Res 112:229–237
12. Bueno CS, Pasuquin E, Tubana B, Lafarge T (2010) Improving sink regulation, and searching for promising traits associated with hybrids, as a key avenue to increase potential of the rice crop in the tropics. Field Crops Res 118:199–207
13. Chapman SC (2008) Use of crop models to understand genotype by environment interactions for drought in real-world and simulated plant breeding trials. Euphytica 161:191–208
14. Chapman SC, Cooper M, Podlich D, Hammer GL (2003) Evaluating plant breeding strategies by simulating gene action and dryland environments. Agron J 95:99–113
15. Chenu K, Cooper M, Hammer GL, Mathews KL, Dreccer MF, Chapman SC (2011) Environment characterisation as an aid to wheat improvement – interpreting genotype-environment interaction by modelling water-deficit patterns in north eastern Australia. J Exp Bot 62:1743–1755
16. Comstock RE (1977) Quantitative genetics and the design of breeding programs. In: Proceedings of the international conference on quantitative genetics. Iowa State University Press, Ames, 16–21 Aug 1976, pp 705–718
17. Condon AG, Reynolds MP, Rebetzke GJ, Ginkel M van, Richards RA, Farquhar GD (2007) Using stomatal aperture-related traits to select for high yield potential in bread wheat. In: Wheat production in stressed environments. Proceedings of the 7th international wheat conference, Mar del Plata, 27 Nov–2 Dec 2005, pp 617–624
18. Dreccer MF, Chapman SC, Ogbonnaya FC, Borgognone MG, Trethowan RM (2008) Crop and environmental attributes underpinning genotype by environment interaction in synthetic bread wheats evaluated in Mexico and Australia. Aust J Agric Res 59:447–460
19. Dreisigacker S, Kishii M, Lage J, Warburton M, Ogbonnaya FC, van Ginkel M, Brettell R (2008) Use of synthetic hexaploid wheat to increase diversity for CIMMYT bread wheat improvement. Aust J Agric Res 59(5):413–420
20. El-Bouhssini M, Street K, Joubi A, Ibrahim Z, Rihawi F (2009) Sources of wheat resistance to Sunn pest, Eurygaster integriceps Puton, in Syria. Genet Resour Crop Evol 56:1065–1069
21. El-Bouhssini M, Street K, Amri A, Mackay M, Ogbonnaya FC, Omran A, Abdalla O, Baum M, Dabbous A, Rihawi F (2011) Sources of resistance in bread wheat to Russian wheat

aphid (Diuraphis noxia) in Syria identified using the Focused Identification of Germplasm Strategy (FIGS). Plant Breeding 130:96–97
22. Ellis MH, Rebetzke GJ, Chandler P, Bonnett DG, Spielmeyer W, Richards RA (2004) The effect of different height reducing genes on early growth characteristics of wheat. Funct Plant Biol 31:583–589
23. FAO (2010) The state of food insecurity in the world. Chief publishing policy and support branch office of knowledge exchange, research and extension FAO, Rome, p57
24. FAO (2010) FAO Statistical yearbook 2010. Economic and social development department, FAO, Rome
25. Fischer RA, Rees D, Sayre KD, Lu Z-M, Condon AG, Saavedra AL (1998) Wheat yield progress associated with higher stomatal conductance and photosynthetic rate and cooler canopies. Crop Sci 38:1467–1475
26. Fitzgerald GJ, Rodriguez D, Christensen LK, Belford R, Sadras VO, Clarke TR (2006) Spectral and thermal sensing for nitrogen and water status in rainfed and irrigated wheat environments. Precision Agric 7:233–248
27. Fitzgerald MA, McCough SR, Hall RD (2009) Not just a grain of rice: the quest for quality. Trends Plant Sci 14:133–139
28. Gregory PJ, Bengough AG, Grinev D, Schmidt S, Thomas WTB, Wojciechowski T, Young IM (2009) Root phenomics of crops: opportunities and challenges. Funct Plant Biol 36:922–929
29. Guan YS, Serraj R, Liu SH, Xu JL, Ali J, Wang WS, Venus E, Zhu LH, Li ZK (2010) Simultaneously improving yield under drought stress and non-stress conditions: a case study of rice (*Oryza sativa* L.). J Exp Bot 61:4145–4156
30. Heffner EL, Sorrells ME, Jannink JL (2009) Genomic selection for crop improvement. Crop Sci 49:1–12
31. Heffner EL, Lorenz AJ, Jannink J-L, Sorrells ME (2010) Plant breeding with genomic selection: gain per unit time and cost. Crop Sci 50:1681–1690
32. Hennessy KJ, Whetton PH, Preston B et al (2010) Climate projections. In: Stokes C, Howden M (eds) Adapting agriculture to climate change-preparing Australian agriculture, forestry and fisheries for the future. CSIRO Publishing, Collingwood, pp 21–48
33. Howden SM, Gifford RG, Meinke H (2010) Grains. In: Stokes C, Howden M (eds) Adapting agriculture to climate change-preparing Australian agriculture, forestry and fisheries for the future. CSIRO Publishing, Collingwood, pp 21–48
34. Horie T, Shiraiwa T, Homma K, Katsura K, Maeda S, Yoshida H (2005) Can yields of low land rice resume the increases that they showed in the 1980s? Plant Prod Sci 8:259–274
35. IPCC (2007) Climate change 2007: impacts, adaptation, and vulnerability. Contribution of working group II to the fourth assessment report of the intergovernmental panel on climate change. Cambridge University Press, Cambridge, UK
36. Jagadish SVK, Craufurd PQ, Wheeler TR (2007) High temperature stress and spikelet fertility in rice (Oryza sativa L.). J Exp Bot 58:1627–1635
37. Ji XM, Shiran B, Wan JL, Lewis DC, Jenkins CLD, Condon AG, Richards RA, Dolferus R (2010) Importance of pre-anthesis anther sink strength for maintenance of grain number during reproductive stage water stress in wheat. Plant Cell Environ 33:926–942
38. Keating BA, Carberry PS, Hammer GL, Probert ME, Robertson MJ, Holzworth D, Huth NI, Hargreaves JNG, Meinke H, Hochman Z, McLean G, Verburg K, Snow V, Dimes JP, Silburn M, Wang E, Brown S, Bristow KL, Asseng S, Chapman S, McCown RL, Freebairn DM, Smith CJ (2003) An overview of APSIM, a model designed for farming systems simulation. Eur J Agron 18: 267–288
39. Jaccoud D, Peng K, Feinstein D, Kilian A (2001) Diversity arrays: a solid state technology for sequence information independent genotyping. Nucleic Acids Res 29:e25
40. Lafarge T, Bueno CS (2009) Higher crop performance of rice hybrids than elite inbreds in the tropics. 2. Does sink regulation, rather than sink size, play a major role? Field Crops Res 114:434–440
41. Lafarge T, Bueno C, Pasuquin E, Wiangsamut B (2009) Biomass accumulation and sink regulation in hybrid rice: consequences for breeding programs and crop management. In: Xie F, Hardy B (eds) Accelerating hybrid rice development. International Rice Research Institute, Los Baños, p 698. Invited oral presentation, international symposium on hybrid rice, Changsha, Hunan, 11–15 Sept 2008, pp 453–474
42. Li Y, Ye W, Wang M, Yan X (2009) Climate change and drought: a risk assessment of crop-yield impacts. Clim Res 39:31–46
43. Meuwissen THE, Hayes BJ, Goddard ME (2001) Prediction of total genetic value using genome-wide dense marker maps. Genetics 157:1819–1829
44. Mitchell PL, Sheehy JE (2000) Performance of a potential C4 rice: overview from quantum yield to grain yield. Stud Plant Sci 7:145–163
45. Montes M, Melchinger AE, Reif JC (2007) Novel throughput phenotyping platforms in plant genetic studies. Trends Plant Sci 12:433–436
46. O'Brien L (1982) Victorian wheat yield trends, 1898–1977. J Aust Inst Agric Sci 48:162–168
47. Palta JA, Kobata T, Turner NC (1994) Carbon and nitrogen in wheat as influenced by postanthesis water deficits. Crop Sci 34:118–124
48. Peñuelas J, Fillela Y (1998) Visible and near-infrared reflectance techniques for diagnosing plant physiological status. Trends Plant Sci 3:151–156
49. Peng S, Cassman KG, Virmani SS, Sheehy J, Khush GC (1999) Yield potential trends of tropical rice since the release of IR8 and the challenge of increasing rice yield potential. Crop Sci 39:1552–1559
50. Peng S, Yang J, Laza MRC, Sanico A, Visperas RM, Son TT (2003) Physiological bases of heterosis and crop management strategies for hybrid rice in the tropics. In: Virmani SS, Mao CX, Hardy B (eds) Hybrid rice for food security, poverty alleviation, and environmental protection. Proceedings of the 4th international symposium on hybrid rice, 14–17 May 2002, Hanoi. IRRI, Los Baños, pp 153–170

51. Peng S, Kush GS, Virk P, Tang Q, Zhu Y (2008) Progress in ideotype breeding to increase rice wheat consortium. Field Crops Res 108:32–38
52. Perry MW, D'Antuono MF (1989) Yield improvement and associated characteristics of some Australian spring wheat cultivars introduced between 1860 and 1982. Aust J Agric Res 40:457–472
53. Pinter PJ, Hatfield JL, Schepers JS, Barnes EM, Moran MS, Daughtry CST, Upchurch DR (2003) Remote sensing for crop management. Photogram Eng Rem S 69:647–664
54. Pinto RS, Reynolds MP, Mathews KL, McIntyre CL, Olivares-Villegas JJ, Chapman SC (2010) Heat and drought adaptive QTL in a wheat population designed to minimize confounding agronomic effects. Theor Appl Genet 121:1001–1021
55. Plant Varieties Journal (2002) Official Journal of Plant Breeder's Rights Australia, 15(1):74
56. Plant Varieties Journal (2004) Official Journal of Plant Breeder's Rights Australia, 17(2):254–261
57. Podlich DW, Winkler CR, Cooper M (2004) Mapping as you go: an effective approach for marker-assisted selection of complex traits. Crop Sci 44:1560–1571
58. Rebetzke GJ, Richards RA, Fischer VM, Mickelson BJ (1999) Breeding long coleoptile, reduced height wheats. Euphytica 106:159–168
59. Rebetzke GJ, Ellis MH, Bonnett DG, Richards RA (2007) Molecular mapping of genes for coleoptile growth in bread wheat. Theor Appl Genet 114:1173–1183
60. Rebetzke GJ, van Herwaarden AF, Jenkins C, Weiss M, Lewis D, Ruuska S, Tabe L, Fettell N, Richards RA (2008) Quantitative trait loci for soluble stem carbohydrate production in wheat. Aust J Agric Res 59:891–905
61. Reynolds MP, Mujeeb-Kazi A, Sawkins M (2005) Prospects for utilising plant-adaptive mechanisms to improve wheat and other crops in drought & salinity-prone environments. Ann Appl Biol 146:239
62. Reynolds MP, Dreccer MF, Trethowan R (2007) Drought adaptive traits derived from wheat wild relatives and landraces. J Exp Bot 58:177–186
63. Reynolds MP, Manes Y, Izanloo A, Langridge P (2009) Phenotyping for physiological breeding and gene discovery in wheat. Ann Appl Biol 155:309–20
64. Reynolds MP, Hays D, Chapman S (2010) Breeding for adaptation to heat and drought stress. In: Reynolds MP (ed) Climate change and crop production. CAB International, Wallingford, pp 71–91
65. Richards RA, Rebetzke GJ, Condon AG, van Herwaarden AF (2002) Breeding opportunities for increasing the efficiency of water use and crop yield in temperate cereals. Crop Sci 42:111–121
66. Rosenzweig C (2009) Climate change and agriculture. In: Meyers RA (ed) Encyclopedia of complexity and systems science., pp 1071–1082. doi:10.1007/978-0-387-30440-3_70, Part 3
67. Semenov MA, Halford NG (2009) Identifying target traits and molecular mechanisms for wheat breeding under a changing climate. J Exp Bot 60:2791–2804
68. Sheehy JE, Ferrer AB, Mitchell PL, Elmido-Mabilangan A, Pablico P, Dionora MJA (2008) How the rice crop works and why it needs a new engine. In: Sheehy JE, Mitchell PL, Hardy B (eds) Charting new pathways to C4 rice. Proceedings of the international workshop, IRRI, Los Baños, pp 3–26
69. Swaminathan MS (2007) Science and shaping the future of rice. In: Aggarwal PK, Ladha JK, Singh RK, Devakumar C, Hardy B (eds) Science, technology, and trade for peace and prosperity. Proceedings of the 26th international rice research conference, 9–12 Oct 2006, New Delhi, pp 3–14
70. Trethowan RM, Reynolds MP, Sayre KD, Ortiz-Monasterio I (2005) Adapting wheat cultivars to resource conserving farming practices and human nutritional needs. Ann Appl Biol 146:404–413
71. Trethowan RM, Mujeeb-Kazi A (2008) Novel germplasm resources for improving environmental stress tolerance of hexaploid wheat. Crop Sci 48:1255–1265
72. Sinclair TR, Purcell LC, Sneller CH (2004) Crop transformation and the challenge to increase yield potential. Trends Plant Sci 9:70–75
73. Sinclair TR, Purcell LC (2005) Is a physiological perspective relevant in a 'genocentric' age? J Exp Bot 56:2777–2782
74. Sirault XRR, James RA, Furbank RTA (2009) A new screening method for osmotic component of salinity tolerance in cereals using infrared thermography. Funct Plant Biol 36:970–977
75. Vandeleur RK, Gill GS (2004) The impact of plant breeding on the grain yield and competitive ability of wheat in Australia. Aust J Agric Res 55:855–861
76. Whan BR (1976) The association between coleoptile length and culm length in semi-dwarf and standard wheats. J Aust Inst Agric Sci 42:194–196
77. Wang J, Chapman SC, Bonnett DG, Rebetzke GJ (2009) Simultaneous selection of major and minor genes: use of QTL to increase selection efficiency of coleoptile length of wheat (Triticum aestivum L.). Theor Appl Genet 119:65–74
78. Wassmann R, Jagadish SVK, Heuer S, Ismail A, Redona E, Serraj R, Singh RK, Howell G, Pathak H, Sumfleth K (2009) Climate change affecting rice production: the physiological and agronomic basis for possible adaptation strategies. Adv Agron 101:59–122
79. Wassmann R, Jagadish SVK, Sumfleth K, Pathak H, Howell G, Ismail A, Serraj R, Redona E, Singh RK, Heuer S (2009) Regional vulnerability of climate change impacts on Asian rice production and scope for adaptation. Adv Agron 102:91–133
80. Yin X, Struik PC (2009) C3 and C4 photosynthesis models: an overview from the perspective of crop modelling. NJAS Wageningen J Life Sci 57:27–38
81. Dreccer MF, van Herwaarden AF, Chapman SC (2009) Grain number and grain weight in wheat lines contrasting for stems soluble carbohydrate concentration. Field Crops Res 112: 43–54
82. Wardlaw IF, Wrigley CW (1994) Heat tolerance in temperate cereals-an overview. Aust J Plant Phys 21:695–703
83. Hibberd JM, Sheehy JE, Langdale JA (2008) Using C-4 photosynthesis to increase the yield of rice - rationale and feasibility. Current opinion Plant Biol 11:228–231

84. Furbank RT, von Caemmerer S, Sheehy JE, Edwards G (2009) C(4) rice: a challnege for plant phenomics. Funct Plant Biol 36:970–977
85. Pinter PJ, Jr, Zipoli G, Reginato RJ, Jackson RD, Idso SB, Hohman JP (1990) Canopy temperature as an indicator of differential water use and yield performance among wheat cultivars. Agric Water Management 18:35–48

Plant Molecular Pharming, Industrial Enzymes

Saifullah Khan[1], Vidya Rajan[2], John Howard[2]
[1]Plant Biotechnology Section, International Center for Chemical and Biological Sciences, HEJ research Institute, University of Karachi, Karachi, Pakistan
[2]Applied Biotechnology Institute, San Luis Obispo, CA, USA

Article Outline

Glossary
Definition of the Subject
Introduction
Historical Background of Industrial Enzymes
Production of Recombinant Proteins in Plants
Regulation of Growth and Use of Transgenic Plants
Plants as Sustainable Sources of Industrial Enzymes
Future Directions
Bibliography

Glossary

Diafiltration Method of cross-flow filtration that separates filtrate from solids.

Industrial enzymes Proteins that are used in commercial applications where very specific catalysts are needed.

Pharmacognosy The study of medicines derived from natural sources.

Plant molecular pharming Production of pharmaceuticals or industrial enzymes from genetically engineered plants.

Sustainability Production to meet present needs without compromising the ability of future generations to meet their own needs.

Transgenic plants Plants genetically engineered by the introduction of foreign genes using recombinant DNA technology.

Definition of the Subject

Plants have been domesticated since around 10,000 years ago in the fertile Babylonian crescent [1] and husbandry and breeding techniques have been applied to increase yield and storage and to retard spoilage [2]. Plants have been used since time immemorial for their medicinal properties, and in ACE 78 Discorides first described 600 medicinal plants in De Materia Medica. Although the first synthetic drug, salicylic acid, entered the market in 1897, plants are still used for pharmacognosy – the preparation of drugs from natural sources [3]. The types of plants used for this purpose, however, are usually distinct from those for food, feed, or fiber. With the advent of molecular techniques, all plants now have the potential to serve as production vehicles for natural or engineered products that were previously limited to other hosts [4, 5]. Plant molecular pharming of industrial proteins refers to recombinant proteins used in industrial processes and produced in plants. Enormous quantities of a variety of enzymes go into the making of products such as paper, leather, detergents, pharmaceuticals, food, beverages, chemicals, and fabric, to name a few, and the economical production of these industrially important enzymes is crucial to commerce. This production must be balanced with the need for sustainability and environmental stewardship.

Sustainable production of industrial enzymes requires that resources are not over-exploited and that the environment is not polluted by wastes. The use of plants as "green" factories can meet both criteria. Plants are a renewable resource and thus generally are not over-exploited and wastes are biodegradable. The problems associated with fertilization runoff, spread of transgenic genes to non-target plants, and crop and land usage must be addressed to allay public concern about the use of transgenic plants. But, combined with modern farming and containment methods, transgenic plants have the potential to produce large quantities of target material safely and sustainably [6, 7].

Introduction

This article provides a review of plant-based production of industrial enzymes as a sustainable solution to increasing demand. The history of interest in sustainable development, industry and industrial enzymes will

set the background for a detailed analysis of how plant-based production systems compare in terms of sustainability to processes that currently exist. A compilation of potentially useful industrial enzymes produced in plants is given and a discussion of the economic, social, and environmental sustainability advantages provided by plant-based production systems is also provided.

Historical Background of Industrial Enzymes

In view of the importance of enzymes to industrial processes, a brief overview of the events leading to this relationship is provided below.

Development of Applications for Industrial Enzymes

Until mechanization and the industrial revolution, most people eked out a subsistence living using human and animal power for agriculture, production, and transport of people and goods. The industrial revolution eventually made possible tremendous increases in commerce, and consequent social upliftment through improved earnings, literacy, and working conditions. There were costs, however, in degradation of the environment through unregulated expansion of industries and consequent pollution. In 1956, the British Parliament enacted the world's first clean air act. Since then, governments have imposed restrictions on locations of industries and the disposal of pollutants and effluents. These measures have helped considerably to alleviate the impact of pollutants on the environment and health [8], but have been costly to the industries themselves. For example, costs imposed on the meat and meat by-products industries, which include industrial enzymes, are passed on to the consumer through increased prices [9] which is often negative for commerce. Thus, the pressure mounts to lower prices across the board.

An assessment of the true cost of product manufacturing is provided by Life Cycle Assessments (LCA) which measures, usually by mass loadings, the cradle-to-grave impact of every stage from resource procurement, inputs for manufacture, and outputs of wastes throughout the process [10]. Although it is often difficult to predict the LCA of a process, especially impacts on biodiversity and environment, key parameters affecting LCA are renewability of the raw material resource and energy inputs. Enzymes lower the activation energy of chemical reactions and are sourced from renewable resources, and thus should lower impact. A theoretical life cycle comparison between the production of biodiesel using inorganic and enzyme catalysis favored the latter as having lower environmental impact, lowered toxicity, and lowered greenhouse gas emissions, all attributed to lower steam heating requirements [11]. Production of large quantities of enzymes therefore comprises a key consideration for future industrial manufacturing processes.

Current Uses of Industrial Enzymes

Today, many industries use enzymes to manufacture a variety of goods (see Table 1) from food to paper to high-value pharmaceuticals. The utilization of industrial enzymes has now extended to almost all industries handling organic compounds. Enzymes are used in the production of detergents, reagents for the analysis of drugs or blood components, food or food additives, for fiber processing or pulp processing in the paper industry, and for environmental purification. The method of enzyme use also varies, for example, as an enzyme preparation, on the surface of an insoluble carrier in a bioreactor, or a biosensor with the enzyme integrated into an electrode. The annual world industrial enzyme market (excluding pharmaceuticals) is in billions of dollars and is composed largely of enzymes used as detergent ingredients and for food processing applications [12, 13]. Thus, enzymes constitute a key lubricant of commercial success in many fields.

Enzymes are formally classified and given an Enzyme Classification (EC) number by the International Union of Biochemistry and Molecular Biology (IUBMB) based on the reaction that they catalyze (http://www.chem.qmul.ac.uk/iubmb/). Each major category is further divided into subclasses and sub-subclasses. Several enzymes with different trivial or common names may share the same EC number based on the type of reaction that they catalyze (see Table 2). For example, lipases and amylases share the same major category, hydrolases, because they catalyze the breakdown of substrate by hydrolysis. However, enzymes of industrial importance are generally referred to by their trivial name, and trivial names will be used in this review. The source of industrial enzymes can be fungal, bacterial, animal, or plant and with the advent

Plant Molecular Pharming, Industrial Enzymes. Table 1 Enzymes used in various industrial segments and their applications (Reprinted from [13]. With permission from Elsevier)

Industry	Industrial enzyme	Industrial effect/application
Detergent laundry and dish wash	Protease	Protein stain removal
	Amylase	Starch stain removal
	Lipase	Lipid stain removal
	Cellulase	Cleaning, color clarification, anti-redeposition (cotton)
	Mannanase	Mannanan stain removal (reappearing stains)
Starch and fuel	Amylase,	Starch liquefication and saccharification
	Amyloglucosidase	Saccharification
	Pullulanase	Saccharification
	Glucose isomerase	Glucose to fructose conversion
	Cyclodextrin-glycosyltransferase	Cyclodextrin production
	Xylanase	Viscosity reduction (fuel and starch)
	Protease	Protease (yeast nutrition-fuel)
Food including dairy	Protease	Milk clotting, infant formulas (low allergenic), flavor
	Lipase	Cheese flavor
	Lactase	Lactose removal (milk)
	Pectin methyl esterase	Firming fruit-based products
	Pectinase	Fruit-based products
	Transglutaminase	Modify visco-elastic properties
Baking	Amylase	Bread softness and volume, flour adjustment
	Xylanase	Dough conditioning
	Lipase	Dough stability and conditioning (in situ emulsifier)
	Phospholipase	Dough stability and conditioning (in situ emulsifier)
	Glucose oxidase	Dough strengthening
	Lipoxygenase	Dough strengthening, bread whitening
	Protease	Biscuits, cookies
	Transglutaminase	Laminated dough strengths
Animal feed	Phytase	Phytate digestability-phosphorus release
	Xylanase	Digestibility
	β-glucanase	Digestibility
Beverage	Pectinase	De-pectinization, mashing
	Amylase	Juice treatment, low calorie beer
	β-glucanase	Mashing
	Acetolactate decarboxylase	Maturation (beer)
	Laccase	Clarification (juice), flavor (beer), cork stopper treatment

Plant Molecular Pharming, Industrial Enzymes. Table 1 (Continued)

Industry	Industrial enzyme	Industrial effect/application
Textile	Cellulase	Denim finishing, cotton softening
	Amylase	De-sizing
	Pectate lyase	Scouring
	Catalase	Bleach termination
	Laccase	Bleaching
	Peroxidase	Excess dye removal
Pulp and paper	Lipase	Pitch control, contaminant control
	Protease	Biofilm removal
	Amylase	Starch coating, de-inking, drainage improvement
	Xylanase	Bleach boosting
	Cellulase	De-inking, drainage improvement, fiber modification
Fats and oil	Lipase,	Transestrefication
	Phospholipase	De-gumming, lyso-lecithin production
Organic synthesis	Lipase	Resolution of chial alcohol and amides
	Acylase	Synthesis of semisynthetic penicillin
	Nitrilase	Synthesis of enantiopure carboxlic acids
Leather	Protease	Unhearing, bating
	Lipase	De-pickling
Personal care	Amyloglucosidase	Antimicrobial (combined with glucose oxidase)
	Glucose oxidase	Bleaching, antimicrobial
	Peroxidase	Antimicrobial

of molecular techniques, many of the genes for these enzymes have been cloned and transformed into organisms that are easy and convenient to grow in an industrial setting. Optimizing gene expression and culture conditions can increase quantities of enzymes produced and consequently lower costs.

In medicine, the prohibitive cost of insulin isolated from human cadavers created a market for porcine insulin despite the negative side effects. Eli Lilly introduced recombinant insulin in 1982, which decreased the cost to a more manageable level through the use of higher-affinity analogs [14], thereby saving innumerable lives. This price decrease is attributed to the use of transgenic bacteria, improved production methods, and also to lower costs of high-purity protease used to cleave the insulin molecule to active form [15].

Another prominent example today is the use of enzymes in the bioconversion of grain to ethanol [16]. In this case the enzymes very efficiently break down starch to fermentable sugars that can then be used to make ethanol. In the near future the hope is that enzymes will also be used to convert cellulosic material into fermentable sugars as well.

The global industrial enzyme market increased from US $1 billion in 1995 to $1.5 billion in the 5-year period to 2000 with growth rates ranging from 2% to 25% annually [13]. The value of the market created by enzyme technology is much higher, at around $80–130 billion. In case studies by the Organization of Economic Cooperation and Development (OECD), the application of biotechnology has generally benefited by improved costs and sustainability, and

Plant Molecular Pharming, Industrial Enzymes. Table 2 Summary of classes of enzymatic reactions and industrial uses

Enzyme class	Reaction catalyzed	Example of industrial enzyme/use
Oxidoreductases	Oxidation or reduction of substrate	Biocatalysis/fine chemical synthesis
Transferases	Transfer of a group from one molecule to another molecule	Transglutaminases/fine chemical synthesis
Hydrolases	Bond cleavage while water is added	Proteases, esterases/food, beverage and paper pulp
Lyases	Non-hydrolytic cleavage of bond and remove group from their substrate	Pectate lyases/food, beverage
Isomerases	Conversion of one isomer to another	Glucose isomerase/food, beverage
Ligases	Joining of two molecules at the expense of chemical energy	Synthetases/fine chemical synthesis

operational costs lowered by between 9% and 90% [12]. It is projected that the enzyme-based biotechnological industries will continue to grow, fuelled by trends including the demand for chiral chemicals, cost savings, emerging technologies, and sustainable industrial development [12, 17]. Novel enzymatic activities can also be generated without prior knowledge of detailed mechanisms [18], providing further impetus for enzyme-based industries.

Enzyme-based industries have certain advantages compared to traditional chemical manufacturing industries. For example, the production of many specialty chemical compounds, especially pharmaceuticals, relies on the use of chirality, or handedness, since many bioactive compounds and receptors show chirality. Chemical processes generally generate a mixture of compounds that are right-handed and left-handed, and separating them is problematic. Enzymes can be rationally designed to produce specific chiral molecules [19–21]. The worldwide market for single enantiomer drugs exceeds $100 billion [22], making this search a worthwhile investment. In addition, enzymes being proteins are biodegradable and not harmful to the environment or difficult to dispose, unlike traditional chemicals which persist in the environment and are sometimes poisonous or bioaccumulate. For example, paper pulp was traditionally whitened using chlorine-based bleaches which are strongly oxidizing. New whiteners incorporate xylanases which are much less harmful than chlorine in the environment [23], and increase chlorine penetration, allowing less chlorine to be used [24, 25]. Many chemicals used in traditional industrial processes are strongly acidic or basic which may skew the pH of the effluents or cause damage to containers. Some enzymes do require extreme pH or temperatures for activity (e.g., some proteases and enzymes from thermophiles) but most industrial enzymes have moderate pH and temperature requirements, overcoming these problems.

Production of Industrial Enzymes

As the source of industrial enzymes varies, so do production procedures. Enzymes sourced from microbes, as well as transgenic enzymes produced in microbes, are usually grown in fermenters and can be extracted from the microbial cells. A preferred method is to secrete the enzyme into the culture media making extraction and purification much easier [26]. Microbial production utilizes microorganisms that have been modified and evaluated for safety and efficient production. Many have been used since historical times in the manufacture of fermented foods such as beer, cheese, soy sauce, and yogurt [13]. The first US patent granted for a transgenic microorganism with an industrial application was US Patent 4,259,444 following a Supreme Court ruling to Ananda Chakrabarty from General Electric Corporation for developing *Pseudomonas* strains harboring plasmids that could degrade aromatic hydrocarbons [27], and subsequently for mixed culture of *Arthrobacter* and *Pseudomonas* suitable "in the biological treatment of a contaminated

material including many persistent compounds of diverse chemical constitution" [28]. The ease of transformation of bacteria with plasmids and protection by patent law catalyzed the development of an industry of selected organisms producing proteins for various purposes.

Methods to optimize gene expression and enhance protein accumulation and purification continue to be developed. The industrial strains used to produce enzymes today are mostly proprietary and are selected for high production and accumulation levels. However, a disadvantage of bacteria is that proteins are not modified post-translationally and are often insoluble and accumulate into inclusion bodies. This can affect activity, especially when the protein is of eukaryotic origin, and methods to recover active proteins from this inactive conglomeration are often tedious [29].

Yeast is often the microbe of choice to express eukaryotic proteins, but hyperglycosylation of transgenic proteins has been observed. Fungal systems are relatively robust, but they have different metabolic pathways, post-translational processing, codon usage, and may form inclusion bodies [30, 31].

Following selection of an efficient microbial producer, the organism is grown in optimized conditions on media which may be solid or liquid. Most industrial enzymes are generally produced in 50–500 m^3 stirred fermenters. A major challenge with fermenters such as these is to maintain sterility, as contamination can cause loss of the entire batch. The integrity of the high producer must also be monitored to ensure that a lower-producing mutant does not outcompete the high-producing strain. But besides operational costs, capital costs can also be high, which makes this system quite expensive [32].

The same considerations apply to cultures of insect and mammalian cell cultures used to overcome the problems of eukaryotic protein expression seen in microorganisms such as glycosylation, folding, subunit association, γ-carboxylation, and cleavage [33]. For cell cultures, each production scale has to be optimized to the product and may vary from high-value, low-demand products being made in small multiple-unit reactors (flasks or roller bottles) and bulk products in large 10,000 L single-unit batch reactors to be cost-effective [34]. In fermenters, cultured mammalian cells are affected by shear forces and are also sensitive to growth conditions such as pH and temperature, metabolites, and dissolved oxygen, which may affect product quantity and quality [5]. Such variation does not permit streamlining or standardization, and makes animal cultures more expensive to operate.

Enzymes such as catalase from liver and rennet from stomach can also be isolated directly from animal tissues, often as byproducts of the meat industry. Transgenic animal sources have the advantages of appropriate modifications of proteins [33], but problems of scale and costs of production, maintenance, and waste disposal. A serious concern with the use of animals is the risk of contamination of end products, especially when they may be used for human therapeutics or consumption, with animal pathogens such as viruses, mycoplasmas, and prions. More recently, Bovine Spongiform Encephalopathy (BSE) or mad cow disease was shown to be transmitted by contamination by small amounts of infective prions in blood and other animal tissues [35]. This had led to fears of contracting this disease by using protein products derived from animals.

Although plants were one of the first sources to be used to produce industrial enzymes such as papain from papaya and β-amylase from barley, only recently have they been developed as recombinant protein production systems [5, 36]. There are several theoretical reasons why plants may be one of the best sources for the long-term supply of exogenous enzymes including: (1) plants represent the least expensive method to produce proteins in general, (2) they do not require the large amount of capital for production compared to microbial fermenters, (3) production can be scaled up or down without major changes in infrastructure, (4) almost any plant in theory can function as a production system, (5) proteins can be targeted to specific compartments allowing for increased accumulation in the desired tissue with little interference in other tissues to reduce potential toxicity to the cell, (6) plants have convenient storage, transport, and processing of component materials; and (7) plants have the potential to combine lines with different enzymes through crossing [37–39].

There are other advantages. Many pharmaceuticals targeted for use in animals are toxic to animal cells. Plants do not share the same receptors and are capable of accumulating such proteins. Since plants do not

form inclusion bodies, the proteins stay soluble and can be purified more easily. Plants can further be engineered to produce protein in specific tissue, allowing the other parts of the plant to be processed to offset the cost of production. Further, the protein is thereby precluded from interfering with metabolism in other parts of the plant. Proteins can also be targeted to subcellular compartments, further reducing the risk of toxicity, as well as increasing production levels. This potential to express different proteins in different locations allows flexibility in storage and purification options [5, 40–42], and will be discussed in more detail below.

One obvious advantage is that plant-produced biologics are free of animal source tissue, thereby eliminating the fear of transmitting animal pathogens. The lower trophic levels plants occupy as producers is advantageous because it indicates that the energy input into plant growth is lower, and therefore the LCA impact is lower compared with microbes and cell lines grown in fermenters and animals on farms. Plants grown in fields require little more than air, rain, soil, and nutrients. Microbes and animals utilize plant material for growth, and unless they can utilize plant resources at 100% efficiency, they can never be as energy proficient as plants themselves. The low cost of production, ability to post-translationally modify proteins and clear growing, handling, and processing knowhow make plants valuable for industrial enzyme production.

In addition to the advantages of plants listed above, plant systems are particularly well suited to inexpensively yield large amounts of a desired product in a relatively small area. For instance, the cost of transgenic seed for extraction of β-glucuronidase in 1998 was estimated to be only $0.20/kg [43], which was considerably less than bacterial cultures [44]. Moreover, because some plant tissues such as seeds can store proteins for years without loss of activity under ambient conditions, a ready supply of material can be manufactured into final form on an as-needed basis [45]. Propagation from stored seed, rapid scale-up, large volumes, and long-term storage are particularly advantageous for industrial enzymes. Low cost combined with the ability to use the raw material directly for industrial processes encourage development in this direction. These advantages have led to a recent increase in use of this technology for the production of new biologics.

While it seems unlikely that one production system could meet all potential needs for the diversity of products, plants do offer some clear theoretical advantages over other systems. A summary of characteristics of different production systems is shown in Table 3.

Production of Recombinant Proteins in Plants

There are a plethora of plants to choose from for heterologous protein production. The choice of the best plant type depends on how the characteristics of the final product complement the characteristics of the plant. Key factors include the ability of certain tissues to accumulate proteins, detrimental compounds such as toxins that may be produced in certain tissues that can co-purify with the protein products, the potential for the industrial crop to inadvertently mix with other food crops or weeds, the ease of purification of the protein from the plant tissue, and the potential to use the plant tissue directly eliminating the need to purify or extract the protein product. Table 4 lists some of the characteristics of different plant systems that can be used for protein production. While most plant systems can be used in theory, the associated cost can make this unsustainable for many industrial proteins. For high volume, the most cost-efficient system is with commodity grains. Grains provide the advantages of high protein content, feasibility for long-term storage, and the ease of downstream processing which give them great potential for future industrial protein production.

While plants are the least expensive source of biomass, they have not been developed to the extent of their microbial counterparts to accumulate proteins. The cost of producing the proteins is inversely related to the amount accumulated in the biomass so this has a direct bearing on the economics. In the past decades, most of the research on plants has focused on improving traditional uses of plants so there has not been much incentive to look at protein accumulation for use as a production vehicle for protein products. Currently high level of expression in plants is usually recognized at levels of 0.1% of the dry weight of the plant tissue. This leaves much room for improvement in the future.

Plant Molecular Pharming, Industrial Enzymes. Table 3 Features of different industrial enzyme production systems

Production system	Bacterial	Fungal	Animal cell lines	Transgenic animals	Plant
Speed of creating transgenic plants	Rapid	Rapid	Rapid	Slow	Moderate
Capital cost to produce raw ingredients (fermenters, chambers)	High	High	Very high	Low to moderate	Low to moderate
Consumables (media and resources)	Moderate	Moderate	High	Moderate	Low
Processing cost	Moderate	Low	Moderate	Moderate	Low
Production issues	Contamination, maintenance of high producers	Contamination	Contamination, animal pathogens	Animal pathogens	

Plant Molecular Pharming, Industrial Enzymes. Table 4 Characteristics of plant systems for the production of transgenic plants (Reprinted from [39]. With permission from Elsevier)

Crop	Advantages	Disadvantages
Wild species	Clearly distinguishable from crops	Low yield
		Outcross to native plants
		Little known about safety
Domesticated species	High yields	Potential to intermix with crops used for other purposes
	Infrastructure and experience exist	
Food	High margin of safety for human health products	Greater potential to intermix with food supply
Non-food	Less potential to intermix with food supply	Greater potential for toxic, antinutritional, or allergenic agents
Fresh tissue	Abundant biomass	Harvest/Transport/Storage
Seed or dry tissue	Harvest/Transport/Storage	
	High protein content	
Hydroponics, cell cultures	Limited exposure to environment	High cost
		Limited knowledge of product safety
Field grown	Low cost	Higher potential to intermix
	Infrastructure in place	
Modified food/feed grain designed for industrial applications	Clearly distinguished by color/shape	Not yet developed
	Non-transferable genetics	
	Low cost	
	Infrastructure and experience transferable from commodity crop	

Commodity plants currently used as a food, feed, or fiber source are being investigated as a production vehicle for industrial proteins. There has been public concern that use of food plants to produce industrial enzymes or pharmaceuticals may lead to inadvertent exposure to these products and cause safety concerns. Production of industrial or pharmaceutical compounds in organisms used in the food chain is far from new. In addition to the many native products isolated from animals, recombinant food organisms such as yeast or eggs play a major role in the production of pharmaceuticals and industrial proteins. There is also precedent in plants for species that produce both food and industrial products. Rapeseed is used primarily for the production of an industrial oil crop while canola seed which was derived from rapeseed, with subtle genetic differences, is used predominantly as a food crop. The key is to keep food and production streams separate [6] and failure to do so can create problems whether the organism is a traditional food or non-food source.

Current government regulations put plants on par with other production systems to prevent inadvertent products entering the food chain or harming the environment. While many of the industrial enzymes in use today are already in the food chain, these added precautions are necessary to limit exposure or can be used to protect against protein products that may not be in the food chain or have not undergone the rigorous or long-term testing needed to give confidence that there are no detrimental effects.

One concern often voiced by the public is that transgenic plants have the potential for dissemination of the transgene through pollen when grown in an open environment. The pollen may be ingested by non-target species, or hybridize with other plants. This situation has been recognized by regulatory agencies and there are strict controls on containment of transgenic plants and pollen. These include physical isolation and temporal delays as well as molecular containment strategies such as pollen and seed sterility and RNA interference have also been adopted to restrict dissemination [46–48]. These measures can lead to increased costs, but are necessary for safety and to allay public unease about transgenic crops.

The types of industrial proteins can include non-enzyme proteins and enzymes that have industrial use for food, feed, or pharmaceutical applications. This also includes proteins used in the making of pharmaceuticals [49], including plantibodies [50–52] and edible vaccines [53, 54]. This may also include pharmaceuticals such as therapeutics and vaccines but these will not be discussed in this contribution.

Like pharmaceutical products, some industrial proteins may require appropriate post-translational modification and folding to be active. Most higher plants can accommodate this in a manner very similar to that which occurs with animal cells with minor modifications. Since plants do not form inclusion bodies, and since many proteins normally harmful to animal cells do not affect plant cells, plants are increasingly and successfully being used for their production.

One of the main limitations in using plants today to produce industrial proteins is the demand that cost must be extremely low compared to pharmaceuticals. This requires that the expression level be high. There are various options in terms of plant type, tissue, and intracellular location, allowing for great potential. However, this versatility also causes uncertainty in the early stages of developing a plant expression system. In addition, the plant's ability to accumulate a particular hydrolytic or oxidative enzyme has the potential for interference with the plant's metabolism and cause damage to the plant long before protein accumulates. While this has been seen in a number of cases, there have also been various ways to overcome this problem by tissue and subcellular targeting. In addition the use of thermophilic [55] and pro-enzymes [56] or the requirement for cofactors lacking in the plant have all been used to increase protein accumulation [57–59]. A list of enzymes from various sources (bacterial, fungal, animal, and synthetic) produced in plants is given in Table 5. This table provides a snapshot of the accumulation levels of specific proteins in selected tissues and the problems that investigators may have encountered by expressing the protein in the tissue.

Options for Plant Transformation

The transformation technology used to express industrial enzymes can have a major impact on the accumulation of the recombinant protein. Therefore, it is important to select the type of transformation protocol that will best fit the application of the enzyme application. As the transformation process is discussed in

Plant Molecular Pharming, Industrial Enzymes. Table 5 List of industrial proteins produced in plants

Enzyme (gene)	Enzyme function; application in industry	Gene source	Host plant	Maximum expression level	Comments	Reference
α-Amylase	Starch degradation; food and beverages, biofuels, textiles, and paper industries	*Bacillus licheniformis*	Tobacco	0.3% total soluble protein (TSP) in leaf	Unaltered plant phenotype Secreted into intercellular space; extra complex sugar chains added; degradation products identical to native protein	[60]
α-Amylase		*Bacillus licheniformis*	*Nicotiana tabacum* SR1	0.4% TSP in seed	Constitutive expression; hydrolysis products identical to purified *B. licheniformis* α-amylase	[61] European Patent 044,9376
Thermostable α-Amylase		*Bacillus licheniformis*	*Vicia norbonnensis* L.	1 mU/mL seed supernatant	Seed specific USP promoter; accumulation in cotyledon protein bodies; post-translationally modified	[62]
α-Amylase OS103		*Oryza sativa* cDNA	*Nicotiana benthamina*	5% TSP in leaf	Viral infection causes mild chlorosisand stunting; moderate glycosylation of protein in plants	[63]
α-Amylase		*Bacillus licheniformis*	*Medicago sativa*	0.01% TSP in leaf	Unaltered phenotype	[64]
Bifunctional thermostable Amylopullula-nase (APU)	Pullulan and amylose degradation; detergent industry	*Thermoanaero-bacter ethanolicus* 39E (ATCC53033)	*Oryza sativa* L. cv Tainung 67	5.7% total soluble protein in seed	Unaltered phenotype; elevation in pullulanase correlates with decrease in amylose; amyloplast location; starch completely hydrolyzed upon heating	[65]
Aprotinin	Inhibitor of trypsin and proteases; medical and research uses	Optimized bovine aprotinin sequence	Maize	0.4% TSP in seed	Multiple copies in genome; ubiquitin promoter; protein accumulation in seed embryo; transgenic protein biochemically identical to native protein	[66]

Plant Molecular Pharming, Industrial Enzymes. Table 5 (Continued)

Enzyme (gene)	Enzyme function; application in industry	Gene source	Host plant	Maximum expression level	Comments	Reference
Aprotinin cDNA fusion with extension signal		Synthetic bovine	*Nicotiana benthamina*	7,100 trypsin inhibitory units/mg extract protein	Transient TMV virion transfection; product biochemically similar to native protein; large-scale production on 1.5 acres open field or 2,500 sq. ft. greenhouse yields 1 kg purified enzyme.	[67]
Arginine decarboxylase (adc) cDNA	Degradation of arginine; medical and research uses	*Datura stramonium*	Rice	2-fold increase in putrescine levels following stress removal	Under drought conditions, wild-type plants are severely affected, whereas transgenic plants have normal phenotype	[68]
Avidin	Irreversibly binds biotin; research uses	Chicken egg white	*Zea mays*	2.3% TSP in seed; 230 mg/kg seed	Partial to complete male sterility in high expressing plants; similar to native glycoprotein; stable during storage for over 3 months	[69]
Endochitinase (ech42) cDNA	Chitin degradation; research and agricultural uses	*Trichoderma atroviride*	Alfalfa	Up to 2,650-fold higher than control plants	Unaltered phenotype; high expression levels do not correlate with higher resistance to pathogen challenge	[70]
Endocellulase E1	Cellulose degradation; biofuels and paper industries	*Acidothermus cellulolyticus*	*Zea mays* L.	Higher levels in ER than mitochondria; max 2.0% total soluble protein	Targeted to ER and mitochondria; ER targeted E1-cellulase called "Spartan Corn 1"	[71]
Endo-1,4-βD-glucanase (E1 cellulase)	Cellulose degradation; biofuels and paper industries	*Acidothermus cellulolyticus*	*Zea mays* L.	6.1% (ER) and 5.6% (vacuole) TSP in seed	No apparent effect on growth; truncated catalytic domain accumulates in ER and vacuole; 16% TSP in single seed indicates high accumulation potential	[41]
Endoglucanase E1		*Acidothermus cellulolyticus*	Lemna minor 8627	0.24% TSP; 0.2 U/mg protein in fresh tissue	Unaltered phenotype	[72]

Endoglucanase E1		*Acidothermus cellulolyticus*	Tobacco	0.25% total soluble protein in leaf (apoplastic targeting)	Unaltered phenotype; stored seeds had 45% more activity after 1 year	[73]
Endoglucanase E1		*Acidothermus cellulolyticus*	Tobacco	Ammonia explosion (AFEX) treatment yielded 35% original activity	AFEX pretreatment is not a suitable method for releasing cellulase enzymes in transgenic plants	[74]
E1 endoglucanase		*Acidothermus cellulolyticus*	*Nicotiana tabacum*	1.35% TSP in leaf	Chloroplast targeting; normal growth and development; activity decreases with leaf age and upon dehydration	[75]
Cellobiohydrolase I (CBHI)	Cellulose degradation; biofuels and paper industries	*Trichoderma reesei*	*Zea mays* L.	3.2% (cell wall) and 4.1% (ER) TSP in seed	Holoenzyme in cell wall; single seed levels of 17.9% indicate high accumulation potential	[41]
Exo-cellobiohydrolase I (CBHI)	Cellulose degradation; biofuels and paper industry	*Trichoderma reesei*	Tobacco	0.11% TSP in leaf and 66.1 μmol/h/g total leaf protein activity; 0.082% TSP in callus and 83.6 μmol h/g total callus protein activity	Unaltered phenotype	[76]
Thermostable (1–3, 1–4) β-glucanase (codon adapted)		*Bacillus* spp.	*Hordeum vulgare* L. (barley)	40 ng enzyme/2 × 105 protoplasts for codon modified constructs compared to none for unmodified constructs	Biolistic transformation; codon usage important for expression; unaltered phenotype; germination induced expression of enzyme in grain	[77]
β (1–3, 1–4)-glucanase		*Bacillus* spp.	*Hordeum vulgare*	1.29 g/mg TS; 5.4% TSP in grain endosperm	Large variations in enzyme levels between transformants; levels stable for 3 years	[78]
Endo-1,4-β -glucanase (EGI, cellulase)		*Trichoderma reesei* egl1	*Hordeum vulgare* L. Kymppi and Golden Promise	0.025% TSP in seed	Plant morphology normal but reduced seed setting in transgenic plants	[79]
Endoglucanase holoenzyme (E1) and catalytic domain (E1cd)		*Acidothermus cellulolyticus*	*N. tabacum*	1.6% TSP in leaf	Unaltered phenotype; apoplast targeting of catalytic domain achieves 500-fold greater expression than cytosolic full length E1	[80]

Plant Molecular Pharming, Industrial Enzymes. Table 5 (Continued)

Enzyme (gene)	Enzyme function; application in industry	Gene source	Host plant	Maximum expression level	Comments	Reference
1,4-β -D-endoglucanase (E1)		*Acidothermus cellulolyticus*	*Solanum tuberosum* L.	2.6% TSP in leaf	Unaltered phenotype; dual crop applications: leaf targeting allows tubers to be used for culinary applications	[81]
Thermostable endo-1,4-β-D-glucanase		*Acidothermus cellulolyticus*	*Nicotiana tabacum*	Not quantified	Targeting to chloroplast in vitro and in vivo	[82]
Modified endoglucanase cellulase (egl)		*Ruminococcus albus*	BY-2 tobacco suspension cells	0.1% TSP; 30-fold greater truncated form activity than endogenous cellulase	Unaltered phenotype; three forms (pre-form; mature form; truncated form); truncated form has highest expression	[83]
Hybrid (1,4) –β-glucanase (cel-hyb1)		*Neocallimastix patriciarum*	Barley grain	1.5% total grain protein	Endosperm targeted; codon optimization leads to 527-fold increase in expression levels; stable during post-harvest storage	[84]
Catalytic domain endo 1,4-β-D-glucanase (E1cd)		*Acidothermus cellulolyticus*	*Zea mays*	2.1% TSP in leaf and 0.845 nmol/μg/min activity; 2.08% TSP in root and 0.835 nmol/μg/min activity	Set seeds at maturity	[85]
Catalytic domain 1,4-β-endoglucanase E1		*Acidothermus cellulolyticus*	*Zea mays*	1.13% TSP	Unaltered phenotype; apoplast targeted; successful conversion of corn stover into glucose following AFEX pre-treatment	[86]
Thermostable catalytic domain endo-1,4-β-glucanase		*Acidothermus cellulolyticus*	*Oryza sativa* L. Japonica cv. Taipei 309	4.9% TSP	Unaltered phenotype; constitutive promoter; capable of hydrolyzing AFEX-treated stover	[87]
Truncated endoglucanase (t-egl)		*Ruminococcus albus*	Tobacco	0.5% TSP	Unaltered phenotype; cell disruption allows cell wall digestion to occur	[88]

Thermostable 1,4 β -D-endoglucanase catalytic domain		Acidothermus cellulolyticus	*Arabidopsis thaliana*	26% TSP in leaf	No abnormal phenotype; apoplast targeting; activity and immunochemically similar to native enzyme	[89]
Thermostable 1,4-β -D-Endoglucanase E2 and E3		*Thermomonospora fusca*	*M. sativa* L.	E2-0.1% TSP	Unaltered phenotype	[90]
			N. tabacum L.	E3 0.02% TSP		
			S. tuberosum L.			
Thermostable cellulases (Cel6A, Cel6B)		*Thermobifida fusca*	Tobacco	4% TSP	Homoplasmic, transplastomic plants using plastid-directed vector; not optimized	[91]
Recombinant hyperthermostable endoglucanase Cel5A		GenBank accession number At3g4890	Tobacco	5.2% TSP in leaf	Unaltered phenotype; chloroplast targeted; stable active enzymes	[92]
Chimeric chymosin (rennin)	Milk curd formation; dairy industry	Bovine	*Brassica napas*	0.5% (w/w) TSP	Seed targeted	[93] US Patent 7,390,936
Coumarate-3-hydroxylase (C3H)	Lignin modification; biofuels	*Medicago sativa*	*Medicago sativa* cv Regen SY	C3H levels 5% of wild type levels	No serious phenotypic impairment	[94]
Hyperthermo-philic α-glucosidase	Breakdown of maltose; brewing and research uses	*Sulfolobus solfataricus*	*Nicotiana tabacum*	0.04% TSP in leaf	Enzyme levels increase at maturity; unaltered phenotype	[95]
			cv. Xanthi			
Glycosyl hydrolase β-glycosidase	Degradation of glycosidic bonds; biofuels and research uses	*Sulfolobus solfataricus*	Tobacco	0.15% TSP in leaf	Enzyme levels increase at maturity; unaltered phenotype	[95]
ADP-glucose pyrophosphory-lase modified (Sh2r6hs)	Starch synthesis; agricultural and research uses	*Zea mays*	*Triticum aestivum*	5-fold greater protein accumulation	Modified large subunits permit greater stability and yield; endosperm specific promoter	[96]

Plant Molecular Pharming, Industrial Enzymes. Table 5 (Continued)

Enzyme (gene)	Enzyme function; application in industry	Gene source	Host plant	Maximum expression level	Comments	Reference
ADP-glucose pyrophosphorylase modified large subunit (Shrunken 2 gene Sh2r6hs)		*Zea mays* L.	*Triticum aestivum* L.	91% more activity in the presence of 10 mM Pi	Transgenic wheat plants produced 38% more seed weight; 31% higher biomass; transgene stable after five generations	[97]
Human placental β-glucosidase (GCase)	Degradation of glycosidic bonds; biofuels and research uses	Human placenta	Tobacco	750 U/kg seed	Seed viability totally impaired above 500 U/kg; taken up by human fibroblasts; free from immunogenic xylose and fucose	[98]
β-glucuronidase (GUS)	Degradation of glucuronic acid residues; research uses	*E. coli*	*Zea mays*	0.7% TSP in seed	Functionally equivalent to native protein; dispersed in cytoplasm; single integration in transformant with highest expression	[99]
β-glucuronidase (GUS) with αAmy8 regulatory and signal sequence		αAmy8 sequences from rice	Rice, tobacco, and potato suspension cells	40% total secreted proteins	Fusion to β-glucuronidase (GUS); inducible by sugar; tunicamycin causes ER accumulation	[100]
Laccase I	Lignin degradation; biofuels, wood, and paper industry	*Trametes versicolor*	*Zea mays*	0.55% TSP 4 ng/mg dry weight (T2) to 70 ng/mg dry weight (T6)	Variable expression levels; breeding and selection increased levels 20-fold in five generations; embryo-preferred promoter with cell wall targeting supports highest expression; germplasm background affects germination frequency	[110]
Laccase		*Trametes versicolor*	*Zea mays*	0.20% of dried, defatted corn germ	Contains both water soluble and immobilized laccase; some laccase is inactive apoenzyme form	[58]

Laccase riceMaL and ricePcyL cDNA		*Melanocarpus albomyces* *Pycanoporus cinnabarinus*	Rice	13 ppm (riceMaL) 39 ppm (ricePycL)	Endosperm targeted; seed production was normal; recombinant protein is biochemically similar to native proteins, but had lower kinetic parameters	[101]
Lipase	Lipid breakdown; dairy, food, biofuels, and detergent uses	Recombinant dog gastric lipase	Tobacco	5% (vacuolar retention signal) and 7% (secretion signal) of acid extractable protein	Active glycosylated protein with similar properties to native protein; specific activity dependent on subcellular compartment; Normal leaf morphology	[102]
Lipase (rDGL)		Recombinant dog gastric lipase	Maize seed endosperm	Specific activities of 3 U/mg protein(grinding); 3.7 U/mg protein (defatting) and 9 U/mg protein (dry milling)	Comparison of relative efficiency of grinding, defatting, and dry milling of seed prior to selective extraction	[103]
Lipase		Dog gastric lipase	Tobacco	360 U/mg protein	Impact of subcellular targeting on glycosylation; transient expression system	[104]
Manganese-dependent lignin peroxidase (MnP)	Lignin degradation; biofuels, wood, and paper industry	*Phanerochaete chrysosporium*	*Medicago sativa* L.	0.5% TSP in leaf	Reduction in dry matter and height related to expression levels; yellow foliage; MnP expression segregates in sexual progeny	[64]
Manganese peroxidase (MnP)	Lignin degradation; biofuels, wood, and paper industry	*Phanerochaete chrysosporium*	Maize	15% TSP in seed 3% TSP in leaf	Cell wall targeting yields full length MnP; cytoplasmic targeting produces truncated products; seed-targeted promoter has higher expression levels and improved plant health outcomes over constitutive promoter	[59]
Anionic peroxidase cDNA	Lignin structural modification; biofuels, wood, and paper industry	cDNA clone for the primary isoenzyme	*N. tabacum*; *N. sylvestris*	$>10\times$ higher peroxidase activity compared to wild type	CMV35S promoter; chronic severe wilting through loss of turgor in leaves initiated at the time of flowering	[105]

Plant Molecular Pharming, Industrial Enzymes. Table 5 (Continued)

Enzyme (gene)	Enzyme function; application in industry	Gene source	Host plant	Maximum expression level	Comments	Reference
Phytase phyA2	Phytic acid breakdown; animal feed uses	*Aspergillus niger*	Maize	2,200 U/kg of seed	Embryo-specific globulin-1 promoter; different glycosylation pattern; stable over four generations; normal transgenic seed germination	[106]
Phytase		*Schwanniomyces occidentalis*	Rice	4.6–10.6 U/g fresh weight in leaves	Stable in silage for 12 weeks	[107]
Rationally designed phytase		*Aspergillus fumigatus*	*Triticum aestivum* L. (wheat)	4,777 FTU/kg seed flour	Vacuole accumulation despite apoplast targeting; unaltered phenotype	[108]
Secretory phytase (PHY)		Synthetic gene	Potato	40% more phosphate in transgenic plants	Trichoblast-specific promoter; healthy plants, but with altered leaf shape	[109]
Chimeric phytase ex::phyA		*Aspergillus niger*	*Nicotiana tabacum*	3.7-fold more phytase secretion and 52% higher P accumulation in transgenic plants	Presence of soil phytate essential	[110]
Phytase phyA		*Aspergillus niger*	*Triticum aestivum* L.	4-fold increase in plants with constructs with a-amylase signal peptide; 56% increase in plants with constructs without signal peptide; Phytase activity 3,000 FTU/kg	Endosperm, but not embryo accumulation; gene stability over three generations	[111]
Phytase gene		*Aspergillus fumigatus*	Rice Japonica var Taipei 309	130-fold increase in grain phytase level	Unchanged phenotype; coexpressed in endosperm with Phaseolus vulgaris ferritin gene and overexpressed endogenous cysteine-rich metallothionein	[112]

Phytase MtPHY1		*Medicago truncatula*	Arabidopsis	12.3- to 16.2-fold higher levels in root apoplast	Dry weight of transgenic plant upto 4.0 times higher than control and P content up to 5.5-fold higher; root-specific and constitutive promoters used	[113]
Phytase		*Aspergillus niger*	Tobacco	1% TSP in seed	Transgenic seed added directly to chicken feed shows improved nutritional quality	[114]
Phytase GmPhy		*Glycine max* L. Merr.	Soybean tissue culture	2–3 fold higher than controls	Novel phytase similar to purple acid phosphatases	[115]
Phytase cDNA		*Aspergillus niger*	*Nicotiana tabacum*	26% dry weight of leaves 14.4% TSP in leaf	Constitutive expression with secretion signal from tobacco pathogen-related protein S; differences in glycosylation compared with native protein	[116]
Phytase phyA		*Aspergillus niger*	*Brassica napus* (Canola)	600 U/g of multi-copy T1seed; 103 U/g in single copy line	Unchanged morphology; seed-specific CruA promoter used; gene-dosage related expression; stable over three generations; no correlation between high expression and seed germination	[117]
Phytase phyA		*Aspergillus niger*	Soybean cell cultures	920 pKat M/g total soluble protein	Secretion and glycosylation may be necessary for activity; transgenic protein smaller than native protein, but has similar biochemical profile	[118]
Phytase SrPf6 (*S. ruminatum*) appA (*E. coli*)		*Selenomonas ruminantium* *Escherichia coli*	*Oryza sativa* L. cv. Tainung 67.	0.6 U/mg (appA); 1.4 U/mg (SrPf6) of TSP in seed; up to 60 times activity of control	No adverse effects; germination-inducible αAmy8 promoter and αAmy8 signal peptide; multiple copy number	[119]
Phytase cDNA		*Aspergillus niger*	*Medicago sativa*	2.0% TSP	Un-glycosylated, but stable	[120]
Transglutaminase (rTGp)	Formation of peptide bonds; food industry	Rat prostate	*Oryza sativa*	0.15 U/mg h leaf	Ca^{2+} dependent enzyme	[121]

Plant Molecular Pharming, Industrial Enzymes. Table 5 (Continued)

Enzyme (gene)	Enzyme function; application in industry	Gene source	Host plant	Maximum expression level	Comments	Reference
Trypsin	Protein hydrolysis; medical and research uses	Bovine pancreas	Zea mays	0.025% seed dry weight	Equivalent to native enzyme. levels suitable for commercial production; produced as zymogen	[56] US Patent 6,087, 558
Xylanase B xynB	Hemicellulose degradation; biofuels, wood, and paper industry	*Streptomyces olivaceoviridis*	Solanum tuberosum L.	5% TSP in leaf	Stable gene expression for several generations	[122]
Xylanase A xynA thermostable catalytic domain xynA1		*Clostridum thermocellum*	Rice	Not quantified	Normal plant phenotype; stable expression in seed and straw; activity in desiccated seed	[123]
Xylanase xynC-oleosin fusion		*Neocallimastix patriciarum*	Canola	2,000 U/kg seed (oil body of seed)	Fusion protein retains optimal temperature, Km, and specificity, but has reduced pH sensitivity	[124]
Xylanase Modified xynC		*Neocallimastix patriciarum*	Barley	0.004% dry weight of seed endosperm	GluB-1 promoter better than Hor2-4 promoter; protein stable during seed maturation, desiccation, and storage; 40% low fertility in one line;	[125]
Xylanase XYLII		*Trichoderma reesei*	*Arabidopsis*	1.2% (cytosol); 3.0% (chloroplast); 1.7% (peroxisome); 4.8% (chloroplast+peroxisome) total soluble protein	Unaltered phenotype; levels highest at flowering; dual targeting to chloroplasts and peroxisomes causes much higher levels than either compartment alone, although RNA levels are similar	[126]

Xylanase xynII		*Trichoderma reesei*	*Arabidopsis*	3.2% TSP in leaf	Chloroplast expression exhibit normal growth, but cytosolic accumulation affected transgenic plant growth	[127]
Xylanase Thermostable, truncated xyn2		*Clostridum thermocellum*	Tobacco	4.1% TSP in leaf	Unaltered phenotype; proteinase II signal peptide used; enzyme enrichment following heat treatment	[128]
Xylanase Thermostable, truncated xyn2		*Clostridum thermocellum*	*Nicotiana tabacum* L. cv Wisconsin	Not quantitated	Clearance zone develops at 3 h	[42]
xylanse (XYLD-A) and β(1-3, 1-4) glucanase (XYLD-C)		*Ruminococcus flavefaciens*	Tobacco	170 μM/min/m^2 xylanase and 2,000 μM/min/m2 glucanase in leaves	Unaltered phenotype; separate constructs; apoplast targeting; glucanase accumulated higher protein levels than xylanase	[129]
1-deoxy-D-xylulose-5-phosphate synthase DXS gene cDNA (CLA1)	Lignin structure modification; biofuels, wood, and paper industry	*Arabidopsis thaliana*	*Arabidopsis thaliana*	Higher or lower levels than wild type	Normal morphology; variable levels of isoprenoid biosynthetic pathway products correlated with increased or decreased enzyme level	[130]

detail elsewhere, only a brief synopsis of how it impacts industrial enzymes is summarized here.

Both stably transformed and transiently expressing plants have been used to express proteins [131]. In stable transformation, the foreign DNA can be targeted to the cytoplasm or a number of different intracellular locations such as the nucleus [132] or into plastid genomes, usually the chloroplast [133]. Mitochondrial targeting is not as well established and has not been pursued in this context. Organelle transformation provides the advantages of high copy number and the transgenes are not passed on by the pollen [6]. This method however is not yet applicable to many types of plants. Stably transformed plants are time consuming to characterize and generate, but once produced, they can be stored as seed. This allows for a ready source upon demand. Transiently expressing foreign DNA can be inserted into somatic tissue with the purpose of short-term expression using viral vectors delivered using Agrobacterium or biolistics [134–136]. Transient expression is useful when a protein needs to be expressed at short notice.

Selection of Plant Species for Transformation

One consideration for industrial protein production is the type of plant used as the production vehicle. The options include: plants grown for their vegetative tissue for large volumes of biomass; plants harvested for grain for their enriched protein and facile storage characteristics; well-established cultivated crops where much is known about growing and processing; wild species that have little use today, making them distinct; food crops that have Generally Regarded as Safe (GRAS) status and pose no safety threat to the crop itself or host protein but have the potential for intermixing with food crops; or a non-food crop with decreased concerns about intermixing with food crops but with greater potential to have compounds that are detrimental or untested with regard to human safety (see Table 3).

Food crops are known to be safe when consumed and they have well-established procedures for growth, harvest, and storage. In cases where the final product may include some or all of the plant tissue as well as the recombinant protein, this has a significant advantage and direct applicability in the case of many industrial enzymes that are used in the food and feed industry.

For example, maize (*Zea mays*; corn) is well accepted as a safe product (GRAS), and is widely used in food, feed, and industrial applications today [137]. The production cost of maize is very low, and the infrastructure can handle large or small acreages for industrial or pharmaceutical products. Storage and transport of seed, and protein purification from flour are compatible and flexible with current practices without special handling. There are no known agents in maize that generally interfere with protein purification. Finally, the grain can be processed with little or no heat inactivation steps without affecting the protein's properties [4, 138, 139].

In addition, maize has an added advantage in that the kernels can be mechanically separated to yield a germ fraction with enriched protein and an endosperm fraction with enriched carbohydrate [137]. This facilitates use of the carbohydrate fraction for industrial applications such as ethanol production [140] or feed. In this way not only is the cost of the raw material reduced but the waste products are conveniently handled as well.

A disadvantage of maize is the fear of inadvertent mixing with the food supply. Intermixing potential can be handled by management practices but will need to gain the public's confidence. While there may be claims that no food source can ever be used to produce pharmaceutical products, it is common knowledge that both eggs and yeast are used to make pharmaceuticals. Not only is there no public outcry of intermixing in these instances, but their perception is that these production systems are distinct from the systems used to make food. This is the perception that food crops must earn as well. Maize as well as other plant systems must build an infrastructure dedicated to industrial protein production, which is as distinct from food production as edible eggs are from vaccine production. Furthermore, this must also be perceived by the public to reduce fears.

One advantage of non-food crops for industrial protein production is that they are less likely to be mistaken for food crops and therefore unlikely to be inadvertently mixed with the food supply. The disadvantage is that non-food crops must be assessed for toxins, allergens, or anti-nutritional agents that may accompany the recombinant protein. For industrial proteins where little purification is performed to keep

the cost down this can be a considerable problem if the protein precuts are to be used in food or feed applications.

Another question that is relevant to selecting a crop for recombinant industrial protein production is whether a cultivated species or wild species is preferred. Cultivated species show "domestication syndrome" and have several advantages for humans than that their wild relatives exhibit through husbandry and selection over thousands of years [141]. Although non-cultivated species have not undergone selection for higher yields or been subject to agronomic practices in past centuries, there may be yield advantages in crossing domesticated plants with wild relatives, with increase in yields of up to 50% in tomato fruit [142]. Finally, the impact of relatively unknown wild species on product safety is unknown. Determination of the degree of this impact would undoubtedly require extensive effort and time, which may be limiting factors for industry.

A further choice is whether to use an open-pollinated or a self-pollinating plant. Self-pollinating plants have the advantage of a lowered risk that pollen will unintentionally transfer onto other plants of the same species. Controlled pollen shed of open-pollinated crops can be used to help alleviate this concern by either physical or genetic means to prevent out-crossing onto weedy species or related food or feed crops [46–48]. The likelihood of gene transfer from engineered to wild plants depends on sexual compatibility, flowering time, and pollen transfer distance between the engineered and wild varieties [143]. This choice is made based on the growing location and the product required.

With a variety of species to select from and the wide variety of products that are possible, it is highly unlikely that any one system will work best for each of these steps and therefore, it is important to select the plant system that best suits the product. Since it is impractical to have thousands of different production systems, it is preferable to adapt a given system to the needs of various products.

Fortunately, some common features exist that will apply to most products enabling a few systems to accommodate most products. The key features include a potential for low cost of goods, maintenance of protein integrity, flexibility with regard to time and temperature for harvest, and maintenance of product safety and environmental safety [144, 145]. Production systems are discussed below as to how they relate to the overall efficiency of the system as well as to the regulatory aspects.

Selection of Plant Growth System

Transgenic plants can be grown in the traditional manner in an open field or in a contained chamber such as a greenhouse [146]. Row-grown transgenic crops are subject to USDA regulations on buffer zones to limit pollen spread and minimize the risk of the intermixing of food crops with "pharma" crops. If the protein source is green tissue, the plants may be harvested before flowering to limit pollen spread. This is also the case when transient transfection is used to express proteins in leaf and other green tissue. When row plants are required to flower and set seed for protein production, such as is the case for grain-targeted proteins, adequate precautions must be taken to avoid pollen transfer. Row plants are capable of higher product accumulation since they are capable of growth to higher biomass [38].

There are strict regulations and permit requirements imposed by APHIS, the branch of USDA with responsibility for animal- and plant-related services (www.aphis.usda.gov). A practical solution proposed for field growth is to dedicate areas to growth of transgenic plants, or to grow transgenic plants in locations within processing areas, such as cellulose-producing plants in a bioethanol production area [140]. This way the material is grown where it is utilized, cutting transportation costs. Alternatively, the transgenic plant can be isolated in greenhouses in soil or in liquid media. This solution is more expensive, but has the advantage of physical isolation of the transgenic plant from the environment.

The potential for inadvertent transfer of the transgene to non-target plants is considerably reduced by containment in a chamber, but production is necessarily limited by cost considerations. Within a chamber, plants can be grown in soil or in liquid growth media where exudates containing the protein of interest may be continuously produced and has similar advantages to plant cell cultures where proteins are secreted into the culture medium [147]. Scalability may also be an

issue. Exudates from roots also facilitate production when secreted into fluid growth medium [40], but chambers for contained growth in liquid medium can be capital intensive and require sterility and media-related expenses. On the other hand, secretion of transgenic proteins into guttation fluid provides a convenient, but labor-intensive method of recovery of secreted proteins. Proof-of-concept was shown with three transgenic proteins in tobacco, [42]. Using this "phyllosecretion" technology, Komaryntsky and colleagues engineered three proteins from different genetic backgrounds (bacterial xylanase, jellyfish green fluorescent protein and human alkaline phosphatase) into *N. tabacum*. The proteins were fused to endoplasmic reticulum signal peptides targeted to leaf apoplast and released into guttation fluid in plants maintained in high humidity conditions. Guttation fluid has lower overall protein content than apoplast fluid, and is also released throughout the plant's life. In addition to continuous production, the process is non-destructive of plants. Levels of up to 1.1 μg/g of leaf dry weight per day, comprising up to 3% TSP, were recovered from the guttation fluid using simplified downstream processing. Although tobacco is not an ideal plant for guttation fluid production, other plants such as tomato and some grasses are highly susceptible to the production of large quantities of guttation fluid and may provide alternative targets for phyllosecretion.

Optimization of Heterologous Protein Production

Because industrial enzymes require a very low cost of production the most critical factor determining the system of choice is the level of accumulation that occurs in the selected tissue. The optimization of expression of heterologous proteins in plants has been studied for various purposes: to improve nutritional value, insect resistance, salt and drought tolerance, and product quality. These other applications however are not nearly as demanding for the level of expression required as for industrial enzymes. Key steps to increase heterologous protein expression are the choice of plant, tissue location, various manipulations of the promoter, codon usage, and compartmentalization of the protein.

After selecting the type of plant, a determination has to be made about which target tissue is best to express the protein. Location of expression is guided by many factors such as the nature of the protein, whether the protein is to be used directly or purified, and accumulation levels desired. Often, strong constitutive promoters such as the CMV 35S promoter are used, and promoter analysis by site-specific mutations has allowed delineation of sequences that modulate expression in tissue-specific locations of this promoter [148]. *Cis*-acting elements in a green-tissue-specific rice promoter P_{D540} acting as activators or suppressors of activity were identified, thereby facilitating control of protein expression in different tissues [149]. Manipulations such as the use of the embryo-specific maize globulin-1 promoter also allow accumulation of proteins in specific locations within tissues [150]. Expression of the heterologous protein can also be controlled by the use of inducible promoters, and a search of patents reveals a plethora of such inducible promoters. A list of promoters in cereals is compared in [151]. Other promoter permutations including the use of inducible promoters, stacking transcriptional units, synthetic bi-directional promoters, global regulatory sequences to recruit transcription factors, and other such approaches have been studied to enhance transcription and are reviewed elsewhere [152].

Further, heterologous gene sequences should be optimized for the plant type and location. For example, chloroplast codon usage is similar to that of prokaryotes, whereas nuclear codon usage varies from plant to plant. Also, RNA silencing is a feature of many plants, and some viruses produce suppressors of silencing, and heterologous protein sequences are often not expressed at high levels because of RNA silencing [49]. This silencing can be turned off by the expression of the heterologous gene together with a suppressor of silencing [153, 154].

In addition to the choice of tissue location, highest expression levels can be obtained when the protein is directed to specific subcellular compartments and especially so if the protein is an enzyme that would interfere with normal cellular activities [38, 41, 152, 155]. Subcellular targeting is critical for accumulation and protein integrity of hydrolytic enzymes. Cell wall targeting allowed expression of full-length manganese peroxidases, but cytoplasmic targeting resulted in truncation of the peptide [41, 59]. In addition, a seed-preferred promoter allowed high accumulation without negative effects on plant health [59]. Interestingly, targeting xylanase to two subcellular locations – the

chloroplast and the peroxisome – accumulated 240% more enzyme than the chloroplast and 160% more than the peroxisome alone. Highest levels also accumulated during flowering time [126]. These are empirical observations, and such permutations may benefit studies of high-level expression of heterologous proteins. Medrano et al. have developed a transient expression system using *Nicotiana* to assess construct efficiency [156], which may be helpful.

Finally, decisions on the expression of a heterologous protein as a fusion or as a free protein depend upon target location and levels of expression desired. For example, fusions to oleosins accumulate in oil bodies in *Brassica napus* seeds [157], and fusions to proteins previously shown to stably accumulate in plant cells may have the effect of stabilizing heterologous proteins as well [158]. Fusions to the C-terminus of ubiquitin also have a stabilizing effect resulting in 10-fold increased levels [159]. Proteins accumulated at high levels may be subjected to cellular protease activity, thus using cell lines with lower protease levels may help stabilize the heterologous protein. The expression of some proteins, such as hydrolytic enzymes, can be detrimental to the cell. The strategy for the protease trypsin was to express it as a zymogen, allowing sufficiently high levels for commercial production, marketed as TrypZean [56].

Product Recovery from Transgenic Plants

The single most important consideration for recovery is whether the protein produced in plants can be used in crude form in the plant extract, or has to be purified prior to use. Obviously, crude extracts are considerably less demanding to make, but the end use of the protein determines the level of purity required. Purification of transgenic proteins is an expensive prospect, regardless of the system, accounting for about 94% of the production cost in the case of maize [44]. Decisions on recovery should form an integral part of assessing production options based on levels of expression, costs, and sustainability. These decisions are based on the nature of protein to be expressed, and include transient or stable expression, type of plant, targeting, and modifications required.

A variety of elegant solutions have been used to overcome the problems of purification, but vary in costs and efficiency. For example, roots have been used to secrete proteins into the growth medium, and guttation liquid produced by plants also provide a useful medium for secretion-based isolation of the transgenic protein, as the growth or secreted liquid can be recovered and filtered for protein recovery [42, 49]. However, they are considerably more labor and energy intensive due to growth in liquid medium as discussed above, and recovery varies based on loss due to dilution factor and protein stability in an extracellular environment [160].

When whole plants are used as production systems, the recovery process depends on the tissue being used for expression. Transient expression in roots or leaves generally requires processing of fresh wet tissue. If stable expression is used, the material may be wet or relatively dry depending on the tissue used. Proteins extracted in fresh tissue are generally unstable and have to be recovered immediately, whereas seed-expressed proteins have shelf-life as long as 3 years [45]. Grain can be subjected to either wet or dry milling followed by separation steps. These include fractionation to obtain enrichment of germ or endosperm in the case of seed, or subcellular compartments targeted for protein accumulation, protein precipitation, adsorption, chromatography, and diafiltration [44]. Methods have been developed to simplify recovery such as post-harvest protein expression using stress-inducible promoters [45, 161] and oleosin-partitioned proteins that can be recovered easily following oil-water separations [124, 162, 163]. A detailed comparison of the economics, processing, and regulatory constraints associated with the most common plant production systems is provided in [145].

In the ideal case, commodity plants that are used for industrial applications would also express the transgenic protein. These transgenic proteins can then be used directly in the industrial process without purification assuming the protein can survive the processing steps. In this best-case scenario, no other inputs are needed to produce, purify, or process the protein leading to lower cost and less detrimental impact on the environment.

Case Study: Economics of Cellulases Produced from Transgenic Plants With the current state of technology for biomass conversion, the overwhelming enzyme

requirement is for cellulases: endo-cellulase, exo-cellulase, and glucosidase [164]. The specific activity of most cellulases is quite low [155, 165] and much effort has focused on increasing their activity levels. However, even with improved enzymes and improved methods of production, the amount of cellulase required to deconstruct the volumes of biomass necessary for 30% replacement of gasoline are in the millions of tons. It has been estimated that 36 billion gallons can require as much as 3.6 million metric tons of cellulase per year [166]. This is an unprecedented challenge in terms of the amount of enzymes and the extreme low cost that is required.

The bioprocessing challenge for ethanol is how to deliver these extremely large volumes to a saccharification facility at an unprecedented low cost. This represents potentially the single greatest application of industrial enzymes.

Currently, cellulases are produced by fungal and bacterial systems, and are a costly component of ethanol production [167]. Plants offer the potential for a production system that can meet the low cost and high volumes required. To do this however, the level of expression needs to be extremely high and the choice of tissue needs careful consideration. There have been many attempts to express cellulase in many types of plants and these have been reviewed elsewhere [37]. Protein and tissue stability, tissue fractionation, protein extraction and formulation, storage, as well as transportation add to this cost and must be considered.

To achieve targeted production cost targets for biomass enzymes the following considerations must be employed: (1) eliminate transportation cost by integrating enzyme processing into biomass conversion facility; (2) minimize fractionation/extraction cost of transgenic material; and (3) reduce the contribution of transgenic plant material to enzyme production cost by capturing plant biomass value through byproduct credits or cellulose. It has been suggested [166] that in order to keep the enzyme cost down, plant production systems that accumulate cellulase in the normally unused or low-value portion of the plants can be competitive when the other parts of the plant are harvested for their traditional use. The obvious example is when the leaves of crops are used to produce the cellulase and the grain is used for food, feed, or other industrial applications. Using the grain for industrial applications is less of a regulatory burden than if the grain is to be used for food or feed. However, according to the US Food and Drug Administration Statement of Policy (http://www.fda.gov/Food/GuidanceComplianceRegulatoryInformation/GuidanceDocuments/Biotechnology/ucm096095.htm) this is still an option, "If plants (or materials derived from plants) used to make nonfood chemicals are also intended to be used for food, producers should consult with FDA to determine whether the non-food chemical would be a food additive requiring an authorizing regulation prior to marketing for food use." These guidelines may change and may vary between countries; therefore, current regulatory practices must be consulted and followed in each case.

A case has been proposed for a fully integrated and synergistic system of ethanol production using maize. Maize grain today is the major source of ethanol production in the USA [168]. Using the stover to make cellulosic ethanol has been proposed as a convenient, economical, and sustainable way to make cellulosic ethanol alongside grain ethanol allowing for lower transportation costs and synergy in the ethanol facilities [170].

Taking this approach one step further, it has been suggested that the leaves themselves can be used to generate the required enzymes [155]. This has great potential if the enzymes can survive in the processing steps and can reach the target levels.

Another option has been proposed using the germ fraction of the grain [140]. In this case the enzymes could be made in the germ which is separated in the dry milling prior to using the endosperm for grain ethanol. The acreage required to grow crops to produce this amount of enzymes has been modeled previously considering the proximity limitations of the lignocellulose biomass to the ethanol facility to avoid large transportation cost. This study demonstrated that if cellulase levels were 0.1% of the dry weight of the seed (1% of germ dry weight), this was more than sufficient to keep the acreage of the cellulase crop less than the acreage needed to supply the lignocellulose biomass. Additional models suggest that when expression levels reach 4% of the dry weight of tissue (0.4% weight of the grain) it may be possible to add the germ tissue without any fractionation [166]. Direct delivery of plant tissue can be the system of choice by eliminating

extraction and purification costs. In addition to the cost of production, this approach allows the entire plant to better utilized without additional acreage or input for growing the plants. There is also no additional stress on the environment due to making or processing the enzymes and this has the potential to meet the current volumes of cellulase projected at a cost below current targets.

The main reason why this is not in use today is that cellulase has not enjoyed the levels of expression required for the models above. However, there is every reason to believe that expression levels will continue to improve in plants as it is a relatively young science compared to microbial production. In maize specifically it has been reported that levels as high as 16% of the total soluble protein were observed [41] and more recently levels of >1% of dry weight in the germ fraction has been achieved [169].

Regulation of Growth and Use of Transgenic Plants

Assuming that one can create plants having industrial enzymes with the characteristics and cost benefits that are desirable, there is still the need to grow these on a commercial scale. The process of growing transgenic plants is highly regulated including those grown for research purposes. However, for research purposes, cost is not a primary concern and the environmental impact is usually minimal due to the small acreage. However, this changes dramatically during scale-up for commercialization. Assuming a yield of 1–10 kg industrial enzyme per acre would require 100–1,000 acres for a relatively low volume of industrial enzymes but this can increase 10- to 1,000-fold for larger volume enzymes. Therefore, the potential for certain individual enzymes to be greater than 100,000 acres creates regulatory scenarios that are much more complex than those addressed in a research environment.

Regulatory systems are a social issue and vary in different countries but they all address human and animal safety as well as environmental implications. They must also address perhaps the most controversial issue, public acceptance. The technical aspects of regulatory concerns are discussed below with the understanding that every country will have its own interpretation and standards for what is acceptable.

Product Safety

The first concern for any product is the inherent safety of the active ingredient. Having a production system different from the native host does not usually change the inherent properties of the enzyme itself. Factors such as exposure to humans, dosage, toxicity, allergenicity, and whether or not the proteins are already a part of the food chain are considered. It is not the intent of this entry to review the regulatory process in detail but rather to point out the difference when using plants as the production vehicle as opposed to other sources. Therefore, the focus is not on the inherent safety of the enzyme but what safety factors arise when produced in plants and what additional challenges are presented with plant production.

For products that have already undergone regulatory approval, it is critical to show, utilizing empirical data, that there is equivalency with the plant-produced process. In many cases plants can produce functionally and chemically equivalent proteins to those made in the native hosts. However, there may be exceptions which in turn can lead to difference in protein structure or function. These differences may be subtle such as a small signal peptide intended to target the protein to the vacuole that is not cleaved and instead retained in the final protein sequence, or carbohydrate structures could be added where none existed before. These types of changes may have no impact on function and may be acceptable in commercial products.

In contrast to that above, some changes may result in proteins that have altered functions or altered safety profiles. As an example, many industrial enzymes are bacterial in origin and therefore are not normally glycosylated proteins. If these bacterial proteins happen to have a glycosylation site that a eukaryote can recognize then that can create a challenge. The possibility exists that the enzyme will be glycosylated when expressed in eukaryotes and potentially lead to a change in function. Fortunately there is little evidence to suggest that glycosylation itself will change enzyme function unless the carbohydrate is added to a key amino acid either in the binding site or catalytic site. An example of this is the bacterial enzyme β-glucuronidase (GUS). GUS protein loses activity due to secretion-specific N-glycosylation of a key amino acid in the protein [171]. Contrary to this

observation, other proteins can be glycosylated such as the bacterial protein organophosphate hydrolase with no significant effect on its biochemical activity [57].

Glycosylation patterns in plants can also be different from those observed in other eukaryotes. Plant glycoproteins contain the same mannose backbone structure found in animal glycoproteins but the additional sugars added to the backbone are usually less complex in plants than animals. Another difference is in β−1-4 linkage versus β−1-6 linkage and the appearance of xylose. In one case the animal protein trypsin was produced in plants and showed evidence of O-glycosylation whereas it is not detected from the native porcine or bovine source [56]. Despite these changes no functional difference in catalytic activity has been observed.

In addition to catalytic activity, there is also the concern that the enzyme may be altered in a way that affects its activity in the desired application. There is little evidence of this for industrial enzymes but there are examples for where carbohydrate structures on proteins can affect their pharmacological properties. In the case of certain pharmaceutical proteins, sialic acid is a terminal sugar on the glycoprotein and leads to a longer half-life in the blood [172]. Since plants do not add sialic acid this leads to an alteration in clearance time in the blood [173]. On the other hand, the plant carbohydrate sequence for antibodies is also critical in vivo but the altered plant sequence appears to work as well as the animal carbohydrate sequence [174]. This demonstrates the need to test the industrial enzymes in the desired application when the composition of matter is different than the native source.

Demonstrating functional equivalency is still not enough from a regulatory standpoint. The addition of carbohydrates has been implicated in a number of studies for allergenicity. This raises the theoretical question of whether plant glycosylation can lead to allergenicity. On the surface this seems highly unlikely since plant proteins are eaten routinely, and plant glycoproteins would seem inherently safe. Therefore, just adding a plant carbohydrate does not make the protein allergenic. On the other hand, there have been reports showing that the carbohydrate sequence of pollen glycoproteins [175] is responsible for an allergenic reaction. Therefore, while generalizing that plant carbohydrates are allergenic is misleading, it is important not only to check whether there is glycosylation but aslo to find out how this may differ from the native source. While there are no current examples where the addition of a plant-specific glycosylation to a transgenic protein has lead to an increase in allergenicity there is still a theoretical concern.

Safety of Host Proteins

While inherent activity is a functionality concern, the addition of extraneous host material is also a regulatory issue. Since most industrial enzymes cannot be purified because of cost restraints, the host material must also be shown to be safe in the final product. For this reason production in plants that already have a proven history of safe use is a great advantage. Certain crops that are known to produce toxins, allergens, antinutritionals, or carcinogens present additional difficulties as hosts. Crops already known to have GRAS (generally regarded as safe) status will be at an advantage because of inherent safety of the crop. In the best case a GRAS enzyme can be produced in a GRAS host greatly reducing the regulatory burden [176].

Environmental Safety

The environmental impact of protein production from a regulatory standpoint can be a concern based on the additional acreage. The consequence of additional inputs, displacement of food crops, and the lack of containment leading to inadvertent exposure to animals and humans must be addressed [177].

Dedicated cropland for the sole purpose of producing industrial enzymes will in most cases be insignificant compared to the acreage already under development for current uses, if produced in tandem with commodity crops. Since expression levels must be high to keep costs low for industrial products, this translates into only a very small percentage (∼1%) of the acreage for even large-volume products. The exception to this scenario is if the by products can be utilized for other, value-added purposes, such as for biomass or feed. In such cases, there is no additional impact either in acreage or inputs.

Of greater concern is the issue of containment and inadvertent exposure. Regulations to evaluate containment of transgenic plants are similar in concept to

those for other hosts, but specifics are very different. One of the areas historically concerning the production process of industrial enzymes is the occurrence of allergenic reactions developed by workers in the production facility. This has led the industry to safer forms of controlling small-particle exposure during microbial production. The concern for plant is that pollen from production fields can act as a carrier of the protein and lead to exposure similar to that observed for microbial production. For this reason, it is suggested that expression of the protein be specific to tissues other than pollen, thereby eliminating this concern.

Field production has the potential to affect wildlife where the crop is grown. Unlike many applied pesticides, transgenic plants are generally non-toxic to wildlife. This may reduce the environmental threat as opposed to many chemicals. The specific protein produced still may have some unwanted effects on wildlife and this aspect needs to be addressed, particularly for endangered species that may be present in the production field. Products that require larger acreage will create more concerns.

The final evaluation and perhaps the most controversial is the potential impact for the industrial enzyme for inadvertent exposure into the food chain. This may occur for several theoretical reasons, including mislabeling of seed, spills during transport, or pollen dissemination into food crops or wild relatives. Pollen dispersion has received the most attention as the other possibilities of inadvertent exposure most likely because the other potential sources are similar to that of other host production systems. To control the flow of pollen several different methods can be employed. These range from male sterility systems and physical isolation of the crops from compatible agricultural crops or weeds. In addition, systems have been proposed for growing transgenic crops within an industrial crop zone thereby further reducing the possibility of inadvertent mixing [140].

The underlying assumption for the production of transgenic proteins produced in plants is that they must be kept at all times isolated from food crops. This is essential for proteins that have the potential for detrimental effects on the population. However, many industrial proteins are used in food processing or derived from material already in the food chain. In these cases the transgenic proteins have the potential to be deregulated. After demonstrating that there is no danger to human safety the strictest of containment conditions may be dropped although some containment may still be desirable, either from a regulatory standpoint or from a commercial necessity.

Plants as Sustainable Sources of Industrial Enzymes

Plants have the potential to provide a sustainable source of industrial enzymes. Most plants can be transformed stably or used to express transiently heterologous proteins at levels that can be used for industrial production. The key sustainable feature of plants is that they are a renewable resource. They do not require intensive efforts for growth and maintenance of sterility, although some may require containment. Even so, the infrastructure and capital investment for growing plants is considerably less than that for fermentation of microbes. In addition, plant waste can be disposed of without intensive treatment, unlike effluents from fermenters. Energy resources for plant growth are also lower than those for maintenance of temperature and sterility of fermenters. In addition, formulations of large volumes of media for culture represent a large input of water, often a limiting resource. Cooling of large fermentation chambers is also energy intensive. These considerations are less severe with plants. Although plants do need regular and sustained watering, they can be grown in traditionally non-irrigated areas or in irrigated land where the input can be spread out using efficient drip hoses and watering procedures over a long period of time, alleviating the need for vast quantities of sterile water at short notice. The water does not need to be sterile, which reduces the energy burden and thereby the LCA.

The projection of 2–25% annual growth of enzyme requirement indicates a massive increase in enzyme production if supply is to keep pace with demand. Large volumes of enzymes imply that a number of fermenters have to be constructed to produce microbial- or cell-culture-based enzymes, or a shift of paradigms to a more efficient supply. Plants can provide the large volumes of enzymes needed with relatively low capital investment, and may represent the only really low-cost option for providing the immense requirements of industrial enzymes anticipated with projected

growth. Depending on the level of purification required, the enzymes can either be used without purification (such as for the production of biofuels) or undergo processing (such as for pharmaceuticals). This decreased processing obviously lowers environmental impact of the procedure. Tissue from plants that are not target for protein accumulation can be processed or disposed of such as to provide a financial buffer to the industrial enzyme production aspect.

The key to using plants for the production of industrial proteins is the increasing expression of transgenic proteins to levels commensurate with economic recovery of protein. A search of the Sigma Aldrich Chemical Company for transgenic-plant-derived products showed that proteins expressed in rice (avidin, lactoferrin, lysozyme), corn (avidin, trypsin), and tobacco (tissue factor proteinase inhibitor II, bovine aprotinin) are commercially marketed. Cell Sciences (www.cellsciences.com) produces over 25 cytokines and growth factors from barley endosperm, especially marketable as they are animal, bacterial, and viral-free. These are fine chemicals produced with high purity, but evidently are also commercially viable, providing a proof of potential. Increasing accumulation levels in plant tissue is an important issue for commercial success.

Storage of enzymes is also energy consuming when produced from microbial fermentation. The protein is usually lyophilized for storage; an energy-intensive process requiring freezing and desiccation simultaneously. Green tissues from plants have to be processed immediately, frozen or dried for protein stability. However, proteins expressed in seeds have been shown to maintain stability, even at room temperature, for at least 3 years without noticeable degradation [45]. This decreases the LCA and increases sustainability, as well as facilitating rapid response to spikes of increased demand.

Plant-based production also results in less waste. The unused portions of the plant body can be funneled into other uses, such as ethanol from biomass, and there is little waste from the recovery process compared to effluents from fermenters, lower waste disposal requirements, and lower net production of greenhouse gases, which is better for environmental sustainability and society.

Future Directions

Plants have historically contributed to industrial processes from dyes and tannins for fabric and leather to drugs for healthcare and pharmaceuticals. The first generation of plant-derived recombinant proteins is now commercially available and the prospects of more products is in the pipeline with many groups working on expressing high levels of laccases, cellulases, plantibodies, and pharmaceutically important proteins. In some cases, enzymes can be directly delivered in the plants, such as cellulolytic enzymes expressed in plants to improve their degradation for production of bioethanol. Alternatively, enzymes can be expressed at high levels and isolated for industrial processes. In order to sustain either process, plants should accumulate proteins in sufficient quantities. Protein targeting to improve expression levels is a topic of major interest and additional studies on inducible expression are being pursued to enhance utility.

Currently, there is a major push to find and utilize renewable energy more efficiently. Plant starch and sugars are major sources of bioethanol, but their production from otherwise discarded lignocellulosic material hold out great promise for fuel production, enabling the real possibility of national fuel self-sufficiency. Plants are a renewable resource, and lower the LCA of processes since energy input into their production is substantially lower than other production systems. In addition, most products of plants can find use elsewhere for feed, silage, or biomass for renewable fuel production. The benefits of large-scale increases with little effort, lower costs, and potential to offset costs with downstream use of waste solely accrue to plants, making this a technology worth investing in.

Bibliography

1. Brown T, Jones M, Powell W, Allaby R (2009) The complex origins of domesticated crops in the fertile crescent. Trends Ecol Evol 24:103–109
2. Hallauer A (2007) History, contribution, and future of quantitative genetics in plant breeding: lessons from maize. Crop Sci 47:S4–S19
3. Raskin I, Ribnicky D, Komarnytsky S, Ilic N, Poulev A, Borisjuk N, Brinker A, Moreno D, Ripoll C, Yakoby N (2002) Plants and human health in the twenty-first century. Trends Biotechnol 20:522–531
4. Giddings G (2001) Transgenic plants as protein factories. Curr Opin Biotechnol 12:450–454

5. Giddings G, Allison G, Brooks D, Carter A (2000) Transgenic plants as factories for biopharmaceuticals. Nat Biotechnol 18:1151–1155
6. Murphy D (2007) Improving containment strategies in biopharming. Plant Biotechnol J 5:555–569
7. Chapotin S, Wolt J (2007) Genetically modified crops for the bioeconomy: meeting public and regulatory expectations. Transgenic Res 16:675–688
8. Hansell A, Knorr-Held L, Best N, Schmid V, Aylin P (2003) Copd mortality trends 1950–1999 in England and Wales – did the 1956 clean air act make a detectable difference? Epidemiology 14:S55
9. Hazilla M, Kopp R (1990) Social cost of environmental quality regulations: a general equilibrium analysis. J Polit Econ 98:853–873
10. Owens J (1997) Life-cycle assessment: Constraints on moving from inventory to impact assessment. J Ind Ecol 1:37–49
11. Harding K, Dennis J, Von Blottnitz H, Harrison S (2008) A life-cycle comparison between inorganic and biological catalysis for the production of biodiesel. J Cleaner Prod 16:1368–1378
12. van Beilen JB, Li Z (2002) Enzyme technology: an overview. Curr Opin Biotechnol 13:338–344
13. Kirk O, Borchert T, Fuglsang C (2002) Industrial enzyme applications. Curr Opin Biotechnol 13:345–351
14. Vajo Z, Fawcett J, Duckworth W (2001) Recombinant DNA technology in the treatment of diabetes: insulin analogs. Endocr Rev 22:706–717
15. Swartz J (2001) Advances in *Escherichia coli* production of therapeutic proteins. Curr Opin Biotechnol 12:195–201
16. Haki G, Rakshit S (2003) Developments in industrially important thermostable enzymes: a review. Bioresour Technol 89:17–34
17. Hatti-Kaul R, Törnvall U, Gustafsson L, Börjesson P (2007) Industrial biotechnology for the production of bio-based chemicals – a cradle-to-grave perspective. Trends Biotechnol 25:119–124
18. Seelig B, Szostak J (2007) Selection and evolution of enzymes from a partially randomized non-catalytic scaffold. Nature 448:828–831
19. Jaeger K, Eggert T (2004) Enantioselective biocatalysis optimized by directed evolution. Curr Opin Biotechnol 15:305–313
20. Bornscheuer U, Pohl M (2001) Improved biocatalysts by directed evolution and rational protein design. Curr Opin Chem Biol 5:137–143
21. Cherry J, Fidantsef A (2003) Directed evolution of industrial enzymes: an update. Curr Opin Biotechnol 14:438–443
22. Jaeger K, Eggert T, Eipper A, Reetz M (2001) Directed evolution and the creation of enantioselective biocatalysts. Appl Microbiol Biotechnol 55:519–530
23. Louwrier A (1998) Industrial products-the return to carbohydrate-based industries. Biotechnol Appl Biochem 27:1–8
24. Zhao J, Li X, Qu Y (2006) Application of enzymes in producing bleached pulp from wheat straw. Bioresour Technol 97:1470–1476
25. Dyer T, Ragauskas A (2002) Developments in bleaching technology focus on reducing capital, operating costs. In: IPST Technical Paper Series Number 929 (Paper, P. a., Ed.)
26. Headon D, Walsh G (1994) The industrial production of enzymes. Biotechnol Adv 12:635–646
27. Chakrabarty A (1981) Microorganisms having multiple compatible degradative energy-generating plasmids and preparation thereof. US Patent No 4,259,444, Google Patents (Office, U. P., Ed.), General Electric Company, United States
28. Chakrabarty A, Kellogg S (1985) Bacteria capable of dissimilation of environmentally persistent chemical compounds. US Patent No 4,535,061. University of Illinois Foundation, United States
29. Sahdev S, Khattar S, Saini K (2008) Production of active eukaryotic proteins through bacterial expression systems: a review of the existing biotechnology strategies. Mol Cell Biochem 307:249–264
30. Twyman R, Schillberg S, Fischer R (2005) Transgenic plants in the biopharmaceutical market. Expert Opin Emerg Drugs 10:185–218
31. Dominguez A, Ferminan E, Sanchez M, Gonzalez F, Perez-Campo F, Garcia S, Herrero A, San Vicente A, Cabello J, Prado M (1998) Non-conventional yeasts as hosts for heterologous protein production. Int Microbiol 1:131–142
32. McAloon A, Taylor F, Yee W, Ibsen K, Wooley R (2000) Determining the cost of producing ethanol from corn starch and lignocellulosic feedstocks. National Renewable Energy Laboratory Report, NREL, Fort Collins, CO
33. Houdebine L (2009) Production of pharmaceutical proteins by transgenic animals. Comp Immunol Microbiol Infect Dis 32:107–121
34. Kretzmer G (2002) Industrial processes with animal cells. Appl Microbiol Biotechnol 59:135–142
35. Prusiner S, Scott M, DeArmond S, Cohen F (1998) Prion protein biology. Cell 93:337–348
36. Ragauskas A, Williams C, Davison B, Britovsek G, Cairney J, Eckert C, Frederick W Jr, Hallett J, Leak D, Liotta C (2006) The path forward for biofuels and biomaterials. Science 311:484
37. Sainz M (2009) Commercial cellulosic ethanol: the role of plant-expressed enzymes. In Vitro Cell Dev Biol Plant 45:314–329
38. Twyman RM, Stoger E, Schillberg S, Christou P, Fischer R (2003) Molecular farming in plants: host systems and expression technology. Trends Biotechnol 21:570–578
39. Howard JA, Hood E (2005) Bioindustrial and biopharmaceutical products produced in plants. Adv Agron 85:91–124
40. Borisjuk N, Borisjuk L, Logendra S, Petersen F, Gleba Y, Raskin I (1999) Production of recombinant proteins in plant root exudates. Nat Biotechnol 17:466–469
41. Hood E, Love R, Lane J, Bray J, Clough R, Pappu K, Drees C, Hood K, Yoon S, Ahmad A (2007) Subcellular targeting is a key condition for high-level accumulation of cellulase protein in transgenic maize seed. Plant Biotechnol J 5:709–719
42. Komarnytsky S, Borisjuk N, Borisjuk L, Alam M, Raskin I (2000) Production of recombinant proteins in tobacco guttation fluid. Plant Physiol 124:927–934

43. Evangelista R, Kusnadi A, Howard J, Nikolov Z (1998) Process and Economic evaluation of the extraction and purification of recombinant β-glucuronidase from transgenic corn. Biotechnol Prog 14:607–614
44. Doran P (2000) Foreign protein production in plant tissue cultures. Curr Opin Biotechnol 11:199–204
45. Fischer R, Stoger E, Schillberg S, Christou P, Twyman R (2004) Plant-based production of biopharmaceuticals. Curr Opin Plant Biol 7:152–158
46. Daniell H (2002) Molecular strategies for gene containment in transgenic crops. Nat Biotechnol 20:581–586
47. Lee D, Natesan E (2006) Evaluating genetic containment strategies for transgenic plants. Trends Biotechnol 24:109–114
48. Lin C, Fang J, Xu X, Zhao T, Cheng J, Tu J, Ye G, Shen Z (2008) A built-in strategy for containment of transgenic plants: creation of selectively terminable transgenic rice. PLoS ONE 3:e1818
49. Lienard D, Sourrouille C, Gomord V, Faye L (2007) Pharming and transgenic plants. Biotechnol Annu Rev 13:115–147
50. Daniell H, Streatfield S, Wycoff K (2001) Medical molecular farming: production of antibodies, biopharmaceuticals and edible vaccines in plants. Trends Plant Sci 6:219–226
51. Stoger E, Sack M, Fischer R, Christou P (2002) Plantibodies: applications, advantages and bottlenecks. Curr Opin Biotechnol 13:161–166
52. Orzáez D, Granell A, Blázquez M (2009) Manufacturing antibodies in the plant cell. Biotechnol J 4:1712–1724
53. Streatfield S, Howard J (2003) Plant production systems for vaccines. Expert Rev Vaccin 2:763–775
54. Lamphear B, Jilka J, Kesl L, Welter M, Howard J, Streatfield S (2004) A corn-based delivery system for animal vaccines: an oral transmissible gastroenteritis virus vaccine boosts lactogenic immunity in swine. Vaccine 22:2420–2424
55. Borkhardt B, Harholt J, Ulvskov P, Ahring B, Jørgensen B, Brinch-Pedersen H (2010) Autohydrolysis of plant xylans by apoplastic expression of thermophilic bacterial endo-xylanases. Plant Biotechnol J 8:363–374
56. Woodard S, Mayor J, Bailey M, Barker D, Love R, Lane J, Delaney D, McComas-Wagner J, Mallubhotla H, Hood E (2003) Maize (*Zea mays*)-derived bovine trypsin: characterization of the first large-scale, commercial protein product from transgenic plants. Biotechnol Appl Biochem 38:123–130
57. Pinkerton T, Howard J, Wild J (2008) Genetically engineered resistance to organophosphate herbicides provides a new scoreable and selectable marker system for transgenic plants. Mol Breed 21:27–36
58. Bailey M, Woodard S, Callaway E, Beifuss K, Magallanes-Lundback M, Lane J, Horn M, Mallubhotla H, Delaney D, Ward M (2004) Improved recovery of active recombinant laccase from maize seed. Appl Microbiol Biotechnol 63:390–397
59. Clough RC, Pappu K, Thompson K, Beifuss K, Lane J, Delaney DE, Harkey R, Drees C, Howard JA, Hood EE (2006) Manganese peroxidase from the white-rot fungus *Phanerochaete chrysosporium* is enzymatically active and accumulates to high levels in transgenic maize seed. Plant Biotechnol J 4:53–62
60. Pen J, Molendijk L, Quax W, Sijmons P, van Ooyen A, van den Elzen P, Rietveld K, Hoekema A (1992) Production of active *Bacillus licheniformis* alpha-amylase in tobacco and its application in starch liquefaction. Nat Biotechnol 10:292–296
61. Pen J, Hoekema A, Sijmons P, Van Ooyen A, Rietveld K, Verwoerd T, Quax W (1991) Production of enzymes in seeds and their use. Gist-Brocades N.V. (Wateringseweg 1 P.O. Box 1, MA Delft, NL-2600, NL) Mogen International N.V. (Einsteinweg 97, CB Leiden, NL-2333, NL) European Patent
62. Czihal A, Conrad B, Buchner P, Brevis R, Farouk A, Manteuffel R, Adler K, Wobus U, Hofemeister J, Bäumlein H (1999) Gene farming in plants: expression of a heatstable *Bacillus* amylase in transgenic legume seeds. J Plant Physiol 155:183–189
63. Kumagai M, Donson J, Della-Cioppa G, Grill L (2000) Rapid, high-level expression of glycosylated rice-amylase in transfected plants by an RNA viral vector. Gene 245:169–174
64. Austin S, Bingham E, Mathews D, Shahan M, Will J, Burgess R (1995) Production and field performance of transgenic alfalfa (*Medicago sativa* L.) expressing alpha-amylase and manganese-dependent lignin peroxidase. Euphytica 85:381–393
65. Chiang C, Yeh F, Huang L, Tseng T, Chung M, Wang C, Lur H, Shaw J, Yu S (2005) Expression of a bi-functional and thermostable amylopullulanase in transgenic rice seeds leads to autohydrolysis and altered composition of starch. Mol Breed 15:125–143
66. Zhong G, Peterson D, Delaney D, Bailey M, Witcher D, Register Iii J, Bond D, Li C, Marshall L, Kulisek E (1999) Commercial production of aprotinin in transgenic maize seeds. Mol Breed 5:345–356
67. Pogue GP, Vojdani F, Palmer KE, Hiatt E, Hume S, Phelps J, Long L, Bohorova N, Kim D, Pauly M, Velasco J, Whaley K, Zeitlin L, Garger SJ, White E, Bai Y, Haydon H, Bratcher B (2010) Production of pharmaceutical-grade recombinant aprotinin and a monoclonal antibody product using plant-based transient expression systems. Plant Biotechnol J 8:1–17
68. Capell T, Bassie L, Christou P (2004) Modulation of the polyamine biosynthetic pathway in transgenic rice confers tolerance to drought stress. Proc Natl Acad Sci USA 101:9909–9914
69. Hood E, Witcher D, Maddock S, Meyer T, Baszczynski C, Bailey M, Flynn P, Register J, Marshall L, Bond D (1997) Commercial production of avidin from transgenic maize: characterization of transformant, production, processing, extraction and purification. Mol Breed 3:291–306
70. Samac D, Tesfaye M, Dornbusch M, Saruul P, Temple S (2004) A comparison of constitutive promoters for expression of transgenes in alfalfa (*Medicago sativa*). Transgenic Res 13:349–361
71. Mei C, Park S, Sabzikar R, Ransom C, Qi C, Sticklen M (2009) Green tissue-specific production of a microbial endo-cellulase in maize *Zea mays* L. endoplasmic-reticulum and mitochondria converts cellulose into fermentable sugars. J Chem Technol Biotechnol 84:689–695

72. Sun Y, Cheng J, Himmel M, Skory C, Adney W, Thomas S, Tisserat B, Nishimura Y, Yamamoto Y (2007) Expression and characterization of *Acidothermus cellulolyticus* E1 endoglucanase in transgenic duckweed *Lemna minor* 8627. Bioresour Technol 98:2866–2872
73. Dai Z, Hooker B, Quesenberry R, Thomas S (2005) Optimization of *Acidothermus cellulolyticus* endoglucanase (E1) production in transgenic tobacco plants by transcriptional, post-transcription and post-translational modification. Transgenic Res 14:627–643
74. Teymouri F, Alizadeh H, Laureano-Pérez L, Dale B, Sticklen M (2004) Effects of ammonia fiber explosion treatment on activity of endoglucanase from Acidothermus cellulolyticus in transgenic plant. Appl Biochem Biotechnol 116:1183–1191
75. Dai Z, Hooker B, Anderson D, Thomas S (2000) Expression of *Acidothermus cellulolyticus* endoglucanase E1 in transgenic tobacco: biochemical characteristics and physiological effects. Transgenic Res 9:43–54
76. Dai Z, Hooker B, Quesenberry R, Gao J (1999) Expression of *Trichoderma reesei* exo-cellobiohydrolase I in transgenic tobacco leaves and calli. Appl Biochem Biotechnol 79:689–699
77. Jensen L, Olsen O, Kops O, Wolf N, Thomsen K, Von Wettstein D (1996) Transgenic barley expressing a protein-engineered, thermostable (1,1,4)-beta-glucanase during germination. Proc Natl Acad Sci USA 93:3487–3491
78. Horvath H, Jensen L, Wong O, Kohl E, Ullrich S, Cochran J, Kannangara C, Von Wettstein D (2001) Stability of transgene expression, field performance and recombination breeding of transformed barley lines. Theor Appl Genet 102:1–11
79. Nuutila A, Ritala A, Skadsen R, Mannonen L, Kauppinen V (1999) Expression of fungal thermotolerant endo-1,4-beta-glucanase in transgenic barley seeds during germination. Plant Mol Biol 41:777–783
80. Ziegelhoffer T, Raasch J, Austin-Phillips S (2001) Dramatic effects of truncation and sub-cellular targeting on the accumulation of recombinant microbial cellulase in tobacco. Mol Breed 8:147–158
81. Dai Z, Hooker B, Anderson D, Thomas S (2000) Improved plant-based production of E1 endoglucanase using potato: expression optimization and tissue targeting. Mol Breed 6:277–285
82. Jin R, Richter S, Zhong R, Lamppa G (2003) Expression and import of an active cellulase from a thermophilic bacterium into the chloroplast both in vitro and in vivo. Plant Mol Biol 51:493–507
83. Kawazu T, Ohta T, Ito K, Shibata M, Kimura T, Sakka K, Ohmiya K (1996) Expression of a *Ruminococcus albus* cellulase gene in tobacco suspension cells. J Ferment Bioeng 82:205–209
84. Xue G, Patel M, Johnson J, Smyth D, Vickers C (2003) Selectable marker-free transgenic barley producing a high level of cellulase (1, 4-ß-glucanase) in developing grains. Plant Cell Rep 21:1088–1094
85. Biswas G, Ransom C, Sticklen M (2006) Expression of biologically active *Acidothermus cellulolyticus* endoglucanase in transgenic maize plants. Plant Sci 171:617–623
86. Ransom C, Balan V, Biswas G, Dale B, Crockett E, Sticklen M (2007) Heterologous *Acidothermus cellulolyticus* 1, 4-beta-endoglucanase E1 produced within the corn biomass converts corn stover into glucose. Appl Biochem Biotechnol 137:207–219
87. Oraby H, Venkatesh B, Dale B, Ahmad R, Ransom C, Oehmke J, Sticklen M (2007) Enhanced conversion of plant biomass into glucose using transgenic rice-produced endoglucanase for cellulosic ethanol. Transgenic Res 16:739–749
88. Kawazu T, Sun J, Shibata M, Kimura T, Sakka K, Ohmiya K (1999) Expression of a bacterial endoglucanase gene in tobacco increases digestibility of its cell wall fibers. J Biosci Bioeng 88:421–425
89. Ziegler M, Thomas S, Danna K (2000) Accumulation of a thermostable endo-1, 4- -D-glucanase in the apoplast of *Arabidopsis thaliana* leaves. Mol Breed 6:37–46
90. Ziegelhoffer T, Will J, Austin-Phillips S (1999) Expression of bacterial cellulase genes in transgenic alfalfa (*Medicago sativa* L.), potato (*Solanum tuberosum* L.) and tobacco (*Nicotiana tabacum* L.). Mol Breed 5:309–318
91. Yu L, Gray B, Rutzke C, Walker L, Wilson D, Hanson M (2007) Expression of thermostable microbial cellulases in the chloroplasts of nicotine-free tobacco. J Biotechnol 131:362–369
92. Kim S, Lee D, Choi I, Ahn S, Kim Y, Bae H (2010) *Arabidopsis thaliana* Rubisco small subunit transit peptide increases the accumulation of *Thermotoga maritima* endoglucanase Cel5A in chloroplasts of transgenic tobacco plants. Transgenic Res 19(3):489–497
93. Rooijen G, Glenn K, Shen, Y, Boothe J (2008) Commercial production of chymosin in plants, United States Patent Application 20080184394
94. Ralph J, Akiyama T, Kim H, Lu F, Schatz P, Marita J, Ralph S, Reddy M, Chen F, Dixon R (2006) Effects of coumarate 3-hydroxylase down-regulation on lignin structure. J Biol Chem 281:8843–8853
95. Montalvo-Rodriguez R, Haseltine C, Huess-LaRossa K, Clemente T, Soto J, Staswick P, Blum P (2000) Autohydrolysis of plant polysaccharides using transgenic hyperthermophilic enzymes. Biotechnol Bioeng 70:151–159
96. Meyer F, Smidansky E, Beecher B, Greene T, Giroux M (2004) The maize Sh2r6hs ADP-glucose pyrophosphorylase (AGP) large subunit confers enhanced AGP properties in transgenic wheat (*Triticum aestivum*). Plant Sci 167:899–911
97. Smidansky E, Clancy M, Meyer F, Lanning S, Blake N, Talbert L, Giroux M (2002) Enhanced ADP-glucose pyrophosphorylase activity in wheat endosperm increases seed yield. Proc Natl Acad Sci U S A 99:1724–1729
98. Reggi S, Marchetti S, Patti T, Amicis F, Cariati R, Bembi B, Fogher C (2005) Recombinant human acid β-glucosidase stored in tobacco seed is stable, active and taken up by human fibroblasts. Plant Mol Biol 57:101–113
99. Witcher D, Hood E, Peterson D, Bailey M, Bond D, Kusnadi A, Evangelista R, Nikolov Z, Wooge C, Mehigh R (1998) Commercial production of β-glucuronidase (GUS): a model system for the production of proteins in plants. Mol Breed 4:301–312

100. Chan M, Chao Y, Yu S (1994) Novel gene expression system for plant cells based on induction of alpha-amylase promoter by carbohydrate starvation. J Biol Chem 269: 17635–17641
101. de Wilde C, Uzan E, Zhou Z, Kruus K, Andberg M, Buchert J, Record E, Asther M, Lomascolo A (2008) Transgenic rice as a novel production system for *Melanocarpus* and *Pycnoporus* laccases. Transgenic Res 17:515–527
102. Gruber V, Berna P, Arnaud T, Bournat P, Clément C, Mison D, Olagnier B, Philippe L, Theisen M, Baudino S (2001) Large-scale production of a therapeutic protein in transgenic tobacco plants: effect of subcellular targeting on quality of a recombinant dog gastric lipase. Mol Breed 7:329–340
103. Zhong Q, Gu Z, Glatz C (2006) Extraction of recombinant dog gastric lipase from transgenic corn seed. J Agric Food Chem 54:8086–8092
104. Mokrzycki-Issartel N, Bouchon B, Farrer S, Berland P, Laparra H, Madelmont J, Theisen M (2003) A transient tobacco expression system coupled to MALDI-TOF-MS allows validation of the impact of differential targeting on structure and activity of a recombinant therapeutic glycoprotein produced in plants. FEBS Lett 552:170–176
105. Lagrimini L, Bradford S, Rothstein S (1990) Peroxidase-induced wilting in transgenic tobacco plants. Plant Cell 2:7–18, Online
106. Chen R, Xue G, Chen P, Yao B, Yang W, Ma Q, Fan Y, Zhao Z, Tarczynski M, Shi J (2008) Transgenic maize plants expressing a fungal phytase gene. Transgenic Res 17:633–643
107. Hamada A, Yamaguchi K, Harada M, Horiguchi K, Takahashi T, Honda H (2006) Recombinant, rice-produced yeast phytase shows the ability to hydrolyze phytate derived from seed-based feed, and extreme stability during ensilage treatment. Biosci Biotechnol Biochem 70:1524–1527
108. Brinch-Pedersen H, Hatzack F, Stoger E, Arcalis E, Pontopidan K, Holm P (2006) Heat-stable phytases in transgenic wheat (*Triticum aestivum* L.): deposition pattern, thermostability, and phytate hydrolysis. J Agric Food Chem 54:4624–4632
109. Zimmermann P, Zardi G, Lehmann M, Zeder C, Amrhein N, Frossard E, Bucher M (2003) Engineering the root-soil interface via targeted expression of a synthetic phytase gene in trichoblasts. Plant Biotechnol J 1:353–360
110. George T, Simpson R, Hadobas P, Richardson A (2005) Expression of a fungal phytase gene in *Nicotiana tabacum* improves phosphorus nutrition of plants grown in amended soils. Plant Biotechnol J 3:129–140
111. Brinch-Pedersen H, Olesen A, Rasmussen S, Holm P (2000) Generation of transgenic wheat (*Triticum aestivum* L.) for constitutive accumulation of an *Aspergillus* phytase. Mol Breed 6:195–206
112. Lucca P, Hurrell R, Potrykus I (2001) Genetic engineering approaches to improve the bioavailability and the level of iron in rice grains. Theor Appl Genet 102:392–397
113. Xiao K, Harrison M, Wang Z (2005) Transgenic expression of a novel M. truncatula phytase gene results in improved acquisition of organic phosphorus by Arabidopsis. Planta 222:27–36
114. Pen J, Verwoerd T, van Paridon P, Beudeker R, van den Elzen P, Geerse K, van der Klis J, Versteegh H, van Ooyen A, Hoekema A (1993) Phytase-containing transgenic seeds as a novel feed additive for improved phosphorus utilization. Nat Biotechnol 11:811–814
115. Hegeman C, Grabau E (2001) A novel phytase with sequence similarity to purple acid phosphatases is expressed in cotyledons of germinating soybean seedlings. Plant Physiol 126:1598–1608
116. Verwoerd T, Van Paridon P, Van Ooyen A, Van Lent J, Hoekema A, Pen J (1995) Stable accumulation of *Aspergillus niger* phytase in transgenic tobacco leaves. Plant Physiol 109:1199–1205
117. Ponstein A, Bade J, Verwoerd T, Molendijk L, Storms J, Beudeker R, Pen J (2002) Stable expression of phytase (phyA) in canola (*Brassica napus*) seeds: towards a commercial product. Mol Breed 10:31–44
118. Li J, Hegeman C, Hanlon R, Lacy G, Denbow D, Grabau E (1997) Secretion of active recombinant phytase from soybean cell-suspension cultures. Plant Physiol 114:1103–1111
119. Hong C, Cheng K, Tseng T, Wang C, Liu L, Yu S (2004) Production of two highly active bacterial phytases with broad pH optima in germinated transgenic rice seeds. Transgenic Res 13:29–39
120. Austin-Phillips S, Koegel R, Straub R, Cook M (1999) Animal feed compositions containing phytase derived from transgenic alfalfa and methods of use thereof. US Patent No 5,900,525, Wisconsin Alumni Research Foundation, Madison, Wisconsin, USA
121. Claparols M, Bassie L, Miro B, Del Duca S, Rodriguez-Montesinos J, Christou P, Serafini-Fracassini D, Capell T (2004) Transgenic rice as a vehicle for the production of the industrial enzyme transglutaminase. Transgenic Res 13:195–199
122. Yang P, Wang Y, Bai Y, Meng K, Luo H, Yuan T, Fan Y, Yao B (2007) Expression of xylanase with high specific activity from *Streptomyces olivaceoviridis* A1 in transgenic potato plants (*Solanum tuberosum* L.). Biotechnol Lett 29:659–667
123. Kimura T, Mizutani T, Tanaka T, Koyama T, Sakka K, Ohmiya K (2003) Molecular breeding of transgenic rice expressing a xylanase domain of the xynA gene from *Clostridium thermocellum*. Appl Microbiol Biotechnol 62:374–379
124. Liu J, Selinger L, Cheng K, Beauchemin K, Moloney M (1997) Plant seed oil-bodies as an immobilization matrix for a recombinant xylanase from the rumen fungus *Neocallimastix patriciarum*. Mol Breed 3:463–470
125. Patel M, Johnson J, Brettell R, Jacobsen J, Xue G (2000) Transgenic barley expressing a fungal xylanase gene in the endosperm of the developing grains. Mol Breed 6:113–124
126. Hyunjong B, Lee D, Hwang I (2006) Dual targeting of xylanase to chloroplasts and peroxisomes as a means to increase protein accumulation in plant cells. J Exp Bot 57:161–169

127. Bae H, Kim H, Kim Y (2008) Production of a recombinant xylanase in plants and its potential for pulp biobleaching applications. Bioresour Technol 99:3513–3519
128. Herbers K, Wilke I, Sonnewald U (1995) A thermostable xylanase from *Clostridium thermocellum* expressed at high levels in the apoplast of transgenic tobacco has no detrimental effects and is easily purified. Biotechnology 13:63–66
129. Herbers K, Flint H, Sonnewald U (1996) Apoplastic expression of the xylanase and (1–3, 1–4) glucanase domains of the xyn D gene from *Ruminococcus flavefaciens* leads to functional polypeptides in transgenic tobacco plants. Mol Breed 2:81–87
130. Estevez J, Cantero A, Reindl A, Reichler S, Leon P (2001) 1-Deoxy-D-xylulose-5-phosphate synthase, a limiting enzyme for plastidic isoprenoid biosynthesis in plants. J Biol Chem 276:22901–22909
131. Vain P (2007) Thirty years of plant transformation technology development. Plant Biotechnol J 5:221–229
132. Tzfira T, Citovsky V (2006) *Agrobacterium*-mediated genetic transformation of plants: biology and biotechnology. Curr Opin Biotechnol 17:147–154
133. Daniell H, Cohill P, Kumar S, Dufourmantel N, Dubald M (2007) Chloroplast genetic engineering. In: Daniell H, Chase C (eds) Molecular biology and biotechnology of plant organelles. Springer, Dordrecht
134. Marillonnet S, Thoeringer C, Kandzia R, Klimyuk V, Gleba Y (2005) Systemic *Agrobacterium tumefaciens*-mediated transfection of viral replicons for efficient transient expression in plants. Nat Biotechnol 23:718–723
135. Sainsbury F, Lomonossoff G (2008) Extremely high-level and rapid transient protein production in plants without the use of viral replication. Plant Physiol 148:1212–1218
136. Ueki S, Lacroix B, Krichevsky A, Lazarowitz S, Citovsky V (2008) Functional transient genetic transformation of *Arabidopsis* leaves by biolistic bombardment. Nat Protoc 4:71–77
137. Watson S (1988) Corn marketing, processing, and utilization. US 9,011,308 (NAL/USDA, A. U., Ed.)
138. Hood E, Kusnadi A, Nikolov Z, Howard J (1999) Molecular farming of industrial proteins from transgenic maize. In: Sahidi F, Kolodziejczyk P, Whitaker J, Munguia A, Fuller G (eds) Chemicals via higher plant bioengineering. Kluwer Academic/Plenum Publishers, New York, pp 127–148
139. Ramessar K, Sabalza M, Capell T, Christou P (2008) Maize plants: an ideal production platform for effective and safe molecular pharming. Plant Sci 174:409–419
140. Howard J, Hood E (2007) Methods for growing nonfood products in transgenic plants. Crop Sci 47:1255
141. Gepts P (2002) A comparison between crop domestication, classical plant breeding, and genetic engineering. Crop Sci 42:1780–1790
142. Gur A, Zamir D (2004) Unused natural variation can lift yield barriers in plant breeding. PLoS Biol 2:1610–1615
143. Dale P (1992) Spread of engineered genes to wild relatives. Plant Physiol 100:13
144. Delaney B, Astwood J, Cunny H, Conn R, Herouet-Guicheney C, MacIntosh S, Meyer L, Privalle L, Gao Y, Mattsson J (2008) Evaluation of protein safety in the context of agricultural biotechnology. Food Chem Toxicol 46:S71–S97
145. Nikolov Z, Hammes D (2002) Production of recombinant proteins from transgenic crops. In: Hood EE, Howard JA (eds) Plants as factories for protein production. Kluwer Academic Publishers, Dordrecht, pp 159–174
146. Horn M, Woodard S, Howard J (2004) Plant molecular farming: systems and products. Plant Cell Rep 22:711–720
147. Hellwig S, Drossard J, Twyman R, Fischer R (2004) Plant cell cultures for the production of recombinant proteins. Nat Biotechnol 22:1415–1422
148. Lam E, Benfey P, Gilmartin P, Fang R, Chua N (1989) Site-specific mutations alter *in vitro* factor binding and change promoter expression pattern in transgenic plants. Proc Natl Acad Sci U S A 86:7890–7894
149. Cai M, Wei J, Li X, Xu C, Wang S (2007) A rice promoter containing both novel positive and negative cis-elements for regulation of green tissue-specific gene expression in transgenic plants. Plant Biotechnol J 5:664–674
150. Belanger F, Kriz A (1991) Molecular basis for allelic polymorphism of the maize Globulin-1 gene. Genetics 129:863–872
151. Jones H, Sparks C (2009) Promoter sequences for defining transgene expression. In: Jones H, Shewry P (eds) Transgenic wheat, barley and oats: production and characterization protocols. Humana, Totowa
152. Streatfield S (2007) Approaches to achieve high-level heterologous protein production in plants. Plant Biotechnol J 5:2–15
153. Vance V, Vaucheret H (2001) RNA silencing in plants – defense and counterdefense. Science 292:2277–2280
154. Baulcombe D (2003) Overcoming and exploiting RNA silencing. In: Vasil IK (ed) 10th IAPTC&B congress. Kluwer Academic Publishers, Orlando, pp 49–58
155. Sticklen MB (2008) Plant genetic engineering for biofuel production: towards affordable cellulosic ethanol. Nat Rev Genet 9:433–443
156. Medrano G, Reidy M, Liu J, Ayala J, Dolan M, Cramer C (2009) Rapid system for evaluating bioproduction capacity of complex pharmaceutical proteins in plants. Meth Mol Biol 483:51–67
157. Van Rooijen G, Moloney M (1995) Structural requirements of oleosin domains for subcellular targeting to the oil body. Plant Physiol 109:1353–1361
158. Rigano M, Alvarez M, Pinkhasov J, Jin Y, Sala F, Arntzen C, Walmsley A (2004) Production of a fusion protein consisting of the enterotoxigenic *Escherichia coli* heat-labile toxin B subunit and a tuberculosis antigen in *Arabidopsis thaliana*. Plant Cell Rep 22:502–508
159. Garbarino J, Oosumi T, Belknap W (1995) Isolation of a polyubiquitin promoter and its expression in transgenic potato plants. Plant Physiol 109:1371–1378
160. Doran P (2006) Foreign protein degradation and instability in plants and plant tissue cultures. Trends Biotechnol 24:426–432

161. Kim K, Kwon S, Lee H, Hur Y, Bang J, Kwak S (2003) A novel oxidative stress-inducible peroxidase promoter from sweetpotato: molecular cloning and characterization in transgenic tobacco plants and cultured cells. Plant Mol Biol 51:831–838
162. Cramer C, Boothe J, Oishi K (1999) Transgenic plants for therapeutic proteins: linking upstream and downstream strategies. Curr Top Microbiol Immunol 240:95–118
163. Moloney M (2003) Oleosin partitioning technology for production of recombinant proteins in oil seeds. In: Vinci V, Parekh S (eds) Handbook of industrial cell culture: mammalian, microbial, and plant cells. Humana Press, Totowa
164. Merino ST, Cherry J (2007) Progress and challenges in enzyme development for biomass utilization. Adv Biochem Eng Biotechnol 108:95–120
165. Jorgensen H, Kristensen JB, Felby C (2007) Enzymatic conversion of lignocellulose into fermentable sugars: challenges and opportunities. Biofuels, Bioprod Biorefin 1:119–134, be
166. Howard JA, Nikolov Z, Hood EE (2011) Enzyme production systems for biomass conversion. In: Hood EE, Nelson P, Powell R (eds) The Plant Biomass Conversion. John Wiley & Sons Inc.
167. Hamelinck C, Hooijdonk G, Faaij A (2005) Ethanol from lignocellulosic biomass: techno-economic performance in short-, middle-and long-term. Biomass Bioenergy 28:384–410
168. Solomon B, Barnes J, Halvorsen K (2007) Grain and cellulosic ethanol: history, economics, and energy policy. Biomass Bioenergy 31:416–425
169. Howard JA, Hood EE (unpublished)
170. Sheehan J, Aden A, Paustian K, Killian K, Brenner J, Walsh M, Nelson R (2003) Energy and environmental aspects of using corn stover for fuel ethanol. J Ind Ecol 7:117–146
171. Groover AT, Fontana JR, Arroyo JM, Yordan C, McCombie WR, Martienssen RA (2003) Secretion trap tagging of secreted and membrane-spanning proteins using Arabidopsis gene traps. Plant Physiol 132:698–708
172. Cohen O, Kronman C, Velan B, Shafferman A (2004) Amino acid domains control the circulatory residence time of primate acetylcholinesterases in rhesus macaques (*Macaca mulatta*). Biochem J 378:117–128
173. Huang J, Sutliff T, Wu L, Nandi S, Benge K, Terashima M, Ralston A, Drohan W, Huang N, Rodriguez R (2008) Expression and purification of functional human α1-antitrypsin from cultured plant cells. Biotechnol Prog 17:126–133
174. Ma J, Hein M (1995) Plant antibodies for immunotherapy. Plant Physiol 109:341–346
175. Garcia-Casado G, Sanchez-Monge R, Chrispeels M, Armentia A, Salcedo G, Gomez L (1996) Role of complex asparagine-linked glycans in the allergenicity of plant glycoproteins. Glycobiology 6:471–477
176. Cockburn A (2002) Assuring the safety of genetically modified (GM) foods: the importance of an holistic, integrative approach. J Biotechnol 98:79–106
177. Peterson R, Arntzen C (2004) On risk and plant-based biopharmaceuticals. Trends Biotechnol 22:64–66

Plant Molecular Pharming, Pharmaceuticals for Human Health

Andreas Schiermeyer, Stefan Schillberg
Department of Plant Biotechnology, Fraunhofer IME, Aachen, Germany

Article Outline

Glossary
Definition of the Subject and Its Importance
Introduction
Plant Transformation
Posttranslational Modification
Downstream Processing
Plant-Derived Vaccines
Plant-Made Pharmaceuticals in Advanced Development
Future Directions
Bibliography

Glossary

Agrobacterium tumefaciens Gram negative phytopathogenic soil bacterium belonging to the family Rhizobiaceae. *A. tumefaciens* naturally infects a variety of dicotyledonous plant species and induces the formation of tumors (galls) by transferring genes located within the T-DNA.

Biopharmaceuticals Drugs, produced using modern biotechnological methods such as recombinant DNA technology, comprising proteins and/or nucleic acids for therapeutic or in vivo diagnostic purposes.

Epigenetic effects Changes caused in gene expression patterns that are not due to changes in the nucleotide sequence of the DNA but due to nucleotide modifications by methylation or RNA-directed mechanisms.

Glycosylation The co- or posttranslational addition of carbohydrate moieties to polypeptides. The carbohydrates may be either N-linked (at asparagine or arginine side chains) or O-linked (at serine, threonine, tyrosine, hydroxylysine, or hydroxyproline side chains).

Immunoglobulin (Ig) Major component of the adaptive immune system with specific antibody activity.

Immunoglobulins are produced by lymphocytes and consist of four polypeptide chains: two identical heavy and two identical light chains. Immunoglobulin G (IgG) is the principal immunoglobulin of the plasma with a molecular weight of 150 kDa. Immunoglobulin A (IgA) is a dimeric 400 kDa molecule secreted by mucosal surfaces. Beside the heavy and the light chains an IgA molecule contains a joining chain and the secretory component. Immunoglobulin M (IgM) is produced early during the immune response. Secreted IgM molecules have a star-shaped pentameric structure.

Molecular farming (also pharming) The production of pharmaceutical or technical proteins in plants or animals.

Monoclonal antibody An immunoglobulin secreted by a single clone of antibody producing cells.

Plastid Plant organelle bound by a double membrane containing its own circular genome. Several types of plastids are known that originate from a common precursor the proplastid. The most prominent form is the chloroplast found in the green tissues.

Posttranslational modification Any modification that occurs once a polypeptide has been synthesized, for example, proteolytic processing, glycosylation, methylation, phosphorylation, and prenylation.

Suspension culture Technique for the cultivation of plant cells or tissues in liquid culture medium under aseptic conditions using shake flasks or fermentation vessels.

T-DNA Transfer DNA. Natural T-DNA is located on large tumor inducing (Ti) or hairy root inducing (Ri) plasmids, although for gene transfer to plants it has been moved onto a smaller, more convenient vector. The T-DNA is transferred to the plant cell with the help of a range of virulence factors, and once in the nucleus it may be stably integrated into the plant genome.

Transformation Transfer of genetic information into a cell by biological (*A. tumefaciens*) or physical means (e.g., gene gun).

Transgene A segment of DNA that is introduced into the genome of a host cell by transformation, and which integrates into the genome so that it is inherited like any other gene.

Transient expression The temporary expression of a transgene within a host cell without stable integration into the host genome.

Vaccine Preparation of immunogenic material that stimulates active immunity in the recipient without causing disease. Vaccines can be based on killed or attenuated microorganisms or isolated components of the disease causing agent (subunit vaccines).

Viral vector Genetic elements derived from viral genomes for the transient expression of transgenes in a host cell. Viral vectors have the ability to replicate autonomously in the host cell and might be able to infect distant cells (depending on the degree of engineering).

Zinc-finger nucleases Chimeric proteins consisting of a zinc-finger domain conferring sequence specific DNA binding and a nuclease domain for the introduction of a double-strand break at the target site.

Definition of the Subject and Its Importance

The demand for therapeutic proteins has increased in recent years and modern biotechnological methods have, until recently, ensured the production of safe and effective biopharmaceuticals to meet this demand. Various production platforms are currently used in the pharmaceutical industry, most based on the fermentation of engineered pro- and eukaryotic microorganisms, insect cells, or mammalian cells. However, the growth of the market for biopharmaceuticals is predicted to outpace production capacity using these platforms in the next decade, so alternatives are necessary. Intact plants and plant cell cultures are suitable production systems for a wide range of therapeutic proteins and could help to fulfill the need for increased production capacity. The production of pharmaceutical proteins in plants began with a monoclonal antibody expressed in transgenic tobacco plants more than 20 years ago. Since then many different plant species have been genetically engineered to produce valuable pharmaceutical proteins using a variety of transformation methods. Major progress has been achieved in transformation and expression technology, the downstream processing of transgenic plant material and the adaptation of regulatory procedures to encompass the new production platforms, allowing the first plant-made pharmaceuticals to begin clinical trials.

Introduction

Plant cells synthesize a vast array of secondary metabolites, many of which are already used as pharmaceuticals. Recombinant DNA technology combined with techniques for plant transformation and the regeneration of transgenic plants have allowed the pharmaceutical exploitation of plants to be extended to include the production of biopharmaceuticals such as subunit vaccines, antibodies, growth factors, cytokines, enzymes, and blood factors. In many cases, these products need to be purified from plant material and formulated in the same way as conventional biopharmaceuticals. However, many plants are "generally regarded as safe" for both topical and oral administration, so they are particularly suitable for the production of vaccines that can be delivered via the oral route or antibodies applied as topical microbicides, especially where such products are required on a large scale. This reflects the fact that plants can be grown inexpensively on an agricultural scale and that plant-derived pharmaceuticals for topical/oral administration would require only minimal processing. This could potentially bring the costs of production and distribution down to levels suitable for deployment in developing countries with limited financial resources and a poor medical infrastructure. This contribution describes the technologies that facilitate biopharmaceutical production in plants and plant cell cultures either through transient expression or stable transformation. It also discusses issues relating to posttranslational modification, extraction and purification, and regulatory compliance, focusing on those plant-derived pharmaceutical products that have advanced the furthest in the clinic. A compilation of selected technical achievements in plant molecular farming is provided in Table 1.

Plant Transformation

Pharmaceutical proteins can be produced in plants or plant cells either through transient expression or stable transformation. In the first case, the DNA encoding the protein is delivered into plant cells by *Agrobacterium tumefaciens* or a viral vector (or a combination of the two) but there is no integration of this DNA into the plant genome and the protein is synthesized for a few hours or days. In the second case, DNA delivered either by *A. tumefaciens* or a physical process such as particle bombardment integrates into the plant genome and becomes a permanent locus, allowing long-term production of the recombinant protein and the transmission of the trait to subsequent generations.

Each method has advantages and disadvantages that need to be evaluated on a case by case basis for each pharmaceutical protein, depending on its intended use and the production scale. The production of an immunoglobulin via stable integration into the nuclear genome was first reported in 1989 when Hiatt and colleagues produced a monoclonal IgG-class antibody in tobacco leaves [1]. They introduced the coding sequences for the gamma heavy chain and kappa light chain of the immunoglobulin into independent tobacco lines and then crossed plants from each line to stack the transgenes in a single plant, which was able to produce the full antibody. The same strategy was used to produce a chimeric secretory (sIgA/G) antibody, although in this case four transgenes were required (encoding the kappa light chain, the chimeric alpha/gamma heavy chain, the joining chain, and the secretory component) and four lines were bred over two generations to generate the final production crop [4]. Later on the assembly of a chimeric secretory sIgA/G antibody could be achieved by simultaneous transformation of all four components in rice plants [20]. These examples clearly show how plant cells can produce even the most complex proteins and modify and assemble them into functional oligomeric structures (two different cell types are required in mammals to produce secretory IgA antibodies). Stable transformation of the nuclear genome enables the combination of several independent expression cassettes into a single transgenic line and also allows the introduction of a transgene from a laboratory cultivar into other varieties of the same species, to yield a germplasm that is particularly suited for a certain purpose. The latter strategy has been used to breed dent and sweet corn varieties that produce the HIV-specific antibody 2G12. The expression cassettes were initially introduced into a laboratory maize cultivar with little agronomic value and low yield [21]. Using conventional breeding transgenes can be transferred to a germplasm that is either inaccessible for direct transformation or that is particularly suited for the cultivation under certain climate conditions.

A drawback of stable nuclear transformation is the time needed to identify and establish a germplasm with

Plant Molecular Pharming, Pharmaceuticals for Human Health. Table 1 Selected research achievements in the field of plant molecular farming between 1989 and 2008

Year	Achievement	Reference
1989	Full-size antibody (mouse IgG) expression in tobacco	[1]
1990	First human protein (HSA) produced in tobacco and potato	[2]
1992	First vaccine candidate (HBsAg) expressed in tobacco	[3]
1995	First secretory antibody (sIgA) produced in tobacco	[4]
1995	Plant seed oilbodies as vehicles for protein production and purification	[5]
1996	Expression of a protein-based polymer in tobacco	[6]
1998	First clinical trial with a vaccine candidate produced in transgenic potato	[7]
1999	Transient expression of an antibody by *Agrobacterium* vacuum infiltration	[8]
1999	N-glycan analysis of a plant-produced antibody	[9]
2000	Human growth hormone produced in tobacco chloroplasts	[10]
2001	N-glycan modification by expression of a human β-1,4 galactosyltransferase	[11]
2004	Knockout mutants of moss lacking plant-specific glycosylation	[12]
2004	Generation of *Arabidopsis* plants lacking plant-specific glycosylation	[13]
2005	*Agrobacterium*-mediated delivery of viral replicons	[14]
2006	Approval of a plant-made vaccine for veterinary medicine	[15]
2007	Production of glucocerebrosidase with terminal mannose residues	[16]
2008	Clinical phase I trial with plant-produced anti-idiotype vaccines	[17]
2008	Engineering of a CMP-sialic acid pathway in plants	[18]
2008	Phase III clinical trial with plant-made glucocerebrosidase	[19]

the desired properties. A large number of primary transformants often need to be screened to identify plants showing high-level transgene expression. These lines then need to be analyzed at the molecular level to determine the number and arrangement of the transgenes. For breeding purposes single-copy integration events or multicopy single locus events with a regular transgene arrangement are preferred [22]. In contrast, multiple transgene copies with a complex integration pattern are likely to suffer from both transcriptional gene silencing (TGS) and posttranscriptional gene silencing (PTGS) [23]. The transgenic plants must also be analyzed for unwanted pleiotropic effects that could be caused by the transgene itself or by the changes that are brought about by its integration, since transgene integration following both *Agrobacterium*-mediated transformation and particle bombardment is a random process. Precise transgene integration at a predefined locus can be achieved by homologous recombination (gene targeting) but this has not been possible for most plant species in the past due to its very low efficiency. A notable exception is the moss *Physcomitrella patens*, where transformation by homologous recombination is a straightforward and robust process [24]. In higher plants, efficient homologous recombination has become possible only recently with the use of zinc-finger endonucleases. These are engineered endonucleases containing zinc-finger motifs that bind precise DNA sequences and introduce double-strand breaks at the target site. This in turn stimulates DNA repair in the host, thereby facilitating homologous recombination. This has enabled the precise engineering of transgenic plants, although there have been no reports thus far concerning applications in molecular farming [25–28].

Another disadvantage of nuclear transgenic plants is that the target protein often accumulates at low levels, making them commercially unfeasible. This has been addressed by the use of plastid transformation, where the transgene is integrated in the circular chloroplast or chromoplast genome, typically by particle bombardment. Unlike nuclear transformation, homologous recombination is an efficient method for transgene integration into the plastid genome, allowing precise gene targeting. Every plastid contains several copies of the genome, and each plant cell contains many plastids [29]; therefore, it is possible in principle to generate plant cells containing several thousand transgene copies (and these are not subject to silencing because the TGS and PTGS mechanisms are not present in the plastid). To ensure the transgene is present in every copy of the plastid genome (the homoplasmic state), the primary transformants must undergo multiple rounds of selection and regeneration. This is generally achieved using the marker gene aminoglycoside 3″-adenylyltransferase, which confers resistance to the antibiotic spectinomycin [30]. The high transgene copy number and absence of silencing allows the accumulation of some target proteins to levels exceeding 10% of the total soluble protein (TSP) in the cell. Furthermore, since plastids are evolutionarily derived from bacteria, it is possible to express multiple genes as operons, producing polycistronic mRNA [31].

Many biopharmaceuticals are complex molecules that require several posttranslational processing steps to achieve a functional state. Plastids are equipped to form disulfide bridges, as demonstrated for the production of the human growth hormone somatotropin [10], and they can also assemble oligomers as demonstrated for the production of cholera toxin B-subunit (CTB), which assembled into functional GM1 ganglioside-binding pentamers [32]. Human serum albumin, which requires posttranslational removal of the N-terminal methionine residue, has also been produced successfully in plastids [33]. The enzyme methionine aminopeptidase cleaves off the initiating N-formylmethionine in plastids depending on the subsequent amino acid sequence context, and this must be considered when dealing with proteins that need to have intact N-termini. Another elegant approach for the production of proteins with a defined N-terminus is the expression of the target protein as an N-terminal ubiquitin fusion protein. Endogenous ubiquitin-specific proteases then remove the ubiquitin moiety precisely, a strategy that has enabled the production of native somatotropin that carries an N-terminal phenylalanine residue [10].

Plastid transformation technique was limited to tobacco for many years but has recently expanded to incorporate certain crop species such as lettuce and tomato [34, 35]. Plastid transformation in crop plants opens new possibilities in the area of oral vaccines, where antigens are produced in the edible parts of plants and delivered via the oral route. A further advantage of plastid transformation is the biosafety aspect, since chloroplasts are inherited maternally in most species and are therefore not present in pollen [36]. However, there are also some limitations. Many biopharmaceuticals need to undergo co- and post-translational glycosylation in order to fold properly or in order to remain functional and stable, but this process does not occur in plastids. Certain target proteins also appear to be unstable or toxic when expressed in plastids, for example, the rotavirus coat protein VP6 and HIV p24 antigen undergo rapid degradation in the chloroplasts of older tobacco leaves, with significant accumulation only possible in the youngest leaves. A codon-optimized HIV p24 construct allowed homogenous expression but all the leaves turned yellow, and rearrangements were observed within the plastid DNA [37].

Transient expression allows more rapid production than stable transformation (nuclear or plastid). DNA encoding the pharmaceutical proteins is either included within a T-DNA cassette carried by an *A. tumefaciens* strain delivered into leaf tissue by vacuum infiltration [38, 39], or inserted into a viral vector that is used to infect the plant [40, 41]. Transient expression can be used for the rapid testing of expression constructs for subsequent stable transformation procedures or can be scaled up for use as production system in its own right. Most of the viral vectors are based on RNA viruses such as *Tobacco mosaic virus* (TMV), *Potato virus X* (PVX), and *Cowpea mosaic virus* (CPMV). These vectors have been used both to produce intact proteins and to produce chimeric virus particles that display peptide antigens on their surface. In such peptide display vectors, the target peptide is fused to the coat protein, and because each

particle has many copies of the coat protein (and hence the antigen), the particles are strongly immunogenic and can be used without additional adjuvants to provoke an immune response. The versatility of this approach has been demonstrated with an experimental rabies vaccine that induced a protective immune response in mice. Furthermore human volunteers who ingested spinach leaves infected with the recombinant virus mounted a humoral immune response [42]. Conventional viral vectors have a limited capacity, and larger transgenes tend to be truncated or eliminated altogether as the virus spreads. This has been addressed by developing a series of deconstructed viral vectors in which the coat protein gene is deleted to provide space for the transgene. In order to deliver these vectors to a maximum number of plant cells the entire recombinant virus genome is incorporated as a DNA copy into a T-DNA cassette and delivered by *A. tumefaciens* via vacuum infiltration [43]. Two similar systems have been developed, one described as the launch vector system [44] and the other as the magnifection system [14]. They both exploit the ability of *A. tumefaciens* to infect a large range of plants, thereby extending the host range of the natural virus and using the efficient viral replication system to amplify the coding sequence of the target protein. In a proof of concept experiment, the accumulation of green fluorescent protein (GFP) peaked at 4 g kg^{-1} fresh weight in *Nicotiana benthamiana* plants transformed by magnifection [14]. The platform has been refined for the production of oligomeric proteins such as antibodies. Full-size IgG1 immunoglobulins have been produced successfully at levels of up to 0.5 g kg^{-1} fresh weight, by introducing the light and heavy chain coding sequences into two independent noninterfering vectors based on TMV and PVX, respectively [45].

Posttranslational Modification

Approximately 30% of all approved biopharmaceuticals contain N-linked glycans, so N-glycosylation is the most important posttranslational modification that needs to be taken into account when manufacturing recombinant biopharmaceuticals in plants. The mechanism of N-glycosylation is conserved between plants and mammals, beginning in the endoplasmic reticulum (ER) with the transfer of an oligosaccharide precursor molecule onto asparagine residues within the sequence motif N-X-S/T (where X is any amino acid except proline). The precursor molecule is subsequently trimmed to yield a structure known as a high-mannose type glycan. The protein then passes into the Golgi apparatus where additional glycan modifications take place.

The final complex type glycan structures differ between plants and mammals (Fig. 1), in that plant glycoproteins contain core β1,2-xylose and α1,3-fucose residues whereas mammalian glycoproteins contain β1,4-galactose and terminal N-acetyl-neuraminic acid (sialic acid) residues [46]. Plant-specific glycosylation patterns have been found to induce an immune response upon injection in some mammalian species [47–49]. To prevent these immune responses several strategies have been explored to avoid the addition of plant-specific sugar residues to the glycan structure. One approach is the attachment of a C-terminal H/KDEL amino acid sequence motif to retain the target protein within the ER, thereby preventing exposure to the Golgi apparatus and the attachment of β1,2-xylose and α1,3-fucose residues [50]. This strategy has been applied successfully in the production of a chimeric mouse/human IgG1 antibody against human chorionic gonadotropin [51]. An alternative strategy is the knockout or knockdown of the endogenous plant β1,2-xylosyltransferase and α1,3-fucosyltransferase genes, which has been achieved in the moss *P. patens* by homologous recombination [12]. The double knockout mutant was used to express human erythropoietin devoid of plant-specific glycan structures [52]. In the model plant *Arabidopsis thaliana*, the β1,2-xylosyltransferase and α1,3-fucosyltransferase genes have been knocked out by T-DNA insertional mutagenesis [13]. This plant line has been used to produce the anti-HIV antibody 2G12 with a humanized glycan structure [53]. In the duckweed *Lemna minor*, the human anti-CD30 antibody MDX-060 was produced without plant glycans by co-introducing inverted repeat transgenes matching the sequences of the β1,2-xylosyltransferase and α1,3-fucosyltransferase genes, so that they were silenced by RNA interference (RNAi) [54]. This antibody also demonstrated stronger antibody-dependent cell-mediated cytotoxicity (ADCC) compared to its counterpart produced in Chinese hamster ovary (CHO) cells, reflecting the tenfold higher affinity of

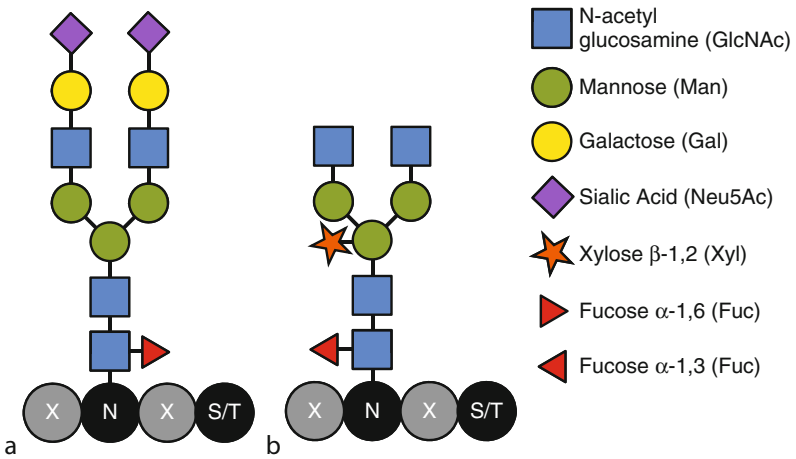

Plant Molecular Pharming, Pharmaceuticals for Human Health. Figure 1
Prototypes of protein N-glycosylation patterns from mammalian (**a**) and plant (**b**) origin. We are grateful to Holger Spiegel (Fraunhofer IME, Aachen, Germany) for the preparation of the graphics

the plant-derived antibody for the human Fcγ receptor [54]. The same phenomenon has been demonstrated for other antibodies produced in the duckweed and moss systems [55, 56].

To further humanize the glycan structure of biopharmaceuticals produced in plants, the coding sequence for human β1,4-galactosyltransferase has been introduced into tobacco [57, 58] and alfalfa plants [59]. The recombinant antibodies produced in these modified host plants not only possessed glycans with terminal galactose residues but they also contained fewer core β1,2-xylose and α1,3-fucose residues. Many human glycoproteins possess terminal sialic acid residues that play a pivotal role in serum stability. For example, erythropoietin usually has a half-life of 5 h in rat serum, but enzymatically trimming off the terminal sialic acid residues reduces the half-life to <2 min [60]. There is consequently an ongoing effort to introduce the CMP-sialic acid biosynthesis pathway into plants and thus far four of the enzymes (α2,6-sialyltransferase, UDP-N-acetylglucosamine 2-epimerase/N-acetylmannosamine kinase, N-acetylneuraminic acid phosphate synthase and CMP-N-acetylneuraminic acid synthetase) have been expressed successfully in *A. thaliana* [18, 61]. Recently, the components of the complete pathway have been transiently expressed in *N. benthamiana* and the co-expressed 2G12 mAb has been shown to become sialylated [62].

There is much less information available about the significance of O-glycosylation in pharmaceutical proteins produced in plants. Endogenous plant proteins tend to undergo O-glycosylation at clustered proline residues that are first converted into hydroxyproline, for example, those found in the extension family of hydroxyproline-rich glycoproteins (HRGPs). Such proline clusters are also present in the hinge region of IgA1 antibodies, so a recombinant IgA1 antibody expressed in maize similarly underwent hydroxylation followed by O-glycosylation [63]. An artificial O-glycosylation motif consisting of 20 tandem repeats of the dipeptide serine/proline has been fused to the C-terminus of human interferon α2b (IFNα2-$(SO)_{20}$) expressed in tobacco suspension cells. The fusion protein accumulated in the culture supernatant at levels two orders of magnitude higher than native IFNα2b, reflecting its more efficient secretion and its greater resistance toward proteolysis [64]. The antiviral activity of the fusion protein was comparable to that of native interferon but its higher molecular weight (75 kDa vs. 19.2 kDa) delayed renal clearance therefore increasing its serum half-life in mice by 13-fold [64].

The unwanted processing of recombinant proteins by endogenous plant proteases is a major obstacle in the field of molecular farming because the overall yield of the recombinant protein is reduced and the resulting protein fragments need to be removed during downstream

processing. Proteolytic degradation has been observed irrespective of the subcellular localization of the target protein but the extracellular compartments (apoplast and culture medium) appear to be particularly rich in proteolytic enzymes [65–68]. This has been addressed using a number of strategies, including the co-expression of protease inhibitors [69–71] and the co-secretion of unrelated proteins that might act as bait for the proteases [72]. Although the proteases responsible for recombinant protein degradation have yet to be identified, there are indications that certain classes of proteases are involved (e.g., aspartic proteases, metalloproteases, and serine proteases) [66, 68]. Once the proteases responsible for recombinant protein degradation are known, knockout and knockdown strategies can be employed to reduce their abundance. However, proteases play a significant role in many aspects of plant development, stress responses, and pathogen defense, so their elimination may only be suitable for cell and tissue cultures that are grown under sterile and controlled conditions in the absence of pathogens.

Downstream Processing

Most biopharmaceuticals are formulated as a purified product so the majority of biopharmaceuticals produced in plants must be extracted from plant tissue and then purified and formulated in the same way as conventional biopharmaceutical products. Regardless of the upstream production platform, downstream processing can account for up to 80% of the total manufacturing costs for a biopharmaceutical protein [73], but the first downstream processing steps are largely determined by the specific production host [74]. If the target protein is produced in plant suspension cells and secreted into the culture medium, the purification process can begin directly after the cells have been removed by filtration or centrifugation. If the protein is produced in an intact plant and/or if it accumulates inside the plant cell, it must be released by mechanical disruption in the presence of an appropriate extraction buffer and the extract must be clarified by filtration and/or centrifugation to remove debris, fibers, and other particulates. Aqueous two-phase partition is a useful initial purification step to remove polyphenols and cell debris from crude plant extracts [75, 76]. The removal of polyphenols is critical to prevent fouling of the chromatography media used in subsequent purification steps [74, 77]. After clarification, the product may be captured from the feed if a suitable affinity chromatography resin is available, allowing a high level of purification in a single step. A wide range of natural affinity ligands and an increasing number of synthetic ligands (e.g., mercaptoethylpyridine, MEP HyperCel™) are available, particularly for the capture of antibodies [78]. After capture, polishing is usually achieved by the application of two or more orthogonal separation methods to achieve maximal purity and contaminant removal, for example, ion exchange, hydrophobic interaction, hydroxyapatite, and size exclusion chromatography [79]. If a capture step is not possible, these chromatography methods may be used for intermediate purification prior to polishing. Purification can be facilitated by engineering the physicochemical properties of the target protein through genetic fusions, although the fusion tag must be removed after purification to yield the authentic protein as a final product (a protease cleavage site adjacent to the tag can be used to achieve separation). A fusion with the hydrophobic plant protein oleosin enables enrichment of the target protein by floating centrifugation [80]. Alternatively, fusing the target protein to elastin-like polypeptides (ELPs) allows the target protein to be isolated by thermal phase transition [81].

Potential contaminants include macromolecules such as host cell proteins and nucleic acids, as well as small molecules such as secondary metabolites (e.g., nicotine). The removal of contaminants derived from plant-associated microbes must also be demonstrated, especially endotoxins from *A. tumefaciens* that can cause inflammatory responses in humans. The successful removal of these substances has recently been demonstrated for a monoclonal antibody that has been produced in *N. benthamiana* by magnifection [82].

Biopharmaceuticals produced for human clinical trials must achieve certain quality criteria that are defined by current good manufacturing practice (cGMP). The regulations for biopharmaceutical manufacture are defined by the Food and Drug Administration (FDA) in the USA and by the European Medicines Agency (EMEA) in the European Union. The production of pharmaceuticals using plant suspension cells is very similar in concept to conventional systems based on mammalian cells, but intact plants

cultivated in the greenhouse or in the open field are very different in concept and in practice. The FDA and EMEA have published guidance documents covering the production of pharmaceuticals in plants, and these might be refined further in the future [83]. Recently the Fraunhofer Institute for Molecular Biology and Applied Ecology in Aachen, Germany, obtained the first GMP license for the production of a plant-made pharmaceutical protein for clinical phase I trials in Europe. Based on this process the anti-HIV antibody 2G12 was produced in transgenic tobacco plants in the greenhouse.

Plant-Derived Vaccines

Plants have been proposed as an alternative production platform for subunit vaccines, with the added advantage that storage tissues such as cereal grains and potato tubers may be used to keep the vaccine stable without the need for a cold chain and could even be used to administer oral vaccines without processing, thus reducing costs.

Antigens embedded in the plant cell matrix are protected against the acidic conditions in the stomach and are released gradually, allowing the induction of a mucosal immune response. Many antigens that could be used as vaccines in humans or farm animals have been produced in plants including the hepatitis B virus surface antigen [3, 84, 85], the Norwalk virus capsid protein [86–88], the *Escherichia coli* heat labile toxin [89–91], and the rabies glycoprotein [42, 92].

Phase I clinical trials in humans have been conducted for some oral vaccines. The coding sequence for the B-chain of the heat labile toxin from enterotoxigenic *E. coli* (LT-B) has been expressed in transgenic potato and maize. Human volunteers who ingested three 50-g or 100-g doses of peeled raw potato slices containing 0.5–1 mg of LT-B developed anti LT serum IgG antibodies (91%) and half of the vaccinees also produced secretory IgA antibodies in their stools [7]. Similarly human volunteers who ingested 2 g of defatted corn germ meal containing 1 mg of LT-B developed anti LT serum IgG and IgA and sIgA in their stools [93].

Transgenic potato tubers producing the major capsid protein of the Norwalk virus (which causes gastroenteritis) were fed to human volunteers in two or three 150-g doses containing ~500 μg of the protein. Higher levels of IgA antibody-secreting cells were observed in more than 90% of the vaccinees, 20% produced serum IgG or IgM responses, and 30% produced anti-NVCP antibodies in their stools [88].

Two phase I clinical trials with plant-derived hepatitis B surface antigen (HBsAg) have been reported. In the first trial, transgenic lettuce (*Lactuca sativa*) was orally administered to seven seronegative individuals in three 200-g doses containing 0.5–1 μg of HBsAg within 5 weeks. After the third dose, all subjects developed serum anti-HB antibodies of up to 6.3 mIU/ml serum [94]. In the second trial, transgenic potato tubers were fed to individuals who had previously been vaccinated against hepatitis B. The vaccinees received two or three 100-g doses of raw peeled potatoes each containing ~800 μg HBsAg. Higher serum anti-HB titers were observed in 60% of the vaccinee group whereas there was no increase in the control group [95].

Recently, H1N1 and H5N1 influenza virus hemagglutinin (HA) have been transiently expressed in *N. benthamiana* [96]. Both proteins assembled into virus-like particles (VLPs) that budded from the plant plasma membrane, a desirable outcome because VLPs are polyvalent and therefore much more immunogenic than soluble subunit vaccines. Mice parenterally immunized with low doses (0.5 μg) of the VLPs were protected against a lethal challenge with influenza virus [96]. A phase I dose escalation study to assess the safety of a plant-derived H5 VLP in healthy volunteers was initiated in 2010 (www.clinicaltrials.gov; NCT00984945).

Although most vaccines are intended to induce an immune response against pathogens, their use is not limited to the prevention of infectious diseases. More recently, vaccines have been developed for the prevention or the treatment of certain types of cancer. A plant-derived vaccine for the treatment of non-Hodgkin's lymphoma (NHL) based on idiotype antibodies has been evaluated in a phase I trial [97]. NHL is a clonal disease of the B-cell lineage and the malignant cells carry specific immunoglobulins (idiotypes) on their surface. These idiotypes can be used to trigger a specific immune response. Because the idiotypes are different in each patient the vaccine has to be manufactured individually for each treated person. Currently the patient's tumor cells are expanded from a biopsy as human/mouse heteromyelomas. The monoclonal idiotype antibody is purified and coupled to an immunogenic carrier protein like keyhole limpet hemocyanin (KLH)

and injected into the patient usually together with granulocyte-macrophage colony stimulating factor (GM-CSF) as an adjuvant [98]. To shorten the time needed to manufacture the patient-specific vaccine a plant-based production system has been developed in which the coding sequences for the variable domains of the idiotype antibody are cloned from the patient's biopsy and inserted into a viral vector for the expression of a single chain antibody (scFv). *N. benthamiana* plants have been infected with such viruses allowing the scFv to be purified from leaves [99, 100]. Sixteen NHL patients who had previously received chemotherapy were treated with two different doses of the tobacco-derived idiotype vaccine either with or without a GM-CSF adjuvant [17]. Most of the treated patients developed a cellular immune response although only three patients developed a humoral immune response. Recently, the Bayer Group announced another phase I clinical trial with idiotype vaccines for NHL using the transient magnifection technology developed by their subsidiary Icon Genetics. The ongoing study will enroll 30 patients with progressive or relapsing NHL. The patients will receive 12 injections over 16 months, each consisting of 1.0 mg of the personalized vaccine. The study is designed as a safety study to evaluate potential toxicity associated with the therapy but will also analyze the relevant immunological parameters of the patients. The final results of the study are expected in 2012 (www.clinicaltrials.gov; NCT01022255).

Plant-Made Pharmaceuticals in Advanced Development

The most advanced plant-derived pharmaceutical in terms of clinical development is glucocerebrosidase manufactured in transgenic carrot suspension cells (prGCD, taliglucerase alpha, Uplyso™). Patients suffering from Gaucher disease, an inherited lysosomal storage disorder, cannot produce active glucocerebrosidase and need enzyme replacement therapy with recombinant glucocerebrosidase, which is currently produced in CHO cells (imiglucerase, Cerezyme™) [101]. This is currently one of the most expensive biopharmaceuticals, with an annual treatment cost of USD 200,000 per patient [102]. The purified recombinant imiglucerase needs to be processed enzymatically to expose terminal mannose residues that are required for the efficient uptake of the enzyme into macrophages. The plant-derived counterpart, taliglucerase alpha, does not require these additional processing steps because it is targeted to the cell vacuole where the complex type N-glycans are trimmed to the paucimannose form exposing terminal mannose residues [16]. A phase III clinical trial with taliglucerase alpha was completed successfully in 2009 (www.clinicaltrials.gov, NCT00376168) and the substance currently awaits market approval from the FDA. Meanwhile patients can get access to taliglucerase alpha under an expanded access protocol [101].

Another plant-derived protein currently in clinical development is alpha-interferon (IFN-α2b) for the treatment of chronic hepatitis C infections. IFN-α2b has a low molecular weight (19 kDa, no glycan chains) and is therefore eliminated rapidly by renal filtration. Special formulations are required to increase its serum half-life, and this is achieved in the current formulation produced in *E. coli* (peginterferone alpha-2b; PEGIntron™), by attachment to polyethylene glycol. The plant-derived protein (Locteron™) is produced in duckweed and formulated in poly(ether-ester) microspheres to achieve controlled release over a defined period [103]. The plant-derived version has been tested successfully in a clinical phase I/II study (www.clinicaltrials.gov, NCT00593151) to establish its safety, tolerability, and efficacy compared to PEGIntron™. Currently two phase IIb clinical trials are underway to determine the optimal dose for the treatment of hepatitis C patients and its efficacy in combination with the antiviral compound ribavirin (www.clinicaltrials.gov, NCT00863239, NCT00953589).

The first recombinant biopharmaceutical on the market was insulin, which received regulatory approval in 1982. A large number of diabetes patients depend on insulin therapy so current demand for the protein exceeds 8 metric tons per year. This demand is currently met by production in *E. coli* and *Saccharomyces cerevisiae* [104, 105]. The successful production of active recombinant human insulin has also been demonstrated in oilseeds, where oleosin fusion can be used to facilitate purification. As stated above, oleosin is a hydrophobic protein component of the seed oilbodies and fusion proteins become concentrated in the oilbodies allowing their purification by floating centrifugation, enzymatic cleavage, and then standard polishing chromatography

methods [106]. For large-scale insulin production, the Canadian company SemBioSys Genetics Inc. uses safflower (*Carthamus tinctorius*) plants [107]. The company recently announced the successful completion of a phase I/II clinical trial with healthy volunteers demonstrating that the safflower-derived insulin (SBS-1000) is equivalent to the recombinant insulin currently on the market [108].

Future Directions

Many biopharmaceutical proteins have been produced successfully in plants and plant cell cultures, clearly demonstrating the utility of plant-based production platforms. The demand for biopharmaceuticals is predicted to rise in the future based on the large number of ongoing clinical trials that involve recombinant pharmaceutical proteins, but current fermenter-based production platforms are already struggling to meet the demand. The enormous flexibility offered by different plant production systems and their specific advantages in terms of cost, safety, and scalability, means that plants could provide an alternative source for recombinant biopharmaceuticals when the capacity of current platforms is exhausted.

To become more competitive with the currently established protein production platforms an increase in productivity for the plant cell factories is mandatory. Therefore future research will aim to boost the protein accumulation levels in plant cells. To achieve this goal different strategies are pursued including, among others, gene amplification, high throughput screening for elite events, targeting the protein of interest to suited storage organelles or even to create them artificially, and to shield the target protein against proteolytic degradation. Systems biology approaches will help to identify cellular targets that can be subsequently engineered to further improve the plant cell as a protein production host. The engineering process itself will be more precise in the future by employing the newly developed techniques to facilitate homologous recombination within the nuclear genome.

Beside the quantity also the quality of the final product will be a major focus of future research and development. Especially the engineering of the glycosylation pattern bears a great potential to optimize the stability and efficacy of the biopharmaceutical product. A critical point with respect to the glycosylation pattern will be the detailed understanding of plant-produced glycoproteins with the mammalian immune system. This will be an important prerequisite for tailoring plant-produced subunit vaccines and to avoid unintended side effects. With respect to oral vaccines reliable formulation and administration protocols have to be defined to ensure the anticipated outcome is achieved.

Further optimization of transient plant expression systems will help to address future needs for the delivery of vaccine, personalized medicine, and biopharmaceuticals for the treatment of orphan diseases. The rapid production cycle will also enable a timely reaction to emerging diseases, pandemics, or biohazards. However, unlike stable transgenic plant production systems, there are currently no specific regulatory guidelines for transient technologies, which are becoming a perceived barrier to their widespread use and commercialization. Therefore, the establishment and harmonization of international regulations for transient expression systems are needed to enable the commercial application of this promising technology.

Bibliography

Primary Literature

1. Hiatt A, Cafferkey R, Bowdish K (1989) Production of antibodies in transgenic plants. Nature 342:76–78
2. Sijmons PC, Dekker BM, Schrammeijer B, Verwoerd TC, van den Elzen PJ, Hoekema A (1990) Production of correctly processed human serum albumin in transgenic plants. Biotechnology 8:217–221
3. Mason HS, Lam DM, Arntzen CJ (1992) Expression of hepatitis B surface antigen in transgenic plants. Proc Natl Acad Sci USA 89:11745–11749
4. Ma JK, Hiatt A, Hein M, Vine ND, Wang F, Stabila P, van Dolleweerd C, Mostov K, Lehner T (1995) Generation and assembly of secretory antibodies in plants. Science 268:716–719
5. van Rooijen GJ, Moloney MM (1995) Plant seed oil-bodies as carriers for foreign proteins. Biotechnology 13:72–77
6. Zhang XR, Urry DW, Daniell H (1996) Expression of an environmentally friendly synthetic protein-based polymer gene in transgenic tobacco plants. Plant Cell Rep 16:174–179
7. Tacket CO, Mason HS, Losonsky G, Clements JD, Levine MM, Arntzen CJ (1998) Immunogenicity in humans of a recombinant bacterial antigen delivered in a transgenic potato. Nat Med 4:607–609
8. Vaquero C, Sack M, Chandler J, Drossard J, Schuster F, Monecke M, Schillberg S, Fischer R (1999) Transient expression of a tumor-specific single-chain fragment and a chimeric antibody in tobacco leaves. Proc Natl Acad Sci USA 96:11128–11133

9. Cabanes-Macheteau M, Fitchette-Laine AC, Loutelier-Bourhis C, Lange C, Vine ND, Ma JK, Lerouge P, Faye L (1999) N-Glycosylation of a mouse IgG expressed in transgenic tobacco plants. Glycobiology 9:365–372
10. Staub JM, Garcia B, Graves J, Hajdukiewicz PT, Hunter P, Nehra N, Paradkar V, Schlittler M, Carroll JA, Spatola L, Ward D, Ye G, Russell DA (2000) High-yield production of a human therapeutic protein in tobacco chloroplasts. Nat Biotechnol 18:333–338
11. Bakker H, Bardor M, Molthoff JW, Gomord V, Elbers I, Stevens LH, Jordi W, Lommen A, Faye L, Lerouge P, Bosch D (2001) Galactose-extended glycans of antibodies produced by transgenic plants. Proc Natl Acad Sci USA 98:2899–2904
12. Koprivova A, Stemmer C, Altmann F, Hoffmann A, Kopriva S, Gorr G, Reski R, Decker EL (2004) Targeted knockouts of *Physcomitrella* lacking plant-specific immunogenic N-glycans. Plant Biotechnol J 2:517–523
13. Strasser R, Altmann F, Mach L, Glossl J, Steinkellner H (2004) Generation of *Arabidopsis thaliana* plants with complex N-glycans lacking β1, 2-linked xylose and core α1, 3-linked fucose. FEBS Lett 561:132–136
14. Marillonnet S, Thoeringer C, Kandzia R, Klimyuk V, Gleba Y (2005) Systemic *Agrobacterium tumefaciens*-mediated transfection of viral replicons for efficient transient expression in plants. Nat Biotechnol 23:718–723
15. Walsh G (2006) Biopharmaceutical benchmarks 2006. Nat Biotechnol 24:769–776
16. Shaaltiel Y, Bartfeld D, Hashmueli S, Baum G, Brill-Almon E, Galili G, Dym O, Boldin-Adamsky SA, Silman I, Sussman JL, Futerman AH, Aviezer D (2007) Production of glucocerebrosidase with terminal mannose glycans for enzyme replacement therapy of Gaucher's disease using a plant cell system. Plant Biotechnol J 5:579–590
17. McCormick AA, Reddy S, Reinl SJ, Cameron TI, Czerwinkski DK, Vojdani F, Hanley KM, Garger SJ, White EL, Novak J, Barrett J, Holtz RB, Tuse D, Levy R (2008) Plant-produced idiotype vaccines for the treatment of non-Hodgkin's lymphoma: safety and immunogenicity in a phase I clinical study. Proc Natl Acad Sci USA 105:10131–10136
18. Castilho A, Pabst M, Leonard R, Veit C, Altmann F, Mach L, Glossl J, Strasser R, Steinkellner H (2008) Construction of a functional CMP-sialic acid biosynthesis pathway in Arabidopsis. Plant Physiol 147:331–339
19. Aviezer D, Almon-Brill E, Shaaltiel Y, Galili G, Chertkoff R, Hashmueli S, Galun E, Zimran A (2008) Novel enzyme replacement therapy for Gaucher disease: on-going phase III clinical trial with recombinant human glucocerebrosidase expressed in plant cells. Mol Genet Metab 93:S15–S15
20. Nicholson L, Gonzalez-Melendi P, van Dolleweerd C, Tuck H, Perrin Y, Ma JKC, Fischer R, Christou P, Stoger E (2005) A recombinant multimeric immunoglobulin expressed in rice shows assembly-dependent subcellular localization in endosperm cells. Plant Biotechnol J 3:115–127
21. Rademacher T, Sack M, Arcalis E, Stadlmann J, Balzer S, Altmann F, Quendler H, Stiegler G, Kunert R, Fischer R, Stoger E (2008) Recombinant antibody 2G12 produced in maize endosperm efficiently neutralizes HIV-1 and contains predominantly single-GlcNAc N-glycans. Plant Biotechnol J 6:189–201
22. Kohli A, Melendi PG, Abranches R, Capell T, Stoger E, Christou P (2006) The quest to understand the basis and mechanisms that control expression of introduced transgenes in crop plants. Plant Signal Behav 1:185–195
23. De Wilde C, Van Houdt H, De Buck S, Angenon G, De Jaeger G, Depicker A (2000) Plants as bioreactors for protein production: avoiding the problem of transgene silencing. Plant Mol Biol 43:347–359
24. Decker EL, Reski R (2004) The moss bioreactor. Curr Opin Plant Biol 7:166–170
25. Cai CQ, Doyon Y, Ainley WM, Miller JC, Dekelver RC, Moehle EA, Rock JM, Lee YL, Garrison R, Schulenberg L, Blue R, Worden A, Baker L, Faraji F, Zhang L, Holmes MC, Rebar EJ, Collingwood TN, Rubin-Wilson B, Gregory PD, Urnov FD, Petolino JF (2009) Targeted transgene integration in plant cells using designed zinc finger nucleases. Plant Mol Biol 69:699–709
26. Durai S, Mani M, Kandavelou K, Wu J, Porteus MH, Chandrasegaran S (2005) Zinc finger nucleases: custom-designed molecular scissors for genome engineering of plant and mammalian cells. Nucleic Acids Res 33:5978–5990
27. Porteus MH (2009) Plant biotechnology: zinc fingers on target. Nature 459:337–338
28. Tovkach A, Zeevi V, Tzfira T (2009) A toolbox and procedural notes for characterizing novel zinc finger nucleases for genome editing in plant cells. Plant J 57:747–757
29. Bendich AJ (1987) Why do chloroplasts and mitochondria contain so many copies of their genome? Bioessays 6:279–282
30. Svab Z, Maliga P (1993) High-frequency plastid transformation in tobacco by selection for a chimeric aadA gene. Proc Natl Acad Sci USA 90:913–917
31. De Cosa B, Moar W, Lee SB, Miller M, Daniell H (2001) Overexpression of the Bt cry2Aa2 operon in chloroplasts leads to formation of insecticidal crystals. Nat Biotechnol 19:71–74
32. Daniell H, Lee SB, Panchal T, Wiebe PO (2001) Expression of the native cholera toxin B subunit gene and assembly as functional oligomers in transgenic tobacco chloroplasts. J Mol Biol 311:1001–1009
33. Fernandez-San Millan A, Farran I, Molina A, Mingo-Castel AM, Veramendi J (2007) Expression of recombinant proteins lacking methionine as N-terminal amino acid in plastids: human serum albumin as a case study. J Biotechnol 127:593–604
34. Lelivelt CL, McCabe MS, Newell CA, Desnoo CB, van Dun KM, Birch-Machin I, Gray JC, Mills KH, Nugent JM (2005) Stable plastid transformation in lettuce (*Lactuca sativa* L.). Plant Mol Biol 58:763–774
35. Ruf S, Hermann M, Berger IJ, Carrer H, Bock R (2001) Stable genetic transformation of tomato plastids and expression of a foreign protein in fruit. Nat Biotechnol 19:870–875
36. Hagemann R (2002) Milestones in plastid genetics of higher plants. In: Esser K, Lüttge U, Beyschlag W, Hellwig F (eds)

Progress in botany: genetics, physiology, ecology, vol 63. Springer, New York, pp 5–51
37. McCabe MS, Klaas M, Gonzalez-Rabade N, Poage M, Badillo-Corona JA, Zhou F, Karcher D, Bock R, Gray JC, Dix PJ (2008) Plastid transformation of high-biomass tobacco variety Maryland Mammoth for production of human immunodeficiency virus type 1 (HIV-1) p24 antigen. Plant Biotechnol J 6:914–929
38. Fischer R, Vaquero-Martin C, Sack M, Drossard J, Emans N, Commandeur U (1999) Towards molecular farming in the future: transient protein expression in plants. Biotechnol Appl Biochem 30:113–116
39. Sheludko YV (2008) Agrobacterium-mediated transient expression as an approach to production of recombinant proteins in plants. Recent Pat Biotechnol 2:198–208
40. Lico C, Chen Q, Santi L (2008) Viral vectors for production of recombinant proteins in plants. J Cell Physiol 216:366–377
41. Pogue GP, Lindbo JA, Garger SJ, Fitzmaurice WP (2002) Making an ally from an enemy: plant virology and the new agriculture. Annu Rev Phytopathol 40:45–74
42. Yusibov V, Hooper D, Spitsin S, Fleysh N, Kean R, Mikheeva T, Deka D, Karasev A, Cox S, Randall J, Koprowski H (2002) Expression in plants and immunogenicity of plant virus-based experimental rabies vaccine. Vaccine 20:3155–3164
43. Marillonnet S, Giritch A, Gils M, Kandzia R, Klimyuk V, Gleba Y (2004) In planta engineering of viral RNA replicons: efficient assembly by recombination of DNA modules delivered by Agrobacterium. Proc Natl Acad Sci USA 101:6852–6857
44. Musiychuk K, Stephenson N, Bi H, Farrance CE, Orozovic G, Brodelius M, Brodelius P, Horsey A, Ugulava N, Shamloul AM, Mett V, Rabindran S, Streatfield SJ, Yusibov V (2007) A launch vector for the production of vaccine antigens in plants. Influenza Other Respi Viruses 1:19–25
45. Giritch A, Marillonnet S, Engler C, van Eldik G, Botterman J, Klimyuk V, Gleba Y (2006) Rapid high-yield expression of full-size IgG antibodies in plants coinfected with noncompeting viral vectors. Proc Natl Acad Sci USA 103:14701–14706
46. Saint-Jore-Dupas C, Faye L, Gomord V (2007) From planta to pharma with glycosylation in the toolbox. Trends Biotechnol 25:317–323
47. Bardor M, Faveeuw C, Fitchette AC, Gilbert D, Galas L, Trottein F, Faye L, Lerouge P (2003) Immunoreactivity in mammals of two typical plant glyco-epitopes, core α(1, 3)-fucose and core xylose. Glycobiology 13:427–434
48. Jin C, Altmann F, Strasser R, Mach L, Schahs M, Kunert R, Rademacher T, Glossl J, Steinkellner H (2008) A plant-derived human monoclonal antibody induces an anti-carbohydrate immune response in rabbits. Glycobiology 18:235–241
49. Bosch D, Schots A (2010) Plant glycans: friend or foe in vaccine development? Expert Rev Vaccines 9:835–842
50. Tekoah Y, Ko K, Koprowski H, Harvey DJ, Wormald MR, Dwek RA, Rudd PM (2004) Controlled glycosylation of therapeutic antibodies in plants. Arch Biochem Biophys 426:266–278
51. Sriraman R, Bardor M, Sack M, Vaquero C, Faye L, Fischer R, Finnern R, Lerouge P (2004) Recombinant anti-hCG antibodies retained in the endoplasmic reticulum of transformed plants lack core-xylose and core-α(1, 3)-fucose residues. Plant Biotechnol J 2:279–287
52. Weise A, Altmann F, Rodriguez-Franco M, Sjoberg ER, Baumer W, Launhardt H, Kietzmann M, Gorr G (2007) High-level expression of secreted complex glycosylated recombinant human erythropoietin in the Physcomitrella Δ-*fuc-t* Δ-*xyl-t* mutant. Plant Biotechnol J 5:389–401
53. Schähs M, Strasser R, Stadlmann J, Kunert R, Rademacher T, Steinkellner H (2007) Production of a monoclonal antibody in plants with a humanized N-glycosylation pattern. Plant Biotechnol J 5:657–663
54. Cox KM, Sterling JD, Regan JT, Gasdaska JR, Frantz KK, Peele CG, Black A, Passmore D, Moldovan-Loomis C, Srinivasan M, Cuison S, Cardarelli PM, Dickey LF (2006) Glycan optimization of a human monoclonal antibody in the aquatic plant *Lemna minor*. Nat Biotechnol 24:1591–1597
55. Gasdaska JR, Sterling JD, Regan JT, Cox KM, Sherwood SW, Dickey LF (2007) Expression of a glyco-optimized anti-CD20 antibody in the aquatic plant *Lemna* with enhanced ADCC activity. Blood 110:697a–697a
56. Schuster M, Jost W, Mudde GC, Wiederkum S, Schwager C, Janzek E, Altmann F, Stadlmann J, Stemmer C, Gorr G (2007) In vivo glyco-engineered antibody with improved lytic potential produced by an innovative non-mammalian expression system. Biotechnol J 2:700–708
57. Bakker H, Rouwendal GJ, Karnoup AS, Florack DE, Stoopen GM, Helsper JP, van Ree R, van Die I, Bosch D (2006) An antibody produced in tobacco expressing a hybrid β-1, 4-galactosyltransferase is essentially devoid of plant carbohydrate epitopes. Proc Natl Acad Sci USA 103:7577–7582
58. Fujiyama K, Furukawa A, Katsura A, Misaki R, Omasa T, Seki T (2007) Production of mouse monoclonal antibody with galactose-extended sugar chain by suspension cultured tobacco BY2 cells expressing human β(1, 4)-galactosyltransferase. Biochem Biophys Res Commun 358:85–91
59. Sourrouille C, Marquet-Blouin E, D'Aoust MA, Kiefer-Meyer MC, Seveno M, Pagny-Salehabadi S, Bardor M, Durambur G, Lerouge P, Vezina L, Gomord V (2008) Down-regulated expression of plant-specific glycoepitopes in alfalfa. Plant Biotechnol J 6:702–721
60. Erbayraktar S, Grasso G, Sfacteria A, Xie QW, Coleman T, Kreilgaard M, Torup L, Sager T, Erbayraktar Z, Gokmen N, Yilmaz O, Ghezzi P, Villa P, Fratelli M, Casagrande S, Leist M, Helboe L, Gerwein J, Christensen S, Geist MA, Pedersen LO, Cerami-Hand C, Wuerth JP, Cerami A, Brines M (2003) Asialoerythropoietin is a nonerythropoietic cytokine with broad neuroprotective activity in vivo. Proc Natl Acad Sci USA 100:6741–6746
61. Wee EG, Sherrier DJ, Prime TA, Dupree P (1998) Targeting of active sialyltransferase to the plant Golgi apparatus. Plant Cell 10:1759–1768
62. Castilho A, Strasser R, Stadlmann J, Grass J, Jez J, Gattinger P, Kunert R, Quendler H, Pabst M, Leonard R, Altmann F, Steinkellner H (2010) In planta protein sialylation through

overexpression of the respective mammalian pathway. J Biol Chem 285:15923–15930
63. Karnoup AS, Turkelson V, Anderson WH (2005) O-linked glycosylation in maize-expressed human IgA1. Glycobiology 15:965–981
64. Xu J, Tan L, Goodrum KJ, Kieliszewski MJ (2007) High-yields and extended serum half-life of human interferon α2b expressed in tobacco cells as arabinogalactan-protein fusions. Biotechnol Bioeng 97:997–1008
65. De Muynck B, Navarre C, Nizet Y, Stadlmann J, Boutry M (2009) Different subcellular localization and glycosylation for a functional antibody expressed in *Nicotiana tabacum* plants and suspension cells. Transgenic Res 18:467–482
66. Delannoy M, Alves G, Vertommen D, Ma J, Boutry M, Navarre C (2008) Identification of peptidases in *Nicotiana tabacum* leaf intercellular fluid. Proteomics 8:2285–2298
67. Doran PM (2006) Foreign protein degradation and instability in plants and plant tissue cultures. Trends Biotechnol 24:426–432
68. Schiermeyer A, Schinkel H, Apel S, Fischer R, Schillberg S (2005) Production of *Desmodus rotundus* salivary plasminogen activator α1 (DSPAα1) in tobacco is hampered by proteolysis. Biotechnol Bioeng 89:848–858
69. Kim TG, Lee HJ, Jang YS, Shin YJ, Kwon TH, Yang MS (2008) Co-expression of proteinase inhibitor enhances recombinant human granulocyte-macrophage colony stimulating factor production in transgenic rice cell suspension culture. Protein Expr Purif 61:117–121
70. Komarnytsky S, Borisjuk N, Yakoby N, Garvey A, Raskin I (2006) Cosecretion of protease inhibitor stabilizes antibodies produced by plant roots. Plant Physiol 141:1185–1193
71. Rivard D, Anguenot R, Brunelle F, Le VQ, Vezina L-P, Trepanier S, Michaud D (2006) An in-built proteinase inhibitor system for the protection of recombinant proteins recovered from transgenic plants. Plant Biotechnol J 4:359–368
72. Baur A, Reski R, Gorr G (2005) Enhanced recovery of a secreted recombinant human growth factor using stabilizing additives and by co-expression of human serum albumin in the moss *Physcomitrella patens*. Plant Biotechnol J 3:331–340
73. Roque AC, Lowe CR, Taipa MA (2004) Antibodies and genetically engineered related molecules: production and purification. Biotechnol Prog 20:639–654
74. Menkhaus TJ, Bai Y, Zhang C, Nikolov ZL, Glatz CE (2004) Considerations for the recovery of recombinant proteins from plants. Biotechnol Prog 20:1001–1014
75. Platis D, Drossard J, Fischer R, Ma JK, Labrou NE (2008) New downstream processing strategy for the purification of monoclonal antibodies from transgenic tobacco plants. J Chromatogr A 1211:80–89
76. Platis D, Labrou NE (2009) Application of a PEG/salt aqueous two-phase partition system for the recovery of monoclonal antibodies from unclarified transgenic tobacco extract. Biotechnol J 4:1320–1327
77. Bai Y, Glatz CE (2003) Bioprocess considerations for expanded-bed chromatography of crude canola extract: sample preparation and adsorbent reuse. Biotechnol Bioeng 81:775–782
78. Low D, O'Leary R, Pujar NS (2007) Future of antibody purification. J Chromatogr B 848:48–63
79. Drossard J (2004) Downstream processing of plant-derived recombinant therapeutic proteins. In: Fischer R, Schillberg S (eds) Molecular farming: plant-made pharmaceuticals and technical proteins. Wiley-VCH, Weinheim, Germany, pp 217–231
80. Parmenter DL, Boothe JG, van Rooijen GJH, Yeung EC, Moloney MM (1995) Production of biologically active hirudin in plant seeds using oleosin partitioning. Plant Mol Biol 29:1167–1180
81. Floss DM, Schallau K, Rose-John S, Conrad U, Scheller J (2010) Elastin-like polypeptides revolutionize recombinant protein expression and their biomedical application. Trends Biotechnol 28:37–45
82. Pogue GP, Vojdani F, Palmer KE, Hiatt E, Hume S, Phelps J, Long L, Bohorova N, Kim D, Pauly M, Velasco J, Whaley K, Zeitlin L, Garger SJ, White E, Bai Y, Haydon H, Bratcher B (2010) Production of pharmaceutical-grade recombinant aprotinin and a monoclonal antibody product using plant-based transient expression systems. Plant Biotechnol J 8:638–654
83. Spok A, Twyman RM, Fischer R, Ma JK, Sparrow PA (2008) Evolution of a regulatory framework for pharmaceuticals derived from genetically modified plants. Trends Biotechnol 26:506–517
84. Kapusta J, Modelska A, Figlerowicz M, Pniewski T, Letellier M, Lisowa O, Yusibov V, Koprowski H, Plucienniczak A, Legocki AB (1999) A plant-derived edible vaccine against hepatitis B virus. FASEB J 13:1796–1799
85. Kong Q, Richter L, Yang YF, Arntzen CJ, Mason HS, Thanavala Y (2001) Oral immunization with hepatitis B surface antigen expressed in transgenic plants. Proc Natl Acad Sci USA 98:11539–11544
86. Mason HS, Ball JM, Shi JJ, Jiang X, Estes MK, Arntzen CJ (1996) Expression of Norwalk virus capsid protein in transgenic tobacco and potato and its oral immunogenicity in mice. Proc Natl Acad Sci USA 93:5335–5340
87. Santi L, Batchelor L, Huang Z, Hjelm B, Kilbourne J, Arntzen CJ, Chen Q, Mason HS (2008) An efficient plant viral expression system generating orally immunogenic Norwalk virus-like particles. Vaccine 26:1846–1854
88. Tacket CO, Mason HS, Losonsky G, Estes MK, Levine MM, Arntzen CJ (2000) Human immune responses to a novel norwalk virus vaccine delivered in transgenic potatoes. J Infect Dis 182:302–305
89. Chikwamba R, Cunnick J, Hathaway D, McMurray J, Mason H, Wang K (2002) A functional antigen in a practical crop: LT-B producing maize protects mice against *Escherichia coli* heat labile enterotoxin (LT) and cholera toxin (CT). Transgenic Res 11:479–493
90. Haq TA, Mason HS, Clements JD, Arntzen CJ (1995) Oral immunization with a recombinant bacterial antigen produced in transgenic plants. Science 268:714–716
91. Rosales-Mendoza S, Soria-Guerra RE, Lopez-Revilla R, Moreno-Fierros L, Alpuche-Solis AG (2008) Ingestion of transgenic carrots expressing the *Escherichia coli* heat-labile enterotoxin B subunit protects mice against cholera toxin challenge. Plant Cell Rep 27:79–84

92. Ashraf S, Singh PK, Yadav DK, Shahnawaz M, Mishra S, Sawant SV, Tuli R (2005) High level expression of surface glycoprotein of rabies virus in tobacco leaves and its immunoprotective activity in mice. J Biotechnol 119:1–14
93. Tacket CO, Pasetti MF, Edelman R, Howard JA, Streatfield S (2004) Immunogenicity of recombinant LT-B delivered orally to humans in transgenic corn. Vaccine 22:4385–4389
94. Kapusta J, Modelska A, Pniewski T, Figlerowicz M, Jankowski K, Lisowa O, Plucienniczak A, Koprowski H, Legocki AB (2001) Oral immunization of human with transgenic lettuce expressing hepatitis B surface antigen. Adv Exp Med Biol 495:299–303
95. Thanavala Y, Mahoney M, Pal S, Scott A, Richter L, Natarajan N, Goodwin P, Arntzen CJ, Mason HS (2005) Immunogenicity in humans of an edible vaccine for hepatitis B. Proc Natl Acad Sci USA 102:3378–3382
96. D'Aoust MA, Lavoie PO, Couture MM, Trepanier S, Guay JM, Dargis M, Mongrand S, Landry N, Ward BJ, Vezina LP (2008) Influenza virus-like particles produced by transient expression in *Nicotiana benthamiana* induce a protective immune response against a lethal viral challenge in mice. Plant Biotechnol J 6:930–940
97. Arntzen CJ (2008) Plant science. Using tobacco to treat cancer. Science 321:1052–1053
98. Sinha R, Shenoy PJ, Flowers CR (2008) Idiotype vaccine strategies for improving outcomes in follicular lymphoma. Expert Opin Biol Ther 8:1213–1223
99. McCormick AA, Kumagai MH, Hanley K, Turpen TH, Hakim I, Grill LK, Tuse D, Levy S, Levy R (1999) Rapid production of specific vaccines for lymphoma by expression of the tumor-derived single-chain Fv epitopes in tobacco plants. Proc Natl Acad Sci USA 96:703–708
100. McCormick AA, Reinl SJ, Cameron TI, Vojdani F, Fronefield M, Levy R, Tuse D (2003) Individualized human scFv vaccines produced in plants: humoral anti-idiotype responses in vaccinated mice confirm relevance to the tumor Ig. J Immunol Meth 278:95–104
101. Hollak CE, vom Dahl S, Aerts JM, Belmatoug N, Bembi B, Cohen Y, Collin-Histed T, Deegan P, van Dussen L, Giraldo P, Mengel E, Michelakakis H, Manuel J, Hrebicek M, Parini R, Reinke J, di Rocco M, Pocovi M, Sa Miranda MC, Tylki-Szymanska A, Zimran A, Cox TM (2010) Force Majeure: therapeutic measures in response to restricted supply of imiglucerase (Cerezyme) for patients with Gaucher disease. Blood Cells Mol Dis 44:41–47
102. Kaiser J (2008) Is the drought over for pharming? Science 320:473–475
103. De Leede LG, Humphries JE, Bechet AC, Van Hoogdalem EJ, Verrijk R, Spencer DG (2008) Novel controlled-release *Lemna*-derived IFN-α2b (Locteron): pharmacokinetics, pharmacodynamics, and tolerability in a phase I clinical trial. J Interferon Cytokine Res 28:113–122
104. Chance RE, Frank BH (1993) Research, development, production, and safety of biosynthetic human insulin. Diab Care 16(Suppl 3):133–142
105. Kjeldsen T (2000) Yeast secretory expression of insulin precursors. Appl Microbiol Biotechnol 54:277–286
106. Nykiforuk CL, Boothe JG, Murray EW, Keon RG, Goren HJ, Markley NA, Moloney MM (2006) Transgenic expression and recovery of biologically active recombinant human insulin from *Arabidopsis thaliana* seeds. Plant Biotechnol J 4:77–85
107. Moloney MM, Boothe J, Nykiforuk C, Kuhlman P, Pollock B (2008) Plant-based production of authentic recombinant human insulin: chemical, biochemical and preclinical evaluation. FEBS J 275:62–62
108. Boothe J, Nykiforuk C, Shen Y, Zaplachinski S, Szarka S, Kuhlman P, Murray E, Morck D, Moloney MM (2010) Seed-based expression systems for plant molecular farming. Plant Biotechnol J 8:588–606

Books and Reviews

Chen Q (2008) Expression and purification of pharmaceutical proteins in plants. Biol Eng 1:291–321

Daniell H, Singh ND, Mason H, Streatfield SJ (2009) Plant-made vaccine antigens and biopharmaceuticals. Trends Plant Sci 14:669–679

De Muynck B, Navarre C, Boutry M (2010) Production of antibodies in plants: status after twenty years. Plant Biotechnol J 8:529–563

Faye L, Gomord V (eds) (2009) Recombinant proteins from plants: methods and protocols. Humana, New York

Fischer R, Schillberg S (eds) (2004) Molecular farming: plant-made pharmaceuticals and technical proteins. Wiley-VCH, Weinheim, Germany

Fischer R, Schillberg S, Twyman RM (2009) Molecular farming of antibodies in plants. In: Kirakosyan A, Kaufman PB (eds) Recent advances in plant biotechnology. Springer, Dordrecht, The Netherlands, pp 35–63

Gomez E, Zoth SC, Berinstein A (2009) Plant-based vaccines for potential human application: a review. Hum Vaccin 5:738–744

Hefferon KL (2009) Biopharmaceuticals in plants: toward the next generation of medicine. CRC, Boca Raton

Hellwig S, Drossard J, Twyman RM, Fischer R (2004) Plant cell cultures for the production of recombinant proteins. Nat Biotechnol 22:1415–1422

Karasev AV (ed) (2009) Plant-produced microbial vaccines. Springer, Berlin

Kempken F, Jung C (eds) (2010) Genetic modification of plants: agriculture, horticulture and forestry. Springer, Berlin

Knäblein J (2004) Biopharmaceuticals expressed in plants. In: Kayser O, Müller RH (eds) Pharmaceutical biotechnology. Wiley-VCH, Weinheim, Germany, pp 35–56

Levine MM (ed) (2009) New generation vaccines, 4th edn. Informa Healthcare, New York

Rader R (2007) Biopharmaceutical products in the US and European markets, 6th edn. Bioplan Associates, Rockville

Rybicki EP (2010) Plant-made vaccines for humans and animals. Plant Biotechnol J 8:620–637

Sharma AK, Sharma MK (2009) Plants as bioreactors: recent developments and emerging opportunities. Biotechnol Adv 27:811–832

Shih SM, Doran PM (2009) Foreign protein production using plant cell and organ cultures: advantages and limitations. Biotechnol Adv 27:1036–1042

Tiwari S, Verma PC, Singh PK, Tuli R (2009) Plants as bioreactors for the production of vaccine antigens. Biotechnol Adv 27:449–467

Twyman RM, Schillberg S, Fischer R (2005) Transgenic plants in the biopharmaceutical market. Expert Opin Emerg Drugs 10:185–218

Walsh G (2009) Market development of biopharmaceuticals. In: Engelhard M, Hagen K, Boysen M (eds) Genetic engineering in livestock: new applications and interdisciplinary perspectives. Springer, Berlin, pp 69–89

Walsh G (ed) (2009) Post-translational modification of protein biopharmaceuticals. Wiley-VCH, Weinheim, Germany

Plant Molecular Pharming, Veterinary Applications

Doreen M. Floss[1], Udo Conrad[2]
[1]Institute of Biochemistry and Molecular Biology II, Heinrich-Heine-University Düsseldorf, Düsseldorf, Germany
[2]Leibniz Institute of Plant Genetics and Crop Plant Research (IPK), Phytoantibodies, Gatersleben, Germany

Article Outline

Glossary
Definition of the Subject
Introduction
Plant-Based Expression Systems
Edible Vaccines and Purification
Future Directions
Acknowledgments
Bibliography

Glossary

Companion animal Animal kept for companionship and enjoyment (household animal).

Edible vaccines Antigenic proteins, which are produced in organs of transgenic plants (e.g., fruits, tubers) and can be directly administered to humans or animals without any purification procedure.

ELP Elastin-like polypeptide containing the hydrophobic amino acids valine, proline, glycine, and guest residues, which shows temperature-dependent, reversible self-aggregation.

ELPylation Genetic C- or N-terminal target protein fusion to elastin-like polypeptides.

Homoplasmy Presence of the transgene in all copies of chloroplast DNA.

Livestock animal Domesticated animal raised in an agricultural setting to produce, e.g., food and fiber.

Molecular pharming The large-scale production and purification of pharmaceutical proteins in plants.

Plant-based expression Process by which information from a transgene is used in the synthesis of a functional protein *in planta*. Different plant-based expression systems are suitable (e.g., transgenic plants, transient expression, and plant cell cultures).

Plantibodies Antibody or antibody derivative produced in genetically engineered plants.

Transgenic plants Genetically engineered plants generated by the biolistic method (particle gun) or by *Agrobacterium tumefaciens* mediated transformation. The introduced transgene, which does not occur naturally in the plant, is transferred to the offspring.

Transient expression Expression of transgenes for a short period of time. In the context of plant-based expression infiltration of recombinant Agrobacteria (Agro-infiltration) or the use of plant viral vectors are the methods of choice to produce a desired protein *in planta*.

Transplastomic plants Introduced transgene is targeted to the chloroplast genome using particle bombardment or other physical DNA delivery techniques.

Zoonotic diseases Infectious disease that can be transmitted from wild and domestic animals to humans.

Definition of the Subject

"Molecular Pharming" refers to the large-scale production and purification of pharmaceutical proteins in plants or plant-based expression systems. Since the successful expression of complete antibodies in transgenic plants in 1989 and the first report of plant-based

vaccine production in 1992, a large number of different vaccines, antibodies, as well as antibody fragments have been produced in plants for medical or veterinary purposes. However, only two plant-produced vaccine-related products have gone all the way through the production and regulatory hurdles, and only one, a plant-made single-chain variable fragment (scFv), is used in the production of a recombinant Hepatitis B Virus (HBV) vaccine in Cuba. Edible vaccines and novel methods of downstream processing such as "ELPylation" have been developed over the past years to facilitate the development of recombinant protein-based therapeutics.

Introduction

Plant-based expression systems possess advantages over conventional eukaryotic expression systems (yeast, insect cells, and mammalian cells), e.g., the ability to obtain complex, correctly folded, and posttranslationally modified proteins [50]. They compete favorably with mammalian cells for the production of vaccines and antibodies because of distinct advantages over conventional systems including cost, safety, and scalability [57]. However, the cost of downstream processing (protein extraction, protein recovery, and protein purification) for recombinant expression systems in general are approximately the same and can represent over 80% of the overall processing costs [30] with the majority of such costs attributed to chromatography and associated materials, labor, and capital equipment [57]. Savings in the upstream components (no need for expensive fermenters, special culture media, and skilled workers) are some of the major benefits for the production of pharmaceutical proteins in plants. Costs of goods sold (COGS) from mammalian cell culture are estimated to be $300 per gram therapeutic protein, whereas the raw material costs for 1 g recombinant protein from plants are in the order of $0.10–$1 (depending on the expression level; [33]). The main technical bottleneck limiting the commercial production of pharmaceuticals in plants is the high cost and inefficiency of downstream processing including purification [34].

One-third of the approved biopharmaceuticals are glycoproteins [56] and the activity of antibodies, blood factors, and interferons is dependent on their glycosylation pattern. Accordingly, biopharmaceuticals are often produced in heterologous expression systems with glycosylation capabilities. Plant-specific glycosylation differs from mammalian glycosylation (for review see [26]) and this aspect explains the major limitation for the use of plant-made pharmaceuticals in therapy. Recently, progress toward the humanization of protein N-glycosylation in plant cells has been made, which focused on the targeted expression of therapeutic proteins, the knock-out of plant-specific N-glycan-processing genes, and/or the introduction of the enzymatic machinery catalyzing the synthesis, transport, and addition of mammalian sugar residues (for review see [27]).

With the development of "edible" vaccines, which can be orally administered in the form of a transgenic fruit or vegetable expressing the appropriate antigen without any prior processing, low-cost production systems and effective delivery systems are expected [40]. One of the easiest ways to get vaccinated against a disease might be eating a bite of banana, full of the virus proteins, as it was contemplated by researchers at the Boyce Thompson Institute for Plant Research at Cornell University in 1997 [25]. In reality, this anticipated development did not occur. Major problems of this technology are low yields, weak antigenicity of plant-produced vaccines and the lack of buy-in by governments and pharmaceutical companies [43].

In this chapter, the historical development of plant-produced vaccines and antibodies, so-called plantibodies, and the development of different stable plant production systems including down-stream processing with a specific focus on the progress of animal therapeutics will be discussed.

Plant-Based Expression Systems

Since the first report of plant-based antibody production [32], different formats have been generated ranging from single variable heavy-chain domain (VHH) antibodies [4] and single-chain molecules (scFvs; [3, 23]) to Fab fragments [10], and complete immunoglobulins [35]. Despite substantial progress in the production of antibodies in plants for human health (for review see [9]), their application to the veterinary field is rather limited (for review see [18]). The development of passive immunization commenced in 1890 with the identification of serum therapy by Emil Behring and

Shibasaburo Kitasato. They identified substances in the blood they called antibodies which were responsible for the immunity against diphtheria and tetanus toxins. Furthermore, the researchers were able to transfer immunity to immunologically naïve animals by injecting serum of animals treated with nonlethal doses of a crude toxin preparation [2]. At the same time, Paul Ehrlich discovered that antibodies can act as so-called magic bullets for the targeting of cancer cells [12]. A century later, the structures of antibodies and the sequences coding for the immunoglobulin chains were elucidated and mouse hybridomas provided highly specific monoclonal antibodies for therapeutic applications [36]. The development of innovative recombinant DNA technologies greatly enhanced the clinical efficiency and safety of mouse-derived monoclonal antibodies. The ability to generate large antibody libraries, and the simplified antibody backbone of a single-chain antibody made antibody phage display a powerful tool for the development of new therapeutic agents (for reviews see [3]).

Production shortfalls and high costs are major incentives for further development of alternative antibody production technologies with a focus on active immunization (vaccination). The defining event for the development of "vaccinology" (from the Latin "vacca," meaning cow) dates back more than 200 years. At that time the smallpox vaccine was discovered by Edward Jenner. He inoculated humans with a less virulent, but antigenic related, Cowpox Virus to confer protection against the related human Smallpox Virus. Criteria for the development of veterinary vaccines are different depending on the particular target animals (for review see [38]). Health and welfare of the individual animal are the primary concerns for companion animal vaccines and thus are comparable to those for humans. In contrast, livestock animal vaccines should be inexpensive, prevent, and control infectious diseases of animals used as food to reduce or eliminate health risks to consumers. In some cases, these vaccines are further used to improve the productivity of livestock. To combat zoonotic diseases which are transmittable to humans, e.g., rabies, vaccination of wildlife animals is the method of choice. Furthermore, veterinary vaccines have a significant impact on public health due to the reduction in the administration of veterinary pharmaceuticals such as hormones.

The pioneering work for the expression of vaccines in plants was described in a patent by Curtiss and Cardineau in 1990. They reported the production of the *Streptococcus mutans* surface protein antigen A (SpaA) in transgenic tobacco plants [6]. Subsequently, Mason and co-workers succeeded in expressing the hepatitis B surface antigen in tobacco [37]. In 1993, Usha and co-workers expressed a peptide representing an epitope of the VP1 envelope protein of the Foot-and-Mouth-Disease Virus (FMDV) on the surface of a plant virus particle [55]. This study was the first report of a plant-derived veterinary vaccine. Following this pioneering work, various veterinary candidate vaccines have been produced in a variety of plant species using different expression systems, and they have proven to elicit humoral and mucosal immune responses against toxins, viruses, bacteria, and parasitic pathogens (for reviews see [18, 29, 44, 52, 57]). There are still no plant-derived veterinary vaccines on the market; however, one major step was made at the beginning of 2006 by Dow AgroSciences (DAS, Indianapolis, USA). Their plant cell–expressed vaccine against the Newcastle Disease Virus (NDV), produced in a suspension-cultured tobacco cell line, has gained regulatory approval by the US Department of Agriculture (USDA) Center for Veterinary Biologics – the final authority for veterinary vaccines in the USA [48]. Regrettably, this vaccine has not been introduced to the market. Dow AgroSciences apparently wished to demonstrate that their Concert™ Plant-Cell-Produced system was useful for the production of safe and effective vaccines, fulfilling the approval requirements of the regulatory system [43]. A year prior to the approval of the DAS vaccine, a plant-made scFv, used in the production of a recombinant Hepatitis B Virus (HBV) vaccine in Cuba [41], progressed through the regulatory system and was commercialized. These are the two plant-produced vaccine-related products which have gone through the production and regulatory hurdles, despite nearly 20 years of plant-derived vaccines [43].

Four plant-based expression systems have been developed thus far (Fig. 1):

- Expression in stably transformed transgenic plants including tissue-specific expression (e.g., in seeds or tubers)
- Expression in transplastomic plants

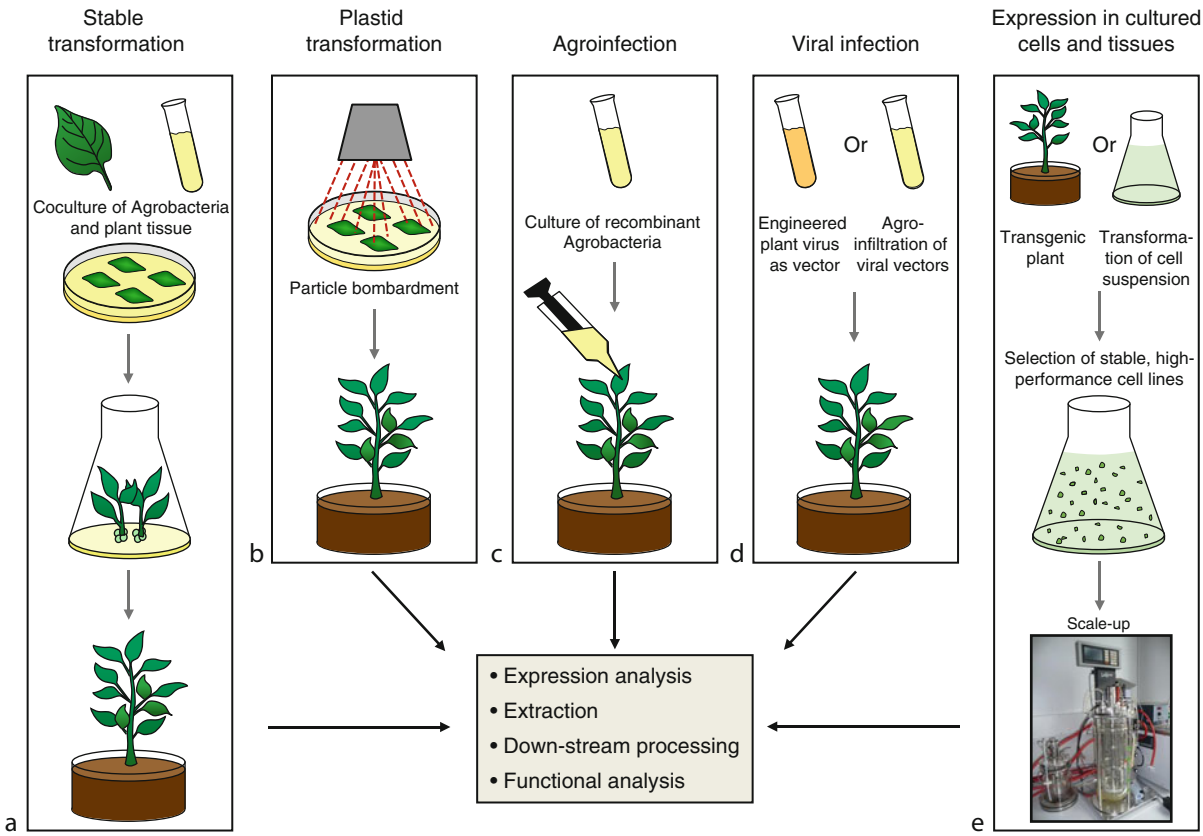

Plant Molecular Pharming, Veterinary Applications. Figure 1

Plant-based expression systems for pharmaceutical proteins. (**a**) Transgenic plants derived by stable transformation, either using *Agrobacterium*-mediated gene transfer [54] or biolistic transformation [1], represent a stable and cheap source for the large-scale production of recombinant proteins. The transgene is genetically fixed and transferred into the next generation. However, the development as well as the selection of a stable transgenic line can take many months. Recombinant proteins may be expressed in the cytoplasm or be localized in other cellular compartments (nucleus, mitochondria, chloroplasts, vacuole, endoplasmic reticulum, or apoplast), or can be produced in different plant tissues (leaves, seeds). (**b**) Transplastomic plants obtained by using particle bombardment often have high yields of the recombinant proteins. However, the system is often not suitable for glycosylated or secreted proteins but this barrier may be overcome soon [27]. (**c**) *Agrobacterium tumefaciens*–mediated transient expression is the standard method for determining if a transgene is expressed *in planta*. Here, a suspension of bacteria is directly injected into the intercellular space of plant leaves either by using a syringe or vacuum. (**d**) Viral vectors can be used for the expression of foreign proteins or of chimeric coat proteins in plants. Two different methods can be used for the delivery of the viral genomes into the plant, either engineered plant viruses (e.g., Tobacco Mosaic Virus) or recombinant Agrobacteria. (**e**) The application of plant cell culture for the production of recombinant proteins is focused on a small number of cell lines, e.g., the tobacco line Bright Yellow-2 (BY-2). Furthermore, transgenic cell lines can be established either from a transgenic plant or by the transformation of cell suspensions either by Agrobacteria or particle bombardment. After selection of stable, high-performance cell lines, the recombinant proteins can be produced in bioreactors under "good manufacturing practice" (GMP)

- Transient expression in tobacco leaves (*Nicotiana tabacum, N. benthamiana*) using either plant viruses, *Agrobacterium tumefaciens*, or both to facilitate high accumulation of vaccines and/or antibodies
- Expression in cultured plant cells and tissues, and lower plants including duck weed and mosses

The first plant virus system used was a recombinant Tobacco Mosaic Virus (TMV) where the capsid protein was fused to a malarial epitope [53] followed by others (for review see [43, 57]). "Agro-infection" has been developed as a versatile tool for a rapid production of vaccines and antibodies in transiently expressing plant tissues, especially tobacco leaves [15, 16]. Simultaneously, a large number of expression constructs could be tested. This method can easily be scaled up by using vacuum-mediated "Agro-infiltration." Lomonossoff and co-workers positioned a gene of interest (GOI) between the 5' leader sequence and 3' untranslated region (UTR) of RNA-2, thereby emulating a presumably stable mRNA for efficient translation. High-level expression could also be achieved in the absence of RNA-1-derived replication functions using *Agrobacterium*-mediated transient expression. Deletion of an in-frame start codon upstream of the main translation initiation site led to a massive increase in foreign protein accumulation (10–20% of total extractable protein; [47]). The magnICON® system (MagniFection) developed by Icon Genetics (Halle, Germany; now a part of Bayer Innovation GmbH, Düsseldorf, Germany) combined significant mRNA expression enhancement by a TMV-based transient expression vector with systemic delivery based on "Agro-infiltration" [24]. A recent press release announced that Bayer started clinical Phase I study with personalized vaccines from tobacco plants, produced with the magnICON® system, for treatment of non-Hodgkin's lymphoma (http://www.icongenetics.com/html/5954.htm). Stable transformants have been widely used to express antibodies (for review see [9]) and vaccines (for review see [52]) in transgenic plants. The expression of recombinant proteins in storage organs such as seeds [13] resulted in functional and stable products that could be stored at room temperature for extended times without significant loss in amount and activity [51]. Stable expression in dicotyledonous seeds could be significantly boosted by specific regulatory sequences as demonstrated for scFvs [8]. Seed tissues therefore represent a very attractive target for production and extraction of pharmaceutical proteins commercially.

In addition to the expression of recombinant proteins in cultured *Nicotiana* cells (for reviews see [14, 31]), expression in duck weed (*Lemna minor*) and in moss bioreactors are alternative interesting systems providing containment during production. The duck weed system [5] and the moss bioreactors (for review see [11]) provide the possibility of glycan optimization as well. Transgenes could also be targeted to the chloroplast, ensuring that they are embedded in a chloroplast DNA homology region. The number of transgene copies after establishment of homoplasmy was shown to be very high leading to increased expression levels [7]. Epigenetic phenomena (e.g., transgene silencing) are apparently absent in chloroplasts, therefore these plant organelles offer ideal prerequisites for the production of functional vaccine antigens. Moreover, chloroplast DNA is absent in pollen, and thus limits the potential for outcrossing. Unfortunately, chloroplasts lack major post-translational modification machineries such as glycosylation (for review see [57]), and accordingly their utility is limited to molecules which do not require glycosylation.

Edible Vaccines and Purification

The basic idea of edible vaccines was to feed animals with genetically engineered grain directly bypassing purification and complicated and expensive downstream processing.

However, this simple approach has been replaced by plant-derived vaccines because of two main reasons. Firstly, the expression level of the antigen in harvestable parts from the same plant can vary substantially. Secondly, a complete segregation of plants for pharmaceutical or veterinary applications from those meant for human or animal consumption is required [52]. However, another interesting approach making use of high-level expression of recombinant antibodies in legume seeds, e.g., peas [45], was the feeding of neutralizing recombinant antibodies against enterotoxic *Escherichia coli* strains to piglets. These antibodies were sufficiently active in the intestine of the fed

animals [28, 46]. A similar approach has been applied for recombinant antibodies against gastrointestinal parasites of chickens, which were expressed in peas [58].

Oral administration is not always the major route for all plant-derived vaccines. In some cases purified antigens are required for injection necessitating the development of specific purification procedures for each product. Two main challenges have to be overcome when purifying proteins from plant material: (1) impurities (proteins, carbohydrates, oils, phenolic compounds, phytic acids, nucleic acids, and other trace products) associated with each plant system must be removed, and (2) low concentrations of the target protein following initial extraction into an aqueous medium have to be avoided. Therefore, special downstream separation units are required to handle large volumes [39]. Specific methods have to be developed to achieve high amounts of vaccines and/or antibodies in a correctly folded and functional form. The successful development of such methods is also dependent on rather high and stable accumulation of the transgenic proteins *in planta*. Here, fusion to elastin-like polypeptides (ELPs) allows both easy and scalable purification as well as enhancement of the accumulation of the recombinant ELP fusion protein. Elastin-like polypeptides are highly biocompatible proteins. They exhibit the useful property of a thermally responsive reversible phase transition. These characteristics improve the efficiency with which recombinant proteins can be purified. ELP fusion proteins also exhibit reversible phase transition property. This new technology, named "ELPylation," has recently been extended to plant cells and several plant-based expression systems have been evaluated for the production of ELPylated proteins (for review see [22]). The approach has been applied to vaccines [19], complete immunoglobulins [17, 20, 21], and antibody derivatives, scFv [49], as well as VHH [4]. For veterinary purposes, where economical features such as low price and easy-to-handle products are major factors of commercial viability, "ELPylation" is a useful component of enrichment and purification strategies.

Future Directions

Over the past years, plant-based production of recombinant proteins has been developed and 11 plant-derived non-pharmaceutical proteins (avidin, trypsin, β-glucuronidase, aprotinin, lactoferrin, lysozyme, thyroid-stimulating hormone receptor, Hantaan and Puumala viral antigens, peroxidase, laccase, and cellulase) have been brought to the market [52] indicating a huge capability of these expression technologies for the production of diagnostic and therapeutic proteins for both human and veterinary medicine. Six years after the commercialization of the first plant-derived recombinant protein, TrypZean, from corn (ProdiGene, USA), only two plant-derived compounds are in late-stage clinical trials: Interferon α-2b made in aquaculture (*Lemna* expression system, LEX system) for the treatment of hepatitis C infections (Biolex Therapeutics, Pittsboro, USA) and taligurase alfa, a form of the enzyme glucocerebrosidase known as prGCD in development for treatment of Gaucher's disease from Protalix Biotherapeutics (Carmiel, Israel). Recently, Pfizer acquired rights to prGCD produced in carrot cells and became the first big pharma company to commit itself to take to the market a biologic plant-produced drug [42].

In view of the new influenza A H1N1 pandemic, plant-based expression systems represent the fastest production for any influenza vaccine as it was demonstrated by two research groups – at Medicago Inc. (Québec, Canada) and at the Fraunhofer Institute (Plymouth, USA) – via the transient expression of the H1 HA protein in tobacco plants [43]. These results underline the advantages of plant-based expression technologies over traditional expression technologies for the production of antigens. This should be essentially true for veterinary purposes, where costs should be generally lower fitting into economical parameters of animal-based food production. Here, the "old" concept of edible vaccines could be verified much easier, because seeds could be used as a source that is an essential and common component of the feed, which do not need to be treated at harsh conditions as baking or cooking. Farm animals grown in high numbers in confined conditions are a suitable target for future attempts to produce veterinary pharmaceuticals using plant-based expression systems. Nevertheless, further improvement of expression levels and development of easy and cheap downstream processes are still needed before decisions about economic viability of transgenic plant-based pharmaceuticals for animal health could be made.

Acknowledgments

The authors thank Stefan Rose-John and Paul Christou for a critical review of the manuscript.

Bibliography

1. Altpeter F, Baisakh N, Beachy R, Bock R, Capell T, Christou P, Daniell H, Datta K, Datta S, Dix PJ, Fauquet C, Huang N, Kohli A, Mooibroek H, Nicholson L, Nguyen TT, Nugent G, Raemakers K, Romano A, Somers DA, Stoger E, Taylor N, Visser R (2005) Particle bombardment and the genetic enhancement of crops: myths and realities. Mol Breed 15:305–327
2. Behring E, Kitasato S (1890) Ueber das Zustandekommen der Diphtherieimmunitaet und der Tetanusimmunitaet bei Tieren. Dtsch Med Wochenschr 16:1113–1114
3. Conrad U, Floss DM (2010) Expression of antibody fragments in transgenic plants. In: Kontermann R, Dübel S (eds) Antibody engineering, vol 2. Springer, Berlin, pp 377–386
4. Conrad U, Plagmann I, Malchow S, Sack M, Floss DM, Kruglov AA, Nedospasov SA, Rose-John S, Scheller J (2010) ELPylated anti-human TNF therapeutic single-domain antibodies for prevention of lethal septic shock. Plant Biotechnol J. doi:10.1111/j.1467-7652.2010.00523.x
5. Cox KM, Sterling JD, Regan JT, Gasdaska JR, Frantz KK, Peele CG, Black A, Passmore D, Moldovan-Loomis C, Srinivasan M, Cuison S, Cardarelli PM, Dickey LF (2006) Glycan optimization of a human monoclonal antibody in the aquatic plant *Lemna minor*. Nat Biotechnol 24:1591–1597
6. Curtiss RI, Cardineau CA (1990) Oral immunization by transgenic plants. World Patent Application, WO 90/02484
7. Daniell H, Chebolu S, Kumar S, Singleton M, Falconer R (2005) Chloroplast-derived vaccine antigens and other therapeutic proteins. Vaccine 23:1779–1783
8. De Jaeger G, Scheffer S, Jacobs A, Zambre M, Zobell O, Goossens A, Depicker A, Angenon G (2002) Boosting heterologous protein production in transgenic dicotyledonous seeds using *Phaseolus vulgaris* regulatory sequences. Nat Biotechnol 20:1265–1268
9. De Muynck B, Navarre C, Boutry M (2010) Production of antibodies in plants: status after twenty years. Plant Biotechnol J 8:529–563
10. De Wilde C, Peeters K, Jacobs A, Peck I, Depicker A (2002) Expression of antibodies and Fab fragments in transgenic potato plants: a case study for bulk production in crop plants. Mol Breed 9:271–282
11. Decker EL, Reski R (2008) Current achievements in the production of complex biopharmaceuticals with moss bioreactors. Bioprocess Biosyst Eng 31:3–9
12. Ehrlich P (1900) On immunity, with special reference to cell life. The Croonian lecture. Proc Roy Soc Lond 66:424–448
13. Fiedler U, Conrad U (1995) High-level production and long-term storage of engineered antibodies in transgenic tobacco seeds. Biotechnology 13:1090–1093
14. Fischer R, Emans N, Schuster F, Hellwig S, Drossard J (1999) Towards molecular farming in the future: using plant-cell-suspension cultures as bioreactors. Biotechnol Appl Biochem 30:109–112
15. Fischer R, Schillberg S (2004) Molecular farming: plant-made pharmaceuticals and technical proteins. Wiley-VCH Verlag GmbH & Co. KGaA, Weinheim
16. Fischer R, Vaquero C, Sack M, Drossard J, Emans N, Commandeur U (1999) Towards molecular farming in the future: transient protein expression in plants. Biotechnol Appl Biochem 30:113–116
17. Floss DM, Conrad U (2010) Expression of complete antibodies in transgenic plants. In: Kontermann R, Dübel S (eds) Antibody engineering, vol 2. Springer, Berlin, pp 489–502
18. Floss DM, Falkenburg D, Conrad U (2007) Production of vaccines and therapeutic antibodies for veterinary applications in transgenic plants: an overview. Transgenic Res 16:315–332
19. Floss DM, Mockey M, Zanello G, Brosson D, Diogon M, Frutos R, Bruel T, Rodrigues V, Garzon E, Chevaleyre C, Berri M, Salmon H, Conrad U, Dedieu L (2010) Expression and immunogenicity of the mycobacterial Ag85B/ESAT-6 antigens produced in transgenic plants by elastin-like peptide fusion strategy. J Biomed Biotechnol 2010:274346
20. Floss DM, Sack M, Arcalis E, Stadlmann J, Quendler H, Rademacher T, Stoger E, Scheller J, Fischer R, Conrad U (2009) Influence of ELP fusions on the quantity and quality of a tobacco-derived HIV-neutralizing antibody. Plant Biotechnol J 7:899–913
21. Floss DM, Sack M, Stadlmann J, Rademacher T, Scheller J, Stoger E, Fischer R, Conrad U (2008) Biochemical and functional characterization of anti-HIV antibody-ELP fusion proteins from transgenic plants. Plant Biotechnol J 6:379–391
22. Floss DM, Schallau K, Rose-John S, Conrad U, Scheller J (2010) Elastin-like polypeptides revolutionize recombinant protein expression and their biomedical application. Trends Biotechnol 28:37–45
23. Gahrtz M, Conrad U (2009) Immunomodulation of plant function by in vitro selected single-chain Fv intrabodies. In: Faye L, Gomord V (eds) Methods in molecular biology: recombinant proteins from plants. Humana Press, Totowa, pp 289–312
24. Gleba Y, Klimyuk V, Marillonnet S (2005) Magnifection – a new platform for expressing recombinant vaccines in plants. Vaccine 23:2042–2048
25. Goldstein D (1997) Banana vaccines. Sci World 53:4
26. Gomord V, Faye L (2004) Posttranslational modification of therapeutic proteins in plants. Curr Opin Plant Biol 7: 171–181
27. Gomord V, Fitchette AC, Menu-Bouaouiche L, Saint-Jore-Dupas C, Plasson C, Michaud D, Faye L (2010) Plant-specific glycosylation patterns in the context of therapeutic protein production. Plant Biotechnol J 8:564–587
28. Hagemann M (2006) Untersuchungen zur Wirksamkeit oral applizierter Antikörper (produziert in transgenen Hefen und Erbsen) gegen enterotoxische *Escherichia coli* (ETEC) bei experimentell infizierten Absetzferkeln. Dissertation, Tierärztliche Hochschule Hannover

29. Hammond RW, Nemchinov LG (2009) Plant production of veterinary vaccines and therapeutics. In: Karasev AV (ed) Plant-produced microbial vaccines. Springer, Berlin, pp 79–102
30. Hassan S, van Dolleweerd CJ, Ioakeimidis F, Keshavarz-Moore E, Ma JKC (2008) Considerations for extraction of monoclonal antibodies targeted to different subcellular compartments in transgenic tobacco plants. Plant Biotechnol J 6:733–748
31. Hellwig S, Drossard J, Twyman RM, Fischer R (2004) Plant cell cultures for the production of recombinant proteins. Nat Biotechnol 22:1415–1422
32. Hiatt A, Cafferkey R, Bowdish K (1989) Production of antibodies in transgenic plants. Nature 342:76–78
33. Hood EE, Woodard SL, Horn ME (2002) Monoclonal antibody manufacturing in transgenic plants – myths and realities. Curr Opin Biotechnol 13:630–635
34. Hussack G, Grohs BM, Almquist KC, McLean MD, Ghosh R, Hall JC (2010) Purification of plant-derived antibodies through direct immobilization of affinity ligands on cellulose. J Agric Food Chem 58:3451–3459
35. Ko K, Brodzik R, Steplewski Z (2009) Production of antibodies in plants: approaches and perspectives. In: Karasev AV (ed) Plant-produced microbial vaccines. Springer, Berlin, pp 55–78
36. Kohler G, Milstein C (1975) Continuous cultures of fused cells secreting antibody of predefined specificity. Nature 256:495–497
37. Mason HS, Lam DMK, Arntzen CJ (1992) Expression of hepatitis B surface antigen in transgenic plants. Proc Natl Acad Sci USA 89:11745–11749
38. Meeusen ENT, Walker J, Peters A, Pastoret PP, Jungersen G (2007) Current status of veterinary vaccines. Clin Microbiol Rev 20:489–510
39. Menkhaus TJ, Roseland J (2008) Recovery of proteins from corn and soybean extracts by membrane adsorption. Biotechnol Prog 24:1075–1084
40. Mor TS, Gomez-Lim MA, Palmer KE (1998) Perspective: edible vaccines – a concept coming of age. Trends Microbiol 6:449–453
41. Pujol M, Ramirez NI, Ayala M, Gavilondo JV, Valdes R, Rodriguez M, Brito J, Padilla S, Gomez L, Reyes B, Peral R, Perez M, Marcelo JL, Mila L, Sanchez RR, Paez R, Cremata JA, Enriquez G, Mendoza O, Ortega M, Borroto C (2005) An integral approach towards a practical application for a plant-made monoclonal antibody in vaccine purification. Vaccine 23:1833–1837
42. Ratner M (2010) Pfizer stakes a claim in plant cell-made biopharmaceuticals. Nat Biotechnol 28:107–108
43. Rybicki EP (2009) Plant-produced vaccines: promise and reality. Drug Discov Today 14:16–24
44. Rybicki EP (2010) Plant-made vaccines for humans and animals. Plant Biotechnol J 8:620–637
45. Saalbach I, Giersberg M, Conrad U (2001) High-level expression of a single-chain Fv fragment (scFv) antibody in transgenic pea seeds. J Plant Physiol 158:529–533
46. Saalbach I, Riehl M, Giersberg M, Kumlehn J, Falkenburg D (2007) Production of recombinant antibodies in pea seeds and their oral application in piglets. In: Xu Z (ed) Biotechnology and sustainable agriculture 2006 and beyond. Springer, The Netherlands, pp 399–402
47. Sainsbury F, Lomonossoff GP (2008) Extremely high-level and rapid transient protein production in plants without the use of viral replication. Plant Physiol 148:1212–1218
48. Santi L (2009) Plant derived veterinary vaccines. Vet Res Commun 33:S61–S66
49. Scheller J, Leps M, Conrad U (2006) Forcing single-chain variable fragment production in tobacco seeds by fusion to elastin-like polypeptides. Plant Biotechnol J 4:243–249
50. Sharma AK, Sharma MK (2009) Plants as bioreactors: recent developments and emerging opportunities. Biotechnol Adv 27:811–832
51. Stoger E, Ma JKC, Fischer R, Christou P (2005) Sowing the seeds of success: pharmaceutical proteins from plants. Curr Opin Biotechnol 16:167–173
52. Tiwari S, Verma PC, Singh PK, Tuli R (2009) Plants as bioreactors for the production of vaccine antigens. Biotechnol Adv 27:449–467
53. Turpen TH, Reinl SJ, Charoenvit Y, Hoffman SL, Fallarme V, Grill LK (1995) Malarial epitopes expressed on the surface of recombinant Tobacco Mosaic Virus. Biotechnology 13:53–57
54. Tzfira T, Citovsky V (2006) *Agrobacterium*-mediated genetic transformation of plants: biology and biotechnology. Curr Opin Biotechnol 17:147–154
55. Usha R, Rohll JB, Spall VE, Shanks M, Maule AJ, Johnson JE, Lomonossoff GP (1993) Expression of an animal virus antigenic site on the surface of a plant-virus particle. Virology 197:366–374
56. Walsh G, Jefferis R (2006) Post-translational modifications in the context of therapeutic proteins. Nat Biotechnol 24: 1241–1252
57. Yusibov V, Rabindran S (2008) Recent progress in the development of plant-derived vaccines. Expert Rev Vaccin 7:1173–1183
58. Zimmermann J, Saalbach I, Jahn D, Giersberg M, Haehnel S, Wedel J, Macek J, Zoufal K, Glunder G, Falkenburg D, Kipriyanov SM (2009) Antibody expressing pea seeds as fodder for prevention of gastrointestinal parasitic infections in chickens. BMC Biotechnol 9:79

Plant Oil Fuels Combined Heat and Power (CHP)

Klaus Thuneke
Technologie- und Förderzentrum im Kompetenzzentrum für Nachwachsende Rohstoffe (TFZ), Straubing, Germany

Article Outline

Glossary
Definition of the Subject
Introduction

Oil Processing and Purification
Fuel-Relevant Properties
Technical Fundamentals of Plant Oil–Fuelled CHP Plants
Case Study: Economic Efficiency
Future Directions
Bibliography

Glossary

Cogeneration Cogeneration, also known as combined heat and power (CHP), describes the simultaneous production of both mechanical energy and useful heat from various sources of energy by a thermodynamic process in a technical plant [1, 2].

Combined heat and power plant (CHP Plant) A combined heat and power plant (CHP plant) or cogeneration plant provides simultaneously electricity and useful heat.

Electricity generation efficiency Electricity generation efficiency or electrical efficiency is the ratio between the electricity output and the energy input of an energy conversion system. Whereas small-scale CHP plants with combustion engines feature electricity generation efficiencies of roughly 30%, large-scale CHP plants obtain up to 45% [3, 4].

Energy conversion efficiency Energy conversion efficiency or overall conversion efficiency is the ratio between the useful energy output and the energy input of an energy conversion system. For CHP plants, energy conversion efficiency is the sum of electricity conversion efficiency and heat conversion efficiency. Electrical and thermal auxiliary power for the CHP plant (e.g., for pumps, control unit, fuel preheating, etc.) has to be deducted [3].

Heat generation efficiency Heat generation efficiency or thermal efficiency is the ratio between the useful heat output and the energy input of an energy conversion system. It is the result of the heat extraction by heat exchangers. Here, the temperature level is decisive [3].

Plant oil fuel Plant oil fuel is derived from oil-containing plant parts for the use in plant oil compatible combustion engines. In Germany, for example, plant oil fuel quality is specified by the national pre-standard DIN V 51623 (publication expected in 2011).

Power-to-heat ratio Power-to-heat ratio is the ratio between produced electrical and useable thermal energy. It is an evaluation criterion of CHP plants and ranges normally between 0.4 and 0.6. Because the power-to-heat ratio is increasing when heat generation efficiency is decreasing, additionally the energy conversion efficiency has to be specified [3].

Rapeseed oil fuel Rapeseed oil fuel is oil extracted from rapeseed, for the use in plant oil compatible combustion engines. In Germany, for example, rapeseed oil fuel quality is specified by the national standard DIN 51605 [5].

Thermal fuel power Thermal fuel power or rated thermal input describes the fuel heat content on basis of the net calorific value feed into an energy conversion system within a defined period of time [3].

Utilization ratio Utilization ratio of an energy conversion system is the ratio between the usable energy and the energy input within a given period of time.

Definition of the Subject

Combined heat and power (CHP) or cogeneration is the simultaneous generation of both useable heat and power in a single process by a heat and power supply station or an engine. The mechanical energy is usually converted into electricity by a generator. The thermal energy can be used for heating or technical processes. CHP is a highly efficient way to use either fossil or renewable fuels and can therefore contribute significantly to reach sustainable energy goals. The benefits of CHP can be of a social, economic, and environmental nature:

- Support of local economy
- Contribution to energy security
- Saving of fossil resources
- Protection of environment and climate

Plant oils are well suited to be used as fuels for CHP with self-ignition engines, using the diesel principle. By using plant oil fuels, additional benefits can be utilized in comparison to fossil fuels. Assuming a sustainable production of the plant oil, this option can help to save fossil resources and to reduce greenhouse gas emissions. Additionally, this possibility can contribute to soil and water protection because of their high biodegradability and low ecotoxicity. Thus, plant oil fuels are

preferably to be used in environmental sensitive areas such as alpine regions or water protection areas. In rural areas with local production and use of the plant oil fuel and the coproduct press cake as fodder, a high level of closed mass flow circles can be obtained.

Plant oil–fuelled CHP plants can play an important role for a decentralized power and heat supply. In case of a favorable legal framework guaranteeing feed-in tariffs for electricity from renewable resources, economic efficiency might be given. However, an appropriate heat use concept has to be incorporated. For a reliable and low-emission operation, various aspects regarding fuel quality and technical equipment (e.g., exhaust gas after-treatment) are to be considered.

Although plant oils can be used as fuel in self-ignition engines, properties vary significantly from those of conventional diesel fuel. This applies particularly for the ignition behavior and the viscosity. To guarantee fine dispersion of the injection spray for a high combustion quality and to minimize deposit formation on injectors and pistons, a technical adaptation of CHP engines and periphery under consideration of the requirements of the plant oil fuel is essential. Measures of adaptation can include:

- Exchange of incompatible materials, fuel pipes, pumps, filter, injectors
- Preheating of fuel, injectors, or cooling water
- Adjustment of injection parameters

Overall technology barriers of plant oil–fuelled CHP plants are low. A high standard in operational reliability has already been achieved. Further research should aim on improvement of plant efficiency, implementation of exhaust gas after-treatment systems, and continuing standardization of promising plant oil fuels at an international level.

Introduction

According to a Communication from the Commission of the European Union (EC) to the European Parliament and the Council, Europe can save more energy by combined heat and power generation. Cogeneration plants can contribute to energy security, sustainable energy supply, a better environment and combating climate change [6]. In addition, technology know-how opens export possibilities and offers opportunities for economic development, particularly at regional and local level. For promotion of a highly efficient combined heat and power technology based on users' heat demand a specific legal framework, the so-called Cogeneration Directive, has been introduced by the EC. Therein possible principles of support by the Member States are established.

As shown in Fig. 1, in 2007, the share of electricity from CHP of the total electricity generation in the EU-27 was 10.9%. However, the percentage varies widely between different Member States. Denmark (42.8%)

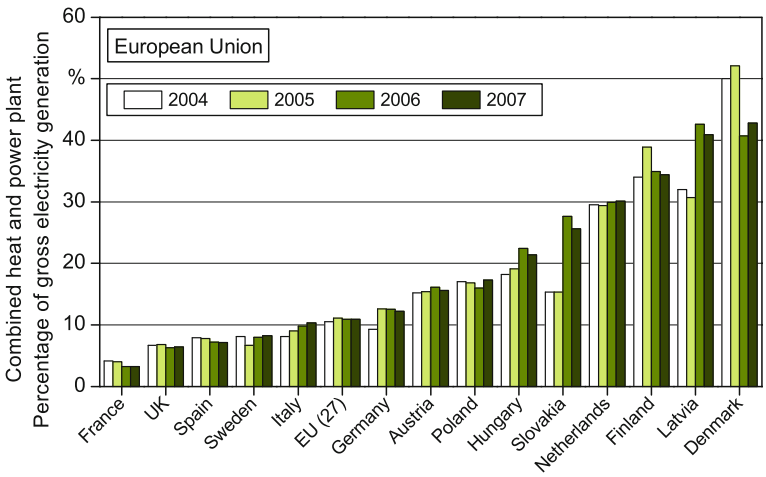

Plant Oil Fuels Combined Heat and Power (CHP). Figure 1
Share of CHP in total electricity generation of European Member States, EU 27 (Data source: EUROSTAT 2010 [1])

and Latvia (40.9%) feature the highest share of electricity from CHP, followed by Finland (34.4%) and the Netherlands (30.3%). Germany ranges with 12.2% in the middle, just above the European average. The share of CHP on electricity generation is lowest in France (3.2%). In Slovakia and Latvia, CHP has considerably increased between 2004 and 2007. In most other Member States, however, none or only little increase was observed.

The installed electrical power of CHP plants can range widely between some hundred megawatts at industrial scale and a few kilowatts in micro-CHP plants for private houses. Big CHP plants usually require extensive heat distribution networks for heat transport from the power station to the end user. Because of the high costs for the network and to minimize heat losses during heat distribution, compact local CHP plants installed close to the place of heat demand can be a reasonable and economic efficient alternative.

The example in Fig. 2 shows that with a fuel energy input of 100 kWh, an internal combustion engine in CHP mode can provide exemplarily about 27 kWh electrical power and 61 kWh heat. This regards to an electrical efficiency of 27%, a thermal efficiency of 61%, and an overall efficiency of 88%. However, efficiency rates vary widely between different plant designs. For example, the electrical power output can reach 40% and more if large-scale diesel engines are used. With increasing electrical efficiency, the thermal energy output is decreasing comparatively. The losses by heat emissions, mainly through the engine system and exhaust gas, can add up to some 12 kWh.

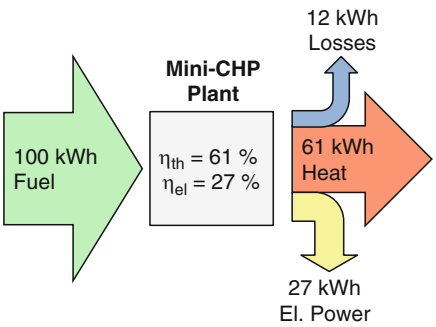

Plant Oil Fuels Combined Heat and Power (CHP). Figure 2
Energy flow schema of combined heat and power (CHP) supply with small-scale CHP plants, using internal combustion engines

In conventional power stations, the heat is not used in most cases. This is due to a remote large-scale production, which does normally not justify the costs of a pipe network for heat transportation and distribution to the end users. To gain the same electrical and usable thermal energy output as in the example of a CHP plant in Fig. 2, by separate heat and power generation, a fuel input of 67 kWh for the heating with burner plus 71 kWh for the power station (altogether 138 kWh) is necessary (Fig. 3). This results in primary energy savings of up to 28% by cogeneration.

CHP plants with electrical power output of less than 1 MW are usually driven by combustion reciprocating piston engines [2]. These engines are widespread, highly developed, and can achieve up to 50,000 operating hours. Compression ignition engines for diesel fuels as drive propulsion systems for CHP plants are far more frequent than Otto-cycle engines due to their higher efficiency [3].

In diesel engines, mostly liquid fuels, such as heating oil, fatty acid methyl esters (FAME), and pure plant oils, are used. These liquid biofuels are common in Europe, even though they gain more importance outside Europe [7].

Plant oil–fuelled CHP plants are characterized by several benefits. Plant oil fuels save fossil resources and reduce greenhouse gas emissions, sustainable production provided. Because of their high biodegradability, plant oil fuels are predestinated to be used in environmental sensitive areas such as alpine regions or water protection areas. In rural areas with local production and use of the plant oil fuel (e.g., rapeseed oil) and the coproduct press cake, a high level of closed mass flow circles can be obtained. This results in high energy-utilization level and positive effects on economic regional development.

Case Study: Plant Oil Compatible CHP Plants in Germany

During the 1970s, engine-driven CHP plants were introduced, enabling decentralized energy supply. Since the liberalization of the energy market in the late 1990s, even private households can act as power contractors [4].

Today, more than 30 mainly medium-sized enterprises provide plant oil compatible CHP units in Germany. After years of increasing plant numbers with the highest growth rates between 2006 and 2007, recently the demand on plant oil compatible CHP plants is decreased strongly. According to Fig. 4, the number of plants dropped from about 2,700 in the year 2007 to 1,400 in the year 2008, resulting in a reduction of installed electrical power from some 400 MW to 310 MW [8]. Presently, this development is continuing [9]. Suppliers of plant oil compatible CHP plants state an almost total absence of orders.

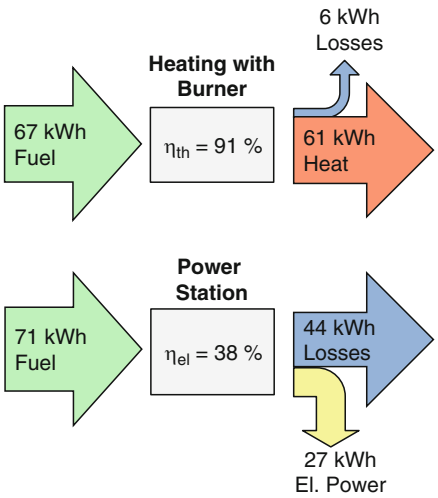

Plant Oil Fuels Combined Heat and Power (CHP). Figure 3
Energy flow schema of separate heat and power generation with burner heating and power station

Reasons for this obvious downturn recorded for all plant sizes up to 1 MW electrical capacity were high prices for plant oil fuels in the year 2008, accompanied with inadequately performed heat use concepts of CHP units. Thus, many plants have been shut down for economic reasons. Additionally, the amendment of the Renewable Energy Act [33] led to a lack of planning reliability, regarding power feed-in tariffs as well as certification issues of sustainable plant oil fuels.

However, operators with favorable long-term contracts for plant oil fuels or CHP plants with a high degree of heat utilization often could hold up an economic viable operation. In general, a tendency from small- to large-scale CHP plants could be noted (Fig. 4).

Figure 5 shows that with 88%, the highest share of the total amount of plant oil that was used in CHP plants in Germany in the year 2007 (ca. 700 Mio. l) was palm oil. With decreasing electrical nominal power, less palm oil and more rapeseed oil as well as some soy oil is used. Small-scale plant oil compatible CHP plants are predominantly fuelled with rapeseed oil.

The main reason for the leading role of palm oil in large-scale CHP plants is the lower market price of

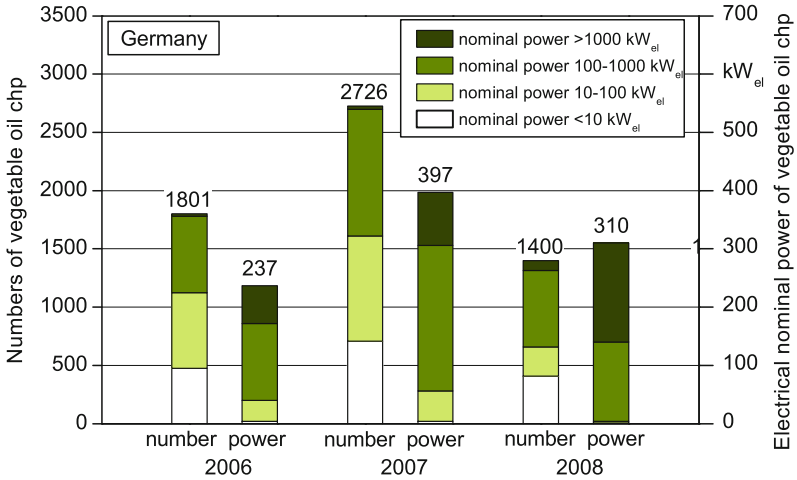

Plant Oil Fuels Combined Heat and Power (CHP). Figure 4
Development of number and installed electrical power of plant oil fuelled CHP plants in Germany (Data source: DBFZ 2009 [8])

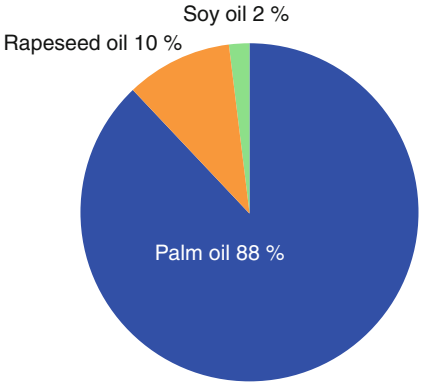

Plant Oil Fuels Combined Heat and Power (CHP). Figure 5
Share of plant oils, used as fuel for plant oil compatible CHP plants (Data source: DBFZ (2009) [8]

palm oil in comparison to rapeseed or soy oil. To ensure flowability of palm oil, extensive technical measures are necessary for heating up the entire fuel system. For small-scale CHP plants, these measures are usually too expensive in terms of installation and operation. Hence, rapeseed oil is the preferred option within the lower power range.

Oil Processing and Purification

In Central Europe, mainly rape and sunflower oilseeds are suited to be used for the production of plant oil fuels. Storable rapeseed for instance contains about 43% oil, 40% crude protein and extractives, 7% water, 5% crude fiber, and 5% ash. The objective of the different ways of oil-processing technologies is to separate the oil content from the seed as effective as possible. Unwanted components of the seed, however, should not be transformed into the oil or need to be excluded from the oil afterwards.

For oil extraction, two different production technologies are available. Mechanical plus solvent extraction of the oilseed in industrial oil mills with processing capacities of up to 4,000 t oilseeds per day and solely mechanical extraction in local small-scale oil mills with processing capacities of 0.5–35 t per day (see [10, 11, 12, 13]).

The process steps of oil processing in industrial plants are:

- Pretreatment of the oilseed (cleaning, drying, optionally hulling, crushing, conditioning)
- Oil processing (mechanical pre-extraction, additional oil separation from extraction residues by solvents)
- After-treatment of the extraction meal (removal and recycling of solvent)
- Refining (removal of unwanted components inserted during mechanical and chemical extraction by degumming, deacidification, bleaching, and deodorization)

In small-scale oil mills, many of these process steps are omitted. Here, oil processing is characterized by following process steps:

- Pretreatment of the oilseed (cleaning, drying, optionally crushing, hulling, rolling)
- Oil extraction by cold pressing (solely mechanical oil separation, mostly by screw presses)
- Oil purification (separation of turbid substances from the oil by sedimentation, filtration, or centrifugation)
- Security filtration

Whereas oil yields in industrial large-scale oil mills obtain 99% of the seeds' oil content, only some 80% are achieved in small-scale oil mills.

Cold pressed rapeseed oil contains about 0.5–6.0% (m/m) solid substances (without oil), derived from the solid components of the oilseed. Solid substances have to be removed from the oil as completely as possible because oil purity is an important quality criteria for fuel use in combustion engines. Oil purification should be carried out at least by two purification steps: main purification and subsequent security filtration.

Because small-scale oil production does not feature any refining, especially oilseed quality, process technology as well as storage conditions have impacts on oil characteristics.

Fuel-Relevant Properties

Rapeseed oil is the predominant plant oil for fuel use in small CHP plants. Pure rapeseed oil consists of 77–78% (m/m) Carbon (C), 11–12% hydrogen (H), and 10–11% oxygen (O). Rapeseed oil is highly biodegradable and shows only little aquatic toxicity in comparison to fossil diesel or gasoline. During storage,

reactions take place depending on storage conditions (storage tank material, temperature, oxygen, light exposure, water). Especially autoxidation and polymerization reactions are relevant. They can be minimized by suitable production and storage conditions. Under favorable conditions (darkness, cold ambient temperature of about 5°C), pure rapeseed oil can be stored at least 12 months without losing quality immoderately.

According to Table 1, characteristics of rapeseed oil according to DIN 51605 differ in important parameters from diesel fuel, heating oil, or fatty acid methyl ester (biodiesel).

In particular, the viscosity of rapeseed oil (Fig. 6), which is 10 times higher compared to fossil diesel fuel, is often responsible for poor injection spray dispersion and insufficient combustion quality in conventional not-adapted diesel engines. As a consequence, especially during low ambient temperatures and cold starts, deposits at injectors, cylinders, pistons, or valves can occur. Similarities in rapeseed oil and diesel characteristics, however, are given among others for the net calorific value. Therefore, due to the little differences, fuel consumption (based on volume) of rapeseed oil is some 4% and in the case of biodiesel some 9% higher than that of diesel fuel or heating oil.

For a long-term reliable engine operation, the fulfillment of minimum requirements of the quality of the plant oil fuel is essential. So far, such requirements are

Plant Oil Fuels Combined Heat and Power (CHP). Table 1 Parameters of various fuels according to DIN standards [5, 14, 15, 16, 17]

Parameter		Rapeseed oil fuel DIN 51605	Diesel fuel DIN EN 590	Heating oil EL DIN 51603–1	FAME for diesel use DIN EN 14214	FAME for heating DIN EN 14213
Density (15°C)	kg/m^3	910–925	820–845	max. 860	860–900	860–900
Kinematic viscosity at 40°C at 20°C	mm^2/s	max. 36.0 ca. 73.1[a]	2.0–4.5	ca. 3.8[a] max. 6.0	3.5–5.0	3.5–5.0
Flashpoint[b]	°C	min. 101	over 55	over 55	min. 101	min. 120
Sulfur content	mg/kg	max. 10	max. 50[c]	>50–1,000	max. 10	max. 10
			max. 10	max. 50[d]		
Acid value	mg_{KOH}/g	max. 2.0	n.s.[e]	n.s.[e]	max. 0.50	max. 0.50
Iodine number	$g_{Jod}/100g$	max. 125	n.s.[e]	n.s.[e]	max. 120	max. 130
Oxidation stability (110°C)	h	min. 6.0	n.r.[f]	n.s.[e]	min. 8.0	min. 4.0
Ash content[b]	% (m/m)	n.s.[e]	max. 0.01	max. 0.01	max. 0.02	max. 0.02
Contamination	mg/kg	max. 24	max. 24	max. 24	max. 24	max. 24
Cetane number[b]	–	min. 40	min. 51	n.s.[e]	min. 51	n.s.[e]
Calorific value net gross	MJ/kg	min. 36[g]	43.1[a]	min. 42.6[a] min. 45.4	37.1[a]	min. 35

[a]Typical value, not specified in standard
[b]Different testing methods
[c]Until 31.12.2008
[d]Low sulfur content heating oil
[e]n.s. = not specified
[f]n.r. = not reported due to different testing methods
[g]Typical value 37.5 MJ/kg

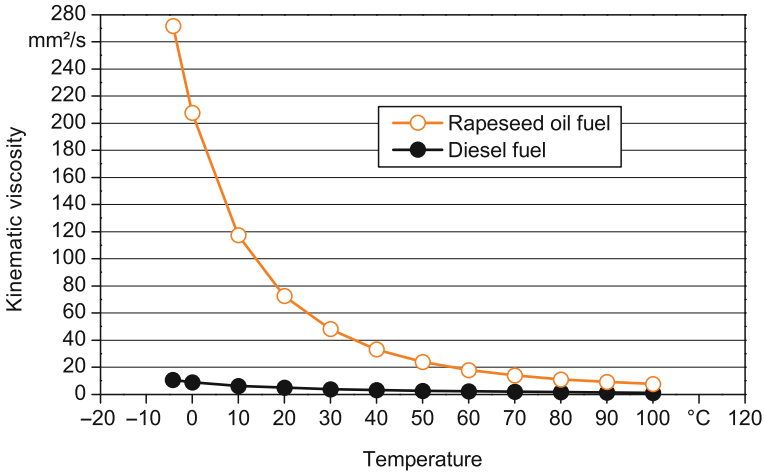

Plant Oil Fuels Combined Heat and Power (CHP). Figure 6
Kinematic viscosity of rapeseed oil and diesel fuel at different temperatures (According to Widmann et al. 1992 [18])

defined only for rapeseed oil fuel in the German standard DIN 51605. Similar to other specifications for heating oil, diesel fuel, or biodiesel, standard DIN 51605 comprises relevant product properties, test methods, and limiting values of rapeseed oil for the use as a fuel in plant oil compatible engines or heating systems.

Besides rapeseed oil, no other plant oils are investigated systematically in depth regarding their fuel-relevant properties, yet. However, many promising experiences were made in practice for palm and soy oil, as well as sunflower and jatropha oil. Table 2 shows analytical results of various plant oil samples in comparison to DIN 51605 for rapeseed oil fuel. These values derive from single analyses; no statement about their representativeness can be given.

Many requirements of DIN 51605 for rapeseed oil fuel are also fulfilled by other plant oils. Various parameters (e.g., element content) could be adjusted by the production process. However, further properties that are not relevant for rapeseed oil need to be considered individually for each type of plant oil (e.g., content of waxes for sunflower oil). This is why a simple comparison of the properties of various plant oils with limiting values defined within DIN 51605 is not sufficient for the evaluation of the suitability of a plant oil to be used as a fuel. Nevertheless, such a comparison might be of help. Palm oil with a high degree of saturation and hence high iodine number has on the one hand high oxidation stability but, on the other hand, poor cold flow characteristics, which results in high viscosity. Thus, an external heating of all components of the fuel system is necessary, when using palm oil as a fuel.

The jatropha oil sample fulfills all limiting values of rapeseed oil fuel listed in Table 2. It could therefore be a promising alternative plant oil for fuel use. However, the specific fatty acid pattern of jatropha oil can restrain applicability. With increasing iodine number, oxidation stability is decreasing, which makes soy, sunflower, false flax, or hemp oil susceptible to oil aging. Technical problems during engine operation can be the consequence.

In order to improve fuel-relevant properties of plant oils, special oil after-treatment or addition of active agents, as it is long-term practice for fossil fuels, can be an option. Further research and standardization work, however, is necessary. Presently, a German DIN standardization committee is developing a national fuel standard for various plant oils. Publication of the pre-standard DIN V 51623 [22] is expected in 2011.

Technical Fundamentals of Plant Oil–Fuelled CHP Plants

Construction

CHP plants with combustion engines comprise one or more CHP modules with superior switchgear, exhaust

Plant Oil Fuels Combined Heat and Power (CHP). Table 2 Properties of various plant oil samples (not representative)

Properties	DIN 51605	Palm oil refined	Jatropha oil cold pressed	Soy oil cold pressed	Soy oil refined	Sunflower oil cold pressed	Sunflower oil refined	False flax oil cold pressed	Hemp oil cold pressed	Hemp oil refined
Reference	[5]	[19]	[20]	[19]	[19]	[19]	[19]	[19]	[21]	[21]
Density at 15°C in kg/dm^3	0.910–0.925	0.93	0.92	0.92	0.92	0.92	0.92	0.92	0.93	0.93
Flash point in °C	min. 101	286	268	250	241	253	265	271	225	238
Kinematic viscosity at 40°C in mm^2/s	max. 36.0	183.5	34.3	30.6	32.4	30.3	31.5	30.0	27.7	28.0
Net calorific value in MJ/kg	min. 36.0	36.7	36.8	37.0	36.9	37.0	37.0	37.1	36.5	36.7
Cetane number	min. 40	–	46	–	–	–	–	–	49	47
Iodine number in g Jod/100 g	max. 125	48	102	137	128	139	132	146	163	163
Sulfur content in mg/kg	max. 10	1.2	<1	28	<1	<1	<1	2.7	<5	<5
Acid value in mg KOH/g	max. 2.0	0.1	1.6	–	0.1	1.5	<0.1	0.3	3.9	0.2
Oxidation stability at 110°C in h	min. 6.0	27.1	10.8	4.5	7.3	3.6	5.0	3.0	2.6	2.5
Water content in mg/kg	max. 750	164	746	581	38	662	37	585	150	185

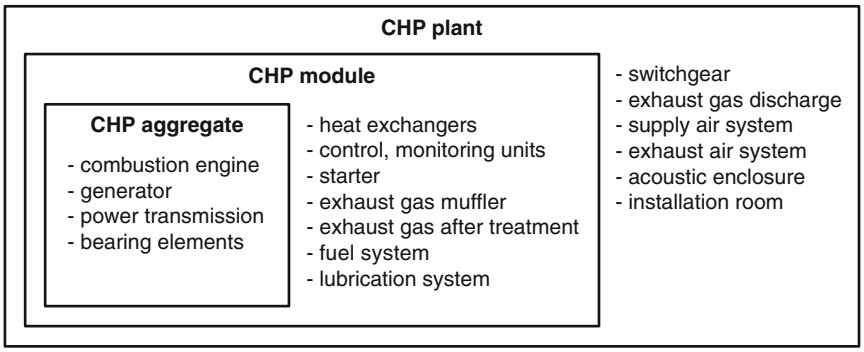

Plant Oil Fuels Combined Heat and Power (CHP). Figure 7
CHP-components – definition [23]

gas discharge, supply and exhaust air system, acoustic enclosure, and installation room (Fig. 7) [23].

The main component of a CHP module is the CHP aggregate consisting of combustion engine and generator with power transmission and bearing elements. Further module components are heat exchangers, control and monitoring units, starter, components of intake and exhaust gas system, fuel and lubrication system [23].

The plant oil compatible CHP plant is installed within an acoustic enclosure. The mechanical energy of the engine is converted into electrical energy by the generator. The released heat of the combustion process from the engine's cooling systems and exhaust gas is partly transferred by heat exchangers through a distribution network to the user.

Usually CHP plants are dimensioned with regard to the heat demand of a user (heat-controlled) and are operated parallel to the public electricity grid. Besides that, it is also possible to operate them power-controlled for full or partly isolated operation independent from the public electricity grid. Important for an economic efficient operation is the careful integration of the heat consumers during facility design. Insufficient heat use due to oversizing of the CHP plant can result in considerable economic losses.

Fuel System

For medium and large-scale CHP plants, the fuel is typically stored in large tanks, which can be installed under or above ground. Depending on the local conditions, an additional intermediate storage of the fuel can take place in smaller tanks close to the engine. Refueling of intermediate storage tanks takes place automatically by pumps and devices regulating the filling level. In small CHP plants with low fuel consumption, transportable containers with capacities of some 1,000 l often serve as fuel storage and supply.

Components of the fuel supply are pipes and flexible tubes, pressure regulators, fuel filters, fuel pumps, injection pumps, and injectors. Here, specific requirements of the plant oil on material and design has to be considered (e.g., fuel pipes and fittings made of chromated or stainless steel, flexible tubes made of flexibilizer poor or free NBR caoutchouc).

Combustion Engine

Since the 1980s, diesel engines for the use of pure plant oil are available on the market. Plant oil compatible engines of former times designed and built especially for the use of plant oil, such as the "Elsbett engine," are no longer available on the market. During recent years, mainly series engines for diesel fuel operation have been adapted for the use of plant oil. The applied retrofitting concepts can be distinguished in single-tank and double-tank systems or single-fuel and dual-fuel systems respectively.

Double-tank systems feature a second fuel tank and fuel supply, which provides highly inflammable fuel, such as heating oil for the cold start phase. When operation temperature is reached, plant oil fuel is supplied from the main tank. Before engine turnoff, fuel from the additional tank is used again to flush the pipes and provide highly inflammable fuel in the injection

system for the following engine start. Such dual-fuel systems are often equipped with fuel preheating devices and electronically controlled fuel changers.

Single-fuel systems operate with only one type of fuel. Therefore, adaptation measures are usually more extensive for modern direct injection engines to guarantee a high spray quality and good ignition behavior of the high viscose plant oil even during cold starts and low ambient temperatures. By appropriate adaptation measures of the fuel system, combustion chamber as well as the engine management system for both direct and indirect injection series engines can be adapted with single-tank systems according to the special demands of plant oil fuel properties.

Following measures are applied in various combinations depending on engine type and adaptation concept at both single- and double-tank solutions [24, 25]:

- Exchange of components with materials not compatible for the use of pure plant oil (e.g., tubes, seals)
- Exchange of fuel pipes with little width for pipes of bigger diameter
- Exchange of fuel filters (i.e., appropriate installation of an (additional) filter)
- Exchange of fuel pump for a pump with higher power, preferably electrically driven
- Exchange or modification of injection pump, with regard to highly viscose fluids
- Exchange or modification of injectors
- Use of alternative stable materials for pistons and cylinder head
- Exchange or modification of preheating relay and heater plug (longer preheating time, placement in fuel stream, for better dispersion)
- Fuel preheating in pipes, filters, pumps, or injectors, either electrically or by warm water or oil carrying heat exchangers
- External preheating of engine by heating up engine cooling water during cold starts
- Modification of combustion chamber or valves
- Recirculation of leakage and excess fuel (possibly degasification)
- Increase of injection pressure
- Adjustment of injection time or delivery start of the pump
- Adjustment of the engine control unit

All professional adaption concepts consider adequate dimensioning and long-term stability of fuel-carrying components, such as pipes, pumps, seals, and filters. Technically sophisticated engines are advisable due to higher operational demands (higher viscosity and higher combustion temperature of plant oils). Contact with catalytic active metals, like copper, needs to be avoided, unless risking an increase of the acid value and decrease of oxidation stability of the plant oil fuel [11].

High-pressure injection systems, such as pump-injector or common rail systems, can be advantageous regarding plant oil operation, due to various possibilities of combustion process adjustment in comparison to low-pressure injection systems. Particularly, electronically regulated injection systems offer high potential of optimization.

For CHP plants, several plant oil compatible engine types are available. Small-scale CHP plants within an electrical power range up to 50 kW usually feature adapted conventional industrial diesel engines of various manufacturers. Plant oil compatible engines for CHP plants up to 500 kW electrical power are also often derived from truck or ship applications.

Emission Reduction

For the reduction of exhaust gas emissions, various techniques are applied. These are for instance exhaust gas recirculation, oxidation catalysts, denitration catalysts, and filter systems for the removal of particulate matter.

For exhaust gas recirculation a defined branch current of exhaust gas is taken and feed into the inlet air of the engine. This leads to a decrease of the oxygen content and lower temperatures within the combustion chamber, resulting in nitrogen oxides reduction rates between 40% and 80%. With increasing recirculation rates, however, soot emissions are increasing due to less available oxygen during combustion. The oxygen content of plant oil usually allows higher recirculation rates than for diesel fuel operation.

Oxidation catalysts reduce the energy level for the induction of oxidation reactions and accelerate the reaction speed. Before the respective oxidation reaction takes place, the oxidizable substances carbon monoxide (CO) and hydrocarbons (HC) as well as oxygen are

adsorbed at the catalytic active layer. Here the molecular bonds are loosened. The optimal operation temperature for CO- and HC-conversion rates higher than 90% ranges between 200°C and 350°C. With oxidation catalysts, also aldehydes held responsible for smelly exhaust gas substances can be reduced by 80% or more. Thus, oxidation catalysts are demanded for all plant oil–fuelled CHP plants. Due to the low sulfur content of plant oils, long-term high efficient reduction rates can be secured if standard conform fuel qualities are used.

With denitration catalysts, nitrogen oxides (NO_x) can be reduced effectively. For this purpose, a fluid or gaseous reduction agent (ammonia, urea or hydrocarbons) is injected into the exhaust gas stream. This so-called selective catalytic reduction (SCR) is the most common denitration technique. However, for cost reason, SCR catalysts are usually applied at engines of higher power range.

Particulate or soot filters can reduce particulate matter emissions by up to 90% and more. Also, the share of very fine particles, which are rated particularly harmful for human health, is decreased significantly. During the soot accumulation process in the filter medium, filtration surface lowers and exhaust gas counter pressure increases. Periodically, whenever the maximum tolerable pressure is reached, the particulate filter has to be regenerated by burning off the soot. The ignition of the soot can be initiated by increasing the exhaust gas temperature. Besides that, regeneration strategies can be based on continuous burning of the soot in the filter by assistance of the exhaust gas component NO_2, whose share is often enlarged by upstream oxidation catalysts. For stationary engines, the injection of burnable gas into the exhaust pipe can be another option for filter regeneration. Noncombustible ash deposits in the filter, derived from the combustion of fuel and engine lubrication oil, have to be removed from time to time by washing or air cleaning.

Filter systems for particulate matter emissions comprise filter medium, regeneration device, as well as a control unit [26]. As filter media high-temperature resistant materials, such as ceramic carrier substances, metals or fiber textures are used. Predominately, ceramic monoliths with alternately closed flow channels, embedded in a steel body, feature as filters (Fig. 8). Filtration takes place by enforced flow-through porous channel walls of the monolith. A catalytic layer on the filter surface can reduce soot ignition temperature considerably, enabling regeneration at lower exhaust gas temperatures.

Exhaust Gas Pipe

The exhaust gas pipe is connected with the CHP engine over a compensator. This prevents vibration transmission and material damage by thermal shocks. The exhaust gas can be fed into an existent chimney if conforming to legal regulations. Otherwise, an isolated exhaust gas pipe of adequate length with a condensate drain has to be provided. Pipes should be of stainless steel to avoid corrosion.

Generator and Electrical Connection

The mechanical energy of the engine is transferred into electrical energy by a generator. To operate a CHP plant independently from the electricity network, for example,

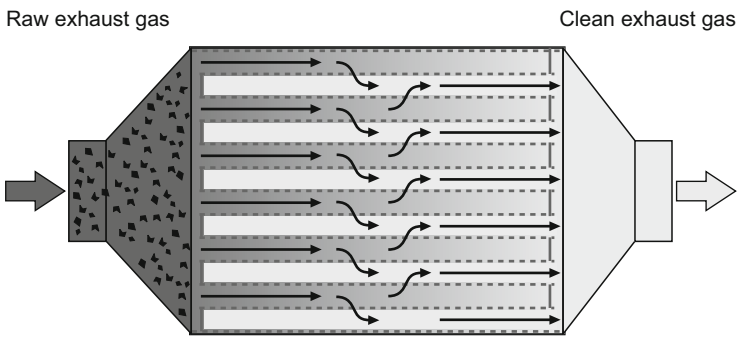

Plant Oil Fuels Combined Heat and Power (CHP). Figure 8
Schema of a particulate filter with alternately closed flow channels

for emergency power supply, a synchronous generator is mainly used. A synchronization device ensures that voltage, frequency, and phase of the generator and grid correspond with each other before connection.

In comparison to synchronous generators, asynchronous generators are often more robust, require less maintenance, and are cheaper in the lower power range. Because asynchronous generators require inductive idle power from the electrical network, they are usually not applicable for stand-alone operation.

The electrical connection can normally take place at the low-voltage power grid if the electrical power of the plant is lower than about 1 MW. Otherwise, a medium-voltage power grid is used.

Heat Exchanger

Besides heat exchangers, which are flown through discontinuously (regenerators), for CHP plants mainly heat exchangers are installed, which are continuously flown through, so-called recuperators. Recuperators are distinguished as counter-flow, co-flow, or cross-flow heat exchangers, depending on the principle of operation. According to demand, they are designed as pipe bundle, plate, bag, or spiral pipe heat exchangers. The dimensioning is done in terms of necessary temperatures of the supply and return flow [3].

CHP plants can feature several heat exchangers in series for transfer of heat from the charge air, the generator cooling water, the engine cooling water, and the exhaust gas into the heating water. Furthermore, heat extraction can also take place in two separate heating circuits for realizing a higher temperature level in one of the circuits.

About 25–30% of the energy contained in the fuel is discharged via the cooling water, and an additional 30% is released as heat of exhaust gas. Heat release via the hot engine surfaces, the oil pan, or exhaust gas pipes is hardly usable. Thus, it is tried to minimize it [3].

Operational deposits in heat exchangers require periodically cleaning of the heat exchange surfaces for an effective heat transmission. Some exhaust gas heat exchangers have to be cleaned with soot brushes regularly. Other types are discontinuously or continuously self-cleaning. Maintenance on exhaust gas heat exchangers can be significantly reduced by installation of exhaust particle filter systems.

Peak Load Boilers

Small size combined heat and power plants are predominantly operated heat-controlled, responding to the basic heat demand. Additionally, installed peak load boilers are switched on when heat delivery of the CHP plant is not sufficient to attain requested temperature in the heating system. To compensate heat peak loads during the day, a heat accumulator is established. Out of this so-called buffer, the heat demand of the users is supplied.

Heat accumulator design depends on the thermal power of the CHP plant, on the heat demand, and the usable temperature difference. The latter is limited by the maximum allowed temperature of the return flow back to the CHP plant. To secure sufficient cooling of the engine, the temperature of the return flow need to range at a maximum of 60–70°C.

Planning and Operation

For planning and design of plant oil compatible CHP plants, generally the same principles apply as for aggregates fuelled with diesel or heating oil. These principles are described for example in the German guideline VDI-Richtlinie 3985 "Grundsätze für Planung, Ausführung und Abnahme von Kraft-Wärme-Kopplungsanlagen mit Verbrennungskraftmaschinen" [23]. However, for economic calculation, different assumptions have to be made in comparison to heating oil aggregates, concerning investment and fuel costs as well as achievable revenues for power feed-in or saving of electricity procurement costs.

The following tasks for planning CHP plants can be specified:

- Conduction of a pilot survey, demand analysis, and inventory
- Preparation of a CHP concept (module selection, operating mode)
- Check of economic efficiency of concepts
- Preliminary planning, schematic design on basis of a preliminary decision
- Interview with approving authority
- Implementation planning and preparation of tender documents and technical specifications
- Obtaining of a technical immission control report, if necessary

Emissions

Due to high utilization of primary energy, less CO_2 is emitted by cogeneration plants than by a separate supply of power and heat. When using plant oil as a fuel, an additional CO_2 reduction is achieved. The emission of further exhaust gas components, like CO, NO_x, HC, and particulate matter, however, has to be considered individually [3].

By combusting plant oil fuels, a different emission behavior is expected compared to conventional fossil fuels. Besides fuel properties, also operation mode, engine and exhaust gas after-treatment, as well as specific fuel related plant design have major influences.

Professional engine adaptation usually results in lower emissions of CO, HC, particulate matter, and PAH when using rapeseed oil fuel. NO_x and aldehydes concentrations are usually little higher compared to diesel or heating oil. During low load operation or by using incompatible engines, also a converse effect can be observed [27, 28, 29, 30, 31, 32].

Case Study: Economic Efficiency

Economic efficiency of CHP plants mainly depends on the achievable prices or credits for generated electricity and heat. The reimbursement for electricity from plant oil–fuelled CHP plants is regulated by law in several countries (e.g., Germany). The rate of reimbursement depends, e.g., on the installed electrical nominal power of the plant, the year of commissioning, the fuel, and the heat use.

All expenses of the CHP plant are usually referred to the heat. The specific heat generation costs result from the total costs per year, less the compensation for the generated energy divided by the produced usable heat quantity per year.

In Table 3, heat generation costs are calculated exemplarily for three scenarios: "CHP 1," "CHP 2," and "CHP 3" (without peak load boiler, buffer vessel, and planning). The three scenarios are characterized by three different plant sizes (8, 20 and 50 kW_{el}). According to Table 3, the heat production costs range from 8.5 Cent/kWh (CHP 3) to 14.1 Cent/kWh (CHP 1).

Plant Oil Fuels Combined Heat and Power (CHP). Table 3 Economic efficiency of plant oil–fuelled CHP plants – model calculation

Assumptions		CHP 1	CHP 2	CHP 3
Assumptions:				
CHP nominal electrical power	kW_{el}	8	20	50
CHP nominal thermal power	kW_{th}	16	35	67
Investment for CHP module[a]	€	20 000	32 000	55 000
Investment for structure (tank, exhaust pipe)[a,b]	€	10 400	26 000	65 000
Costs of maintenance per year for CHP module	% of Invest.	9.0	9.0	9.0
Costs of maintenance per year for structure	% of Invest.	1.5	1.5	1.5
Labor/administrative costs per year[c]	% of Invest.	2.5	2.5	2.5
Insurance costs per year[d]	% of Invest.	1.5	1.5	1.5
Fuel consumption at nominal power	l/h	3.1	6.7	14.0
Fuel costs	€/l	0.80	0.80	0.80
Operating hours at nominal power per year	h	4 000	4 000	4 000
Power feed-in credit (0.2046 €/kWh_{el}) [33]	€/a	6 547	16 368	40 920
Heat generation costs (incl. power feed-in credit)	€/kWh	0.141	0.107	0.085

[a]Interest rate: 6%, assumed useful life 15 years for CHP module and 25 years for structure
[b]Investment for structure: 1,300 €/kW_{el}
[c]Related to investment for CHP module

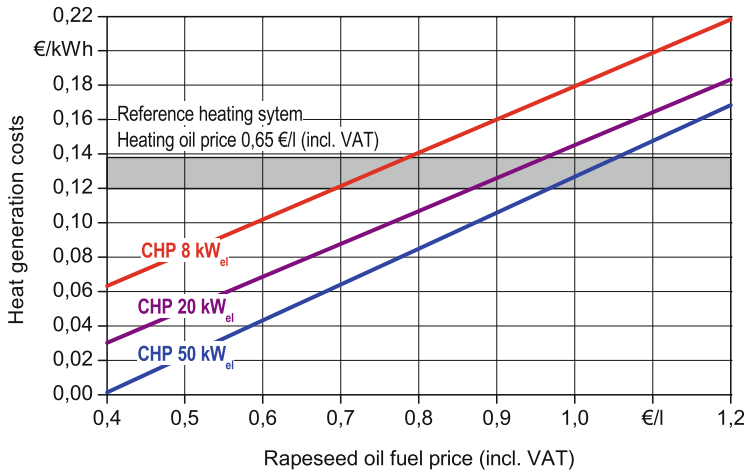

Plant Oil Fuels Combined Heat and Power (CHP). Figure 9
Economic efficiency of plant oil fuelled CHP plants – Influence of the fuel price

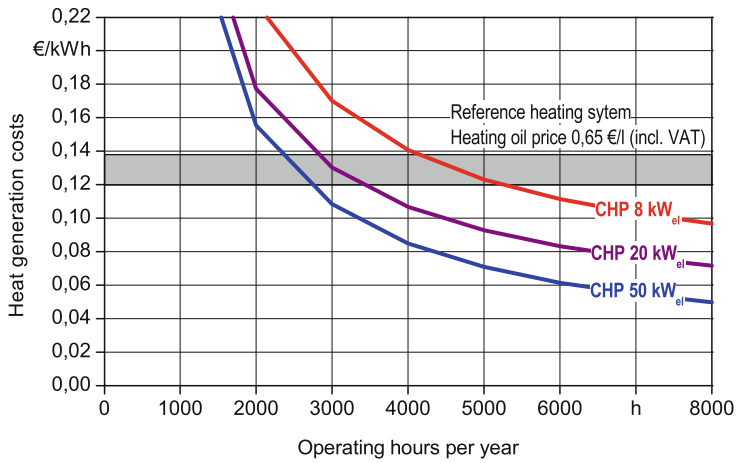

Plant Oil Fuels Combined Heat and Power (CHP). Figure 10
Economic efficiency of plant oil-fuelled CHP plants – Influence of the operating hours

Figure 9 shows heat generation costs for the three scenarios in dependence of the fuel costs. Under the assumptions of the calculation model (Table 3), an increase of rapeseed oil fuel costs of 10 Cent/l results in an increase of the heat generation costs of around 2 Cent/l. The break-even point, where economic efficiency is solely reached by power feed-in payment and heat is virtually available for "free," lies for CHP 3 with 50 kW_{el} as the best option at a fuel price of 40 Cent/kWh. This shows, as expected, that for an economic efficient operation of plant oil compatible CHP plants, heat needs to be of monetary value.

A comparison of the heat generation costs of rapeseed oil–fuelled CHP plants with a reference heating system of the same power range (heating oil price of 65 Cent/l) shows some advantages for CHP plants of a minimum power of 20 kW_{el}. However, CHP plants usually require peak load boilers or buffer vessels for short-time heat storage, which are not included in the calculation. Furthermore, these advantages only apply, when a high number of operating hours per year can be achieved.

Figure 10 shows the influence of the yearly operating hours on the heat generation costs. As it can be

seen, depending on the size of the CHP plant, only at about 3,000–5,000 operating hours per year, heat generation costs of the reference heating system (with fossil heating oil) are obtained. With decreasing operating hours, heat generation costs increase disproportionally. Thus, an economic efficient operation of rapeseed oil–fuelled CHP plants is only possible if the heat use concept is carefully considered.

Future Directions

Climate protection and security of supply with energy sources at reasonable prices is one of the major challenges today. One approach is the extension of the local and regional decentralized energy supply. Cogeneration plants for local heat production contribute to the saving of declining resources and greenhouse gas emissions due to efficient conversion technology with overall conversion efficiencies of up to 90%.

Plant oil–fuelled CHP plants feature also additional environmental benefits. The use of plant oils contribute to soil and water protection. Because of their high biodegradability and low ecotoxicity, plant oils are predestinated to be used in environmental sensitive areas, such as alpine regions or water protection areas.

Market relevance of plant oil–fuelled CHP plants is depending on respective framework conditions. Barriers are economic insecurities due to volatile fuel prices, frequent changes of regulations, and incentive programs. Furthermore, administrative and cost expenses increase, which affect particularly small-scale CHP plants. Besides that, biofuels are still subject to oppositional discussions about social and environmental impacts. Objective debates on the perspectives of all sustainable biofuels with regard to their optimized utilization paths have to be continued. A premature commitment to certain energy sources hinders the development of a stable market for renewable energy supply.

Nevertheless, there is already a broad consensus in the need of implementing measures to reduce GHG-emissions and energy dependency. Plant oil–fuelled CHP plants can make a contribution to meet the renewable energy targets. The high potential of pure plant oils can be utilized in the short term due to existing technology. Sustainably produced plant oil fuels for cogeneration are available.

The technology barriers of plant oil–fuelled CHP are little, and a high standard in operational reliability is already achieved. Depending on the existing frame conditions, economic efficiency is given when the heat can be used reasonably during a long period of the year. Further research should aim on improvement of plant efficiency, implementation of exhaust gas after-treatment systems, and continuation of standardization of promising plant oil fuels.

Bibliography

Primary Literature

1. Eurostat (2010) http://epp.eurostat.ec.europa.eu/portal/page/portal/eurostat/home. Accessed 13 April 2010
2. Schaumann G, Schmitz KW (2010) Kraft-Wärme-Kopplung, 4th edn. Springer, Auflage/Berlin/Heidelberg
3. Klausmann H (2000) Aufbau und Einsatz von anschlussfertigen BHKW-Kompaktmodulen bis 250 kW. Vulkan, Essen, p 344
4. Suttor W, Johler M, Weisenberger D (2009) Das Mini-Blockheizkraftwerk. Eine Heizung, die auch Strom erzeugt., vol 5, Auflage. C. F. Müller, Heidelberg/München/Landsberg/Frechen/Hamburg, p 140
5. Deutsches Institut für Normung (2010) DIN 51605: Kraftstoffe für pflanzenöltaugliche Motoren – Rapsölkraftstoff – Anforderungen und Prüfverfahren. Beuth, Berlin
6. Europäische Kommission (2008) "Mitteilung der Kommission an das Europäische Parlament und den Rat – Mehr Energie einsparen in Europa durch Kraft-Wärme-Kopplung" /*KOM/2008/0771 endg.*/ vom 13.11.2008, Brüssel
7. Thrän D, Müller-Langer F (2008) Bewertung verschiedener flüssiger biogener Kraftstoffe für die stationäre Anwendung – Potenziale, Ökonomie, Ökologie. In: Blockheizkraftwerke 2008. Im Focus biogener Brennstoffe – Technik - Betriebserfahrungen, VDI-Berichte 2046. VDI Verlag, Düsseldorf, p 220
8. Deutsches BiomasseForschungsZentrum (DBFZ) (2009): Monitoring zur Wirkung des Erneuerbare-Energien-Gesetzes (EEG) auf die Entwicklung der Stromerzeugung aus Biomasse – Zwischenbericht "Entwicklung der Stromerzeugung aus Biomasse 2008" im Auftrag des BMU, Eigenverlag, p 59
9. Deutsches BiomasseForschungsZentrum (DBFZ) (2010) Monitoring zur Wirkung des Erneuerbare-Energien-Gesetz (EEG) auf die Entwicklung der Stromerzeugung aus Biomasse – Zwischenbericht im Auftrag des BMU, Eigenverlag, p 91
10. Remmele E (2009) Handbuch. Herstellung von Rapsölkraftstoff. In: Dezentralen Ölgewinnungsanlagen. nachwachsende-rohstoffe.de, 2. Aufl. Gülzow: Fachagentur Nachwachsende Rohstoffe e.V., p 88
11. Widmann B, Kaltschmitt M, Münch EW, Müller-Langer F, Remmele E (2009) Produktion und nutzung von Pflanzenölkraftstoffen. In: Kaltschmitt M, Hartmann H, Hofbauer H (eds) Energie aus Biomasse – Grundlagen, Techniken und Verfahren. 2. Aufl. Springer, Berlin, pp 711–736

12. Brenndörfer M, Graf T (2005) Anlagentechnik der Ölabpressung. In: Kuratorium für Technik und Bauwesen in der Landwirtschaft e. V. (KTBL) (Hrsg.): Dezentrale Ölsaatenverarbeitung, Nr. 427. Landwirtschaftsverlag, Münster, pp 31–36
13. Bockisch M (1993) Nahrungsfette und -öle. Eugen Ulmer, Stuttgart, p 694
14. Deutsches Institut für Normung (2009) DIN EN 590: Kraftstoffe für Kraftfahrzeuge – Dieselkraftstoff - Anforderungen und Prüfverfahren. Beuth, Berlin
15. Deutsches Institut für Normung (2003) DIN EN 14213: Heizöle – Fettsäure-Methylester (FAME) – Anforderungen und Prüfverfahren. Beuth, Berlin
16. Deutsches Institut für Normung (2010) DIN EN 14214: Kraftstoffe für Kraftfahrzeuge – Fettsäure-Methylester (FAME) für Dieselmotoren – Anforderungen und Prüfverfahren. Beuth, Berlin
17. Deutsches Institut für Normung (2008) DIN 51603-1: Flüssige Brennstoffe – Heizöle – Teil 1: Heizöl EL, Mindestanforderungen. Beuth, Berlin
18. Widmann BA, Apfelbeck R, Gessner BH, Pontius P (1992) Verwendung von Rapsöl zu Motorentreibstoff und als Heizölersatz in technischer und umweltbezogener Hinsicht. "Gelbes Heft" Nr. 40. Bayerisches Staatsministerium für Ernährung, Landwirtschaft und Forsten, München, p 650
19. Meierhofer T (2006) Untersuchungen zur Eignung verschiedener Pflanzenöle als Kraftstoff in pflanzenöltauglichen BHKW. Diplomarbeit. Fachhochschule Amberg-Weiden, Fachbereich Maschinenbau/Umwelttechnik. Eigenverlag, p 157
20. ASG Analytik-Service Gesellschaft mbH (2007) Prüfbericht (unpublished)
21. Emberger P, Thuneke K, Haas R, Remmele E (2007) Prüfung von Hanföl hinsichtlich seiner Eignung als Kraftstoff für pflanzenöltaugliche Motoren. Straubing: Technologie- und Förderzentrum im Kompetenzzentrum für Nachwachsende Rohstoffe, 57 Seiten, www.nova-institut.de. Accessed 13 April 2010
22. Deutsches Institut für Normung (2010) DIN V 51623: Kraftstoffe für pflanzenöltaugliche Motoren – Pflanzenölkraftstoff – Anforderungen und Prüfverfahren. Beuth (in preparation), Berlin
23. Verein Deutscher Ingenieure (2004) VDI-Richtlinie 3985: Grundsätze für Planung, Ausführung und Abnahme von Kraft-Wärme-Kopplungsanlagen mit Verbrennungskraftmaschinen. VDI-Gesellschaft Energietechnik (Hrsg.). Beuth, Berlin
24. Remmele E (2002) Standardisierung von Rapsöl als Kraftstoff – Untersuchungen zu Kenngrößen, Prüfverfahren und Grenzwerten. Dissertation an der Fakultät Wissenschaftszentrum Weihenstephan für Ernährung, Landnutzung und Umwelt der Technischen Universität München, Lehrstuhl für Landtechnik, Freising-Weihenstephan, VDI-MEG Schrift Nr. 400, p 194
25. Thuneke K, Remmele E, Widmann B (2002) Pflanzenölbetriebene Blockheizkraftwerke – Leitfaden. Materialien Umwelt & Entwicklung Bayern 170. Bayerisches Staatsministerium für Landesentwicklung und Umweltfragen, München, p 66
26. van Basshuysen R, Schäfer F (2004) Lexikon Motorentechnik. Friedr. Vieweg & Sohn Verlag/GWV Fachverlage GmbH, Wiesbaden, p 1078
27. Thuneke K (2007) Verbrennung und Emissionen von Pflanzenölen in Dieselmotoren – Übersicht zu ausgewählten aktuellen Forschungsergebnissen. In: Nova-Institut GmbH (Hrsg.): Erster Internationaler Kongress zu Pflanzenöl-Kraftstoffen, Tagungsband / Proceedings, Messe Erfurt, 6–7 September 2007. Nova Institut, Hürth, pp 189–204
28. Czerwinski J, Zimmerli Y, Neubert T, Kasper M, Mosimann M (2006) Analysis of (Nano) Particles with GTL, RME & ROR on a Modern HD-diesel engine. Report for Swiss Petrol Union, Zürich, Schweiz. Berner Fachhochschule, Hochschule für Technik und Informatik HTI, Abgasprüfstelle, Nidau (Hrsg.), Eigenverlag, p 40
29. Dobiasch A (2000) Einfluss der chemischen und physikalischen Eigenschaften von regenerativen Kraftstoffen auf das Emissionsverhalten von Verbrennungsmotoren. Fortschritt-Berichte VDI, Reihe 12, Band 428. VDI Verlag GmbH, Düsseldorf, p 173
30. Meyer M (2007) Rapsölkraftstoff in der Schweiz – Statusbericht zur Motorenforschung. In: Tagungsband zum 16. Symposium Bioenergie – Festbrennstoffe, Flüssigkraftstoffe, Biogas. Ostbayerisches Technologie-Transfer-Institut e. V. (OTTI) (Hrsg.), OTTI e. V., Eigenverlag, Regensburg
31. Prankl H, Krammer K, Janetschek H, Roitmeier T (2005) Blockheizkraftwerke auf Pflanzenölbasis. Abschlussbericht zum Forschungsprojekt BLT 012951. Eigenverlag, Wieselburg, p 106
32. Thuneke K (2009) Untersuchungen zu Abgasemissionen und zum Einsatz von Partikelfiltersystemen bei rapsölbetriebenen Blockheizkraftwerken. Dissertation an der Fakultät Wissenschaftszentrum Weihenstephan für Ernährung, Landnutzung und Umwelt der Technischen Universität München, Lehrstuhl für Agrarsystemtechnik. Freising-Weihenstephan. VDI-MEG Schrift Nr. 478, p 191
33. Erneuerbare-Energien-Gesetz vom 25. Oktober 2008 (BGBl. I S. 2074), zuletzt geändert durch das Gesetz vom 11. August 2010 (BGBl. I S. 1170)

Books and Reviews

BINE Informationsdienst FIZ Karlsruhe (2009) Blockheizkraftwerke. Ein Leitfaden für den Anwender., 7th edn. Solarpraxis AG, Berlin

Kaltschmitt M, Hartmann H, Hofbauer H (2009) Energie aus Biomasse. Grundlagen, Techniken und Verfahren., vol 2, Auflage. Springer, Berlin/Heidelberg

Klausmann H (2000) Aufbau und Einsatz von anschlussfertigen BHKW-Kompaktmodulen bis 250 kW. Vulkan, Essen

Mollenhauer KH, Tschöke H (2010) Handbook of diesel engines. Handbuch – Dieselmotoren. 2. Auflage. Springer, Berlin, p 1069

Otto F, Otte J, Raatz A (2009) Untersuchung der Marktchancen, Hemmnisse und Systemoptionen für Strom erzeugende Heizungen vor dem Hintergrund neuer nationaler und internationaler technischer Entwicklungen im Bereich der Kleinst-BHKW im Hinblick auf zukünftig anstehende Neu- und Umstrukturierungen der deutschen Stromversorgung – Abschlussbericht. Fraunhofer IRB Verlag, Stuttgart

Pauleickhoff W (2009) Optimierung der Wirtschaftlichkeit von Miniblockheizkraftwerken. Diplomica Verlag GmbH, Hamburg
Remmele E (2009) Handbuch. Herstellung von Rapsölkraftstoff. In: dezentralen Ölgewinnungsanlagen. 2. Auflage. Fachagentur Nachwachsende Rohstoffe e.V., Gülzow
Suttor W, Johler M, Weisenberger D (2009) Das Mini-Blockheizkraftwerk. Eine Heizung, die auch Strom erzeugt. 5. Auflage. Müller, Heidelberg/München/Landsberg/Frechen/Hamburg
Thomas B (2007) Mini-Blockheizkraftwerke. Grundlagen, Gerätetechnik, Betriebsdaten., vol 1, Auflage. Vogel Buchverlag, Würzburg
VDI-Gesellschaft Energietechnik (2008) Blockheizkraftwerke 2008. Im Focus biogener Brennstoffe. Technik – Betriebserfahrungen. VDI-Berichte 2046. VDI Verlag, Düsseldorf

Plasma-Assisted Waste-to-Energy Processes

Nickolas J. Themelis[1], Armelle M. Vardelle[2]
[1]Earth Engineering Center, Columbia University, New York, NY, USA
[2]Laboratoire Sciences des Procédés Céramiques et de Traitements de Surface, University of Limoges, Limoges Cedex, France

Article Outline

Glossary
Definition of the Subject and Its Importance
Introduction
Composition and Chemical Heat Content of MSW
Thermal Plasma Torches
Energy and Material Balances in Plasma-Assisted Gasification of MSW
Plasma-Assisted Processes for Treating MSW
Environmental Impacts
Future Directions
Bibliography

Glossary

Arc plasma A gas that is heated electrically to temperatures up to 20,000 K by means of an arc struck between two electrodes.

Arc plasma torch Device used to generate a thermal plasma.

Efficiency of energy generation Ratio of net electrical energy generated to chemical heat input, per ton of MSW processed.

MSW Municipal solid waste, mixed waste that is collected by a given collection system.

Non-transferred arc plasma torch The two electrodes located within a water-cooled plasma torch.

Torch thermal efficiency Ratio of enthalpy input to the plasma-forming gas to electrical energy input to the plasma torch.

Transferred arc The material to be processed serves as an electrode.

Vitrification Also called glassification: converting WTE ash to a glassy substance by melting at high temperatures.

WTE Acronym for waste-to-energy, i.e., thermal treatment of solid wastes to recover their chemical energy content.

Definition of the Subject and Its Importance

The thermal plasma technology [1, 2] has been used for over 30 years mainly for surface coating, metal welding and cutting, powder treatment and synthesis, and metal melting and smelting. More recently, thermal plasmas have also been used for the pyrolysis of hazardous liquids and gasses and the compaction of solid wastes [3]. Examples of the latter technology are the destruction of asbestos-contaminated waste materials and the vitrification of the ash by-product of waste-to-energy plants. Efforts to apply plasma in the thermal treatment of municipal solid wastes (MSW), in the absence of partial combustion, have not been successful because of the required high "investment" of electricity per unit of mass treated. Therefore, in this essay, we are examining processes where thermal plasma is used *in conjunction* with partial oxidation and gasification of the organic compounds contained in the MSW, thus reducing the consumption of electricity per ton of material treated. Such processes exist and are in different stages of development. Collectively, they can be called "plasma-assisted WTE" technologies and are the subject of this essay.

Introduction

Although both conventional waste-to-energy (WTE) and plasma-assisted WTE processes involve a certain degree of combustion, there is an important

difference: in conventional WTE, carbonaceous materials are combusted and the heat of combustion is transferred to steam that powers a turbine generator of electricity. Per ton of MSW processed, the ratio of net electric energy generated for the grid/input chemical energy contained in MSW is called the thermal efficiency of energy generation.

In the case of plasma-assisted gasification, the objective is to partially oxidize the carbon content of MSW to carbon monoxide (CO) and produce a synthetic gas that contains as high as possible concentrations of carbon monoxide and hydrogen and, conversely, a very low concentration of carbon dioxide. This synthetic gas or "syngas" can generate electricity in a gas engine or turbine at a higher thermal efficiency than a steam turbine. The heat generated by the plasma torch is used to provide some of the heat for gasification, to break down long hydrocarbons to CO and H_2, and to vitrify the ash product of the gasification process. The syngas product can either be quenched by means of a water stream, or passed through a heat recovery exchanger to produce steam used in a steam turbine to produce additional electricity.

The main difference between traditional combustion and gasification is the amount of oxygen used. Full combustion of the carbonaceous materials in MSW requires a large excess of air, typically 70–100% of the stoichiometric requirement. Gasification is carried out with a sub-stoichiometric amount of oxygen in order to produce mostly carbon monoxide and hydrogen. Of course, in order to utilize the energy content of the syngas, it is necessary to combust it in a gas engine or turbine. The potential advantages of gasification are that a much lower excess oxygen is required, thus simplifying the gas control system; also, the thermal efficiency of the gas engine can be substantially higher than that of the steam turbine used in grate combustion WTE. Figure 1 shows the reaction sequence in gasification systems [4].

Composition and Chemical Heat Content of MSW

The calorific value of MSW varies considerably, depending on their content of food and green wastes, that introduce moisture, and petrochemical wastes, such as plastics and textiles, that are associated with higher calorific values than paper fiber and wood. Metals, glass, and other inorganic materials in the MSW do not contribute to its heating value; in fact they reduce it somewhat. Figure 2 shows the typical composition of U.S. MSW in 2007 [4].

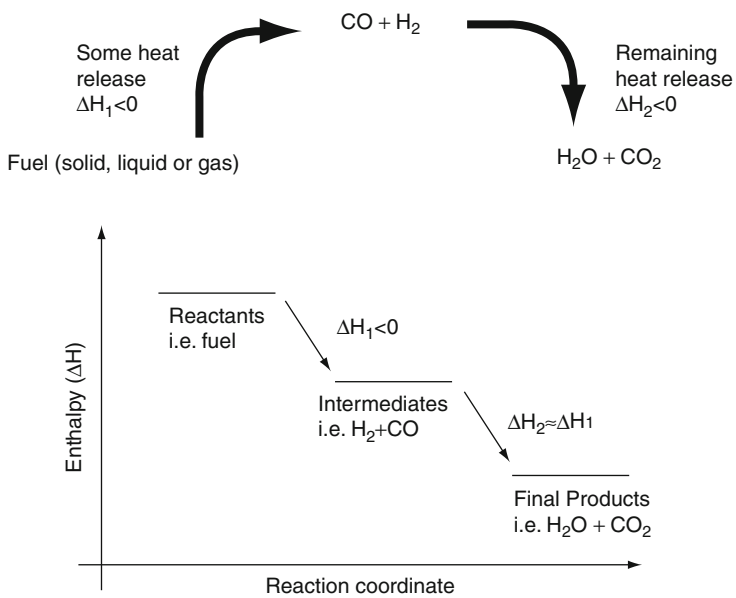

Plasma-Assisted Waste-to-Energy Processes. Figure 1
Conceptual pathway for conversion of carbon fuels to final gaseous products

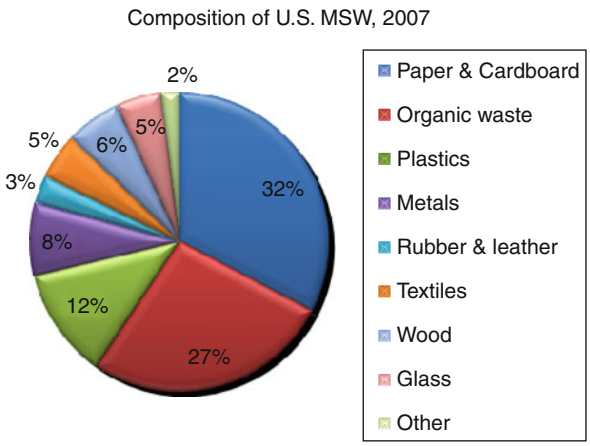

Plasma-Assisted Waste-to-Energy Processes. Figure 2 Composition of the U.S. MSW [4]

On the basis of the MSW composition (e.g., Fig. 2) and the chemical composition of the constituent materials, it has been shown [5] that the chemical structure of *organic* compounds (both biogenic and fossil-based) in MSW can be approximated by the formula $C_6H_{10}O_4$; it is interesting to note that there are about ten organic compounds in nature that have the same chemical structure [6]. In the absence of moisture and inorganic materials, $C_6H_{10}O_4$ would have a calorific value of about 18,500 MJ per kilogram. However, since mixed MSW contains other non-combustible materials, the resulting calorific value can be expressed as follows [5]:

$$\begin{aligned}\text{Heating value of mixed MSW} &= (\text{heating value of combustibles}) \times X_{comb} \\ &\quad - (\text{heat loss due to water in feed}) \times X_{water} \\ &\quad - (\text{heat loss due to glass in feed}) \times X_{glass} \\ &\quad - (\text{heat loss due to metal in feed}) \times X_{metal}\end{aligned}$$

where X_{comb}, X_{water}, etc are the mass fractions of combustible matter, water, etc in the MSW and $X_{comb} + X_{water} + X_{glass} + X_{metal} = 1$.

Substituting numerical values for the heat of reaction, evaporation of moisture, and heat carry over in the WTE ash results in the following equation.

$$\text{Heating value of MSW} = 18.5.X_{comb} - 2.6.X_{water} - 0.6X_{glass} - 0.5X_{metal}\,(\text{MJ/kg})$$

The effect of moisture on the calorific value of several types of solid wastes is shown graphically in Fig. 3.

In the case of conventional WTE processes, the inlet moisture in the MSW is evaporated, the organic compounds in MSW are completely combusted, and the inorganic compounds end up in the WTE ash. The exothermic chemical reaction of U.S. MSW in the combustion chamber can be represented by the following equation:

$$\begin{aligned}&C_6H_{10}O_4 + 6.5O_2 \\ &\quad = 6CO_2 + 5H_2O + 2800 \text{ kWh per ton of MSW}\end{aligned}$$

A study of 97 incinerator power plants in the European Union (Fig. 4, [7]) showed that the average MSW combusted in the E.U. has an average calorific value of 10 MJ/kg (about 2,800 kWh/t of feed). Therefore, a WTE grate combustion facility operating at a net thermal efficiency of 22% would provide 600 kWh/t to the grid. For WTE plants that provide electricity and district heating, as is done in northern European countries, the thermal efficiency can be significantly higher.

Thermal Plasma Torches

The most common way to create a thermal plasma jet is by heating a gas stream to high temperatures (up to 20,000 K) by means of a DC- or AC-sustained electric arc between the cathode and the anode of the torch. The plasma jet is a mixture of ions, electrons and neutral particles and, because of its high temperature, can vaporize and destroy any chemical compound if the material is properly "mixed" with the gas phase. The partly ionized gas exits the plasma torch at high velocity, thus creating what is called a plasma jet. The main advantages of thermal plasma are high energy density, resulting in extremely high heat and mass transfer rates, compact size of the heat source, and rapid start-up and shut down. However, the use of electricity is a drawback since it is an expensive form of energy. Furthermore, the plasma torch needs to be water-cooled, thus introducing a heat loss that ranges from 10% to 40% depending on the torch configuration.

Thermal plasmas can also be generated by radio frequency induction and microwaves. However, for the treatment of waste, plasma is preferentially generated by DC electric discharge with two kinds of torch configurations, non-transferred and transferred arc. Combining classic gasification with plasma technology allows a higher efficiency in the production of

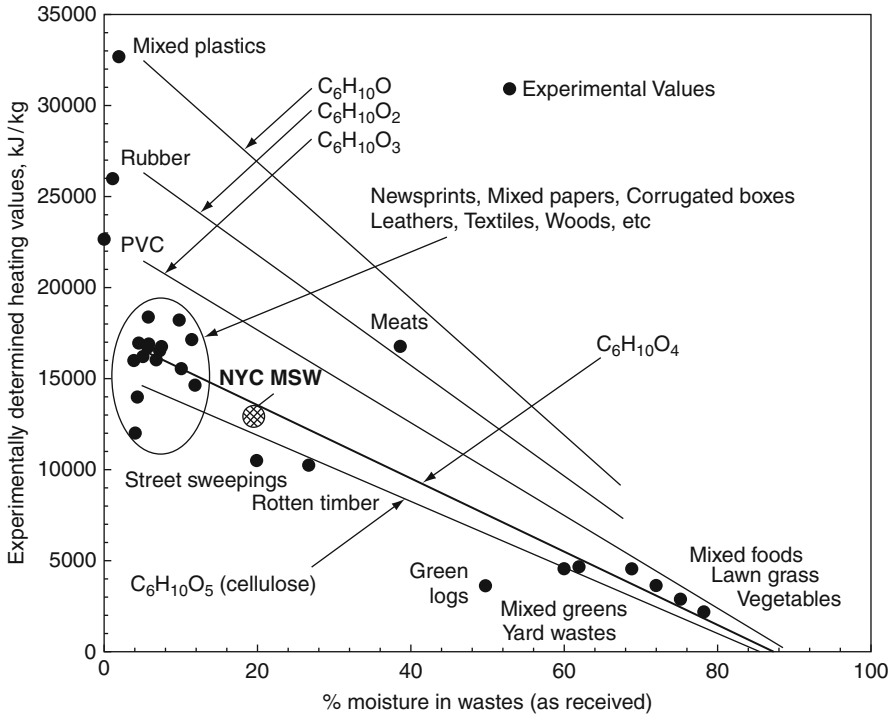

Plasma-Assisted Waste-to-Energy Processes. Figure 3
Effect of constituent materials and moisture on heating value of MSW [5]

the syngas, and lower emissions, as we will see later on. Figure 5 below shows that subjecting the products of gasification to plasma treatment creates a higher quality syngas by increasing the H_2 to CO ratio.

Non-transferred Arc Plasma Torch

Non-transferred arc plasma torches are commonly used in the treatment of wastes. Electricity is transformed into thermal energy by means of an electric discharge between the cathode and the anode contained in a water-cooled torch. This device can be used either with hot (thermo-ionic) rode-type cathode (Fig. 6) and cold tubular water-cooled cathode.

Figure 7 is a schematic of the Europlasma non-transferred plasma torch that utilizes a cold cathode:

Transferred Plasma Arc

In the case of transferred arc, one of the electrodes is external to the torch. The electricity flows through the gas column issuing from the torch into the molten metal or slag below the torch, which is connected to the external electrode (Fig. 8). The peak temperature of the arc plasma can range from 12,000 to over 20,000 K.

Since the plasma is produced outside of the water-cooled body of the torch, this device is thermally more efficient than the non-transferred arc torch. The cathode can be either a water-cooled metal tube or non-cooled graphite tube that is consumed slowly by sublimation. In this case, the thermal loss is reduced, but the cathode needs to be replenished. The anode is generally made from a high thermal conductivity metal that is water cooled at the outer end so as to avoid melting it.

Energy and Material Balances in Plasma-Assisted Gasification of MSW

As described earlier, plasma-assisted gasification volatilizes MSW in an oxygen-deficient environment where the waste materials are decomposed and partially oxidized to the basic molecules of CO, H_2, CO_2 and H_2O. Thus, the organic fraction of the waste is converted into a synthesis gas ("syngas") that contains most of the chemical energy of the waste. Also, the inorganic fraction of the MSW can be converted into an inert vitrified

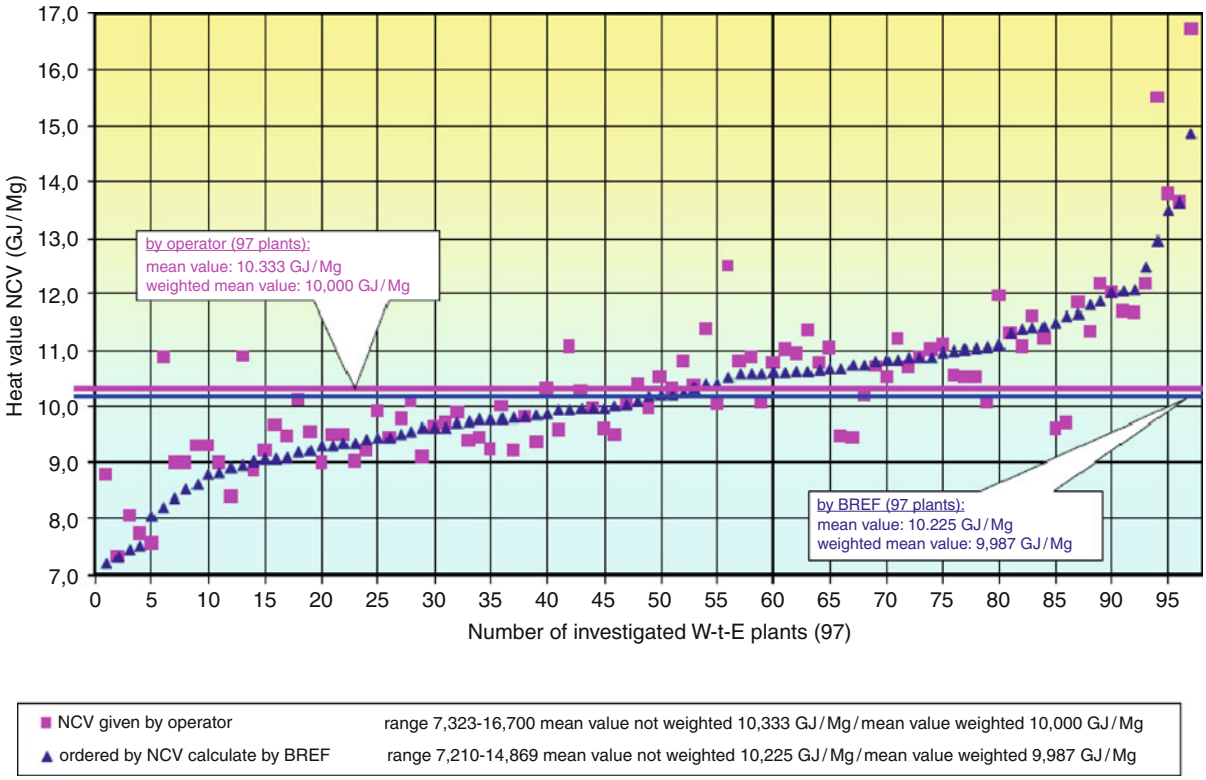

(Reimann 2005)

Plasma-Assisted Waste-to-Energy Processes. Figure 4
Calorific values of MSW of 97 E.U. WTE facilities [7]

glass so that there is no ash remaining to be landfilled. Furthermore, the plasma reactor can treat all waste materials, as the only variable is the amount of energy needed to melt the waste. Any kind of feedstock, other than nuclear waste, can be directly processed. Controlling the temperature of the output gasses by modifying the temperature allows for better control of the syngas composition.

For a typical MSW of total calorific value of 2,800 kWh/t, the two steps of the overall process can be represented by the following chemical equations:

- Gasification by means of partial combustion with oxygen (assuming zero reactor heat loss):

$$C_6H_{10}O_4 + 3O_2 = 3CO + 3CO_2 + 4H_2 + H_2O + 1300 \text{ kWh per ton of MSW} \quad (1)$$

- Gas turbine combustion (assuming zero turbine heat loss):

$$3CO + 4H_2 + 3.5O_2 = 3CO_2 + 4H_2O + 1500 \text{ kWh} \quad (2)$$

Typically, the syngas produced in plasma-assisted gasification has about 30% of the heating value of natural gas.

At an assumed thermal efficiency of 50% of the gas turbine, the electricity generated will be equal to 1,500 kWh × 50% = 750 kWh/t of solid wastes. The oxygen required for partial combustion should be provided in the form of industrial oxygen, to avoid the introduction of about four parts of nitrogen per part of oxygen. The production of 1 t of industrial oxygen (95% O_2) requires about 250 kWh of electricity. Since the gasification reaction (1) requires three moles of oxygen per mole of combustibles, the gasification of 1 t of MSW containing 20% of moisture and 20% of inorganic materials will require

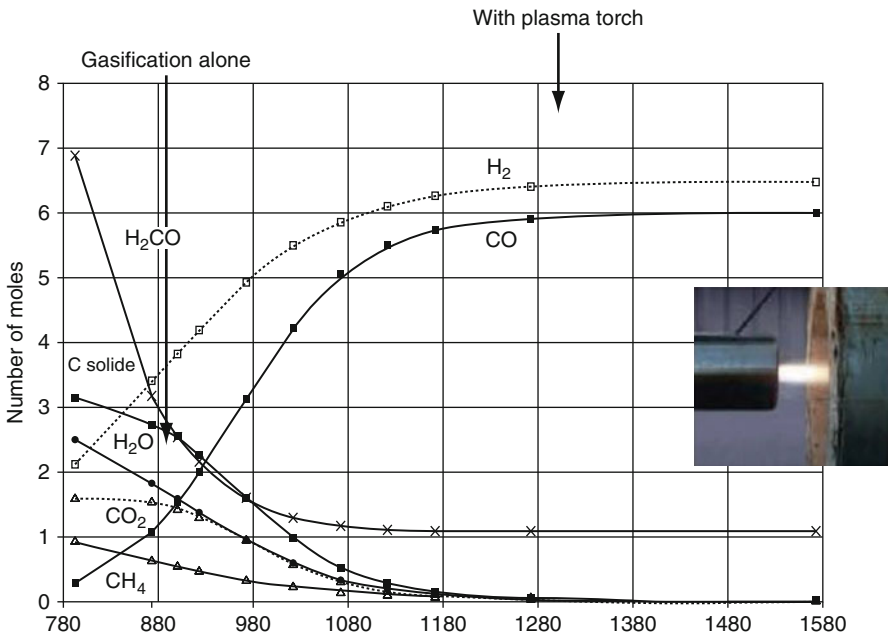

Plasma-Assisted Waste-to-Energy Processes. Figure 5
Effect of plasma on products of gasification [1]

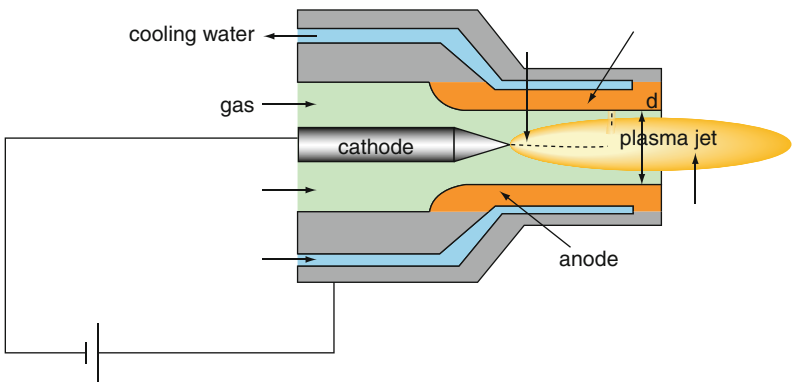

Plasma-Assisted Waste-to-Energy Processes. Figure 6
Non-transferred arc plasma torch [8]

$$1000 \times 60\%/146 \times 96/1000 \times 250 \text{ kWh}$$
$$= 75 \text{ kWh of electricity per ton of MSW processed.}$$

Thermodynamic considerations show that gasification of various types of waste will yield the syngas compositions shown in Table 1. Figure 9 shows the composition of syngas produced by the gasification of a typical MSW.

Plasma-Assisted Processes for Treating MSW

Plasma processes have been used widely for the destruction of asbestos and other hazardous wastes. However, due to their high consumption of electricity, sole use of plasma energy is not viable economically for the treatment of low-value materials, such as MSW. However, *plasma-assisted* gasification processes are being developed and may offer environmental and economic benefits.

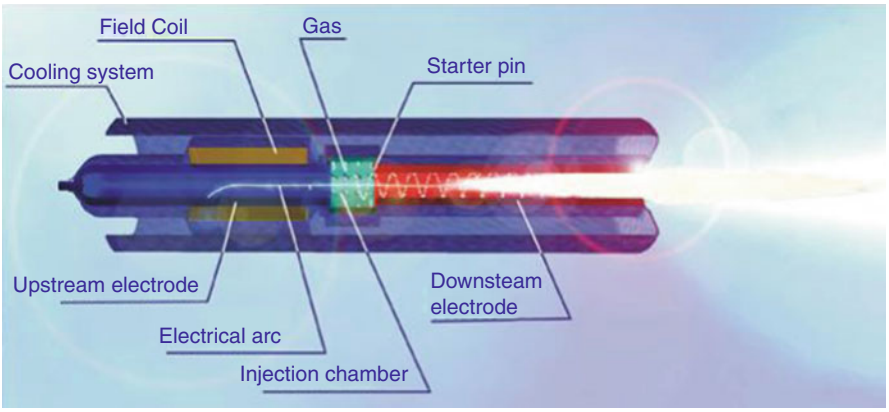

Plasma-Assisted Waste-to-Energy Processes. Figure 7
Europlasma non-transferred arc DC plasma torch [9]

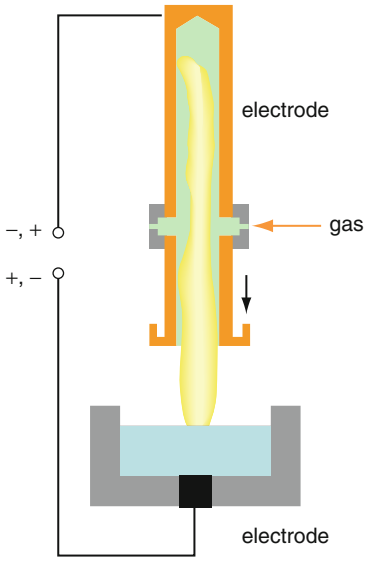

Plasma-Assisted Waste-to-Energy Processes. Figure 8
Transferred arc plasma torch [8]

There are several plasma-assisted gasification technologies where plasma torches are used to accelerate the gasification process, to crack the product of volatilization to CO and H_2, and to vitrify the inorganic component of MSW. The processes to be described in this essay are the gasification process of Alter NRG that is based on the Westinghouse Plasma Technology, and the plasma-assisted process developed by Europlasma. The potential main advantages of plasma-assisted processes, as compared to conventional WTE plants, are the reduction of exhaust gas flow rate, an overall installation with smaller footprint because of more compact equipment, lower capital investment for a given throughput, and faster start-up and shutdown times.

The Alter NRG Westinghouse Plasma Corporation Process

In 2006, Alter NRG acquired the Westinghouse Plasma Corporation (WPC), a leading plasma gasification technology. The non-transferred plasma torch consists of a pair of tubular water-cooled copper electrodes, the operating gas being introduced through an annular space between the electrodes. A schematic diagram of the operation of the torch is shown in Fig. 10. Figure 11 shows two views of the largest plasma torch of Alter NRG that has an operating range of 80–500 kW (Marc 11 plasma torch).

The WPC torches have been used extensively in metal melting cupolas, but their most important applications have been in the destruction of hazardous waste and the vitrification of WTE ash, mostly in Japan. Since the WPC torch is water-cooled, the efficiency of converting electricity into heat ranges from 60% to 75%.

The MSW gasification process developed by Alter NRG is based on a cupola furnace fired by the WPC plasma torches (Fig. 12). This technology is well proven and currently used in several processing plants in Japan. Alter NRG has tested and offers this process for the gasification of MSW, biomass, petroleum coke, and hazardous wastes to produce syngas.

Plasma-Assisted Waste-to-Energy Processes. Table 1 % Molar (volume) composition of the syngas from different feedstocks

	CO	H_2	CO_2	CH_4	H_2O	HCL	H_2S
MSW (typical)	41.0	33.7	13.8	4.1	6.3	0.13	0.13
Carpet	33.2	43.1	6.8	8.8	4.9	0.02	0.03
Tire	56.9	18.9	1.5	22.2	0.3	0.04	0.00
Biomass	27.5	36.1	20.1	1.4	14.7	0.03	0.00
Med waste	27.9	37.8	18.2	1.8	13.7	0.03	0.65
ASR	29.8	37.4	17.3	2.1	12.0	0.00	0.64
Oil	48.8	25.6	2.2	21.1	0.6	1.61	0.00
Bituminous	55.9	23.9	4.1	12.8	1.0	1.71	0.00

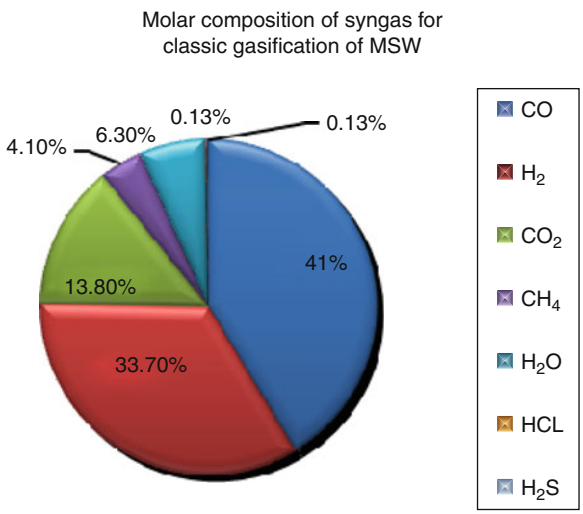

Plasma-Assisted Waste-to-Energy Processes. Figure 9 Composition of syngas from gasification of typical MSW

The Alter NRG-WPC process uses up to six plasma torches at the bottom part of the gasifier. A bed of coke is formed within the cupola using metallurgical coke ("met coke") to absorb and retain the heat energy from the plasma torches and provide a "skeleton" that supports the MSW feed as it descends through the gasification reactor and is converted to gas and liquid slag; this action is similar to the phenomena occurring in an iron blast furnace. The met coke and the MSW are fed from the top of the refractory-lined gasification vessel. Figure 13 is a photograph of the Alter NRG pilot reactor at Madison, Pennsylvania, USA.

In 2010, Alter NRG was using its industrial-size pilot plant at Madison, PA, to gasify wood chips to syngas that is stored in large gas tanks and is then used by another company, located next to the Alter NRG plant, to produce ethanol. There were four industrial plants using the Alter NRG gasifier: two in Japan (one on MSW plus automobile shredder residue; the other on MSW and wastewater sludge) and two in India (Pune and Nagpur) processing hazardous waste. All these plants use the smaller Marc 3 torches (300 kW capacity), quench and clean the syngas, and then combust it with air to generate steam. The largest plant, in Japan, has a nominal capacity of 300 t MSW per day, while the Indian plants are of 72 t/day capacity.

Operating experience has shown that the electrodes of the Marc 3 torch have a lifetime of up to 500 h. Used electrodes are repaired and reused. The largest WPC torch, Marc 11 is currently used in Quebec for metal smelting. The lifetime of this torch is up to 1,200 h. Six Marc 11 torches will be required for a 750 t/day plant processing MSW.

This process can handle any moisture content in the MSW since water is vaporized along with the syngas. However, the feedstock must be less than 25 cm in size to facilitate feeding into the furnace. The process is controlled by maintaining the temperature of the gas exiting the gasifier between 1,000°C to 1,100°C. At the bottom of the cupola, the inorganic components in the MSW are melted into a slag layer and a metal layer underneath the slag. These liquids are tapped intermittently from the furnace.

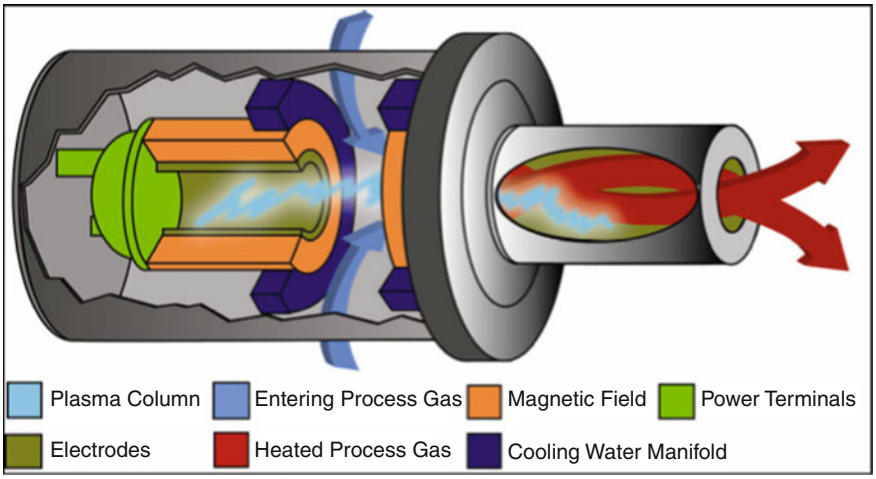

Plasma-Assisted Waste-to-Energy Processes. Figure 10
The WPC non-transferred arc plasma torch [10]

Plasma-Assisted Waste-to-Energy Processes. Figure 11
Side and front view of the Alter NRG Marc 11 plasma torch

The plasma torches are controlled independently of each other, and a torch can be removed for maintenance while the furnace is operating. The gasifier is working at a slightly negative pressure to avoid gaseous leaks. There is a small gap between the torches and the furnace wall so that a small amount of air infiltrates into the furnace (Fig. 14).

As in the case of other gasification processes, the syngas produced contains about one third of the energy content of natural gas. Therefore, the gas turbine used to generate electricity has to be compatible with a lower energy gas. The ultimate goal of Alter NRG is to operate with MSW feed plus 4% of met coke and generate power by means of the Integrated Gasification Combined Cycle (IGCC, Fig. 15).

The largest project for plasma gasification of MSW was announced in 2006 as a partnership between Alter NRG and Geoplasma, at St Lucie, Florida. The initial plan was to construct a plan processing 1 million tons of waste per year. However, due to the lack of investors and public opposition, the project was scaled down to a 500-t/day plant (about 150,000 t/year). This plant will consist of two lines of total nominal capacity of 500 t/day, but maybe increased to 750 t/day. The projected met coke and limestone use will be 4% and 7.9%, respectively. The input materials to the gasification reactor are shown in Fig. 16, and Fig. 17 is a schematic flowsheet of this potential application.

An overall energy balance for such a system was calculated by Caroline Ducharme (Ducharme 2010).

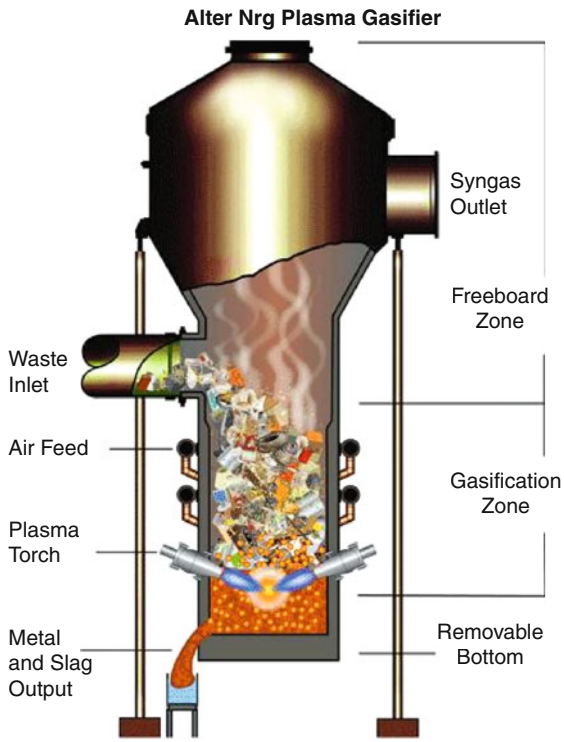

Plasma-Assisted Waste-to-Energy Processes. Figure 12 The Alter NRG plasma gasifier [10]

Plasma-Assisted Waste-to-Energy Processes. Figure 13 The Alter NRG gasification reactor viewed from the bottom [4]

The electricity needed to shred the MSW was estimated at less than 10 kWh/t. As noted earlier, a typical MSW has a calorific value of about 10 MJ/kg which corresponds to 2,800 kWh/t. The energy contained in the

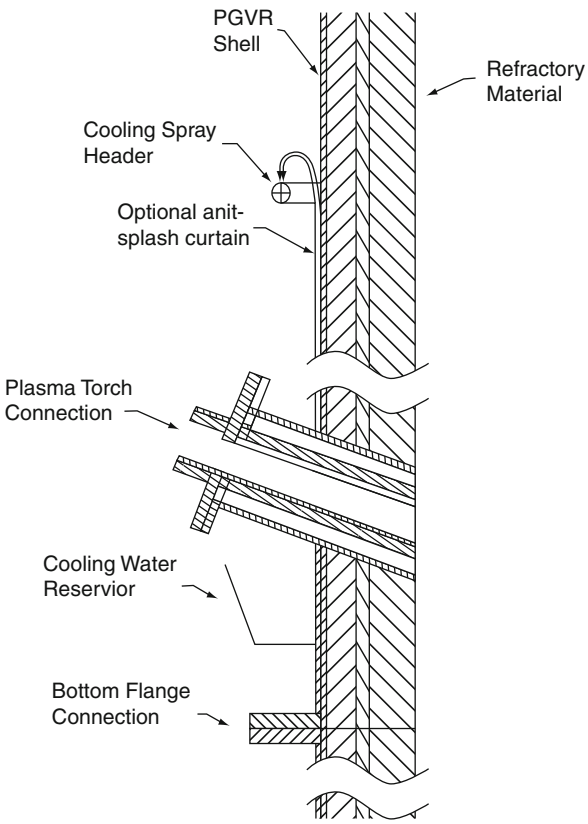

Plasma-Assisted Waste-to-Energy Processes. Figure 14 Schematic diagram showing how torch is introduced through furnace wall

metallurgical coke (LHV: 32.8 MJ/kg) was calculated from

$$\text{One ton of MSW} \times 4\% \times 32.8\text{MJ/kg} \times 1000\,\text{kg/ton} = 1312\ \text{MJ or } 335\ \text{kWh/ton MSW}$$

The thermal energy provided by six 600-kW torches used in the Alter NRG reactor is $6 \times 600 \times 75\% = 2{,}700$ kWh (the plasma torches need to be water-cooled so that their average efficiency of converting electricity to heat is assumed to be 75%). The electricity consumed by the six plasma torches in a plant of 750 t/day (31.25 t/h) would be 3,600 kWh/h, corresponding to about 115 kWh of electricity per ton MSW processed. Table 2 shows the distribution of energy inputs to the gasification plant.

The energy outputs are the heat loss from the reactors, the heat loss in the cooling water of the torches, the heat carryover in the vitrified ash, and the chemical

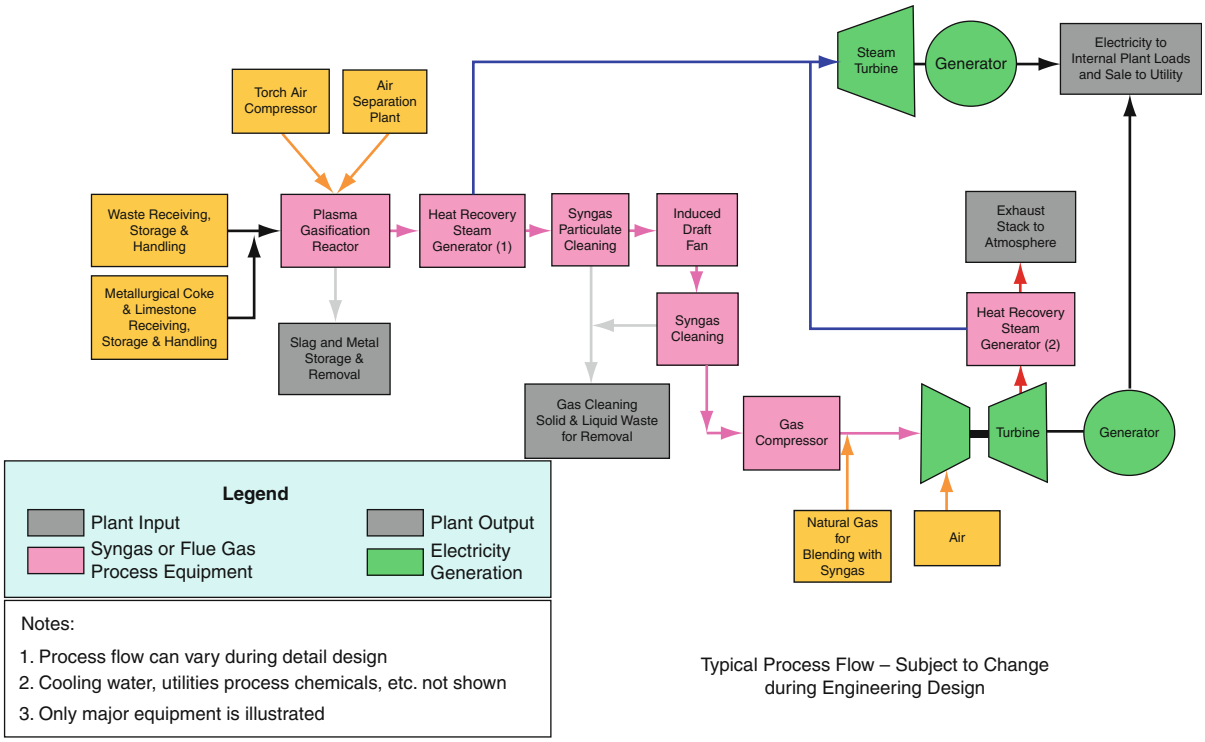

Plasma-Assisted Waste-to-Energy Processes. Figure 15
Integrated Gasification Combined cycle [10]

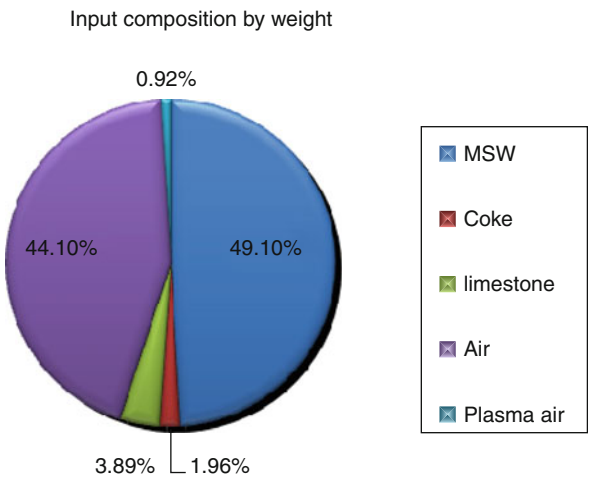

Plasma-Assisted Waste-to-Energy Processes. Figure 16
Input composition to WPC reactor by weight [10]

plus sensible heat in the syngas product. Assuming a 10% heat loss from the gasification reactor plus the water-cooling system of the torches and the vitrified ash, the syngas should carry 90% of the energy input by the MSW, coke, and plasma torches. An estimated 80% of this energy is in the form of chemical energy in the syngas and 20% is thermal energy, in the form of sensible heat. When the syngas is quenched, as in the present Alter NRG process, the sensible heat is not recovered. Therefore, the chemical energy content in the syngas will be: $0.90 \times 0.80 \times 3{,}136 = 2{,}258$ kWh. If the syngas is used to power a gas turbine at 45% efficiency, the gross electrical energy generated will be 1,015 kWh of electricity per ton of MSW. However, some of this energy must be used in the operation of the plant, i.e., shredding of MSW, production of industrial oxygen for combustion, operation of plasma torches, and all other uses of electricity within the plant (Table 2). The consumption of electricity for oxygen production was estimated earlier at 75 kWh/t of MSW.

- Shredding of MSW: 10 kWh/t MSW
- Operation of the Air Separation Unit: as per earlier discussion, an estimated 75 kWh of electricity would be used per ton of MSW processed.

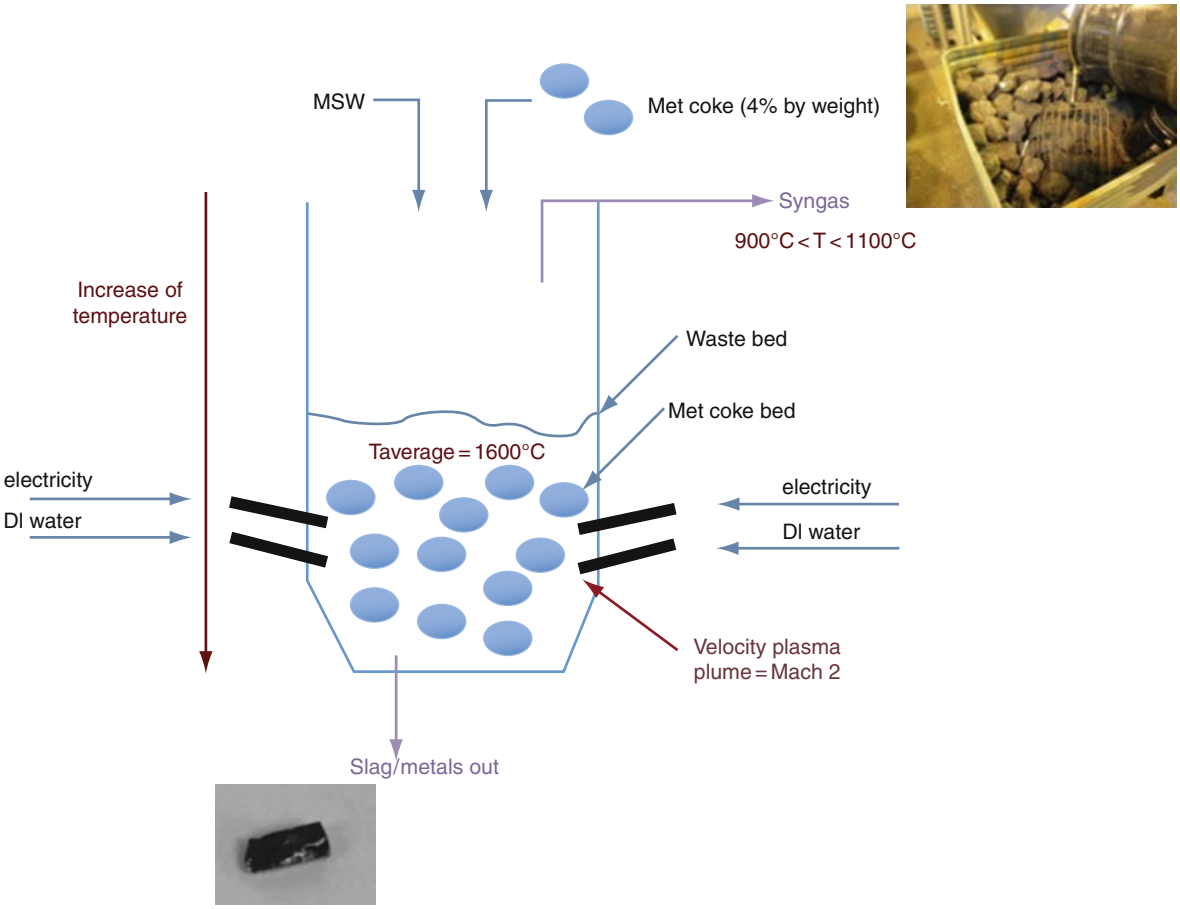

Plasma-Assisted Waste-to-Energy Processes. Figure 17
Flows of materials and energy into the WPC reactor [4]

- Operation of the plasma torches: 115 kWh/t of MSW processed
- All other needs of plant (assumed to be 75% of those of a conventional WTE plant that has to clean a much larger volume of gas): 75 kWh

By subtracting the above internal uses of electricity from the 1,015 kWh generated by the syngas turbine yields the net electricity generated by this plant per ton of MSW processed: 740 kWh. This calculated number is somewhat higher than a conventional grate combustion WTE of the same size that generates 650 kWh per metric ton of MSW containing 2,800 kWh of chemical heat. Figure 18 shows the projected composition of syngas produced by the WPC gasification of MSW.

Plasma-Assisted Waste-to-Energy Processes. Table 2
Energy inputs to Alter NRG plant, per ton of MSW processed

Inputs	In kWh	In % of total inputs
MSW	2,800	85.8
Met coke	335.8	10.3
Energy from torches	115.2	3.5
Total	3,251	100

The Europlasma WTE Process

Europlasma is a French company and one of the world leaders in plasma technology as applied to the thermal treatment of wastes. They have been very successful in

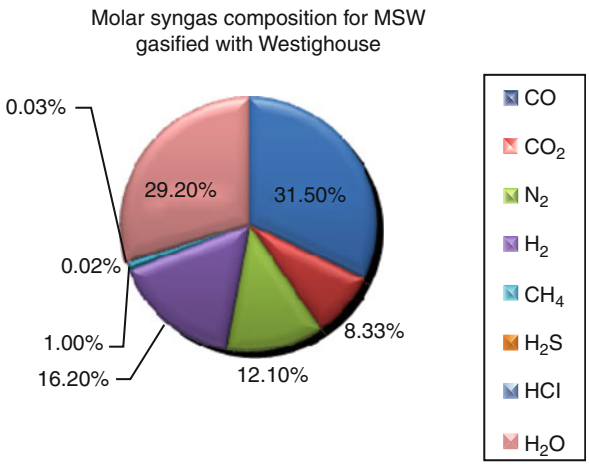

Plasma-Assisted Waste-to-Energy Processes. Figure 18
Syngas composition for MSW gasified by the WPC process

using non-transferred arc torches for vitrifying incinerator residues and have also developed a process for treating asbestos contaminated wastes. The plasma torch consists of two tubular, coaxial, water-cooled, copper electrodes separated by a tubular gap through which flows the plasma forming gas. The thermal efficiency of the Europlasma torches is in the order of 75–80%. Europlasma has also developed a special plasma torch for cracking the gasification syngas, called "TurboPlasma."

Figure 19 shows the Europlasma gasification process. It includes a stoker grate auto-thermal gasifier, a plasma-fired chamber for cracking the gasification gas to hydrogen and carbon monoxide, and a second plasma torch for vitrifying the solid product of gasification; the gas

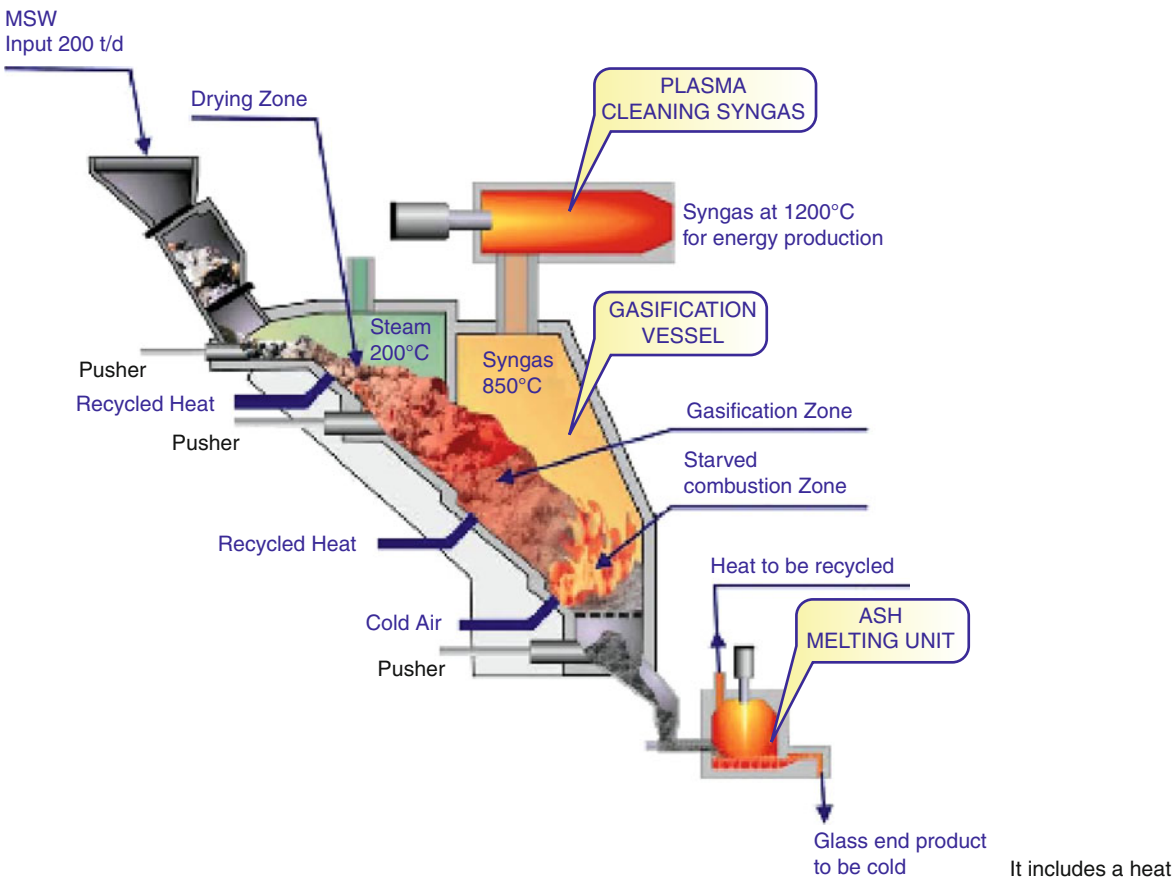

It includes a heat

Plasma-Assisted Waste-to-Energy Processes. Figure 19
The Europlasma process [9]

flow from the vitrification unit flows into the gasification unit and provides the required heat for gasification. The clean syngas may pass through a heat exchanger to recover its sensible heat and then through a scrubber to remove acid gasses and particulate matter; or quenched directly by scrubbing. Figure 20 is a schematic diagram of the processes, such as Europlasma, that use two torches for syngas cracking and ash vitrification.

Europlasma is currently constructing their first MSW gasification plant at Morcenx, France; start up is planned for end of 2011. The plant capacity will be 50,000 t of waste per year.

Since there are no data as yet from the Morcenx plant of Europlasma in France, Ducharme [4] relied on an energy analysis conducted by Sunbeam for Credit Suisse of a proposal to build a Europlasma plant in New Jersey. This plant was to process 400 t/day of MSW mixed with 3% shredded tires. The assumed plant availability was 90% corresponding to a nominal capacity of 120,000 t per year. The LHV of the MSW was 2,800 kWh/t and of the shredded tires 9,690 kWh/ t. Therefore, the MSW-tire mix had an average LHV of 3,090 kWh/t.

According to Sunbeam, the proposed 400 t/day plant would use 4,800 kW for the plasma torches distributed as follows: 4,000 kW (83%) for the syngas polishing torch and 800 kWh (17%) for the ash vitrification torch. Thus, according to the Sunbeam data, the electricity consumption per ton processed would be:

$$4800 \text{ kW} \times 24/400 = 288 \text{ kWh per ton of MSW}$$

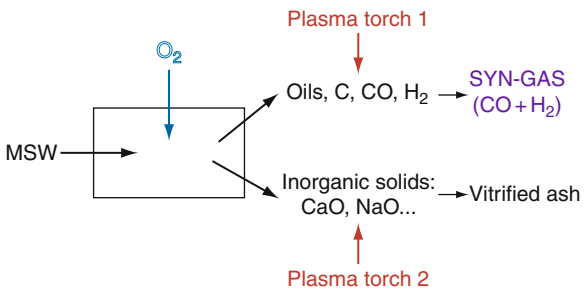

Plasma-Assisted Waste-to-Energy Processes. Figure 20 Flowsheet of plasma assisted-gasification process

On a per ton MSW basis, this projected value is more than double the electricity consumption of the Alter NRG plant and, therefore, questionable. Therefore, it is necessary to wait for operating data after the start-up of the Europlasma plant at Morcenx.

Environmental Impacts

The first noticeable difference of plasma-assisted processes from classic grate combustion is that the syngas is cleaned before combustion, which should be less costly than post-combustion cleaning of WTE flue gas. The final emissions of a plasma-assisted process will depend on the level of cleaning of the syngas, with the exception of NOx that will not be formed during the gasification process. However, some NOx will be formed during combustion in the power generation equipment. Dioxins and furans can be avoided due the high heat of the plasma treatment, but they can form "de-novo" during the cooling of the syngas. However, the dioxin emissions of modern grate combustion WTE plants are so low (less than 0.5 g TEQ per million tons of MSW) that they are insignificant.

In contrast to conventional grate combustion that has no liquid effluents, quenching of the syngas results in an aqueous stream that must be cleaned before discharging.

A definite advantage of plasma-assisted processes is that the vitrified slag is impervious to leaching and can definitely be used for construction.

Future Directions

Plasma torches have been highly developed and are an excellent tool for converting electricity to an extremely high temperature gas. As described in this essay, plasma torches are used for thermally treating hazardous materials such as asbestos and can be used, in combination with partial combustion, for treating any type of solid wastes, including MSW. Such plasma-assisted WTE processes are in operation in Japan and India and an industrial plant is under construction in France. The advantages they offer over conventional grate combustion are a much reduced volume of process gas to clean and the potential of higher thermal efficiency in using

the syngas in a gas turbine, rather than generating steam for a steam turbine, as in the case of conventional grate combustion.

As mentioned in other sections of this Encyclopedia, the major cost factor of thermally treating 1 t of MSW is the repayment of the capital cost. This is where plasma-assisted WTE and other gasification processes can compete with grate combustion and also widen the application of WTE over landfilling: by offering gasification plants that, because of their compactness and higher rates of reaction, will be less costly to build than the giant WTE plants that are based on grate combustion.

With regard to higher energy production, plasma-assisted WTE processes, must "invest" electricity in the operation of the plasma torches. Therefore, it is preferable to use the syngas in a gas turbine that offers higher thermal efficiency than in steam turbines such as those are used by grate combustion processes. An analysis of several plasma-assisted WTE processes at different stages of commercialization by Ducharme [4] showed that most are quoting numbers of electricity generation (e.g., 1,000 kWh/t MSW) that are much higher than the numbers calculated from material and energy balances. Also, the produced syngas has a calorific value equal to one third of natural gas. To overcome this problem, the developing companies have two options, either to blend syngas with natural gas or to use specially adapted turbines.

In conclusion, plasma-assisted gasification of solid wastes is a very interesting process with potential for future application. First, using a reducing atmosphere and producing a relatively smaller amount of process gas facilitates the gas cleaning system. Second, controlling the amount of heat input to the process by means of the plasma torches allows controlling the composition of the syngas. The hydrogen to carbon monoxide ratio can be modified easily, according to the needs of the user. The next decade will show how plasma-assisted gasification of MSW evolves. The plants under planning or construction should provide reliable information on capital and operating costs per ton of solids treated and this technology may provide an alternate route for the thermal treatment of MSW.

Bibliography

Primary Literature

1. Fauchais P, Vardelle A (1997) Thermal plasmas. IEEE T Plasma Sci 5(6):1258–1280
2. Kogelschatz U (2004) Atmospheric-pressure plasma technology. Plasma Phys Control Fusion 46:B63–B75, s.l
3. Heberlein J, Murphy AB (2008) Thermal plasma waste treatment. J Phys D Appl Phys 41:s.l., 053001
4. Caroline D (2010). Technical and economic analysis of plasma-assisted waste-to-energy processes. M.S. Thesis, Earth and Environmental Engineering, Columbia University. www.seas.columbia.edu/earth/wtert/sofos/ducharme_thesis.pdf
5. Themelis NJ, Kim YH (2002) Energy recovery from New York City waste. Waste Manag Res 20:223–233, s.l
6. HSC. Chemistry, 2010. http://www.hsc-chemistry.com
7. Reimann DO (2008). CEWEP energy report (Status 2001–2004). www.cewep.org
8. NOVELECT (2003). Innovative applications of thermal plasmas (in French). s.l.: EDF publication
9. Europlasma. http://www.europlasma.com/
10. Corp, ALter NRG/ Westinghouse Plasma (2010). www.alternrg.ca
11. Igiorno V, De Feo G, Della Rocca C, Napoli R (2003) Energy from gasification of solid wastes. Waste Manag 23:1–15

Books and Reviews

Alexander F (2008) Plasma chemistry. Cambridge University Press, New York

Boulos MI, Fauchais P (1994) Thermal plasmas, fundamentals and applications, 1st edn. Springer, Dordrecht, p 468

Bridgwater AV (1995) The technical and economic feasibility of biomass gasification for power generation. Fuel 74(5): 631–653

Bridgwater AV, Toft AJ, Brammer JG (2002) A techno-economic comparison of power production by biomass fast pyrolysis with gasification and combustion. Renew Sust Energ Rev 6:181–248

Clark BJ, Rogoff MJ (2010). Economic feasibility of a plasma gasification plant. Proceedings of the 18th annual North American waste to energy conference (NAWTEC 18–35), City of Marion, Iowa, 11–13 May 2010

Gomez E, Amutha Rani D, Cheeseman CR, Deegan D, Wisc M, Boccaccini AR (2009) Thermal plasma technology for the treatment of wastes: a critical review. J Hazard Mater 161:614–626

Hackett C, Williams RB, Durbin TD, Welch W, Pence J, Jenkins BM, Aldas R, Salour D (2004) Evaluation of conversion technology processes and products, University of California

Heberlein J (2002) New approaches in thermal plasma technology. Pure Appl Chem 74(3):327–335

Juniper Consulting (2008) Independent waste technology report, the Alter NRG/Westinghouse plasma gasification process
Klein A, Themelis NJ (2003) Energy recovery from municipal solid wastes by gasification. North American waste to energy conference (NAWTEC 11) 11 proceedings, ASME International, Tampa, FL
Kogelschatz U (2004) Atmospheric-pressure plasma technology. Plasma Phys Control Fusion 46:B63–B75
Murphy AB, McAllister T (2001) Modeling of the physics and chemistry of thermal plasma waste destruction. Phys Plasmas 8:2565–2572
Niessen WR, Markes CH, Sommerlad RE (1996) Evaluation of gasification and novel thermal processes for the treatment of municipal solid waste. NREL/TP-430-21612, Aug 1996
Plasco Energy Group. http://www.plascoenergygroup.com/
Solonenko OP. Thermal plasma torches and technologies. Cambridge Science International Publishing, Cambridge
Titus CH, Surma JE (1998). Integrated environmental technologies, LLC, enhanced tunable plasma-melter vitrification systems. Patent number 5,811,752, 22 Sep 1998
Willis KP, Osada S, Willerton KL (2010) Plasma gasification: lessons from ecovalley WTE facility. Proceedings of the 18th annual North American waste to energy conference (NAWTEC 18–3515), Orlando, FL, 11–13 May 2010

Plug-in Hybrid Electric Vehicles

Mehrdad Ehsani
Department of Electrical & Computer Engineering, Texas A&M University, College Station, TX, USA

Article Outline

Glossary
Definition of the Subject
Introduction
Statistics of Daily Driving Distance
Motor and Battery Power
Energy Consumption in Typical Driving Cycles
Operation Strategies
Battery Design
Summary and Future Directions
Bibliography

Glossary

AER All-electric range
CD Charge depletion
CDR Charge-depletion range
CS Charge sustaining
DoD Depth of discharge
EV Electric vehicle
HEV Hybrid electric vehicle
PHEV Plug-in hybrid electric vehicle
SOC State-of-charge

Definition of the Subject

The plug-in hybrid electric vehicle (PHEV) is vehicle that has the capability of accepting part of its propulsion energy from the electric utility grid. However, like the conventional hybrid electric vehicles, it also draws part of its traction energy from its fuel tank. This will afford the plug-in hybrids dual fuel flexibility, electric charge, and fossil fuel. Depending on the design of the vehicle drive train and its operation, the plug-in hybrid vehicle can behave as pure electric, pure engine, or hybrid vehicle.

Introduction

It is now well recognized that the hybrid electric vehicle (HEV) is much more efficient and cleaner than the vehicle powered by gasoline and diesel engine alone [1]. The HEV also has high vehicle performance and more user acceptability than pure battery powered electric vehicle (EV). However, all of the HEV still comes from burning fossil fuel, gasoline, or diesel. On the other hand, the EV has curtain advantages over HEV, mostly zero emission, independence from petroleum, and perhaps low operating cost. However, the major disadvantage of EV is the range limitation and long battery charging time. It should be noted that only fraction of battery energy is used in a conventional HEV, in which the variation of the battery state of charge (SOC) is limited to a narrow band [1]. This fact implies that most of the battery energy just stays there unused.

Using most of the battery energy, drawn from the utility grid, to displace part of petroleum fuel is the major advantage of plug-in hybrid electric vehicles. The plug-in hybrid electric vehicle (PHEV) is a form of hybrid electric vehicle, which is specifically designed and operated to fully use the energy in the battery for period of distance of pure EV operation. It has the advantage of being both pure EV and an HEV. When the battery is in high charge state, after overnight

charging, the vehicle may be operated in pure EV mode: charge-depletion (CD) mode. In this mode, all the traction energy is supplied by the battery. When the state of charge of the battery reaches a certain low level, such as 30%, depending on the characteristics of the battery, the engine is started and the vehicle goes to battery charge-sustaining (CS) mode. In the CS mode, the energy in the battery is maintained around this level till the end of the trip, at which time the battery is charged to its full state through utility grid [2–6].

Thus, the PHEV shares the combined operation characteristics of pure EV and CS HEV. However, the advantages of PHEV over pure EV and HEV are (1) displacement of significant amount petroleum fuel by electric energy that comes from utility grid, (2) longer range than a pure EV, (3) no fuel consumption and emission during pure EV mode, (4) and lower overall fuel consumption and emission.

Statistics of Daily Driving Distance

As mentioned above, using the energy stored in the battery from the utility grid to displace part of petroleum fuel is the major feature of the plug-in hybrid electric vehicles. The fraction of the petroleum fuel displaced by electricity depends mostly upon the amount of electrical energy drawn from the utility grid. That is, the energy capacity of the battery and the total driving distance, which is usually the diurnal driving distance, and electrical traction power usage profiles which is related to the drive cycle features and vehicle control strategies. For optimal PHEV design, especially the battery size, understanding of diurnal driving distance in some detail is very helpful.

Figure 1 shows a histogram of diurnal driving distance distribution and their cumulative frequency in 1995, from National Personal Transportation Survey (NPTS) data [2]. The cumulative frequency or utility factor in Fig.1 represents the percentages of the total driving time (days) during which the daily driving distances are less than or equal to the said distance on the horizontal axis. Figure 1 reveals the fact that about half of daily driving distance is less than 40 miles (64 km). If a vehicle is designed to have 40 miles (64 km) of pure EV range, that vehicle will have half of its total driving distance in pure EV mode. Even if the daily traveling distance is beyond 40 miles, there is still a significant amount of petroleum fuel that can be displaced by electricity, due to the pure EV driving taking a large portion of the daily traveling. Research also shows that even if the pure EV range is less than 40 miles, such as 20 miles (32 km), the portion of petroleum fuel that can be displaced in normal daily driving is still very significant [2].

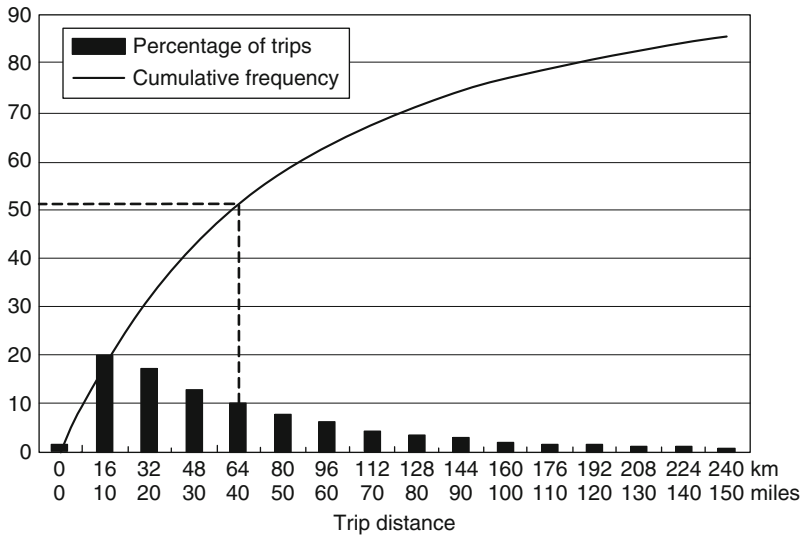

Plug-in Hybrid Electric Vehicles. Figure 1
Diurnal driving distance distribution and cumulative factor

Motor and Battery Power

A PHEV consists of a considerable amount of pure EV operation in which the electric motor and the battery are the sole power plant and the energy source for the vehicle. The motor and battery power must be large enough to stratify the peak power requirement of vehicle. Otherwise, the vehicle cannot accomplish the demanded driving cycle.

The traction power of a vehicle, measured on the drive wheels, can be expressed as:

$$P_t = \frac{V}{1000}\left(Mgf_r + \frac{1}{2}\rho_a C_D A_f V^2 + M\delta\frac{dV}{dt} + Mgi\right)(kW) \quad (1)$$

where M is the vehicle mass in kg, V is vehicle speed in m/s, g is gravity acceleration, 9.81 m/s^2, ρ_a is the air mass density, 1.205 kg/m^3, C_D is the aerodynamic drag coefficient of the vehicle, A_f is the front area of the vehicle in m^2, δ is the rotational inertia factor, dV/dt is the acceleration in m/s^2, and i is the grade of road. In standard driving cycles, road is flat with $i = 0$.

Figure 2 is a diagram showing vehicle speed and traction power measured on the drive wheels versus the travel distance in the FTP 75 urban driving cycle. The vehicle design parameters used in the computation are listed in Table 1.

Figure 2 indicates that the peaking traction power on the drive wheels is around 25 kW. However, there are power losses from the battery to the drive wheels. In order to meet the drive cycle power requirement, the motor output power should be designed to include the power losses from the motor shaft to the drive wheels. Suppose the efficiency from motor shaft to the drive wheels is 90%, then the motor shaft power rating is round 28 kW. It should be noted that this motor power required is related to the vehicle speed at which this peak power occurs. For example, the peaking power in Fig. 2 occurs at the vehicle speed of 50 km/h (31.25 mph). In the motor power design, one must be sure that the motor can produce this peak power at this vehicle speed. Similarly, the peaking power of the battery should include the losses in the electric motor, power electronics, and the mechanical transmission. Suppose the efficiencies of the motor and power electronics are 0.85 and 0.95, respectively. Then, the peak power of the battery must be around 34.7 kW for this example. Table 2 lists the motor power and the battery power in FTP75 urban, highway, LA92 and US06 driving cycles.

Plug-in Hybrid Electric Vehicles. Table 1 Vehicle parameters used in power computation

Vehicle mass (kg)	1,700
Rolling resistance coefficient	0.01
Aerodynamic drag coefficient	0.3
Front area(m^2)	2.2
Rotational inertia factor	1.05

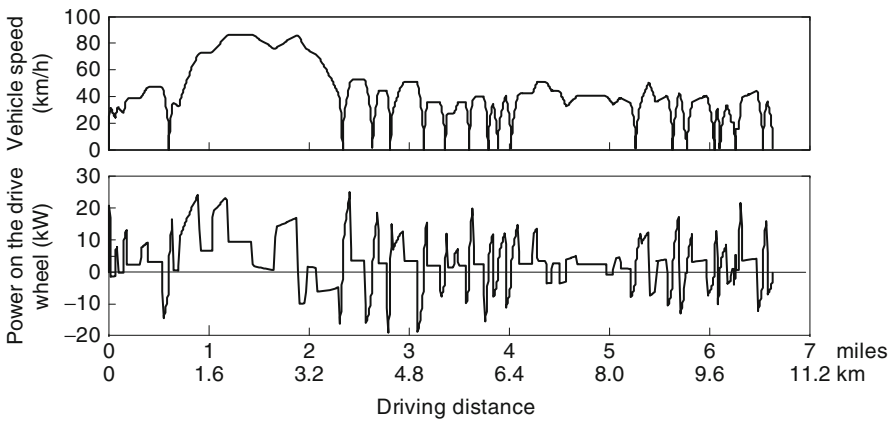

Plug-in Hybrid Electric Vehicles. Figure 2
Vehicle speed and traction power in FPT 75 urban driving cycle

Plug-in Hybrid Electric Vehicles. Table 2 Powers of motor and energy storage in typical driving cycles

	FTP 75 urban	FTP 75 highway	LA92	US06
Motorpower@vehicle speed	28 @50 km/h (31 mph)	32 @72 km/h (57 km/h)	55@57 km/h (36 mph)	98 @117 km/h (73 mph)
Energy storage power	35.7	39	68.5	121

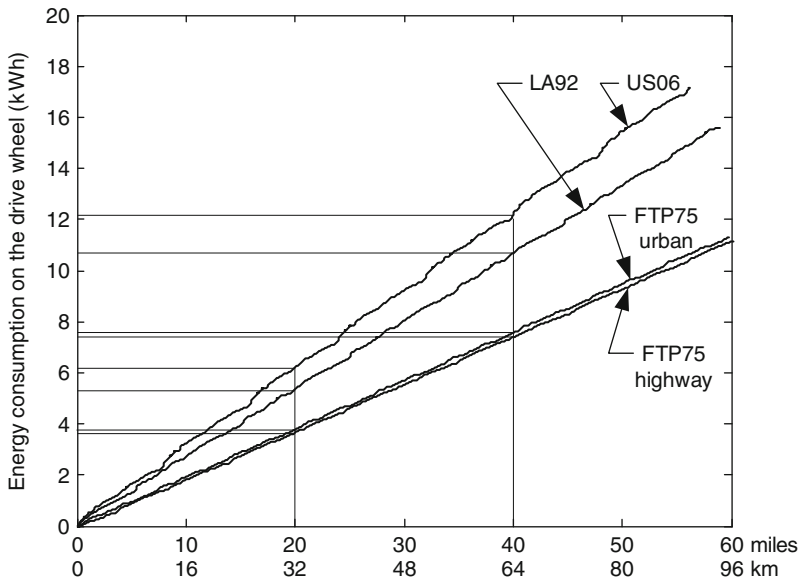

Plug-in Hybrid Electric Vehicles. Figure 3
Energy consumption on the drive wheels versus driving distance in typical driving cycles

Energy Consumption in Typical Driving Cycles

The all-electric range (AER) of a PHEV is determined by the energy capacity of the battery and the energy consumption in drive cycle. The amount of energy consumed in a typical drive cycle can be obtained by integrating (1) over the driving time period, as shown in Fig. 3, in which no regenerative braking is included. Considering the energy losses in the power electronics, motor, and transmission, the usable energy in the battery for 20 and 40 miles (32 and 64 km) of AER in typical drive cycles is listed in Table 3.

In vehicle design, a proper reference drive cycle should be selected. An aggressive drive cycle, such as US06, needs a large motor drive and battery which also leads to good vehicle acceleration and gradeability performance. On the other hand, a mild drive cycle, such as FTP75, needs a small motor drive and battery, but also leads to a sluggish vehicle performance.

Plug-in Hybrid Electric Vehicles. Table 3 Energy consumption in typical driving cycles

	FTP 75 Urban	FTP 75 highway	LA92	US 06
20 miles (32 km)	5.2	5.14	7.29	8.4
40 miles (64 km)	10.4	10.28	14.58	16.8

Operation Strategies

A PHEV may operate in an all-electric range (AER) mode or a blended EV/HEV operation strategy.

AER Mode Operation Strategy

The principle of this operation strategy is to use the energy of the battery exclusively. One possibility is to allow the driver to manually select between the CS HEV

mode and the pure EV mode. The availability of AER with sufficient range allows the vehicle to be driven in areas where emissions are restricted. This strategy provides flexibility for the driver to choose the time when the pure EV mode is used. For example, in a trip that includes a distance where pure EV operation is required, the driver can select the pure EV mode just prior to entering this area in order to have sufficient range. In other places, the vehicle may be operated in pure EV mode or CS HEV mode, depending on the charge status in the battery and the power demand. In normal conditions where the trip does not have an imperative pure EV operation, the driver may select pure EV mode at start of the drip in order to fully use the energy of the battery to save petroleum fuel, until the charge in the battery reaches its design specified level at which the CS HEV mode will start automatically.

The energy drawn from the battery in the pure EV mode can be expressed as

$$E_d = \int_0^T P_d dt, \tag{2}$$

where P_d is the discharging power of the battery, T is the total driving time, P_d is the traction power. During braking, regenerative braking may be used and part of the braking energy is recovered and restored to the battery. The stored energy can be expressed as:

$$E_c = \int_0^T P_c dt, \tag{3}$$

where P_c is the charging power of energy storage during braking. It should be noted that regenerative braking power is smaller than the total braking power of the vehicle and only part of braking energy can be recovered [7–9]. The SOC of the battery can be expressed as

$$\mathrm{SOC} = \mathrm{SOC}_0 - \frac{\mathrm{E_d} - \mathrm{E_c}}{\mathrm{E_t}}, \tag{4}$$

where SOC_0 is the initial value of the SOC that may be equal to 1, and E_t is the total energy of the energy storage with SOC = 1. When the SOC of the battery drops to a specified valued (0.3 for example, depending on the operation characteristics of the battery), the CS mode starts.

In the CS mode, the SOC of the battery should be maintained around the specified value. Here, an engine control constrained to on/off control strategy is used, as described below.

1. When the acceleration pedal traction power command is greater than the engine maximum power (full open throttle), the engine is operated with full open throttle and the electric motor supplies the rest of the power to the drive train. That is,

$$P_{eng} = P_{eng-max}, \tag{5}$$

and

$$P_{mot} = P_{tra} - P_{eng}, \tag{6}$$

where P_{eng} is the engine power, $P_{eng\text{-}max}$ is the engine maximum power with full open throttle, P_{mot} is the motor traction power, and P_{tra} is the commanded traction power of the driver through the acceleration pedal.

2. When the commanded traction power is smaller than the engine maximum power with full open throttle, the engine and motor operation depends on the SOC of the battery, as described below and depicted in Fig. 4.
   (a) When the commanded traction power, represented by point A in Fig.4a, falls in the engine power range of high to medium threshold (labeled by P_{EH} and P_{EM} in Fig. 4a), and the battery SOC is lower than SOC_L, the engine is operated at point a (maximum engine power) so that it has excess power to charge the energy storage. Otherwise if SOC is greater than SOC_L, the engine is operated to produce power that is equal to the commanded power (point A).
   (b) When the commanded traction power, represented by point B in Fig.4a, falls in the engine power range of medium to low (between P_{EM} and P_{EL}) as shown in Fig. 4a, and if battery SOC is lower than SOC_L, the engine is operated at point a with full open throttle so as to quickly raise the battery SOC with a large charging power ($P_{Ea}-P_B$, where P_{Ea} is the engine power at point a and P_B is traction power at point B). Otherwise if the battery SOC is higher than SOC_L but lower than SOC_M, the engine is operated at point b and the relatively small engine power is used to charge the battery ($P_{Eb}-P_B$). However, if the battery SOC is higher than SOC_M, engine alone

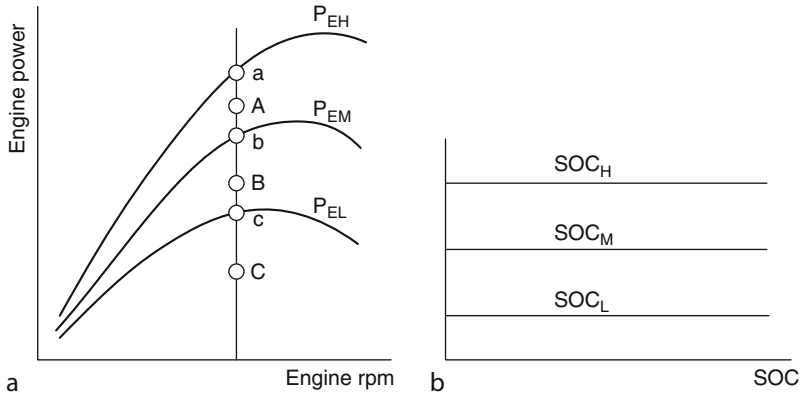

Plug-in Hybrid Electric Vehicles. Figure 4
Constraint engine on/off control strategy, (**a**) engine operating regions, (**b**) energy storage

traction is used, e.g., the engine is controlled to produce power just equal to the commanded traction power and the battery is neither charged nor discharged.

(c) When the commanded traction power, represented by point *C* in Fig.4a, falls in the low power range (below P_{EL} as shown in Fig. 4a) and if the battery SOC is below SOC_L, the engine is operated at point *b* to produce large battery charging power ($P_{Eb}-P_C$). Whereas if the battery SOC is in a range larger than SOC_L, but lower than SOC_M, the engine is operated at point *c*, and the charging power of energy storage is $P_{Ec}-P_C$. However, if the battery SOC is higher than SOC_M, the engine is shut down to avoid low engine operating efficiency, and the vehicle is operated with pure EV mode.

3. When braking is applied, the electric motor is always operated in regenerative braking [7–9].

The thresholds of the engine power (P_{EH}, P_{EM}, and P_{EL} as shown in Fig.4a) are related to the engine fuel consumption characteristics, and should be set such that the battery SOC is maintained in a region lower than SOC_H and higher than SOC_L. The thresholds of battery SOC (SOC_H, SOC_M, and SOC_L) should be set such that it has sufficient power to support motor operation.

The control strategy discussed above is only one of many possible options. Other control strategies may be used.

A PHEV which has the parameters listed in Table 1 has been simulated by using simulation software developed by The Advanced Vehicle Systems Research Program at Texas A&M University. In this simulation, a 400 W electric load for the vehicle accessories is added. The total energy in the fully charged battery is 10 kWh. The simulation sequentially ran nine cycles of FTP75 urban drive cycle, and the pure EV mode was started at the beginning of the simulation until the SOC reached about 30%, beyond which, charge-sustained mode was started.

The simulation results in FTP75 urban drive cycle are shown in Figs. 5, 6, 7. The all-electric range is around 42 km in which about 7 kWh of electric energy is consumed. The engine operating points are placed within the favorite region of the engine fuel consumption map as shown in Fig. 6. The fuel and electric energy consumption are shown in Fig. 7. It can be seen that when the traveling distance is less than four cycles (42 km or 26 miles), the vehicle operates in pure EV mode and completely displaces the petroleum fuel with electricity. The total electric energy consumed is about 7.1 and 15.5 kWh per 100 km, or 4.05 miles/kWh. With the increase in the total traveling distance, the percentage of the fuel displacement decreases since the charge-sustained operation takes a larger percentages of the travel distance. For nine sequential drive cycle (96 km or 60 miles), the fuel and electrical energy consumptions are about 3.2 L/100 km or 74 mpg, and 7.42 kWh/100 km or 8.43 miles/kWh.

Blended Control Strategy

Unlike the AER control strategy, the blended control strategy uses both engine and motor for traction with

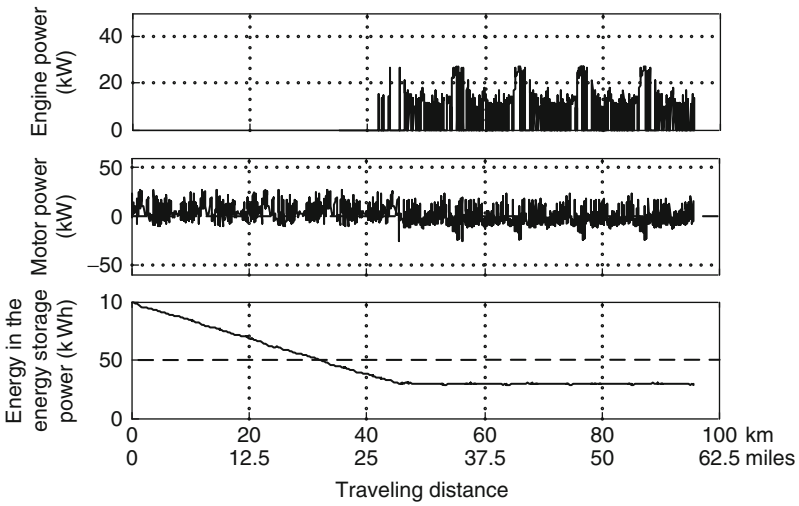

Plug-in Hybrid Electric Vehicles. Figure 5
Profile of engine power, motor power, and energy in the energy storage along with traveling time in FTP75 urban driving cycle

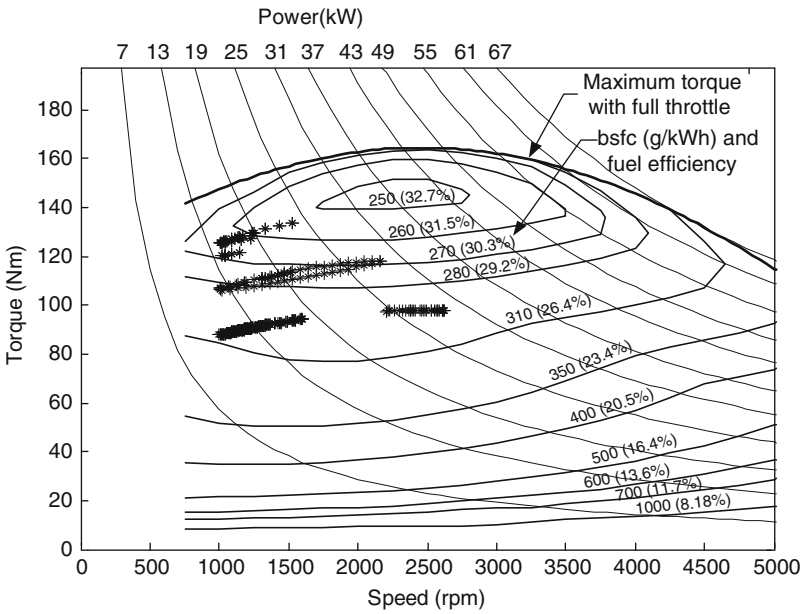

Plug-in Hybrid Electric Vehicles. Figure 6
Engine operating points on the fuel consumption map in FTP75 urban drive cycle

charge-depleting (CD) mode until the battery SOC reaches a specified low level, beyond which the vehicle operates in the charge-sustained (CS) mode.

In the CD mode, both the engine and the motor may operate at the same time. The range before entering CS mode is longer than that with AER control strategy. New control strategies are needed to control the engine and motor to meet the load demand. There are many possible control strategies. The following is one in which the engine and motor alternatively propel

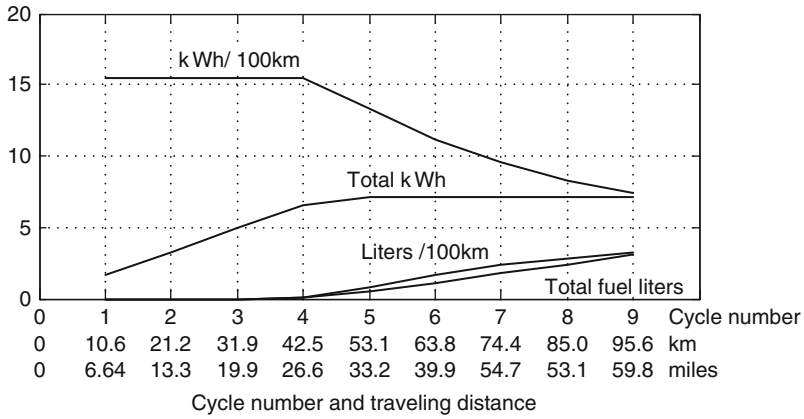

Plug-in Hybrid Electric Vehicles. Figure 7
Fuel and electric energy consumption in FTP75 urban drive cycle

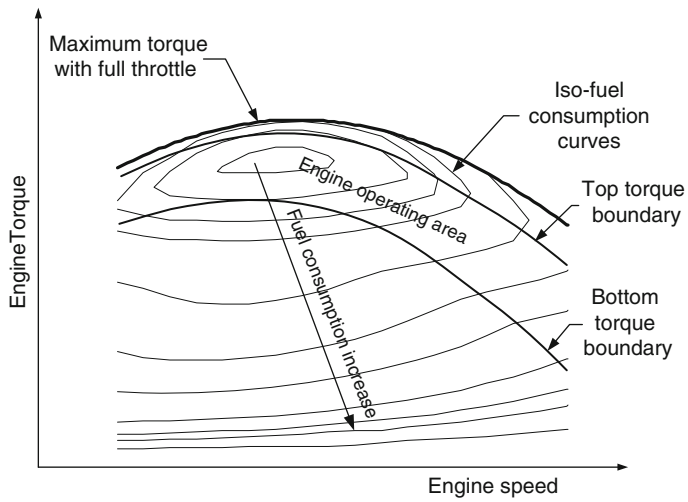

Plug-in Hybrid Electric Vehicles. Figure 8
The operation area of the engine in the CD mode

the vehicle with no battery charging from the engine. The engine is constrained to operate in its optimal fuel economy region. The details are described as follows.

Figure 8 schematically shows the engine operating area. When the requested engine torque is larger than the top torque boundary, the engine is controlled to operate on this boundary and the remaining torque is supplied by the electric motor. When the requested engine torque falls in the area between the top and bottom boundaries, the engine alone propels the vehicle. When the requested engine torque is below the bottom torque boundary, the engine is shut down and the electric motor alone propels the vehicle. In this way, the engine operation is constrained to within its optimal fuel economy region. Since there is no battery charging from the engine, the energy level in the battery continuously drops toward its specified low level. Then the vehicle goes into CS mode, in which the constrained engine on/off control strategy, or some other control strategy, is used as discussed above.

The example vehicle mentioned above has been simulated with the control strategy discussed above in

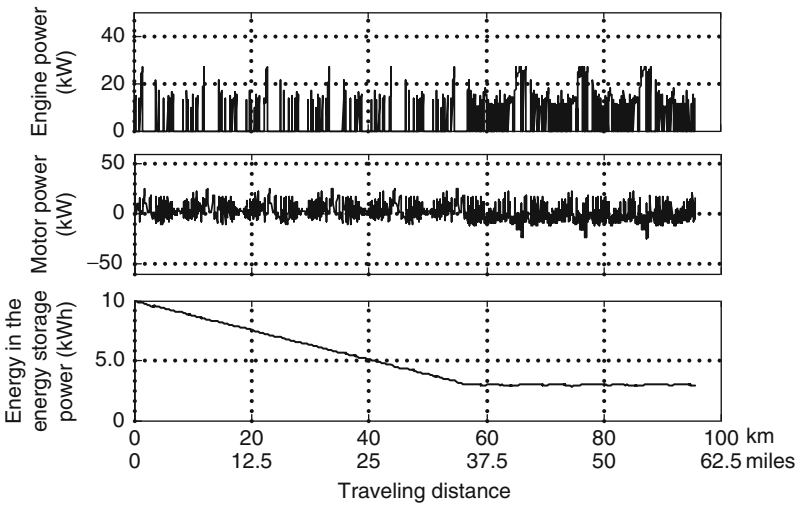

Plug-in Hybrid Electric Vehicles. Figure 9
Profile of engine power, motor power, and energy in the energy storage along with traveling time in FTP75 urban drive cycle

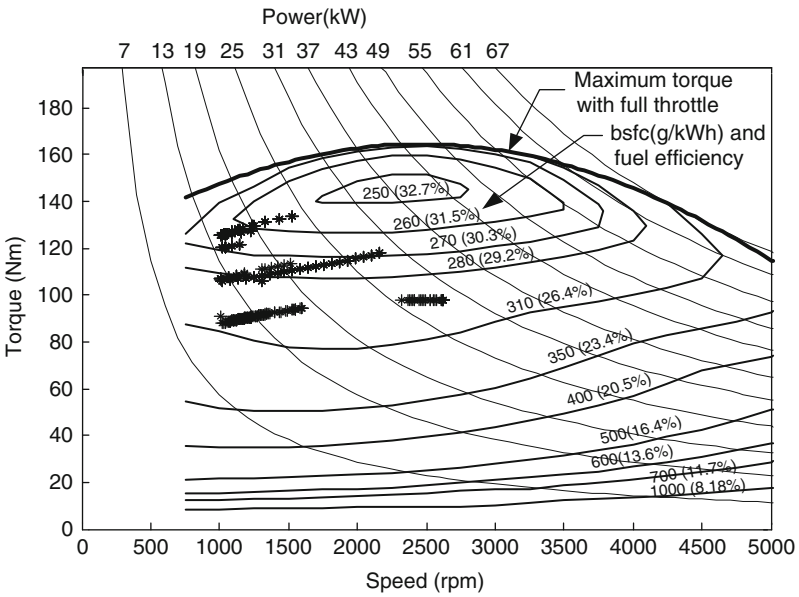

Plug-in Hybrid Electric Vehicles. Figure 10
Engine operating points on the fuel consumption map in FTP75 urban drive cycle

nine sequences of FTP 75 urban driving cycle. The results are presented in Figs. 9, 10, 11. Figure 9 shows that the battery energy continuously drops to the specified value during CD mode, at which point the engine joins the effort traction occasionally, operating in its optimal region as shown in Fig. 8 but does not charge the battery. Figure 9 shows that the CD range is longer than the all-electric range as shown in Fig. 5.

As indicated in Fig. 10, the engine operating points overlap the favored region of the engine fuel consumption map. Figure 11 indicates that the fuel consumption in the CD range (0–53 km) is around

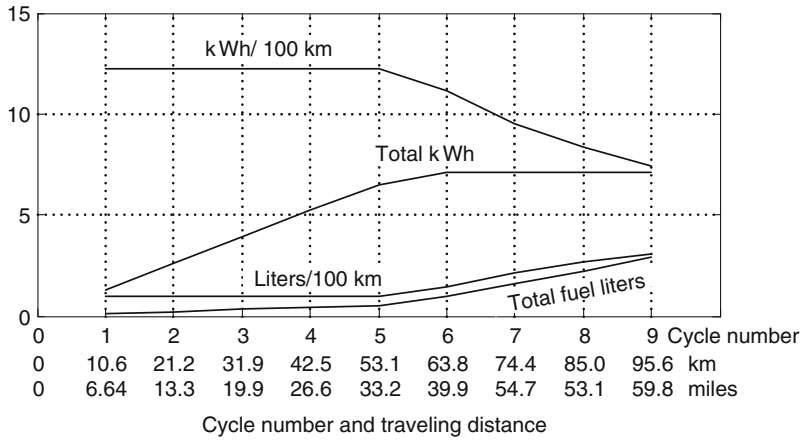

Plug-in Hybrid Electric Vehicles. Figure 11
Fuel and electric energy consumption in FTP75 urban drive cycle

1 L/100 km (235 mpg) and electric energy consumption is around 12.5 kWh/100 km (5 mile/kWh). However, with the increase in the travel distance, the fuel liters per 100 km increases and kWh per 100 km deceases since the ratio of the charge-sustained operation distance to the total trip distance increases.

Battery Design

The amount of energy in the battery determines the all-electric range (AER) or the charge-depletion range (CDR). It is also closely related to fuel consumption, fuel displacement, initial cost, and operating costs. Through simulation, similar to those performed above, the usable energy in the battery can be determined. The total energy capacity can be obtained from

$$E_c = \frac{E_{usable}}{\mathrm{SOC_{top}} - \mathrm{SOC_{bottom}}}, \tag{7}$$

where the E_{usable} is the usable energy in the battery consumed in the AER or CDR modes, SOC_{top} is the top SOC with fully charged battery, which usually equals 1, and SOC_{bottom} is the SOC of the battery at which the operation mode is switched from AER or CDR modes to CS mode. In the example above, the usable energy is about 7 Wh (refer to Figs. 5 and 9). Suppose that the SOC operating window is 0.7 (from 1 to 0.3). Then, the total energy capacity of the battery is about 10 kWh.

It should be noted that the depth of discharge (DoD) of batteries is closely related to battery life. Figure 12 illustrates the cycle life for NiMH and Li-ion batteries [5]. If one deep discharge per day is supposed, a total 4,000+ deep charges would be required for a 10–15 year lifetime. With the characteristics shown in Fig. 12, 70% depth of discharge for NiMH and 50% for Li-ion batteries may be the proper designs.

In the battery design, it should be ensured that the energy storage can supply sufficient power to support the vehicle when its SOC is at a low level (0.3 for NiMH battery and 0.5 for Li-ion battery, for example, as indicated in Fig. 12).

Energy/power ratio of a battery is a good measure of its suitability. The size of the battery will be minimized when its energy/power ratio equals that required. The energy/power ratio is defined as:

$$R_{e/p} = \frac{Total\ Energy}{Power@operating\ \mathrm{SOC}}, \tag{8}$$

In the example vehicle simulated above, the total energy required is around 10 kWh for NiMH battery (0.7DoD) and 14 kWh for Li-ion battery (0.5 DoD). The power required is about 60 kW (refer to Table 2 for LA92 drive cycle) which is defined at 30% of SOC for NiMH battery and 50% of SOC for Li-ion battery. The required energy/power ratio is 0.167 h for NiMH battery at 30% of SOC and 0.233 h for Li-ion battery at 50% of SOC.

Figure 13 shows the energy/power ratio versus the specific power of NiMH and Li-ion batteries [5].

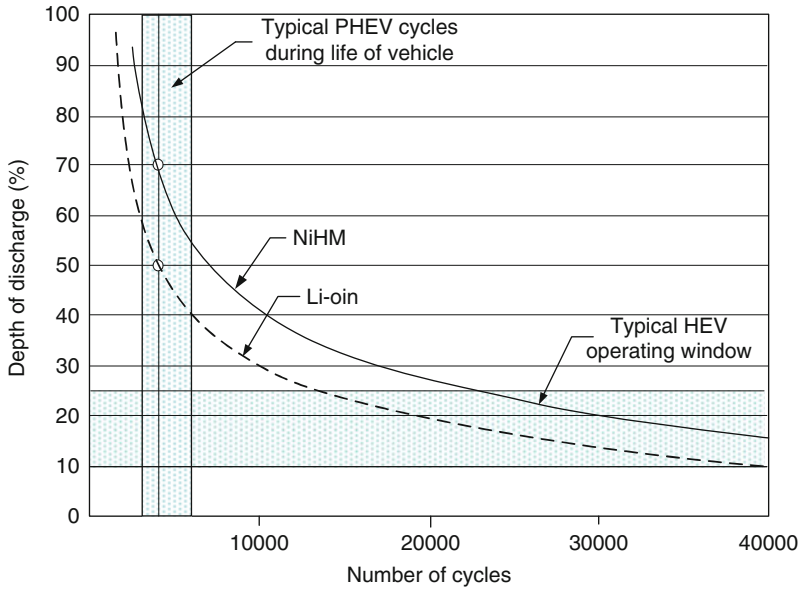

Plug-in Hybrid Electric Vehicles. Figure 12
Cycle life characteristics of Varta battery technologies [5]

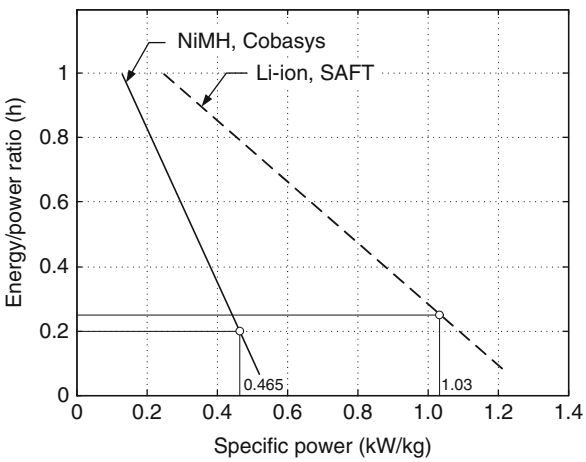

Plug-in Hybrid Electric Vehicles. Figure 13
Typical energy/power ratio versus specific power

A 0.2 h of energy/power ratio (slightly larger than 0.166 h for safety) for Cobasys NiMH battery yields a total weight of 129 kg (60/0.465), which carries 12 kWh of total energy (0.2 × 60). However, 0.25 h (slightly larger when 0.233 for safety) of SAFT Li-ion battery yields a total weight of 58 kg (60/1.03) which carries 15 kWh of energy. Obviously, the SAFT Li-ion battery is superior to the Cobasys NiMH battery. However, other factors have to be considered such as, cost, safety, etc.

Summary and Future Directions

Plug-in hybrid electric vehicle (PHEV) can displace a significant amount of petroleum fuel with electric energy. This technology can significantly change the makeup of transportation fuel supply. Design methodologies presented in this entry can be used to design a drive train that has a specified all-electric range or charge-depletion range. The control strategies developed here can be used in vehicle control to realize all-electric operation, charge depletion, and charge-sustained operations. These control strategies can also operate the engine always within its low fuel consumption region, thus, yielding high overall efficiency. These design methodology and control strategies have been validated by simulation of passenger car driving in FTP 75, a typical urban drive cycle.

Plug-in hybrid vehicles are now being introduced by manufacturers, such as the Chevrolet Volt by GM. It is anticipated that PHEVs will occupy a larger segment of the automotive market in the coming years. These will take various forms and design philosophies to fit the market demands, price points, and fuel and environmental requirements.

Bibliography

1. Ehsani M, Gao Y, Gays SE, Emadi A (2005) Modern electric, hybrid electric and fuel cell vehicle – Fundamentals, theory and design. CRC Press
2. Simpson A (2006) Cost-benefit analysis of plug-in hybrid electric vehicle technology. Presented at the 22nd international battery, hybrid and fuel cell electric vehicle symposium and exhibition (EVS-22), Yokohama, 23–28 Oct 2006
3. Gonder J, Markel T (2007) Energy management strategies for plug-in hybrid electric vehicles. SAE paper # 2007-01-0290, Detroit
4. Markel T, Simpson A (2005) Energy storage systems considerations for grid-charged hybrid electric vehicles. Presented in vehicle power and propulsion, 2005 IEEE conference, Chicago, 7–9 Sep 2005
5. Markel T, Simpson A (2006) Plug-in hybrid electric vehicle energy storage system design. Presented at advanced automotive battery conference, Baltimore, 17–19 May 2006
6. Markel T, Wipke K (2001) Modeling grid-connected hybrid electric vehicles using ADVISOR. Presented in the, The 16th annual battery conference on application and advances, Long Beach, California
7. Gao Y, Ehsani M (2001) Electronic braking system of EV and HEV – Integration of regenerative braking, automatic braking force control and ABS. SAE J Passenger Cars Electron Electr Syst 110. Paper No. 2001-01-2478
8. Gao Y, Chen L, Ehsani M (1999) Investigation of the effectiveness of regenerative braking for EV and HEV. SAE J Passenger Cars 108. Paper No. 1999-01-2901
9. Gao Y, Chu L, Ehsani M (2007) Design and control principle of hybrid braking system for EV, HEV and FCV. In: IEEE on vehicle power and propulsion conference, Arlington, 9–12 Sep 2007

Polio and Its Epidemiology

Lester M. Shulman
Central Virology Laboratory, Laboratory of Environmental Virology at Sheba Medical Center, Public Health Services, Israel Ministry of Health, Department of Epidemiology and Preventive Medicine, School of Public Health, Sackler Faculty of Medicine, Tel Aviv University, Tel Aviv, Israel

Article Outline

Glossary
A Brief Definition of Polio and Its Importance
Introduction
The Epidemiology of Polio
Future Directions: The Endgame Stage of Eradication and Sustainability of Postpolio Eradication
Bibliography

Glossary

ACPE The Advisory Committee on Polio Eradication

AFP Acute flaccid paralysis.

AFP surveillance Characterization of enteroviruses in stool samples from all AFP cases especially in individuals under 15 years of age to rule-in or rule-out etiology by polioviruses.

aVDPV A vaccine-derived poliovirus isolate whose evolutionary path is unknown or ambiguous.

bOPV Bivalent oral polio vaccine (usually containing serotypes 1 and 3).

BSL Biosafety standard level.

Capsid The protein shell that surrounds a virus particle.

Capsomere One of the individual morphological units that make up the viral capsid.

CDC US Centers for Disease Control and Prevention

CD155 or PVr The human encoded cell receptor for poliovirus, a member of the immunoglobulin superfamily.

Codon A sequence of three adjacent nucleotides on a strand of DNA or RNA that specifies which specific amino acid will be incorporated into a protein.

Codon bias Unequal usage of synonymous codons (different codons that specify the same amino acid)

CPE Cytopathic effect.

cVDPV A circulating vaccine-derived poliovirus, that is, a poliovirus that has evolved from vaccine during person-to-person transmission.

eIPV Enhanced inactivated polio vaccine.

Emergence The appearance of a pathogen in a previously pathogen-free area.

Endemic The constant presence of a disease to a greater or lesser extent in a particular locality.

Enteroviruses Any of >80 different species of polioviruses, coxsackie viruses, echoviruses, and enteroviruses belonging to the genus *Enterovirus* in the family *Picornaviridae*.

Environmental surveillance (as related to polioviruses) Investigation of sewage and recreational water for the presence of poliovirus as an

indication of the presence of poliovirus-infected individuals in a community.

EPI Expanded Program on Immunization.

Epidemic A rapid spread of disease into a disease-free area or spread of a disease to more than the usual number of persons affected in a region with disease.

Epitopes The component of an antigen that is recognized by and binds to an antibody.

Eradication The complete elimination of all incidence of disease and/or the presence of the agent that causes the disease.

Evolution Change in the genetic composition of a population or the genome of a given organism during successive generations.

GAP Global action plan for laboratory containment.

GAP I GAP phase I – plan for identifying all known and potential sources of poliovirus especially wild polioviruses within each country.

GAP II GAP phase II – plan for laboratory containment of wild polioviruses.

GAP III GAP phase III – plan to minimize post-eradication poliovirus facility-associated risks.

GAVI Global alliance for vaccines and immunization

Genetic recombination (of polioviruses) A situation where one portion of the genome of a poliovirus is replaced through a covalent linkage with the equivalent segment from another poliovirus or non-polio enterovirus.

Genotype He genetic makeup of an organism as distinguished from its physical characteristics.

GMT Geometric mean titer, usually calculated according to Karber.

GOARN Global Outbreak Alert and Response Network.

GPEI or GEI The Global Poliomyelitis Eradication Initiative of the WHO, adopted in 1988.

GPLN Global Polio Laboratory Network.

Hydrophobic pocket A hydrophobic space located under the binding site for the host encoded viral receptor that is located on the bottom of the canyon surrounding the fivefold axis of symmetry of the enteroviral capsid.

Hydrophobic pocket factors Small hydrophobic molecules that occupy the hydrophobic pocket and that may regulate the host receptor viral capsid interaction.

Immunodeficient Lacking one of the components of the immune system.

Immunogenicity The relative ability of a molecule to elicit an immune response.

i.d. Intradermal or under the skin.

i.m. Intramuscular.

i.n. Intranasal.

i.p. Intraperitoneal.

i.t. Intrathecal.

Infection Establishment and growth of an infectious agent in the body.

IPV Inactivated poliovirus vaccine.

IRES Internal ribosome entry site.

ITD Intratypic differentiation (determination if a virus isolate is vaccine, vaccine-derived, or wild).

iVDPV A vaccine-derived poliovirus that has diverged from its respective oral poliovirus serotype during persistent infection of an immunodeficient host.

Lineages A group of organisms that are closely related genetically.

MAPREC Mutant analysis by PCR and restriction fragment enzyme cleavage to measure reversion of attenuation sites in vaccine strains.

MNVT Monkey neurovirulence test, an in vivo neurovirulence test in monkeys.

mOPV Monovalent OPV.

Neurovirulence The ability of the poliovirus to infect and damage nerve cells causing disease of the nervous system.

Neurovirulence attenuation sites Specific nucleotide positions along the poliovirus genome where the specific nucleotide present at that site will influence whether or not an individual polioviral isolate will be neurovirulent.

Neutralizing antigenic sites Epitopes of the poliovirus that induce neutralizing antibodies.

NID National immunization day.

NSL Non-Sabin-like (wild) virus of vaccine-derived poliovirus (based on results of certain ITD tests).

Major disease Poliomyelitis, AFP, or cases of infection with polio that involves invasion and permanent damage to the nervous system.

Microarray A technology used to study many genes at once using thousands of different short molecular sequences at known position on solid support to hybridize to complementary nucleic acid sequences from different sources.

Minor disease Nonspecific illness caused by poliovirus that may include upper respiratory tract

symptoms (sore throat and fever), gastroenteritis (nausea vomiting, abdominal pain, constipation or diarrhea), and influenza-like illness.

NCCs National Certification Committees.

NGOs Nongovernmental organizations.

NIDs National immunization days.

NPEV Non-polio enteroviruses.

Nonstructural genes Viral genes encoding proteins that are not incorporated into the structure of the capsid.

Oligonucleotide A short sequence of nucleotides frequently synthetic.

OPV Live attenuated oral poliovirus vaccine.

Outbreaks (Under eradication conditions) even the presence of a single case of paralytic poliomyelitis.

Persistent poliovirus infection An infection associated with an immunodeficient host where virus is not cleared but continues to replicate for an indefinite period of time.

Phylogenetic tree A diagram with branches showing the inferred evolutionary relationships among various biological entities.

Picornaviridae A viral family made up of the small (18–30 nm) ether-sensitive single stranded, positive-sense RNA viruses that lack an envelope.

Poliomyelitis The infectious disease caused by poliovirus involving inflammation of motor neurons of the spinal cord and brainstem that leads to acute paralysis followed by atrophy of the muscles enervated by the infected motor neurons.

Poliovirus One of three serotypes of picornaviruses that can cause acute flaccid paralysis and whose cell receptor is CD155.

Polypeptide A small molecule constructed from linked amino acids.

Postpolio syndrome Slow progressive muscle pain and weakness that reappears 30 or 40 years after paralysis caused by a poliovirus infection affecting muscles previously affected by polio as well as muscles that may not have been affected.

Posttranslational processing Any modification of a protein after it has been translated.

Provoked poliomyelitis Poliomyelitis resulting from physical trauma during infection with poliovirus.

Proofreading An enzymatic process that checks whether a newly incorporated nucleotide in a nascent chain is the correct compliment of its corresponding nucleotide in the template.

PVR The poliovirus receptor, CD155.

PVR Tg21 transgenic mouse A mouse that has been genetically modified to express the human poliovirus receptor.

Quasispecies A term used to describe a cluster, cloud, or swarm of viruses with minor differences in nucleotide sequence that arise during replication as a consequence of polymerase incorporation errors.

Rearrangement (in relation to polioviruses) A structural alteration in the genomic sequence occurring during coinfection with two or more viruses resulting in a new genome in which parts are from different parental polio or non-polio enteroviruses

Reemergence Emergence after an absence.

RCC Regional Certification Committees.

RCT Reproductive capacity temperature, the temperature at which viruses can replicate.

RNA-dependent RNA polymerase A viral encoded polymerase that synthesizes a complimentary RNA strand from an RNA template.

RRL Regional Reference Laboratory of the Global Polio Laboratory Network.

SAGE Strategic Advisory Group of Experts on Immunization.

Serotype A group of closely related virus expressing a common set of antigens.

Seroconversion Appearance of antibodies following exposure to antigen in seronegative person, or $\geq$4-fold increase in titer of previously immune person.

Seroconversion index The mean seroconversion rate against all three poliovirus serotypes.

SL Sabin-like poliovirus (based on result from some ITD tests).

SIA Supplemental immunization activities (such as NIDs, SNIDS, and mop-ups).

Silent circulation Person-to-person transmission of virus in a community in the absence of cases of AFP.

Silent infection Asymptomatic infection.

Silent presence The presence of a virus in the absence of clinical cases and the absence of person-to-person transmission.

SNIDS Sub-national Immunization Days.

Stakeholders All governmental and nongovernmental agencies involved in the GPEI.

Structural genes (in relation to polio) Genes encoding viral capsid proteins.

Synonymous nucleotide substitutions Changes in the nucleotide sequence that do not result in a change in encoded amino acid.

TAG Technical Advisory Group.

TD Typic differentiation (determination of the serotype of a poliovirus isolate).

TOPV Trivalent oral polio vaccine containing all three serotypes of attenuated poliovirus.

Transition The substitution of a purine nucleotide with the other purine, or a pyrimidine nucleotide with the other pyrimidine.

Transversions The substitution of a pyrimidine nucleotide by a purine nucleotide or vice versa.

UNICEF United Nations Children's Fund.

Vaccine strains Poliovirus strains approved by the WHO for production of live and inactivated polio vaccines.

VAPP Vaccine-associated paralytic poliomyelitis.

VDPV A vaccine-derived poliovirus that has diverged through evolution from its respective live poliovirus vaccine strain serotype by more than 1% (serotypes 1 and 3) or more than 0.6% (serotype 2) of its respective VP1 capsid protein.

Viremia The presence of virus in the bloodstream during an infection.

VPg Viral protein genome linked – 22 amino acid protein covalently linked to genome and complimentary negative strand.

VP1 Viral capsid protein 1.

VP2 Viral capsid protein 2.

VP3 Viral capsid protein 3.

VP4 Viral capsid protein 4.

WHA World Health Assembly.

WHO World Health Organization.

WPV or wild poliovirus Any poliovirus that is not derived from attenuated oral polio vaccine strains

3'UTR The untranslated region of the polioviral genome that is located 3′ of the open reading frame that encodes the viral polyprotein.

$3D^{pol}$ Viral encoded RNA-dependent RNA polymerase.

5'UTR A highly structured, untranslated area of the polioviral genome located 5′ to the open reading frame that encodes the viral polyprotein. The 5'UTR is covalently linked on its 5′ base to viral protein VPg.

A Brief Definition of Polio and Its Importance

The word "polio" has been used to describe both a disease and the disease agent. Among current methods to measure the importance of or interest in a topic is to run a general web search for the term and to search the scientific literature in PubMed. A Google web search of the word "polio" in Aug 2010 yielded 31,100,000 hits, while a search in PubMed yielded 22,000 articles and 826 review articles. This review will concentrate on those aspects of the epidemiology of polio as it relates to disease eradication and the sustainability of this effort. The terms "polio" and "poliomyelitis" will be used when describing the disease and "poliovirus" and related terms such as "polio vaccine" will be used to describe the agent that causes the disease.

In order to understand the epidemiology of polio, it is important to understand the adversary. Toward this goal, this chapter starts with a detailed physical characterization of polioviruses and the pathological effects caused by poliovirus infections that are most relevant to understanding the epidemiology of polio. This is followed by a description of the global efforts to eradicate poliomyelitis and the viral agent causing the disease, and concludes with a discussion of the future directions needed to achieve and sustain eradication and prevent reemergence. Smallpox was the first human disease to be eradicated and we are currently in the endgame of eradication of polio as the second. Polio eradication is currently the largest public health program in the world and has involved both health professionals and more than ten million volunteers in all countries since the inception of the Global Poliomyelitis Eradication Initiative by the World Health Assembly in 1988 [1].

Introduction

The road toward polio eradication has been long [2] and by no means smooth. Important milestones along the march toward recognition and understanding the disease, identification of its causative agent, and toward prevention and eradication will be briefly discussed in the introduction (see also Fig. 1). A poliovirus isolate is classified as vaccine, vaccine-derived (VDPV), or wild-type poliovirus based on the percent nucleotide sequence homology between its capsid protein VP1

Major milestones along the road towards polio eradication.

1400 BCE	First pictorial record of a person with poliomyelitis.
1789	First modern characterization of polio as a "debility of the lower extremities" by Underwood.
1813	More complete detailed description of polio by Monteggia.
1855	Description of "infantile paralysis by Heine based on systematic investigation of cases started in the 1840's.
1863	Confirmation by biopsy for motor neuron involvement in polio by Cornil.
1870	Detailed description of physiological changes in the anterior horn of the spinal cord by Charcot and Joffroy.
1889	Medin realizes that paralytic cases occur in only a small number of infected individuals during epidemics.
Late 19th Century	The emergence of outbreaks of poliomyelitis.
1905	Recognition of the infectious nature of polio by Wickman confirming Medin's earlier observations.
1908-9	The discovery of poliovirus as the causative agent of poliomyelitis by Landsteiner and Popper.
1920'2	Establishment of the first national rehabilitation center.
1929	Drinker develops the iron lung.
1931	Burnet and MacNamara report more than one non-cross reacting antigenic strain of polio; culminates in the conclusion in 1951 that there were only three serotypes.
1935-36	First clinical trials with inactivated polio vaccine by Brodie and Park and with live attenuated vaccine by Kolmer.
1937	Establishment of the first NGOs to fund support of polio victims and research: The National Foundation of Infantile Paralysis and The March of Dimes.
1939	Armstrong was the first to grow poliovirus in a non-primate (rodent) host.
1940's	Kinny introduces the concept of supportive rehabilitation.
1949	First in vitro passages in tissue cultures by Enders, Weller, and Robbins
1950's	Development and testing of attenuated vaccines by Kaprowski (1950), Sabin (1956-57) and Cox (1958).
1950's	Bottiger and Kaprowski observed that live vaccine spreads to contacts.
1951	Conclusion that there were only three serotypes of poliovirus.
1951-61	Immunizaton of > 11 million children with Sabin and with Kaprowski live oral vaccine strains.
1953-54	Salk develops and tests inactivated poliovirus vaccine licensed for use by 1955.
1954	First use of live vaccine by Kaprowski to control a large outbreak.
1954	Development of standard plaque assays for quantification of virus by Dulbecco and Voigt.
1955	The Cutter Incident in which 400,000 children were immunized with inadequately inactivated wild poliovirus.
1962	Detection of the first persistent infections with vaccine-derived polioviruses.
1968	Introduction of microcarrier cell systems for uniform large-scale vaccine production by van Wezel followed by the use of pathogen cell-free cell systems in the early 1990's.
1979	The development of primate model to test neurovirulence of poliovirus strains.
1979	Last case of wild polio in the Unites States.
1985	Pan Americans Health Organization and CDC establish the Latin American Regional Polio Network.
1986	Development of murine L20B cells transformed with, and expressing the human receptor allowing selective growth of poliovirus while non-permissive for most other human enteroviruses.

Polio and Its Epidemiology. Figure 1
(Continued)

and that of the corresponding OPV vaccine serotype. An isolate with VP1 homology of 99–100% is classified as vaccine virus, 85–99% as VDPV, and > 85% as wild-type poliovirus [3]. This rule of thumb for classifying polioviruses as VDPVs has recently been modified for serotype 2 to include isolates with ≥6 nucleotide

1988	WHO establishes the Global Poliomyelitis Eradication Initiative
1989	Identfication and cloning of the poliovirus receptor by Mendelsohn, Wimmer and Racaniello.
1981	Recombinant nucleic acid techniques used by Racaniello and Baltimore to prepare an infectious clone of poliovirus.
1990's=>	Development of molecular and immunological assays to identify the serotype and determine the vaccine or non-vaccine origin of poliovirus isolates.
1990-91	Development of a transgenic mouse expressing the human encoded poliovirus receptor approved as a non-primate model for neurovirulence testing safety of all three serotypes of live OPV in 1999-2000.
1991	Last case of endogenous wild polio in the Western Hemisphere.
1991	Establishment of a global Polio Laboratory Network to monitor poliovirus infections throughout the world.
1998=>	Isolation and characterization of highly diverged vaccine derived polioviruses from environmental samples excreted by unknown individuals.
1999	Establishment of the Global Action Plan for laboratory containment of all wild polioviruses throughout the world.
1999	Last reported case of poliomyelitis anywhere in the world caused by a wild serotype 2 poliovirus.
2000-01	First prospective recognition that an outbreak was caused by a vaccine-derived poliovirus (in Haiti and the Dominical Republic).
2000	Last case of endogenous wild poliomyelitis in the Western Pacific Region.
2002	Last case of endogenous wild poliomyelitis in the Eastern European Region.
2002	Cello, Paul, and Wimmer synthesize infectious poliovirus from individual nucleotides.
2003	Failure to vaccinate in Nigeria leads to a large increase in the number of cases and exportation of wild polioviruses and vaccine derived -polioviruses to > 21 polio-free countries. This spread is being brought under control by local and regional vaccination campaigns using monovalent, divalent, and trivalent vaccines.
2005	Decision: successful eradication must include cessation of the routine use of OPV.
2010	Large successful clinical trials using fractional sub-dermal doses of IPV.

Polio and Its Epidemiology. Figure 1
Major milestones along the road toward polio eradication

changes (i.e., <1%) and the upper limit of 15% for VP1 divergence has been eliminated (Summary of the 16th Informal Consultation on the Global Polio Laboratory Network, Geneva, Switzerland, 2010).

The earliest record attributed to polio comes from an Egyptian Stele from 1400 BCE that depicts an Egyptian high priest or official with a walking stick and withered leg that bears a striking resemblance to a recent picture of a man with poliomyelitis (Fig. 2). Polio infections from this time to the nineteenth century were endemic and usually occurred in young children where most infections were probably asymptomatic. While early descriptions of "acquired clubfoot" by Hippocrates and Galen were consistent with polio, the first modern medical characterization of polio includes descriptions of "Debility of the Lower Extremities" by Underwood in 1789, polio by Monteggia in 1813, "infantile paralysis" by Heine in 1840, and involvement of motor neurons in infantile paralysis by Duchenne in 1855. Involvement of motor neurons was confirmed by biopsy of the brain and spinal cord of a polio victim by Cornil in 1863 and by a detailed description of physiological changes in the anterior horn of the spinal cord by Charcot and Joffroy in 1870.

A new epidemiological aspect of polio emerged in the nineteenth century, namely, the appearance of outbreaks that increasingly affected adults as well as children [4]. Paradoxically this shift from an endemic to an outbreak pattern of disease transmission may have been facilitated by a "hygiene barrier" derived from improved community sanitation that may have resulted in a shift from fecal–oral to oral–oral transmission, an increase in naïve individuals especially among older cohorts, and primary exposure of increasingly older cohorts where disease manifestation were more severe. These epidemics became more frequent by the mid-twentieth century and involved growing

Polio and Its Epidemiology. Figure 2
Living after paralytic poliomyelitis: then and now. Paralytic poliomyelitis occurs after a biphasic infection where viremia in a small number of systemic infections is followed by infection of the CNS. Paralysis is a direct result of destructive replication of poliovirus in motor neurons followed by atrophy of de-enervated muscles. Both pictures represent men whose skeletal muscles have been affected by infections of nerves in the anterior horn of their spinal cord. The picture on the *left* (**a**) depicts the earliest record of poliomyelitis in a man and comes from a stele from ancient Egypt created around 1500 BCE, and is strikingly similar to the image of the man in the photograph on the *right* (**b**) who has atrophy of the right foot and leg due to polio that was taken in the Far East in 2007 ((**a**) Egyptian Stele at the Ny Carlsberg Glyptotek Museum, Copenhagen, Denmark (GNU free documentation License). (**b**) Photograph #134 Centers for Disease Control and Prevention Public Image Library [CDC/NIP/Barbara Rice])

numbers of people. Wickman described the acute infectious nature of polio in his analysis of a 1905 polio outbreak in New York, confirming Medin's realization in 1889 that paralytic cases were only a small part of epidemics and that even persons with mild illness could infect others. Further complications were the observation by Burnet and MacNamara in 1931 [5] that different strains of poliovirus caused disease, but infection with some strains did not protect against subsequent infection with other strains and the observation in the 1950s that poliomyelitis could be triggered by physical injury during a poliovirus infection and that there was an increased risk of paralysis in limbs that received a mechanical stress or after tonsillectomies [6]. Two important new concepts were the establishment of a national center for treatment of poliomyelitis victims at Warm Springs, Georgia, and the use of professional fund-raisers by President Roosevelt supported by others in the late 1920s. The nonpartisan National Foundation for Infantile Paralysis and the March of Dimes established in 1937 institutionalized this fundraising effort. The iron lung, developed by Drinker in 1929, and the concept of supportive rehabilitation involving the use of hot moist packs to relieve muscle spasm and physiotherapy to maintain strength of unaffected muscle fibers promoted by Kenny in 1940s were important advances for treatment of poliomyelitis.

The study of the pathological organism that caused poliomyelitis was enabled by the discovery of a bacteria-free "filterable" etiological agent, the poliovirus, which could pass disease from one primate to another by Landsteiner and Popper in 1909. Burnet and MacNamara realized in 1931 that there was more than one type of poliovirus since exposure to some isolates did not protect against exposure to others. By 1951, the National Foundation for Infantile Paralysis concluded that there were only three serotypes of poliovirus. The study of poliovirus was aided by (a) the first passages of poliovirus in a non-primate rodent system by Armstrong in 1939, (b) passage in tissue cultures by Enders, Weller, and Robbins in 1949 [7], (c) development of plaque assays for quantification of polio by Dulbecco and Vogt in 1954 [8], (d) the use of microcarrier cell systems for vaccine production by van Wezel in 1967 [9], (e) development of monkey neurovirulence tests in 1979 [10], (f) the use of pathogen-free diploid MRC5 cells (human fetal cells derived from normal lung tissue) and permanent cell lines like Vero (a cell line prepared from the kidney of a normal adult African green monkey) for vaccine production in the early 1990s, (g) identification and cloning of the poliovirus receptor CD155 [11], (h) development of the transgenic PVr-mouse model which expresses the human poliovirus receptor as an alternative to monkeys for neurovirulence testing [12], (i) preparation of a murine cell line, L20B, expressing the human poliovirus receptor for selective growth of poliovirus [13], and (j) the development of the immunological and molecular tools (discussed in detail below) that provide the identity the serotype of the isolate, distinguish whether its origin was from a vaccine or wild strain, and provide phylogenetic information on the evolutionary relationship to other isolates.

Advances in culturing polioviruses outlined in the previous paragraph laid the foundation for developing the vaccines that have turned polio into a vaccine-preventable disease and a candidate for eradication (see below). Early experiments and clinical trials such as those in 1935–1936 with inactivated poliovirus by Brodie and Park [14] and attenuated live vaccine by Kolmer [15] were hampered by lack of awareness until 1951 that there were three serotypes. Afterward, effective inactivated vaccine was developed and tested by Salk and coworkers starting in 1953–1954 [16, 17], while Koproswski, Sabin, and Cox developed and tested attenuated oral vaccines in 1950 [18, 19], 1956–1957 [20], and 1958 [21], respectively. Between 1951 and 1962, 12.9 million children were vaccinated with Koprowski strains and 11 million with Sabin strains [19]. A number of important epidemiological observations were made during that time that continue to guide current vaccination strategies. For attenuated oral vaccines these included (a) the first demonstration by Koprowski of interference between poliovirus serotypes during coinfection [19], (b) a demonstration that maternal antibodies did not prevent an immune response in vaccinees under 6 months of age [19], (c) the observation by Koprowski and especially Bottiger that live vaccine spread to contacts [19], (d) a demonstration of persistence of antibodies at the same levels in vaccinated children for at least 3 years [19], (e) proof of concept by Koprowski that live polio vaccine could be effective in containing large outbreaks [19], and (f) documentation of high vaccine safety with both the Koprowski and Sabin OPV strains [4, 19, 22]. Safety issues relating to both the live and inactivated viral strains will be mentioned in discussions starting on pages 8150 and 8160. After extensive evaluation in hundreds of monkeys at Baylor College of Medicine, and the Division of Biological Standards at the NIH, the Sabin strains were chosen for licensure primarily on the basis of lower neurotropism, but also based on genetic stability on passage in humans and a lower ability to spread to contacts (reviewed in Sutter et al. [4] and Furesz [22]). Efforts to eradicate polio and to prevent reemergence are presented in detail in the following section. Initial paradigms attributed to the different properties of the individual vaccines have not always held true in all circumstances [23].

The Epidemiology of Polio

Epidemiological studies to discover the means of preventing a disease usually begin with the recognition of a new pattern of similar symptoms among those affected and the establishment of a case definition. Discovering means for preventing the disease may start before the disease agent is discovered and characterized, but is certainly accelerated once this characterization becomes available together with the means of quantifying intervention strategies. It is much less

common to start with an agent and then search for a disease as in the case of human anelloviruses [24]. Human anelloviruses are small circular DNA viruses considered to be orphan viruses. They were initially discovered in a patient with hepatitis, but subsequent research indicated no causal link to hepatitis and it has been very difficult to associate them with any other specific disease. However, this section of the review will start with a description of those physical aspects of poliovirus that have the most impact on epidemiology of the disease. This is because there is already a clear case definition for polio and poliomyelitis, polioviruses have been recognized as the causative agents of these diseases, numerous methods for characterizing poliovirus and preventing poliovirus infections have been developed and tested, and the disease is approaching elimination or eradication.

Structural and Functional Organization of the Poliovirus Genome

Polioviruses belong to the *Picornaviridae* virus family. The *Picornaviridae* genome consist of a single strand of positive-sense RNA approximately 7,500 nucleotides located within a protein capsid made up of 60 capsomeres that forms a virion 27–30 nm in diameter. The genome is organized from its 5′ end to its 3′end into a number of functional regions (Fig. 3) that include a 5′ untranslated region (5'UTR) that regulate translation and replication [25], a long open reading frame that encodes a single large polypeptide that is cleaved after translation into four structural capsid proteins and a number of nonstructural proteins including an RNA polymerase, and a short 3′ untranslated region that is attached to a poly-A tail in both viral mRNA and genomic RNA in the virion [25] (see reviews by Wimmer et al. [26], Racaniello [25], and Sutter et al. [4]). The positive-sense single strand of genomic RNA in the virion, serves directly as an mRNA template for translation to viral proteins once the virion penetrates its host cell membrane. Later it serves as a template for synthesis of a complimentary negative sense strand. The current understanding of the physical and genetic aspects of polio was greatly facilitated by the development of and the current commercial availability of methods for easily extracting viral nucleic acids from poliovirus and poliovirus-infected cells and analyzing and manipulating these sequences. Some of these studies led to the unanticipated conclusion that poliovirus capsid proteins and the sequences that encode them define polioviruses, whereas all other elements in the poliovirus genome may be substituted by genomic recombination with equivalent sequences from closely related isolates of enterovirus species C in vivo and even more distantly related rhinoviruses in the laboratory as long as functionality is maintained (reviewed by Kew et al. [3]). Finally, advances in molecular biology also enabled poliovirus to be the first virus to be synthesized from nucleotides in a test tube [27, 28].

The 5'UTR was first subdivided into a highly conserved region (nucleotides 1–650) and a hypervariable region (nucleotides 651–750) based on an analysis of 33 wild-type 3 polioviruses [29]. A series of stem-loop structures with a high degree of secondary structure were proposed to be present within the conserved region by Pilipenko et al. [30] and Skinner et al. [31]. A single nucleotide substitution in a loop structure in stem-loop V of the 5'UTR significantly influenced the neurovirulence of poliovirus isolates from all three serotypes and affected the maximum temperature at which viral isolate replicate efficiently (see reviews by Kew et al. [3] and Sutter et al. [4] and discussions on poliovirus evolution starting on page 8137). The hypervariable region appears to be much less structured, reflecting the high degree of variation and the U nucleotide richness [29].

An Internal Ribosome Entry Site [32, 33], IRES, enables uncapped RNA from *Picornaviridae* to be translated in eukaryotic cells by host ribosomes [25]. One of the first steps in initiation of viral translation is the binding [34] of cellular RNA binding proteins PCB_1 and PCB_2 to stem-loop IV of the IRES. This enables the 40S ribosomal unit to bind to the IRES and continue the process of translation as if the RNA was a capped eukaryotic mRNA. Functional IRES elements can be interchanged among *Picornaviridae* [3]. Nucleotide differences in the conserved 5'UTR among different isolates were unevenly distributed [29] with changes tending to conserve the stem structures. In contrast, the hypervariable region did not seem to have a highly conserved secondary structure and nucleotide differences appeared to be more or less evenly spread throughout [29]. While the length of the hypervariable

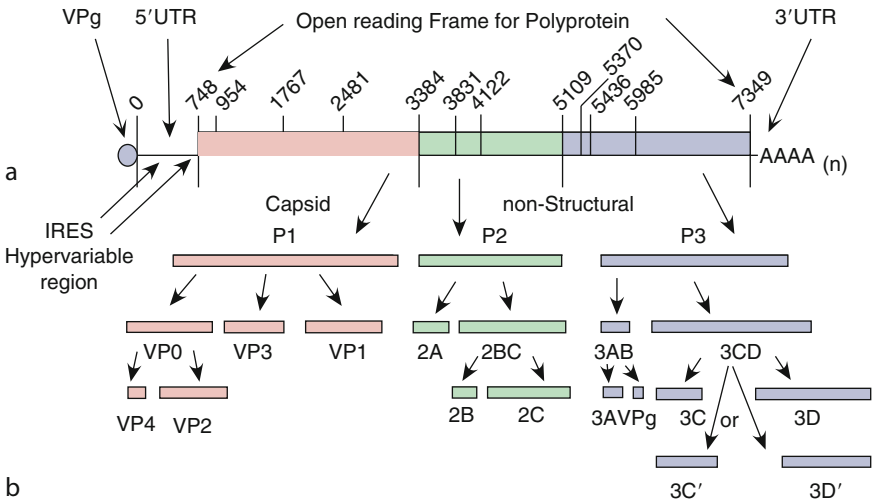

c

Serotype	Nucleotide	Gene	Amino Acid	Temperature Sensitivity
Sabin 1	A480G	5′UTR	Non-coding	Yes
	G935U	VP4	ala 65 ser	-
	U2438A	VP3	lys 225 met	-
	G2791A	VP1	ala 106 thr	-
	C2879U	VP1	leu 134 phe	-
	U6203C	3D	tyr 73 his	Yes
Sabin 2	G481A	5′UTR	Non-coding	Yes
	C2909U	VP1	thr 143 iso	-
Sabin 3	C472U	5′UTR	Non-coding	Yes
	C2034U	VP3	ser 91 phe	-
	U2493C	VP1	iso 6 thre	Yes

Polio and Its Epidemiology. Figure 3

Organization of the polio viral genome, posttranslational processing of the nascent poliovirus polyprotein, and the nucleotide substitutions that differentiate attenuated oral polio vaccine strains from their neurovirulent progenitors. The RNA positive-sense strand genome of Sabin 2 based on GenBank/EMBL/DDBJ entry AY184220 (**a**) is covalently linked to the viral encoded protein VPg. There is a single open reading frame flanked by a 5′ and a 3′ untranslated sequence (UTR). An internal ribosomal entry site (IRES) in the 5′UTR allows the uncapped polio genomic RNA to serve as mRNA for translation on host cell ribosomes. The open reading frame is translated into a single poliovirus polyprotein that undergoes a series of posttranslational proteolytic cleavages (**b**) while it is still being translated. Some of the intermediate products have enzymatic and/or structural functions that differ from those of the final cleavage products. Poliovirus genomic and mRNA terminates in a poly-A tail. The attenuation of neurovirulence in Sabin 2 and the other 2 serotypes, Sabin 1 (GenBank/EMBL/DDBJ entry V01150) and Sabin 3 (GenBank/EMBL/DDBJ entry X00925), of poliovirus strains used for the live polio vaccine result from the nucleotide and amino acid substitutions shown in (**c**). Reversion of these substitutions may restore a neurovirulent phenotype for the progeny of these vaccine strains. Nucleotide substitutions are indicated by the original nucleotide of the parental strain the nucleotide position, and the substituted nucleotide in the vaccine strain (*A*denine *U*racil, *G*uanine, or *C*ytosine). Amino acid substitutions are indicated by the parental amino acid, the position of the amino acid in the final cleavage product, and the amino acid in the vaccine strain (*ala*nine, *his*tidine, *iso*leucine, *leu*cine, *met*hionine, *phe*nylalanine, *ser*ine, *thr*eonine, and *tyr*osine). ((**b**) Based on: [1] Krausslich HG, et al. [37] and [2] Kitamura N, et al. [290]. (**c**) Modified from: Kew OM, et al. [3])

region was generally conserved suggesting an unknown function [29], small deletions were tolerated [35].

Picornaviridae have a genome of approximately 7,200–7,400 nt with a single open reading frame (ORF). While this ORF encodes four capsid proteins and at least seven viral proteins (Fig. 3), these proteins are only produced after the initial translation product, a single polypeptide, is enzymatically cleaved into smaller and smaller polyproteins during and after translation (posttranslational processing). The polypeptide is cleaved in an ordered series of steps (Fig. 3b), by viral encoded protease activity within the nascent polypeptide (self-cleavage) and *in trans* from viral proteases released after cleavage. Interestingly some of the intermediate cleavage products have unique activities by themselves that contribute to the replication cycle of the virus, but which differ from those of the final cleavage products (reviewed by Racaniello [36] and Krausslich et al. [37]). Properties of the polioviral capsid proteins define the epidemiology of polioviruses. The most important aspects of the structure of the four capsid proteins, their assembly into capsomeres and organization within adjacent capsomeres that relate to the epidemiology of polio, will be discussed above on page 8131. The 900–906 nucleotide sequence of the VP1 of polioviruses has become the minimum standard for determining the evolutionary relationship among polioviruses and the rate at which they evolve [4, 38, 39].

Many of the nonstructural proteins and intermediate cleavage products are multifunctional and act at a number of steps in RNA synthesis (reviewed in [4, 25]). Most of the nonstructural proteins will only be mentioned in passing since equivalent nonstructural proteins from other related picornaviruses may replace all of the nonstructural viral proteins as long as functional sites including cleavage recognition sites are maintained (reviewed in [3]). The resultant chimeric recombinants behave as polioviruses. One nonstructural protein, the RNA polymerase, will be discussed in some detail (see page 8135) because of its profound effect on polio epidemiology regardless of its source.

The secondary structure in the 3'UTR that may play a role in translation and replication of picornaviral genomic RNA has been reviewed [25]. A nucleotide difference between Sabin serotype 1 and its wild parent influences the temperature at which serotype 1 can replicate [40]. A poly-A tail is present on both genomic and mRNA that stimulates the cap-independent, internal ribosome entry site (IRES)-driven translation of poliovirus RNA in a mammalian cell-free system by tenfold [41].

Both genomic and minus strand RNA are linked to the small viral encoded protein, VPg, (Fig. 3a) through pUpU bound to tyrosine, the third amino acid from NH terminal end of VPg, by a phosphodiester bond [42]. VPg is also present in infected cells in an unmodified form and bound to pUpU through the same 0^4-phosphotyrosine bond found in the covalently linked forms [42, 43]. The uridylylation of VPg takes place on the opposite side of the polymerase that binds RNA. A host encoded unlinking enzyme that cleaves the 0^4-phosphotyrosine bond between VPg and RNA has been described [44] although its role in replication has not been established. The poliovirus encoded VPg can be replaced by VPg from echoviruses [43].

A mature infectious poliovirus consists of a single sense strand of polyadenylated RNA covalently linked to a viral encoded protein, VPg, surrounded by an icosahedral protein coat, the capsid, made up of 60 capsomeres that each contain a single copy of each of the four viral capsid proteins. Adjacent capsomeres are organized around both fivefold and threefold axes of symmetry and the surface around these axes is organized into a series of regular protrusions and depressions (Fig. 4). The capsid structure is metastable [45] rather than rigid and internal parts of capsid may even be transiently expressed on the surface ([46], review in [25]) exposing additional epitopes such as PALTAVE inVP1 [47].

Capsid proteins are the first viral encoded proteins to appear on the nascent poliovirus polyprotein and are cleaved from the nascent polyprotein into an intermediate polyprotein, P1, by $2A^{pro}$ while the full-length polyprotein is still being synthesized. P1 is processed into final cleavage products VP1 and VP3 and an intermediate cleavage product VP0. VP0 is only cleaved into VP2 and VP4 during the final stages of maturation of the virion. The protein chains of VP1, VP2, and VP3 are arranged in wedge-like structures with extruding loops that interact to form the major (NAgIa, NAgIIa, and NAgIIIa) and minor (NAgIb, NAgIIb, and NAgIIIb) neutralizing antigenic epitopes [48]. Amino

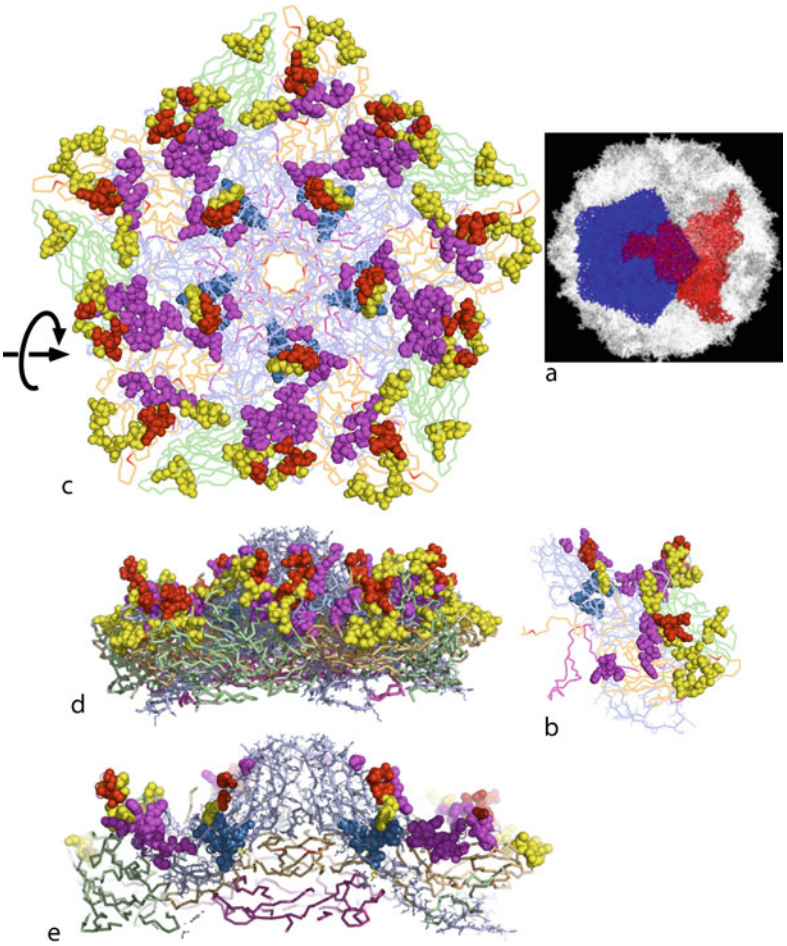

Polio and Its Epidemiology. Figure 4

The hydrophobic pocket and amino acid residues in the neutralizing antigenic epitopes and receptor binding sites of the Sabin 2 polio vaccine strain. The three-dimensional structures represent capsomeres 1–5 from human serotype 2 poliovirus, Genbank/EMBL/DDBJ entry 1eah. The backbones of the amino acid chains of the capsid proteins are represented by *light blue*, *pale green*, *light orange*, and *magenta colored ribbons* for VP1, VP2, VP3, and VP4, respectively. Amino acid residues at the surface of the hydrophobic pocket are represented by *blue spheres*. Amino acid residues within the epitopes recognized by neutralizing antibodies are represented by *yellow spheres*, those involved in receptor recognition and binding are represented by *magenta spheres*, and amino acid residues shared by both antigenic sites and receptor binding sites are represented by *red spheres*. The figure was prepared using the MacPYMOL program (DeLano Scientific LLC, www.pymol.org). Figure (**a**) is a representation of the entire capsid of poliovirus showing the positions of the threefold (in *red*) and fivefold (in *blue*) symmetrical organization of the capsomeres. Each poliovirus capsomere (**b**) contains a single copy of each of the four viral capsid proteins. Five capsomeres are assembled around a fivefold axis of symmetry shown in (**c**) and by *blue* in (**a**). They also assemble around a threefold axis of symmetry shown in *red* in (**a**). Figure (**c**) represents an external view of the five capsomeres at the fivefold axis of symmetry. Figure (**d**) is the side view of the same five capsomeres formed by rotating the figure in (**c**) in the direction of the *circular arrow*, so that the lower structures in (**c**) are nearest the viewer and the internal surfaces of the capsid proteins are facing downward. Figure (**e**) is a transverse section of the figure in (**d**) at the position of the *straight arrow* in (**c**) to more clearly illustrate the topography of the surface of the virion. An animated "Interactive 3D Complement" (I3DC) for the structures in this figure appears in *Proteopedia* at http://proteopedia.org/w/Polio_Epidemiology

acid differences within neutralizing antigenic sites divide polioviruses into three serotypes with limited cross-reactivity [49]. The amino acids of the neutralizing antigenic sites have been mapped onto the three-dimensional structures of the viral capsid of type 2 poliovirus as colored spheres, Fig. 4. Those that are unique to the neutralizing antigenic epitopes are colored yellow. Some amino acid residues in and adjacent to these neutralizing antigenic sites (red spheres in Fig. 4) are also involved in receptor binding and this may have restricted the number of serotypes [50] and influenced evolution in these epitopes in the absence of immunoselection especially during the emergence of vaccine-derived polioviruses (VDPVs) (see page 8159).

The three-dimensional view of the structure of the capsomeres at the fivefold axis of symmetry reveals an elevated central plateau with a hole in the middle surrounded by a depression called the canyon [51, 52]. The fivefold axis of symmetry for type 2 poliovirus is shown in Fig. 4. A number of conserved amino acids and amino acids within and adjacent to the serotype-specific neutralizing epitopes are located on the surface of the canyon walls and have been implicated in interaction with the poliovirus receptor [26, 50].

The human encoded, poliovirus receptor, CD155, belongs to the immunoglobulin super gene family and has one variable and two constant immunoglobulin-like domains (residues 28–337) [11]. This human encoded gene has alternative splice sites that result in two membrane-bound and two secreted isoforms [53]. The variable domain 1 penetrates the canyon and binds to amino acid residues from all three external capsid proteins and the principal binding sites are at the bottom of the canyon above the hydrophobic pocket (blue spheres in Fig. 4) and on the outer side of the canyon rim [50, 54]. The residues of type 1 poliovirus involving receptor virion binding include residues 102–108, 166–169, 213–214, 222–236, 293–297, 301–302 in VP1, residues 140–144, 170–172 in VP2, and 58–62, 93, and 182–186 in VP3. The equivalent residues for serotype 2 poliovirus have been mapped onto the three-dimensional capsid structure as red (shared with neutralizing antigenic epitopes) and magenta spheres for those associated only with the receptor binding sites (Fig. 4). Cryo-electron microscope studies have shown the binding of the poliovirus to the virion to be a two-step process [54]. The initial binding of the receptor to amino acid residues along the canyon wall results in little or no change in virion structure. However, this binding rapidly sets into motion conformational changes leading to the 135 S or A particle state that initiates uncoating and the start of the infections cycle [45, 54].

The human poliovirus receptor has been cloned and used to establish a murine cell line, L20B, where expression of the poliovirus receptor allows infection and growth of polio from clinical and other samples but not most other human non-polio enteroviruses [13, 55, 56]. Transgenic mice, PVR Tg-21 mice that express the human poliovirus receptor, not only support poliovirus infection and present with neurological symptoms, but allow determination of the relative neurovirulence of the isolates [12, 57–59].

A hydrophobic pocket (blue spheres in Fig. 4) located below the canyon floor is normally occupied by pocket factors such as sphingosine-like molecules including palmitic and myristic acids and hydrophobic compounds, that stabilize the capsid, enable receptor docking and whose removal is a necessary prerequisite for uncoating [25, 45, 54, 60].

Small molecules such as pleconaryl and isoflavenes can bind in this hydrophobic pocket and exert antiviral effects by affecting the binding of the receptor or enhancing the stability of the virion and preventing uncoating [25]. Because of the metastable nature of the capsid, mutations distant from the receptor and drug binding sites can compensate mutations in the respective binding sites [45, 61].

Molecular analysis studies of isolates shed during persistent infections of immunodeficient patients [62, 63] and from phylogenetically related aVDPVs from environmental samples help pinpoint amino acid substitutions in capsid proteins that determine antigenicity, receptor recognition, attenuation of neurovirulence, and properties of the hydrophobic pocket. Other changes, some of which are at interfaces between the threefold or fivefold interfaces of capsomeres may also affect these properties indirectly.

In order for single stranded, positive-sense genomic RNA to be incorporated into progeny of the infecting virus, a complimentary negative RNA strand must first be synthesized using the original single stranded positive-sense RNA genome as template, and this

complimentary negative strand must then be used as template for synthesis of new positive-strand RNAs. While some positive-sense copies are incorporated into progeny virions as genomic RNA, other newly synthesized positive-strand RNAs serve as templates to repeat and amplify RNA replication and/or for translation to produce more viral proteins. Eukaryotic cells that serve as the host for poliovirus replication lack a polymerase that can synthesize complimentary RNA from an RNA template. Therefore the virus must encode its own polymerase. Since the single stranded positive-sense RNA genome of the infecting virion is also an mRNA that is immediately translated, the virion does not have to incorporate the polymerase into the virion itself to start replication. The translation product of the $3D^{pol}$ gene (Fig. 3) is the required RNA-primed RNA polymerase. Both the intermediate cleavage products that contain the $3D^{pro}$ and the final cleavage product are multifunctional and the crude replication complex also contains other viral proteins and protein cleavage intermediates such as 2BC, 2C, and 3AB as well as host proteins (reviewed in [4, 25]). The binding site for RNA template and primer are on one face of $3D^{pol}$ and a binding site for the uridylylation of VPg, a prerequisite for covalent linking of VPg to viral RNA, is on the opposite face [25].

One important contrast between genomic DNA replication in eukaryotic host cells and genomic RNA replication in *Picornaviridae* relates to the fidelity of replication. Specifically, there is an elaborate proofreading mechanism combined with pathways for correcting misincorporations during replication of Eukaryotic DNA that is lacking in the RNA-primed RNA polymerase complex for viral replication [64, 65]. This leads to such a high evolutionary rate for polioviruses that it borders on error catastrophe [66, 67] (discussed further below).

Poliovirus Infections in Cells, Individuals, and Populations

This section will deal with the epidemiological aspects of poliovirus infections at three levels, infections in single cells, infections in a single individual, and infections in populations of individuals. The normal infectious cycle of a poliovirus starts with recognition and attachment to poliovirus-specific cell receptors on susceptible cells of human or closely related primate origin. It continues with penetration and uncoating, translation of viral RNA, posttranslational processing of viral polyproteins, replication of viral genomes, assembly and maturation of progeny viruses culminating in the release of infectious polioviruses. During this process, the virus employs and modifies host cell functions to optimize viral yield. The observation that viral RNA and cDNA is infectious when transfected into permissive host cells has allowed recovery of virus from extracted genomic RNA, cloned cDNA or RNA translated from cloned DNA [68–70], genomic RNA immobilized on FTA paper (WHO 16th Informal Consultation Of The Global Polio Laboratory Network, September 2010, Geneva, Switzerland), and from polioviral RNA synthesized in a test tube from individual nucleotides [27, 71]. The infectious cycle has been reviewed extensively. The reader is referred to the following reviews for further reading [4, 25, 72].

Poliovirus Infections at the Level of the Host Cell

All polioviruses recognize a single host cell receptor [50], CD155, also known as the poliovirus receptor (PVR). Identification and cloning of the poliovirus receptor CD155 [11] allowed the creation of cell lines [13] and animal models [58, 59] for the study of polioviral infections in non-primate hosts. The interaction of virion and receptor is complex [25]. The capsid structure is dynamic allowing the transient presence of internal portions and epitopes of capsid proteins on the outer surface of the virion [25, 46] including the N-terminus of VP1 even before uncoating. The shape of the receptor and its position relative to the host cell membrane and the canyon on the virion into which it fits bring the fivefold axis of capsomeres in close proximity to the cell membrane [54].

Conformational changes, induced shortly after the virion–receptor interaction, are required to initiate the uncoating process (reviewed in Racaniello [25]). The capsid begins to disassociate during a transition to the A particle. The A particle contains the viral RNA but has lost its VP4 capsid proteins. The N-terminal of the VP1 externalizes and may insert into the plasma membrane. Viral RNA is believed to enter the cell at or near the fivefold axis through a continuous channel formed in part by VP1 that continues through the cell

membrane [54]. VP4 plays a part in formation of the pore. The pore for poliovirus entry is probably not formed within endosomes [25]. Small molecules that sit in the hydrophobic pocket may influence these conformational changes without affecting receptor binding [61, 73–75].

The only viral proteins in the virion are the four capsid proteins and the VPg covalently linked to the genomic RNA. The internal ribosomal entry site (IRES) on uncoated polioviral RNA enables translation of the viral polyprotein on host cell ribosomes (reviewed in [3, 25]). VPg appears to be cleaved from this RNA and subsequently synthesized viral RNA that will be used as mRNA [44]. Nuclear trafficking of cellular proteins is downregulated shortly after infection resulting in accumulation of host nuclear proteins in the cytoplasm that could function alone or in combination with viral encoded proteins in viral RNA translation, synthesis, and packaging [73]. Downregulation may be due in part to specific degradation of two host transporters, Nup 153 and p62. A full-length polyprotein is not observed in spite of being encoded by the single long open reading frame since posttranslational cleavage of the polyprotein is initiated as soon as the portion encoding the $2A^{pro}$ has been translated. Many of the nonstructural proteins and intermediate cleavage products are multifunctional and act directly or indirectly at a number of steps in the RNA synthesis pathway (reviewed in [4, 25]). One example is the aforementioned viral encoded protease, $2A^{pro}$, that also shuts off host protein synthesis by cleaving eIF4G. eIF4G is required for translation of capped eukaryotic mRNAs, while the C-terminal of the cleavage product enhances IRES activity [25]. $2A^{pro}$ is also important for negative strand but not positive-strand RNA synthesis [76]. Another example is the intermediate cleavage product, $3CD^{pro}$, that also participates in the posttranslational processing of the polyprotein.

The last protein of the polyprotein to be translated is the 3D polymerase. RNA-primed RNA synthesis is initiated once the 3D has been released from the polyprotein reviewed in [25]. VPg-pUpU or VPg itself could act as a precursor for RNA synthesis by hybridizing to template RNA [44, 77]. The binding site for template and primer are on one side and that for VPg is on the other side. A replicate intermediate is formed and consists of a positive-sense RNA with 6–8 nascent negative strand RNAs. The negative sense strand serves in turn as template for synthesis of a 30-fold excess of new sense strand RNAs. Full-length dsRNAs can be isolated from infected cells. Altogether the genomic RNA is amplified up to 50,000-fold. VPg is bound to both genomic RNA and negative sense RNA.

Poliovirus and other picornaviruses employ a quasispecies reproductive strategy [64, 78] where the lack of proofreading rapidly results in a mixture of progeny with modified genomes containing randomly positioned single nucleotide substitutions. Genomic recombination is a second method of evolution where a single event results in substitutions of many nucleotides from a different poliovirus or closely related non-polio enterovirus for the equivalent sequence in the original poliovirus. The majority of single nucleotide substitutions are deleterious or neutral; however some may confer a reproductive advantage for progeny for growth in the current or future host and/or for host-to-host transmission. Evolutionary changes become "fixed" by selective outgrowth of individual members of the quasispecies that pass through bottlenecks within and between hosts [79]. Two evolutionary pathways, the very high number of progeny (>10,000 per infected cell) and outgrowth by chance selection and/or a selective advantage, result in one of the highest observed rates of molecular evolution [39].

RNA is synthesized from four nucleotides, two pyrimidines (uracil and cytosine) and two purines (adenine and guanine). The most common route for polioviral evolution is by nucleotide misincorporation (single nucleotide substitution) in the absence of both proofreading and post-incorporation excision–repair pathways. The nucleotide position that is substituted is probably random but may be influenced to some extent by secondary structure and the adjacent nucleotides. Quasispeciation arises from the fact that the remaining progeny retain the original nucleotide at the position of each unique substitution in an individual progeny virus, while within the cloud of progeny each isolate may have a unique substitution at a different position in the genome.

Among the isolates that make up the quasispecies, substitutions should be found at each position in the genome at an equal frequency, at least in theory.

However, substitutions are much more frequently observed in some positions than in others. Two related factors contribute significantly to the nonuniform distribution (see page 8140) of observed substitutions along the genome. The first is that almost all observations have been made with RNA extracted from the quasispecies that arose during replication of a viable virus directly in the primary host or after amplification of one or more isolates from the quasispecies in vivo in a second host or ex vivo in tissue culture. The second is that substitutions in some positions produce nonviable or less fit offspring that are eliminated during this amplification process.

Sequence-specific variability, based on the individual nucleotide base and its nearest neighbors [67], and inherent characteristics of the polymerase are other factors that contribute to the nonuniform distribution. If misincorporations were unbiased, transversions (the substitution of a pyrimidine by a purine or vice versa) would be expected to occur at twice the rate of transition (the substitution of a purine with a purine or a pyrimidine with a pyrimidine). However empiric observations have revealed a polymerase-based bias of approximately ten to one in favor of transitions [39]. To currently include sequence data from the genomes of nonviable progeny requires either amplification of individual genomes by a process that does not require an active poliovirus infection but that includes high fidelity with proofreading and excision-repair (reverse transcribing the genomic RNA and cloning the cDNA of all viable and nonviable poliovirus progeny into plasmids that can be amplified in bacterial strains with high fidelity, proofreading, and error correction) or by direct sequencing of individual gnomes without amplification (chip/array sequencing technology) [66, 80]. Neither approach is currently very easy to apply since both would require individually processing large numbers of genomes equivalents, although Crotty et al. were able to calculate a rate of 2.1×10^{-2} substitutions per site by direct measurement of mutations in the VP1 of 55 cloned genomes after a single cycle of in vitro virus growth. Massive parallel next-generation sequencing may offer the best approach for analyzing viable and nonviable members of a quasispecies [289].

Wild poliovirus genomes frequently recombine (recombination) with polioviruses and closely related non-polio enterovirus genomes [81, 82]. This recombination can only occur during concurrent infection of a single cell by both parental isolates. Intratypic recombination may occur even within capsid proteins [83–85].

The noncapsid regions of polioviruses are most similar in sequence to other members of the enterovirus C genotype that includes Coxsackie A virus (CAV) serotypes 1, 11, 13, 15, 17, 18, 19, 20, 21, 22, and 24, and these sequences are readily shuffled among polioviruses and the other members of this group [86, 87]. In fact polioviruses show evidence of having evolved from C-cluster Coxsackie A viruses and may reemerge from them after eradication [87]. Interspecific recombination contributes to the phenotypic biodiversity of polioviruses and may favor the emergence of circulating vaccine-derived polioviruses, cVDPVs [88].

Recombination is not site specific, does not require extensive homology between genomes at the crossover site, and most likely occurs by an exchange of templates by the synthesis of complimentary RNA by the RNA-primed RNA polymerase rather than by breakage rejoining [89]. Intratypic (same serotype) and intertypic (different serotype) recombination in in vitro occurred at 1.3×10^{-3} and 7.6×10^{-6}, respectively [89], while recombinations between polio and NPEVs occurred at a frequency of 10^{-6} [87]. Administration of trivalent oral vaccine anywhere and in areas where wild polioviruses and genotype C viruses co-circulate provides the conditions for concurrent infections and polio vaccine-polio vaccine, polio vaccine-wild polio, and polio vaccine-NPEV, as well as endemic wild polio-NPEV recombinations. For examples of such recombinations see molecular analyses of isolates from the cVDPV outbreaks in Haiti and Dominican Republic [90] and Indonesia [91] and in individual cases [92].

Molecular epidemiology is the study of disease and factors controlling the presence or absence of a disease or pathogen using molecular data (DNA, RNA, or protein sequences). The next portion of this section will concentrate on those aspects of molecular epidemiology that impact on the epidemiology of polio.

Polioviruses and other enteroviruses are among the organisms with the highest rate of misincorporation ([67, 78], and reviewed [39]). Misincorporation comes at a high cost, namely, only approximately 10% of

the >10,000 progeny from a single infected cell are viable [67]. This high frequency of misincorporation helps to explain the high ratio of physical to infectious particles [93]. Studies with ribavirin [66, 94], an antiviral drug acting as a nucleoside analogue, have shown that the misincorporation rate of polioviruses is close to the catastrophe error rate, that is, the transition point where a modest increase in misincorporation results in a drastic decrease in viability. In these experiments a 9.7-fold increase in mutagenesis resulted in a 99.3% loss in viral genome infectivity after a single round of replication, while a less than twofold increase in the natural mutational frequency resulted in a 50% loss of viability.

Fitness is based on the overall performance during viral replication [67], a complex process, involving recognition of and binding to the host cell, uncoating/entry, initiation of protein synthesis before RNA replication takes place, regulation of replication and translation once RNA replication is initiated, culminating with assembly, maturation and externalization of mature virus and survivability until subsequent infection of the next host cell or organism. Changes can affect more than one of these processes. For example, an increase in the mutational rate in infections in the presence of the nucleoside analog ribavirin not only led to an increase in nonviable genomes, but also caused a reduction in the total number of viral genomes produced [66]. One of the advantages of the quasispecies nature of poliovirus offspring is that isolates with a selective advantage to new growth conditions may already exist in the population [66]. Studies on mixed infections in PVR Tg21-transgenic mice suggest that random selection may play a role in the selection of which genomic variants within a mixed infection in the gut infect the CNS since virus isolated from the CNS was not always the most neurovirulent [95]. Other experiments showed that increased fidelity of the polymerase reduced viral fitness in the PVR Tg21-transgenic mice [96] or in tissue culture [97]. An alternate explanation for selection was proposed by Andino and colleagues [98]. They provide evidence that the quasispecies is not just a collection of individual variants, but a group of interactive variants and that fitness and selection may occur at the level of the population rather than at the level of individual genomes. In their study, an increase in polymerase fidelity affected viral adaptation and pathogenesis in addition to genome variability. Data supporting the suggestion that minor components can alter the phenotype of quasispecies comes from retroviral infections [99] and studies with VSV [100].

A number of studies have shown that single nucleotide misincorporations by the polio RNA-primed RNA polymerase accumulate at a more or less constant rate that can be used as a "molecular clock" to estimate evolutionary time between isolates and to determine whether sequence differences between two polioviruses isolated within a given time interval are consistent with a shared, direct evolutionary pathway between them [38, 39, 101, 102]. In general, the rate of accumulation and fixation of single nucleotide substitutions appears to be similar for all isolates regardless of kind (all three serotypes of wild, vaccine, or vaccine-derived polioviruses), type of polymerase (original intact polymerase or chimeric or complete recombinant from the same serotype, a different serotype or even a group C non-polio enterovirus), or type of infection (transient in immune competent individuals, persistent in immunodeficient patients, or even in the very elderly where waning immunity may play a role in selection) [4, 39, 79, 90, 101, 103–110]. Moreover, the rate of third codon position synonymous substations appeared to be fairly constant throughout the period of virus excretion in a persistently infected individual [107]. Using molecular observations from full-length genome sequences from viruses isolated during a 10 year long outbreak established from a single imported founder virus, Jorba et al. [39] calibrated five clocks based on five different classes of nucleotide substitutions. The constants for total substitutions (K_t), synonymous third position substitutions in coding regions (K_s), synonymous transitions (A_s), synonymous transversions (B_s), and non-synonymous substitutions (K_a) were $1.03 \pm 0.10 \times 10^{-2}$, $1.00 \pm 0.08 \times 10^{-2}$, 0.96 ± 0.09 _ 10^{-2}, 0.10 ± 0.03 _ 10^{-2}, and $0.03 \pm 0.01 \times 10^{-2}$ substitutions/site/year, respectively. The rates were similar whether calculated using linear regression, a maximum likelihood/single-rate dated tip method, and Bayesian inference. The first two constants were mostly controlled by the third. As for saturation, third position synonymous transitions become evident by 10 years and complete saturate within 65 years while saturation of synonymous transversions was predicted

to be minimal at 20 years and incomplete even at 100 years. This wide variation in calculated time constants depending on the type of substitutions together with differences in the estimated time until all possible changes become saturated, provides a flexibility that allows one or more clock to be applied to characterize the range from evolution in outbreaks between very closely related isolates with short intervals between isolations, to comparison between much more distantly related polioviruses or related enteroviruses. It is interesting to note that the molecular clocks are fairly constant given that intratypic and intrageneous recombination can result in complete or partial substitution of the polymerase whose intrinsic properties presumably govern the rate of misincorporation. Mutations may increase non-synonymous mutation rates [111] while others decrease them [96]. Multiple recombination events [83, 85] must be ruled out or taken into account when calculating time clocks based on the number of nucleotide differences.

Different factors that affect fitness and determine the viability of individual viral offspring result in differences in observed substitution rates and patterns in the different functional elements of the genome shown in Fig. 3. Namely, using the rate of substitutions in the VP1 capsid protein as reference, the rates of substitutions are approximately half in the conserved region of the 5'UTR, approximately threefold higher in the hypervariable region of the 5'UTR, and equivalent or somewhat lower in the remainder of the ORF [4, 39, 101, 109]. The data for nucleotide substitutions in the nonstructural P2 and especially the P3 regions of the ORF and the 3'UTR are less accurate and less informative due to frequent recombinations among polioviruses and between polioviruses and non-polio enteroviruses within these regions.

The genetic code introduces a bias in the position of observed substitutions. Substitutions in the third position of a codon are least likely to result in an amino acid change and these synonymous substitutions are by far the most abundantly observed in wild poliovirus, polio vaccine and VDPV infections [4, 79]. Non-synonymous substitutions that occur in the initial stages of vaccine infections restore replicative fitness and in many cases neurovirulence [3, 112] while those in persistent infections may influence receptor–virus interaction (see page 8133, 8159).

Three-dimensional requirements also bias the observed distribution of substitutions. Maintenance of stem of the stem-loop structure in the conserved region of the 5'UTR especially within the IRES appears to be one of the major constraints on viability. For example, complimentary paired double substitutions that maintained stem structure were frequently found in the loop V of evolutionarily related environmental isolates [109] whereas a single nucleotide substitution in a loop of Loop V is a dominant determinant of attenuation of neurovirulence and growth at elevated temperatures. Other examples of three-dimensional effects are mutations that occur at distances from functional sites that influence the viral response to antiviral drugs in the hydrophobic pocket [61] and mutations that occur at the interfaces between proteins and at the N-terminals of VP1 and VP4 that may affect structural stability and the receptor-induced transitions [45].

Due to the complex nature of polioviral replication and multi-functionality of viral enzymes and viral three-dimensional structures, selective pressures that operate on one structure or function may affect another seemingly unrelated property. One of these apparent paradoxes is the fact that some RNA viruses including poliovirus may diverge antigenically in the absence of immune selection [113]. One of the features that distinguishes polio vaccine evolution during persistent infections in total B-cell deficient immunodeficient patients from evolution during person-to-person transmission in immune competent but naïve individuals is that isolates from the former but not the latter have high numbers of amino acid substitutions in and around neutralizing antigenic sites [3, 4, 62, 114]. Antibody titers tend to wane in the elderly. The finding of amino acid substitutions at or near neutralizing antigenic sites during infection of the elderly with type 1 monovalent mOPV [103] may suggest that waning immunity may create a situation resembling the early stages in establishment of persistence in immunodeficient patients. Since some of the amino acids and structural organizations are shared by neutralizing antigenic sites and receptor binding sites, the high mutation rate in neutralizing antigenic sites is more likely the result from selective pressures governing receptor–virus interaction during establishment and maintenance of persistence than on non-humoral mediated immune selection or selection by variations

in anti-polio antibodies in the IVIg regimens these immunodeficient patients receive to compensate for their B-cell deficiencies. This sharing of functions has also been suggested to be one of the reasons why there are only three serotypes of poliovirus [26, 50]. It is commonly accepted that the evolution of a fourth serotype would require receptor switching of a non-polio enterovirus to the use of the PVR, CD155. A somewhat paradoxical alternative for emergence of a fourth serotype may be through antigenic evolution during persistent infections in immunodeficient individuals as a result of selective pressures relating to receptor binding. Consistent with this is the observation that cohorts of immunized individuals who had high titers against vaccine strains had significantly reduced geometric mean titers against highly diverged neurovirulent vaccine-derived viruses that were isolated from environmental samples [109, 115] and individual titers against some of these isolates were <1:8 in 7% of the adults [109, 116].

Any discussion on molecular evolution of polioviruses and their effects on polio epidemiology would be incomplete without a discussion on vaccine-derived polioviruses, VDPVs (see page 8157 and the section on future directions). Evolution of live attenuated polio vaccine occurs by the same processes as in wild polioviruses, namely, by accumulation of single nucleotide substitutions and through genomic recombination. Evolution of VDPVs occurs during person-to-person circulation in cohorts of naïve or under-immunized individuals especially after interruption of vaccination, or during persistent infections of immunodeficient individuals [3, 80, 106, 114, 117, 118]. The letters "c" or "i" for viruses that evolved during person-to-person circulation or during persistent infections of immunodeficient individuals, respectively, are appended before "VDPV" when the evolutionary pathway is known. The prefix "a" is added instead when the pathway is ambiguous or unknown.

One of the goals of the Global Eradication Initiative (see page 8150) is to reach a stage where all wild poliovirus transmission is terminated and vaccination can be discontinued. "Emergence of VDPVs," "failure to vaccinate," and "vaccine failure" discussed below have been the three major reasons for the delay in achieving eradication of poliomyelitis. Providing that enough money and effort can be mobilized, current vaccines and vaccine strategies are probably sufficient to enable immediate solutions for "vaccine failure" and "failure to vaccinate." Promising alternatives applying experience with adjuvants and better applicators have revived the possibility of using techniques explored in the 1950s such as fractional subdermal doses of inactivated virus, IPV [16, 119–121].

Vaccine-derived viruses consistently emerge as a consequence of the inherent genetic instability of poliovirus [122]. Moreover, many of the first sites that mutate restore replicative fitness, reverse attenuation of neurovirulence, and restrictions on growth at elevated temperatures. cVDPVs behave like wild polio [106, 112]. These cVDPVs clearly present a serious health threat [114]. The minimal amino acid changes in neutralizing antigenic sites that occur during person-to-person transmission of cVDPVs [3, 4, 123] allow rapid control through OPV immunization campaigns [106, 114, 124]. In contrast, iVDPV infections have not always been curable [63, 125], and the numbers and identities of anonymous persistent secretors are unknown [109]. The problem of reemergence of poliomyelitis through cVDPVs and especially iVDPVs requires a coordinated global program to discontinue the use of OPV with substitution of alternative vaccination strategies to prevent the appearance of large cohorts of unimmunized individuals during the period when OPV or cVDPVs may still circulate and iVDPV and aVDPV infections persist [116, 122, 126–128]. In fact, eradication should be redefined to include the elimination of both wild and vaccine-derived viruses [122].

OPV strains, like their wild counterparts, readily recombine the noncapsid encoding portions of their genomes with other polioviruses and related non-polio enteroviruses at very early stages in emergence. Evidence for this comes from analysis of poliovirus RNA from vaccine-associated paralytic poliomyelitis cases, VAPP, where, for example, >50% of polioviruses isolates had recombinant genomes [81, 129–132]. Supporting this is evidence from environmental surveillance where vaccine viruses with minimal divergence (0.5–1%) in their VP1 sequences had already recombined with polio and non-polio enteroviral genomes in regions encoding nonstructural proteins [133]. The ability to simultaneously reverse multiple mutations by recombination could foil efforts to

develop improved oral vaccines. Introducing mutations that decrease the chance for reversal by single nucleotide replacement such as incorporation of polymerases with improved fidelity or a total redesign of the genome of each serotype based on rare codon usage [3] could be bypassed by recombination.

Finally, the general consensus is that selective pressure or a higher mutation rate due to local sequence or secondary structure leads to a higher frequency of mutations at certain "hot spots" [93]. However after reviewing the pattern of changes in substitution frequencies throughout the genome it may be more accurate to think of the real frequency of substitutions as that observed in the so-called hyper variable region of the 5'UTR which may be under minimal selective pressure, and consider all other regions as "cold or colder spots" with lower observed rates of substitution derived from negative selection driven by the requirement for viability.

Virion assembly, maturation, and release in picornaviral infections have been reviewed [25]. The ratio of viral particles to infection particles ranges between 30:1 and 1,000:1. Many of the viral particles are noninfectious due to lethal mutations in their genomic RNA and/or incomplete maturation.

Poliovirus Infections at the Level of the Individual Host

The incidence of poliovirus infections is significantly higher in summer and autumn in temperate zones, becoming less seasonal as the environment becomes more tropical (reviewed in [3]). Improved sanitation and vaccination have reduced natural endemic infections in the very young and together with incomplete vaccine coverage has led to an increasing number of infections in older individuals.

There are two major routes of host-to-host transmission. The most common and most efficient is fecal–oral, followed by oral–oral transmission as Dowdle et al. described for the fate of poliovirus in the environment and their review of the infectious dose for transmission in humans [134]. It has been postulated that there has been a shift from the former to the latter route, as the level of community hygiene improved [56]. The infective dose after ingestion of Sabin vaccine strains is approximately 100-fold higher than that for wild poliovirus, 1000 $CCID_{50}$ compared to 10 $CCID_{50}$, respectively [3, 134, 135]. Nerve damage in the lower spinal cord results in paralysis of the lower limbs (spinal poliomyelitis), whereas damage in the upper spinal cord and medulla may result in bulbar poliomyelitis and paralysis of breathing [72]. The percent of infections ending in paralytic poliomyelitis is further reduced in highly immunized populations. This ratio of asymptomatic cases to paralytic cases has implications for surveillance strategies (see page 8154) based on investigation of all AFP cases. Between these two extremes falls the "minor disease" [72, 136], approximately 5% of infections with wild polio that result in abortive poliomyelitis with fever, fatigue headache, sore throat, and/or vomiting, and another 1–2% result in non-paralytic poliomyelitis with aseptic meningitis, pain, and muscle spasms. The incubation period is between 7 and 14 days but ranges between 2 and 35 days [72]. Virus can be recovered from the throat, blood, and feces by 3–5 days. It was initially thought that viremia was infrequent, but this was based on observations in patients with paralytic poliomyelitis who most likely already had high circulating titers of neutralizing antibodies [72, 137]. However when observations were made early after exposure, for example, in contacts of cases, a high frequency of viremia was demonstrated, implying that the viremia might play a vital role in the development of paralytic poliomyelitis [136, 138]. This was strengthened by concurrent experiments that demonstrated a protective effect against CNS lesions by antiserum in experimentally infected primates. The genetic basis for neurovirulence of poliovirus isolates is addressed below on page 8146.

Paralytic poliomyelitis, encephalitis, and aseptic meningitis occur after a biphasic infection where viremia in some systemic infections is followed by infection of the CNS [136, 138] (Fig. 5). Studies of virus in the CNS and stools in VAPP patients suggested that the virus that invades the CNS was randomly selected [95]. Acute flaccid paralysis (AFP) is a direct result of destructive replication in motor neurons followed by atrophy of de-enervated muscles. Skeletal muscles are affected when nerves in the anterior horn of the spinal cord are infected and bulbar paralysis occurs when cranial nerves are infected [4, 139]. The maximum effect on muscles occurs within a few days after the start of symptoms. Muscle recovery can occur when

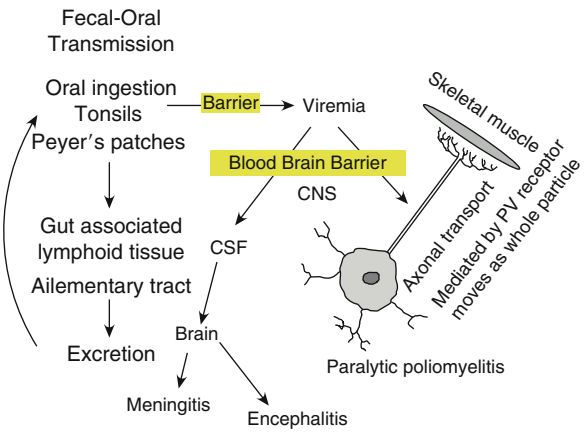

Polio and Its Epidemiology. Figure 5
Poliovirus infections. Poliovirus is transmitted from host-to-host by a fecal–oral and to a lesser extent oral–oral routes of transmission. Virus first infects cells in the tonsils, Peyer's patches, and gut-associated lymphoid tissues and viral progeny are excreted in feces. This phase is followed by a systemic infection during which there is viremia for a short period of time. In some individuals virus crosses the blood-brain barrier by entering the CSF, by axonal transport along nerve cells, and possibly from infected white blood cells that enter the brain. These individuals may develop meningitis, encephalitis, or paralytic poliomyelitis. Destructive viral replication in nerves of the anterior horn of the spinal cord may lead to irreversible atrophy of de-enervated muscles while bulbar paralysis occurs when cranial nerves are infected. Most (>90%) infections of naïve individuals even with the most neurovirulent strains are asymptomatic, 5% result in meningitis, encephalitis, and/or transient paralysis. Only 0.1–1% of the infections will result in permanent paralytic poliomyelitis or death

infection only results in temporary loss of nerve function. Residual paralysis may last from months to the life of the infected individual [72].

Poliovirus infections are not the only cause of AFP. Non-polio AFP occurs with an incidence of 1 per 100,000 children (see page 8153 for the implication this has for surveillance). Guidelines that help epidemiological investigators distinguish AFP caused by polio from AFP caused by other causes are reviewed in Sutter et al. [4]. Final diagnosis requires laboratory confirmation of a poliovirus infection.

Poliovirus infections start as a local infection of cells in the tonsil, intestinal M cells, Peyer's patch of the ileum, and the mesenteric lymph nodes [3, 72]. This replication in the gut results in the excretion of poliovirus during defecation by all individuals with asymptomatic as well as symptomatic infections and is the basis for fecal–oral transmission. It also provides the rational for supplementary environmental sewage surveillance (see page 8154) for poliovirus infections. A review of publications between 1935 and 1995 on excretion of polioviruses by Alexander and associates [140] indicated that in most infections of naïve children, wild polioviruses were excreted for 3–4 weeks with a mean rate of 45% at 28 days, and 25% of the cases were still excreting during the sixth week. In contrast, fewer than 20% excreted vaccine strains after 5 weeks. Excretion of polio ranged from a few days to several months [141]. The highest probability of detecting poliovirus positive stool samples was reported to be at 14 days after the onset of paralysis [140] and is the basis of stool sample collection for diagnosis of polio AFP surveillance (see page 8153). The disappearance of poliovirus from sewage samples and from stool samples of immunized children within 6–8 weeks after an immunization campaign [142] or after transition to exclusive immunization with IPV [143] provides additional confirmation for the short duration of excretion. Persistent poliovirus infections are the exception and will be discussed in more detail below. Interestingly, more than one evolutionarily linked lineage of the same serotype may co-circulate in the gut of such persistently infected individuals [79, 104, 107, 109].

Excretion and the duration of excretion are dependent on host factors and on vaccination history of the infected individual. Immunization history may start with passive immunization from maternal antibodies. However, maternal antibodies have an estimated half-life of approximately 1 month [144]. Based on a comparison between titers in cord blood and at 6 weeks, the half-lives for maternal neutralizing antibodies against type 1, 2, and 3 polio were 30.1 days, 29.2 days, 34.6 days, respectively [119]. Immunization history obviously also includes polio vaccinations and natural exposure to endemically circulating wild poliovirus and waning immunity in aging cohorts.

Skeletal muscle injury, including injury caused from intramuscular injections, increases the likelihood

of poliomyelitis in children infected with wild or vaccine poliovirus. Mouse model studies have suggested that in this provocative poliomyelitis, the muscle injury facilitates viral entry to nerve axons and subsequent damage to the motor neurons in the spinal cord [145].

Some individuals who had poliomyelitis develop new muscle pains, hypoventilation, new or increased weakness or fatigue and paralysis decades later after a period of relative stability. This reappearance of polio-related symptoms is referred to as postpolio syndrome. There is a large body of literature relating to postpolio syndrome that will be left up to the reader to pursue. Suggested starting points include the websites of the Post-Polio Health International (www.post-polio.org), the Mayo Clinic (www.MayoClinic.com), a 1992 paper on the "Epidemilogy of the post-polio syndrome" by Ramlow et al. [146], and a 2010 review on the pathophysiology and management of postpolio syndrome by Gonzalez et al. [147]. There is still a debate whether persistent poliovirus or mutated poliovirus contribute to the development of postpolio syndrome [147]. The risk factors include the extent of permanent residual impairment after recovery from the poliovirus infection, an increased recovery after AFP possibly related to the extra stress on compensatory neural pathways and overuse of weakened muscles, the age of onset of the initial illness, and physical activity performed to the point of exhaustion.

Natural infections with poliovirus stimulate both humoral and cell-mediated immunity (see [149, 150] and reviews [4, 148]). Neutralizing antibodies appear in exposed individuals around the time that paralytic symptoms become evident in the few individuals who develop symptomatic infections [72]. Neutralizing IgG and IgM antibodies are also induced in response to immunization with inactivated polio vaccine. The neutralizing antibodies induced after exposure to live or inactivated poliovirus prevent disease by blocking virus spread to motor neurons of the central nervous system [3]. Once seroconversion occurs after vaccination, individuals are protected from disease for life, although circulating antibody titers may wane late in life and may drop below protective levels against one or more serotype in some individuals.

The epitopes on vaccine-derived and wild poliovirus strains that induce neutralizing antibodies may differ from those on vaccine strains. Neutralizing antibody titers $\geq$1:8 against each of the three Sabin OPV serotypes are considered protective; however higher titers may be needed to compensate for the relatively lower antigenicity of wild and vaccine-derived strains [151]. For example, the highest serum neutralizing antibody titers were recorded from individuals immunized exclusively with OPV or IPV when the live challenge virus was the same as that used in vaccination, slightly lower for the respective heterologous strain, and significantly lower for wild and vaccine-derived strains. Serum from some individuals who had titers of $>$1:50 against Sabin vaccine strains had titers of $<$1:8 against some wild or vaccine-derived of at least one serotype, suggesting that titers of 1:64, 1:32, and 1:16 against Sabin serotypes 1, 2, and 3, respectively, might be more appropriate to ensure minimal protective coverage [151].

Primary infection in the intestinal tract by wild poliovirus or live attenuated polio vaccine induces secretory IgA antibodies in addition to IgM and IgG antibodies. One of the rationales for the use of live attenuated polio vaccine was that while disease would be prevented by humoral antibody production stimulated by either OPV or IPV, the extent of infection or reinfection and shedding would also be reduced by induction of secretory IgA antibodies by active infection of intestinal cells with live vaccine in mimicry of the natural route of infection [148, 152–155]. IgA induced in the gut plays an important role in terminating primary infection in the intestinal tract and the tonsils [3, 152] affecting both fecal–oral and oral–oral transmission. In practice IPV also induce some intestinal immunity although less than OPV and the duration of excretion in individuals immunized with IPV appears to be longer [23, 56, 156–158].

There is some indication that the duration and possibly memory of intestinal protection is relatively short and the time for clearance of virus relatively longer than the 3–6 or 7–14 days incubation period of the minor and paralytic diseases [152, 156, 159]. Complete blockage of replication in the intestines may occur in only 25–40% of fully immunized children [158, 159]. The rapid decline in intestinal immunity means that polio can establish transient infections even in persons with adequate humoral immunity and circulate silently in that community. Lower efficiency of oral vaccines under certain conditions further complicates efforts to break

chains of poliovirus transmission. Passive immunization with maternal antibodies, which has a short half-life, also affects oral vaccine efficacy (see page 8143).

It is not clear what role cell-mediated immunity may play in the control of polioviral infections. Cell-mediated immune responses were observed early after wild poliovirus infections by the macrophage migration inhibition (MIF) technique but were not observed a later time [160], whereas intradermal administration of subfractional doses caused induration and erythema of 3 mm diameter or above, in 14 of 18 vaccinees that indicated a cell-mediated immune response [161]. In addition, at least in a mouse model, all three serotypes stimulated cross-reactive and serotype-specific T helper cell responses detected by both in vitro proliferation and interleukin (IL)-2/IL-4 production [162].

How can poliovirus infections be prevented? The main tools in the global eradication of poliomyelitis have been the introduction of universal vaccination (vaccine) and improvements in hygiene. The primary goal of routine immunization is to protect the individual [163]. The secondary goal is to immunize a high enough proportion of the population so that the entire population will become protected. As eradication approaches completion, it is becoming more and more apparent that additional approaches will need to be employed in parallel with and perhaps instead of vaccination to extinguish the last pockets of endemic person-to-person transmission and persistent infections. All of these approaches will be necessary to prevent and control reemergence of polio after eradication. For more information, the readers are referred to excellent reviews on inactivated poliovirus vaccine by Plotkin and Vidor [164] and live oral poliovirus vaccines by Sutter et al. [4]. Sources for early history can be found in *A History of Poliomyelitis* by Paul [165] and *Polio Vaccine: The First 50 Years and Beyond* edited by E. Griffiths et al. [166].

The road to the development of effective vaccines against poliovirus was long and paralleled the growing understanding and ability to manipulate viral infections in the laboratory. Most of the important early milestones were listed in the last paragraph of the introduction and in Fig. 1. Mass vaccination trials and studies involving millions of vaccinees played an early and important part in acceptance of universal polio vaccination as a means for fighting poliomyelitis [19]. It must be stressed that problems and other difficulties during this progression stimulated numerous basic and epidemiological research studies that have resulted in improvements culminating in the current safe high-potency oral and inactivated vaccines that have reduced the number of annual paralytic poliomyelitis cases from >350,000 per year in 1988 to approximately 1,500 in the last few years. Difficulties in reducing this further are discussed below on page 8166. Criteria for quality control for production of polio vaccines introduced by the WHO in 1962 have been updated in relation to newly acquired knowledge about the epidemiology of poliovirus and polio vaccine. One of the major risks associated with the use of live vaccine is that progenies of the vaccine readily accumulate mutations some of which may reverse attenuation. The highest risk for vaccine-associated paralytic paralysis, VAPP, comes from Sabin 3, the vaccine serotype that also has the highest variability across production lots [3]. However the risk of OPV-associated polio is less than 0.3 per million doses [22] with the risk highest in naive children receiving their first dose [81]. The risk (see page 8156) of not using oral vaccine for global eradication compared to its use at the current stage in the Global Poliovirus Eradication Initiative remains overwhelmingly in favor of its use [1].

Three incidents nearly derailed early efforts to develop and employ effective vaccines. The most glaring of these, primarily from the point of views of negative publicity for use of polio vaccines, was the "Cutter Incident" in 1955 where wild poliovirus was inadequately inactivated probably because of failure to remove clumps that may have sequestered and protected infective vaccine virus, and a nonlinear tailing-off of inactivation at low titers [22, 167, 168]. Altogether more than 400,000 children were inoculated with an inadequately inactivated vaccine batch produced by the cutter vaccine production facility which resulted in 94 cases of poliomyelitis among primary vaccinees, 126 cases in family contacts, and another 40 cases among community contacts and 10 deaths. The publicity caused great concern throughout the world until the cause was discovered and corrective measures applied. The second, apparent failure of early vaccines to protect against subsequent infection and paralytic disease due to an initial lack of awareness in the 1950s that there were three non-cross-reacting serotypes of

polio has already been mentioned. The third problem, the contamination of live polio vaccine with SV40 virus, a simian virus, continues to raise concerns about long-term effects from human zoonotic infection with this virus that was shown to cause cancer in mice [22, 169–171]. The SV40 was inadvertently introduced through the use of SV40-infected simian cell cultures in some early vaccine production batches. So far there is little evidence for any contribution to the incidence of tumors in the humans who received SV40.

The many vaccination formulation and vaccination schedules that have been employed during the effort to eradicate polio and the rational for their use have been reviewed in depth [4, 164]. Changes in schedules and formulations mean that in any one region different cohorts in the total population will have received different vaccine formulations and immunization schedules. This complicates determining duration of protection and interpretation of events. The evolution of vaccination policy in Israel [172–174], a graph showing the history of poliomyelitis in Israel (Fig. 6), and the two disagreeing discussions that were published within the same report on the underlying causes that enabled the last outbreak in Israel in 1988 [175] are a good example of this difficulty.

Isolation of poliovirus with attenuated neurovirulence was a prerequisite for the development of oral polio vaccines (OPV; see reviews [3, 4, 166]). Vaccine candidates were either derivatives of neurovirulent or even highly neurovirulent (e.g., Sabin 3) isolates selected for attenuation after passage in primates, primate cell cultures, and/or non-primate cell cultures or starting from isolates with low neurovirulence (e.g., Sabin 2). Neurovirulence refers to the ability of an isolate to cause an infection adversely affecting functions of the CNS, keeping in mind that for any neurovirulent isolate, only 5% of infections cause transitory adverse CNS effects and less than 1% cause permanent paralytic poliomyelitis. The total number of nucleotide differences between vaccine strains and their respective parental strains was found to be 57 nucleotides and 21 amino acids for serotype 1 [176–178], 2 nucleotide differences and 1 amino acid difference for serotype 2 [179, 180], and 10 nucleotide differences and 3 amino acid differences for serotype 3 [181, 182]. Sequence analysis coupled with genetic manipulation has allowed investigators to pinpoint which of these nucleotide differences between vaccine candidates and vaccine strains account for the loss of neurovirulence (Fig. 3) [93, 183]. "Quantitative determination of the contributions of each substitution is complicated by several factors: (a) The role of minor determinants of attenuation is difficult to measure, (b) some substitutions have pleiotropic effects on phenotype, (c) some Sabin strain phenotypes require a combination of substitutions, (d) second-site mutations can suppress the attenuated phenotype in various ways, and (e) the outcome of experimental neurovirulence tests may vary with the choice of experimental animals (monkeys versus transgenic mice) or the route of injection (intraspinal versus intracerebral)" [3]. The propensity of vaccine to evolve and revert to neurovirulent phenotype is discussed throughout the current review.

The safety and effectiveness of live attenuated polio vaccine strains in preventing poliomyelitis was very clearly demonstrated in large clinical studies involving millions of children in the 1950s [19]. A number of factors including vaccination schedules, the presence of maternal antibodies, hygiene, and nutritional status of the individual influence the efficiency of induction of seroconversion by OPV strains. Early studies showed that viral interference between strains in the trivalent vaccine and from concurrent infections with non-polio enteroviruses also influences vaccination outcome [19]. Multiple doses of OPV are recommended to ensure seroconversion rather than to boost waning immunity [184]. The number of OPV doses that is needed to reach 90–95% seroconversion rates in naïve children is not the same for all populations. For example, three doses will seroconvert 90–95% of naïve children in developing countries, whereas in certain regions within developing countries such as India, the same three doses will only seroconvert a maximum of 60% of vaccinees [184]. Supplemental immunization activities (SIAs) employed sometimes more than once a year are needed to ensure adequate primary vaccination coverage and to fight endemic circulation of wild poliovirus or reintroductions of wild poliovirus. In SIAs, all children in national or subnational regions are immunized in national immunization day (NID) and/or subnational immunization day (SNID) campaigns, respectively, with a dose of OPV irrespective of vaccine history. The costs of the additional doses

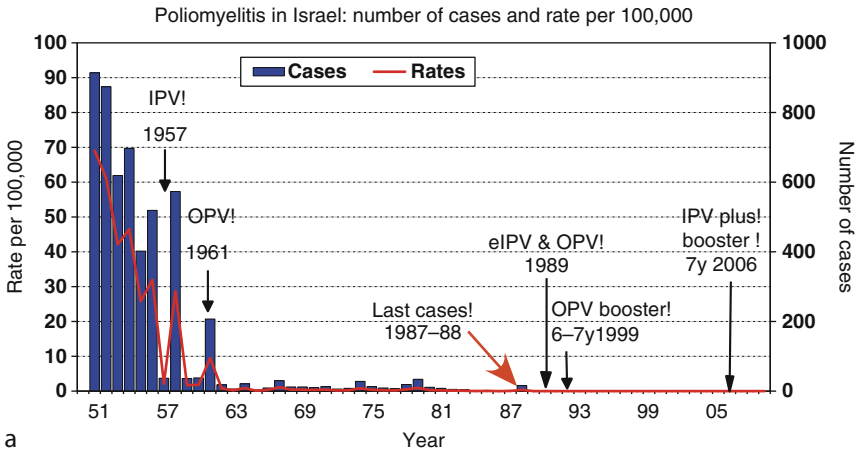

Polio vaccine immunization schedules in Israel 1957–2010

1957–1960 exclusive use of IPV (mainly local production)
- varied number of doss (2 to 4)
- varied quantity of antigen per dose
- initially administered in campaigns then by routine vaccination schedule!
- estimated coverage 75% to 90%

1961–1963 exclusive use of OPV
- coverage 95%
- 1961 mOPV1
- 1962 add mOPV2 and mOPV3
- 1963 tOPV 3 dose schedule (2, 6 and12 months)

1964–1978 4 doses by (2, 4, 6, 24 mo) coverage 81% to 91%

1979–1981 same as in1964–78 plus a supplimental mOPV1 once a year for ages 0–2 yrs

1982–1987 three programs
- a. 4 OPV doses in 12/14 health sub-districts
- b. 4 OPV doses as in a. plus one dose mOPV1 in selected groups at risk
- c. exclusive eIPV 3 doses in 2 of 14 healthsub-districts at least one dose in combination with DTP.

1989–2005 combined eIPV/OPV
- 2 doses of eIPV (2 and 4 mo)
- 2 OPV doses (4 and 6 mo)
- simultaneous IPVplus OPV at 12–16 mo)
- 1990 IPV booster added at 6–7 yr

2006–2010 exclusive use of eIPV
- 4 doses of eIPV (2, 4, 6, 12 mo) plus booster 7 yrs)

1957–2010 Immigration of familes with children who were vaccinated by different vaccination schedules used at their countries of origin.

b

Polio and Its Epidemiology. Figure 6

Prevention of poliomyelitis through universal vaccination and evolving vaccination strategies as illustrated by the history of cases and vaccination schedules in Israel between 1957 and 2010. Figure (**a**) represents the annual number of cases (*blue bars*) of laboratory confirmed poliomyelitis cases and the rate per 100,000 children (*red line*) between 1951 and 2010. The *red arrow* indicates the last cases of poliomyelitis that occurred during an outbreak in 1987–1988. Israel has been poliomyelitis-free since 1989. *Black arrows* indicate major changes in vaccination policy. Previous attack rates of 14.2 and 146.9 per 100,000 in 1949 and 1950, respectively, signaled the transition from endemic to epidemic epidemiology of poliomyelitis in Israel. A full list of vaccination schedules is indicated in (**b**) (Data presented in (**a**) was supplied with permission by the Israel Center for Disease Control. The vaccination schedules were taken from Swartz TA. The Epidemiology of Polio in Israel A Historical Perspective. Tel Aviv: Dyonon Pub. Ltd.; 2008 [172])

needed to raise seroconversion rates to above 90%, significantly raise the cost for effective immunization with OPV and require the coordination and use of many paid and voluntary staff. In fact, in the end it may actually be easier to immunize three times with IPV (even at current costs) than with the additional number of doses of OPV especially when access to populations is difficult and environmental conditions challenge maintenance of viability of the live vaccine. This counters both the lower cost and difficulty of administration rationales for using OPV instead of IPV. Mass immunization campaigns have rapidly boosted herd immunity [3].

The take of OPV is negatively influenced by the presence of maternal antibodies. Nonetheless, when infants are fed OPV at birth, 30–60% excrete virus, 20–40% of infants seroconvert, and the subsequent take of OPV is better when a birth dose is given (reviewed in [184, 185]).

Vaccination formulation must also take into account differences in the efficacy of induction of intestinal immunity by the different vaccine serotypes [155]. For example, type two was 100% effective with two doses, whereas types 1 and 3 needed more than three doses. Since the elimination of wild type 2 in 1999 [186], and the significant decrease in the number of endemic regions where wild type 1 and 3 co-circulate, SIAs have increasingly turned to the use of monovalent and divalent OPV. Monovalent OPV vaccines improve seroconversion rates compared with tOPV [187]. However routine immunization still requires the use of tOPV to prevent the accumulation of large cohorts of individuals who are naïve to type 2 poliovirus and who could serve as a reservoir for transmission of neurovirulent type 2 VDPV as has occurred in Nigeria [106]. New guidelines for the use of mOPV1, mOPV2, and dOVP1+3 have been recently issued [188].

The use of inactivated poliovirus is an alternative approach to vaccination against polio (reviewed in [164]). Salk developed an inactivated polio vaccine, IPV, using neurovirulent strains of the three serotypes of poliovirus. IPV was successfully tested by a placebo-controlled trial in over 400,000 children and in unblinded observations on another 1,000,000 children before certification for use in the mid-1950s [16, 17, 189]. A relatively higher difficulty in production, greater production costs, higher difficulty in administration, and the initial belief that only live vaccine would efficiently evoke intestinal immunity led to the choice of OPV for most routine national vaccination programs [122]. Countries are currently switching to vaccination with IPV in combination with OPV or more often in place of OPV because of its relative safety record (no VAPP cases), improvements in manufacture that have increased effectiveness and reduced the cost difference between a dose of OPV and IPV, and the paradoxical success of OPV in reducing poliomyelitis as an epidemic disease in most countries [164]. Additional motivation has come from the increasing awareness that fully neurovirulent vaccine-derived polioviruses behave like wild polioviruses [133, 190, 191] that must be eliminated and prevented from emerging in order to attain final success for poliomyelitis eradication.

Early studies on genetic and antigenic variation such as a study of Sauket strains, the type 3 used in production of IPV [192] were instrumental in the establishment of rigorous standards for seed stocks for vaccine production. The original IPV formulation has since been improved. This enhanced IPV, eIPV, has a higher immunogenicity and protective efficacy than IPV [157]. A number of factors contributed to this improvement. These included new production protocols, new tissue culture techniques including a microcarrier-based technology, and a more optimal balanced formulation of the three serotypes. It can be administered alone or can be combined with other vaccines such as DTP. The immunogenicity of eIPV was at least as good as that of OPV and there was good long-term immunity [157]. Subdermal administration of fractional doses of IPV was one of the approaches tried in the early 1950s [16]. Subsequently seroconversion rates from fractional doses were shown to be adequate but somewhat lower than for full dose intramuscular injections fractional doses [119, 193]. In another trial, similar seroconversion rates were observed but there were lower median titers in those receiving fractional doses [120]. Fractional doses effectively boost titers in previously immunized individuals [194]; however there is no long-term information on the rate of waning immunity in individuals treated with these fractional doses. Large non-inferiority studies testing subdermal administration of fractional doses of IPV using needle-free devices such as recently by

Mohammed et al. [120] and Resik et al. [119] offer one quite promising practical solution for realizing cessation of use of live OPV with affordable alternative vaccines as recommended by the Advisory Committee on Polio Eradication in 2004 [195].

Antiviral drugs offer a promising complimentary or alternative approach to the use of vaccine to control poliovirus infections especially for persistent infections in immunodeficient individuals, during the final stages of eradication, and for post-eradication reemergence [122]. Presumably theses drugs may also work to control severe infections by non-polio enteroviruses or have been chosen because they have been shown to do so. Drugs with unique virus-specific targets such as capsid proteins, the hydrophobic pocket, the RNA-primed RNA polymerase, protease inhibitors, protein 3A inhibitors, nucleoside analogs, proteinase 2c inhibitors, and compounds with unknown mechanisms of action have been reviewed [196]. There is still a long way to go to find truly effective universal anti-polio or anti-enteroviral drugs, thus only a few examples will be provided.

Pocket factor drugs such as WIN 51711 [74], isoflavenes [61], pleconaryl [197], and capsid inhibitor V-037 [198] prevent viral entry by interfering with receptor binding or by preventing conformational changes needed for viral capsid uncoating. One of the difficulties in developing pocket factor drugs comes from the quasispecies nature of enteroviral infections, where mutants may rapidly emerge [61, 63] or there may be viral isolates already present in the quasispecies that have mutations in the capsid that may either render the isolate resistant or even dependent on the drug for growth. Furthermore these resistance mutations may not even have to be at the drug binding site (see, e.g., [61]).

Ribavirin is a drug that normally interferes with mRNA capping. While enterovirus mRNA is uncapped, the polio polymerase can incorporate ribavirin into both negative and positive-strand progeny RNA molecules increasing mutagenesis above the catastrophe limit causing a decrease in the reproductive capacity of the viruses [66, 94] (discussed above on page 8138).

Passive immunization has also been tested as a means of preventing polio. Administration of immunoglobulin shortly after exposure to polio may reduce the incidence or severity of paralytic disease although its general use is not practical due to the short time during which it is effective [199]. Intravenous preparations of immunoglobulin prepared from human populations exposed to enteroviral infections have however helped to decrease chronic meningoencephalitis infections by these enteroviruses in agammaglobulinemic patients [200]. Regular intravenous treatment may help prevent poliomyelitis in immunodeficient individuals but may not prevent virus replication and shedding [62]. Passive immunization with immunoglobulin or human milk rich in anti-polio IgA together with another antiviral pleconaryl may have helped to resolve at least one persistent poliovirus infection [125]. However, efforts to cure another persistent poliovirus infection with human milk and ribavirin, or other antiviral treatments, did not prove successful [63] and this individual has continued to excrete highly diverged vaccine-derived poliovirus for more than 20 years [62]. Anecdotally, shedding of intestinal mucosa associated with a superinfection with Shigella sonnei may have helped to cure another persistent excretor [62].

Poliovirus Infections in Populations

Poliovirus infections in populations have been the subject of many reviews over the years. The older reviews are still of interest not only because of the information they review but because they also provide a picture of policies and knowledge available at the time. The following paragraphs will concentrate on those aspects of poliovirus infections in populations that impact the most on the endgame strategy of poliomyelitis eradication. The discussion will start with a brief overview of the changing nature of the epidemiology of poliovirus infections. This will be followed by a description of the Global Polio Eradication Initiative and will end with a discussion of the three main problems that have led to a delay in its realization, namely, "failure to vaccinate," "vaccine failure," and "vaccine-derived polioviruses." When reading this section which will highlight some of the current problems and their solutions, the reader must keep in mind the overwhelming success of the Global Polio Eradication Initiation to date: a major reduction in the number of endemic countries where polio is still transmitted from 126 to 4; a decrease in the number of annual cases by >99% that prevented

life-long paralysis in more than five million children between 1988 and 2005; eradication of one wild poliovirus serotype in 1999; and elimination of the majority of wild lineages throughout the world.

The nature of poliovirus infections in populations has gone through a number of phases. Before the appearance of outbreaks of poliomyelitis starting in the nineteenth century, poliovirus circulated endemically. Infections occurred in the very young, and conferred lifelong immunity against reinfections with the same serotype. The epidemics became more frequent, grew in size, and infections included older children and adults who were not naturally immunized. Vaccination has drastically reduced the number of people who have been exposed to natural infection with wild polioviral strains. There also appears to be a shift in person-to-person transmission routes. Oral–oral transmission has increased in importance while fecal–oral transmission decreased as a result of improved hygiene [56]. Control of poliomyelitis requires breaking all chains of wild poliovirus transmission by immunizing all children with three doses of polio vaccine or at least enough children so that herd immunity protects the remaining population. The percent of the population that needs to be immunized for establishment of herd immunity against wild poliovirus is >85% for developed countries and >90–95% in tropical developing countries. In 2010, there were still three groups of countries: four "endemic countries," Afghanistan, India, Nigeria, and Pakistan where the transmission of wild viruses has not yet been completely halted, "polio-free countries" where vaccination has broken all endemic chains of wild poliovirus circulation and there have been no cases other than VAPP within the last 3 or more years, and "importation countries" that were formerly polio-free, but where there are poliomyelitis cases caused by wild poliovirus imported from one of the "endemic countries" and where there may be local transmission of the imported wild poliovirus. Between 2002 and 2006, there were 26 importation counties, 7 with viruses imported from India and 19 with viruses imported from Nigeria [4]. There were 21 importation countries in 2009 and 13 in 2010. These included ongoing outbreaks in Tajikistan and the Russian Federation and apparently expanding outbreaks in Angola and the DRC. The former represents the first cases from wild poliovirus in the European region since regional eradication was declared in 2006 and the latter could potentially spread to polio-free countries in Africa and other regions. The list of importation countries is updated on a weekly and monthly basis and can be accessed at the web page of the Global Polio Eradication Initiative, www.polioeradication.org. Transmission routes are dependent on population movements. One or more outbreak founders may be introduced by infected persons coming from an endemic or importation country or by returning travelers from such countries. One event with very high risk for spreading poliovirus from one country to another is the Hajj in Saudi Arabia. To counter this threat, it is now mandatory for foreign pilgrims coming on Hajj and Umrah to be vaccinated for communicable diseases including polio, especially pilgrims with young children arriving from countries with polio cases. The children must have received a dose of OPV 6 weeks before their arrival and another upon arrival.

Smallpox was eliminated as a circulating human pathogen in 1977 after an 11-year extensive vaccination and surveillance program [201]. Only two sources of smallpox virus have been reserved for research purposes, one in the United States and one in Russia. Final eradication will be achieved when these last two remaining, contained sources of smallpox virus are finally destroyed. Proposing a similar approach in 1988, the World Health Assembly set a goal of eradicating poliomyelitis by the year 2000 (resolution WHA41.28). A group of experts at the global, regional, and country level set the criteria and conduct the process of certification of eradication [202]. These experts must be independent from the vaccine administration and polio laboratories. Global polio eradication, first targeted for completion by 2000, was limited to the eradication of all wild polioviruses with the caveat that "the occurrence of clinical cases of poliomyelitis caused by other enteroviruses, including attenuated polio vaccine viruses, does not invalidate the achievement of wild poliovirus eradication" (Report of the first meeting of the Global Commission for the Certification of the Eradication of Poliomyelitis. Geneva: World Health Organization; 1995. WHO document WHO/EPI/GEN/95.6). OPV vaccination would cease within a few years after eradication of poliomyelitis from wild polio and industrialized nations would save not only the large sums of money needed for the

maintenance and rehabilitation of individuals with paralytic poliomyelitis but the costs of vaccine and vaccine administration as well [203–206].

In order to easily eradicate an infectious agent, (a) the agent should replicate in a single host with no intermediate vector, alternative reservoir species, or carrier state, (b) vaccines and/or anti-infectious agents must be available to break chains of transmission whether directly between susceptible organisms or after exposure to the infectious agent in the environment, (c) if transmission involves environmental exposure, there must be a finite and relatively short survival time for the infectious agents in the environment, (d) all or the majority of infections should be clinically apparent with unique symptoms, and (e) there must be an easy and cost-effective surveillance system for detection of the infectious agent, identifying infected individuals, and for determining the efficacy of treatments in individuals and populations [3, 207]. Deviations from some of these requirements for eradication have made eradication of polio more difficult from the start [56]. In particular, most (>95%) poliovirus infections are clinically asymptomatic while symptoms associated with the few infections that result in poliomyelitis are not unique to poliovirus infections and although effective vaccines were available, there is no easy and cost-effective method to determine the effectiveness of vaccination in vaccinated individuals. This makes surveillance and the identification and isolation of infected individuals much more difficult. When the GPEI resolution was passed in 1988 and even as late as 1996, it was stated [208] that there was no indication of chronic excretors; however, persistent infections (see page 8161) do exist and have emerged as one of the difficulties in achieving eradication. Differences between smallpox and polio have made it relatively more difficult to achieve polio eradication. For example, live polio vaccine is made from three temperature-sensitive serotypes of poliovirus because there were three non-cross-reacting poliovirus serotypes, whereas the vaccine for smallpox was a single more stable unrelated bovine virus. This has complicated vaccine formulation and administration. In addition since the vaccine contains live poliovirus there are also a number of more severe safety issues concerning pre- and post-eradication vaccine production compared with the smallpox vaccine.

Specific eradication strategies for polio included (a) high routine immunization with at least three doses of vaccine for all children and an additional birth dose in countries where polio has remained endemic (b) SIAs, either national or subnational immunization campaigns targeting children under 5 years of age (c) surveillance, primarily investigation of all cases of AFP with an increase in the number of supplementary surveillance programs such as sewage surveillance and enterovirus surveillance as the endgame of eradication approaches, and (d) house-to-house mopping-up immunization campaigns to block final chains of wild polio transmission [1, 163, 203]. The WHO requires genomic sequencing of all isolates of potential interest to the Polio Eradication Initiative. An isolate is of interest when results from either standard immunological and/or molecular tests conducted by accredited laboratories using standard methods (see next section) indicate that the isolate has behaved differently than standard Sabin strains of the corresponding serotype.

A Global Polio Laboratory Network, GPLN, was established to monitor poliovirus infections throughout the world using standardized methods, cell lines, reagents, and reporting methods [209–213]. These standard methods (WHO/EPI.CDS/POLIO/90.1) have been reviewed and revised and improved as knowledge about the epidemiology of polio expands and as new analytical methods become available (Fig. 7). This includes even the flow charts or "algorithms" for culturing viruses, identifying polioviruses, and characterizing the serotype (Typic Differentiation) and determining wild, vaccine, or vaccine-derived virus within specific time frames (Intratypic Differentiation). The current fourth version of the *Polio Laboratory Manual* (WHO/IVB/04.10) was adopted in 2004. The three levels of laboratories, National and Sub-national Laboratories, Regional Reference Laboratories, and Global Specialized Laboratories, are certified each year through on-site visits, after accurate testing and timely reporting of a minimum number of relevant assays, and by results from proficiency tests. The requirements for certification, quality assurance, and safety and the responsibilities of the three types of laboratory are spelled out in the *Polio Laboratory Manual* (WHO/IVB/04.10). By the end of 2009, the GPLN consisted of 146 laboratories of which 139 were fully accredited by the WHO, and another 5 in the process of accreditation (WHO 16th

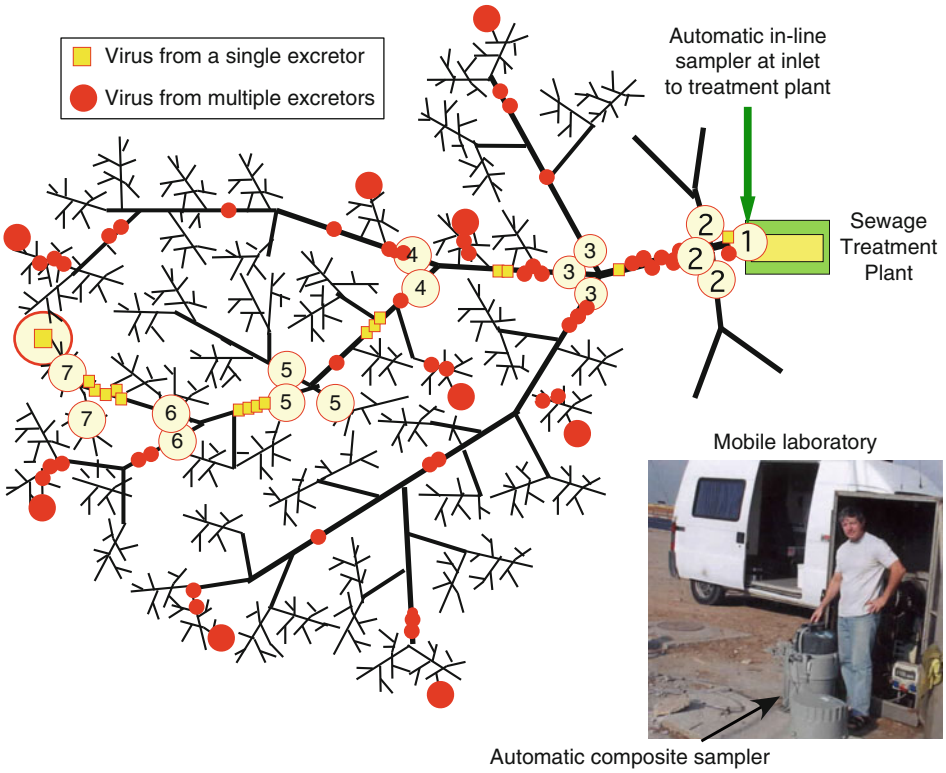

Polio and Its Epidemiology. Figure 7

Population-based environmental surveillance for poliovirus. The figure is a schematic representation of a network of sewage drainage pipes leading to a sewage treatment plant starting from individual homes, schools, or places of work or entertainment (*thinnest lines*) and converging into larger and larger *trunk lines* (*thicker lines*) until entering the treatment plant. There is an in-line automatic sampler at the inlet to the treatment plant (*green arrow*). Portable automatic samplers like those illustrated in the photograph (*black arrow*) can be lowered into sites at branch points to determine which of the branches contain virus detected by downstream sampling sites. *Yellow squares* represent virus excreted by a single infected individual living at the periphery of the system (*large yellow square*). *Large red circles* represent the situation where more than a single individual is infected and the viruses that they excrete are represented by the smaller *red circles*. The incrementally increasing *black numbers in the circles* represent upstream the order in which the portable samplers can be placed at major branch points to approach and determine the location of the single excretor (Adapted from Hovi T et al. [143] and Shulman LM et al. [291])

Informal Consultation Of The Global Polio Laboratory Network, September 2010, Geneva, Switzerland).

The Polio Laboratories are coordinated on a regional basis by Regional Laboratory Coordinators who report to the Global WHO Polio Coordinator in Geneva. Identification tasks such as intratypic differentiation and sequence analysis originally assigned to the more specialized labs are now being certified for use in National and Regional Reference Labs as expertise increases and methods – especially molecular methods are simplified. This trend has been accelerated by the increasing difficulty and costs of shipping material that may contain live infectious wild polioviruses between the different levels of laboratories and the need for decreasing the time between isolation and final notification of characterization of the poliovirus isolates. Rapid identification is especially critical for eradication efforts in endemic regions and for identifying introductions to polio-free regions from these endemic regions.

The laboratories work in close coordination with epidemiologists and medical staff in the investigation

of all cases of AFP and/or supplementary enterovirus surveillance and with municipal employees and epidemiologists where supplemental environmental surveillance is utilized to screen for poliovirus presence and circulation. In late 2010, a commercially available method for preparing noninfective viral RNA suitable for molecular analysis based on automatic nucleic acid extraction, immobilization, and storage on Flinders Technology Associates (FTA) filter papers was being evaluated to increase safety and drastically reduce costs of shipping material between laboratories (Summary and Recommendations of the 16th Informal Consultation Of The Global Polio Laboratory Network, 2010, Geneva). Using this technology, viable virus could be reconstituted from the RNA after it is transfected into eukaryotic cells.

Intratypic differentiation (determination of the serotype of an isolate) was based on results from one immunological ELISA test [214] and one molecular-based test, either probe hybridization [215], diagnostic RT-PCR [216], RT-PCR and RFLP [217], RealTime-RT-PCR [218], or micro-array-based systems [80]. At the 16th Informal Consultation Of The Global Polio Laboratory Network, 2010, Geneva, the recommendation for ITD testing from ITD-accredited laboratories was modified to one of the following three options: (a) two RealTime RT-PCR procedures, one for ITD and one for detecting vaccine-derived poliovirus and sending all non-Sabin-like viruses or Sabin-like viruses with non-Sabin-like VP1 to higher level labs for full-length sequencing and molecular analysis of VP1, (b) one validated ITD method (ITD, or molecular) and shipment of all viruses to higher level labs for full-length sequencing and molecular analysis of VP1 or (c) on-site full-length VP1 sequencing of all isolates or referral of all virus isolates to higher level labs for full-length sequencing and molecular analysis of VP1. Results are confirmed by sequence analysis of the entire VP1 capsid gene. Molecular analysis of the sequences of the genomic RNA encoding the VP1 capsid gene is in fact the definitive method to determine whether an isolate is a vaccine strain, a VDPV, or wild isolate. Sequence analysis of the VP1, all four capsid genes (e.g., P1), and even the entire genome, infers evolutionary relatedness to other isolates in endemic or external reservoirs. The methodology and results from such analyses that help trace the origin of viruses founding outbreaks have been clearly presented in reviews by Kew et al. [101] and Sutter et al. [4]. Sequence data is kept in databases maintained by the specialized laboratories of the Polio Laboratory Network, such as the CDC in Atlanta, GA, Pasteur Institute in Paris, and the HTL in Finland. Phylogenetic comparisons of sequences from new isolates, routinely provided by the CDC, indicate evolutionary relationships to previously isolated polioviruses from the same region and trace importations to or from external reservoirs. Important epidemiological information can be obtained from this phylogenetic analysis. For example, a significant gap between a new sequence and all other known sequences indicates a gap in surveillance while an importation implies that there are cases or silent circulation of related viruses in the region containing the reservoir that it is most closely related to. Knowledge obtained about time clocks [39] for nucleotide substitutions (see page 8139) allow investigators to infer whether nucleotide differences between two isolates are consistent with local transmission or represent separate introductions (e.g., see Manor et al. [102]).

The currently recommended standard method for poliomyelitis surveillance is based on the isolation and molecular and serological analysis of all viruses from all cases of acute flaccid paralysis, AFP, to rule-in or rule-out polioviral etiology [219]. The definition of an outbreak varies depending on whether endogenous poliovirus transmission has remained unbroken or the area has been found to be polio-free. In the latter, given the goal of eradication, a single AFP case can be considered to be an outbreak. The previous section describes what is needed for timely high quality testing of all poliovirus isolates from cases and from other sources such as environmental surveillance. Much time, effort, and money has been spent on maintaining and improving lab quality assurance and performance of laboratories in the Global Laboratory Network. However two factors outside of the control of the laboratories strongly influence the final result. The first is sample collection and the second is the conditions under which the sample is stored and shipped to the first processing lab. The most appropriate sample with the highest probability of detecting poliovirus is a 5-g stool sample. For AFP cases, two stool samples (not rectal swabs) should be collected 1–2 days apart within 14 days of onset of paralysis. This is based on

a review of studies measuring the timing of viral excretion (discussed on page 8143) in infected individuals [140] and the fact that detectable viral excretion is sometimes intermittent. Standardized tissue culture conditions using limited passages of poliovirus sensitive L20B, HEp2C, and RD cells provided by Specialized Laboratories of the Global Polio Laboratory Network are used according to standard operating procedures to isolate polioviruses from clinical samples [219]. An amended algorithm for isolating polioviruses designed to reduce the workload and the time between receipt of sample and identification of viruses of interest has been successfully evaluated in a number of National Poliovirus Laboratories (WHO 16th Informal Consultation Of The Global Polio Laboratory Network September 2010, Geneva, Switzerland). Standard typing and intratypic differentiation assays are based on results from serological assays and molecular assays as described above with final characterization based on the full-length sequence of VP1. Additional regions such as the 5'UTR, the entire P1 region encoding all four capsid proteins, the 3D polymerase, or the entire genome may be sequenced for higher resolution and to determine whether and to what extent genomic recombination has occurred.

Molecular data from any polioviral isolates recovered from the stool samples provides information about the serotype of the isolate or isolates, and differentiates between VAPP, persistent VDPV, and circulating VDPV or wild polioviruses. The different time clocks for single nucleotide substitutions [39] and unique recombination patterns are important tools for these analyses. Timely AFP surveillance also provides the necessary critical information about the temporal and geographic distribution of the isolates for efficient and economical infection and outbreak response. The rational for AFP surveillance is based on the observation that AFP from all non-polioviral causes occurs with an incidence of 1 per 100,000 in children up to the age of 15. When all AFP cases are investigated and the AFP incidence is within the range for non-polio causes, the absence of poliovirus in the stool samples from any AFP case is considered to indicate absence of circulating poliovirus in the region under surveillance. A surveillance area is considered to be wild poliovirus-free when adequate AFP surveillance levels for greater than 3 years indicate absence of wild poliovirus, and entire WHO-designated regions are considered to be free from endogenous wild polioviruses when all countries within that region are wild poliovirus-free.

Wild poliovirus positive AFP cases in previously polio-free areas or WHO regions can occur. Molecular analysis then reveals the most likely external reservoir from which the virus was transmitted [101]. Two recent examples of country-to-country transmission (see page 8156) which have seriously impacted the eradication initiative are the spread of wild polioviruses to >21 polio-free countries [220] as consequences of the temporary cessation of vaccination in Nigeria starting in 2003 and the spread of wild polio into the European region in 2010 [221] enabled by low vaccine coverage in Tajikistan. Sequence analysis of poliovirus isolates from cases in Mumbai confirmed cessation of local chains of transmission and the reintroduction of viral lineages still circulating in the north of India [222].

Most countries employ AFP surveillance. However not all are able to reach the required incidence of AFP investigations. Some of these countries supplement AFP surveillance with enteroviral surveillance and/or environmental surveillance (Fig. 7). Enteroviral surveillance is the systematic identification of the enterovirus genotypes in all clinical infections in general or more specifically from all cases with associated meningitis and encephalitis, symptoms that may appear more frequently than AFP in patients with poliovirus infections (approximately 5% of poliovirus infections compared to 0.5–1% for AFP). In some countries enteroviral surveillance and/or environmental surveillance are used exclusively.

A number of different sampling techniques have been used to obtain environmental samples including grab sampling during peak sewage usage, trapping with silicates or gauze, and automatic composite sampling of sewage aliquots at given time intervals over a 24-h period (Guidelines for environmental surveillance of poliovirus circulation, WHO/V&B/03.03 [223]). All sample storage and shipment must be at low temperatures (4–8°C) to maintain viability since currently certified tests require an amplification step in tissue culture. The FTA technology trial referred to above may eliminate the need for maintaining low temperatures.

The usefulness of L20B cells to isolate polio isolates in the presence of high titers of non-polio

enteroviruses [222] has already been mentioned. It is still important to characterize the viruses that grow since L20B cells can also support growth of some other human and bovine enteroviruses, as well as less well-characterized viruses [56]. Additional steps involving molecular screening and growth at elevated temperatures has enabled investigators to more easily identify and characterize wild and vaccine-derived polio in the presence of high titers of vaccine viruses [102, 215, 216, 218, 224, 225]. Selective growth of non-vaccine poliovirus at elevated temperatures [226] is based on a relative small decrease of titer for these viruses compared to a much higher reduction in yield for vaccine strains at elevated temperatures. The main molecular determinant responsible for this difference is a single nucleotide change in loop V of the 5'UTR which can revert or be modified by other changes, hence some polioviruses of interest may escape detection and some minimally diverged vaccine virus may be included among the selected isolates. Confidence that polioviruses isolated by environmental surveillance reflect circulating viruses comes from the high sequence homology between environmental samples and isolates from cases [38, 143, 227]. One of the major contributions of environmental surveillance reviewed by Hovi et al. [143] is that it can be used to establish the presence and/or circulation of wild or vaccine-derived polioviruses before the appearance of AFP cases [102, 222, 227–229]. Environmental surveillance has also revealed the presence of presumptive primary vaccinees excreting OPV in Switzerland where vaccination is by exclusive use of IPV [56].

Different methods for analyzing environmental samples are also currently employed in different laboratories [223] since unlike AFP surveillance [230] there is as of yet no single standard method. The probability of detecting poliovirus in environmental samples [229] depends on the duration and amount of poliovirus excreted by one or more infected individuals (see page 8143), the effect of physical and mechanical factors on the dilution and survival of poliovirus in the sewage system (reviewed by Dowdle [134]), and the frequency of collection and laboratory processing of the environmental samples [223]. A model based on these factors [229] predicted that environmental surveillance could outperform AFP surveillance for small outbreaks as well as detect circulation before the appearance of cases. The location of the sampling site relative to the excretor and the number of excretors (Fig. 7) also determines the probability of detection [143]. In general polioviruses can be quantitatively recovered from the environment [231]. Decreasing this distance between the excretor and the sample collection site is more effective in increasing the probability of detection and less labor intensive than increasing the sampling frequency [109]. Environmental surveillance is resource and labor intensive and may require large capacity high-speed centrifuges that are not commonly present in most National Poliovirus Laboratories [143]. It requires judicious choice of potential target populations, a competent laboratory, a plan for routine surveillance and reporting, and the cooperation of municipal authorities. The WHO has recommended principles for selecting sites, sampling strategies, and interpretation of results [223]. Lengthy periods of poliovirus-free monitoring are needed to confirm that poliovirus transmission has stopped since even the most comprehensive surveillance covers only subgroups of the entire population of potential excretors [232].

Many poliovirus positive environmental samples contain one or at best a few polioviruses of interest indicating that the surveillance is operating at the lower limits of detection. Thus while negative findings cannot rule-out the presence of polioviruses at levels below detection, they gain significance when they are part of a long sequence of negative results from frequent routine surveillance at the given site. A positive finding of a wild poliovirus or a VDPV can trigger a response ranging from public announcements to remind individuals scheduled for routine vaccinations to be vaccinated in time in areas with high vaccine coverage to scheduling NIDS or SNIDS in regions where immunization coverage is below that required for establishing herd immunity. Sequence analysis can differentiate between multiple importations and local circulation when more than one poliovirus is isolated within a short interval of time [102].

Detection of "orphan polioviruses" or virus that are not closely linked to previously sequenced isolates indicates gaps or suboptimal surveillance. The length of the gap is roughly proportional to 1% single nucleotide divergence per year [39]. Orphan viruses [91, 105, 191] were responsible for most cVDPV outbreaks. This is in contrast to the situation in Nigeria where intensive AFP

surveillance triggered by the circulating wild polioviruses also revealed the initial stages in circulation of multiple lineages of predominantly type 2 cVDPVs [106]. The presence of type 2 cVDPVs, iVDPVs, and aVDPVs is of concern since despite elimination of transmission of wild type 2 in 1999, neurovirulent serotype 2 poliovirus is still among us [124, 128].

A number of countries that switched from OPV or combinations of OPV and IPV to exclusive use of IPV conducted environmental surveillance for OPV after the transition (reviewed in [143]). The OPV rapidly disappeared from the environmental samples but imported OPV-like isolates have been isolated from time to time presumably imported from OPV-using countries [233].

One of the important milestones toward achieving eradication is the containment of all potential sources of the pathogen. In 1999, a process for containing all laboratory stocks of wild poliovirus was initiated by the World Health Assembly entitled *Global action plan for the laboratory containment of wild polioviruses* or GAP 1 (WHO/V&B/99.32). A revised plan, GAP II, included two phases: (1) the identification in all facilities of all known poliovirus stocks and any material that could potentially contain live wild poliovirus, for example, any stool specimens that were collected at times when poliovirus was endemic, and (2) the containment of these stocks by destroying them, rendering them noninfectious, or transferring them to a minimal number of laboratories certified by the WHO as having appropriate BSL3/polio biosafety facilities and justification to work with wild viruses. A draft of the next version, GAP III, extends containment of wild polio to now also include containment of OPV/Sabin strains, and concentrates on minimizing risks associated from facilities that work with polioviruses and vaccine production and storage facilities after eradication of wild poliovirus transmission and cessation of OPV vaccination. Pathways of exposure from these facilities and assessment of the risks from a literature review have been calculated [134]. After risk analysis, a goal was set to reduce the number of such facilities globally to <20 essential facilities that meet required safeguards.

The original target date for polio eradication was not met. By 2001, the WHO Global Commission for the Certification of the Eradication of Poliomyelitis extended eradication to include elimination of circulating VDPVs (Certification of the Global Eradication of Poliomyelitis Report of the sixth meeting of the Global Commission for the Certification of the Eradication of Poliomyelitis. Washington D.C., 28–29 March 2001 WHO/V&B/01.15). The current target date for interruption of all wild poliovirus has been moved to 2013 (Global Polio Eradication Initiative – Programme of Work 2009 and financial resource requirements 2009–2013. WHO/POLIO/09.02). This section will conclude with a discussion of the three major problems that have accounted for the delay in completing the GPEI, "failure to vaccinate," "vaccine failure," and the emergence of "vaccine-derived viruses."

Among the reports available online at the WHO website for polio eradication, www.polioeradication.org, is a report on the annual percentage of children in each country who received a minimum of three doses of polio vaccine annually since 1980. This report provides a complete picture of current polio immunization status. However the variability in coverage between countries and the annual fluctuation within countries illustrates the problem of failure to vaccinate and is also an indication of problems in sustaining the high coverage necessary for successful eradication.

Wild and vaccine-derived poliovirus can penetrate and circulate within areas where vaccination coverage is low or where vaccination has been discontinued [106, 117, 234]. When this occurs this is an example of "failure to vaccinate." The temporary cessation of vaccination in Nigeria in 2003 [235, 236] is usually presented as the classic example for the consequences of a failure to vaccinate. The situation was complicated by suboptimal coverage within Nigeria when vaccination resumed within 12 months and the suboptimal coverage in other countries that had person-to-person contacts with infected Nigerians. Thirteen countries with 52% coverage have had multiple introductions of wild poliovirus from Nigeria, while another eight countries with higher 83% coverage did not have repeated outbreaks [1]. Use of type 1 mOPV was successful in reducing the number of cases from wild type 1 [190, 234] but the decreased use of tOPV lead to a significant increase in cases due to wild type 3. Subsequent use of mOPV1, mOPV3, and bOPV has effectively reduced the number of cases due to wild types 1 and 3 [237]. Unfortunately suboptimal

immunization with any vaccine that contained type 2, presented fertile conditions for the emergence of multiple lineages of type 2 CVDPVs some of which have continued to circulate well into 2010 [106] (see discussion on page 8157, 8161).

A 2010 outbreak that started from a wild type 1 virus imported into Tajikistan from India spread into the Russian Federation. This was the first outbreak due to wild poliovirus in the WHO European region since it was declared polio-free in 2002 [221]. Again failure to vaccinate with coverage sufficient to maintain herd immunity was the main factor that facilitated the outbreak. As of June 2010, wild poliovirus cases from this outbreak accounted for more than 70% of all wild polio cases reported in 2010. Four NIDS with mOPV1 were conducted since the start of the outbreak.

When poliomyelitis occurs in vaccinated individuals it is categorized as "vaccine failure." Current reports on India (20th Meeting of the India Expert Advisory Group for Polio Eradication Delhi, India, 24–25 June 2009 www.polioeraication.org) indicate that most of India is poliomyelitis-free with the exception of the north where both wild type 1 and type 3 still circulate. Type 1 and 3 mOPV have helped to reduce the number of circulating lineages and to constrict the areas within which the wild polioviruses are still circulating and causing cases. However, lack of cases in the south does not mean absence of wild poliovirus as environmental surveillance has revealed silent wild polio in Mumbai. The reservoir is not only a problem for India. Populations with suboptimal coverage in other countries are also at risk, as shown by the 2010 outbreak in Tajikistan and the Russian Federation that was traced back to northern India [221].

Vaccine failure in children in India refers to the finding that antibody response or seroconversion in children required more than the recommended three doses of tOPV [238, 239]. In Uttar Pradesh and Bihar in north India, local conditions exist where even administration of five doses of OPV does not induce the expected seroconversion rates. Approximately 15 doses were required to reach population immunity [240]. The fact that the age when the disease is acquired had not shifted upward was taken as an additional indication of vaccine failure [1]. Various trials of efficacy of mOPVs and bOPV and fractional IPV are underway to evaluate their short-term effectiveness in halting endemic transmission and their long-term performance in maintaining protective titers. In India mucosal immunity in response to vaccination with OPV varied depending on location, serotype, and vaccine formulation [241].

The high number of additional doses needed to achieve herd immunity in some regions such as in northern India combined with the additional cost of OPV in annual and sub-annual vaccination campaigns must be taken into account when comparing the cost effectiveness of OPV and IPV in inducing effective herd immunity.

A less serious type of vaccine failure is based on observations that do not completely confirm the paradigm that OPV prevents replication during subsequent exposures to poliovirus. Israeli children who had concluded a primary immunization schedule consisting of three doses of OPV and three doses of IPV by 18 months of age had seroconverted for all three serotypes with geometric mean titers >1,000 [159]. One month after the last vaccination they were challenged with an additional dose of OPV. Up to 60% of children excreted at least one OPV serotype between 1 and 3 weeks, the upper range of similar studies reviewed in that report. There was no evidence of transmission to siblings or mothers of these children, most likely because of good hygiene [159]. These rates were comparable to other similar studies [159]. Hygiene and high coverage probably also contributed to the fact that there was also no evidence for OPV circulation in IPV-vaccinated populations in the United States living adjacent to OPV-vaccinated populations in Mexico [242].

A number of comprehensive reviews on vaccine-derived polioviruses have been published [3, 62, 79, 105, 114, 243–246]. As described above (page 15), vaccine-derived polioviruses evolve either during person-to-person transmission (cVDPVs) or during relatively rare [247] persistent infections in immunodeficient patients (iVDPVs) (see reviews [3, 4, 105, 114]). To date (2010) there have been 12 cVDPV outbreaks [106]. Using the definition of outbreak in the context of eradication (i.e., even a single case), the number of outbreak may be even higher. For example, in 2009, 21 cases due to cVDPVs were found in four countries in addition to 153 in Nigeria and a case in Guinea traced back to Nigeria [248], and the cases in

Nigeria represent emergence of multiple independent lineages [106].

Most outbreaks caused by cVDPVs have been caused by a single lineage that spread rapidly through a susceptible cohort within the general population. The outbreaks were only discovered after silent circulation of the VDPVs for more than 1 year or more indicating gaps in surveillance. By the time such outbreaks became evident, the genomes of the isolates had usually recombined with those of the progeny of other vaccine serotypes or closely related non-polio enteroviruses. When OPV is introduced or reintroduced into a population with cohorts of naïve individuals as in Nigeria, adequate surveillance revealed that in early stages of reemergence more than one independent lineage may emerge [106]. There is also a potential for recombination of cVDPVs with wild-type viruses in areas where both co-circulate as shown from retrospective molecular analysis of isolates during endemic circulation of wild polioviruses [82]. Luckily from the point of view of eradication, cVDPV outbreaks resemble outbreaks of poliomyelitis from wild polioviruses introduced into polio-free areas and their chains of transmission can be broken by similar vaccination responses [106, 234].

In certain circumstances poliovirus can establish persistent infection in immunodeficient individuals. The types of immune deficiencies of known chronic excretors have been reviewed [3, 4, 62, 105]. The genomes of the Sabin strains are unstable [114] and reversion of nucleotide changes that attenuated neurovirulence appear even among the progeny virus excreted by primary OPV vaccinees. These reversions are believed to improve the replicative fitness of the isolates [123] and are responsible for the rarity of vaccine-associated paralytic poliomyelitis cases (VAPP; 1 per 500,000–1,000,000 vaccinations of naïve infants, and 7,000 times higher for some immunodeficient individuals) and cVDPV outbreaks [3, 105]. Thus it is not surprising that reversion of attenuation also occurs at an early stage in chronic excretors [62]. During 4 months of observation of long-term excretion in a healthy child [62] type 1 virus diverged by 1.1% and evolved toward full reversion to wild-type phenotypic properties similar to the Mahoney parent of the Sabin 1 strain. It is less obvious why these isolates so quickly predominate in the quasispecies of persistently infected immunodeficient individuals. The process by which persistence is established and maintained may present selection through bottlenecks within a single individual that is similar to the bottleneck by which only a single progeny or a subpopulation of the quasispecies is passed onto the next host in person-to-person transmission among immune competent hosts. Selection by passage through bottlenecks was also suggested to explain evolution of wild poliovirus during long-term expression [249]. Examination of the genomes of iVDPV isolates differentiates them from cVDPVs in that significantly fewer heterotypic recombinations occur [4, 110] and intrageneous recombination appears to be largely absent [4, 105]. Interestingly, more than one highly divergent lineage may be recovered from a single stool sample from persistently infected individuals [3, 110]. This suggests that persistence and evolution occur in separate sites although intratypic recombination indicates that some mixed infections in a single cell must occur. Only a single serotype was detected in most (30 of 33) long-term excretors identified between 1962 and 2006 [4] and this pattern has continued to date. Amino acid changes in capsid proteins may allow polo to establish persistence in cells of the CNS [250].

Molecular analysis of phylogenetically related highly diverged (>10%) aVDPVs isolated from sewage in Finland, Slovakia, and Israel reveals a pattern of amino acid substitutions in or near neutralizing antigenic epitopes and lack of intrageneous recombination that resembles the pattern of changes in iVDPVs and is qualitatively different from evolutionary changes in cVDPVs [109, 251]. This pattern and the extended periods of time over which phylogenetically related polioviruses have been isolated from the same sewage systems and surveillance sites within those systems strongly suggests that replication of the related viruses has taken place in one immunodeficient host, or a very limited number of individuals in contact with such a host. Routine monthly sewage surveillance of catchment areas representing 35–40% of the population in Israel intermittently and repeatedly revealed the presence of highly diverged type 2 VDPVs 2 between 1998 and 2010. Phylogenetic analysis indicated that the isolates came from two different and unrelated persistent infections. Isolates form one foci have been isolated intermittently for 12 years and the second for 4 years.

In addition there was a single, respectively, and a single isolation of a highly diverged type 1 VDPV. The situation in Finland is particularly interesting and unusual, since evidence suggests that the infected individual is simultaneously and persistently infected with three highly diverged VDPV serotypes [251].

Most mutations in iVDPVs and aVDPVs are synonymous and are observed in third position codons. These synonymous substitutions occur at similar rates to those for poliovirus during person-to-person transmission [39, 101, 107, 109]. Non-synonymous amino acid substitutions affect antigenicity, neurovirulence, receptor binding motifs, hydrophobic pockets, and drug sensitivity.

The prevalence of aVDPV excretors is unknown, but additional countries with excretors of aVDPVs are being reported as environmental surveillance is introduced into more and more regions [143, 246, 252–256]. Hovi et al. [143] have proposed expanding the suggestion that the GPLN include regular monitoring for cVDPVs [257] through increasing the number of laboratories that employ routine environmental surveillance. It is important to determine the exact nature of the immune status of these types of persistent excretors since it may be different than that for identified persistently infected individuals. Unfortunately the individuals infected with these aVDPS remain unidentified, and will most likely remain so for a long time [143]. The most frustrating attempt to locate such an excretor occurred in Slovakia where moving sampling sites progressively upstream successively restricted the excretor to a population of 500 individuals before detection ceased [143].

There is no consensus on the extent that persistent VDPVs may affect the realization of eradication [133, 163]. Determining the number of unidentified persistent infections is becoming more urgent as eradication of wild polio approaches (WHO 16th Informal Consultation Of The Global Polio Laboratory Network. 22–23 September 2010, Geneva, Switzerland, WHO/HQ. Summary of Discussions and Recommendations). Some researchers believe that VDPVs may pose an insurmountable problem [114, 127] while others feel that the problem is less severe [3, 4, 126]. Most of the identified persistent excretors had primary B-cell-related immunodeficiencies [4, 105]. While molecular epidemiological analysis has indicated that highly diverged neurovirulent anonymous VDPVs isolated from sewage in Finland, Slovakia, and Israel [109, 233, 258] resemble the molecular epidemiology of poliovirus isolates excreted over time by identified excretors of iVDPVs, the exact nature of the immune status that has presumably enabled infection to persist in these aVDPV excretors remains unknown. The time course of excretions, the rate of nucleotide substitutions in virus isolated from identified persistent excretors, and genomic recombination patterns have been consistent with the establishment of persistence and evolution of the virus in these individuals rather than transmission of an iVDPV. Highly diverged iVDPVs (as opposed to cVDPVs and less diverged iVDPVs) have not been found during routine AFP surveillance of cases of immune competent individuals [3]. One clear indication that iVDPV-like aVDPVs are transmissible comes from a study of silent transmission in infected children in an under-vaccinated community in Minnesota [259] where 8 of 23 infants had evidence of type 1 poliovirus of VDPV infection. While this absence of documented transmissibility of very highly diverged VDPVs is encouraging, it may only be circumstantial, since most of the highly diverged neurovirulent aVDPVs have been found in the environment of countries with high vaccine coverage and good hygiene barriers that have also prevented circulation and appearance of wild poliovirus cases even after neurovirulent wild polio was introduced from external reservoirs [102].

The amino acid substitutions in neutralizing antigenic epitopes/receptor binding residues in iVDPVs and iVDPV-like aVDPVs may have helped specialize these virus isolates for microenvironments within the gut during persistent infections. These same changes might affect/reduce transmission via the oral–oral route in communities where there is high vaccine coverage and good hygiene. If true, this might significantly reduce the threat to eradication, despite the highly neurovirulent nature of these isolates in animal model systems and the decreased geometric mean neutralizing antibody titers against some of these excreted iVDPV and aVDPV isolates in the general public in the highly immunized communities where these isolates are found [109, 233]. It must also be taken into account that identified and unknown excretors are free to travel to communities with poor vaccine coverage and

substandard hygiene where the fecal–oral transmission route is more important and continuous person-to-person transmission easier to maintain.

Future Directions: The Endgame Stage of Eradication and Sustainability of Postpolio Eradication

This section will start with an overview of current accomplishments to provide a suitable background for the discussion of future directions and sustainability. One of the best online sources for keeping up to date on eradication can be found at www.polioeradication.org.

There has been a >99% overall reduction in the number of cases since adoption of the Global Poliovirus Eradication Initiative in 1988 [248]. The Region of the Americas (AMR) was certified to be free from all three serotypes of indigenous wild polioviruses in 1994 [260, 261] and the last case anywhere in the world from wild type 2 polio occurred in India in 1999 [186, 262]. Subsequently the Western Pacific Region (WPR) in 2000 [263] and the European Region (EUR) in 2002 [264] have also been certified to be free from indigenous wild polioviruses. These successes have been due to the dynamic nature of the eradication program where vaccination strategies have been adapted in response to specific problems and to changing conditions emerging as the endgame approached [1]. Four countries remain where indigenous poliovirus has continued, Afghanistan and Pakistan in the WHO Eastern Mediterranean Region (EMR), Nigeria in the WHO African Region (AFR), and India in the WHO South-East Asia Region (SEAR).

The accumulated costs for the vaccination program have exceeded 4.5 billion US dollars. National governments (list by alphabetical order: Australia, Austria, Belgium, Canada, Denmark, Finland, Germany, Ireland, Italy, Japan, Luxembourg, the Netherlands, Norway, the United Kingdom, and the United States) have provided a significant portion of the necessary funding. NGOs (WHO, UNICEF, Rotary International, the Bill and Melinda Gates Foundation, and the International Red Cross and Red Crescent societies), the World Bank, and corporate partners (Aventis Pasteur, De Beers) have also made significant contributions toward purchase of vaccines and for applied and basic polio research. In addition to paid professional staff, more than ten million volunteers have assisted in the global vaccination program. Their knowledge of local practices and beliefs has provided a significant asset to the GPEI [1].

One of the goals of eradication was to reach a stage where vaccination could be discontinued, as was the case for smallpox vaccinations after eradication of smallpox [265]. The estimated annual savings would be enormous and could be used to fund other global health initiatives. Similarly the organizational capabilities experience expertise and facilities of member Laboratories in the Global Polio Laboratory Network would also be employed to solve other health-related problems. The three main problems that have delayed eradication originally scheduled for 2000 have been discussed. Among these problems, chronic excretion of vaccine-derived viruses probably remains the most serious obstacle since the number of excretors remains unknown and there are no universally recognized methods of curing chronic excretion in those chronic excretors who have been identified.

Between January 2009 and June 2010, the Global Polio Laboratory Network analyzed 258,000 fecal specimens from 130,000 AFP cases for the presence of poliovirus, and between January 2009 and September 2010 it detected introductions of wild poliovirus into 23 previously "polio-free countries," countries where indigenous polio transmission had been interrupted. Nineteen were in the African region and included seven countries (Burkina Faso, Benin, Chad, Côte d'Ivoire, Mauritania, Niger, and Togo) where the outbreak isolates were related to previous importations into those countries as was the case for Sudan in the Eastern Mediterranean Region. One of the more serious setbacks for eradication was the introduction of wild poliovirus into Tajikistan from Uttar Pradesh in India marking the first outbreak in the European region since it was certified poliovirus-free in 2002 [221]. The large outbreak (>450 confirmed cases) ensued spread into the Russian Federation and resulted in an immediate tenfold increase in the amount of samples that needed to be processed by the Polio Laboratories in the region. In all of these importation countries and/or regions, large-scale coordinated SIAs were conducted. The spread of wild poliovirus to poliovirus-free countries from Nigeria and India via Tajikistan illustrate the need

to maintain high population immunity until all transmission of wild virus has ceased. Similarly, the emergence of multiple lineages of neurovirulent VDPVs in Nigeria and the increasing frequency of isolation of aVDPVs as more countries adopt environmental surveillance reinforce the need to discontinue use of OPV globally in a coordinated effort or staged manner. See Ehrenfeld et al. [266] for a review and discussion of key issues that have affected and will affect the GPEI, including: safety for volunteers in areas of strife, the low efficiency of OPV to induce herd immunity in certain settings, the requirement for maintaining high coverage even after eradication, the inherent mutability of OPV, problems for establishing the safety and efficacy and costs of new vaccines, new vaccine formulations, and scaling up alternatives to OPV.

The saying "*May you live in interesting times*," often attributed to an ancient Chinese proverb or curse, appears appropriate for describing the current status in the quest to eradicate wild polioviruses. Eradication, which is tantalizingly close, will require substantial changes in vaccination policy and practice [117]. It must also include appropriate emergency response measures to control reemergence. "The ideal vaccine choice for the stockpile should be effective in any outbreak scenario, protect all vaccinees with one dose, spread to and protect the unvaccinated population, and have no detrimental effect" [267]. Long-term effects should be considered. While mOPV might be the most effective in rapidly controlling an outbreak and spreading and protecting unvaccinated individuals [267], plans that preferably do not require use of OPV adjacent to areas with high concentrations of unvaccinated individuals would be better in the long run [117, 268]. The reader is referred to the website of poliovirus eradication (www.polioeradication.org) for the latest information on past, current, and future policies.

Three problems have delayed the realization of eradication as has been discussed. Currently available vaccines can overcome "failure to vaccinate," provided that enough doses of vaccines are made available, that there is the political will to use them, and that natural or man-made disasters do not prevent reaching the children for vaccination. Preliminary results from newly approved monovalent and bivalent oral polio vaccines and clinical studies using fractional doses of IPV indicate that there may already be a solution for "vaccine failure" which is exemplified by the poor seroconversion rates for OPV in northern India [240]. The third major problem, "vaccine-derived polioviruses" is more complex, since VDPVs can evolve by person-to-person transmission (cVDPVs) or during persistent infections (iVDPVs). The spread of cVDPVs can be interrupted using the same methods as used to stop transmission of wild poliovirus (paradoxically including use of OPV in vaccination campaigns), since cVDPVs behave like wild virus [106, 234]. Moreover, while it is easy to say that current GPEI plans to coordinate global cessation of the use of OPV will prevent VAPP [206] and emergence of new cVDPVs, at this juncture the actual process is quite complicated and associated with a number of risks. The main problem that will need to be solved is the shedding of highly neurovirulent VDPVs into the environment for prolonged periods by identified and unidentified, persistently infected individuals. There is currently no universal solution to this problem [63, 125]. As long as shedding persists (perhaps as long as some of these individuals remain alive), containment as envisioned in GAP III will be incomplete and high vaccination coverage will need to be maintained. A related but more difficult problem that will need to be solved is (a) to determine the prevalence of unidentified, presumably persistently infected individuals who are responsible for shedding the highly diverged aVDPVs that have been isolated from environmental surveillance, and (b) to identify the presumably persistently infected individuals to determine the physiological conditions that enabled persistence and to try and clear the persistent infection with current or future antiviral treatments. As the endpoint of eradication of wild poliovirus is approached, the number of cases of poliomyelitis will decrease while the number of silent infections may increase as a result of high vaccine coverage. Under these conditions supplemental surveillance programs such as enterovirus surveillance and environmental surveillance will become an even more important tool for providing geographical information for designing NIDS, SNIDS, and final mopping-up campaigns for eradication and for monitoring for post-eradication reemergence.

"Although OPV has been the mainstay of the eradication program, its continued use is ironically

incompatible with the eradication of paralytic disease (since) vaccine-derived viruses consistently emerge as a consequence of the inherent genetic instability of poliovirus [122]." "Eradication of vaccine" suggested in 1997 [204, 205] has become recommended policy on condition that provisions of GAP III for safety in vaccine production and polio laboratories are met [264, 269]. A model describing the impact of cVDPVs on eradication indicated that the probability of eradicating polio with continuous use of OPV was not very likely [270]. Alternative vaccination should be continued during and especially after the transition to maintain high coverage and to avoid the buildup of large susceptible populations during the time when there is the highest risk for reemergence of OPV strains [117, 134, 270–272]. Low population immunity remains the main known risk factor for the emergence and spread of cVDPVs [234, 243]. Since most of the cVDPVs in outbreaks circulated silently for months or years (VP1 divergence >2%) before detection in AFP cases, it is imperative that surveillance be improved and expanded to high-risk regions to detect silent circulation of VDPVs as early as possible.

Endgame vaccination strategies have been reviewed [3, 122, 163, 266, 268] and include (1) indefinite use of OPV, (2) cessation of all polio immunization (3) transition to use of IPV, by synchronous coordinated cessation of all use of OPV with (a) limited use of IPV or (b) replacement of all OPV with IPV, (4) country-by-country cessation of OPV use with options (3a) or (3b), (5) sequential removal of Sabin strains from OPV, as eradication proceeds, (6) development of new vaccines, and (7) indefinite use of IPV or new vaccines. The synchronous cessation of OPV has several problems particularly if inexpensive alternatives are not in place when it occurs, since this vacuum may result in large populations of naïve individuals, in whom, polio could reemerge, after periods of silent circulation, with high force and rapid spread. Such a scenario also does not address the potential risks of unidentified chronic excretors. A gradual shift to IPV may avoid some of the programmatic disadvantages that coordinating a synchronous shift would have on vaccination programs and vaccination production facilities. It also potentially provides a longer window for industry to increase production, integrate information from current fractional vaccine dosage and alternative routes of administration trials, and overcome problems of biocontainment and antigenicity associated with optional use of killed OPV as a substitute for the wild strains used in IPV production.

The WHO and UNICEF regularly consult informally with vaccine manufacturers to discuss the implications and practicality of vaccine policy decisions (summaries are available from the Internet using variations of a search for "WHO/UNICEF Informal Consultation with IPV and OPV Manufacturers"). For example, the 3rd WHO/UNICEF Informal Consultation with IPV and OPV Manufacturers (2003) included a discussion of post-eradication needs and biocontainment requirements and the 5th (2006) included updated information on progress of the GPEI and OPV cessation strategies.

The financial requirements for the transition period are complicated and have been set forth by the WHO (WHO Global Polio Eradication Initiative – Programme of Work 2009 and financial resource requirements 2009–2013 WHO/POLIO/09.02). The bottom line is that alternatives to OPV must be affordable [234]. Three recent reports deal in depth with the economics and practicality of universal replacement of OPV with IPV: (a) Global Post-eradication IPV Supply and Demand Assessment: Integrated Findings, March 2009, and (b) The supply landscape and economics of IPV-containing combination vaccines: Key findings, May 2010, both commissioned by the Bill & Melinda Gates Foundation and prepared by Oliver Wyman, Inc., and (c) Improving the affordability of inactivated poliovirus vaccines (IPV) for use in low- and middle-income countries – An economic analysis of strategies to reduce the cost of routine IPV immunization, April 20, 2010, prepared for PATH by Hickling, Jones, and Nundy. The second report [273] presents a thorough review of the current options and risks for new vaccines and vaccine formulations for achieving and maintaining eradication. New generations of inactivated polio vaccines may need to be developed for post-eradication use [266, 274] and they may have to be used indefinitely.

A number of decisions must be made now, some based on incomplete knowledge, because of the long lead time needed between planning facilities and final production of regulatory agency-approved products. For example, while fractional doses significantly reduce

costs, they are less effective than full doses and there is little data on kinetics of waning, while questions still exist concerning sufficient antigenicity of Sabin IPV. Additional complications involve testing and regulatory approval of new products or formulations (see discussion on regulations and standardization of IPV and IPV combination vaccines in Baca-Estrada and Griffiths [275] and the views of vaccine producers [276, 277]). The good news is that when "new" polio vaccine, type 1 mOPV, was needed, it was produced by two companies and licensed in three countries in a relatively short time, 6 months [135, 278, 279]. (Quotation marks were used around the word new since in actuality millions of monovalent doses of each serotype had been used before introduction of tOPV [280] when old licenses had been left to expire). Licensing was also aided by the fact that monovalent batches were produced and safety tested before being combined to produce tOPV and only qualified tOPV producers were approached to provide mOPVs [279]. Ironically if mOPVs are more effective than respective serotypes in tOPV because of increased titers and longer replication times, the increased number of nucleotide substitutions may increase the potential for cVDPV outbreaks by the serotype used [103] or conversely from the remaining serotypes (or serotype if bOPV is used). Supporting this is the emergence of significantly higher numbers of type 1 viruses with increased antigenic divergence from Sabin 1 after a birth dose of mOPV1 and a second exposure to Sabin 1 [111]. Most (71%) were isolated from stools from infants who did not seroconvert after the birth dose [111]. Rapid licensing of bOPV on January 10, 2010, followed release of efficacy results on June 2009 (issue 6 PolioPipeline, summer 2010). The bad news is that combination vaccines containing IPV cannot be frozen raising questions about long-term stability and appropriate reference standards [275].

There have been a number of attempts to rationally redesign the sequence of vaccine seed strains to make them more stable and safer to use in vaccine production facilities in the post-eradication period [3]. One drawback is that there is no empirical data on how these new viruses will behave in the field especially in relation to genome stability and the ability to recombine with heterotypic or intragenic enteroviruses. Changing codons to equivalent but rarely used synonymous codons based on studies of codon use bias or increasing the frequency of CpG and UpA dinucleotides are methods to change the substitution rate [97, 281, 282]. Others modifications have led to polioviruses that can grow in nonhuman cell lines for production but have very low ability to infect human cells.

Widespread vaccination will continue at least during the 3-year period between the last case due to wild poliovirus and certification that wild poliovirus transmission has been interrupted globally. However, global vaccination should be continued for much longer since by one model [283], after 3 years there would only be a 95% certainty that all silent circulation had in fact ceased and the probability after 5 years ranged between 0.1% and 1%, while a more recent model has predicted a very high probability of reemergence within 10 years after eradication by VDPVs or accidental release of virus from vaccine production facilities, a polio laboratory, or bioterror [272]. Consequently vaccination will need to continue for at least 10 years after eradication. A special issue of the journal Risk Analysis (Volume 26, Issue 6, 2006) has been devoted to risks associated with polioviruses before, during, and after eradication of wild poliovirus. Finally vaccination with IPV may be continued indefinitely at least in countries where aVDPVs continue to be isolated from the environment with attendant risk from a polio vaccine production facility operating in a polio-free era (see discussion above on GAP III). To reiterate, current contingency plans for use of OPV in response to reemergence need to be revised based on the data on circulation of live vaccine strains after temporary and/or partial cessation of vaccination [117].

The final and one of the most important problems that must be successfully dealt with is to answer the question: "How can current achievements and eradication be sustained once the endgame has been concluded?" Ideally a major public health undertaking such as eradication requires a cost-benefit analysis, sufficient funds at the beginning, the means for achievement at hand, and the political and social will to carry the process through to the end. Delays and problems with fund-raising, especially when they occur during the endgame, may derail the entire effort [1]. Some problems with sustainability are associated with management and not scientific problems [1, 284].

However, new unanticipated scientific problems may appear which further delay polio eradication. After all, awareness of the potential problems from cVDPVs in communities with low vaccine coverage and chronic excretors of VDPV primarily appeared during the endgame of eradication when the global burden of cases had decreased by >99% and only after appropriate analytic tools to easily document and confirm VDPV had became widely available [3]. An example is the revelation of the 10-year circulation of cVDPVs in Egypt starting in 1983 [285] by retrospective phylogenetic examination of VP1 sequences.

The means to prevent disease and contain the spread of virus transmission when it emerges are already in hand. Safer and more cost-effective measures are in the pipeline that include schedule reduction and fractional doses, adjuvant use, optimizing of processing, Sabin or modified Sabin IPV, and noninfectious IPV [119, 273]. Sustainability for achieving eradication will depend on vaccine policy decisions made today, on the length of time it takes to eliminate all wild poliovirus transmissions, on political will and advocacy, on the motivation of volunteers and the level of local community involvement, program-related fatigue, and on the absence of complications [286] from bio-error, bioterror, or mother nature [291]. However the major determining factor will probably be the availability of financial resources [135]. Limited resources mean competition between routine immunization and eradication efforts during endgame. A predicted 1.3 billion USD funding gap in June 2010 is already forcing a reprioritization of planned activities (Global Polio Eradication Initiative Monthly Situation Report June 2010 www.polioeracdication.org.) "Even if there are no competing health needs, it is unlikely that immunization could be maintained indefinitely against a non-existent disease at a level that is sufficient to prevent vaccine-derived viruses evolving to cause epidemics"[163]. Programmatic setbacks such as those associated with failure to vaccinate (Nigeria and Tajikistan), vaccine failure (northern India), the frequency of repeated vaccination campaigns, or post-eradication reemergence must not be allowed to derail the current momentum and lead to program-related fatigue [1]. Detailed planning must be made for any post-eradication outbreaks (see Jenkins and Modlin [267] and Tebbins et al. [268]) and provisions to implement them including stockpiling must be in place. Finally it is well worth reading "The pathogenesis of poliomyelitis: what we don't know" by Nathanson [287] and "Gaps in scientific knowledge for the post-eradication world" by Minor [288].

Note

Polio is the second human pathogen for which there is an ongoing global program for eradication that has reached the endgame. The first, smallpox, successfully completed the endgame and is now in the stage of post-eradication sustainability. Bioterror is the main threat to sustainability of smallpox eradication. This chapter will describe some of the difficulties with completing the endgame of polio eradication and then in sustaining postpolio eradication. More than the usual number of items are included in the glossary to make it easier for the reader to follow the progress of eradication as it unfolds in the large number of official documents that deal with a global eradication program and which contain the usual copious number of professional acronyms.

Bibliography

1. Lahariya C (2007) Global eradication of polio: the case for "finishing the job". Bull World Health Organ 85(6):487–492
2. Daniel TM, Robbins FC (1997) A history of poliomyelitis. In: Daniel TM, Robbins FC (eds) Polio. University of Rochester Press, Rochester, pp 5–22
3. Kew OM, Sutter RW, de Gourville EM, Dowdle WR, Pallansch MA (2005) Vaccine-derived polioviruses and the endgame strategy for global polio eradication. Annu Rev Microbiol 59:587–635
4. Sutter RW, Kew OM, Cochi SL (2008) Poliovirus vaccine – live. In: Plotkin SA, Orenstein WA, Offit PA (eds) Vaccines, 5th edn. W.B. Saunders/Elsevier, Philadelphia, pp 631–685
5. Burnet FM, MacNamara J (1931) Immunological differences between strains of poliomyelitic virus. Br J Exp Pathol 12:57–61
6. Wyatt HV (1985) Provocation of poliomyelitis by multiple injections. Trans R Soc Trop Med Hyg 79(3):355–358
7. Enders J, Weller T, Robbins FC (1949) Cultivation of the lansing strain of poliomyelitis virus in cultures of various human embryonic tissues. Science 109(2822):85–87
8. Dulbecco R, Vogt M (1954) Plaque formation and isolation of pure lines with poliomyelitis viruses. J Exp Med 99(2):167–182
9. van Wezel AL (1967) Growth of cell-strains and primary cells on micro-carriers in homogeneous culture. Nature 216(5110): 64–65
10. Cockburn WC (1988) The work of the WHO consultative group on poliomyelitis vaccines. Bull World Health Organ 66(2): 143–154

11. Mendelsohn CL, Wimmer E, Racaniello VR (1989) Cellular receptor for poliovirus: molecular cloning, nucleotide sequence, and expression of a new member of the immunoglobulin superfamily. Cell 56(5):855–865
12. Dragunsky E, Nomura T, Karpinski K, Furesz J, Wood DJ, Pervikov Y et al (2003) Transgenic mice as an alternative to monkeys for neurovirulence testing of live oral poliovirus vaccine: validation by a WHO collaborative study. Bull World Health Organ 81(4):251–260
13. Wood DJ, Hull B (1999) L20B cells simplify culture of polioviruses from clinical samples. J Med Virol 58(2):188–192
14. Brodie M (1935) Active immunization against poliomyelitis. Am J Public Health Nations Health 25(1):54–67
15. Kolmer JA (1936) Vaccination against acute anterior poliomyelitis. Am J Public Health Nations Health 26(2):126–135
16. Salk JE (1953) Studies in human subjects on active immunization against poliomyelitis. I. A preliminary report of experiments in progress. J Am Med Assoc 151(13):1081–1098
17. Salk JE, Bazeley PL, Bennett BL, Krech U, Lewis LJ, Ward EN et al (1954) Studies in human subjects on active immunization against poliomyelitis. II. A practical means for inducing and maintaining antibody formation. Am J Public Health Nations Health 44(8):994–1009
18. Koprowski H, Jervis G, Norton T (1952) Immune responses in human volunteers upon oral administration of a rodent-adapted strain of poliomyelitis virus. Am J Epidemiol 55(1):108–126
19. Koprowski H (2006) First decade (1950–1960) of studies and trials with the polio vaccine. Biologicals 34(2):81–86
20. Sabin AB (1957) Properties and behavior of orally administered attenuated poliovirus vaccine. J Am Med Assoc 164(11):1216–1223
21. Cox HR, Cabasso VJ, Markham FS, Moses MJ, Moyer AW, Roca-Garcia M et al (1959) Immunological response to trivalent oral poliomyelitis vaccine. Br Med J 2(5152):591–597
22. Furesz J (2006) Developments in the production and quality control of poliovirus vaccines – historical perspectives. Biologicals 34(2):87–90
23. John TJ (2001) Anamalous observations on IPV and OPV vaccination. In: Brown F (ed) Progress in polio eradication: vaccine strategies for the end game. Karger, Basel, pp 197–208
24. Davidson I, Shulman LM (2008) Unraveling the puzzle of human anellovirus infections by comparison with avian infections with the chicken anemia virus. Virus Res 137(1):1–15
25. Racaniello VR et al (2007) Picornaviridae: the viruses and their replication. In: Chief E-I, Knipe DM, Howley PM, Editors A, Griffin DE, Lamb RA (eds) Fields virology, 5th edn. Wolters Klewer/Lippincott Williams & Wilkins, Philadelphia, pp 795–838
26. Wimmer E, Hellen CU, Cao X (1993) Genetics of poliovirus. Annu Rev Genet 27:353–436
27. Wimmer E (2006) The test-tube synthesis of a chemical called poliovirus. The simple synthesis of a virus has far-reaching societal implications. EMBO Rep 7:S3–S9
28. Molla A, Paul AV, Wimmer E (1991) Cell-free, de novo synthesis of poliovirus. Science 254(5038):1647–1651
29. Poyry T, Kinnunen L, Hovi T (1992) Genetic variation in vivo and proposed functional domains of the 5′ noncoding region of poliovirus RNA. J Virol 66(9):5313–5319
30. Pilipenko EV, Blinov VM, Romanova LI, Sinyakov AN, Maslova SV, Agol VI (1989) Conserved structural domains in the 5′-untranslated region of picornaviral genomes: an analysis of the segment controlling translation and neurovirulence. Virology 168(2):201–209
31. Skinner MA, Racaniello VR, Dunn G, Cooper J, Minor PD, Almond JW (1989) New model for the secondary structure of the 5′ non-coding RNA of poliovirus is supported by biochemical and genetic data that also show that RNA secondary structure is important in neurovirulence. J Mol Biol 207(2):379–392
32. Pelletier J, Sonenberg N (1988) Internal initiation of translation of eukaryotic mRNA directed by a sequence derived from poliovirus RNA. Nature 334(6180):320–325
33. Jang SK, Krausslich HG, Nicklin MJ, Duke GM, Palmenberg AC, Wimmer E (1988) A segment of the 5′ nontranslated region of encephalomyocarditis virus RNA directs internal entry of ribosomes during in vitro translation. J Virol 62(8):2636–2643
34. Gamarnik AV, Andino R (1997) Two functional complexes formed by KH domain containing proteins with the 5′ noncoding region of poliovirus RNA. RNA 3(8):882–892
35. Liu HM, Zheng DP, Zhang LB, Oberste MS, Kew OM, Pallansch MA (2003) Serial recombination during circulation of type 1 wild-vaccine recombinant polioviruses in China. J Virol 77(20):10994–11005
36. Racaniello VR (2001) Picornaviridae: the viruses and their replication. In: Fields BN, Knipe N, Howley P (eds) Virology, 4th edn. Lippincott Williams & Wilkins, Philadelphia, pp 685–722
37. Krausslich HG, Nicklin MJ, Lee CK, Wimmer E (1988) Polyprotein processing in picornavirus replication. Biochimie 70(1):119–130
38. Shulman LM, Handsher R, Yang CF, Yang SJ, Manor J, Vonsover A et al (2000) Resolution of the pathways of poliovirus type 1 transmission during an outbreak. J Clin Microbiol 38(3):945–952
39. Jorba J, Campagnoli R, De L, Kew O (2008) Calibration of multiple poliovirus molecular clocks covering an extended evolutionary range. J Virol 82(9):4429–4440
40. Bouchard MJ, Lam DH, Racaniello VR (1995) Determinants of attenuation and temperature sensitivity in the type 1 poliovirus Sabin vaccine. J Virol 69(8):4972–4978
41. Bergamini G, Preiss T, Hentze MW (2000) Picornavirus IRESes and the poly(A) tail jointly promote cap-independent translation in a mammalian cell-free system. RNA 6(12):1781–1790
42. Crawford NM, Baltimore D (1983) Genome-linked protein VPg of poliovirus is present as free VPg and VPg-pUpU in poliovirus-infected cells. Proc Natl Acad Sci USA 80(24):7452–7455
43. Kuhn RJ, Tada H, Ypma-Wong MF, Dunn JJ, Semler BL, Wimmer E (1988) Construction of a "mutagenesis cartridge" for poliovirus genome-linked viral protein: isolation and characterization of viable and nonviable mutants. Proc Natl Acad Sci USA 85(2):519–523

44. Ambros V, Pettersson RF, Baltimore D (1978) An enzymatic activity in uninfected cells that cleaves the linkage between poliovirion RNA and the 5′ terminal protein. Cell 15(4):1439–1446
45. Wien MW, Chow M, Hogle JM (1996) Poliovirus: new insights from an old paradigm. Structure 4(7):763–767
46. Li Q, Yafal AG, Lee YM, Hogle J, Chow M (1994) Poliovirus neutralization by antibodies to internal epitopes of VP4 and VP1 results from reversible exposure of these sequences at physiological temperature. J Virol 68(6):3965–3970
47. Harkonen T, Lankinen H, Davydova B, Hovi T, Roivainen M (2002) Enterovirus infection can induce immune responses that cross-react with beta-cell autoantigen tyrosine phosphatase IA-2/IAR. J Med Virol 66(3):340–350
48. Page GS, Mosser AG, Hogle JM, Filman DJ, Rueckert RR, Chow M (1988) Three-dimensional structure of poliovirus serotype 1 neutralizing determinants. J Virol 62(5):1781–1794
49. Bodian D, Morgan IM, Howe HA (1949) Differentiation of types of poliomyelitis viruses; the grouping of 14 strains into three basic immunological types. Am J Hyg 49(2):234–245
50. Harber J, Bernhardt G, Lu HH, Sgro JY, Wimmer E (1995) Canyon rim residues, including antigenic determinants, modulate serotype-specific binding of polioviruses to mutants of the poliovirus receptor. Virology 214(2):559–570
51. Hogle JM, Chow M, Filman DJ (1985) Three-dimensional structure of poliovirus at 2.9 A resolution. Science 229(4720):1358–1365
52. Filman DJ, Syed R, Chow M, Macadam AJ, Minor PD, Hogle JM (1989) Structural factors that control conformational transitions and serotype specificity in type 3 poliovirus. EMBO J 8(5):1567–1579
53. Koike S, Ise I, Nomoto A (1991) Functional domains of the poliovirus receptor. Proc Natl Acad Sci USA 88(10):4104–4108
54. Belnap DM, McDermott BM Jr, Filman DJ, Cheng N, Trus BL, Zuccola HJ et al (2000) Three-dimensional structure of poliovirus receptor bound to poliovirus. Proc Natl Acad Sci USA 97(1):73–78
55. WHO t (1998) Scheme adopted for use for L20B cells. Polio LaB network quarterly update IV(4):1–2
56. Zurbriggen S, Tobler K, Abril C, Diedrich S, Ackermann M, Pallansch MA et al (2008) Isolation of sabin-like polioviruses from wastewater in a country using inactivated polio vaccine. Appl Environ Microbiol 74(18):5608–5614
57. Abe S, Ota Y, Koike S, Kurata T, Horie H, Nomura T et al (1995) Neurovirulence test for oral live poliovaccines using poliovirus-sensitive transgenic mice. Virology 206(2): 1075–1083
58. Horie H, Koike S, Kurata T, Sato-Yoshida Y, Ise I, Ota Y et al (1994) Transgenic mice carrying the human poliovirus receptor: new animal models for study of poliovirus neurovirulence. J Virol 68(2):681–688
59. Ren RB, Costantini F, Gorgacz EJ, Lee JJ, Racaniello VR (1990) Transgenic mice expressing a human poliovirus receptor: a new model for poliomyelitis. Cell 63(2):353–362
60. Smyth M, Pettitt T, Symonds A, Martin J (2003) Identification of the pocket factors in a picornavirus. Arch Virol 148(6): 1225–1233
61. Salvati AL, De Dominicis A, Tait S, Canitano A, Lahm A, Fiore L (2004) Mechanism of action at the molecular level of the antiviral drug 3(2H)-isoflavene against type 2 poliovirus. Antimicrob Agents Chemother 48(6):2233–2243
62. Martin J (2006) Vaccine-derived poliovirus from long term excretors and the end game of polio eradication. Biologicals 34(2):117–122
63. MacLennan C, Dunn G, Huissoon AP, Kumararatne DS, Martin J, O'Leary P et al (2004) Failure to clear persistent vaccine-derived neurovirulent poliovirus infection in an immunodeficient man. Lancet 363(9420):1509–1513
64. Domingo E, Martinez-Salas E, Sobrino F, de la Torre JC, Portela A, Ortin J et al (1985) The quasispecies (extremely heterogeneous) nature of viral RNA genome populations: biological relevance–a review. Gene 40(1):1–8
65. Kinnunen L, Huovilainen A, Poyry T, Hovi T (1990) Rapid molecular evolution of wild type 3 poliovirus during infection in individual hosts. J Gen Virol 71(Pt 2):317–324
66. Crotty S, Cameron CE, Andino R (2001) RNA virus error catastrophe: direct molecular test by using ribavirin. Proc Natl Acad Sci USA 98(12):6895–6900
67. Eigen M (2002) Error catastrophe and antiviral strategy. Proc Natl Acad Sci USA 99(21):13374–13376
68. Racaniello VR, Baltimore D (1981) Cloned poliovirus complementary DNA is infectious in mammalian cells. Science 214(4523):916–919
69. Pollard SR, Dunn G, Cammack N, Minor PD, Almond JW (1989) Nucleotide sequence of a neurovirulent variant of the type 2 oral poliovirus vaccine. J Virol 63(11):4949–4951
70. van der Werf S, Bradley J, Wimmer E, Studier FW, Dunn JJ (1986) Synthesis of infectious poliovirus RNA by purified T7 RNA polymerase. Proc Natl Acad Sci USA 83(8):2330–2334
71. Cello J, Paul AV, Wimmer E (2002) Chemical synthesis of poliovirus cDNA: generation of infectious virus in the absence of natural template. Science 297(5583):1016–1018
72. Melnick JL (1996) Current status of poliovirus infections. Clin Microbiol Rev 9(3):293–300
73. Gustin KE, Sarnow P (2002) Inhibition of nuclear import and alteration of nuclear pore complex composition by rhinovirus. J Virol 76(17):8787–8796
74. Fox MP, Otto MJ, McKinlay MA (1986) Prevention of rhinovirus and poliovirus uncoating by WIN 51711, a new antiviral drug. Antimicrob Agents Chemother 30(1):110–116
75. Zeichhardt H, Otto MJ, McKinlay MA, Willingmann P, Habermehl KO (1987) Inhibition of poliovirus uncoating by disoxaril (WIN 51711). Virology 160(1):281–285
76. Jurgens CK, Barton DJ, Sharma N, Morasco BJ, Ogram SA, Flanegan JB (2006) 2Apro is a multifunctional protein that regulates the stability, translation and replication of poliovirus RNA. Virology 345(2):346–357
77. Takegami T, Kuhn RJ, Anderson CW, Wimmer E (1983) Membrane-dependent uridylylation of the genome-linked protein VPg of poliovirus. Proc Natl Acad Sci USA 80(24): 7447–7451
78. Eigen M (1993) Viral quasispecies. Sci Am 269(1):42–49

79. Gavrilin GV, Cherkasova EA, Lipskaya GY, Kew OM, Agol VI (2000) Evolution of circulating wild poliovirus and of vaccine-derived poliovirus in an immunodeficient patient: a unifying model. J Virol 74(16):7381–7390
80. Cherkasova E, Laassri M, Chizhikov V, Korotkova E, Dragunsky E, Agol VI et al (2003) Microarray analysis of evolution of RNA viruses: evidence of circulation of virulent highly divergent vaccine-derived polioviruses. Proc Natl Acad Sci USA 100(16):9398–9403
81. Guillot S, Caro V, Cuervo N, Korotkova E, Combiescu M, Persu A et al (2000) Natural genetic exchanges between vaccine and wild poliovirus strains in humans. J Virol 74(18):8434–8443
82. Dahourou G, Guillot S, Le Gall O, Crainic R (2002) Genetic recombination in wild-type poliovirus. J Gen Virol 83(Pt 12): 3103–3110
83. Zhang Y, Wang H, Zhu S, Li Y, Song L, Liu Y et al (2010) Characterization of a rare natural intertypic type 2/type 3 penta-recombinant vaccine-derived poliovirus isolated from a child with acute flaccid paralysis. J Gen Virol 91(Pt 2):421–429
84. Tao Z, Wang H, Xu A, Zhang Y, Song L, Zhu S et al (2010) Isolation of a recombinant type 3/type 2 poliovirus with a chimeric capsid VP1 from sewage in Shandong, China. Virus Res 150(1–2):56–60
85. Blomqvist S, Savolainen-Kopra C, Paananen A, El Bassioni L, El Maamoon Nasr EM, Firstova L et al (2010) Recurrent isolation of poliovirus 3 strains with chimeric capsid protein Vp1 suggests a recombination hot-spot site in Vp1. Virus Res 151(2): 246–251
86. Brown B, Oberste MS, Maher K, Pallansch MA (2003) Complete genomic sequencing shows that polioviruses and members of human enterovirus species C are closely related in the noncapsid coding region. J Virol 77(16):8973–8984
87. Jiang P, Faase JA, Toyoda H, Paul A, Wimmer E, Gorbalenya AE (2007) Evidence for emergence of diverse polioviruses from C-cluster coxsackie A viruses and implications for global poliovirus eradication. Proc Natl Acad Sci USA 104(22): 9457–9462
88. Riquet FB, Blanchard C, Jegouic S, Balanant J, Guillot S, Vibet MA et al (2008) Impact of exogenous sequences on the characteristics of an epidemic type 2 recombinant vaccine-derived poliovirus. J Virol 82(17):8927–8932
89. Kirkegaard K, Baltimore D (1986) The mechanism of RNA recombination in poliovirus. Cell 47(3):433–443
90. Kew O, Morris-Glasgow V, Landaverde M, Burns C, Shaw J, Garib Z et al (2002) Outbreak of poliomyelitis in Hispaniola associated with circulating type 1 vaccine-derived poliovirus. Science 296(5566):356–359
91. Estivariz CF, Watkins MA, Handoko D, Rusipah R, Deshpande J, Rana BJ et al (2008) A large vaccine-derived poliovirus outbreak on Madura Island–Indonesia, 2005. J Infect Dis 197(3):347–354
92. Cherkasova EA, Korotkova EA, Yakovenko ML, Ivanova OE, Eremeeva TP, Chumakov KM et al (2002) Long-term circulation of vaccine-derived poliovirus that causes paralytic disease. J Virol 76(13):6791–6799
93. Chumakov KM, Norwood LP, Parker ML, Dragunsky EM, Ran YX, Levenbook IS (1992) RNA sequence variants in live poliovirus vaccine and their relation to neurovirulence. J Virol 66(2):966–970
94. Reyes GR (2001) Ribavirin: recent insights into antiviral mechanisms of action. Curr Opin Drug Discov Devel 4(5): 651–656
95. Georgescu MM, Balanant J, Ozden S, Crainic R (1997) Random selection: a model for poliovirus infection of the central nervous system. J Gen Virol 78(Pt 8):1819–1828
96. Pfeiffer JK, Kirkegaard K (2005) Increased fidelity reduces poliovirus fitness and virulence under selective pressure in mice. PLoS Pathog 1(2):e11
97. Burns CC, Campagnoli R, Shaw J, Vincent A, Jorba J, Kew O (2009) Genetic inactivation of poliovirus infectivity by increasing the frequencies of CpG and UpA dinucleotides within and across synonymous capsid region codons. J Virol 83(19):9957–9969
98. Vignuzzi M, Stone JK, Arnold JJ, Cameron CE, Andino R (2006) Quasispecies diversity determines pathogenesis through cooperative interactions in a viral population. Nature 439(7074):344–348
99. Tao B, Fultz PN (1995) Molecular and biological analyses of quasispecies during evolution of a virulent simian immunodeficiency virus, SIVsmmPBj14. J Virol 69(4):2031–2037
100. de la Torre JC, Holland JJ (1990) RNA virus quasispecies populations can suppress vastly superior mutant progeny. J Virol 64(12):6278–6281
101. Kew OM, Mulders MN, Lipskaya GY, de Silva E, Pallansch MA (1995) Molecular epidemiology of polioviruses. Sem Virol 6:401–405
102. Manor Y, Blomqvist S, Sofer D, Alfandari J, Halmut T, Abramovitz B et al (2007) Advanced environmental surveillance and molecular analyses indicate separate importations rather than endemic circulation of wild type 1 poliovirus in Gaza district in 2002. Appl Environ Microbiol 73(18):5954–5958
103. Boot HJ, Sonsma J, van Nunen F, Abbink F, Kimman TG, Buisman AM (2007) Determinants of monovalent oral polio vaccine mutagenesis in vaccinated elderly people. Vaccine 25(24):4706–4714
104. Kew OM, Sutter RW, Nottay BK, McDonough MJ, Prevots DR, Quick L et al (1998) Prolonged replication of a type 1 vaccine-derived poliovirus in an immunodeficient patient. J Clin Microbiol 36(10):2893–2899
105. Kew OM, Wright PF, Agol VI, Delpeyroux F, Shimizu H, Nathanson N et al (2004) Circulating vaccine-derived polioviruses: current state of knowledge. Bull World Health Organ 82(1):16–23
106. Jenkins HE, Aylward RB, Gasasira A, Donnelly CA, Mwanza M, Corander J et al (2010) Implications of a circulating vaccine-derived poliovirus in Nigeria. N Engl J Med 362(25):2360–2369
107. Martin J, Dunn G, Hull R, Patel V, Minor PD (2000) Evolution of the Sabin strain of type 3 poliovirus in an immunodeficient patient during the entire 637-day period of virus excretion. J Virol 74(7):3001–3010

108. Martin J, Odoom K, Tuite G, Dunn G, Hopewell N, Cooper G et al (2004) Long-term excretion of vaccine-derived poliovirus by a healthy child. J Virol 78(24):13839–13847
109. Shulman LM, Manor Y, Sofer D, Handsher R, Swartz T, Delpeyroux F et al (2006) Neurovirulent vaccine-derived polioviruses in sewage from highly immune populations. PLoS One 1:e69
110. Yang CF, Chen HY, Jorba J, Sun HC, Yang SJ, Lee HC et al (2005) Intratypic recombination among lineages of type 1 vaccine-derived poliovirus emerging during chronic infection of an immunodeficient patient. J Virol 79(20): 12623–12634
111. van der Sanden S, Pallansch MA, van de Kassteele J, El-Sayed N, Sutter RW, Koopmans M et al (2009) Shedding of vaccine viruses with increased antigenic and genetic divergence after vaccination of newborns with monovalent type 1 oral poliovirus vaccine. J Virol 83(17):8693–8704
112. Yakovenko ML, Cherkasova EA, Rezapkin GV, Ivanova OE, Ivanov AP, Eremeeva TP et al (2006) Antigenic evolution of vaccine-derived polioviruses: changes in individual epitopes and relative stability of the overall immunological properties. J Virol 80(6):2641–2653
113. Domingo E, Diez J, Martinez MA, Hernandez J, Holguin A, Borrego B et al (1993) New observations on antigenic diversification of RNA viruses. Antigenic variation is not dependent on immune selection. J Gen Virol 74(Pt 10):2039–2045
114. Agol VI (2006) Vaccine-derived polioviruses. Biologicals 34(2):103–108
115. Blomqvist S, Savolainen C, Laine P, Hirttio P, Lamminsalo E, Penttila E et al (2004) Characterization of a highly evolved vaccine-derived poliovirus type 3 isolated from sewage in Estonia. J Virol 78(9):4876–4883
116. Shulman LM, Manor Y, Sofer D (2010) Poliovirus vaccine and vaccine-derived polioviruses. N Engl J Med 363(19):1870
117. Korotkova EA, Park R, Cherkasova EA, Lipskaya GY, Chumakov KM, Feldman EV et al (2003) Retrospective analysis of a local cessation of vaccination against poliomyelitis: a possible scenario for the future. J Virol 77(23):12460–12465
118. Gumede N, Venter M, Lentsoane O, Muyembe-Tamfum J, Yogolelo R, Puren A et al (2010) Identification of vaccine-derived polioviruses (VDPVS) in the DRC from 2005 to 2010. Commun Dis Sur Bull 8(3):43–45
119. Resik S, Tejeda A, Lago PM, Diaz M, Carmenates A, Sarmiento L et al (2010) Randomized controlled clinical trial of fractional doses of inactivated poliovirus vaccine administered intradermally by needle-free device in Cuba. J Infect Dis 201(9):1344–1352
120. Mohammed AJ, AlAwaidy S, Bawikar S, Kurup PJ, Elamir E, Shaban MM et al (2010) Fractional doses of inactivated poliovirus vaccine in Oman. N Engl J Med 362(25):2351–2359
121. Nirmal S, Cherian T, Samuel BU, Rajasingh J, Raghupathy P, John TJ (1998) Immune response of infants to fractional doses of intradermally administered inactivated poliovirus vaccine. Vaccine 16(9–10):928–931
122. Ehrenfeld E, Glass RI, Agol VI, Chumakov K, Dowdle W, John TJ et al (2008) Immunisation against poliomyelitis: moving forward. Lancet 371(9621):1385–1387
123. Yakovenko ML, Korotkova EA, Ivanova OE, Eremeeva TP, Samoilovich E, Uhova I et al (2009) Evolution of the Sabin vaccine into pathogenic derivatives without appreciable changes in antigenic properties: need for improvement of current poliovirus surveillance. J Virol 83(7): 3402–3406
124. Modlin JF (2010) The bumpy road to polio eradication. N Engl J Med 362(25):2346–2349
125. Buttinelli G, Donati V, Fiore S, Marturano J, Plebani A, Balestri P et al (2003) Nucleotide variation in Sabin type 2 poliovirus from an immunodeficient patient with poliomyelitis. J Gen Virol 84(Pt 5):1215–1221
126. Arita I, Nakane M, Fenner F (2006) Public health. Is polio eradication realistic? Science 312(5775):852–854
127. Chumakov K, Ehrenfeld E, Wimmer E, Agol VI (2007) Vaccination against polio should not be stopped. Nat Rev Microbiol 5(12):952–958
128. Shulman LM, Manor Y, Sofer D, Mendelson E (2009) Type 2 polio still in our midst. Science 324(5925):334
129. Furione M, Guillot S, Otelea D, Balanant J, Candrea A, Crainic R (1993) Polioviruses with natural recombinant genomes isolated from vaccine-associated paralytic poliomyelitis. Virology 196(1):199–208
130. Lipskaya GY, Muzychenko AR, Kutitova OK, Maslova SV, Equestre M, Drozdov SG et al (1991) Frequent isolation of intertypic poliovirus recombinants with serotype 2 specificity from vaccine-associated polio cases. J Med Virol 35(4): 290–296
131. Georgescu MM, Delpeyroux F, Tardy-Panit M, Balanant J, Combiescu M, Combiescu AA et al (1994) High diversity of poliovirus strains isolated from the central nervous system from patients with vaccine-associated paralytic poliomyelitis. J Virol 68(12):8089–8101
132. Minor PD, John A, Ferguson M, Icenogle JP (1986) Antigenic and molecular evolution of the vaccine strain of type 3 poliovirus during the period of excretion by a primary vaccinee. J Gen Virol 67(Pt 4):693–706
133. Shulman LM, Manor Y, Sofer D, Swartz T, Mendelson E (2006) Oral poliovaccine: will it help eradicate polio or cause the next epidemic? Isr Med Assoc J 8(5):312–315
134. Dowdle W, van der Avoort H, de Gourville E, Delpeyroux F, Desphande J, Hovi T et al (2006) Containment of polioviruses after eradication and OPV cessation: characterizing risks to improve management. Risk Anal 26(6):1449–1469
135. Wood DJ (2006) Polio vaccine: the first 50 years and beyond. Summary of the meeting and next steps. Biologicals 34(2): 171–174
136. Horstmann DM, Mc CR, Mascola AD (1954) Viremia in human poliomyelitis. J Exp Med 99(4):355–369
137. Steigman AJ, Sabin AB (1949) Antibody response of patients with poliomyelitis to virus recovered from their own alimentary tract. J Exp Med 90(4):349–372

138. Bodian D, Paffenbarger RS Jr (1954) Poliomyelitis infection in households; frequency of viremia and specific antibody response. Am J Hyg 60(1):83–98
139. Racaniello VR, Ren R (1996) Poliovirus biology and pathogenesis. Curr Top Microbiol Immunol 206:305–325
140. Alexander JP Jr, Gary HE Jr, Pallansch MA (1997) Duration of poliovirus excretion and its implications for acute flaccid paralysis surveillance: a review of the literature. J Infect Dis 175(Suppl 1):S176–S182
141. Minor PD (1992) The molecular biology of poliovaccines. J Gen Virol 73(Pt 12):3065–3077
142. Mas Lago P, Caceres VM, Galindo MA, Gary HE Jr, Valcarcel M, Barrios J et al (2001) Persistence of vaccine-derived poliovirus following a mass vaccination campaign in Cuba: implications for stopping polio vaccination after global eradication. Int J Epidemiol 30(5):1029–1034
143. Hovi T, Shulman LM, van der Avoort H, Deshpande J, Roivainen M, de Gourville EM (2011) Role of environmental poliovirus surveilllance in global polio eradication and beyond, a review. Epidemiol Infect 18:1–13
144. Cohen-Abbo A, Culley BS, Reed GW, Sannella EC, Mace RL, Robertson SE et al (1995) Seroresponse to trivalent oral poliovirus vaccine as a function of dosage interval. Pediatr Infect Dis J 14(2):100–106
145. Gromeier M, Wimmer E (1998) Mechanism of injury-provoked poliomyelitis. J Virol 72(6):5056–5060
146. Ramlow J, Alexander M, LaPorte R, Kaufmann C, Kuller L (1992) Epidemiology of the post-polio syndrome. Am J Epidemiol 136(7):769–786
147. Gonzalez H, Olsson T, Borg K (2010) Management of postpolio syndrome. Lancet Neurol 9(6):634–642
148. Ogra PL (1995) Comparative evaluation of immunization with live attenuated and inactivated poliovirus vaccines. Ann N Y Acad Sci 754:97–107
149. Ogra PL, Karzon DT (1969) Distribution of poliovirus antibody in serum, nasopharynx and alimentary tract following segmental immunization of lower alimentary tract with poliovaccine. J Immunol 102(6):1423–1430
150. Ogra PL, Karzon DT (1969) Poliovirus antibody response in serum and nasal secretions following intranasal inoculation with inactivated poliovaccine. J Immunol 102(1):15–23
151. Sofer D, Handsher R, Abramovitz B, Shilon K, Manor Y, Halmut T, et al (2008) Determining vaccination efficacy: is the current minimum anti-polio neutralization antibody titer of $>$1:8 against Sabin strains high enough? Meeting of the three division of the international union of microbiological societies 5–15 Aug 2008, Istanbul
152. Valtanen S, Roivainen M, Piirainen L, Stenvik M, Hovi T (2000) Poliovirus-specific intestinal antibody responses coincide with decline of poliovirus excretion. J Infect Dis 182(1):1–5
153. Nishio O, Sumi J, Sakae K, Ishihara Y, Isomura S, Inouye S (1990) Fecal IgA antibody responses after oral poliovirus vaccination in infants and elder children. Microbiol Immunol 34(8):683–689
154. Ogra PL, Fishaut M, Gallagher MR (1980) Viral vaccination via the mucosal routes. Rev Infect Dis 2(3):352–369
155. Samoilovich E, Roivainen M, Titov LP, Hovi T (2003) Serotype-specific mucosal immune response and subsequent poliovirus replication in vaccinated children. J Med Virol 71(2): 274–280
156. Onorato IM, Modlin JF, McBean AM, Thoms ML, Losonsky GA, Bernier RH (1991) Mucosal immunity induced by enhance-potency inactivated and oral polio vaccines. J Infect Dis 163(1):1–6
157. Vidor E, Caudrelier P, Plotkin S (1994) The place of DTP/eIPV vaccine in routine paediatric vaccination. Rev Med Virol 4(4):261–277
158. Laassri M, Lottenbach K, Belshe R, Wolff M, Rennels M, Plotkin S et al (2005) Effect of different vaccination schedules on excretion of oral poliovirus vaccine strains. J Infect Dis 192(12):2092–2098
159. Swartz TA, Green MS, Handscher R, Sofer D, Cohen-Dar M, Shohat T et al (2008) Intestinal immunity following a combined enhanced inactivated polio vaccine/oral polio vaccine programme in Israel. Vaccine 26(8):1083–1090
160. Lasch EE, Livni E, Englander T, El-Massri M, Marcus O, Joshua H (1978) The cell mediated immune response in acute poliomyelitis and its use in early diagnosis. Dev Biol Stand 41:179–182
161. Samuel BU, Cherian T, Sridharan G, Mukundan P, John TJ (1991) Immune response to intradermally injected inactivated poliovirus vaccine. Lancet 338(8763):343–344
162. Katrak K, Mahon BP, Minor PD, Mills KH (1991) Cellular and humoral immune responses to poliovirus in mice: a role for helper T cells in heterotypic immunity to poliovirus. J Gen Virol 72(Pt 5):1093–1098
163. Minor PD (2004) Polio eradication, cessation of vaccination and re-emergence of disease. Nat Rev Microbiol 2(6):473–482
164. Plotkin SA, Vidor E (2008) Poliovirus vaccine - inactivated. In: Plotkin SA, Orenstein WA, Offit PA (eds) Vaccines, 5th edn. W.B. Saunders/Elsevier, Philadelphia, pp 605–629
165. Paul J (1971) A history of poliomyelitis. Yale University Press, New Haven
166. Griffiths E, Wood D, Barreto L (2006) Polio vaccine: the first 50 years and beyond. Biologicals 34(2):73–74
167. Nathanson N, Langmuir AD (1963) The cutter incident. Poliomyelitis following formaldehyde- inactivated poliovirus vaccination in the United States during the Spring of 1955. I. Background. Am J Hyg 78:16–28
168. Nathanson N, Langmuir AD (1963) The cutter incident. Poliomyelitis following formaldehyde- inactivated poliovirus vaccination in the United States during the Spring of 1955. II. Relationship of poliomyelitis to cutter vaccine. Am J Hyg 78:29–60
169. Eddy BE, Borman GS, Berkeley WH, Young RD (1961) Tumors induced in hamsters by injection of rhesus monkey kidney cell extracts. Proc Soc Exp Biol Med 107:191–197
170. Shah K, Nathanson N (1976) Human exposure to SV40: review and comment. Am J Epidemiol 103(1):1–12

171. Mortimer EA Jr, Lepow ML, Gold E, Robbins FC, Burton GJ, Fraumeni JF Jr (1981) Long-term follow-up of persons inadvertently inoculated with SV40 as neonates. N Engl J Med 305(25):1517–1518
172. Swartz TA (2008) The epidemiology of polio in Israel an historical perspective. Dyonon, Tel Aviv
173. Tulchinsky T, Abed Y, Handsher R, Toubassi N, Acker C, Melnick J (1994) Successful control of poliomyelitis by a combined OPV/IPV polio vaccine program in the West Bank and Gaza, 1978–93. Isr J Med Sci 30(5–6):489–494
174. Tulchinsky TH, Goldblum N (2001) Polio immunization. N Engl J Med 344(1):61–62
175. Slater PE, Orenstein WA, Morag A, Avni A, Handsher R, Green MS et al (1990) Poliomyelitis outbreak in Israel in 1988: a report with two commentaries. Lancet 335(8699):1192–1195
176. Kawamura N, Kohara M, Abe S, Komatsu T, Tago K, Arita M et al (1989) Determinants in the 5′ noncoding region of poliovirus Sabin 1 RNA that influence the attenuation phenotype. J Virol 63(3):1302–1309
177. Nomoto A, Omata T, Toyoda H, Kuge S, Horie H, Kataoka Y et al (1982) Complete nucleotide sequence of the attenuated poliovirus Sabin 1 strain genome. Proc Natl Acad Sci USA 79(19):5793–5797
178. Christodoulou C, Colbere-Garapin F, Macadam A, Taffs LF, Marsden S, Minor P et al (1990) Mapping of mutations associated with neurovirulence in monkeys infected with Sabin 1 poliovirus revertants selected at high temperature. J Virol 64(10):4922–4929
179. Macadam AJ, Pollard SR, Ferguson G, Skuce R, Wood D, Almond JW et al (1993) Genetic basis of attenuation of the Sabin type 2 vaccine strain of poliovirus in primates. Virology 192(1):18–26
180. Ren RB, Moss EG, Racaniello VR (1991) Identification of two determinants that attenuate vaccine-related type 2 poliovirus. J Virol 65(3):1377–1382
181. Macadam AJ, Arnold C, Howlett J, John A, Marsden S, Taffs F et al (1989) Reversion of the attenuated and temperature-sensitive phenotypes of the Sabin type 3 strain of poliovirus in vaccinees. Virology 172(2):408–414
182. Westrop GD, Wareham KA, Evans DM, Dunn G, Minor PD, Magrath DI et al (1989) Genetic basis of attenuation of the Sabin type 3 oral poliovirus vaccine. J Virol 63(3):1338–1344
183. Minor PD, Macadam AJ, Stone DM, Almond JW (1993) Genetic basis of attenuation of the Sabin oral poliovirus vaccines. Biologicals 21(4):357–363
184. Okonko IO, Babalola ET, Adedeji AO, Onoja BA, Ogun AA, Nkang AO et al (2008) The role of vaccine derived polioviruses in the global eradication of polio-the Nigeria experience as a case study. Biotechnol Mol Biol Rev 3(6):135–147
185. Sutter RW, Cochi SL, Melnick JL (1999) Live attenuated poliovirus vaccines. In: Plotkin S, Orenstein WA (eds) Vaccines, 3rd edn. W.B. Saunders, Philadelphia, pp 364–408
186. Mmwr T (2001) Apparent global interruption of wild poliovirus type 2 trasmission. MMWR Morb Mortal Wkly Rep 50(12):222–224
187. Grassly NC, Wenger J, Durrani S, Bahl S, Deshpande JM, Sutter RW et al (2007) Protective efficacy of a monovalent oral type 1 poliovirus vaccine: a case-control study. Lancet 369(9570):1356–1362
188. WKly Epidemiol Rec (2009) Advisory committee on poliomyelitis eradication: recommendations on the use of bivalent oral poliovirus vaccine types 1 and 3. Wkly Epidemiol Rec 84(29):289–290
189. Salk JE, Krech U, Youngner JS, Bennett BL, Lewis LJ, Bazeley PL (1954) Formaldehyde treatment and safety testing of experimental poliomyelitis vaccines. Am J Public Health Nations Health 44(5):563–570
190. Jenkins HE, Aylward RB, Gasasira A, Donnelly CA, Abanida EA, Koleosho-Adelekan T et al (2008) Effectiveness of immunization against paralytic poliomyelitis in Nigeria. N Engl J Med 359(16):1666–1674
191. Wright PF, Modlin JF (2008) The demise and rebirth of polio–a modern phoenix? J Infect Dis 197(3):335–336
192. Minor PD, Schild GC, Ferguson M, Mackay A, Magrath DI, John A et al (1982) Genetic and antigenic variation in type 3 polioviruses: characterization of strains by monoclonal antibodies and T1 oligonucleotide mapping. J Gen Virol 61(Pt 2):167–176
193. Simoes EA, Padmini B, Steinhoff MC, Jadhav M, John TJ (1985) Antibody response of infants to two doses of inactivated poliovirus vaccine of enhanced potency. Am J Dis Child 139(10):977–980
194. Samuel BU, Cherian T, Rajasingh J, Raghupathy P, John TJ (1992) Immune response of infants to inactivated poliovirus vaccine injected intradermally. Vaccine 10(2):135
195. Wkly Epidemiol Record (2004) Conclusions and recommendations of the Ad Hoc Advisory Committee on Poliomyelitis Eradication, Geneva, 21–22 September 2004. Wkly Epidemiol Rec 79(41):401–407
196. De Palma AM, Purstinger G, Wimmer E, Patick AK, Andries K, Rombaut B et al (2008) Potential use of antiviral agents in polio eradication. Emerg Infect Dis 14(4):545–551
197. Pevear DC, Tull TM, Seipel ME, Groarke JM (1999) Activity of pleconaril against enteroviruses. Antimicrob Agents Chemother 43(9):2109–2115
198. Oberste MS, Moore D, Anderson B, Pallansch MA, Pevear DC, Collett MS (2009) In vitro antiviral activity of V-073 against polioviruses. Antimicrob Agents Chemother 53(10):4501–4503
199. Levy AH (1962) The uses of gamma globulins in the prophylaxis of infection. J Chronic Dis 15:589–598
200. McKinney RE Jr, Katz SL, Wilfert CM (1987) Chronic enteroviral meningoencephalitis in agammaglobulinemic patients. Rev Infect Dis 9(2):334–356
201. Breman JG, Arita I (1980) The confirmation and maintenance of smallpox eradication. N Engl J Med 303(22):1263–1273
202. Smith J, Leke R, Adams A, Tangermann RH (2004) Certification of polio eradication: process and lessons learned. Bull World Health Organ 82(1):24–30
203. Hull HF, Ward NA, Hull BP, Milstien JB, de Quadros C (1994) Paralytic poliomyelitis: seasoned strategies, disappearing disease. Lancet 343(8909):1331–1337

204. Dove AW, Racaniello VR (1997) The polio eradication effort: should vaccine eradication be next? Science 277(5327):779–780
205. Hull HF, Aylward RB (1997) Ending polio immunization. Science 277(5327):780
206. Wood DJ, Sutter RW, Dowdle WR (2000) Stopping poliovirus vaccination after eradication: issues and challenges. Bull World Health Organ 78(3):347–357
207. Wright PF, Kim-Farley RJ, de Quadros CA, Robertson SE, Scott RM, Ward NA et al (1991) Strategies for the global eradication of poliomyelitis by the year 2000. N Engl J Med 325(25): 1774–1779
208. WHO (1996) Field guide for supplementary activities aimed at achieving polio eradication, 1996 Revision: WHO/EPI/GEN/95.01 Rev.1
209. Hull BP, Dowdle WR (1997) Poliovirus surveillance: building the global polio laboratory network. J Infect Dis 175(Suppl 1): S113–S116
210. Wkly Epidemiol Record (2002) Expanding contributions of the global laboratory network for poliomyelitis eradication, 2000-2001. Wkly Epidemiol Rec 77(17):133–137
211. Wkly Epidemiol Record (2003) Laboratory surveillance for wild and vaccine-derived polioviruses, January 2002-June 2003. Wkly Epidemiol Rec 78(39):341–346
212. Wkly Epidemiol Record (2004) Laboratory surveillance for wild and vaccine-derived polioviruses, January 2003-June 2004. Wkly Epidemiol Rec 79(44):393–398
213. de Gourville E, Duintjer Tebbens RJ, Sangrujee N, Pallansch MA, Thompson KM (2006) Global surveillance and the value of information: the case of the global polio laboratory network. Risk Anal 26(6):1557–1569
214. van der Avoort HG, Hull BP, Hovi T, Pallansch MA, Kew OM, Crainic R et al (1995) Comparative study of five methods for intratypic differentiation of polioviruses. J Clin Microbiol 33(10):2562–2566
215. De L, Nottay B, Yang CF, Holloway BP, Pallansch M, Kew O (1995) Identification of vaccine-related polioviruses by hybridization with specific RNA probes. J Clin Microbiol 33(3):562–571
216. Kilpatrick DR, Nottay B, Yang CF, Yang SJ, Mulders MN, Holloway BP et al (1996) Group-specific identification of polioviruses by PCR using primers containing mixed-base or deoxyinosine residue at positions of codon degeneracy. J Clin Microbiol 34(12):2990–2996
217. Balanant J, Guillot S, Candrea A, Delpeyroux F, Crainic R (1991) The natural genomic variability of poliovirus analyzed by a restriction fragment length polymorphism assay. Virology 184(2):645–654
218. Kilpatrick DR, Yang CF, Ching K, Vincent A, Iber J, Campagnoli R et al (2009) Rapid group-, serotype-, and vaccine strain-specific identification of poliovirus isolates by real-time reverse transcription-PCR using degenerate primers and probes containing deoxyinosine residues. J Clin Microbiol 47(6): 1939–1941
219. WHO (2004) Polio laboratory manual 4th edn, 2004. WHO/IVB/04.10 (database on the internet)
220. Wkly Epidemiol Record (2006) Resurgence of wild poliovirus type 1 transmission and effect of importation into polio-free countries, 2002–2005. Wkly Epidemiol Rec 81(7):63–68
221. Wkly Epidemiol Record (2010) Poliomyelitis in Tajikistan - first importation since Europe certified polio-free. Wkly Epidemiol Rec 85(18):157–158
222. Deshpande JM, Shetty SJ, Siddiqui ZA (2003) Environmental surveillance system to track wild poliovirus transmission. Appl Environ Microbiol 69(5):2919–2927
223. WHO (2003) Guidelines for environmental surveillance of poliovirus circulation (database on the internet). WHO, Dept of Vaccines and Biologicals; http://www.who.int/vaccines-documents/DoxGen/H5-Surv.htm. Available from: http://www.who.int/vaccines-documents/DoxGen/H5-Surv.htm
224. Manor Y, Handsher R, Halmut T, Neuman M, Abramovitz B, Mates A et al (1999) A double-selective tissue culture system for isolation of wild-type poliovirus from sewage applied in a long-term environmental surveillance. Appl Environ Microbiol 65(4):1794–1797
225. Shulman LM, Manor Y, Handsher R, Delpeyroux F, McDonough MJ, Halmut T et al (2000) Molecular and antigenic characterization of a highly evolved derivative of the type 2 oral poliovaccine strain isolated from sewage in Israel. J Clin Microbiol 38(10):3729–3734
226. Nakano JH, Hatch MH, Thieme ML, Nottay B (1978) Parameters for differentiating vaccine-derived and wild poliovirus strains. Prog Med Virol 24:178–206
227. Vinje J, Gregoricus N, Martin J, Gary HE Jr, Caceres VM, Venczel L et al (2004) Isolation and characterization of circulating type 1 vaccine-derived poliovirus from sewage and stream waters in Hispaniola. J Infect Dis 189(7):1168–1175
228. Manor Y, Handsher R, Halmut T, Neuman M, Bobrov A, Rudich H et al (1999) Detection of poliovirus circulation by environmental surveillance in the absence of clinical cases in Israel and the Palestinian authority. J Clin Microbiol 37(6):1670–1675
229. Ranta J, Hovi T, Arjas E (2001) Poliovirus surveillance by examining sewage water specimens: studies on detection probability using simulation models. Risk Anal 21(6): 1087–1096
230. WHO (2004) Immunization, vaccines and biologicals. Polio laboratory manual, 4th edn. World Health Organization, Geneva, WHO/IVB/04.10
231. Hovi T, Stenvik M, Partanen H, Kangas A (2001) Poliovirus surveillance by examining sewage specimens. Quantitative recovery of virus after introduction into sewerage at remote upstream location. Epidemiol Infect 127(1):101–106
232. Hovi T (2006) Surveillance for polioviruses. Biologicals 34(2):123–126
233. Roivainen M, Blomqvist S, Al-Hello H, Paananen A, Delpeyreux F, Kuusi M et al (2010) Highly divergent neurovirulent vaccine-derived polioviruses of all three serotypes are recurrently detected in Finnish sewage. Euro Surveill 15(19):pii/19566
234. Wkly Epidemiol Record (2008) Conclusions and recommendations of the Advisory Committee on Poliomyelitis

Eradication, Geneva, 27–28 November 2007. Wkly Epidemiol Rec 83(3):25–35
235. Kapp C (2003) Surge in polio spreads alarm in northern Nigeria. Rumors about vaccine safety in Muslim-run states threaten WHO's eradication programme. Lancet 362(9396):1631–1632
236. Samba E, Nkrumah F, Leke R (2004) Getting polio eradication back on track in Nigeria. N Engl J Med 350(7):645–646
237. Wkly Epidemiol Record (2009) Advisory Committee on Poliomyelitis Eradication: recommendations on the use of bivalent oral poliovirus vaccine types 1 and 3. Wkly Epidemiol Rec 84(29):289–290
238. John TJ (1972) Problems with oral poliovaccine in India. Indian Pediatr 9(5):252–256
239. John TJ (1976) Antibody response of infants in tropics to five doses of oral polio vaccine. Br Med J 1(6013):812
240. Grassly NC, Fraser C, Wenger J, Deshpande JM, Sutter RW, Heymann DL et al (2006) New strategies for the elimination of polio from India. Science 314(5802):1150–1153
241. Grassly NC, Jafari H, Bahl S, Durrani S, Wenger J, Sutter RW et al (2009) Mucosal immunity after vaccination with monovalent and trivalent oral poliovirus vaccine in India. J Infect Dis 200(5):794–801
242. Gary HE Jr, Smith B, Jenks J, Ruiz J, Sessions W, Vinje J et al (2008) Failure to detect infection by oral polio vaccine virus following natural exposure among inactivated polio vaccine recipients. Epidemiol Infect 136(2):180–183
243. Wringe A, Fine PE, Sutter RW, Kew OM (2008) Estimating the extent of vaccine-derived poliovirus infection. PLoS One 3(10):e3433
244. Mmwr T (2007) Update on vaccine-derived polioviruses–worldwide, January 2006-August 2007. MMWR Morb Mortal Wkly Rep 56(38):996–1001
245. MMWR (2009) Update on vaccine-derived polioviruses – worldwide, January 2008-June 2009. MMWR Morb Mortal Wkly Rep 58(36):1002–1006
246. Dowdle W, Kew O (2006) Vaccine-derived polioviruses: is it time to stop using the word "rare?". J Infect Dis 194(5): 539–541
247. Halsey NA, Pinto J, Espinosa-Rosales F, Faure-Fontenla MA, da Silva E, Khan AJ et al (2004) Search for poliovirus carriers among people with primary immune deficiency diseases in the United States, Mexico, Brazil, and the United Kingdom. Bull World Health Organ 82(1):3–8
248. Wkly Epidemiol Record (2010) Progress toward interrupting wild poliovirus transmission worldwide. 2009. Wkly Epidemiol Rec 85(18):178–184
249. Hovi T, Lindholm N, Savolainen C, Stenvik M, Burns C (2004) Evolution of wild-type 1 poliovirus in two healthy siblings excreting the virus over a period of 6 months. J Gen Virol 85(Pt 2):369–377
250. Pelletier I, Duncan G, Pavio N, Colbere-Garapin F (1998) Molecular mechanisms of poliovirus persistence: key role of capsid determinants during the establishment phase. Cell Mol Life Sci 54(12):1385–1402
251. Roivainen M, Blomqvist S, Al-Hello H, Paananen A, Delpeyroux F, Kuusi M et al (2010) Highly divergent neurovirulent vaccine-derived polioviruses of all three serotypes are recurrently detected in Finnish sewage. Euro Surveill 15(19):pii/19566
252. ECDC (2009) Risk assessment from the ECDC on the finding of vaccine-derived polio virus in Finland February 17, 2009. \Documents and Settings\daah\Local Settings\Temporary Internet Files\OLK35A\Risk assessment polio 2009_02_17-JG (2).doc
253. Pavlov DN (2006) Poliovirus vaccine strains in sewage and river water in South Africa. Can J Microbiol 52(8):717–723
254. Yoshida H, Horie H, Matsuura K, Miyamura T (2000) Characterisation of vaccine-derived polioviruses isolated from sewage and river water in Japan. Lancet 356(9240):1461–1463
255. Paximadi E, Karakasiliotis I, Papaventsis D, Papageorgiou G, Markoulatos P (2008) Recombinant Sabin environmental isolates in Greece and Cyprus. J Appl Microbiol 104(4):1153–1162
256. CDC (2009) Update on vaccine-derived polioviruses – worldwide, January 2008-June 2009. MMWR Morb Mortal Wkly Rep 58(36):1002–1006
257. Arya SC, Agarwal N (2007) Global polio laboratory network: future pursuit and commitments. J Clin Virol 38(4):362–363
258. Maderova E, Slacikova M, Cernakova B, Sobotova Z, Nadova K (2005) First isolation of vaccine-derived poliovirus in Slovakia. Euro Surveill 10(8):E050818 3
259. Alexander JP, Ehresmann K, Seward J, Wax G, Harriman K, Fuller S et al (2009) Transmission of imported vaccine-derived poliovirus in an undervaccinated community in Minnesota. J Infect Dis 199(3):391–397
260. MMWR (1994) Certification of poliomyelitis eradication – the Americas, 1994. MMWR Morb Mortal Wkly Rep 43(39):720–722
261. Strebel PM, Sutter RW, Cochi SL, Biellik RJ, Brink EW, Kew OM et al (1992) Epidemiology of poliomyelitis in the United States one decade after the last reported case of indigenous wild virus-associated disease. Clin Infect Dis 14(2):568–579
262. MMWR (2001) Erratum: apparent global interruption of wild poliovirus type 2 transmission. MMWR 50(12):249
263. MMWR (2001) Certification of poliomyelitis eradication–Western Pacific Region, October 2000. MMWR Morb Mortal Wkly Rep 50(1):1–3
264. Wkly Epidemiol Record (2005) Conclusions and recommendations of the Advisory Committee on Poliomyelitis Eradication, Geneva, 11–12 Oct 2005. Wkly Epidemiol Rec 80(47):410–416
265. Heymann DL, Sutter RW, Aylward RB (2006) A vision of a world without polio: the OPV cessation strategy. Biologicals 34(2):75–79
266. Ehrenfeld E, Modlin J, Chumakov K (2009) Future of polio vaccines. Expert Rev Vaccines 8(7):899–905
267. Jenkins PC, Modlin JF (2006) Decision analysis in planning for a polio outbreak in the United States. Pediatrics 118(2): 611–618
268. Tebbens RJ, Pallansch MA, Alexander JP, Thompson KM (2010) Optimal vaccine stockpile design for an eradicated disease: application to polio. Vaccine 28(26):4312–4327

269. WHO (2005) WHO framework for national policy makers in OPV-using countries – Cessation of routine oral polio vaccine (OPV) use after global polio eradication 05.02.: WHO/POLIO/05.02
270. Wagner BG, Earn DJ (2008) Circulating vaccine derived polio viruses and their impact on global polio eradication. Bull Math Biol 70(1):253–280
271. Fine PE, Sutter RW, Orenstein WA (2001) Stopping a polio outbreak in the post-eradication era. Dev Biol (Basel) 105:129–147
272. Tebbens RJ, Pallansch MA, Kew OM, Caceres VM, Jafari H, Cochi SL et al (2006) Risks of paralytic disease due to wild or vaccine-derived poliovirus after eradication. Risk Anal 26(6):1471–1505
273. Oliver Wyman Inc (2010) The supply landscape and economics of IPV-containing combination vaccines: Key findings. May 2010: Commissioned by the Bill & Melinda Gates Foundation
274. Chumakov K, Ehrenfeld E (2008) New generation of inactivated poliovirus vaccines for universal immunization after eradication of poliomyelitis. Clin Infect Dis 47(12):1587–1592
275. Baca-Estrada M, Griffiths E (2006) Regulation and standardization of IPV and IPV combination vaccines. Biologicals 34(2):159–161
276. Duchene M (2006) Production, testing and perspectives of IPV and IPV combination vaccines: GSK biologicals' view. Biologicals 34(2):163–166
277. Graf H (2006) Manufacturing and supply of monovalent oral polio vaccines. Biologicals 34(2):141–144
278. El-Sayed N, El-Gamal Y, Abbassy AA, Seoud I, Salama M, Kandeel A et al (2008) Monovalent type 1 oral poliovirus vaccine in newborns. N Engl J Med 359(16):1655–1665
279. Farag MM (2006) Licensing of monovalent OPV1 vaccine. Biologicals 34(2):145–149
280. Caceres VM, Sutter RW (2001) Sabin monovalent oral polio vaccines: review of past experiences and their potential use after polio eradication. Clin Infect Dis 33(4):531–541
281. Plotkin JB, Dushoff J (2003) Codon bias and frequency-dependent selection on the hemagglutinin epitopes of influenza A virus. Proc Natl Acad Sci USA 100(12):7152–7157
282. Macadam AJ, Ferguson G, Stone DM, Meredith J, Knowlson S, Auda G et al (2006) Rational design of genetically stable, live-attenuated poliovirus vaccines of all three serotypes: relevance to poliomyelitis eradication. J Virol 80(17):8653–8663
283. Eichner M, Dietz K (1996) Eradication of poliomyelitis: when can one be sure that polio virus transmission has been terminated? Am J Epidemiol 143(8):816–822
284. Vashishtha VM (2004) But do we have other options? Indian J Pediatr 71(2):183–184
285. Yang CF, Naguib T, Yang SJ, Nasr E, Jorba J, Ahmed N et al (2003) Circulation of endemic type 2 vaccine-derived poliovirus in Egypt from 1983 to 1993. J Virol 77(15):8366–8377
286. Shulman LM, Manor J, Sofer D, Mendelsohn E (2009) Environmental surveillance for polioviruses in Israel: Bio-error, Bio-terror or just mother nature. In: Marks RS, Lobel L, Amadou SA (eds) Advanced detection of viral pathognes. Neobionics, Omer, Israel, pp 111–121
287. Nathanson N (2008) The pathogenesis of poliomyelitis: what we don't know. Adv Virus Res 71:1–50
288. Minor P (2006) Gaps in scientific knowledge for the post eradication world. Biologicals 34(2):167–170
289. Willerth SM, Pedro HA, Pachter L, Humeau LM, Arkin AP, Schaffer DV (2010) Development of a low bias method for characterizing viral populations using next generation sequencing technology. PLoS One 5(10):e13564
290. Kitamura N, Semler BL, Rothberg PG, Larsen GR, Adler CJ, Dorner AJ et al (1981) Primary structure, gene organization and polypeptide expression of poliovirus RNA. Nature 291(5816):547–553
291. Shulman LM, Manor Y, Sofer D, Mendelson E (2012) Environmental surveillance for poliovirus in Israel. In: Marks RS (eds) Bio-error, Bio-terror, or just mother nature. In viral detection biosensors, Pan Stanford Publishing, Singapore (In press)

Polybenzimidazole Fuel Cell Technology

Max Molleo[1], Thomas J. Schmidt[2], Brian C. Benicewicz[1]
[1]Department of Chemistry and Biochemistry, University of South Carolina, Columbia, SC, USA
[2]General Energy Research, Lab. of Electrochemistry, Paul Scherrer Institute, Villigen-PSI, Switzerland

Article Outline

Glossary
Definition of the Subject
Introduction to Polybenzimidazole Fuel Cell Sustainability
History and Technical Information of Polybenzimidazole Membranes
PBI-PA Fuel Cell Systems and Their Applications
Conclusions and Future Directions
Acknowledgments
Bibliography

Glossary

Polybenzimidazoles (PBIs) A class of polymers recognized for their excellent thermal and chemical stability, PBIs have historically been spun into fibers and woven into thermal protective clothing. In the past decade, PBIs have been cast into membranes and incorporated into fuel cells.

Polymer electrolyte membrane (PEM) Also referred to as Proton Exchange Membranes, PEMs are semi-permeable membranes that conduct and transport protons while preventing the transmission of gases and electrons.

Membrane electrode assembly (MEA) A device that is comprised of a PEM that is sandwiched between two electrodes.

Conventional imbibing The original process of impregnating polymer membranes with dopants. The precast, fully dense membranes are placed in baths of dopants and allowed to absorb the dopant which assists in proton conductivity.

PPA process A recently developed imbibing process, PBIs are polymerized and cast in a polyphosphoric acid (PPA) solvent. Under controlled hydrolysis conditions, Polyphosphoric acid, a good solvent for PBI, is converted into phosphoric acid, a poor solvent for PBI. A mechanically stable PBI gel membrane that is highly doped with phosphoric acid is produced by means of a sol-to-gel transition.

Proton conductivity A measure of how well a material can transfer protons. In fuel cell technology, it is used to gauge the viability of proton exchange membranes.

Combined heat and power (CHP) Stationary fuel cell devices that are used to produce both heat and electricity. High-temperature PBI fuel cell membranes are well suited for this application.

Definition of the Subject

After approximately 10 years of development, polybenzimidazole (PBI) chemistries and the concomitant manufacturing processes have evolved into commercially produced membrane electrode assemblies (MEAs). PBI MEAs can operate reliably without complex water humidification hardware and are able to run at elevated temperatures of 120–180°C due to the physical and chemical robustness of PBI membranes. These higher temperatures improve the electrode kinetics and conductivity of the MEAs, simplify the water and thermal management of the systems, and significantly increase their tolerance to fuel impurities. Membranes cast by a newly developed polyphosphoric acid (PPA) process possessed excellent mechanical properties, higher phosphoric acid (PA)/PBI ratios, and enhanced proton conductivities as compared to previous methods of membrane preparation. *p*-PBI is the most common polymer in PBI-based fuel cell systems, although AB-PBI and other derivatives have been investigated. This chapter reports on the chemistries and sustainable usages of PBI-based high-temperature proton exchange membrane fuel cells (PEMFCs).

Introduction to Polybenzimidazole Fuel Cell Sustainability

Alternative energy is often defined as any energy derived from sources other than fossil fuels or nuclear fission. These alternative energy sources, which include solar, wind, hydro, and geothermal energy, are considered renewable because they are naturally replenished and their supply is seemingly limitless. In contrast, the Earth's supply of fossil fuels is constantly being diminished. Fossil fuels, which include crude oil, coal, and natural gas, continue to be the dominating sources of energy in the world (Fig. 1). Fossil fuels provide more than 86% of the total energy consumed globally [1]. In 2008, over two-thirds of the electrical energy and 97% of the transportation energy in the USA was produced from these nonrenewable sources [2]. It is predicted that the global demand for fossil fuels will continue to increase over the next 10–20 years due to economic growth. One may conclude that the importance of renewable energy will steadily increase as the Earth's supply of fossil fuels continues to be depleted.

Polymer electrolyte membrane (PEM) fuel cells, also known as proton exchange membrane fuel cells (PEMFCs), are energy conversion devices that could provide the world with clean and efficient energy. Due to their excellent energy production, inexpensive starting materials, and lack of pollutant by-products, these cells have exponentially gained in popularity over the past decade. Electricity is produced at the heart of the fuel cell by the membrane electrode assembly (MEA), a component that is comprised of a proton exchange membrane sandwiched between two electrodes. Fueled by a hydrogen-based source, a metal catalyst at the anode splits the hydrogen into protons and electrons. As the protons are transported through the proton electrolyte membrane to the cathode, the electrons provide electrical work by traveling around the membrane through an external circuit from the

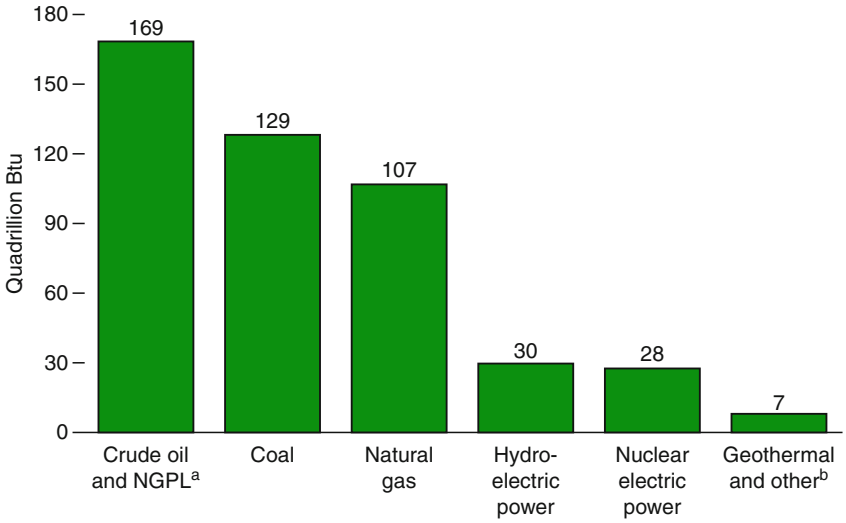

Polybenzimidazole Fuel Cell Technology. Figure 1
Global production of energy in 2006 by source. [a]Natural gas plant liquid. [b]Net electricity generation from wood, waste, solar, and wind [1]

anode to the cathode. The protons and electrons react with an oxidant (typically air or pure oxygen) at the cathode to form water, thereby completing the electrochemical cycle. Hydrogen gas is commonly used as a fuel source for the cells, but other fuels such as methane, methanol, and ethanol have been explored.

PEM fuel cells provide multiple advantages over conventional fossil fuel energy production. Because water is the only by-product of the electrochemical process, these fuel cells are clean and environmentally friendly. If one considers the tremendous amount of carbon dioxide created by energy production on the global scale (Fig. 2), PEM fuel cells offer a method to significantly reduce hazardous gas emissions. Minimal moving parts reduces the amount of maintenance of each cell, and the lack of combustion significantly decreases the amount of harmful pollutants such as sulfur oxides and nitrogen oxides. In addition, PEM fuel cells are much more efficient at producing energy (this is discussed in detail in section "PBI-PA Fuel Cell Systems and their Applications"), and much like a combustion engine, the cell can run continuously as long as fuel and oxidant are provided. Although fuel cells are an environmentally friendly energy conversion device, one must consider the manner in which hydrogen is gathered. Both hydrogen production and conversion from chemical to electrical energy need to be

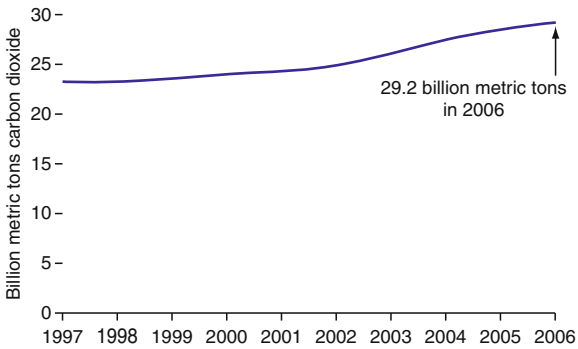

Polybenzimidazole Fuel Cell Technology. Figure 2
Global production of carbon dioxide annually from 1997 to 2006 [3]

sustainable to make the overall process sustainable. Hydrogen production, however, is out of the scope of this chapter.

The efficiency of a PEM fuel cell is largely dependent on the materials used and their arrangement in the cell. Fuel cells use an array of different catalysts, electrodes, membranes, and dopants, each of which function under specific operating conditions. Cells that use low-boiling dopants, such as water, operate at approximately 60–80°C to avoid vaporization of the proton-transfer agent. Large heat exchangers are required to

ensure the heat generated by the cell does not vaporize the electrolyte. Consequently, system complexity is increased as extra components and controls are required to ensure that the membrane remains hydrated during operation. Moreover, cell operation at such low temperatures allows trace amounts of reformate by-products, especially carbon monoxide, to bind to the catalyst. These highly competitive, nonreversible reactions "poison" the catalyst, thereby decreasing and possibly terminating the functionality of the fuel cell. Therefore, low-temperature fuel cells require an extremely pure fuel source.

In contrast to low-temperature cells, high-temperature PEMs use high-boiling dopants, such as phosphoric acid and sulfuric acid, and function at temperatures of 120–200°C. Because the cell is able to run at elevated temperatures, much smaller heat exchangers are required. Operating at higher temperatures allows fuel pollutants to bind reversibly to the catalyst, which helps to prevent catalyst poisoning. Comparatively, high-temperature PEMs can use reformed gases with much higher levels of impurities and lower reformation costs. Furthermore, high temperatures typically improve both the electrode kinetics and operating abilities of the cell. This chapter reports on the chemistries and sustainable usages of PBI-based high-temperature PEMFCs.

History and Technical Information of Polybenzimidazole Membranes

Polybenzimidazoles (PBIs) are a class of polymers recognized for their excellent thermal and chemical stability. PBI is used in multiple applications including matrix resins, high-strength adhesives, thermal and electrical insulating foams, and thermally resistant fibers. PBI fibers were originally synthesized in the early 1960s by a cooperative effort of the US Air Force Materials Laboratory with Dupont and the Celanese Research Company. One of the first PBIs to be widely investigated was poly(2,2′-*m*-phenylene-5,5′-bibenzimidazole), which is commonly referred to as *m*-PBI (Fig. 3). Because *m*-PBI is nonflammable, resistant to chemicals, physically stable at high temperatures, and can be spun into fibers, this polymer has been used in astronaut space suits, firefighter's turnout coats and suits, and high-temperature protective gloves.

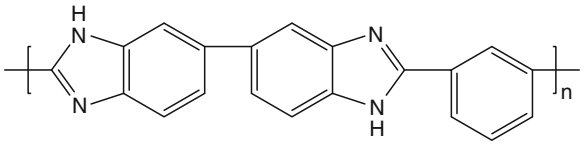

Polybenzimidazole Fuel Cell Technology. Figure 3 Chemical structure of poly (2,2′-*m*-phenylene-5,5′-bibenzimidazole) (*m*-PBI)

Acid-doped polybenzimidazole membranes are excellent candidates for high-temperature fuel cells because of their thermal and chemical stability and proton conducting ability. The stability of PBIs is attributed to its aromatic structure (alternating single and double bonds) and the rigid nature of its bonds [4]. While the acid-doped membrane structure allows protons to flow from one side to the other, it acts as a barrier to the crossover of gases and electrons. The chemical stability of PBIs allows the membranes to withstand the chemically reactive environments of the anode and cathode. Furthermore, the basic nature of the polymer allows it to be highly doped with phosphoric or sulfuric acid. The dopants interact with the polymer matrix and provide a network through which protons can be transported. These acids are used as electrolytes because of their high conductivity, thermal stability, and enhanced proton-transport capabilities. It is important to note that the proton conductivity of PBI membranes without a dopant is negligible. For liquid phosphoric acid, the proton jump rate is orders of magnitude larger than the diffusion of the phosphoric acid molecule as a whole [5]. Additionally, it has been reported that both protons and phosphate moieties have a substantially decreased diffusion coefficient when blended with basic polymers as opposed to liquid phosphoric acid [6]. Therefore, a heterogeneous, two-phase system in which the PBI membrane is phase-separated and imbibed with phosphoric acid has a higher conductivity than its homogeneous counterpart [7]. The partial charges of the phosphate ions involved with proton transfers increases charge delocalization, which lowers the overall energy barrier of proton transfer [8]. The proton-transfer mechanism of large proton vehicle species (such as phosphate ions) can be initiated by local vibrations of the vehicle species. In comparison, the amount of energy required to induce proton transfer small proton vehicle species

such as water is comparable to the amount of energy required to diffuse the entire small proton vehicle.

Synthesis of Polybenzimidazoles

One of the first PBIs membranes investigated for fuel cell use was poly(2,2′-*m*-phenylene-5,5′-bibenzimidazole) (*m*-PBI). At the time, there was a vast amount of research previously reported on *m*-PBI and it was renowned for its excellent thermal and mechanical properties [5]. The polymer is synthesized by the reaction of 3,3′,4,4′-tetraaminobiphenyl (TAB) with diphenylisophthalate (DPIP) during a melt/solid polymerization (Scheme 1). The resulting polymer is extracted and has an inherent viscosity (IVs) between 0.5 and 0.8 dL g^{-1}, which corresponds to a polymer with low to moderate molecular weight. The *m*-PBI is further purified by dissolving it in a solution of N,N-dimethylacetamide and lithium chloride (DMAc/LiCl) under 60–100 psi and 250°C and then filtering; this step removes any cross-linked *m*-PBI. The polymer is then cast as a film and dried at 140°C under vacuum to evaporate the solvent. The *m*-PBI membrane is washed in boiling water to remove any residual DMAc/LiCl solution trapped in the polymer matrix. After the polymer has been dried, an acid bath is used to dope the membrane; the doping level of the membrane can be partially controlled by varying the concentration of acid in the bath. Originally, this conventionally imbibed process created membranes with molar ratios of phosphoric acid/polymer repeat unit (PA/PRU) approximately 6–10 [9]. A "direct acid casting" (DAC) technique was later developed to allow the PBI membrane to retain more PA [10]. Both the conventional imbibing process and DAC were developed following the research performed by Jean-Claude Lassegues, who was one of the first scientists that investigated basic polymeric-acid systems (a summary of his work is reviewed in reference [11]). The DAC technique consists of extracting low molecular weight PBI components from PBI powder, and then dissolving the high molecular weight PBI components in trifluoroacetic acid (TFA). Phosphoric acid is added to the TFA/PBI mixture, which is then cast onto glass plates with a casting blade. One may tune the doping level of the polymer by adjusting the amount of phosphoric acid that is added to the TFA/PBI mixture. However, as one increases the PA doping level of a DAC PBI membrane, its mechanical strength decreases to the point where it can no longer be used in a fuel cell. Modern imbibing processes can increase the PA/PBI ratio to 12–16, and these fuel cell membranes are reported to have proton conductivities as high as 0.08 S cm^{-1} at 150°C at various humidities.

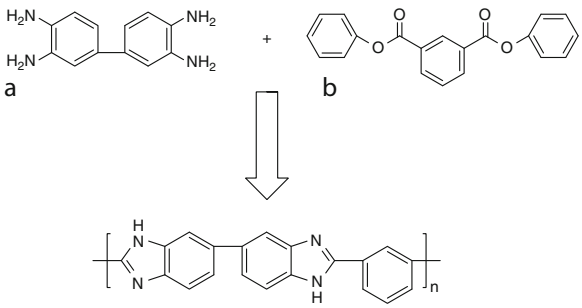

Polybenzimidazole Fuel Cell Technology. Scheme 1 Polymerization of *m*-PBI from 3,3′,4,4′-tetraaminobiphenyl (**a**) and diphenylisophthalate (**b**)

A novel synthetic process for producing high molecular weight PBIs, the "PPA Process" was developed at Rensselaer Polytechnic Institute with cooperation from BASF Fuel Cell GmbH. This process has previously been discussed by Xiao et al. [12]. The general synthesis of PBI by this method requires the combination of a tetraamine with a dicarboxylic acid in polyphosphoric acid (PPA) in a dry environment. The step-growth polycondensation reaction typically occurs around 200°C for 16–24 h in a nitrogen atmosphere, producing high molecular weight polymer. This solution is cast directly from PPA as a thin film on a substrate, and upon absorption of water, the PPA hydrolyzes in situ to form phosphoric acid. Note that PPA is a good solvent for PBI while PA is a poor solvent. Under controlled hydrolysis conditions, a mechanically stable PBI gel membrane that is highly doped with phosphoric acid is produced. The multiple physical and chemical transformations that explain the solution-to-gel phase transition are summarized in Fig. 4.

The PA-doped *m*-PBI fuel cell membrane maintains thermal and physical stability while operating at high temperature. To illuminate the fundamental differences in polymer film architecture, polymers with similar physical characteristics were prepared by the conventional PPA Process (Table 1). Even though the

ratio of phosphoric acid-to-polymer repeat unit (PA/PRU) achieved by both processes were nearly identical, the PPA Process produces membranes with much higher proton diffusion coefficients and conductivities. The higher proton diffusion coefficients of membranes produced by the PPA Process versus conventionally imbibed membranes were confirmed by NMR [13]. One can conclude that the PPA Process creates a membrane with a proton-transport architecture superior to that of the conventionally imbibed PBI membrane. In addition, inherent viscosity data indicates that the PPA process produces polymers of much higher molecular weight [12]. It was subsequently shown that improved membrane morphology and increased molecular weight allow the polymer to retain much more phosphoric acid than traditionally cast PBI membranes. An increased PA doping level typically improves the conductivity of the membrane and may even increase the performance of the cell.

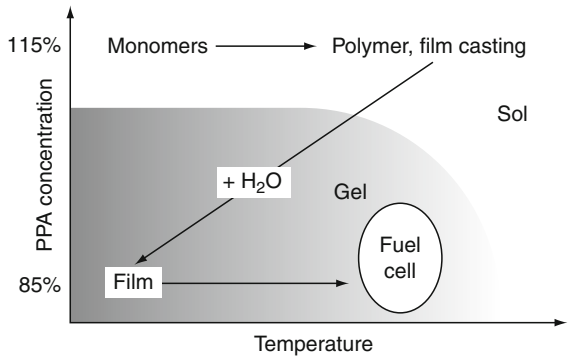

Polybenzimidazole Fuel Cell Technology. Figure 4 State diagram of the PPA Sol-gel process [12]

Properties and Performance of Synthetically Modified PBI

In this chapter, the synthesis of significant PBI membranes (Fig. 5) and their use in fuel cells are described. Synthetically modified PBIs are investigated for enhanced thermo-oxidative stability, solubility, and flexibility; these attributes allow for improved processability and production of membranes with good chemical and mechanical properties. All PBI membranes are produced by means of step-growth polycondensation reactions and are generally imbibed by either the conventional technique or made by the PPA process. To synthesize modified polymers, one may either polymerize modified monomers or use post-polymerization cross-linking or substitution reactions. The following sections briefly detail the syntheses of PBI derivatives and their performances as fuel cell membranes.

***m*-PBI** One of the first PBI membranes investigated for fuel cell use was *m*-PBI (Fig. 5a). As previously discussed, the film can be processed by using either the conventional imbibing method or the PPA process. Using the conventional imbibing method, the inherent viscosity of the membrane is usually between 0.50–1.00 dL g^{-1} at 30°C, which indicates polymers of moderate molecular weight. In contrast, *m*-PBI membranes synthesized and doped via the PPA Process have inherent viscosities of approximately 1.00–2.35 dL g^{-1} at 30°C, which corresponds to higher molecular weight polymers [9]. Using

Polybenzimidazole Fuel Cell Technology. Table 1 Comparison of conventionally imbibed *m*-PBI versus *m*-PBI synthesized from the PPA Process [14]

IV[a] (dL g^{-1})	Film process	Polymer (wt%)	PA (wt%)	Water (wt%)	PA/PBI (Molar ratio)	Proton diffusion coefficient[b] (cm^2 s^{-1})	Conductivity[c] (S cm^{-1})
0.89	Conventionally imbibed	15.6	60.7	23.7	12.2	10^{-7}	0.048
1.49	PPA Process	14.4	63.3	22.3	13.8	3×10^{-6}	0.13

[a]Inherent viscosity (IV) was measured at a polymer concentration of 0.2 g dL^{-1} in concentrated sulfuric acid (96%) at 30°C, using a Canon Ubbelohde viscometer
[b]Estimation of upper bound for conventionally imbibed *m*-PBI at 180°C; PPA-prepared *m*-PBI measured at 180°C
[c]Measured at 160°C after an initial heating to 160°C to remove water

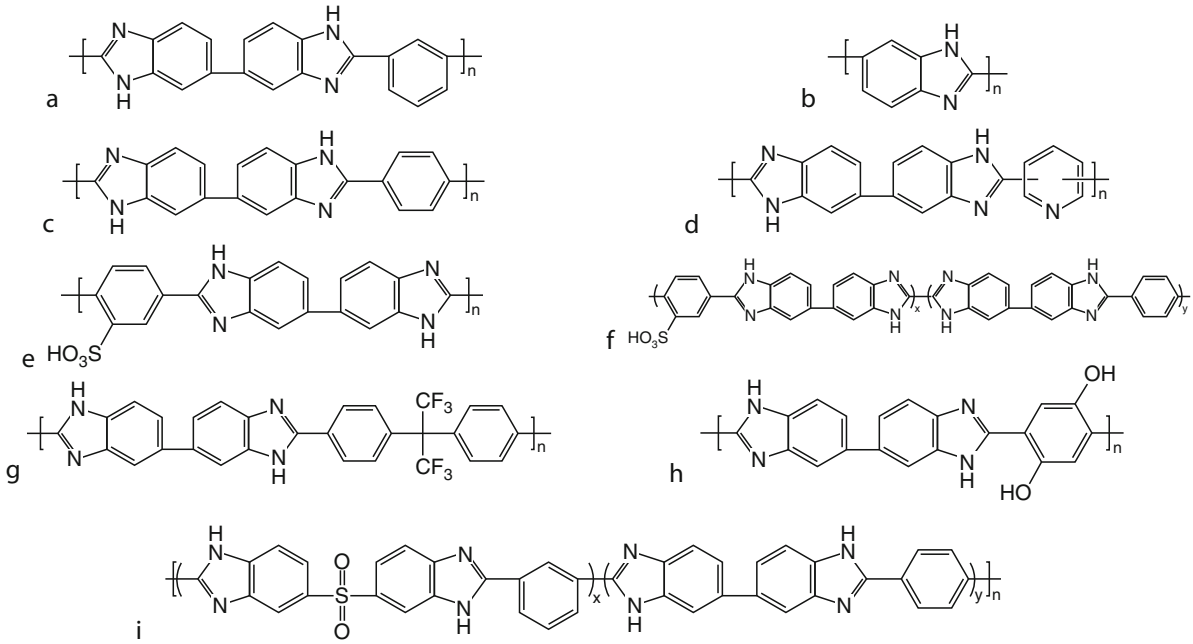

Polybenzimidazole Fuel Cell Technology. Figure 5
Various synthetically modified polybenzimidazoles for use in fuel cells. (**a**) *m*-PBI, (**b**) AB-PBI, (**c**) *p*-PBI, (**d**) py-PBI, (**e**) s-PBI, (**f**) s-PBI/*p*-PBI random block copolymer, (**g**) 6F-PBI, (**h**) 2OH-PBI, and (**i**) *m*-SPBI/*p*-PBI segmented block copolymer

the PPA Process, higher molecular weight polymers have contributed to higher doping levels. Phosphoric acid doping levels for conventionally prepared *m*-PBI ranged from 6 to 10 moles PA/PRU, whereas the doping levels for polymer films prepared via the PPA process range from 14 to 26 moles PA/PRU [4]. Trends show that the mechanical stability of conventionally prepared membranes decrease as the doping level increases and/or as the molecular weight of the polymer decreases. The doping level, casting technique, temperature, and humidity all influence the conductivity of a *m*-PBI membrane. Under various humidities, conventionally prepared *m*-PBI membranes have been reported having conductivities in the range of 0.04–0.08 S cm^{-1} [15]. Using the PPA Process, the conductivity values of *m*-PBI membranes are typically higher than that of the conventionally imbibed process. One study [16] reported *m*-PBI membranes formed by the PPA Process as having a conductivity of 0.13 S cm^{-1} at 160°C under non-humidified conditions.

Phosphoric acid–doped *m*-PBI membranes that have been formed by the conventional imbibing method have been extensively studied for use in fuel cells. Li et al. [17] demonstrated that a membrane with 6.2 PA/PRU doping level obtains a current density of approximately 0.7 A cm^{-2} at 0.6 V using hydrogen and oxygen gases; these results were promising because the gases were not humidified. Zhai et al. [18] studied the degradation mechanisms of the PA/*m*-PBI system by continuously operating it at 0.640 A cm^{-2} at 150°C with unhumidified hydrogen and oxygen for 550 h; the fuel cell was operated intermittently the last 50 h with shutoffs every 12 h. The voltage increased from 0.57 to 0.66 V during the beginning 90 h activation period, and the following 450 h period showed a steady decrease to 0.58 V. The performance of the system rapidly decreased in the following 10 h due to agglomeration of the platinum from the catalyst, leaching of the phosphoric acid, and hydrogen crossover. Kongstein et al. [19] employed use of a dual layer electrode to prevent the oxidation of carbon in the polymer membrane, which can occur in acidic environments at high voltages. This electrode would improve the structural integrity of the polymer and help prevent hydrogen crossover from occurring. The PA/*m*-PBI membrane had a maximum of 0.6 V at 0.6 A cm^{-2} with a maximum power density

of 0.83 W cm^{-2} at 0.4 V. These performances were lower than that of other PEM systems, such as Nafion, but were still impressive because they could be run at much higher temperatures.

Poly(2,5-Polybenzimidazole): AB-PBI Commonly referred to as AB-PBI, poly(2,5-polybenzimidazole) has a much simpler structure than that of *m*-PBI and other polybenzimidazoles (Fig. 5b). Whereas *m*-PBI is synthesized from 3,3′,4,4′-tetraaminobiphenyl and DPIP, AB-PBI is polymerized from a single monomer, 3,4-diaminobenzoic acid (DABA). This monomer is commercially available and is less expensive than the starting materials of *m*-PBI. The polymer membrane can be cast and imbibed with phosphoric acid by the conventional imbibing method in a mixture of methanesulfonic acid (MSA) and phosphorous pentoxide (P_2O_5) [20] or DMAc. It can also be cast by direct acid casting using trifluoroacetic acid (TFA) [10, 15] or by the PPA Process [10, 21–23]. AB-PBI membranes prepared by the conventional imbibing method had IV values around 2.0–2.5 dL g^{-1} as reported by Asensio et al. [23] and 6–8 dL g^{-1} by Litt et al. [15]. Polymers produced from recrystallized DABA by the PPA Process have IV values greater than 10 dL g^{-1} [24]; however, membranes of AB-PBI could not be easily formed via the PPA Process because of the polymer's high solubility in acids.

Because AB-PBI has a high concentration of basic sites (amine and imine groups), it has a high solubility and affinity to acids. Due to this affinity, it can be doped with phosphoric acid and sulfonated with sulfuric acid. Sulfonation of AB-PBI (sAB-PBI) is performed by soaking the precast polymer in sulfuric acid followed by treating the mixture with heat. Asensio et al. [23] reported sAB-PBI-PA membranes having an enhanced conductivity over that of AB-PBI-PA and to be both mechanically strong and thermally stable. Using the direct casting method from MSA-P_2O_5, Kim et al. [20] produced AB-PBI-PA membranes with conductivities similar that of Asensio, having values ranging from 0.02–0.06 S cm^{-1} at 110°C with no humidification. The conductivity values and physical-chemical properties resemble that of *m*-PBI, making it a good candidate for fuel cell use.

Yu [25] synthesized *p*-PBI-block-AB-PBI membranes to lower the membrane's solubility in acids while maintaining a high acid doping level. Different molar ratios of each polymer block were synthesized, and their conductivities and acid doping levels were investigated. As detailed in Table 2, the proton conductivities of the segmented block copolymers were enhanced by an order of magnitude over that of native AB-PBI. Stress–strain studies showed that these block copolymers were strong enough to be used in fuel cell tests. Polarization curves (Fig. 6) of these membranes illustrate that copolymers II, III, and IV have excellent fuel cell properties (approximately 0.6 V at 0.2 A cm^{-2}); polarization curves for copolymer V and VI could not be measured due to poor thermal stability of the membrane (re-dissolution) at 160°C.

Poly(2,2′-(1,4-Phenylene)5,5′-Bibenzimidazole): *p*-PBI Poly(2,2′-(1,4-phenylene)5,5′-bibenzimidazole) (*p*-PBI, Fig. 5c) is one of the highest performing PBI membranes for high-temperature fuel cell use. Due to the

Polybenzimidazole Fuel Cell Technology. Table 2 Percent composition, acid doping level, and proton conductivity data for various *p*-PBI-block-AB-PBI membranes [25]

	Para-PBI/AB-PBI (mole ratio, x/y)	Acid doping level (PA/2 benzimidazole)	Proton conductivity (S/cm @ 160°C)	Membrane composition (%)		
				Polymer	H_3PO_4	Water
I	100/0	42.9	0.25	4.13	60.38	35.11
II	75/25	19.1	0.25	8.68	58.09	33.22
III	50/50	24.1	0.27	6.59	54.53	38.88
IV	25/75	21.8	0.23	7.79	63.31	28.90
V	10/90	17.3	0.15	8.84	63.23	27.94
VI	0/100	N/A	N/A			

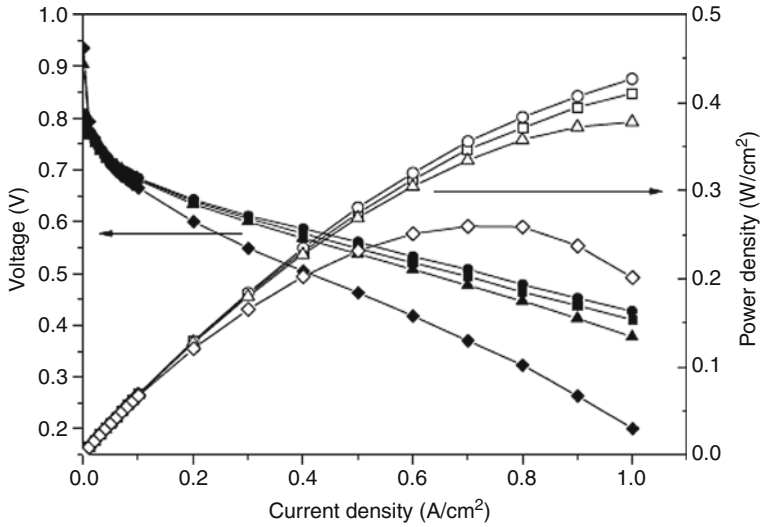

Polybenzimidazole Fuel Cell Technology. Figure 6
Polarization curves (*filled symbols*) and power density curves (*unfilled symbols*) of *p*-PBI (Polymer I, ■) and *p*-PBI-block-AB-PBI membranes (75/25, Polymer II, ●○, 50/50 Polymer III, ▲△, 25/75, Polymer IV, ♦◇) at 160°C with H_2 (1.2 stoic)/Air (2.0 stoic) under atmospheric pressure [25]

rigid nature of *p*-PBI, high molecular weight polymers have typically been difficult to fabricate or process. The first reported high molecular weight *p*-PBI with an IV value of 4.2 dL g^{-1} was synthesized in 1975 by the US Air Force Materials Laboratory [26]. Because it could not be spun into fibers as easily as *m*-PBI, *p*-PBI was not investigated further until after the turn of the century. Using the PPA Process, Xiao et al. [12] and Yu et al. [27] synthesized high molecular weight *p*-PBI with IV values as high as 3.8 dL g^{-1}. The PA doping level of the corresponding polymer membranes was >30 mol PA/PRU, allowing the membrane to achieve a conductivity of 0.24 S cm^{-1} at 160°C. Xiao and Yu showed that *p*-PBI membrane achieves a much higher acid doping level and conductivity than that of *m*-PBI, which only achieves a doping level of 13–16 mol PA/PRU with a conductivity of 0.1–0.13 S cm^{-1}. Because *p*-PBI had excellent mechanical properties at this high doping level, it was a prime candidate for fuel cell performance tests.

The polarization curves of an MEA using *p*-PBI produced by the PPA Process at various temperatures are shown in Fig. 7. Hydrogen was used as the fuel and air was used as the oxidant. The *p*-PBI outperformed the *m*-PBI at all temperatures, and the performance of the MEA increased as the temperature increased. Using a load of 0.2 A cm^{-2}, the cell was able to produce a voltage of 0.606 V at 120°C; upon raising the temperature to 180°C, the voltage increased to 0.663 V. This was especially promising because the gases were unhumidified.

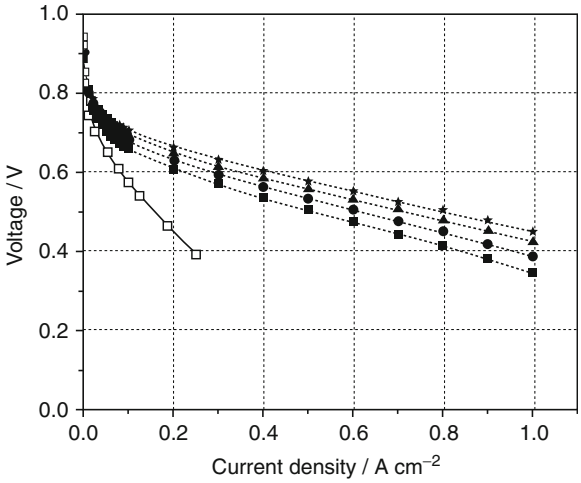

Polybenzimidazole Fuel Cell Technology. Figure 7
Polarization curves of PPA-Processed *p*-PBI MEA using hydrogen/air at 120°C (*squares*), 140°C (*circles*), 160°C (*triangles*), and 180°C (*stars*). Open squares represent DMAc cast *m*-PBI MEA at 150°C [27]

Pyridine-PBI Pyridine polybenzimidazoles (py-PBIs, Fig. 5d) have been investigated for their use in fuel cells because of their high concentration of basic sites (amine and imine groups). Similar to AB-PBI, the high concentration of basic sites allow these polymers to have a high affinity to acids. The pyridine moiety is commonly combined with the traditional PBI structure by including it as part of the backbone structure.

Xiao et al. synthesized an array of py-PBIs that have the pyridine moiety as part of the polymer backbone [12, 28, 29]. These polymers were synthesized by a reaction of 2,4-, 2,5-, 2,6-, or 3,5-pyridine dicarboxylic acid with 3,3′,4,4′-tetraaminobiphenyl (TAB) using the PPA Process. Exceedingly pure monomers were required to polymerize the py-PBIs, and IV values of 1.0–2.5 dL g^{-1} were obtained. The 2,4- and 2,5-py-PBI membranes formed mechanically strong films, whereas the 2,6-py-PBI membrane was mechanically weak and the 3,5-py-PBI was unable to form films due to high solubility in PPA. All of the py-PBI structures were thermally stable in both nitrogen and air in temperatures up to 420°C. The 2,5- and 2,6-py-PBI were reported as having conductivities of 0.2 S cm^{-1} and 0.1 S cm^{-1} at 160–200°C, respectively. The 2,5-py-PBI was found to have the most mechanically robust structure. It was hypothesized that the enhancement of mechanical properties was due to its *para*-orientation as opposed to the other py-PBIs having a *meta*-orientation. In addition, the doping level of 2,5-py-PBI averaged 20 mol of phosphoric acid per polymer repeat unit. Because PPA-Processed 2,5-py-PBI was an extremely good candidate for fuel cell testing, polarization tests of the MEA were performed (Fig. 8). The platinum loading on the anode and cathode was 1.0 mg cm^{-2} with 30% Pt in Vulcan XC-72 carbon black. The active area for the MEA was 10 cm^2. The membranes used non-humidified H_2/O_2 and higher temperatures improved the performances of 2,5-py-PBI MEA.

There have been studies indicating that blends of PBI polymers with pyridine-containing polymers could prove useful in a high-temperature PEM fuel cell. Kallitsis et al. [31] combined commercially supplied *m*-PBI with an aromatic polyether that contained a pyridine moiety in the main chain (PPyPO); these polymer blends were then soaked in 85% wt PA. Dynamic mechanical analysis of a 75/25 PBI/PPyPO

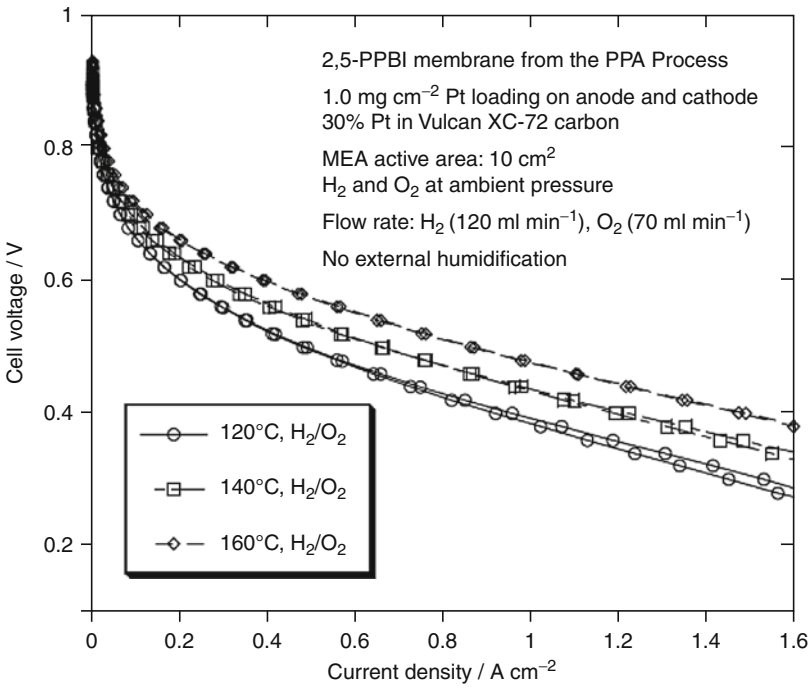

Polybenzimidazole Fuel Cell Technology. Figure 8
Polarization curves under hydrogen and oxygen gases at various temperatures of PA-doped 2,5-py-PBI membranes [30]

block copolymer showed reasonable mechanical strength and flexibility. The conductivity of this copolymer was not reported, but the conductivity of 85/15 PBI/PPyPO block copolymer was 0.013 S cm^{-1} at a relatively low PA doping level. Further investigation of these systems is required to prove its utility as a fuel cell membrane.

Sulfonated PBI Sulfonated aromatic polymers have been widely investigated [32–42] for fuel cell use due to their enhanced physical and chemical robustness, acid and water retention, and conductivity over that of Nafion and other perfluorosulfonic acid-type polymers. Thus, due to the enhanced properties of PBI, it was logical to investigate the physical and chemical properties of sulfonated PBI (s-PBI) membranes. Sulfonation of PBI typically occurs by either direct sulfonation of the polymer backbone [23, 43, 44], grafting sulfonated moieties onto the backbone [23, 45], or by a polycondensation reaction that bonds aromatic tetraamines to sulfonated aromatic diacids [46–48]. Compared to other sulfonation methods, polycondensation reactions provide more control over the degree of sulfonation.

Mader investigated the physical and chemical properties of s-PBI with PA as the dopant (Fig. 5e) [48]. The polymer was synthesized by two different synthetic pathways; the first was a direct polycondensation reaction of 2-sulfoterephthalic acid (s-TPA) and TAB using the PPA Process, and the second was a post-sulfonation reaction of *p*-PBI using concentrated sulfuric acid. The IV values for the polymer membranes derived from the polycondensation reaction ranged from 1 to 2 dL g^{-1}; these polymers had sufficiently high molecular weights to allow strong films to be cast. In addition, these polymer membranes could achieve doping levels between 28 and 53 mol PA/PRU, which resulted in significantly high conductivity values (all above 0.1 S cm^{-1} at all temperatures between 100 and 200°C).

Based on the preliminary data, s-PBI polymer membranes were excellent candidates for fuel cell tests. Polarization tests were run using an s-PBI membrane with an IV value of 1.71 dL g^{-1}, a PA doping level of 52.33 mol PA/PRU, and a conductivity of 0.248 S cm^{-1}; the results are depicted in Fig. 9. The s-PBI membrane exhibited its highest performance at 160°C, producing 0.6788 V at a current density of 0.2 A cm^{-2}. This performance compares well to that of other PBIs produced by the PPA Process, which is typically around 0.6–0.7 V at 0.2 A cm^{-2}.

The s-PBI homopolymer was shown to have both excellent resistance to gas impurities and excellent longevity. A reformate gas composed of 70% hydrogen, 28% carbon dioxide, and 2% carbon monoxide was used as the fuel while air was used as the oxidant. As depicted in Fig. 10, the fuel cell performance increased with increasing temperature; this is explained by the retardation of carbon monoxide poisoning that occurs

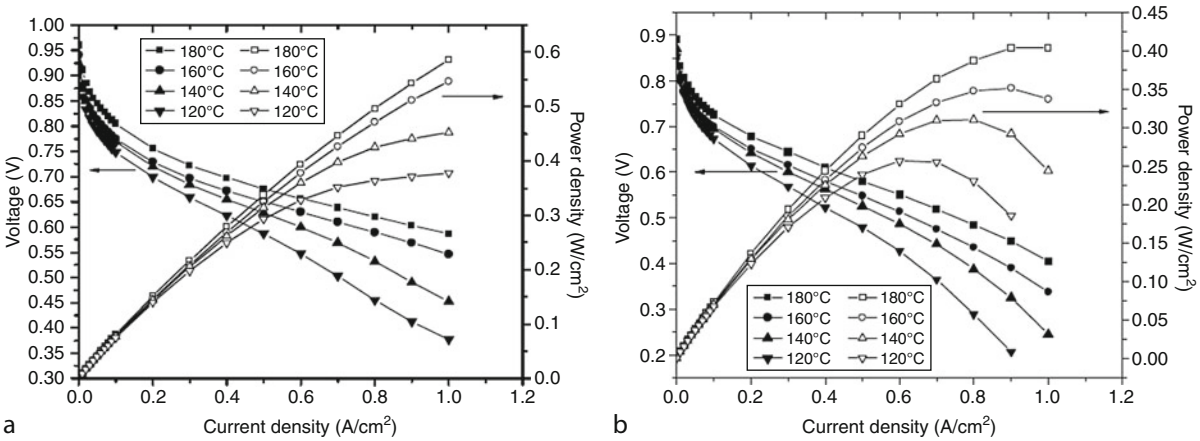

Polybenzimidazole Fuel Cell Technology. Figure 9
Polarization curves (*filled symbols*) and power density curves (*unfilled symbols*) of s-PBI using (**a**) hydrogen and oxygen and (**b**) hydrogen and air [48]

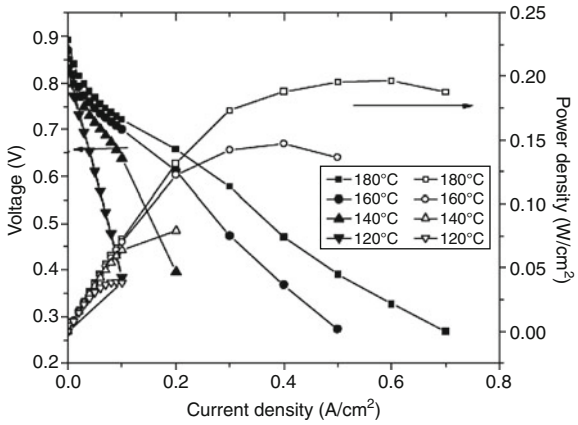

Polybenzimidazole Fuel Cell Technology. Figure 10 Polarization curves (*filled symbols*) and power density curves (*unfilled symbols*) of s-PBI using reformate and air [48]

at high temperatures. The performance loss of s-PBI MEA was measured by holding the MEA at 0.2 A cm^{-2} at 160°C for 1,200 h using H_2/O_2. After reaching stabilization at the 343rd hour, the MEA had a voltage loss of 0.024 mV h^{-1} for the remainder of the test.

Mader also investigated s-PBI/*p*-PBI random copolymers (Fig. 5f) for use in fuel cells [48]. The random copolymer was synthesized by reacting TAB, TPA, and s-TPA in a reaction flask and the membrane was cast via the PPA Process. High molecular weight polymers were achieved with IV values exceeding 1.8 dL g^{-1}; this allowed for mechanically strong films to be cast. As the ratio of s-PBI/*p*-PBI decreased, the molecular weight of the polymer proportionally increased. Higher PA loading was seen at lower s-PBI/*p*-PBI ratios, indicating a stronger attractive force between PA and *p*-PBI than PA and s-PBI. The PA loading values almost directly corresponded to the conductivity of the membranes. The 75/25 s-PBI/*p*-PBI membrane had a PA loading value of 20.32 mol PA/PBI and a conductivity of 0.157 S cm^{-1}, whereas the 25/75 s-PBI/*p*-PBI membrane had a PA loading value of 40.69 mol PA/PBI and a conductivity of 0.291 S cm^{-1}.

Fuel cell performance tests were conducted on the random copolymers. Even though the 25/75 s-PBI/*p*-PBI random copolymer had a higher conductivity than that of *p*-PBI homopolymer, it was found that all of the random copolymers showed lower performance than *p*-PBI. The 50/50 and 75/25 s-PBI/*p*-PBI random copolymers had lower performance than the s-PBI homopolymer at all PA doping levels. However, the 25/75 s-PBI/*p*-PBI random copolymer performed comparably to the s-PBI homopolymer at equivalent PA doping levels.

PBI-Inorganic Composites For conventionally prepared PBI membranes, as the acid doping levels of PBIs increase, the conductivity and overall performance of the PBI membranes also tend to increase. However, as high acid doping levels are reached for PBI membranes, the mechanical strength of the membrane significantly decreases. Inorganic fillers for PBI membranes have been investigated to improve membrane film strength, thermal stability, water and acid uptake, and conductivity. These composite membranes have only been examined using *m*-PBI and the conventional casting method.

He et al. investigated the use of zirconium phosphate (ZrP) in a PA/PBI system [49]. The conductivity of *m*-PBI with a doping level of 5.6 PA/PRU increased from 0.068 S cm^{-1} to 0.096 S cm^{-1} with the addition of 15 wt% ZrP at 200°C and at 5% relative humidity. As seen in Fig. 11, the conductivity of the membrane increased as the relative humidity and temperature of its environment increased. Conductivities of other inorganic fillers, such as phosphotungstic acid, silicotungstic acid, and tricarboxylbutylphosphonate, are comparable or lower than that of ZrP. Unfortunately, there have been no fuel cell performance tests published on these systems. Overall, these inorganic fillers improved the conductivity of *m*-PBI membranes.

Other Modified PBIs Multitudes of other organically modified PBI membranes exist that include, but are not limited to, fluorinated PBI, ionically and covalently cross-linked PBI, PBI blends, and a wide variety of PBI copolymers. Because there are far too many to describe, this subsection will highlight select PBI membranes that have not been included in the prior subsections.

Qian et al. investigated the use of hexafluoroisopropylidene-containing polybenzimidazole (6F-PBI, Fig. 5g) in fuel cells [50]. The polymer was synthesized via the PPA Process through the reaction of TAB with 2,2-Bis(4-carboxyphenyl) hexafluoropropane in PPA. High molecular weight polymer with an IV value of 0.98 dL g^{-1} was achieved. Although the PA doping level

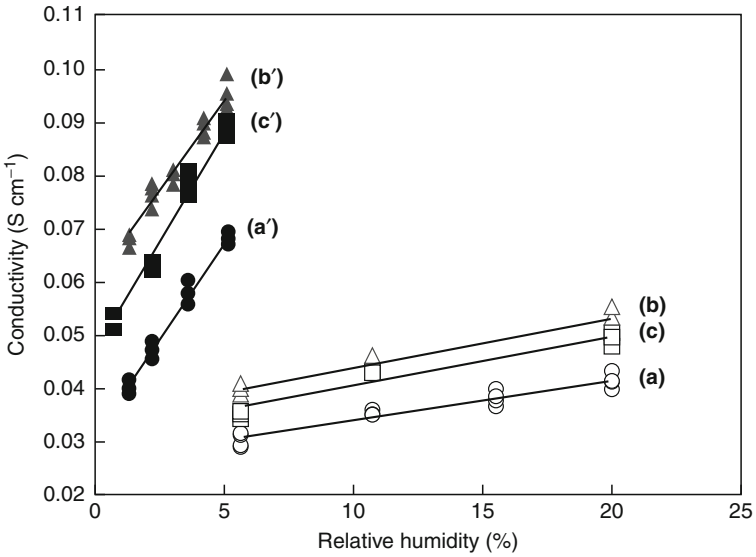

Polybenzimidazole Fuel Cell Technology. Figure 11
Conductivity study of ZrP/*m*-PBI system for (**a**) *m*-PBI at 140°C, (**a′**) *m*-PBI at 200°C, (**b**) 15 wt% ZrP in *m*-PBI at 140°C, (**b′**) 15 wt% ZrP in *m*-PBI at 200°C, (**c**) 20 wt% ZrP in *m*-PBI at 140°C, and (**c′**) 20 wt% ZrP in *m*-PBI at 200°C [49]

of 6F-PBI was considerably high (30–40 mol PA/PRU), the membrane only achieved a peak conductivity value of 0.09 S cm^{-1} at 180°C. This is lower than that of PPA-Processed *p*-PBI that achieved approximately 0.25 S cm^{-1} at 160°C.

The mechanical strength of 6F-PBI at high PA doping levels was strong enough to fabricate a membrane for fuel cell testing. Polarization and power density curves of 6F-PBI using hydrogen and reformate gases as fuel are illustrated in Fig. 12. Using hydrogen as fuel and air as the oxidant, the 6F-PBI MEA achieved a steady-state voltage of 0.58 V at a current density of 0.2 A cm^{-2}. When oxygen was used as the oxidant at the same current density, the steady-state voltage increased to 0.67 V. Additionally, the MEA showed excellent resistance to carbon monoxide poisoning. When a reformate gas comprised of 40% hydrogen, 40.8% nitrogen, 19% CO_2, and 0.2% CO was used as fuel and air was used as the oxidant, the CO poisoning effects produced an approximate 3 mV reduction in voltage. This study illustrates that low levels of CO poisoning have little effect on the 6F-PBI MEA operating at this temperature.

Commonly known as 2OH-PBI (Fig. 5h), poly (2,2′-(dihydroxy-1,4-phenylene)5,5′-bibenzimidazole) is another PBI membrane with extremely promising properties. Yu and Benicewicz [51] synthesized 2OH-PBI homopolymer by combining TAB with 2,5-dihydroxyterephthalic acid (2OH-TPA) in PPA and cast it via the PPA Process. Yu also synthesized the 2OH-PBI/*p*-PBI random copolymer by reacting both 2OH-TPA and TPA simultaneously with TAB; the copolymer membrane was also cast using the PPA Process. It was proposed that the 2OH-PBI homopolymer was significantly cross-linked through phosphoric acid ester bridges. Because of this cross-linking, the polymer was unable to be dissolved and an IV value could not be determined. Upon hydrolysis of the ester bridges by sodium hydroxide, the IV value of the homopolymer was measured as 0.74 dL g^{-1}. The acid doping level of 2OH-PBI homopolymer was approximately 25 PA/PRU, and its conductivity at 160°C was 0.35 S cm^{-1}. It is important to note that at all temperatures between room temperature and 180°C, the conductivity of 2OH-PBI homopolymer was greater than that of *p*-PBI. As the ratio of 2OH-PBI/*p*-PBI decreased in the random copolymer, the doping level and conductivity decreased. It was found that the conductivity of the material was highly dependent on the chemical structure of the PBI membrane and not just the doping level.

Using a Pt anode electrode and a Pt-alloy cathode electrode, polarization tests were performed

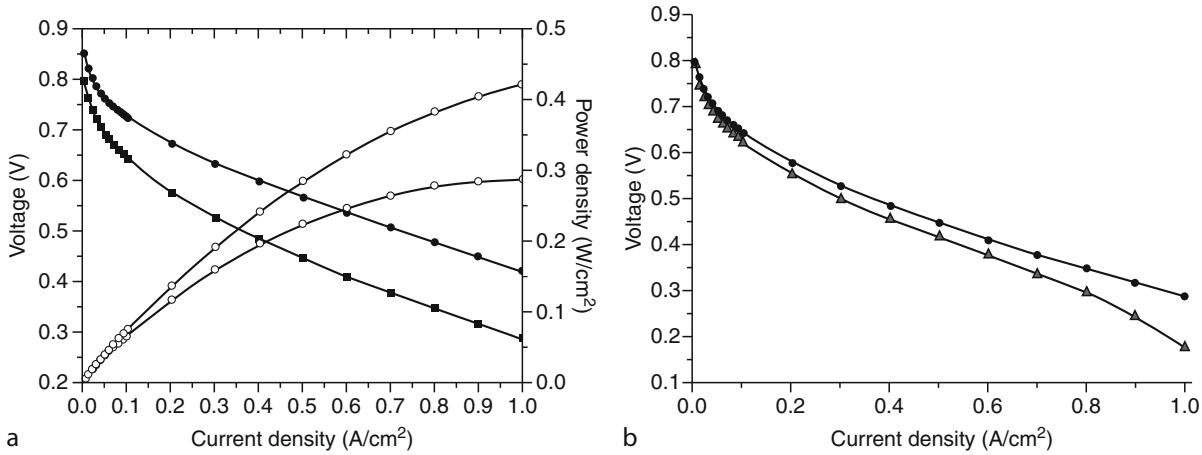

Polybenzimidazole Fuel Cell Technology. Figure 12
Graph (**a**) Polarization curves (filled symbols) and power density curves (unfilled symbols) of 6F-PBI using H_2/air (*squares*) and H_2/O_2 (*circles*). Graph (**b**) Polarization curves of 6F-PBI using H_2/air (*circles*) and reformate/air (*triangles*) [50]

on the homopolymer 2OH-PBI MEA (Fig. 13). The homopolymer produced a voltage of 0.69 V using a load of 0.2 A cm^{-2} at 180°C and H_2/air; this is greater than the 0.663 V produced by *p*-PBI under the same conditions. The high acid doping level and the membrane chemistry significantly contribute to the excellent performance of the 2OH-PBI membrane. Overall, the fuel cell performance of 2OH-PBI is comparable to that of *p*-PBI.

Segmented PBI block copolymers have also been explored for fuel cell use [52]. Scanlon synthesized a 52/48 *p*-PBI/*m*-SPBI (Fig. 5i) segmented block copolymer by polymerizing the oligomer of *p*-PBI with that of *m*-SPBI. The oligomers were polymerized in PPA and cast by the PPA Process. Even with an extremely high PA doping level of 91.5 mol PA/PRU, the polymer film had very strong mechanical properties. Under low humidity at 160°C, the segmented copolymer achieved a conductivity of 0.46 S cm^{-1}. Because of the great results, a *p*-PBI/*m*-SPBI MEA was constructed for use in fuel cell performance tests. The polarization curves of the segmented copolymer MEA displayed a voltage of 0.62 V at 0.2 A cm^{-2} at 160°C and 0.65 V at 0.2 A cm^{-2} at 200°C. As implied by the data, these membranes are excellent candidates for high-temperature fuel cells.

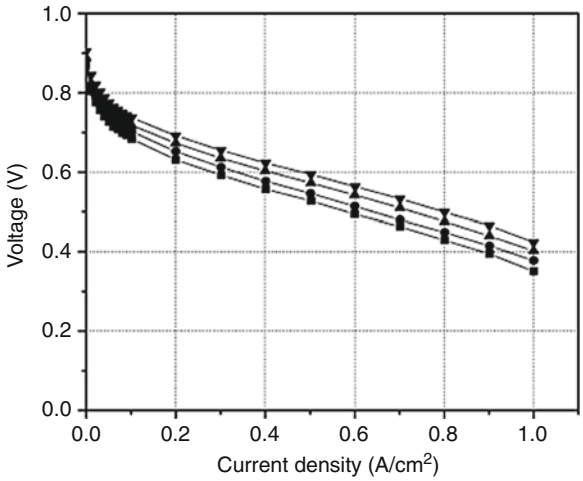

Polybenzimidazole Fuel Cell Technology. Figure 13
Polarization curves of 2OH-PBI using hydrogen as the fuel and air as the oxidant at 120°C (*squares*), 140°C (*circles*), 160°C (*triangles*), and 180°C (*down-triangles*) [51]

Membrane Electrode Assembly Durability As explained in a previous section, a membrane electrode assembly (MEA) consists of the polymer membrane that is sandwiched between an anode and a cathode electrode, respectively. The electrodes are composed of a conductive carbon network that supports a catalyst on a gas diffusion layer. An additive, such as polytetrafluoroethylene (PTFE), helps bind the Pt/C catalyst to the gas diffusion layer. At the anode, the catalyst facilitates the oxidation of hydrogen into its constituent electrons and protons. As the protons are passed

through the acid-doped membrane to the cathode, the electrons are passed through an external circuit, thereby creating electricity. Finally, the electrons and protons react with oxygen at the cathode electrode to form water as the final reaction product.

Although PBI membranes are highly resistant to degradation, it is possible for the membranes to fail. Common degradation modes for PBI membranes at operating temperatures of 120–200°C include membrane thinning and pin-hole formation. If there is too much pressure on the membrane, phosphoric acid could be pushed out of the polymer matrix and "thin out" the membrane. An extreme occurrence of membrane thinning results in pin-hole formations. Both of these occurrences result in increased fuel crossover and reduced fuel cell efficiency. Firm gasket materials help to evenly distribute pressure and prevent over-compression of the membrane [53].

The catalyst-coated electrodes of the MEA must be extremely durable in the presence of harsh physical and chemical environments. The oxidation and reduction processes create immense stress on the electrodes and trigger physical and chemical reactions to occur. A summary of the main MEA and component degradation modes have been previously reported [53, 54]. By means of electrochemical Ostwald ripening, Pt-metal agglomeration causes the loss of electrochemical surface area and decrease of reaction kinetics mainly through a dissolution-recrystallization process [55–57]. Oxidation reactions can also cause corrosion of the gas diffusion layer and carbon components in the electrodes, which would result in acid flooding, an increase in mass transport overpotentials, a decrease reaction kinetics and also, most severely, the loss of the mechanical integrity of the electrodes. Phosphoric acid can dissolve the Pt-metal catalyst and phosphoric acid anions ($H_2PO_4^-$) could adsorb onto the catalyst surface; both of these events would decrease the electrochemical surface area and reaction kinetics. In addition, phosphoric acid evaporation from the catalyst layer would result in similar consequences.

Typical commercial gas diffusion electrodes contain high-surface area carbon supported catalysts, e.g., Pt/Vulcan XC 72. Platinum is typically used as the catalyst at both the anode and cathode electrodes because it facilitates the reduction and oxidation reactions at high efficiency. However, due to the degradation modes previously mentioned, performance of the catalyst is lost over time. Novel platinum-based catalysts have been developed to increase the stability of the electrode catalysts. Compared to a commercial Pt/C (46.6 wt% TKK), Pt_4ZrO_2/C catalysts have been shown to decrease the overall performance loss of the MEA [58]. The Pt_4ZrO_2/C catalyst showed a higher resistance to Pt-sintering than Pt/C following 3,000 cycles of a potential sweep test between 0.6 and 1.2 V versus reversible hydrogen electrode (20 mV s^{-1}). The ZrO_2 is thought to act as an anchor to slow the agglomeration of platinum particles.

In order to improve especially the cathode catalyst kinetics and the catalyst stability, alloying of Pt with a base metal such as nickel or cobalt is widely done. Origins of these alloys date back to early phosphoric acid fuel cell development [59]. These alloys have been reported to typically improve the cathode kinetics for oxygen reduction by roughly 25–40 mV [59] or a factor of 1.5–4 when considered reaction rates. Commercial MEAs using PBI-based membranes also use Pt-base metal alloy catalyst on the cathode [60, 61]. The origin of the kinetic improvements for the Pt-base metal alloys is discussed manifold in literature [62–70]: (1) modification of the electronic structure of Pt (5-d) orbital vacancies), (2) change in the physical structure of Pt (Pt–Pt bond distance and coordination number), (3) adsorption of oxygen-containing species from the electrolyte onto the Pt or alloying element, and/or (4) redox-type processes involving the first-row transition alloying elements. However, as discussed in detail in the recent work by Stamenkovic et al. [70], the main effect is a shift of the Pt d-band center to lower energy values which induces a surface which adsorbs oxygenated and spectator species to a lower extent and therefore makes more active sites available for the oxygen reduction to proceed.

Other additives to platinum-based electrodes, such as tin-oxide (SnOx) [71], have also been shown to significantly improve the catalytic activity of the oxygen reduction reaction. Using a PPA-Processed *m*-PBI membrane with a 7 wt% SnO in Pt/SnO_2/C catalyst under unhumidified H_2/O_2 at 180°C, a voltage of 0.58 V under a load of 0.2 A cm^{-2} was produced. Under the same conditions, a *m*-PBI MEA using a Pt/C catalyst produced only 0.4 V at 0.2 A cm^{-2}.

PBI has also been investigated as an additive to platinum-based electrodes. It is thought that incorporation of PBI in the catalyst layer would provide a better interface for proton conduction between the electrode and membrane. Qian [72] incorporated 6F-PBI into the electrodes by four different methods: formation of a PBI bilayer inserting a thin 6F-PBI membrane between an E-TEK cathode and *p*-PBI membrane, casting 6F-PBI/PPA directly onto the E-TEK electrodes and hydrolyzing to form the gel, spraying a 6F-PBI/DMAc solution onto the electrodes, and coating the electrodes with a mixture of 6F-PBI and catalyst (the PBI replaced PTFE). The bilayer method decreased fuel cell performance, and it is proposed that this occurred by creating a large interface resistance between the two PBI membranes. Both the casting method and the spraying method improved electrode kinetics, and it is postulated that this occurred due to a lower interface resistance. In addition, a significant decrease in fuel cell performance showed that 6F-PBI could not be used to replace PTFE.

As an outlook to further improvements of catalyst kinetics and durability in low- and high-temperature polymer electrolyte fuel cells, several possibilities are currently under investigation [73]: (1) extended large-scale Pt and Pt-alloy surfaces [70]; (2) extended nanostructured Pt and Pt-alloy films [74]; (3) de-alloyed Pt-alloy nanoparticles [75]; (4) precious metal free catalyst as described by Lefèvre et al. [76], e.g., Fe/N/C catalysts; and (5) additives to the electrolyte which modify both adsorption properties of anions and spectator species and also the solubility of oxygen [77]. The latter approach is specific to fuel cells using phosphoric acid as electrolyte.

PBI-PA Fuel Cell Systems and Their Applications

Para-PBI is one of the most common polymers used in commercial PBI-based fuel cell systems. A mechanically strong and chemically stable polymer, *p*-PBI has proved to be one of the most reliable PBI polymers for MEA use. Load, thermal, and shutdown–startup cycling tests performed on the *p*-PBI MEA indicated that high temperatures (180°C and 190°C) and high load conditions slightly increased PA leeching from the MEA system. However, at steady-state fuel cell operation at 80–160°C studies showed that PA loss would not be a significant factor in fuel cell degradation [54, 78]. Long-term studies showed minimal performance degradation over a 2-year span and indicated excellent commercial fuel cell potential [53]. Compared to state-of-the-art phosphoric acid PEMFCs [79], evaporation of phosphoric acid from commercial PBI-based Celtec P1000 MEAs is reduced by a factor of roughly 2–3. This is a key factor of long-term stable operation for PBI-based fuel cells.

For the transition of PBI-based fuel cell science into commercial products, the appropriate manufacturing processes need to be developed. Most companies rely on manual operations [80] for PBI-based MEA fabrication. Only recently have significant efforts been devoted to developing automated production lines because simple changes in MEA materials and architecture could necessitate the use of different manufacturing equipment. To accommodate the evolution of fuel cell science, a flexible modular manufacturing line has been developed. Since 2002, BASF Fuel Cell GmbH (previously PEMEAS) has used the line to accommodate three generations of MEAs. The details of this manufacturing process will be further discussed in section "Advances in PBI MEA Manufacturing".

Commercial PBI-based high-temperature PEMFCs provide energy to a wide array of electronic devices. Hydrogen fuel cell vehicles, both for the private consumer and public transportation, are growing in popularity as pollution and fossil fuel prices continue to increase. Hydrogen offers 2–3 times the overall efficiency in a fuel cell as gasoline does in a typical combustion engine [81]. High-temperature fuel cells are also popular as backup generators and combined heat and power devices for stationary use. These types of systems typically produce 1–10 kW, which is enough energy to power a house or a multifamily dwelling. In addition to providing energy, combined heat and power devices use waste heat to heat water and preheat the fuel cell system components, thereby increasing the overall efficiency of the fuel cell system. Fuel cells also offer applications in mobile electronic devices such as laptops and cell phones. Commonly coupled with a methanol reformer, these fuel cell systems are remarkably portable and can power electronics for hours of continuous use.

In addition to producing electricity, these PEMs have been used as a purification device for hydrogen gas.

Consider the purification device to have the same basic architecture as a fuel cell. A platinum catalyst splits contaminated hydrogen gas into protons and electrons at the anode. Using an external power source, the electrons are driven through an external circuit to the cathode while the protons are allowed to transport across the membrane from the anode to the cathode. The electrons and protons recombine, thereby creating a higher grade hydrogen gas at the cathode while leaving behind the undesired constituents at the anode. These hydrogen pump devices will be further discussed in section "Hydrogen Pump".

In-Depth Analysis of PPA-Processed *p*-PBI MEA

PBI-based high-temperature MEAs offer many benefits over more well-known perfluorosulfonic acid Nafion PEMs. Unlike low-temperature Nafion MEAs, high-temperature PA-doped PBI membranes do not need to be hydrated, and therefore, do not require an external humidification of the gases. Additionally, running at high temperatures generally improve electrode kinetics and proton conductivities while requiring smaller heat exchangers. For PBI fuel cell science to transition into commercially available products, the reliability of PBI fuel cell stacks needs to meet specific requirements. The Department of Energy (DOE) specified durability targets of >5,000 h (>150,000 miles) of automotive fuel cell operation and >40,000 h for stationary applications for 2010. Primarily, the durability of the fuel cell stack dictates the durability of the entire system [82]. In-depth durability studies of PBI MEAs have been performed [53, 54, 61, 78, 83–85] to evaluate the viability of commercial PBI fuel cells. In addition to fuel impurity and PA retention tests, load, thermal, and shutdown–startup cycling tests are commonly performed to evaluate the MEAs.

p-PBI MEAs have displayed a relatively high resistance to carbon monoxide and sulfur contaminants [78, 83, 86, 87]. While Nafion and other traditional low-temperature PEM fuel cells are often poisoned by small amounts of carbon monoxide (5–50 ppm) in the fuel or oxidant, *p*-PBI and other PBI membranes have been shown to perform with minimal voltage loss in 10^4 ppm of carbon monoxide. Operating the fuel cell at 180°C with a load of 0.2 A cm^{-2} with a reformate gas (70% H_2, 1.0% CO, and 29% CO_2), the voltage loss was only 24 mV as compared to pure hydrogen [27]. This decrease in voltage occurred as a result of fuel dilution and carbon monoxide poisoning. As explained in section "Introduction to Polybenzimidazole Fuel Cell Sustainability", the cell is able to resist poisoning because the high operating temperatures allow for reversible binding of carbon monoxide from the catalyst. Details on the CO adsorption isotherms in the presence of hydrogen under fuel cell operation conditions between 150°C and 190°C can be found in literature [87]. Similarly, Garseny et al. [86] reported that a PBI MEA from BASF Fuel Cell GmbH (Celtec-P Series 1000) is 70 times more resistant to sulfur contaminants than Nafion MEAs. Using air contaminated with 1 ppm H_2S or SO_2 as the oxidant, the performance of Nafion decreased by 82.9% while the performance of the Celtec-P MEA decreased by <2%. Garseny et al. proposed that H_2S is converted to SO_2, and that SO_2 adsorbs onto the Pt catalyst surface. At temperatures above 140°C, this SO_2 is desorbed and flushed out of the system. Schmidt and Baurmeister showed that the H_2S tolerance of PBI-based Celtec P1000 MEAs is in the range of 10 ppm [83], a value significantly larger than typical fuel processing catalyst can tolerate. More than 3,000 h operation in reformate with 5 ppm H_2S and 2% CO is proven. Overall, *p*-PBI-based fuel cells can resist contaminant poisoning far better than traditional low-temperature PEM fuel cells, an effect which can mainly be ascribed to the operation temperature between 150°C and 190°C.

Under continuous operation and appropriate stack design and components, the PBI membranes retain phosphoric acid extremely well. Long-term performance tests show that *p*-PBI fuel cells can operate for over 2 years with minimal performance degradation (Fig. 14). This durability is attributed to the unique nature of PBI membrane formed by the PPA Process, which allows it to retain PA under continuous operating conditions. The amount of PA lost from the *p*-PBI MEA per hour was approximately 10 ng h^{-1} cm^{-2}, which is equivalent to a 50 cm^2 cell losing 8.74 mg PA after 2 years of operation. Such a small loss strongly suggests that the life span of a *p*-PBI PEM fuel cell would not be significantly influenced by PA depletion.

Phosphoric acid loss was also monitored during a selection of dynamic durability tests, including load and thermal cycling tests [78]. A single load cycle test

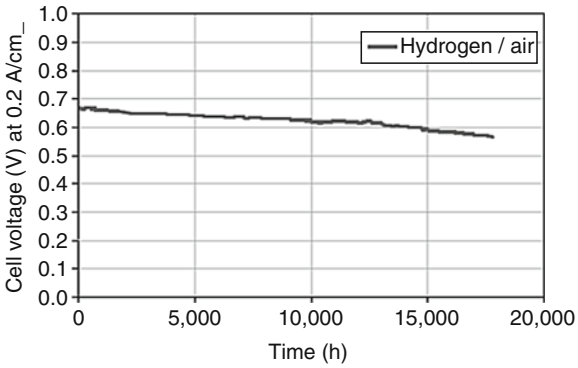

Polybenzimidazole Fuel Cell Technology. Figure 14 Long-term durability test of *p*-PBI MEA at 160°C using hydrogen/air without humidification

involved measuring the voltage at 160°C at three different loads: open circuit voltage (OCV), 0.2 A cm^{-2}, and 0.6 A cm^{-2}. Air and pure hydrogen were supplied to the MEA as oxidant and fuel, respectively. The voltage of the MEA was measured at OCV for 2 min, followed by 0.2 A cm^{-2} for 30 min, and then 0.6 A cm^{-2} for 30 min. A total of 500 load cycles were performed on a *p*-PBI MEA, and the results indicated that larger loads corresponded to an increased PA loss rate (approximately 20 ng h^{-1} cm^{-2}). Thermal cycling tests were performed by measuring the voltage of the MEA with a constant applied current density of 0.2 A cm^{-2} while either cycling the temperature between 120°C and 180°C (for a high-temperature cycle) or between 80°C and 120°C (for a low-temperature cycle). Both the high- and low-temperature cycles were performed 100 times each. The results showed that higher temperatures were associated with an increased PA loss rate (almost 70 ng h^{-1} cm^{-2} for the high-temperature cycle and 20 ng h^{-1} cm^{-2} for the low-temperature cycle). It was proposed that at the higher load and temperature conditions, more water is generated at the cathode. By means of a steam distillation mechanism, an increased amount of PA is lost from the MEA. As indicated by both cycling tests, phosphoric acid loss becomes a significant factor of cell degradation only under extreme conditions.

Shutdown–startup cycling tests have been extensively studied by Schmidt and Baurmeister of BASF Fuel Cell GmbH [54, 61]. Two PBI-based PEFC Celtec-P1000 MEAs were tested under different operation modes; one was run under shutdown–startup cycling parameters (12 h shutdown followed by operation for 12 h at 160°C under a load of 0.2 A cm^{-2}) while the other was continuously operated at 160°C under a load of 0.2 A cm^{-2}. Both MEAs were operated for more than 6,000 h, during which the shutdown–startup cycling MEA underwent more than 270 cycles. While the continuously operating MEA had an average voltage degradation rate of roughly 5 μV h^{-1}, the cycling MEA averaged a voltage degradation of 11 μV h^{-1} or 0.2 mV $cycle^{-1}$. This increase in voltage degradation was attributed to an increased corrosion of the cathode catalyst support, thereby significantly increasing the cathodic mass transport overpotential. The observed corrosion was a result of a reverse-current mechanism that occurs under shutdown–startup cycling conditions [88].

Illustrated by the previously discussed durability tests, *p*-PBI MEAs have been shown to be physically and chemically robust. Highly resistant to fuel contaminants, PBI MEAs are resistant to poisoning effects that would typically expunge a low-temperature Nafion fuel cell system. Long-term steady-state and dynamic durability tests showed that PA loss typically is not a cause of cell degradation. Additionally, Schmidt and Baurmeister showed that PBI MEAs are susceptible to cell degradation under extreme shutdown–startup conditions. Overall, *p*-PBI MEAs have exhibited much potential for use in fuel cell systems.

Advances in PBI MEA Manufacturing

As previously discussed, the manufacturing processes of PBI-based fuel cells need to be improved to make fuel cells a viable commercial product. To put this requirement into perspective, the US Department of Energy has set a goal of producing 500,000 fuel cell cars each year. If these vehicles are powered using current *p*-PBI membranes, this goal requires the production of seven MEAs per second and approximately 250,000 m^2 of electrode per day. Additionally, the performance of each of these MEAs would need to be tested; this is a process called "burn-in testing." A typical test stand is 25 ft^2, costs roughly $50,000, and can only test one stack of MEAs at a time. If each stack requires a 24 h burn-in test, the test facility size would exceed 34,000 ft^2 and house equipment would cost over

$68.5 million. Existing manufacturing processes need to be improved in order to reach this goal.

The Center for Automation Technologies and Systems (CATS) at Rensselaer Polytechnic Institute has developed a flexible manufacturing process for BASF Fuel Cell GmbH to accommodate the evolving science of fuel cells [89–91]. If one changes the fuel cell type, size, materials, MEA architecture, design, or application, the manufacturing line could be significantly affected. Therefore, a modular manufacturing line was developed by CATS in 2002 that could produce a large range of MEA sizes (1–1,000 cm^2), could handle a wide variety of materials (membranes, gaskets, electrodes, etc.), could assemble these materials in different architectures, and could be expanded to integrate additional systems. Each module could be singularly operated or could operate as a subset of the entire process; this modular construction is shown in Fig. 15. Over the past 8 years, this manufacturing line has evolved over three generations of MEA devices.

Members of CATS continue to make great strides in order to reduce costs and improve the overall efficiency of MEA fabrication. Laser cutting and joining of the PBI membranes both uses less power and delivers tighter tolerances than that of conventional cutting and joining. Ultrasonic technology has also been explored to replace the thermal joining of the three components of an MEA. Preliminary results exhibited a significant reduction in pressing time by approximately 90% in addition to using less energy. Additionally, an automated visual inspection of the MEA has been developed using a high precision motion system, multiple cameras and lighting equipment, and software MAT-LAB 7.0 with Image Processing Toolbox [89]. As fuel cell science continues to evolve, so will the manufacturing processes.

Combined Heat and Power

Stationary combined heat and power (CHP) devices are often considered the primary application of high-temperature PBI-based fuel cells. These devices are used to provide both electricity and heat (in the form of hot air or water) to small-scale residential homes or large-scale industrial plants using hydrogen derived from the widely distributed natural gas network. PBI MEAs are ideally situated for combined heat and power devices because they efficiently provide electricity while generating heat as a by-product. Furthermore, these

Polybenzimidazole Fuel Cell Technology. Figure 15
A portion of the 2002 pilot line depicting its modular construction [90]

devices could be used to provide reliable backup power to residential homes, hospitals, servers, etc.

J.-Fr. Hake et al. [92] compared the conventional generation of heat and electricity to that of small-scale combined heat and power generation by high-temperature fuel cells, and the results of which are shown in Fig. 16. The small-scale CHP devices studied were used to provide electricity, space heat, and warm water to both residential and commercial buildings. The conventional generation of electricity is much less efficient than that of small-scale CHP devices due to the issues of transportation and storage. In addition to efficiently converting chemical energy into electrical energy, CHP fuel cell systems further act as a sustainable energy conversion device by reducing the total amount of greenhouse gas emissions. Hake et al. considered the penetration of small-scale CHP fuel cell technology into the US residential sector market starting in 2014 until a saturation point as a logarithmic function. To improve the accuracy of the study, Hake considered the trends of the Japanese small-scale CHP market [92, 93]. A typical CHP device in Japan costs roughly $30,000, but analysts expect the price to drop to $5,000 within 5 years. Analysts also claim that by the year 2050, one in four homes in Japan will run on fuel cells. Also considering current CO_2 emissions, Hake et al. concluded that adoption of this technology in the USA could reduce CO_2 emissions by up to approximately 50 million tons by 2050; this corresponds to a 4% reduction in the residential sector.

As the largest producer of PBI MEAs, BASF Fuel Cell (previously PEMEAS) produces *p*-PBI PEM MEAs for a wide variety of fuel cell applications. The Celtec®-P1000 PEM MEA is typically integrated into either backup or auxiliary power units and can produce from 0.25 to 10 kW. The MEA is also advertised as maintaining performance for over 20,000 h with only a 6 μV h^{-1} voltage drop at 160°C [94]. The Celtec®-P2100 PEM MEA is used in stationary CHP systems and is capable of producing 0.74–10 kW. The MEA has a long-term stability of over 20,000 h under both steady-state and cycling conditions (300 shutdown–startup cycles with 13 μ h^{-1} voltage drop). Polarization curves of a Celtec®-P MEA at 160°C using an active area of 45 cm^2 are shown in Fig. 17. PBI-based CHP devices are commercially available from a variety of companies, including Serenergy, Plug Power, and ClearEdge Power. All of these companies assemble a variety of fuel cell devices using commercially available PBI MEAs.

Plug Power of Latham, New York produces a line of PBI-based small-scale CHP devices including the

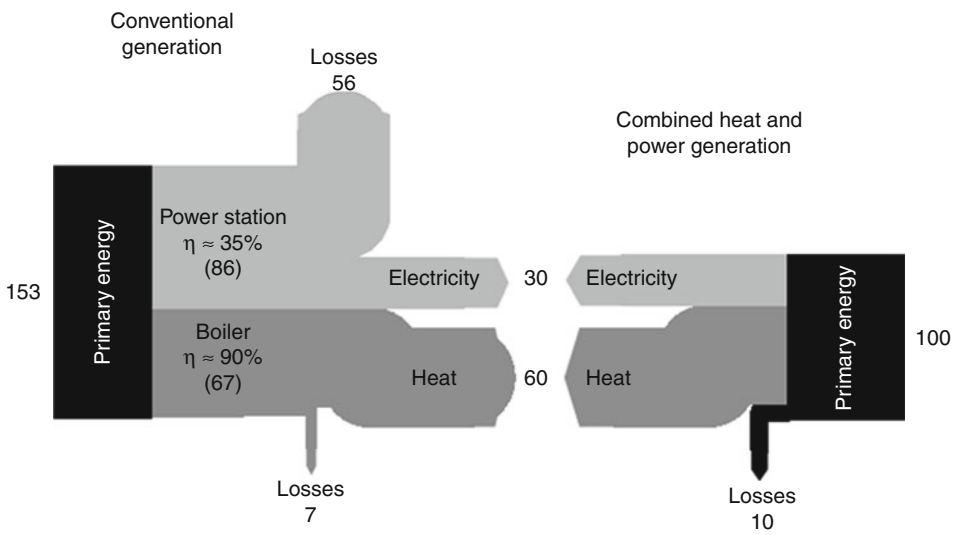

Polybenzimidazole Fuel Cell Technology. Figure 16
Side-by-side comparison of conventional generation of heat and electricity to fuel cell combined heat and electricity generation [92]

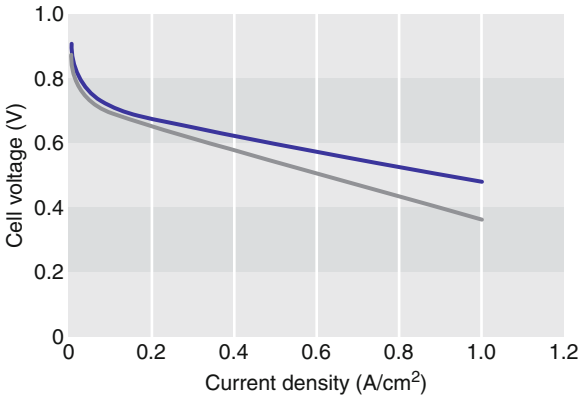

Polybenzimidazole Fuel Cell Technology. Figure 17 Polarization curves of a Celtec®-P MEA [94]. The *blue line* represents using hydrogen/air as fuel/oxidant. The gray line represents a steam reformate of 70% H_2, 29% CO_2, and 1% CO/air

GenSys Blue (Fig. 18) [95]. The GenSys Blue is capable of producing 0.5–5 kW of continuous output and is capable of reducing home energy costs by 20–40%. An autothermal (ATR) reformer reacts natural gas (methane) with oxygen and carbon dioxide to produce hydrogen gas that fuels the PEM stack. An inverter is used to improve the efficiency of the CHP device by specifically supplying enough energy to power the home, thereby minimizing energy losses and reducing CO_2 emissions by 25–35%. Additionally, an integrated peak heater ensures proper heating of the entire home.

Serenergy, which is based in Hobro, Denmark, also produces PBI-based fuel cell CHP devices [96]. Serenergy's Serenus 166 Air C v2.5 and 390 Air C v2.5 micro-CHP modules nominally produce 1 and 3.5 kW, respectively. While the 166 model is comprised of one MEA stack of 65 cells, the 390 model uses three MEA stacks each with 89 cells. Both of these systems are able to tolerate fuel impurities up to 5% CO concentrations and 10 ppm H_2S at 160°C. Because the excess energy can be used to heat up air or water, Serenergy claims that over 80% of the total heat and power generated can be used and that the system efficiency is as high as 57% (the efficiency data was not available). These systems can also be used as auxiliary energy conversion devices.

ClearEdge Power also produces a line of small-scale CHP devices, one of which is the ClearEdge5 [97]. Capable of producing 5 kW h^{-1} and up to 20,000 BTU h^{-1} while running at 150°C, the ClearEdge5 couples a methane reformer to a PBI fuel cell stack using MEAs provided by BASF Fuel Cell GmbH. ClearEdge advertizes that the CHP device can reduce utility bills by up to 50% and cut CO_2 emissions by over 33%. Annually, the device is capable of producing 43,000 kWh in electricity and 50,000 kWh (equivalent) in heat. Similar to other CHP devices, the ClearEdge5 offers at-home production of energy, thereby eliminating the losses associated with transferring the energy. The device is monitored in real-time by ClearEdge Power and can be monitored directly from the owner's smartphone.

Automotive Transportation

Producing 1.9253 billion metric tons of carbon dioxide, which is roughly 33% of USA's total carbon dioxide emissions, the transportation sector was the largest contributor to pollution in 2008 [98]. According to another 2008 study by the US Department of Energy [2], all transportation in the USA consumed approximately 27.8 quadrillion BTUs. Considering both of these facts, one can conclude that a more sustainable energy source could significantly reduce the carbon footprint of the transportation sector. For the transition of fuel cell science into a viable commercial product to occur, the US Department of Energy has set numerous targets for automotive fuel cell systems. Because a typical internal combustion engine costs roughly \$25–35/kW, a fuel cell system will need to cost roughly \$30/kW to become competitive enough to penetrate the US market. Furthermore, the system must be durable enough to operate for at least 5,000 h (or roughly 150,000 miles). Additional issues of system size and management of air, heat, and water will also play a role in automotive fuel cell viability.

Over the past decade, fuel cell technology has been adapted by the major automotive industries as a cleaner, more efficient method of providing energy to vehicles. In addition to the issue of fuel cell automotive viability, issues of hydrogen sources, hydrogen storage, and fueling stations continue to be addressed and solved. The California Fuel Cell Partnership (CaFCP) is a collaboration of auto manufacturers, energy providers, government agencies, and fuel cell technology companies to promote the commercialization of fuel cell vehicles [81]. In 2009, California had

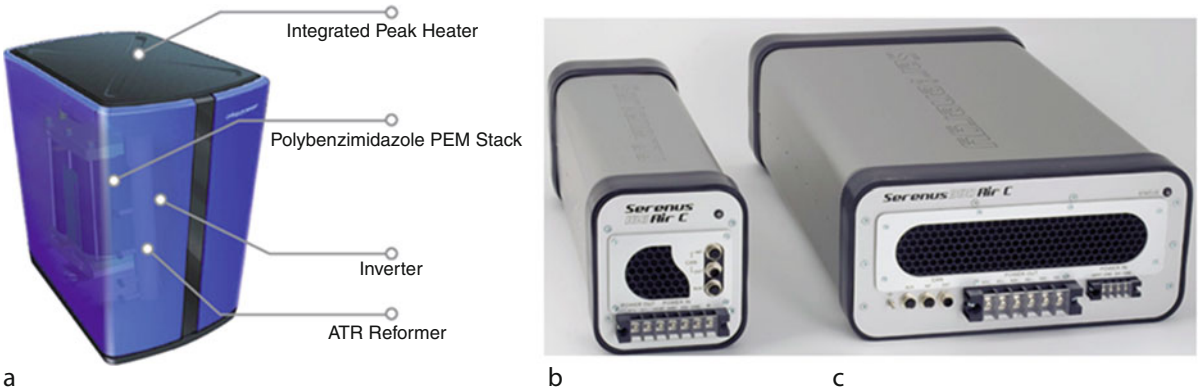

Polybenzimidazole Fuel Cell Technology. Figure 18
Plug Power's GenSys blue (**a**), Serenergy's Serenus 166 air C v2.5 (**b**), and Serenergy's Serenus 390 air C v2.5 (**c**) CHP fuel cell devices [95, 96]

only six public hydrogen fueling stations that were used to fuel roughly 200 vehicles. The CaFCP predicts that in 2014, approximately 5,800 kg of hydrogen will be used to fuel roughly 4,310 fuel cell passenger vehicles and 60 fuel cell busses daily. To accommodate the needs of fuel cell vehicle operators, CaFCP proposed the establishment of 46 new fueling stations by the year 2012. Considering each new station would cost in the range of $1.5–$5.5 million, a predicted $180 million would have to be spent on the fueling station project. Although this "Action Plan" did not specify an amount, this project will provide many new jobs to US residents. The hydrogen used to fuel these stations can be domestically produced as either a low-carbon fuel or potentially as a zero-carbon fuel when produced from renewable sources (such as splitting water into oxygen and hydrogen with solar energy). According to California regulations, at least 33% of the hydrogen must come from such renewable sources.

SunHydro, one of the world's first hydrogen fueling station chains, has set a goal of providing fueling stations along the entire east coast of the USA [99]. Using solar cell technology, every SunHydro station will harvest solar energy to electrolytically split water into hydrogen and oxygen gases. This process is extremely sustainable and will create much less greenhouse gas emissions. This hydrogen highway will stretch from Scarborough, ME, to Miami, FL, and consist of 11 stations. Each station will cost an estimated $2–$3 million to construct and will be paid for by private funders.

Over the past decade, many automotive and fuel cell industries have used PBI technology in the development of fuel cell vehicles. In November of 2008, Volkswagen unveiled the VW Passat Lingyu at a Los Angeles Auto Show [100]. The VW Lingyu uses an AB-PBI-based fuel cell stack that utilizes a trade-secret coating that helps prevent PA from leeching out of the membrane. Metha Energy Solutions, in cooperation with Serenergy, revealed a hybrid electric/fuel cell vehicle in December of 2009 [101]. In this system, a methanol reformer is used to provide hydrogen to the PBI-based fuel cell. It was advertized that this vehicle could travel up to 310 miles on one tank of gas and takes only 2 min to refuel. EnerFuel, a subsidiary of Ener1, has also recently produced a hybrid electric/fuel cell vehicle. The EnerFuel EV uses a reformed methanol PBI fuel cell that works in conjunction with a lithium ion battery. The lithium battery is used to start the vehicle and to power the vehicle while driving, while the fuel cell system produces 3–5 kW to continuously recharge the battery. These fuel cell systems would not generate enough power to drive the vehicle, but would act as a range extender for the battery system. The target market of the EnerFuel EVs is not for those who drive 200+ miles daily, but instead for those with short daily commutes.

In July of 2009, the German Aerospace Center demonstrated that fuel cells have the potential of powering air-transportation vehicles [102, 103]. Designed in cooperation with Lange Aviation, BASF Fuel Cell, DLR Institute for Technical Thermodynamics, and

Serenergy, the Antares DLR-H_2 became the world's first piloted aircraft with a propulsion system powered only by PBI-based fuel cells. Besides creating zero CO_2 emissions during flight, the aircraft also generates much less noise than other comparable motor gliders. Using a fuel cell stack capable of producing up to 25 kW, the Antares DLR-H_2 has a cruising range of 750 km (or 5 h) and can travel at speeds of up to 170 km h^{-1}. Similar fuel cell systems could be coupled with current commercial and military aircrafts as auxiliary power units (APUs) to improve fuel efficiency.

Portable

Microelectricalmechanical (MEM) systems utilizing methanol reformers and PBI fuel cells have been developed for portable use. These devices are generally used to generate power in the range of 5–50 W for laptops, communication systems, and global positioning systems. Compared to batteries that offer equivalent amounts of power, these micro-fuel cell systems are lighter, generate less waste, and are overall more cost effective. Similar to other reformed methanol/PBI fuel cell systems, these MEMS are a sustainable technology as they reduce the amount of greenhouse gases produced per unit of electricity generated.

UltraCell of Livermore, CA, is a well-known producer of PBI MEM fuel cell systems. Funded and field tested by the US Army, the UltraCell XX25 is capable of providing 25 W of continuous maximum power [104]. Depending on the size of the fuel cartridge, the device is capable of delivering 20 W of continuous power from 9 h to 25 days. The fuel cartridge weighs less than a pound and The XX25 MEM system has been shown to power radio gear, mobile computer systems, communication devices, and a variety of other electrical devices. The XX25 provides roughly 70% in weight savings when compared to a typical battery on a 72-h mission (1.24 kg without the cartridge), and is rugged enough to operate in extremely cold or hot environments. In addition, it meets OSHA standards for safe indoor and in-vehicle use. Similar to the XX25, the newly developed UltraCell XX55 is capable of generating 55 W of continuous power for up to 2 weeks using the largest fuel cartridge [105]. Only 0.36 kg heavier than the XX25, the XX55 has an optional battery module that can provide a peak power output of 85 W. Similar to the XX25, it is a very rugged device that can be used essentially in any conditions.

Larger than the Ultracell devices, the relatively new Serenergy Serenus E-350 is a reformed methanol/fuel cell hybrid with an approximate mass of 11 kg. At nominal power levels, it is capable of producing approximately 350 W [106]. The device is fueled by a 60–40 methanol-deionized water mixture. It takes approximately 45 min to start up, at which point it consumes fuel at a rate of 0.45 L h^{-1}.

H_2 Pump

Efficient purification of hydrogen is becoming a common interest in both industrial and energy sectors. In particular, technology which can efficiently purify, pump, and pressurize hydrogen at low to moderate flow rates is needed, but is not readily available. Of course, there are existing methods for hydrogen purification which include various combinations of mechanical compression with cryogenic cleanup, palladium membranes, pressure swing absorption, and passive membrane separators to name a few. However, these technologies are challenged by certain limitations: (1) cryogenic cleanup produces high purity hydrogen, but requires costly refrigeration equipment and is suitable for very-large-scale specialty applications; (2) palladium membrane purification can be fairly simple in design and construction, but requires pressurization to drive the hydrogen separation process and suffers from poor utilization when purifying hydrogen from gases containing low fractions of hydrogen; and (3) pressure swing absorption (PSA) is widely used in high-volume industrial processes and relies on large, mechanical components that are subject to frequent maintenance and inherent inefficiency. Such devices are not easily scaled to smaller sizes or localized generation/purification needs. Furthermore, it is important to state that all of the above processes require expensive, high-maintenance compressors.

Electrochemical pumping is not a new concept and has in fact been utilized as a diagnostic technique within the electrochemical industry for years. General Electric developed this concept in the early 1970s [107]. The use of polymer electrolyte membranes for electrochemical hydrogen compression has been demonstrated in water electrolysis (H_2 generation) devices at

United Technologies Corporation, reaching 3,000 psi_a [108], as well as studied in academic institutions [109]. The electrochemical hydrogen pump, first developed in the 1960s and 1970s, was derived from the original proton exchange membrane fuel cell efforts. The concept is simple, requires little power, and has been shown to pump hydrogen to high pressures. In the original work, the membrane transport medium was a perfluorosulfonic acid (PFSA) material, similar to the material used in many fuel cells today. The process is quite elegant in that like a fuel cell, molecular hydrogen enters the anode compartment, is oxidized to protons and electrons at the catalyst, and then the protons are driven through the membrane while the electrons are driven through the electrically conductive elements of the cell. The major difference in this cell as compared to a fuel cell is that the pump is operated in an electrolytic mode, not galvanic, meaning that power is required to "drive" the proton movement. Once the protons emerge from the membrane at the cathode, they recombine to form molecular hydrogen. Thus, hydrogen can be pumped and purified in a single step with a nonmechanical device. The pump concept builds upon the understanding of proton-transport membranes.

Clearly, the proton conducting membrane properties are critical. Desirable properties include: high proton conductivity, mechanical stability, low solubility and permeability of impurity gases, and sufficient operating temperature to support tolerance to impurities (CO and H_2S) found in reformed gases. The application of the PBI membrane to electrochemical hydrogen pumping provides high proton conductivity (0.2–0.4 S cm^{-1}), mechanical stability, enhanced gas separation, and up to 180°C operation. The high operating temperature eliminates water management difficulties typically experienced with the low operating temperatures of PSFA membranes while also providing tolerance to poisonous gas species such as CO. As such, the PBI membrane and electrode assembly represents a significant new opportunity and paradigm shift in electrochemical hydrogen pumps as well as in advancing the science of hydrogen separation, purification, and pressurization. This concept has been evaluated and demonstrated in recent work using PBI membranes [110]. The hydrogen pump was shown to operate with fairly low power requirements, and generally needed less than 100 mV when operating at 0.2–0.4 A cm^{-2}. This was accomplished without the critical water management commonly encountered in low-temperature, water-based membranes. The cathodic flow of hydrogen from the device was nearly identical to the theoretical Faradic flows. This suggests that the hydrogen pump could have applications as a hydrogen metering device since the hydrogen flow could be easily and accurately controlled by the current of the power source. The initial work reported devices that could operate for several thousand hours with little change in the operating parameters. This would be expected from the related work on PBI membranes for fuel cells which show outstanding long-term durability. In fuel cell applications, the ability to operate at high temperatures provides benefits for gas cleanup and durability on reformed fuels. In hydrogen pump applications, this tolerance to fuel impurities enables the hydrogen pump to purify hydrogen from hydrogen gas feeds containing such impurities. Figure 19 shows the operation of a PBI-based hydrogen pump operating on pure

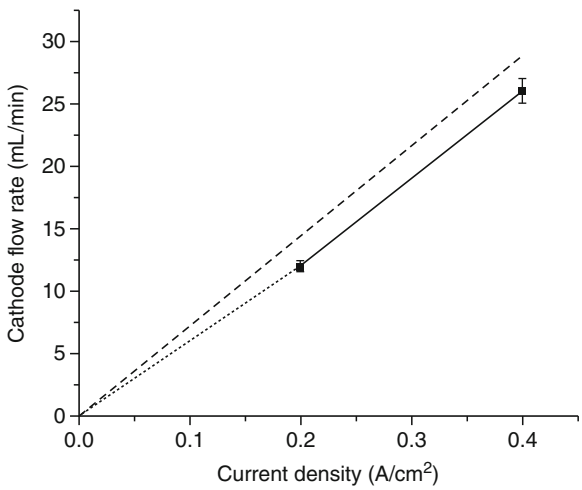

Polybenzimidazole Fuel Cell Technology. Figure 19 The cathodic flow rates of a hydrogen pump operated at 160°C and 0% relative humidity and fueled by pure hydrogen (*unfilled squares*), a reformate gas comprised of 35.8% H_2, 11.9% CO_2, 1,906 ppm CO, and 52.11% N_2 (*filled circles*), and a reformate gas comprised of 69.17% H_2, 29.8% CO_2, and 1.03% CO (*filled triangles*). The values are nearly identical, and thus, the symbols appear superimposed. The *dotted line* represents the theoretical flow rate at 100% efficiency [110]

hydrogen, as well as two different synthetic reformates. The flow rates are nearly unaffected by the composition of the gas feed at the various operating conditions (the data points are superimposed for the different gases). The data demonstrates that the pump was capable of operating at high CO levels (1% in this work) and extracting hydrogen from dilute feed streams (<40% hydrogen). Additionally, the hydrogen pump was capable of producing hydrogen with purities greater than 99%, with the final purity dependent on operating conditions. This device could play a prominent role for both the current industrial hydrogen users, as well as in a future economy that is more heavily reliant on hydrogen as an energy carrier. Commercial development of this device is underway.

Conclusions and Future Directions

After approximately 10 years of development, PBI chemistries and the concomitant manufacturing processes have evolved to produce commercially available MEAs. PBI MEAs can operate reliably without complex water humidification hardware and are able to run at elevated temperatures of 120–180°C due to the physical and chemical robustness of PBI membranes. These higher temperatures improve the electrode kinetics and conductivity of the MEAs, simplify the water and thermal management of the systems, and significantly increase their tolerance to fuel impurities. Membranes cast by a newly developed PPA Process possessed excellent mechanical properties, higher PA/PBI ratios, and enhanced proton conductivities as compared to previous methods of membrane preparation.

The robustness of *p*-PBI membranes cast by the PPA Process has been tested and characterized by a variety of methods. Under a constant load, *p*-PBI has been shown to perform for well over 2 years with very little reduction in performance. Using synthetic reformates, *p*-PBI MEAs have demonstrated excellent resistances to impurities such as CO, CO_2, and SO_2. *p*-PBI membranes have also been shown to retain PA extremely well, and evidence strongly suggests that this small rate of PA loss would not significantly influence the life span of a MEA. Load, thermal, and shutdown–startup cycling tests of *p*-PBI fuel cells have also indicated comparable or improved results over other commercially available fuel cell systems. *p*-PBI is the most common polymer in PBI-based fuel cell systems, although AB-PBI and other derivatives have been investigated. Recently developed 2OH-PBI, which to date has the highest recorded proton conductivity of all other PBIs, offers much potential for future fuel cell use.

Many fuel cell manufacturers are now considering the benefits of high-temperature PBI fuel cells. BASF Fuel Cell, the largest producer of PBI MEAs, has been in operation since March of 2007. BASF offers a wide variety of MEAs for stationary systems (combined heat and power, backup generators, etc.) and portable systems (transportation, microelectricalmechanical systems, etc.). Other companies, such as Plug Power, Serenergy, ClearEdge Power, and UltraCell, incorporate commercially available MEAs into their commercial fuel cell systems. Recently, H_2 Pump LLC has developed electrochemical pumping devices that use PBI membranes for the purification of hydrogen gas. Using various reformate gases, the devices have been shown capable of operating at high gas contamination levels and low hydrogen concentrations. Depending on operating conditions, the purity of the extracted hydrogen gas can be greater than 99%. In transportation applications, PBI-based fuel cells show great promise as APUs or range extenders for battery-powered electric vehicles.

Acknowledgments

The authors would like to acknowledge BASF Fuel Cell GmbH and Dr. Gordon Calundann for technical and financial support of the work at Rensselaer Polytechnic Institute and at the University of South Carolina. The DOE-BES program [DEFG0205ER46258] and DARPA are also acknowledged for partial support in the preparation of the manuscript.

Bibliography

1. Energy Information Administration (2008) World primary energy production by source (2008). Annual Energy Review. http://www.eia.doe.gov/emeu/aer/pdf/pages/sec11_2.pdf. Accessed 1 June 2010
2. U.S. Energy Information Administration (2008) Primary energy consumption by source and sector. Annual Energy Review. http://www.eia.doe.gov/aer/pecss_diagram.html. Accessed 1 June 2010
3. U.S. Energy Information Administration (2008) Carbon dioxide emissions from the consumption and flaring of fossil fuels. Annual Energy Review. http://www.eia.doe.gov/iea/overview.html. Accessed 1 June 2010

4. Wainright J, Wang J, Weng D, Savinell R, Litt M (1995) Acid-doped polybenzimidazoles: a new polymer electrolyte. J Electrochem Soc 142(7):L121–L123
5. Dippel T, Kreuer KD, Lassegues JC, Rodriguez D (1993) Proton conductivity in fused phosphoric acid; a $^{1}H/^{31}P$ PFG-NMR and QNS study. Solid State Ionics 61:41–46
6. Bozkurt A, Ise M, Kreuer KD, Meyer WH, Wegner G (1999) Proton-conducting polymer electrolytes based on phosphoric acid. Solid State Ionics 125:225–233
7. Weber J, Kreuer K-D, Maier J, Thomas A (2008) Proton conductivity enhancement by nanostructural control of poly(benzimidazole)-phosphoric acid adducts. Adv Mater 20:2595–2598
8. Vilciauskas L, Paddison SJ, Kreuer K-D (2009) Ab initio modeling of proton transfer in phosphoric acid clusters. J Phys Chem A 113:9193–9201
9. Mader J, Lixiang X, Schmidt T, Benicewicz BC (2008) Polybenzimidazole/acid complexes as high-temperature membranes. In: Scherer GG (ed) Fuel cells II. Advances in Polymer Science, vol 216. Springer, Heidelberg, pp 63–124
10. Wainright JS, Savinell RF, Litt MH (2003) High temperature membranes. In: Vielstichm A, Lamm H, Gasteiger A (eds) Handbook of fuel cells, vol 3. Wiley, New York, pp 436–446
11. Colomban P (1992) Proton conductors: solids, membranes and gels – materials and devices. Cambridge University Press, Cambridge
12. Xiao L, Zhang H, Scanlon E, Ramanthan LS, Choe EW, Rogers D, Apple T, Benicewicz BC (2005) High-temperature polybenzimidazole fuel cell membranes via a sol-gel process. Chem Mater 17(21):5328–5333
13. Jayakody JRP, Chung SH, Durantino L, Zhang H, Xiao L, Benicewicz BC, Greenbaum SG (2007) NMR studies of mass transport in high-acid-content fuel cell membranes based on phosphoric acid and polybenzimidazole. J Electrochem Soc 154(2):B242–B246
14. Seel DC, Benicewicz BC, Xiao L, Schmidt TJ (2009) High-temperature polybenzimidazole-based membranes. In: Vielstich W, Gasteiger HA, Yokikawa H (eds) Handbook of fuel cells, vol 5. Wiley, Chichester, pp 300–312
15. Litt M, Ameri R, Wang Y, Savinell RF, Wainright JS (1999) Polybenzimidazoles/phosphoric acid solid polymer electrolytes: mechanical and electrical properties. Mater Res Soc Symp Proc 1999:313–323
16. Zhang H (2004) Novel phosphoric acid doped polybenzimidazole membranes for fuel cells. PhD Thesis, Rensselaer Polytechnic Institute, Troy, NY, December 2004
17. Li Q, Hjuler HA, Bjerrum NJ (2001) Phosphoric acid doped polybenzimidazole membranes: physiochemical characterization and fuel cell applications. J Appl Electrochem 31(7):773–779
18. Zhai Y, Zhang H, Liu G, Hu J, Yi B (2006) Performance degradation studies on PBI/H_3PO_4 high temperature PEMFC and one-dimensional numerical analysis. Electrochim Acta 52(2):394–401
19. Kongstein OE, Berning T, Borresen B, Seland F, Tunold R (2007) Polymer electrolyte fuel cells based on phosphoric acid doped polybenzimidazole (PBI) membranes. Energy 32(4):418–422
20. Kim H, Cho SY, An SJ, Eun YC, Kim J, Yoon H, Kweon H, YEW KH (2004) Synthesis of poly(2, 5-benzimidazole) for use as a fuel-cell membrane. Macromol Rapid Commun 25(8):894–897
21. Asensio JA, Gomez-Romero P (2005) Recent developments on proton conducting poly (2, 5-benzimidazole) (AB-PBI) membranes for high temperature polymer electrolyte membrane fuel cells. Fuel Cells 5(3):336–343
22. Li QF, Jensen OJ (2008) Membranes for high temperature PEMFC based on acid-doped polybenzimidazoles. Membr Technol 2:61–96
23. Asensio JA, Borros S, Gomez-Romero P (2004) Polymer electrolyte fuel cells based on phosphoric acid-impregnated poly (2, 5-benzimidazole). J Electrochem Soc 151(2):A304–A310
24. Chen R (2003) Unpublished work
25. Yu S (2006) Novel polybenzimidazole derivatives for high temperature PEM fuel cells. PhD Thesis, Rensselaer Polytechnic Institute, Troy, NY
26. Delano CB, Doyle RR, Miligan RJ (1975) United States air force materials laboratory. Technical report, pp 1974–2022
27. Yu S, Zhang H, Xiao L, Choe EW, Benicewicz BC (2009) Synthesis of poly (2, 2′-(1, 4-phenylene) 5, 5′-bibenzimidazole) (para-PBI) and phosphoric acid doped membrane for fuel cells. Fuel Cells 9(4):318–324
28. Xiao L (2003) Novel polybenzimidazole derivatives for high temperature polymer electrolyte membrane fuel cell application. PhD Thesis, Rensselaer Polytechnic Institute, Troy, NY
29. Xiao L, Zhang H, Jana T, Scanlon E, Chen R, Choe EW, Ramanthan LS, Yu S, Benicewicz BC (2005) Synthesis and characterization of pyridine-based polybenzimidazoles for high temperature polymer electrolyte membrane fuel cell applications. Fuel Cells 5(2):287–295
30. Xiao L, Zhang H, Jana T, Scanlon E, Chen R, Choe EW, Ramanthan LS, Yu S, Benicewicz BC (2004) Synthesis and characterization of pyridine-based polybenzimidazoles for high temperature polymer electrolyte membrane fuel cell applications. Fuel Cells 5(2):287–295
31. Kallitsis JK, Gourdoupi N (2003) Proton conducting membranes based on polymer blends for use in high temperature PEM fuel cells. J New Mat Electrochem Syst 6(4):217–222
32. Faure S, Mercier R, Aldebert P, Pineri M, Sillion B (1996) Gas separation polyimide membranes used to prepare ion-exchange membranes for use in manufacture of fuel cells. French Pat 9605707
33. Watari T, Fang J, Tanaka K, Kita H, Okamoto KI, Hirano T (2004) Synthesis, water stability and proton conductivity of novel sulfonated polyimides from 4, 4′-bis(4-aminophenoxy) biphenyl-3, 3′-disulfonic acid. J Membr Sci 230(1–2):111–120
34. Lufrano F, Gatto I, Staiti P, Antonucci V, Passalacqua E (2001) Sulfonated polysulfone ionomer membranes for fuel cells. Solid State Ionics 145(1–4):47–51
35. Einsla BR, Harrison WL, Tchatchoua C, McGrath JE (2004) Disulfonated polybenzoxazoles for proton exchange membrane fuel cell applications. Polym Prepr 44(2):645–646

36. Gil M, Ji X, Li X, Na H, Hampsey JE, Lu Y (2004) Direct synthesis of sulfonated aromatic poly(ether ether ketone) proton exchange membranes for fuel cell applications. J Membr Sci 234(1–2):75–81
37. Xing P, Robertson GP, Guiver MD, Mikhailenko SD, Kaliaguine S (2004) Sulfonated poly(aryl ether ketone)s containing the hexafluoroisopropylidene diphenyl moiety prepared by direct copolymerization, as proton exchange membranes for fuel cell application. Macromolecules 37(21):7960–7967
38. Gao Y, Robertson GP, Guiver MD, Mikhailenko SD, Kaliaguine S (2004) Synthesis of copoly(aryl ether ether nitrile)s containing sulfonic acid groups for PEM applications. Macromolecules 37(18):6748–6754
39. Xiao GY, Sun GM, Yan DY, Zhu PF, Tao P (2002) Synthesis of sulfonated poly(phthalazinone ether sulfones) by direct polymerization. Polym Prepr 43(19):5335–5339
40. Wang F, Hickner M, Kim YS, Zawodzinksi TA, McGrath JE (2002) Direct polymerization of sulfonated poly(arylene ether sulfone) random (statistical) copolymers: candidates for new proton exchange membranes. J Membr Sci 197(1–2):231–242
41. Hickner MA, Ghassemi H, Kim YS, Einsla BR, McGrath JE (2004) Alternative polymer systems for proton exchange membranes (PEMs). Chem Rev 104(10):4587–4611
42. Kim S, Cameron DA, Lee Y, Reynolds JR, Savage CR (1996) Aromatic and rigid rod polyelectrolytes based on sulfonated poly(benzobisthiazoles). J Polym Sci A 34(3):481–492
43. Ariza MJ, Jones DJ, Roziere J (2002) Role of post-sulfonation thermal treatment in conducting and thermal properties of sulfuric acid sulfonated poly(benzimidazole) membranes. Desalination 147(1–3):183–189
44. Staiti P, Lufrano F, Arico AS, Passalacqua E, Antonucci V (2001) Sulfonated polybenzimidazole membranes – preparation and physico-chemical characterization. J Membr Sci 188(1):71–78
45. Bae JM, Honma I, Murata M, Yamamoto T, Rikukawa M, Ogata N (2002) Properties of selected sulfonated polymers as proton-conducting electrolytes for polymer electrolyte fuel cells. Solid State Ionics 147(1–2):189–194
46. Asensio JA, Borros S, Gomez-Romero P (2002) Proton-conducting polymers based on benzimidazoles and sulfonated benzimidazoles. J Polym Sci A 40(21):3703–3710
47. Sakaguchi Y, Kitamura K, Nakao J, Hamamoto S, Tachimori H, Takase S (2001) Preparation and properties of sulfonated or phosphonated polybenzimidazoles and polybenzoxazoles. Polym Mater Sci Eng 84:899–900
48. Mader J (2010) Novel sulfonated polybenzimidazole derivatives for high temperature fuel cell applications. PhD Thesis, Rensselaer Polytechnic Institute, Troy, NY
49. He R, Li Q, Xiao GY, Bjerrum NJ (2003) Proton conductivity of phosphoric acid doped polybenzimidazole and its composites with inorganic proton conductors. J Membr Sci 226(1–2):169–184
50. Qian G, Benicewicz BC (2009) Synthesis and characterization of high molecular weight hexafluoroisopropylidene-containing polybenzimidazole for high-temperature polymer electrolyte membrane fuel cells. J Polym Sci A 47(16):4064–4073
51. Yu S, Benicewicz BC (2009) Synthesis and properties of functionalized polybenzimidazoles for high-temperature PEMFCs. Macromolecules 42(22):8640–8648
52. Scanlon E (2005) Polybenzimidazole based segmented block copolymers for high temperature fuel cell applications. PhD Thesis, Rensselaer Polytechnic Institute, Troy, NY
53. Schmidt TJ (2006) Durability and degradation in high-temperature polymer electrolyte fuel cells. ECS Trans 1(8):19–31
54. Schmidt TJ (2009) High-temperature polymer electrolyte fuel cells: durability insights. In: Buchi FN, Inaba M, Schmidt TJ (eds) Polymer electrolyte fuel cell durability. Springer, New York, pp 199–221
55. Ross PN Jr (1987) Deactivation and poisoning of fuel cell catalysts. Marcel Dekker, New York
56. Ferreira PJ, la O' GJ, Shao-Horn Y, Morgan D, Makharia R, Kocha S, Gasteiger HA (2005) Instability of Pt/C electrocatalysts in proton exchange membrane fuel cells: a mechanistic investigation. J Electrochem Soc 152(11):A2256–A2271
57. Tang L, Han B, Persson K, Friesen C, He T, Sieradzki K, Ceder G (2010) Electrochemical stability of nanometer-scale Pt particles in acidic environments. J Am Chem Soc 132(2):596–600
58. Liu G, Zhang H, Zhai Y, Zhang Y, Xu D, Shao Z-g (2007) Pt_4ZrO_2/C cathode catalyst for improved durability in high temperature PEMFC based on H_3PO_4 doped PBI. Electrochem Commun 9(1):135–141
59. Landsman DA, Luczak FJ (2003) In: Vielstich W, Lamm A, Gasteiger H (eds) Handbook of fuel cells – fundamentals, technology and applications, vol 4. Wiley, Chicester, pp 811–831
60. Neyerlin KC, Singh A, Chu D (2008) Kinetic characterization of a Pt-Ni/C catalyst with a phosphoric acid doped PBI membrane in a proton exchange membrane fuel cell. J Power Sources 176(1):112–117
61. Schmidt TJ, Baurmeister J (2008) Properties of high-temperature PEFC Celtec-P 1000 MEAs in start/stop operation mode. J Power Sources 176(2):428–434
62. Luczak FJ, Landsman DA (1984) Ordered ternary fuel cell catalysts containing platinum, cobalt and chromium. US Patent 4,447,506
63. Luczak FJ, Landsman DA (1987) Ordered ternary fuel cell catalysts containing platinum and cobalt and method for making the catalyst. US Patent 4,677,092
64. Beard B, Ross PN Jr (1990) The structure and activity of platinum-cobalt alloys as oxygen reduction electrocatalysts. J Electrochem Soc 137(11):3368–3374
65. Glass JT, Cahen GL, Stoner GE (1987) The effect of metallurgical variables on the electrocatalytic properties of platinum-chromium alloys. J Electrochem Soc 134(1):58–65
66. Mukerjee S, Srinivasan S (1993) Enhanced electrocatalysis of oxygen reduction on platinum alloys in proton exchange membrane fuel cells. J Electroanal Chem 357(1–2):201–224
67. Mukerjee S, Srinivasan S, Soriaga MP (1995) Role of structural and electronic properties of Pt and Pt alloys on electrocatalysis of oxygen reduction. An in situ XANES and EXAFS investigation. J Electrochem Soc 142(5):1409–1422

68. Paulus UA, Scherer GG, Wokaun A, Schmidt TJ, Stamenkovic V, Radmilovic V, Markovic NM, Ross PN (2001) Oxygen reduction on carbon-supported Pt-Ni and Pt-Co alloy catalysts. J Phys Chem B 106(16):4181–4191
69. Stamenkovic V, Schmidt TJ, Ross PN, Markovic NM (2002) Surface composition effects in electrocatalysis: kinetics of oxygen reduction on well-defined Pt_3Ni and Pt_3Co alloy surfaces. J Phys Chem B 106(46):11970–11979
70. Stamenkovic V, Fowler B, Mun BS, Wang B, Ross PN, Lucas CA, Markovic NM (2007) Improved oxygen reduction activity on $Pt_3Ni(111)$ via increased surface site availability. Science 315(5811):493–497
71. Parrondo J, Mijangos F, Rambabu B (2010) Platinum/tin oxide/carbon cathode catalyst for high temperature PEM fuel cell. J Power Sources 195(13):3977–3983
72. Qian G (2008) Fluorine-containing polybenzimidazoles for high temperature polymer electrolyte membrane fuel cell applications. PhD Thesis, Rensselaer Polytechnic Institute, Troy, NY
73. Gasteiger H, Markovic NM (2009) Just a dream – or future reality? Science 324(5923):48–49
74. Debe MK, Schmoeckel AK, Vernstrom GD, Atanasoski R (2006) High voltage stability of nanostructured thin film catalysts for PEM fuel cells. J Power Sources 161(2):1002–1011
75. Strasser P (2009) Dealloyed Pt bimetallic electrocatalysts for oxygen reduction. In: Vielstich W, Yokokawa H, Gasteiger HA (eds) Handbook of fuel cells: advances in electrocatalysis, materials, diagnostics, and durability. Wiley, New York, pp 30–47
76. Lefevre M, Proietti E, Jaouen F, Dodelet J-P (2009) Iron-based catalysts with improved oxygen reduction activity in polymer electrolyte fuel cells. Science 324(5923):71–74
77. US Department of Energy (2010) MCFC and PAFC R&D workshop summary report. http://www1.eere.energy.gov/hydrogenandfuelcells/pdfs/mcfc_pafc_workshop_summary.pdf
78. Yu S, Xiao L, Benicewicz BC (2008) Durability studies of PBI-based high temperature PEMFC. Fuel Cells 8(3–4):165–174
79. Okae I, Kato S, Seya A, Kamoshita T (1990) Study of the phosphoric acid management in PAFCs. In: The Chemical Society of Japan 67th Spring Meeting, vol 148, FCDIC Fuel Cell Symposium Proceedings, Japan
80. U.S. Department of Energy (2005) Manufacturing for the hydrogen economy: manufacturing research and development of PEM fuel cell systems for transportation application. http://www1.eere.energy.gov/hydrogenandfuelcells/pdfs/mfg_wkshp_fuelcell.pdf
81. California Fuel Cell Partnership (2009) Hydrogen fuel cell vehicle and station deployment plan: a strategy for meeting the challenge ahead. http://www.fuelcellpartnership.org/
82. Feitelberg AS, Stathopoulos J, Qi Z, Smith C, Elter JF (2005) Reliability of plug power GenSys fuel cell systems. J Power Sources 147(1–2):203–207
83. Schmidt TJ, Baurmeister J (2006) Durability and reliability in high temperature reformed hydrogen PEFCs. ECS Trans 3(1):861–869
84. Mocoteguy P, Ludwig B, Scholta J, Barrera R, Ginocchio S (2009) Long term testing in continuous mode of HT-PEMFC based H_3PO_4/PBI Celtec-P MEAs for u-CHP applications. Fuel Cells 9(4):325–348
85. Mocoteguy P, Ludwig B, Scholta J, Nedellec Y, Jones DJ, Roziere J (2010) Long-term testing in dynamic mode of HT-PEMFC H_3PO_4/PBI Celtec-P based membrane electrode assemblies for micro-CHP applications. Fuel Cells 10(2):299–311
86. Garsany Y, Gould BD, Baturina OA, Swider-Lyons KE (2009) Comparison of the sulfur poisoning of PBI and Nafion PEMFC cathodes. Electrochem Solid State Lett 12(9):B138–B140
87. Schmidt TJ, Baurmeister J (2008) Development status of PBI based high-temperature membrane electrode assemblies. ECS Trans 16(2):263–270
88. Reiser CA, Bregoli L, Patterson TW, Yi JS, Yang JD, Perry ML, Jarvi TD (2005) A reverse-current decay mechanism for fuel cells. Electrochem Solid State Lett 8(6):A273–A276
89. Puffer RH Jr, Rock SJ (2009) Recent advances in high temperature proton exchange membrane fuel cell manufacturing. J Fuel Cell Sci Technol 6(4):041013/1–041013/7
90. Puffer RH Jr, Hoppes GH (2004) Development of a flexible pilot high temperature MEA manufacturing line. J Fuel Cell Sci Technol 2004:573–579
91. Harris TAL, Walczyk D (2006) Development of a casting technique for membrane material used in high-temperature PEM fuel cells. J Manuf Processes 8(1):19–31
92. Birnbaum U, Haines M, Hake J-Fr, Linssen J (2008) Reduction of greenhouse gas emissions through fuel cell combined heat and power applications. 17th World Hydrogen Energy Conference, Forschungszentrum Juelich GmbH, IEA Greenhouse Gas R&D Programme, www.fuelcells.org/info/residentialsavings.pdf
93. Schmidtz R (2009) Japan working toward fuel-cell reality. Marketplace, 8 Dec 2009, p 1
94. BASF Fuel Cell GmbH (2010) Celtec MEAs: membrane electrode assemblies for high temperature PEM fuel cells. http://www.basf-fuelcell.com/en/projects/celtec-mea.html
95. Plug Power (2009) High-temperature fuel cell system for residential applications. http://www.plugpower.com/products/residentialgensys/residentialgensys.aspx
96. Serenergy (2010) Serenus 166/390 Air C v2.5. http://www.serenergy.com/files/assets/documentation/166_390%20Air%20C%20v2.5%20data%20sheet_v1.1-0210.pdf
97. ClearEdge Power (2009) Delivering smart energy today. http://www.clearedgepower.com/
98. U.S. Energy Information Administration (2009) Emissions of greenhouse gases report. http://www.eia.doe.gov/oiaf/1605/ggrpt/#ercde
99. Wired.com (2010) A hydrogen highway for the east coast. http://www.wired.com/autopia/2010/01/east-coast-hydrogen-highway/
100. Telegraph.co.uk, Telegraph Media Group Limited (2008) Driving VW's fuel-cell prototypes. http://www.telegraph.co.uk/motoring/green-motoring/3520714/Driving-VWs-fuel-cell-prototypes.html

101. Renewableenergyfocus.com (2009) Innovative Danish technology uses methanol to make fuel cell vehicles competitive, December 2009. http://www.renewableenergyfocus.com/view/5650/innovative-danish-technology-uses-methanol-to-make-fuel-cell-vehicles-competitive/
102. German Aerospace Center (2009) DLR motor glider antares takes off in Hamburg – powered by a fuel cell. http://www.dlr.de/en/desktopdefault.aspx/tabid-13/135_read-18278/
103. What's next after the dreamliner? Think fuel cells. Design News, 18 Sept 2009. http://www.designnews.com/article/354516-What_s_Next_after_the_Dreamliner_Think_Fuel_Cells.php
104. Ultracell (2008) UltraCell XX25: mobile power for mobile applications. http://www.ultracellpower.com/assets/XX25_Data_Sheet_01-22-2009.pdf
105. Ultracell (2008) UltraCell XX55: extreme mobile power for demanding applications. http://www.ultracellpower.com/assets/XX55_Data_Sheet_01-27-2009.pdf
106. Serenergy (2010) Serenus methanol fuel cell module – 350W. http://www.serenergy.com/files/assets/documentation/Serenus%20H3%20E-350_datasheet_v1.1-0210.pdf
107. Maget HJR (1970) Process for gas purification. US Patent 3489670, 13 Jan 1970
108. McElroy JF (1989) SPE regenerative hydrogen/oxygen fuel cells for extraterrestrial surface applications. In: Energy conversion engineering conference, Washington, DC, Aug 1989. IEEE, Washington, DC, pp 1631–1636
109. Rohland B, Eberle K, Strobel R, Scholta J, Garche J (1998) Electrochemical hydrogen compressor. Electrochim Acta 43(24):3841
110. Perry KA, Eisman GA, Benicewicz BC (2008) Electrochemical hydrogen pumping using a high-temperature polybenzimidazole (PBI) membrane. J Power Sources 177(2): 478–484

Polyculture in Aquaculture

Robert R. Stickney
Texas Sea Grant College Program, Texas A&M University, College Station, TX, USA

Article Outline

Glossary
Definition of Polyculture
Introduction
Key Principles
Polyculture Successes
Future Directions
Bibliography

Glossary

Benthos Organisms that live on or in the sediments in aquatic environments.

Niche A habitat that provides for the needs to support the life or an organism.

Plankton The community of plants and animals suspended in the water column that drift with the currents. They have limited or no swimming ability but may be able to move vertically.

Phytoplankton The plant component of the plankton community.

Zooplankton The animal component of the plankton community.

Definition of Polyculture

Polyculture is the production of two or more cultured species in the same physical space at the same time, often with the objective of producing multiple products that have economic value. They may be a combination of animals, plants and animals, aquatic species only, or aquatic and terrestrial species.

Introduction

Aquaculture has its roots in China, perhaps as long as 4,000 years ago [1]. Interestingly, polyculture was a part of that early history. The Chinese often stocked multiple species of carp together in ponds to take advantage of all the types of food available. The pond would be fertilized, often with terrestrial animal manure, to promote the growth of the food organisms. In addition, terrestrial vegetation might be added. Thus, each of the species stocked occupied its own ecological niche.

Another form of polyculture that has a long history is rice–fish culture. By modifying rice ponds to provide a refuge for fish when a rice paddy is dewatered (usually a trench down one side or in the middle of the paddy), the rice farmer can obtain two types of crops. The most common fishes employed in rice–fish farming are common carp (*Cyprinus carpio*) and tilapia (*Oreochromis* sp.).

Today, polyculture employs a much wider variety of species than those that have been used for millennia in China, and there have been nuances developed in the polyculture approach. In most cases, the species used in polyculture systems need to be compatible, that is, they

need to grow well without interfering with one another. One example is culturing freshwater shrimp (*Macrobrachium rosenbergii*) with tilapia [2]. Exceptions do occur. For example, a predatory species may be stocked to prey on unwanted offspring of the primary culture species. A good example is tilapia culture, where stocked fingerlings may become reproductively active well in advance of reaching desirable market size. A fish predator, such as the snakehead (*Channa* sp.), can be stocked at a size too small to consume the tilapia that are in the system for growout, but large enough to prey upon unwanted tilapia fry.

In marine cage culture, fouling by such organisms as bryozoans and barnacles is often a serious problem. Netting may become so fouled that circulation through the cage is reduced to the point that dissolved oxygen depletions can occur. Depending upon the location of the cage culture operation, such fouling can occur within several days to a few weeks, so frequent cleaning is required. If an animal that will consume the fouling organisms can be found and stocked in the cages, it may be possible to extend the time between manual cleanings. There have also been instances where fish have been stocked in marine cages to consume parasites. One example is the stocking of wrasse (family Labridae) to control sea lice in Atlantic salmon cages in Norway [3]. Another is stocking sea cucumbers (class Holothuroidea) in salmon net pens to feed on fish feces, fouling organisms, and unconsumed feed [4].

Polyculture is primarily used to enhance total production within an aquaculture facility while maintaining and, in many cases, enhancing water quality. Mussels grown in the vicinity of salmon net pens, for example, remove phytoplankton that take up nutrients associated with the degradation of fish feces and unconsumed feed. Adding a seaweed, such as kelp (order Laminariales), to the system can further reduce the levels of dissolved nitrogen and phosphorus in the water. Polyculture of fish, shellfish, and algae together is an example of integrated multitrophic aquaculture [5]. While Atlantic salmon (*Salmo salar*) is the most common fish cultured using the technique, it has also been used with rabbitfish (*Siganus* sp.) [6].

Another specialized case of polyculture is hydroponics (sometimes called aquaponics), wherein terrestrial plants are grown in a nutrient solution rather than being planted in soil. Hydroponics is usually conducted in greenhouses. The water for the terrestrial plants, which are often a combination of vegetables and/or herbs, is fertilized to provide all the proper nutrients for rapid growth and, of course, provided with sufficient natural or artificial light for photosynthesis. In many cases, one or more aquatic species (fish or shellfish) are incorporated into the system.

Many nations culture fish in ponds that receive avian, livestock, or even human waste as fertilizer. The practice is particularly common in developing countries where inorganic fertilizer is expensive and often difficult to obtain. Common carp and tilapia are often grown in ponds that receive the waste from the terrestrial animals.

Key Principles

Polyculture is a Technique that Produces Two or More Compatible Species Within the Same Culture System

Not every species in a polyculture system needs to be aquatic in nature. Combinations of terrestrial and aquatic species are common. One or more of the species in a polyculture system may be a terrestrial or an aquatic plant.

Polyculture Systems can Increase the Profitability of a Culture System

By culturing two or more marketable species together in the same culture system or in close proximity to one another, it is often possible to increase the amount of income generated by a producer. While it may not be economically possible to rear one of the species profitably alone, by polyculturing it with a high-value species, total revenue can be increased. An example is culturing seaweed that is a good source of agar or carrageenan and that could add value to a culture facility if grown in the vicinity of a higher value crop like salmon [7].

Polyculture Systems can Reduce the Environmental Impacts from Aquaculture Systems

Nutrients released from cultured fish and shellfish-culture facilities can be effectively removed from the water by culturing plants such as seaweeds in close proximity to the animals [7]. An alternative approach

would involve the nutrients from such species as fish or shrimp to support phytoplankton that could, in turn, provide a food source for filter feeding Mollusca, such as oysters, scallops, and mussels [5].

Polyculture Successes

As mentioned, polyculture was developed 1000s of years ago [1] and must be considered successful without question since it is still being employed, not only in China, but also in many other countries. The objective of the Chinese system is to stock species that take advantage of the various available food sources in culture ponds. Silver carp (*Hypophthalmichthys molitrix*) consume phytoplankton, bighead carp (*Hypophthalmichthys nobilis*) graze on zooplankton, mud carp (*Cirrhinus molitorella*) feed primarily on detritus, black carp (*Mylopharyngodon piceus*) are mollusc eaters, while grass carp (*Ctenopharyngodon idella*) consume higher vegetation. Grass carp will eat some species of aquatic macrophytes and will also consume various types of terrestrial plants that may be added to the culture pond. Other species that are used in carp polyculture systems are common carp (*Cyprinus carpio*) and tilapia (*Oreochromis* spp.). There are a wide variety of fish, shellfish, and plants that are used in polyculture around the world. In many cases, they are local species, though introduced species are also commonly found – in many cases those were introduced decades ago, such as is the case with tilapia in Asia and the Americas.

Integrated multi-trophic aquaculture systems have a relatively short history, but appear to be highly effective and are a modern approach to polyculture that is being increasingly adopted. Thus, that approach can also be considered a success. The approach typically involves the co-culture of carnivorous species, such as finfish or shrimp, with a filter feeder and a primary producer, typically some kind of algae [8, 9].

Hydroponics can be considered a success, in that the approach can be used to produce a variety of vegetables and other types of plants. While capital intensive, hydroponic systems can be profitable. Various species of aquatic animals have been grown in such systems to provide nutrients that the plants can use and also to produce an additional marketable product. The aquatic animals cannot be counted upon as the only or even the primary nutrient source for the plants, however. The nutrient levels in the aquatic-animal waste products are insufficient in volume and composition, so a nutrient broth needs to be provided.

Future Directions

Biofloc aquaculture is an approach that has been around since the 1970s, but has as yet to be widely adopted. In biofloc systems, the development of high levels of nonpathogenic bacteria in the water is encouraged. Heavy aeration is required to maintain the dissolved oxygen level for the culture species, which is most commonly shrimp, though such systems have also been used in conjunction with tilapia and other fishes. As more experience and research has occurred over the years, the methods for developing and controlling water quality in such systems have advanced. In 2009, one research group was able to produce shrimp at a final density of 9.75 kg/m^3, which is as much as ten times higher than what is typical [10]. It is likely that the approach will be more widely adopted in the future.

Open-ocean aquaculture is expanding rapidly around much of the globe. In the USA, marine aquaculture is largely confined to production of molluscs in coastal waters and salmon cage and net pen culture in protected waters. Once a regulatory framework for the United States Exclusive Economic Zone has been promulgated, there is a likelihood that offshore aquaculture facilities will be developed. It seems reasonable to assume that a polyculture approach similar to the one that is commonly seen with respect to salmon culture, particularly in Chile, will be employed in conjunction with offshore aquaculture as a means of helping prevent water-quality degradation and increasing profitability. Offshore polyculture may involve rearing molluscs suspended from platforms used as support facilities for sea-cage culture operations. Such support structures may provide housing for the culturists, feed, and equipment storage, and may also be used as hatcheries (oil and gas platforms being appropriate once they are out of production and which have been of interest to some prospective aquaculturists). Seaweeds could also be produced, so an offshore operation might employ the multitrophic approach to culture.

Bibliography

1. Stickney RR (2009) Aquaculture: an introductory text. CABI, Wallingford, United Kingdom p 304
2. Brick RW, Stickney RR (1979) Polyculture of Tilapia aurea and Macrobrachium rosenbergii in Texas. Proc World Maricult Soc 10:222–228.
3. Sayer MDJ, Treasurer JW, Costello MJ (1996) Wrasse biology and use in aquaculture. Wiley, New York p 296.
4. Ahlgren MO (1998) Consumption and assimilation of salmon net pen fouling debris by the red sea cucumber *Parastichopus californicus*: implications for polyculture. J World Aquacult Soc 29:133–139
5. Chopin T, Bastarache S (2004) Mariculture in Canada: finfish, shellfish and seaweed. World Aquacult 34(3):37–41
6. Mmochi AJ, Mozes N, Kissil G, Dubi AM, Jiddawi NS, Mwangamilo J (2001) Design and preliminary results of an integrated mariculture pond system (IMPS) at Makoba, Zanzibar. Tanzan Mar Sci Devel In Tanzan East Afr 1:431–450
7. Troell M, Nilsson C, Buschmann A, Kautsky AH, Kautsky N (1997) Integrated marine cultivation of *Gracilaria chilensis* (Gracilariales, Bangiophyceae) and salmon cages for reduced environmental impact and increased economic output. Aquacult 156:45–61
8. Neori A, Troell M, Chopin T, Yarish C (2007) The need for a balanced approach to blue revolution aquaculture. Environ 49:37–43
9. Ridler N, Wowchuk M, Robinson B, Barreington K, Chopin T, Robinson S, Page F, Reid G, Szemerda M, Sewuster J, Boyne-Travis S (2007) Integrated multi-trophic aquaculture (IMTA): a potential strategic choice for farmers. Aquacult Econ Manage 11:99–110
10. Samocha T, Correia E, Hanson T, Wilkenfeld J, Morris T (2010) Opeation and economics of a biofloc-dominated zero exchange system for the production of Pacific white shrimp, *Litopenaeus vannamei,* in greenhouse-enclosed raceways. In: Proceedings of the AES issues forum, Roanoke, 18–19 Aug 2010

Polymer Electrolyte (PE) Fuel Cell Systems

John F. Elter
Sustainable Systems, LLC, Latham, New York, USA

Article Outline

Glossary
Definition of the Subject
Introduction
The PEM Fuel Cell Industry
Fuel Cell Basics
Critical Parameters/Critical Specifications
Recent Advancements
Fuel Cell System Design
Technical Readiness
System Cost and Reliability
Fuel Cell Systems and Sustainability
Future Directions
Bibliography

Glossary

Electrocatalyst A material that enhances the rate of an electrochemical reaction, such as the hydrogen oxidation reaction (HOR) or the oxygen reduction reaction (ORR), without itself being consumed in the reaction. In most PEM fuel cells, the electrocatalysts are nanosized materials made from the precious metals group (PGM), usually platinum, palladium, and ruthenium, or alloys of these materials with nickel, cobalt, and manganese.

Fuel cell system (FCS) The combination of a fuel cell stack and the subsystems that are required to support its operation for the intended application.

Fuel cells (FC) Electrochemical cells that convert chemical energy from a fuel into electrical energy through the controlled transfer of electrical charge driven by the difference in electrochemical potential between two electrodes separated by an electrolyte.

Gas diffusion layer (GDL) A component of the fuel cell used to evenly distribute reactants across the electrode surface.

Membrane electrode assembly (MEA) A manufactured unit consisting of the electrodes, membrane, and gas diffusion layers. Sometimes, the MEA can include the gasket used to seal the fuel cell. The MEA, when placed between two electrically conducting plates with channels to provide the fuel and oxygen, constitute a single cell.

Polymer electrolyte membrane (PEM) Cation- or anion-conducting polymer membrane that separates the two electrodes in a fuel cell. In most PEM fuel cells, the polymer is a cation (proton) conductor and in this case PEM can stand for proton exchange membrane.

Stack A collection of individual fuel cells, separated by electrically conducting "bipolar" plates, connected in series. Stacks can range in size from a few watts as in portable fuel cells to hundreds kilowatts as in stationary fuel cells for combined heat and power.

Triple phase boundary (TPB) The place on the catalyst surface within the fuel cell electrodes where protons, electrons, and the fuel meet in order to oxidize hydrogen or reduce oxygen reactants.

Definition of the Subject

This chapter discusses the subject of fuel cells: how they work and how they are designed and integrated into a collection of subsystems for application in a variety of applications. Particular focus is placed upon systems utilizing polymer electrolyte membranes, and how the properties of the membrane dictate the system design considerations.

Fuel cells themselves were invented over 170 years ago, with the first fuel cell demonstrated by Sir William Robert Grove in 1839. The first commercial use of a PEM fuel cell in a system occurred when General Electric developed the technology with NASA and McDonnell Aircraft for use in the Gemini space program. Since then, fuel cells have been integrated into systems intended for a wide variety of applications, from fuel cells of just a few watts for portable application, to hundreds of kilowatts for applications in transportation.

Introduction

The vision of fuel cells running on renewable hydrogen as an energy carrier derived from water, and producing electricity with only water as a by-product, has long captured the imagination of those concerned with the environment. Since the early days of the use of fuel cells in the Gemini space program, various explorations of the potential use of fuel cells have been conducted by individuals, small firms, and large corporations. In each case, the potential of fuel cells has been validated. The long-term benefits of high efficiency and fuel flexibility are clear, especially in today's context. Energy security and the need to reduce dependence on foreign oil, and the need for sustainable economic development and the reduction of greenhouse gas emissions have been brought into sharp focus by war, weather, and wildlife.

Great progress has been and continues to be made in the development of fuel cells since their first commercial application roughly 50 years ago. This is particularly true of the fuel cells developed for automotive applications, which represents a very demanding application in terms of durability and cost. Progress has been made in other applications as well, particularly for those being developed for motive power and stationary combined heat and power. This chapter will attempt to lay out the status of the technology today, and where it needs to go in the future. First, a brief overview will be given of the fuel cell industry, followed by a review of some of the basic principles underlying the theory of operation. The notion of critical design parameters and specifications will be discussed as a prelude to a review of some recent advancement and to the system design process and some important considerations for fuel cell systems. Finally, there will be a discussion on future directions.

The PEM Fuel Cell Industry

In reality, it is fair to say that the fuel cell industry is nascent. The long-term benefits of high efficiency and potential fuel flexibility are clear, but cost and durability issues are causing a slow adoption timeline. In addition, the nagging issue of the infrastructure needed to provide hydrogen as a fuel has not gone away. Hydrogen availability is still a relevant issue for many of the applications that would have fuel cells as the privileged technology. Other issues include the operational flexibility and lifespan of the incumbent technology. In response to these important issues, fuel cell manufacturers, in need of revenues, are attempting to approach large niche markets for which the technological requirements are suited to current fuel cell capabilities. These markets, such as backup power, indoor forklift trucks, bus fleets, and consumer electronics, each has their own set of adoption issues. Even in these cases, government subsidies are needed to help the industry cope with the slow market penetration associated with product immaturity and the risk-adverse nature of the industries being targeted. Limited revenues from these markets lead to high stock volatility, making valuations difficult, limiting private investment and further exasperating the situation.

The fuel cell industry is itself highly fragmented. Investment bankers such as JP Morgan have limited their coverage to those companies with larger market caps, including Ballard and Plug Power, who focus on backup, forklift, and residential cogeneration systems, and for example Medis Technologies which focuses on the consumer electronics industry with a proprietary direct liquid fuel cell battery charging device. Other players in the fuel cell world include companies with a variety of business models that are aggressively pursuing similar markets. These include pure stack manufacturers, such as Nedstack, fuel cell systems providers such as ClearEdge and IdaTech, companies that supply both stacks and systems to end user and OEM customers, such as Nuvera, and companies that provide stack technology to OEMs such as Intelligent Energy. Feeding fuel cell components to these companies are much larger corporations such as 3M, DuPont, Gore, Asahi Glass, and BASF, as well as a host of large automotive suppliers providing the "balance of plant" components such as blowers, compressors, heat exchangers, and electronics.

One reason for the fragmentation of the fuel cell industry is the wide range of applications to which fuel cells can be applied. As mentioned, these include transportation applications (with the key players being General Motors, Toyota, Honda, UTC, and others), material handling (Ballard, Plug Power, Nuvera, Hydrogenics), telecommunications backup (Plug Power, Ballard, ReliOn, IdaTech), consumer electronics (Samsung, Toshiba, and others) and residential cogeneration (Plug Power, ClearEdge, Toshiba, others). Each of these markets has a well-defined set of operational characteristics and requirements, as defined by the customer. Another and related reason for the fragmentation of the industry is the lack of a dominant design paradigm. Each company has a preferred method of approaching the design of a fuel cell and the system into which it is embedded. Since no single approach has emerged as dominant, there is a lack of standards, de facto or otherwise, around which the industry can capture the benefits of economies of scale and of accumulated knowledge.

On the other hand, it might be argued that there is a de facto dominant design, and it is that standard which, up to now unwittingly adhered to, is limiting the true out-of-the-box thinking needed for step changes in performance at lower cost and improved reliability. In most cases, as will be seen, the commercialization issues around each application are driven to a large extent by this underlying "standard" technology, and its modes of failure in meeting customer requirements. In this chapter, specific attention will be given to these failure modes, and how they drive system complexity. In addition, some attention will be paid to the system design, and how it can be simplified to enable lower costs.

Finally, as will be discussed here, there has been steady progress in lowering costs and improving reliability, due in part to sustained government support of fuel cells over the past decade. Still, there is "a lot of room at the bottom" for scientific and engineering innovation. Indeed, the application of nanotechnology as a means of enabling the fuel cell industry to become a sustainable ecosystem should not be underestimated. There is ample reason for considerable optimism around PEM fuel cell systems for the sustainable energy applications they support.

Fuel Cell Basics

Fuel cells are electrochemical devices that transform chemical energy into electrical energy, much the same way a battery converts chemical potential energy into electrical kinetic energy, except that the chemicals consumed in a fuel cell in the reaction are supplied from external sources. The fuel cell enables the generation of electricity while producing pure water by controlling the combining of hydrogen and oxygen:

$$H_2 + O_2 \rightarrow H_2O \tag{1}$$

Ideally, this reaction would take place at a potential of 1.229 V at standard conditions (25°C and 1 atm) if were it not for losses due to irreversible internal processes. In fact, the reversible potential E_r of this reaction can be expressed in terms of the change in the Gibbs free energy, ΔG:

$$\Delta G = -nFE_r \tag{2}$$

Here n is the number of electrons involved and F is Faraday's constant, which has the value of 96,485 coulombs of charge per mole of electrons. The derivation of Eq. 2 is a straightforward application of thermodynamics, recognizing that in this case the work done is

the product of the amount of charge transferred and the potential. For the case of standard conditions, it is known from thermodynamics that $\Delta G = 237$ kJ/mole when the water is produced as a liquid (corresponding to the higher heating value, HHV) and $n = 2$ for the H_2/O_2 fuel cell reaction. Of course, not all of the energy in the reaction is turned into electricity, and because of this some portion of hydrogen's HHV is converted into heat. The enthalpy change in the reaction is given by the familiar thermodynamic relationship

$$\Delta H = \Delta G + T\Delta S \tag{3}$$

From thermodynamic tables, it is found that at standard conditions $\Delta H = 286$ kJ/mole. It follows that roughly 49 kJ/mole are converted into heat and the theoretical efficiency η_{th} of a fuel cell operating at standard conditions is

$$\eta_{\text{th}} = \Delta G/\Delta H = 237/286 = 83\% \tag{4}$$

There are various additional losses that are due to irreversible processes in the cell itself. These losses, which are intrinsic to the cell and are materials dependent, reduce the fuel cell efficiencies to around 40–60%, depending on the type of fuel cell and its application. There are numerous references that discuss the theory behind fuel cells in detail [1, 2], as well as the other chapters in this encyclopedia. Here only a very cursory overview is given, as the focus of this chapter is on the fuel cell *system*.

In a typical fuel cell, there are two electrodes, an anode from which electrons are removed during the oxidation of hydrogen, a cathode to which electrons flow during the reduction of oxygen, an ion-conducting electrolyte which electrochemically connects the anode and cathode, and an external circuit through which the electrons flow from the anode to the cathode while doing electrical work. In early fuel cells, the electrolyte was generally a liquid such as a solution of KOH, which provided for the flow of OH^- anions. In this case, the fuel cell was termed an "alkaline" fuel cell because of the nature of the electrolyte. In the same way, the electrolyte can be phosphoric acid, in this case providing for the flow of H^+ cations, or protons. Such a fuel cell is called a "phosphoric acid" fuel cell, again in recognition of the electrolyte. In this chapter, polymer electrolyte fuel cell systems will be discussed. In this case, the electrolyte is a polymer in the form of a *membrane*. Hence the term or "polymer electrolyte membrane" or PEM fuel cell. PEM fuel cells, or PEMFCs, are electrochemical devices whose characteristics are determined largely by the properties of the polymer electrolyte. One of the main purposes of this chapter is to illustrate the extent to which the PEMFC's performance is in fact *dominated* by the properties of the polymer electrolyte. It is worth noting that in some cases the acronym PEM is interpreted to mean Proton Exchange Membrane, since in most cases in which the acronym PEM is used, the ion that is transported across the membrane and "exchanged" at the electrodes is the proton. However, here the acronym will be interpreted to mean Polymer Electrolyte Membrane to emphasize the point that it is the polymer electrolyte that to a large extent dictates the characteristics of the system.

In a fuel cell, the two reactants, in this case hydrogen and oxygen, are each directed macroscopically by flow channels molded into electrically and thermally conductive plates. The hydrogen on the anode side and the oxygen at the cathode side are each brought into contact with an electrode by the gas diffusion layer or "GDL" which ensures uniform flow across the cell. As discussed, a polymer membrane is provided that serves as the electrolyte, providing good ionic conductivity while maintaining the separation of these reactant gases, and preventing the flow of electrons. The membrane needs to make intimate contact with the electrodes to ensure efficient charge transfer across the embedded electrode/electrolyte interface. The electrodes are generally porous to allow the diffusion of the reactant gases while providing a support for the catalysts needed to facilitate the electrochemical reactions. The electrodes also need to provide conductive pathways for the ions and electrons. Clearly, the polymer electrolyte membrane, electrodes, and gas diffusion layer have a complex set of interacting functional requirements. These will be discussed in detail, especially from the point of view of their impact on system design.

In most cases, the polymer electrolyte is basically acidic, in which case, the catalysts are usually based upon platinum and its alloys. At the anode electrode, hydrogen gas molecules adsorb onto the supported catalyst material which is used to help strip the

hydrogen of its electron, oxidizing it to become a hydrogen cation, or proton. This proton is transported through the polymer electrolyte membrane to the cathode electrode. Here, oxygen molecules are fed into the cathode electrode, usually by supplying air. Like the active layer at the anode, appropriate nanosized catalyst particles are supported on electrically conducting porous materials. In the current dominant design paradigm, this support is usually a high surface area carbon. Once on the catalyst surface, the oxygen's covalent bonds are broken, forming oxygen anions. The oxygen anions then combine with protons arriving through the membrane and electrons that have been driven through an external circuit by the difference in the anode and cathode potentials. The *critical point* on the catalyst surface at which protons, electrons, and reactant gases must come together is generally called the *triple phase boundary* (TPB). All of the necessary components, the gas diffusion media, the porous electrodes, and the polymer electrolyte membrane, and if desired, even the conformable gasket required to provide sealing around the perimeter of the plate, are manufactured as a "membrane electrode assembly" or "MEA" by various suppliers like 3M, Gore, OMG, and others. Since a typical PEMFC operates at a voltage of less than a volt, multiple cells are electrically connected in series to form a "stack" of cells that can be sized for a particular application. In this case, each thermally and electrically conducting plate is shared between the anode of one cell and the cathode of another, and is thus termed "bipolar." The integrated stack design must accommodate a means for managing the products of the fuel cell reaction: electricity, water, and heat. In smaller systems, the stack can be air cooled, but in larger systems, the plates must incorporate channels that allow for the flow of a liquid coolant.

The electrochemical equation governing the hydrogen oxidation reaction (HOR) at the anode of a single cell is

$$H_2 \leftrightarrow 2H^+ + 2e^+ \qquad E^\circ = 0\ \text{V} \tag{5}$$

This is a thermodynamically reversible reaction, and with platinum as the catalyst, is a standard reference known as the "reversible hydrogen electrode" (RHE), for which the potential is universally chosen as zero volts. The oxygen reduction reaction (ORR) at the cathode, on the other hand, is thermodynamically irreversible, and is generally expressed in terms of the dominant four electron reaction:

$$O_2 + 4H^+ + 4e^- \rightarrow 2H_2O \qquad E^\circ = 1.229\ \text{V(vs. RHE)} \tag{6}$$

In fact, the ORR is an extremely complicated reaction that is dependent upon the electronic structure and number of the active sites on the catalyst surface, which in turn are influenced by many factors including the size and shape of the catalyst particle, the presence of any contaminant species competing for reaction sites, the presence of oxides which may be formed during potential cycling, the effect of the catalyst support, etc. In addition to the 4-electron reaction, there is the possibility for the 2-electron peroxide pathway [3],

$$O_2 + 2H^+ + 2e^- \rightarrow H_2O_2 \qquad E^\circ = 0.695\ \text{V(vs. RHE)} \tag{7}$$

In low-temperature PEMFCs, those that operate in the range of 65–80°C, the peroxide pathway is problematic because if the peroxide is not quickly decomposed into water, it can form radicals that chemically attack the membrane, causing premature failure.

The ORR is a major source of efficiency loss in a PEMFC, but it is not the only source of the so-called overpotential. In general, there are also resistive and mass transport losses. The resistive losses are associated with the finite conductivities of the electrolyte and the electrodes and the contact resistance losses at the plate and GDL interfaces, whereas mass transport losses are associated with the lack of adequate fuel or air reaching the reaction sites within the electrode. For low-temperature PEMFC systems that operate below the boiling point of water, mass transport losses are primarily due to the buildup of liquid water in the electrode or gas diffusion layer (referred to as "flooding"). Mass transport losses are also associated with the tortuous pathways that exist in the porous electrodes and the GDL. Reducing all of these sources of potential losses is important for achieving the highest possible efficiency.

It is perhaps convenient at this point to briefly mention the types of PEM fuel cell that are under development. Low-temperature PEM fuel cells (LTPEMFCs) operate in the range of 65–80°C. These

systems are limited in temperature by the requirement for the membrane to be maintained in a hydrated state in order to have sufficient proton conductivity. Typical of these systems are the perfluorinated sulfonic acid (PFSA) membranes made by DuPont, the standard being Nafion®. 3M, Gore, Asahi, and others make membranes with similar properties and characteristics. Intermediate temperature PEMFCs that are capable of operating above the boiling point of water in the region of 120°C are under development primarily for automotive applications. These are still in the development phase [4], and when available will have a significant impact on PEMFC performance for applications other than just automotive. Still higher temperature PEMFCs (HTPEMFCs) are based upon phosphoric acid–doped materials such as polybenzimidazole (PBI). These proton-conducting polymer electrolyte membranes allow fuel cells to operate at temperatures in the range of 160–200°C, thus providing for a high degree of tolerance to certain fuel cell contaminants such as CO, while at the same time offering a source of high-quality heat [5]. PBI-based systems are discussed in detail elsewhere in this encyclopedia, and will be mentioned briefly below in terms of their potential to simplify system design.

For a basic understanding of PEM fuel cells, it is important to appreciate how the properties of the polymer electrolyte dictate the requirements on the fuel cell, stack, and system design. Here just one but critically important example will be discussed: water management. One of the more well-known and basic properties of the PFSA type of polymer electrolytes is that their protonic conductivity is a strong function of the level of hydration. Sulfonated fluoropolymer membranes are based on a polytetrafluoroethylene (PTFE) backbone that is sulfonated by adding a side chain ending in a sulfonic acid group ($-SO_3H$) to the PTFE backbone. The resulting macromolecule contains both hydrophobic regions associated with the backbone and hydrophilic regions associated with the sulfonic acid group. Thus, a hydrated PFSA membrane forms a two-phase system consisting of a water-ion phase that is distributed throughout a partially crystallized perfluorinated matrix phase. As the membrane adsorbs water, the first water molecules cause the sulfonated group to dissociate, forming hydronium (H_3O^+) ions. The water that hydrates the membrane then forms counterions that are localized on the sulfonated end groups, which act as nucleation sites. As more water is added, the counterion clusters coalesce to form even larger clusters, until a continuous phase is formed with properties that approach those of bulk water. The level of hydration is measured in terms of a parameter λ, which is the equal to the number of absorbed water molecules per sulfonated group. For $\lambda = 0$, there is no water, and this anhydrous form of the membrane is uncommon, since complete removal of water requires temperatures near the decomposition of the polymer. Molecular dynamic simulations indicate that the primary hydration shell around the sulfonated group grows to a level of about λ equal to five waters [6]. As more water is added, for $\lambda > 6$, the added water is screened by the more strongly bound water of the primary hydration shell, and it can be considered a free phase. Saturation occurs in Nafion® at $\lambda = 14$. One of the consequences of this strong coupling is that proton transport within the membrane is accompanied by the transport of water. This effect is known as "electroosmotic drag," and it complicates the required management of the fuel cell by-products: water and heat.

The mechanism and degree of protonic conductivity change as the level of hydration increases. Kreuer [7] has provided an in-depth review of the physics underlying the basic mechanisms of transport in proton conductors. Transport of the proton can occur by two mechanisms: structural diffusion and vehicle diffusion. The structural diffusion mechanism is associated with the proton "hopping" along water molecules (Grotthuss shuttling). Vehicular diffusion is the classical Einstein diffusive motion. The former is viewed as a discrete mechanism, the latter a continuous mechanism. In the nanosized confined hydrophilic spaces within the membrane, both mechanisms are operative, with the diffusion constant of the discrete mechanism being larger and increasing faster than that of the continuous mechanism at higher levels of hydration. At intermediate and low degrees of hydration, the proton mobility is essentially vehicular in nature. What is important here is that the underlying mechanism of transport in proton conducting membranes changes as a function the level of hydration, and it is fundamental to the overall behavior of the fuel cell and therefore the design of the fuel cell system.

Given this fundamental and strong dependence of protonic conductivity with water content, it is necessary to ensure that the polymer electrolyte is safeguarded against localized drying. Indeed, a situation in which the membrane is in a "drying" mode of operation may lead to a catastrophic "death spiral" failure mode, since lower conductivity leads to higher resistances, increased localized temperatures, and therefore an ever-increasing rate of drying, ultimately resulting in membrane failure. In addition, other failure modes, including attack by hydroxyl radicals, are also accelerated at higher temperature and drier membrane conditions, further exasperating the situation.

Hence, it is necessary to maintain the localized level of membrane hydration through "water management," the *active* management of the moisture content of the membrane. One method is to design the system so that the relative humidity (RH) of the reactant streams coming into the stack is nearly saturated; an approach used by Plug Power and other fuel cell manufacturers. Another approach is to provide for water injection, an approach used by Intelligent Energy. Or, one can employ porous plates to distribute the product water generated during operation, a technique used by United Technologies. Each of these techniques requires careful stack and system design. The design approach taken likewise needs to avoid the situation where too much water can cause localized "flooding" within the cell, which in turn results in fuel starvation and subsequent permanent performance degradation. In most cases, the requirement to manage the polymer electrolyte membrane water content adds considerable system complexity and cost, as well as sources of unreliability.

Critical Parameters/Critical Specifications

It is clear that in a typical operating fuel cell, the current–voltage characteristics are dependent on the operating temperature, pressure, flow rate, and composition of the reactant gas streams. These are the system-level *critical parameters* around which the fuel cell system must be designed in order to achieve and maintain the desired electrical state of the system. It is also obvious that the performance of the fuel cell is also dependent on the how well the individual *functional requirements* are met with the *specifications* on the component parts. From a systems design perspective, it is perhaps worthwhile to describe how these terms are related. To motivate this discussion, it is important to note that a system is "technically ready" when all the required critical parameters can be simultaneously achieved through the intended interactions of the buildup of parts whose specifications can be met with ordinary manufacturing methods. It is assumed that the critical parameters are chosen to meet the system specifications, while at the same time avoiding all known failure modes. The extent of the range in the critical parameters under which the system can operate over time, without failure, is called the "operating latitude."

As a simple example, assume that one can write the equations of physics in the linear form

$$F_i = K_{ij} X_j \tag{8}$$

The terms F_i and X_j are termed the *critical parameters*, and the K_{ij} are termed the *critical specifications* that are required to meet the *functional requirements* of the particular component under consideration. The term "critical" is of course an indication that the specification in question is one of the significant few specifications that will be tracked all the way from the voice of the customer down to the factory floor. In a complete PEM fuel cell system, there can be hundreds of specifications that will need to be tracked during the development of the system. Of these, perhaps a few dozen will remain critical even after the product has launched and is in production.

As an example, consider at the conduction of protons across the membrane and for the moment neglect the electroosmotic drag of water with the proton. In this case, Eq. 8 takes the form of Ohm's law:

$$\mathrm{d}\varphi/\mathrm{d}z = -[1/\kappa]i \tag{9}$$

Here $\mathrm{d}\varphi/\mathrm{d}z$ is the potential gradient across the membrane, i is the flux of protons, and κ is the protonic conductivity. The system-level critical parameters (pressure, temperature, flow rate, and composition) establish the conditions for determining the local critical parameters ($\mathrm{d}\varphi/\mathrm{d}z$, i), and these are in turn are determined by the functional requirement that the polymer electrolyte has a protonic conductivity, κ. Typical values lie in the range of 10^{-1} to 10^{-2} S/cm.

Notice that critical parameters are generally *not* dimensions, but are rather forces, and fields, affinities, and fluxes. They are the conditions that are required for operation. Specifications, on the other hand, are the items that an engineer can call out on a drawing: dimensions, conductivities (both electrical and thermal), moduli of elasticity, and so forth. Instead of specifying the protonic conductivity κ, which is fixed by the material chemistry, the design engineer will specify the membrane thickness, thereby affecting not only the resistive losses but also rate the diffusion of gaseous species across the membrane.

As discussed above, the protonic conductivity is known to be a strong function of the moisture content, which again will be influenced by the system-level critical parameters of flow rate, temperature, pressure, and composition. Hence, in reality, a *constitutive equation* of the dependence of conductivity on moisture content is needed to support larger PEM fuel cell models which are essential to account for and keep track of all the complex interactions between the critical parameters and the specifications for the components of the MEA and other critical components. An early constitutive equation defining these interactions was described by Springer et al. [8]. These interactions place stringent demands upon the design of the cell, stack, and ultimately the system. Researchers and engineers have developed sophisticated models in an attempt to describe the current–voltage response of single fuel cells to the significant critical parameters through the specifications of the material properties of the cell components. These models, which are remarkably successful in describing the overall performance of a single cell, are macro-homogeneous in the sense that they use local average properties, such as electrode porosity, conductivity, etc., to describe the materials. Constitutive equations of the conductivity dependence on moisture have been developed to support the fuel cell models [9]. There are also excellent reviews of the models that have been developed to elucidate the various aspects of fuel cell behavior under a variety of conditions, as for example those by Weber and Newman [10] and Wang [11]. In addition, there are specialized models that deal with the root cause of specific failures, such as platinum dissolution [12] and carbon corrosion [13] due to high potentials generated during startup and shutdown [14]. All of these have added considerable insights into how the PEM system runs and how failures are to be avoided. Finally, there are models of the fuel cell system itself. The models predict full system behavior over the range of system-level critical parameters, and are useful in developing the algorithms needed in implementing model predictive control strategies.

Extensive cell/stack/system-level testing is also needed to assess the system's overall performance. In this case, computational fluid dynamics (CFD) is generally used to guide the cell/stack level testing, aiding in the fuel cell system development process. Some of these models have been made commercially available. In particular, models for PEMFCs can be obtained from CD-Adapco [15], Fluent [16], and others. In fact, knowledge of the cell and stack failure modes, and their dependence on the process critical parameters and critical specifications, is fundamental to designing and developing commercially viable fuel cell systems. A more detailed discussion of failure modes will be addressed in what follows. First, however, it is important to understand the current state of the art relative to the component at the heart of the PEM fuel cell, the MEA.

Recent Advancements

The operation of the fuel cell involves complex interactions at the numerous embedded surfaces within the cell, including the triple phase boundary. These embedded surfaces can mask the ability to probe the detailed nature of these interactions. Today, processes at the nanoscale are a fertile ground for research, enabled by the tremendous advances made in computational nanoscience through the convergence of "nano" and "info" technology. These advancements in computation have allowed theoreticians to explore electrochemical and electromechanical processes at the micro, meso, and nanoscales, with meaningful numbers of atoms, thereby improving the theoretical understanding of the basic processes involved. Furthermore, the rapidly expanding field of nanoscience and nanoengineering is being applied in a variety of fields, to include the development and characterization of nanoscale materials and structures that have direct bearing on energy generation, conversion, and storage.

Electrocatalysts

Relatively recent advancements have been made in the understanding of heterogeneous ORR catalysis using the combination of molecular and atomic level simulation tools, nanoscale fabrication methods, and nanoscale characterization techniques. For example, the early experimental work of Markovic [17], combined with the important theoretical work of Nørskov [18], Mavrakakis [19], Neurock [20], and others, has now given a deeper understanding not only of the thermodynamics involved in the ORR, and the likely cause of the associated overpotential, but also how variations in the electronic structure determine trends in the catalytic activity of the ORR across the periodic table. This work, coupled with the insights provided by the seminal work of Adzic [21], Stamenkovic [22], and others in the synthesis and performance characterization of Pt alloys and core-shell architectures, has significantly advanced the understanding of the state-of-the-art catalysts for use in both the HOR and ORR fuel cell reactions.

The exact mechanisms underlying the oxygen reduction reaction are still debatable. However, Nørskov [23] and his group have used density functional theory (DFT) to significantly advance the understanding of the thermodynamics of the various possible reaction pathways, and their dependence on surface properties. In combination with detailed DFT calculations, Nørskov and his team were able to provide a detailed description of the free-energy landscape of the electrochemical ORR over Pt as a function of applied bias. In doing so, they found that adsorbed oxygen and hydroxyl species are very stable intermediates at potentials close to equilibrium, and the calculated rate constant for the activated proton/electron transfer to these adsorbed intermediates accounts for the observed kinetics. On this basis, they were able to account for the trends in the ORR rate for a large number of different transition metals. In particular, they were able to construct "volcano" plots of maximum catalytic activity as a function of the oxygen and hydroxyl adsorption energies, describing known trends and the observed effects of alloying. It is clear that a significant amount of progress has been made in the past several years in the basic understanding of the electrocatalytic processes at the nanoscale. An excellent summary of this and other work has been given in the recent book on fuel cell catalysis by Koper [24].

The high price of platinum has provided the impetus for reducing the platinum loading by improving the kinetics of the ORR reaction. Considerable experimental effort has gone into the research and development of electrodes that incorporate the advantages of new nanomaterials intended to significantly reduce precious metal catalyst loadings, while maintaining high power densities. Chief among these are electrodes that incorporate platinum alloys with transition metals of various types as a means of increasing catalytic activity, thereby allowing a reduction in platinum loading. Currently, Pt_3Co alloys supported on carbon are achieving roughly a $2\times$ improvement over the state-of-the-art Pt/C electrodes. Intermetallic architectures of Pt and other materials have been fabricated by a variety of techniques, some of which yield so-called core-shell and skeleton/skin structures. Some of these, which involve monolayers of Pt particles on Pd cores supported on carbon, are reported to have achieved very significant ($\approx$20) increases in mass activities.

Steady progress has been made experimentally in reducing the platinum loadings, particularly in the hydrogen/air fuel cells used in automotive applications. Gasteiger et al. [25] have discussed the strategies to achieve the nearly fivefold reduction in loading needed in order to achieve automotive cost targets. These strategies, which involve increasing the power density at high voltages by reducing the Pt loading through an increase in the Pt activity, and by reducing mass transport losses in the cell, should also be relevant to backup, motive, and stationary PEMFC applications.

Nanostructure Electrodes

Most porous electrodes are made up of a mixture of ionomer (for proton conduction), high surface area carbon (for electron conduction), and nanoparticles of catalyst all mixed together to form an ink-like random medium. This ink is then either sprayed or doctored onto either a microporous layer on the gas diffusion media, or applied directly to the polymer electrolyte. In either case, the density of triple phase boundaries is to a large extent left determined by the random nature of the ink and application process.

On the horizon, however, lies a new class of electrodes based upon nanoscale structures that enable both increased performance and better utilization of the precious metals. These so-called nanostructured electrodes are highly structured by design, and enable significant improvement in both performance and durability. To date, the most significant of these structures are those under development by Debe [26] at 3M, wherein the structure consists of a dense forest of crystalline organic whiskers with areal densities on the order of three to about ten billion whiskers per cm^2, highly oriented with their long axis normal to the substrate. The whiskers are nanoscale in size (roughly 50 nm by 30 nm by 300–1,000 nm) and provide an interesting support for the Pt catalyst. An image of these whiskers, coated with a platinum catalyst, is shown in Fig. 1 below.

High-resolution TEM studies of the sputter-deposited thin catalyst film on the whiskers indicate that the catalyst films grow as polycrystalline layers that expose highly oriented crystallites. The resulting catalyst "whiskerettes" growing on and at an angle of roughly 70° to the surface of crystalline whiskers represents a very interesting hierarchical nanostructure that is providing significant improvements in performance. As proposed by Debe [27], the source of the activity gain of such a system might have its contribution rooted in the nature of the metal/support interactions.

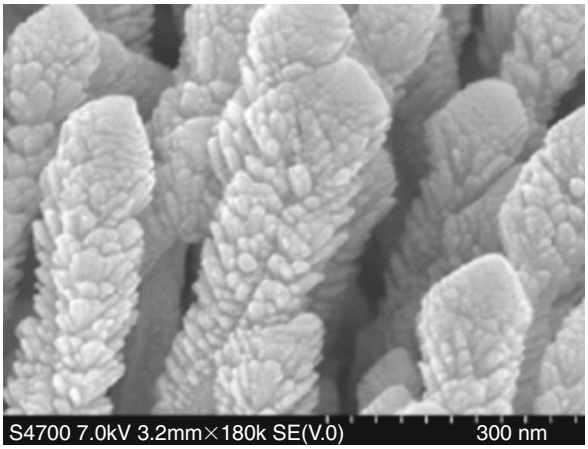

Polymer Electrolyte (PE) Fuel Cell Systems. Figure 1 3M's Pt-coated NSTF electrode [26]

How well do these nanostructured thin-film (NSTF) electrodes meet the expected performance targets? Current DOE maturity targets for light duty vehicle applications specify performance in terms of platinum group metal loading of <0.2 mg/cm_{MEA}^2, a durability target of least 5,000 h (at temperatures <80°C), a mass activity of at least 0.44 A/mg_{Pt} @ 0.9 V_{IRfree}, and a specific activity of 720 $\mu A/cm_{Pt}^2$ @ 0.9 V_{IRfree}. At the most recent DOE Annual Merit Review, 3M reported that they had achieved 0.19 mg_{Pt}/cm_{MEA}^2 loadings on 400 cm^2 in OEM short stacks, 5,000 h of durability (20 μm, 850 EW with no stabilizers), 0.24 A/mg_{Pt} with PtCoMn alloy (0.40 A/mg_{Pt} with a new Pt_3Ni_7 alloy that needs further development), and specific activity of 2,100 $\mu A/cm_{Pt}^2$. This is a substantial improvement in performance over the conventional Pt/C paradigm that has dominated fuel cell MEA designs for the past 15 years. There are water management issues with the thin electrode structure, as the reduced thickness of the electrode results in flooding more easily at cold, humid conditions while at high current density. 3M is studying a unique set of operating conditions and GDL properties on the anode side in order to reduce the impedance of water transport from the cathode to the anode, in order to improve the operating latitude with respect to cathode flooding [28].

It is important to note that in the pursuit of other types of highly ordered nanostructures, researchers are also taking aim on the issue of the catalyst support from the perspective of its stability. As will be discussed below, the usual carbon materials used to support the catalyst nanoparticles corrode under certain operating conditions associated with startup and shutdown of the fuel cell, or conditions of localized fuel starvation, and so it is desirable to have a support which is more stable under these dynamic situations. Accordingly, researchers are developing nanostructures in which the typical carbon material is replaced with materials with greater stability. Included in this set of support materials are the use of carbon nanotubes [29] and ceramic materials such as TiO_2 [30]. It is anticipated that advanced nanostructured electrodes will try to emulate the excellent results and the lessons being learned in the case of the NSTF work underway at 3M, while avoiding problems of water management.

Low and Intermediate Temperature Proton Conducting Polymer Electrolyte Membranes

There is also significant research underway addressing the development of alternative classes of polymer electrolytes for fuel cells. For example, sulfonated aromatic polymers, sulfonated polyimides, proton conducting membranes carrying phosphonic acid groups, and polyphosphazene polymer electrolytes are all being examined as lower cost, more durable alternatives to PFSA-based membranes. There are excellent reviews of the progress being made in the development of these acid-based polymer electrolytes [31].

As noted, PFSA-based polymer electrolyte membranes used in current PEMFCs require thermal and water management systems to control temperature and keep the membrane humidified. These extra components increase the weight and volume of the fuel cell system and add complexity. The cost and complexity of the thermal and water management systems could be minimized if the fuel cell operated at higher temperatures (up to 120°C) and at lower relative humidity (RH). The US Department of Energy has therefore initiated a major effort to develop new membranes that can operate at temperatures up to 120°C without the need for humidification. While it is desired that the fuel cell membrane operate without external humidification, it is recognized that the water generated by the fuel cell itself can be utilized to provide some humidification of the membranes. It is expected that under proper operation, recycling product water from the cathode to the inlet air can provide roughly 25% RH inside a stack operating at 120°C with inlet feeds at a water vapor partial pressure of <1.5 kP_a. This reduces the burden for performance with very low water content, but operation at this low RH still remains a major challenge.

A variety of strategies are being pursued. It is known from extensive molecular level modeling of Nafion® that membrane microstructure has a substantial effect on conductivity. With block copolymers, McGrath [32] has observed that as the block length increases, the performance under partially hydrated conditions increases, suggesting the presence of hydrophilic domains at higher block lengths through which protons can be transported along the sulfonic acid groups and water molecules. Utilizing block copolymers consisting of hydrophilic oligomers and hydrophobic perfluorinated oligomers, McGrath and his coworkers have prepared a block copolymer that exhibited higher proton conductivity than Nafion® 112 at 80°C at all RH values (30–95%).

FuelCell Energy is pursuing a rather sophisticated approach utilizing a four-component composite consisting of a copolymer, a support polymer, a water retention additive, and a protonic conductivity enhancer. The copolymer, which is intended to provide the basic building block for the membrane, is an advanced perfluorosulfonic acid with significantly higher conductivity than state-of-the-art polymers. The support polymer is intended to give a stable cluster structure and to enhance mechanical properties. The functionalized additives are designed to retain water at low RH conditions and to enhance the composite membrane's proton conductivity by providing an alternate proton conduction path for the efficiently transport of proton at high temperature as well as at subfreezing conditions. Progress to date has led to a membrane with conductivity about a factor of 2 better than Nafion® 112 at 120°C [33].

All of these approaches still rely on water for conduction. Systems utilizing phosphonic acids, heteropolyacids, protic ionic liquids, and heterocyclic bases do not rely on water for conduction. One of the major issues for these systems, however, is that the acid or base aiding proton transport is generally water-soluble. The acid or base must be immobilized for use in transportation applications where condensation of liquid water under some of the operating conditions is inevitable. However, enough mobility must be retained by the active group to be able to participate in proton conduction.

In addition to these more advanced studies, progress has been made in developing improvements to the current PFSA polymer electrolyte membranes currently employed in PEMFCs, particularly with regard to degradation caused by peroxide generated either electrochemically or chemically as the result of oxygen crossover to the anode. It is generally accepted that the membrane degradation is the result of the subsequent formation of hydroxyl radicals that attack the side chains of the polymer [34–36]. Here again, dry conditions greatly accelerate the rate of degradation.

What is not generally agreed upon is the location and origin of the hydrogen peroxide formation. Two theories are dominant. One is that the peroxide is formed mainly at the anode due to the diffusion of oxygen across the membrane, at which point the peroxide can form either chemically or electrochemically by the reaction of oxygen with hydrogen. This hypothesis is supported by the fact that the peroxide yield is greatly enhanced in the anode potential region (<0.2 V) of the ORR, as evidenced by rotating ring disc electrode experiments [37]. The other is that the peroxide is formed at the cathode. Experimental results from several sources support this hypothesis. Liu et al. [38], Mittal et al. [39], and Miyake et al. [40] have commonly reported that the membrane degradation rate is higher for an MEA catalyzed only at the cathode side than for one catalyzed only at the anode side. This fact seems inconsistent with the hypothesis that peroxide is formed at the anode. Yu et al. [41], in an effort to identify the origin of the radicals which decompose the membrane, performed a series of experiments after which they concluded, based upon energy dispersive X-ray analysis and IR spectroscopy, that the degradation begins on the cathode and progresses inward. They also found that the formation of radicals within the membrane or near the anode was very low or absent. They postulated the formation of undesirable free radicals involving the catalyst, similar to the hypothesis of Liu and Mittal.

Any model of the degradation process would need to propose that formation of hydrogen peroxide forms by distinct mechanisms in the cathode and anode. The commonly accepted mechanism is that the peroxide then forms radicals through Fenton reactions involving metal-ion impurities. The radicals then participate in the decomposition of reactive end groups in the membrane, to form, among other species, hydrogen fluoride, which can be detected in the product water. Higher fluoride release rates correlate with higher rates of membrane degradation. The degradation occurs through the "unzipping" of the polymer backbone and the cleavage of the polymer side chains. The two conditions that accelerate this degradation mechanism are dry conditions and high temperatures, thinning the membrane until "pin holes" form, allowing gas crossover and cell failure. Therefore, as emphasized earlier, PFSA-like polymer electrolyte materials must be kept under good temperature control and maintained hydrated.

The susceptibility to peroxide radical attack has been attributed to a trace amount of polymer end groups with residual hydrogen-containing terminal bonds [42]. It is at these sites that decomposition is initiated. DuPont has reported that the number of hydrogen-containing end groups can be reduced by treating Nafion® with fluorine gas. 3M has been improving their PEMs by modifying the end groups in the membrane. 3M is investigating modified polymer structures to try to control membrane morphology and has developed a new ionomer with a shorter side chain than standard perfluorosulfonic acid (PFSA) membrane ionomers without the pendant CF_3 group. They have reported that this structure provides a higher degree of crystallinity and allows for lower equivalent weight membranes with improved mechanical properties and durability under hot, dry conditions. Solvay Solexis also has a short side-chain PFSA membrane, Aquivion™, that resists peroxide radical attack. In addition, companies are not only modifying the chemical structure but are also are incorporating proprietary stabilizers to mitigate the effect of peroxide and the attack by its radicals.

High-Temperature Polymer Electrolyte Membranes

Early work on the properties of proton conducting acid polymer blends was carried out by Lassegues et al. [43, 44]. The first detailed study of the effect of doping a high-temperature polymer membrane such as polybenzimidazole (PBI) with a phosphoric acid in order to achieve proton conductivity in a range suitable for use as a fuel cell was conducted at Case Western Reserve [45]. Polymer electrolyte membranes that do not rely on water as the basis of their proton conductivity offer the potential advantage of simplifying the fuel cell system, if these systems can be operated without complex external humidification schemes. Furthermore, because these systems run at high temperature, they can tolerate higher levels of CO in the reformate, thus further simplifying the system in terms of reforming and control. In addition, the higher operating temperature simplifies thermal management issues and provides a source of high-quality heat for combined heat and power applications. Consequently, BASF [46] and other companies are developing PBI-based proton conducting membranes for

high-temperature stationary fuel cell applications. Several companies (for example, Plug Power, ClearEdge) are developing products based upon these materials.

New high-temperature polymer electrolyte membranes based on aromatic polyether polymers and copolymers containing polar pyridine moieties in the main chain have been developed by Advent Technologies for use in HTPEM fuel cells. These are based on the idea of creating acid–base interactions in order to obtain high proton conductivity. The newly developed polymer products are called Advent TPS®. Such materials combine the excellent film-forming properties with high mechanical, thermal, and oxidative stability and the ability to be doped with phosphoric acid. Highly conducting polymer electrolyte membranes were produced after treatment with phosphoric acid amounts that could be controlled by varying the pyridine-based monomer content. The polar pyridine groups strongly retain the phosphoric acid molecules, due to their protonation, thus inhibiting leaching out of the phosphoric acid.

The performance based on Advent TPS® MEA operating at 180°C with pure hydrogen or reformate with different CO contents and air feed gases is shown in Fig. 2. Here again, because of the high operating temperature, this system tolerates up to 2 vol% CO poisoning without a significant decrease of performance.

As is well known, and as discussed by Neyerlin and others, there is an increase in polarization losses with phosphoric acid-based fuel cells, in comparison to low-temperature PFSA-based fuel cells, and this effect is thought to be due to the presence of phosphoric acid and/or its anions that adsorb onto the surface of the catalyst [47]. Because of this, high-temperature stacks based upon phosphoric acid–doped polymer electrolyte membranes are larger in order to get the same power output. The overall question is whether the benefit in system simplification overcomes the need for larger stacks, so that there is an overall net system benefit. Reducing the effect of the adsorbed anion species would, of course, have significant benefit at the stack and system levels.

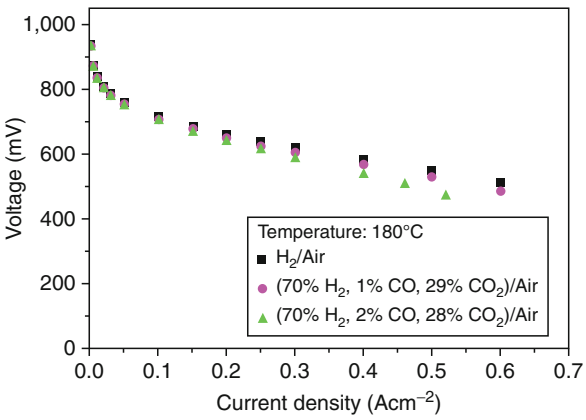

Polymer Electrolyte (PE) Fuel Cell Systems. Figure 2 Polarization curves of Advent TPS® at 180° with H_2 or reformate gas and air, under ambient pressure (λ_{H_2} = 1.2, λ_{air} = 2)

Alkaline Polymer Electrolyte Membranes

There are also efforts underway to develop alkaline-based polymer electrolytes, which enables the replacement of precious metal catalysts by catalysts based on highly inexpensive metals, such as Co, Fe, and Ni. In particular, Cellera Technologies (Caesaria, Israel) is pursuing the development of a new alkaline technology by transitioning from the proton conducting polymer electrolyte membrane and ionomer to an OH- ion conducting membrane and ionomer. The alkaline ion-conducting polymer electrolyte membrane provides a much more benign chemical environment which lowers the risk of instability caused by the corrosion processes prevalent in the highly acidic environment of the PEM fuel cell.

Alkaline-based polymer electrolyte membranes are relative newcomers on the scene. It has been widely believed that the quaternary ammonium hydroxide functional group (RN_4^+, OH^-), which is the one used in most anion exchange membranes, is "self-destructive," because the OH- ion is likely to attack the RN_4^+ cation. In addition, the specific conductivity of an OH^- conducting ionomer was suspected of being at least a factor 3–4 lower than that of the H^+ conducting ionomer, thereby setting a limit on power output. It was also suggested that, as the AEMs developed to date have been based on hydrocarbon, rather than fluorocarbon backbones, the preparation of effective and stable membrane/electrode assemblies would present a significantly tougher challenge versus the case of PFSA ionomers. Historically, there has always been a concern having to do with the effect of CO_2 from

the air feed on the OH- conducting ionomer. Since conversion of the OH- ion in the alkaline ionomer to bicarbonate (and/or carbonate) ion is a very likely process, cell performance could suffer from the effects on both lower ionomer conductivity and, particularly, the kinetics of electrode processes.

Tokuyama, a Japanese company specializing for a long time in membrane technology for electrodialysis and desalination, has undertaken development of AEMs in OH- form, targeting fuel cell applications. Los Alamos National Laboratory researchers have shown that proper selection of the functional group for the AEM could secure stability of the ionomer, maintaining the functional group population under demanding chemical conditions. Cellera has so far proved that factors limiting AEM-FC longevity do not include the chemical stability of the alkaline membrane. Furthermore, the membrane resistivity is not more than two times higher versus Nafion, which is an acceptable level for fuel cell development. Finally, it has apparently been shown that the effects of CO_2 from air on the performance of the AEM-FC can be mitigated by using a combination of tools upstream the stack and in the stack. This is the issue that has plagued most alkaline-based systems which get one of their reactants from the air, including metal/air batteries. The approach developed by Cellera for handling CO_2 upstream of the stack supposedly totally avoids any need of routine replacement of system components. Cellera has so far demonstrated power densities of 200 mW/cm^2 at a cell voltage of 0.4 V, with no platinum catalysts for a hydrogen/air stack, with no addition of liquid electrolyte, and with no humidification from an external source [48].

Fuel Cell System Design

The *process* of designing of a fuel cell system follows the general design process for any commercial product in which a phase-gated, product development process (PDP) guides activities from initial concept to launch. The PDP is one of the most interesting and well-studied business processes, and usually ends up being tailored to each company's appetite for speed and time to market, balanced by its desire to mitigate risk. Product development is very much a social science, one that integrates business, technology, engineering, and human behavior [49]. Many attempts have been made to study its characteristics and improve the manner by which products are brought to market [50]. Even today, it remains a subject of research in most business schools. Before these steps are undertaken, however, usually a *product strategy* is developed which aligns to both the business strategy and the business model of the organization. This product strategy generally takes the form of a *platform strategy*, which shows the relationship between multiple products expected to be developed and launched over a 5–10 years time horizon [51].

System Requirements and Architecture

The design of the fuel cell system really begins with the "Voice of the Customer" (VOC). For fuel cell systems, there can be many potential customers: the end user, the OEM, or an intermediate service provider. In any case, by the voice of the customer is meant that quality expectation taken directly from the customer, properly evaluated, and deployed within the product development process. One such technique for doing this is the well-known Quality Function Deployment (QFD) process which, if properly used, enables the VOC to be deployed all the way to the factory floor. Without knowing and agreeing on the key customer requirements upfront, the fuel cell system design process cannot be successfully completed.

A very much abbreviated and simple example of one of the first steps in the process of developing fuel cell system specifications is shown in Fig. 3. This example is for a residential stationary fuel cell application, but similar requirements are relevant in most other fuel cell applications. Here is shown the high-level VOC, gathered by some technique such as the use of customer interviews or focus groups and the system attributes that will influence their achievement, arranged in order of importance. As shown, some of the key system attributes that are critical to quality (CTQs) and that influence the customer's demand for clean, quiet, safe, and affordable energy are related to meantime between failure, major component life, load-following capability, turndown ratio, operating and maintenance cost, efficiency, startup time, audible noise, and agency compliance. Of course, there are a host of other attributes which need to be specified and met, including the expected ranges in ambient temperature and operating

Developed country end user CTQs	Customer weight	System reliability	FC control and load control	Service provider program	System serviceability	System availability	System design	System kW rating	Cost - capital and installation	System packaging	Cost - O&M	Certification	System efficiency	Customer service	Cost - fuel	System installation
Simple to operate	5	9	9	9	3	9	3		3		3			3		
Safety	5	9	9	9	9	3	9	3	3	9	3	9	1	1		3
Monthly bill </= current utility bill	5	9	9	1	1	3	1	9	9	3	9		9	1	9	1
Supply 100% of electricity needs	5	9	9	9	3	9	3	9	1					3		
Responsive service	4	3	3	9	9	3	3			3	3			3		
Better availability than current alternative energy source	3	9	9	9	9	9	9		3	3	1	1		3		3
Ascetics; appearance and physical size	3	3	3		9		3	9	9	9		9	3			3
Environmentally friendly	2	1					3	1				1	9			
	Totals	230	228	203	170	159	134	134	116	108	90	77	77	61	45	38
	rank	1	2	3	4	5	6	7	8	9	10	11	12	13	14	15

Polymer Electrolyte (PE) Fuel Cell Systems. Figure 3
Example of a limited set of attributes for a residential fuel cell system

altitude, expected number of starts and stops, and the quality of air and water needed for operation. All of these external requirements drive the selection of a technology set which, when optimized, needs to provide for acceptable operating latitude over the life of the system.

One of the key requirements for a successful platform strategy is a well thought-out platform *architecture*. The platform architecture enables that product strategy to be executed. As an example, consider the high-level architecture shown in Fig. 4 below. Here, one sees the functional breakdown of the system into the major components, which in turn defines requirements for each module in the system.

In this figure is shown several major subsystems typical of a PEM system. Included are the reactant processing module (RPM), which determines the pressure, temperature, flow rate, and composition of the reactant streams which are delivered to the power generation module or PGM. Included in the RPM are the desulfurization, reformer and shift reactors, and the required number of heat exchangers which are needed to manage the reforming process. More will be said of this below. The PGM will include the stack and its manifold, and any other subsystems needed to ensure the stack can function properly, such as the subsystems that provide for cathode recirculation and water management. Also shown in this figure is a hydrogen pump module (HPM) that can be used to purify and compress hydrogen for storage in the chemical energy storage module (CESM) for refueling a hydrogen fuel cell car, and a thermal management module (TMM) that provides the methods of capturing and directing the flow of heat to either a heat load (such as the RPM) or heat sink. Electrical energy generated by the fuel cell can either be stored in the electrical energy storage module, EESM, or passed through to the power conditioning module (PCM) where it is converted to high-quality power for alternating current loads. A control module (CM) ensures that the required electrical state of the system is achieved over time, as defined by the energy management module (EMM). The CM provides the proper control of the pressure, temperature, flow rate, and composition of the fuel and air streams going into and out of the system. The result of all of this is made visible to "customer" through an appropriate user interface module (UI).

This is a high-level architecture. If the detailed lower-level subsystem requirements that support this "meta system" are well thought out, it is possible to

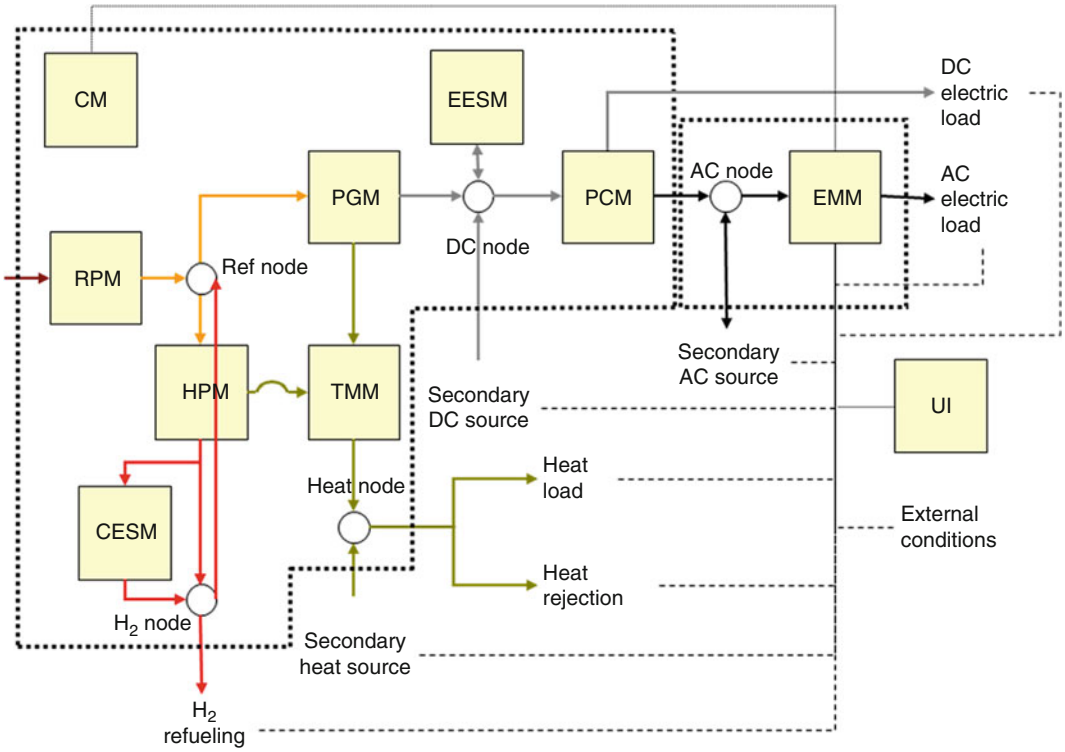

Polymer Electrolyte (PE) Fuel Cell Systems. Figure 4
A high-level fuel cell system architecture [62]

develop *multiple products* off of the same set of hardware and software components, thereby minimizing the product acquisition spending (PAS). For example, at least four products can be derived from this architecture, including a home refueling system, a residential CHP system (eliminating CESM and HPM), a hydrogen fuel cell system for backup applications (further eliminating the RPM system), and a stand-alone hydrogen generator (retaining only the RPM, TMM). Of course, in each case, the controls and user interface have to be modified for the intended application. Furthermore, system-level specifications need to be compatible over the ambient temperature range, etc.

Where the intended range of applications does not allow for a platform architecture at the meta-system level, the platform products then need to be defined at the system level. In fact, the concept of a platform-based architecture can be pursued at the component as well as the system level. Ballard, for example, defines its platforms at the stack level. It is currently advertizing five stack platforms. Each stack platform has a different voltage range, reactant pressure (air and fuel), and cell aspect ratio, optimized for the intended application, whether it be for backup (telecommunications), motive power (forklift trucks), transportation (buses), or residential cogeneration.

While the overall architecture defines the interrelationships among form, fit, and function, *systems engineering* supports the development and achievement of the product specifications. The systems engineering required to enable a product platform strategy is generally quite extensive, requiring many iterations using simulations to guide the final design at the system, subsystem, and component levels. In general, the requirements for a fuel cell system are quite extensive and complex, and these need to be defined, allocated, and enforced all through the development process.

The key steps in the product development process are shown below in Fig. 5. Most activities are focused two types: the systems engineering associated with requirements definition, ending with components

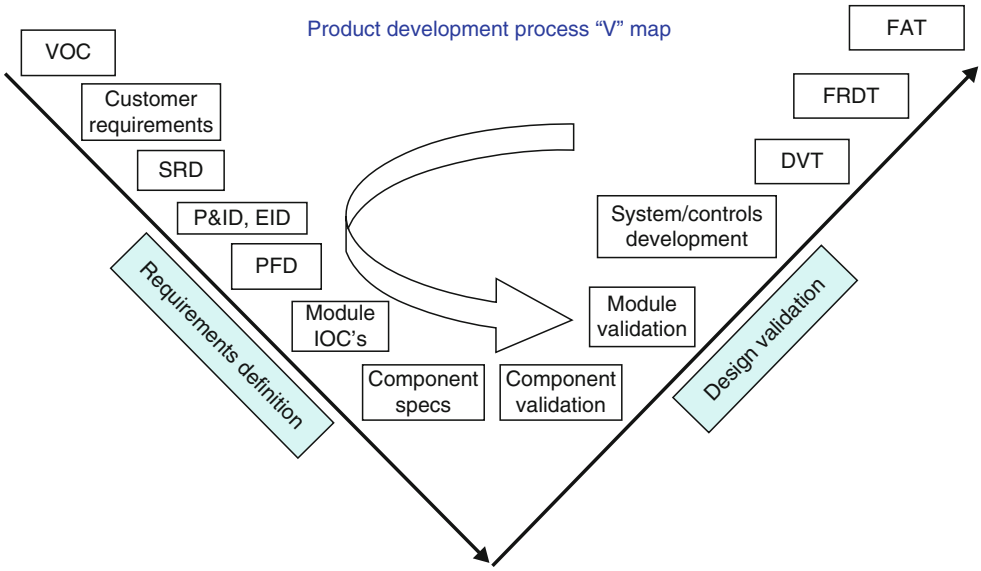

Polymer Electrolyte (PE) Fuel Cell Systems. Figure 5
Product Development Process Map [62]

specifications, and on the actual design and verification process, ending with a successful in-house design verification test (DVT), a field readiness demonstration test (FRDT), and a factory acceptance test (FAT) to validate launch readiness. A key step in the overall process is the development of the systems requirements document (SRD), which enables the development of the process and instrumentation diagram (P&ID), and its companion, the process flow diagram (PFD). The PFD, which is the output of the process engineering analysis using computational tools such as ASPEN®, captures the concepts in flow sheet format and summarizes the heat and material balances characterizing the system design. In short, the PFD, which is the link between concept and reality, defines the critical parameters at each step in the process.

Early on in the process, it is useful to organize the systems engineering effort in pursuit of a collection of interlocking *functionally important topics* which are system-level attributes which need to be allocated to subsystems within the system. One example would be the allocation of efficiency targets between the various major modules. Another high-level example of such an allocation would be the "flow down" of the requirements for cost and reliability. Here, the percentage of total allowed cost and failure rate is allocated among the major modules, based upon an initial test of reasonableness followed by refinement during the development process as further information becomes available. Clearly, the initial allocation of the functionally important topics is important, because it drives engineering behavior and subsequent design modifications and eventually, time to market. The system may have other high-level requirements, such as size, weight, noise, and appearance, and these early requirements are met through systems engineering efforts. Management of the allocation process is achieved through the use of artifacts such as *input/output/constraint* charts (IOCs) that keep track of both functional (signal) and dysfunctional (noise) attributes of each subsystem, subject to the constraints imposed by the overall system. They track the interactions between subsystems in terms of the critical parameters, and are used to define and guide the robust design optimization process, eventually becoming the contract between the subsystem team and the system engineers. Again, a combination of careful testing and simulation is required to ensure convergence to the subsystem and system-level allocations.

Reforming Considerations

In many cases, hydrogen in its pure state is not normally available, in which case it must be obtained by the

reforming process of stripping hydrogen off a hydrocarbon fuel such as methane, propane, ethanol, or liquid petroleum gases (LPG) or kerosene to extract the hydrogen. Generally, there exist sulfur species that are naturally occurring in the fuel (COS, H_2S), or are added as odorants (mercaptans, tetra-hydro-thiophene, THT). Since sulfur poisons the catalysts in the system, the first step in the reforming process generally involves the removal of harmful sulfur-containing species. The level to which sulfur needs to be removed depends upon the operating temperature, but in general it is safe to assume that for PEM systems the level needs to be less than about 50 parts per billion (ppb) [52]. To achieve this level of sulfur impurity, there are several available technologies. At ambient temperatures, these include physical adsorption beds using activated carbon and zeolites, and chemisorption beds incorporating nickel-, copper-, and iron-based sorbents. At higher temperatures, one alternative is to use hydrodesulfurization with Co-, Mo-, and Ni-based catalysts. Another option is thermal swing absorption. Ideally, it is desirable to have a single technology in order to have a fuel flexible system that enables the fuel cell system to be sited in a variety of geographical locations. Seasonal and regional variations in sulfur content, as well as catalyst material cost and toxicity, make this a difficult engineering problem. Each of these technologies is well known, and each has its strengths and weaknesses. All add considerable capital cost and complexity to the system, not to mention annual maintenance cost which can also be a significant expense. Consequently, there is a need for continued research into the discovery and development of effective, low-cost desulfurization for fuel cell applications requiring them.

Assuming that the fuel has been adequately desulfurized, there are essentially three alternative processes for extracting hydrogen: steam reforming (SR), catalytic partial oxidation (CPO), and autothermal reforming (ATR). SR is an endothermic process. Heat must be supplied to the reactor, and this is normally accomplished by combusting an additional amount of fuel in a separate, but thermally integrated reactor. Usually this reactor burns the unused hydrogen which flows through the anode chamber of the fuel cell stack. This component is referred to as the "anode tail gas oxidizer," or ATO. The ATO is generally considered an integral part of the reactant processing module.

The steam reformation reaction is reversible, and the product gas is a mixture of hydrogen, carbon monoxide, carbon dioxide, and water vapor. In the case of methane, the steam reforming step is

$$CH_4 + H_2O \rightarrow CO + H_2O \tag{10}$$

The amount of CO in reformate is a system-level critical parameter, as CO interferes with the hydrogen oxidation reaction by blocking reaction sites on the platinum catalyst surface. To remove the high levels of CO, this reformate stream is then fed to a "shift" reactor which reduces the CO concentration and makes additional hydrogen:

$$CO + H_2O + \rightarrow CO_2 + H_2 \tag{11}$$

Following the "shift" reaction, the reformate is generally passed through a preferential oxidation (PROX) step to further reduce the CO content to an acceptable level so as not to poison the anode catalyst. For low-temperature PEM systems, this level is typically less than 10 ppm. To increase the tolerance to the residual CO, ruthenium is added to the anode catalyst layer, but even this is not sufficient to deal with the amount of CO in the reactant stream. In the case of low-temperature PEM systems, there is generally a small amount of "air bleed" fed into the reactant stream to oxidize any residual levels of CO that adsorb onto the catalyst. It is desirable to keep the air bleed to a minimum to reduce the formation of peroxide. Pulsed air bleed techniques have been studied to achieve this purpose [53]. Depending on the reformer design, there may be a high temperature as well as a low-temperature shift, as well as a single- or two-stage PROX.

Unlike steam reforming, CPO is an exothermic process. It is essentially a combustion, but with a less than stoichiometric amount of oxygen. As in SR, the reformate gas must go through a shift reaction to produce more hydrogen, though a CPO produces less hydrogen than SR, and unlike SR, the product gas contains relatively large amounts of nitrogen from the air used in the process.

Because CPO is an exothermic process, and SR is an endothermic process, these two can be combined in the "autothermal" reforming (ATR) process. The overall reaction of an autothermal process for methane, with the shift reaction included, is

$$CH_4 + \chi O_2 + (2 - 2\chi)H_2O \rightarrow CO_2 + (4 - 2\chi)H_2 \quad (12)$$

In this equation, χ is the number of moles of oxygen per mole of fuel. Its value determines if the reaction (12) is exothermic, endothermic, or thermoneutral. In practice, the value is chosen to avoid the risk of carbon formation in the reactors, and the amount of steam added is usually in excess of that theoretically required. All of these process steps use specially designed catalysts to facilitate the reaction steps. Catalyst designs are in many cases proprietary, although in most cases references to catalyst materials used in similar reactions can be found in the literature.

For many applications requiring the need to reform a logistical fuel, the reactant processing module represents a significant percentage of the total system cost. This is because the reactant processing module must provide reformate with the proper level of humidity over the entire load range, the required level of CO within the constraints of a single stage partial oxidation (PROX) step, have rapid startup and load-following capability with near zero emissions for NO_x, and this all without resulting in coke formation. To meet the efficiency requirements of the overall system, the reactant processing module must also be thermally integrated into the rest of the fuel cell system. This is a very demanding set of requirements, and the cost of the reactant processing module typically ends up being about one-third of the total system cost.

It is well known that most Japanese residential μCHP fuel cell systems use steam reformers, principally due to their high efficiency. Adachi et al. [54] (2009) have recently published the results of their effort to design an autothermal reforming fuel processor for a 1 kW μCHP residential system. They designed and bench tested an ATR system capable of achieving 80% efficiency (on a higher heating value basis) and a reformate containing 48% hydrogen (dry basis) and less than 5 ppm CO. They have studied the ATR principally to address the issues around startup time and the daily start/stop requirements.

A simplified schematic of an ATR-based reformer system is shown below in Fig. 6. Shown in this figure

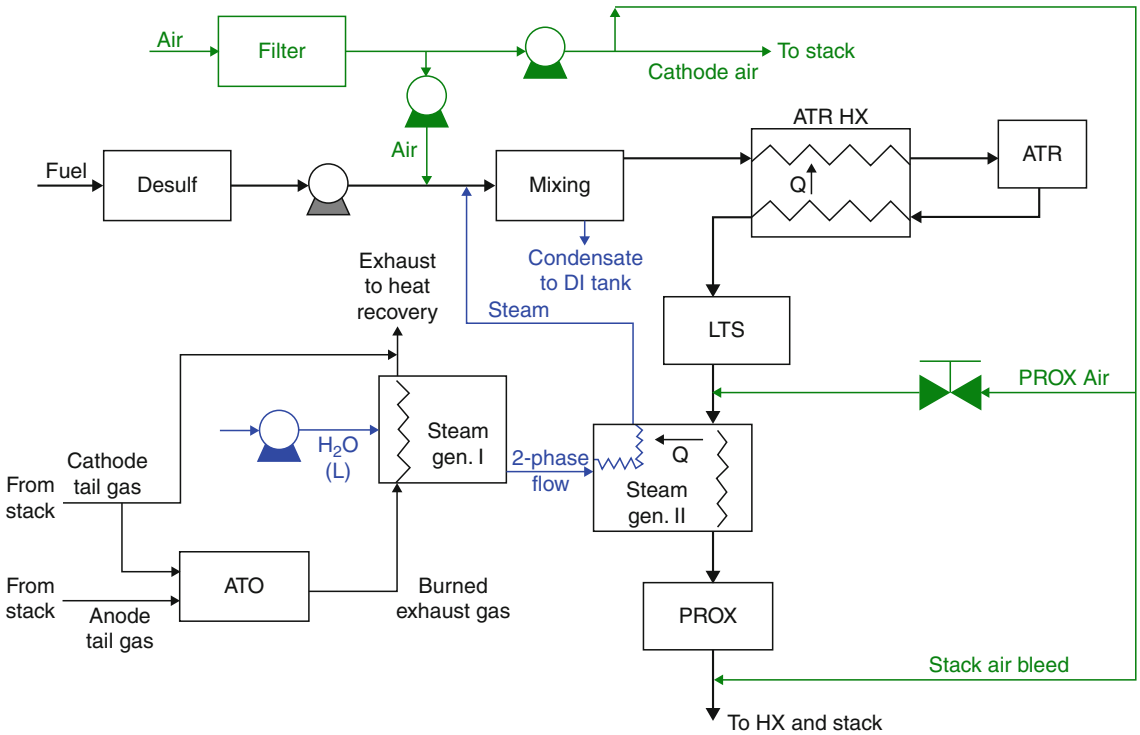

Polymer Electrolyte (PE) Fuel Cell Systems. Figure 6
Simplified schematic of an ATR-based reformer subsystem [62]

are the desulfurization subsystems, the ATR reactor, a low-temperature shift (LTS) reactor, PROX, ATO, low-pressure steam generators to meet the reformate due point requirements, and the appropriate heat exchanges.

In practice, there are several critical operating requirements placed on the reformer system. First, the reformate must contain a negligible amount of carbon monoxide (and oxygen) to avoid poisoning the anode catalyst. Likewise, the fractional conversion of fuel in the reformate needs to be specified in order to minimize unburned hydrocarbon emissions. From a system control perspective, it is also desirable to deliver a predictable amount of hydrogen for a given fuel input. Finally, because of the dependence of the PEM on the level of hydration, the reformate dew point must also be controlled to a specified value. Given these specifications, Feitelberg and Rohr [55] have shown that two variables, the steam to carbon and oxygen to carbon ratios, define a unique "operating line" for the fuel processor. The operating line defines the required relationship between steam-to-carbon and oxygen-to-carbon ratio for a reformer that meets fuel conversion and reformate dew point specifications. An example of the operating line [56] for several dew points is shown in Fig. 7. Operation above this line means that the dew point is greater than that specified, implying that energy has been wasted vaporizing more water than is needed. Operation below the operating line means that the reformate dew point is lower than specified,

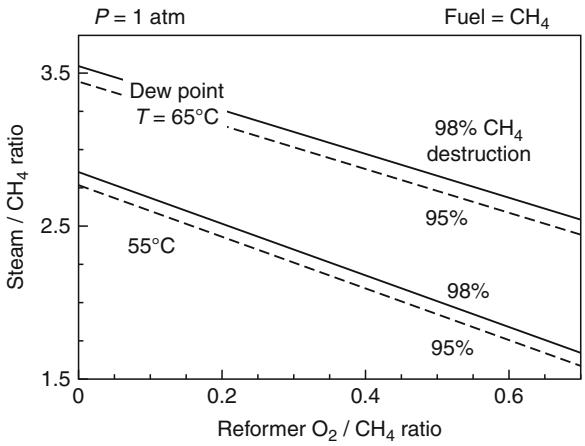

Polymer Electrolyte (PE) Fuel Cell Systems. Figure 7 Reformer operating line analysis [52]

implying that one should expect reduced MEA life or premature failure. When the PEM system is operating on the line, and the heat generated in the ATO just balances the heat consumed in the reformer, the reforming process has achieved the maximum theoretical efficiency.

In this regard, their analysis has shown that the maximum theoretical efficiency of a SR-based system is only about one percentage point higher than the maximum theoretical efficiency of a typical ATR-based fuel processor. Hence, the ATR technology seems to be a good compromise in performance and efficiency.

Technical Readiness

A key milepost in the development of a fuel cell (or any other) system is the achievement of technical readiness; that point in the development cycle when commitments to volume manufacturing can be made with confidence. For this purpose, it is meaningful to define this state of knowledge as:

- Technical readiness is achieved when all critical failure modes are known, and when the critical parameters that are required to avoid those failure modes over the required operating range can be achieved through the intended interaction of specified parts which can be manufactured with acceptable process latitude.

In discussing PEM fuel cells for stationary, transportation, and portable applications, it is worthwhile to do so in terms of defining those conditions needed to not only meet the intended application, but also to avoid the critical failure modes.

Freezing

One of the customer-driven requirements associated with fuel cells intended for stationary and transportation applications is the ability to not only survive subfreezing temperatures, but to gracefully startup from subfreezing conditions and operate over a large number of expected freezing/thaw cycles. Inasmuch as water is the product of the fuel cell reaction, it is normally carried into the stack with humidified reactants, and is fundamental to the transport of protons in the membrane. Most of the work on defining the operating conditions needed for surviving freezing conditions has focused on the behavior of the water within

the principle stack components: manifold, plates, flow fields, and MEA. There are three types of water in PFSA-type polymer electrolyte membranes. Water that has strong interactions with the ionic groups in the polymer can withstand temperatures well below the normal freezing point of water without freezing. Water that finds itself within the nanoscale channels of the polymer electrolyte has a freezing temperature that is dependent on the size and nature of the channel, which in turn is dependent on the degree of hydration of the polymer. This water will therefore have a range of temperatures over which it will freeze, with some of the water having its freezing temperature depressed by the presence of the hydrated ions. Finally, there is "free" water that behaves like bulk water. The result is that there is a distribution of freezing points within the PEM, with no specific "freezing point." The PEM proton conductivity, for example, varies continuously over a wide range of temperatures, depending on the level of hydration. The proton conductivity below freezing can be an order of magnitude lower than that for normal operation [57], indicating that a large fraction of the water in the membrane is frozen. However, even in this state, the polymer electrolyte membrane is capable of carrying current, increasing with increased thawing.

Next to the membrane itself, the most critical components in the fuel cell stack relative to startup from freezing and cool down to subfreezing temperatures are the catalyst layer and the GDL. As previously discussed, the GDL is one of the few critical components in the system that can be designed to affect proper water management, including frozen water that exists during storage or operation from subfreezing conditions. However, only a few studies have been published on the effect of freeze thaw cycles on the properties of the GDL and its subsequent effect on the durability of a PEM fuel cell during cold startup [58, 59]. In fact, due to the wide range of operating conditions and the difference in fuel cell design approaches, reported impacts of freeze thaw cycles on MEA performance vary considerably.

One of the most descriptive accounts of the factors influencing the cold start behavior of low-temperature PEM fuel cells has been given by Mao and Wang [60]. They develop a lumped analysis model of the cold startup of a PEM fuel from subfreezing conditions. The model accounts for the rate of water production, removal and conversion during startup. The condition for a successful startup is to have the fuel cell raise its temperature beyond the freezing point before being shut down by the formation of ice in the catalyst layer. By accounting for the heat and mass balances within the catalyst layer, the authors are able to investigate the conditions under which ice forms in the catalyst layer, thus restricting the flow of oxygen to the reactions sites. In effect, the authors indicate how to calculate the critical parameter requirements for a successful startup from subfreezing conditions. Initial membrane moisture content, heating rate, and thermal masses need to be chosen so that the temperature within the catalyst layer can reach the melting point before ice can fill up the pores within the catalyst layer and the GDL. Clearly, these critical parameters will depend upon the critical specifications of the components within the MEA, as well as the thermal properties of the bipolar plates.

There are a variety of system-level strategies for dealing with freezing, including purging of the stack at shutdown to remove liquid water, heating the stack prior to or during warmup with auxiliary energy sources, preventing freezing conditions from occurring (standby, idling, etc.) Each of these strategies, however, results in a decrease in overall system efficiency.

Start/Stops

Every fuel cell system needs to be started up and shut down in a way that meets the requirements of the customer, and at the same time ensures long-term operation of the system. Frequent starting and stopping can place the system in a severe electrochemical environment. In particular, when the anode side of the fuel cell is filled with air, as would be the case in standby situation, and the system is started up with the flow of a hydrogen rich reactants through the anode, a hydrogen/air boundary forms on the anode side of the cell [61]. This boundary moves from the anode inlet to outlet, and in doing so sets up a high voltage ($\approx$1.4 V) situation across the cell. This potential sets up a reverse current which greatly accelerates the oxidation of carbon, which theoretically can proceed as:

$$\begin{aligned} C + 2H_2O \rightarrow CO_2 + 4H^+ + 4e^- \\ E = 0.207\ \text{V(vs. RHE)} \end{aligned} \tag{13}$$

In fact, this potential driven "corrosion" of carbon can be quite severe, causing substantial loss of the

electrochemically active surface area as the electrode degrades with the loss of the catalyst support. Enhanced fuel cell degradation can occur under the additional stress conditions associated with cold start and hot stopping [62].

In order to deal with the problem of carbon corrosion due to start-stops, it is necessary to understand the critical parameters associated with the start-stop process, as well as the critical specifications that need to be placed upon the materials. What is required to do this is to have a validated model of carbon corrosion and its dependence on the critical parameters: temperature, pressure, flow rate, and composition. Such a model has been developed, to the first order, by Meyers and Darling [63] in which the potentials driving the reaction are linked to the spatial concentrations of oxygen and hydrogen in the flow channels.

Carbon corrosion can also occur due to fuel starvation on the anode, which sometimes happens when flooding is imminent. Again, this situation sets up localized high potentials and reverse currents. Carbon as a catalyst support is problematic, and for this reason control systems need to provide algorithms to deal with the situation when a particular cell in the stack is behaving in an abnormal fashion (so-called stack health algorithms).

Load Following

In most applications involving fuel cells, the load is dynamic, and it is a requirement that the fuel cell system be able to respond to these load transients nearly instantaneously. This requires careful system design. This requirement translates into the need for having rapid delivery of fuel to the catalyst sites within each cell in the stack. Two transient type of operating modes were described above, startup from subfreezing and start/stop. Here focus will be on load changes during operation, and on applications involving both hydrogen and reformate fuel. In the former, emphasis will be placed on the effects of rapid cycling on durability, whereas in the latter, emphasis will be placed upon achievement of the required critical parameters over the expected range in operating parameters.

Hydrogen-air fuel cells, which are used in transportation, backup power, and material handling applications, respond almost instantaneously, provided that they a fed adequate amounts fuel. Control schemes for hydrogen-based fuel cell systems for automotive applications are discussed by Pukrushpan et al. [64] in which the primary focus of the discussion is on control of the supply of air and hydrogen. In some cases, the fuel cell system will be "hybrid" with a battery in the overall system architecture. For example, in telecom backup fuel cell systems, a small battery pack (or supercapacitor) is included to ensure the continuous delivery of power within the first millisecond after the grid drops out. In light duty vehicles, batteries are included as a means of load leveling and energy harvesting during breaking. In forklift applications, batteries offer the opportunity to alleviate the load-following requirements on the stack, thereby extending its operating life. In this regard, it is important from a systems controls perspective that one of the key aspects of achieving adequate load-following capability is to develop a comprehensive stack control scheme that incorporates the relevant system-level components, critical parameters, and their linkage to the critical specifications. In most cases, this control scheme must address both stack health and efficiency.

For reformate-based systems, the control problem becomes particularly difficult because of the strong interactions between subsystems. This is perhaps best seen when considering the function of the ATO. The ATO is designed to oxidize the unreacted anode gas into water for the reformer, as well as to achieve zero emissions from the fuel cell system. On the other hand, the ATO also serves as the heat source for steam generation. Both the stack and the ATO require an air/oxygen source. To minimize cost, improve efficiency, and increase the operating latitude over which the system can be water independent, it is desirable to use a single air blower to provide air to both the stack and the ATO. However, this shared actuator couples the controls for stack, ATO, steam generation and reforming, thereby increasing the complexity of the interaction among the control loops.

Another complexity arises due to the lack of in situ measurement of some of the critical parameters, requiring the inference of the value of the critical parameter from the operation of the system itself. This is particularly true when, by design, the relative humidity of the input reactant streams is near or at saturation. In this situation, RH sensors become unreliable and the RH level needs to be inferred from the system control

parameters. In order to accommodate the strong interactions between the subsystems, a considerable amount of modeling and simulating of system performance is required. This can be accomplished by linking process models in ASPEN Dynamics® with controls models in Matlab®. In this way, nonlinear dependencies in the process can be linearized in a piecewise fashion, and exported to MatLab, an environment in which the order of the model can be systematically reduced together with weighting factors to get time-dependent models that can provide unified descriptions of the fuel cell in both steady state and dynamic environments. An example of the result of such an exercise is shown below in Fig. 8, comparing the performance of the ATO during load transients versus the model predictions. In this particular experiment, the system was run in steady state, and the load-following requirements were simulated by suddenly manipulating the cathode air blower in pseudorandom manner. It is seen that the dynamic model is a remarkably good predictor of the ATO performance [65].

CO Poisoning

One of the challenges facing the fuel cell system is the mismatch in the time constants of the various components in the system. The reformer has the longest time constant, followed by that of the air handling system and stack, and finally the battery. This mismatch can result in large fluctuations in the quality of fuel provided to the stack, and can be the source of unwanted excursions in the amount of CO reaching the stack. With validated advanced simulation tools, it is possible to develop robust control strategies that ensure that the overall system can meet the load-following requirements during large and rapid transients. Shown below in Fig. 9 is the transient response of the Plug Power ATR-based fuel processor to large and sudden step changes in electrical load demand. Here, it is seen the control software is able to keep the CO concentration within performance specifications (<10 ppm). In this case, batteries are used to make up the load demand while the reformer ramps up, illustrating the mismatch in time constants between the stack and reformer subsystems [66].

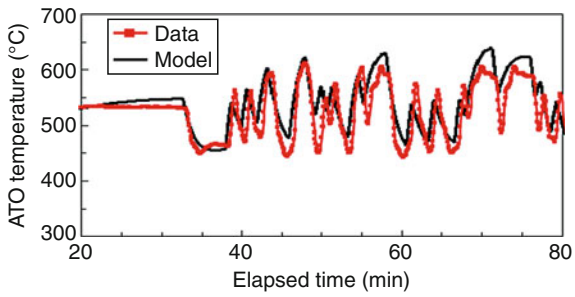

Polymer Electrolyte (PE) Fuel Cell Systems. Figure 8 Model versus data comparison for transient operation of ATO [61]

It is evident that advanced controls, once validated with system verification tests, can be used to maximize the system operational latitude. As shown below in Fig. 10, these controls are used to optimize the operating window for the CO concentration in the reformate stream fed to the stack. Here, it is seen that there is a large operational window, in terms of PROX outlet temperature and CO concentration over which the system can operate within its specification.

It is perhaps important at this point to once again discuss the potential advantages of higher temperature operation. It is well known that fuel cell systems that operate at higher temperatures can tolerate much higher levels of CO. Indeed, tests have shown that stacks at temperatures in the range of 160–200°C can tolerate CO concentrations on the order of 10^3–10^4 ppm. In this case, it is possible to eliminate the PROX and its associated costs and sources of unreliability, while simplifying the controls requirement.

There are of course, many other potential failure modes that need to be addressed. Only a few are mentioned here. Perhaps, the most difficult are those associated with maintenance of the polymer electrolyte's required properties over hours of operation and over a wide range of conditions. Temperature, humidity, and potential cycling place severe stress on the polymer electrolyte and its matching electrodes, and minimizing these through great attention to engineering detail is fundamental to achievement of technical readiness.

System Cost and Reliability

Two key parameters that are obstacles to widespread fuel cell adoption are system cost and reliability. Both are interrelated through the system design, driven mainly by the complexity of the interactions between the stack and the rest of the system, which in turn is determined

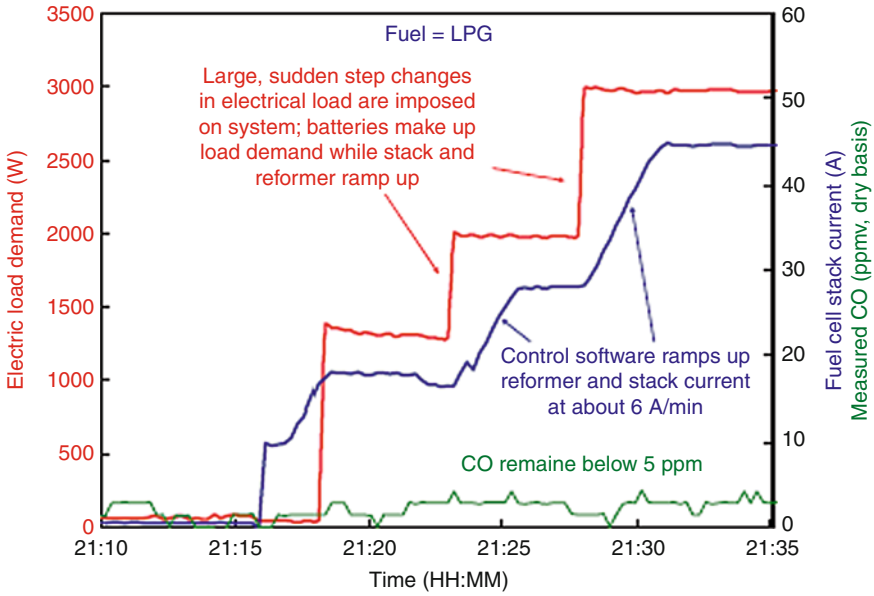

Polymer Electrolyte (PE) Fuel Cell Systems. Figure 9
Fuel processor performance during load transients [61]

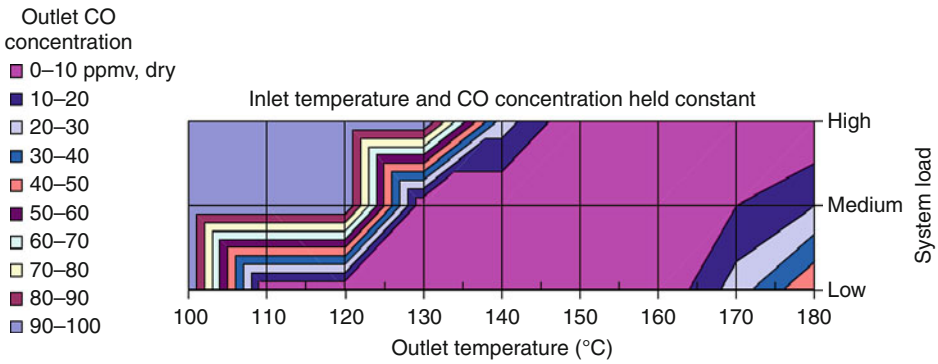

Polymer Electrolyte (PE) Fuel Cell Systems. Figure 10
Prox CO operating latitude in terms of temperature and load [61]

by the nature of the polymer electrolyte. However, system complexity is also determined by the customer-driven system specifications. System specifications can vary widely, depending upon the application, and for this reason it is nearly impossible to make specific claims about costs of fuel cell systems without reference to the detailed requirements driving the design.

The cost and reliability of PEM fuel cell systems for light vehicles are tracked quite closely as automotive manufacturers are making significant investments in developing fuel cell cars for field entry in the next 5–10 years. The US Department of Energy (DOE) has, in conjunction with industry leaders, developed cost and reliability performance targets and tracks progress against those targets in its annual review process. In addition, the DOE has defined a baseline fuel cell system with which to model performance improvements due to advances in technology and to coordinate those findings with the assumptions in the cost projections. In its most recent (2010) Annual Merit Review (AMR), stack cost projections indicate that at low production volumes the membrane dominates the

stack cost, whereas at high-production volumes, the catalyst ink dominates the cost. Cost estimates suggest that in high volume production, stack costs (based upon 3M NSTF nanostructured electrodes) of around \$25/kW$_{e(net)}$ can be achieved, and system costs of around \$51/kW$_{e(net)}$ can be achieved, nearly equal to the 2010 DOE targets [67].

The situation for stationary fuel cells is not as clear. The current 2011 DOE performance targets for integrated stationary fuel systems of \$750/kW$_e$, 40,000 h of durability and 40% electrical efficiency at rated power are difficult targets to meet with a reformate-based system. These targets are under review and will most likely be updated and more clearly aligned with the intended application.

The system requirements for stationary systems can vary widely, depending upon application. In general, however, the key to cost reduction is through system simplification. One way to accomplish this is through good engineering design, including value analysis/value engineering (VA/VE). VA/VE enables one to reduce the number of parts. Another way is to avoid expensive secondary fastening operations by having parts and modules self-align to each other, eliminating adjustments, using gravity wisely, and designing for "Poka Yoke."

Another way to reduce cost and improve reliability is through advances in technology. As mentioned above, the pursuit of polymer electrolytes that are more tolerant to low RH conditions, that do not require external humidification, and that run at higher temperatures is a prime example of how technology can reduce cost and complexity. Elimination of sensors through intelligent and advanced controls is another example.

Currently, stationary fuel cells include the cost burden of the reformer, which makes the achievement of \$750/kW$_e$ difficult. As a percentage of the total system cost, the reactant processing module can be as much as 30% of the total system unit manufacturing and service cost. Whereas the stack can scale downward gracefully as a function of size (kW$_e$ output), the reformer cannot, making low-cost small residential stationary systems even more challenging. For this reason, it is perhaps appropriate to examine *alternative system architectures* that decouple the reformer, and provide the required hydrogen from a shared-use centralized reformer. Such architectures are currently under consideration for use in Japan.

Lastly, it seems appropriate that at this stage fuel cell systems should be developed for large niche markets that are appropriate for the current state technical readiness of the technology. Forklift applications are a prime example of matching requirements versus capability. Large stationary fuel cells that are designed for constant base loads with high combined heat and power utilization requirements is another.

Fuel Cell Systems and Sustainability

The connection between fuel cell systems and sustainability is of course, hydrogen. The lightest and most abundant element on planet Earth is destined to play a central role in the energy landscape of the future. Renewable energy sources can be used to produce hydrogen, which can then be stored as a means of addressing the natural intermittency of the renewable source. In the future, by splitting water with a renewable source of energy such as wind and solar energy, and using the stored hydrogen so produced to produce electricity, one can also return the product water to its source, achieving a sustainable energy paradigm for nearly every nation on earth. This is truly the energy "end game." Indeed, the fact that as an energy carrier hydrogen can play a key role in the storage of energy produced from renewable resources has received renewed interest among a variety of stakeholders.

Since the fuel cell system will play a key role in the pursuit of sustainable energy, whether in electrifying the automobile for transportation, providing energy for buildings, or converting stored hydrogen generated from renewable sources into electricity, the design of the fuel cell itself should consider its impact on the environment. This encyclopedia addresses the subject of life cycle analysis elsewhere. Here, it seems appropriate to note that Cooper et al. [68] have developed a method to assist in the rapid preparation of life cycle assessments of energy generation technologies, and in particular polymer electrolyte fuel cell systems. The method allows one to compare different fuel cell system design approaches, using publically available and peer-reviewed Life Cycle Assessment data, against an environmental impact weighting scheme that reflects various environmental sensitivities. Providing a fuel cell system "designed for the environment," with the

goal that no part ever ends up in a landfill, seems to be a fitting way to approach the objective of truly sustainable energy systems.

Future Directions

Progress in the development of fuel cell systems for transportation, stationary, and motive power applications will continue as long as the incentives around renewable and clean energy continue to receive public support. This support, in turn, needs to be based upon public awareness of the true cost of the incumbent technologies: environmental and social, as well as financial. The rate of progress made in the past 10 years has been accelerating due to the support of governments tending to the longer range needs of their citizens. With a view of the need for a clean energy future clearly in sight, alternative means of energy generation, conversion, and storage will play an increasing role in shaping the future for our children's children, a time not too far away.

To meet this challenge, fuel cell research and development will need to continue to pursue a range of subjects from basic understanding of the key factors governing charge transfer at the nanoscale to enabling the simplification of systems by developing advanced materials that can relax the constraints currently imposed by the polymer electrolyte membrane. Hence, continued examination of the property and structure relationships in electrocatalysis will be needed to point the way to improved catalyst materials. Research on improved and more stable nanostructured electrodes incorporating advanced and lower cost materials will be needed to lower cost while improving durability. The development of new polymer electrolyte membrane materials and structures with broader operating latitudes at higher operating temperatures will be needed to further reduce cost by enabling less complex system designs. In parallel with this, of course, innovative engineering approaches toward reducing cost and increasing durability will be needed to close the gap between today's cost-performance curves and those required to enable penetration of commercial markets. In other words, a broadly based and a steady attack on the issues of cost and durability is necessary to advance the state of the art around PEM systems.

Bibliography

1. Barbir F (2005) PEM fuel cells: theory and practice. Elsevier, Burlington
2. Srinivasan S (2006) Fuel cells: from fundamentals to applications. Springer, New York
3. Vielstich W, Lamm A, Gasteiger HA (eds) (2003) Handbook of fuel cells. Wiley, Chichester
4. Garland N, Kopasz JP (2007) The United States Department of Energy's high temperature, low humidity membrane program. J Power Sources 172:94–99
5. Mader J, Xioa L, Schmidt TJ, Benicewicz BC (2008) Polybenzimidazole/acid complexes as high temperature membrane. In: Fuel cells: advances in polymer science, vol 216. Springer, Berlin, pp 63–124
6. Vishnyakov A, Niemark AV (2000) Molecular study of Nafion membrane solvation in water and methanol. J Phys Chem B 104:4471–4478
7. Kreuer DK, Paddison S, Spohr E, Schuster M (2004) Transport in proton conductors for fuel cell applications: simulations, elementary reactions, and phenomenology. Chem Rev 104:4637–4678
8. Springer TE, Zawodzinski TA, Gottesfeld S (1991) Polymer electrolyte fuel cell model. J Electrochem Soc 138:2334–2341
9. Fimrite J, Carnes B, Struchtrup H, Djilali N (2009) Coupled proton and water management in polymer electroyte membranes. In: Paddison SJ, Promislow KS (eds) Device and materials modeling in PEM fuel cells, vol 113, Series: topics in applied physics. Springer, New York
10. Weber AZ, Newman J (2004) Modeling transport in polymer-electrolyte fuel cells. Chem Rev 104:4679–4726
11. Wang CY (2004) Fundamental models for fuel cell engineering. Chem Rev 104:4727–4765
12. Darling RM, Meyers JP (2003) Kinetic model of platinum dissolution in PEMFCs. J Electrochem Soc 150:A1523–A1527
13. Meyers JP, Darling RM (2006) Model of carbon corrosion in PEM fuel cells. J Electrochem Soc 155:A1432–A1442
14. Reiser CA, Bregoli L, Patterson TW, Yi JS, Yanag JD, Perry MI, Jarvi TD (2005) A reverse current decay mechanism for fuel cells. Electrochem Solid State Lett 8(6):A273–A276
15. www.cd-adapco.com
16. www.fluent.com
17. Markovic N, Gasteiger H, Ross PN (1997) Kinetics of oxygen reduction on Pt (hkl) electrodes: implications of the crystalline size effect with supported Pt electrocatalysts. J Electrochem Soc 144:1591–1597
18. Nørskov JK, Rossmeisl J, Logadottir A, Lindqvist L, Kitchin JR, Bligaard T, Jónsson H (2004) Origin of the overpotential for oxygen reduction at a fuel cell cathode. J Phys Chem B 108:17886–17892
19. Mavrikakis M, Hammer B, Nørskov JK (1998) Effect of strain on the reactivity of metal surfaces. Phys Rev Lett 81:2819–2822
20. Taylor CD, Wasileski SA, Filhol JS, Neurock M (2006) First principles modeling of the electrochemical interface: consideration and calculation of a tunable surface potential from atomic and electronic structure. Phys Rev B 73:65402

21. Adachi H, Ahmed S, Lee SHD, Papadias D, Ahluwaia RK, Bendert JC, Adzic RR et al (2007) Platinum monolayer fuel cell electrocatalysis. Top Catal 46:249
22. Stamenkovic V, Mun BS, Mayrhofer KJJ, Ross PN, Markovic NM, Rossmeisl J, Greely J, Nørskov JK (2006) Changing the activity of electrocatalyst for oxygen reduction by tuning the surface electronic structure. Angew Chem Int Ed 45:2897
23. Norskov JK, Rossmeisl J, Logadottir A, Lindqvist L, Kitchin JR, Bligaard T, Jonsson H (2004) Origin of the overpotential for oxygen reduction at a fuel cell cathode. J Phys Chem B 108:17886–17892
24. Koper MTM (ed) (2009) Fuel cell catalysis. Wiley, Hoboken
25. Gasteiger HA, Kocha SS, Sompali B, Wagner FT (2005) Activity Benchmarks for Pt, Pt-alloy and non-Pt oxygen reduction catalysts for PEMFCs. Appl Catal B 56:9–35
26. Debe MK (2003) Novel catalysts, catalyst support and catalyst coated membrane methods. In: Vielstich MW, Lamm A, Gasteiger HA (eds) Handbook of fuel cells-fundamentals, technology and applications, vol 3. Wiley, New York, Chapter 45
27. Gancs L, Kobayashi T, Debe MK, Atanasoski R, Wieckowski A (2008) Chrystallographic characteristics of nanostructured thin-film fuel cell electrocatalysts: a HRTEM study. Chem Mater 20(7):2444–2454
28. Debe MK (2010) Advanced cathode catalysts and supports for PEM fuel cells. 2010 DOE Hydrogen Program Merit Review and Peer Evaluation, Washington, DC, 11 June 2010
29. Tang JM, Jensen K, Waje M, Li W, Larsen P, Pauley K, Chen Z, Ramesh P, Itkis M, Yan Y, Haddon R (2007) High performance hydrogen fuel cells with ultralow Pt loading carbon nanotube thin film catalysts. J Phys Chem C 111(48):17901–17904
30. Antonlini E, Gonzalez ER (2009) Ceramic Materials as supports for low temperature fuel cell catalysts. Solid State Ionics 180:746–763
31. Scherer GG (ed) (2008) Fuel cells II, vol 216, Advances in polymer science. Springer, Berlin
32. Abhishek R, Yu X, Dunn S, McGrath JE (2009) Influence of mircostructure and chemical composition on proton exchange membrane properties of sulfonated-fluorinated hydrophilic-hydrophobic multiblock copolymers. J Membr Sci 327(1–2):118–124
33. Lipp L (2010) High temperature membrane with humidification independent cluster structure. 2010 DOE Hydrogen Program Merit Review and Peer Evaluation, Washington, DC, 11 June 2010
34. Inaba M (2009) Chemical degradation of perfluorinated sulfonic acid membranes. In: Buechi FN, Inaba M, Schmidt TJ (eds) Polymer electrolyte fuel cell durability. Springer, New York
35. Danilczuk M, Coms FD, Schlick S (2008) Fragmentation of fluorinated model compounds exposed to oxygen radicals: spin trapping ESR experiments and implications for the behaviour of proton exchange membranes used in fuel cells. Fuel Cells 8(6):436–452
36. Ghassemzadeh L, Marrony M, Barrera R, Kreuer KD, Maier J, Mueller K (2009) J Power Sources 186(2):334–338
37. Antoine O, Durand R (2000) J Appl Electrochem 30:839–844
38. Liu H, Gasteiger HA, Laconti A, Zhang J (2006) Electrochemical Soc Trans 1(8):283–293
39. Mittal V, Kunz R, Fenton JM (2006) Electrochemical Soc Trans 1(8):275–282
40. Miyake N, Wakizoe M, Honda E, Ohta T (2006) Electrochemical Soc Trans 1(8):249–261
41. Yu J, Matsuura T, Yoshikawa Y, Islam MN, Hori M (2005) Electrochem Solid State Lett 8:A156–A158
42. Curtin DE, Lousenberg RD, Henry TJ, Tangeman PC, Tisack ME (2004) J Power Sources 131:41–48
43. Lassegues JC, Schoolmann D, Trinquet O (1992) Proton conducting acid polymer blends. In: Balkanski T, Takahashi T, Tuller HL (eds) Solid State Ionics. Elsevier, Amsterdam, pp 443–448
44. Lassègues JC (1992) Mixed inorganic-organic systems: the acid/polymer blends. In: Colomban PH (ed) Proton conductors: solids, membranes and gel – materials and devices. Cambridge University Press, Cambridge, pp 311–328
45. Savinell R, Yeager E, Tryk D, Landau U, Wainright J, Weng D, Lux K, Litt M, Rogers C (1994) A polymer electrolyte for operation at temperatures up to 200°C. J Electrochem Soc 141(4): L46–L48
46. Schmidt TJ (2009) High-temperature polymer electrolyte fuel cells: durability insights. In: Buchi FN, Inaba M, Schmidt TJ (eds) Polymer electrolyte fuel cell durability. Springer, New York
47. Neyerlin KC, Singh A, Chu D (2008) Kinetic Characterization of a Pt-Ni/C catalyst with a phosphoric acid doped PBI membrane in a proton exchange membrane fuel cell. J Power Sources 176:112–117
48. Gottesfeld S, private communication (2010)
49. McGrath MF, Anthony MT, Shapiro AR (1992) Product development. Butterworth-Heinemann, Boston
50. Patterson ML, Fenoglio JA (1999) Leading product innovation. Wiley, New York
51. McGrath M (2001) Product strategy. McGraw-Hill, New York
52. Du B, Pollard R, Elter JF, Ramani M (2009) Performance and durability of a polymer electrolyte fuel cell operating with reformate: effects of CO, CO_2, and other trace impurities. In: Büchi F, Inaba M, Schmidt TJ (eds) Polymer electrolyte fuel cell durability. Springer, New York, pp 341–366
53. Du B, Pollard R, Elter JF (2006) CO-air bleed interaction and performance degradation study in proton exchange membrane fuel cells. Electrochem Soc Trans 3(1):705–713
54. Adachi H, Ahmed S, Lee SHD, Papadias D, Ahluwaia RK, Bendert JC, Kanner SA, Yamazaki Y (2009) A natural gas fuel processor for a residential fuel cell systsem. J Power Sources 168:244–255
55. Feitelberg AS, Rohr DF Jr (2005) Operating line analysis of fuel processors for PEM fuel cell systems. Int J Hydrogen Energy 30:1251–1257
56. Feitelberg A (2003) On the efficiency of PEM fuel cell systems and fuel processors. Presentation at fuel cell seminar, Miami, 3 November 2003
57. Mukundan R, Kim YS, Garzon F, Pivovar B (2006) Freeze/thaw effects in PEM fuel cells. ECS Trans I:403–413

58. Guo QH, Qi ZH (2006) Effect of freeze-thaw cycles on the properties and performance of membrane-electrode assemblies. J Power Sources 160:1269–1274
59. Lee C, Merida W (2007) Gas diffusion layer durability under steady state and freezing conditions. J Power Sources 164:141–153
60. Mao L, Wang C-Y (2007) J Electrochem Soc 154:B139–B146
61. Tang H, Qi Z, Ramani M, Elter JF (2006) PEM Fuel cell cathode carbon corrosion due to the formation of air/fuel boundary at the anode. J Power Sources 158:1306–1312
62. Du B, Pollard R, Ramani M, Graney P, Elter JF (2007) Impact of cold start and hot stop on the performance and durability of a proton exchange membrane (PEM) fuel cell. ECS Trans 5(1):271–282
63. Meyers JP, Darling RM (2006) Model of carbon corrosion in PEM fuel cells. J Electrochem Soc 153(8):A1432–A1442
64. Pukrushpan JT, Stefanopolou AG, Peng H (2005) Control of fuel cell power systems. Springer, London
65. Feitelberg AS, Elter JF (2005) Development, design and performance of plug power's next generation stationary PEM fuel cell system prototype. Presented at 2005 fuel cell seminar, Palm Springs, California, 14–18 November 2005
66. Elter JF (2007) The design and control of fuel cell systems. Presented at the H_2 fuel cells millennium convergence, Bucharest, Romania, 21, 22 September 2007
67. James B (2010) Mass-production cost estimation for automotive fuel cell systems. DOE Annual Merit Review, Washington, DC, June 2010. www.annualmeritreview.energy.gov/
68. Cooper J, Lee S-J, Elter J, Boussu J, Boman S (2009) Life cycle design metrics for energy generation technologies: method, data and case study. J Power Sources 186:138–157

Polymer Electrolyte Membrane (PEM) Fuel Cells, Automotive Applications

Shyam S. Kocha
Hydrogen Technologies and Systems Center, National Renewable Energy Laboratory, Golden, CO, USA
Fuel Cell Laboratory, Nissan Technical Center North America, Farmington Hills, MI, USA

Article Outline

Glossary
Definition of Subject: Automotive PEM Fuel Cells
Introduction
Automotive PEMFCs
Future Directions
Bibliography

Glossary

Automotive PEMFC Proton exchange membrane fuel cell stacks used to power automotive vehicles typically using hydrogen as a fuel and ambient air as the oxidant.

Electrocatalyst The material used on the anode and cathode electrodes of fuel cells to catalyze the fuel oxidation and oxygen reduction reactions to produce electrical power and by-products of heat and water. Amount of electrocatalyst used in the anode or cathode of fuel cells is reported in units of mg/cm^2.

Membrane/PEM The proton conductive polymer electrolyte used to separate the anode and cathode compartments of fuel cells. The membrane replaces the liquid electrolytes used in some fuel cells.

Fuel cell performance The voltage produced by a fuel cell stack at a defined current density. A performance or polarization curve refers to a plot of the cell potential (V) versus current density (I) under specified conditions of pressure, temperature, humidity, and reactant stoichiometry.

Fuel cell durability A measure of the degradation of components of a fuel cell as well as the output power of the entire stack over time. Also defined in terms of the maximum life of the stack before failure or degradation rate of the fuel cell performance in μV/h.

Definition of Subject: Automotive PEM Fuel Cells

Since the discovery of fuel cells in the nineteenth century, they have been designed for operation with liquid alkaline, acid, and solid oxide ion conducting electrolytes in different temperature ranges to produce electrical power for stationary, portable, and automotive applications. The liquid acid that provides ionic conduction has been replaced by fairly thin proton conducting membranes such as polystyrenes and perfluorosulfonic acids (PFSAs) like Nafion and more recently with hydrocarbon-based polymers. These fuel cells incorporating a proton-conducting membrane rather than liquid electrolyte to separate the anode and cathode (forming a 3-layer sandwich or catalyst coated membrane) are referred to as PEMFCs. PEMFCs are preferred for use in automotives for a multitude of reasons including their high volumetric and gravimetric power density.

PEMFCs for automotives have electrodes that are typically constituted of Pt-based catalysts separated by proton-conducting perfluorosulfonic acid (PFSA) or hydrocarbon membranes. The membranes (~25 μm thick) have proton conductivities of about 100 mS/cm and areal resistances of 50 mΩ-cm^2. The anode Pt loadings that catalyze the hydrogen oxidation reaction (HOR) are of the order of 0.05 mg/cm^2 while the cathode Pt loadings that catalyze the oxygen reduction reaction (ORR) fall in the range 0.20–0.40 mg/cm^2. Automotive PEMFCs are operated in the temperature range from ambient to ~90°C at ambient to ~300 kPa and at 30–100% RH. Compressed hydrogen fuel tanks (350–700 kPa) and ambient air pressurized using a compressor are employed as the fuel and oxidant sources. Depending on the size of the vehicle, automotive fuel cell stacks produce 80–140 kW of peak power. Most fuel cell automotives are hybrids and employ a 10–20 kW NiMH or Li ion battery to improve efficiency and to store and provide supplemental power. Automotive PEMFCs are subject to variable operating conditions of high potentials, load cycling, start-up and shutdown cycles, humidity cycles, freeze-thaw cycles, and contamination from ambient air. The main obstacles toward commercialization of PEMFC stacks for automotives are the combination of cost, performance, and durability that are not mutually exclusive. Today's PEMFC-powered automobiles demonstrate driving ranges and lifetimes approaching (~70%) that of ICE vehicles. Major automotive companies have stated that PEMFCs for automotives are slated to arrive at cost levels approaching that necessary for commercialization beginning in 2015.

Currently, ICE-powered vehicles emit ~1.5 billion tons CO_2 equivalent per year at a US urban air pollution cost to society of $30 billion/year. The consumption of fossil fuels by the human species (~6.5 billion) has resulted in challenges of energy sustainability, environmental pollution, and global warming that need to be addressed urgently. Currently, several technologies that lower the green house gas emissions partially such as gasoline-powered hybrid electric vehicles (HEVs) and gasoline plug-in hybrids (PHEVs), biofuel PHEVs, and batteries (BEVs) are being developed in parallel with fuel cells.

PEMFCs can operate on hydrogen fuel and atmospheric air to produce electrical energy, while exhausting only heat and water. Hydrogen is not available on earth as gas; it is found as a compound bound to oxygen as in water or bound to carbon, and in living things as biomass. Hydrogen is a carrier of energy and needs to be generated and stored efficiently; an infrastructure for hydrogen needs to be developed along with more efficient storage of hydrogen carried on board the vehicle. Currently about 9 million metric tons of hydrogen per year are generated in the USA that could power 30 million automobiles. Hydrogen can be produced from fossil fuels such as natural gas, and also, renewable sources, such as hydroelectric, wind, geothermal, solar photovoltaics, direct photoelectrochemical, concentrated solar power ocean (tidal, wave, current, and thermal), etc. The application of H_2|Air PEMFCs in automotives is one of the most important components in a renewable hydrogen economy that has the potential to reduce greenhouse gas emissions (to 80% below 1990 GHG levels), lower pollution, and arrest global warming.

Introduction

Fuel cells have been known to science for more than 150 years. In 1800, British scientists William Nicholson and Anthony Carlisle first demonstrated and explained the phenomena of using electricity to decompose water into hydrogen and oxygen. William Robert Grove (1811–1896), a Welsh scientist who was working on electrolysis of water to hydrogen and oxygen, tested the hypothesis that the reverse might be possible. He placed two platinum strips immersed in dilute sulfuric acid in two separate chambers, one of which was filled with hydrogen and the other with oxygen. A current was found to flow between the two platinum strips and water produced in the chamber confirming the hypothesis [1]. Although Grove was the first to build a working fuel cell, the discovery of the principle and fundamentals of the fuel cell is attributed to Christian Friedrich Schoenbein (1799–1868) [2]. Grove later improved on his original experiments by using a series of four cells to increase the total voltage; he named the device a "gas battery" – now known as a fuel cell stack.

Significant contributions were made in later years on fuel cells powered by various fuels such as that by Mond and Langer [3], Haber, W. V. Jacques [4], Bauer [5], Taitelbaum, Schmid [6], Tobler [7] and others.

In addition to the experimental and practical fuel cell devices, a number of scientists contributed to the science and mechanism of the detailed functioning of fuel cells. Two noteworthy theories were debated to explain the functioning of the fuel cell. One was the "contact" theory originally proposed by Alessandro Volta (1745–1827) to explain his battery and the other was a "chemical" theory that held chemical reactions responsible for the generated power. Both theories had part of the solution which is that reactions that occurred where reactant gases, Pt catalyst, and electrolyte converged. This understanding was advanced by the contributions of Friedrich Wilhelm Ostwald (1853–1932). Other systematic nonempirical contributions were made by Nernst [8], Tafel [9], Erdey-Gruz and Volmer. A history of the development of fuel cell electrodes between 1839 and 1960 can be found in the reviews of Liebhasvsky and Cairns [10], Vielstich [11], Baur [5], Tobler [7], Maget [12], and Liebhavsky and Grubb [13].

In 1932, Francis Thomas Bacon replaced the platinum electrodes with cheaper porous nickel metal and the sulfuric acid with potassium hydroxide to demonstrate the first alkaline fuel cell (AFC). Alkaline fuel cells were demonstrated to produce power for practical applications such as welding machines, tractors, powerlifts, etc., in the 1950s. Improved AFCs (2.3 kW) were engineered by Pratt & Whitney/International Fuel Cells (IFC) and were used by NASA in manned US Apollo space missions (1968–1972) and Skylabs for about 54 missions. High power density AFCs using precious metal-based catalysts, static electrolyte (KOH), and operating on hydrogen and oxygen have been used to power (three 12 kW stacks, 92°C, 400 kPa) space shuttles since 1981 [14]. Other companies that have worked on AFCs include Union Carbide Corp., Siemens AG, and the European Space Agency [15].

Cation exchange resins polymerized as sulfonic acids became available in 1945 for use as de-ionizers. Around 1959, General Electric (Thomas Grubb and Leonard Niedrach) considered the use of these materials (sulfonated polystyrene) to form solid polymer electrodes (SPEs) as membranes for fuel cells; these materials were predicted to eliminate the system complexity involved in using liquid electrolytes and lead to the first PEMFCs [10, 16, 17]. The commercial availability of Teflon® (discovered in 1938 by Roy Plunkett of Dupont®) enhanced the performance of SPEs due to its hydrophobic nature and consequent lowered flooding of electrode pores. Using SPEs, PEM modules were fabricated and used in the Gemini space modules operating under hydrogen and oxygen. The Biosatellite 2 (1967) followed the Gemini program (7 flights, 1962–1966) in which Nafion membrane was used for the first time. GE continued working on PEMFCs and in the 1970s developed PEM water electrolysis technology for undersea life support that was used in US Navy oxygen-generating plants. Some of the technology from GE was acquired by UTC affiliates Hamilton-Standard and IFC in 1984. The British Royal Navy also adopted this technology in the 1980s for their submarine fleet. Siemens A.G. commenced a fuel cell research program on AFCs and in 1984 implemented a 100 kW fuel cell in a German navy submarine; they also have PEMFCs installed in submarines operating with rated power of 34–120 kW with technology that allows a high power density and good thermal management. The efforts described above in all these related areas established the basis and provided the foundation and grounds for pursuing fuel cells for automotive applications.

In 2009, ICE vehicles consumed about 3.5 billion barrels/year gasoline and emitted 1.5 billion tons CO_2 equivalent per year of the greenhouse gases [18]. Figure 1a illustrates the CO_2 emissions over the next century for five different scenarios and Fig. 1b illustrates the well-wheels green house emissions projected for 2010 [19]. In the USA, 28% of the total energy used powers the transportation sector. The fuels commonly used for transportation are gasoline (62%), diesel (22%), jet fuel (9%), natural gas (2%). The by-products (that have an impact on the environment and human health) of petroleum products include CO_2, CO, SO_2, NO_x, volatile organic compounds (VOCs), fine particulate matter (fine PM), lead, benzene, formaldehyde, acetaldehyde, 1,3 butadiene, etc. Automotives produce a large proportion of the pollution and greenhouse gases on earth; with global warming becoming an accepted reality, governments and automakers are finally making an effort to lower green house gas emissions. Although a number of intermediate low-emission technologies are being unravelled, PEMFCs are considered to be the best long-term solution since they can operate on hydrogen

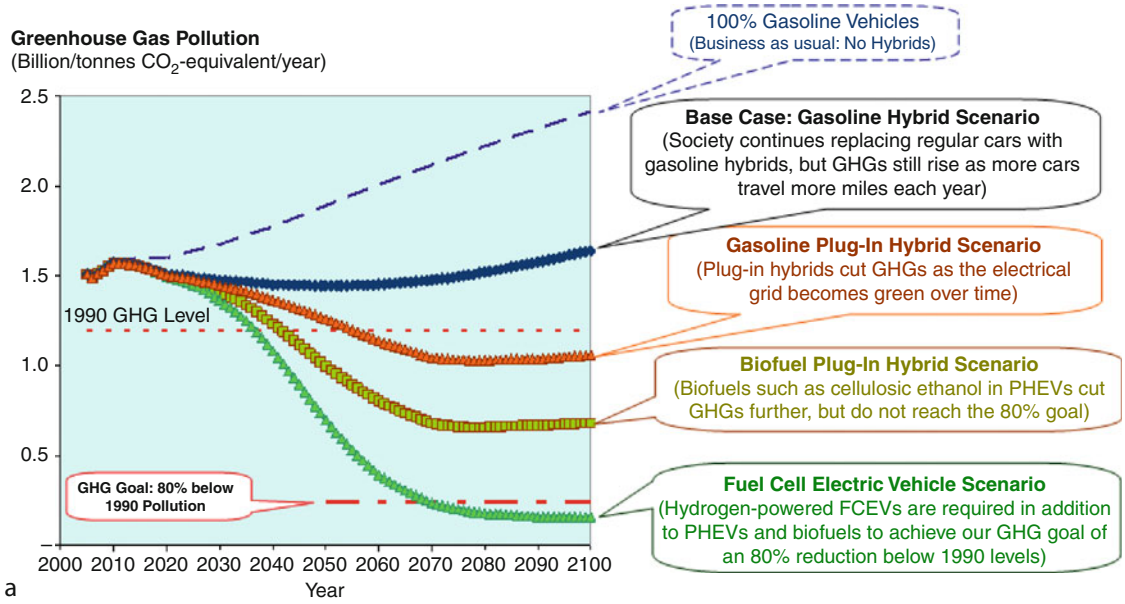

a

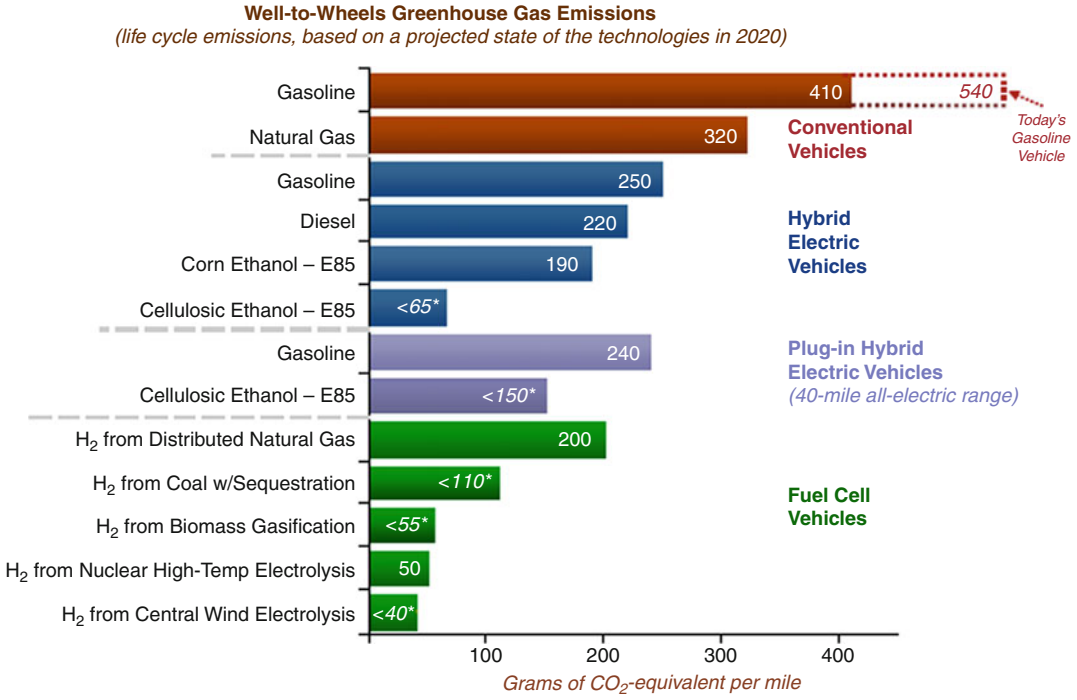

***Net emissions from these pathways will be lower if these figures are adjusted to include:**
* The displacement of emissions from grid power–generation that will occur when surplus electricity is co-produced with cellulosic ethanol
* The displacement of emissions from grid power–generation that may occur if electricity is co-produced with hydrogen in the biomass and coal pathways, and if surplus wind power is generated in the wind-to-hydrogen pathway
* Carbon dioxide sequestration in the biomass-to-hydrogen process

b

Polymer Electrolyte Membrane (PEM) Fuel Cells, Automotive Applications. Figure 1
(**a**) CO_2 emissions over the next century for five scenarios where gasoline vehicles, gasoline-hybrid, gasoline plug-in hybrids, biofuel plug-in hybrids, and fuel cell electric vehicles are used as the power source [18]; (**b**) well-wheels green house gas emissions based on state of technology in 2020 [19]

and atmospheric air to produce electrical energy, while exhausting heat and water with zero emissions.

Although, onboard reforming of methanol, gasoline, etc., was seriously considered and attempted, fitting a miniature chemical plant in the limited space of a fuel cell vehicle was found to be untenable. Hydrogen was unanimously selected as the choice of onboard fuel for automotive vehicles in the early twenty-first century with an understanding of its strengths and weaknesses. Hydrogen is not available on earth as gas; it is found as a compound bound to oxygen as in water or bound to carbon, and in living things as biomass. Hydrogen has the highest energy content of any fuel by weight (hydrogen: 143 MJ/kg, gasoline: 43 MJ/kg) and the lowest by volume. Hydrogen can be produced from fossil fuels such as natural gas, and renewable sources such as hydroelectric, wind, geothermal, solar photovoltaics, direct photo-electrochemical, concentrated solar power ocean (tidal, wave, current, and thermal), etc. Hydrogen is also classified based on criteria such as primary energy sources (hydro, nuclear, wind, solar, natural gas, etc.,); methods of production (reforming, electrolysis, etc.,); renewable/nonrenewable, etc. Currently about 9 million metric tons of hydrogen per year is generated (∼95%–steam methane reforming (SMR) and the rest electrolysis); in the USA, this could in principle, power ∼30 million automobiles.

Historically, there have been concerns about the safety of hydrogen, but in actuality, it is as safe and even safer than other flammable fuels such as gasoline and natural gas. A primary safety advantage of hydrogen is that it has very high diffusivity so that it dilutes rapidly to a nonflammable concentration in a reasonably ventilated space. Additionally, due to the absence of carbon and presence of water vapor in the combustion products of hydrogen, hydrogen fires release less radiant energy thus lowering incidents of secondary fires. The flammability limits, explosion limits, ignition energy, flame temperature, and stoichiometric mixture most easily ignited in air are all well documented for hydrogen. Codes and standards have been established for the safe use of hydrogen. Fuel cell vehicles are subjected to the same safety tests and crash/impact tests as gasoline-powered vehicles and have little trouble passing them.

As the world transitions to a hydrogen economy, a hydrogen infrastructure including a combination of distributed and centralized production is likely to evolve. Hydrogen pipeline networks already exist in some regions, often to provide hydrogen to the refining and food processing industry; transport by trucks is also prevalent. In the USA, at this time, there are 60 hydrogen fueling stations (∼350 world-wide), 1,200 miles of hydrogen pipelines, and ∼9 million tons of hydrogen produced every year. Hydrogen storage is often categorized as physical (or molecular) and chemical (or dissociative) storage. Onboard physical storage methods include compressed gas, liquid hydrogen, and cryo-adsorbed hydrogen; chemical storage includes metal hydrides and liquid organic carriers. Typically, compressed hydrogen (35–70 MPa) in one or two tanks (∼4–8 kg hydrogen depending on the target range) is stored onboard fuel cell vehicles today. Most fuel cell vehicles today closely meet the driving range of their IC engine counterparts.

The application of H_2|Air PEMFCs in automotives is one of the most important components in a renewable hydrogen economy that has the enormous potential to reduce greenhouse gas emissions (to 80% below 1990 GHG levels) and arrest global warming. Based on the Intergovernmental Panel for Climate Change (IPCC) study (Fig. 2) by 2050 well-wheels emissions of CO_2 must be reduced by 70% ∼90% versus 2000 levels [20]. Of all the possible pathways such as gas-electric hybrids, EVs, and fuel cells, only H_2|Air PEMFCs have the ability to reduce emissions to zero. Thus in attempts to reduce greenhouse gas emissions, lower dependence on imported oil, and limit urban air and water pollution, FCVs are expected to play a very central role.

Brief History of Automotive Fuel Cells

Ballard should be recognized for re-igniting the interest in PEMFCs in the late 1980s and 1990s and for the development of improved stacks used today by several companies in their fuel cell vehicles [21]. All the major automotive companies initiated fuel cell research and development programs as well as small-scale demonstration programs between 1998–2010; this was augmented by materials and component development by companies in the area of membranes, catalysts, diffusion media, bipolar plates, etc. In 2003, the US government announced a $1.2 billion FreedomCAR

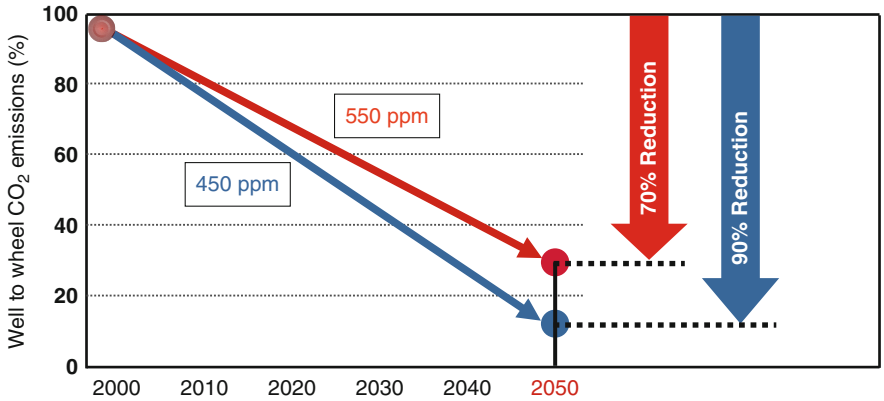

Polymer Electrolyte Membrane (PEM) Fuel Cells, Automotive Applications. Figure 2
Reduction in well-wheels CO_2 emissions recommended for 2050 by the Intergovernmental Panel for Climate Change (IPCC) study [20]

and Hydrogen Fuel Initiative (HFI) to develop hydrogen-powered fuel cells. Together, by 2008, the two initiatives invested about $1 billion to develop hydrogen-powered fuel cells, hydrogen infrastructure, and advanced automotive technologies. Fuel cells suffered a setback due to the 2009 US government policy that projected a longer 10–20-year forecast for automotive fuel cell commercialization. Nevertheless, most of the US, European, and Japanese automakers continue to support the development of PEMFCs for automotives internally as well as in public statements and most of the government funding was later restored. Also, in 2009, the European Union (EU) announced €140 million ($195 million) in available investments for research in energy technology. The funding (European Commission matched by contributions from the private sector) is part of a €1 billion ($1.4 billion) that the EU plans to invest in fuel cell research and development by 2014. In Japan, the Ministry of Economy, Trade and Industry (METI)'s New Energy and Industrial Technology Development Organization (NEDO) has overseen a lot of the funding for fuel cell and hydrogen research, development, and demonstration. The Japan Hydrogen & Fuel Cell Demonstration Project (JHFC) conducts research and activities for the practical use of fuel cell vehicles and hydrogen stations. The JHFC consists of the Fuel Cell Vehicle-Demonstration Study and the Hydrogen Infrastructures-Demonstration Study; the studies are subsidized by the METI. Many countries now have hydrogen corridors or hydrogen highways with a number of hydrogen fueling stations already implemented. In this section, for simplicity, the contributions made by a number of stack developers and automotive companies to advance fuel cell technology for automotives based on publicly available sources will be outlined.

Allis-Chalmers In 1959, a team led by Harry Ihrig developed and demonstrated a 15 kW fuel cell tractor for Allis-Chalmers that was exhibited at state fairs across the USA. The FC stack system used KOH electrolyte and compressed hydrogen and oxygen as the reactants operating at 65°C. The original fuel cell tractor is on display at the Smithsonian. In 1965, Allis-Chalmers further developed hydrogen-powered FC golf carts. Allis-Chalmers is also experimenting with fuel cell stacks to generate power for spot welders and forklift trucks.

General Motors In 1968, GM's Electrovan was the automotive industry's first attempt at an automobile powered by a $H_2|O_2$ 125 kW fuel cell. It took a team of 250 people 2 years to demonstrate the potential feasibility of fuel cell technology. The Electrovan, weighed more than twice as much as a normal van and could travel at speeds up to ~70 mph for 30 s. In the early 1980s Los Alamos National Lab (LANL) initiated a PEMFC program and GM was part of the overview board. In 1996, the program moved from LANL to Rochester, NY, and later to Honeoye Fall, NY, where

a large fuel cell R&D center still operates. In 1997, GAPC was formed globally at Honeoye Falls, NY, Mainz Kastel, Germany, Warren, MI, and Torrance, CA. In 1998, the GM/DOE program was successful in demonstrating a 50 kW methanol fuel processor PEM system and in late 1998 – GM methanol Zafira was displayed at Geneva Auto Show. In 2000, focus shifted to hydrogen fuel and in 2001, HydroGen 3, Zafira was launched. Figure 3 illustrates the history of the various GM FC vehicles from 1968 to 2001 and their latest FCV model. The advancements in volumetric and gravimetric power density of PEMFC stacks designed at General Motors between 1997 and 2004 are depicted in Fig. 4 [22]. Figure 5 is a photograph of their fifth generation stack [23]. Most recently, GM's Chevrolet Equinox FCV passed 1 million miles with customers using the vehicles in everyday real-world conditions [24, 25].

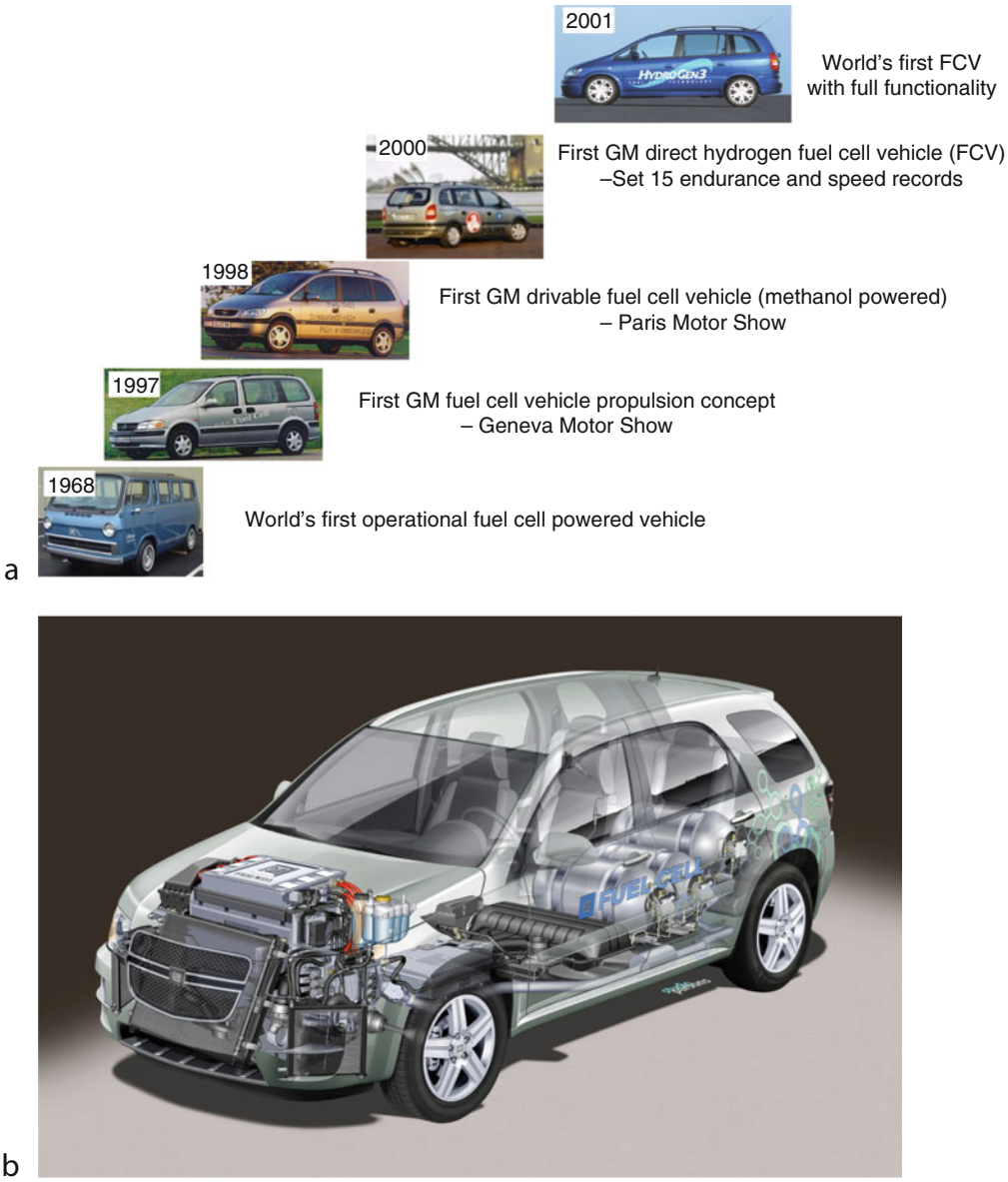

Polymer Electrolyte Membrane (PEM) Fuel Cells, Automotive Applications. Figure 3
(**a**) Timeline of fuel cell vehicle development at General Motors until 2001; (**b**) 2008 Chevy Equinox fuel cell vehicle [24, 25]

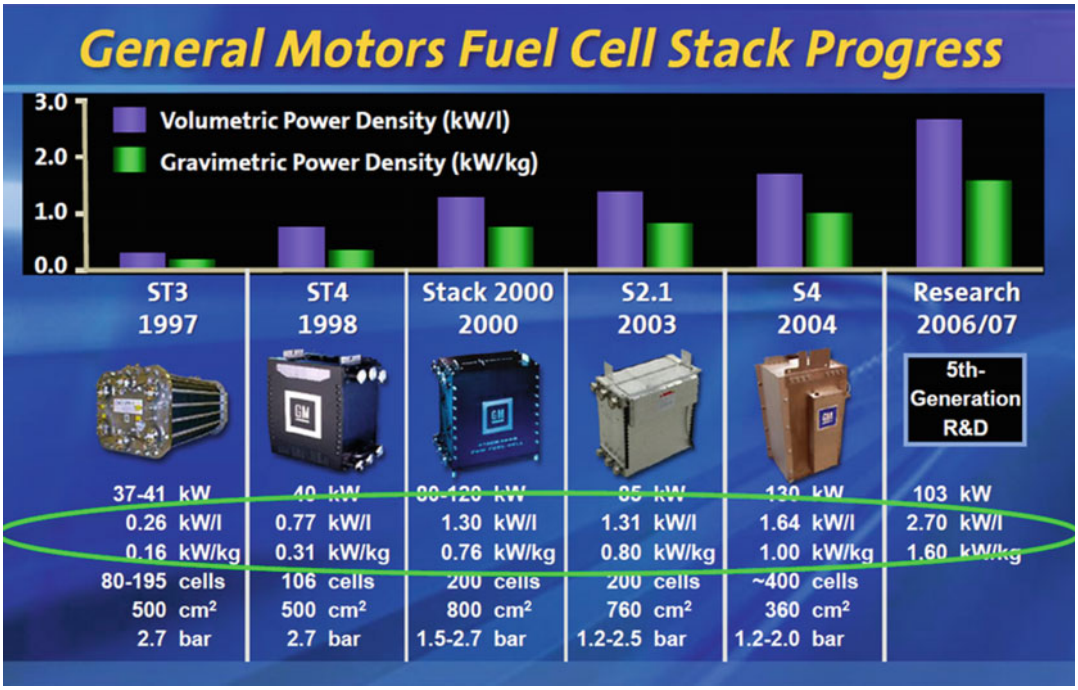

Polymer Electrolyte Membrane (PEM) Fuel Cells, Automotive Applications. Figure 4
Advancements in the development of the fuel cell stacks designed at General Motors from 1997 to 2004 is depicted [22]

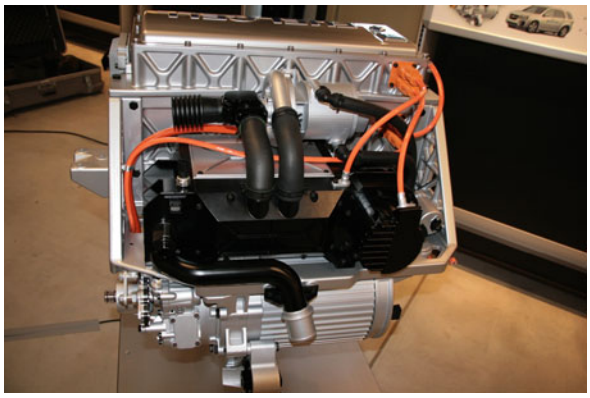

Polymer Electrolyte Membrane (PEM) Fuel Cells, Automotive Applications. Figure 5
Photograph of fifth generation of General Motors PEMFC stack and system [23]

UTC Power/UTC Fuel Cells For the last 40 years, various groups under the umbrella of United Technologies (IFC, UTC Fuel Cells, UTC Power) have been uninterruptedly involved in the research and development of fuel cell stacks such as the commercial PAFC stack-power plant and the AFC PEMFC stacks/power-plant used in the orbiter/space shuttle [26]. Over the last decade, UTC Power collaborated with several automotive companies to integrate their PEMFC stacks into various automotive platforms. Some of the interesting aspects of the UTC- PEMFC stack are that they operate close to ambient pressure and have unique water transport plates or separators; the plates are porous and have internal channels allowing for circulating water or coolant that performs the function of cooling the stack as well as passive water management. The reactants in the anode and cathode flow fields are, in principle, always humidified and improve the performance and durability of the membrane.

Some of the automotive companies they have worked with include: Hyundai-Kia Motor Company, Chevron Technology Ventures, Nissan, BMW, and a few others. UTC Power has also developed PEMFC 5 kW auxiliary power units APUs for BMW installed in BMW 7 series vehicles. The PEMFC stack APU provides energy for the vehicle's on-board electrical requirements. The third generation of the APU has been reported to perform for >3,000 h. UTC Power together with Hyundai-Kia Motor Company developed

an automotive FCV that was capable of starting and functioning under subzero conditions; they were tested in the winter of 2008 in Michigan under the US DOE Hydrogen Fleet and Infrastructure Program. UTC Power also supplied PEMFC stacks for initial generations of Nissan X-TRAIL FCVs.

Ballard/AFCC Ballard Power Systems was originally founded in 1979 as Ballard Research Inc. by Dr. Geoffrey Ballard to conduct research on high-energy lithium batteries. In the late 1980s and 1990s Ballard championed PEMFCs for automotive and other uses and re-invigorated the field. In 1995, Ballard Systems tested PEM cells in buses in Vancouver and Chicago and later in experimental vehicles made by DaimlerChrysler. In late 2007, Ballard pulled out of the hydrogen vehicle sector of its business to focus on fuel cells for forklifts and stationary electrical generation. Established in 2008, the Automotive Fuel Cell Cooperation (AFCC) is a Burnaby, B.C.-based joint-venture private company owned by Daimler AG, Ford Motor Company, and Ballard Power Systems Inc. to develop fuel cell stacks for automotive applications. Today, Daimler and Ford have more than 150 fuel cell vehicles on the road. The fuel cell vehicles of Ford and Daimler are combined together in this subsection since they both generally utilize stacks based on AFCC technology.

DaimlerChrysler unveiled a series of FCVs using Ballard stacks such as the NECAR 1 (50 kW, Compressed H_2, 1994), NECAR 2 (50 kW, Compressed H_2, 1996), NECAR 3 (50 kW, liquid methanol, 1997), NECAR 4 (70 kW, liquid H_2, 1999), and F-Cell (A-class) FCV hybrid delivering 85 k W (Ballard Mark 900) using compressed H_2 in 2002. Most recently, Mercedes announced a series-production of B-class F-Cell powered by an electric motor that generates 136 hp and 214 lb-ft of torque, providing a range of 240 miles, and a refueling time of 3 min [27]. Ford Motor Company has also released a series of vehicles using Ballard stacks such as the P200HFC (1999), Focus FCV (2000), and Advanced Focus FCV (2002).

Toyota Toyota has been developing fuel cells since about 1996 with vehicles such as the RAV 4 FCEV-hybrid (Metal hydride, 1996), RAV 4 FCEV (Methanol, 1997), FCHV-3 (Metal hydride, 2001), FCHV-4 (Compressed H_2, 2001), and FCHV-5 (reformed gasoline, 2001). Their efforts have resulted in the development of the latest Toyota Fuel-Cell Hybrid Vehicle (FCHV), some of which are being tested daily at the University of California in Davis and Irvine. Since 2001, a fleet of 25 FCHVs has accumulated more than 100,000 miles. In 2002, Toyota began limited marketing of the hydrogen-powered TOYOTA FCHV (fuel cell hybrid vehicle) in the USA and Japan [28]. Toyota FCHVs have also been successfully tested under subzero conditions. In real-world driving tests carried out in 2008 in collaboration with the US DOE, Savannah River National Laboratory, and National Renewable Energy Laboratory (NREL), the FCHV-adv averaged the equivalent of ~68 mpg achieving a range of ~430 miles on a single fill of compressed (70 MPa) hydrogen gas. Figure 6 depicts images of Toyota's FCHV and an under the hood look at their PEMFC stack [29].

Nissan Nissan's foray into the development of FCV technology started in 1996 in collaboration with various stack development partners such as Ballard and UTC Fuel Cells. In 1999, testing of a methanol-reforming fuel cell was initiated and in 2000 Nissan participated in the California Fuel-Cell Partnership (CaFP). Since 2004, Nissan has developed and used an in-house PEMFC stack in their FCVs. Their 2005 FCV employs 70 MPa hydrogen fuel tanks that allow the X-Trail FCV to have a driving range of about 300 miles. Figure 7 depicts the timeline for FCV development at Nissan along with metrics of driving range and acceleration time [30]. The range of their current generation vehicle is ~500 km (310 miles) and is comparable to a similar ICE powered vehicle. In 2007, they have developed a new generation of stacks that have significantly lower catalyst loadings, improved durability, high-rated power of 130 kW and a volumetric power density approaching 2 kW/L. Specifications of Nissan's 2005 model FCV are detailed in Fig. 8.

Honda A brief timeline for the development of FCVs by Honda is summarized below. Honda initially employed various 60–85 kW Ballard stacks in their initial FCVs such as the FCX-V1 (Metal hydride, 1999), FCX-V2 (Methanol, 1999), FCX-V3 (Compressed H_2, 2000), FCX-V4 with ultra-capacitors (Compressed H_2, 2001), and the FCX (Compressed H_2, 2002) vehicle that was leased in Los Angeles.

Polymer Electrolyte Membrane (PEM) Fuel Cells, Automotive Applications. Figure 6
Images of Toyota's FCHV-adv installed with their PEMFC stack [29]

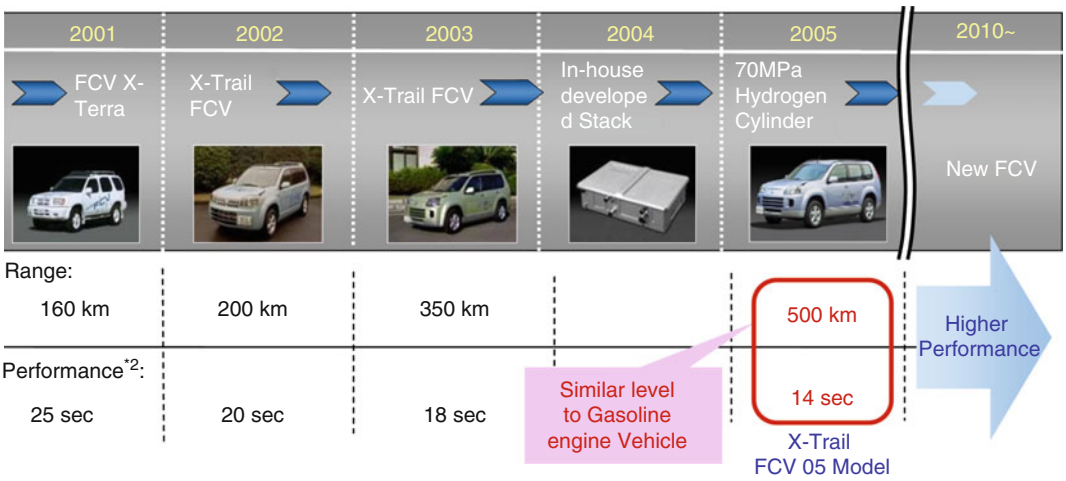

Polymer Electrolyte Membrane (PEM) Fuel Cells, Automotive Applications. Figure 7
Timeline for FCV development at Nissan along with metrics of driving range and 0–100 kmph acceleration time [30]

The US City of Los Angeles became the first FCX customer, leasing the first of five Honda FCX models for fleet use. In 2003, a next-generation fuel cell stack capable of power generation at temperatures as low as –20°C, was announced. In 2005, Honda introduced the second generation FCX and the first to be powered by a Honda FC stack. FCX Clarity FCEV, a dedicated platform hydrogen fuel cell vehicle, debuted at the L.A. Auto Show; the new stack was 20% smaller and 30% lighter than its previous generation. Since 2008, FCX Clarity FCEV has been made available as a leased vehicle for consumer use [31].

Some of the interesting aspects of the Honda fuel cell stack are the so-called V-Flow stack configuration that claims easy drainage of water, higher cell stability, aromatic electrolytic membrane, improved thermal management, and improved packaging. Honda has also reported the use of specialized coatings with impregnated electrical contacts on their bipolar plates that reduced the contact resistance while being corrosion resistant. Figure 9a depicts the conventional stack assembly and Fig. 9b and c illustrate their improved efficient stack packaging design.

Automotive PEMFCs

In this section, the operational modes that fuel cell stacks are subjected to; the 2015 performance, cost,

Classification		X-TRAIL FCV
Vehicle	Overall length / width / height (mm)	4485/1770/1745
	Curb Weight (kg)	1790(1860)
	Seating capacity	5
	Top speed (km/h)	150
	Cruising range (km)	Over 370 (over 500)
Motor	Type	**Co-axial motor integrated with reduction gear**
	Max. power (kw)	**90**
Fuel Cell Stack	Fuel cell	Polymer electrolyte type
	Max. power (kw)	**90**
	Supplier	In-house
Battery	Type	**Compact Lithium-ion Battery**
Fueling System	Fuel type	Compressed hydrogen gas
	Max. pressure (MPa)	35 (70)

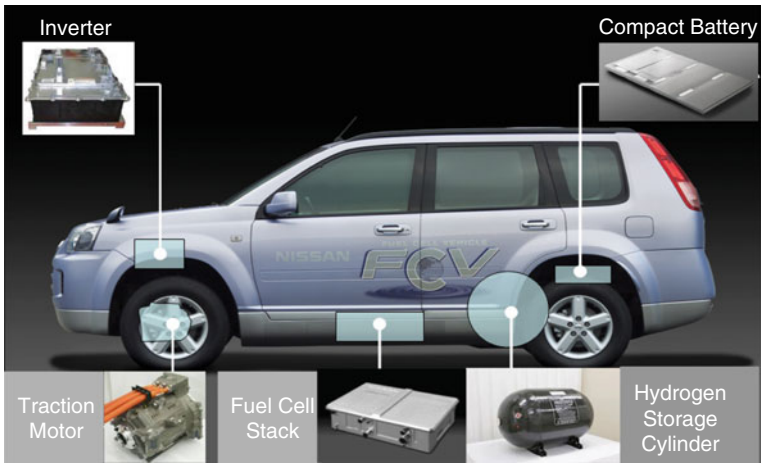

Polymer Electrolyte Membrane (PEM) Fuel Cells, Automotive Applications. Figure 8
Detailed specifications of Nissan 2005 X-Trail FCV along with a layout of components of the fuel cell stack system [30]

and durability targets that fuel cell technology must achieve; and recent advancements made by automotive companies toward achieving the targets for commercialization are discussed.

Operational Modes of Automotive PEMFCs

Unlike residential and stationary fuel cells, automotive PEMFCs undergo the entire slew of aggressive variable loads and environmental conditions that are typically experienced by conventional ICEs. The modes of operation of an automotive PEMFC can simplified to the following [32]: (1) Idling/low load, (2) acceleration-deceleration/load cycling, (3) start-up shutdown, (4) cold temperatures/freeze-thaw cycles, and (5) contamination/impurities from the environments and cell degradation products. The impact of these modes of

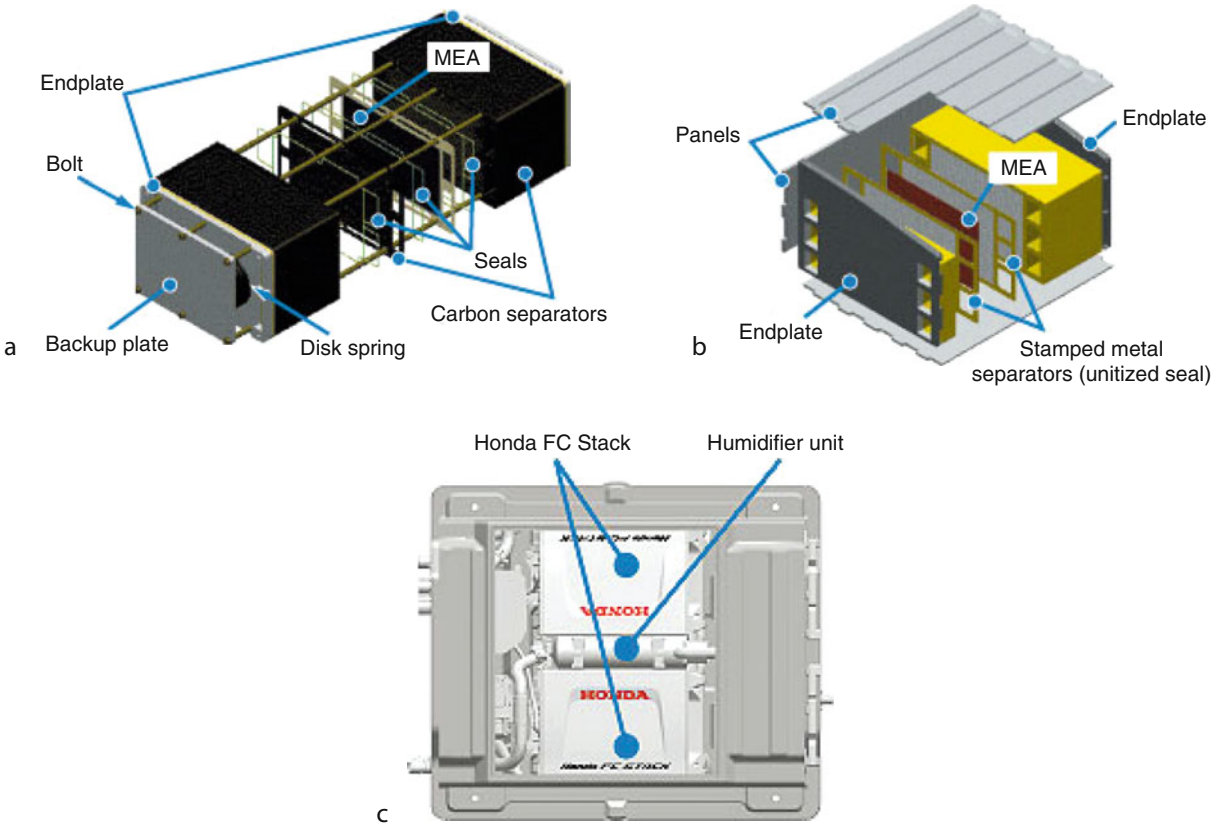

Polymer Electrolyte Membrane (PEM) Fuel Cells, Automotive Applications. Figure 9
(**a**) Illustrates conventional stack package design of previous configurations and (**b**) and (**c**) illustrate Honda's new efficient stack package design [31]

operation on the PEMFC stack is briefly discussed below. Unless otherwise specified, the discussion assumes a Pt nanoparticle–based electrocatalyst on a high-surface-area carbon black support, a perfluorosulfonic acid membrane, hydrogen flow on the anode, air flow on the cathode with the reactants partially humidified at the inlet. Testing is performed on a variety of platforms such as liquid electrolyte-half-cells (~0.198 cm^2), subscale fuel cells (25–50 cm^2), and full-size single cells or short stacks having active areas as high as 400 cm^2. The basic diagnostics techniques and characterization of fuel cell components can be found detailed in the literature [33–35].

Idling/Low Load When a vehicle in operation is at rest, for example, at a stop light, the current drawn by the fuel cell stack is low; essentially power is drawn by the auxiliary equipment in the vehicle. At such low current densities, the cathode potential is high and may approach the open circuit voltage (OCV). Although the thermodynamic reversible potential at 80°C is about 1.18 V, leakage currents (few mA/cm^2) especially due to hydrogen crossover across the (~20–50 μm thick) membrane and electronic shorting lower the OCV to about 0.95 V. This high cathode potential leads to several degradation phenomena in the cells. The Pt-based catalyst dissolves at these potentials and diffuses toward the anode through the membrane and within 48 h forms a band inside the membrane as shown in Fig. 10 [36]. This Pt band formed in the membrane induces chemical degradation of the membrane itself due to formation of $OH^{\cdot}$, hydrogen peroxide, and peroxyl radicals resulting in membrane thinning. The chemical degradation is accelerated under low RH conditions and higher temperatures. Degradation of the membrane leads to an increase in hydrogen crossover and can

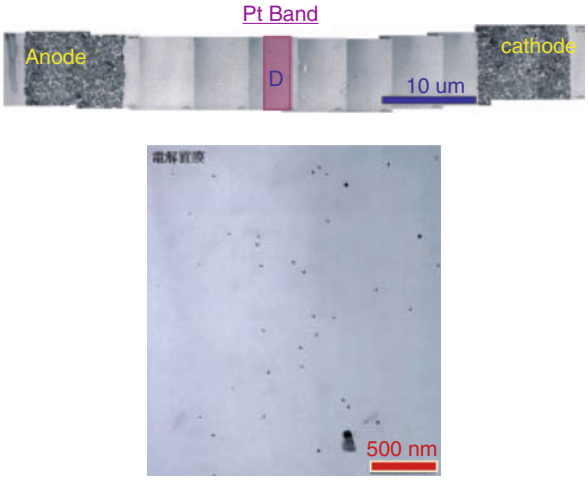

Polymer Electrolyte Membrane (PEM) Fuel Cells, Automotive Applications. Figure 10
Formation of a Pt band (with magnified view of the band) in the membrane when held under OCV conditions over a period of 100 h [36]

result in thinning, pinholes, and eventually catastrophic failure. Figure 11 shows the fluoride and sulfate elution from the exhaust water of a fuel cell during and after OCV testing [37]. About 6% of the fluorine in the membrane is released during 48 h of OCV hold. If the carbon support (on which the catalyst is dispersed) has a high surface area and therefore susceptible to corrosion, it may first become hydrophilic and over time corrode and oxidize leading to some Pt nanoparticle agglomeration which also leads to cell performance loss. If the fuel cell is a hybrid with a 10–20 kW NiMH or Li-ion battery, it may be possible to minimize the deleterious effects of high cathode potentials by using appropriate system controls and algorithms to lower the high potentials.

Acceleration/Deceleration PEMFC stacks in vehicles are subject to variable power demands that depend on environmental conditions such as the grade of the road as well as the driving behavior of the vehicle operator. As the load changes, the current drawn from the fuel cell and hence the cell voltage changes resulting in the cell being subject to load cycles or potential cycles. Thus, the fuel cell is subject to all kinds of potential cycles with the widest potential range being about 0.60–0.95 V [32, 35, 38–41]. The upper potential corresponds roughly to OCV/idling and the lowest potential corresponds to the potential at peak power (about 0.6 V and a few amperes per square centimeter). The upper limit of the voltage is determined by the choice of the membrane (thickness/permeability) and in part by the design of the vehicle system controls. Although peak power is drawn from the stack for only ~5% of the time, it is necessary for the stack to have an electrical efficiency of ~55% (to be competitive with ICEs); also, the size of the stack is partly determined based on the peak power point.

A number of automotive drive cycles (FUDS cycle, US06, NEDC, and Japanese 10–15 mode drive cycles, etc.,) are available to represent the statistical usage of a vehicle and are used to determine the mileage of ICE vehicles. Figure 12 is an example of the Japanese 10–15 drive cycle and Fig. 13 an example of the US06 drive cycle. These drive cycles can be systematically converted into voltage-time profiles and applied to estimate the degradations rates of stacks under simulated driving conditions. A generic individual cycle profile is shown in Fig. 14 that represents a superset of all possible profiles [32]. The five elements of the profile that can be varied are: (1) duration at low potential, (2) duration of the ramp-up from low to high potential (or ramp-up rate), (3) duration at high potential, (4) duration of the ramp-down from high to low potential (or ramp-down rate), and, (5) duration at low potential. The high and low potentials can have infinitely different values between the upper and lower limit in the range 0.6–0.95 V.

It has been determined through a large number of studies that the widest potential cycles of 0.60–0.95 V cause the most degradation of the cathode catalyst layer. Automotives typically undergo 300,000 such cycles over their 5,000 h/10 years lifetime. At potentials above 0.95 V, the Pt surface is highly covered with oxide species while below 0.6 V it is almost free of oxide species as is observable from a typical cyclic voltammogram of platinum in acids or in a PEMFC. Thus the process of cycling in the range 0.60–0.95 V results in the growth (oxidation) and stripping (reduction) of oxide species on the surface and prevents the formation of a stable passivating film. (A more conservative potential regime of 0.70–0.90 corresponding to the iRFree potential that the catalyst layer experiences is sometimes selected.) Figure 15 depicts both the

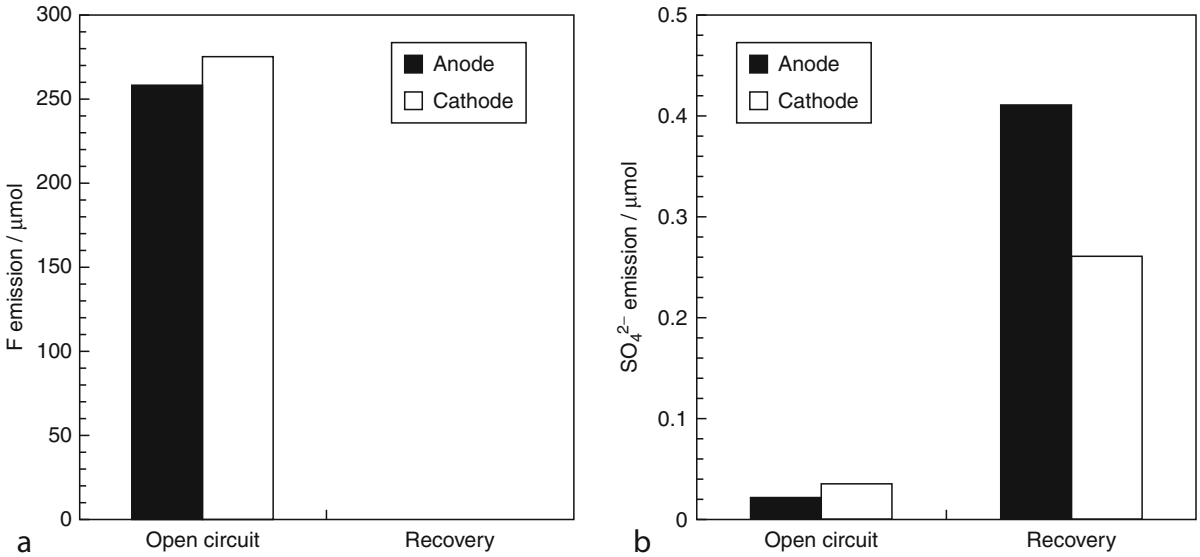

Polymer Electrolyte Membrane (PEM) Fuel Cells, Automotive Applications. Figure 11
Fluoride emission during OCV hold test (6% of fluorine in the membrane is released over a 48 h hold) and sulfate emissions during recovery operation [37]

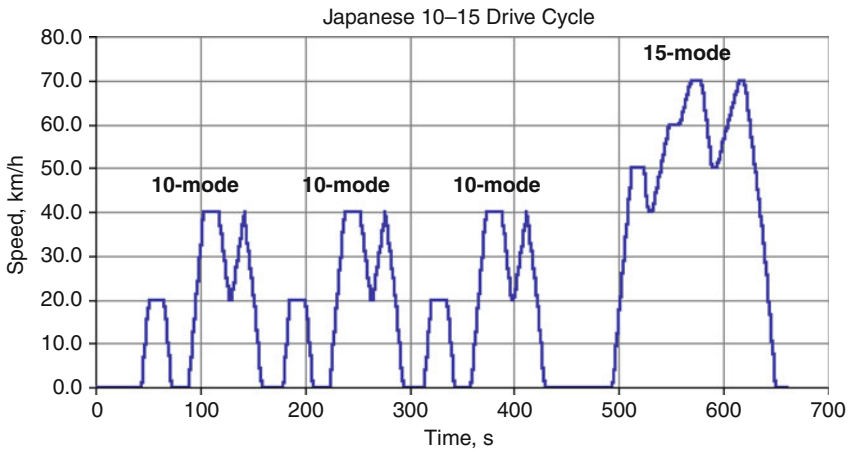

Polymer Electrolyte Membrane (PEM) Fuel Cells, Automotive Applications. Figure 12
Japanese 10–15 drive cycle for automobiles

enhanced activity of PtCo/C electrocatalysts over Pt/C [42] and the surface area loss during cycling [39]. Based on recent research, it appears that exposure of bare (oxide-free) Pt to high potentials during the anodic portion of a scan in a cycle has a high impact on the Pt dissolution and degradation of the cathode catalyst layer. Again, practical methods that involve limiting the number of large cycles with the help of a battery in a hybridized system mitigates the losses partially. Pt-based alloys, heat-treated Pt, and other modifications to the catalyst layer also provide partial material solutions that restrict the losses.

Start-up/Shutdown Automotive PEMFC stacks are shut down and started a number of times depending on the needs of the driver; the number of such occurrences is

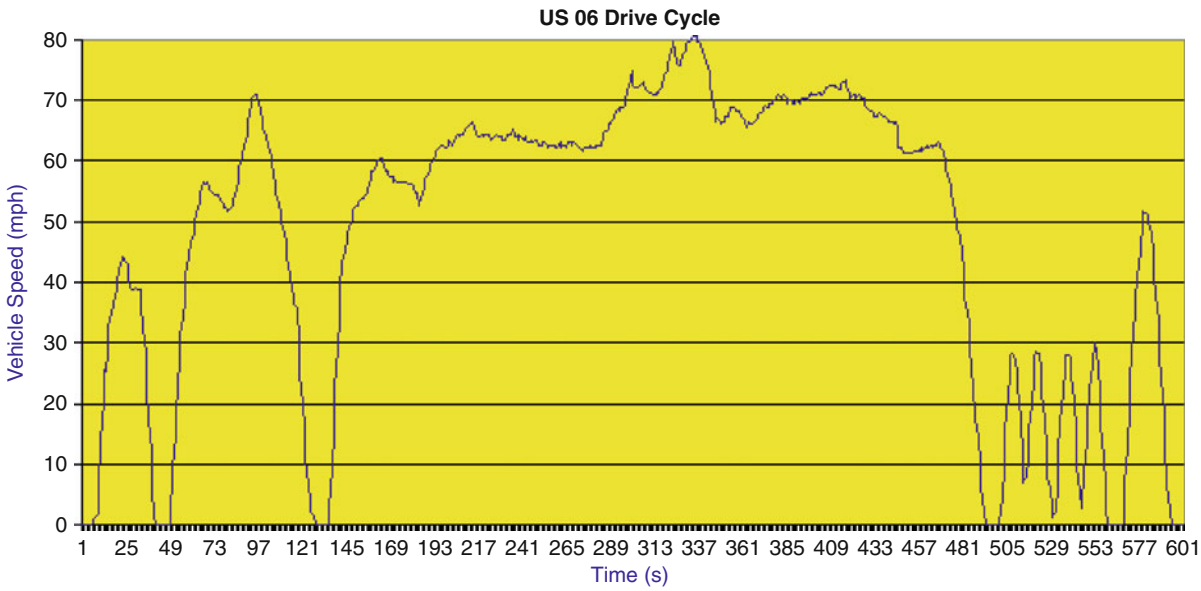

Polymer Electrolyte Membrane (PEM) Fuel Cells, Automotive Applications. Figure 13
US 06 drive cycle for automobiles

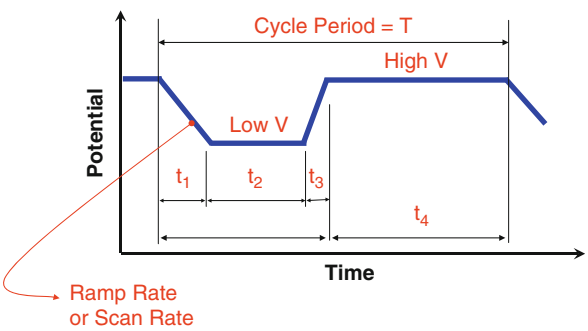

Polymer Electrolyte Membrane (PEM) Fuel Cells, Automotive Applications. Figure 14
Schematic representation of an arbitrary cycle extracted from a complex drive cycle illustrating the various parameters that can be varied in the cycle profile

about ~30,000 over the stack life. When an automotive PEMFC stack is allowed to rest for a period of time, both the anode and cathode chambers get filled with ambient air from the atmosphere. When such a stack filled with air is restarted and hydrogen turned on to flow on the anode side, it pushes out the air leading to the formation of a "H_2-air front." It was discovered around 2001 that frequent starting and shutting down of fuel cells resulted in a peculiar phenomenon where the cathode becomes subject to potential transients as high as 1.5 V [43–45]. At these high potentials, the carbon support of the cathode catalyst layer undergoes precipitous corrosion to carbon dioxide. Loss of the carbon leads to agglomeration of the Pt nanoparticles resulting in a loss in catalyst surface area, severe mass-transport issues, and a precipitous loss in cell performance. No losses are observed if the start-up takes place within a short time of shutdown as long as there is residual hydrogen in the anode of the fuel cell; thus the time interval between start-up and shutdown is an important parameter governing overall degradation rate [46].

Figure 16 below is a schematic of the start-up/shutdown phenomenon and the reactions that occur in the anode and cathode catalyst layers. Interestingly, no damage occurs on the anode-side catalyst layer. Figure 17 depicts the degraded cross section of an MEA (cathode facing up) after ~50 start-up/shutdown cycles. Over the last decade, several mitigation techniques that involve controlling the procedure at start-up and shutdown have been reported and losses have been minimized, albeit at the expense of system complexity. Some of the mitigating solutions include: (1) shorting the stack to minimize the potential spike, (2) purging the anode using high flows of gases to minimize the H_2-air front time (to less than 0.5 s),

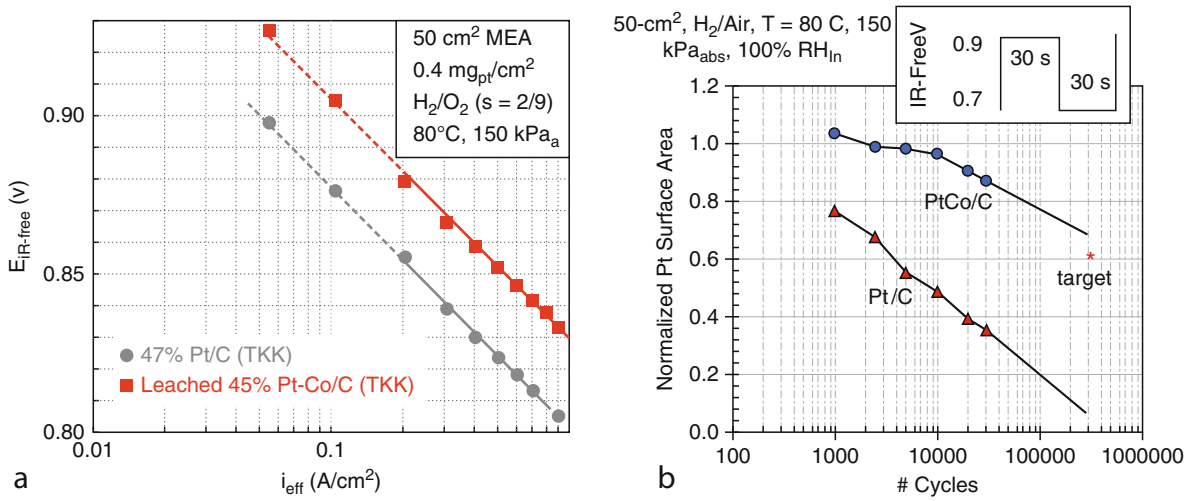

Polymer Electrolyte Membrane (PEM) Fuel Cells, Automotive Applications. Figure 15
(**a**) Enhanced activity (x3) under $H_2|O_2$ for pre-leached PtCo/C electrocatalysts compared to Pt/C as tested in subscale fuel cells [42]; (**b**) electrochemical area loss for Pt/C versus PtCo/C catalysts over 10,000 cycles in subscale fuel cells illustrates lower degradation for the PtCo/C [39]

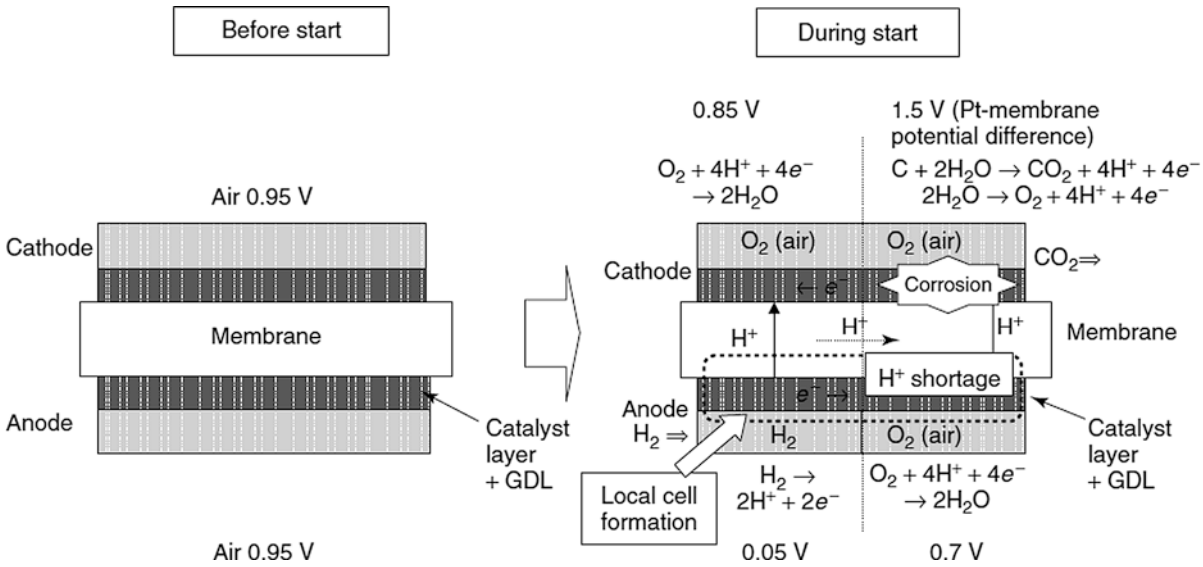

Polymer Electrolyte Membrane (PEM) Fuel Cells, Automotive Applications. Figure 16
Schematic of start-up/shutdown phenomenon before and during passage of the H_2-Air front through the anode chamber [43–46]

(3) drying the stack after shutdown, (4) lowering the Pt loading on the anode side to lower the ORR with a consequent suppression of the COR on the cathode, and (5) lengthening the time for which residual hydrogen remains in the anode, etc. The search for more durable corrosion-resistant supports to replace carbon is underway so that the fuel cell system can be simplified. Oxides, nitrides, carbides, of tungsten, titanium, etc., are promising candidates but they often suffer from poor electronic conductivity, lower surface area

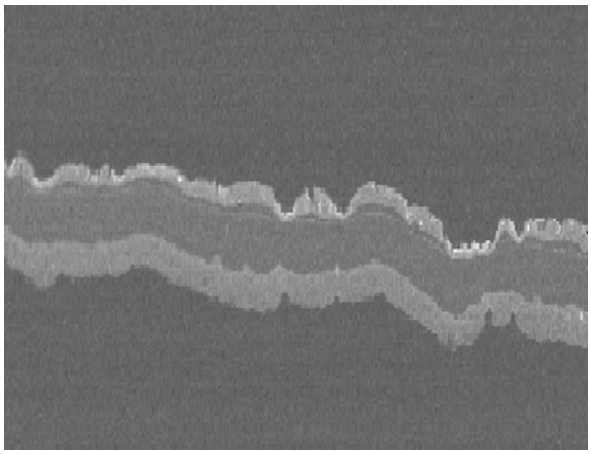

Polymer Electrolyte Membrane (PEM) Fuel Cells, Automotive Applications. Figure 17
SEM cross section of an MEA with the cathode (*top*) layer showing severe corrosion and degradation after about 50 uncontrolled start-up/shutdown cycles. A light band is also observed near the cathode-membrane interface due to the cycling of potential that takes place between 1 and 1.5 V

compared to carbon blacks and it can be difficult to disperse Pt nanoparticles on them [47].

Cold Temperatures Automotive PEMFCs must be capable of enduring cold weather conditions such as freezing temperatures as low as –40°C. Even conventional ICE vehicles need help from engine block warmers, etc., in order to be able to start-up from subzero conditions. Under subzero conditions, an operating fuel cell will generate sufficient heat to prevent water from freezing and will likely show little or no loss in performance. The problem arises when a PEMFC has been idle for a long period of time under subzero conditions and is required to startup.

PEMFCs have the added challenge of liquid water in the system that can freeze, block channels and gas flow paths, and form icicles that may penetrate through the polymer membrane and cause damage. Blockage of channels can lead to fuel starvation, carbon corrosion, and degradation of the anode/cathode catalyst layer. The use of insulation, heaters, and antifreeze coolants are helpful for short periods of time, but the residual water within the fuel cell will eventually freeze forming ice. The catalyst layer and the diffusion media are especially susceptible to repeated freeze-thaw cycles due to their porous nature and the inherent presence of water (loosely bound and free water) that can expand and contract leading to a disruption of the porous structure that is so important for mass-transport. Significant disconnection of the catalyst particles from the ionomer and carbon support could result in degradation in performance due to the loss in protonic and electronic interfacial contact.

Elimination or minimization of the water in the cells by purging with gases or vacuum drying prior to shutting down the stack is a general approach that has been found to be effective. In short, "keeping the stack warm" and "removal of water" are essentially the two main strategies to counter the cold start issue. The principal targets that automotive PEMFC stacks are required to meet are the ability to start unassisted from –40°C and a cold start-up time to 50% of rated power in 30 s (from –20°C) with a start-up energy consumption of <5 MJ [48]. Most automotive manufacturers have claimed to have achieved the targets although research to understand the phenomenon in detail continues.

Contamination/Impurities PEMFCs are very clean systems and act as filters for impurities introduced from ambient air, fuel used, and even degradation products from the cell materials. Both the membrane and the catalyst are susceptible to contamination and poisoning. Electrode degradation of PEMFCs can occur as a result of various impurities found in the fuel feed, air stream, as well as corrosion by-products from fuel cell components such as the bipolar plate, catalysts, or membrane.

Hydrogen for PEMFCs can come from various sources including reformed fossil fuels. Therefore, depending on the reforming technique and degree of posttreatment, small amounts of contaminants such as CO, CO_2, NH_3, H_2S, etc., are expected to be present in the fuel stream [49]. Trade-offs in the level of impurities are unavoidable since ultrahigh purification would lead to elevated costs of hydrogen. The US FreedomCAR technology team has arrived at preliminary fuel mixture specifications that include: >99.9% H_2, 10 ppb H_2S, 0.1 ppm CO, 5 ppm CO_2, and 1 ppm NH_3. Hydrocarbons such as methane, benzene, and toluene are other common impurity by-products from reforming processes.

Atmospheric air contains 78% nitrogen and 20% oxygen with the remainder being a number of trace gases and particulates depending on the local air quality. Pollutants found in the atmosphere include nitrogen oxides (NO and NO_x), hydrocarbons, carbon monoxide (CO), ozone, sulfur dioxide (SO_2), fine primary and secondary particulate matter, and chloride salts from the ocean and deicers. Chloride anions adsorb on Pt, occupy reaction sites, and significantly lower the ORR activity; fortuitously, the loss is recoverable simply by flushing out the anions with generated water. The degradation of performance due to 2.5 and 5 ppm SO_2 in the air stream was reported to be about 50% and 80%, respectively, by Mohtadi et al. [50]. The degradation is due to chemisorption of sulfur species on the Pt catalyst, and oxidation by the application of high potentials (CV) reversed the degradation but operation under normal potentials did not [51]. The poisoning mechanism by NO_2 was reported to be dependent on the time of exposure rather than bulk concentration and could apparently be reversed by operation under clean air for 24 h. Figure 18 depicts the loss in performance of a subscale fuel cell as a result of contamination of the catalyst in the presence of SO_2, H_2S, NO, NO_2, and NH_3 [51]. The PEM is also easily contaminated by cationic impurities that may enter the stack through water, dissolved catalyst cations [52], as well as corrosion products from the bipolar plate. The loss in cell performance is fairly severe due to the lowering of the conductivity of the membrane.

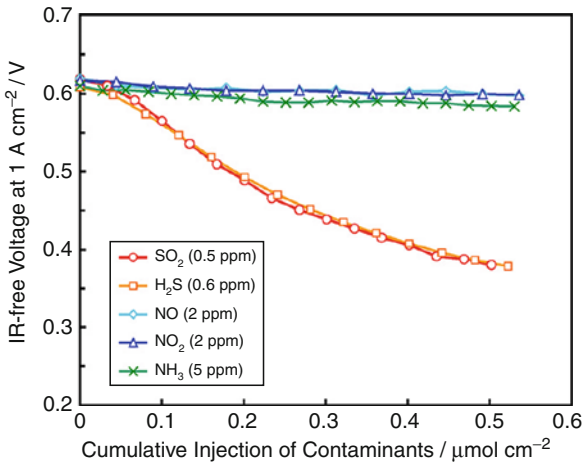

Polymer Electrolyte Membrane (PEM) Fuel Cells, Automotive Applications. Figure 18
The impact of several air contaminants on a fuel cell operated at 1 A/cm^2 [51]

The Status and Targets for Automotive PEMFC Commercialization

The overall status and targets for automotive PEMFC systems as well as hydrogen production, delivery and storage are outlined in Table 1. All of the targets need to be attained for successful commercialization of fuel cell vehicles.

The performance, durability, and cost of PEMFC system and stacks for automotives are approaching levels such that major automotive manufacturers have projected that commercialization will commence around 2015. The US DOE has had cost analysis conducted by independent organizations and estimates assuming 500,000 units/year indicate that system cost has been lowered from $275/kW in 2002 to $73/kW in 2008 [53, 54]. The target for PEMFC system cost in 2015 is $30/kW. The durability of stacks under automotive conditions is currently around 2,500–3,000 h with the target in 2015 being 5,000 h.

In order to achieve commercialization in 2015, the targets of performance, durability, and cost of the fuel cell components (catalyst, membrane, diffusion media, bipolar plates, etc.,) and the system (thermal, fuel, air, and water management, and balance of plant) have to

Polymer Electrolyte Membrane (PEM) Fuel Cells, Automotive Applications. Table 1 Overall status and targets for PEMFC systems, hydrogen storage, production, and delivery [48]

	Status	Target
Fuel cell system cost	$61/kW	$30/kW
Fuel cell system durability	2,000–3,000 h	5,000 h
Hydrogen production	$3–$12/gge	$2–$3/gge
Hydrogen delivery	$2.30–$3.30/gge	$1/gge
Hydrogen storage gravimetric	3.0–6.5 wt.%	7.5 wt.%
Hydrogen storage volumetric	15–50 g/L	70 g/L
Hydrogen storage cost	$15–$23/kWh	$2/kWh

be met simultaneously. For example, high durability can easily be achieved by utilizing high loadings of Pt catalyst, corrosion-resistant bipolar plates with expensive coatings, etc., but this would violate the cost targets. It is required to maintain the performance of PEMFC stacks of today while at the same time lower the precious metal catalyst loadings by a factor of 4–10 and increase the stack durability by a factor of ~2.

Basis for Targets The targets of performance and durability of PEMFC stacks are loosely based on that of IC engines used in automotives today. Durability targets are being addressed by organizations such as the US DOE's Office of Energy Efficiency and Renewable Energy's Hydrogen Fuel Cells and Infrastructure (HFCIT) program in close association with national laboratories, universities, and industry [48], the New Energy and Industrial technology Development Organization (NEDO) in Japan [55] and The European Hydrogen and Fuel Cell Technology Platform (HFP) and Implementation Panel (IP) in Europe. The Fuel Cell Commercialization Conference of Japan (FCCJ) have also published a booklet defining performance, durability, and cost targets in collaboration with Nissan, Toyota, and Honda and a summary has been reported elsewhere [56]. Overall, the general 2015 target for fuel cell stack durability (in cars) is roughly defined to be 5,000 h (150,000 driven miles) at the end of which ~10% performance degradation is allowable. This includes ~30,000 cycles of start-up/shutdown, ~300,000 cycles of wide span load, and hours of idling. So far ~3,000 h of stack life with low degradation rates has been demonstrated and steady progress is being made toward the final goal. An additional durability enhancement by a factor of <2× is needed for attaining the commercialization targets of 2015.

The cost breakdown of PEMFC systems is as illustrated in Fig. 19: The most expensive component (22% of system cost) is the precious metal (~\$40/g_{Pt}) catalyst used on the anode and cathode of each cell. Figure 20 shows the estimated reduction in cost of PEMFC stack system that has been achieved between 2002 and 2009. Figure 21 charts the breakdown of cost by subsystem and component for automotive PEMFC stacks.

Electrocatalyst Targets The amount of Pt currently being used in ultra low emission IC engine automobiles (Pt, Pd, Rh, etc.,) used in automotive catalytic converters can be as high as 6–10 g. This provides a justification for limiting the amount of Pt in a stack to ~10 g (in a typical 100 kW stack) or ~0.1 g_{Pt}/kW. (The target recommended by DOE is ~0.2 g_{Pt}/kW [48]. Recycling of Pt used in fuel cells has been evaluated extensively by Tiax and the conclusion is that more than 90% of the Pt in fuel cell

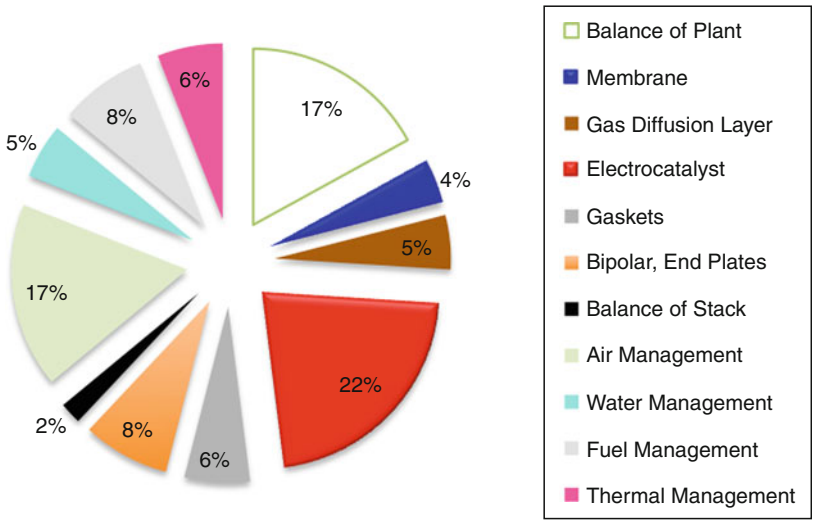

Polymer Electrolyte Membrane (PEM) Fuel Cells, Automotive Applications. Figure 19
Cost structure for automotive PEMFC stack system [53, 54]

stacks is recyclable. Table 2 outlines the latest targets for automotive PEMFC electrocatalyst activity and costs.

Membrane Targets Today's membranes show excellent protonic conductivity (~100 mS/cm) at 100% RH and temperatures below 80°C. PFSA membranes have been improved over the last few years to also achieve durability values that are approaching the target values of 5,000 h. These improvements involve modification of PFSA membranes by varying the casting conditions, thermal pretreatments, forming composites, employing reinforcements, using different lengths of pendant side chains, fluorinating the end groups, etc. In particular, micro-reinforced membranes (such as those from W. L. Gore [57]) allow for the use of thinner membranes that result in the use of less ionomer, improve the back diffusion of water, lower the protonic resistance, and generally result in higher power density fuel cells.

For automotive operation, it would be helpful to have a membrane material that could function with high proton conductivity at a low RH and higher temperatures. It would allow for simplified humidification systems and improved heat rejection (smaller radiator) and improved cell performance (mass transport) is expected due to the absence of liquid water. Membranes that exhibit sufficient conductivity at high temperature by retaining water necessitate the use of higher stack pressures (and higher parasitic compressor-related

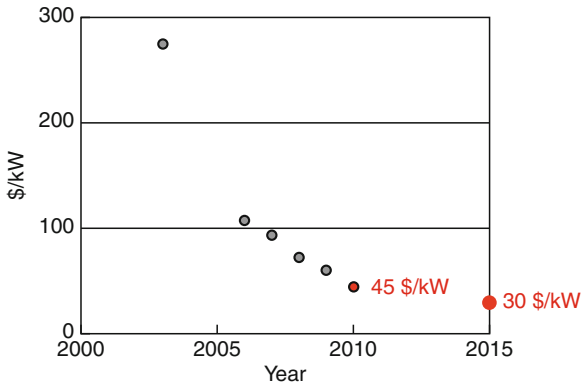

Polymer Electrolyte Membrane (PEM) Fuel Cells, Automotive Applications. Figure 20
Reduction in cost of PEMFC stack system since 2002 and projected values and target for 2010 and 2015 [53]

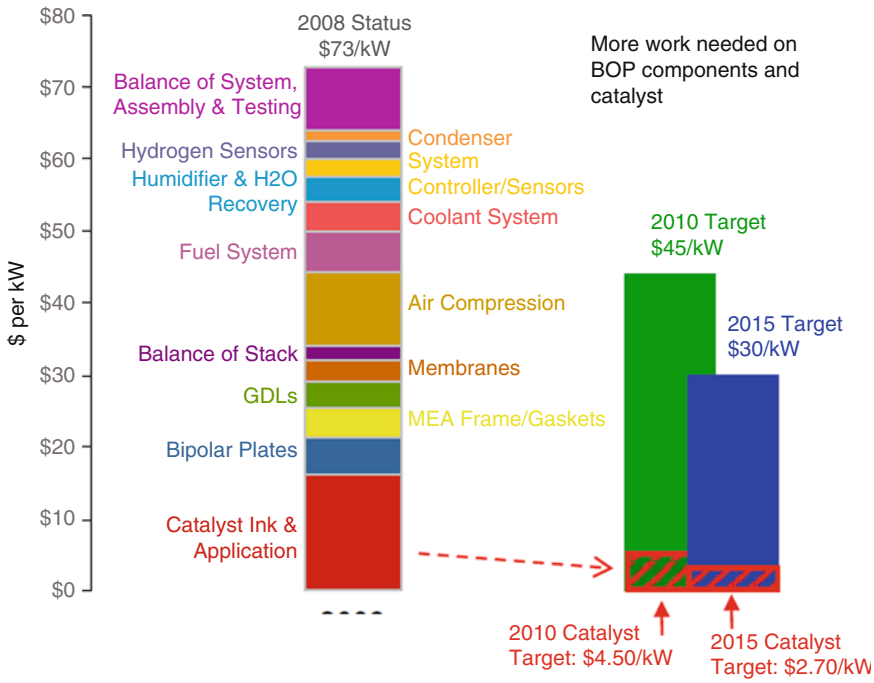

Polymer Electrolyte Membrane (PEM) Fuel Cells, Automotive Applications. Figure 21
Breakdown of cost by subsystem and component for automotive PEMFC stacks [53]

Polymer Electrolyte Membrane (PEM) Fuel Cells, Automotive Applications. Table 2 Targets for automotive PEMFC electrocatalyst activity and costs. Mass Activity @ 0.90 V, $H_2|O_2$, 80°C, P_{H2}, P_{O2} = 100 kPa (based on multiple sources)

	2010 Status	2015 Target
Mass activity	150 mA/mg	450–600 mA/mg
Mass of Pt per 100 kW stack	~30–40 g	~10 g

losses) especially as the temperature exceeds the boiling point of water at ambient pressure.

A cheaper hydrocarbon membrane is also desirable. Hydrocarbon membranes prepared from aromatic block copolymers constituted of alternating rigid sulfonic acid segments with hydrophobic polymeric units that are flexible has been reported. The unique morphology of the membrane provides comparable chemical stability as PFSA commercial membranes with high durability and a wide operating temperature range. Such membranes are already being used by automakers such as Honda. Other hydrocarbon-based membranes that are being actively researched include the use of disulfonated poly(arylene ether) sequenced block and random copolymers [58].

The key requirements for survivability and durability of membranes used in PEMFCs are mechanical durability (RH cycling, subzero start-up, shorting) and chemical durability (OCV holds). Survivability refers to the ability of the membrane to withstand operating conditions without the formation of pinholes that would lead to catastrophic hydrogen crossover and stack failure. Under subzero conditions, membranes can fail if the stack is not designed to eliminate most of the water in the flow fields to prevent formation of ice that can penetrate and damage the membrane on start-up. Durability refers to the slow thinning of the membrane over thousands of hours resulting in increased hydrogen crossover, membrane thinning, and consequent loss of cell performance. The membrane (restrained in a cell) is mechanically stressed (fatigue) when the fuel cell RH cycles between dry and wet conditions; thermal cycles also play a role. In the laboratory, tests have shown that non-reinforced PFSA membranes fail in a few hundred hours or ~6,000 cycles while reinforced membranes last as long as 1,000 h or 60,000 cycles. Shorting is a mechanical degradation leading to electronic leakage currents through the membrane that may occur due to overcompression or penetrating irregularities from the catalyst layer or fibers of the diffusion medium. Shorting failures can be partially mitigated by using lower compression pressures (typically ~1,200 kPa), applying a coating of carbon black–based microporous layer (MPL) on the diffusion medium, etc. Chemical degradation of membranes is accelerated under OCV conditions where the potential is high and no water generated, as well as under generally low RH operation. Chemical degradation of the membrane is measured in terms of the fluoride release rate (FRR in g $F^-/cm^2 \cdot h$) in the collected water; the FRR exhibits Arrhenius dependence with temperature in the range 50–120°C. The FRR is of the order of 1.0×10^{-5} for typical membranes tested under OCV conditions and has been lowered with newer membranes to 1.0×10^{-7}. It should be noted that the mechanism of membrane degradation is not fully understood and is an area of intensive research. The two commonly invoked mechanisms are based on the assumption that hydrogen peroxide formed in the catalyst layer or at the Pt band in the membrane forms a hydroxyl radical which decomposes the membrane/ionomer by unzipping the less stable end groups or by scission of the main polymer chain. In actuality, mechanical and chemical degradation occur simultaneously in fuel cells accelerating the failure of the membrane.

The targets for membrane performance and durability based on figures reported by Nissan, USDOE, and the FCCJ are very similar. In order to be able to design a system that can reject heat at peak power, the fuel cell stack needs to operate for short spurts of time at temperatures as high as 90–95°C. At this time, most fuel cell stacks operate at about 80°C due to the restrictions of system complexity, parasitic (compressor) losses and humidification requirements. The membrane is targeted to operate at temperatures above 100°C (preferably 120°C) at RH <30% while exhibiting a membrane conductivity of >100 mS/cm. The durability targets are similar to that for the complete fuel cell and includes <10% performance loss over 5,000 h/10 years of operation under automotive conditions that include start-up/shutdown, load cycling, freeze (–40°C) and idling. The target cost of the membrane is \$10–20/m^2

for production levels of 10 million m^2/year. More detailed membrane performance targets base on USDOE and other sources are detailed in Table 3.

Bipolar Plate Targets Graphite bipolar plates have been used for a long time and are still being used in some fuel cell stacks. Graphite has a very high electronic conductivity, low interfacial contact resistance (ICR) and high corrosion resistance. Disadvantages of graphite bipolar plates are the high cost of material and machining, increased stack volume, high gas permeability, etc., although high volume manufacturability is somewhat better with polymer–carbon fiber and composite bipolar plates. Graphite–polymer composite plates have also been researched to improve the manufacturability of graphite plates while maintaining conductivity and stability with temperature. Bare metal plates do not have the disadvantages mentioned above but suffer from high ICR and poor corrosion resistance that can lead to metal dissolution and possible poisoning of the PEMFC stack components. The dissolved metal ions can contaminate/lower the conductivity of the membrane by taking up ion exchange sites or adsorb on the catalyst and lower its activity. The stacks are generally tolerant to about 5–10 ppm of metal ion contamination. At the compression forces of relevance to PEMFCs, the USDOE bipolar plate areal resistivity target for ICR is 10 mΩ-cm^2.

Polymer Electrolyte Membrane (PEM) Fuel Cells, Automotive Applications. Table 3 Targets for selected properties of automotive PEMFC membranes [48]

	2015 Targets
Cost	\$5/kW; \$20/m^2
Conductivity/resistance @ Operating T, RH	70 mS/cm; 20 mΩ-cm^2
Conductivity/resistance @ −20 C	10 mS/cm; 200 mΩ-cm^2
Min. electrical resistance	1.0 kΩ-cm^2
Max. O_2 Crossover	<1 mA/cm^2
Max. H_2 Crossover	<2 mA/cm^2
Durability	>5,000 h
Survivability	–40°C to 120°C
RH cycles	20,000
OCV Lifetime	500 h

Stainless steels, as well as Al-, Ni-, and Ti-based alloys have been studied extensively as possible candidates for bipolar plates. One of the most well-studied materials for bipolar plates is SS 316/316L (16–18% Cr, 10–14% Ni, 2% Mo, rest Fe); other candidates are 310,904L, 446, and 2205. Bare stainless steel plates form a passive 2–4 nm chromium oxide surface layer under PEMFC conditions that leads to unacceptably high ICRs. A similar trend is observed for the other alloys and therefore surface modification or surface coatings on selected substrate material has to be considered as a pathway to meet the technical targets of low ICR and high corrosion resistance.

Coatings may be metal based such as gold, TiN, CrN, metal carbides, etc.; carbon-based such as diamond-like carbon, graphite, graphite platelets, carbon–resin composites, conductive tin oxides, etc. Coatings have to be compatible with the substrate bare metal and have good adhesion and peel resistance.

An additional requirement that has to be satisfied is a high level of surface hydrophilicity. Non-wettable plate surfaces result in unstable reactant flows that have to be countered with higher pressure drops and gas stoichiometries and hence higher parasitic power drains. This requirement has lead to the development of hybrid coatings that can provide the low ICR and high wettability. At this time, the bipolar plates account for 75% of the total stack weight and x% of the stack cost. Table 4 summarizes some of the targets for bipolar plates for automotive fuel cells.

Polymer Electrolyte Membrane (PEM) Fuel Cells, Automotive Applications. Table 4 Technical targets for automotive PEMFC bipolar plates [48]

	2015 USDOE Target
Cost	\$3.00/kW
Weight	0.4 kg/kW
Hydrogen permeation @ 80°C	2×10^{-6} $cm^3/cm^2/s$ @ 80 C, 3 bar
Corrosion	1 μA/cm^2
Resistivity	10 mΩ-cm
Flexural strength	25 MPa
Flexibility	3–5% deflection @ midspan

Recent Progress in Fuel Cell Vehicles

Over the last decade, tremendous improvements have been made in PEMFC stacks used in fuel cell vehicles. Table 5 shows the status of selected metrics for the latest generation PEMFC stacks based on information published in the literature and through news announcements. Most of the FCVs produce peak power around 100 kW, use hydrogen compressed at 35 or 70 MPa (4–10 kg), and have a range, top speed, and acceleration that are approaching ICE vehicles. Most of these FCV are hybrids that employ a NiMH or Li-ion battery that helps improve the efficiency by storing energy during regenerative braking and deceleration and supplying energy during acceleration or idling.

In particular, some of the improvements reported by General Motors, Nissan, Toyota, and Honda in their latest generation stacks are discussed.

The main specifications for General Motor's Chevy Equinox are shown in Table 5; additionally, the vehicles employ a 93 kW generator, a 250 V, 35 kW Ni-MH battery and three carbon fiber pressurized (700 bar) hydrogen tanks. As part of a plan called "Project Driveway," 100 of these vehicles were deployed in California, New York, and DC to gage marketability based on customer response. Figure 22 shows schematics of the last two generations: GEN1FCs and GEN2FCS of GM's fuel cell systems comparing the improvements in various metrics. The Pt content in the GEN2FCS stack has been lowered to 30 g from 80 g and the stack and system volume reduced by almost 50%.

The specifications of the Nissan X-Trail FCV can be found in Table 5. Nissan has reported that their latest stacks incorporate reduced Pt catalyst loadings by a factor of 2, almost doubled the power density to 1.9 kW/L and improved the stack durability significantly. A comparison of their latest fuel cell stacks along with specifications is shown in Fig. 23.

Since the first Toyota FCHV launch in 2002, several improvements have been made to the technology. Toyota engineers have extended vehicle range and improved durability and efficiency through improvements in the fuel cell stack and the high-pressure hydrogen storage system, with additional cost reductions in materials and manufacturing. The FCHV-adv boasts a 150% improvement in range compared to the first-generation FCHV. In a real-world driving test carried out in 2008 in collaboration with the US Department of Energy, Savannah River National Laboratory and the National Renewable Energy Laboratory, the FCHV-adv averaged the equivalent of 68 mpg and achieved an estimated range of 431 miles on a single fill of hydrogen compressed gas.

The specifications for Honda's FCX Clarity that is being leased in Southern California can be found in Table 5; additional specs include a DC brushless motor of 100 kW and a 288 V Li-ion battery. Honda has claimed progress in several technologies that they have employed in their FCX Clarity FCV including

Polymer Electrolyte Membrane (PEM) Fuel Cells, Automotive Applications. Table 5 Published metrics (multiple sources including manufacturer websites) for the latest generation of selected fuel cell vehicles

Vehicle/metric	Vehicle model	Power kW/hp	H_2 (kg, MPa)	Range (miles/km)	Time (0–60 mph) (s)	Top speed (mph)
GM	Chevy Equinox	104/140	4.2, 70	190/306	12	100
Nissan	X-Trail FCV	130/174	4.0, 70	310/500	10	95
Toyota	FCHV adv.	90/120	5.7, 70	520/835	10	97
Honda	FCX clarity	100/134	4.0, 35	240/386	9	100
Ford	Explorer FCEV	90/120	10, 70	350/564	18	87
Kia	Borrega FCV	115/154	7.0, 70	426/685	12.8	100
Daimler	F-cell, B-Klasse	90/120	4.1, 70	240/385	11.4	106

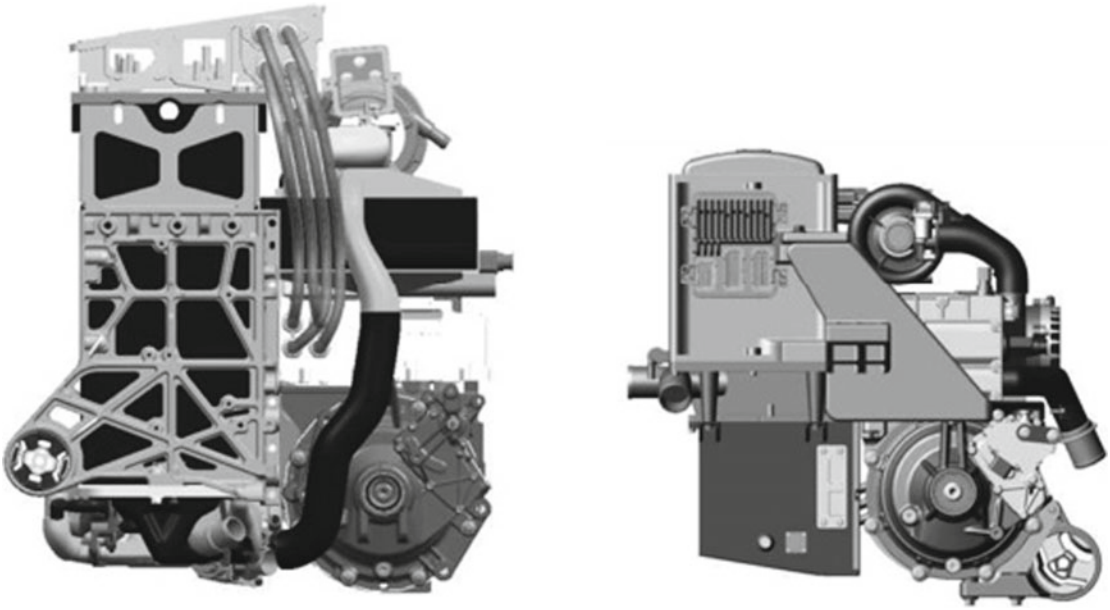

GENI FCS (GMT101X)		GEN2 FCS (GMT/E)
104	Stack Size (L)	64
80	Platinum (g)	30
405	System Size (L)	191
250	System Mass (kg)	130
62	Peak Power @ 150,000 miles (kW)	78
187	System Part Numbers	120
1903	System Part Count	1100

Polymer Electrolyte Membrane (PEM) Fuel Cells, Automotive Applications. Figure 22
Improvements in power density, Pt loading, and system simplification for last two generations of General Motors FCV stacks [24]

Specifications	
Max. Power	90 kW
Volume	90 L
Weight	116 kg

Specifications	
Max. Power	130 kW
Volume	68 L
Weight	86 kg

Polymer Electrolyte Membrane (PEM) Fuel Cells, Automotive Applications. Figure 23
Improvements in stack power density for the last two generations of Nissan's in-house PEMFC stacks [46]

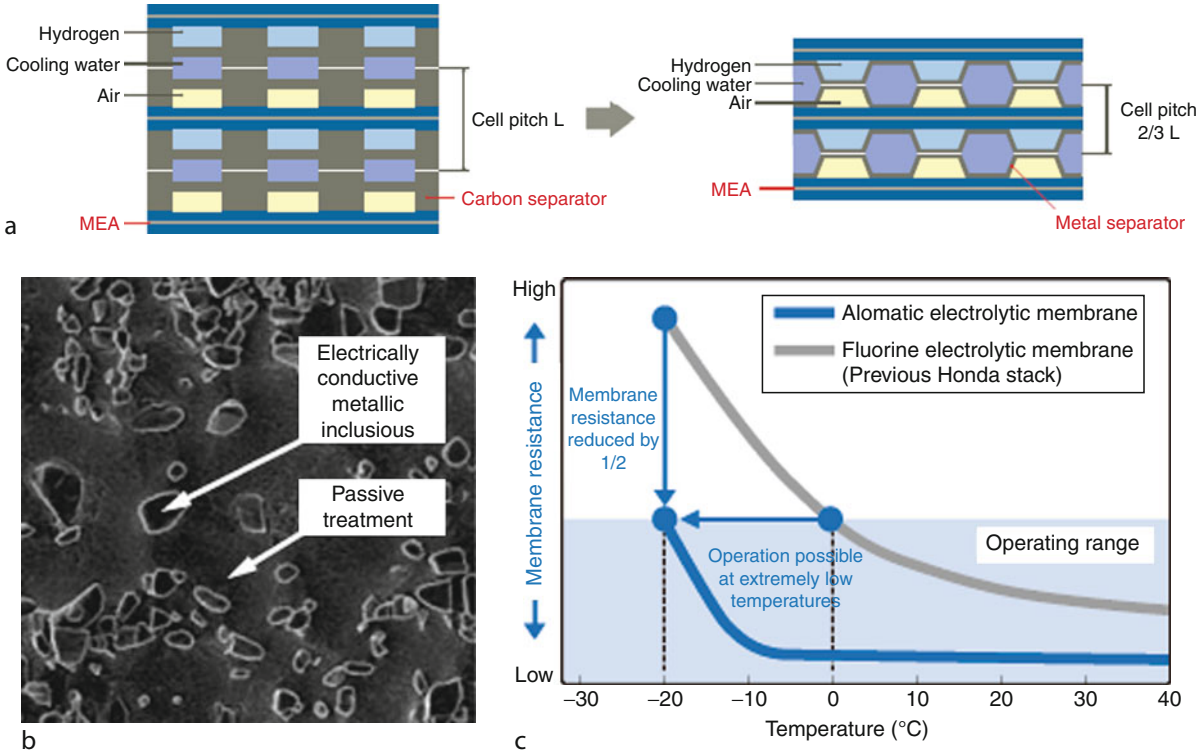

Polymer Electrolyte Membrane (PEM) Fuel Cells, Automotive Applications. Figure 24
Advances in Honda's recent automotive fuel cell stacks components of membrane and bipolar plates [31]

highly conductive aromatic membrane that allows the stack to be operated up to 90°C, thin, stamped metal plates having a high thermal and electrical conductivity. A two sub-stack (V-Flow stacks) configuration takes advantage of the stiffness of the metal separators to generate a structure in which the stack is encased by panels, resulting in efficient packaging. Figure 24 illustrates some of these improved technologies.

Future Directions

Direct hydrogen-fuel-cell-powered vehicles have reached a level of development where the major automotive companies have publicly announced that initiation of commercialization is imminent around 2015. The targets of performance, durability, and cost agreed upon by various organizations, including the US DOE, appear to be achievable in the specified time frame. Well-delineated pathways and strategies have been established to address the barriers of cost and durability of PEMFC stacks and achieve the automotive targets. The principal directions for reduction of cost and enhancement of durability of key fuel cell components, i.e., electrocatalysts, membranes, and bipolar plates are briefly summarized in this section.

Pt-based electrocatalysts will continue to be used in both the anode and cathode of automotive PEMFCs for the next decade. The current status of catalysts in automotive PEMFCs is a Pt-based carbon black–supported catalyst (20–50 wt.% Pt/C, 2–4 nm, 60–90 m^2/g) with a loading of 0.20–0.35 mg_{Pt}/cm^2 on the cathode and about 0.05 mg/cm^2 on the anode. About 30 g of Pt are required for a 100-kW-rated stack. The rated power usually corresponds to a voltage of 0.60 V at 1–2 A/cm^2. The durability of fuel cell stacks under automotive conditions fall in the range of 3,500 h or 75% of the target life.

Progress has already been made over the years in enhancing the activity of the Pt nanoparticles dispersed on carbon support catalysts by alloying Pt with base metals such as Co, Ni, Fe, Rh, Cu, and Ti. The activity enhancements are a factor of 2–4, although the

performance decreases over time. The Pt-alloys/C also fortuitously exhibit improved durability in part due to their larger particle size and heat treatment. This is a conventional pathway that has already been explored and proven over the last few decades in PTFE-bonded electrodes used in PAFCs. A correlation to the improved activity from alloying is that the oxygen binding weakens as the d-band center shifts [59–61]; a volcano plot of various metals can be obtained with Pt sitting at the top [62]. Also, an increased number of neighboring metal atoms, 3d metal neighbors, as well as compressive strain have all been reported to weaken the oxygen binding to Pt. A positive shift in the onset of oxide observed in cyclic voltammograms indicating oxophobic nature of the surface has also been directly correlated to enhanced ORR activity. Larger Pt particles, heat-treated Pt particles, and alloys of Pt exhibit oxophobic tendencies and concomitant improved activities. More recently, the understanding of the impact of d-band center on the metal–oxygen bond strength has been refined [63]; the entire valence band structure (density of states vs binding energy) affects the bond strength and simplification of the band to a single "d-band center" is not valid. To summarize, the same binary and ternary alloys used previously in acid fuel cells are being implemented in PEMFCs using modified electrode structures.

A well-known weakness of the Pt-alloy approach is the leaching out of the base metal from the surface immediately and from the bulk over time. It has been shown by Stamenkovic et al. [64] that almost all the surface base metal is leached off once in contact with electrolyte; a Pt skeleton structure is formed (or Pt-skin for annealed catalysts) that has higher coordinated Pt atoms and a sublayer enriched in the base metal contributes to the higher activity. Nevertheless, as long as the catalyst activity and fuel cell performance is maintained within the target limits over the life of the stack, it remains an acceptable approach. Fundamental studies on single crystal Pt and Pt-alloys through a "materials by design" approach that involves the simultaneous application of a number of surface spectroscopies to a surface undergoing electrochemistry is being pursued by Markovic et al. [65]. Alloys with controlled crystal orientation such as the PtNi (111) have been demonstrated by Stamenkovic et al. [66] to show extremely high specific activities; it remains a fundamentally important yet difficult approach to implement in practical catalysts. Perturbations in the approach to the use of alloy catalysts are the use of voltammetrically de-alloyed catalysts such as dealloyed $Pt_{25}Cu_{75}$ and $Pt_{20}Cu_{20}Co_{60}$ nanoparticles [67]. Pt-rich surfaces and alloy-rich cores of such materials have been shown to exhibit significantly improved activity for oxygen reduction in acidic media due to a reduced Pt–Pt atomic distance (lattice strain) and also possess superior durability to commercial Pt/C.

Two other pathways being explored to further drastically reduce the Pt loading are: (1) raising the catalyst mass activity (mA/mg) by using a core of base metal coated with monolayers of Pt and (2) applying the concept of high specific activity-extended thin films to a practical catalyst electrode system. The catalysts in the first pathway are often referred to as core-shell catalysts [68, 69]. A deposition technique that involves the replacement of a first UPD metal adlayer with a 2D deposit of a nobler metal monolayer to cover the surface uniformly forms the basis of the technique [70]. In addition to the use of expensive Pt only at the surface where reaction takes place, the use of different subsurface materials enhance the specific activity of the surface Pt layer; a Pt–metal mixed surface monolayer may also be used. About 4–10× enhancement in mass activity has been shown using these catalysts. The use of small quantities of gold clusters [71] on the surface has also shown to enhance the durability of the catalysts under potential cycling. Latest work in the area includes the generation of hollow Pt spheres (4–8 nm hollow spheres having 1–2 nm Pt shells) prepared from Ni templates exhibiting 5× enhancement of activity over solid nanoparticles (measured in rotating disk electrode liquid electrolyte half cells) [72]. Scale-up and evaluation in fuel cells of several of these technologies is currently underway.

For decades, discussion on the enhanced specific activity of larger nanoparticles has raged. Larger nanoparticles of Pt have been found to have both a higher activity as well as a higher durability by several groups [38, 73, 74]. In addition, bulk polycrystalline Pt has been shown to have ~10× higher specific activity that Pt nanoparticle in half-cells using ultra pure nonadsorbing liquid electrolytes such as perchloric acid. Over the last decade, the high specific activity of continuous thin films has finally been demonstrated in

practical MEAs of fuel cells especially by 3M with their NSTF catalysts [75, 76]. Two challenges remain in the widespread use of these catalysts in practical fuel cells: the mass specific surface area (m^2/g) which is ten times lower for these films at this time and significant mass transport resistances due to flooding under humidified conditions due to the thinness of the cathode catalyst layer. Essentially, the catalyst films (~30 nm thick) are not thin enough to provide high mass activity and the electrode structure formed with these catalysts is not thick enough to disperse water easily. Both issues are being addressed by programs funded by the US DOE, and in laboratories elsewhere; the next 5 years will determine the degree of success of this approach [77]. The potential for activity enhancement through these methods is predicted to approach a factor of 10; this would be sufficient to achieve the cost reduction target for catalysts used in the electrodes. Figure 25 outlines the main precious metal pathways for future fuel cell electrocatalysts.

Fundamental research related the formation of surface oxides on Pt [78–80] as well as Pt dissolution [81], although studied in the past, has come to the forefront again. This is due to the current understanding that the dissolution/surface area loss of Pt/C in automotive fuel cells is intensified by the cycling of load and hence

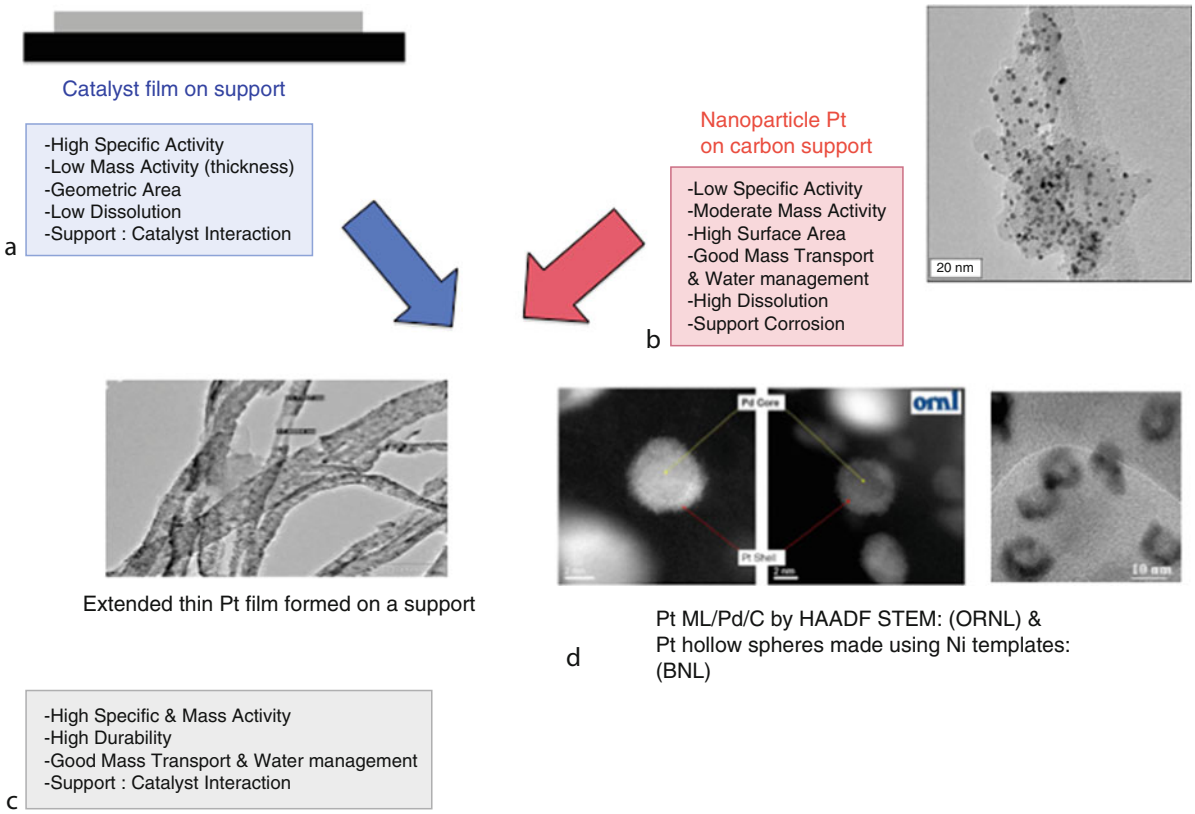

Polymer Electrolyte Membrane (PEM) Fuel Cells, Automotive Applications. Figure 25
Pathways for future electrocatalyst development for automotive PEMFCs. (**a**) Thick films or bulk single crystal and polycrystalline catalysts that are ideal for fundamental studies on surface structure and mechanisms; these materials need to be modified into (**c**) and (**d**) to be applicable to fuel cells. (**b**) Typical commercial nanoparticles (2–4 nm) on a high-surface-area carbon support used in fuel cells at this time; (**c**) Thin continuous films of catalyst on a support such as carbon nanotubes that may provide a physical porous structure for mass transport in a fuel cell; (**d**) Core-shell catalysts where only the shell consists of precious metals and are supported on a typical high-surface-area support [72, 77, 89]

potential [35, 40, 82] along with the trend toward core-shell and nanofilms of catalysts. Operational methods to limit the losses through this understanding of mechanisms as well as material solutions are being actively pursued [32].

An intermediate approach to limit the use of Pt and instead use Pd-based metal alloys has shown reasonable success in activity improvement. Although fairly precious, Pd is currently four times less expensive than Pt. Pd alloyed with Mo, Ta, W, Re, and Cu have all been evaluated. A Pd–Cu (1:1) catalyst composed of 20 nm nanoparticles prepared by co-impregnation showed activity within range of Pt and is being further pursued [63, 83].

Non-precious metal catalysts (non-Pt group metals/non-PGM) research is still in its infancy and lags in activity and durability by a factor of ~10 compared to conventional Pt/C electrocatalysts; they have shown significant progress in terms of improved activity in recently reported work, and research in this field continues as a long-term approach to completely eliminate platinum usage in fuel cells. The target for non-PGM catalyst activity is expressed per unit volume (>130 A/cm^3 @800 mV) since it is the volume/electrode thickness that determines its usability. An example is the C|Fe|N catalyst system that can be synthesized by heat treatment of Fe-N_4 macrocycles as well as individual precursors of the three elements [84, 85]. Lefevre et al. [86] synthesized the catalyst system by utilizing ball-milling to fill microporous carbon with iron ions and pore fillers to obtain higher ORR activity. Carbon supported as well as sputtered transition metal (Cr, Co, Fe)/chalcogens (Se, S) have also been studied with limited success [87]. In research funded by the USDOE, heat-treated, carbon-supported polypyrrole and PANI in the presence of salts of Fe and Co are being investigated in half-cell rotating disk electrodes as well as subscale fuel cells. In comparison to carbon, pyrolyzed carbon, PANI/C, PANI-Co/C, PANI-Fe/C, PANI-Fe_3Co/C exhibited the highest ORR activity of 27 A/cm^3 at 800 mV under $H_2|O_2$; the peroxide yield for PANI-Fe_3Co/C was found to be the lowest at 0.5% [88]. A cyanamide-Fe-C (3.5 mg/cm^2) catalyst has shown catalyst activity in fuel cells of 165 A/cm^3 @ 800 mV in most recent work [89]. Much work is remains to be carried out in the fundamental understanding and characterization of non-PGM catalysts in terms of identification and quantification of the reaction sites and estimating the turnover frequencies and mechanisms for the ORR.

The high-surface-area carbon supports used today enable the use of small nanoparticles of Pt that are well-dispersed; the price paid in using a high-surface-area carbon black is that it tends to be susceptible to corrosion [90–93]. Carbon is thermodynamically susceptible to corrosion in the entire fuel cell operating regime but the kinetics are fortunately very slow. Near and above the open circuit potential of 0.95 V and especially above 1.1 V, the corrosion currents increase. Potentials in the range 1–1.5 V are seen only during uncontrolled start-up and shutdown of fuel cells [43, 94, 95]. Using mitigation techniques based on operating conditions, the highest potential seen is close to the OCV and the losses correspondingly lower. Nevertheless, some carbon corrosion is observed over the life of the fuel cell and material solutions are being actively sought. The material solutions will enable system simplification and lower costs. Alternative non-carbon supports such as titanium, tungsten oxides, nitrides, borides etc., are being studied that can provide a higher corrosion resistance at high potentials and also help anchor the Pt nanoparticles and limit degradation due to particle agglomeration. The main issues with alternative materials is that the corrosion resistance often comes with the cost of lower conductivity, lower surface area, different electrode structure, and the need for new methods to deposit catalysts on them.

Intensive research is being carried out to improve both the membrane performance (conductivity/areal resistance) and durability. The protonic conductivity is typically improved by the use of low EW ionomers; these ionomers swell with water to a greater extent increasing fatigue stresses. Thinner membranes are also being developed to reduce the areal resistance, but often need to be reinforced to provide mechanical strength and suffer from higher reactant permeability and susceptibility to shorting. Thus a trade-off between performance and durability is often unavoidable.

Development of new membrane materials that have the capability of sustaining proton conduction under low RH conditions and at temperatures as high as 120°C has been a struggle. Such a membrane would allow facile water management and also reduce thermal management issues in the stack. Of the two desired

properties, a membrane that operates at low RH with sufficient conductivity is more critical since catalyst (both platinum and carbon) degradation is also suppressed under these conditions.

The approach to synthesizing new membrane material candidates involves obtaining the required properties of conductivity, chemical and mechanical durability by: tailoring or modifying water retention, domain inter-connectivity, lowering the equivalent weight, use of additives such as metal composites and quenchers, stabilizing bonds and end group terminations, use of short side-chains, using reinforcements and cross-linking, raising the glass transition temperature, the use of amphoteric protogenic groups such as imidazole and phosphonic acid, etc. [96, 97]. Inorganics such as titania, silica, and zirconium phosphate have been incorporated into membranes in attempts to maintain conductivity at low RH through tightly bound water in these compounds. The use of amphoteric protogenic groups such as imidazole [98] and phosphonic acid that allow for proton transport in the absence of water has also been pursued [99]. PBI-PA-based membranes at temperatures above 200°C have been investigated by several groups [100] and commercialized by PEMEAS®. These materials suffer from the leaching of phosphoric acid, complex start-up and shutdown, as well as loss of Pt activity due to phosphate anion adsorption. Modifications to this approach include the use of sulfonimides, perfluorinated acids, metal oxides as additives to reduce the anion adsorption and increase the oxygen solubility. Heteropoly acids such as phosphotungstic acid, silicotungstic acid, sulfonated zeolites have been used with partial success [101]. 10–20 wt.% heteropoly acids (not immobilized) were combined with 3 M PFSA ionomers to cast membranes and prepare MEAs; they showed a reduction in the FRR in fuel cell tests under hot dry conditions [100]. Additives in general may not be stable and may leach out over long periods of time and may also change the mechanical properties of the membrane. High-temperature, water-free/water-insoluble, proton-conducting membranes (protic salt polymer membranes) where a salt repeat unit conducts protons with an adjacent unit without the transport of water are also being researched by Gervasio et al. [102]. The membranes are prepared from solvent-free liquid salts known as protic ionic liquids or pILs that are tailored by selecting an acid and base.

Recently, the use of highly electron-poor poly (phenylene) backbones has resulted in ionomers containing sulfone ($-SO_2-$) units connecting the sulfonic acid ($-SO_3H$) functionalized phenyl rings that exhibit high proton conductivity and stability [103]. Some preparation routes have resulted in highly sulfonated material with an exchange capacity of IEC = 4.5 meq/g or an EW of 220 g/eq along with low water transport coefficients. These materials though are water soluble and brittle in the dry state but may still be usable as a component in a PEM. The task of synthesizing and developing such membranes is a difficult task, but even partial success such as obtaining a membrane that can operate at similar temperatures as today but at lower RH will help advance PEMFC stack technology considerably. Hydrophobic-hydrophilic multiblock copolymers ($BPSH_x$-BPS_y; where x = MW of sulfonated poly(arylene ether) and y = MW of poly(arylene ether)) with varying block lengths and controlled morphology that develop order and produce a co-continuous hydrophilic phase for good conductivity at low humidity have also been the subject of research as potential candidates for a new PEM [58].

Incremental engineering modification of membranes is also being carried out with some success. Composite membranes that consist of conductive and nonconductive porous polymer reinforcements have been incorporated for some time into membranes to provide mechanical strength for extremely low thicknesses; they suffer from some loss of conductivity. One approach is to form a composite/polymer blend and decouple the proton conduction from other membrane requirements. Arkema has demonstrated an inexpensive hydrocarbon-based polyelectrolyte blended with polyvinylidene difluoride (PVDF or Kynar) that exhibits similar performance to commercial PFSA membranes [104]. Another approach involves the use of electrospun ionomer fibers embedded in a polymer [105]. 3 M has reported the fabrication of 825 EW non-reinforced membranes with new additives that meet the targets of 20,000 RH cycles and 500 h OCV test in fuel cells [106]. Giner Electrochemical Systems [107] has reported on the development of dimensionally stable membranes (DSM) with

laser-drilled supports composed of polysulfone or polyimide (Kapton) or that lowers the swelling of high acid content PFSA ionomers. Asahi Glass Co., [108, 109] has reported a new polymer composite membrane (based on PFSAs) in PEMFCs operating at 120°C, 50% RH for ~4,000 h; the MEA tested in fuel cells had a degradation rate of 75 μV/h and a FRR of less than 1% of the baseline control. Chemical modification of PFSA membranes is being carried out to minimize the non-fluorinated end groups susceptible to degradation. Additives such as Ce^{3+} and Mn^{2+} ions added in trace quantities into the membrane and ionomer have also been demonstrated to improve the chemical stability.

Although the focus of this article is on PEMs that are being used in automotive fuel cells today, brief mention must be made of work carried out on alkaline anion exchange membranes (AAEMs). Such membranes have the potential to exhibit sufficient activity when used with non-precious metal catalysts, may work with fuels such as methanol and ethylene glycol and provide some of the features that commercial PFSA membranes provide for PEMFCs. A cross-linked, water-insoluble, OH^--conducting, alkaline polymer free of metal ions and consisting of counter ions bound to the quaternary-ammonium containing polymer backbone has been reported with reasonable preliminary results (133–153 μm thick, 0.0092 S/cm @ 30°C, 100%RH) [110]. H_2|Air alkaline membrane fuel cells that showed encouraging preliminary results with Pt and transition metal catalyst cathodes in CO_2 free air have also been reported recently by Acta S.p.A. [111].

Graphite-based bipolar plates have been used in PEMFC stacks, they suffer from drawbacks such as higher manufacturing costs, greater thicknesses, higher gas permeability that is necessary for high power density automotive fuel cell stacks. Metal bipolar plates (stainless steel, Ni, Ti, Al-based alloys) on the other hand possess high thermal conductivity, high mechanical and flexural strength, and facile high volume production but tend to corrode and require corrosion-resistant and conductive coatings that increase their cost [112]. New coatings are under development along with thinner stamped plates with most of the details being proprietary at this time. An example is thermal nitriding of thin (0.1 mm foils, Fe-20Cr-4 V and type 2205) stainless steel plates to generate surface layers of Cr_2N, CrN, TiN, V_2N, etc., that lowers the interfacial contact resistance and raises the corrosion resistance simultaneously [113]. The additional requirement of hydrophilicity to facilitate water management in the flow fields has lead to the development of hybrid coatings that is capable of providing a low ICR and high wettability. Super-hydrophilicity has been shown by layer-by-layer deposition of silica nanoparticles onto bipolar plates, which meets the other requirements [114]. Electrostatic layer-by-layer techniques have been employed to generate 100 nm coating structures that are constituted from 5 to 10 nm graphite platelets and 19 nm silica nanospheres. A low ICR of 4 mΩ-cm^2 and a high degree of hydrophilicity is simultaneously achieved by this method.

Figure 23 in the previous section showed the improvement in Nissans latest generation stack achieved by using metal separators instead of carbon. Figure 24 illustrates schematically novel surface treatments on stainless steel bipolar plates along with electrically conductive inclusions that help maintain high conductivity and corrosion resistance at the same time. Intensive applied research is being carried out to obtain thin, corrosion-resistant conductive bipolar plates modified with coatings that are inexpensive and conducive to high-speed/high-volume manufacturing.

A combination of synergistic improvements in the catalyst, support, gas diffusion layers, membrane, and essentially the entire porous electrode structure in conjunction with bipolar plates/flow fields is expected to improve the mass-transport of reactant gases, protons, and water management. Thus, an increase in the peak current density (A/cm^2) and peak power density (W/cm^2) will result; this in turn will lower the stack volume, the amount of catalyst, and membrane material used and raise the kW/L, kW/kg, and lower the $/kW stack metrics. It should be noted that the rated or peak power for automotive stacks is based in part on maintaining an electrical efficiency of >50%; this dictates that the cell voltage has to be maintained above ~0.60 V. At this time, volumetric power densities of practical stacks in fuel cell vehicles have been reported to be as high as ~2 kW/L [46] and are likely to increase over the next few years contributing to lower stack costs ($/kW).

Trends in short- and longer-term directions for key fuel cell components including electrocatalysts/supports,

membranes, and bipolar plates have been elaborated in this section; improvement of the performance and durability of these components will directly impact the entire automotive fuel cell system requirements, complexity, and cost. Durable catalysts with enhanced ORR activity, durable membranes that perform at very low humidity and durable bipolar plates that have low contact resistance will not only increase the power density and cost of the fuel cell stack but also simplify and lower/eliminate system component costs of the air compressor, humidification systems, recycle pumps, radiator, start-up/shutdown and freeze-start-related components, etc. A combination of advances in all the fuel cell components discussed above, system simplification, governmental policies that are sensitive to sustainable clean energy, and development of a hydrogen infrastructure will enable achieving the projected technical and cost targets needed for automotive fuel cell commercialization.

Bibliography

Primary Literature

1. Grove WR (1842) On gaseous voltaic battery. Phil Mag 3:417
2. Schonbein CF (1839) Phil Mag 14:43
3. Mond L, Langer C (1889) Proc Roy Soc 46:296
4. Jacques WW (1897) Electricity direct from coal. Harpers Mag 94:144–150
5. Baur E, Tobler J (1933) Brennstoffketten Z Elektrochem 39:169–180
6. Schmidt TJ, Paulus UA, Gasteiger HA, Behm RJ (2001) Peroixde rde, anion adsorption effect. J Electroanal Chem 508:41–47
7. Tobler J (1933) Z Elektrochem 39:148
8. Nernst W (1904) Z Phys Chem 47:52
9. Tafel J, Emmert B (1905) Ueber die ursache der spontanen depression des kathodenpotntials bei der eletrolyse verduennter schwefelsaeure. Zeit Phys Chem 50:349–373
10. Liebhavsky HA, Cairns EJ (1968) Fuel cells and batteries. Wiley, New York
11. Vielstich W (1965) Fuel cells. Wiley-Interscience, London
12. Maget HJR (1967) in: Berger C (ed) Handbook of fuel cell technology. Prentice-Hall, Englewood Cliffs, NJ, pp 425–491
13. Liebhavsky HA, Grubb WT Jr (1961) The fuel cell in space. ARS J 31:1183–1190
14. AFC A (2003) Alkaline fuel cells. In: Vielstich W, Lamm A, Gasteiger H (eds) Handbook of fuel cells-fundamentals, technology and applications. Wiley, New York
15. Kordesch KV (1978) 25 years of fuel cell development (1951-1976). J Electrochem Soc 125:77 C–91 C
16. Grubb WTJ (1959) US Patent 2,913,511
17. Niedrach LW, Alford HR (1965) J Elecrochem Soc 112:117
18. Thomas CES (2007) Greenhouse gas results. http://www.cleancaroptions.com/html/greenhouse_gas_results.html
19. DOE US (2010) Well-to-wheels greenhouse gas emissions. http://www.hydrogen.energy.gov/pdfs/9002_well-to-wheels_greenhouse_gas_emissions_petroleum_use.pdf
20. IPCC (2007) The IPCC assessment reports. http://www.ipcc.ch/
21. Koppel T (1999) Powering the future: The ballard fuel cell and the race to change the world. Wiley, New York
22. Taub A (2009) The opportunity in electric transportation. http://www.ncsc.ncsu.edu/cleantransportation/docs/Events/2009_5-27_Taub_GM-EV.pdf
23. GreenCarCongress: GM highlights engineering advances with second generation fuel cell system and fifth generation stack; poised for production around 2015. http://www.greencarcongress.com/2009/09/gm-2gen-20090928.html
24. ChevyEquinox (2010) Chevy equinox fuel cell. http://www.gm.com/vehicles/innovation/fuel-cells/
25. AutoBlogGreen (2010) 2008 chevy equinox fuel cell. http://green.autoblog.com/photos/2008-chevrolet-equinox-fuel-cell/#380179
26. UTCPower (2010) UTC power: Transportation\automotive. http://www.utcpower.com/fs/com/bin/fs_com_Page/0,11491,0151,00.html
27. F-cell M-BB-c (2010) 2010 mercedes-benz b-class f-cell. http://www.caranddriver.com/news/car/09q3/2010_mercedes-benz_b-class_f-cell-car_news
28. FCHV-adv T (2010) Fuel cell technology. http://www2.toyota.co.jp/en/tech/environment/fchv/
29. Pressroom T (2010) Toyota fuel cell vehicle demonstration program expands. http://pressroom.toyota.com/pr/tms/toyota/toyota-fuel-cell-vehicle-demonstration-151146.aspx
30. NissanHistory (2010) The history of Nissan's fuel-cell vehicle development. http://www.nissan-global.com/EN/ENVIRONMENT/CAR/FUEL_BATTERY/DEVELOPMENT/FCV/index.html
31. Honda (2010) Honda: Fuel cell electric vehicle. http://world.honda.com/FuelCell/
32. Uchimura M, Sugawara S, Suzuki Y, Zhang J, Kocha SS (2008) Electrocatalyst durability under simulated automotive drive cycles. ECS Trans 16:225–234
33. Kocha SS (2003) Principles of mea preparation. In: Vielstich W, Lamm A, Gasteiger H (eds) Handbook of fuel cells-fundamentals, technology and applications. John Wiley & Sons, Ltd., New York, pp 538–565
34. Kocha SS, Yang DJ, Yi JS (2006) Characterization of gas crossover and its implications in PEM fuel cells. AIChE J 52:1916–1925
35. Uchimura M, Kocha S (2007) The impact of cycle profile on PEMFC durability. ECS Trans 11:1215–1226
36. Ohma A, Suga S, Yamamoto S, Shinohara K (2007) Membrane degradation behavior during OCV hold test. J Electrochem Soc 154:B757–B760
37. Sugawara S, Maruyama T, Nagahara Y, Kocha SS, Shinohara K, Tsujita K, Mitsushima S, Ota K-i (2009) Performance decay of proton-exchange membrane fuel cells under open circuit conditions induced by membrane decomposition. J Power Sources 187:324–331

38. Gasteiger HA, Kocha SS, Sompalli B, Wagner FT (2005) Activity benchmarks and requirements for pt, pt-alloy, and non-pt oxygen reduction catalysts for PEMFCS. Appl Catal B Environ 56:9–35
39. Mathias MF, Makharia R, Gasteiger HA, Conley JJ, Fuller TJ, Gittleman CJ, Kocha SS, Miller DP, Mittelsteadt CK, Tao X, Yan SG, Yu PT (2005) Two fuel cell cars in every garage? Electrochem Soc Interface 14:24–35
40. Uchimura M, Kocha SS (2007) The impact of oxides on activity and durability of PEMFCS. AIChE Journal Abstract No. 295b
41. Uchimura M, Kocha SS (2008) The influence of Pt-oxide coverage on the ORR reaction order in PEMFCs. ECS Meeting, Honolulu, HI 12–17 Oct 2008
42. Kocha SS, Gasteiger HA (2004) The use of Pt-alloy catalyst for cathodes of PEMFCS to enhance performance and achieve automotive cost targets. Fuel Cell Seminar, San Antonio, TX
43. Reiser CA, Bregoli L, Patterson TW, Yi JS, Yang JD, Perry ML, Jarvi TD (2005) A reverse-current decay mechanism for fuel cells. Electrochem Solid-State Lett 8:A273–A276
44. Reiser CA, Yang D, Sawyer RD (2005) Procedure for shutting down a fuel cell system using air purge. US Patent 6,858,336, 22 Feb 2005
45. Reiser CA, Yang DJ, Sawyer RD (2005) Procedure for starting up a fuel cell system using a fuel purge. US Patent 7,410,712, 12 Aug 2008
46. Shimoi R, Aoyama T, Iiyama A (2009) Development of fuel cell stack durability based on actual vehicle test data: Current status and future work. SAE International 2009-01-1014
47. Merzougui B, Halalay IC, Carpenter MK, Swathirajan S (2006) Conductive matrices for fuel cell electrodes. General Motors, US Patent Application 20060251954
48. DOE US (2007) Fuel cell targets. http://www1.eere.energy.gov/hydrogenandfuelcells/mypp
49. Borup RL, Meyers JP, Pivovar B, Kim YS, Mukundan R, Garland N, Myers DJ, Wilson M, Garzon F, Wood DL, Zelenay P, More K, Stroh K, Zawodizinski TA, Boncella J, McGrath J, Inaba M, Miyatake K, Hori M, Ota K-i, Ogumi Z, Miyata S, Nishikata A, Siroma Z, Uchimoto Y, Yasuda K, Kimijima K-i, Iwashita N (2007) Scientific aspects of polymer electrolyte fuel cell durability and degradation. Chem Rev 107:3904–3951
50. Mohtadi R, Lee WK, Zee JWV (2004) So_2 contamination. J Power Sources 138:216–225
51. Nagahara Y, Sugwara S, Shinohara K (2008) The impact of air contaminants on PEMFC performance and durability. J Power Sources 182:422–488
52. Kocha SS, Gasteiger HA (2004) Platinum alloy catalysts for PEMFCs. Henry B. Gonzalez Convention Center, San Antonio, TX. http://www.fuelcellseminar.com/past-conferences/2004.aspx
53. Satyapal S (2009) Hydrogen program overview. http://www.hydrogen.energy.gov/pdfs/review09/program_overview_2009_amr.pdf
54. Satyapal S (2009) Fuel cell project kickoff. http://www1.eere.energy.gov/hydrogenandfuelcells/pdfs/satyapal_doe_kickoff.pdf
55. NEDO (2007) Nedo homepage. http://www.nedo.go.jp/nenryo/gijutsu/index.html:
56. Iiyama A, Shinohara K, Igushi S, Daimaru A (2009) Membrane and catalyst performance targets for automotive fuel cells. In: Vielstich W, Gasteiger HA, Yokokawa H (eds) Handbook of fuel cells-advances in electrocatalysis, materials, diagnostics and durability. John Wiley & Sons, Ltd.,
57. Cleghorn S, Griffith M, Liu W, Pires J, Kolde J (2007) Gore's development path to a commercial automotive membrane electrode assembly. http://www.fuelcellseminar.com/past-conferences/2007.aspx
58. McGrath J (2007) Advanced materials for proton exchange membranes. DOE Hydrogen Program Merit Review Presentation. http://www.hydrogen.energy.gov/pdfs/review07/fc_23_mcgrath.pdf
59. Luczak FJ (1976) Determination of d-band occupancy in pure metals and supported catalysts by measurement of the liii x-ray absorption threshold. J Catal 43:376–379
60. Mukerjee S, Srinivasan S, Soriaga MP, McBreen J (1995) Role of structural and electronic properties of Pt and Pt alloys on electrocatalysis of oxygen reduction. J Electrochem Soc 142: 1409–1422
61. Nagy Z, You H (2002) Applications of surface x-ray scattering to electrochemistry problems. Electrochim Acta 47:3037–3055
62. Jalan V, Taylor EJ (1983) Importance of interatomic spacing in catalytic reduction of oxygen in phosphoric acid. J Electrochem Soc 130:2299–2302
63. Myers D (2009) http://www.hydrogen.energy.gov/pdfs/review09/fc_20_myers.pdf
64. Stamenkovic VR, Fowler B, Mun BS, Wang G, Ross PN, Lucas CA, Markovic NM (2007) Improved oxygen reduction activity on Pt3Ni(111) via increased surface site availability. Science 315:494–497
65. Markovic NM, Ross PN (2000) Electrocatalysts by design: From the tailored surface to a commercial catalyst. Electrochim Acta 45:4101–4115
66. Stamenkovic VR, Mun BS, Arenz M, Mayrhofer KJJ, Lucas CA, Wang G, Ross PN, Markovic NM (2007) Trends in electrocatalysis on extended and nanoscale Pt-bimetallic alloy surfaces. Nat Mater 6:241–247
67. Neyerlin KC, Srivastava R, Yu C, Strasser P (2009) Electrochemical activity and stability of dealloyed Pt-Cu and Pt-Cu-Co electrocatalysts for the oxygen reduction reaction. J Power Sources 186:261–267
68. Zhang J, Lima FHB, Shao MH, Sasaki K, Wang JX, Hanson J, Adzic RR (2005) Pt monolayer on noble metal-noble metal core core-shell nanoparticle electocatalysts for O_2 reduction. J Phys Chem B 109:22701–22704
69. Zhang J, Mo Y, Vukmirovic MB, Klie R, Sasaki K, Adzic RR (2004) Pt-Pd core-shell. J Phys Chem B 108:10955
70. Brankovic SR, Wang JX, Adzic RR (2001) Metal monolayer deposition by replacement of metal adlayers on electrode surfaces. Surf Sci 474:L173–L179

71. Zhang J, Sasaki R, Sutter E, Adzic RR (2007) Stabilization of platinum oxygen reduction electrocatalysts using gold clusters. Science 315:220–222
72. Adzic RR (2010) Contiguous platinum monolayer oxygen reduction electrocatalysts on high-stability-low-cost supports. http://www.hydrogen.energy.gov/pdfs/review10/fc009_adzic_2010_o_web.pdf
73. Bregoli LJ (1978) The influence of platinum crystallite size on the electrochemical reduction of oxygen in phosphoric acid. Electrochim Acta 23:489–492
74. Makharia R, Kocha SS, Yu PT, Sweikart MA, Gu W, Wagner FT, Gasteiger HA (2006) Durable PEMFC electrode materials: Requirements and benchmarking methodologies. ECS Trans 1:3–18
75. Debe M (2005) Advanced meas for enhanced operating conditions, amenable to high volume manufacture. 2005 DOE Hydrogen Program Review. http://www.hydrogen.energy.gov/pdfs/review05/fc3_debe.pdf
76. Debe M (2008) Advanced cathode catalysts and supports for pem fuel cells. http://www.hydrogen.energy.gov/pdfs/review08/fc_1_debe.pdf
77. Pivovar B (2010) Extended, continuous pt nanostructures in thick, dispersed electrodes. http://www.hydrogen.energy.gov/pdfs/review10/fc007_pivovar_2010_o_web.pdf
78. Conway BE (1995) Electrochemical oxide film formation at noble metals as a surface-chemical process. Prog Surf Sci 49:331–452
79. Conway BE, Barnett B, Angerstein-Kozlowska H (1990) A surface-electrochemical basis for the direct logarithmic growth law for initial stages of extension of anodic oxide films formed at noble metals. J Chem Phys 93: 8361–8373
80. Conway BE, Jerkiewicz G (1992) Surface orientation dependence of oxide film growth at platinum single crystals. J Electroanal Chem 339:123–146
81. Bindra P, Clouser SJ, Yeager E (1979) Pt dissolution in concentrated phosphoric acid. J Electrochem Soc 126:1631
82. Wang X, Kumar R, Myers DJ (2006) Effect of voltage on platinum dissolution relevance to polymer electrolyte fuel cells. Electrochem Solid-State Lett 9:A225–A227
83. Wang X, Kariuki N, Vaughey JT, Goodpastor J, Kumar R, Myers DJ (2008) Bi-metallic Pd-Cu oxygen reduction electrocatalysts. J Electrochem Soc 155:B602–B609
84. Jaouen F, Charreteur F, Dodolet JP (2006) C-n4. J Electrochem Soc 153:A689
85. Medard C, Lefevre M, Dodolet JP, Jaouen F, Lindbergh G (2006) C-n4. Electrochim Acta 51:3202
86. Lefevre M, Proietti E, Jaouen F, Dodolet J-P (2009) Iron-based catalysts with improved oxygen reduction activity in polymer electrolyte fuel cells. Science 324:71
87. Campbell S (2005) Development of transition metal/chalcogen based cathode catalysts for PEM fuel cells. http://www.hydrogen.energy.gov/pdfs/review05/fc13_campbell.pdf
88. Zelaney P (2009) Advanced cathode catalysts. http://www.hydrogen.energy.gov/pdfs/review09/fc_21_zelenay.pdf
89. Zelaney P (2010) Advanced cathode catalysts. http://www.hydrogen.energy.gov/pdfs/review10/fc005_zelenay_2010_o_web.pdf
90. Bett JA, Kinoshita K, Stonehart P (1974) Crystallite growth of Pt dispersed on graphitized carbon black. J Catal 35:307–316
91. Bett JA, Kinoshita K, Stonehart P (1976) Crystallite growth of Pt dispersed on graphitized carbon black ii effect of liquid environment. J Catal 41:124–133
92. Cai M, Ruthkosky MS, Merzougui B, Swathirajan S, Balogh MP, Oh SH (2006) Investigation of thermal and electrochemical degradation of fuel cell catalysts. J Power Sources 160: 977–986
93. Kinoshita K (1988) Carbon electrochemical and physicochemical properties. John Wiley & Sons, New York
94. Yu PT, Gu W, Makharia R, Wagner F, Gasteiger H (2006) The impact of carbon stability on PEM fuel cell start-up and shutdown voltage degradation. ECS 210th Meeting, Abstract 0598.pdf. http://www.electrochem.org/meetings/scheduler/abstracts/210/0598.pdf
95. Yu PT, Kocha SS, Paine L, Gu W, Wagner FT (2004) The effects of air purge on the degradation of PEMFCS during startup an shutdown procedures. Proc AIChE 2004 Annual Meeting, New Orleans, LA, April 25–29 (2004)
96. Kreuer KD, Paddison SJ, Spohr E, Schuster M (2004) PEM review. Chem Rev 104:4637–4678
97. Kreuer KD, Schuster M, Obliers B, Diat O, Traub U, Fuchs A, Klock U, Paddison SJ, Maier J (2008) Short-side-chain proton conducting perfluorosulfonic acid ionomers: Why they perform better in PEM fuel cells. J Power Sources 178:499–509
98. Schuster MFH, Meyer WH, Schuster M, Kreuer KD (2004) Toward a new type of anhydrous organic proton conductor based on immobilized imidazole. Chem Mater 16:329–337
99. Steininger H, Schuster M, Kreuer KD, Kaltbeitzel A, Bingol B, Meyer WH, Schauff S, Brunklaus G, Maier J, Spiess HW (2007) Intermediate temperature proton conductors for PEM fuel cells based on phosphonic acid as protogenic group: A progress report. Phys Chem Chem Phys 9: 1764–1773
100. Larson JM, Hamrock SJ, Haugen GM, Pham P, Lamanna WM, Moss AB (2007) Membranes based on basic polymers and perfluorinated acids for hotter and drier fuel cell operating conditions. J Power Sources 172:108–114
101. Meng FQ, Aieta NV, Dec SF, Horan JL, Williamson D, Frey MH, Pham P, Turner JA, Yandrasits MA, Hamrock SJ, Herring AM (2007) Structural and transport effects of doping perfluorosulfonic acid polymers with the heteropoly acids, h3pw12o40 or h4siw12o40. Electrochim Acta 53:1372–1378
102. Gervasio D (2010) Protic salt polymer membranes. http://www.hydrogen.energy.gov/pdfs/review09/fc_06_gervasio.pdf
103. de Araujo CC, Kreuer KD, Schuster M, Portale G, Mendil-Jakani H, Gebel G, Maier J (2009) Poly(p-phenylene sulfone)s with high ion exchange capacity: Ionomers with unique microstructural and transport features. Phys Chem Chem Phys 11:3305–3312

104. Yi J (2007) Development of low-cost, durable membrane and MEA for stationary and mobile fuel cell applications. http://www.hydrogen.energy.gov/pdfs/review07/fc_9_yi.pdf
105. Pintauro P (2010) Nanocapillary network proton conducting membranes for high temperature hydrogen/air fuel cells. http://www.hydrogen.energy.gov/pdfs/review10/fc038_pintauro_2010_o_web.pdf
106. Hamrock SJ (2010) Membranes and meas for dry, hot operating conditions. http://www.hydrogen.energy.gov/pdfs/review10/fc034_hamrock_2010_o_web.pdf
107. Mittelsteadt CK (2010) Dimensionally stable membranes. http://www.hydrogen.energy.gov/pdfs/review10/fc036_mittelsteadt_2010_o_web.pdf
108. Endoh E (2008) Progress of highly durable mea for PEMFC under high temperature and low humidity conditions. ECS Trans 12:41–50
109. Endoh E, Terazono S, Widjaja H, Takimoto Y (2004) OCV degradation. Electrochem Solid-State Lett 7:A209–AA211
110. Varcoe JR, Slade RCT, Yee E (2006) An alkaline polymer electrochemical interface: A breakthrough in application of alkaline anion-exchange membranes in fuel cells. Chem Commun 1428–1429
111. Piana M, Boccia M, Filipi A, Flammia E, Miller HA, Orsini M, Salusti F, Santiccioli S, Ciardelli F, Pucci A (2010) H_2/air alkaline membrane fuel cell performance and durability, using novel ionomer and non-Pt group metal cathode catalyst. J Power Sources 195:5875–5881
112. Wang H, Turner JA (2010) Reviewing metallic PEMFC bipolar plates. Fuel Cells 10:510–519
113. Brady MP, Wang H, Turner JA, Meyer HM, More KL, Tortorelli PF, McCarthy BD (2010) Pre-oxidized and nitrided stainless steel alloy foil for proton exchange membrane fuel cell bipolar plates: Part 1. Corrosion, interfacial contact resistance, and surface structure. J Power Sources 195: 5610–5618
114. Dadheech G, Elhamid MHA, Blunk R (2009) Nanostructured and self-assembled superhydrophilic bipolar plate coatings for fuel cell water management. Nanotech Conference & Expo 2009, vol 3, Technical Proceedings pp 18–183

Books and Reviews

Alsabet M, Grden M, Jerkiewicz G (2006) Comprehensive study of the growth of thin oxide layers on pt electrodes under well-defined temperature, potential, and time conditions. J Electroanal Chem 589:120–127

Bard AJ, Faulkner LR (1980) Electrochemical methods. John Wiley & Sons Inc., New York

Bockris JO'M, Reddy AKN (1973) Modern Electrochemistry: An Introduction to an Interdisciplinary Area, Vol 1, Springer

Borup RL, Meyers JP, Pivovar B, Kim YS, Mukundan R, Garland N, Myers DJ, Wilson M, Garzon F, Wood DL, Zelenay P, More K, Stroh K, Zawodizinski TA, Boncella J, McGrath J, Inaba M, Miyatake K, Hori M, Ota K-i, Ogumi Z, Miyata S, Nishikata A, Siroma Z, Uchimoto Y, Yasuda K, Kimijima K-i, Iwashita N (2007) Scientific aspects of polymer electrolyte fuel cell durability and degradation. Chem Rev 107:3904–3951

Conway BE (1952) Electrochemical data. Greenwood Press, Westport, CT

Conway BE (1964) Theory of principles of electrode processes. Ronald Press, New York

Conway BE (1995) Electrochemical oxide film formation at noble metals as a surface-chemical process. Prog Surf Sci 49:331–452

Conway BE, Jerkiewicz G (1992) Surface orientation dependence of oxide film growth at platinum single crystals. J Electroanal Chem 339:123–146

Gileadi E (1993) Electrode kinetics. VCH, New York

Kinoshita K (1988) Carbon electrochemical and physicochemical properties. John Wiley & Sons, New York

Kinoshita K (1992) Electrochemical oxygen technology. John Wiley & Sons, New York

Kocha SS (2003) Principles of MEA preparation. In: Vielstich W, Lamm A, Gasteiger H (eds) Handbook of fuel cells-fundamentals, technology and applications. John Wiley & Sons, Ltd., New York, pp 538–565

Kocha SS, Yang DJ, Yi JS (2006) Characterization of gas crossover and its implications in PEM fuel cells. AIChE J 52:1916–1925

Koppel T (1999) Powering the future: The ballard fuel cell and the race to change the world. Wiley, New York

Kreuer KD, Paddison SJ, Spohr E, Schuster M (2004) Pem review. Chem Rev 104:4637–4678

Liebhavsky HA, Cairns EJ (1968) Fuel cells and batteries. Wiley, New York

Markovic NM, Ross PN (2000) Electrocatalysts by design: From the tailored surface to a commercial catalyst. Electrochim Acta 45: 4101–4115

Mathias MF, Makharia R, Gasteiger HA, Conley JJ, Fuller TJ, Gittleman CJ, Kocha SS, Miller DP, Mittelsteadt CK, Tao X, Yan SG, Yu PT (2005) Two fuel cell cars in every garage? Electrochem Soc Interface 14:24–35

Mench MM (2008) Fuel cell engines. John Wiley & Sons Inc., Hoboken, NJ

Pourbaix M (1966) Atlas of electrochemical equilibrium in aqueous solutions, 1st edn. Pergamon Press, New York

Prentice G (1991) Electrochemical engineering principles. Prentice Hall, Englewood, NJ

Savadogo O (1998) Emerging membranes for the electrochemical systems: (i) solid polymer electrolyte membranes for fuel cell systems. J New Mater Electrochem Syst 47–66

Vetter KJ (1963) A general thermodynamic theory of the potential of passive electrodes and its influence on passive corrosion. J Electrochem Soc 110:597–605

Wilson MS, Gottesfeld S (1992) High performance catalyzed membranes of ultra-low Pt loadings for polymer electrolyte fuel cells. J Electrochem Soc 139:L28–L30

Zawodzinski TA, Derouin CR, Radzinski S, Sherman RJ, Smith VT, Springer TE, Gottesfeld S (1993) Water uptake by and transport through nafion 117 membranes. J Elecrochem Soc 140: 1041–1047

Polymer Electrolyte Membrane Fuel Cells (PEM-FC) and Non-noble Metal Catalysts for Oxygen Reduction

Ulrike I. Kramm[1], Peter Bogdanoff[2], Sebastian Fiechter[2]
[1]Brandenburg University of Technology
Applied Physics and Sensors, Cottbus, Germany
[2]Helmholtz-Zentrum Berlin für Materialien und Energie GmbH (HZB), Institut für Solare Brennstoffe und Energiespeichermaterialien, Berlin, Germany

Article outline

Glossary
Definition of the Subject
Introduction
Transition Metal Carbides, Nitrides, and Chalcogenides
Non-noble Metal Catalysts with Molecular Centers
NNMC and Their Potential for PEM-FC Application
Future Direction
Bibliography

Glossary

R(R)DE Rotating (Ring) Disk Electrode. This technique is an electrochemical standard method; in this work, the measurements are performed to determine the catalytic activity towards the oxygen reduction in liquid oxygen–saturated electrolytes. Depending on the rotation rate, the diffusion-limited current changes. Measurements at different rotation rates enable the calculation of the kinetic current by using the Koutecky-Levich equation.

Fe-N-C catalyst Group of catalysts for which it is believed that molecular FeN_4- or FeN_{2+2}-centers are responsible for the reduction of oxygen.

Macrocycle Complex, organic molecule; in the context of this report, usually porphyrins, phthalocyanines, tetraazaannulenes, i.e., characterized by a tetrapyrrole core.

NNMC Non-noble metal catalysts: Catalysts prepared without any noble metals. As a result, the fabrication costs of such materials should be essentially lower as all basic-components are cheap.

ORR Oxygen Reduction Reaction. In this contribution, it stands for the electrochemical reduction of oxygen. The favored pathway is the direct reduction to water whereas the indirect pathway via the formation of peroxides is undesirable for fuel cell application.

Pyrochelates Macrocycles which were heat-treated ($T > 300°C$). During pyrolysis, the initial molecular structure is transferred into a carbon matrix. As also some fractions of the molecular centers of the precursor are preserved, the resulting product is sometimes assigned as pyrochelate.

Site density (S_D) Number of active sites per volume of catalyst. For the calculation of site densities of Me-N-C catalysts, often two assumptions have to be made: (1) the density is similar to other carbon-based catalysts (0.4 g/cm^3) and (2) each metal atom is related to an active site. In some cases, authors determine the exact mass density and/or number of active sites, so that the value becomes more accurate. In all other cases, it is usually overestimated as not all metal atoms are associated with active sites.

Transition metal chalcogenides A chemical compound which is composed of at least one chalcogen (O, S, Se, Te) anion and one or more transition metal cations.

Turnover frequency (TOF) The TOF gives the number of electrons which are transferred from the active site per site and second. Similar to the site density also here often assumptions have to be made.

Definition of the Subject

More efficient energy conversion systems may help to reduce the use of fossil fuels and the emission of greenhouse gases. Polymer Electrolyte Membrane Fuel Cells are such devices which are of particular interest for automotive applications. Unfortunately, cost issues are still limiting the application of this technology in a highly competitive market. An important part of this is the inherently high cost of platinum which is commonly used as electrocatalyst. But recently, the replacement of platinum by NNMC has come into the focus of reach. The most promising approaches – comprising the use of crystalline phases and catalysts with molecular active centers – are described in this entry; limitations of both classes of materials are discussed.

Introduction

Although platinum and platinum alloys are the state-of-the-art electrocatalysts for PEM fuel cell applications,

the platinum loading required to reduce the effective overpotential of the oxygen reduction reaction at high current densities (1–2 A/cm^2) to an acceptable level is still quite high for standard electrode structures (0.2–0.5 mg/cm^2). Therefore, there have been many attempts to improve the dispersion of the nano-scaled platinum particles and to optimize the electronic states of the catalytically active platinum interface with the aim to increase the mass-related activities of the platinum catalysts.

Pt-alloys PtMe (Me = Cr, Mn, Co, Ni, V, Ti) were investigated early on, since they show an increased specific activity with respect to ORR [1, 2]. Enrichments and depletions of alloying metals on the particle interface were found, which influenced the electrochemical activity significantly. Predominant scientific success was achieved in the field of "Pt-monolayer catalysts" [3], the concept of "Pt-skin electrocatalysts" [4], and the concept of "unalloyed Pt bimetallic catalysts" [5].

Some authors report a rise in the mass specific activity of these catalysts by a factor up to 20 in PEM fuel cells [6]. Considering the complex production methods, it remains a question to what extent this concept will effect a real cost reduction. Furthermore, it has to be proven to which extent these sub-nanometer-structured catalysts remain stable in an operating fuel cell under corrosive conditions. Commercial platinum catalysts already show a significant reduction of the active platinum surface especially under changing loading conditions during the long-term operation of a fuel cell due to dissolution and aggregation of Pt particles, which leads to a decline of the fuel cell efficiency [7, 8].

Further challenges remain unsolved concerning the ability of platinum to catalyze the oxidation of the carbon support and the poisoning of the platinum interface in the presence of traces of toxic gases such as CO or H_2S, present in the environment, which arrive at the fuel cell via the cathodic air flow. It needs to be mentioned that novel research activities aim to operate the PEM fuel cells at higher temperatures (>100°C, HT-PEM-FC) in order to obtain enhanced reaction kinetic and, therefore, higher efficiencies. However, due to the elevated temperature, the dissolution of platinum as well as the platinum-catalyzed carbon oxidation both will increase.

In spite of the success in the optimization of platinum catalysts, a major breakthrough in the field of fuel cells is yet to be achieved. Especially, the desire for a significant cost reduction by the replacement of platinum motivates international research activities investigating new catalyst concepts for cathodes. Thereby, the cathodes have to be sufficiently stable under fuel cell conditions; the alternative non-noble metal catalysts (NNMC) need to have a high selectivity for direct reduction of oxygen to water. The US department of energy (DOE) defined 25% of the achievable current density of a commercial platinum catalyst as target value for 2015. For fuel cell application, the catalysts should be producible in such a nano-structured form that suitable gas diffusion structures can be built.

Even if the numerous investigated non-noble material systems cannot yet fulfill all necessary demands, they do highlight new ways and principles in the electroreduction of oxygen, which could become applicable after a further aim-oriented development of these groups of materials. In the next sections, a selection of NNMC will be presented, which constitute a promising potential due to their catalytic properties.

Transition Metal Carbides, Nitrides, and Chalcogenides

As reported so far, one of the best platinum-free ORR catalysts of chalcogenide-type structure is a selenium-modified ruthenium catalyst ($RuSe_x$/C) [9–20]. State-of-the-art catalysts are composed of carbon-supported nano-scaled ruthenium particles whose surface was modified with selenium [9–14]. The modification leads to 10 times higher ORR activity, protects the ruthenium particles against electrooxidation, and suppresses the H_2O_2 formation. As $RuSe_x$/C is insensitive to methanol, it might be particularly suitable as an alternative cathode material in direct methanol fuel cells (DMFC) where platinum shows potential losses due to the methanol crossover [15–18]. However, ruthenium is still a costly and rare noble metal and seems not to be a feasible alternative to platinum. Therefore, readers who are interested in this type of catalyst are referred to the cited literature.

Because of a high electrical conductivity, transition metal carbides and nitrides are promising materials for electrocatalysis. Tungsten carbide has proven to possess platinum-like characteristics in terms of the valence band structure at the Fermi level and the chemisorption of

oxygen and hydrogen [21–24]. Therefore, it was intensively investigated for the electrooxidation of hydrogen and methanol [25–28] as well as for the electroreduction of oxygen. Mazza and Trasatti [29] studied several transition metal carbides (TMe: Ti, Ta, W) in sulfuric acid and selected WC as the most active material for the ORR among the others. However, tungsten carbide revealed poor corrosion stability in acidic electrolytes. More recent investigations on WC by Lee et al. [30] demonstrated that the stability and activity of these catalysts can significantly be increased by the addition of tantalum. They prepared pure WC and WC + Ta layers onto glassy carbon substrates by RF-sputtering and analyzed the electrochemical behavior in a solid state cell with Nafion® 117 as an electrolyte (Fig. 1).

This solid state cell has the advantage that the experimental conditions are close to those in a PEM-FC compared to investigations in an H_2SO_4 electrolyte of conventional electrochemical cells. CV measurements under N_2 atmosphere of WC at 30°C and 60°C showed corrosion with an onset potential of about 0.5 V (DHE), attributed to an oxidation of WC to WO_3 and CO_2. In contrast to this observation, the WC + Ta sample only showed very small anodic currents that points to a significant improved electrochemical stability at both 30°C and 60°C (Fig. 2). In voltammograms, the ORR onset potential of 0.45 V (DHE) for pure WC was shifted to 0.8 V (DHE) for the WC + Ta catalyst, pointing to an improved performance after

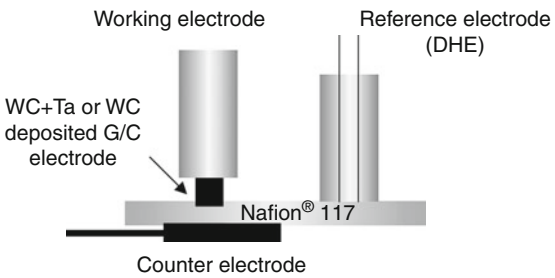

Polymer Electrolyte Membrane Fuel Cells (PEM-FC) and Non-noble Metal Catalysts for Oxygen Reduction. Figure 1

Schematic drawing of the solid state cell as used for the electrochemical measurements of WC and WC + Ta layers by Lee et al.; as counter electrode a platinum foil with platinum black was used. The figure was taken from [30], reproduced with permission of Elsevier

modification with tantalum. X-ray-induced photoelectron spectroscopy (XPS) evidenced that the WC + Ta material consisted of WC, a W-Ta alloy, TaC_x, Ta and carbon (overall composition: $W_{42}Ta_{24}C_{34}$). Among these components, the W-Ta alloy had the highest chemical stability in acidic solutions but exhibited no noteworthy ORR activity [31]. As a reason for the beneficial effect of tantalum, the authors considered that the W-Ta alloy protects the catalytically active WC-phase against corrosion that enabled the WC to reduce oxygen even at those potentials where electrooxidation was observed for the pure material.

Possibly motivated by the high chemical and mechanical stability of metal nitrides as wear- and erosion-resistant coatings [32], the ORR activity of metal nitrides (Me = W, Mo) was investigated by Zhong et al. [33, 34]. The authors prepared tungsten and molybdenum nitrides as cathode catalysts by the following procedure: In the first step, a carbon black (XC-72R) impregnated with an ammonium salt of the respective metal was calcinated (500°C, N_2). Subsequently, nitridation was performed by a temperature-programmed reaction under NH_3 gas flow (T_{final} = 750°C and 700°C for tungsten and molybdenum). X-ray diffraction (XRD) of the final conditioned materials revealed the formation of ß-W_2N and γ-Mo_2N nano-crystals.

From CV measurements in 0.5 M H_2SO_4, the authors concluded a high stability of the β-W_2N/C catalyst under N_2 atmosphere and determined an onset potential for ORR at about 0.6 V, which is inferior compared to the reference measurement with a commercial Pt/C catalyst (onset potential of 1 V (NHE), 20 wt% Pt/C, Johnson Matthey) (Fig. 3a). In PEM-FC measurements at T = 80°C, the β-W_2N/C and γ-Mo_2/C catalysts reached power densities of 39 mW/cm^2 (β-W_2N/C, Fig. 3b) and 65 mW/cm^2, respectively. Both catalysts revealed a good stability within an operating time of ≥ 60 h in galvanostatic tests (120 mA/cm^2 for β-W_2N/C and 200 mA/cm^2 for γ-Mo_2N/C, both at 80°C).

A slightly higher performance in PEM-FC tests was reported by Atanasoski (3 M company) using a C-N_x:Fe catalyst which had been prepared by vapor deposition onto a non-woven carbon support [35, 36]. They achieved 70 mW/cm^2 (0.1 A/cm^2 at 0.7 V, 75°C, H_2/air) and an open circuit potential of 0.9 V which is very

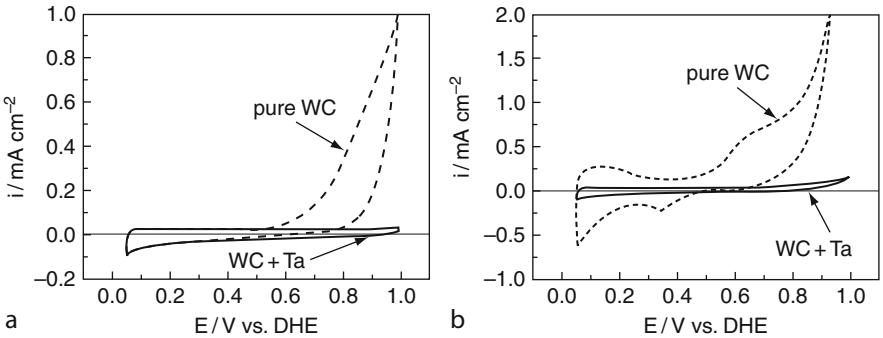

Polymer Electrolyte Membrane Fuel Cells (PEM-FC) and Non-noble Metal Catalysts for Oxygen Reduction. Figure 2 Cyclic voltammograms on Nafion electrolyte under N_2 atmosphere, scan rate 100 mV s^{-1}, measurements were performed at 30°C (**a**) and 60°C (**b**). The figures were taken from [30], reproduced with permission of Elsevier

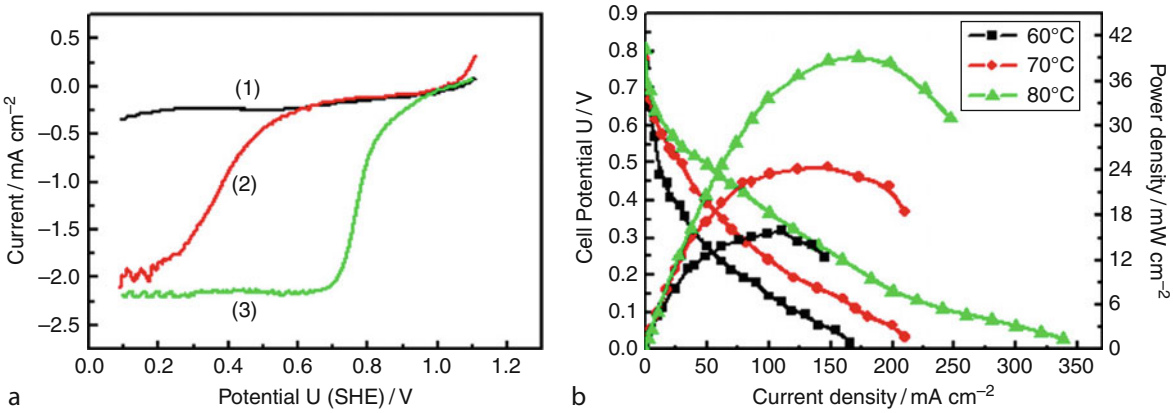

Polymer Electrolyte Membrane Fuel Cells (PEM-FC) and Non-noble Metal Catalysts for Oxygen Reduction. Figure 3 Cyclic voltammograms (**a**) for a W_2N/C (43 mg W_2N) in the 0.5 M H_2SO_4 solution saturated with nitrogen (1) and oxygen (2), respectively. For reasons of comparison, the linear scan of a 20% Pt/C catalyst (12 mg Pt) in oxygen-saturated solution is given (3), all measurements were performed with a scan rate of 5 mV s^{-1} and at T = 25°C. In (**b**), polarization curves as obtained at different temperatures using a W_2N/C catalyst (18% W) as cathode material are shown. Figures were taken from [33], reproduced with permission of Elsevier

close to that of platinum [35]. However, durability tests at 0.65 V revealed a decline of the catalyst's performance to below 10% of the initial value within 10 h. In order to improve the stability, other conductive materials like carbides, silicides, and nitrides were tested as substrates. A considerable improvement in the stability of the catalyst was found by using titanium carbide TiC. No noteworthy decrease of the fuel cell performance within 1,000 h of operation was observed. This remarkable result points out that the interaction between the support and the catalytic sites could be a very crucial factor for the optimization of catalysts.

Concerning the structure of the catalytically active centers in the C-N_x:Fe catalyst, Atanasoski et al. [36] concluded from Extended X-ray Absorption Fine Structure (EXAFS) analysis and Ultraviolet Photoelectron Spectroscopy (UPS) that the iron atoms are coordinated to nitrogen very similar to the FeN_x/C (x = 2, 4) centers which had been detected in pyrolyzed transition metal macrocycles [37–42]. Such pyrolyzed macrocycles and related materials are currently the most active catalysts among all noble metal–free catalysts and will therefore be described in detail in section "Catalysts Prepared by Carbonization of Macrocycles" of this contribution.

Following the idea of pyrolyzed macrocycles, indeed a heat treatment of the vapor-deposited layers at 650°C led to a significantly improved ORR activity. The authors correlated this to an increased atomic order and by the introduction of a second coordination shell around the Fe atom. Similar results have been reported for iron carbon nitride layers prepared by magnetron sputtering in a combinatorial approach [43]. However, the activities are still below that of state-of-the-art pyrolyzed macrocyles. Nevertheless, these explorative works might disclose a new way to prepare similar high catalytically active structures like those known from pyrolyzed macrocycles.

Already in the 1970s, numerous transition metal oxides of perovskite- and spinel-type structure showed promising results for oxygen reduction in alkaline electrolyte; however, only moderate activities and stabilities could be achieved in acidic media. Thus, the interest to use this class of materials for the PEM-FC was nearly abandoned. In 2007, Ota's group investigated metal oxides of type Me_xO_y for Me = Zr, Ti, Nb, Co, Sn, deposited as thin layers by reactive magnetron sputtering on glassy carbon substrates [44]. Significant activities toward ORR in strong acidic media were found for zirconium oxide ZrO_{2-x} with an onset potential of about 0.64 V (NHE) followed by oxides in the sequence Co_3O_{4-x} (0.26 V) > $TiO_{2-x} \approx SnO_{2-x}$ (0.24 V) > Nb_2O_{5-x} (0.14 V). From CV measurements (N_2-saturated 0.1 M H_2SO_4 at 30°C), the authors concluded a sufficiently high electrochemical stability for all oxides in the potential range from 0.65 to 0.85 V (1.15 V for ZrO_{2-x}), except for Co_3O_{4-x}. For ZrO_{2-x}, it was found that with increasing RF-power, the onset potential of the ORR current is shifted to more positive potentials, reaching 0.88 V (NHE) at 175 W RF-power (Fig. 4) [45]. From XPS analysis, the authors concluded that the increased amount of oxygen defects at the surface of the partially reduced ZrO_{2-x} (x = 0.15) might serve as adsorption sites for oxygen, enhancing the ORR activity. Surface defects are discussed by many researchers to be responsible for the adsorption of oxygen molecules on metal oxide surfaces [46–48]. Additionally, the increasing number of defects could be responsible for the observed decrease in the ionization potential and the increase in the conductivity of the n-type material with increasing RF-power.

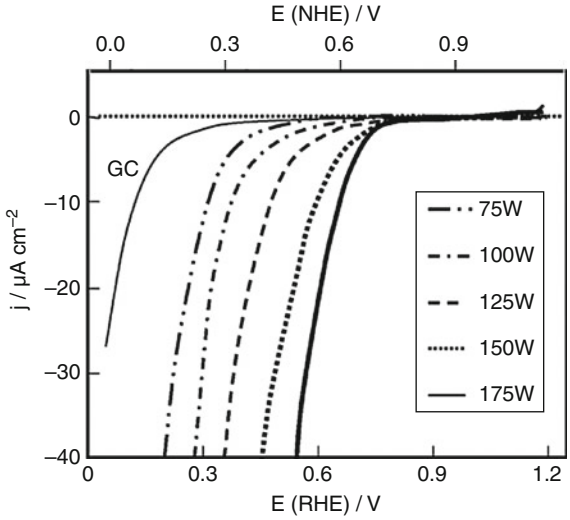

Polymer Electrolyte Membrane Fuel Cells (PEM-FC) and Non-noble Metal Catalysts for Oxygen Reduction. Figure 4

Potential – current curves of glassy carbon (GC) and ZrO_{2-x}-layers deposited at different RF-power (as given in the figure caption) in O_2-saturated 0.1 M H_2SO_4 at 30°C (scan rate: 5 mVs^{-1}). The figure was taken from [45], reproduced with permission of Elsevier

On studying TiO_2 layers, an increasing ORR activity was correlated with an increasing fraction of rutile crystallites characterized by a (110) face habit leading to a decreasing ionization potential of the layers [49]. All these investigations have proven that the catalytic activity of the oxides is dependent on the crystal structure and the degree of crystallinity as well as on the electronic structure at the interface. Unfortunately, no information on the selectivity of the catalysts in the ORR was given. Mentus found on anodically oxidized Ti nanorods that in an acidic electrolyte, oxygen is predominantly reduced via a two-electron transfer pathway while in alkaline electrolytes, a four-electron transfer pathway is preferred [50]. Until now, the observed catalytic activities of these single metal oxides are smaller compared to Pt/C catalysts. Nevertheless, in contrast to Pt/C, these materials show no mixed potentials in the presence of methanol, which could make them attractive for an application in the Direct Methanol Fuel Cell (DMFC).

Based on the results with metal oxides and nitrides, research on the catalytic behavior toward ORR of metal

oxynitrides has been intensified in the last few years. Nitrides and oxynitrides of subgroup IV and V elements have been intensively investigated as photo-catalysts for water oxidation showing remarkable stabilities and electrochemical activities in acidic electrolytes [51, 52]. Due to their partly high metal d-band concentration at the Fermi level, these materials might also be promising as ORR catalysts.

PEM-FC tests with carbon-supported zirconium oxide ZrO_2 and zirconium oxynitrides ZrO_xN_y as cathode catalysts have been reported by Liu et al. [53]. Although the maximum power density of the cell reached only one tenth of a Pt/C reference, the beneficial effect of the nitrogen incorporation into the ZrO_2 lattice on the ORR activity has been clearly demonstrated. Furthermore, a good stability of the nitrogen-modified catalysts can be observed even at operation temperatures of 80°C. Zirconium oxynitrides have also been investigated in detail by Ota´s group [54, 55]. Thin layers were prepared by RF-magnetron sputtering onto heated glassy carbon substrates. As shown in Fig. 5, they observed a strong influence of the substrate temperature on the ORR activity. Up to 500°C, a moderate increase of activity was observed, whereas at higher substrate temperatures, the enhancement was accelerated much stronger (Fig. 5a). This shift in activity increase was attributed to a decrease of the overall activation energy of the ORR at 500°C from 42 KJ mol^{-1} to about 22 KJ mol^{-1} (Fig. 5b); a change in the adsorption enthalpy of O_2 is assumed to be responsible for the change in the activation energy [54]. In accordance with Yeager's group [56], they proposed that the rate-determining step can be attributed to a dissociative adsorption of oxygen, remaining unchanged at approximately unity over the complete investigated temperature range.

Furthermore, the ionization potential can be decreased by introducing nitrogen into monoclinic ZrO_2. However, the nitrogen concentration detected in samples annealed at 800°C was relatively small ($ZrO_{1,7}N_{0,2}$). Similar to Liu's observations [53], CV measurements in 0.5 M H_2SO_4 at 30°C gave no hint on any electrochemical corrosion of ZrO_xN_y. For the most active ZrO_xN_y sample, deposited at a substrate temperature of 800°C, an onset potential for the ORR of about 0.7–0.8 V was stated. More recently, an onset potential of even 0.9 V had been reported for a ZrOCN catalyst which had been prepared by oxidation of ZrCN (potentials with respect to NHE) [55].

It is interesting to compare zirconium oxynitride (ZrO_xN_y) with tantalum oxynitride (TaO_xN_y), which was investigated by Ishihara et al. [57]. The authors reported a remarkable chemical and electrochemical stability for TaO_xN_y in 0.1 M H_2SO_4 at 30°C, that was attributed to the fact that in this oxide, tantalum is present in the highest possible oxidation state Ta^{5+} [57].

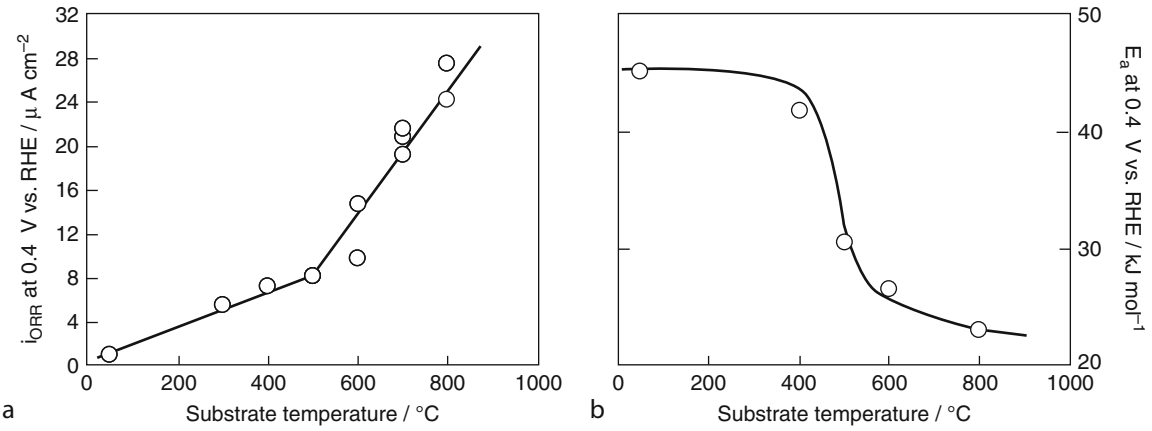

Polymer Electrolyte Membrane Fuel Cells (PEM-FC) and Non-noble Metal Catalysts for Oxygen Reduction. Figure 5 Relationship between the ORR current density at 0.4 V (RHE) (**a**) and the activation energy (**b**), both with respect to the substrate temperature for sputtered zirconium oxynitride thin films. The figures were taken from [54] (figures 6 and 10); reproduced by permission of ECS – The Electrochemical Society

The material was prepared by nitridation of a Ta_2O_5 powder in NH_3 atmosphere. The reaction product consisted of a non-stoichiometric TaO_xN_y (highest activity for x = 0.92 and y = 1.05) that reached a similar high onset potential as ZrO_xN_y of about 0.8 V (NHE) in 0.1 M H_2SO_4. From XRD measurements, it was concluded that the films consisted of a mixture of Ta_3N_5 and ß-TaON. The authors excluded ORR activity for Ta_2O_5 and Ta_3N_5 and concluded that the ß-TaON which crystallizes in the same structure (monoclinic) as ZrO_2 is responsible for the catalytic activity. On the basis of this result, one might assume that the monoclinic ZrO_2 structure type has a promoting effect toward the ORR. On the other hand, in a more recent work, the authors showed good ORR activity (onset potential ≈ 0.8 V [RHE], type of electrolyte not mentioned) for Ta_2O_5 which had been grown onto TaCN by a slight oxidation under low oxygen pressure of 10^{-5} Pa at 1,273 K [58]. By using an adopted conversion electron yield x-ray absorption method (CEY-XAS), they concluded that oxygen vacancies are likely to be responsible for the ORR activity as stated by other groups (see above).

In a recent paper, Domen et al. introduced the use of an arc-plasma gun technique in a controlled O_2/N_2 atmosphere for the preparation of niobium (oxy) nitride catalysts onto carbon blacks [59]. They showed that this technique leads to finely dispersed particles in the nanometer and sub-nanometer range which show excellent activity for the ORR compared to other non-noble metal catalysts (ORR onset potential at 0.8 V (NHE) in 0.1 M H_2SO_4). Also here, oxygen vacancies or reduced sites in the Nb_2O_5 phase were proposed to be responsible for the ORR activity. Highest ORR onset potentials were observed for a N:Nb_2O_5 catalyst (0.86 V (RHE)) which was sputtered in a reactive gas composition of N_2/O_2 = 3:1. A further increase of the nitrogen concentrations led to the formation of less active oxynitride or nitride phases whereas lower nitrogen ratios produced less active niobium oxide (Nb_2O_5) phases. As no nitrogen could be detected by XPS in the most active N:Nb_2O_5 material, only small amounts of nitrogen are obviously causing the promoting effect by doping or by forming defects in the crystalline N:Nb_2O_5 phase. The high deposition rate of this technique enables the rapid synthesis of highly dispersed catalysts onto high surface area substrates that is necessary for an application in fuel cells [59].

In a further paper, they reported on another alternative preparation method called polymerized complex method (PC) for niobium oxynitride supported on carbon (Nb-O-N/CB). The preparation involves the addition of carbon black (CB) during the polymerization process followed by nitridation in ammonia [60]. Such catalysts showed significantly enhanced ORR activity and also a better distribution and homogeneity of the catalyst's nanoparticles compared to a material prepared via conventional impregnation method. They attributed this effect mainly to an improved electrical contact of the catalytic active sites to the carbon substrate [60]. Obviously the use of N_2 instead of O_2 during the required heat treatment step allows the carbonization of organic precursor material which is favorable for contacting the catalyst's particles to the carbon support. Corresponding to this thesis, the authors found improved ORR current densities with increasing heat treatment temperature, probably because of an improved graphitization process.

A further doping of the Nb-O-N/CB catalyst with barium led to a considerable increase of the ORR activity by a factor of about 100 at 0.4 V (NHE) compared to the barium-free sample (Fig. 6). RRDE measurements revealed no H_2O_2 production at potentials positive of 0.25 V (NHE), what points to a direct reduction of O_2 to water (four-electron pathway). Based on XRD, the authors found an increased fraction of niobium oxide Nb_2O_5 crystallites after adding barium to the precursor. This result was confirmed by XPS where in the Ba-Nb-O-N/CB samples, an increased signal of niobium in the oxidation state Nb^{5+} instead of Nb^{4+} had been detected. Therefore, the authors supposed local niobium Nb^{5+} structures close to barium atoms to be responsible for the promoting effect of the ORR activity [60].

As the examples above show, it should be pointed out that it is difficult to compare the different catalytic materials because not only the intrinsic activity but morphological parameters such as particle size, particle distribution, or electronic coupling to the substrate also play an important role in the observed activities. It has to be expected that most of the materials investigated so far can be remarkably improved in catalytic efficiency by optimizing these parameters.

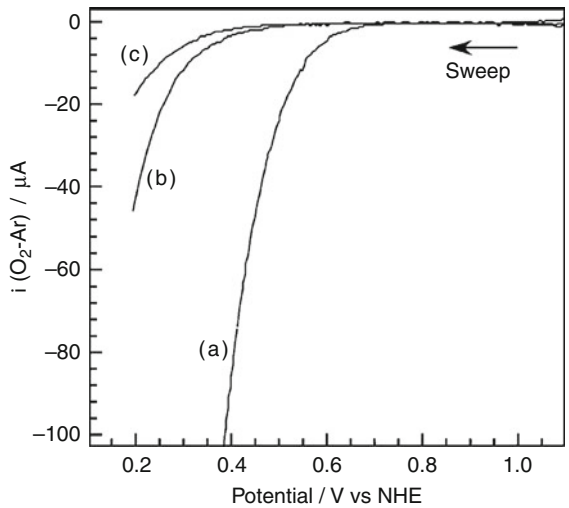

Polymer Electrolyte Membrane Fuel Cells (PEM-FC) and Non-noble Metal Catalysts for Oxygen Reduction. Figure 6

ORR voltammograms for (**a**) Ba-Nb-O-N/CB composit catalyst; (**b**) the Ba-free Nb-O-N/CB catalyst, and (**c**) bare CB. All materials were prepared by two heating steps (N_2 at 773 K, NH_3 at 1,123 K). Measurements in oxygen- and argon-saturated 0.1 M H_2SO_4 were performed with a sweep rate of -5 mV s^{-1}, the vertical axis ($i_{(O2-Ar)}$) denotes the difference in current under O_2 and Ar atmospheres. The figure was taken from [60], reproduced by permission of ECS - The Electrochemical Society

Non-noble Metal Catalysts with Molecular Centers

Already in 1964, Jasinski demonstrated that different metal phthalocyanines (Me: Co, Pt, Ni and Cu) can act as oxygen reduction catalysts in alkaline media [61]. During the following years, it was confirmed that several metallomacrocycles can act as ORR catalysts even in acidic environment. Later, it was found that pyrolysis leads to enormous improvements of the ORR activity even if instead of macrocycles, cheaper and less complex precursors are used [62, 63]. This will be discussed in detail in the section "Alternative Center Generation during Heat Treatment."

The current densities and stabilities of macrocycles are insufficient for fuel cell applications; nevertheless, due to their well-defined molecular structure, they are useful as model systems in order to get a better understanding of the factors that might cause the high oxygen reduction ability of the Me-N-C catalysts prepared via pyrolysis. Therefore, this chapter will first summarize the most important factors that affect ORR activity of non-pyrolyzed macrocycles.

Non-pyrolyzed Macrocycles

In nature, numerous redox and transport processes are associated with metallomacrocycles. As an example, FeN_4-centers of hemoglobin are responsible for the transport of oxygen in blood. In this particular case, oxygen binds reversibly to the FeN_4-unit. Besides the binding, reduction of oxygen to water requires a multi-electron transfer and the reaction with protons. Therefore, (1) all intermediate products have to be bonded strongly (but reversibly) enough to the metal center and (2) the final product of water should only have a weak bonding so that the centers are not blocked and can continue to participate in the reduction process.

The reactivity of a macrocycle will depend on the energetic position of its highest occupied molecular orbital ($HOMO_{Macrocycle}$) related to the lowest unoccupied molecular orbital of the oxygen molecule ($LUMO_{O2}$). A narrow gap between both will make it reactive while a larger gap stabilizes the complex [64, 65].

Jahnke et al. investigated various macrocycles, characterized by different ligands such as nitrogen, oxygen, and sulfur (Me-N_4, Me-S_4, Me-O_4, Me-N_2O_2, Me-N_2S_2), each under the same experimental conditions. For iron and copper, highest kinetic current densities were found if the metal center was fourfold coordinated by nitrogen (FeN_4 and CuN_4 centers); in the case of cobalt, the so-called Pfeiffer complex with a CoN_2O_2-center enabled the best results [62]. If oxygen or sulfur were the only ligands, the complexes were not or only poorly active toward oxygen reduction for all investigated metal centers.

Due to their low electric conductivity, macrocycles were usually impregnated on a conducting substrate, in most cases on a carbon black. Besides electron conductivity, also the active surface area is increased by the impregnation. It was found that quinone and/or carboxyl groups on the carbon surface interact electronically with the metal centers of the macrocycles. This was supposed to enhance the electronic coupling of oxygen toward the active MeN_4-site enabling higher ORR activities [66, 67]. Indeed, with Mössbauer

spectroscopy, Melendres was able to confirm that due to interaction with the carbon support, Mössbauer parameters of iron phthalocyanine (FePc) were changed confirming the different electronic structures of such interacting FeN_4-centers in comparison to FeN_4-sites in pure FePc [68].

An oxygen reduction ability was described for MeN_4-complexes with Fe^{2+}, Fe^{3+}, Co^{2+}, Ni^{2+}, Mn^{2+}, Ru^{2+}, Cu^{2+}, and Zn^{2+} as central ion [62, 64, 66, 67, 69–78].

Best results were found for iron, but also for cobalt, manganese, and nickel [62, 67, 79], which was explained by the 3d electron orbital occupation. It was proposed that MeN_4-centers with $3d^6$ configuration should enable the best oxygen reduction ability [65, 77]. The related volcano plot is given in Fig. 7.

The nature and number of macrocycle substituents and axial ligands are both influencing the electron density at the metal center, leading to variations of the oxidation and/or the spin state and the electron donor capacity of the complex [64, 80–84]. It was shown by STM that macrocycles with a fully occupied $3d_z^2$ orbital are nearly ORR inactive. For the binding of oxygen, this orbital should be either empty or only partially filled [78].

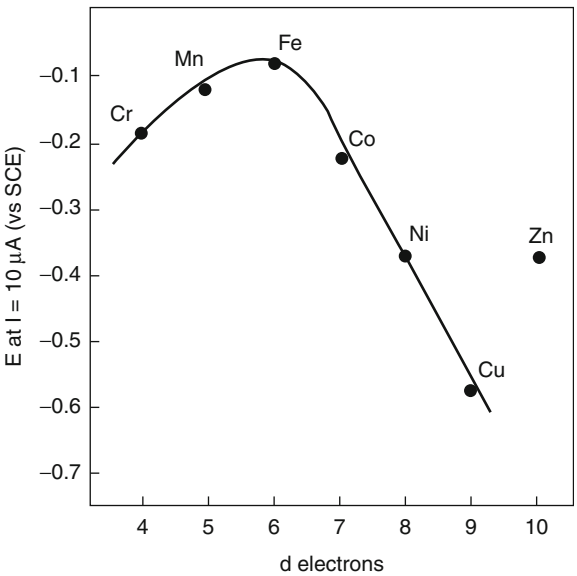

Polymer Electrolyte Membrane Fuel Cells (PEM-FC) and Non-noble Metal Catalysts for Oxygen Reduction. Figure 7

Volcano plot depicting the ORR onset potential of different bivalent Me(II)-TSPs for the oxygen reduction in alkaline media as a function of the number of d electrons (TSP denotes tetrasulphonatophenylporphyrin), the figure was taken from [65], reproduced with permission of Elsevier

Concentrating on complexes with the same metal center, it was shown that the intensity of backbonding to the complex is related to the ORR activity. As a measure for the strength of backbonding, the position of the Co^{3+}/Co^{2+} redox peak was used, i.e., depending on the macrocycle substituents, the redox peak position was shifted in the CV diagrams, the higher the redox potential the higher the kinetic current density was [85, 86].

The electron donor properties of the metal centers are affected by the type of substituents. Donating groups like phenyl or methoxy groups cause an increase of the electron density at the metal center whereas electron-withdrawing groups like sulfinyle have no or even a negative effect [62]. Induced by a higher electron density on the metal center, the oxygen molecule can be more easily activated enabling higher ORR activities [77, 87, 88].

In general, the macromolecular structure enables an extended system of conjugated π-electrons that provides electrons, making multi-electron transfer processes even on monomolecular centers possible. Experimentally, a direct reduction of oxygen to water was confirmed for iron and manganese N_4-macrocycles [65, 67, 79, 88–91]. For non-pyrolzsed cobalt complexes with single CoN_4-centers, only a two-electron reduction to hydrogen peroxide is possible. However, in 1980, it was shown that the so-called face-to-face dicobalt-porphyrins can catalyze a direct reduction of oxygen to water [92]. It was proposed that the oxygen molecule binds to two CoN_4-centers in a trans-configuration, which was suggested as bimolecular center even for pyrolyzed materials [92–97].

The formation of H_2O_2 is crucial for the stability of such complexes. Hydrogen peroxide initiates a weakening or even breaking of the bonds between the tetrapyrrole core and the substituents. The resulting smaller electron donor capacity will cause a decrease of ORR activity [41, 85, 98]. On the other hand, metal ions especially in strong acidic solutions can be removed from the tetrapyrrole core by leaching. It was observed that such demetallation is a further

reason for a decreased activity [71, 99–101]. As discussed in the following, both activity and stability can be enhanced by a heat treatment.

Molecular Centers in Carbonized Materials

In 1976, it was demonstrated that the catalytic activity and stability of carbon-supported macrocycles can be enhanced significantly by a heat treatment [62, 69]. Since the 1980s, it is known that after pyrolysis, some of the metal species formed can be dissolved in acidic solution [41, 42, 63, 71, 79, 98, 102–106]. The remaining MeN_4-centers must either reduce oxygen with a higher turnover frequency or other, more active sites (e.g., N-C-sites) have to be formed. Until now, it is still under debate whether the MeN_4-centers become more active or whether the released metal acts as catalyst during the heat treatment for the formation of a certain active carbon structure (e.g., N-C-sites). It should also be noted that more than one type of catalytic center might be present in the catalysts. Possibly, both MeN_4-centers and metal-free N-C-sites could act as centers for the reduction of oxygen.

In the following, the literature will be discussed separated according to the author's assignment of active site constitution. Hence, one will also find certain metal-containing catalysts, but where the activity was assigned to N-C-sites, already discussed in the following section.

Carbon-Based Materials with Carbon and/or Nitrogen Sites as Active Centers

It is known that the efficiency of catalysts is not only a function of the kind of active site, but also dependent on the constitution of the carbon support, that will influence the overall electronic properties of the catalyst material [96, 107–109]. For platinum-based catalysts, it was shown that by nitrogen doping of the carbon support, the platinum particles are stronger linked to the support material compared to the not-modified carbon. The resultant smaller particles with a more homogeneous distribution enabled higher ORR activity and an improved long-term stability [107, 110].

However, beside the function as a catalyst support, it was reported that nitrogen-doped carbon itself can be active as a metal-free catalyst for the ORR. The nitrogen atoms will (1) change the electronic character of the carbon and (2) the obtained defect structure (in comparison to the inert surface of graphene sheets) might enable an easier adsorption of oxygen and a subsequent reduction to water or hydrogen peroxide.

In 2000, Strelko et al. published theoretical calculations of the electronic character of carbon related to the integration of nitrogen, phosphorous, and boron heteroatoms [111]. In the first step, they investigated the electronic changes that depended on different positions of these atoms in the carbon matrix (i.e., pyridinic, pyrrolic, graphitic). As an example, a scheme of a graphene layer with the different type of nitrogen atoms is given in Fig. 8.

While pyridinic nitrogen atoms only contribute one electron to the π-electron system of the carbon, pyrrolic and graphitic nitrogen atoms increase the π-electron density as they contribute two electrons. Therefore, pyridinic atoms (N, P, B) should be insensitive to an improvement of the electron donor properties of the carbon. For pyrrolic and graphitic nitrogen heteroatoms, a lowering of the graphene bandgap had been calculated, enhancing the electron donor capacity in the order of B < N < P [111].

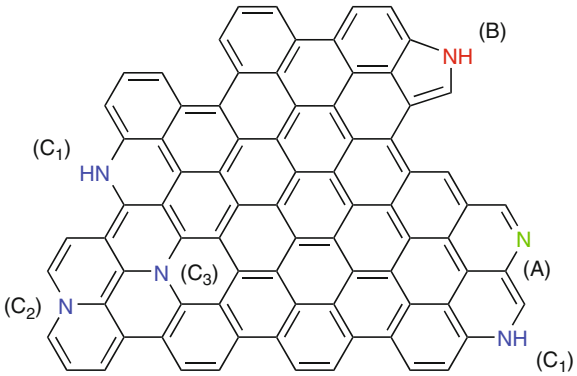

Polymer Electrolyte Membrane Fuel Cells (PEM-FC) and Non-noble Metal Catalysts for Oxygen Reduction. Figure 8

Different types of nitrogen atoms incorporated in a graphene plane. Pyridinic nitrogen atoms (A) only contribute with one electron to the π-electron system of the carbon matrix while pyrrolic (B) and graphitic nitrogen atoms (C) contribute by two electrons. Graphitic nitrogen atoms can be bonded in one C_6-ring (C_1), or between two (C_2) or three (C_3) C_6-rings, respectively. The figure was adapted from figure 3-7 of [112], Südwestdeutscher Verlag für Hochschulschriften

It was first stated by Wiesener that electronically modified carbon itself can act as oxygen reduction catalyst [102]. He measured ORR activity after heat treatment of MeN_4-chelates (without acid leaching). As during long-term measurements, some of the metals were dissolved without significantly affecting the ORR activity, he concluded that the metal could not be a part of active sites but catalyzes the formation of certain active N-C-sites during the heat treatment [98, 102]. Later other authors also assigned the observed ORR activity to the presence of graphitic or pyridinic N-C-sites in carbon-based materials [113–119].

The behavior of graphitic nitrogen atoms integrated in carbon was systematically investigated by Sidik et al. [120]. The catalysts were prepared starting from the soot Ketjen Black EC 300 J, which was treated in HCl and HNO_3 to remove metallic impurities and then heat-treated in NH_3 at 900°C. Induced by nitridation, ORR activity was increased but the high concentration of hydrogen peroxide that was formed (75% H_2O_2 at U = 0.3 V) indicated a predominant two-electron transfer process for this material. At higher overpotentials, H_2O_2 production decreased, which was explained by an ORR process leading to water formation via two two-electron transfer processes. Cluster calculations were performed modeling the nitridation of the basal plane sheet of graphite by substitution of carbon by nitrogen atoms. For carbon atoms at different positions in the graphene sheet, the adsorption energies of reaction intermediates related to ORR were calculated as pointed out in Fig. 9.

On the basis of their calculations, the authors concluded that it is most likely that the oxygen reduction should take place on carbon atoms adjacent to in-plane N-atoms (position a in Fig. 9). With respect to the calculated potentials, for a two-step reduction

$$O_2(g) + H^+(aq) + e^-(U^\circ) \leftrightarrow OOH(ads), \quad U = 0.845V, \tag{1}$$

$$OOH(ads) + H^+(aq) + e^-(U^\circ) \leftrightarrow H_2O_2(aq), \quad U = 0.545V, \tag{2}$$

especially, the second value was in good agreement with their experimental observation of an onset potential of 0.51 V (NHE). Therefore, this work evidences in experiment and theory that carbon doped with graphitic nitrogen indeed is able to reduce oxygen, but only via a two-electron pathway, to hydrogen peroxide at low onset potentials [120].

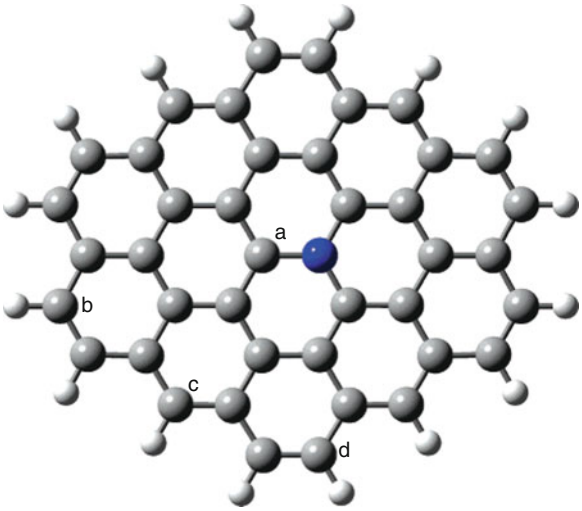

Polymer Electrolyte Membrane Fuel Cells (PEM-FC) and Non-noble Metal Catalysts for Oxygen Reduction. Figure 9
Model cluster used for the calculation of absorption energies on (graphitic) nitrogen-doped carbon. The calculations were performed for carbon atoms at different electronic positions in the N-doped graphene plane as indicated by the letters a, b, c, and d. The figure was taken from [120], reproduced with permission of the American Chemical Society

Table 1 summarizes further attempts to prepare metal-free catalysts for the ORR. Some of these materials were formed by a heat treatment of nitrogen-rich organic precursors (lines 1–2, 6); others are carbon blacks which had been heat-treated in a reactive nitrogen-rich atmosphere at appropriate temperatures (No. 4–5 in Table 1). The highest nitrogen concentration is found for carbon nitride (line 1), in which both graphitic and pyridinic nitrogen atoms have been found. Due to its good electrochemical stability, carbon nitride C_3N_4 has gained interest for several catalytic applications [109, 121–123]. As this material exhibits the largest concentration of nitrogen known for N-C-based materials, it was also suggested to be of interest for the ORR. Lyth et al. investigated the electrochemical reduction of oxygen on C_3N_4 which was prepared by the reaction of cyanuric chloride with sodium azide (in benzene) at 220°C [122]. The achieved catalytic activity was only

Polymer Electrolyte Membrane Fuel Cells (PEM-FC) and Non-noble Metal Catalysts for Oxygen Reduction. Table 1 Comparison of different carbon-based electrocatalysts and their electrochemical characteristics

	Catalyst sample		N content (wt%)	Fe content (wt%)	Onset potential V vs. NHE (@ 0.1 mA/cm^2)	Lit.
1	C_3N_4[a]	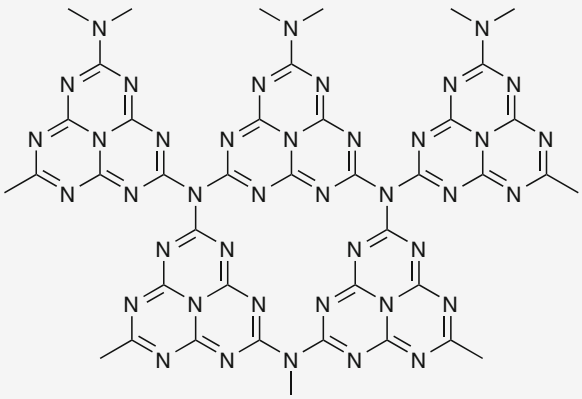	60.9	–	0.4	[122, 123]
2	H_2Pc/PhR[b]	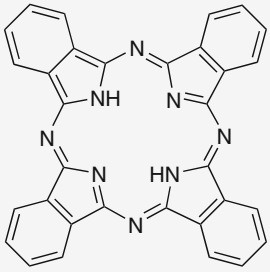	2.0	–	0.53	[124]
3	FePc/PhR[c]	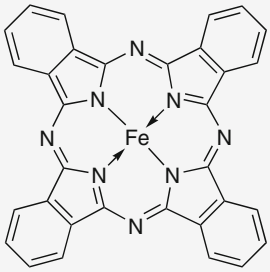	3.75	–	0.77	
4	BP 2000 NH_3 treated[d]	N:CB	1.10	–	0.4	[125]
5	Vulcan + AN[e]	N:CB	4.77	–	no activity	[126]

Polymer Electrolyte Membrane Fuel Cells (PEM-FC) and Non-noble Metal Catalysts for Oxygen Reduction. Table 1 (Continued)

	Catalyst sample		N content (wt%)	Fe content (wt%)	Onset potential V vs. NHE (@ 0.1 mA/cm^2)	Lit.
6	Phen/ AmOx[f]	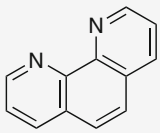	n.d.	0.04	<0.0	[127]
7	Phen/ AmFeOx[g]	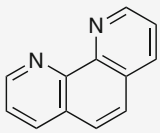	n.d.	13.9	0.82	

[a](cyanuric acid + sodium azide) precipitated at 220°C in benzene
[b](H_2Pc + phenolresin), heat-treated at 700°C for 5 h
[c](FePc + phenolresin), heat-treated at 600°C for 5 h ([a,b]: compare Fig. 3.3)
[d]BP200 heat-treated in NH_3/N_2 at 800°C for 30 min
[e]Vulcan pyrolyzed at 1000°C in acetonitrile-enriched Ar for 2 h, weight gain: 65%
[f]phenanthroline + ammonium oxalate hydrate precursor
[g]phenanthroline + ammonium iron oxalate trihydrate, both samples ([f,g]) were heat-treated at 800°C for 30 min followed by a subsequent acid leaching

slightly better compared to pure carbon black. However, after impregnation of C_3N_4 onto the same carbon black (50/50 C_3N_4/CB, CB not further specified), an enhanced ORR activity was observed. The increased kinetic current density might be related to a higher active surface area and/or an improved electronic conductivity (compare Table 1, No. 1). The authors assigned the catalytic activity which was highest after a 1,000°C pyrolysis to graphitic nitrogen atoms [123]. In contrast to Wiesener [98, 102], they did not observe an improved formation of catalytically active graphitic sites by integration of iron during the heat treatment.

Nabae et al. [124] pyrolyzed iron phthalocyanine mixed with phenolic resin (FePc/PhR) in inert gas at different temperatures, each for five hours, and found best catalytic activity toward ORR at 600°C. A comparison to metal-free H_2Pc/PhR reference samples, as shown in Fig. 10 (a: H_2Pc/PhR, b: FePc/PhR), evidenced significant higher current densities and higher onset potentials for the samples prepared with iron phthalocyanine.

Similar to earlier works [104, 128], the authors observed an increased concentration of nitrogen in the carbon structure for the iron-containing catalysts. They attributed the metal species to be more important in the enrichment of nitrogen rather than in participation in the ORR [124].

Matter et al. [129] and Maldonado and Stevenson [116] attributed the catalytic activity to pyridinic nitrogen atoms at edge-planes of "cub-stacked carbon nanotubes" [129] and carbon nanofibers [116], respectively. The authors proposed that the present metal only enhances the integration of active pyridinic nitrogen atoms.

In order to achieve a high concentration of pyridinic nitrogen atoms – without the presence of any metal source – phenanthroline was pyrolyzed in the presence of ammonium oxalate (Table 1, No. 6) [127]. The oxalate-supported pyrolysis was established for transition metal macrocycles [130–133] (compare section "Catalysts Prepared by Carbonization of Macrocycles"), but works also for metal-free phenanthroline as first shown by Herrmann et al. [134]. If ammonium oxalate is pyrolyzed together with phenanthroline, only a low active carbon-based material was obtained [127]. When the ammonium

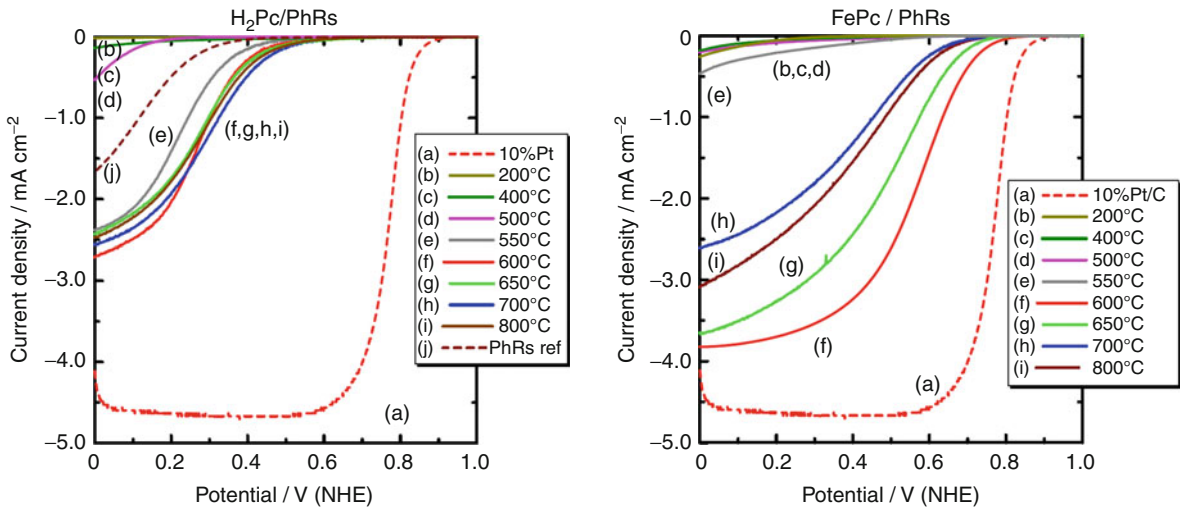

Polymer Electrolyte Membrane Fuel Cells (PEM-FC) and Non-noble Metal Catalysts for Oxygen Reduction. Figure 10 RDE voltammograms (0.5 M H_2SO_4, 1 mV/s, catalyst loading 0.2 mg/cm^2) of (**a**) H_2Pc/PhR and (**b**) the FePc/PhR catalysts, respectively. The FePc/PhR precursor contained 3 wt% Fe, pyrolysis was performed for 5 h for all samples. All given catalysts were not acid-leached after the heat treatment. The figures were taken from [124]; reproduced with permission of Elsevier

oxalate was replaced by an ammonium iron oxalate, however, a highly active catalyst was yielded whose onset potential (at 0.1 mA/cm^2) was shifted to significantly higher values compared to even the best metal-free catalyst of Table 1 (U = 0.8 V compared to 0.5 V). For this iron-containing catalyst, RRDE measurements revealed a predominantly direct reduction of oxygen to water. In this case, however, the much higher activity of the Me-containing catalyst was attributed to the presence of FeN_4-centers [127].

This finding is in accord with theoretical calculations by Kurak and Anderson [135]. Using the VASP code, the authors estimated the extent to which oxygen reduction can take place on carbon, doped with pyridinic nitrogen atoms. Similar to the experimental observation, nitrogen atoms bonded near an edge of a graphene plane magnify the reactivity toward bonding radical molecules in the first step. The strong binding, however, would make large overpotentials necessary in order to enable ORR (often 1.8 V, i.e., $U_{onset} = -0.6$ V). Only for one specific configuration which is shown in Fig. 11, an onset potential of 0.695 V was determined, but only with hydrogen peroxide as product.

The related electron transfer mechanism for the reduction to hydrogen peroxide is shown in Fig. 12. The authors concluded that there are no evidences for a direct reduction to water, but that the integration of transition metals might enhance the catalytic interaction to enable the four-electron transfer process [135].

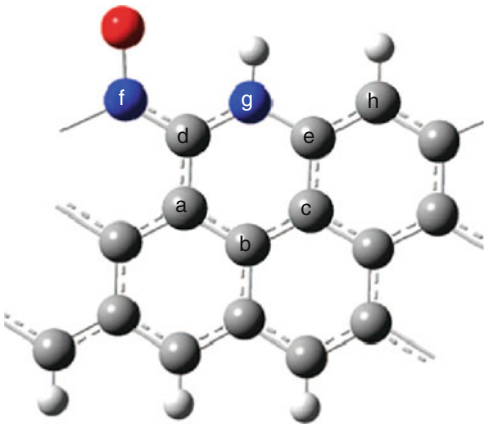

Polymer Electrolyte Membrane Fuel Cells (PEM-FC) and Non-noble Metal Catalysts for Oxygen Reduction. Figure 11
Proposed ON···NH edge sites on graphene sheets as catalytic sites for the oxygen reduction. The figure was taken from [135]; reproduced with permission of the American Chemical Society

Liu et al. prepared catalysts by a multistep preparation [115]. In the first step on either carbon or silica

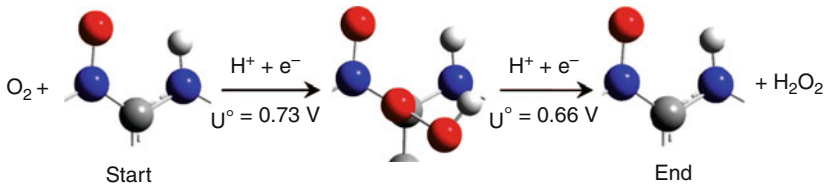

Polymer Electrolyte Membrane Fuel Cells (PEM-FC) and Non-noble Metal Catalysts for Oxygen Reduction. Figure 12 Predicted catalytic cycle for the two-electron reduction on catalytic ON···NH edge sites in pyridinicly doped carbon. The figure was taken from [135]; reproduced with permission of the American Chemical Society

supports, metal complexes were formed by the reaction of $Co(NO_3)_2$ and $FeSO_4$ with ethylendiamine. These precursors were heat-treated twice at 800°C in inert gas whereas after the first pyrolysis, an acid leaching was performed in order to remove soluble metal species. The authors came to the conclusion that in the surface region accessible for ORR, all metal-containing species should have been removed and could therefore be excluded as components of any active sites. The presence of any FeN_4-centers, stable in acidic solution, was excluded, in the first place. XPS confirmed the presence of pyridinic and graphitic nitrogen atoms. The authors proposed both to be catalytically active whereas pyridinic nitrogen atoms should have a higher activity but poorer stability (compare section "Stability") [115].

The results presented so far have shown that in most cases, catalysts reached higher ORR activities and selectivity for a direct reduction when a metal source was present during heat treatment. This makes it difficult to finally assign the role of metals in these catalysts. Nevertheless, unquestionable is the crucial role of nitrogen atoms incorporated in the carbon structure. Even in materials, in which a metal-based MeN_4-center has undoubtedly been identified as the active site, it has been observed that graphitic nitrogen atoms (i.e., not associated to the metal) can enhance the oxygen reduction of the catalysts [136]. Further investigations are necessary to clarify the mechanism of ORR in these materials.

Me-N-C Catalysts with MeN_4 and/or MeN_{2+2}-Centers

Catalysts Prepared by Carbonization of Macrocycles

As already mentioned, one can enhance ORR activity and stability of macrocycle-based catalysts by performing a heat treatment [62]. This result has led to intensive studies of the pyrolysis behavior of different N_4-chelates [37–42, 79, 100, 103, 104, 128, 137–153]. For some carbon-supported macrocycles, the effect of heat treatment on ORR activity is shown in Fig. 13.

Due to the temperature-induced graphitization, an additional carbon support is not needed a priori (see below). Nevertheless, in order to increase the active surface area and thereby the current density, one can use carbon blacks as a substrate. Depending on (1) the choice of the macrocycle, (2) the pyrolysis conditions, and (3) the macrocycle loading, the maximal achievable current density will be obtained during pyrolysis in inert gas flow at temperatures between 600°C and 1,000°C. For such impregnation catalysts, an optimal loading is obtained when a double setting of the available carbon surface is given. In this approximation, the fraction of surface area which is in pores smaller than the macrocycle expansion must not be considered [145, 154]. This explains why the metal content at which highest ORR activity is found varies within the reports.

A comparison of different metal-containing and metal-free macrocycles showed that the metal centers seem to stabilize the tetrapyrrole core [104, 128, 144]. As a result, the second decomposition step is shifted to much higher temperatures compared to the metal-free porphyrin and the overall mass loss is much smaller, as it becomes apparent from Fig. 14. Furthermore, the mass fragments related to the decomposition of the tetrapyrrole core (HCN) are detected at significantly higher temperatures in the coupled mass spectrometer for metal-containing macrocycles compared to the metal-free ones [104, 112, 128, 144].

The disadvantage of the impregnation technique is that above the optimal loading, no further activity increase is possible, even a decline of the activity can be observed [130]. This fact hinders the optimization

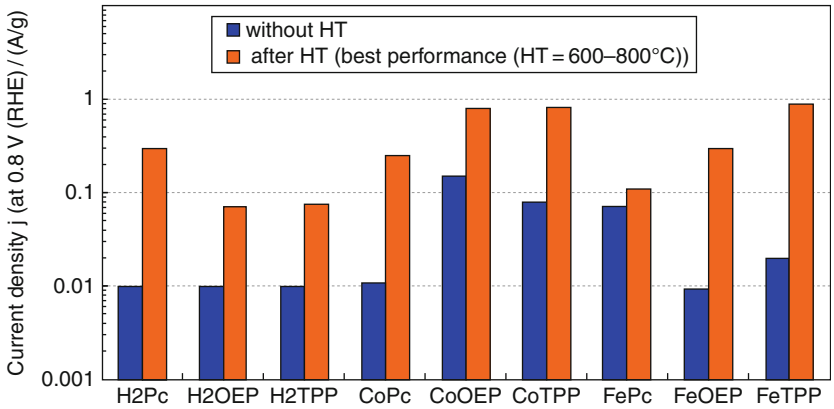

Polymer Electrolyte Membrane Fuel Cells (PEM-FC) and Non-noble Metal Catalysts for Oxygen Reduction. Figure 13 Effect of heat treatment on the kinetic current density for oxygen reduction for some Co, Fe, and metal-free macrocycles (Pc: phthalocyanine, OEP: octaethylporphyrin and TPP: tetraphenylporphyrin). All samples were supported on the same carbon black; for the pyrolyzed samples, the highest kinetic current densities are given, achieved after a heat treatment at temperatures ranging from 600 to 800°C. Current values were taken from [41], figure 1

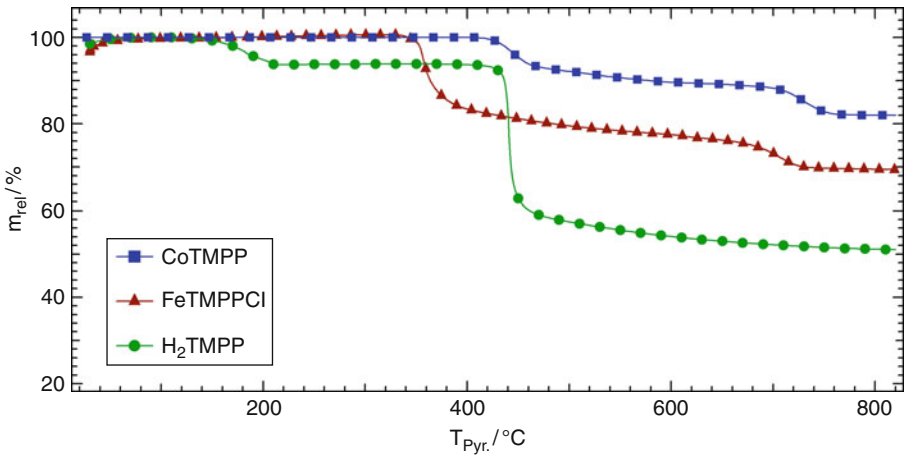

Polymer Electrolyte Membrane Fuel Cells (PEM-FC) and Non-noble Metal Catalysts for Oxygen Reduction. Figure 14 Thermogravimetric measurements of different tetramethoxyphenylporphyrins (TMPP). The metal-free H_2TMPP reveals a much larger mass loss starting at 450°C in comparison to both metal porphyrins. The figure was adapted from figure 5-3 of [112], Südwestdeutscher Verlag für Hochschulschriften

for FC application where higher densities of active sites are required.

For this reason, several alternative production methods were developed which enable higher site densities. In principle, the carbonization can also be reached applying low-temperature plasma. This was first shown by Herrmann et al. in 2005 [155]. The direct comparison to the pyrolyzed equivalent showed that the carbon structure of the final product contained less disordered carbon phases after an Ar-plasma treatment (20 min, 250 W) compared to a pyrolysis at 700°C (for which one of the highest ORR activity was obtained) [156]. Furthermore, as only a local carbonization is reached, a sintering of the macrocycles can be prevented even without carbon support [155–157].

In order to yield higher site densities, macrocycles can either be impregnated on a template or mixed with it prior to a heat treatment. In such a case, it is always

mandatory to remove the template in a subsequent acid leaching. For instance, a sintering of macrocycle molecules is inhibited if fumed silica is used as a template [158–161]. The silica is removed by leaching in HF.

Another template-assisted method that enables high site densities is the so-called oxalate-supported pyrolysis. In this preparation approach, it is utilized that the porphyrine melts shortly before the carbonization takes place [130], whereas in the same temperature range, a decomposition of many metal oxalates occurs [132]. On the one hand, the released CO_2 contributes to a generation of porosity; on the other hand, the metal/metal oxide framework serves as template during the further heat treatment [39, 132, 133, 162, 163]. The advantage of this method is the achievement of a homogenous distribution of active centers over the whole catalyst material [39, 160, 162]. In a second pyrolysis, further porosities can be generated so that due to the surface increase and an increase of participating MeN_4-centers, significant enhancements of kinetic current density can be achieved [39, 162]. It was shown that the addition of sulfur enables much higher current densities due to (1) an easier removal of inactive metal species during the acid leaching, (2) higher site densities, and (3) changed carbon morphology [133]. By in-situ investigation of the pyrolysis process by high-temperature X-ray diffraction (HT-XRD) and TG-MS, it was found that without sulfur addition, iron carbide formation occurs at $T > 580°C$, causing an additional release of HCN fragments (related to MeN_4 decomposition). By the addition of sulfur, the formation of Fe_3C is inhibited as FeS is formed instead. Therefore, a larger fraction of MeN_4-centers remained intact and so higher current densities were gained. Obviously, the carbide formation (or related graphitization) should be excluded during catalyst's preparation [163].

Structural analyses showed that non-leached catalysts are often dominated by decomposition products [37, 38, 41, 42, 104, 116, 164]. In such a case, with TEM, XRD, Mößbauer spectroscopy, and EXAFS analysis, mostly metal particles, carbides, nitrides, and sometimes oxides were detected. In Fig. 15, a Mössbauer spectrum of an as-prepared catalyst (HT 800, 2 h at 800°C in Ar) and its acid-leached product (HT 800, washed) are shown.

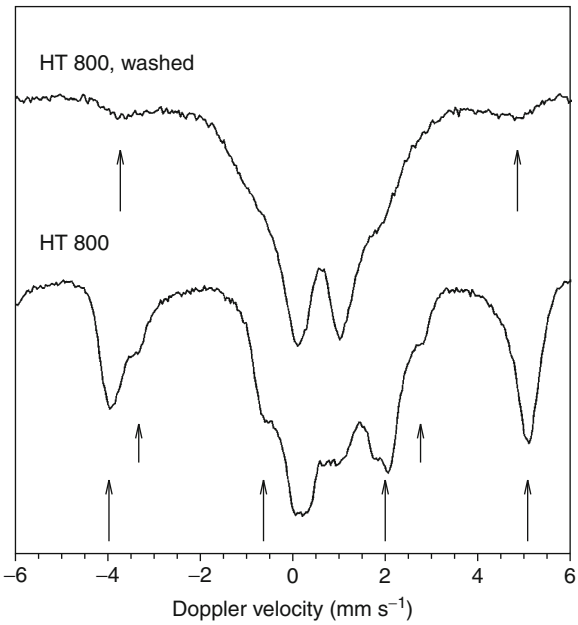

Polymer Electrolyte Membrane Fuel Cells (PEM-FC) and Non-noble Metal Catalysts for Oxygen Reduction. Figure 15
Mößbauer spectra of a catalyst as prepared from carbon-supported FeTPPCl and pyrolyzed at 800°C for 2 h (HT 800) and its acid-leached product (HT 800, washed). The velocity scale is given relative to sodium nitroprusside (0.26 mm/s vs. α-Fe). The figure was adapted from figure 4 of [38]; reproduced with permission of the American Chemical Society

By a sufficient leaching of the catalyst, large amounts of inorganic species can be removed without negatively affecting the kinetic current density [38, 136].

A comparison of both catalysts in Fig. 15 shows that the non-leached catalyst HT 800 is dominated by two sextets (indicated by the two different type of arrays); further Fe-containing species in the material are difficult to assign. Induced by the acid leaching the sextets nearly vanished. Thus, it becomes easier to assign the remaining species which in this case were related to different FeN_4-centers [38]. Several authors have shown that even after a treatment at 1,000°C, about 30% of MeN_4-centers remain intact [37, 38, 41, 42, 136]. These results show clearly that in order to understand the role of metal in the final catalysts, structural analysis should better be performed on the already acid-leached catalysts. As MeN_4-centers are still

remaining, Van Veen et al. concluded that these sites are also responsible for the catalytic activity in the pyrochelates (similar to non-pyrolyzed macrocycles) [41, 42]. The authors proposed that an enhanced electronic structure is the main reason for an increased turnover frequency (TOF) of the remaining MeN_4-centers. In Fig. 16, a model for the processes occurring during heat treatment of porphyrins is shown [38]. According to this observation, even after high-temperature treatments, units of the tetrapyrrole core remain intact but interact with the carbon support.

In 2008, a direct correlation of the ORR activity and the overall concentration of all or at least one specific MeN_4-centre was proven for the first time [42]. In this work by Koslowski et al., the catalysts were produced by the oxalate-supported pyrolysis of FeTMPPCl or H_2TMPP. Variations of ORR activity and concentration of different iron modifications were obtained by different subsequent treatments whereas the heat treatment temperature was always kept constant. It was found that the obtained catalytic activity was proportional to the number of a specific FeN_4-center which is a major hint to the participation of this center in the oxygen reduction process. The correlation is shown in Fig. 17a. In a recent work, carbon-supported FeTMPPCl (FeTMPPCl/KB600) pyrolyzed at different temperatures was thoroughly structurally characterized before and after an acid leaching [136]. The results showed clearly that up to 600°C, the whole nitrogen remained in the system. Due to the carbonization, only a reorganization of the FeN_4-centers was observed, while the pyrolysis at 600°C was sufficient to essentially improve ORR activity [39, 136].

A comparison of XPS and Mößbauer spectroscopic results allows an explanation why significantly higher current densities could be achieved despite a decreasing concentration of active FeN_4-centers. Both, the N1s bonding energy and the isomer shift assigned to the active FeN_4-centers changed with the TOF [136]. The results were interpreted by an increasing bond-strength between iron and the surrounding nitrogen atoms which obviously leads to a higher 3d electron density on the metal center. As a result, oxygen might be activated faster so that higher TOFs can be obtained. A similar relation was already found for non-pyrolyzed macrocycles as discussed in section "Non-pyrolyzed Macrocycles" [65]. The relation between TOF and δ_{ISO} assigned to the active sites is shown in Fig. 17b. According to these results, a mesomerically bonded FeN_4-center with ferrous iron in the low-spin state is assigned as catalytic active center in FeTMPPCl-based catalysts pyrolyzed in inert gas atmosphere [39, 136]. Apart from these findings, graphitic nitrogen atoms seem to enhance the electron donor capacity, thus enabling higher ORR activities [136].

A related positive effect emerged also after a second pyrolysis of Me-N-C catalysts in ammonia [112, 160, 162, 165–167]. Since a huge increase in the concentration of pyridinic nitrogen atoms was observed, it was suggested that either different, but more active sites were formed or an enhanced electronic structure of the carbon matrix enabled the higher ORR activity

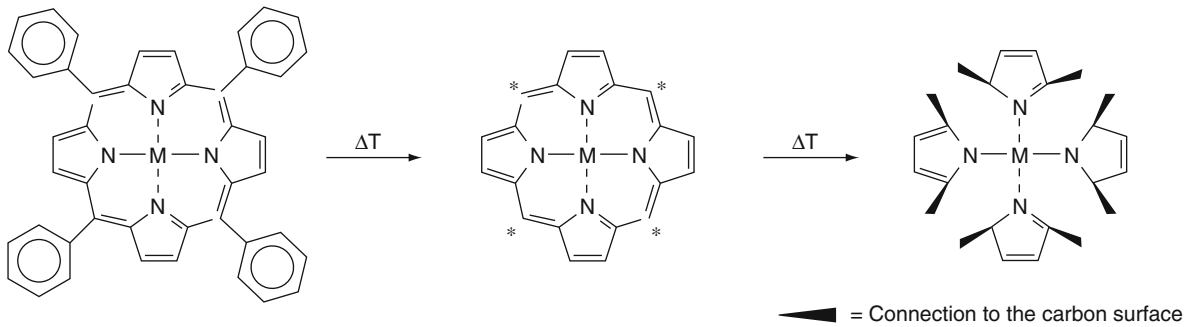

Polymer Electrolyte Membrane Fuel Cells (PEM-FC) and Non-noble Metal Catalysts for Oxygen Reduction. Figure 16 Visualization of the carbonization process of a porphyrin during the heat treatment. The figure was taken from [38]; reproduced with permission of the American Chemical Society. During the first decomposition step of porphyrins (compare figure 14), the substituents are released. In the following heating process, the active centers are integrated into or onto the carbon framework

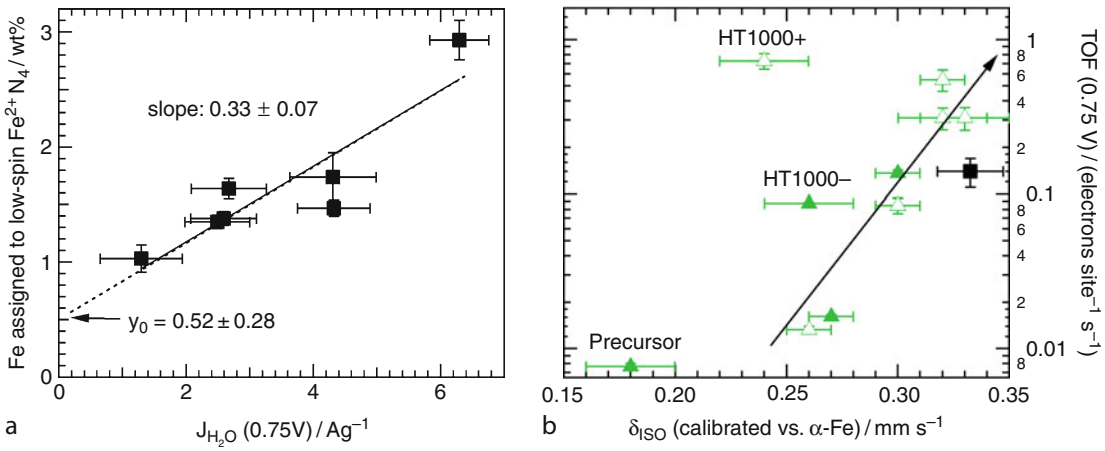

Polymer Electrolyte Membrane Fuel Cells (PEM-FC) and Non-noble Metal Catalysts for Oxygen Reduction. Figure 17 Correlation of the concentration of low-spin $Fe^{II}N_4$-centers with the ORR current density for different Fe-N-C catalysts (**a**). Relation between turnover frequency (TOF) and isomer shift δ_{ISO}. (**b**) The isomer shift δ_{ISO} is related to the electron density at the iron nucleus. In this work, a higher δ_{ISO} is in accord with an increased 3d electron density. The precursor and impregnation catalysts prepared at 1,000°C (HT1000+: acid-leached, HT1,000-: without acid leaching) are indicated. For reasons of comparison, the point ■ related to the catalysts discussed in [39] is added (average values of δ_{ISO} and TOF). Data were taken from [39] and [136], reproduced with permission of the American Chemical Society (for figure a), and permission by ECS – The Electrochemical Society (for figure b), respectively

[115, 117, 118, 126, 129, 165, 168–173]. In general, the utilization of NH_3 allows an alternative generation of catalysts where instead of complex macrocycles, simple and cheap substances can be used. This matter will be discussed in the following.

Alternative Center Generation During Heat Treatment In 1989, Gupta and coauthors showed that highly active catalysts can be prepared from less complex molecules [63]. In their work, they impregnated a carbon black with polyacrylonitril (PAN) and an iron or cobalt acetate. The precursors were heat-treated at different temperatures and the ORR activity was measured. It was found that one can generalize the preparation of Me-N-C catalysts: Whenever a metal precursor is heat-treated with nitrogen and carbon sources at temperatures of ≥600°C (Co) or ≥700°C (Fe), an active catalyst can be obtained. A scheme of their preparation route and the achieved ORR activities (as a function of pyrolysis temperature) are given in Fig. 18.

Since then, this approach was adapted by several working groups [43, 97, 113, 115–118, 126, 152, 165, 166, 168, 171, 173–186]. Extensive studies were made by Dodelet's group, who tested a wide gamut of metal, nitrogen, and carbon sources, in order to find highest current densities by this screening technique. It could be demonstrated that metal acetates and ammonia are especially suited as precursors to achieve highly active catalysts [179, 187]. Besides ammonia, other nitrogen precursors such as acetonitrile (AN), metal-free N_4-macrocycles, phenanthroline (Phen), polypyrrole (PPy), polyanniline (PANI), and others can equally be used as demonstrated by several groups [113, 126, 127, 134, 165, 174, 176–178, 186, 188, 189].

Varying the metal acetate in the precursor, the obtained ORR activity was studied by He et al. [187]. It was found that the kinetic current density increases in the order Ni ($3d^8$ 4s) ≈ Cu ($3d^{10}$ 4s) < Mn ($3d^5$ $4s^2$) < Cr ($3d^5$ 4s) << Co ($3d^7$ $4s^2$) < Fe ($3d^6$ $4s^2$). If the ORR activity is plotted versus the 3d orbital occupation a volcano plot with a maximum at $3d^6$ will be obtained (For the ease of comparison, the electron configuration of the metals is given in brackets). It should be pointed out that this order nearly reflects the relation between ORR onset potentials and the number of 3d electrons as shown for non-pyrolyzed porphyrins in Fig. 7.

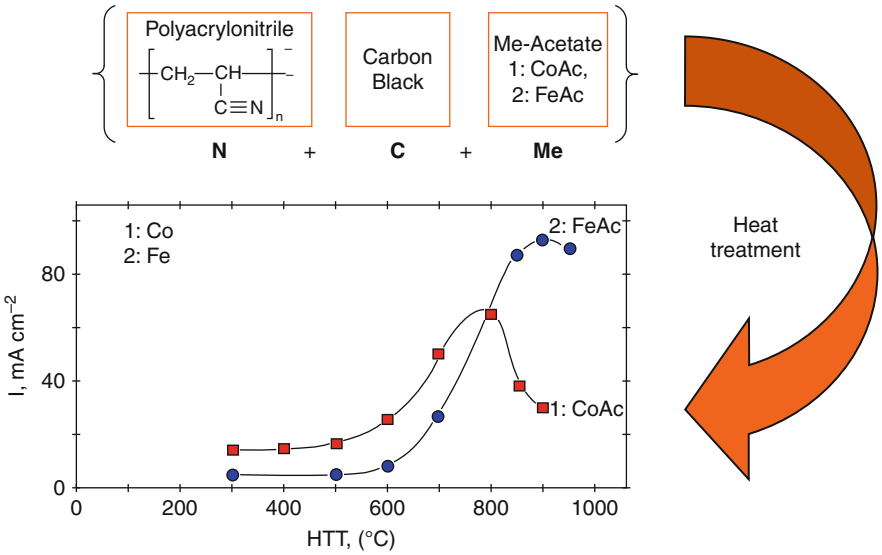

Polymer Electrolyte Membrane Fuel Cells (PEM-FC) and Non-noble Metal Catalysts for Oxygen Reduction. Figure 18 Scheme of Gupta's precursor selection (*top*) and ORR activity of catalysts as a function of the heat treatment temperature and metal precursor, 1: CoAc, ■ and 2: FeAc, ● (*bottom*). ORR activity was measured in 4 M NaOH. The temperature-dependent current curve was taken from [63], Figure 3; reproduced with permission of Springer Publishing Group

It has been observed that besides the type of metal and its content, the fractions of micropores and pyridinic nitrogen atoms play a crucial role for the active site formation. Both are generated during the ammonia treatment [168, 171, 180, 182, 187]. The authors assumed that MeN_{2+2}-centers were built in micropores, a scheme of the center is given in Fig. 19 [168]. Experiments performed with the goal to increase the amount of active centers by annealing the non-porous carbon black impregnated with iron acetate in the presence of NH_3 failed. Even catalysts with more than 0.2 wt% Fe turned out to reveal only smaller turnover frequency. Above 2 wt% iron, the activity dropped remarkably [172].

Mössbauer analysis of such catalysts evidenced that besides less active FeN_4-centers (similar to those in heat-treated porphyrin-based catalysts), a new type of FeN_4-centers was found [190]. This high-spin Fe^{2+}-center was not present in any heat-treated N_4-macrocycle-based catalyst, making it most probable that it is related to the proposed active site. In conclusion, the FeN_{2+2}-centers differ from porphyrin-based ones by the different spin state, the pyridinic coordination of the iron ion and the placement in micropores. The different electronic state might explain why the

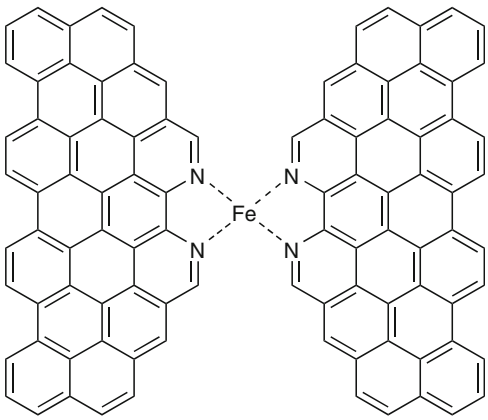

Polymer Electrolyte Membrane Fuel Cells (PEM-FC) and Non-noble Metal Catalysts for Oxygen Reduction. Figure 19
FeN_{2+2}-center embedded in a micropore, as assumed by Charreteur [168]. The figure was taken from [112], figure 3-9; Südwestdeutscher Verlag für Hochschulschriften

FeN_{2+2}-centers can reach much higher turnover frequencies in their "highly active state" (please note: the electron density on iron is higher for Fe^{2+}, HS compared to Fe^{2+}, LS); on the other hand, these centers can

be deactivated, e.g., in contact with acid, as will be discussed in the section "Stability" [190, 191].

Very high activities are obtained when phenanthroline is used as nitrogen source [134, 165, 178]. In 2009, such catalysts exhibited the highest catalytic activity within the system Fe-N-C. The authors assigned their preparation method as pore-filling method (PFM) because especially this step within the preparation process seems to play a crucial role to achieve a high ORR activity [165]. In order to obtain the precursor, a microporous carbon was impregnated with phenanthroline and iron acetate. In the next step, a low-energy ball milling was performed with the aim to press iron acetate and phenanthroline into the micropores. The precursor was pyrolyzed two times (first 1,050°C in Ar, second at 950°C in NH_3) [165]. Highest ORR activities were achieved when the total weight loss from both pyrolysis steps amounted to the weight percentage of phenanthroline, the best having a phenanthroline content of 50 wt% [165, 192].

A homogeneous distribution of active sites was obtained when the phenanthroline is pyrolyzed in the presence of iron oxalate. Such catalysts exhibited an excellent performance in RDE measurements, even without sulfur addition [134]. As indicated by a change of color, already during the mixing of the precursors, a complexation of iron with phenanthroline occurs. These catalysts show similar structural features in Mößbauer spectroscopy and exhibit similar iron contents as those catalysts prepared by the oxalate-supported pyrolysis of porphyrins.

A further preparation approach uses nitrogen-bearing monomers to synthesize catalytic active sites [177, 186, 189], e.g., when pyrrole is impregnated on a carbon black in the presence of a metal source. An oxidation agent induces the polymerization process. Without any heat treatment, only small ORR activity was obtained; however, this catalyst showed a stable performance of more than 500 h in potentiostatic fuel cell tests [177]. Although a heat treatment enhanced the catalyst's activity (similar to the pyrolysis of macrocycles), the stability was moderate. Nevertheless, recent results have shown that by further optimization of the preparation method (including a heat treatment), both, a high activity and a remarkable stability, could be realized [189]. This fact will further be discussed in section "NNMC and Their Potential for PEM-FC Application."

The preparation of catalysts by utilization of monomers with a subsequent polymerization reaction and heat treatment was also applied by other groups [159, 160, 193, 194]. Dahn's team impregnated silica with pyrrole and iron chloride. The polymerization was induced in a hot acid steam. Directly after complete polymerization, the sample was pyrolyzed in Ar at 900°C. The silica template was removed afterward by a doubled leaching in 5% and 40% HF, respectively [159, 160].

Relatively high iron contents are found for self-supported iron-polypyrrole catalysts which were prepared by spray pyrolysis. The authors proposed high site densities; however, comparatively low current densities with respect to other Fe-N-C catalysts make it most probable that only a small fraction of the overall iron is bonded in active sites. Nevertheless, the shape of these catalysts is interesting because porous carbon spheres with diameters of 100 up to 1,000 nm are formed [194].

In conclusion, it can be summarized that active sites in Me-N-C catalysts can be prepared via several different preparation routes. Optimization of each parameter (e.g., amounts of precursors [metal, nitrogen, and carbon], ratios of precursors, annealing temperature, and post treatment) is necessary in order to achieve highest ORR activity. If a heat treatment is performed, one will always achieve a mixture of different metal modifications, whereas it seems that only a fraction of the modifications formed is connected with ORR activity. This observation supports the importance of a subsequent acid leaching and of highly sensitive analysis techniques that can distinguish between the different phases, especially between FeN_4-centers of different oxidation and spin states.

NNMC and Their Potential for PEM-FC Application

With respect to the alternative materials discussed so far, Fe-N-C catalysts seem to be the most promising cathode catalysts for FC application [165, 195]. For that reason, the discussion is focussed on this material system in this chapter. Alternative fuel cell catalysts have to be (1) simple in their preparation, (2) economical in production, and (3) they should generate an

adequately high volumetric current density (J_{vol} in A/cm^3). In order to meet the DOE-target value of the volumetric current density, a certain site density (S_D in sites/cm^3) and a sufficiently high turnover frequency (TOF in electrons sites^{-1}s^{-1}) have to be gained to enable commercial application. Besides, a catalyst stability of several 1,000 h is expected, even under high load conditions of the fuel cell.

Today, catalysts that reach high volumetric current densities often exhibit only low stability while different, less active materials perform nearly stable, even over periods of weeks. Therefore, activity and stability will be discussed separately. The section "Future Direction" will give a final outlook regarding the commercial applicability of NNMC.

Activity

Up-to-date non-noble metal catalysts only partially fulfill the demands in activity for a fuel cell application. To boost activity, the catalyst loading on the cathode can be increased. It was noticed, however, that above a certain layer thickness, mass transport properties hinder a further increase of the current density. For this reason, the specific volumetric activity has to be improved.

The target values for 2010 (the year in which this article was written) and for 2015 are 10% (130 A/cm^3) and 25% (325 A/cm^3), respectively, of the volumetric ORR activity of a commercial Pt/C catalyst [160, 166, 195]. Standard conditions are fulfilled if the measurements are performed at 80°C (T_{CELL} = 80°C) with oxygen and hydrogen partial pressures of 1 bar (p_{02} = 1 bar, p_{H2} = 1 bar) and a relative humidity of RH = 100.

In Table 2, different catalysts are compared with respect to their volumetric ORR activity, site density, kinetic current density, and turnover frequency. The knowledge of these different parameters enables the identification of the factors that have to be further optimized. The catalysts are sorted according to their achieved volumetric current density calculated from fuel cell measurements (column I, Eq. 3). The so far best Fe-N-C catalyst is listed below the DOE-target value followed by the other materials given in the sequence of decreasing volumetric activity. If the authors did not provide any magnitude of the volumetric current density, the value was calculated under the assumption of a catalyst density of ρ = 0.4 g/cm^3 [172, 196].

$$\text{Volumetric current density } J_{vol}\left(\text{in A cm}^{-3}\right): \quad J_{vol} = \frac{J_{A/g}}{\rho_{g/cm^3}}, \tag{3}$$

Presently, none of the Fe-N-C catalysts meet the target value of J_{vol}, even if some of the given data were extrapolated to 0.8 V from the Tafel region of the polarization curve. For highly active catalysts even at 0.8 V, some mass transport limitation is visible so that the measured values of the current density are smaller compared to the extrapolated ones.

An increase of the volumetric current density can be obtained either by enhancing the site density S_D and/or the turnover frequency TOF. Column C in Table 2 lists the site densities of the catalysts as far as the metal content is known. The calculations were made under the assumption that each metal atom is coordinated in an active MeN_4- or MeN_{2+2}-center.

$$\text{Site density } S_D\left(\text{in sites/g}_{cat}{}^{-1}\right): \quad S_D = \frac{[Me]_{wt\%}}{100 \cdot M(Me)_{g/mol}} N_A, \tag{4}$$

In the equation, $[Me]_{wt\%}$ is the concentration of metal species in the catalyst, $M(Me)_{g/mol}$ is the molar mass (if several metal species are present, the average related to the contents of different metals is used), and N_A represents Avogadro's number. Since the density for many of the catalysts is unknown, a weighting related to the volume was neglected.

As described in the section "Non-noble Metal Catalysts with Molecular Centers," it is still controversially discussed, what structural unit (or units) in Me-N-C catalysts causes the oxygen reduction reaction. Furthermore, it was shown for different catalysts that besides the presumably active MeN_4-center also inactive metal-containing modifications exist [39, 40, 117, 129, 131–133, 136, 162, 163, 170, 172, 175, 185, 197, 198]. Consequently, the given site density S_D can merely be regarded as a rough approximate. Nevertheless, it helps to estimate if the site density is a distinct value which has to be adapted.

From the site density S_D and the kinetic current density J_K (at 0.8 V), one can determine the turnover frequency TOF (0.8 V), which is given in Table 2 for

Polymer Electrolyte Membrane Fuel Cells (PEM-FC) and Non-noble Metal Catalysts for Oxygen Reduction. Table 2 Comparison of several catalysts concerning their site density S_D (column C), their kinetic current densities (columns D and E), turnover frequency (columns G and H), and their achieved Volumetric current density (column I). The values in Columns D – I are all given for a potential of 0.8 V. To enable a comparison, for several catalysts values were calculated from the original data as described in the beginning of the chapter Activity

	A	B	C	D	E	F	G	H	I	J
			S_D	RDE	FC	FC/RDE	RDE	FC	FC	
	Shortname	Lit.	$\times 10^{20}$ /sites/$g_{cat.}$	J (0.8 V) /A/g			TOF (0.8 V)/ electrons/ (site s)		vol curr. J_v/(A/cm^3)	Description
1	Target NNMC 2010	DOE							130	
2	Target NNMC 2015	DOE							325	
3	CM-Fe-C	208		–		–	–		127	CM: Cyanamide, Fe-source: $FeSO_4$*$7H_2O$, C-source: sucrose, leaching in KOH
4	PFM1: Fe/Phen/BP-HT1050Ar-HT950NH_3	192	2.2	–	429	–	–	12.42	99	optimized PFM-catalyst, Fe-source: iron acetate
5	PFM2: Fe/Phen/BP-HT1050Ar-HT950NH_3	165	2.2	–	246	–	–	7.12	98.3	catalyst after optimization, Fe-source: FeAc
6	PANI-Fe/EDA-Co-C	208	–	13.75	90	6.55	–		72	PANI-Fe/EDA-Co-C
7	PFM4: Fe/PTCDA/BP-HT1050NH_3 (“M786”)	160	0.8	3	80	26.67	0.23	6.2	32	HT 1050°C, 5 min NH_3, Fe-source: FeAc
8	Fe/Fe/S-HT800N_2-HCl-BM-HT800NH_3	209	5.1	0.71	76.4	107.61	0.01	0.93	30.6	Fe/Fe/S denotes mixture of FeTMPPCl + iron oxalate + sulfur, Leaching in 1 M HCl, 15 min ball milling (BM)
9	Fe/Fe/S-HT800N_2-HCl-HT800NH_3	209	4.3	4.48	31	6.92	0.08	0.45	12.4	Fe/Fe/S denotes mixture of FeTMPPCl + iron oxalate + sulfur, Leaching in 1 M HCl
10	3M-NiANI-HT_NH_3*-HT_NH_3*	166	1.3	–	30	–	–	1.45	12	iron-source: $Fecl_3$, NiANI: Nitroanilin, NH_3*: gas mixture of 25% NH_3 and 75% N_2, HT at 800–1,000°C, same T for both steps

Polymer Electrolyte Membrane Fuel Cells (PEM-FC) and Non-noble Metal Catalysts for Oxygen Reduction. Table 2 (Continued)

	A	B	C	D	E	F	G	H	I	J
			S_D	RDE	FC	FC/RDE	RDE	FC	FC	
	Shortname	Lit.	$\times 10^{20}$ /sites/$g_{cat.}$	J (0.8 V) /A/g			TOF (0.8 V)/ electrons/ (site s)		vol curr. J_v/(A/cm^3)	Description
11	Fe/Fe/S-HT800N_2–HCl–HT800N_2/H_2–HCl–HT800CO_2 ("UK63")	160	3.4	18	20.7	1.15	0.33	0.38	8.3	Leaching in 1 M HCl; N_2/H_2: Forming Gas 10% H_2; Fe/Fe/S denotes mixture of FeTMPPCl + iron oxalate + sulfur
12	PFM3: Fe/Phen/BP-HT1050Ar	165	1.0–2.0	–	13.8	–	–	0.4–0.8	5.5	only heat treatment in Ar, Fe-source: FeAc
13	Co/Fe/S–HT800N_2–HCl–HT800N_2/H_2–HCl–HT800CO_2 ("UK65")	160	3.3	10	10.3	1.03	0.19	0.19	4.1	For leaching 1 M HCl; N_2/H_2: Forming gas with 10% H_2; Co/Fe/S denotes mixture of CoTMPP + iron oxalate + sulfur
14	(PANI–Fe3Co–KB300)–HT900N_2–H_2SO_4	186	2.7	1.3	9.8	7.54	0.03	0.23	3.9	Fe- and Co-sources: hydrated Fe/Co-sulfates, leaching in 0.5 M H_2SO_4
15	μPM1: Fe/npCB–HT950NH_3 ("FC280")	160	0.3	4.2	5.8	1.38	0.92	1.27	2.3	μPM: Micropore method; Fe-source: FeAc; npCB: non-porous carbon black
16	GAdFeCu–HT1000Ar–H_2SO_4 ("GAdFeCu")	160	3.0	0.55	5.7	10.36	0.01	0.12	2.3	G: Glucose, Ad: Adenin, Fe- and Cu-source: hydrated Fe/Cu-gluconate
17	"DAL900c": (DAL900a + Fe)-HT900NH_3	160	1.5	1.1	5	4.55	0.05	0.21	2	DAL900a + Fe: impregnation of DAL900a with FeAc previous to HT
18	CoTMPP/SiO_2–HT700N_2–KOH ("CoTMPP700")	160	6.8	1	3.2	3.20	0.01	0.03	1.3	CoTMPP was impregnated on porous silica previous to HT
19	"DAL900a": ($FeCl_3$/SiO_2 + PPy/HCl)–HT900Ar–HF	160	0.5	0.4	2.7	6.75	0.05	0.36	1.1	PPy/HCl: Polymerization of pyrrole by HCl-vapor; HF: leaching in 5% and 40% HF-solution

Polymer Electrolyte Membrane Fuel Cells (PEM-FC) and Non-noble Metal Catalysts for Oxygen Reduction. Table 2 (Continued)

	A	B	C	D	E	F	G	H	I	J
			S_D	RDE	FC	FC/RDE	RDE	FC	FC	
	Shortname	Lit.	$\times 10^{20}$ /sites/$g_{cat.}$	J (0.8 V) /A/g			TOF (0.8 V)/ electrons/ (site s)		vol curr. J_v/(A/cm^3)	Description
20	Fe/Fe/S–HT800N2–HCl–BM	209	4.3	0.4	2.3	5.75	0.01	0.03	0.9	Fe/Fe/S denotes mixture of FeTMPPCl + iron oxalate + sulfur; BM: 15 min ball milling
21	Hem-HT600Ar–G–HT900CO_2*–H_2SO_4 ("CHb200900")	160	1.2	0.4	2.3	5.75	0.02	0.12	0.9	Hem: grounded Hemoglobin; G: grounded, CO_2*: gas mixture of 10% CO_2 and 90% Ar, leaching in 0.5 M H_2SO_4
22	Co–PPy–C (Vulcan + PPy/H_2O_2) + Co $(NO_3)_2$/($NaBH_4$ + NaOH)	177	4.1	–	1.8	–	–	0.03	0.72	Vulcan was impregnated with pyrrole, polymerization was done by H_2O_2; product was mixed with $Co(NO_3)_2$, which was reduced by $NaBH_4$ + NaOH
23	Fe/Fe/S–HT800N_2–HCl	209	3.9	0.19	1.7	8.95	$<$0.01	0.03	0.7	For leaching 1 M HCl; Fe/Fe/S denotes mixture of FeTMPPCl + iron oxalate + sulfur
24	3 M–NiANI–HT_NH_3*	166	1.3	–	1	–	–	0.05	0.4	iron-source: $FeCl_3$, NiANI:Nitroanilin, NH_3*: gas mixture of 25% NH_3 and 75% N_2, HT at 800–1,000°C
25	$Fecl_3/SiO_2$ + PPy/HCl–HT900Ar–HF	159	2.2	1.3	1	0.77	0.04	0.03	0.4	PPy/HCl: Polymerization of pyrrole by HCl-vapor; HF: leaching in 5% and 40% HF-solution
26	Fe–PPy–MS	194	2.9	0.14	0.4	2.86	0.02	$<$0.01	0.16	Polymerization of pyrrole + $K_3[Fe(CN)_6]$ in H_2O + H_2O_2 induced by $FeCl_3$; US spray pyrolysis (800°C, 2.4 MHz), leaching in 10% HF-solution

Polymer Electrolyte Membrane Fuel Cells (PEM-FC) and Non-noble Metal Catalysts for Oxygen Reduction. Table 2 (Continued)

	A	B	C	D	E	F	G	H	I	J
			S_D	RDE	FC	FC/RDE	RDE	FC	FC	
	Shortname	Lit.	$\times 10^{20}$ /sites/$g_{cat.}$	J (0.8 V) /A/g			TOF (0.8 V)/ electrons/ (site s)		vol curr. J_v/(A/cm^3)	Description
27	((CB–HCl–HNO_3) + Co/Fe/N)–HT900Ar–H_2SO_4	119	6.5	0.28	0.1	0.36	<0.01	<0.01	<0.01	CB–HCl–HNO_3: carbon was first leached in conc. HCl then in conc. HNO_3; Co/Fe/N: $Co(NO_3)_2$+ $FeSO_4$ + Ethylenediamide; final leaching in 0.5 M H_2SO_4
28	GGL–HT1000Ar–H_2SO_4	197	0.5	0.02	0.03	1.50	<0.01	<0.01	<0.01	GGL: Mixture of 0.49:0.49:0.02 mol Glucose:Glycin:Fe-lactate; leaching in 0.5 M H_2SO_4
29	($FePhen_3$ + BP2000)–HT900Ar	174	1.2	0.51	–	–	0.03	–	–	Complexation of phanthroline with hydrated Fe-sulfate

both, RDE as well as fuel cell measurements (columns G and H).

$$\text{Turnover frequency TOF (in electrons site}^{-1}\cdot\text{s}^{-1}\text{)}: \quad \text{TOF} = \frac{J_{K(A/g)}}{S_{D(sites/g)}} \cdot \frac{1}{e}, \tag{5}$$

In this equation, e stands for the elementary charge of the electron.

Fuel cell measurements excellently reflect the actual performance of a catalyst and its applicability. Besides the kinetic behavior, however, the mass transport properties (proton, electron, and oxygen transport as well as water removal) and the internal resistance affect the performance in fuel cells. Thus, it becomes difficult to estimate the kinetic properties of a catalyst just from FC measurements. Rotating (Ring) Disk Electrode (R(R)DE) measurements more precisely reflect the kinetic properties (ORR activity and selectivity). Therefore, in this work also, R(R)DE measurements were taken into account. A comparison of publications showed that measurement conditions (for PEM-FC and R(R)DE) often vary considerably from one laboratory to another, which hinders a direct comparison of the different materials [7, 114, 115, 160, 165, 166, 168–171, 173, 175, 177, 196–206]. In order to enable a better evaluation, F. Jaouen initiated a cross-laboratory comparison of FC and RDE measurements for various Me-N-C catalysts [160]. In Fig. 20, fuel cell measurements of these catalysts are shown.

It was found that the catalysts from different institutes behaved completely different when changing, e.g., the Nafion content or the catalyst loading in FC and RDE tests, as shown for FC measurements in Fig. 20.

Regarding the volumetric current density, best Fe-N-C catalysts yield about 25–40% of the DOE target of 325 A/cm^3 envisaged for 2015 (see lines 3–6, in Table 2) [165, 207, 208]. P. Zelenay's working group published for one of their catalysts a volumetric activity of 40% of the DOE target for 2015 (line 3) [208]. In that preparation route, catalysts were prepared from a mixture of cyanamide, iron sulfate, and sucrose. Further details of the preparation procedure are not yet published. The activity of the so-called PANI-based

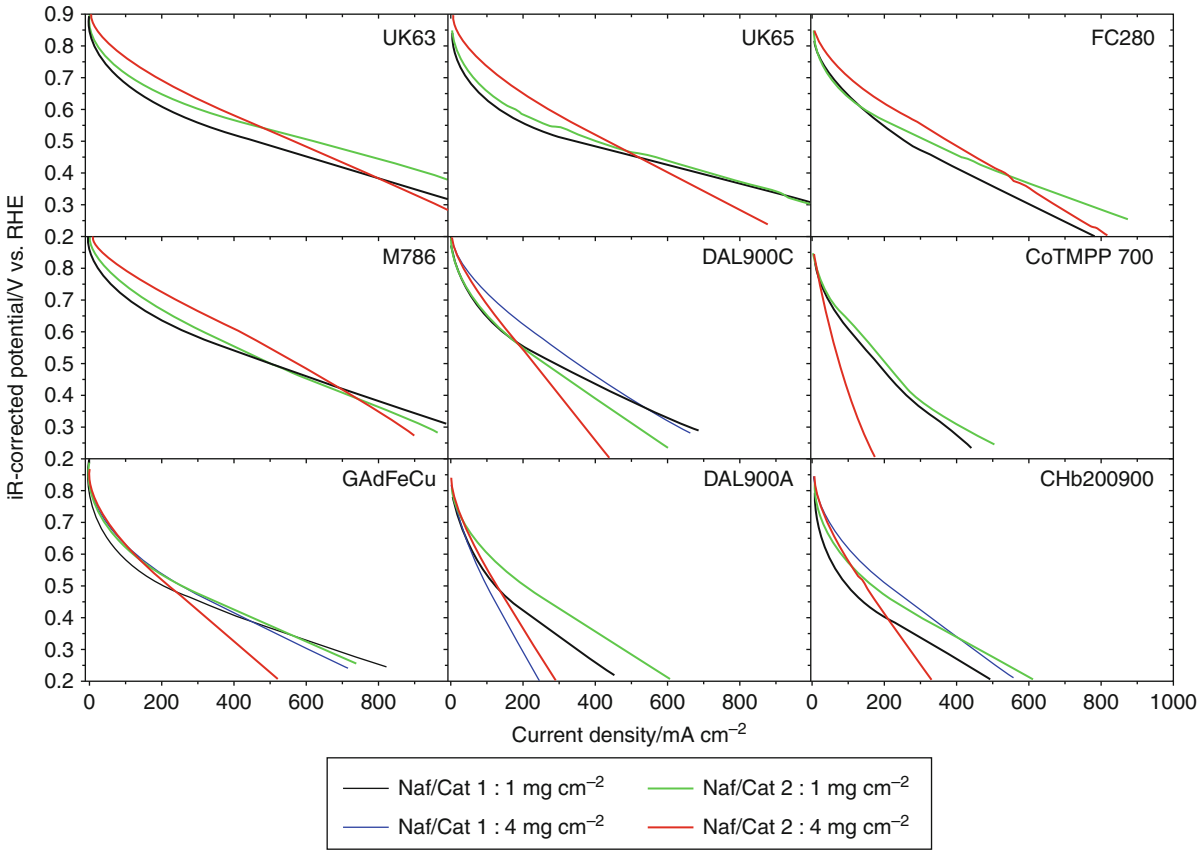

Polymer Electrolyte Membrane Fuel Cells (PEM-FC) and Non-noble Metal Catalysts for Oxygen Reduction. Figure 20 Fuel cell tests of NNMC prepared by different preparation methods (for catalyst's preparation routes, compare Table 2 and [160]). The given FC measurements were made with different Nafion-to-catalyst ratios (Naf/Cat). The figure was taken from [160]; reproduced with permission of the American Chemical Society

catalysts of the same group was boosted by optimization of the preparation steps and the addition of ethylendiamine [189, 207, 208]. Comparing the results of lines 6 and 14, it becomes apparent that by the optimization, the volumetric activity was increased by a factor of 18.

The catalysts in lines 4–5 have been produced via the pore-filling method (PFM) [165]. The preparation is described in the section "Alternative Center Generation During Heat Treatment." A catalyst produced in this manner achieved about 50% of the electron transfer rate of commercial platinum. Similar catalysts, but without ball milling, were already described by Bron et al. in 2002 [174, 178, 188]. The comparison clearly shows that the ball milling has a considerable influence on the achievable activity (lines 4, 5, and 29).

Comparing the volumetric current densities in column I related to the catalyst manufacturing method, it becomes apparent that all catalysts in the upper third of Table 2 were produced in a multistep preparation and/or optimization process. Furthermore, in nearly all procedures, one preparation step is performed in ammonia at $T \geq 800°C$. In 2008, different groups have shown that by performing a second pyrolysis step in ammonia, the kinetic current density can be enhanced drastically [162, 166, 167], a less pronounced improvement was found when other gases (like CO_2, N_2) were used [112, 162]. If previous to the NH_3-treatment a high-energy ball milling is performed, an up to 30-fold increase in current density was achieved as can be learned from columns 8 and 20 in Table 2. The ball milling itself does not affect the kinetics of the

catalyst; however, it can lead to enhanced mass transport properties [209]. Induced by the ball milling, the carbon agglomerates formed during this template-assisted preparation were cracked down allowing subsequently the NH_3 to react more efficiently with the catalyst (compare lines 8 and 9) [209]. Induced by the burn-off, higher site densities are obtained, and a formation of new and/or different catalytic centers might appear [63, 129, 167, 170]. On the other hand, the turnover frequency of the catalysts is improved. To illustrate this behavior, compare lines 4, 5, 12; lines 17, 19; lines 8, 20 and lines 9, 23. Possible reasons for the enhanced kinetics could be (1) the formation of additional, maybe different catalytic centers (i.e., FeN_4 vs. FeN_{2+2} in micropores, compare section "Molecular Centers in Carbonized Materials," Figs. 16 and 19), (2) a general change of the reduction mechanism, or (3) an improvement of the carbon matrix with respect to its electron donor properties [112, 136, 167, 191].

As described in section "Alternative Center Generation During Heat Treatment," some preparation approaches failed by the attempt to increase the site density above a certain critical value [170, 172]. In Table 2, column C, the site densities are listed. It can be deduced that catalysts prepared by the use of a carbon support usually reveal smaller site densities compared to those where exclusively organic precursor molecules were used as carbon sources. In template-assisted preparation processes, an acid leaching (removal of the template) was performed after a first pyrolysis and before the catalyst was further processed [39, 115, 130–133, 159, 160, 162, 177, 186, 189, 197, 201, 209]. The obtained catalysts exhibit site densities of $3{\cdot}10^{20}$ up to $7{\cdot}10^{20}$ centers per gram (compare Table 2). In contrast, the utilization of carbon blacks as support often leads to site densities $<1.5{\cdot}10^{20}$ centers per gram. In these catalysts, the number of active sites should be further increased for FC application.

When high current densities are requested, a lack in the presence of one (or more) of the reactants at the three phase boundary often limits the performance. Another issue concerns the removal of reaction water out of the micro- and mesopore structure which is lowering the kinetics of reactive centers. Thus, in order to optimize the mass transport properties, either the electron or proton conductivity has to be augmented or the pore structure of the catalyst has to be improved to enable better oxygen diffusion to the active centers. Furthermore, the catalyst should be sufficiently hydrophobic in order to guarantee a fast removal of the water to prevent any blocking of active sites. Preferentially, surface groups on the carbon increase the hydrophilicity of the catalyst. Especially disordered carbon can provide higher concentrations of such groups caused by a high number of defects in comparison to well-ordered carbon. Thus, in turn, a high degree of graphitization is beneficial for the water transport properties [207]. As discussed in the next section, graphitic carbon can also enhance the long-term stability.

When switching from RDE to fuel cell measurements, an increase of catalytic activity is expected, simply because of the higher operation temperature. Column F lists the ratio of achieved activities in fuel cell and RDE measurements (J_{FC}/J_{RDE}) at U = 0.8 V. Looking at catalysts, which were produced without commercial carbon support, difficulties in the fuel cell application (as expressed by a low current ratio FC/RDE in column F) can be recognized with the exception of the catalyst in line 8 of Table 2. This catalyst is similar to the one in line 9 except of a ball milling previous to the ammonia treatment. Therefore, a main reason might be the presence of substantially larger carbon agglomerates, which inhibit a homogeneous preparation of the gas diffusion electrode (GDE) [160, 162, 209], as shown in Fig. 21.

Looking at the template-assisted preparation techniques, the physicochemical properties of the in-situ formed carbon could be of lower quality compared to commercial carbon supports. For fuel cell application, an optimization with respect to (1) the electrical conductivity, (2) the agglomerate or particle size, and (3) the transport properties (hydrophilicity) is necessary. However, optimal physicochemical properties of the carbon might not be obtained at the maximum of volumetric current density (determined by S_D and TOF). Therefore, approaches to improve catalysts with an in-situ formed carbon should be also done under utilization of FC measurements in order to evaluate the mass transport kinetics. Nevertheless, optimization remains challenging as a good balance between carbon properties and ORR performance must be found. Not-optimized carbon could not only lower the achievable activity, it could also affect the long-term stability as will be discussed in the following section.

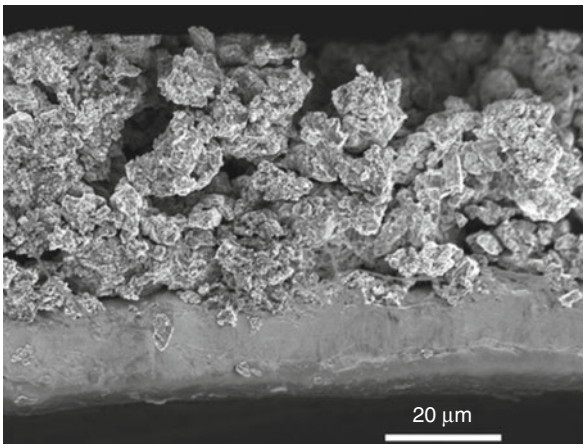

Polymer Electrolyte Membrane Fuel Cells (PEM-FC) and Non-noble Metal Catalysts for Oxygen Reduction. Figure 21
GDE of a catalyst prepared by the oxalate-supported pyrolysis. The figure was taken from [162], reproduced by permission of ECS – The Electrochemical Society

Stability

In this part, possible degradation mechanisms and the currently most promising catalysts with respect to long-term stability will be discussed. For the final implementation, the observed stability is crucial. To optimize the material system, however, it has to be rationalized which processes lead to a decrease of ORR activity.

Regarding non-pyrolyzed macrocycles, hydrogen peroxide formed in the reduction cycle can lead to broken bonds between the substituents and the tetrapyrrole core. Changes in the electronic structure connected therewith cause a decrease of the reduction activity. In acidic conditions as given in PEM-FC, demetallation can also cause an activity decline [71, 87, 98, 102, 210, 211]. Furthermore, carbon monoxide is able to bind irreversibly to the metal centers and thereby deactivating them [212]. With respect to Eq. 7, carbon monoxide might be formed by carbon oxidation during FC operation.

Better stabilities were achieved investigating heat-treated catalysts (section "Molecular Centers in Carbonized Materials"). Nevertheless, in most of the cases, even after the heat treatment, considerable decreases of performance were already observed after a few hours of operation time [69, 159, 168, 184, 188, 213–216]. For catalysts prepared by a heat treatment of either iron porphyrin or iron phthalocyanine, it was shown that they are tolerant toward CO [217, 218]. Therefore, we assume that in general, CO-poisoning can be ruled out as degradation mechanism for carbonized materials. Possible degradation mechanisms could be addressed to (1) a corrosion of carbon as known from platinum catalysts, (2) an inactivation by leaching of active sites, or (3) a deactivation of active species (e.g., by blocking of the centers by intermediates or the final products) [71, 98, 99, 102, 190, 191, 210, 211, 219, 220].

The thermodynamic process of carbon oxidation already starts at potentials >0.21 V. For Pt/C catalysts, SEM cross-sectional images illustrated a significant decrease of the carbon layer thickness, causing a detachment of the platinum particles or an increase of the particle size [8, 110, 220]. In Eqs. 6 and 7, the oxidation reactions of carbon to carbon dioxide (Eq. 6) and carbon monoxide (Eq. 7) are given.

$$C_S + 2H_2O \rightarrow CO_2 \uparrow + 4H^+ + 4e^- \qquad E_0(25°C) = 0.21\ V\ (NHE) \tag{6}$$

$$C_S + H_2O \rightarrow CO \uparrow + 2H^+ + 2e^- \qquad E_0(25°C) = 0.52\ V\ (NHE) \tag{7}$$

Both reactions are initiated by the presence of water. This fact again underlines the importance of an optimized water management. Independent of the nature of the active centers in Me-N-C catalysts, they are presumably integrated into a carbon matrix, either as nitrogen heteroatoms (Fig. 8), MeN_4-centers (Fig. 16), or as MeN_{2+2}-centers in micropores between two adjacent graphene layers (Fig. 19). As discussed above, in N_4-macrocycles, a decrease of the conjugated π-electron system causes a lowering of the ORR activity [41, 42, 80, 81, 221]. It can be assumed that a carbon burn-off in heat-treated materials can cause a similar effect (see below, discussion related to Fig. 25).

Herranz et al. showed that FeN_{2+2}-centers have two different states of catalytic activity depending on whether an NH^+-group or an NH-anion-group is present in its environment [191]. For the first case, very high turnover frequencies are reported. The anion blocking causes a drastic decrease of the turnover frequency and will appear during RDE or FC tests. Nevertheless, it was found that this deactivation process is reversible and that the centers can be activated by performing a thermal or chemical recover

treatment [191]. As such treatments are not applicable during FC operation, however, the effect in general should be inhibited if it is the main reason for activity decay of a specific catalyst.

In 2006, Bashyam and Zelenay published a stable performance of a catalyst entirely produced without heat treatment obtaining stability for a runtime of 100 h. The performance of the catalyst is shown in Fig. 22a. It was prepared by polymerization of pyrrole in the presence of a carbon-supported cobalt salt. Caused by the polymerization, an extended π-electron system was formed leading to good electron conductivity. At that time, the authors suggested that cobalt ions – twofold coordinated by nitrogen atoms – are responsible for the activity [177].

However, the disadvantage of this material was a low catalytic activity (23 A/g at 0.4 V at a catalyst loading of 6 mg/cm^2). Recent approaches of the same group showed that besides pyrrole, also other nitrogen heterocycles and metal salts can be used as nitrogen and metal sources, respectively [189, 208]. Similar to non-pyrolyzed macrocycles, the activity can be enhanced by a heat treatment [177, 189]. A comparison of different nitrogen heterocycles used in the preparation showed that the selection of the polymer significantly affects activity and stability – even after a heat treatment. The Fe/PANI/C-catalyst supported on multiwall carbon nanotubes (MWCNT) achieved an activity of 75 A/g (at 0.4 V) and showed no degradation within the investigated time of 500 h [186, 189]. Therefore, this catalyst is currently the most stable Fe-N-C catalyst, exhibiting even a good catalytic activity (remark: considering catalysts, which have been investigated in fuel cells with respect to their stability). The preparation is similar to that of a pyrrole-based catalyst.

The currently most active catalysts prepared by the Pore-Filling-Method (PFM) from J.-P. Dodelet's group show an average degradation of 0.38%/h for 100 h potentiostatic operation with respect to the initial activity (compare [165, 192]), the related curve is shown in Fig. 22b. The measuring conditions thereby were more or less identical to Bashyam's and Zelenay's experiments. It seems that for the degradation of this PFM-catalyst, one can distinguish an initial fast degradation ($t < 20$ h) which is superimposed by a weaker and slower one ($t > 20$ h: −0.08%/h).

In the work of Wu et al., structural changes of a Fe/PANI/KB300 catalyst were investigated before and after a runtime of 500 h [189]. After a long-term test, the percentage of oxygen in the matrix was drastically increased, that the authors attributed to the oxidation of carbon and nitrogen atoms. Particularly striking were a complete loss of sulfur (which was present in the polymerization agent) and a slight decrease of the

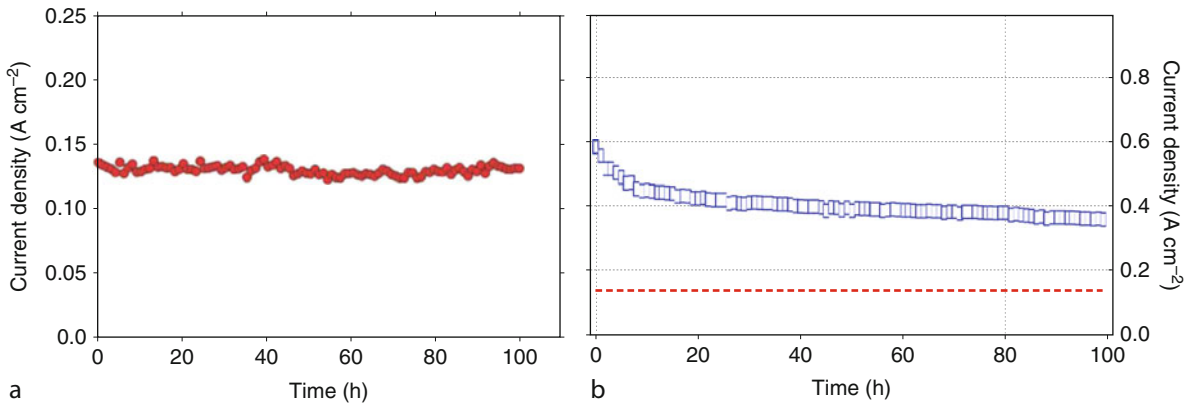

Polymer Electrolyte Membrane Fuel Cells (PEM-FC) and Non-noble Metal Catalysts for Oxygen Reduction. Figure 22 Stability measurements of (**a**) a Co-PPy-CB and (**b**) a Fe/CB-PFM catalysts. Both catalysts were measured under nearly the same conditions at 80°C, backpressures of 2 atm, gases at 100% RH with catalyst loadings of 6 mg/cm^2 and 5.6 mg/cm^2 for the Co-PPy-CB and Fe/CB-PFM catalysts, respectively. The figure in (**a**) was taken from [177]; copyright 2006, reproduced with permission of Nature Publishing Group. The figure in (**b**) was taken from [165], reprinted with permission from AAAS

total nitrogen content (from 6.3% to 5.6%). Changes in the relative composition of the N1s spectra were significant. A comparison of the spectra before and after 500 h fuel cell test time is shown in Fig. 23. It is evident that the long-term performance causes an energetic shift of the nitrogen species toward higher bonding energies. This was mostly attributable to the oxidation of pyridinic nitrogen atoms. In the investigated time-frame, the catalyst lost 17% of its initial activity. Similar shifts in the XPS N1s-spectra were observed by Liu et al. and by Kramm [112, 115].

In the case of Liu et al., significantly higher activity losses compared to Wu et al. were observed (−0.46%/h vs − 0.04%/h), while Kramm did not observe any significant loss (compare Fig. 25). Liu et al. assigned the overall ORR activity to highly active pyridinic and less active graphitic nitrogen atoms (both without iron participation) [115]. They explained their XPS results with a protonation of pyridinic nitrogen atoms in contact with an acidic electrolyte; this process was proposed to be the main reason for the observed deactivation. On the other hand, graphitic nitrogen atoms were assigned to be less active but more stable in acidic environment [115]. Kramm investigated the structural changes of a Fe-N-C catalyst via XPS, NAA and ^{57}Fe Mößbauer spectroscopy [112]. The catalyst was produced by the sulfur-assisted oxalate-supported pyrolysis of FeTMPPCI; in a subsequent acid leaching step, excess iron was removed. Before the long-term measurement was performed, the electrode was kept in distilled water for 24 h in order to initiate a complete swelling of the PTFE previous to the stability test shown in Fig. 24.

The preconditioned electrode showed no loss in activity over a period of 4 weeks and no significant change of the composition in Mößbauer spectra or iron content. The changes of the N1s spectra, however, were similarly pronounced as described by Wu et al. [112, 189]. A comparison of the three references discussed above leads to the conclusion that pyridinic nitrogen atoms might affect the activity of the catalysts up to a certain degree. However, it has been demonstrated that pyridinic nitrogen atoms cannot explain the catalytic activity alone [112].

In an early work of Faubert et al. [140], the influence of the pyrolysis temperature on the stability of MeTPP/C was investigated (Me = Fe, Co). Figure 25 shows the changes of the current density (related to the surface area and the metal content) as a function of performance time. It is evident that catalysts prepared from FeTPP achieve higher current densities and better stabilities than CoTPP-based catalysts. Apart from a pronounced loss in activity within the first 5 min, the FeTPP/C catalysts, produced at 800° and 900° C, demonstrated a nearly stable performance. At even higher pyrolysis temperatures, the stability performance was similar to that of the platinum catalyst (2 wt% Pt/C), which was measured as a reference.

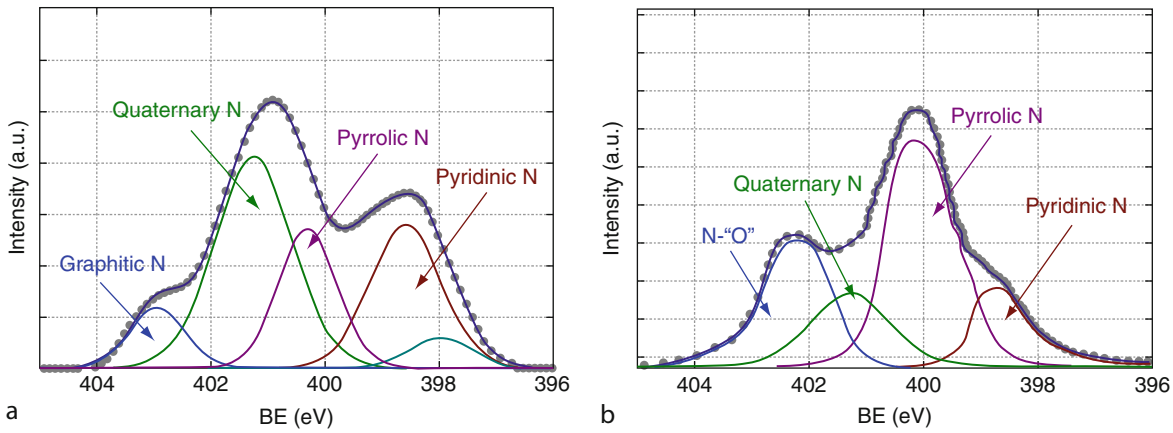

Polymer Electrolyte Membrane Fuel Cells (PEM-FC) and Non-noble Metal Catalysts for Oxygen Reduction. Figure 23 N 1s XP spectra of a Fe-PANI-C catalyst (**a**) before and (**b**) after a 500-h long-term stability test. The figure was taken from [189]; reproduced by permission of ECS – The Electrochemical Society

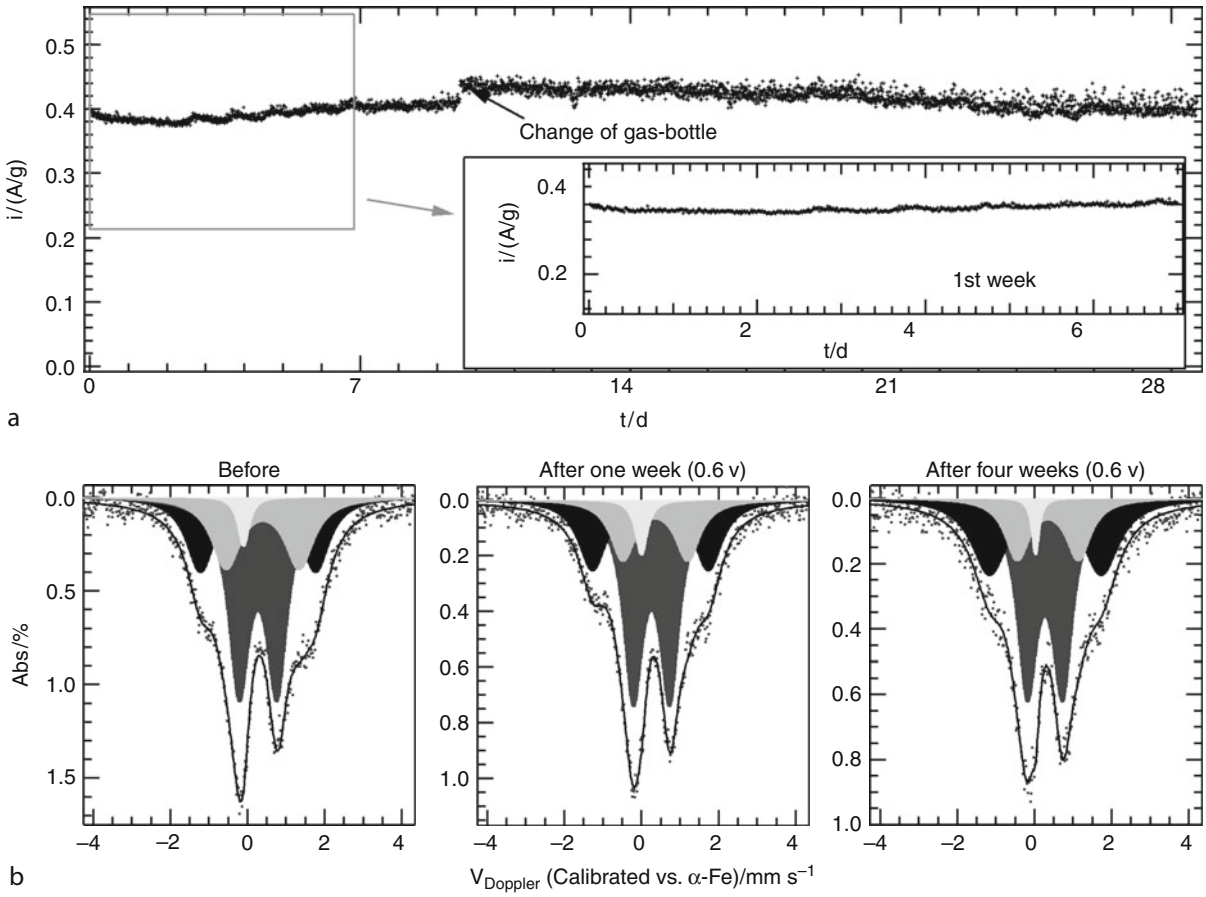

Polymer Electrolyte Membrane Fuel Cells (PEM-FC) and Non-noble Metal Catalysts for Oxygen Reduction. Figure 24 Potentiostatic (U = 0.6 V) long-term stability test in O_2-flushed 0.5 M H_2SO_4 of a Fe-N-C-catalyst at RT (**a**). The insert gives a magnification of the first week of measuring time. The catalyst was prepared by the sulfur-assisted oxalate-supported pyrolysis of FeTMPPCl (800°C, N_2), with acid leaching. The structural features related to iron were studied by Mößbauer spectroscopy at RT; (**b**) before, after 1 week and after 4 weeks of measuring time. The figure is adapted from Figures 7-7 and 7-8 of [112]; copyright 2009 by Südwestdeutscher Verlag für Hochschulschriften

The authors assigned the enhanced stability to an increased amount of graphitic carbon [140].

Recent results published by the same group [222, 223] and the comparison of various carbon-supported Fe/PANI/C catalysts confirm this observation [189]. One might summarize that in fuel cells, obviously the long-term stability seems to depend on the corrosion resistivity of the carbon matrix for both, Fe-N-C and Pt/C catalysts [8, 224].

In order to avoid any activity loss, the catalysts must be stabilized: For Pt/C catalysts, it was shown that the implementation of metal oxide particles into the carbon matrix can enhance the corrosion resistivity substantially. Furthermore, as far as possible, the catalysts should comprise fractions of graphitic carbon which prevent a fast oxidation.

It is believed that the search for alternative supports for Fe-N-C catalysts will become dominant in the future. Especially, different transition metal oxynitrides (TiO_xN_y, TaO_xN_y, ZrO_xN_y), and Nb- or Sb-doped TiO_2 or SnO_2 or PANI appear to be promising in this context [55, 224–227]. It will remain a major challenge to enable the implementation of molecular centers onto the surface of the new support material. It has already been pointed out that PANI possesses a considerable potential with this respect [189]. Since none of the

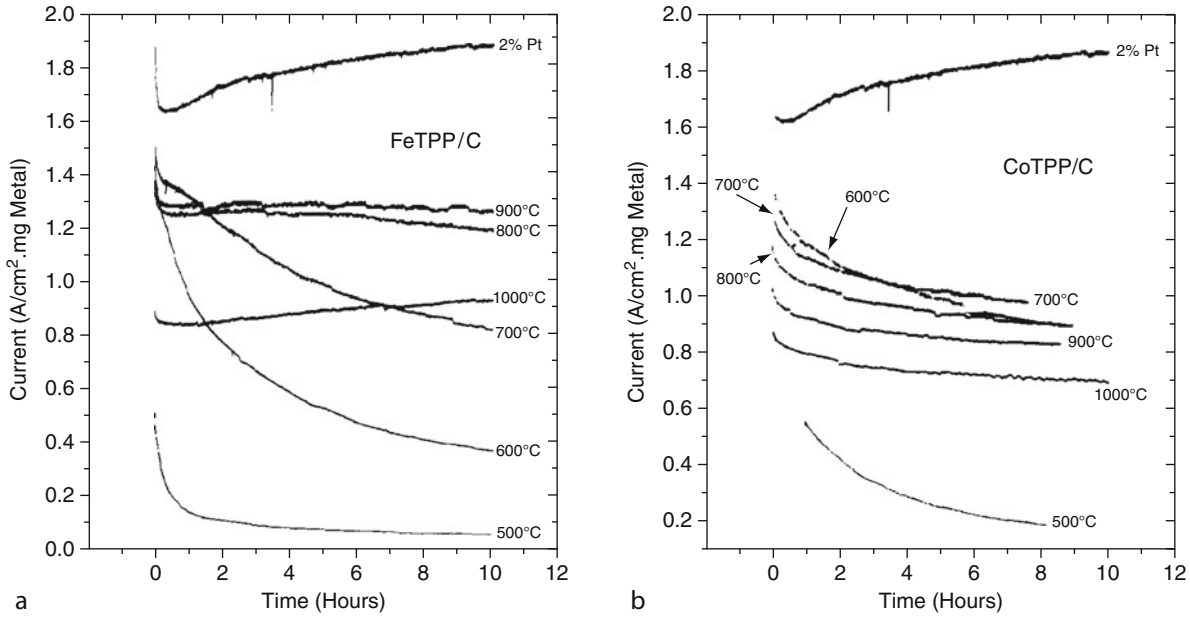

Polymer Electrolyte Membrane Fuel Cells (PEM-FC) and Non-noble Metal Catalysts for Oxygen Reduction. Figure 25 Stability tests of carbon-supported FeTPP (**a**) and CoTPP (**b**), both pyrolyzed at various temperatures as indicated in the graphs. The figures were taken from [140], reproduced with permission of Elsevier

other promising support materials contain carbon, it is questionable how catalytically active Fe-N-C catalysts could be implemented.

With this respect, the work from Atanasoski and coworkers is promising (compare section "Transition Metal Carbides, Nitrides and Chalcogenides") [35]. By performing a heat treatment of their sputtered C-N_x:Fe films, the activity was drastically enhanced but still much lower compared to macrocycle-based catalysts. However, when titanium carbide was used as support instead of carbon, a high stability was obtained. The fact that by changing the support, an essentially better durability was obtained is an important result as it shows that even for catalysts based on molecular centers, alternative support materials can be utilized and that the interaction between the support and the catalytic centers might be crucial for the optimization of those catalysts for a fuel cell application.

However, it has to be kept in mind that a major challenge of these catalysts is to improve their transport properties which are by far not ideal as can be recognized from Tafelplots deduced from RDE measurements. To investigate the water management in platinum-based fuel cells, the use of neutron scattering has meanwhile proven to be an effective tool [228, 229]. Such investigations could also play a major role for further optimization of Fe-N-C catalysts.

Future Direction

Comparing the different types of NNMC, the Fe-N-C catalysts are presently the most promising candidates to replace platinum or other noble metal catalysts. These materials exhibit the highest activities and catalyze with high selectivity the direct reduction of oxygen to water. Since 2009, a significant improvement in comparison to previous results was made; here especially the work of Dodelet and coworkers and Zelenay and coworkers should be mentioned [165, 189]. In general, stable fuel cell performance over periods of up to 1000 h has already been demonstrated (Table 3). Although long-term stability and high catalytic activity appear to be difficult to combine into one material, based on today's knowledge of the structural characteristics that affect activity and/or stability, further improvements of FC performance are expected. One major step to an improved stability may be through alternative support materials.

Polymer Electrolyte Membrane Fuel Cells (PEM-FC) and Non-noble Metal Catalysts for Oxygen Reduction. Table 3
Comparison of different Fe–N–C catalysts with respect to their stability

	A	B	C	D	E	F	G	H
					mW/cm^2			
	Catalyst	Lit.	Conditions	Comm.	Start	End	time/h	Performance (%/h)
1	(FeTMPPCl/non-μpCB)–HT950Ar, 5.2 wt%Fe	222	FC80, H_2/O_2: 1 bar, 2 mg/cm^2	0.6	2.58	6.24	15	9.46
2	(FeTMPPCl/non-μpCB)–HT950Ar–H_2SO_4, 5.2 wt%	222	FC80, H_2/O_2: 1 bar, 2 mg/cm^2	0.6	5.1	6.6	15	1.96
3	PANI–Fe–MWCNT (HT900, N_2–H_2SO_4)	189	FC80, H_2/Air: 2 bar, 4 mg/cm^2	0.4	120	120	500	0.00
4	PPy–Co–C	177	FC80, H_2/Air: 2 bar, 4 mg/cm^2	0.4	56	56	100	0.00
5	PPy–Co–C	177	FC80, H_2/O_2: 2 bar, 6 mg/cm^2	0.7	24.5	24.5	50	0.00
6	Fe/Fe/S–HT800N_2–HCl, 24h_swelling_inH_2O	112	T = 25°C, 0.5 M H_2SO_4, O_2, 4 mg/cm^2	0.6	0.96	0.96	672	0.00
7	3M–NiANI–HT_NH_3*	166	FC80, H_2/O_2: 3/4.3 bar	0.6	0.0024	0.0024	0.5	0.00
8	PANI–Fe_3Co–C (HT900, N_2–H_2SO_4)	189	FC80, H_2/Air: 2 bar, 4 mg/cm^2	0.4	148	132	600	−0.02
9	PANI–Fe_3Co–C (HT900, N_2–H_2SO_4)	186	FC80, H_2/Air: 2 bar, 4 mg/cm^2	0.4	140	130	400	−0.02
10	PANI–Fe–C (HT900, N_2–H_2SO_4)	189	FC80, H_2/Air: 2 bar, 4 mg/cm^2	0.4	120	100	500	−0.03
11	((CB–HCl–HNO_3) + Co/Fe/N) − HT900Ar–H_2SO_4	119	FC80, H_2/O_2, no backpressure	200 mA/cm^2	70	60	450	−0.03
12	PANI–Fe–KB300 (HT900, N_2–H_2SO_4)	189	FC80, H_2/Air: 2 bar, 4 mg/cm^2	0.4	116	90	500	−0.04
13	PANI–Co–C (HT900, N_2–H_2SO_4)	189	FC80, H_2/Air: 2 bar, 4 mg/cm^2	0.4	100	90	180	−0.06
14	Fe/Fe/S–HT800N_2–HCl	112	GDE, T = 25°C, O_2, 4 mg/cm^2	0.6	0.96	0.7032	168	−0.16
15	(Fe,Co)/EDA + SiO_2-HT1000Ar–NaOH–H_2SO_4–HT1000Ar	115	FC75, H_2/Air: 2 bar, 2 mg/cm^2	0.4	140	110	100	−0.21
16	CHb200900	204	FC80, H_2/Air:50/250, 10 mg/cm^2	0.5	–	–	200	−0.22
17	CHb350900C	204	FC80, H_2/Air:50/250, 10 mg/cm^2	0.5	–	–	200	−0.33
18	PFM1: Fe/Phen/BP–HT1050Ar–HT950NH_3	165	FC80, H_2/Air: 2 bar, 5.6 mg/cm^2	0.4	240	150	100	−0.38
19	(Fe,Co)/EDA + SiO_2-HT800Ar-NaOH-H_2SO_4-HT800Ar	115	FC75, H_2/Air: 2 bar, 2 mg/cm^2	0.4	204	120	90	−0.46
20	PPy-Fe-C (HT900, N_2-H_2SO_4)	189	FC80, H_2/Air: 2 bar, 4 mg/cm^2	0.4	196	100	100	−0.49

Polymer Electrolyte Membrane Fuel Cells (PEM-FC) and Non-noble Metal Catalysts for Oxygen Reduction. Table 3 (Continued)

	A	B	C	D	E	F	G	H
					mW/cm^2			
	Catalyst	Lit.	Conditions	Comm.	Start	End	time/h	Performance (%/h)
21	PFM1: Fe/Phen/BP-HT1050Ar-HT950NH$_3$	165	FC80, H_2/O_2: 2 bar, 5.6 mg/cm^2	0.5	385	165	100	−0.57
22	(FePhen3 + BP2000)-HT900Ar	178	GDE, T = 25°C, 0.5 M H_2SO_4, Air	?	13.5	3	40	−1.94
23	(Graphite + BM5)-FeAc-HT950NH$_3$	184	FC80, H_2/O_2: 4/2 bar, 1.1 mg/cm^2	0.3	135	69	24	−2.04
24	(Graphite + BM0.5)-FeAc-HT950NH$_3$	184	FC80, H_2/O_2: 4/2 bar, 1.1 mg/cm^2	0.3	102	37.5	24	−2.63
25	(Graphite + BM10)-FeAc-HT950NH$_3$	184	FC80, H_2/O_2: 4/2 bar, 1.1 mg/cm^2	0.3	43.5	14.4	24	−2.79
26	(FeTMPPCl/non-μpCB)-HT950NH$_3$, 0.4 wt%Fe	222	FC80, H_2/O_2: 1 bar, 2 mg/cm^2	0.6	108	13.2	15	−5.85
27	(FeTMPPCl/non-μpCB)-HT950Ar, 0.4 wt% Fe	222	FC80, H_2/O_2: 1 bar, 2 mg/cm^2	0.6	6	0.66	15	−5.93

Apart from this "hot" topic, one should keep in mind that catalysts based on transition metal chalcogenides, nitrides, and carbides also have the potential to be used without carbon support. Considering the tremendous carbon corrosion problems especially at higher temperature (>110°C), carbon-free electrode structures will be an important aspect of future research.

Bibliography

1. Markovic NM, Radmilovic V, Ross PN (2003) Catalysis and electrocatalysis at nanoparticle surfaces. Marcel Dekker, New York/Basel
2. Mukerjee S, Srinivasan S (1993) Enhanced electrocatalysis of oxygen reduction on platinum alloys in proton exchange membrane fuel cells. J Electroanal Chem 357:201–224
3. Zhang J, Lima FHB, Shao MH, Sasaki K, Wang JX, Hanson J, Adzic RR (2005) Platinum monolayer on non-noble metal-noble metal core-shell nanoparticle electrocatalysts for O_2 reduction. J Phys Chem B 109:22701–22704
4. Stamenkovic VR, Mun BS, Mayrhofer KJJ, Ross PN, Markovic NM (2006) Effect of surface composition on electronic structure, stability and electrocatalytic properties of Pt-transition metal alloys: Pt-skin versus Pt-skeleton surfaces. J Am Chem Soc 128:8813–8819
5. Strasser P, Koh S, Anniyev T, Greeley J, More K, Yu C, Liu Z, Kaya S, Nordlund D, Ogasawara H, Toney MF, Nilsson A (2010) Lattice-strain control of the activity in dealloyed core – shell fuel cell catalysts. Nat Chem 2:454–460
6. Adzic RR, Zhang J, Sasaki K, Vukmirovic MB, Shao M, Wang JX, Nilekar AU, Mavrikakis M, Valerio JA, Uribe F (2007) Platinum monolayer fuel cell electrocatalysts. Top Catal 46:249–262
7. Zhang S, Yuan XZ, Hin JC, Wang H, Friedrich KA, Schulze M (2009) A review of platinum-based catalyst layer degradation in proton exchange membrane fuel cells. J Power Sources 194:588–600
8. Mayrhofer KJJ, Meier JC, Ashton SJ, Wiberg GKH, Kraus F, Hanzlik M, Arenz M (2008) Fuel cell catalyst degradation on the nanoscale. Electrochem Commun 10:1144–1147
9. Delacote C, Bonakdarpour A, Johnston CM, Zelenay P, Wieckowski A (2008) Aqueous-based synthesis of ruthenium – selenium catalyst for oxygen reduction reaction. Faraday Discuss 140:269–281
10. Fiechter S, Dorbandt I, Bogdanoff P, Zehl G, Schulenburg H, Tributsch H, Bron M, Radnik J, Fieber-Erdmann M (2007) Surface modified ruthenium nanoparticles: structural investigation and surface analysis of a novel catalyst for oxygen reduction. J Phys Chem C 111:477–487
11. Guinel MJF, Bonakdarpour A, Wang B, Babu PK, Ernst F, Ramaswamy N, Mukerjee S, Wieckowski A (2009) Carbon-supported, selenium-modified ruthenium – molybdenum catalysts for oxygen reduction in acidic media. ChemSusChem 2:658–664
12. Haas S, Hoell A, Zehl G, Dorbandt I, Bogdanoff P, Fiechter S (2008) Structural investigation of carbon supported Ru-Se based catalysts using anomalous small angle X-ray scattering. ECS Trans 6:127–138
13. Loponov KN, Kriventsov VV, Nagabhushana KS, Boennemann H, Kochubey DI, Savinova ER (2009) Combined in situ EXAFS

and electrochemical investigation of the oxygen reduction reaction on unmodified and Se-modified Ru/C. Catal Today 147:260–269

14. Zehl G, Schmithals G, Hoell A, Haas S, Hartnig C, Dorbandt I, Bogdanoff P, Fiechter S (2007) On the structure of carbon-supported selenium-modified ruthenium nanoparticles as electrocatalysts for oxygen reduction in fuel cells. Angew Chem Int Ed 46:7311–7314
15. Cremers C, Scholz M, Seliger W, Racz A, Knechtel W, Rittmayr J, Grafwallner F, Peller H, Stimming U (2007) Developments for improved direct methanol fuel cell stacks for portable power. Fuel Cells 7:21–31
16. Garsuch A, Michaud X, Böhme K, Wagner G, Dahn JR (2009) Fuel cell performance of templated Ru/Se/C-based catalysts. J Power Sources 189:1008–1011
17. Whipple DT, Jayashree RS, Egas D, Alonso-Vante N, Kenis PJA (2009) Ruthenium cluster-like chalcogenide as a methanol tolerant cathode catalyst in air-breathing laminar flow fuel cells. Electrochim Acta 54:4384–4388
18. Wippermann K, Richter B, Klafki K, Mergel J, Zehl G, Dorbandt I, Bogdanoff P, Fiechter S, Kaytakoglu S (2007) Carbon supported Ru – Se as methanol tolerant catalysts for DMFC cathodes part II: preparation and characterization of MEAs. J Appl Electrochem 37:1399–1411
19. Lee J-W, Popov BN (2007) Ruthenium-based electrocatalysts for oxygen reduction reaction – a review. J Solid State Electrochem 11:1355–1364
20. Zhang L, Zhang J, Wilkinson DP, Wang H (2006) Progress in preparation of non-noble electrocatalysts for PEM fuel cell reactions. J Power Sources 156:171–182
21. Bennett LH, Cuthill JR, McAlister AJ, Erickson NE, Watson RE (1974) Electronic structure and catalytic behavior of tungsten carbide. Science 184:563–565
22. Colton RJ, Huang JJ, Rabalais JW (1975) Electronic structure of tungsten carbide and its catalytic behavior. Chem Phys Lett 34:337–339
23. Levy RB, Boudart M (1973) Platinum-like behavior of tungsten carbide in surface catalysis. Science 181:547–549
24. Ross PN Jr, Stonehart P (1975) Surface characterization of catalytically active tungsten carbide (WC). J Catal 39: 298–301
25. Binder H, Köhling A, Kuhn W, Lindner W, Sandstede G (1969) Tungsten carbide electrodes for fuel cells with acid electrolyte. Nature 224:1299–1300
26. Bronoel G, Museux E, Leclercq G, Leclercq L, Tassin N (1991) Study of hydrogen oxidation on carbides. Electrochim Acta 36:1543–1547
27. Machida K, Enyo M (1990) Preparation of WC_x thin films by RF sputtering and their electrocatalytic property for anodic methanol oxidation. J Electrochem Soc 137:871–876
28. Sokolsky DV, Palanker VS, Baybatyrov EN (1975) Electrochemical hydrogen reactions on tungsten carbide. Electrochim Acta 20:71–77
29. Mazza F, Trassatti S (1963) Transition metal oxides as DMFC cathodes without platinum. J Electrochem Soc 110:847–849
30. Lee K, Ishihara A, Mitsushima S, Kamiya N, Ota K (2004) Stability and electrocatalytic activity for oxygen reduction in WC + Ta catalyst. Electrochim Acta 49:3479–3485
31. Bhattarai J, Akiyama E, Habazaki H, Kawashima A, Asami K, Hashimoto K (1998) The passivation behavior of sputter-deposited W-Ta alloys in 12 M HCl. Corros Sci 40:757–179
32. Chou WJ, Yu GP, Huang JH (2003) Corrosion resistance of ZrN films on AISI 304 stainless steel substrate. Surf Coat Technol 167:59–67
33. Zhong H, Zhang H, Liang Y, Zhang J, Wang M, Wang X (2007) A novel non-noble electrocatalyst for oxygen reduction in proton exchange membrane fuel cells. J Power Sources 164:572–577
34. Zhong H, Zhang H, Liu G, Liang Y, Hu J, Yi B (2006) A novel non-noble electrocatalyst for PEM fuel cell based on molybdenum nitride. Electrochem Comm 8:707–712
35. Atanasoski R (2007) Novel approach to non-precious metal catalysts. DOE hydrogen program FY2007 anual progress report 820–824
36. O´Neill DG, Atanasoski R, Schmoekel AK, Vernstrom GD, O´Brien DP, Jain M, Wood TE (2006) Vacuum deposited non-precious metal catalysts for PEM fuel-cells. Mater Matters 1:17–19
37. Blomquist J, Lang H, Larsson R, Widelöv A (1992) Pyrolysis behaviour of metalloporphyrins: part2: a Mössbauer study of pyrolysed Fe^{III} tetraphenylporphyrin chloride. J Chem Soc Faraday Trans 88:2007–2011
38. Bouwkamp-Wijnoltz AL, Visscher W, van Veen JAR, Boellaard E, van der Kraan AM, Tang SC (2002) On active-site heterogeneity in pyrolysed carbon-supported iron porphyrin catalysts for the electrochemical reduction of oxygen: an in situ Mössbauer study. J Phys Chem B 106:12993–13001
39. Koslowski UI, Abs-Wurmbach I, Fiechter S, Bogdanoff P (2008) Nature of the catalytic centres of porphyrin based electrocatalysts for the ORR – A correlation of kinetic current density with the site density of $Fe\text{-}N_4$ centres. J Phys Chem C 112:15356–15366
40. Lefèvre M, Dodelet J-P, Bertrand P (2002) Molecular oxygen reduction in PEM fuel cells: evidence for the simultaneous presence of two active sites in Fe-based catalysts. J Phys Chem B 106:8705–8713
41. van Veen JAR, van Baar JF, Kroese KJ (1981) Effect of heat treatment on the performance of carbon-supported transition-metal chelates in the electrochemical reduction of oxygen. J Chem Soc Faraday Trans 77:2827–2843
42. van Veen JAR, Colijn HA, van Baar JF (1988) On the effect of a heat treatment on the structure of carbon-supported metalloporphyrins and phthalocyanines. Electrochim Acta 33:801–804
43. Bradley Easton E, Bonakdarpour A, Dahn JR (2006) Fe-C-N oxygen reduction catalysts prepared by combinatorial sputter deposition. Electrochem Sol State Letts 9:A463–A567
44. Liu Y, Ishihara A, Mitsushima S, Kamiya N, Ota K (2007) Transition metal oxides as DMFC cathodes without platinum. J Electrochem Soc 154:B664–B669

45. Liu Y, Ishihara A, Mitsushima S, Ota K (2010) Influence of sputtering power on oxygen reduction reaction activity of zirconium oxides prepared by radio frequency reactive sputtering. Electrochim Acta 55:1239–1244
46. Descorme C, Madier Y, Duprez D (2000) Infrared study of oxygen adsorption and activation on cerium – zirconium mixed oxides. J Catal 196:167–173
47. Lisebigler AL, Lu G, Yates JT (1995) Photocatalysis on TiO_2 surfaces: principles, mechanisms, and selected results. Chem Rev 95:735–758
48. Witko M, Tokarz-Sobieraj R (2004) Surface oxygen in catalysts based on transition metal oxides: what can we learn from cluster DFT calculations? Catal Today 91–92:171–176
49. Kim J-H, Ishihara A, Mitsushima S, Kamiya N, Ota K-I (2007) Catalytic activity of titanium oxide for oxygen reduction reaction as a non-platinum catalyst for PEFC. Electrochim Acta 52:2492–2497
50. Mentus SV (2004) Oxygen reduction on anodically formed titanium dioxide. Electrochim Acta 50:27–32
51. Kudo A, Miseki YCSR (2009) Heterogeneous photocatalyst materials for water splitting. Chem Soc Rev 38:253–278
52. Osterloh FE (2008) Inorganic materials as catalysts for photochemical splitting of water. Chem Mater 20:35–54
53. Liu G, Zhang HM, Wang MR, Zhong HX, Chen J (2007) Preparation, characterization of ZrO_xN_y/C and its application in PEMFC as an electrocatalyst for oxygen reduction. J Power Sources 172:503–510
54. Doi S, Ishihara A, Mitsushima S, Kamiya N, Ota K (2007) Zirconium-based compounds for cathode of polymer electrolyte fuel cell. J Electrochem Soc 154:B362–B369
55. Ohgi Y, Ishihara A, Matsuzawa K, Mitsushima S, Ota K (2010) Zirconium oxide-based compound as new cathode without platinum group metals for PEFC. J Electrochem Soc 57:B885–B891
56. Clouser SJ, Huang JC, Yeager E (1993) Temperature dependence of the tafel slope for oxygen reduction on platinum in concentrated phosphoric acid. J Appl Electrochem 23:597–605
57. Ishihara A, Lee K, Doi S, Mitsushima S, Kamiya N, Hara M, Domen K, Fukuda K, Ota K (2005) Tantalum oxynitride for a novel cathode of PEFC. Electrochem Solid State Lett 8:A201–A203
58. Imai H, Matsumoto M, Miyazaki T, Fujieda S, Ishihara A, Tamura M, Ota K (2010) Structural defects working as active oxygen-reduction sites in partially oxidized Ta-carbonitride core-shell particles probed by using surface-sensitive conversion-electron-yield X-ray absorption spectroscopy. App Phys Lett 96:191905
59. Ohnishi R, Katayama M, Takanabe K, Kubota J, Domen K (2010) Niobium-based catalysts prepared by reactive radio-frequency magnetron sputtering and arc plasma methods as non-noble metal cathode catalysts for polymer electrolyte fuel cells. Electrochim Acta 55:5393–5400
60. Takagaki A, Takahashi Y, Yin F, Takanabe K, Kubota J, Domen K (2009) Highly dispersed niobium catalyst on carbon black by polymerized complex method as PEFC cathode catalyst. J Electrochem Soc 156:B811–B815
61. Jasinski R (1964) A new fuel cell cathode catalyst. Nature (Lond) 201:1212–1213
62. Jahnke H, Schönborn M, Zimmermann G (1976) Organic dyestuffs as catalysts for fuel cells. Top Curr Chem 61:133–182
63. Gupta SL, Tryk D, Bae I, Aldred W, Yeager EB (1989) Heat-treated polyacrylonitride-based catalysts for oxygen electroreduction. J Appl Electrochem 19:19–27
64. Fierro C, Anderson AB, Scherson DA (1988) Electron donor-acceptor properties of porphyrines, phthalocyanines, and related ring-chelats: a molecular orbital approach. J Phys Chem 92:6902–6907
65. Zagal JH (1992) Metallophthalocyanines as catalysts in electrochemical reactions. Coord Chem Rev 119:89–136
66. Kobayashi N, Nishiyama Y (1984) Catalytic electroreduction of molecular oxygen at glassy carbon electrodes with immobilized iron porphyrins containing zero, one, or four amino groups. J Electroanal Chem 181:107–117
67. van Veen JAR, Visser C (1979) Oxygen reduction on monomeric transition metal phthalocyanines in acid electrolyte. Electrochim Acta 24:921–928
68. Melendres CA (1980) Mössbauer and Raman spectra of carbon-supported iron phthalocyanine. J Phys Chem 84:1936–1939
69. Bagotzky VS, Tarasevich MR, Radyushkina KA, Levina OA, Andrusyova SI (1977–1978) Electrocatalysis of the oxygen reduction process on metal chelates in acid electrolyte. J Power Sources 2:233–240
70. Beck F (1977) The redox mechanism of chelate-catalysed oxygen-cathode. J Appl Electrochem 7:239–245
71. Blomquist J, Helgeson U, Moberg LC, Johansson LY, Larsson R (1982) Simultaneous electrochemical and Mössbauer measurements on polymeric iron phthalocyanine oxygen elctrodes. Electrochim Acta 27:1453–1460
72. Brezina M, Khalil W, Koryta J, Musilová M (1977) Electroreduction of oxygen and hydrogen peroxide catalyzed by hemine and phthalocyanines. J Electroana Chem 77:237–244
73. Johansson LY, Mrha J, Larsson R (1973) Elektrokatalyse der O_2-Reduktion in saurer Lösung mit Hilfe der polymeren Phthalocyanine. Electrochim Acta 18:255–258
74. Kazarinov VE, Tarasevich MR, Radyushkina KA, Andreev VN (1979) Some specific features of the metalloporphyrin/electrolyte interface and the kinetics of oxygen electroreduction. J Electroanal Chem 100:225–232
75. Larsson R, Mrha J (1973) Katalytische Sauerstoffelektrode in sauren Lösungen. Electrochim Acta 18:391–394
76. Maroie S, Savy M, Verbist JJ (1979) ESCA and EPR studies of monomer, dimer, and polymer iron phthalocyanines: involvements for the electrocatalysis of O_2 reduction. Inorg Chem 18:2560–2567
77. Zagal JH, Páez M, Tanaka AA, dos Santos JR, Linkous CA (1992) Electrocatalytic activity of metal phthalocyanines for oxygen reduction. J Electroanal Chem 339:13–30
78. Zagal JH, Páez M, Silva JF (2006) Fundamental aspects on the catalytic activity of metallomacrocyclics for the electrochemical reduction of O_2. In: Zagal JH, Bedioui F, Dodelet JP (eds) N_4-macrocyclic metal complexes. Springer, New York, pp 41–82

79. Yeager EB (1984) Electrocatalysts for O_2 reduction. Electrochim Acta 29:1527–1537
80. Ohya T, Kobayashi N, Sato M (1987) Bonding character in tetracoordinate (phthalocyanato) iron(II) complexes with electron-withdrawing substituents as studied by Mößbauer spectroscopy. Inorg Chem 26:2506–2509
81. Ohya T, Sato M (1997) Mössbauer and visible spectra of iron(III) complexes of para-substituted tetraphenylporphyrins - electronic effects of substituents and axial ligands. J Inorg Biochem 67:126, Abstract:126
82. Schlosser K, Hoyer E, Arnold D (1974) Mößbauer Untersuchungen zur π-Rückbindung in Tris(1,2-diimin)eisen (II)chelaten. Spectrochim Acta 30:1431–1436
83. Taube R (1974) New aspects of the chemistry of transition metal phthalocyanines. Pure Appl Chem 38:427–438
84. Walker FA (2003) Pulsed EPR and NMR spectroscopy of paramagnetic iron porphyrinates and related iron macrocycles: how to understand patterns of spin delocalization and recognize macrocycle radicals. Inorg Chem 42:4526–4544
85. Steiger B, Anson FC (1995) Evidence for the importance of back-bonding in determining the behavior of ruthenated cyanophenyl cobalt porphyrins as electrocatalysts for the reduction of dioxygen. Inorg Chem 34:3355–3357
86. Zagal JH, Gulppi M, Isaacs M, Cárdenas-Jirón G, Aguirre MJ (1998) Linear versus volcano correlations between electrocatalytic activity and redox and electronic properties of metallophthalocyanines. Electrochim Acta 44:1349–1357
87. Alt H, Binder H, Lindner W, Sandstede G (1971) Metal chelates as electrocatalysts for oxygen reduction in acid electrolytes. J Electroanal Chem 31:A19–A22
88. Vasudevan P, Santosh MN, Tyagi S (1990) Transition metal complexes of porphyrins and phthalocyanines as electrocatalysts for dioxygen reduction. Transition Metal Chem Lond 15:81–90
89. Kozawa A, Zilionis VE, Brodd RJ (1970) Oxygen and hydrogen peroxide reduction at a ferric phthalocyanine-catalyzed graphite electrode. J Electrochem Soc 117:1470–1474
90. Okunola A, Kowalewska B, Bron M, Kulesza PJ, Schuhmann W (2009) Electrocatalytic reduction of oxygen at electropolymerized films of metalloporphyrins deposited onto multiwalled carbon nanotubes. Electrochim Acta 54:1954–1960
91. Okunola AO, Nagaiah TC, Chen X, Eckhard K, Schuhmann W, Bron M (2009) Visualization of local electrocatalytic activity of metalloporphyrins towards oxygen reduction by means of redox competition scanning electrochemical microscopy (RC-SECM). Electrochim Acta 54:4971–4978
92. Collman JP, Denisevich P, Konai Y, Marrocco M, Koval C, Anson FC (1980) Electrode catalysis of the four-electron reduction of oxygen to water by dicobalt face-to-face porphyrins. J Am Chem Soc 102:6027–6036
93. Biloul A, Coowar F, Contamin O, Scarbeck G, Savy M, van den Ham D, Riga J, Verbist JJ (1993) Oxygen reduction in an acid medium: Electrocatalysis by CoNPc(1,2)-bilayer impregnated on a carbon black support: effect of loading and heat treatment. J Electroanal Chem 350:189–204
94. Collman JP, Wagenknecht PS, Hutchison JE (1994) Cofaciale Bis(metallo)diporphyrine als potentielle molekulare Katalysatoren für Mehrelektronenreduktionen und -oxidationen kleiner Moleküle. Angew Chem 106:1620–1639
95. Liu HY, Weaver MJ, Wang C-B, Chang CK (1983) Dependence of electrocatalysis for oxygen reduction by adsorbed dicobalt cofacial porphyrins upon catalyst structure. J Electroanal Chem 145:439–447
96. Biloul A, Contamin O, Scarbeck G, Savy M, Palys B, Riga J, Verbist JJ (1994) Oxygen reduction in acid media: influence of the activity of conpc(1,2)-bilayer deposits in relation to their attachment to the carbon black support and role of surface groups as a function of heat treatment. J Electroanal Chem 365:239–246
97. Tributsch H, Koslowski U, Dorbandt I (2008) Experimental and theoretical modeling of Fe-, Co-, Cu-, Mn based electrocatalysts oxygen reduction. Electrochim Acta 53:2198–2209
98. Wiesener K, Ohms D, Neumann V, Franke R (1989) N_4 Macrocycles as electrocatalysts for the cathodic reduction of oxygen. Mater Chem Phys 22:457–475
99. Blomquist J, Helgeson U, Moberg LC, Johansson LY, Larsson R (1982) Electrochemical and Mössbauer investigations of polymeric iron phthalocyanine oxygen electrodes. Electrochim Acta 27:1445–1451
100. Scherson DA, Fierro C, Tryk D, Gupta SL, Yeager EB, Eldridge J, Hoffman RW (1985) In situ Mössbauer spectroscopy and electrochemical studies of the thermal stability of iron phthalocyanine dispersed in high surface area carbon. J Electroanal Chem 184:419–426
101. Scherson DA, Fierro C, Yeager EB, Kordesch ME, Eldridge J, Hoffman RW, Barnes A (1984) In situ Mössbauer spectroscopy on an operating fuel cell. J Electroanal Chem 169:287–302
102. Wiesener K (1986) N_4 chelates as electrocatalysts for the cathodic oxygen reduction. Electrochim Acta 31:1073–1078
103. Tanaka AA, Fierro C, Scherson DA, Yeager EB (1989) Oxygen reduction on adsorbed iron tetrapyridinoporphyrazine. Mater Chem Phys 22:431–456
104. Tarasevich MR, Radyushkina KA (1989) Pyropolymers of N_4-complexes: structure and electrocatalytic properties. Mater Chem Phys 22:477–502
105. Franke R, Ohms D, Wiesener K (1989) Investigation of the influence of thermal treatment on the properties of carbon materials modified by N_4-chelates for the reduction of oxygen in acidic media. J Electroanal Chem 260:63–73
106. Joyner RW, van Veen JAR, Sachtler WMH (1982) Extended X-ray absorption fine structure (EXAFS) study of cobalt-porphyrin catalysts supported on active carbon. J Chem Soc Farraday Trans 78:1021–1028
107. Saha MS, Li R, Sun X, Ye S (2009) 3-D composite electrodes for high performance PEM fuel cells composed of Pt supported on nitrogen-doped carbon nanotubes grown on carbon paper. Electrochem Commun 11:438–441
108. Biniak S, Szymanski G, Siedlewski J, Swiatkowski A (1997) The characterization of activated carbons with oxygen and nitrogen surface groups. Carbon 35:1799–1810

109. Lacerda M, Lejeune M, Jones BJ, Barklie RC, Bouzerar R, Zellama K, Conway NMJ, Godet C (2002) Electronic properties of amorphous carbon nitride a-$C_{1-x}N_x$:H films investigated using vibrational and ESR characterisations. J NonCryst Solids 299–302:907–911
110. Chen Y, Wang J, Liu H, Li R, Sun X, Ye S, Knights S (2009) Enhanced stability of Pt electrocatalysts by nitrogen doping in CNTs for PEM fuel cells. Electrochem Commun 11:2071–2076
111. Strelko VV, Kuts VS, Thrower PA (2000) On the mechanism of possible influence of heteroatoms of nitrogen, boron and phosphorus in a carbon matrix on the catalytic activity of carbons in electron transfer reactions. Carbon 38:1499–1503
112. Kramm UI (2009) Strukturelle Untersuchungen alternativer Katalysatoren für die PEM-BZ – Eine Fe-57-Mößbauer-spektroskopische Studie pyrolysierter Eisenporphyrin-Elektrokatalysatoren. Saarbrücken, Südwestdeutscher Verlag für Hochschulschriften
113. Biddinger EJ, Ozkan US (2007) Methanol tolerance of CN_x oxygen reduction catalysts. Top Catal 46:339–348
114. Kothandaraman R, Nallathambi V, Artyushkova K, Barton SC (2009) Non-precious oxygen reduction catalysts prepared by high-pressure pyrolysis for low-temperature fuel cells. Appl Catal B 92:209–216
115. Liu G, Li X, Ganesan P, Popov BN (2010) Studies of oxygen reduction reaction active sites and stability of nitrogen-modified carbon composite catalysts for PEM fuel cells. Electrochim Acta 55:2853–2858
116. Maldonado S, Stevenson KJ (2005) Influence of nitrogen doping on oxygen reduction electrocatalysis at carbon nanofiber. J Phys Chem B 109:4707–4716
117. Matter PH, Biddinger EJ, Ozkan US (2007) Non-precious metal oxygen reduction catalysts for PEM fuel cells. Catalysis 30:338–366
118. Matter PH, Wang E, Millet J-M, Ozkan US (2007) Characterization of the iron phase in CN_x-based oxygen reduction reaction catalysts. J Phys Chem C 111:1444–1450
119. Nallathambi V, Li X, Lee J-W, Popov BN (2008) Developement of nitrogen-modified carbon-based catalysts for oxygen reduction in PEM fuel cells. ECS Trans 16:405–417
120. Sidik RA, Anderson AB, Subramanian NP, Kumaraguru SP, Popov BN (2006) O_2 reduction on graphite and nitrogen-doped graphite: experimental and theory. J Phys Chem B 110:1787–1793
121. Fischer A, Antonietti M, Thomas A (2007) Growth confined by the nitrogen source: synthesis of pure metal nitride nanoparticles in mesoporous graphitic carbon nitride. Adv Mater Weinheim 19:264–267
122. Lyth SM, Nabae Y, Moriya S, Kuroki S, Kakimoto M-a, Ozaki J-i, Miyata S (2009) Carbon nitride as a nonprecious catalyst for electrochemical oxygen reduction. J Phys Chem C 113:20148–20151
123. Lyth SM, Nabae Y, Islam NM, Kuroki S, Kakimoto M-a, Miyata S (2011) Electrochemical oxygen reduction activity of carbon nitride supported on carbon black. J Electrochem Soc 158: B194–B201
124. Nabae Y, Moriya S, Matsubayashi K, Lyth SM, Malon M, Wu L, Islam NM, Koshigoe Y, Kuroki S, Kakimoto M-a, Ozaki K, Miyata S, Ozaki J-I (2010) The role of Fe species in the pyrolysis of Fe phthalocyanine and phenolic resin for preparation of carbon-based cathode catalysts. Carbon 48:2613–2624
125. Plejewski P, Fiechter S (2011) Investigation of the oxygen reduction ability of different metal-free C/N-based materials, in preparation
126. Lalande G, Côté R, Guay D, Dodelet J-P, Weng LT, Bertrand P (1997) Is nitrogen important in the formulation of Fe-based catalysts for oxygen reduction in solid polymer fuel cells? Electrochim Acta 42:1379–1388
127. Martinaiou I, Bogdanoff P, Fiechter S, Kramm UI (2011) Synthesis of nitrogen-rich Fe-N-C catalysts for the oxygen reduction in acidic media, in preparation
128. Scherson DA, Tanaka AA, Gupta GP, Tryk DA, Fierro C, Holze R, Yeager EB, Lattimer RP (1986) Transition metal macrocycles supported on high area carbon: pyrolysis-mass spectroscopy studies. Electrochim Acta 31:1247–1258
129. Matter PH, Zhang L, Ozkan US (2006) The role of nanostructure in nitrogen-containing carbon catatlysts for the oxygen reduction reaction. J Catal 239:83–96
130. Bogdanoff P, Herrmann I, Hilgendorff M, Dorbandt I, Fiechter S, Tributsch H (2004) Probing structural effects of pyrolysed CoTMPP-based electrocatalysts for oxygen reduction via new preparation strategies. J New Mat Elect Syst 7:85–92
131. Herrmann I, Bogdanoff P, Schmithals G, Fiechter S (2006) Influence of the molecular and mesoscopic structure on the electrocatalytic activity of pyrolysed CoTMPP in the oxygen reduction. ECS Trans 3:211–219
132. Herrmann I, Kramm UI, Fiechter S, Bogdanoff P (2009) Oxalate supported pyrolysis of CoTMPP as electrocatalysts for the oxygen reduction reaction. Electrochim Acta 54:4275–4287
133. Herrmann I, Kramm UI, Radnik J, Bogdanoff P, Fiechter S (2009) Influence of sulphur on the pyrolysis of CoTMPP as electrocatalyst for the oxygen reduction reaction. J Electrochem Soc 156:B1283–B1292
134. Herrmann I, Barkschat C, Fiechter S, Bogdanoff P, Iwata N, Takahashi H (2007) Electrode catalyst for fuel cells, a method of preparing an electrode catalyst for fuel cells, and a polymer electrolyte fuel cell. Patent application number PCT/JP2007/074369
135. Kurak KA, Anderson AB (2009) Nitrogen-treated graphite and oxygen electroreduction on pyridinic edge sites. J Phys Chem C 113:6730–6734
136. Kramm UI, Abs-Wurmbach I, Herrmann-Geppert I, Radnik J, Fiechter S, Bogdanoff P (2011) Influence of the electron-density of FeN_4-centers towards the catalytic activity of pyrolysed FeTMPPCl-based ORR-electrocatalysts. J Electrochem Soc 158:B69–B78
137. Biloul A, Coowar F, Contamin O, Scarbeck G, Savy M, Van den Ham D, Riga J, Verbist JJ (1990) Oxygen reduction in acid media on supported iron naphthalocyanine – effect of isomer configuration and pyrolysis. J Electroanal Chem 289:189–201

138. Bouwkamp-Wijnoltz AL, Visscher W, van Veen JAR (1998) The selectivity of oxygen reduction by pyrolysed iron porphyrin supported on carbon. Electrochim Acta 43:3141–3152
139. Faubert G, Côté R, Guay D, Dodelet J-P, Dénès G, Bertrand P (1998) Iron catalysts prepared by high-temperature pyrolysis of tetraphenylporphyrins in polymer electrolyte fuel cells. Electrochim Acta 43:341–353
140. Faubert G, Lalande G, Côté R, Guay D, Dodelet J-P, Weng LT, Bertrand P, Dénès G (1996) Heat-treated iron and cobalt tetraphenylporphyrins adsorbed on carbon black: physical characterization and catalytic properties of these materials for the reduction of oxygen in polymer electrolyte fuel cells. Electrochim Acta 41:1689–1701
141. Gojkovic SL, Gupta S, Savinell RF (1998) Heat-treated iron(III) tetramethoxyphenyl porphyrin chloride supported on high area carbon as an electrocatalyst for oxygen reduction part I: characterization of the electrocatalyst. J Electrochem Soc 145:3493–3499
142. Gojkovic SL, Gupta S, Savinell RF (1999) Heat-treated iron(III) tetramethoxyphenyl porphyrin chloride supported on high area carbon as an electrocatalyst for oxygen reduction part II: kinetics of oxygen reduction. J Electroanal Chem 462:63–72
143. Gojkovic SL, Gupta S, Savinell RF (1999) Heat-treated iron(III) tetramethoxyphenyl porphyrin chloride supported on high area carbon as an electrocatalyst for oxygen reduction part III: detection of hydrogen-peroxide during oxygen reduction. Electrochim Acta 45:889–897
144. Ikeda O, Fukuda H, Tamura H (1986) The effect of heat-treatment on group VIIIB porphyrins as electrocatalysts in the cathodic reduction of oxygen. J Chem Soc Farraday Trans 82:1561–1573
145. Lalande G, Faubert G, Côté R, Guay D, Dodelet J-P, Weng LT, Bertrand P (1996) Catalytic activity and stability of heat-treated iron phthalocyanines for the electroreduction of oxygen in polymer electrolyte fuel cells. J Power Sources 61:227–237
146. Savy M, Coowar F, Riga J, Verbist JJ, Bronoël G, Besse S (1990) Investigation of O_2 reduction in alkaline media on macrocyclic chelates impregnated on different supports: influence of the heat treatment on stability and activity. J Appl Electrochem 20:260–268
147. Sawaguchi T, Itabashi T, Matsue T, Uchida I (1990) Electrochemical reduction of oxygen by metalloporphyrin ion-complexes with heat-treatment. J Electroanal Chem 279:219–230
148. Schulenburg H, Stankov S, Schünemann V, Radnik J, Dorbandt I, Fiechter S, Bogdanoff P, Tributsch H (2003) Catalysts for the oxygen reduction from heat-treated iron(III) tetramethoxyphenylporphyrin chloride: structure and stability of active sites. J Phys Chem B 107:9034–9041
149. Sheng T-C, Rebenstorf B, Widelöv A, Larsson R (1992) Pyrolysis of metalloporphyrins part 1: Fourier-transform infrared study of Fe-tetraphenylporphyrin chloride. J Chem Soc Faraday Trans 88:477–482
150. Sun G-Q, Wang J-T, Gupta S, Savinell RF (2001) Iron(III) tetramethoxyphenylporphyrin (FeTMPP-Cl) as electrocatalyst for oxygen reduction in direct methanol fuel cells. J Appl Electrochem 31:1025–1031
151. Sun G-Q, Wang J-T, Savinell RF (1998) Iron(III) tetramethoxyphenylporphyrin (FeTMPP) as methanol tolerant electrocatalyst for oxygen reduction in direct methanol fuel cells. J Appl Electrochem 28:1087–1093
152. Wang H, Côté R, Faubert G, Guay D, Dodelet J-P (1999) Effect of the pre-treatment of carbon black supports on the activity of Fe-based electrocatalysts for the reduction of oxygen. J Phys Chem B 103:2042–2049
153. Widelöv A (1993) Pyrolysis of iron and cobalt porphyrins sublimated onto the surface of carbon black as a method to prepare catalysts for O_2 reduction. Electrochim Acta 38:2493–2502
154. Lalande G, Côté R, Tamizhmani GD, Dodelet J-P, Dignard-Bailey L, Weng LT, Bertrand P (1995) Physical, chemical and electrochemical characterization of heat-treated tetracarboxylic cobalt phthalocyanine adsorbed on carbon black as electrocatalyst for oxygen reduction in polymer electrolyte fuel cells. Electrochim Acta 40:2635–2646
155. Herrmann I, Brüser V, Fiechter S, Kersten H, Bogdanoff P (2005) Electrocatalysts for oxygen reduction prepared by plasma treatment of carbon-supported cobalt tetramethoxyphenylporphyrin. J Electrochem Soc 152:A2179–A2185
156. Herrmann I, Kramm UI, Fiechter S, Brüser V, Kersten H, Bogdanoff P (2010) Comparative study of the carbonisation of CoTMPP by low temperature plasma and by heat-treatment. Plasma Process Polym 7:515–526
157. Harnisch F, Savastenko NA, Zhao F, Steffen H, Brüser V, Schröder U (2009) Comparative study on the performance of pyrolyzed and plasma-treated iron(II) phthalocyanine-based catalysts for oxygen reduction in pH neutral electrolyte solutions. J Power Sources 193:86–92
158. Atanassov P (2005) Non-platinum electrocatalysts for fuel cells. FC Techn, Aiche
159. Garsuch A, d'Eon R, Dahn T, Klepel O, Garsuch RR, Dahn JR (2008) Oxygen reduction behaviour of highly porous non-noble metal catalysts prepared by a template-assisted synthesis. J Electrochem Soc 155:B236–B243
160. Jaouen F, Herranz J, Lefèvre M, Dodelet J-P, Kramm UI, Herrmann I, Bogdanoff P, Maruyama J, Nagaoka T, Garsuch A, Dahn JR, Olson TS, Pylypenko S, Atanassov P, Ustinov EA (2009) A cross-laboratory experimental review of non-noble-metal catalysts for oxygen electro-reduction. Appl Mater Interfaces 1:1623–1639
161. Olson TS, Chapman K, Atanassov P (2008) Non-platinum cathode catalyst layer composition for single membrane electrode assembly proton exchange membrane fuel cell. J Power Sources 183:557–563
162. Koslowski UI, Herrmann I, Bogdanoff P, Barkschat C, Fiechter S, Iwata N, Takahashi H, Nishikoro H (2008) Evaluation and analysis of PEM-FC performance using non-platinum cathode catalysts based on pyrolysed Fe- and Co-porphyrins – influence of a secondary heat-treatment. ECS Trans 13:125–141

163. Kramm UI, Herrmann I, Fiechter S, Zehl G, Zizak I, Abs-Wurmbach I, Radnik J, Dorbandt I, Bogdanoff P (2009) On the influence of sulphur on the pyrolysis process of FeTMPP-Cl-based electro-catalysts with respect to oxygen reduction reaction (ORR) in acidic media. ECS Trans 25:659–670
164. Maldonado S, Stevenson KJ (2004) Direct preparation of carbon nanofiber electrodes via pyrolysis of iron(II) phthalocyanine: electrocatalytic aspects for oxygen reduction. J Phys Chem B 108:11375–11383
165. Lefèvre M, Proietti E, Jaouen F, Dodelet J-P (2009) Iron-based catalysts with improved oxygen reduction activity in polymer electrolyte fuel cells. Science 324:71–74
166. Wood TE, Tan Z, Schmoeckel AK, O' Neill D, Atanasoski R (2008) Non-precious metal oxygen reduction catalyst for PEM fuel cells based on nitroaniline precursor. J Power Sources 178:510–516
167. Kramm UI, Herrmann-Geppert I, Bogdanoff P, Abs-Wurmbach I, Fiechter S (2011) Effect of an ammonia treatment on the structural composition and ORR activity of Fe-N-C catalysts. J Phys Chem C, in preparation
168. Charreteur F, Jaouen F, Ruggeri S, Dodelet J-P (2008) Fe/N/C Non-precious catalysts for PEM fuel cells: influence of the structural parameters of pristine commercial carbon blacks on their activity for oxygen reduction. Electrochim Acta 53:2925–2938
169. Charreteur F, Ruggeri S, Jaouen F, Dodelet J-P (2008) Increasing the activity of Fe/N/C catalysts in PEM fuel cell cathodes using carbon blacks with a high disordered carbon content. Electrochim Acta 53:6881–6889
170. Dodelet J-P (2006) Oxygen reduction in PEM fuel cell conditions: heat-treated non-precious metal-N_4 macrocycles and beyond. In: Zagal JH, Bedioui F, Dodelet JP (eds) N_4-macrocyclic metal complexes: electrocatalysis,electrophotochemistry & biomimetic electroanalysis. Springer, New York, pp 83–147
171. Herranz J, Lefèvre M, Larouche N, Stansfield B, Dodelet J-P (2007) Step-by-step synthesis of non-noble metal electrocatalysts for O_2 reduction under proton exchange membrane fuel cell conditions. J Phys Chem C 111:19033–19042
172. Jaouen F, Dodelet J-P (2007) Turn-over frequency of O_2 electro-reduction for Fe/N/C and Co/N/C catalysts in PEFCs. Electrochim Acta 52:5975–5984
173. Matter PH, Wang E, Arias M, Biddinger EJ, Ozkan US (2006) Oxygen reduction reaction catalysts prepared from acetonitrile pyrolysis over alumina-supported metal particles. J Phys Chem B 110:18374–18384
174. Bron M, Radnik J, Fieber-Erdmann M, Bogdanoff P, Fiechter S (2002) EXAFS, XPS and electrochemical studies on oxygen reduction catalysts obtained by heat treatment of iron phenanthroline complexes supported on high surface area carbon black. J Electroanal Chem 535:113–119
175. Nallathambi V, Lee J-W, Kumaraguru SP, Wu G, Popov BN (2008) Development of high performance carbon composite catalyst for oxygen reduction reaction in PEM proton exchange membrane fuel cells. J Power Sources 183:34–42
176. Wu T-M, Lin S-H (2006) Characterization and electrical properties of polypyrrole/multiwalled carbon nanotube composites synthesized by in situ chemical oxidative polymerization. J Polym Sci Pol Phys 44:1413–1418
177. Bashyam R, Zelenay P (2006) A class of non-precious metal composite catalysts for fuel cells. Nat Lond 443:63–66
178. Bron M, Fiechter S, Hilgendorf M, Bogdanoff P (2002) Catalysts for oxygen reduction from heat-treated carbon-supported iron phenantroline complexes. J Appl Electrochem 32:211–216
179. Côté R, Lalande G, Guay D, Dodelet J-P (1998) Influence of nitrogen-containing precursors on the electrocatalytic activtiy of heat-treated $Fe(OH)_2$ on carbon black for O_2 reduction. J Electrochem Soc 145:2411–2418
180. Jaouen F, Lefèvre M, Dodelet J-P, Cai M (2006) Heat-treated Fe/N/C Catalysts for O_2 electroreduction: are active sites hosted in micropores? J Phys Chem B 110:5553–5558
181. Jaouen F, Marcotte S, Dodelet J-P, Lindbergh G (2003) Oxygen reduction catalysts for polymer electrolyte fuel cells from the pyrolysis of iron acetate adsorbed on various carbon supports. J Phys Chem B 107:1376–1386
182. Lefèvre M, Jaouen F, Dodelet J-P, Li XH, Chen K, Hay A (2006) Fe-based catalyst for oxygen reduction: functionalization of carbon black and importance of the microporosity. ECS Trans 3:201–210
183. Maruyama J, K-i S, Kawaguchi M, Abe I (2004) Influence of activated carbon pore structure on oxygen reduction at catalyst layers supported on rotating disk electrodes. Carbon 42:3115–3121
184. Proietti E, Ruggeri S, Dodelet J-P (2008) Fe-based electrocatalysts for oxygen reduction in PEMFCs using ball-milled graphite powder as a carbon support. J Electrochem Soc 155:B340–B348
185. Wang P, Ma Z, Zhao Z, Jia L (2007) Oxygen reduction on the electrocatalysts based on pyrolysed non-noble metal/poly-o-phenylenediamine/carbon black composites: new insight into the active sites. J Electroanal Chem 611:87–95
186. Wu G, Chen Z, Artyushkova K, Garzona FH, Zelenay P (2008) Polyaniline-derived non-precious catalyst for the polymer electrolyte fuel cell cathode. ECS Trans 16:159–170
187. He P, Lefèvre M, Faubert G, Dodelet J-P (1999) Oxygen reduction catalysts for polymer electrolyte fuel cells from the pyrolysis of various transition metal acetates adsorbed on 3,4,9,10 perylenetetracarboxylic dianhydride. J New Mater Electrochem Sys 2:243–251
188. Bron M, Fiechter S, Bogdanoff P, Tributsch H (2002) Thermogravimetry/mass spectrometry investigations on the formation of oxygen reduction catalysts for PEM fuel cells on the basis of heat-treated iron phenantroline complexes. Fuel Cells 2:137–142
189. Wu G, Artyushkova K, Ferrandon M, Kropf AJ, Myers D, Zelenay P (2009) Performance durability of polyaniline-derived non-precious cathode catalysts. ECS Trans 25:1299–1311
190. Kramm UI, Herranz J, Arruda TM, Larouche N, Lefèvre M, Jaouen F, Bogdanoff P, Fiechter S, Abs-Wurmbach I, Stansfield B, Mukerjee S, Dodelet JP (2011) The role of

Fe-modifications in the activity of Fe/N/C catalysts for the O_2-reduction in PEM fuel cells, in preparation
191. Herranz J, Jaouen F, Lefevre M, Kramm UI, Proietti E, Dodelet JP, Bogdanoff P, Fiechter S, Abs-Wurmbach I, Bertrand P, Arruda TM, Mukerjee S (2011) Unveiling N-protonation and anion binding effects on Fe/N/C-catalysts for O_2 reduction in PEM fuel cells. J Phys Chem C, submitted (2011-05-10)
192. Lefèvre M, Proietti E, Jaouen F, Dodelet J-P (2009) Iron-based catalysts for oxygen reduction in PEM fuel cells: expanded study using the pore-filling method. ECS Trans 25:105–115
193. Lee K, Zhang L, Lui H, Hui R, Shi Z, Zhang J (2009) Oxygen reduction reaction (ORR) catalyzed by carbon-supported cobalt polypyrrole (Co-PPy/C) electrocatalysts. Electrochim Acta 54:4704–4711
194. Liu H, Shi Z, Zhang J, Zhang L, Zhang J (2009) Ultrasonic spray pyrolyzed iron-polypyrrole mesoporous spheres for fuel cell oxygen reduction electrocatalysts. J Mater Chem 19:468–470
195. Gasteiger HA, Markovic NM (2009) Just a dream – or future reality? Science 324:48–49
196. Gasteiger HA, Kocha SS, Sompalli B, Wagner FT (2005) Activity benchmarks and requirements for Pt, Pt-alloys, and non-Pt oxygen reduction catalysts for PEMFCs. Appl Catal B Environ 56:9–35
197. Maruyama J, Abe I (2007) Fuel cell cathode catalyst with heme-like structure formed from nitrogen of glycine and iron. J Electrochem Soc 154:B297–B304
198. Nallathambi V, Wu G, Subramanian NP, Kumaraguru SP, Lee J-W, Popov BN (2007) Highly active carbon composite electrocatalysts for PEM fuel cells. ECS Trans 11:241–247
199. Bezerra CWB, Zhang L, Liu H, Lee K, Marques ALB, Marques EP, Wang H, Zhang J (2007) A review of heat-treatment effects on activity and stability of PEM fuel cell catalysts for oxygen reduction reaction. J Power Sources 173:891–908
200. Ekström H, Hanarp P, Gustavsson M, Fridell E, Lundblad A, Lindbergh G (2006) A novel approach for measuring catalytic activity of planar model catalysts in the polymer electrolyte fuel cell environment. J Electrochem Soc 153:A724–A730
201. Liu G, Li X, Ganesan P, Popov BN (2009) Development of non-precious metal oxygen-reduction catalysts for PEM fuel cells based on N-doped ordered porous carbon. Appl Catal B Environ 93:156–165
202. Ma Z-F, Xie X-Y, Ma X-X, Zhang D-Y, Ren Q, Heß-Mohr N, Schmidt VM (2006) Electrochemical characteristics and performance of CoTMPP/BP oxygen reduction electrocatalysts for PEM fuel cell. Electrochem Commun 8:389–394
203. Maruyama J, Abe I (2006) Carbonized hemoglobin functioning as a cathode catalyst for polymer electrolyte fuel cells. Chem Mater 18:1303–1311
204. Maruyama J, Fukui N, Kawaguchi M, Abe I (2008) Application of nitrogen-rich amino acids to active site generation in oxygen reduction catalyst. J Power Sources 182:489–495
205. Papakonstantinou G, Daletou MK, Kotsifa A, Paloukis F, Katerinopoulou K, Ioannides T, Neophytides SG (2009) Non noble metal electrocatalysts for high temperature PEM fuel cells. ECS Trans 25:181–189
206. Yang J, Liu D-J, Kariuki NN, Chen LX (2008) Aligned carbon nanotubes with built-in FeN_4 active sites for electrocatalytic reduction of oxygen. Chem Commun 3:329–331
207. Jaouen F, Proietti E, Lefèvre M, Chenitz R, Dodelet J-P, Wu G, Chung HT, Johnston C, Zelenay P (2011) Recent advances in non-precious metal catalysis for oxygen-reduction reaction in polymer electrolyte fuel cells. Energy Environ Sci 4:114–130
208. Zelenay P (2010) Advanced cathode catalysts, hydrogen program annual merit review and peer evaluation meeting. Project ID: fc005
209. Kramm UI, Herrmann-Geppert I, Proietti E, Jaouen F, Lefèvre M, Bogdanoff P, Dodelet J-P, Fiechter S (2011) Effect of a high-energy ball milling on the PEM-fuel-cell performance of Fe-N-C catalysts for the oxygen reduction. J Power Sources, in preparation
210. Beck F (1973) Voltammetrische Untersuchungen an elektrokatalytisch wirksamen Phthalocyaninen und Tetraazaannulenen in konzentrierter Schwefelsäure. Ber Bunsen Ges fuer Phys Chem 77:353–364
211. Meier H, Albrecht W, Tschirwitz U, Zimmerhackl E (1973) Zum Einfluß der Leitfähigkeit von Phthalocyaninen bei der Elektrokatalyse in Brennstoffzellen. Ber Bunsen Ges fuer Phys Chem 77:843–849
212. Bae IT, Scherson DA (1998) In situ X-ray absorption of a carbon monoxide-iron porphyrin adduct adsorbed on high area in an aqueous electrolyte. J Phys Chem B 102:2519–2522
213. Appleby AJ, Savy M, Caro P (1980) The role of transition element multiple spin crossover in oxygen transport and electroreduction in porphyrin and phthalocyanine structures. J Electroanal Chem 111:91–96
214. El Hourch A, Belcadi S, Moisy P, Crouigneau P, Léger JM, Lamy C (1992) Electrocatalytic reduction of oxygen at iron phthalocyanine modified polymer electrodes. J Electroanal Chem 339:1–12
215. Lefèvre M, Dodelet J-P (2003) Fe-based catalysts for the reduction of oxygen in polymer electrolyte membrane fuel cell conditions: determination of the amount of peroxide released during electroreduction and its influence on the stability of the catalysts. Electrochim Acta 48:2749–2760
216. Ziegelbauer JM, Gatewood D, Gullá AF, Ramaker DE, Mukerjee S (2006) X-ray absorption spectroscopy studies of water activation on Rh_xS_y electrocatalyst for oxygen reduction reaction application. Electrochem Solid State Lett 9:A430–A434
217. Bae IT, Tryk DA, Scherson DA (1998) Effect of heat treatment on the redox properties of iron porphyrins adsorbed on high area carbon in acid electrolytes: An in situ Fe K-Edge X-ray absorption near-edge structure study. J Phys Chem B 102:4114–4117
218. Birry L, Zagal JH, Dodelet J-P (2010) Does CO poison Fe-based catalysts for ORR? Electrochem Commun 12:628–631
219. Borup RL, Meyers J, Pivovar B, Kim YS, Mukundan R, Garland N, Myers D, Wilson M, Garzon F, Wood D, Zelenay P, More K, Stroh K, Zawodzinski T, Boncella J, McGrath JE, Inaba M, Miyatake K, Hori M, Ota K, Ogumi Z, Miyata S, Nishikata A,

Siroma Z, Uchimoto Y, Yasuda K, K-i K, Iwashita N (2007) Scientific aspects of polymer electrolyte fuel cell durability and degradation. Chem Rev 107:3904–3951
220. Young AP, Stumper J, Gyenge E (2009) Characterizing the structural degradation in a PEMFC cathode catalyst layer: carbon corrosion. J Electrochem Soc 156:B913–B922
221. Baker R, Wilkinson DP, Zhang J (2008) Electrocatalytic activtiy and stability of substituted iron phthalocyanines towards oxygen reduction evaluated at different temperatures. Electrochim Acta 53:6906–6919
222. Charreteur F, Jaouen F, Dodelet J-P (2009) Iron porphyrin-based cathode catalysts for PEM fuel cells: influence of pyrolysis gas on activity and stability. Electrochim Acta 54:6622–6630
223. Meng H, Larouche N, Lefèvre M, Jaouen F, Stansfield B, Dodelet J-P (2010) Iron porphyrin-based cathode catalysts for polymer electrolyte membrane fuel cells: Effect of NH3 and Ar mixtures as pyrolysis gases on catalytic activity and stability. Electrochim Acta 55:6450–6461
224. Wesselmark M, Lagegren C, Lindbergh G (2009) Degradation studies of PEMFC cathodes based on different types of carbon. ECS Trans 25:1241–1250
225. Ettingshausen F, Weidner A, Zils S, Wolz A, Suffner J, Michel M, Roth C (2009) Alternative support materials for fuel cell catalysts. ECS Trans 25:1883–1892
226. Huang S-Y, Ganesan P, Zhang P, Popov BN (2009) Development of novel metal oxide supported Pt catalysts for Polymer electrolyte membrane and unitized regenerative fuel cells applications. ECS Trans 25:1893–1902
227. Shoyama M, Tomimura T, Okubo Y, Nambu H, Lin M-L, Hara K, Fukuoka A, Ishihara A, K-I O (2009) Synthesis of Ta-oxide based nano-sized cathode catalyst on highly ordered mesoporous carbon for PEM fuel cells. ECS Trans 25:1903–1908
228. Mukundan R, Borup RL (2009) Visualising liquid water in PEM fuel cells using neutron imaging. Fuel Cells 9:499–505
229. Manke I, Hartnig C, Grünerbel M, Kaczerowski J, Lehnert W, Kardjilov N, Hilger A, Banhart J, Treimer W, Strobl M (2007) Quasi-in situ neutron tomography on polymer electrolyte membrane fuel cell stacks. App Phys Lett 90:184101-(01–03)

Poultry Breeding

Yoav Eitan, Morris Soller
Department of Genetics, The Silberman Life Sciences Institute, The Hebrew University of Jerusalem, Jerusalem, Israel

Article Outline

Glossary
Definition of the Subject
Introduction: Animal Breeding in Transition
Brief History of Broiler Breeding and Broiler Production
Roadmap of the Entry
Stage 1: Selection for Juvenile Weight for Age (JWfA)
Stage 2: Combined Selection for JWfA and Feed Conversion Ratio (FCR)
Stage 3: Combined Selection for JWfA, FCR, and Proportion of Breast Meat (PBM)
The Role of Breeding and Management in the Improvement in Performance of the Modern Broiler Chicken
Accounting for the Long-Term Continuous Response to Selection and for the Punctuated and Coordinated Appearance of Secondary Effects
Genetic Improvement of Broiler Production Traits and Broiler Welfare
Future Directions
Conclusions and Interpretation
Abbreviations
Bibliography

Glossary

Breeding value The deviation of trait value of an individual from the overall population mean that is due to genetic factors and hence can be transmitted to the progeny.

Breeding nuclei The closed and pedigreed flocks at the top of the breeding pyramid within which selection is practiced and from which genetic gains are disseminated to the commercial populations.

Feed conversion ratio The weight of food in kg required to produce 1 kg of body weight to market.

Fitness The ability of the animal to reproduce and survive.

Functional traits Traits that contribute to fitness, e.g., reproductive performance, resistance to pathogens and toxins.

Genetic variation Variation in trait expression that is due to variation in structure of the genetic material.

Heritability The proportion of total variation in trait expression that is due to genetic variation.

Index selection Selection based on combination of estimated breeding value of an individual for a number of production and functional traits weighted according to economic importance and genetic correlations to other traits.

Mass selection Selection based on the performance of the individual itself, without consideration of performance of close relatives.

Metabolic heat and water Heat and water produced as a by-product of body metabolism.

Pleiotropic effects Effects of an individual genetic locus on multiple traits.

Primary breeders The commercial organizations that maintain and improve breeding nuclei.

Production traits Traits that contribute directly to production of the animal product that reaches the consumer, e.g., JWfA, FCR, and PBM.

Secondary effect An unintended effect of selection for one trait on some other trait.

Definition of the Subject

Animal breeding today stands on the verge of a methodological revolution that may greatly increase the rate of genetic improvement in production traits. This will modify the physiology of the animals and the genetic architecture of the population at an unprecedented rate. What will be the broader consequences of such extreme modification? What pitfalls and dangers may be encountered as this process unfolds? Beginning about 60 years ago, the broiler chicken has been subject to intense and effective selection for juvenile growth rate (60 generations), feed conversion ratio (40 generations), and body composition (20 generations). This entry describes the ways in which the production and functional traits of the individual bird and accompanying management practices have responded to this unremitting selection, with the objective of suggesting what the future might hold for other agricultural animal species as they enter this new stage of intense and highly effective selection for production traits.

Introduction: Animal Breeding in Transition

Animal breeding today stands in the midst of a methodological revolution based on the availability of microarrays that are capable of genotyping tens and hundreds of thousands of polymorphic markers in a single run, and of low-cost whole genome sequencing that will enable the leading animals in the population to be fully sequenced [1–3]. This has enabled development of deoxyribonucleic acid (DNA)-level diagnostic procedures for highly accurate evaluation of breeding values for production and functional traits. Since DNA can be obtained readily from all animals from birth (and even before) these procedures allow highly effective and intense selection to be implemented at an early age with very high accuracy, and with equal efficiency in males and females; encompassing sex, age, or phenotype-limited characters such as milk and egg production, longevity, and disease resistance. The result will be a quantum leap in the rate of genetic improvement in production traits with consequent far-reaching modification of body development and physiology.

What will be the effects of such intense and effective selection applied to production traits on overall animal performance and capacities? How will management practices and requirements adapt to these changes? The modern broiler chicken, under selection for production traits for over 60 chicken-generations [4] provides an intimation of what to expect [5–9]. The main broiler production traits such as juvenile growth rate, feed conversion ratio, and body composition come to expression in the juvenile bird, are expressed equally in males and females, and have moderate heritabilities, thus enabling highly effective mass selection based on individual phenotype. Introduction of advanced biometrical methods of selection such as Best Linear Unbiased Predictor (BLUP) and Individual Animal Model has made this phenotype-based selection even more effective. Because of the high fecundity of the female chicken, selection for broiler production traits has been intense, and the response to selection has been enormous, converting the broiler chicken from an expensive luxury to a low-cost major meat supplier for the growing human population worldwide [10]. The historical response of the broiler chicken and its management to this selection, models what can be expected from the application of intense and highly effective selection for production traits to other populations of agricultural animals.

Brief History of Broiler Breeding and Broiler Production

The First Commercial Incubator

Keeping a small number of chickens was always a part of the family farm and rural urban household. These were raised primarily for home egg consumption and minor income from sale of surplus eggs and meat. Until the invention of the first commercial incubator in 1875,

replacement chicks had to be hatched by the hens, so that each farm reared its own replacements. With the availability of commercial incubators, specialized breeding farms and hatcheries came into being to supply high-quality chicks to the family farms. Prior to the development of vent sexing by the Japanese in the 1930s, and of sex-linked feather sexing in the 1960s, it was not possible to distinguish male and female chicks by gender until they were a few weeks of age. Consequently, when rearing chicks for egg production, all chicks had to be reared to the age of a month or more when cockerels could be recognized. Having invested this much in the cockerels, it was economically rewarding to rear them to market weight. Thus, each year with the renewal of layer flocks by chicks hatched in the early spring, cockerels for sale provided an important secondary income stream. At this time, therefore, chicken meat was a rather rare and costly commodity generally available only in the spring coincident with layer flock renewal. However, recognizing the potential for additional economic return, some farms began raising an extra hatch of chicks in the summer months for sale as meat birds.

Salmonella pullorum Free Flocks, Vitamin D

Large flocks dedicated to poultry meat production as a main source of farm income do not seem to have become widespread until the 1920s, primarily because of high chick mortality due to *Salmonella pullorum* when large numbers of chicks were reared together. In the early 1920s, a test was developed to identify birds carrying the pathogen, enabling breeders to develop *S. pullorum* free flocks that supplied *S. pullorum*-free chicks. Also about this time (1926), it was found that adding vitamin D to the chick diet in the form of cod liver oil could prevent the development of Rickets in winter broilers. Until then, lack of sunshine had prevented rearing of winter broilers in the Northern states. These two developments made it possible to establish a year round broiler industry [11].

Cornish Breed Males, the "Chicken of Tomorrow Contests," Chick "Sexing"

Growth of the broiler industry was rather slow, and chicken meat remained an expensive specialty item because of the necessity for hand plucking of the feathers. In 1940 the first commercial feather plucker was invented, enabling plucking, evisceration, and packing of broiler carcasses on the same production line. This opened the way to development of a dedicated broiler industry. The use of Cornish breed males to cross with dual-purpose females to produce broiler chicks with higher proportion of breast meat (PBM) was introduced in the 1930s, and by 1942 almost all commercial broiler chicks were crossbreds of "Cornish" males to females of one of the dual-purpose breeds (White Rock, New Hampshire or Barred Rock). In the 1940s, some of the leading White Rock breeders began to develop a bird with high juvenile growth rate specifically for broiler production, while the colored stocks were still bred for the dual-purpose market. From 1946 to 1951, the A&P supermarket chain sponsored a series of "Chicken of Tomorrow" contests [12] in which chicks of leading breeders were reared to 12 weeks of age and compared. By the third of these contests it was clear that the White Rock female, specifically bred for broiler production crossed to Cornish type male was the leading broiler chicken, widely preferred to crosses to dual-purpose colored females. In addition to superior growth rate, the White Rock crosses also gave a clean attractive plucked carcass, in contrast to the unsightly dark-colored pinfeathers remaining on the plucked carcass of the dark-feathered birds.

Thus, by 1952 all the components of the modern broiler chicken were in place. In this year for the first time, specially bred broilers surpassed surplus farm cockerels of the layer flocks as the main source of chicken meat in the USA. With the advent of specialized broiler lines, it was no longer economical to rear layer strain cockerels for meat, as the cockerel of the layer lines, even of dual-purpose breeds, could not achieve the economic returns of the specialized broiler lines. Vent and later feather sexing enabled the male chicks of the layer flocks to be identified at hatch, so that there was no economic incentive to rear these chicks. As a direct consequence, the poultry breeding industry was able to separate into the distinct and completely independent layer and broiler components found today, and intensive broiler breeding focused on the traits of importance for low-cost broiler production commenced in earnest.

Roadmap of the Entry

Broiler breeding experienced three stages with respect to the production traits that were the primary selection

objectives. In the first stage, the primary production objective was rapid juvenile growth rate, with some attention to breast conformation. In the second stage, increasing attention was paid to feed conversion ratio in addition to juvenile growth rate [13]. In the third stage, continuing to the present time, increasing the proportion of breast meat in the carcass was added as a third major production goal. At all stages except the very first, good reproductive performance of the female line and fertility of the male line were strong secondary selection objectives. The need to maintain female reproductive performance led in the 1970s to the introduction of crosses between independent White Rock female lines to provide a heterotic lift to performance. Thus, the typical commercial broiler chick today is the product of a three-way cross: A pair of purebred "female lines, of dual-purpose White Rock origin," is crossed to produce the female parent, and this in turn is crossed to males of a purebred "male line of Cornish breed origin" to produce the commercial chick. With the passage of time, selection for health and welfare traits that were negatively affected by the intense selection for production traits has become an increasingly important component of the broiler selection programs.

Each of these three major stages in genetic development of the modern broiler will be considered in turn, describing first the achievements in terms of the primary production goals, followed by a description of the associated secondary genetic effects on reproductive performance (hatchability and egg numbers) and health (with emphasis on leg and metabolic disorders), and of the management modifications needed to accommodate both the primary genetic effects and their secondary consequences. A common feature of the secondary consequences was inability to predict them in prospect, but ability to explain their appearance in retrospect as a plausible consequence of the changes in primary traits. This will be followed by an overall evaluation of the relative contributions of the breeder and of management to performance of the modern broiler, and a review of possible sources of the genetic variation that has enabled the continuous long-term response to selection for the three major production traits. Welfare issues raised by the genetic and management changes will be addressed, and a framework presented for interpreting the accompanying genetic and management changes in terms of a "resource allocation" model.

Stage 1: Selection for Juvenile Weight for Age (JWfA)

Importance of Juvenile Weight for Age

A day-old chick of one of the dual-purpose breeds that served as the founders for broiler development, typically required up to 90–120 days to reach market weight [4]. This long grow-out period resulted in high feed, labor, veterinary, and capital costs per chick and increased losses by mishap or disease. The number of days to reach market weight is primarily determined by juvenile growth rate – birds growing more rapidly reach market weight earlier. Consequently, increasing juvenile growth rate was the first objective in the development of the modern broiler. The heaviest birds at any given age are obviously the birds that would have reached target weight earliest, so that selection for "age to reach a given target weight" (age for weight) could be achieved by selection for the much more conveniently measured "weight at a given age" (weight for age).

Rapid and Powerful Response to Selection for JWfA

Juvenile weight for age (JWfA) turned out to be an ideal target for selection. The trait had high heritability, meaning that much of the variation in the trait was due to genetic factors. It was easily measured by simply weighing the birds at a given age. It came to expression at an early age equally in males and females. Due to the very high fecundity of hens, only a small proportion of the female chicks and an even smaller proportion of the male chicks produced by a hen had to be retained to renew the breeding population. Consequently, selection was very intense. The response to selection for JWfA was magnificent and continues to the present time yielding a decrease of 1 or 2 days in age for market weight per generation of selection [14] so that the modern broiler reaches market weight at about 35–40 days. This tremendous reduction in market age has reduced broiler-rearing costs in a corresponding manner, bringing chicken from a high-cost luxury food to the lowest-cost meat producer on the market [10]. It should be noted that even during this early period,

attention was also paid to breast conformation of the broiler chick [6]. This was needed in order to produce a more attractive whole carcass with a less prominent keel bone on the supermarket shelf. Usually this was done by "touch," i.e., simply handling the birds already selected on JWfA and rejecting those with the sharpest keel bone.

Secondary Effects of Selection for JWfA (I): Excess Adiposity

The first secondary effect of the selection for JWfA, a marked increase in the adiposity of the commercial broiler at slaughter, was noted by the mid-1960s [6, 15]. This was unexpected, since deposition of a gram of fat is more than twice as costly in caloric terms as deposition of a gram of muscle. Thus, the heaviest birds would be expected to be those that had deposited the least fat. Consequently, selection for JWfA should have reduced the proportion of food intake devoted to fat stores, and in this way reduced the proportion of fat content of the carcass. The situation turned out to be more complex. Depositing body mass in a growing bird requires an excess of food intake over body maintenance requirements. Given unlimited access to feed, the magnitude of this excess is a function of appetite. Thus, JWfA is primarily a function of appetite and gross food intake. The birds with the highest intake put on the most weight. However, this high intake introduces a second factor into the picture. Any excess of intake over maintenance in the juvenile is partitioned between lean body growth (muscle and internal organs) and fat stores. It turns out that the coefficient of partition is itself a function of the excess. When excess is small, almost all goes to build lean body mass (low fat:lean coefficient) but as the excess increases, a greater proportion goes to fat stores (higher fat:lean coefficient). Thus, the animals presenting highest JWfA are primarily those with the highest food intake but these also have the highest fat:lean coefficient, and hence show increased adiposity. The increase in carcass fat content made the carcass unsightly and unattractive to consumers. In addition, the abdominal fat-pad that was discarded in the slaughterhouse represented a waste of feed and was clearly reducing feed conversion ratio on a salable meat basis. This led in the early 1970s to various attempts to select directly against excess fat, e.g., by measuring skin thickness. These approaches were not successful, but control of fat content eventually came from an unexpected direction, as will be seen later.

Secondary Effect of Selection for JWfA (II): EODES in Broiler Breeder Females

A second secondary effect of the intense selection for JWfA was not long in coming and presented as the first of a series of metabolic disorders (see Box 1 for definition and explication) that have afflicted the broiler industry. The disorder manifested as a marked reduction in reproductive performance of the female broiler parent. Egg production dropped precipitously, from over 200 hatching eggs per hen to 120 and below, accompanied by a reduction in fertility and in the hatchability of fertilized eggs. Egg-laying pattern was erratic with many eggs laid outside of the usual time window, and there was a marked increased in double-yolked or otherwise defective eggs. The condition as a whole was termed "Erratic Oviposition Defective Egg Syndrome, EODES" [17]. An outstanding feature was the presence of multiple hierarchies of large yellow follicles in the ovary. The broiler industry was on the verge of collapse, when it was found that restricting (i.e., limiting) feed intake of the broiler pullet during her growth period could completely prevent the problem [18–20]. With this discovery, feed restriction became an essential part of broiler breeder management, both for males and females. With the passage of generations, it has been necessary to increase the degree of feed restriction from 70% of *ad libitum* initially to about 35% of *ad libitum* today. Since EODES is elicited by *ad libitum* feeding and prevented by restricting feed intake, it is plausible that the proximal cause of this disorder was the increased adiposity of the *ad libitum* fed broiler pullet at entry into lay. Excess adiposity is known to interfere with proper reproductive function in many species. The excess adiposity in turn is due at least in part to disruption of the normal homeostatic control over appetite as a consequence of which *ad libitum* fed female-line broiler pullets continue to eat to excess during the entire pullet rearing stage. The hypothalamic appetite control center may not be fully functional in broilers, since lesions of the hypothalamic appetite control center that lead to hyperphagia in layers, do not increase feed consumption in broilers [21].

Box 1 Metabolic Disorders

Metabolism refers to all of the myriad chemical reactions taking place in the cells of a living organism that utilize the chemical and energetic content of ingested food to build and maintain normal body structure and function. These cellular chemical reactions are actively coordinated with one another across the body of the organism and also with the external environment through an intricate network of sensors and regulatory feedback loops so as to maintain life (i.e., stable body function). An outstanding feature of the metabolic system is the ability to actively adapt and modify body structure and function so as to maintain life even under challenging environments.

The metabolic system consists of many thousands of structural, functional, and regulatory components composed of protein or ribonucleic acid (RNA) molecules. All of these are constructed according to instructions coded in the hereditary material of the cell, i.e., its DNA. Mutations in DNA can change the structure or function of the components of the metabolic system. When this happens, the metabolic system may not be able to preserve normal function, and development terminates in the death of the embryo, or in birth of an individual defective in one or more aspects of normal structure and function. Metabolic derangements of this sort are termed "Metabolic Diseases," and there are many hundreds of different hereditary diseases that fall into this category.

Normal metabolism may also be disrupted when the diet does not include essential components that cannot be synthesized by the body but are needed to build the elements of the metabolic system, or conversely, when the diet contains various elements or compounds in toxic excess. Metabolic derangements of this sort are termed "Metabolic deficiency or toxicity disorders". Examples of broiler "Deficiency Disorders" are Rickets, resulting from Vitamin D or mineral deficiencies, and Crazy Chick Disease, resulting from Vitamin E deficiency. Examples of broiler "Toxicity Disorders" are Fluoride and Vanadium toxicity caused by phosphate contamination of feeds, or Selenium toxicity caused by feeding cereals grown on Selenium-rich soil.

The Metabolic Syndrome is a novel form of Metabolic Disorder, which has recently become very prominent in human populations [16]. This is a constellation of pathologies that increase the risk of artherosclerotic vascular disease and Type II (late onset) diabetes. Risk factors for development of Metabolic Syndrome include obesity, psychosocial stress, sedentary lifestyle, and age. There are no identified genetic lesions, dietary deficiencies, or toxins. Thus, all elements of the metabolic system are present and at an individual level appear to be functioning normally. The central role of obesity in the etiology of the syndrome is of special interest. A moderate degree of adiposity is a normal part of body structure. The very high adiposity defining obesity is thus a normal body structure taken to extreme. Apparently, this excess alone unbalances the metabolic system and imposes a regulatory burden to maintain stable function. When the adiposity load is further exacerbated by the regulatory load imposed by psychosocial stress, sedentary life style, and age, the metabolic regulatory system is unable to cope and the pathologies characteristic of the Metabolic Syndrome emerge. This example indicates that whenever some body structure or function is brought to extreme development, this may impose an overload on the metabolic regulatory system resulting in manifestation of Metabolic Regulatory Disorders, with specific pathology depending on the type of overload.

The reduced fertility that accompanied the reduction in egg number apparently resulted in part at least, from impairment of male mating performance, perhaps due to sheer physical difficulty of the obese males and females to handle the mechanics of courting and mating or possibly due to hormonal effects on semen quality of the excess adipose tissue in the male. Feed restriction corrected the reduced fertility as well, so that under pullet and male feed restriction, egg production and fertility returned to high levels.

Secondary Effect of Selection for JWfA (III): Increase in Egg Weight and Hatchability Problems

A third secondary consequence of selection for JWfA was an overall increase in egg weight [14] particularly in older hens. The primary reason for this was the increase in mature size of the broiler female, even

under feed restriction, as a direct consequence of selection for JWfA. In addition, there may have been indirect selection for large egg size, as a larger egg delivers a larger chick at hatch and higher final weight at market age. The increase in egg size had important effects on incubator management, deriving from the dual function of the incubator in embryo development. The small early stage embryo generates very little internal metabolic heat and must be warmed by the incubator, while the larger and rapidly growing later-stage embryo generates large amounts of metabolic heat and water, both of which must be removed by the incubator (see Box 2). Achieving these multiple goals requires careful control of incubator temperature, humidity, and ventilation (THV). Matters are complicated by the fact that even under the best conditions there is variation in the specific THV conditions at different points within the incubator due to variation in airflow over the eggs, and location of the egg with respect to incubator inlets and outlets. There is also variation in egg size and in shell conductance for water and heat. All of these contribute to variation in internal embryo temperature and water content among the population of eggs within the incubator at any given time. As a result, while most eggs will be comfortably within their optimum temperature and water content, others may lie close to outside limits for one or both of these factors.

Larger egg size impacts negatively on all of the multiple incubator functions. At the early embryo stages, the larger egg makes it more difficult to achieve optimal temperature throughout the egg mass. At the later embryo stages, the larger egg accommodates a larger embryo that generates more metabolic heat and water toward the end of embryonic development. At the same time, the surface/volume ratio of the larger egg is reduced making it more difficult for the embryo to dissipate excess metabolic heat and water [22]. Taken together with variability in TMV conditions within the incubator, and in size and shell conductance of the eggs, an increasing proportion of eggs find themselves outside of the optimal parameter range for development and hatching, yielding grade B chicks, and lower overall hatching proportions. This is exacerbated by the increased difference in egg size between young and old breeder hens that increases variability in egg size and shell conductance within the incubator when eggs of different-aged flocks are incubated together. Thus, as egg weight increased, incubators had to be equipped with more effective ventilation systems, and conditions had to be monitored more closely than in the past to ensure minimum variation and close adherence to optimal temperature and humidity throughout the incubator interior.

Box 2 Incubator Management

During the early part of incubation, the embryo generates very little metabolic heat, and must be warmed by the incubator. But during the final week of incubation, the large and rapidly growing embryo generates large amounts of metabolic heat, and must be cooled by the incubator. Both objectives are achieved by setting the incubator air temperature at about 37.5°C. This is sufficient to warm the early embryos, and at the same time, with adequate air movement, will cool the later embryos. Thus, the same incubator (called a "multistage" incubator) was able to accommodate eggs in different stages of development, warming the early embryo eggs and simultaneously cooling the late-embryo eggs. In fact with the multistage incubator, the excess heat produced by the late embryos was used to warm the early embryos.

In addition to producing metabolic heat, the developing embryo also produces water and carbon dioxide. Both carbon dioxide and water escape through the eggshell. However, loss of water must be adjusted carefully. Loss of too much water will dehydrate the chorioallantoic membrane, interfering with importation of oxygen and exportation of metabolic waste, resulting in death of the embryo. It is equally important that the embryo lose more water than it generates (net loss of about 12% of egg weight from beginning to end of incubation). Otherwise, there will be insufficient air space formed for the chick to take its first breath and the chick itself will remain too large to move around inside the shell when trying to pip. In this case, the chick may be unable to break the membrane between itself and the shell, suffocating or drowning to death. Water loss by the embryo is adjusted primarily by adjusting the humidity of the incubation chamber; 50% humidity is close to optimal.

Secondary Effect of Selection for JWfA (IV): Skeletal Problems in Commercial Broiler

Initially, broiler chicks were allowed to free access to feed during daylight hours from the first day post-hatch, with the feed provided in the form of coarsely ground grain ("mash" type feed). However, by the 1970s as growth rate increased, the chicks were unable to consume the amounts of feed needed to meet their growth potential. This was solved by compressing and heating the mash to form pellets, enabling the bird to ingest more feed in a shorter time; and by extending hours of light to 23 h per day to provide more time for feeding. It was later found that equivalent results at lower electricity cost could be obtained by alternating 1–2 h of light with 2–4 h of dark ("intermittent light") with the added advantage of reducing energy expenditure for locomotor activity by the growing broiler. Obviously implementing a light-control program of this sort required a shift to light-controlled housing.

However, as chick growth rate increased, the skeleton could not develop rapidly enough to accommodate the large chick body, resulting in many skeletal and leg problems [13, 23, 24]. These include: infected hocks (from staphylococcus, coliform, or viral infections); twisted legs presenting as valgus distortion (knock-kneed: hocks in feet out) or varus distortion (bow-legged: hocks out, feet in); and tibial dyschondroplasia, in which failure of normal chondrolysis and ossification leaves the end-bone epiphyseal plates at the femoral–tibial junction prone to fracture, infection, and abnormal development resulting in lameness, and swelling of the femoral–tibial joints. These problems did not appear during rearing of broiler parent flocks from day old to maturation with restricted feeding, indicating that the skeletal and leg problems were a result of the very rapid and unbalanced growth rate of the broiler chick, rather than being innate to the animal. This led to more tailored feeding and lighting programs for young broiler chicks, holding growth below the potential in the early part of the growth period, by returning to mash type feed or otherwise decreasing the nutritional content of the diet, and by decreasing hours of light [23, 25]. In the final weeks of the broiler growth period, after the skeleton and body frame were more solidly formed, photoperiod was increased to maximize feed intake, and diet was shifted back to nutritionally dense pelleted form to allow full compensatory growth. Skeletal abnormalities were a leading cause of mortality and carcass condemnations in broiler production in the 1970s. At the present time, however, due to genetic selection to reduce their incidence and formulation of suitable management protocols, skeletal deformities are well controlled.

Stage 2: Combined Selection for JWfA and Feed Conversion Ratio (FCR)

Random sample tests of broiler chickens from different breeding firms were instituted in the 1960s to provide unbiased information as to broiler chick quality. In addition to differences in JWfA, these also showed large differences in feed conversion ratio (FCR) among the various breeders, independent to an appreciable degree of juvenile growth rate. This was surprising, since the metabolic efficiency of feed utilization was thought to be highly correlated with evolutionary fitness and hence it was anticipated that there would be little genetic variation in the trait. Because of the economic importance of FCR, starting in the 1970s breeders included this in their breeding programs as a second major objective along with JWfA, with considerable success.

Further consideration led to the realization that although the metabolic efficiency of catabolism and anabolism may not vary, variation in motor activity, carcass adiposity, and possibly protein turnover rate [14, 26, 27] may all contribute to genetic variation in FCR. Consequently, a positive albeit unexpected secondary effect of selection for reduced FCR was a gradual but steady reduction in carcass adiposity [6, 9], apparently by reducing the fat:lean partition coefficient at high intake. Thus, at the present time, excess broiler fat content of the commercial broiler is no longer considered a problem by the broiler industry.

Secondary Effect of Continued Selection for JWfA and FCR (V): Adverse Effects on Reproductive Performance of Broiler Female and Male Parents

The late 1970s and 1980s, however, brought about a number of additional problems, apparently secondary effects of the continued selection for JWfA and FCR. First of all, female and male reproductive performance again became problematic. As noted, to control EODES, female pullets were reared under feed

restriction. Initially, birds of the reproductive flock were shifted to *ad libitum* feeding to induce entry into lay, and remained on *ad libitum* feeding during the entire reproductive period. However, in the 1970s while peak production remained high, post-peak production dropped rapidly. This was apparently due to continued effects of the loss of appetite control that led to overeating and fat accumulation during the laying period, by both females and males. As a consequence, feed restriction was extended into the laying period itself [18, 19]. This continues to the present time and is effective in maintaining egg production.

The extension of feed restriction to the laying period had a further positive effect in that egg weight is closely related to actual body weight and feed consumption, so that egg weight can be closely controlled by monitoring body weight and feed intake during the reproductive period. Control of egg weight in this manner, however, is limited by the ever-increasing optimum mature body weight of the female parent even under feed restriction. This is due in all likelihood to an increase in threshold weight for sexual maturity that has all along accompanied the increase in JWfA.

Secondary Effect of Continued Selection for JWfA and FCR (VI): Increased Water Consumption, Nipple Drinkers

The increased daily feed consumption of the rapidly growing broiler chick required a proportional increase in water consumption to enable the gizzard and digestive system of the bird to deal effectively with the dry feed. Drinking the additional water from the standard "Bell drinker" resulted in increased water spillage and wet litter causing a host of veterinary and welfare problems, such as foot pad and breast dermatitis, and ammonia production interfering with proper breathing and contributing to pulmonary hypertension syndrome (PHS). This was solved in the early 1980s by the introduction of the "nipple drinker" in which water drops are drawn directly into the chicks' throat in this way greatly reducing spillage and the attendant problems with wet litter.

Secondary Effect of Continued Selection for JWFA and FCR (VII): Delayed Entry into Lay

In the 1980s, a new set of problems arose related to entry of the birds into lay. Under natural conditions, onset of sexual maturity in chickens is controlled by day length (photoperiod). Male and female birds enter sexual maturity in the spring, under the stimulus of gradually increasing photoperiod. Normally, chickens will not enter lay in the fall, due to the negative stimulus of the naturally decreasing photoperiod at this season. In order to have a steady supply of broiler chicks, however, it is necessary to have males and females enter sexual maturity and lay throughout the year. For birds maturing in the fall or winter, this was achieved by extending the photoperiod through the use of supplemental artificial light, added at both ends of the natural day. This produced an artificial spring-type light pattern, and brought the birds into sexual maturity in a reliable manner throughout the year. Beginning in the 1980s, however, onset of sexual maturity was delayed for birds maturing in the fall season of the year, even under the stimulus of supplemental artificial light. Some of the females did not enter lay at all; in others, onset of lay was delayed and peak lay was lower. A management solution was found in the form of "Stimulatory lighting." For this, the chicks are reared in fully enclosed so-called dark-out houses in which photoperiod is under total artificial control, under a regime of 16 h total darkness and 8 h dim light until it is time for them to enter lay. As noted above, during this period they are also under quantitative feed restriction. To bring the birds into lay (generally, at about 6 months of age), they are moved to the laying pens, and exposed to a photoperiod of 14–16 h of daylight, while at the same time feed quantities are increased rapidly (within a few weeks from 100 g/day to over 160 g/day). The combined stimulus of increased photoperiod and feed quantity brings the birds into sexual maturity and lay.

Initially, dark-out rearing and stimulatory lighting were required only for birds entering lay in the fall. However, with the passage of generations, and continued selection for juvenile growth rate and FCR, problems on entering lay appeared even in birds coming to sexual maturity in the spring of the year under optimal natural lighting. At present, therefore, stimulatory lighting to bring the birds into sexual maturity is required at all seasons of the year [28]. Experimental studies showed that the need for stimulatory lighting was due to reduced innate photosensitivity of the broiler chicks [29], as well as to a direct effect of feed

restriction per se on photosensitivity. Apparently the control systems of the bird interpret feed restriction as indicating that environmental conditions are not yet suitable for chick rearing, and delay onset of lay accordingly.

Secondary Effect of Continued Selection for JWfA and FCR (VIII): Male Overfeeding

In the mid-1980s, growth and appetite patterns of males and females began to diverge sufficiently, so that even under feed restriction, the males, when fed together with the females, became overweight and lost fertility. This was resolved by the use of special feeders and feed composition for the males, while using barriers preventing the males from having access to the female feeders.

Secondary Effect of Continued Selection for JWfA and FCR (IX): Heat Distress

Heat is produced by all aspects of body metabolism, including digestion and growth. Producing a given total mass of body weight, therefore, generates a more or less fixed total quantity of metabolic heat to digest the food required to grow this body mass and convert the digested food into body mass. This metabolic heat must be dissipated to avoid symptoms of heat distress. When the grow-out period is long, the daily production of metabolic heat for growth and digestion per unit time is low and readily dissipated by the bird. However, as age to market weight decreases with each generation of selection, this same total metabolic heat is produced in a shorter and shorter grow-out period, so that in each generation the metabolic heat generated per unit time increases [30]. This is particularly true for the final weeks of the grow-out period, when the bulk of body mass is produced.

Generation of metabolic heat interacts strongly with stocking density, a major management determinant of broiler costs through its effect on fixed costs of housing per unit of product. Generally, birds are stocked at a density that gives almost complete ground cover toward the end of the rearing period. Under these conditions, there is maximum radiant heat transmission between birds, and stagnant hot air is trapped between birds and between the birds and the litter. Broilers with slow to moderately rapid growth can be reared in open sheds, with air circulation controlled by opening and closing window flaps or curtains, as the weather dictates. At optimal ambient temperature of 18–22°C, normal air circulation adjusted in this manner is sufficient to dissipate metabolic heat and the birds are comfortable. As ambient temperature increases, the birds cope by generating evaporative heat loss through panting [31]. For broilers with slow to moderately rapid growth, this is ordinarily sufficient to deal with the stress of normal summer peak heat. When peak heat exceeds ability of the bird to cope by panting, metabolic heat can be reduced by reducing food intake during the hottest part of the day, and by artificially "fogging" or "misting" the birds to increase evaporative heat loss when humidity is less than 70%. However, with the increase in growth rate achieved by the early 1980s, metabolic heat production increased to the point where these palliatives were no longer sufficient and the birds exhibited excessive panting and heat distress under conditions that were previously adequate. Heat distress was particularly acute at high stocking densities toward the end of the growing period, when floor cover by the birds was maximal. This led to reduction in growth rate since the birds reduced feed intake during the hottest part of the day, and in some cases to collapse and death of the bird from hyperthermia. To deal with this, fans were introduced into the chicken sheds to create additional circulation of air inside the sheds and to increase exchange of air between the inside and outside of the sheds. This system worked well, and in combination with misting or fogging when outside temperatures were high, enabled rapid growth to continue even under hot summer weather conditions with good FCR and low mortality.

Secondary Effect of Continued Selection for JWfA and FCR (X): Pulmonary Hypertension Syndrome and Sudden Death Syndrome

In 1974, a new pathological condition was reported in broiler birds reared at high altitudes. The condition manifested as sudden death, accompanied by "ascites" (accumulation of protein-rich fluid in the body cavity). Initially, death was attributed to the ascites *per se*, and hence the condition was termed "ascites syndrome." However, further studies showed that the ascites was a secondary consequence of pulmonary hypertension

and the disease is now termed "Pulmonary Hypertension Syndrome" (PHS). With time, PHS manifested in broiler flocks growing at lower altitudes causing high mortality particularly in males of rapidly growing broiler lines from 4 weeks of age. The etiology of the disease has been worked out in detail (Box 3), and it appears to be a direct consequence of continued selection for rapid JWfA, exacerbated by selection for reduced FCR.

At about the same time that PHS manifested, a second metabolic disorder, "Sudden Death Syndrome" (SDS), also became prominent [32, 34, 35]. SDS presents as sudden convulsions, with squawking, violent flapping, and loss of balance. Death ensues within less than a minute from the onset of symptoms, with the bird lying on its back with one or both legs extended. Greatest losses are from 3 to 6 weeks of age, primarily in males. The syndrome is associated with the same factors that induce PHS, namely, high carbohydrate intake, dense housing, very rapid growth, and low feed conversion ratios; but most commonly manifests at an earlier age than PHS. Also similar to PHS, under inducing conditions, SDS can be precipitated by any sudden movements or noises that cause a stress response in the birds. It is plausible therefore, that SDS is an early pathological response to the hypoxia that accompanies rapid growth in broilers (see also Box 3).

From the above, it is clear that incidence of mortality due to PHS and SDS will be increased by any management factor that increases oxygen demands of the animal, such as social stress, low ambient temperature, feeding high-energy food in pellet form that stimulates growth rate; or that limits oxygen supply, such as overcrowding and poor air circulation or avian respiratory disease. Although a major problem in the 1980s, and still a problem today when circumstances combine, by the mid-1990s PHS and SDS were brought under control by a combination of family-based genetic selection against the condition, and careful management minimizing the external factors that contribute to hypoxia.

Stage 3: Combined Selection for JWfA, FCR, and Proportion of Breast Meat (PBM)

From the early 1970s, selection of birds with a less-pronounced keel bone was a part of broiler selection,

Box 3 Etiology of Pulmonary Hypertension Syndrome and Sudden Death Syndrome

The causal sequence leading from selection for JWfA and FCR to PHS is thought to be as follows: Selection for rapid juvenile growth rate increases metabolic rate for growth resulting in increased need for oxygen in tissues. At the same time, selection for decreased FCR caused the relevant regulatory, circulatory, and hormonal systems to reduce oxygen consumption by the tissues resulting in effective hypothyroidism, and also reduced the proportion of oxygen-supplying organs (lung and heart) relative to oxygen-demanding tissue (muscle). The combination of these two factors results in tissue hypoxia that leads, via the kidney and erythropoietin, to increased production of red blood cells that increases blood viscosity, and also to constriction of pulmonary arterioles to ensure blood flow to all parts of the lungs so as to increase pulmonary oxygen exchange. The result of these two factors was increased lung arteriole pressure leading to increased workload on the heart and hypertrophy of the right (pulmonary) ventricle. This in turn resulted in incomplete closure of the right arterial valve with consequent backup of blood pressure to the hepatic and portal veins generating pulmonary hypertension and impaired uptake of fluid by the lymphatic system. Pulmonary hypertension results in fluid leakage and accumulation of fluid in the lungs (hypertensive lung syndrome) and in the abdominal and pericardial cavities (Ascites), and inability of the heart to supply body oxygen needs through left ventricle heart failure. Any of these final syndromes can result in death of the chick from PHS.

The detailed etiology of SDS differs [34, 35]. Electrocardiograms of broilers in the last stages of SDS show the immediate cause of death in SDS to be acute cardiac arrhythmia terminating in ventricular fibrillation. It is thought that under conditions of hypoxia the myocardium may become hyperirritable, serving as a secondary pacemaker and interfering with normal cardiac rhythms. Indeed, studies of rapidly growing broilers show that they manifest a high rate of cardiac arrhythmia under "normal" high growth-rate conditions, and are highly susceptible to stress-induced cardiac arrhythmia. Thus, under normal high growth-rate conditions, any additional stress may be sufficient to tip the heart from simple arrhythmia to ventricular fibrillation and sudden death [32, 33].

with primary aim of producing a finished product having a fuller appearance that was more attractive to the consumer. This had a secondary result of selecting birds with more breast meat. With an increasing percentage of birds sold as individual parts, a major price differential between chicken breast "white" meat and chicken leg and thigh "dark" meat became apparent. This meant that the income of the broiler producer was primarily a function of the amount of breast meat produced. In the mid-1980s, realization of this economic fact by the breeders led to the addition of specific selection for a high proportion of breast meat in the broiler carcass as a third major breeding goal in addition to JWfA and FCR. This continues to the present time.

Secondary Effect of Selection for JWfA and PBW (XI): Heat Stress (Again)

The major secondary effect of selection for PBW in the broiler was an additional increase in heat stress effects, due to the increased metabolic load induced by the high metabolic cost of muscle mass synthesis. As a result, the modern broiler could no longer cope with even small deviations from the neutral temperature zone without a significant loss of meat yield. It became clear that the typical broiler-rearing shed of minimal structure with open sides plus fan-ventilation could no longer deal successfully with the enormous metabolic heat produced by the modern broiler flocks. This led the industry to adopt a closed shed and a shift to "tunnel ventilation" with further option of cooling the air by drip technology. During the 2000s, "tunnel ventilation" with "drip cooling pads" for broilers became an obligatory feature of broiler rearing.

Secondary Effect of Selection for PBM (XII): Quasi-EODES at Entry to Lay

A secondary effect of the selection for PBM was the appearance of a new "quasi-EODES" syndrome at the onset of lay in the broiler breeder female parent, with symptoms very similar to classical EODES but to a less-pronounced degree [36]. This "quasi-EODES" syndrome was characterized by high mortality at entering lay, caused mainly by cloacal prolapse, internal lay, and inflammation of the oviduct. For the surviving birds, the quasi-EODES syndrome has marked negative effects on peak lay and eggshell quality resulting in a lower proportion of hatching eggs out of all eggs and lower hatch of healthy chicks from fertile eggs. The overall result is a marked reduction in chick production. Practical experience of hatchery flock managers, supported by later research revealed that the quasi-EODES syndrome is induced by even minor "overfeeding" during the critical weeks of forced sexual maturation. The modern female breeder became very sensitive to even a slight deviation from optimal feed restriction.

Two factors appear to have combined to generate the quasi-EODES syndrome. The first, is the continued increase in the degree of feed restriction during the pullet growth period, needed for preventing EODES, going, as noted above, from about 70% of *ad libitum* consumption during the 1970s to about 35% of *ad libitum* consumption at present. The second is the continued increase in threshold weight for onset of sexual maturity of the female broiler breeder, as a direct result of the selection for higher JWfA and PBM. For example, recommended 24-week body weight for out-of-season "Cobb 500" female broiler breeders increased from 2700 g in 1987 to 3160 g in 2005 [37] with a higher proportion of body mass as muscle tissue. Thus, the actual gap between the pullet lean mass attained at the point where light and feed stimulation is initiated, and the threshold lean mass required for entering lay has progressively increased, and with it the time required from initiation of light and feed stimulation to actual onset of lay. Attempting to cover this gap more rapidly by increasing feeding levels exceeds the ability of the pullet to rebuild breast mass and results in a surplus of nutrients causing the ovary to behave as if fed *ad libitum* and leading to development of quasi-EODES. Thus, the modern broiler breeder pullet entering lay is delicately balanced at a feeding schedule that will induce lay as rapidly as possible, yet will not induce quasi-EODES. Consequently, the bird is very unforgiving of any deviation from optimum feeding schedule in the direction of overfeeding.

Secondary Effect of Selection for PBW (XIII): Hatchability Problems (Again)

A further secondary effect of the selection for increased proportion of breast meat was a reemergence of hatchability problems. These appeared even though

continued selection for rapid JWfA did not result in appreciable further increase in egg weight. Stability of egg weight was achieved due to increasing feed restriction of the broiler mother targeted specifically at controlling egg weight (which responds very rapidly to feed restriction) and to conscious selection against excessive egg size by the breeders. Thus, the situation was unchanged throughout the 1990s. However, the intense selection for increased muscle mass that began in the mid-1980s resulted in an increase in the proportion of muscle mass in the late developing embryo. As noted, the metabolic energy expended in development of muscle is greater than for other body tissues, because of the high metabolic cost of protein synthesis. Hence, this resulted in a further increase in metabolic heat production by the late embryo [38–41]. This additional excess heat was beyond the capacity of multistage incubators, no matter how carefully managed. Consequently, hatchability began to fall again, owing to increased late mortality and decreased yolk uptake leading to an increased proportion of weak chicks, and more grade B chicks [42], and negative effects on broiler bone development and leg health [43, 44].

To meet this challenge, the industry began shifting to "single-stage" incubators [40]. In these incubators, all eggs from flocks of about the same age and same average egg weight are loaded into the incubator on the same day. They are then incubated together until they hatch. Thus, they are all at the same stage of development at any given time (hence the name "Single-Stage" incubator). This makes it possible to better adjust incubation temperature, according to the stage of the embryos [42] – somewhat warmer at the early embryo stages, when the embryo requires external heat to reach desired internal temperature, and cooler at the later embryo stages, when the embryo needs to rid itself of excess heat. Similarly, humidity can also be adjusted so as to achieve optimal egg water loss across the incubation period [41]. This has proven to be a satisfactory solution, and hatchability and chick quality have improved accordingly.

Secondary Effect of Selection for PBW (XIV): Reduced Locomotor Activity

The very large breast of the modern broiler chick results in an animal that is unbalanced between breast weight and leg and thigh muscles [45]. Consequently, it is difficult for the animal to move, and locomotor activity is much reduced. Toward the end of the growth period, the broiler chick spends over 90% of its time sitting and lying, resting its overdeveloped breast on the litter, and basically moving only to eat and drink. Selection for reduced FCR may also have contributed to the reduction in locomotor activity, since this is one way to reduce metabolic expenditure of the animal. As a result, the animal is very susceptible to contact dermatitis, including footpad lesions and breast blisters. These conditions can be well controlled by meticulous attention to litter quality, specifically litter temperature and humidity, but are exacerbated and can reach high levels when litter quality is poor.

The Role of Breeding and Management in the Improvement in Performance of the Modern Broiler Chicken

Achievements of the Modern Commercial Broiler with Respect to the Three Main Production Traits and the Associated Secondary Traits

The extraordinary improvement in broiler performance for the three main production traits (JWfA, FCR, and PBW) over the past 60 years is best captured by the following table (Table 1), which compares the performance (average of males and females) of representative commercial broiler stocks of 1957, 1991, and 2001.

Poultry Breeding. Table 1 Comparison of performance of broiler stocks of 1957, 1991, and 2001[a]

Trait	1957	1991	2001
Age at sale (d)	84	42	42
Live weight at sale (g)	1646	2132	2672
Feed conversion ratio	3.26	2.04	1.63
Breast meat (%)	12.9	15.0	20.0
Carcass fat (%)	14.7	14.1	13.7
Heart+lungs (%)	1.242	ND	1.023
Mortality to market (%)	2.52	9.70	3.57

[a]Based on [6–9]; data for 1957 average of [6 and 8 and 7 and 9] for birds fed the commercial feed formulations of 1991 [6, 7] and 2001 [8, 9].

It is evident that in the period 1957–2001 enormous improvement has been achieved in the three major production traits. Days to market weight and FCR have been reduced by half, while JWfA has almost doubled, and PBW has increased by almost 30%. Improvement in all traits was continuous, with no indication of reduced rate of gains in the latter decade.

When compared using the feed formulations of 1957, gains in JWfA and FCR were only a bit less. There is no doubt therefore, that genetic selection by the primary breeders was by far the main driving force leading to the gains in these traits. The increase in PBM from 1991 to 2001 is particularly impressive and can be attributed almost completely to the attention devoted to this trait by the primary breeder beginning in late 1980s. However, JWfA and FCR also increased strongly during this period showing the ability of the breeder to deal simultaneously and effectively with the three major production traits.

Along with the phenomenal improvement in production traits, the broiler industry was able to cope successfully with all of the deleterious secondary effects detailed in the preceding sections that accompanied the genetic gains in the three main production traits. Through a combination of genetic selection on the one hand, and continual adjustment and innovation in broiler and breeder flock management and physical facilities on the other, the industry succeeded in maintaining male and female reproductive performance at very high levels, while keeping losses due to heat sensitivity, skeletal problems, and metabolic disorders at very low levels.

Relative Contribution of Genetics and Management to Modern Broiler Performance

The relative contribution of genetics and management to these achievements depends on the specific trait. In particular, it seems clear that the shift to progressively more active ventilation culminating in the tunnel ventilation with drip cooling in general use at present was the main means for coping with the heat sensitivity of the modern broiler. Similarly, changes in incubator management and the more recent shift from multistage to single-stage incubators together with flock management to reduce egg weight were the main factors maintaining high hatchability rates. However, selection played some role in both cases, since families that display low hatchability and high sensitivity to heat stress are generally culled from the breeding population.

With respect to reproductive performance, feed restriction during pullet growth and the hen laying period, and dark-out housing of the parent stock pullets with stimulatory lighting and feeding at entry into lay, were critical management factors contributing to maintaining reproductive performance in male and female broiler parent stock. However, selection for reproductive performance within this overall management scheme played an important secondary role, as attested by the appreciable differences between genetic stocks in reproductive performance under optimal feeding and lighting schedules. In the same way, while appropriate management is essential to control skeletal problems and metabolic disorders, the effective selection applied to these conditions appears to have been crucial in reducing their incidence in well-managed flocks to present-day low single-digit proportions.

Thus, although the improvement in production traits of the modern broiler compared to its original founder populations can be attributed almost entirely to genetic improvement achieved by selection, the bird that results is able to achieve optimal production and functional performance as broiler and parent stock primarily due to major modifications in broiler housing, and in parent flock and incubator management coupled with a greater or lesser contribution by selection, depending on the trait. Be that as it may, one can only stand in awe at the combined ability and synergistic work of the major players in the industry to overcome the challenges as they arose while maintaining continual progress in overall efficiency of the broiler enterprise.

Breeding Methods for Genetic Improvement

In large part, this is due to the fact that the methods practiced by the primary broiler breeders increased in sophistication in accord with the complexity of the breeding challenges that they faced [46]. In the first stage of broiler genetic improvement, JWfA was the main trait under selection, with a minor goal of improved breast conformation. This was achieved by simple two-step tandem mass selection, the first step

being selection for JWfA followed by a second step of selection for breast conformation. Flocks were not pedigreed at this stage. With the addition of reproductive performance, FCR and reduction of adiposity and skeletal problems as breeding objectives in the second stage of broiler genetic improvement, simple mass selection was no longer effective and multiple-stage tandem selection no longer feasible. To meet the new challenges, breeders changed to fully pedigreed flocks to provide information on reproductive performance, FCR, and skeletal problems, and to index selection based on individual and close relatives to combine information on the various traits in an optimal manner. Finally, in the third stage of broiler genetic improvement, with the addition of PBM and reduction of metabolic disorders to the breeding objectives, breeders adopted BLUP and Individual Animal Model statistical methodologies for estimating breeding values for the various traits under selection, based on individual data for the entire current and past population. At the same time, the primary breeders adopted phenotyping procedures that increased the completeness and accuracy with which the traits of importance were evaluated. For example, individual skeletal problems are now assessed by x-ray scanning of bird joints and individual cardiovascular function is assessed by blood oximeter machine. At present, over 50 traits are recorded on the individuals in the breeding nuclei, about half of these relating to various aspects of broiler health.

At all stages, breeding nuclei were kept very large in order to avoid inbreeding and maintain genetic variation. With the advent of genome-wide procedures for estimation of breeding values [1–3], all of the major primary breeders have instituted in-house experimental studies to evaluate the use of these methodologies in their practical breeding programs. Although very promising in initial studies, the results in practice in commercial breeding nuclei remain to be seen.

Accounting for the Long-Term Continuous Response to Selection and for the Punctuated and Coordinated Appearance of Secondary Effects

Commercial breeding nuclei have been under intense and effective directional selection for JWfA for 60 generations, for FCR for 40 generations, and for PBM for 25 generations. Two remarkable features characterize the response to this selection. The first and most striking is that the direct response of the target traits to selection has been positive and continuous for all three traits, with no indications of having reached a selection plateau for any of them. This continued response to selection requires explanation. Since selection acts on all relevant loci at the same time, the intense directional selection for the target traits should have exhausted the existing genetic variation in the original dual-purpose chicken founder populations rather rapidly, leading to selection plateaus for the various traits. The second remarkable feature is the rather sudden manifestation of the secondary effects of the response to selection at about the same time period in the stock of all leading breeders, even though their respective breeding nuclei are effectively isolated from one another. This "punctuated" (i.e., "relatively sudden") and "coordinated" (i.e., relatively universal and synchronous) manifestation of the secondary affects requires explanation. If due to genetic correlations or pleiotropic effects of the initial genetic variation of the founder populations, they would be expected to manifest in a more linear and gradual manner. If due to pleiotropic effects of new mutations, they would be expected to manifest in a more sporadic manner, affecting only stock of one or two of the various breeders.

Sources of Genetic Variation for the Long Continued Response to Selection

Based on classical population genetics, three sources can be envisaged with respect to sources of genetic variation to serve as a substrate for selection. The first is the genetic variation present in the original founder populations of the broiler stocks. Recent research in mapping of the loci responsible for genetic variation in production traits in farm animals (the so-called Quantitative Trait Loci or QTL) indicates that tens of QTL may contribute to genetic variation of such traits. This genetic variation present in the founder populations would have provided the basis for the first decades of response. The second source comprises rare alleles with positive effects on the target traits that were present at low frequency in the founder populations. The primary breeders maintain large breeding nuclei, and these

could have included an appreciable number of such loci. In the early generations, because of their low frequency these loci would not have contributed materially to genetic variation in the target traits, or to the response to selection. However, after several decades of intense selection, their frequency would have increased to the point where they could serve as useful targets for the middle stages of selection. Finally, new mutations or rare recombinants would supply a steady stream of new genetic variation that would come into play in the later stages of selection.

Punctuated and Coordinated Appearance of Deleterious Secondary Effects

Similarly, a number of explanations can be offered within classical frameworks, for the punctuated and coordinated appearance of deleterious secondary effects. Some of these effects may be due to non-linear secondary effects of selection interacting with downstream threshold effects. For example, adiposity can be presumed to have increased more or less linearly with selection for JWfA, but the effect on egg production was virtually nil for the first 10–15 generations of selection, and then suddenly became very severe – in the few years just before the introduction of feed restriction in the late 1960s, yearly egg production had fallen by almost 100 eggs per laying hen. Such effects would be expected to manifest in flocks of all breeders at about the same time, as their breeding populations reached more or less the same degree of expression of the primary traits. Other secondary effects may be due to the introduction of new primary target traits. Thus, an entire group of new secondary effects manifested following the introduction of FCR, and again following the introduction of PBM as targets for selection. Since the primary breeders introduced the same new target traits for selection at more or less the same time, these secondary effects would be expected to manifest in flock of all breeders at about the same time.

Difficulties with the Explanations Within the Classical Framework of Population Genetics

Rare mutations are often those that are held at low frequencies because of deleterious pleiotropic effects on fitness. Similarly, new mutations generally affect numerous traits, with deleterious fitness effects on one or more of them. Intense selection can increase the frequency of genes with strong positive effect on the target trait in spite of negative effects on fitness, but in a long-term selection program this should result in reduced overall functional fitness of the population. Furthermore, because of their low frequency in the founder populations, rare alleles would not distribute uniformly among different breeding populations derived from the same founders. The same would certainly hold for the genes that were affected by mutation. Consequently, fitness traits should be differentially affected in different breeding populations, according to the specific low-frequency genes that were inherited or mutated in each population. This does not appear to have been the case. Similarly, although in almost all cases it was possible to trace in retrospect a causal chain leading from selection for the primary trait to the manifestation of the secondary trait it is somewhat unexpected that the specific form of these manifestations (e.g., PHS, SDS, quasi-EODES, reduced photosensitivity) was the same in stocks of all breeders. If much genetic variation is due to initially rare or mutated loci that are necessarily specific and different in different breeding populations, specific manifestations of secondary traits would be expected to differ as well.

Selection-Induced Genetic Variation (SIGV)

The difficulties with the explanations proposed within the classical framework for long-term response to selection and for punctuated and coordinated appearance of the secondary manifestations have led to a recent proposal for a new previously unrecognized source of genetic variation in ongoing selection programs: selection-induced genetic variation (SIGV) [47]. The SIGV hypothesis is based on the observation that the individual QTL determining genetic variation in production traits often exhibit strong epistatic interactions with one another and with the genetic background. Consequently, a segregating locus with zero effect on the target trait in one genetic background might have a strong effect on the trait in a different genetic background.

The intense continued directional selection, changes the frequency of many alleles in many loci and by means of “hitchhiking effects” of their closely

linked neighboring genes as well. This changes the genetic architecture of a population to a marked degree. Thus, some loci that were neutral in their effect on the target trait at the beginning of the selection program, may transform into sources of genetic variation as the selection program progressively modifies the genetic architecture of the population. As the positive alleles at these loci are caught up and brought to high frequency by the ongoing selection, the genetic architecture of the population becomes modified again, and new previously neutral loci come into play as sources of genetic variation. In this way, the population under selection would continually generate new genetic variation to serve as a substrate for the next phase of the directional selection process, with no obvious limit in place.

Since the loci involved in the SIGV process are loci that were present at appreciable frequencies in the original founder populations, they would be present in all breeding stocks, and would be expected to come into play at about the same stage in the selection process in the individual flocks. Thus, genetic progress in the various breeder populations would not depend on rare alleles or new mutations, which would be specific to each population, but on segregating loci already present in the population at useful frequencies, that come into play in a programmed manner, as the genetic architecture of the population changes. On this hypothesis, the genetic architecture of all breeding populations under the same general selection regime would be similar at all stages of the selection process, and hence the specific form of any secondary effects would also be similar in the different populations. Strong secondary effects on fitness would not be expected, since the loci involved are loci historically present in the populations, and hence have survived the screening effect of natural selection.

Thus, the SIGV hypothesis provides plausible explanations both for the long-term response to selection and for the punctuated and coordinated appearance of secondary effects. Indeed, recent experimental studies analyzing crosses between layers and broilers, and between two-way single-trait selection lines for JWfA, provide significant experimental support for this hypothesis [48, 49]. The SIGV hypothesis emphasizes the importance of epistatic interactions in genetic variation and encourages the development of statistical and genomic methodologies that can exploit these interactions.

Genetic Improvement of Broiler Production Traits and Broiler Welfare

In the previous sections, it was seen that the modern broiler is greatly modified developmentally and physiologically from the original dual-purpose breeds from which it was developed. Furthermore, to achieve optimal economic performance the modern broiler and its parent flocks must be reared, managed, and housed under conditions very different from the husbandry conditions of the founder parent lines. Various aspects of these genetic and management changes impinge on animal welfare, in the sense that they can lead to distress or pain of the individual. These can be considered in two main categories. Those where the distressful situation is unavoidable, and those where the distressful situation is avoidable under good management, but manifests under less than optimal management. There is a third category, which considers aspects where the bird is comfortable and not in distress, but where it is thought that its life might be more joyful if living under different conditions, for example, on free range or scrounging for food in the jungle or farmyard, instead of in a closed shed. This latter raises more profound issues of the morality and ethics of animal agriculture in general and industrial animal agriculture in particular, and will not be considered here.

Unavoidable Distress

The negative effect of excess adiposity on reproductive performance and survival of the modern broiler parent female or male is dramatic and extreme. Consequently, stringent feed restriction of the parent flock pullets and males during the rearing and laying period is essential, if the birds are to achieve optimal reproductive performance. This appears to be the only aspect of the broiler enterprise that causes distress, but is unavoidable. An animal that is fed only 35% of its *ad libitum* consumption, and can be seen to eat ravenously when feed is available, must surely be feeling hunger pangs. The period of stringent feed restriction is rather short, however, from about 4–14 weeks of age, and while it can be presumed to be uncomfortable, does not affect the overall health of the individuals in any way. Indeed, allowing the animal to eat *ad libitum* and become grossly obese would probably entail much more distress over the entire life span of the animal including

mortality. The much milder feed restriction that is in effect during lay would not seem to pose a welfare problem, as it is ordinarily sufficiently generous to even allow for some increase in body weight over the course of the laying period.

Avoidable Distress

A review of the preceding sections, however, reveals a considerable list of conditions to which the modern broiler is susceptible due to its changed genetic constitution. These include: quasi-EODES at entry into lay that can result in death from cloacal prolapse or from internal lay; heat stress, skeletal abnormalities, PHS which often manifests as ascites, SDS, and various forms of contact dermatitis. SDS, in which death of the animal occurs within less than a minute from the onset of first symptoms of distress, would seem to occur too rapidly to be a source of significant pain or distress. But the other conditions can be presumed to be moderately to severely painful, according to their respective natures and degree of severity. As emphasized in the previous sections, thanks to the selective work of the breeder on the one hand, and innovative management of the industry on the other, when broiler commercial or parent flocks are managed with care and attention to detail, all of the above can be kept at very low single-digit levels [46, 50].

Importance of Stocking Density

In this context, stocking density, an aspect of management that was not previously emphasized becomes important [45]. Stocking density interacts with the susceptibilities of the modern broiler in two ways: increasing heat stress and decreasing litter quality with consequent increase in the incidence of contact dermatitis. When stocking density is high, the bodies of the chicks cover the entire floor area, forming a barrier between the litter surface and the ventilated area of the shed. In addition, higher stocking density provides additional nitrogen and moisture to the litter increasing heat production due to microbial growth and metabolism. Taken together, these two factors can generate an appreciable differential between temperature at broiler level and temperature a meter above the floor. High stocking density also limits air movement and increases radiant heat transfer between birds, further increasing heat stress. The increase in litter temperature, humidity, and ammonia concentration resulting from high stocking density also interacts with the limited locomotor activity of the broilers to increase the incidence of contact dermatitis. Accordingly, proper control of stocking density is essential for optimal broiler welfare, and may be less than the economic optimum.

From Farm to Market

The handling of the bird on its final path from shed to slaughterhouse is another case in point. Because of the young age of the broiler at market weight, and its minimal locomotor activity, the long bones of the legs and wings are fragile relative to body weight. Moving the birds from the grow-out shed to the slaughter line is low-wage work with high personnel turnover and great pressure to get the work done with minimal labor costs. Consequently, the birds may be roughly handled at this time resulting in leg and wing bone breakage when they are captured and moved from the pen to the transport crates, and again from the transport crates to the slaughter line [51, 52]. Such breakage results in direct losses to the farmer and hence normally efforts are expended to reduce this to a minimum through mechanization, proper design of facilities, and training of personnel [53].

Welfare and Society

Apparent from the above paragraphs is the critical dependence of broiler welfare on meticulous flock and personnel management. Due to the work of the breeder, with proper management the susceptibilities of the bird remain latent. But there is little room for error. The bird is unforgiving of even slight deviations from optimal management, and will react to such deviations by manifesting one or other of its innate susceptibilities. The modern chicks that manifest any of the conditions above are a net loss to the farmer, and management conditions conducive to such manifestation are often inimical to optimal growth and reproduction. Consequently, for the most part, the welfare of the chick and the economic interests of the farmer correspond. However, achieving optimal management has its costs as well, and economic maximization may result in a management program that is somewhat less than optimal for the bird.

Society as a whole has benefited greatly from the improved production characteristics of the modern broiler, which has added a low-cost highly nutritious staple to the menu at minimal environmental footprint. Along with these benefits comes responsibility for the welfare of the bird in those instances where economic interests of the farmer and the quality of life of the broiler are not perfectly aligned. This is true throughout the broiler enterprise; nowhere more than in the final hours of the chick's life. Happily, society is accepting these responsibilities by designing facilities based on understanding of livestock behavior [53], and by defining acceptable production standards, and embodying these in appropriate regulatory legislation [54, 55].

Future Directions

One stands in awe of the magnificent achievements of the primary broiler breeders who have succeeded in improving the production characteristics of the modern broiler manifold relative to the initial dual-purpose founder populations, while at the same time dealing successfully with the many secondary functional problems that arose along the way, maintaining high reproductive performance together with very low incidence of health problems. This was not the achievement of the breeder working alone, of course, and at all stages involved combined contributions by all components of the industry in devising novel management programs and physical facilities such as feed restriction and stimulatory photoperiods, dark-out housing, and tunnel ventilation that enabled optimal functional performance of the birds.

The Resource Allocation Model

These results are all the more remarkable, because they differ from what would be expected on the widely accepted resource allocation model for interpreting the effects of selection for production traits on functional traits [56, 57]. The basic assumption of this model is that under the conditions of intensive agriculture, the energy resources available to an animal are fixed. The animal must then allocate these resources to maintenance, to production traits including growth, and to functional traits including reproduction, regulation of physiology and metabolism, and defense against pathogens and toxins. Selection for production traits diverts resources preferentially to these traits, leaving less for the functional traits. Consequently, functional traits are expected to suffer. Indeed, many experimental studies show that production traits suffer when resources are preferentially allocated genetically or experimentally to functional traits, and functional traits suffer when resources are preferentially allocated to production traits. Amazingly, the broiler industry appears to have been able to circumvent this negative correlation, achieving high levels in both production and functional traits.

Management and Biological Costs of the Performance Achievements of the Broiler Industry

More detailed consideration, however, shows these achievements have incurred two costs. The first is the cost of more sophisticated physical facilities and complexity of management. These include sheds with tunnel ventilation and drip cooling for broiler rearing; dark-out houses for pullet rearing; feed restriction, single-stage incubators; and all of the many management and nutritional modifications required for optimum performance. The second cost is the apparent loss of buffering capacity of the animal regulatory systems, resulting in ever-increasing fragility or sensitivity of the animal to environmental challenges. This sensitivity expresses itself as reduced production and functional performance, and increased incidence of health problems as a consequence of even minor deviations from optimum management and environment. The result is not only loss of economic value, but also harmful impact on animal welfare. Because of the high metabolic cost of protein synthesis, a provocative hypothesis suggests that selection for productivity in general, and FCR in particular may reduce protein turnover rate. Since protein synthesis is essential to meet new conditions, this may be the underlying cause for the general loss in buffering capacity [58]. The primary broiler breeders today are attempting to decrease the sensitivity of their populations to environmental insults by testing under multiple environments and selecting for "robustness", as they would select for any other positive health trait. Will they succeed? Or will the future broiler require an increasingly narrow and complex multidimensional management path for optimal performance, with steep losses outside of this path?

The coming years will tell, with strong implications for the broiler industry, and for animal breeding in general.

Conclusions and Interpretation

Be that as it may, the broiler experience teaches that deleterious effects on functional traits are almost certain to arise in the course of selection, and can take unexpected forms. The industry, whatever the species, must be alert to this possibility, so as to seek solutions as early as possible. The broiler experience also teaches that the breeder and the industry acting in concert can indeed find these solutions to these problems, enabling a joint genetic-management program that provides very high productive performance together with high functional performance within a framework of innovative physical facilities and increased management complexity. Based on past experience, therefore, as animal breeding enters a new genomic phase with greatly accelerated improvement in production traits, the future can be looked at with appropriate confidence in the ability of the breeder and industry working together to achieve sustained genetic improvement in production traits while maintaining high levels of functional and health performance.

Abbreviations

BLUP	Best linear unbiased predictor
DNA	Deoxyribonucleic acid
EODES	Erratic oviposition defective egg syndrome
FCR	Feed conversion ratio
JWfA	Juvenile weight for age
PBM	Proportion of breast meat
PHS	Pulmonary hypertension syndrome
QTL	Quantitative trait locus
RNA	Ribonucleic acid
SDS	Sudden death syndrome
SIGV	Selection-induced genetic variation

Bibliography

Primary Literature

1. Hayes BJ, Bowman PJ, Chamberlain J, Goddard ME (2009) Invited review: genomic selection in dairy cattle: progress and challenges. J Dairy Sci 92:433–443
2. Tier B (2010) Editorial: genomic selection: promise and propriety. J Anim Breed Genet 127:169–170
3. Meuwissen T, Goddard M (2010) Accurate prediction of genetic values for complex traits by whole-genome resequencing. Genetics 185:623–631
4. Hartmann W (1989) From Mendel to multi-national in poultry breeding. Worlds Poult Sci J 45:5–26
5. Schmidt CJ, Persia ME, Feierstein E, Kingham B, Saylor WW (2009) Comparison of a modern broiler line and heritage line unselected since the 1950's. Poult Sci 88:2610–2619
6. Havenstein GB, Ferket PR, Scheideler SE, Rives DV (1994) Carcass composition and yield of 1957 vs 1991 broiler when fed "typical" 1957 and 1991 broiler diets. Poult Sci 73: 1795–1804
7. Havenstein GB, Ferket PR, Scheideler SE, Larson BT (1994) Growth, livability and feed conversion of 1957 vs 1991 broiler when fed "typical" 1957 and 1991 broiler diets. Poult Sci 73:1785–1794
8. Havenstein GB, Ferket PR, Qureshi MA (2003) Growth, liveability and feed conversion of 1957 vs 2001 broilers when fed representative 1957 and 2001 broiler diets. Poult Sci 82:1500–1508
9. Havenstein GB, Ferket PR, Qureshi MA (2003) Carcass composition and yield of 1957 versus 2001 broilers when fed representative 1957 and 2001 broiler diets. Poult Sci 82:1509–1518
10. F.A.O. Food outlook global market analysis (2010). http://www.fao.org/docrep/012/ak349e/ak349e00.pdf. Accessed April 2010
11. Anonymous (1996) The history of Hubbard Farms. Hubbard Farms, Walpole
12. National Chicken Council. US chicken industry history. http://www.nationalchickencouncil.com/. Accessed April 2010
13. Emmerson DA (1997) Commercial approaches to genetic selection for growth and feed conversion in domestic poultry. Poult Sci 76:1121–1125
14. Siegel PB, Wolford JH (2003) A review of some results of selection for juvenile body weight in chickens. Poult Sci J 40:81–91
15. Soller M, Eitan Y (1984) Why does selection for live weight gain increase fat deposition? A model. Worlds Poult Sci J 40:5–9
16. Wikipedia The metabolic syndrome. http://en.wikipedia.org/wiki/Metabolic_syndrome. Accessed April 2010
17. Jaap RG, Muir FV (1968) Erratic oviposition and egg defects in broiler type pullets. Poult Sci 47:417–423
18. Katanbaf MN, Dunnington EA, Siegel PB (1989) Restricted feeding in early and late feathering chickens 2. Reproductive response. Poult Sci 68:352–358
19. Robinson FE, Robinson NA, Scott TA (1991) Reproductive performance, growth rate and body composition of full fed versus feed restricted broiler breeder hens. Can J Anim Sci 71:549–556
20. Hocking PM, Waddington D, Walker MA, Gilbert AB (1989) Control of the development of the ovarian follicle hierarchy in broiler breeder pullets by food restriction during rearing. Br Poult Sci 30:161–174
21. Nir I, Nitsan Z, Dror Y, Shapira N (1978) Influence of over feeding on growth, obesity and intestinal tract in young chicken of light and heavy breeds. Br J Nutr 39:27–35

22. Boerjan M (2004) Genetic progress inspires changes in incubator technology. World Poult 5:16–17
23. Leach RM (1992) Leg weakness in broilers – complex situation involving many factors. Poult Dig 3:24–27
24. Oviedo-Rondon EO, Ferket PR, Havenstein GB (2006) Understanding long bone development in broilers and turkeys. Avian Poult Biol Rev 17(3):77–88
25. Nicholson D (1998) Research: is it the broiler industry's partner into the new millennium. World's Poult Sci J 54:271–278
26. Tomas FM, Pym RA, Johnson RJ (1991) Muscle protein turnover in chickens selected for increased growth rate, food consumption or efficiency of food utilization: effects of genotype and relationship to plasma IGF-I and growth hormone. Br Poult Sci 32:363–376
27. Skinner-Noble DO, Teeter RG (2003) Components of feed efficiency in broiler breeding stocks: energetics, performance, carcass composition, metabolism and body temperature. Poult Sci 82:1080–1090
28. Lewis P (2009) Proper lighting for broiler and turkey breeders. World Poult 25(12):18–21
29. Eitan Y, Soller M (1994) Selection for high and low threshold body weight at first egg in broiler strain females. 4. Photoperiodic drive in the selection lines and in commercial layers and broiler breeders. Poult Sci 73:769–780
30. Teeter RG (1994) Optimizing production of heat stressed broilers. Poult Dig 53:10–27
31. Yahav S (2010) Alleviating heat stress in domestic fowl: different strategies. Worlds Poult Sci J 65:719–732
32. Leeson S (2007) Metabolic challenges: past, present and future. J Appl Poult Res 16:121–125
33. Decuypere E, Buyse J, Buys N (2000) Ascites in broiler chickens: exogenous and endogenous structural and functional causal factors. Worlds Poult Sci J 56:367–377
34. Moghadam HK, NcMillan I, Chambers JR, Julian RJ, Tranchant CC (2005) Heritability of sudden death syndrome and its associated correlations to ascites and body weight in broilers. Br Poult Sci 46:54–57
35. Olkowski AA, Classen HL (1997) Malignant ventricular dysrhythmia in broiler chickens dying of sudden death syndrome. Vet Rec 140:177–179
36. Eitan Y, Soller M (2009) Problems associated with broiler breeder entry into lay: a review and hypothesis. Worlds Poult Sci J 65:641–648
37. Cobb-Vantress (2005, 2008) Cobb 500 breeder management guide. Cobb-Vantress, Arkansas
38. Taylor G (1999) High yield breeds require special incubation. World Poul 15(3):27–29
39. Hill D (2000) Multistage incubation and yield genetics. Poult Dig 10–11:14–20
40. Boerjan M (2004) Single stage incubation is the most natural choice. World Poult 20(7):18–20
41. Tona K, Bamelis F, Coucke W, Bruggeman V, Decuypere E (2001) Relation between Broiler Breeder's age and egg weight loss and embryonic mortality during incubation in large-scale conditions. J App Poult Res 10:221–227
42. Meijerhof R (2002) Incubation by embryo temperature. World Poult 18(6):36–37
43. Oviedo-Rondon EO, Wineland MJ, Funderburk S, Small J, Cutchin H, Mann M (2009) Incubation conditions affect leg health in large high yield broilers. J Appl Poult Res 18:640–646
44. Oviedo-Rondon EO, Wineland MJ, Small J, Cutchin H, McElroy A, Barry A, Martin S (2009) Effect of incubation temperatures and chick transportation conditions on bone development and leg health. J Appl Poult Res 18: 671–678
45. Bessei W (2006) Welfare of broilers: a review. Worlds Poult Sci J 62:455–466
46. Katanbaf MN, Hardiman JW (2010) Primary broiler breeding – striking a balance between economic and well-being traits. Poult Sci 89:822–824
47. Eitan Y, Soller M (2004) Selection induced genetic variation: a new model to explain direct and indirect effects of sixty years of commercial selection for juvenile growth rate in broiler chickens. In: Wasser SP (ed) Evolutionary theory and processes: modern horizons. Papers in honor of Eviatar Nevo. Kluwer, Dordrecht, pp 153–176
48. Deeb N, Lamont SJ (2002) Genetic architecture of growth and body composition in unique chicken populations. J Hered 93:107–118
49. Carlborg O, Jacobsson L, Ahgren P, Siegel P, Andersson L (2006) Epistasis and the release of genetic variation during long-term selection. Nat Genet 38:418–420
50. Flock DK, Laughlin KE, Bentley J (2005) Minimizing losses in poultry breeding and production: how breeding companies contribute to poultry welfare. Worlds Poult Sci J 61:227–237
51. Nicol CJ, Scott GB (1990) Pre-slaughter handling and transport of broiler chickens. Appl Anim Behav Sci 28:57–73
52. Grandin T, Johnson C (2009) Animals make us human - Creating the best life for animals. Houghton Mifflin Harcourt, Boston/New York
53. Grandin T, Deesing M (2008) Humane livestock handling: understanding livestock behavior and building facilities for healthier animals. Storey Publ., North Adams
54. Shane S (2009) Broiler welfare symposium – The balance between producers' and consumers' standards. World Poult 25(12):32–34
55. Blokhuis HJ (2004) Recent developments in European and international welfare regulations. Worlds Poult Sci J 60:469–477
56. Gross WB, Siegel PB (1997) Why some get sick. J Appl Poult Res 6:453–460
57. Siegel PB, Honaker CF (2009) Impact of genetic selection for growth and immunity on resource allocations. J Appl Poult Res 18:125–130
58. Rauw WM, Knap PW, Varona L, Gomez-Raya L, Noguera J (2002) Does selection for high production affect protein turnover rate? Communication No. 10-03, 7th world congress on genetics applications to livestock production, Montpellier, France

Books and Reviews

Falconer DS, Mackay TFC (1996) Introduction to Quantitative Genetics, 4th edn. Longman Group Ltd., Harlow

Weller JI (2009) Quantitative Trait Loci Analysis in Animals, 2nd edn. CAB International, Wallingford

Proton Exchange Membrane Fuel Cells: High-Temperature, Low-Humidity Operation

Steven J. Hamrock[1], Andrew M. Herring[2]
[1]Fuel Cell Components Program, 3M Company, St Paul, MN, USA
[2]Department of Chemical Engineering, Colorado School of Mines, Golden, CO, USA

Article Outline

Glossary
Definition of the Subject
Introduction
Proton Exchange Membrane Fuel Cells
Electrolyte Membranes
PFSAs
Non-fluorinated or Hydrocarbon PEMs
Mechanical Stabilization of Low EW Membranes
Stabilizing Low EW Membranes Through Chemical Modification of the Ionomer
Conductivity Enhancing/Stabilizing Inorganic Additives
Electrodes
Future Directions
Acknowledgments
Bibliography

Glossary

3 Phase boundary Region in the electrode where protons from the ionomer, electrons from the electrically conducting Pt and/or carbon, and reactant gases meet.

Electrolyte membrane A solid polymer ion-conducting membrane used in the center of the fuel cell membrane electrode assembly.

Fuel cell electrocatalyst A catalyst that catalyzes either the oxidation of the fuel or the reduction of oxygen in a fuel cell.

Equivalent weight A measure of the acid content of an ionomer in the units of grams of polymer per mole of acid.

Gas diffusion layer A carbon paper or cloth used as a current collector in fuel cells that can allow the passage of reactant gases and product water to and from the electrodes.

Hydrogen oxidation reaction (HOR) Electrochemical oxidation of H_2 at the anode.

Ionomer A copolymer of an ion-containing monomer and a nonionic monomer, typically not soluble in water.

Membrane electrode assembly (MEA) An ion-conducting membrane sandwiched between two electrodes, an anode at which fuel oxidation occurs and a cathode at which oxygen reduction occurs.

Oxygen reduction reaction (ORR) Electrochemical reduction of O_2 at the cathode.

Flooding Liquid water collecting within the electrodes or current collectors, impeding the flow of gases to the catalyst surface.

Perfluorinated sulfonic acid containing polymer (PFSA) A fluorinated sulfonic acid containing ionomer. The most commonly used polymer in proton exchange fuel cell membranes today.

Definition of the Subject

Proton exchange membrane fuel cells (PEMFCs) together with hydrogen represent an important storage and utilization technology for energy generated from renewable sources such as wind, solar, geothermal, or hydroelectric. This is due in part to their high energy density, low operating temperature, rapid start-up, modular design, flexibility of scale (a few watts to hundreds of kilowatts), and the absence of any point-of-use emissions. One barrier to commercialization and widespread acceptance of this technology is cost, a situation fairly common with the introduction of a new technology. Over the past decade much work has been done, and very significant progress has been made, in bringing down the manufacturing cost of fuel cell systems [1]. Manufacturing processes have been optimized, volumes manufactured have increased, less expensive materials have been demonstrated, system efficiencies and power outputs have been increased, and the amount of precious metal catalyst required to

generate a kilowatt of power has been reduced dramatically. All of these features have contributed to significant cost reductions. In the case of the precious metal catalysts, one of the major costs, a fuel cell stack that can generate enough power for an automobile can now be built using less than 30 g of platinum catalyst (about 3–4 times as much precious metal as is used in vehicles today), and the auto industry target of 10 g per vehicle appears within reach [2, 3].

There is still work to be done. One area where important improvements are currently being made is in developing materials and constructions that address the need of today's PEMFC systems for high levels of humidification during operation. Materials currently used in PEMFCs require water for optimum performance. The electrolyte membranes require a relatively high level of hydration to provide sufficient conductivity for high performance. The electrodes in use also require water, both to provide ionic conductivity within the electrode and between the electrode and the electrolyte, as well as to maintain high electrocatalytic activity for high efficiency.

This thirst for water within the fuel cell requires strict water management, imposing limitations on the system design and adversely affecting manufacturing cost. Reactant gases entering the cell often must be humidified, adding the expense of humidification equipment and the parasitic power loss from its operation. In addition, cell temperature must be carefully controlled, as overheating can cause the cells to dry out, and so larger cooling systems or radiators are required. This must be balanced with the fact that excess cooling or over humidification can cause water vapor formed in the electrochemical reaction to liquefy and collect within the electrodes or current collectors, impeding the flow of gases to the electrodes, a phenomenon called flooding. These requirements of careful control of humidification and temperature in fuel cells are not consistent with the need for a robust, inexpensive power source. New materials, including new membrane materials and catalysts that are less dependent on water, are needed to address this limitation.

Introduction

For the last few years, there has been a growing, worldwide public focus on the increasing use of energy. One cannot pick up a newspaper or watch a television news program without being exposed to stories about the growth in the need for energy, and the economic and environmental cost of that growth. Concerns about energy cost, energy security, and environmental factors (notably climate change) are driving many toward a shift to cleaner, cheaper, and more sustainable methods of generating and using energy. Much of this discussion has centered on the generation of energy, through the more efficient use of fossil fuels, nuclear energy generation, or renewables such as solar and wind energy. There is also growing recognition that if a movement to more sustainable methods of generating energy is to be made, a change in the way of transporting and storing energy will also be required.

An important area of energy technology that has received attention is the area of energy storage. Advanced batteries, capacitors, pumped hydroelectric, compressed air, flywheels, and other methods of energy storage are being considered [4]. As stated above, many believe that proton exchange membrane fuel cells (PEMFCs) together with hydrogen represent an important energy storage and utilization technology for a number of application areas to allow the transition away from fossil fuels. For this reason, significant research and investment in this technology have taken place over the last two decades. PEMFCs are beginning to find use in certain emerging applications, such as backup and primary power supplies for telecommunications, powering material handling fork-trucks and providing electricity in remote, off-grid locations. While these represent relatively low volumes of systems in the greater energy market, they are an enabling first step, which is important for the introduction of fuel cells into a marketplace where they must compete with established technologies.

Another application of PEMFCs that has received much media attention and many research dollars over the past few years is transportation. While fuel cell–powered vehicles are still limited to a few hundred prototypes, they are seen by many as the "end game" for renewable-energy-powered vehicles [3]. Hydrogen fuel cells for powering automobiles are attractive for several reasons. Their high energy density can provide driving ranges of 250 miles or more, and compressed hydrogen tanks can be refilled easily in less than 5 min. This allows automakers to provide vehicles with

essentially the same functionality as drivers enjoy today. However, the strict limitation on weight and volume in automotive applications, as well as the variation in power requirements during use, mean that these systems must run efficiently and reliably under a wide range of temperatures and humidification levels. The current limitations on temperature and humidification require excessively large cooling systems, or radiators, and humidifiers, which make meeting cost and efficiency targets more difficult.

In addition to the utility of hydrogen for storing energy from renewables such as wind or solar, the conversion of hydrocarbon feedstocks such as renewably derived methane or biomass into hydrogen can be an energy-efficient way of utilizing these resources. Currently, the least expensive route to hydrogen is from the reforming of natural gas, a process that initially produces a mixture of hydrogen gas, water, and carbon dioxide with a high carbon monoxide (CO) content. At the current relatively low temperature of operation of the PEM fuel cell, 80°C, CO is a severe poison to the Pt catalyst on the fuel cell anode. It is, therefore, necessary to reduce the CO content of the hydrogen fuel to a few parts per million by use of water gas shift reactors and a final gas clean up stage that may be a hydrogen selective membrane, pressure swing adsorption, or a preferential oxidation reactor. Each of these additional unit operations adds expense to the hydrogen production process. If hydrogen from the reforming of biomass is to be cost competitive, then the tolerance for CO on the catalyst must be improved so that less expensive less pure hydrogen can be utilized. One method of doing this is to operate the fuel cell at elevated temperature, e.g., a phosphoric acid fuel cell operating at >180°C can tolerate a reformed hydrogen fuel containing 2% of CO. The operation of PEM fuel cells at elevated temperatures would, therefore, enable the utilization of biomass-derived hydrogen at a price competitive fuel cost.

For the rate of commercialization of PEMFCs to continue to increase, system costs must continue to decrease. One way to do this is to eliminate the fuel cell temperature and humidification requirements described above, allowing operation over a wide range of temperatures without the need for humidification of the incoming gases. To do this, new materials are needed. These include new ion-conducting materials for membranes and electrodes and new catalysts that can function with less water. This entry will review how these materials function in a PEMFC and some of the approaches to new materials that may overcome the humidification and temperature barriers.

Proton Exchange Membrane Fuel Cells

A fuel cell is an electrochemical cell that oxidizes a fuel to provide electrical energy. It is similar to an engine in that you provide fuel and air to generate energy, and it is similar to a battery in that it is an electrochemical cell that produces electricity. A variety of fuels can be used depending on the type of fuel cell. High temperature fuel cells, such as solid oxide fuel cells, can use a wider assortment of fuels because the electrocatalysts are more efficient and less prone to poisoning at these higher temperatures, up to 1,000°C. These fuels include hydrogen, alcohols, and hydrocarbons. Fuel cells that operate at lower temperatures are typically restricted to using fuels that are more easily oxidized, such as hydrogen or methanol. PEMFCs fall into this class. PEMFCs use a polymeric ion exchange membrane as an electrolyte and operate at lower temperatures, typically up to about 80°C.

A schematic of the cross section of a single cell, often called a *membrane electrode assembly* (MEA), is shown in Fig. 1. The electrolyte membrane is at the center of two porous, catalyst-containing electrodes. The electrodes are typically formed from carbon-supported platinum particles. These carbon particles are held together by a small amount of an ion-conducting polymer, which act as both a binder and an ion conductor, allowing protons to move through the electrode. Newer types of electrode structures that allow for improved catalyst efficiency and durability are being introduced [5]. This three-layer construction is then positioned between two porous gas diffusion layers that act as current collectors. Hydrogen is supplied to the negative electrode, or anode, and oxygen, usually in the form of air, is supplied to the positive electrode, or cathode. The product water is formed at the cathode.

A PEMFC system typically comprises a fuel cell stack where MEAs are stacked between electrical conductive bipolar plates that have flow fields embedded in them, allowing the reactive gases to be supplied to the catalyst surface and allowing the reactant water to be

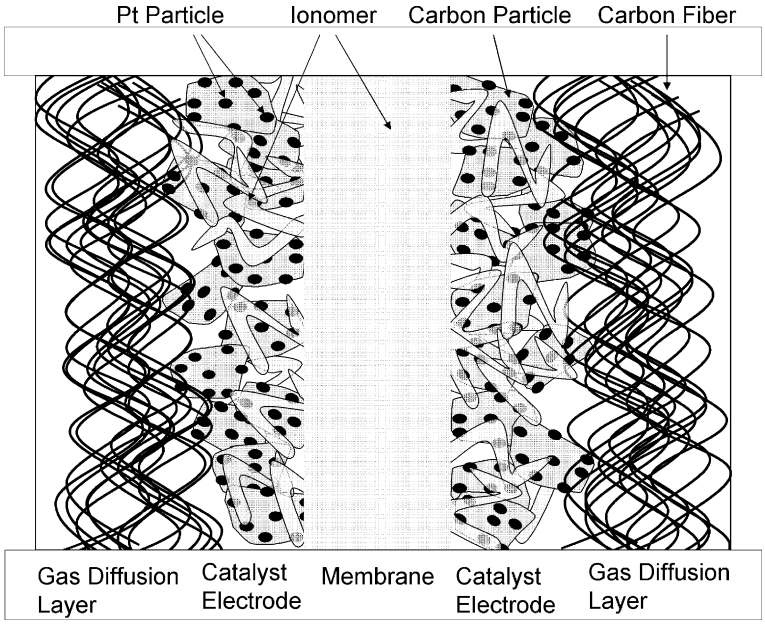

Proton Exchange Membrane Fuel Cells: High-Temperature, Low-Humidity Operation. Figure 1
A schematic representation of the cross section of an MEA

carried away. The area of the MEA determines the amount of current that can be passed through a cell and the number of cells in the stack determines the voltage. Together, these define the power the stack is capable of providing.

To allow PEM fuel cells to operate under the hotter, drier conditions required for widespread use in applications such as automobiles, new materials are needed. These include new electrolytes with higher proton conductivity and improved durability at low relative humidity (RH) and at higher temperatures. New electrodes that can provide adequate performance with less water are needed.

Electrolyte Membranes

The electrolyte in a PEMFC, as the name implies, is a proton exchange membrane, or PEM. It functions by allowing transport of protons from the negative to positive electrode, and as a physical barrier to prevent shorting of the electrodes and crossover of the reactant gases. The requirements for an electrolyte membrane in a PEMFC typically include the following:

- High proton conductivity
- Low permeability to reactant gases
- Good mechanical properties both dry and equilibrated with water
- Stability toward leaching of components by liquid water
- Excellent chemical stability (Hydrolytic and oxidative)
- Reasonable cost
- The ability to form stable intimate interfaces with the electrodes

A variety of types of materials have been used in electrolyte membranes for PEM fuel cells. Most of these fall into two classes: basic polymers that have been imbibed with an acid and polymers with acidic groups attached.

In the first category, the most commonly used polymers for this are polybenzamidazole (PBI) or analogs imbibed with phosphoric acid [6]. This type of membrane was developed at Case Western Reserve University in the mid-1990s [7]. These membranes are known to have good conductivity at very high temperatures, up to 200°C, and membranes with high phosphoric acid contents, and increased conductivity combined with good mechanical properties have been prepared [8]. MEAs comprising such membranes are commercially available from the BASF company.

There are drawbacks to using PBI/Phosphoric acid-based membranes in many fuel cell applications. The highly water-soluble phosphoric acid can be easily leached out of the membrane by liquid water, preventing use in applications where the cell could experience higher humidifications or lower temperatures. The phosphoric acid also absorbs to the platinum catalyst surface, inhibiting the electrode kinetics, particularly on the oxygen electrode. To overcome this, high levels of expensive platinum catalysts are required for adequate fuel cell performance. It should be stressed that while PBI/Phosphoric acid-based membranes have drawbacks that prevent their widespread use, they are the only commercially available membranes that can be used in the temperature range between about 120°C and 200°C.

The majority of PEMs used today are from the second class of polymers, those with pendent acidic groups. Specifically, most polymers currently used in PEMs are typically members of a class of polymers called *ionomers*. An ionomer is a copolymer of a strong acid containing monomer and a nonionic, neutral monomer [9]. When the neutral monomer is relatively nonpolar, ionomers will adapt a phase-separated morphology, where the ionic groups can bind tightly together into ionic aggregates or clusters. These clusters have a significant impact on the physical properties of the ionomer, often behaving as physical cross-links and stiffening the polymer [10]. A few examples of ionomers of this type are commercially available, such as DuPont's Surlyn™, a copolymer of ethylene and a salt of methacrylic acid, which is used in several applications, including the coating on the outside of golf balls.

In order for the protonated form of an ionomer to be suitable for use in a fuel cell, it must be chemically and mechanically stable enough to survive the chemically aggressive, oxidizing environment of a fuel cell. Oxidizing species such as peroxides can be formed during operation, which attack and chemically degrade the membrane [11]. Simultaneously, the membrane is mechanically stressed from the fluxuations in water content resulting from variations in current density and temperature. These combined can cause the membrane to fail, leading to gases crossing over and catastrophic cell failure. For this reason, ionomers used in fuel cells today fall into two categories of polymers that have sufficient chemical stability and mechanical properties. These are perfluorinated sulfonic acid containing polymers (PFSAs) and aromatic-backbone polymers with pendent sulfonic acid groups.

PFSAs

Perfluorinated sulfonic acid containing polymers (PFSAs) are the most commonly used membrane materials in fuel cells today. Membranes made from these ionomers provide the benefits of highly acidic pendant acid groups for high proton conductivity, good mechanical properties, excellent chemical stability, and fairly low cost. The first PFSA used in PEMFCs was DuPont's Nafion™, originally developed in the 1960s for brine electrolysis to produce chlorine [12]. Since then, several other PFSA membranes have been developed and introduced for use in fuel cells [13]. All of these are copolymers of tetrafluoroethylene (TFE) and a sulfonic acid containing monomer. The chemical structures of some of these polymers are shown in Fig. 2.

When enough acid groups are present in the ionomer, the very hydrophilic sulfonic acid aggregates will absorb water. These hydrated acid groups can provide a continuous, acid-rich, hydrated pathway through the polymer. For PFSAs, in addition to the ionic regions, the TFE segments in the backbone provide another structural feature of the polymer. If the ratio of TFE units to acid containing monomers is high enough to provide TFE runs of sufficient length (about 4 or more TFE monomer units) these can crystallize, much like the highly crystalline polymer, polytetrafluoroethylene. These crystallites in the hydrophobic region of the polymer provide significant mechanical stabilization to the membrane. The amount of acid contained in the membrane is typically expressed as *equivalent weight* (EW), the number of grams of polymer required to provide one mole of acidic protons. For traditional PFSAs such as Nafion™, this value is in the range of 1,000–1,100. This gives a ratio of TFE to acidic monomers of about 5.5–6.5, enough to provide some stabilizing backbone crystallinity. Such polymers have a good combination of proton conductivity and mechanical properties when fully hydrated. Much work has been done over the years to provide a detailed understanding of the structure of PFSAs, and this is

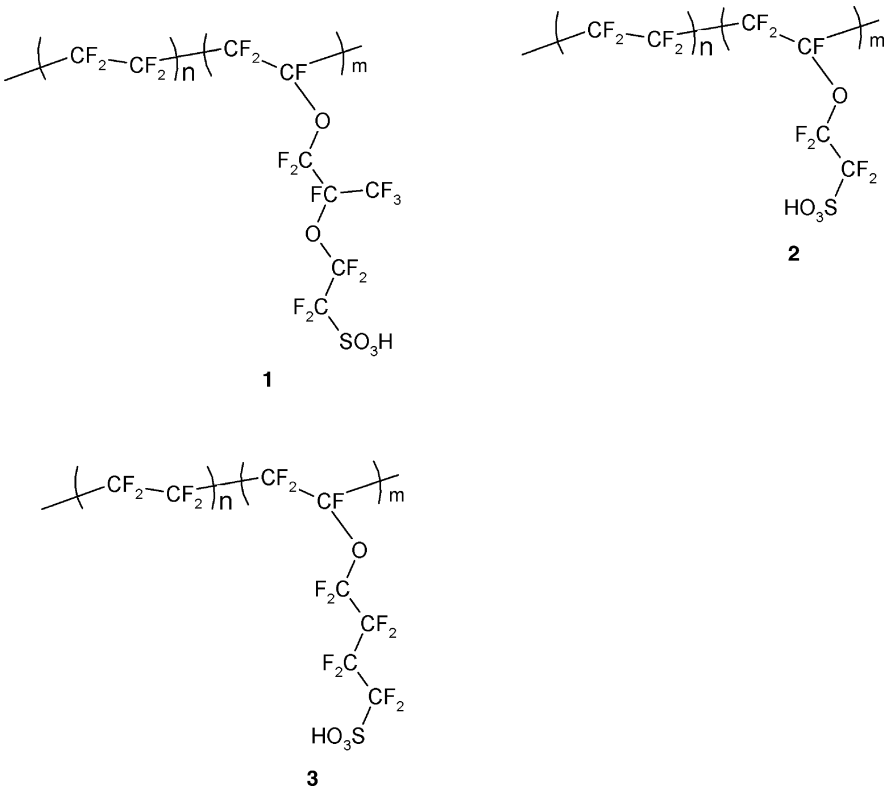

Proton Exchange Membrane Fuel Cells: High-Temperature, Low-Humidity Operation. Figure 2
Structures of some perfluorinated sulfonic acid containing polymers (PFSAs). Polymer 1 is available from DuPont (Nafion™), Asahi Glass (Flemion™), and others; Polymer 2 is the short-side-chain ionomer developed at Dow, currently available from Solvacore; and Polymer 3 is the ionomer available from 3M Company

still an active area of research. A comprehensive review on the subject has been written by Mauritz and Moore [14]. A generalized representation of a hydrated PFSA structure is shown in Fig. 3.

The amount of water present in the hydrated channels of the membrane is a function of the number of sulfonic acid groups present in the membrane and the humidity of the reactant gases [15]. In a typical PFSA membrane, at a given relative humidity the ratio of water molecules to sulfonic acid groups (referred to as lambda, λ) is fixed. At low %RH, there are a few tightly bound water molecules. As the %RH is increased, more water is absorbed and these additional water molecules are less tightly bound and more mobile. It is thought that the less tightly bound, more mobile water molecules that are farther from the sulfonic acid groups are more able to contribute to proton transport [16]. When the temperature is increased, or humidity levels in the reactant gases are decreased, the membrane will dry out and the conductivity drops. This represents an increase in the resistance of the cell and causes a loss in efficiency and performance.

One method of maintaining high conductivity with less water is to lower the EW, increasing the concentration of sulfonic acid groups in the membrane.

Figure 4 shows the conductivity as a function of relative humidity for several different EW membranes. Lower EW membranes do provide a significant increase although conductivity still drops off at lower relative humidity.

Another way to consider the impact of membrane conductivity on fuel cell performance is shown in Fig. 5. Figure 5a shows the conductivity of a few different EW membranes as a function of temperature with the atmosphere inside the conductivity cell held at a fixed dew point of 80°C [17]. When the conductivity cell is at 80°C, the %RH is 100%. As the temperature of the cell increases, the %RH at a fixed dew point

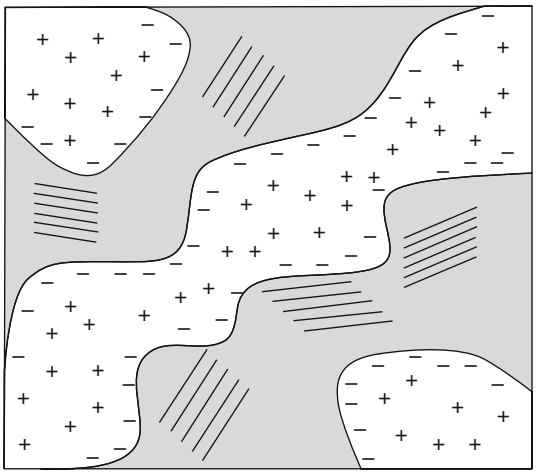

Proton Exchange Membrane Fuel Cells: High-Temperature, Low-Humidity Operation. Figure 3
A general representation of the morphology of a hydrated PFSA. The + represents the hydrated protons and the − represents the sulfonate groups at the edges of the hydrated region. These hydrated regions are thought to have the dimensions of 2–3 nm. The parallel lines represent the crystallites formed from the tetrafluoroethylene (TFE) groups of the backbone

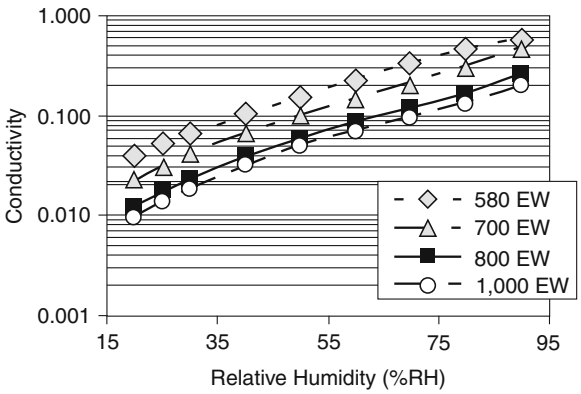

Proton Exchange Membrane Fuel Cells: High-Temperature, Low-Humidity Operation. Figure 4
Conductivity vs. relative humidity for several different 3M Ionomers (Polymer 3) measured by AC impedance spectroscopy at 80°C

decreases, causing a decrease in the membrane conductivity. This is similar to the situation in some PEMFC applications where the cell temperature may rise while the humidity level of the incoming gases remains constant. The graph in Fig. 5b uses the same data. Here the conductivity is used to calculate the resistance of a 25 μm membrane, and using Ohms law, that resistance is used to calculate the voltage loss (ohmic loss) one would see in a fuel cell at a 0.6 A/cm^2 current density [17]. This represents the fuel cell performance loss due to the loss of membrane conductivity (certainly not the only performance loss under these conditions!).

At 80°C, 100% RH, the performance loss is low, about 10 mV. Further, the performance difference between the different EW membranes is also quite low, less than 4 mV. As the temperature increases, the performance losses also increase and the effect of the different EW ionomers becomes apparent. At 120°C, the 1,000 EW membrane has a large ohmic loss of about 180 mV. This represents a $\geq$ 20% loss in the operating voltage of a typical PEMFC at this current density, or about $\geq$ 15% of the energy contained in the hydrogen fuel being converted to heat. The lower EW membranes do provide a significant improvement, but even at the lowest EW shown here, 650, the ohmic loss is still 6 times that of the fully humidified cell.

Lowering the EW of the ionomer does seem to provide at least a partial solution to this problem. This suggests the possibility that even lower EW ionomers could allow performance equivalent to the fully hydrated membranes even under these dry conditions. In the case of typical PFSAs, this is not a practical approach. This is due in part to the lack of the backbone crystallites mentioned above. At an EW of below about 700, these polymers do not have enough TFE to provide sufficient backbone crystallinity. This renders the membrane effectively water soluble, and thus not useful in most PEMFC applications [18]. The solubility of the 3M ionomer as a function of EW is shown in Fig. 6.

PFSA ionomers with lower MW side chains should allow additional crystallinity at a given EW. The Polymer 2, shown in Fig. 2, has a side chain that is 100 MW units lower than the 3M ionomer, so it may allow a more stable membrane at somewhat lower EW.

Non-fluorinated or Hydrocarbon PEMs

A variety of non-fluorinated or partially fluorinated ionomers have been evaluated as alternatives to PFSAs for PEM fuel cells. These are typically sulfonated

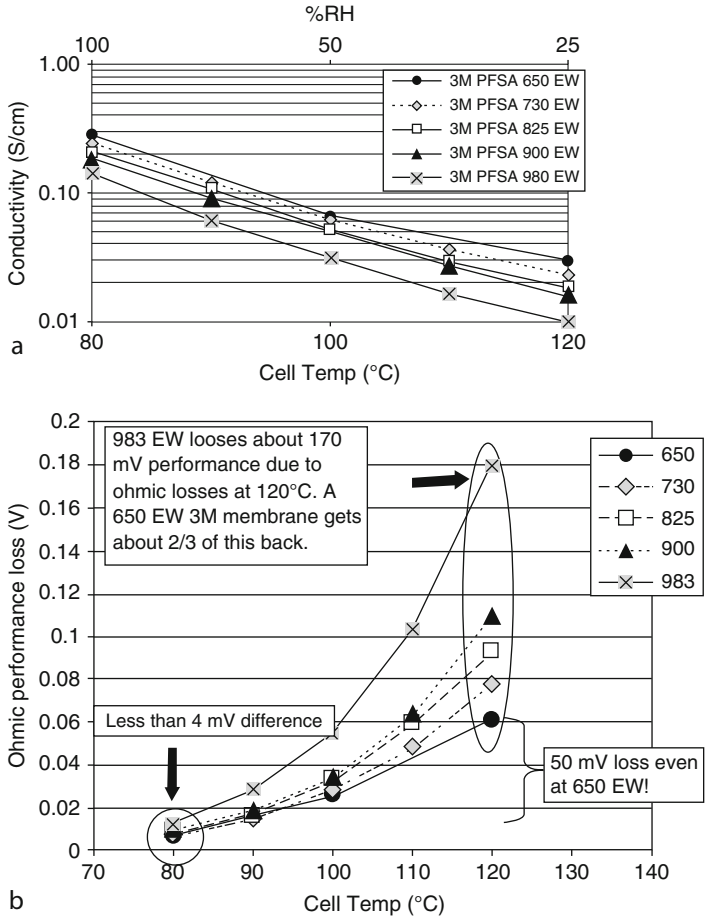

Proton Exchange Membrane Fuel Cells: High-Temperature, Low-Humidity Operation. Figure 5
(**a**) Conductivity of various equivalent weight (EW) 3M ionomer membranes (Polymer 3) as a function of temperature in an atmosphere with an 80°C dew point. (**b**) Calculated performance loss due to membrane ohmic losses at 0.6 A/cm2 for these membranes at 25 μm thickness

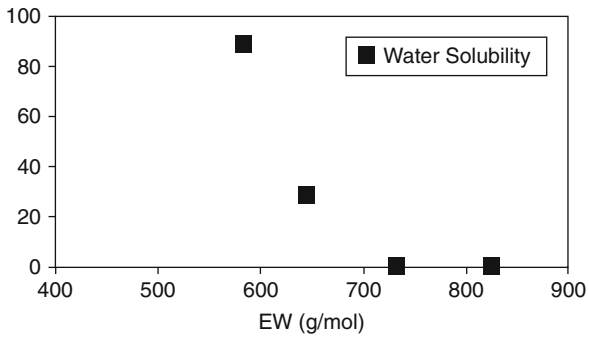

Proton Exchange Membrane Fuel Cells: High-Temperature, Low-Humidity Operation. Figure 6
Water solubility of 3M ionomers (Polymer 3) as a function of EW. The samples were boiled for 3 h

aromatic hydrocarbon polymers. Examples include sulfonated engineering thermoplastics such as polyimides [19], polyetherketones [20], and polysulfones [21] as well as polyphosphazines [22], or sulfonated polystyrene grafted to fluoroplastics such as polyvinylidene fluoride [23]. Some of the observed or proposed advantages of these membrane materials include lower cost, increased toughness or improved mechanical properties, and lower permeability to oxygen and fuels [24]. Permeation of oxygen through the membrane is thought to lead to formation of hydrogen peroxide on the hydrogen electrode, contributing to chemical degradation of the membrane [25]. One significant advantage of hydrocarbon-based ionomers

that PFSAs do not have, is their inherent synthetic versatility, allowing one to more easily design the polymer structure one needs for optimum conductivity, physical and mechanical properties, and chemical stability (of course, this assumes one knows what structure one needs).

Many examples of hydrocarbon ionomers have been prepared by exposing aromatic-backbone polymers to sulfonating agents, producing ionomers with sulfonic acid moieties attached to the most electron-rich positions on the aromatic rings. By controlling the degree of sulfonation, ionomers can be prepared by this method with suitable swelling characteristics and high proton conductivity at high relative humidity. It should be pointed out that due to the lower density of hydrocarbon-based polymers compared to fluoropolymers; a lower EW is needed in a hydrocarbon ionomer to provide an equivalent volumetric density of acid groups of a PFSA. Differences in the volumetric density of acid groups are more useful when comparing the conductivity of ionomers based on different classes of polymers [26]. Unfortunately, many studies have shown that randomly sulfonated hydrocarbon ionomers often suffer from lower conductivity at low relative humidity compared to PFSAs [20]. This is likely a consequence of a less favorable microstructure for proton transport as well as the lower acidity of the sulfonic acid groups bound to the aromatic ring (pKa = *ca.* −2 to −4) compared to the sulfonic acid groups of the PFSA (pKa = *ca.* −5.5) [20, 27].

Synthetic methods that allow attachment of sulfonic acid groups to more electron-deficient sites on aromatic rings can produce polymers where these groups are not only more acidic, but also more stable toward thermal desulfonation [28]. Kreuer and coworkers have prepared such polymers in sulfonated polysulfones with a variety of EWs [29]. The structure is shown as Polymer 4 in Fig. 7. These ionomers have high thermal stability, high conductivity at low levels of hydration, and surprisingly low water solubility. These sulfonated polysulfones are not water soluble at 100°C at EW values of down to 430. The improved conductivity at low hydration is likely due in part to the low electron density of the aromatic rings of the polysulfone, and also possibly due in part to a favorable microstructure for proton transport. To further increase conductivity under very dry conditions, some highly sulfonated hydrocarbon polymers have been show to have very high proton conductivity, even at low relative humidity. The Kreuer group has also prepared a completely sulphonated polysulfone, that is polysulfone with a sulfonic acid group on every aromatic ring (EW = 220). While this ionomer is water soluble, it has conductivity substantially higher than 1,100 EW Nafion™, even under dry conditions [30]. Litt and coworkers have prepared highly sulfonated polyphenylenes with one and two sulfonic acid groups per aromatic ring, shown as polymers 5 and 6 in Fig. 7 [31]. The latter has an EW of 118! Both of these ionomers are also water soluble and have very high proton conductivity at low %RH. These ionomers have been shown to hold more water at lower %RH than other sulfonic acid–based ionomers. This observation was explained by an increase in the "frozen-in

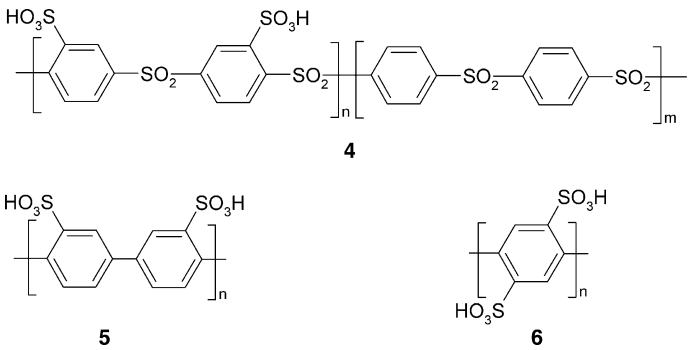

Proton Exchange Membrane Fuel Cells: High-Temperature, Low-Humidity Operation. Figure 7
Structures of some hydrocarbon ionomers. Polymer 4 is from reference 30 and Polymers 5 and 6 are from reference [32]

free volume" in these ionomers, that is that the rod-like morphology of the polymer hindered close packing. Removal of the last few waters of hydration in the voids between these rods would force them closer together into a higher energy state, effectively increasing the heat of vaporization of the bound water molecules.

The studies mentioned above show that through control of the electronic and structural features of hydrocarbon ionomers, increased conductivity can be achieved. However, this is often at the expense of the mechanical stability of the polymer to the point where these materials cannot be used in fuel cells. One potential method of stabilizing these materials is to incorporate them into a stable multiphase or segmented system. A variety of synthetic methods exist that allow generation of different branched or block copolymers and these have been applied to the synthesis of PEMs [32]. This allows control over the morphology of the phase-separated structures to create interconnected proton-conducting channels that may allow increased proton conductivity. McGrath and coworkers have prepared and evaluated sulfonated multiblock poly arylene ether sulfones with conductivity at low relative humidity equivalent to a Nafion™ membrane [33, 34]. The conductivity has been shown to be a function of the length and the chemistry of both the hydrophilic and the hydrophobic blocks.

Mechanical Stabilization of Low EW Membranes

One way of mechanically stabilizing low EW ionomer membranes is to generate a composite membrane using a porous film as an internal reinforcing structure [35, 36]. A PFSA membrane reinforced with a thin expanded polytetrafluoroethylene layer is available from W.L Gore. Reinforced membranes of this type have been shown to have increased strength and lower in-plane swelling upon hydration, lowering the potential of damage due to stresses generated during fuel cell operation. This should result in increased fuel cell durability [37]. Composite membranes have also been formed by using the porous phase as the conducting phase and filling the pores with a reinforcing phase. Pintauro and coworkers have made membranes using microfibers of sulfonated polyether sulfone filled with an inert filler to provide a membrane with good mechanical properties and proton conductivity when fully hydrated [38]. This group then used low EW PFSA fibers in this process, which gave a membrane with low swelling and very good conductivity at relatively low % RH (0.10 S/cm conductivity at 80°C and 50% RH, about 2–3 times higher than a 1,100 EW Nafion™ membrane) [39].

Mechanical stabilizing membranes in this way can allow significant stabilization of low EW ionomers. However, since many applications of PEM fuel cells require not only hotter and/or drier operation conditions but also require that the membrane to be insoluble in liquid water (often hot!) at times during operation, there is a limit to how low this method will allow one to go. In order to allow very low EW ionomers to be feasible, a change in the polymer chemistry will also probably be required.

Stabilizing Low EW Membranes Through Chemical Modification of the Ionomer

One possible method of chemically stabilizing low EW ionomers's toward excessive swelling and dissolution in water is to cross-link the ionomer. Some attempts are being made to cross-link low EW ionomers. [40, 41]. Generally, there are two "regions" in which ionomers can be cross-linked, in the hydrophilic, conducting region, near the acid groups and in the hydrophobic region, near the backbone. In the case of the former, one method that has been studied is forming a bis-sulphonyl imide from two of the pendent sulfonyl halide groups on the ionomer precursor [42]. Bis-sulphonyl imides are known to have highly acidic protogenic hydrogens and excellent chemical stability [43]. This method has the advantage that the cross-links formed have similar acidity to the acid groups consumed. A generalized representation of this method is shown in Fig. 8.

Methods in which the backbone of the polymer can be cross-linked include radiation grafting [44] and through the preparation of a cross-linkable terpolymer by including a reactive third monomer in the polymerization of the ionomer, followed by curing in film form [45–47].

Another approach to providing ionomers with lower EW and suitable mechanical and solubility properties is to have more than one acidic proton per side

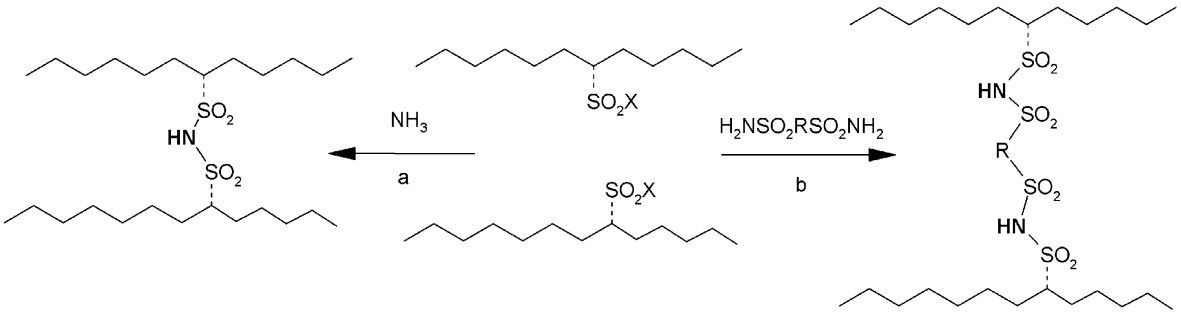

Proton Exchange Membrane Fuel Cells: High-Temperature, Low-Humidity Operation. Figure 8
General method of synthesizing bis-sulphonyl imide containing cross-links from polymers with pendent sulfonyl halide groups

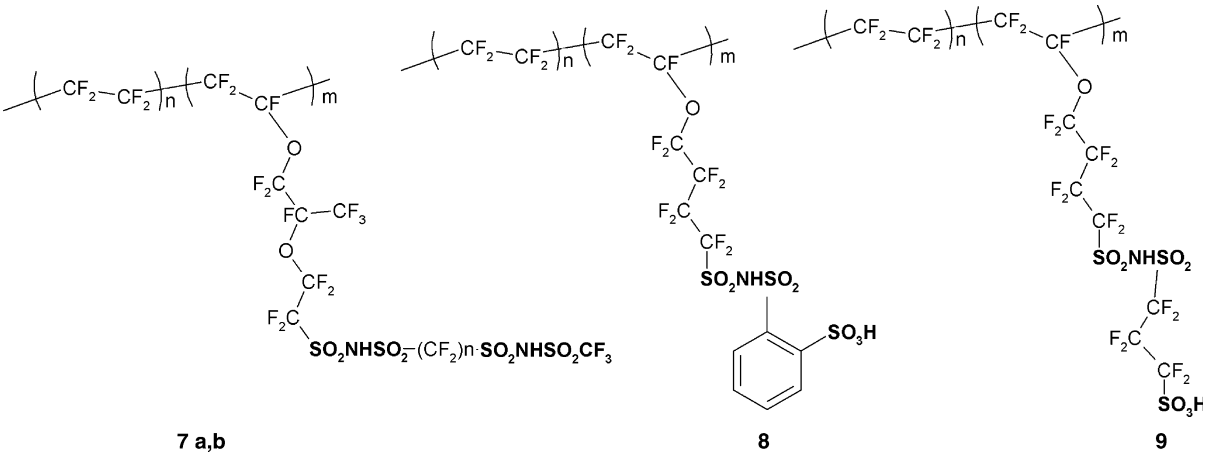

Proton Exchange Membrane Fuel Cells: High-Temperature, Low-Humidity Operation. Figure 9
The structure of 3 multi acid side-chain ionomers. Polymer 7a, n = 4, 7b n = 2 are from reference 49, Polymers 8 and 9 are from reference [50]

chain. If the side chain has additional protogenic groups, a low EW ionomer can be prepared having a higher degree of backbone crystallinity, and hopefully increased stability toward liquid water. One way to prepare such ionomers is to include a highly acidic bis-sulfonyl imide acid in the side chain. Such materials were prepared by Desmarteau (Polymers 7a,b) and more recently at 3M (Polymers 8 and 9) [48, 49, 51]. The structures of some of these materials are shown in Fig. 9.

The relationship between the number of TFE units that form the backbone crystallites and EW is shown in Fig. 10. The slope of each line gives the EW of the ionomer/the ratio of TFE units to protons in the polymer, and the intercept is the MW of the acid functional monomer/the number of protons. This shows the utility of having multiple protogenic groups on each side chain in providing polymers having high crystallinity and low EW.

In the case of Polymers 8 and 9, it has been demonstrated that low EW ionomers with higher conductivity, low swelling in boiling water, and good mechanical properties can be prepared [50].

Conductivity Enhancing/Stabilizing Inorganic Additives

Another approach to overcome the inherent deficiencies of ionomers under hot, dry operating conditions

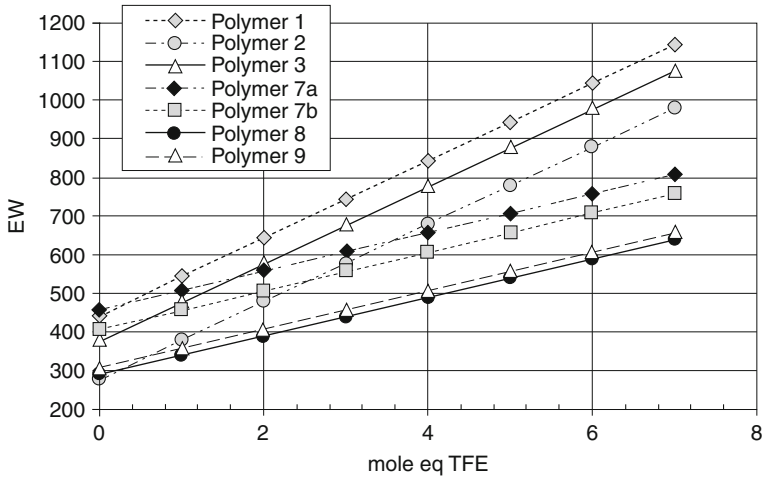

Proton Exchange Membrane Fuel Cells: High-Temperature, Low-Humidity Operation. Figure 10
Plot of EW vs. the number of TFE units in the backbone of selected ionomers

has been to investigate the use of inorganic additives to form composites membranes [51]. Three basic functionalities are invoked:

1. Additives that are hygroscopic and designed to retain additional water in the membrane so that no loss of performance is observed when the fuel cell is operated under conditions of reduced RH. If the fuel cell spends significant time under dry operations, these approaches inevitably fail.
2. Additives that have enhanced acidity and can facilitate proton transport and so enhance performance under drier conditions.
3. Additives that are designed to decompose peroxide in situ in the membrane to increase the membrane chemical durability.

A number of additives also have combined functionality.

Probably every common hygroscopic inorganic oxide has at some time been used to prepare a composite membrane for fuel cell use. The perceived benefit of an insoluble inorganic additive is from a surface interaction between the additive particle and the ionomer and so nano-sized individual particles or meso-porous materials into which the ionomer can penetrate have the larger benefit. Larger particles give no additional benefit and simply reduce the EW of the ionomer. The inorganic materials are either preformed before being mixed with the ionomer or are formed in situ, typically by a solgel process. Of the oxides that can be formed in situ, the most commonly used additive has been silica, but it is unstable to acid and so its suitability for fuel cell operation is questionable [52]. Titania and zirconia composites would appear to have more promise from a stability viewpoint [53], although they have mostly been found to enhance membrane mechanical properties, as ultimately the water in these additives will also be lost on sustained dry operation. Recently improved performance has been observed under drier operation by combining tin oxide with titania [54]. Clays both natural and synthetic have also been used, but again their benefit to fuel cell under RH cycling is also questionable.

More promising are approaches using either acid-functionalized particles [55] or super acidic inorganic materials that are designed to increase proton mobility. Of these, the two most promising are zirconium phophonates and the heteropoly acids (HPAs) [56–58]. The effect of these may simply that they are more hygroscopic, or that the phenomena is simply a proton concentration effect, essentially lowering the equivalent weight. However, as they also lower the activation energy for proton transport it seems that they also act as an effective proton transport promoter, perhaps more effective than the sulfonic acids.

Figure 11 shows proton conductivity data at 100°C for the 3M ionomer doped with various HPAs. Two observations are immediately apparent: (1) that the

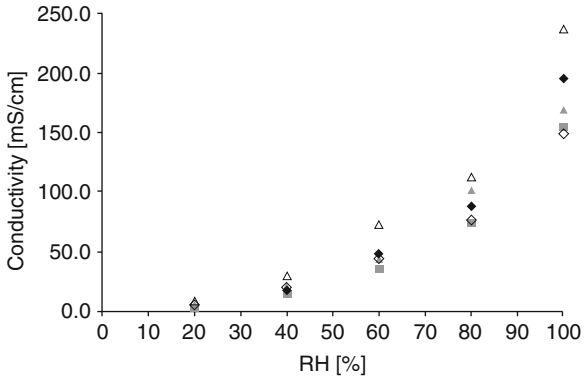

Proton Exchange Membrane Fuel Cells: High-Temperature, Low-Humidity Operation. Figure 11
Proton conductivity at 100°C for the 3M ionomer (■) and the 3M ionomer doped with (◊) 1% HPW, (♦) 5% HPW, (Δ) 1% HSiW, and (▲) 5% HSiW at 20–100% RH. From reference [59]

structure and amount of the additive have a strong influence and (2) that the effect becomes dramatically less as the RH is lowered. Similar results are shown for zirconium phosphonate composites with PFSA ionomer [59].

Hydrogen peroxide decomposition catalysts can be added to ionomer membranes in small amounts to slow down the decomposition of the ionomer during fuel cell operation. Additions of cerium and manganese, in both oxide and ionic forms, have been shown to increase the oxidative stability of membranes by orders of magnitude, and fuel cells prepared with such membranes have shown substantial increases in lifetime under aggressive hot and dry operation [60–62]. Unfortunately, these metal ions and oxides can consume ion exchange capacity and negatively impact fuel cell performance.

The ideal additive would enhance proton conductivity and stability. One demonstration of this was in a composite PFSA membrane using Pt nanoparticles supported on titania or silica [63]. The composite membranes when employed in MEAs demonstrated unhumidified fuel cell performance comparable to that of a similar humidified fuel cell. Whether adding Pt to the membrane will help durability or hurt it is still a matter of some debate [64, 65]. Unfortunately, it is not commercially feasible at this time to add additional Pt to the MEA and so this approach while novel is not practical. The HPAs are known peroxide decomposition catalysts and so these inorganic oxides have been demonstrated to improve performance and decompose peroxide in fuel cells and if they could be immobilized would present a practical solution to this problem [66].

Electrodes

As stated above, the membrane acts as the proton transporting medium, is an electrical insulator, and separates the reactant gases from direct chemical reaction. On either side of this membrane are placed two electrodes. The anode at which hydrogen is consumed in the hydrogen oxidation reaction (HOR) and the cathode in which oxygen from air is consumed in the oxygen reduction reaction (ORR). The two half-cell reactions and the overall reaction are shown below.

$$2H_2 \rightarrow 4H^+ + 4e^- \quad \text{HOR}$$

$$O_2 + 4H^+ + 4e^- \rightarrow 2H_2O \quad \text{ORR}$$

$$2H_2 + O_2 \rightarrow 2H_2O \quad \text{Overall reaction}$$

The electrons flow around an external circuit and do work, while the protons pass through the fuel cell membrane. This overall reaction represents the combustion of hydrogen that produces heat I, one reason why the membranes function to separate the two reactant gases is critical. Not only would a leak lead to fuel cell inefficiency, but also a hot spot would develop at the site of the leak, which would result in potential damage to the MEA. Unfortunately, the ORR is not 100% efficient and a $2e^-$, $2H^+$ reaction results in the formation of hydrogen peroxide as shown below:

$$O_2 + 2H^+ + 2e^- \rightarrow H_2O_2$$

This reaction is currently unavoidable and appears to be favored at hot and dry operating conditions of the fuel cell. The peroxide decomposition forms reactive radials such as hydroxyl, $^{\bullet}OH$, and peroxyl, $^{\bullet}OOH$, that cause oxidative degradation of both the fuel cell membrane and catalyst support [67]. Both electrodes currently use Pt or Pt alloys to catalyze both the HOR and ORR reactions. The catalyst particles are typically supported on a high surface area, heat-treated carbon to both increase the effectiveness of the catalyst and to provide a path for the electrons to pass through to the external circuit via the gas diffusion media (which is

typically also made of carbon) and the current collecting bipolar plates. In addition, the catalyst particles are coated in ionomer to facilitate proton transport; however, the electrode structure must also be porous to facilitate reactant gas transport. A schematic of a typical PEM MEA is shown in Fig. 1. A boundary condition exists at the catalyst particle where protons from the ionomer, electrons from the electrically conducting Pt and carbon, and reactant gases meet. This is usually referred to as the *three-phase boundary*. The transport of reactants, electrons, and protons must be carefully balanced in terms of the properties, volume, and distribution of each media in order to optimize operation of the fuel cell.

Typically, a good proton conductor is thought to be one where the proton conductivity is ≤ 0.1 S cm^{-1}, however, from the point of view of fuel cell operation it is the area-specific resistance (ASR) of the MEA that is more important. If one was to consider the MEA as a series of resistances an anode resistance would be observed, an interfacial resistance between the membrane and the anode, a membrane resistance, an interfacial resistance between the membrane and the cathode, and a cathode resistance. It is assumed here that the resistance of electrical connection between the anode and the current collectors is negligible compared to those described above, however, this too can be compromised if there is insufficient pressure between the bipolar plates and the gas diffusion media. All of these resistances must be optimized in order to lower the area-specific resistance of the fuel cell. The effect of the resistances, or ohmic losses on the overall performance and efficiency of the fuel cell is illustrated in Fig. 5. While a large amount of current work is concerned with optimizing membrane ionomers for hotter and drier operation, little thought has to date been put into optimizing the electrode ionomer, the ionomer catalyst interface, or the catalytic reactions at the anode or cathode for higher temperature, lower RH operation. If the ionomer in the membrane is not well matched and linked to that in the fuel cell electrodes, a large ASR can result. Of course part of the reason for this, until recently, has been the lack of suitable hot, dry ionomers for practical fuel cell testing.

As stated above, in a conventional, fully humidified fuel cell, part of the reactant gas stream is diluted by water vapor and the cathode suffers from formation of liquid water blocking the pores, or flooding, as the water is being produced in a water-saturated environment. To overcome this problem, hydrophobic fillers such as Teflon™ may be added to the electrode to facilitate water rejection [68]. These systems have been to a large extent already optimized, and great deal of art pertains to electrode fabrication [69]. One advantage of running a fuel cell hot and dry is that the electrode flooding issue is eliminated. In these fuel cells, there is still water produced on the cathode, but possibly not enough to saturate the PFSA polymer in the electrode layer, and potentially leaving the anode side of the fuel cell under humidified. However, as it is likely that polymers with low EW will be used for high temperature operation, back diffusion of water should be increased improving the chance that the anode will not be dried out. With less water in the fuel cell system, freeze issues on start-up in cold climates may also be partially mitigated.

Each of the electrode components is now considered in terms of hot and dry operation, what is known, and what needs to be accomplished to realize these systems.

It is generally thought that as temperature increases so do reaction kinetics. However, the situation in a fuel cell, an electrochemical device, is far more complicated. The reaction mechanism will depend on the surface environment of the catalyst particle and the potential at which the reaction is taking place. The electrode overpotential associated with the ORR represents the largest voltage loss in fully humidified fuel cells and so it is important that the situation not be exacerbated in running fuel cell under hot and dry conditions. In the kinetically controlled region of the fuel cell operation, the performance can be described by the Tafel equation:

$$E = E_{\text{rev}} + b\log i_0 - b\log i$$

$$b = -2.3\frac{\text{RT}}{\alpha nF}$$

where E, E_{rev}, b, i, i_0, n, and α are the electrode potential, reversible potential, Tafel slope, current density, exchange current density, the number of electrons transferred in the rate determining step, and the transfer coefficient, respectively [70, 71]. The first observation is that increasing the fuel cell temperature from 60 to 120°C, while maintaining a constant relative

humidity (RH), causes the theoretical opened circuit voltage (OCV) to decrease from 1.22 to 1.14 V due to the increase in water partial pressure [72] and so again it is desirable to operate the fuel cell at reduced RH. The Tafel slope, a measure of the potential loss of the electrode due to reaction kinetics, is the logarithmic decrease in current density with applied voltage. It is therefore desirable to have as small a Tafel slope as possible. The Tafel slope varies with current density as the surface of the platinum varies with voltage. At high voltage or low current density, the Pt is oxide coated (Temkin adsorption conditions) and the Tafel slope is 60 mV/decade; at lower voltage, higher current density the Pt is oxide free (Langmurian adsorption conditions) and the Tafel slope is 120 mV/decade. So above 100°C, the reaction mechanism may change if the surface coverage is compromised by the lack of water. Experimentally it has been shown for a water-saturated electrode that the Tafel slope increases with temperature at high voltage but is invariant at low voltage [73].

There are very few studies of the ORR under hot and dry fuel cell operating conditions. Recently, methods have been devised to separate the mass transport effects from the kinetic effects [74, 75], but none of these have been applied to hot and dry fuel cell operation. These studies showed that, under fully humidified conditions up to 70°C, oxygen reduction had a tenfold higher specific performance for platinum black at 0.90 V compared to Pt on carbon as has been previously reported in the literature [76]. However, this significant benefit of platinum black is shown to rapidly decrease when the potential is shifted to lower, more fuel cell relevant potentials. This is manifested in the Tafel slope, which decreased from ~360 to ~47 mV/decade in the region where the overpotential was <0.35 V. The effect of hot and dry conditions has been studied in a 5 cm^2 MEA where mass transport and kinetics are difficult to separate [73]. At 120°C, the Tafel slope is found to increase inversely with RH. It is speculated that this is due to the decrease in ionic conductivity in the electrode. RH can also influence water oxidation to form Pt-OH and Pt-O and thereby change the surface condition of the platinum crystals.

It has been shown that the current exchange density increases up to 70°C, but there is no data for this above 100°C, again there is a critical need to measure this under real fuel cell conditions. Much work is being undertaken in precious metal alloy catalysts where Pt is combined with one or more other metals and in non-precious metal catalysts [77]. These new catalytic materials are being studied in aqueous acid or in MEAs at 100% RH, very little data exists on how these materials will behave under hot and dry conditions. In fact the development of new catalyst for fuel cells run under hot and dry conditions may require there optimization outside of aqueous or water-saturated systems.

H_2 can be produced from fossil hydrocarbons such as natural gas or renewable biomass via reforming to produce syn gas (H_2 + carbon monoxide, CO), which can be converted to a H_2-rich gas via the water gas shift reaction. These processes, while commonplace in chemical engineering practice, do not produce pure H_2, the last 1,000 ppm or so of CO must be removed by expensive and/or inefficient unit operations such as partial oxidation, pressure swing adsorption, or membrane technology. The great advantage for the fuel cell electrodes in terms of high temperature operation is on the anode where the effected of adsorbed contaminants that slow the HOR are mitigated. This allows the anode to operate with H_2 contaminated with increasing levels of CO, a by-product of hydrocarbon reforming. At 80°C, CO levels as low as 10 ppm can cause significant degradations in performance but at 130°C, the fuel cell anode can tolerate 1,000 ppm of CO allowing the cost of H_2 produced from hydrocarbons to be dramatically reduced.

The optimum particle size for Pt in the catalyst layer is 3–5 nm [78]. Another issue is that the Pt both agglomerates and suffers from dissolution and re-precipitation. Both processes are expected to increase at higher temperature and result in higher particle sizes, lowering the rate of the ORR [79]. As described above, in a typical electrode the precious metal catalyst is supported on a carbon support that is susceptible to corrosion. It has been shown that the carbon corrodes rapidly if the electrode is held at relatively high potentials and that the reaction is first order with respect to water vapor. Carbon corrosion obviously increases with temperature and Pt loading, Fig. 12 [80]. Doping carbon with N is expected to increase the durability of the carbon.

Another solution to both the carbon support and the ionomer contact issue is to use a Pt catalyst that has no support and is embedded in the membrane such as

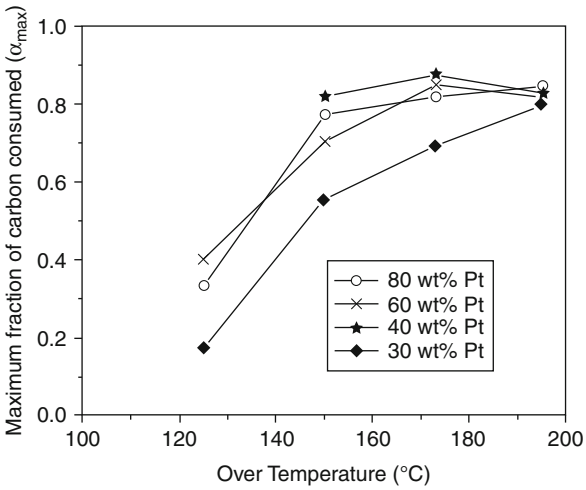

Proton Exchange Membrane Fuel Cells: High-Temperature, Low-Humidity Operation. Figure 12
Maximum fraction of carbon consumed as a function of temperature for samples with 30–80 wt.% Pt. From reference [81]

Proton Exchange Membrane Fuel Cells: High-Temperature, Low-Humidity Operation. Figure 13
Nano-structured thin film (NSTF) catalyst as fabricated and before transfer to a PEM. Plan view at 50,000× original. The scale bar indicates 600 nm. From reference [5]

the Nano-structured thin film (NSTF) catalyst being developed by 3M [5, 81]. A SEM of the NSTF-Pt catalyst is shown in Fig. 13. In addition to not having a carbon support to corrode, this catalyst system is much less susceptible to Pt dissolution because the small whiskers are coated with a continuous layer of Pt, not Pt nanoparticles, and so behaves more like bulk Pt.

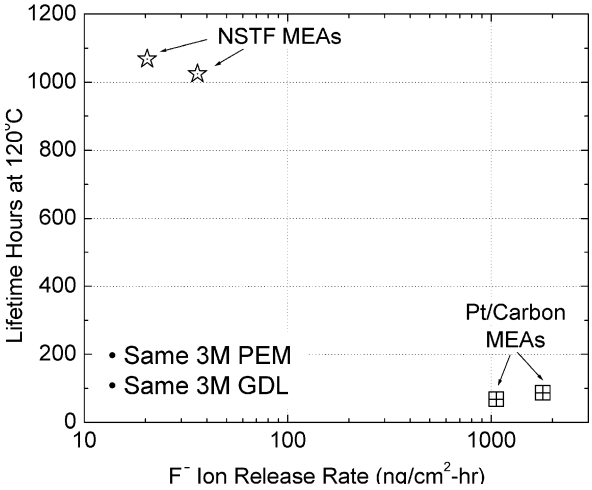

Proton Exchange Membrane Fuel Cells: High-Temperature, Low-Humidity Operation. Figure 14
Hours of lifetime at 120°C (before catastrophic failure of the PEM) versus fluoride ion release rates (by IC) for NSTF and Pt/C catalyst-based membrane electrode assemblies (MEAs) having the same type PEM and GDL. Cells of 100 cm2 were operated at 0.4 A/cm2, 120°C, 300 kPa, 61/84% inlet relative humidity (RH). Electrochemical surface area and crossover were measured daily at 75°C. Total lifetimes were ~1,800 h for the NSTF MEAs due to diagnostic testing at 75°C. End-of-life criteria were severe falloff of cell voltage and corresponding ramp-up of F-ion release indicative of membrane pinhole formation. From reference [5]

MEAs made with these electrodes also produce less F^- in the effluent water coming from the fuel cell under hot and dry operating conditions, as shown in Fig. 14. The fluoride content in the effluent water coming from the cell is a common diagnostic for the rate of membrane degradation. Materials known to decompose peroxide have also been added to PEM fuel cell catalyst layer such as MnO_2 [82], CeO_2 [83], and HPA [84], and all have shown a decrease in fluoride emission rates of the fuel cell under hot and dry conditions.

Nafion™ and other PFSA ionomers work very well in conventional PEMFC electrodes because they form a thin layer that allows both gas diffusion and proton transport. For this reason, they are still the ionomer of choice in fuel cell electrodes for hot and dry operation, although under these conditions, the PFSA used usually has a much lower EW to increase proton

conductivity at the drier conditions. While the approach of adding a lower EW PFSA ionomer works well for hot and dry operating conditions, the increased swelling and hydrophilicity at lower EW leads to serve flooding if the same fuel cell is operated under high RH. As new ionomers for hot and dry operation are developed, they must be capable of extending their proton connectivity into the electrode without a large interfacial loss due to material incompatibility at the boundary of the electrode and membrane. The consequence of a change in ion-conducting material is that proton transport to and from the catalyst layer may be compromised if conventional ionomers are employed. It is true that at the current time little work has been done to develop new, stable ionomers suitable for high temperature applications that will also allow high proton conductivity and high gas permeability in the fuel cell electrodes. One may consider using stable, lower EW version of the new ionomers, functionalizing the carbon support with suitable functional groups or developing new ionomers with higher gas permeability for use as binders in the electrode. It may be necessary to completely redesign fuel cell electrodes for high temperature, low relative humidity operation using materials that are stable to oxidation, enhance the ORR, proton conductivity, and gas permeability, while maintaining suitable electrical conductivity to maintain the three-phase boundary condition during operation.

Future Directions

This entry is by no means comprehensive. It is intended to show important examples of the approaches being taken to address the need for new materials to allow the robust operation of fuel cells under hotter and drier conditions than possible today.

At this point, there are no membranes or ionomers commercially available that will meet both the performance and durability requirements outlined above, although much progress has been made in the development of polymer membranes, which have improved conductivity and durability under these conditions. More radical approaches to the development of new fuel cell electrolytes including the development of ionomers with a variety of different protogenic groups are being explored [85, 86]. Using imidazole, ionic liquids and other replacements for water to allow completely dry operation is also being studied [87–89]. The next few years should see significant technical advances and the introduction of improved electrolyte membranes into the marketplace.

Optimization of the electrodes for these fuel cell systems has just started. Work has been done on the optimization of electrode structure for operation under hot, dry conditions, but less has been done to study catalysis under these conditions. Part of the reason for this is that as stated above there are no commercially available polymeric materials available for the development of new electrodes studies. It is hoped that until commercially available materials for this application become available that researchers offer to share their materials. This will, however, be insufficient as the ionomers developed for catalyst layers need different properties than ionomers developed to act as fuel cell membranes. The other major issue is that catalysts for fuel cells run under conditions of water saturation have been developed using liquid phase electrochemical methods. It will be extremely important that new catalyst for fuel cells to be operated under hot, dry conditions be developed by solid-state electrochemistry. New methods must also be developed so that electrodes containing compatible ionomers can be tested.

Acknowledgments

We gratefully acknowledge the support of numerous coworkers and collaborators. AMH would like to acknowledge support provided by the National Science Foundation MRSEC program under Grant No. DMR-0820518 at the Renewable Energy MRSEC.

Bibliography

1. Epping Martin K, Kopasz JP, McMurphy KW (2010) Status of fuel cells and the challenges facing fuel cell technology today. In: Herring AM, Zawodzinski TA Jr, Hamrock SJ (eds) Fuel cell chemistry and operation, ACS symposium series. American Chemical Society, Washington, DC, pp 1–13
2. Ohnsman A (2010) Toyota targets $50,000 price for first hydrogen car. Bloomberg Businessweek, 6 May 2010. http://www.businessweek.com/news/2010-05-06/toyota-targets-50-000-price-for-first-hydrogen-car-update2-.html
3. Kranz R (2010) Industry expects fuel cell on U.S. highways in 2015. Automotive News, p 20H
4. Chen H, Cong NC, Yang W, Tan C, Li Y, Ding Y (2009) Progress in electrical energy storage systems: a critical review. Prog Nat Sci 19:291–312

5. Debe MK, Schmoeckel AK, Vernstrom GD, Atanasoski R (2006) High voltage stability of nanostructured thin film catalysts for PEM fuel cells. J Power Sources 161:1002–1011
6. Wainwright JS, Litt MH, Savinell RF (2003) High temperature membranes. In: Vielstien W, Gasteiger HA, Lamm A (eds) Handbook of fuel cells: fundamentals, vol 3, Technology and applications. Wiley, West Sussex, pp 436–446
7. Savinell R, Yeager E, Tryk D, Landau U, Wainright J, Weng D, Lux K, Litt M, Rogers C (1994) A polymer electrolyte for operation at temperatures up to 200°C. J Electrochem Soc 141: L46–L48
8. Mader J, Xiao L, Schmidt TJ, Benicewicz BC (2008) Polybenzimidazole/acid complexes as high-temperature membranes. Adv Polym Sci 216:63–124
9. Pinery M, Eisenberg A (1987) Structure and properties in ionomers, vol 198, NATO Advanced Study Institute Series. D. Reidel, Dordrecht
10. Bazuin CG, Eisenberg A (1981) Ion-containing polymers: ionomers. J Chem Educ 58:938–943
11. Laconti AB, Hamdan M, McDonald RC (2003) Mechanisms of membrane degradation. In: Vielstien W, Gasteiger HA, Lamm A (eds) Handbook of fuel cells: fundamentals, vol 3, Technology and applications. Wiley, West Sussex, pp 647–662
12. Doyle M, Rajendran G (2003) Perfluorinated membranes. In: Vielstien W, Gasteiger HA, Lamm A (eds) Handbook of fuel cells: fundamentals, vol 3, Technology and applications. Wiley, West Sussex, pp 351–395
13. Hamrock SJ, Yandrasits MA (2006) Proton exchange membranes for fuel cell applications. Polym Rev 46:219–244
14. Maritz KA, Moore RB (2004) The state of understanding of nafion. Chem Rev 104:4535–4585
15. Mittelsteadt CK (2010) U.S. department of energy hydrogen program 2010 annual merit review proceedings http://www.hydrogen.energy.gov/pdfs/review10/fc036_mittelsteadt_2010_o_web.pdf
16. Paddison SJ, Paul R (2002) The nature of proton transport in fully hydrated nafion. Phys Chem Chem Phys 4:1158–1163
17. Emery M, Frey M, Guerra M, Haugen G, Hintzer K, Lochhaas KH, Pham P, Pierpont D, Schaberg M, Thaler A, Yandrasits M, Hamrock S (2007) The development of new membranes for proton exchange membrane fuel cells. ECS Trans 11:3–14
18. Yandrasits MA, Hamrock SJ (2010) Membranes for PEM fuel cells. In: Herring AM, Zawodzinski TA Jr, Hamrock SJ (eds) Fuel cell chemistry and operation, ACS symposium series. American Chemical Society, Washington, DC, pp 15–29
19. Faure S, Cornet N, Gebel G, Mercier R, Pineri M, Sillion B, (1997) Sulfonated polyimides as novel proton exchange membranes for H_2/O_2 fuel cells. In: Proceedings of the second international symposium on new materials for fuel cell and modern battery systems, Montreal, pp 818–825
20. Kreuer KD (1997, 2001) On the development of proton conducting materialspolymer membranes for technological applications. Solid State Ionicsi 97:1–15; Hydrogen and methanol fuel cells. J Membr Sci 185:29–39
21. Noshay LM, Robeson J (1976) Sulfonated polysulfone. J Appl Polym Sci 20:1855–1903
22. Guo Q, Pintauro PN, Tang H, O'Conner S (1999) Sulfonated and cross-linked polyphosphazine-based proton-exchange membranes. J Membr Sci 154:175–181
23. Buchi FN, Gupta B, Halim J, Haas O, Scherer GG (1994) A new class of partially fluorinated fuel cell membranes. Proc Electrochem Soc 23:220–235
24. Hickner MA, Ghassemi H, Kim YS, Einsla BR, McGrath JE (2004) Alternative polymer systems for proton exchange membranes (PEM's). Chem Rev 104:4587–4612
25. Sethuraman VA, Weidner JW, Haug AT, Protsailo LV (2008) Durability of perfluorosulfonic acid and hydrocarbon membranes: effect of humidity and temperature. J Electrochem Soc 155:B119–B124
26. Kim YS, Pivovar BS (2009) Comparing proton conductivity of polymer electrolytes by percent conducting volume. ECS Trans 25:1425–1431
27. King JF (1991) Acidity. In: Patai S, Rappoport Z (eds) The chemistry of sulphonic acids, esters and their derivatives. Wiley, New York, p 249
28. Iley J (1991) Rearrangements. In: Patai S, Rappoport Z (eds) The chemistry of sulphonic acids, esters and their derivatives. Wiley, New York, p 453
29. Schuster M, Kreuer KD, Andersen HT, Maier J (2007) Sulfonated poly(phenylene sulfone) polymers as hydrolytically and thermooxidatively stable proton conducting ionomers. Macromolecules 40:598–607
30. de Araujo CC, Kreuer KD, Schuster M, Portale G, Mendil-Jakani H, Gebel G, Maier J (2009) Poly(p-phenylene sulfone)s with high ion exchange capacity: ionomers with unique microstructural and transport features. Phys Chem Chem Phys 11:3305–3312
31. Litt M, Granados-Focil S, Kang J (2008) Rigid rod polyelectrolytes with frozen-in free volume: high conductivity at low RH. In: Herring AM, Zawodzinski TA Jr, Hamrock SJ (eds) Fuel cell chemistry and operation, ACS symposium series. American Chemical Society, Washington, DC, pp 49–63
32. Higashiharaa T, Matsumotoa K, Ueda M (2009) Sulfonated aromatic hydrocarbon polymers as proton exchange membranes for fuel cells. Polymer 50:5341–5357
33. Ghassemi H, McGrath JE, Zawodzinski TA (2006) Multiblock sulfonated–fluorinated poly(arylene ether)s for a proton exchange membrane fuel cell. Polymer 47:4132–4139
34. Roy A, Hickner MA, Yu X, Li Y, Glass TE, McGrath JE (2006) Influence of chemical composition and sequence length on the transport properties of proton exchange membranes. J Polym Sci B Polym Phys 44:2226–2239
35. Penner RM, Martin CR (1985) Ion transporting composite membranes. J Electrochem Soc 132:514–515
36. Cleghorn S, Kolde J, Liu W (2003) Catalyst coated composite membranes. In: Vielstien W, Gasteiger HA, Lamm A (eds) Handbook of fuel cells: fundamentals, vol 3, Technology and applications. Wiley, West Sussex, pp 566–575

37. Tang Y, Kusoglu A, Karlsson AM, Santare MH, Cleghorn S, Johnson WB (2008) Mechanical properties of a reinforced composite polymer electrolyte membrane and its simulated performance in PEM fuel cells. J Power Sources 175:817–825
38. Choi J, Lee KM, Wycisk R, Pintauro PN, Mather PT (2008) Nanofiber network ion-exchange membranes. Macromolecules 41:4569–4572
39. Pintauro P (2009) U.S. department of energy hydrogen program 2009 annual merit review proceedings. http://www.hydrogen.energy.gov/pdfs/review09/fc_09_pintauro.pdf
40. Kerres JA (2005) Blended and cross-linked ionomer membranes for application in membrane fuel cells. Fuel Cells 5:230–247
41. Yang Y, Holdcroft S (2005) Synthetic strategies for controlling the morphology of proton conducting polymer membranes. Fuel Cells 5:171–186
42. Mao SS, Hamrock SJ, Ylitalo DA (2000) US Patent 6,090,895 crosslinked ion conductive membranes
43. Koppel IA, Taft RW, Anvia F, Zhu SZ, Hu LQ, Sung KS, DesMarteau DD, Yagupolskii LM, Yagupolski YL, Ignat'ev V, Kondratenko NV, Volkonskii AY, Slasov VM, Notario R, Maria PC (1994) The gas-phase acidities of very strong neutral Bronsted acids. J Am Chem Soc 116:3047–3057
44. Gubler L, Gürsel SA, Scherer GG (2005) Radiation grafted membranes for polymer electrolyte fuel cells. Fuel Cells 5:317–335
45. Sauguet L, Ameduri B, Boutevin B (2006) Fluorinated, crosslinkable terpolymers based on vinylidene fluoride and bearing sulfonic acid side groups for fuel-cell membranes. J Polym Sci A Polym Chem 44:4566–4578
46. Yandrasits MA, Hamrock SJ, Grootaert WM, Guerra MA, Jing N (2006) US Patent 7,074,841 polymer electrolyte membranes crosslinked by nitrile trimerization
47. Yandrasits MA, Hamrock SJ, Hintzer K, Thaler A, Fukushi T, Jing N, Lochhaas KH (2007) US Patent 7,265,162 bromine, chlorine or iodine functional polymer electrolytes crosslinked by e-beam
48. Desmarteau DD (1995) Novel perfluorinated ionomers and ionenes. J Fluorine Chem 72:203–208
49. Hamrock SJ (2010) U.S. department of energy hydrogen program 2010 annual merit review proceedings. http://www.hydrogen.energy.gov/pdfs/review10/fc034hamrock_2010_o_web.pdf
50. Schaberg MS, Abulu J, Haugen GM, Emery M, O'Conner SJ, Xiong PN, Hamrock SJ (2010) New multi acid side-chain ionomers for proton exchange membrane fuel cells. ECS Trans 33:627–633
51. Herring AM (2006) Inorganic polymer composite membranes for proton exchange membrane fuel cells. Polym Rev 46: 245–296
52. Iler R (1979) The chemistry of silica. Wiley, New York
53. Mauritz KA, Hassan MK (2007) Nanophase separated perfluorinated ionomers as sol-gel polymerization templates for functional inorganic oxide nanoparticles. Polym Rev 47:543–565
54. Abbaraju RR, Dasgupta N, Virkar AV (2008) Composite nafion membranes containing nanosize TiO2/SnO2 for proton exchange membrane fuel cells. J Electrochem Soc 155: B1307–B1313
55. Kreuer K-D, Paddison SJ, Spohr E, Schuster M (2004) Transport in proton conductors for fuel-cell applications: simulations, elementary reactions, and phenomenology. Chem Rev 104:4637–4678
56. Alberti G, Casciola M (2003) Composite membranes for medium-temperature PEM fuel cells. Annu Rev Mater Res 33:129–154
57. Malhotra S, Datta R (1997) Membrane-supported nonvolatile acidic electrolytes allow higher temperature operation of proton-exchange membrane fuel cells. J Electrochem Soc 144: L23–L26
58. Meng F, Aieta NV, Dec SF, Horan JL, Williamson D, Frey MH, Pham P, Turner JA, Yandrasits MA, Hamrock SJ, Herring AM (2007) Structural and transport effects of doping perfluorosulfonic acid polymers with the heteropoly acids, $H_3PW_{12}O_{40}$ or $H_4SiW_{12}O_{40}$. Electrochim Acta 53:1372–1378
59. Alberti G, Casciola M, Capitani D, Donnadio A, Narducci R, Pica M, Sganappa M (2007) Novel Nafion-zirconium phosphate nanocomposite membranes with enhanced stability of proton conductivity at medium temperature and high relative humidity. Electrochim Acta 52:8125–8132
60. Coms FD, Han Liu H, Owejan JE (2008) Mitigation of perfluorosulfonic acid membrane chemical degradation using cerium and manganese ions. ECS Trans 16:1735–1747
61. Trogadas P, Parrondo J, Ramani V (2008) Degradation mitigation in polymer electrolyte membranes using cerium oxide as a regenerative free-radical scavenger. Electrochem Solid State Lett 11:B113–B116
62. Frey MH, Hamrock SJ, Haugen GM, Pham PT (2009) US Patent 7,572,534 fuel cell membrane electrode assembly
63. Watanabe M, Uchida H, Seki Y, Emori M, Stonehart P (1996) Self-humidifying polymer electrolyte membranes for fuel cells. J Electrochem Soc 143:3847–3852
64. Endoh E, Hommura S, Terazono S, Widjaja H, Anzai J (2007) Degradation mechanism of the PFSA membrane and influence of deposited Pt in the membrane. ECS Trans 11:1083–1091
65. Cipollini NE (2007) Chemical aspects of membrane degradation. ECS Trans 11:1071–1082
66. Haugen GM, Meng F, Aieta NV, Horan JL, Kuo M-C, Frey MH, Hamrock SJ, Herring AM (2007) The effect of heteropoly acids on stability of PFSA PEMs under fuel cell operation. Electrochem Solid State Lett 10:B51–B55
67. Liu H, Coms FD, Zhang J, Gasteiger HA, LaConti AB (2009) Chemical degradation: correlations between electrolyzer and fuel cell findings. In: Büchi FN, Inaba M, Schmidt TJ (eds) Chemical degradation: correlations between electrolyzer and fuel cell findings polymer electrolyte fuel cell durability. Springer, New York, pp 71–117
68. Friedmann R, Van Nguyen T (2010) Optimization of the microstructure of the cathode catalyst layer of a PEMFC for two-phase flow. J Electrochem Soc 157:B260–B265

69. Litster S, McLean G (2004) PEM fuel cell electrodes. J Power Sources 130:61–76
70. Shao Y, Yin G, Wang Z, Gao Y (2007) Proton exchange membrane fuel cell from low temperature to high temperature: material challenges. J Power Sources 167:235
71. Zhang J, Xie Z, Zhang J, Tang Y, Song C, Navessin T, Shi Z, Song D, Wang H, Wilkinson DP, Liu ZS, Holdcroft SJ (2006) High temperature PEM fuel cells. Power Sources 160:872
72. Xu H, Song Y, Kunz HR, Fenton JM (2005) Effect of elevated temperature and reduced relative humidity on ORR kinetics for PEM fuel cells. J Electrochem Soc 152: A1828–A1836
73. Parthasarathy A, Srinivasan S, Appleby AJ, Martin CR (1992) Temperature dependence of the electrode kinetics of oxygen reduction at the Platinum/Nafion® Interface: a microelectrode investigation. J Electrochem Soc 139:2530
74. Chen YX, Li MF, Liao LW, Xu J, Ye S (2009) A thermostatic cell with gas diffusion electrode for oxygen reduction reaction under fuel cell relevant conditions. Electrochem Commun 11:1434–1436
75. Kucernak AR, Toyoda E (2008) Studying the oxygen reduction and hydrogen oxidation reactions under realistic fuel cell conditions. Electrochem Commun 10:1728–1731
76. Gasteiger HA, Kocha SS, Sompalli B, Wagner FT (2005) Activity benchmarks and requirements for Pt, Pt-alloy, and non-Pt oxygen reduction catalysts for PEMFCs. Appl Catal B 56:9–35
77. Thompsett D (2003) Pt alloys as oxygen reduction catalysts. In: Vielstien W, Gasteiger HA, Lamm A (eds) Handbook of fuel cells: fundamentals, vol 3, Technology and applications. Wiley, West Sussex, pp 467–480
78. Tada T (2003) High dispersion catalysts including novel carbon supports. In: Vielstien W, Gasteiger HA, Lamm A (eds) Handbook of fuel cells: fundamentals, vol 3, Technology and applications. Wiley, West Sussex, pp 481–488
79. Shao Y, Yin G, Gao Y (2007) Understanding and approaches for the durability issues of Pt-based catalysts for PEM fuel cell. J Power Sources 171:558
80. Stevens DA, Dahn JR (2005) Thermal degradation of the support in carbon-supported platinum electrocatalysts for PEM fuel cells. Carbon 43:179–188
81. Debe MK, Schmoeckel AK, Hendricks SM, Vernstrom GD, Haugen GM Atanasoski RT (2006) Durability aspects of nanostructured thin film catalysts for pem fuel cells. ECS Trans 1:51–66
82. Trogadas P, Ramani V (2007) Pt/C/MnO_2 hybrid electrocatalysts for degradation mitigation in polymer electrolyte fuel cells. J Power Sources 174(1):159–163
83. Trogadas P, Parrondo J, Ramani V (2008) Degradation mitigation in polymer electrolyte membranes using cerium oxide as a regenerative free-radical scavenger. Electrochem Solid State Lett 11(7):B113–B116
84. Brooker RP, Baker P, Kunz HR, Bonville LJ, Parnas R (2009) Effects of silicotungstic acid addition to the electrodes of polymer electrolyte membrane fuel cells. J Electrochem Soc 156:B1317–B1321
85. Paddison SJ, Kreuer KD, Maier J (2006) About the choice of the protogenic group in polymer electrolyte membranes: Ab initio modelling of sulfonic acid, phosphonic acid, and imidazole functionalized alkanes. Phys Chem Chem Phys 8:4530–4542
86. Horan JL, Genupur A, Ren H, Sikora BJ, Kuo MC, Meng F, Dec SF, Haugen GM, Yandrasits MA, MA HSJ, Frey MH, Herring AH (2009) Copolymerization of divinylsilyl-11-silicotungstic acid with butyl acrylate and hexanediol diacrylate: synthesis of a highly proton-conductive membrane for fuel-cell applications. ChemSusChem 2:226–229
87. Doyle M, Choi SK, Proulx G (2000) High-temperature proton conducting membranes based on perfluorinated ionomer membrane-ionic liquid composites. J Electrochem Soc 147:34
88. Zhou Z, Li S, Zhang Y, Liu M, Li W (2005) Promotion of proton conduction in polymer electrolyte membranes by 1*H*-1,2,3-triazole. J Am Chem Soc 127:10824–10825
89. Jia L, Nguyen D, Halleý JW, Pham P, Lamanna W, Hamrock S (2009) Proton transport in HTFSI–TFSI–EMI mixtures: experiment and theory. J Electrochem Soc 156:B136–B151

Pulverized Coal-Fired Boilers and Pollution Control

David K. Moyeda
GE Energy, Irvine, CA, USA

Article Outline

Glossary
Definition of the Subject
Introduction
Air Pollutant Emissions from Coal Combustion
Particulate Matter Control Technologies
SO_2 Emissions Control Technologies
NO_x Emissions Control Technologies
Future Directions
Bibliography

Glossary

Anthracite Coal which typically contains 86–97% carbon. Anthracite is considered the highest rank of coal as it has the highest energy content of all coals.

Ash Inorganic residues remaining after combustion.

Baghouse See fabric filter.

Bituminous coal Coal which typically contains 45–86% carbon. Bituminous coal lies between subbituminous coal and anthracite in terms of rank, and

is commonly divided into additional subgroups dependent upon the content of volatile material.

Calorific value Corresponds to the amount of heat per unit mass when combusted. Can be expressed as gross calorific value, which is the amount of heat liberated during combustion under standardized conditions at constant volume so that all of the water in the products remains in liquid form, or as net calorific value, which is the maximum achievable heat release obtainable in a furnace at constant pressure.

Carbon dioxide (CO_2) A heavy, colorless gas that results from the combustion of fossil fuels and from natural sources.

Carbon monoxide (CO) A colorless, odorless gas produced by incomplete combustion of fossil fuels.

Coal A solid fossil fuel consisting primarily of carbon, hydrogen, nitrogen, oxygen, sulfur, and nitrogen. Coal also contains ash, minerals which do not burn, and moisture. Coal is typically classified or ranked by its volatile matter, fixed carbon content, and calorific value.

Dry FGD A process that removes sulfur oxides from the flue gas and results in the formation of a dry product or waste.

Electrostatic precipitator (ESP) A device for removing particulate from a gas stream based upon using an electric field to charge the particles in the gas and move them to a collecting surface.

Fabric filter A device for removing particulate from a gas stream based upon filtering the gas through a filer media.

Flue gas desulfurization (FGD) Technologies that are used to remove sulfur oxides from the flue gas.

Lignite Coal which contains 25–35% carbon and which has a lower calorific value than subbituminous and bituminous coals and typically higher moisture and volatile content. Lignite is the lowest range of coal.

Low-NO_X burners (LNB) Technology for reducing NO_X emissions by controlling fuel and air mixing in the flame.

Nitric oxide (NO) A colorless gas resulting from the combustion of fossil fuels.

Nitrogen dioxide (NO_2) A reddish-brown gas that can be emitted from the combustion of fossil fuels or is formed by atmospheric reaction of nitric oxide (NO) and oxygen (O_2).

NO_X Refers to the total nitric oxide (NO) and nitrogen dioxide NO_2 concentration.

Overfire air (OFA) Technology that reduces NO_X emissions based upon air staging.

Reburning Technology that reduces NO_X emissions based upon staging fuel in a fashion that permits fuel fragments to reduce (or reburn) nitric oxide (NO) in the flue gas.

Selective catalytic reduction (SCR) Technology that reduces NO_X emissions by mixing ammonia into the flue gas and reacting the ammonia with NO_X over a catalyst.

Selective noncatalytic reduction (SNCR) Technology that reduces NO_X emissions by mixing an amine-based reagent into the flue gas at a temperature which selectively promotes the reaction of amine (NH_2) with nitric oxide to form molecular nitrogen (N_2)

Subbituminous coal Coal which typically contains 35–45% carbon and which typically has a lower calorific value than bituminous coal and higher moisture and volatile content.

Sulfur dioxide (SO_2) A colorless, irritating gas resulting from the combustion of sulfur contained in fossil fuels, particularly coal.

Sulfur oxides Refers to sulfur dioxide (SO_2) and sulfur trioxide (SO_3).

Volatile matter Non-moisture component of coal that is liberated at high temperature in the absence of air.

Wet FGD A process that removes sulfur oxides from the flue gas and results in the formation of a product or waste that is a solution or slurry.

Definition of the Subject

Fossil fuels, such as coal, natural gas, and fuel oil, are used to generate electric power for industrial, commercial, and residential use. Due to its relatively low cost and abundance throughout the world, coal has historically played a significant role in energy production and approximately 41% of the world power generation was supplied by coal-fired power plants in 2008 [1]. While increased discoveries of natural gas and fuel oil resources, and growth in renewable energy sources, such as wind, solar, and geothermal energy is projected to reduce the use of coal for power generation, energy

from coal will continue to be used to satisfy the world's energy demands.

One drawback in the use of coal for power production is that it produces high levels of air pollutants, such as particulate, sulfur oxides, and nitrogen oxides. Coal also produces higher carbon dioxide emissions than other fossils such as natural gas and fuel oil. In addition, due to the large quantities of coal that are used for power production, emissions of toxic metals, such as mercury, which are contained in very small quantities in the coal, can also be a concern.

Over the past several decades, a number of technologies have been developed to reduce the air pollutant emissions formed from coal combustion. Modern power plants can be equipped with advanced technologies that reduce particulate, sulfur oxide, and nitrogen oxide emissions to the most stringent levels. These technologies are the focus of this entry.

Introduction

The abundance of coal throughout the world led to its use in China as early as 1000 B.C. and by the Romans in Britain before 400 A.D. [2]. While the use of coal in Briton largely disappeared when the Romans left in the fifth century, coal use in England increased in the thirteenth century, and by the beginning of the seventeenth century, coal was the dominate source of energy [3]. During the industrial revolution of the eighteenth and nineteenth century, the invention and development of the steam engine led to an increase in coal production and use for industrial processes and transportation [4–6]. In the late nineteenth century, advances in electricity and the invention of a reliable incandescent lamp set the stage for the use of coal to generate electrical power with the first coal-fired central generating plant in the USA established in 1882 [7, 8]. The growing demand for electrical power led to further developments in steam-generating boiler technology, such as pulverizing the coal prior to introducing it to the boiler furnace. Pulverized coal firing enabled the construction of larger boilers and power plants and became the predominant firing method for large steam-generating power plants beginning in the late 1920s [9, 10].

The air pollution associated with coal combustion was recognized in England as early as the thirteenth century, where the burning of coal in urban areas created a smoky environment and led to bans on coal use [11]. While improvements in combustion methods and the use of chimneys or stacks to disperse the smoke overcame some of the objections to coal burning, fundamentally, the growing need for low-cost energy offset public concerns over the unhealthy aspects of coal combustion, and such bans were largely ignored [3]. As the world entered the twentieth century, widespread industrialization and the increased use of coal resulted in degraded air quality in London and other English cities [12]. By the middle of the century, severely degraded air quality in Los Angeles, California [13], and air quality disasters in London, England [14, 15], and Donora, Pennsylvania [16], heightened public awareness of the dangers of air pollution and government recognition of the need for research to understand the formation of and problems associated with air pollutants and for the development of regulations to limit their emissions [17].

For coal combustion, the primary air pollutants of concern are particulate matter (PM), sulfur dioxide (SO_2), and oxides of nitrogen (NO and NO_2, which are referred to as NO_X) [18]. These pollutants originate from the ash, sulfur, and nitrogen species present in the coal. Particulate matter reduces visibility and contributes to regional haze. In addition, "coarse" particles (from 2.5 to 10 μm in diameter, PM_{10}) and "fine" particles (smaller than 2.5 μm in diameter, $PM_{2.5}$) can accumulate within different areas of the respiratory system and aggravate health problems such as asthma or lead to increased respiratory symptoms and disease [19–21]. Exposure to sulfur and nitrogen oxides in sufficient concentration can lead to respiratory symptoms, particularly for those susceptible to these problems [22, 23]. In addition, sulfur and nitrogen oxide emissions can react with water in the atmosphere to form acids that deposit in lakes and soils leading to acidification [24–26], which is referred to as "acid rain." Nitrogen oxides also react with volatile organic compounds to form photochemical oxidants, such as ozone (O_3), which present a hazard to human health and plants in high concentrations and which cause visible "smog" in urban areas [27, 28].

This article will introduce how PM, $_{SO2}$, and NO_X emissions are formed during coal combustion and will discuss the technologies that have been developed to

control these emissions from pulverized coal-fired power plants. The technology discussion will focus on the primary technologies that have been applied and are available on a commercial scale.

Air Pollutant Emissions from Coal Combustion

The primary air pollutants regulated from coal-fired power plants worldwide are carbon monoxide (CO), sulfur dioxide (SO_2), oxides of nitrogen (NO and NO_2, which are referred to as NO_X), and particulate matter (PM) [29]. In general, CO emissions from pulverized coal-fired power boilers are low (<50–200 ppmv) as the combustion system tends to be operated with sufficient excess air to maximize combustion efficiency [30]. Local standards, rather than national standards, are generally established to limit CO emissions and can vary widely. SO_2 and NO_X emissions are regulated as both can be a health hazard in high concentrations [22, 23] and are contributors to dry and wet acid deposition [24–26]. In addition, NOx emissions contribute to ground-level ozone formation through the reaction with volatile organic compounds [27, 28]. Particulate emissions can lead to reduced visibility and degraded air quality. Small particulates emitted from combustion (<10 μm) or formed by reactions of SO_2 and NO_X in the environment (<2.5 μm) are associated with increased respiratory symptoms and disease [19–21].

In addition to these primary pollutants, since the early 1990s, there has been significant interest in the emissions of hazardous air pollutants (HAPs), such as toxic organic compounds, acid gases, and metals, from coal combustion. Based upon comprehensive studies performed to characterize HAPs from fossil fuel–fired power plants [31, 32], the US Environmental Protection Agency (EPA) identified mercury as the primary HAP of concern due to the contribution of coal-fired power plants to the total anthropogenic emissions of this compound and to the risk of exposure to methylmercury through the consumption of contaminated fish [33]. Methylmercury is a highly toxic neurotoxin that bioaccumulates up the food chain [34]. The concern over mercury emissions from coal combustion is shared in other developed areas of the world [35–37]. In addition to mercury, other HAPs of concern from coal-fired power plants due to their levels of emissions and potential health risks include carcinogenic metals, such as chromium, nickel, and arsenic, and acid gases, including hydrogen chloride (HCl) and hydrogen fluoride (HF), which are soft-tissue irritants and can cause respiratory disease [38].

A by-product of the combustion of fossil fuels is the generation of carbon dioxide (CO_2). In the atmosphere, CO_2 and other gases, such as water vapor, absorb and reemit infrared radiation reflected from the earth's surface, resulting in a "greenhouse" effect that raises surface temperature of the earth [39]. Since coal has a higher carbon-to-hydrogen ratio than other fossil fuels, such as natural gas and fuel oil, CO_2 emissions from coal combustion are higher than those from the combustion of other fossil fuels [40, 41]. The high carbon footprint of coal-fired power plants has led to an increased demand for the generation of power from alternative sources, such as cleaner fuels (e.g., natural gas) and renewable sources (e.g., biomass, wind, and solar), to the development of high-efficiency coal-fired power plants (e.g., integrated gasification combined cycle (IGCC)), and to the research and development of methods for carbon capture and sequestration from large coal-fired power plants [42, 43].

This article focuses on the primary pollutants from coal. The levels of SO_2, NO_X, and PM from coal-fired power plants vary widely and are determined by the coal type and combustion system design. Table 1 compares the major properties of several coals, low, medium, and high-sulfur bituminous coals; subbituminous coal; and lignitic coal. As can be seen in the table, the sulfur, nitrogen, and ash content contained in coals can vary significantly. Bituminous coals are characterized by a higher heating value in terms of energy release per mass of fuel consumed than lower rank subbituminous coal and lignite, which have higher moisture contents in comparison to bituminous coal. Bituminous coals also tend to have higher sulfur and nitrogen content in comparison to the low-rank coals. In the remainder of this entry, the impacts of coal ash, sulfur, and nitrogen content and boiler design and operation on emissions from coal-fired power plants will be discussed.

Particulate Emissions

Particulate emissions from pulverized coal combustion result primarily from the mineral matter included in

Pulverized Coal-Fired Boilers and Pollution Control. Table 1 Typical coal properties

Property	Units	Bituminous low sulfur	Bituminous medium sulfur	Bituminous high sulfur	Subbituminous	Lignite
Ultimate analysis						
Carbon	% dry	69.36	70.06	62.08	65.54	66.15
Hydrogen	% dry	5.32	5.00	4.44	4.15	4.20
Nitrogen	% dry	1.50	1.66	1.07	0.95	0.96
Sulfur	% dry	1.04	3.08	7.40	0.79	0.37
Oxygen	% dry	12.73	7.54	6.15	14.00	20.72
Ash	% dry	10.05	12.66	18.86	14.57	7.60
Proximate analysis						
Volatile matter	% a.r.	42.97	38.15	34.87	31.16	27.02
Fixed carbon	% a.r.	43.21	43.10	42.79	34.88	33.38
Ash	% a.r.	9.62	11.77	18.05	11.26	4.97
Moisture	% a.r.	4.20	6.98	4.29	22.70	34.63
Dry, ash-free basis						
Nitrogen	% d.a.f.	1.67	1.90	1.32	1.11	1.04
Sulfur		1.16	3.53	9.12	0.92	0.40
Volatile matter		49.86	46.95	44.90	47.18	44.74
Fixed carbon		50.14	53.05	55.10	52.82	55.26
Gross heating value						
	kJ/kg	27,244	27,386	25,663	20,002	16,866
	Btu/lb	11,713	11,774	11,033	8,599	7,251

a.r. as received
d.a.f. dry, ash-free

the coal. The mineral matter can be classified as being inherent (chemically bound into the coal matrix), included (present in the coal matrix), or extraneous (soil and rock mixed into the coal during mining) [44]. The composition of the mineral matter varies according to the geographic location, type of coal, and how much extraneous material is entrained into the coal during mining. The primary minerals in coal are quartz, aluminosilicates, iron sulfides, and carbonates [45]. These minerals can be broken down into the major ash constituents shown in Table 2 [46]. The primary constituents are silica and alumina oxides (SiO_2 and Al_2O_3). The iron (Fe) and alkali metal (calcium (Ca), magnesium (Mg), and sodium (Na)) content vary widely but are important as these metals have a major influence on the slagging and fouling characteristics of the resulting ash [47]. Slagging refers to the buildup of molten or partially fused ash on the furnace walls or radiant heat transfer surfaces of the boiler. Fouling refers to the deposit of ash on the convective heat transfer surfaces such as the superheater and reheater.

During combustion, the mineral matter in coal undergoes several transformations to become particulate matter that is entrained in the flue gas. The size and composition of the particulate matter depends upon the mineral composition, how it is included in the coal, the presence of other species, and the time-temperature history of the coal particles as they are being burned [48]. There are two primary mechanisms for ash

Pulverized Coal-Fired Boilers and Pollution Control. Table 2 Major constituents in ash for typical US coals

State coal type		Pennsylvania bituminous	Utah bituminous	Wyoming subbituminous	North Dakota lignite
Ash composition					
SiO_2	wt.%, S-free	45.3	60.0	43.3	22.0
Al_2O_3		24.2	22.7	17.2	20.4
Fe_2O_3		20.3	4.1	6.3	11.8
TiO_2		1.2	1.2	1.4	0.5
O_2O_5		0.6	1.5	2.5	0.1
CaO		4.8	4.6	22.7	30.3
MgO		1.1	1.9	4.0	8.0
Na_2O		1.4	1.1	1.7	5.1
K_2O		1.3	1.8	0.5	1.4

formation during combustion. First, ash may remain with the burning coal particle, melt at high temperature and coalesce to form liquid droplets, and then agglomerate with other ash particles [49]. Fragmentation of the coal char leads to the formation of additional ash particles smaller than the parent particle [50]. Second, at high temperatures, the more volatile metals will vaporize [51]. These vapors can then undergo homogeneous nucleation to form very fine particulate that grow larger by the condensation of additional volatile species onto the particle surface or can form larger particles by coagulation and chain agglomerate formation. Ash particles formed by the first mechanism represent the bulk of the fly ash mass and are greater than 1 μm in diameter, with a typical size range of 3–50 μm, and those by the second mechanism are less than 0.5 μm in diameter, with a peak around 0.1 μm.

The total particulate emissions in the flue gas from a coal-fired boiler depend upon the design of the combustion system and the amount of unburned carbon resulting from incomplete combustion. For pulverized coal-fired boilers, 70–90% of the ash will typically end up in the flue gas (fly ash), and the remaining 10–30% of the ash will collect on the walls of the boiler and end up as ash removed from the bottom of the boiler (bottom ash) [9]. Cyclone-fired boilers and other boilers with wet bottom designs collect more bottom ash and generate approximately 15–30% fly ash. Boiler load can also impact particulate emissions with lower boiler loads resulting in lower emission rates depending upon boiler design and fuel characteristics [52]. Periodic cleaning of heat transfer surfaces, such as the superheater, reheater, economizer, and air preheater, via soot blowing can lead to short-term increases in particulate loading in the flue gas.

Sulfur Oxides Formation

Sulfur is present in coal in inorganic and organic forms. The primary inorganic form is as iron sulfide (FeS_2), which is typically in pyrite (cubic) form. A small amount of sulfur is also present as inorganic sulfates, typically as salts of minerals such as calcium and iron ($CaSO_4 \bullet 2H_2O$ and $FeSO_4 \bullet 7\ H_2O$). The organic compounds containing sulfur are larger chain hydrocarbons and are believed to consist of thiols, sulfides, and thiophenes [53]. The proportions of inorganic and organic sulfur vary depending upon the coal; however, organic sulfur typically comprises between 30% and 50% of the total sulfur [54]. The remainder is primarily pyrite, as inorganic sulfates are typically less than 0.1% of the total sulfur.

During the combustion process, the inorganic and organic sulfur is released and converted to sulfur dioxide, SO_2. For pyrite, this process involves decomposition to FeS and subsequent oxidation [55]. For the organic sulfur, this process involves decomposition

and oxidation of the parent compound to release the sulfur-bearing species. The gas-phase sulfur chemistry is complex [56], but in fuel-lean flames, the released sulfur species are readily oxidized to SO_2. Under fuel-rich conditions, hydrogen sulfide (H_2S) and carbonyl sulfide (COS) are also present in low concentrations [57, 58], but these species are readily oxidized to SO_2 in the high-oxygen environment of practical combustion systems.

For bituminous and subbituminous coals, nearly all of the sulfur in the coal (90–95%) is released as sulfur oxides, both SO_2 and sulfur trioxide, SO_3, with the remainder ending up as sulfates in the ash. For pulverized coal-fired boilers, emissions of SO_2 are independent of the boiler design and operating conditions [59]. For lignitic and subbituminous coals containing ash with a high alkali (calcium and sodium) content, a higher fraction of the sulfur is retained in the ash. Sulfur oxide emissions from lignites can be correlated with the sulfur, sodium oxide (Na_2O), and silica (SiO_2) content of the ash [60].

The fraction of sulfur that is emitted as SO_3 is small and is typically 0.5–1.5% of the total sulfur in the coal [61]. While equilibrium favors the formation of SO_3 at low temperatures, the reaction kinetics are too slow to permit appreciable SO_3 to form prior to the flue gas exiting the stack [49]. The SO_3 that does form is a concern as, at low temperatures, it reacts with moisture to form sulfuric acid, which can condense out of the flue gas and cause corrosion. The coal sulfur content and fly ash composition and boiler design and operating variables, such as excess oxygen and flue gas residence time-temperature profile, are all factors that can influence the concentration of SO_3 that is emitted [62].

Nitrogen Oxides Formation

During combustion, NO_X emissions can form through three main mechanisms. The first process is fixation of nitrogen in the air (atmospheric nitrogen) via the overall reaction:

$$N_2 + O_2 \rightarrow 2NO \tag{1}$$

The detailed reaction is believed to be initiated by a free oxygen atom (O) attacking the very stable nitrogen molecule (N_2) to form NO and a free nitrogen atom (N), which can then attack O_2 [63]. As this chain reaction can only be initiated at high temperatures, NO formed from this process is referred to as "thermal NO_X." The second mechanism is through the reaction between hydrocarbons in the flame front with molecular nitrogen [64]. As this reaction can produce NO levels higher than those expected from thermal NO formation alone within the initial stages of combustion, it is referred to as "prompt NO_X." The third mechanism is through oxidation of fixed nitrogen species present in the fuel. NO formed from this process is referred to as "fuel NO_X." For pulverized coal combustion, the majority of the NO_X emissions result from fuel nitrogen rather than thermal NO_X formation [65, 66]. Prompt NO_X is estimated to be less than 5% [67].

The nitrogen content in coal typically varies between 1% and 2%, with some coals having nitrogen contents higher and lower than this range. Analytical techniques suggest that the majority of the nitrogen is contained in five-member (pyrrolic) or six-member (pyridinic) aromatic ring structures [68, 69], with pyrrolic nitrogen being the dominate form for all coal ranks. A smaller fraction of nitrogen is present in other species which may include quaternary nitrogen (i.e., a nitrogen molecule with four bonds) or aromatic amines [70]. The form and distribution of nitrogen within the coal matrix is expected to impact how the nitrogen is released during the combustion process and the potential for its conversion to NO.

As a coal particle devolatilizes during combustion, a fraction of the nitrogen is released with the volatiles, while a fraction of the nitrogen stays in the coal char [71]. The volatile nitrogen may be contained in tars or in the form of cyanic and amine species, which are believed to be the products of rapid secondary pyrolysis of the hydrocarbon forms. As the tars undergo further breakdown, a fraction of the nitrogen is released primarily in the form of HCN [72], and a fraction is incorporated into soot compounds [73]. The nitrogen species released during devolatilization can undergo oxidation to form NO via the overall reactions:

$$HCN + O_2 \rightarrow NO + CO + H \tag{2}$$

$$NH_3 + O_2 \rightarrow NO + \frac{1}{2}H_2O + H_2 \tag{3}$$

In the absence of oxygen, the fixed nitrogen species can be reduced to N_2. After the volatiles are released,

further nitrogen species, primarily as HCN, can be released from the coal char by thermal dissociation of the remaining organic solids. As the coal char burns, NO can be formed by heterogeneous oxidation of nitrogen remaining in the char [74].

Pilot-scale studies to evaluate the impacts of coal type and combustion conditions on the formation of NO_X emissions from pulverized coal combustion have shown that as the total fuel nitrogen content increases, NO_X emissions increase, but that the fraction of fuel nitrogen evolved with the volatiles also impacts NO_X emissions [75]. Large differences in NO_X emissions can result from coals having similar nitrogen contents and burned under the same conditions when fuel nitrogen is evolved at different rates. Fuel and air contacting also has a strong influence on NO_X emissions with rapid and intimate contact of air with the fuel during devolatilization leading to higher NO_X emissions than those which result from the slow mixing processes typical of a diffusion flame [76]. The staging inherent in a diffusion flame lowers NO_X emissions by allowing fuel nitrogen to evolve in an oxygen-free environment where it can be reduced to N_2 rather than being oxidized to NO [77]. In a practical pulverized coal flame, coals which evolve fuel nitrogen early in the combustion process tend to produce lower NO_X emissions than those that retain more nitrogen in the char.

The coal type and the boiler design and combustion system all impact the NO_X emissions produced from pulverized coal-fired power plants [75, 78]. Low-rank coals (i.e., subbituminous and lignite) produce lower NO_X emissions than high-rank coals (i.e., bituminous and anthracite). This is primarily due to the lower nitrogen and higher volatile content of the low-rank fuels. For power generation, the majority of pulverized coal fired boilers use either an array of circular burners located on one or two walls of the furnace (i.e., wall or opposed wall firing) or columns of burners arranged on the furnace corners firing in a tangential pattern (i.e., tangential firing). Tangential firing results in longer, slower mixing flames and produces lower NO_X emissions than wall-fired boiler designs, which tend to have shorter, faster mixing flames. Other firing system designs, such as cyclone and arched-fired boilers, that are designed to remove the coal ash in a molten state tend to produce the highest NO_X emissions due to intense fuel and air mixing and higher temperatures. For a given boiler design, firing configuration, and coal, NO_X emissions can be approximately correlated with the total heat liberation per unit of cooled surface area [79]. Older boiler designs tend to have a high ratio of heat release per surface area resulting in high NO_X emissions, while more modern designs use a lower ratio to reduce NO_X emissions.

Particulate Matter Control Technologies

To remove dust from a gas stream, such as fly ash contained in boiler flue gas, a force must be applied that causes the particles to divert from the flow direction of the gas long enough for the particles to contact a collecting surface. The collecting force can be gravitational, centrifugal, inertial, direct interception, diffusional, or electrostatic [80]. Some collection devices may use a combination of these forces. The effectiveness of the collecting force depends upon the characteristics of the particulate matter to be collected; hence, the particulate matter size distribution and chemical and physical characteristics must be known to select the most appropriate collecting device [81].

Modern coal-fired power plants use two primary devices to remove and collect fly ash: electrostatic precipitators and fabric filters. Older boilers and industrial boilers may also use mechanical collectors, such as cyclones, to remove larger fly ash particles prior to the remaining particulate being collected in an electrostatic precipitator or fabric filters. Venturi scrubbers have also been used for large coal-fired boilers; however, these are less common and would not be used for compliance with current emissions regulations. The remainder of this section will provide an introduction to electrostatic precipitators and fabric filters.

Electrostatic Precipitator

If a dust-laden gas is passed through a strong electrical field, the dust will become charged and will begin to flow in the direction of the ion flow, enabling them to be removed from the gas. To apply this phenomenon in practice requires four steps: (1) the particles need to be charged, (2) the particles need to be collected on a surface, (3) the particles need to be removed from the surface in a fashion that minimizes their reentrainment into the gas flow, and (4) the particles need to be removed from the device [82]. The collecting device

that accomplishes these steps is typically referred to as an electrostatic precipitator (ESP). As shown in Fig. 1, in an ESP, an electric potential is set up between a discharge electrode and a collection electrode, and the dust laden gas is passed between the electrodes at a relatively low velocity. When the potential is high enough, corona discharge is generated near the discharge electrode that begins to ionize the gas molecules; these molecules then migrate to the lower potential collecting electrode. In the process, the molecules attached themselves to the dust particles which then also migrate to the electrode. Upon reaching the electrode, the particles lose their charge and stick to the electrode. As the dust layer on the collection electrode builds up, the electrical current is reduced, and it becomes necessary to vibrate the plate to remove the particles. This is accomplished through a rapper system that strikes the top of the collection plate periodically to remove the dust. The dust then falls into the collection hopper where it can be removed.

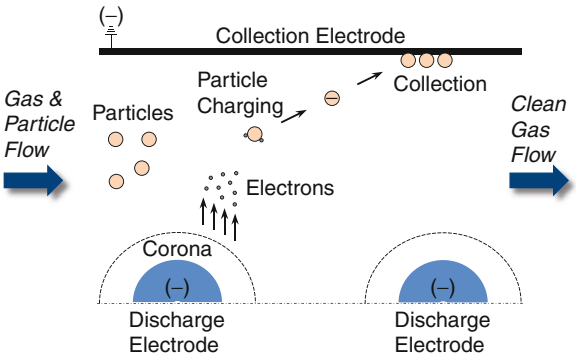

Pulverized Coal-Fired Boilers and Pollution Control. Figure 1
Principle of electrostatic precipitator operation

ESPs are generally classified by the method in which the particulate is removed from the collection electrode, e.g., wet versus dry, and by the geometry of the electrodes, e.g., wire in tube or wire and plates. The most common design for coal-fired power plants is the dry, wire, and plate type as illustrated in Fig. 2. The main components of an ESP are a gas-tight casing or outer shell, discharge electrodes, collection electrodes, a high-voltage transformer rectifier or high-frequency power supply for application of electrical power, rappers to remove particulate from the collection electrode, and pyramidal-shaped hoppers to remove particulate from the system [83]. The collection electrodes or plates are arranged in multiple mechanical fields, where each field consists of a series of equally spaced plates perpendicular to the gas flow.

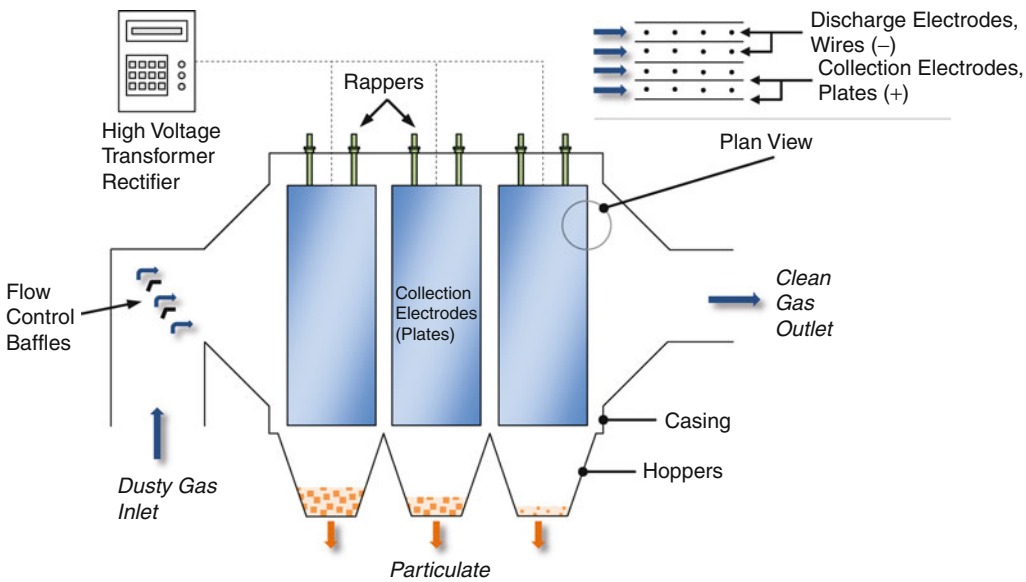

Pulverized Coal-Fired Boilers and Pollution Control. Figure 2
Overview of electrostatic precipitator

The discharge electrodes or wires are suspended in the gas passage between each pair of plates. An ESP will have one or more mechanical fields. A high-voltage pulsed direct current or direct current is applied to the discharge electrode. When the voltage is high enough, a corona discharge will be generated that causes particles to be moved to the collection electrode.

The performance of an ESP is impacted by the design of the ESP, the strength of the electric field, and the particle characteristics. The theoretical collection efficiency of an electrostatic precipitator can be expressed by the Deutsch-Anderson equation [84]:

$$\eta = 1 - e^{-\left(\frac{A}{V}\right)\omega} \tag{4}$$

where η is the collection efficiency for a given particle size, A is the surface area of the collecting electrode, V is the volumetric gas flow rate, and ω is the migration velocity of the particle. The term (A/V) is referred to as specific collection area (SCA) of the ESP. Equation 4 shows that the collection efficiency of an ESP can be improved by either increasing the surface area of the collecting electrodes or decreasing the volume of gas to be treated. The theoretical migration velocity of the particle can be calculated by comparing the electrostatic forces on the particle to the drag force and, with simplifying assumptions, can be expressed as [85]:

$$\omega = \frac{E_c E_p d}{4\pi\mu_g} \tag{5}$$

where E_c is the charging field strength, E_p is the precipitating (collecting) field strength, d is the particle diameter, and μ_g is the gas viscosity. Equation 5 shows that the particle migration velocity is proportional to both the electric potential and the particle size. As particle size is reduced, voltage must be increased to maintain migration velocity and collection efficiency. Equation 5 suggests that continuing to increase the electric field will continue to increase the particle migration velocity and, hence, the ESP collection efficiency. While this is true, a practical limit is reached where the field breaks down and sparking between the electrodes occurs [80]. Sparking destroys the electrical field and lowers the collection efficiency.

The electrical conductivity of the particulate matter has an impact on the electrical field between the discharge and collection electrodes. The resistance to electrical conductivity is called the "resistivity" [86]. As the dust layer builds up on the collection electrode, the voltage at which sparking occurs is lowered due to the increased electrical field at the dust layer. If the resistivity of the ash is too high, charge will build up on the collected particles and can become high enough to cause an electrical breakdown which causes ions of the opposite polarity to be injected back into the gap which reduces the charge on the particles in the gas flow and which can cause sparking. This breakdown is referred to as "back corona" [87]. The resistivity of fly ash is a function of the particle composition, gas temperature, and concentrations of water vapor and SO_3 in the flue gas [88].

Properly designed and operating ESPs can remove between 99% and 99.9% of the total particulate matter. Older equipment is generally less efficient. As noted above, the primary factors that influence the ESP performance are the particle resistivity, the particle size distribution, and the flue gas temperature and flow rate [83]. As these parameters vary from the conditions assumed in designing the ESP, the ESP collection efficiency can be impacted. Other factors that can impact the ESP performance are the electrical conditions in the ESP, the gas flow distribution, and the particle reentrainment during rapping [89]. The applied voltage in each field of the ESP needs to be optimized to maximize the acceptable spark rate with the specific ash characteristics. The gas flow distribution entering the ESP should be optimized to ensure a uniform flow distribution between the collecting plates, and the ESP should be designed to minimize the potential for gas flow to bypass the plates (sneakage). The rapping system design and frequency should be optimized to minimize the reentrainment of particles into the gas stream.

Fabric Filter Baghouse

If a dust-laden gas is passed through a fiber bed or filter, the dust will be removed from the gas and will collect on the filter. The principle mechanisms of filtration include impaction, interception, and diffusion, which are related to the relative particle and fiber size and velocity through the filter [90]. These mechanisms are illustrated in Fig. 3. Particles will impact on a fiber when they are too large to follow the gas streamlines

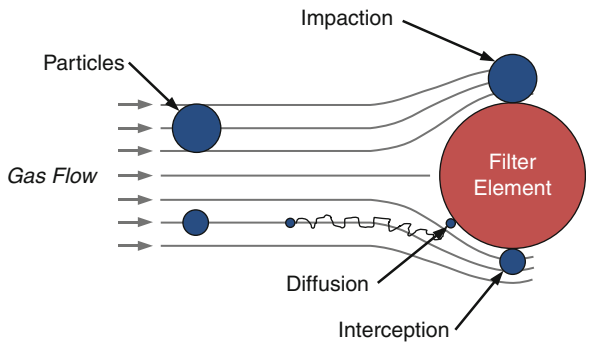

Pulverized Coal-Fired Boilers and Pollution Control. Figure 3
Principal mechanisms involved in fabric filtration

around the filter. Interception will occur when a particle follows a streamline close to a fiber and is attracted to the surface by van der Waals forces. Particles that are very small are influenced by Brownian diffusion and can come into contact with the fiber and be removed from the gas. Other forces, such as electrostatic and gravity, can also play a role in removing particulate from the gas.

The filtration media can be flat and supported in a frame or in bags which are supported on cages. As bags are most common for large systems, the containing device is commonly called a baghouse. In a baghouse or fabric filter, the dust-laden gas passes through the suspended filtration media. Particles impact on the filter and are held. As collection proceeds, a deposit begins to build up that also serves as a means of collecting particulate. Eventually, the deposit must be removed or the pressure drop will be too high. As this can be accomplished by several means, baghouses are most commonly classified by the cleaning method [91]. Typical cleaning methods include mechanical, reverse airflow, and pulse-jet cleaning. Mechanical cleaning typically involves flowing the gas on the inside of the bag, stopping the gas flow, and shaking the bag to remove particulate. Reverse airflow cleaning consists of periodically flowing gas in the opposite direction to the normal gas flow to remove the particulate buildup from the filter. In a pulse-jet system, the gas flows from the outside to the inside of the bag. Periodically, a pulse of compressed air is injected down the center of the bag to flex the bag and remove particulate.

Reverse airflow and pulse-jet baghouses have been applied to coal-fired boilers throughout the world [92, 93]. Simplified overviews of the cleaning methodology and main components for reverse airflow and pulse-jet fabric filters are illustrated in Figs. 4 and 5. The similar components for each type of fabric filter include a gas-tight casing, fabric filters, supporting frames, and pyramidal-shaped hoppers to remove particulate from the unit. Large-scale systems will be designed with multiple compartments to facilitate cleaning and maintenance. Reverse airflow baghouses include a fan and ductwork and valves for flowing cleaned gas back through the unit. Pulse-jet baghouses include a compressed air header and distribution plenum to periodically introduce compressed air into the throat of the filter bags. While significant experience exists with the use of reverse airflow baghouses on large utility boilers, interest in pulse-jet baghouses is increasing since this design uses higher air-to-cloth ratios than the reverse airflow design, resulting in smaller equipment size and lower capital costs [94].

The filtration media used in fabric filters can be woven or felted. Woven fabrics are typically used in shaker-type baghouses as they have good mechanical strength. Felted fabrics tend to be used for reverse air and pulse-jet fabric filters [95]. For proper operation, the type of fabric must be matched to the specific application. The gas stream temperature and chemical composition are critical factors that influence the fabric selection. For coal-fired power plants, the baghouse is installed after the air preheater, where normal gas temperatures are in the range of 120–175°C (250–350°F) and where the presence of sulfur oxides and moisture increases the potential for corrosion. In this application, the utility industry has primarily used coated fiberglass fabrics for reverse airflow baghouse designs as these fabrics are resistant to chemical attack and can withstand temperatures up to 260°C [96]. The primary coating in use today is polytetrafluoroethylene (PTFE), which improves bag lifetime and provides resistance to acidic attack and thermal excursions. For pulse-jet baghouses equipped units fired with low-sulfur coal, the bags are typically made of polyphenylene sulfide (PPS) [97].

The performance of a fabric filter is impacted by the particle properties, fabric properties, operating characteristics, cleaning method, and interrelationships

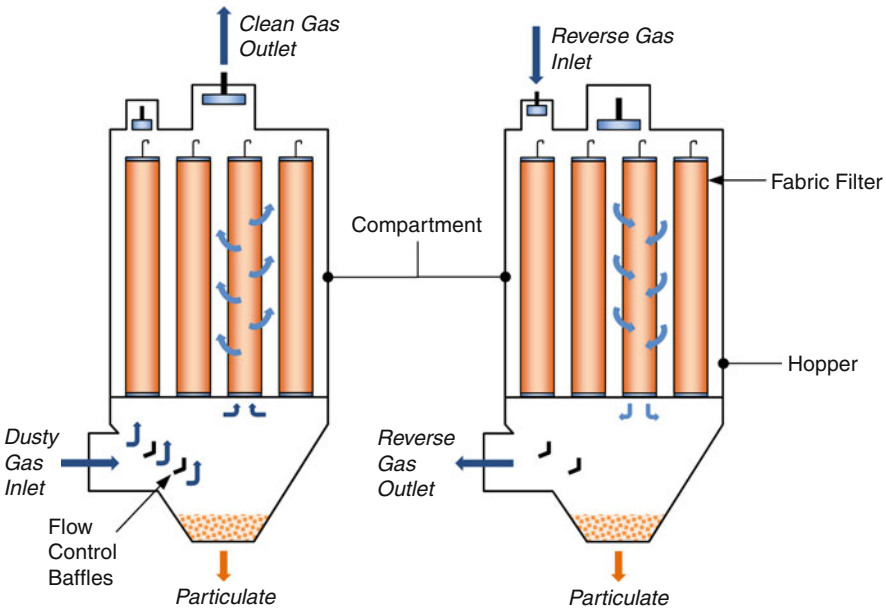

Pulverized Coal-Fired Boilers and Pollution Control. Figure 4
Reverse air flow baghouse features

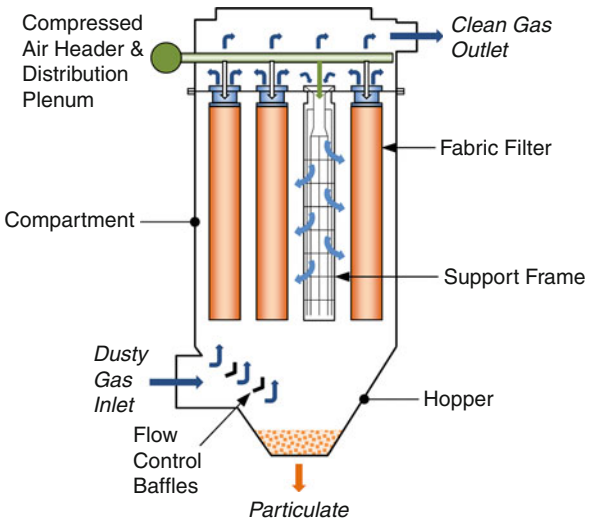

Pulverized Coal-Fired Boilers and Pollution Control. Figure 5
Pulse jet baghouse features

between these parameters [98]. While the fundamental mechanisms involved in removing particles from the gas are understood, the highly complex nature of the collection process and the participation of the dust layer in the collection process make the design of fabric filters more empirical in nature. The two primary design and operating parameters are the air-to-cloth ratio, which sets the velocity ratio passing through the filter and, hence, the relative size of the unit, and the pressure drop, which sets the energy consumption requirements [99]. These two parameters are related as baghouses with a small A/C ratio will have a lower pressure drop than baghouses with a higher A/C ratio, resulting in a trade-off between capital and operating costs. The bag cleaning method influences the A/C ratio and pressure drop as more energetic cleaning methods can reduce the A/C ratio (and unit size) for a given pressure drop [100].

Fabric filters are highly efficient collection devices for both coarse and fine particulate, with typical efficiencies of 99–99.9%. Due to the collection mechanisms involved in fabric filtration, particle removal performance is not as sensitive to particle size for these devices as with ESPs. In comparing the costs of fabric filters to ESPs, fabric filters become more economic where highly efficient removal of submicron particles are required [101]. As noted above, the design A/C ratio and operating pressure drop impact fabric filter performance. Fabric filter performance is also impacted by flue gas and particle characteristics.

The flue gas temperature impacts the volume of the flue gas and, hence, the operating A/C ratio, while the flue gas moisture content and composition can impact the characteristics of the dust cake. The particle size impacts the buildup (and removal) of the dust cake on the filter and, along with the particle composition, impacts the adhesion of particles to the filter surface and the cohesion of particles to each other. Reactions between the particles and constituents of the gas can also impact the cohesiveness of the dust cake. Finally, the cleaning cycle interval and intensity will also impact the overall performance of a fabric filter.

SO_2 Emissions Control Technologies

The primary mechanisms for removal of a gaseous pollutant from a gas stream involve (1) absorption into a liquid, (2) gas/solid reaction, and (3) adsorption onto a solid. The first two mechanisms are the primary methods for removal of sulfur dioxide from coal-fired boiler flue gas. Commercial processes based upon these mechanisms can be categorized into whether the process is regenerable, where the sulfur compound is separated from the absorbent, or nonregenerable, where the sulfur compounds are thrown away with the absorbent [102]. The product from regenerable processes can be concentrated SO_2, hydrogen sulfide, elemental sulfur, or sulfuric acid. SO_2 removal processes can be further characterized into wet processes, where the product is a solution or slurry, and dry processes, where a dry product is produced [103]. The majority of non-regenerable processes produce a throwaway waste; however, some wet processes can be modified to produce a gypsum by-product that can be sold if site-specific conditions permit.

The primary technologies for removing sulfur dioxide from coal-fired power plants are wet limestone ($CaCO_3$) and dry lime ($Ca(OH)_2$) scrubbing [104], typically referred to as wet and dry flue gas desulfurization (FGD). The preference for these technologies over regenerable processes is largely driven by the low cost and high availability of limestone and lime, by the relative simplicity of these processes in comparison to other tail end processes, and by the fact that power plants are not chemical companies. For wet scrubbing, limestone tends to be preferred over lime due to lower cost, particularly if a ready supply is located close to the power plant. In comparison to lime, limestone requires finer grinding, has higher transportation costs, requires larger equipment, and is less responsive with respect to pH control [105]. Thus, absorbent selection is done by performing a comparison based upon site-specific technical and economic factors. For wet FGD systems that produce gypsum, which will be sold for wallboard manufacturing, the use of hydrated lime rather than limestone can lead to improvements in the product quality in some cases [106]. In dry scrubbing, lime is required due to the need for rapid reaction times as lime has a higher reactivity than limestone.

A wide variety of wet and dry FGD processes exist, but the basic processes are similar [107–109]. In addition to or instead of lime and limestone, several processes introduce sodium compounds, such as sodium carbonate (e.g., trona), where these materials are available locally to improve process efficiency [110]. Seawater scrubbing, which uses seawater to remove the SO_2 and discharge in into the ocean, has also been applied to coal-fired power plants located in a coastal environment [111]. While wet and dry scrubbing are highly efficient technologies, they have high capital and operating costs. This has led to interest in lower capital cost SO_2 removal technologies such as furnace sorbent injection [112, 113]. The remainder of this section will discuss the basic wet limestone and dry lime scrubbing processes.

Wet Flue Gas Desulfurization

In wet FGD, flue gas containing SO_2 is input into a scrubbing tower or absorber where it is brought into contact with an alkaline solution or slurry containing partially dissolved limestone ($CaCO_3$). The SO_2 is absorbed into the solution where it reacts to form calcium sulfite ($CaSO_3$) and calcium sulfate ($CaSO_4$). The detailed chemistry of the process is complex and depends upon the composition of the slurry and extent of dissolution of the limestone [105]. The primary steps involved in the process are gas/liquid mass transfer of the SO_2, dissolution of the limestone, oxidation of SO_3 to SO_4 in solution, and crystallization of $CaSO_3$ and $CaSO_4$. By controlling the solution pH and concentration of $CaCO_3$ in the solution, high levels of SO_2 removal can be achieved. As SO_2 absorbs into the solution as bisulfate (HSO_3^-), the primary product

from the process is calcium sulfite. However, due to the high oxygen content of flue gas (3–10% by volume), a fraction of the calcium sulfite will oxidize to calcium sulfate. Typically, the product from this process is a waste sludge. It is possible to force oxidation of calcium sulfite into calcium sulfate by bubbling air through the solution which improves the ability to remove water from the waste and permits the material to be upgraded for use for gypsum ($CaSO_4 \cdot 2HO$).

The basic components of the limestone wet scrubbing process are illustrated in Fig. 6. Flue gas from the particulate control device (ESP or baghouse) enters the bottom of an absorber tower (typically a spray tower) and flows upward. The absorbing solution is sprayed into the gas stream. The SO_2 is absorbed into the solution where it reacts with the limestone to form solids. The resulting slurry is then captured in an effluent holding tank where ground limestone slurry and recycled solution are added. This solution is then recycled to the absorber. A portion of the solution is sent to the thickener to concentrate the waste solids as a sludge. The sludge from the thickener is then dewatered in a vacuum filter to produce a filter cake, which is mixed with fly ash to stabilize the waste prior to sending it to a landfill. Enhancements to the basic process include the use of a pre-scrubber upstream of the main absorber to quench the flue gas and protect the materials used in the absorber, incorporation of a second scrubbing loop into the pre-scrubber, and blowing air into the effluent holding tank to force oxidation of calcium sulfite to calcium sulfate [114]. This latter improvement minimizes scale formation, improves the characteristics of the sludge, and eliminates the need for adding fly ash for stabilization. Forced oxidation is also used to produce solids that can be used to produce gypsum for wallboard manufacturing. If lime rather than limestone is used, forced oxidation is not required for scale control. The cleaned flue gas exiting the absorber after passing through a mist eliminator designed to remove entrained droplets from the gas, passes through a reheater, and is then sent to the stack. A reheater is used to protect equipment downstream of the scrubber from condensation and corrosion, to reduce the visible plume, and to improve rise and dispersion of the stack gas.

The performance of a wet FGD system is impacted by a number of design and operational factors, most of which are related [114]. The design of the absorber tower must provide for effective contacting of the flue

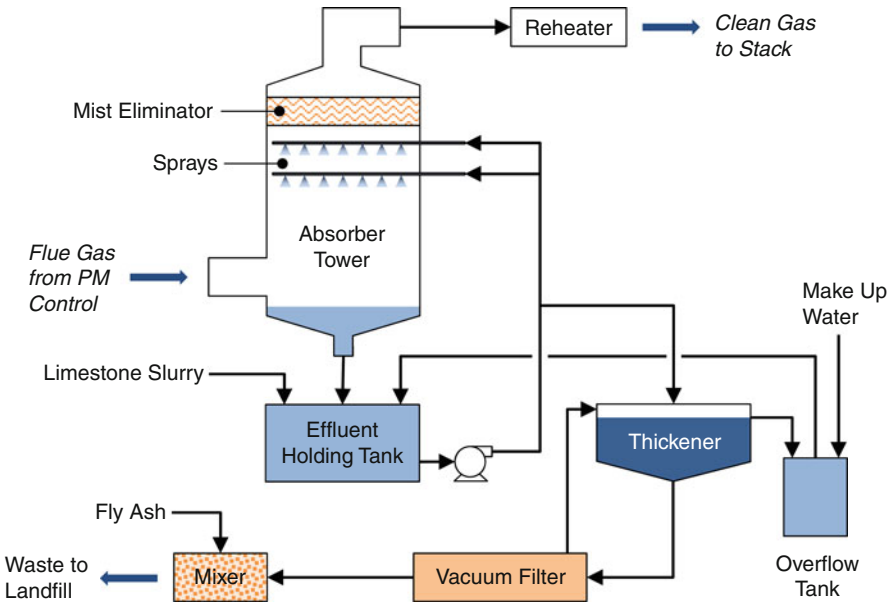

Pulverized Coal-Fired Boilers and Pollution Control. Figure 6
Basic limestone wet scrubbing process

gas with the absorber solution and for separation of the cleaned gases from the liquid. From an economic standpoint, the size of the tower is linked closely to the process chemistry and the relative flows of flue gas and absorber solution, which is typically expressed as the liquid-to-gas ratio. Operational factors that impact performance include the SO_2 concentration in the flue gas, pH of the slurry, solids concentration in the slurry, concentration of other components in the slurry such as magnesium and chloride ions, residence time of the slurry in the reaction tank, and degree of slurry oxidation [105, 115]. High utilization of the limestone (or lime) is important and most systems operate with a calcium-to-sulfur molar ratio of close to 1:1. Liquid pH is monitored and used to control the limestone addition rate to maximum limestone utilization, to minimize the potential for scale in the system, and to reach a specific emissions target. The limestone grind fed to the FGD system can also be important, with finer grinds leading to a smaller-sized reaction tank, higher SO_2 removals, and an increase in gypsum purity [116].

Wet FGD systems are capable of achieving over 95% SO_2 removal, with some systems being designed for 96–98%, and can be applied to both low and high sulfur coals. As discussed above, a number of parameters can impact system performance and must be optimized to ensure effective SO_2 control as well as maintain system reliability and availability. Overall, wet FGD systems represent a significant capital, operating, and maintenance expense for a coal-fired power plant. The main operating and maintenance (O&M) costs differ for various designs and should be considered in selecting an FGD process [117]. Experience with existing plants has led to a number of equipment improvements, such as large, single-tower, absorbers with higher flue gas velocities and improved mist eliminator designs, and process improvements, such as the use of fine limestone and solution buffers [103]. These improvements can lead to higher SO_2 removal efficiencies, lower capital costs, and reduced O&M costs.

Dry Flue Gas Desulfurization

In dry FGD, flue gas containing SO_2 is input into a spray dryer absorber where it is brought into contact with an alkaline solution containing hydrated lime ($Ca(OH)_2$). The SO_2 is absorbed into the solution where it reacts with the alkali material to form solid calcium sulfite ($CaSO_3$). Absorption and reaction occur while the thermal energy of the flue gas vaporizes the water in the droplets to produce a fine powder. The primary processes involved in spray drying consist of atomization of the alkaline slurry into a spray of droplets, contacting of the spray with the flue gas, absorption of SO_2 into the droplets, reaction with the suspended alkali material, drying of the spray by evaporation of the moisture in the droplets, and, finally, separation of the solids from the gas [118]. Due to the high oxygen concentrations of the flue gas, a fraction of the $CaSO_3$ will be oxidized into $CaSO_4$.

An overview of the lime dry scrubbing process is shown in Fig. 7. Hot flue gas from the air preheater outlet enters the top of the cylindrical spray dryer where an atomizer sprays the alkaline slurry from the feed preparation system into the flue gas. SO_2 is absorbed into the spray droplets where it reacts with the lime to form a solid. The water in the droplet evaporates leaving a fine powder that can be collected from the spray dryer and in a subsequent particulate collection device. Twin fluid and rotary or spinning disk atomizers can be used; however, most large utility applications use a rotary atomizer. Typically, fabric filters are used for removal of the fly ash and spent absorbent. Collection of the solids on the fabric filter permits additional SO_2 removal to occur resulting in increased sorbent utilization.

The spray dryer absorber needs to be designed to maximize SO_2 removal, yet produce a dry product. Since absorption and reaction of SO_2 is fastest when surface liquid is present, it is necessary to operate as close to the saturation point of the flue gas as possible and to maximize the residence time available for reaction while still yielding dry solids at the absorber walls and outlet [119]. The quality of water that can be used for the slurry is limited by the boiler outlet temperature, which is set by the boiler thermal efficiency, and the desired approach to saturation. The concentration of solids in the slurry is limited by the viscosity of the material which impacts the practical aspects of handling and atomizing the material. These two factors constrain the SO_2 removal that can be achieved for a given inlet SO_2.

Dry FGD systems are capable of achieving over 95% SO_2 removal and are typically applicable to low and

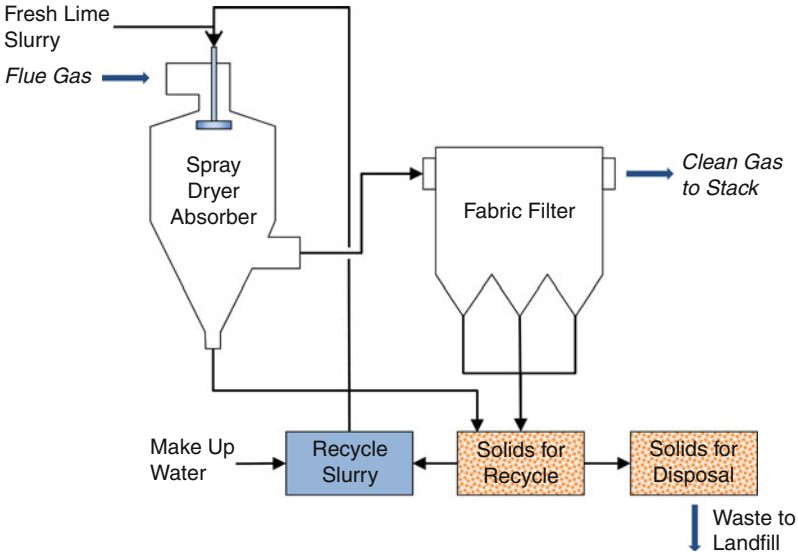

Pulverized Coal-Fired Boilers and Pollution Control. Figure 7
Basic lime dry scrubbing process

medium sulfur coals. There are technical constraints on the application of this technology to high sulfur coals as an increase in sulfur content requires an increase in the solids' content of the slurry and a point can be reached where the viscosity of the material is too high for proper pumping and atomization [103].

NO_x Emissions Control Technologies

Technologies to reduce NO_X emissions from combustion systems can be placed into two broad categories: (1) combustion modification technologies which reduce the formation of NO_X during combustion and (2) postcombustion technologies which eliminate NO_X from the flue gas following combustion [28]. Combustion modification techniques will generally seek to lower flame temperature or to control the flame stoichiometric ratio depending upon whether thermal NO_X or fuel NO_X emissions are being targeted. For pulverized coal combustion, as discussed previously, the majority of the NO_X emissions result from the nitrogen in the fuel; hence, the most effective combustion modifications are those which control the stoichiometric ratio during coal devolatilization. Postcombustion techniques tend to rely on the use of additives to reduce the NO_X to molecular nitrogen, N_2. Removal of NO_X by wet scrubbing is difficult due to the insolubility of NO and poor solubility of NO_2. Scrubbing technologies that can be applied to industrial plants have not been widely applied to large pulverized coal-fired power plants due to high capital and operating costs and the low initial NO_X concentrations [120].

For coal-fired power plants, the primary combustion modification techniques are low-NO_X burners, overfire air, and reburning technology [121]. Each of these technologies relies on controlling the combustion process in the furnace. The primary postcombustion technologies are selective noncatalytic reduction (SNCR) and selective catalytic reduction (SCR) [122]. These technologies involve the use of a reagent that reduced NO_X to N_2. Combustion modification technologies are generally the most cost-effective when evaluated against postcombustion technologies on a cost per mass of pollutant removed [123]. SCR technology is the most expensive technology but also provides the highest level of NO_X emission reduction. SNCR technology provides a modest level of NO_X reduction, with cost-effectiveness typically between that of combustion modifications and SCR.

In retrofitting existing units with NO_X emissions control technologies, selection of the most cost-effective technology or set of technologies generally

requires a boiler-specific analysis that includes assessment of the NO_X emission goals or limits and the expected performance and costs of the specific technologies. Retrofit costs for NO_X control technologies are very site specific and depend upon the ease of the retrofit and the boiler design and operating characteristics, such as the furnace size, firing configuration, and the condition of existing equipment [124]. The remainder of this section will provide an introduction to NO_X control technologies.

Low-Nox Burners

Low-NO_X burners reduce NO_X formation in the combustion process by delaying the mixing of fuel and air in the flame [125]. One means of aerodynamically staging fuel and air mixing in a coal flame for a wall-fired boiler is illustrated in Fig. 8. In this low-NO_X burner design, the mixing of fuel and air is controlled by dividing the combustion air into multiple streams, with separate control over each stream. Coal entering the flame is initially burned in a fuel-rich core which gradually becomes fuel lean as air is progressively mixed into the flame. Staging of the air into the flame permits volatile nitrogen compounds released in the early portion of the flame to be processed in a reducing environment, resulting in lower NO_X emissions. Staging of the flame also reduces peak flame temperatures and, therefore, can reduce thermal NO_X formation as well.

For wall-fired boilers, low-NO_X burner designs vary from manufacturer to manufacturer [126–128], but all tend to have similar features, including separate control over the combustion air split into two or more passages, control over the degree of swirl imparted to the air streams, and a flame stabilizing device. The inner and outer air split and swirl settings are adjusted to generate a stable low-NO_X emissions flame for a specific coal. These settings can also be adjusted to ensure that the flames do not impinge on the side or rear walls of the boiler.

For tangentially fired boilers, low-NO_X burner designs typically consist of alternating passages of air and fuel [129]. The fuel nozzles direct the fuel into the center of the furnace, while the air nozzles direct the air closer to the furnace walls. Offsetting the air from the fuel generates a fuel-rich flame in the center of the furnace which leads to low-NO_X emissions. The offset air also provides a measure of protection along the wall from rich conditions that can lead to wall corrosion. Additional air staging is achieved by adding a fraction of the combustion air through air ports located on the top of the burner stack. The air added to the top of the burner is typically called "close-coupled overfire air" or CCOFA.

The performance of low-NO_X burners in a particular application is very dependent upon the boiler and coal characteristics. Low-NO_X burners generally produce longer flames than the original equipment; hence, the trade-off between optimal burner performance and acceptable carbon-in-ash levels is strongly tied to the furnace geometry. NO_X control levels for the application of low-NO_X burners to wall-fired utility boilers typically range from 40% to 50%.

Overfire Air

Overfire air is a combustion modification technology that, like low-NO_X burners, stages the combustion process to reduce NO emissions [130]. To apply

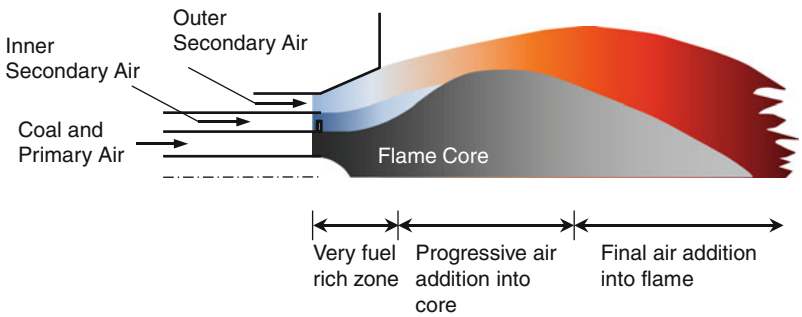

Pulverized Coal-Fired Boilers and Pollution Control. Figure 8
Typical low-NO_X burner design approach

overfire air to a coal-fired boiler, combustion air is diverted from the main combustion zone and is injected through ports located on the walls above the burners. In this process, the primary zone is operated slightly less fuel lean than usual, and fuel and air mixing is delayed. This delay reduces the formation of fuel NO and also reduces peak flame temperatures, resulting in a reduction in thermal NO formation as well. Overfire air is added to complete combustion of unburned fuel.

For pulverized coal-fired boilers, the performance of overfire air is dependent upon the overfire air system design and the burner/boiler characteristics. Optimal NO_X control for a particular system can be achieved provided that the overfire air jets mix effectively, that good control over the main flame can be maintained as combustion air is diverted to the overfire air system, and that there is sufficient residence time in the furnace for carbon burnout to occur. As with low-NO_X burners, the NO_X control performance of overfire air is limited by acceptable carbon-in-ash. For pulverized coal-fired industrial boilers, NO_X reductions between 15% and 30% are generally expected with the application of overfire air.

Reburning

Reburning is a combustion modification technology that removes NO_X from combustion products by using fuel as the reducing agent [131]. As illustrated in Fig. 9, application of reburning to a coal-fired boiler conceptually divides the furnace into three zones (primary zone, reburning zone, and burnout zone) which are typically defined as follows:

Primary Zone: The primary zone consists of the normal firing system and constitutes the bulk (typically 80–90%) of the total heat release. This zone is operated fuel lean at an excess air level which is close or slightly below normal operation. NO_X formed in this zone enters the reburning zone.

Reburning Zone: The reburning fuel is injected downstream of the primary zone to create a slightly fuel-rich, NO_X reduction zone. The reburning fuel provides the remainder, normally 10–20%, of the total heat input. In this zone, hydrocarbon radicals generated during breakdown of the reburning fuel react with NO molecules to form other reactive nitrogenous species, such as HCN, which react with other NO molecules to form molecular nitrogen, N_2.

Burnout Zone: In this final zone, combustion air is added to complete the oxidation of the reburning fuel and to bring the boiler back to a normal operating excess air level.

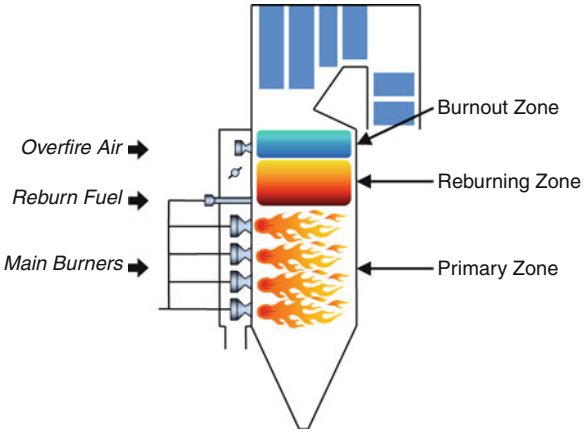

Pulverized Coal-Fired Boilers and Pollution Control. Figure 9
Application of reburning to a utility boiler

Studies of the reburning process have shown that natural gas, fuel oil, and coal can be used as reburning fuels [132]. As shown in Fig. 10, hydrocarbon fuels with low fuel-bound nitrogen, such as propane or natural gas, provide the lowest NO_X emissions since nitrogen in the reburning fuel tends to contribute to the final NO_X exiting the process. In Fig. 10, the reburning zone stoichiometric ratio is defined as the ratio of the total air supplied to the primary and reburning zones to the total stoichiometric air requirements of the primary and reburning fuels. The parameters which control the performance of the reburning process have been defined through an extensive series of experimental studies [133]. For boiler applications, the most critical parameters are the reburning zone stoichiometric ratio and the initial NO_X level. As shown in Fig. 10, most fuels exhibit a maximum NO_X reduction (i.e., minimum NO_X emissions) at a reburning stoichiometric ratio of about 0.9, which corresponds to a reburning fuel input of approximately 18–19% of the total heat input at a primary zone excess air level of 10%. NO_X reduction with reburning increases as the NO_X level from the primary zone increases.

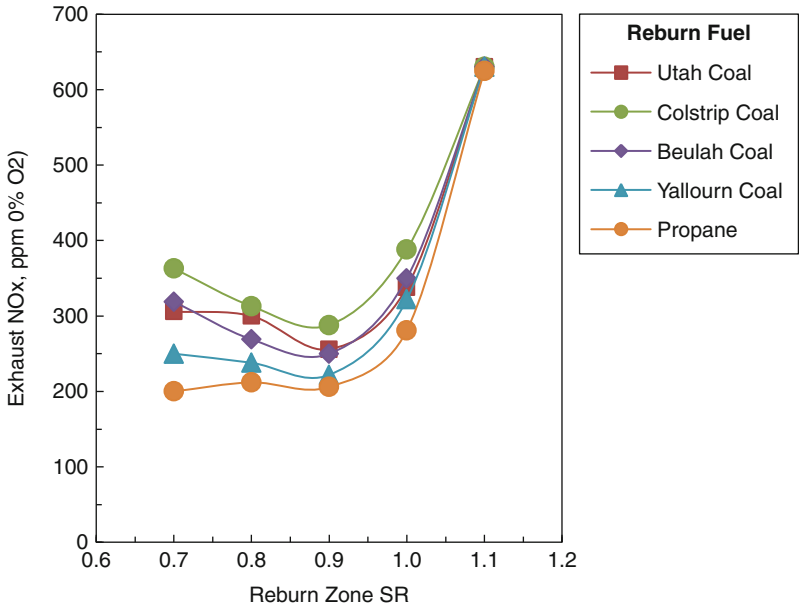

Pulverized Coal-Fired Boilers and Pollution Control. Figure 10
Impacts of reburning zone stoichiometry and fuel on reburning performance

Similar to other combustion modification techniques, the most significant factors which limit the performance of reburning in full-scale applications are the design of the reburning system and the boiler characteristics. The boiler geometry must permit adequate mixing of the reburning fuel and overfire air to be achieved and must provide adequate residence time for the process to be implemented above the primary combustion zone. Reliable methodologies for scaling the reburning process to boilers with varying characteristics have been developed [134]. The use of these methodologies has led to NO_X control levels between 50% and 70% for application of reburning to full-scale utility boilers, independent of the firing configuration.

Selective Noncatalytic Reduction

Selective noncatalytic reduction is a flue gas treatment process in which an amine-containing agent, such as ammonia (NH_3) or urea ($CO(NH_2)_2$), is injected into combustion gases to react with and reduce NO formed during the combustion process [135, 136]. At the proper temperature, NH_2, generated from decomposition of the injected reagent, reacts with NO via a complex set of reactions to form N_2. The chemistry of the SNCR process is illustrated in the following global reactions that are based upon the use of ammonia as the reagent:

$$NH_3 + OH \rightarrow NH_2 + H_2O \quad (6)$$

$$NH_2 + NO \rightarrow H + OH + N_2 \quad (7)$$

$$H + OH \rightarrow H_2O \quad (8)$$

Initially, the injected ammonia is activated by OH to form a reactive amine, NH_2, radical. This radical then selectivity reacts with NO to form molecular nitrogen, N_2, and H and OH radicals. The OH radical can help to activate additional ammonia or can react with H radicals to form water, H_2O.

Figure 11 shows the impacts of gas temperature on the NO_X reduction achieved with urea or ammonia in tests performed in a pilot-scale combustion facility. As shown in this figure, at the proper flue gas temperature (approximately 950–1,000°C), the injected reagent selectively reduces NO to molecular nitrogen, N_2. As temperatures increase, NO_X reduction performance is reduced and a portion of the reagent can be oxidized to NO. As temperatures decrease, a portion of the reagent exits the process unconverted. The unconverted reagent exiting the process is referred to as ammonia slip.

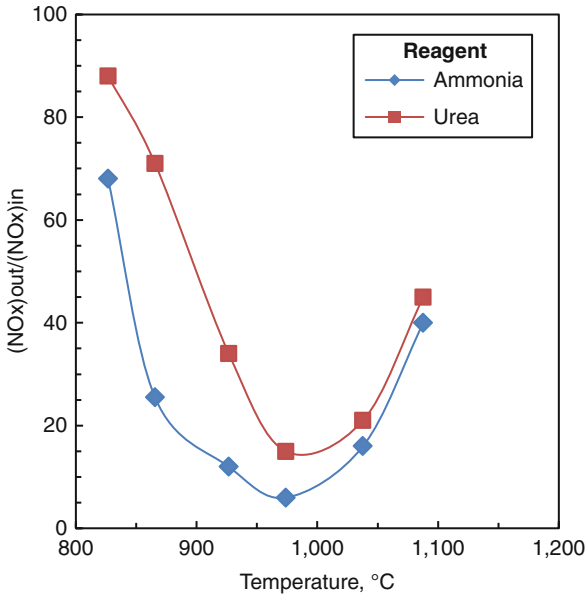

Pulverized Coal-Fired Boilers and Pollution Control. Figure 11
Impacts of gas temperature in SNCR performance

The performance of SNCR on utility boilers depends upon the reagent used, the quantity of reagent injected, and the boiler design and operating characteristics [137]. For maximum performance, the injection system must be designed to provide effective mixing of the reagent within the optimal temperature window. In addition, the boiler design should provide adequate residence time at the proper temperatures. For pulverized coal-fired boilers, the optimal temperature window generally resides within the convective heat transfer sections, where access is limited and quench rates are high [138]. Wide variations in temperature at the point of injection due to stratification or to changes in load can also limit performance. Multiple injection locations can help to reduce the negative impacts of temperature variations. Due to concerns over the handling and storage of anhydrous ammonia, aqueous ammonia or urea is generally preferred for application of SNCR to utility boilers.

Application of SNCR to coal-fired boilers is expected to reduce NO_X emissions by 30–60% from uncontrolled levels. The higher levels of reduction are generally achieved in boilers with slower quench rates (temperature decay versus residence time) in the upper furnace and with good access to the optimal temperature window.

Selective Catalytic Reduction

Selective catalytic reduction is a high-efficiency flue gas treatment process in which ammonia is added to the flue gas to react with NO over a catalyst [139]. The primary overall reactions for this process can be expressed as:

$$4NO + 4NH_3 + O_2 \xrightarrow{\text{Catalyst}} 4N_2 + 6H_2O \quad (9)$$

$$2NO_2 + 4NH_3 \xrightarrow{\text{Catalyst}} 3N_2 + 6H_2O \quad (10)$$

SCR catalysts are made of a solid ceramic material that contains active catalytic components. The ceramic may be in the form of a honeycomb monolith or it may be wash coated onto a ceramic, metal, or fiber substrate [140]. The typical operating temperature range for available catalysts is shown in Fig. 12. Noble metal catalysts, such as platinum-palladium formulations, function at lower temperatures (150–290°C; 300–550°F) than base metal and zeolite catalysts but are susceptible to deactivation by sulfur oxides. Base metal catalysts, such as vanadium-titanium formulations, function at temperatures in the range of 260–490°C (500–900°F) and are more resistant to sulfur deactivation. Zeolite catalysts operate at a temperature range above that of the other catalysts (340–590°C, 650–1,100°F) and have shown a good resistance to poisoning from trace elements in coal such as arsenic. The majority of SCR technology applications to pulverized coal-fired boilers use vanadia-titania catalysts as they are widely available and have good resistance to deactivation by sulfur oxides in the flue gas. Catalyst formulations are specific to the catalyst manufacturer and may include the addition of other base metal oxides to increase the catalyst activity, to increase poison resistance, to minimize ammonia slip, and to reduce SO_2 oxidation to SO_3.

To meet the temperature requirements for vanadia-titania catalysts, the catalyst needs to be installed in the flue gas path between the boiler economizer and air preheater. The arrangement for both new and retrofit SCR systems depends upon the boiler and balance of plant equipment arrangement [141, 142]. Typically,

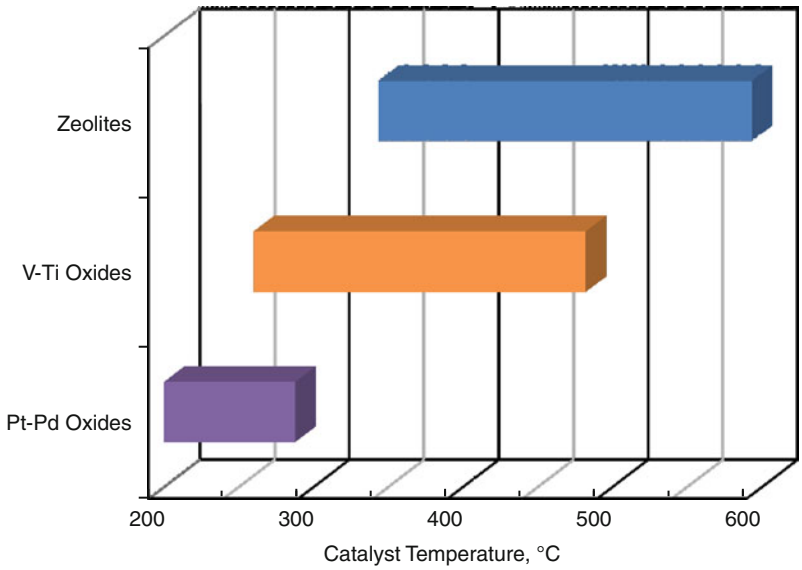

Pulverized Coal-Fired Boilers and Pollution Control. Figure 12
Operating range for various SCR catalyst formulations

one or two layers of catalyst are incorporated into a catalyst housing or reactor. Flue gas from the economizer exit is either routed in a horizontal duct to the top of the reactor where it then flows downward over the catalyst. Alternatively, the ductwork arrangement may need a vertical upward duct followed by a 180° transition into the top of the reactor. Ammonia is injected into the flue gas upstream of the SCR reactor using an ammonia injection grid that typically consists of a series of injection lances spaced across the duct and designed to provide good mixing of the ammonia with the flue gas. Static mixers and flow conditioning devices such as turning vanes are used to ensure uniform distribution of the ammonia and flue gas within the ductwork.

A number of factors need to be considered in designing an SCR system, including reactor location and design, catalyst type and configuration, and the location and design of the ammonia injection grid. The catalyst space velocity and uniformity of ammonia and flue gas distribution all influence system performance. Coal properties are an important consideration for catalyst selection [143]. In general, since the SCR system is separate from the combustion process and since the extensive retrofit requirements permit the design to be optimized, the overall control performance is less influenced by boiler characteristics than the other NO_X control technologies described previously. On the other hand, the cost of installing an SCR system is very sensitive to site-specific factors due to the extensive retrofit requirements [144]. NO_X reduction in the range of 70–90% is expected for application of SCR to coal-fired boilers.

Future Directions

Significant steps have been taken to reduce air pollutant emissions from coal-fired power plants throughout the developed countries in the world. Promulgation of more stringent emission limits in various counties will require further application of these technologies to smaller power plants and place constraints on new power plants. The cost of the air pollution control technologies is a challenge with both retrofit and new technologies and, hence, research and technology development is focused on reducing both the capital and operating costs of these technologies, on improving performance to meet stricter standards, and on improving equipment reliability and availability. In addition, due to concerns over emissions of air toxic compounds from coal-fired power plants, the potential positive and negative impacts of existing air pollution control equipment on these emissions is an area of active investigation.

Bibliography

1. International Energy Agency (2010) World energy outlook 2010. International Energy Agency, Paris
2. World Coal Insitute (2009) The coal resource, a comprehensive overview of coal. World Coal Insitute, London
3. Freese B (2003) Coal: a human history. Perseus, Cambridge, MA
4. Stuart R (1824) A descriptive history of the steam engine. John Knight and Henry Lacey, London
5. Burn RS (1854) The steam engine. H. Ingram, London
6. Thurston RH (1903) A history of the growth of the steam engine, 4th edn. D. Appelton, New York, Revised
7. Tagliaferro L (2003) Thomas Edison: inventor of the age of electricity. Lerner, Minneapolis
8. Woodside M (2007) Thomas A. Edison: the man who lit up the world. Sterling, New York
9. Babcock & Wilcox Company (1992) Steam: its generation and use, Fortieth edition. Babcock & Wilcox, Barberton
10. Combustion Engineering, Inc (1981) Combustion: fossil power systems, 3rd edn. Combustion Engineering, Windsor
11. Heidorn KC (1978) A chronology of important events in the history of air pollution meteorology to 1970. Bulletin of the American Meteorological Society, vol 59, issue 12. American Meteorological Society, Toronto, pp 1589–1597
12. Thorshiem P (2006) Inventing pollution: coal, smoke, and culture in Britain since 1800. Ohio University Press, Athens
13. Jacobs C, Kelly WJ (2008) Smogtown: the lung-burning history of pollution in Los Angeles. The Overlook Press, New York
14. Brimblecombe P (1987) The big smoke: a history of air pollution in London since medieval times. Methuen, London
15. Greater London Authority (2002) 50 years on: the struggle for air quality in London since the great smog of December 1952. Greater London Authority, London
16. Davis DL (2002) When smoke ran like water: tales of environmental deception and the battle against pollution. Basic Books, New York
17. Reitze AW (2005) Stationary source air pollution law. Environmental Law Institute, Washington, DC
18. Martineau RJ, Novello DP (2004) The clean air act handbook. American Bar Association, Chicago
19. U.S. Environmental Protection Agency (2005) Review of the National Ambient Air Quality Standards for particulate matter. Policy assessment of scientific and technical information. OAQPS staff paper. EPA-425/R-05-005a. Office of Air Quality Planning and Standards, Research Triangle Park
20. U.S. Environmental Protection Agency (2009) Integrated science assessment for particulate matter. Office of Research and Development, Research Triangle Park. EPA/600/R-08/139F
21. U.S. Environmental Protection Agency (2004) Air quality criteria for particulate matter. EPA/600/P-99/002aF. Office of Research and Development, Research Triangle Park
22. U.S. Environmental Protection Agency (2008) Integrated science assessment for sulfur oxides – health criteria. EPA/600/R-08/047F. Office of Research and Development, Research Triangle Park
23. U.S. Environmental Protection Agency (2008) Integrated science assessment for oxides of nitrogen – health criteria. EPA/600/R-08/071. Office of Research and Development, Research Triangle Park
24. Glass NR (1979) Environmental effects of increased coal utilization: ecological effects of gaseous emissions from coal combustion, vol 33. U.S. National Institute of Environmental Health Sciences, Research Triangle Park, pp 249–272
25. Bennett DA, Goble RL, Linhurst RA (1985) The acidic deposition phenomenon and its effects: critical assessment document. EPA/600/8-85/001. U.S. Environmental Protection Agency, Office of Research and Development, Research Triangle Park
26. National Acid Precipitation Assessment Program (2005) National Acid Precipitation Assessment Program report to Congress: an integrated assessment. National Acid Precipitation Assessment Program
27. U.S. Environmental Protection Agency (1997) Nitrogen oxides: impacts on Public Health and the Environment. EPA-452-R-97-002. Office of Air and Radiation, Research Triangle Park
28. U.S. Environmental Protection Agency (1999) Nitrogen oxides (NOx), why and how they are controlled. EPA-456/F-99-006R. Office of Air Quality Planning and Standards, Research Triangle Park
29. McConville A (1997) Emissions standards handbook. IEACR/96. IEA Coal Research, London
30. U.S. Environmental Protection Agency (2000) Air quality criteria for carbon monoxide. EPA 600/P-99/001F. Office of Research and Development, Washington, DC
31. U.S. Environmental Protection Agency (1998) Study of hazardous air pollutant emissions from Electric Utility Steam Generating Units. Final report to congress, vols 1 and 2. EPA-453/R-98-004a, b. Office of Air Quality Planning and Standards, Research Triangle Park
32. U.S. Environmental Protection Agency (1997) Mercury study report to congress, vols I–VII. EPA-452/R-97-003, 010. Office of Air Quality Planning and Standards, Research Triangle Park
33. U.S. Environmental Protection Agency (2000) Regulatory finding on the emissions of hazardous air pollutants from Electric Utility Steam Generating Units, vol 65(245). Federal Register, Research Triangle Park, pp 79825–79831
34. National Research Council (2000) Toxicological effects of methylmercury. National Academy Press, Washington, DC
35. European Commission (2001) Ambient air pollution by mercury (Hg). Position paper. Office for Official Publications of the European Communities, Luxembourg
36. Environment Canada (2010) Risk management strategy for mercury
37. UNEP Chemicals Branch, DTIE (2010) The global atmospheric mercury assessment: sources, emissions and transport. United Nations Environment Programme, Geneva
38. US Environmental Protection Agency (2011) National Emission Standards for Hazardous Air Pollutants from Coal and Oil-Fired Electric Utility Steam Generating Units and Standards of

Performance for Fossil Fuel-Fired Electric Utility, Industrial-Commercial- Institutional, and Small Industrial-Commercial-Institutional Steam Generating Units, vol 76(85). Federal Register, Research Triangle Park, pp 24976–25147
39. Mitchell JFB (1989) The "Greenhouse" effect and climate change, vol 27, No 1. American Geophysical Union, Washington, DC, pp 115–139
40. U.S. Environmental Protection Agency (1995) Compliation of air pollutant emissions factors, 5th edn. AP-42. Office of Air Quality Planning and Standards, Research Triangle Park
41. Eggleston HS, Buendia L, Miwa K, Ngara T, Tanabe K (eds) (2006) 2006 IPCG guidelines for National Greenhouse Gas Inventories. National Greenhouse Gas Inventories Programme. Intergovernmental Panel on Climate Change, Hayama, Kanagawa
42. Ciferno JD, Fout TE, Jones AP, Murphy JT (2009) Capture carbon from existing coal-fired power plants, Chemical Engineering Progress. American Instutite of Chemical Engineers, New York, pp 33–41
43. IRA Greenhouse R&D Programme (2007) CO_2 capture ready plants. Report No. 2007/4. International Energy Agency, Cheltenham
44. Newton GH, Schieber C, Socha RG, Kramlich JC (1990) Mechanisms governing fine particulate emissions from coal flames. DOE/PC/73743-T8. U.S. Department of Energy, Pittsburgh
45. Gluskoter HJ (1978) An introduction to the occurrence of mineral matter in Coal. [ed.] Richard W. Bryers. Ash deposits and corrosion due to impurities in combustion gases. Hemisphere Publishing Department, Washington, DC, pp 3–19
46. Chen Y, Shah N, Huggins FE, Huffman GP, Linak WP, Andrew Miller C (2004) Investigation of primary fine particulate matter from coal combustion by computer-controlled scanning electron microscopy, vol 85. Fuel Processing Technology, Elsevier, Amsterdam, pp 743–761
47. Folsom BA, Heap MP, Pohl JH (1986) State-of-the-art review summary and program plan. Effects of coal quality on power plant performance and costs, vol 1. Report No. CS-4283. Electric Power Research Institute, Palo Alto
48. Miller CA, Linak WP (2002) Primary particles generated by the combustion of heavy fuel oil and coal. Review of research results from EPA's National Risk Management Research Laboratory. EPA-600/R-02-093. U.S. Environmental Protection Agency, Office of Research and Development, Research Triangle Park
49. Flagan RC, Seinfeld JH (1988) Fundamentals of air pollution engineering. Prentice Hall, Englewood Cliffs
50. Flagan RC (1978) Submicron particles from coal combustion. In: Proceedings of the seventeenth symposium (international) on combustion. The Combustion Institute, Pittsburgh, pp 97–104
51. Kramlich JC, Chenevert B, Park J, Hoffman DA, Butcher EK (1996) Suppression of fine ash formation in pulverized coal flames. Final Technical Report prepared for DOE Grant No. DE-FG22-92PC92548. U.S. Department of Energy, Pittsburgh Energy Technology Center, Pittsburgh
52. Acurex Environmental Corporation (1993) Emission factor documentation for AP-42 Section 1.1 bituminous and subbituminous coal combustion. U.S. Environmental Protection Agency, Office of Air Quality Planning and Standards, Research Triangle Park
53. Attar A, Dupuis F (1979) Data on the distribution of organic sulfur functional groups in coal. Preprints of the Papers of the Spring National Meeting of the Division of Fuel Chemistry, vol 24(1). American Chemical Society, Honolulu, pp 166–177
54. Pershing DW, Silcox GD (1988) SO_x fundamentals. Combustion of solid fuels – a one week intensive course. International Flame Research Foundation, Noordwijkerhout
55. Davis K, Dissel A, Valentine J (2001) The evolution of pyritic and organic sulfur from pulverized coal particles during combustion. The 2nd joint meeting of the US Sections of The Combustion Institute. The Combustion Institute, Oakland
56. Muller III CH, Schofield K, Steinberg M, Broida HP (1978) Sulfur chemistry in flames. In: Proceedings of the seventeenth symposium (international) on combustion. The Combustion Institute, Pittsburgh, pp 867–879
57. Kramlich JC, Malte PC, Grosshandler WL (1981) The reaction of fuel-sulfur in hydrocarbon combustion. In: Proceedings of the eighteenth symposium (international) on combustion. The Combustion Institute, Pittsburgh, pp 151–161
58. Shao D, Hutchinson EJ, Heidbrink J, Pan W-P, Chou C-L (1994) Behavior of sulfur during coal pyrolysis. J Anal Appl Pyrolysis 30:91–100. Elsevier, Amsterdam
59. Castaldini C, Angwin M (1977) Boiler design and operating variables affecting uncontrolled sulfur emissions from pulverized-coal-fired steam generators. EPA-450/3-77-047. U.S. Environmental Protection Agency, Research Triangle Park
60. Folkedahl BC, Zygarlicke CJ (2004) Sulfur retention in North Dakota lignite coal ash. Preprints of the papers of the spring national meeting of the Division of Fuel Chemistry, vol 49(1). American Chemical Society, Anaheim, pp 167–168
61. Blythe G, Dombrowski K (2004) SO3 mitigation guide update. Report No. 1004168. Electric Power Research Institute, Palo Alto
62. Srivastava RK, Miller CA, Erickson C, Jambhekar R (2004) Emissions of sulfur trioxide from coal-fired power plants. J Air Waste Manag Assoc 54:750–762. Air and Waste Management Association, Pittsburgh
63. Glassman I (1987) Combustion, 2nd edn. Academic, Orlando
64. Fenimore CP (1971) Formation of nitric oxide in premixed hydrocarbon flames. In: Proceedings of the thirteenth symposium (international) on combustion. The Combustion Institute, Pittsburgh, pp 373–389
65. Pershing DW, Wendt JOL (1977) The influence of flame temperature and coal composition on thermal and fuel NO_x. In: Proceedings of the sixteenth symposium (international) on combustion. The Combustion Institute, Pittsburgh, pp 389–399
66. Sarofim AF, Beér JM (1990) The fate of fuel nitrogen and ash during combustion of pulverized coal, Chapter 4. In: Lemieux PM, Air and Energy Engineering Research Laboratory (eds)

Pulverized coal combustion: pollutant formation and control, 1970–1980. U.S. Environmental Protection Agency, Air and Energy Engineering Research Laboratory, Research Triangle Park
67. Hayhurst AN, Vince IM (1980) Nitric oxide formation from N2 in flames. Prog Energy Combust Sci 6:35–51. Elsevier, Amsterdam
68. Kelemen SR, Gorbaty ML, Vaughn SN, Kwiatek PJ (1993) Quantification of nitrogen forms in argonne premium coals. Preprints of the papers of the spring national meeting of the Division of Fuel Chemistry, vol 38(2). American Chemical Society, Denver, pp 384–392
69. Mitra-Kirtley S,. Mullins OC, Branthaver J, Van Elp J, Cramer SP (1993) Nitrogen XANES studies of fossil fuels. Preprints of the papers of the fall national meeting of the Division of Fuel Chemistry, vol 38(3). American Chemical Society, Chicago, pp 762–768
70. Solomon PR, Fletcher TH (1994) Impact of coal pyrolysis on combustion. In: Proceedings of the twenty-fifth symposium (international) on combustion. The Combustion Institute, Pittsburgh, pp 463–474
71. Pohl JH, Sarofim AF (1977) Devolatilization and oxidization of coal nitrogen. In: Proceedings of the sixteenth symposium (international) on combustion. The Combustion Institute, Pittsburgh, pp 491–501
72. Rees DP, Smoot LD, Hedman PO (1981) Nitrogen oxide formation inside a laboratory pulverized coal combustor. In: Proceedings of the eighteenth symposium (international) on combustion. The Combustion Institute, Pittsburgh, pp 1305–1311
73. Chen JC, Niksa S (1992) Suppressed nitrogen evolution from coal-derived soot and low-volatility coal chars. In: Proceedings of the twenty-fourth symposium (international) on combustion. The Combustion Institute, Pittsburgh, pp 1269–1276
74. Zhang H (2001) Nitrogen evolution and soot formation during secondary coal pyrolysis. PhD dissertation, Brigham Young University
75. Pohl JH, Chen SL, Heap MP, Pershing DW (1983) Correlation of NOx emissions with basic physical and chemical characteristics of coal. In: Proceedings of the 1982 joint symposium on NOx control, vol 2. Electric Power Research Institute, Palo Alto
76. Pershing DW, Heap MP, Chen SL (1990) Bench-scale experiments on the formation and control of NOx emissions from pulverized coal combustion, Chapter 9. In: Pulverized coal combustion: pollutant formation and control, 1970–1980. U.S. Environmental Protection Agency, Air and Energy Engineering Research Laboratory, Research Triangle Park
77. Chen SL, Heap MP, Pershing DW, Martin GB (1982) Influence of coal composition on the fate of volatile and char nitrogen during combustion. In: Proceedings of the nineteenth symposium (international) on combustion. The Combustion Institute, Pittsburgh, pp 1271–1280
78. Bartok W, Crawford AR, Piegari GJ (1971) Systematic field study of NOx emission control methods for utility boilers. APTD-1163. U.S. Environmental Protection Agency, Office of Air Programs, Research Triangle Park
79. Payne R, Heap MP, Pershing DW (1981) NOx formation and control in pulverized-coal flames. In: Proceedings of the low rank coal technology development workshop, 17–18 June 1981. San Antonio
80. Licht W (1980) Air pollution control engineering, basic calculations for particulate collection. Marcel Dekker, New York
81. Strauss W (1975) Industrial gas cleaning, 2nd edn. Pergamon Press, New York
82. Kinsey JS, Schliesser S, Englehart PJ (1985) Control technology for sources of PM10. Draft report prepared for EPA Contract No. 68-02-03891, work assignment 4. U.S. Environmental Protection Agency, Office of Air Quality Planning and Standards, Research Triangle Park
83. U.S. Environmental Protection Agency (1982) Control techniques for particulate emissions from stationary sources, vol 1. EPA-450/3-81-005a. Emissions Standards and Engineering Division, Research Triangle Park
84. White HJ (1977) Electrostatic precipitation of fly ash. J Air Pollut Control Assoc 27(1):15–21. Air Pollution Control Association, Pittsburgh
85. U.S Environmental Protection Agency (2011) Electrostatic precipitator plan review. APTI Course No. SI:412B. U.S. Environmental Protection Agency, Research Triangle Park
86. White HJ (1977) Electrostatic precipitation of fly ash. Fly ash and furnace gas characteristics. J Air Pollut Control Assoc 27(2):114–120. Air Pollution Control Association, Pittsburgh
87. Turner JH, Lawless PA, Yamamoto T, Coy DW, Mckenna JD, Mycock JC, Nunn AB, Greiner GP, Vatavuk WM (2002) Electrostatic precipitators. In: Mussatti DC (ed) EPA Air pollution control cost manual. U.S. Environmental Protection Agency, Office of Air Quality Planning and Standards, Research Triangle Park. Chapter 3 in Section 6, Particulate matter controls
88. Szabo MF, Shah YM (1979) Inspection manual for evaluation of electrostatic precipitator performance. EPA-340/1-79-007. U.S. Environmental Protection Agency, Division of Stationary Source Enforcement, Washington, DC
89. White HJ (1977) Electrostatic precipitation of fly ash. Precipitator design. J Air Pollut Control Assoc 27(3):206–217. Air Pollution Control Association, Pittsburgh
90. National Air Pollution Control Administration (1969) Control techniques for particulate air pollutants. NAPCA Publication No. AP-51. National Air Pollution Control Administration, Washington, DC
91. Turner JH, Lawless PA, Yamamoto T, Coy DW, Mckenna JD, Mycock JC, Nunn AB, Greiner GP, Vatavuk WM (2002) Baghouses and filters. In: Mussatti DC (ed) EPA air pollution control cost manual. U.S. Environmental Protection Agency, Office of Air Quality Planning and Standards, Research Triangle Park. Chapter 1 in Section 6, Particulate matter controls
92. Cushing KM, Merritt RL, Chang RL (1990) Operating history and current status of fabric filters in the utility industry. J Air Waste Manage Assoc 40(7):1051–1058. Air and Waste Management Association, Pittsburgh
93. Belba VH, Theron Grubb W, Chang R (1992) The potential of pulse-jet baghouses for utility boilers. Part 1: a worldwide survey of users. J Air Waste Manage Assoc 42(2):209–217. Air and Waste Management Association, Pittsburgh

94. Sloat DG, Gaikwad RP, Chang RL (1993) The potential of pulse-jet baghouses for utility boilers. Part 3: comparative economics of pulse-jet baghouse precipitators and reverse-gas baghouses. J Air Waste Manage Assoc 43:120–128. Air and Waste Management Association, Pittsburgh
95. EC/R Incorporated (1998) Stationary source control techniques document for fine particulate matter. Report prepared for EPA Contract No. 68-D-98-026, Work Assignment No. 0-08. U.S. Environmental Protection Agency, Research Triangle Park
96. Felix LG, Cushing KM, Grubb WT, Giovanni DV (1988) Fabric filters for the electric utility industry. In: Guildelines for fabrics and bags, vol 3, CS-5161. Electric Power Research Instutute, Palo Alto
97. Electric Power Research Instutute (2005) Utility boiler baghouse update. Report No. 1010367. Electric Power Research Instutute, Palo Alto
98. Dennis R (1974) Collection efficiency as a function of particle size, shape and density: theory and experience. J Air Pollut Control Assoc 23(12):1156–1161. Air Pollution Control Association, Pittsburgh
99. Carr RC, Smith WB (1974) Fabric filter technology for utility coal-fired power plants. J Air Pollut Control Assoc 34(1):79–89. Air Pollution Control Association, Pittsburgh
100. Carr RC, Cushing KM, Gallaer CA, Smith WB (1992) Fabric filters for the electric utility industry. In: Guidelines for fabric filter design, vol 5, CS-5161. Electric Power Research Institute, Palo Alto
101. Bustard CJ, Cushing KM, Pontius DH, Smith WB (1988) Fabric filters for the electric utility indistry. In: General concepts, vol 1, CS-5161. Electric Power Research Institute, Palo Alto
102. Devitt T, Gestle R, Gibbs L, Hartman S, Klier R (1978) Flue gas desulfurization system capabilities for coal-fired steam generators, vol II. Technical report. U.S. Environmental Protection Agency, Office of Research and Development, Washington, DC, EPA-600/7-78-032b
103. Wojciech J, Singer C, Srivastava RK, Tsirigotis PE (1999) Status of SO_2 scrubbing technologies. EPRI-DOE-EPA combined utility air pollution control symposium. TR-113187-V1. Electric Power Research Institute, Palo Alto
104. Srivastava RK (2000) Controlling SO_2 emissions: a review of technologies. EPA/600/R-00/093. U.S. Environmental Protection Agency, Office of Research and Development, Washington, DC
105. Kohl A, Riesenfeld F (1985) Gas purification, 4th edn. Gulf, Houston
106. Weiler H, Ellison W (1997) Wet gypsum-yielding FGD experience using quicklime reagent. EPRI-DOE-EPA combined utility air pollutant control symposium. The mega symposium. TR-108683-V2. Electric Power Research Institute, Palo Alto
107. United Engineers and Constructors, Inc (1991) Economic evaluation of flue gas desulfurization systems. GS-7193, vol 1. Electric Power Research Institute, Palo Alto
108. United Engineers and Constructors, Inc (1992) Economic evaluation of flue gas desulfurization systems. GS-7193, vol 2. Electric Power Research Institute, Palo Alto
109. United Engineers and Constructors, Inc (1995) Economic evaluation of flue gas desulfurization systems. GS-7193-V3, vol 3. Electric Power Research Institute, Palo Alto
110. Fox MR, Hunt TG (1990) Flue gas desulfurization using dry sodium injection. Presented at the EPA/EPRI 1990 SO_2 control symposium. s.n., New Orleans
111. Radojevic M (1991) Scrubbing of flue gases with sea-water. Presented at the AFRC/JFRC international conference on environmental control of combustion processes, 7–10 October 1991. s.n., Honolulu
112. Zhou W, Maly P, Brooks J, Nareddy S, Swanson L, Moyeda D (2010) Design and test furnace sorbent injection for SO_2 removal in a tangentially fired boiler. Environmental Engineering Science, vol 27, Number 4, Mary Ann Liebert, New Rochelle, pp 337–345
113. Nolan PS (1996) Emission control technologies for coal-fired power plants. Presented at the People's Republic of China Ministry of Electric Power seminar, 22–25 April 1996, s.n., Beijing
114. Henzel DS, Laseke BA, Smith EO, Swenson DO (1982) Handbook for flue gas desulfurization scrubbing with limestone. Noyes Data Corporation, Park Ridge
115. Miller SF, Miller BG, Scaroni AW (1997) Limestone performance in a pilot-scale forced oxidation scrubber. EPRI-DOE-EPA combined utility air pollutant control symposium. The mega symposium. TR-108683-V2, Electric Power Research Institute, Palo Alto
116. Brogen C, Klingspor JS (1997) Impact of limestone grind size on WFGD performance, August. EPRI-DOE-EPA combined utility air pollutant control symposium. The mega symposium. TR-108683-V2. Electric Power Research Institute, Palo Alto
117. Blythe G, Horton B, Rhudy R (1999) EPRI FGD operating and maintenance cost survey. EPRI-DOE-EPA combined utility air pollution control symposium. TR-113187-V1, Electric Power Research Institute, Palo Alto
118. Masters K (1985) Spray drying handbook, 4th edn. Wiley, New York
119. Burnett TA, Anderson KD (1981) Technical review of dry FGD systems and economic evaluation of spray dryer FGD systems. EPA-600/7-81-014. U.S. Environmental Protection Agency, Office of Research and Development, Washington, DC
120. Lachapelle DG, Brown JS, Stern RD (1974) Overview of environmental protection agency's NOx control technology for stationary combustion sources. Presented at the 67th annual meeting American Insitute Of Chemical Engineers
121. Srivastava RK, Hall RE, Khan S, Culligan K, Lani BW (2005) Nitrogen oxides emission control options for coal-fired electric utility boilers. J Air Waste Manage Assoc 55:1367–1388. Air and Waste Management Association, Pittsburgh
122. Hjalmarsson A-K (1990) NOx control technologies for coal combustion. IEACR/24. IEA Coal Research, London
123. U.S. Environmental Protection Agency (1992) Evaluation and costing of NOx controls for existing utility boilers in the NESCAUM region. EPA-453/R-92-010. Office of Air Quality Planning and Standards, Research Triangle Park

124. U.S. Environmental Protection Agency (1994) Alternative control technologies document: NOx emissions from utility boilers. EPA-453/R-94-023. Office of Air Quality Planning and Standards, Research Triangle Park
125. Heap MP, Folsom BA (1990) Optimization of burner/combustion chamber design to minimize NOx formation during pulverized coal combustion, Chapter 10. In: Pulverized coal combustion: pollutant formation and control, 1970–1980. U.S. Environmental Protection Agency, Air and Energy Engineering Research Laboratory, Research Triangle Park
126. Sommer TM, Jensen AD, Melick TA, Orban PC, Christensen MS (1993) Applying European low NOx burner technology to U.S. installations. Presented at the 1993 EPRI/EPA joint symposium on stationary combustion NOx control, 24–27 May 1993. EPRI/EPA, Miami Beach
127. LaRue AD (1989) The XCL burner – latest developments and operating experience. Presented at the 1989 EPRI/EPA joint symposium on stationary combustion NOx control, 6–9 Mar 1989. EPRI/EPA, San Francisco
128. Vatsky J, Sweeney TW (1991) Development of an ultra-low NOx pulverizer coal burner. Presented at the 1991 EPRI/EPA joint symposium on stationary combustion NOx control, 25–28 Mar 1991. EPRI/EPA, Washington, DC
129. U.S. Department of Energy (1996) Reducing emissions of nitrogen oxides via low-NOx burner technologies. Topical report number 5. U.S. Department of Energy, Pittsburgh
130. Campbell LM, Stone DK, Shareef GS (1991) Sourcebook: NOx control technology data. U.S. Environmental Protection Agency, Research Triangle Park
131. Wendt JOL, Sternling CV, Matovich MA (1973) Reduction of sulfur trioxide and nitrogen oxides by secondary fuel injection. In: Proceedings of the fourteenth symposium (international) on combustion. The Combustion Institute, Pittsburgh, pp 897–904
132. U.S. Environmental Protection Agency (1996) Control of NOx emissions by reburning. EPA/625/R-96/001. U.S. Environmental Protection Agency, Cincinnati
133. Chen SL, McCarthy JM, Clark WC, Heap MP, Seeker WR, Pershing DW (1986) Bench and pilot scale process evaluation of reburning for in-furnace NOx reduction. In: Proceedings of the twenty-first symposium (international) on combustion. The Combustion Institute, Pittsburgh, pp 1159–1169
134. Payne R, Moyeda DK (1994) Scale up and modeling of gas reburning. In: Moussa A, Presser C, Rini MJ, Weber R, Woodward G, Gupta AK (eds) Combustion modeling, scaling and air toxins. ASME FACT, vol 18. American Society of Mechanical Engineers, New York, pp 115–122
135. Lyon RK (1987) Thermal DeNOx, controlling nitrogen oxides emissions by a noncatalytic process. Environ Sci Technol 21(3):231–236. American Chemical Society, Washington, DC
136. Jødal M, Nielsen C, Hulgaard T, Dam-Johansen K (1990) Pilot-scale experiments with ammonia and urea as reductants in selective non-catalytic reduction of nitric oxide. In: Proceedings of the twenty-third symposium (international) on combustion. The Combustion Institute, Pittsburgh, pp 237–243
137. Muzio L, Quartucy G (1993) State-of-the-art assessment of SNCR technology. Topical Report No. TR-102414. Electric Power Research Institute, Palto Alto
138. Berg M, Bering H, Payne R (1993) NOx reduction by urea injection in a coal fired utility boiler. Presented at the 1993 EPRI/EPA joint symposium on stationary combustion NOx control, 24–27 May 1993. EPRI/EPA, Miami Beach
139. U.S. Department of Energy (2005) Selective catalytic reduction (SCR) technology for the control of nitrogen oxide emissions from coal-fired boilers. Topical Report Number 23. U.S. Department of Energy, Pittsburgh
140. Pereira CJ, Amiridis MD (1995) NOx control from stationary sources: overview of regulations, technology, and research frontiers, Chapter 1. In: Umit S, Agarwal SK, Marcelin Ozkan G (eds) Reduction of nitrogen oxide emissions. American Chemical Society, Washington, DC, pp 1–13
141. Nischt W, Woolridge B, Bigalbal J (1999) Recent SCR retrofit experience in coal-fired boilers. Presented at POWER-GEN international, 30 Nov–2 Dec 1999. New Orleans
142. Tonn DP, Uysal TA (1998) 220 MW SCR installation on new coal-fired project. Presented at the Institute of Clean Air Companies ICAC forum '98, 18–29 Mar 1998, Durham
143. Khan S, Shroff G, Tarpara J, Srivastava R (1997) SCR applications: addressing coal chacteristics concerns. EPRI-DOE-EPA combined utility air pollutant control symposium – the mega sumposium. Technical report TR-108683-V1. Electric Power Research Institute, Palo Alto
144. Foerter D, Jozewicz W (2001) Cost of selective catalytic reduction (SCR) application for nox control on coal-fired boilers. EPA/600/R-01/087. U.S. Environmental Protection Agency, Office of Research and Development, Washington, DC

PV Policies and Markets

Wolfgang Palz
Former EU Commission Official, World Council for Renewable Energy (WCRE), Brussels, Belgium

Article Outline

Glossary
Definition of the Subject
Introduction
State of PV Solar Electricity Today: An Overview
Historical Political Development: Initiating a Market Explosion
Future Directions: PV's Promise in a 100% Renewable Energy Strategy
Bibliography

Glossary

Energy and power Power is the capacity to generate electric energy. The power capacity is measured in Watts, kW (1,000 W), MW, GW, etc. The energy is measured in "Watt hours," kWh, etc.

Feed-in tariff, FiT or FIT It is a tariff imposed by national legislation that grid operators have to pay for PV electricity delivered on their net by the PV generator operators. It is measured in cents/kWh. It is mostly employed in the European Union.

Green certificates In some countries such as the UK, some US states, and Belgium, the kWh of PV sold to the grid are paid with certificates whose value is defined by legislation. Those can be traded on the market place.

Inverters Inverters are electronic devices that convert the DC (direct current) generated in the PV modules into AC (alternating current).

National REAP in the EU In the frame of its Directive "Energy and Climate," the European Union has agreed with all 27 EU Member Countries the REAP, i.e., the "Renewable Energy Action Plans." They are mandatory obligations and must be implemented by 2020. In this frame each country has a particular target for PV implementation.

Plus-energy buildings Buildings whose energy consumption is more than compensated by internal energy production. This is generally achieved by means of PV integrated onto the buildings.

PV cells, modules, systems *PV cells* are made from silicon or other semiconductor materials. They are less than 0.5 mm thin. When interconnected by metal strips, cells are integrated into *PV modules*. They have typically a power rating of up to 200 W and may be 2 m^2 large. *PV systems* are power generators ready for use to produce electricity for a given purpose: feeding into an electric grid, supplying any appliance, in particular a whole building with power.

PV: photovoltaics Semiconductor plates that generate DC electricity when exposed to light, namely, the Sun's radiation.

Thin-film cells, a-silicon (a-Si), mc-silicon (mc-Si) *Thin-film cells* are 100 times thinner than crystalline silicon cells. They do not come as individual cells but are integrated into larger modules during the deposition of the thin semiconducting layers on a substrate. *Amorphous silicon* has no crystalline structure but one that is similar to glass; it contains a few percentages of hydrogen. *mc-Si layers* are made of silicon microcrystals in the range of a few nanometers. Layers of mc-Si are often deposited on top of an a-Si layer.

Definition of the Subject

The large-scale generation of solar electricity by means of photovoltaics (PV) was traditionally considered excessively expensive and particularly problematic because of the Sun's intermittency and the claim that the PV areas needed for deployment were prohibitively large.

Nevertheless, starting from a low level some 30 years ago, the global PV markets never stopped growing. In this very year 2011, the level of 60 GW of power will be exceeded globally for the first time. In the longer run, a major share of all the world's electricity demand could eventually be supplied by PV. The reasons for the new market success of PV are manifold and are presented in detail in this article.

Introduction

Large-scale power generation by means of photovoltaic conversion of the Sun's rays into electricity is a newcomer in the global electricity markets. The underlying reasons for this new interest are associated with the growing concern about the global effects of climate change and additionally with the challenge of security of energy supply. This has recently been illustrated again by the problems and new concerns raised after the nuclear accident in Japan and the threat of continuously growing oil prices on the world markets.

PV is one of the solutions to address these problems. The Sun that supplies the fuel for PV power generation is accessible everywhere. In concert with the other forms of renewable energies, PV can play an ever-growing role with the prospect of achieving ultimately a 100% renewable energy supply worldwide.

The intermittency problems of PV power can be solved in combination with hybrid power supply systems associated with the development of electricity storage in batteries and other devices resulting from the increased interest in electric cars and electric transport in general.

Further, PV has the particular interest of making it possible to go progressively to a more decentralized electricity supply system and reducing the needs for larger transport and distribution networks of power.

The entry starts by providing a comprehensive update on the PV's status today around the world. Emphasis is being put on the tremendous developments that occurred in particular during the last 2 years, 2009 and 2010. Investments in new module production lines in the GW range have induced tremendous decreases of costs and prices and consequently an explosion of the world markets.

A particular analysis is addressed to the national market support schemes. The reasons why "PV tariff" systems – involving many billions of $ – are positively viewed in some countries and in others not are for the first time analyzed in detail in such a publication.

Before attempting an outlook in the short and longer term future, the entry goes back for a moment to recall the historical events and the political fighting that was needed to kick start the market growth that the world has seen since the early years of 2000.

The article is closed by a comprehensive overview of PV references with emphasis of the many currently available sources from publications on the Internet.

State of PV Solar Electricity Today: An Overview

Global PV Markets

In 2010 a PV power capacity of 18,000,000 kW or 18,000 MW, i.e., 18 GW was newly installed. This is reported by the British Market research company IMS [1]. For the first time ever, more than 10 GW of PV capacity were globally installed and connected to an electric grid in one single year. 18 GW represent an overall collector area of over 120 km^2 – as 1 kW of "peak power" corresponds typically to a module area of some 7 m^2.

They stand for a global market volume of 70 billion USD or 50 billion €, just for the modules. On average the PV modules make up for 50% of the total cost of a turnkey system. When including the balance of system, installation costs, etc., global PV business attained a total market value of 100 billion € in 2010.

Over 80% of the global new PV capacity was installed in Europe. For the first time Europe set up more PV than wind power that year and more than any other form of conventional power.

To measure what has been achieved in the last 30 years it should be reminded that in the year 1980 world sales of PV amounted to just 4 MW [2], that is 4,500 times less than now. During the last 30 years the global PV market never stopped growing but with a rate of 130%, last year was also exceptional from this point.

IMS [1] announced also for 2010 a global PV cell and module manufacturing capacity of 34.5 GW in place. But only a part of it was in full production. A total area of 22 GW were actually produced, of which next to the 18 GW that were sold in the markets, some 4 GW went to inventory.

With *annual capacities* of 7.4 GW, 3.5 GW, and 1.36 GW installed during 2010 Germany, Italy, and the Czech Republic were globally number 1, 2, and 3 on the global hit list. All other nations including the USA had less than 1 GW newly connected during 2010. In summary this is the following ranking of new PV installations for the single year 2010:

1. Germany 7.4 GW
2. Italy 3.5 GW
3. Czech Republic 1.36 GW
4. Japan 991 MW
5. USA 878 MW
6. France 720 MW
7. Belgium 355 MW

This is a snapshot for 2010: It is already clear by now that this order is going to change in the future because of the restrictions in some countries that are similar to those Spain had taken in 2009.

The *cumulated* PV capacity installed worldwide looks like this:

In total a world PV capacity of over 38 GW is by now in early 2011 connected to the electricity networks. With this, some 6 GW of stand-alone PV must be included in the global account [3]. In total there was at year's end 2010 some 44 GW of PV in all sizes installed worldwide. As it is expected that more than 20 GW will be newly added worldwide in 2011, the global PV capacity will have reached 65 GW in early 2012.

Almost half of all globally grid-connected PV was in place in Germany: 17.3 GW. Next to Germany, Italy

stands out as a brilliant second with a total of 7 GW installed – even though part of it was not yet grid-connected at the end of 2010 (Although the orders of magnitude were different it is interesting to note that in the 1990s the national R&D budgets for European PV came in the same order: Germany first and Italy second [4]). The Czech Republic had a *cumulated* capacity of 1.82 GW at the end of 2010.

On March 22, 2011, Germany had at one time more PV capacity feeding electricity to the grids, i.e., 12.1 GW than all nine atomic power plants in operation with 12 GW; it was a breakthrough.

The market in Germany favors decentralized PV deployment: In total 860,000 individual PV generators were in operation there at the end of 2010. Of them 230,000 have been installed just in the last year [5]. Fifty eight percent of the newly installed PV capacity went for systems with a capacity under 100 kW – most of those had a capacity between 10 and 100 kW [6].

In Italy 250,000 plants were widely distributed over the country at the end of 2010 [7].

Of Japan's 991 MW PV market in 2010, an overwhelming majority was installed on 200,000 residential households (803 MW) [8].

In early 2011, there is a total worldwide installation of well over 1.5 million individual PV plants connected to the electricity grids.

Even though a high number of PV plants were attached to a building envelope, the proper "building integrated PV, BIPV" in the architectural sense remained in an early stage of development. Keeping in mind that in particular in Europe national policies are moving now in favor of the so-called plus energy buildings and hundreds of thousands of them are going to be built, BIPV will have a great future: A building's energy balance where it produces more energy than it consumes is difficult to achieve without proper integration of PV.

It is true to say, however, that currently the ground-mounted utility-scale projects take a considerable share of the global PV market: In the USA about half of the capacity installed in 2009 was for system sizes of over 100 kW [9]. The reasons for this preference for larger plants are in general, among others, local bureaucracy and the kind of administrative regulations that make the procedures for small systems cumbersome. The same was true when Spain had its big PV boom before 2009.

The largest single PV project identified in 2010 [10] was Sarnia with 97 MW in Ontario, Canada; not far behind came Montalto di Castro in Italy with 84 MW. In Arizona, a 290 MW PV installation is currently being built in Agua Caliente, and in China are talks in progress of a 2 GW PV system that would be built in steps in the next few years.

PV power plants are indeed unique as they cover a range of over 12 orders of magnitude of capacity: mW for watches and pocket calculators, some Watts for street lights, solar-home systems, SHS, in the poor villages, kW for building integration, and MW and GW, the sizes of conventional centralized power plants.

China currently dominates the world market of PV modules: half of the PV modules sold in 2010 were manufactured in China; plus some 8% in Taiwan [11]. This impressive proportion did increase all the time over the last few years. Virtually all of it is exported as China has by now no significant home market for PV.

What are the reasons for China's competitive edge in current world markets? This author believes that it is certainly true that the Chinese industry is very effective in bringing products of high quality to the market; but the essential reason for its market dominance seems rather to be the undervaluation of the Chinese currency, the Yuan. In the end this very situation was – together with the national support schemes for PV in some countries – the driving force that triggered a revolutionary decrease of cost and prices on the world's PV markets and correspondingly the developments of these markets as have been seen over the last few years.

As could be expected, many nations such as the USA and France are unhappy with the dominance of imported PV products on their home markets. Some try to react with "local content rules" imposing that 50% or more should come from domestic production [12]. Germany being a world's leading export nation, makes a point of following a liberal route and accepts all the PV imports: But still, German PV industry has a strength of its own and was able to keep a share of 40% in its domestic market while 50% came from China [13].

In terms of technology, thin film modules had a share of 13% of global PV market in 2010 while a year earlier that share stood at 17% [11]. This may

look disappointing for the "thin-film enthusiasts" but it still means an increase in absolute terms. The reason for the ongoing dominance of crystalline silicon in the markets has to do with the vitality of the Chinese producers who are not so much interested in thin films for the time being; another reason is maybe that it took more time than previously thought to bring cells of the young CIS/CIGS family from laboratory to mass production.

PV's Role in General Electricity Supply

A PV array of 1 kW will typically generate an electric energy of between 1,000 and 2,000 kWh over a whole year; in the winter months production will generally be about half of what can be expected in the summer. Details will obviously depend on the climate at the place of installation, if the array is fixed-plate or tracking the sun, and other constraints. As an order of magnitude, a PV generator produces per kW and year in terms of energy only half of that of a wind turbine at a "typical" wind regime. It also produces less per kW than most conventional power plants.

But what counts in the end is the kWh cost.

In that respect, latest reports in the media tend to become most optimistic about PV's competitiveness with some of the key electricity providers of today: two scientists of the Duke University in North Carolina came recently to the conclusion that PV is indeed getting competitive with modern nuclear plants [14]; also in the United Kingdom an industry participant has claimed that the proposed atomic plants foreseen for construction in the country will not be able to match the price of solar electricity [15]. Concerning the outlook for competition with natural gas – arguably the cheapest electricity in the market today – it is noteworthy that the utility Southern California Edison filed recently the request of approval for a total of 250 MW of PV at lower price than electricity from combined-cycle natural gas plants [16].

With respect to other renewable sources of electricity, too, "expensive PV" as conservative politicians like to call it, started recently to look a lot more attractive: The cost information about "concentrating solar plants CSP" is traditionally much more opaque than that for PV, but the message is eventually spreading that CSP's promise should be seen with caution [17].

A significant revolution with respect to wind energy occurred also in 2010 in Germany: 7.4 GW of PV were installed in the country and only 1.55 GW of wind power. Traditionally the relation used to be the other way around. Some years ago when Germany was a world leader for wind power, PV deployment was yet at an embryonic stage. As far as off-shore wind is concerned, latest cost figures also indicate that PV is getting competitive here faster than previously thought.

As of today a relevant region with a particularly high contribution of PV to its overall electricity consumption is the German "Free State of Bavaria": With over 6 GW of installed PV capacity Bavaria has since 2011 exceeded a 7% PV electricity supply to its overall consumption. By the end of 2011 this proportion will no doubt go to 10%: When buying a BMW or an AUDI car that are actually Bavarian products, the fact is that solar energy has already now a nice share embedded in these cars.

Germany as a whole draws now on average 3% of its electricity demand from its PV plants. On favorable days the PV plants produce more than 8 of the country's 14 nuclear power plants [18]. Other countries with significant PV contributions of over 2.5% to their national electrical consumption are Italy and Spain; all other nations stay for the moment well below 1%.

As to transport and distribution of electricity, PV plants are currently well integrated into the low-voltage grids: thanks to local production and consumption, transport over long distances must not be necessary. In that respect PV plants are different from most conventional ones. Even for wind power, long-distance electricity transport is often essential as the consumption centers do not always coincide with the regions of sufficiently high-wind regimes, namely, when offshore wind on the sea is being talked of. For PV that is much less an issue, even though in Germany in areas of high PV deployment the capacity of the medium and low voltage distribution grids may currently become stressed and may need reinforcement. . .

National Policies and the Role of Financial Support

In 1983, it was written [2]: there is a "chicken-and-egg situation: new technology such as PV will not reach large-scale, low-cost commercialisation unless a market

is perceived by the producer. . .. Manufacturers learn to make a cheaper product as output increases. . .. The problem is particularly acute for high capital cost/low running-cost systems such as PV. Another paradox is that, even when economic break-even cost levels have been reached potential customers may still decide to wait in anticipation of further cost reductions. . ..” It was also written: “The only alternative would be for governments to provide the necessary support and turn what is technically feasible into an established fact.”

Another anomaly with respect to PV deployment of those days was the trend to offer “clean solar electricity” at real cost. This cost was and still is obviously higher than the market price of conventional electricity from fossil and atomic sources, but as people declared they were ready to pay more if the electricity was clean – it looked for some promoters as an option. Even though there was never a level-playing field in the electricity market. Subsidies are distorting all market prices in this sector, above all those for the conventional energies: the International Energy Agency IEA in Paris declared that in the year 2009 global subsidies for the fossil energies had been 312 billion USD – not mentioning those for nuclear electricity – compared to 57 billion USD for all forms of renewable energy of which PV was only a small part in that year. In particular from an ethical point of view, higher market prices for solar electricity are an absurdity; it cannot be that one pays less for polluting and unsustainable electricity than for PV: PV has a wealth of environmental and social merits together with those of unlimited supply that make it institutionally desirable everywhere. The external costs of conventional electricity production and supply do have to be included in market prices to compensate what economists call a “market failure” [19].

The market explosion for PV started actually in 2004 with the introduction of the “feed-in tariff, the FiT” in Germany. Elsewhere in this paper the details of the political decision process in those days would be discussed. No doubt, the FiT is at the origin of a global PV market of some 60 GW connected to the grids at the end of 2011. Still in the 1980s and 1990s nobody would have expected such a thrilling success. And in all logic it is currently Germany where the political initiative started that leads the world markets.

The FiT in *Germany* is actually not a subsidy: this was a decision by the highest European Court in a dispute with the German electric utilities. The reason is that the favorable tariffs for the PV electricity that is supplied to the grids are paid by the grid operators and are not coming from public financing sources.

The situation may be different in other countries such as for instance Spain where electricity is anyway partially subsidized by the government and where the tariff payment for PV comes on top of the ongoing subsidy.

The essential features of the FiT are the following: (a) the grid operators have the obligation – unless it is technically just not feasible in a certain situation – to buy any kWh from PV (and other forms of renewable electricity that are specified in the law) that is offered to them at any time; (b) the operators have to pay from their own budget the particular tariff that was decided previously by the government.

There is a large consensus across German society and the industry that the FiT legislation or “EAG EE” as it is called after the latest revision in March 2011 has great value: It allows for reasonable planning and administrative approval schemes, a stable and accountable policy, and last not least attractive “returns on investments” of 8% and more. The FiT system has only winners; everybody gains money with it: the investors, the banks, the communities, the PV industry and its commerce. The money inflow comes from the electric utilities, i.e., eventually from all electricity consumers – with the exception of some industries. In early 2011 all customers, with their exception, contributed for some 8% of the tariff applicable to all electricity they bought from the net. But in reality the part of the FiT in everybody’s electricity bill is only a smaller fraction of all the extras the utilities have added to these bills: between 2002 and 2011 the tariff for consumers was increased by 12 € cents of which the FiT part represented just a quarter [20].

The share of the FiT in the general tariffs is expected to stabilize at about 8% in the future: While the number of plants in the country will keep growing, the FiT is decreasing by decision of the government in line with the decrease of the PV module and system prices (the PV FiT is being cut by 50% between 2009 and 2012) – that is the new agreement reached between the German Government and the PV industry. This decision is a breakthrough as in the past PV investors in Germany made excessive profits when the module prices

decreased faster than the feed-in tariff; that happened in particular in 2009. Since the beginning of 2011, the FiT regulation will be frequently adapted just in phase with the development of the German PV market volume. In this way it can be avoided that profits together with the market volume grow excessively: the target is to keep the market below 5 or 4 GW/year.

As mentioned before, one of the beneficiaries of the PV deployment in Germany are the municipalities: in 2010 the value created in villages, towns, and cities by PV through tax and leasing revenues, corporate earnings, jobs, and saving of conventional fuels reached a new record of 5.8 billion €.

At the beginning of 2011 Germany had 133,000 jobs associated with production and deployment of PV. Half of them were linked to various suppliers and module manufacturing; the rest was for installation services, mechanical engineering, etc.

PV plays also a considerable role in Germany's regional development. South of Berlin, in the declined economies of what was previously Eastern Germany's GDR, a "Solar Valley" has developed as a brilliant success of the country's effort to make the regions' economies "blossoming" again. Most German PV module and silicon feedstock manufacturers have settled in the "Solar Valley." Here a win-win situation is seen: Whereas the regions in difficulty get enormous new hope to see their economies developing again, the PV industry benefits from low labor cost that prevails in these areas. In addition, the industry benefits from considerable subsidies for their manufacturing plant investments on behalf of the European Union's "Structural funds."

Since the revision of the German FiT regulation in 2009, the ecologists are a lot more happy as new plants can no more be built on agricultural land.

Another interesting addition was the purpose of promoting self-consumption by a storage system: When more than 30% of the PV electricity produced is consumed "in-house," the paid tariff is increased by 8%. It is a first step, but a lot more would be necessary to stimulate the combination of storage capacity with the PV installation to weaken the role of the electric grid and its domination of the whole deployment structure.

A remaining deficiency of the German FiT is the fact that the PV tariff is presently not modulated following the regional differences of solar irradiation in the country. Most PV plants are now installed in the South where the income is higher. Typically, Bavaria in the South had in 2010 four times the PV capacity installed in Lower Saxony in the North.

To complete the facts and figures on the German market leader for PV one should mention two additional financial benefits.

The investment of PV plants is supported by favorable credits from the state-owned KfW bank. Since February 2011 the interest rate of a KfW credit for PV plants stands at 3.5% with a duration of 20 years, of which 10 years at a fixed rate and 3 years amortization free [21].

Building integrated PV systems can be amortized by tax credits over 20 years [22].

Interesting innovations have recently been offered by the German industry for combining PV with heating of the building. Some propose a combination of PV, solar heat collectors, and intelligent windows. Others propose systems that make use of PV rejected heat for house heating by means of a heat pump.

In summary, there are many reasons why Germany has become a market leader of global PV. First of all, PV has gained support, more than any other form of energy – even among the renewables – across all parts of German society. Support remained unchanged when the Federal Government changed in the mid of the last decade from social democratic "left/green" to conservative "right/liberal." There is no prevailing complaint about an excessive financial burden for PV like in other countries.

The government made it clear that PV is a clear winner for everybody and society at large when including the external effects of energy generation and supply. For 2009 the net cost of PV support amounted officially to less than 6 billion €. But the financial benefits to compensate it were actually a multiple of that cost. They are listed as follows:

- Billions of euros saved on environmental degradation
- Carbon certificates gained in the European carbon market
- 5 billion € saved on energy imports
- 4 billion € for "Merit order," a cost saving on the European electricity spot market in Leipzig. It takes

account of the effect that at certain times renewable electricity is available at the lowest cost of all electricity on offer; the price difference with the next dearer "conventional electricity" is the "Merit Order"
- 5 billion € as value created in the municipalities through tax income and others
- Value created through export of products and services, 130,000 new jobs, technological stimulation

It is said that the FiT was adopted by over 60 nations by now. But in most cases countries were facing considerable teething problems to get their legal regulations right. In their new enthusiasm for PV, many legislators were too generous, put the PV tariffs too high, added very favorable tax regulations and found themselves eventually confronted with mountain-high financial burdens of billions of euros to be borne by the national budgets. No wonder that investors had been rushing into the new business where return on investments could exceed 20%. It happened first in Spain in 2008/2009; France, Italy, Czech Republic, the UK, and others followed. Emergency measures had to be taken by the legislators. The options were either to impose a cap on the yearly PV capacity to be financially supported for installation and grid connection or to decrease radically the PV tariffs and the tax credits, or to do both.

And to make things worse, investors had to go through a national tendering process to get approval.

Spain and Czech Republic even imposed retroactive restrictions.

Italy had the second biggest PV market worldwide in 2010. There had been discussions, however, if really 3.5 GW had been installed in that singular year to reach a total of 7 GW. There were complaints about fraud, a possible involvement of the mafia that had already intervened previously in the Italian wind market; the question was raised, too, if not a major part of the PV installations were not yet grid connected. After discussion between the government and the Italian PV associations, new measures will no doubt make the national support system more sustainable. Measures in the pipeline are an annual cap, a reduction of the PV FiT down to 25 € cents/kWh, auctions, etc., [23].

Spain has almost 4 GW of PV capacity installed, but since 2009 the national market came almost to a complete stop. A 500 MW annual cap and a new auction mechanism for future contracts were decided. The PV FiT is being strongly reduced. As a result, PV industry in Spain is losing companies and up to 40,000 jobs. The background for the restrictions is the fact that Spain has since 2002 set up 22 GW of combined-cycle gas plants. As the demand of electricity has weakened, these plants are partly lying idle. To ease the overcapacity, Spain is exporting electricity as much as it can. At the end of 2010, the government has taken emergency measures: While freezing electricity prices for the five million poorest families, the incomes of all PV plants in the country are trimmed by 30% – for a duration of 3 years. The reduction is achieved not by reducing the FiT height but rather by paying it for a lower number of hours than the kWh produced over the year.

France had 720 MW of PV newly installed in 2010 – almost three times more than California that year. 152,000 PV systems were set up. France used to be a pioneer for rooftop PV installations; they had a considerable bonus in the financial support system.

By the end of 2010, construction and grid connection permits of 3.4 GW had been issued; then the government imposed a moratorium. As a result most of these systems were not going to be built. In March 2011 dramatic changes in the French PV regulations were introduced: an annual cap of 500 MW was imposed; systems of 100 kW and more are subject of a tendering procedure and they will receive not more than 12 € cents/kWh; the FiT for smaller systems were reduced by 20% immediately in March and a further 10% every following quarter to reach a reduction by 40% end 2011.

Talking about reductions and restrictions one must not omit the decrease of the French tax credit for private investors in PV that went from 50% to 22.5%, effective 1 January 2011 [24].

The United Kingdom is a latecomer for PV promotion by FiTs. The market still is very small. But Britain did not want to stand back in the recent wave of PV market restrictions. PV systems over 50 kW will see their tariff capped from 30 pence/kWh to between 8.5 pence and 19 pence/kWh [25]. . ..

Japan has a very long record in PV promotion but it is another latecomer in terms of PV promotion by means of the FiT scheme. The Japanese FiT is called "Excess Electricity Purchasing Scheme"; it stood in

early 2011 at 42 Yen/kWh. To better promote MW-scale PV plants, the PV FiT for such systems was increased from 24 to 40 Yen/kWh [8]. PV is also locally promoted in Japan by the "School New Deal" project by the Ministry of Education, by introduction measures by METI, by local governments, etc.

A special case among the European countries in terms of PV market support is "little" *Belgium* in the heart of Europe. It has a market promotion system of its own that is not linked to the FiT. It is similar to those in the USA, but for the time being more successful. Hence, it is worth a closer look.

Belgium has installed in 2010 355 MW, i.e., 40% more than California that year [26]. 95% of all installations were residential; Brussels, the capital of Europe, had 2,000 roof-mounted PV systems grid connected. Many industrial promoters are in competition on the Belgian PV market. They guarantee a rate of return on investment of 8%. The profitability comes from the conventional electricity that is saved, a 40% tax credit on the investment, and the income from "green certificates." The regional governments pay a number of certificates in units of 1,000 kWh fed into the grid. Those have a minimum value that is increased by a trading system in which the electric utilities buy those certificates as needed for achieving the quota of green electricity imposed on them.

In late 2010 the Flanders Government decided to decrease the value of the certificates they issue in 3-month steps by some 10% each time.

Self-consumption gets promotion as systems over 1 MW with less than 50% self-consumption will receive green certificates of much lower value.

It is also interesting to notice that the Belgian system includes a bonus for low-income investors: for building integrated PV the subsidy for such families can reach 1 €/W up to a total of 30% of the installed system cost.

The *USA* has a long record of PV development and enthusiasm for its deployment. However, by international standards, the current American PV markets as of 2011 are relatively small. 878 MW had been installed in 2010 at a market value of $6 billion [27]. In the USA the FiT scheme is not employed, but as shown for the example of Belgium where it is not employed either, the FiT alone cannot explain the difference.

The American PV market environment is obviously more complex than, for instance, the German one. PV system prices on the markets are blown up through numerous effects.

It is mentioned that in the US "balance of system" costs are twice of what they are in Germany; even module prices are higher there so that American installers are not fully benefiting from the favorable price developments on the global markets. "Permitting issues and delays resulting from the USA's jurisdictions" are problems that cost money [28]. Access to critical financing is also a difficulty.

American support for PV includes several original elements. Firstly, there is the "net metering" that allows delivering PV electricity into the net at the same price as the usual sales tariffs to customers. Secondly, there was still in 2011 a federal 30% cash grant for all investors in communities, from banks, private parties. Thirdly, the renewable Portfolio Standards RPS in the States. It is a requirement on retail electric suppliers to supply a percentage of their retail load with PV or another form of renewable electricity; they are often associated with a tradable renewable energy credit, REC. Each state has a different arrangement for it.

And much of the remaining support is linked to tradable tax credits in various forms. "Many developers are borrowing against the cash grant to raise money for construction, then handing the payment over to the construction lender when the project is completed" [29]. "The off-take agreements, the 'power purchase agreements' or PPA are essential to lock in revenue streams from the power plants, and lenders will not consider projects that do not have a PPA in place" [30].

"Bloomberg New Energy Finance" estimates that commercial-scale PV systems can obtain returns of 8–14% in certain states.

One may also mention the subsidies given by the Department of Agriculture to farmers and ranchers to install PV and other clean energies.

In California there are new initiatives to install PV for the benefit of low-income families.

Last not least, a note about *China*, the giant in PV module production with 120,000 PV jobs in place [31], and almost a dwarf in domestic installations: 0.8 GW existed in total at the end of 2010. So far China was lacking a PV promotion scheme that worked.

In March 2009 the government launched the "Golden Sun" Programme. It has as far as one can know two routes.

One concerns the setting up of larger system blocks in the west of the country. After tendering, just a few hundred MW are supposed to be built for an incredibly low prices down to 8 € cents/kWh [32]. One will have to wait for implementation to see if this is realistic.

The second approach looks very original and promising; it focuses on PV implementation in the "nonresidential sector" [33]. The idea is the following:

- In industrial and commercial zones, administrative quarters and educational buildings energy demand is better in phase with solar generation during the day; no net-metering and feeding into the public grid is necessary, all PV generated electricity is for self-consumption.
- In China currently the kWh price from the grid is twice as high for the industry than it is for residential use. For Europeans this is surprising as in Germany, etc., the national industry benefits from the lower electricity tariffs for protection and many of the companies are not even sharing the cost of the FiT like all the residential grid customers do. Hence it is a fact that in China the incentive for PV utilization is higher in the nonresidential area
- The government provides the PV modules and the inverters at half price with a 50% subsidy
- The government buys the modules in a large tendering exercise. Central procurement will further lower the PV module prices
- All PV systems are to be quality controlled and certified after installation

Also impressive are the favorable credits of some 20 billion $ that the Chinese banks provide to the Chinese module manufacturers.

PV Industry, Products, Costs, Prices

The following module manufacturers were leading the global markets in 2010 [34]:

1. Suntech Power (China) 1.57 GW
2. JA Solar (China) 1.46 GW
3. First Solar (USA) 1.41 GW
4. Q-Cells (Germany) 1.01 GW
5. Motech (Taiwan) 0.85 GW
6. Gintech (Taiwan) 0.72 GW
7. Sharp (Japan)
8. Kyocera (Japan)

They all sell crystalline silicon cells and modules, except First Solar which is the market leader for CdTe thin-film solar cells, and Sharp that markets next to crystalline silicon also amorphous (a-Si) and microcrystalline silicon (mc-Si).

The ranking is actually rather volatile. Years ago, Sharp was for a long time the global leader; later it became Q-Cells. The latter went through a crisis when in one single year it accumulated a deficit of 1.5 billion €. First Solar took the helm in the following year 2009.

In terms of technology, a provisional ranking came for 2010 from Paula Mints of Navigant Consulting [35]:

- Monocrystalline Si +/−43%
- Multicrystalline Si +/−43%
- CdTe 9%
- CIS/CIGS 2%
- a-Si/mc-Si 2%

There is consensus among experts that the family of CIS cells, the "Copper Indium Diselenide," is particularly promising among the thin-film cells. Numerous companies worldwide are working on it. The latest example was the announcement of Solar Frontier, a company of the Shell Oil Group in Japan, in last April 2011 that it opened a new factory for CIS modules in Japan. It targets a manufacturing capacity of 1 GW within months.

In general terms, there is no type of cell or module that could be given preference for matters of principle.

GaAs cells have the highest efficiencies: Lately over 43% have been achieved. But because of their high cost they only found a market on space satellites and on concentrating PV systems, the CPV.

Crystalline silicon cells, as far as they are concerned, offer today still higher conversion efficiencies than thin-film cells; over 18% are now readily available for Si modules on the commercial markets. The American SunPower is the leader with up to 25% efficiency. It is not unfair to say that the efficiency development on silicon cells did not see a major breakthrough in the last 40 years: in 1972 the USA already had the "violet cell" with 16% efficiency and 2 years later the "black cell" with 19% [36]. On the more negative side, one could mention the higher complexity of the silicon technology and hence a somewhat higher production cost.

Most thin-film cells are a factor of 100 thinner than the massive silicon ones implying a gain in material

consumption and cost. Today's market leader is CdTe. Typical efficiencies for this material go up to "only" 12%. It is interesting to note that a very thin additional intermediate layer of CdS does contribute to this efficiency [37]. The simpler thin-film technology leads to attractive manufacturing costs: First Solar announced one half € per Watt. But this cell has its own enemies because of the cadmium it uses. In particular in Japan, this raises a problem as the country had a bad record with cadmium pollution in the past.

No wonder then that – as mentioned before – Japan has turned its attention toward the CIS family of cells and a-Si cells. Among the many labs currently working on CIS, the Japanese company "Solar Frontier" mentioned before has claimed a record efficiency of over 15%. NREL in the USA has recently measured 15.5% on a 30 × 30 cm CIS cell of the US company Avancis. The problem looming around the corner is the "scarcity" of indium in nature; it is an essential compound in the cell. It could become a problem in case of mass production.

Finally there is a-Si and mc-Si. A new record has been reported here also by NREL, the US Institute which is an international reference in this field. On 400 cm^2, 12% efficiency has been observed. Since the days of tremendous stability problems linked to the Stabler–Wronski effect in hydrogenated a-Si, there has been great progress thanks to the combination with mc-Si layers, a newcomer developed in Switzerland. This type of cells is now also among the promising ones.

Many cell and module manufacturers today are "GW" companies. As the economy of scale is the determining factor for achieving competitive and low-cost market products, smaller factories are disadvantaged. All experts, from the early days on, were unanimous to see the future for PV in large GW-size production [38].

From this short list of global module manufacturers, it might be wrong to hastily conclude that just these few companies dominate the entire PV business. Typically, a company such as SolarWorld is not even included on the larger list of 12 module manufacturers even though it is highly profitable and a darling on the stock markets: It is one of those "vertically integrated" PV companies that put under one roof all business from silicon feedstock to plant installation.

There is also a large fraction of PV companies specializing in silicon material production, such as Hemlock in the USA, Wacker in Germany, and many others in Norway, China, Japan, Korea, etc. The global silicon feedstock capacity was estimated at 0.23 million tons in 2010 [8]. Nowadays more silicon goes into PV module production than in the electronic chip business. The business exceeds globally the 15 billion € mark.

A major part of the global PV business involves the specialized equipment providers, those who sell turnkey automated cell and module manufacturing plants. An example is the German Roth & Rau that just recently changed ownership. Solarbuzz [39] mentions for 2011 a global business of over $15 billion for the equipment needed for a capacity expansion of the ingot, wafer, cell, and module manufacturing. Thirty percent is expected to go for crystalline silicon and the majority of 70% for thin-film modules. Almost 80% of this year's thin-film investments might go to the CIS family of technology and the amorphous/microcrystalline silicon group of materials and structures.

At the end of 2011 a new production capacity record for a single company is expected: 3 GW for silicon cell producer JA in China.

And last not least, there is a global $6 billion market for solar inverters. Very high DC/AC conversion efficiencies above 98% are international commercial standard today. One of the leaders is SMA in Germany that has a long-standing record for specializing particularly in this sector.

To conclude this chapter, *PV's market economics* should be briefly reviewed. In that respect it is convenient to look at the case of Germany. Its solar resource is relatively low: What holds true for Germany then is also applicable for most other regions that benefit from a more favorable solar irradiation. On the other hand, the FiT tariff is a good image of the PV's market value. If it were not profitable at a certain FiT value in place, investors would certainly not go for it.

At the end of 2010 one could find on the Internet in Germany the following wholesale prices per Watt for solar modules, all TÜV certified:

- CdTe modules 1.38€, 80 cents on the spot market
- Si modules from China 1.55€, 1.24€ on the spot market
- Si modules European origin 1.75€

As mentioned before, it is no secret that the cost advantage of the Chinese modules reflects very well the

undervaluation of the Chinese currency with respect to the euro.

System prices (without storage) varied between 2.10€ and 2.90€; they were the lower, the larger the system. On the spot market prices down to 1.60€ could be found. In 2006, those prices stood still at 5€ in Germany.

Since early 2011, the German FiT was set at 28.74 cents/kWh for building integrated systems and 21.11 cents/kWh for ground-mounted ones.

Two conclusions follow:

1. The PV electricity cost from large in-field systems is currently still two to three times higher than electricity from the high-voltage grid. It will need many more years to get competitive in pure monetary terms. This will be achieved for a smaller part because of lower PV costs and for a larger part as a result of the need for more "sustainable" electricity on the networks and hence higher commercial costs there.
2. PV looks a lot more favorable for decentralized power supply. Consider this: The German FiT is expected to be lowered in the course of 2011 to +/−25 € cents/kWh while the average cost of conventional electricity sold to every consumer will this year increase from 23.70 cents/kWh by 8%. In conclusion, the crossover of both – the German "grid parity" – will be at around 25 € cents and it is going to happen in the course of this year 2011.

Historical Political Development: Initiating a Market Explosion

To stimulate the PV markets, political authorities have first tried the so-called Solar Roof Programmes. The German Government put the first one in place in 1989/1990; the responsible official in Bonn was W. Sandtner. In 1994 the Japanese Government's Cabinet decided another one that was larger in size (+/−70 MW). A third one, a 100,000 Roof Programme was eventually decided in Germany by the Minister of Finance O. Lafontaine, the KfW Bank, and a few Parliamentarians, namely, H. Scheer, H-J Fell, and others. It started on 1 January 1999.

The driving force in Germany was the late Hermann Scheer, Member of the Bundestag. All that followed was, as H. Scheer called it, a "High Noon Story" until the real thing, the FiT was in place in Germany in 2004, with over 60 other nations following suite since then – and the market explosion that has been seen.

The whole story is explained in Ref [38], its Preface of H. Scheer and on page 77. It will only be summarized in the following.

The German PV Roof Programme was a zero-interest scheme in which these interests and also the final installment were borne by public finance. Contrary to the later FiT, investors could not count on any profit, on the contrary. It was just a subsidy for less than one third of the total investment.

As a next step, the Bundestag decided – after a harsh fighting – an additional "feed-in-tariff" of 99 German Pfennige (about 50 € cents) – but only for the investors of the PV Roof Programme. This Act became effective on 1st April 2000. On this, the EU Commission in Brussels filed a law suite against Germany at the European Court of Justice. In March 2001 the law suite was dismissed.

This arrangement of a FiT paid on top of the investment subsidy lasted until 2003 when a total of 300 MW had been newly installed in Germany. As the 100,000 Roof limit had actually been exhausted at that point, it was time to establish a simple FiT on its own right, called EEG. Before this was going to happen in 2004, the preparatory process was bridged by a "Transitional Law" put forward by Hermann Scheer and eventually imposed by the Parliament against the will of the responsible Minister J. Trittin.

Eventually, the EEG including the FiT was decided in April 2004. That was the kickoff date for modern PV.

The value of some PV companies on the stock markets soared from one day to the other. Since then many people around the globe – not only in Germany – became PV millionaires.

To conclude this story it is important to mention that a cap of 750 MW always existed in the German FiT; it was eventually removed only in 2009, i.e., just 2 years ago.

It is interesting to add at this point a note on certification of PV products. For the FiT and the US or Belgian "green certificates" scheme, certification is being taken care of by the inherent interest of the investors: If the investor does not make sure he got a certified product, he will lose an income with the

kWh payment. Not so with the PV subsidies for roof-mounted systems. Here an additional certification must be superimposed. If not the subsidy sponsor may be the loser.

Future Directions: PV's Promise in a 100% Renewable Energy Strategy

The European Union, with a population of 500 million in 27 Member Countries, is globally the only major region or nation that has a precise and binding target for the implementation of the renewable energies by 2020. The legal instrument is the EU Directive "Energy and Climate."

The EU has the plan, on average over all its Member Countries, to double the renewable energies' share from 10% in 2010 to 20% in 2020. The EU Member Countries have defined their own particular shares inside this target in the so-called national Renewable Energy Action Plans or "nREAPs." Details can be found on the EU Commission's web site or [40, 41], and others.

Following the nREAPs, the EU's share of electricity consumption from renewable sources like hydro, solar, wind, etc. will increase from 19% in 2010 to 34% in 2020.

Within the frame of the nREAPs, the EU projects a cumulated PV capacity of 84 GW within its borders by 2020, more than half of it in Germany.

The hit list of the eight leading countries is the following:

- Germany 51.7 GW
- Spain 8.4 GW
- Italy 8.0 GW
- France 5.4 GW
- UK 2.7 GW
- Greece 2.2 GW
- Czech Rep. 1.7 GW
- Belgium 1.4 GW

These figures were put together in the course of 2010 by the bureaucracies in the national governments. In some cases, the targets are already obsolete by now. In particular after the nuclear catastrophe in Japan, there are reasons to believe that the real markets may in many cases be larger.

As it stands, Germany's role looks preponderant. The national grid operators in Germany see already for 2015 a total installed PV capacity of 39 GW in the country – against 17.3 GW at the end of 2010. Following the roadmap of the German Solar Industry Association, the PV capacity could well attain 52–70 GW by 2020. In agreement with the competent Ministry of the Environment, the contribution of PV-generated electricity as part of total consumption could increase from 2% in the course of 2010 to 10% by that year.

Outside Europe, "Bloomberg New Energy Finance" sees a realistic goal of a 30 GW total capacity installed in the USA by 2020.

China originally aimed at 20 GW of Solar Electricity installed by 2020. But in the wake of the nuclear accident in Japan, the government is considering the option to raise the targets for 2015 from 5 to 10 GW and for 2020 to 50 GW [42].

Osamu Ikki of the RTS Corp. in Tokyo anticipates for Japan a cumulated PV capacity of 28 GW by 2020 [43].

In summary, the cumulated PV capacity to be installed and grid-connected globally by 2020 may become the following:

- Germany 52 GW
- China 50 GW
- EU without Germany 32 GW
- USA 30 GW
- Japan 28 GW

The sum of 192 GW for these leading countries may well be a minimum. And there is a high probability that PV will spread to many other nations worldwide. For instance, the analyst Ikki mentioned before sees on that horizon a total grid-connected PV capacity of 340 GW.

That would be almost 10 times the global capacity seen at the end of 2010 with 38 GW.

The *annual* PV market might reach 60 GW in 2020 – compared to 17 GW in 2010. For 2011 and 2012 analysts expect a global market volume of slightly over 20 GW. By 2030 it might increase to 200 GW, Ikki speculates [43].

Solar industry associations from Europe, the USA, and others presented to COP 16, the last Climate summit in Cancun in 2010, the report "Seizing the Solar Solution" [44]. The profession advocates a global capacity of 980 GW by 2020.

The International Energy Agency IEA in Paris, known rather for their conservative opinion in energy matters, speculates that by 2050 a quarter of the world's electricity needs could be covered by PV [45].

In summary, the years 2009/2010 have brought a turning point for the implementation of PV on a large scale. In particular in Europe, PV has now become a leader of all power investment. Across the board, no other type of power generation, not even wind power, saw the same level of investment, leaving alone nuclear energy that has been left far behind.

There are important consequences for global power generation in the longer run. Again in Europe, a large consensus has grown in the last few years that on the horizon of 2050, "green house gas" emissions must be reduced by at least 80%. The option of atomic power in this perspective is losing ground all the time, in particular after the accident in Fukushima. The only option that remains then for "carbon-free" power generation are the renewable energies. That reasoning does not even take into account that the conventional energies are finite resources and solar energy is not. As a consequence, it is essential to move in the next few decades to a 100% supply scenario with these "natural energies" that are all derived from the Sun.

In this situation, the good news is that PV becomes at last a credible contender. It is not unreasonable to believe that PV could eventually meet between one third and one half of all electricity demand in our countries. It is actually PV that opens a new door to a better energy world, one that is decentralized, with less need for high-voltage power lines than more, and higher energy self-sufficiency for everybody.

PV's promise used to be a dream – now it has become a very solid political and industrial business model. As mentioned here above, Germany has taken the driving seat in modern PV market implementation. There is a large political consensus in German society and across all political parties. Germany is happy with the experience it had thus far with the development of its PV markets – and the hardest is behind as grid parity in Germany is readily around the corner. And the German commitment for PV has a solid base as its economy, Europe's largest, is strong and booming.

The second pillar of PV's high credibility is the new PV industry that was built on hundreds of $ billions of investment, a young and enthusiastic work force of over 200,000 people around the world, and last not least, a highly motivated R&D community.

Bibliography

1. Wang J (2011) IMS Research. In: 6th AsiaSolar PV industry forum, Shanghai, 5–7 May 2011
2. Starr MR, Palz W (1983) Photovoltaic power for Europe, an assessment study. Reidel, Dordrecht. ISBN 90-277-1556-4
3. Neue Energie Berlin, 4 Apr 2011, p 55
4. Wrixon GT, Rooney A-ME, Palz W (1993) Renewable energy-2000. Springer, New York. ISBN 0-387-56882-4
5. Bundesverband Solarwirtschaft (2010) sonnenseite.com/Franz Alt: 1-1-2011
6. German Bundesnetzagentur quoted in guntherportfolio.com 3-23-2011
7. Neue Energie Berlin, 3 Mar 2011
8. RTS Corp. Tokyo (2011) PV activities in Japan and global PV highlights, vol 17, 3 Mar 2011
9. Lawrence Berkeley Nat. Lab. Dec 2010: PV installed cost trends
10. renewableenergyworld.com: 4-1-2011
11. Paula Mints (2010) electroiq.com: 10-22-2010
12. Bloomberg, VIP briefing Feb-2011 newenergyfinance.com
13. sonnenseite.com/Franz Alt: 1-17-2011
14. Systèmes Solaires Paris Nov/Dec 2010, p 65
15. renewableenergyworld.com Jan 2011
16. renewableenergyworld.com Feb 2011
17. renewableenergyworld.com March 11
18. Fell HJ, (2010) MP private communication
19. Letendre SE, The Grid Parity Fallacy, Renewable Energy World, 9-16-2010
20. Seltmann Th sonnenseite.com 1-30-11
21. enbausa.de 3-10-2011
22. enbausa.de 7-5-2010
23. pv-magazine.com 3-22-2011
24. pv-magazine.com 3-8-2011
25. newenergyworldnetwork.com 3-21-11
26. thesolarfuture.com March 2011
27. greentechmedia 3-10-2011
28. greentechmedia 3-4-2011
29. renewableenergyworld.com 7-5-2010
30. reuters.com 3-3-2011
31. RENEWABLES 2011, draft Global Status Report, REN 21, Paris, copyright GTZ/GIZ, Germany
32. solarnovus.com 3-8-2011
33. Haiyan QIN (2011) DG China General Certification Center, Beijing May 2011, personal communication
34. Solarbuzz, cited by pv-tech.org Mar 2011, and RTS Corp. Tokyo PV activities in Japan, vol 17, 4 Apr 2011

35. electroiq.com 2/23 2011
36. Palz W (1978) Solar electricity. UNESCO, Paris. ISBN 92-3-101427-7
37. Böer KW (2011) p-type emitters covered with a thin CdS layer show a substantial improvement of V_{oc} and FF. Sol Energy Mater Sol Cells 95:786
38. Palz W et al (2010) Power for the world. Pan Stanford, Singapore. ISBN 978-981-4303-37-8
39. solarbuzz.com, 4-25-2011
40. European Environment Agency eea.europa.eu
41. ECN, Petten, NL, ecn.nl
42. Sicheng W (2011) Energy Res. Inst. Beijing. In: 6th AsiaSolar PV industry forum, Shanghai, 5-7-2011
43. RTS Corp. Tokyo PV activities in Japan, vol 16, 12 Dec 2010
44. SolarCOP16 seia.org
45. reuters.com 4-19-2011 © Wolfgang Palz, Brussels, May 2011

R

Radioactivity in the Marine Environment

Jordi Vives i Batlle
Biosphere Impact Studies Unit, Belgian Nuclear Research Centre, Mol, Belgium

Article Outline

Glossary
Definition of the Subject and Its Importance
Introduction
Radionuclide Speciation in Seawater
Radionuclide Interactions In the Water Column
Radionuclides in Sediments
Behavior of Radionuclides in Estuaries
Cycling in the Foodweb
Radiological Implications of the Marine Environment
Conclusions
Future Directions
Bibliography

Glossary

Absorbed dose Quantity of energy imparted by ionizing radiation to unit mass of matter, such as tissue – Units of Gray, 1 Gy = 1 J Kg^{-1}.

Activity concentration The activity of radionuclides incorporated in a particular material per unit mass or volume – Units of Bq kg^{-1}, Bq m^{-3}.

Allometric scaling The power relationship of average body mass with the rates of many metabolic processes.

Analogue radionuclide Radionuclide which has similar environmental behavior to another.

Bioavailability Fraction of a substance that can be taken up by living organisms, depending both on chemical properties of the substance and the physiological status of the organism.

Bioindicator Biological species whose presence or absence may be characteristic of environmental conditions in a particular area of habitat.

Biokinetic studies Studies of the dynamic exchange of substances between organisms and their surrounding environment.

Biological half-life The time that it takes for a substance incorporated in an organism to lose half of its concentration by natural processes of elimination.

Bioturbation Stirring or mixing of sediment or soil by organisms, resulting in the remobilization of radionuclides.

Broken arrow An accidental event that involves the loss of nuclear weapons or nuclear components but which does not create the risk of nuclear war.

Colloid Substance dispersed as small particles in water, typically 5–200 nm in diameter. Electrostatic surface forces are the key factor in determining their properties.

Concentration factor Equilibrium parameter quantifying the capacity of an organism to concentrate a specific radioelement, expressed as the ratio of activity concentration in an organism (Bq kg^{-1}, fresh weight) to activity concentration in water (Bq m^{-3}). Units of m^3 kg^{-1}.

Distribution coefficient (K_d) Equilibrium parameter used to quantify the partition of a radioelement between solid (soil or sediment) and liquid phases (overlaying or interstitial water), expressed as the ratio of activity concentration in solids (Bq kg^{-1}) to activity concentration in water (Bq m^{-3}). Units of m^3 kg^{-1}.

Dose conversion coefficient Dose rate received by an organism exposed to radiation, relative to activity concentration of the source. Units of Gy s^{-1} per Bq kg^{-1} (or Bq m^3).

Robert A. Meyers (ed.), *Encyclopedia of Sustainability Science and Technology*, DOI 10.1007/978-1-4419-0851-3,
© Springer Science+Business Media, LLC 2012

Ecosystem The system formed by a biological community and its nonliving surroundings.

Foodweb A succession of organisms in an ecosystem that is linked by predator–prey relationships, transferring mass and energy from one to another.

Global fallout Residual radiation hazard from the atmospheric nuclear explosions of the 1940s to 1960s, with slowly declining global presence in the planet up to the present day.

NORM Radionuclides from naturally occurring radioactive materials released to the environment by industrial processing, e.g., mineral extraction and processing, oil and gas, phosphogypsum by-products, and fertilizers.

OSPAR The Convention for the Protection of the Marine Environment of the Northeast Atlantic, a mechanism by which 15 Governments of the western coasts and catchments of Europe, together with the European Community, cooperate to protect the marine environment of the Northeast Atlantic.

Radiation weighting factor Factor representing the relative effectiveness of different radiation types relative to X- or gamma-rays, in producing biological effects of significance.

Remobilization The return of a radionuclide to circulation within an ecosystem, such as return to the water column of radionuclides which had been locked in sediments.

Scavenging Removal of substances from the water column by the action of settling particles and/or organic matter.

Sediment mixing Mixing of sediment and water at the interface between the two, by processes such as bioturbation and water turbulence.

Speciation Partitioning of an element amongst defined species in a chemical system.

Definition of the Subject and Its Importance

The sea is a complex system containing different components (water column, suspended particulates, colloids, sediments, and organic matter) and inhabited by life forms at multiple scales (from plankton to large mammals), undergoing complex interactions.

With the arrival of nuclear technology in the late 1940s, a variety of man-made radionuclides have entered the marine environment, either as a result of military operations, industrial discharges, medical releases, or nuclear accidents. This has resulted in their widespread distribution, cycling across the sea and uptake by biota, both locally (in the vicinity of discharge points) and globally.

Studies of the different ways radioactive substances interact with the marine environment fall into the domain of marine radioecology. In the 1950s and 1960s, this discipline focused on studying how the global fallout from nuclear weapons testing and satellite burn-up entered the oceans and was distributed within the water column, reaching the seabed sediments and the food chain. Radionuclides of interest were the relatively long-lived plutonium (Pu), americium (Am), radiocesium (Cs), and radiostrontium (Sr), the fission products from nuclear detonations.

From the late 1970s to 1980s, more studies explored the interaction mechanisms of radionuclides with sediments, suspended particulates, and marine colloids. A key focus for marine radioecology research at that time was the input from European reprocessing plants to the seas of the northern hemisphere. Most significantly, the marine discharges from the reprocessing plants at Sellafield, UK, and La Hague, France resulted in enhanced radionuclide levels in the Irish Sea and English Channel/North Sea respectively. Fundamental to investigations at this time was to understand the chemical speciation of the transuranic radionuclides, predominantly plutonium and americium, and the mechanisms of how they concentrated in sedimentary deposits and how they became remobilized.

A key driver for this phase was the estimation of radiation doses to humans arising from the consumption of contaminated marine foodstuffs. However, beyond the purely radiological protection point of view, substantial understanding was sought and gained on the potential of radionuclides as tracers in the study of marine and coastal processes, as well as understanding the transfer of radionuclides to the local communities of animals and plants.

The Chernobyl accident in 1986 resulted in a global release of radionuclides. Although in the Irish and North Seas the main influence continued to be the input from reprocessing plants, the Baltic and Black Seas became affected by the Chernobyl accident, with ^{90}Sr, ^{134}Cs, ^{137}Cs, and ^{239,240}Pu entering these

environments. Meanwhile, during the 1990s, Irish Sea studies shifted focus to the ^{99}Tc discharges arising from the Enhanced Actinide Removal Plant (EARP) in Sellafield, with ^{99}Tc discharges reaching their peak between1994 and 1996. As a result, levels of ^{99}Tc in organisms such as lobsters found off the coast of Sellafield reached their highest levels in the late 1990s and early 2000s. During this time, transuranium discharges decreased several orders of magnitude below their peak discharge rates of the mid-1970s.

Before the Fukushima accident in Japan in 2011, there were no more major releases of radioactivity into the marine environment. In a period marked by concerns on long-term environmental sustainability came the realization that radionuclides persist in the marine environment for long periods of time. Research addressed in more detail the interaction of radionuclides with individual organisms and foodwebs, striving for a global understanding at a species and ecosystem level. The traditionally anthropocentric view of radiological protection was replaced by a more ecocentric approach. There was a realization that, even if humans are protected, the environment is not necessarily protected because marine organisms inhabit areas where humans cannot reach. This called for the development of an international system of radiological protection for the environment, and new studies of the transfer of radionuclides to marine biota.

Recently, dynamic situations such as accidental scenarios, decommissioning discharges and NORM releases from offshore oil operations have attracted scientific interest. These situations are characterized by irregular discharge patterns, requiring dynamic modeling of the transfer of radionuclides to marine organisms. There is also interest in low-level ionizing radiation effects to biota, and it is felt that Radioecology needs to be applied in a world of multiple contaminants, exerting their combined stress on interdependent species and entire ecosystems. A number of collaborative international projects are developing in this direction.

Radioactivity in the marine environment is here to stay, and there is an onus to gain a scientific understanding of its implications, as part of a drive to preserve the quality of this environment for future generations.

Introduction

Artificial radioactivity reaches the world's oceans from various sources: releases from nuclear power plants and reprocessing facilities connected to coastal areas directly or via waterways, the worldwide fallout from nuclear weapons tests, dumping of waste to the seafloor or accidental situations such as satellite burn-up, "broken arrow" situations, or the sinking of nuclear submarines.

The historical sources of radioactivity into the environment, detailing natural radioactivity, global fallout, accidents, and NORM and discharges from the nuclear industry to the marine environment have been abundantly described elsewhere [1–8], so they will only be summarized briefly.

Historically, one of the most significant inputs with relevance to the marine environment is the worldwide fallout of nuclear weapons tests, resulting in the global inventory of man-made radioactivity in the world's oceans [9, 10], to which one must add accidents involving space satellites [11, 12] and lost nuclear weapons [2, 13–16]. The earliest weapons tests provided in fact the first opportunities to investigate at close quarters the impact of man-made radionuclides in the marine ecosystem [17–19].

Nuclear accidents represent another source of radioactivity to the marine environment. The Chernobyl accident affected indirectly several marine areas [20–23]. The two major nuclear accidents in 1957, Kyshtym and Windscale, also affected the marine environment to some degree, but they are not believed to have been a major source of contamination to the marine environment [6]. At the time of writing this article (April 2011), it is too early to evaluate the impact of the 2011 nuclear accident at the Fukushima plant (Japan), though it is clear that this event resulted in the direct release of radionuclides to sea, chiefly ^{131}I and ^{137}Cs.

Routine operations from the nuclear industry have been a source of radioactive contamination to sea since the early 1950s. The most important contribution is from the reprocessing of spent nuclear fuel in purpose-built facilities discharging waste to sea. The importance of the Sellafield site discharges to the Irish Sea has resulted in numerous radioecological studies being performed, examples of which are described

here [24–28]. Another significant reprocessing site which has been extensively studied from the marine discharges point of view is the La Hague reprocessing plant in France [29, 30]. In the Arctic Ocean, run-off from contaminated sediment in the Ob and Yenisey river system connected to the Mayak, Krasnoyarsk, and Tomsk nuclear facilities and the Semipalatinsk test site has also become a well-studied source of radionuclides [31].

Lastly, historical dumping of radioactive waste [32] has been a controversial source of radioactivity release into the world's oceans. Between 1946 and 1982, packaged low-level radioactive waste (LLW) was dumped at more than 50 sites in the northern part of the Atlantic and Pacific Oceans. Beta-gamma emitters represented the majority of the total radioactivity in that waste, but alpha-emitters such as plutonium and americium were also disposed of by this method [33].

By the above means, an extensive list of man-made radionuclides has been introduced to the marine environment in varying amounts. This article cannot cover every one of them. Due to their availability in the environment, their radiological importance, and the amount of environmental data available, the four radionuclides to be considered further are ^{99}Tc, ^{137}Cs, Pu (as the α-emitters ^{238}Pu and $^{239+240}$Pu, as well as the β-emitter ^{241}Pu), and ^{241}Am. These radionuclides can be grouped broadly into two categories: those behaving as dissolved in the water column (Tc and Cs) and those with a strong affinity for suspended particulates and sediments (Pu and Am).

In sea water, almost all of the naturally occurring elements are present in variable quantities. The concentrations of the major constituents are found to be directly proportional to the salinity of the water. The more soluble Tc and Cs radionuclides follow the same behavior, and so they are termed "conservative." The sediment-seeking Pu and Am are classed as "nonconservative" radionuclides. The residence time within the seabed for these non-conservative radioelements will generally be longer than the hydrological transit time following release or remobilization from the sediments.

After radionuclides have entered the water, physicochemical changes will occur, followed by dilution and dispersion further afield by the action of oceanographic processes. However, it is also possible for radionuclides to become accumulated in certain parts of the marine environment, such as sediments, through the processes of scavenging and particle deposition, as well as becoming biologically concentrated. A conceptual representation of the key processes is given in Fig. 1.

Whether radionuclides from a specific source are associated with particles, colloids, or various chemical species in the water depends on the type of source and conditions prevailing in a particular environment [7, 34]. For example, plutonium from global fallout is mainly associated with submicron iron oxide particles; in fallout from surface tests in the Marshall Islands, plutonium was mainly attached to calcium hydroxide particles [35]; Pu in effluents from nuclear reprocessing plants are associated with particulate material or colloids [36].

Ultimately, the transport, distribution, and biological uptake of radionuclides in the marine environment depends heavily on the physicochemical forms of radionuclides (i.e., their speciation) in the discharged effluents, as well as on the transformation processes that occur after entering coastal waters. For this reason, this article will cover in some detail radionuclide speciation, a "hot topic" in the aquatic environment where trace metals are concerned.

Trace element speciation in the marine environment is different from speciation under freshwater conditions. This is due to varying features such as salinity, pH, dissolved organic carbon and the size of particulates in the water column, ranging from nanocolloids to micron-sized particulates. Many reviews on radionuclide speciation concentrate on particle size considerations, i.e., physical speciation. In this entry, consideration will be given to the actual chemical speciation, which refers to the molecular form of the radionuclides in the marine environment.

Radionuclide Speciation in Seawater

Conservative radio elements, like ^{90}Sr, ^{137}Cs, and ^{99}Tc, have a relatively low (but measurable) capacity for adsorption onto solid particles. They readily disperse upon release to the marine environment, and therefore can be used as tracers for oceanographic processes.

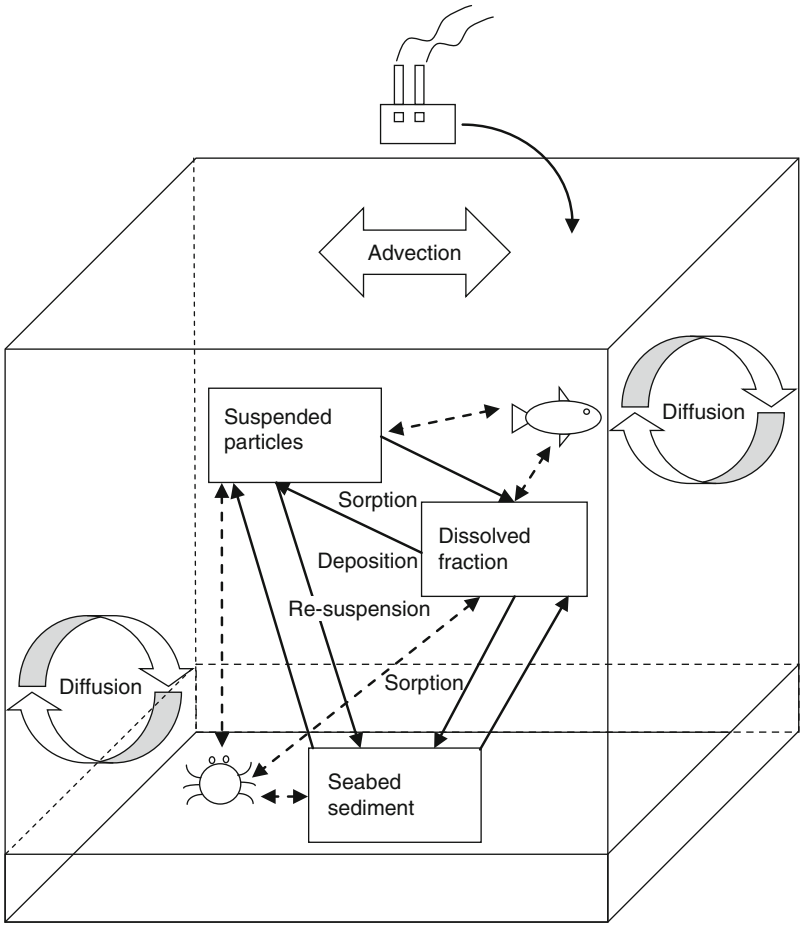

Radioactivity in the Marine Environment. Figure 1
Conceptual representation of the processes occurring when radionuclides enter the marine environment

On the other hand, transuranium elements, like plutonium and americium, are not efficiently dispersed away from the source point but, instead, are more efficiently carried onto the seabed by scavenging particles, becoming incorporated onto sediment for protracted periods of time. ^{241}Am is a special case as additional quantities will be formed by the decay of ^{241}Pu if this radionuclide is present.

The above picture is somewhat simplified, and becomes more complicated by the fact that certain radionuclides, such as plutonium, can have different chemical forms, or species, capable of coexisting in varying proportions in the water column. Some of these species actually have low particle reactivity, behaving conservatively, whereas others can have a high affinity for sediment and behave nonconservatively. In this section, the speciation of Pu and ^{241}Am is compared on one hand, and ^{99}Tc and ^{137}Cs on the other, to illustrate how this phenomenon affects their environmental behavior.

Plutonium and Americium Speciation

It is well known that, in aqueous solution, plutonium can exist in the oxidation states +3, +4, +5, and +6 [37]. In the absence of complexing agents, these oxidation states form the chemical species Pu^{3+} and Pu^{4+} (the "reduced," or Pu(III,IV) group) and PuO_2^{+} and PuO_2^{2+} (the "oxidized," or Pu(V,VI) group), respectively. These two oxidation state groups of plutonium exhibit very

different sediment sorption properties, with reduced plutonium possessing an affinity for sediment approximately two orders of magnitude higher than oxidized plutonium, relative to concentration in seawater.

Such species can be interconverted from one to another by means of oxidation–reduction reactions, coexisting in equilibrium in the aquatic environment [9, 38–41]. Theoretical calculations show that in a pure aqueous solution (without suspended particles or colloidal matter) PuO_2^+ is, by far, the predominant form [42–45]. The insolubility of $Pu(OH)_4$ is the limiting factor of the net solubility of plutonium in oxic natural waters, making $Pu(V)O_2^+$ the most stable oxidation state [46].

Americium in aqueous solution can also exist in the oxidation states +3, +4, +5, and +6 but the oxidation state +4 is stable only in the presence of concentrated H_3PO_4, $K_4P_2O_7$ and fluoride solutions [47]. In the absence of complexing agents, the oxidation states +3, +5, and +6 can occur in the form of the hydrated ions Am^{3+}, AmO_2^+, and AmO_2^{2+}. However, AmO_2^+ and AmO_2^{2+} are quickly reduced to Am^{3+}. Hence, the chemical speciation of americium, as well as its environmental behavior, is less complex than that of plutonium and Am^{3+}, likely to be in the form of a hydroxide, is the predominant species of americium in seawater [48].

Understanding the environmental behavior of plutonium in seawater requires consideration of the complex interactions of Pu (III,IV) and Pu (V,VI) within a heterogeneous water column where two distinct solid phases (particulate and colloidal) coexist, as well as interactions with seabed sediments. The situation is fully described elsewhere [49, 50]. Environmental factors such as the physical nature of the discharge (i.e., particulate vs. soluble radionuclides in the original effluent), salinity [51], the presence of dissolved organic carbon [52], suspended particulate load and colloids [53] can alter the balance, increasing the proportion of the "reduced" species in the water column [50, 54, 55].

The above can be illustrated with the following example. If plutonium is released in an insoluble, particulate form in a relatively shallow coastal area, it will likely be incorporated in the seabed sediments, with the relatively smaller oxidized fraction traveling farther afield. The result is that the percentage of oxidized plutonium in seawater will increase over the first few kilometers away from the outlet, in the direction of the dispersion. This is the case of the Sellafield reprocessing discharges where plutonium releases occurred in particulate form and the bulk of the historical inventory is incorporated into sedimentary deposits [48, 50]. However, if plutonium is released in oxidized form, this oxidized fraction will dominate throughout the dispersion pathway. For americium, the situation is much simpler, since the oxidized form Am(VII) is unstable and most of the Am in seawater is reduced. Hence, this radionuclide will largely be incorporated into particles and sedimentary deposits.

It therefore follows that most of the plutonium in open waters (well removed from source terms) is to be found in the oxidized form Pu(V,VI), behaving like a conservative tracer which can be transported within the dissolved phase by advection-dispersion processes. This has been verified experimentally in the open waters of the Irish Sea [37, 50, 56, 57], semi-enclosed seas and shallow continental shelf waters such as the Mediterranean Sea [41, 50], the benthic environments of Bikini and Eniwetok Atolls [9, 58], the northwest Greenland continental shelf [55], and the English Channel [59]. In contrast, ^{137}Cs and the similarly behaved ^{99}Tc are readily dispersed, with relatively little quantity residing in sediments compared with plutonium and americium [60–62].

A smaller fraction of the plutonium in open waters is in a reduced form, and this is partly associated with suspended particulate matter. This scenario becomes somewhat complicated by the fact that Pu(IV) in seawater can reoxidize to Pu (V, VI) simultaneously with the slower opposite reaction, with rates of the order of 10^{-1} and 10^{-2} days^{-1}, respectively [49, 59]. In contrast, all of the americium in open waters is in a reduced form, characterized by a strong affinity for suspended particulate matter, colloids and sedimentary deposits.

It follows from the above that, although it is true that they have an affinity for sediments [63–66], the fate and transport of plutonium and americium depend heavily on oceanographic considerations as well as the nature of the discharges themselves. In addition, intermixing of the different fractions of Pu (oxidized and reduced) takes place over long timescales.

Technetium and Radiocesium Speciation

The speciation of the conservative elements ^{99}Tc and ^{137}Cs is relatively simple compared with Pu and Am. The effect of technetium chemistry on its environmental behavior has been the subject of numerous studies and reviews [67–76], from which the following summary may be derived.

The pertechnetate anion TcO_4^-(VII), a soluble species, is the form most likely to be discharged in low active liquid effluents from nuclear fuel reprocessing facilities and, thus, the dominant form of technetium in the marine environment [77]. Strong reducing conditions are required to overcome the inherent stability of TcO_4^-, forming the particle reactive species technetium dioxide TcO_2(IV). For instance, these conditions can be found in oxygen-depleted sediments, but the difficulty in reducing Tc(VII) means that reduced Tc(IV) may only be found where pH and redox conditions permit it. Once reduced, technetium may exist as insoluble technetium dioxide or technetium sulfide species. Environmental Tc(IV) can also be stabilized by organic matter. Precipitation or association with humic acids may occur in sediments.

Given its chemical behavior, the dominant "oxidized" species of technetium, TcO_4^-, behaves as a soluble compound. As such, it has a high mobility throughout the environment. In contrast, "reduced" Tc(IV) behaves as an insoluble compound and is much less mobile.

^{137}Cs is a Group I metal existing as the monovalent cation Cs^+, its only environmentally available oxidation state. Speciation studies carried out in the Baltic Sea confirm that water-soluble cesium constitutes most (60–99%) of the total ^{137}Cs in seawater, predominantly as Cs^+, both in near–shore and open waters. The remainder of radiocesium in the water column is in particulate form, varying between 1 and 30% depending on environmental conditions [78]. The uptake of Cs onto suspended matter and sediment is proportional to the illite content of the sediments, probably involving an ion-exchange reaction with potassium [79]. Hence ^{137}Cs is stably bound by crystalline minerals, more so than by organic matter [80].

For the above reasons, technetium and radiocesium are considered to be long-distance tracers in the marine environment, more suitable for following hydrodynamic transport processes than their actinide counterparts. In contrast to Pu and Am, they have the ability to disperse readily in seawater [60–62]. In the Irish Sea, e.g., these radionuclides are advected, principally in a northerly direction, associated with the mean flow of water currents, leaving the area via the North Channel with a mean transit time of about 1 year [81].

Iodine is of renewed interest due to the recent Fukushima accident. This radionuclide is generally soluble in seawater, and poorly adsorbed onto particulates and sediment. Both iodide (I^-) or iodate (IO_3^-) anions can be present, but the latter predominates [82]. In this way, IO_3^-can be broadly classed as analogous to Cs and Tc in the marine environment.

Radionuclide Interactions In the Water Column

When radionuclides are released into seawater, physicochemical processes such as polymerization, disproportionation and the formation of precipitates can occur. As a result, there takes place a redistribution between the amount of radionuclide in solution and the insoluble forms partially attaching to solid surfaces. At trace concentrations, the dominant process for this attachment is primary adsorption, where a monomolecular layer of the adsorbed substance is formed on the surface of a particle. Simultaneously, radionuclides are dispersed by turbulent mixing and advective currents, undergoing significant dilution in the process.

Interactions with Suspended Particulates

Radionuclides initially released in an ionic form may undergo molecular dispersion as simple compounds. However, after some time, low solubility forms of these simple compounds can become adsorbed onto the surfaces of suspended particulate material, e.g. the fine suspended matter present in estuaries.

Varying proportions of Pu and Am are associated with the particulate phase [50, 83–85]. In the surface waters of the North Pacific and the Mediterranean, the proportion of particulate to total Pu is less than 10%, whereas in the deep waters of the Pacific it is less than 2% [86]. In coastal and estuarine environments, this

proportion can be much higher [87]. This contrasts with ^{90}Sr, ^{137}Cs, and ^{99}Tc, which have lower fractions in suspension.

Since the soluble and particulate forms of these radionuclides behave quite differently, it is important to know the partitioning between the aqueous phase and the solid phase (suspended particulates or sediment) on a radionuclide by radionuclide basis. For simplicity, this is represented by an equilibrium ratio, the distribution coefficient or K_d, which include implicitly the complex processes involved:

$$K_d(\mathrm{L\ kg^{-1}}) = \frac{\text{Activity concentration per unit mass of solid (Bq/kg dry weight)}}{\text{Activity concentration per unit volume of water (Bq/L)}}$$

K_d values for the various elements in seawater are provided in the literature, duly compiled by the International Atomic Energy Agency (IAEA) on the basis of best estimates and empirical data for various environments [88]. A summary of representative K_ds for Cs, Tc, Am, and Pu in open oceans and coastal environments is given in Table 1.

As explained previously, plutonium has different chemical forms. Pu(III,IV) has a K_d one order of magnitude higher than given in Table 1, of the order of 10^3 $m^3\ kg^{-1}$, similar to the K_d for americium [37, 45, 50]. In contrast, the IAEA recommends a K_d for technetium of 10^{-1} $m^3\ kg^{-1}$ for both pelagic clays and coastal sediments [88, 89], derived from Irish Sea measurements [90]. This K_d may be taken to represent the most oxygenated marine sediments, but higher values should be applied to anoxic sediments with high organic matter content [67]. For radiocesium, measured K_ds are in the range of 10^0–10^1 $m^3\ kg^{-1}$ (IAEA recommended value = 3.5×10^0 $m^3\ kg^{-1}$) [88, 89].

The K_d is a somewhat crude simplification of reality, since time is required for complete equilibration to be attained between the aqueous and solid phases. Typically, for suspended particulate concentrations in the order of 10^{-3}–10^{-2} g L^{-1}, adsorption equilibrium is achieved within seconds to minutes, but processes other than sorption may considerably delay the adjustment between the soluble and the suspended load phases. In such cases, a so-called effective K_d can be derived, which should not be interpreted simply as an equilibrium adsorption parameter [45].

When effluent released in particulate form travels away from its source, the K_ds for plutonium and americium will decrease with distance from the outfall. In the Irish Sea, an order of magnitude exponential fall has been observed in transit between the eastern and the western regions, as the partitioning between liquid and solid fractions re-equilibrates [45, 50]. Sediment resuspension and dissolution continue to influence the dispersion of Pu along the route [91].

For seabed sediments, equilibration takes much longer to be achieved. Some understanding of the relevant mechanisms can be gained by a simple model involving two compartments: water column and sediment, with uptake and release rates R_s and R_w mediating between them (Fig. 2). The processes to consider are: depletion of radionuclides adsorbed onto suspended particulates (particle scavenging), molecular diffusion, pore water mixing and bioturbation, i.e., the disturbance of sediment by living organisms, modeled effectively as a diffusive process.

Radioactivity in the Marine Environment. Table 1
Representative K_d values for Cs, Tc, Am, and Pu in open oceans and coastal environments [88]

Radionuclide	K_d value ($m^3\ kg^{-1}$)	
	Open waters	Coasts and estuaries
Cs	2×10^0	4×10^0
Tc	1×10^{-1}	1×10^{-1}
Pu	1×10^2	1×10^2
Am	2×10^3	2×10^3

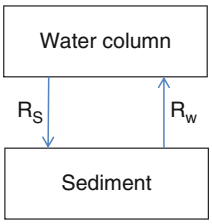

Radioactivity in the Marine Environment. Figure 2
Simplified representation of the exchange of radionuclides between surface sediment and the water column [92, 93]

Previous investigators [92, 93] have given the basic equations describing the combined transfer rates for these processes:

$$\begin{aligned} R_s &= \text{Particle scavenging} \\ &\quad + \text{Molecular diffusion} + \text{Pore water mixing} \\ &\quad + \text{Particle mixing} \\ &= \frac{1}{d_w(1+K_d\alpha)} \\ &\quad \times \left(SK_d + \frac{D + h^2\varepsilon R_T + R_W K_d \rho h(1-\varepsilon)}{h}\right) \\ R_w &= \text{Molecular diffusion} + \text{Pore water mixing} \\ &\quad + \text{Particle mixing} \\ &= \frac{1}{h\varepsilon\left(1 + K_d\rho\frac{(1-\varepsilon)}{\varepsilon}\right)} \\ &\quad \times \left(\frac{D + h^2\varepsilon R_T + R_W K_d \rho h(1-\varepsilon)}{h}\right) \end{aligned}$$

where S is the sedimentation rate, d_w the water layer depth, α the suspended sediment load, D the diffusion coefficient, h the thickness of the sediment layer, R_T the pore water turnover rate, R_W the sediment reworking rate, ε the porosity, and ρ the density. In the case where there is no suspended load (and hence, no sedimentation) and the sediment is assumed to be a simple solid surface (zero porosity), the ratio between the uptake and turnover rates equals the quotient between the activity, in Bq, in the sediment relative to the water:

$$\frac{R_s}{R_w} = \frac{\rho h}{d_w} K_d$$

In reality, the adsorption behavior of radionuclides is influenced by a number of environmental factors including salinity, temperature, depth, size distribution and composition of the suspended load, biological productivity, trace metal concentrations, and the presence of colloids and organic pollutants.

Interaction with Colloids

Another associative mechanism for particle-seeking nuclides initially in ionic form is the attachment to colloidal and pseudo-colloidal matter. Colloids are nanoparticles and macromolecules in the size range 1–10 kDa (or 5–200 nm) [50, 87], held apart by the mutual repulsion of their negative charge [94]. Colloids are in fact abundant in both shelf and open ocean surface waters, with a total surface area of about 8 m^2/m^3 of sea water [95–97]. Given the high surface per unit mass of colloidal systems and the electric charge available, it is inevitable that they will be efficient in fixing radionuclides that have low solubility per se. This means that particle-reactive radionuclides released in an "insoluble" chemical form (such as Pu(III,IV) or americium) could potentially behave as if they were soluble, dispersing away with the water.

Colloidal and pseudo-colloidal particles can be inorganic (polyhydroxy complexes or polysilicates) [98] or organic, i.e., colloidal organic carbon (COC), which is composed of combined amino acids, carbohydrates, and lipids. There are even higher molecular weight components such as humic acids and their compounds, which have a high capacity to strongly and specifically complex metals. These components are formed upon the degradation of organic matter within the water column and the seabed. The resulting products are stable over protracted periods of time and exist in a wide range of sizes: in sea water, dissolved organic carbon (DOC), comprises structures with molecular weights varying from $<10^3$ to over 2×10^5.

It is known that part of this DOC exists in a colloidal form [45]. Typical concentrations of colloidal organic carbon in unpolluted ocean surface waters are about 1–5 $\times$ 10^{-3} kg of organic matter per m^3 [99, 100], similar to typical suspended particulate matter concentrations. In these environments, the percentage of plutonium which appears to be bound to COC seldom exceeds 20% [45].

In coastal regions and estuaries, colloidal particles are likely to be present at higher concentrations, explaining perhaps the increased percentage of reduced plutonium in apparent solution in these environments. Conversely, in the open waters of temperate environments, the percentage of colloidal plutonium seldom exceeds 15% [50]. In the subsurface waters at Thule (northwest Greenland) there appears to be little, if any, plutonium associated with colloidal species [55].

The effects of DOC on the sorption properties of plutonium in natural water systems have been studied in some detail [52, 101], and it has been demonstrated that DOC plays an important role in regulating the binding of plutonium (and presumably americium)

to particulate matter. Furthermore, it has been shown that the K_d for reduced plutonium is strongly correlated with DOC according to an equation that is almost constant for very low COC concentrations, quasi-linear at intermediate levels and parabolic at high concentrations:

$$\frac{1}{K_d} = \frac{1}{K_d^0} + \frac{K_1}{K_s}[\mathrm{COC}] + \frac{K_2}{K_s}[\mathrm{COC}]^2$$

where K_d^0 is the limiting distribution coefficient, that is to say, the K_d value for [COC] = 0. This behavior has been reproduced in several laboratory experiments [102].

In coastal waters with high levels of colloidal and dissolved organic carbon (COC/DOC), Pu(III,IV) and americium may have a significant fraction in colloidal form, as a result of the repartitioning of radionuclides between the dissolved and the particulate phases due to competition for adsorption sites with COC/DOC. However, for some radionuclides exhibiting complex speciation, the proportion attached to particulate matter can actually increase. This has been observed experimentally for plutonium and it is due to the reduction of plutonium(V) to plutonium(IV) in such environments [50, 103].

In open waters, virtually all of the plutonium, including the fraction in a reduced chemical form, is present as a fully dissolved species [104]. This implies that long-range transport of radionuclides via a colloid pathway is unlikely, but the possibility of radionuclide interaction with some colloidal matter like naturally occurring complexing ligands, actually contributing to the overall transport of radionuclides, cannot be discounted [58].

Contrasting with the potential of ^{239,240}Pu(III,IV) and ^{241}Am to be in a colloidal state, laboratory experiments on dilution of radioactive effluent into sea water indicate that ^{90}Sr, ^{137}Cs, and ^{239,240}Pu(V) do not have such an ability to persist in colloidal form [36]. This is due to the lower chemical reactivity of these radionuclides, hence mechanisms for their binding to colloids are passive, and consequently weaker [105, 106].

Colloids are not always inherently stable and will tend to form aggregates, particularly at high salinity, resulting in coagulation of the material and the eventual deposition of radionuclides to the seabed [107]. This process appears to be biphasic, i.e., represented by the sum of two exponential functions, with an initial fast phase (0–5 h) transitioning to a slower process (5–120 h), and rate constants of 2.1×10^{-2} and 3.5×10^{-3} h^{-1}, respectively [49]. Since only ~25% of the colloidal phase coagulates via the initial fast phase, a coagulation half-time of 8.25 days (corresponding to the rate constant of 3.5×10^{-3} h^{-1}) and a "colloidal" K_d of 10^4 m^3 kg^{-1}can be used to represent the overall process at long timescales [108].

Scavenging from the Water Column

As suspended particulates and coagulated colloids sink to the bottom by the action of gravity, the radionuclides attached to them are gradually removed from surface waters. Hence, fallout plutonium and americium concentrations in surface waters have been decreasing over the decades, with preferential removal of americium with respect to plutonium.

In the Mediterranean Sea, e.g., mean residence times for plutonium and americium in surface waters are about 15 and 3 years, respectively, so only a small fraction of the fallout is still in the water column [109]. For conservative radionuclides such as Sr, Tc, and Cs the process is much slower, but after time a significant fraction of those radionuclides has also deposited onto the seabed. To give an idea of the difference between conservative and nonconservative radionuclides, average residence times of ^{90}Sr (^{137}Cs) and ^{239,240}Pu in surface waters of the world are calculated to be 27 ± 2 and 13 ± 1 years, respectively [6].

Radionuclide depletion from the water column occurs by direct precipitation or by absorption on suspended particles and their aggregates, which sink to the bottom at rates of the order of 70–400 m year^{-1} [110]. Another important mechanism for the removal of radioelements from surface water is a biological one: scavenging by biological aggregates such as marine snow and plankton fecal pellets. Studies have shown that such fecal pellets are relatively rich in plutonium and americium. Metal binding on copepod fecal pellets and marine snow appears to be generally greater than on euphausiid fecal pellets [111].

The process of decomposition and release of trace elements from zooplankton debris has been investigated in some detail [112]. Release rates of metals/metalloids (^{65}Zn, ^{75}Se, and ^{241}Am) in the context of

carbon release appear to decrease exponentially over time, with the most pronounced decreases occurring within the first 6 days. The retention half-time of ^{241}Am in fecal pellets is in the order of 50 days, compared with 1–10 days for the other elements in this study. This result helps to explain the enrichment of scavenged transuranics in fecal pellets and their short residence times in surface waters.

Overall, the mechanism of fecal pellet sinking and degradation is an important factor in the vertical transport of many radionuclides from surface to bottom waters [111, 113–115]. In fact, zooplankton grazing in the surface layers and concentration of particle-reactive radionuclides into large and dense (hence rapidly sinking) fecal pellets is the plausible mechanism whereby Chernobyl-derived radioactivity (particularly the rare earths) entering the Mediterranean was rapidly transported to 200 m in the few days after the accident [116]. This has potential implications for the recent Fukushima nuclear accident in Japan, which discharged during spring time into the Pacific coast off the island of Honshu, a moderately high productivity ecosystem of complex oceanography [117–119]. In this area, radionuclides have the potential to be entrapped in the gyres formed by the interplay between the Kuroshio and Oyashio currents, which hypothetically limit the dispersion of radionuclides from the area while driving them partially to the seabed, with increased exposure to benthic organisms.

In shelf seas, relatively high inventories of plutonium can accumulate in the continental shelf sediments, attributed to high-density particle scavenging, and contrasting with deep areas where particulate inputs from the shelf are generally low [120]. In the open oceans, particle scavenging by falling biogenic particles can generate a distinct concentration front (subsurface maximum) at depths of 100–1,000 m for plutonium and americium [121], as observed in the Northeast Pacific [122, 123], North Atlantic [124, 125], western Mediterranean [50, 126], Norwegian and Greenland Seas [127] and the central Arctic Ocean [128, 129]. The radionuclide profile in the water column generally exhibits a typical pattern with a surface minimum, a mid-depth maximum and gradual decrease with increasing depth. As time passes, this subsurface maximum tends to sink. For example, in the central Northwest Pacific Ocean, the fallout ^{239,240}Pu subsurface maximum has moved from about 500 m in the early 1970s down to 800 m by the late 1990s, as a result of these processes [130].

Following deposition, radionuclides can migrate through the sediment column, either by diffusion through pore water or its expulsion from compacted sediments, groundwater discharges through the seabed, turbulent mixing in shallow areas or the action of burrowing organisms (bioturbation). In addition, sediment-dwelling species can play a significant role in the remobilization process, as they may redistribute radionuclides from sediments by mixing and agitation [131]. In estuaries where abundant sedimentation occurs it is this, rather than diffusion, that becomes the dominant process [132].

Radionuclides in Sediments

The high Pu and Am K_d's in Table 1 exemplify how strong the affinity of these radionuclides for sediments is. Particle size is a major influence, with a greater tendency for adsorption onto the smaller particles found in mud and silts [133]. To a lesser extent, the same affinity for fine particles applies to Tc and radiocesium [73, 134–136].

Despite its predominantly conservative behavior, a certain proportion of the radiocesium also absorbs onto sediments ($K_d = 2–4 \times 10^0$ m^3 kg^{-1}, see Table 1). For this reason, a radiocesium inventory still resides in areas such as the Irish Sea, along with the transuranium radionuclides. Anionic technetium adsorbs poorly onto particulate matter, which has almost exclusively cationic sorption sites [137]. However, sediments with a high organic content can also retain technetium, especially under reducing conditions. There is a possible link with the presence of bacteria [138], as it has been suggested that the organic polymers that coat the cells of microorganisms may be responsible for technetium sorption [139].

Technetium VII may be reduced to technetium IV forming insoluble compounds such as $TcO_2.2H_2O$, co-precipitated with metallic sulfides or precipitated as Tc_2S_7 [140, 141]. The above studies show that the technetium is most likely reduced at quite a fast rate to insoluble and relatively immobile technetium dioxide by biogenic iron in sediments [142]. It is, therefore, postulated that technetium remains

relatively immobile in sediments beneath the depth at which reduction occurs [68].

Radionuclide Inventories in Sediments

Of the many instances of radionuclide bioaccumulation in sediments, the Irish Sea is noteworthy due to the amount of studies published, which serve to illustrate the environmental processes at play. Over the past 4 decades, the reprocessing discharges from Sellafield have peaked and are now in decline [25, 29, 81, 84]. The sediment inventory from historic discharges has, therefore, become the dominant source to the water column [66, 136, 143–145]. In particular, the mud patch located in the immediate vicinity of the Sellafield outfall remains significant as a repository of plutonium, americium, and radiocesium from the site.

At least 85% of the sediment-bound plutonium and americium in the Irish Sea lies within this coastal strip, approximately 30-km wide, near the Cumbrian coast, buried at mid-depth (~50-cm), and only a small fraction (<7%) of the plutonium discharged annually from Sellafield leaves the area [49, 50, 65]. Accumulation in such a small zone can be explained by local water movements and the fact that most of the plutonium and americium were originally associated with particulate matter in the effluent itself [48].

The distribution of plutonium, americium, and radiocesium in the sub-tidal sediments and interstitial waters of the northeastern Irish Sea has been assessed through major surveys in the late 1970s to mid-1990s [144, 146]. A budget of Pu(alpha) based on these published observations totals 460–540 TBq, or 64–75% of the reported discharge still residing in the zone of fine sediment. The solid phase profiles of plutonium and americium have major subsurface peaks that appear to reflect the history of discharges from Sellafield. In contrast, the inventory of ^{137}Cs in sub-tidal sediments of the whole Irish Sea in 1988 was 1500 TBq, reducing to 960 TBq by 1995 [147], and it has been estimated that only about 40 TBq of ^{99}Tc are still associated with the sediments of the Irish Sea, down to a depth of 50 cm [148, 149].

There remains some shortfall between the estimated inventories and the reported, decay-corrected discharge. Although part of this can be accounted for by the total loss through the North Channel, it is likely that a significant proportion of the unaccounted fraction is situated in sub-tidal and intertidal sandy deposits below the sampling depth achieved in most published studies [144, 149]. Consequently, more recent publications have updated the radionuclide budget estimation for the eastern Irish Sea [150].

Plutonium in the sediments is reported to be complexed with high-molecular-weight humic and low-molecular-weight fulvic compounds [103, 151]. There appears to be evidence for the reduction of Pu(V) to Pu(III) in anoxic waters, whereupon this reduced plutonium becomes complexed with DOC/COC in the form of humic and fulvic acids. This is a naturally slow reaction in pure water, but its speed increases rapidly in the presence of sediments, in proportion to sediment concentration [103]. Particle surfaces also have the capacity to change the oxidation state of the adsorbed species [152]. Such processes have been verified experimentally in fine sediments under different lighting [145, 153] and in sandy muds collected from the mud-patch near the Cumbrian coast in the vicinity of Sellafield [133].

^{137}Cs uptake kinetics has been studied in the laboratory, demonstrating that uptake by suspended matter occurs immediately after introduction of the isotope and attains equilibrium within a few hours [154]. It would appear that biotite and organic carbon are the most important factors controlling ^{137}Cs fixation onto sediments [155]. In the arctic, ^{137}Cs in surface sediments also correlates with total organic carbon content and is stronger in finer sediment [156].

In contrast with plutonium, americium, and radiocesium, uptake of ^{99}Tc from seawater onto sediment is minimal, and likely to occur only onto anoxic sediments where it may be biogeochemically reduced from $^{99}Tc(VII)O_4^-$ to insoluble Tc(IV). Conversely, Tc uptake is unlikely in oxidizing sediments low in organic matter [157].

Redissolution from Sediments

The realization that sediments can act not just as a sink but also a potential source of contaminants to the overlying waters has major implications for the assessment of the environmental impact of radioactive discharges into the marine environment [64, 65, 81].

Thus, redissolution rates constitute an important source of information.

The rate of redissolution from sediments is relatively fast for radiocesium, with a predicted desorption rate constant for suspended particles of 1.2 $days^{-1}$ [105]. However this rate is much slower for plutonium and americium [49]. Overall, the "halving time" (time taken for the radionuclide inventory to drop by 50% by considering radioactive decay and rate of removal) is of the order of 10 years for ^{137}Cs, 100 years for $^{239,240}Pu$, and 1,000 years ^{241}Am [64–66, 133, 144, 145, 147, 158]. Hence the actinides will persist in the sediments for a considerable time, and in the case of the Irish Sea the water flowing out of the area is one of the sources of transuranics to the shelf seas of Northwest Europe and beyond [81].

That remobilization of plutonium from the sediments of the northeastern Irish Sea is the predominant source for plutonium in this region over the last 2 decades or so has been amply verified [45, 50, 65, 66, 145, 158–160]. An evaluation of the time scales involved in the remobilization of radionuclides from this mud patch (i.e., hold-up/residence times and transport times) is a complex exercise, but it confirms that there is a "hold-up" of plutonium within the eastern Irish Sea sediments of at least a decade [50, 63].

According to an experimental study, the proportions of plutonium and americium available for redissolution from seabed and suspended sediment are rather low at 0.02–1% [133]. This is possibly because plutonium in sediments is predominantly associated with strongly bound sesquioxide and organic complex fractions, while americium is associated mainly with the organic complex fraction, with a significant fraction in carbonate form [133]. The reaction half-time for Pu(V) species to obtain "equilibrium" between solid and liquid phases in sandy sediments is quite short, about 8 h [133]. According to the same study, the process can be accelerated by stirring, which releases 2.5 times more plutonium and americium into seawater, indicating the importance disturbance of the seabed may have on redissolution.

It has also been verified that ^{137}Cs is also desorbing from Irish Sea sediments as a consequence of the general reduction in seawater concentrations [85, 147]. A part of the radiocesium discharged from Sellafield made its way and is probably still to be found in the Arctic Ocean, between Canada and Greenland, with a recorded transit time from Sellafield to Baffin Bay of approximately 8 years [161]. This is not surprising, since monovalent Cs^{+} is less strongly adsorbed than plutonium and americium and therefore it is more easily transported by tides and currents. In poor circulation areas, radiocesium can be remobilized by ion-exchange displacement by cations such as NH_4^{+}, Fe^{+2}, and Mn^{+2} released under anaerobic conditions [162].

Desorption of ^{99}Tc from contaminated sediment into uncontaminated seawater appears to be highly variable depending on sediment type. Redissolution from oxidizing sediment is rapid, whereas for anoxic sediment it is very slow [157]. In the Irish Sea, where much of the ^{99}Tc discharged appears to be in a truly dissolved form [36], the impact of ^{99}Tc remobilization from Irish Sea sediments upon levels in the water column is thought to be minimal [148]. This is a consequence of the fact that these sediments are mildly reducing, while the overlaying water remains well oxidized during the year [146, 163].

Influence of Bioturbation

Important evidence has been acquired, indicating that bioturbation of radionuclides stored within the sediments is significant, even at some depth [164]. This is important because biological and physical mixing in the upper layers of the sediment column by processes such as bioturbation or gas leakage can disturb the stratigraphic record [165, 166], effectively burying "older" sediment under "younger" deposits [25, 66, 84, 164]. Variations in concentration by as much as a factor of 100 have been observed within a single core [167], making the vertical distribution of sediments notoriously difficult to predict.

Experimental evidence points to the echurian worm *Maxmuelleria lankesteri* as the main agent responsible for altering the vertical profiles of plutonium and americium in the sediment column of the eastern Irish Sea. The ragworm *Nereis diversicolor* also plays a role in the redistribution of particle-bound radionuclides deposited at the sediment-water interface, with the ability to redistribute ~35% of ^{137}Cs deposited on the sediment surface to ~10 cm depth over a period of just 40 days [168]. The depth distributions of $^{239,240}Pu$ in deep waters of the Northeast Atlantic Ocean exhibit

pronounced subsurface maxima caused by sediment reworking by benthic fauna such as *Sipunculida* worms [169]. These alterations are produced by the organisms feeding on surface sediment and depositing fecal pellets within excavated burrows. The extensive and heterogeneous bioturbation to which sediments are subject, is, undoubtedly, responsible for the variability observed in the vertical profiles of various radio elements [25, 48].

Modeling Studies

It is clear from the foregoing that the sediments of regions like the Irish Sea will continue to be a significant source of plutonium and americium for many centuries [65, 145]. Hence, it is important to model the uptake and redissolution process, predicting the fate of these sediment-locked inventories. The simplest approach is to assume that the sediment is in equilibrium with the surrounding water on an annual basis, applying the concept of mean time of availability, i.e., the average time for which the radionuclide is effectively available to the environment [170]. With this simple method it is possible to reconstruct the deposition history of some radionuclides to a first approximation.

A better approach is to apply compartmental modeling [61, 85, 171, 172]. Irish Sea modeling results confirm the decline of ^{137}Cs and Pu concentrations in water and surface sediments as a result of remobilization and transfer further afield, albeit for the latter radionuclide the process would occur at a much slower rate. The same models predict that the plutonium inventory in deep sediment has not yet peaked, and that this would not be expected to occur for thousands of years.

A process-based model for representing the partitioning of dissolved, colloidal, particulate, and sediment fractions of plutonium and radiocesium has recently been developed [49] (Fig. 3). This model

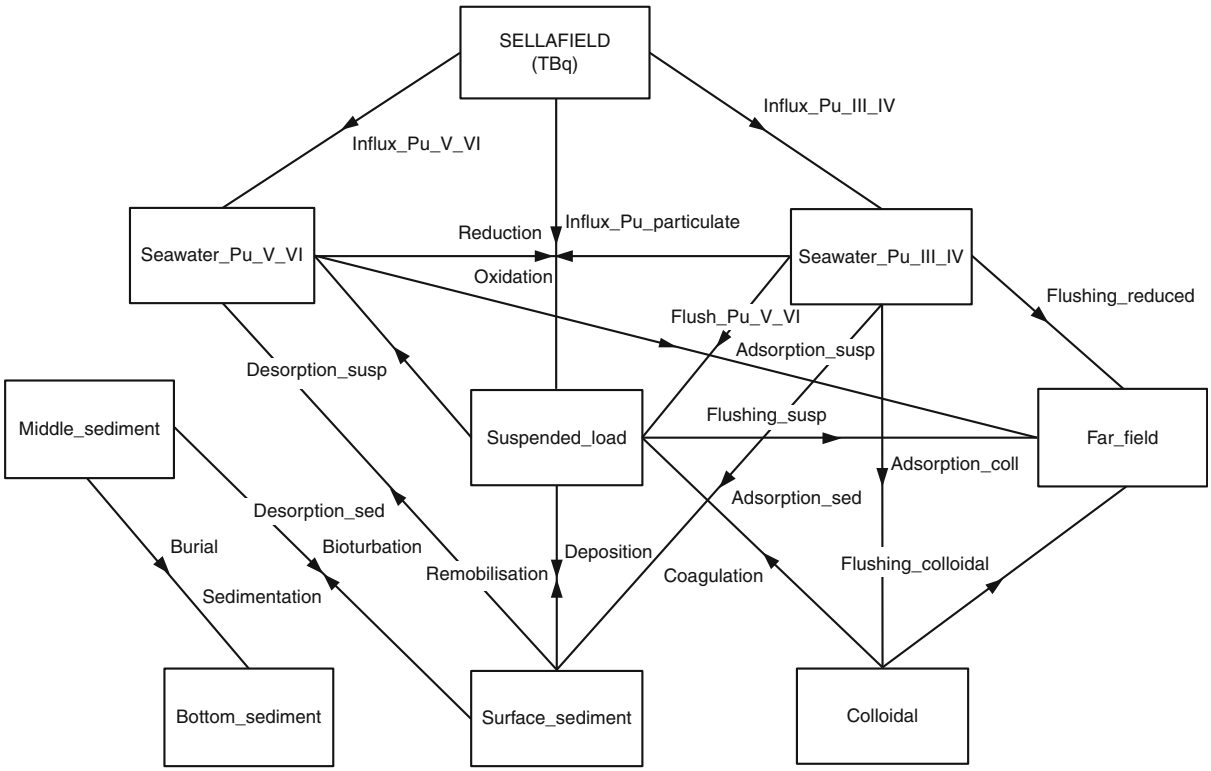

Radioactivity in the Marine Environment. Figure 3
Schematic of speciation model for plutonium and radiocesium [49]. For clarity, radioactive decay is not represented

represents basic biogeochemical processes including a three-layer representation of the seabed, based on previous studies [92, 93]. It confirms the experimental observation that, although in the Cumbrian coastal area near the Sellafield outfall the majority of plutonium in the water column is in a (reduced) particulate form, the majority of the water-borne fraction is in the oxidized state group Pu (V, VI). The model also confirms that most of the plutonium and radiocesium inventories are presently at a depth between 0.1 and 2 m, with the particulate flux from sedimentary deposits to the water column being the main source term for plutonium in the area [85]. Most importantly, the model also predicts the consolidation of the bottom layer inventory over a period of thousands of years.

Behavior of Radionuclides in Estuaries

The environmental behavior of radionuclides depends not only on the nature of the release or source term, but also on the geochemical features of the receiving environment. Considerable variations in the physicochemical behavior of the radionuclides are to be expected in coastal areas, estuaries being a case in point. These behavioral variations are compounded by the fact that the input of inorganic particles, such as clays and metal oxides, can induce important local changes in water chemistry when first entering the sea via estuaries.

There are reports of a wide range of K_d's in tidal estuaries, illustrating the nonequilibrium nature of such systems [51, 173]. Estuaries are highly dynamic environments in which there is a substantial influx of riverine waters, so salinity levels are low. This is accompanied by pH changes and the considerable presence of colloids and suspended particulate matter, competing for the uptake of environmentally available, particle-seeking radionuclides.

In zones where bottom circulation is heavily restricted, such as fjords, there will be a significant depletion in dissolved oxygen levels due to the oxidation of organic matter in bottom waters which are thus converted into an anoxic environment. This results in the reduction of oxidized Pu species reaching the anoxic zone, as observed experimentally in the Framvaren and Hellvik fjords in Norway [174]. Another special case is regions which are shallow and warm by nature, whereupon calcium carbonate tends to form precipitates, which may induce the co-precipitation of radionuclides.

For radionuclides such as plutonium, a redistribution between the dissolved and particulate phase occurs as a consequence of major salinity changes. K_d values can increase substantially when salt concentrations decrease [175]. Consequently, the affinity of particle-seeking radiouclides for suspended sediments is enhanced in these low-salinity environments. Conversely, it has been proposed that small nanoparticles, or colloids, can be important remobilization agents at high salinity [176, 177].

Two cases in point are the Esk Estuary, UK, situated at close proximity to the Sellafield outfall, and the Seine Estuary, which receives an input of plutonium from the Cap de La Hague reprocessing plant. In the Esk Estuary, activity versus salinity plots show higher activities in the dissolved phase below a salinity of 18‰, probably due to the rapid desorption of a labile form of plutonium from suspended particles and sediment in the low salinity in the waters of the estuary [51, 102, 178–180]. The process seems to be associated with a rapid exchange reaction involving competition between plutonium species, protons, and major cations for available solid surfaces [179]. Additional evidence that this is the case comes from measurements of the isotopic quotient, $^{238}Pu/^{239,240}Pu$. It has been found that the average quotient in high salinity dissolved fractions is characteristic of contemporaneous discharges, while in the particulate fraction it is characteristic of historical discharges. This has been attributed to the admixture of reworked older estuarine sediment with the original particulate input [51].

Interestingly, the mixing behavior of plutonium in the Esk Estuary at low salinities is the reverse of that observed in the Seine Estuary, where it has been reported that plutonium is lost from the dissolved phase over a wide range of salinities [181]. Suggestions as to the mechanism/s controlling behavior in the Seine Estuary include scavenging of plutonium from solution by reworked uncontaminated estuarine sediments and removal of plutonium from the freshwater input via coagulation with humic acid and iron. This exemplifies the environmental variability of estuaries and the need to understand the processes affecting radionuclide cycling in particular environments.

Other factors besides salinity changes may affect the behavior of radionuclides in estuaries. As discussed previously, enhanced levels of DOC can lead to relatively low plutonium K_d's due to favorable competition of colloids versus suspended particulates for adsorption sites [182]. Differences in the pH of river water compared with seawater may result in particle-seeking radionuclides (chiefly plutonium) arriving from the open sea to redissolve [179]. Another study appears to confirm that, in intertidal sediments, plutonium speciation is influenced by pH changes within estuarine waters [183]. Biological recycling in estuarine intertidal sediments can lead to additional variation through formation of organoliths with a relatively high radionuclide content, following a seasonal pattern [184].

The existence of "hot particles" in estuaries located near reprocessing plant outfalls, known to persist in the environment for months before dissolving [185], can further complicate the picture by increasing the apparent K_d's for particle-seeking radionuclides, such as plutonium and americium [88, 186]. For these reasons, the behavior of radionuclides in the waters of estuaries is difficult to study.

Cycling in the Foodweb

It is clear from previous discussions that life needs to be regarded as an active agent of radionuclide cycling in the marine environment. There is significant biomass in coastal areas, from phytoplankton and zooplankton at the base of the food chain to the higher vertebrates. Radionuclides can be removed from the marine environment by aquatic biota, either by sorption from seawater or by ingestion/egestion of food and sediment. Some species have a high affinity for particular radionuclides, and so they are regarded as biological markers (or bioindicator species) for radiological contamination. They are important aids to help map the transport and distribution of both conservative and nonconservative radionuclides in the marine environment.

Concentration Factors

To express uptake and accumulation of radionuclides by aquatic biota, concentration factors (CFs) are generally used. The concentration factor is the ratio of radionuclide concentration in biological tissue to that in the surrounding water environment:

$$\mathrm{CF} = \frac{\text{Radionuclide concentration in biota (Bq kg}^{-1}\text{ wet weight)}}{\text{Radionuclide concentration in water (Bq m}^{-3}\text{)}}$$

A summary of concentration factors and half-times of elimination ($T_{B1/2}$) for some marine organisms, based on two recent surveys [187, 188], is given in Table 2.

Certain species of brown seaweed (e.g., *Fucus vesiculosus*) have a high concentration capacity for ^{99}Tc. For example, in the Irish Sea, CFs for *Fucus* in excess of 1×10^5 have been recorded [190]. Other species of brown seaweed, such as *Fucus serratus*, also exhibit high concentration factors for technetium, radiocesium, and the transuranics [232, 251–256], leading to their use as bio-indicators. Uptake of ^{99}Tc by the common lobster and the Norwegian lobster is also very significant [199, 200].

Presently, interest on ^{131}I in coastal environments has risen, due to the Fukushima accident. The highest affinity of this radionuclide is for brown seaweed, zooplankton, and phytoplankton, with CFs in the order of 15, 3, and 0.6 $m^3\ kg^{-1}$, respectively. In molluscs ^{131}I has an affinity for the byssus, operculum, and shell of the molluscs [257, 258]. Iodine $T_{B1/2}$s are in the order of 1–5 days for these species, and a few tens of days for fish and molluscs [187].

Independently from the degree of conservativeness, different elements are incorporated into biota and subsequently depurated at different rates, depending on their chemical and biochemical behavior inside the organism. This means that conservative elements will have low K_d's, but not necessarily low concentration factors or $T_{B1/2}$s in biota. This makes analogue generalizations with regards to biological behavior difficult.

Limitations of the Concentration Factor Approach

The data from Table 2 reflects several decades of work deriving concentration factors for input into models, recognizing the state of equilibrium for the best use of these data in many situations. However, there are limitations to the equilibrium approach. CFs are calculated by comparison of organism activities, which are time integrated, with an average of several

Radioactivity in the Marine Environment. Table 2 Concentration factors (m^3 kg^{-1}) and biological half-lives (d) for selected marine organisms [187, 188]

Species	Data	Tc	Cs	Pu	Am	Source
Cod (*Gadus morhua*)	CF $T_{B1/2}$	2.4E-02 N/A	8.0E-02 N.A.	4.0E-02 N/A	5.0E-02 N/A	Tc: [88, 89, 189, 190]; Cs: [88, 89, 191, 192]; Pu & Am: [88, 89]
Plaice (*Pleuronectes platessa*)	CF $T_{B1/2}$	1.9E-02 3.5E + 01	2.9E-02 6.5E + 01	4.0E-02 N/A	5.0E-02 N/A	Tc: [88, 89, 193]; Cs: [88, 89, 192, 194, 195]; Pu & Am: [88, 89, 196]
Lobster (*Homarus gammarus*)	CF $T_{B1/2}$	3.0E + 00 1.6E + 02	2.2E-02 N/A	3.0E-01 N/A	5.0E-01 N/A	Tc: [88, 89, 140, 193, 197–204]; Cs: [88, 89, 205, 206]; Pu: [88, 89, 198, 200, 202, 203, 207–210]; Am: [88, 89, 198, 202, 206, 208, 211, 212]
Crab (*Cancer pagurus*)	CF $T_{B1/2}$	1.6E-02 6.3E + 01	3.0E-02 N/A	3.0E-01 N/A	5.0E-01 N/A	Tc: [88, 89, 197, 201, 213]; Cs: [88, 89]; Pu: [208]; Am: [88, 89, 208]
Winkle (*Littorina littorea*)	CF $T_{B1/2}$	2.2E + 00 1.4E + 02	3.8E-02 8.6E-01	1.9E + 00 1.2E + 02	7.3E-01 1.8E + 02	Tc: [88, 89, 200, 214, 215]; Cs: [45, 88, 89, 216–220]; Pu & Am: [45, 88, 89, 216, 217, 219–223]
Cockle (*Cardium edule*)	CF $T_{B1/2}$	1.7E + 00 N/A	3.0E-02 N/A	1.4E-01 6.5E + 00	2.4E-01 2.0E + 01	Tc: [88, 89, 140]; Cs: [88, 89]; Pu & Am: [88, 89, 223, 224]
Mussel (*Mytilus edulis*)	CF $T_{B1/2}$	9.8E-01 N/A	2.1E-02 1.8E + 01	1.9E + 00 7.1E + 02	1.2E + 00 3.0E + 02	Tc: [88, 89, 200]; Cs: [45, 88, 89, 217, 219, 220, 223, 225]; Pu: [45, 88, 89, 217, 219, 220, 222, 223, 226]; Am: [45, 88, 89, 219, 220, 222, 223, 226, 227]
Brown seaweed (*Fucus vesiculosus*)	CF $T_{B1/2}$	2.2E + 01 1.3E + 02	5.4E-02 5.4E + 01	3.0E + 00 N/A	4.3E + 00 1.4E + 02	Tc: [88, 89, 140, 200, 215, 228, 229]; Cs: [45, 88, 89, 140, 218–220, 230–234]; Pu: [45, 88, 89, 218–220, 235]; Am: [45, 88, 89, 219, 220, 232, 236, 237]
Zooplankton	CF $T_{B1/2}$	5.5E-02 N/A	3.0E-02 1.3E + 01	5.5E-01 N/A	1.1E + 00 3.4E + 01	Tc: [88, 89, 238]; Cs: [88, 89, 239]; Pu: [88, 89, 113, 238, 240, 241]; Am: [88, 89, 240–243]
Phytoplankton	CF $T_{B1/2}$	6.3E-03 2.1E + 00	2.0E-02 2.6E + 01	2.8E + 02 6.1E + 00	2.2E + 02 1.3E + 01	Tc: [88, 89, 238, 244, 245]; Cs: [88, 89, 246]; Pu: [88, 89, 241, 247, 248]; Am: [241, 247, 249, 250]

instantaneous seawater results (or even a single result). This problem can be compounded by the large range of seawater activity typical of many coastal inputs [215].

Although aquatic organisms equilibrate more rapidly than terrestrial organisms with radionuclide concentrations in the surrounding media [259], there are cases in which equilibrium cannot be assumed, the timeframe of interest being the limiting factor. For example, after a short-term pulsed release of Tc activity, the activity concentration in lobsters along the dispersion path begins to increase gradually. Lobsters have a long biological half-life of elimination for technetium (66 days for uptake from food and 200–300 days for uptake from seawater) [203]. However, technetium is soluble in seawater and will clear quickly from the area where lobsters live, aided by tides and currents, so its concentration in seawater is likely to decrease sharply within a few days. If a lobster has been sampled within days of the discharge, it may appear to have an anomalously high "concentration factor" because it still retains the technetium that it absorbed, while the initial Tc pulse has cleared from the surrounding water.

In other words, if equilibrium has not been reached, the measured CF will only reflect the concentration ratio at a given point in time rather than the steady-state CF that can be measured in the laboratory under controlled conditions. This is why uptake of radionuclides such as ^{99}Tc in the field has occasionally been

observed to exceed that which has been reported in laboratory studies [260].

Despite the above shortcomings, if used correctly, concentration factors can be used to effectively illustrate trends and differences between species. If the timeframe of interest is long (e.g., years or decades of planned authorized discharges, involving continuous releases or gradual changes in discharge concentrations) then the CF approach may well suffice. If the timeframe of the assessment is short (e.g., hours, days, or weeks, such as in emergency or unplanned release scenarios involving abrupt changes in discharge concentrations) dynamic models of the radionuclide transfer to biota are a better assessment tool. This is especially true for organisms that respond slowly to a change in ambient radioactivity concentration.

Bio-Accumulation as a Dynamic Process

The assumption of equilibrium in marine ecosystems can lead occasionally to erroneous estimations of radionuclide transfer to biota. As an illustration, Jackson et al. [215] made the observation that concentrations of ^{99}Tc in seawater off the Cumbrian coast after episodic discharges of ^{99}Tc from Sellafield decreased relatively rapidly, while those in seaweed (*Fucus vesiculosus*) and winkles (*Littorina littorea*) did not. This demonstrates the limitations of using an equilibrium factor to predict radionuclide uptake under discharges of an intermittent nature.

Several methods have been developed to derive activity concentrations in biota under nonequilibrium conditions. One aspect of the dynamic process approach is that these models can very quickly become data "hungry," requiring many terms and parameters that are difficult to measure. However, relatively simple biokinetic models based on first-order exchange kinetics between the medium and the organism are a good improvement. These models use relatively few data: the biological half-life of elimination and the CF (which, as an equilibrium parameter, still has a role to play in the calculations) to deduce the exchange rates between the medium and the organism [188, 261–266].

The simplest approach is to assume a two-compartment first-order kinetic model with constant rates of uptake and excretion from water (k_u and k_{el}), as shown in Fig. 4. With such a simple model, it is possible

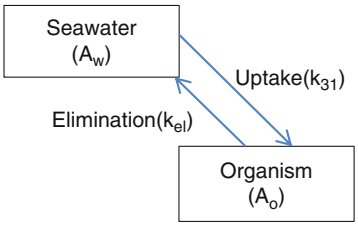

Radioactivity in the Marine Environment. Figure 4 Simple 2-compartment biokinetic model

to deduce the CF for the steady-state as a function of the model rate constants:

$$\mathrm{CF} = \frac{k_u}{k_{el}} \frac{V}{m}$$

where m and V are the mass of the organism (kg) and the volume of water (L) in which the organism is immersed. The kinetic rates k_u and k_{el} can be simply written in terms of the biological half-life of elimination after uptake from water ($T_{B1/2}$), which is the length of time required for all combined physiological processes to cause the loss of half of the bio-accumulated radionuclide from an organism. Hence:

$$k_{el} = \frac{\ln 2}{T_{B1/2}} \quad \text{and} \quad k_u = \frac{\ln 2}{T_{B1/2}} \frac{m}{V} \mathrm{CF}$$

This simple way to calculate the uptake and release rates allows an estimation of the response time for biota exposed to a discharge of radioactivity. For example, it takes some 1–1.5 years for activity in winkles (*Littorina littorea*) and lobsters (*Homarus gammarus*) to peak, following an increase in generalized ^{99}Tc levels in seawater [188, 260].

The above explanation is somewhat simplified because radionuclide turnover by marine organisms can be multiphasic, i.e., with an initial fast release followed by a slower, longer-term release, with a point in time marking the transition from one phase to another. There are many instances of this, such as the biphasic release of Tc in seaweed with $T_{B1/2}$s of ~1 and ~100 days, respectively [140, 200, 229]; Tc and Pu in European lobsters [193, 201, 209, 260]; ^{241}Am and ^{237}Pu from contaminated mussels (*Mytilus galloprovincialis*) [226], or the typical multiphasic release curve representing the depuration of ^{131}I from *Littorina*

littorea [267–269] (Fig. 5), to quote but a few examples. Details of other occurrences are given elsewhere [187, 188].

Recent modeling studies have attempted to represent organ assimilation, direct excretion, and delayed excretion, capturing multiphasic release in the process. A typical improvement with respect to Fig. 2 involves adding more compartments with linear transfer rates between different organs [260, 270, 271]. An adequate compromise is a three-compartment model which makes the working simplification that marine organisms absorb radionuclides mainly from the surrounding seawater, allowing to relate their radioactivity concentration to their environment (Fig. 6).

The above model includes direct exchange with seawater of specific activity A_w through both a fast compartment of activity A_f and a slow compartment of activity A_s:

$$\frac{dA_w}{dt} = k_{el}^{f}A_f + k_{el}^{s}A_s - (k_u^f + k_u^s)A_w$$

$$\frac{dA_f}{dt} = k_u^f A_w - k_{el}^f A_f; \frac{dA_s}{dt} = k_u^s A_w - k_{el}^s A_s$$

Such a model incorporates biphasic release, being sufficiently simple to be solved analytically without recourse to numerical computation. The model requires relatively few parameters, rendering the approach practical for use in radiological assessments [188].

The biological half-life of a radionuclide in an organism is not always constant. It can be affected by factors such as: the fed or starved state, resulting in slower turnover for the latter (observed for ^{99}Tc in gastropods) [214]; temperature, with higher depuration rates at higher values (observed for ^{99}Tc in shrimps [272] and Pu in lobsters [209]); the physical and chemical speciation of the radionuclide; physiological characteristics (size, age, stage of development, sex, habitat); and certain physiological processes associated with molting in crustaceans, which tend to temporarily increase the uptake rate. The latter has been observed for Tc [197, 204] and Pu [209] in crabs and lobsters.

Allometry

The introduction of the biological half-life as an additional transfer parameter is not without its difficulties, as data are not always available. Allometric approaches provide some guidance when estimating transfer rates for use in models [261, 273–275], as well as providing a tool for data interpretation [276]. It has been observed that most metabolic parameters, including basal metabolic rates, ingestion rates, biological half times, etc., are proportional to a simple power function of organism mass. This was first formulated by Kleiber [277, 278], who predicted that the metabolic rate B_r of an organism of mass M is proportional to a quartile power of the mass M:

$$B_r = aM^b; \quad b = 0.75$$

Various radionuclides in marine biota exhibit allometric relationships with respect to the CF and the $T_{B1/2}$, relating to metabolism [279]. A recent study found

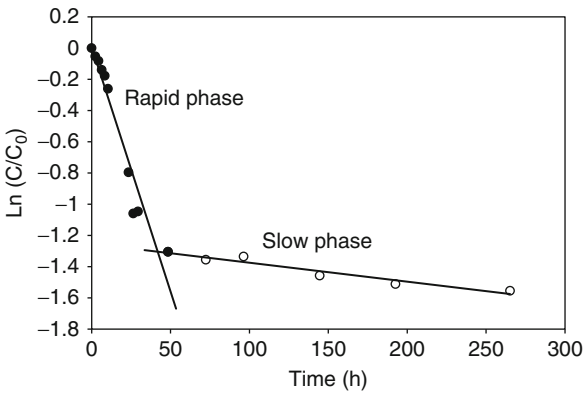

Radioactivity in the Marine Environment. Figure 5 Multicomponent release curve for ^{131}I depuration from *Littorina littorea* [268]

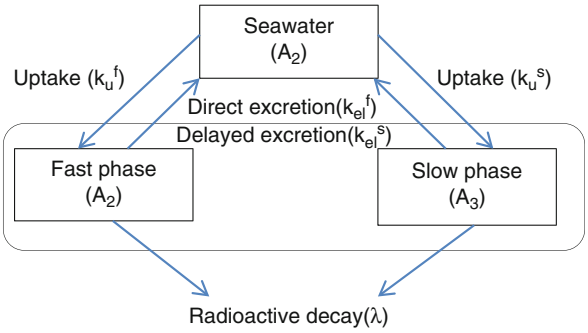

Radioactivity in the Marine Environment. Figure 6 Basis of a dynamic model for the transfer of radionuclides to marine biota [188]

power-like allometric associations between the biological half-life (^{137}Cs, ^{99}Tc) or the concentration factor (Pu, ^{241}Am) on the one side, and size in marine biota [187, 280], as shown in Table 3.

This same study found an association of the independent term of the allometric power function (b) with the K_d, at least for particle-seeking lanthanides and actinides.

It is not surprising that, on average, the CF correlates with mass to the power of about −0.26, since the CF relates to ingestion rate per unit mass, and the ingestion rate is proportional to the metabolic rate, hence CF $\sim M^{0.75} \times M^{-1}$or $M^{-0.25}$. The relationship between $T_{B1/2}$ and metabolic rate is more difficult to explain, but it can be derived using a dynamic model developed for the prediction of radionuclide activity concentrations in Arctic marine species (ECOMOD) [281]. This approach considers that, for a growing organism of total mass $M(t)$, the radionuclide activity concentration y (Bq kg^{-1}, fresh weight) in a given tissue changes according to:

$$\frac{dy}{dt} = -\left(\lambda + \varepsilon_a \frac{B_r}{M} + \frac{1}{M}\frac{dM}{dt}\right) y + \frac{Q_1^A}{Q_0^A}\left(\frac{1}{M}\frac{dM}{dt} + \varepsilon_a \frac{B_r}{M}\right) X(t)$$

where λ is the radioactive decay constant (s^{-1}); ε_a is a proportionality coefficient between the rate of biological loss of a radionuclide from a deposit tissue and the general metabolic rate of the organism; B_r is the metabolic rate (kg s^{-1}); $X(t)$ is the radionuclide activity concentration in food (Bq kg^{-1}, fresh weight) or in water (Bq L^{-1}) when bio-assimilation occurs directly from water at time t, and Q_1^A,Q_0^A are the stable element concentrations in a given tissue and in food or water (mg kg^{-1}), respectively.

For the depuration case, in which $X(t) = 0$, if assuming that the mass of the organism is constant and neglecting radioactive decay, the above equation returns $y(t) = y(0)e^{-\varepsilon_a \frac{B_r}{M} t}$. According to this model, the concentration halving time, or biological half-life of elimination, is $T_{B1/2} = \frac{\ln(2)M}{\varepsilon_a B_r}$. Hence, $T_{B1/2} \sim M \times M^{-0.75} \sim M^{0.25}$, consistent with the prediction that turnover times generally change with a quartile power of the mass [280, 282].

Food Chain Transfer and Biomagnification

The transfer of radionuclides through the marine food chain opens the potential for biomagnification, i.e, the build-up of concentration of certain contaminants, such as toxic metals and persistent halogenated organic compounds, in the bodies of organisms at higher trophic levels. As smaller organisms are ingested by larger ones within the food chain (Fig. 7), biomagnification could theoretically result in higher concentrations of the substance than would be expected if water were the only exposure mechanism.

The potential problem caused by biomagnification has been relatively under-investigated. A modeling study was carried out in the Arctic under the INCO-Copernicus EPIC program [281]. According to this study, ^{137}Cs biomagnification could be occurring for the lower trophic levels (e.g., benthic food chains), similar to what has been observed for other elements such as Cd, methyl-mercury (MeHg), and Po in a chain

Radioactivity in the Marine Environment. Table 3 Allometric relationships for CF and $T_{B1/2}$ in marine biota [280]

	$\log_{10}$[CF(m^3 kg^{-1})]								$\log_{10}$[$T_{B1/2}$(d)]			
Parameter	Ru	Ce	Pm/Eu	Ra	Th	Pu	Am	Cm	Tc	Cs	Pu	Am
$\log_{10}$a	−1.54	−0.33	0.19	−1.07	−0.25	−0.68	−0.60	−0.44	1.99	1.73	2.80	2.40
b	−0.46	−0.25	−0.18	−0.11	−0.27	−0.30	−0.28	−0.27	0.15	0.17	0.20	0.13
r^2	0.75	0.72	0.72	0.79	0.89	0.80	0.78	0.85	0.72	0.92	0.91	0.76
SE($\log_{10}$a)	0.37	0.22	0.17	0.08	0.14	0.22	0.21	0.17	0.20	0.08	0.39	0.22
SE(b)	0.10	0.06	0.04	0.02	0.04	0.06	0.06	0.04	0.05	0.04	0.06	0.04
p-value	0.002	0.004	0.004	0.001	0.0002	0.001	0.002	0.0004	0.03	0.04	0.2	0.05
N	9	9	9	9	9	9	9	9	6	4	3	5

Note: SE, Standard error of the mean

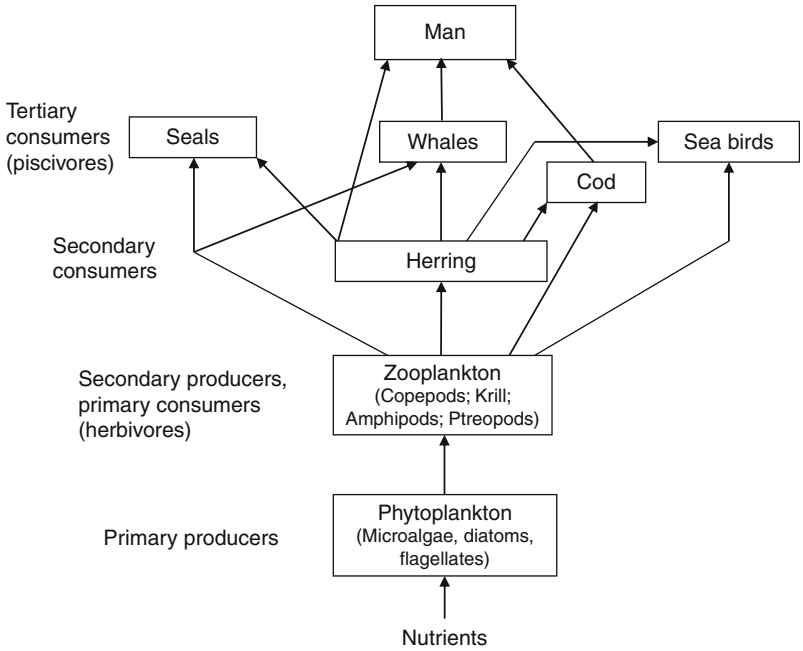

Radioactivity in the Marine Environment. Figure 7
Example of a simple marine food chain containing the basic trophic levels. Adapted from [283]

from plankton to killifish [284]. However, this study suggests that the same is not happening at the highest trophic levels. For ^{239}Pu, transfer to successively higher trophic levels is shown to be low – there is a fall of several orders of magnitude between primary producers, represented by phytoplankton, and higher trophic levels, e.g., cod. Further investigations on polar foodwebs in the waters of the Barents Sea also concluded that transport of ^{137}Cs upward through the food chain does not take place [285]. On the basis of this limited information, it is unlikely that radionuclides from the Fukushima accident will be magnified up in marine food chains, except possibly for the lower trophic levels.

Biodiminution of metals in the planktonic food chain (phytoplankton to copepods to fish) has been attributed to the outflow of metals by copepods and the very low capacity of marine fish to assimilate metals [286]. However, there may be some exceptions to this rule, such as whales, whose diet is based on zooplankton (which have a relatively high concentration capacity for plutonium) [281]. Nevertheless, the potential for the biomagnification of many radionuclides appears to be low. This is likely to be due to biological discrimination against uptake of elements having limited biochemical usefulness, an argument which may not apply to chemical analogues which are incorporated as nutrients into living organisms.

Radiological Implications of the Marine Environment

Human Radiological Exposure

The worldwide fallout from nuclear weapons tests led to the transfer of radionuclides via the marine food chain and an internal dose rate to man through ingestion of the species responsible for human exposure: fish, shellfish, and seaweed, as well as external exposure to beaches and fishing nets. It has been calculated that the corresponding dose rates are very low compared with the dose rates received by general populations from the terrestrial environment. For general populations depending heavily on fish consumption, dose rates could have been at most in the order of 4 μ-sieverts per year (μSv y^{-1}) to the whole body [132].

Radiologically, the seas most affected by the Chernobyl accident were the Baltic and Black Seas, where enhanced ^{137}Cs was observed in aquatic food. However,

the dose rates to the public from ingestion of ^{137}Cs from Chernobyl in aquatic food have been estimated to be low, at least an order of magnitude lower than those due to natural ^{210}Po [287]. The highest dose from the Chernobyl accident was delivered to the critical group in the Baltic Sea region, who received a maximum dose of 0.08 mSv during 1986 [288].

Exposures to routine discharges from the nuclear industry to coastal sites have generally given rise to dose rates of a few tens of μSv per year for the majority of power stations. Some examples in the 1985–2000 period are: 10 μSv y^{-1} in Bradwell, UK, arising from the consumption of ^{137}Cs in fish (1996); 10 μSv y^{-1} in Heysham, UK, arising from external gamma exposure to ^{60}Co (1991); 70 μSv y^{-1} for Paluel, France, arising from consumption of crustaceans and molluscs contaminated with ^{110m}Ag in 1987; and 15 μSv y^{-1} for Dounreay power station, UK, from ^{137}Cs in fish in 1987 [289]. An up-to-date account of exposures due to discharges from the UK nuclear industry in 2009 gives total dose rates to the public for liquid releases from the site of <5, 49 and 11 μSv y^{-1} for Bradwell, Heysham and Douneray, respectively [290]. The dominant contribution is due to gamma dose rates to adult occupants over sediment (only Sellafield has an exposure contribution from the consumption of seafood).

The two most important contributions over the time period 1985–2000 in terms of human dose were the reprocessing plants at Sellafield (UK) and Cap de la Hague (France). According to a modeling study, in Cap de la Hague, dose rates dropped steadily from 170 μSv y^{-1} in 1987 to 19 μSv y^{-1} in 1996, being dominated throughout this period by the consumption of molluscs contaminated with ^{106}Ru and ^{241}Pu and external exposure to gamma-rays from ^{60}Co in sediments.

The radiological impact of Sellafield releases to the Irish Sea environment has been studied in detail using monitoring data and habits surveys [4, 23]. According to a thorough review [291], during the 1950s and 1960s, the highest dose rates from Sellafield were received by individuals consuming Cumbrian *Porphyra* and laverbread, with peak dose rates around 1 mSv y^{-1}. A maximum dose rate of 3.5 mSv y^{-1} (arising principally from ^{137}Cs discharges) would have been reached by 1981.

The maximum dose rate of 3.5 mSv y^{-1} for Sellafield has been revised in line with a reassessment of the porphyra/laverbread ingestion pathway. It is now thought that the critical pathway was fish and shellfish consumption, particularly actinides in molluscs, which tend to concentrate transuranics to a considerably greater extent than do crustaceans, in turn accumulating more than fish. Peak exposures to the critical group of about 2 mSv y^{-1} would have been received in the mid-1970s [292].

By the mid-1980s dose rates from Sellafield decreased to about 0.5 mSv y^{-1}, arising mainly from ingestion of Pu and Am. Exposures then decreased to 187 μSv y^{-1} in 1987 and further down to 114 μSv y^{-1} in 1996, in line with reductions in the transuranic discharges [289].

After the enhanced actinide removal plant (EARP) began operations in 1994, ^{99}Tc discharges from Sellafield increased by almost two orders of magnitude, reaching a maximum in 1995. This resulted in relatively elevated critical group dose rates arising from the consumption of Tc in shellfish (mainly lobsters), 50 μSv y^{-1} in 1997 [293]. As the backlog of Tc effluent was processed by the plant and the soluble Tc began to clear from the Sellafield coastal area, these dose rates decreased sharply [294].

Since then, dose rates from Sellafield to all critical groups have continued to decline [81], currently being very low compared to the peak discharge periods of 1995 for ^{99}Tc, 1975 for ^{137}Cs, 1973 for ^{239,240}Pu, and 1974 for ^{241}Am. In 2009, e.g., a combined dose rate of 0.28 mSv y^{-1} for Sellafield and LLWR sites (^{239,240}Pu and ^{241}Am) on the one hand, and the phosphate processing works in Whitehaven (^{210}Po) on the other, was reached [290]. The Pu and Am contribution at the time, majorly attributable to Sellafield, was about 0.15 mSv y^{-1}. The main pathway continues to be adult crustacean and mollusc consumption.

Along the Irish coast, dose rates have been much lower. Starting from 14 μSv y^{-1} in the early 1980s when the Sellafield discharges were close to their peak, exposures have decreased sharply to <0.1 μSv y^{-1} at present, arising mainly from Pu and Am from consumption of fish and shellfish [295]. ^{99}Tc dose rates to Irish typical and heavy seafood consumer groups in the period 1996–1998 were low at 0.061 and 0.24 μSv y^{-1}, respectively [296].

Long-range transports of radionuclides originating from fallout and from reprocessing plants (including

remobilization of Pu and Cs from Irish Sea sediments) are still the main sources of man-made radionuclides to the Norwegian marine environment. An additional source was outflow of Chernobyl ^{137}Cs-labeled waters from the Baltic Sea [297]. Using an average consumption rate for a Norwegian individual and average concentration compiled for a suite of radionuclides (including anthopogenic and naturally occurring radionuclides) from Norwegian marine areas, an approximate annual dose rate of 0.1 mSv has been derived from the consumption of fish and other seafood. Some 99% of the dose contribution is from naturally occurring radionuclides [298].

The Marina Med project [22] assessed doses in the Mediterranean region for a generalized critical group with high fish and shellfish consumption rates, using measured seawater concentrations and the known biota concentration factors. It was calculated that the critical group received doses of 0.5 μSv y^{-1} from ^{137}Cs and 540 μSv y^{-1} from ^{210}Po in 1990 [288]. The Mediterranean also received an additional input of ^{137}Cs as a consequence of the Chernobyl accident. Calculations showed that, by that time, the critical Mediterranean group was receiving an integrated effective dose from Chernobyl ^{137}Cs in marine food of about 7.5 μSv y^{-1}, about five times lower than the Black Sea critical group and two times lower than Baltic critical group [23].

In the northwestern Pacific Ocean, the average individual dose rates from seafood ingestion in the early 2000s were estimated to be 0.03 μSv y^{-1} from ^{137}Cs and 9 μSv y^{-1} from ^{210}Po. The calculated annual dose of ^{137}Cs for a hypothetical critical group of heavy fish and shellfish consumers was 3 μSv y^{-1}, while the contribution from ^{210}Po would be 160 μSv y^{-1}[299].

In the Arctic generally, by the late 1990s dose rates to humans from the consumption of seafood were dominated by ^{137}Cs and estimated to be 2.6 μSv y^{-1} due to seafood from the Barents Sea and 4.2 μSv y^{-1} via seafood from the Kara Sea [300]. Meanwhile, in the Antarctic Ocean, the individual dose to a critical group consuming molluscs as a result of NEA dumping activities was modeled to be 0.1 μSv y^{-1}, arising mainly from ^{239}Pu and ^{241}Am [301].

Overall, the various sources of anthropogenic radionuclides in the marine environment, such as global fallout, nuclear weapons testing, releases from nuclear facilities, radioactive waste dumping, the Chernobyl accident and nuclear submarine and aircraft accidents, give individual dose rates from ingestion of marine food which are presently a few μSv y^{-1}. For comparison, the annual dose rate for a heavy consumer of fish and shellfish due to the naturally occurring ^{210}Po would be 150–160 μSv y^{-1} [302, 303].

Given the abundance of dosimetric studies on coastal sources of radioactivity, this summary is not comprehensive. However, it is clear that for most situations dose rates from coastal inputs of radioactivity are well below the annual average dose rate of ~3 mSv received by members of the general population from all sources of radiation, except for external irradiation in a few contaminated spots [304]. The dominant contribution to dose actually derives from natural ^{210}Po in fish and shellfish, compared with which the contribution from anthropogenic ^{137}Cs (mainly originating from nuclear weapons tests and the nuclear industry) is generally lower [305, 306].

In the early 1990s, the IAEA MARDOS study confirmed that the dominant contribution to marine dose rates to man comes from natural ^{210}Po in fish and shellfish and that the contribution of anthropogenic ^{137}Cs (mostly from fallout) is negligible, as are the marine dose rates from other man-made radionuclides occurring in the oceans [307]. This confirms that, taken globally, radiation dose rates to humans from exposure to the marine environment and its foodstuffs have little radiological significance.

Radiological Protection of Non-Human Biota

A particular problem surrounding the assessment of radiation dose to non-human biota is that, unlike for humans, an internationally accepted system for the radiological protection of animals and plants is still under development, although the need for such a system to demonstrate that the environment is protected from ionizing radiation is now broadly recognized [308–310]. The old tenet that if humans are protected biota are also protected is no longer accepted [311, 312]. For example, renewed dumping of low-level radioactive waste to the sea would result in low dose rates to humans due to the high dilution in transit from remote areas, but there could be effects in biota that live at the dumping sites. In another example, the maximum radiation dose rate to the marine mammals in

coastal waters around the UK (mainly from radiocesium) is estimated to have been higher than dose rates previously assessed for critical groups of humans living near Sellafield, while the maximum dose rate from plutonium is comparable to the dose rates for humans [313].

As the need to ensure explicit radiological protection of the environment is felt, several national and international bodies have developed or are developing assessment methodologies for nonhuman biota [188, 259, 266, 275, 308, 314–320]. The current state of knowledge underpinning these methodologies is being continually improved and cross-compared [321], but it is generally accepted that prediction of the transfer of radionuclides to organisms (as explained previously) is a major source of uncertainty [322, 323].

Compounded with the above are the challenges posed by the derivation of benchmarks with which to evaluate the scale of radiation doses to nonhuman biota. There is a general consensus on dose rate levels that are unlikely to cause effects to flora and fauna: Brown et al. [324] concluded that only minor effects on biota are to be found for dose rates $<100\ \mu Gy\ h^{-1}$, while the EC ERICA project, based on a detailed statistical analysis, proposed a benchmark level of $10\ \mu Gy\ h^{-1}$ [316]. UNSCEAR concluded that dose rates up to $400\ \mu Gy\ h^{-1}$ to a small proportion of individuals in aquatic populations would not have a detrimental effect at the population level [325]. In their revised recommendations, the International Commission on Radiological Protection (ICRP) proposed a "derived consideration reference level" (DCRL) of 4–40 $\mu Gy\ h^{-1}$ for the most sensitive reference animals and plants [318]. A generic screening value of $10\ \mu Gy\ h^{-1}$ seems reasonably robust, on the basis of current knowledge [326], and is within range of natural background doses for aquatic organisms of up to a few tens of $\mu Gy\ h^{-1}$.

Nevertheless, knowledge on *what effects may be expected* at radiation dose rates in excess of $10\ \mu Gy\ h^{-1}$ is currently very sparse, and there is little known in respect of long-term effects to entire populations. This limits the assessment of the implications of exceeding a "screening dose rate" and, given the amount of data that would be required, such limitation is unlikely to be resolved in the near future.

During recent years, a number of studies have been performed to estimate radiation doses to marine biota. Such estimates are generated using purposely developed assessment tools or models, a fact that should be borne in mind given the evolving scientific position in the dose-to-biota assessment field. However, actual experiments to measure doses to biota have also been carried out. For example, in a pioneering study [327] plaice were tagged with dosimeters and released into the eastern Irish Sea environment in an attempt to generate "measured" exposure rates of biota in their natural state.

In the Sellafield zone, dose rates for ^{239}Pu in benthic molluscs were calculated to have been $10^{-2}\mu Gy\ h^{-1}$ in the 1950s. They increased to about $7\ \mu Gy\ h^{-1}$ in the late 1970s, when transuranium discharges were at their peak. By 2005, plutonium doses had diminished to about $0.1\ \mu Gy\ h^{-1}$. For ^{99}Tc in lobsters it has been estimated that, in the 1950–1970s, dose rates were less than $10^{-2}\ \mu Gy\ h^{-1}$. Then, in the late 1970s, they rose to a peak of about $0.1\ \mu Gy\ h^{-1}$. Between 1980 and the early 1990s Tc doses decreased to pre-1970s levels. Finally, in the early 1990s, they peaked again to above $0.1\ \mu Gy\ h^{-1}$, due to the treatment of EARP plant effluent, before falling again to low levels at present [328].

Another study gives doses of the order of 1.3×10^{-2}, 0.17 and 17 $\mu Gy\ h^{-1}$ for fish, crustaceans, and molluscs over the period 1986–2001 [329]. With the exception of molluscs, these values are low compared with doses to biota local to the Whitehaven phosphate plant, UK (where enhanced levels of naturally occurring radioactive material were processed until 1992), or 4×10^{-2}, 0.4 and 0.8 $\mu Gy\ h^{-1}$ for fish, crustaceans and molluscs by the early 1990s [329].

It can be concluded that in the Irish Sea near Sellafield, even during the period of maximum discharges, dose rates to marine biota were below those which would cause any measurable effect at the population level [84, 330], with exposures expected to decline significantly as a result of the dispersion and mixing of water and sediments in the presence of falling discharges [81].

Dose rates to marine biota in the Cap de la Hague coastal area have been calculated to be somewhat lower than those at Sellafield. During the period 1986–2001, for which a major international assessment exercise was performed [329], the most exposed organisms were molluscs and crabs, with beta and gamma dose rates

varying between 6×10^{-3} to 6×10^{-1} μGy h^{-1}. For Pu-isotopes the dose rate (weighted by radiation weighting factor) was estimated to be 0.6–1.7 μGy h^{-1} for mussels and 8×10^{-3} to 2×10^{-2} μGy h^{-1} for fish [329]. Subsequently, there has been a general tendency for doses to decrease, with contributions from ^{3}H, ^{14}C, ^{60}Co, ^{90}Sr, radiocesium, Pu, and Am to crustaceans, molluscs, fish, and algae reaching levels not in excess of 5×10^{-2} μGy h^{-1} by 2003 [331].

In the fjords of the Novaya Zemlya archipelago (Abrosimov and Tsivolki Fjords) where some of the world's largest radioactive waste dumping sites are located, radiation dose rates to the local marine biota in 1992–1994 (predominantly from α-emitters) appear to have been small (in the order of 0.2, 0.6, and 3.7 μSv y^{-1} for zooplankton, molluscs, and fish, respectively), with maximum external dose rates up to 3 mSv y^{-1} for molluscs living within small contaminated spots on the seabed [304]. These dose rates would have not been exceeded by biota from the Kara Sea generally.

By the end of the 1990s, dose rates for biota in the Barents Sea, where the main contributors to ^{137}Cs contamination are the European reprocessing plants and Chernobyl fallout draining through the Baltic Sea, were also low at 0.1–0.3 μGy h^{-1}. The factor driving the dose was external exposure from ^{137}Cs in bottom water and sediments [285]. More recent data suggests that, in remote areas of the Barents Sea, doses of 0.8–3×10^{-4} μGy h^{-1} exist for fish, crustaceans and molluscs, with crustaceans dominating [329].

Overall, for the whole of the nuclear industry operating across the OSPAR region, a range of 10^{-4}–10^{-1} μGy h^{-1} was estimated for exposures in macroalgae, crustaceans, and vertebrates by 2005 [332]. Other sources of radioactivity appear to pose lower impact on marine biota. For example, NORM radionuclides in oil and gas rigs in Norway ($^{226/228}Ra$, ^{210}Pb, ^{210}Po) have given rise to doses to fish, molluscs, phytoplankton, and zooplankton of as little as 5×10^{-3}–7×10^{-2} μGy h^{-1} by 1996 [333].

A recent development in studies of impact to nonhuman biota is the incorporation of dynamic transfer of radionuclides as part of the assessment, to address situations in which ambient concentrations change rapidly and $T_{B1/2}$s are protracted, such as in the vicinity of coastal inputs where equilibrium is almost never reached. One such study [328] predicts lower dose rates than calculated with the equilibrium CF approach when ambient activities are rising, and the opposite when they are decreasing. For example, using the Environment Agency (UK) R&D 128 dose to biota assessment tool [259], which is equilibrium based, peak ^{99}Tc dose rates in the Drigg area near Sellafield during the period 1997–1999 were calculated to be 7 μGy h^{-1} for brown seaweed (*Fucus vesiculosus*) and 0.7 μGy h^{-1} for gastropod (*Littorina littorea*). These doses correspond to a ^{99}Tc pulse released around January 25, 1998. An alternative dynamic model generates lower predictions of 3.5 and 0.1 μGy h^{-1}, respectively. This effect should be borne in mind when assessing the radiation dose to marine biota under pulsed discharges of radioactivity.

On the basis of the above, it can be concluded that doses to biota above a level of 10 μGy $h^{-1}$are hardly achieved under planned exposure situations [334], though the same cannot be concluded for accidents. It is necessary to continue investigating the radiological impact to benthic organisms inhabiting the sediments, because sediments constitute the eventual sink for many radionuclides entering the marine environment and these habitats may be sensitive, due to the presence of sediment-dwelling organisms such as polychaete worms.

Conclusions

It is clear from this overview that a considerable body of knowledge has been accumulated over the years on the behavior of radionuclides discharged into the marine environment, including the transfer processes responsible for their cycling and their impact on wildlife. The present review cannot be exhaustive, given the many and distinguished investigations carried out in this field of research, but it suffices to illustrate the amount of effort that has gone into understanding the physicochemical speciation, bioavailability, and radiological impact of radionuclides in marine systems, through numerous field and laboratory studies.

From the evidence presented, it can be concluded that, by the complexity of their physical and chemical properties, radionuclides have invaded every component of marine ecosystems: soluble fraction, particulates, colloids, suspended and seabed sediments, and the life forms inhabiting therein. The circulation and

fate of these radionuclides is inextricably linked to the marine processes occurring in a uniquely complex environment, and thus radionuclides are very useful as tracers in the study of marine processes.

The key chemical factor determining radionuclide behavior in the marine environment appears to be its oxidation state distribution, i.e., speciation. The key factors affecting horizontal transport are advection and tidal currents, whereas vertical transport is driven by uptake and scavenging by organic and inorganic particulate matter, having a strong capacity to remove radionuclides from the water column. The importance of this process varies considerably depending on the environment, whether it be shallow coastal areas, intermediate depth, or the deep ocean [121, 335]. In shelf areas, radionuclides are removed from the water column more quickly by the deposition of fine grain sediments. In open oceans the key mechanism may be in falling fecal matter from plankton.

The ultimate fate of radionuclides in the environment is to disperse globally across the oceans, with a certain fraction of the inventory depositing in seabed sediments, down to considerable depths. There, the radionuclides are far from being permanently immobilized, since a number of physical and biological processes conspire to bring some of the material back to the water column, in an ongoing biogeochemical cycle.

In the post-Chernobyl years, the geographical distribution of radionuclides in coastal waters was governed by marine processes rather than input processes [86]. Consequently, radionuclide cycling through the oceans and marine foodwebs gained prominence, with more studies on the uptake of radionuclides in aquatic organisms, the derivation of kinetic transfer parameters for use in modeling and, as of recent times, novel mathematical models to represent dynamically the transfer of radionuclides to the biota. The recent Fukushima accident will likely reopen some of these lines of study.

In terms of radiological impact, man-made radionuclides deposited into the marine environment have been found to pose relatively little radiological significance to humans, except in very specific situations. However, the recent emphasis on long-term radiological protection of marine biota has reawakened an interest on the bioaccumulation, potential biomagnification and radiological effects on whole species and ecosystems. The possibility that some species inhabit contaminated locations where humans are not present, and consequently could be more radiologically exposed, merits special attention.

Modeling studies currently underway hold the key for something that up to now has eluded investigators: the development of a meaningful benchmark level for radioactivity in a whole marine ecosystem. Such work may ultimately be able to consider the distortions introduced by radiation on the balance of different species populations, opening new perspectives for the future of radioecology as a science.

Future Directions

Despite an abundance of field research, presently, marine radioecology is singularly lacking in underlying theories and principles that are experimentally testable. Some of the work has an inherent weakness in that it tries to combine data from various sources to derive results, without a clear underlying theoretical basis. It is necessary to improve this situation, studying the behavior of radioactive contaminants in the seas and the radiological impact of substances on man and environment from a "first-principles," classical science basis. This is particularly important (and necessary) if future reliance on nuclear energy, and all of its potential risks to the marine environment (however small), become the accepted way worldwide.

A direction of particular importance is carrying out laboratory and field studies of radionuclide transfer in marine biota. The concentration factor approach to bioaccumulation (still the most commonly used) is not applicable to dynamic situations, as it does not provide a mechanistic approach to transfer. Biokinetic models can better represent radionuclide transfer to biota in nonequilibrium situations, bringing more realism to predictions of the impact on marine biota arising from pulsed discharges. Such models are required for quantifying the activity retained and how quickly it is cycled and cleared within the marine environment. Much scope for understanding the dynamics of transfer is offered by these modeling and field investigations.

Studies of the speciation of radionuclides in the oceans and the interplay between their different physicochemical forms were initiated in the late 1980s and

continue to this date. Much scope is left for such studies in complex and highly dynamic environments such as fjords and estuaries, especially in the vicinity of inputs, which have not been sufficiently investigated.

Subtropical and tropical environments also offer scope for future research, because tropical countries and small islands are among the most active in terms of urbanization and industrialization. Tracking the behavior of heavy metals through their radiotracers offers a way to study threats to such environmentally fragile ecosystems [336, 337].

The long-term fate of the radionuclide inventory in the oceans (especially transuranics) in fine sedimentary deposits is also of interest, and much work remains to be done in this area by providing models and parameters to better understand the stability and final fate of radionuclide inventories.

The current emphasis on investigating the radiological impact of radionuclides on marine ecosystems and risk to nonhuman biota is likely to increase. It is frequently asserted that measures to protect the environment from radiation exposures should focus on the population rather than the individual [338]. An answer to this need is to use population models, and recent studies have begun to focus on the application of such models for the calculation of doses to populations of marine biota in response to chronic radiation-induced changes [338–341]. Population models can be used to study how radiation effects could alter the natural balance of the ecosystem due to the differing radiation sensitivity between predator and prey species in marine food chains [340].

In terms of environmental conservation and sustainability generally, there is a perceived need to integrate protection from ionizing radiation with the approaches adopted for nonradioactive contaminants. Possible integrated assessment approaches are already being outlined, another obvious trend for future research [342].

In the past, radiotracers have helped the scientific community to understand water circulation and marine processes generally. Given the present concerns on climate change, the use of radioactive tracers as indicators of ocean-climate coupling offer potentially a fruitful line of research. The high sensitivity of radionuclide tracers and their chronological ability (using isotope activity ratios) could be used to track changes in thermohaline circulation, which can affect significantly the global climate [343].

Finally, the directions that marine radioecology may take may depend on unforeseen nuclear events. As this article was written, the accident at the Fukushima nuclear power plant in Japan resulted in the dispersal of radionuclides to the Pacific Ocean, in the context of a possible multi-contaminant situation. This may provide an important new direction for radioecology in the future.

Bibliography

Primary Literature

1. Waller EJ (2011) Sources of radiation in the environment including natural radiation, naturally occurring radioactive materials (NORM), technically enhanced materials, weapon tests and nuclear accidents. Encyclopedia of sustainability science and technology. Springer
2. Eisenbud M, Gesell T (1997) Environmental radioactivity – from natural, industrial and military sources, 4th edn. Academic Press, Toronto, Canada
3. Alexakhin RM (2006) Radioecology: history and state-of-the-art at the beginning of the 21(st) century. In: Cigna AA, Druante M (eds) Radiation risk estimates in normal and emergency situations. Springer, Dordrecht, pp 159–168
4. Aarkrog A (1998) A retrospect of anthropogenic radioactivity in the global marine environment. Radiat Prot Dosim 75(1–4):23–31
5. Povinec PP (2003) Worldwide marine radioactivity studies (WOMARS) – Preface. Deep-Sea Res (Part II Top Stud Oceanogr) 50(17–21):2595–2595
6. IAEA (2005) Worldwide marine radioactivity studies (WOMARS) – Radionuclide levels in oceans and seas – Final report of a coordinated research project. In: Povinec P (ed) IAEA-TECDOC-1429, International Atomic Energy Agency, Vienna, 187 pp
7. Lindahl P, Lee S-H, Worsfold P, Keith-Roach M (2010) Plutonium isotopes as tracers for ocean processes: a review. Mar Environ Res 69(2):73–84
8. Solomon KA (1988) Sources of radioactivity in the ocean environment: from low level waste to nuclear powered submarines. J Hazard Mater 18(3):255–262
9. Noshkin VE, Wong KM (1979) Plutonium mobilization from sedimentary sources to solution in the marine environment. Nuclear energy agency seminar on marine radioecology, Tokyo, Japan, 1 Oct 1979
10. Hardy EP, Krey PW, Volchok HL (1973) Global inventory and distribution of fallout plutonium. Nature 2412:444–445
11. Gummer W, Campbell F, Knight G, Richard J (1980) Cosmos 954 – The occurrence and nature of recovered debris. Atomic Energy Control Board AECB- INFO-0006

12. Hardy EP, Krey PW, Volchock HL (1972) Global inventory and distribution of 238Pu from SNAP-9A. United States Atomic Energy Commission Report HASL-250-250 (TID-4500), New York
13. Gascó C (1991) Estudio de la Distribución de Plutonio en el Ecosistema Marino de Palomares Después de una Descarga Accidental de un Aerosol de Transuránidos. PhD Thesis, Universidad Complutense de Madrid, 375 pp
14. Aarkrog A, Dahlgaard H, Nilsson K, Holm E (1984) Studies of plutonium and americium at Thule, Greenland. Health Phys 46:29–44
15. Povinec PP, Gayol J, Togawa O (1999) Global marine radioactivity database (GLOMARD), IAEA-TECDOC-1094, International atomic energy agency, Vienna, pp 481–482
16. Espinosa A, Aragon A, Stradling N, Hodgson A, Birchall A (1998) Assessment of doses to adult members of the public in palomares from inhalation of plutonium and americium. Radiat Prot Dosim 79:161–164
17. Nevissi A, Schell WR (1975) Distribution of plutonium and americium in Bikini Atoll Lagoon. Health Phys 28:539–547
18. Schell WR, Watters RL (1975) Plutonium in aqueous systems. Health Phys 29:589–597
19. Nevissi A, Schell WR (1975) 210Po and 239Pu, 240Pu in biological and water samples from the Bikini and Eniwetak Atolls. Nature 255:321–323
20. Ilus E (2007) The Chernobyl accident and the Baltic Sea. Boreal Environ Res 12:1–10
21. HELCOM (1995) Radioactivity in the Baltic Sea 1984–1991, Helsinki commission and Baltic marine environment protection commission, Baltic sea environment proceedings no. 61, ISSN 0357–2994
22. EC (1994) The radiological exposure of the population of the European community from radioactivity in the Mediterranean Sea. Radiation Protection 70 MARINA-MED Project Report EUR 15564, Luxembourg
23. EC (1990) The radiological exposure of the population of the European community from radioactivity in north European marine waters project MARINA. Radiation protection 47 MARINA-MED project report EUR 12483, Luxembourg
24. Dunster HJ (1998) An historical perspective of radioactive effluents: discharges from Sellafield to the Irish Sea. Radiat Prot Dosim 75(1–4):15–21
25. Kershaw PJ, Woodhead DS, Malcolm SJ, Allington DJ, Lovett MB (1990) A sediment history of Sellafield discharges. J Environ Radioact 12:201–241
26. Leonard KS, McCubbin D, McDonald P, Service M, Bonfield R, Conney S (2004) Accumulation of technetium-99 in the Irish Sea. Sci Total Environ 322(1–3):255–270
27. McCartney M, Kershaw PJ, Woodhead DS, Denoon DC (1994) Artificial radionuclides in the surface sediments of the Irish Sea, 1968–1988. Sci Total Environ 141:103–138
28. Sellafield Ltd (2009) Monitoring our environment. Discharges and monitoring in the United Kingdom. Annual report 2008, Sellafield Ltd., UK, 62 pp
29. Bailly Du Bois P, Boust D, Fievet B, Maro D, Gandon R (1997) Etude de l'impact des rejets de la Hague sur l'environment des mers du nord est de l'Europe
30. Bailly du Bois P, Gueguenait P (1999) Quantitative assessment of dissolved radiotracers in the English Channel: sources, average impact of la Hague reprocessing plant and conservative behaviour (1983, 1986, 1988, 1994). Cont Shelf Res 19:1977–2002
31. Lind OC, Oughton DH, Salbu B, Skipperud L, Sickel MA, Brown JE, Fifield LK, Tims SG (2006) Transport of low 240Pu/239Pu atom ratio plutonium-species in the Ob and Yenisey Rivers to the Kara Sea. Earth Planet Sci Lett 251:33–43
32. Yablokov A (2001) Radioactive waste disposal is seas adjacent to the territory of the Russian federation. Mar Pollut Bull 43(1–6):8–18
33. Calmet DP (1989) Ocean disposal of radioactive waste: status report, in IAEA Bulletin 4/1989. IAEA, Vienna, pp 47–50
34. Salbu B (2001) Actinides associated with particles. In: Kudo A (ed) Plutonium in the environment. Radioactivity in the environment. Elsevier, Oxford, pp 121–138
35. Buesseler KO (1997) The isotopic signature of fallout plutonium in the North Pacific. J Environ Radioact 36:69–83
36. Leonard KS, McCubbin D, Lovett MB (1995) Physico-chemical characterisation of radionuclides discharged from a nuclear establishment. Sci Total Environ 175:9–24
37. Nelson DM, Lovett MB (1978) Oxidation state of plutonium in the Irish Sea. Nature 276:599–602
38. Riglet C, Robouch P, Vitorge P (1989) Standard potentials of the (MO22+/MO2+) and (M4+/M3+) redox systems for neptunium and plutonium. Radiochim Acta 46:85–94
39. Leonard BR (1980) Properties of plutonium isotopes. In: Wick OJ (ed) Plutonium handbook (a guide to technology), vol 1. American Nuclear Society, Illinois, pp 1–8
40. Brown PL (1989) Prediction of formation constants for actinide complexes in solution. Talanta 36(3):351–355
41. Fukai R, Yamato A, Thein M, Bilinski H (1981) Speciation of plutonium in the Mediterranean environment, in techniques for identifying transuranic speciation in aquatic environments. International Atomic Energy Agency, Vienna, pp 37–41
42. Sillén LG, Martell AE (1964) Stability constants of metal-ion complexes. Special publication 17, Chemical Society, London, pp 51–53
43. Rabideau SW, Kline RJ (1958) Kinetics of oxidation-reduction reactions of plutonium. The reaction between plutonium (VI) and plutonium (III) in perchlorate solution. J Phys Chem 62:617–620
44. Rabideau SW (1953) Equilibria and reaction rates in the disproportionation of Pu(IV). J Am Chem Soc 75:798–801
45. Vives i Batlle J (1993) Speciation and bioavailability of plutonium and americium in the Irish Sea and other marine ecosystems. PhD dissertation, Department of Experimental Physics, University College Dublin, Dublin p 347
46. Choppin GR, Bond AH, Hromadka PM (1995) Redox speciation of plutonium. J Radioanal Nucl Chem 219(2):203–210

47. Schulz W (1976) The chemistry of americium. Technical information center, Energy Research and Development Administration, U.S. Department of Commerce, Springfield, 290 pp
48. Pentreath RJ, Woodhead DS, Kershaw PJ, Jefferies DF, Lovett MB (1986) The behaviour of plutonium and americium in the Irish Sea. Rapports et Proces-verbaux des Réunions du Conseil International pour l'Éxploration de la Mer, pp 60–69
49. Vives i Batlle J, Bryan S, McDonald P (2008) A process-based model for the partitioning of soluble, particulate and sediment fractions of plutonium and radiocaesium in the Eastern Irish Sea near Sellafield. J Environ Radioact 99(1):1464–1473
50. Mitchell PI, Vives i Batlle J, Downes AB, Condren OM, Vintro LL, Sanchez Cabeza JA (1995) Recent observations on the physico-chemical speciation of plutonium in the Irish Sea and the Western Mediterranean. Appl Radiat Isotopes 46(11):1175–1190
51. Assinder DJ, Kelly M, Aston SR (1985) Tidal variations in dissolved and particulate phase radionuclide activities in the Esk Estuary, England, and their distribution coefficients and particulate activity fractions. J Environ Radioact 2(1):1–22
52. Nelson DM, Penrose WR, Karttunen JO, Mehlhaff P (1985) Effects of dissolved organic carbon on the adsorption properties of plutonium in natural waters. Environ Sci Technol 79:127–131
53. Nevissi A, Schell WR (1976) Efficiency of a large volume water sampler for some radionuclides in salt and fresh water. In: Cushing CE Jr (ed) Radioecology and energy resources. Dowden, Hutchinson and Ross, Stroudsburg, PA, pp 277–282
54. Nelson DM, Orlandi KA (1985) The role of natural dissolved organic compounds in determining the concentrations of americium in natural waters. In: Bulman RA, Cooper JR (eds) Speciation of fission and activation products in the environment. Elsevier, London, pp 262–268
55. McMahon CA, León Vintró L, Mitchell PI, Dahlgaard H (2000) Oxidation-state distribution of plutonium in surface and subsurface waters at Thule, northwest Greenland. Appl Radiat Isot 52:697–703
56. Lovett MB, Nelson DM (1980) Determination of some oxidation states of plutonium in sea water and associated particulate matter. In: Proceedings of the symposium on techniques for identifying transuranic speciation in aquatic environments. Ispra, Italy. IAEA, Vienna
57. Pentreath RJ, Jefferies DF, Lovett MB, Nelson DM (1980) The behaviour of transuranic and other long-lived radionuclides in the Irish Sea and its relevance to the deep sea disposal of radioactive wastes. In: Marine radioecology, proceedings of 3rd symposium, Tokyo, Japan. OECD, Paris
58. Noshkin VE, Wong KM (1981) Plutonium mobilization from sedimentary sources to solution in the marine environment. In: Proceedings of the marine radioecology, 3rd nuclear energy agency seminar, Paris, 1979, pp 165–178
59. Boust D, Mitchell PI, Garcia K, Condren OM, Leon Vintro L, Leclerc G (1996) A comparative study of the speciation and behaviour of plutonium in the marine environment of two reprocessing plants. Radiochim Acta 74:203–210
60. Jefferies DF, Preston A, Steele AK (1973) Distribution of caesium 137 in British coastal waters. Mar Pollut Bull 4(8):118–122
61. Jefferies DF, Steele AK (1989) Observed and predicted concentrations of caesium-137 in seawater of the Irish Sea 1970–1985. J Environ Radioact 10:173–189
62. Jefferies DF, Steele AK, Preston A (1982) Further studies on the distribution of ^{137}Cs in British coastal waters - I. Irish Sea. Deep-Sea Res Part A 29(6A):713–738
63. Hunt GJ (1985) Timescales for dilution and dispersion of transuranics in the Irish Sea near Sellafield. Sci Total Environ 46:261–278
64. Hunt GJ, Kershaw PJ (1990) Remobilisation of artificial radionuclides from the sediment of the Irish Sea. J Radiol Prot 10(2):147–151
65. Cook GT, MacKenzie AB, McDonald P, Jones SR (1997) Remobilization of Sellafield-derived radionuclides and transport from the north-east Irish Sea. J Environ Radioact 35(3):227–241
66. MacKenzie AB, Cook GT, McDonald P, Jones SR (1998) The influence of mixing timescales and re-dissolution processes on the distribution of radionuclides in northeast Irish Sea sediments. J Environ Radioact 39(1):35–53
67. Bishop GP, Beetham CJ, Cuff YS (1989) Review of literature for chlorine, technetium, iodine and neptunium. Nirex radioactive waste disposal safety studies report NSS/R193, UK Nirex Ltd. Harwell
68. Beasley TM, Lorz HV (1986) A Review of the biological and geochemical behaviour of technetium in the marine environment. J Environ Radioact 3:1–22
69. Rudin MJ, Stanton C, Patterson RG, Garcia RS (1992) National low-level waste management program radionuclide report series. Vol 2: Technetium-99. Idaho national engineering laboratory report, EG and G Idaho Inc., Idaho Falls, 16 pp
70. Schulte EH, Scoppa P (1987) Sources and behaviour of technetium in the environment. Sci Total Environ 64:163–179
71. Sparkes ST, Long SE (1988) The chemical speciation of technetium in the environment - a literature survey, AERE R12743, HMSO, London
72. Wildung RE, McFadden KM, Garland TR (1979) Technetium sources and behaviour in the environment. J Environ Qual 8:156–161
73. Nicholson S, Howorth JM, Sanders TW, Blaine LM (1992) Technetium-99 in the Irish Sea. Department of the environment report no. DOE/HMIP/RR/92.008
74. Leonard KS, McCubbin D, Brown J, Bonfield R, Brooks T (1997) Distribution of technetium-99 in UK coastal waters. Mar Pollut Bull 34(8):628–636
75. McCubbin D, Leonard KS, Brown J, Kershaw PJ, Bonfield RA, Peak T (2002) Further studies of the distribution of technetium-99 and caesium-137 in UK and European coastal waters. Cont Shelf Res 22:1417–1445
76. McCubbin D, Leonard KS, McDonald P, Bonfield R, Boust D (2006) Distribution of Technetium-99 in sub-tidal sediments of the Irish Sea. Cont Shelf Res 26(4):458–473

77. Till JC, Hoffmann O, Dunning DE (1979) A new look at ^{99}Tc releases to the atmosphere. Health Phys 29:695–699
78. Lujanienė G, Šilobritienė B, Jokšas K, Morkūnienė R (2004) Behaviour of radiocesium in marine environment. Environ Res Eng Manage 2(28):23–32
79. Aston SR, Duursma EK (1973) Concentration effects on 137-Cs, 65-Zn, 60-Co and 106-Ru sorption by marine sediments with geological implications. Neth J Sea Res 6(1–2):225–240
80. Ueda S, Hasegawa H, Kondo K (1999) Concentration and speciation of 137Cs in the surface sediments in Brackish Lake Obuchi, Rokkasho village. Radioisotopes 48(11):683–689
81. León Vintró L, Smith KJ, Lucey JA, Mitchell PI (2000) The environmental impact of the Sellafield discharges. In: SCOPE-RADSITE workshop, Brussels, 4–6 Dec 2000, 27 pp
82. Pentreath RJ (1985) General review of literature relevant to water discharges. In: Behaviour of radionuclides released into coastal waters. IAEA-TECDOC-329. International Atomic Energy Agency, Vienna
83. Pentreath RJ, Harvey BR, Lovett MB (1986) Chemical speciation of transuranium nuclides discharged into the marine environment. In: Bulman RA, Cooper JR (eds) Speciation of fission and activation products in the environment. Elsevier, London, pp 312–325
84. Kershaw PJ, Pentreath RJ, Woodhead DS, Hunt GJ (1992) A review of radioactivity in the Irish Sea. A report prepared for the marine pollution monitoring group, Ministry of agriculture, fisheries and food aquatic environment monitoring report 32. MAFF, Directorate of Fisheries Research, Lowestoft, UK, 65 pp
85. Mitchell PI, Condren OM, Vintro LL, McMahon CA (1999) Trends in plutonium, americium and radiocaesium accumulation and long-term bioavailability in the western Irish Sea mud basin. J Environ Radioact 44(2–3):223–251
86. Hirose K (2009) Plutonium in the ocean environment: its distributions and behavior. J Nucl Radiochem Sci 10(1):R7–R16
87. Mitchell PI, Downes AB, León-Vintró L, McMahon CA (2001) Studies of the speciation, colloidal association and remobilisation of plutonium in the marine environment. In: Kudo A (ed) Plutonium in the environment. Elsevier, London, pp 79–104
88. IAEA (2004) Sediment distribution coefficients and concentration factors for biota in the marine environment, Technical reports series no. 422, International Atomic Energy Agency, Vienna
89. IAEA (1985) Sediment Kd's and concentration factors for radionuclides in the marine environment. International Atomic Energy Agency, Vienna
90. Harvey BR, Kershaw PJ (1984) Physico-chemical interactions of long-lived radionuclides in coastal marine sediments and some comparisons with the deep sea environment. In: International symposium on the behaviour of long-lived radionuclides in the marine environment. 1984. Commission of the European Communities, Luxembourg
91. Lansard B, Grenz C, Charmasson S, Schaaff E, Pinazo C (2006) Potential plutonium remobilisation linked to marine sediment resuspension: first estimates based on flume experiments. J Sea Res 55(1):74–85
92. Lepicard S, Raffestin D, Rancillac F (1998) POSEIDON: a dispersion computer code for assessing radiological impacts in a European sea water environment. Radiat Prot Dosim 75(1–4):79–83
93. Simmonds JR, Bexon AP, Lepicard S, Jones AL, Harvey MP, Sihra K, Nielsen SP (2004) Update of the MARINA project on the radiological exposure of the European community from radioactivity in North European marine waters. Annex D: radiological impact on EU member states of radioactivity in north European waters. European Commission report, 190 pp
94. Starik IE (1959) Principles of radiochemistry. Doklady Akademii Nauk SSSR, Translation series AEC-tr-6314, U.S. Atomic Energy Commission
95. Wells ML, Goldberg ED (1991) Occurrence of small colloids in sea water. Nature 353:342–344
96. Wells ML, Goldberg ED (1992) Marine submicron particles. Mar Chem 40:5–18
97. Wells ML, Goldberg ED (1993) Colloid aggregation in seawater. Mar Chem 41:353–358
98. Salbu B (1987) Radioactive tracer techniques in speciation studies. Environ Technol Lett 8:381–392
99. Guo L, Santschi PH, Warnken KW (1995) Dynamics of dissolved organic carbon (DOC) in oceanic environments. Limnol Oceanogr 40:1392–1403
100. Santschi PH, Burd AB, Gaillard J-F, Lazarides A (2005) Transport of materials and chemicals by nanoscale colloids and micro- to macroscale flocs in marine, freshwater, and engineered ecosystems. In: Droppo I, Leppard G, Liss S, Milligan T (eds) Flocculation in natural and engineered environmental systems. CRC Press, Boca Raton, FL
101. Nelson DM, Larsen RP, Penrose WP (1987) Chemical speciation of plutonium in natural waters. In: Pinder JE III, Alberts JJ, McLeod KW, Schreckhise RG (eds) Environmental research on actinide elements. U.S. Department of Energy, Washington, DC, pp 27–48
102. Mudge SM, Hamilton-Taylor J, Kelly M, Bradshaw K (1988) Laboratory studies of the chemical behaviour of plutonium associated with contaminated estuarine sediments. J Environ Radioact 8(3):217–237
103. Penrose WR, Metta DN, Hylko JM, Rinckel LA (1986) The reduction of plutonium (V) by aquatic sediments. J Environ Radioact 5:185–208
104. León Vintró L, Mitchell PI, Smith KJ, Kershaw PJ, Livingston HD (2005) Chapter 3 Transuranium nuclides in the world's oceans. In: Livingston HD (ed) Marine radioactivity. Radioactivity in the environment, vol 6. Elsevier, UK, pp 79–108
105. Nyffeler UP, Li YH, Santschi PH (1984) A kinetic approach to describe trace-element distribution between particles and solution in natural aquatic systems. Geochim Cosmochim Acta 48:1513–1522
106. Oughton DH, Borretzen P, Salbu B, Tronstad E (1997) Mobilisation of ^{137}Cs and ^{90}Sr from sediments: potential sources to Arctic waters. Sci Total Environ 202:155–165
107. Förstner U, Wittmann GTW (1979) Metal pollution in the aquatic environment. Springer, New York, 486 pp

108. Quigley MS, Santschi PH, Guo L, Honeyman BD (2001) Sorption irreversibility and coagulation behavior of 234Th with marine organic matter. Mar Chem 76:27–45
109. Leon Vintro L, Mitchell PI, Condren OM, Downes AB, Papucci C, Delfanti R (1999) Vertical and horizontal fluxes of plutonium and americium in the western Mediterranean and the Strait of Gibraltar. Sci Total Environ 237–238:77–91
110. Noshkin VW, Bowen VT (1973) Concentrations and distributions of long-lived fallout radionuclides in open ocean sediments. In: Radioactive contamination of the marine environment. IAEA, Vienna, pp 671–868
111. Fisher NS, Nolan CV, Fowler SW (1991) Scavenging and retention of metals by zooplankton fecal pellets and marine snow. Deep-Sea Res Part A: Oceanogr Res Pap 38(10):1261–1275
112. Lee B-G, Fisher NS (1992) Decomposition and release of elements from zooplankton debris. Mar Ecol Prog Ser 88:117–128
113. Higgo JJW, Cherry RD, Heyraud M, Fowler SW (1977) Rapid removal of plutonium from the oceanic surface layer by zooplankton faecal pellets. Nature 266:623–624
114. Krishnaswami S, Baskaran M, Fowler SW, Heyraud M (1985) Comparative role of salps and other zooplankton in the cycling and transport of selected elements and natural radionuclides in Mediterranean waters. Biogeochemistry 1(4): 353–360
115. Rodriguez y Baena AM, Fowler SW, Migel JC (2007) Particulate organic carbon: natural radionuclide ratios in zooplankton and their freshly produced fecal pellets from the NW Mediterranean (MedFlux 2005). Limnol Oceanogr 52(3): 966–974
116. Fowler SW, Buat-Menard P, Yokoyama Y, Ballestra S, Holm E, Nguyen HV (1987) Rapid removal of Chernobyl fallout from Mediterranean surface waters by biological activity. Nature 329(6134):56–58
117. Shiomoto A, Hashimoto S, Murakami T (1998) Primary productivity and solar radiation off Sanriku in May 1997. J Oceanogr 54:539–544
118. Alekseev AV, Khrapchenkov FF, Baklanov PJ, Blinov YG, Kachur AN, Medvedeva IA, Minakir PA, Titova GD (2006) Oyashio current – GIWA regional assessment 31: regional definition. Global International Waters Assessments (GIWA) Regional Report, pp 13–21. Available from http://www.unep.org/dewa/giwa/areas/reports/r31/regional_definition_giwa_r31.pdf. Accessed 4 May 2011
119. Terazaki M (1989) Recent large-scale changes in the biomass of the Kuroshio current ecosystem. In: Sherman K, Alexander LM (eds) Biomass yields and geography of large marine ecosystems. AAAS selected symposium 111, Westview, Boulder, pp 37–65
120. Papucci C, Charmasson S, Delfanti R, Gascó C, Mitchell PI, Sánchez Cabeza JA (1996) Chapter 8. Time evolution and levels of man-made radioactivity in the Mediterranean Sea. In: Guegueniat P, Germain P, Metivier H (eds) Radionuclides in the oceans: inputs and inventories. IRSN, France, pp 177–197
121. León Vintró L, Mitchell PI, Smith KJ, Kershaw PJ, Livingston HD (2004) Transuranic radionuclides in the world's oceans. In: Livingston HD (ed) Marine radioactivity, radioactivity in the environment, vol 6. Elsevier, Amsterdam, pp 79–107
122. Fowler SW, Ballestra S, La Rosa J, Fukai R (1983) Vertical transport of particulate-associated plutonium and americium in the upper water column of the northeast pacific. Deep-Sea Res Part A: Oceanogr Res Pap 30(12):1221–1233
123. Bowen VT, Noshkin VE, Livingston HD, Volchok HL (1980) Fallout radionuclides in the Pacific Ocean: vertical and horizontal distributions, largely from GEOSECS stations. Earth Planet Sci Lett 49:411–434
124. Cochran JK, Livingston HD, Hirschberg DJ, Surprenant LD (1987) Natural and anthropogenic radionuclide distributions in the northwest Atlantic Ocean. Earth Planet Sci Lett 84:135–152
125. Nyffeler F, Cigna AA, Dahlgaard H, Livingston HD (1996) - Chapter 1. Radionuclides in the Atlantic Ocean: a survey. In: Radionuclides in the ocean: inputs and inventories. Les Editions de Physique, France
126. Fukai R, Holm E, Ballestra S (1979) A note on vertical distribution of plutonium and americium in the Mediterranean Sea. Oceanol Acta 2(2):129–132
127. Herrmann J, Nies H, Goroncy I (1998) Plutonium in the deep layers of the Norwegian and Greenland Seas. Radiat Prot Dosim 75(1–4):237–245
128. Livingston HD, Kupferman SL, Bowen VT, Moore RM (1984) Vertical profiles of artificial radionuclide concentrations in the Central Arctic Ocean. Geochim Cosmochim Acta 48:2195–2203
129. Smith JN, Ellis KM (1995) Radionuclide tracer profiles at the CESAR Ice Station and Canadian Ice Island in the western Arctic Ocean. Deep-Sea Res 42(6):1149–1470
130. Livingston HD, Povinec PP, Ito T, Togawa O (2001) The behaviour of plutonium in the Pacific Ocean. Radioactiv Environ 1:267–292
131. Ryan TP (2002) Transuranic biokinetic parameters for marine invertebrates–a review. Environ Int 28:83–96
132. NAS (1971) Radioactivity in the marine environment. National Academy of Sciences, Washington, DC, 272 pp
133. McDonald P, Vives i Batlle J, Bousher A, Whittall A, Chambers N (2000) The availability of plutonium and americium in Irish Sea sediments for re-dissolution. Sci Total Environ 267:109–123
134. Clifton J, McDonald P, Plater A, Oldfield F (1997) Relationships between radionuclide content and textural properties in Irish Sea intertidal sediments. Water Air Soil Pollut 99(1–4): 209–216
135. He Q, Walling DE (1996) Interpreting particle size effects in the adsorption of ^{137}Cs and unsupported ^{210}Pb by mineral soils and sediments. J Environ Radioact 30(2):117–137
136. MacKenzie AB, Cook GT, McDonald P (1999) Radionuclide distributions and particle size associations in Irish Sea surface sediments: implications for actinide dispersion. J Environ Radioact 44(2–3):275–296

137. Higgo JJW (1990) Radionuclide Interactions with marine sediments. Nirex radioactive waste disposal safety studies report NSS/R142, UK Nirex Ltd., London
138. Scoppa P, Schulte EH, Secondini A (1982) Chemical form and behaviour of technetium in the marine environment. J Nucl Med Allied Sci 26(3):156
139. Pignolet L, Myttenaere C, Vandercasteele CM, Moreau Z, Cogneau M (1984) Behaviour of technetium in the marine environment: uptake and distribution of Tc into sediments and sedimentary microorganisms. In: Cigna A, Myttenaere C (eds) International symposium on the behaviour of long-lived radionuclides in the marine environment, Proceedings symposium. La Spezia, CEC Report
140. Masson M, Patti F, Colle C, Roucoux P, Grauby A, Saas A (1989) Synopsis of French experimental and in situ research on the terrestrial and marine behaviour of Tc. Health Phys 57(2): 269–279
141. Schreiner F, Fried S, Friedman A (1982) Diffusion of neptunyl (V)- and pertechnetate ions in marine sediments'. In: Topp SV (ed) The scientific basis for nuclear waste management. Elsevier, New York, pp 273–277
142. Burke IT, Livens F, Lloyd JR, Brownd AP, Law GTW, McBeth JM, Ellis BL, Lawson RA, Morris K (2010) The fate of technetium in reduced estuarine sediments: combining direct and indirect analyses. Appl Geochem 25(2):233–241
143. McDonald P, Cook GT, Baxter MS, Thomson JC (1990) Radionuclide transfer from Sellafield to south-west Scotland. J Environ Radioact 12:285–298
144. Kershaw PJ, Denoon DC, Woodhead DS (1999) Observations on the redistribution of plutonium and americium in the Irish Sea Sediments, 1978 to 1996 concentrations and inventories. J Environ Radioact 44:191–221
145. Leonard KS, McCubbin D, Blowers P, Taylor BR (1999) Dissolved plutonium and americium in surface waters of the Irish Sea, 1973–1996. J Environ Radioact 44:129–158
146. Malcolm SJ, Kershaw PJ, Lovett MB, Harvey BR (1990) The interstitial water chemistry of ^{239,240}Pu and ^{241}Am in the sediments of the North-East Irish Sea. Geochim Cosmochim Acta 54:29–35
147. Poole AJ, Denoon DC, Woodhead DS (1997) The distribution and inventory of ^{137}Cs in sub-tidal sediments of the Irish Sea. Radioprotection – Colloques 32(C2):263
148. Leonard KS, McCubbin D, Jenkinson SB, Bonfield RA, McMeekan IT (2008) An assessment of the availability of Tc-99 to marine foodstuffs. Cefas Contract C2170 FOR FSA Project R01062, 81 pp
149. Jones DG, Roberts PD, Strutt MH, Higgo JJ, Davis JR (1999) Distribution of ^{137}Cs and inventories of ^{238}Pu, $^{239/240}$Pu, ^{241}Am and ^{137}Cs in Irish Sea intertidal sediments. J Environ Radioact 44:159–189
150. Jones DG, Kershaw PJ, McMahon CA, Milodowski AE, Murray M, Hunt GJ (2007) Changing patterns of radionuclide distribution in Irish Sea subtidal sediments. J Environ Radioact 96(1–3):63–74
151. Baxter MS, Fowler SW, Povinec PP (1995) Observations on plutonium in the oceans. Appl Radiat Isot 46(11):1213–1223
152. Morse JW, Choppin GR (1986) Laboratory studies of plutonium in marine systems. Mar Chem 20(1):73–89
153. McCubbin D, Leonard KS (1996) Photochemical dissolution of radionuclides from marine sediment. Mar Chem 55(3–4): 399–408
154. Knapińska-Skiba D, Bojanowski R, Radecki Z, Łotocka M (1995) The biological and physico-chemical uptake of radiocesium by particulate matter of natural origin (Baltic Sea). Aquat Ecol 29(3–4):283–290
155. Kim Y, Kim K, Kang H-D, Kim W, Doh S-H, Kim D-H, Kim BK (2007) The accumulation of radiocesium in coarse marine sediment: effects of mineralogy and organic matter. Mar Pollut Bull 54(9):1341–1350
156. Cooper LW, Grebmeier JM, Larsen IL, Dolvin SS, Reed AJ (1998) Inventories and distribution of radiocaesium in arctic marine sediments: influence of biological and physical processes. Chem Ecol 15(1–3):27–46
157. Leonard KS, McCubbin D (2004) Accumulation and remobilisation of 99Tc in the eastern Irish Sea. Environment Report RL 01/04, Centre for Environment, Fisheries and Aquaculture Science, Lowestoft Laboratory, UK, 65 pp
158. McCubbin D, Leonard KS, Emerson HS (1999) The role of thermal and photochemical reactions upon the remobilisation of Pu from an Irish Sea sediment. J Environ Radioact 44:253–273
159. MacKenzie AB, Scott RD, Allan RL, Ben Shaban YA, Cook GT, Pulford ID (1994) Sediment radionuclide profiles: implications for mechanisms of Sellafield waste dispersal in the Irish Sea. J Environ Radioact 23:39–69
160. McCubbin D, Leonard KS (1997) Laboratory studies to investigate short-term oxidation and sorption behaviour of neptunium in artificial and natural seawater solutions. Mar Chem 56(1–2):107–121
161. Aarkrog A, Boelskifte S, Dahlgaard H, Duniec S, Hallstadius L, Holm E, Smith JN (1987) Tc-99 and cesium-134 as long-distance tracers in Arctic waters. Estuar Coast Shelf Sci 24(5):637–647
162. Evans DW, Alberts JJ, Clarke RA (1983) Reversible ion-exchange fixation of caesium-137 leading to mobilization from reservoir sediments. Geochim Cosmocim Acta 47(6):1041–1049
163. Harvey BR (1981) Potential for post depositional migration of neptunium in Irish Sea sediments. In: Impacts of radionuclide releases into the marine environment, IAEA-SM-248/104, IAEA, Vienna, pp 93–103
164. Kershaw PJ, Swift DJ, Pentreath RJ, Lovett MB (1983) Plutonium redistribution by biological-activity in Irish Sea sediments. Nature 306(5945):774–775
165. Officer CB (1982) Mixing, sedimentation rates and age dating for sediment cores. Mar Geol 46:261–278
166. Croker PF (1995) Shallow gas accumulation and migration in the western Irish Sea. In: Croker PF, Shannon PM (eds)

The petroleum geology of Ireland's offshore basins. Geological Society Special Publication No. 93, pp 43–58
167. Pentreath RJ (1984) Alpha-emitting nuclides in the marine environment. Nucl Instrum Methods Phys Res 223:493–501
168. Cournane S, León Vintró L, Mitchell PI (2010) Modelling the reworking effects of bioturbation on the incorporation of radionuclides into the sediment column: implications for the fate of particle-reactive radionuclides in Irish Sea sediments. J Environ Radioact 101:985–991
169. Norton Smith J, Boudreau BP, Noshkin V (1986) Plutonium and 210Pb distributions in northeast Atlantic sediments: subsurface anomalies caused by non-local mixing. Earth Planet Sci Lett 81(1):15–28
170. Nicholson MD, Hunt GJ (1995) Measuring the availability to sediments and biota of radionuclides in wastes discharged to the sea. J Environ Radioact 28:43–56
171. Camplin WC, Durance JA, Jefferies DF (1982) A marine compartment model for collective dose assessment of liquid radioactive effluents. Sizewell enquiry series 4. MAFF Directorate of Fisheries Research, Lowestoft, UK, pp 1–22
172. Gleizon P, McDonald P (2010) Modelling radioactivity in the Irish Sea: from discharge to dose. J Environ Radioact 101:403–413
173. Abril JM, Fraga E (1996) Some physical and chemical features of the variability of Kd distribution coefficients for radionuclides. J Environ Radioact 30(3):253–270
174. Sanchez AL, Gastauda J, Holm E, Roos P (1994) Distribution of plutonium and its oxidation states in Framvaren and Hellvik fjords, Norway. J Environ Radioact 22(3):205–217
175. Pennders RMJ, Prins M, Frissel MJ (1985) The influence of environmental factors on the solubility of Pu, Am and Np in soil-water systems. In: Bulman RA, Cooper JR (eds) Speciation of fission and activation products in the environment. Proceedings CEC-NRPB speciation-85 seminar. Elsevier Applied Science, London, pp 38–46
176. Schell WR, Nevissi A, Huntamer D (1978) Sampling and analysis for Pu and Am in natural waters. Mar Chem 6:143–153
177. Schell WR, Lowman FG, Marshall RP (1980) Geochemistry of transuranium elements at Bikini Atoll. In: Hanson WC (ed) Transuranium elements in the environment. U.S. Department of Energy Publication USDOE/TIC-2280, pp 541–577
178. Assinder DJ, Hamilton-Taylor J, Kelly M, Mudge M, Bradshaw K (1990) Field and laboratory measurements of the rapid remobilisation of plutonium from estuarine sediments. J Radioanal Nucl Chem Art 138:417–424
179. Hamilton-Taylor J, Kelly M, Mudge M, Bradshaw K (1987) Rapid remobilisation of plutonium from estuarine sediments. J Environ Radioact 5(6):409–423
180. Kelly M, Mudge S, Hamilton-Taylor J, Bradshaw K (1988) The behaviour of dissolved plutonium in the Esk Estuary, UK. In: Guary JC, Guéguéniat P, Pentreath RJ (eds) Radionuclides – A tool for oceanography. Elsevier, London/New York, pp 321–330
181. Sholkowitz ER (1983) The geochemistry of plutonium in fresh and marine water environments. Earth Sci review 19:95–161
182. Baskaran M, Ravichandran M, Bianchi TS (1997) Cycling of 7Be and 210Pb in a high DOC, shallow, turbid estuary of southeast Texas. Estuar Coast Shelf Sci 45(2):165–176
183. Lucey JA, Gouzy A, Boust D, Vintro LL, Bowden L, Finegan PP, Kershaw PJ, Mitchell PI (2004) Geochemical fractionation of plutonium in anoxic Irish Sea sediments using an optimised sequential extraction protocol. Appl Radiat Isot 60(2–4):379–385
184. Hamilton EI (1989) Radionuclides and large particles in estuarine sediments. Mar Pollut Bull 20(12):603–607
185. Hamilton EI (1981) Alpha-particle radioactivity of hot particles from the Esk Estuary. Nature 290(5808):690–693
186. Hamilton EI, Williams R, Kershaw PJ (1991) The total alpha particle radioactivity for some components of marine ecosystems. In: Kershaw PJ, Woodhead DS (eds) Radionuclides in the study of marine processes. Elsevier, London, pp 234–244
187. Vives i Batlle J, Wilson RC, McDonald P (2007) Allometric methodology for the calculation of biokinetic parameters for marine biota. Sci Total Environ 388(1–3):256–269
188. Vives i Batlle J, Wilson RC, Watts SJ, Jones SR, McDonald P, Vives-Lynch S (2008) Dynamic model for the assessment of radiological exposure to marine biota. J Environ Radioact 99:1711–1730
189. Brown J, Kolstad AK, Lind B, Rudjord A, Strand P (1998) Technetium-99 contamination in the North Sea and in Norwegian Coastal Areas 1996 and 1997. Strålevern Report 1998: 3. Available at http://www.nrpa.no/dav/07f3957104.pdf. Accessed 7 July 2011
190. Smith V, Ryan RW, Pollard D, Mitchell PI, Ryan TP (1997) Temporal and geographical distributions of 99Tc in inshore waters around Ireland following increased discharges from Sellafield. Radioprotection – Colloques 32:71–77
191. Kasamatsu F, Ishikawa Y (1997) Natural variation of radionuclide 137Cs concentration in marine organisms with special reference to the effect of food habits and trophic level. Mar Ecol Prog Ser 160:109–120
192. Steele AK (1990) Derived concentration factors for cesium-137 in edible species of North Sea fish. Mar Pollut Bull 21(12):591–594
193. Aprosi G, Masson M (1984) Evaluation of experimental studies on technetium transfers to sediments and benthic marine species, and comparison with in situ data. Radioprotection 19(2):89–103
194. Jefferies DF, Hewett CJ (1971) The accumulation and excretion of radioactive caesium by the plaice (Pleuronectes platessa) and the thornback ray (Raia clavata). J Mar Biol Assoc UK 51:411–422
195. Preston A, Jefferies DF (1969) Aquatic aspects in chronic and acute contamination situations. IAEA-SM-117, Report no. STI/PUB/226, IAEA, Vienna, pp 183–211
196. Pentreath RJ, Lovett MB (1978) Transuranic nuclides in plaice (*Pleuronectes platessa*) from the North-Eastern Irish Sea. Mar Biol 48:19–26
197. Smith DL, Knowles JF, Winpenny K (1998) The accumulation, retention, and distribution of ^{95m}Tc in crab (*Cancer pagurus* L.)

and lobster (*Homarus gammarus* L.). A comparative study. J Environ Radioact 40(2):113–135
198. Barnes RD (1974) Invertebrate zoology, 3rd edn. WB Saunders, Philadelphia, 870 pp
199. Busby RG, McCartney M, McDonald P (1997) Technetium-99 concentration factors in Cumbrian Seafood. Radioprotection – Colloques 32(C2):311–316
200. Busby R (1998) The behaviour of technetium-99 in the Irish Sea. PhD thesis, Scottish Universities Research and Reactor Centre, University of Glasgow
201. Knowles JF, Smith DL, Winpenny K (1998) A comparative study of the uptake, clearance and metabolism of techetium in lobster (*Homarus gammarus*) and edible crab (*Cancer pagurus*). Radiat Prot Dosim 75(1–4):125–129
202. Loo LO, Baden SP, Ulmestrand M (1993) Suspension feeding in adult Nephrops norvegicus (L.) and Homarus gammarus (L.) (Decapoda). Neth J Sea Res 31:291–297
203. Pentreath RJ (1981) The biological availability to marine organisms of transuranium and other long-lived nuclides. In: Impacts of radionuclide releases into the marine environment, IAEA STI/PUB/565, Vienna, pp 241–272
204. Swift DJ (1985) The accumulation of ^{95m}Tc from sea water by juvenile lobsters (*Homarus gammarus* L.). J Environ Radioact 2(3):229–243
205. BNFL (1999) Annual report on discharges and monitoring of the environment, environment, health and safety. BNFL, Risley, Warrington, p 152
206. Durand JP, Milcent MC, Goudard F, Paquet F, Germain P, Nafissi T, Pieri J (1994) Chemical behaviour of three radionuclides (cesium, americium and technetium) and their uptake at the cytosolic level in aquatic organisms. Biochem Mol Biol Int 33:521–534
207. BNFL (1998) Annual report on radioactive discharges and monitoring of the environment 1998. British Nuclear Fuel Plc Ltd., UK
208. Miramand P, Germain P, Trilles JP (1989) Histo-autoradiographic localisation of americium (241Am) in tissues of European lobster Homarus gammarus and edible crab Cancer pagurus after uptake from labelled seawater. Mar Ecol Prog Ser 52:217–225
209. Swift DJ (1992) The accumulation of plutonium by the European Lobster (Homarus gammurus L.). J Environ Radioact 16:1–24
210. Ward EE (1966) Uptake of plutonium by the Lobster Homarus vulgaris. Nature 209:625–626
211. Goudard F, Paquet F, Durand J-P, Milcent M-C, Germain P, Pieri J (1994) Biodynamic study of Americium-241 accumulation in the cytosol of the hepatopancreas of the lobster Homarus gammarus. Biochem Mol Biol Int 33:841–851
212. Paquet F, Goudard F, Durand J-P, Germain P, Pieri J (1993) Accumulation of 241Am in subcellular stuctures of the hepatopancreas of the lobster Homarus gammarus. Mar Ecol Prog Ser 95:155–162
213. Conversi A (1985) Uptake and loss of technetium-95m in the crab *Pachygrapsus marmoratus*. J Environ Radioact 2:161–170
214. Swift DJ (1989) The accumulation and retention of Tc-95m by the Edible Winkle (Littorina-Littorea L). J Environ Radioact 9(1):31–52
215. Jackson D, Vives i Batlle J, Parker TG, Whittall AJ, McDonald P (2001) Considerations in optimising the marine discharge regime for ^{99}Tc. In: Proceedings of the British nuclear energy society conference on radiation dose management in the nuclear industry, Windermere, England, 14–16 May 2001
216. Jackson D, Rickard A (1998) The influence of body size and food preparation practices on the uptake and loss of radionuclides in Cumbrian winkles. Radiat Prot Dosim 75(1–4): 155–159
217. McDonald P, Baxter MS, Fowler SW (1993) Distribution of radionuclides in mussels, Winkles and Prawns.1. Study of organisms under environmental-conditions using conventional radio-analytical techniques. J Environ Radioact 18(3):181–202
218. McDonald P, Cook GT, Baxter MS (1992) Natural and anthropogenic radioactivity in coastal regions of the UK. Radiat Prot Dosim 45(1–4):707–710
219. Mitchell J, Vives Batlle J, Ryan TP (1992) Artificial radioactivity in Carlingford Lough. Radiological Protection Institute of Ireland, Dublin
220. Mitchell PI, Vives Batlle J, Ryan TP, McEnri C, Long S, O'Colmain M, Cunningham JD, Caulfield JJ, Larmour RA, Ledgerwood FK (1992) Plutonium, americium and radiocaesium in seawater, sediments and coastal soils in Carlingford Lough. In: Kershaw PJ, Woodhead DS (eds) Radionuclides in the study of marine processes. Elsevier, Amsterdam, pp 265–275
221. Swift DJ (1995) A laboratory study of 239,240Pu, 241Am and 243,244Cm depuration by edible winkles (Littorina Littorea L.) from the Cumbrian Coast (NE Irish Sea) radiolabelled by Sellafield discharges. J Environ Radioact 27(1):13–33
222. Marshall C (1996) Concentration factors for plutonium and americium for mulluscs in the Irish Sea. MSc Dissertation, Environmental Pollution Control Management, Department of Mechanical and Chemical Engineering, Heriot-Watt University, UK
223. Clifton R, Stevens H, Hamilton E (1983) Concentration and depuration of some radionuclides present in a chronically exposed population of mussels (*Mytilus edulis*). Mar Ecol Prog Ser 11:245–256
224. Miramand P, Germain P (1985) Sea water uptake, sediment transfer and histo-autoradiographic study of plutonium (239Pu) and americium (241Am) in the edible cockle Cerastoderma edule. Mar Ecol Prog Ser 22:59–68
225. Dahlgaard H, Nolan C (1999) Long-term rates of radioisotopes of cobalt, zinc, ruthenium, caesium and silver by Mytilus edulis under field conditions. Marine Pollution, IAEA-TECDOC-1094, pp 19–24
226. Guary JC, Fowler SW (1981) Americium-241 and plutonium-237 turnover in mussels (Mytilus galloprovincialis) living in field enclosures. Estuar Coast Shelf Sci 12:193–203

227. Wang WX, Fisher NS, Luoma SN (1996) Kinetic determinations of trace element bioaccumulation in the mussel Mytilus edulis. Mar Ecol Prog Ser 140(1–3):91–113
228. Bonotto S, Robbrecht V, Nuyts G, Cogneau M, Van der Ben D (1988) Uptake of technetium by marine algae autoradiographic localization. Mar Pollut Bull 19(2):61–65
229. Topcuoglu S, Fowler SW (1984) Factors affecting the biokinetics of technetium (Tc-95m) in marine macroalgae. Mar Environ Res 12(1):25–43
230. Gutknecht J (1965) Uptake and retention of ceasium-137 and zinc-65 by seaweeds. Limnol Oceanogr 10(1):58–66
231. Polikarpov GG (1965) Radioecology of aquatic organisms: the accumulation and biological effect of radioactive substances. North Holland, Amsterdam, 314 pp
232. Boisson F, Hutchins DA, Fowler SW, Fisher NS, Teyssie JL (1997) Influence of temperature on the accumulation and retention of 11 radionuclides by the marine alga Fucus vesiculosus (L.). Marine Pollut Bull 35(7–12):313–321
233. Carlson L, Erlandsson B (1991) Effects of salinity on the uptake of radionuclides by fucus vesiculosus L. J Environ Radioact 13:309–322
234. Carlson L, Erlandsson B (1991) Seasonal variation of radionuclides in fucus vesiculosus L. from the Öresund, Southern Sweden. Environ Pollut 73:53–70
235. McDonald P, Cook GT, Baxter MS (1990) A radiological assessment of Scottish edible seaweed consumption. Environ Manage Health 1:17–26
236. Carvalho FP (1985) Experimental studies on biokinetics of americium in benthic marine organisms. In: Bulman JA, Cooper JR (eds) Speciation of fission and activation products in the environment. Elsevier, London, pp 297–315
237. Carvalho FP, Fowler SW (1985) Americium adsorption on the surfaces of macrophytic algae. J Environ Radioact 2:211–317
238. Fowler SW, Benayoun G, Parsi P, Essa MWA (1981) Experimental studies on the bioavailability of technetium in selected marine organisms. In: Proceedings of the international symposium on the impacts of radionuclide releases into the marine environment, Vienna (Austria), 6 Oct 1980. IAEA-SM-248/113
239. Yamamoto T, Fujita T, Ishibashi M (1970) Chemical studies on the seaweeds (25): vanadium and titanium contents in seaweeds. Rec Oceanogr Works Jpn 10:125–135
240. Fisher NS, Nolan CV, Fowler SW (1991) Assimilation of metals in marine copepods and its biogeochemical implications. Mar Ecol Prog Ser 71:37–43
241. Fisher NS, Bjerregaard P, Fowler SW (1983) Interactions of Marine Plankton with transuranic elements.I. Biokinetics of neptunium, plutonium, americium, and californium in phytoplankton. Limnol Oceanogr 28(3):432–447
242. Fisher NS, Rheinfelder JR (1991) Assimilation of selenium in the marine copepod Acartia tonsa studied with a radiotracer method. Mar Ecol Prog Ser 70:157–164
243. Rheinfelder JR, Fisher NS (1991) The assimilation of elements ingested by marine copepods. Science 251:794–797
244. Beasley TM, Gonor JJ, Lorz HV (1982) Technetium - uptake, organ distribution and loss in the mussel, *Mytilus californianus* (Conrad) and the Oyster *Crassostrea gigas* (Thunberg). Mar Environ Res 7(2):103–116
245. Fisher NS (1982) Bioaccumulation of technetium by marine phytoplankton. Environ Sci Technol 16:579–581
246. Warnau M, Fowler SW, Teyssie JL (1996) Biokinetics of selected heavy metals and radionuclides in two marine macrophytes: the seagrass Posidonia oceanica and the alga Caulerpa taxifolia. Mar Environ Res 41(4):343–362
247. Fisher NS, Bjerregaard P, Huynh-Ngoc L (1983) Interactions of marine plankton with transuranic elements. II. Influence of dissolved organic compounds on americium and plutonium accumulation in a diatom. Mar Chem 13:45–56
248. Wilson RC, Watts SJ, Batlle JVI, McDonald P (2009) Laboratory and field studies of polonium and plutonium in marine plankton. J Environ Radioact 100(8):665–669
249. Fisher NS, Bjerregaard P, Fowler SW (1983) Interactions of marine plankton with transuranic elements. III. Biokinetics of americium in euphausiids. Mar Biol 75:261–268
250. Fisher NS, Wente M (1993) The release of trace-elements by dying marine-phytoplankton. Deep-Sea Res (Part I-Topical Stud Oceanogr) 40(4):671–694
251. McCartney M, Rajendran K (1997) 99Tc in the Irish Sea: recent trends. Radioprotection 32:359–364
252. Hamilton EI, Clifton RJ (1980) Concentration and distribution of the transuranium radionuclides Pu-239 + 240, Pu-238 and Am-241 in Mytilus Edulis, Fucus vesiculosus and surface sediment of the Esk estuary. Mar Ecol Prog Ser 3:267–277
253. Nawakowski C, Nicholson MD, Kershaw PJ, Leonard KS (2004) Modelling Tc-99 concentrations in fucus vesiculosus from the north-east Irish sea. J Environ Radioact 77(2): 159–173
254. Ryan TP, Dowdall AM, Long S, Smith V, Pollard D, Cunningham JD (1999) Plutonium and americium in fish, shellfish and seaweed in the Irish environment and their contribution to dose. J Environ Radioact 44(2–3):349–369
255. Thompson N, Cross J, Muller R, Day JP (1982) Alpha and gamma radioactivity in fucus vesiculosus from the Irish sea. Environ Pollut 3:11–19
256. Van der Ben D, Cogneau M, Robbrecht V, Nuyts G, Bossus A, Hurtgen C, Bonotto S (1990) Factors influencing the uptake of technetium by the brown alga fucus-serratus. Mar Pollut Bull 21(2):84–86
257. Sombrito EZ, Banzon RB, de la Mines AS, Bautista E (1982) Uptake of iodine-131 in mussel (*Mytilus smaragdinus*) and algae (*Caulerpa racemosa*). Nucleus J Radioisotope Soc Philippines 22(1):83–89
258. Shunhua C, Qiong S, Xiaokui K (1997) Effects of body size on accumulation and distribution of ^{125}I in the green mussel (*Perna viridis*). China Nuclear Information Centre, Beijing, China
259. Copplestone D, Bielby S, Jones SR, Patton D, Daniel CP, Gize I (2001) Impact assessment of ionising radiation on wildlife. R&D Publication 128, Environment Agency, UK

260. Olsen YS, Vivesi Batlle J (2003) A model for the bioaccumulation of 99Tc in lobsters (*Homarus gammarus*) from the West Cumbrian coast. J Environ Radioact 67(3):219–233
261. Brown J, Børretzen P, Dowdall M, Sazykina T, Kryshev I (2004) The derivation of transfer parameters in the assessment of radiological impacts to arctic marine biota. Arctic 57(3):279–289
262. Fiévet B, Plet D (2003) Estimating biological half-lives of radionuclides in marine compartments from environmental time-series measurements. J Environ Radioact 65:91–107
263. Heling R, Bezhenar R (2009) Modification of the dynamic radionuclide uptake model BURN by salinity driven transfer parameters for the marine foodweb and its integration in POSEIDON-R. Radioprotection 44(5):741–746
264. Lepicard S, Heling R, Maderich V (2004) POSEIDON/RODOS models for radiological assessment of marine environment after accidental releases: application to coastal areas of the Baltic, Black and North Seas. J Environ Radioact 72:153–161
265. Rowan DJ, Rasmussen JB (1996) Measuring the bioenergetic cost of fish activity in situ using a globally dispersed radiotracer (137Cs). Can J Fish Aquat Sci 53:734–745
266. EPIC (2003) The "EPIC" impact assessment framework. Towards the protection of the Arctic Environment from the effects of ionising radiation. In: Brown J, Thorring H, Hosseini A (eds) EPIC (Environmental Protection from Ionising Contaminants) Report ICA2-CT-2000-10032: Østerås, Norway, 175 pp. http:wiki.ceh.ac.uk/display/rpemain/EPIC+reports/. Accessed 7 July 2011
267. Wilson RC, Vives Batlle J, Watts SJ, McDonald P, Parker TG (2007) Uptake and depuration of ^{131}I from labelled diatoms (*Skeletonema costatum*) to the edible periwinkle (*Littorina littorea*). J Environ Radioact 96:75–84
268. Wilson RC, Vives i Batlle J, McDonald P, Parker TG (2005) Uptake and depuration of ^{131}I by the edible periwinkle Littorina littorea: uptake from labelled seaweed (Chondrus crispus). J Environ Radioact 80(3):259–271
269. Vives i Batlle J, Wilson RC, McDonald P, Parker TG (2005) Uptake and depuration of ^{131}I by the edible winkle Littorina littorea: uptake from seawater. J Environ Radioact 78(1):51–67
270. Vives i Batlle J, McDonald P, Parker TG (2002) Studies on the uptake of ^{99}Tc by the edible winkle (*Littornia littorea*). In: Proceedings of the International Conference on Radioactivity in the Environment, Monaco
271. Vives i Batlle J, Wilson RC, McDonald P, Parker TG (2006) A biokinetic model for the uptake and release of radioiodine by the edible periwinkle Littorina littorea. In: Povinec PP, Sanchez-Cabeza JA (eds) Radionuclides in the environment, vol 8. Elsevier, Amsterdam, pp 449–462
272. Schulte EH, Scoppa P, Secondini A (1982) Accumulo e rilascio del tecnezio da parte di alcuni organismi marini: (1) Palaemon elegans. Boll Soc Ital Biol Sper 58:1361–1367
273. West GB, Brown JH, Enquist BJ (1997) A general model for the origin of allometric scaling laws in biology. Science 276(5309):122–126
274. Higley KA, Domotor SL, Antonio EJ (2003) A kinetic-allometric approach to predicting tissue radionuclide concentrations for biota. J Environ Radioact 66(1–2):61–74
275. USDOE (2002) A graded approach for evaluating radiation doses to aquatic and terrestrial biota. Technical Standard DOE-STD-1153-2002. Department of Energy, Washington, DC
276. Carvalho FP, Oliveira JM, Alberto G, Vivesi Batlle J (2010) Allometric relationships of 210Po and 210Pb in mussels and their application to environmental monitoring. Mar Pollut Bull 60(10):1734–1742
277. Kleiber M (1932) Body size and metabolism. Hilgardia 6:315–351
278. Kleiber M (1947) Body size and metabolic rate. Physiol Rev 27(4):511–541
279. Cherry RD, Heyraud M (1991) Polonium-210 and lead-210 in marine organisms: allometric relationships and their significance. In: Kershaw PJ, Woodhead DS (eds) Radionuclides in the study of marine processes. Elsevier, London/New York, pp 309–331
280. Vives i Batlle J, Wilson RC, Watts SJ, McDonald P, Craze A (2009) Derivation of allometric relationships for radionuclides in marine phyla. Radioprotection 44(5):47–52
281. Barnett CL, Kryshev I, Kryshev A, Iospje M, Børretzen P, Golikov V, Shutov V, Kravtsova O, Galeriu D, Vives Lynch SM, Vives i Batlle J, Arkhipov A (2003) Transfer and uptake models for reference arctic organisms. In: Beresford NA, Wright SM, Brown JE, Sazykina T (eds) Environmental protection from ionising contaminants (EPIC) report, European Commission Inco-Copernicus Programme Contract No.: ICA2-CT-2000-10032, May 2003, 75 pp
282. Hendriks AJ (2007) The power of size: a meta-analysis reveals consistency of allometric regressions. Ecol Modell 205(1–2):196–208
283. Lars Føyn L, Heldal HE, Varskog P (2000) Radionuclide uptake and transfer in pelagic food chains of the Barents Sea. In: Brown JE (ed) Radionuclide uptake and transfer in pelagic food chains of the Barents Sea and resulting doses to man and biota, project report under the Transport and Effects Programme. Norwegian Radiation Protection Authority, Oslo, Norway
284. Mathews T, Fisher NS (2008) Evaluating the trophic transfer of cadmium, polonium, and methylmercury in an estuarine food chain. Environ Toxicol Chem 27(5):1093–1101
285. Kryshev I, Sazykina T, Kryshev A, Brown J (2000) Ecological dosimetry models. In: Brown JE (ed) Radionuclide uptake and transfer in pelagic food chains of the Barents Sea and resulting doses to man and biota, project report under the transport and effects programme. Norwegian Radiation Protection Authority, Oslo, Norway
286. Wang WX (2002) Interactions of trace metals and different marine food chains. Mar Ecol Prog Ser 243:295–309
287. Povinec PP, Fowler SW, Baxter MS (1996) Chernobyl and the marine environment: the radiological impact in contex. In: IAEA Bulletin 1/1996, 22 pp

288. Nielsen SP, Keith-Roach M (2004) Update of the MARINA project on the radiological exposure of the European community from radioactivity in North European marine waters. Annex E: critical group exposure. European Commission report, 30 pp
289. Smith JG, Bexon AP, Boyer FHC, Harvey MP, Jones AL, Kindler T, Mercer J, Haywood SM, Verhoef NB, Haverkate BRW, Artmann A (2002) Assessment of the radiological impact on the population of the European Union from European Union nuclear sites between 1987 and 1996. European Commission Radiation protection Report 128, Luxembourg, 38 pp
290. Environment Agency, Food Standards Agency, Northern Ireland Environment Agency and Scottish Environmental Protection Agency (2010) Radioactivity in food and the environment, 2009, RIFE-15 report, 254 pp
291. Jackson D, Lambers B, Gray J (2000) Radiation doses to members of the public near to Sellafield, Cumbria, from liquid discharges 1952–98. J Radiol Prot 20:139–167
292. Hunt GJ, Smith BD (1999) The radiological impact of actinides discharged to the Irish Sea. J Environ Radioact 44(2–3):389–403
293. BNFL (1993–2002) Discharges and monitoring of the environment in the UK (Annual reports – 1993–2002). British Nuclear Fuels Ltd., UK
294. Sellafield Ltd (2010) Monitoring our environment. Discharges and monitoring in the United Kingdom. Annual report 2009, Sellafield Ltd., UK, 65 pp
295. Fegan M, Currivan L, Dowdall A, Hanley O, Hayden E, Kelleher K, Long SC, McKittrick L, Somerville S, Wong J, Pollard D (2010) Radioactivity monitoring of the Irish environment 2008. Report RPII 01/10, Radiological Protection Institute of Ireland, Dublin, 36 pp
296. Smith V, Fegan M, Pollard D, Long S, Hayden E, Ryan TP (2001) Technetium-99 in the Irish marine environment. J Environ Radioact 56:269–284
297. Kershaw PJ, Heldal HE, Mork KA, Rudjord AL (2004) Variability in the supply, distribution and transport of the transient tracer Tc-99 in the NE Atlantic. J Mar Syst 44(1–2):55–81
298. Alexander J, Frøyland L, Hemre G-I, Jacobsen BK, Lund E, Meltzer HM, Skåre JU (2006) Et helhetssyn på fisk og annen sjømat i norsk kosthold. Norwegian Scientific Committee for Food Safety Report – Vitenskapkomiteen for mattrygghet, Oslo, 171 pp
299. Hong GH, Baskaran M, Povinec PP (2004) Artificial radionuclides in the Western North Pacific: a review. In: Shiyomi M, Kawahata H, Koizumi H, Tsuda A, Awaya Y (eds) Global environmental change in the ocean and on land. Terra Scientific Publishing Company, Tokyo, pp 147–172
300. Sazykina TG, Kryshev II (1997) Current and potential doses from Arctic seafood consumption. Sci Total Environ 202(1–3): 57–65
301. NEA (1996) Co-ordinated research and environmental surveillance programme related to sea disposal of radioactive waste. CRESP Final Report 1981–1995, OECD, Paris
302. Pollard D, Long SC, Hayden E, Smith V, Ryan TP, Dowdall A, McGarry A, Cunningham JD (1996) Radioactivity monitoring of the Irish marine environment, 1993 to 1995. Radiological Protection Institute of Ireland, Dublin, 41 pp
303. Livingston HD, Povinec PP (2000) Anthropogenic marine radioactivity. Ocean Coast Manage 43(8–9):689–712
304. Sazykina TG, Kryshev II, Kryshev AI (1998) Doses to marine biota from radioactive waste dumping in the Fjords of Novaya Zemlya. Radiat Prot Dosim 75(1–4):253–256
305. Aarkrog A, Baxter MS, Bettencourt AO, Bojanowski R, Bologa A, Charmasson S, Cunha I, Delfanti R, Duran E, Holm E, Jeffree R, Livingston HD, Mahapanyawong S, Nies H, Osvath I, Pingyu L, Povinec PP, Sanchez A, Smith JN, Swift DJ (1997) A comparison of doses from 137Cs and 210Po in marine food: a major international study. J Environ Radioact 34(1):69–90
306. Togawa O, Povinec PP, Pettersson HBL (1999) Collective dose estimates by the marine food pathway from liquid radioactive wastes dumped in the Sea of Japan. Sci Total Environ 237–238:241–248
307. Aarkrog A (1998) Review of the state of the oceans for radioactivity. In: IAEA 42nd session of the general conference. Scientific forum "Nuclear technology in relation to water resources and the aquatic environment." Available from http://www.iaea.org/About/Policy/GC/GC42/SciProg/gc42-scifor-9.pdf Accessed 22 Mar 2011
308. ICRP (2003) A framework for assessing the impact of ionising radiation on non-human species. ICRP Publication 91, Annals of the ICRP 33(3). Pergamon Press, Oxford
309. IAEA (2005) Proceedings of the IAEA international conference on protection of the environment from the effects of ionising radiation, 6–10 October 2003, Stockholm, Sweden. IAEA CN109/37, International Atomic Energy Agency, Vienna
310. Pentreath RJ, Woodhead DS (2001) A system for protection of the environment from ionizing radiation: selecting reference fauna and flora, and the possible dose models and environmental geometries that could be applied to them. Sci Total Environ 277:33–43
311. ICRP (1991) The 1990 recommendations of the international commission on radiological protection, vol 21, no 1–3. Annals of the ICRP, ICRP 60, Pergamon Press, Oxford
312. Copplestone D, Jones S, Allott R, Merrill P, Vivesi Batlle J (2007) Protection of the Environment from Exposure to Ionising Radiation. In: Shaw G (ed) Radioactivity in the Terrestrial Environment (Radioactivity in the Environment Vol. 10). Pergamon Press, Oxford, 300 pp
313. Watson WS, Sumner DJ, Baker JR, Kennedy S, Reidd R, Robinson I (1999) Radionuclides in seals and porpoises in the coastal waters around UK. Sci Total Environ 234(1–3):1–13
314. Copplestone D, Wood MD, Bielby S, Jones SR, Vivesi Batlle J, Beresford NA (2003) Habitat regulations for stage 3 assessments: radioactive substances authorisations. R&D technical report P3-101/SP1a. Environment Agency, Bristol, 100 pp
315. FASSET (2003). Handbook for assessment of the exposure of biota to ionising radiation from radionuclides in the environment. In: Brown J, Strand P, Hosseini A, Børretzen P (eds)

FASSET deliverable 5 report for the EC 5th framework programme contract FIGE-CT-2000-00102, Norwegian Radiation Protection Authority, Østerås, Norway, 101 pp. https://wiki.ceh.ac.uk/display/rpemain/ERICA+reports. Accessed 7 July 2011

316. Beresford N, Brown J, Copplestone D, Garnier-Laplace J, Howard B, Larsson C-M, Oughton D, Pröhl G, Zinger I (2007) D-ERICA: an integrated approach to the assessment and management of environmental risks from ionising radiation. A deliverable of the ERICA project (FI6R-CT-2004-508847), Swedish Radiation Protection Authority (SSI). Stockholm. Available via http://wiki.ceh.ac.uk/download/attachments/115017395/D-Erica.pdf?version=1. Accessed 4 May 2011
317. Brown JE, Alfonso B, Avila R, Beresford NA, Copplestone D, Pröhl G, Ulanovsky A (2008) The ERICA tool. J Environ Radioact 99(9):1371–1383
318. ICRP (2008) Environmental protection – the concept and use for reference animals and plants for the purposes of environmental protection. In: Valentin J (ed) ICRP publication 108, Annals of the ICRP, Elsevier, Oxford, vol 38 Issue 4–6, 76 pp
319. Kryshev AI, Sazykina TG, Kryshev II, Strand P, Brown JE (2001) Radioecological modelling and the computer codes for calculations of doses to marine biota and man in the Arctic. Environ Modell Softw 16:697–709
320. EC & HC (2003) Canadian environmental protection act 1999. Priority substances list assessment report releases of radionuclides from nuclear racilities (Impact on non-human biota). Environmental Canada, Health Canada Report, 117 pp. Available from: http://www.chemicalsubstanceschimiques.gc.ca/about-apropos/assess-eval/radionuclides-eng.pdf Accessed 1 April 2011
321. Vives i Batlle J, Balonov M, Beaugelin-Seiller K, Beresford NA, Brown J, Cheng J-J, Copplestone D, Doi M, Filistovic V, Golikov V, Horyna J, Hosseini A, Howard BJ, Jones SR, Kamboj S, Kryshev A, Nedveckaite T, Olyslaegers G, Pröhl G, Sazykina T, Ulanovsky A, Vives-Lynch S, Yankovich T, Yu C (2007) Inter-comparison of unweighted absorbed dose rates for non-human biota. Radiat Environ Biophys 46(4):349–373
322. Beresford NA, Barnett CL, Brown J, Cheng JJ, Copplestone D, Filistovic V, Hosseini A, Howard BJ, Jones SR, Kamboj S, Kryshev A, Nedveckaite T, Olyslaegers G, Saxén R, Sazykina T, Vives i Batlle J, Vives-Lynch S, Yankovich T, Yu C (2008) Inter-comparison of models to estimate radionuclide activity concentrations in non-human biota. Radiat Environ Biophys 47(4):491–514
323. Beresford NA, Barnett CL, Brown JE, Cheng JJ, Copplestone D, Gaschak S, Hosseini A, Howard BJ, Kamboj S, Nedveckaite T, Smith JT, Vives I, Batlle J, Vives-Lynch S, Yu C (2010) Predicting the radiation exposure of terrestrial wildlife in the Chernobyl exclusion zone: an international comparison of approaches. J Radiol Prot 30:341–373
324. Brown J, Strand P, Hosseini A, Børretzen P (2003) Handbook for assessment of the exposure of biota to ionising radiation from radionuclides in the environment. FASSET (Framework for assessment of environmental impact) deliverable 5 report, contract no FIGE-CT-2000-00102, 101 pp
325. UNSCEAR (1996) Sources and effects of ionizing radiation. Scientific annex: effects of radiation on the environment, United Nations scientific committee on the effects of atomic radiation report to the general assembly, United Nations, New York, 86 pp
326. Andersson P, Garnier-Laplace J, Beresford N, Copplestone D, Howard B, Howe P, Oughton D, Whitehouse P (2009) Protection of the environment from ionising radiation in a regulatory context (PROTECT): proposed numerical benchmark values. J Environ Radioact 100:1100–1108
327. Woodhead DS (1984) Contamination due to radioactive materials. In: Kinne O (ed) Marine ecology, vol v, part 3: pollution and protection of the seas – radioactive materials, heavy metals and oil. Wiley, New York, NY, pp 1111–1287
328. Vives Batlle J, Wilson RC, Watts SJ, Jones SR, McDonald P, Vives-Lynch S (2008) Dynamic model for the assessment of radiological exposure to marine biota. J Environ Radioact 99(1):1711–1730
329. Sazykina TG, Kryshev II (2002) MARINA II – update of the MARINA project on the radiological exposure of the European community from radioactivity in North European marine waters. Annex F: assessment of the impact of radioactive substances on marine biota of North European waters. EC Radiation Protection Report 132, Directorate-General Environment, Brussels, 44 pp
330. Woodhead DS (1980) Marine disposal of radioactive waste. Helgolander Meeresunters 33:122–137
331. Chambers D, Muller E, Saint-Pierre S, Le Bar S (2005) Assessment of marine biota doses arising from radioactive discharges to the sea by the Cogema La Hague facility – a comprehensive case study. In: Proceedings of the international conference on protection of the environment from the effects of ionizing radiation, Stockholm, 6–10 Oct 2003, pp 159–174
332. OSPAR (2008) Assessment on impact of anthropogenic sources of radioactive substances on marine biota, Radioactive substances series, OSPAR commission report no. 381, 978-1-906840-22
333. Beresford N, Howard B (2005) Application of FASSET framework at case study sites, ERICA deliverable D9. Available from wiki.ceh.ac.uk/display/rpemain/ERICA + reports Accessed 22 March 2011
334. Proehl G, Telleria D, Louvat D (2010) The activities of the IAEA in developing standards on radiological protection of the environment. In: Proceedings of the third European IRPA congress 2010 June 14–16, Helsinki, Finland, 11 pp
335. Livingston HD, Povinec PP (2002) A millennium perspective on the contribution of global. Fallout radionuclides to ocean science. Health Phys 82(5):656–668
336. IAEA (2004) Discovering bio-indicator species for heavy metals in the lagoon of New Caledonia. In: Marine

Environment News, Newsletter of the IAEA marine Environmental Laboratory, Monaco, vol 2, no 1, March 2004
337. Aarkrog A (1994) Past and recent trends in radioecology. Environ Int 20(5):633–643
338. Woodhead DS (2003) A possible approach for the assessment of radiation effects on populations of wild organisms in radionuclide-contaminated environments? J Environ Radioact 66:181–213
339. Vives i Batlle J, Wilson RC, Watts SJ, McDonald P, Jones SR, Vives-Lynch SM, Craze A (2009) Approach to the assessment of risk from chronic radiation to populations of European lobster, *Homarus gammarus* (L.). Radiat Environ Biophys doi:10.1007/s00411-009-0251-y
340. Wilson RC, Vivesi Batlle J, Watts SJ, McDonald P, Jones SR, Vives-Lynch SM, Craze A (2010) Approach to the assessment of risk from chronic radiation to populations of phytoplankton and zooplankton. Radiat Environ Biophys 49:87–95
341. Kryshev AI, Sazykina TG, Sanina KD (2008) Modelling of effects due to chronic exposure of a fish population to ionizing radiation. Radiat Environ Biophys 47(1): 121–129
342. Copplestone D, Howard BJ, Brechignac F (2004) The ecological relevance of current approaches for environmental protection from exposure to ionizing radiation. J Environ Radioact 74:31–41
343. Kershaw PJ (2004) Radiotracers as new barometers of ocean-climate coupling. In: Marine Environment News, Newsletter of the IAEA marine environmental laboratory, Monaco, vol 2, no 1, March 2004

Books and Reviews

Ancellin J, Guegueniat P, Germain P (1979) Radioecologie marine: etude du devenir des radionucleides rejetes en milieu marin et application a la radioprotection. Eyrolles, Paris

Guegueniat P, Germain P, Metivier H (1996) Radionuclides in the oceans: inputs and inventories. Institut de Protection et de Surete Nucleaire, IPSN, France, ISBN 2-86883-285-7

Jones SR (2000) Marine radioecology – five decades of research in the Irish Sea. In: Inaba J, Hisamatsu S, Ohtsuka Y (eds) Proceedings of the international workshop on distribution and speciation of radionuclides in the environment, Rokkasho, Aomori, Japan 11–13 October 2000. Institute for Environmental Sciences, Japan, pp 85–92

Livingston HD (2004) Marine radioactivity. Pergamon Press, Oxford, 310 pp

Matishov DG, Matishov GG (2010) Radioecology in Northern European Seas. Springer, Berlin, 337 pp

Stone R (2002) Radioecology's coming of age – or its last Gasp? Science 297:1800–1801

Sheppard SC (2003) An index of radioecology, what has been important? J Environ Radioact 68:1–10

Whicker FW, Schultz V (1982) Radioecology: nuclear energy and the environment, vol II. CRC Press, Boca Raton, 228 pp

Radiation Assessment, Use of Transfer Parameters

Nicholas A. Beresford
Radioecology Group, Centre for Ecology & Hydrology – CEH Lancaster, Lancaster Environment Centre, Bailrgg, Lancaster, UK

Article Outline

Glossary
Definition of the Subject
Introduction
Application of Transfer Parameters in Human Food Chain Modeling
Radiological Assessment of the Environment
Future Directions
Bibliography

Glossary

Aggregated transfer parameter ($T_{ag}m^2\,kg^{-1}$) Ratio of the activity concentration in an organism (its tissues or milk) and the activity concentration in soil expressed on a per unit area basis (Bq m^{-2}).

Concentration ratio (CR) Ratio of radionuclide activity concentrations in any two compartments. Often used to describe relationship between organism activity concentrations and those in appropriate medium (soil, air, or water) and being recommended as approach to describe relative activity concentrations in animal tissues/milk/egg and those in the animals' diet.

Transfer coefficient ($F_f\,d\,kg^{-1}F_m\,d\,L^{-1}$) The ratio of the activity concentration of a radionuclide in the tissues (F_f) or milk (F_m) of an animal to the daily intake of radionuclide in the diet.

Wildlife Wildlife is defined here to include all non-domesticated plants, animals, and other organisms including feral species (i.e., non-native self-sustaining populations).

Definition of the Subject

There had been some consideration of radioactivity from natural sources within the environment prior to World War II. However, the study of the behavior of

radionuclides in the environment, driven by the need to assess potential impacts on humans and the environment, has largely evolved since the 1940s following the first atomic bomb tests and subsequent testing programs (predominantly in the 1950s–1960s), and the development of nuclear technologies.

Historically, radiological protection has concentrated on ensuring that humans are protected from the effects of ionizing radiation. Until comparatively recently there has been little regulatory requirement to actively demonstrate the protection of wildlife specifically. In order to assess the contribution of foodstuffs to the internal doses received by humans a number of models have been developed. Many such models rely upon "transfer parameters" which are typically ratios describing the relative activities or activity concentrations between two compartments. Considerable effort has gone into defining such parameters over the last 50–60 years, and compendia of recommended values are published by bodies such as the International Atomic Energy Agency (IAEA).

Starting in the 1990s the anthropogenic focus of radiological protection has been increasingly challenged and there is now legislation in some countries (e.g., UK, USA, Canada, Finland and Sweden) requiring radiological assessment of wildlife. In response to this a number of models/software packages have been developed for application in environmental assessment. These of course require parameterization. The vast numbers of radionuclides and species which may require consideration present challenges to those developing environmental assessment approaches.

Introduction

Exposure of humans and other species to ionizing radioactivity as a result of nuclear power production may occur as a result of planned (authorized) or unplanned releases of radioactive substances from all stages of the nuclear fuel cycle (i.e., from mining to disposal). Other exposure routes include: discharges from facilities that use radioactive substances (e.g., hospitals); industries such as oil and gas extraction and the burning of coal, which release naturally occurring radionuclides to the environment; legacies of nuclear weapons testing and historical accidents; and exposure to radionuclides (such as ^{40}K, ^{238}U-series, ^{232}Th-series, etc.), which are present naturally within the environment.

Methods to assess the risk from these sources of ionizing radiation to humans and other species are required. While exposure to radiation may result from both external and internal sources, this entry considers the estimation of the transfer of radionuclides to human foodstuffs and wildlife (i.e., an essential step in estimating internal exposure). [Readers interested in the methods applied to estimate absorbed dose rates from external and internal sources should consult ICRP [1–4] (for consideration of humans) and Ulanovsky et al. [5] (for consideration of wildlife)]. While ideally sufficient measurements of the radionuclide activity concentrations in human foodstuffs and wildlife would be available to enable robust assessment of internal dose rates, this is not always feasible not least because assessments often need to consider future planned releases. Therefore, models to predict radionuclide concentrations in foodstuffs and wildlife are required. Depending upon their aim such models may need to encompass many processes including: dispersion modeling; interaction with abiotic components of the environment; deposition and interception by vegetation surfaces; surface runoff; and biological uptake and loss. However, many models utilize transfer parameters which are empirical ratios of typically the activities or activity concentrations in different compartments. These can then be used to estimate the radionuclide concentration in a human foodstuff or wild species from a known activity concentration. For instance, the concentration ratio for freshwater fish flesh may be defined as:

$$\mathrm{CR} = \frac{\text{Radionuclide activity concentration in flesh (Bq kg}^{-1}\text{ fresh mass)}}{\text{Radionuclide activity concentration in water (Bq L}^{-1}\text{)}}$$

Therefore, if the activity concentration in water is known then the activity concentration in fish flesh can be estimated as:

$$\mathrm{CR} \times \text{Radionuclide activity concentration in filtered water}$$

As will be evident from the above definition such empirical ratios are a simplification which encompass the many processes described in other entries

(Seaman and Roberts, this section, Rowan this section). The concentration ratio and virtually all of the other empirical ratios discussed below are defined as being at equilibrium. The degree of equilibrium will influence the apparent CR value if measurements are made when equilibrium is not established (e.g., activity concentrations on the tissues of an animal that has been consuming a contaminated diet for a short period will not be equilibrated with those in the diet and hence a low apparent CR value would be derived; plants sampled soon after an atmospheric deposition event will have residual intercepted activity and hence a high apparent CR value would be estimated).

The derivation, application, problems, and advantages of such ratio based approaches are discussed in this entry. The subsequent section presents an overview of transfer parameters for the human food chain focusing on agricultural foodstuffs. The focus of the remainder of the entry is a discussion of the approaches taken to developing models to estimate the transfer of radionuclides to wildlife.

Application of Transfer Parameters in Human Food Chain Modeling

Over the years there have been many compilations of transfer parameters for human foodstuffs which, most notably, include the compilations of Ng and coworkers from Lawrence Livermore Laboratory (USA) in the 1970s and 1980s [6–9] and, more latterly, the IAEA, which has published handbooks of transfer parameters for marine [10], and terrestrial and freshwater environments [11, 12]. The recent update of the terrestrial and freshwater handbook [12] is supported by detailed information on the derivation of the transfer parameter values [13] including extensive publication in the refereed literature (including [14, 15]). The update of the IAEA handbook also prompted the publication of a series of reviews of studies previously only been documented in Russian language publications [16–19] and also consideration of tropical/subtropical ecosystems [20], whereas the previous handbook had only presented data for temperate ecosystems [11].

Soil to Plant Concentration Ratios

Concentration ratios are the most common approach to estimating the transfer of radionuclides from soil to the edible parts of plants consumed by humans or herbivorous animals. In this instance, CR is most typically defined as:

$$\mathrm{CR} = \frac{\text{Radionuclide activity concentration in plant (Bq kg}^{-1}\text{ dry weight)}}{\text{Radionuclide activity concentration in soil (Bq kg}^{-1}\text{ dry weight)}}$$

Following the recommendations of the International Union of Radioecologists, the IAEA [12] defines CR as being based upon soil activity concentrations determined to a soil depth of 10 cm for grass and 20 cm for all other sample types.

The recent collation of IAEA [12] presents radionuclide CR values for a range of crop types. Where possible, IAEA [12] presents CR values for each crop type by soil textural category (i.e., sand, loam, clay, and organic) in addition to overall summary values by radionuclide and group. Figure 1 presents a comparison of CR values for a selection of the crops and radionuclides from IAEA [12]. Given that CR amalgamates many parameters it is not surprising that for a given radionuclide-crop CR values range over more than two orders of magnitude [13].

For radionuclides with low root uptake rates, measured plant concentrations, and consequently CR values determined in the field, may be dominated by

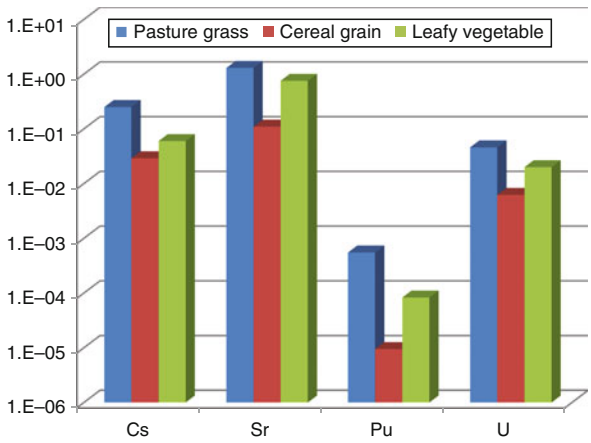

Radiation Assessment, Use of Transfer Parameters. Figure 1
A comparison of recommended plant CR values for different radionuclides and crops from IAEA [12]

adherent soil. For instance, assuming soil comprises 1% of a vegetation sample on a dry matter basis for a radionuclide with a soil-plant CR of <0.01, the adherent soil will contribute >50% of the activity concentration of the sample; where soil-plant CR values are <0.001 the adherent soil at 1% by dry matter will contribute >90% of the samples activity concentration. Adherent soil can contribute considerably more than 1% by dry matter of pasture grass samples depending upon stocking rate, sward height, and soil type, with values >20% having been recorded [21].

The root uptake of radionuclide generally occurs through soil solution. Interactions of chemical species in soil solution including complexation and precipitation reactions, oxidation-reduction transformations and interactions with soil components (including soil microorganisms) determine the mobility of radionuclides in soils and hence the value of soil-plant CR. The soil-plant CR is therefore influenced by many factors including chemical and physical soil characteristics (percentage clay, percentage organic matter, available stable element concentrations, pH) and land management (e.g., fertilization rates). Soil solution concentrations of Ca and K influence the root uptake of Sr and Cs, respectively. Consequently, lime (calcium carbonate) and potassium fertilizers were successfully used to reduce the uptake of ^{90}Sr and ^{134,137}Cs in agriculturally managed areas affected by the Chernobyl accident [22].

The solid–liquid distribution coefficient (K_d) is used to describe the relative activity concentrations in soil solution and on soil solids, where:

$$K_d(\mathrm{L\ kg^{-1}}) = \frac{\text{Activity concentration in solid phase (Bq kg}^{-1}\text{)}}{\text{Activity concentration in liquid phase (Bq L}^{-1}\text{)}}$$

A collation of K_d values can be found in IAEA [12] and a more detailed discussion of the concept in accompanying documentation Vidal et al. [23–26].

Quantifying Radionuclide Transfer to Farm Animals

Since the mid-1960s the most common parameter used to estimate the transfer of radionuclides to farm animals has been the transfer coefficient. This was first proposed by Ward et al. [27] to describe the transfer of radiocesium from the diet to milk of dairy cattle. Ward et al. defined the transfer coefficient (F_m) as:

$$F_m(\mathrm{d\ L^{-1}}) = \frac{^{137}\text{Cs activity concentration in milk (Bq L}^{-1}\text{)}}{\textit{Daily dietary intake of } ^{137}\textit{Cs (Bq d}^{-1}\textit{)}}$$

The originators reported that the transfer coefficient exhibited less variability between animals within the herd they had studied than expressing transfer as the total amount of radiocesium excreted in milk as a percentage of radiocesium intake. Subsequently, the same workers [28] proposed the transfer coefficient for meat (F_f) as:

$$F_f(\mathrm{d\ kg^{-1}}) = \frac{^{137}\text{Cs activity concentration in meat (Bq kg}^{-1}\text{ fresh weight)}}{\text{Daily dietary intake of } ^{137}\text{Cs (Bq d}^{-1}\text{)}}$$

The transfer coefficient was adopted by other researchers and modelers as the method of determining transfer for all radionuclides to the milk, meat, and eggs of farm animals; the definition in later publications being the equilibrium ratio of the activity concentration in an animal product to the daily radionuclide intake. In the late 1970s to early 1980s, compendia of recommended transfer coefficient values were being published (e.g., [6–9]) and in 1994, the IAEA included tables of recommended transfer coefficient values in its *Handbook of transfer parameter values for the prediction of radionuclide transfer in temperate environments* [11]. Transfer coefficient values as recommended in such publications were incorporated into many predictive human food chain models (e.g., [29–32]).

Ward and Johnson [33] suggested that this wider use of F_m was justified and that factors such as milk production rate, metabolic rate, soil intake, and stable element intake could be ignored.

In an update to their transfer parameter handbook, IAEA [12] presents recommended transfer coefficient values for: (1) the meat (muscle) of sheep, goats, cattle, pigs, and poultry; (2) the milk of cattle, sheep, and goats; and (3) eggs. In agreement with many other publications the recommended transfer coefficients were generally higher for smaller animals than large

animals. This is demonstrated in Figs. 2 and 3, which present a comparison of recommended transfer coefficients for the milk and meat of different animals, respectively, for a few example radionuclides.

For some radionuclides the transfer coefficient for commonly eaten tissues is higher than that to meat. For instance, comparatively high transfer coefficients for liver have been determined for a number of radionuclides such as Pu, Am, Co, and Ag [34–36], while the transfer of Ru to kidney is higher than that to other tissues [35, 36].

While Ward and Johnson [33] suggested the wide use of transfer coefficients was justified, in Ward and Johnson [37] they also noted that these conclusions were based predominantly on data for the transfer of Cs to cow milk. Subsequently many factors have been demonstrated to influence the transfer coefficient; some examples are described in the following section.

Factors Demonstrated to Influence Transfer Coefficient Values Radiocesium is one of the most studied radionuclides with respect to transfer to farm animals, and factors affecting radiocesium transfer coefficients were the subject of considerable research following the 1986 Chernobyl accident. The dietary source of radiocesium has been demonstrated to have a considerable influence on estimated transfer coefficient values in a number of studies [38–44]. Subsequent research has confirmed that these differences were the consequence of the degree of absorption of radiocesium across the gut [45]. Other studies have demonstrated that the radiocesium transfer coefficient is influenced by lactation [46, 47] and dry matter intake rate [47–49]. However, there is no evidence to suggest that dietary potassium (a chemical analog of cesium) has any significant effect on the transfer of radiocesium to animal-derived food products.

The behavior of radiostrontium in animals has long been known to be determined by that of its chemical analog Ca which is an essential element under homeostatic control (e.g., [50–53]). The absorption of calcium from the diet is inversely proportional to the dietary intake of calcium at a given calcium requirement [54] and an inverse relationship between calcium intake and radiostrontium absorption has been demonstrated in farm ruminants [45]. Howard et al. [55] suggested that the transfer coefficient for radiostrontium to milk (F_{mSr}) could be described by:

$$F_{mSr}(\mathrm{d\ L^{-1}}) = \frac{OR_{milk\text{-}diet} \times [Ca]_{milk}(\mathrm{g\ kg^{-1}})}{\text{Daily dietary intake of Ca } (\mathrm{g\ d^{-1}})}$$

where $OR_{milk\text{-}diet}$ is the observed ratio of the comparative transfers of strontium and calcium from the diet to milk which had previously been shown to be relatively constant with a value of approximately 0.11 [52, 56].

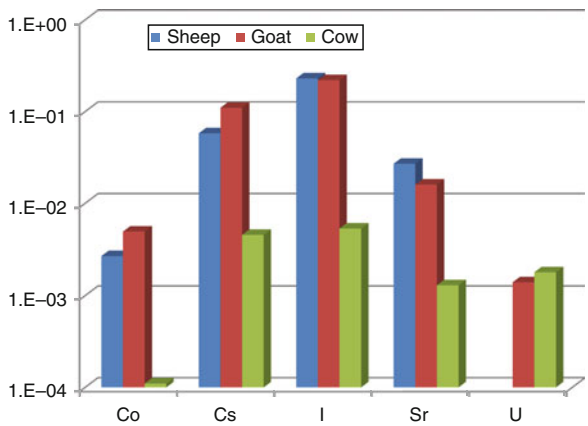

Radiation Assessment, Use of Transfer Parameters. Figure 2
A comparison of recommended milk F_m values for different radionuclides and dairy animals from IAEA [12]

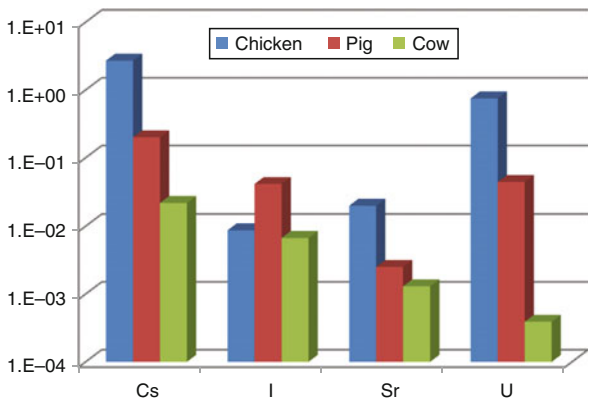

Radiation Assessment, Use of Transfer Parameters. Figure 3
A comparison of recommended meat (muscle) F_f values for different radionuclides and farm animals from IAEA [12]

Assuming a value of calcium in cow milk of 1.15 g kg^{-1}, Howard et al. [55] compared predicted F_{mSr} values with data from a number of published studies and demonstrated a good agreement. Subsequently Beresford et al. [57] demonstrated that the relationship could also be used to predict F_{mSr} for sheep and goat milk sources (assuming appropriate Ca concentrations in the milk of these animals) (Fig. 4). Unlike for radiocesium the dietary source of radiostrontium appears to be relatively unimportant in determining absorption from the gastrointestinal tract and subsequently F_m [45].

The transfer of radioiodine to milk can be one of the most important routes of exposure to humans in the event of accidental release of radioactivity, for instance, after the 1986 Chernobyl [58, 59] and 1957 Windscale accidents [60]. The absorption of radioiodine from the gastrointestinal tract of ruminant animals is generally complete regardless of stable iodine intake rate of dietary source [45, 61]. The iodine milk transfer coefficient is dependent upon the degree of transfer of absorbed radioiodine from the circulatory system to milk. This appears to be determined by the requirements of the thyroid for iodine [62]. At dietary intake rates below requirement levels low transfer coefficients can be expected compared to animals on diets with optimal levels of iodine [62, 63]. At high rates of iodine intake the transfer of radioiodine to milk increases as the requirements of the thyroid reduce; at extremely high intake rates the transfer of radioiodine to milk is reduced as transfer across the mammary gland saturates [62, 63] (Fig. 5).

The transfer coefficient is defined as the ratio between the activity concentration in an animal-derived food product to the daily radionuclide *intake at equilibrium*. For many radionuclides, activity concentrations in milk reach equilibrium relatively rapidly (e.g., [64, 65]). The uptake rate of some radionuclide to animal tissues is also relatively quick with biological half-lives of a few tens of days [66]. However, the rates of uptake and loss of some radionuclides are comparatively slow such that equilibrium is unlikely to be reached in tissues and even milk within the lifetime of the animal (e.g., [67–69]). For such radionuclides the concept of an "equilibrium" transfer coefficient is therefore questionable (e.g., Pu-isotopes and ^{241}Am).

The transfer of technetium to farm animals has been studied in a number of experimental feeding trials [69–76]. While the main isotope of interest in radiological assessments is the long-lived ^{99}Tc, most

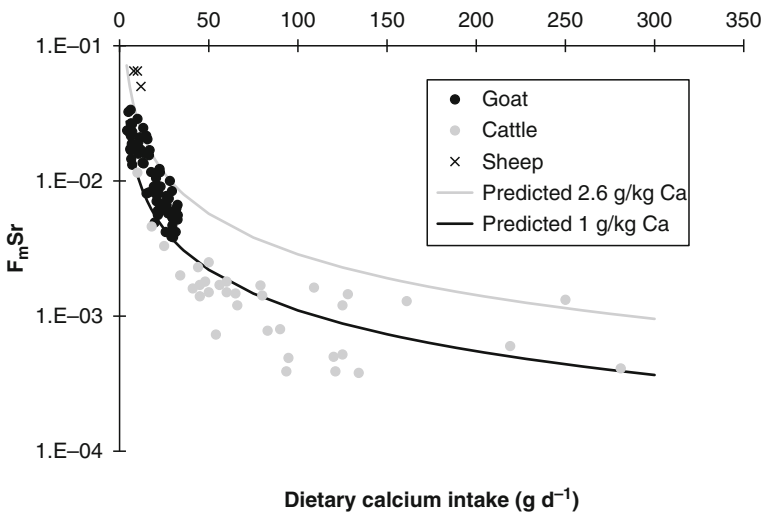

Radiation Assessment, Use of Transfer Parameters. Figure 4
Relationship between calcium intake and F_m for strontium adapted from Beresford et al. [57]; the lines represent predicted values from equation derived by Howard et al. [55] based upon calcium contents in milk of 1 g kg^{-1} (typical for cattle) and 2.6 g kg^{-1} (typical for sheep) respectively

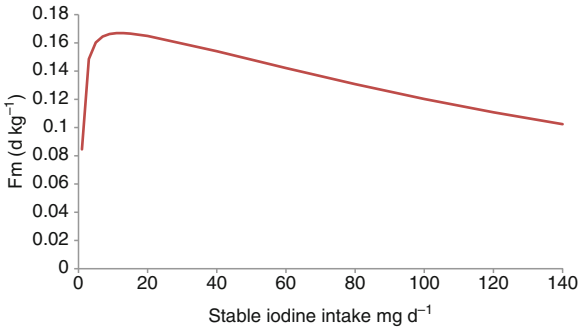

Radiation Assessment, Use of Transfer Parameters. Figure 5
Variation in the radioiodine transfer coefficient for the milk of dairy goats, as predicted by the model of Crout et al. [62]. The stable iodine intakes span suboptimal dietary levels, normal intake rates (1–20 mg day^{-1}), and maximal tolerable intake rates (50 mg kg^{-1} dry matter of feed)

experimental studies have used the short-lived gamma-emitting radioisotopes ^{99m}Tc and ^{95m}Tc. However, the studies of Ennis et al. [69–71] demonstrate variation in the transfer coefficients determined for goat milk for the three technetium radioisotopes. The F_m values of 1.5×10^{-4} d L^{-1} for ^{99m}Tc, 8.5×10^{-4} d L^{-1} for ^{95m}Tc, and 1.1×10^{-2} d L^{-1} for ^{99}Tc were inversely proportional to the specific activity of the three technetium radioisotopes. The authors suggested that this was the consequence of differential rates of reduction of pertechnate to a less available form in the rumen. As a consequence of these isotopes-specific differences in transfer and the lack of data for ^{99}Tc, IAEA [12] does not present recommended transfer coefficient values for technetium [77].

Tritium and ^{14}C are radioactive isotopes of essential macro-elements which constitute the building blocks of animal tissues and feed components; this makes them unusual compared to other radionuclides. Given their potential radiological significance there are relatively few measured transfer coefficients for the two radionuclides. Galeriu et al. [78] presented an approach for the derivation of tritium transfer coefficients based on an understanding of the metabolism of hydrogen in animals and which separately accounted for transfer to and from free (i.e., water) and organically bound tritium. Predictions of the approach compared well to the available data for a range of animal species and products. In Galeriu et al. [79] the approach was expanded to also consider ^{14}C. However, Galeriu et al. cautioned that predicted transfer coefficients for any animal product could not be considered a constant but were dependent upon the animal's metabolic status (see further discussion below). The IAEA [12] does not present transfer coefficient values for ^{3}H and ^{14}C but rather recommend the approach described by Galeriu et al. [78, 79].

Is Transfer Coefficient the Correct Parameter? As already discussed the transfer coefficient has been the accepted parameter to describe the transfer of radionuclides to products of farm animals since the mid-1960s. There has been considerable effort put into understanding the factors which influence transfer coefficients and it is generally accepted that transfer coefficient values for smaller animals are higher than those for larger animals (e.g., see Figs. 2 and 3 above) and those for young animals are higher than those for adults (e.g., [18]). However, the logic of the transfer parameter has increasingly been questioned [9, 36, 47, 77, 80, 81]. In the early 1980s, Ng et al. [9] suggested that size-related differences in estimated transfer coefficients were the consequence of the transfer coefficient incorporating dry matter intake rate which increases with animal size. Consequently, the denominator of the transfer coefficient equation (radionuclide activity concentration in feed × daily dry matter intake rate) will, for instance, be approximately an order of magnitude higher for cattle grazing the same pasture as sheep. However, the elemental composition of the meat and milk of different farm animals does not differ proportionally to size. For instance, Smith et al. [80] considered radiocesium transfer coefficients for the milk of three species and the meat of four species. The milk transfer coefficients they compared ranged from 8×10^{-3} d L^{-1} (cow) to 1×10^{-1} d L^{-1} (goat) while those for meat ranged from 5×10^{-2} d kg^{-1} (beef) to 10 d kg^{-1} (chicken). Rearranging the transfer coefficient equation to derive a food product to dietary concentration ratio (CR), that is:

$$\text{CR} = \text{Dry matter intake rate} \times \text{transfer coefficient}$$

and assuming typical daily dry matter intake rates (taken from [11]), they demonstrated that the CRs for both milk and meat varied by less than twofold.

In a study of the transfer of ^{137}Cs to female sheep throughout a breeding cycle significantly higher F_f values were found for sheep when their lambs had been weaned (F_f *circa* 0.7 d kg^{-1}) than during pregnancy (F_f *circa* 0.3 d kg^{-1}) and lactation (F_f *circa* 0.2 d kg^{-1}) [47]. Documented relationships between dry matter intake rates and protein turnover could credibly explain some of the difference observed in the study. However, when the same data were expressed as concentration ratios the highest value determined was 0.8 d kg^{-1} for lactating sheep with two lambs compared to values in the range 0.3–0.5 for pregnancy and postweaning. This is simply because the dry matter intake rate of the sheep producing milk sufficient to support two lambs was the highest of any experimental group, and therefore this group has the highest denominator in the transfer coefficient equation.

As noted above Galeriu et al. [78, 79] stated that the transfer coefficient for ^{3}H and ^{14}C could not be considered a constant but depends upon metabolic status. For instance, a high yielding dairy animal will ingest more feed and water (and hence C and H) than an animal producing little milk. However, the H and C content of milk and meat will be virtually the same regardless of yield/intake rate, and consequently the transfer coefficient will be lower for high yielding animals. The authors demonstrated that the ratio of the concentration between ^{3}H and ^{14}C activity in meat or milk and the diet is a more robust parameter as it remains relatively constant regardless of the metabolic status of the animal (given that the H and C concentrations in feed and milk/meat remain relatively constant).

The transfer coefficient can therefore be misleading (e.g., a high transfer coefficient value for one species compared to another does not imply the activity concentrations in this species will be higher). Moreover, as the concentrations of many elements are broadly similar in the milk and meat of different animal species a concentration ratio estimated for one species should give a reasonable estimate of transfer to a species for which there are no data. Howard et al. [81] derived CR values for a number of elements (using radionuclide and stable element data) for: (1) the milk of cattle, goats, sheep, and horses; and (2) the meat of cattle, sheep, and pigs. The resultant CR values were found to differ little between species whereas transfer coefficient values varied across the species by more than an order of magnitude (see Fig. 6 that compares CR and F_m for a number of radionuclides). The CR values estimated by Howard et al. have been included as recommended values in IAEA [12]. However, unfortunately, many radioecological studies do not present data in a manner in which a CR value can be estimated and hence for many radionuclides-animal products, transfer coefficient values still have to be relied upon.

The "Aggregated Transfer Parameter"

Some relatively simple models express transfer to plant- and animal-derived foodstuffs as the aggregated transfer factor (T_{ag}) where:

$$T_{ag}(m^2\ kg^{-1}) = \frac{\text{Activity concentration in foodstuff (Bq kg}^{-1}\text{ dry matter (plant) or fresh weight (animal))}}{\text{Soil activity concentration (Bq m}^2\text{)}}$$

The aggregated transfer parameter is simplification incorporating many processes it tends to be primarily used for seminatural ecosystems including for game, berries and fungi [12]. The T_{ag} is time dependent (e.g., as a consequence of movement down the soil profile) and is often used in association with ecological half-life

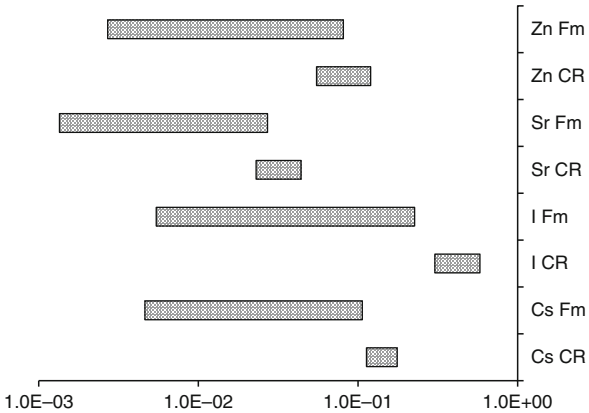

Radiation Assessment, Use of Transfer Parameters. Figure 6

A comparison of the range in CR and F_m values [81] for Zn, Sr, I, and Cs to the milk of different animals (ranges include data for cow, sheep, goat, and horse). The figure demonstrates the considerably greater variation in F_m values between species than that in CR values

estimates. As with soil-plant CR values there have been some attempts to categorize T_{ag} values on the basis of broad soil type (e.g., Fesenko et al. [82]); Wright et al. [83] related the radiocesium grass T_{ag} to soil organic matter and time after deposition to derive a model to apply in a geographical information system.

Radiological Assessment of the Environment

Although there have been studies to quantify both the exposure of wildlife to ionizing radiation and the potential effects of this exposure (e.g., see Bird this section and Tracy this section), protection of the environment per se has not been a focus of radiation protection until relatively recently. Rather the ICRP [2] statement "the Commission believes that the standards of environmental control needed to protect man to the degree currently thought desirable will ensure that other species are not put at risk" had been relied upon. However, the need to actually demonstrate that the environment is protected is now recognized by a number of international organizations (e.g., [84–87]) and national regulators. In some instances this has been driven by the need to meet conservation legislation [88]. The need for a system to demonstrate environmental protection is recognized in the latest ICRP Recommendations [85].

Approaches to estimate the exposure of wildlife to ionizing radiation have been developed in a number of countries including: the USA [89], England and Wales [90, 91], Korea [92], France [93], Lithuania [94], and Canada [95–97]. Within Europe there have been a series of EC EURATOM funded projects including, most notably, FASSET [98] and subsequently, ERICA [99]. The ICRP have also started to develop a framework for environmental protection based on their reference Animal and Plants concept [100].

An element that all assessment approaches require is a method to predict the transfer of radionuclides to wildlife to be able to determine internal exposure. The most common approaches to doing this are described in this section.

Estimating the Transfer of Radionuclides to Wildlife

All of the current approaches use, at least for some organism, equilibrium ratios between whole-organism activity concentrations and those in environmental media (see [101]), where the whole-organism concentration ratio (CR_{wo}) value is defined for terrestrial ecosystems as:

$$CR_{wo-soil} = \frac{\text{Activity concentration in biota whole organsim (Bq kg}^{-1}\text{ fresh weight)}}{\text{Activity concentration in soil (Bq kg}^{-1}\text{ dry weight)}}$$

with exceptions, in some models [89, 102], for chronic atmospheric releases of some gaseous radionuclides (such as ^{3}H and ^{14}C), where:

$$CR_{wo-soil} = \frac{\text{Activity concentration in biota whole organsim (Bq kg}^{-1}\text{ fresh weight)}}{\text{Activity concentration in air (Bq m}^{-3}\text{)}}$$

For aquatic ecosystems the majority of approaches calculate CR_{wo} as:

$$CR_{wo-water} = \frac{\text{Activity concentration in biota whole organsim (Bq kg}^{-1}\text{ fresh weight)}}{\text{Activity concentration in water (Bq L}^{-1}\text{)}}$$

If sediment concentrations are known but data for water are lacking, then distribution coefficient (K_d) values are used to estimate concentrations in water. The K_d can also be used to estimate sediment activity concentrations from filtered water concentrations which may be necessary to calculate external dose from sediment. The K_d, which is defined at equilibrium, is determined as:

$$k_d(\text{L kg}^{-1}) = \frac{\text{Activity concentration in sediment (Bq kg}^{-1}\text{ dry weight)}}{\text{Activity concentration in filtered water (Bq L}^{-1}\text{)}}$$

The K_d will not be discussed here in detail, however, while models currently source K_d values from existing publications (most especially [10–12]), which summarize data predominantly for application in human assessments. However, most often these consider suspended sediments whereas, for application in assessments of exposure to wildlife it is bed sediments which are of interest. Therefore, the existing reviews may not be ideal for wildlife assessments although

IAEA [103] suggests that the activity concentration of bed sediments is approximately 10% of that of suspended sediments.

There are some models that do not rely solely on organism-media CR_{wo} values but which for some, generally higher, organism types utilize allometric expression relating radionuclide transfer or biological half-life to body mass (e.g., [104–106]) or retention functions (e.g., [106]). Allometric relationships are discussed further in section on "Allometry".

Application of Concentration Ratio in Models and Available Databases

Environment assessment could potentially require the consideration of a large number of organisms. Most of the available environmental radiological assessment approaches have simplified this issue by considering a set of default organisms for which transfer, dosimetric and effects data are collated (e.g., [89, 90, 102]). Some approaches refer to these as "reference organisms" [102, 107, 108]. In selecting these organisms a number of factors have been considered such that they encompass various criteria such as: organisms most likely to be exposed; different tropic levels; organisms sensitive to radioactivity; and protected species. Data are therefore often collated by broad wildlife group such as benthic feeding fish, carnivorous mammal, broadleaf tree, bivalve mollusc, etc.

The ICRP [100] have opted to use a similar approach which they suggest parallels that of the Reference Person [85] approach proposing a set of 12 Reference Animals and Plants (RAPS) (see Table 1) for which effects and transfer, data are being collated and dosimetric parameters estimated. However, the ICRP approach places more emphasis on life stages than the other methodologies considered, with ICRP [100] presenting dose conversion coefficient values for a number of life-stages for some of the RAPs. The RAPs are suggested as "points of reference" for drawing comparisons with sets of information on other organisms. It is acknowledged that the RAPs may not be the direct objects of protection per se and that it may be necessary to establish a "secondary set of Reference Organisms for a specific purpose or geographical area." Since there are no internationally accepted "rules" on classification above Family (or "Super Family") level, the ICRP have suggested that this constitutes the most suitable level of generalization. A RAP is defined as: "a hypothetical entity, with the assumed basic biological characteristics of a particular type of animal or plant, as described to the generality of the taxonomic level of Family, with defined anatomical, physiological, and life-history properties, that can be used for the purposes of relating exposure to dose, and dose to effects, for that type of living organism" [100]. The RAPs are defined in more specific terms than the simplified organisms included in most other approaches (e.g., [91, 103, 109]).

Radiation Assessment, Use of Transfer Parameters.
Table 1 ICRP reference animals and plants (RAPs) by three generic habits and the taxonomic family level at which they are defined

RAP	Habitat	Family
Bee	Terrestrial	Apidea
Brown seaweed	Marine	Fucaceae
Crab	Marine	Cancridae
Deer	Terrestrial	Cervidae
Duck	Terrestrial, freshwater	Anatidae
Earthworm	Terrestrial	Lumbricidae
Flatfish	Marine	Pleuronectidae
Frog	Terrestrial, freshwater	Ranidae
Pine tree	Terrestrial	Pinaceae
Rat	Terrestrial	Muridae
Trout	Freshwater, marine	Salmonidae
Wild grass	Terrestrial, freshwater	Poaceae

Most of the current approaches are applied in some form of tier, or iterative, assessment consistent with methods used for other stressors. Such tiered assessments begin with a highly conservative screening tier and progress, if required, to more refined assessments. This is in common with assessment methodologies used for other stressors such as chemicals. In the more comprehensive models the tiered structure is in-built into the software [102, 110]. The different assessment tiers place different requirements on the collation of CR_{wo} values. The highly conservative screening tier typically utilizes maximum or 95th percentile CR_{wo} values. If site-specific data are not

available subsequent tiers require best estimate (mean or geometric mean) values, and if the model has probabilistic functionality an associated probability distribution (pdf) (which may also be required to derive 95th percentile values for application in initial screening tiers).

Since 2000 there have been a number of collations of radionuclide transfer data for wild species to support the developing model codes. Subsequent works have generally replaced earlier outputs such that a number of compilations have quickly become out of date. The databases [109, 111] complied for the ERICA Tool (Brown et al. [102]; software freely available from http://www.project.facilia.se/erica/download.html) incorporated those of the earlier European funded FASSET [112] and EPIC [113] projects. Where appropriate they also utilized limited database data compiled for the model (referred to as R&D128]) developed in England and Wales (Copplestone et al. [90, 91]; model spread sheets available from: http://wiki.ceh.ac.uk/x/9wHbBg).

The RESRAD-BIOTA code [110] which implements the USDOE *Graded Approach* [89] contains a default CR database for four generic organisms (terrestrial animal, terrestrial plant, riparian animal, aquatic animal) which was compiled primarily for the initial screen assessment only. Values are generally the maximum CR values (termed B_{iv} in RESRAD-BIOTA) identified by the model developers for any species falling within the appropriate broad organism category (i.e., the value for one radionuclide in a freshwater ecosystem may be for a fish while for another radionuclide the value may be for an invertebrate). For more refined assessments the latest release of RESRAD-BIOTA (code freely available from http://web.ead.anl.gov/resrad/home2/biota.cfm) has some probabilistic functionality and largely recommends the default CR values and associate pdfs from the ERICA Tool. A database of CR values developed to support application of the USDOE Graded Approach can be found online (see http://homer.ornl.gov/nuclearsafety/env/bdac/bcfs.html). However, this is very limited with, in some instances, the denominator not having been specified and its use is not recommended.

Model intercomparison exercises (see further discussion below) have clearly demonstrated that the largest contribution to variability between model predictions, and comparison with available data, is the parameterization of the model transfer components [114–119]. Other studies are in agreement with this conclusion [105, 120]. Based on such observations an IAEA working group recommended that there was a clear need to better share knowledge on the transfer of radionuclides to biota and to provide authoritative collations of those data which are available [101]. Subsequently, the IAEA established a working group to produce a handbook of radionuclide transfer parameters to wildlife (http://www-ns.iaea.org/projects/emras/emras2/working-groups/working-group-five.asp). At the time of writing the handbook is anticipated to be submitted for publication in early 2011 [121]. An online database was established to collate data for the handbook and this will be maintained and updated subsequent to IAEA, the handbook being produced (see https://wiki.ceh.ac.uk/display/rpemain/Wildlife+transfer for links to the database and associated guidance documents). The database has also been utilized by the ICRP to derive CR_{wo} values for their RAPs (a draft report on transfer values for RAPS was released for consultation in July 2010 – see www.ICRP.org). The online database and previous collations (e.g., [109, 111]) utilize stable element data in addition to environmental measurements of radionuclide transfer; typically it is assumed that transfer is element and not isotope dependent.

Data Availability

Current assessment approaches determine whole-organism activity concentrations to subsequently estimate whole-organism dose rates (rather than consideration of target tissues). This approach enables comparison with the available effects data which originate from studies of external gamma exposure (see for instance, Garnier-Laplace et al. [122]). However, many of the available radioecological data for wild species originate from measurements taken for human food chain assessments. These are, therefore, for tissues consumed by humans (most typically muscle). Yankovich et al. [123] provide a series of lookup tables presenting whole-organism: tissue-specific concentration ratios for terrestrial, freshwater, and marine animals which can be used to convert tissue-specific data to whole-organism activity concentrations for the purposes

of environmental assessment. While models such as the ERICA Tool [102] nominally estimate whole-organism dose rates for all organism types the geometries used for dosimetric calculations are typically for above ground parts only and CR_{wo} for plants are derived from a variety of above ground plant parts with no attempt to derive a whole-organism activity concentration.

At the time of writing neither the IAEA handbook of wildlife parameters nor the ICRP report presenting CR_{wo} values for their RAPs are finalized and consequently these documents cannot be discussed in any detail. Given this the most comprehensive database of CR_{wo} values for wildlife is that compiled for the ERICA Tool and described by Beresford et al. [112] and Hosseini et al. [113]. The ERICA Tool considers 31 elements and 37 organisms (13 terrestrial organisms, 12 freshwater organisms, and 12 marine organisms); it therefore required 1147 CR_{wo} values. The total number of CR_{wo} values which could be derived from data available in the literature was 453 (i.e., <40% of those required). For some radionuclides and organisms the IAEA handbook [121] and the wildlife transfer database (https://wiki.ceh.ac.uk/display/rpemain/Wildlife+transfer) will considerably expand the amount of data available to those conducting assessments. However, realistically, there will never be a complete set of transfer parameters for all of the potential radionuclide – organism that may be required in assessments. A number of approaches have been derived and used to parameterize existing models [89, 91, 102] to overcome this lack of data. In most cases the resultant parameters are only intended to be used in initial screening tier assessments which aim to be conservative. However, some prospective assessments or the need to consider protected species may require robust extrapolation approaches for application in more refined assessments. As it will present data specifically for species belonging to the taxonomic Family for which each RAP is defined, the amount of data for some RAP-radionuclide combinations will be limited (e.g., there are comparatively large amounts of data available for terrestrial mammals) but very few for species belonging to the Family *Muridae* (i.e., the Reference Rat). Consequently, the ICRP will also need to rely upon extrapolation techniques to provide a complete set of CR_{wo} values.

The next section describes the extrapolation approaches which have been used or suggested for use in radiological assessments of wildlife.

Extrapolation Approaches to Address Lack of Data

A number of extrapolation approaches which have been used to provide values for environmental assessment models are described below. Those having to use such approaches will often have more than one option available to them and will need to make a judgment about which is the most robust based upon the available information they will be applying it to. With the few exceptions which are noted below it is not appropriate here to suggest that any one approach is better than another.

Allometry Allometry, or more properly biological scaling, is the consideration of the effect of size on biological variables. The dependence of a biological variable Y on a body mass M is typically characterized by allometric equations of the form:

$$Y = aM^b$$

where a and b are constants.

There are a number of publications summarizing allometric relationships for a wide range of biological variables (e.g., [124]). Many biological phenomena scale as quarter powers of the mass [125, 126], for example: metabolic rates scale as $M^{0.75}$; rates of cellular metabolism and maximal population growth rate, as $M^{-0.25}$; lifespan and embryonic growth and development, as $M^{0.25}$; cross sectional areas of mammalian aortas and tree trunks, as $M^{0.75}$.

Allometric relationships for the biological half-life and dietary transfer coefficient for some radionuclides have been derived [89, 104, 120, 127–129]. While terrestrial mammals and birds have received most attention, Vives i Batlle et al. [104, 129] and Cherry and Heyraud [128] derived allometric relationships between body mass and radionuclide biological half-life and concentration ratio for a number of radionuclides in marine organisms.

In agreement with observations for many other biological parameters the radioecological allometric relationships often scaled to quartile values. Higley et al. [120] and USDOE [89] derived allometric

biological half-life relationships for Cs, Sr, I, Co, H, Am, Eu, Pu, Ra, Sb, Tc, Th, U, Zn, and Zr. Of these Cs, Co, Ra, Sb, Sr, U, Zn, and Zr had an exponent of approximately 0.25. Notable exceptions are provided by the actinide elements which scale to about 0.8. Macdonald [127] derived allometric relationship for the tissue-diet transfer coefficient (i.e., F_f as discussed in section on "Application of Transfer Parameters in Human food chain Modeling" for farm animals) for Cs and I for wild animals and birds. The exponent for both elements approached −0.75. For marine organisms Vives i Battle et al. [104] report that (organism-water) CR values for Ru, Ce, Pm/Eu, Ra, Th, Pu, Am, and Cm all scaled allometrically with an exponent of approximately −0.25. However, for marine organisms, while significant, biological half-life values for Tc, Cs, Pu, and Am scaled in the range 0.13–0.2 (Vives i Batlle et al. [104]).

As already noted Macdonald [127] derived allometric relationships describing the transfer coefficient (F_f) of cesium and iodine from feed to the tissues of wild mammals and birds which had similar exponents in the range −0.66 to −0.78. Based on these observations Sheppard [130] hypothesized that the derivation of relationships for other radionuclides required only the estimation of the multiplicand.

Allometric relationships for radionuclide biological half-life [89, 120] were used in the parameterization of the RESRAD-Biota model [110]. The model also allows users to create simple food chain models using these relationships combined with other allometric relationships for dry matter intake and water consumption rates among other parameters. The allometric relationships presented by Higley et al. have been used to provide CR_{wo} values for other models when data are lacking (e.g., [109, 131]).

In the literature discussing allometric relationships in general, there is discussion with regard to both the reasoning for the observation of quarter-power scaling the value of the exponent (e.g., does basal metabolic rate scale to 0.75 or 0.67) (see discussion in Higley and Bytwerk [132]). However, for the purposes of application within radioecological models these nuances are largely of academic interest. Of more relevance in further exploiting the phenomenon is perhaps to understand why some radionuclides and organisms do not scale to approximately quartile values: does this represent a real difference or simply lack of data? Radioecological allometric relationships represent qualitative trends over order of magnitude ranges in body mass and can be used as general predictors across species. They appear fit for this purpose and where predictions using allometric approaches have been compared to available data and/or predictions of other models, they perform adequately [116, 117, 133].

Although some biological traits for plants can be described by allometric functions (e.g., [134, 135]), Higley [136] recently reported that evidence to support the concept of using allometric scaling functions to estimate radionuclide activity concentrations in plants was inconclusive.

Does Size Matter? By algebraic derivation, Beresford et al. [133] suggested that there should be no effect of animal mass on the ratio between the activity concentration in body tissues and feed (for some radionuclides), as the combination of allometric relationships for either biological half-life or F_f with that for dry matter intake (which scales to *circa* 0.75 [137]) removes any mass dependent component from the resulting expression derived for the tissue/organism to diet activity concentration ratio. Considering the allometric relationship for biological half-life, then:

$$\frac{d[WB]}{dt} = \frac{f_1 \times [Diet] \times DMI}{M} - \frac{0.693}{T_{1/2b}} \times [WB]$$

where [WB] is the wholebody activity concentration of a radionuclide in an animal (Bq kg^{-1} fresh weight), t is time (d), $T_{1/2b}$ is the radionuclide biological half-life (d), DMI is the daily dry matter intake of feed (kg day^{-1}), f_1 is the fraction of ingested radionuclide absorbed from the gastrointestinal tract (dimensionless), and M is body mass (kg). At equilibrium and substituting DMI and $T_{1/2b}$ for allometric relationships assuming scaling factors of 0.75 and 0.25, respectively, this can be rearranged to:

$$\frac{0.693 \times [WB]}{a_1 M^{0.25}} = \frac{[Diet] \times a_2 M^{0.75}}{M}$$

which can be rearranged to give a wholebody to dietary activity concentration ratio:

$$\frac{[WB]}{[Diet]} = \frac{a_1 M^{0.25} \times a_2 M^{0.75}}{0.693M} = \frac{a_1 a_2}{0.693}$$

where a_1 and a_2 are the multiplicands of the allometric expressions for $T_{1/2b}$ and DMI, respectively.

Similarly starting from the equation for F_f presented in section on "Application of Transfer Parameters in Human Food Chain Modeling" and the allometric relationship suggested assuming a scaling factor of −0.75:

$$F_f = \frac{[WB]}{a_1 M^{0.25} \times [Diet]} = a_3 M^{-0.75}$$

can be rearranged to give a wholebody to dietary activity concentration ratio:

$$\frac{[WB]}{[Diet]} = a_1 a_2$$

where a_3 the multiplicand of the allometric expressions for F_f. Consequently, while F_f and biological half-life for radionuclides may vary considerably, concentration is relatively independent of size [133, 136] as demonstrated in Table 2. This is in agreement with the suggestion made in section on "Application of Transfer Parameters in Human Food Chain Modeling" that the dietary CR is a more robust parameter for estimating transfer to farm animals than the transfer coefficient. However, as should be apparent from Table 2, while the equilibrium activity concentration is relatively constant across a wide range of body masses the time taken to reach that concentration will increase with size.

The assumption of a constant CR value between wholebody and dietary activity concentrations was used to provide default CR_{wo} values for some terrestrial vertebrates in the ERICA Tool [109].

Radiation Assessment, Use of Transfer Parameters.
Table 2 Allometric predictions of radiocesium biological half-life, F_f, and equilibrium activity concentration for organisms of increasing mass

Body mass (kg)	Biological half-life (d)	F_f (d kg^{-1})	Bq kg^{-1}
0.001	2.6	1,400	0.46
0.01	4.4	260	0.47
0.1	7.7	48	0.48
1.0	13.2	8.9	0.49
10	22.8	1.7	0.50
100	39.8	0.31	0.51
1,000	68.0	0.06	0.52

Assume Value for a Similar Organism Where data are lacking for an organism-radionuclide combination the CR_{wo} value for a "similar" organism may be assumed. This approach was used in the ERICA model [109, 111] and Copplestone et al. [91]. For instance, if there are no data for ^{241}Am transfer to birds then a model may assume the CR_{wo} for mammals may be applied (both being warm-blooded vertebrates with a similar trophic levels).

Such decisions are obviously subjective but they can perhaps be given some scientific grounding. Differences in CR values between vascular plant species have been shown to be related to their evolutionary history, or phylogeny [138]. Broadley et al. [139] demonstrated that variation in the accumulation of radiologically relevant metals (Ni, Pb, Zn, Cd, Cr, and Cu) occurred at classification of the order or above. Willey [138] demonstrated significant phylogenetic signals for soil-plant transfer for Cs, Sr, Co, Cl, and Ru with monocots being found to have lower transfer than eudicots. A similar finding was reported in Willey et al. [140] for ^{99}Tc.

For marine organisms Jeffree et al. [141] demonstrated that the rates of uptake of nine radionuclides from water by three species of *chondrichthyans* differed to that by one species of *pleuronectiform* and two species of *perciform teleost* species.

Put simply, a significant phylogenetic signal demonstrates that transfer of the element is likely to be more similar for organisms which are close to each other evolutionary than those which are distant. Willey [138] presents the statistical coding to perform phylogenetic analyses. However, the analysis is rather data hungry.

Based upon an analysis of tree and crop data, Tagami and Uchida [142] suggest that CR values derived for crops (which are relatively numerous) could be applied to predict radionuclide transfer to trees if data for the latter are lacking.

Analog Elements Some approaches have assumed that where CR data are lacking an appropriate value for an element with similar biogeochemical behavior can be assumed. This generally entails consideration of placement on the periodic table and knowledge that the

elements behave in a similar manner. For instance, to provide a complete set of CR_{wo} values for the ERICA Tool assumptions such as applying Am values for Pu, Ce values for La, U values for Th, etc., were made if data were not available for a given element [109, 111].

Higley [136] suggests that soil-plant transfer could better be predicted using ionic potential citing work by Railsback [143] and Tyler [144]. Ionic potential is the ratio of ionic charge of a cation or anion to its ionic radius (see http://www.gly.uga.edu/railsback/PT.html). Considering 50 cationic elements Tyler [144] demonstrated a strong correlation ($R^2 = 0.6$) between ionic potential and CR for roots.

However, it is likely that in most instances selecting analog elements based upon period table grouping/prior knowledge of comparative behaviors or ionic potential would result in a similar element being selected.

Specific Activity Models As for human food chain transfer models (see section on "Quantifying Radionuclide Transfer to Farm Animals") conventional modeling techniques used for the majority of elements may not be appropriate to determining the transfer of ^{3}H and ^{14}C to wildlife. Some approaches [90, 102, 113] therefore use specific activity models which given these two radionuclides are primarily present as reversible gases ($^{14}CO_2$ and ^{3}HHO) relate activity concentrations in wildlife to those in air (Bq m^{-3}) for terrestrial systems. The derivation of the ^{3}H and ^{14}C approach adopted in the ERICA Tool is described in Galeriu et al. [145]. Currently, the approach taken by the ERICA Tool for aquatic ecosystems is inconsistent with that taken for terrestrial ecosystems in that empirical CR_{wo} values are used.

"Extreme" Assumptions In order to provide complete CR_{wo} datasets some approaches have used assumptions which could be considered as rather extreme. These include using the kd value for aquatic organisms if no CR_{wo} values are available [91]; applying the maximum available CR_{wo} for the given element regardless of organism [91, 109, 111]; and using a CR_{wo} for the organism-radionuclide from a different ecosystem [111]. Readers are reminded that such assumptions are used to enable initial screening level assessments to be conducted and are intended to yield conservative CR_{wo} values; such default values should not be used in more realistic assessments.

Problems with Providing "Complete" Sets of Cr_{wo} Value As noted in the previous sections, some radiological environmental assessment models in an attempt to enable users to be able to conduct initial screening tier assessments have used various extrapolation techniques to derive CR_{wo} values where data are unavailable. In some cases default values derived by such models are clearly identified in the model and/or accompanying documentation [91, 102].

However, there is a potential problem in providing complete sets of CR_{wo} values in that users may ignore caveats on their application. There is some published evidence that this is occurring [119, 146].

The derivation of transfer parameters where data are lacking is not restricted to assessments of wildlife exposure; IAEA [10] derives values for some radionuclide-organisms using similar approaches for application in assessments of human exposure via seafood consumption. And IAEA [12] presents a discussion of the application of analog elements and species for application in terrestrial and freshwater foodstuff models.

How are Environmental Assessment Models Performing?

The IAEA initiated a working group under its Environmental Modeling for Radiation Safety (EMRAS) program in 2004 to compare and validate models being used and developed to demonstrate protection of the environment (see IAEA [101]) These activities are currently continuing under the IAEA EMRAS II program (see http://www-ns.iaea.org/projects/emras/emras2/working-groups/working-group-four.asp).

The working groups have conducted (and continue to conduct) a number of model-model and model-data intercomparisons. Two of these exercises considered the estimation of dose under assumed conditions of unit activity concentration in medium or organism [114, 115]. Together with the other exercises these demonstrated that for consideration of simplified organism-medium geometries, the differences in dosimetry between the various models add little to the overall uncertainty in radiological assessments of

wildlife. However, comparisons of predicted activity concentrations assuming 1 Bq per unit media showed variability in predictions which for some organism-radionuclide combinations varied by more than three orders of magnitude [116]. Predictions were often the most variable for poorly studied organisms (e.g., amphibians, ducks, aquatic mammals). Some of the most extreme variability could be attributed to some users applying default model values derived using the extrapolation approaches described above. In some models the application of such techniques to provide default values aim to be conservative and in most instances comparatively high (i.e., conservative) predictions were made.

Yankovich et al. [119] reports the EMRAS working groups predictions of ^{60}Co, ^{90}Sr, ^{137}Cs, and ^{3}H activity concentrations in a variety of wildlife in Perch Lake (Ontario, Canada). Key findings were:

- Models parameterized using CR_{wo} values derived from laboratory experiments tended to under predict
- Models accounting for water calcium concentrations (see example below) better predicted ^{90}Sr activity concentrations in fish than models applying generic CR_{wo} values
- Predictions were generally poor for aquatic mammals and herpetofauna

An example of the relationships between CR_{wo} and water calcium concentrations used is that of Kryshev [147]:

$$CR_{wo}Sr = \frac{3940}{[Ca^{2+}]}$$

where $[Ca^{2+}]$ is calcium concentration in water (mg L^{-1}).

A similar intercomparison was made for terrestrial organisms in the Chernobyl Exclusion Zone with predictions being made for ^{137}Cs, ^{90}Sr, Pu-isotopes, and ^{241}Am [117]. In many instances predictions were found to be within an order of magnitude of the observed data, however, some predictions were under- or overestimates by more than two orders of magnitude. Two models applied in the exercise applied allometric biological half-life relationships (see "Allometry"); overall these models performed similarly to those using simple CR approaches.

It is envisaged that the majority of assessed sites will require only a screening assessment. An initial screening levels assessment is designed to be simple requiring minimal inputs and provide conservative results, with the aim of being able to identify sites of negligible concern and to remove them from further consideration with a high degree of confidence. As an example within England and Wales, 600 out of approximately 700 sites with authorizations to discharge radioactivity were identified as not requiring more detailed assessment (i.e., they were "screened" out) [148]. Beresford et al. [118] compared the screening level application of the R&D128 model, RESRAD-BIOTA and the ERICA Tool models, which are available for use by any user (see section on "Application of Concentration Ratio in Models and Available Databases" for links to download software) to data for seven sites. The outputs of the three models varied considerably for a given assessment with different conclusions being inferred with regard to the requirement if the site required any more detailed assessment. A number of factors were identified as contributing to this variability including: CR_{wo} and K_d values, input options, secular equilibrium assumptions, and geometry and exposure scenario. Such wide variation in screening application results gives some concern as to if they can be used with a high degree of confidence.

Future Directions

Many states currently face a number of radiological issues associated with: (1) long-term waste storage; (2) likely expansion of nuclear power productions; (3) legacy sites (most often associated with mining and mineral processing operations); (4) emergency planning (including potential malevolent use of radioactive sources); and (5) adapting to new recommendations and regulation (e.g., recent developments to explicitly demonstrate that the environment is protected). Recent reviews, such as IAEA [12], demonstrate that knowledge of the transfer of some radionuclides, including those identified as of concern with regard to some of these issues, is poor.

The majority of the parameters discussed above are relatively simplistic equilibrium ratios (although these may often be used within models having some dynamic parameters). These offer a pragmatic approach to

predicting radionuclide concentrations in human foodstuffs and wildlife. However, they often amalgamate many biological-chemical-physical processes and hence have a high degree of associated uncertainty.

In some instance these simplistic approaches have been refined and uncertainty reduced by categorizing transfer parameters on the basis of environmental variables (e.g., the categorization of soil-plant CR in IAEA [12] on the basis of soil type). Derivation of relationships between the transfer of Sr to milk and the dietary calcium intake represents a relatively simple approach to making best use of scientific knowledge (see section on "Factors Demonstrated to Influence Transfer Coefficient Values"). Similarly, CR values for freshwater fish have been related to water Ca and K concentrations for Sr and Cs, respectively [149, 150].

An essential first step in defining future research requirements is to assess where current models are fit for purpose. It is highly unlikely that detailed mechanistic knowledge will be gained for all radionuclides which require assessment. However, is such knowledge required for all radionuclides or is it probable that some which have to be assessed (as they constitute authorized discharges) are unlikely to contribute significantly to dose rates? Similarly, it may be that an equilibrium CR_{wo} is adequate for use in assessments of exposure of wildlife for the long time frames and exposure routes considered in assessments for waste repositories. However, some element of dynamic modeling may be required when considering chronic atmospheric release as a consequence of interception on vegetation surfaces [151].

The application of foodstuff, or organism, to medium concentration ratios will always have associated uncertainty. Depending upon the purposes of the assessment, or radionuclide and exposure pathway considered, such uncertainty may be acceptable. However, there will be circumstances where there is a requirement to better predict/understand radionuclide behavior. The development of models which utilize readily available/measurable environmental parameters should be encouraged as these will lead to models which can be applied globally. A good example of such a model for terrestrial systems is that described by Gillett et al. [152] which uses soil parameters such as exchangeable K concentration, pH, percentage clay, and percentage organic matter to predict the uptake of radiocesium by vegetation. For other radionuclides it is likely that environment chemistry models developed for stable elements (e.g., [153]) could provide a basis for the development of radioecological models.

As resources will always be limited well founded extrapolation approaches should be pursued. These will be especially useful to provide parameters for models predicting transfer to wildlife although they also have application in human food chain models (e.g., dietary CR represents a more generic approach than does the generally accepted transfer coefficient) (see section on "Is Transfer Coefficient the Correct Parameter?").

Sensitive analytical techniques such as ICP-MS, ICRP-OES, and neutron activation offer the possibility of obtaining data for a large number of elements of relevance to radiological assessments from the same sample and such approaches are increasingly being used (e.g., Higley [136], Takata et al. [154]; Tagami and Uchida [142]). Such techniques offer a cost- and resource-effective approach to obtaining data for poorly studied radionuclides. However, there is perhaps a requirement to more fully assess any limitations to the application of stable element data in models of radionuclide behavior (Uchida et al. [155] considers this for transfer to rice).

Where possible research to improve human food chain and wildlife assessment models should be integrated as the key processes determining transfer will often be the same (e.g., water chemistry, soil characteristics).

The potential implications of climate change on radiological assessments have to date received little consideration. While there may be some circumstances where climate directly impacts on radionuclide transfer (e.g., period of soil freezing in Arctic regions; ^{3}H transfer), largely the impact of climate is likely to be indirect (e.g., influence of climate on soil, land use, crop types, farm animals, and their management). However, the existing data are biased toward northern temperate ecosystems.

This entry focused on the "transfer parameters" used in radiological assessments. Other parameters (weathering rates, interception factors, resuspension rates, gastrointestinal absorption coefficients, dispersion coefficient, biological half-lives, etc.) are used in models and an overview of many of these can be found in IAEA [13].

Bibliography

Primary Literature

1. International Commission on Radiological Protection (ICRP) (1977) Recommendations of the international commission on radiological protection, ICRP publication 26. Pergamon, Oxford
2. International Commission on Radiological Protection (ICRP) (1991) Recommendations of the international commission on radiological protection, ICRP publication 60; Annals of the ICRP 21. Pergamon, Oxford
3. International Commission on Radiological Protection (ICRP) (1990) Age-dependent doses to members of the public from intake of radionuclides: Part 1, vol 20/2, ICRP publication 56; Annals of the ICRPl. Pergamon, Oxford
4. International Commission on Radiological Protection (ICRP) (1996) Age-dependent doses to members of the public from intake of radionuclides: Part 5 compilation of ingestion and inhalation dose coefficients, vol 26/1, ICRP publication 72; Annals of the ICRPl. Pergamon, Oxford
5. Ulanovsky A, Pröhl G, Gomez-Ros JM (2008) Methods for calculating dose conversion coefficients for terrestrial and aquatic biota. J Environ Radioactiv 99:1440–1448
6. Ng YC (1982) A review of transfer factors for assessing the dose from radionuclides in agricultural products. Nucl Safety 23:57–71
7. Ng YC, Colsher CS, Quinn DL, Thompson SE (1977) Transfer coefficients for the prediction of the dose to man via the forage-cow-milk pathway from radionuclides released to the biosphere, UCRL-51939. Lawrence Livermore Laboratory/University of California, Livermore/California, 94550
8. Ng YC, Colsher CS, Thompson SE (1979) Transfer factors for assessing the dose from radionuclides in agricultural products. In: Proceedings of an international symposium on the biological implications of radionuclides released from nuclear industries, IAEA-SM-237/54. International Atomic Energy Agency, Vienna
9. Ng YC, Colsher CS, Thompson SE (1982) Transfer coefficients for assessing the dose from radionuclides in meat and eggs: final report, NUREG/CR-2976. US Nuclear Regulatory Commission, Washington, DC
10. International Atomic Energy Agency (IAEA) (2004) Sediment distribution coefficients and concentration factors for biota in the marine environment, Technical Reports Series No. 422. International Atomic Energy Agency, Vienna
11. International Atomic Energy Agency (IAEA) (1994) Handbook of parameter values for the prediction of radionuclide transfer in temperate environments, Technical Reports Series No. 364. International Atomic Energy Agency, Vienna
12. International Atomic Energy Agency (IAEA) (2010) Transfer to animals. In: Handbook of parameter values for the prediction of radionuclide transfer in terrestrial and freshwater environments. Technical Reports Series No. 472. International Atomic Energy Agency, Vienna
13. International Atomic Energy Agency (IAEA) (2009) Quantification of radionuclide transfer in terrestrial and freshwater environments for radiological assessments, IAEA-TECDOC-1616. International Atomic Energy Agency, Vienna
14. Beresford NA, Howard BJ, Voigt G (2007) Transfer of radionuclides to food producing animals. J Environ Radioactiv 98:1–3
15. Calmon P, Fesenko S, Voigt G, Linsley G (2009) Quantification of radionuclide transfer in terrestrial and freshwater environments. J Environ Radioactiv 100:671–674
16. Fesenko S, Isamov N, Howard BJ, Voigt G, Beresford NA, Sanzharova N (2007) Review of Russian language studies on radionuclide behaviour in agricultural animals: Part 1 gut absorption. J Environ Radioactiv 98:85–103
17. Fesenko S, Howard BJ, Isamov N, Voigt G, Beresford NA, Sanzharova N, Barnett CL (2007) Review of Russian language studies on radionuclide behaviour in agricultural animals: part 2 transfer to milk. J Environ Radioactiv 98:104–136
18. Fesenko S, Isamov N, Howard BJ, Beresford NA, Barnett CL, Sanzharova N, Voigt G (2009) Review of Russian language studies on radionuclide behaviour in agricultural animals: part 3 transfer to muscle. J Environ Radioactiv 100:215–231
19. Fesenko S, Howard BJ, Isamov N, Beresford NA, Barnet CL, Sanzharova N, Voigt G (2009) Review of Russian language studies on radionuclide behaviour in agricultural animals: part 4 poultry. J Environ Radioactiv 100:815–822
20. Velasco H, Juri Ayub J (2009) Root uptake: tropical and subtropical environments. In: International Atomic Energy Agency (ed) IAEA quantification of radionuclide transfer in terrestrial and freshwater environments for radiological assessments, IAEA-TECDOC-1616. International Atomic Energy Agency, Vienna, pp 207–238
21. Beresford NA, Howard BJ (1991) The importance of soil adhered to vegetation as a source of radionuclides ingested by grazing animals. Sci Total Environ 107:237–254
22. Fesenko SV, Alexakhin RM, Balonov MI, Bogdevich IM, Howard BJ, Kashparov VA, Sanzharova NI, Panov AV, Voigt G, Zhuchenka Yu (2007) An extended critical review of twenty years of countermeasures used in agriculture after the Chernobyl accident. Sci Total Environ 383:1–24
23. Vidal M, Rigol A, Gil-Garcia CJ (2009) Soil-radionuclide interactions. In: International Atomic Energy Agency (ed) Quantification of radionuclide transfer in terrestrial and freshwater environments for radiological assessments, IAEA-TECDOC-1616. International Atomic Energy Agency, Vienna, pp 71–102
24. Gil-Garcia C, Rigol A, Vidal M (2009) New best estimates for radionuclide solid-liquid distribution coefficients in soils, Part 1: radiostrontium and radiocaesium. J Environ Radioactiv 100:690–696
25. Vandenhove H, Gil-Garcia C, Rigol A, Vidal M (2009) New best estimates for radionuclide solid-liquid distribution coefficients in soils, Part 2: naturally occurring radionuclides. J Environ Radioactiv 100:697–703
26. Gil-Garcia C, Tagami K, Uchida S, Rigol A, Vidal M (2009) New best estimates for radionuclide solid-liquid distribution coefficients in soils, Part 3: miscellany of radionuclides (Cd, Co, Ni,

Zn, I, Se, Sb, Pu, Am, and others). J Environ Radioactiv 100: 704–715
27. Ward GM, Johnson JE, Stewart HF (1965) Cesium-137 passage from precipitation to milk. In: Klement AW (ed) Proceedings of the second conference on radioactive fallout from nuclear weapons tests. National Technical Information Service, Springfield, pp 703–710
28. Ward GM, Johnson JE (1965) The caesium-137 content of beef from dairy and feed lot cattle. Health Phys 11:95–100
29. Brown J, Simmonds JR (1995) Farmland: a dynamic model for the transfer of radionuclides through terrestrial foodchains, NRPB-R275. National Radiological Protection Board, Chilton
30. Müller H, Pröhl G (1993) ECOSYS-87 – a dynamic-model for assessing radiological consequences of nuclear accidents. Health Phys 64:232–252
31. Nuclear Regulatory Commission (NRC) (1977) Calculation of annual doses to man from routine releases of reactor effluents for the purpose of evaluating compliance with 10 CFR 50. Appendix I. Regulatory Guide 1.109. Nuclear Regulatory Commission, Office of Standards Development, Washington, DC
32. Yu C, Zielen AJ, Cheng J-J, LePoire DJ, Gnanapragasam E, Kamboj S, Arnish J, Wallo A III, Williams WA, Peterson H (2001) Users manual for RESRAD version 6. ANL/EAD-4. US Department of Energy, Office of scientific and technical information, Oak Ridge, http://web.ead.anl.gov/resrad/documents/resrad6.pdf
33. Ward GM, Johnson JE (1989) Assessment of milk transfer coefficients for use in prediction models of radioactivity transport. Sci Total Environ 85:287–294
34. Voigt G (1988) The transfer of ^{60}Co from feed into vitamin B12 in cow liver, milk and beef. J Environ Radioactiv 8:209–215
35. Beresford NA, Crout NMJ, Mayes RW, Howard BJ, Lamb CS (1998) Dynamic distribution of radioisotopes of cerium, ruthenium and silver in sheep tissues. J Environ Radioactiv 38: 317–338
36. Beresford NA, Howard BJ, Mayes RW, Lamb CS (2007) The transfer of radionuclides from saltmarsh vegetation to sheep tissues and milk. J Environ Radioactiv 98:36–49
37. Ward GM, Johnson JE (1986) Validity of the term transfer coefficient. Health Phys 50:411–414
38. Solheim Hansen H, Hove K (1991) Radiocaesium bioavailability: transfer of Chernobyl and tracer radiocaesium to goat milk. Health Phys 60:665–673
39. Howard BJ, Mayes RW, Beresford NA, Lamb CS (1989) Transfer of radiocaesium from different environmental sources to ewes and suckling lambs. Health Phys 57:579–586
40. Beresford NA, Lamb CS, Mayes RW, Howard BJ, Colgrove PM (1989) The effect of treating pastures with bentonite on the transfer of Cs-137 from grazed herbage to sheep. J Environ Radioactiv 9:251–264
41. Assimakopoulos PA, Ioannides KG, Karamanis DT, Pakou AA, Stamoulis KC, Mantizios AS, Nikolaou E (1993) Radiocaesium transfer to sheep's milk as a result of soil ingestion. Sci Total Environ 136:13–24
42. Belli M, Blas M, Capra E, Drigo A, Menegon S, Piasentier E, Sansone U (1993) Ingested soil as a source of ^{137}Cs to ruminants. Sci Total Environ 136:243–249
43. Belli M, Sansone U, Piasentier E, Capra E, Drigo A, Menegon S (1993) ^{137}Cs transfer coefficients from fodder to cow milk. J Environ Radioactiv 21:1–8
44. Voigt G, Müller H, Paretzke HG, Bauer T, Rohtmoser G (1993) ^{137}Cs transfer. Health Phys 65:141–146
45. Beresford NA, Mayes RW, Cooke AI, Barnett CL, Howard BJ, Lamb CS, Naylor GPL (2000) The importance of source dependent bioavailability in determining the transfer of ingested radionuclides to ruminant derived food products. Environ Sci Technol 34:4455–4462
46. Assimakopoulos PA, Ioannides KG, Karamanis DT, Pakou AA, Stamoulis KC, Mantizios AS, Nikolaou E (1994) Variation of the transfer coefficient for radiocaesium transport to sheep's milk during a complete lactation period. J Environ Radioactiv 22:63–75
47. Beresford NA, Mayes RW, Barnett CL, Howard BJ (2007) The transfer of radiocaesium to ewes through a breeding cycle – an illustration of the pitfalls of the transfer coefficient. J Environ Radioactiv 98:24–35
48. Beresford NA, Mayes RW, Barnett CL, MacEachern PJ, Crout NMJ (1998) Variation in the metabolism of radiocaesium between individual sheep. Radiat Environ Biophys 37: 277–281
49. Beresford NA, Mayes RW, Barnett CL, Lamb CS (2002) Dry matter intake- a generic approach to predict the transfer of radiocaesium to ruminants? Radioprotection colloques 37:373–378
50. Comar CL, Wasserman RH, Lengemann FW (1966) Effect of dietary calcium on secretion of strontium into milk. Health Phys 12:1–6
51. Comar CL, Wasserman RH, Twardock AR (1961) Secretion of calcium and strontium into milk. Health Phys 7:69–80
52. Comar CL (1966) Radioactive materials in animals – entry and metabolism. In: Russell RS (ed) Radioactivity and human diet. Pergamon, Oxford, pp 127–156
53. Lengemann FW (1963) Overall aspects of calcium and strontium absorption. In: Wasserman RH (ed) Transfer of calcium and strontium across biological membranes. Academic, London, pp 85–96
54. Agricultural Research Council (ARC) (1980) The nutrient requirements of ruminant livestock, Technical review by an Agricultural Research Council Working Group. CAB International, Wallingford
55. Howard BJ, Beresford NA, Mayes RW, Hansen HS, Crout NMJ, Hove K (1997) The use of dietary calcium intake of dairy ruminants to predict the transfer coefficient of radiostrontium to milk. Radiat Environ Biophys 36:39–43
56. Van den Hoek J (1989) European research on the transfer of radionuclides to animals – an historical perspective. Sci Total Environ 85:17–27
57. Beresford NA, Mayes RW, Hansen HS, Crout NMJ, Hove K, Howard BJ (1998) Generic relationship between calcium

intake and radiostrontium transfer to milk of dairy ruminants. Radiat Environ Biophys 3:129–131
58. Kazakov VS, Demidchik EP, Astakhova LN (1992) Thyroid cancer after Chernobyl. Nature 359:21
59. Likhtarev IA, Gulko GM, Sobolev BG, Kairo IA, Chepurnoy NI, Prohl G, Henrichs K (1994) Thyroid dose assessment for the Chernigov region (Ukraine): estimation based on ^{131}I thyroid measurements and extrapolation of the results to districts without monitoring. Radiat Environ Biophys 33:149–166
60. Jackson D, Jones SR (1991) Reappraisal of environmental countermeasures to protect members of the public following the Windscale Nuclear Reactor accident 1957. In: CEC (ed) Proceedings of a seminar on comparative assessment of the environmental impact of radionuclides released during three major nuclear accidents: Kyshtym, Windscale, Chernobyl, vol II. Commission of the European Communities, EUR 13574, Luxembourg, pp 1015–1040
61. Howard BJ, Beresford NA, Barnett CL, Fesenko S (2009) Gastrointestinal fractional absorption of radionuclides in adult domestic ruminants. J Environ Radioactiv 100:1069–1078
62. Crout NMJ, Beresford NA, Mayes RW, MacEachern PJ, Barnett CL, Lamb CS, Howard BJ (2000) A model of radioiodine transfer to goat milk incorporating the influence of stable iodine. Radiat Environ Biophys 39:59–65
63. Voigt G, Kiefer P (2007) Stable and radioiodine concentrations in cow milk: dependence on iodine intake. J Environ Radioactiv 98:218–227
64. Assimakopoulos PA, Ioannides KG, Pakou AA (1989) A study of radiocaesium contamination and decontamination of sheep's milk. Sci Total Environ 85:279–285
65. Howard BJ, Beresford NA, Mayes RW, Lamb CS (1993) Transfer of ^{131}I to sheep milk from vegetation contaminated by Chernobyl fallout. J Environ Radioactiv 19:155–161
66. Howard BJ, Voigt G, Beresford NA (2001) Transfer to food producing animals. Parts A and B. In: Van der Stricht E, Kirchmann R (eds) Radioecology, radioactivity and ecosystems. Fortemps, Liege, pp 58–169
67. Howard BJ, Beresford NA, Gashchak S, Arkhipov A, Mayes RW, Caborn J, Strømann G, Wacker L (2007) The transfer of $^{239/240}$Pu to cow milk. J Environ Radioactiv 98:191–204
68. Beresford NA, Mayes RW, Crout NMJ, MacEachern PJ, Dodd BA, Barnett CL, Lamb CS (1999) The transfer of cadmium and mercury to sheep tissues. Environ Sci Technol 33: 2395–2402
69. Ennis ME, Johnson JE, Ward GM, Voigt GM (1988) A specific activity effect in the metabolism of technetium. Health Phys 54:157–160
70. Ennis ME, Ward GM, Johnson JE, Boamah KN (1988) Transfer coefficients of selected radionuclides to animal products, 2. Hen eggs and meat. Health Phys 54:167–170
71. Ennis ME, Ward GM, Johnson JE, Boamah KN (1989) Technetium metabolism by lactating goats. Health Phys 57:321–330
72. Johnson JE, Ward GM, Ennis ME Jr, Boamah KN (1988) Transfer coefficients of selected radionuclides to animal products, 1. Comparison of milk and meat from dairy cows and goats. Health Phys 54:161–166
73. Jones BEV (1989) Technetium metabolism in goats and swine. Health Phys 57:331–336
74. Bondietti EA, Garten CTJ (1988) Transfer of I-131 and Tc-95 m from pasture to goat milk. In: Desmet G, Myttenaere C (eds) Technetium in the environment. Elsevier Applied Science, London, pp 339–347
75. Von Wiechen A, Heine K, Hagemeister H (1983) A contribution to the question of the transfer of technetium-99 into milk. Atomkernenerg Kerntech 42:199–200, In German
76. Voigt G, Henrichs K, Prohl G, Paretzke HG (1988) Measurements of transfer coefficients for ^{137}Cs, ^{60}Co, ^{22}Na, ^{131}I, and ^{95m}Tc from feed into milk and beef. Radiat Environ Biophys 27:143–152
77. Howard BJ, Beresford NA, Barnett CL, Fesenko S (2009) Radionuclide transfer to animal products: revised recommended transfer coefficient values. J Environ Radioactiv 100:263–273
78. Galeriu D, Crout NMJ, Melintescu A, Beresford NA, Peterson SR, van Hees M (2001) A metabolic derivation of tritium transfer coefficients in animal products. Radiat Environ Biophys 40:325–334
79. Galeriu D, Melintescu A, Beresford NA, Takeda H, Crout NMJ (2009) The dynamic transfer of ^{3}H and ^{14}C in mammals: a proposed generic model. Radiat Environ Biophys 48:29–45
80. Smith J, Beresford NA, Shaw GG, Moberg L (2005) Radioactivity in terrestrial ecosystems. In: Smith JT, Beresford NA (eds) Chernobyl, catastrophe and consequences. Springer/Praxis, Chichester, pp 81–137
81. Howard BJ, Beresford NA, Barnett CL, Fesenko S (2009) Quantifying the transfer of radionuclides to food products from domestic farm animals. J Environ Radioactiv 100: 767–773
82. Fesenko SV, Colgan PA, Sanzharova NI, Lissianski KB, Vazquez C, Guardans R (1997) The dynamics of the transfer of caesium-137 to animal fodder in areas of Russia affected by the Chernobyl accident and resulting from the consumption of milk and milk products. Radiat Prot Dosim 69: 289–298
83. Wright SM, Smith JT, Beresford NA, Scott WA (2003) Monte-Carlo prediction of changes in areas of west Cumbria requiring restrictions on sheep following the Chernobyl accident. Radiat Environ Biophys 42:41–47
84. International Atomic Energy Agency (IAEA) (2006) Fundamental safety principles. IAEA Safety Standards Series No. SF-1. International Atomic Energy Agency, Vienna, p 37
85. International Commission on Radiological Protection (ICRP) (2007) Recommendations of the international commission on radiological protection, vol 2–3, ICRP publication 103; Annals of the ICRP 37. Pergamon, Oxford
86. International Union of Radioecology (IUR) (2000) Dose and effects in non-human systems. Summary of the work of the action group of IUR. IUR Report 01. International Union of Radioecology Osteras, Norway. Available at www.iur-uir.org

87. Nuclear Energy Agency (NEA) (2007) Scientific issues and emerging challenges for radiological protection: report of the expert group on the implications of radiological protection sciences, No. 6167. Nuclear Energy Agency, France. ISBN 978-92-64-99032-6
88. Howard BJ, Beresford NA, Andersson P, Brown JE, Copplestone D, Beaugelin-Seiller K, Garnier-Laplace J, Howe PD, Oughton D, Whitehouse P (2010) Protection of the environment from ionising radiation in a regulatory context—an overview of the PROTECT coordinated action project. J Radiol Prot 30:195–214
89. United States Department of Energy (USDOE) (2002) A graded approach for evaluating radiation doses to aquatic and terrestrial biota, Technical standard DOE-STD-1153-2002, Modules 1-3. United States Department of Energy, Washington, DC
90. Copplestone D, Bielby S, Jones SR, Patton D, Daniel CP, Gize I (2001) Impact assessment of ionising radiation on wildlife, R&D Publication 128. Environment Agency and English Nature, Bristol
91. Copplestone D, Wood MD, Bielby S, Jones SR, Vives i Batlle J, Beresford NA (2003) Habitat regulations for stage 3 assessments: radioactive substances authorisations. R&D Technical Report P3- 101/SP1a. Environment Agency, Bristol
92. Keum D-K, Jun I, Lim K-M, Choi Y-H (in press) External dose conversion coefficients to assess the radiological impact of an environmental radiation on aquatic and terrestrial animals. J Nucl Sci Tech
93. Beaugelin-Seiller K (2006) EDEN version 2 – User's manual. Report ECRE/06-29. IRSN/DEI, pp 38
94. Nedveckaite T, Filistovic V, Marciulioniene D, Remeikis V, Beresford NA (2007) Exposure of biota in the cooling pond of Ignalina NPP: hydrophytes. J Environ Radioactiv 97:137–147
95. Garisto NC, Cooper F, Fernandes SL (2008) No-effect concentrations for screening assessment of radiological impacts on non-human biota. NWMO TR-2008-02. Nuclear Waste Management Organisation, Toronto. Available at www.nwmo.ca
96. Chouhan SL, Yankovich TL, Davis PA (2009) Environmental radionuclide concentrations below which non-human biota experience no effects. Radioprotection 44:107–114
97. Environment Canada, Health Canada (2003) Releases of radionuclides from nuclear facilities (Impact on non-human biota): final report May 2003, Priority substances list assessment report: Canadian Environmental Protection Act 1999. Minister of Public Works and Government Services Canada, Ottawa
98. Williams C (ed) (2004) Framework for assessment of environmental impact (FASSET) of ionising radiation in European ecosystems. J Radiol Prot 24
99. Howard BJ, Larsson C-M (2008) The ERICA integrated approach and its contribution to protection of the environment from ionising radiation. J Environ Radioactiv 99:1361–1363
100. International Commission on Radiation Protection (ICRP) (2008) Environmental protection: the concept and use of reference animals and plants, ICRP Publication 108; Ann. ICRP 38. International Commission on Radiation Protection, Oxford
101. International Atomic Energy Agency (IAEA) (in-press) Modelling radiation exposure and radionuclide transfer for nonhuman species. Report of the biota working group of the EMRAS theme 3: environmental modelling for radiation safety (EMRAS) programme. International Atomic Energy Agency, Vienna. http://www-ns.iaea.org/downloads/rw/projects/emras/final-reports/biota-final.pdf
102. Brown JE, Alfonso B, Avila R, Beresford NA, Copplestone D, Pröhl G, Ulanovsky A (2008) The ERICA tool. J Environ Radioactiv 99:1371–1383
103. International Atomic Energy Agency (IAEA) (2001) Generic models for use in assessing the impact of discharges of radioactive substances to the environment, IAEA Safety Reports Series 19, STI/PUB/1102. International Atomic Energy Agency, Vienna
104. Vives i Batlle J, Wilson RC, Watts SJ, McDonald P, Craze A (2009) Derivation of allometric relationships for radionuclides in marine phyla. Radioprotection 44:47–52
105. Avila R, Beresford NA, Agüero A, Broed R, Brown J, Iospje M, Robles B, Suañez A (2004) Study of the uncertainty in estimation of the exposure of non-human biota to ionizing radiation. J Radiol Prot 24:A105–A122
106. Olyslaegers G (in-press) Modelling radiation exposure and radionuclide transfer for non-human species, Appendix IV DosDiMEco. Report of the biota working group of the EMRAS theme 3: environmental modelling for radiation safety (EMRAS) programme. International Atomic Energy Agency, Vienna. http://www-ns.iaea.org/downloads/rw/projects/emras/final-reports/biota-final.pdf
107. Beresford NA, Wright SM, Sazykina T (2001) Reference Arctic organisms. Contract deliverable under EPIC Inco-copernicus Project ICA2-CT02000-10032. Centre for Ecology and Hydrology: Merlewood, Grange-over-Sands. https://wiki.ceh.ac.uk/display/rpemain/EPIC+reports
108. Strand P, Beresford NA, Avila R, Jones SR, Larsson C-M (eds) (2001) Overview of radiation exposure pathways relevant for the identification of candidate reference organisms. FASSET Deliverable 1, Identification of candidate reference organisms from a radiation exposure pathways perspective. EC 5th framework programme Contract No. FIGE-CT-2000-00102. Including Appendix 1 and 2 on ecological characteristics of European terrestrial (App.1) and aquatic (App. 2) ecosystems. Norwegian Radiation Protection Authority, Østerås. https://wiki.ceh.ac.uk/display/rpemain/FASSET+reports
109. Beresford NA, Barnett CL, Howard BJ, Scott WA, Brown JE, Copplestone D (2008) Derivation of transfer parameters for use within the ERICA tool and the default concentration ratios for terrestrial biota. J Environ Radioactiv 99:1393–1407
110. United States Department of Energy (USDOE) (2004) RESRAD-BIOTA: a tool for implementing a graded approach to biota evaluation: User Guide Version 1, DOE/EH-0676. United States Department of Energy, Springfield

111. Hosseini A, Thørring H, Brown JE, Saxén R, Ilus E (2008) Transfer of radionuclides in aquatic ecosystems – default concentration ratios for aquatic biota in the ERICA tool. J Environ Radioactiv 99:1408–1429
112. Brown JE (ed) (2003) Environmental protection from ionising contaminants in the Arctic: Project ICA2-CT-2000-10032. Second annual report for EPIC (01.11.2001 – 31.10.2002). Norwegian radiation Protection Authority, Østerås. https://wiki.ceh.ac.uk/display/rpemain/EPIC+reports
113. Brown J, Strand P, Hosseini A, Borretzen P (eds) (2003) Handbook for assessment of the exposure of biota to ionising radiation from radionuclides in the environment. FASSET Deliverable 5. Norwegian Radiation Protection Authority, Østerås. https://wiki.ceh.ac.uk/display/rpemain/FASSET+reports
114. Vives i Batlle J, Balonov M, Beaugelin-Seiller K, Beresford NA, Brown J, Cheng J-J, Copplestone D, Doi M, Filistovic V, Golikov V, Horyna J, Hosseini A, Howard BJ, Jones SR, Kamboj S, Kryshev A, Nedveckaite T, Olyslaegers G, Pröhl G, Sazykina T, Ulanovsky A, Vives Lynch S, Yankovich T, Yu C (2007) Inter-comparison of unweighted absorbed dose rates for non-human biota. Radiat Environ Biophys 46:349–373
115. Vives i Batlle J, Beaugelin-Seiller K, Beresford NA, Copplestone D, Horyna J, Hossein, A, Johansen M, Kamboj S, Keum D-K, Kurosawa N, Newsome L, Olyslaegers G, Vandenhove H, Ryufuku S, Vives Lynch S, Wood MD, Yu C (2011) The estimation of absorbed dose rates for non-human biota: an extended inter-comparison. Radiat Environ Biophys 50:231–251
116. Beresford NA, Barnett CL, Brown J, Cheng J-J, Copplestone D, Filistovic V, Hosseini A, Howard BJ, Jones SR, Kamboj S, Kryshev A, Nedveckaite T, Olyslaegers G, Saxen R, Sazykina T, Vives i Batlle J, Vives-Lynch S, Yankovich T, Yu C (2008) Inter-comparison of models to estimate radionuclide activity concentrations in non-human biota. Radiat Environ Biophys 47:491–514
117. Beresford NA, Barnett CL, Brown JE, Cheng J-J, Copplestone D, Gashchak S, Hosseini A, Howard BJ, Kamboj S, Nedveckaite T, Olyslaegers G, Smith JT, Vivesi Batlle J, Vives-Lynch S, Yu C (2010) Predicting the radiation exposure of terrestrial wildlife in the Chernobyl exclusion zone: an international comparison of approaches. J Radiol Prot 30:341–373
118. Beresford NA, Hosseini A, Brown JE, Cailes C, Beaugelin-Seiller K, Barnett CL, Copplestone D (2010) Assessment of risk to wildlife from ionising radiation: can initial screening tiers be used with a high level of confidence? J Radiol Prot 30:265–284
119. Yankovich TL, Vives i Batlle J, Vives-Lynch S, Beresford NA, Barnett CL, Beaugelin-Seiller K, Brown JE, Cheng J-J, Copplestone D, Heling R, Hosseini A, Howard BJ, Kamboj S, Kryshev AI, Nedveckaite T, Smith JT, Wood MD (2010) An international model validation exercise on radionuclide transfer and doses to freshwater biota. J Radiol Prot 30: 299–340
120. Higley KA, Domotor SL, Antonio EJ (2003) A kinetic-allometric approach to predicting tissue radionuclide concentrations for biota. J Environ Radioactiv 66:61–74
121. International Atomic Energy Agency (IAEA) (in-preparation) Handbook of transfer parameters for the prediction of radionuclide transfer to wildlife. Technical Report Series No. XX. International Atomic Energy Agency, Vienna
122. Garnier-Laplace J, Della-Vedova C, Andersson P, Copplestone D, Cailes C, Beresford NA, Howard BJ, Howe P, Whitehouse P (2010) A multi-criteria weight of evidence approach for deriving ecological benchmarks for radioactive substances. J Radiol Prot 30:215–233
123. Yankovich TL, Beresford NA, Wood MD, Aono T, Andersson P, Barnett CL, Bennett P, Brown J, Fesenko S, Hosseini A, Howard BJ, Johansen M, Phaneuf M, Tagami K, Takata H, Twining J, Uchida S (2010) Whole-body to tissue concentration ratios for use in biota dose assessments for animals. Radiat Environ Biophys 49:549–565
124. Peters RH (1983) The ecological implications of body size. Cambridge University Press, Cambridge
125. Brown JH, West GB, Enquist BJ (2000) Patterns and processes, causes and consequences scaling in biology. In: Brown JH, West GB (eds) Scaling in biology. Oxford University Press, New York, pp 1–24
126. West GB, Brown JH, Enquist BJ (2000) The origin of universal scaling laws in biology. In: Brown JH West GB, West JH (eds) Scaling in biology. Oxford University Press, New York, pp 7–112
127. Macdonald CR (1996) Ingestion rates and radionuclide transfer in birds and mammals on the Canadian shield, Report TR-722 COG-95-551. AECL, Ontario
128. Cherry RD, Heyraud M (1991) Polonium-210 and lead-210 in marine organisms: allometric relationships and their significance. In: Kershaw PJ, Woodhead DS (eds) Radionuclides in the study of marine processes. Elsevier Applied Science, London, pp 309–318
129. Vives i Batlle J, Wilson RC, McDonald P (2007) Allometric methodology for the calculation of biokinetic parameters for marine biota. Sci Total Environ 388:256–269
130. Sheppard SC (2001) Toxicants in the environment: bringing radioecology and ecotoxicology together. In: Brechignac F, Howard BJ (eds) Radioactive pollutants impact on the environment. EDP Sciences, France, pp 63–74
131. Brown J, Børretzen P, Dowdall M, Sazykina T, Kryshev I (2004) The derivation of transfer parameters in the assessment of radiological impacts to arctic marine biota. Arctic 57:279–289
132. Higley KA, Bytwerk DP (2007) Generic approaches to transfer. J Environ Radioactiv 98:4–23
133. Beresford NA, Broadley MR, Howard BJ, Barnett CL, White PJ (2004) Estimating radionuclide transfer to wild species – data requirements and availability for terrestrial ecosystems. J Radiol Prot 24:A89–A103

134. Enquist BJ, Kerkhoff AJ, Stark SC, Swenson NG, McCarthy MC, Price CA (2007) A general integrative model for scaling plant growth, carbon flux, and functional trait spectra. Nature 449:218–222
135. Niklas KJ (2006) Plant allometry, leaf nitrogen and phosphorus stoichiometry and interspecific trends in annual growth rates. Ann Bot 97:155–163
136. Higley KA (2010) Estimating transfer parameters in the absence of data. Radiat Environ Biophys 49:645–656
137. Nagy KA (2001) Food requirements of wild animals: predictive equations for free-living mammals, reptiles and birds. Nutr Abstr Rev B 71:1R–12R
138. Willey NJ (2010) Phylogeny can be used to make useful predictions of soil-to-plant transfer factors for radionuclides. Radiat Environ Biophys 49:613–623
139. Broadley MR, Willey NJ, Wilkins J, Baker AJM, Mead A, White P (2001) Phylogenetic variation in heavy metal accumulation in angiosperms. New Phytol 152:9–27
140. Willey NJ, Tang S, McEwen A, Hicks S (2010) The effects of plant traits and phylogeny on soil-plant transfer of 99Tc. J Environ Radioactiv 101:757–766
141. Jeffree RA, Oberhansli F, Teyssie J-L (2010) Phylogenetic consistencies among chondrichthyan and teleost fishes in their bioaccumulation of multiple trance elements from seawater. Sci Total Environ 408:3200–3210
142. Tagami K, Uchida S (2010) Can elemental composition of crop leaves be used to estimate radionuclide transfer to tree leaves? Radiat Environ Biophys 49(4): 583–590
143. Railsback LB (2003) An earth scientist's periodic table of the elements and their ions. Geology 31:737–740
144. Tyler G (2004) Ionic charge, radius, and potential control root/soil concentration ratios of fifty cationic elements in the organic horizon of a beech (*Fagus sylvatica*) forest podzol. Sci Total Environ 329:231–239
145. Galeriu D, Beresford NA, Melintescu A, Avila R, Crout NMJ (2003) Predicting tritium and radiocarbon in wild animals. In: International Atomic Energy Agency (ed) International conference on the protection of the environment from the effects of ionizing radiation (IAEA-CN-109), Stockholm, 6–10 October 2003. International Atomic Energy Agency, Vienna, pp 186–189
146. Smith KL, Robinson CA, Jones SR, Vives i Batlle J, Norris S (2008) Assessment of impact to non-human biota from a generic waste repository in the UK. In: Strand P, Brown J, Jølle T (eds) Proceeding of international conference on radioecology and environmental radioactivity: oral and poster presentations, part 2, Bergen, 15–20 June 2008. Norwegian Radiation Protection Authority, Østerås, pp 415–418
147. Kryshev AI (2006) ^{90}Sr in fish: a review of data and possible model approach. Sci Total Environ 370:182–189
148. Allott R, Copplestone D (2008) Update on habitats assessments for England and Wales. National Dose Assessment Working Group. Paper 13-04. http://www.ndawg.org/documents/Paper13-04.pdf
149. Smith JT, Kudelsky AV, Ryabov IN, Hadderingh RH (2000) Radiocaesium concentration factors of Chernobyl-contaminated fish: a study of the influence of potassium and "blind" testing of a previously developed model. J Environ Radioactiv 48:359–369
150. Smith JT, Sasina NV, Kryshev AI, Belova NV, Kudelsky AV (2009) A review and test of predictive models for the bioaccumulation of radiostrontium in fish. J Environ Radioactiv 100:950–954
151. Copplestone D, Brown JE, Beresford NA (2010) Considerations for the integration of human and wildlife radiological assessments. J Radiol Prot 30:283–297
152. Gillett AG, Crout NMJ, Absalom SM, Wright SM, Young SD, Howard BJ, Barnett CL, McGrath SP, Beresford NA, Voigt G (2001) Temporal and spatial prediction of radiocaesium transfer to food products. Radiat Environ Biophys 40:227–235
153. Tipping E (1994) WHAM – a chemical equilibrium model and computer code for waters, sediments and soils incorporating a discrete-site electrostatic model of ion-binding by humic substances. Comput Geosci 20:973–1023
154. Takata H, Aono T, Tagami K, Uchida S (2010) Concentration ratios of stable elements for selected biota in Japanese estuarine areas. Radiat Environ Biophys 49:591–601
155. Uchida S, Tagami K, Shang ZR, Choi YH (2009) Uptake of radionuclides and stable elements from paddy soil to rice: a review. J Environ Radioactiv 100:739–745

Books and Reviews

Eisenbud M, Gesell T (1997) Environmental radioactivity from natural, industrial and military sources, 4th edn. Academic, San Diego

International Atomic Energy agency (IAEA) (2005) Protection of the environment from the effects of ionizing radiation. In: International Atomic Energy agency (IAEA) (ed) Protection of the environment from the effects of ionizing radiation: Proceedings of an International conference, Stockholm, 6–10 October 2003. International Atomic Energy agency, Vienna

Kathren RL (1984) Radioactivity in the environment: sources, distribution and surveillance. Harwood Academic Publishers, Switzerland

Scott EM (ed) (2003) Modelling radioactivity in the environment. Elsevier, Amsterdam

Smith JT, Beresford NA (eds) (2005) Chernobyl, catastrophe and consequences. Springer/Praxis, Chichester

van der Stricht E, Kirchmann R (eds) (2001) Radioeology, radioactivity & ecosytems. International Union of Radioecology (IUR), FORTEMPS, Liege, Belgium

Whicker FW, Schulz V (1982) Radioecology: nuclear energy and the environment, vol 1&2. CRC Press, Boca Raton

Radiation Effects on Caribou and Reindeer

Bliss L. Tracy
Radiation Protection Bureau, Health Canada 6604C, Ottawa, ON, Canada

Article Outline

Glossary
Definition of the Subject
Introduction
The Species *Rangifer terandus*
The Sources of Radionuclides in the Environment of Caribou/Reindeer
Radionuclide Levels in Lichens
Radionuclide Levels in *Rangifer tarandus*
Effects in *Rangifer tarandus*
Impacts on Human Populations
Future Directions
Bibliography

Glossary

Absorbed dose The amount of radiation energy absorbed per unit mass of tissue.

Alpha radiation A form of ionizing radiation, consisting of tightly bound particles containing two protons and two neutrons. This is the least penetrating form of ionizing radiation and can be stopped by a sheet of paper or by a layer of skin.

Becquerel (Bq) The SI (Système International) unit of activity, defined as one disintegration per second.

Beta radiation A form of ionizing radiation consisting of positively or negatively charged electrons. This is a moderately penetrating form of ionizing radiation and can be stopped by 1 mm of aluminum.

Equivalent dose The absorbed dose multiplied by a radiation weighting factor, equal to one for beta and gamma radiation, 20 for alpha radiation, etc.

Gamma radiation A form of ionizing radiation consisting of very-high-frequency electromagnetic waves. This is the most penetrating form of ionizing radiation and requires 10 cm of lead to significantly reduce its intensity.

Gray (Gy) The SI (Système International) unit of absorbed dose, equal to 1 J/kg. One Gray = 1,000 milligrays (mGy).

Half-life The time required for the number of radioactive atoms in a substance to decrease to one half of its initial value.

Ionizing radiation Radiation capable of stripping electrons from atoms as it passes through matter, hence creating ions. Normally emitted by the nuclei of radioactive elements.

Nuclear fission A process in which a heavy nucleus (e.g., ^{235}U) splits into two lighter fragments with the release of a large amount of energy. The resulting fragments are usually radioactive.

Radioactivity The property of the nuclei of certain elements to undergo disintegration, with the emission of one or more particles of ionizing radiation.

Radionuclide A radioactive substance characterized by the number of protons and neutrons in its nuclei. For example, the radionuclide cesium 137 (^{137}Cs) is characterized by 55 protons and 82 neutrons, giving a total mass of 137.

Sievert (Sv) The SI (Système International) unit of equivalent dose, equal to absorbed dose in grays multiplied by a radiation weighting factor. One Sievert = 1,000 millisieverts (mSv).

Definition of the Subject

Since the 1960s, extensive studies have been conducted on the uptake and retention of radionuclides in the lichen → caribou → human food chain. The reported concentrations of radioactivity in caribou and reindeer have been higher than in any other large terrestrial mammal. The results from these studies need to be brought together to address a fundamental question: Are these elevated levels of radioactivity having any measurable impact on the health of the animals? A supplementary question to be answered is: What is the impact on human populations?

Introduction

It has been known since the early 1960s that caribou and reindeer are particularly vulnerable to radioactive fallout and other airborne contaminants. To understand why this is so, one must examine the position and role of these animals in the ecosystem.

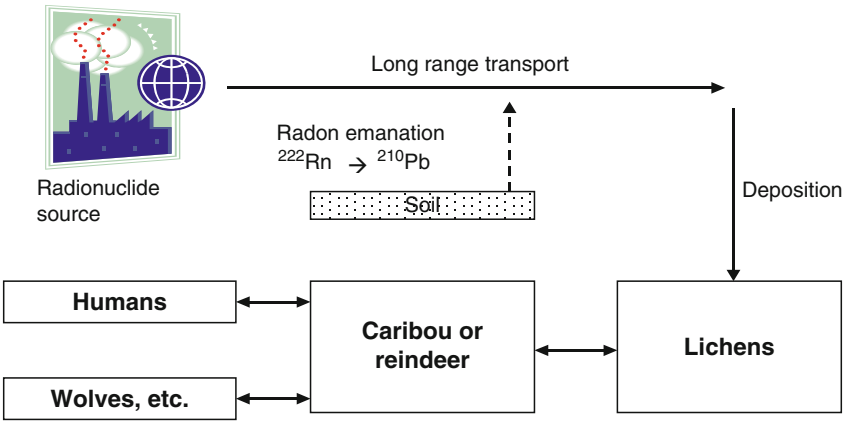

Radiation Effects on Caribou and Reindeer. Figure 1
A schematic diagram of the radioecology of caribou and reindeer

Figure 1 provides a simplified view of the caribou/reindeer ecosystem, emphasizing those features responsible for the uptake of radionuclides.

Sources of radioactivity in the environment may be natural (e.g., radon emanation from the ground) or artificial (e.g., a nuclear reactor or nuclear explosion). Radioactivity released into the atmosphere as a fine aerosols may be transported hundreds or thousands of kilometers from its original source by prevailing winds and global circulation patterns.

Gravitational settling and washout by precipitation eventually cause the radioactive aerosols to be deposited on the ground and on vegetation surfaces.

One vegetation class of particular importance are the lichens, which have large surface areas and no root systems. They depend on the atmosphere for many of their nutrients and thus are efficient collectors of a wide range of airborne pollutants, including radionuclides. Furthermore, lichens are not renewed annually, like grasses or deciduous leaves, but live for decades, which means they can accumulate contaminants over long periods of time.

Caribou and reindeer (*Rangifer tarandus*) are the only mammalian species that can subsist on a diet of lichens during the long winter months. This accounts for their reproductive success and proliferation in harsh northern climates and also for their vulnerability to ecosystem contamination. In order to obtain sufficient nourishment, they must graze the lichens over a large area and thus become integrators of radioactive fallout, both in space and in time. Caribou and reindeer serve as food for both humans and natural predators, which are often in competition with one another.

The relationship between *Homo sapiens* and *Rangifer tarandus* is a very ancient one, as attested to by cave paintings and artifacts found in southern Europe from 17,000 years ago (Fig. 2). Arctic and subarctic peoples, including the Sami of Fennoscandia and the Nenets of northern Siberia, have herded reindeer since the Middle Ages. Reindeer are raised for their meat, hides, antlers, and, to a lesser extent, for milk and for use as draft animals or beasts of burden.

The ancestors of the North American Indians migrated across the Bering Strait land bridge 10,000–12,000 years ago in search of game animals such as caribou. Today, caribou are still the most important dietary source of protein in many communities of Alaska and northern Canada. In the late nineteenth century, reindeer were introduced into Alaska as semi-domesticated livestock as a means of providing a livelihood for native peoples. Descendants of that herd populate several game farms in Canada today.

Recent studies are beginning to show that populations of caribou are on the decline. The reasons for this decline are still poorly understood. It is likely due to a combination of factors – climate change, natural predators, overhunting by humans, disruptions of migration routes by highways and oil pipelines from northern development, and, last but not least, environmental contaminants. It is debatable whether

Radiation Effects on Caribou and Reindeer. Figure 2
A modern reindeer and a cave painting from 17,000 years ago

exposures to environmental contaminants alone can explain the decline, but contaminants may interact with other environmental stressors and weaken the overall ability of the animals to survive.

To gain further understanding of one major class of contaminants, this entry traces the origins and transport of both natural and artificial radionuclides in the environment. It documents their uptake and concentration levels in lichens and caribou/reindeer. The question of possible effects on the animals is addressed in light of the latest knowledge on radiation effects. The impacts on human populations who depend on caribou/reindeer are discussed as well.

The Species *Rangifer terandus*

Both caribou and reindeer are members of the same species, *Rangifer tarandus*, which in turn belongs to the *cervidae* or deer family. There are a number of distinct subspecies of *Rangifer*, but caribou and reindeer do not fall neatly into these categories. In fact, the variability within these two types is greater than the difference between them. The main distinction is probably etymological. Essentially, "caribou" is a New World term for the *Rangifer tarandus* that are native to North America and "reindeer" is an Old World term for the ones that inhabit northern Europe today. The term "caribou" comes, through French, from Mi'kmaq *qalipu*, meaning "snow shoveler," and refers to the animals' habit of pawing through the snow for food [1]. The English word "reindeer" comes from the Norwegian *reinsdyr* [old Norse *hreinn* + *dyr* ("animal")].

Since 1961, *Rangifer* has been divided into two major groups: tundra with six subspecies and woodland with three subspecies.

Tundra *Rangifer tarandus*

- Arctic Reindeer (*R. tarandus eogroenlandicus*), an extinct subspecies found until 1900 in eastern Greenland
- Peary Caribou (*R. tarandus pearyi*), found in the northern islands of the Nunavut and the Northwest Territories of Canada
- Svalbard Reindeer (*R. tarandus platyrhynchus*), found on the Svalbard islands of Norway, the smallest subspecies
- Mountain/Wild Reindeer (*R. tarandus tarandus*), found in the Arctic tundra of Eurasia, including the Fennoscandia peninsula of northern Europe
- Porcupine Caribou or Grant's Caribou (*R. tarandus granti*), found in Alaska, the Yukon, and the Northwest Territories of Canada. Very similar to *R. tarandus groenlandicus* described below, and

probably better regarded as a junior synonym of that subspecies

- Barren-ground Caribou (*R. tarandus groenlandicus*), found in Nunavut and the Northwest Territories of Canada and in western Greenland

Woodland *Rangifer tarandus*

- Finnish Forest Reindeer (*R. tarandus fennicus*), found in the wild in only two areas of Fennoscandia – Finnish/Russian Karelia and a small population in central south Finland
- Migratory Woodland Caribou (*R. tarandus caribou*), or Forest Caribou, once found in the North American taiga (boreal forest) from Alaska to Newfoundland and Labrador and as far south as New England, Idaho, and Washington. Woodland Caribou have disappeared from most of their original southern range and are considered threatened where they remain, with the notable exception of the Migratory Woodland Caribou of northern Quebec and Labrador
- Queen Charlotte Islands Caribou (*R. tarandus dawsoni*), which became extinct at the beginning of the twentieth century

Rangifer tarandus is widely distributed throughout the circumpolar region and range as far south as 46° North Latitude (Fig. 3). It was once believed that *Rangifer* evolved in Europe and Asia, and moved into North America during the time of the land bridge across the Bering Strait (10,000–20,000 years ago). However, *Rangifer* bones dating back 1.5 million years have been found in the Fort Selkirk area of the Yukon. It now seems likely that *Rangifer tarandus* evolved in North America, moved to Europe and Asia, and then moved back into North America across the land bridge.

It is an oversimplification to state that all caribou are wild and all reindeer domesticated. Reindeer are not considered fully domesticated, as they generally roam

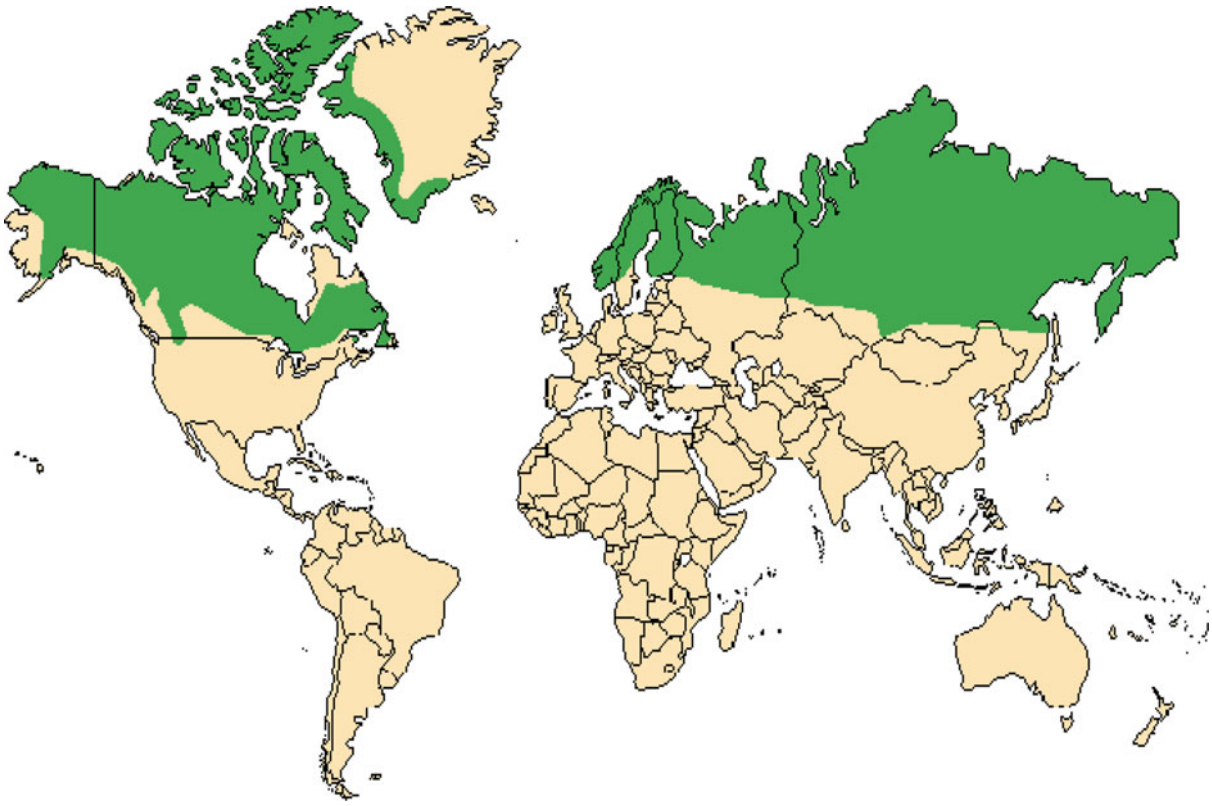

Radiation Effects on Caribou and Reindeer. Figure 3
World distribution of *Rangifer tarandus* shown in green

free on pasture grounds and they have never been bred in captivity. In traditional nomadic herding, reindeer herders migrate with their herds between coast and inland areas according to an annual migration route, and herds are keenly tended. Furthermore, truly wild reindeer do exist in Norway. They number about 25,000 animals and are found in 23 more or less separated areas in the mountainous southern part of the country. A total of 4,817 animals, or about 20% of the population, was harvested in 2005. Also, a diminutive subspecies of wild reindeer occurs throughout the unglaciated parts of the Svalbard Archipelago. Although no exact count has been carried out, these reindeer are believed to number several thousands.

Rangifer are ruminants, having a four-chambered stomach. They eat mainly lichens in winter, especially reindeer moss. However, they also eat the leaves of willows and birches, as well as sedges and grasses. Some populations of the North American caribou migrate the furthest of any terrestrial mammal, traveling up to 5,000 km in 1 year. They normally travel about 20–60 km per day while migrating, but can run at speeds of 60–80 km/h. During the spring migration, smaller herds will group together to form larger herds of 50,000–500,000 animals but during autumn migrations, the groups become smaller and the caribou begin to mate.

Rangifer tarandus is the only species of deer in which both sexes have antlers. Males are significantly larger than females, with weights ranging from 100 to 200 kg and occasionally exceeding 300 kg. Female weights vary from 80 to 120 kg. Male caribou compete for access to females during the fall rut, which occurs in October and early November. During this time, males may engage in battles that leave them injured and exhausted. Dominant males restrict access to small groups of 5–15 females. Males stop feeding during this time and lose much of their body reserves. Calves are born the following May or June. After 45 days, the calves are able to graze and forage but continue suckling until the following autumn and become independent from their mothers.

Although populations of *Rangifer* have been relatively stable in the past, there is some evidence of declining caribou herds, especially in Canada's Northwest Territories. A Territorial government survey released in September 2009 indicated that the Bathurst herd population had decreased from 128,000 to 32,000 animals between 2003 and 2009 [2]. In the mid-1980s, this herd numbered nearly 500,000 animals. The Cape Bathurst and Bluenose herds showed similar decreases over this period. The causes of these declines are not well understood. A number of possible causes have been put forward, including climate change, natural predators, overhunting by humans, disruptions of migration routes by highways and oil pipelines from northern development, and environmental contaminants.

The Sources of Radionuclides in the Environment of Caribou/Reindeer

Artificial Radionuclides

Two of the most important artificial radionuclides are cesium 137 (^{137}Cs) and strontium 90 (^{90}Sr). Both are produced with high yields in nuclear fission; both have half-lives of about 30 years, and thus persist in the environment for long periods of time; and both are highly radiotoxic. Cesium is a chemical analogue of potassium and is readily taken up by all living organisms where it becomes more or less uniformly distributed throughout the body of the organism. Strontium is an analogue of calcium and becomes concentrated in the bones and teeth of animals where it may remain for years.

The major source of these radionuclides in the global environment has been fallout from the atmospheric testing of nuclear weapons. Figure 4 shows the annual global deposition of ^{137}Cs since 1951 [3]. Fallout declined sharply after 1963, when the United States, the Soviet Union, and the United Kingdom signed a treaty banning the testing of nuclear weapons in the atmosphere. France and China, non-signatories of the treaty, continued some atmospheric testing up until 1980, leading to a continuing input of fission products at a reduced level. A large amount of ^{137}Cs and ^{134}Cs were injected into the atmosphere following the accident in 1986 at the Chernobyl nuclear power station in the Ukraine. Fallout radiocesium was significantly augmented over large areas of Europe and Asia during the year of the accident. The less-volatile ^{90}Sr was not emitted to the same degree.

Figure 5 shows the cumulative distribution of ^{137}Cs deposition worldwide, integrated over 10° latitude

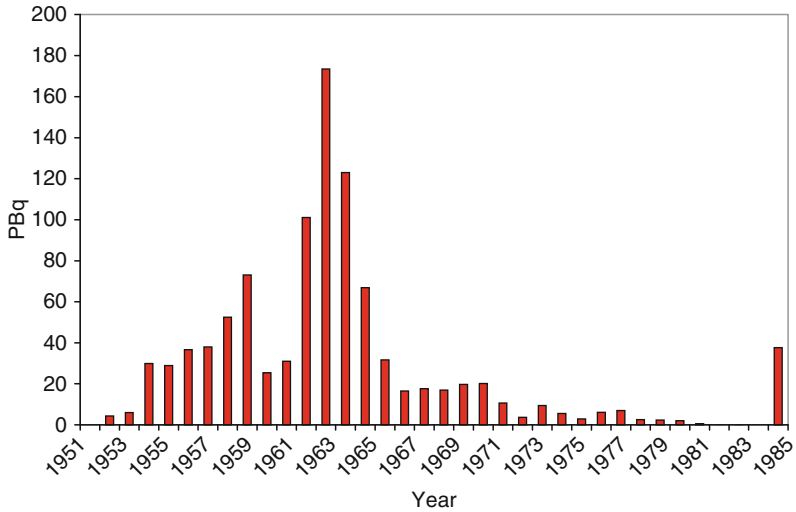

Radiation Effects on Caribou and Reindeer. Figure 4
Annual global deposition of ^{137}Cs from 1951 to 1986. The large spike in 1986 is due to the Chernobyl accident. The units are Petabecquerels = 10^{15} Bq (Based on data from UNSCEAR [3])

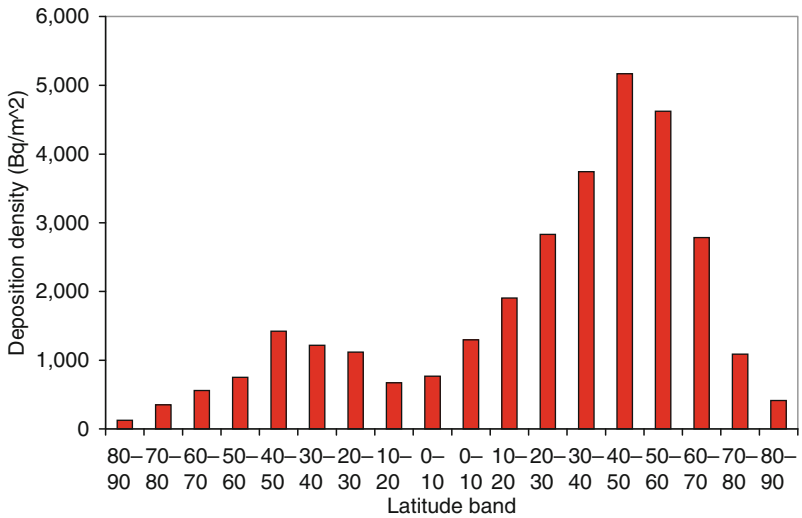

Radiation Effects on Caribou and Reindeer. Figure 5
Cumulative deposition density of ^{137}Cs from 1951 to 1985, averaged over each 10° latitude band. The contribution from the Chernobyl accident in 1986 is not included, since this deposition was very nonuniform (Based on data from UNSCEAR [3])

bands [3]. Fallout was higher in the Northern Hemisphere than the Southern Hemisphere, and higher in temperate zones than polar zones. However, fallout was still significant from Latitude 50° to 70° N, where most of the world's caribou and reindeer reside.

Natural Radionuclides

The natural radioactive elements uranium and thorium are present at average levels of 20–40 Bq/kg in the earth's crust, although higher levels are observed in zones of significant mineralization. These elements

normally remain locked in rocks and soils, until they are brought to the surface by mining operations. However, an important exception occurs in nature. One of the decay products of both uranium and thorium is radon gas, which readily diffuses out of the soil. Normally, it disperses quickly in outdoor air but can build up to hazardous levels in buildings and underground mines. One of the decay products of radon 222 (^{222}Rn) is lead 210 (^{210}Pb), which is important in the caribou/reindeer ecosystem. Lead 210 in turn decays to polonium 210 (^{210}Po), a highly toxic, alpha-emitting radionuclide. The reader may recall that ^{210}Po was the poison used in the famous Russian spy case of 2006 [4]. The partial decay scheme leading to these radionuclides is shown below. Half-lives are shown in brackets.

^{238}U (4.5 billion years) → intermediate products → ^{222}Rn (3.824 days) → short-lived products (∼minutes) → ^{210}Pb (21 years) → ^{210}Bi (5.01 days) → ^{210}Po (138.4 days) → ^{206}Pb (stable)

With a half-life of 22 years, ^{210}Pb can be transported over long distances and then be deposited on lichens, where it builds up over decades. The average residence time of ^{210}Pb in air is about 10 days [5], which is sufficient for global transport. Once deposited, ^{210}Po soon grows into equilibrium with ^{210}Pb and the two radionuclides are ingested by caribou and reindeer which graze on the lichens.

Radionuclide Levels in Lichens

Lichens are composite organisms consisting of a symbiotic association of a fungus (the mycobiont) with a photosynthetic partner (the photobiont or phycobiont), usually either a green alga or cyanobacterium. Lichens do not have roots and do not need to tap continuous reservoirs of water like most higher plants, thus they can grow in locations impossible for most plants, such as bare rock, sterile soil, or sand. Lichens occur in some of the most extreme environments on earth – arctic tundra, hot deserts, rocky coasts, and toxic slag heaps. Lacking a root system, their primary source of most nutrients is the air. Therefore, elemental levels in lichens often reflect the accumulated composition of ambient air. Lichens are widespread and can live for decades; however, they are vulnerable to environmental pollution and do not fare well in most urban environments.

Several factors account for the high concentrations of radionuclides found in Arctic lichens.

- They have a large surface area to mass ratio. Total deposited radioactivity depends on surface area, so this leads to a high radionuclide concentration per unit mass.
- Their lack of a root system makes them efficient at absorbing trace elements from air.
- With a lifetime of decades, they can accumulate pollutants over a long period of time.
- In northern environments, the growing season is short and vegetation turnover is generally slow. This leads to long-term retention times of pollutants in lichens.

^{137}Cs

As early as 1959, Gorham [6] noted the ability of lichens to concentrate radionuclides in the environment. Hofmann et al. [7] stated that this is due to the absorption of cesium by the mycobiont, that is, the fungal part of the lichen, in order to satisfy its potassium requirements.

Hanson [8] reported ^{137}Cs levels in lichens from four locations in Alaska between 1962 and 1979. He noted a dramatic increase during the peak of nuclear testing 1962–1963, reaching levels of 25–30 nCi kg^{-1} (900–1,100 Bg kg^{-1}) dry weight. He determined a caribou intake of 4.5–5.0 kg dry lichens day^{-1}, which would lead to a radiocesium intake of up to 5,000 Bq day^{-1}. The ^{137}Cs content of lichens declined only very slowly over subsequent years. In a separate experiment, he determined the retention half-time of cesium on lichens to be 5 ± 2 years, quite close to currently accepted values.

Enormous increases in radiocesium concentrations in lichens were observed in Europe after the Chernobyl accident of 1986. Hofmann et al. [7] measured the enhancement factors of 23–547 for ^{137}Cs in Austrian lichens before and after Chernobyl, showing the extreme vulnerability of this plant. White et al. [9] observed a more modest increase of 75% for lichens in the Fairbanks area of Alaska, which was less affected by Chernobyl fallout.

In 1980, Hutchison-Benson, Svoboda, and Taylor [10, 11] measured ^{137}Cs concentrations in vegetation

and top soil along a south–north transect in Canada from 58° to 82° N. They found concentrations in lichens up to 2,000 Bg kg^{-1} dry weight – five times higher than in vascular plants from the same locations. The concentrations in all plants followed a bell-shaped distribution curve with latitude, reaching a maximum between 60° and 70° N, farther north than the maximum in ^{137}Cs fallout shown in Fig. 5. The authors attributed this northward shift to the slower vegetation turnover rates at higher latitudes. They found that the effective ^{137}Cs half-life in the lichen species *Alectoria nigricans* increased from about 4 years at 50° N to 8 years at 82° N.

The above findings have important implications for the study of radiocesium in *Rangifer*. First of all, the latitude band 60°–70° N is where the majority of world's caribou and reindeer herds are found – in Alaska, Canada, Fennoscandia, and Siberia. Second, the effective half-life of ^{137}Cs in the caribou/reindeer ecosystem is driven by its retention time in vegetation, particularly lichens.

^{210}Pb and ^{210}Po

The detection of enhanced ^{137}Cs uptake by lichens led some investigators to suspect that naturally occurring airborne radionuclides, such as ^{210}Pb and ^{210}Po, might also be concentrated by this mechanism. In the 1960s, Holtzman [12] measured these two radionuclides in a suite of biota and human specimens from Alaska. He found ^{210}Pb levels in Alaskan lichens of 420–2,500 Bq kg^{-1} dry weight, whereas Beasley and Palmer [13] reported 170 Bq kg^{-1} wet weight for a composite lichen sample from Alaska.

Kauranen and Miettinen [14] measured ^{210}Po and ^{210}Pb concentrations in lichens collected from various locations in Finland between 1961 and 1967. Their results are reproduced here in Table 1 to illustrate the

Radiation Effects on Caribou and Reindeer. Table 1 ^{210}Po and ^{210}Pb content (Bq kg^{-1} dry weight) of lichen samples (*Cladonia alpestris*) from different parts of Finland from [14]. (Units in the original publication were pCi g^{-1} dry weight)

Date of collection	Locality	^{210}Po	^{210}Pb	$^{210}Po/^{210}Pb$
	Lapland			
August 1961	Inari	–	310	–
July 1964	Inari	250	270	0.92
July 1966	Enontekiö	350	380	0.93
July 1966	Inari	210	210	0.98
	Average	270	290	0.92
	Southern Finland			
October 1964	Tuusula	220	270	0.80
July 1965	Pielisjärvi	220	240	0.92
August 1965	Porvoo	180	200	0.91
October 1966	Helsinki	180	230	0.82
October 1966	Virolahti	210	260	0.84
October 1966	Loppi	170	190	0.90
April 1967	Helsinki	200	260	0.78
April 1967	Virolahti	260	300	0.86
May 1967	Loppi	200	230	0.85
	Average	200	240	0.85

consistency of these concentrations over time and space. It is notable that the $^{210}Po/^{210}Pb$ ratios are only slightly less than 1.00, indicating that the ^{210}Po in lichens is nearly in secular equilibrium with ^{210}Pb.

Jaworowski [15] measured ^{210}Pb in lichens along a south–north transect from 41° to 77° N and found higher values in the Arctic (200–500 Bq kg^{-1}dry weight) than in the temperate zone (30–120 Bq kg^{-1}). He also observed an increase in ^{210}Pb levels in samples from Polish glaciers dated between 1952 and 1965. A likely explanation for this increase is anthropogenic input from nuclear weapons testing, specifically from the reaction $^{208}Pb(2n, \gamma)^{210}Pb$ in the intense neutron flux created by the nuclear explosion.

Persson [16] reported ^{210}Pb concentrations in archived lichen samples from Sweden, collected between 1882 and 1972. Although there were considerable fluctuations in the data, no consistent trends were apparent during this long time period. More intensive sampling from 1962 to 1972 gave a range of ^{210}Pb concentrations between 100 and 300 Bq kg^{-1} dry weight.

Table 2 shows more recent results from Skuterud et al. [17] on three radionuclides in Norwegian lichens – ^{90}Sr, ^{137}Cs, and ^{210}Po. The ^{210}Po concentrations were not notably different from the values obtained in Finland 40 years earlier.

In short, the ^{210}Pb content of Arctic lichens varies from about 100 to 300 Bq kg^{-1} dry weight, with the ^{210}Po almost in secular equilibrium with ^{210}Pb. These levels are not insignificant, compared to the ^{137}Cs levels from fallout, especially when one considers that ^{210}Po, an alpha emitter, could be 10–20 times more radiotoxic than ^{137}Cs for the same level of activity. Apart from a small temporary increase during the period of intensive nuclear weapons testing in the 1960s, the ^{210}Pb levels appear to have been constant in time over the past 130 years.

Radionuclide Levels in *Rangifer tarandus*

^{137}Cs

Monitoring of radiocesium in the caribou and Inuit of Alaska began in 1962. At that time, Hanson and Palmer [18] observed a close correlation between body burdens in animals and in people over the next 3 years. In a later paper, Hanson [8] established that there was a clear annual cycle in the ^{137}Cs levels in caribou flesh, with low values occurring in the fall months and highest values in the spring month after feeding

Radiation Effects on Caribou and Reindeer. Table 2 Activity concentrations of ^{90}Sr, ^{137}Cs, and ^{210}Po in the living part of *Cladonia arbuscula* at different locations in Vågå and Østre Namdal (Bq kg^{-1} DM)

District	Location	Sampling date	^{90}Sr	^{137}Cs	^{210}Po
Vågå	1	August 2001	9.1 ± 1.1	3470 ± 280	121 ± 4
	2	August 2001	12.1 ± 1.5	1,460 ± 120	-
	3	August 2001	-	1,115 ± 96	104 ± 3
	7	August 2001	22.6 ± 2.8	1,910 ± 160	192 ± 6
	11	August 2001	12.0 ± 1.5	3,060 ± 250	70 ± 2
	12	September 2002	-	1,890 ± 160	212 ± 5
Østre namdal	D-2	September 2001	6.0 ± 0.7	1,930 ± 160	119 ± 3
	D-4	September 2001	9.7 ± 1.2	1,380 ± 120	171 ± 4
	0	July 2003	7.9 ± 1.0	3,180 ± 250	111 ± 3
	1	July 2003	-	3,510 ± 270	154 ± 3
	S-1	July 2003	5.5 ± 0.7	1,430 ± 110	-
	J-3	July 2003	-	1,570 ± 120	151 ± 4

on lichens over the winter. The highest value in caribou meat occurred during the period 1964–1972, with spring maxima reaching about 7,000 Bq kg^{-1} dry weight during some years.

During the early 1960s, Norway began investigations of possible high exposures to ^{137}Cs in the Sami population of Finnmark, due to substantial fallout registered in this region and due to the habits of the reindeer breeders [19]. They reported that radiocesium levels in reindeer meat had decreased from a high of 3,000 Bq kg^{-1} wet weight in 1966 to a value of 350 Bq kg^{-1} by 1983. This implies a T_{eff} of about 7 years for ^{137}Cs in reindeer meat. Rissanen and Rahola [20] have published similar data for reindeer in Finland.

The Chernobyl accident of 1986 introduced a huge flux of radiocesium fallout into northwestern Europe, which had a profound effect on the lichen → reindeer → food chain. Fallout in some parts of Scandinavia exceeded 60,000 Bq m^2. Åhman and Åhman [21] reported levels of 20,000 Bq kg^{-1} wet weight in Swedish reindeer in the year of the accident, and values as high as 80,000 Bq kg^{-1} the following year. The results showed a strong seasonality, with the lowest values in September and highest from January through April. Åhman and Åhman followed the decline in ^{137}Cs concentrations from 1986 to 1992, and derived effective halftimes of 2.3–5.0 years, depending on seasonality and locations. These halftimes are significantly lower than the values obtained from global nuclear weapons fallout.

The impact of Chernobyl fallout was much less in North America. Using the signature from ^{134}Cs (found in reactor emissions but not nuclear weapons fallout), Macdonald et al. [22] estimated that Chernobyl fallout contributed only an additional 10–20% to the radiocesium burdens in Canadian caribou herds. White et al. [12] predicted that the impact on Alaskan herds could have been as high as 75%.

Macdonald et al. [22] recently published a comprehensive review of all radiocesium data in caribou and reindeer across Canada, Alaska, and Greenland over the 40-year period from 1960 to 2000. Canada began sampling of caribou meat in 1963 onward, with measurements in northern peoples following shortly thereafter. The program was largely terminated after 1969, but was restarted after the Chernobyl accident of 1986 and continued sporadically throughout the 1990s. Concentrations of ^{137}Cs in some Canadian caribou herds reached levels of 2,000–3,000 Bq kg^{-1} in the 1960s, with one value of 6,400 Bq kg^{-1}. At the time of the Chernobyl accident, there were still some Canadian caribou showing ^{137}Cs concentrations above 1,000 Bq kg^{-1}. By the late 1990s, levels had decreased to a few hundred Bq kg^{-1} at most.

Figure 6 compares radiocesium levels in the various herds and demonstrates how they changed over a 20-year period from the mid-1960s to the mid-1980s. Figure 7 shows the decrease in radiocesium levels from the height of nuclear testing to the late 1990s. A fit to the data yielded an effective half-life of 6.1 years – not out of line with other estimates. Rissanen and Rahola [23] derived ecological half-lives for ^{137}Cs in reindeer meat of 4.9 ± 1.1 years in western Russia, 8.3 ± 4.7 years in eastern Russia, 5.4 ± 1.1 years in Finland, and 7.2 ± 1.3 years in Norway.

A similar review of radiocesium data in reindeer in the Eastern Hemisphere is available in the 1998 assessment report of the Arctic Monitoring and Assessment Programme (AMAP) [24]. Figure 8 shows the time trends for ^{137}Cs in caribou from 1960 to 1995 for five regions in Eurasia – Arctic Norway, Arctic Finland, Greenland, western Russia, and eastern Russia. The trends are quite similar to those in North America, with high values during the period of intensive atmospheric weapons testing in the 1960s followed by a gradual decline toward the present. The spike from the Chernobyl accident in 1986 is much more evident in the European data than the North American data. The map in Fig. 9 shows the average concentrations of ^{137}Cs in caribou and reindeer meat after 1990 at locations throughout the circumpolar region.

A number of studies have been conducted on the uptake, tissue distribution, and retention time of ^{137}Cs in caribou and reindeer. Hollemann et al. [25] injected experimental reindeer with radiocesium and also fed reindeer with lichens containing known radiocesium concentrations. They obtained a radiocesium absorption factor of 0.24 ± 0.031 for reindeer and retention times varying from 7 days in summer to 18 in winter. Applying these results to radiocesium levels in caribou in late spring, they estimated a lichen consumption rate of 3 kg dry weight per day.

Macdonald et al. [22] reported results for ^{137}Cs concentrations in caribou liver, kidney, and heart.

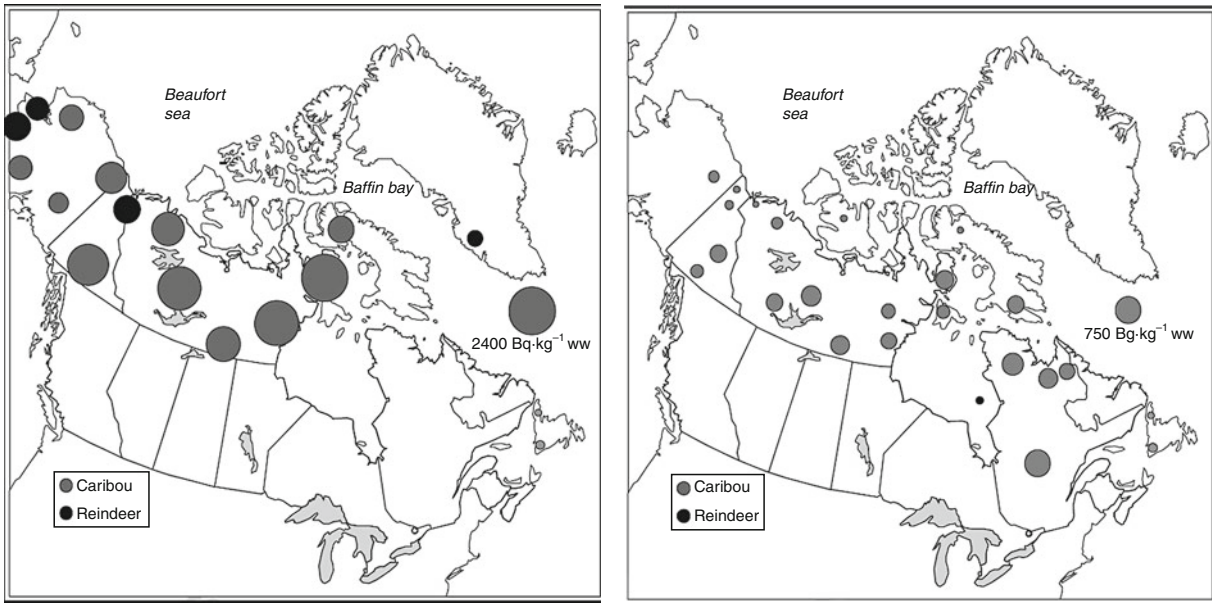

Radiation Effects on Caribou and Reindeer. Figure 6
Spatial distribution of ^{137}Cs in North American caribou and reindeer during the 1960s (*left*) and the 1980s (*right*). The area of each circle is proportional to the pooled mean of all winter/spring concentrations for a given herd during the decade (From Macdonald et al. [22])

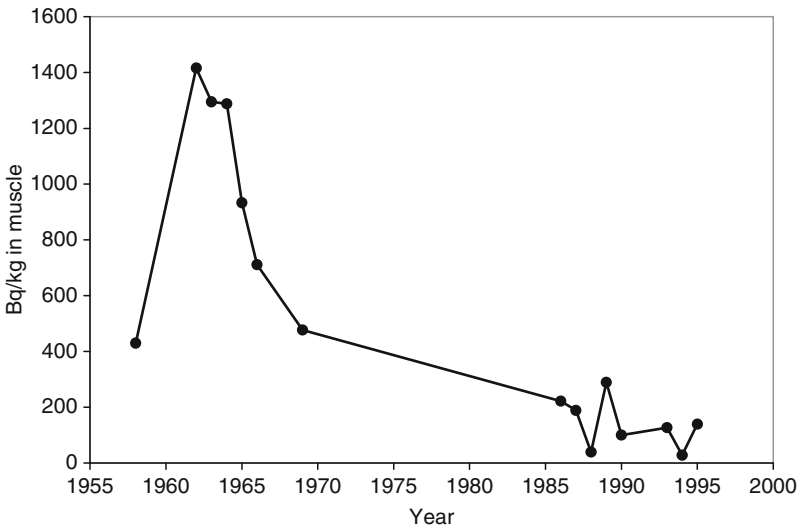

Radiation Effects on Caribou and Reindeer. Figure 7
Decline in ^{137}Cs concentrations in caribou muscle of Canadian herds from the 1960s to the 1990s. Each circle represents the geometric mean concentration of ^{137}Cs for all caribou herds in a given calendar year (Based on data from Macdonald et al. [22])

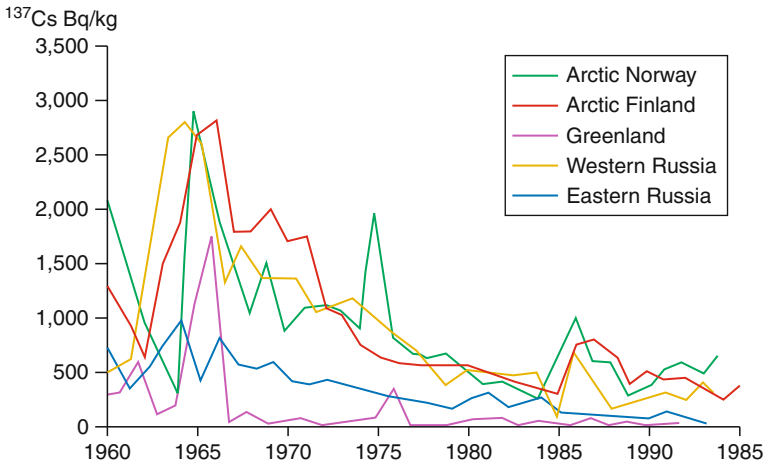

Radiation Effects on Caribou and Reindeer. Figure 8
Changes with time in activity concentration of ^{137}Cs in reindeer meat in Arctic Norway, Arctic Finland, Greenland, and Arctic Russia (From AMAP [24])

In general, ^{137}Cs concentrations were up to 30% higher in kidney than in muscle, whereas values in liver averaged about half those in muscle. In the three herds for which heart tissue was analyzed, the ^{137}Cs concentrations in heart were slightly lower than that in skeletal muscle. Macdonald et al. did not observe any significant correlation between ^{137}Cs concentration and age of the animals.

^{90}Sr

Much less has been reported on ^{90}Sr in caribou and reindeer. Certainly, ^{90}Sr was spread worldwide by global fallout in approximately the same amount as radiocesium. Like cesium, strontium can be transferred through the lichen → caribou → human food chain. However, strontium tends to be more mobile in the environment, and is not retained to the same degree in lichens. Being a chemical analog of calcium, strontium tends to accumulate in the bones of caribou and reindeer, which are not part of the human diet. Hence, less attention has been devoted to this radionuclide in Arctic food chains.

In 1962, Shulert [26] reported measurements of ^{90}Sr in the antlers and bones of Alaskan caribou. He obtained an average value of 7.7 Bq g^{-1} Ca for antlers, and values of 6.6 and 5.8 Bq g^{-1} Ca for the bones of two different caribou.

^{210}Pb and ^{210}Po

The accumulation of the naturally occurring radionuclides ^{210}Pb and ^{210}Po have been studied extensively in caribou and reindeer as well as in lichens. During the 1960s, ^{210}Pb and ^{210}Po were measured in Alaskan caribou by Beasely and Palmer [13], Blanchard and Kearney [27], and Blanchard and Moore [28]. They were also measured in Scandinavian reindeer by Kaurenen and Miettinen [14] and by Perrson [16]. More recently, results have been reported for Canadian caribou by Macdonald et al. [29] and by Thomas et al. [30]. These data are summarized in Table 3.

It is apparent from Table 3 that there is a major redistribution of ^{210}Pb and ^{210}Po within the body of the animal, with ^{210}Pb concentrating primarily in bone and ^{210}Po in soft tissues, particularly liver and kidney. This is quite different from the situation in the lichens, where ^{210}Po is nearly in secular equilibrium with ^{210}Pb (Table 1). Data from Alaska and Scandinavia are quite similar to one another, but the Canadian values are consistently higher. This may be due to a number of factors. The air concentrations of ^{210}Pb can build up to higher levels over the large Canadian land mass than over Alaska or Scandinavia which are more influenced by coastal air currents. Also, the ^{137}Cs levels in caribou have

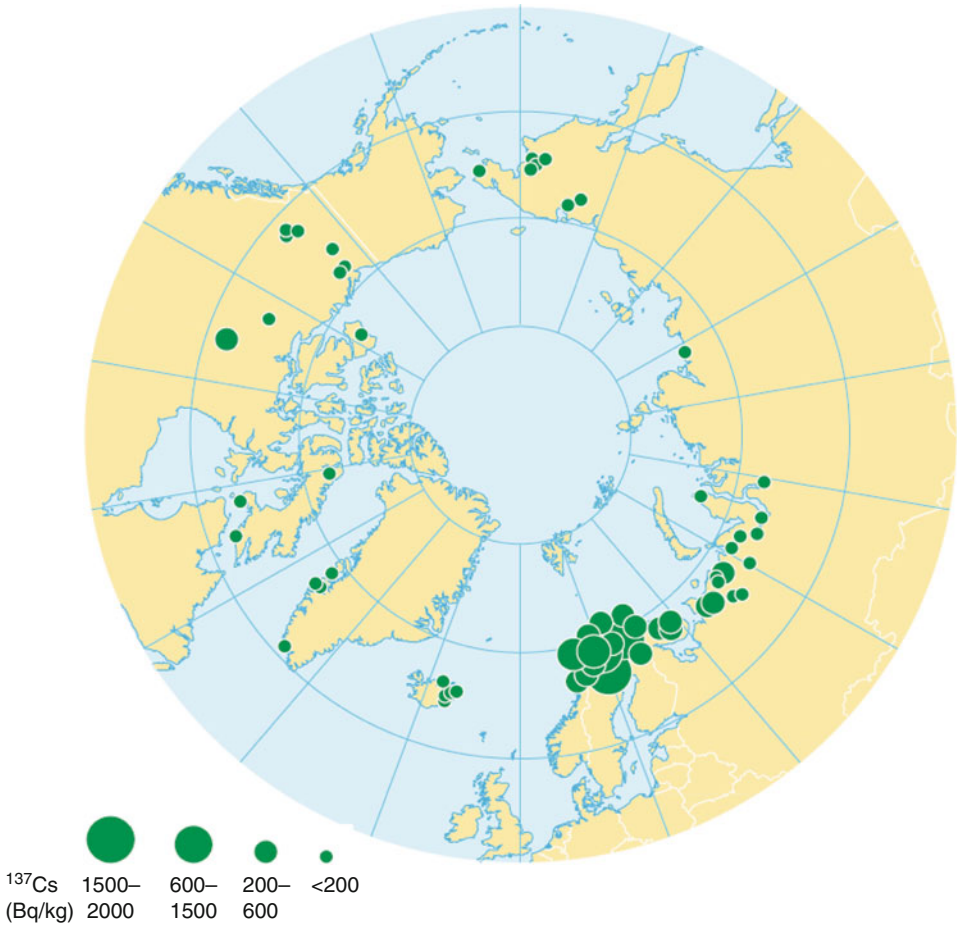

Radiation Effects on Caribou and Reindeer. Figure 9
Average activity concentrations of ^{137}Cs in reindeer meat after 1990 (From AMAP [24])

been consistently higher over Canada than Alaska (Figs. 4 and 5), which indicates differing deposition patterns and uptake by vegetation.

Major variations in ^{210}Pb and ^{210}Po concentrations were observed among different caribou herds in Canada. Macdonald et al. reported [29] ^{210}Pb concentrations in bone from the high Arctic Islands that were an order of magnitude less than in the central Arctic. A more detailed comparison is available from Thomas et al. [30], who studied complete tissue distributions of ^{210}Pb and ^{210}Po in 24 caribou taken by local hunters in each of the two Arctic communities – Baker Lake (Qamani'tuaq) in Nunavut Territory and Snowdrift (Łutsel K'e) in the Northwest Territories. Baker Lake lies in the tundra and relies on the Wager Bay and Kaminuriak herds; Snowdrift is located in boreal and scrub forest, and relies on caribou largely from the Beverly herd. Their results are summarized in Table 4. The concentrations in Baker Lake caribou were in most cases about twice those in Snowdrift caribou.

^{210}Pb and ^{226}Ra

Blanchard and Moore [28] reported measurements of ^{210}Pb and ^{226}Ra from five archived caribou bone samples collected in Canada before 1951. The ^{210}Pb concentrations in pre-1951 bone (240 ± 209 Bq kg^{-1}) were

Radiation Effects on Caribou and Reindeer. Table 3 A summary of ^{210}Pb and ^{210}Po measurements (Bq kg^{-1}) in caribou tissues. Standard deviations are given in brackets

Radionuclide and location	Muscle	Liver	Kidney	Bone
LEAD-210				
Alaska 1960s [13]	1.1	48 (27)	19 (3)	161 (35)
Alaska 1960s [28]	–	–	–	187 (85)
Alaska 1960s [27]	0.34 (0.12)	–	–	172 (67)
Finland 1960s [14]	0.22 (0.08)	25 (18)	–	169 (29)
Sweden 1970s [16]	0.48	26	10	192
Canada 1990s [29]	–	187 (168)	56 (21)	664 (308)
Canada 1990s [30]	–	136 (66)	71 (26)	793 (419)
POLONIUM-210				
Alaska 1960s [13]	13 (3)	171 (27)	145 (16)	140 (42)
Alaska 1960s [27]	7.5 (4.8)	–	–	131 (53)
Finland 1960s [14]	5.8 (3.9)	103 (59)	–	76 (2)
Canada 1990s [29]	–	431 (281)	227 (163)	387 (232)
Canada 1990s [30]	16 (9)	299 (147)	214 (108)	403 (266)

Radiation Effects on Caribou and Reindeer. Table 4 Concentrations of ^{210}Pb and ^{210}Po in the organs of caribou taken near two northern Canadian communities, from Thomas et al. [30]. Standard deviations are given in brackets

	Baker lake		Snowdrift	
Organ	Pb 210	Po 210	Pb 210	Po 210
Bone	1,023 (402)	531 (235)	562 (120)	274 (125)
Rumen	103 (24)	191 (39)	77 (16)	166 (54)
Kidney	84 (18)	259 (88)	57 (19)	168 (62)
Liver	158 (22)	374 (122)	113 (62)	224 (82)
Muscle		17 (8)		15 (5)
Placenta	2.7 (0.8)	26 (7)	1.9 (0.6)	11 (3)
Fetus	11 (7)	5.8 (2.0)	6.5 (1.9)	2.3 (0.6)
Fetal liver	25 (11)	16 (15)	10 (5)	35 (19)

not greatly different from the Alaskan data of 1965–66 (187 ± 85 Bq kg^{-1} in Table 3). These results confirm that the ^{210}Pb in the lichen → caribou food chain is likely of natural rather than anthropogenic origin. The concentrations of ^{226}Ra in the bone (6.5 ± 3.1 Bq kg^{-1}) are much lower, demonstrating that ^{210}Pb in bone is not supported by ^{226}Ra decay but originates from radon gas in the atmosphere.

^{40}K

Macdonald et al. [22] reported potassium 40 concentrations in Canadian caribou taken since 1986.

The mean concentrations and standard deviations in different organs were as follows:

Muscle	109 (22)
Liver	11 (26)
Kidney	122 (34)
Heart	93 (10)

The values were quite similar for all animals and organs, which is not surprising since potassium is homeostatically regulated in the bodies of animals.

Effects in *Rangifer tarandus*

The question now arises as to what are the health effects, if any, to the animals from these radionuclide levels. This question is addressed here in three steps. First, absorbed doses in organs and tissues are calculated based on the measured radionuclide concentrations. Then, the literature is surveyed to ascertain whether radiation effects might be expected at these levels of dose. Finally, a number of studies are examined from areas of high radioactive fallout, which suggest possible effects on caribou and reindeer.

Radiation Doses to Caribou and Reindeer

The primary factor governing radiation effects in living organisms is the absorbed dose, defined as the amount of radiation energy absorbed per kg of tissue. The SI unit for absorbed dose is the Gray (Gy), equal to 1 J of energy absorbed per kg. A quantity often used in human assessments is the equivalent dose which recognizes that some types of ionizing radiation are more detrimental than others. The equivalent dose in Sv is defined as absorbed dose in Gy multiplied by a radiation weighting factor equal to one for beta and gamma radiation, 20 for alpha radiation, 5 for protons, and 5–20 for neutrons.

A simple calculation of the absorbed dose in an organ or tissue relies can be carried out with the assumption that the radioactivity is uniformly distributed throughout an infinite medium. This assumption requires only that the range of the emitted radiation is small compared to the dimensions of the organ. It works well for alpha and beta radiation, but may slightly overestimate the dose from gamma radiation, some of which may escape from the tissue. According to this assumption, the amount of radiation energy absorbed per unit volume of tissue must equal the amount of energy generated per unit volume, or else there would be a net flow of energy from one part of the tissue to another. The energy generated per unit volume is readily calculated from the radionuclide concentration in Bq kg^{-1} and the expression for absorbed dose becomes

Dose (mGy $year^{-1}$) = radionuclide concentration (Bq kg^{-1}) $\times$ radiation energy (MeV) $\times$ 1.602 $\times$ 10^{13} (joules MeV^{-1}) $\times$ 86,400 (s day^{-1}) $\times$ 365.25 (d $year^{-1}$) $\times$ 1,000 (mGy Gy^{-1}).

The amount of radiation energy (MeV) per disintegration is given below for each of the relevant radionuclides considered here:

^{137}Cs	0.937 (mixed β and γ)
^{210}Pb	0.753 (mixed β and γ; includes decay of ^{210}Bi)
^{210}Po	5.305 (pure α)
^{40}K	0.570 (mixed β and γ)

The resulting doses to caribou organs and tissues are shown in Table 5. The measured distributions of ^{210}Pb and ^{210}Po in caribou tissues from Baker Lake (Table 4) were used, since these data have some of the highest values in Canadian caribou. Since ^{137}Cs concentrations in meat have varied widely over time and location, a range of values has been assumed for this radionuclide. The natural radionuclide ^{40}K was taken to be present in all tissues at about 100 Bq kg^{-1}. It was assumed here that all measured concentrations represent a steady state and are maintained at these levels for an entire year. Lead and polonium are grouped together in this table, since they are closely correlated. Cesium and potassium are grouped together because of their chemical similarity.

In the absence of fallout from nuclear weapons testing, the greatest contributors to doses in caribou have been the naturally occurring radionuclides – ^{210}Pb and ^{210}Po. The organs most greatly affected are bone, liver, and kidney, with doses to muscle an order of magnitude lower. It is notable that doses to placenta, fetus, and fetal liver are quite low, indicating that the lead and polonium activities are not passing on

Radiation Effects on Caribou and Reindeer. Table 5 Annual doses to caribou organs and tissues based on the measured concentrations of radionuclides

Organ	Concentrations (Bq kg^{-1})		Doses (mGy year^{-1})		
	Pb 210	Po 210	Pb 210	Po 210	Pb + Po
Bone	1,023	531	3.90	14.24	18.14
Kidney	84	259	0.32	6.95	7.27
Liver	158	374	0.60	10.03	10.63
Muscle	–	17	–	0.46	0.46
Placenta	2.7	26	0.01	0.70	0.71
Fetus	11	5.8	0.04	0.16	0.20
Fetal liver	25	16	0.10	0.43	0.52
	Cs 137	K 40	Cs 137	K 40	Cs + K
Muscle	80,000[a]	100	378.95	0.57	379.52
	20,000[b]	100	94.74	0.57	95.31
	7,000[c]	100	33.16	0.57	33.73
	3,000[d]	100	14.21	0.57	14.78
	1,000[e]	100	4.74	0.57	5.31
	200[f]	100	0.95	0.57	1.52

[a]Highest Swedish value from Chernobyl
[b]Typical Swedish value from Chernobyl
[c]Highest single value in North America
[d]Highest herd values in Canada, 1960s
[e]Highest herd values in Canada, 1980s
[f]Highest values in Canada, today (2010)

significantly to the developing fetus. The doses from ^{137}Cs range from a high of over 300 mGy year^{-1} (in Scandinavian reindeer after the Chernobyl accident) down to present-day values of about 1 mGy year^{-1} and approaching the doses from naturally occurring ^{40}K.

Dose–Effect Relationships in Animals

In recent years, there has been a paradigm shift in the protection of nonhuman biota from radiation. Before the early 1990s, it was generally assumed if radiation standards were set low enough to protect humans, then all other species would automatically be protected. The primary goal in radiation standard-setting is the protection of individual humans from stochastic effects such as cancer, where the risks are assumed to be directly proportional to radiation dose with no threshold (linear no threshold or LNT hypothesis). For nonhuman biota, it is the survival of the species (or the local subpopulation of that species) that is important. This places the focus on deterministic effects, such as cell death and reproductive failure, that will definitely occur but not below a certain dose threshold. This logic leads to the conclusion that other species can withstand more radiation than humans.

Today, there is an increased awareness of situations where the old paradigm may break down, either because there are no humans present in the immediate environment or because a certain species is supersensitive to the effects radiation at some stage in its life cycle. The lichen–caribou/reindeer ecosystem may represent one such situation. These animals wander over large stretches of remote territory which may be heavily contaminated by radioactive fallout.

Humans may not be immediately exposed to these high-contamination levels. In the previous section, it was seen how radionuclide concentrations can build up to high levels in caribou and reindeer.

In the past 2 decades, there has been a considerable effort to establish dose criteria that will protect all species. In a recent review, Real et al. [31] scanned a database of over 1,000 references on radiation effects in plants and animals. They concluded that no effects could be observed in plants, fish, or mammals for dose rates less than 0.1 mGy h^{-1} (1 Gy $year^{-1}$), but that effects were becoming clear for lifetime exposures at dose rates above 1 mGy h^{-1} (10 Gy $year^{-1}$). UNSCEAR [32] concluded that irradiation at chronic dose rates of 1 mGy day^{-1} to even the most radiosensitive species does not appear likely to cause observable changes in terrestrial animal populations.

Historically, most of the ^{137}Cs doses in caribou and reindeer have been well below these threshold values (Table 5). However, doses in Scandinavian reindeer did rise to several hundred mGy $year^{-1}$ after the Chernobyl accident and were approaching threshold values.

These results should be evaluated in light of the doses from the natural radionuclides ^{210}Pb and ^{210}Po, which can reach 18 mGy $year^{-1}$ in bone and 7–10 mGy $year^{-1}$ in kidney and liver. Although well below the thresholds noted above, most of this dose is due to alpha radiation from ^{210}Po, known to be more damaging than beta or gamma radiation for the same dose. The choice of an alpha radiation weighting factor for nonhuman biota has been the topic of much discussion. The value of 20 used in human dosimetry is probably too high, since it was designed to protect against stochastic effects such as cancer. Chambers et al. [33] recommend an alpha weighting factor of 5 for nonhuman biota, with a range of 1–10. Thomas et al. measured the relative biological effectiveness of ^{210}Po alpha radiation in comparison to 250 kVp X-rays in bovine [34] and porcine [35] endothelial cells, and found values up to 10 for cell survival and clonogenic assay. These are large mammals and may exhibit responses to radiation that are similar to caribou. If a weighing factor of 10 were applied to the ^{210}Po doses in Table 5, then the equivalent doses to bone, kidney, and liver from this natural radionuclide could exceed 100 mSv $year^{-1}$. Since caribou have flourished for tens of thousands of years with this background radiation dose, it is unlikely that a similar dose from ^{137}Cs in the short term would have major consequences for the health of the animals.

Possible Effects in Reindeer

It is difficult to establish experimentally whether these borderline radiation doses are having any measurable effect on caribou and reindeer populations. Most of the knowledge on radiation effects in animals is based on laboratory experiments with large numbers of small mammals such as mice and rats. It is not feasible to carry out similar experiments on the numbers of large mammals that would be needed to establish statistically meaningful results. The best that can be done is to examine natural populations that have been exposed to high levels of radioactivity.

There is some evidence of chromosome aberrations in Norwegian reindeer calves exposed to fallout from the Chernobyl accident. In a study of peripheral blood lymphocytes from 24 calves taken from high-fallout areas in Norway and 26 calves from low-fallout areas, Røed et al. [36] found three dicentrics, two rings, and three translocations in calves from the exposed area, but no dicentrics or rings and only one translocation from the control area. Dicentrics and rings are two types of chromosome aberrations most frequently associated with radiation exposure. The authors cautiously conclude "that certain genetic effects have occurred as a result of the Chernobyl accident in Norwegian reindeer in the most contaminated areas."

In a later study, Røed and Jacobsen [37] reported results from 192 Norwegian reindeer in four herds heavily affected by the accident and three herds only lightly affected. They found significant heterogeneity in the distribution of chromosome aberrations between herds, but concluded that the pattern of chromosome aberration frequencies was not related to the variation in radiocesium exposure. They did confirm that within the most contaminated areas, reindeer born in 1986 showed significantly more chromosome aberrations than those born both before and after 1986.

Impacts on Human Populations

Given the close interrelationship between humans and reindeer/caribou, it is fitting to conclude this chapter

with a brief discussion of the impacts on human populations dependent on these animals. Tracy et al. [38] published an assessment of all radiocesium body burden measurements carried out from 1963 to 1990 on indigenous peoples of the Canadian Arctic. The results varied widely with time, geographical location, age, and sex. Average radiocesium concentrations in people for each community were strongly correlated with the concentrations in local caribou herds available in the local community. A comparison of results from the 1960s and 1980s showed that body burdens in people were declining faster than the radiocesium levels in caribou. The authors attributed this rapid decline to a shift from traditional foods to market foods during this period. The cumulative radiocesium doses in people over the entire period varied from 0.3 to 40 mSv (average for each community) with an Arctic-wide average of 12 mSv. It is unlikely that any health effects to humans would be observable at these doses, given that the average worldwide exposure to natural background radiation is about 2 to 3 mSv year^{-1}.

With regard to exposures from ^{210}Po in caribou meat, Thomas [39] estimated average radiation doses of 0.3 mSv year^{-1} and 0.4 mSv year^{-1} to residents in the two communities studied. She obtained the doses to the caribou and wolves to vary from 7 to 20 mSv year^{-1}, assuming a weighting factor of 20 for ^{210}Po alpha radiation.

Because of concerns about heavy Chernobyl fallout over northern Europe, a number of epidemiological studies have carried out on reindeer herders. Kurttio et al. [40] examined the cancer incidence in a cohort of 34,653 people from northern Finland. A total of 1,580 cancer cases were observed versus 1,948 expected on the basis of incidence rates in Northern Finland [standardized incidence ratio (SIR) = 0.81 with 95% confidence interval (CI) = 0.77–0.85]. No association between the lifetime cumulative radiation exposure from global radioactive fallout and cancer incidence in the Arctic population was found.

With regard to the effects of fallout from atmospheric weapons testing before the Chernobyl accident, Wiklund et al. [41] studied cancer incidence from 1961 to 1984 in a cohort of 2,034 Swedish reindeer breeders and found 100 cancer cases observed versus 163 expected. No increased risk was found for the cancer sites considered to be most sensitive to radiation.

From the above, it appears that no observable health effects are likely to occur in human populations dependent on caribou or reindeer. Perhaps the greatest impacts are economic and cultural. In the year following the Chernobyl accident, 73,000 reindeer had to be destroyed in Sweden alone because of high radiocesium levels. This placed a severe economic burden on the Sami people and on the national governments who had to compensate the Sami for losses.

Although the actual amounts of Chernobyl fallout in Canada were minimal, fears of radioactive contamination likely contributed to the decline in traditional food consumption of many northern Canadians. The replacement of traditional foods by market foods places a greater economic burden on northerners who are eking out a marginal existence at the best of times. Futhermore, the hunting and sharing of caribou meat has played a major role in the culture of Canada's aboriginal peoples for thousands of years. This perspective can best be summed up in the words of an Inuit caribou hunter, Pauloosie Kilabuk, from Nunavut Territory:

> I don't hunt just for me. I hunt for other people. I go out and get a caribou and feel good about myself. It keeps me close to the men I hunt with. I make my parents, kids, relatives and friends happy because they don't have caribou sometimes, and we all come together and share the meat. Caribou is more important than seal to keep my family and community together. With a caribou you can get four or five families together. What is a community feast without a caribou?

Future Directions

Radiocesium levels became elevated in the environment during the latter half of the twentieth century as a result of atmospheric nuclear weapons testing and the Chernobyl nuclear reactor accident. This fallout has been persistent in northern ecosystems, particularly the lichen → caribou/reindeer → human food chain. Radiocesium is disappearing from this system with an effective halftime of 5–10 years and has now decreased to insignificant levels, expect for occasional pockets of high contamination in some parts of northern Europe. Radiocesium contamination of caribou/reindeer will not be considered a problem in the twenty-first

century, unless there is another major nuclear event comparable to Chernobyl. If this should occur, there will be a large body of available knowledge gleaned from the twentieth-century investigations.

High levels of the natural radionuclides ^{210}Pb and ^{210}Po have always been present in caribou/reindeer. The available evidence shows that these levels have been constant, at least for the past century. However, global warming, especially in polar regions, could affect this situation. Melting permafrost could lead to higher radon emanation rates from soil, and this could lead to a buildup of higher ^{210}Pb and ^{210}Po levels in the environment.

These natural radionuclides should continue to be monitored in the environment generally and in the lichen → caribou/reindeer → human food chain particularly as harbingers of climate change.

The question of possible radiation effects in caribou/reindeer cannot be answered unequivocally at present. Recent levels of radioactivity have been just below the known threshold values for possible effects. It is possible that contaminants including radionuclides could interact with other stressors to weaken the survivability of caribou and reindeer in the wild. This complex ecosystem should be the subject of ongoing study.

Bibliography

Primary Literature

1. Flexner SB, Hauck LC (eds) (1987) The Random House Dictionary of the English Language, 2 (unabridged)th edn. Random House, New York, pp 315–316
2. Department of the Environment and Natural Resources, Government of the Northwest Territories (September 2009). www.enr.gov.nt.ca. See also the globe and mail, Wednesday, 5 May 2010, p A4
3. United Nations Scientific Committee on the Effects of Atomic Radiation (UNSCEAR) (2004) Exposures of workers and the public from various sources of radiation. Report to the general assembly
4. Cornett J, Tracy B, Kramer G, Whyte J, Moodie G, Auclair JP, Thomson D (2009) Polonium-210: lessons learned from the contamination of individual Canadians. Radiat Prot Dosim 134(3–4):164–166
5. Francis W, Chesters G, Haskin LA (1970) Determination of the ^{210}Pb mean residence time in the atmosphere. Environ Sci Technol 4:586
6. Gorham E (1959) A comparison of lower and higher plants as accumulators of radioactive fallout. Can J Bot 37:327
7. Hofmann W, Attarpour N, Lettner H, Turk R (1993) ^{137}Cs concentrations in lichens before and after the Chernobyl accident. Health Phys 64(1):70–73
8. Hanson W (1982) ^{137}Cs concentrations in northern Alaskan Eskimos, 1962-79: Effects of ecological, cultural, and physical factors. Health Phys 42(4):433–447
9. White RG, Holleman DF, Allaye-Chan AC (1986) Radiocesium concentrations in the lichen-reindeer/caribou food chain: before and after Chernobyl. Rangifer Appendix 1:24–29
10. Hutchison-Benson E, Svoboda J, Taylor HW (1985) The latitudinal inventory of ^{137}Cs in vegetation and topsoil of Northern Canada, 1980. Can J Bot 63:784–791
11. Taylor HW, Hutchison-Benson E, Svoboda J (1985) Search for latitudinal trends in the effective half-life of fallout ^{137}Cs in vegetation of the Canadian Arctic. Can J Bot 63: 792–796
12. Holtzman RB (1966) Natural levels of lead-210, polonium-210 and radium-226 in humans and biota of the Arctic. Nature 210:1094–1097, June 11
13. Beasley TM, Palmer HE (1966) Lead-210 and polonium-210 in biological samples from Alaska. Science 152:1062–1063
14. Kauranen P, Miettinen JK (1969) ^{210}Po and ^{210}Pb in the Arctic food chain and the natural radiation exposure of Lapps. Health Phys 16:287–295
15. Jaworowski Z (1966) Temporal and geographical distribution of radium D (lead-210). Nature 212:886–889
16. Perrson RBR (1973) Stable lead and ^{210}Pb in the food chain lichen-reindeer-man. IAEA-SM-175/18
17. Skuterud L, Gwynn JP, Gaare E, Steinnes E, Hove K (2005) ^{90}Sr, ^{210}Po and ^{210}Pb in lichen and reindeer in Norway. J Environ Radioact 84(3):441–456
18. Hanson WC, Palmer HE (1965) Seasonal cycle of ^{137}Cs in some Alaskan natives and animals. Health Phys 11: 1401–1406
19. Westerlund EA, Berthelsen T, Bertig L (1987) Cesium-137 body burdens in Norwegian Lapps, 1965-1983. Health Phys 52(2):171–177
20. Rissanen K, Rahola T (1990) Radiocesium in lichens and reindeer after the Chernobyl accident. Rangifer (Special issue 3): 55–61
21. Åhman B, Åhman G (1994) Radiocesium in Swedish reindeer after the Chernobyl fallout: seasonal variations and long-term decline. Health Phys 66(5):505–512
22. MacDonald CR, Elkin BT, Tracy BL (2007) Radiocesium in caribou and reindeer in northern Canada, Alaska and Greenland from 1958 to 2000. J Environ Radioact 93:1–25
23. Rissanen K, Rahola T (1996) Radioactivity levels in foodstuffs in Finnish Lapland. In: Proceedings of the 11th Meeting of the Nordic Society for Radiation Protection, Reykjavik
24. Arctic Monitoring and Assessment Programme (1998) AMAP Assessment report: arctic pollution issues, chapter 8. Radioactivity. ISBN 82-7655-061-4
25. Holleman DF, Luick JR, Whicker FW (1971) Transfer of radiocesium from lichen to reindeer. Health Phys 21(5): 657–666

26. Shulert AR (1962) Alaskan Eskimos for whom the caribou is a dietary staple have a high strontium-90 concentration. Science 136(3511):146–148
27. Blanchard RL, Kearney JW (1967) Natural radioactivity and ^{137}Cs in Alaskan caribou and reindeer samples. Environ Sci Technol 1:932–939
28. Blanchard RL, Moore JB (1970) ^{210}Pb and ^{210}Po in tissues of some Alaskan residents as related to consumption of caribou or reindeer meat. Health Phys 18:127–134
29. Macdonald CR, Ewing LL, Elkin BT, Wiewel AM (1996) Regional variation in radionuclide concentrations and radiation dose in caribou (*Rangifer tarandus*) in the Canadian Arctic; 1992-94. Sci Total Environ 182:53–73
30. Thomas P, Sheard JW, Swanson S (1994) Transfer of ^{210}Po and ^{210}Pb through the lichen-caribou-wolf food chain of northern Canada. Health Phys 66(6):666–677
31. Real A, Sundell-Bergman S, Knowles JF, Woodhead DS, Zinger I (2004) Effects of ionising radiation exposure on plants, fish and mammals: relevant data for environmental radiation protection. J Radiol Prot 24:A123–A137
32. United Nations Scientific Committee on the Effects of Atomic Radiation (UNSCEAR) (1996) Sources and effects of ionising radiation. Report to the general assembly, Supplement No. 46 (A/51/46), Annex: "Effects of Radiation on the Environment," United Nations Sales No. E96.IX.3)
33. Chambers DB, Osborne RV, Garva AL (2006) Choosing an alpha radiation weighting factor for doses to non-human biota. J Environ Radioact 87(1):1–14
34. Thomas PA, Tracy BL, Ping T, Wickstrom M, Sidhu N, Hiebert L (2003) Relative biological effectiveness (RBE) of ^{210}Po alpha-particles versus X-rays on the lethality of bovine endothelial cells. Int J Radiat Biol 79(2):107–118
35. Thomas PA, Tracy BL, Ping T, Baweja A, Wickstrom M, Sidhu N, Hiebert L (2007) Relative biological effectiveness of alpha radiation in cultured porcine aortic endothelial cells. Int J Radiat Biol 83(3):171–179
36. Røed KH, Eikelmann IMH, Jacobsen M, Pedersen Ø (1991) - Chromosome aberrations in Norwegian reindeer calves exposed to fallout from the Chernobyl accident. Hereditas 115(3):201–206
37. Røed KH, Jacobsen M (1995) Chromosome aberrations in Norwegian reindeer following the chernobyl accident. Mutat Res Lett 346(3):159–165
38. Tracy BL, Kramer GH, Zielinski JM, Jiang H (1997) Radiocesium body burdens in residents of northern Canda from 1963-1990. Health Phys 72(3):431–442
39. Thomas PA (1994) Dosimetry of ^{210}Po in humans, caribou, and wolves in northern Canada. Health Phys 66(6):678–690
40. Kurttio P, Pukkala E, Ilus T, Rahola T, and Auvinen A (2010) Radiation doses from global fallout and cancer incidence among reindeer herders and Sami in northern Finland. In: Proceedings of Third European IRPA Congress, 14—16 June, Helsinki, Finland
41. Wiklund K, Holm LE, Eklund G (1990) Cancer risks In Swedish Lapps who breed reindeer. Am J Epidemiol 132(6):1078–1082

Books and Reviews

Advisory Committee on Radiological Protection (2002) Protection of non-human biota from ionizing radiation. Canadian Nuclear Safety Commission INFO-0730

Arctic Monitoring and Assessment Programme (2002) AMAP Assessment 2002: radioactivity in the arctic. Available on-line from the AMAP web site http://www.amap.no. Accessed July 2010

Indian and Northern Affairs Canada (2003) Canadian arctic contaminants assessment report, ISBN-10-0662334663. Library of Congress TD182.4.N67 C36 2003

Indian and Northern Affairs Canada (2009) Canadian arctic contaminants heath assessment report. Available on-line at http://www.ainc-inac.gc.ca/nth/ct/ncp/pubs/har/har-eng.asp. Accessed July 2010

Muir DCG, Shearer RG, Van Oostdam J, Donaldson SG, Furgal C (2005) Contaminants in Canadian arctic biota and implications for human health: preface. Sci Total Environ 351–352:1–3

Thomas DJ, Tracy B, Marshall H, Norstrom RJ (1992) Arctic terrestrial ecosystem contamination. Sci Total Environ 122:135–164

United Nations Scientific Committee on the Effects of Atomic Radiation (UNSCEAR) (2006) Report to the general assembly, vol 1. Effects of ionizing radiation

Williams TM, Heard DC (1986) World status of wild Rangifer tarandus populations. Rangifer 1:19–28

Radiation in the Environment, Sources of

Edward J. Waller
University of Ontario Institute of Technology, Oshawa, ON, Canada

R

Article Outline

Glossary
Definition of the Subject and Its Importance
Introduction
Sources of Radioactivity in the Environment
Future Directions
Bibliography

Glossary

Anthropogenic Created or generated by human activity.

Atmosphere The term atmosphere derives from the Greek *atmosphaira* (atmos = vapor + sphaira = sphere) and on Earth is defined by seven layers

extending from the surface of the Earth as follows: troposphere, tropopause, stratosphere, stratopause, mesosphere, mesopause, and thermosphere. Above the thermosphere is normally termed exoatmospheric.

Atoll String of tightly packed small coral islands that enclose or almost enclose a shallow lagoon.

Biocenosis A group of interacting organisms that live in a particular habitat forming an ecological community.

Critical group The target population for an environmental dose assessment. Generally, the members of a population most sensitive to radiation exposure.

Cosmogenic Pertaining to origin, structure, and dynamic behavior of the universe.

Decay chain A series of radioactive transformations, starting with an initial radioisotope that decays into another radioisotope and so on, until a final stable end isotope is reached.

Environment Components of the Earth, and includes (a) land, water, and air, including all layers of the atmosphere; (b) all organic and inorganic matter and living organisms; and (c) the interacting natural systems that include components referred to in (a) and (b).

Half-life The time it takes for a large quantity of radioactive atoms to fall to half of their initial quantity.

HBRA High background radiation area. A region or locality which has levels of natural background radiation in excess of the current limit for radiation workers of 20 mSv a^{-1}. The highest of these areas may be termed very high background radiation areas (VHBRA) when their estimated potential public exposure may exceed 50 mSv a^{-1}.

HLNRA High levels of natural radiation area. Same as HBRA.

Isotope Atom with the same number of protons (Z) as another atom, but different number of neutrons (N), giving it a different atomic mass (A).

JCO Formerly the Japan Nuclear Fuel Conversion Co., a subsidiary of Sumitomo Metal Mining Co.

NORM Naturally occurring radioactive material.

TENORM Technologically enhanced NORM.

Primordial Existing from the beginning.

Pyrophoric A material which can spontaneously combust in air.

Radioactive Unstable isotope that decays by emitting ionizing radiation.

Radioisotope Radioactive isotope; also termed radionuclide.

Radionuclide Same as radioisotope.

RDD Radiological dispersal device.

RORSAT Radar Ocean Reconnaissance Satellite (USSR).

RTG Radioisotopic thermoelectric generator.

SNAP Systems for Nuclear Auxiliary Power.

Spallation A nuclear reaction in which a high energy particle strikes another particle and causes it to fragment into multiple pieces.

Terrestrial Pertaining to the Earth (or more generally, pertaining to land).

TNT Trinitrotoluene (chemical explosive).

Definition of the Subject and Its Importance

Radioactivity in the environment is ubiquitous. From the first moments of time during formation of the universe, elementary particles (protons, neutrons, and electrons) underwent nuclear reactions to produce elements and isotopes, forming all matter in the universe, on a time frame that extends billions of years. Elementary particles formed into nuclear configurations (atoms), consisting of protons and neutrons in the central core (nucleus) surrounded by electrons. By convention, configurations with the same number of protons in the nucleus are termed elements, which are the building blocks of all matter. All elements have members with varying numbers of neutrons in the nucleus, termed isotopes. Some configurations are stable, meaning that they had achieved an optimum number of protons and neutrons in the nucleus. Some configurations were formed with excess protons or excess neutrons in the nucleus, making them unstable. To become stable, these configurations release energy as particles, energy quanta or both. The release of energy as particles or quanta is termed radiation, and these isotopes are termed radioisotopes (or radionuclides). Thus, in the creation of the universe, as atoms formed into more complex structures, a certain amount of radioactive and nonradioactive material made up the structures. As a result, it may be speculated that most structures in the universe have varying levels of naturally occurring radioactive material, which was

incorporated into their formation from the beginning of time. The Earth, for example, is a planet consisting of large quantities of naturally occurring radioactive material.

In the past approximately 100 years, humans have learned to utilize the power of the atom for generation of electrical power, performing medical treatment and diagnosis, application to industrial techniques that are not readily achievable through other means, and for the production of weapons. All of these applications give rise to potential introduction of anthropogenic radioisotopes into the environment. The significance of radioisotopes in the environment is multi-faceted. Since radioisotopes were naturally ubiquitous from the beginning of time, it may be thought that evolution of life on Earth has been influenced, in part, by the natural radiation environment that all living organisms were, and are, exposed continuously. All sources of radiation can potentially produce a radiation dose and subsequent biological effect in both human and nonhuman biota. It is known that extremely large doses of radiation can be biologically harmful to living organisms. At low doses of radiation exposure, there is no consistent body of knowledge to describe the biological significance on living organisms. There exists evidence to suggest that low-level radiation exposure may be beneficial, and there is contradictory evidence to suggest that low-level radiation exposure may be harmful. As a result, it is important to continually assess and understand the sources of radiation that exist in the environment and to estimate exposure to human and nonhuman biota. One fact is certain: There will continue to be natural radiation sources in the environment that expose all living organisms on Earth, and in space radiation environments that will expose all future space explorers.

Introduction

Radioisotopes are fundamentally as old as the universe itself. However, the study of radioisotopes, radiation, and effects on the environment is a little over a century old. As such, environmental radioactivity as a science is a very young field dealing with very old phenomena as the Earth is estimated to be over 4.5 billion years old. It is well known that the Earth is rich in radioisotopes that occur naturally. In addition to the radioisotopes that made up the Earth from primordial formation, natural nuclear reactors existed on the Earth approximately 2 billion years ago, which produced radioactive by-products via nuclear fission of natural uranium. Also, it is also known that radioisotopes are produced on Earth via cosmic ray interactions in the atmosphere. Humans live in a complex radiation environment simply from natural sources, termed naturally occurring radioactive material (NORM). Early investigations in mining materials that contain radioisotopes produced some of the first anthropogenic sources introduced into the environment. Although these sources were natural in origin, their processing and accumulation are such that they do not strictly satisfy the condition of being purely natural, and are often called technologically enhanced naturally occurring radioactive materials (TENORMs). This category of environmental sources can come from many industries such as mining, fertilizer, pulp and paper, and petroleum. Another significant source of radionuclides detected in the environment is from nuclear weapons, specifically historical nuclear weapons testing. Many of the isotopes detectable at low levels in environmental samples are a direct result of nuclear weapons testing, and would not otherwise be present in environmental samples. A routine industrial-origin radionuclide source in the environment is from nuclear reactor operations. Nuclear reactors release low levels of radionuclides into the environment, as allowed by regulatory bodies. Nuclear reactor operations have the distinction of being one of the safest industries, and accidents are rare events. However, nuclear reactor accidents are another potential source of radionuclides in the environment. The only reactor accident that has introduced significant and widespread (compared to natural background) levels of radionuclides to the environment is from the Chernobyl NPP Unit 4 accident in the Ukraine. Commercially produced radioisotopes that may be introduced into the environment comprise the categories of medical and industrial radioisotopes. Medical radioisotopes are routinely released to the environment via nuclear medicine procedures, whereas industrial radioisotopes are typically only released when used in tracer studies. Lost or orphan sources comprise an increasingly more important sector of environmental radioactivity insofar as there are thousands of anthropogenic sources worldwide that are not

accounted for that either exist in the environment or may impact the environment. A final category of potential environmental source is that from a radiological dispersal device, or a "dirty bomb." This is a special case insofar as the use of radioisotopes as a weapon suggests targeting of both human and nonhuman biota.

The current breakdown in the USA of collective dose is shown in Fig. 1. This plot is demonstrative of the fact that natural background and medical exposure contribute the majority of dose to humans. It is worthy to note that the actual percentages will vary from country to country on a collective basis. In less technologically advanced countries, the natural radiation component will be much larger than depicted in Fig. 1.

The complex sources of radiation on Earth can be discussed in terms of naturally occurring radiation, radiation originating from nuclear technology origins, and enhanced radiation originating from nonnuclear technologies. The following sections detail the variety of sources of radiation that may have an impact on human and nonhuman biota.

Sources of Radioactivity in the Environment

Of primary importance to the study and early interest in environmental sources of radioactivity were the discovery of x-rays by Wilhelm Röntgen in 1895, radioactivity by Henri Becquerel in 1896, and radium by Marie and Pierre Curie in 1898. The further discovery of nuclear fission by Otto Hahn, Lise Meitner, and Fritz Straßmann in 1938 initiated the atomic age and widespread development of anthropogenic sources of radiation. As such, the study of anthropogenic sources of radioactivity in the environment rapidly became important.

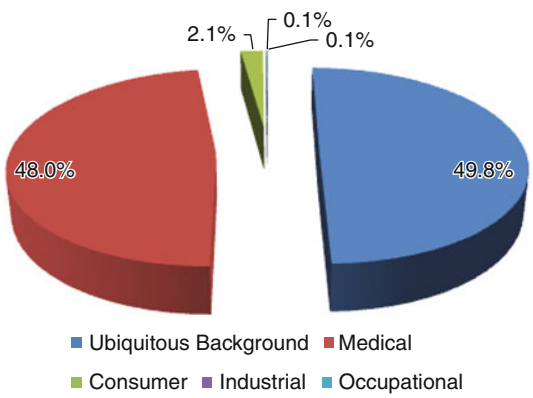

Radiation in the Environment, Sources of. Figure 1 Breakdown of collective dose in the USA (Adapted from NCRP [1])

All anthropogenic radionuclides in the environment have their origins in nuclear technology, through production in nuclear reactors, particle accelerators, mining operations, or nuclear weapon use. Some radionuclides that are natural in origin get concentrated through industrial and chemical processes and are termed "technologically enhanced naturally occurring radioactive material." Radioactivity in the environment can therefore be broken down into two primary categories: (1) naturally occurring and (2) nuclear technology origins. The following sections discuss the various forms of natural and anthropogenic radioactivity and place them into context of sources of radiation in the environment.

Natural Radiation

There are two primary sources of natural radiation on Earth. The first is radioactive material in the Earth itself that originated from planetary formation (terrestrial radiation) and the second is the contribution from radionuclides that have origins from extraterrestrial events (cosmogenic radiation). A third source of environmental radioactivity that is an extension of the cosmogenic component is the radiation environment in aircraft at altitude. Finally, a fourth source, which is important for human space activities, is the natural space radiation environment. Some of the more important radionuclides with respect to human exposure will be discussed, including:

- H-3 (tritium)
- Be-7
- C-14
- Na-22
- K-40
- Rb-87
- Uranium decay series
- Thorium decay series
- Actinium decay series

The order of discussion will begin with the radiation source furthest away from the collective human receptor: the space environment. This outward-in approach is appropriate since (a) all terrestrial radiation originated from events that happened in space, (b) the Earth is completely surrounded by radiation, and (c) over the past 50 years human activities have extended further into space, and the likelihood is high that human space exploration beyond the Earth-moon system will take place within the next 50 years. Following the space environment, the cosmogenic environment, which is the transition between the space and terrestrial environment, will be discussed. Next, a modification to the cosmogenic environment, the high altitude aircraft radiation environment, will be considered as there are implications on flight crew exposure. Lastly, the discussion culminates to consider the terrestrial environment.

Space Radiation Environment By conventional definition of the "environment," exoatmospheric exposures are not typically included. However, as humans (and nonhuman biota) venture further from the immediate vicinity of planet Earth, the effect of the space radiation environment becomes important for exposure profiles, and is therefore discussed herein.

The natural space radiation environment consists of electrons, protons, and heavy ions of various energies, either trapped by the Earth's magnetic field or passing through typical spacecraft trajectories or orbits. The near-earth geospace or magnetosphere is a geomagnetic cavity formed by the Earth's magnetic field as it passes through the solar wind. The cavity is asymmetric, ranging from a 10–12 R_E ("earth-radius," R_E is approximately equal to 6,500 km) hemisphere (sun-side) to a 60 R_E cylinder (night-side). As the Earth penetrates the solar wind, it generates a "wake" or "magnetotail" path in the solar wind for approximately 500 R_E.

The Earth's total magnetic field is the algebraic sum of the Earth's internal magnetic field (molten core and crust residual magnetism) and the net external effects established by solar wind–magnetosphere interactions. The total field is nonconstant, due to slow variations in the internal component, with erratic (random solar flares) and cyclic (solar cycle, seasonal tilt, diurnal effects) variations in the external component.

Although to a first approximation the total magnetic field is dipolar, non-dipolar contributions are important and are best described by numerical models that also account for the offset (approx. 11°) and tilt (approx. 500 km into the Western Pacific) of the geomagnetic axis with respect to the rotational axis. This offset and tilt brings the plasmasphere, also known as the Van Allen radiation belts, to very low altitudes over the coast of Brazil, creating the "South Atlantic Anomaly" (SAA). The SAA is directly responsible for nearly all trapped radiation dose received by space vehicles in low-earth orbits (LEO). Conversely, axial offset and tilt causes the radiation belts to move to higher altitudes (180° longitude from the SAA) over the coasts of Thailand and Vietnam, creating the Southeast Asian Anomaly.

Trapped Radiation Energetic charged particles trapped in the Earth's radiation belts or plasmasphere routinely interact with spacecraft operating in near-earth orbits. The composition, energy, and strength of the trapped particle populations are functions of many variables, the most important being the location at which the radiation is encountered within the trapped radiation belts. At altitudes greater than approximately 80 km, the magnetosphere contains relatively large numbers of trapped electrons and protons, as well as smaller numbers of low-energy heavy ions. The particles interact electromagnetically with the Earth's magnetic field: (1) by gyrating around and traveling along field lines, reflecting between regions of maximum field strength on the lines (conjugate mirror points), and (2) with positively charged protons and heavy ions drifting westward and negatively charged electrons drifting eastward across field lines, around the Earth. Calculation of radiation fluxes integrated over the magnetic field and dipole shell coordinates ("*B*–*L*" plots) of the orbits provide realistic means of quantification of the trapped radiation component of the natural space environment. The strong dependence of trapped particle fluxes upon particle location is primarily an altitude and latitude dependence. Importantly, specific boundaries exist in radiation trapping regions of the magnetosphere, but these boundaries (particle energy-dependent) are typically smeared areas, quite sensitive to magnetospheric perturbations or variations.

Energetic electrons populating the plasmasphere can be divided into two groups or belts: (1) inner and (2) outer electrons. The inner belt extends to approximately 2.4 R_E on the equator. A region known as the "slot" is found between 2.4 and 2.8 R_E on the equator, wherein the trapped electron, temporally dependent population varies directly with the degree of solar activity. Beyond 10–12 R_E, geomagnetic field intensity has fallen and continuous, steady-state trapping is no longer possible. The intensity and energy bounds of outer belt electrons are greater than those of inner electrons, with peak outer belt fluxes approximately ten times those of inner belt fluxes and with electron outer belt maximum energies approximately two orders of magnitude larger than inner belt energies (10^7 MeV compared with 10^5 MeV). Distant outer belt electrons are brought to low altitude at high latitudes, creating relatively low-intensity and low-energy trapped electron "polar horns."

The proton trapping region of the magnetosphere extends to approximately 4 R_E on the equator. The spatial distribution of these protons varies inversely and monotonically with proton energies, directly opposing trends observed for trapped electrons. Thus, one would expect spacecraft in low-altitude equatorial orbits to encounter the most intense and energetic severe proton fluxes. Unlike lightweight electrons, heavy protons cannot follow the steeply gradated high-latitude geomagnetic field lines, thereby precluding formation of trapped proton polar horns.

The magnetosphere exhibits both short-term and long-term variations in the dynamic behavior of its trapped electron and proton populations. These variations are caused by terrestrial magnetic anomalies, diurnal effects, seasonal tilt, chronology of the 11-year solar (sunspot) cycle and the random occurrences of solar flares.

Transiting Radiation Transiting radiation included in the discussion of the natural space radiation environment has both a solar and an interstellar component. These radiations are termed cosmic rays (CR) and are composed of all the nuclei found in the periodic table (of GeV energies and in various stages of ionization) and energetic (hundreds of MeV) electrons. The distinction between galactic cosmic rays (GCR) and solar cosmic rays (SCR) is made based upon the source and energies of the radiation, rather than its composition.

Galactic cosmic rays are composed mainly of energetic (100–1,000 GeV/nucleon) charged particles such as helium, oxygen, carbon, iron, and nitrogen (and a proportionately low proton and electron component), produced in the interstellar void and arriving omnidirectionally at the surface of the magnetosphere after diffusing through space. Spatial variations in the GCR flux are attributable to variations in the strength and location of the source with respect to the Earth, and the location and depth at which the GCR particles penetrate the magnetosphere. Also, for target locations within 400 km of the Earth's surface, the incident GCR flux is physically shielded on the earth-side by the Earth's shadow.

Solar cosmic rays are energetic charged particles randomly emitted into interplanetary space from events occurring in disturbed regions on, or close to, the surface of the Sun. These particles escape the Sun's near-gravitational field and diffuse throughout the interplanetary medium, traveling along in the solar wind and reaching the magnetosphere within minutes to hours after the solar energetic particle (SEP) event. Solar energetic particle events usually occur in conjunction with solar flares and are composed primarily of 90% energetic protons, 3% alpha particles, and 2% energetic heavy ions and electrons.

Secondary Ionizing Radiation Energetic protons and/or electrons may interact with spacecraft structural materials and cause secondary emissions of an ionizing nature. Proton nuclear capture interactions followed by transmutation and subsequent emission of X and gamma rays can cause ionization in other space-borne materials. Spacecraft design can be used to minimize this secondary radiation hazard. Electron interactions with spacecraft materials can cause more serious problems. For electron energies encountered in the magnetosphere essentially all incident electrons are attenuated by spacecraft walls and shielding layers, ionizing materials and/or causing atomic electron (secondary) excitation. Photo-de-energization of these excited states occurs, with photons possessing a continuous X-ray spectrum emitted approximately along the direction of electron incidence. These bremsstrahlung fluxes typically average one-third that

of the incident electron energies, varying linearly with the host material atomic number and with the square of the incident electron energy.

Cosmogenic Environment The space radiation environment consists of energetic charged particles (atomic nuclei, protons, alpha and beta particles) as well as high-energy photons, originating from events from the Sun and beyond the solar system. After entering the Earth's atmosphere, cosmic rays collide with atoms in the atmosphere, resulting in secondary radiation. For example, the interaction of cosmic rays with oxygen and nitrogen results in the production of numerous cosmogenic radionuclides, such as C-14. Cosmogenic radionuclides are therefore those produced continuously in the upper atmosphere via cosmic ray interactions.

The composition and reactions of cosmic rays interacting with the Earth's atmosphere is complex; however, it is dominated by proton and He nuclei interactions (Table 1).

The composition of the atmosphere at sea level is approximately 78% N, 21% O, and 1% other constituents, which is fairly uniform up to approximately 100 km altitude. Therefore, cosmic ray interactions with nitrogen and oxygen are most probable. The high-energy interactions in the upper atmosphere tend to be more exotic than the reactions typically considered on Earth. For example, protons can interact with oxygen or nitrogen via a process called spallation to generate neutrons, protons, and pions. The neutrons and protons can generate further nuclear reactions, generating the cosmogenic radionuclides. For example, a very important reaction involves production of C-14 as follows:

$$ {}_{0}^{1}n + {}_{7}^{14}N \rightarrow {}_{6}^{14}C + {}_{1}^{1}H $$

Radiation in the Environment, Sources of. Table 1
Galactic radiation abundance entering atmosphere

Particle	Mean abundance (%)
Protons	87
He Nuclei	11
Nuclei with $Z > 2$	1
Electrons	1

Source: Adapted from [2].

The importance of C-14 is that it is ubiquitous in the environment and it has a long half-life. This makes it important from both a biological dose standpoint and the fact that C-14 is utilized in carbon dating of organic materials. Carbon dating is possible because while flora and fauna are alive, there is a constant C-14 load within the organism. Upon death, no further C-14 is taken in, and therefore the elimination of carbon is due solely to radioactive decay. Therefore, the age of an organism can be estimated by the C-14 signature.

The principal radionuclides produced via cosmic ray interactions, with half-lives greater than a few hours and sorted by half-life, are presented in Table 2.

The radionuclides produced via cosmic ray interactions eventually settle on Earth through atmospheric dispersion and deposition, as well as through precipitation processes, and become the cosmogenic component of terrestrial radiation.

Aircraft Radiation Environment The Earth is surrounded and continually bombarded by radiation. The extraterrestrial environment has impact both on manned space missions, for generation of cosmogenic radionuclides, and for contribution of human exposure

Radiation in the Environment, Sources of. Table 2
Principal cosmogenic radionuclides

Radionuclide	Half-life	Decay mode
^{10}Be	1.6 million years	β
^{26}Al	0.72 million years	β^+
^{36}Cl	0.3 million years	β
^{14}C	5,730 years	β
^{32}Si	330 years	β
^{39}Ar	269 years	β
^{3}H	12.3 years	β
^{22}Na	2.6 years	β^+
^{35}S	87 days	β
^{7}Be	53 days	EC
^{33}P	25 days	β
^{32}P	14.3 days	β
^{28}Mg	20.9 h	β
^{24}Na	15 h	β

at aircraft altitude. The exposure due to cosmic radiation is highly variable; however, it may be generally said to increase as both a function of altitude above the Earth's surface due to decreased atmospheric shielding, and increase in latitude from the equator, due to decreased geomagnetic shielding [3].

The dose rate from cosmic radiation increases with depth into the atmosphere to a maximum value (known as the Pfotzer maximum) at approximately 20 km (60,000 ft), whereupon it decreases with decreasing altitude to the Earth's surface [4]. The principal constituents of the dose at aircraft altitudes are neutrons (55%), electrons/positrons (20%), protons (15%), energetic photons (5%), and muons (5%), whereas at surface level almost all dose from cosmic ray origins is attributable to muons.

At altitudes from 3 to 25 km (10,000–80,000 ft), neutrons are the dominant component to the dose [5]. These neutrons are produced through complex cascades involving spallation processes induced by primary cosmic particles (principally protons) entering the atmosphere [6]. The dose to humans in aircraft from the primary neutron spectrum is complicated by interactions of neutrons and other particles within the aircraft aluminum structure and other materials within the aircraft.

Terrestrial Environment The natural terrestrial radiation environment has two principal components: (1) primordial and (2) cosmogenic (discussed in section on "Cosmogenic Environment"). Primordial radionuclides have, by definition, been present since Earth, as a terrestrial body, formed. During the Earth's formation approximately 4.5 billion years ago, a great number of isotopes were introduced as part of the mass generation. Only radioisotopes with long half-lives persist in the Earth to this day. There are a number of long-lived radionuclides that make up the primordial family, presented in Table 3. As may be seen, most of the primordial radionuclides all have half-lives much greater than the estimated age of the Earth.

Besides the single radionuclides presented in Table 3, there are also three principal and very important radionuclide chains that are primordial:

1. U-238 decay chain (uranium series)
2. Th-232 decay chain (thorium series)
3. U-235 decay chain (actinium series)

Radiation in the Environment, Sources of. Table 3
Primordial radionuclides and half-lives

Nuclide	Half-life (billion years)	Decay mode
^{40}K	1.3	β
^{50}V	600,000	β
^{87}Rb	47	β
^{113}Cd	9,000,000	β
^{115}In	460,000	B
^{123}Te	12,000	EC
^{138}La	110	β
^{142}Ce	50,000,000	α
^{144}Nd	2,380,000	α
^{147}Sm	110	α
^{148}Sm	7,000,000	α
^{152}Gd	110,000	α
^{156}Dy	200,000	α
^{176}Lu	27	β
^{174}Hf	2,000,000	α
^{180}Ta	16,000	β
^{187}Re	50	β
^{190}Pt	700	α
^{204}Pb	140,000,000	α
^{238}U	4.5	α
^{235}U	0.7	α
^{232}Th	14.0	α

The natural decay series are presented in Figs. 2–4. In the figures, parent radionuclides that undergo alpha decay are above their progeny (sometimes termed "daughter" products), while parents that undergo beta decay are to the left of their progeny. Under each radionuclide identifier, the radiological half-life is presented in brackets. All decay series are seen to eventually decay to stable lead isotopes.

The most important radionuclides from an environmental exposure perspective are K-40 and the uranium and thorium series decay chains. The actinium decay chain is less important due to its lower abundance compared to the other chains. K-40 is ubiquitous in the environment, and is an important radionuclide

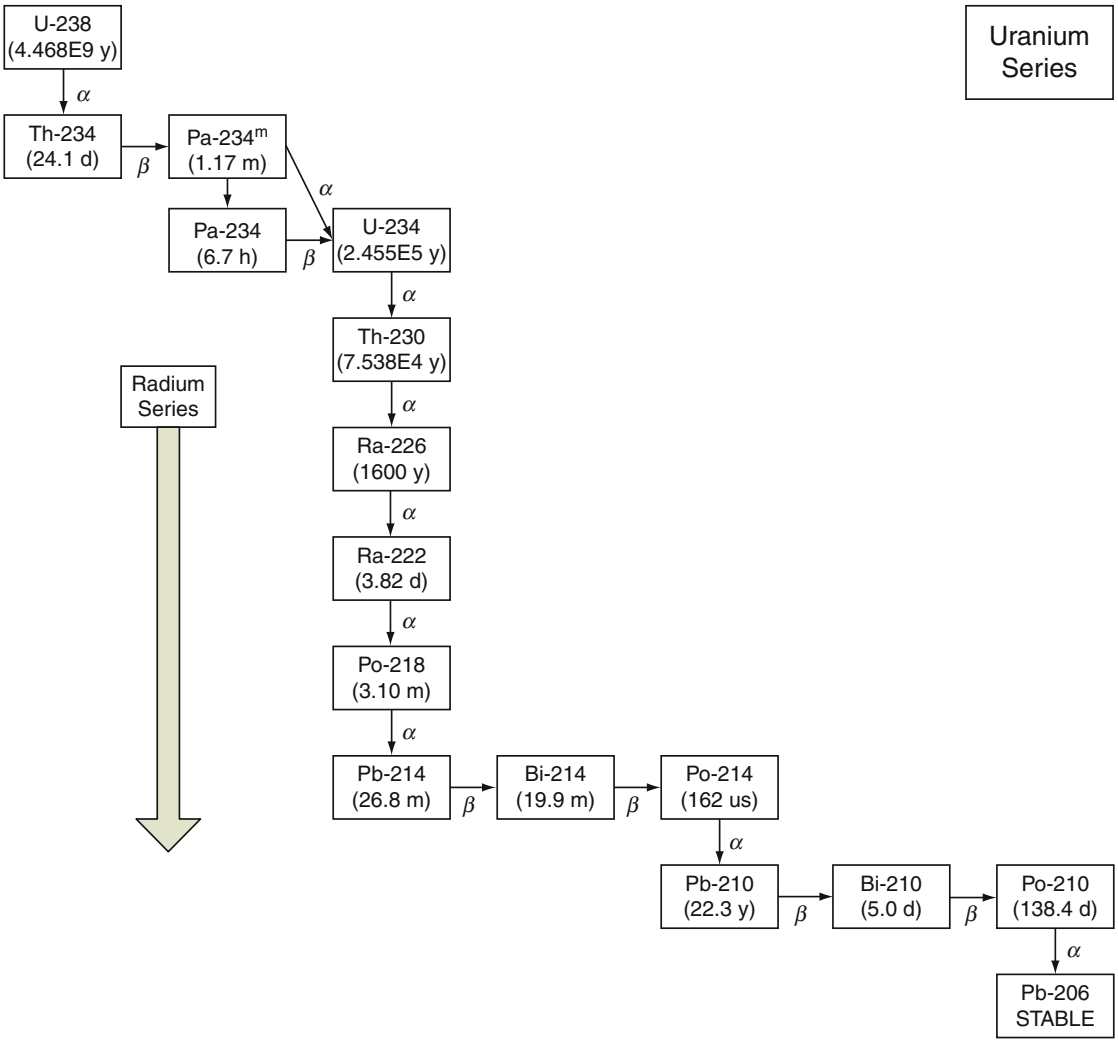

Radiation in the Environment, Sources of. Figure 2
Uranium decay series

in humans, with an average activity concentration in the body of approximately 60 Bq kg^{-1} [7]. Humans have a continual uptake of K-40 through ingestion of food, as the average quantity of natural potassium consumed is approximately 2.5 g day^{-1}, where K-40 makes up 0.017% of naturally occurring potassium. From an environmental monitoring standpoint, K-40 is important as an indicator radionuclide. That is, a primordial radionuclide that is almost always expected to be detected in environmental samples. The uranium and thorium series are also ubiquitous and very important to terrestrial radiation due to the progeny. Of greatest importance from the perspective of dose to humans is the radon component commonly termed "radon gas" or "radon" (Rn-222) in the uranium decay chain. There is also a radon component in the thorium series, commonly termed "thoron gas" or "thoron" (Rn-220), but is less significant for dose to humans due to its short half-life of under 1 min. The decay chains are interesting in the fact that the top of the chain is matter in solid form and all progeny are solid matter until radon, which is a gas, and decays back to solid form progeny until the series finally reach stable lead isotopes. This gas form is the reason for the

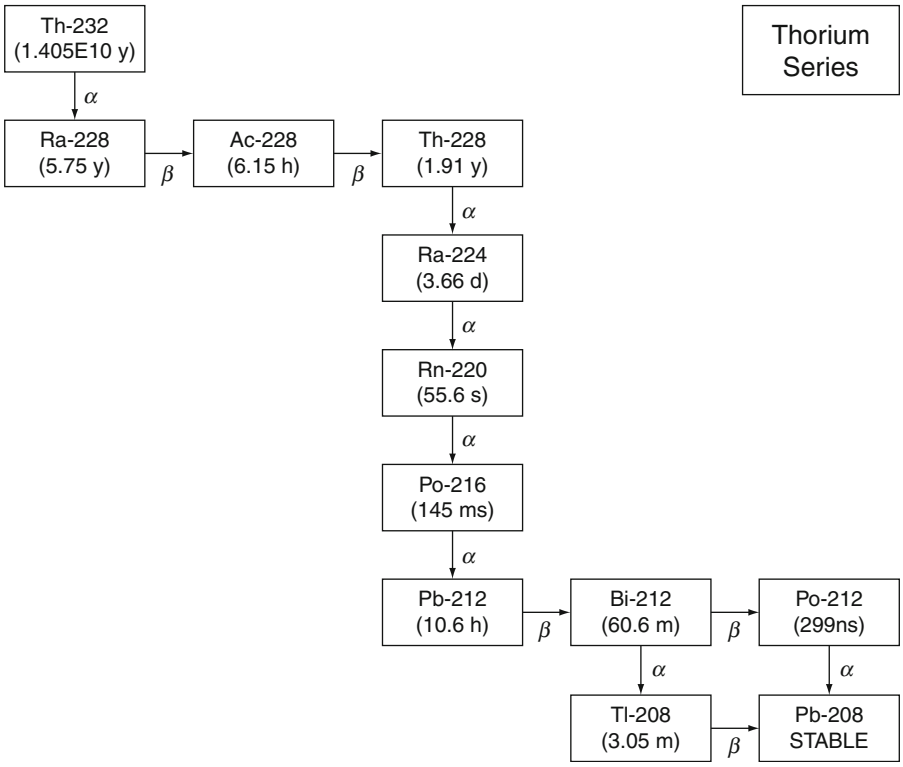

Radiation in the Environment, Sources of. Figure 3
Thorium decay series

high human dose, as it is available for inhalation and instillation in the respiratory tract where it will decay via alpha emission and generate alpha-, beta-, and gamma-emitting progeny. Also, natural series are important as sources of environmental radiation through mining and industrial use of some of the isotopes (e.g., Ra-226 used in luminescent materials, Th-232 used in lantern mantels, and U-235/238 used for nuclear fuel). Some of these uses will be discussed in subsequent sections.

Natural Reactors In 1972, a French physicist named H. Bouzigues made an unexpected discovery during routine measurement of uranium concentrations in the fuel supplied to French nuclear reactors obtained from Oklo in Gabon, West Africa. These concentrations are basically a constant at any given time, changing only through their characteristic half-lives. The U-235 concentration in 1972 was 0.7202 ± 0.00004% and Perrin measured 0.7171%, the first measurement ever recorded outside this range. Other discrepancies were to follow, with some uranium samples depleted to half their normal concentrations. In addition, the presence of some trace levels of fission products was also observed [8]. The observations were explained by a theory that a number of coincidental physical factors merged at Oklo approximately 2 billion years ago to create a natural fission reactor. In fact, in the areas of Oklo and nearby Bangombé, at least 17 uranium deposits are hypothesized to have acted as natural fission reactors [9]. There were a number of prerequisite conditions required to make a natural fission reactor, stated as follows:

1. Sufficient U-235 – At the time of the natural reactors (2 billion years ago), the amount of U-235 in natural uranium was approximately 3% (as opposed to the 0.72% currently). At 3% enrichment, a chain reaction is sustainable (in fact, this is the approximate enrichment in commercial light water–moderated reactors).

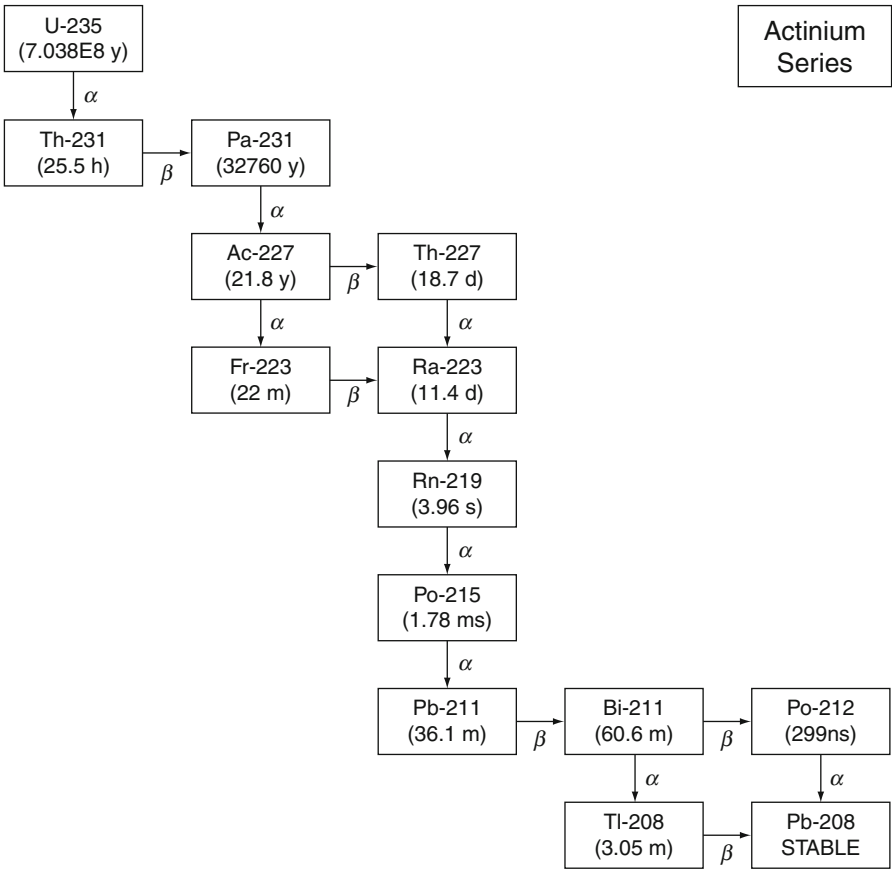

Radiation in the Environment, Sources of. Figure 4
Actinium decay series

2. Sufficient physical size – If the "reactor" was too small, then too many fission-produced neutrons would escape, and a chain reaction would not be possible. One of the most studied natural reactors around Oklo is of dimensions 12 m × 18 m × 0.5 m [9].
3. Sufficient moderator – Fast neutrons produced from fission must slow down by colliding with other nuclei. An effective moderator is water, and therefore if the uranium (uranium dioxide, or UO_2) had formed into a porous matrix, then water could impregnate the pores and provide the moderator required to sustain the chain reaction.

Thus it is believed that over 2 billion years ago, natural uranium deposits formed into porous matrices of sufficient size to allow critical reactors to form in this region. Based upon observations of fission product concentrations (especially Xe and Kr) in surrounding mineral deposits, it has been estimated that the reactors ran with 30 min active pulses, separated by 2.5 h dormant periods, continuously cycling for approximately 150,000 years [10]. This cycling occurred when (a) water entered the pores and a chain reaction started, resulting in (b) energy liberated through the chain reaction heating the surroundings and evaporating the water or turning it to steam, thus stopping the chain reaction, until (c) the surroundings cooled and more water could enter, thereby restarting the chain reaction [9].

There is modern interest in studying these ancient natural reactors as they provide a naturally aged laboratory in which to study migration of fission products through the environment, which is a very important area of study in radioactive waste management [11].

Radon Radon was discovered in the early 1900s in Germany by Friedrich Ernst Dorn. Radon is a ubiquitous, odorless, colorless, tasteless, and dense noble gas. Radon is heavier than air, and it is soluble in water. Because it is a noble gas, radon is chemically inert and electrically uncharged. It is a naturally occurring radioactive material which originates from the U-238 decay chain. When uranium, thorium, or actinium atoms decay, other radioactive atoms are formed. One of these is radium. Radium is the immediate source of radon. The radium isotope of principal interest is Ra-226 which decays through alpha emission to produce radon gas (Rn-222). There are 33 isotopes of radon listed in the chart of the nuclides [12], 3 of which are naturally occurring. All of the three emit alpha particles when they decay, and they all have short half-lives. Rn-222 is commonly known as "radon" and is the most stable isotope with a 3.8 day half-life. Rn-220 (or "thoron" as it is referred to in historical context) is a member of the thorium decay series and has a much shorter half-life (55.6 s). Rn-219 (historically referred to as "actinon") is a member of the actinium series and has the shortest half-life of the three isotopes at 4.0 s. Because it is naturally occurring, radon is found almost everywhere, including air, soil, groundwater, granite, pumice, clay, brick, and other construction materials such as concrete made from fly ash and industrial slag.

The primary human health hazard from radon is indoor exposure. Radon can enter into buildings by several pathways. The surrounding composition of soil and concentration of uranium is the basis for varying levels of radon from location to location. Indoors, the basement is the cause for concern where radon can diffuse through the foundation and travel through cracks, remaining for longer periods of time due to lack of ventilation and minimal exit paths. The building structure plays an important role as mentioned for cracks in the foundation along with wall joints which present a likely entry path for the gas. Cracks in the landscape surrounding a home can also accelerate the entrance of radon into the atmosphere and home.

The World Health Organization (WHO) has estimated average indoor radon concentrations for a number of countries, presented in Table 4. It may be seen that there is significant variation in the average radon concentrations globally.

Radiation in the Environment, Sources of. Table 4
Average global radon concentrations

Country	Average concentration (Bq m^{-3})
Canada	11.4
Czech Republic	140
Finland	123
Germany	50
Ireland	60
Japan	20
Lithuania	37
Norway	51–60
Russia	19–250
Sweden	108
Switzerland	70
UK	20
USA	46

Source: Adapted from [13].

The effective dose calculated for a radon exposure of 200 Bq m^{-3} is 3 mSv a^{-1}, whereas at 600 Bq m^{-3}, the effective dose is 10 mSv a^{-1} [14]. The International Commission on Radiological Protection recommends action levels be established between 200 and 600 Bq m^{-3}, where an action level would indicate a point where remedial action should be taken to reduce the radon concentration.

For nonhuman biota, outdoor concentrations of radon are important as these organisms spend most of their lives in more direct contact with the source of radon gas (i.e., uranium and thorium bearing ores). Although radon gas disperses rapidly in open-air environments [7], closed environments, such as for burrowing animals, may yield elevated radon concentrations.

Considering environmental pathways, radon (Rn-220/222) is the most important terrestrial radionuclide, whereas polonium (Po-210) is the most important radionuclide in aquatic environments. From a yearly dose standpoint, radon gas is the most important environmental radionuclide for human exposure.

High Background Radiation Areas Regions on Earth that have elevated levels of natural radiation compared

to the global average may be termed high background radiation areas (HBRA), very high background radiation areas (VHBRA) or high levels of natural radiation areas (HLNRA). The levels of natural radiation can vary greatly depending on location, with the annual effective radiation dose from natural radiation for the world population being approximately 2.4 mSv. Some prominent and inhabited areas with high levels of natural radiation (leading to average local doses much higher than the world average) are found in the following locations (approximate population in brackets):

- Ramsar, Iran (2,000)
- Kerala, India (100,000)
- Tamil Nadu, India (30,000,000)
- Mombasa, Kenya (500,000)
- Guarapari, Brazil (100,000)
- Morro do Ferro, Brazil (500)
- Yangjiang, China (3,000,000)

Focus: Ramsar, Iran

Ramsar, a town of 2,000 people, has a long history of being a vacation destination, with approximately 50 hot springs, 9 of which have for centuries been used as recreation and health facilities by the local population and visitors alike. The soil in Ramsar has elevated levels of Ra-226, compared with world average expected values, and the hot springs bring terrestrial radium to the surface, where it precipitates. The radiation fields in Ramsar are heterogeneous with hotspots having dose rates as high as 100 μGy h^{-1}. In some areas of Ramsar, people receive an effective radiation dose of hundreds of mSv a^{-1}, which tends upward of 100 times the average global value [15].

There are two significant pathways for human exposure in Ramsar: building materials and hot springs, both primarily due to radium dissolved in mineral water. Since the raw materials utilized to build the structures come directly from the soil, they are concentrated in Ra-226. In addition, local produce contributes to the effective dose through plant sequestering of Ra-226 and progeny. The typical pathway of exposure from environmental radiation in Ramsar, Iran, is depicted in Fig. 5. It may be seen that the pathways for exposure are varied and complex.

The average and maximum dose rates from various areas around the world are presented in Table 5 (adapted from [16]).

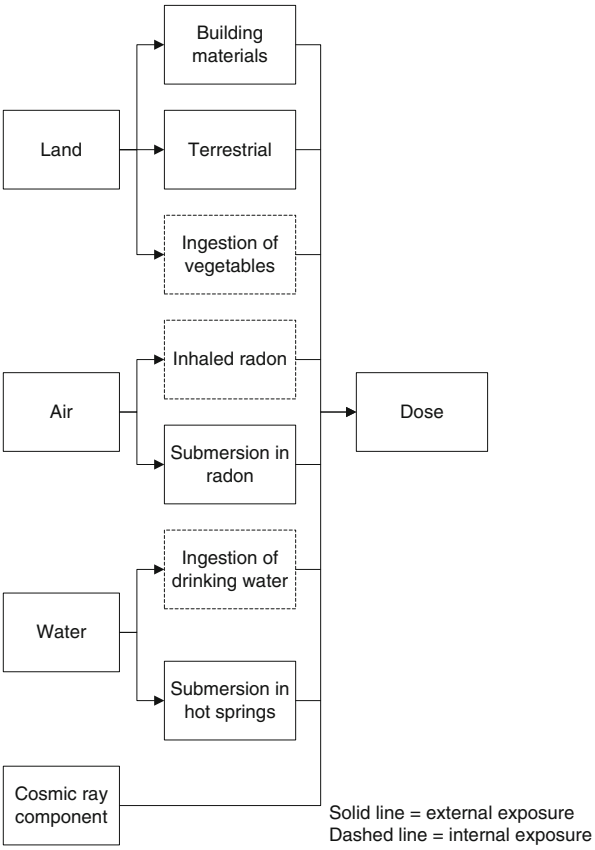

Radiation in the Environment, Sources of. Figure 5 Typical exposure pathways for a resident of Ramsar, Iran

It may be seen that the dose received by persons living in very high background areas can be as high as 100 times the global average dose. Of interest is the fact that in the very high background radiation areas such as Ramsar, no indication of excess cancer in the population has been observed [15].

Naturally Occurring Radioactive Material (NORM) and Technologically Enhanced NORM (TENORM)

Naturally occurring radioactive material (NORM) is germane to the discussion of sources of radioactivity in the environment. NORM, as a source of environmental radioactivity, has been discussed in the section on "Natural Radiation", and does not include anthropogenic radionuclides. It is difficult to separate discussions on NORM from other categories of environmental radioactivity, as there is significant overlap. The fact

Radiation in the Environment, Sources of. Table 5
Average and maximum dose rates for comparison

Location	Average (mSv a^{-1})	Maximum (mSv a^{-1})
High Background		
Ramsar (Iran)	10.2	260
Guarapari (Brazil)	5.5	35
Kerala (India)	3.8	35
Yangjiang (China)	3.5	5.4
Normal Background		
Norway	0.63	10.5
China	0.54	3.0
India	0.48	9.6
Germany	0.48	3.8
Japan	0.43	1.26
USA	0.40	0.88
Denmark	0.33	0.45

that NORM has natural origins does not suggest that NORM cannot have high levels of radioactivity. In fact, through technological processes (technologically enhanced NORM, or TENORM), naturally occurring radionuclides (uranium and thorium decay series, as well as other natural radionuclides, such as K-40) can concentrate to yield reasonably large specific activities in materials, and through recycling of materials NORM can become a significant source of exposure.

NORM is defined as [17]:

- Any of the primordial radionuclides or radioactivity present in soils, rocks, and materials undisturbed as a result of human activities

In contrast, the definition of TENORM is somewhat more complicated [17]:

- Naturally occurring radioactive material disturbed or altered from natural settings or present in a technologically enhanced state due to past or present human activities and practices, which may result in a relative increase in radionuclide concentrations, radiation exposures and risks to the public, and threat to the accessible environment above background radiation levels. "Technologically enhanced" means that the radiological, physical, and chemical properties of the radioactive material have been altered such that there exists a potential for: (a) redistribution and contamination of environmental media (soil, water, air, and biota), (b) increased environmental mobility in soils, surface water and ground water, (c) incorporation of elevated levels of radioactivity or increased accessibility in products and construction material, or (d) improper disposal or use of disposal methods that may result in unnecessary or elevated exposures to individuals and populations via the accessible environment.

Accountability for naturally occurring radioactive material (NORM) and TENORM (technologically enhanced NORM) has been coming under increased scrutiny since the publication of the 1990 International Commission on Radiological Protection recommendations [18] for a public dose limit reduction from 5 to 1 mSv a^{-1}. There are numerous sources of TENORM that are generated through industrial processes and may become available for recycling (Table 6), thereby placing the exposure closer to environmental and human receptors [19].

Although, by definition, NORM is "natural," this does not belay the fact that in a large enough quantity it may become hazardous (the toxicology principle that "the dose makes the poison"). For NORM to be considered hazardous in the recycling industry, there must be a pathway from the NORM to humans and/or the environment from recycling.

Recycled landfill material that is rich in uranium and thorium is one pathway for NORM or TENORM to contribute to public dose. Another significant pathway is through metal recycling, when the metals have been in contact with NORM, usually for significant periods of time (years), such that small quantities of radioactive material have been allowed to collect on surfaces (such as scaling or sludge). It is possible that recycling metal with this type of NORM will result in contaminated metal, or at the very least, contaminated equipment. Another important issue regarding steel recycling is the possibility of having an anthropogenic source (e.g., from a nuclear gauge) mixed in with a shipment containing NORM. If the recycler regards an indication of radiation from this type of shipment as

Radiation in the Environment, Sources of. Table 6
Industrial activities that generate TENORM

Industrial activity	Recycled forms
Uranium mining	Tailing residue
Phosphate fertilizer	Scale, slag
Coal combustion	Fly ash, bottom ash, slag
Oil and natural gas production	Scale, sludge, contaminated water
Municipal water treatment	Sludge, radium-selective resins
Metal mining and processing	Slag, leachate, tailings
Geothermal energy production	Scale, brine-pond deposits
Pulp and paper production	Scale
Metal casting	Ceramic shells
Former radium processing facilities	Contaminated soils

being caused by the NORM, and determines to recycle the scrap, they may inadvertently smelt the gauge source and contaminate all the recycled material.

The risk from recycling NORM (e.g., scaling on steel pipes) would generate insignificant and nonmeasurable contamination due to dilution, and ideally portal monitors and other recycling plant–detection equipment would ignore NORM altogether. However, separating the detection of NORM from non-NORM would be very challenging in the recycling environment, and would likely require a radiation specialist on site. Many recycling companies have radiation detection equipment installed at entry points and/or various locations in the plant. In general, most recyclers have a "zero tolerance" policy for accepting radioactive material. The policy is based upon the alarm indication as provided by the radiation detection equipment, which in turn depend upon the discrimination and sensitivity of the equipment. Therefore, if NORM alarms the radiation detection equipment, this is reason enough to refuse acceptance of a shipment. When a shipment is refused, some sort of action must be taken. The action will clearly depend upon the individual circumstances. The recycling company often initiates the NORM (re)action based upon "blind" instrument alarms, and has very little culpability with respect to this action. In fact, the recycling company has no requirement to accept any given load of material. Litigation and economic penalties surrounding the transport and disposal of materials containing NORM or TENORM are of great concern to many industries that have not previously needed to address the NORM issue [20].

Tobacco Product Tobacco leaf, by virtue of the fact that it is manufactured into smoking product, deserves special consideration. Its categorization here as a technologically enhanced NORM resides in the fact that production of tobacco products is a technological activity, yet the radioactive material is sequestered naturally by the tobacco leaf. Natural radioactivity, primarily Polonium-210 (Po-210) and Lead-210 (Pb-210), are sequestered by tobacco plants from two principal pathways: (1) through the root system by absorption through the ground, or (2) by leaf deposition from the atmosphere. These naturally occurring radioisotopes originate from the terrestrial uranium decay chain found in soil. Regarding environmental radionuclides and impact to human health, Po-210 is one of the most radiotoxic nuclides to humans [21] and is volatile at the temperature of burning tobacco (500–700°C), making it highly available for transport and deposition throughout the human respiratory tract via smoking. The main source of Po-210 and Pb-210 in the atmosphere, which subsequently deposits on tobacco leaves, is Rn-222. The radon gas originates as the progeny of Ra-226 which is present in soil. A second pathway for Po-210 and Pb-210 to enter the plants is via the tobacco plant root systems, again from the uranium decay chain. The concentration of Po-210 and Pb-210 in the soil depends on the humus content of the soil [22]. Soil with higher humus content will generate a higher concentration of these radionuclides in the tobacco plant. The concentration of these radionuclides in tobacco leaves depends on many factors, including the type of soil the plant is grown in, the weather conditions during the time the tobacco is growing and the variety of the tobacco and the storage methods. The importance of radionuclides in tobacco can be illustrated as follows. Depending upon the method of smoking and filtration used, the tobacco

used may contain tens of mBq of Po-210 which is vaporized, inhaled, and deposited along the tracheobronchial lining in the smoker, where it can irradiate the sensitive epithelial cells [23]. If a person smokes a single pack (20 cigarettes) per day for 50 years, they will have inhaled from 365,000 cigarettes. Assuming 10 mBq Po-210 per cigarette, and 100% inhalation efficiency (i.e., no effect of filter and no loss of Po-210) the total amount of Po-210 inhaled over 50 years will be 3.65 kBq. This relatively large quantity of Po-210 to the lungs would be expected to increase the risk of lung cancer. Even when the smoking product is filtered, a significant portion of radionuclides are still exposed to the respiratory tract. The risk scales up or down as a function of activity per unit tobacco product, amount smoked, and duration of smoking.

From an epidemiological perspective, there have been no conclusive correlations that tobacco radioisotopes are a major contributor to lung and esophagus cancer from smoking, although it has been well proven that smoking increases radiation dose to the people who smoke, or are exposed to "second-hand" smoke. However, it is well known that smoking is related strongly to lung cancer and therefore it is highly probable that this technologically enhanced environmental radioactivity, which is concentrated in the lungs through smoking, is one of the contributors (amongst a number of other nonradioactive contaminants found in cigarette tobacco) to excess cancer risk observed in the smoking population and likely in the "second-hand smoke" cohort [24]. Infants and children are more radiosensitive to tobacco smoke, as well as persons with weakened immune systems.

Nuclear Reactor Operations

There are three principal components to nuclear reactor operations that can contribute sources of radionuclides to the environment: (1) releases from mining, milling, processing/reprocessing operations; (2) operational releases; and (3) waste storage. Currently, radioactive waste is not a large contributor to sources of environmental radioactivity. However, due to the fact that waste storage solutions are actively being pursued worldwide, this category deserves discussion. Accidental releases related to nuclear power generation are discussed in section on "Nuclear Material Accidents".

It is worthy to note that commercial nuclear power contributes to a very small proportion of the collective effective dose to the population. For example, Fig. 6 shows the breakdown of collective dose to the US population from industrial exposure [1]. It is noted that nuclear power generation is responsible for 15% of the total industrial exposure, where the average effective dose for the exposed population ranges from 1 to 10 μSv, which is, at maximum, approximately 0.05% of the total yearly exposure from natural background radiation.

The nuclear generation component can be further broken down into constituents, as presented in Fig. 7 [1]. It may be seen that uranium mining and milling are the largest contributors (87.2%) to the collective dose

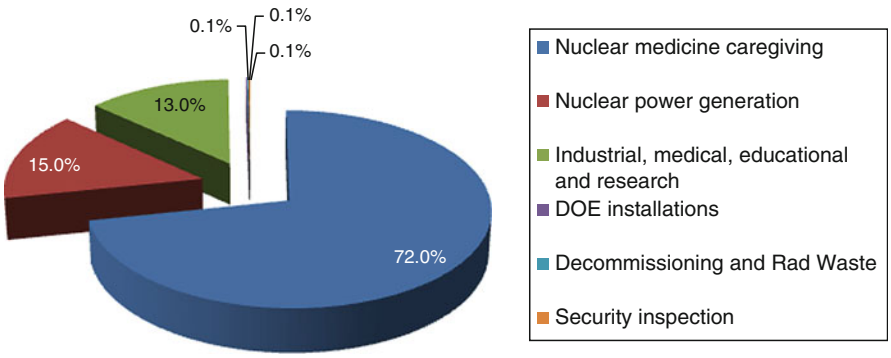

Radiation in the Environment, Sources of. Figure 6
Industrial exposure breakdown of the US population (Adapted from [1])

of the US population, whereas operation of nuclear plants is responsible for only 3.5%.

The following section discusses the three principal contributors to environmental sources of radioactivity from nuclear power generation.

Mining, Milling, and Processing of Uranium The approximate geographic breakdown of the world's supply of natural uranium is depicted in Fig. 8.

The life cycle of uranium for use in nuclear power generation slightly differs depending upon whether

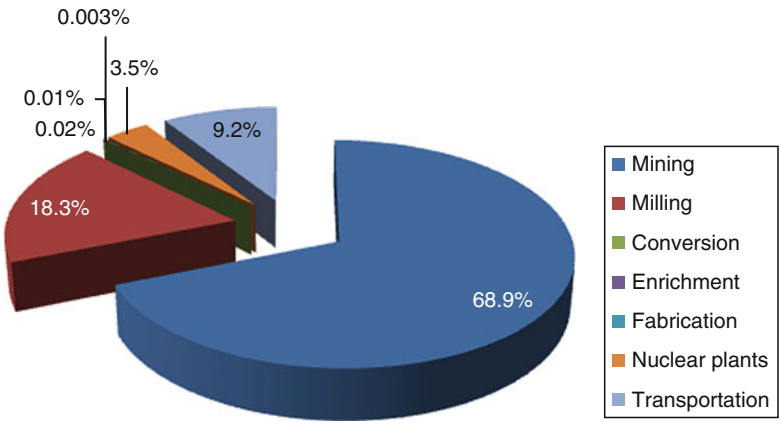

Radiation in the Environment, Sources of. Figure 7
Breakdown of nuclear power collective dose (Adapted from [1])

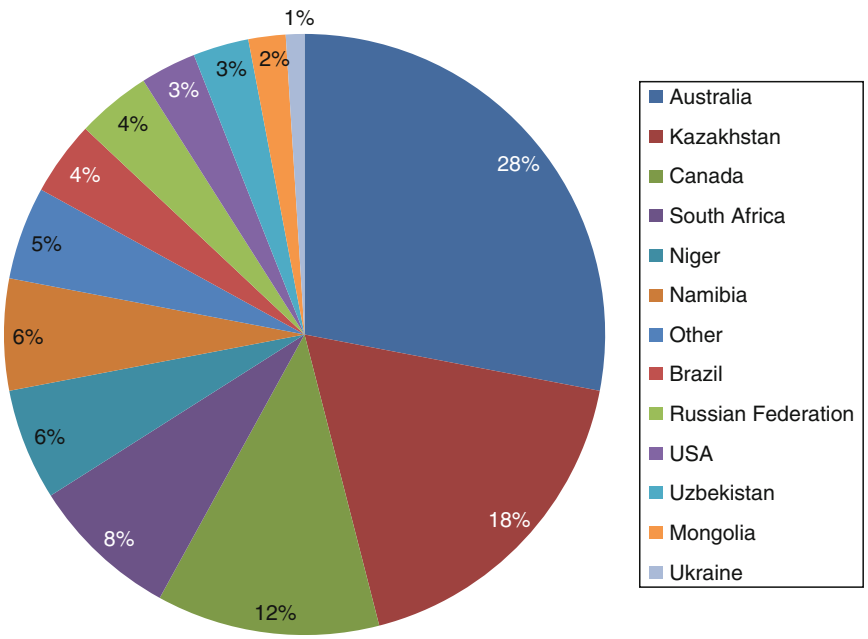

Radiation in the Environment, Sources of. Figure 8
World's supply of uranium

nuclear fuel is to be enriched, and whether fuel reprocessing activities will take place. The generic steps in the nuclear fuel cycle are provided in Table 7.

To start the cycle, an adequate location for uranium mining must be identified. Mining operations generate dust which includes uranium and progeny, and radon is present in large concentrations in the mining environment. Both are contributors to human exposure in and around the mining site. An alternate method of extracting uranium from ore deposits is by in situ leaching (ISL), which is the process of recovering uranium by dissolving it in a leaching agent and extracted via pumps. ISL requires the ore body be permeable to liquids and located such that ground water cannot be contaminated away from the ore body. The main advantage to ISL is that it does not produce tailings. Milling refers to the process of removing unwanted minerals from the ore (including radioactive minerals) to generate the required U_3O_8 product (termed "Yellowcake"). The tailings can contain many undesirable by-products including trace quantities of the mined ore (uranium), other radioactive materials and chemical used in the mining and leaching processes to separate the useful ore. The tailings may be stored above ground, below ground, or in ponds. The potential environmental impact from tailings include (1) radon gas, (2) atmospheric dispersion of tailing material, and (3) potential use of tailing material for building material or landfill [25]. It is worthy to note the fact that tailings have historically been unsecured, suggesting that potential spread of tailing material from the source of generation is not insignificant, and that both human and nonhuman biota are potential receptors. Enrichment and fabrication into fuel both involve chemical processing regardless of whether the end product will be natural or enriched fuel. Chemical processing always produces a waste stream, and therefore environmental spread of uranium and progeny will occur. Significantly, the removal of radium and progeny from the uranium production stream has lead to environmental contamination at some sites [26]. The predominant radionuclides acting as environmental sources of radiation from mining, milling, and processing of reactor fuel are natural uranium isotopes (and progeny), natural thorium isotopes (and progeny) and explicitly Ra-226 and Rn-222, all of which are naturally occurring species.

Radiation in the Environment, Sources of. Table 7
Generic nuclear fuel cycle

Step	Activity	Comment
1	Exploration	Test digs, aerial survey, etc.
2	Mining	Extraction of uranium ore
3	Milling	Yellowcake produced (U_3O_8)
4	Conversion to UO_2 (natural) or UF_6 (for enrichment)	Complex chemical processing
5	*Enrichment (if applicable)*	Increasing U-235 content
6	Fuel fabrication	Into fuel elements or bundles
7	Reactor operation	Depletion of U-235
8	*Reprocessing of spent fuel (if applicable)*	Back to enrichment/fuel fabrication
9	Spent fuel storage	High-level "waste"

It must be noted that radionuclides generated as a by-product of mining and milling processes may be considered technologically enhanced naturally occurring radioactive material (TENORM), which was discussed in section on "Naturally Occurring Radioactive Material (NORM) and Technologically Enhanced NORM (TENORM)".

Routine Operational Releases Nuclear power plants have multiple barriers to prevent release of radionuclides to the environment. However, under normal operation, routine releases of radionuclides occur as allowed by the regulatory body in the country in which the nuclear power plant is operating. Gaseous forms of radionuclides may vent from locations within the plant. For example, tritium (hydrogen atom) formed in cooling and moderating water can easily move through engineered barriers. Volatile radionuclides that exist in gaseous form such as radioisotopes of xenon, krypton, and iodine can leak from the fuel and ultimately be purged through the filtered air discharge system of the reactor building. The release of radionuclides to the environment is a function of reactor type in use. Data for normalized releases of radionuclides from nuclear power plants are provided

Radiation in the Environment, Sources of. Table 8 Nuclear power plant radionuclide releases

Plant type	TBq GW(e)$^{-1}$ a^{-1}						
	Noble gas	H-3 (gas)	C-14	I-131	Particulate (gas)	H-3 (liquid)	Other liquids
PWR	13	2.4	0.22	0.0002	0.0001	19	0.008
BWR	180	0.86	0.51	0.0003	0.35	0.87	0.01
CANDU	250	330	1.6	0.0001	0.00005	340	0.044
RBMK	460	26	1.3	0.007	0.008	11	0.006
FBR	210	49	0.12	0.0002	0.001	1.7	0.023

in Table 8 (adapted from [8]). The types of reactors considered are PWR (Pressurized Water Reactor), BWR (Boiling Water Reactor), CANDU (CANadian Deuterium Uranium), RBMK (Reaktor Bolshoy Moschnosti Kanalniy *(Russian)*, meaning high power channel-type reactor), and FBR (Fast Breeder Reactor).

As is evidenced by the collective dose component of nuclear power from Fig. 7, radionuclides released from nuclear power generation do not contribute an appreciable exposure.

Nuclear Versus Coal It has long been known that burning coal releases radionuclides to the environment [27]. When comparing the emissions of radioactivity from nuclear power plants with those from coal-fired power plants, it is crucial to understand the radionuclides involved and their source. For coal-fired power plants the source of the radioactivity is the naturally occurring radioactive material within the coal itself. The main radionuclides present include the U-238 series, Th-232 series, and K-40 with typical concentrations of 20, 20 and 50 Bq kg^{-1}, respectively [28]. These values, however, can vary widely depending on the type of coal. During the combustion process a by-product known as fly ash forms. Radionuclides can either be encased within the fly ash or attached to the surface of the fly ash. As coal burns, some of the more volatile radionuclides can escape as gas but most will escape on the fly ash. Activity concentration on the fly ash is about ten times higher than the feed coal. In modern coal-fired power plants, approximately 99.5% of the fly ash is prevented from escaping to the atmosphere (compared to <90% in older plants). Doses of approximately 1.0 μSv a^{-1} from a new efficient plant and approximately 20 μSv a^{-1} for an older inefficient plant to a member of a critical group have been estimated [29]. The normalized collective effective doses for 1 year produced from a 1,000 MW(e) plant are as follows: 0.5 person-Sv per GW year for a typical modern plant, 6.0 person-Sv per GW year for a typical old plant, and 50 person-Sv per GW year for the typical plant operating in China, with the global average being approximately 20 person-Sv per GW year [30].

By way of comparison, radionuclides from nuclear plant operations that are released to the environment tend to be noble gases, carbon-14 and tritium. These have a different impact on uptake in the body and the effective dose received. These radionuclides are formed through fission in the uranium fuel and also by neutron activation that occurs in and around the reactor vessel. These radionuclides are released from the nuclear plant in varying levels depending on the reactor type. The most common reactor types, PWR and BWR, deliver an effective dose of 5 and 10 μSv, respectively [31]. When using global averages for all reactor types, the normalized collective effective dose is 0.43 person-Sv per GW year [31], which is slightly less than the suggested value for typical modern coal-fired power plants and significantly less than the global average of 20 person-Sv per GW year.

When comparing the radionuclide emissions and effects on the environment from nuclear power plants and coal-fired power plants, it is found that direct comparisons are difficult because of the differences in radionuclide type, plant designs, and assessment methodologies. Radionuclides emitted from coal-fired plants tend to be alkali metals and rare earths such as those from the U-238 and Th-232 series. Radionuclides released from nuclear plant operations to the environment tend

to be noble gases, carbon-14 and tritium, which have a different impact regarding uptake of the radionuclides into the body and the effective dose received. McBride [27] shows the bone dose significantly greater from a coal-fired power plant compared with a nuclear plant of the same size. For the 1,000 MW(e) plants modeled the committed effective bone doses were 2.25 person-Sv for coal-fired power plants and 0.21 person-Sv for nuclear power plants. Therefore, direct comparisons can only be made when the parameters of study are carefully specified. It is certain, however, that for as long as coal-fired plants are operating there will be radionuclide releases to the environment from their operation.

Radioactive Waste The International Atomic Energy Agency (IAEA) has established a set of principles based on the basic objective that "*radioactive waste is dealt with in a manner that protects human health and the environment now and in the future without imposing undue burdens on future generations*" [8]. Radioactive waste has been disposed by many different countries in many different ways. Disposal of low-level wastes has been carried out in 20-m deep trenches and capped with a semi-impermeable cover; medium-level wastes have been disposed of in shallow burial facilities, although deep geological burial is considered more appropriate; high-level waste requires isolation from the biosphere in deep repositories [8].

There are numerous possible classifications for radioactive waste. The International Atomic Energy Agency [32] recommends a minimum waste classification system defined as follows:

1. Exempt
   Waste released from regulatory control in accordance with local exemption or clearance levels (generally, waste activity below concentrations established by government regulators).
2. Low- and intermediate-level waste (LILW)
   Generally defined as waste above exemption or clearance levels (i.e., above exempt) with low thermal powers.
3. High-level waste (HLW)
   Waste with long-lived radionuclides (>30 year half-life) above specified concentration levels and high thermal powers.

In addition to the above classifications, there are a number of descriptive waste classifications that may be utilized to further subdivide categories. Some other possible classifications [32] are listed in Table 9.

A more comprehensive approach to radioactive waste classification has been adopted [33] which incorporates defined categories as a function of waste activity and half-life. A qualitative depiction of this is presented in Fig. 9 (adapted from [33]).

It is clear from Fig. 9 that radioactive waste may have different potential environmental impact based upon its classification and storage or disposal criteria. The lower the activity and half-life of the waste, the more immediate impact there can potentially be on the environment, due to the fact that for lower activity and half-life the material is disposed closer to human and nonhuman biota receptors. For higher activity and half-life, the disposal and storage solutions are engineered for long-term security that may last thousands of years, suggesting that any potential environmental impact will be far into the future.

There are two general types of radioactive waste disposal: (1) land disposal (or storage) and (2) ocean disposal. Land disposal may also be considered storage, since the waste will usually be in a condition whereby it could be recovered if needed. Ocean disposal of radioactive waste would generally not be retrievable due to the extreme depths involved. A third type of disposal that has been discussed in the past is nuclear waste disposal in space [34]. Investigations into this method of disposal are not being actively pursued due to high cost of disposal and potential launch risks.

All radionuclides that are found in used nuclear fuel and that are produced through nuclear power generation to be utilized for commercial, industrial, medical, or research purposes may be found in radioactive

Radiation in the Environment, Sources of. Table 9
Descriptive radioactive waste classifications

Cladding	Long lived	Primary/raw	Transuranic
Alpha bearing	Short lived	Secondary	Nuclear application
NORM	Heat generating	Mining and milling	Very low level
Mixed	Solidified	Reactor	Vitrified

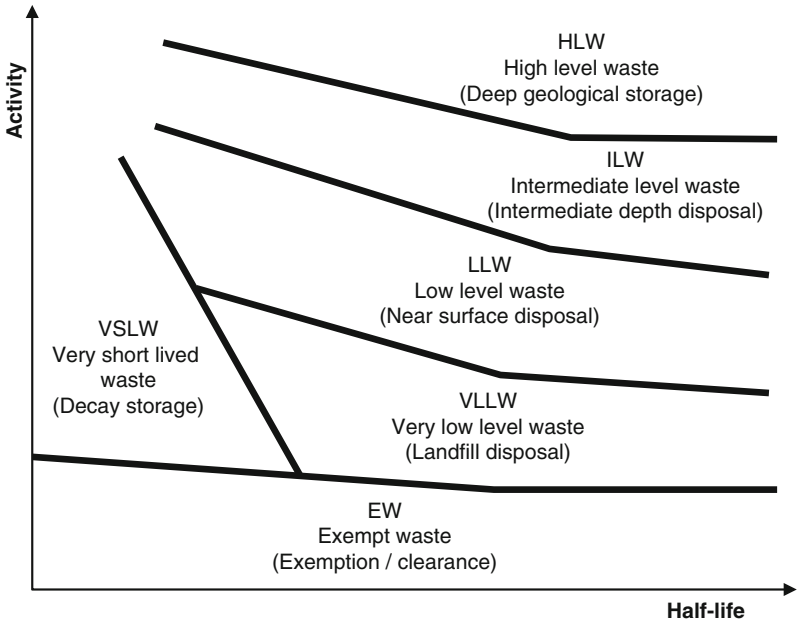

Radiation in the Environment, Sources of. Figure 9
Radioactive waste classification schemes

waste. Wastes that are stored in landfills or municipal waste storage facilities are de facto introduced into the environment. However, their designation as low-level waste is strictly regulated to ensure protection of both human and nonhuman biota. High-level waste (e.g., from nuclear reactor spent fuel) has engineered barriers and its storage employs defense-in-depth strategies to prevent release to the environment.

Ocean Dumping of Radioactive Waste In the past, the disposal of radioactive waste at sea was allowed and regulated by the terms of the 1972 Convention of the Prevention of Marine Pollution by Wastes and other Matter (London Convention). In 1985, a decision was passed at the London Convention that suspended radioactive waste dumping at sea, and in 1993 the suspension was converted into an indefinite ban [8].

Historical dumping of radioactive waste into the oceans has taken place from 1946 through at least 1991 [35]. From 1946 through 1970, the USA dumped radioactive waste into the Atlantic Ocean, Pacific Ocean, and Gulf of Mexico [36]. The greatest amount of radioactive waste was, however, disposed by the former Soviet Union between the years of 1959 and 1991. Both solid and liquid radioactive wastes ranging from liquid effluent, containers, large objects, and entire vessels have been disposed into the Baltic, White, Barents, and Kara seas as well as other Arctic locations [35]. The sinking of Soviet submarines is covered in section "Nuclear-Powered Vessel Accidents". A summary of the estimated total activity introduced into the seas adjacent to the former Soviet Union is provided in Table 10 [35]. It must be noted that the activities presented represent the best estimates of activity at the time of disposal, and therefore represent a maximum bound.

There have been no measurements of dangerous levels of radioactivity in the surface seawater near any of the dumping sites [35]. However, this does not suggest that continuing monitoring and numerical prediction of release and consequences should not take place. It has been calculated that the global radiological impact of the radioactive waste dumping in the Arctic seas will be much less than that of the other forms of anthropogenic radionuclides already in existence [37]. The future impact remains to be verified through a continual environmental monitoring program near ocean radioactive waste dump sites.

Radiation in the Environment, Sources of. Table 10
Activity introduced into the maritime Arctic environment

Waste type	Activity (TBq)
Liquid radioactive waste	903
Solid radioactive waste (low and intermediate level)	590
Objects with spent nuclear fuel	85,100
Objects without spent nuclear fuel	Up to 3,700

Nuclear Weapons Testing

The world's first nuclear test detonation occurred on July 16, 1945 (Code Name: Trinity), at the Alamagordo Proving Ground Site in New Mexico, USA, and is the earliest form of anthropogenic radioactivity having potential for global environmental impact. The nuclear weapon tested was an implosion type device placed on top of a 30.5 m (100 ft) steel tower (Fig. 10). The device contained 6 kg Pu-239 and the nuclear yield was approximately 21 kT, where a kiloton (kT) is the explosive energy release expressed in equivalent tons of the chemical explosive trinitrotoluene (TNT) [38]. The explosion at 15 s post detonation and the resulting crater created at the Trinity site are seen in Fig. 11. The heat of the explosion fused elements of the device, tower, and soil into a glassy material known as Trinitite. Sixty years after the first nuclear explosion, samples of Trinitite have been analyzed [39] and determined to contain fission products (Sr-90 and Cs-137), activation products (Co-60, Ba-133, Eu-152, Eu-154, Pu-238, and Pu-241), as well as fuel remnants (Pu-239 and Pu-240). A sample of Trinitite is shown in Fig. 12. The characteristic green hue is observed, and it is noted that the side facing the heat from the nuclear device blast is smooth, whereas the side away from the blast is rough.

The Trinity test was the prelude for the only wartime use of nuclear weapons; when in World War II, the USA detonated two nuclear weapons against Japan: the first on August 6, 1945 (Code Name: Little Boy), and the second on August 9, 1945 (Codename: Fat Man). The Little Boy weapon was a gun-type nuclear device, producing a nuclear yield of approximately 13 kT, whereas the Fat Man weapon was an implosion device producing a nuclear yield of approximately 22 kT [40]. These first acts of exploiting the massive energy release associated with nuclear technology opened the so-called Atomic Age [41].

Radiation in the Environment, Sources of. Figure 10
Trinity tower (Photo courtesy of National Nuclear Security Administration/Nevada Site Office)

In general terms, the objectives of a nuclear test program are to ensure the operational readiness of stockpiled nuclear weapons, test new designs and to study the nature and effect of radiation fields generated by the weapons. The characteristics (such as design, weapon yield, and burst type) of nuclear weapons are important in understanding the potential distribution to and impact on the environment, and are discussed in the next section.

Characteristics of Nuclear Weapons Prior to discussing nuclear weapons testing, it is worthwhile to discuss environmental impact from the manufacture of nuclear weapons. Nuclear weapons production involves, in broad categories, the following seven steps in the fissile material production [42]:

1. Uranium mining
2. Milling

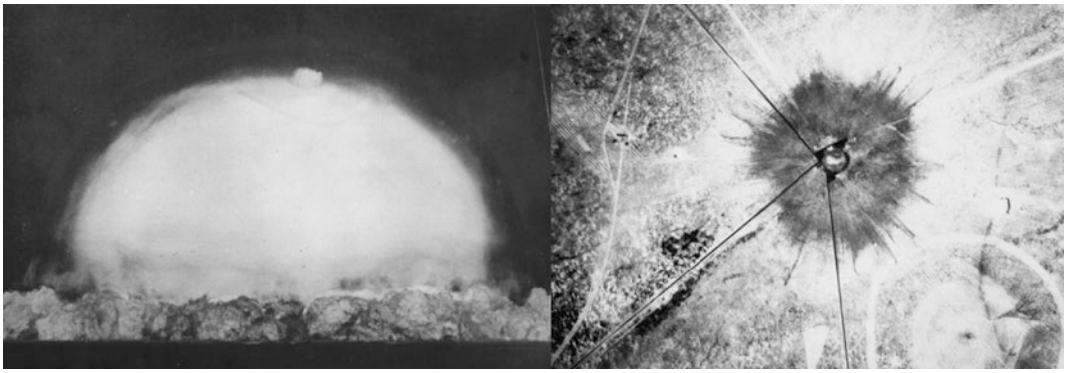

Radiation in the Environment, Sources of. Figure 11
The Trinity explosion at 15 s post detonation (*left*) and the resulting crater (*right*) (Photo courtesy of National Nuclear Security Administration/Nevada Site Office)

Radiation in the Environment, Sources of. Figure 12
Trinitite, blast side (*left*) and ground side (*right*) (Photo courtesy of E. Waller, UOIT)

3. Refining
4. Enrichment
5. Fuel and target fabrication
6. Reactor operations
7. Chemical separations

Approximately 85% of the radioactive waste generated through weapons production occurs at the chemical separations stage. For example, regarding the US Nuclear Weapons Complex, most of the environmental contamination is confined to production facilities at Hanford, Savannah River, K-25, Portsmouth, and Paducah [42] and all are under remediation.

The two principal types of nuclear weapons are (1) nuclear fission based and (2) thermonuclear fusion based. Fission weapons can be further subdivided as gun type and implosion type. The fission-based weapons were the first nuclear weapons developed and have an energy yield in the range of <1–500 kT. Subsequently, fusion-based weapons were developed (which usually involve two stages: a fission detonation

rapidly followed by the fusion reaction) and capable of energy release that can exceed 50 MT.

There are numerous physical designs of nuclear weapons, which tend to depend upon the delivery system they are designated for. Different delivery systems include free-fall bomb (from aircraft), missile (as part of rocket package), torpedo (from submarine), shell (from artillery delivery), and stationary (i.e., emplacement of the weapons package statically). There are four principal categories of nuclear weapons detonation (hence testing), which include (a) exoatmospheric, (b) atmospheric, (c) underground, and (d) underwater. Each category of detonation has a different potential impact on the environment, as described below [40]:

Exoatmospheric: The primary reason to detonate in this fashion is to destroy command and communication, via disruption of satellites. First, the direct radiation can destroy sensitive electronics systems. Second, radiation generated through an exoatmospheric burst can generate a satellite phenomenon called system-generated electromagnetic pulse (SGEMP) which can destroy electronics within the satellite. Finally, it can increase the radiation density in and around the Van Allen belts, thereby increasing the probability of disabling satellite systems. The environmental impact on Earth from radiation emitted during an exoatmospheric detonation is minimal; however, the impact on the space environment can be severe.

Atmospheric: The primary reason to detonate in this fashion is to maximize damage to target(s). The spread of ground contamination is reduced with increasing height of burst from surface to near-exoatmospheric, since the interaction of the weapon radiation and material with the ground material will be reduced as the height of burst increases. The distribution of weapon energy from an atmospheric detonation at low to moderate altitudes is given in Fig. 13. Although most damage is introduced through thermal and blast effects, instantaneous neutron radiation will be responsible for activation of structural materials, and residual radiation (fallout) will be responsible for persistent environmental radiation. In addition, at very high altitude (>50 km) a very strong electromagnetic field (EMP) will be generated, which is capable of disabling electronics on ground and in the air. In addition, a number of atmospheric tests conducted by the USA

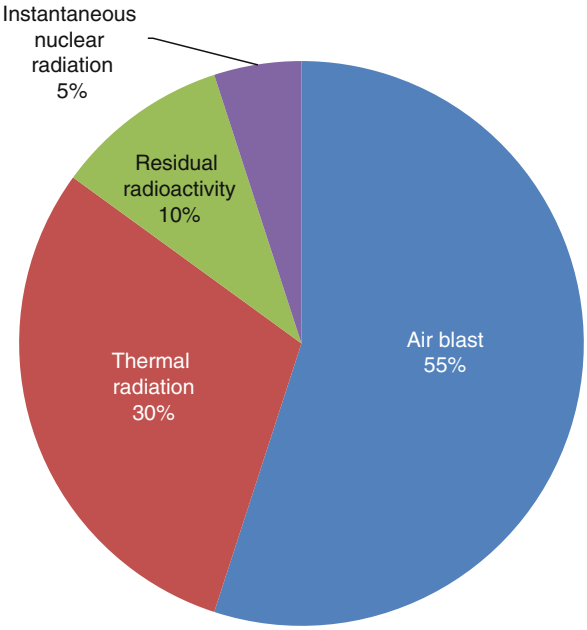

Radiation in the Environment, Sources of. Figure 13 Distribution of energy in a nuclear weapon atmospheric explosion (Adapted from [44])

(22 tests), UK (12 tests), and France (5 tests) can be classified as safety tests, or "shots" [31]. These shots were conducted to test the safety features of nuclear weapons to inadvertent detonation of the warhead (e.g., through Broken Arrow accidents). A safety shot, by design, has a desired effect of no nuclear yield, and therefore contamination should purely be a result of damage and dispersion of the weapon materials [43].

Underground: This type of testing was introduced when test ban treaties were signed by the major nations testing nuclear weapons in the atmosphere. Except for weapons testing and the possibility of generating a large shock wave to destroy underground structures, there is little reason to detonate a nuclear weapon underground.

Underwater: An underwater burst can send large shock waves (both atmospheric and subsurface) to great distances, disrupting sea-going vessels of all kinds.

Nuclear radiation is emitted from both fission and fusion reactions in a thermonuclear weapon. Initial, or prompt, radiation is that generated within approximately 1 min post detonation. This includes neutrons, gamma rays, x-rays, alpha particles, and beta particles.

Only neutrons are capable of producing persistent radioactivity in the environment through neutron activation of materials. Residual radiation, primarily in the form of fission products, is manifest approximately 1 min post detonation [45]. It is this residual radiation that becomes a source of environmental radioactivity.

Global Nuclear Weapons Testing The worldwide total number of nuclear weapons tests recorded to date is 2,421, including the atomic bombs dropped on Hiroshima and Nagasaki and all safety shots [31]. A summary of the tests is provided in Table 11. Only two categories are considered: atmospheric (including all atmospheric and exoatmospheric tests), and underground (including all underground and underwater tests).

As is evidenced in Table 11, the USA and USSR conducted hundreds of nuclear weapons tests since 1945. The great quantities of measureable radioactive fallout from these tests, coupled with the unstable political situation of the 1962 Cuban Missile Crisis, lead to the development of the Limited Test Ban Treaty (LTBT) of 1963, which banned nuclear detonations in the atmosphere, exoatmosphere, and underwater. The ban did not extend to underground testing. Although the USA, UK, and USSR were signatories to this treaty, France and China were not and continued to test in the atmosphere until 1980. In 1974, the Threshold Test Ban Treaty (TTBT) came into effect and limited underground nuclear weapons tests to less than 150 kT yield. Two years later in 1976 the Peaceful Nuclear Explosions Treaty (PNET) extended the ban from weapons to include nuclear explosions for peaceful purposes. Throughout this period, a Comprehensive Test Ban Treaty (CTBT) was developed with the goal to ban all nuclear weapon testing. The treaty became available for signature in 1996, and most of the world's nations have signed (if not ratified) the treaty [46].

Of greatest importance to the injection of anthropogenic sources of radioactive material into the global environment is atmospheric nuclear testing. This is due to the fact that the fission and fusion processes generate radioactive by-products that are introduced with high energy into global atmospheric circulation patterns, and can travel aloft globally in the troposphere and stratosphere. The radionuclides distributed globally from atmospheric testing that are important from a dosimetry standpoint are presented in Table 12 [31]. The significance to environmental sources of radioactivity is clear, as many of the isotopes have been released in great abundance or have relatively long half-lives.

In the following sections, specific important nuclear weapon test sites are discussed with relevance to their environmental impact and global distribution of radionuclides.

Radiation in the Environment, Sources of. Table 11
Summary of all nuclear weapons testing

Country	Number of tests		
	Atmospheric	Underground	Total
USA	219	908	1,127
USSR	219	750	969
France	50	160	210
UK	33	24	57
China	22	22	44
India		6	6
Pakistan		6	6
North Korea		2	2
Total	543	1,878	2,421

Marshall Islands, Pacific Ocean The Pacific Proving Ground was located in The Republic of the Marshall Islands (RMI), and is composed of 1,225 islands and inlets including 29 atolls and 5 solitary, low coral islands. Centrally located in the Pacific Ocean, the Republic of Marshall Islands covers more than 5,025,000 km^2; however, only 181.3 km^2 or about 0.01% of the republic is dry land. The two primary atolls utilized for nuclear weapons testing were Bikini and Enewetak. Bikini Atoll is the largest atoll in the Republic of the Marshall Islands (RMI) and consists of 23 islands and 187 km^2 of coral reefs [47]. The atolls of the RMI were formed when fringing reefs began to establish and grow around emergent volcanoes. While the volcanic peaks slowly sank and reduced in size, the fringing reefs continued to grow and eventually coral atolls formed after the volcanoes disappeared entirely beneath the sea [47]. In the period between 1945 and 1962, a total of 5 underwater and 101 atmospheric nuclear weapon tests were conducted here.

Radiation in the Environment, Sources of. Table 12 Global release of radionuclides from atmospheric nuclear weapons testing

Radionuclide	Half-life	Global release (PBq)
H-3	12.33 a	186,000
C-14	5,730 a	213
Mn-54	312.3 d	3,980
Fe-55	2.73 a	1,530
Sr-89	50.53 d	117,000
Sr-90	28.78 a	622
Y-91	58.51 d	120,000
Zr-95	64.02 d	148,000
Ru-103	39.26 d	247,000
Ru-106	373.6 d	12,200
Sb-125	2.76 a	741
I-131	8.02 d	675,000
Ba-140	12.75 d	759,000
Ce-141	32.50 d	263,000
Ce-144	284.9 d	30,700
Cs-137	30.07 a	948
Pu-239	24,110 a	6.52
Pu-240	6,563 a	4.35
Pu-241	14.35 a	142

The Bikini and Enewetak Atolls were the first nuclear testing grounds after World War II. Starting in 1946 and ending in 1958 the USA tested 23 surface and subsurface thermonuclear devices at Bikini Atoll with an additional test conducted approximately 100 km from the atoll [48]. The total magnitude of the Bikini nuclear tests was 76.3 MT, accounting for 72% of the total yield tested in both atolls [7]. These tests caused great damage to Bikini's physical and ecological landscape creating five craters, the biggest one being the BRAVO crater which is 73 m deep [47]. The BRAVO test has been termed the "BRAVO accident" by some researchers due to the fact that the test, conducted on March 1, 1954, had a yield of 15 ± 2 MT, but prior to detonation was estimated to yield 6 ± 2 MT [49]. The creation of the BRAVO crater caused the destruction of three small islands and moved millions of tons of sand, coral, plant, and sea life from Bikini's reef [50]. Observed short-term effects in native and military populations from the BRAVO shot included nonfatal depression of blood cell production, localized skin burns from beta-emitting fallout, and internal contamination (hence dose) from fission products [49]. In addition, observance of leukemia in exposed persons has been made, as well as deleterious effects to thyroid function due to I-131 [49]. As a final consequence to the Marshallese populations living on the Bikini Atoll, major psychological trauma from repetitive relocations (due to areas being inhabitable from fallout) was observed [49].

The long-term consequences of nuclear weapons testing from chronic and large-scale anthropogenic disturbances for biodiversity are not very well understood in the Marshall Islands, to either inhabitants or the ecosystem. As a result of the nuclear weapons testing, the following principal radionuclides were released into the environment in the Marshall Islands: Cs-137, Sr-90, Pu-239,240, and Am-241 [51]. For example, soil samples from mid-Pacific global fallout are estimated to be approximately 400–800 Bq m^{-2} for Cs-137 and 0.2–0.4 Bq kg^{-1} for Pu-239,240 [48]. Distribution of radionuclides varies widely amongst the islands of the various atolls and also as a function of latitude [48]. Nuclear weapons testing also altered the natural sediment distribution by redistributing a higher amount of the fine material over the surface of the sediment, which impacts the local ecosystem [52]. The testing caused a great disturbance to the Marshall Islands environment and to local and global distribution of anthropogenic radionuclides.

Nevada Test Site, USA A number of locations within the continental USA were used for nuclear weapons testing [53], presented in Table 13. The most utilized testing site by far was the Nevada Test Site (NTS). The NTS is located approximately 105 km northwest of Las Vegas, NV. The site encompasses 3,500 km^2 and is bordered by the Nellis Air Force Range and Tonopah Test Range. The three US federally controlled areas total approximately 14,200 km^2 of unpopulated land.

After the Trinity test and the dropping of the two nuclear weapons on Hiroshima and Nagasaki in 1945, testing was moved to the Bikini and Enewetak Atolls in

Radiation in the Environment, Sources of. Table 13 Location and number of nuclear weapon tests in the continental USA

Location	Number of tests
Alamogordo, NM	1
Amchitka, AK	3
Bombing Range, NV	5
Carlsbad, NM	1
Central Nevada	1
Fallon, NV	1
Farmington, NM	1
Grand Valley, CO	1
Hattiesburg, MS	2
Nevada Test Site, NV	928
Rifle, CO	1
Total	945

the Pacific Ocean, where five nuclear weapons were tested between 1945 and 1951 [53]. Due to the large logistical effort, support, cost, and time required to perform testing at these remote locations and the requirement to accelerate nuclear weapons testing and production, a decision was made to develop a weapons testing capability within the continental USA. A number of sites were considered, and some nuclear weapons were tested at candidate sites (see Table 13). However, the primary site selected for continued testing, both atmospheric and underground, was the Nevada Test Site. The Nevada site was selected for atmospheric testing based upon its remote setting, favorable year-round weather/wind patterns, and restricted access. In addition, for underground testing, the NTS is characterized by favorable conditions for excavating deep geological trenches, slow-moving groundwater, and arid climate [54]. Atmospheric testing (199 tests) was conducted at the NTS between January 1951 and October 1958. From 1958 through 1961, nuclear testing was suspended by an international voluntary moratorium. Underground testing (approximately 809 tests) was conducted there from 1962 through 1992 (although underground testing is still allowed under test ban treaties, no nuclear weapons testing has been conducted at NTS since 1992 as the US Government adopted a second voluntary testing moratorium). Radionuclide contamination in and around the Nevada test site and neighboring states was monitored during and after each test. Numerous monitoring devices, such as ion chambers, Geiger counters, and air samplers (Fig. 14), were used to characterize the fallout. Aircraft were routinely decontaminated after flying near the plumes (Fig. 15).

The environmental radionuclide source term from the NTS has two components: atmospheric testing fallout (until October 1958) and underground testing radionuclide inventories (until October 1992). Fallout from atmospheric testing consists primarily of a large array of fission products. An estimate of the total radionuclide deposition in the continental USA from some of the more important fission products generated by NTS tests is given in Table 14 [55].

Underground testing was performed such that the majority of the radionuclides produced were contained in the deep geological formations in which the nuclear devices were tested. As such, there is no appreciable fallout. However, there is potential impact to the environment through migration of the radionuclides into the water table at the NTS. The primary radionuclide constituents involve fission products, unspent fuel actinides, tracer elements, residual tritium primarily from thermonuclear detonation, and activation products both in the weapon casing and the soil. Measurements and calculations have been performed to estimate the total radionuclide inventory below the water table at the primary NTS testing sites. An estimate of some of the principal radionuclides (decay corrected to September 23, 1992) is provided in Table 15 [49, 54].

Native American Exposure at Duckwater, Nevada A reservation was established in 1940 for the Duckwater Shoshone tribe (21 families) in Duckwater, Nevada, located approximately 160 km (100 miles) north of what was to become the Nevada Test Site (NTS). Historical wind directions from most bomb tests indicate that fallout would tend to travel predominantly north and east of the NTS, which directed fallout into populated Native American territories [56]. It has been reported that during the period of nuclear weapons testing, no health protective measures were attempted and only minimal efforts

Radiation in the Environment, Sources of. Figure 14
Two airmen check a T-33 jet airborne filter units used for collecting plume particulate (Photo courtesy of National Nuclear Security Administration Nevada Site Office)

Radiation in the Environment, Sources of. Figure 15
Decontamination of a B-50 Superfortress (Photo courtesy of National Nuclear Security Administration/Nevada Site Office)

Radiation in the Environment, Sources of. Table 14 NTS fallout radionuclides

Radionuclide	Total deposition (PBq)
^{137}Cs	2.3
^{90}Sr	1.8
^{95}Zr	220
^{103}Ru	430
^{140}Ba	1,400
^{141}Ce	500
^{144}Ce	40
^{106}Ru	24
^{89}Sr	330
^{131}I	1,500
$^{239+240}Pu$	0.13
^{241}Pu	0.54

Radiation in the Environment, Sources of. Table 15 NTS radionuclide inventory from underground testing

Radionuclide	Total deposition (PBq)
^{3}H	4,647
^{137}Cs	106
^{90}Sr	81
^{85}Kr	7
^{152}Eu	6
$^{239+240}Pu$	8
^{241}Pu	22

were made to inform people about the testing and the associated risks [57]. As a result, members of this tribe were exposed to fission products, especially volatile fission products.

A model was designed to follow a specific fission product, I-131, through a rabbit consumption scenario based upon tribal member activity. Researchers estimated that during the fall 3.2 rabbits were eaten per week, and during the rest of the year, 1.5 rabbits were eaten per week per person [57]. The pathway from the initial deposition of I-131 through to the consumption of rabbit by an adult is summarized as follows: (a) I-131 is deposited on plant surfaces from nuclear weapons testing, where it can either be reduced via weathering or by radioactive decay. (b) When a rabbit eats the vegetation, the I-131 is absorbed by the thyroid in the rabbit, with reduction occurring via radioactive decay and excretion. (c) Seasonal consumption of the rabbits by humans occurs whereby the I-131 goes to the human thyroid. (d) I-131 can also be transferred by breast milk to infant. In addition, the mobility of the Duckwater Shoshone tribe members was taken into account, insofar as they tended to hunt over a wide area. Twenty-five test events were reported to have deposited fallout in Duckwater or within 50 miles of Duckwater [57]. Dose estimates and thyroid cancer excess relative risk (ERR) estimates were derived based upon the largest events. Elevated ERR estimated were generated for the vulnerable population (<15 years of age when exposed), although there is no epidemiological data to support excess observed thyroid cancers to date. Of interest to the subject of sources of radioactivity in the environment, this study depicts an environment exposed to multiple fission products, extending numerous decades of weapons testing, which has elements of vulnerable populations (children), and has relatively stationary ecosystem members (rabbits), as well as highly mobile target populations (adults), which all point to the complexity of establishing environmental pathways for identified groups. Significant whole body exposures (upward of 10 mSv) have been estimated to residents of Duckwater and other Native American communities in the environs surrounding the NTS. As well, estimates of up to 200 mSv thyroid dose (from I-131) to these populations have been made [56].

Maralinga Test Site, Australia The UK conducted nuclear weapons testing between 1952 and 1957 on the Australian continent. The tests were conducted at Monte Bello Island, Western Australia (3 tests), Emu Field, Southern Australia (2 tests), and Maralinga Range, South Australia (7 tests). The nuclear weapons tests ranged in nuclear yield from approximately 1 to 60 kT. In addition to the above nuclear weapons tests, the UK conducted a number of "minor trials" designated primarily as safety shots, producing little to no nuclear yield. The safety shots were designed to explore

the potential dispersion of material from a nuclear weapon under conditions of burning and explosive dispersal.

The most used test site was the Maralinga range, which hosted seven nuclear weapon detonations and hundreds of safety shots. The radionuclides released from the weapons tests were standard fission and activation products, many of which rapidly decayed away. However, the safety shots generated large areas of plutonium and uranium contamination in Maralinga, and specifically the area of Taranaki became the most contaminated region in Maralinga [58]. The principal limiting radionuclide for environmental exposure is Pu-239 and studies have been performed to characterize the plutonium contamination [59]. Soil concentrations around Maralinga are estimated on average at a level of 10 Bq g^{-1} [60] and annual effective doses to members of critical groups (typically aboriginal peoples residing in the area) have been conservatively estimated to approach 0.5 Sv [58]. Rehabilitation of some of the areas at Maralinga (including Taranaki) has been performed by collecting contaminated soils, placing in trenches, and covering with 5 m of clean soil. The Maralinga site rehabilitation effort is ongoing [61].

Mururoa, French Polynesia Early (1960–1966) French nuclear weapon testing (17 tests) was conducted in French Algeria [62]. As a result of Algeria gaining independence in 1962, the French moved testing to the Mururoa and Fangatuafa Atolls in French Polynesia. A total of 178 nuclear weapon tests were conducted in the Atolls along with 15 safety shots at Mururoa [63], as presented in Table 16. It may be seen that Mururoa was the most utilized test location.

The Atolls are largely uninhabited and as a result there was little potential impact to human exposure. Studies have been performed to quantify the levels of certain fission products such as Cs-137 [64] and actinides such as Pu-239 and Pu-240 [65]. In general, long-lived fission products and actinides have been observed in the lagoon sediments. The largest potential contributor to environmental exposure is plutonium, which is decreasing over time due to removal from the sediments and dilution in a large Pacific Ocean volume [66]. Tritium has also been measured in the lagoons; however, it is estimated that any dose contribution from the tritium is negligible [66]. The estimated inventories of some important radionuclides from the lagoons of the Atolls are presented in Table 17 [67].

Semipalatinsk Test Site, Kazakhstan The former Soviet Union (USSR) conducted nuclear tests from 1949 to 1990 primarily at the Semipalatinsk test site (456 tests) in Kazakhstan and the Novaya Zemyla test site (130 tests) in the Arctic Archipelago [68]. In addition, three other locations hosted nuclear weapons tests, specifically (1) missile test range, Astrakhan region; (2) firing grounds, Soviet Ministry of Defense, Totsk; and (3) near Aralsk. The former Soviet Union conducted peaceful nuclear explosions (119 tests) in a number of locations around the former Soviet Union. All nuclear weapon and peaceful use tests are outlined in Table 18 [68].

It is clear that the Semipalatinsk test site was the most utilized of all nuclear test sites. A total of 111 atmospheric detonations (86 air and 25 surface) were conducted between 1949 and 1963 at Semipalatinsk, causing the majority of contamination to the environment and most exposure to the public. Four of the tests, occurring in 1949, 1951, 1953, and 1956, are estimated to have contributed to more than 95% of

Radiation in the Environment, Sources of. Table 16
French nuclear weapon tests

Location	Atmospheric	Underground	Total
Mururoa	37	127	178
Fangataufa	4	10	
Safety shot	5	10	15

Radiation in the Environment, Sources of. Table 17
Radionuclide inventories from Mururoa and Fangataufa Atolls

Radionuclide	Total activity (TBq)
$^{238+239+240}Pu$	30
^{241}Am	<1
^{137}Cs	<1
^{152}Eu	<1
^{60}Co	<1

the dose to the population surrounding the Semipalatinsk test site [70].

Considerable levels of contamination can be found in and around the Semipalatinsk test site, as demonstrated in Table 19 [71, 72]. "Ground Zero" refers to the area immediately under the first thermonuclear test in 1953, and Chagan (sometimes referred to as Bolapan) refers to a crater formed by a 1965 underground nuclear explosion. The total inventory of radionuclides important as environmental contaminants near the Semipalatinsk test site is provided in Table 20 [68].

Radiation in the Environment, Sources of. Table 18 Location and number of nuclear weapon tests in the former USSR

Location	Number of tests
Semipalatinsk	456[a]
Novaya Zemlya	130
Russian federation (European)	59
Russian federation (Asian)	32
Ukraine	2
Kazakhstan	33
Uzbekistan	2
Turkmenia	1
Total	715

[a] This number is sometimes quoted as 498, which takes into account unsuccessful nuclear explosions that contributed to spread of contamination [69].

Numerous studies have been conducted on the population and ecology of the former Soviet Union, especially near the Semipalatinsk test site. Radionuclides have been detected in the terrestrial environment, members of the food chain, and efforts have been made to retrospectively calculate the dose to surrounding populations (see, e.g., [73, 74]). The investigations will continue for many decades.

Nuclear Material Accidents

There are six main categories of nuclear accidents considered herein with respect to release of radioactive material to the environment:

1. Nuclear reactor accidents
2. Fuel processing accidents
3. Nuclear weapon accidents
4. Nuclear-powered vessel accidents
5. Depleted uranium munitions
6. Space nuclear power source accidents

Accidents and incidents involving medical, industrial, and lost/orphan sources are discussed in their respective sections. Although not accidents per se, depleted uranium munitions use is included herein since the controversy surrounding depleted uranium use in the battlefield was not anticipated a priori.

It is worthy to note that, due to the secrecy surrounding nuclear reactor and nuclear weapon capability in many countries, there may be many more undocumented minor releases to the environment or lost nuclear weapons. It is expected that most major releases to the environment will be detected by

Radiation in the Environment, Sources of. Table 19 Radionuclide contamination (Bq kg^{-1}) in and around Semipalatinsk

Radionuclide	On-site [71]		Nearby village [72]
	Ground zero	Chagan	Dolon
^{137}Cs	108–83,300	1,500–22,600	2.8–71.4
^{60}Co	<2–5,410	356–21,840	–
^{152}Eu	17–96,100	321–17,200	–
^{154}Eu	<6–2,910	585–11,430	–
$^{239+240}$Pu	488–27,900	192 – 8,850	1.7–94.9
^{241}Am	52–520	24–1,056	–

appropriate metrology, although the potential impact of historical releases that have not been documented may never be known, or their impact has not yet been realized.

Nuclear Reactor Accidents Nuclear reactor accidents are amongst the least common of all industrial accidents. There have only been a few accidents that have resulted in radioactive releases to the environment and/or death, compared with environmental impact and accidents from other industries such as chemical processing, mining, or manufacturing.

A list of nuclear reactor accidents contributing to environmental source terms is provided in Table 21. The table only describes accidents where there were measured releases of radioactive material to the environment, and not core releases that were contained within the reactor environs.

Three Mile Island Unit 2 The interest in the TMI-2 accident is not as much in its environmental releases (which were minimal) but in the damage it did to the nuclear industry in the USA and abroad. The accident has been well analyzed [75], and the details will not be discussed herein.

On March 28, 1979, a combination of equipment and operator errors culminated in the core of the reactor partially (approximately 50%) melting. This led to stack venting of built-up noble gases and volatile iodine [25]. The activities of principal radionuclides released as a result of the TMI-2 accident are shown in Table 22 (adapted from [2]). There is no environmental impact from the releases since all principal radionuclides have short half-life. In addition, there was no significant radiation exposure to any workers or members of the public.

Chernobyl NPP Unit 4 Special discussion must be given to the Chernobyl (also known as Chornobyl) Nuclear Power Plant Unit 4 accident as it is responsible for the single greatest release of anthropogenic radioactive material into the environment from a nuclear reactor accident. A great number of essays, treatises, and books have been written about the technical, political, sociological, and health impacts of the Chernobyl accident, and as such this section makes no attempt to cover these issues in any detail. A brief summary of the accident follows, with an overview of the sources of radiation introduced into the environment from this accident.

The Chernobyl Nuclear Power Plant (NPP) is located in Northern Ukraine, in relatively close

Radiation in the Environment, Sources of. Table 20 Total radionuclide inventory of important radionuclides near Semipalatinsk

Radionuclide	Total activity (TBq)
$^{238+239+240}Pu$	0.15
^{90}Sr	1
^{137}Cs	1.5

Radiation in the Environment, Sources of. Table 21 Nuclear reactor accidents with environmental releases

Date	Reactor	Release to environment
December 12, 1952	NRX, Chalk River, Ontario, Canada	Fission products, principally Pu, Xe, Te, I, Cs and Ru
October 10, 1957	Windscale Pile 1, Cumbria, UK	Fission products, principally I-131, Cs-137, Sr-89,90 and Po-210
July 26, 1959	Sodium Reactor Experiment, Santa Barbara, California, USA	Radioactive gases released from containment
January 3, 1961	SL-1, near Idaho Falls, Idaho, USA	I-131
January 21, 1969	"Experimental nuclear reactor," Lucens Vaud, Switzerland	Reactor was housed in a natural cavern under a hill. No radioactivity was released from cavern
March 28, 1979	TMI-2, Middletown, Pennsylvania, USA	Noble gas fission products and I
April 26, 1986	Chernobyl Unit-4, Chernobyl, USSR (now Ukraine)	Fission and activation products, discussed below

Radiation in the Environment, Sources of. Table 22
Estimated activity of radionuclides released from 1979 TMI-2 accident

Nuclide	Activity (PBq)
^{88}Kr	1.4
^{133}Xe	55.5
^{133m}Xe	8.5
^{135}Xe	11.1
^{135m}Xe	0.9
^{131}I	0.00056

proximity to both Russia and Belarus. The nuclear plant site is situated near the Pripyat River, which feeds into the larger Dnieper River that flows south to the capital city of Kiev. The site hosted six nuclear plants: units 1–4 were operational, whereas units 5 and 6 were under construction at the time of the accident. The reactors were of the RMBK type, which are water-cooled, graphite-moderated reactors. Each reactor was capable of producing approximately 3,200 MW_t, or 1,000 MW_e energy. The reactor was designed with no containment, which suggests that under a severe accident scenario, there would be no barrier between the radioisotopes produced in the fuel and the environment. Unfortunately, in the early hours of April 26, 1986, the Chernobyl NPP Unit 4 had a "beyond design basis" accident, which included a power excursion to at least 300,000 MW_t that produced two major steam explosions within the reactor, blowing the 1,000 t top plate off, destroying all 2,000 fuel channels and releasing massive quantities of radioactive material into the environment.

Activity of the principal radionuclides released in the accident may be found in Table 23. The values presented in the table are averages of a number of estimates made in 1996 [31].

Although only about 3.5% of the core was ejected from the reactor during the accident, extremely large quantities of fission products were released into the atmosphere with much of it being distributed globally. In addition, high percentages of core inventory of certain volatile radionuclides were released, notably approximately 30% of Cs-137 and 50% of I-131 core inventories [31]. The principal dose-producing

Radiation in the Environment, Sources of. Table 23
Estimated activity of radionuclides released from 1986 Chernobyl accident

Radionuclide	Activity (PBq)
^{85}Kr	33
^{89}Sr	92
^{90}Sr	9
^{99}Mo	189
^{95}Zr	169
^{103}Ru	153
^{106}Ru	43
^{131}I	1,753
^{133}I	2,500
^{132}Te	1,075
^{133}Xe	6,500
^{134}Cs	51
^{137}Cs	85
^{140}Ba	190
^{141}Ce	172
^{144}Ce	115
^{239}Np	1,323
^{238}Pu	0.033
^{239}Pu	0.031
^{240}Pu	0.046
^{241}Pu	6
^{242}Cm	1

radionuclides emitted from the Chernobyl accident were Xe-133, I-131, Cs-137, Sr-90, and Pu-239 [25]. Of those, Xe-133 and I-131 were dispersed quickly and have short half-lives, thereby mitigating their concern as long-term environmental contaminants. The Pu-239 and Sr-90 were found to predominantly deposit in the near (<30 km) vicinity of the release, and therefore may be considered a local environmental concern (although most of the contaminated soil was stripped and stored at the Chernobyl NPP4 site). Cesium-137 is significant because of its substantial contribution to lifetime effective dose, its relatively long radiological half-life (30.2 years), and its ease of measurement in

environmental samples (through gamma spectroscopy). Therefore, Cs-137 has been historically chosen as the key indicator radionuclide for environmental contamination [31].

Ground deposition of radioactive material was found in virtually every country in the northern hemisphere. No contamination due to the accident was detected in the southern hemisphere, although interhemispheric transport of contamination occurred through a small extent from human activities, such as shipping materials and food [31]. The predominant radionuclide found globally in the environment from the accident is Cs-137, due to its volatile nature and long half-life. Iodine-131 was important in the early stages of the accident, due to its volatile nature and its impact on the human thyroid. However, with a short half-life of 8 days, it is not a persistent environmental radionuclide. Contributions from Chernobyl to local distributions of Cs-137 have been detected and confirmed in the environment using ratios of Cs-134 to Cs-137 (e.g., [76]). To illustrate the widespread dispersion of radioactivity into the environment, the distribution of Cs-137 around Europe in terms of surface contamination is depicted in Fig. 16. Areas of elevated contamination around the accident site are observed, as well as other isolated areas generated by atmospheric deposition around the time of the accident. Specifically, Finland, Norway, Sweden, Austria, and Bulgaria all recorded elevated levels of Cs-137 [31]. Prior to the Chernobyl accident, all environmental Cs-137 was due to nuclear weapons fallout.

In the area around Chernobyl NPP4, known as the exclusion zone, environmental sampling is conducted to help assess the long-term impact of the accident. Soil and vegetation sampling (Fig. 17) routinely takes place to monitor radionuclide (specifically Cs-137) movement and soil-vegetation transfer factors. Measurable quantities of long-lived radionuclides may be found in local biota. Figure 18 shows a beta particle detector reading above background levels on a moose bone. The beta radiation is likely from Sr-90, which has a half-life of 30 years, is a strong beta emitter and was released in abundance from the accident. Strontium acts similar to calcium when taken into the human body, and tends to accumulate where calcium accumulates, hence the elevated bone reading.

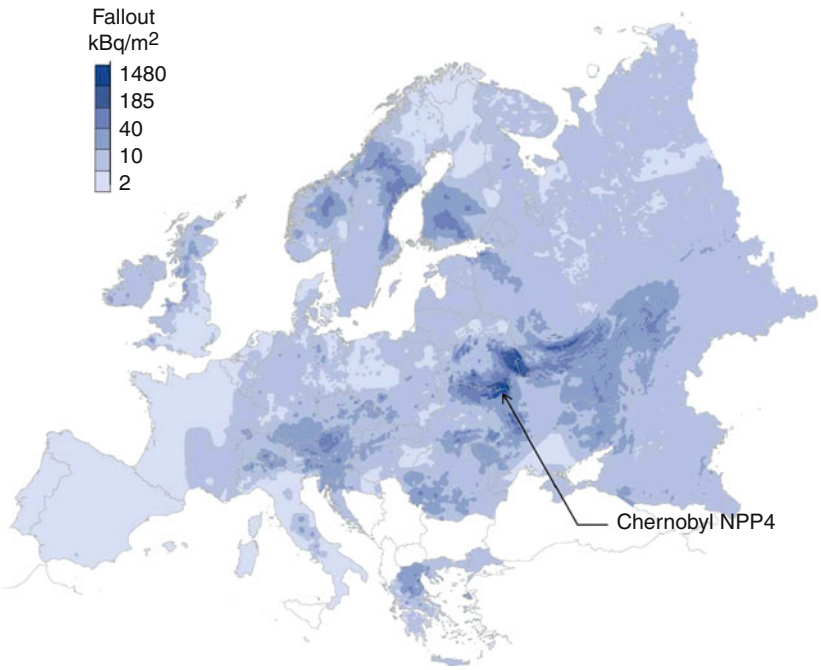

Radiation in the Environment, Sources of. Figure 16
Distribution of Cs-137 around Europe in May 2006 (Figure modified from [77] based on original from EU/IGCE)

Radiation in the Environment, Sources of. Figure 17
Environmental sampling in the Chernobyl NPP4 exclusion zone (Photo courtesy of E. Waller, UOIT)

Radiation in the Environment, Sources of. Figure 18
Beta radiation readings on bone fragment (Photo courtesy of E. Waller, UOIT)

The entrance to the exclusion zone is strictly controlled by monitoring entrance and exit points, which are under control of shelter maintenance and emergency services (Fig. 19 depicts the signage circa 1999). This mitigates problems surrounding movement of contamination to areas outside of the exclusion zone. Regarding the radiological state of the reactor, in mid-May 1986 the decision was made to cover the destroyed Unit 4 with a barrier to prevent further environmental contamination and improve the radiological situation of the Chernobyl NPP4 site [78]. In just over 200 days, by the end of November 1986, the massive concrete and

Radiation in the Environment, Sources of. Figure 19
Sign entering Chernobyl (Photo courtesy of E. Waller, UOIT)

steel structure, known as the "shelter" or "sarcophagus" was constructed. Figure 20 shows the shelter (darker gray) over the original structure (lighter gray).

The shelter was never intended to be a permanent structure, and as such has been in a constant state of deterioration since initial fabrication. As a result, in the mid-1990s plans were made to construct a new permanent structure. The goals of this structure, termed the "New Safe Confinement," were to (a) transform Unit 4 into an environmentally safe system, (b) reduce weathering and corrosion of the existing Unit 4 and shelter structure, (c) mitigate the consequences of a Unit 4 structural collapse, and (d) facilitate safe deconstruction of the unstable Unit 4 structures. The New Safe Confinement is designed to be emplaced over the existing Unit 4 and shelter. It is currently scheduled for completion in 2012.

Fukushima Daiichi Units 1–6 On 11 March 2011, an earthquake and subsequent tsunami off the east coast of Japan caused destabilization of a number of nuclear reactors north of Tokyo, resulting in the release of radioactive material to the environment. This accident will be discussed in the section "Future Directions" – Risk Assessment.

Fuel Processing Accidents There have been a small number of significant environmental releases of radioactivity associated with nuclear fuel processing/reprocessing facilities. In November 1959, there was a chemical explosion at the Oak Ridge National Laboratory radiochemical processing pilot plant, which contaminated the pilot plant building and nearby streets with plutonium [25]. Although the plutonium escaped the confines of the plant, the area was cleaned and no persistent environmental contamination ensued. On September 30, 1999, a prompt criticality occurred at the JCO fuel processing facility in Tokaimura, Japan, resulting in the deaths of two

Radiation in the Environment, Sources of. Figure 20
Chernobyl NPP4 shelter (circa 1999) (Photo courtesy of E. Waller, UOIT)

workers and small releases of radioactivity (principally I-131 and noble gases) to the nearby environment. Due to the short half-lives of the radionuclides released, there is no persistent impact on the environment. A number of other process criticality accidents have occurred over the past 60 years [79] that have produced minor venting of radionuclides to the environment. Two separate facilities in the former Soviet Union/Russian Federation are worthy of special mention here, due to the significant environmental releases associated with both: Siberian Chemical Enterprises in Tomsk, and the MAYAK Production Center in the Ural Mountains.

Tomsk-7 An accident occurred at a Siberian Chemical Enterprises nuclear fuel reprocessing plant, known as Tomsk-7, located near Tomsk in the Russian Federation on April 6, 1993. An overpressure occurred in a tank containing uranium nitrate and a number of radionuclides. The most likely cause of the accident was improper mixing of various solutions that were present in the tank, causing stratified layers of organic material, radioisotopes and uranium nitrate [80]. Nitric acid introduced into this non-mixed solution caused oxidation and nitration of the organic layer (so-called red oil), ultimately resulting in an exothermic reaction [81]. This exothermic reaction increased the tank pressure to 17 atm and resulted in the tank exploding. As a result, approximately 10% of the tank contents were released to the environment, contaminating approximately 135 km^2. The estimated activity and composition of the radionuclides released is given in Table 24.

There was environmental impact both in the environs around the plant, and extending outward to the nearby village of Georgievka and to a lesser extent Naumovka [80]. Relatively low-level contamination was measured in both air and to a lesser extent surface water samples taken around the time of the accident near the accident site. It is estimated that up to 30% of the fallout activity deposited on forest canopies, in the same ratio as presented in Table 24. Many buildings, roads, and infrastructure around the Tomsk-7 site were decontaminated, and waste was buried in a disposal site at Tomsk-7. The relatively short half-lives of the principal radionuclides (except for Pu-239), ensured that the radioactivity associated with the waste dropped off fairly rapidly. Radioactive contamination

Radiation in the Environment, Sources of. Table 24 Estimated activity of principal radionuclides released from the 1993 Tomsk-7 accident

Radioisotope	% Composition in fallout	Estimated activity released (TBq)
^{95}Zr	20.4	6.5
^{95}Nb	44.0	14.3
^{103}Ru	1.4	0.36
^{106}Ru	31.4	9.5
^{125}Sb	0.4	0.1
^{141}Ce	1.5	0.37
^{144}Ce	0.9	0.24
^{239}Pu	0.01	6.3e-3

Source: Adapted from [80].

(of the composition presented in Table 24) was measured around the neighboring village of Georgievka, and this area was also decontaminated. The long-term impact of the accident is limited to the environmental deposition of the longest-lived radionuclide, Pu-239, which was a small percentage of the total fallout. The major constituents of the fallout have relatively short half-lives and decayed fairly rapidly.

Mayak The Mayak Production Association, located in the Chelyabinsk region of the southern Ural mountains, was opened in June 1948 as a critical component of the nuclear weapons complex in the former USSR. The primary mission of the facility was to produce plutonium (Pu-239) for nuclear weapons. The Mayak facility encompassed 90 km^2 surrounded by a buffer zone of 250 km^2 [82]. The facility consisted of uranium-graphite reactors (seven reactors over the years spanning from 1948; five reactors decommissioned), radiochemical plants, and waste storage. Since 1962, Mayak has reprocessed nuclear fuel and has been a significant supplier of radioisotopes. A number of accidents and incidents have occurred over the years at this facility that have resulted in significant releases to the environment and significant dose to both Mayak workers and the general population around the facility.

In the time frame 1951–1967, gaseous aerosol releases in the form of noble gases, I-131, and other volatile materials were emitted from the reactor and radiochemical plant side. Also within this time frame, both planned and unplanned liquid waste releases were introduced into the Techa River from facility operation. A significant accident occurred on September 29, 1957, at the Kyshtym high-level waste storage tank. An equivalent 100 t TNT chemical explosion resulted in significant spread of contamination over 20,000 km^2 in a narrow band extending from Kyshtym to the north eastern village of Kamyshlov [59]. In addition to the above, a number of "wild overflows" occurred in the liquid waste storage tanks resulting in significant environmental contamination of the Techa river. In 1951 an open liquid waste reservoir known as Karachay Lake began operation. In 1967, during a hot spring following a dry winter, the lake partially dried up and large quantities of radioactive sediment underwent wind-driven resuspension and were transported away from the lake. It is impossible to determine with certainty all of the releases that have occurred with respect to operation of the Mayak facility, due to the secrecy of the operation, incomplete record keeping, extended timeline over which the releases occurred, and absolute magnitude of the releases. Some of the more significant environmental releases, and approximate radioisotope activities, are presented in Table 25.

International Nuclear Event Scale To aid in determining the severity of nuclear and radiological incidents, the International Atomic Energy Agency (IAEA) devised the International Nuclear and Radiological Event Scale (INES). The purpose of the INES is to facilitate communication between the technical community, the media and the public on the significance of nuclear or radiological events [83]. The rating system takes into account the impact on workers, the public and the environment. The position on the scale is determined from the highest of three numerical scores from examining on-site effects, off-site effects, and degradation of the defense-in-depth principle. The INES scale is depicted in Fig. 21. Some of the higher INES-level events are the Chernobyl NPP4 accident (INES Level 7); the Mayak Kyshtym explosion (INES Level 6); the Windscale fire, TMI-2 accident, and Goiania accident (INES Level 5); and the SL-1 accident and Tokaimura accident (INES Level 4).

Radiation in the Environment, Sources of. Table 25 Estimated releases to the environment from the Mayak Production Association facility

Release	Date(s)	Principal radioisotope(s)	Activity released (PBq)
Gaseous aerosol releases	1951–1967	^{131}I	20.0
Liquid waste releases including wild overflows	1949–1956	Rare earth elements	27.0
		$^{103,106}Ru$	26.0
		$^{95}Zr/Nb$	14.0
		^{137}Cs	12.0
		$^{89,90}Sr$	20.0
Kyshtym accident	September 29, 1957	Rare earth elements	70.0
		^{90}Sr	3.75
Karachay Lake Resuspension	April–May 1967	^{137}Cs	0.011
		^{90}Sr	0.004

Source: Adapted from [8, 82].

Nuclear Weapon Accidents There have been relatively few nuclear weapon accidents or incidents since the development of nuclear weapons in 1945. The major threat from an accident involving a nuclear weapon is not a nuclear detonation, but rather a spread of contamination through the environment via explosion and/or fire associated with an accident. The reason for this is simply that nuclear weapons require a number of systematic initiation steps including physical insertion of materials and setting of interlocks prior to their use as weapons. Also, typically, accidents occur when weapons are being ferried in a not fully functional state or are in an otherwise relatively inert state. That being said, nuclear weapons contain significant quantities of conventional explosives which can detonate in an accident, spreading the nuclear material (e.g., U-235, Pu-239, H-3, and depleted uranium) into the environment. For the purpose of this section, discussion will include accidents involving nuclear weapons (bombs, missiles, etc.). Nuclear-powered sea-going vessels that also often serve as nuclear weapon platforms will be discussed in section on "Nuclear-Powered Vessel Accidents".

Unplanned events involving nuclear weapons can be categorized as either accidents or incidents. A nuclear weapon accident can be broadly categorized as unauthorized launching, unexpected detonation or burning, release of contamination from an event, or theft/loss. A nuclear weapon incident can be broadly categorized as an event leading to increased possibility of explosion or contamination, errors/malfunction in the weapon system (not leading to an accident), or any force majeure resulting in damage of a weapon, facility, or component. In terms of severity, a nuclear accident is more severe than a nuclear incident. Similar to the INES accident severity scale (Fig. 21), the US Navy devised further subdivisions to clarify the magnitude of the event. These subdivisions are as follows:

1. Nucflash: Any accidental or unauthorized incident involving a possible detonation of a nuclear weapon by US Forces that could create the risk of nuclear war.
2. Broken Arrow: The accidental or unauthorized detonation, or possible detonation of a nuclear weapon (other than war time) including the non-nuclear detonation or burning of a nuclear weapon; radioactive contamination; and seizure, theft, or loss of a nuclear weapon or component (including jettisoning).
3. Bent Spear: Any nuclear-weapon-significant incidents other than accidents or war detonations.
4. Dull Sword: Any nuclear weapon incident other than significant incidents.
5. Faded Giant: Any nuclear reactor or radiological accidents involving equipment used in connection with naval nuclear reactors or other naval nuclear energy devices while such equipment is under the custody of the Navy.

In this section, only events related to introduction or release of radioactivity to the environment are considered, and are therefore classified as Broken Arrows.

Accidents Involving Nuclear Weapons The majority of accidents involving nuclear weapons have occurred during military aircraft operations during the Cold War between the USA and former Soviet Union (1947–1991). Due to extreme secrecy of the former

Radiation in the Environment, Sources of. Figure 21
INES Scale (Adapted from [83])

Soviet nuclear weapons program, there is very little known in the open literature regarding Soviet nuclear weapon accidents, and therefore are not discussed herein. The most prominent US nuclear weapon accidents (Broken Arrows) involving release of radionuclides to the environment are listed below:

1. B-36 bomber ditching with nuclear weapon off the coast of British Columbia (February 13, 1950). A B-36 bomber carrying a nuclear weapon with a "dummy" warhead (uranium instead of plutonium) ditched off the coast of British Columbia. The nuclear weapon was jettisoned and the weapon's conventional explosives detonated on impact with the ocean.
2. B-50 bomber jettison and detonation of nuclear weapon near Rivière-du-Loup, Québec (November 10, 1950). A B-50 bomber upon having engine problems over the St. Lawrence River in Canada jettisoned its nuclear weapon which was set to self-destruct at 760 m (2,500 ft). There was no plutonium in the weapon; however, approximately 45 kg (100 lb) of depleted uranium was dispersed around Rivière-du-Loup.
3. B-47 bomber loss over the Mediterranean Sea (March 10, 1956). Two capsules of nuclear weapons material were on board the aircraft when it disappeared. The aircraft was never found, and was presumed to have crashed into the sea. The states of the two nuclear weapons capsules are unknown.
4. B-36 bomber inadvertent jettison of weapon at Kirtland Air Force Base, New Mexico (May 27, 1957). A (non-armed) nuclear weapon was inadvertently released at low altitude, and upon striking, the ground was destroyed through detonation of its convention explosives. Low levels of radioactivity were detected in the impact crater.
5. C-124 Globemaster II cargo aircraft jettison of weapons off the coast of New Jersey (July 28, 1957). Three nuclear weapons and one fissile core were being transported when the aircraft

lost power and the crew jettisoned two of the nuclear weapons. The states of the two nuclear weapons are unknown.

6. B-47 bomber take-off roll accident and fire in Morocco (January 13, 1958). A B-47 performing a simulated take-off while carrying a nuclear weapon experienced a ruptured fuel tank and subsequent fire. The nuclear weapon high explosives did not detonate, although low-level alpha contamination was detected in the vicinity of the accident.
7. B-47 bomber jettison of weapon off the Atlantic Coast near Savannah, Georgia (February 5, 1958). A mid-air collision damaged the bomber, forcing it to jettison the single nuclear weapon it was carrying over the Atlantic Ocean. The state of the nuclear weapon is unknown.
8. C-124 Globemaster II cargo aircraft destruction of weapon at Barksdale Air Force Base, Louisiana (July 6, 1959). The transport aircraft crashed on take-off carrying one nuclear weapon. The fire destroyed the aircraft and weapon, and a small amount of radioactive contamination was discovered in the immediate vicinity of the crash.
9. BOMARC nuclear missile destroyed by explosion at McGuire Air Force Base, New Jersey (June 7, 1960). A fire at a BOMARC air defense missile facility lead to the destruction of the nuclear payload, leading to release of plutonium to the atmosphere and local contamination of the site.
10. B-52 bomber mid-air explosion loss of weapons near Goldsboro, North Carolina (January 24, 1961). A B-52 carrying two nuclear weapons suffered a mid-air explosion, causing its two nuclear weapons to come free during the aircraft breakup. One weapon was recovered relatively intact. The other weapon broke up upon contact with the ground. Most of the thermonuclear stage and enriched uranium was never located, and the area of impact was purchased by the US Air Force and secured. The area is routinely monitored for evidence of environmental contamination.
11. Thor rocket with nuclear payload destruction near Johnson Atoll, Pacific Ocean (June 4, 1962). A Thor rocket carrying a nuclear device for a high-altitude nuclear test was destroyed after control of the rocket was lost. It is believed that the nuclear device vaporized through the destruction. The nuclear material would have been dispersed through the atmosphere and mostly settled in the Pacific Ocean.
12. Thor rocket with nuclear payload destruction near Johnson Atoll, Pacific Ocean (June 20, 1962). A Thor rocket carrying a nuclear device for a high altitude nuclear test was destroyed after the booster rocket shutdown prematurely. The nuclear device is believed to have fallen into the Pacific Ocean. The state of the device is unknown.
13. B-58 bomber accident and destructive ground fire at Grissom Air Force Base, Indiana (December 8, 1964). A B-58 bomber slid off a taxiway and caught fire with five nuclear weapons on board, which were damaged as a result. Contamination was detected and confined to the immediate vicinity of the accident. A B-58 Hustler, exhibiting the large nuclear weapons payload capability, is shown in Fig. 22. A large nuclear device (multi-color weapon near bottom center of Fig. 22) is wrapped within the fuel pod (termed the "two component pod"), and the four smaller weapons are attached directly to hard-points under the wings. Operationally, after the final refueling before target, the aircraft would burn the fuel from the pod tank and jettison the pod from the aircraft, leaving the large nuclear weapon for delivery. Therefore, an aircraft fully fueled prior to take-off in this configuration would be of great concern in the event of fire on the ground.
14. A-4E attack aircraft lost from carrier with nuclear weapon near the Ryukyu Islands, Japan (December 5, 1965). An A-4E armed with a nuclear weapon rolled off the deck of the USS Ticonderoga and sank to a depth of approximately 4,875 m (16,000 ft). The state of the weapon is unknown.
15. B-52 bomber with nuclear weapons mid-air collision near Palomares, Spain (January 17, 1966). A B-52 collided while refueling with a KC-135 tanker, destroying both aircraft. The conventional explosives on two of the four nuclear weapons detonated upon impact with the ground spreading low levels of radioactive contamination over the countryside around Palomares. See detailed description below.

Radiation in the Environment, Sources of. Figure 22
B-58 Hustler nuclear capable strategic bomber (Photo courtesy of Lt. Col. BJ Brown, US Air Force (Ret))

16. B-52 bomber destruction while carrying four nuclear weapons at Thule Air Force Base, Greenland (January 21, 1968). A fire in the navigator's compartment caused a B-52 to attempt an emergency landing. The aircraft crashed in the attempt and the fire caused at least one of the nuclear weapon's conventional explosives to detonate. The explosion spread contamination (primarily plutonium) around the accident site. Although there are conflicting reports, it is anticipated that four of the weapons were destroyed. There is conjecture that one of the weapons actually fell through the ice to the ocean floor, but this is unsubstantiated.

It is clear that there are two generic categories of Broken Arrow accidents: (1) lost and (2) destroyed nuclear weapons. The environmental impact of a destroyed nuclear weapon is immediate, whereas the impact of a lost weapon in unknown, with the impact possibly occurring at some time in the future (note that lost weapons may be destroyed, but with no way to confirm). In all destroyed weapon accidents, there were decontamination efforts to mitigate or eliminate potential effects. A summary of the US nuclear weapon accidents resulting in either lost radioactive material or destruction of weapon is presented in Table 26.

Accident at Palomares, Spain The Palomares Broken Arrow incident is of special interest since it was responsible for widespread radionuclide contamination of the environment. On January 17, 1966, a B-52 bomber of the US Strategic Air Command collided with a KC-135 tanker while trying to perform an airborne refueling operation at 31,000 ft above Palomares, Spain. The collision destroyed both aircraft, and the four Mk-28 thermonuclear weapons were expelled from the aircraft during the B-52 breakup. Three of the weapons were recovered within 24 h on land (of which two had undergone detonation of their high explosive charges, dispersing radioactive material into the environment), while the fourth weapon landed at sea and was the focus of an extensive deep sea search and recovery operation [84]. The fourth weapon was recovered relatively intact with no release of radioactivity to the environment.

Radiation in the Environment, Sources of. Table 26 US broken arrow accidents with environmental impact

No.	Date	Location	Weapons lost	Weapons destroyed
1	February 13, 1950	Coast off British Columbia, Canada		1
2	November 10, 1950	Rivière-du-Loup, Québec, Canada		1
3	March 10, 1956	Mediterranean Sea	2	
4	May 27, 1957	Kirtland Air Force Base, New Mexico, USA		1
5	July 28, 1957	Coast off New Jersey, USA	2	
6	January 31, 1958	Air Base, Sidi Slimane, French Morocco		1
7	February 5, 1958	Coast off Savannah, Georgia, USA	1	
8	July 6, 1959	Barksdale Air Force Base, Louisiana, USA		1
9	June 7, 1960	McGuire Air Force Base, New Jersey, USA		1
10	January 24, 1961	Goldsboro, North Carolina, USA		1
11	June 4, 1962	Johnson Atoll, Pacific Ocean		1
12	June 20, 1962	Johnson Atoll, Pacific Ocean	1	
13	December 8, 1964	Grissom Air Force Base, Indiana, USA		5
14	December 5, 1965	Ryukyu Islands, Japan	1	
15	January 17, 1966	Palomares, Spain		2
16	January 21, 1968	Thule Air Force Base, Greenland		4[a]
TOTAL			7	19

[a] Official US Air Force position is that fragments of all four nuclear weapons were found at Thule. There has been conjecture that one of the bombs melted through the ice and was lost on the sea bottom. An abundance of aircraft fragment was confirmed to be on the sea bottom. There is no readily available evidence to support the lost weapon hypothesis.

A contaminated area of 640 acres of hillside, village, and farmland was determined, of which 319 acres were cultivated farmland [84]. An aerial overview of a typical soil cleanup operation, depicting plow tractors, water dousing vehicles, and dump trucks removing soil, is provided in Fig. 23. Decontamination and cleanup criteria were based upon instrument readings which related to surface contamination of plutonium (Pu-239). Contaminated areas were assessed using portable alpha detectors (PAC-1S) as depicted in Fig. 24. An agreement was reached between governments of the USA and Spain that above a plutonium contamination level of 462 μg m^{-2}, soil was to be lifted, packaged, and transported from Spain to the USA. For lower levels of surface contamination, plowing and/or watering was deemed sufficient to mitigate the impact of the residual plutonium [85]. Contaminated soil, vegetation, and hot spots were packed into 4,810 barrels (Fig. 25) and shipped to Savannah River Nuclear Processing Facility for storage. Contaminated vegetation below an estimated 462 μg m^{-2} was removed to a dry riverbed and burned.

Environmental monitoring of the plutonium contamination in and around Palomares started immediately after the accident and continues to this day. Air monitoring (e.g., see Fig. 26) and soil and water sampling are performed on a continuing basis, as well as monitoring of local foodstuffs. Studies have shown persistent plutonium contamination in soils near the locations where weapons were destroyed [86]. Assessments of public doses from the event have been performed [87] and the estimates indicate that no member of the public would exceed the International Commission on Radiological Protection guidance level of 1 mSv a^{-1}.

Nuclear-Powered Vessel Accidents Nuclear powered vessels are floating, compact sources of large quantities

Radiation in the Environment, Sources of. Figure 23
Aerial view of soil cleanup site (Photo courtesy of Capt. Lewis B. Melson, US Navy (Ret))

Radiation in the Environment, Sources of. Figure 24
Airman conducting soil contamination survey (Photo courtesy of Capt. Lewis B. Melson, US Navy (Ret))

Radiation in the Environment, Sources of. Figure 25
Waste barrels with contaminated soil awaiting shipment to USA (Photo courtesy of Sandia National Laboratory)

Radiation in the Environment, Sources of. Figure 26
Chain link fence enclosing an air sampling station in Palomares (circa 2007) (Photo courtesy of Barbara Moran)

of fixed and loose radioactive material. In addition, unlike land-based commercial nuclear power plant counterparts, their operation is shrouded in secrecy. Many events, including the details of nuclear weapons as part of the vessels' armament inventory, are generally unavailable or speculative. As a result, the full magnitude of environmental releases of radionuclides from nuclear powered vessel accidents and incidents will never be known. It is known that a certain amount of radioactive material, from gases to coolant to resins, were (and possibly are) routinely released to marine environments during operation of these vessels. Also, nuclear-powered vessels often have tender ships that are utilized for, amongst other duties, reception of radioactive waste materials, which may lead to leakage to the environment under abnormal transfer. As a final environmental legacy of nuclear-powered vessel operations, it is well known that the former Soviet Union routinely disposed of decommissioned nuclear vessel components and reactors at sea, making the future environmental impact difficult to predict.

A list of known nuclear submarine accidents (all involving either the USA or USSR/Russian Federation) with known or potential environmental impact is provided in Table 27. It is quite possible that there are other accidents or incidents not included in this table that were never reported or remain classified to this day. A similar table for surface vessels is provided in Table 28. It is worthy to reiterate that under normal operations for these vessels, small routine releases occur.

The two principal threats to the environment from sunken nuclear vessels are (1) fission products in reactor fuel and (2) weapons material (primarily plutonium). It is worthy to note, however, that despite

Radiation in the Environment, Sources of. Table 27 Significant nuclear submarine with environmental impact

No.	Date and vessel	Location	Nuclear weapons lost	Reactor or fuel sunk	Radiation discharge
Submarines					
1	April 18, 1959, SSN-575 USS Sea Wolf	190 km east of Maryland, Atlantic Ocean		1 (scuttled reactor)	Possible
2	July 4, 1961, K-19 "*Hiroshima*"	South of Greenland, North Atlantic			Probable
3	April 10, 1963, SSN-593 USS Thresher	50 km east of Cape Cod, Massachusetts		1 (sunk)	Probable
4	May 22, 1968, SSN-589 USS Scorpion	740 km southwest of Azores, Portugal	2	1 (sunk)	Probable
5	March 8, 1968, K-129 Golf-II (NATO)	1,390 km northwest of Oahu, Hawaii	3 (sunk)		Possible
6a	May 24, 1968, K-27 "*Project 645*"	Reactor problem; location unknown			Probable
6b	September 6, 1982, K-27 "*Project 645*"	Scuttled in Kara Sea, north of Siberia		1 (scuttled vessel)	Possible
7	April 11, 1970, K-8 "*Project 627*"	490 km northwest of Spain, Bay of Biscay	4	2 (sunk)	Probable
8	October 6, 1986, K-219 Yankee I (NATO)	1,090 km northwest of Bermuda	16	2 (sunk)	Possible
9	April 7, 1989, K-278 Komsomolets	Barents Sea, Arctic Ocean	2	1 (sunk)	Yes
10	August 12, 2000, K-141 Kursk	Barents Sea, Arctic Ocean		2 (sunk)	Probable
11	August 30, 2003, K-159 Kit (NATO)	Barents Sea, Arctic Ocean		1 (scuttled fuel)	Possible
TOTAL			27	12	

Radiation in the Environment, Sources of. Table 28 Significant nuclear surface vessel with environmental impact

No.	Date and vessel	Location	Vessel category	Radiation discharge
Surface vessels				
1a	February 1965, NS Lenin	Unknown; Probably at shipyard	Nuclear-powered icebreaker (civilian)	Possible
1b	1967, NS Lenin	Unknown; Probably at shipyard	Nuclear-powered icebreaker (civilian)	Possible
2	December 12, 1971, AS-11 USS Fulton	Thames River, New Haven, Connecticut	Submarine tender	Yes
3	October 1975, AS-19 USS Proteus	Apra Harbor, Guam	Submarine tender	Yes

the moderate number of nuclear vessel accidents, no significant marine environmental contamination has been measured from these events. This is, in part, due to the depth at which these vessels sink or are scuttled, typically many thousands of meters, the large dispersion volume the oceans allow, and the complex pathway from release to receptor. It is likely that nuclear vessel reactors and weapons sunk or scuttled to great depths will remain in their sunken locations for as long as their local environment remains relatively static, although there are no universal models for evaluating either the short- or long-term impact of these events [88].

Depleted Uranium Munitions Depleted uranium (DU) is a mix of naturally occurring uranium isotopes in which the fissionable isotope U-235 is depleted compared to its abundance in natural uranium, as presented in Table 29.

DU has a high mass density (approximately 19 g cm^{-3}) and corresponding high electron density, which makes it ideal for radiation shielding, or any application that requires a large mass in a small volume. There are numerous uses for depleted uranium including radiation shielding, field trimmers for radiotherapy machines and aircraft control surface counterweights [89]. Therefore, on any aircraft crash where there is high velocity impact and/or fire, it is possible to get environmental contamination from DU. However, these are rare events and relatively small masses of DU, and are therefore of minimal environmental concern.

Radiation in the Environment, Sources of. Table 29 Percentage (by weight) of typical natural and depleted uranium

Isotope	Natural uranium (%)	Depleted uranium (%)
U-238	99.3	99.8
U-236		0.0003
U-235	0.72	0.2
U-234	0.006	0.0006

The utilization of depleted uranium in munitions and the subsequent dispersal into the environment is not an accident. However, the controversy surrounding the use of these munitions and their potential effect of both humans and the environment was not fully realized until the Persian Gulf War ("Gulf War I," 1990–1991). Subsequently, DU ammunition was utilized extensively during the wars in Bosnia-Herzegovina (1992–1995), Kosovo (1999), Afghanistan (2002), and Iraq ("Gulf War II," 2003).

Depleted uranium (DU) is a by-product of the enrichment of natural uranium process. It has the same chemical properties as natural uranium with approximately one third of the radioactivity. Its high density, pyrophoric properties, and low cost make it an ideal metal for military applications, wherein it is used for armor piercing ammunition. A typical DU penetrator (MK149-2) that is used, for example, in a Phalanx Close-in-Weapon System (CIWS), is shown in Fig. 27. This ammunition has a total length of

approximately 5.4 cm (including a 1.5 cm plastic tip used to increase the stability of the ammunition in flight [90]), maximum diameter of approximately 1.2 cm with a mass of approximately 70 g. Other DU weapon systems, such as those utilizing anti-tank penetrators, are much larger (and have a much larger mass of DU) than the ammunition depicted in Fig. 27.

Other common DU ammunition types used by the US military are listed in Table 30. It is worthy to note that DU munitions are or have been used by a variety of countries other than the USA, and therefore the introduction of these sources into the environment either by military tactical use or in training is a worldwide issue.

When DU penetrators impact a hard target surface, the resultant high temperature causes small DU particulate to ignite both outside and inside the target. When the weapon penetrates the target, it generates shards and spall that can incapacitate the crew. As a result, a large amount of DU dust in the respirable range (<10 micron AMAD) is generated and dispersed. The DU fragments can be incorporated into humans through the shrapnel process, and/or DU dust may be inhaled by personnel in the vicinity of ammunition impact. Dust that is deposited in the environment can become mixed with surface layers of soil or sand, and can also become resuspended via wind or mechanical mixing. Once mixed with soils, DU will be sequestered in plants, and may enter the food chain this way (as natural uranium will) or may enter potable water supplies. When DU penetrators miss their targets, they embed into the ground and can contaminate the local surroundings [91].

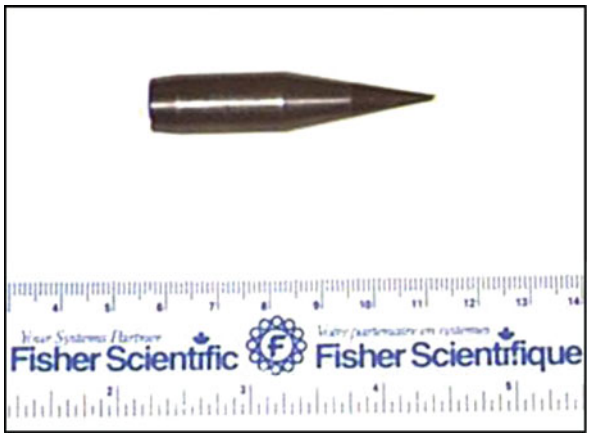

Radiation in the Environment, Sources of. Figure 27 Depleted uranium armor piercing shell (Photo courtesy of E. Waller, UOIT)

Extensive environmental studies on air, soil, and water have been performed in military conflict regions in which DU has been used. Generally speaking, no detectable widespread contamination has been found in these regions. Contamination from DU tends to be limited to areas below penetrators that have missed targets and impacted soft soil or sand [92]. It has been suggested that the long-term effects of military use of DU on both local populations and the environment is not likely to be significant from either a chemical or radiological toxicity perspective [93].

Space Nuclear Power Source Accidents A historical and potential source of anthropogenic radioactive material being introduced into the environment is from the destruction on launch or reentry of a spacecraft utilizing a nuclear power source.

Radiation in the Environment, Sources of. Table 30 Depleted uranium ammunitions

Ammunition designation	Caliber (mm)	DU weight (g)	Used by
M829A1,A2	120	5,350	Tanks (M1 Abrams)
M900	105	4,246	Tanks (M1 Abrams)
PGU-14	30	298	Aircraft (A-10 Warthog)
M919	25	97	Armored personnel carriers (Bradley, LAV)
PGU-20	25	148	Heavy machine gun (MK-38)
			Aircraft (AV-8 Harrier)
MK149-2	20	70	Missile defense guns (Phalanx CIWS)

The two types of nuclear power sources that have been used on spacecraft are nuclear fission reactors and radioisotopic thermoelectric generators (RTGs). The mechanisms of operation vary greatly between the two. A space nuclear fission reactor works similarly to a commercial nuclear reactor, whereby the fission process generates heat, which may be used through a heat exchanger to run a turbine and generator (dynamic generation), or coupled to a transducer (similar to a thermocouple), which directly converts heat to electricity (static generation). An RTG, on the other hand, utilizes the properties of radioactive decay to generate heat which can be directly converted through a transducer to electricity (static generation). The advantage of both sources is that they can provide reliable and maintenance-free energy to power electronic systems in spacecraft, which is especially important in unmanned missions. Radiologically, in the case of a nuclear fission reactor (typically based on U-235), radioactive fission products are produced, as well as neutron activation of some surrounding materials. In the case of an RTG, the power source itself is highly radioactive. In both cases, destruction of the power source either at launch or through reentry can disperse radioisotopes over a large area, depending upon the position in the atmosphere where the breakup occurs.

To date, there have been eight verified accidents and two possible accidents involving space nuclear power source systems [94, 95]. All accidents have involved either USA or USSR (Russian after 1991) spacecraft, and are outlined in Table 31.

Of the few accidents involving space nuclear power systems, the two accidents known to have widely spread radionuclides into the environment are the Transit-5BN-3 and Cosmos-954 reentries, discussed below.

Transit-5BN-3 Reentry On April 21, 1964, the US Transit-5BN-3 navigation satellite was launched from Vandenburg Air Force base in California, but the rocket failed to boost the satellite into orbit. As a result, the payload reentered the southern atmosphere and the SNAP-9A RTG burned up [96]. The SNAP-9A RTG contained approximately 629 TBq of Pu-238, which is believed to have mainly deposited on the Earth's

Radiation in the Environment, Sources of. Table 31 Space nuclear power system accidents

Accident date	Launch country	Spacecraft	Power source	Release to environment
Verified accidents				
April 21, 1964	USA	Transit-5BN-3	RTG (Pu-238)	Yes (see discussion below)
May 18, 1968	USA	Nimbus-1	RTG (Pu-238)	No (RTGs retrieved)
April 17, 1970	USA	Apollo 13	RTG (Pu-238)	No (RTGs never retrieved from ocean)
April 25, 1973	USSR	RORSAT	Unknown; probable nuclear reactor	Unknown (possible)
January 24, 1978	USSR	Cosmos 954	Nuclear Reactor (U-235)	Yes (see discussion below)
February 7, 1983	USSR	Cosmos 1402	Nuclear Reactor (U-235)	Unknown (possible)
September 30, 1988	USSR	Cosmos 1900	Nuclear Reactor (U-235)	No (reactor boosted to higher orbit)
November 16, 1996	Russia	Mars-96	RTG (Po-210)	Unknown (RTGs never recovered)
Possible accidents				
January 25, 1969	USSR	Unknown, possible RORSAT	Unknown; probable nuclear reactor	Unknown
September 23 and October 22, 1969	USSR	Unknown; unmanned moon probes	Unknown; possible Po-210 RTG source	Probable

surface [94]. This deposition was estimated to have almost tripled the global deposition of Pu-238 by 1970 (the prior contribution being from global nuclear weapons testing).

Cosmos-954 The USSR Cosmos-954 (also known as Kosmos-954) was launched on September 18, 1977 (Fig. 28). The satellite was postulated to be powered by an approximately 20 kg U-235 nuclear fission reactor.

On January 24, 1978, the satellite reentered the atmosphere with the nuclear reactor core on-board, partially burning up over a 1,000 km long path extending primarily over the Canadian Northwest Territories, and partially into the provinces of Alberta and Saskatchewan. A large-scale search was conducted for potential contamination over approximately 124,000 km^2 extending from January to October 1978. In Fig. 29, a radiation surveyor is seen performing duties in the harsh Arctic environment, which slowed recovery efforts. Figure 30 shows two persons packaging radioactive material for removal from recovery site.

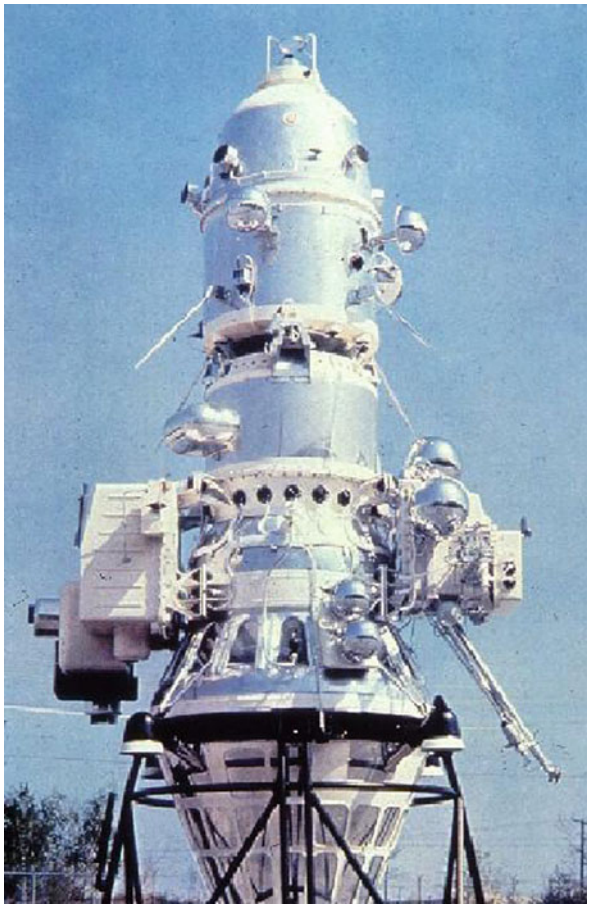

Radiation in the Environment, Sources of. Figure 28 Cosmos satellite (Adapted from http://gsc.nrcan.gc.ca. Reproduced with the permission of the Minister of Public Works and Government Services, 2010)

At the time of reentry, the core was estimated to contain approximately 3.1 TBq Sr-90, 180 TBq I-131, and 3.2 TBq Cs-137 [25]. The reentry generated a dispersion of radioactive fragments and particles from large chunks (Fig. 31) to particles less than 100 μm in diameter (Fig. 32). The fragments depicted in Fig. 31 were termed the "antlers," as from a distance they were originally thought to be Caribou antlers. The "antlers" were believed to be part of the reactor control mechanism [97]. An additional large piece of debris, termed the "stovepipe" due to its shape (Fig. 33), was found to be nonradioactive and likely the only material found that was not part of the reactor structure. Numerous beryllium rods were discovered (Fig. 34), which were hypothesized to be part of the neutron reflector system [97].

The Cosmos 954 satellite is believed to have weighed 4–5 t; however, only 65 kg total mass of material was recovered [97]. It is estimated that approximately 75% of the original material remained in the upper atmosphere. Approximately 0.1% of the particulate dispersed is estimated to have been recovered by the search efforts. Most of the recovered material was radioactive, suggesting that it was part of the reactor structure. A summary of the recovered debris is provided in Table 32 (adapted from [97]).

The most radioactive fragment (Fig. 35), which was most certainly a piece of the reactor core, was found to have a dose rate of approximately 5 Gy h^{-1} near contact.

Analysis of the fragments and particles identified a number of fission and activation products characteristic of an enriched U-235 reactor (Table 33).

Based upon the difficulty of finding small radioactive particles dispersed over a large area, it is highly probable that radioactive particles, and perhaps fragments, from the reentry of Cosmos-954 remain in Northern Canada to this day as environmental contamination. From the list outlined in Table 33, it is likely that the principal isotopes detectable over

Radiation in the Environment, Sources of. Figure 29
Radiation surveyor approaching piece of Cosmos 954 debris (Photo courtesy of Canadian Nuclear Safety Commission [97])

Radiation in the Environment, Sources of. Figure 30
Radiation surveyors packaging debris from Cosmos 954 (From http://gsc.nrcan.gc.ca. Reproduced with the permission of the Minister of Public Works and Government Services, 2010)

Radiation in the Environment, Sources of. Figure 31
Large piece of satellite debris nicknamed the "antlers" (Reproduced from www.nsarchive.org with the permission of the National Security Archive)

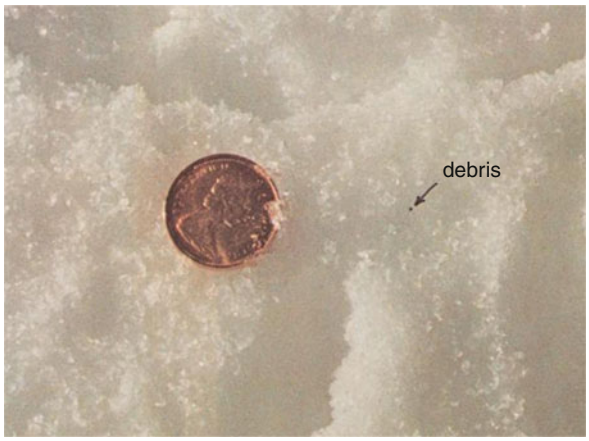

Radiation in the Environment, Sources of. Figure 32
Small radioactive particle of fuel (Photo courtesy of Canadian Nuclear Safety Commission [97])

Radiation in the Environment, Sources of. Figure 33
The "stovepipe" debris (Photo courtesy of Canadian Nuclear Safety Commission [97])

30 years post crash would be H-3, Cs-137, Sr-90, and Pu-239. Of the four principal radionuclides identified, the only one that would be readily detectable in a field survey due to its gamma emission would be Cs-137.

Medical, Industrial, Commercial, and Research Sources

There are numerous types and categories of radioactive materials used for medical, industrial, commercial, or research uses. The sources can be gaseous, liquid, or solid in form. Sources that are in gas or liquid form can directly enter the environment as they are inherently mobile. Sealed sources (generally in solid form) can only enter the environment if there is a disruption to their source capsule. On a basis of specific activity, sealed sources generally have the highest activity.

Figure 36 graphically depicts the range of source activity for common sealed radiation sources [98]. The activity of these sources varies from hundreds of Bq to the PBq range.

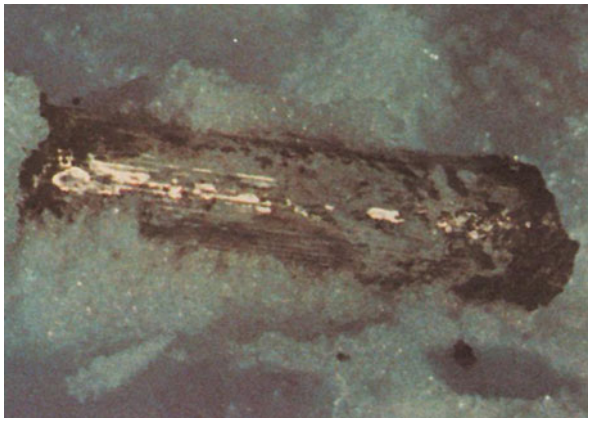

Radiation in the Environment, Sources of. Figure 34 Beryllium rod found in snow (Photo courtesy of Canadian Nuclear Safety Commission [97])

Radiation in the Environment, Sources of. Table 32 Summary of recovered debris from Cosmos 954

Item(s)	Mass (g)	Max. Measured dose rate (Gy h^{-1}) on contact
Large Debris		
Steel plate fragments (x4)	272 (max)	2
Beryllium rods (x41)	51 each	1
Beryllium cylinders (x6)	3,600 each	0.15
Tubes/rods/plate ("antlers")	20,000 total	0.15
Steel tube ("stovepipe")	18,200 total	Not detectable
Chunks/flakes/slivers	Variable	5
Small Debris		
~4,000 particles	1E-4 to 5E-3	1E-3

Details of these sources are briefly discussed below.

Teletherapy units are commonly found in medical institutions, such as hospitals or clinics. The physical dimensions of the source are relatively small, with generally a cylindrical (few centimeters in diameter by several centimeters long) shape. The source is contained inside a large shielding device.

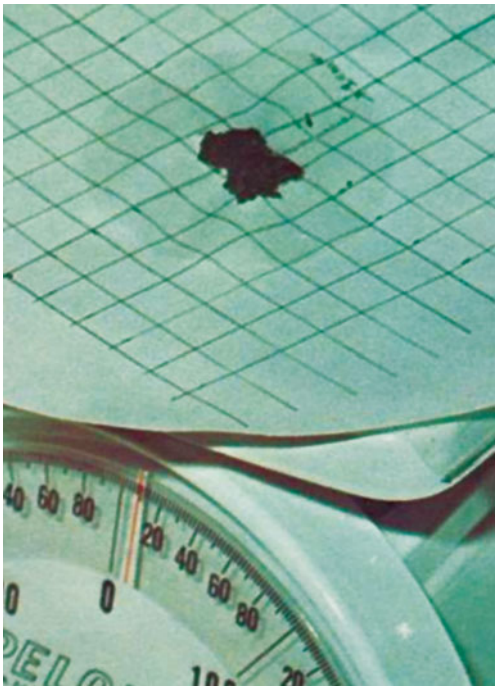

Radiation in the Environment, Sources of. Figure 35 Most radioactive fragment found from Cosmos 954 (Photo courtesy of Canadian Nuclear Safety Commission [97])

Irradiator facilities are relatively few in number, and contain very high activity sources to sterilize foodstuffs, medical products and supplies, and for other specialized applications. The sources used in performing the irradiation of the material vary in physical size, some being large or others being pencil sized, and each facility will contain many such sources.

Portable industrial radiography sources and their devices are generally small in terms of physical size, although the devices are usually heavy due to the shielding contained in them. The sources themselves are very small, less than 1 cm in diameter, and only a few centimeters long, and are attached to specially designed cables for their proper operation. The use of radiography sources and devices is very common, and their portability may make them susceptible to theft or loss. The small size of the source allows for unauthorized removal by an individual, and such a source may be placed into a pocket of a garment. Industrial radiography may also be performed in fixed installations, either using

the same small portable devices, or using larger machines which may appear to be similar to teletherapy units.

Brachytherapy sources are of two slightly different varieties. These are generally referred to as Low Dose Rate (LDR) brachytherapy and High Dose Rate (HDR) brachytherapy. Both applications use sources that may be small physically (less than 1 cm in diameter, only a few cm long) and, thus, are susceptible to being lost or misplaced. HDR sources, and some LDR sources, may be in the form of a long wire attached to a device (a remote afterloading device). The afterloading device may be heavy, due to the shielding for the sources when not in use, and the device may be on wheels for transport within a facility. The remote afterloading device may also contain electrical and electronic components for its operation, and pneumatic systems for source transfer. Brachytherapy sources are located in hospitals, clinics, and similar medical institutions, and such facilities may have a large number of sources.

Well logging sources and devices are generally found in areas where exploration for minerals is occurring, such as searching for coal, oil, natural gas, or similar uses. The sources are usually contained in long (1–2 m, typically) but thin (<10 cm in diameter) devices which also contain detectors and various electronic components. The actual size of the sources inside the devices is generally small. The devices are heavy, due to the ruggedness needed for the environments in which they are used.

Industrial sources (gauges) are of various shapes and sizes, and are either fixed or portable. These devices are generally designed for many years of operation

Radiation in the Environment, Sources of. Table 33
Fission and activation products detected in Cosmos 954 debris

Fission product	Activation product
^{89}Sr	^{51}Cr
^{90}Sr	^{54}Mn
^{95}Zr	^{58}Co
^{95}Nb	^{60}Co
^{99}Mo	^{59}Fe
^{137}Cs	^{182}Ta
^{140}Ba	^{46}Sc
^{140}La	^{124}Sb
^{141}Ce	^{239}Pu
^{144}Ce	^{3}H
^{103}Ru	
^{106}Ru	
^{132}Te	
^{131}I	
^{147}Nd	

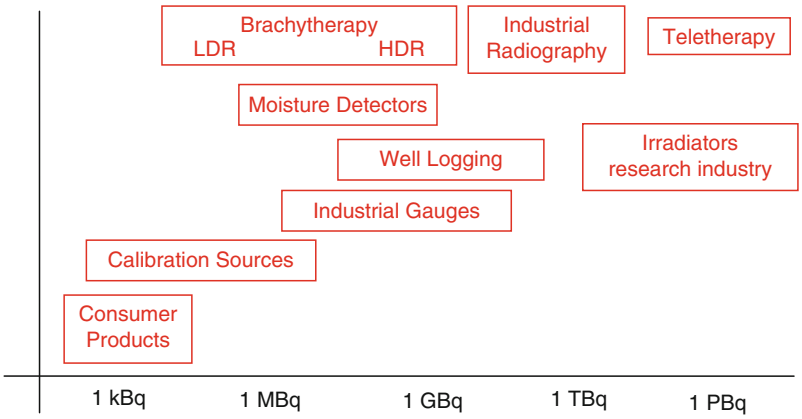

Radiation in the Environment, Sources of. Figure 36
Activity range of common sealed sources used in medicine and industry

with little or no special tending. They may be used for control over a process, for measurement of flow, volume, density, material presence, and may be placed in locations unsuitable for continuous human presence. Consequently, they may accumulate layers of dirt, grime, grease, oil, material, etc., covering any warning labels that may have been present. Depending upon the specific application, industrial gauges may contain relatively small quantities of radioactive material, or may contain sources with activities approaching 1 TBq.

Moisture/density devices are types of industrial gauges which are small and portable. These devices contain the sources, detectors, and electronic gear necessary for the measurement undertaken. The source is physically small in size, typically a few cm long by a few cm in diameter, and may be located either completely within the device or at the end of a rod/handle assembly.

Calibration sources are typically small sealed sources that are used to calibration and verification of the operation of radiation detection equipment.

Consumer products include any commercially available item that utilizes a radionuclide source to operate. A common example is a smoke detector.

Table 34 lists a number of sealed source categories by application, radioisotope, and typical radioactivity level [99]. The source categories (Category 1, 2, and 3) are for those requiring the most stringent control (Category 1) to the least (Category 3) as determined by the IAEA [100]. There is generally no pathway to the

Radiation in the Environment, Sources of. Table 34
Common sources, categories, and activities

Application	Radioisotope	Typical radioactivity (GBq)
Category 1		
Radioisotope thermoelectric generators	Sr-90	1E+06 – 1E+07
Teletherapy	Co-60	5E+04 – 1E+06
	Cs-137	5E+05

Radiation in the Environment, Sources of. Table 34 (Continued)

Application	Radioisotope	Typical radioactivity (GBq)
Blood irradiation	Cs-137	2E+03 – 1E+05
Industrial radiography	Ir-192	1E+02 – 9E+03
	Co-60	1E+02 – 9E+03
Sterilization and food preservation (irradiators)	Co-60	1E+05 – 4E+08
	Cs-137	1E+05 – 4E+08
Other irradiators	Co-60	1E+03 – 1E+06
	(Cs-137 rare)	1E+03 – 1E+06
Category 2		
High dose rate remote afterloading brachytherapy	Co-60	1E+01
	Cs-137	3E-05 – 1E-02
	Ir-192	4E+02
Low dose rate brachytherapy (manual or remote)	Cs-137	5E-02 – 5E-01
	Ra-226	3E-02 – 3E-01
	Co-60	5E-02 – 5E-01
	Sr-90	5E-02 – 1E+00
	Pd-103	5E-02 – 1E+00
Well logging	Cs-137	1E+00 – 1E+02
	Am-241/Be	1E+00 – 8E+02
	Cf-252 (rare)	5E+01
Level gauge	Cs-137	1E+01 – 1E+03
Thickness gauge	Co-60	1E+00 – 1E+01
Conveyor gauge	Am-241	1E+01 – 4E+01
Moisture/density detector (portable, mobile units)	Am-241/Be	1E-01 – 2E+00
	Cs-137	$\leq$ 4E-02
	Ra-226/Be	1E+00
	Cf-252 (rare)	3E+00
Category 3		
Level gauge	Cs-137	1E-01 – 2E+01
Density gauge	Co-60	1E-01 – 1E+00
Thickness gauge	Kr-85	1E-01 – 3E+00
	Am-241	1E+00 – 1E+01
	Sr-90	1E-01 – 4E+01
	Tl-204	4E+0

environment for these sealed source categories unless they are (a) destroyed, (b) tampered with, or (c) intentionally dispersed maliciously.

Medical Sources Introduction of large sealed medical sources into the environment from, for example, teletherapy units would generally only occur through complete destruction of the source via fire or explosion, or theft of the source and inadvertent or intentional dispersion. Such a scenario is considered in section on "Lost and Orphan Sources" and is not further considered here.

Medical sources of radiation are routinely introduced into the environment from nuclear medicine procedures. Isotopes utilized in nuclear medicine diagnostic imaging are characterized by their short radiological half-lives and relatively low energies of gamma emission. Common sources used in nuclear medicine are presented in Table 35. A more detailed discussion of nuclear medicine pharmacy can be found in [101].

Radionuclides can be used in pure form, or attached with some other chemical molecule to perform a specific body function (termed "labeling" or "radiolabeling"). Radionuclides used in medicine are called radiopharmaceuticals, and consists of two components: the radionuclide and the pharmaceutical. The design of a radiopharmaceutical is based upon two characteristics: (1) its ability to preferentially locate in a desired organ or for its participation in a physiological function, and (2) the emission of radiation that will either be detected (for imaging) or deposit energy (for treatment). Approximately 95% of radiopharmaceuticals are used for diagnostic imaging, while the remaining 5% are used for therapy. Of the diagnostic imaging radiopharmaceuticals, approximately 80% are Tc-99m-labeled compounds [101].

Technetium has become the most widely used radionuclide for diagnostic nuclear medicine. It has advantageous physical characteristics of short half-life, low energy of its mono-energetic gamma ray and ease of chelation. It is formed from the decay of a parent radionuclide, molybdenum-99, which through this parent–daughter process, can be provided in a convenient, readily available and mobile form, the Technetium Generator. Tc-99m is formed when molybdenum-99 (^{99}Mo, popularly called "Molly") emits radioactivity. Molly has a half-life of 66 h and is easily bound to the cartridge. As Molly gradually disintegrates, ^{99m}Tc is formed which does not bind as well to the cartridge and can be washed out as needed with sterile salt water. The cartridge is delivered to the customers in a lead container which protects against radiation exposure. These are called technetium generators, or "cows," as they can be "milked" repeatedly as needed. The technetium is combined with a "label" and injected into the patient. After a waiting period to allow the Tc-99m-labeled compound to be distributed to target organs, the patient is scanned with an imaging device. Almost all of the technetium leaves the body via urine or radiologically decays within the body.

Radiation in the Environment, Sources of. Table 35 Some common radionuclides used in nuclear medicine studies

Element	Radionuclide	Half-life	Energy gamma (keV)	Energy beta (keV)
Phosphorus	^{32}P	14.3 days		1,700
Chromium	^{51}Cr	27.7 days	320	
Gallium	^{67}Ga	78.3 h	93, 184, 300	
Strontium	^{89}Sr	50.5 days		1,480
Yttrium	^{90}Y	64.1 h		2,280
Technetium	^{99m}Tc	6.02 h	140	
Indium	^{111}In	2.8 days	171, 245	
Iodine	^{131}I	8.0 days	364	606
	^{123}I	13.2 h	159, 35	
Thallium	^{201}Tl	73.1 h	68–82 (x-rays) 167	

The Tc-99m that is excreted via urine enters the municipal sewer system and ultimately enters the aquatic environment. Due to the short radiological half-life, low energy of the decay emissions, and the fact that hospital delivery is regulated to acceptable release levels, environmental impact of Tc-99m on the environment is minimal.

Another nuclear medicine radionuclide that is sometimes observed in the environment is I-131. Radioactive iodine can be observed in aquatic plants near harbors where hospitals perform thyroid imaging or treatment using radioactive iodine [76]. Although the radiological half-life of I-131 is only 8 days, a constant introduction into the environment can yield a steady state burden of I-131 in aquatic plants. In addition, I-131 as well as other nuclear diagnostic radionuclides have been observed in river sediment downstream from hospitals performing nuclear medicine procedures [102]. It is noted that radionuclides in the environment from medical procedures far exceed equivalent releases from nuclear power plants [102]. No known deleterious effects of these radionuclides have been observed in either human or nonhuman biota, primarily due to the fact that their release is regulated to levels below regulatory concern. These radionuclides do, however, make up part of the food chain for both human and nonhuman biota and must be taken into account in total dose estimates.

Industrial Sources Although there are various industrial applications of radioactive sources, the most common classifications are:

1. Radiography sources
2. Nuclear gauges
3. Irradiator sources
4. Radioactive tracers

Except for tracers, all of the above categories of sources are sealed activity, and therefore their introduction into the environment requires damage or intentional removal of the source material from its protecting capsule. The sealed sources are briefly discussed below.

Industrial radiography sources come in a wide variety of packaging. Some are in the form of cameras (which work on a shutter mechanism) and some are in the form of a projector Teleflex cable. Industrial radiography requires relatively high activity sources that emit energetic gamma rays. Examples of radioisotopes commonly used in radiography include ^{60}Co, ^{137}Cs, ^{192}Ir, and ^{169}Yb. The source for a projector-type industrial radiography device is typically located at the end of a Teleflex pigtail. The pigtails have quick-release connectors for ease of source replacement. Typically, the source is encapsulated within two welded stainless steel capsules. The source material is often radioactive metal (cobalt or iridium), or embedded on nonsoluble ceramics (called microspheres) that minimize the potential of inhalation if the source encapsulation is breached. For transportation from source manufacturer to end user, the capsule is typically positioned at the center of a drum, surrounded by lead and shock-absorbent packing.

The basic principle of a nuclear gauge is that a radiation source is placed on one side of a material or container that requires a measurement (such as mass density, level of material, etc.), and a detector is placed on the other side. For example, a source is placed on one side of a pipe, and the detector on the other side. The amount of attenuation of the primary beam is proportional to the material between the source and detector. Therefore, this type of arrangement is useful for mass flow rate or mass density measurements. The source for this type of application is generally a photon source on the order of tens of gigabecquerel. Another popular type of gauge is the Troxler™ density and moisture gauge (Fig. 37). The Troxler device uses two types of radiation sources: gamma (~296 MBq ^{137}Cs) for measuring density and neutron (~1.5 GBq ^{241}Am-Be or ~2.2 MBq ^{252}Cf) for measuring moisture content.

An irradiator is a radiation device containing radioactive material, usually ^{137}Cs or ^{60}Co, in the form of a sealed source. The activity of the source is relatively high, often ten to hundreds of petabecquerel. These sealed sources are used to deliver very high radiation doses to objects and biological materials for various purposes. For example, irradiators are used to (a) sterilize blood, soil, medical instruments, and food; (b) to calibrate radiological instruments; (c) to extend the potency of cells; (d) in the treatment/eradication of cancer; or (e) to measure the density and detect deficiencies of various materials. There are two basic categories of irradiators: self-contained (enclosed beam) and non-self-contained (open beam or panoramic)

Radiation in the Environment, Sources of. Figure 37 Troxler™ density and moisture gauge (Photo courtesy of E. Waller, UOIT)

irradiators. Examples of open-beam irradiators are teletherapy, large wet-source-storage (pool-type), and panoramic dry-source-storage. Self-contained irradiators are devices in which the primary radiation beam is completely shielded during use and storage conditions. Consequently, under normal conditions of use, there are no high levels of radiation within the irradiator room. An example of a self-contained irradiator is the MDS Nordion Gammacell 220. The unit is 193 cm high, 107 cm diameter, and mass of approximately 5,680 kg. The sample is placed in a chamber 20 cm high by 15 cm diameter and lowered into the cell. This type of irradiator uses ^{60}Co, and the activity (new) can range from 89 to 890 TBq. The central dose rate delivered to a sample ranges (based on activity) from approximately 2 to 20 kGy h^{-1}. The dose rate at 5 cm from the outer surface of this irradiator is on the order of hundreds of μSv h^{-1}. Non-self-contained or panoramic irradiators are devices in which the primary radiation beam is not shielded during irradiator use. It is shielded only when the source is in storage position. The type of shielding used depends on the type of irradiator. For example, water in the form of a storage pool is the shielding material for pool-type or wet storage irradiators whereas lead and concrete are often used for dry-source-storage and teletherapy-type irradiators. During use, the source is not shielded and there are very high radiation levels in the irradiator room. In a typical irradiation facility used for sterilization of medical supplies, cartons are moved to a central location, and high activity gamma sources are raised into an irradiate position. An example is the MDS Nordion JS 10000 hanging-tote irradiator. This irradiator uses up to 1.85 PBq ^{60}Co sources in the form of racked pencils, and is capable of delivering tens to hundreds of thousands of gray per hour, depending upon the configuration.

Radionuclides are used as tracers since they emit a characteristic radiation signature at very low material mass. Tracers are useful when transport of material is being characterized in terms of flow velocity, direction, and interaction with the environment. Another extremely useful application of tracers is determination of a leak in a closed system. For example, consider a pipe carrying a liquid where it is suspected that there is a leak in the pipe. A radionuclide is introduced at an upstream position in the pipe and a radiation detection instrument is used to find an area of large signal, indicating an accumulation of flow material, which includes the radionuclide (Fig. 38).

Specific uses of radionuclide tracers include [7]:

- Chemical process investigations, such as flow rate and residence time determination
- Mixing time and optimization
- Maintenance investigations, such as leak detection
- Wear and corrosion investigations, including lubrication studies

Generally speaking, industrial sources are only an environmental issue when they are disrupted, as non-sealed source introduction into the environment is done with very low level of activity using short-lived isotopes.

Commercial Sources There are various applications of radionuclides for commercial purposes. For example, historically, radium (Ra-226) was used in self-luminous light sources. Today, tritium (H-3) is found for the same application in watches, emergency lighting, and any location where a light indicator is required without a power source. Some consumer products containing radionuclides that may find their way into the environment due to the principal fact that they are uncontrolled substances once released to the consumer, are presented in Table 36 [103]. Modern consumer

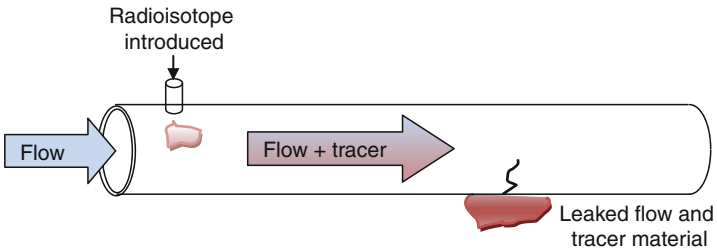

Radiation in the Environment, Sources of. Figure 38
Application of tracer for leak detection

Radiation in the Environment, Sources of. Table 36 Consumer items containing radionuclides

Consumer product	Radionuclide(s)	Comment
Smoke detectors	^{241}Am	In older smoke detectors, ^{90}Sr was also used.
Watches/clocks	^{3}H	Historically (pre-1970s), ^{226}Ra was the predominant radionuclide used.
Ceramics	Uranium chain	Older (pre-1960s) ceramics can contain significant quantities of uranium and progeny.
Glassware	Uranium chain	Historical glass ("Vaseline glass") often contained uranium for coloring.
Lenses	Thorium chain	Some lenses produced from 1950s through 1970s used ^{232}Th as a coating.
Lantern mantles	Thorium chain	Historically, many gas lantern mantles contained significant quantities of ^{232}Th.
Food	Natural radionuclides	Food is a commodity that inherently contains radionuclides, sequestered from the environment.
Fertilizer	^{40}K, uranium chain	Fertilizer is high in potassium naturally and can contain phosphates with elevated uranium concentrations.
Historical items	Primarily ^{226}Ra	Many historical items, "quack cures" and the like around the beginning of the twentieth century employed radioactivity for various purposes.

products utilizing radioactive material are highly regulated to ensure no appreciable dose to the public from either their use or disposal. Historical items and artifacts that may still be found in homes, antique shops, museums, or on Internet auction sites may still contain significant quantities of radioactive material (often as uranium/radium decay series). The historical items can become sources of radioactivity if disposed improperly.

The two most common consumer products containing anthropogenic radioactivity are described below.

Gaseous Tritium Light Sources Tritium may be obtained in relatively large quantities as gaseous tritium light sources (GTLS). These sources are commonly used in emergency lighting systems and watches (Fig. 39).

Tritium gas is readily oxidized or exchanges with other hydrogen isotopes forming HTO or tritium oxide which can remain in the atmosphere for a time or precipitate to the Earth [2]. However, given the relatively small risk associated with the ingestion of tritium (short biological half-life and weak beta emitter), it is not a significant environmental source of radioactivity in this form.

Smoke Detector Modern ionization-based smoke detectors use ^{241}Am (half-life ~432 years,) which decays by alpha emission. A typical detector uses an activity of approximately 37 kBq. The ^{241}Am source is located in an ionization chamber consisting of two plates with a voltage across them, and the source near one plate. The alpha particles ionize the oxygen and

Radiation in the Environment, Sources of. Figure 39
GTLS in wristwatch (Photo courtesy of E. Waller, UOIT)

nitrogen atoms of the air in the chamber. The electrons from the ionizations are attracted to the plate with a positive voltage, and the positively charged atom is attracted to the plate with a negative voltage plate. The electronics in the smoke detector sense the small amount of electrical current that these electrons and ions moving toward the plates represent. When smoke enters the ionization chamber, it disrupts this current – the smoke particles attach to the ions and neutralize them. The smoke detector senses the drop in current between the plates, and alarms accordingly.

Research Sources In university and research settings, virtually any category of radioactive source may be utilized, dependent upon the nature of the research. Radionuclides are used in medicine, biology, physics, chemistry, geology, and engineering studies. Very common research sources used in research settings are presented in Table 37 [104].

Laboratories and research activities are generally well regulated such that environmental releases and radioactive waste disposal are governed by the license conditions to hold the isotopes.

Radiation in the Environment, Sources of. Table 37
Common research radionuclides

Radionuclide	Typical use
^{3}H	Biological tracer studies
^{14}C	Biological tracer studies
$^{32,33}P$	Biochemical labeling studies
$^{125,131}I$	Medical research
^{60}Co	Irradiation and physics studies
^{137}Cs	Physics studies
^{252}Cf	Neutron studies

Lost and Orphan Sources

The IAEA (2002) estimates that millions of radioactive sources have been distributed globally over the past 50 years. In addition, the IAEA estimates over 20,000 operators of significant radiation sources, including radiotherapy units (more than 10,000), industrial radiography sources (more than 12,000) and approximately 300 irradiator facilities [105]. Given the vast quantity of sources distributed globally, the variable regulations and regulatory guidance over the past 50 years and regulatory differences from country to country, it is not implausible that some of these sources have become lost, stolen, or orphan.

A "lost source" is a source that has been misplaced, has become detached from a shielded unit, has been stolen, or otherwise has departed from positive control of a responsible party. The term "orphan source" refers to a sealed source of radioactive material contained in a small volume, but not radioactively contaminated soils and bulk metals, in any one or more of the following conditions:

- In an uncontrolled condition that requires removal to protect public health and safety from a radiological threat.
- Controlled or uncontrolled, but for which a responsible party cannot be readily identified.
- Controlled, but the material's continued security cannot be assured. If held by a licensee, the licensee has few or no options for, or is incapable of providing for, the safe disposition of the material.
- In the possession of a person, not licensed to possess the material, who did not seek to possess the material.
- In the possession of a radiological protection program for the sole purpose of mitigating a radiological threat because the orphan source is in one of the conditions described in one of the first four

bullets, and for which the program does not have a means to provide for the material's appropriate disposition.

There have been a significant number of lost and orphan sources estimated worldwide. The USA estimates that 1,500 sources have been lost since 1996 with more than half never being recovered, and that currently approximately 375 sources per year are reported lost or stolen [106]. The European Union estimates up to 70 sources per year are lost from regulatory control [105]. Any one of these source, if tampered with, can introduce anthropogenic radionuclides into the environment which can result in harm to human and nonhuman biota, as well as cause significant psychological, social, and economic burden. A number of source incidents impacting the environment are discussed in the next section.

Specific Source Incidents The incidents discussed below do not represent all lost or orphan source accidents, although they do represent some major accidents and the potential consequence. Generally speaking, when a lost source is found, it is relatively straightforward to mitigate the effects. However, it is probable that there are many lost or orphan sources that may have breached source capsules and are leaking radioactivity into the environment.

- January 2002 (Tbilisi, Georgia) Two orphan ^{90}Sr sources (~1.11 PBq each) used as portable electrical generators known as "radioisotopic thermoelectric generators" were recovered from the forest near Tbilisi (Lja). The sources had been found by woodsmen, who used them to keep warm (all three suffered varying degrees of radiation injury). At least two similar Sr-90 units are believed to be missing in Georgia.
- January–February 2000 (Samut Prakan, Thailand) A number of teletherapy heads were in unauthorized storage in a warehouse. Thieves accessed the site and partially disassembled one unit containing a ^{60}Co source (15.7 TBq). The thieves removed the head to their residence and continued to disassemble, which resulted in the source capsule falling out of its housing unnoticed. A number of people received high doses, and three people died of radiation exposure.
- May 2000 (Cairo, Egypt) A ^{192}Ir (3 TBq) radiography source fell from the back of a truck transporting it, and a farmer and his son found it in a ditch. They took the item home and a number of family members were exposed to high doses of radiation. The farmer and his son died of radiation exposure.
- February 1999 (Yanango, Peru) An industrial radiographer failed to notice that his ^{192}Ir (1.17 TBq) had disconnected from its Teleflex cable and was lost in the area in which he had been working. Another worker picked up the object and removed it to his residence. The worker, his wife, and baby were exposed to the source. The worker received extremely high doses and subsequently lost his leg due to the exposure.
- December 1998–January 1999 (Istanbul, Turkey) Three used ^{60}Co teletherapy sources that were meant to be shipped back to point of origin in the USA, were left in storage for 5 years. Tracking on the packages was lost and two of the packages were subsequently sold for scrap metal. The scrap merchants opened the source container (~3.3 TBq activity) and were exposed. A number of people received doses from 0.1 and 3.0 Gy. The third source package of 23.5 TBq was never found.
- October 1997 (Lilo, Georgia) A large number of ^{137}Cs and ^{226}Ra sources, abandoned at a former Russian training center, were found in the clothing of Georgian military personnel at the Lilo Training Facility, and around the grounds and local environment. The sources, many of which were in close contact with the soldiers for extended periods of time, caused varying degrees of radiation injury to the personnel involved.
- 1983 (Juarez, Mexico) An orphaned ^{60}Co teletherapy source (37 GBq) from a hospital was sold as scrap metal. During transport some small source pellets scattered along the road, and the unit was subsequently smelted and used in building materials (rebar). A number of people received doses ranging from 0.25 to 7 Gy. A total of 814 homes were demolished, generating 16,000 m^3 of soil waste and 4,500 t of metal waste.

A highly publicized and dramatic example of the potential for environmental and human catastrophe

from lost or orphan sources is the Goiânia accident, discussed below.

Goiânia Accident (1987) Possibly the most well-known orphan source case leading to injury, death, and environmental contamination is the Goiânia accident. In 1985, the Instituto Goiano de Radioterapia in Goiânia, Brazil, moved to new premises, taking with it a ^{60}Co teletherapy unit and leaving in place a ^{137}Cs teletherapy unit without notifying the licensing authority as required under the terms of the institute's license. The former premises were subsequently partly demolished and as a result, the ^{137}Cs teletherapy unit became unsecured. On September 13, 1987, two people entered the premises and, not knowing what the unit was but thinking it might have some scrap value, removed the source assembly from the radiation head of the machine and tried to dismantle it at home. In the attempt the source capsule was ruptured. The radioactive source was in the form of ^{137}CsCl (cesium chloride salt) which is highly soluble and readily dispersible. The source activity was 50.9 TBq, with a total source plus inert matrix mass of 93 g [107] and estimated ^{137}CsCl mass of 22 g. For scale, approximately 22 g of (nonradioactive) CsCl is depicted in the hand of the author in Fig. 40.

Contamination of the environment ensued with the external irradiation and internal contamination of several persons. After the source capsule was ruptured, the remnants of the source assembly were sold for scrap to a junkyard owner. Fragments of the source, the size of rice grains, were distributed to several families who were fascinated that the material glowed blue in the dark. This contact with the source continued for 5 days, by which time a number of people were showing gastrointestinal symptoms arising from their exposure to radiation from the source. The symptoms were not initially recognized as being due to irradiation. However, one of the persons irradiated connected the illnesses with the source capsule and took the remnants to the public health department in the city. This action began a chain of events which led to the discovery of the accident [107]. Many individuals incurred external and internal exposure. In total, approximately 112,000 persons were monitored, of whom 249 were contaminated either internally or externally, and 4 died from their exposures. Some suffered very high internal and external contamination owing to the way they had handled the ^{137}CsCl powder, such as daubing their skin and eating with contaminated hands, and via contamination of buildings, furnishings, fittings, and utensils. Massive amounts of resources were utilized both for the initial response, follow-up, and environmental remediation. Hundreds of personnel were required to perform initial radiological assessments on thousands of people and to remediate the city. The response also generated large quantities of radioactive waste. A temporary waste storage site was chosen 20 km from Goiânia. Wastes were classified into nonradioactive (below 74 kBq kg^{-1}), low level (below 2 mSv h^{-1}) and medium level (between 2 and 20 mSv h^{-1}). Various types of packaging were used, according to the levels of contamination. The waste packaging required 3,800 metal drums (200 L), 1,400 metal boxes (5 t), 10 shipping containers (32 m^3), and 6 sets of concrete packaging. The temporary storage site was designed for a volume of waste of 4,000–5,000 m^3 encapsulated in about 12,500 drums and 1,470 boxes. The final total volume of waste stored was 3,500 m^3. The economic burden of such levels of waste is enormous [107], and long-term socioeconomic effects were devastating. Goiânia suffered a 20% drop in gross domestic product, which took 5 years to return to normal levels. Tourism in the tropical town dropped to zero and Goiânia found itself the victim of economic

Radiation in the Environment, Sources of. Figure 40 Simulated ^{137}CsCl powder source of mass 22 g in hand (Photo courtesy of E. Waller, UOIT)

discrimination, as demand for food and other products from the area plummeted. Even with careful monitoring and accounting, the estimate of activity in the recovered contaminated materials is approximately 44 TBq, whereas the activity of the ^{137}Cs as stored in the teletherapy head is known to be 50.9 TBq. This suggests that even with careful analysis, survey and recovery, it is very difficult to recover all of a widely distributed source. It is also worthy to note that the people in and around Goiânia were considered pariahs around Brazil. People were afraid both of the people from the area and the area itself. The local fear and anxiety generated by this event was widespread and lasting.

Radiological Dispersal Devices

A radiological dispersal device (RDD), sometimes referred to as a "dirty bomb," is a terrorist weapon. Terrorism may be defined as the systematic use of terror or unpredictable violence against governments, public, or individuals to attain a political objective. Terrorism has been used by political organizations with both rightist and leftist objectives, by nationalistic and ethnic groups, by revolutionaries, and by government armies and secret police.

The basic concept behind an RDD is to disperse radioactive material in a location that will cause human health and environmental health harm, generate denial of access to areas, create confusion, disrupt command and communications, produce psychological harm in a population, and ultimately generate large detrimental economic consequences. The material can be dispersed into the atmosphere energetically by destroying a source package with conventional explosives (the typical "dirty bomb"), or a liquid/powder could be dispersed using sprayers. In addition to dispersal into the atmosphere, sources would also be dispersed in water supplies or members of the food chain. Although not a dispersal, a source could be covertly emplaced with the intent of irradiating people. Nuclear weapons or improvised nuclear devices are not discussed herein as their effects to the environment are discussed in sections on "Nuclear Weapons Testing" and "Nuclear Material Accidents".

The common elements for the most typical use of radionuclides for terrorist activities are shown in Fig. 41.

Technical Considerations for Environmental Contamination A radiological dispersal device (RDD) may be defined as:

> Any device, including any weapon or equipment, other than a nuclear explosive device, specifically designed to employ radioactive material by disseminating it to cause destruction, damage, or injury by means of the radiation produced by the decay of such material.

Almost any radioactive material can be used to construct an RDD, including fission products, spent fuel from nuclear reactors, and relatively low-level materials, such as medical, industrial, and research waste. Weapons grade materials (i.e., highly enriched uranium or plutonium) are not needed (nor desired) although they could be used. An RDD is designed to scatter radioactive material over a wide area, thereby contaminating the area.

It is assumed that a quantity of radioactive material is in the possession of an individual or individuals for the purpose of constructing an RDD. That is, an individual is able (through some process) to obtain and store a source of radioactive material. Next, it is assumed that in order for an RDD to be effective in doing harm to human health, it must have a relatively large activity within a relatively small exposed population. Based upon the above assumptions, the following source classifications are high risk for an RDD:

- Large industrial-use sources of radioactive material (such as nondestructive testing gamma sources, thickness indicators, moisture detectors, and tank level monitors)
- Gamma sources used in radiotherapy medical facilities
- Various large sources of radioactivity used in government and commercial applications

It is worthy to note, however, that small, low-activity sources that would be ineffective at producing human bodily harm or environmental damage are capable of generating significant psychological damage to affected populations, and therefore even small radioisotope sources may be considered a threat.

There are four broad classifications with respect to exposure pathway:

1. Passive irradiation
2. Dissemination into a food or water chain directly

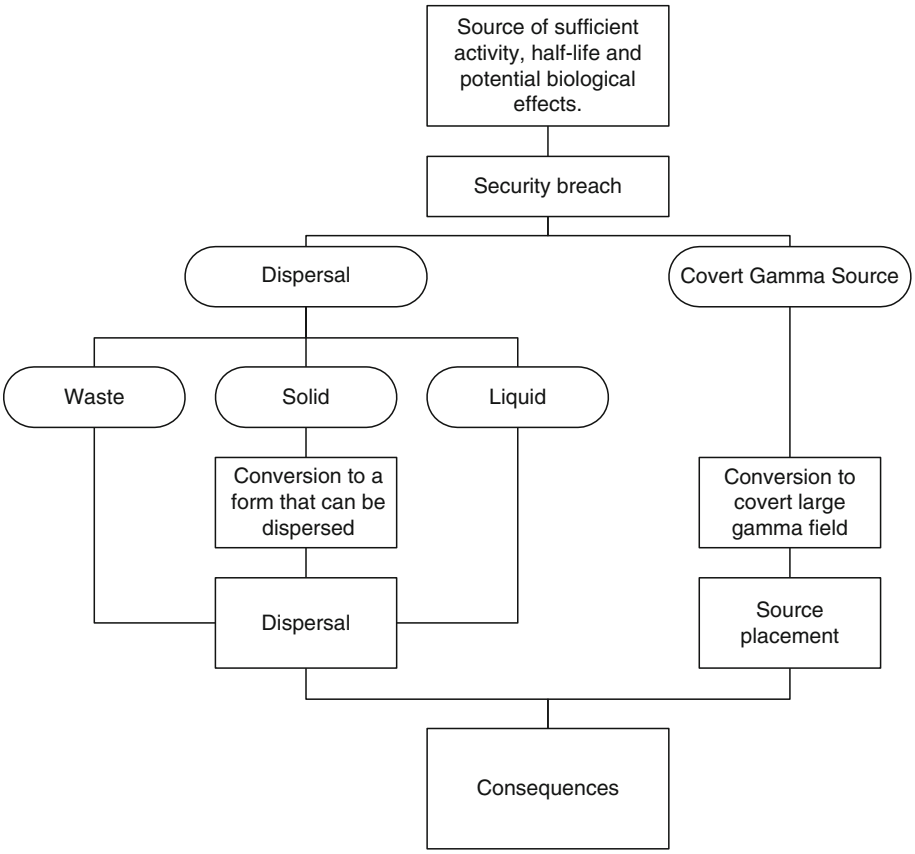

Radiation in the Environment, Sources of. Figure 41
Flowchart for possible terrorist activity involving radioactive material

3. Explosive aerosol dispersal
4. Nonexplosive aerosol dispersal

Passive irradiation involves placing a source in covert manner, as irradiating individuals or a population. This scenario affects a relatively small population and is readily detectable. The health physics theory behind external irradiation is well developed and readily applied to postulated scenarios. Dissemination into a food or water chain poses an ingestion threat to potentially large populations. Valued ecosystem component (VEC) analysis of radiological species is a well-developed science, primarily through pathways analysis as used in nuclear power plant operations. Explosive aerosol dispersal of radionuclide sources is a relatively undeveloped field of study. There are many parameters requiring investigation for explosive dispersal, including source metallurgical form, source encapsulation and explosive configuration. Nonexplosive dispersal of radiological contaminants is a relatively well-developed field of study, from the perspective of nuclear reactor accident plume characterization.

A large number of common radioisotopes have potential for generating either a radiological or psychological threat. Some of these are presented in Table 38. Although any radioisotope could be used in an RDD, the usefulness is usually determined by the availability, total activity, and radiological half-life.

A radiological dispersal device has never been used in war or terrorist act, and as such there is no operational data as to the effects on the environment. It would be expected that the effects would be similar to those from analogous events, such as nuclear material accidents (discussed in section on "Nuclear Material Accidents"), although targeted for optimum harm.

Radiation in the Environment, Sources of. Table 38
Potential industrial radioisotopes for RDD use

Radioisotope	Primary emission considered (secondary)	Typical use
H-3	β	Gaseous luminous light sources
Am-241	α (γ)	Smoke detectors
Cs-137	γ (β)	Irradiators
Co-60	γ (β)	Irradiators
Ir-192	γ (β)	Industrial radiography
Pu-238	α	Radioisotopic thermoelectric generators (RTG)
Ra-226	α (β, γ through progeny)	Historical medical and light sources
Sr-90	β	Radioisotopic thermoelectric generators (RTG)
Cf-252	Neutron (α, γ)	Oil well logging
Am-241/Be	Neutron (α, γ)	Oil well logging
Pu-238/Be	Neutron (α, γ)	Oil well logging

Future Directions

Environmental science is a constantly growing and adapting field. Although radionuclides have been in the environment since the origins of the universe, human understanding and impact assessment of environmental radionuclides has only taken place for approximately the past 100 years. Protection of the environment and stewardship over planetary resources is of great global concern. Some areas in which there is current and future need for research and development are listed below.

Dose–response models – Radionuclide environmental assessment ultimately relies upon risk estimation. Risk estimation has been, and continues to be, driven by the linear non-threshold (LNT) model. Despite the fact that it is widely acknowledged that LNT model has little data to support it below about 100 mGy dose, it continues to be used and drives all aspects of radiation protection from environmental restoration criteria, to human dosimetry, to the fundamental interactions with naturally occurring radioactive material. There is much research to be done to generate bona fide risk estimates from exposure at low dose (generally, the regime of environmental radioactivity).

Nuclear weapon reduction – Since the inception of nuclear weapons in 1945, there was a strong buildup and leveling off. Work is still being performed to completely ratify the Comprehensive Test Ban Treaty, with numerous political hurdles to overcome. Nuclear weapons have been the major contributor to worldwide distribution of anthropogenic radionuclides to the environment, so any efforts to eliminate testing are crucial to eliminate future introduction of anthropogenic radionuclides.

Radon dosimetry and mitigation – Radon is the major natural contributor to background dose, and, as such, efforts to measure radon both spatially and temporally will aid in radon mitigation strategies. Understanding radon dosimetry and the relationship with lung cancer and smoking is needed to determine if any detriment exists (observed, not calculated) from radon at low dose exposure.

TENORM – The issue of technologically enhanced naturally occurring radioactive material is both technical and regulatory in nature. There is much research to be done to reduce TENORM from chemical and industrial processes, as well as determining action and remediation levels in a reasonable and cost-effective manner.

Radioactive waste management – This has been one of the most studied areas related to environmental radioactivity for the past 30 years, and will continue to be a significant research area. Fundamental research is required in storage systems and strategies, modeling the fate of radionuclide transport far into the future, and dealing with issues such as transmutation of waste, waste reprocessing and recycling, and public acceptance issues. Other esoteric areas, such as revisiting the concepts of disposal in space or deep ocean disposal, require further exploration.

Nonhuman biota – Radiation protection principles have always worked on the belief that safe levels of radiation for humans did de facto protect the environment. More research is required examining explicit pathways, radionuclides, and environmentally valued ecosystem components to determine if this is indeed the case. Special attention must be given to vulnerable ecosystem populations.

Human and societal effect – Further research is required for understanding low dose radiation effects on populations, and exploring the paradoxes of high background radiation area populations and low cancer incidence. The health of the population (and nonhuman ecosystem components) requires complete epidemiological quantification, taking into account all endpoint confounders.

Contaminated ecosystem remediation – Decontamination and remediation of contaminated urban and rural environments is not a well-developed field, and there are a number of issues surrounding remediation efficacy, collection of remediated material, resuspension of contamination, and restoration guidelines all requiring further research. Immediate work is needed into assessing and quantifying sites of large introductions of historical anthropogenic radionuclides, such as the Arctic Ocean environment.

Modeling of the environment – Increases in computing power are related to increased ability to model complex systems such as the atmosphere and marine and terrestrial environments. There is much research to be done to model these complex systems. High-performance computing will enable complex compartmental systems to be modeled, which will enable prediction of environmental radioactivity transport over large spatial and temporal scales.

Mitigation of ground-level cosmogenic effects – There are numerous documented reports of solar storm activity disrupting ground-level electrical systems [108]. One major solar storm in 1859 allowed telegraph operators to continue utilizing their equipment despite unhooking them from battery power sources. Major solar storm activity is predicted for the 2012–2013 time frame, which in the worst case could disable numerous satellites, disrupt ground based communications, and trip electrical power distribution systems. The implications of losing electrical power, Internet, and audio/visual communications on a large public and governmental scale is obvious in a technology-driven society, and therefore strategies must be continuously developed for circumvention and mitigation of the effects in light of increasing advances in communication and electronics technology.

Orphan sources – Although largely an administrative issue, there are areas of research involving intelligent systems, data fusion, and other data analysis techniques that may assist in identifying probabilities of locating orphan sources, and for protecting against lost or orphan sources in the future.

Risk assessment - On 11 March 2011 an earthquake of magnitude 9 on the Richter scale struck off the east coast of Japan, proximal to Sendai. The earthquake, and subsequent tsunami, severely damaged the reactor buildings and control infrastructure for boiling water reactor (BWR) Units 1–6 at the Fukushima Daiichi nuclear reactor power facility. At the time of the event, Units 1–3 were operational and the earthquake triggered automatic shutdown of these units. Units 4–6 were off-line for inspection at the time of the incident, and unit 4 was completely defueled. Various hydrogen explosions occurred within the reactors' external structures and lack of water cooling caused damage to the reactors' fuel. Workers on-site were exposed to radioactivity primarily in contaminated water, and various isotopes were measured in and around environmental samples taken near the Fukushima Daiichi plant site [109]. The accident has been rated as Level 7 on the INES scale, which is the same level as was assigned to the Chernobyl NPP-4 accident. This "beyond-design-basis" accident is prompting regulators to reevaluate risk assessment models. Future work in redefining the design basis schema and details of consequence analysis from natural catastrophic events will be required for comprehensive protection of the environment as greater utilization of nuclear power is established.

In summary, radiation has provided much benefit to mankind over the past 100 years. Strong global stewardship and support is required to ensure that the supply of radionuclides, and the benefits of nuclear technology, remains safe into the future.

Bibliography

Primary Literature

1. NCRP (2009) Ionizing radiation exposure of the population of the United States. National Council on Radiation Protection and Measurements Report No. 160, Bethesda
2. Kathren R (1984) Radioactivity in the environment: sources, distribution and surveillance. Harwood Academic, London
3. Kendall G (2005) Factors affecting cosmic ray exposures in civil aviation. Int Congr Ser 1276:129–132
4. Bartlett D (2004) Radiation protection aspects of the cosmic radiation exposure of aircraft crew. Radiat Prot Dosim 109(4):349–355

5. Goldhagen P (2000) Overview of aircraft radiation exposure and recent ER-2 measurements. Health Phys 79(5): 526–544
6. Schraube H, Leuthold G, Roesler S, Heinrich W (1998) Neutron spectra at flight altitudes and their radiological estimation. Adv Space Res 21(12):1727–1738
7. Valković V (2000) Radioactivity in the environment. Elsevier Science, Amsterdam
8. Cooper J, Randall K, Sokhi R (2003) Radioactive releases in the environment: impact and assessment. Wiley, Etobicoke
9. Coogan L, Cullen J (2009) Did natural reactors form as a consequence of the emergence of oxygenic photosynthesis during the Achean? GSA Today 19(10):4–10
10. Meshik A, Hohenberg C, Pravdivtsea O (2004) Record of cycling operation of the natural nuclear reactor in the Oklo/Okelobondo area in Gabon. Phys Rev Lett 93(18):182302-1–182302-4
11. Gauthier-Lafaye F, Holliger P, Blanc P (1996) Natural fission reactors in the Franceville Basin, Gabon: a review of the conditions and results of a "critical event" in a geological system. Geochim Cosmochim Acta 60(23):4831–4852
12. Baum E, Knox H, Miller T (2002) Nuclides and isotopes, 16th edn. Lockheed Martin-Knolls Atomic Power Laboratory, Schenectady
13. WHO (1996) Indoor air quality: a risk-based approach to health criteria for radon indoors. WHO, Copenhagen
14. ICRP (1994) Protection against Radon-222 at home and at work. International Commission on Radiological Protection. ICRP Publication 65
15. Ghiassi-Nejad M, Beitolahi M, Fallahian N, Saghirzadeh M (2005) New findings in the very high natural radiation area of Ramsar, Iran. Int Congr Ser 1276:13–16
16. Magill J, Galy J (2005) Radioactivity radionuclides radiation. Springer, New York
17. ANSI (2009) Control and release of technologically enhanced naturally occurring radioactive material (TENORM) ANSI/HPS N13. American National Standards Institute
18. ICRP (1990) Recommendations of the International Commission on Radiological Protection. ICRP Publication 60. International Commission on Radiological Protection, Pergamon, Oxford
19. Goldstein B, Eisenbud M, Gesell T, Ibrahim S, Kocher D, Landa E, Pashoa A (1999) Evaluation of guidelines for exposures to technologically enhanced naturally occurring radioactive materials. National Academic, Washington, DC
20. Karam A, Vetter B (2009) Naturally occurring radioactive materials (NORM) and technologically enhanced NORM (TENORM). Medical Physics, Madison
21. Khater A (2004) Polonium-210 budget in cigarettes. J Environ Radioactiv 71:33–41
22. Skwarzec B, Ulatowski J, Struminska D, Borylo A (2001) Inhalation of Po-210 and Pb-210 from cigarette smoking in Poland. J Environ Radioactiv 57:221–230
23. Evans G (1993) Cigarette Smoking = Radiation hazards. Pediatrics 92(3):464–465
24. Abd El-Aziz N, Khater AEM, Al-Sewaidan HA (2005) Natural radioactivity contents in tobacco. Int Congr Ser 1276: 407–408
25. Eisenbud M, Gesell T (1997) Environmental radioactivity – from natural, industrial and military sources, 4th edn. Academic, Toronto
26. Landa E (1984) Geochemical and radiological characterization of soils from former radium processing sites. Health Phys 46(2):385–394
27. McBride J, Moore R, Whiterspoon J, Blanco R (1978) Radiological impact of airborne effluents of coal and nuclear plants. Science 202(4372):1045–1050
28. UNSCEAR (1988) Sources, effects and risks of ionizing radiation. United Nations Scientific Committee on the Effects of Atomic Radiation (UNSCEAR), 1988 Report to the General Assembly, with scientific annexes, United Nations, New York
29. Hedvall R (1996) Radioactivity concentrations in non-nuclear industries. J Environ Radioactiv 32(1–2):19–31
30. UNSCEAR (1993) Sources and effects of ionizing radiation. United Nations Scientific Committee on the Effects of Atomic Radiation (UNSCEAR), 1993 Report to the General Assembly, with scientific annexes, United Nations, New York
31. UNSCEAR (2000) Sources and effects of ionizing radiation, vol I and II. United Nations, New York
32. IAEA (2003) Radioactive waste management glossary. International Atomic Energy Agency. STI/PUB/1155, Vienna
33. IAEA (2009) Classification of radioactive waste. International Atomic Energy Agency. General Safety Guide GSG-1, Vienna
34. Salkeld R, Beichel R (1980) Nuclear waste disposal in space: implications of advanced space transportation. Acta Astronaut 7:1373–1387
35. Yablokov A (2001) Radioactive waste disposal is seas adjacent to the territory of the russian federation. Mar Pollut Bull 43(1–6):8–18
36. Champ M, Brooks J, Gomez L, Palmer H, Makeyev V, Betz F (2001) Ocean storage of nuclear waste? Experiences from the Russian Arctic. Mar Pollut Bull 43(1–6):1–7
37. Baxter M, Harms I, Osvath I, Povinec P, Scott E (1998) Modelling the potential radiological consequences of radioactive waste dumping in the Kara Sea. J Environ Radioactiv 39(2):161–181
38. Widner E, Flack S (2010) Characterization of the world's first nuclear explosion, the trinity test, as a source of public radiation exposure. Health Phys 98(3):480–497
39. Parekh P, Semkow T, Torres M, Haines D, Cooper J, Rosenberg P, Kitto M (2006) Radioactivity in trinitite six decades later. J Environ Radioactiv 85:103–120
40. Glasstone S, Dolan P (1977) The effects of nuclear weapons, 3rd edn. US DoD, Washington, DC
41. Geddes D (1945) The atomic age opens. Pocket Books, New York
42. Loeber C (2002) Building the bombs: a history of the nuclear weapons complex. Sandia National Laboratories, Albuquerque
43. Salbu B (2008) Nuclear risks in Central Asia. In: Radioactive particles released from different nuclear sources: with focus

on nuclear weapons tests. Springer Science and Business Media, New York, Chapter 2
44. AFSWP (1951) Radiological defense, vol. II – the principles of military defense against atomic weapons. Armed Forces Special Weapons Project
45. Messenger G, Ash M (1986) The effects of radiation on electronic systems. Van Nostrand Reinhold, New York
46. CTBT Data obtained via Comprehensive Test Ban Treaty Organization. http://www.ctbto.org
47. Berger M, Jacobson D, Pinca S, Richards Z, Hess D, Hariss F, Page C, Peterson E, Baker N (2008) The state of coral reef ecosystems of the Marshall Islands. NOAA/NCCOS Center for Coastal Monitoring and Assessment's Biogeography Team, Silver Spring
48. Simon SL, Graham JC (1997) Findings of the first comprehensive radiological monitoring program of the Republic of the Marshall Islands. Health Phys 73(1):66–85
49. Cronkite EP, Conard RA, Bond VP (1997) Historical events associated with fallout from Bravo Shot–Operation Castle and 25 Y of medical findings. Health Phys 73(1):176–186
50. Richards ZT, Beger M, Pinca S, Wallace CC (2008) Bikini Atoll coral biodiversity resilience five decades after nuclear testing. Mar Pollut Bull 56(3):503–515
51. Robison WL, Conrado CL, Bogen KT, Stocker AC (2003) The effective and environmental half-life of 137Cs at Coral Islands at the former US nuclear test site. J Environ Radioactiv 69(3):207–223
52. Noshkin VE, Robison WL, Wong KM, Brunk JL, Eagle RJ, Jones HE (1997) Past and present levels of some radionuclides in fish from Bikini and Enewetak atolls. Health Phys 73(1):49–65
53. NCI (1997) Estimated exposures and thyroid doses received by the American people from Iodine-131 in fallout following Nevada atmospheric nuclear bomb tests. National Cancer Institute, Bethesda
54. Bowen S, Finnegan D, Thompson J, Miller C, Baca P, Olivas L, Geoffrion C, Smith D, Goishi W, Esser B, Meadows J, Namboodiri N, Wild J (2001) Nevada test site radionuclide inventory, 1951-1992. Los Alamos National Laboratory, LA-13859-MS, Los Alamos
55. Miller C, Bouville A (2005) Report on the feasibility of a study of the health consequences to the American population from nuclear weapons tests conducted by the Unites States and other nations. Centers for Disease Control, Atlanta
56. Frohmberg E, Goble R, Sanchez V, Quigley D (2000) The assessment of radiation exposures in native American communities from nuclear weapons testing in Nevada. Risk Anal 20(1):101–111
57. Russ A, George P, Goble R, Crema S, Liu C, Sachez D (2005) Native American exposure to 131I from nuclear weapons testing in Nevada. Hum Ecol Risk Assess 11(5):1047–1063
58. Haywood S, Smith J (1992) Assessment of potential doses at the Maralinga and emu test sites. Health Phys 63(6):624–630
59. Cooper M, Burns P, Tracy B, Wilks M, Williams G (1994) Characterization of plutonium contamination at the former nuclear weapons testing range at Maralinga in South Australia. J Radioanal Nucl Chem 177(1):161–184
60. Weber J, Till J (1999) Final report – Task 1: cleanup levels at other sites, radionuclide soil action level oversight panel. Risk Assessment Corporation, Neeses
61. Woollett S (2003) Rehabilitating Maralinga. Clean Air Environ Qual 37(4):31–33
62. Carter M, Moghissi A (1977) Three decades of nuclear testing. Health Phys 33:55–71
63. De Planque G (1998) The Mururoa study. IAEA Bull 40(4):21–23
64. Bourlat Y, Martin G (1992) Precise determination of the concentration of radiocesium in the water of Mururoa Lagoon. J Environ Radioactiv 17:13–29
65. Bourlat Y, Millies-Lacroix J, Nazard R (1995) Determination of plutonium radioactivity in Mururoa Lagoon water. J Radioanal Nucl Chem 192(2):387–408
66. Linsley G, McEwan A (1998) Potential doses at the atolls. IAEA Bull 40(4):38–42
67. Danesi P, Moreno J, Makarewicz M, Radecki Z (2002) Residual radioactivity in the terrestrial environment of the Mururoa and Fangataufa atolls nuclear weapons test sites. J Radioanal Nucl Chem 253(1):53–65
68. Egorov N, Novikov V, Parker F, Popov V (2000) The radiation legacy of the Soviet nuclear complex. Earthscan, London
69. Gusev B, Abylkassimova Z, Apsalikov K (1977) The Semipalatinsk NUCLEAR TEST SITE: a first assessment of the radiological situation and the test-related radiation doses in the surrounding territories. Radiat Environ Biophys 36:201–204
70. Grosche B (2002) Semipalatinsk test site: introduction. Radiat Environ Biophys 41:53–55
71. Carlsen T, Petersen L, Ulsh B, Werner C, Purvis K, Sharber A (2001) Radionuclide contamination at Kazakhstan's Semipalatinsk test site: implications on human and ecological health. Hum Ecol Risk Assess 7(4):943–955
72. Sakaguchi A, Yamamoto M, Hoshi M, Imanaka T, Apsalikov K, Gusev B (2006) Radiological situation in the vicinity of Semipalatinsk nuclear test site: Dolon, Mostik, Cheremushku and Budene settlements. J Radiat Res 47(Suppl A):A101–A116
73. Simon S, Baverstock K, Lindholm C (2003) A summary of evidence on radiation exposures near to the Semipalatinsk nuclear weapons test site in Kazakhstan. Health Phys 84(6):718–725
74. Balmukhanov S (2006) Medical effects and dosimetric data from nuclear tests at the Semipalatinsk test site. Defense Threat Reduction Agency. DRTA-TR-06-23, Fort Belvoir
75. Kemeny J (1979) Report of the President's commission on the accident at three mile Island – the need for change: the legacy of TMI., Library of Congress Catalog Card No. 79-25694. ISBN 0-935758-00-3
76. Waller E, Cole D (1999) An environmental radionuclide baseline study (ERBS) near three Canadian Naval Ports. Health Phys 77:37–42
77. Strålskyddsnytt (2006) Tjernobyl 20 år. Strålskyddsnytt 1, 11.
78. Borovoy A, Beskorovainyi V, Bogatov S, Vysotskiy E, Gavrilov S, Ivanov A, Kotovich V, Krinitsyn A, Molodykh V, Nemchinov Y,

Pazukhin E, Rudko V, Sharovarov G, Shcherbin V (1998) The shelter's current safety status and situation development forecasts (updated version). Tacis Services DG IA, Brussels
79. McLaughlin T, Monahan S, Pruvost N, Frolov V, Ryazanov B, Sviridov V (2000) A review of criticality accidents. Los Alamos National Laboratory, Los Alamos
80. IAEA (1998) The radiological accident in the reprocessing plant at Tomsk. International Atomic Energy Agency. STI/PUB/1060, Vienna
81. Usachev V, Markov G (2003) Incidents caused by red oil phenomena at semi-scale and industrial radiochemical units. Radiochemistry 45(1):1–8
82. Anspaugh L, Degteva M, Vasilenko E (2002) Mayak production association: introduction. Radiat Environ Biophys 41:19–22
83. IAEA (2009) INES: The international nuclear and radiological event scale user's manual, 2008 ed. IAEA, Vienna
84. Moran B (2009) The day we lost the H-Bomb: cold war, hot nukes and the worst nuclear weapons disaster in history. Ballantine Books, New York
85. Place W, Cobb F, Defferding C (1975) Palomares summary report. Field Command, Defense Nuclear Agency, Technology and Analysis Directorate, Kirtland Air Force Base, New Mexico
86. Jiménez-Ramos M, García-Tenorio R, Vioque I, Manjón G, García-León M (2006) Presence of plutonium contamination in soils from Palomares (Spain). J Environ Radioactiv 142:487–492
87. Espinosa A, Aragon A, Stradling N, Hodgson A, Birchall A (1998) Assessment of doses to adult members of the public in Palomares from inhalation of plutonium and Americium. Radiat Prot Dosim 79(1–4):161–164
88. Erisken V (1990) Sunken nuclear submarines – a threat to the environment? Norwegian University Press, Oslo
89. Waller E, Cole D, Jamieson T (2008) Radiation protection issues related to Canadian museum operations. Health Phys 94(2 Suppl 1):S155–S159
90. NCRP (2007) Development of a biokinetic model for radionuclide-contaminated wounds and procedures for their assessment, dosimetry and treatment. National Council on Radiation Protection and Measurements. Report No. 156, Bethesda
91. Burkart W, Danesi P, Hendry J (2005) Properties, use and health effects of depleted uranium. Int Congr Ser 1276:133–136
92. Papastefanou C (2002) Depleted uranium in military conflicts and the impact on the environment. Health Phys 83(2):280–282
93. McLaughlin J (2005) Public health and environmental aspects of DU. Int Congr Ser 1276:137–140
94. Aftergood S (1989) Background on space nuclear power. Sci Glob Secur 1:93–107
95. Bennett G (2006) Space nuclear power: opening the final frontier, American Institute of Aeronautics and Astronautics AIAA 2006-4191. In: Presentation at 4th international energy conversion engineering conference and exhibit (IECEC), San Diego, pp 12–13
96. Hardy E, Krey P, Volchok H (1973) Global inventory and distribution of fallout plutonium. Nature 241:244–245
97. Gummer W, Campbell F, Knight G, Richard J (1980) Cosmos 954 – the occurrence and nature of recovered debris. Atomic Energy Control Board. AECB- INFO-0006
98. IAEA (2000) Categorization of radiation sources. International Atomic Energy Agency. IAEA GOV/2000/34-GC(44)/7 Attachment 3, Vienna
99. NN (2003) RDD Report offers steps to reduce threat. *Nuclear News* 03/2003, 37
100. Ferguson C, Kazi T, Perera J (2003) Commercial radioactive sources: surveying the security risks. Occasional Paper No. 11, Centre for Non-Proliferation Studies, Monterey Institute of International Studies, Monterey
101. Saha G (1998) Fundamentals of nuclear pharmacy, 4th edn. Springer, New York
102. Fischer H, Ulbrich S, Pittauerová D, Hettwig B (2009) Medical radioisotopes in the environment – following the pathway from patient to river sediment. J Environ Radioactiv 100(12):1079–1085
103. NCRP (1987) Radiation exposure of the US population from consumer products and miscellaneous sources. National Council on Radiation Protection and Measurements. Report No. 95, Bethesda
104. Bevelacqua J (1995) Contemporary health physics: problems and solutions. Wiley-Interscience, Toronto
105. IAEA (2002) Inadequate control of world's radioactive sources. International Atomic Energy Agency. IAEA Press Release 2002/09, Vienna
106. IAEA (2004) Strengthening control over radioactive sources in authorized use and regaining control over orphan sources – national strategies. International Atomic Energy Agency. IAEA-TECDOC-1388, Vienna
107. IAEA (1988) The radiological accident in Goiania. International Atomic Energy Agency. STI/PUB/815, Vienna
108. Boteler D, Pirjola R, Nevanlinna H (1998) The effects of geomagnetic disturbances on electrical systems at the Earth's surface. Adv Space Res 22(1):17–27
109. Fukushima (2011) Special report: Fukushima Daiichi after the earthquake and tsunami. Nuclear News 54:17–18b, 83–84b

Books and Reviews

Aycik G, Ercan A (1997) Radioactivity measurements from coals and ashes from coal fired power plants from the southwestern part of Turkey. J Environ Radioactiv 35:23–35

Bailey R, Clark H, Ferris J, Krause S, Strong R (2002) Chemistry of the environment, 2nd edn. Academic, New York

Baryakhtar V, Kukhar V, Los I, Poyarkov V, Kholosha V, Shestopalov V (1998) Comprehensive risk assessment of the consequences of the chernobyl accident. Science and Technology Center in Ukraine – Ukrainian Radiation Training Centre. Project No. 369. Kiev, Ukraine

Brodsky A (1996) Review of radiation risks and uranium toxicity with application to decisions associated with decommissioning clean-up criteria. RSA, Hebron

Bussard RW, DeLauer RD (1958) Nuclear rocket propulsion. McGraw Hill, Toronto
Calomet D (1989) Ocean disposal of radioactive waste: status report. IAEA Bull 4:47–50
Cember H, Johnson T (2009) Introduction to health physics, 4th edn. McGraw Hill, Toronto
Chernobyl (2005) Chernobyl's legacy: health, environmental and socio-economic impacts and recommendations to the Governments of Belarus, the Russian Federation and Ukraine. The Chernobyl Forum: 2003-2005, 2nd rev edn
Crick MJ, Linsley GS (1982) An assessment of the radiological impact of the windscale reactor fire, October 1957. Report NRPB-R135, National Radiological Protection Board, Chilton
Dai L, Wei H, Wang L (2007) Spatial distribution and risk assessment of radionuclides in soils around a coal-fired power plant: a case study from the city of Baoji. China Environ Res 104: 201–208
Fry RJ (2000) Radiation protection guidance for activities in low-earth orbit. National Council on Radiation Protection and Measurements. NCRP Report No. 132, Bethesda
Gomez M (1981) Radiation hazards in mining: control, measurement, and medical aspects. Society of Mining Engineers. American Institute of Mining, Metallurgical and Petroleum Engineers, New York
Heaps L (1978) Operation morning light. Ballantine Books, Toronto
IAEA (1996) Issues in radioactive waste disposal – second report of the working group on principals and criteria for radioactive waste disposal. International Atomic Energy Agency. IAEA-TECDOC-909, Vienna
IAEA (1999) Protection of the environment from the effects of ionizing radiation – a report for discussion. International Atomic Energy Agency. IAEA-TECDOC-1091, Vienna
Journal of Environmental Radioactivity. Elsevier Science, Maryland Heights, MO. ISSN: 0265-931X
Lamarsh J, Baratta A (2001) Introduction to nuclear engineering, 3rd edn. Prentice Hall, Toronto
Lehr J, Hyman M, Gass T, Seevers W (2002) Handbook of complex environmental remediation problems. McGraw Hill, Toronto
Lewis WB, Ward AC (1953) An appreciation of the problem of reactor shut-off rods with special reference to the NRX reactor. Atomic Energy of Canada Limited. AECL No. 590, Chalk River
Louvar J, Louvar B (1998) Health and environmental risk analysis. Prentice Hall, Toronto
Mangeno J, Steele J, Betschart J (1991) Environmental monitoring and disposal of radioactive wastes from U.S. Naval nuclear-powered ships and their support facilities 1990. Naval Nuclear Propulsion Program, Department of the Navy. Report NT-91-1
Mangeno J, Tyron A, Burrows C (1991) Occupational radiation exposure from U.S. Naval nuclear propulsion plants and their support facilities. Naval Nuclear Propulsion Program, Department of the Navy. Report NT-91-2
May J (1989) The Greenpeace handbook of the nuclear age. McClelland and Stewart, Toronto
McCracken G, Stott P (2005) Fusion: the energy of the universe. Elsevier Academic, New York
Messenger GC, Ash MS (1997) Single event phenomena. Chapman & Hall, Toronto
Moeller D (2005) Environmental health, 3rd edn. Harvard University Press, Cambridge
Moeller D (2005) Environmental health physics: 50 years of progress. Health Phys 88:676–696
Moore T, Dietrich D (1987) Chernobyl and its legacy. EPRI J 5:21
Oberg J (1999) The probe that fell to Earth. *New Scientist* 6 March 1999
Paić G (1988) Ionizing radiation: protection and dosimetry. CRC, Boca Raton
Reese H (1986) DoD nuclear mishaps. Armed Forces Radiobiology Research Institute. AFRRI SP86-2, Bethesda
Rippon S (1986) Chernobyl: The Soviet report. Nucl News 1:8
Scott RL (1971) Fuel-melting incident at the fermi reactor on Oct 5, 1966. Nucl Saf 12:123–134
Silva P, Camargo I, Mazzilli B (2006) Radioactivity of coal and ashes from figueira coal power plant in Brazil. J Radioanal Nucl Chem 270:597–602
Simon SL (1997) A brief history of people and events related to atomic weapons testing in the Marshall Islands. Health Phys 73(1):5–20
Till J, Grogan H (2008) Radiological risk assessment and environmental analysis. Oxford University Press, Toronto
Turner J (1995) Atoms, radiation and radiation protection, 2nd edn. Wiley Interscience, Toronto
Tykva R, Berg D (eds) (2004) Man-made and natural radioactivity in environmental pollution and radiochronology. Kluwer, Dordecht/Holland
Zeevaert T, Sweeck L, Vanmarcke H (2006) The radiological impact from airborne routine discharges of a modern coal-fired power plant. J Environ Radioactiv 85:1–22

Radiation Shielding

J. Kenneth Shultis[1], Richard E. Faw[2]
[1]Department of Mechanical & Nuclear Engineering, Kansas State University, Manhattan, KS, USA
[2]Department of Mechanical & Nuclear Engineering, Kansas State University, Winston Salem, NC, USA

Article Outline

Glossary
Definition of the Subject
Introduction
History of Shielding
Practice of Radiation Shielding
Basic Analysis Methods

Intermediate Methods for Photon Shielding
Intermediate Methods for Neutron Shielding
Gamma-Ray and Neutron Reflection
Radiation Streaming Through Ducts
Gamma-Ray and Neutron Skyshine
Transport Theory
Future Directions
Bibliography

Glossary

Albedo A quantity describing how neutrons or photons incident on the surface of some medium (e.g., a wall) are reflected or reemitted from the surface.

Buildup factor A factor to account for production of secondary photons in a shield. The transmitted dose from only uncollided photons times the buildup factor equals the dose from all photons, uncollided plus secondary photons.

Dose A general term for the energy transferred from radiation to matter. Specifically, the absorbed dose is the amount of energy imparted to matter from ionizing radiation in a unit mass of that matter. Units are the gray (Gy) and rad, respectively, equivalent to 1 J/kg and 100 ergs/g.

Flux A measure of the intensity of a radiation field. Specifically, it equals the number of radiation particles entering, in a unit time, a sphere of cross-sectional area ΔA divided by ΔA, as $\Delta A \to 0$. The flux, integrated over a specified time interval is called the *fluence*.

Interaction coefficient A quantity, denoted by μ, describing how readily a photon or neutron interacts with a given medium. Specifically, it is the probability a radiation particle of energy E will interact in a specified manner per unit distance of travel, for infinitesimal distances. It thus has units of inverse length. The total interaction coefficient $\mu = \sum_i \mu_i$ where μ_i is the coefficient for the ith type of interaction (e.g., scattering, absorption).

Neutron A neutral subatomic particle that collectively with positively charged protons forms an atomic nucleus. Although both are composite particles composed of quarks and gluons, for the energies considered in this entry they can be viewed as fundamental unchangeable particles.

Photon A quantum of electromagnetic radiation with energy $E = h\nu$, where h is Planck's constant and ν is the frequency. Photons produced by a change in the structure of the nucleus are called *gamma photons* and those produced by atomic electron rearrangement are called *x-rays*.

Skyshine A term for the radiation that reaches some point of interest after being scattered by the atoms in the atmosphere back to the point of interest.

Transport equation Also known as the linearized Boltzmann equation, it describes rigorously the spatial, energy, and angular distribution of neutrons or photons in any medium with arbitrary source distributions. From its solution, the radiation flux or dose anywhere in the medium can be determined.

Definition of the Subject

We live in a world that abounds in radiation of all types. Many radiations, such as the neutrinos or visible light from our sun present little risk to us. Other radiations, such as medical x-rays or gamma rays emitted by radioactive materials, have the potential to cause us harm. In this entry, only the transport of *indirectly ionizing radiation* is considered. These radiations consist of chargeless particles such as neutrons or photons that, upon interacting with matter, produce energetic secondary charged particles called *directly ionizing radiation*. It is these secondary charged particles that, through ionization and excitation of ambient atoms along their paths, cause radiation damage to biological tissues or other sensitive materials.

To mitigate radiation damage, a *shield* is often interposed between a source of ionizing radiation and the object to be protected so that the radiation levels near the object are reduced to tolerable levels. Typically, a shield is composed of matter that effectively diminishes the radiation that is transmitted. (However, there are noncorporeal shields such as magnetic fields that deflect moving charged particles. The earth's magnetic field serves as such a shield to protect us from charged particles reaching earth from outer space.) The term *radiation shielding* refers usually to a system of shields constructed for a specific radiation protection purpose. The term also refers to the study of shields – the topic of this entry.

Introduction

The origins of shielding go back to the science of optics in which the exponential attenuation of light was long recognized. The exponential attenuation of radiation rays is still widely used for neutron and photon shielding. Also the governing field equation that describes how radiation migrates through matter was introduced in 1872 by Ludwig Boltzmann who used it to study the kinetic theory of gas. All this occurred before the discovery of ionizing radiation! The *radiation transport equation* is just a special case of the Boltzmann equation applied to situations in which radiation particles do not interact among themselves.

The study of shielding has many aspects: transport of (deeply penetrating) indirectly ionizing radiation in the shield, the production of very slightly penetrating secondary (directly ionizing) radiation in the shield and its surroundings, the radiation levels in the vicinity of the shield, deposition of heat in the shield, radiation penetration through holes in the shield, radiation scattered around the shield, selection of shielding materials, optimization of the shielding configuration, and the economics of shield design. It also involves understanding of related matters such as radiation source characteristics, radiation protection standards, and the fundamentals of how radiation interacts with matter.

The restriction of this entry to indirectly ionizing radiation is of a practical nature. Sources of charged particles, such as the alpha and beta particles emitted in some types of radioactive decay, can and do cause biological damage, particularly if the radioactive material is ingested. Here, however, it is assumed that the radiation sources are external to the body or the sensitive material of interest. Such external sources also usually emit far more penetrating indirectly ionizing radiation, and any shield that is effective against indirectly ionizing radiation is usually more than adequate to stop the directly ionizing radiation.

History of Shielding

To appreciate better the current state of shielding practice, it is important to understand how the discipline developed and what were the driving forces that caused it to mature. In this section, a brief overview of the history of shielding is presented. (A greatly expanded version of the following synopsis is provided by Shultis and Faw [1].)

Early History

The hazards of x-rays were recognized within months of Roentgen's 1895 discovery, but dose limitation by time, distance, and shielding was at the discretion of the individual researcher until about 1913. Only then were there organized efforts to create groups to establish guidelines for radiation protection. And it was not until about 1925 that instruments became available to quantify radiation exposure.

In 1925, Mutscheller [2] introduced important concepts in x-ray shielding. He expressed the erythema dose (An *ED* value of unity represents a combination of time, distance, and beam current just leading to a first-degree burn) *ED* quantitatively in terms of the beam current i (mA), exposure time t (min), and source-to-receiver distance r (m), namely, $ED = 0.00368it/r^2$, independent of x-ray energy. Mutscheller also published attenuation factors in lead as a function of lead thickness and x-ray average wavelength.

Evolutionary changes to x-ray shielding were made during the decades preceding World War II. These included consideration of scattered x-rays, refinements in shielding requirements in terms of x-ray tube voltages, recommendations for use of goggles (0.25-mm Pb equivalent) and aprons (0.5-mm Pb equivalent) for fluoroscopy, and specifications for tube-enclosure shielding and structural shielding for control rooms.

The other major source of ionizing radiation before World War II was the medical and industrial use of radioactive radium discovered by Marie and Pierre Curie in 1898. Not until 1927 were lead shielding standards recommended for radium applicators, solutions, and storage containers. For example, the International X-Ray and Radium Protection Committee recommended that tubes and applicators should have at least 5 cm of lead shielding per 100 mg of radium. It was not until 1941 that a tolerance dose for radium, expressed in terms of a maximum permissible body burden of 0.1 μCi, was established. This was done largely in consideration of the experiences of early "radium-dial" painters and the need for standards on safe handling of radioactive luminous compounds [3].

Manhattan Project and the Early Postwar Period

Early reactor shielding. During World War II, research on nuclear fission, construction of nuclear reactors, production of enriched uranium, generation of plutonium and its separation from fission products, and the design, construction, testing, and deployment of nuclear weapons all were accomplished at breakneck speed in the Manhattan Project. Radiation sources new in type and magnitude demanded not only protective measures such as shielding but also examination of biological effects and establishment of work rules.

The construction of nuclear reactors for research and for plutonium production required shield designs for both gamma rays and neutrons. However, with only sparse empirical data and large uncertainties about how neutrons and gamma rays migrate through shields, shield designers acted very conservatively. For example, shielding for both Fermi's 1943 graphite pile in Chicago and the 1947 X-10 research reactor at what is now Oak Ridge National Laboratory was adequate for gamma rays and overdesigned for neutrons. Operation of the X-10 reactor, built to provide data for the design of plutonium-production reactors, revealed problems with streaming of gamma rays and neutrons around access holes in the shield. The water-cooled graphite plutonium-production reactors at Hanford, Washington used iron thermal shields and high-density limonite and magnetite concrete as biological shields.

By the 1940s, the importance of scattered gamma rays was certainly known from measurements, and use of the term *buildup factor* to characterize the relative importance of scattered and unscattered gamma rays had its origin during the days of the Manhattan Project. Neutron diffusion theory and Fermi age theory were established, but shielding requirements for high-energy neutrons were not well understood. Wartime radiation shielding was an empirical, rule-of-thumb craft.

Nuclear reactors for propulsion. The Atomic Energy Act of 1946 transferred control of nuclear matters from the Army to the civilian Atomic Energy Commission (AEC). That same year, working with the AEC, the US Navy began development of a nuclear powered submarine and the US Air Force, a nuclear powered aircraft. Both of these enterprises demanded minimization of space and weight of the nuclear-reactor power source. Such could be accomplished only by minimizing design margins and that required knowledge of mechanical, thermal, and nuclear properties of materials with greater precision than known before.

Research reactors were constructed at various national laboratories in the USA and Britain to provide the much needed shielding data. The first such research program was begun in 1947 at Oak Ridge National Laboratory with the construction of the X-10 graphite reactor. The X-10 graphite reactor had a 2-ft square aperture in its shielding from which a neutron beam could be extracted, the intensity being augmented by placement of fuel slugs in front of the aperture. Attenuation of neutrons could then be measured within layers of shielding materials placed against the beam aperture. Early measurements revealed the importance of capture gamma rays produced when neutrons were absorbed. Improved experimental geometry was obtained by using a converter plate containing enriched uranium instead of relying on fission neutrons from fuel slugs. A broadly uniform beam of thermal neutrons incident on the plate generated a well-defined source of fission neutrons. A water tank was adjacent to the fission source, with shielding slabs and instrumentation within the tank. This *Lid Tank Shielding Facility*, LTSF, was the precursor of many so-called *bulk-shielding facilities* incorporated into many water-cooled research reactors.

Although a nuclear powered aircraft never flew, the wealth of information gained on the thermal, mechanical, and shielding properties of many special materials is a valuable legacy. To obtain shielding data in the absence of ground reflection of radiation, several specialized facilities were constructed. A test reactor was suspended by crane for tests of ground reflection. Then an aircraft shield test reactor was flown in the bomb-bay of a B-36 aircraft to allow measurements at altitude. The Oak Ridge tower shielding facility (TSF) went into operation in 1954, and remained in operation for almost 40 years. Designed for the aircraft nuclear propulsion program, the facility allowed suspension of a reactor hundreds of feet above grade and separate suspension of aircraft crew compartments. In its long life, the TSF also supported nuclear defense and space nuclear applications.

Streaming of radiation through shield penetrations and heating in concrete shields due to neutron and gamma-ray absorption were early shielding studies conducted in support of gas-cooled reactor design.

Additional efforts were undertaken soon thereafter at universities as well as government and industrial laboratories. Shielding material properties, neutron attenuation, the creation of capture and inelastic scattering gamma rays, reflection and streaming of neutrons and gamma rays through ducts and passages, and radiation effects on materials were major research topics.

The Decade of the 1950s

This era saw the passage in the USA of the Atomic Energy Act of 1954, the Atoms for Peace program, and the declassification of nuclear data. During this decade, many simplified shielding methods were developed that were suitable for hand calculations. The first digital computers appeared and were quickly used for radiation transport calculations. The US Air Force also started a short-lived nuclear rocket program.

Advances in neutron shielding methods. These advances resulted from measurements at the LTSF and other bulk-shielding facilities. One advancement was the measurement of point kernels, or Green's functions, for attenuation of fission neutrons in water and other hydrogenous media. The other was the discovery that the effect of water-bound oxygen, indeed the effect of homogeneous or heterogeneous shielding materials in hydrogenous media, could be modeled by exponential attenuation governed by effective "removal" cross sections for the non-hydrogen components. The LTSF allowed measurement of removal cross section for many materials.

Advances in gamma-ray shielding methods. As the decade began, researchers at the National Bureau of Standards investigated electron and photon transport. Much of this effort dealt with the moments method for solving the transport equation describing the spatial, energy, and angular distributions of radiation particles emitted from fixed sources. From such calculations, *buildup factors* to account for scattered photons were determined for various shielding media and shield thicknesses. Various empirical formulas were also developed to aid in the interpolation of the buildup-factor data.

Advances in Monte Carlo computational methods. The Monte Carlo method of simulating radiation transport computationally has its roots in the work of John von Neumann and Stanislaw Ulam at Los Alamos in the 1940s. Neutron-transport calculations were performed in 1948 using the ENIAC digital computer which had commenced operations in 1945. In this decade, major theoretical advances in Monte Carlo methods were made and many clever algorithms were invented to allow Monte Carlo simulations of radiation transport through matter. Little did the pioneers of this transport approach realize that Monte Carlo techniques would become indispensable in modern shielding practice.

The Decade of the 1960s

The 1960s saw the technology of nuclear-reactor shielding consolidated in several important publications. Blizard and Abbott [4] edited and released a revision of a portion of the 1955 Reactor Handbook as a separate volume on radiation shielding, recognizing that reactor shielding had emerged from nuclear-reactor physics into a discipline of its own. In a similar vein, the first volume of the Engineering Compendium on Radiation Shielding [5] was published. These two volumes brought together contributions from scores of authors and had a great influence on both practice and education in the field of radiation shielding.

This exciting decade also saw the beginning of the Apollo program, the start of the NASA NERVA (Nuclear Engine for Rocket Vehicle Application) program, the deployments in space of SNAP-3, a radioisotope thermoelectric generator in 1961, and SNAP-10A nuclear-reactor power system in 1965. It also saw the Cuban missile crisis in October 1962 and a major increase in the cold-war apprehension about possible use of nuclear weapons. The Apollo program demanded attention to solar flare and cosmic radiation sources and the shielding of space vehicles. Cold-war concerns demanded attention to nuclear-weapon effects, particularly structure shielding from nuclear-weapon fallout. Reflection of gamma rays and neutrons and their transmission through ducts and passages took on special importance in structure shielding. The rapid growth in access to digital computers allowed introduction of many computer codes for shielding design and fostered advances in solving various approximations to the Boltzmann transport equation for neutrons and gamma rays. Similar advances were made in treating the slowing down and transport of charged particles.

Space shielding. Data gathered over many years revealed a very complicated radiation environment in space. Two trapped-radiation belts had been found to surround the earth, an inner proton belt and an outer electron belt. Energy spectra and spatial distributions in these belts are determined by the earth's magnetic field and by the solar wind, a plasma of low-energy protons and electrons. The radiations pose a risk to astronauts and to sensitive electronic equipment. Uniform intensities of very-high-energy galactic cosmic rays demand charged-particle shielding for protection of astronauts in long duration missions. The greatest radiation risk faced by Apollo astronauts was from solar flare protons and alpha particles with energies as great as 100 MeV for the former and 400 MeV for the latter. The overall subject of space radiation shielding is treated by Haffner [6].

Structure shielding. Structure shielding from nuclear-weapon fallout required careful examination of the atmospheric transport of gamma rays of a wide range of energies and expression of angular distributions and related data in a manner easily adopted to analysis of structures. There was a need to assess, at points within a structure, the ratios of interior dose rates to that outside the building, called *reduction factors*. These factors were measured experimentally and also calculated with the transport moments method which had been used so successfully in calculation of buildup factors.

Other shielding advances. Of great importance to structure shielding, but also of interest in reactor and nuclear plant shielding, were the development of simplified methods to quantify neutron and gamma-ray streaming through ducts and voids in shields. This decade saw the development of removal-diffusion methods to describe quite accurately the penetration and slowing down of fast fission neutrons in shields. Finally, a simplified approach was developed to describe how gamma rays or neutrons incident on some material are scattered back. The central concept in this approach is the *particle albedo*, a function that describes how radiation incident on a thick medium, a concrete wall for example, is reemitted or reflected back from the surface. Measurements, theoretical calculations, and approximating formulas for both neutron and gamma-ray albedos were developed in this decade.

Digital computer applications. Radiation transport calculations are by nature very demanding of computer resources. The community of interest in radiation transport and shielding has been served magnificently for more than 4 decades by the Radiation Safety Information Computational Center (RSICC). Established in 1962 as the Radiation Shielding Information Center (RSIC) at Oak Ridge National Laboratory, RSICC's mission is to provide in-depth coverage of the radiation transport field to meet the needs of the international shielding community.

The 1960s saw many new "mainframe" computer codes developed and disseminated. Among these codes were gamma-ray "point-kernel" codes such as ISOSHLD and QAD, with versions of both still in use after almost 4 decades. The discrete-ordinates method of solving the Boltzmann transport equation was devised in the 1950s and put into practice in the 1960s in a series of computer codes, such as DTF, DOT, and ANISN. The spherical harmonics method of treating neutron spatial and energy distributions in shields was advanced by Shure [7] in one-dimensional P_3 calculations. Progress in Monte Carlo methods advanced in pace with discrete-ordinates methods, and the multigroup Monte Carlo code for neutron and gamma-ray transport, MORSE, was introduced at the end of the decade. The continuous energy Monte Carlo code, now known as MCNP, also began in this decade at Los Alamos National Laboratory. A general-purpose particle-transport code MCS was written in 1963 to be followed by the MCN code for three-dimensional calculations written in 1965.

The Decade of the 1970s

The Nuclear Non-Proliferation Treaty (NPT) of 1968 and the National Environmental Policy Act (NEPA) of 1969 had major impacts on the radiation shielding field in the 1970s and succeeding decades. The NPT precluded nuclear fuel reprocessing and led to ever-increasing needs for on-site storage of spent fuel at nuclear power plants. NEPA required exhaustive studies of off-site radiation doses around nuclear power plants and environmental impacts of plant operations. Early in the 1970s, there were major disruptions in oil supplies caused by the OPEC embargo. The response in the USA was an energy policy that forbade electricity production using oil or natural gas. The result was placement of many orders for nuclear power plants

despite NPT and NEPA constraints. In the field of radiation shielding, special attention was given to plant design issues such as streaming of neutrons and gamma rays through voids, passageways, and shield penetrations, and to operational issues such as fission-product inventories in fuels and gamma-ray skyshine, particularly associated with ^{16}N sources.

Information essential for plant design, fuel management, and waste management is data tracking radionuclide activities in reactor fuel and process streams, and corresponding strengths and energy spectra of sources, including fission products, activation products, and actinides. To accomplish this, the ORIGEN codes were developed at Oak Ridge National Laboratory and the CINDER code was developed at Los Alamos National Laboratory. Assessment of radiation doses from airborne beta-particle emitters was also studied for the first time. Although the ETRAN Monte Carlo code for electron transport was available at the National Bureau of Standards, work began in the mid-1970s at Sandia Laboratory on the TIGER code and at Stanford Linear Accelerator Center on the EGS code, both for coupled photon and electron transport by the Monte Carlo method.

Design needs brought new attention to buildup factors and to attenuation of broad beams of neutrons and gamma rays. Definitive compilations were made of buildup factors and also the attenuation and reflection by shields obliquely illuminated by photons. Detailed results were also obtained for transmission of neutrons and secondary gamma rays through shielding barriers. This decade also saw the publication of two important NCRP reports [8,9] dealing with neutron shielding and dosimetry and with design of medical facilities that protected against effects of gamma rays and high-energy x-rays.

Design and analysis needs also fostered continuing attention to computer codes for criticality and neutron-transport calculations. A series of more robust discrete-ordinates transport codes were developed. Advances in Monte Carlo calculations were also made. The MCN code was merged with the MCG code in 1973 to form the MCNG code for treating coupled neutron–photon transport. Another merger took place with the MCP code in 1977, allowing detailed treatment of photon transport at energies as low as 1 keV. This new code was known, then and now, as MCNP.

The 1980s and 1990s

These years saw the consolidation of resources for design and analysis work. In the 1980s, personal computers allowed methods such as point-kernel calculations to be programmed. In the 1990s, personal computers took over from the mainframe computers in even the most demanding shielding design and analysis. Comprehensive sets of fluence-to-dose conversion factors became available for widespread use. Radionuclide decay data became available in databases easily used for characterizing sources. Gamma-ray buildup factors were computed with precision and a superb method of data fitting was devised. All these carried point-kernel as well as more advanced shielding methodology to a new plateau.

Databases. Kocher [10] published radioisotope decay data for shielding design and analysis that largely supplanted earlier compilations. Then a new MIRD compendium [11] and ICRP-38 database became the norms, with the latter especially useful for characterizing low-energy x-ray and Auger electron emission. Today a wealth of nuclear structure and decay data is available on the web from the National Nuclear Data Center at Brookhaven National Laboratory (http://www.nndc.bnl.gov/index.jsp).

Advances in buildup factors. Refinements in the computation of buildup factors continued to be made over the years. Computer codes now could account for not only Compton scattering and photoelectric absorption, but also positron creation and annihilation, fluorescence, and bremsstrahlung. Calculation of buildup factors incorporating all these sources of secondary photon radiation was made leading to a comprehensive set of precise buildup factors standardized for use in design and analysis [12]. Also a new five-parameter buildup-factor formulation, called the *geometric progression* formula, was introduced. Although difficult to use for hand calculations, it is an extraordinarily precise formula and is today used in most modern point-kernel codes. Both the calculated buildup factors and the coefficients for the geometric progression buildup factors are tabulated in the design standard [12].

Cross sections and dose conversion factors. Authoritative cross-section data are now available in the ENDF/B

(evaluated nuclear data file) (http://www.nndc.bnl.gov/exfor/endf00.htm) database containing evaluated cross sections, spectra, angular distributions, fission product yields, photo-atomic and thermal scattering law data, with emphasis on neutron-induced reactions. The National Institute of Science and Technology (NIST) has long been the repository for gamma-ray interaction coefficients. The Institute also sponsors the XCOM cross-section code, which may be executed on the NIST Internet site (http://physics.nist.gov/PhysRefData/Xcom/Text/XCOM.html) or downloaded for personal use.

Gamma-ray fluence-to-dose conversion factors for local values of exposure or kerma may be computed directly from readily available energy transfer or energy absorption coefficients for air, tissue, etc. Neutron conversion factors for local values of tissue kerma were computed by Caswell et al. [13]. As the second century of radiation protection begins, there are two classes of fluence-to-dose conversion factors in use for neutrons and gamma rays. One very conservative class is to be used for operational purposes at doses well below regulatory limits. This class is based on doses at fixed depths in 30-cm diameter spherical phantoms irradiated in various ways. The other class is to be used for dose assessment purposes, and not for personnel dosimetry. This class is based on the anthropomorphic human phantom and weight factors for effective dose equivalent [14] or effective dose [15].

Computer applications. The 1980s and 1990s were decades of revolution for the computational aspects of radiation shield design and analysis. The advent of inexpensive personal computers with rapidly increasing speeds and memory freed the shielding analyst from dependence on a few supercomputers at national laboratories. Many shielding codes that could previously run only on large mainframe computers were reworked to run on small personal computers, thereby, allowing any shielding analysts to perform detailed calculations that only a privileged few were able to do previously.

At the same time, many improvements were made to the transport codes and their algorithms. MCNP has gone through a series of improvements adding new capabilities and improvements, such as new variance reduction methods, tallies, and physics models. It has also spun off a second version MCNPX with a capability of treating 34 types of particles with energies up to 150 MeV. Also in these decades many other Monte Carlo transport codes were developed by researchers in many nations. Each version has unique features and capabilities. General-purpose discrete-ordinates codes were also extensively improved with many novel acceleration schemes introduced to improve their speeds. An excellent review of many such improvements is given by Adams and Larsen [16].

Practice of Radiation Shielding

Shielding design and shielding analysis are complementary activities. In design, the source and maximum target dose are specified, and the task is to determine the type and amount of the shielding required to reduce the target dose to that specified. In analysis, the source and shielding are identified and the task is to determine the dose at some point(s) of interest. Whether one is engaged in a hand calculation or in a most elaborate Monte Carlo simulation, one is faced with the tasks of (1) characterizing the source, (2) characterizing the nature and attenuating properties of the shielding materials, (3) evaluating at a target location the radiation intensity and perhaps its angular and energy distributions, and (4) converting the intensity to a dose or response meaningful in terms of radiation effects.

Source Characterization

Source geometry, energy, and angular distribution are required characteristics. Radionuclide sources, with isotropic emission and unique energies of gamma and x-rays are relatively easy to characterize. Activity and source strength must be carefully distinguished, as not every decay results in emission of a particular gamma or x-ray. Careful consideration must be given to a low-energy limit below which source particles may be ignored, else computation resources may be wasted. Similarly, when photons of many energies are emitted, as in the case of fission-product sources, one is compelled to use a group structure in source characterization, and much care is needed in establishing efficient and appropriate group energy limits and group average energies. When the source energies are continuously distributed, as is the case with fission neutrons and gamma rays, one option is to use a multigroup approach, as might be used in point-kernel calculations. Another option, useful in Monte Carlo

simulations, is to sample source energies from a mathematical representation of the energy spectrum.

A point source is very often an appropriate approximation of a physical source of small size. It is also appropriate to represent a line, plane, or volume source as a collection of point sources, as is done in the point-kernel method of shielding analysis. Radionuclide and fission sources are isotropic in angular distribution; however, there are cases for which it is efficient to identify a surface and to characterize the surface as a secondary source surface. Such surface sources are very often non-isotropic in angular distribution. For example, consider the radiation emitted into the atmosphere from a large body of water containing a distributed radiation source. The interface may be treated approximately, but very effectively, as a plane source emitting radiation not isotropically, but with an intensity varying with the angle of emission from the surface.

Attenuating Properties

The total microscopic cross section for an element or nuclide, $\sigma(E)$, multiplied by the atomic density, is the linear interaction coefficient $\mu(E)$, also called the macroscopic cross section, the probability per unit (differential) path length that a particle of energy E interacts with the medium in some way. Its reciprocal, called the *mean free path*, is the average distance traveled before interaction. Usually, the ratio μ/ρ, called the mass interaction coefficient, is tabulated because it is independent of density. Various subscripts may be used to designate particular types of interactions, for example, $\sigma_{\mathrm{a}}(E)$ for absorption or $\sigma_{\mathrm{f}}(E)$ for fission. Likewise, additional independent variables may be introduced, with, for example, $\sigma_{\mathrm{s}}(E, E')\mathrm{d}E'$ representing the cross section for scattering from energy E to an energy between E' and $E' + \mathrm{d}E'$. Information resources for attenuating properties are described in this entry's historical review, as are resources for radionuclide decay data.

Intensity Characterization

The intensity of a neutron or photon field is usually described in terms of radiation crossing the surface of a small spherical volume V. The *fluence* Φ is defined, in the limit $V \to 0$, as the expected or average sum of the path lengths in V traveled by entering particles divided by the volume V. Equivalently, Φ is, again in the limit $V \to 0$, the expected number of particles crossing the surface of V divided by the cross-sectional area of the volume. The time derivative of the fluence is the fluence rate or *flux density* Φ. Note that the fluence, though having units of reciprocal area, has no reference area or orientation. Note too that the fluence and flux are point functions. The fluence, a function of position, may also be a distribution function for particle energies and directions. For example, $\Phi(r, E, \Omega)\,\mathrm{d}E\mathrm{d}\Omega$ is the fluence at $\mathbf{r}$ of particles with energies in $\mathrm{d}E$ about E and with directions in solid angle $\mathrm{d}\Omega$ about the direction $\mathbf{\Omega}$. When a particular surface, with outward normal $\mathbf{n}$, is used as a reference, it is useful to define radiation intensity in terms of the flow $J_n(\mathbf{r}, E, \mathbf{\Omega})\,\mathrm{d}E\mathrm{d}\Omega \equiv \mathbf{n} \cdot \mathbf{\Omega}\Phi(\mathbf{r}, E, \mathbf{\Omega})\,\mathrm{d}E\mathrm{d}\Omega$ across the reference surface.

Fluence-to-Dose Conversion Factors

Whether the shield designer uses the simplest of the point-kernel methods or the most comprehensive of the Monte Carlo or discrete-ordinates methods, fluence-to-dose conversion factors generally have to be used. The radiation attenuation calculation deals with the particle fluence, the direct measure of radiation intensity. To convert that intensity into a measure of radiation damage or heating of a material, to a field measurement such as *exposure*, or to a measure of health risk, conversion factors must be applied.

The shielding analysis ordinarily yields the energy spectrum $\Phi(\mathbf{r}, E)$ of the photon or neutron fluence at a point identified by the vector $\mathbf{r}$. Use of a Monte Carlo code normally yields the energy spectrum as a function of energy, whence the dose or, more generally, response $R(\mathbf{r})$ is given by the convolution of the fluence with the fluence-to-dose factor, here called the response function $\mathcal{R}(E)$, so that

$$R(\mathbf{r}) = \int_E \mathrm{d}E\mathcal{R}(\mathbf{r}, E)\Phi(\mathbf{r}, E). \tag{1}$$

Point-kernel, or other energy-multigroup methods yield the energy spectrum at discrete energies, or in energy groups, and the dose convolution is a summation rather than an integration.

While the fluence is most always computed as a point function of position, the response of interest

may be a dose at a point (called a *local* dose) or it may be a much more complicated function such as the average radiation dose in a physical volume such as an anthropomorphic phantom. Local and phantom-related doses are briefly discussed later.

Suppose the local dose of interest is the kerma, defined as the expected sum of the initial kinetic energies of all charged particles produced by the radiation field in a mass m, in the limit as $m \to 0$. Then the response function is given by

$$\mathcal{R}_{\mathcal{K}}(E) = \kappa \sum_i \frac{N_i}{\rho} \sum_j \sigma_{ji}(E)\varepsilon_{ji}(E). \quad (2)$$

in which ρ is the mass density, N_i is the atoms of species i per unit volume (proportional to ρ), $\sigma_{ji}(E)$ is the cross section for the jth interaction with species i, and $\varepsilon_{ji}(E)$ is the average energy transferred to secondary charged particles in the jth interaction with species i. A units conversion factor κ is needed to convert from, say, units of MeV cm^2/g to units of rad cm^2 or Gy cm^2. For neutrons, a quality factor multiplier $Q(E)$ is needed to convert to units of *dose equivalent* (rem or Sv). For photons, Eq. 2 reduces to

$$\mathcal{R}_{\mathcal{K}}(E)\ (\text{Gy cm}^2) = 1.602 \times 10^{-10} E[\mu_{\text{tr}}(E)/\rho], \quad (3)$$

where E is in MeV and μ_{tr}/ρ is the mass energy transfer coefficient in units of cm^2/g for the material to which energy is transferred.

More related to radiation damage is the local *absorbed dose*, defined as the expected energy imparted, through ionization, excitation, chemical changes, and heat, to a mass m, in the limit as $m \to 0$. Under conditions of *charged-particle equilibrium*, the neutron or gamma-ray kerma equals the absorbed dose, less the energy radiated away as bremsstrahlung. Such equilibrium is approached in a region of homogeneity in composition and uniformity in neutron or photon intensity. Then the absorbed dose is given by Eq. 3 with μ_{tr} replaced by the energy absorption coefficient μ_{en} to account for any bremsstrahlung losses.

The second type of response function or dose is that related to the local dose within a simple geometric phantom or some sort of average dose within an anthropomorphic phantom. The phantom dose, in fact, is a point function and serves as a standardized reference dose for instrument calibration and radiation protection purposes. Even though the radiation fluence, itself a point function, may have strong spatial and angular variation as well as energy variation, it is still possible to associate with the radiation fluence a phantom-related dose. The procedure is as follows. The fluence is treated, for example, as a very broad parallel beam of the same intensity as the actual radiation field, incident in some fixed way on the phantom. This is the so-called expanded and aligned field. For a geometric phantom, the dose is computed at a fixed depth. For an anthropomorphic phantom, the dose is computed as an average of doses to particular tissues and organs, weighted by the susceptibility of the tissues and organs to radiation carcinogenesis or hereditary illness. Many phantoms have been used with various directions of incident radiation. The calculated response functions are then tabulated as a function of the radiation energy. Additional details of phantom doses and their tabulations are given by Shultis and Faw [17].

Basic Analysis Methods

To say modern shielding practice has been reduced to running large "black-box" codes is very misleading. Randomly varying model parameters, such as shield dimensions, placement, and material, is a very inefficient way to optimize shielding for a given situation. Using the concepts and ideas behind the earlier simplified methods often allows a shield analyst to select materials and geometry for a preliminary design before using large transport codes to refine the design. In this section, fundamental methods for estimating neutron or photon doses are reviewed. Such indirectly ionizing radiation is characterized by straight-line trajectories punctuated by "point" interactions. The basic concepts presented here apply equally to all particles of such radiation.

It should be noted that throughout this entry, calculated doses are the *expected* or *average* value of the stochastic measured doses, that is, the mechanistically calculated dose represents the statistical average of a large number of dose measurements which exhibit random fluctuations as a consequence of the stochastic nature of the source emission and interactions in the detector and surrounding material.

Uncollided Radiation Doses

In many situations, the dose at some point of interest is dominated by particles streaming directly from the

source without interacting in the surrounding medium. For example, if only air separates a gamma-ray or neutron source from a detector, interactions in the intervening air or in nearby solid objects, such as the ground or building walls, are often negligible, and the radiation field at the detector is due almost entirely to uncollided radiation coming directly from the source.

In an attenuating medium, the uncollided dose at a distance r from a point isotropic source emitting S_p particles of energy E is

$$D^o(r) = \frac{S_p \mathcal{R}}{4\pi r^2} e^{-l}, \tag{4}$$

where l is the total number of mean-free-path lengths of material a particle must traverse before reaching the detector, namely, $\int_0^r ds\, \mu(s)$. Here $\mathcal{R}$ is the appropriate response function. The $1/(4\pi r^2)$ term in Eq. 4 is often referred to as the *geometric* attenuation and the e^{-l} term the *material* attenuation. Equation 4 can be extended easily to a source emitting particles with different discrete energies or a continuous spectrum of energies.

Point Kernel for Uncollided Dose

Consider an isotropic point source placed at $\mathbf{r}_s$ and an isotropic point detector (or *target*) placed at $\mathbf{r}_t$ in a homogeneous medium. The detector response depends not on $\mathbf{r}_s$ and $\mathbf{r}_t$ separately, but only on the distance $|\mathbf{r}_s - \mathbf{r}_t|$ between the source and detector. For a unit strength source, the detector response is (cf. Eq. 4)

$$\mathcal{G}^o(\mathbf{r}_s, \mathbf{r}_t, E) = \frac{\mathcal{R}(E)}{4\pi|\mathbf{r}_s - \mathbf{r}_t|^2} e^{-\mu(E)|\mathbf{r}_s - \mathbf{r}_t|}. \tag{5}$$

Here $\mathcal{G}^o(\mathbf{r}_s, \mathbf{r}_t, E)$ is the *uncollided dose point kernel* and equals the dose at $\mathbf{r}_t$ per particle of energy E emitted isotropically at $\mathbf{r}_s$. This result holds for any geometry or medium provided that the material through which a ray from $\mathbf{r}_s$ to $\mathbf{r}_t$ passes has a constant interaction coefficient μ.

With this point kernel, the uncollided dose due to an arbitrarily distributed source can be found by first decomposing (conceptually) the source into a set of contiguous effective point sources and then summing (integrating) the dose produced by each point source.

Applications to Selected Geometries

The results for the uncollided dose from a point source can be used to derive expressions for the uncollided dose arising from a wide variety of distributed sources such as line sources, area sources, and volumetric sources [4, 5, 18, 19]. An example to illustrate the method is as follows:

An isotropic disk source of radius a emitting isotropically S_a particles per unit area at energy E is depicted in Fig. 1. A detector is positioned at point P a distance h above the center of the disk. Suppose the only material separating the disk source and the receptor at P is a slab of thickness t with a total attenuation coefficient μ.

Consider a differential area dA between distance ρ and $\rho + d\rho$ from the disk center and between ψ and $\psi + d\psi$. The source within dA may be treated as an effective point isotropic source emitting $S_a dA = S_a \rho d\rho d\psi$ particles which produces an uncollided dose at P of dD^o. The ray from the source in dA must pass through a slant distance of the shield $t \sec\theta$ so that the dose at P from particles emitted in $d\rho$ about ρ is

$$dD^o(P) = \frac{\mathcal{R} S_a \rho d\rho d\psi}{4\pi r^2} \exp[-\mu t \sec\theta], \tag{6}$$

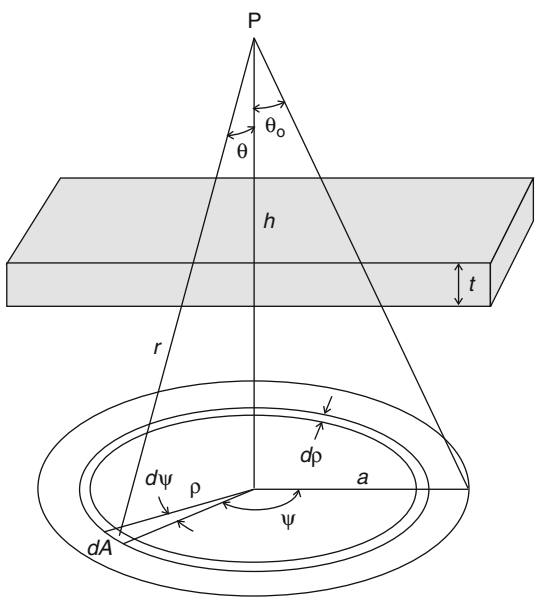

Radiation Shielding. Figure 1
An isotropic disk source is shielded by a parallel slab shield of thickness t

where $\mathcal{R}$ and μ generally depend on the particle energy E. To obtain the total dose at P from all differential areas of the disk source, one then must sum, or rather integrate, $\mathrm{d}D^{\mathrm{o}}$ over all differential areas. Thus, the total uncollided dose at P is

$$D^{\mathrm{o}}(P) = \frac{S_a\mathcal{R}}{4\pi}\int_0^{2\pi}\mathrm{d}\psi\int_0^a \mathrm{d}\rho\,\frac{\rho exp[-\mu t\sec\theta]}{r^2}. \tag{7}$$

Because h is fixed, $\rho\mathrm{d}\rho = r\mathrm{d}r$, and from Fig. 1 it is seen that $r = h\sec\theta$. Integration over ψ and changing variables yields

$$D^{\mathrm{o}}(P) = \frac{S_a\mathcal{R}}{2}\int_h^{h\sec\theta_{\mathrm{o}}}\mathrm{d}r\,r^{-1}\mathrm{e}^{-\mu rt/h} \tag{8}$$

$$= \frac{S_a\mathcal{R}}{2}\int_{\mu t}^{\mu t\sec\theta_o}\mathrm{d}x\,x^{-1}\mathrm{e}^{-x} \tag{9}$$

$$= \frac{S_a\mathcal{R}}{2}[E_1(\mu t) - E_1(\mu t\sec\theta_{\mathrm{o}})], \tag{10}$$

where the *exponential integral function* E_n is defined as $E_n(x) \equiv x^{n-1}\int_x^\infty \mathrm{d}u\,u^{-n}\mathrm{e}^{-u}$ and is tabulated in many compilations [4, 5, 17].

Intermediate Methods for Photon Shielding

In this section, several special techniques are summarized for the design and analysis of shielding for gamma and x-rays with energies from about 1 keV to about 20 MeV. These techniques are founded on very precise radiation transport calculations for a wide range of carefully prescribed situations. These techniques, which rely on buildup factors, attenuation factors, albedos or reflection factors, and line-beam response functions, then allow estimation of photon doses for many frequently encountered shielding situations without the need of transport calculations.

Buildup-Factor Concept

The total photon fluence $\Phi(\mathbf{r}, E)$ at some point of interest $\mathbf{r}$ is the sum of two components: the *uncollided* fluence $\Phi^{\mathrm{o}}(\mathbf{r}, E)$ of photons that have streamed to $\mathbf{r}$ directly from the source without interaction, and the fluence of *scattered* and *secondary* photons $\Phi^{\mathrm{s}}(\mathbf{r}, E)$ consisting of source photons scattered one or more times, as well as secondary photons such as x-rays and annihilation gamma rays.

The buildup factor $B(\mathbf{r})$ is defined as

$$B(\mathbf{r}) \equiv \frac{D(\mathbf{r})}{D^{\mathrm{o}}(\mathbf{r})} = 1 + \frac{D^{\mathrm{s}}(\mathbf{r})}{D^{\mathrm{o}}(\mathbf{r})}, \tag{11}$$

where $D(\mathbf{r})$ is the total dose equal to the sum of the uncollided dose $D^{\mathrm{o}}(\mathbf{r})$ and the scattered or secondary photon dose $D^{\mathrm{s}}(\mathbf{r})$. For a monoenergetic source this reduces to

$$B(E_{\mathrm{o}}, \mathbf{r}) = 1 + \frac{1}{\Phi^{\mathrm{o}}(\mathbf{r})}\int_0^{E_{\mathrm{o}}}\mathrm{d}E\,\frac{\mathcal{R}(E)}{\mathcal{R}(E_{\mathrm{o}})}\Phi^{\mathrm{s}}(\mathbf{r}, E). \tag{12}$$

In this case, the nature of the dose or response is fully accounted for in the ratio $\mathcal{R}(E)/\mathcal{R}(E_{\mathrm{o}})$. By far the largest body of buildup-factor data is for point, isotropic, and monoenergetic sources of photons in infinite homogeneous media. Calculation of buildup factors for high-energy photons requires consideration of the paths traveled by positrons from their creation until their annihilation. Such calculations have been performed by Hirayama [20] and by Faw and Shultis [21] for photon energies as great as 100 MeV. Because incoherent scattering was neglected in many buildup-factor calculations, coherent scattering should also be neglected in calculating the uncollided dose, a significant consideration only for low-energy photons at deep penetration.

Buildup-Factor Geometry Generally, buildup factors depend on the source and shield geometries. For a given material thickness between source and detector, buildup factors are slightly different for point isotropic sources in (a) an infinite medium, (b) at the surface of a bare sphere, and for a slab shield between source and detector. However, the use of buildup factors for a point isotropic source is almost always conservative, that is, the estimated dose is greater than that for a finite shield [17]. Adjustment factors for buildup factors at the surface of a finite medium in terms of the infinite-medium buildup factors is illustrated in Fig. 2.

Buildup factors are also available for plane isotopic (PLI) and plane monodirectional (PLM) gamma-ray sources in infinite media. Indeed, Fano et al. [22], Goldstein [23], and Spencer [24], in their moments-method calculations, obtained buildup factors for plane sources first and, from these, buildup factors for point sources

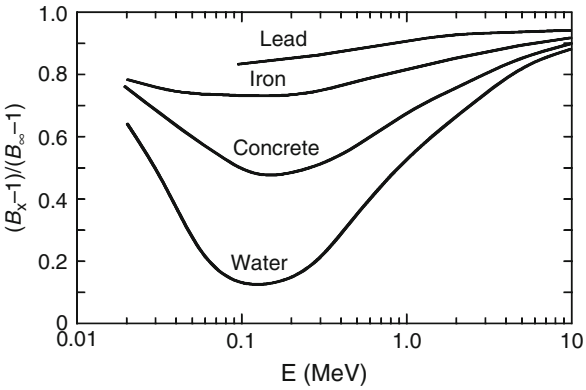

Radiation Shielding. Figure 2
Adjustment factor for the buildup factor B_x at the boundary of a finite medium in terms of the infinite-medium buildup factor B_∞ for the same depth of penetration (EGS4 calculations courtesy of Sherrill Shue, Nuclear Engineering Department, Kansas State University)

were derived. Buildup factors at depth in a half-space shield are also available for the PLM source, that is, normally incident photons [20, 25, 26]. The use of buildup factors for a point isotropic source in an infinite medium is conservative, that is, overpredictive, for the PLI and PLM geometries.

Buildup Factors for Stratified Shields Sometimes shields are stratified, that is, composed of layers of different materials. The use of the buildup-factor concept for such heterogeneous shields is, for the most part, of dubious merit. Nevertheless, implementation of point-kernel codes for shielding design and analysis demands some way of treating buildup when the ray from source point to dose point is through more than one shielding material. However, certain regularities do exist, which permit approximate use of homogeneous-medium buildup factors for stratified shields. Many approximate buildup methods have been suggested, as described by Shultis and Faw [17]; however, they are of little use in most point-kernel codes and are not needed at all for shielding analysis based on transport methods.

Point-Kernel Computer Codes

There are many codes in wide use that are based on the point-kernel technique. In these codes, a distributed source is decomposed into small but finite elements and the dose at some receptor point from each element is computed using the uncollided dose kernel and a buildup factor based on the optical thickness of material between the source element and the receptor. The results for all the source elements are then added together to obtain the total dose. Some that have been widely used are MicroShield [27], the QAD series [28], QADMOD-GP [29], QAD-CGGP [30], and G^3 [31].

Broad-Beam Attenuation

Often a point radionuclide or x-ray source in air is located sufficiently far from a wall or shielding slab that the radiation reaches the wall in nearly parallel rays. Further, the attenuation in the air is usually quite negligible in comparison to that provided by the shielding wall. Shielding design and analysis for such broad-beam illumination of a slab shield are addressed by NCRP Report 49 [9], Archer [32], and Simpkin [33]. The dose at the surface of the cold side of the wall can be computed as

$$D = D^{\mathrm{o}} A_{\mathrm{f}}. \tag{13}$$

For a radionuclide source of activity $\mathcal{A}$, the dose D^{o} without the wall can be expressed in terms of the source energy spectrum, response functions, and distance r from the source to the cold side of the wall. Then,

$$D = D^{\mathrm{o}} A_{\mathrm{f}} = \frac{\mathcal{A}}{r^2} \Gamma A_{\mathrm{f}}, \tag{14}$$

where Γ, called the *specific gamma-ray constant*, is the dose rate in vacuum at a unit distance from a source with unit activity, and A_{f} is an *attenuation factor* which depends on the nature and thickness of the shielding material, the source energy characteristics, and the angle of incidence θ (with respect to the wall normal). Values for Γ and A_{f} are provided by NCRP [9].

Oblique Incidence Attenuation factors for obliquely incident beams are presented in NCRP Report 49 [9]. For such cases, special three-argument slant-incidence buildup factors should be used [17]. For a shield wall of thickness t mean free paths, slant incidence at angle θ with respect to the normal to the wall, and source energy E_{o}, the attenuation factor is in function form $A_{\mathrm{f}}(E_{\mathrm{o}}, t, \theta)$. However, a common, but erroneous,

practice has been to use a two-argument attenuation factor based on an infinite-medium buildup factor for slant penetration distance $t\sec\theta$, in the form $A_f(E_o, t\sec\theta)$. This practice can lead to severe underprediction of transmitted radiation doses.

X-ray Beam Attenuation For x-ray sources, the appropriate measure of source strength is the electron-beam current i, and the appropriate characterization of photon energies, in principle, involves the peak accelerating voltage (kVp), the wave form, and the degree of filtration (e.g., beam half-value thickness). If i is the beam current (mA) and r is the source-detector distance (m), the dose behind a broadly illuminated shield wall is

$$D(P) = \frac{i}{r^2} K_o A_f, \tag{15}$$

in which K_o, called the *radiation output (factor)*, is the dose rate in vacuum (or air) per unit beam current at unit distance from the source in the absence of the shield. Empirical formulas for computing A_f are available for shield design [34, 35].

Intermediate Methods for Neutron Shielding

Shielding design for fast neutrons is generally far more complex than shielding design for photons. Not only does one have to protect against the neutrons emitted by some source, one also needs to protect against primary gamma rays emitted by most neutron sources as well as secondary photons produced by inelastic neutron scattering and from radiative capture. There may also be secondary neutrons produced from $(n, 2n)$ and fission reactions. In many instances, secondary photons produce greater radiological risks than do the primary neutrons. Fast-neutron sources include spontaneous and induced fission, fusion, (α, n) reactions, (γ, n) reactions, and spallation reactions in accelerators, each producing neutrons with a different distribution of energies.

Unlike photon cross sections, neutron cross sections usually vary greatly with neutron energy and among the different isotopes of the same element. Comprehensive cross-section databases are needed. Also, because of the erratic variation of the cross sections with energy, it is difficult to calculate uncollided doses needed in order to use the buildup-factor approach. Moreover, buildup factors are very geometry dependent and sensitive to the energy spectrum of the neutron fluence and, consequently, point-kernel methods can be applied to neutron shielding only in very limited circumstances.

Early work led to kernels for fission sources in aqueous systems and the use of removal cross sections to account for shielding barriers. Over the years, the methodology was stretched to apply to nonaqueous hydrogenous media, then to non-hydrogenous media, then to fast-neutron sources other than fission. Elements of diffusion and age theory were melded with the point kernels. Today, with the availability of massive computer resources, neutron shielding design and analysis is largely done using transport methods. Nevertheless, the earlier methodologies offer insight and allow more critical interpretation of transport calculations.

Also, unlike ratios of different photon response functions, those for neutrons vary, often strongly, with neutron energy. Hence, neutrons doses cannot be converted to different dose units by simply multiplying by an appropriate constant. The energy spectrum of the neutron fluence is needed to obtain doses in different units. Consequently, many old measurements or calculations of point kernels, albedo functions, transmission factors, etc., made with obsolete dose units cannot be converted to modern units because the energy spectrum is unknown. In this case, there is no recourse but to repeat the measurements or calculations.

Capture Gamma Photons

A significant, often dominant, component of the total dose at the surface of a shield accrues from capture gamma photons produced deep within the shield and arising from neutron absorption. Of lesser significance are secondary photons produced in the inelastic scattering of fast neutrons. Secondary neutrons are also produced as a result of (γ, n) reactions. Thus, in transport methods, gamma-ray and neutron transport are almost always coupled.

Historically, capture gamma-ray analysis was appended to neutron removal calculations. Most neutrons are absorbed only when they reach thermal energies, and, consequently, only the absorption of thermal neutrons was considered. (Exceptional cases include

the strong absorption of epithermal neutrons in fast reactor cores or in thick slabs of low-moderating, high-absorbing material.) For this reason, it is important to calculate accurately the thermal neutron fluence $\Phi_{th}(\mathbf{r})$ in the shield. The volumetric source strength of capture photons per unit energy about E is then given by

$$S_\gamma(\mathbf{r}, E) = \Phi_{th}(\mathbf{r})\mu_\gamma(\mathbf{r})f(\mathbf{r}, E), \tag{16}$$

where $\mu_\gamma(\mathbf{r})$ is the absorption coefficient at $\mathbf{r}$ for thermal neutrons and $f(\mathbf{r}, E)$ is the number of photons produced in unit energy about E per thermal neutron absorption at $\mathbf{r}$.

Once the capture gamma-ray source term $S_\gamma(\mathbf{r}, E)$ is known throughout the shield, point-kernel techniques using exponential attenuation and buildup factors can be used to calculate the capture gamma-ray dose at the shield surface.

Neutron Shielding with Concrete

Concrete is probably the most widely used shielding material because of its relatively low cost and the ease with which it can be cast into large and variously shaped shields. However, unlike that for photon attenuation in concrete, the concrete composition, especially the water content, has a strong influence on its neutron attenuation properties. Other important factors that influence the effectiveness of concrete as a neutron shield include type of aggregate, the dose–response function, and the angle of incidence of the neutrons.

Because concrete is so widely used as a shield material, its effectiveness for a monoenergetic, broad, parallel beam of incident neutrons has been extensively studied, both for normal and slant incidence, and many tabulated results for shields of various thickness are available [36–40]. These results, incorporated into design and manufacturing standards (standards are available from professional societies such as the American Nuclear Society and the American Society of Mechanical Engineers) are extremely useful in the preliminary design of concrete shields.

Gamma-Ray and Neutron Reflection

Until now only shielding situations have been considered in which the radiation reaching a target contains an uncollided component. For these situations, point-kernel approximations, in principle, may be used and concepts such as particle buildup may be applied. However, in many problems encountered in shielding design and analysis, only scattered radiation may reach the target. Radiation doses due to reflection from a surface are examples that arise in treatment of streaming of radiation through multi-legged ducts and passageways. Treatment of radiation reflection from surfaces of structures is also a necessary adjunct to precise calibration of nuclear instrumentation. Skyshine, that is, reflection in the atmosphere of radiation from fixed sources to distant points is another example of this class of reflected-radiation problems. All such reflection problems are impossible to treat using elementary point-kernel methods and are also very difficult and inefficient to treat using transport-based methods. For reflection from a surface of radiation from a point source to a point receiver, the *albedo function* has come to be very useful in design and analysis. The same can be said for use of the *line-beam response function* in treatment of skyshine. Both are discussed below.

Albedo Methods

There are frequent instances for which the dose at some location from radiation reflected from walls and floors may be comparable to the line-of-sight dose. The term *reflection* in this context does not imply a surface scattering. Rather, gamma rays or neutrons penetrate the surface of a shielding or structural material, scatter within the material, and then emerge from the material with reduced energy and at some location other than the point of entry.

In many such analyses, a simplified method, called the *albedo method*, may be used. The albedo method is based on the following approximations. (1) The displacement between points of entry and emergence may be neglected. (2) The reflecting medium is effectively a half-space, a conservative approximation. (3) Scattering in air between a source and the reflecting surface and between the reflecting surface and the detector may be neglected.

Application of the Albedo Method

Radiation reflection may be described in terms of the geometry shown in Fig. 3. Suppose that a point isotropic and monoenergetic source is located distance r_1

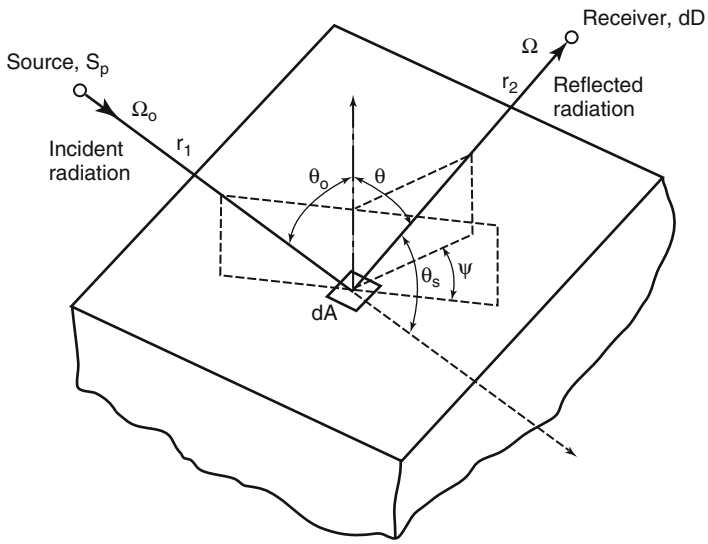

Radiation Shielding. Figure 3
Angular and energy relationships in the albedo formulation

from area dA along incident direction Ω_o and that a dose point is located distance r_2 from area dA along emergent direction Ω. Suppose also the source has an angular distribution such that $S(\theta_o)$ is the source intensity per steradian evaluated at the direction from the source to the reflecting area dA. Then the dose dD_r at the detector from particles reflected from dA can be shown to be [17]

$$\mathrm{d}D_r = D_o \alpha_D(E_o, \theta_o; \theta, \psi) \frac{\mathrm{d}A \cos\theta_o}{r_2^2}, \tag{17}$$

in which D_o is the dose at dA due to incident particles. Here $\alpha_D(E_o, \theta_o; \theta, \psi)$ is the *dose albedo*. Determination of the total reflected dose D_r requires integration over the area of the reflecting surface. In doing so one must be aware that, as the location on the surface changes, all the variables θ_o, θ, ψ, r_1, and r_2 change as well. Also, it is necessary to know $\alpha_D(E_o, \theta_o; \theta, \psi)$ or, more usefully, to have some analytical approximation for the dose albedo so that numerical integration over all the surface area can be performed efficiently.

Gamma-Ray Dose Albedo Approximations

A two-parameter approximation for the photon dose albedo was first devised by Chilton and Huddleston [41] and later extended by Chilton et al. [42]. Chilton [43] later proposed a more accurate seven-parameter albedo formula for concrete. Brockhoff [44] published seven-parameter fit data for albedos from water, concrete, iron, and lead. Two examples of this dose albedo approximation are shown in Fig. 4.

Neutron Dose Albedo Approximations

The dose albedo concept is very useful for streaming problems that involve "reflection" of neutrons or photons from some material interface. However, unlike photon albedos, the neutron albedos are seldom tabulated or approximated for monoenergetic incident neutrons because of the rapid variation with energy of neutron cross sections. Rather, albedos for neutrons with a specific range of energies (energy group) are usually considered, thereby, averaging over all the cross-section resonances in the group. Also unlike photon albedos, neutron albedos involve reflected dose from both neutrons and secondary capture gamma rays.

There are many studies of the neutron albedos in the literature. Selph [45] published a detailed review. Extensive compilations of neutron albedo data are available, for example, SAIL [46] and BREESE-II [47]. Of more utility are analytic approximations for the albedo based on measured or calculated albedos. Neutrons albedos are often divided into three types: (1) fast-neutron albedos ($E \geq 0.2$ MeV), (2) intermediate-energy albedos, and (3) thermal-neutron albedos. Selph [45] reviews early

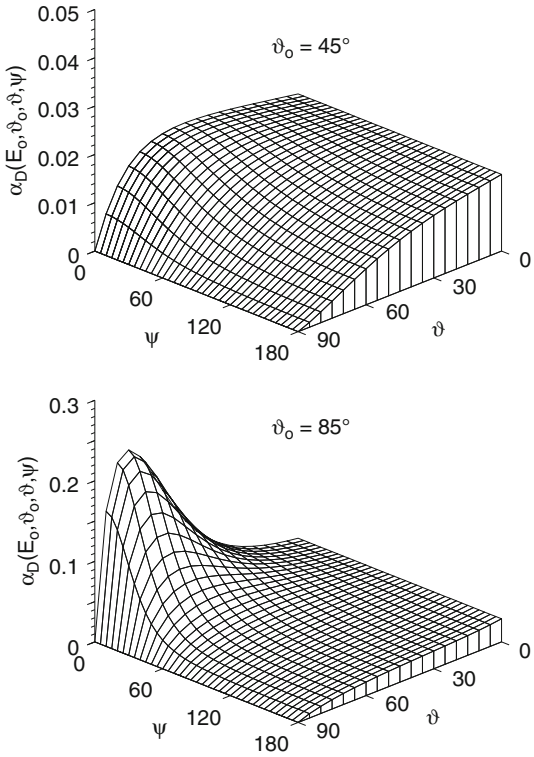

Radiation Shielding. Figure 4
Ambient-dose-equivalent albedos for reflection of 1.25-MeV photons from concrete, computed using the seven-term Chilton–Huddleston approximation

approximations for neutron albedos, among which is a 24-parameter approximation developed by Maerker and Muckenthaler [48]. Newly computed and more accurate fast-neutron albedos, based on different 24-parameter approximations, have been computed by Brockhoff [44] for several shielding materials.

For neutrons with energy less than about 100 keV, the various dose equivalent response functions are very insensitive to neutron energy. Consequently, the dose albedo α_D is very closely approximated by the number albedo α_N. Thus, for reflected dose calculations involving intermediate or thermal neutrons, the number albedo is almost always used. Coleman et al. [49] calculated neutron albedos for intermediate-energy neutrons (200 keV to 0.5 eV) incident monodirectionally on reinforced concrete slabs and developed a nine-parameter formula for the albedo.

Thermal neutrons entering a shield undergo isotropic scattering that, on the average, does not change their energies. For one-speed particles incident in an azimuthally symmetric fashion on a half-space of material that isotropically scatters particles, Chandrasekhar [50] derived an exact expression for the differential albedo. A purely empirical and particularly simple formula, based on Monte Carlo data for thermal neutrons, has been proposed by Wells [51] for ordinary concrete, namely,

$$\alpha_N(\theta_o;\theta,\psi) = 0.21\cos\theta(\cos\theta_o)^{-1/3}. \tag{18}$$

Radiation Streaming Through Ducts

Except in the simplest cases, the analysis of radiation streaming requires advanced computational procedures. However, even within the framework of Monte Carlo transport calculations, albedo methods are commonly used, and special data sets have been developed for such use [46, 47, 52].

Elementary methods for gamma-ray streaming are limited to straight cylindrical ducts, with incident radiation symmetric about the duct axis and uniform over the duct entrance. Transmitted radiation generally may be subdivided into three components: line-of-sight, lip-penetrated, and wall scattered. The first two may be treated using point-kernel methodology. The last requires use of albedo methods to account for scattering over the entire surface area of the duct walls. Selph [45] reviews the methodology of duct transmission calculations and LeDoux and Chilton [53] devised a method of treating two-legged rectangular ducts, important in analysis of structure shielding.

Neutron streaming through gaps and ducts in a shield is much more serious for neutrons than for gamma photons. Neutron albedos, especially for thermal neutrons, are generally much higher than those for photons, and multiple scattering within the duct is very important. Placing bends in a duct, which is very effective for reducing gamma-ray penetration, is far less effective for neutrons. Fast neutrons entering a duct in a concrete shield become thermalized and thereafter are capable of scattering many times, allowing the neutrons to stream through the duct, even those with several bends. Also, unlike gamma-ray streaming, the duct need not be a void (or gas filled) but can be any part of a heterogeneous shield that is "transparent" to neutrons. For example, the steel walls of a water pipe embedded in a concrete shield (such as the cooling

pipes that penetrate the biological shield of a nuclear reactor) act as an annular duct for fast neutrons.

There is much literature on experimental and calculational studies of gamma-ray and neutron streaming through ducts. In many of these studies, empirical formulas, obtained by fits to the data, have been proposed. These formulas are often useful for estimating duct-transmitted doses under similar circumstances. As a starting point for finding such information, the interested reader is referred to Rockwell [18], Selph [45], and NCRP [54].

Gamma-Ray and Neutron Skyshine

For many intense localized sources of radiation, the shielding against radiation that is directed skyward is usually far less than that for the radiation emitted laterally. However, the radiation emitted vertically into the air undergoes scattering interactions and some radiation is reflected back to the ground, often at distances far from the original source. This atmospherically reflected radiation, referred to as *skyshine*, is of concern both to workers at a facility and to the general population outside the facility site.

As alternatives to rigorous transport-theory treatment of the skyshine problem several approximate procedures have been developed for both gamma-photon and neutron skyshine sources [54]. This section summarizes one approximate method, which has been found useful for bare or shielded skyshine sources. The *integral line-beam skyshine method*, is based on the availability of a *line-beam response function* $\mathcal{R}(E, \phi, x)$, which gives the dose (air kerma or ambient dose) at a distance x from a point source emitting a photon or neutron of energy E at an angle ϕ from the source-to-detector axis into an infinite air medium. The air–ground interface is neglected in this method. This response function can be fit over a large range of x to the following three-parameter empirical formula, for a fixed value of E and ϕ [55]:

$$\mathcal{R}(E, \phi, x) = \kappa(\rho/\rho_o)^2 E[x(\rho/\rho_o)]^b \exp[a - cx(\rho/\rho_o)], \tag{19}$$

in which ρ is the air density in the same units as the reference density $\rho_o = 0.0012\ \mathrm{g/cm^3}$. The constant κ depends on the choice of units.

The parameters a, b, and c in Eq. 19 depend on the photon or neutron energy and the source emission angle. These parameters have been estimated and tabulated, for fixed values of E and ϕ, by fitting Eq. 19 to values of the line-beam response function, at different x distances, usually obtained by Monte Carlo calculations. Gamma-ray response functions have been published by Lampley [56] and Brockhoff et al. [57]. Neutron and secondary gamma-ray response functions have been published by Lampley [56] and Gui et al. [58]. These data and their method of application are presented by Shultis and Faw [17].

To obtain the skyshine dose $D(d)$ at a distance d from a bare collimated source, the line-beam response function, weighted by the energy and angular distribution of the source, is integrated over all source energies and emission directions. Thus, if the collimated source emits $S(E, \Omega)$ photons, the skyshine dose is

$$D(d) = \int_0^\infty \mathrm{d}E \int_{\Omega_s} \mathrm{d}\Omega\, S(E, \Omega)\mathcal{R}(E, \phi, d), \tag{20}$$

where the angular integration is over all emission directions Ω_s allowed by the source collimation. Here, ϕ is a function of the emission direction Ω. To obtain this result, it has been assumed that the presence of an air–ground interface can be neglected by replacing the ground by an infinite air medium. The effect of the ground interface on the skyshine radiation, except at positions very near a broadly collimated source, has been found to be very small.

The presence of a shield over a skyshine source, for example, a building roof, causes some of the source particles penetrating the shield to be degraded in energy and angularly redirected before being transported through the atmosphere. The effect of an overhead shield on the skyshine dose far from the source can be accurately treated by a two-step hybrid method [59,60]. First a transport calculation is performed to determine the energy and angular distribution of the radiation penetrating the shield, and then, with this distribution as an effective point, bare, skyshine source, the integral line-beam method is used to evaluate the skyshine dose.

The integral line-beam method for gamma-ray and neutron skyshine calculations has been applied to a variety of source configurations and found to give generally excellent agreement with benchmark calculations and experimental results [59]. It has been used as the basis of the microcomputer code *MicroSkyshine* [61]

for gamma rays. A code package for both neutron and gamma-ray calculations is available from the Radiation Safety Computation Information Center. (Code package CCC-646: SKYSHINE-KSU: Code System to Calculate Neutron and Gamma-Ray Skyshine Doses Using the Integral Line-Beam Method, and data library DLC-188: SKYDATA-KSU: Parameters for Approximate Neutron and Gamma-Ray Skyshine Response Functions and Ground Correction Factors.)

Transport Theory

For difficult shielding problems in which simplified techniques such as point kernels with buildup corrections cannot be used, calculations based on transport theory must often be used. There are two basic approaches for transport calculations: *deterministic* transport calculations in which the linear Boltzmann equation is solved numerically, and *Monte Carlo* calculations in which a simulation is made of how particles migrate stochastically through the problem geometry. Both approaches have their advantages and weaknesses. Because of space limitations, it is not possible to give a detailed review of the vast literature supporting both approaches. What follows is a brief explanation of the basic ideas involved and some general references are supplied.

Deterministic Transport Theory

The neutron or photon flux $\phi(\mathbf{r}, E, \mathbf{\Omega})$ for particles with energy E and direction $\mathbf{\Omega}$ is rigorously given by the linear Boltzmann equation or, simply, the transport equation

$$\mathbf{\Omega} \cdot \nabla\phi(\mathbf{r}, E, \mathbf{\Omega}) + \mu(\mathbf{r}, E)\phi(\mathbf{r}, E, \mathbf{\Omega}) = S(\mathbf{r}, E, \mathbf{\Omega}) + \int_0^\infty \mathrm{d}E' \int_{4\pi} \mathrm{d}\mathbf{\Omega}'\, \mu_s(\mathbf{r}, E', \mathbf{\Omega}' \to E, \mathbf{\Omega})\phi(\mathbf{r}, E', \mathbf{\Omega}'), \tag{21}$$

where S is the volumetric source strength of particles. This equation can be formally integrated to yield the integral form of the transport equation, namely,

$$\phi(\mathbf{r}, E, \mathbf{\Omega}) = \phi(\mathbf{r} - R\mathbf{\Omega}, E, \mathbf{\Omega})f(R) + \int_0^R \mathrm{d}R' q(\mathbf{r} - R'\mathbf{\Omega}, \mathbf{\Omega})f(R'), \tag{22}$$

where $f(x) \equiv \exp\left[-\int_0^x \mu(\mathbf{r} - R''\mathbf{\Omega}, E)\,\mathrm{d}R''\right]$ and q is given by

$$q(\mathbf{r}, E, \mathbf{\Omega}) \equiv S(\mathbf{r}, E, \mathbf{\Omega}) + \int_0^\infty \mathrm{d}E' \int_{4\pi} \mathrm{d}\mathbf{\Omega}'\mu_s(\mathbf{r}, E', \mathbf{\Omega}' \to E, \mathbf{\Omega})\phi(\mathbf{r}, E', \mathbf{\Omega}'). \tag{23}$$

Unfortunately, neither of these formulations of the transport equation can be solved analytically except for idealistic cases, for example, infinite medium with monoenergetic particles or a purely absorbing medium. Numerical solutions must be used for all practical shielding analyses. Many approximations of the transport equation are used, such as diffusion theory, to allow easier calculations. Also the energy region of interest is usually divided into a few or even hundreds of contiguous energy subintervals and average cross sections are calculated for each group using an assumed energy spectrum of the radiation. In this manner, the transport equation is approximated by a set of coupled equations in which energy is no longer an independent variable. Even with an energy-multigroup approximation, numerical solutions are still computationally formidable.

The most widely used deterministic transport approach is the discrete-ordinates method. In this method, a spatial and directional mesh is created for the problem geometry, and the multigroup form of the transport equation is then integrated over each spatial and directional cell. The solution of the approximating algebraic equations is then accomplished by introducing another approximation that relates the cell-centered flux densities to those on the cell boundaries, and an iterative procedure between the source (scattered particles and true source particles) and flux density calculation is then used to calculate the fluxes at the mesh nodes. For details of this method, the reader is referred to Carlson and Lathrop [62], Duderstadt and Martin [63], and Lewis and Miller [64].

Discrete-ordinates calculations can be computationally expensive because of the usually enormous number of mesh nodes and the fact that the convergence of an iterative solution is often very slow. A subject of great interest in the last 30 years has been the development of numerous methods to accelerate convergence of the iterations. Without convergence acceleration schemes,

discrete-ordinate solutions would be computationally impractical for many shielding problems. An excellent description of the various acceleration schemes that have been used is provided by Adams and Larsen [16].

Mature computer codes based on the discrete-ordinates method are widely available to treat one-, two-, and three-dimensional problems in the three basic geometries (rectangular, spherical, and cylindrical) with an arbitrary number of energy groups [65,66].

Although discrete-ordinates methods are widely used by shielding analysts, these methods do have their limitations. Most restrictive is the requirement that the problem geometry must be one of the three basic geometries (rectangular, spherical, or cylindrical) with boundaries and material interfaces placed perpendicular to a coordinate axis. Problems with irregular boundaries and material distributions are difficult to solve accurately with the discrete-ordinates method. Also, in multidimensional geometries, the discrete-ordinates method often produces spurious oscillations in the flux densities (the *ray effect*) as an inherent consequence of the angular discretization. Finally, the discretization of the spatial and angular variables introduces numerical truncation errors, and it is necessary to use sufficiently fine angular and spatial meshes to obtain flux densities that are independent of the mesh size. For multidimensional situations in which the flux density is very anisotropic in direction and in which the medium is many mean-free-path lengths in size, typical of many shielding problems, the computational effort to obtain an accurate discrete-ordinates solution can become very large. However, unlike Monte Carlo calculations, discrete-ordinates methods can treat very-deep-penetration problems, that is, the calculation of fluxes and doses at distances many mean-free-path lengths from a source.

Monte Carlo Transport Theory

In Monte Carlo calculations, particle tracks are generated by simulating the stochastic nature of the particle interactions with the medium. One does not even need to invoke the transport equation; all one needs are complete mathematical expressions of the probability relationships that govern the track length of an individual particle between interaction points, the choice of an interaction type at each such point, the choice of a new energy and a new direction if the interaction is of a scattering type, and the possible production of additional particles. These are all stochastic variables, and in order to make selections of specific values for these variables, one needs a complete understanding of the various processes a particle undergoes in its lifetime from the time it is given birth by the source until it is either absorbed or leaves the system under consideration.

The experience a particle undergoes from the time it leaves its source until it is absorbed or leaves the system is called its *history*. From such histories expected or average values about the radiation field can be estimated. For example, suppose the expected energy $\langle E \rangle$ absorbed in some small volume V in the problem geometry is being sought. There is a probability $f(E)\mathrm{d}E$ that a particle deposits energy in $\mathrm{d}E$ about E. Then the expected energy deposited is simply $\langle E \rangle = \int Ef(E)\mathrm{d}E$. Unfortunately, $f(E)$ is not known *a priori* and must be obtained from a transport calculation. In a Monte Carlo analysis, $f(E)$ is constructed by *scoring* or tallying the energy deposited E_i in V by the ith particle history. Then in the limit of a large number of histories N

$$\langle E \rangle \equiv \int Ef(E)\mathrm{d}E \simeq \overline{E} \equiv \frac{1}{N}\sum_{i=1}^{N} E_i. \tag{24}$$

The process of using a computer to generate particle histories can be performed in a way completely analogous to the actual physical process of particle transport through a medium. This direct simulation of the physical transport is called an *analog* Monte Carlo procedure. However, if the tally region is far from the source regions, most analog particle histories will make zero contribution to the tally, and thus a huge number of histories must be generated to obtain a statistically meaningful result. To reduce the number of histories, *nonanalog* Monte Carlo procedures can be used whereby certain biases are introduced in the generation of particle histories to increase the chances that a particle reaches the tally region. For example, source particles could be emitted preferentially toward the tally region instead of with the usual isotropic emission. Of course, when tallying such biased histories, corrections must be made to undo the bias so that a correct score is obtained. Many biasing schemes have been developed, and are generally called *variance*

reduction methods since, by allowing more histories to score, the statistical uncertainty or variance in the average score is reduced.

The great advantage of the Monte Carlo approach, unlike discrete-ordinates, is that it can treat complex geometries. However, Monte Carlo calculations can be computationally extremely expensive, especially for deep-penetration problems. The stochastic contribution a single history makes to a particular score requires that a great many histories be simulated to achieve a good estimate of the expected or average score. If a tally region is many mean-free-path lengths from the source, very few histories reach the tally region and contribute to the score. Even with powerful variance reduction techniques, enormous numbers of histories often are required to obtain a meaningful score in deep-penetration problems.

Those readers interested in more comprehensive treatments of the Monte Carlo method will find rich resources. A number of monographs address Monte Carlo applications in radiation transport. Those designed for the specialists in nuclear-reactor computations are Goertzel and Kalos [67], Kalos [68], Kalos et al. [69], and Spanier and Gelbard [70]. More general treatments will be found in the books by Carter and Cashwell [71] Lux and Koblinger [72], and Dunn and Shultis [73]. Coupled photon and electron transport are addressed in the compilation edited by Jenkins et al. [74]. A very great deal of practical information can be gleaned from the manuals for Monte Carlo computer codes. Especially recommended are those for the EGS4 code [75], the TIGER series of codes [76], and the MCNP code [77].

Future Directions

In many respects, radiation shielding is a mature technological discipline. It is supported by a comprehensive body of literature and a diverse selection of computational resources. Indeed, the present availability of inexpensive computer clusters and the many sophisticated transport codes incorporating the most detailed physics models, modern data, and the ability to model complex geometries has reduced shielding practice in many cases to brute force calculation. Many shielding problems require such a computer approach; however, there are many routine shielding problems that can be effectively treated using the simplified techniques developed in the 1940s–1970s. Point-kernel methods are still widely used today. However, there are shielding problems for which no simplified approach is effective and transport methods must be employed. These include transmission of radiation through ducts and passages in structures, reflection of gamma rays from shielding walls and other structures, and transmission of beams of radiation obliquely incident on shielding slabs.

Despite the relative maturity of the discipline, one must not become complacent. There will continue to be advances in many areas. Undoubtedly, new computational resources will allow much more detailed 3-D graphical modeling of the shielding geometries and their incorporation into the transport codes. Likewise 3-D displays of output will allow much better interpretations of results. New capabilities will be added to Monte Carlo and discrete-ordinates codes. Hybrid codes employing both Monte Carlo and deterministic techniques will also be developed. More nuclear data will become available that will, for example, allow detailed analysis of actinides in spent fuel and correlation effects in nuclear data will allow better sensitivity analyses of results. Likewise, more information on material properties, especially in radiation resistance, will become known. Advances in microdosimetry will provide better understanding of cellular responses to single radiation particles and the effects of low-level radiation doses. A better understanding of radiation hormesis effects may lead to changes in radiation standards that will better reflect health effects of radiation. New sources of radiation in research and medicine will include energetic protons and neutrons. These developments require continuing attention and adoption into the radiation-shielding discipline.

Bibliography

Primary Literature

1. Shultis JK, Faw RE (2005) Radiation shielding technology. Health Phys 88:297–322
2. Mutscheller A (1925) Physical standards of protection against Roentgen-ray dangers. Am J Roentgenol Radiat Ther 13:65–70

3. National Council on Radiation Protection and Measurements (1941) Safe handling of radioactive luminous compounds. NBS handbook 27. NCRP report 5. US Government Printing Office, Washington, DC
4. Blizard EP, Abbott LS (eds) (1962) Reactor handbook, vol III, Part B, Shielding. Wiley, New York
5. Jaeger RH (ed) (1968) Engineering compendium on radiation shielding, vol 1, Shielding fundamentals and methods. Springer, New York
6. Haffner JW (1967) Radiation and shielding in space. Academic, New York
7. Shure K (1964) P-3 multigroup calculations of neutron attenuation. Nucl Sci Eng 19:310
8. National Council on Radiation Protection and Measurements (1971) Protection against neutron radiation. NCRP report 38. National Council on Radiation Protection and Measurements, Washington, DC
9. National Council on Radiation Protection and Measurements (1976) Structural shielding design and evaluation for medical use of x-rays and gamma rays of energies up to 10 MeV. NCRP report 49. National Council on Radiation Protection and Measurements, Washington, DC
10. Kocher DC (1981) Radioactive decay tables. Technical Information Center, U.S. Department of Energy; DOE/TIC 11026, Washington, DC
11. Weber DA, Eckerman KE, Dillman LT, Ryman JC (1989) MIRD: radionuclide data and decay schemes. Society of Nuclear Medicine, Medical Internal Radiation Dose Committee, New York
12. ANS (American Nuclear Society) (1991) American national standard gamma-ray attenuation coefficients and buildup factors for engineering materials. ANSI/ANS-6.4.3-1991. American Nuclear Society, La Grange Park
13. Caswell RS, Coyne JJ, Randolph ML (1980) Kerma factors for neutron energies below 30 MeV. Radiat Res 83: 217–254
14. International Commission on Radiological Protection (1987) Data for use in protection against external radiation. Publication 51. Annals of the ICRP 17(2/3). Pergamon, Oxford
15. International Commission on Radiological Protection (1996) Conversion coefficients for use in radiological protection against external radiation. Publication 74. Annals of the ICRP 26(3/4). Pergamon, Oxford
16. Adams ML, Larsen EW (2002) Fast iterative methods for discrete-ordinates particle transport calculations. Prog Nucl Energy 40(1):3–159
17. Shultis JK, Faw RE (2000) Radiation shielding. American Nuclear Society, La Grange Park
18. Rockwell T III (ed) (1956) Reactor shielding design manual. Van Nostrand, Princeton
19. Schaeffer NM (1973) Historical background. In: Schaeffer NM (ed) Reactor shielding. TID-25951. US Atomic Energy Commission, Washington, DC
20. Hirayama H (1987) Exposure buildup factors of high-energy gamma rays for water, concrete, iron, and lead. Nucl Technol 77:60–67
21. Faw RE, Shultis JK (1993) Absorbed dose buildup factors in air for 10–100 MeV photons. Nucl Sci Eng 114:76–80
22. Fano U, Spencer LV, Berger MJ (1959) Penetration and diffusion of x rays. In: Encyclopedia of physics, vol 38, Part 2. Springer, Berlin
23. Goldstein H (1959) Fundamental aspects of reactor shielding. Addison-Wesley, Reading
24. Spencer LV (1962) Structure shielding against fallout radiation from nuclear weapons. Monograph 42. National Bureau of Standards, Washington, DC
25. Takeuchi K, Tanaka S, Kinno M (1981) Transport calculation of gamma rays including bremsstrahlung by the discrete ordinates code PALLAS. Nucl Sci Eng 78:273–283
26. Takeuchi K, Tanaka S (1984) Buildup factors of gamma rays, including bremsstrahlung and annihilation radiation for water, concrete, iron, and lead. Nucl Sci Eng 87:478–489
27. Negin CA, Worku G (1998) Microshield v.5 user's manual. Grove Software, Lynchburg
28. Malenfant RE (1967) QAD: a series of point kernel general-purpose shielding programs. LA-3573. Los Alamos National Laboratory, Los Alamos
29. Price JH et al (1979) Utilization instructions for QADMOD-G. RRA-N7914. Radiation Research Association, Fort Worth. Available from RSICC as CCC565/QADMOD-GP
30. Litwin KA et al (1994) Improvements to the point kernel code QAD-CGGP: a code validation and user's manual. RC-1214 COG-94-65. AECL Research, Canada. Available from RSICC as CCC-645/QAD-CGGP-A
31. Malenfant RE (1990) G^3: a general purpose gamma-ray scattering code. LA-5176. Los Alamos National Laboratory, Los Alamos. Available from RSICC as CCC-564/G33-GP
32. Archer BR (1995) History of the shielding of diagnostic x-ray facilities. Health Phys 69:750–758
33. Simpkin DJ (1989) Shielding requirements for constant-potential diagnostic x-ray beams determined by a Monte Carlo calculation. Health Phys 56:151–154
34. Archer BR, Conway BJ, Quinn PW (1994) Attenuation properties of diagnostic x-ray shielding materials. Med Phys 21:1499–1507
35. Simpkin DJ (1995) Transmission data for shielding diagnostic x-ray facilities. Health Phys 68:704–709
36. Chilton AB (1971) Effect of material composition on neutron penetration of concrete slabs. Report 10425. National Bureau of Standards, Washington, DC
37. Roussin RW, Schmidt FAR (1971) Adjoint Sn calculations of coupled neutron and gamma-ray transport through concrete slabs. Nucl Eng Des 15:319–343
38. Roussin RW, Alsmiller RG Jr, Barish J (1973) Calculations of the transport of neutrons and secondary gamma rays through concrete for incident neutrons in the energy range 15 to 75 MeV. Nucl Eng Des 24:250–257

39. Wyckoff JM, Chilton AB (1973) Dose due to practical neutron energy distributions incident on concrete shielding slabs. Proceedings of 3rd international congress IRPA, American Nuclear Society, La Grange Park
40. Wang X, Faw RE (1995) Transmission of neutrons and secondary gamma rays through concrete slabs. Radiat Prot Dosim 60:212–222
41. Chilton AB, Huddleston CM (1963) A semi-empirical formula for differential dose albedo for gamma rays on concrete. Nucl Sci Eng 17:419–424
42. Chilton AB, Davisson CM, Beach LA (1965) Parameters for C-H albedo formula for gamma rays reflected from water, concrete, iron, and lead. Trans Am Nucl Soc 8:656
43. Chilton AB (1967) A modified formula for differential exposure albedo for gamma rays reflected from concrete. Nucl Sci Eng 27:481–482
44. Brockhoff RC (2003) Calculation of albedos for neutrons and photons. Ph.D. dissertation, Department of Mechanical and Nuclear Engineering, Kansas State University, Manhattan
45. Selph WE (1973) Albedos, ducts, and voids. In: Schaeffer NM (ed) Reactor shielding. TID-25951. US Atomic Energy Commission, Washington, DC
46. Simmons GL, Albert TE, Gritzner DM (1979) The SAI/EPRI information library. Report SAI-013-79-525-LJ. Science Applications Inc, La Jolla
47. Cain VR, Emmett MV (1979) BREESE-II: auxiliary routines for implementing the albedo option in the MORSE Monte Carlo code. ORNL/TM-6807. Oak Ridge National Laboratory, Oak Ridge
48. Maerker RE, Muckenthaler FJ (1966) Measurements and single-velocity calculations of differential angular thermal-neutron albedos for concrete. Nucl Sci Eng 26:339
49. Coleman WA, Maerker RE, Muckenthaler FJ, Stevens PJ (1967) Calculation of doubly differential current albedos for epicadmium neutrons incident on concrete and comparison of the subcadmium component with experiment. Nucl Sci Eng 27:411–422
50. Chandrasekhar S (1960) Radiative transfer. Dover, New York
51. Wells MB (1964) Reflection of thermal neutrons and neutron capture gamma rays from concrete. USAEC report RRA-M44. Radiation Research Associates, Fort Worth
52. Gomes IC, Stevens PN (1991) MORSE/STORM: a generalized albedo option for Monte Carlo calculations. ORNL/FEDC-91/1, TN. Oak Ridge National Laboratory, Oak Ridge
53. LeDoux JC, Chilton AB (1959) Gamma ray streaming through two-legged rectangular ducts. Nucl Sci Eng 11:362–368
54. National Council on Radiation Protection and Measurements (2003) Radiation protection for particle accelerator facilities. NCRP report 144. National Council on Radiation Protection and Measurements, Washington, DC
55. Lampley CM, Andrews MC, Wells MB (1988) The SKYSHINE-III procedure: calculation of the effects of structure design on neutron, primary gamma-ray, and secondary gamma-ray dose rates in air. RRA-T8209A. Radiation Research Associates, Fort Worth
56. Lampley CM (1979) The SKYSHINE-II procedure: calculation of the effects of structure design on neutron, primary gamma-ray, and secondary gamma-ray dose rates in air. RRA-T7901. Radiation Research Associates, Fort Worth
57. Brockhoff RC, Shultis JK, Faw RE (1996) Skyshine line-beam response functions for 20- to 100-MeV photons. Nucl Sci Eng 123:282–288
58. Gui AA, Shultis JK, Faw RE (1997) Response functions for neutron skyshine analysis. Nucl Sci Eng 125:111–127
59. Shultis JK, Faw RE, Bassett MS (1991) The integral line-beam method for gamma skyshine analysis. Nucl Sci Eng 107:228–245
60. Stedry MH (1994) A Monte Carlo line-beam calculation of gamma-ray skyshine for shielded sources. MS thesis, Kansas State University, Manhattan
61. Negin CA (1987) The microskyshine manual. Grove Software, Lynchburg
62. Carlson BG, Lathrop KD (1968) Transport theory, the method of discrete ordinates. In: Greenspan H, Kelber CN, Okrent D (eds) Computing methods in reactor physics. Gordon and Breach, New York
63. Duderstadt JJ, Martin WR (1979) Transport theory. Wiley, New York
64. Lewis EE, Miller WF (1984) Computational methods of neutron transport theory. Wiley, New York
65. Rhoades WA, Childs RL (1987) The TORT three-dimensional discrete ordinates neutron/photon transport code. ORNL-6268. Oak Ridge National Laboratory, Oak Ridge
66. Alcouffe RE, Baker RS, Dahl JA, Turner SA (2002) PARTISN user's guide. CCS-4, LA-UR-02-5633. Los Alamos National Laboratory, Transport Methods Group, Los Alamos
67. Goertzel G, Kalos MH (1958) Monte Carlo methods in transport problems. In: Progress in nuclear energy, ser 1, vol 2. Pergamon, New York
68. Kalos MH (1968) Monte Carlo integration of the adjoint gamma-ray transport equation. Nucl Sci Eng 33:284–290
69. Kalos MH, Nakache NR, Celnik JC (1968) Monte Carlo methods in reactor computations. In: Greenspan H, Kelber CN, Okrent D (eds) Computing methods in reactor physics. Gordon and Breach, New York
70. Spanier J, Gelbard EM (1969) Monte Carlo principles and neutron transport problems. Addison-Wesley, Reading
71. Carter LL, Cashwell ED (1975) Particle-transport simulation with the Monte Carlo method. TID-26607. Los Alamos National Laboratory, Los Alamos
72. Lux I, Koblinger LK (1991) Monte Carlo particle transport methods: neutron and photon calculations. CRC Press, Boca Raton
73. Dunn WL, Shultis JK (2011) Exploring the Monte Carlo method. Elsevier, Amsterdam
74. Jenkins TM, Nelson TM, Rindi A (1988) Monte Carlo transport of electrons and photons. Plenum, New York
75. Nelson WR, Hirayama H, Rogers DWO (1985) The EGS4 code system. SLAC-265. Stanford Linear Accelerator Center, Menlo Park

76. Halbleib JA, Kensek RP, Mehlhorn TA, Valdez GD, Seltzer SM, Berger MJ (1992) ITS Version 3.0: the integrated TIGER series of coupled electron/photon Monte Carlo transport codes. SAND91-1634. Sandia National Laboratories, Albuquerque
77. X-5 Monte Carlo Team (2003) MCNP—a general Monte Carlo n-particle transport code, version 5. LA-UR-03-1987 (vol 1: Overview and theory), LA-UR-03-0245 (vol 2: User's guide). Los Alamos National Laboratory, Los Alamos

Books and Reviews

Blizard EP, Abbott LS (eds) Reactor handbook, vol 3, Part B, Shielding. Wiley, New York
Faw RE, Shultis JK (1999) Radiological assessment: sources and doses. American Nuclear Society, La Grange Park
Goldstein H (1959) Fundamental aspects of reactor shielding. Addison-Wesley, Reading
Haffner JW (1967) Radiation and shielding in space. Academic, New York
ICRP (2007) The 2007 recommendations of the international commission on radiological protection. Report 103. Annals of the ICRP 37:2–4
ICRP (2008) Nuclear decay data for dosimetric calculations. Report 107. Annals of the ICRP 38(3):1–96
ICRU (1993) Quantities and units in radiation protection dosimetry. Report 51. International Commission on Radiation Units and Measurements, Bethesda
ICRU (1998) Fundamental quantities and units for ionizing radiation. Report 60. International Commission on Radiation Units and Measurements, Bethesda
Jaeger RG (ed) (1968–1975) Engineering compendium on radiation shielding. Shielding materials and design, vol 1; Shielding materials and designs, vol 2; Shield design and engineering, vol 3. Springer, New York
NCRP (2003) Radiation protection for particle accelerator facilities. Report 144. National Council on Radiation Protection and Measurements, Bethesda
NCRP (2005) Structural shielding design for medical x-ray imaging facilities. Report 147. National Council on Radiation Protection and Measurements, Bethesda
NCRP (2005) Structural shielding design and evaluation for megavoltage x- and gamma-ray radiotherapy facilities. Report 151. National Council on Radiation Protection and Measurements, Bethesda
Rockwell T III (ed) (1956) Reactor shielding design manual. Van Nostrand, Princeton
Schaeffer NM (ed) (1973) Reactor shielding. TID-25951, U.S. Atomic Energy Commission, Washington, DC
Shultis JK, Faw RE (2000) Radiation shielding. American Nuclear Society, La Grange Park
UN (1977, 1982, 1988, 1993, 2000) Reports of the United Nations Scientific Committee on the Effects of Atomic Radiation, New York. http://www.unscear.org/unscear/en/publications.html

Radiation Sources

Richard E. Faw[1], J. Kenneth Shultis[2]
[1]Department of Mechanical & Nuclear Engineering, Kansas State University, Winston Salem, NC, USA
[2]Department of Mechanical & Nuclear Engineering, Kansas State University, Manhattan, KS, USA

Article Outline

Glossary
Definition of the Subject
Introduction
Radiation-Producing Reactions
Radioactivity
Sources of Neutrons
Sources of Gamma Photons
Sources of X-rays
Cosmic Rays, Solar Radiation, and Trapped Radiation Belts
Radiation Sources Used in Human Activities
Future Directions
Bibliography

Glossary

Absorbed dose A general term for the energy transferred from radiation to matter. Specifically, the absorbed dose is the amount of energy absorbed in a unit mass of matter from ionizing radiation. Units are the gray (Gy) and rad, respectively, equivalent to 1 J/kg and 100 ergs/g. Thus, 1 Gy equals 100 rad.

Activity The decay rate (expected number of nuclear transformations per unit time) in a radioactive sample. Units are the becquerel (Bq) equal to one decay per second, and the curie (Ci) equal to 3.7×10^{10} decays per second.

Alpha particle The nucleus of a ^{4}He atom, composed of two neutrons and two protons and denoted by α.

Committed dose The dose equivalent accumulated over the rest of a person's life following the ingestion or inhalation of radioactive material into the body.

Coulomb force The electrostatic force between two charges. It is proportional to the product of the charges and inversely proportional to the square of

the distance between them. The force is attractive if the charges are of opposite sign, and repulsive if of like sign.

Dose equivalent A measure of the health risk associated with the absorption of radiation locally in the human body. It equals the local absorbed dose multiplied by a *quality factor* to correct for the relative biological effect associated with different radiations. Units are the sievert (Sv) or rem.

Effective dose An overall measure of the risk of cancer or hereditary illness associated with radiation exposure. It is a weighted average dose to multiple organs and tissues of the body, with weighting over both quality factor and the relative sensitivity of each organ or tissue. Units are the sievert (Sv) or rem for the dose in grays and rads, respectively.

Hadron A subatomic particle that reacts via strong nuclear forces. Hadrons include mesons (e.g., pions and kaons) and baryons (e.g., protons and neutrons). Hadrons do not include bosons (e.g., photons) and leptons (e.g., electrons, muons, and neutrinos).

Meson A subatomic particle, a subclass of hadrons, composed of an even number of other subatomic particles called quarks. Most important are the pi meson (pion) and K meson (kaon).

Nuclide A term used to refer to a particular atom or nucleus with a specific neutron number N and atomic (proton) number Z. The nuclide with N neutrons and Z protons and electrons is denoted as ${}^{A}_{Z}\mathrm{X}$ where X is the chemical symbol (determined by Z) and $A = Z + N$ is the mass number. If the nuclide is radioactive, it is called a *radionuclide*.

Photon A quantum of electromagnetic radiation with energy $E = h\nu$ where h is Planck's constant and ν is the frequency. Photons produced by changes in the structure of a nucleus are called *gamma photons*, and those produced by atomic electron rearrangement are called *x-rays*.

Positron The antiparticle of the electron with the same mass m_e but with a positive charge equal in magnitude to the negative charge of the electron. A positron, denoted by β^+, quickly after its formation annihilates with an ambient electron converting the two electron masses into two photons each with energy $m_e c^2 = 0.511$ MeV.

Definition of the Subject

This entry treats sources of only ionizing radiation, such as electrons, protons, high-energy photons, neutrons, and similar radiations that have the ability to cause ionization, either directly or indirectly, and, thus, to induce chemical and physical changes along their passages through materials. Not included are sources of relatively lower frequency electromagnetic radiation from radio waves to ultraviolet light.

Characterization of sources requires characterization of radiations as well. Many sources encountered are radioactive isotopes of elements in the periodic table. These sources, as they decay radioactively, emit ionizing radiation. Some of the ionizing radiation is in the form of alpha particles, gamma rays, and x-rays, all characteristically monoenergetic in nature. Some is in the form of beta particles, distributed in energy but with well-defined maxima. Other sources are not directly associated with radioisotopes. X-ray machines and accelerators release ionizing radiation generally distributed in energy but with some monoenergetic components. The radiation belts surrounding the earth are composed of electrons and protons distributed in energy. Solar radiation and galactic cosmic rays are ionizing radiations widely distributed in type and energy. The nuclear fission process results in prompt emission of gamma rays and neutrons very widely distributed in energy. Fission also yields an extremely wide range of *fission products*, which radioactively decay over long periods of time.

Characterization of sources, to be meaningful, also begs discussion of radiation doses and radiation effects. There are acute effects accompanying high exposures. There are also known carcinogenic effects of human exposure and suspected mutational and hereditary effects. Therefore, a portion of this entry is devoted to examination of health effects associated with exposure to ionizing radiation.

This entry is divided into two parts. In the first several sections, the quantitative technical characterization of physical processes that produce ionizing radiation are reviewed. In latter sections, a qualitative examination is given of the various types of radiation sources encountered in the environment, workplace, laboratory, or medical facility.

Introduction

Throughout our lives, ionizing radiation is ever present, though rarely sensed. Radioactive sources are present in the food we eat, in the water we drink, and in the air we breathe. Most of these sources have but brief sojourns in our bodies, but some are taken up in bone and permanently retained. These sources, isotopes of elements in the periodic table, decay radioactively, emitting ionizing radiation most often in the form of gamma and x-rays, alpha particles, beta particles, and electrons. The ionization taking place in the body accounts for biological effects, good and bad.

Radiation also reaches us from sources outside our bodies. Radioactivity is present in our soils and minerals, and in our construction materials. Electromagnetic radiation of all wavelengths, including radio waves, microwaves, radar, and light, of both man-made and natural origins, constantly, bombard us. Photons are far more prevalent in number than atoms in our universe; for every nucleon there are about 10^9 photons. Cosmic rays and the subatomic debris they create during interactions in the atmosphere also impinge on us. Neutrinos from fusion reactions in our sun reach us in such numbers that tens of billions per second pass through every square centimeter of our skin. Most of this radiation, for example, neutrinos and radio waves, fortunately, passes harmlessly through us. Other radiation such as light and longer wavelength electromagnetic radiation usually interacts harmlessly with our tissues. However, shorter wavelength electromagnetic radiation, for example, ultraviolet light, x-rays and gamma rays, and charged particles produced by nuclear reactions can cause various degrees of damage to our cells.

The types and sources of radiation just described may be naturally occurring, may be a legacy of the era of nuclear weapons testing, or may be a result of human enterprise, for example, uranium in coal ash, radium in mine tailings, medical wastes, and fission or activation products in wastes from nuclear power production. All vary with latitude, longitude, and altitude – even on a small scale.

There are also population groups especially affected, but in different ways, by exposure to ionizing radiation from many sources. First among these in importance are patients and providers of medical radiation exposures. In the USA, as of 2006, collective effective doses to patients accruing from medical exposure, about 900,000 person-Sv annually, amount to almost half the total for the entire population. Computed tomography and nuclear medicine procedures dominate the exposure, with fluoroscopy and radiology accounting for about 230,000 person-Sv annual effective dose. Interventional fluoroscopy, while of great value to the patient, contributes in a major way to provider dose. Brachytherapy and beam therapy using photons, electrons, and protons lead to high therapeutic radiation exposures to patients, of course. Modern beam therapy utilizes exquisite beam shielding techniques to minimize doses to off-target patient tissues. Of all occupational groups, medical workers are greatest in number and accrue the highest collective doses, namely, 549 person-Sv annually in the USA. However, recordable individual worker annual doses are about 0.75 mSv as compared to 1.87 mSv for the fewer workers in commercial nuclear power.

Another population group consists of astronauts and aviation flight crews especially in high-altitude, international flights. Radiation from solar and galactic sources lead to high occupational radiation exposures. For astronauts, the life-threatening risk of solar-flare radiation exposures is a major concern.

Radiation sources used in industry affect another significant occupational group. Industrial radiography using x-ray, gamma-ray, or even neutron sources is an important component of occupational exposure. Other sources find wide use in measurement devices and sensor appliances.

For radiation to produce biological damage, it must first interact with tissue to alter molecular bonds and change the chemistry of the cells. Likewise, for radiation to produce damage in structural and electrical materials, it must cause interactions that disrupt crystalline and molecular bonds. Such radiation must be capable of creating ion–electron pairs and is termed *ionizing* radiation. Fast-moving charged particles, such as alpha particles, beta particles, and fission fragments, can directly ionize matter. Neutral particles, such as photons and neutrons, cannot interact directly with the electrons of the matter through they pass; rather they cause interactions that transfer some of their

energy to charged secondary particles, which in turn produce ionization as they slow.

Radiation-Producing Reactions

Origins of Ionizing Radiation

Ionizing radiation is invariably the consequence of physical reactions, involving subatomic particles, at the atomic or nuclear level. The possible radiation-producing reactions are many, and usually, although not always, involve altering the configuration of neutrons and protons in an atomic nucleus or the rearrangement of atomic electrons about a nucleus. These reactions can be divided into two categories:

Radioactive decay. In the first type of radiation-producing reaction, the nucleus of an atom spontaneously changes its internal arrangement of neutrons and protons to achieve a more stable configuration. In such spontaneous *radioactive* transmutations, ionizing radiation is almost always emitted. The number of known different atoms, each with a distinct combination of Z and A is about 3,200. Of these, only 266 are stable and 65 are long-lived radioisotopes all of which are found in nature. The remaining nuclides have been made by humans and are radioactive with lifetimes much shorter than the age of the solar system. Both naturally occurring and manufactured radionuclides are the mostly commonly encountered sources of ionizing radiation.

Binary reactions. The second category of radiation-producing interactions involves two impinging atomic or subatomic particles that react to form one or more reaction products. Examples include neutrons interacting with nuclei of atoms, or photons interacting with nuclei or atomic electrons. Many binary reactions, in which an incident subatomic particle x strikes an atom or nucleus X, produce only two reaction products, typically a residual atom or nucleus Y and some subatomic particle y. These binary two-product reactions are often written as $X(x,y)Y$, for example, ${}^{14}_{7}\mathrm{N}(\alpha, p){}^{17}_{8}\mathrm{O}$.

Energetics of Radiation-Producing Reactions

In any nuclear reaction, total energy must be conserved. The total energy (kinetic plus rest-mass energy) of the initial particles must equal the total energy of the final products, that is, $\sum_i [E_i + m_i c^2] = \sum_i \left[E_i' + m_i' c^2\right]$, where E_i (E'_i) is the kinetic energy of the ith initial (final) particle with a rest mass m_i (m'_i), and c is the speed of light.

Any change in the total kinetic energy of particles before and after the reaction, ΔE, must be accompanied by an equivalent change in the total rest mass of the particles before and after the reaction, Δm, that are related by Einstein's famous equation $\Delta E = \Delta m c^2$. To quantify this change in the kinetic or rest-mass energies, a so-called Q-value is defined as

$$\begin{aligned} Q &= (\text{rest mass of initial particles})c^2 \\ &\quad - (\text{rest mass of final particles})c^2 \\ &= (\text{KE of final particles}) - (\text{KE of intial particles}) \end{aligned}$$

The Q value of a nuclear reaction may be either positive or negative. If the rest masses of the reactants exceed the rest masses of the products, the Q value of the reaction is positive with the decrease in rest mass being converted into a gain in kinetic energy. Such a reaction is *exoergic*. Radioactive decay is such a spontaneous exoergic nuclear reaction in which the Q-value energy is converted into the kinetic energy of the products.

Conversely, if Q is negative, the reaction is *endoergic*. For this case, kinetic energy of the initial particles is converted into rest-mass energy of the reaction products. The kinetic energy decrease equals the rest-mass energy increase. Such reactions cannot occur unless the colliding particles have at least a certain amount of kinetic energy, the so-called *threshold energy* for the reaction. For the binary, two-product reaction $X(x,y)Y$, the threshold kinetic energy of x incident on a stationary X is, neglecting Coulombic barrier effects, given approximately by

$$E_{th} \simeq -\left(1 + \frac{m_x}{m_X}\right) Q.$$

In any reaction, linear momentum must also be conserved. Thus, the momentum of the reaction products must equal that of the reactants. For two-product nuclear reactions, conservation of linear momentum requires that the products, depending on their recoil directions, have very definite amounts of kinetic energy. By contrast, for reactions with three or more products, there is no unique division of the reaction

energy, and the products generally have a continuous distribution of kinetic energies.

Physical Characterization of Sources

The most fundamental type of source is a *point source*. Clearly, no real source can have zero size, but a real source can be approximated as a point source provided (1) that the volume is sufficiently small, that is, with dimensions much smaller than the dimensions of the attenuating medium between source and detector, and (2) that there is negligible interaction of radiation with the matter in the source volume. The second requirement may be relaxed if source characteristics are modified to account for source self-absorption and other source–particle interactions.

In general, a point source may be characterized as depending on energy, direction, and time. In almost all cases, time is not treated as an independent variable because the time delay between a change in the source and the resulting change in the radiation field is usually negligible. Therefore, the most general characterization of a point source used here is in terms of energy and direction. Most radiation sources treated in shielding practice are isotropic, so that source characterization requires only knowledge of energy dependence. Radioisotope sources are certainly isotropic, as are fission sources and capture gamma-ray sources.

A careful distinction must be made between the activity of a radioisotope and its source strength. *Activity* is precisely defined as the expected number of atoms undergoing radioactive transformation per unit time. It is *not* defined as the number of particles emitted per unit time. Decay of two very common laboratory radioisotopes illustrate this point. Each transformation of ^{60}Co, for example, results in the emission of two gamma rays, one at 1.173 MeV and the other at 1.333 MeV. Each transformation of ^{137}Cs, accompanied by a transformation of its decay product ^{137m}Ba, results in emission of a 0.662-MeV gamma ray with probability 0.85.

The SI unit of activity is the becquerel (Bq), equivalent to one transformation per second. In medical and health physics, radiation source strengths are commonly calculated on the basis of *accumulated activity*, Bq s. Such time-integrated activities account for the cumulative number of transformations in some biological entity during the transient presence of radionuclides in the entity. Of interest in such circumstances is not the time-dependent dose rate to that entity or some other nearby region, but rather the total dose accumulated during the transient. Similar practices are followed in dose evaluation for reactor transients, solar flares, nuclear weapons, and so on.

Radiation sources may be distributed along a line, over an area, or within a volume. Source characterization requires, in general, spatial and energy dependence. Occasionally, it is necessary to include angular dependence. This is especially true for effective area sources associated with computed angular flows across certain planes. Energy dependence may be discrete, such as for radionuclide sources, or continuous, as for bremsstrahlung or fission neutrons and photons.

Radioactivity

Radioactive Decay Dynamics

The decay of a radioactive nuclide is a stochastic phenomenon. The time an individual radionuclide decays cannot be predicted; rather, only the probability of decay in a specified time interval can be predicted. The rate at which a sample of a large number of identical radionuclides decays is determined by the *radioactive decay constant* λ for the nuclide. This constant is the probability, per unit time, that a radionuclide decays in an infinitesimal time interval. That λ is constant for a given radionuclide species implies that the expected number of radionuclides, $N(t)$, at time t is $N(t) = N(0)e^{-\lambda t}$, where $N(0)$ is the initial number of radionuclides in the sample. The exponential decay of radionuclides is sometimes called the *radioactive decay law*.

Generally, the number of radionuclides in a sample is not of interest. Rather the *activity* $A(t)$ or rate at which a radionuclide sample decays, $\mathrm{d}N(t)/\mathrm{d}t$, is desired since this quantity determines the rate of radiation emission from the sample. From the radioactive decay law, it is found that $\mathrm{d}N(t)/\mathrm{d}t = \lambda N(t) \equiv A(t)$, so that the activity of a radionuclide sample also decays exponentially, that is, $A(t) = A(0)e^{-\lambda t}$. The standard unit of activity is the becquerel (Bq) equal to one radioactive decay per second. The traditional unit is the curie (Ci) = 3.7×10^{10} Bq (approximately the activity of 1 g of ^{226}Ra).

The rate at which a radioactive sample decays is commonly described by its *half-life* $T_{1/2}$. The half-life is the time required for half of the sample to decay, or, equivalently, for the sample activity to halve. From the radioactive decay law, it is found $T_{1/2} = \ln 2/\lambda \simeq 0.693/\lambda$.

Types of Radioactive Decay

There are several types of spontaneous changes (or *transmutations*) that can occur in radioactive nuclides. In each transmutation, the nucleus of the parent atom ${}^{A}_{Z}\mathrm{P}$ is altered in some manner and one or more particles of radiation are emitted. If the number of protons in the nucleus is changed, then the number of orbital electrons in the daughter atom D must subsequently also be changed, either by releasing an electron to or absorbing an electron from the ambient medium. The most commonly encountered types of radioactive decay are

Gamma decay (γ) ${}^{A}_{Z}\mathrm{P}^{*} \rightarrow {}^{A}_{Z}\mathrm{P} + \gamma$: An excited nucleus decays (usually within 10^{-8} s) to its ground state by the emission of one or more gamma photons. The excited parent is often the product of radioactive decay or a binary nuclear reaction.

Isomeric transition (IT) ${}^{Am}_{Z}\mathrm{P}^{*} \rightarrow {}^{A}_{Z}\mathrm{P} + \gamma$: This is a special case of gamma decay, in which the excited parent has a lifetime much greater than usual nuclear lifetimes (10^{-8} s), ranging from seconds to thousands of years. Such a long-lived excited nucleus is said to be *metastable* and is called an *isomer*.

Internal conversion (IC) ${}^{A}_{Z}\mathrm{P}^{*} \rightarrow [{}^{A}_{Z}\mathrm{P}]^{+1} + \mathrm{e}^{-}$: The excitation energy of a nucleus is used to eject an orbital electron (usually a *K*-shell electron).

Alpha decay (α) ${}^{A}_{Z}\mathrm{P} \rightarrow {}^{Z-4}_{Z-2}\mathrm{D} + \alpha$: An α particle is emitted leaving the daughter with 2 fewer neutrons and 2 fewer protons than the parent. The transition often is to an excited nuclear state of the daughter which decays by emission of one or more gamma photons.

Beta decay (β^{-}) ${}^{A}_{Z}\mathrm{P} \rightarrow {}^{A}_{Z+1}\mathrm{D} + \beta^{-} + \bar{\nu}$: In effect, a neutron in the nucleus decays to a proton. An electron (β^{-}) and antineutrino ($\bar{\nu}$) are emitted, which share the decay energy. The daughter is often produced in an excited nuclear state and subsequently emits gamma photons.

Positron decay (β^{+}) ${}^{A}_{Z}\mathrm{P} \rightarrow {}^{A}_{Z-1}\mathrm{D} + \beta^{+} + \nu$: In effect, a proton in the nucleus changes into a neutron. A positron (β^{+}) and neutrino (ν) are emitted, which share the decay energy. If the daughter is produced in an excited state, gamma decay results. The emitted positron, after slowing in the ambient medium, annihilates with an ambient electron producing two 0.511-MeV gamma rays.

Electron capture (EC) ${}^{A}_{Z}\mathrm{P} \rightarrow {}^{A}_{Z-1}\mathrm{D}^{*} + \nu$: An orbital electron is absorbed by the nucleus, converts a nuclear proton into a neutron, emits a neutrino (ν), and, generally, leaves the nucleus in an excited state, which decays by the emission of one or more gamma photons.

Spontaneous fission (SP) ${}^{A}_{Z}\mathrm{P} \rightarrow {}^{A_H}_{Z_H}\mathrm{D}_H + {}^{A_L}_{Z_L}\mathrm{D}_L + n({}^{1}_{0}\mathrm{n}) + m(\gamma)$: A heavy nucleus spontaneously splits or fissions into a heavy (H) and light (L) fission fragment. The fission fragments are produced in highly excited nuclear states and decay by prompt neutron and gamma photon emission within 10^{-13} s of the fission event, releasing, on the average, n neutrons and m γ photons. The resulting *fission products* are usually radioactive and undergo a chain of β^{-} decays releasing several delayed gamma photons and beta particles until a stable nucleus is reached. In some instances, ternary rather than binary fission takes place, releasing a light product such as tritium.

Many radionuclides decay by more than a single decay mechanism. For example, electron capture is always in competition with positron decay. An example of a radionuclide that decays by three mechanisms is ${}^{64}\mathrm{Cu}$ whose decay scheme is shown in Fig. 1.

In any radioactive decay that alters the proton number Z, electron rearrangements necessarily result. The resulting cascade of orbital electrons to lower energy levels results in emission of x-rays and, in competition, ejection of what are called *Auger electrons*.

Naturally Occurring Radionuclides

Singly Occurring Primordial Radionuclides Of the many radioactive species present when the earth was formed, only those very few with half-lives comparable to the age of the earth remain in the environment. Of these few primordial radionuclides not belonging to a decay chain, only ${}^{40}\mathrm{K}$ and ${}^{87}\mathrm{Rb}$ contribute

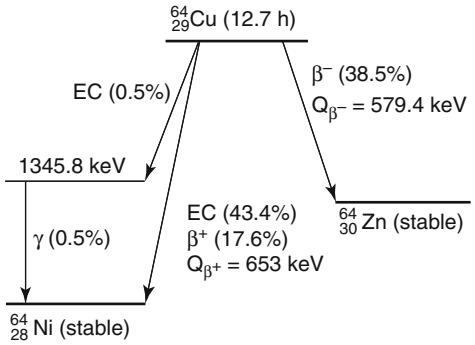

Radiation Sources. Figure 1
The radioactive decay scheme for ^{64}Cu per decay, on average a beta particle of maximum energy 0.579 MeV is emitted with a probability of 0.385, a positron of maximum energy 0.653 MeV is emitted with a probability of 0.176, and a gamma ray of energy 1.346 MeV is emitted with a probability of 0.005. Source: NUDAT 2.5, National Nuclear Data Center, Brookhaven National Laboratory

significantly to human exposure. Of minor consequence are the nuclides ^{138}La, ^{147}Sm, and ^{176}Lu. The radionuclide ^{87}Rb has a half-life of 4.8×10^{10} years and decays by beta-particle emission. In the human body, its main impact is on bone-surface cells. The radionuclide ^{40}K is a major contributor to human exposure from natural radiation. Present in an isotopic abundance of 0.0118%, it has a half-life of 1.227×10^9 years, decaying both by electron capture and beta-particle emission. Annual human doses are about 140 μGy to bone surface, 170 μGy on average to soft tissue, and 270 μGy to red marrow [1]. ^{40}K also contributes in a major way to external exposure. The population-average specific activity of the nuclide in soil is 420 Bq/kg [2]. Based on a soil density of 1,600 kg/m^3, and dose conversion factors from [3], ^{40}K in the soil contributes 120 μSv effective dose annually.

Decay Series of Terrestrial Origin Two actinide decay series, identified by the long-lived parents ^{238}U and ^{232}Th contribute appreciably to human exposure to natural radiation. Another series headed by ^{235}U contributes very little. Members of the two important series are listed in Table 1. Many of the radionuclides in these series decay by emission of alpha particles with energies from 4 to 6 MeV. Others in the series emit beta particles accompanied by gamma rays. With long-lived parent radionuclides and short-lived daughter products, the chain might be thought to exist in a state of secular equilibrium, that is, each component having the same decay rate per unit volume of the host medium. However, some of the chain members are more soluble than others, and some are gaseous. Thus, unless the host medium is a rigid solid, such as granite, decay rates are far from equilibrium state.

Ingestion of elements in the uranium and thorium decay chains is unavoidable. Table 2 illustrates the consequences in terms of the committed effective dose incurred by ingestion but perhaps experienced long thereafter.

The portions of the series headed by the gases ^{220}Rn and ^{222}Rn are of special importance in public health. The gases escape from soil and rock into the atmosphere and into the airspace within homes. Their daughter products, some of which emit alpha particles, may be inhaled, with risk of radiation damage to radiation-sensitive cells in the lungs potentially leading to lung cancer. ^{222}Rn and its daughters ordinarily present a greater hazard than ^{220}Rn (thoron) and its daughters, largely because the much shorter half-life of ^{220}Rn makes decay more likely prior to release into the atmosphere. Globally, the mean annual effective dose equivalent due to ^{222}Rn daughters is about 1 mSv (100 mrem) while that due to ^{220}Rn daughters is estimated to be about 0.2 mSv (20 mrem).

Cosmogenic Radionuclides Cosmic-ray interactions with constituents of the atmosphere, sea, or earth, but mostly with the atmosphere, lead directly to radioactive products. Capture of secondary neutrons produced in primary interactions of cosmic rays, leads to the formation of many more radionuclides. Of the nuclides produced in the atmosphere, only ^{3}H, ^{7}Be, ^{14}C, and ^{22}Na contribute appreciably to human radiation exposure.

Over the past century, combustion of fossil fuels and the emission of carbon dioxide not containing ^{14}C has diluted the cosmogenic content of ^{14}C in the environment. Moreover, since World War II, artificial introduction of ^{14}C, ^{3}H, and other nuclides into the environment by human activity has been significant, especially as a result of atmospheric nuclear tests. Consequently, these radionuclides no longer exist in natural equilibria in the environment.

Radiation Sources. Table 1 Principal radioisotopes in two naturally occurring primordial decay series. Source: NUDAT 2.5, National Nuclear Data Center, Brookhaven National Laboratory

Thorium series			Uranium series		
Nuclide and decay mode		Half-life[a] $T_{1/2}$	Nuclide and decay mode		Half-life[a] $T_{1/2}$
$^{232}_{90}$Th	α	**14.05 Gy**	**$^{238}_{92}$U**	α	**4.468 Gy**
$^{228}_{88}$Ra	β	5.75 years	$^{234}_{90}$Th	β	24.10 days
$^{228}_{89}$Ac	β	6.15 h	$^{234m}_{91}$Pa	β	1.159 min
$^{228}_{90}$Th	α	1.912 years	$^{234}_{92}$U	α	245.5 ky
$^{224}_{88}$Ra	α	3.66 days	$^{230}_{90}$Th	α	75.4 ky
$^{220}_{86}$Rn	α	55.6 s	$^{226}_{88}$Ra	α	1,600 years
$^{216}_{84}$Po	α	0.145 s	$^{222}_{86}$Rn	α	3.8235 days
$^{212}_{82}$Pb	β	10.64 h	$^{218}_{84}$Po	α, β	3.098 min
$^{212}_{83}$Bi	α, β	60.55 min	$^{214}_{82}$Pb	β	26.8 min
$^{212}_{84}$Po	α	0.299 μs	$^{214}_{83}$Bi	α, β	19.9 min
$^{208}_{81}$Ti	β	3.053 min	$^{214}_{84}$Po	α, β	164 μs
$^{208}_{82}$Pb		∞	$^{210}_{82}$Pb	β	22.2 years
			$^{210}_{83}$Bi	α, β	5.012 days
			$^{210}_{84}$Po	α	138.4 days
			$^{206}_{82}$Pb		∞

[a]Gy = 10^9 years, ky = 10^3 years, μs = 10^{-6} s

Radiation Sources. Table 2 Annual intake and effective dose from ingestion of uranium, thorium, and daughters. For population weighted averages, apply 5% infants, 30% children, and 65% adults

Nuclide	Activity intake (Bq/year)			Committed effective dose (μSv/year)		
	Infants	Children	Adults	Infants	Children	Adults
^{238}U	1.9	3.8	5.7	0.23	0.26	0.25
^{234}U	1.9	3.8	5.7	0.25	0.28	0.28
^{230}Th	1.0	2.0	3.0	0.42	0.48	0.58
^{226}Ra	7.8	15	22	7.5	12	8.0
^{210}Pb	11	21	30	40	40	28
^{210}Po	21	39	58	180	100	85
^{232}Th	0.6	1.1	1.7	0.26	0.32	0.36
^{228}Ra	5.5	10	15	31	40	21
^{228}Th	1.0	2.0	3.0	0.38	0.30	0.25
^{235}U	0.1	0.2	0.2	0.011	0.011	0.011
Total				260	200	110

Source: Reference [2].

The tritium ^{3}H nuclide is produced mainly from interactions of neutrons with nitrogen and oxygen. Tritium has a half-life of 12.3 years and, upon decay, releases one low-energy beta particle of mean energy 5.7 keV. Tritium exists in nature almost exclusively in water form (HTO) but, in foods, may be partially incorporated into organic compounds. The nuclide ^{14}C is produced mainly from the interactions of neutrons with nitrogen in the atmosphere. It exists in the atmosphere as CO_2, but the main reservoir is the ocean. It has a half-life of 5,700 years and decays by beta particle emission of mean energy 49.5 keV.

^{7}Be is also produced by cosmic ray interactions with nitrogen and oxygen in the atmosphere. It decays by electron capture, 10.4% of which events yield a 0.478-MeV gamma ray. ^{22}Na decays by positron emission (90%) and electron capture (10%). The positron emission yields two annihilation photons as well as a positron of mean energy 215 keV. Both the positron emission and electron capture yield a 1.275-MeV gamma ray. Table 3 lists natural inventories, atmospheric concentrations, and effective doses to populations. Note that 1 PBq = 10^{15} Bq.

Sources of Neutrons

Fission Neutrons

Many heavy nuclides fission after the absorption of a neutron, or even spontaneously, producing several energetic fission neutrons. Almost all of the fast neutrons produced from a fission event are emitted within 10^{-14} s of the fission event, and are called *prompt neutrons*. Generally, less than 1% of the total fission neutrons are emitted as *delayed neutrons*, which are produced by the neutron decay of fission products at times up to many seconds or even minutes after the fission event. As the energy of the neutron which induces the fission in a heavy nucleus increases, the average number of fission neutrons also increases. For example, the fission of ^{235}U by a thermal neutron (average energy 0.025 eV) produces, on the average, 2.43 fission neutrons. A fission caused by a 10-MeV neutron, by contrast, yields 3.8 fission neutrons. For ^{239}Pu, fission by thermal or 10 MeV neutrons yield 2.87 or 4.2 neutrons. The fission of ^{238}U is induced only by fast neutrons, a 10-MeV neutron yielding 3.9 fission neutrons.

Since the advent of fission reactors, many transuranic isotopes have been produced in significant quantities. Many of these isotopes have appreciable spontaneous fission probabilities, and consequently they can be used as very compact sources of fission neutrons. For example, 1 g of ^{252}Cf releases 2.3×10^{12} neutrons per second, and very intense neutron sources can be made from this isotope, limited in size only by the need to remove the fission heat through the necessary encapsulation. Almost all spontaneously fissioning isotopes decay much more frequently by α emission than by fission.

The energy dependence of the fission neutron spectrum has been investigated extensively, particularly for the important isotope ^{235}U. All fissionable nuclides produce prompt-fission neutrons with energy frequency distributions that go to zero at low and high energies, reaching a maximum at about 0.7 MeV, and have an average energy of about 2 MeV. The fraction of prompt fission neutrons emitted per unit energy about E, $\chi(E)$, can be described quite accurately by a Watt distribution

$$\chi(E) = ae^{-E/b}\sinh\sqrt{cE},$$

where the parameters a, b, and c depend on the fissioning isotope. For example, a = 0.5535 MeV, b = 1.0347 MeV, and c = 1.6214 MeV^{-1} for thermal-neutron fission of ^{235}U, whose fission-neutron spectrum is often used as an approximation for other fissioning isotopes.

Radiation Sources. Table 3 Cosmogenic radionuclides and consequential mean doses to the population

Nuclide	Half-life	Global inventory (PBq)	Troposphere conc. (mBq/m^3)	Annual effective dose (μSv/year)
^{3}H	12.32 years	1,275	1.4	0.01
^{7}Be	53.22 days	413	12.5	0.03
^{14}C	5,700 years	12,750	56.3	12
^{22}Na	2.602 years	0.44	0.0021	0.15

Source: Reference [2].

Fusion Neutrons

Neutrons can be produced as products of nuclear reactions in which energetic charged particles hit target atoms. Most such reactions require accelerators to produce the energetic charged particles and, hence, such neutrons are to be encountered only near accelerator targets.

One major exception to the insignificance of charged-particle-induced reactions are those in which light elements fuse exoergically to yield a heavier nucleus and which are accompanied quite often by the release of energetic neutrons. The resulting fusion neutrons are usually the major source of radiation to be shielded against. The two neutron-producing fusion reactions of most interest in the development of thermonuclear fusion power are

$$^{2}\mathrm{H} + {}^{2}\mathrm{H} \rightarrow {}^{3}\mathrm{He}(0.82\ \mathrm{MeV}) + {}^{1}n(2.45\ \mathrm{MeV})$$

$$^{2}\mathrm{H} + {}^{3}\mathrm{H} \rightarrow {}^{4}\mathrm{He}(3.5\ \mathrm{MeV}) + {}^{1}n(14.1\ \mathrm{MeV}).$$

When these reactions are produced by accelerating one nuclide toward the other, the velocity of the center of mass must first be added to the center-of-mass neutron velocity before determining the neutron energy in the laboratory coordinate system. In most designs for fusion power, the velocity of the center of mass is negligible, and the concern is with monoenergetic 2.45- or 14.1-MeV fusion neutrons. The 14.1-MeV fusion neutrons are also produced copiously in a thermonuclear explosion.

A beam of relatively low-energy deuterons (100–300 keV) incident on a deuterium or tritium target can produce a significant number of thermonuclear neutrons. Thus, these D–D or D–T reactions are used in relatively compact accelerators, called *neutron generators*, in which deuterium ions are accelerated through a high voltage (100–300 kV) and allowed to fall on a thick deuterium- or tritium-bearing target. Typically, in such devices, a 1-mA beam current produces up to 10^9 14-MeV neutrons per second from a thick tritium target.

Photoneutrons

A gamma photon with energy sufficiently large to overcome the neutron binding energy (about 7 MeV in most nuclides) may cause a (γ,n) reaction. Very intense and energetic photoneutron production can be realized in an electron accelerator where the bombardment of an appropriate target material with the energetic electrons produces intense bremsstrahlung (see "Sources of X-rays") with a distribution of energies up to that of the incident electrons. The probability a photon will cause a (γ,n) reaction increases with the photon energy, reaching a maximum over a broad energy range of approximately 20–23 MeV for light nuclei ($A \lesssim 40$) and 13–18 MeV for medium and heavy nuclei. The peak energy of this broad (often called *giant*) nuclear resonance can be approximated by 80 $A^{-1/3}$ MeV for $A > 40$. The width of the resonance varies from about 10 MeV for light nuclei to 3 MeV for heavy nuclei. Consequently, in medical or accelerator facilities that produce photons with energies above about 15 MeV, neutron production in the surrounding walls can lead to a significant neutron field.

However, the gamma photons produced in radioactive decay of fission and activation products in nuclear reactors generally have energies too low, and most materials have a photoneutron threshold too high for photoneutrons to be of concern. Only for the light elements ^{2}H, ^{6}Li, ^{7}Li, ^{9}Be, and ^{12}C are the thresholds for photoneutron production sufficiently low that these secondary neutrons may have to be considered. In heavy-water- or beryllium-moderated reactors, the photoneutron source may be very appreciable, and the neutron field deep within an hydrogenous shield is often determined by photoneutron production in deuterium, which constitutes about 0.015 atom percent of the hydrogen. Capture gamma photons arising from neutron absorption have particularly high energies, and thus may also cause a significant production of energetic photoneutrons.

The photoneutron mechanism can be used to create laboratory neutron sources by mixing intimately a beryllium or deuterium compound with a radioisotope that decays with the emission of high-energy photons. Alternatively, the encapsulated radioisotope may be surrounded by a beryllium- or deuterium-bearing shell. A common reactor photoneutron source is an antimony–beryllium mixture, which has the advantage of being rejuvenated by exposing the source to the neutrons in the reactor to transmute the stable ^{123}Sb into the required ^{124}Sb isotope (half-life of 60.2 days).

One very attractive feature of such (γ,n) sources is the nearly monoenergetic nature of the neutrons if the photons are monoenergetic. However, in large sources, the neutrons may undergo significant scattering in the source material and thereby degrade the nearly monoenergetic nature of their spectrum. These photoneutron sources generally require careful use because of their inherently large photon emission rates. Because nominally only one in a million high-energy photons actually interacts with the source material to produce a neutron, these sources generate gamma rays that are of far greater biological concern than are the neutrons.

Alpha-Neutron Sources

Many compact laboratory neutron sources use energetic alpha particles from various radioisotopes (*emitters*) to induce (α,n) reactions in appropriate materials (*converters*). Although a large number of nuclides emit neutrons if bombarded with alpha particles of sufficient energy, the energies of the alpha particles from radioisotopes are capable of penetrating the potential barriers of only the lighter nuclei.

Of particular interest are those light isotopes for which the (α,n) reaction is exoergic ($Q > 0$) or, at least, has a low threshold energy. For endoergic reactions ($Q > 0$), the threshold alpha energy is $-Q(1 + 4/A)$. Thus, for an (α,n) reaction to occur, the alpha particle must (1) have enough energy to overcome the repulsive Coulombic force field of the nucleus, and (2) exceed the threshold energy for the reaction. Converter materials used to make practical (α,n) sources include lithium, beryllium, boron, carbon, fluorine, and sodium.

The converter nuclides ^{18}O and ^{19}F are responsible for neutron production in many areas of the nuclear fuel cycle. Alpha particles emitted by uranium and plutonium range between 4 and 6 MeV in energy and can cause (α,n) neutron production when in the presence of oxygen or fluorine. In particular, (α,n) neutrons often dominate the spontaneous fission neutrons in UF_6 or in aqueous mixtures of uranium and plutonium such as found in nuclear waste.

A neutron source can be fabricated by mixing intimately a light converter element, such as lithium or beryllium, with a radioisotope that emits energetic alpha particles. Most of the practical alpha emitters are actinide elements, which form intermetallic compounds with beryllium. Such a compound, for example, $PuBe_{13}$, ensures both that the emitted alpha particles immediately encounter converter nuclei, thereby producing a maximum neutron yield, and that the radioactive actinides are bound into the source material, thereby reducing the risk of leakage of the alpha-emitting component.

The neutron yield from an (α,n) source varies strongly with the converter material, the energy of the alpha particle, and the relative concentrations of the emitter and converter elements. The degree of mixing between converter and emitter and the size, geometry, and source encapsulation may also affect the neutron yield. For example, a $^{239}Pu/Be$ source has an optimum neutron yield of about 60 neutrons per 10^6 primary alpha particles.

The energy distributions of neutrons emitted from (α,n) sources are continuous below some maximum neutron energy with definite structure at well-defined energies determined by the energy levels of the converter and the excited product nuclei. The use of the same converter material with different alpha emitters produces similar neutron spectra with different portions of the same basic spectrum accentuated or reduced as a result of the different alpha-particle energies. Average energies of neutrons typically are several MeV. For example, the neutrons produced by a $^{239}Pu/Be$ source have an average energy of 4.6 MeV.

Activation Neutrons

A few highly unstable nuclides decay by the emission of a neutron. The delayed neutrons associated with fission arise from such decay of the fission products. However, there are nuclides other than those in the fission-product decay chain which also decay by neutron emission. Only one of these nuclides, ^{17}N, is of importance in nuclear reactor situations. This isotope is produced in water-moderated reactors by an (n,p) reaction with ^{17}O (threshold energy, 8 MeV). The decay of ^{17}N by beta emission (half-life 4.4 s) produces ^{17}O in a highly excited state, which in turn decays rapidly by neutron emission. Most of the decay neutrons are emitted within ± 0.2 MeV of the most probable energy of about 1 MeV, although neutrons with energies up to 2 MeV may be produced.

Spallation Neutron Sources

In a spallation neutron source, pulses of very energetic protons (up to 1 GeV), produced by an accelerator, strike a heavy metal target such as mercury or liquid bismuth. Such an energetic proton when it strikes a target nucleus "spalls" or knocks out neutrons. Additional neutrons boil off as the struck nucleus heats up. Typically, 20–30 neutrons are produced per spallation reaction. These pulses of neutrons are then slowed down or thermalized by passing them through cells filled with water, or even liquid hydrogen if very slow neutrons are needed.

Sources of Gamma Photons

Radioactive Decay

Radioactive sources serve a wide variety of purposes in educational, medical, research, industrial, governmental, and commercial activities. The radionuclides in these sources almost always leave their decay daughters in excited nuclear states whose subsequent transitions to lower-energy states usually result in the emission of one or more gamma photons.

Prompt Fission Photons

The fission process produces copious gamma photons either within the first 6×10^{-8} s after the fission event (the *prompt fission gamma photons*) or from the subsequent decay of the fission products. These photons are of extreme importance in the shielding and gamma-heating calculations for a nuclear reactor. Consequently, much effort has been directed toward determining their nature.

Most investigations of prompt fission gamma photons have centered on the thermal-neutron-induced fission of ^{235}U. For this nuclide, it has been found that the number of prompt fission photons is 8.13 ± 0.35 photons per fission over the energy range 0.1–10.5 MeV, and the energy carried by this number of photons is 7.25 ± 0.26 MeV per fission. The energy spectrum of prompt gamma photons from the thermal fission of ^{235}U between 0.1 and 0.6 MeV is approximately constant at 6.6 photons MeV^{-1} fission^{-1}. At higher energies, the spectrum falls off sharply with increasing energy. The measured energy distribution of the prompt fission photons can be represented by the following empirical fit over the range 0.1–10.5 MeV:

$$N(E) = \begin{cases} 6.6 & 0.1 < E < 0.6 \text{ MeV} \\ 20.2e^{-1.78E} & 0.6 < E < 1.5 \text{ MeV} \\ 7.2e^{-1.09E} & 1.5 < E < 10.5 \text{ MeV}, \end{cases}$$

where E is in MeV and $N(E)$ is in units of photons MeV^{-1} fission^{-1}.

Investigation of ^{233}U, ^{239}Pu, and ^{252}Cf indicates that the prompt fission photon energy spectra for these isotopes resembles very closely that for ^{235}U, and hence for most purposes, it is reasonable to use the ^{235}U spectrum for other fissioning isotopes.

Fission-Product Photons

With the widespread application of nuclear fission, an important concern is the consideration of the very long lasting gamma activity produced by the decay of fission products.

In the fission process, most often two fragments are produced (*binary fission*) with a distribution in mass shown in Fig. 2. About 0.3% of the time, a third light fragment is produced (*ternary fission*), most often ^{3}H. As seen in Fig. 2, the mass distribution or *fission-product chain yield* is bimodal, with many products

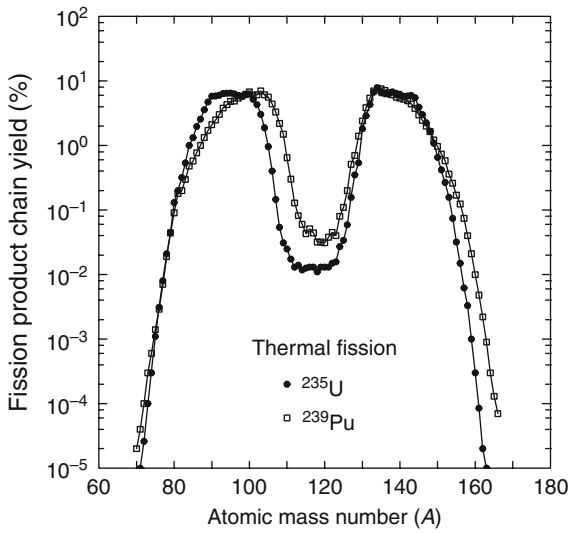

Radiation Sources. Figure 2
The probability (%) that a fission product with mass number A is produced in the thermal-neutron-induced fission of ^{235}U and ^{239}Pu

having atomic mass number around 95 and around 140. Among the former are the important long-lived radionuclide ^{90}Sr, several isotopes of the halogen bromine, and various isotopes of the noble gas krypton. Among the heavy fragments are the important long-lived radionuclide ^{137}Cs, radioisotopes of halogen iodine, notably ^{131}I, and isotopes of the noble gas xenon. The fission-products are neutron-rich and decay almost exclusively by β^- emission, often forming long decay chains. From the range of mass numbers produced (see Fig. 2), about 100 different decay chains are formed. An example of a short chain is

$$^{140}_{54}\mathrm{Xe} \xrightarrow[16\,\mathrm{s}]{\beta^-} {}^{140}_{55}\mathrm{Cs} \xrightarrow[66\,\mathrm{s}]{\beta^-} {}^{140}_{56}\mathrm{Ba} \xrightarrow[12.8\,\mathrm{days}]{\beta^-}$$

$$^{140}_{57}\mathrm{La} \xrightarrow[40\,\mathrm{h}]{\beta^-} {}^{140}_{58}\mathrm{Ce(stable)}.$$

The total gamma-ray energy released by the fission product chains is comparable to that released as prompt fission gamma photons. The gamma-ray energy release rate declines rapidly in the time after fission. About three-fourths of the delayed gamma-ray energy is released in the first 1,000 s after fission. In most calculations involving spent nuclear fuel, the gamma activity at several months or even years after removal of fuel from the nuclear reactor is of interest and only the long-lived fission products need be considered.

It has been found that the gamma energy released from fission products is relatively independent of the energy of the neutrons causing the fissions. However, the gamma-ray energy released and the photon energy spectrum depend significantly on the fissioning isotope, particularly in the first 10 s after fission. Generally, fissioning isotopes having a greater proportion of neutrons to protons produce fission-product chains of longer average length, with isotopes richer in neutrons and hence with greater available decay energy. Also, the photon energy spectrum generally becomes less energetic as the time after fission increases.

For very approximate calculations, the energy spectrum of delayed gamma photons from the fission of ^{235}U, at times up to about 500 s, may be approximated by the proportionality $N(E) \sim e^{-1.1E}$, where $N(E)$ is the delayed gamma yield (photons MeV^{-1} fission^{-1}) and E is the photon energy in MeV. The time dependence for the total gamma photon energy emission rate $F(t)$ (MeV s^{-1} fission^{-1}) is often described by the simple decay formula $F(t) = 1.4\ t^{-1.2}$, 10 s $< t <$ 10^7 s, where t is in seconds. More complicated (and accurate) expressions for $F(t)$ have been obtained from fits to experimental data; but for preliminary calculations the simpler result is usually adequate. It is observed that both ^{235}U and ^{239}Pu have roughly the same total gamma-ray-energy decay characteristics for up to 200 days after fission, at which time ^{235}U products begin to decay more rapidly until at 1 year after fission, the ^{239}Pu gamma activity is about 60% greater than that of ^{235}U.

For accurate calculations involving fission products, the variation with time after fission of the energy spectra of the photons must be taken into account. Often the energy spectra are averaged over discrete energy intervals and the energy emission rate in each energy group is considered as a function of time after fission. Computer codes, based on extensive libraries of radionuclide data, have been developed to compute the abundances and decay rates of the hundreds of fission-product radionuclides. An example of such calculations is shown in Fig. 3.

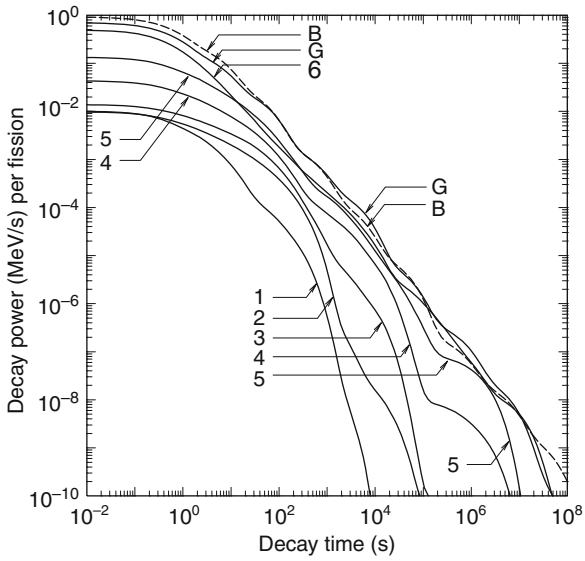

Radiation Sources. Figure 3
Total gamma-ray (G) and beta-particle (B) energy emission rates as a function of time after the thermal fission of ^{235}U. The curves identified by the numbers 1–6 are gamma emission rates for photons in the energy ranges 5–7.5, 4–5, 3–4, 2–3, 1–2, and 0–1 MeV, respectively

Capture Gamma Photons

The compound nucleus formed by neutron absorption is initially created in a highly excited state with excitation energy equal to the kinetic energy of the incident neutron plus the neutron binding energy, which averages about 7 MeV. The decay of this nucleus, usually within 10^{-12} s, and usually by way of intermediate states, typically produces several energetic photons. Generally, the probability a neutron causes an (n,γ) reaction is greatest for slow-moving *thermal neutrons*, that is, neutrons whose speed is in equilibrium with the thermal motion of the atoms in a medium. At high energies, it is more likely that a neutron scatters, thereby losing some of its kinetic energy, and then slows toward thermal energies.

Capture photons may be created intentionally by placing a material with a high thermal-neutron (n,γ) cross section in a thermal neutron beam. The energy spectrum of the resulting capture gamma photons can then be used to identify trace elements in the sample. More often, however, capture gamma photons are an undesired secondary source of radiation.

Inelastic Scattering Photons

The excited nucleus formed when a neutron is inelastically scattered decays to the ground state within about 10^{-14} s, with the excitation energy being released via one or more photons. Because of the constraints imposed by the conservation of energy and momentum in all scattering interactions, inelastic neutron scattering cannot occur unless the incident neutron energy is greater than $(A + 1)/A$ times the energy required to excite the scattering nucleus to its first excited state. Except for the heavy nuclides, neutron energies above about 0.5 MeV are typically required for inelastic scattering.

The detailed calculation of secondary photon source strengths from inelastic neutron scattering requires knowledge of the fast-neutron fluence, the inelastic scattering cross sections, and spectra of resultant photons, all as functions of the incident neutron energy. The cross sections and energy spectra of the secondary photons depend strongly on the incident neutron energy and the particular nuclide. Such inelastic scattering data are known only for the more important structural and shielding materials, and even the known data require extensive data libraries. Fortunately, in most situations, these secondary photons are of little importance compared to the capture photons. Although inelastic neutron scattering is usually neglected with regard to its secondary-photon radiation, it is a very important mechanism in the attenuation of fast neutrons, better even than elastic scattering in some cases.

Activation Photons

For many materials, absorption of a neutron produces a radionuclide with a half-life ranging from a fraction of a second to many years. The radiation produced by the subsequent decay of these activation nuclei may be very significant for materials that have been exposed to large neutron fluences, especially structural components in a reactor or accelerator. Many radionuclides encountered in research laboratories, medical facilities, and industry are produced as activation nuclides from neutron absorption in some parent material (see Table 4). Such nuclides decay, usually by beta emission, leaving the daughter nucleus in an excited state, which usually decays quickly to its ground state with the emission of one or more gamma photons. Thus, the apparent half-life of the photon emitter is that of the parent (or activation nuclide), while the number and energy of the photons are characteristic of the nuclear structure of the decay daughter.

Although most activation products of concern in shielding problems arise from neutron absorption, there is one important exception in water-moderated nuclear reactors. The ^{16}O in the water can be transmuted to ^{16}N in the presence of fission neutrons by an (n,p) reaction with a threshold energy of 9.6 MeV. ^{16}N decays with a 7.4-s half-life emitting gamma photons of 6.13 and 7.10 MeV (yields of 0.69 and 0.05 per decay). This gamma-ray source is very important in coolant channels of power reactors.

Positron Annihilation Photons

Positrons, generated either from the positron decay of radionuclides or from pair production interactions induced by high-energy photons, slow down in matter within about 10^{-10} s and are subsequently annihilated with electrons. With rare exception, the rest-mass

Radiation Sources. Table 4 Important radioisotopes produced by reactors and accelerators for use in medical, research, and industrial applications. Those isotopes commercially available for medical use are shown in bold. Decay data from NUDAT 2.5, National Nuclear Data Center, Brookhaven National Laboratory

Nuclide	Half-life	Decay modes[a]	Nuclide	Half-life	Decay modes[a]
^{3}H	12.33 years	β^- *	^{81m}Kr	13.1 s	EC IT
^{11}C	20.39 min	β^+ EC	^{85}Kr	10.76 years	β^-
^{13}N	9.965 min	β^+ EC	**^{82}Sr**[b]	25.6 days	EC *
^{14}C	5,730 years	β^- *	**^{89}Sr**	50.5 days	β^-
^{15}O	122.2 s	β^+ EC	**^{90}Sr**[c]	28.90 years	β^- *
^{18}F	109.8 min	β^+ EC	**^{99}Mo**[d]	65.94 h	β^-
^{22}Na	2.602 years	β^+ EC	^{103}Pd	16.99 days	EC
^{26}Al	7.17E5 years	β^+ EC	^{110m}Ag	249.8 days	β^- IT
^{28}Mg	20.91 h	β^-	**^{111}In**	2.80 days	EC
^{32}Si	153 years	β^- *	^{113m}In	99.48 min	IT
^{32}P	14.26 days	β^- *	**^{123}I**	13.27 h	EC
^{33}P	25.3 days	β^- *	**^{125}I**	59.40 days	EC
^{35}S	87.51 days	β^- *	**^{131}I**	8.025 days	β^-
^{36}Cl	3.01E5 years	$\beta^\pm$ EC	**^{133}Xe**	5.243 days	β^-
^{46}Sc	83.79 days	β^-	^{137}Cs[e]	30.1 years	β^- *
^{51}Cr	27.70 days	EC	^{140}La	1.679 days	β^-
^{54}Mn	312.1 days	β^- EC	^{148}Gd	70.9 years	α *
^{57}Co	271.7 days	EC	**^{153}Sm**	46.3 h	β^-
^{57}Cu	196 ms	β^+ EC	^{159}Gd	18.48 h	β^-
^{57}Cr	21.1 s	β^- *	^{169}Yb	32.02 days	EC
^{59}Fe	44.50 days	β^-	^{170}Tm	128.6 days	β^- EC
^{60}Co	5.271 years	β^-	^{186}Re	89.25 h	β^- EC
^{64}Cu	12.70 h	$\beta^\pm$ EC	^{191}Os	15.4 days	β^-
^{65}Zn	244.1 days	β^+ EC	^{192}Ir	73.83 days	β^- EC
^{67}Ga	3.261 days	EC	^{198}Au	2.696 days	β^-
^{68}Ga	67.71 min	β^+ EC	**^{201}Tl**	73 h	EC
^{75}Se	119.8 days	EC	^{204}Tl	3.78 years	β^- EC *
^{81}Rb	4.570 h	β^+ EC	^{210}Pb	22.2 years	$\alpha\beta^-$
^{82}Rb	1.273 min	β^+ EC	^{241}Am	432.6 years	α

[a]Decays without any gamma photon emission are denoted by *
[b]In equilibrium with decay product ^{32}Rb (1.273 min, β^+ EC)
[c]In equilibrium with decay product ^{90}Y (64 h, β^-)
[d]In equilibrium with decay product ^{99m}Tc (6.01 h, IT)
[e]In equilibrium with decay product ^{137m}Ba (2.552 min, IT)
Source: References [4, 5].

energy of the electron and positron is emitted in the form of two annihilation photons, each of energy $m_e c^2$ (= 0.511 MeV).

Sources of X-rays

The interaction of photons or charged particles with matter leads inevitably to the production of secondary x-ray photons. The x-rays in many applications have energies $\lesssim$100 keV, and hence are easily attenuated by any shield adequate for the primary radiation. Consequently, the secondary x-rays are often completely neglected in analyses involving higher-energy photons. There are many cases, though, when the energies of x-rays and Auger electrons must be accounted for as well as those of the x-rays. An example is the evaluation of radiation dose to the total body, or an organ of the body, after a radionuclide intake. This is a situation in which the source and receiver volumes may be the same.

There are important situations in which x-ray production is the only source of photons. To estimate the intensity, energies, and doses from the x-ray photons, it is necessary to understand how the x-rays are produced and some characteristics of the production mechanisms. There are two principal methods whereby secondary x-ray photons are generated: the rearrangement of atomic electron configurations leads to characteristic x-rays, and the deflection of charged particles in the nuclear electric field results in bremsstrahlung.

Characteristic X-rays and Fluorescence

The electrons around a nucleus are arranged in shells or layers, each of which can hold a maximum number of electrons. The two electrons in the innermost shell (K shell) are the most tightly bound, the six electrons in the next shell (L shell) are the next most tightly bound, and so on outward for the M, N,... shells. If the normal electron arrangement around a nucleus is altered, say by ejection of an inner electron, the electrons begin a complex series of transitions to vacancies in the inner shells (thereby acquiring higher binding energies) until the unexcited state of the atom is achieved. In each electronic transition, the difference in binding energy between the final and initial states is either emitted as a photon, called a *characteristic x-ray*, or given up to another electron which is ejected from the atom, called an *Auger electron*. The discrete electron energy levels and the transition probabilities between levels vary with the Z number of the atom, and thus the characteristic x-rays provide a unique signature for each element.

The number of x-rays with different energies is greatly increased by the multiplicity of electron energy levels available in each shell (1, 3, 5, 7, ... distinct energy levels for the K, L, M, N, ... shells, respectively). To identify the various characteristic x-rays for an element, many different schemes have been proposed. One of the more popular uses the letter of the shell whose vacancy is filled together with a numbered Greek subscript to identify a particular electron transition (e.g., $K_{\alpha 1}$ and $L_{\gamma 5}$).

Production of Characteristic X-Rays There are several methods whereby atoms may be excited and characteristic x-rays produced. A photoelectric absorption leaves the absorbing atom in an ionized state. If the incident photon energy is sufficiently greater than the binding energy of the K-shell electron, which ranges from 14 eV for hydrogen to 115 keV for uranium, it is most likely (80–100%) that a vacancy is created in the K shell and thus that the K series of x-rays dominates the subsequent secondary radiation. These x-ray photons produced from photoelectric absorption are often called *fluorescent radiation* and are widely used to identify trace elements in a sample by bombarding the sample with low-energy photons from a radioactive source or with x-rays from an x-ray machine and then observing the induced fluorescent radiation.

Characteristic x-rays can also arise following the decay of a radionuclide. In the decay process known as *electron capture*, an orbital electron, most likely from the K shell, is absorbed into the nucleus, thereby decreasing the nuclear charge by one unit. The resulting K-shell vacancy then gives rise to the K series of characteristic x-rays. A second source of characteristic x-rays which occurs in many radionuclides is a result of *internal conversion*. Most daughter nuclei formed as a result of any type of nuclear decay are left in excited states. This excitation energy may be either emitted as a gamma photon or transferred to an orbital electron which is ejected from the atom. Again, it is most likely that a K-shell electron is involved in this internal conversion process.

X-Ray Energies To generate a particular series of characteristic x-rays, an electron vacancy must be created in an appropriate electron shell. Such vacancies are created only when sufficient energy is transferred to an electron in that shell so as to allow it to break free of the atom or at least be transferred to an energy level above all the other electrons. The characteristic x-rays emitted when electrons fill a vacancy in a shell always have less energy than that required to create the vacancy. The most energetic x-rays arise from an electron filling a *K*-shell vacancy and, since the binding energy of *K*-shell electrons increases with the atomic number *Z*, the most energetic x-rays are *K*-shell x-rays from heavy atoms. For example, the K_α x-ray energy varies from only 0.52 keV for oxygen ($Z = 8$) to 6.4 keV for iron ($Z = 26$) to 98 keV for uranium ($Z = 92$). By comparison, the *L* series of x-rays for uranium occurs at energies around 15 keV. Thus, in most shielding situations, only the *K* series of x-rays from heavy elements are sufficiently penetrating to be of concern.

X-Ray Yields The *fluorescent yield* of a material is the fraction of the atoms with a vacancy in an inner electron shell that emit an x-ray upon the filling of the vacancy. The fluorescent yield increases dramatically with the *Z* number of the atom. For example, the fluorescent yield for vacancies in the *K* shell increases from 0.0069 for oxygen ($Z = 8$) to 0.97 for uranium ($Z = 92$). Thus, the secondary fluorescent radiation is of more concern for heavy materials.

Bremsstrahlung

A charged particle gives up its kinetic energy either by collisions with electrons along its path or by photon emission as it is deflected, and hence accelerated, by the electric fields of nuclei. The photons produced by the deflection of the charged particle are called *bremsstrahlung* (literally, "braking radiation"). For a given type of charged particle, the ratio of the rate at which the particle loses energy by bremsstrahlung to that by ionizing and exciting the surrounding medium is

$$\frac{\text{Radiation loss}}{\text{Ionization loss}} \simeq \frac{EZ}{700}\left(\frac{m_e}{M}\right)^2,$$

where *E* is in MeV, m_e is the electron mass, and *M* is the mass of the charged particle. From this result, it is seen that bremsstrahlung is more important for high-energy particles of small mass incident on high-*Z* material. In shielding situations, only electrons ($m_e/M = 1$) are ever of importance for their associated bremsstrahlung. All other charged particles are far too massive to produce significant amounts of bremsstrahlung. Bremsstrahlung from electrons, however, is of particular radiological interest for devices that accelerate electrons, such as betatrons and x-ray tubes, or for situations involving radionuclides that emit only beta particles.

Energy Distribution of Bremsstrahlung The energy distribution of the photons produced by the bremsstrahlung mechanism is continuous up to a maximum energy corresponding to the maximum kinetic energy of the incident charged particles. The exact shape of the continuous bremsstrahlung spectrum depends on many factors, including the energy distribution of the incident charged particles, the thickness of the target, and the amount of bremsstrahlung absorbed in the target and other masking material.

For monoenergetic electrons of energy E_o incident on a target thick compared to the electron range, the number of bremsstrahlung photons of energy *E*, per unit energy and per incident electron, emitted as the electron is completely slowed down can be approximated by the Kramer distribution

$$N(E_o, E) \simeq 2kZ\left(\frac{E_o}{E} - 1\right), \qquad E \leq E_o,$$

where $k \simeq 0.0007\ \text{MeV}^{-1}$ is a normalization constant. The fraction of the incident electron's kinetic energy that is subsequently emitted as bremsstrahlung can then be calculated from this approximation as kZE_o, which is usually a small fraction. For example, about 10% of the energy of a 2-MeV electron, when stopped in lead, is converted into bremsstrahlung.

Angular Distribution of Bremsstrahlung The angular distribution of bremsstrahlung is generally quite anisotropic and varies with the incident electron energy. Bremsstrahlung induced by low-energy electrons ($\lesssim$100 keV) is emitted over a relatively broad range of directions around the direction of the incident electron. As the electron energy increases, the direction of the peak intensity shifts increasingly toward the forward direction until, for electrons above a few

MeV, the bremsstrahlung is confined to a very narrow forward beam. The angular distribution of radiation leaving a target is very difficult to compute since it depends on the target size and orientation. For thin targets, the anisotropy of the bremsstrahlung resembles that for a single electron–nucleus interaction, while for thick targets multiple electron interactions and photon absorption in the target must be considered.

X-ray Machines The production of x-ray photons as bremsstrahlung and fluorescence occurs in any device that produces high-energy electrons. Devices that can produce significant quantities of x-rays are those in which a high voltage is used to accelerate electrons, which then strike an appropriate target material. Such is the basic principle of all x-ray tubes used in medical diagnosis and therapy, industrial applications, and research laboratories.

Although there are many different designs of x-ray sources for different applications, most designs for low-to-medium voltage sources ($\lesssim$180 kV) place the electron source (cathode) and electron target (anode) in a sealed glass tube. The glass tube acts as both an insulator between the anode and cathode and a chamber for the necessary vacuum through which the electrons are accelerated. The anodes of x-ray tubes incorporate a suitable metal upon which the electrons impinge and generate the bremsstrahlung and characteristic x-rays. Most of the electron energy is deposited in the anode as heat rather than being radiated away as x-rays, and thus heat removal is an important aspect in the design of x-ray tubes. Tungsten is the most commonly used target material because of its high atomic number and because of its high melting point, high thermal conductivity, and low vapor pressure. Occasionally, other target materials are used when different characteristic x-ray energies are desired. For most medical and dental diagnostic units, voltages between 40 and 150 kV are used, while medical therapy units may use 6–150 kV for superficial treatment or 180 kV to 50 MV for treatment requiring very penetrating radiation.

The energy spectrum of x-ray photons emitted from an x-ray tube has a continuous bremsstrahlung component up to the maximum electron energy, that is, the maximum voltage applied to the tube. If the applied voltage is sufficiently high as to cause ionization in the target material, there will also be characteristic x-ray lines superimposed on the continuous bremsstrahlung spectrum. Absorbing filters are used to minimize low-energy x-rays, which are damaging to skin. As the beam filtration increases, the low-energy x-rays are preferentially attenuated and the x-ray spectrum *hardens* and becomes more penetrating. These phenomena are illustrated in Fig. 4. Calculated exposure spectra of x-rays are shown for the same operating voltage but for two different amounts of beam filtration. As the filtration increases, lower energy x-rays are preferentially attenuated; the spectrum hardens and becomes more penetrating. Readily apparent in these spectra are the tungsten $K_{\alpha 1}$ and $K_{\alpha 2}$ characteristic x-rays.

The characteristic x-rays may contribute a substantial fraction of the total x-ray emission. For example, the *L*-shell radiation from a tungsten target is between 20% and 35% of the total energy emission when voltages between 15 and 50 kV are used. Above and below this voltage range, the *L* component rapidly decreases in importance. However, even a small degree of filtering of the x-ray beam effectively eliminates the low-energy portion of the spectrum containing the *L*-shell x-rays. The higher-energy *K*-series x-rays from a tungsten target contribute a maximum of 12% of the

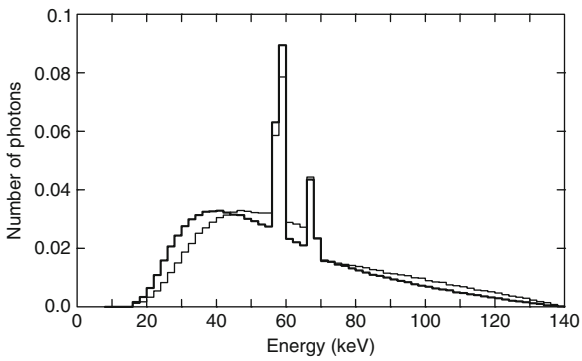

Radiation Sources. Figure 4
Measured photon spectra from a Machlett Aeromax x-ray tube (tungsten anode) operated at a constant 140 kV potential. This tube has an inherent filter thickness of 2.50-mm aluminum equivalent and produces the spectrum shown by the thick line. The addition of an external 6-mm aluminum filter hardens the spectrum shown by the thin line. Both spectra are normalized to unit area. Data are from [6]

x-ray emission from the target for operating voltages between 100 and 200 kV.

Synchrotron Photons

When a charged particle moving in a straight line is accelerated by deflecting it in an electromagnetic field, the perturbation in the particle's electric field travels away from the particle at the speed of light and is observed as electromagnetic radiation (photons). Such is the origin of bremsstrahlung produced when fast electrons (beta particles) are deflected by the electric field of a nucleus.

This same mechanism can be used to produce intense photon radiation by deflecting an electron beam by magnetic fields. In a special accelerator called a *synchrotron*, highly relativistic electrons are forced to move in a circular path inside a storage ring by placing *bending magnets* along the ring. Photons are emitted when the beam is accelerated transversely by (1) the bending magnets (used to form the circular electron beam), and by (2) insertion device magnets such as *undulators*, *wigglers*, and *wavelength shifters*.

Because the electrons are very relativistic, the synchrotron radiation is emitted in a very narrow cone in the direction of electron travel as they are deflected. Undulators cause the beam to be deflected sinusoidally by a weak oscillatory magnetic field, thereby producing nearly monochromatic photons. By contrast, a wiggler uses a strong oscillatory magnetic field which, because of relativistic effects, produces distorted sinusoidal deflections of the electron beam and synchrotron radiation with multiple harmonics, that is, a line spectrum. If very strong magnetic fields are used, many harmonics are produced that merge to yield a continuous spectrum ranging from the infrared to hard x-rays. By placing undulators or wigglers at a specific location in the storage ring, very intense and narrowly collimated beams of photons with energies up to a few keV can be produced to use, for example, in x-ray diffraction analysis.

Cosmic Rays, Solar Radiation, and Trapped Radiation Belts

The earth is subjected continuously to radiation with sources in our sun and its corona, from sources within our galaxy, and from sources beyond our galaxy. In addition, surrounding the earth are belts of trapped particles with solar origins. Radiation reaching the earth's atmosphere consists of high-energy electrons and atomic nuclei. Hydrogen nuclei (protons) constitute the major component, with heavier atoms decreasing in importance with increasing atomic number. The highest energy particles originate in our galaxy and more distant galaxies and are referred to as galactic cosmic radiation (GCR). Cascades of nuclear interactions in the atmosphere give rise to many types of secondary particles. Of much lower energy are particles of solar origin, which are highly variable in time and are associated with solar activity. Sources of these particles are sometimes associated with solar flares but are more generally identified with solar particle events (SPE) or coronal mass ejections (CME). The number of solar flare events and SPE emissions fluctuate with the 11-year cycle associated with solar activity. GCR intensity is modulated by SPE emissions, being minimal when solar activity is maximal.

Galactic Cosmic Radiation

At the earth's surface, cosmic radiation dose rates are largely due to muons and electrons. The intensity and angular distribution of galactic radiation reaching the earth is affected by the earth's magnetic field and perturbed by magnetic disturbances generated by solar flare activity. Consequently, at any given location, cosmic ray doses may vary in time by a factor of 3. At any given time, cosmic ray dose rates at sea level may vary with geomagnetic latitude by as much as a factor of 8, being greatest at the pole and least at the equator. Cosmic ray dose rates also increase with altitude. At geomagnetic latitude 55°N, for example, the absorbed dose rate in tissue approximately doubles with each 2.75 km (9,000 ft) increase in altitude, up to 10 km (33,000 ft). Figure 5 illustrates the relative importance, in terms of dose rate, for cosmic rays and their reaction products in the atmosphere. Cosmic ray dose rates affecting populations vary strongly with latitude. Table 5 describes this variation. The outdoor and indoor average effective dose rates for space radiation in the most heavily populated urban areas in the USA are 45 and 36 nSv/h [7]. Population averaged annual doses are about the same in the northern and southern hemispheres, and globally amount to 31 nSv/h for

charged particles plus 5.5 nSv/h for neutrons. GCR energies span a vast range and there is no way of shielding astronauts from GCR effects. On the earth's surface, the GCR presence results in a source of steady low-dose-rate radiation.

As a result of nuclear reactions of cosmic rays with constituents of the atmosphere, secondary neutrons, protons, and pions, mainly, are produced. Subsequent pion decay results in electrons, photons, and muons. Muon decay, in turn, leads to secondary electrons, as do scattering interactions of charged particles in the atmosphere. Cosmic ray debris that reaches the surface of the earth consists mainly of muons and electrons with a few neutrons. Except for short-term influences of solar activity, galactic cosmic radiation has been constant in intensity for at least several thousand years. The influence of solar activity is cyclical and the principal variation is on an 11-year cycle. The geomagnetic field of the earth is responsible for limiting the number of cosmic rays that can reach the atmosphere thus accounting for the strong effect of latitude on cosmic-ray dose rates.

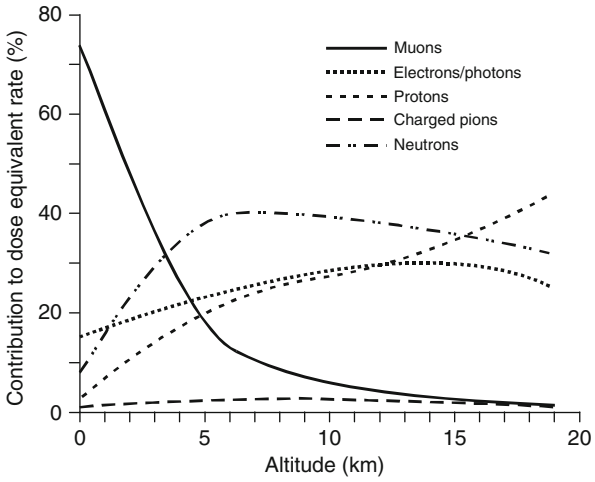

Radiation Sources. Figure 5
Components of the dose equivalent rate from cosmic rays in the atmosphere (Reproduced from [2], derived from [5])

Solar Particle Events

Both SPE and CME emissions are mainly hydrogen and helium nuclei, that is, protons and alpha particles, predominantly the former. Electrons are thought to be emitted as well, but with energies less than those of protons by a factor equal to the ratio of the rest masses. Energy spectra are highly variable, as are temporal variations of intensity. A typical course of events for a flare is as follows. Gamma and x-ray emission takes place over about 4 h as is evidenced by radio interference. The first significant quantities of protons reach the earth after about 15 h and peak proton intensity occurs at about 40 h after the solar eruption.

Solar particle events are closely related to solar flares associated with sunspots with intense magnetic fields linking the corona to the solar interior. CME emissions are not directly connected to flares, but originate in the corona driven by the energy of the sun's

Radiation Sources. Table 5 Cosmic ray dose rate variation at sea level as a function of latitude for the northern and southern hemispheres

Latitude (deg N–S)	Population% in latitude band (N–S)	Effective dose rate (nSv/h)	
		Charged particles	Neutrons
60–70	0.4–0	32	10.9
50–60	13.7–0.5	32	10
40–50	15.5–0.9	32	7.8
30–40	20.4–13	32	5.3
20–30	32.7–14.9	30	4
10–20	11–16.7	30	3.7
0–10	6.3–54	30	3.6

Source: Reference [2].

magnetic field. While of too low energy to contribute to radiation doses at the surface of the earth, these radiations, which fluctuate cyclically with an 11-year period, perturb earth's magnetic field and thereby modulate galactic cosmic-ray intensities with the same period. Maxima in solar flare activity lead to minimal GCR intensity. SPE and CME emissions, in comparison to galactic cosmic rays, are of little significance as a hazard in aircraft flight or low orbital space travel. On the other hand, these radiations present considerable, life-threatening risk to personnel and equipment in space travel outside the earth's magnetic field. Protection of astronauts in space missions beyond low-earth orbit is addressed in [8].

Trapped Radiation Belts

Released continuously from the sun, as an extension of the corona, is the solar wind, a plasma of low-energy protons and electrons. The solar wind does not present a radiation hazard, even in interplanetary space travel. However, it does affect the interplanetary magnetic field and the shape of the geomagnetically trapped radiation belts. These radiation belts are thought to be supplied by captured solar-wind particles and by decay into protons and electrons of neutrons created by interactions of galactic cosmic rays in the atmosphere. The trapped radiation can present a significant hazard to personnel and equipment in space missions.

The earth's geomagnetically trapped radiation belts are also known as Van Allen belts in recognition of James A. Van Allen and his coworkers who discovered their existence in 1958. There are two belts. The inner belt consists of protons and electrons, the protons being responsible for radiation doses in the region. The outer belt consists primarily of electrons. The particles travel in helical trajectories determined by the magnetic field surrounding the planet. They occur at maximum altitude at the equator and approach the earth most closely near the poles. At the equator, the inner belt extends to about 2.8 earth radii. The center of the outer belt is at about 5 earth radii. The solar wind compresses the trapped radiation on the sunny side of the earth and the compression is enhanced by solar flare activity. In the earth's shadow, the belts are distended as the solar wind sweeps the magnetosphere outward. In a plane through the earth, perpendicular to the earth–sun axis, the proton and electron belts are maximum in intensity at altitudes of about 3,000 and 18,000 km, respectively.

In the southern Atlantic Ocean, there is an eccentricity of the geomagnetic field with respect to the earth's center, and magnetic field lines dip closer to earth. This region, the South Atlantic Anomaly, is the primary source of radiation exposure to astronaut crew members in low-altitude and low-inclination missions. Radiation protection guidance for low-earth orbit missions is found in [9] and [10].

Radiation Sources Used in Human Activities

Life on earth is continually subjected to radiation of natural origin. Exposure is from sources outside the body, arising from cosmic radiation and radionuclides in the environment, and from sources inside the body, arising from ingested or inhaled radionuclides retained in the body. Natural sources are the major contributors to human radiation exposure and represent a reference against which exposure to man-made sources may be compared. Table 6 summarizes radiation doses to man resulting from natural sources. Listed in the table are both doses to individual organs or tissues of the body and the effective dose equivalent, which is a composite dose weighted by the relative radiation sensitivities of many organs and tissues of the body.

Since the early 1980s, there has been negligible change in exposure to naturally occurring radiation, an increase estimated from 3 to 3.1 mSv annually. However, in the USA, medical diagnostic exposures have increased by a factor of 5.5 by 2006, an increase from 0.53 to 3 mSv annually. Of the 3 mSv total, 1.47 mSv is from computed tomography (CT) scans, 0.43 mSv for interventional fluoroscopy, 0.77 mSv for nuclear medicine procedures, and 0.33 mSv for conventional radiography and fluoroscopy (10).

Sources in Medicine

Very shortly after their discoveries at the end of the nineteenth century, radium and x-rays were used for medical purposes – radium sources being concentrated from natural materials and x-rays being generated using new technology. These were the only radiation sources seeing significant use until the 1930s, when

Radiation Sources. Table 6 Summary of US annual doses from natural background radiation

Radiation source	Average annual dose equivalent (mrem)				
	Bronchial epithelium	Other soft tissues	Bone surfaces	Bone marrow	Effective dose equivalent
Cosmic radiation	27	27	27	27	27
Cosmogenic nuclides	1	1	1	3	1
External terrestrial	28	28	28	28	28
Inhaled nuclides	2,400				200
Nuclides in the body	36	36	110	50	39
Totals (rounded)	2,500	90	170	110	300

Source: Reference [11].

research into nuclear fission began and when high-energy particle accelerators were developed for nuclear research. In the first half of the twentieth century, x-rays revolutionized diagnostic medicine. In the second half, accelerator radiation and radionuclides produced by accelerators and nuclear reactors established radiography, radiation therapy, and nuclear medicine, both diagnostic and therapeutic, as mature medical sciences. Table 4 lists the radioisotopes commonly used in medicine and industry. Some of these radionuclides are produced in nuclear reactors, either as products of fission or as products of neutron absorption. Nuclei of these isotopes are rich in neutrons and tend to decay by emission of negative beta particles, thereby becoming more positive in charge and more stable. Other isotopes are produced in accelerators. These generally have nuclei deficient in neutrons and tend to decay either by emission of a position or capture of an electron, either process leaving the nucleus more negative and more stable.

There are three broad categories of medical procedures resulting in human radiation exposure: (1) diagnostic x-ray examinations, including mammography and computed tomographic (CT) scans, (2) diagnostic nuclear medicine, and (3) radiation therapy.

Diagnostic X-Rays Of all the radiation exposures to the general public arising from human activity, the greatest is due to medical procedures, and collective exposures from diagnostic x-rays dominate all other medical exposures. Also, the population subgroup receiving diagnostic x-rays is not small. In the USA, about 250 million medical x rays are delivered annually, as are about 70 million CT scans. About 900 thousand persons receive radiation therapy annually [2, 7].

Diagnostic Nuclear Medicine Internally administered radionuclides are used medically for imaging studies of various body organs and for non-imaging studies such as thyroid uptake and blood volume measurements. Such uses present hazards for both patients and medical staff. Radiopharmaceuticals are also used for in vitro studies such as radioimmunoassay measurements and thus are of potential hazard to medical staff. Frequencies of procedures, while steadily increasing, vary widely from country to country. As of 2000, in industrialized countries, about 10–40 examinations involving radiopharmaceuticals are carried out annually per 1,000 population. In developing countries, annual frequencies are on the order of 0.2–2 examinations per 1,000 population. In the USA in 2006, for example, some 18 million radionuclide administrations were performed annually for diagnostic purposes [2, 7].

Radiation Therapy There are three broad categories of radiation therapy– teletherapy, brachytherapy, and therapy using administered radiation sources. *Teletherapy* involves external beams from sources such as sealed ^{60}Co sources, x-ray machines, and accelerators that generate electron, proton, neutron, or x-ray

beams. *Brachytherapy* involves sources placed within body cavities (*intracavitary* means) or placed directly within tumor-bearing tissue (*interstitial* means). In the USA, Europe, and Japan, the frequencies for teletherapy and brachytherapy procedures exceed 2,000 annually per million population.

Thyroid disorders, including cancer, for many years have been treated by ^{131}I, usually by oral administration. Introduced about 1980, in association with the development of techniques for producing monoclonal antibodies, were new cancer diagnosis and treatment methodologies called radioimmunoimaging and radioimmunotherapy. The therapy involves administration of large doses of antibodies tagged with radionuclides and selected to bind with antigens on the surfaces of tumor cells. Imaging involves administration of very much smaller doses, with the goal of detecting the presence of tumor cells using standard camera and scanner imaging techniques. Imaging requires the use of radionuclides such as ^{99m}Tc, which emit low-energy gamma rays. Therapy involves the use of radionuclides emitting beta particles and electrons, with minimum emission of gamma rays, thus limiting radiation exposure, to the extent possible, to tumor cells alone. Among radionuclides used in radioimmunotherapy are ^{75}Se, ^{90}Y, ^{111}In, ^{125}I, ^{186}Re, and ^{191}Os.

Occupational Medical Exposure A world survey conducted by the United Nations for the years 1990–1994 reports the annual average effective dose 1.39 mSv to some 550,000 workers receiving measurable doses (2.3 million total). Of this group, the greatest number were involved in diagnostic radiology (350,000 at 1.34 mSv). Overall, exposures were in the range of 0.9–1.7 mSv annually [2].

Accelerator Sources

The earliest particle accelerators were the x-ray tubes of the late nineteenth century. Indeed, the radio and television (cathode-ray) tubes of the twentieth century are low-voltage electron accelerators. As electrons beams are stopped, x-rays are produced, inadvertently in the case of radio tubes, and deliberately in the case of x-ray generators.

Modern charged-particle accelerators date from the early 1930s, when Cockroft and Walton in England, and Lawrence and Livingston in America developed particle accelerators for research purposes using beams of electrons or ions. Over the years, steady advances have been made in types of accelerators, in the energies of the particles accelerated, and in the magnitude of the current carried by the charged particle beams. Accelerators continue to serve at the frontiers of atomic and nuclear physics as well as the materials sciences. Moreover, accelerators play an ever more important role in diagnostic and therapeutic medicine and in industrial production processes such as radiography, analysis of materials, radiation processing, and radioisotope production.

Particle accelerators may be classified technologically as direct (potential drop) accelerators and indirect (radio-frequency, plasma) accelerators. Among the former are the Van de Graaff and Cockroft-Walton devices. Among the latter are linear accelerators, betatrons, cyclotrons, and synchrotrons. In the linear accelerator, the particles travel in straight lines, accelerated by the electric fields along their paths. In cyclic accelerators, magnets are used to direct particles into approximately circular paths, along which they may pass through the same accelerating electric fields many times along their paths. The ultimate energies reached by the accelerated particles have increased from about 10^6 eV in the accelerators of the 1930s to 10^{12} eV in modern research accelerators.

By their very nature and function, accelerators are intense radiation sources. In certain applications, accelerated beams of charged particles are extracted from accelerators and directed onto external receivers. Medical applications and radiation processing see this use of accelerators. In other applications, charged particle beams impinge on internal target receivers designed to act as desired sources of secondary radiations such as x-rays or neutrons. In all cases, beams are stopped by targets within which secondary x-rays, neutrons, and other particles such as mesons may be produced as undesirable but unavoidable by-product radiations. Radiation shielding integral with the accelerator as well as structural radiation shielding surrounding the accelerator are necessary for personnel protection.

The production of secondary radiations arises mainly from three phenomena, direct nuclear reactions of ions or electron with accelerator components, electromagnetic cascades, and hadronic cascades.

Among the secondary radiations are neutrons, which in turn may be absorbed in accelerator and structural materials thereby leading to capture gamma rays and radioactive reaction products.

Representative of the direct nuclear reactions are those of relatively low-energy proton or deuteron beams in light-element targets. A popular method of generating energetic neutrons, for example, involves interactions of deuterons accelerated to 150 keV with tritium atoms in a target. The resulting reaction, $^{3}H(d,n)^{4}He$, produces an approximately isotropic and monoenergetic source of 14-MeV neutrons. Other such reactions include $^{3}H(p,n)^{3}He$, $^{2}H(d,n)^{3}He$, and $^{7}Li(p,n)^{7}Be$.

The electromagnetic cascade involves exchanges of the kinetic energy of an electron to electromagnetic energy of multiple photons in the bremsstrahlung process, followed by creation of the rest-mass and kinetic energies of an electron–positron pair in the pair-production process experienced by the photons. As the positrons and electrons lose kinetic energy radiatively, more photons are produced, and the cascade continues. The cascade is quenched when photons have insufficient energy to generate the rest masses of the electron–positron pair and when electron radiative energy losses fall below collisional energy losses.

In high-energy electron or proton accelerators, hadronic cascades may be produced when particles collide with atoms in the accelerator target or, inadvertently, with some other accelerator component, giving rise to many reaction products, including pions, kaons, protons, and neutrons. There is also exchange with the electromagnetic cascade via photodisintegration reactions and by production of energetic gamma rays upon decay of π^0 mesons. Propagation of the hadronic cascade occurs through reactions of the secondary protons and neutrons, and is especially important for nucleon energies of 150 MeV or greater. The cascade process produces most of the induced radioactivity at high-energy accelerators. Many reaction-product nuclei are in highly excited nuclear states and relax by emission of neutrons, whose subsequent absorption leads, in many cases, to radioactive by-products.

Water, plastics, and oils in the radiation environs of high-energy accelerators yield ^{7}Be and ^{11}C. Aluminum yields these same radionuclides plus ^{18}F, ^{22}Na, and ^{24}Na. Steel, stainless steel, and copper yield all the aforementioned, plus a very wide range of radionuclides, especially those of V, Cr, Mn, Co, Fe, Ni, Cu, and Zn. Neutron absorption in structural concrete also leads to a wide range of radionuclides, among which ^{24}Na is a major concern. This nuclide has a half-life of 15 h and, in each decay, emits high-energy beta particles and gamma rays.

Industrial Isotope Sources

Radionuclides used in industry contribute very little to collective population doses, although individual occupational exposures may be significant. The largest sources are those used in radiography, typically comprising 10–100 Ci of ^{192}Ir, ^{137}Cs, ^{170}Tm, or ^{60}Co. Borehole logging is accomplished using somewhat lower activity gamma-ray sources and neutron sources such as mixtures of plutonium, americium, or californium with beryllium. Much lower activity sources, often $^{90}Sr - {}^{90}Y$ beta-particle sources, are used for various instrumentation and gaging applications.

There are many consumer products containing radiation sources. While these sources are very weak and no one individual receives significant radiation exposure, many persons are involved. For example, the soil, water supplies, and building materials contain low concentrations of naturally occurring radionuclides. Electronic devices emit very low levels of x-rays, and devices ranging from luminous timepieces to smoke detectors contain weak radiation sources. Even the use of tobacco exposes smokers to alpha particles from naturally occurring ^{210}Po in the tobacco leaf.

Various modern technologies have led to human radiation exposures in excess of those which would have occurred in the absence of the technologies. For example, the mining of coal and other minerals and their use is responsible for increased releases of naturally occurring radionuclides to the environment. World production of coal is about 4 billion tonnes annually. About 70% is used in generation of electricity, the balance mainly in domestic heating and cooking. Coal contains ^{40}K, and the ^{238}U and ^{232}Th decay chains in widely varying concentrations. Depending on the nature of combustion, radionuclides are partitioned between fly ash and bottom ash. The smaller-sized fly ash particles are more heavily enriched with

radionuclides, particularly ^{210}Pb and ^{210}Po. The average ash content of coal is about 10% by weight, but may be as high as 40%. Efficiency of ash removal in power plants is quite variable– from only 80% removal to as much as 99% removal, the average being about 97.5%. In domestic use of coal, as much as 50% of the total ash is released into the atmosphere. In terms of doses to individual tissues, the main impact of atmospheric releases during combustion is the dose to bone surface cells accruing from inhalation of ^{232}Th present in the downwind plumes of particulates from plants.

Annually, some 1.4 billion tonnes of phosphate rock are mined and processed for use in production of fertilizers and phosphoric acid. By-product (phospho)gypsum finds wide use in the construction industry. The USA produces about 38% of the phosphate rock, the former Soviet Union 19%, and Morocco 14%. Sedimentary phosphate rock contains high concentrations of radionuclides in the ^{238}U decay chain. Most airborne radioactivity releases are associated with dust produced in strip mining, grinding, and drying of the ore. Utilization of the phosphates leads to both internal and external radiation exposure, the greatest exposure resulting from use of by-product gypsum in construction.

The Nuclear Power Industry

In mid-2008, there were 439 nuclear power plants operating around the world, with a total electrical generating capacity of 372,000 MW. An additional 42 nuclear plants were under construction in 15 countries. Most of the generating capacity consisted of pressurized-water and boiling-water reactors, which use ordinary water as coolant. Gas-cooled reactors, heavy-water reactors, light-water graphite reactors, and sodium-cooled reactors provided the balance of the capacity.

Nuclear Power Reactors The fission process and production of neutrons associated with reactor operation lead to a wide array of radioactive fission products and activation products arising from neutron absorption. Moreover, large quantities of uranium and plutonium are fissioned in modern nuclear power plants (typically 3 kg/day) to produce the thermal energy needed to produce electricity. Consequently, large quantities of fission products are produced and accumulate in the fuel. Also contained within the fuel are actinides produced by cumulative neutron absorption in uranium, thorium, and plutonium fuels. The actinides are characterized by spontaneous fission in competition with alpha-particle decay, and require sequestration to the same degree as the fission products.

One way of categorizing the generated radionuclides is by their physical–chemical behavior, namely, (1) noble gases (2) ^{3}H and ^{14}C, (3) halogens, and (4) particulates. These divisions are based on the relative ease of isolation of the radionuclides from airborne effluents. The noble gases include the many isotopes of the krypton and xenon fission products as well as the activation product ^{41}Ar. These elements cannot be removed from a gas stream by filtration. Halogens include the many isotopes of the bromine and iodine fission products. If they are present in a gas stream, they are likely to be in a chemical form unsuitable for filtration, and effective removal requires adsorption on a material such as activated charcoal. Other radionuclides and the halogens in ionic form may be removed from a gas stream by filtration. In aqueous liquids, the particulates may be isolated by evaporation, filtration, or ion exchange. The halogens, unless in ionic form, cannot be isolated by evaporation or filtration, nor can noble gases. Special cases are ^{3}H in the form of tritiated water and ^{14}C as carbon dioxide. The tritium can be isolated only with very great difficulty, and CO_2 removal requires chemical treatment.

There are two sources of radionuclides in reactor coolant, leakage from defective fuel rods and activation products produced by neutron interactions in the coolant itself or with fuel and structure in contact with the coolant. Activation product sources are inevitable, and include a number of radionuclides which may be produced in the coolant. For example, ^{16}N is produced as a result of neutron interactions with oxygen, ^{41}Ar as a result of neutron absorption in naturally occurring argon in the atmosphere and ^{3}H as a result of neutron absorption in deuterium and, especially in pressurized-water reactors, by neutron-induced breakup of ^{10}B. Of course, in a sodium-cooled fast reactor, activation of natural sodium to short-lived ^{24}Na is an important consideration for in-plant radiation protection. Other activation products include isotopes of iron, cobalt,

chromium, manganese, and other constituents of structural and special-purpose alloys. The radionuclides are leached into the coolant stream. They then may be adsorbed on surfaces or trapped as particulates in the boundaries of coolant streams within the plant, only later to be resuspended in the coolant. These sources can be minimized by carefully specifying the alloy and trace-element concentrations in plant components.

Uranium Mining and Fuel Fabrication In the preparation of new fuel for nuclear reactors, the radiation sources encountered are natural sources associated with the uranium and thorium decay chains.

The principal release of radiation sources associated with uranium mining, underground or open pit, is release of natural ^{222}Rn to the atmosphere. Airborne particulates containing natural uranium daughter products also arise from open pit mining and from ore crushing and grinding in the milling process. Mill tailings can also become a long-term source of radiative contamination due to wind and water erosion, leaching, and radon release, the degree depending on the tailing-stabilization program followed. Mining and milling operations are generally conducted in remote areas, and liquid releases containing dissolved uranium daughter products are of little impact on human populations.

The product of milling is U_3O_8 "yellow cake" ore concentrate. In this phase of the nuclear fuel cycle, the concentrate is purified and most often converted to UF_6 for enrichment in ^{235}U via gaseous diffusion or centrifuge processes. Prior to fuel fabrication, the uranium is converted to the metallic or the ceramic UO_2 form suitable for use in fuel elements. Large quantities of uranium depleted in ^{235}U are by-products of the enrichment process. Under current practice, the depleted uranium is held in storage as being potentially valuable for use in breeder reactors. In this stage of the nuclear fuel cycle, there are relatively minor liquid and gaseous releases of uranium and daughter products to the environment.

Fuel Reprocessing As nuclear fuel reaches the end of its useful life in power generation, there remain within the fuel recoverable quantities of uranium and plutonium which may be extracted for reuse in the fuel reprocessing stage of the nuclear fuel cycle. Whether or not the fuel is reprocessed is governed by economic and political considerations. Among the former are costs of reprocessing as compared to costs of mining, milling, conversion, and enrichment of new stocks of uranium. Among the latter are concerns over the potential diversion of plutonium to nuclear-weapons use.

In the reprocessing of oxide fuels, the spent fuel is first dissolved in nitric acid. Plutonium and uranium are extracted into a separate organic phase from which they are ultimately recovered and converted into the oxide form. The aqueous phase containing fission and activation products is then neutralized and stored in liquid form pending solidification and ultimate disposal. Because one reprocessing plant may serve scores of power plants, inventories of radionuclides in process may be very great and extraordinary design features and safety procedures are called for. Because of the time delays between removal of fuel from service and reprocessing, concerns are with only relatively long-lived radionuclides, notably ^{3}H, ^{14}C, ^{85}Kr, ^{90}Sr, ^{106}Ru, ^{129}I, ^{134}Cs, and ^{137}Cs.

During the dissolution step of reprocessing, all the ^{85}Kr, the bulk of the ^{14}C (as CO_2), and portions of the ^{3}H and ^{129}I appear in a gas phase. This gas is cleaned, dried, and released through a tall stack to the atmosphere. All the ^{85}Kr is thus released; however, the major part of the ^{3}H is removed in the drying process and the bulk of the ^{129}I and ^{14}C is removed by reaction with caustic soda. The ^{14}C may then be precipitated and held as solid waste. Depending on the degree of liquid-effluent cleanup, some of the ^{129}I and other fission products subsequently may be released to the environment.

Waste Storage and Disposal Wastes generated in the nuclear fuel cycle fall into the broad categories of high-level wastes (HLW) and low-level wastes (LLW). The former, comprising unprocessed spent fuel or liquid residues from fuel reprocessing, accounts for only about 1–5% of the waste volume, but about 99% of the waste activity. The latter is comprised of in-reactor components, filter media, ion-exchange resins, contaminated clothing and tools, and laboratory wastes. For the most part, LLW consists of short-lived beta-particle and gamma-ray emitters. Wastes of low specific activity, but containing long-lived alpha-particle

emitters, for example, ^{239}Pu, require special handling more in the nature of that required for HLW.

In the USA, fuel elements from commercial reactors are presently not processed. By the year 2000, the cumulative spent fuel reached about 16,000 m^3, amounting to 40,000 t of uranium and fission products. Most of this spent fuel will be stored at the plant sites where it is generated which are primarily in eastern states.

Nuclear Power and Occupational Exposure Table 7 summarizes a United Nations survey of occupational exposures as well as public exposures based on nuclear power operations in the 1990s. Improvements continue to be made and US occupational annual committed occupational doses have by 2007 declined from about 3 to 1.1 person Sv per GWy(e).

Nuclear Explosives

Large fractions of radioactive debris from atmospheric nuclear weapons tests are distributed globally, and the radionuclides remain in the biosphere indefinitely. The hazard is better characterized by the long-term dose commitment than by the dose rate at any instant and location. The fusion and fission energy released in a nuclear-weapon explosion is usually measured in units of megatons (Mt). One megaton refers to the release of 10^{15} cal of explosive energy– approximately the amount of energy released in the detonation of 10^6 metric tons of TNT. The quantity of fission products produced in a nuclear explosion is proportional to the *weapon fission yield*. For a 1-Mt weapon fission yield, there must be the complete fissioning of about 56 kg of uranium or plutonium. The quantities of ^{3}H and ^{14}C, which are produced in the atmosphere by interactions of high-energy fission neutrons, are also proportional to the *weapon fusion yield*. There are several fusion reactions used in thermonuclear devices, with a 1-Mt weapon fusion yield requiring, for example, the fusion of 7.4 kg of tritium with 4.9 kg of deuterium.

The disposition of weapon debris may be divided into three categories, local fallout, tropospheric fallout, and stratospheric fallout. Local fallout, comprising as much as 50% of the debris and consisting of large particles, is defined as that deposited within 100 miles of the detonation site. Depending on detonation altitude and weather conditions, a portion of the weapon's

Radiation Sources. Table 7 Collective doses incurred by the public and workers from the nuclear fuel cycle, normalized to unit electrical energy generation

Operation	Committed dose (person Sv) per GWy(e)		
	General population		Occupational
	Local/regional	Waste/global[a]	
Mining	0.19	–	1.72
Milling	0.008	–	0.11
Mine tailings	0.04	7.5	–
Fuel fabrication	0.003	–	0.1
Reactor operation	0.44	0.5	3.9
Fuel reprocessing	0.13	0.05	3.0
Transportation	<0.1	–	–
Global dispersion	–	40	–
Research	–	–	1.0
Enrichment	–	–	0.02
Total	0.91	50	9.8

[a]For solid waste and global dispersion, committed dose is for 10,000 years
Source: Reference [2]: (1995–1997 general, 1990–1994 occupational).

debris is injected into the stratosphere and a portion remains in the troposphere. These two atmospheric regions are separated by the tropopause (about 16 km altitude at the equator and 9 km at the poles). Temperature decreases with elevation in the troposphere. This hydrodynamically unstable condition leads to the development of convective weather patterns superimposed upon generally westerly winds. In the stratosphere, temperature is more nearly constant or, in equatorial regions, even rises with elevation. Vertical convective motion is relatively slight and the tropical temperature inversion restricts transfer of material in the stratosphere from hemisphere to hemisphere.

Debris in the troposphere is distributed in longitude but remains within a band of about 30° of latitude. The mean lifetime of radioactive debris in the troposphere is about 30 days and tropospheric fallout is important for radionuclides with half-lives of a few days to several months. Over the years, the bulk of the radioactive debris from weapons tests has been injected into the stratosphere in the northern hemisphere and at altitudes less than 20 km. Mechanisms for transfer of the debris to the troposphere and thence to fallout on the earth's surface are complex. At elevations less than 20 km, the half-life for transfer of aerosols between hemispheres is about 60 months, while the half-life for transfer to the troposphere is only about 10 months, with little material crossing the tropopause in equatorial regions. Consequently, the bulk of the fallout from any one test occurs over the hemisphere of injection and in temperate regions. In terms of the megatons of fission energy, in the period prior to 1980, 78% of the debris was injected into the stratosphere– 70% into the northern hemisphere and 8% into the southern.

Eight radionuclides contribute significantly to the committed effective dose equivalent to the population. These are ^{137}Cs, ^{131}I, ^{14}C, ^{239}Pu, ^{90}Sr, ^{106}Ru, ^{144}Ce, and ^{3}H. Because of its long half-life, 5,730 years, the commitment from ^{14}C extends over many human generations. The collective effective dose equivalent commitment into the indefinite future due to weapons tests to date is equivalent to about four extra years of exposure of the current world population to natural background radiation.

High-level radioactive wastes generated in the USA in the production of nuclear weapons have accumulated for decades. The wastes are stored at three sites, one in the state of Washington, one in Idaho, and one in South Carolina. The approximately 9,000 t of waste has a volume of 380,000 cubic meters and there are plans to dispose of this waste in a repository used also for disposal of spent fuel for nuclear power plants.

Future Directions

Accelerators

Research, materials processing, and teletherapy accelerators employ higher and higher energy beams and beam currents. The production of secondary radiations associated with beam interactions with targets and structure lead to radiation sources of new types and increased magnitudes. Proton-beam accelerators grow in use for specialized radiation therapy. Synchrotrons deliver beams of protons with energies up to 250 MeV, with increased demands for new and better radiation surveillance, shielding, and dosimetry. Minimization of radiation damage to accelerator components calls for more precise beam simulation in the design process as well as more robust components.

Space Activities

In low-earth orbit, galactic cosmic rays (GCR) properties are well known except for short-term enhancements caused by solar particle events (SPE), especially in polar regions [10]. Consequences may be important in extravehicular activities (EVA) outside the Space Shuttle or International Space Station. There is a need for real-time measurement of instantaneous absorbed dose and effective dose rates as well as cumulative doses. Improved modeling of the space environment is needed so that longer-term predictions may be of conditions in orbit.

For activities beyond low-earth orbit, there is also a need for improved forecasting capabilities [8] for SPE. There is also a need for development and validation of space radiation transport codes, accounting for neutrons, protons, light and heavy ions, mesons, and electromagnetic cascades. Radiation spectrometers are needed for combined measurements of neutron doses and doses from high-energy charged particles. As to biological effects, there is need for more sophisticated

risk assessment methodology – at one extreme addressing late somatic and carcinogenic effects – at the other extreme addressing thresholds for symptoms affecting mission requirements, namely, central nervous system effects, dermal and immune issues.

Nuclear Power

Extending the operating lives of nuclear power plants brings on the need for increased attention to maintenance, corrosion control, and surveillance of piping and components. Similarly, extending the in-core operating life of individual fuel assemblies places intense demands on design, manufacturing, and quality assurance. Likewise, greater fuel "burnup" requires increased attention to actinide source inventories and secondary neutron production in spent fuels. Plant operating lives of 60 or more years need support of strong technical and manufacturing infrastructure.

No doubt the future will also see new generations of plants operating with radically advanced designs, with breeding capability, and using mixed $^{235}U/^{239}Pu$ fuels as well as fuels utilizing the ^{232}Th fuel cycle. These changes will bring on new design and operational challenges as well as the continued support of the physics community in broadening the evaluated nuclear data files (ENDF) and the evaluated nuclear structure data files (ENSDF).

Methods of storage and disposal of spent nuclear fuel continues to involve a complex mixture of technical, economic, political, and emotional issues. Resolution of the political and emotional issues seems to be the more demanding challenge.

Medical Applications

Challenges in nuclear medicine vary from nation to nation, but a recent survey [4] identified a number of universal concerns.

Hybrid imaging, employing dual use of CT, PET, MRI, and SPECT methods, introduces new combinations of radiation sources – positron emitters for PET, x-rays for CT, and gamma ray emitters for SPECT. Accounting for these mixed sources brings new challenges in facility design, treatment planning, patient and staff protection, as well as management of wastes. The same is true for radionuclides used in nuclear-medicine therapy such as delivery of radionuclides to malignant tumor cells using monoclonal antibody and related techniques.

In many countries, there is a need for improvement of domestic medical radionuclide production to alleviate the shortage of accelerator- and nuclear reactor–produced medical radionuclides available for research, diagnosis, and treatment. Finally, improvements in detector technology, image reconstruction algorithms, and advanced data processing techniques are needed to facilitate translation from research laboratory to the clinic.

Industrial and Commercial Activities

Sources of ionizing radiation find use in a very broad array of applications, examples being radiography and tracer techniques in manufacturing and density and moisture gauging in highway construction. Sources find their way into the home via ^{241}Am in smoke detectors and into public buildings via ^{3}H in exit signs. There is a very sad history of injury and death caused by the loss, abandonment, and theft of such sources. Better control of inventory, use, storage, and disposal of such sources is badly needed as well as better oversight by regulatory bodies.

Bibliography

Primary Literature

1. UN (1982) Sources and effects of ionizing radiation. Reports of the United Nations Scientific Committee on the effects of atomic radiation. United Nations, New York
2. UN (2000) Sources and effects of ionizing radiation. Reports of the United Nations Scientific Committee on the effects of atomic radiation. United Nations, New York
3. Eckerman KF, Ryman JC (1993) External exposure to radionuclides in air, water, and soil. Federal guidance report 12, EPA-402-R-93-081. U.S. Environmental Protection Agency, Washington, DC
4. National Research Council (2007) Advancing nuclear medicine through innovation. Committee on State of the Science of Nuclear Medicine. National Academy of Sciences, Washington, DC
5. World Nuclear Association (2006) Radioisotopes in industry (Information paper). www.world-nuclear.org/info/inf56.html
6. Fewell TR, Shuping RE, Hawkins KR (1981) Handbook of computed tomography and X-ray spectra. Report HHS (FDA) 81-8162
7. NCRP (2009) Ionizing radiation exposure of the population of the United States. Report no 160. National Council on Radiation Protection and Measurements, Bethesda

8. NCRP (2006) Information needed to make radiation protection recommendations for space missions beyond low-earth orbit. Report no 153. National Council on Radiation Protection and Measurements, Bethesda
9. NCRP (2000) Radiation protection guidance for activities in low-earth orbit. Report no 132. National Council on Radiation Protection and Measurements, Bethesda
10. NCRP (2002) Operational radiation safety program for astronauts in low-earth orbit. Report no 142. National Council on Radiation Protection and Measurements, Bethesda
11. NCRP (1987) Exposure of the population in the United States and Canada from natural background radiation. Report no 94. National Council on Radiation Protection and Measurements, Bethesda

Books and Reviews

Cohen BL (1986) A national survey of ^{222}Rn in U.S. homes and correlating factors. Health Phys 51:175–183

Cohen BL, Shah RS (1991) Radon levels in United States homes by states and counties. Health Phys 60:243–259

Eisenbud M (1987) Environmental radioactivity, 3rd edn. Academic, Orlando

Faw RE, Shultis JK (1999) Radiological assessment: sources and doses. American Nuclear Society, La Grange Park

Firestone RB, Shirley VS (eds) (1996) Table of isotopes, 8th edn. Wiley-Interscience, Malden

Haffner JW (1967) Radiation and shielding in space. Academic, New York

Glasstone S, Dolan PJ (eds) (1977) The effects of nuclear weapons. United States Departments of Energy and Defense, Washington, DC

ICRP (1987) Radiation dose to patients from radiopharmaceuticals. ICRP publication 53. Annals of the ICRP 18(1–4). International Commission on Radiological Protection, Pergamon Press, Oxford

Kocher DC (1981) Radioactive decay tables. Report DOE/TIC-11026. National Technical Information Service, Springfield

NAS (1971) Radioactivity in the marine environment. Report of the panel on radioactivity in the marine environment. Committee on Oceanography, National Research Council, National Academy of Sciences, Washington, DC

NAS (1988) Health risks of radon and other internally deposited alpha-emitters. Report of the BEIR Committee [The BEIR-IV Report]. National Research Council, National Academy of Sciences, Washington, DC

NAS (1990) Health effects of exposure to low levels of ionizing radiation. Report of the BEIR Committee [The BEIR-V Report]. National Research Council, National Academy of Sciences, Washington, DC

NCRP (1975) Natural background radiation in the United States. Report no 45. National Council on Radiation Protection and Measurements, Washington, DC

NCRP (1977) Radiation protection design guidelines for 0.1–100 MeV particle accelerator facilities. Report no 51. National Council on Radiation Protection and Measurements, Bethesda

NCRP (1984) Exposures from the Uranium Series with Emphasis on Radon and its Daughters. Report no 77. National Council on Radiation Protection and Measurements, Washington, DC

NCRP (1987a) Ionizing radiation exposure of the population of the United States. Report no 93. National Council on Radiation Protection and Measurements, Washington, DC

NCRP (1987b) Radiation exposure of the U.S. population from consumer products and miscellaneous sources. Report no 95. National Council on Radiation Protection and Measurements, Bethesda

NCRP (1989a) Exposure of the U.S. population from diagnostic medical radiation. Report no 100. National Council on Radiation Protection and Measurements, Bethesda

NCRP (1989b) Exposure of the U.S. population from occupational radiation. Report no 101. National Council on Radiation Protection and Measurements, Bethesda

NCRP (1989c) Radiation protection for medical and allied health personnel. Report no 105. National Council on Radiation Protection and Measurements, Bethesda

NCRP (2003) Radiation protection for particle accelerator facilities. Report no 144. National Council on Radiation Protection and Measurements, Bethesda

Shultis JK, Faw RE (2000) Radiation shielding. American Nuclear Society, La Grange Park

Slaback LA Jr, Birky B, Schleien B (1997) Handbook of health physics and radiological health. Lippincott Williams & Wilkins, Hagerstown

UN (1977/1982/1988/1993/2000) Report of the United Nations Scientific Committee on the effects of atomic radiation. United Nations, New York

Weber DA, Eckerman KF, Dillman LT, Ryman JC (1989) MIRD: radionuclide data and decay schemes. Society of Nuclear Medicine, New York

Radioactive Waste Management: Storage, Transport, Disposal

Audeen W. Fentiman
School of Nuclear Engineering, Purdue University, West Lafayette, IN, USA

Article Outline

Glossary
Definition of the Subject
Introduction

High-level Radioactive Waste – Including Used (Spent) Nuclear Fuel (SNF)
Low-level Radioactive Waste
Transuranic Waste
Future Directions
Bibliography

Glossary

Fission Process by which a nucleus splits into two smaller nuclei, emitting two or three neutrons and energy.

Half-life The time required for half of the nuclei in a sample of a radioactive isotope to emit radiation and be transformed to another isotope.

High-level radioactive waste (HLW) Used nuclear fuel or the highly radioactive materials that are generated when used nuclear fuel is reprocessed.

Low-level radioactive waste (LLW) Radioactive waste that is not high-level radioactive waste, used nuclear fuel, or mill tailings.

Transuranic waste (TRU) Wastes that are not classified as high-level waste and contain more than 100 nCi/g of alpha-emitting transuranic isotopes ($Z > 92$) with half-lives of more than 20 years.

Used nuclear fuel or spent nuclear fuel (SNF) Terms used to designate nuclear fuel that has been irradiated in a reactor to produce power.

Definition of the Subject

Radioactive materials are widely used in our society, and when they are, radioactive wastes can be produced. In addition to being used to generate about 20% of the electricity used in the USA and 17% of the electricity used worldwide, radioactive materials are important in medicine, industry, and research. For example, radioactive materials are used to help diagnose and treat disease, as thickness gages in manufacturing, as components of some smoke detectors, to kill bacteria in food, to trace the movement of nutrients through plants, and to power spacecraft leaving the solar system. Just as there are many uses of radioactive materials, there are many types of radioactive waste, each of which must be stored for a time, treated (prepared either for disposal or recycling), transported, and ultimately disposed of in a licensed facility. Some radioactive materials are utilized in weapons production, an activity which also results in generation of radioactive wastes, although this chapter shall focus on civilian uses of radioactive materials. Proper management of radioactive wastes is essential to ensure that society continues to realize the benefits of radioactive materials without undue risk to human health or the environment, and all aspects of radioactive waste management are highly regulated.

Introduction

This chapter addresses four types of radioactive waste, used nuclear fuel, high-level radioactive waste (HLW), low-level radioactive waste (LLW), and transuranic waste (TRU). Used nuclear fuel (sometimes called spent nuclear fuel) is fuel that has reached the end of its useful life and has been taken out of a nuclear power plant. It is highly radioactive. High-level waste is a category of radioactive waste that includes used nuclear fuel and the highly radioactive wastes that are generated when used nuclear fuel is reprocessed. These two materials are expected to be disposed of in the same facility and thus are lumped together in one category. As the name implies, this waste is highly radioactive. Low-level radioactive waste is material that is not HLW or TRU; LLW typically consists of items with low concentrations of radioactive materials with relatively short half-lives (<100 years). There are several categories of low-level radioactive material, and the category assigned to any particular container of low-level waste depends on the type and amount of contamination on the waste material. Finally, transuranic waste is a very specialized type of waste containing materials that have an atomic number greater than that of uranium. One section of this chapter is devoted to each type of waste, and within each section, methods for storing, treating, transporting, and disposing of the waste will be discussed.

High-level Radioactive Waste – Including Used (Spent) Nuclear Fuel (SNF)

One hundred and four nuclear power plants in the USA generate about 20% of the electricity used each year [1]. Worldwide, over 435 nuclear power plants generate about 17% of the electricity [2]. Some countries rely heavily on nuclear power. For example, over 75% of the electricity in France is generated by nuclear power

plants, and over 40% of the electricity in Sweden, Belgium, and Slovakia is from nuclear power [3].

The fuel for the nuclear power plants is uranium dioxide (UO_2), which is typically pressed into ceramic pellets. About 5% of the uranium in the fuel is ^{235}U which fissions, releasing energy that is ultimately converted to electricity. The other 95% of the uranium in the fuel is ^{238}U which is mostly inert although a small fraction of the ^{238}U atoms is converted to plutonium while the reactor is operating and another small fraction fissions. The ceramic UO_2 pellets are small cylinders about 0.6 in. long and 0.4 in. in diameter [4]. Stacks of pellets are sealed in zircaloy tubes about 12 ft long, and a 17 × 17 array of rods constitutes one typical fuel assembly. About 180 fuel assemblies are loaded into an average-sized pressurized water reactor. The other type of nuclear reactor commonly used in the USA, the boiling water reactor, is fueled with about 500–750 smaller fuel assemblies.

As the reactor operates, ^{235}U nuclei fission, after they absorb a neutron, breaking into two smaller nuclei. A small number of neutrons emitted during fission strike other ^{235}U atoms, causing more fissions, and releasing more energy. This process is known as a chain reaction. Eventually, most of the ^{235}U atoms in a fuel assembly have fissioned, and there are not enough of those atoms remaining to sustain the chain reaction. At that point, about one third of the fuel assemblies is removed from the reactor and fresh ones inserted in their place. Most nuclear power plants operate for 18–24 months before they need to be refueled. The fuel assemblies that are removed during refueling are referred to as used nuclear fuel or spent nuclear fuel.

The composition of the used nuclear fuel is shown in Table 1. Approximately 95% of the used nuclear fuel is ^{238}U. Less than 1% of the used fuel is plutonium. Some plutonium isotopes, primarily ^{239}Pu, fission and can be incorporated into new fuel rods. The reminder of the used fuel consists of fission products, that is, the atoms created when the ^{235}U atoms split, and minor actinides which were formed when some ^{238}U atoms absorbed neutrons. Many fission products are highly radioactive and emit penetrating gamma rays.

When the used nuclear fuel is removed from the reactor, it is transferred to the spent fuel pool in a structure adjacent to the reactor building. The spent fuel pool is an in-ground, concrete, steel-reinforced, stainless steel-lined pool that is filled with at least 20 ft of water [6]. Used fuel assemblies are placed vertically in the pool. Water in the pool cools the fuel assemblies and serves to shield workers and equipment in the area of the pool from the radiation emitted by the fuel assemblies.

Radioactive Waste Management: Storage, Transport, Disposal. Table 1 Composition of used nuclear fuel [5]

Material	Percent of used fuel (%)
Uranium (^{235}U and ^{238}U)	95.6
Plutonium (all isotopes)	0.9
Minor actinides	0.1
Stable fission products	2.9
Radioactive fission products	0.5

Perhaps surprisingly, the spent fuel pool at a nuclear power plant is not designed to be large enough to hold all of the used fuel that will be discharged from the nuclear power plant over its lifetime. A nuclear power plant's initial license is for 40 years. By early 2010, over half of the nuclear power plants in the USA had been granted license extensions of 20 years [7]. Thus, nuclear power plants are expected to operate at least 60 years, and it will be necessary to store some used fuel outside of the spent fuel pool. At the time the first nuclear power plants were built in the 1960s, it was presumed that used nuclear fuel would be reprocessed and recycled after the fuel assemblies had cooled for several years. Thus there was no need to build a spent fuel pool to hold all of the discharged fuel. In April 1977, US policy on reprocessing was changed when President Carter issued a statement that the USA would "defer indefinitely the commercial reprocessing and recycling of plutonium" [8]. The Nuclear Waste Policy Act of 1982 mandated construction of a geologic repository for permanent disposal of used nuclear fuel and required the Department of Energy to begin disposing of the used nuclear fuel not later than January 31, 1998 [9]. Once again, it did not appear that the spent fuel pool would need to hold all of the used nuclear fuel from a nuclear power plant, since there would be a place to send the used fuel for disposal. However, the geologic repository has not been built, and spent fuel pools at many of the older nuclear power plants are full or nearly full.

Many power plants are now moving some of their older used fuel assemblies that have been cooling in the spent fuel pool for many years to dry storage casks to make room in the pool for more fuel coming out of the reactor. The typical dry storage cask is a cylinder about 19 ft high and 8 ft in diameter made of concrete or steel. Dry storage casks come in different sizes, but they usually hold approximately 30 fuel assemblies and weigh about 100 t when loaded [10]. Spent fuel assemblies are sealed in an inner canister which is then placed in the dry storage cask. Some of the dry storage casks are designed to sit vertically on a concrete pad near the reactor building. In other dry storage systems, the casks are placed horizontally into a concrete bunker near the reactor building.

Across the USA, as of 2010, there are about 60,000 t [11] of used nuclear fuel stored either in spent fuel pools or dry storage casks at the nuclear power plants where it was generated. (Because uranium is a very dense material (19.05 g/cm^3), denser even than lead (11.35 g/cm^3), a ton of used fuel does not occupy much space. If all of the used fuel assemblies that have been discharged from US nuclear power plants since they began to operate were stacked on a football field 100 yards long and 53⅓ yards wide, the stack would be about 6½ yards high.) The Nuclear Regulatory Commission which is responsible for overseeing safety at the nuclear power plants has said that the used fuel can be safely stored at the power plant where it was generated for up to 100 years [12].

Ultimately, the used nuclear fuel must be disposed of permanently or reprocessed with as many of the constituents as possible being recycled and reused and the remainder being disposed of permanently. Until a decision about the final disposition of used nuclear fuel is made, the used fuel will continue to be stored either at the power plants where it was generated or at central storage facilities. Regardless of where the fuel is stored or whether it is reprocessed or buried, a system for transporting the used nuclear fuel will be required. Regulations governing the transportation system have been in place for decades, and some used fuel has been moved in licensed transportation casks. The next several paragraphs will describe recent US policy for disposing of used nuclear fuel, the options for central storage of used fuel if the fuel currently in dry storage casks is moved from the reactors to a central location, and the transportation system in place to move that used fuel.

Current US policy for disposal of used nuclear fuel was set by the Nuclear Waste Policy Act of 1982 and its 1987 amendments which provided for permanent disposal of used nuclear fuel in a deep geologic repository. The repository was to hold 70,000 t of used nuclear fuel and vitrified high-level waste from Department of Energy (DOE) facilities. The DOE was responsible for designing, building, and operating the repository, and the DOE was to begin taking used fuel from nuclear power plants by January 31, 1998. The Office of Civilian Radioactive Waste Management was established within DOE to manage both the repository and the transportation system for used nuclear fuel. In addition, the law required a monitored retrievable storage facility (MRS) where used fuel from reactors throughout the USA could be stored temporarily and then put into standard packages for disposal. The bill also established the Nuclear Waste Fund to pay for the design, construction, and operation of the used nuclear fuel management system. A charge of one mill (one tenth of a cent) for every kilowatt hour of electricity generated by a nuclear power plant is the source of money for the Nuclear Waste Fund. Between 1982 and 2007, $27.3 billion dollars were collected for the Nuclear Waste Fund [13].

Three possible sites for the deep geologic repository were identified, and each was to be characterized to determine whether it was an appropriate location for nuclear waste disposal. The sites were in (1) Deaf Smith County, Texas, (2) Richland, Washington, on the Hanford Site, and (3) Yucca Mountain, Nevada, near the Nevada Test Site where nuclear weapons had been tested underground. Each of the three sites offered a different type of rock in which the repository would be located. The Texas site was in salt, the Washington site in basalt, and the Nevada site in tuff. Local opposition to construction of a nuclear waste repository was strong in all three locations, and efforts to characterize the sites were often thwarted. Little progress was made toward identifying the best location for the repository.

In 1987, the US Congress passed the Nuclear Waste Policy Amendments Act. This law identified the Yucca Mountain site in the Nevada desert as the location of the nation's deep geologic repository. The law established a position of Nuclear Waste Negotiator to find a volunteer site for the MRS since the site in Tennessee identified pursuant to the 1982 Nuclear Waste Policy Act was rejected.

The geologic repository for used nuclear fuel was required to be licensed by the Nuclear Regulatory Commission (NRC). Following passage of the 1987 law, work began at the Nevada site to gather scientific evidence required to prepare an application for a license to construct and operate the geologic repository. Information required for the license application is specified in 10 CFR Part 60, Disposal of High-Level Radioactive Wastes in Geologic Repositories [14]. Scientists working on the application needed to show that they understood not only the characteristics of each of the components of the repository, but also how the components would interact and perform over time. Since the repository was to accommodate both used nuclear fuel from commercial nuclear power plants and vitrified high-level waste from nuclear weapons programs, data on composition of both waste forms as well as chemical and physical properties were required. Information required on packages that confined the waste included proposed materials, dimensions, and response to heat, pressure, radiation, water, and other possible corrosive chemicals in the rock and soil. Detailed information on the design of the engineered repository was required. DOE had to show that the repository would be safe for workers while the waste was being emplaced, that any specific container of buried waste could be retrieved for 50 years after it had been emplaced, and that the repository would confine the waste over a specified period. Data required for the site, itself, included characteristics of the rocks and soil, groundwater speed and direction, and an inventory of flora and fauna species in the area of the repository.

Between 1987 and 2007, the team of scientists characterizing Yucca Mountain spent approximately $7 billion gathering data on the site and preparing the required documents including an environmental impact statement and the license application. The repository design called for a network of tunnels approximately 1,200 ft below the surface. Each tunnel was to be reinforced with steel supports to keep the rock from collapsing onto the waste packages. Rails on the floor of each tunnel would allow casks to be moved into place. Casks designed to hold about 30 used fuel assemblies or half a dozen cylinders of vitrified waste from DOE facilities would be made of thick steel. An inverted U-shaped titanium shield was proposed to cover the casks in each tunnel to divert any water that might reach the repository from the desert above.

On June 3, 2008, DOE delivered to the Nuclear Regulatory Commission the application for a license to construct and operate the nuclear waste repository at Yucca Mountain. According to the Nuclear Waste Policy Act, the NRC had 3 years to review the application but could request an additional year. Following the presidential election in 2008, funding for the Yucca Mountain Project was reduced, and March 2010, the DOE withdrew its application for a license for a nuclear waste repository at Yucca Mountain "with prejudice." At almost the same time, the DOE created the Blue Ribbon Commission on America's Nuclear Future. The charter of this Commission was "to conduct a comprehensive review of policies for managing the back end of the nuclear fuel cycle, including all alternatives for the storage, processing, and disposal of civilian and defense used nuclear fuel, high-level waste, and materials derived from nuclear activities." The Commission is to complete its report in 24 months.

The Blue Ribbon Commission is likely to consider both direct disposal of used nuclear fuel assemblies in a deep geologic repository and reprocessing of used nuclear fuel followed by recycling of many of the components and utilization, treatment, or disposal of the remaining materials. Direct disposal in a geologic repository was discussed earlier. Reprocessing of used nuclear fuel is briefly addressed here.

Reprocessing of used nuclear fuel currently involves chopping up the used fuel rods, dissolving the fuel in a concentrated nitric acid solution, and chemically separating the various elements in the used fuel. The uranium and plutonium, which constitute about 96% of the used fuel, can be recycled and used in fabricating new fuel rods. The remaining material is typically dried, mixed with glass frit, melted, and poured into metal cylinders. Many countries that rely heavily on nuclear power either reprocess their own used nuclear fuel or send it to other countries that have reprocessing facilities. The USA does not reprocess used fuel from commercial nuclear power plants.

The reprocessing method currently used in most countries is the PUREX method which was developed in the USA to reprocess fuel from government-run reactors to recover plutonium for use in nuclear weapons.

A small amount of used fuel from commercial nuclear power plants was reprocessed at a facility in West Valley, New York, between 1966 and 1972, but the facility was shut down because it was not economical. Since the USA decided not to reprocess used nuclear fuel in 1977, no additional reprocessing of commercial nuclear fuel has occurred. One objection to use of the PUREX method was that it isolates plutonium from other materials in the used fuel, supposedly making it easier for terrorists to divert the plutonium.

Research is being conducted in the USA on reprocessing methods that would not isolate plutonium. Some of the methods under consideration are for reprocessing used fuel from the light water reactors that are currently operating in the USA. Other methods are being developed for different types of fuel that might be used in the next generation of reactors (commonly referred to as Generation IV) now being designed for use around the world. Reprocessing facilities are complex and expensive to build. Japan completed construction of a nuclear fuel recycling facility in Rokkasho at a cost of approximately $20 billion [15]. It is likely that US policy makers will want more information on the types of nuclear power plants that will be operating in the USA over the next century and results of research programs on reprocessing methods in hand before deciding what type of reprocessing facility, if any, to build in the USA.

Since it appears that the USA will not be disposing of used nuclear fuel or reprocessing it in the near future, storage of used nuclear fuel at a central facility (or facilities) is being studied. Central storage is not a new concept. The Nuclear Waste Policy Act of 1982 called for establishing a Monitored Retrievable Storage (MRS) facility, and the Nuclear Waste Policy Amendments Act of 1987 provided for a person to seek a community willing to host the MRS. No MRS has been sited. A consortium of utilities, called Private Fuel Storage, negotiated with the Skull Valley Band of the Goshute Indian Tribe to establish a central used fuel storage facility on the Tribe's land in Utah. An application was submitted on the NRC for a license to construct and operate the storage facility, and on February 21, 2006, the NRC granted a license, but said that construction could not begin until it obtained "necessary approvals from other agencies, including the Bureau of Land Management, the Bureau of Indian Affairs, and the Surface Transportation Board" [16]. Neither the Bureau of Land Management nor the Bureau of Indian Affairs has approved the site. At the request of Senators Barbara Boxer, Harry Reid, and John Ensign, the US General Accountability Office did a study of a central storage facility option and an on-site storage facility option, along with the Yucca Mountain repository. The study, which was issued in November 2009, concluded that while a centralized interim storage facility could be built relatively quickly, finding a site could be difficult, and since the facility would not be a final disposal site, any waste going to the centralized storage facility would have to be transported twice [17]. The Blue Ribbon Commission on America's Nuclear Future is also likely to consider options for a central storage facility.

Eventually, the used nuclear fuel currently stored at the nuclear power plants must be transported to a central storage facility, a processing facility, or a permanent disposal site. Some used nuclear fuel has been transported in the USA, for example, between nuclear power plants owned by the same company or from a power plant to a government research facility. Both the NRC and the US Department of Transportation have regulations governing transportation of used nuclear fuel. The NRC regulation is Title 10, Part 71 of the Code of Federal Regulations (10 CFR Part 71) [18], which specifies requirements for the packages that carry the highly radioactive material, called Type B packages. The regulation also specifies how packages for transporting used nuclear fuel are to be approved. Each Type B package must have a Radioactive Material Package Certificate of Compliance from the NRC. Procedures for applying for the Certificate of Compliance can be found in NUREG-1617, "Standard Review Plan for Transportation Packages for Spent Nuclear Fuel" [24]. Packages for used nuclear fuel are designed for transportation by truck and by rail.

To receive a Certificate of Compliance, a Type B package, which is often called a shipping cask, must undergo a series of tests that simulate accident conditions a cask might encounter en route. The first four tests, conducted sequentially on a single cask, are:

1. Drop test. Drop the cask from 30 ft onto a hard, unyielding surface in an orientation most likely to damage the cask.

2. Puncture test. Drop the cask from 40 in. onto a 6-in. diameter shaft in an orientation most likely to result in damage.
3. Fire test. Engulf the cask fully in a fire at least 1,475°F for 30 min.
4. Immersion test. Place the cask under 3 ft of water for 30 min [19].

In order to receive the Certificate of Compliance, the cask must not release any radioactive materials during or following the series of tests. A new, undamaged cask must pass a fifth test, immersion in water at a pressure equivalent to that exerted by water 50 ft deep, before the Certificate can be issued.

Several different shipping casks have been designed to be transported by truck. Those casks carry between 1 and 9 used fuel assemblies. A typical rail cask carries 36 fuel assemblies, but the number varies because there are different sizes of fuel assemblies. The shipping casks are usually cylindrical with their walls made of several layers of different materials. The innermost and outermost layers are usually steel to provide structural strength. One layer of material between the steel shells is designed to absorb gamma rays emitted by the used fuel. Steel, lead, and depleted uranium are some materials that are used to absorb gamma rays. Another layer is made of a material that slows down and absorbs neutrons. *The Radioactive Materials Packaging Handbook*, [20] written at the Oak Ridge National Laboratory in 1998 contains detailed information required to design and manufacture a shipping cask for used nuclear fuel.

NRC regulations govern routes to be used for transporting used nuclear fuel and physical protection for the shipments. The Department of Transportation regulations specify methods for selecting routes (49 CFR 397) and labeling of the shipping casks (49 CFR 172). In addition, drivers of trucks transporting radioactive materials must meet training and experience requirements and undergo a background investigation.

Low-level Radioactive Waste

Low-level radioactive waste is defined in the Low Level Radioactive Waste Policy Act of 1980 as radioactive waste that is not high-level radioactive waste, spent nuclear fuel, or mill tailings [21]. There are four classes of low-level radioactive waste (LLW) based on the concentration of radioisotopes with short half-lives and the concentration of radioisotopes with longer half-lives in the waste. The classes are designated as A, B, C, and Greater Than Class C (GTCC). Tables 1 and 2 in 10 CFR Part 61 are used to determine the class of LLW in a particular container.

LLW is generated by almost any activity that involves radioactive material. Some examples of LLW are lab coats and shoe covers worn when working with radioactive materials, medical equipment involved in treating a patient with radiopharmaceuticals, and laboratory supplies and equipment used in experiments involving radioactive tracers. Radioactive tracers are very commonly used. They are radioactive isotopes that move through a system (e.g., the human body, a growing plant, or an ecosystem) along with the material being studied. Since small amounts of radiation can be detected, the researchers can measure radiation from the tracer to determine how the substance of interest is moving through the system. For example, tracers are used in the development of virtually all new medicines to study how the medicine or its metabolites move through the body. Hospitals, universities, and research laboratories operated by corporations or government agencies often generate LLW.

The largest amount of commercial LLW is generated by industry, including the nuclear power industry. Equipment and materials from power plant maintenance activities, samples collected during environmental monitoring, and protective clothing are disposed of as LLW. In addition, LLW is generated during the various stages of nuclear fuel fabrication.

Often LLW is initially in liquid form. For example, it is sometimes more cost-effective to wash protective clothing than to dispose of it. Likewise, it may be more economical to decontaminate some equipment using a solvent than to dispose of the equipment. In these cases, the wash water and the solvent become LLW. Environmental samples are routinely dissolved in a liquid for analysis, yielding liquid LLW. Since LLW disposal facilities will not accept large amounts of liquid wastes, most liquid LLW must be solidified. Several methods can be used including evaporation, ion exchange, flocculation, and filtration. The liquid waste could simply be mixed with a solidifying agent such as concrete. However, since the cost of disposal is

determined, in part, by the volume of the waste, methods that minimize the volume are usually preferred.

Dry LLW is typically treated to reduce its volume prior to packaging for shipment to a disposal facility. Compaction, which results in a volume reduction to one half or one third of the initial volume, or super-compaction, which can result in a volume reduction to one tenth of the original volume are commonplace. Incineration can reduce the volume to 1% of the original and is especially useful for combustible materials like wood that cannot be compacted easily.

Three disposal facilities for commercial LLW are currently operating in the USA. They are in Barnwell, South Carolina, Richland, Washington, and Clive, Utah. Another one has been proposed in Texas. LLW disposal sites have been available since the early 1960s. Four early sites have been closed. They were in Sheffield, Illinois, Maxey Flats, Kentucky, West Valley, New York, and Beatty, Nevada.

While LLW disposal facilities have been operating in the USA since the 1960s, the law which currently governs LLW disposal was not passed by the US Congress until 1980. The Low-Level Radioactive Policy Act of 1980 made each state responsible for arranging for disposal of its own LLW. States were encouraged to form compacts, groups of states that could collaborate to build one LLW disposal facility to serve all of the compact's members. If a state within a compact built a LLW disposal facility, that facility would not be required to accept LLW from any state outside of the compact. States that did not belong to a compact and chose to build their own disposal facility would not be able to exclude waste from other states. The law required states to form compacts by 1986. States did not meet that deadline, and in 1985, the Low Level Radioactive Waste Policy Amendments Act was passed. It gave the states until 1992 to form compacts. At one time, all states have belonged to a compact. Some have left the compact, and some compacts have been reconstituted. However, no compact has built a new LLW disposal facility.

Until 2008, the lack of new disposal facilities did not impact LLW generators' ability to dispose of their waste. The Richland, Washington, facility accepted Class A, B, and C waste from the Northwest and Rocky Mountain compacts, and the Barnwell, South Carolina, facility accepted Class A, B, and C waste from the rest of the country. The Clive, Utah, facility accepted only Class A waste, but it had applied for a revised license to accept Class B and C waste. The Barnwell facility announced that after July 1, 2008, it would not accept Class B and C waste from states outside of the Atlantic Compact. As of early 2010, the Clive, Utah, facility did not yet have a license to accept Class B and C waste. Thus, as of July 2008, the 36 states that had previously been served by the Barnwell facility have had no place to send their Class B and C wastes. Since nearly 99% of commercial LLW is Class A waste and can be sent to a disposal facility, most generators have only small amounts of Class B and C waste and will have space to store that waste until a new facility can be built or some other solution can be found [22].

Packaging requirements are specified for each class of LLW in 10 CFR Title 61.56. Some requirements for Class A waste are: no cardboard or fiberboard containers may be used, wastes cannot be explosive or pyrophoric, emit toxic gases, or contain biological pathogens or infectious material and if the package contains liquids, it must also have enough absorbent material to absorb twice the volume of liquid present. Packing for Class B waste must meet all of the requirements for Class A waste packaging plus a stability criterion which ensures that packages will remain intact when other packages are stacked on top of them. Class C waste packaging must meet all of the requirements of Class B waste packaging plus provide a barrier to inadvertent intrusion.

Low-level radioactive waste is typically disposed of in shallow land burial facilities. A facility must be designed to minimize contact of the buried waste with water. A trench about 30 ft deep and 100 ft wide is excavated in soil that drains well. Containers are placed in the trench in a way that minimizes void space, and any voids that are created are filled with sand. When a portion of the trench is full, it is covered with a cap that is designed to divert any water that falls on it away from the waste.

Transuranic Waste

Transuranic wastes are defined in 40 CFR 191, Environmental Standards for the Management and Disposal of Spent Nuclear fuel, High Level and Transuranic Waste, as wastes that are not classified as high-level

waste but contain more than 100 nCi/g of alpha-emitting transuranic isotopes (materials with $Z > 92$) with half-lives of more than 20 years. Transuranic isotopes are generated in a reactor when U-238 absorbs neutrons. Most transuranic waste in the USA has been generated during weapons production when used nuclear fuel from government-operated reactors was reprocessed to recover plutonium for weapons. If the USA begins to reprocess used nuclear fuel from commercial nuclear power plants, transuranic wastes will be generated at the commercial fuel reprocessing facilities as well.

Most transuranic (TRU) waste is solid. Typical wastes are protective clothing or equipment that has been contaminated with transuranic isotopes. TRU waste is packaged in steel, concrete, or wooden boxes. Since most of the transuranic isotopes emit alpha particles which cannot penetrate a sheet of paper, most TRU waste (about 97%) is referred to as Contact Handled TRU, meaning that people can handle the packages. Only 3% of the TRU must be handled remotely [23].

Transuranic waste is disposed of in the Waste Isolation Pilot Plant (WIPP). WIPP is a deep geologic repository in salt located near Carlsbad, New Mexico. It has been accepting and disposing of TRU waste since 1999. The US Department of Energy Report DOE-WIPP-069, Waste Acceptance Criteria for the Waste Isolation Pilot Plant, outlines requirements for TRU waste shipped to the facility for disposal. They include specifications for the container, data to accompany the package, and radiologic, physical, chemical, and gas generation properties of the waste.

TRU waste is transported to WIPP in Type B packages which are certified by the Nuclear Regulatory Commission after undergoing the rigorous tests described in the section on used nuclear fuel.

Future Directions

Future directions for radioactive waste management in the USA vary depending on the type of radioactive waste. Transuranic wastes are likely to continue to be shipped to the Waste Isolation Pilot Plant (WIPP) for disposal. For decades, low-level radioactive wastes have been disposed of in shallow land burial facilities. Currently, several states do not have a location for disposal of Class B and C wastes, but those constitute only about 1% of the low-level wastes and can be stored at the generation site until a disposal facility is available. Efforts to open new or expand existing low-level waste disposal facilities are ongoing.

High-level radioactive waste disposal policy in the USA is being reviewed. The Blue Ribbon Commission on America's Nuclear Future has been established (2010) to consider the alternatives. Meanwhile, used nuclear fuel is being stored at reactor sites and can be kept there for several decades while the federal government adopts a policy for its disposal and constructs the facilities required to carry out the policy. The nation has experience with all of the components of the system required to treat and dispose of HWL. Transportation casks for HLW have been built, certified, and used to transport that material. Used nuclear fuel belonging to the federal government and some used commercial fuel have been reprocessed. Research on advanced reprocessing methods is being conducted at national laboratories and universities. Research done at Yucca Mountain and experience at WIPP have provided extensive data on deep geologic repositories, which are the type of facility in which used nuclear fuel or reprocessing waste is likely to be placed. Several other countries that rely heavily on nuclear power for their electricity are currently reprocessing used nuclear fuel and conducting research on geologic repositories. Technical information related to treatment, storage, transportation, and disposal of high-level radioactive waste will be available when the policy decisions are made.

Bibliography

Primary Literature

1. US Energy Information Administration (2009) United States percent of electricity from nuclear. http://www.eia.doe.gov/cneaf/electricity/epm/epm_sum.html. Accessed 15 Mar 2010
2. World Nuclear Association (2008) World nuclear power reactors & uranium requirements. http://www.world-nuclear.org/info/reactors.html. Accessed 15 Mar 2010
3. World Nuclear Association (2008) Nuclear shares of electricity generation. http://www.world-nuclear.org/info/nshare.html. Accessed 15 Mar 2010
4. Murray RL (1988) Nuclear energy. Pergamon Press, Oxford
5. Ryskamp JM (2003) Nuclear fuel cycle. http://nuclear.inel.gov/docs/papers-presentations/nucle_fuel_CYCLE_3-5-03.PDF. Accessed Jun 2008

6. US Nuclear Regulatory Commission (2007) Spent fuel pools. http://www.nrc.gov/waste/spent-fuel-storage/pools.html. Accessed Mar 2010
7. US Nuclear Regulatory Commission (2010) Nuclear power plant license extensions. http://www.nrc.gov/reactors/operating/licensing/renewal/applications.html#completed. Accessed Mar 2010
8. PBS Frontline (2010) Carter nuclear fuel reprocessing. http://www.pbs.org/wgbh/pages/frontline/shows/reaction/readings/keeny.html. Accessed Mar 2010
9. Nuclear Waste Policy Act of 1982 as amended (2010) http://www.nrc.gov/reading-rm/doc-collections/nuregs/staff/sr0980/v2/sr0980v2.pdf#pagemode=bookmarks&page=141. Accessed Apr 2010
10. Board on Radioactive Waste Management (2006) Safety and security of commercial spent nuclear fuel storage: public report. National Academies Press, Washington
11. How many tons of spent nuclear fuel on hand – in what year http://epw.senate.gov/public/index.cfm?FuseAction=Minority.PressReleases&ContentRecord_id=f2cbe309-802a-23ad-4925-643845f220b5&Region_id=&Issue_id
12. Waste Confidence Decision, 49 FR 34694, August 31, 1984, as amended at 55 FR 38474, September 18, 1990; 72 FR 49509, August 28, 2007, Federal Register
13. Congressional Budget Office Testimony on the Federal Government's Liabilities under the Nuclear Waste Policy Act (2007) Nuclear waste fund balance. http://www.cbo.gov/doc.cfm?index=8675&type=0. Accessed Mar 2010
14. US Nuclear Regulatory Commission (1981) 10 CFR Part 60, disposal of high-level radioactive wastes in geologic repositories
15. vonHippel F (2009) Why reprocessing persists in some counties and not in others: the costs and benefits of reprocessing – for the Non-Proliferation Education Center. www.npec-web.org/.../vonhippel%20-%20TheCostsand-Benefits.pdf. Accessed Mar 2010
16. US Nuclear Regulatory Commission press release No. 06-028 (2006) Private Fuel Storage license application. http://www.nrc.gov/reading-rm/doc-collections/news/2006/06-028.html. Accessed Mar 2010
17. US General Accountability Office (2009) Nuclear waste management: key attributes, challenges, and costs for the Yucca mountain repository and two potential alternatives. GAO-10-48
18. US Code of Federal Regulations (CFR) (2010) 10 CFR Part 71 http://www.nrc.gov/reading-rm/doc-collections/cfr/part071. Accessed Mar 2010
19. Kutz M (2009) Environmentally conscious materials handling. Wiley, Hoboken
20. Arnold ED, Shappert LB, Bowman SM (1998) Radioactive materials packaging handbook: design, operations, and maintenance. Department of Energy, Oak Ridge National Laboratory, Oak Ridge
21. Low-level Radioactive Waste Policy Amendments Act of 1985. http://www.nrc.gov/reading-rm/doc-collections/nuregs/staff/sr0980/v2/sr0980v2.pdf#pagemode=bookmarks&page=15. Accessed Apr 2010
22. US General Accounting Office (2004) Low-level radioactive waste: disposal availability adequate in the short term but oversight needed to identify any future shortfalls. GAO-04-604
23. Saling JH, Fentiman AW (2002) Radioactive waste management. Taylor & Francis, New York
24. US Nuclear Regulatory Commission (2000) NUREG-1617 Standard Review Plan for Transportation Packages for Spent Nuclear Fuel. http://www.nrc.gov/reading-rm/doc-collections/nuregs/staff/sr1617/. Accessed Mar 2010

Books and Reviews

Office of Civilian Radioactive Waste Management Website (2010). http://www.ocrwm.doe.gov/. Accessed Mar 2010

Ohio State University Extension (2010) Low-level radioactive waste fact sheets. http://ohioline.osu.edu/rer-fact/index.html. Accessed Mar 2010

US Department of Energy (2002) Final environmental impact statement for a geologic repository for the disposal of spent nuclear fuel and high-level radioactive waste at Yucca mountain, Nye County, Nevada. DOE/EIS-0250

US General Accountability Office (2008) Low-level radioactive waste: status of disposal availability in the United States and other countries. GAO-08-813T

US General Accountability Office (2007) Low-level radioactive waste management: approaches used by foreign countries may provide useful lessons for managing US Radioactive Waste. GAO-07-221

US Nuclear Regulatory Commission Website, Radioactive Waste (2010). http://www.nrc.gov/waste.html. Accessed Mar 2010

Waste Isolation Pilot Plant Website (2010). http://www.wipp.energy.gov/index.htm. Accessed Mar 2010

Radionuclide Fate and Transport in Terrestrial Environments

John C. Seaman[1], Kimberly A. Roberts[2]
[1]Environmental Geochemistry, Savannah River Ecology Laboratory, The University of Georgia, Aiken, SC, USA
[2]Radiological Performance Assessment, Savannah River National Laboratory, Aiken, SC, USA

Article Outline

Glossary
Definition of the Subject
Introduction
Radiochemistry Background

R

Radionuclide Sources
Soils as the Repository for Radioactive Waste
Important Soil Processes
Models for Describing Radionuclide Sorption and Plant Uptake
Characteristics of Specific Radionuclides
Future Directions
Acknowledgments
Abbreviations
Bibliography

Glossary

Actinides Row of elements in the periodic table and so-called 5f elements with atomic number 89 (actinium) through 103 (lawrencium).

Amphoteric The ability to act as either an acid or a base depending on conditions.

Biological half-life ($t_{\frac{1}{2}}^{bio}$) A measure of the rate at which radionuclides are excreted from an organism defined as the time required for the twofold decrease in activity resulting from processes other than radioactive decay.

Ecological half-life ($t_{\frac{1}{2}}^{eco}$) A measure of the rate at which the exposure and bioavailability of a radionuclide decreases with time due to processes other than radioactive decay.

Lanthanides Fourteen elements with atomic numbers 58 through 71 generally forming trivalent cations.

Radioactive half-life ($t_{1/2}$) The time required for the activity of an isotope to be reduced by half.

Transuranics Elements with atomic number 92 (uranium) and greater.

Definition of the Subject

The soil environment becomes the ultimate repository for radioactive waste in terrestrial systems, whether intentional or not. Therefore, a fundamental understanding of radionuclide migration and cycling in the soil environment is critical to the development of environmental policies that are protective of both human health and the environment. Radionuclides may be assimilated and/or immobilized into the organic matter pool within the soil microbiota and absorbed by the roots of higher order plants as the first steps in trophic transfer in terrestrial systems. An added complication in dealing with radionuclides is that decay and fission processes result in radioactive products with significantly different chemical properties from the parent material. The primary objective of this chapter is to describe the physical and chemical processes that impact the fate and transport of radionuclides in the soil environment, including a discussion of the results from recent studies and the identification of appropriate reference material for more in-depth analysis. For the current discussion, the term "soil" will be used in a generic sense to represent unconsolidated geologic material, including both vadose (unsaturated) and saturated groundwater systems, as the underlying processes are the same.

Introduction

In addition to nuclear weapons testing and accidental releases, natural and anthropogenic radioactive substances may enter the terrestrial environment from natural uranium (U) ore deposits, U mining and processing, waste discharges and disposal efforts. Thus, various soil processes as impacted by the chemical speciation of the radionuclide of interest control both ecosystem exposure (i.e., wildlife, human, etc.) and the success of any waste containment or remediation effort. In the USA, remediation efforts have generally focused on limiting radiation exposure to humans under the assumption that such an approach is also protective of the general environment, while the European community has applied more of an ecosystem approach to environmental policy [1, 2].

In recent years the interest in nuclear energy has been renewed due to concerns over the rise of greenhouse gasses and their impact on global climate change, the cost and availability of fossil fuel sources, and political instability and conflict within oil exporting countries. Since 2006, the US Nuclear Regulatory Commission (NRC) has received preliminary licensing applications for the construction of more than 30 new reactors. However, acceptance of nuclear power in the USA in particular is still limited by the public's perception of adverse safety, environmental, and health effects associated with nuclear facilities [3].

Despite improvements in reactor design, several important environmental issues face the nuclear power industry. Proposed expansion could exacerbate environmental concerns associated with U mining and

processing [4]. Furthermore, the disposition of spent nuclear fuel (SNF) remains a major impediment to industry expansion in the USA with the future of the Yucca Mountain repository still in question. Currently, 54,000 metric tons of SNF are stored on site at existing nuclear facilities in the USA, with plans to require new facilities to provide enough on-site storage to accommodate the entire inventory of SNF generated during the 60-year lifetime of current reactor designs [5, 6]. Furthermore, the growing inventory of SNF at existing power stations in the USA will likely exceed the legislatively defined capacity for the Yucca Mountain repository within the next decade or so, even without expansion of the nuclear industry [7]. The eventual disposition of such waste remains unclear as debate continues regarding the cost and technical limitations associated with long-term storage as opposed to various SNF reprocessing technologies that increase the risk of nuclear proliferation [5, 6, 8].

Radiochemistry Background

Before further discussion concerning the fate of radionuclides in soils, a limited review of radiochemistry is warranted. Interested readers seeking a more thorough discussion are directed to one of several comprehensive texts that are currently available, i.e., [9–11]. Isotopes of an element differ by mass but display the same chemical properties, except for minor mass-dependent differences. Most readers are familiar with the conventions for distinguishing various isotopes of a given element:

$$ {}^{A}_{Z}X \tag{1} $$

where the mass number A represents the sum of protons (Z) and neutrons (N) within the nucleus of the element in question, X, with Z often omitted because it is defined by the element symbol [12, 13].

Radioactive decay is a spontaneous, irreversible process that releases energy, the magnitude of which depends on the element and mode of decay, as unstable isotopes transform to a lower energy state. Unlike other chemical reactions/transformations, radioactive decay is insensitive to environmental conditions, like temperature and pressure. When an isotope is radioactive, it is referred to as a radionuclide. The standard SI unit for radioactivity is the Becquerel (Bq), which is equivalent to one disintegration per second. For environmental samples, radioactivity is often reported in terms of picocuries (1 pCi = 10^{-12} Curies), with 1 pCi equivalent to 0.037 Bq.

Each radionuclide decays at a constant rate. The decay constant, λ, is the probability of decay per unit time and is related to half-life ($t_{1/2}$), the time required for the activity of an isotope to be reduced by half. For a more detailed discussion on the mathematics of radioactive decay, the reader is referred to Ivanovich [14]. In an ecological context, the biological half-life ($t_{\frac{1}{2}}^{bio}$) is a measure of the rate at which the radioactivity within an organism decreases by processes other than decay after the exposure source has been removed. Furthermore, the ecological half-life ($t_{\frac{1}{2}}^{eco}$) refers to the processes of redistribution and "aging" in the soil environment that control exposure levels for a given organism.

Another useful term in discussing radionuclides is specific activity which is the number of decays per unit time per amount of substance (usually mass). The shorter the half-life, the higher the specific activity and the more radioactive an isotope is considered. The concept of specific activity is important in terms of assessing radioactivity in the environment. A radionuclide with a long half-life may not be a concern, but could have short-lived daughters and thus considered to be more highly radioactive.

Alpha (α), beta (β), and gamma (γ) are the most common forms of radioactive decay. Other decay modes such as electron capture and proton and neutron emission are far less common, and beyond the current general discussion. Alpha decay is the emission of helium ions (${}^{4}_{2}He$) and generally observed for elements heavier than lead (Pb) on the periodic table, most actinides and some lanthanide elements. For example:

$$ {}^{A}_{Z}X \rightarrow {}^{A-2}_{Z-4}X + {}^{4}_{2}He \tag{2} $$

with α particles generally having kinetic energy in the range of 3–9 MeV (mega-electron volts; 10^6 eV), but displaying very limited ability to penetrate matter because of their large mass and charge. A sheet of paper or skin is all that is needed to prevent penetration of α particles. Thus, the big health threat from α decay

is through inhalation or ingestion, as the particles trapped inside the body can damage sensitive tissue.

Although derived from the nucleus, β particles are essentially electrons with a mass of 5.49×10^{-4} amu (atomic mass units), and a charge of -1. For isotopes with an unstable N/Z ratio, β decay is a spontaneous exothermic process where

$$ {}^{A}_{Z}X \rightarrow {}_{z+1}{}^{A}X + \beta^{-} + \text{decay energy} \quad (3) $$

resulting in an increase in Z with no change in A. Due to the limited energy release, β decay is commonly measured by liquid scintillation counting. In terms of penetration, β particles are intermediate between α particles and γ rays. Plexiglas is typically sufficient shielding for these particles. Tritium (^{3}H) is an example of a β emitter.

The two decay processes discussed above, i.e., α and β decay, may leave the nucleus in its ground state, or more frequently in an excited state. The excited nucleus may then release energy through the emission of electromagnetic radiation known as γ radiation in returning to the ground state. Although somewhat similar to x-rays, γ rays display a very high frequency ($\sim 10^{19}$ Hz) and a shorter wavelength than x-rays, with energies ranging from a few thousand keV to 10 MeV. Gamma rays are produced from transitions within the nucleus, while x-rays are emitted from the electron shell. Two additional processes, internal conversion and de-excitation are means by which the excited nucleus may return to the ground state. All three processes are known as γ transitions because no change in A or Z is observed. In an example of γ decay

$$ {}^{A}X^{*} \rightarrow {}^{A}X + \gamma \quad (4) $$

X^{*} represents a nucleus in an excited state. Gamma decay can occur between multiple lower energy states before reaching the ground state. Since γ rays carry no charge, their interaction with matter is limited and depends on the density of the absorber, with much greater penetration than observed for α or β radiation [10, 15]. Lead (Pb) is commonly used as a shield for γ rays.

Fission Products

The isotopes ^{235}U and ^{239}Pu have the unique ability to split into two atoms (i.e., fission products) when impacted by a slow moving neutron, releasing additional neutrons plus a significant amount of energy:

$$ {}^{235}U + {}^{1}n_{O} \rightarrow \text{fission fragments} + 2 \text{ to } 3 \text{ neutrons} + \text{energy} \quad (5) $$

In a nuclear reactor, the heat generated by this process is used to produce steam for powering a turbine generator. Conventional reactors typically use fuel rods that are enriched with ^{235}U to a level of 2–4%. A portion of the neutrons produced in fission are sorbed by the more plentiful ^{238}U, eventually leading to the formation of fissile ^{239}Pu, contributing about one-third of the energy produced in the reactor. Within about 3 years the buildup of fission products within the nuclear fuel interferes with the transfer of neutrons, reducing the efficiency to the point where the fuel must be removed [10, 13]. There are two groups of fission fragments: relatively short-lived, highly radioactive isotopes (^{137}Cs and ^{90}Sr) and longer-lived isotopes (^{99}Tc, ^{135}Cs, and ^{129}I). Both groups are major contributors to radioactive waste streams, and need to be assessed in terms of their behavior in the environment when developing a waste disposition policy.

Radionuclide Sources

Natural Sources

Some natural radionuclides are primordial in origin (e.g., $\approx$ 10 ppm Th and $\approx$ 4 ppm U) with half-lives generally exceeding 10^{9} years. Other natural radionuclides are generated by continuous bombardment of the earth and atmosphere by cosmic rays, including ^{14}C which is important in radiometric dating, as well as ^{3}H, ^{7}Be, and ^{10}Be (see Table 1) [10, 12]. In addition to naturally occurring radionuclides, anthropogenic sources in terrestrial systems include fallout from the atmospheric testing of nuclear weapons, nuclear material mining, and processing activities for defense and industrial uses, nuclear power generation and fuel reprocessing and disposal, and biomedical wastes. Some recognition of natural background radiation levels is essential in defining the boundary of contaminated sites and establishing an appropriate threshold for cleanup levels [16].

Uranium mining and milling efforts generate the largest volume of radioactive waste, often containing

Radionuclide Fate and Transport in Terrestrial Environments. Table 1 Source, characteristics and examples of the various nuclide classes [10, 12]

Class	Sources	Characteristics	Examples
Stable	Found in nature		^{12}C, ^{14}N, ^{16}O
Primary natural radionuclides	Initial forming of the universe	≈26 known radionuclides with generally very long half-lives	^{40}K (1.28 × 10^9 y), ^{238}U (4.47 × 10^9 y), ^{235}U (7.13 × 10^8 y)
Secondary natural radionuclides	Decay products of natural radionuclides	≈38 known; short half-lives	^{226}Ra (1,600 y), ^{234}Th (24.1 d)
Induced natural radionuclides	Cosmogenic formation in troposphere	≈10 known	^{3}H (12.3 y), ^{14}C (5730 y), ^{7}Be, ^{10}Be, ^{22}Na, ^{32}P, ^{33}P, ^{35}S, ^{39}Cl
Anthropogenic radionuclides	Man made	≈2,000 known	^{60}Co (5.3 y), ^{137}Cs (30.2 y)

Values in parentheses represent radioactive half-lives.

additional hazardous metals and sulfides, which generate acidity upon oxidation that enhances contaminant release. However, the relative environmental footprint associated with U mining for nuclear energy is orders of magnitude less than coal for an equivalent unit of energy production. Under the Uranium Mill Tailings Remedial Action (UMTRA) program, the US Department of Energy (DOE) has made considerable progress in the remediation of 24 U mining and milling sites in 10 states. Nonetheless, U mining and milling will likely increase within the next decade as current fuel stockpiles are exhausted [4, 17, 18]. Other important sources of naturally occurring radioactive materials (NORM) include waste generated from the phosphate fertilizer industry, the scales from oil and gas extraction, ash from conventional coal-based power generation, and the waste from metal mining and processing facilities [19].

Nuclear Weapons Development, Testing, and Production

Since the first nuclear test in New Mexico in 1945, more that 2,400 nuclear test explosions have occurred, including more than 500 atmospheric tests, resulting in the global dispersal of ^{239}Pu, ^{137}Cs, ^{14}C, ^{90}Sr, ^{131}I, ^{3}H, and much lower quantities of numerous short-lived radionuclides. The Former Soviet Union (FSU) conducted more than 460 nuclear tests at the Semipalatinsk test site in Kazakhstan [7, 18, 20]. The total radioactivity released to the atmosphere from nuclear weapons testing has been estimated to be over 2 × 10^8 TBq [21]. Even now, there are still approximately 27,000 nuclear weapons spread among the various nuclear powers, and the USA and Russia each have an inventory of about 40 metric tons of Pu [22].

Beyond the releases associated with weapons testing, nuclear weapons development and production has resulted in the generation of large stockpiles of nuclear waste and extensive contaminated areas [23], the disposition of which is still in question. For example, about 2 million m^3 of high-level waste currently stored in 177 underground tanks was produced at the two Pu processing lines at the DOE Hanford Facility, with 67 of the tanks having leaked at some point [7]. In another example, considerable environmental contamination occurred at the Mayak nuclear facility in the FSU, with substantial volumes of accumulated high-level waste (>350 million Ci) awaiting final disposition [24].

Nuclear Energy

Currently, about 17% of the world's electricity is derived from nuclear power. A 1,000 MWe nuclear reactor generates about 27 metric tons of waste a year (globally ≈ 12,000 metric tons $year^{-1}$), compared to the 400,000 metric tons of waste generated by a coal-fired plant producing the same amount of electricity [17]. The USA currently has 103 of the 443 nuclear power reactors worldwide, France has 59, and Japan has 54, with much of the expansion in nuclear power generation set in Asia and the developing world.

The three major producers combined represent about 57% of the world's total electrical production from nuclear power. However, France (70% of domestic electricity), Slovakia (57%), and Belgium (54%) are the countries most dependent on nuclear power [7]. Most if not all of the nuclear power reactors in the USA have or will petition the NRC to extend their initial 40-year operational limit.

More than 200 radionuclides are produced during the operation of a typical nuclear power reactor. As discussed previously, reactor fuel must be routinely replaced because of fission product buildup that disrupts neutron transfer, inhibiting fission and energy production. Many of the SNF radionuclides have relatively short half-lives and decay within the first few decades [7]. Important fission products associated with the SNF include ^{135}Cs, ^{137}Cs, ^{129}I, ^{90}Sr, and ^{99}Tc, representing about 3% of the residual SNF weight. The fission products ^{137}Cs and ^{90}Sr account for much of the SNF radioactivity for the first 10–100 years of storage. Despite the public's reservations concerning the safety of nuclear power, controlled and uncontrolled releases of radioactivity from the operation of commercial nuclear reactors represents less than 3% of the amount released from atmospheric nuclear weapons testing [21]. Furthermore, the atmospheric emission of radioactivity in the form of U and Th from a conventional coal-fired plant can exceed the atmospheric release from nuclear power when compared on an equivalent energy output basis [25, 26].

In Europe and Japan, much of the SNF fuel is reprocessed to remove the fissile material (U and Pu) for subsequent reuse. For instance, the French facility at La Hague recycles SNF for France, Germany, Belgium, Switzerland, and the Netherlands, with the recovered waste returned to the originating country for disposal. Another commercial SNF reprocessing facility serving multiple countries is housed at the Sellafield nuclear facility in England, with additional reprocessing facilities in India, Japan, Russia, and China [7]. However, fuel reprocessing is not without its limitations and drawbacks. Contaminants such as Cm and Am build up in the recycled SNF and limit continued reprocessing. Eventually, both high-level waste removed during reprocessing and the recycled SNF will require disposal in a geologic repository [22]. Although deep geologic containment has largely been accepted as the primary disposal strategy for commercially derived high-level waste, no country to date has completed the design and construction of such a repository [7]. Given the limited mass of ^{239}Pu required to create a nuclear bomb (≈7–10 kg), the potential diversion of fissile materials in SNF destined for reprocessing is viewed as a potential route to expedited nuclear weapons proliferation.

In contrast to Europe, the USA currently practices a once-through nuclear fuel cycle due to concerns over proliferation, with much of the SNF remaining in storage pools housed on the reactor sites awaiting the opening of the Yucca Mountain repository or the choice of an alternate disposal strategy. However, the USA is constructing a facility for combining the surplus inventory of Pu originally produced for nuclear weapons with U to produce a mixed-oxide fuel for use in commercial nuclear reactors. In addition, fourth-generation nuclear reactors currently in development offer several potential advantages, including a closed fuel cycle that produces little or no long-lived radioactive waste and reduces the generation of materials that aid in nuclear proliferation, i.e., enriched U and ^{239}Pu [27].

Nuclear Accidents

Accidental discharges at both government and commercial nuclear facilities have played an important role in shaping public opinion concerning the relative safety of nuclear energy. In 1957, a fire within the graphite core of a reactor at the British nuclear facility at Windscale, known now as Sellafield, released significant amounts of ^{131}I and ^{137}Cs to the countryside. The Windscale facility produced ^{239}Pu for the British nuclear weapons program. Following the fire, a second Windscale reactor of similar design was shut down, and the damaged reactor unit was essentially decommissioned in place. The same year, the Kyshtym disaster, known for the name of a local town, occurred at the Mayak nuclear facility, the center for nuclear weapons production in the FSU. The cooling system associated with a series of nuclear waste storage tanks failed, resulting in a nonnuclear explosion that released significant levels of ^{90}Sr and ^{137}Cs throughout the adjacent countryside known since as the East-Ural Radioactive Trace [24, 28].

Three Mile Island and Chernobyl

In 1979, a mechanical failure in the cooling water loop at the Three Mile Island (Dauphin County, PA) reactor resulted in a lowering of the water level within the reactor core which exposed the upper section of the fuel rods. While nuclear fission within the reactor ceased in the absence of the water moderator, the temperature of the power rods increased rapidly due to the ongoing decay of existing fission products, resulting in a partial meltdown of the fuel rods. Contaminated water from the primary cooling loop was released within the plant facility, and noble gases (e.g., ^{135}Xe and Kr) and fission products (^{129}I and ^{131}I) were released into the environment. There was concern at the time that the zirconium alloy coating the rods would react with the steam to produce H_2 that could potentially react with O_2 to produce an explosion, resulting in additional dispersion of reactor fuel materials and fission products in the environment [10].

Another serious accident occurred in 1986 at the Chernobyl power station near Kiev, Ukraine, when the control rods were removed from the reactor during a systems test, accelerating the chain reaction. The buildup of heat eventually vaporized the cooling water, causing the core to explode. As in the accident at Three Mile Island, nuclear fission ceased due to the lack of the moderator, but the graphite within the exposed reactor ignited, releasing additional transuranics ($\approx$ 800 Ci ^{238}Pu, $\approx$700 Ci ^{239}Pu, $\approx$1,000 Ci ^{240}Pu) and fission products into the environment, i.e., ^{137}Cs, ^{134}Cs, ^{90}Sr, and ^{131}I. Because of the danger in approaching the burning facility, the fire was eventually extinguished using helicopters and the reactor was entombed in concrete [10, 29].

Soils as the Repository for Radioactive Waste

Reactive Soil Components

Excluding radioactive decay, the major chemical, physical, and biological processes governing the fate and transport of radionuclides in the soil system include aqueous speciation/complexation, sorption/desorption, convection/dispersion, resuspension and erosion, and redox state and other chemical species transformations. In terms of biological reactions, radionuclides may be assimilated/immobilized into the living organic matter within the soil microbiota and absorbed by the roots of higher order plants as the first steps in trophic transfer in terrestrial systems.

Before discussing the reactions controlling the fate and transport of specific radionuclides of interest, it is important to review the physical and chemical properties of soils that control reactivity. Soils consist of three phases; the solids account for about 40–50% of the soil volume, and the aqueous and gaseous phases account for the remaining balance. As the degree of saturation increases, the relative volume of the gaseous phase decreases. The degree of saturation is an important variable controlling solute fate and transport in soil and vadose systems, including advective/dispersive transport and the buildup and transfer of volatile constituents that impact biotic activity and soil redox state (i.e., O_2, CO_2, NH_3, CH_4, etc.). Although the term "soil" is generally restricted to the top meter or so of the earth's crust, the current discussion concerning various soil processes controlling radionuclide fate and transport is generally relevant to the vadose zone and saturated groundwater systems.

Phyllosilicate Clays

Surface area is a major factor controlling the reactivity of a solid phase, including soil materials. Therefore, discussion will focus on the clay fraction (<2 μm) that tends to dominate soil reactivity because of the large surface to volume ratio. However, the term "clay" can also be used in reference to a specific soil textural class or classes based on the relative proportion of sand (2 mm −50 μm), silt (<50 μm to 2 μm), and clay-sized (<2 μm) materials, or a specific type of mineral that consists of repeating silicate sheets, i.e., phyllosilicate clays. All three definitions are relevant to the current discussion of soil reactivity.

Minerals are generally classified based on the dominant anion or anionic group within the structure, e.g., halides, carbonates, sulfides, phosphates, oxides/hydroxides/oxyhydroxides, and silicates [30]. Much of the current discussion will focus on phyllosilicates and metal oxides. However, other soil mineral classes will be discussed in relation to processes controlling the behavior of specific radionuclides as warranted. Readers are directed to Dixon and Schulze [31] for

a more thorough introduction to the complexities of soil mineralogy.

Silicates are an extremely diverse mineral class accounting for well over 90% of the earth's crust. In discussing clay structure, the octahedral and tetrahedral layers will be referred to as sheets, while the term "layer" refers to the fundamental clay unit representing the combination of the sheets. The fundamental structural unit for silicates is the SiO_4 tetrahedron, consisting of four O^{2-} ions surrounding a single Si^{4+} ion. For the layer silicates, the three basal oxygens are shared with other Si-tetrahedral units to form a sheet. The second primary structural unit in phyllosilicate clays is the octahedron consisting of Al^{3+} (also Fe^{2+} and Mg^{2+}) surrounded by six hydroxyl groups, OH^-, which also combine to form a sheet structure [31].

Phyllosilicate clays are divided into 2:1 and 1:1 type minerals based on the number and sequence of tetrahedral and octahedral sheets in the layer structure. The 2:1 clay minerals consist of an octahedral sheet sandwiched between and sharing the apical O^{2-} ions of two Si-tetrahedral sheets. The 2:1 clay minerals display a net surface charge due to imperfections in the crystal structure derived from the substitution of a lower valence cation for a higher valence cation, termed isomorphic substitution. Isomorphic substitution generally results from the substitution of Al^{3+} for Si^{4+} in the tetrahedral sheet and Mg^{2+} or Fe^{2+} for Al^{3+} in the octahedral sheet, resulting in diffuse permanent negative charge that is compensated by the attraction of common alkali and alkali-earth cations to the clay surface, i.e., cation exchange capacity (CEC). Isomorphic substitution is insensitive to conditions in the solution environment, and therefore termed constant charge. In addition to the external siloxane oxygens of the basal tetrahedral planes for each layer, terminal aluminol (AlOH) and silanol (SiOH) groups are found along the edge boundaries of the clay layers. In addition to the diffuse cation exchange capacity resulting from isomorphic substitution, the edges can serve as sorption sites depending on pH and other solution conditions, just like other variable-charge sites to be discussed below.

The 2:1 mineral class can be further categorized based on the location and degree of isomorphic substitution within the mineral structure, i.e., micas (illites), vermiculites, and smectites (Fig. 1a). The terms "illite" and "hydrous mica" are often used to refer to weathered micas. Layer charge is defined as the magnitude of charge derived from isomorphic substitution per mineral formula unit for a given clay, with the layer charge for mica > illite > vermiculite > smectite. However, the general distinction between these groups of 2:1 clays and the 1:1 kaolin group discussed below is operationally defined by their response in terms of interlayered spacing to various cation saturation, heating, and desiccation treatments, as determined by x-ray diffraction (XRD) according to standardized criteria [32].

Increasing layer charge results in increasing interlayer bonding as adjacent clay layers tightly share interlayer cations that balance the charge resulting from isomorphic substitution. For instance, smectites have a relatively low layer charge when compared to vermiculites and micas, with much of the charge residing in the octahedral layer; however, smectites display a higher CEC and reactive surface area than mica because cations, water, and other polar molecules can be exchanged between the clay interlayer and the bulk solution due to the weaker interaction of adjacent clay layers (Fig. 1a). In contrast, micas have a high degree of isomorphic substitution within the tetrahedral layer, resulting in more localized charge distribution, but display limited CEC. Cations with ionic radii similar to the ditrigonal cavity formed by six corner sharing Si tetrahedra present on the exterior planar surface of 2:1 clay minerals (i.e., K^+, NH_4^+, and Cs^+) are strongly bound between mica layers because of the close proximity to the origin of charge in the tetrahedral layer. This strong interaction, represented by K in Fig. 1a, limits the ability of water or cations from the bulk solution to penetrate the mica clay interlayer. Vermiculites display an intermediate behavior, with cations like K^+, NH_4^+, and Cs^+ held within the interlayer becoming non-exchangeable under certain conditions.

Although larger than a clay-sized particle (i.e., > 2 μm), the clay mineral displayed in the SEM micrograph Fig. 1b can serve to illustrate the heterogeneous surfaces present on clay minerals, despite the fact that sorption processes occur at a much more refined scale than apparent in this macroscopic representation of various clay features. Distinguishing various external planar, interlayer, and edge sites will become important when discussing ^{137}Cs and ^{90}Sr behavior in soil.

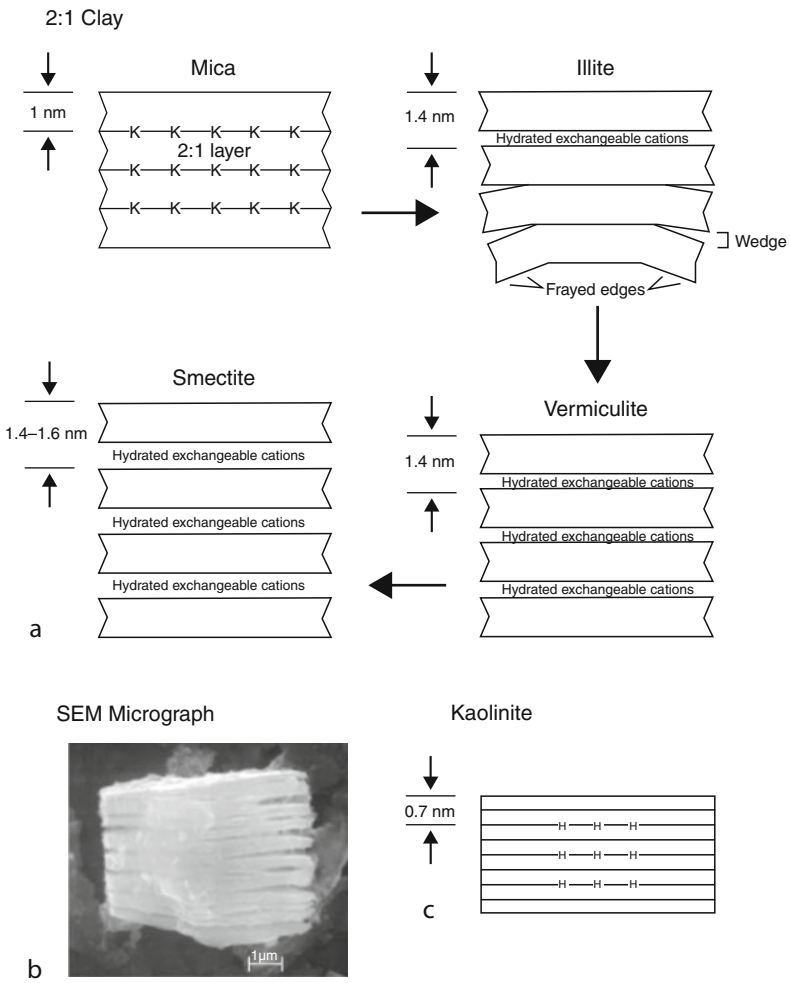

Radionuclide Fate and Transport in Terrestrial Environments. Figure 1
(**a**) Weathering transition and interlayer expansion properties of 2:1 clays from mica to smectite. (**b**) SEM micrograph of 2:1 clay illustrating planar surface, interlayer and edge character apparent at a larger scale (20 kV, Seaman unpublished). (**c**) Kaolinite clay with no interlayer expansion because of hydrogen bonding between 1:1 sheets (A and C revised from NCRP [156])

Due to their high reactivity and surface area, and swelling properties, smectites have been evaluated for use as engineered barriers or back-fill materials for proposed high-level nuclear waste repositories (HLNWR) in Japan and Europe. However, recent evidence suggests that high levels of radiation (i.e., alpha recoil and ionizing radiation from fission products) can induce amorphization, altering both the solubility and sorptive properties of the smectites [33]. Therefore, the impact of radiation on natural environmental sorbents, such as soil clays, warrants greater research attention.

In some highly weathered soils like those of the southeastern USA, polymeric $Al(OH)_n^{(3-n)+}$ sheets often occupy portions of the interlayer of 2:1 clays, blocking cation exchange sites and limiting interlayer expansion and collapse in response to cation saturation and hydration conditions. These clays are commonly classified as hydroxyl-interlayered smectites (HIS) or hydroxyl-interlayered vermiculites (HIV) based on the degree to which interlayer expansion and collapse are restricted [34]. Although the $Al(OH)_n^{(3-n)+}$ polymers reduce CEC and limit interlayer collapse, their presence

can result in sorption sites that potentially display unique preferences for soil contaminants.

In 1:1 phyllosilicates there are three anion planes: the basal siloxane plane associated with the tetrahedral sheet, the middle layer associated with O^{2-} ions within both the tetrahedral and octahedral sheets, including apical tetrahedral O^{2-} ions shared with the octahedral sheet, and the hydroxyls associated with the remaining planar surface of the octahedral sheet (Fig. 1c). Kaolinite consists of a series of stacked 1:1 structural layers with Al^{3+} in the octahedral sheets and Si^{4+} in the tetrahedral sheets. Although structurally neutral due to limited isomorphic substitution, the adjacent 1:1 layers are restricted from expanding by hydrogen bonding associated with the aluminol planar surface of the octahedral sheet and the basal siloxane surface of the next kaolinite layer. In general, surface charge in kaolinite is derived from the amphoteric functional groups on the edges of the clay layers.

Zeolites

Zeolites are framework aluminosilicates consisting of extended three-dimensional networks of linked SiO_4 and AlO_4 tetrahedra. Zeolites derive cation exchange capacity from Al^{3+} substitution for Si^{4+} with the size of the channel determining the type of cation that is preferred [35, 36]. In nature, zeolites are found in significant concentrations associated with sedimentary materials of volcanic origin [37]. Although not common in soils, zeolites are important because of their use as selective sorbents for removing radionuclides from waste streams, treating contaminated systems, and backfilling to buffer radioactive waste storage systems [38]. Zeolites possess unique interconnected channels or voids that form selective sorption sites for water and alkali and alkali-earth metals, including $^{135/137}Cs^{+}$ and $^{90}Sr^{2+}$ [39]; however, zeolites display a limited sorption affinity for metals that tend to hydrolyze or form strong complexes with carbonate (e.g., Np, Th, and U) [39–41].

Metal Oxides and Hydroxides

Soil minerals are further characterized as either being primary or secondary in nature, with primary referring to minerals that were formed at elevated temperatures, and then derived from igneous or metamorphic rock. Secondary minerals are formed at lower temperatures and derived from sedimentary minerals or soil weathering processes. As primary soil minerals break down and weather, ionic constituents are released into solution that may recombine and form other minerals, i.e., secondary minerals. Iron, Al, Mn, and Ti released during the weathering of primary minerals tend to persist and form stable oxides/oxyhydroxides that are resistant to continued weathering, with the metal cation occupying octahedral sites [42, 43]. In general, the term "oxide" will be used in reference to any metal-oxide, hydroxide, or oxyhydroxide mineral.

Gibbsite (γ-$Al(OH)_3$) is the most common Al hydroxide found in soils. Gibbsite is structurally analogous to the $Al(OH)_n^{(3-n)+}$ found in the interlayers of HIS and HIV, and consists of parallel layers of Al in octahedral coordination with OH anions, with every third cation center remaining vacant. Ion adsorption by gibbsite occurs at the edge surfaces of the layer sheets. Goethite (α-FeOOH) and hematite (α-Fe_2O_3) are the most common Fe oxides found in soils and sediments. The poorly ordered ferrihydrite ($Fe(OH)_3$) is also quite common, but its limited crystallinity precludes identification based on XRD. However, the crystalline and amorphous Fe oxide contents for soils are typically estimated by selective extraction using the citrate-dithionite-bicarbonate (CDB) and ammonium-oxalate (AO) extractions, respectively [44]. Several metal cations, including Al^{3+}, have the ability to substitute for Fe within Fe oxide structures [45].

Although generally found in lower concentrations than Fe and Al oxides, Mn(III/IV) oxides are strong sorbents and highly important in surface-mediated redox reactions [46, 47]. Manganese oxides are difficult to study because of their complicated mineralogy and highly variable structure, with various stable and metastable phases found in soils.

Organic Matter

Soil organic matter (SOM) is a complex, polymeric mixture of aliphatic and aromatic compounds derived from the decomposition of plants and animals by heterotrophic microorganisms. SOM possesses a wide range of organic functional groups that bind with radionuclides, including hydroxyl (OH), carboxyl (COOH), sulfite (SO_3), sulfide (S), and amine (NH_2) functionalities. Soil organics can enhance the dissolution of

minerals through the complexation of metals, and can prevent the formation of Fe and Al oxides by forming strong organic complexes that hinder precipitation. Binding to SOM also plays a large role in controlling the bioavailability and toxicity of metals [48]. Furthermore, SOM can facilitate redox transformations at mineral surfaces, and alter the charge properties of soil clays, generally enhancing soil aggregation [49].

SOM can occur in the particulate phase, colloidal phase, or dissolved in solution. This division is operationally defined by the methods used to separate the fractions. Typically, 0.45 μm is the filter pore size used to separate particulates from what is traditionally considered "dissolved." The filtrate can be further separated to isolate the colloidal fraction. The colloidal fraction can play a significant role in the mobilization/immobilization of soil contaminants [50–52]. For example, U-humic colloids have been observed to constitute > 75% of the soluble U found in groundwater around the Gorleben salt domes in Germany [53, 54]. Microbes and microbially produced substances also play a significant role in the migration of radionuclides because of their influence on redox status which can affect speciation and thus the ultimate fate of redox-sensitive radionuclides, such as U and Pu, in the environment [55].

Important Soil Processes

Radionuclide Partitioning

In discussing soil processes, the term "sorption" is used to describe a decrease in the concentration of a given constituent in the aqueous phase, in this case a specific radionuclide, without implying a specific partitioning mechanism, such as surface complexation, precipitation, or ion exchange. The use of such a generic term is a reflection of the complexity of the soil environment, and the difficulty in experimentally distinguishing between an array of "sorption" mechanisms using standard wet-chemical analysis techniques [56–58]. In recent years, Monitored Natural Attenuation (MNA) has received considerable attention as an alternative to more invasive remediation strategies that can be highly destructive to functioning, contaminated ecosystems, even for addressing radionuclide contamination [59]. However, a thorough understanding of radionuclide partitioning mechanisms is critical to the effective application of MNA for contaminated sites where expensive, invasive remediation is unlikely to greatly lessen environmental risks.

Chemical Speciation

Radionuclides released in global fallout display a wide range of chemical properties that impact their behavior in the environment, including both cationic and anionic species and redox-sensitive elements. Initially, radionuclide speciation in the environment is highly dependent on the form in which it was released, often becoming less labile over time. Some of the actinides display very complex redox speciation (e.g., Pu), with the possibility for multiple redox states to coexist. Further, fission products resulting from nuclear power generation represent every group in the periodic table [10]. The form of the radionuclide (i.e., chemical species) and the physical and chemical properties of the soil materials largely control the fate and transport of the contaminant, including solid-phase partitioning, bioavailability, and subsequent trophic transfer [58, 60–62]. When limited data are available, the understanding of radionuclide behavior in the environment is based on that of a biogeochemical analogue/surrogate, either an element with similar chemical properties (i.e., ^{137}Cs vs K) or a stable or longer-lived isotope of the element of concern, like ^{135}Cs for ^{137}Cs [61, 63, 64].

Most common analytical techniques, such as mass- or radiolytic-based methods, provide estimates of total isotope concentration, but are insensitive to chemical speciation. Spectroscopic methods, such as x-ray absorption spectroscopy, are generally required to determine chemical speciation [65]. Goldberg et al. [58] provide an extensive review of spectroscopic techniques for evaluating structural features of both sorbent surfaces and adsorbed species. Such information is critical in validating a mechanistic description of reactive solute partitioning. However, the detection limits for solid-phase speciation techniques are often inadequate for their application to radionuclide concentrations associated with environmental samples, and special care must be taken to ensure that various changes in chemical speciation do not occur as a result of sample collection and storage before analysis, or even as a result of the analysis method itself. Colloidal

suspensions are particularly sensitive to artifacts associated with storage and handling [66, 67].

Sequential extraction procedures, such as the widely used Tessier et al. [68] and Miller et al. [69] methods, can provide information concerning contaminant partitioning and bioavailability. Such methods were first developed for the solid-phase speciation of metals, using a series of progressively more-aggressive extractants to isolate metals or radionuclides presumably associated with various contaminant partitioning mechanisms, i.e., water soluble, ion exchangeable, sorbed to Fe oxides, etc.; however, sequential extraction methods are operational in nature and suffer from limitations associated with the non-specificity of extractants and problems related to re-adsorption of metals during the extraction process [70, 71]. From an environmental assessment standpoint, sequential extractions can provide useful information concerning specific conditions under which a contaminant may be mobilized (i.e., acidic, reducing, etc.), and evaluating changes in solid-phase associations resulting from a given remediation treatment [72–74].

Cation Exchange Reactions

Cation exchange is one of the most common types of sorption reactions occurring in soils [75]. Using Sr^{2+} as an example, a typical cation exchange reaction can be formulated as:

$$2(R^{-} - Na^{+}) + Sr^{2+}_{aq} \Leftrightarrow (R^{2-}_{2} - Sr^{2+}) + 2Na^{+}_{aq} \qquad (6)$$

where R^{-} represents an exchange site associated with the solid phase, and Na^{+} and Sr^{2+} are exchangeable cations. Such reactions are quite rapid and fully reversible. Although cation exchange can be written as mass action equations, the resulting selectivity coefficients are not thermodynamic constants because of the difficulty in correcting for activities associated with the exchanger phase [76]. The CEC of a soil material is generally assumed to represent the charge associated with isomorphic substitution within phyllosilicate clays plus the exchange capacity associated with SOM. CEC is generally reported in units of equivalent cations sorbed per unit mass of soil, i.e., centi-moles of charge per kilogram of soil ($cmol_{(+)}\ kg^{-1}$).

For cation exchange sites resulting from isomorphic substitution, the relative exchange affinity increases with valence, i.e., bivalent cations are sorbed preferentially to monovalent cations. However, the selectivity tends to decrease with increasing ionic strength. Thus, dilution increases the bivalent to monovalent cation ratio on the exchange complex. For cations of the same valence, the relative affinity for cation exchange sites increases with the non-hydrated radii of the ion: $Cs^{+} > K^{+} > Na^{+} > Li^{+}$ and $Ba^{2+} > Sr^{2+} > Ca^{2+} > Mg^{2+}$. However, differences in cation selectivity as a function of ionic size indicate that additional factors beyond coulombic attraction contribute to such preferences.

In Fig. 2a, a simplified diagram of a 2:1 clay is presented with the negative signs representing the charge (i.e., cation exchange capacity) derived from isomorphic substitution. The right side of Fig. 2a is a diagram illustrating the impact of pH on surface charge (solid line). Since the charge is derived internally, it remains unchanged with variations of soil pH. However, terminal OH functional groups located on the edges of 2:1 clays are responsive to soil pH, and an increase in net negative charge (i.e., CEC) can be observed with increasing pH. The phyllosilicate edges can also act as "specific" sorption sites for both cationic and anionic species as discussed below for other variable-charge surfaces.

Variable Charge and Surface Complexation

In contrast to charge resulting from isomorphic substitution, amphoteric surfaces on soil minerals and ionizable functionalities on SOM are sensitive to the conditions in the solution environment (i.e., pH, ionic strength, counterion valence, etc.), and therefore termed variable-charge sites/minerals. The oxides and oxyhydroxides of Al, Fe, Ti, Mn, and other metals display this type of charging mechanism, e.g., $\equiv M - OH$, where M represents the primary metal and OH is a surface hydroxyl filling the coordination sphere of the metal (Fig. 2b). The surface charge of the oxide becomes more positive with increasing acidity, and more negative with increasing alkalinity. As noted before, the silanol and aluminol edges of phyllosilicate clays (Fig. 2a) also display this type of charge behavior, with the CEC for kaolinite largely derived from amphoteric edge sites because of the limited isomorphic substitution within the clay structure.

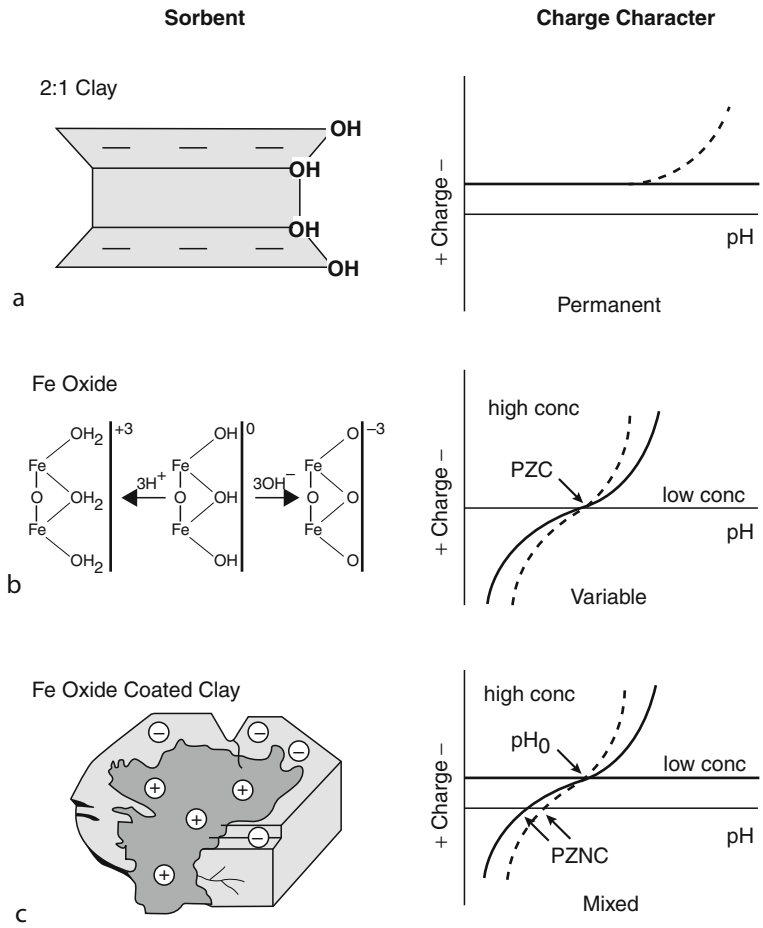

Radionuclide Fate and Transport in Terrestrial Environments. Figure 2
Common mineral sorbent types found in soils and electrostatic charge expression as a function of solution conditions (i.e., pH and ionic strength): (**a**) constant charge, (**b**) variable charge, and (**c**) a combination of constant and variable-charge types

For variable-charge minerals, the reactivity of the mineral surface will depend on the structure of the metal hydroxide, the mineral surface area and surface reactive site density, and the point of zero charge (PZC). The PZC (pH_{pzc}) is defined as the pH at which positive and negative surface charges are equal, i.e.,

$$\equiv M - OH_2^+ \quad \text{equals} \quad \equiv M - O^- \tag{7}$$

which also corresponds to the pH value for the minimum solubility of the metal-oxide/oxyhydroxide in question, and to conditions that facilitate the rapid coagulation of oxide suspensions [76]. Conceptually, the acid/base equilibrium at the mineral surface can be represented by the following:

$$\equiv M - OH_2^+ \Leftrightarrow \equiv M - OH^0 + H^+ \qquad K_{a1} \tag{8}$$

$$\equiv M - OH^0 \Leftrightarrow \equiv M - O^- + H^+ \qquad K_{a2} \tag{9}$$

where K_{a1} and K_{a2} are the apparent acidity constants, with the surface charge becoming more positive as the pH decreases and more negative as the pH increases (Fig. 2b). In contrast to an amphoteric solute, the mineral surface provides a degree of structural constraint to the acid/base functionalities that alters the apparent dissociation constants, constraining

subsequent protonation and deprotonation, causing the dissociation constants to express more variable amphoteric character. At a specific pH, however, the surface charge of a variable-charge mineral will increase with increasing ionic strength, as illustrated by the two charge curves on Fig. 2b.

As a consequence of this amphoteric behavior, both anions and cations may be electrostatically sorbed to the charged oxide surface. Such electrostatic bonds in which the sorbed ion remains hydrated are termed "outer sphere" complexes. Using the same convention, hydrous oxides can form stronger "inner sphere" surface complexes with metal ions resulting in the displacement of a proton and the generation of excess positive charge, which may in term attract an anion:

$$\equiv Fe-OH+Pb^{+2} \Leftrightarrow \equiv Fe-OPb^{+}+H^{+} \qquad (10)$$

A similar reaction can be written for the "inner sphere" sorption of an anion by ligand exchange with a surface OH^- or H_2O group:

$$\equiv Fe-OH+A^{n-} \Leftrightarrow \equiv Fe-A^{(n-1)}+OH^{-} \qquad (11)$$

where A^{n-} represents the anion in solution. As indicated by the previous equations, surface complexation reactions are competitive processes that depend on the pH and the sorbate in question. Such reactions will be discussed further in the context of Surface Complexation Modeling (SCM).

It is important to note that soils generally contain a combination of constant charge clays, variable-charge oxides, and SOM with various reactive functionalities. Figure 2c represents a phyllosilicate clay impacted by an oxide coating. Although the term "coating" is widely used to describe the interactions between Fe oxides and phyllosilicate clays, it is somewhat misleading as the Fe oxides often display a very discrete, fine-grained morphology that is best described as armoring the clay surface [77]. As the charge diagram on the right illustrates (Fig. 2c), a fixed level of negative charge derived from isomorphic substitution is present at all times, with an additional variable-charge component that is responsive to pH and ionic strength. In such systems, the variable-charge oxides may actually block a portion of the CEC in a manner similar to the way $Al(OH)_n^{(3-n)+}$polymers can block interlayer exchange sites in 2:1 clays. For systems with limited CEC, the pH conditions may be such that the positive charge (anion exchange capacity, AEC) derived from the oxides may be equivalent to or even exceed the CEC.

Redox Reactions

By convention, redox reactions are written in terms of the reductive half reaction. For instance, the reduction of Fe(III),

$$Fe^{3+}+e^{-} \Leftrightarrow Fe^{2+} \qquad (12)$$

where e^- represents the electron. To be complete, reactions such as Eq. 12 must be balanced by an appropriate oxidation reaction:

$$4H^{+}+O_{2(g)}+4e^{-} \Leftrightarrow 2H_2O \qquad (13)$$

Reaction 13 is reversed and balanced to represent the overall redox reaction:

$$Fe^{3+}+\frac{1}{2}H_2O \Leftrightarrow Fe^{2+}+H^{+}+\frac{1}{4}O_{2(g)} \qquad (14)$$

with the electrons from the two half reactions canceling each other out [13]. In a more relevant example, the two prominent redox states of U (IV and VI) in soils are linked by

$$UO_2^{2+}+4H^{+}+2e^{-} \Leftrightarrow U^{4+}+2H_2O \qquad (15)$$

with the subsequent precipitation of the sparingly soluble $UO_{2(S)}$ [78]. Uranium (VI), originally thought to be reduced abiotically, can also be reduced by microbially mediated processes [79, 80]. For example, microbially produced acetate can reduce U(VI) to U(IV) as seen in reaction 16.

$$CH_3COO^{-}+4U(VI)+4H_2O \rightarrow 4U(IV) + 2HCO_3^{-}+9H^{+} \qquad (16)$$

Redox conditions may control the relative solubility of a contaminant by altering its chemical speciation and/or the properties of the sorptive phase. For instance, the reduced form of U, U(IV), is much less soluble than the oxidized form, U(VI) [13]. Furthermore, reducing conditions may lead to the dissolution of important sorbents such as goethite (α-FeOOH), releasing both adsorbed contaminants as well as contaminants that may have substituted for Fe within the mineral structure.

Precipitation/Dissolution

Dissolution and precipitation reactions are likely to dominate in highly contaminated systems, such as waste disposal facilities, or where steep pH and oxidation/reduction gradients persist [81, 82]. A full treatment of mineral equilibrium interactions is beyond the scope of the current chapter. For more detail the reader is directed to references [76] and [83]. The Gibbs free energy of a reaction is

$$\Delta G_r = RT \ln \frac{Q}{K_{eq}} \tag{17}$$

where R is the gas constant, T is the standard temperature (K), Q is the ion activity product (IAP) of soil solution components, and K_{eq} is the equilibrium product, i.e., the solubility product (K_{sp}) for the precipitate of interest. At equilibrium for a given system, $Q = K_{sp}$. The saturation index (SI) with respect to a specific solid phase is defined as

$$SI = \log_{10}\left(\frac{Q}{K_{eq}}\right) \tag{18}$$

A SI < 0 (i.e. negative value) indicates that the solution is under-saturated, while a SI > 0 indicates the solution is supersaturated with respect to a specified solid phase. A SI of 0 indicates that the solution is in equilibrium with a given solid.

At equilibrium with a solid phase, the aqueous-phase activity of the soluble components is independent of the amount of the precipitate present. In contrast to adsorption reactions, precipitation involves nucleation and then solid-phase growth in three dimensions. Coprecipitation occurs when an element is incorporated within a precipitate as a trace or minor component, with metal substitution readily observed for Fe oxides [45]. In a relevant example, the precipitation of U(VI) with secondary Al-phosphates has been observed when apatite ($Ca_5(PO_4)_3OH$) was added to an ultisol contaminated with U and other metals, rather than sorbing to residual apatite or the formation of a discrete U phosphate [74, 84].

Before concluding the detailed discussion of soil mineralogy and reactive sites, it is important to note that the properties of natural soil minerals are often quite different from their pure mineral specimens or synthetic analogues on which much of the fundamental contaminant partitioning studies are based. Recent studies have elucidated the role of less abundant mineral and organic substrates as important surface chemical modifiers and have demonstrated the complex coupling of reactivity between permanent-charge phyllosilicates and variable-charge Fe-oxyhydroxide phases [77, 85–87].

Models for Describing Radionuclide Sorption and Plant Uptake

Empirical Partitioning Isotherms

Partitioning isotherms are often used to describe solute behavior in recognition of the simplistic, empirical methods by which solute–surface interactions are commonly evaluated. The three most commonly used equilibrium sorption models include the Linear, Freundlich, and Langmuir equations. When used to describe solute transport, the sorption behavior described by the three isotherms is assumed to be both rapid and fully reversible. The Linear isotherm equation is

$$S = K_d C \tag{19}$$

where S is the amount sorbed, K_d is the linear distribution/partition coefficient (L kg^{-1}), and C is the solute concentration in equilibrium with the sorbent phase. For radionuclides, the K_d is often calculated in terms of Bq within both the aqueous (Bq L^{-1}) and solid phases (Bq kg^{-1}), resulting in the same final units as above, i.e., L kg^{-1}. A large K_d value is indicative of a greater tendency for a solute to partition to the solid phase; thus, a greater degree of infiltration and leaching will be required for the contaminant to move through the soil and vadose system into the underlying groundwater, and then migrate down gradient.

Several relevant databases have been developed for using the linear partitioning function to describe radionuclide transport [64, 81, 88–92]. The US Environmental Protection Agency (EPA) in collaboration with DOE issued a series of comprehensive reports discussing the underlying geochemical processes controlling contaminant sorption, including several key radionuclides (i.e., Am, Cs, ^{3}H, I, Np, Pu, Ra, Rn, Sr, Tc, Th, U), and the often-cited limitations associated with using the linear partitioning coefficient (i.e., K_d) to describe contaminant migration in the subsurface environment. A major recommendation noted

throughout the reports is the necessity to derive site-specific K_d values to better understand a given contaminant transport scenario. The use of literature-derived K_d values should be restricted to preliminary screening calculations of contaminant transport when additional data is not readily available. EPA did, however, produce a concise table listing important aqueous and solid-phase parameters that impacted the sorption behavior of each inorganic contaminant discussed in the reviews (see Table 2) [81, 89, 90]. It is interesting to note that field-derived K_d values are often much higher than lab estimates because extended exposure tends to reduce the apparent contaminant solubility, often described as aging.

In 2010, the International Atomic Energy Agency (IAEA) released an extensive compendium of estimated partition coefficients that could be used in evaluating the impact of both routine discharges and accidental releases. The IAEA report covers a more extensive list of radionuclides than the previous EPA reports, and further distinguishes transfer parameters based on soil properties, such as texture and organic matter content (Table 3). The classification of soil texture is limited to three main groups (sand, loam and clay), compared to 12 textural classes in the US Department of Agriculture system. A fourth class defined as organic soils is reserved for soils with >20% organic matter content. The IAEA report also distinguishes K_d values based on additional key soil properties, termed cofactors, that control radionuclide partitioning, in many respects consistent to the parameters identified by the EPA in Table 2.

Radionuclide Fate and Transport in Terrestrial Environments. Table 2 Important aqueous- and solid-phase parameters that influence radionuclide partitioning in the soil environment [89, 90]

Element	Important aqueous- and solid-phase parameters influencing contaminant sorption
Am	Clay content, Fe/Al oxide content, pH
Cs	Clay content, Fe/Al oxide content, (NH_4^+), CEC, mica/illite clay content, pH, (K^+)
I	Dissolved halides, OM content, pH, redox, volatilization
Pu	Clay content, Fe/Al oxide content, (CO_3^{2-}, F^-, SO_4^{2-}, PO_4^{3-}), OM content, pH, redox
Ra	Clay content, Fe/Al oxide content, $BaSO_4$ coprecipitation, (dissolved alkaline earth elements), CEC, ionic strength, OM content, pH
Rn	None
Sr	CEC, (Ca), (CO_3^{2-}), pH, (Sr)
Tc	OM content, redox
Th	Fe/Al oxide content, (CO_3^{2-}), OM content, pH
^3H	None
U	Clay content, Fe/Al oxide content, (CO_3^{2-}, F^-, SO_4^{2-}, PO_4^{3-}), OM content, pH, redox, (U)

CEC cation exchange capacity, *OM* organic matter
Parentheses represent aqueous concentrations

In addition to the Linear partitioning coefficient (K_d), the Freundlich and Langmuir isotherms are widely used in describing solute partitioning in the soils. For comparison, an example data set with the three common isotherms is provided in Fig. 3. The Freundlich isotherm is

$$S = K_F C^n \tag{20}$$

where S and C are the same as defined above, K_F is the Freundlich partition coefficient (L kg^{-1}), and n is the dimensionless heterogeneity parameter that describes the nonlinearity of the sorption process (n is typically ≤ 1). Note that when $n = 1$ the Freundlich equation is identical to the Linear isotherm. A plot of log S versus log C should yield a straight line with a slope of n and an intercept of log K_F. Although it describes the reduction in contaminant sorption often observed with increasing concentration, the Freundlich equation fails to account for the sorption maximum that is often observed.

Originally used to describe the adsorption from gases to solids, the Langmuir isotherm is

$$S = \frac{S_m K_L C}{1 + K_L C} \tag{21}$$

where S_m is the maximum adsorption per unit mass of sorbent, K_L is the Langmuir affinity parameter, and, as above, C is the solute concentration in equilibrium (Mol L^{-1}, mg L^{-1}, etc.) with the sorbent phase. Values for K_L and S_m are typically derived from batch sorption data using various linear transformations of the Langmuir equation or nonlinear least squares error fitting routines [58].

Radionuclide Fate and Transport in Terrestrial Environments. Table 3 Partition coefficients (K_d) for radionuclides as a function of soil texture [64, 107]

Element	Soil group	N^a	Mean[b]	GSD[c]	Minimum	Maximum
Sr	All soils	255	5.2×10^1	5.9	4.0×10^{-1}	6.5×10^3
	Sand	65	2.2×10^1	6.4	4.0×10^{-1}	2.4×10^3
	Loam + clay + organic	176	6.9×10^1	5.4	2.0	6.5×10^3
Cs	All soils	469	1.2×10^3	7.0	4.3	3.8×10^5
	Sand	114	5.3×10^2	5.8	9.6	3.5×10^4
	Loam + clay	227	3.7×10^2	3.6	3.9×10^{-1}	3.8×10^5
	Organic	108	2.7×10^2	6.8	4.3	9.5×10^4
U	All soils	178	2.0×10^2	12	7.0×10^{-1}	6.7×10^4
	Mineral	146	1.8×10^2	13	7.0×10^{-1}	6.7×10^4
	Organic	9	1.2×10^3	6.1	3.3×10^2	7.6×10^3
Th	All soils	46	1.9×10^3	10	1.8×10^1	2.5×10^5
	Mineral	25	2.6×10^3	10	3.5×10^1	2.5×10^5
	Organic	5	7.3×10^2	44	1.8×10^1	8.0×10^4
I	All soils	250	6.9	5.4	1.0×10^{-2}	5.8×10^2
	Mineral	196	7.0	5.2	1.0×10^{-2}	5.4×10^2
	Organic	11	3.2×10^1	3.3	8.5	5.8×10^2

[a]Number of data sets
[b]Geometric mean
[c]Geometric standard deviation

As apparent in Fig. 3, both the Freundlich and Langmuir isotherms provide a good description of the entire data set, accounting for an initial high level of sorption that decreases with increasing concentration. In this instance, the slope of the Linear partitioning coefficient was chosen to intersect with the two other isotherms. The Linear isotherm could have more accurately described initial solute partitioning at relatively low surface coverages. However, the choice of an arbitrary solution concentration (or surface coverage) for evaluating K_d is a drawback to the Linear partitioning approach. Other inherent limitations of the empirical sorption isotherms will become more apparent when discussing solute transport.

Mechanistic Adsorption Models: Surface Complexation Modeling

Surface complexation models (SCM) address some of the inherent uncertainties in the empirical partitioning (K_d) approach by describing sorption in terms of surface functional groups, with formation constants, reaction stoichiometries, and in some cases sorption site densities determined by fitting batch sorption data, or exhaustive physicochemical characterization of the sorptive material. Several approaches to SCM have been developed (e.g., Constant Capacitance Model, Double Layer Model, Triple Layer Model, etc.), generally differing in the manner in which they describe the mineral/water interface, and account for columbic interactions that impact the mass action equations. SCM models generally conform to the four following principles: (1) reactive surfaces are composed of surface functional groups that react with dissolved solutes to form surface species in a manner similar to complexation reactions that occur in solution; (2) surface acidity reactions that generate charge can be described by SCM, and the resulting surface charge can be invoked based on electrical double-layer theory; (3) the apparent mass action binding constants describing sorption

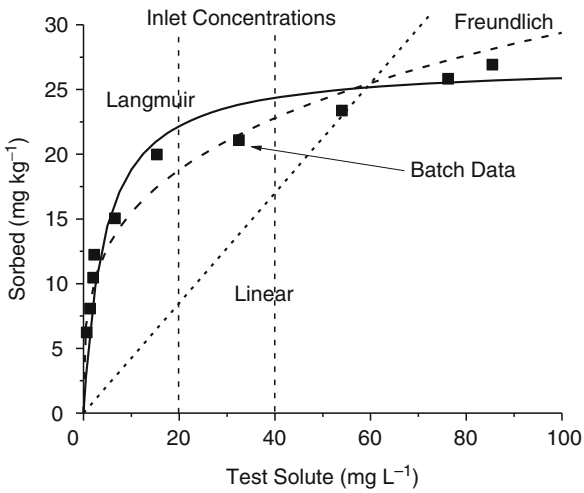

Radionuclide Fate and Transport in Terrestrial Environments. Figure 3
Example batch sorption data described using the three most common empirical sorption isotherms, Linear, Freundlich, and Langmuir. The dashed lines at 20 and 40 mg L^{-1} reflect the two inlet column concentrations used in generating the breakthrough curves presented in Fig. 4

reactions are empirical parameters that can be related to thermodynamic constants through the use of activity coefficients for the surface species; and (4) the electrical charge at the mineral surface is determined by the reactions of surface function groups [58, 86, 93–95].

As discussed previously for amphoteric surface functionalities, surface charge and electrical potential in SCM are derived from the consequences of surface complexation for protons, hydroxyls, and other sorbates, with specific surface reactive sites defined as *MOH* (Eq. 7), where M represents the metal ion of the oxide mineral (i.e., Fe, Al, etc.) that is bound to the reactive surface hydroxyl. For phyllosilicate clays, the edges form the sites for surface complexation reactions through aluminol and silanol groups [57]. Protonation and deprotonation reactions are described as follows:

$$MOH + H^+ \leftrightarrow MOH_2^+ \tag{22}$$

$$MOH \leftrightarrow MO^- + H^+ \tag{23}$$

Reaction 22 and 23 are somewhat simplistic in that potentiometric titrations of oxide minerals often fail to display clear inflection points because surface acidity is a function of surface protonation and site heterogeneity even in fairly ideal monomineralic systems [86]. One approach for addressing such site heterogeneity is the use of strong and weak coordination sites, as in the Diffuse Double Layer Model (DDLM) of Dzombak and Morel (1990, ref. [96]). Even so, the thermodynamic equilibrium for Eq. 23 can be written as:

$$K = \frac{[MO^-](H^+)\gamma_{\mathrm{MO}}}{[MOH]\gamma_{\mathrm{MOH}}} \tag{24}$$

where the brackets refer to concentration, and parenthesis refer to activity, and γ is the activity coefficient for the respective species. Instead of defining more sites, the consequences of surface site heterogeneity discussed above are often addressed within the activity corrections in order to limit the number of site types that are modeled. Equilibrium constants derived for surface complexation reactions, such as the one described in Eq. 24, differ from aqueous reactions in that the surface activity terms represent corrections for the electrostatic energy at the mineral solution interface, i.e., the electrical double layer (*edl*):

$$K = K_C \times edl \tag{25}$$

where K_C is a conditional equilibrium constant written in terms of the activities for aqueous species, concentrations for surface sites, and the *edl* term is a model-dependent means of accounting for the surface potential or potential within the adsorptive plane [97]. One limitation in applying SCM to natural systems is the difficulty of characterizing the electrical double-layer properties of heterogeneous soils and aquifer sediments where sorbed ions, organic matter, and oxide coatings alter mineral surface charge properties, i.e., pH_{pzc}, in a manner that is difficult to predict and evaluate experimentally [77, 86, 87, 93, 98]. Goldberg et al. (2007) provide an excellent review of the experimental techniques used in validating a mechanistic understanding of contaminant sorption processes [58].

Two distinct approaches to the application of SCM to describe contaminant sorption to soil and aquifer materials have developed: the Component Additivity (CA) approach and the Generalized Composite (GC) approach. In the CA approach, one assumes the sorption behavior of heterogeneous natural materials can be described using a relative combination of the individual reactive components, with specific mass law

equations accounting for each phase of the mixture based on sorption experiments conducted on individual synthetic or ideal mineral analogs. For highly idealized systems, the CA approach can be quite effective in describing sorption behavior and even multicomponent solute transport [99]. For example, Table 4 provides the surface species and stability constants for UO_2^{2+} sorption to the poorly crystalline Fe oxyhydroxide, i.e., ferrihydrite, utilizing weak and strong binding sites [95, 100]. Although defining "strong" and "weak" sites enhances the ability to account for surface heterogeneity, it also doubles the number of adjustable site parameters, i.e., protonation/deprotonation constants, contaminant complexation constants, etc. However, the application of the CA approach to describing sorption behavior for natural materials has achieved only limited success [58, 101].

In contrast, the GC approach assumes that the sorption behavior of natural materials is far too complex to be described using the contributions of each sorptive phase. Furthermore, GC is often invoked in a non-electrostatic manner that considers adsorption purely in terms of surface equilibria without correcting for electrostatics, the influence of which is included to some degree in the resulting binding constants. As such, the resulting model may favor surface reactions that lack stoichiometric or spectroscopic validity, while providing an accurate description of the macroscopic sorption behavior. When the semiempirical GC approach is invoked, the specific protonation of the reactive surfaces does not have to be explicitly included, as it is grossly included within the contaminant specific sorption reactions [58, 93, 98, 101].

Vegetation Transfer Factors

Similar to the soil partition coefficient (K_d), the soil-to-plant transfer factor (TF), sometimes referred to as the Concentration Ratio (CR), is often used to quantify the bioavailability or plant uptake of a given soil contaminant. More mechanistic approaches to predicting plant accumulation of soil radionuclides based on nutrient uptake models have been developed. However, the inherent complexity of the rhizosphere and difficulty in parameterizing such models have limited their application [102].

The TF is the concentration of the radionuclide in dried plant tissue (Bq kg^{-1}) divided by the concentration of the radionuclide in the dried soil (Bq kg^{-1}) supporting the plant of interest, where the units cancel out yielding a dimensionless transfer term. Since mobility is a key factor controlling plant uptake of radionuclides, the TF is inversely correlated with K_d as expected [103]; however, the degree of correlation is often insufficient for predictive purposes. The TF is largely assumed to be associated with root uptake, as resuspension and foliar deposition are generally assumed to be minor [64, 104]. However, contaminated

Radionuclide Fate and Transport in Terrestrial Environments. Table 4 Stability constants for U(VI) sorption to Fe oxides (ferrihydrite) in component additivity (CA) modeling approach [95, 100]

Surface Species	Log K
$TOH + H^+ \leftrightarrow TOH_2^+$	6.51
$WOH + H^+ \leftrightarrow WOH_2^+$	6.51
$TOH \leftrightarrow TO^- + H^+$	−9.13
$WOH \leftrightarrow WO^- + H^+$	−9.13
$T(OH)_2 + UO_2^{2+} \leftrightarrow TO_2UO_2^0 + 2H^+$	−2.57
$W(OH)_2 + UO_2^{2+} \leftrightarrow WO_2UO_2^0 + 2H^+$	−6.28
$T(OH)_2 + UO_2^{2+} + H_2CO_3 \leftrightarrow TO_2UO_2CO_3^{2-} + 4H^+$	−13.031
$W(OH)_2 + UO_2^{2+} + H_2CO_3 \leftrightarrow WO_2UO_2CO_3^{2-} + 4H^+$	−17.103

T and *W* refer to strong and weak binding sites, respectively.

particulates are often a major part of the initial source term and risk associated with past nuclear reactor accidents [62, 105].

Although similar to the K_d, the TF depends on numerous factors, including the initial source of contamination (i.e., fallout, liquid waste, etc.), the duration since introduction, specific characteristics of the radionuclide, soil properties, soil management practices, nutrient status, and plant species, to name a few [104, 106, 107]. Microbial processes independent of plants also influence speciation, mobility, and plant availability of soil-borne radionuclides, particularly through the control of soil redox status. As observed for essential trace nutrients, mycorrhizal fungi can also facilitate root uptake of radionuclides, such as ^{137}Cs and ^{90}Sr [108, 109]. In addition, the calculated TF will depend to a large degree on how the rooting zone is defined for the purposes of soil sampling and analysis. The International Union of Radioecologists (IUR) has established a standard for estimating TF, with the upper 10 cm chosen as the rooting depth for grass species, and the upper 20 cm for all other crops, including fruit trees [106, 110]. The 2010 IAEA report also provides uptake transfer factors for 14 plant groups reflecting a range of crop species. The reader is directed to IAEA (2009) for a more comprehensive discussion of the complete data set and methods used in deriving the IAEA (2010) transfer parameters [64, 107].

Transfer factors tend to decrease with time after source introduction as the bioavailability of the radionuclide decreases. In recognition that soil properties, organic matter turnover, and nutrient cycling differ in response to the predominant environmental conditions, the IAEA [64] further divided the TF data into tropical, subtropical, and temperate systems based on site climate. As an example, an abbreviated list of the TF values for $^{90}Sr^{2+}$ associated with cereal grain production under various climatic conditions is presented in Table 5. As evident in Table 5, far less data are available for the subtropical and tropical systems in general. Furthermore, a specific set of TF values have been derived for rice production because of its importance as major food source in the humid tropics, and the unique flooded conditions under which it is grown. The fluctuating redox conditions associated with rice production can impact the speciation of redox-sensitive radionuclides, such as U, Pu, I, Tc, as well as the stability and sorption capacity of Fe

Radionuclide Fate and Transport in Terrestrial Environments. Table 5 Transfer factor (TF) values for $^{90}Sr^{2+}$ in cereal crops under various climatic conditions [64, 107]

Element	Plant group	Plant compartment	Soil group	N	Mean/value	GSD/SD	Minimum	Maximum
Temperate								
Sr	Cereals	Grain	All	282	1.1×10^{-1}	2.7	3.6×10^{-3}	1.0
			Sand	123	1.4×10^{-1}	3.0	3.6×10^{-3}	1.0
			Loam	71	1.1×10^{-1}	2.4	1.6×10^{-2}	7.2×10^{-1}
			Clay	72	7.8×10^{-2}	2.4	5.3×10^{-3}	7.1×10^{-1}
			Organic	10	9.7×10^{-2}	4.1	1.2×10^{-2}	3.6×10^{-1}
Subtropical								
Sr	Cereals	Grain	Loam	8	5.1×10^{-2}	1.3	3.6×10^{-2}	6.5×10^{-2}
		Stems, shoots	Loam	7	1.5×10^{-1}	2.5	4.2×10^{-2}	4.2×10^{-1}
Tropical								
Sr	Cereals	Grain	All	2	6.0×10^{-1}		4.4×10^{-1}	7.6×10^{-1}
			Sand	1	4.4×10^{-1}			
			Loam	1	7.6×10^{-1}			

N number of entries, *GSD/SD* geometric standard deviation/standard deviation

oxyhydroxides like goethite (α-FeOOH) and ferrihydrite ($Fe(OH)_3$), important sorbents in soil systems.

Radionuclide Migration

To date, contaminant transport research and modeling efforts have generally focused on improving the understanding of water movement while much less attention has been placed on the interrelated biological and geochemical reactions that impact solute partitioning, treating such complex processes in a rather simplistic manner that can be easily implemented within a multidimensional flow model [59, 111, 112]. However, numerous studies have demonstrated the inherent limitations in applying simplistic empirical partitioning expressions to describing contaminant migration at the field scale. Although coupling various reactive partitioning mechanisms to a transport model can be numerically challenging, a major limitation to the implementation of more mechanistic solute partitioning in transport models is the defensible parameterization of the model [59, 113].

For simplicity, radionuclide partitioning and transport in soil will be discussed in terms of the one-dimensional, steady-state convection dispersion equation (CDE):

$$\frac{\partial C}{\partial t} = D\frac{\partial^2 C}{\partial z} - v\frac{\partial C}{\partial z} - \frac{\rho}{\theta}\frac{\partial S}{\partial t} \qquad (26)$$

Terms 1 2 3

where C is the concentration of the solute in the aqueous phase ($M\ L^{-3}$), S is the sorbed concentration per unit mass of solid phase ($M\ M^{-1}$), ρ is the porous media bulk density ($M\ L^{-3}$), θ is the volumetric water content ($L^3\ L^{-3}$), v is the flow velocity ($L\,T^{-1}$), t or T is time (sec., min., days, etc.), z is distance (L), and D is the dispersion coefficient ($L^2\ T^{-1}$). Starting from the left, the CDE indicates that changes in the concentration of a solute with time are a reflection of the hydrodynamic dispersion (term 1), linear convective flow velocity (term 2), and sorption (term 3). In some form, the CDE has been widely applied to the description of radionuclide migration in soils, e.g., [64, 114–116]. Additional terms can be added to the equation to account for multiple flow domains, biodegradation, first-order decay, and other related processes. Also, preferential flow, physical and chemical soil heterogeneity, fluctuating θ, and/or facilitated transport may account for the rapid migration that is often observed for a small fraction of radionuclides following initial release to the soil environment [61, 115, 117].

The dispersion coefficient ($L^2\ T^{-1}$) can be further defined as:

$$D = \lambda v + D_e \qquad (27)$$

where λ is the dispersivity (L), and D_e is the effective diffusion coefficient ($L^2\ T^{-1}$). A non-sorbing solute, also referred to as a conservative tracer, is transported convectively in the flow stream and spreads by dispersion, a combination of molecular diffusion and mechanical dispersion resulting from differences in pore-water velocity and flow path. Thus, dispersion serves to dilute the solute plume (i.e., radionuclide) over the course of migration.

Understanding the physics of water movement is essential to correctly describing the migration behavior of a reactive solute, and interpreting the underlying mechanisms [118–120]. Dispersivity, generally considered a scale-dependent function of the physical heterogeneity encountered during solute migration, is a key factor in describing the physical aspects of contaminant migration in the subsurface environment. In addition to transport scale, different λ values have been reported as a function of varying degrees of saturation, θ. The transmissive path for convective transport is altered by changes in the degree of saturation that may control reaction kinetics and the type of surfaces available for sorption (i.e., phyllosilicate clays, Fe oxides, etc.) [120, 121]. Extensive breakthrough tailing observed under any flow regime can result from both physical and/or chemical disequilibria that may be conveniently, although incorrectly, described by the dispersion coefficient or even multiple flow domains, especially when applying a transport model that lacks the ability to explicitly account for nonlinear sorption behavior [122–124].

Assuming one understands the flow regime, linear sorption (i.e., n = 1) can be described as $S = K_d C$ (Eq. 19), and the CDE equation (Eq. 26) can be further simplified:

$$R\frac{\partial C}{\partial t} = D\frac{\partial^2 C}{\partial z} - v\frac{\partial C}{\partial z} \qquad (28)$$

where R represents the dimensionless retardation factor as it relates to K_d, ρ_{BD} is the matrix bulk density (M L^{-3}), and the volumetric water content, θ:

$$R = 1 + \frac{\rho_{BD} K_d}{\theta} \tag{29}$$

Retardation of a given solute can be more generally defined as

$$R = \frac{v_w}{v_s} \tag{30}$$

where v_w is the travel velocity for water, and v_s is the travel velocity of the solute of interest. A value other than 1 indicates that the solutes interact with the soil in some way, with R > 1 indicative of sorption and R <1 indicating some form of pore-water exclusion that results in the solute traveling faster than water.

Differences in K_d values observed for batch equilibration and flow-through systems have been attributed to: (1) differences in soil:solution ratio inherent to each system; (2) failure to remove or account for competitive reaction products in batch studies; (3) limitations in the availability of sorption sites in batch versus column experiments; (4) colloid-facilitated transport; (5) inherent limitations in the linear distribution coefficient to account for temporal and spatial variations in groundwater chemistry; (6) partitioning reactions controlled by solubility and/or redox conditions; and (7) rate-limited geochemical reactions and physical nonequilibrium present under flowing versus static conditions [62, 120, 125–130]. Under complex field conditions, several of these limitations may be operative at the same time. However, flow-through techniques can provide a better representation of field conditions than batch sorption experiments by accounting for temporal and spatial nonequilibrium.

When radionuclide sorption can be described using the K_d, the CDE equation (Eq. 28) can be solved analytically given appropriate boundary conditions, such as pulse-like or step input histories. More complex reaction schemes and variable boundary conditions can be invoked within the transport equation through numerical solutions. Figure 4 illustrates the breakthrough behavior observed for the three different sorption isotherms presented in Fig. 3, i.e., Linear, Freundlich, and Langmuir. In discussing the modeled breakthrough results, the term "rad" will be used to identify the hypothetical radionuclide solute. In each case, the rad is introduced at one of two different inlet concentrations (20 and 40 mg L^{-1}) to illustrate the impact of solute concentration on breakthrough for the three different sorption isotherms. For both cases the inlet rad concentration (C_o) remains constant for two pore volumes (PV), followed by several PV of rad-free water. In Fig. 4a, piston flow behavior for a nonreactive solute is included for comparison to illustrate the influence of both sorption and dispersion on contaminant transport. For piston flow, the solute displays 100% breakthrough (i.e., $C/C_o = 1$) after exactly 1 PV of leaching, and the leach-out breakthrough occurs exactly 1 PV after the inlet source is removed, i.e., 3 PV in the present example. As a result of sorption and hydrodynamic dispersion, the reactive solute breakthrough is both delayed and diluted with respect to the piston flow example, with maximum breakthrough of about 60% ($C/C_o = 0.6$) occurring at slightly less than 3 PV. However, the breakthrough behavior is exactly the same for the two different inlet concentrations, and the total rad mass applied to the column is recovered in the effluent.

Similar breakthrough is observed for both the Freundlich (Fig. 4b) and Langmuir (Fig. 4c) isotherms at each of the two different inlet concentrations, with both earlier and higher relative breakthroughs observed with increasing inlet concentration. Differences between the two nonlinear isotherms would be more evident at higher inlet concentrations where the Langmuir isotherm has leveled off at the sorption maximum, while the Freundlich isotherm continues to predict increasing sorption. Also, extensive breakthrough tailing observed for both nonlinear isotherms is a consequence of the higher relative degree of sorption observed at lower concentrations when compared to the Linear isotherm. Despite such different breakthrough histories, the total rad mass applied is recovered in the column effluent for all three isotherms, assuming sufficient leaching.

As illustrated by the previous example, the interpretation of contaminant migration behavior suffers from the same limitations inherent in the interpretation of sorption behavior in laboratory batch studies. Even in relatively simple one-dimensional column studies, similar contaminant migration patterns can be derived from different combinations of chemical

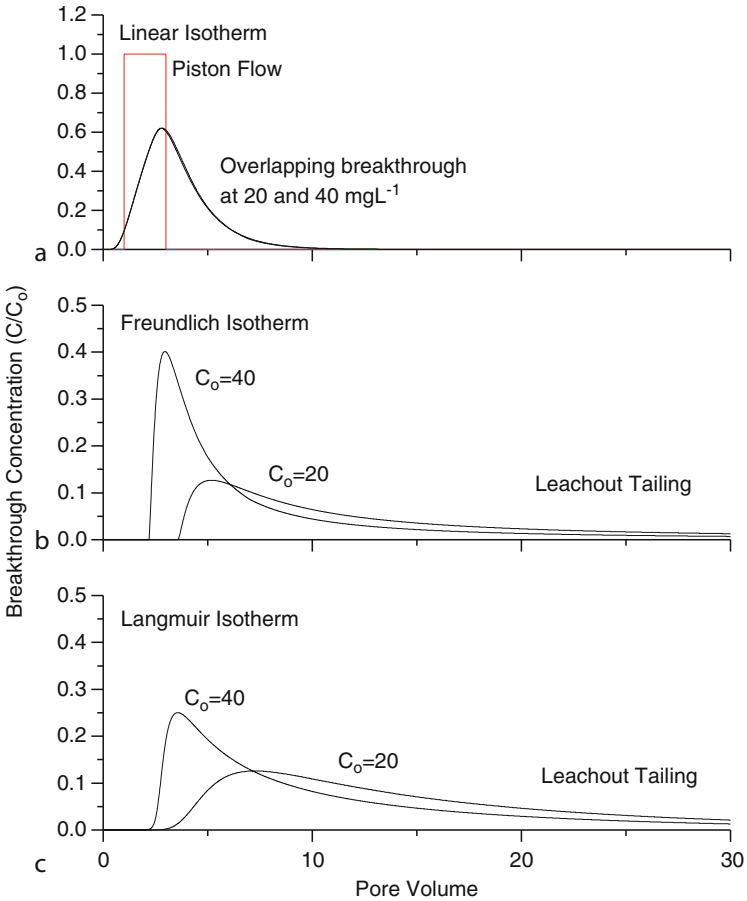

Radionuclide Fate and Transport in Terrestrial Environments. Figure 4
Relative outlet concentration (i.e., C/Co) as a function of time (pore volume) for a reactive solute (2 PV pulse) based on sorption isotherm: (**a**) Linear, (**b**) Freundlich, and (**c**) Langmuir partitioning (based on isotherms in Fig. 3)

retardation processes (e.g., reaction kinetics, nonlinear sorption behavior, sorption competition, etc.) and physical transport phenomena, such as mass transfer kinetics [118, 120, 126, 131, 132]. At a fundamental level, the mathematical equations used to describe physical and chemical nonequilibrium are identical, and thus distinguishing such processes based on the transport behavior of a reactive solute requires the presence of a "conservative" tracer for comparison. Reactive solutes often display complex transport behavior that can be misinterpreted in terms of multiple chemical and physical processes in the absence of an a priori understanding of the solute sorption behavior [122, 124, 133–136].

A transient flow model that accounts for changes in soil θ, usually through the use of Richards' equation to describe water flow, can improve transport predictions for radionuclides displaying low to moderate partitioning to the immobile soil matrix [137, 138]. For radionuclides displaying very high K_d values, movement in the soil environment may be insensitive to transient fluctuations in θ, and thus migration can be described by the steady-state CDE based on the average rate of water movement down the profile. As before, the dispersion term accounts for a combination of mechanisms that tend to spread the solute plume in a manner analogous to diffusion. Furthermore, various forms of the CDE equation can be used to describe radionuclide distribution in the soil profile without considering contaminant partitioning based on "apparent" convection and dispersion coefficients that describe the center of mass and distribution, respectively, without

accounting for actual water flux or θ. This approach yields an apparent site-specific migration rate (i.e., cm y^{-1}) and an apparent dispersion coefficient that can be readily used for comparing the behavior of various radionuclides [115, 116, 139–141]. The application of the steady-state CDE model to unsaturated soil systems often under predicts an initial period of rapid migration when applied to the transport of radionuclides with high K_d values, generally assumed to reflect physical or chemical nonequilibrium.

Compartmental models, also called "residence time" models, offer a more "black box" alternative to the CDE for describing radionuclide migration in the soil and vadose zone. The soil profile is split into "compartments" that are conceptually consistent with natural soil horizonization, providing a means for accounting for vertical soil heterogeneity. However, model compartment dimensions are often established based on an arbitrary sampling scheme rather than soil properties.

Radionuclide transport in a compartment model is controlled by a system of linear first-order differential equations representing each layer [139, 142]. The change in concentration (i.e., activity) of a radionuclide, C, in a given layer, i, can be described as:

$$\frac{\Delta C_i}{\Delta t} = K_{i-1}C_{i-1} - K_i C_i \tag{31}$$

where K_i is the transfer rate from one layer to another. The resulting migration velocity for the compartmental model reflects a combination of both convective and diffusive transport processes, yielding a migration rate that differs from the effective convection velocity in the CDE. In the compartmental model, the dispersive effect is a function of layer thickness in that the accuracy of radionuclide distribution is limited to the thickness of layers homogenized for soil analysis [115, 139, 143, 144]. As with the CDE, both analytical and numerical methods are available depending on the complexity of both the compartmental layers and the underlying boundary conditions.

Although the SCM approach has been used extensively to describe batch sorption data [96], extension of the approach to the description of reactive solute migration has been limited. To date, the SCM approach has been reasonably successful in describing U, zinc (Zn), phosphate (PO_4^{3-}), and molybdate (MoO_4^{2-}) migration in saturated materials, and boron (B) in an irrigated agricultural field [93, 98, 101, 145–148]. As discussed above for even relatively simple solute transport models, the development of mechanistic transport models must be constrained in a manner to minimize the number of model parameters that can lose their mechanistic significance when applied to the complexities of the field.

Characteristics of Specific Radionuclides

In discussing the properties of radionuclides that impact their behavior in soils, it is important to note that the physical and chemical processes that control solubility, sorption, and migration have no impact on the isotopes decay mechanism or radioactivity. Information about the total amount of a given radionuclide in a soil system provides little information concerning its form, i.e., chemical speciation, or bioavailability [16]. Furthermore, radionuclides do represent a unique hazard when compared to other environmental contaminants (i.e., heavy metals, organic solvents, etc.) in that intimate contact, inhalation, and ingestion are not necessarily prerequisites for exposure. Formed by neutron capture reactions, actinides (e.g., Pu, Am, and Np) exhibit complex speciation chemistry with multiple stable oxidation states, each of which can form complexes and solid phases with unique stability characteristics [13, 82]. Because of such complexity, a thorough discussion of actinide speciation chemistry is beyond the scope of the current chapter.

Americium

Americium, an actinide with no stable isotopes, has mainly been introduced in the environment through atmospheric weapons testing in the 1950s and 1960s. Nineteen isotopes of Am have been identified with atomic masses ranging from 231 to 249, most of which have very short half-lives. Americium-241 ($t_{1/2}$ = 432.2 y) and ^{243}Am ($t_{1/2}$ = 7,370 y) are the only isotopes with half-lives long enough to persist as radioactive waste in SNF. Plutonium-241 ($t_{1/2}$ = 14.4 y) results from multiple neutron adsorption events for ^{238}U, which then decays via β emission to form ^{241}Am. Americium-241 primarily decays by α emission to ^{237}Np plus a strong γ emission that is useful as a source for γ radiography. Americium is also used as a source of ionization in smoke detectors [90, 149].

Similar to several other actinides (Pa, U, Np, Pu), Am can occur in several oxidation states (III–VI), although the +3 form dominates with a speciation chemistry similar to trivalent lanthanides. All other oxidation states are strong oxidizing agents and are therefore unstable in the presence of other oxidizable compounds. As with other actinides, Am forms strong complexes with oxygen-donating ligands (OH^-, PO_4^{3-}, and CO_3^{2-}) and relatively weak complexes with monovalent anions, Cl^-. The Am^{3+} cation dominates under acidic conditions, with various hydrolysis products forming with increasing pH. It is usually considered to be fairly immobile, displaying relatively high K_d values; however, this can make facilitated transport more likely. For instance, Artinger et al. [150] found that a small fraction of Am was preferentially transported in association with DOC, while the largest fraction remained sorbed to immobile Fe oxides. Similar to U, the Am-carbonate complexes are generally more important with increasing pH, forming anionic complexes that increase solubility under alkaline conditions. Americium also forms strong complexes with humic substances [12, 50, 82, 90, 149].

In a relevant example of Am partitioning in soils, leaking storage drums at the Rocky Flats DOE site released ^{241}Am and ^{239,240}Pu. Both Am and Pu were found to be largely associated with Fe oxides and to lesser degree with SOM. Column and batch experiments indicated that reducing conditions in the presence of strong complexing agents were effective at recovering a large fraction of the total α activity from the Rocky Flats soil [151]. Another study at Rocky Flats measured ^{239,240}Pu and ^{241}Am in storm-water runoff and pond-water discharge in different size fractions [50]. The actinides were found to be primarily associated with the particulate phase (>0.5 μm), but a significant colloidal fraction was able to pass through the filter.

Cesium

Cesium, with ^{133}Cs as the only stable isotope, is ubiquitous in the soil environment and exists in the +1 oxidation state, forming very few stable aqueous complexes. The most important radioactive Cs^+ isotopes include: ^{134}Cs ($t_{1/2}$ = 2.05 y), ^{135}Cs ($t_{1/2}$ = 3 × 10^6 y), and ^{137}Cs ($t_{1/2}$ = 30.2 y). Cesium-137, a nuclear fission product, decays by β^- emission with ≈ 85% forming the metastable ^{137m}Ba which subsequently decays within minutes by γ emission (0.66 MeV) [10, 12].

As a chemical surrogate for K^+, Cs^+ behavior is governed by similar metabolic and geochemical processes in the environment. Like K^+, Cs^+ tends to serve as a biochemical electrolyte rather than a structural component in plant or animal tissues. However, Cs^+ concentrations and Cs^+/K^+ ratios have been observed to increase by a factor of 2–3 for each increase in the trophic level. Despite similar uptake rates, the apparent bioaccumulation of Cs^+ has been attributed to the longer biological retention times when compared to K^+, with a biological half-life in humans that is two to five times that of K^+ [152].

Despite its high solubility, Cs^+ can be selectively adsorbed and strongly bound to zeolites and certain 2:1 phyllosilicate clays, often resulting in contamination being restricted in close proximity to the point of deposition [61, 153–157]. As discussed earlier, polyvalent ions tend to sorb to a greater degree than monovalent ions on soil clays; however, there is a distinct exception when discussing monovalent ions with low hydration energy, such as Cs^+, Rb^+, and K^+ (also NH_4^+). Micas (illites) and vermiculites, 2:1 phyllosilicate clays possessing relatively high layer charge, have the ability to irreversibly fix or "sorb" certain elements and molecules within the clay interlayer, significantly reducing their mobility and bioavailability in the soil environment.

Interlayer sorption followed by cation dehydration can induce interlayer collapse known as fixation, which is to some degree irreversible [153, 158–160]. Such high-affinity interlayer sorption sites are called frayed edge sites (FES selectivity $Cs^+ > Rb^+ > NH_4^+ > K^+$) [161, 162]. The specific Cs^+ sorption capacity for soil and clay materials has been operationally defined by use of the silver thiourea (Ag-TU) method. The Ag-TU complex displays a high affinity for cation exchange sites on the outer planar surfaces of soil clays, blocking their ability to retain common soil cations; however, the Ag-TU complex is unable to access "frayed edge sites" because of its size [163]. Other factors such as the soil moisture content, the presence of organic acids and cations of similar ionic radius (K^+ and NH_4^+) can affect Cs^+ sorption and fixation by soil clays [158, 164–166].

This suggests that the relative effectiveness interlayer fixation of Cs^+ as a stabilization method depends on factors such as background solution composition (i.e. predominant cation), soil pH, clay mineralogy, and SOM content [166].

Recognizing the widespread distribution of 2:1 clays and their ability to strongly sorb ^{137}Cs, the National Council on Radiological Protection and Measurement (NCRP) recommends a default value for the TF of 0.1 for risk calculations. However, TF values reported for the DOE Savannah River Site (SRS) facility, located near Aiken, SC, are much higher, with mean values ranging from ≈ 3 to 15 [167–169]. The poor retention in SRS soils has been attributed to their coarse texture and a clay fraction dominated by Fe oxides (i.e., goethite) and kaolinite, a 1:1 layer phyllosilicate with no capacity for interlayer fixation [73]. The poor retention of Cs may be exacerbated in riparian and wetland systems where anoxic conditions can result in the buildup of NH_4^+ that competes with Cs^+ for FES sorption sites [167, 170, 171].

In systems that display a limited intrinsic ability to fix $^{137}Cs^+$, the addition of illitic clays can effectively reduce the mobility and bioavailability of $^{137}Cs^+$ [73]. Using a limno-corral system that isolates the water column above the contaminated pond sediments, Hinton et al. [170, 172] further demonstrated that the addition of illites can reduce $^{137}Cs^+$ availability in aquatic systems. However, the widespread use of such a remediation technique is limited by the need to incorporate the sorptive materials within the contaminated soils, a practice that would drastically disturb a functioning, albeit contaminated, ecosystem.

Greenhouse and field studies have demonstrated the ability of zeolites to reduce the uptake of $^{137}Cs^+$ in plants [41, 173]. Certain zeolites, e.g., clinoptilolite, display high ion exchange selectivities for Cs^+ and Sr^{2+} [41], even in the presence of Ca^{2+} and Mg^{2+}, and are naturally abundant enough for use as low-cost sorbents. Selectivity for Cs^+ and Sr^{2+} is generally highest under slightly acidic conditions (pH 5.0–6.0), but drops off dramatically at lower pH values due to competition with hydrogen for exchange sites. The presence of strong ligands, such as the synthetic chelate EDTA or citrate and tartate, can also reduce Cs^+ and Sr^{2+} sorption [174]. One advantage of zeolites is that they possess high sorption capacity even in larger particle-size fractions due to the internal reactive voids. This makes the material ideal for systems where hydraulic conductivity must be maintained, such as reactive flow-through barriers. Zeolites can also be incorporated into bentonite clay liners in minor amounts to improve the sorptive capacity of the liner without overly enhancing hydraulic conductivity. However, the larger particle size can have a negative impact on the kinetics of sorption [174]. In addition, zeolites are not effective sorbents for transuranic species, such as uranyl (UO_2^{2+}), that are commonly found at sites with elevated Cs^+ and Sr^{2+} levels [39].

Iodine

Iodine (I) has many short-lived isotopes (including ^{131}I and ^{125}I), one long-lived isotope, ^{129}I ($t_{1/2}$ = 1.6 million y), and one stable isotope, ^{127}I. Due to its long half-life, tendency to accumulate in the thyroid, and perceived high mobility in the environment, ^{129}I is often a key radionuclide of environmental concern [175]. There are many sources of ^{129}I to the environment. Naturally, ^{129}I can be produced from cosmic-ray spallation of Xe in the atmosphere and spontaneous fission of ^{238}U in the earth's crust. Anthropogenic inputs of ^{129}I to the environment include atmospheric weapons testing, the Chernobyl reactor accident, and SNF reprocessing, with the major contributors being Sellafield (formerly Windscale) and LaHague [176].

Iodine occurs in several oxidation states with −1, +5, and molecular I_2 being the most environmentally relevant [81]. Iodide (I^-), iodate (IO_3^-) and organic iodine are the main species of iodine in the environment. Although I^- and IO_3^- dominate in environmental waters, organic iodine is common in soils and sediments [177]. Iodine forms negatively charged species and thus, like ^{99}Tc, is assumed to be highly mobile in neutral to alkaline environments. This behavior is of particular concern at contaminated sites such as the DOE-SRS. The F-Area Basins on the SRS were used for the disposal of large volumes of low-level acidic waste. After basin closure, remediation efforts first involved pump-and-treat to control the spread of the mobile groundwater contaminants, i.e., ^3H_2O, ^{129}I, etc. More recently, base injection to neutralize the low pH (~3.5) groundwater has been successfully applied to sequester contaminant metals; however, such treatment can

mobilize ^{129}I associated with variable-charge minerals as a result of the increase in pH. Current studies are underway to better understand I speciation and to help develop successful remediation strategies [178–180].

Historically, total ^{129}I has been measured by accelerator mass spectrometry and neutron activation. More recently, analytical methods have involved the use of high performance liquid chromatography and inductively coupled plasma mass spectrometry coupled with ion chromatography and gas chromatograph mass spectrometry to better evaluate the dynamics of I speciation [177, 180–182].

Plutonium, Pu

The current environmental inventory of Pu is largely derived from nuclear weapons testing and accidental releases, such as the reactor fire at Windscale in 1957 and the Chernobyl explosion in 1986 [10, 28]. However, minor amounts of Pu were generated from neutron capture by ^{238}U within the U ore of the Oklo natural reactor in Gabon. There are 15 known Pu isotopes, the three most common of which are ^{239}Pu (94%; $t_{1/2}$ = 24,000 y), ^{240}Pu (6%; $t_{1/2}$ = 6,560 y), and ^{241}Pu (0.4%; $t_{1/2}$ = 14.4 y). Plutonium-239 and ^{240}Pu decay by α emission, forming ^{235}U and ^{236}U, respectively. The generation of fissile ^{239}Pu from the more plentiful ^{238}U associated with nuclear fuel contributes about one-third of the energy produced in the reactor. Plutonium is a major proliferation hazard because a limited mass of ^{239}Pu (≈ 7–10 kg) is required to create a nuclear bomb. When ingested, Pu tends to concentrate in the bones and liver [10, 12].

Oxidation-reduction reactions are critical in controlling Pu behavior in the environment, with four common redox states (i.e., III, IV, V, and VI) possible under typical pH and redox conditions. In fact, multiple Pu redox states can coexist in solution. Iron oxides such as goethite (α-FeOOH), hematite (α-Fe_2O_3), and magnetite (Fe_3O_4) have been shown to facilitate the reduction from Pu(V) to Pu(IV) across a broad pH range, from 3 to 8, with sorption to the oxide required in many instances for reduction to occur [183, 184]. Plutonium (IV) is less soluble and sorbs readily. Plutonium forms very strong carbonate and hydroxyl complexes that enhance solubility at pH > 7 [21, 82, 89, 185, 186].

Radium-226 and Radon-222

There are two products within the U-Th decay series that warrant special attention, Radium-226 (^{226}Ra, $t_{1/2}$ = 1,600 y) and its daughter Radon-222 (^{222}Rn, $t_{1/2}$ = 3.8 d), because they represent a significant fraction of the background internal radiation dose to humans. Radium (Ra^{2+}), an alkali-earth metal, behaves similarly to Ca^{2+} and Ba^{2+}, and is often found associated with U-bearing minerals. Radium may coprecipitate with various sulfate and carbonate minerals, and readily sorbs to phyllosilicate clays and Fe and Al oxides in a fairly reversible manner. Radium is considered to be more mobile in the soil environment than U and more subject to plant uptake [12, 59].

Radon (Rn) is a colorless and odorless inert gas that is water soluble, insensitive to aqueous speciation, and displays negligible interaction (i.e., $K_d \approx 0$) with soil components. However, the generation of ^{222}Rn depends on the presence of the parent elements (i.e., U, Th, Ra) that are subject to various soil processes, i.e., sorption, precipitation, etc. Radon-222 ($t_{1/2}$ = 3.8 d) is derived from ^{226}Ra via decay in the ^{238}U decay series. Twenty isotopes of Rn have been identified, all of them radioactive, many with very short half-lives [89]. The inert ^{222}Rn gas displays a negligible ability to accumulate in the body; however, the short half-life results in the significant potential for α decay to occur while exposed to the sensitive tissues within the lungs, accounting for approximately two-thirds of the natural radiation dose within the USA. Furthermore, Rn exposure has been estimated to account for 6–12% of the cases of lung cancer observed in the USA [10].

Strontium-90

Strontium (Sr), a chemical analog for Ca^{2+}, is generally present in the soil environment in the +2 oxidation state. Nuclear fuel processing and weapons testing are the primary sources for the radioactive fission products, $^{89}Sr^{2+}$ ($t_{1/2}$ = 52 d) and $^{90}Sr^{2+}$ ($t_{1/2}$ = 29 y). Because of the short half-life of $^{89}Sr^{2+}$, $^{90}Sr^{2+}$ represents the more persistent environmental problem. As with other alkaline earth cations, Sr^{2+} partitioning is primarily controlled by the CEC of the soil, and competition with other common exchangeable cations (i.e., Ca^{2+}, Mg^{2+}, Na^{+}, K^{+}, etc.), as well as stable Sr^{2+}. Solution pH

and ionic strength are also important factors controlling Sr^{2+} partitioning [187–189].

On an equivalence basis, cation exchange experiments have shown that stable Sr^{2+} will dominate cation exchange site in competition with alkaline and alkaline earth cations, i.e., $Sr^{2+} > Ca^{2+} > Mg^{2+} > K^{+} > NH_4^{+} > Na^{+}$; however, the concentration of $^{90}Sr^{2+}$ in soil systems is typically several orders of magnitude lower than Ca^{2+}. Consistent with cation exchange as a sorption mechanism, $^{90}Sr^{2+}$ does not become more recalcitrant with extended equilibration time, and is therefore subject to desorption when in the presence of competing cations [190]. However, other studies have reported that some fraction of $^{90}Sr^{2+}$ may become less exchangeable with extended soil equilibration, presumably due to substitution within calcium-bearing minerals. Under high pH conditions, $^{90}Sr^{2+}$ may coprecipitate with calcite ($CaCO_3$) or anhydrite ($CaSO_4$), or precipitate as strontianite, $SrCO_3$ [89, 191]. Strontium does not form strong complexes with either organic or inorganic ligands, with the possible exception of $Sr\text{-}CO_{3(aq)}$ under high pH conditions [192]. As an analog of Ca^{2+}, Sr^{2+} is readily taken up by plants and tends to accumulate in the bone and bone marrow of animals [12].

Technetium-99

Technetium-99 (^{99}Tc), with a half-life of 210,000 years, is a neutron fission product of ^{235}U and ^{239}Pu [12]. Under oxidizing conditions, Tc persists in the environment as the pertechnetate anion (TcO_4^{-}), with Tc in the +7 oxidation state. As an anion, pertechnetate is generally assumed to sorb poorly to many soil clays that display significant negative surface charge (i.e., cation exchange capacity) resulting from isomorphic substitution [12, 193]. Technetium-99 also appears to be readily translocated in plants from the roots to leaves.

Pertechnetate (TcO_4^{-}) sorption is generally associated with variable-charge soil (i.e., amphoteric) minerals, like Fe and Al oxides/oxyhydroxides. However, TcO_4^{-} is subject to competition for sorption sites from other common soil anions, such as Cl^{-}, NO_3^{-}, PO_4^{3-}, and SO_4^{2-}. Sheppard and Thibault (1990) reported Tc (VI) K_d values in the range from 0.1 to 1.0 depending on texture and SOM content [92]. In contrast, Kaplan et al. (2008) reported higher K_d values for materials rich in Fe oxides [194]. Under anoxic conditions, Tc (VII) can be reduced to the sparingly soluble Tc(IV) oxidation state, which in the absence of strong complexing agents is subject to additional sorption to soil minerals and organic matter and may form the sparingly soluble $TcO_2 \cdot nH_2O$ [195–197]. Heterogeneous reduction of Tc(VI) by sorbed Fe(II) is faster than homogeneous reduction by soluble Fe(II). Such reactions are somewhat reversible as recent studies have shown that Fe(III) can serve as an oxidant for Tc(IV) under acidic condition [196].

Thorium

Thorium (Th) is ≈ three times more abundant in the earth than U, and exists in the +4 oxidation state, forming hydroxide and carbonate species in the soil environment. Thorium has several isotopes with atomic masses ranging from 212 to 236, all of which are unstable [10, 12, 89]. In addition to its greater abundance than U, interest in the use of Th for nuclear power generation has increased in recent years because it represents less of a nuclear proliferation threat, and produces fewer long-lived actinides (i.e., Np, Am, and Cs). For use in a nuclear reactor, ^{232}Th requires a neutron source to produce the fissile ^{233}U; however, ^{232}Th can replace natural uranium (i.e., mixture of 0.7% ^{235}U and 99.3% ^{238}U) in the reactor fuel with less enriched U required as an initial neutron source. Once the process has started, Th-based fuel has the potential to maintain (i.e., breed) the production of ^{233}U without requiring any additional enriched U. Further, the use of a fuel mixture of Th and natural U reduces the production of ^{239}Pu and complicates the potential extraction of fissile ^{233}U, further limiting nuclear proliferation when compared to current fuel practices [17].

Tritium, ^{3}H

Tritium (^{3}H) is one of the three isotopes of hydrogen, which include the stable isotopes hydrogen (^{1}H; 99.984% abundance) and deuterium (^{2}H; 0.016% abundance). As an isotope of hydrogen, ^{3}H can exist in ionic, gaseous, solid, and liquid forms. Small quantities of ^{3}H are produced naturally in the stratosphere by cosmic-ray interaction with ^{14}N to form ^{12}C in addition to ^{3}H. Nuclear fallout and discharges from nuclear power facilities reflect a greater source of ^{3}H

than cosmic rays. Tritium is produced by fission and thermal neutron reactions with ^{6}Li in nuclear reactors. Tritium has a half-life of 12.3 y, and readily combines with oxygen to form tritiated water ($^{3}H_2O$), with a $K_d \approx 0$. Tritium decays to ^{3}He by means of low-energy β^- emission (18.6 keV) that is commonly determined by liquid scintillation analysis. Atmospheric nuclear weapons testing has released 2.4×10^{20} Bq of ^{3}H into the environment [10].

Tritium has several industrial uses including luminous paints, non-powered light sources, and as a radioactive tracer in chemical, geological, and biological experiments [12]. Because $^{3}H_2O$ water travels at the same rate as groundwater (i.e., $K_d \approx 0$ and R = 1), it is often used as a conservative tracer in natural recharge and solute transport experiments to differentiate between multiple complex physical and chemical processes that impact the migration of a "reactive" solute [88, 188]. Although subject to possible substitution for stable H on oxides and clays, such reactions are deemed to be minor because of the relative low concentration of ^{3}H compared to the other isotopes of hydrogen, ^{1}H and ^{2}H, indicating that ^{3}H would need to be highly preferred to see significant retention, as indicated by the lack of an effective ion exchange method for separating $^{3}H^+$.

Tritiated water can be incorporated into the body by several pathways, including inhalation of vapor, absorption through the skin, and ingestion, by far the dominant uptake pathway [198, 199]. Once inside the body, $^{3}H_2O$ is generally distributed in the bodily fluids, with a limited fraction incorporated into various body compartments, and predominant excretion through urine and feces. A small fraction of ingested ^{3}H is tightly bound to organic structures, i.e., organically bound tritium (OBT), which can be released by decomposition or combustion, complicating liquid scintillation analysis [200]. With continuous exposure, $^{3}H_2O$ reaches a steady-state concentration in body fluids, and removal of the source allows for depuration [198, 201, 202]. The human biological half-life for ingested $^{3}H_2O$ within body fluids ranges from about 9.5 to 12 days compared to $\approx$ 2.26 days for rodents [12, 203, 204].

Uranium

For a comprehensive discussion of U geochemistry the readers are directed to Burns and Kinch [205]. Uranium is the most common radionuclide soil contaminant throughout the DOE weapons complex [23]. Furthermore, thermodynamically unstable $UO_{2(s)}$ represents greater than 90% of SNF, which upon oxidation forms $UO_{3(s)}$ corrosion products at relevant environmental temperatures [206]. In nature, U exists primarily as three isotopes, ^{238}U (99.3% abundance; $t_{1/2} = 4.5 \times 10^9$ y), ^{235}U (0.71%; $t_{1/2} = 7.13 \times 10^8$ y), and ^{234}U (0.0057%; $t_{1/2} = 2.47 \times 10^5$ y). However, ^{235}U is of primary interest for nuclear weapons and power generation because of its fissile capacity [10, 12]. Uranium exists in multiple oxidation states (from +4 to +6), with U(IV) and U(VI) dominating under reducing and oxidizing conditions, respectively. Under oxidizing conditions, U(VI) hydrolyzes instantly to form the uranyl cation (UO_2^{2+}). In the absence of carbonates, UO_2^{2+} forms various hydrolysis species in response to pH, UO_2OH^+, $UO_2(OH)_2^o$, $UO_2(OH)_2^-$, etc. [95]. Soil parameters such as OM content, Fe oxide content, and pH play a strong role in controlling U partitioning [207].

The U-carbonate species tend to dominate at neutral and higher pH conditions. Uranium also forms strong complexes with fluoride (F^-), phosphate (PO_4^{3-}), sulfate (SO_4^{2-}), and DOC [205, 208–211]. Cation exchange studies suggest that UO_2^{2+} displays similar affinity to the fully hydrated Ca^{2+} for interlayer cation exchange sites; however, surface complexation reactions tend to dominate with increasing U concentrations and pH > 4 [212]. In a biological setting, U tends to accumulate in the bones and bone marrow of animals, with a biological half-life of $\approx$ 300 d. Long-lived radionuclides, like natural and depleted U (i.e., mostly ^{238}U), may display greater chemical rather than radiological toxicity [12, 213].

Most remediation efforts focus on altering U speciation to favor the formation of insoluble/immobile U phases. Amonette et al. [214] provide an in-depth review of various methods for assessing the environmental availability of U as a means of evaluating the relative effectiveness of such efforts. Uranium reduction in situ has been widely evaluated as a potential remediation strategy [215–219]. In recognition of the fact that many actinides and other heavy metals form relatively insoluble phosphates under a range of pH conditions, the addition of apatite ($Ca_5(PO_4)_3OH$) and other PO_4 sources has been evaluated as a means

of remediating U and other metal-contaminated sites [73, 74, 84, 120, 211, 220–224]. For example, Arey et al. (1998) demonstrated in batch studies that minor additions (<5% by wt.) of hydroxyapatite to a highly weathered contaminated soil from the DOE-SRS significantly reduced water-soluble U, as well as a number of other environmentally important metals, such as nickel (Ni) and lead (Pb). Although directly correlated to DOC, U solubility in apatite-amended soil was found to be less than that expected for the common U phosphate mineral, autunite, with TEM analysis revealing U to be largely associated with secondary Al-phosphate precipitates rather than residual apatite [74, 84].

Future Directions

In concluding the discussion of processes controlling the fate and transport of radionuclides in terrestrial systems, it is important to note critical areas warranting greater research attention. As mentioned previously, a good deal of site-specific data is required for the development of both empirical and mechanistic models (both conceptual and numerical) for describing radionuclide partitioning in the presence and absence of corrective measures, and their impact on receptor exposure. The development of efficient geophysical methods for evaluating physical and chemical heterogeneity that impact radionuclide partitioning at the field scale is critical in site characterization and identifying an appropriate remediation strategy, including MNA and institutional control. Such characterization efforts should be a component of a systematic, iterative process designed to minimize uncertainty associated with performance assessment and waste disposition.

Additional research is needed concerning the aqueous and solid-phase speciation of transuranics in complex environmental samples, including aqueous complex formation and their incorporation at trace levels within mineral phases. Assessing the impact of facilitated transport (i.e., mobile colloids and DOC) for strongly sorbing/insoluble radionuclides requires additional consideration. Further development and refinement of a consistent thermodynamic database for radionuclides that can be used within mechanistic speciation, transport, and exposure models will aid in reducing uncertainties associated with environmental impact assessments. Even when the use of mechanistic partitioning schemes within contaminant transport models is impractical, a better understanding of the partitioning mechanisms can certainly help to constrain the use of appropriate empirical parameters for a given transport scenario. Continued focus on reaction and partitioning kinetics is warranted as many environmental systems are not at chemical equilibrium. An expanded focus on the ecological impact of radionuclides in combination with other anthropogenic contaminants (i.e., metals, organic solvents, etc.) is warranted, as contaminated sites usually contain a complex mixture of various hazardous agents as part of a multi-stressor approach.

Acknowledgments

Preparation of this manuscript was partially funded by Cooperative Agreement DE-FC09-07SR22506 between the University of Georgia and the Department of Energy. The authors would like to acknowledge the assistance of T. Murphy and L. Lee with revising the manuscript and reproducing the figures.

Abbreviations

AO	Ammonium-oxalate
AEC	Anion exchange capacity
amu	Atomic mass units
CEC	Cation exchange capacity
CDB	Citrate-dithionite-bicarbonate
CA	Component additivity
CDE	Convection dispersion equation
DOE	Department of Energy
DDLM	Diffuse Double Layer Model
EPA	Environmental Protection Agency
FES	Frayed edge sites
GC	Generalized composite
HLNWR	High-level nuclear waste repository
HIS	Hydroxyl-interlayered smectite
HIV	Hydroxyl-interlayered vermiculite
IAEA	International Atomic Energy Agency
IUR	International Union of Radioecologists
IAP	Ion activity product
MCL	Maximum contaminant limit
MNA	Monitored natural attenuation
NCRP	National Council on Radiological Protection and Measurement

NORM	Naturally occurring radioactive materials
NRC	Nuclear Regulatory Commission
OBT	Organically bound tritium
OM	Organic matter
PV	Pore volume
SI	Saturation index
SRS	Savannah River Site
SEM	Scanning electron microscope
Ag-TU	Silver thiourea
SOM	Soil organic matter
TF	Soil-to-plant transfer factor
SNF	Spent nuclear fuel
SCM	Surface complexation modeling
TCLP	Toxicity Characteristic Leaching Procedure
UMTRA	Uranium Mill Tailings Remedial Action
XRD	X-ray diffraction

Bibliography

1. Strand P, Brown J (2009) The international conference on radioecology and environmental radioactivity. J Environ Rad 100:999–1001
2. Fuma S, Ishii N, Takeda H, Miyamoto K, Yanagisawa K, Doi K, Kawaguchi I, Tanaka N, Inamori Y, Polikarpov GG (2009) Effects of acute γ-irradiation on the aquatic microbial microcosm in comparison with chemicals. J Environ Rad 100:1027–1033
3. Pennington CW (2007) Exposing America: Comparative assessments of ionizing radiation doses to U.S. populations from nuclear and non-nuclear industries. Prog Nucl Energy 49:473–85
4. Abdelouas A (2006) Uranium mill tailings: Geochemistry, mineralogy and environmental impact. Elements 2(6):335–341
5. APS (2007) Consolidated interim storage of commercial spent nuclear fuel- A technical and programmatic assessment, Am Phys Soc. 19
6. NRC (2008) Review of DOE's nuclear energy research and development program, Committee on review of DOE's nuclear energy research and development program, National Research Council. p 102
7. Hu QH, Weng JQ, Wang JS (2010) Sources of anthropogenic radionuclides in the environment: A review. J Environ Rad 101:426–437
8. Peters MT, Ewing RC, Steefel CI (2008) GNEP waste form campaign science & technology and modeling & simulation program: Roadmap with rationale & recommendations, Global Nuclear Energy Partnership. p 51
9. Lieser KH (2001) Nuclear and radiochemistry: Fundamentals and applications, 2nd edn. Wiley-VCH, Weinheim, Federal Republic of Germany, 462
10. Loveland W, Morrissey DJ, Seaborg GT (2006) Modern nuclear chemistry. Wiley-Interscience, Inc, Hoboken, NJ
11. Rydberg J, Liljenzin JO, Choppin G (2001) Radiochemistry and nuclear chemistry. Elsevier Science, Woburn, MA, p 720
12. Zhang PC, Krumhansl JL, Brady PV (2002) Introduction to properties, sources and characteristics of soil radionuclides. In: Zhang PC, Brady PV (eds) Geochemistry of soil radionuclides. Soil Science Society of America, Madison, WI, pp 1–20
13. Langmuir D (1997) Aqueous environmental geochemistry. Prentice Hall, Upper Saddle River, NJ, p 600
14. Ivanovich M (1982) The phenomenon of radioactivity. In: Ivanovich M, Harmon RS (eds) Uranium series disequilibrium: Applications to environmental problems. Clarendon Press, Oxford, pp 1–32
15. Friedlander G, Kennedy JW, Macias ES, Miller JM (1981) Nuclear and radiochemistry, 3rd edn. John Wiley & Sons, New York, p 684
16. Elless MP, Lee SY (2002) Radionuclide-contaminated soils: A mineralogical perspective for their remediation. In: Dixon JD, Schulze DG (eds) Soil mineralogy with environmental applications. Soil Science Society of America, Madison, WI, pp 737–763
17. Macfarlane AM, Miller M (2007) Nuclear energy and uranium resources. Elements 3:185–192
18. Linsley G (2001) International advice and experience relevant to chronic radiation exposure situations in the environment. In: Brechignac F, Howard BJ (eds) Radioactive pollutants: Impact on the environment. EDP Sciences, France, pp 105–129
19. IAEA (2003) Extent of environmental contamination by naturally occurring radioactive materials (NORM) and technological options for remediation. International Atomic Energy Agency, Vienna
20. Aarkrog A (2001) Thoughts on radioecology by the millennium shift. In: Brechignac F, Howard BJ (eds) Radioactive pollutants: Impact on the environment. EDP Sciences, France, pp IX–XXI
21. Choppin GR (2003) Actinide speciation in the environment. Radiochim Acta 91:645–649
22. Ewing RC (2006) The nuclear fuel cycle: A role for mineralogy and geochemistry. Elements 2(6):331–34
23. Riley RG, Zachara JM, Wobber FJ (1992) Chemical contaminants on DOE lands and selection of contaminant mixtures for subsurface science research. DOE, Washington, DC, p 77
24. Glagolenko YV, Drozhko YG, Rovny SI (2009) Experience in rehabilitating contaminated land and bodies of water around the Mayak production association. In: Schweitzer GE, Parker FL, Robbins K (eds) Cleaning up sites contaminated with radioactive materials. NRC, Washington, DC, pp 81–91
25. Garwin RL (2001) Can the world do without nuclear power? Can the world live with nuclear power? Interdiscip Sci Rev 26(4):265–271
26. McBride JP, Moore RE, Whitherspoon JP, Blanco RE (1978) Radiological impact of airborne effluents of coal and nuclear plants. Science 8:1045–1050
27. Kharecha PA, Kutscher CF, Hansen JE, Mazria E (2010) Options for near-term phaseout of CO_2 emissions from coal in the United States. Environ Sci Technol 44(11):4050–4062
28. Jones S (2007) Windscale and Kyshtym: A double anniversary. J Environ Radioact 99:1–6

29. IAEA (2005) Chernobyl's legacy: Health, environmental and socio-economic impacts and recommendations to the governments of Belarus, the Russian federation and Ukraine. International Atomic Energy Agency, Vienna
30. Klein C, Hurlbut CS (1993) Manual of mineralogy, 21st edn. John Wiley & Sons, New York, NY
31. Dixon JB, Schulze DG (eds) (2002) Soil mineralogy with environmental applications. Soil Science Society of America, Madison, WI, p 866
32. Harris W, White GN (2008) X-ray diffraction techniques for soil mineral identification. In: Methods of soil analysis Part 5–Mineralogical methods. Soil Science Society of America, Madison, WI, pp 81–115
33. Fourdrin C, Allard T, Monnet I, Menguy N, Benedetti M, Calas G (2010) Effect of radiation-induced amorphization on smectite dissolution. Environ Sci Technol 44:2509–2514
34. Barnhisel RI, Bertsch PM (1989) Chlorites and hydroxy-interlayered vermiculite and smectite. In: Minerals of the soil environment. Soil Science Society of America, Madison, WI, pp 729–788
35. Breck DW (1974) Zeolite molecular sieves. Krieger Publishing Company, Malabar, FL
36. Sparks DL, Huang PM (1985) Physical chemistry of soil potassium. In: Munson RD (ed) Potassium in agriculture. American Society of Agronomy, Madison, WI, pp 201–276
37. Ming DW, Mumpton FA (1989) Zeolites in soils Ch. 18. In: Dixon JB, Weed SB (eds) Minerals in the soil environment. Soil Science Society of America, Madison, WI, pp 973–997
38. Dyer A (2000) Application of natural zeolites in the treatment of nuclear wastes and fall-out. In: Cotter-Howells JD, Campbell LS, Valsami-Jones E, Batchelder M (eds) Environmental mineralogy: Microbial interactions, anthropogenic influences, contaminated land, and waste management. The Mineralogical Society of Great Britain and Ireland Oxford, UK
39. Vaniman DT, Bish DL (1995) The importance of zeolite in the potential high-level radioactive waste repository at Yucca Mountain, nevada. In: Ming DW, Mumptom FA (eds) Natural zeolites, '93 occurrence, properties, use. International committee on natural zeolites, Brockport, NY, pp 533–546
40. Boettinger JL, Ming DW (2002) Zeolites. In: Dixon JB, Schulze DG (eds) Soil mineralogy with environmental applications. Soil Science Society of America, Madison, WI, pp 585–610
41. Chelishchev NF (1995) Use of natural zeolite at Chernobyl. In: Ming DW, Mumptom FA (eds) Natural zeolites, '93 occurrence, properties, use. International committee on natural zeolites Brockport, NY, pp 525–532
42. Schulze DG (2002) An Introduction to soil mineralogy: Chapter 1. In: Dixon JB, Schulze DG (eds) Soil mineralogy with environmental applications. Soil Science Society of America, Madison, WI, pp 1–35
43. Schwertmann U, Taylor RM (1989) Iron oxides. In: Dixon JB, Weeds SB (eds) Minerals in the soil environment. Soil Science Society of America, Madison, WI, pp 379–438
44. Jackson ML, Lin CH, Zelazny LW (1986) Oxides, hydroxides, and aluminosilicates. In: Klute A (ed) Methods of soil analysis, vol 1, Physical and mineralogical methods. American Society of Agronomy Inc, Madison, WI, pp 101–150
45. Gerth J (1990) Unit-cell dimensions of pure and trace metal-associated goethites. Geochim Cosmochim Acta 54: 363–371
46. Eary LE, Rai D (1987) Kinetics of chromium (III) oxidation to chromium (VI) by reaction with manganese dioxide. Environ Sci Technol 21:1187–1193
47. Manceau A, Charlet L, Boisset MC, Didier B, Spadini L (1992) Sorption and speciation of heavy metals on hydrous Fe and Mn oxides. From microscopic to macroscopic. Appl Clay Sci 7:201–223
48. Kinniburgh DG, vanRiemsdijk W, Koopal L, Borkovec M, Benedetti M, Avena M (1999) Ion binding to natural organic matter: Competition, heterogeneity, stoichiometry and thermodynamic consistency. Colloids Surf, A 151:147–66
49. Deng Y, Dixon JB (2002) Soil organic matter and organic-mineral interactions. In: Dixon JB, Schulze DG (eds) Soil mineralogy with environmental applications. Soil Science Society of America, Madison, WI, pp 69–107
50. Santschi PH, Roberts KA, Guo LD (2002) Organic nature of colloidal actinides transported in surface water environments. Environ Sci Technol 36(17):3711–3719
51. McCarthy JF, Zachara JM (1989) Subsurface transport of contaminants. Environ Sci Technol 23:496–502
52. Kersting AB, Efurd DW, Finnegan DL, Rokop DJ, Smith DK, Thompson JL (1999) Migration of plutonium in groundwater at the Nevada test site. Nature 397:56–59
53. Zeh P, Czerwinski KR, Kim JI (1997) Speciation of uranium in Gorleben groundwaters. Radiochim Acta 76:37–44
54. Dearlove JPL, Longworth G, Ivanovich M, Kim JI, Delakowitz B, Zeh P (1991) A study of ground-water colloids and their geochemical interactions with natural radionuclides in gorleben aquifer systems. Radiochim Acta 52/53:83–89
55. Xu C, Santschi PH, Zhong JY, Hatcher PG, Francis AJ, Dodge CJ, Roberts KA, Hung C-C, Honeyman BD (2008) Colloidal cutin-like substance cross-linked to siderophore decomposition products mobilizing plutonium from contaminated soils. Environ Sci Technol 42(22):8211–8217
56. Sposito G (1984) The surface chemistry of soils. Oxford University Press, New York, 234
57. Goldberg S (2005) Chapter 10: Equations and models describing adsorption processes in soils. In: Tabatabai MA, Sparks DL (eds) Chemical processes in soils. Soil Science Society of America, Madison, WI, pp 489–517
58. Goldberg S, Criscenti LJ, Turner DR, Davis JA, Cantrell KJ (2007) Adsorption-desorption processes in subsurface reactive transport modeling. Vadose Zone J 6:407–435
59. IAEA (2006) Applicability of monitored natural attenuation at radioactively contaminated sites. International Atomic Energy Agency, Vienna, p 105
60. Brady PV, Jove-Colon CF, Carr G, Huang F (2002) Soil radionuclide plumes. In: Zhang PC, Brady PV (eds) Geochemistry of soil radionuclides. Soil Science Society of America, Madison, WI, pp 165–190

61. Alexakhin RM, Krouglov SV (2001) Soil as the main compartment for radioactive substances in terrestrial ecosystems. In: Brechignac F, Howard BJ (eds) Radioactive pollutants: Impact on the environment. EDP Sciences, France, pp 149–174
62. Salbu B (2009) Challenges in radioecology. J Environ Radioact 100:1086–1091
63. Varga B, Leclerc E, Zagyvai P (2009) The role of analogues in radioecology. J Environ Rad 100:802–805
64. IAEA (2010) Handbook of parameter values for the prediction of radionuclide transfer in terrestrial and freshwater environments. International Atomic Energy Agency, Vienna, p 194
65. Runde W, Neu MP, Conradson SD, Li D, Lin M, Smith DM, VanPelt CE, Xu Y (2002) Geochemical speciation of actinides in soil and solution. In: Zhang PC, Brady PV (eds) Geochemistry of soil radionuclides. Soil Science Society of America, Madison, WI, pp 45–59
66. Seaman JC, Guerin M, Jackson BP, Bertsch PM, Ranville JF (2003) Analytical techniques for characterizing complex mineral assemblages: Mobile soil and groundwater colloids. In: Selim HM, Kingery WL (eds) Geochemical and hydrological reactivity of heavy metals in soils. Lewis Publishers, New York, pp 271–309
67. McCarthy JF, Degueldre C (1993) Sampling and characterization of colloids and particles in groundwater for studying their role in contaminant transport: Chapter 6. In: Buffle J, Leeuwen HPv (eds) Environmental particles. Lewis Publishers, Ann Arbor, MI
68. Tessier A, Campbell PGC, Bisson M (1979) Sequential extraction procedure for the speciation of particulate trace metals. Anal Chem 51:844–850
69. Miller WP, Martens DC, Zelazny LW (1986) Effect of sequence in extraction of trace metals from soils. Soil Sci Soc Am J 50:598–601
70. Clark SB, Johnson WH, Malek MA, Serkiz SM, Hinton TG (1996) A comparison of sequential extraction techniques to estimate geochemical controls on the mobility of fission product, actinide, and heavy metal contaminants in soils. Radiochim Acta 74:173–179
71. Rigol A, Roig M, Vidal M, Rauret G (1999) Sequential extractions for the study of radiocesium and radiostrontium dynamics in mineral and organic soils from western europe and Chernobyl areas. Environ Sci Technol 33(6):887–895
72. Voegelin A, Barmettler K, Kretzschmar R (2003) Heavy metal release from contaminated soils: Comparison of column leaching and batch extraction results. J Environ Qual 32:865–875
73. Seaman JC, Meehan T, Bertsch PM (2001) Immobilization of ^{137}Cs and U in contaminated sediments using soil amendments. J Environ Qual 30(4):1206–1213
74. Arey JS, Seaman JC, Bertsch PM (1999) Immobilization of uranium in contaminated sediments by hydroxyapatite addition. Environ Sci Technol 33:337–342
75. Evangelou VP, Phillips RE (2005) Cation exchange in soils. In: Chemical processes in soils. Soil Science Society of America, Madison, WI, pp 343–410
76. Stumm W, Morgan JJ (1995) Aquatic chemistry: An introduction emphasizing chemical equilibria in natural waters, 3rd edn. Wiley-Interscience, New York
77. Bertsch PM, Seaman JC (1999) Characterization of complex mineral assemblages: Implications for contaminant transport and environmental remediation. P Natl Acad Sci 96:3350–3357
78. Grenthe I, Fuger J, Konings RJM, Lemire RJ, Muller AB, Nguyen-Trung C, Wanner H (1992) Chemical thermodynamics of uranium. North Holland, Amsterdam
79. Lovley DR, Phillips EJP, Gorby YA, Landa ER (1991) Microbial reduction of uranium. Nature 350(April 4):413–416
80. Gorby YA, Lovley D (1992) Enzymatic uranium precipitation. Environ Sci Technol 26:205–207
81. USEPA (1999) Understanding variation in partition coefficient, K_d, values- Volume I: The K_d model, measurement, and application of chemical reaction codes. US Environmental Protection Agency, Washington, DC
82. Runde W (2002) Geochemical interactions of actinides in the environment. In: Zhang PC, Brady PV (eds) Geochemistry of soil radionuclides. Soil Science Society of America, Madison, WI, pp 21–44
83. Karathanasis AD (2002) Mineral equilibria in environmental soil systems. In: Soil mineralogy with environmental applications. Soil Science Society of America, Madison, WI, pp 109–151
84. Seaman JC, Arey JS, Bertsch PM (2001) Immobilization of Ni and other metals in contaminated sediments using soil amendments. J Environ Qual 30(2):460–469
85. Zachara JM, Smith SC, Resch CT, Cowan CE (1992) Cadmium sorption to soil separates containing layer silicates and iron and aluminum oxides. Soil Sci Soc Am J 56:1074–1084
86. Davis JA, Kent DB (1990) Surface complexation modeling in aqueous geochemistry. Rev Mineralog 23:177–260
87. Coston JA, Fuller CC, Davis JA (1995) Pb^{2+} and Zn^{2+} adsorption by a natural aluminum- and iron-bearing surface coating on an aquifer sand. Geochim Cosmochim Acta 59(17):3535–3547
88. Thibault DH, Sheppard MI, Smith PA (1990) A critical compilation and review of default soil solid/liquid partition coefficients, Kd, for use in environmental assessments. Atom Energy Canada Ltd AECL10125:1–112
89. USEPA (1999) Understanding variation in partition coefficient, K_d, values- Volume II: Review of geochemistry and available Kd values for cadmium, cesium, chromium, lead, plutonium, radon, strontium, thorium, tritium, and uranium. US Environmental Protection Agency, Washington, DC
90. USEPA (2004) Understanding variation in Partition coefficient, K_d, values Volume III: Review of geochemistry and available Kd values for americium, arsenic, curium, iodine, neptunium, radium, and technetium, Office of Air and Radiation, Washington, DC
91. Looney BB, Grant MW, King CM (1987) Estimation of geochemical parameters for assessing subsurface transport at the Savannah River Site. E.I. du Pont de Nemours & Co, Aiken, SC
92. Sheppard MI, Thibault DH (1990) Default soil solid/liquid partition coefficients, K_dS, for four major soil types: A compendium. Health Phys 59:471–482

93. Davis JA, Coston JA, Kent DB, Fuller CC (1998) Application of the surface complexation concept to complex mineral assemblages. Environ Sci Technol 32(19):2820–2828
94. Sposito G (1983) On the surface complexation model of the oxide-aqueous solution interface. J Colloid Interface Sci 91:329–340
95. Davis JA, Payne TE, Waite TD (2002) Simulating the pH and pCO_2 dependence of uranium(VI) adsorption by a weathered schist with surface complexation models. In: Zhang PC, Brady PV (eds) Geochemistry of soil radionuclides. Soil Science Society of America, Madison, WI, pp 61–86
96. Dzombak DA, Morel FMM (1990) Surface complexation modeling: Hydrous ferric oxide. John Wiley & Sons, Inc, New York, p 393
97. Zachara JM, Westall JC (1998) Chemical modeling of ion adsorption in soils. In: Sparks DL (ed) Soil physical chemistry. CRC Press, Boca Raton, FL, pp 47–95
98. Davis JA, Randall JD (2003) Application of surface complexation modeling to describe uranium (VI) adsorption and retardation at the uranium mill tailings site at Naturita, Colorado. U. S. Nuclear Regulatory Commission Office of Nuclear Regulatory Research, Washington, DC, pp 1–223
99. Meeussen JCL, Scheidegger A, Hiemstra T, Riemsdijk WHV, Borkovec M (1996) Predicting multicomponent adsorption and transport of fluoride at variable pH in a goethite-silica sand system. Environ Sci Technol 30:481–488
100. Waite TD, Davis JA, Payne TE, Waychunas GA, Xu N (1994) Uranium (VI) adsorption to ferrihydrite: Application of a surface complexation model. Geochim Cosmochim Acta 58(24):5465–5478
101. Davis JA, Meece DE, Kohler M, Curtis GP (2004) Approaches to surface complexation modeling of uranium(VI) adsorption on aquifer sediments. Geochim Cosmochim Acta 68(18): 3621–3641
102. Casadesus J, Sauras T, Gonze MA, Vallejo R, Brechignac F (2001) A nutrient-based mechanistic model for predicting the root uptake of radionuclides. In: Brechignac F, Howard BJ (ed) Radioactive pollutants: Impact on the environment. EDP Sciences, France, pp 209–239
103. Sheppard SC, Sheppard MI (1989) Impact of correlations on stochastic estimates of soil contamination and plant uptake. Health Phys 57:653–657
104. Vandenhove H, Olyslaegers G, Sanzharova N, Shubina O, Reed E, Shang Z, Velasco H (2009) Proposal for new best estimates of the soil-to-plant transfer factor of U, Th, Ra, Pb and Po. J Environ Radioact 100:721–732
105. Salbu B, Lind OC, Borretzen P, Oughton DH (2001) Advanced speciation techniques for radionuclides associated with colloids and particles. In: Brechignac F, Howard BJ (ed) Radioactive pollutants: Impact on the environment. EDP Sciences, France, pp 243–260
106. IAEA (2000) Radiation legacy of the 20th century: Environmental restoration, in RADLEG 2000. International Atomic Energy Agency, Moscow, Russian Federation, 64 p
107. IAEA (2009) Quantification of radionuclide transfers in terrestrial and freshwater environments for radiological assessments. International Atomic Energy Agency, Vienna p 616
108. Tamponnet C, Plassard C, Parekh N, Sanchez A (2001) Impact of micro-organisms on the fate of radionuclides in rhizospheric soils. In: Brechignac F, Howard BJ (eds) Radioactive pollutants: Impact on the environment. EDP Sciences, France, pp 175–185
109. Strandberg M, Johansson M (1998) ^{134}Cs in heather seed plants grown with and without mycorrhiza. J Environ Rad 40(2):175–184
110. IUR (1992) Protocol developed by the working group on soil to plant transfer, International Union of Radioecology, France
111. Tebes-Stevens CL, Espinoza F, Valocchi AJ (2001) Evaluating the sensitivity of a subsurface multicomponent reactive transport model with respect to transport and reaction parameters. J Contam Hydrol 52:3–27
112. Steefel CI, DePaolo DJ, Lichter PT (2005) Reactive transport modeling: An essential tool and a new research approach for the earth sciences. Earth Planet Sc Lett 240:539–558
113. Davis JA, Yabusaki SB, Steefel CI, Zachara JM, Curtis GP, Redden GD, Criscenti LJ, Honeyman BD (2004) Assessing conceptual models for subsurface reactive transport of inorganic contaminants. EOS 85(44):449
114. Bossew P, Kirchner G (2004) Modelling the vertical distribution of radionuclides in soil. Part 1: The convection–dispersion equation revisited. J Environ Radioact 73:127–150
115. Kirchner G, Strebl F, Bossew P, Ehlken S, Gerzabek MH (2009) Vertical migration of radionuclides in undisturbed grassland soils. J Environ Radioact 100:716–720
116. Ivanov YA, Lewyckyj N, Levchuk SE, Prister BS, Firsakova SK, Arkhipov NP, Arkhipov AN, Kruglov SV, Alexakhin RM, Sandalls J, Askbrant S (1997) Migration of ^{137}Cs and ^{90}Sr from Chernobyl fallout in Ukrainian, Belarussian and Russian soils. J Environ Radioact 35(1):1–21
117. Pontedeiro EM, van Genuchten MT, Cotta RM, Simunek J (2010) The effects of preferential flow and soil texture on risk assessments of a NORM waste disposal site. J Hazard Mat 174:648–655
118. Gamerdinger AP, Kaplan DI (2000) Application of a continuous-flow centrifugation method for solute transport in disturbed, unsaturated sediments and illustration of mobile-immobile water. Water Resour Res 36(7):1747–1755
119. Seyfried MS, Rao PSC (1987) Solute transport in undisturbed columns of an aggregated tropical soil: Preferential flow effects. Soil Sci Soc Am J 51:1434–1444
120. Wellman DM, Gamerdinger AP, Kaplan DI, Serne RJ (2008) Effect of particle-scale heterogeneity on uranium(VI) transport in unsaturated porous media. Vadose Zone J 7(1):67–78
121. Zachara JM, Davis JA, McKinley J, Wellman D, Liu C, Qafoku N, and Yabusaki S (2005) Uranium geochemistry in vadose zone and aquifer sediments from the 300-area uranium plume, Pacific Northwest National Laboratory, Richland, WA, p 113

122. Pickens JF, Jackson RE, Inch KJ, Merritt WF (1981) Measurement of distribution coefficients using a radial injection dual-tracer test. Water Resour Res 17(3):529–544
123. Seaman JC, Bertsch PM, Miller WP (1995) Ionic tracer movement through highly weathered sediments. J Contam Hydrol 20:127–143
124. Seaman JC, Bertsch PM, Wilson M, Singer J, Majs F, Aburime SA (2007) Tracer migration in a radially divergent flow field: Longitudinal dispersivity and anionic tracer retardation. Vadose Zone J 6:373–386
125. Porro I, Newman ME, Dunnivant FM (2000) Comparison of batch and column methods for determining strontium distribution coefficients for unsaturated transport in basalt. Environ Sci Technol 34(9):1679–1686
126. Gamerdinger AP, Kaplan DI, Wellman DM, Serne RJ (2001) Two-region flow and decreased sorption of uranium (VI) during transport in Hanford groundwater and unsaturated sands. Water Resour Res 37(12):3155–3162
127. Maraqa MA, Wallace RB, Voice TC (1999) Effect of water saturation on retardation of ground-water contaminants. J Environ Eng 125(8):697–704
128. Phillippi JM, Loganathan VA, McIndoe MJ, Barnett MO, Clement TP, Roden EE (2007) Theoretical solid/solution ratio effects on adsorption and transport: Uranium(VI) and carbonate. Soil Sci Soc Am J 71:329–335
129. Reardon EJ (1981) Kd's - Can they be used to describe reversible ion sorption reaction in contaminant migration? Ground Water 19(3):279–286
130. Brusseau ML, Srivastava R (1999) Non-ideal transport of reactive solutes in heterogeneous porous media: 4. Analysis of the Cape Cod natural-gradient field experiment. Water Resour Res 35(4):1113–1125
131. Curtis GP, Davis JA, Naftz DL (2006) Simulation of reactive transport of uranium(VI) in groundwater with variable chemical conditions. Water Resour Res 42:WO4404 1–15
132. Ma R, Zheng C, Prommer H, Greskowiak J, Liu C, Zachara J, Rockhold M (2010) A field-scale reactive transport model for U (VI) migration influenced by coupled multirate mass transfer and surface complexation reactions. Water Resour Res 46:17p
133. Boggs MJ, Adams EE (1992) Field study in a heterogeneous aquifer 4. Investigation of adsorption and sampling bias. Water Resour Res 28(12):3325–3336
134. Seaman JC (1998) Retardation of fluorobenzoate tracers in highly weathered soil and groundwater systems. Soil Sci Soc Am J 62:354–361
135. McCarthy JF, Howard KM, McKay LD (2000) Effect of pH on sorption and transport of fluorobenzoic acid ground water tracers. J Environ Qual 29:1806–1813
136. Seaman JC, Bertsch PM, Korom SF, Miller WP (1996) Physicochemical controls on non-conservative anion migration in coarse-textured alluvial sediments. Ground Water 34(5): 778–783
137. Jacques D, Šimůnek J, Mallants D, and Van Genuchten MT (2005) Long term uranium in agricultural field soils following mineral P-fertilization, in the 10th International Conference on Environmental Remediation and Radioactive Waste Management Glascow, Scotland. p 6
138. Jacques D, Šimůnek J, Mallants D, Van Genuchten MT (2008) Modeling coupled hydrologic and chemical processes: Long-term uranium transport following phosphorus fertilization. Vadose Zone J 7(2):698–711
139. Smith JT, Elder DG (1999) A comparison of models for characterizing the distribution of radionuclides with depth in soils. J Europ Soil Sci 50(2):295–307
140. Cernik M, Federer P, Borkovec M, Sticher H (1994) Modeling of heavy metal transport in a contaminated soil. J Environ Qual 23:1239–1248
141. Bossew P, Gastberger M, Gohla H, Hofer P, Hubmer A (2004) Vertical distribution of radionuclides in soil of a grassland site in Chernobyl exclusion zone. J Environ Radioact 73:87–99
142. Bunzl K, Forster H, Kracke W, Schimmack W (1994) Residence times of fallout $^{239+240}$Pu, ^{238}Pu, ^{241}Am and ^{137}Cs in the upper horizons of an undisturbed grassland soil. J Environ Radioact 22:11–27
143. Coughtrey PJ (1988) Models for radionuclide transport in soils. Soil Use Manag 73:87–99
144. Kirchner G (1998) Applicability of compartmental models for simulating the transport of radionuclides in soil. J Environ Radioact 38(3):339–352
145. Kent DB, Wilke JA, Davis JA (2007) Modeling the movement of a pH perturbation and its impact on adsorbed zinc and phosphate in a wastewater-contaminated aquifer. Water Resour Res 43(7):W07440
146. Stollenwerk KG (1998) Molybdate transport in a chemically complex aquifer: Field measurements compared with solute-transport model predictions. Water Resour Res 34(10):2727–2740
147. Parkhurst DL, Stollenwerk KG, Colman JA (2003) Reactive-transport simulation of phosphorus in the sewage plume at the Massachusetts military reservation, Cape Cod, Massachusetts. Air Force Center for Environmental Excellence, Northborough, MA, pp 1–33
148. Vaughan PJ, Shouse PJ, Goldberg S, Suarez DL, Ayars JE (2004) Boron transport within an agricultural field: Uniform flow versus mobile-immobile water model simulations. Soil Sci 169:401–412
149. Silva RJ, Nitsche H (1995) Actinide environmental chemistry. Radiochim Acta 70/71:377–396
150. Artinger R, Schuessler W, Scherbaum F, Schild D, Kim J (2002) ^{241}Am migration in a sandy aquifer studied by long-term column experiments. Environ Sci Technol 36(22): 4818–4823
151. Lu N, Kung KS, Mason CFV, Triay IR, Cotter CR, Pappas AJ, Pappas MEG (1998) Removal of plutonium-239 and americium-241 from Rocky Flats soil by leaching. Environ Sci Technol 32(3):370–374
152. Whicker W, Schultz V (1982) Radioecology: Nuclear energy and the environment. CRC Press, Boca Raton, FL

153. Sawhney BL (1966) Kinetics of cesium sorption by clay minerals. Soil Sci Soc Am J 30:565–569
154. Mahara Y (1993) Storage & migration of fallout strontium-90 and cesium-137 for over 40 years in the surface soil of Nagasaki. J Environ Qual 22:722–730
155. Zygmunt J, Chibowski S, Klimowicz Z (1998) The effect of sorption properties of soil minerals on the vertical migration rate of cesium in soil. J Radionchem Nucl Chem 231(1–2): 57–62
156. NCRP (2006) Cesium-137 in the environment: Radioecology and approaches to assessment and management. National Council on Raditation Protection and Measurement, Bethesda, MD, p 382
157. McKinley JP, Zeissler CJ, Zachara JM, Serne RJ, Lindstrom RM, Schaef HT, Orr RD (2001) Distribution and retention of ^{137}Cs in sediments at the Hanford Site, Washington. Environ Sci Technol 35(17):3433–3441
158. Comans RN, Haller M, Pretter PD (1991) Sorption of cesium on illite: Non-equilibrium behaviour and reversibility. Geochim Cosmochim Acta 55:433–440
159. Comans RNJ, Hockley DE (1992) Kinetics of cesium sorption on illite. Geochim Cosmochim Acta 56:1157–1164
160. Komarneni S (1978) Cesium sorption and desorption behavior of kaolinites. Soil Sci Soc Am J 42:531–532
161. deKoning A, Comans RNJ (2004) Reversibility of radiocaesium sorption on illite. Geochim Cosmochim Acta 68(13): 2815–2823
162. deKoning A, Konoplev AV, Comans RNJ (2007) Measuring the specific caesium sorption capacity of soils, sediments and clay minerals. Appl Geochem 22:219–29
163. Cremers A, Elsen A, DePreter P, Maes A (1988) Quantitative analysis of radiocaesium retention in soils. Nature 335: 247–250
164. McLean EO, Watson ME (1985) Soil measurement of plant-available potassium. In: Potassium in agriculture. American Society of Agronomy, Madison, WI, pp 277–308
165. Hsu CN, Chang KP (1994) Sorption and desorption behavior of cesium on soil components. Appl Radiat Isot 45(4): 433–437
166. Stauton S (1997) On the mechanisms which determine the fate of radiocaesium in soil. Analusis Mag 25:24–28
167. Pinder JE III, Garten CT Jr, Paine D (1980) Factors affecting radiocesium uptake by plants inhabiting a contaminated floodplain. Acta Ecologica 1(1):3–10
168. Hinton TG, Bell CM, Whicker FW, Philippi T (1999) Temporal changes and factors influencing ^{137}Cs concentration in vegetation colonizing an exposed lake bed over a three-year period. J Environ Rad 44:1–19
169. Seel JF, Whicker FW, Adriano DC (1995) Uptake of ^{137}Cs in vegetable crops grown on a contaminated lakebed. Health Phys 68:793–799
170. Hinton T, Knox A, Kaplan D, Serkiz S (2001) An in situ method for remediating ^{137}Cs-contaminated wetlands using naturally occurring minerals. J Radioanalytical Nucl Chem 249(1): 197–202
171. Pinder JE III, Hinton TG, Whicker FW, Smith JT (2009) Cesium accumulation by fish following acute input to lakes: A comparison of experimental and Chernobyl-impacted systems. J Environ Radioact 100:456–467
172. Hinton TG, Kaplan DI, Knox AS, Coughlan DP, Nascimento RV, Watson SI, Fletcher DE, Koo B (2006) Use of illitic clay for the in situ remediation of ^{137}Cs-contaminated water bodies: Field demonstration of reduced biological uptake. Environ Sci Technol 40(14):4500–4505
173. Leppert D (1990) Heavy metal sorption with clinoptilolite zeolite: alternatives for treating contaminated soil and water. Min Eng 42(6):604–608
174. Tsitsishvili GV, Andorikashvili TG, Kirov GN, Filizova LD (1992) Natural zeolites. Ellis Horwood, New York, 296
175. Zhang PC, Brady PV (eds) (2002) Geochemistry of soil radionuclides. Soil Science Societyof America, Madison, WI, p 252
176. Moran JE, Oktay S, Santchi PH, Schink DR (1999) Atmospheric dispersal of ^{129}I from nuclear fuel reprocessing facilities. Environ Sci Technol 33(15):2536–2542
177. Hou X, Aldahan A, Nielsen SP, Possnert G (2009) Time series of ^{129}I and ^{127}I speciation in precipitation from Denmark. Environ Sci Technol 43:6522–6528
178. Schwehr KA, Santschi PH, Kaplan DI, Yeager CM, Brinkmeyer R (2009) Organo-iodine formation in soils and aquifer sediments at ambient concentrations. Environ Sci Technol 43:7258–7264
179. Kaplan DI, Serne RJ, Parker KE, Kutnyakov IV (2000) Iodide sorption to subsurface sediments and illitic minerals. Environ Sci Technol 34:399–405
180. Hu Q, Zhao P, Moran JE, Seaman JC (2005) Sorption and transport of Iodine species in sediments from the Savannah River and Hanford Sites. J Contam Hydrol 78: 185–205
181. Li HB, Xu XR, Chen F (2009) Determination of iodine in seawater: Methods and applications. In: Comprehensive handbook of iodine: Nutritional, biochemical, pathological and therapeutic aspects. Elsevier Academic Press, New York, pp 2–13
182. Schwehr KA, Santschi PH (2003) Sensitive determination of iodine species, including organo-iodine, for freshwater and seawater samples using high performance liquid chromatography and spectrophotometric detection. Anal Chim Acta 482:59–71
183. Powell BA, Field RA, Kaplan DI, Coates JT, Serkiz SM (2004) Pu(V)O^{2+} adsorption and reduction by synthetic magnetite (Fe_3O_4). Environ Sci Technol 38:6016–6024
184. Powell BA, Field RA, Kaplan DI, Coates JT, Serkiz SM (2005) Pu (V)O^{2+} adsorption and reduction by synthetic hematite and goethite. Environ Sci Technol 39:2107–2114
185. Kim JI (1986) Chemical behaviour of transuranic elements in natural aquatic systems. Handbook on the Phys Chem Actinides 4:413–455
186. Kim JI, Kanellakopulos B (1989) Solubility product of Pu(VI) oxide and hydroxide. Radiochim Acta 48:145–150

187. Routson RC, Barney GS, Smith RM (1980) Hanford site sorption studies for the control of radioactive wastes: A review. Rockwell Hanford Operations, Richland, WA
188. Ames LL, McGarrah JE, Walker BA, Salter PF (1982) Sorption of uranium and cesium by Hanford basalts and associated secondary smectites. Chem Geol 35:205–225
189. Strenge DL, Peterson SR (1989) Chemical databases for the multimedia environmental pollutant assessment system, PNL-7145, Pacific Northwest National Laboratory Richland, WA
190. Serne RJ, LeGore VL (1996) Strontium-90 sorption-desorption properties and sediment characterization at the 100 -Area. Pacific Northwest National Laboratory, Richland, WA
191. Lefevre R, Sardin M, Schweich D (1993) Migration of strontium in clayey and calcareous sandy soil: Precipitation and ion exchange. J Contam Hydrol 13:215–229
192. Stevenson FJ, Fitch A (1986) Chemistry of complexation metal ions with soil solution organics. In: Huang PM, Schnitzer M (eds) Interactions of soil minerals with natural organics and microbes. Soil Science Society of America, Madison, WI
193. Wildung RE, McFadden KM, Garland TR (1979) Technetium sources and behavior in the environment. J Environ Qual 8(2):156–161
194. Kaplan DI, Roberts K, Shine G, Grogan K, Fjeld R, and Seaman J (2008) The range and distribution of technetium Kd values in the SRS subsurface environment, WSRC-STI-2008-00286 Aiken, SC. p 45
195. Peretyazhko T, Zachara JM, Heald SM, Jeon BH, Kukkadapu RK, Liu C, Moore D, Resch CT (2008) Heterogeneous reduction of Tc(VII) by Fe(II) at the solid-water interface. Geochim Cosmochim Acta 72:1521–1539
196. Peretyazhko T, Zachara JM, Heald SM, Kukkadapu RK, Liu C, Plymale AE, Resch CT (2008) Reduction of Tc(VII) by Fe(II) sorbed on Al (hydr)oxides. Environ Sci Technol 42:5499–5506
197. Wildung RE, Gorby YA, Krupka KM, Hess NJ, Li SW, Plymale AE, McKinley JP, Fredrickson JK (2000) Effect of electron donor and solution chemistry on products of dissimilatory reduction of technetium by shewanella putrefaciens. Appl Environ Microbiol 66(6):2451–2460
198. Murphy CE Jr (1993) Tritium transport and cycling in the environment. Health Phys 65(6):683–698
199. Okada S, Momoshima N (1993) Overview of tritium: Characteristics, sources and problems. Health Phys 65(6):595–609
200. Pointurier F, Baglan N, Alanic G, Chiappini R (2003) Determination of organically bound tritium background level in biological samples from a wide area in the south-west of France. J Environ Rad 68:171–189
201. van den Hoek J (1986) Tritium metabolism in animals. Radiat Prot Dosim 16:117–121
202. Moghissi AA, Bretthauer EW, Patzer RG (1987) Biological concentration of ^{3}H. Health Phys 53:385–388
203. Richmond CR, Langham WH, Trujillo TT (1962) Comparative metabolism of HTO by mammals. J Comp Physiol 59:45–53
204. Kelsey-Wall A, Seaman JC, Jagoe CH, Dallas CE (2006) Biological half-life and oxidative stress effects in mice with low-level, oral exposure to tritium. J Toxicology Environ Health Part A 69(3):201–213
205. Burns PC. and Finch R, eds. (1999) Uranium: Mineralogy, geochemistry, and the environment. Reviews in Mineralogy, vol 38. The Mineralogical Society of America: Washington, DC, p 679
206. Finn PA, Hoh JC, Wolf SF, Slater SA, Bates JK (1996) The release of uranium, technetium, and iodine from spent fuel under unsaturated conditions. Radiochim Acta 75:65–71
207. Vandenhove H, Hees MV, Wouters K, Wannijn J (2007) Can we predict uranium bioavailability based on soil parameters? Part 1: Effect of soil parameters on soil solution uranium concentration. Environ Pollut 145:587–595
208. Sandino A, Bruno J (1992) The solubility of $(UO_2)_3(PO_4)_2$-$4H_2O$ (s) and the formation of U(VI) phosphate complexes: their influence in uranium speciation in natural waters. Geochim Cosmochim Acta 56:4135–4145
209. Langmuir D (1978) Uranium solution-mineral equilibria at low temperatures with applications to sedimentary ore deposits. Geochim Cosmochim Acta 42:547–569
210. Artinger R, Rabung T, Kim JI, Sachs S, Schmeide K, Heise KH, Bernhard G, Nitsche H (2002) Humic colloid-borne migration of uranium in sand columns. J Contam Hydrol 58:1–12
211. Shi Z, Liu C, Zachara JM, Wang Z, Deng B (2009) Inhibition effect of secondary phosphate mineral precipitation on uranium release from contaminated sediments. Environ Sci Technol 43:8344–8349
212. Boult KA (1998) Towards an understanding of the sorption of U(VI) and Se(IV) on sodium bentonite. J Contam Hydrol 35:141–150
213. Sheppard SC (2001) Toxicants in the environment: Bringing radioecology and ecotoxicology together. In: Brechignac F, Howard BJ (eds) Radioactive pollutants: Impact on the environment. EDP Sciences, France, pp 63–74
214. Amonette JE, Holdren GR, Krupa KM, Lindenmeier CW (1994) Assessing the environmental availability of uranium in soils and sediments. Pacific Northwest Laboratory, Richland, WA, p 101
215. Fredrickson JK, Zachara JM, Kennedy DW, Duff MC, Gorby YA, Li SW, Krupka KM (2000) Reduction of U(VI) in goethite (α-FeOOH) suspensions by a dissimilatory metal-reducing bacterium. Geochim Cosmochim Acta 64(18):3085–3098
216. Lloyd JR, Lovley DR (2001) Microbial detoxification of metals and radionuclides. Curr Opin Biotechnol 12:248–253
217. Gu B, Wu W, Ginder-Vogel MA, Yan H, Fields MW, Zhou J, Fendorf S, Criddle CS, Jardine PM (2005) Bioreduction of uranium in a contaminated soil column. Environ Sci Technol 39(13):4841–4847
218. Cummings DE, Fendorf S, Singh N, Sani R, Peyton B, Magnuson T (2007) Reduction of Cr(VI) under acidic conditions by the facultative Fe(III)-reducing bacterium acidiphilium cryptum. Environ Sci Technol 41(1):146–152
219. Ginder-Vogel M, Criddle CS, Fendorf S (2006) Thermodynamic constraints on the oxidation of biogenic UO_2 by Fe (III) (hydr)oxides. Environ Sci Technol 40(11):3544–3550

220. Seaman JC, Hutchison J, Jackson BP, Vulava VM (2003) In situ treatment of metals in contaminated soils using phytate. J Environ Qual 32(1):153–161
221. Nash KL, Jensen MP, Schmidt MA (1998) Actinide immobilization in the subsurface environment by in-situ treatment with a hydrolytically unstable organophosphorus complexant: Uranyl uptake by calcium phytate. J Alloys Compounds 271–273:257–261
222. Nash KL, Jensen MP, Hines JJ, Friedrich SA, Redko M (1997) Phosphate mineralization of actinides by measured addition of precipitating anions. Chemistry Division-Argonne National Laboratory Argonne, IL, p 22
223. Nash KL, Jensen MP, Schmidt MA (1998) In-situ mineralization of actinides for groundwater cleanup: Laboratory demonstration with soil from the fernald environmental management project. In: Schulz WW, Lombardo NJ (eds) Science and technol. for disposal of radioactive tank waste. Plenum Press, New York, pp 507–518
224. Wellman DM, Pierce EM, Bacon DH, Oostrom M, Gunderson KM, Webb SM, Bovaird CC, Cordova EA, Clayton ET, Parker KE, Ermi RM, Baum SR, Vermeul VR, and Fruchter JS (2008) 300-Area treatability test: Laboratory development of polyphosphate remediation technology for in situ treatment of uranium contamination in the vadose zone and capillary fringe, PNNL, Richland, WA, p 110

Radionuclide Migration from Catchments, Modeling

Luigi Monte
ENEA, CR Casaccia, Rome, Italy

Article Outline

Glossary
Definition of the Subject and Its Importance
Introduction
Empirical Background
Principles for Developing Models of Radionuclide Migration from Catchments
Conclusions
Future Directions
Bibliography

Glossary

Catchment A delimited geographical area that collects water from rain and melting snow and ice flowing to a point of discharge into a water body.

Deposit Radionuclide inventory in a catchment, often expressed as radionuclide per square meter ($\mathrm{Bq\,m^{-2}}$).

Radionuclide deposition The process of migration to exposed surfaces of a radionuclide dispersed in the atmosphere.

Radionuclide washout The process of migration of a radionuclide transported by runoff waters from the catchment to a water body.

Runoff The portion of precipitation on a catchment that is discharged into a water body.

Transfer function (of radionuclide deposited over a catchment) The amount of radionuclide flowing per unit time from upstream drainage basin to a water body following a single-pulse deposition of radioactive substance.

Definition of the Subject and Its Importance

A catchment, or drainage basin, is a delimited geographic area that collects water from rain and melting snow and ice flowing to a point of discharge into a water body. Catchments are complex ecosystems of significant economic, social, and environmental value. They play a major role in determining the water quality of streams, rivers, lakes. The portion of waters flowing through the catchment that reaches the point of discharge, the so-called runoff, transports dissolved and particulate substances, such as minerals, nutrients, eroded soil particles, that significantly influence the chemical and the biological characteristics of the water body that receives the runoff.

Catchments comprise terrestrial and aquatic ecosystems including forests, grasslands, ponds, etc., whose behavior is influenced by a great many natural and nonnatural factors that depend on geographic, geological, and climatic conditions and on the impact on the environment of the human activities.

The flow and the balance of the water in a catchment are controlled by many complex processes such as the interception of precipitation by the above ground vegetation, evapotranspiration (the conversion to the vapor state of waters on surfaces, soils, vegetation), storage in catchment depressions, snow and ice accumulation, infiltration through the soil and the rocks, overland flow, interflow, and the groundwater flow through the saturated and the unsaturated zones of the watershed.

Contaminants deposited over the catchment surface can be transported to the water ecosystems contributing to persistent levels of pollution in rivers, lakes, coastal areas, and seas. The complex processes of radionuclide migration through a drainage area depend on the characteristics of the radioactive substances and of the catchment. More specifically, these processes are chiefly controlled by the hydrology of the drainage basin and by the mechanisms of interaction of radionuclides with soils and bedrocks.

The radioactive pollution of a catchment can be caused by events occurring at different scales. However, the contamination of large geographical areas following the introduction of radionuclides into the atmosphere is of particular significance in view of the possible radioecological impact on water bodies and the relevant consequences for the human health. On the medium and long term, radionuclides migrating from catchments can be important sources of contamination for the water bodies and, consequently, of radiation doses to man.

In particular, the global fallout of radionuclides from the nuclear weapon tests in atmosphere carried out in the early 1960s and severe cases of environmental pollution like the Chernobyl accident caused the radioactive contamination of large catchments.

Modeling the transfer of radionuclides from drainage areas to water bodies is essential to evaluate the consequences of accidental releases of radioactive substance into the environment and to develop environmental management plans in view of the social, economic, and ecological values of freshwater ecosystems.

A variety of models for predicting the migration of toxic substances from catchments have been developed. The main aim of these models is to determine, following the introduction of contaminants into the catchment, the amount of radionuclides migrating, per unit time, from the drainage area to the freshwater body or to the marine environment. This is a major challenge for modelers owing to the complicated web of processes that control the migration of toxic substances through the complex freshwater environment.

Introduction

The complex hydrological processes (Fig. 1) controlling the runoff from a drainage area depend on the topography, the geology, the environmental conditions, etc., of the catchment.

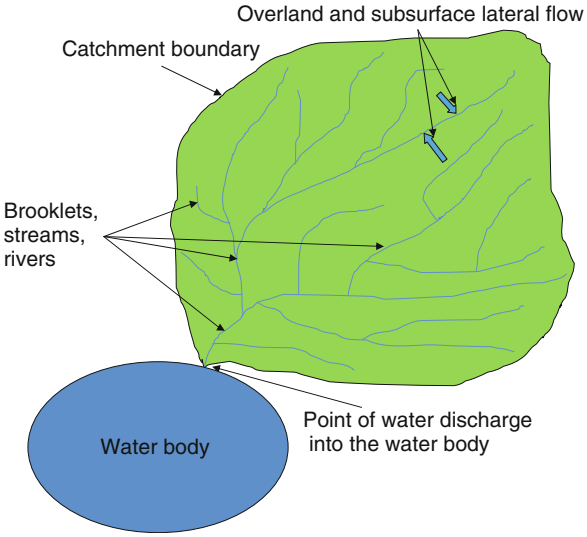

Radionuclide Migration from Catchments, Modeling. Figure 1
Simplified scheme of a catchment and of the main water fluxes

For the purpose of the present entry, it is sufficient to pay attention to the schematic representation of the main water fluxes depicted in Fig. 2. Precipitation is intercepted by the vegetation cover and by the soil surface, then infiltrates from the water unsaturated zone (strata of rocks, sand, gravel, etc., where available spaces are not completely filled with water) and percolates to the saturated zone. A portion of the water is returned to the atmosphere by evaporation and transpiration, whereas the remaining part flows to water bodies.

Runoff waters that reach the point of discharge carry dissolved substances and particulate materials of natural origin, but can also transport contaminants that have been released into the environment.

The evaluation of the transfer of contaminants from catchments to aquatic ecosystems is of paramount importance for the proper assessment of the aftermath of events of accidental introduction of pollutants into the biosphere. In particular, the pollution of large geographical areas following the release of pollutants into the atmosphere can be an event with severe consequences for aquatic ecosystems.

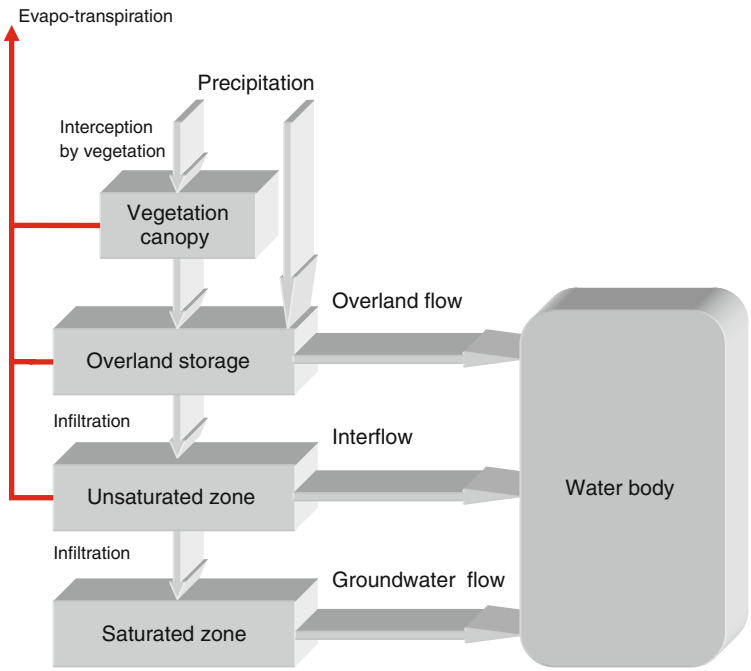

Radionuclide Migration from Catchments, Modeling. Figure 2
Main water fluxes that control the migration of toxic substances through a catchment

A contaminant discharged into the atmosphere is deposited on the ground surface through processes of particle settling (dry deposition), through the direct adsorption onto exposed surfaces of pollutants in the gaseous phase, and, chiefly, as wet deposition caused by precipitation scavenging. A further mechanism of contaminant migration to the ground is the so-called cloud deposition that is caused by the deposition of contaminated droplets in low clouds and mist on exposed surfaces. Generally, this last mechanism, although dissimilar from precipitation scavenging, is also classified as wet deposition. The deposited contaminant is partially adsorbed onto the exposed surface in the catchment (vegetation cover, rocks, soils, etc.) and is transported by runoff waters to the point of discharge in dissolved form or attached to eroded particles (radionuclide washout).

Basically, the migration of a contaminant within the catchment is governed by water flow, sediment erosion, and the complex physical and chemical processes of contaminant interaction with the exposed surfaces in the catchment (in particular, with the soil particles). These processes depend on the characteristics of the catchments and of the pollutant.

Radionuclides transported by runoff waters are often transformed into different chemical/physical forms ("speciation") following the interaction with different kinds of rocks and soil particles in a complex geochemical environment. However, it is commonly assumed that these forms can be grouped in two broad categories, "particulate" and "dissolved," according to a simplified and conventional approach based on an operational definition of "dissolved substances" – the material passing a 0.45 μm membrane filter [1] (correspondently, the "particulate form" is the suspended material that can be collected by such filters). Schematically, radionuclides are transported throughout the catchment into the water body by: (a) the overland flow, (b) the interflow (the water flowing through the upper part of the unsaturated zone), and (c) the groundwater flow. As it will be described in the following sections, the above mentioned flows contribute in different measure to the contaminant washout, depending on the chemical properties of the radionuclide that control the interaction of the pollutant with the particulate matter and the rocks in the catchment.

The amount of radionuclide migrating from the catchment is a significant component of the

mass-balance equation for predicting the time behavior of the radioactive contamination of a water body. The mass conservation law requires that:

$$\frac{dT}{dt} = DR + IR + CR - OR - RDR \quad (1)$$

where

T is the total amount of radionuclide in the water body (Bq)
DR is the rate of deposition of radionuclide over the water body surface
IR is the rate of direct introduction of radionuclide into the water body (from sources other than the water body catchment)
CR is the rate of radionuclide migrating from the catchment to the water body
OR is the rate of radionuclide outflow from the water body (for instance, through the outlet of a lake)
RDR is the radioactive decay rate of the contaminant in the water body
t is time

All the terms in the right-hand side of the previous equation are expressed in $Bq\,s^{-1}$.

In particular, the contribution of contaminant from the catchment of an aquatic system characterized by a relatively short mean water retention time, such as a river, can be one of the most important components of the contaminant mass balance in the water body.

The present contribution focuses on the description and the analysis of the most common methodological techniques to develop models for predicting the migration of radionuclides from catchments to water bodies. Before discussing the modeling approaches, the empirical background and the main methods adopted to analyze the available experimental data will be reviewed. This can help in understanding the motivation of the principles underlying the different classes of models described.

Empirical Background

Experimental Results Following the Environmental Contamination Caused by the Nuclear Weapon Explosions in the Atmosphere

Since the beginning of the 1960s, a great deal of research has been carried out to investigate the transfer of radionuclides from catchments to water bodies on the basis of available experimental data.

The worldwide fallout of radioactive substances following the peacetime testing of nuclear weapons was a source of copious experimental data for studying the process of migration of radionuclides through the environment. The radioactive debris released by the nuclear explosions reached the troposphere and the stratosphere, were widely dispersed through the atmosphere and returned to the earth as "global fallout" [2, 3].

Research on the migration of radionuclides from catchments was initiated as soon as the fallout from nuclear weapon tests in atmosphere caused the contamination of large geographical areas [4, 5]. These studies were aimed at establishing possible relationships between the radionuclide concentration in runoff water at the point of water discharge and the contaminant deposition over the catchment.

Yamagata et al. [5] tried to evaluate the washout of ^{137}Cs and ^{90}Sr deposited over the catchments of rivers in Japan by fitting empirical data of radionuclide concentration C ($Bq\,m^{-3}$) in river water to the expression:

$$C = C_d + p_r \cdot C_r \quad (2)$$

where C_r ($Bq\,m^{-3}$) is the concentration of radionuclide in the rain water, p_r (dimensionless) is a proportionality factor ($p_r \cdot C_r$ corresponds to the process of instantaneous transfer of deposited contaminant to the runoff water) and C_d ($Bq\,m^{-3}$) is the radionuclide concentration in the river water associated with the cumulative deposition stored in the catchment. Equation 2 was based on a simple conceptual scheme of the mechanisms of transfer from the whole catchment to the water body of deposited radionuclides. The results of the regression analyses suggested that, approximately, 1.3% of deposited ^{137}Cs and 7.2% of deposited ^{90}Sr were quickly removed from the catchment.

Furthermore, let D denote the cumulative radionuclide deposit on the ground ($Bq\,m^{-2}$), F the radionuclide runoff from the catchment ($Bq\,s^{-1}$), λ_w (s^{-1}) the removal rate of the cumulative ground deposit and A (m^2) the surface area of the catchment. Then it is possible to write:

$$F = \lambda_w \cdot D \cdot A \quad (3)$$

From the application of Eq. 3 to the available empirical data, Yamagata et al. [5] estimated that the

removal rates λ_w of ^{137}Cs and ^{90}Sr from catchments were of the order of $1.9 \times 10^{-11}\ s^{-1}$ and $9.8 \times 10^{-11}\ s^{-1}$, respectively, concluding that those values were significantly lower than the radioactive decay constants.

It is worthwhile to note that the deposition caused by the nuclear weapon tests in the atmosphere was a continuous process. It was impossible to isolate the input of radionuclide into the environment from each single explosion. Moreover, the dynamics of deposition over the ground surface of radionuclides from an atmospheric nuclear weapon test showed a complex time behavior as a significant amount of contaminant was introduced into the stratosphere and returned slowly to the troposphere and the earth [2].

The main problems with the above mentioned evaluations were the difficulty of determining the transfer rates from data of environmental contamination caused by the dynamics of continuous deposition and, chiefly, the high uncertainty levels of the estimates of radionuclide deposition on the whole catchment and of the contaminant runoff.

Experimental Results Following the Chernobyl Accident

Following the accident on 26 April 1986 at the Chernobyl Nuclear Power Plant located in Ukraine, radioactive substances were dispersed into the environment. The Chernobyl accident represented a line of demarcation between research carried out following the environmental contamination due to the nuclear weapon tests in the atmosphere and the new results from a single contamination event. The releases of contaminants occurred over a few weeks period and the radionuclides spread across Europe. Vast regions were affected by the consequences of the accident and whole large river catchments were contaminated [6]. The accident can be classified as a pulse-type event of radionuclide release, at least in relation to those environmental migration processes that occur over periods of time of the order of months or years such as the migration on the medium and long term of radionuclides from a catchment.

Following the accident, a variety of studies focused on the evaluation of the quantitative behavior of radionuclide in catchments [7–9]. Some results from the analysis of contamination data collected by various European laboratories [10–17] are analyzed and discussed below.

The main assumption of the above mentioned studies was that, following a pulse of radionuclide deposition D ($Bq\,m^{-2}$) occurred at time t=0, the flux of radionuclide, $F(t)$ ($Bq\,s^{-1}$), transported by the river water at instant t can be expressed as D multiplied by a "radionuclide transfer function per unit deposition" $TF(t)$ ($m^2\ s^{-1}$)

$$F(t) = D \cdot TF(t) \tag{4}$$

Generally, function TF was fitted to the sum of time-dependent exponential components $e^{-(\lambda+\lambda_i)t}$ which account for environmental effects and other first-order processes, such as the radioactive decay, that influence the time behavior of the pollutant concentration in the water flowing through the catchment:

$$TF(t) = \sum_i A_i^* \, e^{-(\lambda+\lambda_i)t} \tag{5}$$

A_i^* are multiplicative factors, λ_i are empirical parameters controlling the decay of radionuclide concentration in water due to environmental effects (s^{-1}) and λ is the radioactive decay constant (s^{-1}).

We can assume that, in given hydrological conditions (water fluxes, amount and characteristics of suspended matter in water, environmental conditions due to seasonal effects, such as the fraction of catchment area covered by snow, ice, etc.), the initial concentration $C(0)$ of radionuclide in water is proportional to the deposition pulse D:

$$C(0) = \varepsilon\, D \tag{6}$$

where ε is a coefficient (m^{-1}) that depends on the radionuclide, on the catchment characteristics, and on the above mentioned conditions. In principle, coefficients A_i^* may depend on the water fluxes $\Phi(t)$ and the relationships between A_i^* and $\Phi(t)$ can be nonlinear. It is useful to "normalize" the water flux and the radionuclide migration rate to the initial conditions. By such a "normalization," it is possible to fit the empirical data of contaminant flux to the function $(F(t)/F(0))$ that characterizes the time behavior of the radionuclide transfer from the catchment:

$$\frac{F(t)}{F(0)} = \sum_i A_i \left(\frac{\Phi(t)}{\Phi(0)}\right)^{\alpha_i} e^{-(\lambda_i+\lambda)t} \tag{7}$$

α_i are empirical exponents (dimensionless) that give reason for the above mentioned possible nonlinearity of $F(t)$ as a function of the water flux from the catchment. Coefficients A_i (dimensionless) are the relative weights of the exponential components in the transfer function.

The use of the ratios $(F(t)/F(0))$ and $(\Phi(t)/\Phi(0))$ assures that coefficients A_i are dimensionless and that $\sum_i A_i = 1$, as it can be easily demonstrated by putting t=0 in Eq. 7.

The flux of radionuclide at instant t can be simply expressed in terms of D and ε. Indeed, in view of

$$C(t) = \frac{F(t)}{\Phi(t)} \tag{8}$$

and of Eq. 6, we can write for t=0:

$$F(0) = \varepsilon D \Phi(0) \tag{9}$$

Consequently, by accounting for Eq. 9, Eq. 7 is transformed as follows:

$$F(t) = \varepsilon D \sum_i [\Phi(t)]^{\alpha_i} \beta_i A_i e^{-(\lambda_i+\lambda)t} \tag{10}$$

or, in view of Eq. 8,

$$C(t) = \varepsilon D \sum_i [\Phi(t)]^{\alpha_i - 1} \beta_i A_i e^{-(\lambda_i+\lambda)t} \tag{11}$$

where

$$\beta_i = [\Phi(0)]^{1-\alpha_i} \tag{12}$$

are "normalization" coefficients

The main advantage of formula (7) is that Eq. 10 can be fitted to the experimental data of radionuclide fluxes by using the empirical dimensionless estimates of variables $(F(t)/F(0))$ and $(\Phi(t)/\Phi(0))$ in order to determine the values of parameters ε, λ_i, A_i, and α_i.

If the effects of the seasonal variations of the water flow on the radionuclide concentration in water are not accounted for (for instance, if the data analysis is based on yearly average of the water fluxes), we can put α_i=1. With such an assumption, from Eqs. 11 and 12, we obtain

$$C(t) = \varepsilon D \sum_i A_i e^{-(\lambda+\lambda_i)t} \tag{13}$$

As Eq. 13 shows, the yearly average concentration in water comprises two terms:

- A multiplicative "scaling factor" ε
- The sum:

$$\sum_i A_i e^{-(\lambda+\lambda_i)t} \tag{14}$$

Expression (14) characterizes the "shape" of the curve (i.e., the time behavior of the migration process).

The scaling factor ε, the ratio between the initial concentration of radionuclide in water and the total deposition, determines the "position" of the curve in the graph "radionuclide concentration in water versus time" [18]. From the available experimental data collected over the course of 5–7 years following the Chernobyl accident, it was possible to identify short-term and long-term components for periods of few months and of several years, respectively.

The above described notion of transfer function can be applied to the dissolved, the particulate, and the total (particulate+dissolved) concentration of radionuclide in water. A review of available empirical evaluations of the effective decay constants, of the coefficient A_2 and of the exponent α_2 are reported in Table 1.

Examples of applications of Eq. 11 are shown in Figs. 3 and 4. The concentrations of ^{137}Cs and ^{90}Sr in the River Prypiat (Ukraine) are reported as functions of time and are compared with the values calculated by Eq. 11.

The values of α_2 are higher than 1 for strontium, a radionuclide that is chiefly in dissolved form. This suggests that the concentration in water of such a radionuclide is positively correlated with the water flux. A possible explanation of this effect is the different contributions of dissolved radionuclide from soil layers at different depth. Following deposition of a radionuclide, the upper part of soil is heavily contaminated and significantly contributes to the contamination of the surface runoff waters. When the flux of water in the catchment increases due to the effects of heavy precipitation or snow melting, the water saturation of soils in the catchment implies that a larger fraction of water flows as surface runoff and interacts with the more contaminated upper soil layers. There is no similar effect for dissolved cesium, (α_2 ranges from 0.53 to 1.08 and, in most cases, the correlation coefficient

Radionuclide Migration from Catchments, Modeling. Table 1 Measured values of some parameters in the transfer function

River	Radionuclide	Period of collection of fitted data (following the accident)	A_2 (dimensionless)	α_2 (dimensionless)	Standard deviation of α_2	$\lambda_1+\lambda$ (s^{-1})	Standard deviation of $\lambda_1+\lambda$	$\lambda_2+\lambda$ (s^{-1})	Standard deviation of $\lambda_2+\lambda$	Reference
Po[a]	^{137}Cs	Few months				2.3×10^{-7}	5.5×10^{-8}			[9][c]
Rhine[a]	137Cs	< 2 years	0.052	0.53	0.3	6.5×10^{-7}	1.3×10^{-7}	2.7×10^{-8}	0.6×10^{-8}	[9]
Prypiat[a]	^{137}Cs	≈5 years	0.035	1.08	0.06	5.2×10^{-7}	6.5×10^{-7}	1.8×10^{-8}	0.7×10^{-9}	[9]
Dnieper[a]	^{137}Cs	≈5 years	0.028	0.86	0.06	8.8×10^{-7}	1.1×10^{-7}	1.1×10^{-8}	0.7×10^{-9}	[9]
Teterev[a]	^{137}Cs	≈5 years		0.96	0.15			8.2×10^{-9}	$2.\times10^{-9}$	[9]
Uzh[a]	^{137}Cs	≈5 years		1.02	0.1			1.5×10^{-8}	1.8×10^{-9}	[9]
Inlets of Devoke Water[b]	^{137}Cs	few years		1.0–1.3				1.2×10^{-8}		[7]
Inlets of lakes	^{137}Cs	≈6 years				$.6\times10^{-7}$–1.5×10^{-7}		$7.\times10^{-9}$–$2.\times10^{-8}$		[13]
Hillesjön and Salgsjön[b] Garonne, Meuse, Moselle, Rhône, Seine	^{137}Cs	≈18 years						3.6×10^{-9} –$8.\times10^{-9}$		[14][d]
Kemijoki, Kymijoki Tornionjoki, Kokemaenjoki, Oulujoki[b]	^{137}Cs	≈15 years						1.2×10^{-8} –4.9×10^{-8}		[15]

Po[a]	^{131}I	Few months				1.1×10^{-6}	6.5×10^{-8}			[9][c]
Po[a]	^{103}Ru	Few months				4.7×10^{-7}	4.0×10^{-8}			[9][c]
Prypiat	^{90}Sr	≈5 years	0.048	1.55	0.08	9.0×10^{-7}	1.1×10^{-7}	4.9×10^{-9}	0.9×10^{-9}	[9]
Dnieper	^{90}Sr	≈5 years	0.166	1.4	0.08	5.2×10^{-7}	1.5×10^{-7}	5.5×10^{-9}	0.9×10^{-9}	[9]
Teterev	^{90}Sr	≈5 years		1.12	0.14			3.6×10^{-9}	2.1×10^{-9}	[9]
Uzh	^{90}Sr	≈5 years		1.31	0.09			5.9×10^{-9}	1.8×10^{-9}	[9]
Irpen	^{90}Sr	≈15 years						1.6×10^{-9}	–	[16]
Ilya	^{90}Sr	≈15 years						2.7×10^{-9}	–	[16]
Sakhan	^{90}Sr	≈15 years						3.8×10^{-9}	–	[16]
Glinitsa	^{90}Sr	≈15 years						1.9×10^{-9}	--	[16]

[a]Dissolved radionuclide
[b]Total ^{137}Cs (particulate+dissolved)
[c] Data fitted to a single exponential function
[d]Assesses from contamination decline in sediment and biota

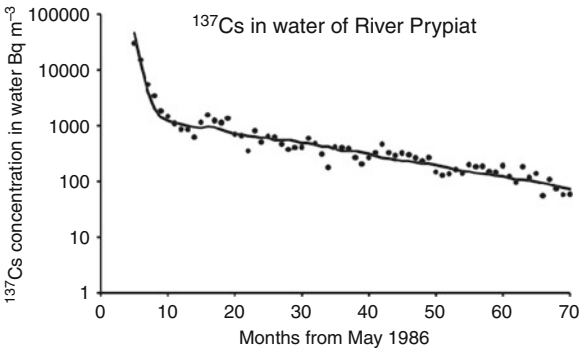

Radionuclide Migration from Catchments, Modeling. Figure 3
Empirical values of ^{137}Cs concentration in water of River Prypiat (dissolved form) compared with the results of Eq. 11

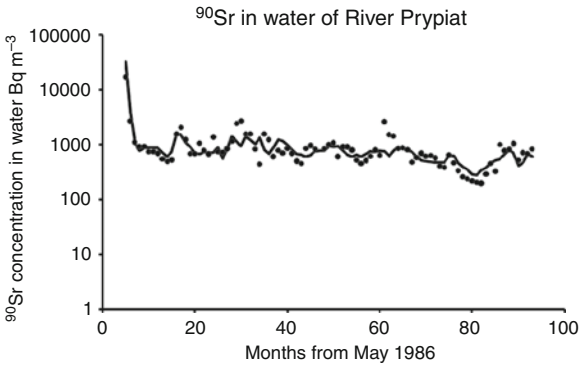

Radionuclide Migration from Catchments, Modeling. Figure 4
Empirical values of ^{90}Sr concentration in water of River Prypiat compared with the results of Eq. 11

between ^{137}Cs in dissolved form and the water flux is <0.1). This is due to the fast fixation of these radionuclides to soil particles and to the dilution in the river waters that, generally, show lower levels of contamination. Indeed, a significant amount of the radionuclide is removed from the water column as a consequence of the intense interaction with settling suspended matter and bottom sediments.

Table 2 shows the values of some measured parameters of the transfer function, TF, for particulate cesium. It is worthwhile to note that the values of α_2 are higher than 1 probably as a consequence of the significant amounts of suspended matter in river water during periods of high water fluxes.

As Tables 1 and 2 show, several experimental evaluations of the effective decay rates and of the values of the exponential components of the TF were obtained. However, comparatively few experimental assessments are available for the transfer coefficient ε. Among the parameters in the transfer function, ε is the one that most significantly influences the uncertainty of the predictions. This parameter depends on many factors of environmental significance. Consequently, its values vary within a wide range. It is extremely important to evaluate ε for the specific environmental conditions of the catchment in order to perform reliable assessments of the radionuclide migrating from the drainage area. Smith et al. [18] analyzed the correlations between ε and several environmental characteristics of the catchments of 25 rivers in Europe and Asia. The analysis showed a significant dependence of ε on the percentage of "inland water" in the catchment. The "inland water" percentage (I_{WP}) values were obtained from the Advanced Very High Resolution Radiometer (AVHRR) database. As high values of reflectance from water surface correspond to very wet land areas, the "inland water" percentage provides a good estimate of the area of a catchment that can be more actively involved in the contaminant migration owing to possible higher levels of surface runoff. A linear relation between ε and I_{WP} was suggested:

$$\varepsilon = a \cdot I_{WP} + b \tag{15}$$

The estimated values of the multiplicative coefficient "a" were 0.011 and 0.14 m^{-1} for ^{137}Cs and ^{90}Sr, respectively. The values of "b" were 0.063 m^{-1} (^{137}Cs) and 0.55 m^{-1} (^{90}Sr). The values for strontium are higher than the corresponding values for cesium as the former radionuclide is more mobile than the latter in the aquatic environment.

Principles for Developing Models of Radionuclide Migration from Catchments

The migration of radioactive substances from drainage areas is influenced by complex processes of hydraulic, geochemical, sedimentological, ecological, and anthropogenic nature. Broadly speaking, a model for

Radionuclide Migration from Catchments, Modeling. Table 2 Measured values of some parameters in the transfer function from catchments (particulate cesium) [17]

River	α_2	95% up of α_2	95% down of α_2	$\lambda_2+\lambda$ (s^{-1})	95% up of $\lambda_2+\lambda$ (s^{-1})	95% down of $\lambda_2+\lambda$ (s^{-1})
Danube	2.44	1.90	2.98	1.4×10^{-8}	2.2×10^{-8}	6.7×10^{-9}
Uzh	1.02	0.65	1.39	1.1×10^{-8}	1.8×10^{-8}	4.0×10^{-9}
Teterev	1.34	0.97	1.77	1.2×10^{-8}	1.8×10^{-8}	6.0×10^{-9}
Prypiat	1.52	1.34	1.7	1.4×10^{-8}	1.6×10^{-8}	1.3×10^{-8}
Dnieper	1.24	1	1.37	1.2×10^{-8}	1.4×10^{-8}	1.1×10^{-8}
Desna	1.11	0.83	1.39	8.9×10^{-8}	1.3×10^{-8}	4.7×10^{-9}
Rhine	1.12	0.27	1.97	1.7×10^{-8}	2.4×10^{-8}	1.0×10^{-8}
Geometric mean	1.34			1.2×10^{-8}		

predicting the migration of radionuclides from catchments should account for [19]:

1. Hydrological processes
   (a) Water fluxes
   (b) Sediment erosion, dispersion, and deposition
2. Physicochemical processes of interaction of radionuclides with the exposed surfaces in the catchment and, in particular, with soils and eroded particles and the consequent partition of the contaminant in dissolved and particulate phases
3. The migration of dissolved and particulate contaminants transported by the waters flowing through the catchment

A great deal of work has been done in past decades to investigate the above processes.

The hydrologic cycle and the surface water runoff and balance have been thoroughly studied and many models have been developed. The evaluations of water runoff, of erosion rates and of the fluxes of water within the various vertical horizons of the catchment can be performed, at least in principle, by using equations that are copiously described in the scientific literature [20, 21].

The physicochemical processes of the interaction of radionuclides dissolved in water with soil and bedrock have been the subject of many studies in past decades [22, 23]. An extensive review of similar investigations, whose results chiefly refer to nonradioactive substances but that can be also applied, at least conceptually, to radionuclides, can be found in the specialized literature [24].

Finally, the evaluation of the migration of radionuclides transported, in dissolved and particulate forms, by waters flowing through the catchment is based on the application of the contaminant mass balance equation and on the assessment of the complex processes of radionuclide dispersion such as diffusion and transport [25].

The overwhelming complexity of the previously mentioned processes requires the application of suitable strategies to develop models for practical use [26–28].

In principle, the models for predicting the behavior of complex environmental processes can be classified as reductionistic or aggregated.

As all the above mentioned classes of hydrological, physicochemical, and migration processes have been copiously studied, it seems, at first sight, that the appropriate linking of the corresponding sub-models makes it possible to develop a comprehensive general model of the behavior of radionuclides migrating from catchments to water bodies. This is the well-known principle that governs the so-called reductionistic approach for modeling natural phenomena.

Reductionistic models are aimed at predicting the behavior of complex environmental systems by accounting for as many processes as reasonably possible. The term reductionism emphasizes the fact that the functioning of the considered system is modeled

according to primary laws from fundamental disciplines such as physics and chemistry. [29].

A reductionistic model, in principle, accounts for a great deal of processes and, consequently, makes use of a copious number of parameters and variables in the equations controlling these processes. For instance, one of these models [30] predicts the migration of radiocaesium from lake catchments by accounting for the following processes and the relevant parameters: interception of rain and radionuclides by vegetation; infiltration through soil layers; effects of catchment slope, of soil density, porosity, and soil particle size; effects of washout from vegetation; etc. The model includes sub-models to determine the overload flow, the water depth of channeled flow, the water flow velocity, the overland flow of particulate matter, etc.

An alternative method consists in developing models based on the aggregation of processes and parameters. The aggregation occurs not only at level of processes but also by spatial integration over entire subregions of the catchment. It is assumed that the behavior of a complex system can be predicted, with acceptable approximations (at least in relation to those target variables that are deemed of interest in view of the specific problem), by means of more or less simple models that make use of a limited set of information, data, and parameters to describe the dynamics of the contaminant in the environment.

In the following sections, the main principles of the above mentioned modeling strategies will be described and discussed.

Principles Underlying Reductionistic Models

Several reductionistic models for predicting the fluxes of radionuclides from complex catchments to water bodies have been developed. These models simulate the dynamics of waters flowing to the water body and the resulting radionuclide migration. In principle, they are based on complicated hydrological equations, accounting for precipitation, water infiltration, interception of rain by the vegetation canopy, evapotranspiration, etc., and assessing the consequent dispersion of radionuclides through the different catchment components [31–33].

Reductionistic models make use of many parameters that are frequently assessed by specific sub-models and account for the spatial variability of the catchment hydrologic and geophysical characteristics. In several cases, appropriate hypotheses make it possible to simplify the approaches for evaluating the complex dynamics of the many involved processes.

The application of a reductionistic model requires the knowledge of the catchment characteristics and of the model parameters at levels of spatial resolution appropriate for modeling the processes with the required precision. It is beyond the scope of this entry to describe in detail such models. The main aim of the present section is to review the most important principles underpinning the reductionistic modeling approach.

It is worthwhile to remind the reader of the meaning of certain terms as to their *particular usage* in this entry. "Transport" is the ordered movement of the contaminant transported by the water current, while "dispersion" denotes the disordered movement of the pollutant caused by chaotic processes such as the molecular diffusion and the turbulent motion of water. The expression "radionuclide migration" defines the overall process of contaminant movement caused by both transport and dispersion processes.

A reductionistic model accounts for the dispersion and the transport of radionuclides through the saturated and the unsaturated zones of the aquifer (Fig. 2).

The dispersion implies the movement of a pollutant from regions of space of high contaminant concentration to regions of low concentration. The radionuclide flux, $\mathbf{F}$ ($\mathrm{Bq\,m^{-2}\,s^{-1}}$) (bold characters denote vectors or tensors), is related to the concentration gradient according to the Fick's first law:

$$\mathbf{F} = -\mathbf{K}\,\mathbf{grad}C \tag{16}$$

where **grad** is the gradient of C ($\mathbf{grad}C = \mathbf{i}\frac{\partial}{\partial x}C + \mathbf{j}\frac{\partial}{\partial y}C + \mathbf{k}\frac{\partial}{\partial z}C$), C ($\mathrm{Bq\,m^{-3}}$) is the dissolved radionuclide concentration in water and $\mathbf{i}$, $\mathbf{j}$, and $\mathbf{k}$ are the unit vectors along the coordinate axes x, y, and z. $\mathbf{K}$ is a 3×3 component symmetric tensor (the diffusion tensor).

Tensor $\mathbf{K}$ in Eq. 16 highlights that, in principle, diffusion is a non-isotropic process occurring in the three dimensions.

The radionuclide flux due to the ordered motion caused by the water current is related to the

concentration C of radionuclide and to the water velocity $\mathbf{V}$ (ms^{-1}) by the following equation:

$$\mathbf{F} = \mathbf{V}\ C \tag{17}$$

From the Mass Conservation Law and Eqs. 16 and 17 that control the contaminant flux, it is possible to derive the equation governing the behavior of the concentration of a radionuclide in the water flowing through the catchment.

Let θ ($m^3\ m^{-3}$) denote the volumetric content of water, at point of coordinate (x, y, z), in the substrate (for instance, the sand, the gravel, etc.) that adsorbs the contaminant. The value of θ depends on the volume of water filling the pores of the substrate components. It is lower than 1 $m^3\ m^{-3}$ and reaches this maximum value in surface water where the volume of particulate matter per unit volume is negligible. The total flux $\mathbf{F}$ (Bq $m^{-2}s^{-1}$) of radionuclide in dissolved form at point x is:

$$\mathbf{F} = (-\mathbf{K} \times\ \mathbf{grad}C + \mathbf{v}\ C)\theta \tag{18}$$

The application of the contaminant mass balance equation over a finite region of space and the following transformation of the surface integral of flux $\mathbf{F}$ in a volume integral yield, in view of Eq. 18:

$$\frac{\partial}{\partial t}(\theta C + \delta C_s) + \lambda(\theta C + \delta C_s) + div\mathbf{F} = 0 \tag{19}$$

where C_s ($Bqkg^{-1}$) is the concentration of radionuclide attached to the firm substrate, δ (kgm^{-3}) is the mass of substrate per cubic meter and λ is the radioactive decay constant.

To determine C and C_s from Eq. 19 requires an appropriate sub-model for predicting the dynamics of the interaction of radionuclide in dissolved form with particulate matter.

The most common and simple approach to model this interaction with substrate matter is based on the hypothesis of a reversible rapid equilibrium between the dissolved and the adsorbed phases. More specifically, if the substrate is composed of particulate matter like sand or clay, the ratio between the radionuclide concentration in particulate form (Bq per unit mass of particulate) and the radionuclide in dissolved form (Bq per unit volume of water) is the so-called distribution or partition coefficient k_d (m^3kg^{-1}) [34]:

$$\frac{C_s}{C} = k_d \tag{20}$$

The distribution coefficient may be used as a first approach to evaluate the behavior of pollutants like radionuclides and heavy metals in the system water-soil when the ratio of the pollutant concentration in soil (particulate phase) and the pollutant concentration in interstitial water (dissolved phase) quickly reaches the equilibrium value k_d. The value of the partition coefficient depends on the radionuclide and the physical and geochemical conditions of the system particulate matter–water.

From Eqs. 19 and 20 we obtain that, in the regions of the drainage area where k_d, θ, and δ are constant, the contaminant concentration is governed by the following equation:

$$\frac{\partial C}{\partial t} = \mathbf{div}\,\mathbf{K}^* \times\ \mathbf{grad}C - \mathbf{div}\,\mathbf{V}^*\ C - \lambda C \tag{21}$$

where

$$\mathbf{K}^* = \frac{\mathbf{K}}{R} \tag{22}$$

and

$$\mathbf{V}^* = \frac{\mathbf{V}}{R} \tag{23}$$

R is the so-called retardation factor:

$$R = 1 + k_d\frac{\delta}{\theta} \tag{24}$$

The migration of radionuclides is "retarded" by the processes of interaction with particulate matter. Indeed, the components of the effective velocity and of the dispersion tensor $\mathbf{V}^*$ and $\mathbf{K}^*$ in the two phases system water–particulate matter are lower than the corresponding values of $\mathbf{V}$ and $\mathbf{K}$ in water ($R>1$). This effect is more marked for contaminants characterized by higher values of k_d.

Equation 19 can be also used to predict the radionuclide migration in the over land waters flowing through the catchments provided that θ is assumed approximately equal to 1 $m^3\ m^{-3}$ and the dissolved concentration C of radionuclide in Eq. 18 to calculate flux $\mathbf{F}$ is replaced by the total radionuclide concentration (dissolved + particulate form).

As previously noted, the above described approach is based on the essential hypothesis of a quick and complete equilibrium between the dissolved and the attached phases. Furthermore, it is assumed that, in

spite of the heterogeneous composition of the substrate, the use of an average value of the partition coefficient is sufficiently appropriate for assessing the ratio between the radionuclide phases. Unfortunately, such hypotheses underlying Eq. 20 are not generally held. The equilibrium is not instantaneously achieved and, moreover, the adsorption–desorption processes are not ever reversible and may depend on the characteristics of the different components of the substrate.

Many authors have discussed and analyzed the dynamic behavior of sorption–desorption processes of dissolved pollutants with sediments and solid matter [35]. Several multiphase dynamics models accounting for complex sorption–desorption kinetics and nonreversible interaction processes have been developed [36].

As formulae (22), (23), and (24) show, when the interaction of a radionuclide with particulate matter is negligible (very low values of k_d as in the case of ^3H) the retardation factor R is approximately equal to 1 and the migration velocity and the dispersion coefficient of the contaminant are equal to the corresponding values in Eqs. 16 and 17.

To model the transport of a contaminant by the water flowing through a catchment is complicated by the necessity of accounting for the complex geometry of channels and fractures in the rocks. Moreover, at least in principle, the sub-catchment should be subdivided in "cells" each characterized by specific geological, geochemical, and environmental properties that influence the contaminant migration.

Frequently, discretization of the model equations is performed along the vertical axis. Many models account for several compartments corresponding to different soil layers to assess the vertical migration of radionuclides. A typical multi-compartment model was proposed by Korhonen [37], in which soil in the drainage area was subdivided into layers of various thicknesses. The migration of radionuclides was evaluated accounting for the fluxes of infiltrating water.

However, as experienced for many other kinds of models, increasing the level of detail in the description of the processes does not guarantee greater accuracy of model performance [29]. Indeed, the overall uncertainty of a model is significantly influenced by the contribution of nonnegligible uncertainties from a large number of parameters whose values cannot be known with a sufficient accuracy at site-specific level [38].

It is commonly assumed that two main factors can affect the reliability of a model for predicting the behavior of complex systems:

- The lack of detailed knowledge at the level of the actual processes
- The lack of parameter values necessary for the quantitative assessment of the processes

It has been frequently argued that reductionistic models require a vast amount of data and information and, consequently, may be difficult to apply in practical circumstances. Nevertheless, the reductionistic approach provides a theoretical basis for understanding the role of the fundamental processes involved in the migration of radionuclides through the environment.

Reductionistic models have the undoubted merit of framing the available knowledge concerning the behavior of radionuclides in catchments in a coherent system of logical assumptions, helping the understanding of the functioning of the complex process of contaminant migration from drainage areas.

Principles Underlying Aggregated Models

The alternative strategy for developing models to predict the behavior of contaminants in complex environmental systems is based on the aggregation of processes and parameters. Aggregated models assume that the many different processes of migration of radioactive substances from catchments can be grouped in terms of radionuclide storage, retention, and release by spatially distributed components that, in spite of the heterogeneity of their constituent parts, can be assumed as functional units playing specific roles in the overall migration process.

The radionuclide flux to the water body is a function of time and depends on the rate of deposition of contaminant onto the catchment surface. One of the most simple (or, probably, the most simple) aggregated model was described by Carlsson [39]. Such a model was developed by accounting for the empirical information obtained before the Chernobyl accident. The approach assumes that an initial fraction $k_1 D(t)$ of radionuclide deposited ($D(t)$) per unit time and

per unit surface at instant t is instantaneously transferred by runoff waters to the water body (k_1 is dimensionless). Thereafter, the remaining part of deposited radionuclide accumulates in some catchment compartments, such as soils, snowpack, glaciers, etc., that act as "storage units." The amount $S(t)$ of radionuclide per square meter in the storage compartment is available for delayed release and is washed off at a rate $k_2S(t)$ where k_2 (s^{-1}) is a multiplicative factor. Therefore, the flux of radionuclide from the catchment per square meter, $F_R(t)$ ($Bq\,m^{-2}s^{-1}$), can be calculated as follows:

$$F_R(t) = k_1\,D(t) + k_2\,S(t) \tag{25}$$

The model (Fig. 5) corresponds to the conceptual scheme adopted by Yamagata and coworkers [5] that accounts for the fraction of the deposition that is instantaneously transferred to the runoff water and for the removal of radionuclide from the ground deposit.

The coefficient k_2 corresponds to λ_w in Eq. 3. Estimates of k_1 and k_2 were obtained from experimental data available for chronic releases (the fallout from the nuclear weapon tests in the atmosphere). The results of a review by Helton and coworkers [40] suggested that the values of k_1 varied from 0.5×10^{-2} to 12.2×10^{-2} and from 0.1×10^{-2} to 1.9×10^{-2} for ^{90}Sr and ^{137}Cs, respectively. Estimates of k_2 ranged from 2.2×10^{-11} s^{-1} to 1.0×10^{-9} s^{-1} for ^{90}Sr and from 2.1×10^{-12} s^{-1} to 1.8×10^{-10} s^{-1} for ^{137}Cs. For plutonium isotopes, the order of magnitude of k_2 was 10^{-11} s^{-1}.

It is possible to derive the following differential equation controlling the time behavior of $S(t)$ from the radionuclide balance in the catchment:

$$\frac{dS(t)}{dt} = -(\lambda + k_2)S(t) + (1 - k_1)D(t) \tag{26}$$

where λ is the radioactive decay constant (s^{-1}).

It is worthwhile to note that k_2 in Eq. 26 corresponds to λ_2 in Eq. 10 as can be easily realized by solving Eq. 26 for a pulse deposition and accounting for Eq. 25.

Unfortunately, as previously noted, before the Chernobyl accident, the contamination of large catchments was essentially caused by chronic releases of radionuclides from the weapon nuclear tests in the atmosphere. This made particularly difficult the evaluation of the parameters in the proposed models. For instance, the estimated values of removal rates (k_2) for strontium are higher that the corresponding values for cesium. Therefore, according to these estimates, the concentration of radiostrontium in runoff water should decline faster than the concentration of radiocaesium. This is in disagreement with the experimental evidence as the empirical evaluations of the TF parameters reported in Table 2 show (note that the values of λ_2 for ^{137}Cs are significantly higher than the corresponding values for ^{90}Sr). Moreover, the effective decay rates of ^{137}Cs concentration in water determined following the Chernobyl accident range from

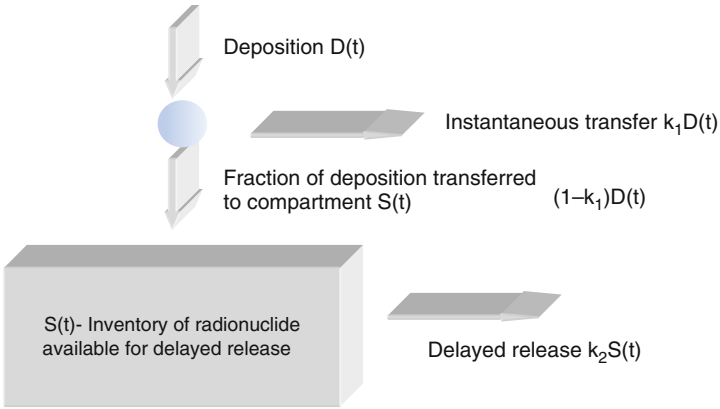

Radionuclide Migration from Catchments, Modeling. Figure 5
Structure of a simple model for predicting the migration of radionuclides from catchments

3.6×10^{-9} to 2.7×10^{-8} s^{-1}. These values are significantly higher than those reported in the studies performed before the accident [5, 40].

The chronic contamination caused by radionuclide fallout from nuclear weapon tests in atmosphere prevented an accurate evaluation of the time behavior (and consequently of the effective decay parameters) of radionuclides in water. Moreover, these assessments were based on the assumption that radionuclides accumulated in the catchment storage compartments $S(t)$ were fully available for migration. This hypothesis implies a significant underestimate of k_2 when such a parameter is evaluated from the radionuclide balance in the catchment by accounting for the total deposit and for the radionuclide washout as it was performed by pre-Chernobyl assessments.

A Technique to Derive the Radionuclide Migration Model from the Transfer Function The mathematical characteristics of the radionuclide transfer function (10) derived from the analysis of the available empirical data suggest a technique to develop an empirically based aggregated model for assessing the migration of radionuclides from catchments.

Before embarking upon complicated technical matters, it is useful to remind some mathematical notions that are of importance for the following discussion.

Let $GF(t, \tau)$ be the flux ($\mathrm{Bq\,s^{-1}}$), at time t, of contaminant from the catchment to a water body following a single unit pulse (1 $\mathrm{Bq\,m^{-2}}$) of radionuclide deposition at instant τ. Let $\delta(t-\tau)$ denote the so-called Dirac's delta function, representing a unit pulse function at time τ. Following a deposition pulse $D \cdot \delta(t-\tau)$, the amount of contaminant $G(t, \tau)$ ($\mathrm{Bq\,s^{-1}}$) flowing from the catchment is:

$$G(t, \tau) = D \cdot GF(t, \tau) \tag{27}$$

Equation 27 simply states that the radionuclide flux is proportional to the deposition (it is assumed that the process is linear). A chronic deposition $D(t)$ ($\mathrm{Bq\,m^{-2}\,s^{-1}}$) can be interpreted as a continuous series of pulses $D(\tau) \cdot \delta(t-\tau)$ occurring at infinitesimal intervals of time $\mathrm{d}\tau$. Consequently, $G(t)$, the radionuclide flux from the catchment due to the deposition rate $D(t)$, can be obtained by integrating (27) over the domain of τ (we assume that $D(t)$ is different from 0 when $t>0$):

$$G(t) = \int_0^t GF(t, \tau) \cdot D(\tau) \mathrm{d}\tau \tag{28}$$

Equation 28 shows that it is possible to determine the radionuclide flux from a catchment for any chronic deposition rate $D(t)$ if function $GF(t, \tau)$ is known. In principle, $GF(t, \tau)$ definitely characterizes all the features of the dynamics of the radionuclide migration process that are necessary for assessing the pollutant flux from a contaminated catchment. It should be noted that $GF(t, \tau)$ corresponds to the so-called transfer function $F(t)$ that was defined in section "Experimental Results Following the Chernobyl Accident." In other words, $F(t)$ should be interpreted as an "empirical estimate" of $G(t, \tau)$ for $\tau=0$ (the instant of radionuclide pulse deposition).

As previously described, the analysis of contamination data collected following the Chernobyl accident showed that the measured radionuclide flux from a catchment can be fitted to Eq. 10. Consequently, accounting for Eq. 28 and for the equivalence between $GF(t,\tau)$ and $F(t)$ it is possible to write:

$$G(t) = \varepsilon \int_0^t D(\tau) \sum_i \Phi(t)^{\alpha_i} \beta_i A_i \mathrm{e}^{-(\lambda_i+\lambda)(t-\tau)} \mathrm{d}\tau \tag{29}$$

(as usual, we have assumed that the deposition rate $D(t)$ is different from 0 for $t>0$). In principle, $GF(t, \tau)$ depends on the specific characteristic of the catchment. However, the empirical results previously presented suggest that this function shows a general mathematical form though the values of the parameters in Eq. 29 can be site specific. Putting:

$$S_i(t) = \int_0^t A_i e^{-(\lambda_i+\lambda)(t-\tau)} D(\tau) dt \tag{30}$$

it is possible to write:

$$G(t) = \varepsilon \sum_i \Phi(t)^{\alpha_i} \beta_i S_i(t) \tag{31}$$

It can easily be shown that S_i are solutions of the following system of differential equations:

$$\frac{\mathrm{d}}{\mathrm{d}t} S_i(t) = -(\lambda_i + \lambda) S_i(t) + A_i D(t) \tag{32}$$

with the initial conditions $S_i(0)=0$. Although Eqs. 31 and 32 were obtained from Eq. 29 by a mere mathematical artifice, S_i can be interpreted as the amount of radioactive substance ($\mathrm{Bq\,m^{-2}}$) accumulated in the ith radionuclide storage compartment of the catchment and available for migration to the water body. λ_i account for all those processes, such as the radionuclide fixation to soil, that makes the removal of the radioactive substances from the catchment by the runoff waters less effective. Parameters A_i are the fractions of deposited radionuclide accumulated in the ith compartment and the products $\varepsilon\Phi(t)^{\alpha_i}\beta_i(\mathrm{m^2\,s^{-1}})$ are the transfer factors of radionuclide from the ith compartment to the runoff water at instant t. It is worthwhile to note that the instantaneous transfer of deposited radionuclide in the Carlsson–Yamagata model corresponds to a storage compartment characterized by a value of λ_i that tends to infinity.

According to Håkanson [41], two main storage compartments correspond to the fast and slow components in the transfer function (10): (a) a fast component – wetlands dominated by a fast turnover of substances and horizontal migration processes; (b) a slow component – dryland dominated by vertical migration processes, through the soil horizons, and by the ground water dispersion.

The described aggregated model is based on the assumption that ε, A_i, and β_i are independent of time. In principle, alternative formulations are possible in view of the seasonal effects that can influence the migration of radionuclide from catchments and, therefore, the values of the model parameters. It is important to note that the available empirical information refers, almost exclusively, to the environmental contamination caused by the Chernobyl accident that occurred during spring when particular and typical seasonal processes like snow and ice melting occurred.

Theoretical Basis of "Aggregated" Models The amount F_R ($\mathrm{Bq\,s^{-1}}$) of radionuclide removed, per unit time, by the runoff waters from a catchment is:

$$F_R = A\phi C \tag{33}$$

where A is the surface of the catchment ($\mathrm{m^2}$), ϕ is the yearly average flux of water per square meter flowing through the catchment ($\mathrm{m^3\,s^{-1}\,m^{-2}}$) and C, as usual, is the concentration of contaminant in water. ϕ is the sum of two components: the infiltrating water (ϕ_2) and the surface runoff (ϕ_1). Due to the relatively high values of k_d and, consequently, of the retardation factors of radionuclides such as ^{137}Cs and ^{90}Sr, it is reasonable to assume that ϕ_2 does not contribute significantly to the migration of the contaminant to the water body.

The time behavior of the radionuclide inventory per square meter, I ($\mathrm{Bq\,m^{-2}}$), in the catchment is controlled by the following first-order differential equation:

$$A\frac{\mathrm{d}I}{\mathrm{d}t} = -F_R - \lambda \cdot A \cdot I \tag{34}$$

Let K ($\mathrm{m^{-1}}$) be the ratio of the radionuclide concentration in water divided by the radionuclide inventory:

$$K = \frac{C}{I} \tag{35}$$

K is the so-called entrainment coefficient used by several authors [27, 42, 43] to investigate, by quantitative approaches, the migration of radionuclides from catchments.

The radionuclide activity balance requires that:

$$\frac{\mathrm{d}I}{\mathrm{d}t} = -\phi \cdot K \cdot I - \lambda \cdot I \tag{36}$$

thus

$$I = I_0\,\mathrm{e}^{(-\phi Kt - \lambda t)} \tag{37}$$

and, from Eqs. 33 and 35,

$$F_R = I_0\,A\phi K\mathrm{e}^{(-\phi Kt - \lambda t)} \tag{38}$$

where I_0 is the value of I at instant $t=0$.

The radionuclide flux, F_1, due to the surface runoff is:

$$F_1 = I_0\rho A\phi K\mathrm{e}^{(-\phi Kt - \lambda t)} \tag{39}$$

where ρ is ϕ_1/ϕ.

In particular, the concentration in the surface runoff water is:

$$C = I_0\,K\mathrm{e}^{(-\phi Kt - \lambda t)} \tag{40}$$

The above results were obtained from a simple application of a general notion of entrainment coefficient K

without any particular assumption concerning the mechanisms of interaction of the radionuclide with the different kinds of rock and soil substrata in the catchment (however, K should be assumed independent of time).

To fix the ideas it can be useful to evaluate K under the hypothesis that the partition coefficient approach can be applied to determine the radionuclide concentration in water [44]. The contaminant transported through the catchment by the surface runoff is, prevailingly, confined in an upper layer of soil of thickness ζ (m). Such a hypothesis is valid when the contaminant strongly interacts with the soils and the rocks in the catchment as it occurs for radionuclides characterized by high values of the partition coefficient k_d.

The inventory I may be calculated as follows:

$$I = C\zeta(\theta + \delta k_d) \tag{41}$$

where θ ($m^3 m^{-3}$) is the water content of soil and δ ($kg m^{-3}$) is the soil density. As for the mentioned radionuclides:

$$\delta k_d >> \theta \tag{42}$$

from formula (35), it follows:

$$K = \frac{1}{\zeta \delta k_d} \tag{43}$$

It is worthwhile to note that the flux of radionuclide F_1 is expressed by a single exponential function when values of the parameters ρ, ϕ, and K averaged over the whole catchment are used in Eq. 39. This result is in disagreement with the empirical data available following the Chernobyl accident. Indeed, Figs. 3 and 4 clearly show that at least two exponential components can be observed over a period of several years. Moreover, since K is proportional to the reciprocal of k_d, the calculated values (Eq. 43) of the entrainment coefficient for Cs are significantly lower than the corresponding values for Sr. Consequently, Eq. 40 predicts a faster decline of the concentration in water of the latter radionuclide in disagreement with the empirical evidence as already noted in section "Principles Underlying Aggregated Models."

However, the characteristics that control the migration of a radionuclide through a catchment can be very variable on a spatial scale. For instance, the values of the distribution coefficient depend on the soil characteristics and on the chemical properties of the pollutant. Of course, in a complex catchment, the values of k_d for a particular pollutant may vary within a large range in view of the spatial variability of the geological properties of the soils. The assessment of the flux of radionuclide transported by runoff waters requires that the catchment is subdivided in subregions, each of which is characterized by particular values of ρ, ϕ, and K. The overall migration process can be modeled by integrating the fluxes of radionuclide from each subcatchment over the whole drainage area.

Putting $\phi K = \omega$, the pollutant flux can be evaluated as follows:

$$F_1 = I_0 A \bar{\rho} e^{(-\lambda t)} \int_0^\infty \omega f(\omega) e^{(-t\omega)} d\omega \tag{44}$$

where $f(\omega)$ is the distribution function of ω ($\bar{\rho}$ is the average of ρ over the catchment). Equation 44 is valid if ρ and ω are statistically independent.

The effective decay rate, $\lambda^*(t)+\lambda$, of radionuclide concentration in water at time t is:

$$\lambda^*(t) + \lambda = -\frac{1}{C}\frac{dC}{dt} = -\frac{1}{F_1(t)}\frac{dF_1(t)}{dt} \tag{45}$$

$\lambda^*(t)$ controls the decay of radionuclide concentration in runoff water due to environmental effects.

After boring but easy calculations and an integration by parts, we get:

$$\lambda^*(t) = \frac{1}{t} + \frac{1}{t}\frac{\int_0^\infty \omega g'(\omega) e^{(-t\omega)} d\omega}{\int_0^\infty g(\omega) e^{(-t\omega)} d\omega} \tag{46}$$

where $g(\omega) = \omega \cdot f(\omega)$. The second term in the right hand side of the previous equation may scarcely affect the order of magnitude of $\lambda^*(t)$ due to the presence of $g'(\omega)$ in the integral at numerator. Such a derivative reaches, indeed, both positive and negative values that may mutually compensate when the function is integrated over $(0, \infty)$.

$\lambda^*(t)$ can be evaluated for some simple distribution functions. Several examples show that such a function depends prevailingly on the observation time t but may be less sensitive to the environmental conditions and to the pollutant characteristics [17, 45].

If we hypothesize that ω is log-normally distributed:

$$f(\omega) = \frac{1}{\sigma\sqrt{2\pi}}\frac{1}{\omega}\exp\left[-\frac{1}{2\sigma^2}(\ln\omega - \mu)^2\right] \tag{47}$$

we obtain:

$$\lambda^*(t) = \frac{\phi(t)}{t} \tag{48}$$

where

$$\phi(t) = 1 + \frac{1}{\sigma^2}\left(\mu - \frac{\int_0^\infty \exp\left(-\frac{(\ln\omega-\mu)^2}{2\sigma^2}\right)\ln\omega\exp(-\omega t)\mathrm{d}\omega}{\int_0^\infty \exp\left(-\frac{(\ln\omega-\mu)^2}{2\sigma^2}\right)\exp(-\omega t)\mathrm{d}\omega}\right) \tag{49}$$

μ and σ are, respectively, the mean value and the standard deviation of the distribution of the natural logarithm of ω. $\phi(t)$ is close to 1 when σ is very large ($\lim_{\sigma\to\infty}\phi(t) = 1$).

The statistical aggregation of the contaminant migration fluxes from different points of a catchment can lead to slight variability in the dynamics of the overall migration process. Equation 48 shows that the value of $\lambda^*(t)$ depends on the observation time. In particular, the average value of $\lambda^*(t)$ over an interval of time centered around t should be of the order of $\langle\phi(t)/t\rangle$ (the angular brackets denote the time average).

Function (49) can be evaluated for ^{137}Cs and ^{90}Sr using the experimental log-normal distribution of k_d. For values of the parameters in Eq. 43 and in the distribution function (47) commonly measured for Cs and Sr in soils [46], $\phi(t)$ is almost independent of time (at least when t is of the order of months or years). Therefore, it is possible to write:

$$\lambda^*(t) \approx \frac{k}{t} \tag{50}$$

where k is a dimensionless constant of the order of 1. The previous results explain several characteristics of the time behavior of radionuclide concentration in runoff waters. Indeed, the experimental evaluations of λ_1 and λ_2 in Table 2 show that, following a single pulse of radionuclide deposition, the values of such parameters are approximately of the order of the reciprocal of t (the time since the accidental release of radionuclide occurred) averaged over the period of observation (months for the first exponential component and few years for the second) in agreement with Eq. 50. The empirical values of the effective environmental decay rates λ_1 and λ_2 (Table 2) are slightly variable despite the large range of characteristics of the catchments and the significantly different chemical properties of radionuclides like ^{137}Cs and ^{90}Sr. For instance, the values of λ_2 for ^{90}Sr are less than one order of magnitude lower than the corresponding values for ^{137}Cs, whereas the values of k_d for these radionuclides differ up to several orders of magnitude. Note that $\langle\lambda^*(t)\rangle$ is an estimate of λ_1 and λ_2 when the average is calculated over the above mentioned periods of time.

All the previous calculations are based on several assumptions and simplifications (for instance, ϕ_1, the yearly average surface runoff, is independent of time). However, the conceptual approach of the model sheds light on the role played by sub-catchments characterized by different radionuclide entrainment properties. It seems reasonable that, around a given instant t, the catchment areas characterized by values of the product ϕK of the order of $1/t$ contribute more effectively to the radionuclide migration. Indeed, the contributions from areas with $\phi K >> 1/t$ are negligible in view of the high value of the exponent in Eq. 38, whereas, if $\phi K << 1/t$, the contribution is negligible in view of the low value of the multiplicative factor ϕK in the equation.

Modeling Particular Processes of Radionuclide Migration from Catchments

Analyses based on process and system aggregations at level of the whole catchment can be useful as it has been shown in the previous sections. However, it is essential to define the most appropriate spatial scale and resolution time in view of the applications of this kind of models.

It is important to note that the described aggregated models are essentially aimed at assessing the radionuclide fluxes in hydrological conditions representing the average situation throughout the whole catchment. For a reliable and proper application of the models, the spatial resolution should be based on the identification of the areas in the catchment where particular

hydrologic processes may significantly influence the radionuclide migration. For instance, the role of river floodplains should be, in some circumstances, carefully accounted for in view of radionuclide removal and remobilization when such areas are significantly contaminated. For example, the peak concentration of ^{90}Sr in water of Prypiat River showed in Fig. 4 at instant "t = 62nd month" corresponds to the inundation, in January 1991, of the heavily polluted Prypiat floodplain in the vicinity of the Chernobyl Nuclear Power Plant. The flooding was caused by an "ice jam" formed in the Prypiat River channel between the Yanov bridge and the town of Chernobyl. The consequent washout of the radionuclide from the flooded area into the river water resulted in a significant increase of ^{90}Sr concentration [47] that cannot be properly predicted by Eq. 11 and by the corresponding model (section "A Technique to Derive the Radionuclide Migration Model from the Transfer Function") when the aggregation is performed at level of the whole catchment of the river.

Further, sub-catchment areas covered with snow and glaciers play a particular role in the radionuclide transfer process. For instance, it was found [48] that, in connection with the high water fluxes caused by ice and snow melting, the concentrations of dissolved cesium in water can significantly increase. For example, in spring, the concentrations of ^{137}Cs of Chernobyl origin in the water of the Dora Baltea River, whose catchment in Northwest Italy comprises high mountain areas in the Alps, were at least one order of magnitude higher than the concentrations measured in the other seasons. On the contrary, the high water fluxes in the river following the heavy precipitation in autumn were not associated with a similar corresponding increase of dissolved radionuclide concentration in water. A direct application of Eq. 11 is not appropriate to predict such a behavior as the modeled levels of radionuclide concentration in water are not correlated to the water flux in the river due to the low values of α_2. However, in order to properly predict the different radionuclide contributions associated with the sub-catchments covered by ice and snow, the catchment of the river can be subdivided in subregions characterized by different values of the transfer coefficient ε. The values of ε in the sub-catchments covered by ice and snow should be assumed significantly higher than the corresponding values in the other areas of the drainage basin. With these assumptions, the different levels of dissolved radionuclide concentration in river water during the flow peaks in spring and autumn can be easily explained by the different proportions of the rain runoff and of the melting waters flowing from areas covered by ice and snow.

Conclusions

The migration of radionuclides from the terrestrial to the aquatic environment involves complex processes of hydrological, physical, and geochemical nature. In principle, the models aimed at predicting the transfer of radioactive substances from catchments to water bodies can be classified as reductionistic and aggregated. However, most of the models developed for practical applications are hybrids that profit from both techniques to assess the complex behavior of radionuclide migrating from drainage areas.

Reductionistic models are aimed at predicting the migration of radionuclides according to primary laws from fundamental disciplines such as physics and chemistry and by accounting for as many detailed processes as reasonably possible. On the contrary, aggregated models are based on the identification of environmental units and processes whose behaviors can be explained by laws that are derived from empirical observations and that concern each unit as a whole (this could justify the term "holistic" occasionally used to define aggregated models). It is important to emphasize that, in this entry, the word "aggregation" refers to a conceptual empirical approach rather than to the mathematical techniques commonly used to simplify the structure of a model.

The advantages and the disadvantages of reductionistic and aggregated models for predicting the migration of radionuclides through the aquatic environment have been extensively analyzed and discussed in the scientific literature chiefly in view of applications for the management of environmental emergencies [26–28, 49–51]. It is generally recognized that reductionistic models have the merit of framing in a rational scheme the many processes controlling the transfer of radionuclides from catchments to water bodies and, therefore, are helpful for understanding the different roles of the migration mechanisms and their reciprocal interactions. Aggregation is a useful strategy for developing

models that can be easily applied for practical purposes and especially in emergence situations where model input data is limited without extensive collection of empirical data in the field.

Future Directions

A Discussion Including Potential Impacts on the Development of Certain Areas of Science

Radioecology and radiological modeling are traditional scientific disciplines that have been the subject of a great many studies carried out during the past decades. Pulse-type accidents of environmental contamination at continental scale are infrequent and the experiences gained following the Chernobyl accident are somewhat unique in environmental sciences. It is reasonable to think that the results from these experiences can be useful for addressing similar problems concerning the migration from catchments of other kinds of pollutants such as heavy metals.

As for many other radioecological studies, the investigations of the migration of radionuclide from catchments have produced several consolidated results that are widely accepted by most experts. However, some further model improvements are still necessary. The available aggregated models have been applied and validated chiefly for two radionuclides, ^{137}Cs and ^{90}Sr, that can significantly contribute to radiological doses to man from the aquatic pathway as demonstrated by the environmental consequences of the Kysthym and the Chernobyl accidents. It can be of interest, however, to extend the investigations to other radionuclides in view of other kinds of accidents causing releases of radioactive substances into the environment.

The analysis of the mathematical structure of the transfer function raises a variety of questions relevant to the quantitative assessment of radionuclide migration from catchments, such as the dependence of the function coefficients from the seasonal conditions during accidental releases. Further, the possible occurrence of nonlinearity effects caused by the water flux deserves to be better investigated, chiefly in relation to the early period following an accident.

Both reductionistic and aggregated models require calibration and customization for the applications to the specific catchments of interest. This can entail a significant effort for complex reductionistic models. It is desirable that appropriate strategies are developed in the future to solve such complex problems.

In general, models to simulate radionuclide migration through and from catchments are available. However, a major difficulty is the lack of suitable model input data at the appropriate scale. A profitable strategy for developing models aimed at assessing the radionuclide behavior in catchments is based on the identification of emerging processes and on their parameterization accounting for the specific environmental conditions and situations that influence migration processes.

Bibliography

Primary Literature

1. Horowitz AJ, Lum KR, Garbarino JR, Hall GEM, Lemieux C, Demas CR (1996) Problems associated with using filtration to define dissolved trace element concentrations in natural water samples. Environ Sci Technol 30:954–963
2. Eisenbud M (1963) Environmental radioactivity. McGraw-Hill, New York/San Francisco/Toronto/London
3. Fowler EB (1965) Radioactive fallout, soils, plants, foods, man. Elsevier, Amsterdam/London/New York
4. Menzel RG (1960) Transport of strontium-90 in runoff. Science 13:499–500
5. Yamagata N, Matsuda S, Kodaira K (1963) Run-off of caesium-137 and strontium-90 from rivers. Nature 200:668–669
6. De Cort M, Dubois G, Fridman D, Germenchuk M, Izrael YA, Janssen A, Jones AR, Kelly GN, Kvasnikova EV, Matveenko II, Nazarov IM, Pokumeiko YM, Sitak VA, Stukin ED, Tabachny LY, Tsaturov YS, Avdyushin SI (1998) Atlas of caesium deposition on Europe after the Chernobyl accident. EUR Report 16733, Luxemburg
7. Hilton J, Livens FR, Spezzano P, Leonard DRP (1993) Retention of radioactive caesium by different soils in the catchment of a small lake. Sci Total Environ 129:253–266
8. Santschi PH, Bollhander S, Zingg S, Luck A, Farrenkothen K (1990) The self-cleaning capacity of surface waters after radioactive fallout. Evidence from European Waters after Chernobyl, 1986–1988. Environ Sci Technol 24:519–527
9. Monte L (1995) Evaluation of radionuclide transfer functions from drainage basins of fresh water systems. J Environ Radioactiv 26:71–82
10. Kaniviets VV, Voitcekhovich OV (1992) Scientific report: Radioecology of water systems in zone of consequences of Chernobyl accident. Report of Ministry of Chernobyl Affairs of Ukraine. Contract Number 1/92 (in Russian)
11. Mundschenk H (1992) Ueber Nachwirkungen des Reaktorunfalls in Tschernobyl im Bereich der "alten" Bundeswasserstrassen. (On long term effects of the Accident of the Nuclear Power Plant in Chernobyl in the German

Federal Waterways) Sonderdruck aus: Deutsche Gewaesserkundliche Mitteilungen 36:7–19 (in German)
12. Maringer FJ (1994) Das Verhalten von Radionukliden im Wasser, Schwebstoff und Sediment der Donau. Dissertation, Technischen Universität Wien (in German)
13. Sunblad B, Bergström U, Evans S (1991) Long term transfer of fallout from the terrestrial to the aquatic environment. In: Moberg L (ed) The Chernobyl fallout in Sweden. Results from a research program on environmental radiology. The Swedish Radiation Protection Institute, Stockholm
14. Vray F, Debayle C, Louvat D (2003) Long-term flux of Chernobyl-derived ^{137}Cs from soil to French rivers: A study on sediment and biological indicators. J Environ Radioactiv 68:93–114
15. Smith JT, Clarke RT, Saxén R (2000) Time-dependent behaviour of radiocaesium: a new method to compare the mobility of weapons test and Chernobyl derived fallout. J Environ Radioactiv 49:65–83
16. Smith JT, Konoplev AV, Bulgakov AA, Comans RNJ, Cross MA, Kaminski S, Khristuk B, Klemt E, de Koning A, Kudelsky AV, Laptev G, Madruga M-J, Voitsekhovitch OV, Zibold G (2002) Simplified models for predicting ^{89}Sr, ^{90}Sr, ^{134}Cs, ^{137}Cs, ^{131}I in water and fish of rivers, lakes and reservoirs, AQUASCOPE Technical Deliverable. CEH Centre for Ecology and Hydrology, Natural Environment Research Council, United Kingdom
17. Monte L (1997) A collective model for predicting the long-term behaviour of radionuclides in rivers. Sci Total Environ 2001:17–29
18. Smith JT, Wright SM, Croos MA, Monte L, Kudelsky A, Saxen R, Vakulovsky A, Timms D (2004) Global analysis of the riverine transport of ^{90}Sr and ^{137}Cs. Environ Sci Technol 38:850–857
19. Kivva SL, Zheleznyak MI (2000) Hydrological and physico-chemical processes determining radionuclide redistribution. In: van der Perck M, Svetlitchnyi AA, den Basten J, Wielinga A (eds) SPARTACUS, Spatial redistribution of radionuclides within catchments. Final report EC Contract n° IC15CT980215. Utrecht University, The Netherlands
20. Håkanson L (2006) Suspended particulate matter in lakes, rivers, and marine systems. The Blackburn Press, Caldwell
21. Wanielista PM (1990) Hydrology and water quality control. Wiley, New York
22. Benes P, Picat P, Gernik M, Quinault S (1992) Kinetics of radionuclide interaction with suspended solids in modeling the migration of radionuclides in rivers. (Part I and II). J Radioanal Nucl Chem 159:175–200
23. Cremers A, Henrion PN (1984) Radionuclide partitioning in sediments: theory and practice. In: Seminar on the Behaviour of Radionuclides in Estuaries, Renesse (The Netherlands), 17–21 September 1984. Commission of the European Communities, XII/380/85-EN: 1–25
24. Delle Site A (2000) Factors affecting sorption of organic compound in natural sorbent/water systems and sorption coefficients for selected pollutants. A review. J Phys Chem Ref Data 29(6):1–253
25. Zheleznyak M, Demchenco R, Khursin S, Kuzmenko Yu, Tkalich P, Vitjuk N (1992) Mathematical modelling of radionuclide dispersion in the Prypiat-Dnieper aquatic system after the Chernobyl accident. Sci Total Environ 112:89–114
26. Garcia-Sanchez L (2008) Watershed wash-off of atmospherically deposited radionuclides: review of the fluxes and their evolution with time. J Environ Radioactiv 99:563–573
27. Garcia-Sanchez L, Konoplev AV (2009) Watershed wash-off of atmospherically deposited radionuclides: a review of normalized entrainment coefficients. J Environ Radioactiv 100:774–778
28. Monte L, Brittain EJ, Håkanson L, Smith JT, van der Perk M (2004) Review and assessment of models for predicting the migration of radionuclides from catchments. J Environ Radioactiv 75:83–103
29. Håkanson L, Monte L (2003) Radioactivity in Lakes and Rivers. In: Scott EM (ed) Modelling radioactivity in the environment. Elsevier Science, Oxford
30. Agüero A, García-Olivares (2000) CIEMAT model results for Esthwaite water. In: Modelling of the transfer of radiocaesium from deposition to lake ecosystems. Report of the VAMP Aquatic Working Group. IAEA-TECDOC-1143, International Atomic Energy Agency, Vienna
31. Bäverstam U, Fraser G, Kelly GN (eds) (1997) Decision making support for off-site emergency management. Radiat Prot Dosim 73:1–317
32. BIOMOVS II (1996) Wash-off of Sr-90 and Cs-137 from two experimental plots: model testing using Chernobyl data. Technical report No. 9. Swedish Radiation Protection Institute, Stockholm
33. Heling R, Zheleznyak M, Raskob W, Popov A, Borodin R, Gofman D, Lyashenko G, Marinets A, Pokhil A, Shepeleva T, Tkalich P (1997) Overview of the modelling of hydrological pathways in RODOS. Radiat Prot Dosim 73:67–70
34. International Atomic Energy Agency (IAEA) (2010) Handbook of parameter values for the prediction of radionuclide transfer in terrestrial and freshwater environments. Technical Reports Series no. 472. Vienna
35. Karickoff SW (1986) Pollutant sorption in environmental systems. In: Brock Nelly W, Blau GE (eds) Environmental exposure from chemicals, vol I. CRC Press, Boca Raton
36. Comans RNJ, Hockley DE (1992) Kinetics of cesium sorption on illite. Geochim Cosmochim Acta 56:1157–1164
37. Korhonen R (1990) Modeling transfer of ^{137}Cs in a large Finnish watercourse. Health Phys 59:443–454
38. Håkanson L (1995) Optimal size of predictive models. Ecol Modell 78:195–204
39. Carlsson S (1978) A model for the movement and loss of ^{137}Cs in a small watershed. Health Phys 34:33–73
40. Helton JC, Muller AB, Bayer A (1985) Contamination of surface – water bodies after reactor accidents by the erosion of atmospherically deposited radionuclides. Health Phys 48:757–771
41. Håkanson L (2004) A new generic sub-model for radionuclide fixation in large catchments from continuous and single-pulse fallouts, as used in a river model. J Environ Radioactiv 77:247–273
42. Bulgakov A, Konoplev A, Popov V, Scherbak A (1991) Removal of long-lived radionuclides from the soil by surface runoff near the Chernobyl nuclear power station. Sov Soil Sci 23:124–131

43. Konoplev A, Bulgakov A, Popov V, Bobovnikova TI (1992) Behaviour of long-lived Chernobyl radionuclides in a soil–water system. Analyst 117:1041–1047
44. Joshi SR, Shukla BS (1991) The role of water/soil distribution coefficient in the watershed transport of environmental radionuclides. Earth Planet Sci Lett 105:314–318
45. Monte L (1998) Predicting the migration of dissolved toxic substances from catchments by a collective model. Ecol Modell 110:269–279
46. Sheppard MI, Thibault DH (1990) Default soil solid/liquid partition coefficients, k_ds, for four major soil types: a compendium. Health Phys 59:471–482
47. Monte L, Periañez R, Kivva S, Laptev G, Angeli G, Barros H, Zheleznyak M (2006) Assessment of state-of-the-art models for predicting the remobilisation of radionuclides following the flooding of heavily contaminated areas: the case of Pripyat River floodplain. J Environ Radioactiv 88: 267–288
48. Spezzano P, Bortoluzzi S, Giacomelli R, Massironi L (1994) Seasonal variations of ^{137}Cs activities in the Dora Baltea River (Northwest Italy) after the Chernobyl Accident. J Environ Radioactiv 22:77–88
49. Monte L, Brittain JE, Håkanson L, Heling R, Smith JT, Zheleznyak M (2003) Review and assessment of models used to predict the fate of radionuclides in lakes. J Environ Radioactiv 69:177–205
50. Monte L, Boyer P, Brittain JE, Håkanson L, Lepicard S, Smith JT (2005) Review and assessment of models for predicting the migration of radionuclides through rivers. J Environ Radioactiv 79:273–296
51. Monte L, Håkanson L, Periañez R, Laptev G, Zheleznyak M, Maderich V, Angeli G, Koshebutsky V (2006) Experiences from a case study of multi-model application to assess the behaviour of pollutants in the Dnieper-Bug Estuary. Ecol Modell 195:247–263

Books and Reviews

Moldan B, Černý B (eds) (1994) Biogeochemistry of small catchments: a tool for environmental research. SCOPE 51. Wiley, England, pp 419

Sir Warner F, Harrisson RM (eds) (1993) Radioecology after Chernobyl. Biogeochemical pathways of artificial radionuclides. SCOPE 50. Wiley, England, pp 367

Scott EM (ed) (2003) Modelling radioactivity in the environment. Elsevier Science, Oxford, p 427

Degens ET, Kempe S, Richey JE (eds) (1991) Biogeochemistry of major world rivers. SCOPE 42. Wiley, England, pp 356

Wanielista M (1990) Hydrology and water quality control. Wiley, New York, p 565

Håkanson L (2006) Suspended particulate matter in lakes, rivers, and marine systems. Blackburn Press, Caldwell, p 319

Shukla SB (1993) Watershed, river, and lake modeling through environmental radioactivity. Environmental Research & Publications Inc, Hamilton, p 227

Radionuclides as Tracers of Ocean Currents

Pavel P. Povinec[1], Katsumi Hirose[2]
[1]Faculty of Mathematics, Physics and Informatics, Comenius University, Bratislava, Slovakia
[2]Faculty of Science and Technology, Sophia University, Chiyodaku, Tokyo, Japan

Article Outline

Glossary
Definition of the Subject
Introduction
Hydrography Background
Sources of Radionuclides in the Marine Environment
Sampling and Analytical Techniques
Distribution and Transport of Radionuclides in Seawater – Tracing Ocean Currents
Future Directions
Acknowledgments
Bibliography

Glossary

Anthropogenic radionuclides Radionuclides produced by human activities (e.g., in nuclear weapons tests, in nuclear reactors, in particle accelerators).

Global fallout Radioactive contamination from atmospheric nuclear weapons tests, which was widely dispersed in the atmosphere and then deposited on land and sea.

Ocean current A continuous, directed movement of ocean water generated by wind, Coriolis force, temperature and salinity differences, breaking waves, and tides caused by the gravitational pull of the Moon and the Sun.

Ocean gyre A large system of rotating ocean currents associated with large wind movements.

Thermocline A layer in the water column in which temperature changes more rapidly with depth than it does in the layers above or below, separating the upper mixed layer from the calm deep water below.

Thermohaline circulation A large-scale circulation of water masses in the ocean driven by global density gradients created by surface heat and freshwater fluxes.

The southern ocean The southernmost part of the World Ocean, south of 60°S latitude, encircling Antarctica.

Definition of the Subject

Global fallout radionuclides after their main injection from atmospheric nuclear weapons tests on the ocean surface have been used for about 5 decades for studying processes in the marine environment. Conservative (^{3}H, ^{14}C, ^{90}Sr, ^{129}I, ^{137}Cs, and others) as well as nonconservative (^{238}Pu, ^{239}Pu, ^{240}Pu, ^{241}Am, and others) radionuclides have been available for surface-, medium-, and deepwater studies. Using the recent data obtained in the framework of several international projects, it has been possible to study recent trends in the circulation of ocean water masses in the Atlantic, Pacific, and Indian Oceans, as well as interocean exchange. Subtropical gyres, which accumulate radionuclide tracers and other contaminants on timescales of decades, are of environmental importance for the protection of the marine environment from land-based contamination sources.

Introduction

There are four main sources of environmental radionuclides that can be found in the marine environment [1]:

(i) Natural – cosmogenic radionuclides – results of interactions of cosmic rays with atoms in the atmosphere, and their subsequent deposition on the ocean surface (e.g., ^{3}H, ^{7}Be, ^{10}Be, ^{14}C, ^{26}Al, ^{53}Mn).

(ii) Natural – primordial radionuclides (e.g., ^{40}K, ^{238}U, ^{232}Th) and their decay products (e.g., ^{226}Ra, ^{230}Th) found in the earth crust; due to radon emanation its decay products are also found in the atmosphere, and then after deposition in the terrestrial and marine environments (e.g., ^{210}Po, ^{210}Pb).

(iii) Anthropogenic – global fallout radionuclides – produced during atmospheric tests of nuclear weapons (e.g., ^{3}H, ^{14}C, ^{90}Sr, ^{137}Cs, Pu isotopes, ^{241}Am).

(iv) Anthropogenic – radionuclides released from nuclear installations – mostly from reprocessing nuclear facilities (e.g., ^{3}H, ^{14}C, ^{90}Sr, ^{99}Tc, ^{129}I, ^{137}Cs).

This entry concentrates mostly on global fallout radionuclides as they have been most frequently used in oceanic studies. They were injected onto the ocean surface from the atmosphere after large-scale U.S. and former USSR atmospheric nuclear weapons tests carried out mainly during the 1950s and early 1960s [2, 3]. The peak concentrations of the anthropogenic radionuclides in the atmosphere of the Northern Hemisphere were observed in 1963, and with 1 year delay in surface waters of northern oceans and seas [4]. Mapping of this deposition revealed that the major injection on the ocean surface occurred at midlatitudes of the western North Pacific [5]. Global fallout radionuclides in seawater have been measured since the 1960s with the aim to assess radiological impact from nuclear weapons tests [6], and later they were used as transient tracers to investigate oceanographic processes [3, 7–10]. Radionuclides released from nuclear installations, especially from European nuclear reprocessing facilities in Sellafield (UK) and La Hague (France) have also been extensively used for tracing water masses in the eastern North Atlantic ocean and adjacent seas [11–14]. Radioecological studies were carried out to investigate the possible impact of dumped radioactive wastes in the Barents and Kara Sea [15–18], as well as in the Japan Sea and the Northwest Pacific Ocean [19–21]. The collected radionuclide data have been recently stored in marine radionuclide databases (GLOMARD/MARIS [22, 23], www.iaea.org/maris), and HAM [24] radionuclide databases).

There have been two important breakthroughs in the oceanographic research. Firstly, national and/or regional investigations have been shifted to global projects, such as GEOSECS (Geochemical Ocean Sections Study) program, WOCE (World Ocean Circulation Experiment) (www.WOCE.org), or more recently CLIVAR (www.CLIVAR.org) and GEOTRACES (www.GEOTRACES.org). The WOCE program, which was carried out during the 1990s represents the most extensive ^{3}H and ^{14}C sampling carried out in the World Ocean till now. Secondly, new highly sensitive analytical techniques have been implemented. In the case of shorter-lived ^{137}Cs, it was the development of underground facilities for ultra-low-level gamma-ray spectrometry [25–29]. For long-lived radionuclides (e.g., ^{239}Pu, ^{240}Pu), it was a total change in the philosophy of analysis as a shift from counting of radioactive

decays (and thus waiting for them) to the direct counting of atoms using mass spectrometry techniques such as Accelerator Mass Spectrometry (AMS) [30–33], Inductively Coupled Plasma Mass Spectrometry (ICPMS) [34–37], Thermal Ionization Mass Spectrometry (TIMS) [38], and Resonance Ionization Mass Spectrometry (RIMS) [39] has been made.

Several radionuclides have extensively been used as tracers in oceanographic studies. Tritium is an ideal tracer because it is directly incorporated into the water molecule. However, its short half-life (12.32 year) restricts its use only for studies of relatively short-term transport processes. ^{3}H is produced either naturally by interactions of cosmic rays with nitrogen and oxygen in the upper atmosphere, but it has also been produced in large amounts in atmospheric nuclear weapons tests. The ^{3}H concentration peaked in the atmospheric moisture in 1963, when it was almost 1,000 times higher than its natural cosmogenic concentration. ^{3}H has also been released in large quantities from nuclear reprocessing facilities, mainly in Sellafield and in La Hague. The penetration of bomb tritium from surface waters into deeper layers of the ocean has been used to study pathways and timescales of deep and bottom water formation [40, 41]. Cosmogenic ^{14}C is produced by cosmic rays in the upper atmosphere, mainly in the reaction ^{14}N(n,p)^{14}C. Its levels in the environment have also been disturbed by bomb-produced ^{14}C, when in 1963 they were by a factor of 2 higher than natural (cosmogenic) levels observed in atmospheric carbon dioxide. Large quantities of ^{14}C have also been produced in nuclear reprocessing facilities. Because of its long half-life (5,730 year), specific stratosphere–troposphere–biosphere interactions, exchange of carbon dioxide between air and surface ocean, and sequestration of carbon dioxide into the ocean interior, ^{14}C became the most frequently studied environmental radionuclide, important for a better understanding of climate change [42, 43]. Oceanic radiocarbon data contributed to a better understanding of thermohaline circulation in the World Ocean known as a Great Ocean Conveyor Belt [44]. Other global fallout radionuclide tracers extensively used in water circulation studies are ^{90}Sr (half-life 28.78 year) and ^{137}Cs (half-life 30.17 year). Both were released in large quantities during atmospheric nuclear weapons tests, as well as from nuclear reprocessing facilities. They are found in seawater mostly in a dissolved phase, following well the movement of water masses. Their removal from the water column is mainly due to their radioactive decay and diffusion [45, 46]. ^{129}I has been introduced to the World Ocean mainly from nuclear reprocessing facilities, and because of its long half-life (15.7×10^{6} year) it represents an alternative tracer to global fallout radionuclides for studies of long-term transport and circulation processes [47]. On the other hand, anthropogenic tracers such as ^{238}Pu (half-life 87.74 year), ^{239}Pu (half-life 2.44×10^{4} year), ^{240}Pu (half-life 6.58×10^{3} year), and ^{241}Am (half-life 458 year) are particle reactive, and due to their chemically reactive nature, significant portions of these radionuclides in the World Ocean have reached marine sediments [8, 48–50].

GEOSECS program [7–9], carried out during the 1970s, was the first large-scale project devoted to investigation of the distribution of global fallout radionuclides (^{3}H, ^{14}C, ^{137}Cs, ^{239,240}Pu) in the ocean basins. ^{3}H and ^{14}C were also used during the most comprehensive tracer program WOCE, which was carried out during the early 1990s [51]. Both programs covered the World Ocean. Some radionuclides, such as ^{137}Cs, ^{90}Sr, and ^{239,240}Pu, were investigated in GEOSECS, International Atomic Energy Agency – Marine Environment Laboratories (IAEA-MEL) and national programs, for example, in the Pacific Ocean [3, 4, 8, 10, 48–50, 52, 53], in the Indian Ocean [54–58], and in the Atlantic and Arctic Oceans [59–61]. Financial support required for large volume water sampling, needed for analysis of ^{137}Cs and ^{239,240}Pu, was a limiting factor for their wider applications in large-scale studies.

One of the most recent and the most comprehensive open ocean studies of anthropogenic radionuclides in the water column has been the IAEA-MEL research program on Worldwide Marine Radioactivity Studies (WOMARS). The primary objective was to develop an understanding of the present open ocean distribution of radionuclides in the water column and sediment, and to contribute to scientific knowledge of the processes, which affect radionuclide behavior in the marine environment. Any contributions over established background levels due to additional nuclear discharges or accidents could then be easily identified [4, 62]. Three anthropogenic radionuclides (^{90}Sr, ^{137}Cs, and ^{239,240}Pu)

were chosen as the most important and radiologically typical of each class of marine radioactivity. They are the most abundant anthropogenic radionuclides present in the marine environment, and they may lead to the highest radiation doses to humans and marine biota. The project was thus filling the existing gap in the WOCE program that covered only ^{3}H and ^{14}C. The project was carried out in collaboration with several laboratories in Denmark, France, Germany, India, Italy, Japan, Republic of Korea, New Zealand, Sweden, UK, and USA. New data for ^{3}H, ^{14}C, ^{90}Sr, ^{129}I, ^{137}Cs, ^{238}Pu, ^{239,240}Pu, and ^{241}Am were obtained for the western North Pacific Ocean [10, 63–66] and the adjacent seas [67, 68], for the North and South Indian Ocean [55], including the Arabian Sea [56, 57], and for the Northeastern Atlantic Ocean [69].

This entry reviews the distribution of global fallout radionuclides in World Ocean waters about 5 decades after their main injection from atmospheric nuclear weapons tests on the ocean surface. The entry focuses on waters, because the main idea is to apply radionuclide tracers in studies of ocean currents. The presented results are mainly based on the work carried out in IAEA-MEL and collaborating institutions. Results obtained from the WOMARS project, as well as from the SHOTS (Southern Hemisphere Ocean Tracer Studies) project are compared with some previous measurements. Water samples included in the SHOTS project were collected during the "around-the-globe" BEAGLE2003 expedition (organized by JAMSTEC [70, 71]), which sampled seawater along 20°S–30°S latitude covering the Pacific Ocean [72], the Atlantic Ocean [73], and the Indian Ocean [74]. It was the first time that many radionuclide tracers were used in such a large-scale project producing high-density radionuclide data for water profiles.

Hydrography Background

Pacific Ocean

The Pacific Ocean is the largest ocean, spreading from the northern boundary of the Bering Sea near 50°N to the boundary of the Southern Ocean at 60°S (Fig. 1). A typical global thermohaline circulation transports cold Circumpolar Bottom Waters (CBW) from the South Pacific to the North Pacific, and upwells deep water to shallower water in the North Pacific Ocean. Warm surface waters in the western North Pacific Ocean move to the Indian Ocean via the Indonesian Seas.

The current system in the western North Pacific Ocean comprises the Kuroshio Current, which is a typical western boundary current consisting of a part of the North Pacific subtropical circulation, and the Oyashio Current, which is included in the North Pacific Subpolar Gyre system. In the eastern North Pacific, the major currents are the Alaska Current included in the Alaskan Gyre, and the California Current, which is a part of the North Pacific Subtropical Gyre. The equatorial current system in the Pacific is complicated as it consists of the North Equatorial Current (NEC), the North Equatorial Countercurrent (NECC), the Northern Subsurface Countercurrent (NSCC), the Equatorial Undercurrent (EUC), the Southern Subsurface Countercurrent (SSCC), and the South Equatorial Current (SEC). Nevertheless, west- and eastward flows are prevailing in the equatorial Pacific Ocean. In the South Pacific Ocean, the South Pacific Subtropical Gyre primarily governs the South Pacific current system, including the East Australian Current (EAC) and the Peru Current.

There is no formation of deep waters in the North Pacific due to freshwater supply, in contrast to the North Atlantic Ocean. However, more complicated subsurface processes, including formation of water masses occur in the North Pacific Ocean. The hydrographic analysis in the North Pacific Ocean suggests that several water masses are formed in the Kuroshio Current and the Kuroshio Extension region. The water mass with high salinity (about ~35) and σ_θ of 23–25, which has been named as the North Pacific Tropical Water (NPTW) [75], is produced in the midlatitude region of the central North Pacific (west of 160°W) as a result of high evaporation and low precipitation. The produced high salinity water is then subducted under the subtropical North Pacific, and transported from the central North Pacific to the western subtropical North Pacific Ocean [76, 77]. The North Pacific Subtropical Mode Water (NPSTMW), which is formed by deep convection in winter, just south of the Kuroshio Current, is defined as a voluminous water mass with an isothermal layer of 16.5°C, σ_θ of approximately 25.5, and a potential vorticity minimum [78]. The North Pacific Central Mode Water (NPCMW), defined as water mass with σ_θ in the range of 26.0–26.4, is formed

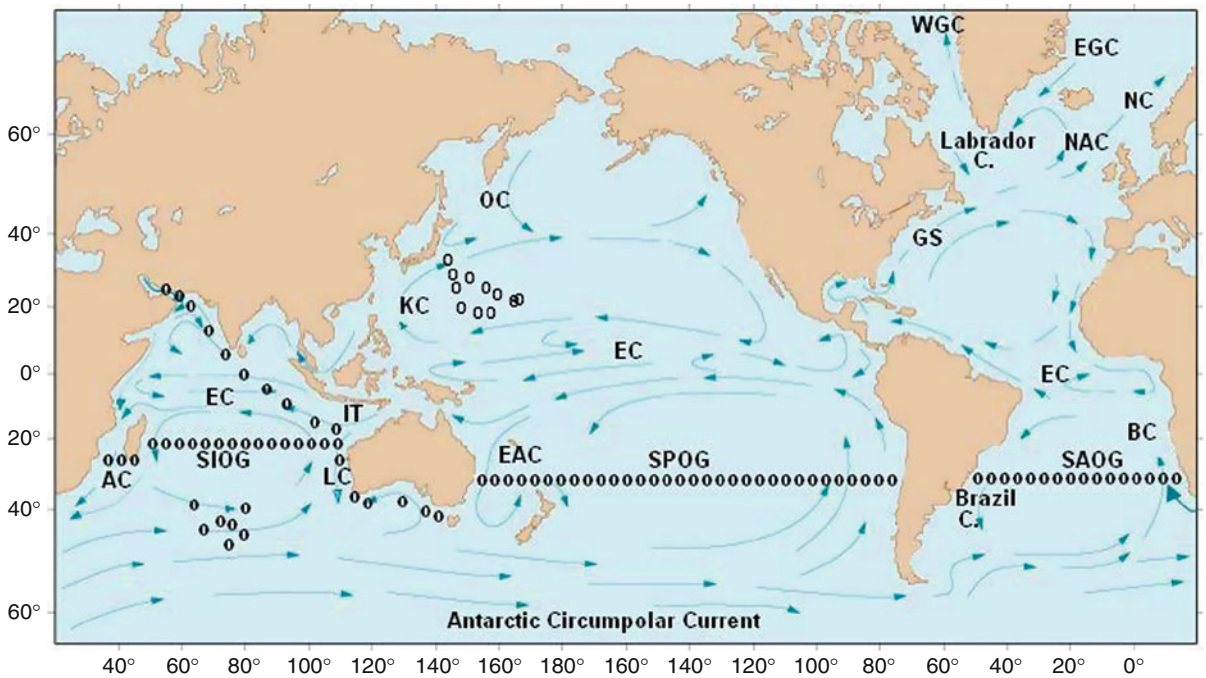

Radionuclides as Tracers of Ocean Currents. Figure 1

The main surface currents in the World Ocean with sampling sites visited in the framework of the WOMARS project [62] and the BEAGLE2003 expedition [70, 71] (along 20°S in the Indian Ocean, 32.5°S in the Pacific, and 30°S in the Atlantic Oceans). AC – Agulhas Current; SIOG – South Indian Ocean Gyre; EC – Equatorial Countercurrent; IT – Indonesian Throughflow; LC – Leeuwin Current; KC – Kuroshio Current; Oyashio Current; SPOG – South Pacific Ocean Gyre; EAC – East Australia Current; SAOG – South Atlantic Ocean Gyre; BC – Benguela Current; GS – Gulf Stream; NAC – North Atlantic Current; WGC – West Greenland Current; EGC – East Greenland Current; NC – Norwegian Current (modified from www.AmericanMeteorologicalSociety.org)

around 34°N–41°N and 160°E–165°W [79]. On the other hand, the shallow salinity minimum water (SSM) is present in the eastern North Pacific. The SSM, which may be produced by the subduction of low-salinity surface water in the northern outcropping zone due to Ekman pumping, turns southwestward with the eastern boundary current near 20°N, and spreads between 10°N and 20°N from 130°W to 170° W°W in the density range of 25.4–25.7 $\sigma_\theta\sigma_\theta$ [80, 81]. These water masses, formed in the North Pacific Ocean are closely related to tracer transport in the Pacific Ocean interior.

Indian Ocean

The Indian Ocean is the smallest ocean when compared with the Atlantic and Pacific Oceans as it is limited northward to 25°N (Fig. 1). The southern boundary of the Indian Ocean is set at 60°S, where it becomes the Southern Ocean. A global thermohaline circulation transports warm surface waters from the western North Pacific through the Indonesian throughflow into the Indian Ocean. On the south, the Indian Ocean is via the cold Antarctic Circumpolar Current (ACC) system connected with the Pacific Ocean, and via the Agulhas Current (AC) system with Atlantic Ocean waters [82]. It represents therefore the most fragile part in the global ocean circulation system, important for global climate change studies. As it is surrounded by highly populated continents, there is also a real danger of contamination from land-based sources. The equatorial current system of the Indian Ocean is strongly influenced by the seasonal variation in the winds north of the Equator [82]. From

November to March these winds blow from the northeast (Northeast Monsoon), while from May to September they blow from the southwest (Southwest Monsoon). The change of wind direction north of the Equator then results in a change of currents there. During the Northeast Monsoon season, the North Equatorial Current (NEC) flows westward from 8°N to the Equator; the Equatorial Countercurrent (ECC) flows eastward from the Equator to 8°S and the South Equatorial Current (SEC) flows westward from 8°S to 15°S–20°S. During the Southwest Monsoon the flow north of the Equator is reversed, and a part of the SEC turning north supplies the Somali Current up to the east coast of Africa. The SEC, the Somali Current, and the Monsoon Current then comprise a strong wind-driven gyre in the northern Indian Ocean. Strong upwelling occurs at this time along the Somali and Arabian coasts.

An important feature is a transport of warm water masses (10–15 Sv) from the western North Pacific Ocean via the Indonesian throughflow to the eastern Equatorial Indian Ocean, and their further transport to the South Indian Ocean [83]. The South Indian Ocean Subtropical Gyre is the most important current system influencing water circulation between 20°S and 40°S [82]. Along the eastern boundary of the Indian Ocean, off western Australia, the Leeuwin Current flows poleward along the continental shelf break from about 22°S to 35°S, and then turns eastward. The Leeuwin Current is warm and of relatively low salinity, low dissolved oxygen, and high phosphate content. It transports a significant amount of heat to the south [82].

The southern part of the Indian Ocean (Crozet Basin) is well known for its strong physical currents, which form in this area one of the most dynamic places of the World Ocean. The banded structure of the ACC consists there of narrow jets associated with sharp fronts due to the presence of the Crozet and Kerguelen Islands.

Several frontal systems that meet there, such as Agulhas Front (AF), Subtropical Front (STF), Subantarctic Front (SAF), and Polar Front (PF), represent narrow zones with sharp changes in temperature and salinity [84] (Fig. 2). The dominant current affecting the circulation in the Crozet Basin is the AF,

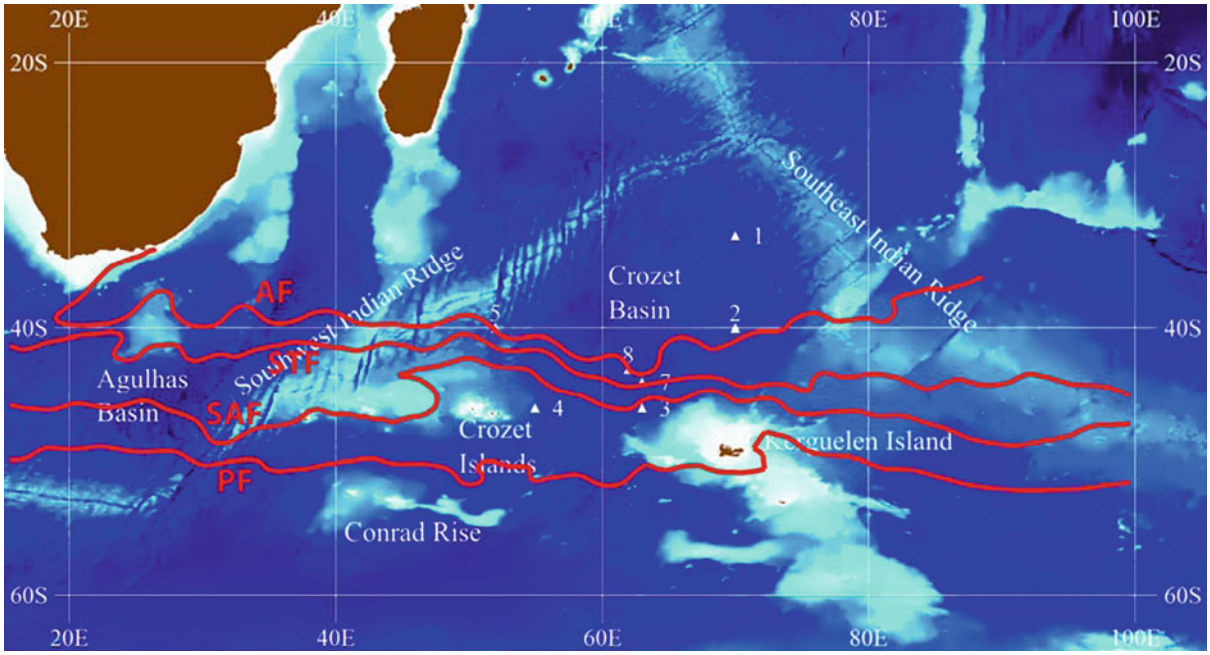

Radionuclides as Tracers of Ocean Currents. Figure 2
The main currents in the South Indian Ocean (AF – Agulhas Front; STF – Subtropical Front; SAF – Subantarctic Front; PF – Polar Front; modified from [84]), and ANTARES-4 sampling stations [58]

characterized by warm and saline water. Extending eastward into the basin, up to 60°E, AC recirculates to the north, as a part of an anticyclonic Subtropical Gyre [84]. The distribution of tracers in the South Indian Ocean has therefore been controlled by the banded structure of the fronts [85]. The Southern Ocean region has also been documented as a major sink of CO_2, and is thus a highly productive area.

Atlantic Ocean

The Atlantic Ocean is a unique ocean linking with the Arctic Ocean at the north side, with Mediterranean at the east side and with the Weddell Sea in the south side. The main circulation patterns in the Atlantic Ocean are represented by the thermohaline circulation [44] that is part of the global ocean circulation known as the Great Ocean Conveyor Belt (Fig. 3). Warm surface waters from the western South Indian Ocean are advected southward along the eastern African coast by the Agulhas current. A fraction enters the South Atlantic around South Africa forming a branch of the Agulhas Current that does not complete its retroflection, also called the Agulhas leakage [82]. These waters are advected further north and westward, as a part of the Subtropical Gyre of the South Atlantic Ocean, mainly with large eddies or Agulhas rings. A part of these waters continue northward along the western African coast as the Benguela Current, which is responsible for an intergyre water transport to the Central Atlantic Ocean (Fig. 1). The dominant surface water circulation system in the South Atlantic is thus represented by the Subtropical Gyre with the Benguela Current system at the east, and the Brazil Current system at the west (Fig. 1). In the Antarctic Ocean (>60°S), the Weddell Sea Gyre is part of the Polar Current system.

In the Central Atlantic Ocean, the tropical circulation is formed by the Atlantic Equatorial Current system, which consists of the North Equatorial Current (NEC), the North Equatorial Countercurrent (NECC), the Equatorial Undercurrent (EUC), the North Brazil Current (NBC), the Southern Equatorial Countercurrent (SECC), and the South Equatorial Current (SEC). Similarly to the Equatorial Pacific Ocean, west- and eastward zonal flows prevail in the equatorial Atlantic Ocean.

A surface flow in the North Atlantic Ocean, a typical western boundary current, is the Gulf Stream System (Fig. 1), flowing along the Blake Plateau between the Straits of Florida (at ~20°N) and Cape Hatteras (at ~35°N), leaving the continental slope, and after that following the North Atlantic Current as a northeastward branch and the Azores Current as an eastward branch. Much of the water in the North Atlantic Current with the Azores Current water turns southeastward to contribute to the Canary Current. This current system consists of the North Atlantic Subtropical Gyre. In the northern North Atlantic (>50°N), the North Atlantic Subpolar Gyre governs the current system including the Labrador Current and the branch of the North Atlantic Current.

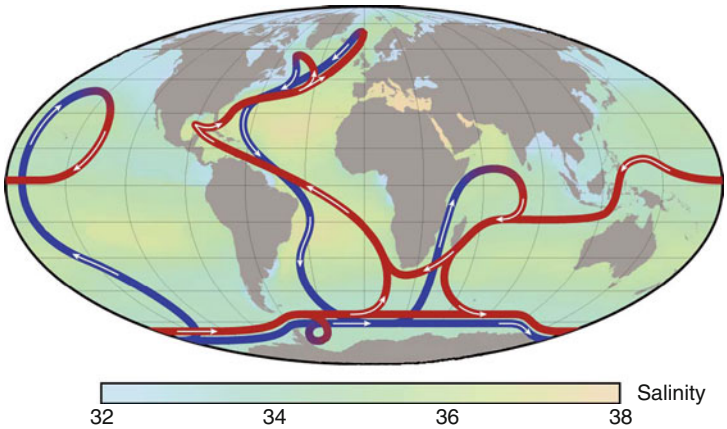

Radionuclides as Tracers of Ocean Currents. Figure 3
Great Ocean Conveyor Belt (modified from www.Wikipedia.org)

The Mediterranean Sea supplies high salinity water (>36) to the North Atlantic Ocean intermediate layer (~1,000 m), whereas the Arctic Ocean is a source of low-salinity water. Deep water formation that drives the global thermohaline circulation occurs in the Nordic (Greenland, Norwegian and Iceland) Seas and the Labrador and Weddell Seas. It represents therefore the most important part in the global ocean circulation system closely linked with global climate change studies [86]. The North Atlantic Deep Water (NADW) formed in the Nordic and Labrador Seas spreads southward near 50°S, following a flow path near the western boundary. The Antarctic Bottom Water (AABW) formed in the Weddell Sea exits in the region of >30°S. The Antarctic Intermediate Water (AAIW) formed near the Antarctic Polar Frontal Zone intrudes near 1,000 m from 50°S to near the Equator.

Several water masses are formed in the Atlantic Ocean. The North Atlantic Subtropical Mode Water (NASTMW) with properties centered at 18°C, salinity at 36.5 and 26.5σ_θ is formed just south of the Gulf Stream Extension. The NASTMW is advected southward out of the Gulf Stream Extension region. The Madeira Mode Water (MMW) with temperature and potential density ranges between 16°C and 18°C and 26.5–26.8σ_θ is associated with the warm side of the Azores Front, offshore of the coastal upwelling area. The MMW is advected southwestward from its formation region and joins the thermocline as part of the North Atlantic Central Water. The Subpolar Mode Water (SPMW), which is high-density mode water (density range: 26.9–27.75σ_θ) in the North Subtropical Gyre and the Subpolar Gyre, originates as thick layers at 14–15°C in the North Atlantic Current loop. The SPMW is advected eastward south of the North Atlantic Current to the eastern Atlantic. The Labrador Sea Water (LSW), which is the fresh intermediate water of the North Atlantic Ocean, arises from convection in the western Labrador Sea. It is advected throughout the subpolar Atlantic, as well as into the subtropical Atlantic.

Sources of Radionuclides in the Marine Environment

Global Fallout Background

The main source of anthropogenic radionuclides in the World Ocean has been global fallout from atmospheric tests of nuclear weapons. A total of 543 nuclear weapons tests have been carried out in the atmosphere with fission yield of 189 Mt of TNT equivalent [2]. The tests with the highest yields were carried out mainly in the late 1950s (1952–1958) and early 1960s (1961–1962). As radionuclides produced in weapons tests with 29 Mt fission yield were not globally dispersed, but were deposited as local fallout (mostly from Bikini and Enewetak atolls); hence only 160 Mt was available for global fallout [2]. The global fallout from the atmospheric nuclear weapons tests has by now been transferred from the atmosphere to the surface of Earth. Since about 70% of the surface of the planet is ocean, much of this mixture of anthropogenic radionuclides has ended up there. Despite the fact that most atmospheric nuclear weapons tests took place in the Northern Hemisphere, it can be shown from the proportions of land and ocean in each hemisphere, and from the latitudinal fallout patterns over time, that over two thirds of the fallout entered the ocean. Following entry to the ocean, the behavior of global fallout radionuclides was determined by their physical and chemical properties and their fate by oceanic physical and biogeochemical processes. As in the terrestrial environment, the postdelivery behavior of these fallout radionuclides provided a unique opportunity to gain insights into the nature of the processes controlling their fate. The great depth and dynamic nature of the oceans have resulted in substantially greater dispersion and dilution than on land.

Initially, the marine radionuclide studies were driven by the need to assess the impact and fate of fallout radionuclides on marine life and associated transfer to man through marine exposure pathways [6]. Subsequently, fallout radionuclides were widely used as oceanic process tracers, due to their unique time-marker labeling of sea water, marine organisms, and sediments according to their individual chemical properties. In this sense, they contributed to the broad growth of knowledge of the intricate physical, chemical, biological, and sedimentological processes, which occur in the oceans. The main periods of delivery of fallout to the oceans were the years following the two intense series of atmospheric tests in the mid-1950s and the early 1960s. The scale of testing by countries that continued atmospheric tests after the 1962 Test Ban Treaty represented a relatively small input. The majority of the fallout produced in atmospheric tests was

injected into the stratosphere and then through the specific stratosphere–troposphere mixing returned to Earth's surface as global fallout. Some tests, especially in the earlier test series in the 1950s, were conducted at or near ground level and produced tropospheric fallout with a regional impact. The oceanic impact of ground-level tests was significant from testing at oceanic locations such as those on Pacific islands – especially the U.S. test series at the Pacific Test Site in the Marshall Islands [87]. So this regional impact was largely confined to the western North Pacific. Minor traces of tropospheric fallout from the U.S. Nevada Test Site were identified in the Atlantic Ocean and Mediterranean Sea [88].

The typical depositional pattern with maxima at mid-latitudes and minima toward the Equator and the poles, observed on the land, was also expected on the ocean surface. The patterns of surface seawater concentrations observed during peak fallout years proved rather complex due to seasonal fluctuations in delivery, ocean mixing, and nonstandard observational networks [5, 89]. A convincing demonstration of oceanic distributions came more than a decade later, and relied on water column inventory patterns of ^{137}Cs [90]. The interesting point about these inventory patterns was that not only did they show a latitudinal pattern similar to overland fallout patterns, but that these patterns still were preserved later – despite the dynamic nature of the ocean, with the active gyral circulation of surface and subsurface currents.

The behavior of radionuclides in the marine environment has been classified as either "conservative" or "nonconservative" [90]. The conservative group includes radionuclides having a very small affinity for particles and whose behavior consequently is controlled by the physics of ocean circulation and mixing. Examples of these include ^{3}H, ^{90}Sr, ^{85}Kr, and (in most situations) ^{137}Cs. The nonconservative group includes radionuclides with a range of strengths of particle association and whose ultimate behavior is linked to these affinities. Examples of these include ^{55}Fe, ^{147}Pm, plutonium and americium isotopes, etc. It is important to note that, despite this classification, the timescales over which such behavioral differences may be observed are also important to keep in mind. For example, it is well established that the association of nonconservative radionuclides with plankton blooms provides a mechanism by which reactive fallout nuclides can be removed from surface seawater and released through remineralization processes below the euphotic zone. This can occur over seasonal timescales and produces separation of nonconservative and conservative fallout radionuclides. But as even reactive radionuclides can have oceanic residence times of hundreds to thousands of years, physical circulation processes can dominate in the short term – at least in the open ocean that received the major part of the fallout input.

However, the use of global fallout radionuclides as a tool for ocean science has been limited by the availability and state of development of analytical measurements, sampling technologies, and suitable observation systems. The lack of fixed observational systems covering the oceans (in contrast to the global fallout monitoring on the land), and the enormous area of the oceans, meant that only a very few systematic observations of global fallout delivery to the surface ocean were made. It was noticed [89] that the pattern of seasonal deposition, with a pronounced maximum each spring, was not found generally in over-ocean measurements and that processes of deposition other than precipitation could deliver fallout to the ocean. However, other factors marked the course of the larger-scale studies. These included the way in which ocean science was changing over the years. In the period between 1950 and 1970, ocean studies were carried out largely at the national and institutional level. A new approach to ocean science began later when large-scale projects integrated suites of measurements covering major ocean areas, thus producing in a short time a much better global description of ocean properties or processes. For ocean fallout studies, the GEOSECS project [7–9, 91] was a milestone in marine chemistry and was a major event in the history of ocean fallout studies and their application as tracers of ocean physical and biogeochemical processes. This project spanned the decade of the 1970s with the objective of obtaining a global inventory of chemical components in the world oceans with special emphasis on the deep waters. Intensive sampling was carried out in the Atlantic in 1972–1973, the Pacific in 1973–1974, and the Indian Ocean in 1977–1978. The GEOSECS project produced a comprehensive data set for the fallout radionuclides ^{137}Cs, ^{90}Sr, ^{239,240}Pu (and limited ^{241}Am) for the Atlantic and Pacific Oceans, which permitted inventory estimates for each ocean to be compared with global

fallout inputs [8]. Even more detailed data sets on the distributions of ^{3}H and ^{14}C in all three oceans were produced during the GEOSECS project [7, 9].

WOCE was an even larger-scale project, carried out during the early 1990s. It produced the highest data density of ^{3}H [48] and ^{14}C [49] in the World Ocean with important impact not only on the ocean science, but also on general climate change studies [93]. The GEOSECS and WOCE projects led to the specific use of the conservative tracer radionuclides by the physical oceanographic community, and their valuable contributions to ocean science have been widely acknowledged.

The global fallout radionuclides were dispersed horizontally following the main ocean currents, as well as vertically due to specific biogeochemical processes in the water column. During the 1970s, new sources of radionuclides impacted the ocean, and their study and assessment have been made against the preexisting global fallout signal. A comparison of sources of main radionuclide tracers in the World Ocean, represented by cosmogenic radionuclides, global fallout from atmospheric nuclear weapons tests carried out predominantly until 1963, and discharges from nuclear facilities is presented in Table 1.

The distribution of ^{90}Sr, ^{137}Cs, and $^{239,240}Pu$ in the World Ocean and adjacent seas was treated in the framework of the IAEA WOMARS project [62]. For this purpose, the World Ocean was divided into latitudinal belts for which average radionuclide concentrations were estimated. ^{90}Sr, ^{137}Cs, and $^{239,240}Pu$ concentrations in surface waters were found to vary considerably, still preserving the latitudinal dependence observed in the 1960s, with lowest values in the southern and highest values in the northern latitudes. The results confirm that the main source of these radionuclides in the marine environment is still global fallout. Time trends in radionuclide concentrations (^{90}Sr, ^{137}Cs, and $^{239,240}Pu$) were studied and mean residence times of radionuclides in surface waters of the World Ocean were estimated as well (Table 2). The results confirm a similar residence time for ^{90}Sr and ^{137}Cs in surface waters of 22 ± 2 year. A lower value of 12 ± 1 year has been obtained for $^{239,240}Pu$. Average radionuclide concentrations in surface waters estimated for oceans and seas, adjusted to the year 2010, are presented in Table 3. Higher radionuclide concentrations observed in the northeast Atlantic Ocean (the Irish and North Seas) and the Arctic are due to the release and transport of the radionuclides from Sellafield and La Hague reprocessing plants. The Baltic, Black, and Mediterranean Seas were the main reservoirs for radionuclides released after the Chernobyl accident. The ^{90}Sr distribution in surface waters shows a similar pattern to that of ^{137}Cs, confirming the average global fallout $^{137}Cs/^{90}Sr$ ratio of 1.6 ± 0.1,

Radionuclides as Tracers of Ocean Currents. Table 1 Radionuclide inventories in the World Ocean (after [62])

Nuclide	Half-life (year)	Natural inventory (PBq)	Global fallout inventory		Discharges from reprocessing facilities	
			Total inventory (PBq)	Inventory in 2010 (PBq)	Total inventory (PBq)	Inventory in 2010 (PBq)
^{3}H	12.32	2,200	113,000	8,000	410	45
^{14}C	5,730	1	130	130	2.5	2.5
^{90}Sr	28.78		380	100	7	3
^{137}Cs	30.17		600	170	40	26
^{129}I	15.7×10^{6}	0.6×10^{-3}	0.3×10^{-3}	0.3×10^{-3}	0.04	0.04
^{238}Pu	87.74		0.6	0.4	Regional only	
^{239}Pu	24,110		4	4		
^{240}Pu	6,560		2.5	2.5		
^{241}Pu	14.35		85	8		

with the exception of seas affected by radioactive discharges and the Chernobyl accident.

This entry, however, focuses on those aspects of marine radionuclide studies which contributed to a better understanding of the transport of water masses in ocean basins, as well as transport between the oceans.

Radionuclides as Tracers of Ocean Currents. Table 2 Mean residence time of ^{137}Cs, ^{90}Sr, and $^{239,240}Pu$ in Pacific, Indian, and Atlantic Ocean surface waters (after [62])

Area	Mean residence time (year)	
	^{137}Cs, ^{90}Sr	$^{239,240}Pu$
Pacific Ocean	23±4	11±2
Indian Ocean	29±3	13±2
Atlantic Ocean	31±4	13±1
World Ocean	28±2	12±1

Pacific Ocean

Due to specific deposition patterns [5] and the large size of the Pacific Ocean, the largest reservoir of global fallout radionuclides is in this ocean. The depositional situation in the Pacific turned out to be considerably more complex than in the Atlantic. Both the GEOSECS data sets [8], Japanese measurements [94, 95], as well as studies in the USA [96, 97] revealed substantial excesses of measured inventories of ^{137}Cs, ^{90}Sr, and $^{239,240}Pu$ at many locations in the western North Pacific Ocean compared with the estimated delivery from global fallout. It has become clear that the 68 near-surface nuclear tests [87] conducted at Bikini and Enewetak

Radionuclides as Tracers of Ocean Currents. Table 3 Average radionuclide concentrations in surface waters estimated for oceans and seas, adjusted to the year 2010 (modified after [62])

Sea area	^{90}Sr (mBq L^{-1})	^{137}Cs (mBq L^{-1})	$^{239,240}Pu$ (μBq L^{-1})
North Pacific	0.8±0.1	1.7±0.2	1.2±0.5
Equatorial Pacific	0.9±0.2	1.5±0.2	1.5±0.3
South Pacific	0.6±0.3	0.9±0.4	1.4±0.8
Antarctic	<0.1	<0.1	0.5±0.3
Sea of Japan	0.9±0.2	1.7±0.3	2.4±0.9
Arabian Sea	0.6±0.1	1.0±0.2	0.7±0.4
Indian Ocean	0.8±0.1	1.5±0.2	1.5±0.7
Southern Ocean	0.4±0.2	0.6±0.4	0.2±0.2
Arctic	1.3±0.5	8±4	2.4±0.6
Barents Sea	1.1±0.2	2.2±1.2	7.3±4.4
Baltic Sea	6.2±1.6	37±12	1.3±0.9
North Sea	2.2±0.7	4.1±0.5	5.5±3.7
Irish Sea	27±47	35±33	180±150
English Channel	2.3±0.8	2.6±0.9	4.8±2.9
North N. Atlantic	1.2±0.5	2.6±1.6	13±6
Black Sea	9±3	15±2	1.9±0.8
Mediterranean Sea	0.9±0.1	1.6±0.2	5.2±1.5
North Atlantic	0.7±0.3	1.0±0.5	1.8±1.1
Central Atlantic	0.4±0.1	0.8±0.1	1.0±0.5
South Atlantic	0.2±0.1	0.4±0.1	0.7±0.2

produced not only local fallout but regionally deposited tropospheric fallout, which led to a widespread deposition to the western North Pacific Ocean on a scale similar to that from global fallout. Its presence has been detected not only by the substantial increments to fallout nuclide inventories and concentrations, but also by the distinctive enriched $^{240}Pu/^{239}Pu$ signature in Pacific seawater and sediments over a wide area [38]. The western North Pacific Ocean is, therefore, unique in the history of atmospheric nuclear weapons test fallout in that it is the one area of the globe where fallout was substantially enhanced over the patterns globally observed.

Contributions from nuclear facilities discharging directly to the Pacific Ocean were negligible when compared with global fallout. They were mostly concentrated on the Japanese coast where a small reprocessing facility operated in Tokai. Recently, a large reprocessing facility has been constructed in Rokkasho area, on the Pacific coast of northern Japan.

A small, but measurable contribution in the ^{137}Cs radioactivity of western North Pacific Ocean surface waters was derived from the Chernobyl accident [25].

Indian Ocean

There were two significant inputs of anthropogenic radionuclides to the Indian Ocean, namely, global fallout and the SNAP-9A satellite RTG burnup [1]. The Indian Ocean because of its smaller size received only 14% of global fallout, in comparison to 52% for the Pacific and 33% for the Atlantic Ocean. Because of the greater spatial coverage of southern latitudes of the Indian Ocean, the global fallout inputs were distributed according to one third part in the northern and two thirds parts in the southern Indian Ocean. Additionally, the Indian Ocean has been receiving global fallout radionuclides by advection of surface waters from the Pacific Ocean via the Indonesian Seas.

The most important contribution of Pu from accidents to global fallout was from the SNAP-9A satellite, which burned up over the Mozambique Channel of the Indian Ocean in 1964 and deposited about 0.6 PBq of ^{238}Pu [98]. This input increased the local surface $^{238}Pu/^{239,240}Pu$ fallout ratio by a factor of 10 [55].

Discharges from nuclear industry around the Indian Ocean are expected to be small relative to those received by the other oceans. A possible source may be controlled releases from the nuclear facilities at Trombay, near Mumbai (Bombay), which include several research reactors, radioisotope laboratories, and most significantly a nuclear fuel reprocessing plant. The releases peaked in 1971 at 14 TBq of ^{90}Sr equivalent and subsequently decreased below 0.4 TBq [99]. Compared to the releases from Sellafield or Cap de La Hague fuel reprocessing plants, the Trombay inputs seem to have been very small and are probably important only for coastal waters.

Atlantic Ocean

While the Central and South Atlantic Oceans have received inputs of anthropogenic radionuclides only from global fallout, important North Atlantic contributions were made from authorized liquid radioactive discharges from European nuclear fuel reprocessing plants at Sellafield and La Hague, and from the Chernobyl accident. In addition to these sources, nuclear power stations, fuel production facilities, nuclear research facilities, and dumping of low-level radioactive waste in the deep NE Atlantic Ocean [100] may contribute to the contamination of the immediate environments. The discharges or releases from these sources are not detectable in the open marine environment and their impact on the local environment is monitored by the competent authorities [101]. Accidental losses of radionuclide sources on the seabed, including the wreck of the vessel "Carla" on November 30, 1997, close to the Açores with two medical ^{137}Cs sources of 330 TBq and nuclear powered vessels (e.g., Thresher, Komsomolets) carrying nuclear weapons, represent additional potential sources. The nuclear submarine Komsomolets sank on April 7, 1989, in the Norwegian Sea in a depth of 1,680 m with one nuclear reactor and two torpedoes containing about 16 TBq of Pu. However, the limited monitoring which was carried out demonstrated that the contamination was minor and localized [100].

The major source of anthropogenic radionuclides in the NE Atlantic Ocean has been released from two nuclear fuel reprocessing plants. They are the Sellafield plant on the Irish Sea on the northwest coast of England, and the La Hague facility on the northwest coast of France on the English Channel. A third

reprocessing plant at Dounreay, on the north coast of the Scottish mainland, also discharges directly into the sea. In general, contamination from this facility has been localized and has tended to have been masked by the Sellafield signal. The first discharge from the Sellafield reprocessing plant (formerly Windscale) took place in 1952 when waste with a total activity of about 370 TBq was discharged to the NE Irish Sea. The overall composition of the discharges has been available since 1960 and more comprehensive data were published by BNFL from 1978 onward and in recent years by the UK Government. This topic has been reviewed in several papers [2, 102]. The discharges of most radionuclides peaked in the mid- to late 1970s, with the peak annual value of 5.2 PBq of ^{137}Cs discharged to the Irish Sea in 1975. A total of 41 PBq of ^{137}Cs were released from 1952 up to the end of 1998. The other long-lived radionuclide discharges totaled about 60 PBq of ^{3}H, 6 PBq of ^{134}Cs, 0.6 PBq of ^{90}Sr, 0.1 PBq of ^{238}Pu, 0.6 PBq of ^{239,240}Pu, 22 PBq of ^{241}Pu, and 1 PBq of ^{241}Am. Most of the plutonium and americium has been retained in the seabed sediments of the Irish Sea. Cesium also became incoporated into sediments and since the mid-1980s, the sediment remobilization has represented a ^{137}Cs source [103].

The La Hague nuclear fuel reprocessing facility has been discharging into the English Channel since 1966 [104]. The discharge levels for most of the radionuclides have been decreasing from a peak value of 243 TBq of ^{137}Cs observed in 1971. Recent discharges are about 2 orders of magnitude lower, with the exception of ^{129}I, which has increased substantially in the past decade. The total ^{137}Cs releases have been estimated at 1 PBq. When compared with Sellafield discharges, the contribution of La Hague to the marine inventory of radionuclides, expressed as a percentage of Sellafield releases, is about 2% for ^{137}Cs, 12% for ^{90}Sr, and 0.4% for ^{239,240}Pu. However, for other radionuclides such as ^{3}H, ^{125}Sb, and ^{129}I, the accumulated discharges from La Hague have been higher by a factor of 2–4. For example, La Hague discharges of ^{129}I amount to about 11 TBq compared to Sellafield's 5 TBq (up to the year 1998). Dispersion of La Hague releases in the English Channel and the North Sea have been reviewed in several papers, and used as tools for the validation of numerical hydrodynamic models [105].

The Chernobyl nuclear accident in April 1986 was the largest nuclear accident to date and has had a significant impact on the marine environment. The total activity of nuclear debris released was high (about 1,100 PBq) and the radioactive fallout was widely distributed after the accident and dominated environmental radionuclide levels in various parts of the world. The total releases of ^{137}Cs were estimated to be about 85 PBq [106]. Of the more than 20 radionuclides that were released in significant quantities during the Chernobyl accident, only a few have been studied in the marine environment. Among the Chernobyl radionuclides, the most important are ^{134}Cs and ^{137}Cs. The cesium isotopes were the most widespread, most abundant, and most investigated of those released. The sea most affected by the Chernobyl accident was the Baltic Sea, as the first radioactive clouds from Chernobyl traveled to the north and caused high deposition over the Scandinavian region. The ^{137}Cs inventory in the Baltic Sea due to the Chernobyl accident increased to about 4.5 PBq [107], higher by at least a factor of 10 than the pre-Chernobyl value. Because of the semi-enclosed nature of this sea, and its limited exchange of water with the North Sea, the levels of ^{137}Cs in the Baltic Sea have remained the highest in Europe, 125 Bq/m^{3} in the reference year of 1990 [108]. The North Sea received about 1.2 PBq of ^{137}Cs by direct deposition. The total Chernobyl inventory in the NES waters was estimated to be about 6 PBq of ^{137}Cs.

In the Arctic Ocean various potential sources exist, such as dumped radioactive wastes in the Kara Sea, discharges from nuclear installations on the Kola Peninsula, and nuclear submarines awaiting decommissioning [15]. Arctic sources include (1) nuclear tests on Novaya Zemlya (NZ), (2) dumping of fully fueled nuclear reactors from submarines and icebreakers in eastern NZ fjords, (3) dumping of liquid wastes in Barents Sea, (4) underwater nuclear tests on NZ, (5) discharges from upstream nuclear facilities on Ob and Yenesey Rivers into Kara Sea, (6) discharges from Murmansk from Russian naval and civilian nuclear facilities, and (7) minor contamination from Kursk accident in Barents Sea.

When comparing the main radionuclide sources in the North Atlantic Ocean it can be seen that the total input due to global fallout was 68 PBq of ^{90}Sr, corresponding to 102 PBq of ^{137}Cs, derived using the

$^{137}Cs/^{90}Sr$ fission yield ratio of 1.5. The estimated values for the region of the North European Seas (NES) are 8 PBq for ^{90}Sr and 12 PBq for ^{137}Cs. The dominant source in NES has been ^{137}Cs from the Sellafield reprocessing plant with about a 68% contribution to the ^{137}Cs inventory [14].

Sampling and Analytical Techniques

This entry reviews radionuclide data obtained from several sampling campaigns carried out in the Pacific, Indian, and Atlantic oceans (Fig. 1). Surface seawater sampling was carried out by pumping 100–200 L of seawater from an average depth of 4 m. Water column samples were taken at different depths from the surface to the bottom either by large volume (200 L) samplers, or by 12 L Niskin bottles. Samples for tritium, radiocarbon, and ^{129}I analyses were stored in 1 L glass bottles with air-tight covering so that no exchange with the surrounding air was possible. Radiocarbon samples were poisoned by adding mercury chloride to prevent any biological activity.

Tritium was measured either by the ^{3}He in-growth method at the University of Miami (USA) or by liquid scintillation spectrometry (after an electrolytic enrichment) at the Institute of Geological and Nuclear Sciences (Lower Hutt, New Zealand) and the IAEA's Isotope Hydrology Laboratory (Vienna, Austria). Tritium results are expressed in Tritium Units (1 TU = 118 mBq L^{-1} of water).

Stable isotopes of hydrogen and oxygen (δD, $\delta^{18}O$) were also measured in Lower Hutt and Vienna laboratories. $\delta^{18}O$ analyses were performed using the CO_2-H_2O equilibration procedure. δD analyses were done using the H_2O-Zn reduction method. The isotopic analyses were reported against the international standard VSMOW (Vienna Standard Mean Ocean Water) using conventional delta (δ notation in ‰). The precision of measurements (1σ) was ± 0.1‰ for $\delta^{18}O$ and ± 1‰ for δD.

Radiocarbon in the form of dissolved inorganic carbon (DIC) was extracted either in the Arizona University AMS facility or in IAEA-MEL [108] by acidification of the water sample to pH ~ 3. The released carbon dioxide was then (in a flow of high purity oxygen gas) collected in a trap cooled by liquid nitrogen. After purification, the carbon dioxide was finally converted to graphite over a Fe catalyst. The radiocarbon activity in seawater samples is expressed by $\Delta^{14}C$ defined as $\Delta^{14}C = (F_m - 1)10^3$, where F_m (a fraction of modern carbon) is the measured AMS ratio of ^{14}C–^{13}C, normalized to $\Delta^{14}C$ of 25‰.

Iodine samples were prepared either at IAEA-MEL or at the IsoTrace Laboratory of the University of Toronto [108]. NaI carrier (10 mg) was added to the sample, and after several steps AgI was obtained. This was used as a target for AMS measurements carried out in the IsoTrace Laboratory. The AMS measurements were normalized with respect to ISOT-2 reference material ($^{129}I/^{127}I = 1.174 \pm 0.022$) 10^{-11}. No background subtraction was required as the machine background was below 2×10^{-14}. The results of ^{129}I analyses of seawater samples are expressed in atom L^{-1}.

Onboard pre-concentration procedures (sequentional extraction) were carried out to separate ^{90}Sr, ^{137}Cs, Pu, and ^{241}Am from the collected water samples (MnO_2 co-precipitation). ^{90}Sr was separated by co-precipitation with oxalic acid, and determined in IAEA-MEL by ^{90}Y in-growth method followed by beta-ray counting. Cesium was separated by absorption onto ammonium molybdophosphate and counted in surface or underground gamma-ray spectrometry laboratories. Transuranics were purified using anion exchange resins and extraction chromatography. The samples were then either electrodeposited on stainless steel disks for alpha-ray spectrometry or used for ICPMS or AMS analysis (except ^{241}Am). IAEA reference material, Irish Sea water [109], was analyzed simultaneously with collected samples to ensure high quality of results. A detailed description of the applied procedures used in IAEA-MEL, MRI, and UNIBA is given elsewhere [110–118].

Distribution and Transport of Radionuclides in Seawater – Tracing Ocean Currents

One of the major oceanographic achievements in which radionuclide oceanic tracers played an important role was the development of a model of general circulation between the oceans [44], namely, the Great Ocean Conveyor Belt (Fig. 3). The conveyor belt transfers warm water from the Pacific Ocean to the Atlantic as a shallow current. Passing Europe the surface water evaporates and the ocean water cools, releasing heat to

the atmosphere. Colder water with increased salinity becomes dense, and sinks thousands of meters below the surface as it flows from the Nordic Seas into the deep North Atlantic. Cold water from the Atlantic is then transported as a deep current to the Indian Ocean and then to the Pacific Ocean, that flows further to the north up to 1,600 years later. A global ocean circulation between deep, colder water and warmer, surface water strongly influences regional climates around the world. Although this very simplified model was has been further refined, it has helped to understand links between the ocean basins, and the ocean's role in shaping the Earth's climate.

Studies of the evolving three-dimensional distribution of soluble fallout tracers provided a basic set of reference data against which the contrasting behavior of particle active tracers can be compared. For example, the distributions over depth and time of ^{90}Sr and ^{137}Cs have evolved in a tightly coupled way in the open ocean, at least, and can be taken as tracing their dispersion from the ocean surface by physical processes. The behavior of radionuclides in the water column will be further illustrated using radionuclide time series that were developed for a few stations in the Pacific Ocean. By revisiting some of the GEOSECS stations, it was possible to evaluate water column radionuclide data over time. As an example, Fig. 4 compares ^{90}Sr and ^{239,240}Pu profiles for the western North Pacific Ocean as obtained from the GEOSECS expedition [8], from the Hakuho Maru expedition [94], and from the IAEA'97 Pacific Ocean Expedition [10]. Both the ^{90}Sr and ^{239,240}Pu profiles show typical behavior for these radionuclides in the water column. Twenty-four years later, the subsurface ^{239,240}Pu maximum had become much smaller and less pronounced (a decrease by about a factor of 4) and had moved to deeper layers (from 450 to 850 m). The decline in the ^{90}Sr maximum is clearly seen as well (the data were decay corrected to January 1, 1997), although the decrease 24 years later is less than a factor of 2. This observation would emphasize that the observed changes in plutonium over time could not only be caused by the association of

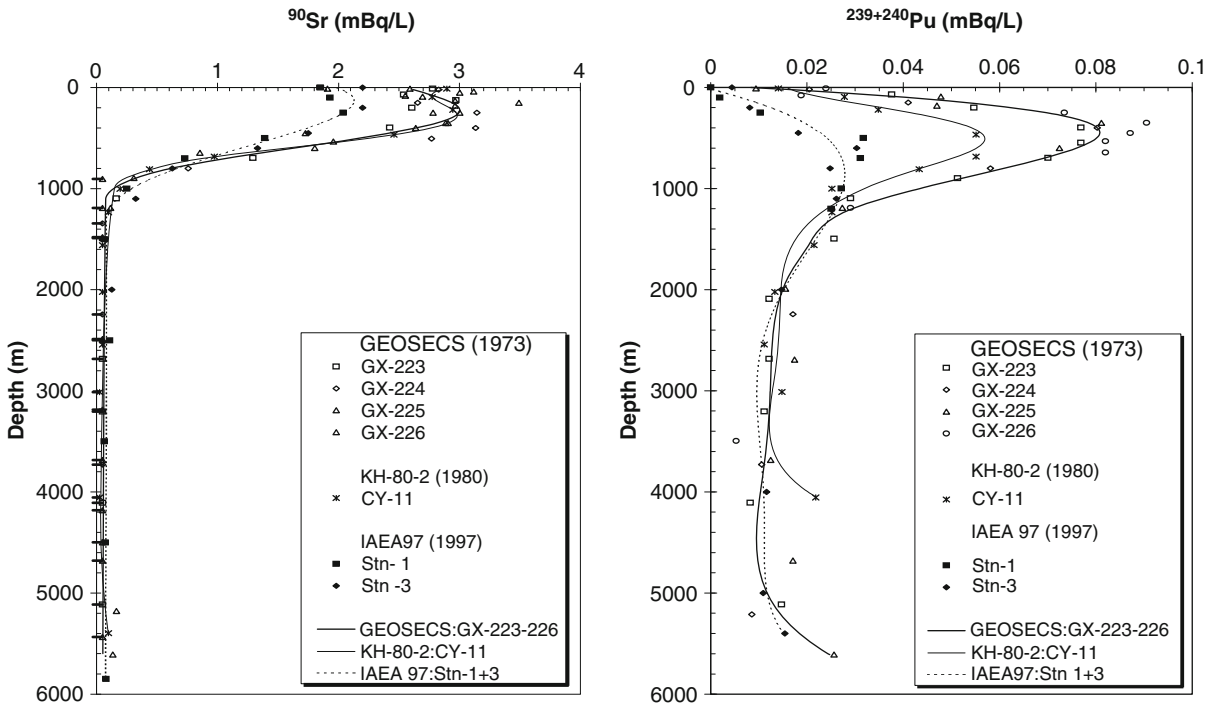

Radionuclides as Tracers of Ocean Currents. Figure 4
Comparison of ^{90}Sr and ^{239,240}Pu profiles as measured by GEOSECS [8], Hakuho Maru [94] and IAEA'97 [10] expeditions in the western North Pacific Ocean (decay corrected to January 1, 1997)

plutonium with sinking particles, but also could be due to physical circulation in the upper water column, which has brought water masses bearing significantly lower levels of fallout radionuclides advectively into the region.

It can be seen from Fig. 4 that the distributions of ^{90}Sr (and similarly for ^{137}Cs) in the water column decline to undetectable levels below 1,000 m, that is, in the main thermocline. In contrast, ^{239,240}Pu continues to be found at depth down to 5,000 m. Due to specific biochemical processes, the major fraction of the ^{239,240}Pu inventory is found therefore in the deep water below the depths containing the major part of the ^{90}Sr and ^{137}Cs inventories. The second broad group of studies was directed specifically to illustrate or quantify specific features of physical mixing [119, 120]. However, the direction of real growth of these studies came in the use of ^{3}H in the large international ocean projects ushered in with the GEOSECS project like Transient Tracers in the Oceans (TTO) in 1981–1983 and South Atlantic Ventilation Experiment in 1988–1989 in the Atlantic Ocean. This could be characterized as the start of recognition by the physical oceanographic community of the potential and power of the use of global fallout ocean tracers in conjunction with standard physical property measurements.

A typical example of the high-density tritium profiles of the World Ocean as obtained from the WOCE program is presented in Fig. 5. The tritium transect was constructed using the WOCE data along 32.5°S in the Pacific Ocean, along 20°S in the Indian Ocean, and along 30°S in the Atlantic Ocean (www.noc.soton.ac.uk/OTHERS/woceipo/atlas_webpage/index.html). In the Pacific Ocean, it is possible to see two tritium maxima: at 155°E (in the Tasman Sea at the western side of the South Pacific Subtropical Gyre), and at 120°W, with penetration depth over 1,000 m. Two ^{3}H maxima (~1.2 TU) at 100°E and 60°E and penetration of ^{3}H down to 1,000 m water depth can also be seen in the Indian Ocean. The surface maxima coincide with the Subtropical Gyre flow (Fig. 1), maintaining there high ^{3}H levels, comparable with those observed in the western North Pacific Ocean [145]. In the Atlantic Ocean, local, tritium maxima at 5°E and 33°W, which should be associated with the South Atlantic Subtropical Gyre can be seen as well. The tritium penetration depth is over 1,000 m.

In addition to fallout ^{3}H (and its radiogenic progeny ^{3}He), chlorofluorocarbons (CFCs), chemically inert man-made compounds, began to be used in parallel applications as physical tracers. CFCs have been injected into the ocean surface by air–sea gas exchange with an input function that has some similarities to the atmospheric input function of ^{3}H [121]. However, it is noteworthy that the atmospheric history of CFCs, which shows an increase from the 1950s to the end of the 1980s, largely differs from that of ^{3}H. When used together, these tracers have seen the greatest level of adoption for physical tracer use. Both have the advantage that sampling and analysis developed rapidly, permitting the collection of quite high resolution two- and three-dimensional data sets, which found ready assimilation to the physical oceanographic modeling community. As an example of such high-resolution data sets, Schlosser et al. [121] has described the tritium (^{3}He) data sets being developed in the framework of the WOCE program. They give as an example, the north–south line at about 135°W in the Pacific. It is a beautiful snapshot of the near century end distribution of this tracer in the eastern Pacific Ocean and illustrates the application of this fallout tracer in a most impressive way. The WOCE program was strongly connected to ocean/climate studies so the application of the ^{3}H (^{3}He) method as part of this program demonstrates one of the most striking contributions of global fallout to advances in marine science. The ^{3}H (^{3}He) technique has also contributed very specifically and precisely to particular aspects of the study of ocean circulation, namely, the "age" of given water mass. This age, the so-called ^{3}H/^{3}He age, is a measure of time that has elapsed since the last equilibrium of a given water mass with the atmosphere [122]. It rests on the resetting of this ^{3}H/^{3}He clock when a surface mass degasses any helium and the clock begins to record ^{3}He ingrowth when, for example, the body water becomes isolated from the surface by convective cooling and sinking. A classic application of the method was a study on ventilation of water masses in the deep western North Atlantic [123].

Pacific Ocean

Anthropogenic radioactivity monitoring in the 1960s [124] revealed a subsurface maximum of ^{137}Cs

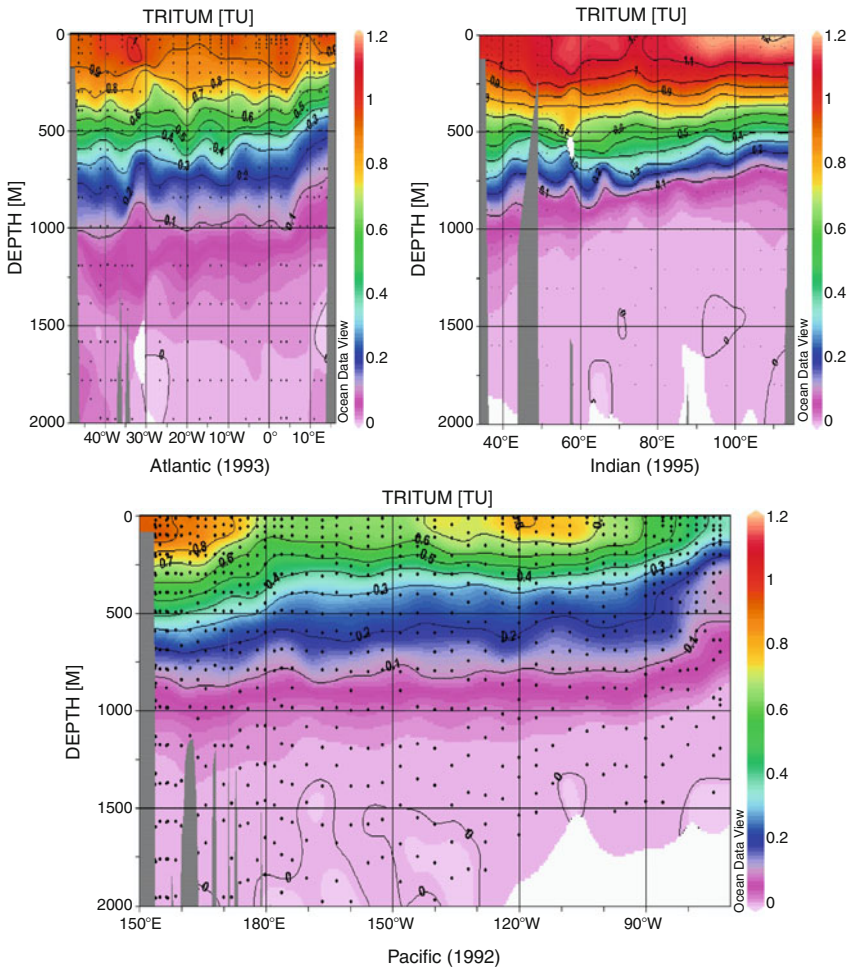

Radionuclides as Tracers of Ocean Currents. Figure 5
Distribution of ^{3}H in the Atlantic Ocean (along 30°S), Indian Ocean (along 20°S), and Pacific Ocean (along 32.5°S) waters (WOCE data: www.noc.soton.ac.uk/OTHERS/woceipo/atlas_webpage/index.html)

(100–200 m depth) in the central and eastern North Pacific water column, which was a first view of subduction in the North Pacific by tracers. The ^{137}Cs and ^{3}H measurements in the Pacific water columns for GEOSECS [8] found that subsurface maxima in the latitudinal vertical sections occurred in the midlatitude and subtropical regions in the North Pacific. A transect of vertical profiles of ^{137}Cs using a composite data set of ^{137}Cs concentrations from the surface to 500-m depth in the western North Pacific (along about 160°W) in the 1970s based on the HAM database [125] indicated that a core water mass with higher ^{137}Cs concentrations exists in a subsurface layer from 10°N to 20°N in the western North Pacific [126], which corresponds to the NPTW with a higher salinity of ~35. In the eastern North Pacific, the occurrence of a subsurface maximum of bomb ^{3}H in the Subtropical Gyre has been recognized [127]. The water mass with higher ^{3}H seems to correspond to the SSM. A water mass with higher ^{3}H, which was a winter outcrop in the midlatitude of the eastern North Pacific in the early 1960s, penetrated into the eastern subtropical North Pacific. The 1970s ^{137}Cs section in the eastern North Pacific [128] suggested that cores of water masses with higher ^{137}Cs concentrations exist as a subsurface layer (~100 m depth) from 10°N to 20°N in the eastern subtropical North Pacific, which corresponds to the SSM with lower salinity.

A 1991 ^{3}H section along 135°W (P13C line of WOCE) traces the equatorial transport from the subtropical North Pacific by the ^{3}H tongue, which extends more than 3,000 km meridionally. The ^{3}H tongue extended southward following isopycnals ($26.0 < \sigma_\theta < 26.5$), rising in depth from about 250 m at 30°N to around 75 m at 10°N, and deepening about 100 m at the Equator [129]. A 2002 ^{137}Cs vertical section along 165°E [130] revealed that several cores of ^{137}Cs maxima occurred at 250–500 m depth. A pronounced high ^{137}Cs concentration region, near 500 m depth ($\sigma_\theta \approx 26.0$) at around 20°N marks a major core that corresponds to NPCMW produced in the central North Pacific and a second core near 250 m depth ($\sigma_\theta \approx 25.0$) at 20°N coincides with NPSTMW. Figure 6 shows the schematic diagram of formation, subduction, and transport of NPSTMW and NPCMW.

A Global Ocean Circulation Model (OGCM) can provide information on the subsurface movement of water masses in the North Pacific. The transport of global fallout ^{137}Cs in the Pacific has been studied by Lagrangian trajectory analysis following OGCM streamline [131]. The Lagrangian trajectory analysis suggests that the 1975 subsurface ^{137}Cs maximum water near 10°N along 165°E [126] is identified as the transport of the eastern subtropical Mode Water (EMW), which is formed in the eastern North Pacific around 30°N and 140°W [132], rather than NPSW. The 2002 subsurface ^{137}Cs maximum water near 20°N along 165°E [130] almost coincides with NPCMW, although the Lagrangian particles in 2002 around 20°N spread from the top of the NPCMW-derived water to the bottom of the NPTW-derived water. The tracer experiments reveal that water masses formed in the Kuroshio Current and Kuroshio Extension region are subducted and moved southwestward following the North Pacific subtropical circulation, although the depth of subduction and timescale of subducted water transport depend on the formation region of water mass.

The 1991 ^{3}H and ^{3}He meridional sections along 135°W [129] showed that a strong front exists at the Equator for $24 < \sigma_\theta < 26.5$. This feature is a consequence of the strongly asymmetric global fallout pattern for nuclear explosion–derived radionuclides [125]. There is no obvious indication of cross Equator transport of tracers although ^{3}H isopleths above $\sigma_\theta = 24$ appear to splay, presumably in response to Ekman divergence flow at the Equator. The BEAGLE2003 expedition [72] provided a new view of the ^{137}Cs cross section along 32.5°S, which revealed that an enhanced ^{137}Cs region exists in the Tasman Sea. The higher ^{137}Cs concentration in the Tasman Sea cannot be explained by global fallout and by contamination due to nuclear activities such as French nuclear explosions conducted in the French Polynesia. A possible cause of the enhanced ^{137}Cs in the Tasman Sea is cross Equator transport of ^{137}Cs from the North Pacific to the South Pacific, taken into account temporal changes of surface ^{137}Cs in each sea area of the Pacific,

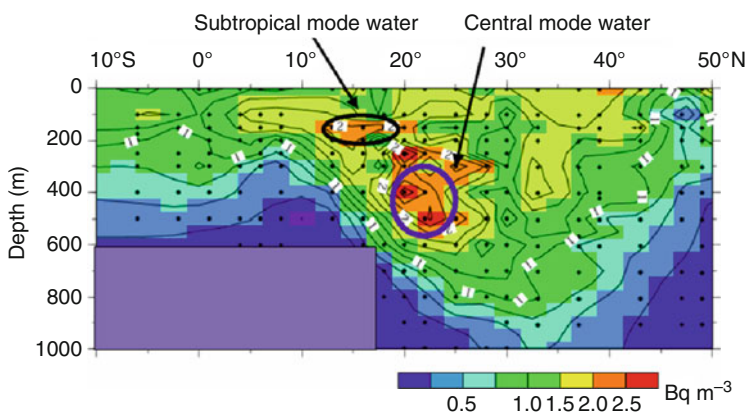

Radionuclides as Tracers of Ocean Currents. Figure 6
Formation and subduction areas of the North Pacific Subtropical Mode Water (NPSTMW) and the Lighter Central Mode Water (LCMW) (modified from [130])

which suggests Equator ward movement of ^{137}Cs [125]. The Lagrangian trajectory analysis [131] reveals cross Equator pathway from the North Pacific to the South Pacific. The ^{137}Cs in the North Pacific midlatitude region enters the equatorial region through the interior pathways described in previous sections and the Mindanao Current. After that, the ^{137}Cs flows eastward along the EUC and finally enters the eastern South Pacific equatorial region by Ekman transport. A part of ^{137}Cs is transported to the South Pacific Subtropical Gyre via the SEC and East Australian Currents, although ^{137}Cs entering the South Pacific returns to the equatorial region. This pathway is shown in Fig. 7.

Anthropogenic radionuclides and CFCs are strong tools to detect deep water formation, for example, in the Labrador Sea. However, these tracers are insufficient to follow the flow of mid-depth and deep waters in the Pacific because spatial and temporal resolution of concentration contours is too low due to low concentrations to detect water motion. Radionuclide tracers such as ^{3}He and ^{14}C are effective to detect the motion of the mid-depth and deep waters in the Pacific. Submarine hydrothermal fluids that are injected into the ocean interiors from deep-sea ridges and from active seamounts contain enriched ^{3}He comparable to that in the atmosphere. Valuable ^{3}He/^{4}He measurements can be used to follow water movement in mid-depth layers. The larger fraction of excess ^{3}He in the Pacific is injected at the crust of the East Pacific Rise at depths of 2,000–2,500 m, in the eastern equatorial Pacific and eastern South Pacific. A comprehensive excess ^{3}He map in the Pacific was depicted based on WOCE data and others [133]. Two intense ^{3}He-rich jets in the 2,500 m depth surface extend westward into the Pacific basin from the crest of the East Pacific Rise at ≈10°N and ≈15°S with a marked minimum between these plumes centered on the Equator. This feature suggests that westward flow exists at 2,500 m depth in ≈10°N and ≈15°S of the Pacific and eastward flow may be present at the Equator. On the other hand, there is weak indication of southwestward flow in the eastern North Pacific midlatitude region. Another mantle helium injection occurs at hydrothermally active seamounts. Loihi Seamount, on the southeastern flank of the island of Hawaii, has released ^{3}He from active hydrothermal vents centered at 1,100 m depth [134]. The δ^{3}He map at a 1,100-m depth surface reveals that the Loihi ^{3}He extends eastward as a continuous plume

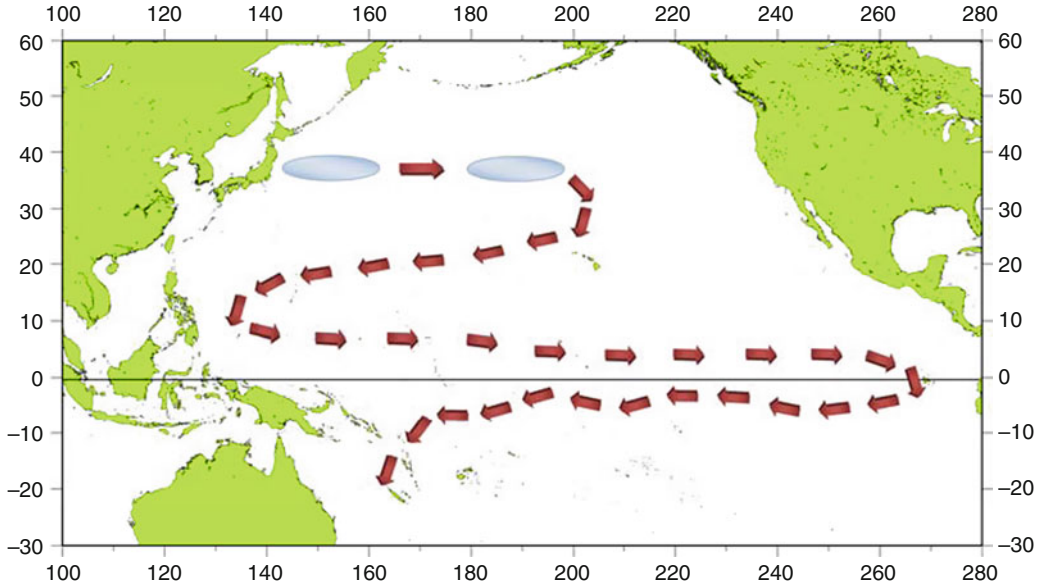

Radionuclides as Tracers of Ocean Currents. Figure 7
Schematic diagram of possible water pathway from the North Pacific midlatitude region (the input region from global fallout) to the Tasman Sea via the Equator

to the coast of Mexico. The helium distribution pattern in the mid-depth of the Pacific is consistent with the circulation pattern predicted by Reid [135] on the basis of a steric height analysis of hydrographic data.

^{14}C is an ideal tracer to study the long-term mean of the deep water flow pattern. The GEOSECS Pacific expedition depicted the meridional $\Delta^{14}C$ section in the Pacific, which indicated deep water flow circumpolar water to the North Pacific and allowed us to estimate a net transport of circumpolar water to the North Pacific of 25 Sv [136]. The WOCE Pacific measurements [129] confirmed the GEOSECS data and provided more useful flow pattern data, in which the primary pathway is northward flow as a deep western boundary current passing along the Tonga-Kermadec trench suggested by hydrographic data and the OGCM model. The WOCE $\Delta^{14}C$ data can trace the North Pacific deep water flow, which turns westward after across the Equator and then moves clockwise around the basin and finally reaches the Aleutian Island Arch [137]. The bottom water flow in the Pacific is restricted by bottom topography.

In addition to global fallout, there has also been a contribution (especially for plutonium) from close-in fallout from nuclear weapons tests carried out at Bikini and Enewetak Atolls [138]. As many of these tests were conducted at/or near ground level, much of the resultant radionuclides were delivered to the troposphere with substantial fallout to regional areas of the Pacific Ocean, with subsequent transport to the eastern North Indian Ocean. Other Pacific tests conducted at Christmas Island and at Johnson Atoll were carried out at high altitudes, and are unlikely to have contributed significantly to close-in tropospheric fallout in comparison to Enewetak and Bikini tests [3]. A significant amount of close-in fallout Pu was transported in deep layers and dissolved in deep water. As a result, an area with enhanced $^{239,240}Pu$ derived from Bikini exists in the deep water of the western North Pacific [139]. However, there is no precious map of $^{239,240}Pu$ in deep layers (>2,000 m depth) of the North Pacific Ocean due to scant observation of deep $^{239,240}Pu$. The map of $^{239,240}Pu$ in deep layers of the North Pacific Ocean would be a valuable tool for tracing deep water flow in the North Pacific Ocean, because deep plutonium behaves as a conservative tracer due to low biological activity in deep waters.

Indian Ocean

Higher radionuclide concentrations were expected to be observed in the areas around 45°N and 30°S–40°S, with values decreasing to the Equator and to the Poles, if the global deposition patterns would have the main impact on radionuclide concentrations [140]. However, from the first comprehensive radionuclide study carried out in the Indian Ocean in 1978 in the framework of the GEOSECS program [9], it was already observed that the latitudinal trend in tritium distribution did not reflect the fallout deposition pattern. Low levels characterized the area south of 40°S, while the highest concentrations were found between 30°S and 10°S. Toward the north, tritium concentration regularly decreased around the Equator, to 10°N and leveled in the Arabian and Red Seas.

The range of observed ^{137}Cs and Pu concentrations in surface waters of the Indian Ocean was between 1.5 and 6 $mBqL^{-1}$ for ^{137}Cs, 0.7–7 μBqL^{-1} for $^{239,240}Pu$ and 0.6–1.4 μBqL^{-1} for ^{241}Am [54]. These results demonstrated for the first time that a direct transport of ^{137}Cs, $^{239,240}Pu$, and ^{241}Am from the Northwest Pacific to the Indian Ocean is feasible via the Indonesian Seas. The data also indicated a radionuclide transport from the eastern Equatorial Indian Ocean via the Leeuwin Current to the eastern South Indian Ocean. A few ^{137}Cs data were obtained during the 1970s [141] (values from 2.8 to 2.9 Bq/m^3) and the early 1990s [142] when the ^{137}Cs concentrations ranged between 1.6 and 2.3 Bq/m^3, while the ^{90}Sr ranged from 1.1 to 1.5 Bq/m^3. Only three results were reported for plutonium isotopes. Again, the lowest levels of ^{137}Cs and $^{239,240}Pu$ characterized the area south of 30°S. A similar latitudinal trend as obtained for GEOSECS tritium [9] with the smallest values around 60°S and the highest between 10°S and 35°S was observed for the concentration of ^{137}Cs in surface waters. Higher average ^{137}Cs level (2.1 ± 0.3 $mBqL^{-1}$) was found for the South Indian Ocean, while for the North Indian Ocean, the estimated average concentration is 1.6 ± 0.3 $mBqL^{-1}$. Low ^{137}Cs concentrations (1.1–1.8 $mBqL^{-1}$) characterized the whole area south of Australia, at latitudes ranging between 40°S and 35°S. Proceeding northwest, all other stations showed higher ^{137}Cs concentrations (2.1–2.2 $mBqL^{-1}$). Upwelling near the Equator is probably responsible for the decrease in concentrations

in the latitudinal band 10°S and 10°N. ^{239,240}Pu data show a similar latitudinal dependence as do the other radionuclides. The Arabian and Red Seas are characterized by radionuclide concentrations, in the range of 1.4–1.7 Bq/m^3 for ^{137}Cs and 0.9–1.4 for ^{90}Sr. The mean ratio ^{137}Cs/^{90}Sr is 1.63 ± 0.19. As all investigated radionuclides show similar latitudinal trends with the smallest values in the southern box and the highest in the center box between 10°S and 35°S, the broken latitudinal dependence in radionuclide concentrations in surface water (as expected from the global fallout deposition) must be due to specific circulation patterns in the Indian Ocean.

The time-series ^{137}Cs data in the North Pacific show decreasing surface ^{137}Cs concentrations during the past 4 decades, although their decrease rates have been depending on the sea area, being larger in the North Pacific than in the equatorial and South Pacific [10, 143]. As ^{137}Cs after deposition on the ocean surface is affected only by advection, diffusion, and radioactive decay, and there has not been significant transport of ^{137}Cs to bottom waters and to sediments [8, 63, 144], these findings suggest that a significant amount of ^{137}Cs has been transported from the North Pacific Ocean to the Indian Ocean. The observed latitudinal trend, particularly in the Southern Hemisphere, does not reflect that of the integrated deposition density of global fallout radionuclides [3]. Apparently, the system of equatorial currents, the monsoon-induced circulation, transport of water masses from the Mediterranean and from the western North Pacific, outflow to the South Atlantic Ocean, and the Subtropical Gyre have been playing an important role in maintaining radionuclide concentrations in the Indian Ocean surface waters which differ from global fallout.

A comparison of WOMARS tritium data [55, 56] obtained during the late 1990s with GEOSECS (1978) decay corrected values for the Arabian Sea [9] showed unexpectedly high ^{3}H levels at surface and subsurface water depths (0.5–1 TU, i.e., higher almost by a factor of 2). This may be explained by the supply of water masses with higher ^{3}H levels from the Mediterranean Sea, where levels around 2 TU were found [55]. On the eastern side of the Sea there may be also a contribution from the Indonesian throughflow from the western North Pacific Ocean where corresponding ^{3}H levels as high as 1.5 TU were measured [145]. The second interesting feature of this comparison is a deeper penetration of surface ^{3}H into the Indian Ocean water column [56], variable in the depth range of 500–1,500 m. An estimated penetration rate on the basis of ^{3}H and ^{14}C data is around 60 m/year [57]. As there are no water profile data for ^{137}Cs or ^{90}Sr available from the GEOSECS or other cruises, no direct comparison can be made for the Indian Ocean. However, it is possible to compare the ^{137}Cs profiles calculated from the measured GEOSECS ^{3}H profiles using the ^{137}Cs/^{3}H ratio. The observed average ^{137}Cs/^{3}H ratio in the Indian Ocean waters is 0.019 ± 0.004 (the correlation coefficient is 0.74 ± 0.09). This comparison confirms again that higher ^{137}Cs (^{90}Sr) levels were found than expected from the decay corrected ^{3}H GEOSECS data.

Typical profiles of ^{239,240}Pu and ^{241}Am observed in the open ocean have minimum values at the surface, and subsurface maxima at medium water depths. Pu isotopes and ^{241}Am because of their particle-reactive nature are attached to particles, effectively scavenged from surface water, and released again at medium depths by biogeochemical mineralization [7, 10, 146]. The observed Arabian Sea ^{239,240}Pu profiles have maxima at water depths between 400 and 800 m, reflecting different position of sampling sites characterized by slower or faster vertical transport. A similar pattern was observed for the vertical distribution of ^{241}Am, except that the concentrations were lower, and the penetration depths deeper [56]. As Am is more particle reactive than Pu, it reaches deeper depths than Pu because of preferential particulate scavenging and downward transport [143].

As an example for the South Indian Ocean, ^{129}I water profiles as obtained from the ANTARES-4 cruise will be compared with those measured during the IAEA'97 expedition in the western North Pacific Ocean [145]. Figure 8 documents that similar ^{129}I concentrations in surface seawater were measured during both expeditions. The differences observed in medium depth and deep water samples are due to specific advection conditions observed in the Crozet Basin, where NADW and AABW are manifested, as will be discussed later.

A similar picture on the accumulation of anthropogenic radionuclides in the Subtropical Gyre is presented in Fig. 9. Here, ^{137}Cs profile along 20°S as obtained in the framework of the SHOTS project [74] is showed. This is the first high-density ^{137}Cs profile

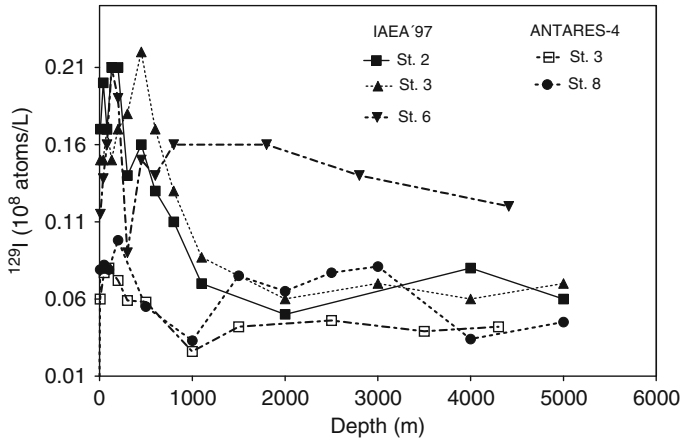

Radionuclides as Tracers of Ocean Currents. Figure 8
Comparison of ^{129}I water profile results as obtained during the IAEA'97 expedition in the western North Pacific Ocean with those measured during the ANTARES-4 cruise in the South Indian Ocean (modified from [145])

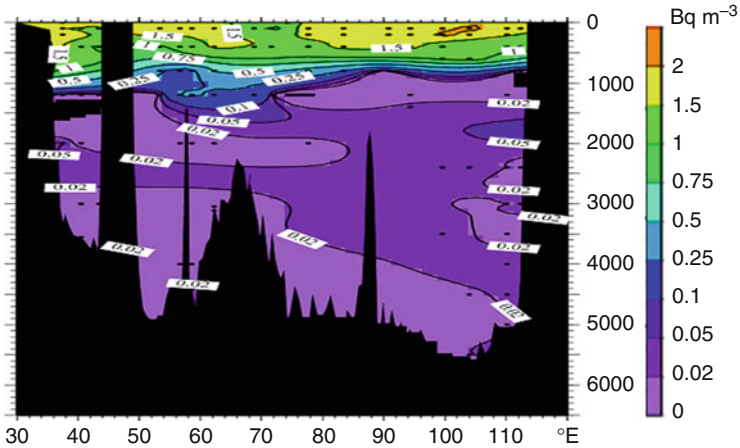

Radionuclides as Tracers of Ocean Currents. Figure 9
Distribution of ^{137}Cs in South Indian Ocean waters along 20°S (data from [74])

obtained thanks to underground gamma-spectrometry analysis of 10–20 L water samples collected during the BEAGLE2003/2004 expedition in the Indian Ocean. The profile shows surface ^{137}Cs maxima at 100°E and 60°E, and deep penetration of ^{137}Cs down to 1,500 m. However, tracers of ^{137}Cs are visible even at depths around 4,000 m. The ^{137}Cs transect is copying the cross section of the gyre (Fig. 1), crossing the main eastern gyre stream roughly at 20°S–100°E. The western gyre, predicted to be at 55°E, has been shifted to 60°E. The central part of the gyre, outside of the main streams, should have the lowest ^{137}Cs concentrations, which is confirmed by observation of lower ^{137}Cs values (1.4 mBq L^{-1}) at 20°S–70°E. This confirms again that transport of water masses from the western North Pacific (where comparable ^{137}Cs were observed 10) occurs via Indonesian Seas to the southern Indian Ocean. The high ^{137}Cs concentration observed in the Madagascar channel (1.95 mBq L^{-1} at 37°31′E) should be due to the Red Sea Overflow Water (Fig. 1), carrying higher ^{137}Cs levels from the Mediterranean Sea [55].

It has been noticed from the ANTARES-4 results (Crozet Basin) that AF, STF, and SAF control radionuclide distribution in surface and subsurface waters with

the highest ^{3}H levels observed at the Subtropical Gyre [58, 85]. However, several other water masses can be identified in medium and deep waters [148]. Figure 10 shows the relationship between ^{3}H levels and heavy oxygen isotope content. The intermediate layer (1,000 ±500 m) with decreasing ^{3}H levels represents the Antarctic Intermediate Water (AAIW), which is also characterized by a minimum in ^{129}I at 1,000 m (Fig. 8). The elevated ^{3}H levels around 40°S at water depths 1,500–2,500 may indicate a presence of the North Indian Deep Water (NIDW), which originates from the northern Indian Ocean where comparable ^{3}H levels were observed [55]. The ^{3}H concentrations decrease dramatically below 1,500 m down to 3,000 m, a depth range where the Circumpolar Deep Water (CDW) layer exists. This may be due to the influence of the North Atlantic Deep Water (NADW), which is known to be the most important contributor to the CDW [82]. As measurable ^{3}H concentrations (and negligible levels of ^{129}I) were observed in bottom waters, an injection of Antarctic Bottom Water (AABW) might be considered as the most plausible source of ^{3}H in bottom waters. A major formation area of the AABW is the Weddell Sea, where it is produced by sinking of cold, dense shelf waters. Surface ^{3}H levels in samples collected in 2003 in the Weddell and Ross Seas showed 0.4–0.5 TU, which is consistent with ^{3}H levels found in bottom waters of the Crozet Basin (taking into account a transit time and ^{3}H decay). As the NADW has too low ^{3}H concentrations, and the NIDW is located well above the bottom layer, higher ^{3}H levels found in bottom waters may represent the AABW. This is also confirmed by the fact that the AABW is depleted both in ^{2}H and ^{18}O in comparison with surface waters [85].

The distribution study of radionuclide deposition from nuclear weapons tests clearly showed that the idealized deposition (peaks at 45°N and S) has been interrupted in a few regions, such as western North Pacific Ocean, mainly due to higher precipitation rates [5], impact of close-in fallout from Bikini and Enewetak Atolls, and due to specific seawater circulation patterns. The observed radionuclide levels in the Indian Ocean were significantly influenced by circulation patterns in the North, as well as in the South. Combining the ^{14}C data presented in this work together with WOCE data (www.noc.soton.ac.uk/OTHERS/woceipo/atlas_webpage/index.html), it has been possible to construct a ^{14}C distribution map for

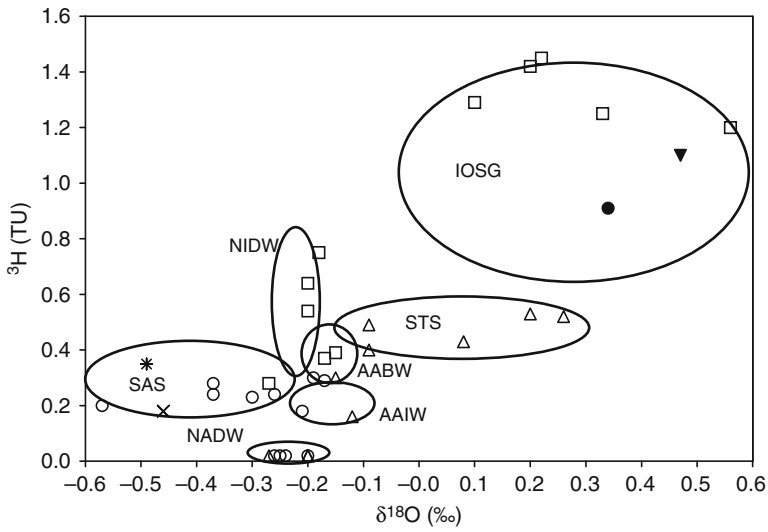

Radionuclides as Tracers of Ocean Currents. Figure 10
Water masses present in the Crozet Basin of the South Indian Ocean (IOSG – Indian Ocean Subtropical Gyre, STS – Subtropical Surface water, SAS – Subantarctic Surface water, NIDW – North Indian Deep Water, NADW – North Atlantic Deep Water, AABW – Antarctic Bottom Water, AAIW – Antarctic Intermediate Water

the southern Indian Ocean (Fig. 11). High ^{14}C concentrations can be seen along the Subtropical Gyre (20°S–40°S), with a sharp decrease south of 40°S. This observation has also been confirmed by ^{3}H, ^{90}Sr, and ^{129}I data [85]. When comparing the recent (1997–2003) ^{137}Cs, $^{239,240}Pu$, and ^{241}Am levels with those observed in 1976–1978 [54], it can be seen that there were not big changes in radionuclide concentrations. The ^{137}Cs concentrations observed in surface waters southwest of Australia (influenced by Leeuwin Current) decreased by about a factor of 2 only, in agreement with the estimated mean residence time of ^{137}Cs in the Indian Ocean (29 ± 3 year; Table 2).

A different situation is the case for transuranics, where the observed $^{239,240}Pu$ concentrations are lower by about a factor of 2 than previously reported (the mean residence time of $^{239,240}Pu$ is 13 ± 2 year; Table 2). In the case of ^{241}Am they decreased only by ~30%, in spite of a relatively shorter effective half-life of ^{241}Am (~3 years). A slower decrease in transuranics levels may be due to their additional transport from the Marshall Islands testing grounds, and in the case of ^{241}Am also due to its ingrowth from the decay of ^{241}Pu (half-life 14.4 year).

The main feature observed in the South Indian Ocean is the action of the Subtropical Gyre, which concentrates radionuclides between 20°S and 40°S on a timescale of several decades. The Subtropical Gyre due to fresh supply of water masses from the northern latitudes, and their circulation within the Gyre, acts as a reservoir, maintaining higher radionuclide concentrations there.

Atlantic Ocean

The radionuclide tracing of ocean currents in the Atlantic Ocean will be focused on the eastern North Atlantic (Fig. 12), where most of the radionuclide data including tritium, ^{137}Cs, ^{129}I, and ^{99}Tc are available. Although ^{137}Cs is the most frequently analyzed radionuclide in surface waters, the data density has not been high enough for the computer evaluation of data on yearly basis and their presentation in the form of isoline maps. The ^{137}Cs data therefore were grouped in 5-year

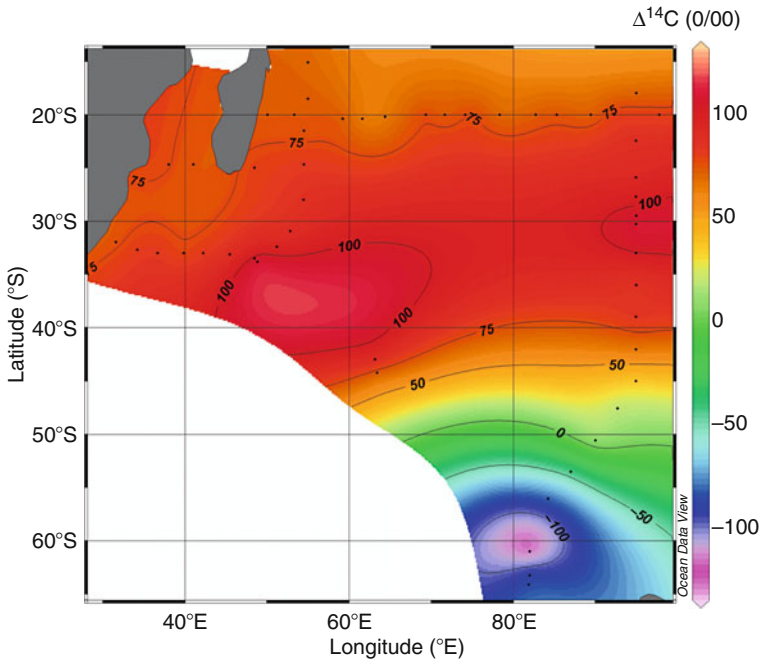

Radionuclides as Tracers of Ocean Currents. Figure 11
Spatial distribution of ^{14}C in surface waters of the South Indian Ocean (combined data of WOCE (www.noc.soton.ac.uk/OTHERS/woceipo/atlas_webpage/index.html) and ANTARES-4 [85])

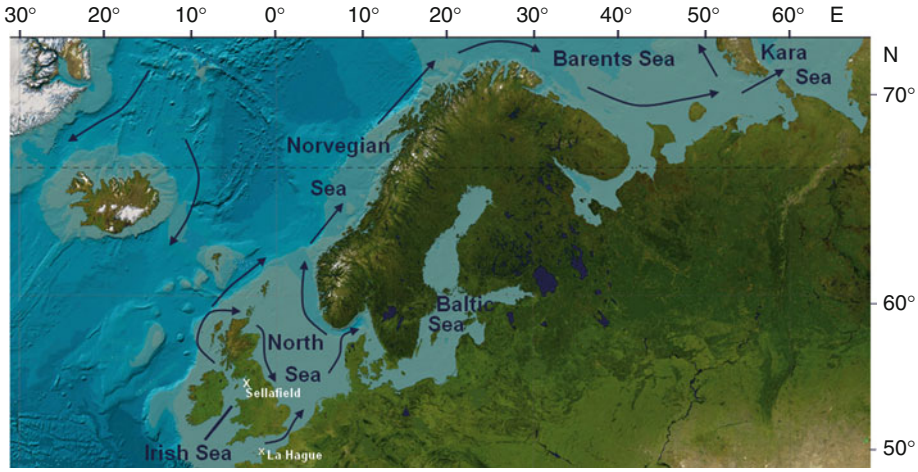

Radionuclides as Tracers of Ocean Currents. Figure 12
Transport of ^{137}Cs from the Sellafield and La Hague reprocessing nuclear facilities in the eastern North Atlantic Ocean (the map after www.gebco.org)

intervals and evaluated. ^{137}Cs isoline maps computed by data interpolation are presented in Fig. 13, which clearly show the movement of ^{137}Cs contaminated water masses from the Irish Sea through the North Channel to the North Sea, the Norwegian, Barents, and Kara Seas, and onward to the Arctic Ocean. A branch of the North Atlantic Current (NAC) with low (global fallout) ^{137}Cs concentrations entering the northern North Sea is pushing Sellafield contaminated waters to the south, along the east coasts of Scotland and England, before moving eastward, in accordance with the ocean and seafloor topography (Fig. 1). It is because of this specific current system that the ^{137}Cs concentrations along the Scottish, English, and Norwegian coasts are much higher than in the open North and Norwegian Seas. Further, the strong Norwegian Current (NC) keeps the ^{137}Cs concentrations along the coast uniform with high gradients to the west, in contrast to the open Norwegian Sea, where the ^{137}Cs concentrations have been about one order of magnitude lower. This is because of the fact that the open Norwegian Sea is controlled by (NAC), keeping high gradients between ^{137}Cs of NAC and NC waters. The NC receives water from the Baltic and North Seas and from the Norwegian coast. It is a result of wind forcing and freshwater fluxes and it is influenced by bathymetry and the wind-driven cyclonic circulation in the North Sea [149]. Therefore, the transit time necessary for the ^{137}Cs contaminated waters to reach the central Norwegian Sea is much longer. The fast movement of water masses with the NC explains the relatively short transit time to the western South Barents Sea. In the western Barents Sea both NAC and NC warm waters are mixed together, so the west–east ^{137}Cs concentration gradient is lower. The ^{137}Cs lower concentrations observed in the Greenland Sea may be associated with the Greenland Sea Gyre and ventilation of deep waters [150]. At this latitude, a certain portion of the Sellafield-contaminated waters may be transported to the East Greenland, and then transferred back to the Atlantic Ocean through the Denmark Strait [11, 13] (Fig. 12). By comparing the ^{137}Cs release rates from Sellafield and La Hague reprocessing plants with the observed ^{137}Cs distribution, it is possible to derive a transit time for the movement of ^{137}Cs from the Irish Sea to the Nordic Seas (Fig. 12). The transit time of water movement from Sellafield to the North Channel of the Irish Sea can be estimated as 0.5 ± 0.1 year; 2.0 ± 0.2 year to the north of Scotland, 2.5 ± 0.2 year to the east coast of England, 3.0 ± 0.5 year to the southern North Sea, and 4.0 ± 0.5 year to the central and eastern North Sea. In the western Baltic Sea, the signal is detected in 5 ± 1 year after the release into the Irish Sea. Further to the north, peak ^{137}Cs concentrations are found along the Norwegian coast, as well as in the Southwestern Barents Sea, at 4.5 ± 0.5 year after the

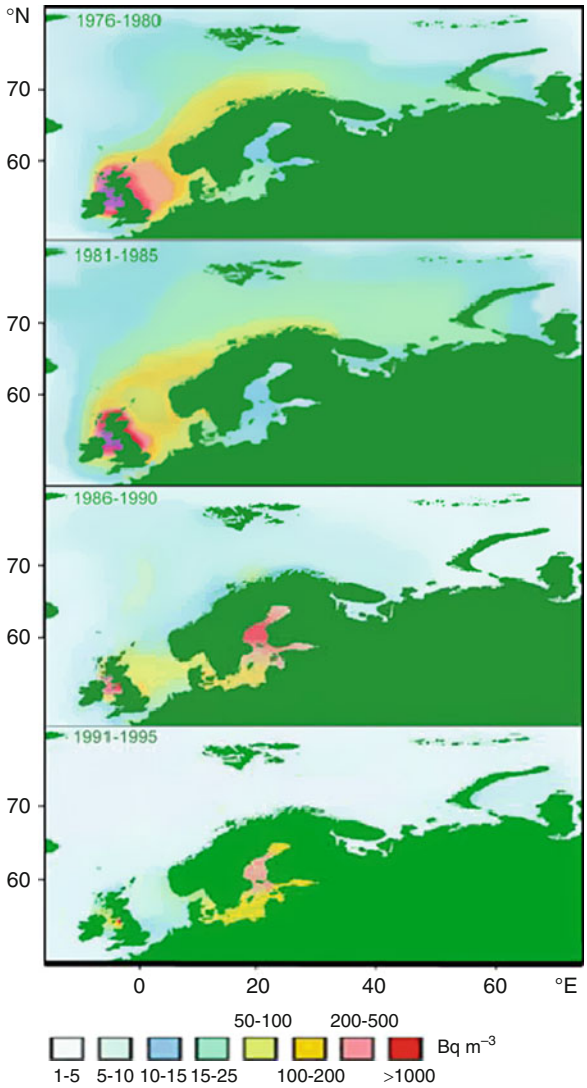

Radionuclides as Tracers of Ocean Currents. Figure 13 Distribution of ^{137}Cs from the Sellafield and La Hague reprocessing nuclear facilities (1976–1995) and the Chernobyl accident (1986–1995) in the eastern North Atlantic Ocean and its adjacent seas (modified from [10])

Sellafield discharges. The transit time to the central Barents Sea, as well as to Svalbard is 5 ± 1 year, and 6 ± 1 year to the Kara Sea. The Arctic Ocean was contaminated with ^{137}Cs of Sellafield origin 8 years later. The estimated transit time for ^{137}Cs from the La Hague facility to the North Sea, the Norwegian Sea, etc., would be 2 years less than the transit time estimated from the Sellafield facility. The transit time for water movement south from the Irish Sea to the Celtic Sea is 1.5±0.2 year, and 2.0±0.2 year to the English Channel. The estimated transit times are more precise, and in reasonable agreement with previous estimations [60, 151, 152].

Tritium, ^{129}I, and ^{99}Tc are useful transient tracers as does ^{137}Cs. The GEOSECS 1972 tritium section through the western basin of the North Atlantic [9] highlights the penetration of bomb tritium into the basin over decade timescales, which is the most dramatic evidence for the validity of the "Ocean Conveyer Belt" [44]. This means that recent formed overflow water enters to the Labrador Sea basin from the Greenland/Norwegian Seas and deep convection occurred. ^{129}I and ^{99}Tc have been used to track water flows and NADW formation because discharge of both radionuclides from the Sellafield and La Hague reprocessing plants increased abruptly in the 1990s [153–157]. A marked increase of the ^{129}I concentrations in the Labrador Sea around 2000 reveals that the leading edge of the ^{129}I tracer front derived from the European reprocessing discharge has passed through the Nordic Seas and is entering in NADW via Labrador Sea [158]. The ^{129}I and CFC-11 data in 2001 provide about 2 years for a transit time in Denmark Strait Overflow Water, which is longer than estimates in 1999. This suggests general weakening in the subpolar gyre of the North Atlantic during the 1990s, which may be an indication of oceanic response accompanied with recent climate change.

A specific feature of the water circulation in the North Atlantic is the influence of the Arctic Ocean, which is the smallest, and shallowest of the world's five major oceanic divisions, located mostly in the Arctic north polar region. The Arctic Ocean is partly covered by sea ice throughout the year, and almost completely in winter. Its salinity is the lowest on average of the five major oceans, due to low evaporation, heavy freshwater inflow from rivers, and limited connection with surrounding oceanic waters with higher salinities. The Arctic Ocean contains a major choke point in the southern Chukchi Sea, which provides access to the Pacific Ocean through the Bering Strait between Alaska and Eastern Siberia. The greatest inflow of water comes from the Atlantic via the Norwegian Current, which then flows along the Eurasian coast. Water also enters from the Pacific via the Bering Strait.

The East Greenland Current carries the major outflow. Recently, radionuclide tracers and the water circulation in the North Atlantic and the Arctic Ocean were of interest due to possible transport of radioactive wastes dumped in the Kara Sea [1, 13, 15, 16].

Anthropogenic radionuclide data for the Central and South Atlantic Ocean are very sparse when compared with that in the North Atlantic Ocean. The BEAGLE2003 expedition provided an opportunity to have ^{137}Cs and plutonium data in water columns in the midlatitude region of the South Atlantic Ocean. The ^{137}Cs transect along 30°S shows a core with higher ^{137}Cs concentrations, accompanied with deep intrusion [73]. This ^{137}Cs core corresponds to the Agulhas eddy, which is formed in the Agulhas Current south of South Africa, injected into the Benguela Current and finally carried away northwestward into the South Atlantic Ocean. The ^{137}Cs transect reveals that the Indian Ocean–derived ^{137}Cs trapped in the eddy is transported into the South Atlantic. This is an indication of surface conveyor belt transport from the western North Pacific Ocean to the South Atlantic Ocean via the Indonesian throughflow and the Indian Ocean on a timescale of several decades.

Future Directions

Even 50 years after the first measurements of ^{3}H, ^{14}C, ^{137}Cs, ^{90}Sr, and ^{239,240}Pu were made in the marine environment, there is not at hand a suitable data set (except for ^{3}H and ^{14}C), which could be used for a complex evaluation of radionuclide tracers in the World Ocean. A first look at the global distribution of anthropogenic radionuclides in the water column has been presented in this entry; however, the data density is still too low to allow a more detailed evaluation.

In the Pacific Ocean, tracer (^{3}H, ^{14}C, ^{137}Cs) studies have revealed decadal-scale transport of global fallout radionuclides, which includes ocean interior transport such as subduction and interocean transport. ^{137}Cs has been found to be the most effective tool to trace motion of labeled waters for more than 50 years because of its longer physical half-life and improvement of analytical techniques. New ^{137}Cs data have been accumulated by the Meteorological Research Institute of Tsukuba and by the University of Kanazawa (including data obtained in the framework of the SHOTS project [72]). The ^{137}Cs data set shows new high-resolution latitudinal and longitudinal sections in the Pacific Ocean, in addition to the latitudinal section (at 165°E) and longitudinal sections, obtained from the SHOTS project (at 32.5°S). Another important feature is that the ^{137}Cs data give a constraint to validate the OGCM. The coupling of the OGCM with the ^{137}Cs observations assists in showing the pathway of tracer transport via subsurface currents, including the cross Equator pathway. However, there is still only a vague figure of the tracer transport in deep Pacific waters using tracers due to the low resolution of tracer contours. Another powerful tracer in the Pacific Ocean is ^{239,240}Pu, which has two major sources of global fallout injected in the midlatitude region (30°N–40°N), and close-in fallout in the western subtropical Pacific. Only surface ^{239,240}Pu data have been obtained till now in the SHOTS project for the South Pacific Ocean along 32.5°S latitude [65, 72, 159]. Plutonium behaves as a biogeochemical tracer in shallower layers because of its particle-reactive properties, whereas in deep layers it may move analogously to conservative tracers due to its low biological activity in deep waters. Denser observation of ^{239,240}Pu will be a key factor in solving biogeochemical processes and deep water transport in the Pacific Ocean.

In the Indian Ocean, the ^{137}Cs concentrations observed in surface waters southwest of Australia decreased by about a factor of 2 when compared with 1976–1978 data, in agreement with the estimated mean residence time of ^{137}Cs (29 ± 3 year) in the Indian Ocean. A different situation is in the case of transuranics, where the observed ^{239,240}Pu concentrations are by about a factor of 2 lower than previously reported. In the case of ^{241}Am they decreased only by ~30%, in spite of a relatively shorter mean residence time of ^{241}Am. A slower decrease in transuranics levels may be due to their additional transport from Marshall Islands testing grounds, and in the case of ^{241}Am also due to its ingrowth from the decay of ^{241}Pu. The water column ^{3}H and ^{14}C data obtained during the WOCE program show reasonable density, and new data sets have been obtained by revisiting WOCE stations during the BEAGLE2003 [160] and GEOTRACES expeditions. In the case of ^{137}Cs, only one transect along 20°S latitude was obtained [74]. For ^{239,240}Pu only surface water data are available [159]. It is hoped therefore that more data will be available soon. The dominant circulation system in

the South Indian Ocean is represented by the Subtropical Gyre, which accumulates radionuclides on a decadal timescale, as confirmed by ^{3}H and ^{137}Cs observations. This fact is of environmental concern and suggests that the protection of the Indian Ocean against contamination from land-based sources must be considered.

In the Atlantic Ocean, the most comprehensive data set has been obtained for ^{137}Cs in surface waters of the eastern North Atlantic. The dominant actions of the North Atlantic and the Norwegian Currents caused a widespread of ^{137}Cs into the Arctic Ocean. By comparing the ^{137}Cs release rates from the Sellafield and La Hague reprocessing plants with the observed ^{137}Cs distribution, it has been possible to derive a transit time for the movement of ^{137}Cs labeled waters from the Irish Sea to the Arctic Ocean and its adjacent seas. For example, 3 years were required to observe the signal in the southern North Sea, 4 years in the central and eastern North Sea, 5 years in the western Baltic Sea, 6 years in the Kara Sea, and 8 years for the Arctic Ocean. For the South Atlantic Ocean, a first data set on the distribution of ^{137}Cs in surface waters along 30°S latitude obtained in the framework of the SHOTS project [73] has clearly shown transport of western North Pacific waters via Indonesian Seas to the South Indian Ocean, and then via Agulhas Current to the southern Atlantic on a timescale of about 20 years, where they become part of the Benguela Current system and the South Atlantic Subtropical Gyre. For $^{239,240}Pu$, only surface water data are available, which also document transport of Pu from the western North Pacific Ocean via Indian Ocean to the South Atlantic Ocean [161].

It is hoped that new developments in radioanalytical techniques based on underground counting systems (e.g., for ^{137}Cs analysis) and on mass spectrometry systems (Accelerator Mass Spectrometry for long-lived radionuclides), which considerably improve the detection sensitivity, and simultaneously permit a smaller sample size, will further stimulate work on radionuclide oceanic tracers. New international projects tracing radionuclides in the World Ocean (e.g., GEOTRACES) will further improve information on oceanic processes, and provide a better understanding of climate change and the protection of the marine environment.

Acknowledgments

Many colleagues contributed significantly to the production of the radionuclide data sets evaluated in the present entry. It is great pleasure to acknowledge long-term collaboration with M. Aoyama (Meteorological Research Institute at Tsukuba), A.J.T. Jull (Arizona University at Tucson), W.E. Kieser (Toronto University), M. Groening (IAEA, Vienna), K. Fiefield (Australian National University of Canberra), U. Morgenstern (Institute of Geological and Nuclear Sciences, Lower Hutt), H. Nies (Bundesamt für Seeschiffahrt und Hydrographie, Hamburg), P. Roos (Risø National Laboratory), B.L.K. Somayajulu (Physical Research Laboratory, Ahmedabad), Z. Top (University of Miami), and former IAEA-MEL directors (M.S. Baxter, H.D. Livingston, R.F.C. Mantoura) and colleagues (J. Gastaud, T. Honda, Y. Ikeuchi, T. Ito, S.-H. Lee, I. Osvath, J. La Rosa, I. Levy, M. Nakano, B. Oregioni, H. Pettersson, O. Togawa, E. Wyse) at Monaco, as well as at the University of Bratislava, and the Meteorological Research Institute of Tsukuba. PPP acknowledges a support provided by the EU Research & Development Operational Program funded by the ERDF (project n. 26240220004).

Bibliography

Primary Literature

1. Livingston HD, Povinec PP (2000) Anthropogenic marine radioactivity. Ocean Coast Manag 43:689–712
2. UNSCEAR (2000) Sources and effects of ionizing radiation. United Nations, New York
3. Livingston HD, Povinec PP (2002) A millennium perspective on the contribution of global fallout radionuclides to ocean science. Health Phys 82:656–668
4. Povinec PP, Hirose K, Honda T, Ito T, Scott ME, Togawa O (2004) Spatial distribution of ^{3}H, ^{90}Sr, ^{137}Cs and $^{239,240}Pu$ in surface waters of the Pacific and Indian Oceans – GLOMARD database. J Environ Radioact 76:113–137
5. Aoyama M, Hirose K, Igarashi Y (2006) Re-construction and updating our understanding on the global weapons tests ^{137}Cs fallout. J Environ Monit 8:431–438
6. Aarkrog A, Baxter MS, Bettencourt AO, Bojanowski R, Bologa A, Charmasson S, Cunha I, Delfanti R, Duran E, Holm E, Jeffree R, Livingston HD, Mahapanyawong S, Nies H, Osvath I, Pingyu L, Povinec PP, Sanchez A, Smith JN, Swift D (1997) A comparison of doses from ^{137}Cs and ^{210}Po in marine food: a major international study. J Environ Radioact 34:69–90

7. Broecker WS, Peng TH, Östlund G (1986) The distribution of tritium in the Ocean. J Geophys Res 91:14331–14344
8. Bowen VT, Noshkin VE, Livingston HD, Volchok HL (1980) Fallout radionuclides in the Pacific Ocean; vertical and horizontal distributions, largely from GEOSECS stations. Earth Planet Sci Lett 49:411–434
9. Ostlund HG, Brescher R (1982) Tritium laboratory data report no. 2. University of Miami, Miami, USA
10. Povinec PP, Livingston HD, Shima S, Aoyama M, Gastaud J, Goroncy I, Hirose K, Huyhn-Ngoc L, Ikeuchi Y, Ito T, La Rosa J, Liong Wee Kwong L, Lee S-H, Moriya H, Mulsow S, Oregioni B, Pettersson H, Togawa O (2003) IAEA'97 expedition to the NW Pacific Ocean – results of oceanographic and radionuclide investigations of the water column. Deep-Sea Res II 50:2607–2638
11. Nyffeler F, Cigna AA, Dahlgaard H, Livingston HD (1996) Radionuclides in the Atlantic Ocean: a survey. In: Guéguéniat P, Germain P, Metivier H (eds) Radionuclides in the Oceans. Les Editions de Physique, IPSN, Les Ulis, pp 177–197
12. Kershaw PJ, McCubbin D, Leonard KS (1999) Continuing contamination of north Atlantic and Arctic waters by Sellafield radionuclides. Sci Total Environ 237/238:119–132
13. Nies H, Harms IH, Karcher MJ, Dethleff D, Bahe C (1999) Anthropogenic radioactivity in the Arctic Ocean – review of the results from the German project. Sci Total Environ 237/238:181–191
14. Povinec PP, Bailly du Bois P, Kershaw PJ, Nies H, Scotto P (2003) Temporal and spatial trends in the distribution of ^{137}Cs in surface waters of Northern European Seas – a record of 40 years of investigations. Deep-Sea Res II 50:2785–2802
15. Sjoblom K-L, Salo A, Bewers JM, Cooper J, Dyer RS, Lynn NM, Mount ME, Povinec PP, Sazykina TG, Schwarz J, Scott EM, Sivintsev YV, Tanner JE, Warden JM, Woodhead D (1999) International Arctic Seas Assessment Project. Sci Total Environ 237/238:153–166
16. Povinec PP, Osvath I, Baxter MS, Harms I, Huynh-Ngoc L, Liong Wee Kwong L, Pettersson HBL (1997) IAEA-MEL's contribution to the investigation of Kara Sea radioactivity and radiological assessment. Mar Pollut Bull 35:235–241
17. Baxter MS, Harms I, Osvath I, Povinec PP, Scott EM (1997) Modelling the potential radiological consequences of radioactive waste dumping in the Kara Sea. J Environ Radioact 39:161–181
18. Osvath I, Povinec PP, Baxter MS (1999) Kara Sea radioactivity assessment. Sci Total Environ 237/238:167–179
19. Hirose K, Amano H, Baxter MS, Chaykovskaya E, Chumichev VB, Hong GH, Isogai K, Kim CK, Kim SK, Miyao T, Morimoto T, Nikitin A, Oda K, Petterson HBL, Povinec PP, Seto Y, Tkalin A, Togawa O, Veletova NK (1999) Anthropogenic radionuclides in seawater in the East Sea/Japan Sea: results of the first-stage Japanese–Korean–Russian expedition. J Environ Radioact 43: 1–13
20. Ikeuchi Y, Amano H, Aoyama M, Berezhnov VI, Chaykovskaya E, Chumichev VB, Chung CS, Gastaud J, Hirose K, Hong GH, Kim CK, Kim SH, Miyao T, Morimoto T, Nikitin A, Oda K, Pettersson HBL, Povinec PP, Tkalin A, Togawa O, Veletova NK (1999) Anthropogenic radionuclides in seawater of the far Eastern Seas. Sci Total Environ 237/238:203–212
21. Pettersson HBL, Amano H, Berezhnov VI, Chaykovskaya E, Chumichev VB, Chung CS, Gastaud J, Hirose K, Hong GH, Kim CK, Kim SH, Lee SH, Morimoto T, Nikitin A, Oda K, Povinec PP, Suzuki E, Tkalin A, Togawa O, Veletova NK, Volkov Y, Yoshida Y (1999) Anthropogenic radionuclides in sediments in the NW Pacific Ocean and its Marginal Seas. Results of the 1994–1995 Japanese–Korean–Russian expeditions. Sci Total Environ 237/238:213–224
22. Povinec PP, Hirose K, Honda T, Ito T, Marian Scott E, Togawa O (2004) Spatial distribution of ^{3}H, ^{90}Sr, ^{137}Cs and ^{239,240}Pu in surface waters of the Pacific and Indian Oceans – GLOMARD database. J Environ Radioact 76:113–137
23. Povinec PP, Scotto P, Osvath I, Ramadan H (2006) The marine information system. In: Povinec PP, Sanchez-Cabeza JA (eds) Isotopes in environmental studies. IAEA, Vienna, pp 68–69
24. Aoyama M, Hirose K (2004) Artificial radionuclides database in the Pacific Ocean: HAM database. Sci World J 4:200–215
25. Povinec PP, Comanducci JF, Levy-Palomo I (2004) IAEA-MEL's underground counting laboratory in Monaco – background characteristics of HPGe detectors with anti-cosmic shielding. Appl Radiat Isot 61:85–93
26. Povinec PP, Comanducci JF, Levy-Palomo I (2005) IAEA-MEL's underground counting laboratory (CAVE) for the analysis of radionuclides in the environment at very low-levels. J Radioanal Nucl Chem 263:441–445
27. Povinec PP, Comanducci JF, Levy-Palomo I (2006) IAEA-MEL's underground counting laboratory – the design and main characteristics. In: Povinec PP, Sanchez-Cabeza JA (eds) Radionuclides in the environment. Elsevier, Amsterdam, pp 538–553
28. Hirose K, Aoyama M, Igarashi Y, Komura K (2005) Extremely low background measurements of ^{137}Cs in seawater samples using an underground facility (Ogoya). J Radioanal Nucl Chem 263:349–353
29. Hirose K, Aoyama M, Igarashi Y, Komura K (2008) Improvement of ^{137}Cs analysis in small volume seawater samples using the Ogoya underground facility. J Radioanal Nucl Chem 276:795–798
30. Tuniz C, Bird JR, Fink D, Herzog GF (1998) Accelerator mass spectrometry: ultrasensitive analysis for global science. CRC, Boca Raton
31. Kutschera W (2005) Progress in isotope analysis at ultra-trace level by AMS. Int J Mass Spectrom 242:145–160
32. Fifield LK (2008) Accelerator mass spectrometry of long-lived heavy radionuclides. In: Povinec PP (ed) Analysis of environmental radionuclides. Elsevier, Amsterdam, pp 263–295
33. Jull AJT, Burr GS, Beck JW, Hodgins GWL, Biddulph DL, McHargue LR, Lange TE (2008) Accelerator mass spectrometry of long-lived light radionuclides. In: Povinec PP (ed) Analysis of environmental radionuclides. Elsevier, Amsterdam, pp 240–262
34. Lee S-H, Gastaud J, La Rosa JJ, Liong Wee Kwong L, Povinec PP, Wyse E, Fifield LK, Hausladen PA, De Tada LM, Santos GM (2001) Analysis of plutonium isotopes in marine samples by radiometric, ICP-MS and AMS techniques. J Radioanal Nucl Chem 248(3):757–764

35. Wyse EJ, Lee SH, La Rosa J, Povinec PP, de Mora SJ (2001) ICP-sector field mass spectrometry analysis of plutonium isotopes: recognizing and resolving potential interferences. J Anal At Spectrom 16:1107–1111
36. Povinec PP, Betti M, Jull AJT, Vojtyla P (2008) New isotope technologies for environmental physics. Acta Phys Slov 58:1–154
37. Roos P (2008) Analysis of radionuclides using ICP-MS. In: Povinec PP (ed) Analysis of environmental radionuclides. Elsevier, Amsterdam, pp 295–330
38. Buesseler KO (1993) Thermal ionization mass spectrometry. In: Development and evaluation of alternative radioanalytical methods, including mass spectrometry for marine materials. IAEA-TECDOC-683. IAEA, Vienna, pp 45–52
39. Erdmann N, Passler G, Trautmann N, Wendt K (2008) Resonance ionization mass spectrometry for trace analysis of long-lived radionuclides. In: Povinec PP (ed) Analysis of environmental radionuclides. Elsevier, Amsterdam, pp 331–354
40. Weiss W, Roether W (1980) The rates of tritium input into the oceans. Earth Planet Sci Lett 49:435–446
41. Roether W (1994) Studying thermohaline circulation of the ocean by means of tracer data. In: Malanotte-Rizzoli P, Robinson AR (eds) Ocean processes in climate dynamics: global and Mediterranean examples. Kluwer, Dordrecht, pp 157–171
42. Stuiver M, Ostlund HG (1983) GEOSECS Indian Ocean and Mediterranean radiocarbon. Radiocarbon 25:1–29
43. Bard E, Arnold M, Toggweiler JR, Maurice P, Duplessy JC (1989) Bomb ^{14}C in the Indian Ocean measured by accelerator mass spectrometry: oceanographic implications. Radiocarbon 31:510–522
44. Broecker WS (1991) The great ocean conveyor. Oceanography 4:79–89
45. Broecker WS, Bonebakker ER, Rocco GG (1966) The vertical distribution of cesium 137 and strontium 90 in the oceans. J Geophys Res 71:1999–2003
46. Aoyama M, Hirose K (2003) Temporal variation of ^{137}Cs water column inventory in the North Pacific since the 1960s. J Environ Radioact 69:107–117
47. Raisbeck GM, Yiou F (1999) ^{129}I in the oceans: origins and applications. Sci Total Environ 237/238:31–42
48. Livingston HD, Povinec PP, Ito T, Togawa O (2001) The behaviour of plutonium in the Pacific Ocean. In: Kudo A (ed) Plutonium in the environment. Elsevier, Amsterdam, pp 267–292
49. Baxter MS, Fowler SW, Povinec PP (1995) Observations of plutonium in the oceans. Appl Radiat Isot 46:1213–1223
50. Hong GH, Baskaran M, Povinec PP (2004) Artificial radionuclides in the western North Pacific: a review. In: Shiyomi M (ed) Global environmental change in the ocean and on land. Terrapub, Tokyo, pp 147–172
51. Key RM (1996) WOCE Pacific Ocean Radiocarbon Program. Radiocarbon 38:415–423
52. Aoyama M, Hirose K, Miyao T, Igarashi Y, Povinec PP (2001) Temporal variation of ^{137}Cs inventory in the western North Pacific. J Radioanal Nucl Chem 248:785–787
53. Povinec PP, Woodhead D, Blowers P, Bonfield R, Cooper M, Chen QJ, Dahlgaard H, Dovlete C, Fox V, Froehlich K, Gastaud J, Gröning M, Hamilton T, Ikeuchi Y, Kanisch G, Krüger A, Liong Wee Kwong L, Matthews M, Morgenstern U, Mulsow S, Pettersson HBL, Smedley P, Taylor B, Taylor C, Tinker R (1999) Marine radioactivity assessment of Mururoa and Fangataufa Atolls. Sci Total Environ 237/238:249–267
54. Miyake Y, Saruhashi K, Sugimura Y, Kanazawa T, Hirose K (1988) Content of ^{137}Cs, plutonium and americium isotopes in the Southern Indian Ocean waters. Pap Meteorol Geophys 39:95–113
55. Povinec PP, Delfanti R, Gastaud J, La Rosa J, Morgenstern U, Oregioni B, Pham MK, Salvi S, Top Z (2003) Anthropogenic radionuclides in the Indian Ocean surface waters – the Indian Ocean transect 1998. Deep-Sea Res II 50:2751–2760
56. Mulsow S, Povinec PP, Somayajulu BLK, Oregioni B, Liong Wee Kwong L, Gastaud J, Top Z, Morgenstern U (2003) Temporal (3H) and spatial variations of ^{90}Sr, ^{239,240}Pu and ^{241}Am in the Arabian Sea: GEOSECS stations revisited. Deep-Sea Res II 50:2761–2776
57. Bhushan R, Dutta K, Mulsow S, Povinec PP, Somayajulu BLK (2003) Distribution of natural and man-made radionuclides during the reoccupation of GEOSECS stations 413 and 416 in the Arabian Sea: temporal changes. Deep-Sea Res II 50:2777–2784
58. Lee SH, Povinec PP, Gastaud J, Oregioni B, Coppola L, Jeandel C (2009) Radionuclides as tracers of water fronts in the South Indian Ocean – ANTARES IV results. J Oceanogr 65:397–406
59. Holm E, Roos P, Persson RBR, Bojanowski R, Aarkrog A, Nielsen SP, Livingston HD (1992) Radiocaesium and plutonium in Atlantic surface waters from 73°N to 72°S. In: Kershaw PJ, Woodhead DS (eds) Radionuclides in the study of marine processes. Elsevier Applied Science, London, pp 3–11
60. Kershaw PJ, Baxter AJ (1995) The transfer of reprocessing waste from northwest Europe to the Arctic. Deep-Sea Res II 42:1413–1448
61. Livingston HD, Kupferman SL, Bowen VT, Moore RM (1984) Vertical profile of artificial radionuclide concentrations in the central Arctic Ocean. Geochim Cosmochim Acta 48:2195–2203
62. IAEA (2005) Worldwide Marine Radioactivity Studies (WOMARS): radionuclide levels in oceans and seas. IAEA-TECDOC-1439. IAEA, Vienna
63. Moon D-S, Hong G-H, Kim YI, Baskaran M, Chung CS, Kim SH, Lee H-J, Lee S-H, Povinec PP (2003) Accumulation of anthropogenic and natural radionuclides in bottom sediments of the Northwest Pacific Ocean. Deep-Sea Res II 50: 2649–2674
64. Hirose K, Aoyama M, Povinec PP (2003) Concentration of particulate plutonium in surface and deep-water samples collected during the IAEA'97 expedition. Deep-Sea Res II 50: 2639–2647
65. Hirose K, Aoyama M, Fukasawa M, Kim CS, Komura K, Povinec PP, Sanchez-Cabeza JA (2007) Plutonium and ^{137}Cs in surface water of the South Pacific Ocean. Sci Total Environ 381:243–255
66. Lee S-H, Gastaud J, Povinec PP, Hong G-H, Kim S-H, Chung C-S, Lee K-W, Pettersson HBL (2003) Distribution of plutonium and americium in the marginal seas of the northwest Pacific Ocean. Deep-Sea Res II 50:2727–2750

67. Lee S-H, Gastaud J, Povinec PP, Hong G-H, Kim S-H, Chung C-S, Lee K-W, Pettersson HBL (2003) Distribution of plutonium and americium in the marginal seas of the northwest Pacific Ocean. Deep-Sea Res II 50:2727–2750
68. Ito T, Povinec PP, Togawa O, Hirose K (2003) Temporal and spatial variations of anthropogenic radionuclides in Japan Sea waters. Deep-Sea Res II 50:2701–2711
69. Baxter MS, Ballestra S et al (1995) Marine radioactivity studies in the vicinity of sites with potential radionuclide releases. In: Impact of radioactive releases. IAEA, Vienna, pp 125–142
70. Uchida H, Fukasawa M (eds) (2005) WHP P6, A10, I3/I4 Revisit Data Book Blue Earth Global Expedition 2003, vol 1, 2. Aiwa, Tokyo, www.jamstec.org
71. Uchida H, Fukasawa M (eds) (2007) WHP P6, A10, I3/I4 Revisit Data Book Blue Earth Global Expedition 2003, vol 3. Aiwa, Tokyo, www.jamstec.org
72. Aoyama M, Fukasawa M, Hirose K, Hamajima M, Kawano T, Povinec PP, Sanchez-Cabeza J-A. ^{137}Cs in the South Pacific Ocean based on the results of BEAGLE2003 cruises – cross Equator transport of ^{137}Cs from North Pacific Ocean to South Pacific Ocean. Prog Oceanogr, in print for publication
73. Sanchez-Cabeza JA, Levy I, Gastaud J, Eriksson M, Osvath I, Aoyama M, Povinec PP, Komura K. Transport of North Pacific ^{137}Cs labeled waters to the south-eastern Atlantic Ocean. Prog Oceanogr, in print
74. Povinec PP, Aoyama M, Fukusawa M, Hirose K, Komura K, Sanchez-Cabeza J-A, Gastaud J, Ješkovský M, Levy-Palomo I, Sýkora I (2008) Profiles of ^{137}Cs in South Indian Ocean water along the 20°S latitude – an evidence for accumulation of pollutants in the subtropical gyre. Prog Oceanogr, in print
75. Fine RA, Lukas R et al (1994) The equatorial Pacific: a water mass crossroads. J Geophys Res 99:25063–25080
76. Cannon GA (1966) Tropical waters in the western Pacific Ocean, August–September 1957. Deep-Sea Res 13:1139–1148
77. Tsuchiya M (1968) Upper waters of the intertropical Pacific Ocean. Johns Hopkins Oceanographic Study 4:50
78. Suga T, Hanawa K, Toba Y (1989) Sub-tropical mode water in the 137°E section. J Phys Oceanogr 19:1605–1618
79. Suga T, Takei Y, Hanawa K (1997) Thermostat distribution in the North Pacific subtropical gyre: the general mode water and the subtropical mode water. J Phys Oceanogr 27: 140–152
80. Reid JL (1973) The shallow salinity minima of the Pacific Ocean. Deep-Sea Res 20:51–68
81. Yuan X, Talley LD (1992) Shallow salinity minima in the North Pacific. J Phys Oceanogr 22:1302–1316
82. Tomczak M, Godfrey JS (1994) Regional oceanography: an introduction. Pergamon, New York, 422 pp
83. Gordon AL, Susanto RD, Vranes K (2003) Cool Indonesian throughflow as a consequence of restricted surface layer flow. Nature 425:824–828
84. Park YH, Pollard RT, Pollard RT, Read JF, Leboucher V (2002) A quasi-synoptic view of the frontal circulation in the Crozet Basin during the ANTARES-4 cruise. Deep-Sea Res II 49: 1823–1842
85. Povinec PP, Breier R, Coppola L, Groening M, Jeandel C, Jull AJT, Kieser WE, Lee S-H, Liong Wee Kwong L, Morgenstern U, Park Y-H, Top Z (2011) Tracing of water masses using a multi isotope approach in the southern Indian Ocean. Earth Planet Sci Lett, in print
86. Srocker TF, Wright DG (1991) Rapid transitions of the ocean's deep circulation induced by changes in surface water fluxes. Nature 351:729–732
87. Robinson WL, Noshkin VE (1999) Radionuclide characterization and associated dose from long-lived radionuclides in close-in fallout delivered to the marine environment at Bikini and Enewetak Atolls. Sci Total Environ 237/238:311–327
88. Buesseler KO, Sholkovitz ER (1987) The geochemistry of fallout plutonium in the North Atlantic: II. ^{240}Pu/^{239}Pu ratios and their significance. Geochim Cosmochim Acta 51:2623–2637
89. Volchok HL, Bowen VT, Folsom TR, Broecker WS, Schuert EA, Bien GS (1971) Oceanic distributions of radionuclides from nuclear explosions. In: Radioactivity in the marine environment. National Academy, Washington, DC, pp 42–89
90. Livingston HD, Jenkins WJ (1982) Radioactive tracers in the sea. In: The future of oceanography. Springer, New York, pp 163–191
91. Craig H, Turekian KK (1980) The GEOSECS program: 1976–1979. Earth Planet Sci Lett 49:263–265
92. Kupferman SL, Livingston HD, Bowen VT (1979) A mass balance for ^{137}Cs and ^{90}Sr in the North Atlantic Ocean. J Mar Res 37:157–199
93. Schlosser P, Bullister JL, Fine R, Jenkins WJ, Key R, Lupton J, Roether W, Smethie WM (2001) Transportation and age of water masses. In: Siedler GJ, Church J, Gould J (eds) Ocean circulation and climate. Academic, London, pp 431–452
94. Nagaya Y, Nakamura K (1984) ^{239,240}Pu, ^{137}Cs and ^{90}Sr in the central Pacific. J Oceanogr Soc Jpn 40:416–424
95. Nagaya Y, Nakamura K (1987) Artificial radionuclides in the western Northwest Pacific (II): ^{137}Cs and ^{239,240}Pu inventories in water and sediment columns observed from 1980 to 1986. J Oceanogr Soc Jpn 43:345–355
96. Noshkin VE, Bowen VT (1973) Concentrations and distributions of long-lived fallout radionuclides in open ocean sediments. In: Radioactive contamination of the marine environment. IAEA symposium SM-158/45. IAEA, Vienna, pp 671–686
97. Noshkin VE, Robison WL, Wong KM, Eagle RJ (1998) Behavior of plutonium isotopes in the marine environment of Enewetak Atoll. J Radioanal Nucl Chem 234:243
98. National Academy of Sciences (1971) Radioactivity in the marine environment. National Academy of Sciences, Washington, DC. ISBN 0-309-01865-X
99. Patel B, Patel S, Pawar S (1978) Desorption of radioactivity from nearshore sediment. Est Coastal Mar Sci 7:49–58
100. Baxter MS, Ballestra S, Gastaud J, Hamilton TF, Harms I, Huynh-Ngoc L, Osvath I, Parsi P, Pettersson H, Povinec PP, Sanchez A (1996) Marine radioactivity studies in the vicinity of sites with potential radionuclide releases. In: Proceedings of the environmental impact of radionuclide releases. IAEA, Vienna, pp 125–141

101. CEC (1994) The radiological exposure of the population of the European community from radioactivity in the Mediterranean Sea – Project "MARINA-MED". Report MARINA-MED. In: Cigna A (ed) European Commission Report XI-094-93. Brussels
102. Mackenzie AB (2000) Environmental radioactivity: experience from the 20th century – trends and issues for the 21st century. Sci Total Environ 249:313–329
103. Mitchell PI, Condren ON, Leon Vintro L, McMahon CA (1999) Trends in plutonium, americium and radiocaesium accumulation and long-term bioavailability in the western Irish Sea sediment. J Environ Radioact 44:221–250
104. Guéguéniat P, Kershaw P, Herrmann J, Bailly du Bois P (1997) New estimation of La Hague contribution to the artificial radioactivity of Norwegian waters (1992–1995) and Barents Sea (1992–1997). Sci Total Environ 202:249–266
105. Bailly du Bois P, Salomon JC, Guéguéniat P, Gandon R (1995) A quantitative estimate of English Channel water fluxes into the North Sea from 1978 to 1992 based on radiotracer distribution. J Mar Syst 6:457–481
106. WHO (1989) Health hazards from radiocaesium following the Chernobyl nuclear accident. J Environ Radioact 10:257–295
107. HELCOM (1995) Radioactivity in the Baltic Sea 1984–1991. Baltic Sea environment proceedings no. 61. Helsinki Commission, Hamburg. ISSN: 0357-2994
108. Povinec PP, Oregioni B, Jull AJT, Kieser WE, Zhao X-L (2000) AMS measurements of ^{14}C and ^{129}I in seawater around radioactive waste dump sites. Nucl Instrum Meth Phys Res B172:672–678
109. Povinec PP, Badie C, Baeza A, Barci-Funel G, Bergan TD, Bojanowski R, Burnett W, Eikenberg J, Fifield LK, Serradell V, Gastaud J, Goroncy I, Herrmann J, Hotchkis MAC, Ikaheimonen TK, Jakobson E, Kalimbadjan J, La Rosa JJ, Lee S-H, Liong Wee Kwong L, Lueng WM, Nielsen SP, Noureddine A, Pham MK, Rohou J-N, Sanchez-Cabeza A, Suomela J, Suplinska M, Wyse E (2002) Certified reference material for radionuclides in seawater IAEA-381 (Irish Sea Water). J Radioanal Nucl Chem 251:369–374
110. Povinec PP (2004) Developments in analytical technologies for marine radioactivity studies. In: Livingston HD (ed) Marine radioactivity. Elsevier, Amsterdam, pp 237–294
111. La Rosa J, Burnett W, Lee S-H, Levy I, Gastaud J, Povinec PP (2001) Separation of actinides, cesium and strontium from marine samples using extraction chromatography and sorbents. J Radioanal Nucl Chem 248:765–770
112. Lee SH, Gastaud J, La Rosa JJ, Liong Wee Kwong L, Povinec PP (2001) Analysis of plutonium isotopes in marine samples by radiometrics, ICPMS and AMS techniques. J Radioanal Nucl Chem 248:757–764
113. Povinec PP, La Rosa JJ, Lee SH, Mulsow S, Osvath I, Wyse E (2001) Recent developments in radiometric and mass spectrometry methods for marine radioactivity measurements. J Radioanal Nucl Chem 248:713–718
114. Povinec PP (2005) Ultra-sensitive radionuclide spectrometry: radiometrics and mass spectrometry synergy. J Radioanal Nucl Chem 263:413–417
115. Hirose K, Aoyama M, Igarashi Y, Komura K (2005) Extremely low background measurements of ^{137}Cs in seawater samples using an underground facility (Ogoya). J Radioanal Nucl Chem 263:349–353
116. Aoyama M, Hirose K (2008) Radiometric determination of anthropogenic radionuclides in seawater. In: Povinec PP (ed) Analysis of environmental radionuclides. Elsevier, Amsterdam, pp 137–162
117. Povinec PP (2008) Low-level gamma-ray spectrometry for environmental samples. J Radioanal Nucl Chem 276:771–777
118. Levy I, Aoyama M, Hirose K, Povinec PP, Sanchez-Cabeza JA, Azemard S, Eriksson M, Gastaud J, Hamajima Y, Kim CS, Komura K, Osvath I, Roos P, Yim SA. Marine anthropogenic radiotracers in the Southern Hemisphere: new sampling and analytical strategies. Prog Oceanogr, in print
119. Broecker WS (1966) Radioisotopes and the rate of mixing across the main thermocline of the ocean. J Geophys Res 71:5827–5836
120. Rooth CG, Ostlund HG (1972) Penetration of tritium into the Atlantic thermocline. Deep-Sea Res 19:481–492
121. Schlosser P, Bayer R, Boenisch G, Cooper LW, Ekwurzel B, Jenkins WJ, Khatiwala S, Pfirman S, Smethie WM (1999) Pathways and residence times of dissolved pollutants in the ocean derived from transient tracers and stable isotopes. Sci Total Environ 237/238:15–30
122. Jenkins WJ, Clarke WB (1976) The distribution of ^{3}He in the western Atlantic Ocean. Deep-Sea Res 23:481–494
123. Jenkins WJ (1988) The use of anthropogenic tritium and helium-3 to study subtropical gyre ventilation and circulation. Philos Trans R Soc Lond A325:43–61
124. Folsom TR, Grismore R (1970) Survey of Oceanic fallout traces using cesium absorbers. IEEE Trans Nucl Sci 17:202–212
125. Inomata Y, Aoyama M, Hirose K (2009) Analysis of 50-y record of surface ^{137}Cs concentrations in the global ocean using the HAM-global database. J Environ Monit 11:116–125
126. Hirose K, Aoyama M (2003) Analysis of ^{137}Cs and $^{239,240}Pu$ concentrations in surface waters of the Pacific Ocean. Deep-Sea Res II 50:2675–2700
127. Fine RA, Peterson WH, Ostlund HG (1987) The penetration of tritium into the tropical Pacific. J Phys Oceanogr 17:553–564
128. Hirose K, Aoyama M et al (2006) Plutonium isotopes in seawater of the North Pacific: effect of close-in fallout. In: Povinec PP, Sanchez-Cabeza JA (eds) Radionuclides in the environment, pp 67–82
129. Schlosser P, Bullister JL et al (2001) Transformation and age of water masses. In: Siedler G et al (eds) Ocean circulation & climate, observing and modelling the global ocean, vol 77, International geophysics series. Academic, New York, pp 431–452
130. Aoyama M, Hirose K et al (2008) Water masses labeled with global fallout ^{137}Cs formed by subduction in the North Pacific. Geophys Res Lett 35:L01604
131. Nakano H, Motoi T et al (2010) Analysis of ^{137}Cs concentration in the Pacific using a Lagrangian approach. J Geophys Res (in press)

132. Hautala S, Roemmich DH (1998) Subtropical mode water in Northeast Pacific Basin. J Geophys Res 103:13055–13066
133. Lupton JE (1998) Hydrothermal helium plumes in the Pacific Ocean. J Geophys Res 103:15853–15868
134. Lupton JE (1996) A far-field helium plume from Loihi Seamount. Science 272:976–979
135. Reid JL (1997) On the total geotrophic circulation of the Pacific: flow patterns, tracers, and transports. Prog Oceanogr 39:263–352
136. Stuiver M, Quay PD, Ostlund HG (1983) Abyssal water carbon-14 distribution and the age of the world oceans. Science 219:849–851
137. Key RM, Kozyr A, Sabine CL, Lee K, Wanninkhof R, Bullister JL, Feely RA, Millero FJ, Mordy C, Peng T-H (2004) A global ocean carbon climatology: Results from Global Data Analysis Project (GLODAP), Global Biogeochem Cycles, 18:GB4031. doi:10.1029/2004GB002247
138. Mittelstaedt E, Osvath I, Povinec PP, Togawa O, Scott EM (1999) Transport of radionuclides from the Mururoa and Fangataufa Atolls through the marine environment. Sci Total Environ 237/238:301–309
139. Hirose K, Aoyama M, Kim CS, Kim CK, Povinec PP (2006) Plutonium isotopes in seawater of the North Pacific: effect of close-in fallout. In: Povinec PP, Sanchez-Cabeza JA (eds) Radionuclides in the environment, IAEA, Vienna, pp 67–82
140. Aarkrog A (2003) Input of anthropogenic radionuclides into the World Ocean. Deep-Sea Res II 50:2597–2606
141. Holm E, Roos P, Josefsson D, Persson B (1996) Radioactivity from the North Pole to the Antarctic. In: Guéguégnat P, Germain P, Métivier H (eds) Radionuclides in the oceans, inputs and inventories. Les Editions de Physique, Les Ulis, pp 59–74
142. Bourlat Y, Millies-Lacroix J-C, Le Petit G, Bourguignon J (1996) ^{90}Sr, ^{137}Cs and $^{239+240}$Pu in world ocean water samples collected from 1992 to 1994. In: Guéguégnat P, Germain P, Métivier H (eds) Radionuclides in the oceans, inputs and inventories. Les Editions de Physique, Les Ulis, pp 75–93
143. Livingston HD, Povinec PP, Ito T, Togawa O (2001) The behaviour of plutonium in the Pacific Ocean. In: Kudo A (ed) Pu in the environment. Elsevier, Amsterdam, pp 267–292
144. Lee S-H, Povinec PP, Wyse E, Pham MK, Hong G-H, Chung CS, Kim S-H, Lee HJ (2005) Distribution and inventories of ^{90}Sr, ^{137}Cs, ^{241}Am and Pu isotopes in sediments of the Northwest Pacific Ocean. Mar Geol 216:249–263
145. Povinec PP, Lee SH, Liong Wee Kwong L, Oregioni B, Jull AJT, Kieser WE, Morgenstern U, Top Z (2010) Tritium, radiocarbon, ^{90}Sr and ^{129}I in the Pacific and Indian Oceans. Nucl Instrum Meth Phys Res B268:1214–1218
146. Yamada M, Zheng J, Wang Z-L (2006) ^{137}Cs, $^{239+240}$Pu and ^{240}Pu/^{239}Pu atom ratios in the surface waters of the western North Pacific Ocean, eastern Indian Ocean and their adjacent seas. Sci Total Environ 366:242–252
147. Hirose K, Aoyama M, Povinec PP (2009) ^{239,240}Pu/^{137}Cs ratios in the water column of the North Pacific: a proxy of biochemical processes. J Environ Radioact 100:258–262
148. Coppola L, Roy-Barman M, Mulsow S, Povinec PP, Jeandel C (2005) Low particulate organic carbon export in the frontal zone of the Southern Ocean (Indian sector) revealed by ^{234}Th. Deep-Sea Res I 52:51–68
149. Mork M (1981) Circulation phenomena and frontal dynamics of the Norwegian coastal current. Philos Trans R Soc Lond Ser A 302:635–647
150. Livingston HD (1988) The use of Cs and Sr isotopes as tracers in the Arctic Mediterranean Seas. Philos Trans R Soc Lond Ser A 325:161–176
151. Kautsky H (1998) Determination of distribution processes, transport routes and transport times in the North Sea and the Northern North Atlantic using artificial radionuclides as tracers. In: Guary JC, Guéguéniat P, Pentreath RJ (eds) Radionuclides: a tool for oceanography. Elsevier, Amsterdam, pp 271–280
152. Dahlgaard H (1993) Where does all the Cs and Sr in Greenland waters come from? In: Proceedings of the environmental radioactivity in the Arctic and Antarctic. NRPA, Osteras, pp 121–124
153. Edmonds HN, Smith JN, Kilius LR, Livingston HD, Edmond JM (1998) ^{129}I in archived seawater samples: source functions and tracer comparisons. Deep-Sea Res I 45:1111–1125
154. Brown JE, Isojpe M, Kolstad AK, Lind B, Rudjord AL, Stand P (2002) Temporal trends for ^{99}Tc in Norwegian coastal environments and spatial distribution in the Barents Sea. J Environ Radioact 60:49–60
155. Karcher MJ, Gerland S, Harms I, Isojpe M, Heldal H, Kershaw PJ, Sickel M (2004) The dispersion of technecium-99 in the Nordic Seas and the Arctic Ocean: a comparison of model results and observation. J Environ Radioact 74:185–198
156. Smith JN, Ellis KM, Kilius LR (1998) ^{129}I and ^{137}Cs tracer measurements in the Arctic Ocean. Deep-Sea Res I 45(6):959–984
157. Smith JN, Ellis KM, Boyd TM (1999) Circulation features in the Central Arctic Ocean revealed by nuclear fuel reprocessing tracers from SCICEX 95 and 96. J Geophys Res 104(C12): 29,663–29,677
158. Smith JN, Jones EP, Moran SB, Smethie WM Jr, Kieser WE (2005) ^{129}I/CFC-11 transit times for Denmark Strait overflow water in the Labrador and Irminger Seas. J Geophys Res 110: C05006. doi:10.1029/2004JC002516
159. Hirose K, Kim CS, Yim SA, Aoyama M, Fukasawa M, Komura K, Povinec PP, Sanchez-Cabeza J-A. Vertical profiles of plutonium in the central South Pacific. Prog Oceanogr, in print
160. Kumamoto Y, Murata A, Watanabe S, Fukasawa M. Temporal and spatial variations in bomb-produced radiocarbon along BEAGLE2003 lines – revisits of WHP P06, A10 and I03/I04 in the Southern Hemisphere oceans. Prog Oceanogr, in print
161. Gastaud J, Povinec PP, Aoyama M, Hirose K, Sanchez-Cabeza JA, Levy I, Roos P, Eriksson M, Bosc E. Long-term scavenging of Pu from surface waters of the Southern Hemisphere Oceans. Prog Oceanogr, in print

Books and Reviews

Aoyama M, Povinec P, Sanchez-Cabeza JA (eds) (2010) South Hemisphere ocean tracer studies. Prog Oceanogr, submitted (special issue)

Broecker WS, Peng WH (1982) Tracers in the sea. Eldigo, New York, 690 pp
IAEA (2005) Worldwide Marine Radioactivity Studies (WOMARS): radionuclide levels in oceans and seas. IAEA-TECDOC-1439. IAEA, Vienna
Livingston HD (ed) (2004) Marine radioactivity. Elsevier, Amsterdam, 301 pp
Povinec P (ed) (1986) Low-level counting. Proceedings of low radioactivities '85. Nucl Instrum Meth Phys Res B17:377–588
Povinec P (ed) (1987) Low-level counting and spectrometry. VEDA, Bratislava, 308 pp
Povinec P (ed) (1991) Rare nuclear decays and fundamental physics. J Phys G 17(special issue):543
Povinec P (1992) Rare nuclear processes. World Scientific, Singapore, 441 pp
Povinec PP (ed) (1999) Marine environment – understanding and protecting for the future. Sci Total Environ 237/238(special issue):1–526
Povinec PP (ed) (2008) Analysis of environmental radionuclides. Elsevier, Amsterdam
Povinec PP, Sanchez-Cabeza JA (eds) (2006) Isotopes in environmental studies. IAEA, Vienna, 710 pp
Povinec PP, Sanchez-Cabeza JA (eds) (2006) Radionuclides in the environment. Elsevier, IAEA, Vienna, 646 pp
Povinec PP, Betti M, Jull AJT, Vojtyla P (2008) New isotope technologies for environmental physics. Acta Phys Slov 58:1–154
Rahmstorf S (2006) Thermohaline ocean circulation. In: Elias SA (ed) Encyclopedia of quaternary sciences. Elsevier, Amsterdam
Tomczak M, Godfrey JS (1994) Regional oceanography: an introduction. Pergamon, New York, 422 pp
Tuniz C, Bird JR, Fink D, Herzog GF (1998) Accelerator mass spectrometry: ultrasensitive analysis for global science. CRC, Boca Raton, 371 pp
UNSCEAR (1993) Sources and effects of ionizing radiation. United Nations, New York, 922 pp
UNSCEAR (2000) Sources and effects of ionizing radiation. United Nations, New York

Rainwater Harvesting

Sangho Lee, Reeho Kim
Department of Water Resources and Environmental Research, Korea Institute of Construction Technology, Goyang-Si, Gyeonggi-Do, Republic of Korea

Article Outline

Glossary
Definition of the Subject
Introduction
Describing Rainwater Harvesting
Technologies for Rainwater Harvesting
Future Directions
Bibliography

Glossary

Catchment A surface that collects rainwater, which is to be used in a beneficial manner.

Cistern Storage tank.

Detention Detention systems provide a temporary storage of runoff for subsequent release.

First flush Initial surface runoff of a rainfall.

First flush effect Rapid changes in water quality (pollutant concentration or load) that occur in the initial stage of a rainfall.

Health risk assessment An evaluation of the potential for adverse health effects to occur as a result of actual or potential exposures to chemicals.

Hydrological cycle Hydrological cycle (also know as Hydrologic cycle or water cycle) Continuous movement of water on, above, and below the surface of the Earth.

Irrigation Supply of land or crops with water.

Nonpotable water Water intended for uses other than potable purposes.

Nonpoint source pollution Pollution whose sources cannot be pinpointed but rather is washed from the land surface in a diffuse manner by stormwater runoff.

Pathogens Disease-causing organisms capable of inflicting damage on a host it infects.

Rainwater harvesting Direct collection of precipitation falling on the roof or onto the ground without passing through the stage of surface runoff on land. The collected rainwater is mostly used for non-potable but may be used for potable use after proper treatment steps.

Reclaimed water Municipal wastewater that has gone through various treatment processes to meet specific water quality criteria with the intent of being used in a beneficial manner.

Potable water Water deemed safe for human consumption, food preparation, and bathing.

Rainwater Water that has fallen as rain

Rainwater storage tank A tank that stores collected rainwater prior to its beneficial use.

Retention Retention systems retain stormwater without subsequent surface discharge.

Rooftop The outer surface of a roof.

Stormwater Precipitation that is discharged across the land surface or through conveyances to one or more waterways and that may include storm water runoff, snow melt runoff, and surface runoff and drainage.

Surface runoff Water flow that occurs when soil is infiltrated to full capacity and excess water from rain, snowmelt, or other sources flows over the land.

Sustainability The principle of optimizing the benefits of a present without compromising the ability of future generations to meet their own needs.

Trace organics Organic compounds detected at very low (minute) levels by the use of sophisticated instrumentation capable of measuring concentrations in the range of 10^{-12}–10^{-3} mg/L.

Wastewater Used water discharged from homes, business, cities, industry, and agriculture. Various synonymous uses such as municipal wastewater (sewage), industrial wastewater, and stormwater.

Water reuse The use of treated wastewater for a beneficial use, such as agricultural irrigation and industrial cooling. A process or a system for producing renewable water source, which is to be used in human activity such as agriculture, shower, flushing, and drinking, from wastewater treatment.

Definition of the Subject

Rainwater harvesting is a term covering all those techniques whereby rain is captured and used close to where it first reaches the earth [1, 2]. It includes the collecting, storing, and use of rainwater as non-potable and potable water from rooftop and other impermeable surface. The term has been also applied to arrangements to cause rainfall to infiltrate into the ground rather than run off its surface, to forms of flood control, to the construction of small reservoirs to capture runoff water so that it can be used for irrigation, and to the treatment of runoff from road and pavement surface to control nonpoint source pollutions.

Rainwater harvesting is regarded as one of the best available ways for sustainable water supply and also effective to recover natural hydrological cycles in urban area [3]. Rainwater harvesting systems provide a source of ongoing water supply and reduce reliance on other water sources [4, 5]. Moreover, rainwater harvesting not only allows an effective control of stormwater runoff by storing and infiltrating rainwater [6] but also aids the control of nonpoint source pollution in urban areas.

Introduction

Global freshwater resources are being increasingly polluted and depleted, threatening sustainable development and human and ecosystem health [7]. Water stress has been causing adverse effects and limiting economic and social development in many countries of the world. Thus, concern about the clean and safe water is a strong motivation to understand the water demands and the consequences of water use under the rapid population growth condition. It is necessary to introduce new concepts, policies, and measures for sustainable water use and management [8].

There is also a growing consensus that the way that cities and infrastructures are constructed is seriously out of step with natural hydrological and ecological processes [9, 10]. Recent environmental problems in urban areas arise from this nonresponsiveness of urban development to natural systems and processes. For example, urbanization has increased impermeable areas that have lost functions of rainwater storage and infiltration, leading to water-related disasters including urban floods and droughts [11, 12]. Increases in population and water use are resulting in increased pressures on water resources, and traditional planning concepts for water supply in urban area have a limit [13, 14]. Creating cities that are more responsive to the natural water cycle is therefore a preventative measure that will contribute to the long-term solution for water control and supply problems [10].

Rainwater harvesting is recognized as a sustainable method to overcome the problems of water shortage and urban environmental problems related to hydrological cycle. The term rainwater harvesting refers to direct collection of precipitation falling on a surface known as catchment without passing through the stage of surface runoff on land. Rainwater may be harvested from roofs, ground surfaces as well as from ephemeral watercourses and stored in physical structures or within the soil profile. Generally, rainwater harvesting involves all the activities such as collection of rainwater

from roofs and other surfaces, its storage, infiltration into the ground, and subsequent use.

Almost all water used by human beings derives from rainfall. However, it is always necessary to store water, so that it can be used when rain is not actually falling, and it is often necessary to transport it from where it falls to where the user is located. Rainwater harvesting differs from other water supplies in that there is no need to transport water, since it is used where it falls as rain. Accordingly, rainwater harvesting is a means to supply water in a decentralized manner.

Rainwater harvesting provides the long-term answers to the problem of water scarcity [15]. It offers an ideal solution in areas where there is sufficient rain but inadequate ground water supply and surface water resources are either lacking or are insufficient. On the other hand, it has not been widely employed in industrialized societies that rely primarily on centralized water distribution systems. However, the role of rainwater harvesting is being reassessed in urban regions. Rainwater harvesting can be adopted in cities to provide supplemental water for the city's requirements, to increase soil moisture levels for urban greenery, to increase the ground water table through artificial recharge, to mitigate urban flooding, and to improve the quality of groundwater.

Rainwater harvesting may be implemented as a means to mitigate the adverse effect of global warming. Predictions regarding global warming could have a major effect in significantly increasing water demand in many cities [15]. At the same time, increased evaporation from reservoirs and reduced river flows in some areas may decrease the available surface water supplies. A greater uncertainty regarding yields from major reservoirs and well fields is likely to make investments in the diversification of water sources, better water management, and water conservation even more prudent in future. The role of rainwater harvesting systems as sources of supplementary, back-up, or emergency water supply will become more important, especially in view of increased climate variability and the possibility of greater frequencies of droughts and floods in many areas. This will particularly be the case in areas where increasing pressure is put on existing water resources.

Rainwater harvesting is not a new idea. Rainwater harvesting and utilization systems have been used since ancient times and evidence of roof catchment systems date back to early Roman times [15]. Roman cities were designed to take advantage of rainwater as the principal water source for drinking and domestic purposes since at least 2000 B.C. In the Middle East, archaeological evidence of water harvesting structures appears in Jordan, Israel, Palestine, Syria, Iraq, the Negev, and the Yemen [16]. In many countries in Africa and Asia, rainwater harvesting was an important method to obtain water until the centralized water distribution system was introduced. Various technologies to harvest rainwater have been in use for over 4,000 years B.C.

There are two types of rainwater harvesting, direct rainwater harvesting and indirect rainwater harvesting. Direct rainwater harvesting implies the collection and storage of precipitated water for immediate use. Thus, it includes the rooftop water harvesting and similar systems. On the other hand, indirect rainwater harvesting means the collection and infiltration of rainfall into ground water aquifer for future use. Artificial recharge of rainwater is an example of indirect rainwater harvesting. The primary goal of direct rainwater harvesting is to supply collected rainwater as an alternative water source although excess rainwater may be infiltrated. Indirect rainwater focuses on the control of urban runoff and restoration of the hydrological cycle.

Rainwater harvesting offers a number of benefits compared with other competing technologies. It provides inexpensive supply of water and reduces stormwater runoff. Nonpoint source pollution related to stormwater can be controlled and hydrological cycles in urban areas may be recovered. In addition, rainwater needs little treatment for irrigation or non-potable indoor uses. However, there are also problems and barriers. First, the supply of rainwater is limited and unpredictable. Rainwater is often contaminated by toxic pollutants and microbes. Although rainwater is free, the initial setup costs are high. In addition, many people don't understand the importance of rainwater collection.

Rainwater harvesting system consists of several components (see Fig. 1):

- Catchment: The surface upon which the rain falls; the roof has to be appropriately sloped preferably toward the direction of storage and recharge.
- Storage: Reservoirs, tanks, etc. where collected rain water is safely stored.

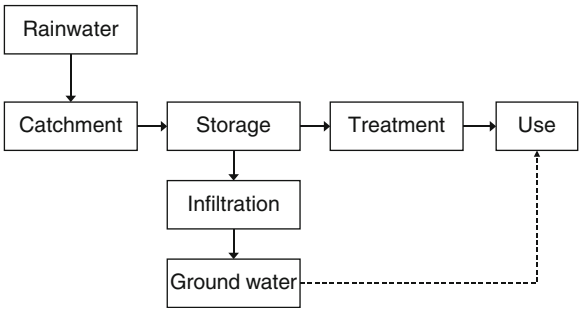

Rainwater Harvesting. Figure 1
Key components of rainwater harvesting

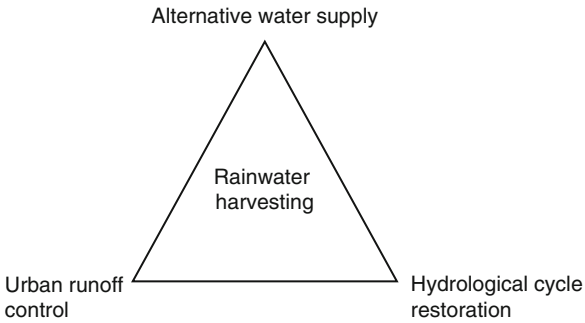

Rainwater Harvesting. Figure 2
Basic functions of rainwater harvesting

- Infiltration: Recharging of the stored rainwater into the ground water through open wells, bore wells, or percolation pits, etc.
- Treatment: Filters and other devices to remove solids and organic material and equipment, and additives to settle, filter, and disinfect.
- Others: Conveying (the delivery system for the treated rainwater, either by gravity or pump) and other equipments.

Describing Rainwater Harvesting

As shown in Fig. 2, rainwater harvesting has three basic functions: provision of an alternative water source; control of urban runoff; and restoration of hydrological cycle that is distorted by urbanization.

Alternative Water Supply

At least one third of the population in developing countries has no access to safe drinking water, which results in major health problems due to waterborne diseases [17]. The two major water problems are inadequate supplies and insufficient treatment, which are particularly serious in developing nations [18]. Accordingly, it is essential to search for alternative approaches, including the use of decentralized water supply systems and low-cost, low-energy water technologies. Rainwater harvesting provides the long-term answers to the problem of water scarcity [15]. It helps to mitigate variation in water availability by collecting the rain and storing it more efficiently. In doing so, rainwater harvesting assures a continuous and reliable access to water. A water harvesting system collects and stores water within accessible distance of its place of use. The rainwater collected can be stored for direct use or can be recharged into the ground water.

Rainwater harvesting may offer a clean source for good quality water. This is relevant for areas where ground water or surface water is contaminated by harmful chemicals or pathogenic bacteria or pesticides and/or in areas with saline surface water. Rainwater collected using various methods has less negative environmental impacts compared to other technologies for water resources development. Rainwater is relatively clean and the quality is usually acceptable for many purposes with little or even no treatment [15]. Rainwater harvesting technologies are flexible and can be built to meet almost any requirements. Construction, operation, and maintenance are not labor intensive.

Especially, poor countries suffering or facing water shortages as a result of climate change have a massive potential in rainwater harvesting. According to a report, about a third of Africa is deemed suitable for rainwater harvesting if a threshold of 200 mm of arrival rainfall, considered to be at the lower end of the scale, is used [19]. Widely deployed, rainwater harvesting can act as a buffer against drought events for these people while also significantly supplementing supplies in cities and areas connected to the large-scale water infrastructures.

Rainwater harvesting is not only useful in poor communities but also in urban regions. Water conservation makes good economic sense and is sometimes law for private and public commercial buildings, educational facilities, and homes. There is plenty of rainfall that can be harvested and used to supplement the demands for non-potable purposes. In urban areas of the developed world, at a household level, harvested rainwater can be used for flushing toilets and washing

laundry. It can also be used for showering or bathing after proper treatment. Indeed, in hard water areas, it is superior to mains water for this. Water used for non-potable purposes does not require the same level of treatment as water that must meet drinking water quality standards. In order to safely serve these needs, this water must have, however, appropriate quality depending on its specific purpose of use.

Rainwater has an advantage over reclaimed water in that it generally contains fewer pollutants and is easier to collect, and there are few regulatory barriers to outdoor uses. It can also easily be treated for more uses inside a building such as showers, hand washing, and even drinking. However, the greatest drawback to the development of rainwater harvesting systems is that the supply is not guaranteed. To compensate, storage volume must be significantly greater than that required for grey water. In addition, rising environmental pollution requires that rainwater be treated before storage and use for indoor purposes, and storage of rainwater intended for human contact can present problems with bacteria. A possible solution for this problem is to integrate rainwater harvesting and water reclamation into one system [20].

Urban Runoff Control

Rainfall inevitably creates stormwater runoff in your watershed. If precipitation occurs faster than it can infiltrate the soil or if the soil is saturated, it becomes runoff. Runoff remains on the surface and flows into streams, rivers, and eventually large bodies such as lakes or the ocean. However, urban development has dramatically changed the natural system of stormwater runoff when it rains [21]. Impervious surfaces such as driveways, sidewalks, and streets block rainfall and other precipitation from infiltrating naturally into the ground. Thus, rainfall is directed rapidly into pipes and channels instead of being absorbed by vegetation and soil. Movement of this stormwater across the soil causes urban flood and erosion.

Every time there is concentrated heavy rain, there is an overflow of water from drains, and small- and medium-sized rivers and streams repeatedly flood [2]. These conditions can often lead to an outpouring of sewage into rivers and streams from sewer outlets and sewer pumping stations, thus contaminating the quality of urban streams and rivers. Stormwater can also carry and deposit untreated pollutants, such as sediment, nutrients, and pesticides, into surface water bodies as a form of nonpoint source pollution.

Implementing a rainwater harvesting system is one way to decrease the amount of stormwater runoff and minimize the problems associated with it. By collecting and storing rainwater from roof, rainwater harvesting systems reduce stormwater runoff taking significant pressure off stormwater infrastructure and the environment. This means reduced need for investment in stormwater infrastructure (fewer, smaller pipe systems required) and reduced maintenance of stormwater infrastructure (ponds, wetlands, and pollutant traps).

Rainwater harvesting also helps to reduce the contamination of surface water. Nonpoint source pollution from urban areas represents a serious threat to water quality. Rainwater carries chemicals, nutrients, sediments, and other forms of nonpoint source into water bodies such as rivers and lakes. Rainwater harvesting allows control of stormwater runoff, thereby reducing the nonpoint source pollution.

Hydrological Cycle Restoration

Due to the rapid pace of urbanization, many of the world's large cities are facing problems related to the hydrological cycle [2]. The impermeable surfaces of concrete and asphalt structures of cities have tended to disrupt the natural hydrological cycle, and reduce the amount of rainwater permeating underground. A decrease in the area where water can penetrate speeds up the surface flow of rainwater causes water to accumulate in drains.

The hydrological cycle is closely related to heat cycle, which is also affected by impermeable surfaces. Cities can be several degrees warmer than surrounding regions due to the built environment and the concentration of human activity, a phenomenon referred to as an urban heat island [22]. Pavements have become an important contributor to this effect by altering landcover over significant portions of an urban area. The urban heat island phenomenon alters the city's natural hydrological cycle and ecological environment in a big way.

In order to achieve a comprehensive solution to this problem, new approaches to urban development are

required, emphasizing sustainability and the restoration of the urban hydrological cycle. Traditionally, storm sewer facilities have been developed based on the assumption that the amount of rainwater drained away will have to be increased [2]. From the standpoint of preserving or restoring the natural water cycle, it is important to retain rainwater and to facilitate its permeation.

The natural hydrological cycle in urban areas can be rehabilitated through rainwater harvesting, which is of great importance for sustainable development of cities. Low Impact Development (LID) is a design and site development methodology that allows newly developed and/or existing sites to hydrologically mimic predevelopment conditions. For example, if a forested area is developed for commercial purposes, one LID goal would be to mimic some of the hydrological functions of trees and encourage cleansing and infiltration of site rainwater runoff. Capturing rain and encouraging it to soak into the ground as close to the location where it falls, is another goal of LID. A rainwater harvesting system can act as a large buffer, storing water for later use. The water can then be released at a slower rate via landscape watering. Stormwater retention requirements can be partially achieved by incorporating rainwater harvesting as an integral part of the design.

Technologies for Rainwater Harvesting

There are a number of types of systems to harvest rainwater ranging from very simple to the complex industrial systems. Generally, rainwater is either harvested from the ground or from a roof. The rate at which water can be collected from either system is dependent on the plan area of the system, its efficiency, and the intensity of rainfall.

Key to success in implementing rainwater harvesting is to adopt appropriate technologies. Engineering aspects including design, implementation, construction, and operation form the cornerstones of success for rainwater harvesting. Material and technique developments lead to improved and appropriate construction practices, and proper operation ensures optimal use. Water quality, sustainability, cost, and performance of rainwater harvesting systems are major areas of concern.

Catchment

The catchment area of a water harvesting system is the surface, which receives rainfall directly and contributes the water to the system. It can be a paved area like a terrace or courtyard of a building, or an unpaved area like a lawn or open ground. Temporary structures like sloping sheds can also act as catchments.

The catchment methods are listed as [15]:

- Rooftops: If buildings with impervious roofs are already in place, the catchment area is effectively available and they provide a supply at the point of consumption. The quality of collected rainwater is high compared with other catchment methods. However, the size of rooftop area is often limited and the collected rainwater may not be sufficient.
- Paved and unpaved areas: Roads and pavements and other open areas can be effectively used to harvest the runoff. The main advantage is that water can be collected from a larger area. This is particularly advantageous in areas of low rainfall. However, the collected rainwater may be contaminated by the pollutants in such surfaces.
- Storm water drains: Most of the residential colonies have proper network of stormwater drains. If maintained neatly, these offer a simple and cost-effective means for harvesting rainwater.

Runoff harvested water, which is collected from pavement surfaces and stormwater drains, should only be used for non-potable uses because of the increased risk of contamination. For in-house uses, rooftop harvested rainwater is safer for drinking purposes than the runoff harvested water.

Water quality from different roof catchments is affected by the type of roof material [23]. To be suitable for rainwater harvesting, the catchment should be made of some hard material that does not absorb the rain or pollute the runoff. Thus, tiles, metal sheets, and most plastics are suitable, while grass and palm leaf roofs are generally not suitable. The surface texture affects the quantity of rainwater that can be collected from a given roof, the smoother the better [15]. In addition, roof catchment materials should resist corrosion for extended periods of time. Roof materials that could leach toxic materials into the rainwater as it touches the roof surface are recommended only for

non-potable water uses (i.e., composite asphalt, asbestos, and some painted roofs).

The rainwater reaching a roof in a year can be estimated as the annual rainfall times the roof's plan area. However, some of the rainwater is typically lost to evaporation and overflow. In areas of low annual rainfall, the available roof area is not big enough to capture enough water to meet all the water needs. In this case, either the roof must be extended, or rooftop water harvesting is combined with other sources of water. In fact, getting water from more than one source is the usual practice in developing countries, and is reviving in popularity in richer countries.

One of the most challenging issues in rainwater catchment is the control of first flush effect. First flush is the initial surface runoff of a rainstorm. During this phase, water pollution is typically more concentrated compared to the remainder of the storm. Consequently, the rainwater collected in early stage of rainfall contains high concentrations of pollutants compared with that collected in later stage. The first flush effect is attributed to one or a combination of the following three processes [24]: (1) matter deposited on the catchment surface during preceding dry period is washed off by the falling rain [25]; (2) weathering and corrosion products of the catchment surface and drainage system are washed off [26]; and (3) concentrations in falling rain itself are decreasing with increasing rainfall depth due to scavenging of particles, aerosols, and gases by rain droplets [27].

To collect rainwater of high quality, rejection or treatment of first flush rainwater is essential. A first flush (foul flush) device is a valve that ensures that runoff from the first spell of rain is flushed out and does not enter the system [15]. This needs to be done since the first flush of rain carries a relatively larger amount of pollutants from the air and catchment surface. Roof washing, or the collection and disposal of the first flush of water from a roof, is of particular concern if the collected rainwater is to be used for human consumption, since the first flush picks up most of the dirt, debris, and contaminants, such as bird droppings that have collected on the roof and in the gutters during dry periods. There are a number of commercially available devices to divert or filter the first flush rainwater.

In rooftop water harvesting systems (see Figs. 3 and 4), the arrangement for leading water from the roof to the water store is usually called "guttering" or "gutters and downpipes." The gutters are open channels carrying water sideways under the edge of the roof to a point just above the water store; the downpipes are tubes leading water down from the gutters to the entrance of the water store. There are many ways of achieving the transfer of water from roof to store. However, guttering is the most popular method because it helps keep runoff water clean.

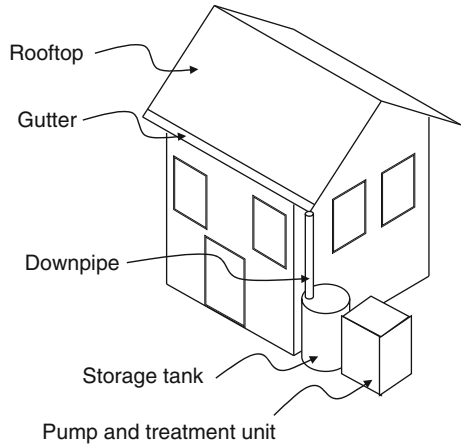

Rainwater Harvesting. Figure 3
Typical rooftop water harvesting system in a house

Storage

The storage tank or cistern generally is the most important design of a component of a rainwater harvesting system. In most cases, it is permanent and its placement should be carefully thought out. Storage tanks for collecting rainwater may be located either above or below the ground. They may be constructed as part of the building, or may be built as a separate unit located some distance away from the building. Tank location is dependent on aesthetics, climate, and soil conditions. The design considerations vary according to the type of tank and other factors. Many types of rainwater storage facilities are found in practice. Depending on the material of tanks, their characteristics are different (Table 1).

Although the level of contamination in the collected rainwater may decrease during the catchment process, it is still necessary to properly manage the rainwater storage tank to maintain high quality of water. Rainwater is usually stored for more than a week to several months before usage and thus has potential of

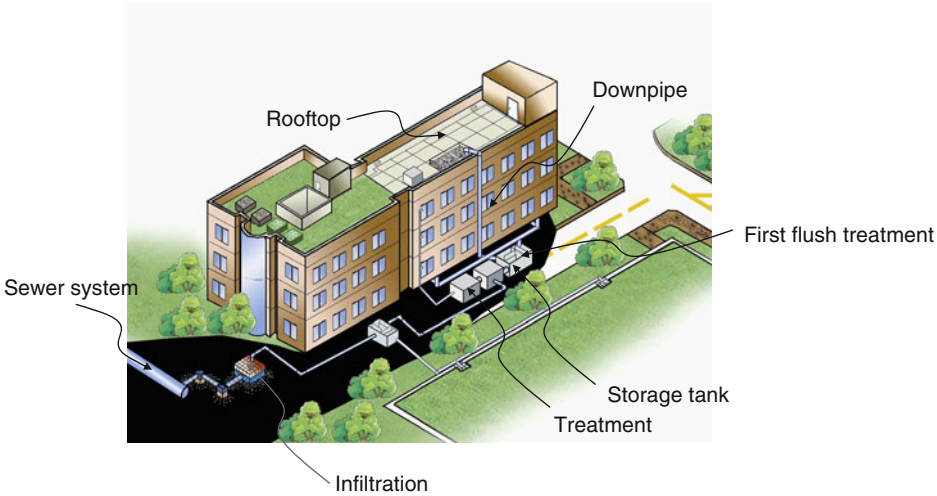

Rainwater Harvesting. Figure 4
Typical rooftop water harvesting system in a commercial building

Rainwater Harvesting. Table 1 Comparison of tank materials [15, 23, 28]

Tank material		Advantages	Disadvantages
Concrete		• Durable and long lasting • Ability to decrease the corrosiveness of rainwater by allowing the dissolution of calcium carbonate from the walls and floors • Install above or below ground	• Potential to crack and leak • Ongoing maintenance required • Poured in place
Plastic	Fiberglass	• Lightweight, affordable, long lasting, little maintenance • Commercially available in various sizes	• Light penetration that may promote algae growth
	Polyethylene	• Moderate price • Lightweight, low price, long lasting, little maintenance • Commercially available in various sizes • Cheap price • Easy to clean • Relatively easy to repair	• UV-degradable (Painting is required for below ground installation) • Light penetration that may promote algae growth
Metal	Galvanized steel	• Commercially available in various sizes • Moderate price	• Corrosion and rust must be lined for potable use • Only above ground use

contamination during storage. Microbial contamination is of great concern for long-term storage because it may deteriorate water quality seriously.

Infiltration

Urban rainwater cannot only be used as water supplement for daily residential use but also for improving the rate of natural rainwater infiltration and, more importantly, to rehabilitate the natural hydrological cycle. Rainwater infiltration is an approach to surface water drainage, which aims to utilize rainwater as a water supply, recharge groundwater, increase base flow levels of nearby streams, reduce flood risk, and control pollution [29]. The objective is to retain water on-site and where possible, clean it and make it available for reuse.

Infiltration is the most effective means of controlling stormwater runoff since it reduces the volume discharged to receiving waters and the negative impacts associated with it [30]. Infiltration is also an important mechanism for pollutant control. As runoff infiltrates into the ground, particulates and contaminants such as metals and nutrients are removed by filtration through the soil, and dissolved constituents are removed by adsorption. Infiltration techniques have been used for many years to control stormwater quality and flooding. Decentralized stormwater infiltration can be an additional and cost-efficient alternative resource to conventional stormwater treatment measures, which can be applied on-site close to the runoff area.

Rainwater infiltration gives rise to several benefits in relation to water quality, biodiversity, and vegetation. It is useful to reduce the amount of stormwater discharged into the sewer system and recirculate water back to the natural water cycle [29, 30]. The combination of rainwater storage and rainwater infiltration offers technical benefits and exerts positive effects on the environment and the local water balance. A hydraulic load reduction can minimize hydraulic peak loads in the sewer network significantly. In addition, infiltration of rainwater over a long period can increase and/or stabilize the groundwater reserves. The main benefits on an individual level are the complete uncoupling from the public sewer. Construction costs will be also reduced if rainwater harvesting and rainwater infiltration systems are planned together in addition to a reduction in the wastewater fees.

Infiltration is governed by two forces: gravity and capillary action. While smaller pores offer greater resistance to gravity, very small pores pull water through capillary action in addition to and even against the force of gravity. The rate of infiltration is affected by soil characteristics including ease of entry, storage capacity, and transmission rate through the soil. The soil texture and structure, vegetation types and cover, water content of the soil, soil temperature, and rainfall intensity all play a role in controlling infiltration rate and capacity. A soil hydraulic conductivity in the range of 10^{-6}–10^{-3} m/s is generally considered appropriate to achieve reasonable infiltration rates. For long-term infiltration, a fall-off due to gradual clogging of the soil must be taken into account. Moreover, the process of infiltration can continue only if there is room available for additional water at the soil surface [29, 30].

Infiltration systems are designed to capture a volume of stormwater and infiltrate this water into the ground over a period of several hours or even days. Different types of systems can be employed, which retain water safely on site, including: pervious pavements, infiltration basins, vegetated swales, ponds and wetlands, and green roofs [29].

- Infiltration basins: They are designed to capture stormwater runoff, hold this volume, and infiltrate it into the ground over a period of days. Thus, they are useful to reduce peak flows to receiving waters. Infiltration basins exhibit a high pollutant removal rate through mechanisms such as filtration, adsorption, and biodegradation. Infiltration basins may or may not be lined with plants. Vegetated systems are advantageous because they can reduce pollutants and increase the infiltration efficiency.
- Infiltration trenches: They are long, narrow gravel-filled trenches designed to infiltrate stormwater into the ground. Runoff is stored in the void space between the gravel and infiltrates through the bottom and into the soil matrix. Infiltration trenches typically capture a small amount of runoff and therefore may be designed to capture the first flush of a runoff event. Infiltration trenches efficiently remove suspended solids, particulates, bacteria, organics, and soluble nutrients.
- Vegetated swales: Swales are channels with vegetation designed to convey stormwater runoff. Vegetated swales can be applied for infiltration of not only low-polluted runoffs from roof surfaces but also high-polluted stormwater from pavement surfaces in new development areas. Except for the space requirements, they can be adapted for use in most residential, commercial, and industrial land development projects.
- Trough–trench systems: This is a combination of surface infiltration in a trough and subsurface percolation from a gravel-filled trench. The topsoil between the trough and the trench filters and purifies the infiltrating stormwater. Runoff delay is achieved through a short-term storage in the trough and long-term storage in the trench.

- Porous pavement: It is a permeable pavement surface with a stone reservoir underneath. The reservoir temporarily stores surface runoff before infiltrating it into the subsoil. Runoff is thereby infiltrated directly into the soil and receives some water quality treatment. Porous pavement often appears the same as traditional asphalt or concrete but is manufactured without "fine" materials, and instead incorporates void spaces that allow for infiltration. [29].

Treatment

Although rainwater can provide clean, safe, and reliable water, rainwater collected in many locations still contains various pollutants. Once rain comes in contact with a roof or collection surface, it can wash many types of bacteria, molds, algae, protozoa, and other contaminants into the cistern or storage tank [31]. Indeed, some samples of harvested rainwater have shown detectable levels of these contaminants. Health concerns related to bacteria, such as salmonella and e-coli, and to physical contaminants, such as pesticides, lead and arsenic, are the primary criteria for drinking water quality analysis. Falling rain is generally free of most of these hazards. But, if the rainwater is intended for use inside the household, either for potable uses such as drinking and cooking or for non-potable uses including showering and toilet flushing, appropriate filtration and disinfection practices should be employed. Therefore, in order to ensure quality of water, the collection systems will have to be properly built and maintained and the water shall also have to be treated appropriately for intended uses.

If the rainwater is to be used outside for landscape irrigation, where human consumption of the untreated water is less likely, the presence of contaminants may not be of major concern and thus treatment requirement can be less stringent or not required at all. Depending on where the system is located, the quality of rainwater itself can vary, reflecting exposure to air pollution caused by industries such as cement kilns, gravel quarries, crop dusting, and a high concentration of automobile emissions.

Rainwater quality varies for a number of reasons [15]. While there are widely accepted standards for drinking water, the development of approved standards for water when it is used for non-potable applications would facilitate the use of rainwater sources [2]. In terms of physical–chemical parameters, collected roof water, rainwater, and urban stormwater tend to exhibit quality levels that are generally comparable to the World Health Organization (WHO) guidelines for drinking water. However, low pH rainwater can occur as a result of sulfur dioxide, nitrous oxide, and other industrial emissions. Hence, air quality standards need to be reviewed and enforced. In addition, high lead values can sometimes be attributed to the composition of certain roofing materials – thus, it is recommended that for roof water collection systems, the type of roofing material should be carefully considered. A number of collected rainwater samples have exceeded the WHO values in terms of total coliform and fecal coliform. The ratios of fecal coliform to fecal streptococci from these samples indicated that the source of pollution was the droppings of birds, rodents, etc.

Before making a decision about what type of water treatment methods to use, water should be got tested by an approved laboratory and determine whether the water can be used for potable or non-potable uses. The types of treatment discussed are filtration, disinfection, and buffering for pH control. Dirt, rust, scale, silt and other suspended particles, bird and rodent feces, airborne bacteria, and cysts will inadvertently find their way into the cistern or storage tank even when design features such as roof washers, screens, and tight-fitting lids are properly installed. Water can be unsatisfactory without being unsafe; therefore, filtration and some form of disinfection is the minimum recommended treatment if the water is to be used for human consumption (drinking, brushing teeth, or cooking). The types of treatment units most commonly used by rainwater systems are filters that remove sediment, in consort with either ultraviolet light or chemical disinfection. Advanced treatment such as reverse osmosis may be applied for special purposes (see Fig. 5).

A filter is an important part of the inflow structure of a rainwater harvesting system. Once screens and roof washers remove large debris, other filters are available, which help improve rainwater quality. Keep in mind that most filters available in the market are designed to treat municipal water or well water. Therefore, filter selection requires careful consideration. Screening,

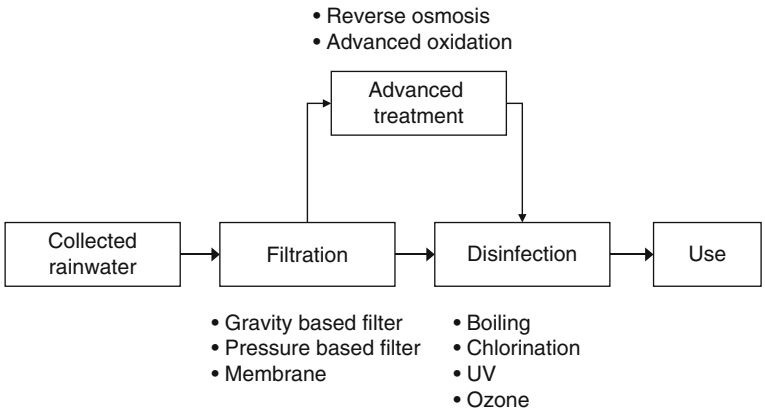

Rainwater Harvesting. Figure 5
Schematics of rainwater treatment system

sedimentation, and pre-filtering occur between catchment and storage or within the tank [15, 23, 28].

- Gravity-based filter: This consists of construction of an underground/above ground filtration chamber consisting of layers of fine sand/coarse sand and gravel. Alternatively, only fine sand can also be used along with the gravel layer. Further deepening of the filter media shall not result in an appreciable increase in the rate of recharge and the rate of filtration is proportional to the surface area of the filter media. A unit sq.m. surface area of such a filter shall facilitate approx. 60 l/h of filtration of rainwater runoff. In order to determine the optimum size of the surface area, just divide the total design recharge potential with this figure. A system of coarse and fine screen is essential to be put up before the rainwater runoff is allowed to flow into the filtration pit. A simple charcoal can be made in a drum or an earthen pot. The filter is made of gravel, sand, and charcoal, all of which are easily available. The common types of filters are:
- Sand filters: Sand filters are commonly available, easy and inexpensive to construct. These filters can be employed for treatment of water to effectively remove turbidity (suspended particles like silt and clay), color, and microorganisms. These filters are manufactured commercially on a wide scale.
- Pressure-based filter: Pressure-based filters facilitate a higher rate of filtration in a pressurized system. Being a pressure-based system, it involves a pump of capacity 0.5–1 hp. The rate of filtration is evidently high and the quality of water is than those by gravity-based filters. They are successful for areas with larger rainwater runoff and limited space availability. Also, these filters can be put in combination with an existing tube well so as to recharge water into the same bore.
- Membrane filters: Low pressure membrane such as microfiltration and ultrafiltration can be applied for removing particles and colloids from harvested rainwater [20]. It allows direct removal of pathogens without using chemicals, although disinfection is still recommended for potable use. However, the capital and operational cost of membrane filtration is more expensive than those of other filtration systems.

To reduce the risk of microbial contamination, disinfection is needed after filtration. If the harvested rainwater is used to wash clothes, water plants, or other tasks that do not involve direct human consumption or contact, treatment beyond screening and sedimentation removal is optional. However, if the water is plumbed into the house for general indoor use such as for drinking, bathing, and cooking, disinfection is needed. While filtering is quite common in private water systems, disinfection is less common for these reasons. There are many options for disinfecting rainwater prior to use [15].

- Boiling: Boiling is a very effective method of purification and very simple to carry out. Boiling water

for 10–20 min is enough to remove all biological contaminants.

- Chlorination: Chlorination is done with sodium hypochlorite or calcium hypochlorite. Chlorination can kill all types of bacteria and make water safe for drinking purposes. Chlorine is the most common disinfectant because of its dependability, water solubility, and availability. However, chlorine is disliked due to taste, fear associated with trihalomethanes (THMs), and other concerns.
- Chlorine tablets: Chlorine tablets are easily available commercially. One tablet of 0.5 g is enough to disinfect 20 l (a bucketful) of water.
- Ultraviolet (UV) light water disinfection: It kills most microbiological organisms that pass through them. Since particulates offer a hiding place for bacteria and microorganisms, pre-filtering is necessary for UV systems. To determine whether the minimum dosage is distributed throughout the disinfection chamber, UV water treatment units should be equipped with a light sensor. Either an alarm or shutoff switch is activated when the water does not receive the adequate level of UV radiation. The UV unit must be correctly calibrated and tested after installation to insure that the water is being disinfected. Several systems in US utilize ultraviolet light.
- Ozone: Ozone is a strong disinfectant that readily kills microorganisms and oxidizes organic matter in the water. Any remaining ozone reverts back to dissolved oxygen in the water. Recent developments have produced compact ozone units for home use. Since ozone is produced by equipment at the point of use with electricity as the only input, it is easier to handle than chlorine or other chemicals. Ozone can also be used to keep the water in cisterns without microbial growth.

When a disinfectant such as chlorine is added to rainwater, an activated carbon filter at the tap may be used to remove the chlorine prior to use. It should be remembered that activated carbon filters are subject to becoming sites of bacterial growth. Chemical disinfectants such as chlorine or iodine must be added to the water prior to the activated carbon filter. If ultraviolet light or ozone is used for disinfection, the system should be placed after the activated carbon filter. Many water treatment standards require some type of disinfection after filtration with activated carbon. Ultraviolet light disinfection is often the method of choice.

Currently, water quality control in roof water collection systems is limited to diverting first flushes and occasional cleaning of cisterns. Boiling, despite its limitations, is the easiest and surest way to achieve disinfection, although there is often a reluctance to accept this practice as taste is affected. Chlorine in the form of household bleach can be used for disinfection. However, the cost of UV disinfection systems is usually prohibitive.

System Design

The effectiveness of rainwater harvesting depends on various factors including climate conditions, geographic information, water usage patterns, and the major purpose of collected rainwater. Therefore, the design of rainwater harvesting systems is of primary importance.

The rate at which water can be collected is dependent on the plan area of the system, its efficiency, and the intensity of rainfall. Thus, the basic system design of rainwater harvesting systems should be determined based on the size and nature of the catchment areas, water quality of collected rainwater, and whether the systems are in urban or rural settings. Some of the systems are described below [15]:

- Simple roof water collection systems: This system is suitable for household use of rainwater. While the collection of rainwater by a single household may not be significant, the impact of thousands or even millions of household rainwater storage tanks can potentially be enormous. The main components in a simple roof water collection system are the cistern itself, the piping that leads to the cistern and the appurtenances within the cistern.
- Larger systems for educational institutions, stadiums, airports, and other facilities: When the systems are larger, the overall system can become a bit more complicated, for example, rainwater collection from the roofs and grounds of institutions, storage in underground reservoirs, treatment, and then use for non-potable applications.

- Roof water collection systems for high-rise buildings in urbanized areas: In high-rise buildings, roofs can be designed for catchment purposes and the collected roof water can be kept in separate cisterns on the roofs for non-potable uses.
- Land surface catchments: Rainwater harvesting using ground or land surface catchment areas can be a simple way of collecting rainwater. Compared to rooftop catchment techniques, ground catchment techniques provide more opportunity for collecting water from a larger surface area. By retaining the flows (including flood flows) of small creeks and streams in small storage reservoirs (on surface or underground) created by low-cost (e.g., earthen) dams, this technology can meet water demands during dry periods. There is a possibility of high rates of water loss due to infiltration into the ground, and because of the often marginal quality of the water collected, this technique is mainly suitable for storing water for agricultural purposes.
- Collection of storm water in urbanized catchments: The surface runoff collected in stormwater ponds/reservoirs from urban areas is subject to a wide variety of contaminants.

A basic goal for sizing any rainwater harvesting system is to balance the volume of water that can be captured and stored (supply), compared to the volume of water used (demand). In order to balance the system, the supply must equal or exceed the demand. This is easiest to understand if broken down on a monthly basis.

If rainfall is fairly evenly distributed throughout the year, the storage capacity may be smaller than in other areas of the country where rainfall occurs more seasonally. Storage capacity needs to be sufficient to store water collected during heavy rain events to last through dry periods. Some residences might be constrained by the size of the collection surfaces and/or the volume of storage capacity that can be installed due to space or costs.

There are many ways to determine the amount of rainfall, the estimated demand, and how much storage capacity is needed to provide enough rainwater to meet the demand. The simplest way to size the rainwater storage tank is to multiply catchment area with a certain factor (0.01$\sim$ 0.1m). Although this method is widely used, it does not consider the usage rate, leading to an inefficient design. Therefore, a design method based on simulation is preferred. A few softwares for simulating rainwater harvesting, such as MUSIC (http://www.toolkit.net.au/Tools/MUSIC), STORM (http://www.azstorm.org), and RainCity (http://www.rainwater.re.kr), are commercially available. These softwares may consider many factors including target function, catchment type, catchment area, and economic feasibility.

Operation and Maintenance

Operation and maintenance are also important steps to ensure high efficiency of rainwater harvesting. Appropriately designed rainwater harvesting systems require little maintenance. However, like any household component, it should be checked periodically to ensure it is operating efficiently and appropriately [28]. As a matter of fact, many problems related to rainwater harvesting arise from improper operation and maintenance. There are a few general guidelines:

- Catchment: The catchment surface should be as clean as possible for use of collected rainwater. Periodic cleaning of the catchment surface is recommended.
- Storage: The storage tank should be regularly cleaned to prevent contamination by sediments and microorganisms. In rooftop water system, the cleaning frequency is once a year. However, the cleaning frequency should be determined based on the characteristics of collected rainwater. If a first flush filter is not used, tanks will require periodic cleaning to remove organic debris buildup. If a first flush filter is used, tanks will not require frequent cleaning.
- Infiltration: The infiltration system may be blocked by pollutants in rainwater. Cleaning is often inefficient to recover the initial infiltration rate. Thus, the water flowing into the infiltration system should be properly treated to reduce the amount of particles.
- Treatment: The quality of treated water should be regularly monitored.

Future Directions

Rainwater harvesting has recently gained popularity as a way to secure sustainable water resource. This is

becoming widespread all over the world. Rainwater harvesting may be implemented to supply clean water in developing countries such as Africa and Asia. It may be applied in cities to lessen the load of municipal water system, control urban flood, and recover natural hydrological cycle. Rainwater harvesting has been also identified as a technology with the potential of contributing immensely as a coping mechanism for climate change and variability.

However, rainwater harvesting has some limitations. The supply from rainwater harvesting is not guaranteed. In urban areas, separate systems of rainwater harvesting are not effective to reduce runoff and recover water cycle. Moreover, the understanding on rainwater harvesting is hampered by the lack of scientifically sound principles and research.

Accordingly, technologies for rainwater harvesting will be developed in many ways in the future. Rainwater harvesting will continue to be combined with wastewater reclamation for stable supply of high-quality water. Rainwater harvesting will be systematically considered in urban design to maximize its effect on runoff control and water cycle restoration. It will be an essential part of a decentralized infrastructure for water management.

Bibliography

1. Thomas TH, Martinson DB (2007) Roofwater harvesting: a handbook for practitioners. IRC, Delft
2. UNEP (2002) Rainwater harvesting and utilisation: an environmentally sound approach for sustainable urban water management: an introductory guide for decision-makers. UNEP, Osaka
3. Kim RH, Lee S, Kim YM (2003) Development of rainwater utilization system in Korea. In: 11th IRCSA, Mexico City, Mexico
4. Bambrah GK (1993) Rainwater catchment systems and technologies – An overview. In: 6th international conference on rainwater catchmant systems "Participation in rainwater collection for low-income communities and sustainable development", Nairobi, Kenya
5. Herrmann T, Hasse K (1998) Ways to get water: rainwater utilization or long-distance water supply? A holistic assessment. Water Sci Technol 36(8–9):313–318
6. Fewkes A (1999) The use of rainwater for WC flushing: the field testing of a collection system. Build Environ 34(6): 765–772
7. Furumai H (2008) Rainwater and reclaimed wastewater for sustainable urban water use. Phys Chem Earth, Parts A/B/C 33(5):340–346
8. Wagner W et al (2002) Sustainable watershed managment: an international multi-watershed case study. Ambio 31(1):2–13
9. Coombes P, Donovan I, Cameron C (1999) Water sensitive urban development: Implementation issues for the lower hunter and central coast. Lake Macquarie City Council, Lake Macquarie City, p 99
10. Weigert FB, Steinberg CEW (2002) Sustainable development: assessment of water resource management measures. Water Sci Technol 46(6–7):55–62
11. Kim RH (2002) Rainwater utilization for urban establishment of new paradigm. In: A joint conference with Korea society of water and wastewater and Korea society on water quality, Goyang
12. Kim RH (2000) Rainwater utilization and functional changes in building roof. Construct Technol Rev 220:13–19
13. Konig KW (2001) Rainharvesting in building. Wilo Brain, Dortmund
14. Masaru T (2002) Strategies toward buidling "Green" society. Central law publishing Co, London
15. Ray K (2005) Rainwater harvesting and utilisation. UN-HABITAT
16. Prinz D (2002) The role of water harvesting in alleviating water scarcity in arid areas. In: International conference on water resources management in arid regions. Kuwait Institute for Scientific Research, Kuwait
17. WHO (2004) Facts and figures: water, sanitation and hygiene links to health. WHO, New York
18. Murinda S, Kraemer S (2008) Exploring the potential of solar water disinfection as a household water treatment method in peri-urban Zimbabwe. Phys Chem Earth, Parts A/B/C 33:8–13
19. Calabria K (2006) Devastating rains may hold solution to Africa's water woes: report in Agence France Presse
20. Kim R-H et al (2007) Reuse of greywater and rainwater using fiber filter media and metal membrane. Desalination 202(1–3): 326–332
21. Lampe L, Andrews H, Kinsinger K (1996) 10 Issues in urban stormwater pollution control. American City and County, pp 36–53
22. Cambridge Systematics I (1005) Cool pavement report: EPA cool pavements study – Task 5, EPA
23. Krishna HJ (2005) The texas manual on rainwater harvesting. Texas Water Development Board, Austin
24. Zobrist J et al (2000) Quality of roof runoff for groundwater infiltration. Water Res 34(5):1455–1462
25. Yaziz MI et al (1989) Variations in rainwater quality from roof catchments. Water Res 23(6):761–765
26. Zhang X et al (2002) Determination of instantaneous corrosion rates and runoff rates of copper from naturally patinated copper during continuous rain events. Corros Sci 44(9): 2131–2151
27. Zinder B, Schuman T, Waldvogel A (1988) Aerosol and hydrometer concentrations and their chemical composition during winter precipitation along a mountain slope – II. Enhancement below cloud scavenging stably stratified atmosphere. Atmos Environ 22(12):2741–2750

28. LaBranche A et al (2007) Virginial rainwater harvesting manual. The Cabell Brand Center, Salem
29. Khoury-Nolde N (2008) Rainwater infiltration. European Rainwater Catchment Systems Association
30. CSIRO (2006) Urban stormwater: best practice environmental management guidelines. CISRO, Collingwood
31. Pressman A (2007) Architectural graphic standards. American Institute of Architects. Wiley, New Jersy

Rating Systems for Sustainability

Raymond J. Cole
School of Architecture & Landscape Architecture, University of BC, Vancouver, BC, Canada

Article Outline

Glossary
Definition of the Subject
Introduction
Environmental Assessment Methods
Sustainability Assessment
Future Directions
Acknowledgments
Bibliography

Glossary

Building Environmental Assessment Method (system or scheme) Technique that has environmental assessment as one of its core functions but may be accompanied by third party verification before issuing an overall performance rating or label.

Assessment process Use of assessment methods, including deployment by the design team and engagement of other stakeholders as the basis for making informed decisions.

Certification Third party verification and scrutiny of a performance assessment that adds to the overall credibility of the assessment process but invariably brings additional layers of constraints, bureaucracy, and costs.

Environmental (or green) assessment Assessment of resource use, ecological loadings, and indoor environmental quality.

Framework Organization or classification of environmental performance criteria in a structured manner with assigned points or weightings.

Rating (labeling) Extended output from the assessment process, typically in the form of a singular, easily recognizable designation, for example, "Gold" or "Excellent."

Sustainability assessment Assessment that expands the range of performance criteria to include social and economic considerations.

Weighting Assigning the relative significance of the environmental criteria to permit their aggregation into an overall single score.

Definition of the Subject

Voluntary building environmental assessment methods have emerged as a legitimate means to evaluate the performance of buildings across a broad range of environmental considerations – most typically resource use, ecological loadings, and indoor environmental quality. An underlying premise of these voluntary assessments is that if the market is provided with improved information and mechanisms, a discerning client group can and will provide leadership in environmental responsibility, and that others will follow suit to remain competitive.

The increase in development and application of building environmental assessment methods over the past 20 years has provided considerable theoretical and practical experience on their contribution in furthering environmentally responsible building practices. An important indirect benefit is that the broad range of issues incorporated in environmental assessments require greater communication and interaction between members of the design team and various sectors with the building industry, that is, environmental assessment methods encourage greater dialogue and teamwork. Although the developers of assessment tools continue to refine their scope, structure, and metrics, key issues are the interpretation placed on the final environmental profile or label by the "market," its significance alongside other design requirements, and the changing relationship between voluntary and regulatory mechanisms to improve building environmental performance. Moreover, while the term

"sustainable" building is increasingly used and social and economic criteria are being added to the assessments, few current assessment methods have been designed and structured from the outset to embrace these considerations.

Introduction

Until the release of the *Building Research Establishment Environmental Assessment Method* (BREEAM) in 1990 [1] little, if any, attempt had been made to establish an objective and comprehensive means of simultaneously assessing a broad range of environmental considerations. Building environmental rating methods offer a means to demonstrate that a building has been successful at meeting an expected level of performance in a number of declared criteria. They provide building owners with a credible and objective means to communicate to prospective tenants the environmental qualities of the building they are leasing and, by emphasizing more demanding performance goals and the benefits over typical practice, they offer the potential for reframing expectations.

Building environmental assessment methods typically consist of three major components:

- A declared set of environmental performance criteria organized in a logical fashion – the *structure*
- The assignment of a number of possible points or credits for each performance issue that can be earned by meeting a given level of performance – the *scoring*
- A means of showing the overall score of the environmental performance of a building or facility – the *output*

Deriving a final aggregate "score" invariably requires some form of "weighting" – either implicitly or explicitly – being applied to the constituent criteria to reflect their relative significance within the overall measure of performance. This weighting process, which can profoundly influence the final overall building performance designation, has consistently represented a key part of discussions on building environmental performance. Key issues here relate to need to establish a more rational basis for the derivation of weightings, how these reflect regional priorities, and whether they should be implicit or explicit in the scoring process.

The development of assessment methods has, for the main part, been driven by the scoping and structuring of performance criteria. Although it is generally accepted that environmental criteria must be organized in ways that facilitate meaningful dialogue and application, the structuring of criteria within the assessment method is most important during the *output* of the performance evaluation, when the "story" of the performance must be told in a coherent and informative way to a variety of different recipients. Gann et al. [2] indicate that the "methods by which results are depicted has a direct bearing on how the indicators are used and understood – and by whom." The Japanese *Comprehensive Assessment System for Building Environmental Efficiency* (CASBEE) [3], for example, explicitly distinguishes between the way that performance information is organized during the assessment process and how it is transformed to communicate a variety of different outputs. It uses a variety of different output formats, providing the opportunity to tell different "stories" about a building's performance – an overall performance as well as more detailed descriptions. Moreover, CASBEE, while employing an additive/weighting approach, breaks away from the simple addition of points achieved in *all* performance areas to derive an *overall* building score, which has been the dominant feature of all previous methods. It distinguishes between the *Environmental Loading* (resource use and ecological impacts) and *Environmental Quality and Performance* (indoor environmental quality and amenities), scoring them separately to determine the Building Environmental Efficiency, that is, the ratio of *Environmental Quality and Performance* to *Environmental Loading*. As such, the structure of the CASBEE itself conveys an eco-efficiency view of assessment.

Given that assessment methods function as voluntary, market place mechanisms, ensuring that the methods are simple, practical, and inexpensive in both use and maintenance is deemed paramount. This simple characterization of building environmental issues has both positive and negative impacts on building design. For owners and design teams beginning to address environmental issues, the simplicity provides

a straightforward means of discovering what is important and what is not important. As such assessment methods can be an instrument for changing design practice by identifying a new standard of performance that encourages architects and engineers to break old habits and design norms. However, building environmental methods may, indirectly, detract from a more fundamental professional commitment to environmental responsibility. Currently, design teams and owners use assessment methods to collectively establish an overall desired "score" – a BREEAM "Excellent" or "Very Good," or a US Leadership in Energy and Environmental Design (LEED®) [4] "Gold" or "Silver" rating – and then review the range of individual performance criteria to identify those seen as being attainable. There is concern that "checklist" type environmental assessment methods may drive the product and process where simply achieving a high score, with many important gains, may prove more important than aspiring to the best overall product.

Environmental Assessment Methods

Assessment implies measuring how well or poorly a building is performing, or is likely to perform, against a declared set of criteria. Most current building assessment methods attempt to measure improvements in the environmental performance of buildings relative to current typical practice or requirements and have the following general characteristics:

- Are technically framed and emphasize the assessment of resource use, ecological loadings, and health and comfort in individual buildings
- Are primarily concerned with mitigation – reducing stresses on natural systems by improving the environmental performance of buildings
- Assess performance relative to explicitly declared or implicit benchmarks and, as such, measure the extent of improvement rather than proximity to a defined, desired goal
- Assess design intentions and potential as determined through prediction rather than actual real-world performance
- Structure performance scoring as a simple additive process and use explicitly declared or implicit weightings to denote priority
- Offer a performance summary, certificate, or label that can be part of leasing documents and promotional documents

Building environmental assessment is now a distinct and important realm of research and inquiry that seeks to develop greater refinement and rigor in performance indicators, weighting protocols, and, where appropriate, the potential incorporation of Life Cycle Assessment (LCA) approaches to refine the constituent measures. Moreover, it has provided numerous side-by-side comparisons of the more notable methods and tools (e.g., BREEAM, LEED®, CASBEE, and the Australian Green Star) to illustrate areas of convergence and distinction, typically as a starting point for generating applicable methods in other regions or countries seeking to develop new assessment schemes. Within this debate, the scope of comparison and analysis is typically based only on technical content (e.g., the framework) and makes little or no reference to the organizational or market context within which the methods operate; that is, comparisons are made indiscriminately between tools and methods. This represents a serious problem since the context within which an assessment method has been designed to operate profoundly affects the effective scope, emphasis, and rigor of an assessment.

Although initially introduced to perform a specific assessment role as a means to counter-act unverified claims of building performance – "green-wash" – building environmental assessment methods play a qualitatively different role in today's context. There are several emerging issues that increasingly frame the use of building assessment methods:

- Assessment methods have moved beyond voluntary market place mechanisms. Performance thresholds in the assessment methods (e.g., LEED® Gold) are increasingly being specified by public agencies and other organizations as performance requirements, and are being considered as potential incentives for development approval, bonus density, and other concessions.
- Building environmental assessment is increasingly being recognized by banking, financial, and insurance companies as a basis for risk and mortgage appraisals and real estate valuations.

- With more widespread adoption of assessment tools, compliance with performance requirements increasingly affects associated manufacturing industries. While some industries use this as an opportunity to reevaluate production processes, some become increasingly resistive.
- The range of building types seeking certification is increasing and this, in turn, is creating the need either to develop generic systems that can recognize distinctions on an as-needed basis for specific situations or to create a suite of related methods and tools, each of which uniquely addresses a particular building type.
- The need to permit easy access to tools and methods, and to enable assessments to be made quickly and cheaply, is spurring the increased deployment of Web-based methods and electronic submission processes to attain certification.
- The aggregate effect of individual buildings has enormous consequence for community infrastructure design and operation. This, together with the inherent limitation of analyzing individual buildings as the basis to understand ecological impacts, has generated interest in creating and linking assessment methods and tools across a variety of scales.
- Increased awareness of the inevitability of climate change has extended the approach from solely one of mitigation to now embrace adaptation to changing conditions and the conscious restoration of previously degraded natural systems.

Proliferation of Building Environmental Assessment Methods

The field of building environmental assessment has matured remarkably quickly since the introduction of BREEAM, and the interim period has witnessed a rapid increase in the number of methods either in use or being developed worldwide. Within this relatively short time period, successive generations of systems have evolved as a result of accumulated experience, new conceptual insights, and theoretical propositions. Different systems have greater strengths and weaknesses than others, and later systems draw on these to include features and elements that permit more effective use. The past decade has witnessed a proliferation of building environmental assessment methods by countries worldwide for application within their respective domestic markets (see Table 1). Many of these systems have made considerable conceptual advances over early, more established methods. To date, however, with the exception of three or four systems, the number of assessed buildings in many countries using the domestic systems remains modest. This lack of traction is primarily due to the lack of the organizational and financial resources required to support the necessary educational, management, and certification programs.

There is little doubt that building environmental assessment methods have contributed enormously to furthering the promotion of higher environmental expectations and are directly and indirectly influencing the performance of buildings. Assessment methods have enjoyed considerable success and their widespread awareness has created the critical mass of interest necessary to cement their role in creating positive change. "Success" is used here in reference to the way that assessment methods have entered the parlance of the building industry rather than the number of actual "assessed" and "certified" projects – which is still relatively low compared to the total number of buildings constructed annually [5].

A number of factors have collectively generated the early momentum of assessment methods:

- The prior absence of any means to both discuss and evaluate building performance in a comprehensive way left open a distinct niche within an emerging European and North American "culture of performance assessment."
- The simple, seemingly straightforward declaration of the requirements of a discrete number of performance measures presented a complex set of issues in a manageable form.
- By offering a recognizable structure for environmental issues, they provided a focus for the debate on building environmental performance.
- Public sector building agencies have used them as a means of demonstrating commitment to emerging environmental policies and directives.
- Manufacturers of "green" building materials and products have been given the opportunity to make direct and indirect associations with the relevant performance criteria, to support the sales of

Rating Systems for Sustainability. Table 1 Building environmental assessment methods and tools in use worldwide

Region	Country	Name	Owner/Management
Europe	France	HQE Method	HQE (*Haute Qualité Environnementale)*
	Finland	PromisE	VTT (Technical Research Centre of Finland)
	Germany	Sustainable Building Certificate	German Sustainable Building Council
	Italy	Protocollo ITACA	iiSBE Italia
	Norway	Envir. Programming of Urban Development	SINTEF (Skandinavias største uavhengige forskningsorganisasjon)
	Portugal	LiderA (Leadership for the Environment in Sustainable Building)	Instituto Superior Técnico, Lisbon
	Spain	VERDE	Spanish GBC
	Sweden	EcoEffect	Royal Institute of Technology
	Netherlands	BREEAM-NL	Dutch GBC
	UK	BREEAM (Building Research Establishment Environmental Assessment Method)	Building Research Establishment
	Europe	LEnSE (Label for Environmental, Social & Economic building)	Belgian Building Research Institute
N. America	United States	LEED® (Leadership in Energy and Environmental Design)	United States GBC
		GreenGlobes	Green Building Initiative
	Canada	LEED-Canada	Canada GBC
		GreenGlobes	ECD Canada
	Mexico	SICES	Mexico GBC
Asia	China	GHEM (Green Housing Evaluation Manual)	Ministry of Construction
		GOBAS (Green Olympic Building Assessment Scheme)	Ministry of Science & Technology
		ESGB (Evaluation Standards of Green Building)	Ministry of Housing and Urban-Rural Construction
	Hong Kong	BEAMPlus	HK-BEAM Society
		CEPAS (Comprehensive Environmental Performance Assessment Scheme)	HK Building Department
	India	TERI-GRIHA (Green Rating for Integrated Habitat Assessment)	TERI (The Energy & Research Institute)
		LEED-India	Indian GBC
	Japan	CASBEE (Comprehensive Assessment System for Building Environmental Efficiency)	Japan Sustainable Building Consort.
	Korea	GBCC (Green Building Certification Criteria)	Korean Korea Institute of Energy Research

Rating Systems for Sustainability. Table 1 (Continued)

Region	Country	Name	Owner/Management
	Singapore	Green Mark	Singapore Building & Construction Authority (BCA)
	Taiwan	EEWH (Ecology, Energy, Waste and Healthy)	ABRI (Architecture and Building Research Institute)
	Vietnam	LOTUS	Vietnam GBC
Southern H.	Australia	Green Star	Australian GBC
		NABERS (National Australian Building Environmental Rating Scheme)	
	Brazil	LEED-BRAZIL	GBC Brazil
		HQE	Fundação Vanzolini
	New Zealand	Green Star NZ	New Zealand GBC
	S. Africa	Green Star SA	South African GBC
		SBAT (Sustainable Building Assessment Tool)	CSIR (Council for Scientific and Industrial Research)
Generic		GBTool/SBTool	iiSBE (International Initiative for a Sustainable Built Environment)
		SPeAR (Sustainable Project Assessment Routine)	Ove Arup Ltd.

GBC – Green Building Council

"high" performance products. The range of environmental goals has led to the engagement of diverse professional expertise early in the design process with collaborative decision-making processes emerging.

Because of this momentum, building environmental assessment methods have dwarfed all other mechanisms for instilling environmental awareness within the building industry. Indeed, over the past decade they have been positioned as the most potent mechanism for affecting change.

Sustainability Assessment

The majority of current building environmental methods assess *environmental* performance improvements *relative* to typical practice, either implicitly or explicitly. They are also set within the parlance of marketing practice, and the intentions for such systems and the individual assessment credits that comprise them are understandable by all the stakeholders. Since its introduction in 1987, "sustainability" has emerged as a widely held and necessary overarching notion to frame and guide all future human activity and enterprise. An emerging debate on building assessment relates to shift from environmental or "green" performance to this larger goal of sustainability.

The need to develop methods of deliberation and decision making that actively engage the relevant interests of stakeholders will become increasingly important to infuse sustainability considerations into day-to-day conduct and practice. Robinson [6] suggests that the "power of sustainability lies precisely in the degree to which it brings to the surface these contradictions and provides a kind of discursive playing field in which they can be debated" and subsequently encourage the "development of new modes of public consultation and involvement intending multiple views to be expressed and debated." Again, the parallel debate in building environmental assessment is becoming increasingly evident. Kaatz, Root, and Bowen [7], for example, advocate the implementation of a broader participatory approach in building assessment, including consideration of process design, definition of desired outputs and outcomes, etc.

Sustainability relates to a suite of concepts and embraces notions other than environmental

performance, and as such is open to wider interpretation. However, it has two implicit requirements. Firstly, within the constituent dimensions of sustainability – environmental, social, and economic – is a responsibility to inter- and intra-generational equity. Secondly, sustainability, and any discussion of it, requires thinking long-term and assuming responsibility to the future. However, the ideal of the principles of sustainability is one thing, their assimilation and practice within the building industry is somewhat different. Whereas it is possible to define "green" and even "greener" as well as the incremental process for improving performance, it is currently difficult to envision and articulate a sustainable future – either in general terms or as related to the configuration of human settlement. It is therefore difficult to have confidence in the design of effective assessment systems when it is not possible to link them to final results. Moreover, short-sighted economic priorities and gains have always compromised environmental and social considerations in building.

Although the building development industry is fundamentally risk averse, this tendency is not evident in either recognizing or responding to larger environmental issues. Despite powerful arguments on the importance of environmental issues and evidence on the multiple benefits of early adoption of higher performance standards, the construction industry procrastinates in making changes that are perceived to increase initial cost. While the fundamental idea of economic sustainability relates to long-term and shared economic benefit, the short-term mind-set of the building industry is using the language of sustainability to maintain the status quo. What is increasingly evident at the level of the individual building is the notion of "economic sustainability" being appropriated as simply dealing with the costs of building production, and thereby relegating environmental performance issues to being included only if they make economic sense.

Sustainability Assessment Methods

The Living Building Challenge (LBC) [8], launched in August 2006, is emerging in North America as a recognized and complementary performance aspiration to LEED®. Rather than permitting choice of credits to attain an overall performance score, the LBC requires 20 demanding performance requirements – including net-zero energy – to be met before the designation of Living Building is granted. However, while it references natural systems and uses a flower/petals metaphor, there is no recognizable organization of the issues based on ecological or systems theory. Similar to LEED® and the majority of other current assessment methods, the structure is simply a list of required performance requirements set within a defined set of categories.

A number of assessment tools have been introduced that expand on the range of performance issues to explicitly include social and economic criteria and thereby attempt to provide a measure of "sustainable" performance:

- *Ove Arup's Sustainable Project Assessment Routine SPeAR®* [9]: Functions as a project assessment methodology within Ove Arup's consulting projects to enable a rapid review of the sustainability of projects, plans, products, and organizations. Performance criteria are organized in four general sustainability categories: *Environment (*Air Quality, Land Use, Water, Ecology and Cultural Heritage, Design and Operation, and Transport); *Natural Resources* (Materials, Water, Energy, Land Utilization, and Waste Hierarchy); *Economic* (Social Benefits and Costs, Transport, Employment/Skills, Competition Effects, and Viability); and *Societal* (Health and Welfare, User Comfort/Satisfaction, Form and Space, Access, Amenity, and Inclusion). The SPeAR® diagram combines, in a graphical format, the diverse issues that need to be considered in sustainable design, including social, economic, natural resource, and environmental issues, acknowledging both negative and positive results. SPeAR® can be used to highlight areas where a project/design/development performs poorly in terms of sustainability principles, and to identify opportunities to optimize performance, integrate best practice, or utilize new technology. SPeAR® provides a basis for evaluating a project's sustainability performance not in comparison with that of other buildings, but relative to strengths and weaknesses within a particular context. This permits a greater level of subjectivity in the definition of performance criteria and their interpretation during scoring.

- *iiSBE's Sustainable Building Tool (SBTool)* [10]: The current version of *SBTool* is arranged in seven Performance Issues: Site Selection, Planning, and Development; Energy and Resource Consumption; Environmental Loadings; Indoor Environmental Quality; Service Quality; Social and Economics Aspects; and Cultural and Perceptual Aspects. Whereas previous versions had focused on three distinct building types – Office buildings, Multi-Unit Residentials, and Schools – the current version allows a more generic description of buildings with multiple occupancies.
- *South African Sustainable Building Assessment Tool (SBAT)* [11]: Since the social and economic concerns in developing countries are far more pressing than those in developed countries, domestic constraints on environmental progress are therefore qualitatively different. SBAT explicitly introduces performance criteria that acknowledge social and economic issues [12]. A total of 15 performance areas are identified, equally divided within the overarching sustainability framework of environmental, social, and economic categories, each described through 5 performance criteria. Further, SBAT considers how it could become an integral part of, and subsequently influence, the building production process by relating its application to a nine-stage process based on the typical life cycle of a building: Briefing, Site Analysis, Target Setting, Design, Design Development, Construction, Handover, Operation, and Reuse/Refurbish/Recycle.
- *German Sustainable Building Council's Certificate Program* [13]: Five general sustainability "quality" categories are assessed and they form the overall aggregate building score: Ecological; Economic; Socio-cultural and Functional; Technical; and Process. A sixth quality with six sub-criteria – location – is evaluated and presented separately. Criteria within these performance areas are evaluated individually and aggregated to determine an overall performance designation of gold, silver, or bronze.

Robinson [6] suggests that if sustainability is to mean anything, "it must act as an integrating concept" and will require "new concepts and tools that are integrative and synthetic, not disciplinary and analytic; and that actively creates synergy, not just summation." When judged against these criteria, most current assessment methods and tools are left wanting in their ability to provide either insights or effective guidance on sustainability. A sustainable building is likely to be judged by the way that various systems fulfill multiple functions and, indeed, it is typically only possible to achieve high environmental performance within demanding cost and time constraints through the creative integration of systems. Similarly, while the three domains of environmental, social, and economic are typically used to frame sustainability, it is their points of intersection that are equally critical, that is, the ways and extent to which they positively or negatively influence each other. Simply adding social criteria to the current mix of environmental performance measures may not necessarily expose the way that one influences and is influenced by others. It can only do so if the method or tool is used as part of the deliberations between various stakeholders, that is, synergies are achieved through active, cross-disciplinary use of the tool, rather than simply the structure of the tool itself. That stated, it is important to ensure that environmental and social goals are not, yet again, compromised within this process.

Cross-Scale Assessment At a more pragmatic level, the notion of assessing the sustainability of an "individual" building is clearly problematic. Although one can assess the relative extent to which measures have been taken in an individual building to reduce resource use and ecological loadings, it is not possible to identify their effectiveness at addressing or furthering economic and social progress by relating them to regional or national indicators. Indeed, Gibberd suggests that "there is no such thing as a sustainable building – only buildings that enable people to live and work in sustainable ways" [14]. Assessing the ways and extent that buildings contribute progress toward sustainability will require understanding linkages across a range of scales.

Existing environmental assessment methods were primarily conceived to assess *individual* buildings, and performance issues are bounded by those factors that influence and are influenced by them. Many of the major building environmental assessment methods offer a suite of products each targeted at a specific building type or situation. The sequence in the

development of assessment methods is important in revealing the increasing acknowledgment of a broader context. The majority began with a version for new office buildings and then subsequently expanded the range of products to include existing office buildings, multi-unit residentials, and then other broader applications – schools, homes, etc. Several existing systems have recently introduced versions that address a broader context, for example, USGBC's *LEED for Neighbourhood Development (LEED-ND®), CASBEE for Urban Development (CASBEE-UD)* and *BREEAM Communities*. The fact that these were developed *after* gaining experience with assessing individual buildings is remarkably telling – development has been from the scale of individual buildings upward to that of a neighborhood scale rather than setting building performance within the overarching context of a neighborhood, community, or city.

Future Directions

There are several emerging trends that will shape the future design, roles, and use of assessment tools.

Voluntary and Regulatory Mechanisms

Given the pressing time-scale of anticipated significant climate change, it is difficult to imagine that a sustainable system of production and consumption will emerge from simply tweaking current practice. A key issue, therefore, lies in the considerable difference between the levels of change that the scientific community is advocating and those that are socially and politically acceptable. Similar arguments relate to the difficulties of making significant leaps forward in achieving widespread sustainable building practices within the acknowledged conservative and cost-sensitive context of the building industry. The majority of current "green" environmental assessment methods are voluntary in their application and have the primary objective of stimulating market demand for buildings with improved environmental performance. Indeed, the "acceptance" of current assessment methods currently derives largely from their voluntary application. However, the voluntary nature of existing methods significantly compromises both their comprehensiveness and rigor. Voluntary building environmental assessment methods must serve two conflicting requirements – they must function as an objective and sufficiently demanding metric to have credibility within the environmental community, while simultaneously being attractive to building owners who wish to have something positive to show for *any* effort that they have placed on environmental performance. Satisfying these twin requirements invariably compromises both the number of criteria that are assessed, where the benchmarks are set before performance points are earned and what is presented as the most demanding performance target.

Higher environmental performance requirements are increasingly being mandated bringing into question the ways that voluntary assessment methods will have to be cast within a broader array of mechanisms for creating necessary change. Here, the current success that assessment methods enjoy within both research and practice has potentially adverse consequences. By being almost the sole focus of the debate, too much expectation may be being placed on their ability to create the necessary change.

Given the practical (and incentive) constraints on setting demand targets and dependency on market acceptance, it is uncertain whether voluntary mechanisms will ultimately be sufficient to create the necessary improvements in environmental performance of buildings needed to meet broader national environmental or sustainability targets. As such, the relationship between building environmental assessment methods and other change instruments, both regulatory and incentive based, will gain in importance [15]. Historically, regulation provided minimal acceptable performance requirements, and the voluntary mechanisms offer the complementary high performance aspiration. Recently, the mandates of far reaching performance requirements such as carbon neutrality will profoundly change these roles. In Europe, for example, demanding energy and carbon emission standards for buildings are now being introduced requiring phased reductions to net-zero energy performance [16, 17]. In North America, the recent development of ASHRAE 189.1-2009 [18] jointly by the American Society of Heating, Refrigeration, and Air Conditioning Engineers (ASHRAE), the Illuminating Engineers Society (IES), and the US Green Building Council (USGBC) sets green building performance criteria within a regulatory framework.

Achieved Performance

The assessment of building environmental performance of new buildings is typically made at the design stage and based on default patterns of occupant behavior and building operation. There is sufficient evidence to show that a building's performance in use is often markedly different from that anticipated or predicted during design and this discrepancy has initiated a shift toward basing assessments on achieved performance.

The owners and developers of any of the major assessment systems are actively seeking data on the actual performance of buildings, particularly energy and water use, and energy-related emissions. The Canada Green Building Council (CaGBC), for example, adopted the 2030 Challenge which aims for net-zero buildings by 2030 [19] and has set targets of 50% measured reductions in energy and water use from a 2005 baseline for 100,000 buildings and 1,000,000 homes by 2015. These targets cover existing and new building stock, and represent 20% of all buildings in Canada, two-thirds of total building space, and 10% of all Canadian homes. To meet these targets, the CaGBC introduced the Green Building Performance Initiative in 2008 that involves performance benchmarking, auditing, action planning and verification have informed the development and testing. GREEN UP – Canada's Building Performance Program – is providing online tools, standards, and continuously updated performance information to building owners and managers across Canada [20]. The current program is addressing performance in energy and water use, and energy-related emissions, using monthly utility billing as the data source.

Building Valuation

The need to establish a business case for the development of "green" or/and sustainable commercial properties within the real estate industry has paralleled the technical development and application of building environmental assessment methods [21]. Although the possible capital cost premiums associated with attaining higher building environmental performance has been a recurring issue over the past 20 years, the emphasis of these economic considerations has changed considerably. Initially, the business case was framed around the added benefit and reduced revenue costs to the building owner. Today, however, the business case is increasingly rooted in the added value associated with higher building environmental performance and the demonstration that green buildings may be "worth more" to investors, owners, and tenants [22].

Whereas the cost arguments have consistently referenced building environmental assessments, for example, the cost of LEED [23, 24], very little attention has been directed at connecting green rating to value. CASBEE is the first system to introduce a version explicitly linking building environmental performance assessment with real estate appraisal. CASBEE for Property Appraisal [25] is an "appraisal support tool that measures the impact degree of [design for the environment] on the property value" that when widely applied will significantly increase the demand for green buildings.

Regionalization and Standardization

The past decade or so has witnessed many countries worldwide now either having or in the process of developing domestic systems. This carries the implicit expectation for domestic systems to encourage green building practices appropriate to their specific climatic and cultural contexts. Moreover, many of these systems include innovative conceptual advances over the earlier more established methods. With the exception of iiSBE's *SBTool* and the more recent *LEnSE* project [26] that have generic core frameworks and criteria but were designed from the outset to permit regional customization, the majority of recognized assessment methods are country or context specific. All assessment tools carry the values and priorities of their authors, either implicitly or explicitly, raising questions regarding the ways and extent that – without significant adaptation – they can be meaningfully adopted by other countries. Moreover, the organizational context in which assessment methods reside, that is, who owns and manages them, is critical in terms of the credibility of the method for the broad range of industry and client stakeholders, and the human and financial resources available to maintain and implement the method. These attributes are equally significant in the marketing and widespread use of systems internationally.

Similar to the necessity and value of developing standardized Life Cycle Assessment protocols for building materials and products, that is, universal criteria for establishing boundary conditions, data quality, etc., there is increased activity in defining standardized requirements for building assessment methods (e.g., ISO TG59/SC17: Sustainability in Building Construction) [27].

Given the proliferation of domestic assessment systems worldwide over the past 15 years, a number of developments are now pushing toward increased standardization. A primary driver for this development is organizations seeking a common international vocabulary for building environmental assessment that can then facilitate communication between stakeholders and inter-building and inter-country comparisons [28]. A recent development in Europe has been the establishment of the *Sustainable Building Alliance* (SBA) [28] and the *International Sustainability Alliance* (ISA) [29]. The French *Centre Scientifique et Technique du Bâtiment* (CSTB), UK *Building Research Establishment* (BRE), and others launched the *Sustainable Building Alliance* (SBA) in April 2008 with the aim of establishing common metrics for key issues so as to provide transparency between rating systems while, importantly, still recognizing regional and national differences.

The BRE initiated the International Sustainability Alliance (ISA) in late 2009 to "drive the development of common international standards for real estate" by providing an international governance structure that "join forces with international companies, Green Building Councils, research institutes and other stakeholders in the real estate chain toward an international sustainability standard for the built environment" [30]. ISA stated goals include:

- Driving toward one single European certification standard, adaptable to local market conditions
- Expanding on the current BREEAM system and creating a third Generation System for the market and industry

Methods are owned and operated by a wide range of private and public sector organizations. However, one of the most significant developments regarding the organizational context for building environmental assessment methods is the increase in the number of *Green Building Councils* [31], their linkage through the *World Green Building Council (WorldGBC)* [32], and their sharing experiences with using assessment methods. Two aspirations with the World GBC's mission are to ensure Green Building Councils are successful and have the tools necessary to advance and to support effective green building rating systems. The ways and extent to which the various member Councils favor certain assessment tools remain uncertain at this time.

Branding

An often-stated role and expectation is that the widespread adoption of assessment methods could ultimately transform the market in its expectation and demand for buildings with higher environmental performance. Almost all current building environmental assessment methods are voluntary in their application and have the primary objective of stimulating market demand for buildings with improved environmental performance. This has been accompanied by the notion of "branding" the names of LEED® and BREEAM to building owners, purchasers, and lessors to make them synonymous with high levels of environmental performance and companion mechanisms such as the LEED Accredited Professional program to "transform" expectations and valuation of skills and knowledge of design professionals. While "branding" the assessment methods domestically is obviously a necessary process for their promotion and adoption, there is also a clear shift to the support for a few international "brand-name" systems. The primary drivers here include:

- Multinational companies who have building/development projects worldwide and who are expected to adhere to numerous national environmental assessment methods
- Corporations/companies that need to acquire green buildings when they are operating internationally to fulfill their corporate sustainability requirements
- Manufacturers of green building products who are expected to adhere to numerous national environmental assessment methods

BREEAM and LEED® are two of the oldest and most widely internationally recognized systems and, by virtue of this, have the greatest presence outside

their countries of origin. They are also being increasingly positioned as being in competition within a global market [33, 34].

BREEAM Abroad Early in its development, there was a declared aspiration that BREEAM would have an international presence. In 1997, Doggart and Baldwin reported that "BREEAM type schemes have now been developed in other countries and regions, such as Hong Kong and Canada" and that "BREEAM versions are also being developed in Denmark, Norway, Australia, New Zealand and USA" [35]. While this did not materialize, the need for some level of regional adaptation was also explicitly referenced.

BRE Global now presents BREEAM as "the world's leading environmental assessment method for buildings and now communities" [36] with over 110,000 buildings certified and over half a million registered for certification [37]. BREEAM is currently having influence internationally in terms of using *BREEAM Bespoke International* or country-specific versions. Versions of BREEAM have been created for Europe and the Gulf, a country-specific version for the Netherlands, and Memorandum of Understanding has been signed between BRE Global and a group in Spain and with the Russian and Turkish GBCs, for the introduction into those respective countries.

LEED Abroad LEED® is having influence beyond the USA in terms of various countries adapting the system for their own markets or through overseas owners having buildings assessed through the USGBC:

- The Canadian and Indian Green Building Councils have created adaptations of LEED®, while groups in Brazil, Argentina, Italy, and a dozen other countries are developing/using adaptations of LEED® [38].
- The recent creation of the Green Building Certification Institute (GBCI) – established with the support of the USGBC – allows for "balanced, objective management of the LEED Professional Accreditation program, including exam development, registration, and delivery." As of January 2010, the GBCI's website records that LEED Accredited Professions are currently in 84 countries worldwide, the largest being: USA, 126,750; Canada, 1,314; China (including Hong Kong), 936; UAE, 622; UK, 280; India, 267; South Korea, 212; Mexico, 106 [39].

While the picture is not entirely clear regarding the extent of use of the BREEAM and LEED® internationally, with registered/certified projects in 103 countries the LEED® "brand" appears to currently have the greater uptake globally. Domestic and international property developers appear to be becoming increasingly interested in certifying their buildings to LEED® in order to attract these companies to move in. It is anticipated that as more and more companies move into the China market, the demand for LEED® certified buildings will further increase.

Building environmental assessment and labeling programs are considered one of the most potent and effective means to both improve the performance of buildings and transform market expectations and demand. Indeed, the environmental performance assessment of buildings is now a major business, with significant revenues generated through the certification process, licensing of the systems, training and education, and the accrediting of professionals. Many countries around the world clearly have domestic methods that will remain the sole or dominant system within their respective markets, for example, Green Star in Australia and New Zealand, CASBEE in Japan, and Green Mark in Singapore. However, there are many other countries and regions where BREEAM, LEED®, and other systems will expand their presence over the next decade as a result of increased demand and active promotion. Market forces and "branding" will, in the fullness of time, invariably play a role in dictating the extent to which voluntary systems become de facto international approaches. While there are numerous benefits for consistency in how certain performance measures are defined and evaluated, such as energy and carbon emissions, the ways and extent that methods both recognize and accommodate cultural and contextual differences when deployed internationally will remain decisive in shaping a positive outcome.

Given the increased deployment of the major systems internationally and the significance of global building practices, it is also highly likely that there will be some level of harmonization between the major tools to enable international benchmarking, especially in relation to greenhouse gas emissions,

that is, the introduction of a commonly recognized standard/metric for measuring and recording energy use and carbon emissions, which could be adopted by multiple tools.

The benefits of assessment methods have been considerable: providing more comprehensive performance goals for buildings, supporting collaborative design processes, changes in economic investment, changes in industry, international collaboration, etc. They will continue to evolve in response to a host of current challenges such as ensuring that delivered performance matches design intentions, accommodating community and regional goals and priorities, and supporting a more comprehensive integration of human and natural systems.

Acknowledgments

In addition to the specific references, the content of this article draws on following previous published works:

Cole RJ (2005) Building Environmental Assessment Methods: Redefining Intentions and Roles, Building Research & Information, 35:5, pp 455–467

Cole RJ (2006) The Coexistence of Building Environmental Assessment Methods in Common Markets, Building Research & Information, 34:4, pp 357–371

Cole RJ (2009) Chapter 18: Environmental Assessment: Shifting Scales, IN: Designing High-Density Cities for Social & Environmental Sustainability, Ed: Edward Ng, Earthscan Press, pp 273–282

Cole RJ (2010) Building Environmental Assessment in a Global Market, International Journal of Sustainable Building Technology and Urban Development, 1:1, pp 11–14

Bibliography

1. Baldwin R, Leach SJ, Doggart J, Attenborough M (1990) BREEAM version 1/90: an environmental assessment for new office designs. Building Research Establishment, Garston
2. Gann DM, Salter AJ, Whyte JK (2003) The design quality indicator as a tool for thinking. Build Res Inform 31(5):318–333
3. CASBEE, Comprehensive assessment system for building environmental efficiency, Japan Sustainable Building Consortium Corps
4. Leadership in energy and environmental design (LEED) Green building rating System, US green building council
5. Cole RJ (2005) Building environmental assessment methods: redefining intentions and roles. Build Res Inform 35(5):455–467
6. Robinson J (2004) Squaring the circle? some thoughts on the idea of sustainable development. Ecol Econ 48: 369–384
7. Kaatz E, Root D, Bowen P (2004) Implementing a participatory approach in a sustainability building assessment tool. In: Proceedings of the sustainable building Africa 2004 conference, Stellenbosch, South Africa (CD Rom, Paper No. 001), 13–18 Sept 2004
8. LBC (2010) Living building challenge version 2.0. International Living Building Institute, Seattle, WA
9. Sustainable Project Assessment Routine (SPeAR®) http://www.arup.com/environment/feature.cfm?pageid=1685
10. iiSBE (International Initiative for a Sustainable Built Environment) (2010) Sustainable building tool. http://www.iisbe.org
11. Gibberd J (2001) The sustainable building assessment tool – assessing how buildings can support sustainability in developing countries. Continental shift 2001 – IFI international conference, Johannesburg, South Africa, 11–14 Sept 2001
12. Gibberd J (2005) Paper 04–001, Assessing sustainable buildings in developing countries – The Sustainable Building Assessment Tool (SBAT) and The Sustainable Building Lifecycle (SBL). The 2005 world sustainable building conference, Tokyo 27–29 Sept 2005
13. German Sustainable Building Council's Certificate Program. http://www.gesbc.org/
14. Gibberd J (2001) The opinion of Gibberd. Sustain Build (3):41
15. Cole RJ (1999) Building environmental assessment methods: clarifying intentions. Build Res Inform 27(4/5):230–246
16. European Parliament (2009) Press release. www.europarl.europa.eu/sides/getDoc.do?pubRef=–//EP//TEXT+IM-PRESS+20090330IPR52892+0+DOC+XML+V0//EN&language=EN. Last accessed Sept 2009
17. Department for Communities and Local Government (2006) Code for sustainable homes: a step-change in sustainable home building practice. www.communities.gov.uk.
18. ASHRAE/USGBC/IES, Standard 189.1-2009, Standard for the design of high-performance green buildings (Except low-rise residential buildings), American society of heating, Ventilation and air conditioning engineers, Atlanta, Georgia
19. 2030 Challenge, The 2030 Challenge was issued by Architecture 2030, a non-profit organization. www.architecture2030.org.
20. Jarvis IA (2009) Closing the loops – how real building performance data drives continuous improvement. Intell Build Int 1(4):269–276
21. Lorenz D, Lützkendorf T (2008a) Sustainability in property valuation – theory and practice. J Property Investment Finance 26(6):482–521
22. Sayce S, Sundberg A, Mohd A (2009) Sustainable property: a premium product? A working paper, Paper presented at ERES Conference 2009, Stockholm, 24–27 June 2009
23. Kats, Gregory (2003b) The costs and financial benefits of green building: a report to california's sustainable building task force. California: Capital E. October. www.usgbc.org/Docs/News/News477.pdf

24. Matthiessen Lisa F, Peter M (2004) Costing green: a comprehensive cost database and budgeting methodology. Davis Langdon Adamson, Los Angeles
25. CASBEE for property appraisal, Japan Sustainable Building Consortium Corps. December 2009
26. LEnSE (Methodology Development towards a Label for Environmental, Social and Economic Buildings) (2006). "Stepping Stone's 1,2 & 3," LEnSE Partners, November 2006
27. ISO CD 21931, Framework for methods for assessment of environmental performance of construction works – Part 1 – Buildings, international organization for standardization, standard under development ISO TG59/SC17: sustainability in building construction
28. Visier JC (2009) Common metrics for key issues. SB alliance annual conference Paris, 5 Nov 2009
29. Sustainable Building Alliance. http://www.sballiance.org/
30. International Sustainability Alliance. http://www.bre.co.uk/page.jsp?id=2019
31. Green Building Councils. Country based members of the World Green Building Council – either established members, emerging members or prospective members
32. World Green Building Council founded in (1999) http://www.worldgbc.org/
33. Julien A (2009) Assessing the assessor: BREEAM VS LEED. Sustain Mag 9(6):30–33
34. Online (2009) BREEAM V LEED, Onoffice Magazine, May 2009
35. Doggart J, Baldwin DR (1997) BREEAM international: regional similarities and differences of an international strategy for environmental assessment of buildings. In: Proceedings second international conference: buildings and the environment, Paris, pp 83–90
36. BRE Global (2010) http://www.bre.co.uk/page.jsp?id=1763
37. BRE Global (2009) BREEAM – The environmental system for buildings around the world
38. LEED International Program. http://www.usgbc.org/DisplayPage.aspx?CMSPageID=2346
39. Numbers of LEED Accredited Professionals worldwide.http://www.gbci.org/DisplayPage.aspx?CMSPageID=113

Rechargeable Batteries, Separators for

Shriram Santhanagopalan, Zhengming (John) Zhang
Celgard, LLC, Charlotte, NC, USA

Article Outline

Glossary
Definition of the Subject
Introduction and Scope
Separator and Batteries
Separator Classification
Separators for Lithium-Ion Batteries
Separator for Lithium Polymer Batteries
Separator for Lithium-Ion Gel Polymer Batteries
Separator for Aqueous Batteries
Mathematical Modeling of Separators
Summary
Future Directions
Acknowledgments
Bibliography

Glossary

Dry process A process used to make a separator, which involves melting a polyolefin resin and extruding it into a film, thermal annealing to increase the size and amount of lamellar crystallites, and stretching to form tightly ordered micro pores.

Gurley A measure of time taken for a predetermined quantity of air (or other specified fluid) to permeate across a porous membrane.

Nonwoven separators Sheet, web, or matt of directionally or randomly oriented fibers, bonded by friction, and/or cohesion, and/or adhesion excluding paper and products which are woven, tufted, stitch-bonded incorporating binding yarns or filaments, or felted by wet milling.

Separator A porous membrane placed between electrodes of opposite polarity, permeable to ionic flow but preventing electronic contact between the electrodes.

Shutdown separator A separator that responds to increasing heat within a cell, by closure of the pores, such that it stops ionic flow between the anode and cathode, during a thermal event.

Wet process A process used to make a separator that involves a solvent.

Definition of the Subject

The battery industry has undergone tremendous growth over the last couple of years – both in terms of technological growth as well as in the variety of applications. The need to optimize battery materials to meet the increasing demand for energy as well as to extend the operating range continues to be a challenge – more so now than ever before. Correspondingly, the demand for novelty in separator membranes

to match the newer battery chemistries and geometries continues to grow.

A separator is a porous membrane placed between electrodes of opposite polarity, permeable to ionic flow but preventing electronic contact between the electrodes [1, 2]. A variety of separators have been used in batteries over the years – from cedar shingles and sausage casing to present-day microporous flat sheet membranes made from polymeric materials. Their main function, however, continues to be the same – to keep the positive and negative electrodes apart. They should be very good electronic insulators and have the capability of conducting ions by either intrinsically being an ionic conductor or by soaking an electrolyte. They should minimize any processes that adversely affect the electrochemical energy efficiency of the batteries.

The separator is among the components that have sustained maximum growth in the battery industry with minimal changes to the material ingredients. Not much attention has been given to separators even in publications reviewing batteries [1–7]. The number of reviews on separators [8–17] is minimal compared to those on cell fabrication, their performance, and application in real life. Kinoshita et al. have reviewed different types of membranes/separators used in different electrochemical systems, including batteries [9]. Zhang presented a more recent review of the various separators used in liquid electrolyte systems [10]. This chapter is largely based on the work of Arora and Zhang [4].

The majority of the separators currently used in batteries were typically developed as spin-offs of existing technologies. They were usually not developed specifically for those batteries and thus were not completely optimized for battery systems in which they are currently used. One positive result of adapting existing technologies is that the separators are produced in high volumes at relatively low cost. The availability of low-cost separators is an important consideration in the commercialization of batteries, since the battery industry traditionally operates with thin profit margins and relatively small research budgets.

Introduction and Scope

The battery industry has seen enormous growth over the past few years in portable, rechargeable battery packs. The majority of this surge can be attributed to the revolution in the use of multimedia in mobile phones and personal digital assistants (PDAs), as well in laptop computers and other wireless electronics devices. The introduction of vehicles implementing rechargeable batteries has increased the demand for batteries by several-fold. Batteries remained the mainstream source of power for systems ranging from mobile phones and personal digital assistants (PDAs) to electric and hybrid electric vehicles. The world market for batteries was approximately $41 billion in 2000, which included $16.2 billion primary and $24.9 billion secondary cells [20]. In 2010, the global demand was placed at $71 billion.

The Freedonia group estimates [21, 22] the aggregate US demand for primary and secondary batteries to be $16.8 billion in 2012 and that China will surpass the USA as the largest market with an estimated average annual growth at 7%. This growth will be driven by strong demand for battery-powered electronic devices like digital cameras and 3G wireless phones, increasing production of electrical and electronic equipment and the expansion in the automotive sector in the near future. The secondary battery demand has outpaced the primary battery market gains benefiting from strong growth in the use of high-drain portable electronic devices.

The tremendous progress in lithium-ion cells is clearly visible with as much as a threefold increase in the volumetric and gravimetric energy storage capability for both 18650 and prismatic cells between their initial introduction in the early 1990s and 2010. In last few years the lithium-ion production has expanded in South Korea (Samsung SDI, LG Chemical, etc.), China (ATL BYD, B&K, and Lishen, among others), and Japan. Several Japanese (Sanyo, Sony, MBI, NEC, etc.) and Korean (LG Chemical) manufacturers have also moved their manufacturing plants to China [23]. Japan, which controlled 94% of the global rechargeable battery market in 2000, has seen its market share drop to less than 50% of the global market [22, 24, 25]. The continued growth in lithium-ion battery market has led to a strong demand for battery separators. All the major separator manufacturers (Celgard, Asahi, and Tonen) have continually increased their capacity since 2003 [24, 26–29]. The industry has also witnessed the emergence of several new entrants [30–33].

There is not much information available on battery separator market in the literature. In 2009, it was estimated that about 50% of the rechargeable lithium battery market is the size of the components market, and separators constitute about 17% of this volume [22]. The Freedonia Group reported that the US demand for battery separators increased to $410 million in 2007 from $237 million in 1977, and $300 million in 2002, respectively [21, 22, 25].

The purpose of this chapter is to describe separators used in secondary batteries and characterization of their chemical, mechanical, and electrochemical properties, with particular emphasis on separators for lithium-ion batteries. The separator requirements, properties, and characterization techniques are described with respect to lithium-ion batteries. Despite the widespread use of separators, a need still exists for improving the performance, increasing its life, and extending the operating range.

Separator and Batteries

Batteries are built in many different shapes and configurations – button, flat, prismatic (rectangular), and cylindrical (AA, AAA, C, D, 18650 etc.). The cell components (including separators) are designed to accommodate a particular cell shape and design. The separators are either stacked between the electrodes or wound together with electrodes to form jellyrolls as shown in Fig. 1. Stacked cells are generally held together by pressure from the cell container. The lithium-ion gel polymer stacked cells are prepared by bonding/laminating layers of electrodes and separators together. The separator properties should not change significantly during the bonding process. In some cases, the separators are coated to help in bonding process and reduce the interfacial resistance [34, 35].

In the conventional way of making spirally wound cells, two layers of separators are wound along with the positive and negative electrodes, resulting in separator/negative/separator/positive configuration. They are wound as tightly as possible to ensure good interfacial contact. This requires the separators to be strong to prevent any contact between the electrodes through the separator. The separator also must not yield and reduce in width, or else the electrodes may contact each other. Once wound, the jellyroll is inserted into a can and filled with electrolyte. The separator must be wetted quickly by the electrolyte to reduce the electrolyte filling time. A header (cap) is then crimped onto the cell to cover the can top. In some prismatic cells, the electrode stack is pressed at high temperatures and pressures and then inserted into thin prismatic (rectangular) cans. A typical 18650 lithium-ion cell uses around 0.07–0.09 m^2 of separator, which is approximately 4–5% of the total cell weight [36].

A number of factors must be considered in selecting the best separator for a particular battery and application. The characteristics of each available separator must be weighed against the requirements and one selected that best fulfills these needs. A wide variety of properties are required of separators used in batteries. These include:

- Electronic insulator
- Minimal electrolyte (ionic) resistance
- Mechanical and dimensional stability
- Sufficient mechanical strength to allow easy handling
- Chemical resistance to degradation by electrolyte, impurities, and electrode reactants and products
- Effectiveness in preventing migration of particles between the two electrodes
- Readily wetted by electrolyte
- Uniformity in properties such as thickness, resistance, etc.

The above list presents a broad spectrum of requirements for separators in batteries. The order of importance of the various criteria varies, depending on the battery applications. In many applications, a compromise in requirements for the separator must be made to optimize performance, safety, cost etc. For example, batteries that are characterized by small internal resistance and consume little power require separators that are highly porous and thin; but the need for adequate physical strength may require that they be thick.

In addition to the above general requirements each battery type may have other specific requirements essential for good performance and/or safety. One typical example is that the separator used in sealed Nickel Metal Hydride (NiMH) batteries should be permeable to gas molecules for overcharge protection.

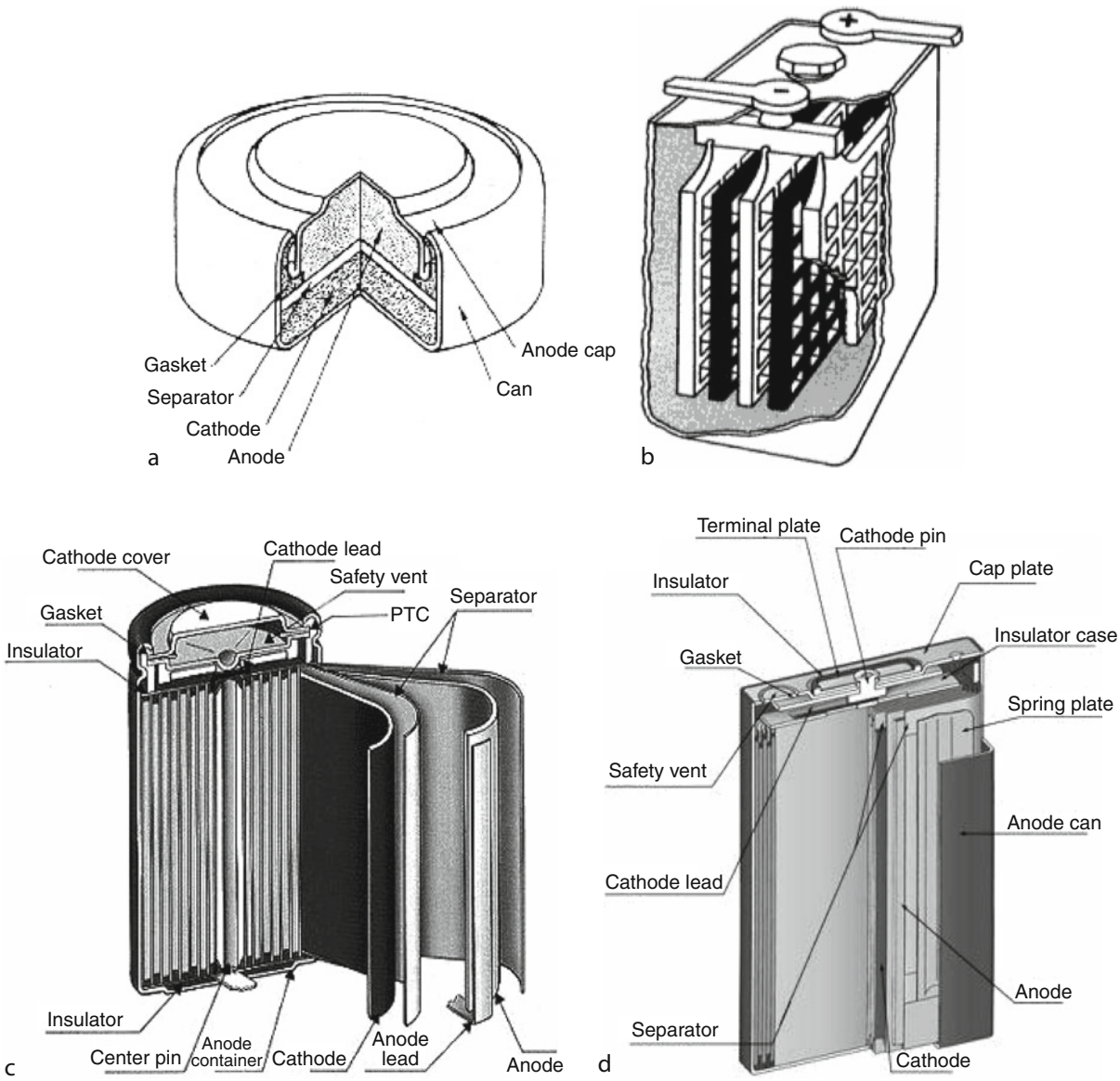

Rechargeable Batteries, Separators for. Figure 1
Typical battery configurations (**a**) button cell, (**b**) stack lead acid, (**c**) spiral wound cylindrical lithium-ion; (**d**) spiral wound prismatic lithium-ion

Separator Classification

Separators for batteries can be divided into different types, depending on their physical and chemical characteristics. They can be molded, woven, nonwoven, microporous, bonded, papers, or laminates. In recent years, there has been a trend to develop solid and gelled electrolytes that combine the electrolyte and separator into a single component.

In most batteries, the separators are either made of nonwoven fabrics or microporous polymeric films. Batteries that operate near ambient temperatures usually use separators fabricated from organic materials such as cellulosic papers, polymers, and other fabrics, as well as inorganic materials such as asbestos, glass-wool, and SiO_2. In alkaline batteries, the separators used are either regenerated cellulose or microporous

polymer films. The lithium batteries with organic electrolytes mostly use microporous polymer films.

For the sake of discussion, the separators have been divided into six types – microporous films, nonwovens, ion-exchange membranes, supported liquid membranes, solid polymer electrolytes, and solid ion conductors. A brief description of each type of separator and their application in batteries are discussed below.

Microporous Separators

Separators are fabricated from a variety of inorganic, organic, and naturally occurring materials and generally contain pores that are greater than 50–100 Å in diameter. Materials such as nonwoven fibers (e.g., nylon, cotton, polyesters, glass), polymer films (e.g., polyethylene (PE), polypropylene (PP), polytetrafluoroethylene (PTFE), polyvinyl chloride (PVC)), and naturally occurring substances (e.g., rubber, asbestos, wood) have been used as microporous separators in batteries that operate at ambient and low temperatures (−40°C to 100°C). The microporous polyolefins (PP, PE, or laminates of PP and PE) are widely used in lithium-based nonaqueous batteries. More recently, other polymers have been employed, especially to enhance the window of temperature across which the polymer remains stable.

Nonwovens

Nonwovens are textile products that are manufactured directly from fibers. They are defined as a manufactured sheet, web, or matt of directionally or randomly oriented fibers, bonded by friction, and/or cohesion, and/or adhesion excluding paper and products which are woven, tufted, stitch-bonded incorporating binding yarns or filaments, or felted by wet milling whether or not needed. The fibers may be of natural or man-made origin. They may be staple or continuous filaments or maybe formed in situ [37].

The macroporous fibrous matrix is either dry laid, meltblown, or wet laid. The wet laid process is very similar to papermaking process. The fibers are bonded together by chemical or thermal bonding. The meltblown process is a binderless process and there the polymer fiber web is extruded. Typical pore size of fibrous matrix varies from 1 to 100 μm.

Nonwovens are widely utilized as separators for several types of batteries. Light-weight, wet laid nonwovens made from cellulosic, polyvinyl alcohol, and other fibers have achieved considerable success as separators for popular primary alkaline cells of various sizes. The key nonwoven attributes include consistently uniform basis weight, thickness, porosity, and resistance to degradation by electrolytes. Nonwovens are also successfully employed as separators in NiCd cells.

The materials used in nonwoven fabrics include a single polyolefin, or a combination of polyolefins, such as polyethylene (PE), polypropylene (PP), polyamide (PA), polytetrafluoroethylene (PTFE), polyvinylidine fluoride (PVdF), and polyvinyl chloride (PVC). Nonwoven fabrics have not been able to compete with microporous films in lithium-ion cells. This is primarily because of the inadequate pore-size structure and difficulty in making thin (<25 μm) nonwoven fabrics with acceptable physical properties. However, nonwoven separators have been used in button cells and bobbin cells when thicker separators and low discharge rates are acceptable.

Ion-Exchange Membranes

These membranes are generally fabricated from polymeric materials containing pores with diameters of less than 20 Å. The transport properties of ions in these membranes are characterized by strong interactions between the permeating species and the molecular structure of the polymer. This interaction is due to the presence of ion-exchange groups in the membrane, which allows the membrane to discriminate between permeating or migrating ions by virtue of their specific charge.

Radiation grafted membranes such as Permion® manufactured by RAI Research Corporation are ion-exchange membranes. Such membranes are used as battery separators in alkaline batteries. They are made from PE, PP, or Teflon-based films, which have excellent oxidation resistance and superior chemical resistance to alkali media. However, they are totally impervious to electrolyte flow, and therefore, have almost infinite resistance as a separator in this form. By using radiation grafting and cross-linking techniques, however, selected chemical species are grafted as pendant chains to the base structure of the linear

polymer without altering the inert backbone. This modification imparts desirable hydrophilic properties to the films without materially impairing their excellent chemical resistance. This chapter provides a very limited discussion on ion-exchange membranes, as their application in batteries is very limited.

Supported Liquid Membranes

These types of separators consist of a solid matrix and a liquid phase, which is retained in the microporous structure by capillary forces. To be effective for batteries, the liquid in the microporous separator, which generally contains an organic phase, must be insoluble in the electrolyte, chemically stable, and still provide adequate ionic conductivity. Several types of polymers, such as polypropylene, polysulfone, polytetrafluoroethylene, and cellulose acetate, have been used for porous substrates for supported liquid membranes. The PVdF-coated polyolefin-based microporous membranes used in gel polymer lithium-ion battery fall into this category. Gel polymer electrolytes/membranes are only discussed briefly.

Polymer Electrolyte

Polymer electrolytes (e.g., poly(ethylene oxide), poly (propylene oxide)) have attracted considerable attention for batteries in recent years. These polymers form complexes with a variety of alkali metal salts to produce ionic conductors that serve as solid electrolytes. Its use in batteries is still limited due to poor electrode/electrolyte interface and poor room temperature ionic conductivity. Due to its rigid structure it can also serve as the separator. Polymer electrolytes are discussed briefly in the section Separators for Lithium-Ion Batteries.

Solid Ion Conductors

They serve as both separator and electrolyte. These are generally inorganic materials that are impervious barriers to gases and liquids. They allow one or more kinds of ions to migrate through their lattice when a potential gradient or a chemical gradient is present. These types of separators are beyond the scope of this article.

Separators for Lithium-Ion Batteries

All lithium-based batteries use nonaqueous electrolytes because of the reactivity of lithium in aqueous solution and because of electrolyte's stability at high voltage. The majority of these cells use microporous membranes made of polyolefins. In some cases, nonwovens made of polyolefins are either used alone or with microporous separators. This section will mainly focus on separators used in secondary lithium batteries.

Lithium secondary batteries can be classified into three types, a liquid-type battery using liquid electrolytes, a gel-type battery using gel electrolytes mixed with polymer and liquid, and a solid-type battery using polymer electrolytes. The types of separators used in different types of secondary lithium batteries are shown in Table 1. The liquid lithium-ion cell uses microporous polyolefin separators while the gel polymer lithium-ion cells either use PVdF separator (e.g., PLION® cells) or PVdF-coated microporous polyolefin separators. The PLION® cells use PVdF loaded with silica and plasticizer as separator. The microporous structure is formed by removing the plasticizer and then filling with liquid electrolyte. These are also characterized as plasticized electrolyte. In solid polymer lithium-ion cells, the solid electrolyte acts as both electrolyte and separator.

Sony's introduction of the rechargeable lithium-ion battery in the early 1990s precipitated a need for new

Rechargeable Batteries, Separators for. Table 1 Types of separators used in different types of secondary lithium batteries

Battery system	Type of separator	Composition
Lithium-ion (liquid electrolyte)	Microporous	Polyolefins (PE, PP, PP/PE/PP)
Lithium-ion gel polymer	Microporous	PVdF
	Microporous	Polyolefins (PE, PP, PP/PE/PP) coated with PVdF or other gelling agents
Lithium polymer (e.g., Li-V_6O_{13})	Polymer electrolyte	Polyethylene oxide with lithium salt

separators that provided good mechanical and electrical properties. Since then, separators have played a significant role in improving the performance as well as safety of lithium battery technology. In 2010, 90% of the total rechargeable battery markets for mobile communication devices use lithium-based batteries whereas the nickel metal hydride batteries continue to dominate the automotive sector and a significant factor in the camera market as well as alternate to the alkaline primary cell.

The microporous polyolefin separator has been used extensively in lithium-ion batteries, since it is difficult for most other conventional separator materials to satisfy the characteristics required in lithium-ion batteries. In lithium-ion batteries two layers of separators are sandwiched between positive and negative electrodes and then spirally wound together in cylindrical and prismatic configurations. The pores of the separator are filled with an ionically conductive liquid electrolyte.

Microporous polyolefin membranes (see Fig. 2) in current use are thin (<30 μm) and are made of polyethylene (PE), polypropylene (PP), or laminates [38] of polyethylene and polypropylene. Polyolefin materials are preferred because they provide excellent mechanical properties, chemical stability, and acceptable cost [39, 40]. They have been found to be compatible with the cell chemistry and can be cycled for several hundred cycles without significant degradation in chemical or physical properties.

Commercial membranes offer pore size in the range of 0.03–0.1 μm, and 30–50% porosity. The low melting point of PE enables their use as a thermal fuse. As the temperature approaches the melting point of the polymer, 135°C for PE and 165°C for PP, the porosity of the membrane is lost. The trilayer material (PP/PE/PP) [41] has been developed by Celgard® where a PP layer is designed to maintain the integrity of the film, while the low melting point of PE layer is intended to shutdown the cell if an over-temperature condition is reached [42]. Asahi Kasai's flat-film membrane "Hipore™" is available in thicknesses ranging from 20 μm to several hundred micrometers, and with highly uniform pore sizes ranging from 0.05 to 0.5 μm [43]. The major manufacturers of lithium-ion battery separators along with their typical products are listed in Table 2.

In recent years there has been a strong demand for higher-capacity lithium-ion cells because of the strong growth in portable electronics. One way to achieve higher capacity is by reducing the thickness of separators. At present, battery manufacturers routinely use separators 16 μm or thinner in higher-capacity (>2.6 Ah) cylindrical cells and 9 μm separators in lithium-ion gel polymer cells.

Separator Development

The process for making lithium-ion battery separators can be broadly divided into dry and wet processes. Both processes usually employ one or more orientation steps to impart porosity and/or increase tensile strength. Dry process involves melting a polyolefin resin, extruding it into a film, thermal annealing to increase the size and amount of lamellar crystallites, and precisely stretching to form tightly ordered micropores [44–48]. In this

Rechargeable Batteries, Separators for. Figure 2
Polyolefin separators used in lithium-ion batteries

Rechargeable Batteries, Separators for. Table 2 Major manufacturers of lithium-ion battery separators along with their typical products

Manufacturer	Structure	Composition	Process	Trade name
Asahi Kasai	Single layer	PE	Wet	HiPore
Celgard Inc	Single layer	PP, PE	Dry	Celgard
	Multilayer	PP/PE/PP	Dry	Celgard
	PVdF coated	PVdF, PP, PE, PP/PE/PP	Dry	Celgard
Entek Membranes	Single layer	PE	Wet	Teklon
Mitsui Chemical	Single layer	PE	Wet	
Nitto Denko	Single layer	PE	Wet	
DSM	Single layer	PE	Wet	Solupur
Tonen	Single layer	PE	Wet	Setela
Ube Industries	Multilayer	PP/PE/PP	Dry	U-Pore

process, a row lamellar crystal structure is generated in the polymer in the initial extrusion step. This nonporous structure is highly oriented as a result of extrusion and annealing conditions. The films are then stretched to form micropores. This microporous structure is continuous throughout the bulk interior of the membrane [49].

Polypropylene and polyethylene microporous films obtained by this method are available from Celgard, [44, 46, 50, 51] and Ube [52]. The dry process is technologically convenient and environmentally benign because no solvents are required. However, biaxial stretching has been met with limited success to date and, as a result, the pores are slit-like in shape, and the mechanical properties of films are anisotropic. The tensile strength in the lateral direction is relatively low.

Wet process (phase inversion process) [53, 54] involves mixing of hydrocarbon liquid or some other low-molecular-weight substance generally with a polyolefin resin, heating and melting the mixture, extruding the melt into a sheet, orientating the sheet either in the machine direction (MD) or biaxially, and then extracting the liquid with a volatile solvent [55, 56]. Separators made by wet process are available from Asahi Kasei [57], Tonen [58–60], Mitsui Chemicals [57], and more recently from Polypore/Membrana and Entek [31]. The structure and properties of the membranes can be changed by controlling the composition of the solutions and the evaporation or removal of solvents in the gelation and solidification processes. The separators made by wet process use ultrahigh-molecular-weight polyethylene (UHMWPE). The use of UHMWPE gives good mechanical properties as well as some degree of melt integrity.

Ihm et al. have given an overview of the wet process by preparing a separator with polymer blends of high-density polyethylene (HDPE) and ultrahigh-molecular-weight polyethylene (UHMWPE) [54]. They showed that the mechanical strength and drawing characteristics are influenced by the content and the molecular weight of the UHMWPE contained in a polyolefin blending solution. The manufacturing process of typical microporous film by dry and wet process is compared in Table 3.

A simplified flowchart for separator manufacturing process is shown in Fig. 3 [61]. The virgin polymer is prepared and mixed with processing aids (e.g., antioxidants, plasticizer, etc.) and then extruded. The extruded polymer then goes through different steps, which vary from process to process. For dry process, it can involve film annealing and stretching, while for wet process, it can involve solvent extraction and stretching. The finished film is then slit into required widths and packed into boxes and shipped to the battery manufacturers. With the advent of thinner separators, the film handling during manufacturing steps has become very important for the final quality of the film.

Rechargeable Batteries, Separators for. Table 3 Manufacturing process of typical microporous film

Process	Mechanism	Raw material	Properties	Typical membranes	Manufacturers
Dry process	Drawing	Polymer	Simple process Anisotropic film	PP, PE, PP/PE/PP	Celgard, Ube
Wet process	Phase separation	Polymer + Solvent	Isotropic film	PE	Asahi, Tonen
		Polymer + Solvent + Filler	Large pore size High porosity	PE	Asahi

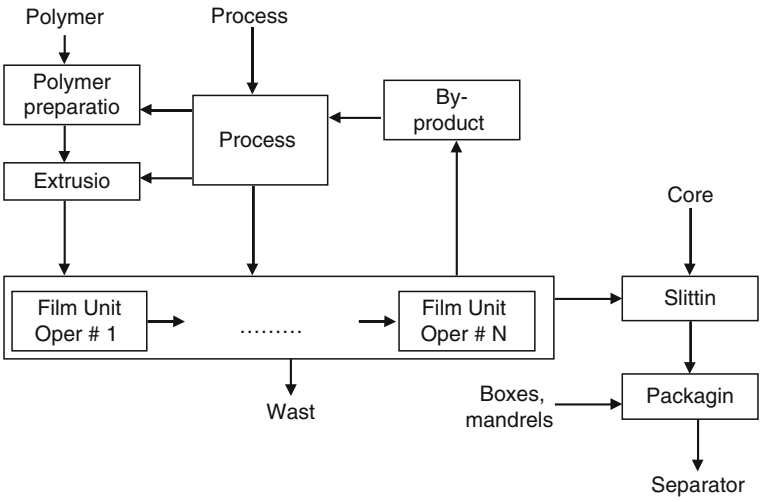

Rechargeable Batteries, Separators for. Figure 3
Generalized process for lithium-ion separator manufacturing [61]. Each step of the separator manufacturing process has online detection systems to monitor the quality of the separator

Each step of the separator manufacturing process has online detection systems to monitor the quality of the separators.

Uniaxially oriented films generally have high strength in only one direction, whereas biaxially oriented films are relatively strong in both machine direction (MD) and transverse direction (TD). However, biaxial orientation often tends to introduce TD shrinkage. This shrinkage, at elevated temperatures, can allow electrodes to contact each other. The separator must have sufficient strength in the machine direction so that it does not decrease in width or break under the stress of winding. The typical requirement for the mechanical strength in a 25-μm separator is 1,000 kg/mm^2 [54].

The typical properties of some commercial microporous membranes are summarized in Table 4. Celgard 2730 and Celgard 2400 are single-layer PE and PP separators, respectively, while Celgard 2320 and 2325 are Trilayer separators of 20 and 25 μm thickness. Asahi and Tonen separators are single-layer PE separators made by wet process. Basic properties such as thickness, Gurley, porosity, melt temperature, and ionic resistivity are reported in Table 4. These properties are defined in a subsequent section.

Efforts have been made to find a new route for dry process using biaxial stretching techniques for preparing polypropylene microporous films, which may have submicron pore size and narrow size distribution, high permeability to gasses and liquids combined with good mechanical properties. The biaxially stretched polypropylene microporous films (Micpor®) were made by using nonporous polypropylene films of high beta-crystal content [62]. The porosity of these films can be as high as 30–40%, with an average pore size of

Rechargeable Batteries, Separators for. Table 4 Typical properties of some commercial microporous membranes

Separator/properties	Celgard 2730	Celgard 2400	Celgard 2320	Celgard 2325	Asahi Hipore	Tonen Setela
Structure	Single Layer	Single layer	Trilayer	Trilayer	Single layer	Single layer
Composition	PE	PP	PP/PE/PP	PP/PE/PP	PE	PE
Thickness (um)	20	25	20	25	25	25
Gurley (s)	22	24	20	23	21	26
Ionic resistivity[a] (Ω-cm^2)	2.23	2.55	1.36	1.85	2.66	2.56
Porosity (%)	43	40	42	42	40	41
Melt temperature (°C)	135	165	135/165	135/165	138	137

[a]In 1 M $LiPF_6$ EC:EMC (30:70 by volume)

approximately 0.05 μm. The pores on the surface were almost circular in shape compared to slit-like pores observed in uniaxial stretched samples and exhibited high permeability to fluids with good mechanical properties and almost circular pore shape with narrow pore-size distribution [63–65].

The PP/PE bilayer [38] and PP/PE/PP trilayer separators were developed by Celgard. Multilayer separators offer advantages of strength and combine the lower melting temperature of PE with the high-temperature strength of PP. Nitto Denko has also patented a single-layer separator made from a blend of PE/PP by the dry stretch process [66]. According to the patent, the separator has microporous regions of PE and PP. On heating in an oven, the impedance of the separator increases near the melting point of PE and the impedance remains high until beyond the melting point of PP. However, battery performance data have not been presented.

Microporous polyethylene separator material composed of a combination of randomly oriented thick and thin fibrils of ultrahigh-molecular-weight polyethylene (UHMWPE), Solupur®, manufactured by DSM Solutech, is also an interesting separator material for lithium-ion batteries. Solupur® is fabricated in standard grades with base weights ranging from 7 to 16 g/m^2 and mean pore size ranging from 0.1 to 2.0 μm and a porosity of 80–90% [67]. Ooms et al. carried out a study on a series of DSM Solupur materials with different permeability. Rate capability and cycling tests of these materials were compared with commercial available separators in CR2320-type coin cells. Solupur® materials showed low tortuosity, high strength and puncture resistance, excellent wettability, good high rate capability and low-temperature performance because of its high porosity and UHMWPE structure [68].

Nitto Denko has also developed a battery separator made by a wet process that had high puncture strength and high heat rupture resistance [69]. They used a polyolefin resin with a high-molecular-weight rubber as its main component material and cross-linked through oxidation in air. The melt rupture temperature, as measured by thermomechanical analysis, was over 200°C in this material. They also tried cross-linking ultrahigh-molecular-weight polyethylene with electron-beam and ultraviolet irradiation, but this had the side effect of causing deterioration in the polyolefin including rupture of the main chains and therefore resulted in reduced strength.

ENTEK Membranes LLC has developed Teklon™ – a highly porous, ultrahigh-molecular-weight polyethylene separator for lithium-ion batteries. At the writing of this publication, the separator is available in small quantities. Pekala et al. characterized Celgard™, Setela™, and Teklon™ separators in terms of their physical, mechanical, and electrical properties [70].

Celgard's separators are the best-characterized battery separators in literature as they have been widely used in numerous battery systems. Bierenbam et al. [55] has described the process, physical, and chemical properties, and end-use applications. Fleming and Taskier [71] described the use of Celgard microporous membranes as battery separators. Hoffman et al. [72]

presented a comparison of PP and PE Celgard microporous materials. Callahan discussed a number of novel uses of Celgard membranes. Callahan and coworkers [73] also characterized Celgard membranes by SEM image analysis, mercury porosimetry, air permeability, and electrical resistivity, and later characterize the puncture strength and temperature/impedance data for Celgard membranes [38]. Spotnitz et al. reported short-circuit behavior in simulated, spirally wound cells, as well as impedance/temperature behavior and thermomechanical properties [42]. Yu [74] found that a trilayer structure of PP/PE/PP Celgard™ microporous membranes provided exceptional puncture strength.

Nonwoven materials such as cellulosic fibers have never been successfully used in lithium batteries. This lack of interest is related to the hygroscopic nature of cellulosic papers and films, their tendency to degrade in contact with lithium metal, and their susceptibility to pinhole formation at thickness of less than 100 μm.

Asahi Chemical Industry carried out an exploratory investigation to determine the requirements for cellulose-based separators for lithium-ion batteries [75]. In an attempt to obtain an acceptable balance of lithium-ion conductivity, mechanical strength, and resistance to pinhole formation, they fabricated a composite separator (39–85 μm) that consists of fibrilliform cellulosic fibers (diameter 0.5–5.0 μm) embedded in a microporous cellulosic (pore diameter: 10–200 nm) film. The fibers are intended to reduce the possibility of separator meltdown under exposure to heat generated by overcharging or internal short circuiting. The resistance of these films was equal to, or lower than, the conventional polyolefin-based microporous separators. The long-term cycling performance was also very comparable.

Pasquier et al. [76] used paper-based separators in flat pouch-type lithium-ion batteries and compared the performance with cells made with Celgard-type polyolefin-based separators. The paper separators had good wetting properties, good mechanical properties, but did not provide the shutdown effect essential for large lithium-ion batteries. Their resistance was similar to polyolefin separators and when all water traces were removed from paper, their cycling performance was similar to Celgard separators. The paper-based separators can be used in small flat pouch-type cells where high strength and shutdown behavior is not required. For larger spherically wound cells, which require strong separators with shutdown feature, paper-based separators cannot be used.

Recently Degussa announced that they have developed Separion® separators for lithium batteries by combining the characteristics of flexible polymeric separators with the advantages of chemical and thermally resistant and hydrophilic ceramic materials. Separion® is produced in a continuous coating process. Ceramic materials, e.g., alumina, silica, and/or zirconia, are slip coated and hardened onto a support [77, 78]. According to Degussa, Separion separators have an excellent high temperature stability, superior chemical resistance, and good wettability, especially at low temperatures. They tested the performance and safety behavior of Separion separator in 18,650 cells and found the performance to be comparable to polyolefin-based separators [79].

The potential use of polymeric ion-exchange membranes in the next generation single-ion secondary lithium polymer batteries was shown by Sachan et al. [80, 81]. Conductivities exceeding 10^{-4} S/cm with transference numbers of unity were achieved for Nafion converted to Li^{+} salt form. However, little work has continued to introduce ion-exchange membranes in lithium batteries. The cost associated with the manufacturing of such membranes has been a significant barrier to their commercial viability.

To obtain a thin (less than 15 μm) separator for lithium batteries, Optodot has taken a different approach of high-speed coating of a metal oxide sol gel coating on a smooth surface followed by a delamination step to provide the free-standing separator. Using this approach, separator with thicknesses from 6 to 11 μm was made on large-scale production coating equipment [82]. They found that the sol gel separators with a thickness in the middle of this range of 8–9 μm have the preferred combination of thinness and strength. The metal oxide sol gel coating is water based with no organic solvents present. The coating formulations include a polymer and a surfactant. The polymer provides improved coating rheology, mechanical strength, and other properties. The surfactant provides improved wetting properties on the substrate. The films prepared were around 11 μm thick, with 45% porosity, completely wettable in nonaqueous

electrolyte, and melt temperature greater than 180°C. While these films are relatively thin and should help in increasing the capacity, they may not be strong enough for use in tightly wound cells. Moreover, the shutdown temperature of the separator seems to be very high and thus not suitable for existing lithium-ion chemistries.

Gineste et al. carried out the grafting of hydrophilic monomers onto PP or PE separators to improve the wettability of separators used in secondary lithium batteries with a lower content of wetting agents [83, 84]. They used a PP film (Celgard 2505) of 50 μm thickness after irradiating in air by electron beams with a dose ranging from 0.5 to 4 Mrad. The irradiated film was grafted by a monofunctional monomer (acrylic acid, AA), in the presence of difunctional cross-linking agent (diethyleneglycol dimethacrylate, DEGDM). The separators start losing mechanical properties, when the grafting ratio is higher than 50%.

Separator Requirements

In lithium-based cells, the essential function of battery separator is to prevent electronic contact, while enabling ionic transport, between the positive and negative electrodes. It should be usable on high-speed winding machines and possess good shutdown properties. The most commonly used separators for primary lithium batteries are microporous polypropylene membranes. Microporous polyethylene and laminates of polypropylene and polyethylene are widely used in lithium-ion batteries [85]. These materials are chemically and electrochemically stable in secondary lithium batteries. A key requirement for the separators for lithium primary batteries is that their pore size be small enough to prevent dendritic lithium penetration through them.

The general requirements [86] for lithium-ion battery separators are given below:

1. *Thickness* – The lithium-ion cells used in consumer applications use thin microporous separators (<25 μm). The separators being developed for EV/HEV applications will require thicker (~40 μm) separators. The thicker the separator, the greater the mechanical strength and the lower the probability of punctures during cell assembly, but reduce the amount of active materials that can be placed in the same size can. The thinner separators lower the internal resistance, take up less space, and permit the use of longer electrodes for increased capacity and rate capability.
2. *Permeability* – The separators should not limit the electrical performance of the battery under normal conditions. Typically the presence of separator increases the effective resistivity of the electrolyte by a factor of 6–7. The ratio of the resistivity of the separator filled with electrolyte divided by the resistivity of the electrolyte itself is called MacMullin number. The rate capability of the battery is inversely proportional to the MacMullin number; however, it has been shown that increase in resistance across the electrode material has a larger impact on the cell performance for comparable changes made to the separator [87].
3. *Gurley* (*air permeability*) – Air permeability is proportional to electrical resistivity, for a given separator morphology. It is used in place of electrical resistance (ER) measurements once the relationship between Gurley and ER is established. The separator should have low Gurley values for good electrical performance.
4. *Porosity* – It is implicit in the permeability requirement; typically lithium-ion battery separators have a porosity of 40%. Control of porosity is very important for battery separators. Specification of percent porosity is commonly an integral part of separator acceptance criteria. The porosity of separators used in alkaline zinc MnO_2 cells is typically around 80–90%.
5. *Wettability* – The separators should wet out quickly and completely in typical battery electrolytes. The lack of wetting results in localized spots of high resistance.
6. *Electrolyte absorption and retention* – A separator should be able to absorb and retain electrolyte. Electrolyte absorption is needed for ion transport. The microporous membranes usually do not swell on electrolyte absorption.
7. *Chemical stability* – The separators should be stable in battery for a long period of time. It should be inert to both strong reducing and strong oxidizing conditions and should not degrade or loose mechanical strength or produce impurities, which can interfere with the function of the battery. The separator must be able to withstand the strong

oxidizing positive electrode and the corrosive nature of the electrolyte at temperatures as high as 75°C. The greater the oxidation resistance, the longer the separator will survive in a cell. Polyolefins (e.g., polypropylene, polyethylene) exhibit high resistance to most of the conventional chemicals, good mechanical properties, and moderate temperature range for application making it one of the ideal polymers for lithium-ion battery separators. Polypropylene separators exhibit better mechanical properties and minimal oxidation when in contact with the positive electrode in a lithium-ion cell. Thus, the performance of trilayer (PP/PE/PP) separators with PP as the outside layer and PE as inner layer are superior.

8. *Dimensional stability* – The separator should lay flat and should not curl at the edges when unrolled as this can greatly complicate cell assembly. The separator should also not shrink when exposed to electrolyte. The cell winding should not affect the porous structure in any adverse way.
9. *Puncture strength* – The separators used in wound cells require high puncture strength to avoid penetration of electrode material through the separator. If particulate material from the electrodes penetrates the separator, an electrical short will result and the battery will be rejected. The separators used in lithium-ion batteries require more strength then the one used in lithium primary batteries. The primary lithium batteries have only one rough electrode and thus it requires less strength. As empirically observed, for most applications, the puncture strength should be at least 400 g/mil for separators used in lithium-ion cells. Mix penetration strength is a better measure of separator strength in a battery compared to puncture strength.
10. *Mix penetration strength* – The susceptibility of separators to particle penetration is characterized by mix penetration strength [45]. During the winding of the spiral wrap construction considerable mechanical pressure is applied to the cathode–separator–anode interface. Any loose particle could be forced through the separator and short the cell. The mix penetration strength should be at least 100 kgf/mil for separators used in lithium-ion cells.
11. *Thermal stability* – Lithium-ion batteries can be poisoned by water and so materials going into the cell are typically dried at 80°C under vacuum. Under these conditions, the separator must not shrink significantly and definitely must not wrinkle. Each battery manufacturer has specific drying procedures. The requirement of less than 5% shrinkage after 60 min at 90°C (in vacuum) in both MD and TD direction is a reasonable generalization.
12. *Pore size* – A key requirement of separators for lithium batteries is that their pores be small enough to prevent dendritic lithium penetration through them. Membranes with submicron pore sizes have proven adequate for lithium batteries.
13. *Tensile strength* – The separator is wound with the electrodes under tension. The separator must not elongate significantly under tension in order to avoid contraction of the width. A tensile strength specification is sometimes given, but the key parameter is Young's Modulus in the machine direction. Since Young's Modulus is difficult to measure, 2% offset yield is a good measure; less than 2% offset at 1,000 psi is acceptable for most winding machines.
14. *Camber* – Ideally, when a strip of separator is laid out, the separator should be straight and not bow or skew. In practice, however, some camber is often observed. If sufficiently extreme, this can cause misalignment between the electrodes and separator. Camber can be measured by laying the separator flat on a table parallel with a straight meter stick. The camber should be less than 0.2 mm/m of separator.
15. *Shutdown* – Lithium-ion battery separators provide some margin of protection against short circuit and overcharge in lithium-ion cells. The separators exhibit a large increase in impedance at temperature about 130°C that effectively stops ionic transport between the electrodes [88, 89]. The greater the mechanical integrity of the separator above 130°C, the greater the margin of safety the separator can provide. If the separator looses mechanical integrity, then the electrodes can come into direct contact, react chemically, and result in thermal runaway. The shutdown behavior of a separator can be characterized by heating the

separator (saturated with electrolyte) to high temperatures and simultaneously monitoring the electrical resistance of the separator [42, 89].

16. *High temperature stability* – A separator might provide an extra margin of safety if it can prevent the electrodes from contacting one another at high temperatures. Separators with good mechanical integrity at high temperatures can provide a greater margin of safety for lithium-ion cells. Thermal Mechanical Analysis (TMA) can be used to characterize the high temperature stability of separators. Utilizing TMA, the separator is held under constant load and the degree of elongation versus temperature is measured; the temperature at which the separator loses mechanical integrity, the elongation increases dramatically.
17. *Electrode interface* – The separator should form a good interface with the electrodes to provide sufficient electrolyte flow.

In addition to the above properties, the separator must be essentially free of any type of defects (pinholes, gels, wrinkles, contaminants, etc.). All of the above properties have to be optimized before a membrane qualifies as a separator for a lithium-ion battery. The general requirements for lithium-ion battery separators are also summarized in Table 5.

Separator Properties/Characterization

Separators are characterized by structural and functional properties; the former describes what they are and the latter how they perform. The structural properties include chemical (molecular) and microcrystalline nature, thickness, pore size, pore-size distribution, porosity, and various chemical and physical properties such as chemical stability, and electrolyte uptake. The functional properties of interest are electrical resistivity, permeability, and transport number. It is useful to characterize separator materials in terms of their structural and functional properties, and to establish a correlation of these properties with their performance in batteries. A variety of techniques are used to evaluate separators. Some of these techniques are discussed in this section.

Gurley Number Separator permeability is usually characterized by air permeability. The Gurley number expresses the time required for a specific amount of air to pass through a specific area of separator under a specific pressure. The standard test method is described in ASTM-D726 (B).

The Gurley number is used to characterize separators because the measurement is accurate and easy to make, and deviations from specific values are a good indication of problems. Air permeability (Gurley) is proportional to electrical resistance (ER), for a given separator morphology [90]. Gurley can be used in place of ER measurements once the relationship between Gurley and ER is established. A lower Gurley value means higher porosity, lower tortuosity, and accordingly lower ER.

Electrical Resistance The measurement of separator resistance is very important to the art of battery manufacture because of the influence the separator has on electrical performance. Electrical resistance is a more comprehensive measure of permeability then the Gurley number, in that the measurement is carried out in the actual electrolyte solution. The ionic resistivity of the porous membrane is essentially the resistivity of the electrolyte that is embedded in the pores of the separator. Typically, a microporous separator, immersed in an electrolyte, has an electrical resistivity about six to seven times that of a comparable volume of electrolyte, which it displaces. It is a function of the membrane's porosity, the tortuosity, the resistivity of the electrolyte, the thickness of the membrane, and the extent to which the electrolyte wets the pores of the membrane [83]. The electrical resistance of the separator is the true performance indicator of the cell. It describes a predictable voltage loss within the cell during discharge and allows one to estimate rate limitations.

Classical techniques for measuring electrical resistivity of microporous separators have been described by Falk and Salkind [5] and Robinson and Walker [42]. The resistivity of an electrolyte is more accurately determined by AC methods since DC can polarize the electrodes and cause electrolysis of the solution. Modern AC impedance measuring systems allow rapid measurements of cell resistance over a wide range or frequencies from which resistance can be calculated free of capacitance effects. Compared to the DC techniques, the equipment required and the theory

Rechargeable Batteries, Separators for. Table 5 General requirements for lithium-ion battery separator [86]

Parameter	Goal
Thickness[a,b] (μm)	<25
Electrical resistance (MacMullin No.[c], dimensionless)	<8
Electrical resistance (ohms-cm^2)	<2 Ω-cm^2
Gurley[d] (s)	~25 ml
Pore size[e] (μm)	<1
Porosity (%)	~40
Puncture strength[f] (g)	>300 g/mil
Mix penetration strength (kgf)	>100 kgf/mil
Shrinkage[g] (%)	<5% in both MD and TD
Tensile strength[h]	<2% offset at 1,000 psi
Shutdown temperature (°C)	~130
High temperature melt integrity (°C)	>150
Wettability	Complete wet out in typical battery electrolytes
Chemical stability	Stable in battery for long period of time
Dimensional stability	Separator should lay flat; be stable in electrolyte
Skew	<0.2 mm/m

[a]ASTM D5947-96, "Standard test methods for physical dimensions of solid plastics specimens," ASTM International.
[b]ASTM D2103, "Standard specification for polyethylene film and sheeting," ASTM International.
[c]Caldwell DL, Poush KA (1984) US Patent 4,464,238
[d]ASTM D726, "Standard test methods for identification of fibers in textiles," ASTM International.
[e]ASTM E128-99, "Standard test method for maximum pore diameter and permeability of rigid porous filters for laboratory use," ASTM International.
[f]ASTM D3763, "Standard test method for high-speed puncture properties of plastics using load and displacement sensors," ASTM International.
[g]ASTM D1204, "Standard test methods for linear dimensional changes of nonrigid hermoplastic sheeting or film at elevated temperatures," ASTM International.
[h]ASTM D882, "Standard test method for tensile properties of thin plastic sheeting," ASTM International.

necessary to interpret the AC techniques are more complex; however, AC measurements yield information about long-range migration of ions and polarization phenomena occurring within the cell. In an AC measurement, a sinusoidal voltage is applied to a cell, and the sinusoidal current passing through the cell as a result of this perturbation is determined. A four-electrode cell is usually used for resistivity measurements. The outer two electrodes serve to apply a sinusoidal potential, and the resulting current passing through the inner two electrodes is measured. This technique is employed to avoid the complications arising from a nonuniform potential field near the outer two electrodes. An excellent review of experimental techniques for measuring electrical resistivity in aqueous solution is available [91, 92].

The separator resistance is usually characterized by cutting small pieces of separators from the finished material and then placing them between two blocking electrodes. The separators are completely saturated with the electrolyte. The resistance (Ω) of the separator is measured at a certain frequency by AC impedance techniques. The frequency is chosen so that the separator impedance is equal to the separator resistance. In order to reduce the measurement error, it is best to do multiple measurements by adding extra layers.

The average resistance of single layer is determined from multiple measurements. The specific resistivity, ρ_s (Ω-cm), of the separator saturated with electrolyte is given by

$$\rho_s = \frac{R_s A}{l} \tag{1}$$

where R_s is the measured resistance of separator in Ω, A is the electrode area in square centimeters and l is the thickness of membrane in centimeters. Similarly, the specific resistivity of the electrolyte, ρ_e (Ω-cm), is given by

$$\rho_e = \frac{R_e A}{l} \tag{2}$$

where R_e is the measured resistance of electrolyte in ohms. The ratio of the resistivity of a separator membrane to that of the electrolyte is called MacMullin number, N_m, which can be used to predict the influence of the separator on battery performance [93].

$$N_m = \frac{\rho_s}{\rho_e} = \frac{\tau^2}{\varepsilon} \tag{3}$$

where τ is the tortuosity and ε is the porosity of the separator. The MacMullin number describes the relative contribution of a separator to cell resistance. It is almost independent of electrolyte used and also factors out the thickness of the material. It assumes that the separator wets completely in the electrolyte used for the test. From Eqs. 1 and 3 the electrical resistance of a microporous membrane is given by the following [5, 94]:

$$R_m = \rho_e \left(\frac{\tau^2 l}{\varepsilon A} \right) \tag{4}$$

It has been shown for Celgard membranes that the membrane resistance can be related to the Gurley number by Eq. 5. where R_m is the membrane resistance (Ω), A is the membrane area (cm^2), ρ_e is the specific electrolyte resistance (Ω-cm), t_{gur} is the Gurley number (10 cm^3 air, 2.3 mmHg), d is the pore size, and 5.18×10^{-3} a scaling factor [90].

$$R_m A = \frac{\rho_e}{5.18 \times 10^{-3}} t_{gur} d \tag{5}$$

The usual procedure for characterizing battery separators is to cut several test samples from the finished material. Thus, only a small portion of the separator is actually examined. Ionov et al. has proposed an alternative technique to measure the resistance of a separator over a large separator area [95]. In this technique the separator material is passed through an electrolyte bath between electrical resistance measuring transducers. The set of transducers installed in the bath transverse to the moving sheet of separator material examines the whole surface of the material. If the production process ensures good uniformity in the physicochemical properties of the separator material over the whole surface, the transducer outputs will be close to one another. A nonuniform separator will cause significant deviations from the average value at various sections of the material examined. In this case, the sections having lower or higher resistance compared with the average value should be regarded as flawed.

Porosity The porosity is important for high permeability and also for providing a reservoir of electrolyte in the cell. A higher and uniform porosity is desirable for unhindered ionic current flow. Nonuniform porosity leads to nonuniform current density and can further lead to reduced activity of the electrodes. Cell failure can result, if during discharge, some areas of the electrodes work harder than other.

Porosity of a separator is defined as the ratio of void volume to apparent geometric volume. It is usually calculated (Eq. 6) from the skeletal density, basis weight, and dimensions of the material and so may not reflect the accessible porosity of the material.

$$\text{Porosity}(\%) = 1 - \frac{\left(\frac{\text{Sample weight}}{\text{Sample volume}}\right)}{\text{Polymer density}} \times 100\% \tag{6}$$

The standard test method is described in ASTM D-2873. The actual or accessible porosity can also be determined by the weight of liquid (e.g., Hexadecane) absorbed in the pores of the separator. In this method, the separator weight is measured before and after dipping in Hexadecane solvent and the porosity is calculated (Eq. 7) by assuming that volume occupied by Hexadecane is equal to the porous volume of the separator.

$$\text{Porosity}(\%) = \frac{\text{Volume occupied by Hexadecane}}{\text{Volume of Polymer Volume occupied by Hexadecane}} \times 100 \tag{7}$$

Tortuosity Tortuosity is the ratio of mean effective capillary length to separator thickness. The tortuosity factor τ of a separator can be expressed by

$$\tau = \frac{l_s}{d} \tag{8}$$

where l_s is the ion path through the separator and d is the thickness of the separating layer.

Tortuosity is a long-range property of a porous medium, which qualitatively describes the average pore conductivity of the solid. It is usual to define τ by electrical conductivity measurements. With knowledge of the specific resistance of the electrolyte and from a measurement of the sample membrane resistance, thickness, area, and porosity, the membrane tortuosity can be calculated from Eq. 3.

This parameter is widely used to describe the ionic transport by providing information on the effect of pore blockage. A tortuosity factor $\tau = 1$, therefore, describes an ideal porous body with cylindrical and parallel pores, whereas values of $\tau > 1$ refer to more hindered systems. Higher tortuosity is good for dendrite resistance but can lead to higher separator resistance.

Pore Size and Pore-Size Distribution For any battery applications, the separator should have uniform pore distribution to avoid performance losses arising from nonuniform current densities. The submicron pore dimensions are critical for preventing internal shorts between the anode and the cathode of the lithium-ion cell, particularly since these separators tend to be as thin as 25 μm or less. This feature will be increasingly important as battery manufacturers continue to increase the cell capacity with thinner separators. The pore structure is usually influenced by polymer composition, and stretching conditions, such as drawing temperature, drawing speed, and draw ratio. In the wet process, the separators produced by the process of drawing after extraction (as claimed by Asahi Chemical and Mitsui Chemical) are found to have much larger pore size (0.24–0.34 μm) and wider pore-size distribution than those produced by the process of extraction (0.1–0.13 μm) after drawing (as claimed by Tonen) [54].

The testing of battery separators and control of their pore characteristics are important requirements for proper functioning of batteries. Mercury porosimetry has been historically used to characterize the separators in terms of percentage porosity, mean pore size, and pore-size distribution [96]. In this method, the size and volume of pores in a material are measured by determining the quantity of mercury, which can be forced into the pores at increasing pressure. Mercury does not wet most materials and a force must be applied to overcome the surface tension forces opposing entry into the pores.

The hydrophobic (e.g., polyolefins) separators are also characterized with Aquapore (nonmercury porosimetry) technique, where water is used in place of mercury. This is a very useful technique for characterizing polyolefin-based separators used in lithium batteries [97]. Porosimetry gives pore volume, surface area, mean pore diameter, and pore-size distribution. In a typical experiment, the sample is placed in the instrument and evacuated. As the pressure increases, the quantity of water forced into the pores increases in proportion to the differential pore volume, the size of the pores corresponding to the instantaneous pressure. Thus, increasing the pressure on a membrane having a given pore-size distribution results in a unique volume versus pressure or pore diameter curve. The pressure required for intrusion of water into a pore of diameter D is given by following equation

$$D = \frac{4\gamma \cos\theta}{p} \tag{9}$$

where D is the diameter of the pore assuming the pore to be cylindrical, p is the differential pressure, γ is the surface tension of the nonwetting liquid, water, and θ is the contact angle of water. The pores generally are not of spherical shape or a constant diameter. They usually vary in their form and size. Thus, statements of any pore diameter are always to be viewed with the above in mind.

Another technique, Capillary Flow Porometry has been developed by Porous Materials Inc. [98] to characterize battery separators [99, 100]. The instrument can measure a number of characteristics of battery separators such as size of the pore at its most constricted part, the largest pore size, pore-size distribution, permeability, and envelope surface area [101].

Scanning electron microscopy (SEM) is also used to examine separator morphology. SEM pictures of some commercial membranes are shown in Figs. 4–6.

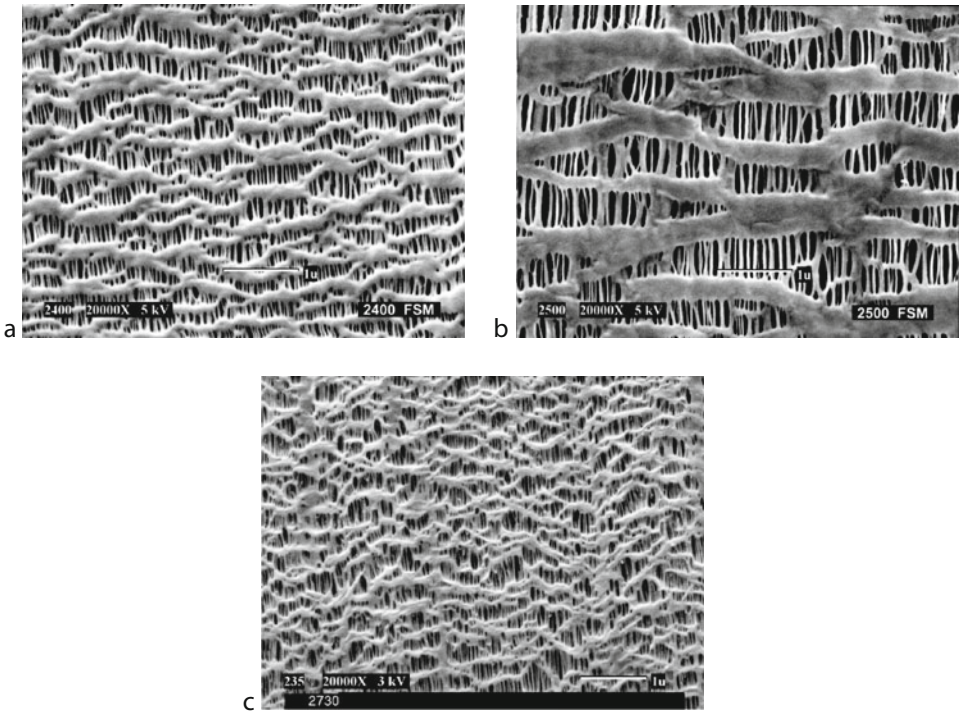

Rechargeable Batteries, Separators for. Figure 4
Scanning electron micrographs of surface of single-layer Celgard separators used in lithium batteries (**a**) 2400 (PP), (**b**) 2500 (PP), and (**c**) 2730 (PE)

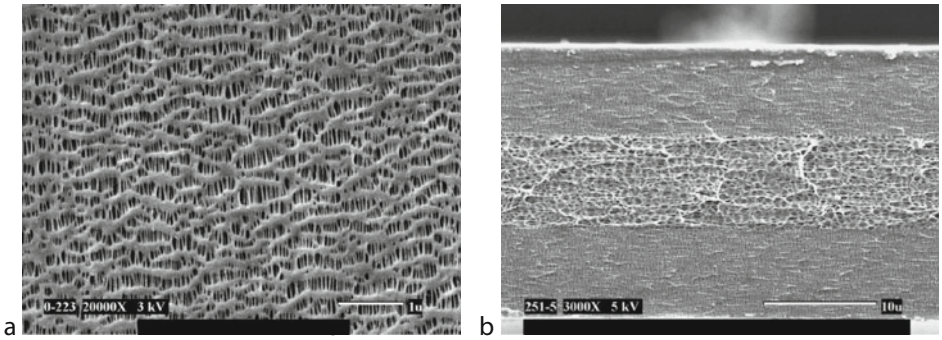

Rechargeable Batteries, Separators for. Figure 5
Scanning electron micrographs of Celgard trilayer separator (2325) used in lithium-ion batteries (**a**) surface SEM; (**b**) cross-section SEM

The surface SEM of Celgard 2400, 2500, and 2730 are shown in Fig. 4. It is clear from the images that the pores are uniformly distributed. Both Celgard 2400 and 2500 are single-layer PP separators, but the pore size of Celgard 2500 is substantially larger than Celgard 2400. Thus, it has lower resistance and is more suited for high rate applications. Fig. 5 shows the surface SEM and cross-section SEM of Celgard 2325. The surface SEM only shows the PP pores while the PE pores are visible in the cross-section. It is clear from the image that all three layers are of equal thickness. The SEM pictures of separators made by wet process are shown in Fig. 6.

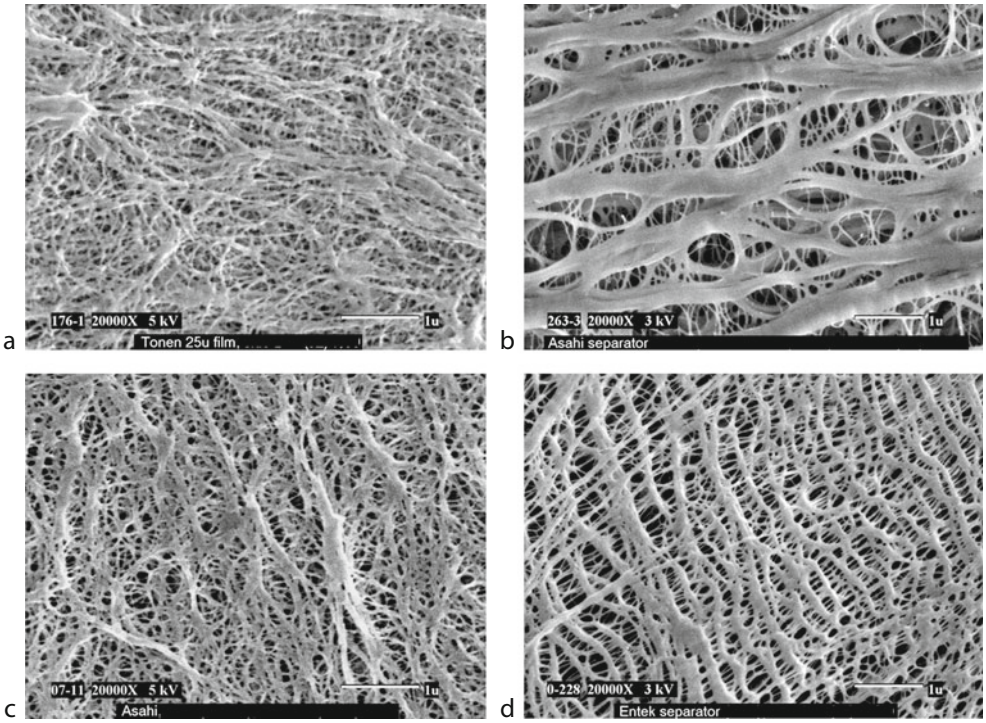

Rechargeable Batteries, Separators for. Figure 6
Scanning electron micrographs of separators made by wet process and used in lithium-ion batteries (**a**) Setela (Tonen), (**b**) Hipore–1 (Asahi), (**c**) Hipore-2 (Asahi), and (**d**) Teklon (Entek)

The pore structure of all of these membranes is very similar. Asahi-1 (Fig. 6b) separator has significantly larger pores compared to the other membranes.

Image analysis has been used to characterize the pore structure of synthetic membrane materials [102]. The films can also been characterized by scanning tunneling microscopy, atomic force microscopy, and field emission scanning electron microscopy [49, 103]. The pore size of the membranes can also be calculated from Eq. 5, once the MacMullin number and Gurley values are known.

Puncture Strength A separator is required to have sufficient physical strength to endure the rigors of cell assembly and day-to-day charge–discharge cycling. Physical strength is required to withstand basic handling, cell blocking/assembly, physical shock, punctures, abrasion, and compression.

The Puncture Strength (PS) is the weight that must be applied to a needle to force it completely through a separator [55, 104]. It has been used to indicate the tendency of separators to allow short circuits in a cell that may occur due to holes generated in the separator by the rough surface of an electrode during the battery assembly and charge–discharge cycle. The PS requirement for lithium-ion batteries is higher them lithium-foil batteries, because the separator must contend with two rough surfaces. Commercially available puncture strength machines made for textiles tend to give meaningless results when testing battery separator membranes. More reproducible results can be obtained with a load frame (such as an Instron Machine). The mix penetration strength is a better measure of mechanical strength for battery separators as it measures the force required to create a short through the separator when electrode mix is pushed through it.

The strength of the separator depends greatly on the materials used and the manufacturing method. The wet-biaxial method simultaneously stretches in the

MD and TD directions and thus achieves a material that has tensile modulus and rupture strength in both directions. Both high polymer entanglement and stretching help increase the physical strength of the separator.

Mix Penetration Strength The force required to create a short through a separator due to mix (electrode material) penetration defines mix penetration strength. In this test, force (with a ½-inch diameter ball) is applied on the positive electrode/separator/negative electrode sandwich and the force at which the mix penetrates through the separator and creates an electronic short is called mix penetration force. Mix penetration strength is used to indicate the tendency of separators to allow short circuits during battery assembly. The mix penetration resistance test is more closely related to particle penetration resistance compared to puncture resistance [45].

Tensile Strength The tensile strength measurements (e.g., Young's Modulus, Percent offset strength, elongation at break, stress at break) can be made by utilizing widely known standard procedures. These tests are carried out in both MD and TD directions. The tensile properties are dependent on the manufacturing process. The Uniaxially oriented films have high strength in only one direction, whereas biaxially oriented films are more uniformly strong in both MD and TD directions. ASTM test method D882-00 "Standard test method for tensile properties of thin plastic sheeting" is an appropriate test.

The separator should be strong enough to withstand mechanical handling during cell winding and assembly. It should be dimensionally stable and should not neck down during winding. The decrease in width will allow the electrodes to touch each other and create a short. Thus, the tensile property of the separator should be very strong in MD direction compared to TD direction.

Shrinkage Shrinkage test is carried out on both MD and TD directions. In this test, the dimensions of separators are measured and then stored at 90°C for a fixed time. The shrinkage is then calculated from the change in dimensions as shown in Eq. 10,

$$\text{Shrinkage}(\%) = \frac{L_i - L_f}{L_i} \times 100 \tag{10}$$

where L_i is the initial length and L_f is the final length of separator after high temperature storage. The uniaxially stretched separators tend to shrink in MD direction only, while the biaxially stretched separators shrink in both MD and TD directions. The shrinkage of separators can also be compared by carrying out Thermal Mechanical Analysis (TMA) test at a constant load and rate.

Shutdown Separator shutdown is a useful and essential mechanism for limiting temperature and preventing venting in short-circuited cells [42]. It usually takes place close to the melting temperature of the polymer when the pores collapse turning the porous ionically conductive polymer film into a nonporous insulating layer between the electrodes. At this temperature, a significant increase in cell impedance occurs and passage of current through the cell is restricted. This prevents further electrochemical activity in the cell, thereby shutting the cell down before an explosion can occur.

The ability of the PE-based separator to shutdown the battery is determined by its molecular weight, percent crystallinity (density), and process history. Material properties and processing methods might need to be tailored so that the shutdown response is spontaneous and complete. The optimization needs to be done without affecting the mechanical properties of the material in the temperature range of interest. This process is easier to do with the trilayer separators, since one material is utilized for the shutdown response and another for the mechanical properties. Polyethylene containing separators, in particular trilayer laminates of polypropylene, polyethylene, and polypropylene, appear to have the most attractive properties for preventing thermal runaway in lithium-ion cells [101–105]. The shutdown temperature of 130°C is usually sufficient to control the cell heating and avoid thermal runaway in lithium-ion cells. A lower temperature shutdown will be desirable if it does not affect the separator mechanical properties or high temperature cell performance in any adverse way.

The shutdown property of separators is determined by measuring the impedance of a separator while the

temperature is linearly increased [42, 89]. Figure 7 shows actual measurement for Celgard® 2325 membrane. The heating rate was around 60°C/min and the impedance was measured at 1 kHz. The rise in impedance corresponds to a collapse in pore structure due to melting of the separator. A 1,000-fold increase in impedance is necessary for the separator to stop thermal runaway in the battery. The drop in impedance corresponds to opening of the separator due to coalescence of the polymer, and/or to penetration of the separator by the electrodes; this phenomenon is referred to as a loss in "melt integrity." This test is fairly reliable in indicating the temperature at which the impedance rises, but some variability in characterizing the subsequent drop in impedance may occur.

In Fig. 7, the shutdown behavior of a multilayer (PP/PE/PP) separator (Celgard 2325) is shown. The impedance rise occurred near the melting point of polyethylene (130°C) and remained high until such time as the melting point of polypropylene (165°C) is attained. The shutdown temperature of the separator is governed by the melting point of the separator material. At the melting point, the pores in the separator collapse to the form a relatively nonporous film between the anode and the cathode. This was confirmed by DSC. The DSC scan in Fig. 8 gives a peak melting temperature of 135°C for Celgard 2730, 168°C for Celgard 2400, and 135/165°C for Celgard 2325. The shutdown behavior of thinner separators (<20 μm) is very similar to thicker separators. The battery manufacturers have been very successful in using the thinner separators without compromising on the shutdown behavior of the separators.

Laman et al. introduced the use of impedance measurements as a function of temperature to characterize shutdown separators [89]. Using a temperature scan rate of 1°C/min they found that the impedance increased several orders of magnitude near the melting point of the separator. They verified the patent claims of Lundquist et al. [106] that bilayer separators of PE and PP gave a temperature window of high impedance extending approximately between the melting point of the polymers. The concept of using separators consisting of distinct layers, one of which could act as a fuse, was developed by Lundquist et al. [106, 107]. Laman's results have been corroborated by Geiger et al. [38] and Spotnitz et al. [94]. Spotnitz et al. developed a thin layer cell which allowed temperature scan rates of 5°C/min and higher and obtained results similar to those of Laman et al.

Prior work related with shutdown separators also involved application of waxes on membranes [108, 109]. In these cases, the wax or low melting polymers were coated on the polyolefin separator. The disadvantage of this technique is that the coating can block the pores of the separator and thus can affect the performance by increasing separator resistance. Moreover, the coating level has to be very high to get complete shutdown.

The shutdown characteristic provides protection from external short circuit and during cell overcharge. It provides little protection from internal shorts should

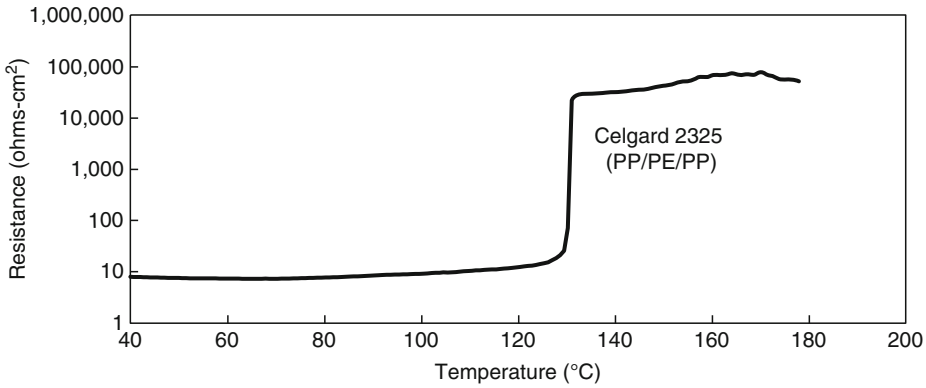

Rechargeable Batteries, Separators for. Figure 7
Internal impedance (at 1 kHz) of Celgard 2325 (PP/PE/PP) separator as a function of temperature. Heating rate: 60°C/min

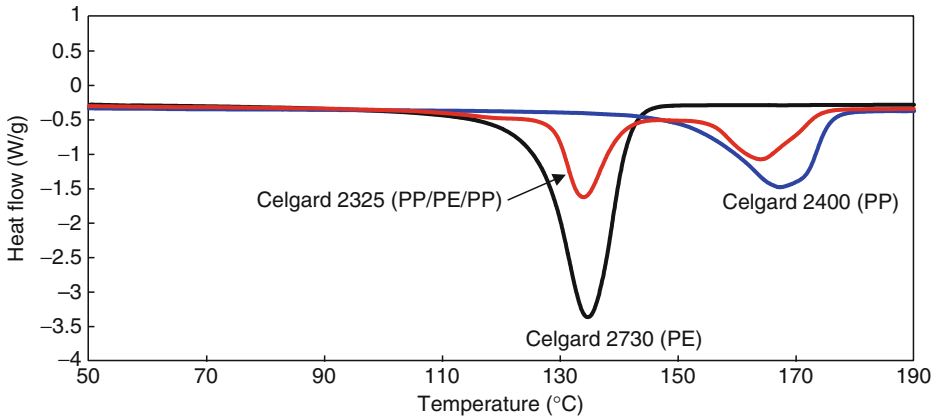

Rechargeable Batteries, Separators for. Figure 8
DSC of Celgard 2730 (PE), 2400 (PP), and 2325 (PP/PE/PP)

they occur. Should the electrodes touch each other or become shorted from a dendritic growth of soluble impurity or other dendrite forming soluble material, the separator only helps in avoiding delayed failures. In case of an instant failure during internal short circuit, the heating rate is too high and the separator shutdown is not fast enough to control the heating rate.

Melt Integrity The separators used in lithium-ion batteries should have high temperature melt integrity. The separator should maintain its melt integrity after shutdown so that the electrodes do not touch and create a short. This helps in avoiding the thermal runaway even when the cell is exposed to high temperatures. Thermal Mechanical Analysis (TMA) is a very good technique to measure the high temperature melt integrity of separators.

TMA involves measuring the shape change of a separator under load while the temperature is linearly increased. Typically, separators show some shrinkage, and then start to elongate and finally break as shown in Fig. 9. This test utilizes a small separator sample (about 5–10 mm length (MD) and about 5 mm width), which is held in mini-instron-type grips. The sample is held with a constant 2 g load while the temperature is ramped at 5°C/min past the melting point until the tension ruptures the film. Three parameters are reported from TMA test – shrinkage onset temperature, melt temperature, and melt rupture temperature. TMA has proven to be a more reproducible measure of melt integrity of the separator [107].

Figure 9 shows the TMA data for two different Celgard membranes. The shrinkage onset temperature, deformation temperature, and rupture temperature are summarized in Table 6. The single-layer PP membrane (Celgard 2400) showed a higher softening temperature (∼121°C), a deformation temperature around 160°C, and a very high rupture temperature around 180°C. The multilayer polypropylene/polyethylene/polypropylene separator (Celgard 2325) combined the low-temperature shutdown property of polyethylene with the high temperature melt integrity of polypropylene, resulting in a separator with softening (∼105°C) and melt temperature (∼135°C) very similar to PE and rupture temperature (∼190°C) very similar to PP.

Separators with melt integrity greater than 150°C are desirable for lithium-ion cells. The Trilayer separators with polypropylene on the outside helps in maintaining the melt integrity of the separators at higher temperatures compared to single-layer PE separators. The choice of a shutdown separator for bigger lithium-ion cells being developed for hybrid and electric vehicles is highly specific to the design of the cell.

Wettability and Wetting Speed Two physical properties of separators, which are important to the operating characteristics of a battery, are electrolyte absorption and electrolyte retention. Any good separator should be able to absorb a significant amount of electrolyte and also retain the absorbed electrolyte when the cell is in operation. These are more important in sealed cells where no free electrolyte is present.

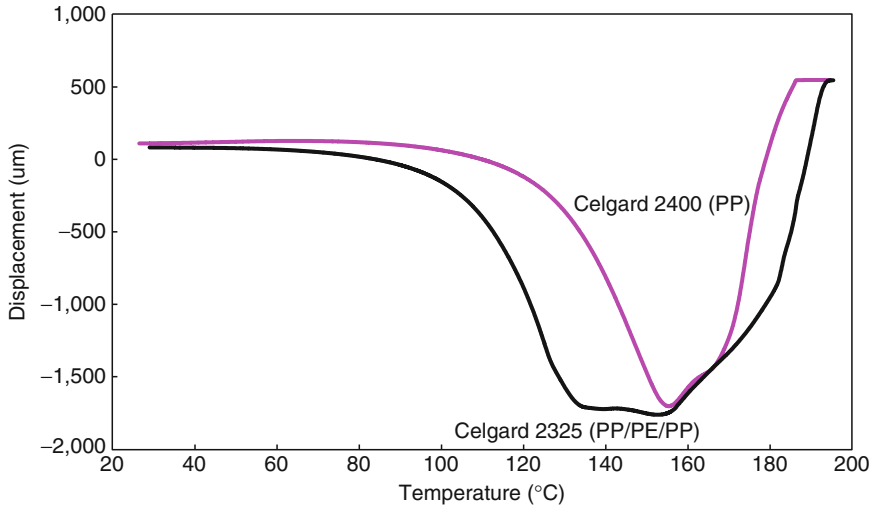

Rechargeable Batteries, Separators for. Figure 9
TMA of Celgard 2400 (PP) and 2325 (PP/PE/PP). A constant load (2 g) is applied while the temperature is ramped at 5°C/min

Rechargeable Batteries, Separators for. Table 6 TMA data for typical Celgard separators

	Celgard 2730	Celgard 2400	Celgard 2325
Shrinkage onset temperature (°C)	100	121	106
Deformation temperature (°C)	125	156	135, 154
Rupture temperature (°C)	140	183	192

A maximum amount of electrolyte in the separator is desirable to achieve minimum cell internal resistance. Quite often separator dry-out or lack of sufficient amount of electrolyte is misinterpreted as inadequate wetting of the separator.

The separator wettability can limit the performance of batteries by increasing the separator and cell resistance. Separator wetting speed can be correlated with electrolyte filling time in real cells. The wetting speed is determined by the type of polymer (surface energy), pore size, porosity, and tortuosity of the separators. There is no generally accepted test for separator wettability. However, a simple wicking test by placing a drop of electrolyte onto the separator is a good indication of wettability. Standard dyne-solutions of known surface tension values exist and can be used to adjust the surface tension of the electrolyte as to expedite wetting. The contact angle is also a good measure of wettability. The uptake of electrolyte by many hydrophobic polymer separators can be enhanced either by wetting agents or ionic-functional groups (e.g., ion-exchange membranes).

Effect of Separator on Cell Performance and Safety

Although the material of a battery separator is inert and does not influence electrical energy storage or output, its physical properties greatly influence performance and safety of the battery. This is especially true for lithium-ion cells and, thus, the battery manufacturers have started paying more attention to separators while designing the cells. The cells are designed in such a way that separators do not limit the performance, but if the separator properties are not uniform, or if there are other issues, it can affect the performance and safety of cells. This section will focus on the effect of the separator properties on cell performance and safety. Table 7 shows different types of safety and performance tests for lithium-ion batteries and the corresponding important separator property and how it affects performance and/or safety.

To achieve good performance of lithium-ion cells, the separators should have low resistance and low shrinkage and strength across the thickness.

Rechargeable Batteries, Separators for. Table 7 Safety and performance tests for lithium-ion batteries and the corresponding important separator property and its affect on the cell performance and/or safety

Cell property	Separator property	Comments
Cell capacity	Thickness	Cell capacity can be increased by making the separator thinner
Cell internal resistance	Resistance	Separator resistance is a function of thickness, pore size, porosity, and tortuosity
High rate performance	Resistance	Separator resistance is a function of thickness, pore size, porosity, and tortuosity
Fast charging	Resistance	Low separator resistance will aid in overall faster charging by allowing higher and/or longer constant current charging
High temperature storage	Oxidation resistance	Oxidation of separators can lead to poor storage performance and reduce performance life
High temperature cycling	Oxidation resistance	Oxidation of separators can lead to poor cycling performance
Self-discharge	Weak areas, pinholes	Soft shorts during cell formation and testing can lead to internal current leakage
Long-term cycling	Resistance, shrinkage, pore size	High resistance, high shrinkage, and very small pore size can lead to poor cycling performance
Overcharge	Shutdown behavior; high temperature melt integrity	Separator should completely shutdown and then maintain its melt integrity at high temperatures
External short circuit	Shutdown behavior	Separator shutdown stops the cells from overheating
Hotbox	High temperature melt integrity	Separator should be able to keep the two electrodes apart at high temperatures
Nail crush	Shutdown (to stop delayed failure)	In case of internal shorts, the separator may be the only safety device to stop the cell from overheating.
Bar crush	Shutdown (to stop delayed failure)	In case of internal shorts, the separator may be the only safety device to stops the cell from overheating.

The separator with high resistance will perform poorly during high rate discharge and will also increase the cell charging time. Low shrinkage is a very important characteristic for separators, especially for higher capacity cells. These cells are used in high-speed laptop computers, which can experience higher temperatures (~70–75°C) under certain conditions [110]. This can lead to shrinkage of separators and ultimately higher cell resistance and poor long-term cycling. The shrinkage in TD direction can lead to safety issues because of an internal short between the electrodes. Larger pores can lead to shorts during cell manufacturing or can fail during Hipot testing. Larger pores will allow more soft shorts and higher self-discharge, especially during high temperature storage. Very small pore size can lead to higher resistance and poor cycle life during high temperature cycling and storage. Thus, the pore size of the separator should be optimized to achieve good strength and performance.

One of the ways to increase cell capacity is by decreasing the thickness of separators. The newer high capacity cells (>2.6 Ah) generally use 16 and 12 μm separators as compared to 20–25 μm separators used in cells with 2.2–2.4 Ah capacity. The thinner separators offer lower resistance and help in increasing the capacity; but the amount of electrolyte they can

hold is less and their mechanical strength is often not as high as thicker separators. Thus, appropriate changes should be made in cell design to keep the cell safe. The handling and manufacturing of thinner separators is also a challenge for the separator manufacturers. They are required to maintain the same electrical and mechanical properties and better quality for thinner separators. The separator manufacturers have installed better controls and quality standards. Many battery experts are of the opinion that the 16 μm is the thinnest that can be used while still maintaining the stringent performance and safety requirements of lithium-ion cells. The use of thinner separators has often resulted in voluminous battery recalls [111].

The separators inside the lithium-ion batteries experience extreme oxidizing environment on the side facing the positive electrode and extreme reducing environment on the side facing the negative electrode. The separators should be stable in these conditions during long-term cycling especially at high temperatures. Separators with poor oxidation resistance can lead to poor high temperature storage performance and poor long-term cycling behavior. The oxidation resistance properties of trilayer (PP/PE/PP) separators with PP as the outside layer and PE as inner layer is superior compared to polyethylene separators. This is because of the better oxidation resistance properties of polypropylene in contact with the positive electrode in a lithium-ion cell.

The products formed by the decomposition of the electrolyte can also block the pores of the separator, leading to increase in cell resistance. The separators with lower resistance also help in better low-temperature performance. At very low temperatures, the resistance of the electrolytes is very high and thus smaller contribution from separator helps in keeping the cell resistance low.

The lithium-ion cells have demonstrated power loss when aged and/or cycled at high temperatures. Norin et al. [112] demonstrated that the separator is at least partly responsible for the power loss due to the intrinsic increase in its ionic resistance. They showed that impedance increased significantly upon cycling and/or aging of lithium-ion cells at elevated temperatures and that separators account for about 15% of the total cell impedance rise. They later reported that the loss in ionic conductivity of the separator was due to blocking of the separator pores with the products formed due to electrolyte decomposition, which was significantly accelerated at elevated temperatures [113].

There are several groups that regulate, or provide testing, to verify safe operation of lithium-ion cells under abuse conditions. The US Department of Transportation (DOT) classifies all lithium-ion batteries as hazardous materials for shipping in the same category as lithium metal primary batteries [114]. The DOT grants exceptions based on the cell capacity and ability of the cells to pass specified tests. In addition, the UL Laboratories [115, 116], the International Electrotechnic Commission [117], and the United Nations (UN) [118] have developed standardized safety testing procedures. These tests are designed to assure that cells are safe to ship and are resistant to typical abuse conditions such as internal shorting, overcharge, overdischarge, vibration, shock, and temperature variations that may be encountered in normal transportation environments.

Underwriters Laboratories (UL) requires that consumer batteries pass a number of safety tests (UL 1642 [119] and UL-2054 [120]). There are similar recommendations from UN for transport of dangerous goods, [121] the International Electrotechnical Commission (IEC), and the Japan Battery Association [122]. An abnormal increase in cell temperature can occur from internal heating caused by either electrical abuse – overcharge or short circuit – or mechanical abuse – nail penetration or crush. Higher cell temperature could also be a result of external heating. For this reason, lithium-ion cells used in battery packs are designed with safety control circuits that have redundant safety features (PTC, CID, vent, thermal fuse, etc.). Shutdown separators are one of the safety devices inside the cell and act as a last line of defense. The separator shutdown is irreversible, which is fine for polyethylene-based separators, which melt around 130°C.

The impedance of the separator increases by two to three orders of magnitude due to an increase in cell temperature, resulting from cell abuse (e.g., short circuit, overcharge). The separator should not only shutdown around 130°C, but it should also maintain its mechanical integrity at higher temperatures, preferably at temperatures as high as 200°C. If the separator does not shutdown properly then the cell will continue to

heat during an overcharge test and can lead to thermal runaway. The high temperature melt integrity of separators is also a very important property to keep the cell safe during extended overcharge or during extended exposure to higher temperatures.

Figure 10 shows a typical short-circuit curve for an 18650 lithium-ion cell with shutdown separator, $LiCoO_2$ positive electrode, and MCMB carbon negative electrode. For the results shown in Fig. 10, the cell tested did not have other safety devices (e.g., CID, PTC), which usually work before separator shutdown. As soon as the cell is short circuited externally through a shunt resistor, the cell starts heating because of the large current drained through the cell. The shutdown of the separator, which occurs around 130°C, stops the cell from heating further. The current decrease is caused by increase of battery internal resistance due to separator shutdown. The separator shutdown helps in avoiding the thermal runaway of the cell.

Cells can be overcharged when the cell voltage is incorrectly detected by the charging control system, or when the charger breaks down. When this happens, the lithium ions remaining in the cathode are removed and more lithium ions are inserted into the anode then under standard charging conditions. If the lithium insertion ability of the carbon anode is limited, lithium metal in the form of dendrites may be deposited on the carbon and cause a drastic reduction in thermal stability. At higher charging rates, the heat output increases greatly because the joule heat output is proportional to I^2R. Several exothermic reactions (e.g., reaction between lithium and electrolyte, thermal decomposition of anode and cathode, thermal decomposition of electrolyte, etc.) occur inside the cell as its temperature increases. Separator shutdown happens when cell temperature reaches melting point of polyethylene as shown in Fig. 11. The CID and PTC of the 18650 cells were removed, to identify the role of the separator. The current decrease is caused by increase of battery internal resistance due to separator shutdown. Once the pores of the separator have closed due to softening, the battery cannot continue to be charged or discharged, and thus thermal runaway is prevented. During continued overcharge, the separator should maintain its shutdown feature and should not allow the cell to heat again. It should also maintain its melt integrity and should not allow the two electrodes to touch each other.

The separator should also not allow any dendrite to penetrate through the separator to avoid internal

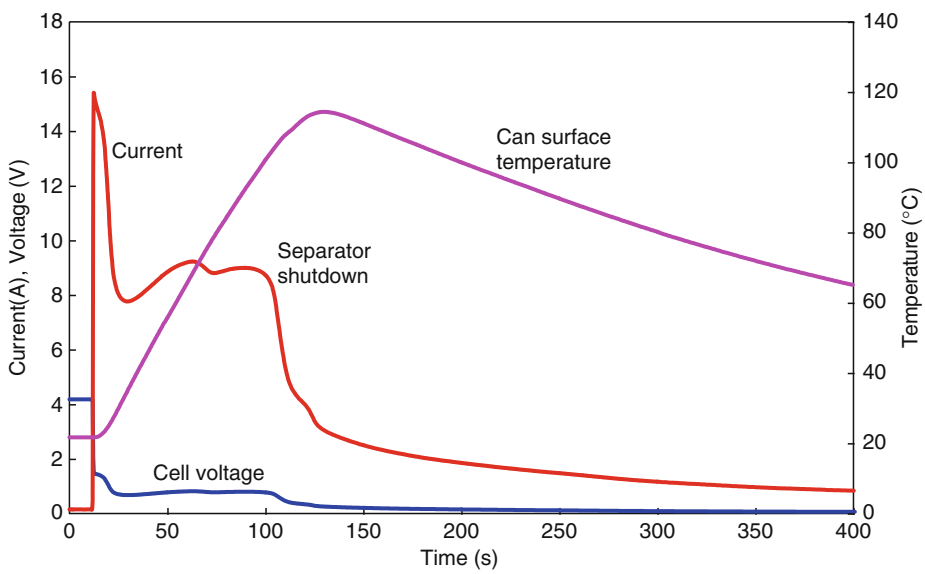

Rechargeable Batteries, Separators for. Figure 10
Typical short-circuit behavior of a 18650 lithium-ion cell with shutdown separator and without PTC (positive temperature coefficient) and CID (current interrupt device). This test simulates external short circuit of cell

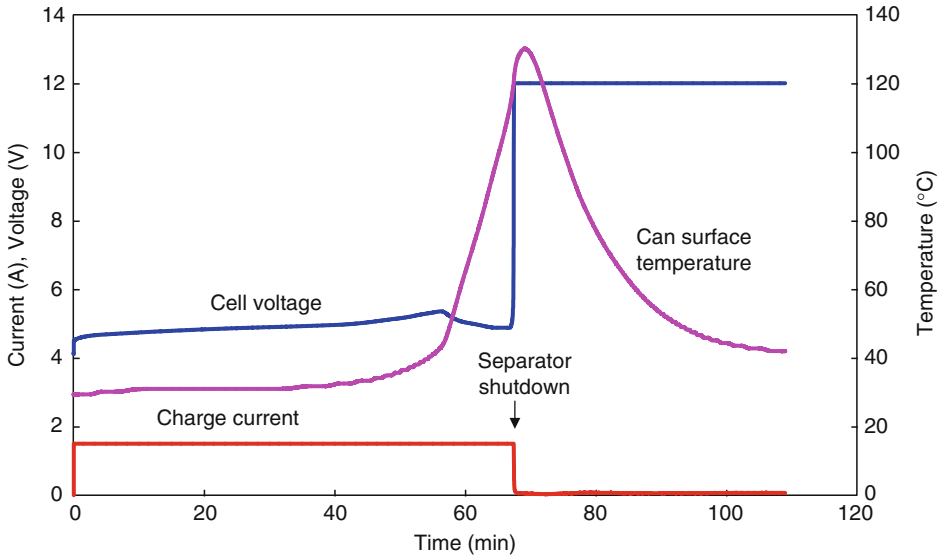

Rechargeable Batteries, Separators for. Figure 11
Typical overcharge behavior of a 18650 lithium-ion cell with shutdown separator. The PTC (Positive Temperature Coefficient) and CID (Current Interrupt Device) were removed from the cell header

shorts. During an internal short, separator is the only safety device, which can stop the thermal runaway. If the heating rate is not too high then the separator shutdown can help in controlling the heating rate and stop thermal runaway. In a nail penetration test, an instantaneous internal short results the moment the nail penetrates into battery. Enormous heat is produced from current flow (double-layer discharge and electrochemical reactions) in the circuit by the metal nail and electrodes. Contact area varies according to depth of penetration. In general, the shallower the penetration depth, the smaller the contact area and therefore the greater are the local current density and heat production. Thermal runaway is likely to take place as local heat generation induces electrolyte and electrode materials to decompose. On the other hand, if the battery is fully penetrated, the increased contact area would lower the current density, and the cell could pass the nail penetration test. A detailed investigation of various internal short-circuit scenarios is presented by Santhanagopalan et al. [229]. Internal short-circuit tests are more difficult to pass than the external short-circuit tests described earlier, because the nature of the short cannot be determined a priori.

Figure 12 shows the typical nail penetration behavior of an 18650 lithium-ion cell with shutdown separator, $LiCoO_2$ positive electrode, and MCMB carbon negative electrode. Clearly, there was a voltage drop from 4.2 to 0.0 V, instantaneously, as the nail penetrated through (when internal short circuit occur), and temperature rose. When the heating rate is low the cell stops heating when the temperature is close to separator shutdown temperature as shown in Fig. 12a. If the heating rate is very high, then the cell continues to heat and fails the nail penetration test as shown in Fig. 12b. In this case, the separator shutdown is not fast enough to prevent thermal runaway. Thus, separator only helps in avoiding delayed failures in case of internal short circuit as simulated by nail and bar crush tests. Separators with high temperature melt integrity and good shutdown feature (to avoid delayed failures) are needed to pass internal short-circuit test. Thinner separators (<20 μm) used in high capacity cells should offer similar shutdown and high temperature melt integrity properties as thicker separators. The decrease in separator strength should be balanced with changes in cell design. The separator properties across the length and width should be very uniform to keep the cell safe during abnormal use.

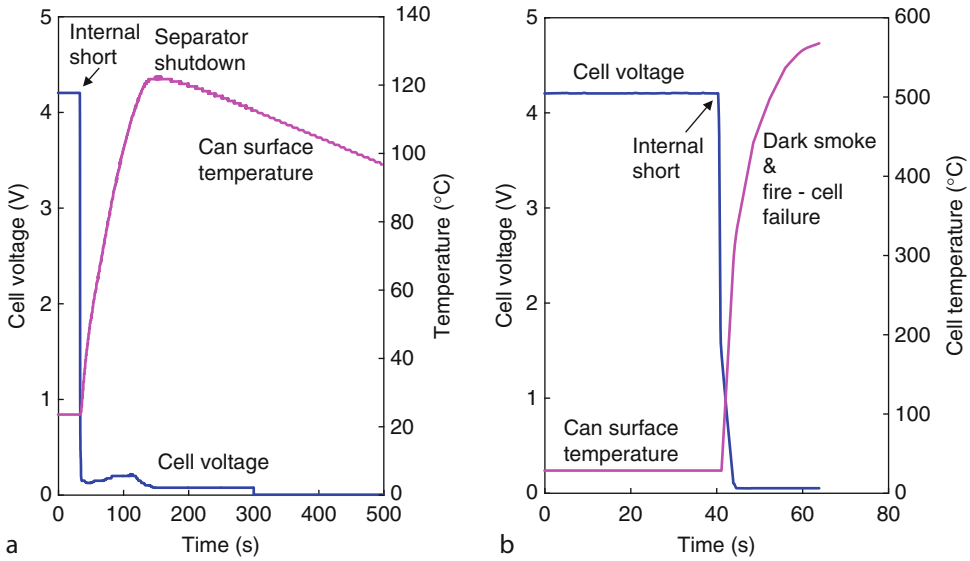

Rechargeable Batteries, Separators for. Figure 12

Typical nail penetration behavior of an 18650 lithium-ion cell with shutdown separator. This test simulates internal short circuit of a cell. (**a**) Cell passed nail penetration test; (**b**) cell failed nail penetration test

The mechanism and characteristics of thermal cut-off devices in several prismatic lithium-ion cells was studied by Venugopal [124] by monitoring the impedance at 1 kHz and the Open Circuit Voltage (OCV) of the cells as a function of temperature. All the cells studied contained PE-based separators with a shutdown temperature between 130°C and 135°C. Within this narrow temperature range, the shutdown separators caused a sharp and irreversible rise in impedance of the cell. Single-layer PE separators were effective up to around 145°C, above which they demonstrated a meltdown effect. Trilayer separators had meltdown temperatures as high as 160°C because of the presence of additional layers of higher melting PP. It was found that the separators, alone, are not able to shutdown the cell completely. In case of an overcharged test, the cell could continue to charge at lower currents even after the shutdown event, rendering the cell a potential hazard if not disposed of immediately and safely. This usually does not become an issue in commercial cells because the cell manufacturers have addressed this issue by including multiple cut-off devices within a single cell. The use of inorganic coatings and fillers has also drawn considerable attention in order to prevent cell failure in such cases [78, 125].

Development efforts are under way to displace the use of microporous membranes as battery separators and instead use gel or polymer electrolytes. Polymer electrolytes, in particular, promise enhanced safety by eliminating organic volatile solvents. The next two sections are devoted to solid polymer and gel-polymer-type lithium-ion cells with focus on their separator/electrolyte requirements.

Separator for Lithium Polymer Batteries

Due to their high theoretical capacity, lithium polymer batteries have long been identified as a very promising technology to meet the requirements of upcoming applications such as standby power and electric vehicles. Research and development of polymer electrolytes for ambient-temperature rechargeable lithium batteries has always been very active. Rapid progress for the past two decades in this field has led to numerous monographs and reviews [126–131]. These polymers

are generally polyethers, poly(ethylene oxide) (PEO), or poly(propylene oxide) (PPO).

Solid polymer electrolytes serve two principal roles in rechargeable lithium batteries. Not only do they function as the traditional electrolyte, i.e., the medium for ionic transport, but also as the separator which insulates the cathode from the anode. Consequently, the polymer electrolyte must have sufficient mechanical integrity to withstand electrode stack pressure and stresses caused by dimensional changes, which the rechargeable electrodes undergo during charge/discharge cycling.

Lithium polymer electrolytes formed by dissolving a lithium salt LiX (where X is preferably a large soft anion) in poly(ethylene oxide) PEO can find useful application as separators in lithium rechargeable polymer batteries [132–134]. Thin films must be used due to the relatively high ionic resistivity of these polymers. For example, the lithium-ion conductivity of PEO-Li salt complexes at 100°C is still only about 1/100 the conductivity of a typical aqueous solution.

A polymer electrolyte with acceptable conductivity, mechanical properties, and electrochemical stability has yet to be developed and commercialized on a large scale. The main issues that must be resolved for a completely successful operation of these materials are the reactivity of their interface with the lithium metal electrode and the decay of their conductivity at temperatures below 70°C. Croce et al. found an effective approach for reaching both of these goals by dispersing low-particle-size ceramic powders in the polymer electrolyte bulk [135, 136]. They claimed that this new "nanocomposite polymer electrolytes" had a very stable lithium electrode interface and an enhanced ionic conductivity at low temperature, combined with good mechanical properties. Fan et al. [137] has also developed a new type of composite electrolyte by dispersing fumed silica into low to moderate molecular weight PEO.

The gel-type polymer electrolyte prepared by dispersing ceramic powders (e.g., Al_2O_3) into a matrix formed by a lithium salt solution contained in a poly(acrylonitrile) (PAN) network was reported by Appetecchi et al. [138] These new types of composite gel electrolytes had high ionic conductivity, wide electrochemical stability, and particularly, high chemical integrity even at temperatures above ambient. Kim et al. [139] used a blend of PVdF-HFP and PAN as a matrix polymer to attain high ionic conductivity and good mechanical strength. The PAN can give mechanical integrity and structural rigidity to a porous membrane without inorganic fillers. The high ionic conductivity was due to the high volume of pores and a high affinity of the membrane for electrolyte solution [140].

Separator for Lithium-Ion Gel Polymer Batteries

The solid polymer electrolyte approach provides enhanced safety, but the poor ambient-temperature conductivity excludes their use for battery applications, which requires good ambient-temperature performance. In contrast, the liquid lithium-ion technology provides better performance over a wider temperature range, but electrolyte leakage remains a constant risk. Midway between the solid polymer electrolyte and the liquid electrolyte is the "hybrid polymer" electrolyte concept leading to the so-called gel polymer lithium-ion batteries. Gel electrolyte is a two-component system, namely, a polymer matrix swollen with a liquid electrolyte. The gel polymer electrolyte approach to the lithium-ion technology combines the positive attributes of both the liquid (high ionic conductivity) and solid polymer electrolytes (elimination of leakage problems).

Gel polymer lithium-ion batteries replace the conventional liquid electrolytes with an advanced polymer electrolyte membrane. These cells can be packed in light-weight plastic packages as they do not have any free electrolyte and they can be fabricated in any desired shape and size. They are now increasingly becoming an alternative to liquid electrolyte lithium-ion batteries, and several battery manufacturers, such as Sanyo, Sony, and Panasonic, have started commercial production [141, 142]. Song et al. [143] have recently reviewed the present state of gel-type polymer electrolyte technology for lithium-ion batteries. They focused on four plasticized systems, which have received particular attention from a practical viewpoint, i.e., poly (ethylene oxide) (PEO), poly (acrylonitrile) (PAN) [144],

poly (methyl methacrylate) (PMMA) [145, 146], and poly (vinylidene fluoride) (PVdF) based electrolytes [147–150].

One particular version of the lithium-ion gel polymer cells, also known as plastic lithium-ion cell (PLION™), was developed by Bellcore [151–153]. In this case, Gozdz et al. developed a microporous plasticized PVdF-HFP-based polymer electrolyte that served both as separator and electrolyte. In PLION™ cells, the anode and cathode are laminated onto either side of the gellable membrane. Good adhesion between the electrodes and the membranes is possible because all three sheets contain significant amounts of a PVdF copolymer that can be melted and bonded during the lamination step.

The PVdF-HFP separators used in PLION™ cells were around 3 ml thick, and had poor mechanical properties. It has been reported that the major source of rate limitation in PLION™ cells was the separator thickness [154]. The rate capability of these cells can be significantly improved by decreasing the separator thickness to that typically used in liquid electrolyte system. Moreover, in the absence of shutdown function, the separator does not contribute to cell safety in any way. Park et al. reported that the HFP content in separators did not have any significant impact on cell performance [155]. The Bellcore process has proven to be an elegant laboratory process but is difficult to implement in large-scale production.

To overcome the poor mechanical properties of polymer- and gel-polymer-type electrolytes, microporous membranes impregnated with gel polymer electrolytes, such as PVdF, PVdF-HFP, and other gelling agents, have been developed as an electrolyte material for lithium batteries [156–166]. Gel-coated and/or gel-filled separators have some characteristics that may be harder to achieve in the separator-free gel electrolytes. For example, they can offer much better protection against internal shorts when compared to gel electrolytes and can therefore help in reducing the overall thickness of the electrolyte layer. In addition the ability of some separators to shutdown at a particular temperature allows safe deactivation of the cell under overcharge conditions.

The shutdown behavior of PVdF-coated Celgard a trilayer membrane is shown in Fig. 13. The shutdown

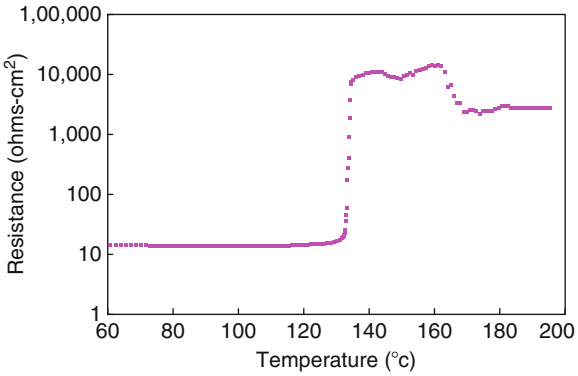

Rechargeable Batteries, Separators for. Figure 13 Internal impedance (at 1 kHz) of PVdF-coated Celgard trilayer separators as a function of temperature. Heating rate: 60°C/min

is defined by the sharp increase in resistance around 130°C. The PVdF coating should be porous and should not block the pores to maintain similar ionic conductivity. The scanning electron micrographs of PVdF-coated membrane is shown in Fig. 14. The cross-section SEM of Celgard 3300 provides visual evidence that the coating is porous and is not blocking the pores of the top PP layer.

Abraham et al. [158] were the first ones to propose saturating commercially available microporous polyolefin separators (e.g., Celgard®) with a solution of lithium salt in a photopolymerizable monomer and a nonvolatile electrolyte solvent. The resulting batteries exhibited low discharge rate capability due to the significant occlusion of the pores with the polymer binder and the low ionic conductivity of this plasticized electrolyte system. Dasgupta and Jacobs [157, 168] patented several variants of the process for the fabrication of bonded-electrode lithium-ion batteries, in which a microporous separator and electrode were coated with a liquid electrolyte solution, such as ethylene-propylene-diene (EPDM) copolymer and then bonded under elevated temperature and pressure conditions. This method required that the whole cell assembling process be carried out in scrupulously anhydrous conditions, which make this approach difficult, and expensive.

The later methods, proposed by Motorola [159, 170] and Mitsubishi Electric [171] researchers, differ

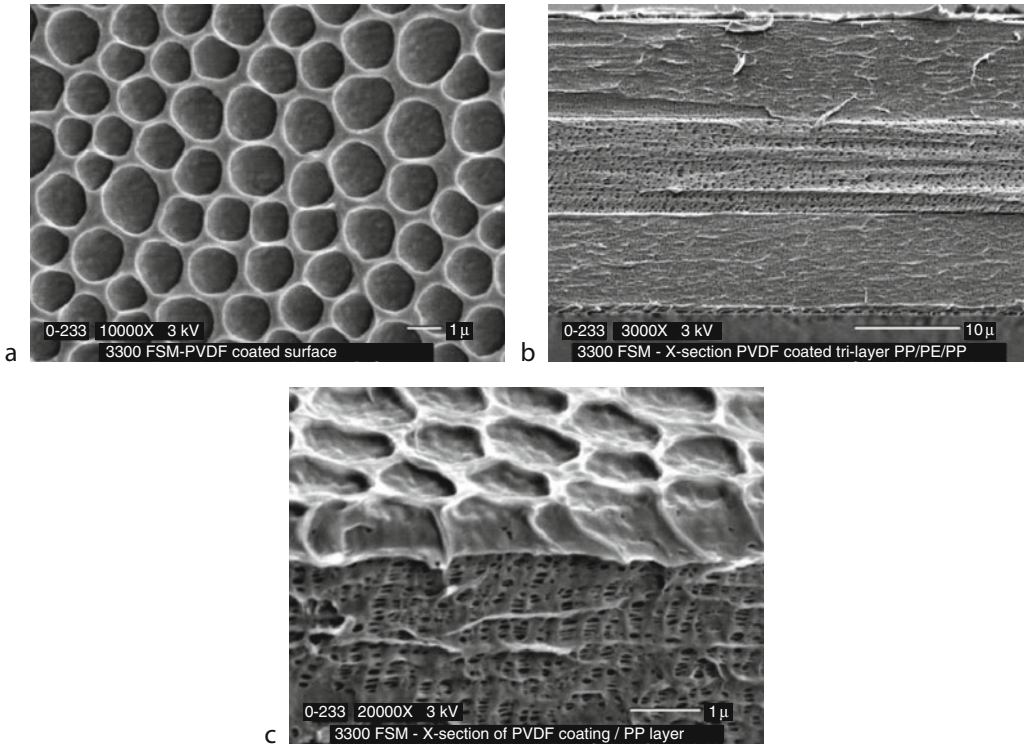

Rechargeable Batteries, Separators for. Figure 14
Scanning Electron Micrographs of Celgard PVdF-coated separators used in lithium gel polymer batteries (**a**) surface SEM, (**b**) cross-section SEM of coated layer, and (**c**) cross-section of PVdF coating

in implementation details, but they share a common feature in that a separate adhesive layer (PVdF) is applied to the separator and used to bond the electrode and the separator films, using in the first case the hot, liquid electrolyte as an in situ PVdF plasticizer. Sony [172, 173] researchers described the use of thin, liquid electrolyte-plasticized polyacrylonitrile layer directly applied either to the electrode or the separator surfaces as an effective ion-conductive adhesive. Sanyo [174, 175] investigators, on the other hand, used thermally polymerizable additives to gel, or solidify, liquid electrolyte solutions in a wound, packaged battery.

The ceramic fillers (e.g., Al_2O_3, SiO_2, TiO_2) can greatly influence the characteristics and properties of polymer electrolyte by enhancing the mechanical stability and the conductivity [135, 175–178]. Prosini et al. [179] in a PVdF-HFP polymer matrix used γ-$LiAlO_2$, Al_2O_3, and MgO as fillers to form self-standing, intrinsically porous separators for lithium-ion batteries. The MgO-based separators showed the best anode and cathode compatibilities.

Liu et al. [180] has successfully prepared a PVdF-HFP/PE composite gel electrolyte by cast method. They showed that when the PE content was over 23 wt.%, the electrical impedance of the composite gel electrolyte increased rapidly by several orders, around the melting point of PE. The SEM pictures showed that the PE particles were fused and formed into a continuous film at or near the PE melting point, which cuts off the ion diffusion. This shutdown feature of the composite gel electrolyte can help in preventing the cell runaway under abusive usage. Similarly, Kim et al. [181] prepared polyethylene oxide (PEO)-coated separators by coating PEO onto a microporous PE separators. The ionic conductivity of PEO-coated membranes was higher than the base film. Kim et al. prepared the polymer electrolytes by coating

polyethylene oxide (PEO) and polyethylene glycol dimethacrylate (PEGDMA) onto a microporous polyethylene membrane (Asahi Kasei, 25 um, 40% porosity) [182]. They showed that the relative weight ratio of PEO and PEGDMA coated onto the microporous membrane played a critical role in determining the uptake of electrolyte solution and ionic conductivity.

Separator for Aqueous Batteries

The aqueous batteries use water-based electrolytes (e.g., KOH electrolyte for NiCd, NiMH, and H_2SO_4 electrolyte for Lead acid), which are less resistive than nonaqueous electrolytes. Polyolefin materials are generally suitable for use in the manufacture of separators for these batteries, but they are not inherently wettable by aqueous electrolytes. Such electrolytes are therefore unable to penetrate the pores of a separator formed from such a material, so that ion migration through the pores in solution will not occur without modification. This problem is sometimes overcome by treating the polyolefin material with a surfactant, which allows an aqueous electrolyte to wet the material. However, such surfactant can be removed from the surfaces of the polyolefin material when electrolyte is lost from the device, for example during charging and discharging cycles, and it is not subsequently replaced on the material when the electrolyte is replenished.

This problem has also been addressed by modifying the surface properties of the polyolefin materials used to form polymeric sheets, by graft copolymerizing a monomeric substance to its surface, which, after copolymerization, confers hydrophilic properties, and, in some cases ion-exchange properties. This technique has been found to be practical when the porous substrate is formed from PE, which lends itself well to a graft-copolymerization reaction of this kind. However, it has been found that, when such a reaction is attempted using polyolefin materials other than PE, the rate of the grafting reaction is reduced significantly.

Graft polymerization is a convenient method for the modification of the physical and chemical properties of polymer materials and is of particular interest for synthesis of the hydrophilic membranes. Graft copolymerization can be achieved by various methods such as an exposure to ionizing radiation or ultraviolet light and the use of chemical initiators. Ionizing radiation is one of the most promising methods because of its rapid and uniform formation of active sites for initiating grafting throughout the matrix. Under appropriate experimental conditions, modifications of polymer properties can be accomplished not only on the surface but also throughout the polymer.

There have been several reports on radiation grafting of acrylic and methacrylic acid onto various substrates. These include both the direct grafting method and the pre-irradiation method to synthesize ion-exchange membranes. Two cation exchange membranes modified with the carboxylic acid group for battery separator was prepared by radiation-induced grafting of acrylic acid (AA) and methacrylic acid (MA) onto a polyethylene film by Choi et al. [183]. They found that KOH diffusion flux of AA-grafted PE membrane and MA-grafted PE membrane increased with an increase in the degree of grafting. AA-grafted PE membrane had a higher diffusion flux then MA-grafted PE membrane. Electrical resistance of both membranes decreased rapidly with an increase in the degree of grafting up to 120%, and then leveled off.

Battery separators having carboxylic acid group were prepared by radiation-induced grafting of acrylic acid onto a polyolefin nonwoven fabric (PNF). The PNF comprised of approximately 60% polyethylene and 40% polypropylene. It was found that the wetting speed, electrolyte retention, thickness, and ion-exchange capacity increased, whereas the electrical resistance decreased with increasing grafting yield [184]. The surface characteristics of the separators can also be modified by plasma discharge.

The subsequent subsections discuss separators used in lead acid and nickel metal hydride batteries.

Separators for Lead Acid Batteries

It has been a long time since the invention of the lead acid battery, but it still represents the most important secondary chemical power source – both in number of types and diversity of application. The lead acid battery has maintained its leading role for so many decades due to its competitive electrical characteristics and price, and due to its adaptability to new applications. It is manufactured in a variety of sizes and designs, ranging from less than 1 Ah to over 10,000 Ah [185].

Lead acid batteries can be classified into three major types or categories, namely, automotive (SLI), stationary, and motive power (industrial). In addition, there are many special batteries that cannot be easily categorized as either of the above types. These types of batteries are constructed with different materials and designed to meet the requirements of their intended end uses, each with a particular separator requirement with specific material composition, mechanical design, and physical, chemical, and electrochemical properties, tailored for the battery and its relevant specific uses. These batteries are generally available in flooded electrolyte or valve regulated (sealed) versions. In this section the types and properties of separators used for lead acid batteries are reviewed. The reader is referred to recent reviews published by Boehnstedt [12, 186, 187] and others [188–190] for detailed descriptions of lead acid separators.

Flooded Electrolyte Lead Acid Separators currently used in lead acid batteries can be classified based on their materials of construction into four major types: plastic (PE/silica, PVC/silica, Sintered PVC), paper (phenolic resin impregnated cellulose), glass (glass fiber mat), and rubber (hard rubber/silica, flexible rubber/silica, coated rubber/silica) separators. Table 8

Rechargeable Batteries, Separators for. Table 8 Typical separators used in lead acid battery systems

Separator	Class	Manufacturing process	Properties
Wood	Paper	Cellulosic separators are made from cotton linters or craft pulp and generally coated with phenolic resin for acid resistance and strength	Comparatively large pore size and relatively high electrical resistance
Hard rubber	Rubber	Made by mixing natural rubber, rehydrated precipitated silica, and sulfur. This is then extruded and calendared, vulcanized under water, and dried.	Finer pore diameter (0.2 μm average), relatively lower electrical resistance, excellent oxidation resistance, retards antimony transfer
Flexible rubber	Rubber	Made by mixing natural rubber, rehydrated precipitated silica. This is then extruded and calendared, irradiated with an ionizing electron beam and dried.	Flexible, fine pore structure (0.06 μm average), retards antimony transfer
Glass mat rubber	Rubber/ glass mat	Made by mixing polymeric emulsion, precipitated silica, and rubber. This is then coated on a fiberglass mat and finally cured and dried.	Finer pore diameter (<0.2 μm average), high porosity, excellent thermal dimensional stability
Sintered PVC	Plastic	Made by sintering PVC powder of a particle size ranging between 10 and 20 μm	Medium pore size (10–20 μm), generally good chemical resistance
Synthetic PVC	Plastic	Made from mixture of PVC, silica fine powder, and a solvent, and then extruded, calendared, and extracted	Small to medium average pore size and relatively low electrical resistance
Synthetic pulp with glass mat	Plastic/ glass	Made from blending PE synthetic pulp, synthetic fiber, and fine silica powder, and then heat treated	Medium pore size, low electrical resistance, and long service life at high temperatures; more difficult to process and assemble
Polyethylene (PE)	Plastic	Made from a mixture of UHMW PE powder, fine silica powder, and mineral oil. The mixture is extruded as a film, calendered, and made porous by extraction	Fine pore size, low electrical resistance, high puncture resistance, and strongly resistant to oxidation
Glass fiber mat	Glass	Deposition on a single sheet, a mixture of fibers dispersed in an aqueous solution	Excellent wettability, durable in an acid environment, good resiliency, high temperature stability, more difficult to process and assemble

shows the different types of separators used in batteries along with their manufacturing process and main features. Glass, paper, and sintered PVC separators can be classified as macroporous separators having an average pore diameter greater than 10 μm while all other separators can be classified as microporous separators having an average pore diameter smaller than 1 μm. All of these separators can be utilized as leaf separators in battery construction. Polyethylene can be used also as enveloped separators around either the positive or the negative plate. The use of "envelope" separators is popular in small, sealed cells, SLI, motive power, and standby batteries to facilitate production and to control lead contamination during manufacturing.

The environment of the lead acid battery (e.g., automotive battery) has been increasing in severity in recent years. The improvements and development of the separators have proceeded in accordance with the changes in the specifications for the batteries which were first made with wooden separators (preferred wood was Oregon Ceder as it contained small amounts of Lignin that enhances the performance of lead negative), then progressed through microporous rubber separators, cellulose separators and synthetic pulp separators (SPG) with glass mats, PVC separators, and now polyethylene separators have evolved. This sequential change in separator technology has provided continuous improvements in the charge and discharge efficiency of batteries and has given high vehicle-starting capability and reliability. Moreover, short circuits (caused by particles of active material dislodged from the battery plates) are prevented due to the smaller pores and excellent electrochemical oxidation resistance of the PE separator. These features contributed greatly to the improvement in battery life.

Rubber separators have good voltage characteristics, ability to retard antimony transfer, properties to retard dendrite growth, and good electrochemical compatibility [191]. Due to the hydrophilic properties of the rubber composition, the separators are highly wettable and renewable for the dry-charging process. Paik et al. showed that ACE-SIL (sulfur cured, hard rubber) separators performed well in industrial stationary or traction batteries, FLEX-SIL (electron-beam-cured, flexible rubber separator) separators are suited for deep-cycling batteries, and MICROPOR-SIL (a coated, glass mat, rubber separator) separators have been found to be a good choice for high rate discharging or cranking applications and for various types of gel cells [192]. Recently Daramic® DC UHMW PE has demonstrated excellent performance in these applications, as well.

Polyvinylchloride (PVC) and polyethylene (PE) separators have been the most commonly used separators in automotive batteries for the last 20 years. Polyethylene separators have a narrow pore-size distribution. The PVC separator is built up by sintering PVC powder in general of a particle size ranging between 10 and 20 μm. The decrease of particle size in the sintered product is negligible compared to the particle size of the raw materials. The pores are dispersed homogenously with a medium size ranging between 10 and 20 μm. Since a PVC separator exclusively consists of PVC, it exhibits advantageously good chemical resistance against acid and alkaline solutions. Unlike PE, PVC is disadvantaged due to its brittleness. The decline in PVC separators in recent years is in part due to their tendency to yield chloride ions from chemical attack.

The battery separators currently used by most flooded-cell-type lead acid battery manufacturers are of the microporous PE type. It was invented in the late 1960s by W.R. Grace & Co. [193]. The term "polyethylene separators" is somewhat misleading, since such a separator consists mainly of agglomerates of precipitated silica, being held within a network of extremely long-chain UHMWPE [194]. A typical PE separator formulation comprises precipitated silica (~60 wt.%), UHMW PE (~20 wt.%), mineral process oil (~15 wt.%), as well as some processing aids, like antioxidants and/or proprietary surface tension modifiers [195, 196].

The microporous PE separator is commercially manufactured by passing the ingredients through a heated extruder, passing the extrudate generated by the extruder through a die and into the nip formed by two heated calendar rolls to form a continuous web, extracting a substantial amount of the processing oil from the web by use of a solvent, drying the extracted web, slitting the web into lanes of predetermined width, and winding the lanes into rolls [195].

Rechargeable Batteries, Separators for. Table 9 Comparison of properties of different separators used in lead acid batteries

Property	Rubber	Cellulose	PVC	PE	Glass fiber
Year available	1930	1945	1950	1970	1980
Electrical resistance	Very poor	Poor	Poor	Very good	Very good
Porosity	Sufficient	Good	Poor	Good	Very good
Battery performance (cold crank)	Poor	Sufficient	Sufficient	Very good	Very good
Maximum pore size	Good	Poor	Sufficient	Very good	Poor
Mean pore diameter	Good	Poor	Poor	Very good	Poor
Purity	Good	Fair	Good	Good	Good
Resistance to shorting	Good	Poor	Poor	Very good	Poor
Corrosion resistance	Very good	Poor	Good	Very good	Good
Oxidation resistance	Fair	Poor	Good	Very good	Very good
Envelopable (sealability)	Very poor	Very poor	Sufficient	Very good	Very poor
Flexibility	Brittle	Brittle	Brittle	Excellent	Good

The PE separators have excellent microporous structure for electrolyte flow with minimal lead particle deposits; excellent ductility, strength, and toughness for envelopability and plate puncture resistance; excellent oxidation, chemical, and thermal resistance to resist premature deterioration; good manufacturability with high production efficiency and relatively low raw material cost which reduces overall manufacturing costs [196]. The PE pocket separation is in almost all aspects significantly superior to leaf separation. Only PE separators can be enveloped and can develop good sealability. These have low electrical resistance, sufficient porosity, small pore size, and great resistance to both shorting and corrosion. The PE separator, by virtue of its low electrical resistance, generally provides better cold cranking performance. They are very flexible and offer excellent oxidation resistance if the residual oil content is controlled and/or proprietary chemical modifiers have been incorporated. A comparison of the properties of different types of separators is given in Table 9.

PE separators have contributed to improved battery specific energy and specific power, increased battery cycle life, and higher temperature operating capabilities. PE separators have gained in popularity and have generally replaced PVC, cellulose, glass fiber, and other conventional separators. The transition to microporous PE envelope separators started in the USA in the 1970s, followed by Europe in 1980s. Today, PE separators have captured almost 100% of the US market and more than 70% of the remaining worldwide automotive markets [197].

In a flooded-cell-type lead acid battery, the battery separator typically has "ribs" or protrusions extending from at least one planer face of the separator. Such ribs are either formed integrally with the backweb of the separator, or they can be subsequently applied to the backweb as a bead of the same or different material as the backweb, or they can be formed by embossing the backweb. The ribs function is to provide proper spacing between the plates and to provide a space wherein free electrolyte resides. The ribs also provide pressure to hold the electrodes in contact with the separator. This reduces the need for precise dimensional control on the cell components. Microporous PE separators typically have a configuration comprising a backweb having a predetermined thickness, and a plurality of parallel or patterned ribs spaced apart by a predetermined

distance and extending outwardly from one planar surface of the backweb. The ribs extend continuously in a longitudinal direction parallel to the edges of the separator material. The thickness of the backweb and height and spacing of the ribs is specified to the separator manufacturer by the battery manufacturer; based on specifications designed to maximize certain battery characteristics desired by the battery manufacturer. SLI batteries tend to have separators that are thinner than "industrial" lead acid batteries used for standby power sources and traction devices.

Endoh [198] has reported that one reason for the occasionally shortened life of batteries assembled with PE pocket separators is the development of internal short circuits at the bottom part of the PE separator due to anodic corrosion causing active material to shed from the positive plates and leak through the separators. He also found that when synthetic pulp (SP) separators with glass mats are used, it is possible to not only restrain the shedding from positive plates, but also to protect the separators against intensive oxidation so that no internal short circuits develop on charge. He concluded that the use of SP separators with glass mat is required to produce long service-life batteries, especially in tropical regions.

Higashi et al. [199] carried out endurance test under high temperature conditions on automotive batteries made with three different types of separators. One group was assembled with PE pocket separators for the negative plates, another with PE pocket separators with glass mats for the positive plates, and a third with leaf-type synthetic pulp separators with glass mats. They concluded that battery assembly with PE pocket separators with glass mat is an effective way to achieve good endurance (i.e., life extension at high temperature) and leaf-type synthetic pulp separators with glass mats are the best approach for hot climatic conditions.

Valve Regulated Lead Acid (VRLA) The valve regulated lead acid battery is an important development in lead acid battery technology. These batteries operate on the principle of oxygen recombination, using a "starved" or immobilized electrolyte. The oxygen generated at the positive electrode during charge can, in these battery designs, diffuse to the negative electrode, where it can react, in the presence of sulfuric acid, with freshly formed lead. The separator material should provide innumerable gas channels between the plates through which oxygen can flow from the positive to the negative electrode. These batteries differ from its flooded electrolyte precursor in a number of important ways [200]. They have been manufactured for many years with microfiber glass separators, also called absorptive glass mat (AGM). They are inherently resistant to acid stratification and have the additional important advantage of being essentially maintenance free. The separator is a crucial component in determining the useful life of a VRLA cell. While a prime function of the VRLA cell separator is to hold the cell's electrolyte in place, it must also offer characteristics that prevent major failure mechanisms occurring in the cell's positive and negative plates.

The microglass separator, since its discovery by McClelland and Devitt, has been the material of choice for VRLA designs [201, 202]. It is a wet laid nonwoven (glass fiber) "paper" and is manufactured on a paper machine. The type of paper machine used by the manufacturer can influence the separator properties. Three properties – porosity, uniformity, fiber directionality – are important attributes that can be influenced by the type of fiber used. The glass fiber, which has a zero contact angle with the acid, is durable in the acid environment, and the fine fiber structure also has good resiliency to allow for a sustained pressure against the plate. The microglass separator has a porosity in the 90–95% range and is very conformable. It can adapt to imperfections in the plate surface. The separator also has high temperature stability. Recent studies have shown that higher levels of fine fiber and higher separator compression provide improved cycle performance in VRLA batteries [203–206].

On the other hand, AGM separators offer little control over the oxygen transport rate or the recombination process. The arrival of too much oxygen to the negative plate could result in overheating, hindrance of the battery's ability to recharge, or even a loss of capacity. Furthermore, AGM separators exhibit low puncture resistance.

Nickel Systems

The nickel-based systems have traditionally included the following systems – nickel-iron (Ni/Fe), nickel-cadmium (NiCd), nickel metal hydrides (NiMH), nickel hydrogen (Ni/H_2), and nickel-zinc (Ni/Zn). Of these, the metal hydride chemistry has been the most successful in the secondary battery market. All nickel systems are based on the use of a nickel oxide active material (undergoing one valence change from charge to discharge or vice-versa). The electrodes can be pocket type, sintered type, fibrous type, foam type, pasted type, or plastic roll-bonded type. All systems use an alkaline electrolyte, KOH.

The sealed nickel metal hydride battery uses hydrogen, absorbed in a metal alloy, for the active negative material. The NiMH batteries have a higher energy density and are considered environmentally friendly than the NiCd battery. However, the sealed NiMH battery has limited rate capability and is less tolerant of overcharge. The self-discharge rate is generally higher when conventional nylon separators are used [207]. The presence of oxygen and hydrogen gases cause the polyamide materials to decompose, producing corrosion products which poison the nickel hydroxide, promoting premature oxygen evolution and also forming compounds capable of a redox shuttle between the two electrodes which further increases the rate of self-discharge [208]. Ikoma et al. carried out a detailed investigation to study the self-discharge mechanism and contribution of separators [209]. They used nonwoven fabric made of conventional polyamide (PA), PP (with surfactant), and a nonwoven fabric whose main material was sulfonated-PP (hydrophilic) as separators. When nonwoven fabric made of chemically stable sulfonated-PP is used as a separator instead of a conventional polyamide separator, the self-discharge rate of the NiMH battery was strongly depressed, to the same level as that for the NiCd battery [208, 210, 211].

Nagarajan et al. [212] used differential scanning calorimeter (DSC) to study the materials used as separators in commercial AA cells. They found that Sanyo and Matsushita cells containing nonwoven fabrics fabricated from conventional polyamide as separators exhibited substantially higher self-discharge due to the shuttle reaction of the ammonia and amine. Scimat Ltd. has shown that acrylic acid grafted nonwoven polyolefin separators have the ability to absorb chemical impurities, for example ammonia, from the alkaline environments. It has been shown that by using a grafted polyolefin separator the free ammonia present inside a NiMH cell is trapped by the separator resulting in a reduction in self-discharge to levels normally associated with NiCd cells [213]. In October 2002, Scimat Ltd. announced the launch of the next generation of separators for NiMH and NiCd cells using its second-generation grafting technology [214].

The commonly used separator material now is the surface-treated polypropylene. The surface treatment helps in making the polypropylene permanently wettable. Surface treatments involve the grafting of a chemical such as acrylic acid to the base fibers to impart wettability and are accomplished using a variety of techniques such as UV or cobalt radiation. Another method of imparting wettability to the polypropylene is a sulfonation treatment where the base fiber material is exposed to fuming sulfuric acid. The separator surface is designed to be made hydrophilic to the electrolyte.

Cheng et al. [215] carried out the impedance study on a foam-type NiMH battery with nonwoven PP separator to determine the main causes of early cycle deterioration. Their data indicated that the decrease in the voltage characteristic of the battery was due to drying out of the separator that increases the ohmic resistance of the battery, and that decay of the total discharge capacity is due to an inactive surface that increases the charge-transfer resistance of the battery.

Mathematical Modeling of Separators

Computer simulations have been used as an important tool for understanding and optimizing battery performance since the 1970s [216–218]. Continued progress in computational tools has enabled ever-increasing sophistication in battery modeling and a steady increase in the number of systems to which modeling has been applied. Today, it is possible to obtain simulation codes for all of the major rechargeable batteries, some of which are available in the public domain [219].

The mathematical models of different types of batteries (lead acid [220, 221], NiMH [222],

lithium-ion [223, 224]) have been developed during the last few years [219]. This has led to a better understanding of those systems. The present models consider usually, the thickness and porosity of the separators. Very little has been done in incorporating the effect of physical and chemical properties of separators on the performance and safety of batteries. This is also because the microstructure of separators and their effect on transport properties in batteries are generally known only qualitatively.

A thorough understanding of the microstructure of separators would be beneficial for modeling studies and optimization of electrochemical systems. This will help in making the battery model predictions more practical and reliable. The separator pore structure is usually very complex. It consists of a porous network of interconnected pores, which are filled with liquid electrolyte. A complete description of the pore structure would require a very intricate model. Simulations are only practically possible if a simplified quasi-continuum model involving a few parameters represents the structure. In such an approach, the "effective" electrolytic conductivity, σ_{eff}, is often defined by [93]

$$\sigma_{\text{eff}} = \varepsilon^{\alpha}\sigma_0, \alpha \approx 1.5 \tag{11}$$

where σ_0 is the bulk ionic conductivity of the electrolyte, ε is the void volume fraction of separator filled with electrolyte, and α is the Bruggeman exponent. The general applicability of alpha $\sim$1.5 appears questionable because separator pores are never of an ideal shape. Fan and White [224] chose a α value of 2.5 for separators in NiCd batteries and Doyle et al. [225] used 3.3 for lithium-ion batteries. Arora et al. [226] measured the value as 2.4 for PVdF-based separators by measuring the separator and electrolyte conductivity at different salt concentration. Doyle et al. used an even higher Bruggeman exponent of 4.5 for quantifying the ionic conductivity of their plasticized electrolyte membrane [86].

Patel et al. showed that a Bruggeman exponent of 1.5 is often not valid for real separator materials, which do not have uniform spherical shape [227]. Porous networks based on other morphologies such as oblate (disk-type) ellipsoids or lamella increase the tortuous path for ionic conductivity and result either in a significant increase of the exponent α, or in a complete deviation from the power law. They showed that spherical or slightly prolate ellipsoidal pores should be preferred for separators, as they lead to higher ionic conductivity separators.

Tye [122] explained that separator tortuosity is a key property determining transient response of a separator and steady-state electrical measurements do not reflect the influence of tortuosity. He recommended that the distribution of tortuosity in separators be considered; some pores may have less tortuous paths than others. He showed mathematically that separators with identical average tortuosity and porosities could be distinguished by their non-steady-state behavior if they have different distributions of tortuosity.

Doyle et al. [86] used a mathematical model to examine the effect of separator thickness for the PVDF:HFP gel electrolyte system and found that decreasing separator thickness below 52 μm caused only a minor decrease in ohmic drop across the cell. The voltage drop in the electrodes was much more significant. Mao and White [228] developed a mathematical model for discharge of a Li/TiS_2 cell. Their model predicted that increasing the thickness of the separator from 25 to 100 μm decreased the discharge capacity from 95% to about 90%; further increasing separator thickness to 200 μm reduced discharge capacity to 75%. These theoretical results indicate that conventional separators (25–37-μm thick) do not significantly limit mass transfer of lithium. Santhanagopalan et al. [229] studied the influence of the separator on several internal short-circuit scenarios.

The use of electroactive polymers for overcharge protection has been recently reported for lithium-ion batteries [230, 231]. The electroactive polymer incorporated into a battery's separator is an attractive new option for overcharge protection. Thomas et al. [233] developed a mathematical model to explain how electroactive polymers such as polythiophene can be used to provide overcharge protection for lithium-ion batteries. The model shows that, as the cell potential exceeds the oxidation potential of the polymer, the cell is transformed, over a time scale of a few minutes, from a battery into a resistor, after which a steady-state overcharge condition is attained.

Summary

The ideal battery separator would be infinitesimally thin, offer no resistance to ionic transport in electrolytes, provide infinite resistance to electronic conductivity for isolation of electrodes, be highly tortuous to prevent dendritic growths, and be inert to chemical reactions. Unfortunately, such a product is not commercially feasible. Actual separators are electronically insulating membranes whose ionic resistivity is brought to the desired range by manipulating the membranes thickness and porosity.

It is clear that no single separator satisfies all the needs of battery designers, and often, optimization is performed on a case-by-case basis. It is ultimately the application that decides which separator is most suitable. This chapter is intended to be a useful tool to help battery manufacturers in selecting the most appropriate separators for their batteries and respective applications. The information provided is purely technical and does not include other very important parameters, such as cost of production, availability, etc.

There has been a continued demand for thinner battery separators to increase battery power and capacity. This has been especially true for lithium-ion batteries used in portable electronics. However, it is very important to ensure the continued safety of batteries, and this is where the role of the separator is greatest. Thus, it is essential to optimize all the components of battery to improve the performance while maintaining the safety of these cells. Separator manufacturers continue to work along with the battery manufacturers to create the next generation of batteries with increased reliability and performance, but always keeping safety in mind.

This chapter has attempted to present a comprehensive review of literature on separators used in various batteries. It is evident that a wide variety of separators are available, and that they are critical components in batteries. In many cases, the separator is one of the major factors limiting the life and/or performance of batteries. Consequently, development of new improved separators would be very beneficial for the advanced high capacity batteries.

Future Directions

Up until the last few years, most of the separators and membranes historically used had not been customized for specific battery applications. Thus, future research should be aimed at developing custom-separators that are specifically tailored for the individual battery applications. For example, the form factor of batteries has drastically changed since 2005 – with the advent of sleek consumer electronic devices, and large format batteries and packs for automotive applications. Efforts toward better heat dissipation, extended operating windows, and more stringent requirements on long-term durability have significantly expanded. The general objectives of separator research should be: (a) to find new and cost-effective separators, (b) to understand the separator properties in batteries, and (c) to optimize separator properties related to specific cell performance, life, and safety. The battery separators for tomorrow will demand more than just good insulation and mechanical filtration; they will require unique electrochemical properties. More work focusing on precise control of the membrane properties guided by fundamental insight into the membrane behavior will set the trend for the next generation separators.

Acknowledgments

The authors would like to acknowledge numerous colleagues and staff members at Celgard, LLC and Polypore, International Inc. for their help with the preparation and publication of this chapter.

Bibliography

Primary Literature

1. Linden D, Reddy TB (2002) Handbook of batteries, 3rd edn. McGraw Hill, New York
2. Besenhard JO (ed) (1999) Handbook of battery materials. Weimheim, Wiley-VCH
3. Berndt D (2003) Maintenance free batteries, 3rd edn. Research Studies Press, Taunton, Somerset
4. Arora P, Zhang Z (2004) Chem Rev 104:4419
5. Brodd RJ, Friend HM, Nardi JC (eds) (1995) Lithium ion battery technology. ITE-JEC Press, Brunswick
6. Wakihara M, Yamamoto O (eds) (1998) Lithium ion batteries, fundamentals and performance. Wiley-VCH, New York
7. Yoshino A (1995) Chem Ind 146:870

8. Schalkwijk WAV (ed) (2002) Advances in lithium ion batteries. Kluwer, New York
9. Kinoshita K, Yeo R (1985) Survey on separators for electrochemical systems. LBNL, January 1985
10. Zhang SS (2007) J Power Sources 164 (1):351
11. Benett J, Choi WM (1995) Developments in small cell separators. In: Proceedings of the 10th annual battery conference on applications & advances, IEEE, New York, 10–13 Jan 1995, p 265
12. Boehnstedt W (1999) In: Besenhard JO (ed) Handbook of battery materials. VCH Wiley, Amsterdam
13. Spotnitz R (1999) In: Besenhard JO (ed) Handbook of battery materials. VCH Wiley, Amsterdam
14. Shirai H, Spotnitz R (1996) In: Kozawa A, Yoshio M (eds) Lithium ion secondary battery – materials and applications. Nikkan Kogyo Shin-bun, Tokyo, p 91 (in Japanese)
15. Shirai H, Spotnitz R, Atsushi A (1997) Characterization of separators for lithium ion batteries – a review. Chem Ind 48:47 (in Japanese)
16. Hiroshi T, In: Ogumi Z (ed) (1997) The latest technologies of the new secondary battery materials. CMC, Tokyo, p 99 (in Japanese)
17. Hiroshi T, In: Oyama N (ed) (1998) Advanced technologies for polymer battery. CMC, Tokyo, p 165 (in Japanese)
18. Koichi K, In: Oyama N (ed) (1998) Advanced technologies for polymer battery. CMC, Tokyo, p 174 (in Japanese)
19. Kiyoshi K, In: Kanamura K (ed) (2004) Lithium secondary battery technology for the 21st century. CMC, Tokyo, p 116
20. Brodd RJ, Bullock KR, Leising RA, Middaugh RL, Miller JR, Takeuchi EJ (2004) Electrochem Soc 151:K1
21. http://www.freedoniagroup.com/Batteries.html. Accessed Feb 2010
22. About Edison batteries, Inc. http://www.optodot.com/sys-tmpl/htmlpage/. Accessed Feb 2010
23. Industry News: Looking Back, Looking Forward. Battery & EV Technology, January 2004, 28:2
24. Advanced rechargeable battery industry 2001/2002. Nomura Research Institute Limited, Japan
25. Battery and fuel cell components (2009) The Fredonia Group, Cleveland, OH
26. Pilot C (2004) The worldwide rechargeable battery market. Presented at Batteries 2004, 6th edn, Paris, 2–4 June 2004
27. Celgard Inc. http://www.celgard.com. Accessed Feb 2010
28. http://www.celgard.com/news-room/press-releases/2010/celgard-expansion.asp. Accessed Feb 2010
29. http://www.asahi-kasei.co.jp/asahi/en/ir/supplement/1003transcript.pdf. Accessed Feb 2010
30. Advanced Battery Technology, February 2004, 40:22
31. Pekala RW, Khavari M (2003) US Patent 6,586,138
32. www.porouspower.com. Accessed Feb 2010
33. http://www.sumitomo-chem.co.jp/english/division/itrc.html. Accessed Feb 2010
34. Hamano K, Yoshida Y, Shiota H, Shiraga S. Aihara S, Murai M, Inuzuka T (2003) US Patent 6,664,007 B2
35. Sun L (2003) US Patent 2003/0152828A1
36. Johnson BA, White RE (1998) J Power Sources 70:48
37. Hoffman HG (1995) In: Proceedings of the tenth annual battery conference on applications and advances, LongBeach, 10–13 Jan 1995, IEEE, New York, p 253
38. Geiger M, Callahan RW, Diwiggins CF, Fisher HM, Hoffman DK, Yu WC, Abraham KM, Jillson MH, Nguyen TH (1994) The eleventh international seminar on primary and secondary battery technology and application, Fort Lauderdale, FL, 28 Feb–3 Mar 1994, Florida Educational Seminars, Boca Raton
39. Tanba H (1999) Molding Process 11:759
40. Adachi A, Spotnitz RM et al (1997) Osaka chemical marketing center. Osaka, Japan, p 69
41. Callahan RW, Nguyen KV, McLean JG, Propost J, Hoffman DK (1993) In: Proceedings of the 10th international seminar on primary and secondary battery technology and application, Fort Lauderdale, 1–4 Mar 1993. Florida Educational Seminars, Boca Raton
42. Yu WC, Hux SE (1999) US Patent 5,952,120
43. Hipore. http://www.asahikasai.co.jp/memrbane/english/tradenm/t07.html. Accessed Feb 2010
44. Druin ML, Loft JT, Plovan SG (1974) US Patent 3,801,404
45. Schell WJ, Zhang Z (1999) In: The fourteenth annual battery conference on applications and advances, Long Beach, 12–15 Jan 1999. IEEE, New York, p 161
46. Isaacson RB, Bierenbaum HS (1971) US Patent 3,558,764
47. Kamei E, Shimomura Y (1986) US Patent 4,563,317
48. Yu TH (1996) Processing and structure-property behavior of microporous polyethylene – from resin to final film. Ph.D. Dissertation, Virginia Polytechnic Institute and State University, Virginia
49. Sarada T, Sawyer LC, Ostler MI (1983) J Membr Sci 15:97
50. Bierenbaum HS, Daley LR, Zimmerman D, Hay IL (1974) US Patent 3,843,761
51. Hamer EAG (1986) US Patent 4,620,956
52. Hiroshi K, Tetuo A, Akira K (1997) US Patent 5,691,047
53. Kesting RE (1985) Synthetic polymeric membranes, 2nd edn. Wiley, New York
54. Ihm DW, Noh JG, Kim JY (2002) J Power Sources 109:388
55. Bierenbaum HS, Isaacson RB, Druin ML, Plovan SG (1974) Ind Eng Chem Prod Res Dev 13:2
56. Norimitsu K, Kotaru T, Koichi K, Hidehiko F (2000) US Patent 6,153,133
57. Michiyuki A (1996) Japan Patent 8064194
58. Kotaro T, Koichi K, Tatsuya T, Kenkichi O (1991) US Patent 5,051,183
59. Koichi K, Kotaro T, Mamoru T, Tatsuya T (1996) Japan Patent 8012799
60. Akinao H, Kazuo Y, Hitoshi M (2000) US Patent 6,048,607
61. Userguide (2003) FreedomCar separator costing document, February 2003
62. Xu M, Hu S, Guan J, Sun X, Wu W, Zhu W, Zhang X, Ma Z, Han Q, Liu S (1992) US Patent 5,134,174

63. Fisher HM, Wensley CG (2002) US Patent 6,368,742
64. Zhu W, Zhang X, Zhao C, Zu W, Hou J, Xu M (1996) Polym Adv Tech 7:743
65. Sadamitsu K, Ikeda N, Hoki M, Nagata K, Ogino K (2002) World Patent Application 02066233A1
66. Higuchi H, Matsushita K, Ezoe M, Shinomura T (1995) US Patent 5,385,777
67. Calis GHM, Daemen APM, Gerrits NSJA, Smedinga JT (1997) J Power Sources 65:275
68. Ooms FGB, Kelder EM, Schoonman J, Gerrits N, Smedinga J, Calis G (2001) J Power Sources 97–98:598
69. Yamamura Y, Ooizumi S, Yamamoto K (2001) Separator for rechargeable lithium-ion batteries with high puncture strength and high melt rupture temperature, Nitto Denko Technical Report, vol 39, p 39. http://www.nitto.com/rd/rd6_1.html. Accessed Feb 2010
70. Pekala RW, Khavari M, Dobbie G, Lee D, Fraser-Bell G (2000) In: 17th international seminar & exhibit on primary and secondary batteries, Fort Lauderdale, 6–9 Mar 2000. Florida Educational Seminars, Boca Raton
71. Fleming R, Taskier H (1990) Prog Batt Sol Cells 9:58
72. Hoffman D, Fisher H, Langford E, Diwiggins C (1990) Prog Batt Sol Cells 9:48
73. Spotnitz R, Ferebee M, Callahan RW, Nguyen K, Yu WC, Geiger M, Dwiggens C, Fischer H, Hoffman D (1995) In: Proceedings of the 12th international seminar on primary and secondary battery technology and applications, Fort Lauderdale, 6–9 Mar 1995. Florida Educational Seminars, Boca Raton
74. Yu WC, Callahan RW, Diwiggins CF, Fischer HM, Geiger MW, Schell WJ (1994) In: North America membrane society conference, Breckenridge, CO
75. Kuribayashi I (1996) J Power Sources 63:87
76. Pasquier AD, Gozdz A, Plitz I, Shelburne J (2002) In: 201st meeting, The Electrochemical Society, Philadelphia, 12–17 May 2002
77. Augustin S, Volker H, Gerhard H, Christian H (2002) Desalination 146:23
78. http://www.separion.com. Accessed Feb 2010
79. Hying C (2004) Separion separators for lithium batteries – safety & performance. In: Batteries 2004, 6th edn. Paris, 2–4 June 2004
80. Sachan S, Ray CA, Perusich SA (2002) Polym Eng Sci 42:1469
81. Sachan S, Perusich S (1999) In: Electrochemical Society Meeting, Seattle
82. Carlson SA (2004) Membrane & separation technology news. 22, 8
83. Abraham KM (1993) Electrochim Acta 38:1233
84. Gineste JL, Pourcell G (1995) J Membr Sci 107:155
85. Hoffman DK, Abraham KM (1991) In: Proceedings of the fifth international seminar on lithium battery technology and applications, Deerfield Beach. Florida Educational Seminars, Boca Raton, FL
86. Fuller TF, Doyle M, Newman J (1994) J Electrochem Soc 141:1
87. USABC (2001) Development of low cost separators for lithium-ion batteries, RFPI 2001
88. Laman FC, Sakutai Y, Hirai T, Yamaki J, Tobishima S (1992) Extended abstract. In: 6th International meeting lithium batteries, Münster, Germany, 10–15 May 1992, p 298
89. Laman FC, Gee MA, Denovan J (1993) J Electrochem Soc 140:L51
90. Robinson RG, Walker RL (1963) In: Collins DH (ed) Batteries. MacMillan, New York, p 15
91. Lander JJ, Weaver RD, Salkind AJ, Kelley JJ (1964) In: Cooper JE, Fleischer A (eds) Characteristics of separators for alkaline silver oxide zinc secondary batteries. Screening methods. NASA Technical Report NAS 5–2860
92. Kilroy WP, Moynihan CT (1978) J Electrochem Soc 125:520
93. MacMullin RB, Muccini GA (1956) AIChE J 2:393
94. Spotnitz R, Ferebee MW (1996) Meeting abstracts, 6–11 Oct 1996. The Electrochemical Society Inc., vol 96-2, Fall Meeting, San Antonio, TX
95. Ionov VV, Isakevitch VV, Katalevsky EE, Chernokoz AJ (1990) J Power Sources 30:321
96. Lowell S, Shields E (1991) Powder surface area and porosity, 3rd edn. Chapman and Hill, New York
97. PMI conference 2000 proceedings (2000) PMI short course, Ithaca, NY, 16–19 Oct 2000
98. Porous materials Inc. http://www.pmiapp.com. Accessed Feb 2010
99. Jena AK, Gupta KM (1999) J Power Sources 80:46
100. Jena AK, Gupta KM (2001) J Power Sources 96:214
101. Venugopal G, Moore J, Howard J, Pendalwar S (1999) J Power Sources 77:34
102. Zeman L, Denault L (1992) J Membr Sci 71:221
103. Chen RT, Saw CK, Jamieson MG, Aversa TR, Callahan RW (1994) J Appl Polym Sci 53:471
104. Fujii T, Mochizuki T (1998) US Patent, 5,759,678
105. Venugopal G (1997) The role of plastics in lithium-ion batteries. In: Proceedings of the 3rd annual conference on plastics for portable and wireless electronics, Philadelphia, 14–15 Oct 1997, p 11
106. Lundquist JT, Lundsager CB, Palmer NL, Troffkin HJ, Howard J (1998) US Patent 4,731,304
107. Lundquist JT, Lundsager CB, Palmer NI, Troffkin HJ (1987) US Patents 4,650,730
108. Faust MA Suchanski MR, Osterhoudt HW (1988) US Patent No. 4,741,979
109. Matthias U, Dieter B, Heinrich R, Thomas B (2003) US Patent 6,511,517
110. Maleki H, Shamsuri AK (2003) J Power Sources 115:131
111. http://www.cpsc.gov/cpscpub/prerel/prhtml07/07011.html. Accessed Feb 2010
112. Norin L, Kostecki R, McLarnon F (2002) Electrochem Solid State Lett 5:A67
113. Kostecki R, Norin L, Song X, McLarnon F (2004) J Electrochem Soc 151:A522

114. Hazardous materials regulations, Code of Federal Regulations, CFR49 173.185
115. UL1640, Lithium batteries, Underwriters Laboratories, Illinois
116. UL2054, Household and commercial batteries, Underwriter Laboratories, Illinois
117. Secondary lithium cells and batteries for portable applications, International Electrotechnic Commission, IEC 61960–1 and IEC 61960–2
118. Recommendations on the transport of dangerous goods (1999) Manual of Tests and Criteria, United Nations, New York
119. Safety Standard for Lithium Batteries (1995) UL 1642, 3rd edn. Underwriters Laboratories Inc, Illinois
120. Standard for Household and Commercial Batteries (1993) UL 2054. Underwriter Laboratories, Illinois
121. UN Recommendations on the Transport of Dangerous Goods, December 2000
122. Tye FL (1983) J Power Sources 9:89
123. Japan Battery Association (1997) A guideline for the safety evaluation of secondary lithium cells. Japan Battery Association, Tokyo
124. Venugopal G (2001) J Power Sources 101:231
125. Kim MH (2008) LG Li-Ion technology for automotive applications. Presented at the AABC 2008, Tampa, FL
126. Alamgir M, Abraham KM (1994) Chapter 3. In: Pistoia G (ed) Lithium batteries: new materials, developments and perspectives, vol 5, Industrial Chemistry Library. Elsevier, New York
127. Gray FM (1997) Polymer electrolytes, RSC materials monograph. The Royal Society of Chemistry, Cambridge
128. Fauteux D, Massucco A, McLin M, Van Buren M, Shi J (1995) Electrochim Acta 40:2185
129. North M, Markin TL, Hooper A, Tofield BC (1984) In: Second international meeting on lithium batteries, Extended Abstracts #19, Paris, France, 25–27 Apr 1984
130. Appetecchi GB, Dautzenberg G, Scrosati BJ (1996) J Electrochem Soc 143:6
131. Armand M (1983) Solid State Ionics 9/10:745
132. Lightfoot P, Mehta MA, Bruce PG (1993) Science 262:883
133. Vincent CA, Scrosati B (1993) Modern batteries. An introduction to electrochemical power sources. Arnold, London
134. Appetecchi GB, Passerini S (2002) J Electrochem Soc 149:A891
135. Croce F, Appetecchi GB, Persi L, Scrosati B (1998) Nature 394:4496
136. Croce F, Persi L, Ronci F, Scrosati B (2000) Solid State Ionics 135:47
137. Fan J, Fedkiw PS (1997) J Electrochem Soc 144:399
138. Appetecchi GB, Romagnoli P, Scrosati B (2001) Electrochem Commun 3:281
139. Kim DW, Sun YK (2001) J Power Sources 102:41
140. Chojnacka J, Acosta JL, Morales E (2001) J Power Sources 97–98:819
141. Nishi Y (2002) In: van Schalkwijk W, Scrosati B (eds) Advances in lithium ion batteries. Kluwer/Plenum, New York
142. EE Times.com. http://www.eet.com/story/OEG19990121S0013. Accessed Feb 2010
143. Song JY, Wang YY, Wan CC (1999) J Power Sources 77:183
144. Min HS, Ko JM, Kim DW (2003) J Power Sources 119–121:461
145. Jo SI, Sohn HJ, Kang DW, Kim DW (2003) J Power Sources 119–121:478
146. Kim HS, Kum KS, Cho WI, Cho BW, Rhee HW (2003) J Power Sources 124:221
147. Abraham KM, Alamgir M (1994) Solid State Ionics 70–71:20
148. Schmutz C, Tarascon JM, Gozdz AS, Schumtz CN, Warren PC, Shokoohi FK (1995) In: Proceeding electrochemical society, 1995. Rechargeable lithium and lithium ion batteries, vol 94–28, pp 330–335
149. Murata K, Izuchi S, Yoshihisa Y (2000) Electrochim Acta 45:1501
150. Jiang Z, Carroll B, Abraham KM (1997) Electrochim Acta 42:2667
151. Song JY, Cheng CL, Wang YY, Wan CC (2002) J Electrochem Soc 149:A1230
152. Gozdz AS, Schmutz CN, Tarascon JM, Warren PC (1995) US Patent 5,456,000
153. Gozdz AS, Tarascon JM, Schmutz CN, Warren PC, Gebizlioglu OS, Shokoohi F (1995) In: Tenth annual battery conference on advances and applications, Long Beach, 10–13 Jan 1995. IEEE, New York, p 301
154. Tarascon JM, Gozdz AS, Schumtz CN, Shokoohi FK, Warren PC (1996) Solid State Ionics 86–88:49
155. Pasquier AD, Waren PC, Culver D, Gozdz AS, Amatucci G, Tarascon JM (1999) Electrochem Soc Proc 99(24):360
156. Park CK, Kakirde A, Ebner W, Manivannan V, Chai C, Ihm DJ, Shim YJ (2001) J Power Sources 97–98:775
157. Dasgupta S, Jacobs JK (1995) US Patent 5,437,692
158. Abraham KM, Alamgir M, Hoffman DK (1995) J Electrochem Soc 142:683
159. Pendalwar SL, Howard JN, Venugopal G, Oliver M (1998) US Patent 5,716,421
160. Gozdz AS, Plitz I, Du Pasquier A, Zheng T (2001) In: Proceedings of the 200th ECS meeting, Phoenix, AZ, vol 2000–2001, Fall 2001, p 336
161. Gozdz AS (2001) US Patent 6,328,770
162. Kim DW, Oh B, Park JH, Sun YK (2000) Solid State Ionics 138:41
163. Wang Y, Sejdic JT, Steiner R (2002) Solid State Ionics 148:443
164. Gozdz AS, Plitz I, DuPasquier A, Zheng T (2007). Presented at the 198th meeting of the electrochemical society, Phoenix, AZ, 22–27 Oct 2000
165. Spotnitz RM, Wensley CG (2000) US Patent 6,322,923
166. Fabrice C, Bradford R (2002) WO 02/50929 A2
167. Jeong YB, Kim DW (2004) J Power Sources 128:256
168. Dasgupta S, Jacobs JK (1996) US Patent 5,498,489
169. Balsara N (2010) Block copolymer separators for lithium batteries. In: Presented at the 2010 annual merit review of the vehicle technologies program. http://www1.eere.energy.gov/vehiclesandfuels/pdfs/merit_review_2010/electrochemical_storage/es088_balsara_2010_p.pdf. Accessed Feb 2010
170. Eschbach FO, Oliver M (1997) US Patent 5,681,357
171. Hamano K, Shiota H, Shiraga S, Aihara S, Yoshida, Y, Murai M, Inuzuka T (1999) US Patent 5,981,107
172. Akashi H (1997) US Patent 5,658,686

173. Akashi H (1996) Paper presented at the international symposium on polymer electrolytes, ISPE-5, Uppsala, Sweden, 11–16 Aug 1996
174. Fujii T (2000) In: Proceeding of 17th international seminar & exhibit on primary and secondary batteries, Boca Raton, 6–9 Mar 2000. Florida Educational Seminars, Boca Raton
175. Nakane I, Narukawa S (2000) Power 2000. In: The 8th annual international conference on power requirements for mobile computing and wireless communications, San Diego, CA, 24–27 Sept 2000
176. Kim KM, Ryu KS, Kang SG, Chang SH, Chung IJ (2001) Macromol Chem Phys 202:866
177. Kim KM, Park NG, Ryu KS, Chang SH (2002) Polymer 43:3951
178. Kim KM, Ko JM, Park NG, Ryu KS, Chang SH (2003) Solid State Ionics 161:121
179. Prosini PP, Villano P, Carewska M (2002) Electrochim Acta 48:227
180. Liu X, Kusawake H, Kuwajima S (2001) J Power Sources 97–98:661
181. Kim DW, Ko JM, Chun JH, Kim SH, Park JK (2001) Electrochem Comm 3:535
182. Kim DW, Noh A, Chun JH, Kim SH, Ko JM (2001) Solid State Ionics 144:329
183. Choi SH, Park SY, Nho YC (2000) Radiat Phys Chem 57:179
184. Choi SH, Kang HJ, Ryu EN, Lee KP (2001) Radiat Phys Chem 60:495
185. Mardegain SB (2003) Battery Power Prod Technol 1:12
186. Boehnstedt W (1996) J Power Sources 59:45
187. Boehnstedt WJ (2004) J Power Sources 133:59
188. Lander JJ (1974) In: Proceedings of the symposium on battery separators. The Electrochemical Society, Columbus, OH, p 4
189. Prout L (1993) J Power Sources 46:117
190. Vinal GW (1945) Storage batteries. Wiley, New York
191. Butherus AD, Lindenberger WS, Vaccaro FJ (1970) Lead-acid battery: electrochemical compatibility of plastics. Bell Syst Tech J 49(7):1377–1392
192. Paik SL, Terzaghi G (1995) J Power Sources 53:283
193. Kung J (1994) J Power Sources 48:129
194. Wang LC, Harvey MK, Stein HL, Scheunemann U (1997) The role of UHMW-PE in microporous PE separators. In: Proceedings of the 12th annual battery conference on applications & advancesIEEE, New York, 14–17 Jan 1997, p 69
195. Larsen DW, Kehr CL (1996) US Patent 3,351,495
196. Boehnstedt W (2001) J Power Sources 95:234
197. Wang LC, Harvey MK, Ng JC, Scheunemann U (1998) J Power Sources 73:74
198. Endoh H (1996) J Power Sources 599:51
199. Higashi T, Endoh H (1998) J Power Sources 73:110
200. Rand DAJ, Woods R, Dell RM (1998) Batteries for electric vehicles. Research Studies Press, Taunton, UK. ISBN. ISBN 0-86380-205-0
201. McClelland DH, Devitt JL (1975) US Patent 3,862,861
202. Zguris GC (1998) J Power Sources 73:60
203. Zguris GC (1997) J Power Sources 67:307
204. Zguris GC (1996) J Power Sources 59:131
205. Pavlov D, Ruevski S, Naidenov V, Sheytanov G (2000) J Power Sources 85:164
206. Ferreira AL (1999) J Power Sources 78:41
207. Fetcenko MA, Venkatesan S, Ovshinsky S (1992) In: Proceedings of the symposium on hydrogen storage materials, batteries & electrochemistry. Electrochemical Society, Pennington, NJ, p 141
208. Wada M (1994) Polymer role in advanced battery technology. Polym Adv Tech 5:645–652
209. Ikoma M, Hoshina Y, Matsumoto L, Iwakura C (1996) J Electrochem Soc 143:1904
210. Ikoma M, Takahashi O, Tsuboi R, Matsumoto L (1993) Denki Kagaku 61:997
211. Furukawa N (1994) J Power Sources 51:45
212. Nagarajan GS, Van Zee JW (1998) J Power Sources 70:173
213. Cook JA, Lancaster IM (1998) Electrochem Soc Proc 98–15:55
214. Scimat's latest separators (2002) Batteries International, October 2002
215. Cheng S, Zhang J, Liu H, Leng Y, Yuan A, Cao C (1998) J Power Sources 74:155
216. Newman J, Tiedemann W (1975) AIChE J 21:25
217. Newman JS (1991) Electrochemical systems, 2nd edn. Prentice-Hall, Englewood Cliffs
218. Vidts PD, White RE (1997) J Electrochem Soc 144:1343
219. Ceder G, Doyle M, Arora P, Fuentes Y (2002) Computational modeling and simulation for rechargeable batteries. MRS Bull 27(8):619–623
220. Newman J, Tiedemann W (1997) J Electrochem Soc 144:3081
221. Gu H, Nguyen TV, White RE (1987) J Electrochem Soc 134:2953
222. Vidts PD, Delgado J, White RE (1995) J Electrochem Soc 142:4006
223. Doyle M, Fuller TF, Newman J (1993) J Electrochem Soc 140:1526
224. Fan D, White RE (1991) J Electrochem Soc 138:17
225. Doyle M, Newman J, Gozdz AS, Schumtz CN, Tarascon JM (1996) J Electrochem Soc 143:1890
226. Arora P, Doyle M, Gozdz AS, White RE, Newman J (2000) J Power Sources 88:219
227. Patel KK, Paulsen JM, Desilvestro J (2003) J Power Sources 122:144
228. Mao Z, White RE (1993) J Power Sources 43–44:181
229. Santhanagopalan S, Ramadass P, (Zhengming) Zhang J (2009) Analysis of internal short-circuit in a lithium ion cell. J Power Sources 194(1):550–557
230. Denton F, Howard JN, Anani AA, Fernandez JM (2001) US Patent 6,228,516
231. Takita K, kono K, Takashima T, Okamoto K (1991) US Patent 5,051,183
232. Mao H, Wainwright DS (1990) US Patent 6,074,766
233. Thomas-Alyea KE, Newman J, Chen G, Richardson TJ (2004) A concentrated solution theory model of transport in solid-polymer-electrolyte fuel cells. J Electrochem Soc 151: A509

Recreational Water Risk: Pathogens and Fecal Indicators

Alexandria B. Boehm[1], Jeffrey A. Soller[2]
[1]Environmental and Water Studies, Department of Civil and Environmental Engineering, Stanford University, Stanford, CA, USA
[2]Soller Environmental, LLC, Berkeley, CA, USA

Article Outline

Glossary
Definition of the Subject and Its Importance
Introduction
Pathogens in Coastal Waters
Assessing Risk: Epidemiology and Indicator Organisms
Assessing Risk: Quantitative Microbial Risk Assessment (QMRA) Modeling
Future Directions
Bibliography

Glossary

Microbial pollution Pathogens.
Quantitative microbial risk assessment Assessment of risk from exposure to pathogens.
Epidemiology The study of human health in response to a treatment.
Recreational waterborne illness Illness resulting from exposure to microbial pollution, includes gastroenteritis, respiratory illness, ear, nose, eye, and throat ailments, and skin rash.
Bacterial pathogens Pathogens that are bacterial.
Viral pathogens Pathogens that are viruses.
Protozoan pathogens Pathogens that are protozoa.

Definition of the Subject and Its Importance

Pathogens can enter recreational waterbodies (lakes, rivers, ocean beaches) from a number of different sources. The illness acquired by swimmers after exposure to pathogen-polluted recreational waters is termed recreational waterborne illness (RWI). Since many RWI go unreported to health care agencies, the true number of RWI each year can only be estimated; however, numbers are believed to be high – over one million in southern California alone. The risk of RWI from exposure to recreational waters can be measured using epidemiological studies and estimated using quantitative microbial risk assessments.

Introduction

Exposure to microbially polluted recreational waters can cause a variety of adverse health effects in humans including neurological infections, skin infections, earaches, eye infections, gastrointestinal illnesses, and respiratory infections [1]. Microbial pollution refers to the presence of organisms that cause illness in humans either through the production of toxins or their colonization of the human body.

It is estimated that globally, exposure to coastal waters polluted with wastewater results in an excess 120 million gastrointestinal and 50 million severe respiratory illnesses per year [2], including illnesses acquired through consumption of contaminated shellfish. In southern California, there are an estimated 1.5 million cases of gastrointestinal illnesses each year due to recreational exposure to polluted waters [3]. Moreover, there were 259 recreational water outbreaks that occurred in the USA between 1970 and 2000 [4].

Estimating the number of individuals acquiring illness through exposure to recreational waters is challenging. Typically, individuals who acquire recreational waterborne illness (RWI) do not seek medical attention because most of the illnesses tend to be mild and self-limiting. In addition, most RWIs are not reportable, so incidence levels are highly uncertain. The estimates mentioned previously were obtained using a variety of assumptions about the contamination of water and exposures. Epidemiology studies and quantitative microbial risk assessments (QMRA) are two scientifically rigorous methods that are used to estimate rates of RWI as a function of water quality.

This chapter provides a brief overview of the pathogens present in coastal waters. Readers are referred to other references for more information on these topics [5–7]. The two most common methods of assessing risk of exposure to pathogens in coastal waters, epidemiology studies, and QMRA, are also described. Example applications of these methods to assess risk of illness from exposure to pathogen-polluted coastal waters are presented. Critical research gaps are identified and summarized.

Pathogens in Coastal Waters

Pathogens present in coastal waters can be characterized into two broad groups. The first group consists of autochthonous pathogens that have an ecological niche in recreational waters. The other group is composed of allochthonous pathogens that come from human and animal wastes that have been discharged into these waterbodies.

Autochthonous pathogens include harmful algae, organisms in the genus *Vibrio*, and some protozoa such as *Naeglaria fowleri*. Harmful diatoms and dinoflagellates can cause a variety of ailments in humans from their production of toxins [8, 9]. *Vibrio vulnificus* and *V. parahaemolyticus* can infect open wounds and cause gastroenteritis if ingested from seawater. Other *Vibrio* species (such as *V. cholerae* and *V. mimicus*) can be pathogenic and cause similar ailments. *N. fowleri* is primarily found in freshwater, and when it enters the human body, can cause a rare but serious brain infection. While these organisms are extremely important from a human health perspective, this chapter will not discuss risks associated with autochthonous pathogens.

The focus of this chapter is allochthonous pathogens (Table 1) including the eight pathogens that cause a large proportion (>95%) of all non-foodborne illnesses in the USA [10]: the viruses norovirus, rotavirus, and adenovirus; the bacteria *Campylobacter*, *Salmonella* and pathogenic *Escherichia coli*; and the protozoans *Cryptosporidium* spp. and *Giardia lamblia*. Other pathogens that are important etiologies of RWI include enteroviruses, *Staphylococcus aureus*, and methicillin-resistant *S. aureus* (MRSA). All these pathogens, with the exception of *S. aureus* and MRSA, cause gastrointestinal illness. *Staphylococcus* causes skin infections.

Recreational Water Risk: Pathogens and Fecal Indicators. Table 1 Allothchonous human pathogens detected in coastal waters

	Concentration/Occurrence	Reference
Viruses		
Enteroviruses	Present in 9 of 72 1-liter samples using RT-PCR at Avalon Beach, CA[a]	[81]
Adenoviruses	Present in 15 of 30 250-liter samples using PCR at Silver Beach, MI[a]	[63]
Hepatitis A	105–30,771 viral particles/l using Q-RTPCR at Imperial Beach, CA[a]	[82]
Norovirus	2 of 19 samples in 110-liters using RT-PCR at Key West sites (FL)[a]	[83]
Rotavirus (reovirus)	2 of 19 sites with 2–5 MPN/L at Italian coastline	[84]
Bacteria		
Campylobacter	Detected in 25 of 192 100 – 1,000 mL Spanish marine recreational water samples using culture-based methods	[85]
Salmonella	Detected in 70–100% of samples from a lagoon in Brazil using culture-based methods, volume assayed not reported	[86]
Staphylococcus	60–70% of approx. 100 mL seawater samples from Doheny and Avalon Beach, CA using culture-based methods	[13]
Pathogenic *Escherichia coli*	2 of 377 *E. coli* isolates from North Carolina and Southern California coastal waters using combined culture and PCR methods	[87]
Shigella	100% of algal mat samples from Lake Michigan near Burns Ditch by PCR	[18]
Protozoa		
Cryptosporidium	13.7 ± 1.7 oocysts/L on weekends at Chesapeake Bay beach, MD	[88]
Giardia	9.1 ± 1.1 cysts/L on weekends at Chesapeake Bay beach, MD	[88]

[a]Volumes reported do not account for the fact that a fraction of water sample was used during polymerase chain reaction (PCR), reverse-transcriptase (RT-)PCR, or quantitative (Q)PCR.

Adenoviruses can cause gastrointestinal illness, as well as eye and respiratory infections.

The detection of pathogens in environmental matrices is methodologically challenging. Allochthonous pathogens are rare microbes in the environment. In seawater there are on the order of one million autochthonous bacteria and 10 million autochthonous viruses in a milliliter. Whereas allochthonous pathogens may be present at levels of 1 per 10 liters l or lower. Thus, enumerating the allochthonous pathogens is particularly difficult because the presence of all the other organisms in the sample can interfere with the detection of the rare target. Because the field of pathogen detection is still evolving and because allochthonous pathogens densities are typically low, there are limited data on pathogen concentrations and occurrence in recreational waters. In many cases, authors only provide data on the presence or absence of pathogens in recreational waters and do not provide concentrations. Some example concentrations are provided in Table 1.

Treated and untreated wastewater, human and other animal feces, stormwater and urban runoff, and agricultural runoff can all contain microbes that are pathogenic to humans [11, 12]. When discharged to coastal waters, concentrations of pathogens may be high and can pose high levels of human health risks.

Pathogens are also found in environmental reservoirs that in some cases may serve as a source of pathogens to recreational waters. Beach sands can harbor *Campylobacter, Salmonella*, and *S. aureus* [13–16]. Aquatic sediments can accumulate bacteria, protozoa, and viruses [17]. Marine and lacustrine kelp species may also harbor bacterial pathogens including pathogenic *E. coli*, *Salmonella*, and *Campylobacter* [18, 19].

Assessing Risk: Epidemiology and Indicator Organisms

The monitoring of recreational waters for all RWI pathogens to assess the safety of swimming is not scientifically or economically feasible [20]. Microbial indicator organisms have been used for centuries as indicators of the presence of human pathogens. Internationally, many countries use fecal and total coliforms as a basis for their recreational water quality criteria, standards, or guidelines [21]. Other countries rely on measurements of enterococci (or fecal streptococci), *E. coli*, or both for their recreational waters, most based on guidelines provided by World Health Organization [22] and/or the US Environmental Protection Agency (EPA). These organisms were chosen as indicators because their concentrations are high in human wastewater and feces, they are relatively simple to measure, and their presence in coastal waters is correlated to adverse health outcomes in swimmers through epidemiology studies conducted in wastewater-impacted waters [23–26]. The epidemiology studies that correlate indicator concentration to adverse health outcomes are key to the use of indicators to assess risk.

Epidemiology studies evaluate illness resulting from exposure to a particular contaminant or activity. When applied to RWI, epidemiology studies evaluate the illness rates in swimmers versus non-swimmers, and characterize illness rates as a function of indicator organism concentration. The studies involve the collection of health and behavior data contemporaneously with concentrations of indicator organisms. RWI epidemiology studies are either case-control randomized trial or prospective cohort designs. In case-control studies, swimmer and non-swimmer activities are prescribed by randomization at the onset of the study. In these studies, exposures are well controlled. Subject recruitment is done in advance of the study. In prospective cohort studies, subjects are recruited at the study site and are enrolled when they arrive at the shoreline. Exposures are self-prescribed by subjects and behavioral data on exposure is collected using self-reports at the end of the day. In the prospective cohort design, there is less control over exposure, but the exposures are more realistic as they are not prescribed by the study design. Additional types of studies that have been employed to study RWI include cross-sectional studies and event studies. The former is similar in design to a cohort study; the latter takes advantage of a sporting event, for example, for data collection.

Since the 1950s, numerous epidemiological studies have been conducted throughout the world to evaluate the association between recreational water quality and RWI (including GI symptoms; eye infections; skin complaints; ear, nose, and throat infections; and respiratory illness) [23–26]. Most of these studies investigated wastewater effluent-impacted marine and

estuarine waters alone or in combination with freshwater. Several investigated freshwater recreational environments or non-wastewater effluent-impacted waters. These studies indicate that the rates of some adverse health outcomes are higher in swimmers compared with non-swimmers [23].

Taken as a whole, the weight of evidence from these studies indicates that fecal indicator bacteria (fecal streptococcus/*Enterococcus*, in particular) are able to predict GI and in some cases, respiratory illnesses from exposure to recreational waters [23, 25, 26]. This broad base of information stems from studies conducted throughout much of the developed world (Table 2, Adapted from [27]).

Several meta-analyses and/or systematic reviews have summarized the available recreational water epidemiology studies [23, 25, 26]. Pruss et al. [23] conducted a systematic review to initiate development of new WHO guidelines for recreational use of the water environment. The comprehensive review of 22 published studies on sewage pollution of recreational water and health outcomes concluded that the epidemiological basis had been laid to develop WHO guidelines on fecal pollution based on a causal association between GI illness symptoms and increased concentrations of bacterial indicators (i.e., enterococci for marine, enterococci and *E. coli* for fresh) in recreational waters.

Zmirou et al. [26] examined 18 published studies to provide a scientific basis for establishing new standards for the microbial quality of marine and fresh recreational waters to replace the 30 year-old European Union bathing water quality guidelines [28]. The researchers provided four major results: (1) increased concentrations of fecal coliforms or *E. coli* and enterococci in both fresh and marine recreational waters are associated with increased risks of acute GI illness, with enterococci eliciting four to eight times greater excess risks than fecal coliforms or *E. coli* at the same concentrations; (2) GI illness risks associated with enterococci occur at lower indicator concentrations in marine versus fresh recreational waters; (3) increased concentrations of total coliforms have little or no association with GI illness risk; and (4) no evidence exists of a concentration threshold of indicator microorganisms below which there would be no GI illness risk to bathers.

Wade et al. [25] conducted a systematic review and meta-analysis of 27 published studies to evaluate the evidence linking specific microbial indicators of recreational water quality to specific health outcomes under non-outbreak (endemic) conditions. The study was conducted at the request of the United States National Academy of Sciences. Secondary goals included identifying and describing critical study design issues and evaluating the potential for health effects at or below the current regulatory criteria [29]. They concluded that (1) enterococci and, to a lesser extent, *E. coli* are adequate indicators (predictors) of GI illness in marine recreational waters, but fecal coliforms are not; (2) the risk of GI illness is considerably lower in studies with enterococci and *E. coli* densities below those established by EPA [29], thus providing support for their regulatory use; (3) *E. coli* is a more reliable and consistent predictor of GI illness than enterococci or other indicators in fresh recreational waters; and (4) studies that used a non-swimming control group and that focused on children found elevated GI illness risks.

Based on these meta-analyses, the weight of evidence indicates that there is a relationship between levels of specific indicator bacteria and RWI in coastal waters impacted by wastewater. However, as discussed earlier there are many sources of indicator bacteria to coastal waters, and many of these sources contain different pathogens with diverse health risks. Along coastlines with good sewage infrastructure and regulated anthropogenic discharges, wastewater is unlikely to be contributing substantial amounts of indicator organisms to the swimming areas on a regular basis [27]. Important sources of indicator organisms and pathogens are probably nonpoint in nature, emanating from soils, animal feces, urban runoff, stormwater runoff, or agricultural runoff.

There are only a few epidemiology studies that examine the link between RWI and fecal indicator organisms in recreational waters polluted with sources other than wastewater. Review of these studies suggests the relationship between indicator concentration and RWI risks are equivocal. On one hand, Colford et al. [30] found that the incidence of swimmer illness was greater than the incidence of non-swimmer illness, but swimmer illness was not associated with any of the bacterial indicator organisms at a marine beach where bacterial contamination was not attributable to

Recreational Water Risk: Pathogens and Fecal Indicators. Table 2 Recreational water epidemiology studies included in reviews by Prüss [23], Wade et al. [25], and Zmirou et al. [26]. Location refers to geographic location of study. Water Type refers to whether the study was conducted at a marine or fresh water. Study design denotes whether to study was a cohort, randomized trial, cross section, or event study

Reference	Location	Water type	Study design	Review article
Alexander et al. [89]	UK	Marine	Cohort	Wade, Zmirou
Bandaranayake [90]	New Zealand	Marine	Cohort	Prüss
Brown et al. [49]	UK	Marine	Cohort	Zmirou
Cabelli [38]	USA	Marine	Cohort	Wade, Prüss, Zmirou
Cabelli [44]	Egypt	Marine	Cohort	Wade, Prüss
Calderon et al. [31]	USA	Fresh	Cohort	Wade
Cheung et al. [36]	Hong Kong	Marine	Cohort	Wade, Prüss, Zmirou
Corbett et al. [52]	Australia	Marine	Cohort	Wade, Prüss, Zmirou
Dufour [39]	USA	Fresh	Cohort	Wade, Prüss, Zmirou
Fattal et al. [42]	Israel	Marine	Cohort	Wade, Prüss, Zmirou
Ferley et al. [47]	France	Fresh	Cohort	Wade, Prüss, Zmirou
Fewtrell et al. [91]	UK	Fresh	Event	Wade, Zmirou
Fewtrell et al. [92]	UK	Marine	Cohort	Wade, Zmirou
Kay et al. [71]	UK	Marine	Randomized trial	Wade
Fleisher et al. [93]	UK	Marine	Randomized trial	Prüss
Foulon et al. [48]	France	Marine	Cross-sectional	Wade
Haile et al. [34, 94]	USA	Marine	Cohort	Wade, Prüss, Zmirou
Kay et al. [71]	UK	Marine	Randomized trial	Wade, Prüss, Zmirou
Kueh et al. [95]	Hong Kong	Marine	Cohort	Wade, Prüss
Lee et al. [96]	UK	Fresh	Event	Wade
Lightfoot [97]	Canada	Fresh	Cohort	Wade, Prüss
Marino et al. [98]	Spain	Marine	Cohort	Wade
McBride et al. [33]	New Zealand	Marine	Cohort	Wade
Medema et al. [99]	The Netherlands	Fresh	Event	Wade
CSIR [100]	South Africa	Marine	Cohort	Prüss
Mujeriego et al. [46]	Spain	Marine	Cohort	Prüss
Philipp et al. [101]	UK	Marine	Event	Wade, Zmirou
Pike [102]	UK	Marine	Cohort	Wade, Prüss, Zmirou
Prieto et al. [103]	Spain	Marine	Cohort	Wade
Seyfried et al. [40]	Canada	Fresh	Cohort	Wade, Prüss, Zmirou
Stevenson [104]	USA	Fresh	Cohort	Wade, Prüss, Zmirou
UNEP/WHO [105]	Israel	Marine	Cohort	Prüss
UNEP/WHO [106]	Spain	Marine	Cohort	Prüss

Recreational Water Risk: Pathogens and Fecal Indicators. Table 2 (Continued)

Reference	Location	Water type	Study design	Review article
Van Asperen et al. [107]	The Netherlands	Fresh	Event	Wade, Zmirou
Van Dijk et al. [108]	UK	Marine	Cohort	Prüss
Von Schirnding et al. [109]	South Africa	Marine	Cohort	Wade, Zmirou

wastewater discharges. Similarly, Calderon et al. [31] found no statistically significant association between swimmers' illness risk and indicator concentrations in a freshwater pond where agricultural runoff was the source of contamination. McBride [32] suggested that if more swimmers had been included in the Calderon et al. [31] study, achieving statistically significant results would have been possible, however. At a marine bathing study in New Zealand, McBride et al. [33] indicated that RWI risks posed by animal versus human fecal material were not substantially different; however, the study's limited range of indicator organisms' concentrations precluded the development of a detailed statistical model of health risks versus indicator density.

In the first study to be conducted in waters directly impacted by urban runoff, Haile et al. [34] reported associations between swimmer health and indicator densities. However, this nonpoint runoff source was known to contain human sources of fecal contamination, based on the presence of human enteric viruses. Dwight and colleagues [35] found that surfers exposed to Southern California urban runoff had higher illness rates than surfers exposed to Northern California rural runoff. The results from a Hong Kong marine water study [36] and a German freshwater study [37] are more difficult to interpret regarding risks from human versus nonhuman sources because in both studies, the analyses combined the results from sites with different predominant contamination sources.

An additional meta-analysis examined the differential risks associated with exposure to human and nonhuman animal fecal material [24]. Illness risk associated with bathing in water polluted primarily with human fecal material was reviewed based on studies from the USA [38, 39], Canada [40, 41], Israel [42, 43], Egypt [44, 45], Spain [46], France [47, 48]; the UK [49, 50], Hong Kong [51], and Australia [52, 53]. Most of these studies showed a positive correlation between GI illness and fecal indicator density; there was little equivalent evidence from waters polluted primarily with animal feces. The only study specifically designed to address swimming-associated illness in animal-impacted waters was that of Calderon et al. [31] who found no statistically significant association between GI illness and fecal indicator bacteria densities. Based on this observation, Sinton and colleagues [24] concluded that reliable epidemiological evidence was lacking, and that other sources of information were needed to identify and apportion human and nonhuman fecal inputs to natural waters.

Given these studies, there are not sufficient epidemiological data to conclude that concentration of indicator organisms in coastal waters not impacted by wastewater are predictive of health risks in all cases. More epidemiology data may help address the lack of information. However, fecal contamination in coastal waters not impacted by wastewater is likely to be highly variable and emanate from a complex mix of sources. Other approaches may be more useful for addressing the relationship between indicators and health risk along these shorelines. Despite the lack of epidemiological evidence for a relationship between indicator organism concentration and health risk, it is well established in the outbreak literature that water contaminated with animal feces can cause illness in humans [4].

Assessing Risk: Quantitative Microbial Risk Assessment (QMRA) Modeling

QMRA is a health risk modeling approach that translates microbial exposures into infection or illness risk estimates. For RWI, the dose received by individuals is derived from estimates of the volume of water ingested during an exposure event and concentration of

pathogen(s) in that volume of water. Once a dose (number of pathogens per exposure) is determined then a risk of infection or illness is derived from applying published dose-response models for specific pathogens [54], which are derived from human feeding trials or outbreak data [55, 56].

Estimations of key model parameters (such as ingested volume of water and pathogen concentration) are generally described as probability density functions (PDFs) (i.e., distributions to account for the stochastic nature of the parameter) to help account for inherent variability as well as various methods and model uncertainties. The characterized risk is best described as a distribution as well, to capture variability and uncertainty as best as possible. This characterized risk can then be compared to "tolerable risk" or a site benchmark for the recreational water (e.g., 8 or 19 gastrointestinal illnesses per 1,000 bathers as used in the 1986 EPA criteria for freshwater and marine recreation, respectively).

An initial screening-level risk assessment for a site may start by only using point estimates to describe model parameters (e.g., WHO, 2004). Then, to reduce uncertainties in the risk estimate, more complexity is built into a QMRA model using PDFs to better represent a specific site, in what is called a "static" model. An alternative approach known as "dynamic QMRA" takes into account secondary infections to the broader community, as well as addressing the susceptibility versus nonsusceptibility of individuals to infection and illness [57–59].

QMRA can be useful for a number of purposes. First, it can be used to look at hypothetical risks under different scenarios of pathogen sources and/or recreational activities and exposure routes [60, 61]. This can provide a human health interpretation of environmental pathogen concentrations, or it can provide guidance for decision-making with respect to alternative management options. Second, QMRA can be used to augment the understanding of recreational water epidemiology studies [62]. A number of studies have evaluated pathogen risks in recreational waters using QMRA [60, 61, 63–70]. A handful of these are reviewed below.

Diallo et al. [69] examined the risk associated with recreational exposure to canals in Thailand containing *Giardia*, *Cryptosporidum*, and diarrhegenic *E. coli*. They found the predicted risk of illness from the protozoa was two orders of magnitude higher than the actual protozoan infection rate in the region of Thailand, while the rate of gastrointestinal illness predicted from diarrhegenic *E. coli* matched actual observed rates of the disease in the region. The authors suggest that the illness rates predicted for the protozoa are much higher due to immunity in the community, which was not considered in the QMRA modeling. Another possibility is massive under-reporting of protozoa illness rates, which is a documented issue for diarrheal diseases.

Ashbolt and Bruno [65] used QMRA in conjunction with the published relationship between enterococci concentrations and probability of gastrointestinal illness and acute respiratory illness observed during a UK beach epidemiology study [71]. The authors showed that by assuming that the etiology of illnesses was viral, a fixed ratio between enterococci and viruses of 1–175, a volume of water ingested of 50 mL, and 50% illness rate of those infected with virus, they were able to model the observed illness rates (at exposures greater than 60 CFU/100 mL enterococci) assuming viruses had an exponential dose-response curve. Further, they were able to model the observed acute respiratory illness using the dose-response curve of adenovirus.

Gerba et al. [70] estimated risk of exposure to rotavirus in bathing waters using the few previously reported data available at the time on rotavirus concentrations in bathing waters. They found the risk of illness to be 1/10–1/100 with a one time bathing event. These authors chose to use rotavirus as a model pathogen because it is one of the most infectious viruses for which a dose-response model is available. A major limitation to their study is the lack of data on concentrations of rotavirus in bathing waters. Surface water concentrations were estimated to be between 0.24/L and 29/L. Ingested volumes used were 100 mL for recreational exposure.

Schoen and Ashbolt [67] explored the relative risk associated with exposure to seagull feces, poorly treated sewage, and a mixture of both sources in seawater with enterococci at levels of 35 CFU/100 mL (a USEPA standard). Authors assumed that seagull feces contained *Campylobacter* and *Salmonella*, while sewage contained norovirus, *G. intestinalis*,

Cryptosporidium spp., and *Salmonella*. A distribution of ratios of enterococci to pathogen concentrations were considered to reflect the uncertainty in this parameter. The authors showed that when enterococci came exclusively from seagull feces, the risk of illness is less than the benchmark of 0.01 on which US standards are based.

Soller et al. [61] examined the risk of viral gastroenteritis associated with recreational and non-recreational use of a river downstream of a wastewater treatment plant discharge. Two wastewater treatment scenarios were compared with the goal of evaluating the public health benefit of increased treatment of the effluent. The authors employed a health protective approach by assuming that the etiology of illness would be a virus with clinical features identical to those of rotavirus. They also assumed that removal of the virus in treatment facilities would mirror that of coliphage and that coliphage and the virus occurred in a ratio that varied from 0.001 to 1. Exposures were informed by a hydrologic model of the area and observations of swimmer behavior. Unlike the other models discussed above, this model incorporated secondary transmission by allowing illness to be passed from person to person.

Steyn et al. [68] compared the risks in recreational surfaces waters in South Africa expected from measured *E. coli* concentrations (applying epidemiology study-derived dose-response curves) and measured *Salmonella* concentrations (applying the QMRA method and the *Salmonella* dose-response curve assuming ingestion of 100 mL of water for exposure). The researchers found that risks derived from the *Salmonella* QMRA model were higher than those derived from the *E. coli* concentrations. Their results suggest using *E. coli* to assess risk from exposure to *Salmonella* may be inadequate.

Wong et al. [63] estimated risk from exposure to adenoviruses during recreation contact with water at Great Lakes beaches impacted by point sources of treated wastewater. The authors measured adenoviruses using an MPN culture-dependent assay at their study site, assumed an adenovirus dose-response model, and an ingestion rate of 100 mL of water. The authors found that 0.24–2.4 illnesses per 1,000 swimmers were likely to have occurred from adenoviruses, a range of frequencies below the EPA guideline of 8 illnesses per 1,000 swimmers. Although an epidemiology study was done at the same time as their study, the epidemiology data were not available for comparison of actual illness rates.

Soller et al. [62] used QMRA to understand more fully the reported epidemiologic results from studies conducted on the Great Lakes in the US during 2003 and 2004 by identifying pathogens that could have caused the observed illnesses in those studies. The reference pathogens used for this analysis were *Norovirus*, rotavirus, adenovirus, *Cryptosporidium* spp., *G. lamblia, Campylobacter jejuni*, *Salmonella enterica, and E. coli* O157:H7. Two QMRA-based approaches were used to estimate the pathogen combinations that would be consistent with observed illness rates: in the first, swimming-associated gastrointestinal (GI) illnesses were assumed to occur in the same proportion as known illnesses in the US due to all non-foodborne sources, and in the second, pathogens were assumed to occur in the recreational waters in the same proportion as they occur in disinfected secondary effluent. The results indicated that human enteric viruses and in particular, norovirus could have caused the vast majority of the observed swimming-associated GI illnesses during the 2003/2004 water epidemiology studies [72, 73]. Evaluation of the time to onset of illness strongly supports the principal finding, and sensitivity analyses support the overall trends of the analyses even given their substantial uncertainties. These results are notable because little is known about the specific microbial agents that are responsible for the observed illnesses in swimmers. While several studies have attempted to collect biological specimens (blood or stool) as part of epidemiologic research at beach sites, these efforts have to date been largely unsuccessful in identifying the agents responsible for the observed increase in GI symptoms among swimmers [50].

Soller et al. [74] conducted a QMRA investigation to determine whether estimated risks following exposure to recreational waters impacted by gull, poultry, pig, or cattle fecal contamination are substantially different from those associated with waters impacted by human sources such as treated wastewater. Previously published QMRA methods were employed and extended to meet these objectives [67]. Health outcomes used in the analyses were infection via reference pathogens by water ingestion during recreation and subsequent GI illness. Illness risks from the reference

pathogens were calculated for exposure to contaminated recreational water with fecal indicator bacterial densities at the U.S. regulatory limits: 35 CFU/100 mL enterococci and 126 CFU/100 mL *E. coli*. The probabilities of GI illness from reference pathogens were calculated using dose-response relationships from the literature and Monte Carlo simulations. The primary findings from the analysis were that: (1) GI illness risks associated with human exposure to recreational waters directly impacted by fresh cattle feces are not substantially different from those impacted by human sources; and (2) the risks associated with human exposure to recreational waters impacted by fresh gull, poultry, or pig feces are substantially lower than those impacted by human sources.

Several observations may be drawn from the QMRA studies summarized above. First, the assembled studies focused on a small subset of the pathogens potentially important in waterborne exposure during recreation. The pathogen analyzed most frequently is rotavirus, primarily due to its high infectivity and the availability of dose-response data. It is likely that future QMRAs will also focus on norovirus [62, 67, 74] now that a published dose-response relationship is available [75].

Second, modeling variability in pathogen source density appears to be hampered by scarcity of both data and analysis techniques. Two common methods for accounting for source variability among studies are (1) use of empirical distributions for pathogen density based on relatively short time series, and (2) assumption of log-normal distribution of pathogen densities. There are advantages and drawbacks to both of these approaches. Drawbacks to the use of empirical distributions are inconsistency in sampling strategies used to develop databases, frequent non-detects, constraint of pathogen densities to those observed in a limited number of samples, and lack of availability of pathogen concentration data. Use of distributions to describe pathogen density in sources overcomes some of the constraints associated with use of empirical distributions, but choosing a distributional family can be problematic. Among the studies reviewed, many studies employed point estimates for pathogen density. Among studies using distributions to describe pathogen variability, the following distributions were employed: normal, triangular, log-normal, negative binomial, uniform, and Poisson.

Third, most of the studies reviewed do not account for variability and uncertainty in dose-response model parameters. As with variability in exposure, this observation likely indicates that high quality and diverse dose-response model data are not available. The use of a small number of dose-response models may indicate that some QMRA modelers chose the pathogens to model based on the availability of dose-response models. Lack of dose-response models for many pathogens of concern and for differing routes of exposure (i.e., cutaneous exposure to *S. aureus*) is a major data gap. The need for dose-response models corresponding to different exposure routes (i.e., ingestion, inhalation, etc.) arises from the ability of some waterborne pathogens such as adenovirus to initiate infection via multiple routes.

Finally, secondary transmission and immunity are often neglected in risk estimation. Studies that have included secondary transmission and waterborne illnesses [57, 58, 60, 76–78] have demonstrated that consideration of secondary transmission and immunity can influence overall risk associated with exposure to pathogens significantly and in unintuitive ways.

Future Directions

Health data collected from recreational swimmers confirm measurable health effects from exposure to contaminated coastal waters. To adequately protect the health of swimmers and others who recreate in coastal waters or consume fish and shellfish from coastal waters, it is essential to understand the microbial hazards present and the risks they represent to human health. While there are data available on microbial hazards and risks, many aspects remain poorly understood and characterized.

Research is needed to further characterize microbial hazards in recreational waters. Pathogen detection techniques that allow detection of infectious pathogens rapidly in environmental waters are needed. There are a number of pathogen and indicator detection technologies that are in development or have been recently developed [79, 80]. However, many of these have not been applied to natural waters, or are just in the "proof of concept" stage. Work is needed to transit new detection technologies that work at the bench-scale to the field scale – to detect pathogens in environmental

waters. Once this is accomplished, they should be applied to a wide array of waterbodies to fully understand pathogen and indicator occurrence, concentrations, fate, and transport.

A better understanding of the risks of exposure to pathogens from different sources is needed. Some QMRA studies have addressed this issue, but further research is needed to ground truth the QMRA results with epidemiology data, or data on infection rates and etiologies, as determined through analysis of bodily fluid from individuals with RWI. Gastroenteritis is the most well-studied RWI; more work is needed to understand the importance of other RWI including skin infections and respiratory ailments. More dose-response data for a wider array of pathogens are needed to provide more refined estimates of risk using QMRA. The importance of secondary infections and immunity for RWI should also be further characterized.

Finally, better surveillance systems are needed for RWI so that prediction systems can be developed. As global climate changes in the coming decades, the scientific community needs to be able to anticipate how this might change the burden of RWI. Microbial pollution of coastal waters is expected to change as temperatures, runoff frequency and volumes, and rainfall pattern change. A thorough understanding of the occurrence of RWI, and the distribution, fate, and transport of waterborne pathogens will enable us to better anticipate the effects of climate change.

Bibliography

1. CDC http://www.cdc.gov/healthywater/swimming/rwi.html (5 January)
2. Shuval H (2003) Estimating the global burden of thalassogenic diseases: human infectious diseases caused by wastewater pollution in the environment. J Water Health 1:53–64
3. Given S, Pendleton LH, Boehm AB (2006) Regional public health cost estimates of contaminated coastal waters: a case study of gastroenteritis at Southern California beaches. Environ Sci Technol 40:4851–4858
4. Craun GF (2003) Causes of waterborne outbreaks in the United States. Wat Sci Tech 24:17
5. Santo-Domingo JW, Hansel J (2008) Waterborne diseases and microbial water quality monitoring for recreational water bodies using regulatory methods. In: Walsh PJ, Smith SL, Fleming LE, Solo-Gabriele HM, Gerwick WH (eds) Oceans and human health. Academic, San Diego
6. Griffin DW, Donaldson KA, Paul JH, Rose JB (2003) Pathogenic human viruses in coastal waters. Clin Microbiol Rev 16(1):129–143
7. Maier RM, Pepper IL, Gerba CP (2000) Environmental microbiology. Academic, San Diego
8. Boehm AB, Bischel HN (2010) Oceans and human health. In: Nriagu J (ed) Encyclopedia of environmental health. Elsevier, New York, NY
9. Walsh PJ, Smith SL, Fleming LE, Solo-Gabriele HM, Gerwick WH (2008) Oceans and human health. Academic, San Diego
10. Mead PS, Slutsker L, Dietz V, McCaig LF, Bresee JS, Shapiro C, Griffin PM, Tauxe RV (1999) Food related illness and death in the United States. Emerg Infect Dis 5(5):607–625
11. Olivieri AW, Boehm AB, Sommers CA, Soller JA, Eisenberg JNS, Danielson R (2007) Development of a protocol for risk assessment of separate stormwater system microorganisms; Water Environment Research Foundation. Project 03-SW-2, Final Project Report
12. U.S. EPA (2009) Review of published studies to characterize relative risks from different sources of fecal contamination in recreational water, EPA 822-R-09-001. In Lett Appl Microbiol, Office of Science and Technology, Washington
13. Goodwin KD, Pobuda M (2009) Performance of CHROMagar™ Staph aureus and CHROMagar™ MRSA for detection of Staphylococcus aureus in seawater and beach sand – Comparison of culture, agglutination, and molecular analyses. Water Res 43(19):4802–4811
14. Bolton F, Surman SB, Martin K, Wareing DR, Humphrey TJ (1999) Presence of Campylobacter and Salmonella in sand from bathing beaches. Epidemiol Infect 122:7–13
15. Elmanama AA, Fahd MI, Afifi S, Abdallah S, Bahr S (2004) Microbiological beach sand quality in Gaza Strip in comparison to seawater quality. Environ Res 99:1–10
16. Obiri-Danso K, Jones K (2000) Intertidal sediments as reservoirs for hippurate negative campylobacters, salmonellae and faecal indicators in three EU recognized bathing waters in North West England. Water Res 34:519–527
17. LaBelle RL, Gerba CP, Goyal SM, Melnick JL, Cech I, Bogdan GF (1980) Relationships between environmental factors, bacterial indicators, and the occurrence of enteric viruses in estuarine sediments. Appl Environ Microbiol 39(3):588–596
18. Ishii S, Yan T, Shivley DA, Byappanahalli MN, Whitman RL, Sadowsky MJ (2006) Cladophora (Chlorophyta) spp. harbor human bacterial pathogens in nearshore water of Lake Michigan. Appl Environ Microbiol 72:4545–4553
19. Byappanahalli MN, Sawdey R, Ishii S, Shively DA, Ferguson JA, Whitman RL, Sadowsky MJ (2009) Seasonal stability of Cladophora-associated Salmonella in Lake Michigan watersheds. Water Res 43:806–814
20. U.S. EPA (2009) Review of published studies to characterize relative risks from different sources of fecal contamination in recreational water, EPA 822-R-09-001. In Office of Science and Technology, Washington
21. WHO (1999) Health-based monitoring of recreational waters: the feasibility of a new approach (The 'Annapolis Protocol'); WHO/SDE/WSH/99.1, World Health Organization, 1999

22. WHO (2003) Guidelines for safe recreational-water environments, coastal and fresh-waters, vol 1. World Health Organization, Geneva
23. Prüss A (1998) Review of epidemiological studies on health effects from exposure to recreational water. Int J Epidemiol 27(1):1–9
24. Sinton LW, Finlay RK, Hnnah DJ (1998) Distinguishing human from animal faecal contamination in water: a review. NZ J Mar Freshw Res 32:323–348
25. Wade TJ, Pai N, Eisenberg J, Colford JM (2003) Do US EPA water quality guidelines for recreational waters prevent gastrointestinal illness? A systematic review and meta-analysis. Environ Health Perspect 111(8):1102–1109
26. Zmirou D, Pena L, Ledrans M, Letertre A (2003) Risks associated with the microbiological quality of bodies of fresh and marine water used for recreational purposes: summary estimates based on published epidemiological studies. Arch Environ Health 58(11):703–711
27. Boehm AB, Ashbolt NJ, Colford JM, Dunbar J, Fleming LE, Gold MA, Hansel JA, Hunter PR, Ichida AM, McGee CD, Soller JA, Weisberg SB (2009) A sea change ahead for recreational water quality criteria. J Water Health 7:9–20
28. EEC (1976) Bathing water quality: Directive 76/160/EEC, 1–6
29. U.S. EPA (1986) Ambient water quality criteria for bacteria, EPA440/5-84-002, Office of Water, Washington
30. Colford JM Jr, Wade TJ, Schiff KC, Wright CC, Griffith JF, Sandhu SK, Burns S, Sobsey M, Lovelace G, Weisberg SB (2007) Water quality indicators and the risk of illness at beaches with nonpoint sources of fecal contamination. Epidemiology 18(1):27–35
31. Calderon R, Mood E, Dufour A (1991) Health effects of swimmers and nonpoint sources of contaminated water. Int J Environ Health Res 1:21–31
32. McBride GB, Calderon RL, Mood EW, Dufour AP (1991) Health effects of swimmers and non-point sources of contaminated water. Int J Environ Health Res 1:21–31
33. McBride GB, Salmond CE, Bandaranayake DR, Turner SJ, Lewis GD, Till DG (1998) Health effects of marine bathing in New Zealand. Int J Environ Health Res 8(3):173–189
34. Haile RW, Witte JS, Gold M, Cressey R, McGee C, Millikan RC, Glasser A, Harawa N, Ervin C, Harmon P, Harper J, Dermand J, Alamillo J, Barrett K, Nides M, Wang GY (1999) The health effects of swimming in ocean water contaminated by storm drain runoff. Epidemiology 10(4):355–363
35. Dwight RH, Baker DB, Semenza JC, Olson BH (2004) Health effects associated with recreational coastal water use: urban versus rural California. Am J Public Health 94(4):565–567
36. Cheung WH, Chang KC, Hung RP, Kleevens JW (1990) Health effects of beach water pollution in Hong Kong. Epidemiol Infect 105(1):139–162
37. Wiedenmann A, Kruger P, Dietz K, Lopez-Pila JM, Szewzyk R, Botzenhart K (2006) A randomized controlled trial assessing infectious disease risks from bathing in fresh recreational waters in relation to the concentration of Escherichia coli, intestinal enterococci, Clostridium perfringens, and somatic coliphages. Environ Health Perspect 114(2):228–236
38. Cabelli VJ (1983) Health effects criteria for marine recreational waters, EPA-600/1-80-031. USEPA, Cincinnati
39. Dufour A (1984) Health effects criteria for fresh recreational waters; EPA-600 1-84-004. US EPA, Cincinnati
40. Seyfried PL, Tobin RS, Brown NE, Ness PF (1985) A prospective study of swimming-related illness. I. Swimming-associated health risk. Am J Public Health 75(9):1068–1070
41. Seyfried PL, Tobin RS, Brown NE, Ness PF (1985) A prospective study of swimming-related illness. II. Morbidity and the microbiological quality of water. Am J Public Health 75(9):1071–1075
42. Fattal B, Peleg-Olevsky E, Yoshpe-Purer Y, Shuval H (1986) Association between morbidity among bathers and microbial quality of seawater. Water Sci Technol 18(11):59–69
43. Fattal DB, Peleg-Olevsky E, Agursky T, Shuval PHI (1987) The association between seawater pollution as measured by bacterial indicators and morbidity among bathers at Mediterranean bathing beaches of Israel. Chemosphere 16(2/3):565–570
44. Cabelli V (1983) Public health and water quality significance of viral diseases transmitted by drinking water and recreational water. Water Sci Technol 15:1–15
45. El-Sharkawi HF (1979) The relation between the state of pollution in Alexandria swimming beaches and the occurrence of typhoid among bathers. Bull High Inst Public Health 9:337–351
46. Mujeriego R, Bravo J, Feliu M (1982) Recreation in coastal waters: public health implications. Vier Journee Etudes Pollutions, 585–594
47. Ferley JP, Zmirou D, Balducci F, Baleux B, Fera P, Larbaigt G, Jacq E, Moissonnier B, Blineau A, Boudot J (1989) Epidemiological significance of microbiological pollution criteria for river recreational waters. Int J Epidemiol 18(1):198–205
48. Foulon G, Maurin J, Quoi N, Martin-Boyer G (1983) Relationship between the microbial quality of water and health effects. Revue des Sciences de L'Eau 2:127–143
49. Brown JM, Campbell EA, Rickards AD, Wheeler D (1987) Sewage pollution of bathing water. Lancet 2(8569): 1208–1209
50. Jones F, Kay D, Stanwell-Smith R, Wyer M (1991) Results of the first pilot-scale controlled cohort epidemiological investigation into the possible health effects of bathing in seawater at Langland Bay, Swansea. Water Environ J 5(1):91–98
51. Holmes P (1989) Research into health risks at bathing beaches in Hong Kong. J Inst Water Environ Manage 3:488–495
52. Corbett SJ, Rubin GL, Curry GK, Kleinbaum DG (1993) The health effects of swimming at Sydney beaches. The Sydney beach users study advisory group. Am J Public Health 83(12):1701–1706
53. Harrington JF, Wilcox DN, Giles PS, Ashbolt NJ, Evans JC, Kirton HC (1993) The health of Sydney surfers: an epidemiological study. Water Sci Technol 27:175–181

54. Haas CN (1983) Estimation of risk due to low doses of microorganisms: a comparison of alternative methodologies. Am J Epidemiol 55:573–582
55. Haas CN, Rose JB, Gerba CP (1999) Quantitative microbial risk assessment. Wiley, New York
56. McBride G, Till D, Ryan T, Balll A, Lewis G, Palmer S, Weinstein P (2002) Pathogen occurrence and human health risk assessment analysis. In: Freshwater Microbiology Research Programme, Ministry for the Environment, Ministry of Health, New Zealand
57. Soller JA (2009) Potential implications of person-to-person transmission of viral infection to US EPA's Groundwater Rule. J Water Health 7(2):208–223
58. Soller JA, Eisenberg JNS (2008) An evaluation of parsimony for microbial risk assessment models. Environmetrics 19(1): 61–78
59. Eisenberg JNS, Seto EYW, Olivieri AW, Spear RC (1996) Quantifying water pathogen risk in an epidemiological framework. Risk Anal 16(4):549–563
60. Soller JA, Eisenberg J, DeGeorge J, Cooper R, Tchobanoglous G, Olivieri A (2006) A public health evaluation of recreational water impairment. J Water Health 4(1):1–19
61. Soller JA, Olivieri AW, Crook J, Cooper RC, Tchobanoglous G, Parkin RT, Spear RC, Eisenberg JN (2003) Risk-based approach to evaluate the public health benefit of additional wastewater treatment. Environ Sci Technol 37(9):1882
62. Soller JA, Bartrand T, Ashbolt NJ, Ravenscroft J, Wade TJ (2010) Estimating the primary aetiologic agents in recreational freshwaters impacted by human sources of faecal contamination. Water Res 44(16):4736–4747
63. Wong M, Kumar L, Jenkins TM, Xagoraraki I, Phanikumar MS, Rose JB (2009) Evaluation of public health risks at recreational beaches in Lake Michigan via detection of enteric viruses and a human-specific bacteriological marker. Water Res 43(4): 1137–1149
64. Ashbolt A, Reidy C, Haas CN (1997) In Microbial health risk at Sydney's coastal bathing beaches. In: 17th Australian Water and Wastewater Association meeting, AWWA, Melbourne, 1997, pp 104–111
65. Ashbolt N, Bruno M (2003) Application and refinement of the WHO risk framework for recreational waters in Sydney, Australia. J Water Health 1(3):125–131
66. Roser D, Ashbolt N (2007) Source water quality assessment and the management of pathogens in surface catchments and aquifers. Research report 29, Bolivar
67. Schoen ME, Ashbolt NJ (2010) Assessing pathogen risk to swimmers at non-sewage impacted recreational beaches. Environ Sci Technol 44(7):2286–2291
68. Steyn M, Jagals P, Genthe B (2004) Assessment of microbial infection risks posed by ingestion of water during domestic water use and full-contact recreation in a mid-southern African region. Water Sci Technol 50(1):301–308
69. Diallo MB, Anceno AJ, Tawatsupa B, Houpt ER, Wangsuphachart V, Shipin OV (2008) Infection risk assessment of diarrhea-related pathogens in a tropical canal network. Sci Total Environ 407(1):223–232
70. Gerba CP, Rose JB, Haas CN, Crabtree KD (1996) Waterborne rotavirus: a risk assessment. Water Res 30(12):2929–2940
71. Kay D, Fleisher JM, Salmon RL, Jones F, Wyer WD, Godfree AF, Zelenauch-Jacquotte Z, Shore R (1994) Predicting likelihood of gastroenteritis from sea bathing: results from randomised exposure. Lancet 344:905–909
72. Wade TJ, Calderon RL, Brenner KP, Sams E, Beach M, Haugland R, Wymer L, Dufour AP (2008) High sensitivity of children to swimming-associated gastrointestinal illness: results using a rapid assay of recreational water quality. Epidemiology 19(3):375–383
73. Wade TJ, Calderon RL, Sams E, Beach M, Brenner KP, Williams AH, Dufour AP (2006) Rapidly measured indicators of recreational water quality are predictive of swimming-associated gastrointestinal illness. Environ Health Perspect 114(1):24–28
74. Soller JA, Schoen ME, Bartrand T, Ravenscroft J, Ashbolt NJ (2010) Estimated Human Health Risks from Exposure to Recreational Waters Impacted by Human and Non-human Sources of Faecal Contamination. Water Res 44(10):4674–4691
75. Teunis PF, Moe CL, Liu PSEM, Lindesmith L, Baric RS, Le Pendu J, Calderon RL (2008) Norwalk virus: how infectious is it? J Med Virol 80(8):1468–1476
76. Eisenberg JNS, Soller JA, Scott J, Eisenberg DM, Colford JMJ (2004) A dynamic model to assess microbial health risks associated with beneficial uses of biosolids. Risk Anal 24(1):221–236
77. Eisenberg JNS, Moore K, Soller JA, Eisenberg D, Colford JMJ (2008) Microbial risk assessment framework for exposure to amended sludge projects. Environ Health Perspect 116(6):727–733
78. Eisenberg JNS, Seto EYW, Colford JM, Olivieri AW, Spear RC (1998) An analysis of the Milwaukee cryptosporidiosis outbreak based on a dynamic model of the infection process. Epidemiol 9(3):255–263
79. Vikesland PJ, Wigginton KR (2010) Nanomaterial enabled biosensors for pathogen monitoring - A review. Environ Sci Technol 44(10):3656–3669
80. Goodwin KD, Litaker RW (2008) Emerging Technologies fir monitoring recreational waters for bacteria and viruses. In: Walsh PJ, Smith SL, Fleming LE, Solo-Gabriele HM, Gerwick WH (eds) Oceans and human health. Academic, San Diego
81. Boehm AB, Yamahara KM, Love DC, Peterson BM, McNeill K, Nelson KL (2009) Covariation and photoinactivation of traditional and novel indicator organisms and human viruses at a sewage – impacted marine beach. Environ Sci Technol 43:8046–8052
82. Gersberg RM, Rose MA, Robles-Sikisaka R, Dhar AK (2006) Quantitative detection of hepatitis A virus and enteroviruses near the United States-Mexico border and correlation with levels of fecal indicator bacteria. Appl Environ Microbiol 72(12):7438–7444
83. Griffin DW, Gibson CJ, Lipp EK, Riley K, Paul JH, Rose JB (1999) Detection of viral pathogens by reverse transcriptase

PCR and of microbial indicators by standard methods in the canals of the Florida Keys. Appl Environ Microbiol 65(9): 4118–4125
84. Aulicino FA, Orsini P, Carere M, Mastrantonio A (2001) Bacteriological and virological quality of seawater bathing areas along the Tyrrhenian coast. Int J Environ Health Res 11:5–11
85. Alonso JL, Alonso MA (1993) Presence of Campylobacter in marine waters of Valencia. Spain Water Res 27(10):1559–1562
86. Gonzalez AM, Paranhos R, Lutterbach MS (2010) Relationships between fecal indicators and pathogenic microorganisms in a tropical lagoon in Rio de Janeiro, Brazil. Environ Monit Assess 164(1–4):207–219
87. Lang AL, Tsai Y-L, Mayer CL, Patton KC, Palmer CJ (1994) Multiplex PCR for Detection of the Heat-Labile Toxin Gene and Shiga-Like Toxin I and II Genes in Escherichia coli Isolated from Natural Waters. Appl Environ Microbiol 60(9): 3145–3149
88. Graczyk TK, Sunderland D, Tamang L, Lucy FE, Breysse PN (2007) Bather density and levels of Cryptosporidium, Giardia, and pathogenic microsporidian spores in recreational bathing water. Parasitol Res 101(6):1729–1731
89. Alexander LM, Heaven A, Tennant A, Morris R (1992) Symptomatology of children in contact with sea water contaminated with sewage. J Epidemiol Community Health 46(4):340–344
90. Bandaranayake DR, Turner SJ, McBride GB, Lewis G, Till D (1995) Health effects of bathing at selected New Zealand marine beaches. New Zealand Department of Health, Wellington
91. Fewtrell L, Godfree AF, Jones F, Kay D, Salmon RL, Wyer MD (1992) Health effects of white-water canoeing. Lancet 339:1587–1589
92. Fewtrell L, Kay D, Salmon R, Wyer M, Newman G, Bowering G (1994) The health effects of low-contact water activities in fresh and estuarine waters. J Inst Water Environ Manag 8:97–101
93. Fleisher JM, Kay D, Salmon RL, Jones F, Wyer MD, Godfree AF (1996) Marine waters contaminated with domestic sewage: nonenteric illnesses associated with bather exposure in the United Kingdom. Am J Public Health 86(9):1228–1234
94. Haile RW, Witte JS, Gold M, Cressey R, McGee C, Millikan RC, Glasser A, Harawa N, Ervin C, Harmon P, Harper J, Dermand J, Alamillo J, Barrett K, Nides M, Wang G.-Y (1996) An epidemiological study of possible adverse health effects of swimming in Santa Monica Bay. Santa Monica Bay Restoration Project, Santa Monica, CA, 70pp
95. Kueh CSW, Tam TY, Lee T, Wong SL, Lloyd OL, Yu ITS, Wong TW, Tam JS, Bassett DCJ (1995) Epidemiological study of swimming-associated illnesses relating to bathing-beach water quality. Water Sci Technol 31:1–4
96. Lee JV, Dawson SR, Ward S, Surman SB, Neal KR (1997) Bacteriophages are a better indicator of illness rates than bacteria amongst users of a white water course fed by a lowland river. Water Sci Technol 35:165–170
97. Lightfoot N (1989) A prospective study of swimming related illness at six freshwater beaches in southern Ontario. University of Toronto, Toronto
98. Marino F, Morinigo M, Martinez-Manzanares E, Borrego J (1995) Microbiological-epidemiological study of selected marine beaches in Malaga (Spain). Water Sci Technol 31:5–9
99. Medema G, Van Asperen I, Klokman-Houweling J, Nooitgedagt A, Van de Laar M (1995) The relationship between health effects in triathletes and microbiological quality of freshwater. Water Sci Technol 31:19–26
100. Medical Research Council & Council for Scientific and Industrial Research (CSIR) (1995) Pathogenic microorganisms/epidemiological microbiological study. Final report (1991–1995), South Africa
101. Philipp R, Evans EJ, Hughes AO, Grisdale SK, Enticott RG, Jephcott AE (1985) Health risks of snorkel swimming in untreated water. Int J Epidemiol 14(4):624–627
102. Pike E (1994) Health effects of sea bathing (WMI 9021), phase III—final report to the department of the environment. Water Research Centre, Medmenham
103. Prieto M, Lopez B, Juanes J, Revilla J, Llorca J, Delgado-Rodriguez M (2001) Recreation in coastal waters: health risks associated with bathing in sea water. J Epidemiol Community Health 55(6):442–447
104. Stevenson AH (1953) Studies of bathing water quality and health. Am J Public Health Nations Health 43:529–538
105. United Nations Environment Programme/World Health Organization (1991) Epidemiological studies related to environmental quality criteria for bathing waters. Shellfish-growing waters and edible marine organisms (Activity D). Final report on project on relationship between microbial quality of coastal seawater and rotavirus-Induced gastroenteritis among bathers (1986–88). United Nations Environment Programme, Athens, Greece
106. United Nations Environment Programme/World Health Organization (1991) Epidemiological studies related to environmental quality criteria for bathing waters, Shellfish-growing waters and edible marine organisms (Activity D). Final report on epidemiological study on bathers from selected beaches in Malaga, Spain (1988–1989). United Nations Environment Programme, Athens, Greece
107. van Asperen IA, Medema G, Borgdorff MW, Sprenger MJ, Havelaar AH (1998) Risk of gastroenteritis among triathletes in relation to faecal pollution of fresh waters. Int J Epidemiol 27(2):309–315
108. van Dijk PAH, Lacey RF, Pike EB (1996) Health effects of sea bathing—further analysis of data from UK beach surveys. Department of the Environment, WRc pic, Medmenham
109. von Schirnding YE, Kfir R, Cabelli V, Franklin L, Joubert G (1992) Morbidity among bathers exposed to polluted seawater. A prospective epidemiological study. S Afr Med J 81(11):543–546

Recycling Collection and Materials Separation

Matthew J. Franchetti
Department of Mechanical, Industrial, and Manufacturing Engineering, University of Toledo, Toledo, OH, USA

Article Outline

Glossary
Definition of the Subject and Its Importance
Introduction
The Hierarchy of Solid Waste Management
Benefits from Recycling
Fundamentals of Recycling Processes
Common Problems and the Human Factors of Recycling
Solid Waste and Recycling Assessments
Recycling Collection Systems and Methods
Separation Methods and Equipment by Material
Financial Analysis
Case Study
Industrial Ecology and Solid Waste Exchanges
Future Directions
Bibliography

Glossary

Source reduction Source reduction is the reduction of materials coming into the system. The US Environmental Protection Agency (EPA) defines source reduction as "activities designed to reduce the volume or toxicity of waste generated, including the design and manufacture of products with minimum toxic content, minimum volume of material, and/or a longer useful life." The two interesting components of this definition are *volume* and *toxicity*. This means that an organization does not have to solely focus on reducing volumes for source reduction initiatives, but could focus efforts on reducing the negative impacts on the environment of those same volumes. This may mean a reduction of pallets entering a building or of flash being generated from a mold.

Reuse Reuse is the actual reuse of a material in its present form. Some examples are printing draft copies on the back side of previously used paper, using incoming pallets as outgoing pallets, or using incoming boxes as collection containers for recyclables.

Recycling Recycling is a type of reuse which involves changing the composition or properties of the material in one way or another. For example, this can be accomplished by melting it down, chipping, or grinding the materials. A broad definition of recycling is taking a product or material at the end of its useful life and turning it into a usable raw material to make another product. There are three types of recycling, as discussed in the hierarchy of waste management: in-process, on-site, and off-site.

Pollution prevention Pollution prevention is the broadest and most difficult term to concisely define. In essence, it is the overall process of reducing waste and preventing pollution from entering the environment through the air, water, or ground. It encompasses both the aspects of source reduction and waste reduction. The EPA has defined pollution prevention as follows: Pollution prevention means source reduction, as defined under the Pollution Prevention Act, and other practices that reduce or eliminate the creation of pollutants through: Increased efficiency in the use of raw materials, energy, water, or other resources, or Protection of natural resources under conservation.

Definition of the Subject and Its Importance

A broad definition of recycling is taking a product or material at the end of its useful life and transforming it into a usable raw material to make another product. Recycling collection and separation is concerned with the infrastructure, resources, and processes required for gathering, transporting, separating, and consolidating materials for the recycling process. Recycling collection and material separation are critical components of solid waste minimization and aid in conserving natural resources, maintaining healthier environments, and reducing greenhouse gas emissions. In addition, many organizations can achieve economic benefits and public image enhancements by developing strong recycling programs.

Introduction

In the year 2006, US residents, businesses, and institutions generated more than 228 million metric tons (251 million US tons) of solid waste, which is approximately 2.1 kg (4.6 pounds) of waste per person per day, up from 1.2 kg (2.7 pounds) per person per day in 1960 [1]. From this total, 32.5% is recovered and recycled or composted, 12.5% is burned at combustion facilities, and the remaining 55% is disposed of in landfills [1]. Source reduction can be a successful method of reducing waste generation. Practices such as grass recycling, backyard composting, two-sided copying of paper, and transport packaging reduction by industry have yielded substantial benefits through source reduction. Source reduction has many environmental benefits. It prevents emissions of many greenhouse gases, reduces pollutants, saves energy, conserves resources, and reduces the need for new landfills and combustors.

Recycling, including composting, diverted 74 million metric tons (82 million US tons) of material away from disposal in 2006, up from less than 14 million metric tons (15 million US tons) in 1980, when the recycle rate was just 10% and 90% of MSW was being combusted with energy recovery or disposed of at landfills [1]. Typical materials that are recycled include automobile batteries, recycled at a rate of 99%, paper and paperboard at 52%, and yard trimmings at 62%. These materials and others may be recycled through curbside programs, drop-off centers, buyback programs, and deposit systems.

International Waste Generation Comparison Rates

As discussed in the book "Germany, Garbage, and the Green Dot" by Bette Fishbein, it is very difficult to make international comparisons regarding waste generation [2]. For example, Ms. Fishbein points out that "according to the data published by the Organization of Economic Cooperation and Development, waste generation in Germany is 318 kg per person per year as compared to 864 kg per person per year in the United States. This might suggest that the average person in the United States generates two or three times as much garbage as the average person in Germany. However, data from the two countries are not comparable: the German data do not include materials collected from recycling, nor do they include some commercial waste, both of which are included in U.S. data. International comparisons of waste generation are usually unreliable because countries use different data collection methodologies and different definitions of waste."

Recycling is a critical component to help increase these material recovery rates. This section provides an overview of the hierarchy of solid waste management and the benefits of recycling. Next, an overview of the fundamentals of recycling processes is discussed, along with common problems and human factors of recycling systems. Accurate data are critical when developing recycling systems, and a brief overview of solid waste and recycling assessments is provided. Then, a discussion of collection methods and separations equipment is provided, followed by a discussion regarding the financial analyses related to recycling process decisions. A case study is also provided to demonstrate these analyses. Finally, an overview of industrial ecology and waste exchanges is provided and a discussion of future directions in this field.

The Hierarchy of Solid Waste Management

When approaching solid waste analysis and minimization, there is an accepted hierarchy, or order of solution approaches, that should be deployed when analyzing an organization's waste streams. This hierarchy is given before a discussion of definitions of solid waste management terms because it makes the definitions more meaningful and easier to understand. This hierarchy has been defined in the US Pollution Prevention Act of 1990 as follows:

The Congress hereby declares it to be national policy of the United States that pollution should be prevented or reduced at the source whenever feasible; pollution that cannot be prevented should be recycled in an environmentally safe manner, whenever feasible; pollution that cannot be prevented or recycled should be treated in an environmentally safe manner whenever feasible; and disposal or release into the environment should be employed only as a last resort and should be conducted in an environmentally safe manner.

Based on that definition, the solid waste management solutions, in order of preference, are:

1. Source reduction
2. In-process recycling
3. On-site recycling

4. Off-site recycling
5. Waste treatment to render the waste less hazardous
6. Secure disposal
7. Direct release to the environment

These terms may be easier to understand with an example. A very straightforward and simple example involves a company that receives incoming raw material in cardboard packaging. Suppose the company is a metal stamping plant for the automobile industry. Below are situations where the company could apply the hierarchy:

1. Source reduction – eliminate the waste through engineering process modifications. For example, the company could work with the vendor to eliminate the use of cardboard containers and switch to returnable plastic containers. This is the most preferred method and completely eliminates the problem of waste management and need for recycling.
2. In-process recycling – if waste is generated, develop a separation method to use the waste as a raw material for the same process. For example, the company could collect the metal scrap from the stamping process and attempt to process it again in the same process.
3. On-site recycling – if waste is generated, develop a separation method to use the waste as a raw material for another in-house process. For example, the company could use the cardboard packages to ship their own final products.
4. Off-site recycling – if waste is generated, develop a separation method and transport the waste to another organization so that another company could use the waste as a raw material. For example, the company could transport the cardboard to a third-party processor for recycling.
5. Waste treatment to render the waste less hazardous – if waste is generated, develop a separation method and treat the waste so it is less harmful before releasing it to the environment. This solution applies mostly to chemical processes, such as treating waste water and releasing it to the public sewer.
6. Secure disposal – dispose of the waste at a secure landfill. The company could have their waste hauler transport the cardboard to a local landfill.
7. Direct release to the environment – when waste is generated, develop a separation method and release the waste directly to the environment. In this final scenario, the company could stage the cardboard in an outside area to allow it to biodegrade.

Benefits from Recycling

The purpose of a project, plan, or initiative (solid waste minimization or otherwise) is to achieve measurable results that can be tied into the original goal. These results or benefits are often critical in determining the feasibility or acceptance of a project proposal. These benefits are also the key selling points used when promoting solid waste minimization to stakeholders and decision makers. The benefits of solid waste minimization and recycling can be separated into four areas:

- Environmental
- Economic
- Corporate image
- Personal and social

Ideally, an organization would like to create a situation where multiple benefits can be realized from a single project. This synergistic approach allows for the creation of win-win situations when applied appropriately using the system approach discussed in this book. Specifically, the company will realize cost benefits and enhanced public image, the environment will be protected, and the stakeholders of the organization (including employees) often gain a sense of well-being and harmony with the environment as the organization is protecting the greater good for society. This chapter discusses in greater detail these benefits and includes examples that may be used to promote solid waste minimization to decision makers.

Environmental Benefits

Waste minimization efforts are a big step forward in moving toward a sustainable environment. The results are clear: cleaner air and water, less pollution, more forested land and open space, and reduced greenhouse gases. It is obvious that recycling translates into less trash entering landfills. But the greatest environmental benefits of recycling are not related landfills, but to the conservation of energy and natural resources and the prevention of pollution when a recycled material, rather than a raw

material, is used to make a new product. Since recycled materials have been refined and processed once, manufacturing the second time around is much cleaner and less energy intensive than the first. The following list summarizes the key benefits to the environment that can be derived from solid waste minimization:

- Conservation of natural resources (water, trees, energy, and land)
- Healthier environment via landfill emissions reductions (carbon dioxide, methane, and leachate)
- Global warming reduction
- Conservation of habitats

The primary environmental benefit of solid waste minimization is resource conservation. The Medical University of South Carolina (MUSC) reports that the college recycled 1,151 metric tons (1,269 US tons) of paper, metals, organics, and other materials in 2003. Based on the school's calculations, this saved a total of about 14,513 kJ (13,756 BTU) of energy, enough energy to power nearly 137 homes for 1 year. In addition, products made using recovered rather than virgin or raw materials use significantly less energy. Less energy used means less burning of fossil fuels such as coal, oil, and natural gas. When burned, these fuels release pollutants, such as sulfur dioxide, nitrogen oxide, and carbon monoxide, into the air. By using recycled materials instead of trees, metal ores, minerals, oil, and other raw materials harvested from the earth, recycling-based manufacturing conserves the world's scarce natural resources. This conservation reduces pressure to expand forests cutting and mining operations.

Recycling and composting in the USA diverted nearly 63.5 million metric tons (70 million US tons) of material away from landfills and incinerators in 2000 as reported by the National Recycling Coalition. This total is up from 31 million metric tons (34 million US tons) in 1990, which is doubling in just 10 years. Below are some interesting facts about the relationship between recycling and resource conservation. These facts can have great emotional appeal when promoting waste minimization and can serve as part of a comprehensive strategy to promote recycling.

- Every US ton of paper that is recycled saves 17 trees.
- The energy that is saved when one glass bottle is recycled is enough to light a light bulb for 4 h.
- Recycling benefits the air and water by creating a net reduction in ten major categories of air pollutants and eight major categories of water pollutants.
- In the USA, processing minerals contributes almost half of all reported toxic emissions from industry, sending 1.4 million metric tons of pollution into the air and water each year. Recycling can significantly reduce these emissions.
- It is important to reduce our reliance on foreign oil. Recycling helps the nation accomplish this by saving energy.
- Manufacturing with recycled materials, with very few exceptions, saves energy and water and produces less air and water pollution than manufacturing with virgin materials.
- It takes 95% less energy to recycle aluminum than it does to make it from raw materials. Making recycled steel saves 60%, recycled newspaper 40%, recycled plastics 70%, and recycled glass 40%. These savings far outweigh the energy created as by-products of incineration and landfilling.
- In 2000, recycling resulted in an annual energy savings equal to the amount of energy used in six million homes (over 696 trillion kJ [660 trillion BTU]). In 2005, recycling is conservatively projected to save the amount of energy used in nine million homes (950 trillion kJ [900 trillion BTU]).
- A national recycling rate of 30% reduces greenhouse gas emissions as much as removing nearly 25 million cars from the road.
- Recycling conserves natural resources, such as timber, water, and minerals.
- Every bit of recycling makes a difference. For example, 1 year of recycling on just one college campus, Stanford University, saved the equivalent of 33,913 trees and the need for 577 metric tons (636 US tons) of iron ore, coal, and limestone.
- When one US ton of steel is recycled, 1,134 kg (2,500 pounds) of iron ore, 635 kg (1,400 pounds) of coal, and 54.4 kg (120 pounds) of limestone are conserved.
- Brutal wars over natural resources, including timber and minerals, have killed or displaced more than 20 million people and are raising at least $12 billion a year for rebels, warlords, and repressive governments. Recycling eases the demand for the resources.

- Mining is the world's most deadly occupation. On average, 40 mine workers are killed on the job each day, and many more are injured. Recycling reduces the need for mining.
- Tree farms and reclaimed mines are not ecologically equivalent to natural forests and ecosystems.
- Recycling prevents habitat destruction, loss of biodiversity, and soil erosion associated with logging and mining.

Solid waste minimization also aids in creating a healthier environment by reducing landfill emissions. As discussed in the environmental concerns section of this chapter, landfills emit a liquid called leachate. Leachate is liquid that is generated from a landfill that is created from decomposing waste, created after rainwater mixes with the chemical waste in a landfill, or liquids present in the landfill. Once it enters the environment, the leachate is at risk for mixing with groundwater near the site which can have very negative effects. This liquid can be treated in a similar manner to sewage, and the treated water can then be safely released into the environment. One study reports that landfills are responsible for 3.8% of the global warming damage from human sources in the USA. Municipal solid waste landfills are the largest source of human-related methane emissions in the United States, accounting for about 25% of these emissions in 2004 [1]. This gas consists of about 50% methane (CH_4), the primary component of natural gas; about 50% carbon dioxide (CO_2); and a small amount of nonmethane organic compounds. In 2003, US landfills generated 131.2 teragrams methane in terms of carbon dioxide (CO_2) equivalents (where a teragram is 1 million metric tons). Reducing the amounts of solid waste disposed in landfills would reduce methane generation and subsequently reduce global warming. Although it is difficult to accurately quantify habitat loss, many animal species are displaced by the creation of landfills and the effects of deforestation. By minimizing solid waste levels and increasing recycling, available habitats for animals will not be disrupted by the development or expansion of landfills and the effects of deforestation to acquire virgin raw materials.

The Medical University of South Carolina reported that in 2003, recycling reduced overall air emissions by 22.6 metric tons (24.9 US tons) (excluding carbon dioxide and methane) and reduced waterborne waste by 3.8 metric tons (4.2 US tons). By reducing air and water pollution and saving energy, recycling offers an important environmental benefit: It reduces emissions of greenhouse gases, such as carbon dioxide, methane, nitrous oxide, and chlorofluorocarbons, that contribute to global climate change. Recycling and composting reduce greenhouse gas by:

- Decreasing the energy needed to make products from raw materials
- Reducing emissions from incinerators and landfills, which are the largest source of methane gas emissions in the USA
- Slowing the harvest of trees, thereby maintaining the carbon dioxide storage benefit provided by forests

Recycling prevents the emission of many greenhouse gases and water pollutants, saves energy, supplies valuable raw materials to industry, creates jobs, stimulates the development of greener technologies, conserves resources for our children's future, and reduces the need for new landfills and combustors.

Recycling also helps reduce greenhouse gas emissions that affect global climate. In 1996, recycling of solid waste in the United States prevented the release of 30 million metric tons (33 million US tons) of carbon into the air – roughly the amount emitted annually by 25 million cars. The number of landfills in the United States is steadily decreasing – from 8,000 in 1988 to 1,754 in 2006. The capacity, however, has remained relatively constant. New landfills are much larger than in the past.

Economic Benefits

The economic benefits of waste minimization are often one of the key selling points when promoting environmentally conscious initiatives to businesses. Other than regulatory compliance, the cost benefits from waste minimization can turn an "environmental decision" into a wise business decision that will increase an organization's financial statements. Often times, when promoting a solid waste minimization program to the decision makers of an organization, the most influential benefits are the cost savings and potential revenue generated from the program. Often, when the creation

of a recycling program is first discussed with management, the first response is "we do not have a budget for recycling." This is far from the truth; the budget does exist, and the starting point is the funds that the company is currently paying for waste hauling and removal. The systems approach to solid waste minimization explores for cost-effective methods to better utilize these funds and protect the environment. The three areas for cost benefits are usually derived from:

- Cost avoidance in solid waste hauling and disposal
- Cost savings in material purchases due to reuse and reduction
- Revenue generation from the sale of recyclable material

Many organizations are surprised to learn that recycling and waste minimization can make strong business sense. A common environmental adage is "become green to make green." The Business Waste Reduction Assistance Program at The University of Toledo has identified over $3.1 million in annual savings for Northwest Ohio businesses in the 70 waste assessments that the program has completed. For example, at a plastic manufacturer with 100 employees, approximately $16,000 in annual cost benefits were identified via increased plastic, paper, and cardboard recycling. The waste stream amounts and revenues also cost justified the purchase of a baling system.

In the state of Pennsylvania, recycling adds significant value to the state's economy. In the state, collection and processing, the first step in the recycling process, involves sorting and aggregating recyclable materials. It includes municipal and private collectors, material recovery and composting facilities, and recyclable material wholesalers. These activities employ nearly 10,000 people in Pennsylvania, with a payroll of $284 million and annual sales of $2.3 billion. Recycling manufacturing involves the actual conversion of recyclables into products. The primary recycling manufacturers in Pennsylvania in order of magnitude are steel mills, plastic converters, paper and paperboard mills, and nonferrous metal manufacturers. Recycling manufacturing employs over 64,000 people with a payroll of almost $2.5 billion and annual sales of over $15.5 billion. Reuse and remanufacturing focuses on the refurbishing and repair of products to be reused in their original form. The largest activities are retail sales of used merchandise and reuse of used motor vehicle parts. The amount of value that can be added via this process is limited because of competition from new products. Nevertheless, reuse and manufacturing contributes over 7,000 jobs, a payroll of $115 million, and sales of over half a billion dollars.

On a national scale, the recycling industry continues to grow at a rate greater than that of the economy as a whole. According to the Institute for Local Self-Reliance, total employment in the recycling industry from 1967 to 2000 grew by 8.3% annually while total United States employment during the same period grew by only 2.1% annually. The recycling industry also outperformed several major industrial sectors in regard to gross annual sales as its sales rose by 12.7% annually during this period. Furthermore, the number of recycling industries in the United States increased from 8,000 in 1967 to 56,000 in 2000. These facilities employ 1.1 million people across the country.

For many items, recycling can be more cost effective versus disposal. The list below provides a summary of select construction materials based on survey results of 63 companies:

- Average cost to recycle
  - Asphalt debris: $5.70 per US ton
  - Concrete rubble: $4.85 per US ton
  - Used bricks and blocks: $5.49 per US ton
  - Trees and stumps: $37.69 per US ton
  - Wood scrap: $46.43 per US ton
- Average cost of disposal
  - Over $75.00 per US ton and can be as high as $98.00 per US ton

Recycling saves money for manufacturers by reducing energy costs. In 2001, New Jersey's recycling efforts saved a total of 135 kJ (128 trillion BTU) of energy, equal to nearly 17.2% of all energy used by industry in the state, with a value of $570 million.

The sale of recycled products is an increasingly important component of the retail sector and commerce in general. There are over 1,000 different types of recycled products on the market, and due to changes in technology and increased demand, today's recycled products meet the highest quality standards. Recycled products are also more readily available than ever before and are affordable. By purchasing recycled products, consumers are helping to create long-term

stable markets for the recyclable materials that are collected from New Jersey homes, businesses, and institutions.

The economic value of clean air, water, and land is significant, but difficult to quantify. Since recycling plays an important role in protecting these natural resources, it must be attributed an economic value in this context as well.

Corporate Image Benefits

Corporate imaging and product branding play a critical role in the profitability of any organization. Successfully maintaining and strengthening these concepts is one of the chief duties of any marketing department, and environmental initiatives can go a long way to bolster them. Specifically, by focusing on solid waste minimization and publicizing these efforts, an organization can:

- Increase sales by attracting environmentally conscious consumers
- Improve the recruitment of employees that share similar values
- Attract environmentally conscious partners
- Attain free corporate publicity
- Increase employee involvement gateway to other programs (heart and mind)
- Maintain cleaner facilities

Personal and Social Benefits

Solid waste minimization also offers personal and social benefits. Although many of these benefits are somewhat intangible and difficult to measure, they are worth mentioning. They are worth mentioning because they can be selling points when promoting an environmental program. Below is a list of some of these benefits:

- Personal satisfaction for helping the environment
- Sustainable environment for future generations
- Cleaner facilities
- Buy-in at work programs (employee involvement)
- Healthier environments and a higher standard of living
- Generation of money to assist local programs such as the sale of aluminum cans to benefit a children's burn unit at a hospital

Fundamentals of Recycling Processes

An understanding of the recycling industry and the related processes can be very beneficial when evaluating recycling system options. In addition, a basic understanding can aid managers and engineers in making better decisions in regard to recycling and disposal options. Following is a brief summary of some of these benefits:

1. Gaining a better understanding of recycling options and the different roles that material recovery facilities, processors, and material brokers play in the process
2. Gaining an understanding of the recycling process and the process flow for materials as they leave a facility
3. Gaining an understanding of the material separation needs based on the recycling process for each material type
4. Gaining an understanding of the recycling process to design better processes and products to reduce the environmental impact
5. Learning more about the LCA process and develop more accurate inventory audits

This section provides an overview of the recycling industry which includes brief discussions of the business entities operating in the field. In addition, overviews of the recycling processes for major waste items are also provided. The intent of this section is to expose the reader to basic terms and processes in the field, not to provide a detailed or comprehensive analysis.

Recycling Industry Overview

The recycling industry is comprised of five primary entities that work together to get recyclable materials from the point of generation as a by-product or waste to the stage where they can be used again as raw materials.

These entities are:

- Haulers – these companies transport materials between entities, including the generation facility, consolidation points, and processing facilities. Often times, these companies will lease a semitruck trailer to the generating facilities to consolidate and store recyclable materials before transportation to a consolidator or depot.

- Material recovery facilities (MRF) – an MRF is a specialized plant that receives, separates, and prepares recyclable materials for marketing to end-user manufacturers [3]. There are two types of MRFs: clean and dirty MRFs. A clean MRF accepts recyclable materials that have been collected as commingled wastes from curbside collection or drop-off sites (Fig. 2). The most common clean MRF is a two-stream MRF, where source-separated recyclables are delivered in the form of a mixed commingled container stream (typically glass, ferrous metal, aluminum and other nonferrous metals, PET [No. 1] and HDPE [No. 2] plastics) and a mixed paper stream. A dirty MRF accepts a mixed (recyclable and nonrecyclable) solid waste stream and then proceeds to separate recyclable materials via a combination of manual and mechanical sorting [3] (Fig. 1). The sorted recyclable materials may undergo further processing required to meet technical specifications established by end markets while the balance of the mixed waste stream is sent to a disposal facility such as a landfill [3].
- Consolidators and depots – a consolidator or depot is similar to an MRF, but it does not perform any sorting operations. These entities hold or store materials until a specified batch size is reached or when a recycling processing facility is ready to process the material.
- Material brokers – material brokers buy recyclable materials from cities, businesses, depots, or MRFs and sell the materials to a processing facility.
- Processing facilities – these facilities perform the actual processes to recycle materials. Many different processing facilities exist for different materials, such as metals, glass, and papers.

Aluminum Recycling

Aluminum recycling can be broken down into three steps:

- Sorting
- Baling
- Compressing

A United Kingdom Web site (rethink.sita.co.uk) provides an overview of aluminum recycling and is summarized in the following paragraphs [4]:

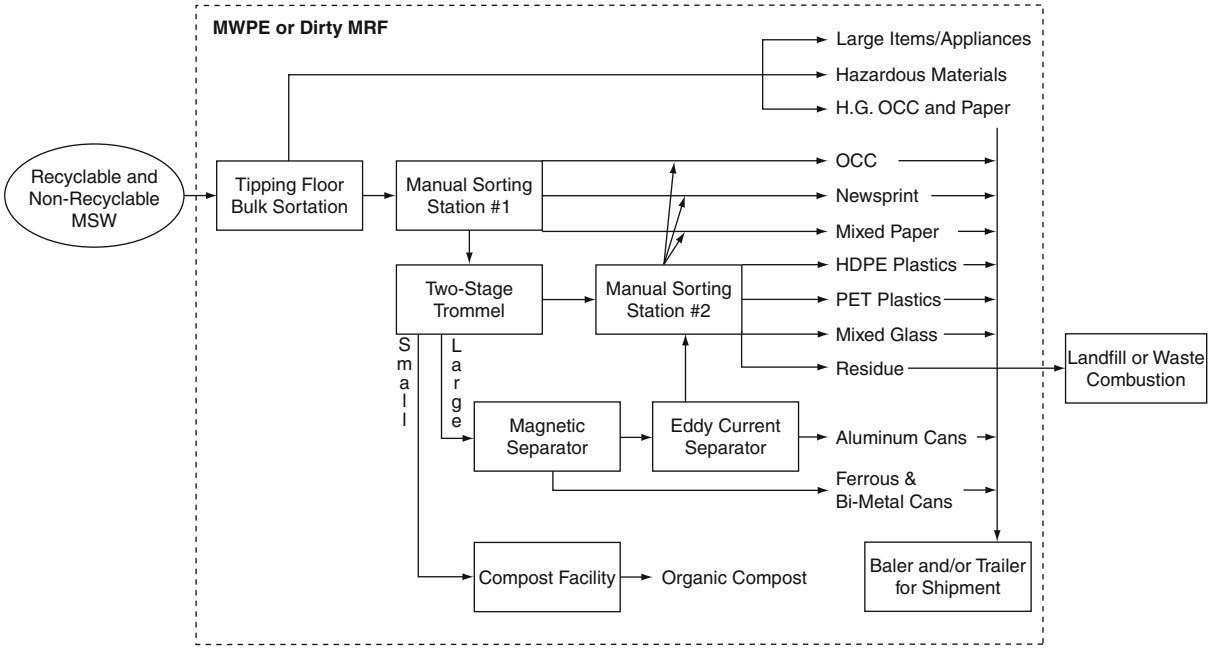

Recycling Collection and Materials Separation. Figure 1
Dirty MRF overview

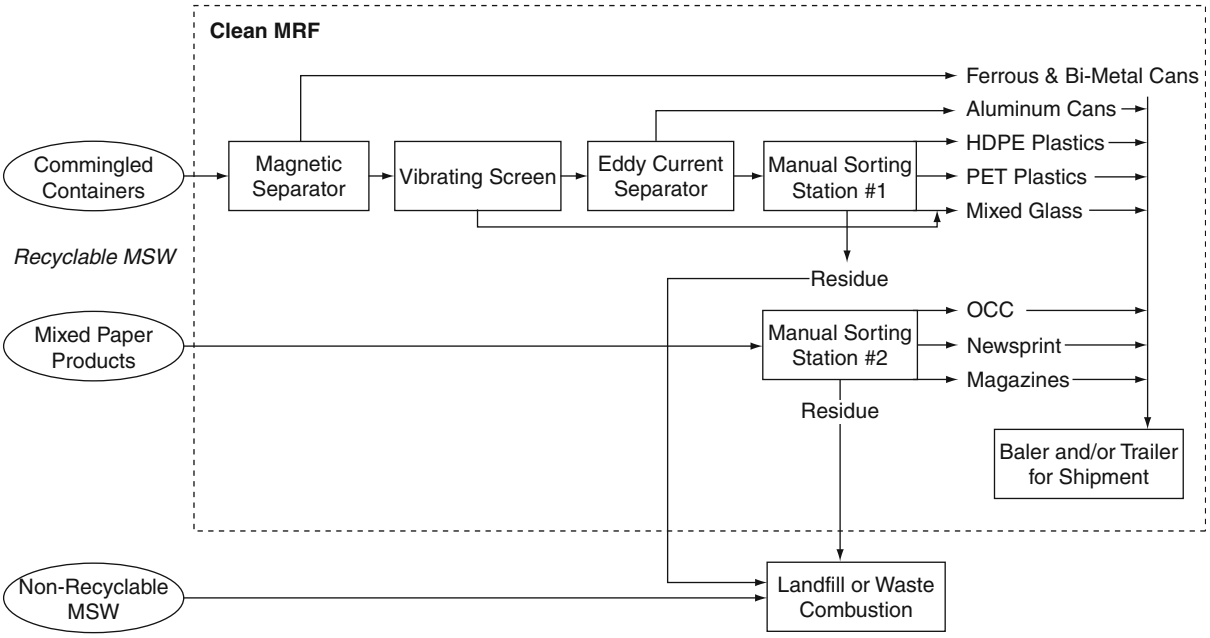

Recycling Collection and Materials Separation. Figure 2
Clean MRF overview

Before being transported to an aluminum recycling facility, the material is passed under a magnet to remove any steel. Aluminum is a non-ferrous metal, so it is not magnetic. Steel is a ferrous metal, so it is magnetic. The magnet picks up the steel cans and separates them from aluminum. The remaining cans are then crushed and compressed to form bales and transported to the aluminum recycling facility.

Once at the facility, the cans are shredded into small pieces about 2.5 cm in diameter. These pieces then pass through a magnet which removes any remaining ferrous metals such as steel. The shredded aluminum then travels to a de-coater, where hot air (at 500°C/930°F) removes any coating or decoration.

The hot cans go straight from the de-coater to the furnace, where they are melted at a temperature of 700°C/1,300°F. Once melted, the liquid aluminum is transferred to a holding furnace which clears any remaining contaminants, and a degasser which removes any gas.

The liquid aluminum is poured into cooled rectangular shaped moulds. The cooling transforms the aluminum back into a solid metal. This solid metal is taken to a saw where the ends are made square and transported to the rolling facility. At the rolling facility the aluminum is rolled into large sheets to be used a raw material.

Glass Recycling

Different types of glass go through different recycling processes. For example, cookware melts at a much higher temperature than container glass and must be processed separately. This section follows the typical recycling process of container glass (such as beverage bottles). There are four types of glass as related to recycling processes [5]:

- Container glass (wine and beer bottles)
- Float glass (windows)
- Cookware (plates and dishes)
- Automotive glass (windshields)

Glass for recycling is mostly collected from businesses, curbside collection, or community drop-off sites. Trucks collect the bottles and transport them to be stored at a depot. When a processing batch of glass has been collected and delivered to the depot, it is all transported to a glass recycling facility [5].

Once at the recycling facility, the glass is crushed (crushed glass is "cullet"). Cullet goes through various processes to remove nonglass items. To remove ferrous metal, the cullet is passed through a strong magnet which removes the ferrous metals such as steel and iron [5]. To remove nonferrous metals, the cullet passes by powerful air jets which separate the metal pieces from the cullet [5]. To remove lightweight items, such as paper, the cullet goes through a vacuum [5]. To remove any remaining items that are not glass, such as ceramics, the cullet passes under a laser which rejects them [5]. The cullet is now ready to be made into new glass. To make new glass, the cullet goes into a furnace where it is melted at a temperature of 1,500°C/2,700°F [5]. The high temperature turns the cullet into a liquid called molten glass. The molten glass is shaped into molds to become bottles or jars. Recycled glass is melted at a lower temperature than virgin glass, which saves 30% of the energy used [5].

Paper Recycling

Collected paper must be sorted before being recycled. The recycling process itself can be separated into eight steps [6]:

- Sorting
- Baling
- Pulping
- Screening
- De-inking
- Pouring
- Rolling
- Packing

This section provides a brief overview of each of these steps. Paper recycling can be challenging because there are over 50 grades of wastepaper. The main four groups are [6]:

- Low grade (mixed paper, corrugated board)
- De-inking grade (newspapers, magazines, office paper)
- Kraft grade (unbleached brown backing)
- High grade (printer cutoffs and unprinted paper)

Large amounts of paper, including shredded paper, are baled before being transported to a paper mill. Once at the paper mill, the paper is placed into a large vat and mixed with water. The process breaks down the paper into tiny strands of cellulose fibers. Eventually, this turns into a mushy mixture called pulp.

The pulp is then filtered and screened. The screens are made of a series of holes and slots of different shapes and sizes, and remove any remaining contaminants such as bits of plastic of glue. For certain uses, pulp must also be de-inked. There are two main methods of de-inking [6]:

1. Washing – Chemicals can be used to separate the ink from the paper, and the ink is washed away with water. Although this process requires the use of chemicals and water, the quantities used are much less than the manufacture of new paper and the water can often be cleaned and reused.
2. Floatation – Air can be passed through the pulp to produce foam. The foam holds at least half of the ink and can be skimmed off.

Pulp is poured into a huge flat wire screen. On the screen, water starts to drain from the pulp and the recycled fibers quickly begin to bond together to form a watery sheet. The sheet, which now resembles paper, passes through a series of heavy rollers, which squeeze out more water; some heated cylinders, which dry the paper; and an iron roller, which irons the paper [6]. Next, the paper is wound into a large roll. One roll can be as wide as 9 m (30 ft) and weigh as much as 18 metric tons (20 US tons). The roll of paper is cut into smaller rolls, or sometimes sheets, before being dispatched for use.

Plastic Recycling

Plastic recycling can be separated into six steps [7]:

- Sorting
- Shredding
- Cleaning
- Melting
- Extrusion
- Pelletizing

Plastics are synthetic polymers made from oil and natural gas and are one of the world's most used raw materials [7]. Plastics are blended in different formulas and modified with additives to create the 40 categories of plastic and the several specific grades within these

formulas [7]. Most consumer plastics in waste are labeled with an Identification Code, numbered 1–7. Before plastics are processed, they are sorted into seven different polymer types. The polymer type indicates both the properties and characteristics of the material, such as the melt temperature and its suitability for recycling [7]. The symbols used to classify the different polymer types can be found on the plastic items as follows:

Number 1: PETE or PET (polyethylene terephthalate)
- Used typically for beverage bottles, plastic wrap, and frozen food trays.
- Recycled PETE is commonly used to make new clothing fibers, furniture, new beverage containers, and carpet.

Number 2: HDPE (high-density polyethylene)
- Used typically for milk jugs, juice jugs, liquid detergent bottles, trash and shopping bags, and cereal box liners.
- Recycled HDPE is commonly used to make detergent, oil and vitamin bottles, drain pipes, recycling bins, dog houses, and other plastic lumber.

Number 3: Vinyl (PVC)
- Used in clear food packaging, shampoo bottles, and medical tubing. It is also used in construction building.
- Recycled PVC is used to make packaging, binders, mats, decks, paneling, roadway gutters, mud flaps, and speed bumps.

Number 4: LDPE (low-density polyethylene)
- Used in food packaging (especially bread), frozen food bags, shrink wrap, dry cleaning bags, and squeezable bottles.
- Recycled LDPE is used to make mailing envelopes, trash cans, trash liners, furniture, floor tiles, paneling, and compost bins and lumber.

Number 5: PP (polypropylene)
- Used to make ketchup and medicine bottles, some dairy containers, and molded automobile parts.
- Recycled PP is commonly used to make signal lights, car battery components, brooms, brushes, oil funnels, ice scrapers, bike racks, pallets, storage bins, and trays.

Number 6: PS (polystyrene)
- Used to make packing foam, egg cartons, meat trays, aspirin bottles, plates, CD jackets, and food service items.
- Recycled PS is used to make thermometers, switch plates, insulation, egg cartons, vents, office supplies, foam packaging, and containers.

Number 7: Other plastics
- Typical examples are 3- and 5-gallon reusable water bottles, some citrus juice and ketchup bottles.

Once sorted, the plastics are baled before being transported to a plastic reprocessing plant. Once at the reprocessing plant, the plastic is shredded into small pieces which are then washed. After washing, the plastic pieces are passed under a metal detector to remove any metal, and a de-dusting unit which removes any lighter particles [7].

The clean plastic pieces are dried and melted so they can be made into new shapes. The melted plastic is then filtered to remove any remaining contaminants and extruded to form fine strands. The plastic strands are then cut into pellets, cooled in water, then dried and stored ready to be processed and molded as new plastic items [7].

Common Problems and the Human Factors of Recycling

There are many common problems involved in creating a successful recycling program. The two biggest problems found in the duration of this research were material misplacement and hindrances inherent in the company itself.

Material Misplacement

One problem often encountered when companies attempt to separate out recyclables is employee involvement. At most sites surveyed, containers dedicated to certain materials were found to contain other materials as well. This often results in higher costs for the companies. For instance, at one company, recyclable material was found in a dumpster dedicated for hazardous wastes and therefore costs more to dispose. However, wood, Old Corrugated Containers (OCC), and other recyclables were finding their way into this dumpster.

At another company, recyclables were found in the landfilled trash stream even though there were recycling containers nearby. One such example was in a warehouse. The warehouse had recycling containers

for shrink wrap and clean cullet (broken glass) positioned throughout the aisles, and yet the shrink wrap, glass, and wood were all found in the garbage cans which were also throughout the aisles. In addition, there were aluminum collection barrels containing glass, glass collection barrels containing aluminum, and other miscellaneous trash mixed into the bins labeled for recyclables.

A third company, a heavy manufacturer and assembly plant, also encountered this problem of material misplacement. Upon a preliminary tour of the plant, it was noted that in clearly marked recycling containers, other materials such as expanded polystyrene cups, paper, and mixed trash were found. Similarly, in a large office building with over 600 employees, the paper collection boxes also contained film plastic, OCC, and mixed trash.

These observations raised several serious questions. First, why do people place the wrong materials into collection containers or place recyclables into a landfill stream even when the appropriate container is located within close proximity? What is the motivation which causes some people to obey the recycling policies and what is the motivation that causes others not to? What can be done to improve involvement and deter carelessness in regard to recycling? What human factors come into play in determining the signs which should be used to mark collection containers and in the placement of containers? Finally, what motivational ideas work best in regard to recycling, trash separation, and waste minimization?

It has been noted that when recycling containers are distinctive according to acceptable material, the employees are much more likely to place the proper material in the container. This may involve a difference in the type of container used, the color of the recycling container, or the size and shape of the opening or of the container itself. For instance, some companies use large wire bins which are always for recyclables only. Other used colored containers to designate the end point of the materials. Still others use containers of different shapes and sizes for each different material. Often, the same types of similar containers are used with only a difference in size and shape of the opening for each material.

It is also obvious that when there are clear signs designating the acceptable materials for each container, accidental wrong placement of materials is much less likely. These signs usually work better if they are in color, have pictures, and are placed in easy sight. The signs must be easily recognizable and distinguishable in order to facilitate employee involvement. People do not like to be bothered by extra time and energy needed in order to recycle. If it requires extra effort, people will often not participate.

In a similar venue, the collection containers must be properly placed or people will not bother to find them. Individuals who have a personal interest in recycling will hold on to recyclables until they can be properly disposed of or placed in the proper container. Such people have often been found to do such things as take aluminum cans home from work if the company does not recycle them. These people will take the added time and energy necessary to get the materials in their proper containers. However, if one does not have such personal convictions, then in fast-paced society, taking the extra time and effort to find the proper recycling container is often too time-consuming and problematic to bother with.

If there is a motivation to recycle, the outcome is much better. There is not one cure-all for motivating employees, but there are some highly successful motivation factors. These include money, fun, and free time. There three motivation factors can be utilized in a variety of ways. One option is to keep track of recycling by department and then to award the best department(s) with cash, a party, or a paid afternoon off. There are countless other creative options available. The feasibility of these options depends on the particular company and its schedule, policies, and recycling revenue.

According to human nature, there will always be some people who are too careless, apathetic, or lazy to obey recycling mandates. However, the proper use of human factors and motivation can minimize the number of such people and in turn minimize the incidents of contamination of recyclables and recycling collection containers.

Observed Common Hindrances

There are many common hindrances to recycling which occur on a higher level than employee involvement. These include management perceptions,

company policies, union rules and regulations, poor past performance in recycling attempts, and many other reasons. These hindrances must be overcome or successful recycling will be impossible. It is often very difficult to overcome these hindrances. Very often, they are due to a misunderstanding or wrong perceptions. This makes it vitally important for the assessment team to understand the hindrances and how to combat them.

Though it may seem impossible to overcome policies or company rules, recommendations may still be made which do not conform to the problematic rules. The recommendations can be provided as win-win situations and may go a long way to adjusting the policies inhibiting recycling practices. The most important issue is that the economically and ecologically best scenario is chosen. This can always be accomplished with win-win situations if those participating are willing to be creative. In short, the assessment team cannot direct the company to change its policies but can present alternatives which allow the company, management, or union to see the downfall in the policy and the benefits of alterations.

Solid Waste and Recycling Assessments

The process used for the assessment was expanded from a waste assessment manual provided by the US EPA [8]. This EPA manual was also used by Petek to reduce waste water emissions by 24% at a textile facility in Slovenia [9]. To initiate the waste audit process, the company was given a Pre-assessment Questionnaire to complete. This is done to allow the researchers the opportunity to have a general understanding of the company before gathering data on the walk-through. The questionnaire gives the researchers an opportunity to investigate the processes beforehand if needed. Figure 3 summarizes the nine-step waste assessment process.

Process step	Description
1. Pre-Assessment Questionnaire	The purpose of the pre-assessment questionnaire is to obtain information about the company, which is needed for the research team to perform a comprehensive and efficient waste assessment.
2. Pre-Assessment Meeting	The purpose of the pre-assessment meeting is to take notes of the questions which may arise during the review of the pre-assessment questionnaire and to discuss the responsibility of each member for the waste assessment so that the assessment tasks are evenly distributed throughout the team members.
3. In Plant Data Collection	The team leader will introduce the team members to the client. Then the company gives a detailed explanation of the primary business processes. Next a "walk though" is performed by the assessment team. During the walk through the assessment group will gather raw data on what they observed as well as record the location and the main purpose of each dumpster. The team also examines the company's mainproduction, the waste flow in the facility, number of waste streams in the facility, and draws a process and material flow diagram.
4. Data Analysis	Each person writes up a summary from walk through. Brain storming and discussion are used to establish major waste minimization opportunities. Recyclers and waste handlers are called and a time line is developed.
5. Additional Data Collection	A second trip to the plant is performed to collect detailed or more specific information. The detailed wasteassessment includes performing trash sorts, obtaining additional manufacturing and waste stream information, and asking questions. At the facility the waste sort information is entered into a standardized Waste Composition Table to track each waste stream. Waste data is entered into a software program called "Tabulator". The "Tabulator" consists of several-linked Excel spreadsheets, which will calculate the amount of waste disposed. Next local recyclers and equipment vendors are located. In addition a financial analysis is performed.
6. Research Progress Meeting	All team members will discuss how to target each of the waste streams and come up with final recommendations and conclusions for the waste assessment.
7. Waste Assessment Research Report Writing	The purpose of the waste assessment research report is to give the company information about the volume and content of the waste generated and also to give recommendations for reusing, reducing and recycling waste generated by the company.
8. Presentation	A presentation is prepared for the company or for people who don't have time to read the full report and to give an opportunity for a question and answer period.
9. System Feedback	Four to five months after the waste assessment, a letter or telephone call survey is used to determine the success of the project and gather data on information to improve the process.

Recycling Collection and Materials Separation. Figure 3
Waste assessment process overview

Recycling Collection Systems and Methods

Advances in technology, changes in recycling laws, trends in recycling markets, and other variables have had a large impact on recycling collection systems and methods. The public and businesses now have more options to aid them in increasing recycling levels. So, it is important for organizations to periodically evaluate their recyclables collection system to determine if it is the most cost-effective and efficient program. Several widely used programs include:

- Curbside programs (single stream, multiple stream, and pay-as-you-throw)
- Automated collection
- Drop-off centers
- Incentive programs

Curbside Recycling

Curbside recycling now serves half of the US population, providing the most convenient means for households to recycle a variety of materials [10]. While individual curbside programs differ, the most commonly collected materials are "The Big Five," which includes aluminum cans, glass bottles, paper, plastic, and steel/tin cans. Curbside recycling exists in several ways [10]. They include:

- Dual-stream recycling
- Single-stream recycling
- Pay-as-you-throw

Dual-stream recycling is probably the most popular form of curbside recycling in the USA [11]. Used containers (plastics and metals) are placed into one bin, and papers (such as newspaper, magazines, and direct mail) go in another bin. Both bins are set out on the curb on pickup day. Most communities that offer this service use special trucks divided into two compartments so workers can sort at the truck.

Single-Stream Recycling is a method that is growing, but somewhat controversial. It provides one cart (65 or 94 gal) where materials are commingled [12]. Households do not have to separate any materials. Haulers favor single-stream because it involves less trucks and pickups [12]. Evidence suggests that single-stream increases the quantity of household recyclables, and many cities have implemented single-stream programs as a result [12].

Pay-as-you-throw (PAYT) is a trash collection program that encourages curbside recycling [13]. Residents are charged per trash bag, and curbside recycling is offered at no or a reduced cost. There are several benefits to PAYT programs as discussed by the EPA [13]:

- Decreases waste: The US EPA says municipalities often see 25–35% less nonrecyclable waste.
- Increases recycling: If residents can pay for trash or recycle for "free," they are much more watchful about what gets trashed; one California PAYT program saw recycling volumes triple, literally overnight.
- Control of waste costs: Residents have a direct effect on what they spend on disposal.
- More information about who supports PAYT is available from the US EPA. Over 5,000 communities across the country currently have a PAYT program.

Automated Collection

Many communities are moving toward automated collection using a specialized vehicle that lifts, empties, and returns a cart to the curb. The driver controls the entire process from the cab of the vehicle and does not leave the vehicle [10]. This can reduce labor costs and on-the-job injuries, thereby reducing worker's compensation claims [10]. Automated systems utilize specialized trucks equipped with mechanical extensions that automatically lift and empty trash and recycling containers without the driver leaving the vehicle. This is a system designed to improve the efficiency and makes the task of putting out garbage easier and cleaner for the residents [10].

Drop-off Centers

Drop-off centers can be a cost-effective way for smaller or rural communities to collect recyclables [10]. It can also be effective for urban communities to offer businesses, apartment buildings, and condominiums access to recycling [10]. In most cases, drop-off centers have lower operating costs versus curbside collection due to lower resource requirements in terms of labor and fuel.

Drop-off centers, like curbside programs, can offer full source separation (multiple bins), commingled materials (fewer bins), or a single-stream (fully commingled) approach for collecting recyclables [10].

Dual-Stream Versus Single-Stream Collection

Single-stream recycling collection: "Single-stream" recycling collection (fully commingled) programs allow participants to put all recyclable materials (e.g., paper, bottles, cans) into one collection container. In the case of paper, all grades are mixed together along with cardboard and rinsed food containers at the curb and/or bin at a municipal transfer station.

The fully commingled recyclable materials are then transferred to a central point such as a materials recovery facility (MRF) where the recyclables are separated using handpicking and/or automation. Paper collected in single-stream systems may be further separated into various paper grades (e.g., high-grade white paper, newsprint, cardboard). For single-stream recycling to work, the processing facility must sort the recyclable materials properly and thoroughly to meet market specifications [14].

Single-stream collection has become popular for the following reasons:

- Many residents find it convenient, since no sortation is required by them.
- The convenience has resulted in higher recycling participation rates [3].
- New materials can be added to the collection system with minimal change to the collection system and process.
- It is found to increase the amount of recyclables collected [3].
- Reduces the number of collection trucks needed because single-stream programs usually lead to changing to automated or semiautomated curbside collection [3].

Dual-stream or multi-stream recycling collection programs require participants to place each recyclable material in the appropriate collection bin when they first discard the item. Separate containers collect glass, metal, plastic, newsprint, and magazines.

Recovered paper can be collected separately by grade (e.g., white office paper, newspapers, magazines, and corrugated cardboard boxes) or, more commonly, collected as mixed paper separated from other recyclable materials. If different grades of paper are commingled, they are sorted at a central point, such as a materials recovery facility (MRF). If paper is separated at the source, the different grades of paper can be marketed separately for the highest return.

Benefits of dual- or multi-stream (sorted) collection include [3]:

- Lower levels of contamination at the source.
- Higher-quality materials.
- Materials are more valuable and may result in higher financial returns.
- Lower costs to process the recovered paper.

Single-stream recycling collection allows residents to "fully commingle" all their recyclables (mixed paper and mixed food containers together) at the curb, transfer station, or recycling center [10]. The materials are separated during processing, at a resource recovery or materials recovery facility, and prepared for recycling markets [10]. Single-stream curbside collection programs are most often implemented with automated or semiautomated collection [10].

Incentive Programs

The following is a list of several incentive programs that have been implemented to increase recycling levels for communities:

"Recycle Man" Rewards Residents with Grocery Gift Cards [10]

Polk County, Florida – Officials recently conducted a 6-week recycling incentive program. Each recycling day, the county recycling coordinator, also known as "the Recycle Man" and his supervisor canvassed local communities with low recycling rates to encourage residents to recycle. For each bin they observed that was properly prepared, they awarded the resident with a $20 gift card to their local grocery store. While full results are pending, the county did receive a notable increase in calls for bins as a result, and their MRF reported an increase in recycling volume [10].

Recyclebank [10]

RecycleBank provides coupons to residents that participate in curbside recycling programs.

RecycleBank calculates and records quantity (weight) of recyclables collected at curb (requires automated collection using bar code on recycling container) in exchange for coupons for products and services for local businesses. In 2008, the City of Hartford, CT implemented a 1-year pilot program that included using RecycleBank [10].

Door Prizes Encourage Participation at County Drop-off Center [10]

Hanover, Pennsylvania – Hanover, Pennsylvania, was ordered by the PA Department of Environmental Protection to make curbside recycling mandatory for all residents in the summer of 2004. The city immediately began looking for ways to track and promote recycling participation [10].

One method officials used was to issue a card with a bar code to each resident subscribed to the recycling service. Residents swipe the card when they take recyclables to the recycling center. The cards help the borough keep track of residents' participation in the recycling program [10].

To create incentive for residents to continue dropping off recycled materials at the center, the borough began issuing door prizes at random to people using the recycling center starting in May 2006. More than 800 cards were swiped at the recycling center during the first 2 weeks of March [10].

Separation Methods and Equipment by Material

A materials recovery facility (MRF) or materials reclamation is a specialized plant that receives, separates, and prepares recyclable materials for marketing to end-user manufacturers. As previously discussed, there are two different types – clean and dirty MRFs.

The percentage of residuals (unrecoverable recyclable or nonprogram materials) from a properly operated clean MRF supported by an effective public outreach and education program should not exceed 10% by weight of the total delivered stream, and in many cases, it can be significantly below 5% [3]. A dirty MRF recovers between 5% and 45% of the incoming material as recyclables [3]; then, the remainder is landfilled or otherwise disposed. A dirty MRF can be capable of higher recovery rates than a clean MRF, since it ensures that 100% of the waste stream is subjected to the sorting process, and can target a greater number of materials for recovery than can usually be accommodated by sorting at the source [3]. However, the dirty MRF process is necessarily labor intensive, and a facility that accepts mixed solid waste is usually more challenging and more expensive to site [3]. The following sections provide additional details regarding the recycling processes for common materials.

Newspaper

The generalized process for newspaper collection involves:

- Newspaper is collected and consolidated from drop-off sites, curbside collection, or business collection.
- The material is baled at a material recovery facility.
- The baled material is sold to a paper mill.
- The paper mill recycles the newspaper and creates raw material to be used as newspapers or other products.

Old newspaper is an essential material in the paper remanufacturing process; as the paper mills are concerned about both quality (cleanliness, type of paper) and quantity of the supply, they usually issue purchasing contracts to dealers rather than buying small amounts of paper from the public [15].

The equipment and recycling process are summarized in the following paragraph:

At the paper mill, de-inking facilities separate ink from the newspaper fibers through a chemical washing process. A slusher turns the old paper into pulp, and detergent dissolves and carries the ink away. Next, screens remove contaminants like bits of tape or dirt. The remaining pulp is bleached and mixed with additional pulp from wood chips to strengthen it. The watery mixture is poured onto a wire, a continuously moving belt screen which allows excess moisture to drain through. By the time the mixtures gets to the end of the belt, it's solid enough to be lifted off and fed through steam-heated rollers which further dry and flatten it into a continuous sheet of paper. This paper machine produces finished newsprint at the rate of 915 m (3,000 ft) per minute [15].

Cardboard

The generalized process for cardboard or Old Corrugated Container (OCC) recycling is very similar to

newspaper recycling. The equipment and recycling process are summarized in the following paragraph:

While some corrugated cardboard is recycled at curbside, the bulk of it comes from commercial rather than residential sources. At the paper mill, the corrugated containers are pulped and blended with additional pulp from wood chips. Old fibers, which are broken, shorter and weaker, as compared to new fibers, are blended with the new pulp. Recycled paper fibers and new pulp are then blended to make linerboard. Next, the linerboards are shipped to a boxboard plant, where the manufacturing process is finished. The paper is corrugated by specially-geared machines, the linerboards are glued on, and the resulting flat pieces, called mats, are trimmed to size and creased along a pattern of folds. The mats are shipped flat to customers who set them up into boxes. Then the boxes are used to package products for shipping [15].

Glass

The generalized process for glass recycling also involves collection and consolidation. Glass recycling poses additional challenges over other materials because it is fragile and breaks easily during transportation and consolidation. This can cause safety and separation issues for transportation and hauling companies. The equipment and recycling process are summarized in the following paragraph:

At the plant, a mechanical processing system breaks the glass into small pieces called cullet. Magnets, screens and vacuum systems separate out metals, labels, bits of plastic, metal rings and caps. The cullet then is blended in measured amounts with silica sand, soda ash, and limestone, and placed in a furnace which melts it into molten glass [10].

Steel (Tin) Cans

The equipment and recycling process are summarized in the following paragraphs:

After the cans are collected, the volume of cans collected and type of transportation arrangements available will determine whether the load will go through a dealer or directly to a de-tinning plant. At the plant, a chemical de-tinning solution flows into and drains the cans more easily, which results in better recovery of the tin during the reclaiming process. The process consists of a series of chemical and electrical steps which separate, purify, and recover the steel and tin. In the batch process of de-tinning, the cans first are loaded into perforated steel drums and dipped into a caustic chemical solution which dissolves the tin from the steel. The de-tinned steel cans are drained, rinsed, and baled into 14”x14”x30” 181 kg (400 pound) blocks. Then they are sold to steel mills to be made into new products [10].

Meanwhile, the liquid with the tin, a salt solution called sodium stannate, is filtered to remove scraps of paper and garbage. Then it’s chemically treated to eliminate other metals. Next, the solution is transferred to an electrolysis bath. When electricity is applied, tin forms on one of the plates in the solution. After the plate is covered, the tin is melted off and cast into ingots. The ingots are at least 99.98% pure tin and are used in the chemical and pharmaceutical industries. Pure tin also is alloyed with other metals to make solder, babbitt, pewter, and bronze products [10].

Aluminum

The equipment and recycling process are summarized in the following paragraph:

After the aluminum is collected and consolidated it is transported to a smelter, where it may be shredded or ground into small chips before being melted and cast into ingots. The ingots are sent on to manufacturing plants where they are rolled into sheets of aluminum and used to manufacture end products ranging from cans to castings to car bodies. The major markets for shredded aluminum are exports (comprising a variety of end users) and domestic smelters [10].

Financial Analysis

If this section were to be reduced into one key idea, it would be the application of the three R’s and the two E’s as they apply to solid waste minimization. From a technical and regulatory standpoint, the hierarch mentioned in the previous section is excellent, but it does not hit home with the leadership of many organizations and does not promote the full benefits of solid waste minimization [16]. In terms of communicating and promoting solid waste minimization, the three R’s and the two E’s have served as a very effective tool. The three R’s are:

- *R*educe
- *R*euse
- *R*ecycle

The three R's are a summary of the hierarchy discussed in the previous section. In terms of the hierarchy, the first item discussed, "source reduction," has been separated into two components, "reduce" and "reuse." Reuse has been added to emphasize the fact that many items that are being disposed of at a landfill by organizations could have been reused, such as cardboard containers, plastic caps, or rubber bands [16]. Finally, all recycling methods, in-process, on-site, and off-site, have been lumped into one category for simplicity.

And the two E's are:

- *E*nvironment
- *E*conomics

The concept is to apply the three R's at an organization to help the two E's. The three R's provide the solutions to the solid waste problem based on the hierarchy of solid waste management. The two E's communicate the goals of these efforts: to lessen the environmental impact of an organization and improve an organization's economics or bottom line. This simple phrase is easy to understand and has served as a great "tag line" or "catch phrase" to promote solid waste reduction. By emphasizing economic benefits, solid waste reduction and minimization benefits are much easier to sell to the decision makers because the efforts are placing attention on the financial health of the organization as well. A plant manager of a battery manufacturing firm located in Toledo, Ohio, bluntly summarized this concept when he stated that his company "is in the business of producing and selling batteries, not recycling" [16]. It is easy to get caught up in the good feelings associated with helping the environment, but unless there is a financial incentive, many organizations may give environmental concerns only "lip service" [16]. A buzzword that is now emerging is "green washing," which is a situation in which a company publicly and verbally promotes their environmental efforts to bolster corporate images, but falls short of the actions associated with the public statements. The goal of emphasizing the three R's and two E's is to bridge the gap between public statements and corporate actions by demonstrating that environmental concerns make business sense.

A common misconception of organizations is that they do not have funds in their budgets for recycling or environmental initiatives. The fallacy in this thinking is that virtually all companies have a starting point or a "budget" for recycling and waste reduction: the annual expenses for trash removal and janitorial efforts [16]. The paradigm shift requires considering the amount of money expended per year as the "environmental" or "recycling" budget and devising creative methods and processes to minimize impacts to the environment. Many organizational leaders are surprised to learn the potential cost avoidance or revenue generated from becoming more environmentally conscious. A financial case study is discussed later in this section highlighting some of the typical benefits.

Economic benefits from solid waste analysis and minimization can be achieved a variety of ways. The most common economic benefits derived from solid waste minimization are listed below [16]:

- Cost avoidance – Organizations can save money by diverting solid waste streams from the landfill to back within the company in terms of reuse or off-site to a recycler. The monetary savings are derived from no longer paying a waste hauler to remove the trash and dispose of it at the landfill.
- Recycling revenue – Substantial additional revenue can be earned by selling recyclables to third-party processors or recycling commodity brokers. For example, one US ton of baled cardboard sells for $100–$180 on the market.
- Reduced raw material costs – When an organization is able to utilize in-process or on-site recycling, they reduce their raw material needs directly by replacing virgin material purchases with in-house scrap, rework, or process by-products.
- Reduced energy costs – By reducing the amount of materials within a facility through reduction and reuse, material handling costs can be minimized.
- Increased sales – Many consumers and businesses look favorably on organizations that are environmentally conscious and purchase products or services from them.
- Increased productivity – As workers are engaged in efforts that they see as meaningful, many of them take pride and put additional efforts into their work. In addition, absenteeism may reduce as well.

The case study discussed in the following section highlights the financial aspects of a decision by the

Lucas County Solid Waste Management District to build and operate a government-owned material recovery facility.

Case Study

Solid waste minimization and recycling goals for municipalities are achievable through the installation of material recovery facilities (MRFs), and in certain solid waste management systems, government-owned and government-operated MRFs are feasible and cost justified. This section demonstrates a process to evaluate and determine the operational and economic feasibly of a government-owned MRF [17]. A case study from Lucas County, Ohio, is provided that demonstrated this analysis process. The key findings from the case study indicate that the municipality will achieve a payback period of approximately 4 years, and a 10-year internal rate of return of 20.5%, versus the current system of outsourcing [17].

In 2007, the Lucas County Solid Waste Management District (District) purchased a material recovery facility (MRF) to sort and sell nearly 9,000 metric tons (10,000 US tons) recyclable materials that were collected per year from its municipal recycling programs. Currently, the county recycles two classes of materials, commingled fiber and commingled used beverage containers. In 2006, the District recycled 9,755 US tons of materials [17]: 7,280 US tons were commingled fiber (mixed office paper, newspaper, and OCC) and 2,475 were commingled used beverage containers (plastic bottles and aluminum cans).

The first phase of the analysis process involved estimating the current recycling levels in terms of materials compositions and volumes (annual tonnages). These data were collected from District records from the 2006 fiscal year and included operating cost and revenue data [17]. Once combined, this information provided a complete baseline of the operations of the current system utilizing outsourced processing. This baseline was used to compare the cost structure of acquiring a county-owned and county-operated MRF. The baseline data all annualized costs and revenues associated with the drop-off recycling program, specifically [17]:

- Revenue paid from third-party processors for recyclable materials
- Third-party processing fees
- Labor costs
- Administrative costs
- Vehicle costs (fuel, maintenance, repair)
- Drop-off container and material costs

The second phase involved indentifying potential MRF sites. A local business realtor was contacted for assistance. Upon the identification of the MRF site, a complete annual cost and revenue projection was conducted to operate the MRF over a 20-year period [17]. This analysis included the following annualized costs and revenues:

- Revenue paid from third-party recycling material commodity brokers
- Building purchase cost (including realtor fees)
- Building modification and renovation costs
- Equipment and inspection/repair costs
- Labor costs (including driver and processors)
- Administrative costs
- Utility costs
- Vehicle costs (fuel, maintenance, repair)
- Drop-off container and material costs

This financial projection of the proposed MRF was compared with the current system baseline. In essence, the analysis answered the question whether the additional revenue earned from the sale of the processed recyclable materials will outweigh the additional capital and operating costs over the projected 20-year life of the project at a 15% minimum attractive rate of return [17]. To accomplish this analysis, a net present worth (NPW) was conducted. The NPW is the difference between the present worth of all cash inflows and outflows of a project. Since all cash flows are discounted to the present, the NPW method is also known as the discounted cash flow technique. This method allows not only the selection of a single project based on the NPW value but also a selection of the most economical project from a list of more than one alternative projects, in the case of this research, the existing system of outsourcing versus purchasing and operating a government-owned MRF.

This section demonstrated the process for municipalities to economically justify the purchase and operation of a government-owned MRF. Key findings from this research revolve around a case study from the 2007 purchase of a government-owned MRF in Toledo,

Ohio, USA [17]. The key findings were demonstrated through a complete financial analysis. Specifically, the financial analysis indicated that the municipality will achieve a payback period of approximately 4 years and a 10-year internal rate of return of 20.5% [17]. The consequences of these findings, stemming from the economic and operational justification, led to the actual purchase of the MRF site and subsequent operation in 2007 through early 2008. This research may serve as an example or model for other local governments considering the implementation of such a system [17].

Industrial Ecology and Solid Waste Exchanges

Industrial ecology is the field of research that studies waste generation from a macrolevel for entire industries. From a solid waste standpoint, industrial ecology is concerned with the conversion or reuse of undesirable materials into something useful for another company or industry, in other words, waste exchanges and material efficiency. Material efficiency is defined as the percentage of process by-products that are recycled or reused divided by the total by-product generation for a company or industry. Industrial ecology and waste exchanges examine the material efficiency and methods to improve that efficiency. Whereas waste audits examine an individual company's ability to reduce, reuse, or recycle, waste exchanges examine an entire industry's or region's ability to reduce, reuse, or recycle. In essence, waste exchanges examine methods for one company to use another company's by-products as a raw material, diverting this material from entering a landfill. Waste exchanges are a great tool that can enhance a company's recycling levels and generate economic benefits as part of the solid waste auditing process. Waste streams identified during a solid waste audit that the company cannot reduce or reuse could be sent to another company using one of many solid waste exchanges operating around the world.

With increased pressures on companies to improve profitability and reduce environmental impacts, waste exchanges are more popular than ever. Many companies and nonprofit organizations are turning to these exchanges to bolster corporate images and reduce costs. The Internet has simplified, streamlined, and reduced the costs associated with the administration of waste exchanges as well. Information is available in real time, 24 h/day, which makes such systems more accurate and user friendly, while allowing the exchanges to reach a larger client base.

History and Background

Waste commodity exchange is defined as the ability of a company or organization to use another company's waste as its raw material. As the old adage goes, "One person's trash is another person's treasure." Instead of sending seemingly worthless items or process by-products away to a landfill, the goal of the waste commodity exchange is to find a company that may get more use out of the product.

A good household example of this is garage sales, which are an excellent way to reuse products. Another alternative is to find different ways to reuse items. Baby food jars, for example, can be reused to store miscellaneous nuts, bolts, and washers in a workshop.

Waste exchanges have been around for over 60 years [18]. The British Government established the earliest documented industrial waste exchange, called the National Industrial Materials Recovery Association, in 1942 [18]. This waste exchange was created to conserve materials for the war effort during World War II. The first North American waste exchange was started in Canada in 1974 for hazardous waste [18]. The National Industrial Materials Recovery Association is no longer active as it disbanded after the war. The Canadian waste exchange is still active as the Canadian Waste Materials Exchange (CWME).

Waste commodity exchanges are reuse and recycling services that help these types of material exchanges occur on a much larger scale for businesses. These services help businesses save money as well as help the environment by diverting waste into usable raw materials.

Waste Commodity Exchanges in North America

Over 200 waste commodity exchanges are currently operating in North America. These exchanges differ in terms of the service area, materials exchanged, exchange processes, and fee structures [19]. Many of these exchanges are coordinated by state and local governments, while others are for-profit businesses. The US Environmental Protection Agency (Washington)

provides an excellent reference list of waste exchanges and contact information [19].

More than 35 national and 150 state-specific waste exchanges exist in the USA, and Canada has more than seven national waste exchanges [19]. The majority of the waste exchanges are specific to certain regions or states. The drawback to regional or state-specific exchanges is that they expose the available materials to fewer potential companies. The benefits of regional exchanges, though, are that they significantly reduce transportation costs, especially for heavy or bulky items and large quantities.

Regional exchanges are appealing to companies that may continually exchange waste items over an extended period of time due to longstanding process by-products. An example of this is plastic scrap from a manufacturing process. Another company may be able to grind the scrap, use it as a raw material, and establish dedicated routes to transport the material. On the other hand, national exchanges expose materials to a much larger number of companies, but transportation fees may make some options infeasible.

The material and waste focus of the various exchanges differs significantly. Some are very broad and deal with a wide variety of materials. For example, in terms of the national exchanges, Recycler's World (www.recycle.net) and the Reuse Development Organization (www.redo.org) handle any waste that users post on the Web site.

Alternatively, some exchanges are very narrowly focused. Good national examples of this are the American Plastics Exchange (www.apexq.com), which deals solely with plastics, and Planet Salvage (www.planetsalvage.com), which deals only with used automobile parts. Overall, any material that is available from one business and wanted by another can become an exchange item, and a waste exchange most likely exists for it.

Materials that are available for exchange are generated from a variety of sources, which include:

- By-products
- Damaged materials
- Expired products
- Obsolete and off-specification goods
- Overstock virgin products
- Surplus

Common materials that are available and wanted for exchange include categories such as:

- Acids
- Agricultural by-products
- Alkalis
- Ash and combustion by-products
- Chemicals
- Computers and electronics
- Construction and demolition debris
- Durables and furniture
- Glass
- Metals
- Miscellaneous
- Oils and waxes
- Paints and coatings
- Paper
- Plastics
- Refractory material
- Rubber
- Sand
- Services
- Shipping materials
- Solvents
- Textiles and leather
- Wood

Waste exchanges are used by a variety of organizations, including private sector waste generators, government agencies, solid waste district staff, recycling organizations, and material brokers. Materials exchange users can be anyone who handles surplus or unwanted materials, such as architects, administrative assistants, buyers, engineers, residents, consultants, custodians, environmental managers, government employees, procurement specialists, purchasing representatives, recycling brokers, shipping clerks, and storeroom managers.

Differences in the business models and processes for the waste commodity exchanges are also evident. Many of these exchanges serve as a meeting place for companies that would like to list materials and potential respondents, who then work out the details of payment, transportation, and storage themselves to facilitate exchanges. Some exchanges have an eBay-type Web posting system, whereas others produce printed periodicals. Some handle requests via the phone or fax; however, most utilize the Internet.

According to the EPA materials exchange, "Typically, the exchanges allow subscribers to post materials available or wanted on a Web page listing. Organizations interested in trading posted commodities then contact each other directly. As more and more individuals recognize the power of this unique tool, the number of Internet-accessible materials exchanges continues to grow, particularly in the area of national commodity-specific exchanges" [20].

Finally, the major difference among the exchanges dealt with the fee structures. Most exchanges are no cost, but some charge periodic membership fees or fees per transaction. Overall, waste exchanges have very minimal fees – just enough to cover the administrative costs. The American Plastics Exchange, for example, is the most expensive waste exchange, with a $360-per-year membership fee and $0 per exchange – still, a very cost-effective exchange. The typical per exchange fee, for those that did charge, was $5–$10 [20].

Success Stories

Waste exchanges have played an important role in assisting companies to identify and implement recycling and reuse opportunities. These efforts result in lower operating costs, reduced purchasing costs, reduced storage costs, enhanced corporate images, diminished demand for landfill space and incinerator capacity, and, ultimately, a cleaner environment.

"It is estimated that, by promoting the reuse and recycling of industrial materials through waste exchanges, the industry currently saves $27 million in raw material and disposal costs and the energy equivalent of more than 100,000 barrels of oil annually," as determined by the National Materials Exchange Network operating in Silver Spring, Maryland [21]. These savings often translate directly to the companies' bottom lines with stronger financial performance [21].

In 1998, its first year of operation, the Ohio Materials Exchange (Columbus, Ohio) exceeded initial expectations by exchanging over 2,600 US tons of waste and saving Ohio businesses $103,000 in disposable costs [22]. According to Dale Gallion, manager of quality assurance at Diamond Products (Elyria, Ohio), the company used to pay to have leftover metal powder scrapped [22]. After joining the waste exchange program, Diamond Products sold 8,000 pounds of metal powder for $14/pound. Additionally, the company accumulates about 1,000 pounds of metal powder each month and plans to continue using the exchange [22].

Another good example is the Massachusetts Materials Exchange [23]. "In the past 4 years, the Massachusetts Materials Exchange has moved over 2,000 US tons of materials, saving participants more than $100,000 in avoided disposal and purchasing costs" [23].

Waste exchanges are a cost-effective means of helping businesses save money, as well as helping to divert waste into usable raw materials. Advances in information technology over the past decade have served as a catalyst to promote the exchanges, and further allow exchanges to provide current information on both the materials available for use and the materials wanted, which helps business make better environmental and financial decisions [20].

These exchanges also play an important role in assisting waste generators in identifying and implementing recycling and reuse opportunities. For example, since the inception of the Ohio Materials Exchange, businesses using the service reported savings of over $13.5 million in disposal costs and diverted over 308,000 metric tons (340,000 US tons) from landfills [22]. These efforts result in lower operating costs and diminished demand for landfill space and burning capacity, which all lead to a cleaner environment. Natural resources are limited, and resources need to be conserved as much as possible [22]. The fewer raw materials used, the greater supply for future generations, and waste exchanges are helping achieve this goal.

Future Directions

The current trends within recycling collection and separation revolve around discovering more cost-effective methods and ways to enhance participation. Automated collection systems are gaining a great deal of popularity and will continue to proliferate as many organizations seek to reduce long-term costs.

Bibliography

Primary Literature

1. USEPA (2008) Municipal solid waste in the United States: 2007 facts and figures, EPA-350-R-08-101, Washington, DC
2. Fishbein B (1994) Germany, garbage, and the green dot: challenging the throwaway society. Inform Publishing, New York

3. Stessel R (1996) Recycling and resource recovery engineering: principles of waste processing. Springer, Berlin/Heidelberg/New York
4. Where it goes: aluminum recycling processes. SITA, UK, http://rethink.sita.co.uk/where-it-goes/aluminium/. Accessed 15 Nov 2010
5. Fix A (1997) Glass: reduce, reuse, recycle. Heinemann/Raintree, Chicago, IL
6. McKinney R (1994) Technology of paper recycling. Springer, Berlin
7. Goodship V (2008) Introduction to plastics recycling. Smithers Rapra Press, Akron, OH
8. USEPA (1988) Waste minimization assessment manual. Hazardous Waste Engineering Research Laboratory, Cincinnati
9. Petek J, Glavic P (1996) An integral approach to waste minimization in process industries. Resour Conserv Recycl 17: 169–188
10. Recycling collection systems, State of Connecticut, Department of Energy and Environmental Protection. http://www.ct.gov/dep/cwp/. Accessed 15 Nov 2010
11. Granger T (2007) Types of Curbside Recycling Programs. Earth911, http://earth911.com/recycling/curbside-recycling/. Accessed 31 Dec 2007
12. Curbside recycling, Earth911, http://earth911.com/recycling/curbside-recycling/. Accessed 20 Nov 2010
13. Wastes – resource conservation – conservation tools – pay-as-you-throw. The U.S. EPA, http://www.epa.gov/osw/conserve/tools/payt/. Accessed 20 Nov 2010
14. The U.S. EPA (2010) Wastes – resource conservation – common wastes & materials – paper recycling. http://www.epa.gov/osw/conserve/materials/paper/basics/grade.htm. Accessed 20 Nov 2010
15. The recycling process after collection what happens to materials when you recycle, The University of Oregon. http://pages.uoregon.edu/recycle/after_collection.html. Accessed 20 Nov 2010
16. Franchetti M (2009) Solid waste analysis and minimization. McGraw-Hill, New York
17. Franchetti M (2009) Case study: determination of the economic and operational feasibility of a material recovery facility for municipal recycling. Resour Conserv Recycl 52:535–543
18. (1994) A review of industrial waste exchanges. The U.S. EPA, solid waste and emergency response (5305), EPA-530-K-94-003
19. The U.S. EPA (2010) Recycling market development. www.epa.gov/epaoswer/non-hw/recycle/jtr/comm/exchange.htm. Accessed 20 Nov 2010
20. The U.S. EPA (2010) Waste and material exchange. www.epa.gov/epaoswer/non-hw/recycle/jtr/comm/exchange.htm. Accessed 20 Nov 2010
21. The National Material Exchange Network (2010) Waste exchange directory http://www.cftech.com/BrainBank/MANUFACTURING/WasteExchgs.html. Accessed 25 Nov 2010
22. The Ohio Material Exchange (2010) The Ohio material exchange: background. http://www.myomex.com/about.aspx. Accessed 25 Nov 2010
23. The Massachusetts Material Exchange (2010) Materials exchange: the benefits of recycling. http://www.materialsexchange.org/. Posted 13 Sept 2010

Books and Reviews

Avsar E, Demirer G (2008) Cleaner production opportunity assessment study in SEKA Balikesir pulp and paper mill. J Cleaner Prod 16(4):422–431

Beck RW (2004) Lycoming county material recovery facility evaluation. Pennsylvania Department of Environmental Protection, Final report

Berenyi EB (2002) 2001–2002 materials recycling and processing in the United States, 4th edn. Governmental Advisory Associates, Westport

Birgisdottir H (2006) Environmental assessment of solid waste systems and technologies: EASEWASTE. Waste Manage Res 24:3–15

Chang N, Wang SF (1995) The development of material recovery facilities in the United States: status and cost structure analysis. Resour Conserv Recycl 13:115–128

Covey SK (2000) Building partnerships – the Ohio materials exchange. Resour, Conserv Recycl 28(3):265–277

Covey SK (2000) Building partnerships – the Ohio materials exchange. Resources, Conserv Recycling. 28(3): 265–277

Davila E, Chang N (2005) Sustainable pattern analysis of a publicly owned material recovery facility in a fast-growing urban setting under uncertainty. J Environ Manage 75:337–351

De Alessi M, The dirty MRF. http://www.pacificresearch.org/pub/sab/. Accessed 20 Nov 2010

Diaz LF, Savage GM, Eggerth LL, Golueke CG (1993) Composting and recycling municipal solid waste. Lewis, Boca Raton

Dowie W, McCartney D, Tamm J (1998) A case study of an institutional solid waste environmental management system. J Environ Manage 53:137–146

enviro/05_enviroindex/25_toxics.html. Accessed 20 Nov 2010

EPA (1988) Waste minimization opportunity assessment manual. US Environmental Protection Agency, Cincinnati

Franchetti M (2008) One company's trash is another company's treasure: with the rising volumes of recyclable materials entering the waste stream, waste commodity exchanges have started receiving increased interest from companies looking trim their bottom line. Resource Recycling: N Am Recycling Compost J, Vol. 28, pp 40–42, February 2008

Franklin and Associates for the EPA (2000) Municipal solid waste generation, recycling, and disposal in the United States: 2000 facts and figures. June 2002

Haman W (2000) Total assessment audits (TAA) in Iowa. Resour Conserv Recycl 28:189–198

Harris E (2000) Cornell waste management institute update June 2000. Ithaca

Lui H (2003) Waste minimization at a nitrocellulose manufacturing facility. J Environ Studies 60:353–61

McCartney D (2003) Auditing non-hazardous wastes from golf course operations: moving from a waste to a sustainability framework. Resour Conserv Recycl 37:283–300

Mixed waste processing. NC division of pollution prevention and environmental assistance. http://www.p2pays.org/ref/01/00028.htm, Jan 1997. Accessed Feb 2006
Modern marvels: history of garbage (2004) Video produced by The History Channel
Ohio EPA (1997) Governor's pollution prevention award recipient: mahoning county's industrial waste minimization project. Fact Sheet #41
PEER Consultants and CalRecovery (1993) Material recovery facility design manual. CRC Press, Boca Raton
Petrell R, Duff S, Felder M (2001) A solid waste audit and directions at the University of British Columbia, Canada. Waste Manage Res 19:354–365
Rathje W, Murphy C (2001) Rubbish!: the archeology of garbage.
Rhyner CR, Schwartz LJ, Wenger RB, Kohrell MG (1995) Waste management and resource recovery. Lewis, Boca Raton
Ryding S (1994) International experiences of environmentally sound product development based on life cycle assessment. Swedish Waste Research Council, ARF Report 36, Stockholm, May 1994
Schianetz K, Kavanagh L, Lockington D (2007) Concepts and tools for comprehensive sustainability assessments for tourism destinations: a comprehensive review. J Sustain Tour 15:369–389
Shimberg SJ (1985) The hazardous and solid waste amendments of 1984: what congress did ... and why. The Environmental Forum. March 1985, pp 8–19
(2001) State solid waste management plan 2001. Ohio EPA – Division of Solid and Infectious Waste Management, Columbus
Strong DL (1997) Recycling in America, 2nd edn. ABC-CLIO, Santa Barbara
The Environmental Industries Associations Garbage then and now (2003) Washington, DC
The league of women voters (U. S.) Garbage primer (1993) Washington, DC
Tompkins JA, White JA, Bozer YA, Tanchoco JMA (2003) Facilities planning. Wiley, Hoboken
U.S. Department of Energy, Office of Energy Efficiency and Renewable Energy (2001) Industrial Assessment Center Brochure 2001. Washington, DC
U.S. Environmental Protection Agency (1990) The nation's hazardous waste management program at a crossroads. Report no. EPA/530-SW-90-069. EPA, Washington, July 1990, 114 p
U.S. Environmental Protection Agency (1998) Household hazardous waste management: a manual for one-day community collection programs. Washington, DC
United States Congress of Technology Assessment (US Congress OTA) (1992) Green products by design: choices for a cleaner environment. OTA-E-541. U.S. Government Printing Office, Washington, DC
United States Environmental Protection Agency (2003) Municipal solid waste generation, recycling, and disposal in the United States: facts and figures for 2003. United States Environmental Protection Agency, Washington, DC
United States Environmental Protection Agency (2006) Municipal solid waste – basic facts. http://www.epa.gov/epaoswer/non-hw/muncpl/facts.htm. Accessed Feb 2006
United States Environmental Protection Agency (2006) Decision maker's guide to solid waste management, volume II. http://www.epa.gov/epaoswer/non-hw/muncpl/dmg2.htm, 1995. Accessed Feb 2006
United States Environmental Protection Agency (2006) Full cost accounting for municipal solid waste management. http://www.epa.gov/epaoswer/non-hw/muncpl/fullcost/docs/fca-hanb.pdf. Accessed March 2006
US Department of Energy, Office of Energy Efficiency and Renewable Energy (2001) Industrial assessment center brochure. Washington, DC
US Environmental Protection Agency (2006) Full cost accounting for municipal solid waste management. US EPA, Washington, DC
Wang Q, Dong L, Xi B, Zhou B, Huang Q (2006) The current situation of solid waste management in China. J Mater Cycles Waste Manage 8:63–69

Recycling Technologies

Giuseppe Bonifazi, Silvia Serranti
Dipartimento di Ingegneria Chimica Materiali Ambiente Sapienza, Università di Roma Via Eudossiana, Rome, Italy

Article Outline

Glossary
Definition of the Subject and Its Importance
Introduction
Recycling and Materials to Recycle
Future Directions: Innovative Control/Sorting Devices/Logics Integration in Recycling Plants
Bibliography

Glossary

Ceramic glass Transparent ceramic products with an appearance similar to that of glass. They are characterized by an amorphous phase and one or more crystalline phases.

Classification Set of mechanical actions carried out in dry or wet conditions, designed to perform a "classification" of particles systems according to their morphometrical (e.g., size-shape) attributes.

Comminution Set of mechanical actions carried out to reduce waste materials in particles of suitable size and shape to be properly handled and processed in order to liberate/remove contaminants.

Cullet Particulate solid product resulting from collection-comminution of waste glass.

De-inking Mechanical process that removes "ink particles" and "stickies" from waste paper.

Ferrous metal Magnetic metals mainly composed of iron.

Flotation Mechanical process that selectively separates hydrophobic from hydrophilic materials. Hydrophobic materials are forced to adhere to bubbles and float.

Fluff Fine fractions resulting from automotive shredder residue (ASR). *Fluff* is constituted by materials characterized by intrinsic low specific gravity (e.g., plastics, rubber, synthetic foams, textiles, etc.).

Municipal solid waste (MSW) All non-hazardous waste resulting from the collection of household, commercial, and institutional waste materials.

Non-ferrous metal Metals that contain no iron (e.g., aluminum, copper, brass, bronze, etc.)

Separation Set of mechanical actions carried out in dry or wet conditions, designed to perform a "separation" of particles systems according to their physical attributes (e.g., density, surface properties, electrostatic properties, magnetic properties, color, etc.)

Sorting Waste particle separation, usually carried out with optical-electronic recognition devices and logics.

Definition of the Subject and Its Importance

Recycling technologies can be defined as the whole of procedures designed to set up physical-chemical actions, at an industrial scale, that perform the recovery of materials and end-use products resulting from the collection of household or industrial wastes. The materials to be recovered and recycled, obviously, influence both processing technologies and plant layouts. In this section an in-depth analysis of the problems arising when suitable recycling technologies must be designed, implemented, and set up is presented with particular reference to paper, glass, metals, plastics, and textiles (not organics or **C***onstruction* and **D***emolition* (C&D) waste). Recycling technologies must be approached from a processing perspective, that is, by defining a sequence of steps and actions where the waste flow stream feed, and the different products resulting from the different sequential processing steps, are handled in order to produce one or more outputs of materials to reuse. Obviously, processing strategies and equipment must be selected with both low environmental impact and positive economic perspectives in mind. Dealing with waste often means dealing with complex products, that is, products constituted of one or more materials of interest but also of polluting material. The economic value, per unit of weight, of the materials to recover is usually low: recycling technologies thus must assure high production, while minimizing plant investments and management costs. From this perspective, a full characterization of the input waste streams and complete control of the different phases of the recycling process are a key issue when recycling technologies are selected and applied. In this section, for each of the different materials, methodologies, procedures, and logics are presented to preliminarily identify and quantitatively assess recycling technologies according to the characteristics of the materials to be recovered.

Introduction

The concept of recycling is an intrinsic part of nature. The different forms of life, at the end of their life cycle, decompose in the soil and become "compost," which helps plants grow. Furthermore, the organic materials resulting from decomposition of vegetation are food for bacteria and fungi. Bacteria and fungi are a food for earthworms, and earthworms are food for ants, beetles, and so on. This recycling chain can be framed in the theory of conservation of mass, originally stated by Heraclitus (530–470 BCE) [1]:

- πάντα χωρεῖκαὶ οὐδὲν μένει: everything changes and nothing remains still

and after by Nasir ad-Din Tusi (1201–1274) [2]:

- a body of matter cannot disappear completely. It only changes its form, condition, composition, color and other properties and turns into a different complex or elementary matter

and finally clearly outlined and formalized by M. Lomonosov (1711–1765) and A. Lavoisier (1743–1794) [3]:

- the mass of a closed system (in the sense of a completely isolated system) will remain constant over time.

Recycling can thus be considered as something related to nature, and as consequence, to humans. Since the beginning of time people have needed to find a way to dispose of and/or to recycle waste. Obviously, technology influenced and continues to influence recycling strategies. In early pre-industrial times waste was mainly constituted of combustion residues, wood, bones, bodies, and vegetable waste. A simple recycling approach, mimicking what happens in nature, was to dispose of these wastes in the ground. Wastes thus became compost, helping to improve soil. Nearly 4,000 years ago there was a recovery and reuse system of bronze scrap in Europe. Composting is known to have been a part of life in China (2000 BCE). Ancient rubbish dumps excavated in archeological digs reveal only tiny amounts of ash, broken tools, and pottery. In Knossos (Crete, Greece), traces of landfill sites exist, dating from 3000 BCE, where waste was placed in large pits and covered with earth at various levels. The evolution of humans from nomadic hunter-gatherers to farmers increased waste production. Waste could no longer be left behind, and it soon became a growing problem.

The First World War, the Great Depression, and the Second World War each contributed to recycling. Recycling, in fact, was a necessity for many people to survive or for a nation to support the war effort. Nylon, rubber, and many metals began to be recycled during this period. The practice of recycling continued in many countries after the Second World War came to an end, especially those nations with a high dependence on resources, such as Japan. However, in other countries, with the post-war years' economic boom, consciousness about the importance of applying policies addressed to recycling and recovering materials and products at the end of their life cycle rapidly decreased. In the 1960s and 1970s, the importance of recycling returned with the Environmental Movement (e.g., the first celebration of Earth Day was in 1970), and a constant and continuous growth followed.

The mass production of the Industrial Age is the main cause of the past low level of consciousness about the importance of recycling: when products can be produced, and/or purchased, at low cost, at least if compared with the income, it often seems more economical to just throw away old items and purchase new ones. This "disposable goods" mentality and the corresponding problems of waste disposal have created environmental problems that today all countries face today when adopting recycling technologies.

What are the benefits related to a wider use of recycling technologies?

The first benefit is obviously related to the reduction of the environmental impact of human activities. The possibility of significantly decreasing the industrial use of non-renewable resources, such as primary raw materials and fossil fuels, by utilizing products resulting from recycling represents an important step forward toward environmental protection and energy savings; both aspects strongly contribute to a reduced exploitation of natural resources. The second benefit is the reduction of the environmental impact related to waste dumping. Less waste disposed of means less natural sites to select and manage for waste storage and less risk to the environment in terms of soil contamination and surface water and groundwater pollution. The third benefit is related to better design and manufacturing of products, from the simplest (e.g., paper, glass, metals, or plastic containers) to more complex ones (e.g., household appliances, cars, etc.) from the perspective of recycling (e.g., ease in dismantling) at the end of their life cycle.

What problems are to be faced in increasing the use of recycling technologies both quantitatively and qualitatively?

The lack of the public acceptance toward recycling and the subsequent low growth of the related **W***aste*-**D***erived*-**P***roduct***s** (WDPs) market are the main factors negatively affecting recycling in quantitative terms [4]. Such problems have progressively decreased thanks to (1) the definition of a clear traceability route of the WDPs, (2) the technical-economical improvement of recycling products, and (3) new legislation at the national and/or international level stimulating recycling and utilization of recycled products. In qualitative terms, an obstacle to wider "up-to-date" utilization of recycling technologies is related to

concerns about the application of innovative technologies inside existing recycling layouts. Today, a great amount of equipment (e.g., comminution, classification, and separation units), and related operative technologies, is easily available on the market. Sometimes, lack of knowledge of specific control tools, necessary for correct handling and control of the equipment, can affect final recycling plant layouts and overall quality of the plant itself in terms of capacity to adapt to new possible future market requirements. From this perspective, the utilization of equipment and inspection tools for waste products quality control are fundamental for a modern, efficient, and profitable recycling technologies implementation. Both equipment and control device systems must be selected and fully integrated according to: (1) waste feed attributes, (2) possible feed variation, and (3) required final products characteristics. These three aspects must always be taken into account in the definition and analysis of the recycling technologies utilized for all the materials described in this section.

For paper, glass, metals, plastic, and textiles, the above-mentioned aspects play a different role and assume a different importance. In paper recycling feed characteristics are relatively easy to control. Final product characteristics, that is, the quality of the recovered fibers, is preeminent. In glass recycling, the main problem is feed quality, especially for the recycling of glass collected from **M***unicipal* **S***olid* **W***aste* (MSW), where the presence of "ceramic glass" can strongly impact the further processing and final quality of recovered glass fragments. With metal recycling, the aim is to maximize the "correct" recovery of non-ferrous metal alloys. The achievement of this goal strongly influences the development of innovative sorting/detection logic in order to assure the requested final products' characteristics. In plastic recycling, both feed and final products influence the selection of the separation devices and strategies, as well as the sensing technologies required for quality assessment during the different processing stages. Finally, dealing with fiber recycling requires maximizing source material identification and its preliminary separation. Process and technologies are quite different for textiles and carpets; carpets are much more difficult to recycle than textiles. Here, we have briefly outlined the different problems that must be taken into account in the recycling and recovery of the most common waste materials. In the following, such procedures will be analyzed and the related processing/control devices and actions illustrated.

Recycling and Materials to Recycle

Recycling Technologies: Paper

Paper is usually made from raw material wood pulp and fiber. Vegetable fibers are mixed and "cooked" until the fibers are sufficiently softened, chemicals (e.g., lye) are added to enhance and accelerate softening. The pulp is then "screened" over a screening media. Water is dropped off and/or evaporated. The material is then pressed for further water removal in order to obtain the "paper sheet." The quality and arrangement of the fibers affects the overall quality of the final manufactured paper material [5]. With this in mind, recycling technologies applied to waste paper are primarily aimed at maximizing recovery of the fibers.

Paper production dates back to the ancient Egyptians (e.g., papyrus paper). Around 200 BCE Cai Lun, a Chinese court official, made paper from tree bark and old fish netting. Its production was considered as a remarkable secret and only 500 years later were the Japanese able to acquire the secret. Papermaking spread to the West when some Chinese paper makers were captured by Arabs after the defeat of the Tang troops in the Battle of Talas River (751 AD). The first European paper mill was built at Jativa (Valencia, Spain) around 1150. From that time to the fifteenth century, paper mills were located mainly in Italy, France, Germany, and England; by the end of sixteenth century they were located all over Europe. In 1719, Rene de Reaumur, a French scientist, observed wasps chewing slivers of wood and building their nest starting from such a fiber paste. The use of wood fibers for papermaking started from this observation.

One of the key points in papermaking is an appropriate handling of connected fibers. They can come from a number of sources including cloth rags and cellulose fibers from plants and trees. The use of cloth in the papermaking has always produced high-quality paper. The presence of cotton and linen fibers in the mix creates papers for special uses. From this perspective, cotton and linen rags can be profitably re-utilized for fine-grade papermaking (e.g., bank notes,

certificates, letterhead, resume paper, etc.). Rags are usually cuttings and wastes from textile and garment mills. Also, the paper itself can be profitably recycled. The constituting fibers can be reused five to seven times before they become too short and brittle. Many paper-based-products can be manufactured from recycled waste paper: fruit trays, corrugated cardboard, egg cartons, ceiling tiles, plasterboard, sound insulation panels, etc. Waste paper collection and recycling produces a number of positive environmental effects:

- Less timber is used for wood pulp production, which has a positive impact on biodiversity, that is preservation of valuable wildlife habitats and ecosystems, such as old-growth forests that are not replaced by managed plantations, very often constituted by allochthonous species, usually fast-growing conifers
- Waste disposal reduction
- Energy and water savings, as there is no need for pulping to turn wood into paper. Such a savings depends on paper grade, processing, mill operation, and proximity to a waste paper source and markets
- Considerable reduction of emissions into the air and water (no bleached is usually required in recycled paper)
- Lower greenhouse gas production; the larger the amount of waste paper re-used, the lower the emissions will be

The main problems faced in waste paper recycling are as follows:

- Collection criteria addressed to simplify waste paper handling and further processing
- Identification of polluting elements and suitable processing strategies in place to remove them
- Quantity and the quality of pollutants (e.g., effluents) discharged to water

Waste Paper Characteristics Waste paper mainly originates from pre-sorting and collection of consumer waste and/or industrial waste. The following attention will be primarily addresses consumer waste, which is mainly constituted by:

- Newspapers, magazines, telephone directories, and pamphlets
- Cardboard
- Mixed or colored paper
- White office paper
- Computer printout paper

Waste paper is usually subjected to sorting according to its origin and characteristics. Such characteristics have been quantified at in Europe with the definition of the European List of Standard Grades of Recovered Paper and Board [6]. Waste graded papers are then pressed and handled as bales. Bales can be thus assumed as the secondary raw materials fed to waste paper recycling plants.

Different waste paper processing strategies will be thus adopted according to the presence of contaminants, to collected paper grade, and to their final re-use. Waste papers contaminants are usually constituted by:

- Materials and/or products not directly utilized in paper manufacturing, such as metals (e.g., nuts, screws, foil, cans), plastics (e.g., films, bags, envelopes), cloth, yard waste, leather, and dirt;
- Materials and/or products directly utilized in paper manufacturing, such as:
  - Inks and toners.
  - "Stickies" (e.g., adhesives, coatings, pitch, resins, etc.): these tend to deposit inside paper manufacturing equipments (e.g., wires, press felts, dryer fabrics, calendar rolls, etc.) causing problems, mainly machine down-time. Furthermore, they are difficult to remove due to their neutral density and resulting particles flow characteristics.
  - Coatings: these are usually constituted by inorganic fillers (e.g., $CaCO_3$, TiO_2, clay, etc.) and polymeric binders. Fillers have to be removed from the pulp and lower the overall yield of the recycling process. The presence of wax-treated papers (e.g., cardboard) negatively affects recycled paper quality in terms of weak and slippery properties. Furthermore, wax tends to deposit on equipment.
  - Fillers (e.g., $CaCO_3$, TiO_2, clay, etc.): their removal is compulsory when specific paper product, as tissue paper, have to be produced.
  - Papermaking additives (e.g., starch, gums, dyes, etc.): among the most difficult to handle are dyes. Their incorrect removal can affect recycled

paper new coloring. In some cases, wet strength additives can prejudice the further waste paper re-use.

As a result, waste paper characterized by high quality grades (e.g., paper-mill production scrap and office waste) requires simpler processing and can be profitably applied as a primary paper pulp substitute in applications such as paper printing and tissues. Waste paper of intermediate grades (e.g., newspapers) must be subjected to a stronger processing, mainly for de-inking, and can be used again by the newspaper industry. Finally, waste paper of lower grade is utilized for packaging and board.

Waste Paper Recycling Technologies In waste paper recycling the selection and the sequence of the processing units is strongly influenced, as previously outlined, by the characteristics of the waste paper (e.g., grade) and the presence and typologies of contaminants [7]. The latter influence the process, not only by their composition, but also by their chemical-physical attributes (e.g., size, shape, density, surface properties, solubility, strength, etc.). In the following, the main units, related actions, and/or potential problems are reported and described with reference to waste paper processing:

- Re-pulping, "to pulp" waste paper
- Screening, for fine contaminant removal
- Cleaning, for contaminant removal
- De-inking
- Water and solid waste treatment

Re-pulping The re-pulping operation is the first and one of the most important processing stages in paper recycling. Correct re-pulping is a pre-requirement for efficient downstream operations (e.g., cleaning, screening, flotation, etc.). Incorrect re-pulping can damage fibers, preventing their "correct" re-use [8]. A re-pulper is thus a device that converts recovered paper into a slurry of well-separated fibers and other waste paper components by performing mechanical, chemical, and thermal actions [9]. In order to fulfill this goal, a re-pulper has to satisfy specific conditions, that is:

- Contaminant detachment from fibers, without performing comminution (the larger the contaminant, the easier its removal)
- Correct mixing between waste paper, H_2O, and chemicals to liberate fibers, limiting at the same time their cutting
- Contribution to large debris removal

Re-pulping can be carried out in batch or continuous conditions. In batch conditions waste paper, H_2O, and chemicals are all charged at the beginning of the process and are removed, all at once, at the end of the process, then the process starts again. In continuous conditions waste paper, H_2O, and chemicals are continuously added to the pulper, as the pulped product is continuously removed.

Screening Screening is usually performed by forcing the pulp to pass through a sieve. The sieving surface is characterized by holes and slots of different sizes and shapes. The main goal of this phase is removing contaminants (e.g., bits of plastic, glue globs, etc.) and at the same time to realize a first separation of "short" fibers. Screening performances are influenced by many variables, the most important being:

- Feed pulp characteristics: fiber size and shape, quantity and quality of debris
- Screening device characteristics and operative conditions: screen surface (e.g., flat or cylindrical), screen hole size and shape, screen surface cleaning mechanism, fed pulp flow rate, solid-water ratio, stock temperature, etc.

Cleaning Cleaning is mainly applied to remove heavy contaminants. Separation is usually based on centrifugal forces, frequently using hydrocyclones. These devices are constituted by a cone-shaped (e.g., tapered) cylinder. Pulp is fed under pressure to the device, the rotational movement produces, inside the hydrocyclone, two vortexes create the separation: heavier particles are thus recovered in the bottom part and the lighter ones in the upper part. During this stage, metals, inks, sand, and dirt, are usually removed. The cleaning stage is influenced by many variables, including:

- Fiber and contaminant characteristics (e.g., size, shape, density, and quantity);
- Selected device architecture and setting: cylinder/cone size, inlet and/or outlet geometrical

characteristics, vortex finder diameter and length, cylindrical section height, cone angle, feeding pressure, pulp dilution, etc.

Deinking Pulp deinking removes printing ink and "stickies" (sticky materials like glue residue and adhesives). Deinking is usually performed in two steps: (1) washing and (2) flotation. Small particles of ink are thus preliminarily rinsed from the pulp with water by washing, then large particles and "stickies" are removed with the help of chemicals and air bubbles by flotation.

Froth flotation technology has been developed and used for many decades in the mineral processing industry before the technology was adopted by the pulp and paper industry for the deinking of waste papers at the beginning of the 1960s [10]. A flotation process is based on the surface properties of particulate solids systems when suspended in a fluid. Particles according to their, natural or caused, hydrophobic or hydrophilic characteristic tend to adhere to bubbles and float. During flotation deinking, pulp is thus fed to one, or to a bank of, flotation cells, where air (e.g., bubbles) and chemicals (e.g., surfactants) are also present. The surfactants cause flotation of the ink and sticky materials. Air bubbles carry the ink particles to the top of the cell/s, where the foam is continuously removed, realizing the required pulp deinking.

The most significant differences between deinking flotation and mineral flotation are specifically linked to the particular characteristics of waste paper pulp suspensions [10], that is:

- The large size class distribution and shape of the particles to float (e.g., ink particles), as well as their surface properties. Ink particles, in fact, can vary from about 1 μm–1 mm, they are generally hydrophobic, except for water-based inks. Large particles are usually flat shaped, and other techniques, as previously outlined, such as screening, with slots down to 0.1 mm and centrifugal cleaning, are also used to remove the various impurities of waste paper pulp suspensions (e.g., pressure sensitive adhesives, hot melt glues, plastic films, etc.)
- The low density of the particles to be removed from the deinking pulp: polymeric particles with specific gravity close to that of the water. Mineral particles (e.g., fillers, kaolin, and $CaCO_3$, utilized for paper coating), in the size range of about 1 mm, should generally not be removed
- The presence of flocs or networks (e.g., cellulose fibers typically of 1–3 mm in length and 10–30 μm in diameter according to wood essences originally utilized) that tend to flocculate up to constitute about 1% of the volume, in the separation zone of deinking cells, as the turbulence level is decreased
- The need to add chemicals to the re-pulped waste papers, both to realize a better release of the ink particles from the fibers, at the same time enhancing the flotation process (e.g., calcium soap and caustic soda or other deinking chemicals to be used under alkaline or neutral conditions) and the various chemicals introduced with the waste papers (e.g., surfactants used in the coating color)

After flotation, if necessary, pulp is further beaten, or "refined," in order to separate, as much as possible, fibers, avoiding fibers bundles. When white recycled paper is required, pulp is bleached with hydrogen peroxide or chlorine dioxide.

Water and Solid Waste Treatment Production of both virgin and recycled paper gives rise to pollutants that are discharged to water (e.g., effluents). Studies providing comprehensive comparative evaluation of the environmental impact linked to the effluents generated from recycling plants and those from paper mills demonstrated the environmental impact of the former is lower than that of the latter. In any case, environmental problems related to paper waste recycling are, with reference to the other recycling technologies, further described in this chapter, those presenting a higher impact [7]. The different waste paper processing stages, and related utilized technologies, are, in fact, always carried out in wet conditions and with a large quantities of water and chemicals.

Water. Four key parameters have to be fully monitored in the waste water resulting from waste paper processing: total suspended solids (TSS), biological oxygen demand (BOD), chemical oxygen demand (COD), and chlorinated organic compounds (AOX). De-inking is the main cause of TSS and BOD, and sometimes these parameters are comparable with the same produced processing virgin pulp. On the other

hand, COD and AOX are always lower in effluents resulting from waste paper processing. Waste water must be properly processed before it can be re-utilized or before release in the environment. The significant decrease, in recent years, of Cu, Cr, Pb, Ni, and Cd in printing inks dramatically contributed to reduce heavy metal presence in waste water, sludge, and final recycled-paper-based-products.

Solid wastes. The sludge resulting from waste paper processing contains a solid fraction ranging between 30% and 50%. It is mainly constituted by short fibers, fillers, and ink from the de-inking process. Their relative proportion depends on waste paper source characteristics and processing strategies applied to obtain a final product of the required characteristics. Usually the wastes are sent to dumps. In recent years, different attempts have been made to further process and/or re-use them: composting [11], and removal of clay [12] and other fillers [7] for re-use or their utilization for energy production [13].

Emissions to air. Direct emissions from the process of making recycled paper itself are minimal and considered to be relatively insignificant, although little research has been done in this field. Gaseous and particulate emissions to air are produced when the thermal utilization of sludge generated by the pulp and paper-making processes is carried out. Combustion presents many advantages [13], including reduction of the disposed solid mass and volume leading to lower disposal costs, destruction or reduction of the organic matter present in the sludge, and energy recovery. Critical points related to the adoption of this solution are:

- The **L***ow* **H***eating* **V***alue* (LHV) characterizing wet sludge, requiring preliminary dewatering and/or drying treatments to bring solids content above 30–35% in order to enable a self-sustained combustion and
- The presence of potentially hazardous elements (e.g., sulfur, chlorine, cadmium, and fluorine), that requires a complete gas cleaning

At the end of all the above-described processing stages recycled pulp fiber finally enters the machine for manufacturing recycled paper sheets. Waste-paper-recovered-fibers can be used alone, or blended with virgin ones to achieve better strength, or smoothness, of the final paper product.

Recycling Technologies: Glass

Glass is made of three relatively simple raw materials, silica sand, limestone, and sodium carbonate, which are melted together at high temperatures (about 1,500°C). Additives can be included to modify some properties, such as color, refractive index, durability, etc. [14].

Examples of glass manufactured goods can be found from several thousand years BCE, when such material was used for ornaments. In the Renaissance period, glass use increased. Vessels, bottles, and other glass containers started to be produced and utilized for both decorative and everyday use. At that time glass manufactured goods were expensive to produce. Large-scale production started with the Industrial Revolution and mass production of glass containers began at the onset of the twentieth century. Together with the increase in production and larger use came the problem of handling glass waste. Glass manufacturers produce a large quantity of products of different characteristics that are addressed to different uses. Glass's physical properties, at high temperature, are close to that of a viscous fluid, and as a consequence it can be worked, by craftsmen or on an industrial scale, to obtain final products of practically nearly infinite number of shapes and characteristics. For this reason glass can be found in, according to its composition and use, several products, ranging from those commonly used at home (e.g., bottles, vases, jars, mirrors, etc.), to those utilized in the automotive sectors (e.g., windscreen) and in industry (e.g., fiberglass for the production of G*lass* R*einforced* P*lastics* (GRP), G*lass* R*einforced* C*ement* (GRC), special thermal and/or acoustic insulating panels, X-Ray and cathode tubes, etc.). It is thus easy to understand that waste glass production, and its recycling to produce mainly "new" glass containers, assumes great importance.

Glass is one of the materials that is most often recycled. It presents a series of positive characteristics: it is non-absorbent and does not confer flavors and odors; it resists high temperatures, such as those required for cleaning after its use; its strength and mechanical resistance are indispensable for multiple fillings and reuse. These characteristics make glass containers suitable to be used over and over again. Selective waste glass collection and recycling provide great benefits:

- Reduction of environmental impact related to its disposal

- Conservation of the non- renewable raw materials (quartz sands) required for its production
- Energy savings
- Reduction in the quantity of solid urban waste

The problems to face in glass recycling can be summarized as follows:

- The definition of collecting criteria able to simplify the further processing
- The identification of polluting materials and the set up of suitable processing strategies to remove them
- The separation of "broken glasses" (*cullet*) according to their color

Recycled glass mainly comes from the selective collection of solid urban waste (bottles, jars, various containers, etc.), usually done by citizens, and only partially from the refuse of glass goods manufacturing and/or glass-based products at the end of their life-cycle. As a consequence, waste glass collection represents one of the most critical steps of the entire recycling process, and the following recycling technologies and separation strategies are strongly conditioned by the criteria and the methods followed during collection. The quality of the collected materials can be quite different, according to the level of knowledge and, more generally, the "education" of the people involved. As a matter of fact, the quality of the glass collected for recycling can strongly differ from region to region or, in the same city, from district to district.

The following discussion is based on urban waste collection as the source of the glass. It is important to consider the final destination of the recycled glass, which can be identified by the classical market categories where glass in commonly utilized, that is: (1) container production, (2) construction industry, (3) special concrete production (e.g., partial substitution of aggregates by glasses), (4) road pavement (e.g., special asphalt where the coarse fraction is partially substituted by glass), (5) abrasive products, (6) wool glass, etc.

The recycling technologies described for glass recycling will be primarily addressed to producing an economically valuable *cullet* to use to make new containers. Recycled glass is not equally re-utilized in all the above-mentioned market sectors. Only a small fraction is, in fact, re-utilized in fiberglass, bricks, concrete, and asphalt production. This is mainly for two reasons: (1) *cullet* quality sometimes does not fit well with the quality standards required in some of the these sectors and (2) the glass container industry is the most interested in waste glass reuse (due to the high cost of primary raw materials versus the relatively lost cost of each single glass container).

Cullet characteristics must satisfy strict conditions to be re-utilized for container production. These characteristics are primarily related to both presence of polluting elements and color of the fragments. Furthermore cullet size class distribution is another important parameter to control. Usually particles around 1 or 2 cm are preferred both for handling and quality control purposes.

Contaminant removal and *cullet* color sorting are the main goals when recycling glass. Furthermore, such goals must be reached using a process that does not produce too fine particles. As a consequence recycling technologies must be designed to fulfill these goals.

***Cullet* Contaminants Definition** There are two classes of contaminants: materials not constituted by glass (e.g., ceramics, stones, masonry, organics, and heavy metals) and glass fragments of the wrong color, that is *cullets* whose color characteristics are different from that of the class they belong to (cross-contamination).

Non-glass materials. Ceramics and stones, which have melting points higher than that of the glass, remain un-melted inside the vitrified matter and as a consequence, even if present in a small amounts, degrade the mechanical characteristics (resistance) of the manufactured products (bottles, jars, etc.). Furthermore, they can seriously damage glass processing equipment, increasing maintenance costs. Lead and heavy metals, according to their high volume weight, settling on the bottom of the fusion crucibles and have a corrosive effect on the refractory material, causing, in some conditions, the perforation of the refractory material itself. Optical sorting devices are commonly used to identify and automatically remove *non-glass materials*. Among polluting materials special attention has been addressed, in recent years, to ceramic glass. This material rapidly increased its presence in waste glass products, mainly due to the introduction on the market of a large amount of ceramic glass manufactured goods, such as dishware,

cookware, etc. [15]. Such material, even if seems quite similar to classic glass, is characterized by a different behavior (i.e., higher fusion point) when melted inside glass furnaces, where cullets are usually fed together with natural raw materials (quartz sands) [16]. As a consequence, the presence of ceramic glass reduces the production rates of the furnace, which needs to be shut down to be cleaned more frequently, and sometimes causes damage that requires the furnace to be rebuilt or replaced. Classical optical sorting devices are practically "blind" to ceramic glass, as its physical-chemical characteristics are similar to those of glasses.

Cullet cross-contamination by color. Glass has, according to its color, a different destination of use and, as a consequence, different market value. The use affects the value of the glass containers; as a consequence, white glasses have higher value than the so-called half-white or colored glass (brown, yellow, green). *Cullet*s, that are collected without distinction of color can be primarily used for the production of green glass and only in part for the production of yellow glass. The production of white glass requires that only *cullet* of that color be employed. Cross-contamination can thus represent a problem because it always contributes to depreciate the *cullet's* value. For this reason *cullet* optical sorting by color is extensively utilized.

***Cullet* Recycling Technologies** On the basis of the previously mentioned washing goals, specific processing layouts have to be defined. Each of them will be constituted by one or more units, in series and/or in parallel, and each one specialized to perform a specific action. In the following the main units, and related actions, are reported and described with reference to waste glass fragments (*cullet*) processing:

- Hoppers and conveyor belts, to perform *cullet* handling
- Manual sorting of macro-contaminants (e.g., ceramics, metals, plastics, stones, etc.)
- Crushing and screening, to reduce glass fragments in two or three size fractions, avoiding the production of fines, for a better handling of the glass waste, and to perform, in some cases, also a separation of contaminants
- Ferrous and non-ferrous metals separation, respectively, by electro-magnets and eddy-current separators, for metals and non-metals not manually sorted
- Light contaminant (e.g., paper and plastic) removal
- *Cullet* fine contaminants and color sorting by magnetic and/or optical devices, to define different *cullet* quality classes according to market specifications

Hoppers and Conveyor Belts Storage-feeding and conveying equipment constitutes the skeleton of the plant providing glass waste transportation for the action performed. Conveyors thus assume an important role because they have to operate continuously to assure a constant feed to the different units of the recycling plant. *Cullets* are strongly abrasive, so conveying, and related mechanical devices, are subject to strong abrasive actions. Furthermore, *cullet* handling produces fine particles and dusts. These aspects, if not fully controlled (e.g., sealed bearings, enclosed gear boxes and other moving parts protection, suction units for dusts collection) can produce severe damage to conveying units, as well as severe environmental working conditions in the plant. Table 1 are details some of the characteristics that a conveyor belt has to satisfy to be correctly utilized inside a glass recycling plant.

Manual Sorting of Macro-Contaminants Human-based sorting continues to be commonly applied on the coarser fraction. Manual sorting allows removing the larger pieces of contaminants, easily detectable and removable by trained personnel. Today, this phase is often performed by automatic sorting equipment, utilizing different principles, mainly optical, for contaminant detection. Among macro-contaminants, in recent years, ceramic glass has become a problem. As its machine-based identification is difficult, manual sorting continues to be utilized to perform its removal.

Crushing Waste glass comminution, usually performed by crushing equipment, is carried out to reduce the collected waste glass materials to particles of suitable size and shape in order to be properly handled and processed to remove contaminants and to separate glass into suitable classes of colors to produce new containers or other products. After crushing a sieving stage is usually carried out. *Cullet*s are thus "sorted" according to their size.

Recycling Technologies. Table 1 Conveyor belt design principles and/or maintenance good practices with reference to waste glasses handling

Cleats	Conveyors without cleats are preferred, because they can represent an obstacle to conveyor surface cleaning by scrapper bar. Their presence is negative if moisture is present.
Bearings	Bearings and other revolving parts (e.g., pulleys) have to be regularly cleaned or, better, should be sealed.
Drivers	Drivers should be selected in order to assure flexibility according to end markets variability.
Surface	Belt constituting materials have to be selected taking into account cullets' abrasive characteristics and related wear effects. Rubber belt are the most commonly utilized but wearing effects are severe, for this reason vibratory conveyors are more and more utilized. They are less subject to wearing but can represent a further source of pollution (e.g., presence of fine metallic parts in the final cullet concentrate).
Moisture and/or organic residues	Moisture can severely affect *cullet* handling, especially with reference to sorting operations.

Glass, different from aggregates, when subjected to comminution (e.g., crushing) tends to produce, for its chemical-physical characteristics, a lot of fines (pieces smaller than 1–2 mm); such a behavior increases if comminution equipment is not properly selected, that is, if the comminution unit and its operative conditions do not take into account glass mechanical characteristics. A comminution unit usually develops its action through the application of four forces on the materials: impact, shear, abrasion, and compression. The quantitative relationships among them, in terms of cause-effect, strongly differ according to the equipment. For glass comminution, impact forces are those to be primarily applied, allowing a low production of fines. The production of fines causes several problems: (1) loss of product (e.g., recycled glass fragments below 2–3 mm are usually rejected from the market), (2) a double loss of money (e.g., unsold material and rejected fines have to be disposed of), and (3) higher costs for comminution equipment maintenance. Glass fines are extremely abrasive; they can enter the gears and bearings of traditional comminution equipment and cause serious damage. Furthermore, the presence of fines produces the same mechanical problems in the other equipment constituting the processing layout. When selecting a comminution unit it is thus important to evaluate not only the capacity, but also the degree of flexibility characterizing the crusher, that is, the ability to vary power and speed. These two parameters can be modified according to changes in required crushed glass characteristics in respect of the initial feed and possible requirements of the end market. Table 2 describes some of the impact crushing equipment most commonly used to perform waste glass comminution.

Screening and Air Classification Screening and air classification are usually performed for two purposes: (1) particle size control and (2) contamination removal. The proper use of screening and air classification is to cut *cullets* into particles belonging to different size class ranges. Such a division can be performed both to facilitate *cullets*' further processing and to obtain final marketable products characterized by a population of specific and well-defined particle size. Screens and air classifiers can be profitably utilized as "separators" when polluting elements (e.g., wood, paper, iron, steel, aluminum, plastics, etc.) are characterized by a size and/or a shape different from the cullet population to classify. In this case, the setting of a "threshold," for the geometrical attributes, allows separating pollutants from glass. Furthermore, when air classifiers are used, the different densities of the polluting materials, compared to those of glass, represent an important factor in performing an improper "air classifier based separation." In both cases, moisture is a restricting factor for both classification and separation efficiency.

In the selection of screening and/or air classification devices some important factors have to be taken into account: (1) particle size distribution of the feed, (2) particle size distribution after the different classification stages, and (3) market tolerance, that is,

Recycling Technologies. Table 2 Characteristics of the comminution units mainly utilized to perform waste glass crushing

Comminution units	Characteristics
Hammer Mills (HM)	Movable hammers mounted on a rotating shaft hit and/or throw glass against mill chamber or other glass. As a result comminution is realized. Cullets are recycled inside the hammer until they do not reach a size lower than the aperture of a grid installed at the exit of the mill chamber. Comminution is efficient, that is, a relatively small size glass grain can be achieved in just one comminution stage. The wear rate of the hammer is high.
Rotating Drums (RD)	A spinning rotor with bars attached to the outside is responsible for the comminution. Glass particles breakage is mainly due to: (1) the impact of the rotating bars on glass and (2) the glass projection against "special plates" installed on the inside the chamber. Crushed material is finally discharged when particles size is lower than the space, adjustable, between the rotating bar and the plates. The wear rate is lower in comparison to hammer mills.
Vertical Shaft Impactor (VSI)	Crushing is performed by a revolving vertical rotor. The material is fed from the top. The mechanical actions resulting for the interaction of the revolving rotor with the glass and with the chamber walls produce the requested glass size reduction. A screening system, in a closed loop with the impactor, allows obtaining the desired *cullet* size. VSI allows obtaining large productions, but a pre-broken feedstock, usually obtained utilizing as primary crusher an HM, is required. The wear rate is minimized; the resulting *cullets* are round shaped.
Impact Crusher (IC)	IC utilizes a continuous breaker bar which is mounted horizontally in the rotor. Glass is fed and blown against *adjustable* aprons. Replaceable liners are installed inside unit. The broken product passes through an open discharge. As for VSI, IC allows to efficiently handle a large volume of throughput of product below 10 mm. *Cullets*, according to IC comminution actions, are characterized by an angular or sub-angular shape.

precision required with respect to end-user tolerance versus possible presence of under-/over-size in the final classified product. Table 3 describes some of the screening and air classification devices commonly utilized in the waste glass recycling sector.

Ferrous and Non-ferrous Metal Separation Ferrous (e.g., metals containing iron) and non-ferrous metals (e.g., aluminum, copper, lead, zinc, tin) are among the most common contaminants in waste glass. Their origin can be related to the presence of caps, lids, special labels, bottle neck wrap, etc. The presence of these materials even at low level can produce severe damage to the production process (e.g., deposits and chemical reactions in the furnaces, presence of hot spots, clogging or jamming of the injection devices, etc.) and can compromise the final product (container) mechanical characteristics and quality.

Ferrous contaminants are easily removed by magnetic separation. Usually magnetic separation is performed in two stages. A first stage, at the beginning of the recycling process, in order to remove ferrous contaminant before the further processing stages (comminution, classification, sorting by color, etc.) and a later stage, where usually it is applied to remove the finer particles of metals not separated during the previous processing stages. The selection of a magnetic separator is strongly influenced by: (1) waste feed rate, (2) amount of ferrous contaminants, (3) *cullet* stream depth, (4) contaminants size, and (5) value of the magnetic field to apply to perform separation. Non-ferrous metal contaminants are not affected by the presence of a magnetic field; for this reason eddy current separators are usually utilized for their collection [17] [18]. Eddy current separation devices and related separation strategies are strongly influenced by non-ferrous metal particles size, shape, and conductivity. In this latter case, different from magnetic separation, particles' attributes play a preeminent role. Table 4 details the equipment commonly utilized to perform ferrous and non-ferrous metal separation.

Light Contaminants Removal Light contaminants such as plastic, paper, wood, corks, etc. do not

Recycling Technologies. Table 3 Characteristics of the classification units mainly utilized in the waste glass recycling sector

Classification units	Characteristics
Tro*mmels* (TRO)	A TRO is a rotating cylinder whose surface is characterized by apertures of a specific size and shape where *cullets* can pass through according to their size. For its characteristics TRO can play both as a classifier and a separation unit. Contaminants as plastic bottles or bags are not able to pass through trommel surface apertures and can thus be easily removed. A trommel can be designed to fit practically any size glass processing operation. In some cases hot air is blown to facilitate waste glass feed drying, helping the screening and the following processing stages.
V*ibratory S*creens (VS)	VS usually work in a closed loop with crushing unit. As for TRO *cullets* can pass through, or not, the sieving surface, according to their size, usually larger particles are fed again (closed loop) to the comminution unit (crusher) or rejected if recognized as pollutants. According to the requested *cullets* size class characteristics, vibratory screens can allow to classify particles population up to – 75 μm. When such dimensional grades are requested obviously throughputs are lower. Usually multi-deck VS, up to five, are utilized when the final *cullet* product has to be divided in several dimensional classes.
A*ir C*lassifiers (AC)	These types of classifiers are based on the utilization of air flow to classify particles. Different from sieving, particles are thus classified/separated according to their size, shape, and density. An AC is a vessel where an air flow is generated. Wastes are usually fed from the top, coarse (larger or heavier) and fine (smaller or light) particles follow a different path according to flow characteristics, that can be set to achieve the required classification/separation. Classification/separation can be achieved simply utilizing gravity or/and free or forced vortex generated by static vanes or a dynamic classifier wheel. The equilibrium between the forces determines the "cut point." ACs represent a good alternative to screening, especially when the materials to classify are characterized by the presence of large fraction of fines (particles below 250 μm). When a well classified coarse fraction is requested, air classifiers are utilized prior to screening.

constitute, at least in principle, a problem in glass recycling. They burn and volatize at the temperatures of the glass furnaces. Today, new applications requiring granular products are sensitive even to the presence of small amounts of "organics"; for this reason the recycling processes have to take into account the removal of these kinds of contaminants. Such a goal is easily reached by simple screening or by air-screening, that is creating a sort of fluidized bed where heavier particles, *cullet*, remain on the site and lighter or finer particles can be easily removed by air flow.

Fine Contaminants and Color Originally *cullet* optical sorting was performed following an optical-based analogical approach. It was developed and implemented to perform control-separation actions:

- To remove all contaminants not removed in the previous physical processing stages (e.g., venting, classification, eddy current separation, magnetic separation, etc.)
- To perform a separation of *cullet* by color

Normally, ceramics, stones, and opaque particles are sorted before color sorting is applied. In recent years, the increasing presence, inside waste glass, of ceramic glass, which is almost impossible to separate via classical recycling technologies, has resulted in research related to optical sorting to solve this problem with a new class of devices based on X-rays and/or H*yperS*pectral I*maging* (HSI) technology.

Sorting was originally performed manually. Such an approach is labor-intensive. Being based on human senses it is strongly affected by human sorter experience, by the size of the materials to sort, and by time: the level of attention of the worker is strongly affected by time. With technological developments, *cullet* sorting was, and in some cases continues to be, adopted as detection unit, laser beam technology based devices, and scan line cameras. Table 5 describes the devices, and related architectures, commonly utilized to perform *cullets* sorting.

Sorting device characteristics. These are related to the optic detector/s size and arrangement. The final

Recycling Technologies. Table 4 Characteristics of the separation units commonly utilized to perform ferrous and non ferrous contaminants separation in the waste glass recycling sector

Separation units	Characteristics
Overhead/Cross Belt Magnets (O/CBM)	The magnet is usually installed above the glass waste flow stream (e.g., conveyor belt). The overhead magnetic field has a belt moving across its surface at approximately a 90° angle to the materials flow. Metals particles are thus attracted, removed from cullets and discharged as the moving belt of the separator turns away from the magnetic field the metals particles. Sometimes, especially when O/CBM strategy is applied to control the possible presence of ferrous particles in the final product, "simple" high intensity magnets are utilized. Collected particles are thus discontinuously removed.
Magnetic Head Pulleys (MHP)	MHP is usually installed at the end of a conveyor belt, beneath the belt. Ferrous particles are thus held to the belt while cullets can be discharged. With the decrease of the magnetic field ferrous particles leave the belt and can be properly recovered.
Magnetic Drums (MD)	MD commonly installed inside feeder chutes, between chutes and conveyors. Their behavior is similar to MHP. Glass waste stream passes over the magnetic drum, ferrous metals are held by the drum, as non-magnetic materials continue their flow. Ferrous materials hold to the drum until a divider provides to its discharge.
Eddy Currents Separators (ECS)	ECS is realized by spinning a magnetic rotor with alternating polarity at high speed. The magnetic drum of the ECS induces electric currents (eddy currents) within the volume of each particle flowing in the proximity of the drum. The effect is that non-ferrous metals passing over the drum are subjected to an ejecting force that throws away non-ferrous metals pollutants from the waste glass stream. The main difference from ordinary magnetic separation is that the magnetization of particles is not induced by the alignment of the internal magnetic domain with the external field. The efficiency of the eddy current separation process is highly dependent on the size of the feed particles.

sensing architectures, in fact, are influenced by optical information acquisition and its further handling: both factors dramatically influence the sorting architectures, usually based on a pneumatic blast, enabling the modification of the *cullet's*, and/or polluting particle's, trajectory, after recognition. Furthermore, flow characteristics can influence the selection. To realize an optical sorting (Table 5), the flow has to be, at least in principle, constituted by particles forming a mono-layer (e.g., *cullet* fed to the color-sorting unit by a vibrating conveyor belt, which keeps the glass in a thin layer). In these conditions glass fragments can be analyzed by the laser beams. Recent equipments are so fast that they can test, according to its dimension, the same cullet several times. As a consequence the larger the glass fragment, the better its control can be carried out. The influence of the "anomalies" can be thus reduced when each cullet is analyzed by more than one detector and more than one time. This is not possible with smaller pieces: they can pass, for their dimension and for the flowing conditions, unsorted, or diffraction/refraction effects (e.g., presence of marked cleavage or surface anomalies) can be so strong that detectors are practically unable to analyze them. As a consequence, such a technique cannot be profitably used with the entire size range of cullets. Materials of smaller dimensions, less than 2 mm, resulting from the processing-cleaning stages, not being correctly investigated, are usually disposed of, with the resulting financial loss and negative environmental impact. For this reason, in recent years, a new class of sorting devices based on imaging has been developed and implemented (Table 5). Imaging allows breaking down the investigation limits, with detection resolution linked to array detector resolution and optics magnification. Obviously the geometrical constraints, linked to the presence of the pneumatic devices, for particle removal remain; however, the imaging approach constitutes a big step forward allowing: (1) a better detection and (2) the potential to perform *on-line* certification of products.

Recycling Technologies. Table 5 Characteristics of the detectors, and related logics, commonly utilized to perform *cullet* sorting

Sorting units	Characteristics
Laser Beam Technology Based (LBTB)	Detection is based on the evaluation of the "characteristics" of the energy and the spectra received by a detector after the *cullets*, and/or polluting particles, were crossed by a suitable laser beam light. Such an approach presents two technological limits, related to: (1) the constructive characteristics of the equipment and (2) the material characteristics. The sorting logic is mainly analogical. An *on-off* logic is applied.
Image Analyzers (IA)	IA allow to perform sorting on the basis of the *cullets'* detected colors. CCD (**C***harged* **C***oupled* **D***evice*) scan line cameras are utilized. They present the advantage, in comparison with LBTB, that practically do not have any detection limitation in terms of geometrical resolution, being the investigated scan line dimension is the only function of the lens. Furthermore, colors are better detected.

Material characteristics versus their optical recognition. Cullet attributes, surface status (e.g., dirty or clean) and characteristics (e.g., fragments of bottle neck or jar with or without thread, bottle or jar bottom, etc.) can strongly interfere with the measurements. Measurements are, in fact, based on the evaluation of the transmitted energy received by a detector after the *cullets* are crossed by an energizing source (e.g., standard or laser beam light). In these measures surface characteristics and the status of each cullet play a decisive role in the further response of the detector (Fig. 1).

Ceramic glass recognition. As previously outlined, the frontier in *cullet* optical sorting is represented by ceramic glass recognition. The only two strategies extensively used and designed to reduce the presence of ceramic glass contaminants are source reduction and manual sorting. The problem with reduction at the source is that usually citizens, in spite of public education campaigns, confuse transparent-glass-like contaminants with normal glass, invalidating both curbside and door-by-door collection. As a consequence, some steps of the sorting process are still carried out manually by "trained personnel" who try to recognize ceramic glass fragments prior to crushing, looking at their shape or evaluating their reflective characteristics. Such an approach is expensive, unreliable, and represents a real and important problem for the whole glass recycling sector. Infrared sensors are sometimes used to detect opaque cullet within the "dirty" recyclable glass in order to separate ceramic/ceramic glass and stone fragments from glass cullet. No entirely effective and low-cost solution has been found to date for ceramic glass *on-line* automatic sorting in recycling plants. X-ray sorting techniques have been recently proposed as a solution for ceramic glass identification [19]. Anyway, it must be considered that the use of X-ray equipment in a plant requires appropriate shielding and must follow strict rules to protect workers from exposure, with an increase in costs and environmental and safety problems. Glass sorting, originally based on analog devices, utilizing laser beam technology, has moved towards digital image techniques [20, 21]. Scan line color cameras are thus seeing greater use in this sector to implement selection strategies addressed to identify opaque objects inside the flow stream and/or to separate cullets according to their color [22]. Technology in this field, although sophisticated, remains practically "blind" with regard to the identification of ceramic glass materials. Spectrophotometers should be able, at least in principle, to identify these contaminants; however, they are usually only able to work on a point-by-point basis and are not able to cope with real-time sampling/sorting architectures such as those required in glass recycling plants [23]. They are used, in several industrial fields, mainly at the laboratory scale. A new class of sensing devices based on HSI has recently created new potential for the *on-line* recognition of glass and ceramic glass fragments inside glass recycling plants [24]. A more detailed description of such a technique is reported in the later section Future Directions.

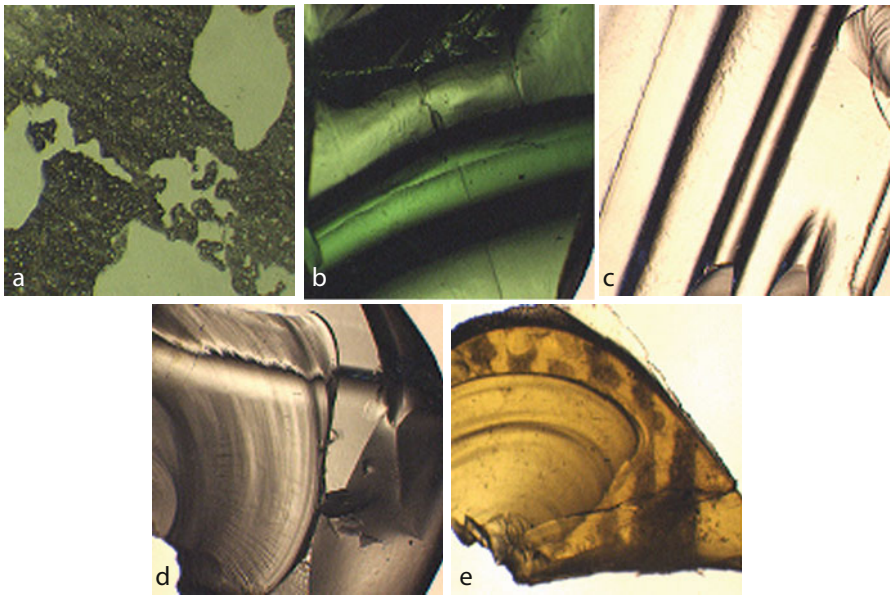

Recycling Technologies. Figure 1
The spectral response of the cullets, suitably energized, is based on the evaluation of the transmitted energy received by the detectors. The detected energy is thus influenced by the status (dirty or clean) and the characteristics (fragments of bottle neck or vase with or without thread, bottle or vase bottom etc.) of the cullet surface. (**a**) 16 × 16 mm image field of dirty *light green cullet*. (**b**) 16 × 16 mm image field of *dark green cullets* (*bottle bottom*). (**c**) 2 × 2 mm image field of *white cullets* (*threaded bottle neck*). (**d**) 2 × 2 mm image field of *half-white cullets* (*bottle bottom*) and (**e**) 2 × 2 mm image field of *brown cullets* (*bottle bottom*)

Recycling Technologies: Metals

Human history and progress are linked to the discovery and utilization of metals [25]. Thanks to these materials, humans have been able to interact and modify the environment, performing advances in agriculture, warfare, transport, etc. The Industrial Revolution, from steam to electricity, was conditioned by metals. Even what, and how, people eat was and is strongly influenced by metals.

The first use of metals dates back to about 7000 BCE in Anatolia (Turkey), where some Neolithic communities started to replace handmade stone knives and sickles with "hammering" native copper. The tools worked as well as their stone equivalents and lasted far longer. The first examples of extractive activities belongs to 4000 BCE. Deep shafts were cut into the hillside at Rudna Glava, in the Balkans, to excavate copper ore. Mining was considered a sort of ritual activity; as thank for the exploited metals, fine pots, bearing produce from the daylight world, were placed in the mines as a form of recompense to propitiate the spirits of the dark interior of the Earth [26]. Thousands of years later, humans started again to understand the importance of preserving the environment and, together with more stringent economic reasons, started to apply more metal recycling.

Metals present many advantages; they can easily be recycled because a specific material can melted several times without losing its properties. Metals commonly utilized in the recycling sectors mainly derive: (1) from the collection and processing of post-consumer metal products and (2) from metal industrial wastes (e.g., working residues, metallic scraps, etc.). Recycling strategies are strongly affected by the previously mentioned origins of the metals. Furthermore, metals' value is strongly affected by several costs, that is, the quality of recovered products (e.g., composition, contaminants residues, etc.), (3) recycled product market, and

(4) metal market value. Together with these costs, their processing (e.g., collection, transport, sorting, etc.) and waste disposal settlements also play an important role. Metals to recycle can be divided in two different families, that is: ferrous and non-ferrous metals. Such a distinction is important because it dramatically influences recycling strategies and related adopted technologies. Ferrous metals scraps are mainly constituted of iron and steel scraps, primarily obtained from automotive dismantling and household appliances (e.g., large kitchen appliances, washers and dryers, etc.). Such waste is usually collected and preliminarily sorted in different classes of products of different grade before being sent to a recycling plant or directly to metal refiners. Wastes resulting from their processing (e.g., wood, plastics, fibers, etc.) are, according to their quantity and physical characteristics, totally or partially recovered; the unrecovered fraction is sent to a landfill. Another lesser source of ferrous metals results from the processing of the bottom ashes produced by incinerators.

Non-ferrous metals scraps are mainly constituted by aluminum, copper, zinc, and lead. Aluminum is the main scrap deriving from household waste (e.g., cans, containers, etc.); the others primarily result from waste from industrial and commercial activities.

Ferrous Metals Iron and steel are the main materials utilized in many industrial sectors: building and construction, automotive, chemical, operative equipments, etc. These materials are so common in use for several reasons: (1) relatively low costs, (2) high availability, (3) good mechanical attributes, (4) easiness in working, and (5) because they can also, at least in principle, be easily recycled, the main reason being linked to the ease in recovering them due to their magnetic properties.

Iron and steel are obtained from raw materials (e.g., iron ores) and/or 2) from recycling. Different production methods are thus utilized: **B***last* **F***urnace* (BF) and **B***asic* **O***xygen* **F***urnace* (BOF), when primary raw materials are utilized, and **E***lectric* **A***rc* **F***urnace* (EAF) when recycled products are employed. Metal scrap recycling allows reduction of both energy-production costs (e.g., less energy is required for produced unit of weight when scraps are re-melted instead of using iron ore) and environmental impact (e.g., reduced exploitation of primary raw materials such as iron ores, limestone, and coal necessary when primary metals are produced by BF or BOF). Furthermore, a corresponding decrease of CO_2 emission is achieved, with a further environmental benefit.

Metal recycling is a well-established practice and it will continue to grow with the increased availability of automotive-derived scraps. In the future, however, this source will probably be reduced as more motor vehicles are designed with plastics and/or polymeric-based composites. In a quantitative way, steel represents the most recycled product, more than aluminum, paper, and glass together and greater than all other metals combined (e.g., aluminum, copper, nickel, chromium, zinc).

Metal Scraps' Sources and Characteristics Metal scraps can be obtained from many sources:

- *Home scrap*, that is, the scrap (e.g., working production waste, defective parts, etc.) derived from a manufacturing process. In this case, waste is directly re-melted. There are no problems related to metal scrap quality, as the material is constituted only of the metal to recycle
- *Industrial scrap* usually consists of the wastes produced in iron- and/or steel-manufacturing plants, mainly leftover product resulting from specific manufacturing actions. Such wastes are usually sold and re-used in foundries
- *Post-consumer scrap* is metal waste derived from products that have reached the end of their life-cycle (e.g., industrial equipment, cars, metals structures, home appliances, etc.). In this class of scrap, contamination, mainly the presence of non-ferrous metals (e.g., aluminum, copper, zinc, and lead), can represent, in some circumstances, an important problem to face and solve

Other iron and steel intermediary products, and/or waste, play an important role as recycled products: steel-making slag and flue dust (resulting from BF, BOF, and EAF), waste sludge and filter cake (resulting from BF and BOF), spent pickle liquor, and mill scale.

One of the most important steps in the development and set-up of metals recycling systems is creating appropriate strategies to identify and sort metals into

groups presenting similar characteristics. Such a "grouping" must be carried out according to specific rules defined by steel-makers and market requirements.

Ferrous Metals Recycling Technologies On the basis of what has been previously outlined, specific processing layouts have to be defined. Each is constituted by one or more units, in series and/or in parallel, and each is specialized to perform a specific action. The main actions, and related units, are reported and described below with reference to ferrous metal wastes processing:

- Manual sorting (e.g., non-metal miscellaneous material detachment, large non-ferrous metal separation) and preparation (e.g., cutting of large metal manufactured goods, removal and dismantling of specific metal unit, etc.)
- Crushing and screening, to reduce metal scraps to easy-to-handle pieces to be directly fed into furnaces or subjected to further classification-separation actions
- Separation of the different metal fractions into groups characterized by similar composition attributes
- Testing and/or sorting of the different resulting ferrous metals end-life-goods-derived-material, to characterize and certify different classes of products according to market requirements

Manual Preparation and Sorting Metal manufactured goods to recycle are usually constituted of units of large dimensions (e.g., automobiles, metal structures, etc.); for this reason they must first be reduced to easy-to-handle pieces, both for further processing and/or for direct re-use inside furnaces. For these reasons, shears, hand-held cutting torches, crushers, or shredders are commonly utilized. After this preliminary stage, manual sorting, if required according to ferrous metal waste to recycle, is carried out. At this early stage of the process large contaminants that are easily detectable with human senses (e.g., car batteries, plastics, foams, wood, non-metallic elements, etc.) are removed.

Materials Handling Conveying units are mainly usually conveyor belts. For the characteristics of the feed, especially at the early stages of ferrous metals handling (e.g., relatively large pieces of materials), handling equipment is of rough construction. Ferrous wastes are usually stockpiled and the primary feeding, after the preliminary operation outlined in the previous paragraph, is realized by cranes. Ferrous metals are abrasive; as a consequence, all the different parts of the equipment utilized for conveyors are subject to strong abrasive actions; also, the presence of fine particles and dusts must be carefully checked and reduced to avoid mechanical problems and to assure good environmental working conditions.

Comminution After manual preparation and sorting, further size reduction actions are applied to scraps. Comminution actions are different according to destination of the materials, that is: (1) direct feeding to the furnaces or (2) further processing. In the first case, large scrap materials are milled utilizing shears, flatteners, and torch-cutting and turning crushers. The resulting pieces are then compacted by baling or briquetting in order to increase the apparent density of the scrap aggregates to re-melt, trying to avoid their possible floating in the mold. In the second case, crushing actions are usually applied, the goal being to reduce scraps to suitable dimensions to allow their processing (further crushing stages, sieving, separation, sorting, etc.).

A comminution unit usually develops its action through the application on the materials of four forces: impact, shear, abrasion, and compression. The quantitative relationships among them, in terms of cause-effect, strongly differ according to the equipment. For ferrous metals comminution, impact, and shear forces are those to be primarily applied, in order to optimize metal scraps and minimize fine particle production. Coarser fractions are mainly constituted by iron and steel, finer fractions usually contain the residues. Finer fractions can be divided in heavy and light (*fluff*) fractions. They present different characteristics in composition according to constituting particles weight. **A***utomotive* **S***hredder* **R***esidue* (ASR) can be considered as the main source of metals. ASR heavy fraction mainly contains aluminum, stainless steel, copper, zinc, and lead. ASR *fluff*, for quantities and characteristics, represents an important class of ferrous metals end-life-goods-derived material of particular interest for the recycling sector. *Fluff* represents about 25% of

the weight of a car. It is usually constituted by materials characterized by intrinsic low specific gravity (e.g., plastics, rubber, synthetic foams, textiles, etc.). When processed to perform their recovery, they pollute the materials presenting higher specific gravity (i.e., copper, aluminum, brass, iron, etc.), constituting parts of the electrical devices of the vehicle that, for their shape, size (e.g., wires, metal straps, slip rings, wipers, etc.) and utilization remain concentrated in the lighter products. Such "polluting agents," for their intrinsic characteristics, are not well removed by classical separation techniques. The development and application of efficient washing strategies for *fluff* could dramatically reduce waste and environmental pollution, allowing, at the same time, an increase in energy recovery through pure sorted polymer re-use. Furthermore, the potential to use finer *fluff* fractions to produce energy could contribute to increasing the full recovery of such kinds of products. To reach this goal the quantity and the quality of the metal contaminants have to be strongly controlled in order to not prejudice the quality of the final fluff-based fuel. Always with reference to car dismantling, ASR heavy fractions contain large quantities of both ferrous and non-ferrous metals. Their recovery is usually performed adopting recycling technologies based on heavy media and eddy current separation.

Shredding is usually the main comminution action applied. Processing layouts, embedding this phase, are usually applied to automobile hulks and to the so-called white goods, that is, stoves, refrigerators, washing machines, etc. The most utilized class of shredders are those based on the use of **S***wing*-**H***ammer* **S***hredders* (SHS), subordinately, **R***otating* **D***rums* (RD), are also employed. The main characteristics of both types of equipments are described in Table 6.

Recycling Technologies. Table 6 Characteristics of the comminution units mainly utilized to perform ferrous metals shredding

Comminution units	Characteristics
Swing-Hammer Shredders (SHS)	The input material is fed from the side. Fed material flow is controlled according to the energy required for comminution, usually greater of one order of magnitude in respect of minerals. Material is transported into the relatively narrow gap between the impacting tools and the lower part of housing, where it is subject to an intense deformation and comminution. The material, which has become sufficiently small, is discharged from the chamber of comminution by means of grates. The configuration of the discharge grates can vary. Normally grate is placed above the rotor and in some cases a second one below it. According to different comminution chamber size and shape, rotating of the rotor in respect of the feed, grates position and configuration, different comminution actions can be thus performed. In the last decade a lot of efforts have been addressed to investigate to utilize SHS with vertical mounted rotors. Such comminution units are actually mainly utilized in the processing of metallic cuttings, waste wood, paper waste, etc. Their possible full and systematic use in ferrous metal recycling sector could embed several advantages, that is: (1) a lower residence time of the metal particles inside the comminution chamber (e.g., higher flow rate and less energy consumption), (2) a better liberation and (3) a lower compaction of the liberated thin-walled metal pieces. A more systematic utilization of SHS, with vertical mounted rotors, is strongly linked to a further development of shredders' mechanical architectures and utilized materials characteristics.
Rotating Drums (RD)	A spinning rotor with chains or bars attached to the outside is responsible for the comminution. Ferrous metals fragmentation is mainly due to: (1) the impact of the rotating chains or bars on metals and (2) metals projection against "special plates" installed on the inside the chamber. Crushed material is finally discharged when particles size is lower than the space, that can be properly set, between the "rotating unit" and the wall. This equipment is commonly utilized as the primary crusher. For their characteristics do not allow the degree of flexibility in terms of operative conditions as those allowed by SHS.

Separation Separation technologies are applied when the shredded materials to recover are composed of different families of particles characterized by different physical-chemical attributes and different relative composition, texture, and shape. For these reasons automatic and in-series handling-separation strategies are required, as simple manual sorting or separation are unable to recover in an efficient and economically profitable way the different materials. Table 7 lists the equipment commonly utilized to perform separation of end-life-goods-derived products; those resulting from car dismantling represent the main source of complex ferrous metal waste to recover. Because they are constituted of different particles of different magnetic properties, specific weight, color, chemical composition, etc., they require different separation strategies [27–29].

Testing Different from other recycling-derived materials, the possibility of performing a rapid test on samples collected from the different recycled ferrous metal flow streams is particularly important, especially with reference to alloys. Alloys of similar grades and composition are usually difficult to discriminate. Specific attributes are thus evaluated both by expert personnel and by specific tests. Recognition, via

Recycling Technologies. Table 7 Characteristics of the separation units commonly utilized to perform separation in the ferrous metal recycling sector, with particular reference to ASR

Separation units	Characteristics
Belt Magnets (BM) *and Drum Magnets* (DM)	BM and DM are usually utilized in the first stage of processing, which is on coarser fractions as they result from primary crushing. Permanent and/or electromagnets are usually utilized. Separation is realized adopting BM and DM. In the first case the magnet is located between pulleys around which a continuous belt travels. In the second case the magnet is installed inside the rotating shell, metals particles are attracted, removed from the other non magnetic fractions and discharged as the moving belt of the separator turns away from the magnetic field the metals particles. Following this approach iron and steel cannot be separated from nickel and magnetic stainless steels. An improper separation can negatively influence the further melting stage. For this reason, hand sorting, to reduce the contamination of the ferrous products, is usually performed after this stage.
Eddy Currents Separators (ECS)	ECS is realized passing the waste products to separate into magnetic field, as a result, eddy current induced in the non-ferrous metals, produces ejecting forces that throw away non-ferrous metals the waste feed flow. ECS is commonly applied after the first magnetic separation stage (e.g., DM or DM). The most utilized ECS architecture is based on an inclined ramp. The material is thus fed to the ramp. The ramp surface is usually constituted by stainless steel. Under the ramp surface a series of magnets is positioned. Due to the eddy current non-ferrous metals are deflected sideways. Separation is realized according to the trajectory followed by the different classes of materials. Other separation architectures are based on the use of a rotating cylinder or a conveyor belt: magnets are positioned around the rotating axis of the cylinder or fitted inside the head pulley, respectively. As in the previous case separation is realized according to materials trajectory variations.
Heavy Media Separators (HMS)	HMS are based on the utilization of a medium constituted by a finely milled solid (e.g., magnetite or ferrosilicon) and water. According to the solid/water ratio the density of the medium can vary. Usually such a value is between the value of the specific gravity of the two classes of materials to separate, so that a sink and a float product is obtained. In this process the recovered materials are then washed and dried. The fine particles of the heavy media are recovered, by magnetic separation, from the slurry resulting from product washing and re-utilized inside the process. Decreasing the size of the particles to separate, also separation efficiency decreases for the increasing effect of viscosity, in this case cycloning is utilized.

human senses and analytical equipment, is thus performed to evaluate characteristics such as color (e.g., copper and brass distinction), apparent density and hardness (e.g., lead distinction from copper and brass), magnetic properties (e.g., iron and stainless steel), presence and attributes of spark patterns as they results from abrasion test, chemical reaction to reagents, chemical and X-ray spectrographic analysis (e.g., alloys composition), thermal behavior (e.g., melting point), etc. All the above-mentioned approaches are expensive and are difficult to implement *on-line*.

Sorting As outlined in a previous paragraph, sorting is important because it allows removal of contaminants from the different ferrous metal flow streams handled in the recycling plant. Different sorting strategies addressed to recognize different metal scrap constituents have been developed and used. Table 8 lists the devices, and related architectures, commonly used to perform metal scrap sorting.

Non-ferrous Metals Aluminum is the main non-ferrous metals being recovered and recycled. The main source of aluminum scraps comes from the packaging, transport and homeware industries. Aluminum can be "infinitively" recycled. Its re-melting achieves several environmental goals: considerable energy savings (about 95%) in comparison with the energy required to produce it from bauxite ore, a consequent reduction of primary non-renewable raw materials exploitation, and a reduction of overall emissions (airborne dusts and CO_2). The automotive sector significantly increased, in recent years, its use of aluminum; for this reason scraps from end-of-life vehicles represent the main source of aluminum for recovery

Recycling Technologies. Table 8 Characteristics of the sorting units commonly utilized to perform sorting in the ferrous metal recycling sector, with particular reference to ASR

Detection units utilized for sorting	Characteristics
Portable Optical Emission Spectrometers (POES)	POES can be utilized to perform the on-site sorting and identification of metals. Such an approach, even if not reaching the precision of the corresponding laboratory device, is quite useful to perform fast quality control, usually well satisfying recovered products grade requirements. POES is able to detect up to 90% of the currently produced grades of steel.
Image Analyzers (IA)	IA allow to perform sorting on the basis of the detected color. IA belongs to the first class of devices utilized for metal scraps sorting. Adopting this approach, zinc, copper, brass, and stainless steel are commonly well sorted. Even with technological improvements, both in terms of speed of processing (the same pieces can be checked several times), sensor quality (better discrimination in terms of recognizable colors), and resolution (minimum identifiable scrap piece), IA is not efficient when slightly different alloys have to be recognized.
Laser-Induced Breakdown Spectroscopy (LIBS)	The detection architecture is based on the analysis of the optical spectrum, or fingerprint, of a small spot on each metal particle that is evaporated using powerful laser pulses. Even though very powerful, the techniques show some limitations. The most important thing is that it is particularly sensitive to the status of the scrap surface. Presence can negatively influence measurements because laser pulses can penetrate for just few Å in the surface.
X-ray Fluorescence Spectroscopy (XRF)	XRF is based on the emission of X-rays emission inside an XRF unit. The fluorescence radiation generated by the atoms when they release the energy, after the excitation stage is collected and analyzed. Both emitted wavelengths, and the energy released are functions of the elements constituting the waste sample. Correlating the emission intensity it is thus possible to evaluate the content of a specific element within the sample.

and reuse. Other non-ferrous metals commonly recycled are copper, zinc, and lead, but as outlined in the previous paragraph the recycled quantities are not comparable with aluminum and they are also relatively easy to recover. For this reason, the following recycling technologies will be described with reference to automotive aluminum scraps.

Aluminum from Automotive Scraps Aluminum scrap is usually classified into two categories: cast and wrought aluminum alloys. Recycling of aluminum scrap introduces several technical problems to the secondary ingot market. Because of its high reactivity, aluminum cannot be refined pyrometallurgically, as with copper or iron scrap. Therefore, the aluminum scrap can be recycled only by blending and dilution in order to obtain a specific alloy. Wrought aluminum alloys contain low percentages of alloying elements (e.g., silicon, magnesium, copper, and zinc), less than about 4% of the total. Casting aluminum alloys contain the same elements as wrought, but in greater amounts (the silicon content in cast alloys can range up to 22%).

Actual scrap sorting technologies produce mixtures of cast and wrought aluminum not suitable for recycling in wrought alloy production.

The wrought fraction of these mixtures has a higher value; if selectively collected its reuse as wrought aluminum alloys would prevent unnecessary downgrading. Moreover, aluminum alloys, used in vehicle manufacturing, are increasing and the recovery of aluminum alloys is quite interesting. Considerable efforts have been devoted to substitution of steel and cast iron with lighter materials such as aluminum alloys and polymers. Steel replacement by aluminum alloys could have a counterbalancing effect in the case of success in selection of cast and wrought aluminum.

Non-ferrous Metals Recycling Technologies The same processing steps and strategies previously described for ferrous metals can be also applied for non-ferrous metals scraps. Such phases, for scrap originating from end-of-life vehicles (one of the main non-ferrous metals sources, in particular aluminum) can be synthetically identified in:

- Collection, dismantling (e.g., removal of re-usable vehicle parts as engines, doors, glass, seats, etc. and hazardous parts as batteries, fluids, etc.) and/or manual sorting (e.g., metal miscellaneous material detachment, large ferrous metal separation)
- Crushing and screening, to reduce non-ferrous metal scraps in pieces easy to handle for further processing
- Separation of the different non-ferrous materials in classes of products characterized by composition attributes
- Testing and/or sorting

Collection, Dismantling, and/or Manual Sorting Non-ferrous metal manufactured goods to recycle can be constituted by pieces of different dimensions, ranging from aluminum cans up to a "jet airliner," thus, according to their size, they can be directly handled or must be cut to be properly handled. Often, non-ferrous metal parts are linked (e.g., bolted, welded, etc.) with other materials and have to be liberated. Hand dismantling and/or sorting in some cases is necessary, but in many cases it is time consuming and inefficient for the dimension and the degree of locking of the different constituting materials. For these reasons comminution/separation actions must be applied adopting specific processing layouts.

Materials Handling Conveying units are mainly conveyor belts of rough construction. Non-ferrous wastes are usually stockpiled and the primary feeding, after collection, dismantling, and/or manual sorting is done by cranes. Ferrous metals are abrasive, and as a consequence all the parts of the equipment used for conveyors are subjected to strong abrasive actions. The presence of fine particles and dusts also has to be carefully monitored and reduced to avoid mechanical problems and to assure good environmental working conditions. Furthermore, problems related to explosive characteristics of aluminum dust have to be taken into account.

Comminution and Screening Comminution and screening are currently applied to reduce metal scrap to different size classes that are sent for proper processing and recovery of the different materials constituting the feed. The considerations developed with reference to ASR metal fraction comminution, in terms of equipment and characteristics (Table 9), can also be directly applied to ASR non-ferrous metals.

Recycling Technologies. Table 9 Characteristics of the comminution units mainly utilized to perform non-ferrous metals size reduction

Comminution units	Characteristics
Alligator (AS) and/or *Guillotine Shears* (GS)	AS mimics, to perform cutting, the behavior of an alligator mouth. The device is constituted by two jaws, one fixed and the other mobile. The main advantage in the use of AS is its versatility in terms of different aluminum scraps it is (e.g., ship, aircraft, automotive vehicles and in general large objects) able to cut. Furthermore better detachment is allowed of different metals constituting a specific piece to dismantle. When a GS is utilized, aluminum scrap is placed underneath a cutting blade, which drops down onto the scrap creating the cut. GS are characterized by higher power ratings and productivity than AS.
Impact Shredders (IS)	IS as *hammer mills* are among the most used devices for aluminum scrap size reduction. Fragmentation is realized for two co-occurring effects: (1) hammers impact being the main one, and (2) scraps projection the secondary one, against mill chamber internal surface. *Impact crushers* are often also utilized. They use the same milling actions but invert the relative effects.
Rotary Shredders (RS)	RS utilized, as main milling actions: (1) cutting and (2) impact for their architecture are normally utilized to process light metal scraps (e.g., foil and beverage cans and containers).

Separation Aluminum-based material separation technologies are mainly based on magnetic [27], eddy current [17], air [28], and sink-float separation [29]. The main characteristics of the different separation units, based on the previously mentioned physical principles, are reported in Table 10.

Among the different separation approaches, sink-float separation (S&FS) plays an important role when non-ferrous metals products have to be separated and/or refined before the final re-melting stages. Such products, in fact, are usually composed of a wide range of materials characterized by different density, shape, and size class distribution, strongly affecting sink-float separation. For this reason separation is performed in different stages. After a preliminary removal of *non-magnetic-fine fractions*, a two- or three-stage density separation is carried out. With a typical three-stage density separation, low-density plastics, foam, and wood are usually preliminary removed (*cut-off* density: 1 g/cm^3), then, utilizing a *cut-off* density, 2.5 g/cm^3, high-density plastics, magnesium, and hollow aluminum alloys are recovered in the floating fraction and then processed again utilizing ECS. The "remaining" sink fraction is constituted by brass, zinc, lead, copper, and so on. One of the main limits of S&FS is that it is not capable of performing a good separation of cast from aluminum alloys or differentiating among the different alloy groups. Furthermore, S&FS present other limitations, namely:

- Cost, the process is expensive both at technical (e.g., heavy media costs, complexity of the processing circuit, etc.) and environmental levels (e.g., strict control of the heavy media with reference to possible environmental pollution, water recovery and cleaning, etc.)
- Media recovery, separated scraps are obviously contaminated by heavy media, thus they have to be cleaned and the media recovered (e.g., utilization of specific processing circuits)
- Separation is strongly influenced by particulate solids' morphological and morphometrical attributes

To attempt to totally or partially solve address these issues, in recent years innovative separation/sorting technologies have been successfully proposed and adopted in many recycling plants.

Sorting The main role of sorting strategies is to perform a sort of further refining of non-ferrous metals as they result from the previous separation stages. From this perspective, sorting is mainly addressed at realizing greater discrimination

Recycling Technologies. Table 10 Characteristics of the separation units commonly utilized to perform separation in the non-ferrous metal recycling sector

Separation units	Characteristics
Magnetics Drum Separators (MDS)	MDS is usually constituted by a stationary drum with half of its surfaced lined with NdFeB magnets installed inside a rotating cylinder that is set up as a conveyor belt. Ferromagnetic particles are attracted, removed from the other non magnetic fractions and discharged as the moving belt of the separator turns away from the magnetic field ferromagnetic particles.
Eddy Currents Separators (ECS)	ECS is realized passing the waste products to separate into magnetic field, as a result, eddy current induced in the non-ferrous metals, producing a forward thrust (F) and torque (T) on the particles resulting in their ejection from the stream of non-metallic materials. Separation is realized according to the trajectory followed by the different classes of materials. ECS is commonly applied after the first magnetic separation stage (e.g., MDS). Other eddy current based separation architectures are based on the use of a rotating cylinder or a conveyor belt: magnets are positioned around the rotating axis of the cylinder or fitted inside the head pulley, respectively. As in the previous case separation is realized according to materials trajectory variations.
Air Separators (AS)	AS is usually applied to preliminary recover light fractions contained in the feed or on *non-magnetic-fractions* as they result from previous MDS and ECS. Light fractions (e.g., plastics, rubbers, foams, fibers, etc.) are usually sucked by a nozzle positioned above the conveyor.
Sink and *Float Separators* (S&FS)	S&FS are based on the utilization of a medium constituted by a finely milled solid (e.g., magnetite or ferrosilicon) and water. According to the solid/water ratio the density of the medium can vary. Usually such a value is between the value of the specific gravity of the two classes of materials to separate, so that a sink and a float product is obtained. In this process, the recovered materials are then washed and dried. The fine particles of the heavy media are recovered, by magnetic separation, from the slurry resulting from product washing and re-utilized inside the process. Decreasing the size of the particles to separate, separation efficiency also decreases for the increasing effect of viscosity, in this case cycloning is utilized.

between different families of alloys and different classes inside the families. The technology utilized to fulfill this goal is based on two different approaches: color sorting (**I***mage* **A***nalysis*: IA) and **L***aser*-**I***nduced* **B***reakdown* **S***pectroscopy* (LIBS). For IA, a new process applied to aluminum scrap allows enhancement of IA performance. It consists of a selective etching of the scraps in different solutions that produces, as a result, the coloring of the scrap according to the presence and quantities of specific alloys agent. LIBS allows determination of the chemical composition of each scrap in a reliable and cost-effective way. The main limitation of this approach is linked to the characteristics of the investigated surface (e.g., presence of paints, lubricants, adhesives, or other polluting substances) since the laser pulse laser can only penetrate to a depth of 30 Å or less on the surface of the aluminum. Table 11 lists the devices and related architectures commonly utilized to perform non-ferrous metal scrap sorting.

A new class of sensing devices based on **H***yper***S***pectral* **I***maging* (HSI) has recently opened new interesting scenarios for the *on-line* recognition of the different products resulting from both ferrous and non-ferrous metal waste processing. A more detailed description of this technique is given in the section Future Directions.

Recycling Technologies: Plastics

Re-utilization of waste plastics has increased with "new" plastic polymers; such re-utilization has increased not only quantitatively but also qualitatively (e.g., a larger range of recycled polymers). Plastics can be roughly divided in two types: thermoplastics, which soften when heated and harden again when cooled, and thermosets, which harden by curing and cannot

Recycling Technologies. Table 11 Characteristics of the sorting units commonly utilized to perform sorting in the non-ferrous metal recycling sector, with particular reference to products resulting from S&FS

Detection units utilized for sorting	Characteristics
Image Analyzers (IA)	IA allow to perform sorting on the basis of the detected color. IA belongs to the first class of devices utilized for non-ferrous metal scrap color sorting. Adopting this approach, zinc, copper, brass, and stainless steel are commonly well sorted. Thanks to great technological improvements, both in terms of speed of processing (the same pieces can be checked several times), sensor quality (better discrimination in terms of recognizable colors) and resolution (minimum identifiable scrap piece), recent studies demonstrated that IA allows good separation of magnesium alloys from hollow aluminum products.
Laser-Induced Breakdown Spectroscopy (LIBS)	The detection architecture is based on the analysis of the optical spectrum, or fingerprint, of a small spot on each metal particle that is evaporated using powerful laser pulses. Even if, at least in principle, very powerful, the techniques show some limitations. The most important is that it is particularly sensitive to the status of the scrap surface. Presence can negatively influence measurements because laser pulses can penetrate for just few Å in the surface.

be re-molded. Thermoplastics are by far the most common types of plastic, comprising almost 80% of the plastics used in Europe, and they are also the most easily recyclable. It is easy to understand that when collection-recycling strategies are set up, mixing between thermoplastics and thermosets has to be strictly avoided.

Plastic materials can be considered relatively modern, but some "natural" polymers exist in nature (e.g., amber, tortoiseshell, and horn) that behave very similarly to "modern" manufactured plastics and were used in the past in similar ways. For example, horn, which becomes transparent and pale yellow when heated, was used in the eighteenth century to replace glass.

The first plastic material produced for industrial-scale applications was the Parkesine, later named Xylonite. This material was invented by Alexander Parkes, who exhibited it as the world's first plastic in 1862. It was used for such objects as ornaments, knife handles, and boxes, and for flexible products such as cuffs and collars. Since that time great steps forward have been made and today plastics are widely produced and utilized, creating massive problems with litter and waste disposal.

Plastics are continuously replacing other materials in a number of applications. From greenhouses, mulches, coating, and wiring, to packaging, films, covers, bags, and containers. It is only reasonable expect to find a considerable amount of **P***lastic* **S***olid* **W***aste* (PSW) in the final stream of **M***unicipal* **S***olid* **W***aste* (MSW). In the EU countries, over 250 × 10^6 t of MSW are produced each year, with an annual growth of 3%. In 1990, each individual in the world produced an average of 250 kg of MSW generating in total 1.3 × 10^9 t of MSW [1]. Ten years later, this amount almost doubled at 2.3 × 10^9 t. In the United States, PSW found in MSW has increased from 11% in 2002 [2] to 12.1% in 2007 [3]. Increasing cost and decreasing space in landfills have forced considerations of alternative options for PSW disposal [4]. Years of research, study, and testing have resulted in a number of treatment, recycling, and recovery methods for PSW that can be economically and environmentally viable [5]. The plastic industry has successfully identified workable technologies for recovering, treating, and recycling of waste from discarded products. In 2002, 388.000 t of polyethylene (PE) were used to produce various parts of textiles, of which 378.000 t were made from PE discarded articles [6].

The better solution "to recover" plastic goods should be, when possible, to re-use them as they are. Such a choice can be adopted, for example, for crates or other plastic-manufactured containers, which can be used several times for products and/or materials transportation and handling. Re-using is better than

recycling because less energy and resources are required (JCR, 2006). In any case both re-use and/or recycling present several important advantages, related to:

- Reduced use of fossil fuels
- Energy savings
- Reduced emissions of CO_2, SO_2, and NO_x

The main problems in plastic recycling are mainly related to the difficulties of developing and setting up reliable automatic sorting architectures and systems able to perform an efficient selection of the different polymers. These problems can synthetically be divided in two classes, that is: single and multiple type and color plastic separation. In the first case (e.g., bottle, container, etc.) separation is relatively easy, the main problem being related to correct polymer recognition independent of the presence of fillers and other chemical additives. In the second case (e.g., cellular phones, electrical and electronic devices, automotive parts, etc.) separation is more complex, as the objects are constituted by different types of plastics characterized by the presence of different fillers and chemical additives. In the latter case, both separation and recognition strategies have to be sequentially applied.

Waste Plastics Sources and Characteristics Used plastic packaging and other plastic items can be valuable resources in the manufacture of new products and in the generation of energy. It is important that a society aims to make the best affordable use of these valuable plastic resources. This is good for the environment, for the economy, and for the international community. Analyses by the European Community (EU) indicate that besides their ecologic importance, raw materials and energy are also the most important competitiveness factors for EU industries. Therefore, the need to increase recycling, improving at the same time the quality and homogeneity of recycled materials to minimize environmental pollution and usage of resources, is thus an important topic the EU. There is a strong drive to recycle polymers from end-of-life products and avoid their ending up in landfills and waste incinerators because plastics recycling reduces CO_2 emission and saves resources. The worldwide production of plastics was 230 million tons in 2005 [30]. In Europe, 53.5 million tons were produced in total. Out of 22 million tons of post-consumer plastic waste in Europe in 2005, 53% was disposed, 29% was used for energy recovery, and 18% was recycled [30]. According to the last EU Directive 2004/12/EC on packaging and packaging waste, the recycling level of plastics should dramatically increase in the next years. New, more cost-effective separation technology can thus provide an important incentive to increase recycling rates. The recycling of polymers that are present in relatively pure streams such as post-industrial waste and separately collected containers of food and beverage is generally well-developed in Europe. The situation is very different for the large and complex stream of post-consumer waste, including wastes such as **W***aste* **E***lectrical* and **E***lectronic* **E***quipment* (WEEE), household waste, and **A***utomotive* **S***hredder* **R***esidue* (ASR). Effective recycling of these wastes is possible, as has been demonstrated at some places in Europe, by large investments in logistics and dismantling (cars, electronic equipment) or hand-sorting (household waste). Such strategies are expensive, however, and they are therefore not widely applied.

There are about 50 different groups of plastics, with hundreds of different varieties [31]. All types of plastic are recyclable. To make sorting and thus recycling easier, the American Society of the Plastics Industry developed a standard marking code to help consumers to identify and sort the main types of plastic. An example of these types and their most common uses are reported in Table 12.

All separation-sorting techniques are based on the identification of one or more physical properties to utilize to discriminate the materials to process in order to establish classes of physical attributes and to set up appropriate technologies to address materials inside these classes. One of the most utilized properties is the density. Unfortunately, such a parameter is not particularly useful when plastics have to be separated because this value is similar for the different polymers to recycle.

Technologies that address these resources need to be extremely powerful, as they must be relatively simple in order to be cost-effective, but also accurate enough to create high-purity products and able to valorize a substantial fraction of the materials, present in the waste, into useful products of consistent quality in order to be economical. On the other hand, the potential market for such technologies is large, and environmental regulations along with oil price increases have

Recycling Technologies. Table 12 Example of most common types of plastics and use

1	PET	*Polyethylene terephthalate* – Fizzy drink bottles and oven-ready meal trays.
2	HDPE	*High-density polyethylene* – Bottles for milk and cleaning liquids.
3	PVC	*Polyvinyl chloride* – Food trays, cling film, bottles for squash, mineral water and shampoo.
4	LDPE	*Low density polyethylene* – Carrier bags and bin liners.
5	PP	*Polypropylene* – Margarine tubs, microwaveable meal trays.
6	PS	*Polystyrene* – Yogurt containers, foam meat or fish trays, hamburger boxes and egg cartons, vending cups, plastic cutlery, protective packaging for electronic goods and toys.
7	OTHER	*Any other plastics* that do not fall into any of the above categories. An example is melamine, which is often used in plastic plates and cups.

increased the interest in many industries both in waste sorting technologies, for the production of high quality secondary polymers, as well as in developing automatic sensors for quality assessment of waste-derived secondary polymers. This latter aspect is particularly crucial because: "*no matter how efficient the recycling scheme is, sorting is the most important step in recycling loop.*" Fast, accurate, and reliable identification of the primary plastics and the polluting materials in the feed is thus essential to set up suitable mechanical actions on PSW and optimal sorting strategies on the resulting products. The attainment of this goal is thus fundamental for companies that buy recycled plastics, because they obviously want those recycled plastics have the same characteristics as virgin ones. Otherwise, it is not efficient, and sometimes dangerous, to use recycled plastics materials. A simple example is the case of polyethylene theraphalate (PET) and polyvinylchloride (PVC), which are sometimes indistinguishable by sight. These two resins are contaminants to each other. Combinations of PVC and PET resins can result in the release of hydrochloric gases. The PET resin will be ruined even with only a few parts per million of PVC resin.

Waste Plastics Recycling Technologies From what has been previously reported, it is clear that correct plastic recycling is not an easy task. Among all the different wastes materials and products analyzed in this section, plastics are probably the most difficult to separate and recover. Preliminary and efficient plastics sorting, as well as a continuous monitoring of the different waste plastics flow streams, are both key issues to develop optimal PSW products recycling strategies. From this perspective plastics recycling technologies can be divided into four main categories [32]:

- Re-extrusion, that is, the re-introduction inside an extrusion cycle of plastics presenting the same characteristics

- Mechanical, developed to recover different plastic products by a physical processing
- Chemical, addressed to produce feedstock chemicals for the chemical industry
- Energy recovery, that is, complete or partial waste plastics materials oxidation to produce heat, power, and/or gaseous fuels, oils, and/or materials to be disposed of (e.g., ashes)

In the following, particular attention will be addressed to mechanical recycling, one among the four mentioned approaches that maximizes "waste plastics recovery," producing lower environmental impact.

Re-extrusion The main assumption with re-extrusion is that the utilized waste scraps have to be constituted by polymers presenting the same characteristics as the original product. Manufactured products resulting from this process that do not satisfy quality composition constraints are usually addressed to a use where mechanical properties are more important than compositional ones (e.g., crates).

Mechanical Recycling When mechanical recycling strategies are applied, sorting, at the different stages of the processing, represents an important issue. Despite great technological developments, most current plastic sorting continues to be done by hand. *Manual sorting* is a simple process that needs very little technology. It is a labor-intensive, costly, and inefficient method for sorting materials and more specifically plastics. For this reason, as previously outlined, the Society of the Plastics Industry instituted a voluntary labelling system. The system created a set of codes (Table 12) for each of the six most commonly used resin types. Even with this labeling system, it is still difficult to manually distinguish polymer types due to the condition of the plastics as they reach the separation facility. Plastic containers, in fact, may be crushed, cracked, or covered, rendering the resin label practically useless. In any case, systematic and extensive manual sorting of plastic parts, bottles, and the like is counterproductive since accurate, high-speed flake-sorting technology exists to separate one plastic from another; in fact, a number of automated sorting strategies have been investigated, developed, and implemented in recent years. They can be divided in two categories according to the size of plastics objects to sort:

- *Macro-sorting* deals with the separation of bottles or containers, as a whole. Such an approach has the advantage that it does not require any specific preparation of the sample before sorting. Specific polymers' attributes have been detected and according to their characteristics further separated, usually following air-blow-based strategies.
- *Micro-sorting* is applied after the plastic materials have been milled into pieces. This system has the advantages of lower handling costs and larger volume processing. A more sophisticated technology is required: a real mechanical processing sequence (e.g., comminution, classification, separation, etc.) has to be set up and applied.

Macro-sorting Plastic *macro-sorting* is addressed to separate plastics manufactured goods as recovered after their use. Strategies have to be thus addressed to recognize big targets. The main problem to face, following this approach, is to set up a suitable processing line that is able to handle large pieces and consequently large and cumbersome stocks. Different techniques have been investigated in the past years and are currently utilized, some of them are outlined below:

- Near-infrared spectroscopy
- X-rays analysis
- Laser aid identification
- Marker systems

Near-infrared spectroscopy (NIR). This techniques is one of the most utilized to perform an automated sorting of post-consumer plastic containers. NIR has the advantage that direct or close contact between the detector and the sample is not necessary. NIR instruments are also compatible with flexible fiber-optic probes. It is based on the energizing of the unsorted, unidentified plastic with near-infrared waves (600–2,500 nm). When the infrared light reflects off the surface of the plastic, the different resins' characteristic infrared absorption bands can be measured. The detected bands are then compared to known polymer spectral bands response, in the same wavelength range, to determine the plastic type. Such an approach is characterized by many advantages. The most

significant one is the detection/identification speed. Because of the great scanning speed allowed by spectroscopic devices, many readings of one sample can be taken in short periods of time; a multiple check of the same object is thus possible, allowing set up of proper and reliable identification strategies. Detection speed also allows an increased volume of plastics sorted in smaller amounts of time. The second advantage is the lack of specimen preparation. Labels or other obstructions like dirt do not significantly interfere with readings thanks to the option of performing multiple checks. Finally this detection architecture presents another advantage: color does not interfere with proper resin identification. Except for black, the readings are independent of the color of the resin. Black containers represent a problem, because their color is a strong absorber in the near-infrared region. As a result, black plastic produces a featureless spectrum that, in many cases, does not allow proper identification [33].

X-rays analysis. This sorting approach is based on the study of the transmitted or reflected wavelengths in the X-ray region. This technology is mainly applied for PVC sorting. Chlorine atoms in PVC give a unique peak in the X-ray spectrum that is readily detectable. X-ray fluorescence (XRF), based on energy level variations of core electrons of atoms, can be used to detect elements in plastics, except for H, C, N, and O, that are usually detectable utilizing infrared spectroscopy. XRF presents many advantages: ease of use, rapid preparation and analysis of the sample, a large range of element detection, etc. It can be thus utilized *on-line*. Furthermore, it allows one to quantitatively determine the presence and characteristics of fillers, pigments, and flame retardants.

Laser aid identification. With this approach the detection architecture identifies plastics by shining a laser beam onto the surface to be identified and then analyzing the material's response. Utilizing an infrared thermographic system, various material properties including absorption coefficient, thermal conductivity, thermal capacity, and surface temperature distribution can be thus determined. The detected properties can then be analyzed to identify plastic type. The resulting system is suitable for quick analysis and identification of various plastics. The approach presents some advantages, that is: (1) different thickness, forms, and surface structures of plastics containers do not play any role in the identification and (2) printing and different additives (softeners) also do not play any role. The limits are related to (1) the presence, in terms of quantity and quality (particularly of carbon), of fillers, (2) difficulty in classification of plastics due to the evaluation of the maximum temperatures directly after laser radiation and, as a consequence of (1) and (2), a lower identification speed, in comparison with spectroscopy and X-ray, wherein checking of plastic containers can be carried out within *only* 1/10 s.

Marker systems. This approach entails marking either the container or the resin itself with something readily detectable. There are no barriers standing in the way of an automated sorting system that would read a hidden marker and identify resin type. Many studies and attempts were carried out in the 1990s, but with low success, mainly due to problems arising both at the production and recycling levels. Every packaging production line would have to install a marking system on their line. Also, each recycler would need to install a machine to scan for the marking on the containers.

Micro-sorting Plastic *micro-sorting* separate post-consumer plastics after a combination of comminution/separation processes specifically addressed to remove contaminants (e.g., non-plastic materials) and to increase bulk density, lowering storage requirements and shipping/transport costs, ease material handling and conveying, and liberating materials. Comminution is thus a fundamental and critical step when complex plastic waste streams have to be processed. Waste feed size reduction, in fact, has to satisfy comminution-liberation requirements and at the same time not produce too much fine fractions, which represent a problem in the further separation stages. According to the recycling plant "input" feedstock, different comminution strategies (e.g., number of comminution stages, utilized equipment, and operative conditions: dry or wet) have to be selected. Table 13 describes some of the comminution units commonly used to perform waste plastics shredding.

After comminution, plastic wastes are reduced in dimension but obviously maintain their original composition, that is plastics and contaminants (e.g., ferrous and non-metals, nonferrous, foams, film, rubber, labels, paint and coatings, metallic foils, glass, rocks,

Recycling Technologies. Table 13 Characteristics of the comminution units mainly utilized to perform waste plastics shredding

Comminution units	Characteristics
Hammer Mills (HM)	Movable hammers mounted on a rotating shaft hit and/or throw plastic against mill chamber or the other waste fed material. As a result comminution is realized. Particles are recycled inside the hammer until they do not reach a size lower than the aperture of a grid installed at the exit of the mill chamber. HM can handle without problems metal contaminants, high energy is required, milled particles are not uniform and the process produces a lot of noise.
Ring Mills (RM)	A RM is usually constituted by a steel rolling blade. This blade chops and grinds the plastic that is placed inside the roller. After it has been ground up to the desired size, it falls through the small holes located beneath the rolling blade.
Shear Shredders (SS)	This machine uses one or more rotating shafts, each with a set of cutting disks or knives mounted closely together on the shaft(s) that sits in a chamber at the bottom of a feed hopper. As the shaft rotates, the cutting devices pull the material down through the small spaces between the cutting disks/knives and the surrounding chamber.
Two or *Four Shaft Shear Shredders* (TSSS or FSSS)	The equipment can be composed by two- or four-shafts shredder with rotary blades (e.g., sharp-corners disks provided with hooks) and spacer combs, that keep the tools clean and make material unloading easy. Once the material goes into the hopper, the shredder catches the material and begins to cut it grossly. Thanks to the high cutting torque and the different conformation of the cutters group it is possible to shred pieces made of different materials. FSSS can handle metal contaminants, relatively low energy is required, particles are well liberated, good size control, throughput rate is lower in comparison with conventional shredding machine without screen, high maintenance cost.
Granulators (Gn)	The main feature of Gn is represented by the rotor conformation provided with short blades with staggered arrangement. During rotation every tool scratches the material and makes the final shredding. Gn are particularly efficient when material characterized by high thickness and resistance has to be cut. They realize a good liberation of the materials, a high throughput, they cannot handle metals (e.g., contaminants) and are characterized by high maintenance costs.
Cryogenic Comminution Units (CCU)	CCU realize a fine grinding by using liquid nitrogen, usually the material is blended with liquid nitrogen to provide sub-zero temperature level up to −150°C, to cool the material in a grinding mill. The cryogenic process produces fairly smooth fracture surfaces. Little or no heat is generated in the process. This results in less degradation of the rubber. Even if the price of liquid nitrogen has come down significantly, recently the process is always characterized by high operative costs. CCU are thus ideal for fine pulverizing of thermo plastic and heat sensitive materials, they also allow to reach an excellent liberation of the materials.

sand, dirt, etc.). Contaminant removal has thus to be carried out adopting different classification/separation strategies strictly linked to the size class distribution of the flow streams and to the contaminants' characteristics, with respect of the polymer/s to recover. For waste plastic recycling, different from what is usually carried out in the recycling sector, some separation stages are carried out in wet conditions, that is, using a fluid, usually water and sometimes heavy-media, to enhance separation devices' efficiency. In some cases, when the feedstock is particularly contaminated (e.g., automotive shredder residue), the recycling process starts with a water or heavy media-based separation stages in order to

remove as much contaminants as possible, as metal, rocks, glass, and sand that could damage size reduction equipment could negatively affect the further recycling stages.

To fulfil the previously mentioned classification/separation goals different techniques are currently used:

- Air classification
- Magnetic and eddy current separation
- Density-based separation processes:
  - Sink-float separation (wet process)
  - Jigging (wet process)
  - Hydrocycloning (wet process)
  - Centrifuge-based separation (wet process)
  - Air table classifiers and gravity table separators (dry process)
- Surface-based separation processes:
  - Electrostatic separation (dry process)
  - Flotation (wet process)
- Selective dissolution

Air classification. Air classification is commonly used to remove, in dry conditions, light contaminants such as dust, small foam particles, paper, glass powders, etc. Usually aspirators or air-cyclones are used [28]. Air classifiers are, in principle, simple devices, their control can vary according to feed characteristics. Equipment has to be correctly set for each stream of material. Separation of material is based on differences in terminal velocities in an airstream and is dependent on particle density as well as morphological and morphometrical attributes. An air-cyclone provides a simple and economical means for most medium to coarse and/or heavier particle collection applications. The centrifugal action and gravitational forces are the operative principles of cycloning. The air flow containing the particles to classify/separate goes through a high-velocity inlet, forcing particles to the collector wall in spiral motion. This, together with gravitational pull, forces the heavier particles downward, while the lighter ones travel upward via the inner vortex and out the air outlet on the top side. Air-based classification represents a fundamental step in any plastics recycling facility, handling complex plastic-rich parts from end-of-life durables (e.g., automotive derived parts, electronic and electrical devices, and appliances, etc.).

Magnetic and eddy current separations. These separation techniques are utilized both at the beginning of the recycling process, as well as after different handling stages. Usually ferrous (e.g., low-grade stainless steel, nickel alloys, etc.) and non-ferrous metals (e.g., aluminum) are removed using magnets [27] and eddy current [17] and/or electrostatic separators [29], respectively. The characteristics of these separation devices are described in the section dealing with metal recycling. The magnetic separators commonly utilized are belt magnets, magnetic pulleys, and drum magnets. The refining/control of the final products is usually carried out by high-intensity permanent magnets.

Density separation processes. Density separation is the most frequently applied technique to recover different plastics from a mixed plastics-pollutants streams. Such an approach can be also be profitably used to separate polymers belonging to the same family but containing different additives. Density-based separation techniques are more reliable than those "only" based on plastics surface characteristics. Bulk plastic properties, in fact, are less sensitive to possible alteration linked to specific environmental conditions (e.g., lighting, oxidation, etc.) or contaminant presence (e.g., oil, dirt, various costing, etc.). When density separation is applied, waste materials to be separated are placed in a medium characterized by a density that is intermediate between two or more densities of the particles constituting the waste. Following this approach, the fluid and/or recovered solid fractions have to be further processed for environmental and cleaning purposes, respectively.

Sink and float process. Sink and float separation systems are very common. They represent a simple and robust approach to separate materials characterized by different densities. The method simply involves depositing the materials in a tank filled with water or other liquid at a specific density. The lighter materials float and the heavier ones sink. For a sink and float system to work efficiently the materials' densities must differ greatly from one another (e.g., polypropylene, PP: 0.96 g/cm^3, high-density polyethylene, HDPE: 0.94 g/cm^3, medium-density polyethylene, MDPE: 0.926–0.940 g/cm^3, low-density polyethylene, LDPE: 0.915–0.925 g/cm^3, linear low-density polyethylene, LLDP: 0.91–0.94 g/cm^3). Furthermore, even when applied the process is difficult to handle because chemicals have to be added to water, to modify density, or specific heavy liquids [34],

as bromoform ($CHBr_3$) (2.87 g/cm^3), TBE: 1,1,2,2-tetrabromoethane $C_2H_2Br_4$ (2.95 g/cm^3) and methylene iodide (3.31 g/cm^3), have to be utilized. Such liquids are highly toxic, require stringent conditions to minimize exposure to workers and create plastics contaminated fraction that have to be further cleaned [34, 35]. Furthermore, the presence of possible contaminants and bubbles on the plastic surface, plastics particle size and shape, and characteristics of fillers and additives also strongly affect separation.

Jigging. Jigging is based on the application of repetitive pulsation actions to a particle bed by a current of water in stratification of plastic waste particles of different specific gravity. A jig operates in a cyclic manner where one cycle consists of four stages, namely, inlet, expansion, exhaust, and compression. In the inlet stage the bed lifts up en-masse. Near the end of the lift stroke the particles at the bottom of the bed start falling resulting in loosening of the bed which, in turn, causes its expansion or dilation. During the third and fourth stages of the jig cycle, the particles resettle through the fluid, and the bed collapses back to its original volume. The pulsation and suction is repeated to bring about stratification with respect to specific gravity across the bed height.

Hydrocyclones. Hydrocyclones are an economical and effective tool for separating mixed plastics and for removing many contaminants from a target plastic. A hydrocyclone transfers fluid pressure energy into rotational fluid motion. This rotational motion causes relative movement of materials suspended in the fluid thus permitting separation of the materials from one another [36]. The mixed fluid enters tangentially at the inlet, which causes the material to rotate within the vessel and ultimately to form a vortex. As this vortex of fluid spirals within the cyclone, heavier materials are forced outward by centrifugal force and down from the barrel section into the cone section. The materials more dense than the fluid flow down the inner wall and exit through the apex and out the underflow port with a portion of the fluid. Lighter materials are swept into the center vortex by inward fluid motion, and are carried vertically up through. Different from classical applications (e.g., mineral processing, food industry, pharmaceutical industry, etc.), when hydrocyclones are utilized in plastics waste recycling, two factors have to be carefully taken into account: (1) the tendency of recycled plastic particles to assume a plate-like shape and (2) the low differences usually existing between different plastics. Hydrocyclones can be considered intermediate density based separation units. For their characteristics, in fact, can be placed between a classical sink-float and a centrifugal process. Hydrocyclones present several advantages: they require very little space, are quite efficient, and outputs can be high; on the other hand, they require a more complex fluid-dynamic circuit (e.g., presence of pumps) and stricter control of feed characteristics (e.g., water solids ratio), etc.

Centrifuges. These equipments are very efficient; they balance optimal separation performances with a reasonably high separation rate. Morphological and morphometrical particle attributes affect in a limited way this separation, because of the applied centrifugal fields characterized by high values. This technique is particularly efficient when fibers and/or film-like particles have to be recovered.

Air table classifiers and gravity table separators. These devices come from mineral processing and metal recycling industries (e.g., automotive derived waste containing plastics). Their application is quite limited.

Surface based separation processes: *Electrostatic separation*. When this separation is applied usually the particle charging method is based on the triboelectric effect. Such an effect is based on a simple principle: when dissimilar materials, for example, particles of two different plastics, are rubbed together they transfer electrical charge and the resulting surface electrical charge differences can be used to separate the two plastics in an electric field; usually charged plastics fall down freely in the area between two electrodes. The particles are drawn to either positive or negative electrode according to the polarity of the charge. According to their trajectory they are thus collected and separated. Many plastics can be separated with this technique: ABS (Acrylonitrile Butadiene Styrene) and HIPS (High Impact Polystyrene) from end-of-life electronic devices, ABS and PMMA (Polymethyl Methacrylate) from automotive waste, PE (Polyethylene) and PP (Polypropylene), PET, (Polyethylene Terephthalate) and nylon, PVC (Polyvinylchloride) and PE from cable scrap, PVC and PC (polycarbonate) from bottles, etc. Electrostatic separation has two main advantages: it

can be carried out in dry conditions and the separation architectures and equipments are relatively simple. The main disadvantages are related to the shape of the particles, which influences their surface charge and separation effect. Furthermore when electrostatic separation is applied particles' humidity and moisture have to be strictly controlled.

Flotation. Froth-flotation is another possible method to perform plastics *micro-sorting*. Flotation works similarly to sink and float systems. Froth-flotation is based on the plastic particles surfaces' chemical-physical attributes; for this reason it is particularly suitable for when plastics of similar densities but different surface properties have to be separated. As outlined in [31] a specific plastic can be separated from a complex waste stream by flotation after treating the waste in alkaline solution [32, 33]. Separation of mixed plastic, according to different plastic typologies, can be achieved utilizing appropriate collectors. A large literature exits on this topic [31, 37, 38]. Furthermore, specific wetting agents can be also used to prepare a hydrophobic property [36, 39]. Due to the conditioning some plastics that normally sink (hydrophilic behavior), adhere, according to their composition, to air bubbles generated by a controlled air flow pumped into the system. As a result such particles float to the surface. Materials that are not affected by the bubbles sink to the bottom. Collection systems at the top and bottom of the system can then recover the separated fractions. Other parameters affecting froth flotation are particle size and shape. The main advantages linked to the utilization of froth flotation in plastic recycling are that the technique is well known and settled from a technological point of view and that it is quite flexible in terms of application possibilities. The limitations are primarily related to plastic particle surface status (e.g., dirtiness and/or pollutants) and to the difficulty in defining precise control logics because of plastic waste variability and important factors that have to be taken into account.

Selective dissolution. Selective dissolution is a plastic sorting option that was investigated in depth, as the markers for macro-sorting purposes, in the early 1990s. The process separates mixed or commingled plastics waste into nearly pure reusable polymers without any mechanical pre-sorting techniques. The selective dissolution is based on two different principles: temperature-dependent solubility of different plastics in a single solvent and solvent-dependent solubility of different plastics at a specified temperature. These technologies are not cost-effective for commodity polymers but are sometimes the only solution for the liberation of different coatings associated with PP, such as paint or skin.

Chemical Recycling Chemical recycling, using a depolymerization process, is applied to convert waste plastics, utilizing heat or heat and catalyst, in smaller molecules (e.g., gases, liquids, solid waxes, etc.), that can be used as a feedstock to produce new plastics or other chemical products. The term chemical is thus used, because an alteration is bound to occur in the chemical structure of the polymer. In recent years, a lot of attention has been addressed to this recycling approach (e.g., non-catalytic thermal cracking, catalytic cracking, and steam degradation) in order to produce different fuel fraction from plastic waste products. Several polymers can be profitably processed adopting this approach. Polyethylene terephthalate (PET), certain polyamides (nylon 6 and 6.6), and polyurethanes (PURs) can be efficiently depolymerized. The resulting chemicals can then be used to make new plastics that can be indistinguishable from the initial virgin polymers [40]. Polyethylene (PE) has been targeted as a potential feedstock for fuel (gasoline) producing technologies [41]. The two cited cases are just an example of chemical recycling potentialities. A great deal of literature exists on this topic, because a lot of research efforts and technologies development have been addressed to improve the utilization of this recycling technology. Chemical recycling, in fact, presents, at least in principle, a big advantage with the possibility of treating heterogeneous and contaminated polymers with limited use of pre-treatment [42]. An excellent review and analysis of this technique is reported in Al-Salem et al. [41].

Energy Recovery Energy recovery is based on using waste plastics to produce energy in the form of heat, steam, and electricity. Deriving from crude oil, waste plastics when burned generate a high calorific value. Furthermore, producing water and carbon dioxide upon combustion, plastics behave similarly to other petroleum-based fuels [43]. Such a solution can be

considered technically and economically correct when the other recycling strategies (e.g., sorting, mechanical, chemical, etc.) cannot be profitably applied. A typical example is represented by *fluff*, which is the light fine fraction resulting from car dismantling. *Fluff* is constituted of plastics, rubber, synthetic foams, etc. and well fulfils the concept of *waste-to-energy* product. This material, after a "washing" stage, (e.g., polluting materials removal: copper, aluminum, brass, iron, etc.), can be profitably utilized as fuel. Energy production can thus dramatically contribute to increase the full recovery of such a kind of secondary waste with a lower environmental impact (e.g., landfill reduction). Recent studies demonstrated that when plastic waste energy recovery is performed, foams and granules contribute to destroy CFCs and other harmful blowing agents present [44]. However, several environmental problems related to the emissions have to be faced when such an approach is followed, mainly the presence of (1) volatile organic compounds (VOCs), (2) particulate solids, (3) particulate-bound heavy metals, (4) polycyclic aromatic hydrocarbons (PAHs), (5) polychlorinated dibenzofurans (PCDFs), and (6) dioxins. Finally, the presence of flame-retardants (FRs) can influence the combustion process.

All the considerations previously outlined refer to thermoplastics. When thermoset plastics have to be recycled several problems arise. They, in fact, cannot be readily dissolved, melted, re-compounded, and reshaped like thermoplastics. Specific recycling strategies have to be set up. Mechanical recycling is thus primarily addressed to fine grind them for a further re-use as fillers in new thermoset resins or thermoplastic compositions or to recover natural filler or fibers originally utilized in the original thermoset product. In any case, chemical recycling as well as energy recovery processes can be applied to large range of thermoset materials.

Recycling Technologies: Fibers (Textiles and Carpets)

Fibers, both natural and artificial, are commonly utilized in daily life, as well as in technical applications. Also with reference to fiber-based apparels, legislation fixed severe constraints about their disposal at the end of their life-cycle; as a consequence proper recycling systems must be adopted. Recycling can be carried out via two different approaches: (1) to recover energy or (2) to recover fiber materials for their further reuse.

The energetic utilization of end-of-life fibers is not particularly efficient, because the energy generated from burning is less than the energy required for fiber manufacturing. This approach makes sense, from an ecological point of view, since proper combustion results in energy gains without significant air pollution and the consumption of resources. However, the production of synthetic fibers is more expensive compared to non-fibrous plastics. Also the production of natural fibers, like cotton, requires a large use of resources (e.g., water). Hence, product recycling of fibers will increase the sustainability of products and processes. With reference to cotton its caloric value is about 17 MJ kg [45], on the other hand, the energy demand for producing 1 kg of raw cotton is between 38 and 46 MJ kg [45] considering an oil consumption of 1 kg. As a consequence, any recycling process is more convenient than thermal utilization. If the same considerations are applied to man-made fibers, a different fiber-related-energetic-balance can be drawn. The water consumption for the production of synthetic fibers is significantly lower (about 1/10) compared to cotton. For acrylic fibers, for example, the demand ranges between 0.3 and 15 l H_2O per 1 kg of fibers [46]. Energy consumption for polymerization, spinning and finishing is between 369 and 432 MJ kg [45] [46]. Given a caloric value of crude oil between 38 and 46 MJ kg it can be concluded that for 1 kg of fiber about 11 kg of crude oil is necessary. However, during thermal utilization only the caloric value can be used that is about the same or slightly lower compared to crude oil. From this it is obvious that thermal utilization should be replaced by any other process.

Technologies actually available for textile and carpet recycling do not offer satisfying solutions in terms of economic and ecologic demands, this fact is mainly linked to the difficulty of developing a correct separation, first, and a full characterization, after, of fibers, and other polluting materials. Fiber composition as well as their morphological and morphometrical attributes represent important factors to develop optimal re-utilization strategies, this last aspect being particularly relevant in carpet recycling. Recycling technologies have been developed, in terms of

logics and complexity, dealing with textiles and carpets, respectively.

Textiles Systematic textile recycling originated in the Yorkshire Dales (Great Britain) about 200 years ago, and the *rag and bone men* of days past were the predecessors of the actual "textile recycling businesses." They collected not only clothing, but also handbags, shoes, bedding, and curtains for re-use. These materials were then often sold abroad, as second hand clothing, but also to provide raw materials to the "wiping" and "flocking" manufacturers and for fibers reclamation to make new garments. Furthermore, it is well known that textiles were and are recycled for papermaking. Textiles recycling can follow different rules according to "recycled textile function":

- The original product function (e.g., clothing reused again as clothes)
- The textile material properties (e.g., absorbency in a wiper, fire retardant non-woven in a mattress spring cover, etc.)

According to their reutilization, recycled textiles can be up-cycled or down-cycled. In the first case they are used for more technically demanding application (higher value); in the second case, they are utilized for less demanding application (lower value). In these two cases, original textiles have to be mechanically processed, adopting specific comminution, classification, and separation strategies in order to recover the constituting fibers from the other materials (contaminants). Products resulting from these approaches are usually: shoddy (e.g., fabric made from the recycling of knitted products), mungo (e.g., fabric made from the recycling of woven products), cotton rag paper made from recycled cellulosic fabrics, etc.

As previously outlined, textile fibers can be classified into natural (e.g., cotton and wool) and synthetic. Recycled fibers demand is strongly influenced by several factors as:

- Fibers composition and characteristics. The presence of fiber blends (e.g., elastic polyurethane) that make recycling more difficult, or the presence of polymers not commonly recycled (e.g., acrylics and polyesters) negatively impact on fiber recycling process
- The possibility to identify new industrial sectors where recycled fiber products can be utilized

Textiles Source and Characteristics Textile wastes can be originated by industry and/or consumers.

Textiles industrial wastes are originated during the processing, production, and/or the manufacturing phase. Such wastes are easy to recycle, the fiber composition and characteristics being known. Contaminants are usually not present.

Textiles consumer wastes are more difficult to recycle. They are usually constituted by fiber mixtures and contain "contaminants" (e.g., non-fibrous materials such as buttons, buckles, or other metal parts).

Waste textiles are usually collected by charitable organization. End-of-life apparel is then sorted according to a possible re-use, that is:

- As re-wearable, cleaning and wiping clothes, short cut for nonwovens as well as for the paper and cardboard industry [45]
- As recovered fibers, in this latter case a mechanical processing has to be applied in order to produce fibers of desired length for their further re-use

Textiles Recycling Technologies According to the considerations previously outlined recycling technologies are applied when "recycled fibers" have to be produced. Waste textiles processing is usually carried out in dry conditions. Such an approach presents two advantages: (1) low energy consumption (e.g., drying is not required) and (2) no water treatment. In this perspective the main actions and the related equipments are reported in the following:

- Human based sorting (e.g., separation of the different apparels typologies)
- Milling and classification, to obtain fibers of the requested morphological and morphometrical attributes
- Separation of the different fibrous and non-fibrous material according to their physical-chemical attributes
- Fiber tailoring and characterization

Manual Preparation and Sorting A human based sensing approach is commonly followed to recognize

and preliminary separate the different apparels according to the different types of fibers. After this phase of sorting/grading, clothes are then packed as bales. Each bale is obtained by pressing and identified in terms of average fiber composition and weight. Each bale is thus assumed as the minimal identifiable raw material unit to address to different possible recycling phases, that is:

- Second-hand clothing
- Wiping and polishing cloths for industry
- New products in the reclamation sector (e.g., component for new high-quality paper, upholstery, insulation, even building materials, etc.)
- Filling materials (e.g., car insulation, seat stuffing, etc.)

Milling and Classification Textiles milling is usually carried out utilizing equipment where cutting actions are maximized and the possible comminution effects on hard components (e.g., buttons, zippers, etc.) are minimized to reduce the presence of fine particles contaminants. Classification is usually carried out to recover/remove fine fractions before the further tailoring stage/s. Usually zig-zag classifier and/or pneumatic tables are utilized. As a result of this processing non-ferrous metal and plastics, if present, can also be recovered for further recycling.

Separation Separation is usually addressed to recover the non-textiles materials inside the milled textiles products. Separation is usually carried out adopting magnetic separators (e.g., hump magnet, magnetic pulley, etc.). Metallic fractions (e.g., button, zippers, etc.) are thus recovered.

Fibers Tailoring and Characterization Tailoring is a process specifically addressed to produce individual fibers and to disintegrate all residual textiles and yarns. At this stage of the process the main target is thus to develop a processing sequence able to progressively produce fibers from fabric. A *three-in-one* process, finalized to separate fibers from fabric, is usually applied, that is: picking, pulling, and tearing. Such a goal is usually reached adopting a series of drums with spiked surfaces characterized by an increasing number of finer spikes. Fibers classification is then carried out adopting air classifiers, their characteristics can vary according to classification goals. Tailoring can produce rather long (greater than 2 mm, e.g., new "long fiber" textiles making, nonwovens, etc.) or short (less than 1 mm, e.g., viscosity modification, composite reinforcement, concrete, mortars, adhesives, etc.), fibers according to their re-use. Tailoring process has to be quantitatively and qualitatively assessed, performing a morphometrical and morphological fibers characterization. Fibers morphological and morphometrical attributes (e.g., fiber length, width, and profile structure) thus represent important factors to develop optimal recycled fibers re-utilization strategies, allowing correct identification and new potential applications. Most of the literature describing the recycling of fibers does not provide any details about fiber characterization. Recently, a procedure (MorFi), originally developed for pulp characterization [47], was successfully applied for short fiber characterization [48]. Following this procedure, the length of fibers (*FL*) was measured automatically adopting an imaging-based approach: a suspension flowing through a flat cell observed by a digital CCD video-camera. The analysis of morphological properties of fibers performed by MorFi provided arithmetical average length of fiber (the value most sensitive to the effect of shortening of degraded fibers during their mechanical treatment), expressed by the equation

$$FL = \frac{\sum z_i l_i}{\sum z_i}$$

where z_i is the number of fibers in a given class of length, and l_i is the mean length of fibers in the given class.

Carpets Differently from textiles, carpets represent a more difficult product to recycle, the reason being linked to its compositional characteristics. A carpet, in fact, is usually constituted by a two-layers backing of polypropylene. In between the layers styrene-butadiene latex rubber (SBR) is joined by calcium carbonate ($CaCO_3$) and the fibers are tufted into the rubber (the majority being nylon 6 and nylon 6.6 textured yarns). The SBR adhesive is a thermoset material, which cannot be re-melted or re-shaped. Nylon generally performs the best among all synthetic fibers as carpet face yarn, but it is also the most expensive. This also explains why most of the recycling effort is on nylon

recovery. Due to the "complexity" of carpet, at least in comparison with textiles, if fibers have to be recovered, more complex comminution-classification-separation strategies have to be applied. It is possible to recover fibers, mainly polypropylene, from the backing that range from 3 to 25 mm in length. On the other hand, a fraction originating from the pile yarn is obtained. The latter fibers are between 12 to 25 mm in length [49–53]. The composition of this fraction is reported to have 36% PP (fibers from the backing), 18% nylon (fibers from the pile yarn), and 46% (non-fibrous) SBR and $CaCO_3$ [50, 51]. An extensive literature exists on different possible positive re-use of recycled carpet fibers in concrete and soil reinforcement and several other applications [49–53].

Carpet Source and Characteristics Carpet wastes can be originated by industry and/or consumers. Different from textiles, post-consumer-waste carpets represent the larger source. Carpet can be considered a sophisticated product. It is, as previously described, constituted by many materials assembled to assure the durability of final manufactured product, the consequence is that its disassembly and recovery is difficult and requires complex technology and suitable separation control actions to properly recover and certify the different constituents. Carpet-derived products, both fibers and polymeric materials, can be thus originate lower or higher value recycled products, according to the adopted recycling strategies.

Carpets Recycling Technologies As for waste textiles, carpets recycling technologies are carried out in dry conditions. The main processing steps are outlined in the following:

- Preliminary fiber identification and sorting
- Comminution and classification
- Separation
- Solvent extraction of nylon
- Nylon depolymerization
- Melt processing

Fiber Identification and Sorting Carpet recycling strategies have to be set up according to upper surface fiber characteristics. Fiber identification thus represents a key issue to properly address carpet to different downstream recycling tracks [54]. Usually portable infra-red (IR) spectrophotometers are utilized; they usually allow a fast and reliable recognition of nylon 6, nylon 6.6, polypropylene, polyester, and wool fibers. Sorting is usually applied in the collection point; sometimes such a control is centralized in the stocking facilities of the recycling plant. This last solution is usually more efficient.

Comminution Shredding and/or grinding are the commonly applied size reduction actions [45, 55]. These actions are usually performed by a mill with rotary drums equipped with hardened blades. The material after shredding is then sieved by a grid installed at the exit of the mill chamber. The material, which has become sufficiently small, is thus discharged from the mill chamber, the other remains in the mill chamber for re-cutting. Comminution usually produces an increment of the temperature, such a fact can negatively affect milled materials characteristics, for this reason comminution equipments are usually designed to realize a high torque and a low rotational speed. Studies have been carried out to perform carpet cryogenic milling [56]. Following this strategy comminution results are particularly efficient because the *freezing action* of liquid nitrogen, or CO_2, changing the mechanical behavior of the different carpet components allows their better milling and liberation of the different constituents. Costs are usually higher than classical blade based milling and as a consequence the use of this technology is limited. In some cases milling is also realized utilizing water jet [57].

Separation Carpets constituents separation is usually carried out adopting different processing strategies based on a series of combined comminution-classification stages and a further density based separation utilizing both the "simple" gravitational and/or centrifugal field. The second approach is usually adopted to enhance the differences existing between the different materials to separate. Following these strategies filler, nylon and polypropylene can be recovered. A detailed description of this approach is reported in two papers from J. Herlihy [58] and H. P. Kasserra [59]. In some cases the separation of the different carpet components is realized without comminution [60, 61]. Waste carpet is thus subjected

to a preliminary clipping of the exposed fiber, a further bombardment of air and steam of the carbonate-filler latex backing and a combination of peeling and picking. The combination of these actions allows recovery of up to 95% of the face fibers.

Solvent Extraction of Nylon Such an approach is utilized when high value nylon has to be recovered from carpet at the end of its life-cycle. Solvents commonly utilized are aliphatic alcohol [62], alkyl phenols [63], and hydrochloric acid [64]. A preliminary comminution of the carpet is always required. The optimal size-class ranges between 1 and 5 cm. Solvents utilization presents both advantages and disadvantages. The advantages are that the use of solvents allows to good recovery of nylon (yield about 90%) characterized by a relatively low degradation. The disadvantages are those related to the use of chemicals and their further recovery and/or re-use, when possible. Furthermore, process temperature and the time required for nylon extraction are other constraints to take into account. Their values change according to the dissolution process adopted. Sometimes **S***uper* **C***ritical* **F***luids* (SCF) are utilized [65, 66]. The process is commonly carried out in batch conditions at high or low pressure and temperatures according to the fluid utilized: CO_2 [65] or formic acid [66], respectively.

Nylon Depolymerization Depolymerization is usually applied to recover nylon, from nylon carpets, because nylon resin has a remarkable higher value than the other polymers commonly utilized in carpet manufacturing [67]. A typical depolymerization process [68] is based on a preliminary carpet sorting and a further mechanical shredding, the recovered nylon six face fibers are sent to a depolymerization reactor and treated with superheated steam in the presence of a catalyst to produce a distillate containing caprolactam, that is the single monomer that after polymerization originates nylon 6. The crude caprolactam is then distilled and re-polymerized to produce again nylon 6 [69]. Another process to obtain caprolactam is based on the utilization of a two-stage pyrolysis process. The ground nylon carpet, without separation, is dissolved with high-pressure steam and then continuously hydrolyzed with super-heated steam to form caprolactam [70, 67].

Melt Processing Melting and compounding are two other processes currently carried out for carpet recycling. Both require a preliminary size-reduction process. By melting, a thermoplastic polymer is converted by extrusion in resin pellets [45, 55], if more polymers are blended together and then extruded a compounding process is applied. For its characteristics, the products resulting from comminution have to be "compacted" before the extrusion process; they, in fact, are quite bulky. Specific equipment (crammer-compactor feeder) is thus utilized. Extruders can vary, ranging from single screw, twin-screw co-rotating, or twin-screw counter rotating architectures according to feed and required products characteristics. The melted-extruded products are then cooled and cut to obtain pellets. Usually ring, strand or underwater pelletizers are utilized. In Table 14 are synthetically reported some of the characteristics of pelletizing devices commonly utilized for waste-carpets-based melted-extruded products chopping.

Melted-extruded products present different characteristics and market values according to the characteristics of the original feed-stocks [71]. When carpets are constituted by polymers as plastic and polypropylene [72], the resulting pellets (e.g., compounds) are of low quality due to the fact that they are thermodynamically unstable when melt-mixed [73, 74]. They must be thus stabilized to prevent coalescence during melt processing [75]. This process of stabilizing polymer blends is commonly called *compatibilization*. It usually consists of the addition of a premade block copolymer composed of blocks that are each miscible with one of the homopolymers [76].

A melting plant is relatively simple to utilize and maintain. Its main limits are primarily related to its operating principle, that is, low flexibility in terms of possible modification of final products characteristics. Furthermore, the presence of water represents a further environmental processing problem (e.g., H_2O filtering, temperature control and re-circulation to face when melting is applied).

Pellets resulting from the previously described melt-based process are commonly utilized in the

Recycling Technologies. Table 14 Characteristics of the pelletizing equipment utilized for waste-carpets-based melted-extruded products chopping

Equipment	Characteristics
Water Ring Pelletizer (WRP)	A WRP is commonly utilized for liquid polymers in which pellets fall from cutter knives into an annulus on the surface of a body of cooling liquid. The velocity and trajectory of the pellets are controlled by the projection of a spray of cooling liquid radially across the dies from which the pellets are severed. Band heaters in proximity to the dies maintain the polymer in a liquid state prior to extrusion. WRP is particularly suitable to be applied for polymers characterized by a low melt flow index (e.g., polyethylene).
Strand Pelletizer (SP)	In a SP polymer strands discharging from the die head are sent to cooling water-based-device. The water "wetting" the polymer strands is eliminated utilizing an "air knife." The dry, solidified polymer strands are then delivered towards a strand pelletizer where cutting is applied. One of the main disadvantages of SP is that a large floor space and particular care has to be addressed to control possible strands breakage. Polymers as nylon, polyester terephthalate, and polypropylene are commonly processed by SP.
UnderWater Pelletizer (UWP)	UWP is usually constituted by an extruder that conveys the polymer melt to the die plate through the start-up valve. The melt stream is then divided into a ring of strands that flow through the annular die into a cutting chamber flooded with process water. A rotating cutter head in the water stream cuts the polymer strands into pellets, which are immediately conveyed out of the cutting chamber. The pellets are cooled and transported in a slurry to the centrifugal dryer. Pellets are then separated by water through rotating paddles. Polymers as nylon, polyester terephthalate, and polypropylene are commonly processed by UWP.

molding process, as they result from recycling or are blended with virgin polymers. Other common applications are in glass fiber-reinforced composites, where they are utilized as matrices [77].

Future Directions: Innovative Control/Sorting Devices/Logics Integration in Recycling Plants

The different recycling technologies described and analyzed for the different waste materials (e.g., paper, glass, metals, plastics and textiles) clearly demonstrate that improvements in comminution-classification strategies, and further separation technologies (e.g., magnetic, electrostatic, sink-float separation, flotation, etc.) can be mainly carried out by introducing innovative control devices and architectures, as equipment technology and characteristics have reached a very high level of quality and reliability. Such classes of innovative devices can be also utilized as detection systems to realize innovative sorting architectures. Single and/or combined control/sorting actions can be thus developed, taking into account different aspects: (1) waste streams physical-chemical characteristics, (2) market requirements for concentrates of specific quality, and (3) related innovative control/sorting device/logics operating at different scale, that is, at single equipment and/or plant scale.

Waste Feed Streams Characteristics

Processing actions applied to different particular solids waste streams, constituted by different materials (e.g., paper, glass, metals, plastics and textiles), usually perform a change of some physical attributes of the wastes, these changes depend on the intrinsic characteristics of the constituting materials and the actions applied. For example, comminution produces a reduction of the size class distribution of waste, originating smaller particles of different morphological and morphometrical characteristics and producing the liberation of the different materials originally locked (e.g., mixed particles). On the other hand, separation actions allow grouping together of particles according to a specific property (e.g., density, conductivity, magnetic, color, texture, etc.), originating a concentrate.

What are the strategies to apply to make improvements in terms of a correct utilization of waste streams characteristics versus *adopted recycling technologies finalized to a higher recovery of concentrates?*

The answer is in principle very simple, being related to the correct application of recycling technologies taking fully into account waste streams' physical-chemical characteristics. For example, the definition of proper comminution strategies addressed to obtain adequate size class distribution, minimizing the presence of fines and ultrafine particles, is obviously related to a correct knowledge of wastes. With reference to plastics, milling actions based on cutting represent the best solution; on the other hand, impact actions better realize comminution for glasses. Lack of knowledge of the composition of the waste materials to process, in terms of constituents and their time variation, can strongly impact the quality and quantity of the final recovered products. Waste materials present a high degree of compositional variability. Batch sampling, as usually performed on feeds and processed flow streams, does not allow performance of a full and continuous monitoring of the materials flow. Low-cost, reliable, and robust waste streams' physical-chemical characteristics detection devices, realizing continuous monitoring, could represent the solution to performing a *full-time-independent-evaluation* of waste materials streams handled in the plant.

Waste Derived Concentrates Recovery and Quality Assessment

Concentrate quality affects its value and, as consequence, the economic revenue of the recycling process. The possibility to realize a continuous full monitoring of concentrate characteristics is important: (1) to apply correct waste processing strategies to quantitatively and qualitatively maximize recovery, (2) to build a production data base embedding produced product characteristics, and (3) to perform a full products certification.

Recovery maximization is one of the key issues when recycling technologies are applied. Waste products are usually constituted by different materials of different characteristics. An optimal target could be represented to set up recycling actions addressed to separate and recover all the different waste constituents. In this case "the zero-waste" target should be fully reached. If successful, this strategy could allow re-integrating all the wastes in new production cycles. Such a goal is almost impossible to reach, but the strong scientific development, the related technological innovation and the larger attention of new generations towards environmental problems has and will continue to contribute to introduce new technologies for a more efficient recovery. To maintain a trace of when and what is produced in terms of WDPs is another key issue. The achievement of this goal allows establishment of a time correlation between waste feed and resulting concentrate. Correlations are useful not only in technical terms, for a better understanding of plant behavior with respect to waste feed variations, but also because they provide useful information about consumption and related waste production, contributing this way to better waste collection and handling strategies prior to the application of recycling technologies. Finally, product certification in the recycling sector sometimes represents a negative point. The proposed approach could strongly contribute to solving this problem, allowing at the same time a big step forward in product quality detection performed continuously and not on a batch basis.

Control Actions and Logics

As outlined in the previous paragraphs, one of the key points related to a systematic introduction of control logics, inside processing layouts, is to define simple, reliable, robust, efficient, and low-cost architectures able to perform a full characterization of the different flow streams in terms of waste feed and/or resulting product composition, that is, grade of the recovered materials and presence and characteristics of pollutants. The two aspects are intimately linked to the definition of suitable *process-control-strategies* and to the subsequent certification of the recovered materials.

How can control actions and logics be fully introduced and widely utilized in waste recycling?

Each material is characterized by specific attributes; these attributes are usually detected, with sensing devices able to collect one or more piece of information related to the characteristics of handled materials. Information is then processed following logics oriented to maximize the positive effects of the single and/or or group of actions. Control actions can be commonly categorized in four groups:

- *Feedback control*: a control system that monitors its effect on the resulting product. On the basis of the

collected information, tuning actions are applied on equipment, recycling plant sections, and operative variables in order to modify the output (product) accordingly.

- *Feedforward control*: a control in which changes are detected at the process input (waste feed) and an anticipated correction signal is applied before process output (concentrate) is affected.
- *Cascade control*: an automatic control system in which various control units are linked in sequence, each control unit regulating the operation of the next control unit in line.
- *Ratio control*: a control procedure in which a predetermined ratio between two or more variables is maintained.

Feedback and feedforward controls are most commonly utilized in recycling.

Waste recycling flow streams are usually constituted by complex particulate solids systems. A particle is thus the minimum portion of material that can be processed. Each particle is characterized by different attributes: size, shape, composition, texture, etc. To define a control logic means identifying one or more rules to handle one or more of the previous mentioned attributes as they have been collected inside a particle flow stream, with the specific aim of verifying whether processing has produced an output satisfying the expected requirements of these attributes, both qualitatively and quantitatively, in the concentrate. In plastic recycling, for example, if a recovery of PP and/or PE has to be carried out, the presence of other plastics materials as PET or PVC, or other pollutants, as metals, glass, etc., must be avoided. In this case, the attribute composition plays a pre-eminent role in control logic definition. Actions to perform are related to: (1) the characteristics of equipment/s generating the PP or PE concentrate and (2) the parameters allowing their operation. Relationships existing between equipment/s operative conditions (processing parameters set up) and quality of the output, for a specific feed, have to be clearly investigated and formalized, constituting the basis for control logic implementation. A quantitative evaluation of the composition of PP and PE concentrate is thus fundamental to set up the logic in a quantitative way. In this case, as when recycling technologies have to be applied to other waste products, the quantitative collection of the attributes qualifying, or certifying, an intermediate and/or a concentrate product is not easy in terms of economically acceptable devices. This problem is common in waste recycling, where the value per unit of weight of product is usually low. To be economical, a process requires the processing of large quantities of waste and the production of a corresponding high amount of waste-derived concentrate. Often this condition does not match with the adoption of sensing devices that, to fulfill the previous requirements, are usually very expensive. A different approach has thus to be followed. If composition can be correlated with other parameter/s, easily detectable, a transposition logic can be applied: that is, the correlated property can be assumed as the control parameter and new control logics applied. Such an approach is particularly meaningful when *on-line* control logics have to be defined. The possibility to apply transposition logics sometimes produces a strong simplification in control. An example of what is described is reported in the following where different examples of sensing architectures based on **H***yper***S***pectral* **I***maging* (HSI) techniques are reported with reference to some of the materials taken into account in this section.

Plant Scale Control

The application of control actions and logics, on a recycling plant scale, can be considered a common practice. Originally performed, and in some cases also today applied, following a human senses-based approach, with the technological development "humans" have been and are being replaced by sensing devices. The first step to implement a plant scale control consists of the identification of some key points inside the plant where product characteristic detection can give useful information about the process. According to the values of the detected parameters, and utilizing pre-assigned rules, the equipment operative variables are modified accordingly. These actions can usually be performed with a feedback or a feedforward approach, more rarely adopting a cascade control. Approaches vary according to waste materials characteristics, control objectives, and implementation modalities: (1) introduction of control logics inside an existing plant or (2) in new ones.

In this latter case, a large flexibility in control architecture design can be performed, not existing predefined plant architectural constraints.

Single Equipment Control

Following this approach, control actions and logics play at single equipment scale. Process and product parameters detection is carried out before (feedforward) and/or after (feedback) the single processing unit and control logics act accordingly. Such an approach is very promising, especially for future improvements in the recycling sector. The "intelligent processing machine," is equipment able to "understand" how it works, according to feed flow stream and resulting product characteristics, and able to modify its "behavior" accordingly, adopting pre-assigned and/or time-dependent learning rules. This is particularly relevant in recycling, where very often handled materials do not show constant compositional characteristics, affecting equipment performance.

Innovative Sensing Technologies in the Waste Sector

In recent years a lot of innovative sensing technologies and related control logics have been proposed in recycling. A sensing station is usually constituted by a conveying device (e.g., conveyor belt, vibrating channel, etc.) for the separation and steadying of the material, and a detection unit, positioned underneath or above the conveying device or at the material discharge area. Collected information can be then utilized to quantitatively assess material characteristics (certification) or to modify operative conditions of the equipment handling the materials before or after sensing (control) or to develop separation actions by actuators, e.g., valve bank blowing out materials constituents according to specific component characteristics (sorting). In the following, some sensing devices and their operative principles, together with possible application fields, are described.

E*lectronic* I*maging* (EI) Vis*ible* (VIS) Wavelength Based EI-based sensing devices and algorithms [78] are the most widely used in recycling. They belong to the first class of control device utilized in this sector. EI application in recycling technologies comes from architectures developed in mineral processing and food control sectors. Such a technology moves from black & white (B&W) to color sensing systems. Actually color is widely applied in many recycling sectors: glass, WEEE, metals scraps, fluff, wood, etc. Color-based sensing is based on the collection and analysis of materials surface characteristics. Such an approach can represent sometimes a limitation because the collected information "only" relates to the surface (e.g., varnished objects in principle cannot be detected in a material-related way). In many cases, for the relatively low cost of this approach, EI will solve many control/sorting/quality assessment problems when the materials to check have passed shredding stages beforehand that remove the existing surface coatings or that break up the material in a way that with utmost probability uncoated fracture faces can be observed [79]. EI-based detection architectures are commonly constituted by an energizing source (lighting system), a CCD, matrix, or single array camera. Single array-based devices are particularly suitable to be utilized in waste material quality control because the detection principle (scan line) and the target of investigation (waste particles) moves towards each other with a constant speed. Waste particles can thus be fully investigated adopting different time-scale-related sampling strategies according to control/quality actions to apply.

E*lectronic* I*maging* (EI) n*ear* I*nfrared* (NIR) Based The principle that is at the basis of NIR technology is the measurement of object reflectivity within a wavelength ranging between 1.100 and 2.100 nm [80]. In this wavelength range, materials such as plastics, paper, and textiles are characterized by specific spectral firms allowing their recognition. This range of wavelengths is not visible to the human eye. This is also the reason that optical sorting systems must be used. The new generation of NIR-based detection devices can operate a good plastics distinction (e.g., PP, PS, PET, EPS, PC, or PVC) [81], as well as allow identification of materials such as paper, card, cardboard. or wood and natural fibers. A recognition limit of such a procedure is in the identification of materials that cannot be identified due to a lack of individual stone, porcelain, or dark materials, that, for the low level of reflectance, in the investigated wavelength range, do not allow recognition.

X-*Ray* F*luorescence* S*pectroscopy* (XRF) XRF is based on X-ray emission by a radioactive source or X-ray tube inside an XRF unit. X-rays emitted are absorbed by the atoms in the waste sample generating fluorescence as the atoms relax and release energy. The emitted wavelengths, as well as the energy released, are a function of the elements constituting the waste sample. Emission intensity is correlated to the content of a specific element within the sample. Such a technique was and is widely used in many recycling sectors as: metal/alloys, glass, plastics, wood (detection of arsenic, chromium, and copper in treated wood [82] and treated wood waste [83–85]), WEEE, waste-derived-fuels, etc.

D*ual* E*nergy* X-R*ay* T*ransmission* (DE-XRT) DE-XRT is similar to that applied for luggage inspection and medical applications. Waste products are transported by a conveying belt. Waste material is energized, from the bottom, by X-rays. Transmitted radiation is collected by X-ray line detectors [86]. In order to separate the effects of density of the X-rayed object and the material thickness, the radiation intensity is generally measured in two different energy ranges. Following this approach thickness influence is eliminated and the radiation that passes through the material allows performance of materials recognition according to its density. The sensing approach allows classification of the material on volume basis. Different from EI or NIR techniques, surface characteristics (e.g., dust, water, small quantities of pollutants) do not practically influence recognition.

L*aser-I*nduced B*reakdown S*pectroscopy* (LIBS) The system analyzes the optical spectrum, or fingerprint, of a small spot on each metal particle that is evaporated using powerful laser pulses. LIBS has been widely used as a diagnostic technique for the analysis of both surfaces and gaseous streams for metals [87, 88]. LIBS uses a high-power laser that is directed towards the sample through a series of mirrors and lenses that create a small micro-plasma on the surface of the targeted material. Due to the extremely high temperatures produced within the plasma (greater than 20,000°C) the atoms within the plasma emit light (or energy) characterized by different wavelengths. Certain wavelengths of energy are unique to different elements. The system then analyzes the optical spectrum, or fingerprint, of the micro-plasma collected and re-directed toward a fiber optic cable, which then feeds the signal to a spectrometer. The intensity of the emission is directly proportional to the amount of that element present in the sample. The costs and complexity of the system, as well as limitations in efficiency, are the main reason why LIBS is only applied in a number of very specialized operations, commonly for surface contamination. Applications have been developed with reference to wood waste contaminated with chromated copper arsenate sorting [89] and scrap metals [90].

H*yperspectral* I*maging* (HSI) HSI, known also as chemical or spectroscopic imaging, is an emerging technique that combines the imaging properties of a digital camera with the spectroscopic properties of a spectrometer able to detect the spectral attributes of each pixel in an image. Thus, a hyperspectral image, is a three-dimensional dataset with two spatial dimensions and one spectral dimension.

HSI was originally developed for remote sensing applications [91], but has found a large utilization in such diverse fields as astronomy [92, 93, agriculture [94–96], pharmaceuticals [97–99], medicine [100, 101], and in recent years in the recycling sector [24, 102, 103], where important projects were also sustained by the European Union [104, 105].

Among the previous mentioned sensing techniques HSI can be considered one of the most interesting and subject to a wider and wider utilization inside the recycling sector. HSI, in fact, presents some advantages related to its intrinsic characteristics:

- Continuous monitoring, with HSI-based devices as scan line cameras,
- Utilization of different time-scale-related sampling strategies, according to the control/quality actions to develop,
- Implementation of fast and reliable recognition logics, strongly linked to HSI detectors characteristics (e.g., possibility handle spectra as images),
- Null environmental impact of the device,
- Relatively low costs of the devices.

Furthermore, HSI devices, and related operative architectures can be easily integrated inside existing recycling plants, or implemented in new ones, with an optimal cost-benefit ratio. HSI, for its intrinsic

properties, can thus be profitably utilized, both as a smart detection engine for sorting and as flow stream quality control, that is, certification of recovered materials and/or products. HSI is fast, accurate, affordable, and it can strongly contribute to lowering the economic threshold above which recycling is cost efficient. For its characteristics it can be meaningfully and reasonably developed, and applied, with reference to many solid waste-handling-sectors ranging from inorganic to organic waste sources.

Different cases studies describing the potentialities of HSI integration inside recycling technologies are reported in the following section.

H*yperspectral* I*maging* (HSI) Based Applications

An HSI system is typically constituted by optics, a spectrograph, a camera, an acquisition system, a translation stage, an energizing source (lighting device), and a control unit (PC). The camera, spectrograph, and illumination conditions determine the spectral range of the detection architecture. The sample/target is usually diffusely illuminated by a tungsten-halogen or LED source. A line of light reflected from the sample enters the objective lens and is separated into its component wavelengths by diffraction optics contained in the spectrograph. A two-dimensional image (spatial versus wavelength dimension) is then formed on the camera and saved on the computer. The sample is moved past the objective lens on a motorized stage and the process is repeated. Two-dimensional line images acquired at adjacent points on the object are stacked to form a three-dimensional hypercube that may be stored on a PC for further analysis.

The applications described in the following are based on sensing devices working in two different wavelength spectral ranges, from 400 to 1,000 nm (VIS-NIR range) and from 1,000 to 1,700 nm (NIR range). The first consists of a CCD camera, a line scan spectrograph (ImSpector™ V10E, SpecIm™, Finland), a lighting architecture, the spectrograph ImSpector™ V10E operates in the spectral range of 400–1,000 nm with a spectral resolution of 2.8 nm. The details of the acquisition architecture are reported in Table 15. The second is a SpecIm NIR spectral camera consisting of an ImSpector N17E imaging spectrograph for the wavelength region 1,000–17,000 nm and a temperature-stabilized InGaAs camera and a lighting architecture (Table 16).

Recycling Technologies. Table 15 Technical characteristics of the ImSpector™ V10E

Sensor	– 2/3″ CCD Array 780 × 580
	– Firewire digital output
	– Pixel resolution: 12 bit
Spectral range	400–1,000 nm
Spectral resolution	2.8 nm
Smile	< 1.5 μm
Keoneyst	< 1 μm
Entrance slit	30 μm × 14.2 μm
Image size	6.5 mm × 14.2 mm
Numerical aperture	F/2.4
Illuminant	– Anodized aluminum cylinder – Barium sulfate internal coating – d/O illumination and viewing conditions – Adjustable height and distance – 150 W cooled halogen lamp – Stabilized power source

Both equipments are installed to perform the inspection of the waste materials on a laboratory scale conveyor belt (Fig. 2). The two devices are fully controlled by a PC unit equipped with the Spectral Scanner™ v.2.3 [106] acquisition/pre-processing software.

Sample Set Selection The waste or derived products investigated belong to some of the classes of materials analyzed in this Section and characterized by different specific attributes, different sorting-selection problems, and quality requirements. From this perspective, waste glass fragments (*cullet*), light fraction derived from car shredding residues (*fluff*), and complex plastics-based waste streams have been selected. Results show that the HSI approach allows development and set up of strategies able to reduce analytical costs, improving the speed of the waste streams characteristics detection/analysis, and/or simplifying the

Recycling Technologies. Table 16 Technical characteristics of the ImSpector™ N17E

Sensor	– TE-cooled INGaAs photodiode array 640 × 512 – 14 bit, USB_2, LVDS, CameraLink
Spectral range	900–1,000 nm ± 10 nm
Spectral resolution	2.6 nm
Spatial resolution	Rms spot radius < 15 μm
Aberrations	Insignificant astigmatism, smile or keystone
Effective slit length	12.8 mm
Numerical aperture	F/2.0
Stray light	< 0.5% (halogen lamp, 1,400 nm notch filter)

procedures in terms of possible *on-line* implementation of fast and robust classification procedures oriented to develop innovative control strategies "human judgments and error free" as well as innovative certification criteria.

Spectra Acquisition and Detection Logics Implementation Spectra related to the different investigated can be acquired adopting the acquisition architecture described in Fig. 2. Such a strategy is adopted because it mimics, at laboratory scale, the real behavior of the control architecture at an industrial scale, that is, the progressive and continuous horizontal translation of the sample and the "synchronized" acquisition of the spectra at a pre-established step, allowing a tuning of the detection/inspection frequency of the waste materials according to their characteristics. Analyses can thus be performed to verify the fulfillments of different goals:

First goal: the possibility to identify specific spectral attributes for each of the constituents of the different waste streams according to their intrinsic chemical-physical characteristics. Starting from this information, analysis can be carried out performing a characterization of the "shape" of the entire detected spectra and/or identifying, at specific wavelengths, peaks or valleys characterizing the detected spectral firm.

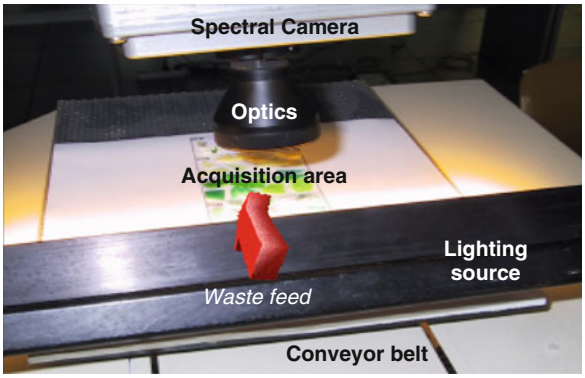

Recycling Technologies. Figure 2 Particulars of the architecture set-up utilized to perform a progressive and continuous waste samples spectra acquisition based on the ImSpector™ series devices

Second goal: the definition of fast, reliable, and robust recognition-classification procedures, based on different logics as: (1) spectral firms correlation, (2) single band intensity comparison at specific wavelengths, and (3) specific wavelengths intensity ratio analysis, in order to perform the discrimination of the different constituents inside a specific waste stream and to allow to reach a certification of the different products in terms of their composition.

Third goal: the possibility to perform a correlation among detected spectra, sample textural attributes, presence, characteristics, and localization of "pollutants": this latter aspect being of great interest to develop innovative sorting strategies. To validate the efficiency of the HSI-based technique to perform a topological assessment of the different materials an approach based on Principal Component Analysis (PCA) can be also adopted.

Case Studies Tests reported are referred to different solid waste materials characterized, as previously outlined, by a different nature and physical-chemical attributes and "affected" by different processing-separation and/or control problems. For each investigated waste product, a synthetic overview of the target to reach by the HSI approach (*Issues*) and current status of the related utilized characterization approaches (*State of the art*) is reported.

Case Study No. 1: Ceramic Glass Identification Inside Waste Glass Products (cullets). *Issues*: The amount of ceramic glass in post consumer glass waste stream is strongly increased in recent years, mainly for the introduction on the market of many ceramic glass manufactured goods [15]. These products constitute a new generation of consumer household goods used for their thermal-shock resistant properties. It can be argued that, considering the typology of ceramic glass products, contamination involves both the main production lines of glass recycling plants, e.g., the flat glass cullet and the container glass cullet. Due to its physical properties, similar to those of glass, ceramic glasses are almost impossible to detect adopting the automated optical technologies, commonly utilized for cullet color sorting [107]. Therefore, identifying and removing ceramic glass from the glass waste stream has long been a challenge for recyclers of glass.

State of the art: The two actions usually carried out to realize transparent ceramic contaminant removal are source reduction and manual sorting. Therefore, there is the need for the development and the implementation of a system able to realize a real-time identification of ceramic glass in the cullet stream. Sorting techniques based on X-ray [79] and FT-IR spectroscopy [24] have been proposed as methods for ceramic glass detection, but both are expensive and difficult to implement for safety and efficiency reasons, respectively.

The HSI approach clearly has potential in developing innovative sorting strategies. In the visible range (400–700) nm the technique presents a high discrimination power for classical cullet separation by color, allowing the possibility to decrease the minimum size of sorted glass particles, on the other hand, in the visible range the recognition of glass from ceramic glass is almost impossible. Moving in the wavelength range between (700–1,000) nm and (1,000–1,700) nm it is possible the architecture allows discrimination between glass (Fig. 3) and ceramic glass fragments (Fig. 4). Such a discrimination is relatively easy for clear samples; darker samples are more difficult to discriminate. Color, in fact, seems to affect the reflectance levels. Amber glasses show reflectance values near zero, green glasses present intermediate reflectance values, whereas clear glasses display higher reflectance values. A two-steps sorting, a first based on HSI acting between (700–1,700) nm and the second in the (700–1,000) nm range, could thus allow good preliminary *cullet* sorting targeted to ceramic glass contaminant identification/removal and a further *cullet* color-based separation. Application of this technique, in the waste glass sector, can thus allow development of innovative

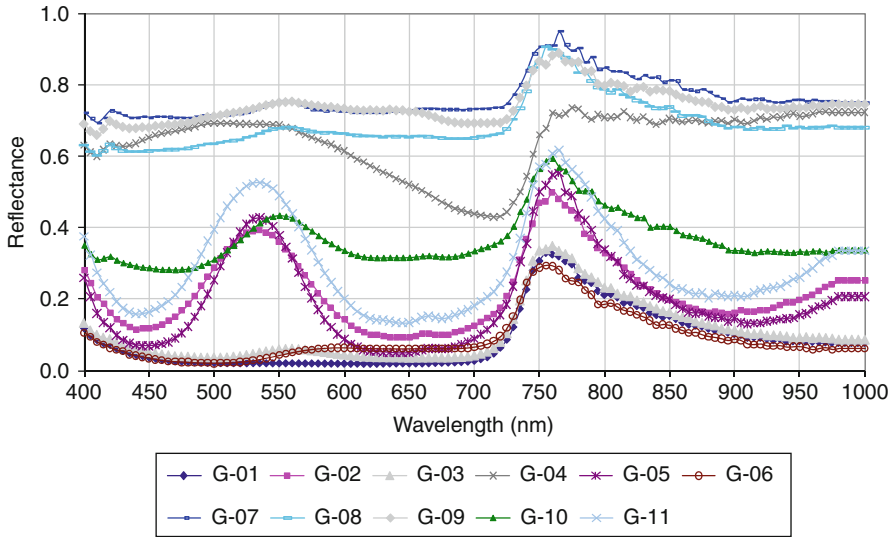

Recycling Technologies. Figure 3
Spectral plots in the VIS–NIR field (400–1,000 nm) of glass samples

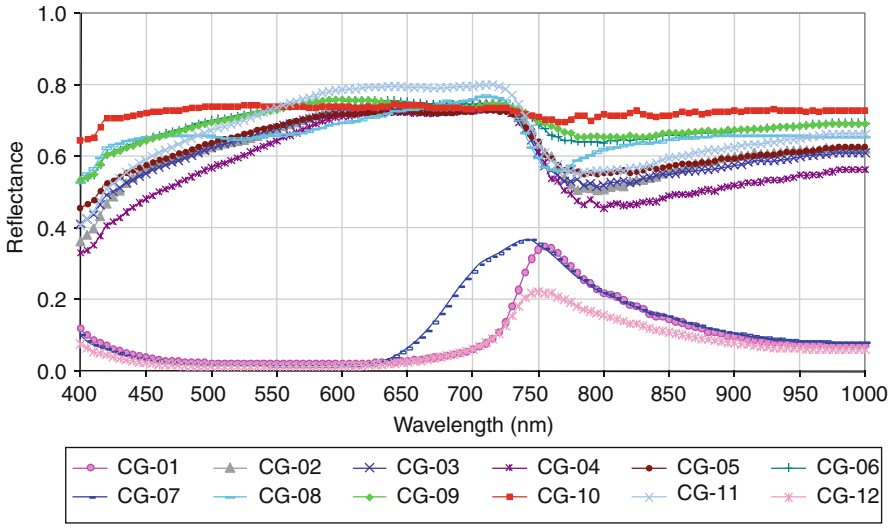

Recycling Technologies. Figure 4
Spectral plots in the VIS–NIR field (400–1,000 nm) of ceramic glass samples

sorting logics: (1) specific attributes can be associated to particulate solid materials, (2) classification procedures based on wavelengths intensity ratio can be defined to perform sorting, and (3) the elements to sort can be topologically assessed adopting a Principal Component Analysis (PCA) [108]. An example related to this last point is outlined in Fig. 5. The HSI devices for their hardware architecture can be easily installed both to integrate and/or to substitute classical sorting imaging-based devices.

Case Study No. 2: Light Fraction Resulting from Car Dismantling (Fluff) Characterization. *Issues*: *Fluff* represents about 25% of the weight of a car and is usually constituted by materials characterized by intrinsic low specific gravity (i.e., plastics, rubber, synthetic foams, etc.). When processed to perform its recovery, *fluff* is polluted by materials presenting higher specific gravity (i.e., copper, aluminum, brass, iron, etc.), constituting parts of the electrical devices of the vehicle that, for their shape, size (i.e., wires, metal straps, slip rings, wipers, etc.) and utilization remain concentrated in the lighter products. Such "polluting materials," for their intrinsic characteristics, are not well removed by classical separation techniques.

State of the art: *Fluff* is usually produced after different comminution-classification stages. The final classification is usually carried out by cycloning or venting (air suction or blowing systems), in order to separate the light material. A good separation could contribute to reducing the waste disposal and environmental pollution, and increasing the energy recovery through pure sorted polymer re-use. Furthermore, the possibility to utilize finer *fluff* fractions to produce energy could dramatically contribute to increase the full reutilization of such products. To reach this goal the quantity and the quality of the metal contaminants have to be strongly controlled in order to not prejudice the quality of the final fluff based fuel. The need to develop both efficient selection and control strategies to obtain contaminant-free, or almost free, fine *fluff* products thus assumes a fundamental role in all the processing and control stages of the recycling chain.

Results show the HSI proposed architecture allows identification of all *fluff* constituents and polluting materials (Fig. 6). The discriminating power is high in the region between (400–1,000) nm, this is a quite important result being thus possible to utilize, for *fluff* inspection, a single device (ImSpector™ V10E) sorting/control unit, with considerable costs reduction. From this perspective, the HSI approach can be profitably applied utilizing "simple" band intensity comparison, at specific wavelengths, among unknown *fluff* particles and a reference library of spectra, previously

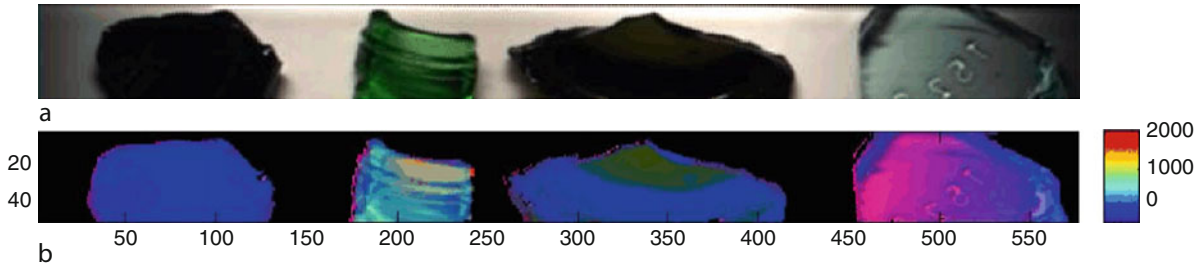

Recycling Technologies. Figure 5
Representation of the HSI data set, as acquired (**a**), of different *cullets* resulting from a recycling process. The fragment on the right end side of the image is ceramic glass. (**b**) Corresponding false color image embedding the results of all the three score plots, (image of scores on PC1: 97.46, image of scores on PC2: 1.82 and image of scores on PC3: 0.43) related to PC1, PC2, and PC3 components as resulting from the application of the PCA. Contaminant (ceramic glass) can be easily identified

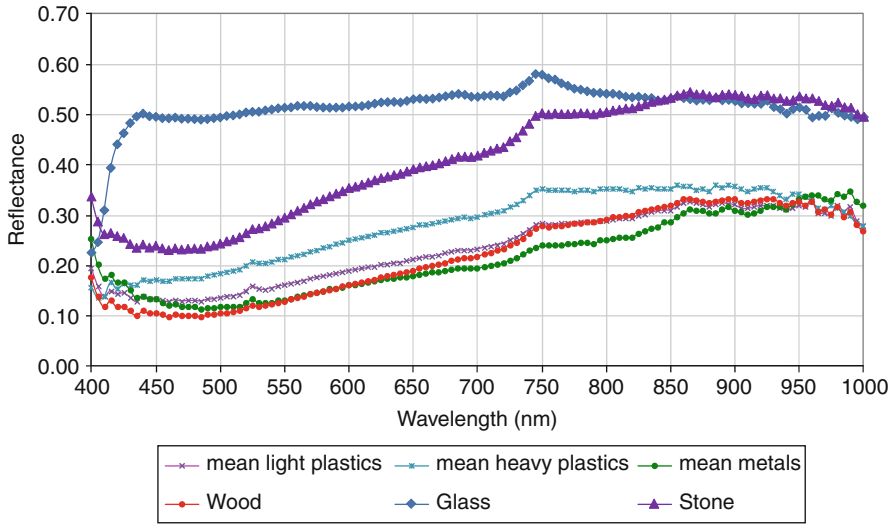

Recycling Technologies. Figure 6
Spectral plots in the VIS–NIR field (400–1,000 nm) of *fluff* materials. The HSI approach clearly allows discrimination between the different light materials constituting *fluff*

built, embedding the different waste materials spectra constituting the light fractions to investigate. The approach is particularly flexible to use because *fluff* of different origin and/or composition can be sorted/controlled adopting the same logic, but working on different specifically spectra library, built according to new materials characteristics to detect.

Case Study No. 3: Polyolefins Recognition-Separation. Issues: Polyolefin recovery from complex waste streams is a challenging issue that has not yet been profitably solved. Furthermore, polypropylene (PP), high density polyethylene (HDPE), and low density polyethylene (LDPE) together are both difficult to separate and chemically incompatible. In order to produce high-purity granulates from these concentrates, of a quality comparable to materials produced from post-industrial waste, the mixture must be sorted very accurately, and in order to be economically and ecologically sound, most of the polyolefins should end up

in a useful product. Such accurate and efficient separations exist, but they involve multiple separations. They are therefore expensive, difficult to control, and often do not allow the production of good concentrates. The possibility to develop efficient and low-cost recognition logics to control the process and certify the products thus represents a key issue in polyolefin recovery.

State of the art: Innovative processing plant layouts have been realized to process complex plastic-based wastes by shredding and sink-floating to produce polyolefin concentrates of varying quality. Analysis of such concentrates generally shows a mixture of polyolefins, rubbers, foams, fibers, and wood, next to varying amounts of materials heavier than water. Currently available separation techniques, based on the difference in flotation proprieties in water, can be used to separate lighter types of plastic such as PP, HDPE, and LDPE from the heavier types such as polyethylene terephthalate (PET) and polyvinyl chloride (PVC). A known method is to separate the mixtures into five fractions using separation media with densities

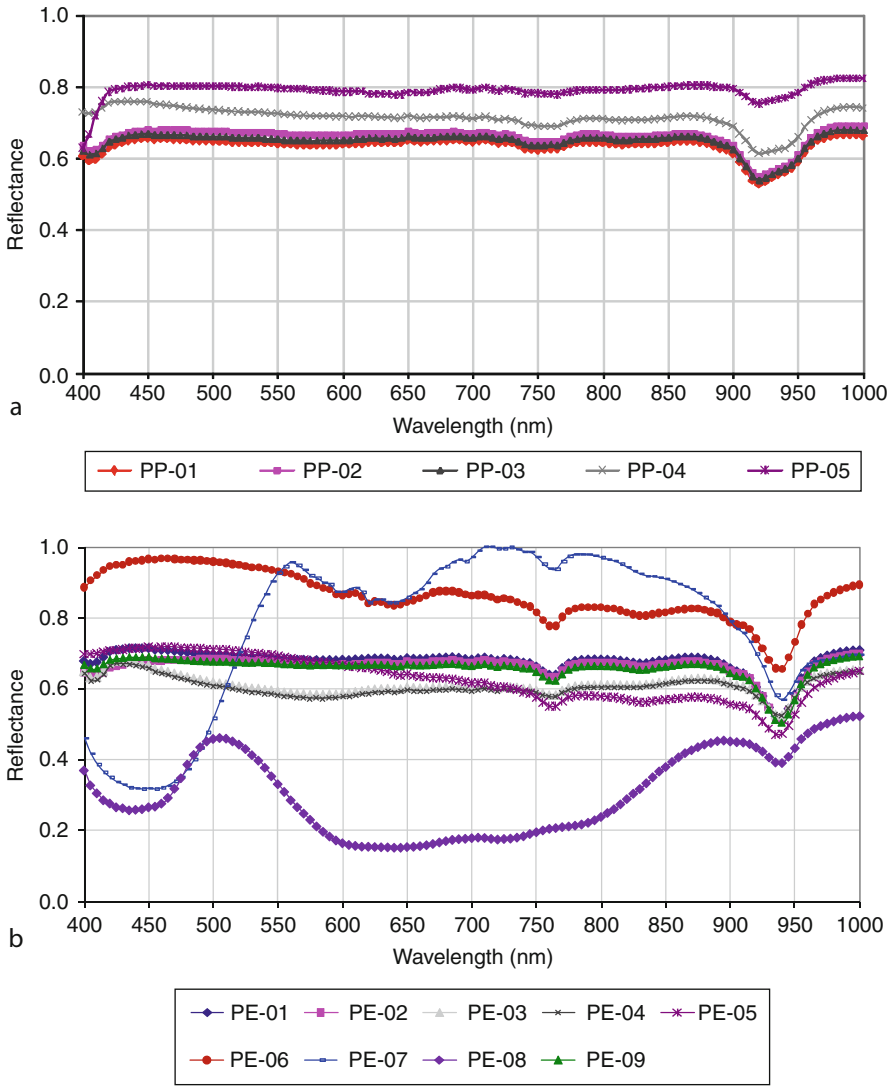

Recycling Technologies. Figure 7
Spectral plots in the VIS–NIR field (400–1,000 nm) of polyolefins: PP (**a**) and PE (**b**)

of 880, 920–930, 940, and 970 kg/m^3. Such a procedure will create high-purity PP and HDPE products, whereas foams, most of the wood and rubbers, LDPE, filled PP, and residual heavy materials will end up in relatively small residue fractions. Certain expensive liquids have been specially designed to separate at one of the target densities for polyolefin recycling. Other technologies, such as electrostatic separation and thermal adhesion, have been able to create only a single relatively pure product.

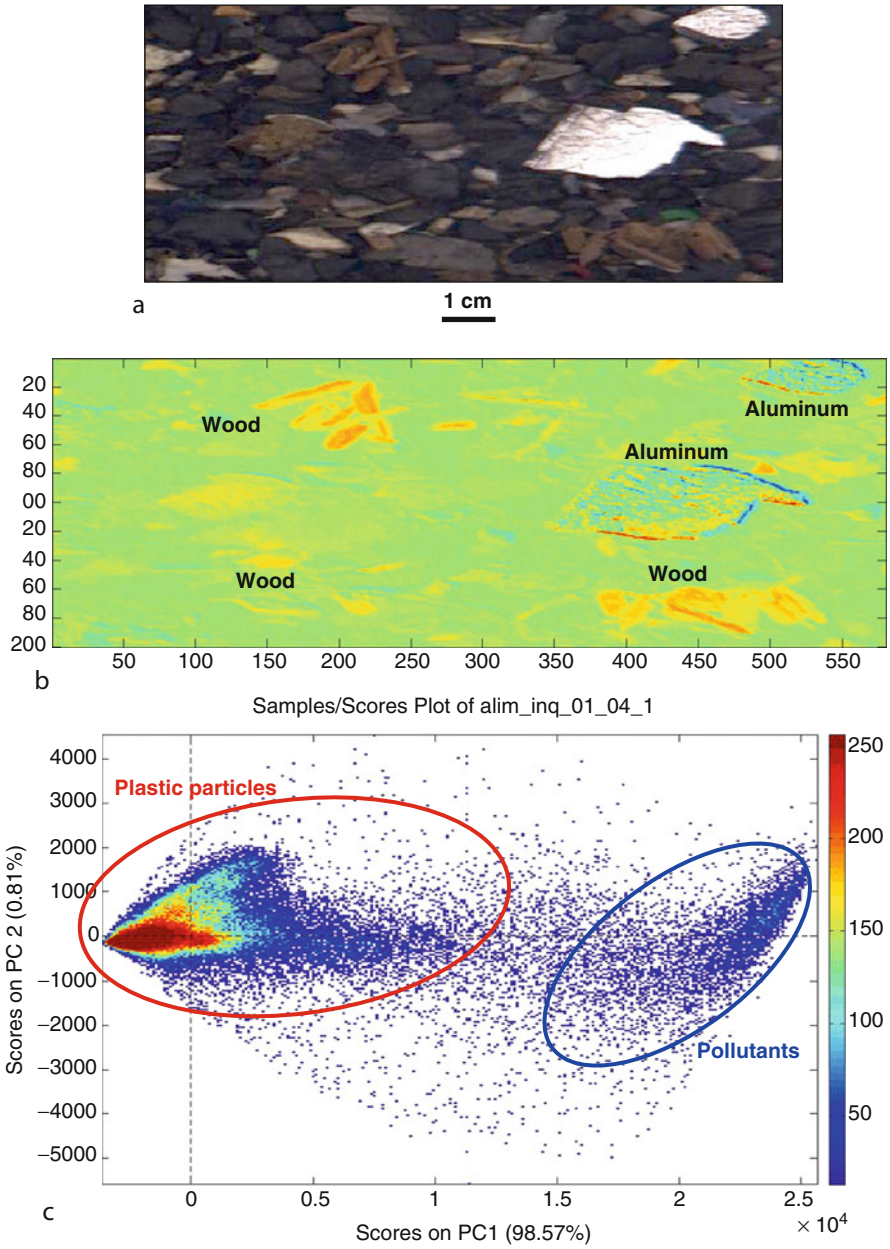

Recycling Technologies. Figure 8

Image on scores on PC2:0.81 (**b**) of the HSI data set of (**a**). Samples/Scores Plot PC1-PC2 clearly outlines the correspondence existing among typology of contaminants and their "mapping" inside the plot (**c**)

Analyses show PP and PE recognition is strongly influenced, in the visible region, by the color of the samples. Based on the analysis of HSI spectra, it is evident the possibility to define specific parameters useful for recognition of the two polyolefins, as, for example, the slope of the spectrum in a selected wavelength range or a band ratio among two different wavelengths. Analyses show PP and PE spectra present significant differences in regions around 750 nm and (900–950) nm (Fig. 7). It is important to note that the best and most precise recognition logic, especially for polluting particles detection and their topological assessment inside plastic waste feed, should be based on more sophisticated and complex statistical analyses, such as (PCA) (Fig. 8), Partial Least Square (PLS), Neural Network (NN), etc., that usually require long computation time. Considering that in most industrial applications the fast response of the detecting/sorting device is one of the main constraints, as, for example, when particles are moving on a conveyor belt and they are sorted *on-line*, the adoption of simplified logics, working properly, is preferred. This latter approach (multiple bands intensity comparison at specific wavelengths) can be profitably applied for recovered polyolefins quality control.

The examples clearly outline the importance of HSI in recycling technologies as an innovative, flexible, and low-cost tool that, combining imaging and reflectance spectroscopy, can profitably allow performance of both waste feed and recovered products characterization, control, and certification. HSI-based technology through the detection of the spectral signature of waste and waste-derived products, of different nature and composition, allows to extract and quantify those physical-chemical attributes influencing their characteristics and behavior. Results demonstrated as the proposed technique, and the related recognition logics, will have a greater impact on the development of recycling technologies finalized to implement *on-line* innovative sorting strategies, as well as new control procedures. The possibility to reach a primary goal in recycling, that is a full control, at a low cost, of the quality of the different flow streams inside the plant, according to the different processing stages, can strongly contribute to develop *innovative-inside-processing* products certification.

Bibliography

Primary Literature

1. Kahn CH (1979) The art and thought of Heraclitus. Cambridge University Press, Cambridge
2. Mamedbeii GD (1959) Muhammed Nasir al-Din al-Tusi on the theory of parallel lines and the theory of ratios. (Azerbaijani), Izdat. Akad. Nauk Azerbaijzansk. SSR (Baku)
3. Dumas M (1955) Lavoisier, théoricien et expérimentateur. Presses Universitaires de France, Paris
4. Heijungs R, Huppes G, Guinée JB (2010) Life cycle assessment and sustainability analysis of products, materials and technologies. Toward a scientific framework for sustainability life cycle analysis. Polym Degrad Stab 95(3):422–428
5. Bartl A, Hackl A, Mihalyi B, Wistuba M, Marini I (2005) Recycling of fibre materials. Process Safety Environ Protect 8(B4):351–358
6. Confederation of European Paper Industries (2009) CEPI sustainability report. Brussels, Belgium
7. Ochoa JAG (2008) Feasibility of recycling pulp and paper mill sludge in the paper and board industries. Resour Conserv Recycl 52(7):965–972
8. Wiegand PS, Unwin JP (1994) Alternative management of pulp and paper industry solid wastes. Tappi J 77:91–97
9. Wolfer EP, Venkat WB, Maroju BV, Martiny A (1997) Method for recovering fiber from effluent streams. U.S. Patent 5, pp 593–542
10. Saint Amand FJ (1999) Hydrodynamics of deinking flotation. Int J Miner Process 56:277–316
11. Tandy S, Healey JR, Nason MA, Williamson JC, Jones DL (2009) Heavy metal fractionation during the co-composting of bio-solids, deinking paper fibre and green waste. Bioresour Technol 100(18):4220–4226
12. Moo-Young HK Jr, Zimmie TF (1997) Waste minimization and re-use of paper sludges in landfill covers: a case study. Waste Manag Res 15(6):593–605
13. Werther J, Ogada T (1999) Sewage sludge combustion. Prog Ener Combust Sci 25(1):55–116
14. Safeglass (Europe) Limited, Nasmyth Building, Nasmyth Avenue. East Kilbride. UK G75 0Q. http://www.breakglass.org/Glass_making.html
15. Höland W, Beall G (2002) Glass–ceramic technology. The American Ceramic Society, Westerville, p 372
16. Pannhorst W (1997) Glass ceramics: state of the art. J Non-Cryst Solids 219:198–204
17. Rem PC (1999) Eddy current separation. Delft University of Technology, Delft
18. Bonifazi G, D'Addetta A, Massacci P (2002) Classification by neural net of a particle stream in an eddy-current drum separator. Int J Part Part Syst Charact 19:96–102
19. Jong TPR, de Dalmijn WL (2002) X-ray transmission imaging for process optimisation of solid resources. In: R02, 6th World congress on integrated resources management, Geneva, Switzerland, CD-Paper 173

20. Bonifazi G (2000) Imaging based sorting logic in solid waste recycling. In: Proceedings of the 16th international conference on solid waste technology and management, vol 6, Philadelphia, USA, pp 14–26
21. Bonifazi G, Massacci P (2000) Cullets (glass fragments) quality control by artificial vision: a textural based approach. In: 4th World Congress R00 – Recovery, recycling, re-integration, Toronto, Canada, CD-Paper 31, pp 723–728
22. Bonifazi G, Massacci P (1998) Cullets (glass fragments) quality control by artificial vision: a color based approach. In: Proceedings of international conference on quality control by artificial vision, Takamatsu, Japan, pp 94–99
23. Serranti S, Bonifazi G, Pohl R (2006) Spectral cullet classification in the mid-infrared field for ceramic glass contaminants detection. Int J Waste Manag Res 24:48–59
24. Bonifazi G, Serranti S (2006) Imaging spectroscopy based strategies for ceramic glass contaminants removal in glass recycling. Int J Waste Manag 26:627–639
25. Cramb AW (1996) A short history of metals. Dept. of Materials Science and Engineering. Carnegie Mellon University. http://neon.mems.cmu.edu/cramb/Processing/history.html
26. Gascoigne B (2001) History of metallurgy. HistoryWorld. Ongoing. http://www.historyworld.net/wrldhis/PlainTextHistories.asp?historyid=ab16
27. Alter H (1977) Magnetic separation – Recovery of salable iron and steel from municipal solid waste. Environmental Protection Agency, Cincinnati
28. Shapiro M, Galperin V (2005) Air classification of solid particles: a review. Chem Engin Process 44:279–285
29. Wills BA (1997) Mineral processing technology, 6th edn. Butterworth-Heinmann, Boston, pp 232
30. Bradley D (1965) The hydrocyclone. Pergamon, New York
31. Takoungsakdakun T, Pongstabodee S (2007) Separation of mixed post-consumer PET–POM–PVC plastic waste using selective flotation. Sep PurifTechnol 54:248–252
32. Buchan R, Yarar B (1995) Recovering plastics for recycling by mineral processing techniques. J Miner Met Mater Soc 47:52–55
33. Drelich J, Kim JH, Payne T, Miller JD, Kobler RW (1999) Purification of polyethylene terephthalate from polyvinyl chloride by froth flotation for the plastics (soft-drink bottle) recycling industry. Sep Purif Technol 15:9–17
34. Kang H, Schoenung JM (2005) Electronic waste recycling: a review of US infrastructure and technology options. Resour Conserv Recycl 45(4):368–400
35. Veit HM, Pereira C, Bernardes AM (2002) Using mechanical processing in recycling printed wiring board. J Miner Met Mater Soc 54(6):45–47
36. Askvik KM, Hetlesæther S, Sjobölm J, Stenius S (2001) Properties of the lignosulfonate–surfactant complex phase. Colloids Surf A Physicochem Eng Aspects 182:178–189
37. Singh BP (1998) Wetting mechanism in the flotation separation of plastics. Filtration Sep 35:525–527
38. Shen H, Pugh RJ, Forssberg E (2002) Floatability, selectivity and flotation separation of plastics by using a surfactant. Colloids Surf A Physicochem Eng Aspects 196:63–70
39. Fraunholcz N (2004) Separation of waste plastics by froth flotation – a review. Part I, Miner Engin 17:261–268
40. Andrady AL (2003) Plastics and the environment. Wiley, Hoboken, pp 792
41. Al-Salem SM, Lettieri P, Baeyens J (2009) Thermal pyrolysis of high density polyethylene (HDPE). In: Proceedings of the 9th European gasification conference: clean energy and chemicals, Düsseldorf, Germany
42. Scheirs J (1998) Polymer recycling: science, technology and application, 1st edn. Wiley-Blackwell, New York
43. Dirks E (1996) Energy recovery from plastic waste in waste incineration plants. In: Brandrup J, Bittner M, Menges G, Michaeli W (eds) Recycling and recovery of plastics, 1st edn. Hanser, Munich, pp 746–769
44. Zia KM, Bhatti HN, Bhatti IA (2007) Methods for polyurethane and polyurethane composites, recycling and recovery: a review. React Funct Polym 67(8):675–692
45. Hawn K (2001) An overview of commercial recycling technologies and textile applications for the products. In: 6th annual conference on recycling of polymer, textile and carpet waste, Dalton, USA
46. Cupit MJ (1996) Opportunities and barriers to textile recycling, AEA Technology, Report 0113, Oxfordshire, UK
47. Passas R, Voillot C, Tarrajat G, Caucal G, Khelifi B, Tourtollet G (2001) Morfi as a novel technology for morphological analysis of fibers. Recents Progres en Genie des Procedes 15: 259–264
48. Bartl A, Mihalyi B, Marini I (2004) Applications of renewable fibrous materials. Chem Biochem Engin 18:21–28
49. Wang Y (1995) Reuse of carpet industrial waste for concrete reinforcement. In: RILEM Proceeding (Disposal and recycling of organic and polymeric construction materials), vol 27, London, pp 297–306
50. Wang Y (1997) Properties of concrete reinforced with recycled carpet waste fibers. In: Proceedings of International symposium on brittle matrix composites 5, Warsaw, pp 179–186
51. Wang Y (1999a) Ecotextile'98: sustainable development. In: Proceedings of the Conference, Bolton, pp 165–171
52. Wang Y (1999) Utilization of recycled carpet waste fibers for reinforcement of concrete and soil. Polym Plast Technol Engin 38:533–546
53. Wang Y (2002) Recycling of automotive fibers. In: Proceedings of Joint INDA-TAPPI Conference, Atlanta, pp 160–167
54. Bohnhoff A, Petershans J (2002) De-centralised technology for the sorting of textile floor coverings. In: 7th annual conference on recycling of polymer, textile and carpet waste, Dalton, USA
55. Strzelecki C (2004) Modern solutions for shredding, grinding and re-pelletizing post-industrial fiber, nonwovens and carpet scrap. In: Annual conference on recycling of polymer, textile and carpet waste, Dalton, USA
56. Bacon FC, Holland WR, Holland LH (1998) Method and machine for recycling discarded carpets. U. S. Patent 5, 704, 104
57. Howe MA, White SH, Locklear SG (2001) Method and apparatus for reclaiming carpet components. US Patent 6, 182, 913

58. Herlihy J (1997) Recycling in the carpet industry. Carpet and Rug Industry, pp 17–25
59. Kasserra P (1998) Recycling of polyamide 6.6 and 6. In: Prasad PN et al (eds) Science and technology of polymers and advanced materials. Plenum, New York, pp 629–635
60. Hagguist JAE, Hume RM (1993) Carpet reclaimer, U.S. Patent 5, 230, 473
61. Schut JH (1995) Big plans for carpet. Plast World 53:25
62. Booij M, Hendrix JAJ, Frentzen YH (1997) Process for recycling polyamide-containing carpet waste, European Patent 759, 456
63. Frentzen YH, Thijert MP, Zwart RL (1997) Process for the recovery of caprolactam from waste containing nylon by extraction with alkyl phenol, World Patent 97, 03, 04
64. Sarian AK, Handerman AA, Jones S, Davis EA, Adbye A (1998) Recovery of polyamide from composite articles, U.S. Patent 5, 849, 80
65. Sikorski ME (1993) Recycling of polymeric materials from carpets and other multi-component structures by means of supercritical fluid extraction, U.S. Patent 5, 233, 021
66. Griffith AT, Park Y, Roberts CB (1999) Separation and recovery of nylon form carpet waste using a supercritical fluid antisolvent technique. Polym Plast Technol Engin 38(3):411–432
67. Honeywell Nylon Inc (2005) http://www.infinitynylon.com
68. Elam CC, Evan RJ, Czernik S (1997) An Integrated approach to the recovery of fuels and chemicals from mixed waste carpets through thermocatalytic processing, Preprint papers - American Chemical Society. Div Fuel Chem 42(4):993–997
69. Bajaj P, Sharma ND (1997) In: Gupta VB, Kothari VK (eds) Reuse of polymer and fibre waste in manufactured fibre technology. Chapman & Hall, New York, pp 615
70. Brown T (2001) Infinity nylon - a never-ending cycle of renewal, 6th annual conference on Recycling of polymer, Textile and Carpet Waste, Dalton, GE, USA. http://hdl.handle.net/1853/10385
71. Schut JH (1993) A recycling first: carpets! Plast Technol :22–25
72. Young D, Chlystek S, Malloy R, Rios I (1998) Recycling of carpet scrap, U.S. Patent 5,852,115
73. Hagberg CG, Dickerson JL (1997) Recycling nylon carpet via reactive extrusion. Plast Engin 53:41–43
74. Datta RJ, Polk MB, Kumar S (1995) Reactive compatibilization of polypropylene and nylon. Polym Plast Technol Engin 34(4):551–560
75. Dagli SS, Xanthos M, Biesenberger JA (1992) Blends of nylon 6 and polypropylene with potential applications in recycling, effects of reactive extrusion variables on blend characteristics. ACS Symp Ser 513:241–257
76. David DJ, Dickerson JL, Sincock TF (1994) Thermoplastic composition and method for producing thermoplastic composition by melt blending carpet, U. S. Patent 5, 294, 384
77. Muzzy J, Wang Y, Hagberg C, Patel P, Jin K, Samanta S, Bryson L, Shaw B (2004) Long fiber reinforced post-consumer carpet. In: ANTEC 2004, Annual Technical Conference of the society of plastics engineers, Chicago, USA
78. Jähne B (1993) Digital image processing; concepts, algorithms, and scientific applications, 2nd edn. Springer, Berlin
79. de Kattentidt HUR, Jong TPR, Dalmijn WL (2003) Multi-sensor identification and sorting of bulk solids. Control Engin Pract 11:4147
80. Bearmann GH, Levenson RM, Cabib D (eds) (2002) Spectral imaging: basic principles and prospective applications. Kluwer, Dordrecht
81. Leitner R, Mairer H, Kercek A (2003) Real-time classification of polymers with NIR spectral imaging and blob analysis. Real-Time Imag 9:245–251
82. American Wood Preservers' Association (AWPA) (1999) American wood preservers' association book of standards. American Wood Preservers' Association, Grandbury
83. Blassino M, Solo-Gabriele HM, Townsend T (2002) Pilot scale evaluation of sorting technologies for CCA treated wood waste. Waste Manag Res 20:290–301
84. Kormienko M (1999) Sorting technologies for CCA-treated wood waste. Master of Science Thesis, University of Miami, Coral Gables, USA
85. Solo-Gabriele H, Townsend T, Kormienko M, Stook K, Gary K, Tolaymat T (2000) Alternative chemicals and improved disposal-end management practices for CCA-treated wood. Final Technical Report #00-03. Florida center for solid and hazardous waste management, Gainesville, USA
86. de Jong TPR, Dalmijn WL (2002) X-ray transmission imaging for process optimisation of solid resources. In: Proceedings of R'02 congress, Geneva, pp 1–6
87. Hahn DW, Flower WL, Hencken KR (1997) Discrete particle detection and metal emissions monitoring using laser-induced breakdown spectroscopy. Appl Spectrosc 51: 1836–1844
88. Hahn DW (1998) Laser-induced breakdown spectroscopy for sizing and elemental analysis of discrete aerosol particles. Appl Phys Lett 72:2960–2962
89. Radziemski LJ, Cremers DA (1989) Laser-induced plasmas and applications. Marcel Dekker, New York
90. de Mesina MB, Jong TPR, Dalmijn WL (2007) Automatic sorting of scrap metals with a combined electromagnetic and dual energy X-ray transmission sensor. Int J Miner Process 82:222–232
91. Goetz AFH, Vane G, Solomon TE, Rock BN (1985) Imaging spectrometry for earth remote sensing. Science 228: 1147–1153
92. Hege E, O'Connell D, Johnson W, Basty S, Dereniak E (2003) Hyperspectral imaging for astronomy and space surveillance. Proceedings of the SPIE 5159:380–391
93. Wood KS, Gulian AM, Fritz GG, Van Vechten D (2002) A QVD detector for focal plane hyperspectral imaging in astronomy. Bull Am Astron Soc 34:1241
94. Monteiro S, Minekawa Y, Kosugi Y, Akazawa T, Oda K (2007) Prediction of sweetness and amino acid content in soybean crops from hyperspectral imagery. ISPRS J Photogram Remote Sens 62(1):2–12
95. Smail V, Fritz A, Wetzel D (2006) Chemical imaging of intact seeds with NIR focal plane array assists plant breeding. Vibrational Spectroscopy 42(2):215–221

96. Lyon RC, Lester DS, Lewis EN, Lee E, Yu LX, Jefferson EH (2002) Near-infrared spectral imaging for quality assurance of pharmaceutical products: analysis of tablets to assess powder blend homogeneity. AAPS Pharm Sci Tech 3(3):17
97. Rodionova O, Houmøller L, Pomerantsev A, Geladi P, Burger J, Dorofeyev V (2005) NIR spectrometry for counterfeit drug detection: a feasibility study. Anal Chim Acta 549(1–2):151–158
98. Roggo Y, Edmond A, Chalus P, Ulmschneider M (2005) Infrared hyperspectral imaging for qualitative analysis of pharmaceutical solid forms. Anal Chim Acta 535(1–2):79–87
99. Ferris D, Lawhead R, Dickman E, Holtzapple N, Miller J, Grogan S (2001) Multimodal hyperspectral imaging for the non invasive diagnosis of cervical neoplasia. J Low Genit Tract Dis 5(2):65–72
100. Kellicut D, Weiswasser J, Arora S, Freeman J, Lew R, Shuman C (2004) Emerging technology: hyperspectral imaging. Perspect Vasc Surg Endovasc Ther 16(1):53–57
101. Zheng G, Chen Y, Intes X, Chance B, Glickson JD (2004) Contrast-enhanced near-infrared (NIR) optical imaging for subsurface cancer detection. J Porphyrins Phthalocyanines 8(9):1106–1117
102. Serranti S, Bonifazi G (2009) Hyperspectral imaging detection architectures for polyethilene (PE) and polypropylene (PP) identification inside plastic waste streams. In: Proceedings of waste-to-resources, III International symposium MBT&MRF. Hanover, Germany, pp 463–474
103. Serranti S, Bonifazi G, Bonoli A, Dall'Ara A (2009) Composting products quality assessment and monitoring by hyperspectral imaging based logics. In: Proceedings of waste-to-resources, III International symposium MBT&MRF. Hanover, Germany, pp 584–597
104. W2Plastics (2008) Collaborative Project 212782 - FP7-ENV-2007-1: magnetic sorting and ultrasound sensor technologies for production of high purity secondary polyolefins from waste
105. HYSPIMGLASS (2002) CRAFT Programme: CRAF-1999-71817: development of a Novel and high speed spectral imaging system to detect glass-like contaminants in the recyclable, cost-effectively increasing glass recycling and avoiding landfilling
106. SSOM (2008) Spectral scanner operative manual (Version 2.0). DV Optics S.r.l., Italy http://www.dvoptic.com/index.html
107. Bonifazi G (2000) Imaging based sorting logic in solid waste recycling. In: The Sixteenth international conference on solid waste technology and management – session 6A: recycling and source reduction. Philadelphia, USA, pp 6.14–26
108. Geladi P, Isaksson H, Lindqvist L, Wold S, Esbensen K (1989) Principal components analysis of multivariate images. Chemometr Intell Lab Syst 5(3):209–220

Books and Reviews

An good paper presenting an excellent review of recent progress in the recycling and recovery of P*lastic* S*olid* W*aste* (PSW), with particular emphasis "*on waste generated from polyolefinic sources, which makes up a great percentage of our daily single-life cycle plastic products*" is: Al-Salem SM, Lettieri P, Baeyens J (2009) Recycling and recovery routes of plastic solid waste (PSW): a review. Waste Manag 29:2625–2643

Beede DN, Bloom DE (1995) Economics of the generation and management of MSW. NBER Working Papers 5116. National Bureau of Economic Research, Inc, Cambridge, MA

Caputo AC, Pelagagge PM (2001) Waste-to-energy plant for paper industry sludges disposal: technical-economic study. J Hazard Mater 81(3):265–283

Cofie O, Kone D, Rothenberger S, Moser D, Zubruegg C (2009) Co-composting of faecal sludge and organic solid waste for agriculture: process dynamics. Water Res 43(18): 4665–4675

El Haggar S (2007) Sustainable industrial design and waste management: cradle-to-cradle for sustainable development. Academic, St. Louis, pp 424

Galperin V, Shapiro M (1999) Separation of solid particles in a fluidized bed air classifier. Powder Handling Process 11:2

Gesing A, Berry L, Dalton R, Wolanski R (2002) Assuring continued recyclability of automotive aluminium alloys: grouping of wrought alloys by color, X-ray absorption and chemical composition-based sorting. In: Proceedings annual meeting on automotive alloys and aluminium sheet and plate rolling and finishing technology, Seattle, USA

Gesing A, Steward C, Wolanski R, Dalton R, Berry R (2000) Scrap preparation for aluminium alloy sorting. In: Proceedings TMS fall extraction and process metallurgy meeting, Pittsburgh, USA

Hosokawa Micron Group (2011) http://www.hmicronpowder.com/application/classification

Huth-Fehre Th, van den Broek W (1995) NIR-Remote sensing and artificial neural networks for rapid identification of post consumer plastics. J Mol Struct 348:143–146

Johansson JE (2007) Plastics – the compelling facts and figures. 6th IdentiPlast Biennial Conference on the Recycling and Recovery of Plastics. Brussels, Belgium

Kunii D, Levenspiel O (1991) Fluidization engineering, 2nd edn. Butterworth, Heinmann, pp 233

Marques GA, Tenorio JAS (2000) Use of froth flotation to separate PVC/PET mixtures. Waste Manag 20:265–269

Méndez A, Fidalgo JM, Guerrero F, Gascó G (2009) Characterization and pyrolysis behaviour of different paper mill waste materials. J Anal Appl Pyrolysis 86(1):66–73

Oshitani J, Kiyoshima K, Tanaka Z (2003) Continuous dry material separation from automobile shredder residue. Kagaku Kogaku Ronbunshu 29:8–14

Pascoe RD (2005) The use of selective depressants for the separation of ABS and HIPS by froth flotation. Miner Eng 18:233–237

Sekito T, Matsuto T, Tanaka N (2006) Application of a gas–solid fluidized bed separator for shredded municipal bulky solid waste separation. Waste Manag 26:1422–1429

Sekito T, Tanaka N, Matsuto T (2006) Batch separation of shredded bulky waste by gas–solid fluidized bed at laboratory scale. Waste Manag 26:1246–1252

Svoboda J (2004) Magnetic techniques for the treatment of materials, Kluver Academic Publisher, New York, USA. pp. 656.

http://www.springer.com/earth+sciences+and+geography/book/978-1-4020-2038-4
Van Nieuwenhuijzen A, Van der Graaf J (2010) Handbook on particle separation processes. IWA, London, UK, pp 400
World Bank (2007) Environmental, health, and safety guidelines for pulp and paper mills. Draft technical document. Environment and Social Development Department, International Finance Corporation, Washington, DC
Yoshida M, Oshitani J, Kaname K, Gotoh K (2006) Fluidized bed medium separation (FBMS) of Cl-containing plastics in home electric appliance shredder residue. Kagaku Kogaku Ronbunshu 32:115–121

Regenerative Braking

Yimin Gao
Department of Electrical and Computer Engineering, Texas A&M University, College Station, TX, USA

Article Outline

Glossary
Definition of the Subject
Introduction
Braking Energy
Hybrid Brake System
Future Directions
Bibliography

Glossary

Antilock braking system (ABS) Safety system that prevents the wheels on a vehicle from locking up while braking.

Brake-by-wire Technology to replace the traditional mechanical and hydraulic control systems with electronic control systems using electromechanical actuators and human–machine interfaces.

Brake controller A microchip-based device which receives brake strength command from driver and feedback signals and generates control signals to control the mechanical and electric brake systems.

Braking energy The energy consumed by the brake system of a vehicle.

Hybrid brake system A vehicle brake system that uses both regenerative braking and mechanical fictional brake.

Regenerative braking Braking device of a vehicle which can absorb vehicle braking energy and store the absorbed braking energy into an energy storage and then uses it for later traction.

Definition of the Subject

Regenerative brake system is a newly developed brake system used in electric, hybrid electric, and fuel cell vehicles which can convert part of braking energy into electric energy using an electric motor/generator. For braking safety, the traditional mechanical brake is still required. The electric and mechanical brake systems constitute a hybrid braking system. In the design and control of such a system, the braking force distribution on front and rear wheels has to meet the braking regulation for braking safety, and meantime, a braking force distribution on mechanical and electric brake system design should be able to recover as much braking energy as possible.

Introduction

One of the most important features of electric, hybrid, and fuel cell vehicles is the ability of recapturing part of braking energy, which can save significant amount of fuel, especially for the vehicles driving mostly with stop-and-go pattern.

Brake system of a vehicle is most important for vehicle safety, which has to meet the demands of quickly slowing down the vehicle and maintaining the vehicle stability. In normal driving, braking force requirements widely vary from slightly retarding vehicle to emergency braking, depending on the traffic situation. Heavy braking needs a huge braking force that regenerative brake cannot produce, consequently, a mechanical brake has to be engaged. This forms a hybrid brake system. As in a hybrid propulsion system, there are many options in configurations and control strategies. An advanced hybrid braking system may be a braking-by-wire system with intelligent control.

Braking Energy

Percentage of Braking Energy to Propelling Energy

Braking force has to be applied to a vehicle while slowing down its speed or descending a grade. The kinetic

energy ($1/2M\,V^2$) or potential energy ($M\,g\,h$, where, h is the vertical height of the vehicle descent) is dissipated through vehicle brake system. For relative flat roads, most of the braking energy is consumed for slowing down the vehicle speed, especially, driving in urban areas. Thus, discussion in this section focuses on the urban stop-and-go driving pattern. The stop-and-go driving pattern is interpreted by typical driving cycles, such as those of EPA FTP 75 urban, LA 92, US 06, ECE-15, and New York city. Of course, other driving cycles can also be used.

While a vehicle driving on a flat road, the braking force measured on drive wheels for developing a deceleration j (m/s^2) can be expressed as

$$F_b = M\delta j - F_r - F_w, \tag{1}$$

where, M is the vehicle mass in kg, δ is the equivalent mass factor, which is a factor that equivalently converts the rotating inertia into translational inertia, F_r is the rolling resistance, and F_w is the aerodynamic drag of the vehicle. Correspondingly, the braking power can be expressed as

$$P_b = \frac{V}{1000}(M\delta j - F_r - F_w),\ (kW) \tag{2}$$

where, V is vehicle speed in m/s. The energy consumed by braking can be obtained as

$$E_b = \int P_b\,dt. \tag{3}$$

Figure 1 shows the propelling and braking energy profiles of 1,500 kg passenger car while driving in EPA FTP 75 urban driving cycle. It can be seen that, propelling energy consumed on the wheels in a whole cycle is about 1.13 kWh, in which, about 0.63 kWh is consumed in braking. The braking energy is about 55.4% of the total propelling energy which comes from the power sources of the vehicle. Table 1 lists the energy scenario of the 1,500 kg passenger car in the driving cycles of FTP 75 urban, LA92, US06, ECE-15, and New York city. The data in Table 1 shows a significant percentage of the energy consumed by braking. It also hints the importance of an effective regenerative brake system in energy saving.

Braking Energy Distribution over Vehicle Speed

Understanding the braking energy distribution over vehicle speeds is helpful for an effective generative brake system design. For example, in regenerative brake system design, attempts may be made for maximizing regenerative braking capability in the speed range in which most significant braking energy appears. In other speed ranges with less braking energy, other braking performance may be the major concern without significant scarification of energy recovery.

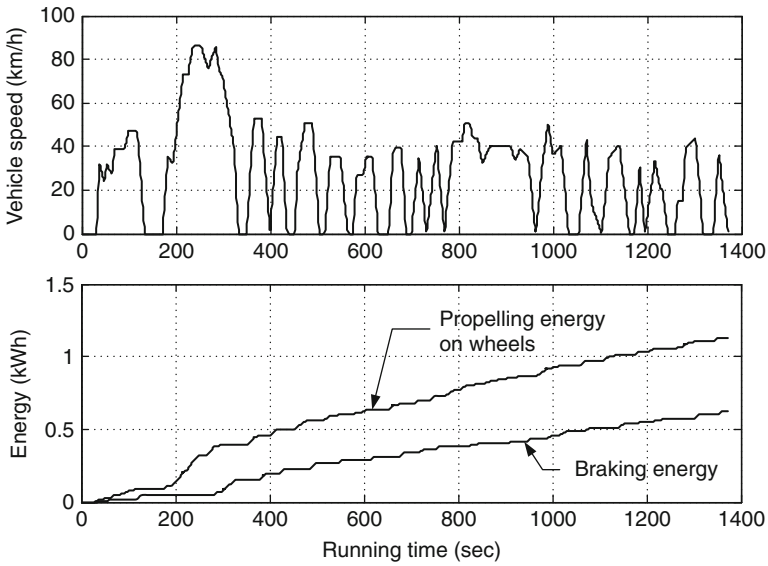

Regenerative Braking. Figure 1
Significant percentage of propelling energy consumed in braking [1]

Regenerative Braking. Table 1 Braking energy scenario of 1,500 kg passenger car in FTP 75 urban drive cycle [1]

	FTP75 urban	LA92	US06	ECE-15	New York city
Maximum speed (km/h)	86.4	107.2	128.5	120	44.6
Average speed (km/h)	27.9	39.4	77.5	49.9	12.2
Traveling distance per cycle (km)	10.6	15.7	12.8	7.95	1.9
Propelling energy (kWh)					
Per cycle	1.129	2.356	2.266	0.969	0.296
Per km	0.106	0.15	0.177	0.122	0.156
Braking energy (kWh)					
Per cycle	0.625	1.337	0.923	0.330	0.243
Per km	0.059	0.087	0.072	0.042	0.127
Percentage of braking energy to propelling energy	55.4	58.0	40.7	34.1	81.9

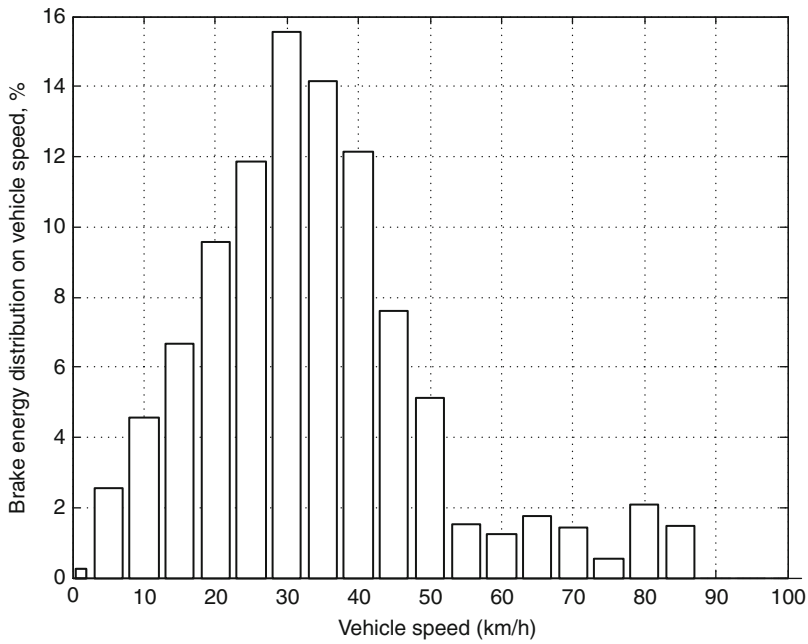

Regenerative Braking. Figure 2
Braking energy density over vehicle speeds in FTP75 urban driving cycle

In calculation of the braking energy distribution over vehicle speeds, the whole speed range is divided into a serial of speed interval, ΔV_j ($j = 1, 2, \ldots, n$). The braking energy in the speed interval ΔV_j can be obtained by integrating the powers falling into the speed interval ΔV_j, with respect to time, as

$$\Delta E_b^j = \int_{\Delta V_j} P_b^j dt, \tag{4}$$

where ΔE_b^j and P_b^j are the braking energy and braking power in the speed interval of ΔV_j. Figure 2 shows

Regenerative Braking. Table 2 Braking energy scenario of 1,500 kg passenger car in FTP 75 urban drive cycle [1]

	FTP 75 urban	LA92	US06	ECE-15	NY city
Braking energy @ speeds <15 km/h (%)	10.93	5.51	3.27	4.25	21.32

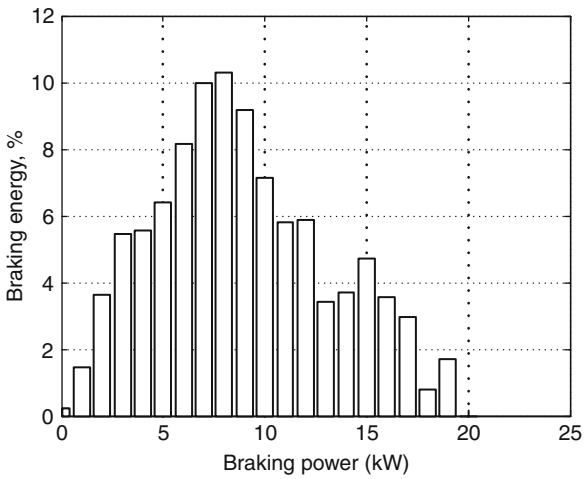

Regenerative Braking. Figure 3
Braking energy distribution over braking power in FTP75 urban driving cycle

Regenerative Braking. Table 3 Braking range in which 85% of braking energy falls dissipated in typical urban driving cycles [1]

	FTP 75 urban	LA92	US06	ECE-15	NY city
Power range in which 85% of total energy falls (kW)	<14.4	<44.5	<46.5	<33.5	<18.5

a vehicle braking energy distribution diagram over vehicle speeds in FTP 75 urban driving cycle. It can be seen that most of the braking energy are consumed in the speed range of 15–50 km/h and very small amount falls into the speed range of less than 15 km/h and larger than 50 km/h. It has been known that electric motor has a poor performance for generation in low speed due to its low back electromagnetic force (EMF). Thus, in regenerative brake system design, regenerative braking may be cancelled and only mechanical braking is applied at low speed, which will not sacrifice much braking energy recovery. Table 2 shows the braking energy consumed in the speed range of less then 15 km/h in typical driving cycle.

Braking Energy Distribution over Braking Power

Braking energy distribution over braking power can supply useful information for the power capacity design of an electric, especially, for mild hybrid vehicle, in which a small electric motor is usually used and for battery design, so that they can recover most of the braking energy.

Similar to the braking energy distribution on vehicle speeds, the braking power is divided into a series of power intervals ΔP_j and the braking energy in a power interval ΔP_j is calculated by

$$\Delta E_b^j = \int_{\Delta P_j} P_b^j dt, \tag{5}$$

where ΔE_b^j and P_b^j are the braking energy and braking power interval of ΔP_j. Figure 3 shows the braking power distribution over braking powers of a 1,500 kg passenger car, in which 85% of braking energy falls into the power range of less than 15 kW. Table 3 gives the power ranges in which 85% of the braking is consumed in the driving cycles of FTP 75 urban, LA92, US06 ECE-15, and New York city.

Hybrid Brake System

A brake-by-wire system is conceptually illustrated in Fig. 4. A brake pedal simulator is connected to a brake pedal. The brake simulator is a mechanical or hydraulic device that produces a "braking feel" for the driver. Instead of generating a braking force, the brake simulator generates a braking command signal which represents driver's desired braking force. The braking controller controls a brake regulator for producing a correct thrust force for the brake actuator. The brake actuator pushes the master cylinder rod. A brake power buffer may be used for supplying brake thrust force and a brake power source

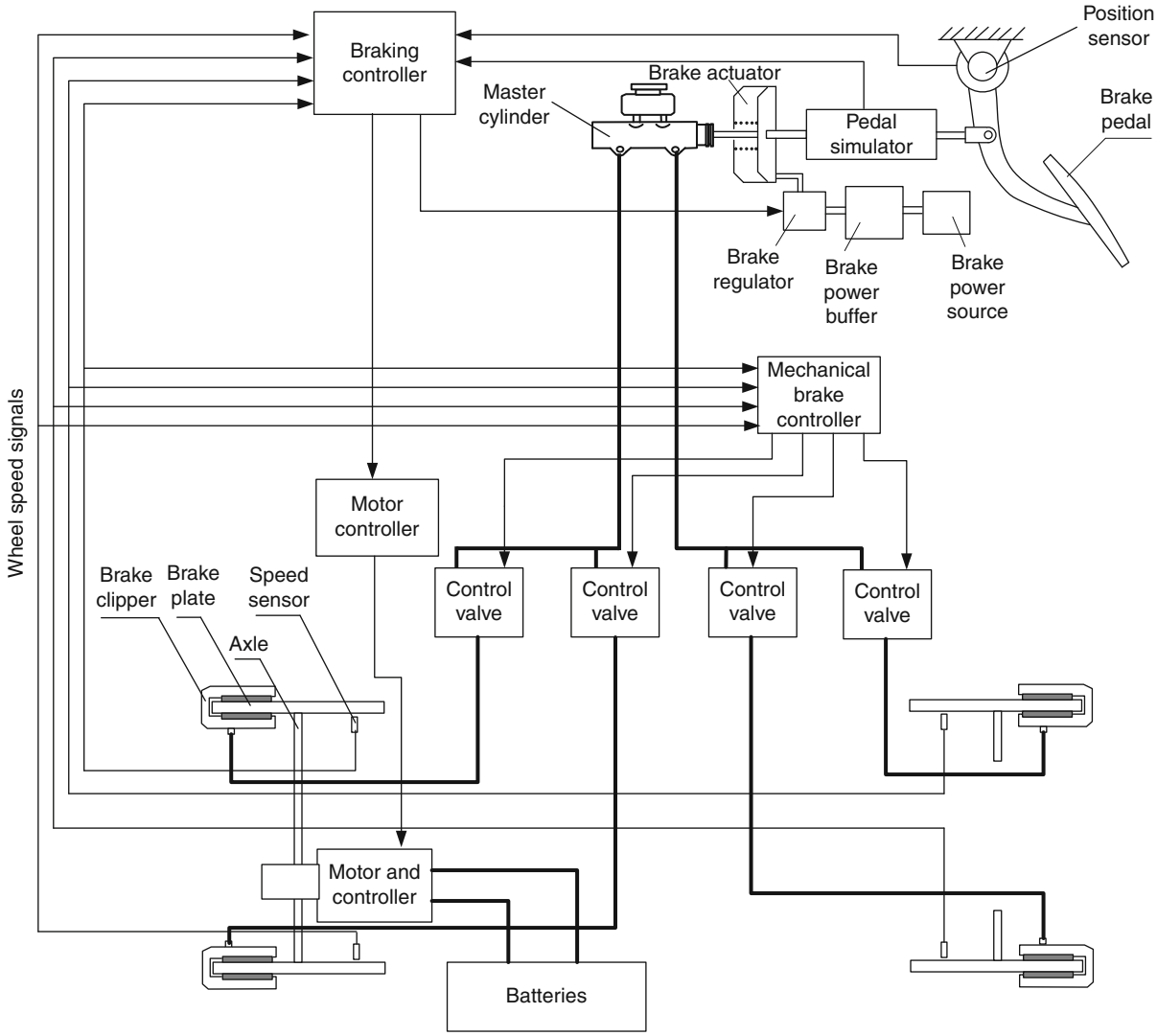

Regenerative Braking. Figure 4
A brake-by-wire hybrid braking system

powers the brake system. This system may be pneumatic, which includes an air solenoid as the brake actuator, air pressure regulator as the brake regulator, a compressed air storage as the brake power buffer, and an air compressor as the brake power source.

A brake position sensor is also attached to the brake pedal to sense its position. Based on receiving braking command and feedback speed signals, the computing algorithm embedded in the brake controller generates control commands to the electric motor and the pressure regulator. In the case of failure of the electric system, the brake simulator can directly apply its force to the master cylinder to generate a mechanical braking force.

The mechanical brake controller operates very similar to the controller of a conventional anti-lock brake system (ABS), which operates the control values to produce correct mechanical brake torque to each of the wheels to preventing wheels from lockup.

The braking controller functions for correctly allocating total braking force to electric regenerative

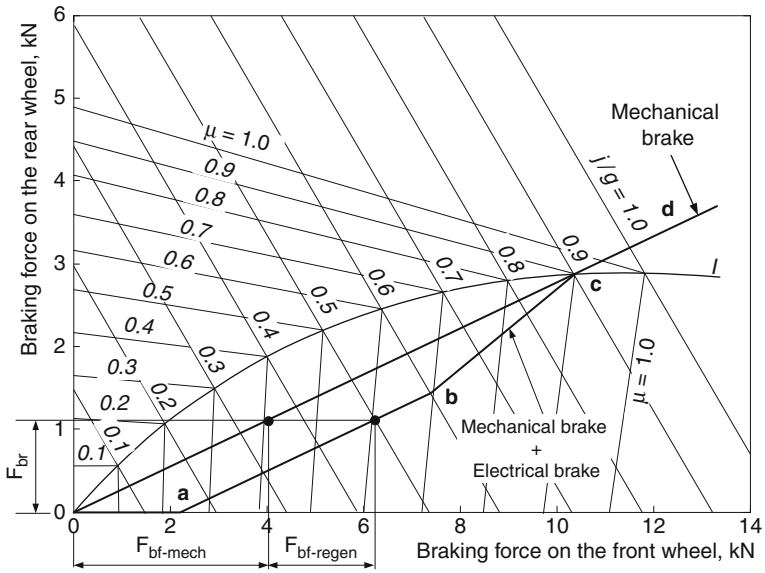

Regenerative Braking. Figure 5
Braking forces varying with braking strength

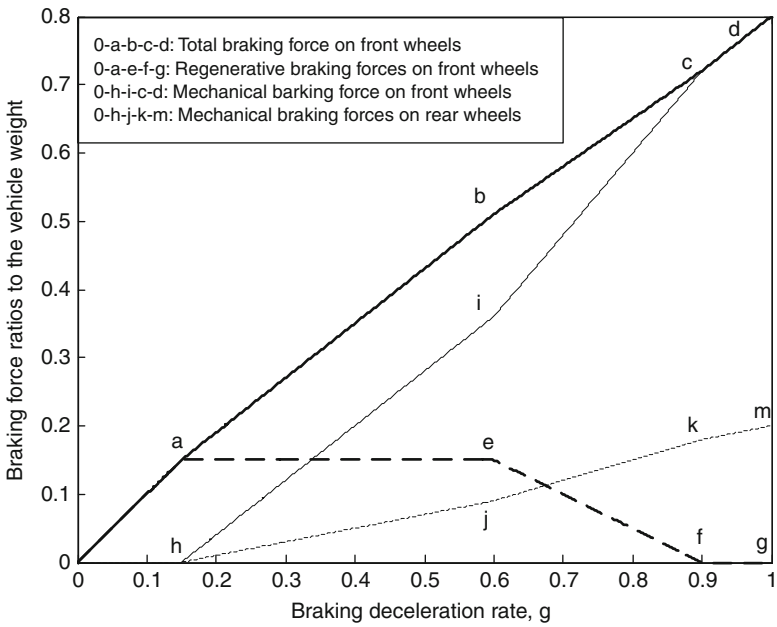

Regenerative Braking. Figure 6
Braking force ratios relative to the vehicle weight versus braking strength [1]

braking and mechanical braking. There are several control strategies for this purpose.

A simple control strategy is shown in Fig. 5, where, front wheels are braked by both regenerative and mechanical brakes, and rear wheels only by mechanical brake. This control strategy is explained as below.

With a slight braking strength, for example, less than 0.15 g, only regenerative braking on front wheels

is applied. This operation is simulating the engine retarding effect. Actually, in normal driving, the braking strength falls in this range in most of driving time [1]. Since no mechanical braking is applied to both the front and the rear wheels, the braking torque generated by the electric machine may be commanded by the position of the brake pedal. However, at low speed, the mechanical braking may be needed due to the weak regenerative braking capability. Furthermore, the electric motor should have sufficient torque to fulfill this braking action.

Regenerative Braking. Table 4 The percentage of the total braking energy available for recovering

	FTP 75 urban	LA 92	US 06	New York	ECE-15
Percentage of the total braking energy available for recovering	89.69	82.92	86.55	76.16	95.75

When strong braking is required, both mechanical and regenerative brakes are needed to be applied to front wheels and only mechanical braking is applied to rear wheels. The braking force distribution on the front and rear wheels follows the lines of a–b–c–d and mechanical braking distribution follows the straight line a–d. In the braking strength range of 0.15–0.6 g, the regenerative braking part is a constant as shown in Fig. 6. When the braking strength is greater than 0.6 g, the regenerative braking is gradually reduced to zero at a high braking strength of 0.9 g. At high braking strength, mechanical brake is more reliable. Figure 6

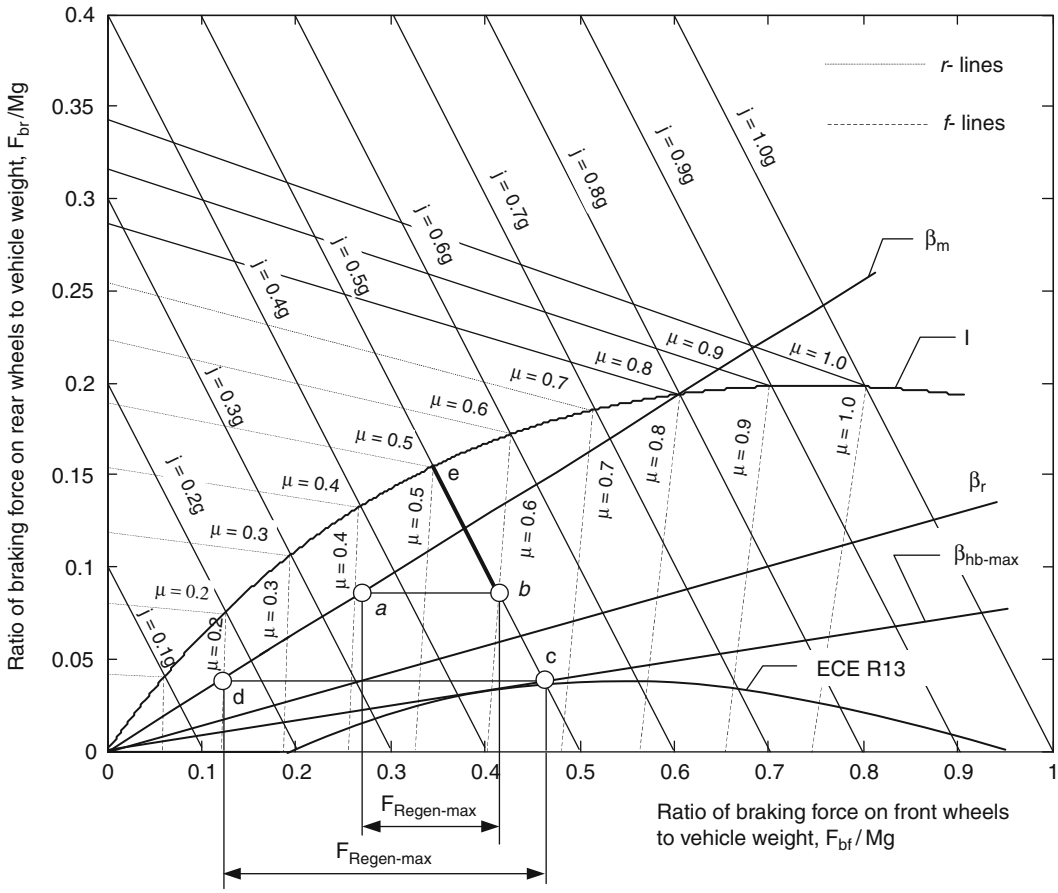

Regenerative Braking. Figure 7
Illustration of braking force distribution on the front wheels (electrical + mechanical) and rear wheels

shows an example of total braking force scenarios. Table 4 shows the calculation results of the percentage of the braking energy that can be recovered by this control strategy in typical urban driving cycles [1].

A control strategy that focuses on maximum regenerative braking may be applied. This braking control strategy follows the rule of allocating the total braking force to front wheels as much as possible within the range stipulated by regulation, for example, ECE R13 regulation. The ECE R13 regulation stipulates a braking force distribution zone, which is in between curves *I* and ECE R13 as shown in Fig. 7. For control simplicity, a straight line, $\beta_{hb\text{-}max}$ may replace the ECE R13 curve.

For certain braking strength commanded by the driver (e.g., 0.5 g) on a road with adhesive coefficient (e.g., 0.6), the braking force distribution can be at any point in the segment of b–e as shown in Fig. 7. Obviously, operating at point b, front wheels obtain its maximum braking force. In this case, the available regenerative braking force on the front wheels is the segment of a-b, depending on the motor torque capacity. The mechanical brake works at point a. If the road coefficient increases to 0.7 and still with braking strength 0.5 g, the braking force distribution can be at any point between points c–e. Obviously, the maximum available braking force on the front wheels is at point c, limited by the ECE R13 regulation. The mechanical brake works at point d and available regenerative braking force is the segment of c–d. This control strategy can be summarized as a rule such that, if the road adhesion and motor torque permit, operate the total braking force distribution on the line $\beta_{hb\text{-}max}$. Obviously, line $\beta_{hb\text{-}max}$ stands for the extreme case. In practice, a margin would be set, for example, line β_r as shown in Fig. 7.

Future Directions

A fully electronic controlled, brake-by-wire hybrid braking system is still under development. In this system, the electric motor/generator and mechanical braking force on individual wheels can be independently and coordinately controlled. While driving on any road, the road adhesive capacity can be fully used for quickly stopping the vehicle, maintaining the vehicle stability, and meanwhile recovering braking energy as much as possible. The braking system is coordinately controlled with steering system for vehicle driving stability.

Bibliography

Primary Literature

1. Ehsani M, Gao Y, Emadi A (2010) Modern electric, hybrid and fuel cell vehicles-fundamentals, theory and design. CRC, Boca Raton

Books and Reviews

Cikanek SR, Bailey KE (1995) Energy recovery comparison between series and parallel braking system for electric vehicle using various drive cycles, DSC vol 56/DE, 86. Advanced Automotive Technologies, American Society of Mechanical Engineers (ASME), New York, pp 17–31

Gao H, Gao Y, Ehsani M (2001) Design issues of the switched reluctance motor drive for propulsion and regenerative braking in EV and HEV. Proceedings of the SAE 2001 future transportation technology conference, Costa Mesa, CA, paper No. 2001-01-2529

Gao Y, Chu L, Ehsani M (2007) Design and control principle of hybrid braking system for EV, HEV and FCV, 2007 IEEE VPPC

Shu J, Zhang Y, Yin CL (2009) Longitudinal control of hybrid electric buses using traction motor and pneumatic braking system. WSEAS Trans Circuits Syst 8(11):873–882

Regenerative Development and Design

Pamela Mang[1], Bill Reed[2]
[1]Regenesis Group and Story of Place Institute, Santa Fe, NM, USA
[2]Regenesis Group and Story of Place Institute, Arlington, MA, USA

Article Outline

Glossary
Definition of the Subject and Its Importance
Introduction
Regenerative Development and Design–Redefining Sustainability
Overview: Ecological Sustainability and Regenerative Development and Design

Regenerative Approaches to Sustainable Development and Design – Key Framework Premises and Practice Methodologies Overview
Future Directions
Bibliography

Glossary

Biomimicry Sometimes called biomimetic design, an emerging design discipline that looks to nature for sustainable design solutions [1].

Cradle to Cradle® Framework for designing manufacturing processes "powered by renewable energy, in which materials flow in safe, regenerative, closed-loop cycles," and which "identifies three key design principles in the intelligence of natural systems, which can inform human design: *Waste Equals Food*; *Use Current Solar Income*; *Celebrate Diversity*" [2, 3].

Ecoliteracy The ability to understand the natural systems that make life on earth possible, including understanding the principles of organization of ecological communities (i.e., ecosystems) and using those principles for creating sustainable human communities [4, 5].

Ecological sustainability A biocentric school of sustainability thinking that, based on ecology and living systems principles, focuses on "the capacity of ecosystems to maintain their essential functions and processes, and retain their biodiversity in full measure over the long term"; contrasts with technological sustainability based on technical and engineering approaches to sustainability [4].

Ecology The interdisciplinary scientific study of the living conditions of organisms in interaction with each other and with the surroundings, organic, as well as inorganic.

Ecosystem "The interactive system of living things and their nonliving habitat" [6].

Ecosystem concept "A coherent framework for redesigning our landscapes, buildings, cities, and systems of energy, water, food, manufacturing, and waste" through "the effective adaptation to and integration with nature's processes." It has been used more to shape an approach than as a scientific theory [7].

Living systems thinking A thinking technology, using systemic frameworks and developmental processes, for consciously improving the capacity to apply systems thinking to the evolution of human or social living systems [8].

Locational patterns The patterns that depict the distinctive character and potential of a place and provide a dynamic mapping for designing human structures and systems that align with the living systems of a place.

Pattern literacy Being able to read, understand, and generate ("write") appropriate patterns.

Permaculture A contraction of *permanent agriculture* or *permanent culture*, permaculture was developed as a system for designing ecological human habitats and food production systems based on the relationships and processes found in natural ecological communities and the relationships and adaptations of indigenous peoples to their ecosystems [9].

Place The unique, multilayered network of ecosystems within a geographic region that results from the complex interactions through time of the natural ecology (climate, mineral, and other deposits, soil, vegetation, water, and wildlife, etc.) and culture (distinctive customs, expressions of values, economic activities, forms of association, ideas for education, traditions, etc.).

Regenerate American Heritage Dictionary of the English Language and Merriam Webster Dictionary

- To give new life or energy; to revitalize; to bring or come into renewed existence; to impart new and more vigorous life
- To form, construct, or create anew, especially in an improved state; to restore to a better, higher or more worthy state; refreshed or renewed
- To reform spiritually or morally; to improve moral condition; to invest with a new and higher spiritual nature
- To improve a place or system, especially by making it more active or successful

Regenerative design A system of technologies and strategies based on an understanding of the inner working of ecosystems that generates designs to regenerate rather than deplete underlying life support systems and resources within socioecological wholes.

Regenerative development A system of technologies and strategies for generating the patterned whole-system understanding of a place, and developing the

strategic systemic thinking capacities and the self-organizing and self-evolving stakeholder engagement/commitment required to ensure regenerative design processes achieve maximum systemic leverage and support.

Restorative design Sometimes called restorative environmental design, a design system that combines returning "polluted, degraded or damaged sites back to a state of acceptable health through human intervention" [10] with biophiliac designs that reconnect people to nature.

Source to sink Simple linear flows from resource sources (farms, mines, forests, watershed, oilfields, etc.) to sinks (air, water, land) that deplete global sources and overload/pollute global sinks [11].

Systems thinking A framework for seeing interrelationships rather than things and for seeing patterns of change rather than static "snapshots." It addresses phenomena in terms of wholeness rather than in terms of parts [5].

Definition of the Subject and Its Importance

The emerging field of regenerative development and design marks a significant evolution in the concept and application of sustainability. Practices in sustainable or green design have focused primarily on minimizing damage to the environment and human health, and using resources more efficiently, in effect, slowing down the degradation of earth's natural systems. Advocates of a regenerative approach to the built environment believe that a much more deeply integrated, whole-systems approach to the design and construction of buildings and human settlements (and nearly all other human activities) is needed. Regenerative approaches seek not only to reverse the degeneration of the earth's natural systems but also to design human systems that can coevolve with natural systems – evolve in a way that generates mutual benefits and greater overall expression of life and resilience. The field of regenerative development and design, which draws inspiration from the self-healing and self-organizing capacities of natural living systems, is increasingly seen as a source for achieving this end. This field is redefining the way that proponents of sustainability are thinking about and designing for the built environment, and even the role of architecture as a field.

Introduction

Chronology

Early Roots In the 1880s, Ebenezer Howard wrote *To-morrow: A Peaceful Path to Social Reform*. Reissued in 1902 as *Garden Cities of To-Morrow*, with an introductory essay by Lewis Mumford, the book was an early and influential expression of ecological thinking applied to human settlement. It sought to reconnect humans to nature, and featured use of natural rather than engineered processes to build the health of the system. His description of a utopian city in which man lives harmoniously together with the rest of nature stimulated the founding of the garden city movement and the establishment of several Garden Cities in Great Britain in the early twentieth century [11, 12].

In 1915, Patrick Geddes published his study of the urban growth patterns stimulated by the mass movement of people into cities [13]. Geddes, a biologist, saw cities as living organisms. He believed that addressing the problems of unsustainable growth required understanding a city's context – the surrounding landscape's natural features, processes, and resources – and called for a solid analytic method for developing that understanding. His conclusion would influence regional planning movements across Europe and the United States. Geddes applied the terms *Paleotechnic* and *Neotechnic* to distinguish the industrial era producing this destructive growth of human settlements from the era he predicted would follow its demise. These terms would be picked up by John Tillman Lyle, some 80 years later, to differentiate industrial era and regenerative technologies. Some trace the origins of ecological design to the work of Patrick Geddes [7, 11].

Development of the Ecosystem Concept and Ecological Perspective In 1935, Arthur Tansley introduced an entirely new concept to ecology in his work, "The Use and Abuse of Vegetational Concepts and Terms" [6]. He proposed the term *ecosystem* as a name for the interactive system of living things and their nonliving habitat and the application of systems science as a way to bring more scientific rigor to the study of nature's complexity and the effect of human activities on that complexity. Tansley and other organismic biologists of the period were the first to formulate a systems view of life. Seeking a more accurate depiction of how life

ordered and organized itself within a particular landscape or geographic location, he posited that neither a living organism nor its physical environment could be thought of as separate entities: "we cannot separate them from their special environment, with which they form one physical system." Two of the most significant implications of this depiction of how life structures itself were the deconstruction of the human/nature dichotomy that had shaped Western design thinking and the establishment of the premise that all species are ecologically integrated with each other, as well as with the abiotic constituents of their biotope or habitat. For Tansley and other ecologists concerned about the increasing impact of humans on natural systems, the ecosystem offered a valuable framework for analyzing the effect of human activities on natural systems and resources. In later years, the concept was further defined or clarified to explicitly include a social complex (human social institutions and actions) and a built complex (structures and infrastructures) and became a framework for sustainable urban planning and development [14, 15].

In the 1950s and 1960s, Eugene and Howard Odum laid the foundation for the development of ecology into a modern science, based on the core concept of the ecosystem as the fundamental ordering structure of nature. They published the first textbook on ecology, *The Fundamentals of Ecology*, in 1953. Their work brought attention to the importance of understanding how the earth's ecological systems interact with one another. Howard Odum further developed a number of key theoretical concepts and methodologies including his "energy systems language," a set of symbols used to compose energy flow diagrams for any scale system [16]. His study of wetlands pioneered the now widespread approach of using wetlands as water quality improvement ecosystems and served as an important contribution to the beginnings of the field of ecological engineering [17].

New Foundations for Systems Theory and Systems Thinking In 1968, biologist and systems theoretician Ludwig von Bertalanffy published his *General System Theory: Foundations, Development, Applications*. General systems theory (GST) introduced the concept of open systems, emphasized the difference between physical and biological systems, and introduced evolutionary thinking – thinking focused on change, growth, and development [18]. GST opened the door to a new science of complexity. The recognition that complex systems cannot be understood through simple analysis led to the emergence of systems thinking as a major scientific field, a profound change from the analytic, reductionist mode that had dominated Western scientific thinking since the time of Descartes, Newton, Galisteo, and Bacon. GST also laid the basis for the development of living systems science, for Charles Krone's development of living systems thinking and their application to natural systems, as well as to human social systems. His work strongly influenced Howard Odum's ecosystem modeling and energetics, which, in turn, influenced John Tillman Lyle's work on regenerative design technologies.

In the 1960s–1970s – systems theorist and architect of organizational processes and structures, Charles Krone developed living systems thinking as a developmental technology for consciously improving systems thinking capacity. His work drew on and greatly extended GST and *Systematics*, a discipline developed by mathematician John Bennett that uses systemic frameworks to understand complex wholes within which people are participants rather than observers. The systemic frameworks and developmental processes Krone generated were applied and evolved within businesses. Their purpose was to create an understanding of businesses, communities, and nature as living systems and to build the consciousness required to create reciprocally beneficial relationships through better integration of industrial, community, and natural processes. His work served as a core foundation for Regenesis Collaborative Development Group as they developed and evolved regenerative development processes and technologies, starting in the 1990s [19, 20, 21]. Of particular importance for regenerative development was Krone's framework depicting four orders or levels of work that living systems of all scales need to carry out. Ranging over four levels from basic operations up through regenerative work, it allows practitioners to design for the integrated evolution of all levels of work in support of a regenerative change process.

Ecological Sustainability – Foundations of Regenerative Development and Design In 1969, Landscape architect Ian McHarg published *Design with Nature*, pioneering a technology for ecological land-use

planning based on understanding natural systems [22]. His book became a foundational textbook for the ecological view of urban landscape design, and its basic concepts were later developed into the geographic information systems (GIS) – a critical tool for ecological development.

In 1978, Bill Mollison, an Australian ecologist, and one of his students David Holmgren coined the word permaculture from a contraction of *permanent agriculture* or *permanent culture*. They developed the field of permaculture as an ecological design system to promote design of human habitats and food production systems based on the relationships and processes found in natural ecological communities. Much of its inspiration was drawn from the relationships and adaptations of indigenous peoples to their ecosystems [9]. Like ecological practitioners such as Ian McHarg, Mollison and Holmgren espoused integration of human and natural environments, but they also developed design technologies and practices for increasingly self-sufficient human communities and food production systems. By creating "man-made ecosystems," permaculture demonstrated how to provide for a host of human needs while reducing dependence on environmentally destructive industrial practices. While earlier iterations of ecological design promoted integration of human and natural systems for more sustainable development, permaculture was the first ecological design system to introduce the concept of a regenerative effect as a new standard of ecological performance for the built environment – the generation of a surplus or overabundance of energy and resources that could be reinvested to evolve natural and human living systems as an integrated whole. In support of that goal, Mollison's *Permaculture: a designers' manual*, published in 1988, introduced a hierarchy of investment (regenerative, generative, and degenerative) as a framework for assessing the value of potential actions for building regenerative capacity in a system [9].

Also in the 1980s, Robert Rodale, son of organic agriculture pioneer J. I. Rodale, advanced the use of the word *regenerative* in relation to the use of land, calling for going "beyond sustainability, to renew and to regenerate our agricultural resources" [23]. Rodale used the term to describe the continuing organic renewal of the complex living system that he saw as the basis for healthy soil and, in turn, for healthy food and healthy people. He later applied the same principle of ongoing self-renewal to regenerative economic development [24]. While his work did not extend to the built environment, his principles influenced John Tillman Lyle's work and are foundational in the subsequent conceptualization and application of regenerative methodologies to all of the systems that support life.

In 1984, John Tillman Lyle published *Design of Human Ecosystems* [25] in which he argued that "designers must understand ecological order operating at a variety of scales and link this understanding to human values if we are to create durable, responsible, beneficial designs." He defined human ecosystems as "places in which human beings and nature might be brought together again" for mutual benefit and posited conscious ecosystemic design as essential to a sustainable future. The book introduced several key concepts that laid the basis for his subsequent work on regenerative design (below). These included (1) "shaping ecosystems, just like shaping buildings," requires a set of organizing principles drawn from "strong concepts of an underlying order that holds the diverse pieces and all their hidden relations together." (2) In ecosystem design, "these underlying concepts of order are drawn from ecology" and principles for ecosystem design draw from the "need to comprehend and envision the ecosystem the designer is seeking to shape as a dynamic (living) whole," and (3) ecological concepts are "more or less analogous to the laws of mechanics in architecture in that they provide us with organizing principles for shaping ecosystems much as architects shape buildings."

Ecological Design Systems Proliferate The 1990s was a period of intense creative ferment for ecological design thinking. A number of foundational books were published laying out both the practical and theoretical bases of design for ecological sustainability, including *Ecological literacy: education and the transition to a postmodern world* by David Orr (1992), *From Eco-Cities to Living Machines: Principles of Ecological Design* by Nancy Jack Todd & John Todd (1993), *The web of life: A new scientific understanding of living systems* by Fritjoff Capra (1995), *Ecological Design* by Sim van der Ryn and Stuart Cowan (1996), and *The ecology of place: Planning for environment, economy, and community* by Timothy Beatley (1997).

In 1992, educator David Orr and physicist Fritjof Capra coined the term ecological literacy (also referred to as *ecoliteracy*) to describe the ability to understand the natural systems that make life on earth possible, including understanding the principles of organization of ecological communities (i.e., ecosystems) and using those principles for creating sustainable human communities [4].

Also in the 1990s, new ecological and living system-based metric systems were introduced, including the revision of architect Malcolm Wells' Wilderness-Based Check-list for Design and Construction 1999 by the Society of Building Science Educators (SBSE) to address site and building issues. Their work acknowledged John Tillman Lyle's idea that sustainable design is merely breaking even, while regenerative design renews earth resources [20]. On a larger scale, Pliny Fisk's work on EcoBalance land-use planning and design method employed the principle of life cycles as a framework for sustaining basic life supporting systems, balancing human needs with their ability to manage the environment using technologies for augmenting natural processes [26].

Emergence of Regenerative Development and Design as Distinct Disciplines In 1996, John Tillman Lyle published *Regenerative Design for Sustainable Development*, the first comprehensive articulation of, and handbook for, regenerative design [11]. Written as a practical guide to the theory and design of regenerative systems, it laid out the framework, principles, and strategies for a design technology aimed at reversing the environmental damage caused by what Lyle called industrial land-use practices. The book reflected the continuing evolution of the thinking he had been pursuing as a landscape architect, architect and educator. He established the Center for Regenerative Design at California State Polytechnic University, Pomona to test, demonstrate, and further evolve this technology.

Deeply concerned about conventional industrial development's resource depletion and environmental degradation – consequences embedded in "the design of our twentieth century landscape," Lyle believed that at the core of growing environmental crises lay the simplification of living systems caused by "paleo" design and technologies (a term he adopted from Patrick Geddes to depict their relative crudity). "Where nature evolved an ever-varying, endlessly complex network of unique places adapted to local conditions," he wrote, ". . .humans have designed readily manageable uniformity." This creates relatively simple patterns and forms designed to be easily replicable anywhere. Most important, in his view, was the replacement of nature's continual cycling and recycling of materials and energy – processes "core to the earth's operating system" – with one-way linear flows from source to sink. "Eventually a one-way system destroys the landscapes on which it depends," Lyle observed. "The clock is always running and the flows always approaching the time when they can flow no more. In its very essence, this is a degenerative system, devouring its own sources of sustenance." The degenerative patterns caused by these linear, one-way flows he believed, demanded a fundamentally different approach that he named regenerative design. Accordingly, Lyle defined regenerative design as the replacement of linear systems of throughput flows with "cyclical flows at sources, consumption centers, and sinks." The resulting systems provide for "continuous replacement, through (their) own functional processes, of the energy and materials used in their operation" [11].

Lyle died just 4 years after publication of *Regenerative Design for Sustainable Development*. While he called redesign of the degenerative systems created by industrial linear flows as the "first order of work," it is clear from the larger body of his work and other writings [19] that he saw regenerative design as encompassing far more than this basic operational goal, as fundamental as it was. While much attention has been given to his models and techniques for designing self-renewing resource and energy flows, Lyle always saw the heart of his work, and the work of regenerative design, as the conscious design of whole ecosystems. His concern with the importance of developing a different nature of thinking as the basis for regenerative design, which was addressed in introductory chapters of the book, was also left without further development. Unfortunately, the narrow definition of the term regenerative as simply "self-renewing" came to define the focus of regenerative design for many architects and landscape architects.

In 1995, the authors of this chapter and the Regenesis Collaborative Development Group began developing the theoretical and technological foundation for regenerative development – enabling human communities to coevolve with the natural living systems they inhabit while continuously regenerating

environments and cultures. Regenesis founders had practiced biocentric design, inspired by natural processes, in a variety of arenas for a number of years and knew the power of this approach. They agreed that development projects needed to be sources of ecological health, even "engines of positive or evolutionary change for the systems into which they are built" [27]. While agreeing with the ends of ecological sustainability, they felt that the primary cause driving unsustainable patterns was not being addressed by ecological design systems. They saw environmental problems as symptoms of a fractured relationship between people and the living web of nature, and argued that the core issue was cultural and psychological, rather than technological. Like Lyle, they believed that addressing this issue required a fundamental transformation in how humans saw their relationship and role with regard to the planet – moving from the current view of standing apart from and using (or protecting) nature to seeing a "coevolutionary whole, where humans exist in symbiotic relationship with the living lands they inhabit" [28].

For regenerative design to take hold and be successfully applied, they reasoned, a radical shift in thinking and understanding would be required among design professionals, stakeholders, and all the human inhabitants of a place. They proposed the term regenerative development for the more comprehensive work of creating the conditions and building the capacities required for achieving this shift, with the aim of making development a source of harmonious integration with nature [27, 29].

Regenerative Development and Design–Redefining Sustainability

Introduction

Sustainable development and design has been described as falling broadly into two streams – one primarily technical and engineering based (technological sustainability) and the other based in ecology and living systems principles (ecological sustainability) [4, 7]. Green or high-performance building, sometimes called eco-efficient design, emerged out of the first stream, and regenerative development and design out of the second. Green building, like the conventional building field before it, defined the built environment as "all the structures people have built when considered as separate from the natural environment" (MacMillan Dictionary). It defined a sustainable built environment as one that is resource efficient and has minimal or neutral environmental impact. While that definition is evolving, the primary aim of green building continues to be increasing the efficiency of energy, water, and material use while reducing local and global impacts on the natural environment.

However, as Sarah Jenkin and Maibritt Pedersen Zari note in their 2009 research paper, "Rethinking the Built Environment," "The definition of a sustainable built environment is changing rapidly. While aiming for neutral or reduced environmental impacts in terms of energy, carbon, waste or water are worthwhile targets, it is becoming clear that the built environment must go beyond this. It must have net positive environmental benefits for the living world" [10].

The rising field of regenerative development and design, which emerged from the ecological stream, is not only leading the charge to redefine sustainability but also redefining what the built environment encompasses and what its role must be. Advocates of a regenerative approach to the built environment believe that a much more comprehensive, deeply integrated, and whole-systems approach is needed. They propose that eco-efficient design technologies and strategies be integrated within an ecologically based approach that reverses the degeneration of both the earth's natural systems and the human systems that inhabit them. The methodology of this approach focuses on the development of human settlements that partner with natural systems and processes to actively regenerate the health of their place as a whole and the spirit of the people who inhabit it (Fig. 1).

The philosophical and technical foundations for regenerative development and design as a distinctive field within ecological sustainability were laid in the 1990s, though they draw from scientific and technological advances reaching back into the early part of the last century (see "Chronology"). The practices emerging from that body of work are still evolving and expanding to cover an increasingly broad and sophisticated spectrum of sustainability concerns. Held together by a common philosophical core, they extend beyond the traditional aspects of design to address the

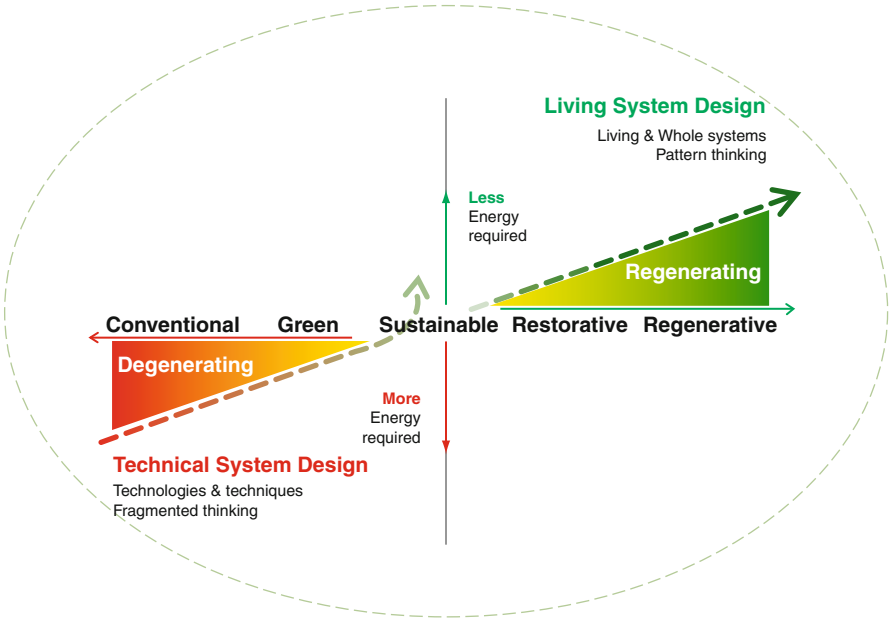

Regenerative Development and Design. Figure 1
Graphic contrast of Technical System Design and Living System Design. © Regenesis Group. Reprinted with permission

different nature of thinking and interactivity that is required to design and engage in a regenerative process.

While regenerative approaches are attracting growing interest among sustainability design practitioners, transitioning from green building to a regenerative practice has presented a number of challenges. The holistic and deeply integrated nature of the regenerative approach does not lend itself to a "menu approach" – picking one or two regenerative technologies without understanding the underlying principles that assure a regenerative outcome. Another challenge is reconciling the two radically different worldviews shaping technological and ecological sustainability within the way one's practice is carried out. Few architects and engineers are familiar with, let alone trained in an ecological paradigm. Yet as David Orr notes:.

- *Ecological problems are in many ways design problems: our cities, cars, houses, and technologies often do not fit in the biosphere. Ecological design requires the ability to comprehend patterns that connect, which means looking beyond the boxes we call disciplines to see things in their larger context. Ecological design is the careful meshing of human purposes with the larger patterns and flows of the natural world; it is the careful study of those patterns and flows to inform human purposes. Competence in ecological design requires spreading ecological intelligence—knowledge about how nature works.* [30]

Still, another challenge lies in the lack of a universally agreed upon definition for regenerative development and design and a tendency to blur or confuse regenerative approaches with the range of other design systems that emerged in pursuit of ecological sustainability in the 1990s.

This confusion around the distinctive nature of regenerative development and design has been due in part to being an emerging field lacking universal understanding of the meaning of regeneration, especially as it applies to design of the built environment. The distinction between regenerative development and regenerative design must also be further clarified if this field's potential contribution to sustainability is to be fully realized.

Overview: Ecological Sustainability and Regenerative Development and Design

Ecological Sustainability

Ecological sustainability has been defined as the "capacity of ecosystems to maintain their essential functions and processes, and retain their biodiversity in full measure over the long-term" (www.businessdictionary.com).

While accurate and straightforward, the seeming simplicity of this definition is deceptive. To understand and then deliver what is required to "maintain" and "retain" requires first understanding the nature of ecosystems and the nature of the ecological world in which they exist. That, in turn, requires understanding the ecological perspective – the use of ecological concepts from biology as a metaphor for understanding and designing environments.

All development of the built environment involves changing the landscape and, perforce, the natural systems embedded within it – modifying and adapting them for human purposes. The design of that change is ultimately based on the designer's understanding of the "nature of nature"– how nature works and, concomitantly, humans' relationship to it. That understanding, in turn, is shaped by the fundamental model or paradigm held by the larger culture – the metaphor used to depict how the world works. In the same way, technologies reflect a culture and how it understands nature [7, 11, 25].

The divergent definitions of ecological and technological sustainability can be attributed in large part to their being grounded in very different worldviews. Ecological sustainability as a field and the design systems within it emerged from the profound shift in worldview that occurred over the last century as a result of advances in both the physical and biological sciences. Fritjof Capra has described this as a shift from the mechanistic worldview of Descartes and Newton. In that paradigm, the dominant metaphor for understanding the world (and all organisms within it) was that of a machine composed of separate parts. In contrast, the ecological worldview sees the world as a self-organizing, continuously evolving, interdependent web of living systems, and the concept of ecosystem is the dominant metaphor for understanding its workings. The ecosystem concept, as it has been evolved and informed by living systems science, has been particularly influential in shaping ecological and regenerative understanding of the world and the role of humans within it, with profound implications for sustainability and development [5, 14, 15].

The industrial era metaphor of machine was particularly influential in shaping much of the built environment in the developed world and continues to play a significant role even today. By the first decade of the twenty-first century, however, Le Corbusier's image of the modern house as a "machine for living" was being challenged by the image of living buildings and communities as ecosystems.

As the ecosystem emerged as a new "governing concept of relationship between humanity and nature" [14], it confronted some of the most basic premises of the technologies, processes, and goals of the design field at the time, including the role of buildings, the definition of the built environment, the role of designers, and even the role of humans on the planet. As designers concerned about sustainability began to explore the implications of this new paradigm, it became clear that new ways of thinking and working, along with new forms of technology and new standards of ecological performance were required. The ecological sustainability stream, and within that stream, regenerative development and design, grew out of the work of the pioneering designers, educators, and scientists who took up the challenge of changing their design practice, themselves, and ultimately, their field in order to meet these requirements.

While many have written about different aspects of ecological sustainability during and since the 1990s, some of the most comprehensive articulations of the key premises that shaped the distinctive character of the broader field as a whole can be found in the writings of Sim Van der Ryn, Stuart Cowan, David Orr, and Fritjoff Capra [4, 5, 7, 30].

Regenerative Development and Design Overview

A number of ecological strategies for sustainability were developed during the 1980s and 1990s that were organized around the core set of philosophical, theoretical, and scientific concepts that underlie the ecological perspective of reality. All were aligned around a commitment to net positive goals for the built environment and to integrate human structures, processes, and infrastructures with natural living systems to that end. They differed in the systemic scope they encompassed, falling into four broad categories along a spectrum of comprehensiveness (Fig. 2).

1. Biomimetic – Cradle to Cradle and Biomimicry are design philosophies that fit into this category:

   Biomimetic approaches look to nature as inspiration. It is a *functional* approach that uses

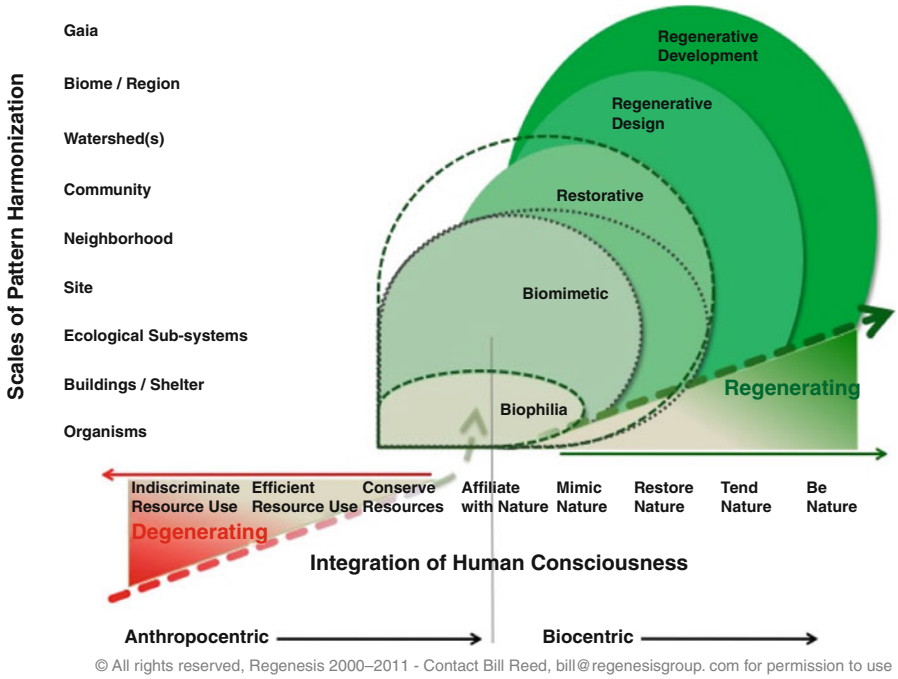

Regenerative Development and Design. Figure 2
Levels of Ecological Strategies for Sustainability. © Regenesis Group. Reprinted with permission

nature – its forms and its processes – as a model for humans to follow – an anthropocentric perspective. Technical product design, buildings, manufacturing processes, agriculture, and human activity will function best and be more in harmony with ecological processes if nature is used as a model and guide. Nature's services and techniques are generally much more effective and certainly more sustainable than technical engineering approximations [31].

The principles guiding biomimetic thinking are essentially derived from an ecological understanding of how life works and provide a conceptual starting point to move into more whole and regenerative systems scope.

2. Biophilia – A general term, meaning "urge to affiliate with other forms of life" [32].

As a design philosophy, biophilia is *relational* in its approach – it is somewhat passive in its engagement with life and is anthropocentric in its purpose. It acknowledges that humans will, if given a choice between nature and a human-made context, choose an environment or situation that utilizes, or is in contact with, living systems and their processes. Human health is positively influenced in relation to life and diminished if separated from living system connectivity. The design fields that use biophiliac approaches consciously use Literal Connections to natural features and elements; Facsimile Connections in terms of the use of nature imagery and materials; and Evocative Connections that use the qualities and attributes of nature in design such as sensory variability, prospect and refuge, serendipity, discovered complexity [33].

3. Restorative – Reestablishes the self-organizing and evolving capability of natural systems.

This is an approach that acknowledges that humans have a role to play. It is more highly *integrated* than biomimetic approaches and more *active* than biophilic approaches – yet it generally is an episodic and finite engagement. This approach typically intervenes on an initial basis to reestablish the health of a subsystem of an ecosystem and community – such as wetlands, woods, riparian corridors, beach dune systems, social systems, and so on. It is

a biocentric approach. When the intervening human role is finished, however – once the capacity of the system to self-organize is set in motion – the humans leave the engagement and are expected to [34].

4. Regenerative

   Acknowledges that humans are "nature," and there is greater hope of evolutionary potential in a state of intentional interrelationship. Humans have a positive role to play in nature. In order to create sustained ecological health, humans must evolve a conscious and *integral* interrelationship where humans and nature are in a mutually beneficial being and becoming relationship – one that is always aware of evolutionary potential. It is a fully conscious awareness that the health of an ecosystem is dependent on human health and human health is dependent on the health of the whole ecology. It is coevolutionary. This might be termed a process of *biobecoming* – the development of a whole system of interrelated living consciousness – a new mind. "Design inevitably instructs us about our relationships to nature and people that makes us more or less mindful and more or less ecologically competent. The ultimate object of design is not artifacts, buildings, or landscapes, but human minds" [4].

M. Kat Anderson supports this way of being in "Tending the Wild": *Wilderness is a negative label for land that has not been taken care of by humans for a long time...California Indians believe that when humans are gone from an area long enough, they lose the practical knowledge about correct interaction, and the plants and animals retreat spiritually from the earth or hide from humans. When intimate interaction ceases, the continuity of knowledge passed down through generations, is broken, and the land becomes "wilderness"* [35].

Together, regenerative development and design provide a framework for creating, applying, adapting, and integrating a blend of modern and ancient technologies to the design, management, and continuing evolution of sustainable built environments, accomplishing positive ecological and social results that include:

- Improving the health and vitality of human and natural communities – physical, psychological, economic, and ecological.
- Producing and reinvesting surplus resources and energy to build the capacity of the underlying relationships and support systems of a place needed for resilience and continuing evolution of those communities.
- Creating a field of caring, commitment, and deep connection to place that enables the changes required for the above to take place and to endure and evolve through time [10, 28].

The first comprehensive articulation of the theoretical and practical basis of regenerative approaches to the built environment emerged separately for regenerative development and regenerative design in the mid-1990s from two separate sources – the work of Regenesis Collaborative Development Group and John Tillman Lyle. Their respective bodies of work each reflected a convergence of disciplines in addition to architecture including, landscape ecology, geohydrology, landscape architecture, permaculture, regenerative agriculture, general systems theory and cybernetics, living systems theory and thinking, and developmental psychology.

Regenerative development and design, as articulated by Regenesis and Lyle, recognizes that "humans, human developments, social structures and cultural concerns are an inherent part of ecosystems" [10], making humans integral and particularly influential participants in the health and destiny of the earth's web of living systems. According to this view, the sustainability of the real estate development industry, which works directly on these webs, is largely determined by whether humans participate in them as partners or as exploiters [11, 25, 27, 28, 36, 37].

In his paper, "New Context, New Responsibilities: Building Capability" [38], Ray Cole articulated some of the key implications of a regenerative approach, including:

- Seeing the responsibility of design as "designing the 'capability' of the constructed world to support the positive coevolution of human and natural systems" versus designing "things" (buildings, infrastructure, etc.) and defining sustainable buildings as "buildings that can support sustainable patterns of living."
- Emphasizing the "role of building in positively supporting human and natural *processes*" versus "building as *product*."
- Positioning "building as central in creating higher levels of order and, as such, creating increased variety and complexity."

- Seeing the building as within and connected to a larger system – place, shifts "the current emphasis of greater energy self-reliance at the individual building level" to "opportunities for positive connections and creative synergies with adjacent buildings and surrounding natural systems."

A Note on the Distinction Between Regenerative Development and Regenerative Design For ecological sustainability to succeed, it requires a far broader and deeper scope of engagement than an individual building or even community design [39]. Yet the structure of the development and construction industry, for the most part, works to narrow the designers' role and scope, often as a result of decisions made before the design process even begins. Regenerative development was developed, in part, to address this concern. Regenerative approaches view development and design as two distinct yet synergistic processes, both of which play an essential role in ensuring that greater scope, neither of which is sufficient without the other.

The following dictionary definitions provide insight into the different roles of development and design:

Development: *O.Fr. desveloper, "an unfolding, bringing out the latent possibilities," from des- "undo" + veloper "wrap up"* a state in which things are improving; the act of improving by expanding or enlarging or refining; progression from a simpler or lower to a more advanced, mature, or complex form or stage; an unfolding; the discovering of something secret or withheld from the knowledge of others; disclosure.

Design: *L. designare "mark out, devise," from de- "out" + signare "to mark,"* an act of working out the form of something; to create or contrive for a particular purpose or effect.

Jenkin and Pedersen Zari, in their study, "Rethinking the Built Environment," write that "Regenerative development . . . investigates how humans can participate in ecosystems through development, to create optimum health for both human communities (physically, psychologically, socially, culturally and economically) and other living organisms and systems." They describe regenerative development as defining the desired outcome, and regenerative design as the means of achieving it. In contrast, John Tillman Lyle [25] defined design within the context of the built environment as giving form to physical processes [ref], and regenerative design as the replacement of linear systems of throughput flows with "cyclical flows at sources, consumption centers, and sinks." The resulting systems provide for "continuous replacement, through (their) own functional processes, of the energy and materials used in their operation" [11].

Regenerative development works at the intersection of understanding and intention, generating the patterned, whole-system understanding of a place, and developing the strategic, systemic thinking capacities and the stakeholder engagement required to ensure the design process achieves maximum systemic leverage and support. To that end, it integrates building, human, and natural development processes within the context of place. Regenerative development also creates an environment that greatly enhances the effect and effectiveness of restorative and biomimetic designs.

The roles of regenerative development, more specifically, are to:

1. Determine the *right* phenomena to work on, or to give form to, in order to inform and provide direction for regenerative design solutions that can realize the greatest systemic potential.
2. Build a field of commitment and caring in which stakeholders step forward as cocreators and ongoing stewards of those solutions.

Regenerative design then follows directly to offer a system of technologies and strategies based on an understanding of the inner working of ecosystems. Regenerative design solutions regenerate rather than deplete underlying life support systems and resources, are grown from the uniqueness of place, and work to integrate the flows and structures of the built and natural world "across multiple levels of scale, reflecting the influence of larger scales on smaller scales and smaller on larger" [40].

Regenerative Approaches to Sustainable Development and Design – Key Framework Premises and Practice Methodologies Overview

Key Premises

The following four premises are drawn from the work of Regenesis and Lyle. They offer key elements for

framing regenerative approaches [11, 25, 27, 29, 37]. The four premises work as a system to integrate and align motivation and means, providing the framework within which methodologies and approaches from other ecological design systems can be integrated into a regenerative practice (Fig. 3). The first two define and shape motive and motivation in a regenerative project. The last two relate to how a project is carried out to ensure that ends and means stay congruent and that the process stays on course toward a regenerative result.

1. *Place and potential* – Understanding and conceptualizing right relationship to place. Starting with the richest possible understanding of the evolutionary dynamics of a place in order to identify the potential for realizing greater health and viability as a result of human presence in that place [41].
2. *Goals focus on regenerative capacity.* Regenerative project goals are defined by the capacity that must be developed and locally embedded to support ongoing coevolution of the built, cultural and natural environments, and the humans who utilize and tend to them toward higher (more complex, diverse, and generative) levels of order for all their constituent members as well as for the larger systems they are a part of and depend on [12, 37].
3. *Partnering with place.* Implementing a regenerative project requires taking on a new role, moving from a "builder of systems we control" to a gardener, working in partnership with a place and its processes [42].
4. *Progressive harmonization.* Regenerative approaches seek to catalyze a process of continually increasing the pattern harmony between human and natural systems and require indicators and metrics that can track dynamic, holistic, and evolving processes [43].

Place and Potential

- Potential: "the inherent capacity for growth, development or coming into being." (American Heritage Dictionary of the English Language)

William McDonough often describes design as an expression of human intention. Both that intention and the resultant design, however, are shaped by the potential the designer sees and seeks to realize for a particular project. Regenerative potential is defined as the ability to leverage human interventions to achieve greater systemic health through time for the place they occupy and depend on [27].

Many projects fail to achieve a regenerative effect because the potential they target is too limited – focused on an element or a problem without seeing its systemic connections. Others fail because they seek to realize potential defined by human ideals but fail to recognize and are thus unable to align with the essence of a place and the larger patterns of life that make it work. When a project is grounded in a rich patterned understanding of its place and a vision of its role and potential within that place guides its design, even small interventions can ripple out into large systemic transformations – what Curitiba's long-time mayor Jaime Lerner called "urban acupuncture" [44], with ecological as well as social and economic ramifications.

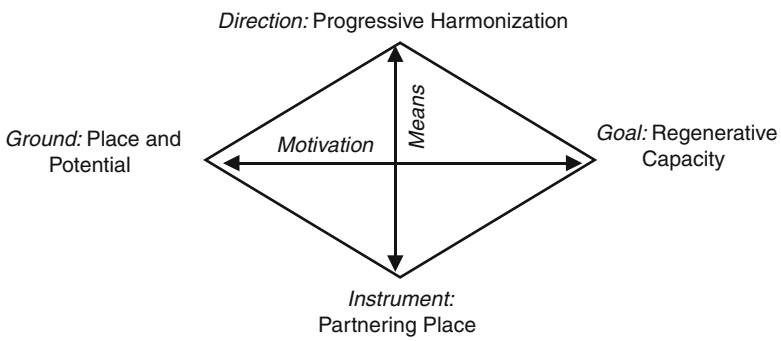

Regenerative Development and Design. Figure 3
Framework depicting key premises and processes characterizing regenerative approaches. © Regenesis Group. Reprinted with permission

"Place" in regenerative development is alive, a living system or entity that is "...a unique constellation of patterns nested within patterns, interwoven with other patterns in families and guilds and social relationships, all endlessly changing, cycling, evolving and building to greater levels of complexity over time ... an incredibly dynamic and complex being" [43]. A unique, multilayered dynamic network of natural and human ecosystems within a geographic region, this network forms a socioecological whole that is the result of complex interactions through time between and within its constituent ecosystems. The natural ecosystems include wildlife and vegetation, local climate, mineral and other deposits, soil, water geologic structures, etc.; human ecosystems include distinctive customs, expressions of values, economic activities, forms of association, ideas for education, traditions, physical artifacts such as buildings and constructed infrastructure, etc. [11, 28, 36, 37, 45, 46].

Regenerative Capacity: *Defining Goals for Realizing Regenerative Potential* The central element for regenerative development and design is the performance not of a single building, but rather of its living context – the unique socioecological system or "place" in which the building is just one of many interdependent and interactive elements and dynamics. Within that context, regenerative goals are set, and performance measured in terms of the intended contribution of the built environment to the regenerative capacity of that larger living context – (i.e., its capacity to realize and express more of its full potential as a source of increasingly healthy life for all its constituent members as well as for the larger systems it is a part of and depends on).

Characteristics of regenerative goals include:

- Place-sourced and place specific.
- Evolutionary, going beyond improving current systemic performance (what is often called restorative) to embedding into the system the capacity to continue to improve performance through time and through varying environmental conditions.
- Goes beyond functional performance goals. Recognizing "human aspiration and will as the ultimate sustaining source of our activities" [28], they address qualitative and spirit dimensions that shape the quality and degree of caring humans bring to their place and its capacity to continue to thrive.
- Focus on the processes physical structures enable as central.

Growing Capacity Versus Producing Things Regenerative projects set place and project specific goals that address all three aspects of regenerative built environments:

- Operational capacity.
- Organizational capacity.
- Aspirational capacity.

Operational capacity goals: Operational goals focus on systemic functional effectiveness in growing the potential of the underlying resource base – energy, materials, and support systems that enable the evolution of life in a place. Regenerative projects set goals for ensuring that the energies and nutrients flowing through it are used and invested optimally to grow the health of the system and all the life it supports.

Organizational capacity goals: Organizational capacity focuses on "who" a place is and addresses two dimensions – what is core to how this place works as a living system (what one can "mess" with and what one cannot) and what is the core qualitative character (its essence or distinctiveness, not data alone) or nature that humans can connect to at a heart level. Goals for this aspect deal with how to utilize the built environment and the design process to both illuminate and enhance the distinctive character of a place as something to be cherished. Historic codes and zones are often used to this end, but they tend to focus on surface appearance rather than essence, and over time, the code and its restrictions come to take the center stage, overshadowing the living core of the place they intended to protect [38].

Aspirational goals: Growing the systemic regenerative capacity of a place requires an integration of human aspirations with the distinctive ecosystems of that place and their drive to evolve their own health and generativity. This means harnessing inherent human creativity and aligning it with the creativity of nature and creating opportunities for people to experience themselves as able to make significant and meaningful contributions to their place [11, 47].

Partnering with Place – A New Role for Humans and Buildings In an ecological paradigm, sustainability requires a fundamental shift in how humans conceive of and carry out their role on the planet. In the words of Joshua Ramo, people must "change the role we imagine for ourselves from architects of a system we can control and manage to gardeners in a living, shifting ecosystem. For hundreds of years now we have lived in our minds as builders: constructing everything from nations to bridges . . . In a revolutionary age, with rapid change all around us, our architects' tools are deadly. It is time for us to put them down and follow (Nobel Laureate Friedrich von) Hayek's injunction to live and to think as gardeners."– gardeners who see themselves as partners in coevolution with the living system in which they work, cultivating "growth by providing the appropriate environment, in the manner a gardener does for his plants" [42, 48].

Successful regenerative development ultimately requires all the stakeholders in a place, not just the development/design team to move from the role of "builder" to "partner-gardener," with the first step a different nature of understanding that enables people to see the places they inhabit as alive.

A whole-systems assessment looks at a wide range of patterns covering multiple scales of systems and a number of different facets. The place intelligence it develops is a resource that can be mined to inform each stage of design to help ensure that the patterns generated by the project harmonize with the larger patterns of place. Another nature of understanding, however, is required to generate the experience of connection and caring that creates a relationship of partnership with a place. This understanding conveys "who" a place is as a living being in addition to how it functions. Every living system – whether a person, a tree, or a place – has an ongoing and distinctive core from which it organizes the complex arrays of relationships that produce its activities, its growth, and its evolution. Being able to grasp and share the distinctive core or *essence* of a place among and between the design team and local stakeholders provides an enduring basis for strong partnering relationships; in the same way, it builds strong human partnerships.

► A New Way of Thinking:

Learning how to apply a regenerative approach begins not with a change of techniques but rather with a change of mind—a new way of thinking about how we plan, design, construct, and operate our built environment [27].

Growing stakeholders and designing and constructing projects that can work as "place gardeners" requires bringing and developing whole-systems thinking that is able to and capable of comprehending and ordering and organizing the systemic complexity and dynamism of a living place and its multiple scales of nested systems, interactions of multidisciplinary teams over extended periods, and extensive local stakeholder participation [14, 15, 49]. This nature of systems thinking is characterized by:

- Being grounded in ecoliteracy and pattern literacy. Ecoliteracy applies an understanding the fundamental principles that govern how living systems work to specific situations and conditions. Pattern literacy involves being able to read, understand, and generate appropriate patterns that harmonize with and enable a place and its inhabitants to more fully realize what they can be [43].
- Requiring the practitioners to see what they are working on as a system of energies or life processes rather than as things – illuminating the constant reaching toward being more whole and being more alive inherent in living systems that is the fuel for regeneration [29, 50].
- Enabling a diversity of participants to grow their own systems thinking capacity in order to take on more challenging, value-adding roles [21, 50].

A new way of working: Regenerative development and design does not end with the delivery of the final drawings and approvals, or even with build out of a project. The responsibility of a regenerative designer includes putting in place, during the development and design process, what is required to ensure that the ongoing regenerative capacity of the project, and the people who inhabit and manage it, is sustained through time. Regenerative development employs *Developmental Design Processes.* They encompass integrative design (integrative, interdisciplinary beyond traditional building disciplines, open, and participatory) [51] and go beyond to embed self-managed learning processes into the work of conceptualizing, designing, constructing, managing, and evolving regenerative projects. They integrate the traditional focus of organizing for task

accomplishment with the development of new thinking capacities required to design processes not things, make ecologically sound place-appropriate decisions, and create the being connection to and emotional resonance with place that generates the will required to follow through on those decisions.

Progressive Harmonization The "pole star" or overarching source of direction for regenerative projects derives from the ultimate effect every regenerative project seeks to achieve: an enduring and mutually beneficial relationship between the human and natural systems in a particular place. Pattern is the language of relationship, and regenerative development and design in a living system is a process of patterning human communities to align with the energetic patterns of a place in a way that both humans and the place coevolve. Christopher Alexander was speaking of pattern harmony when he wrote, "When you build a thing, you cannot merely build that thing in isolation, but must also repair the world around it, and within it, so that the large world at that one place becomes more coherent, and more whole; and the thing which you make takes its place in the web of nature, as you make it" [52]. While his initial work focused primarily on the pattern relationship between a building and the human community and life surrounding, his later work has increasingly encompassed all living systems. Wendell Berry, in his essay Solving for Pattern, speaks to creating pattern harmony between human communities and activities and the biosphere they take place in [53]. "A bad (design) solution is bad," Wendell Berry notes, "because it acts destructively upon the larger patterns in which it is contained. . . most likely, because it is formed in ignorance or disregard of them. A good solution is good because it is in harmony with those larger patterns . . . A bad solution acts within the larger pattern the way a disease or addiction acts within the body. A good solution acts within the larger pattern the way a healthy organ acts within the body" [53].

Pattern harmony, however, is not a stable state; a good solution today may become a bad one in a few years, so solving for pattern requires a progressive rather than one-time harmonization, a continuous repatterning. Theoretical biologist Stuart Kauffman called this mutually beneficial relationship "co-evolving mutualism" – co-evolving because "its ecosystems are always in the process of self-organization and reorganization, increasing in complexity, definition, and information content" [25, 54, 55].

Practice Methodologies

The following is an example of how these premises can translate into a regenerative practice. The methodologies were developed from over 15 years of fieldwork by Regenesis during which collaborative members explored, practiced, and evolved regenerative development. The diagram in Fig. 4 was developed as a depiction of the essential elements of this practice – three phases and three developmental processes that are considered key to creating and sustaining an evolutionary spiral, growing systemic capacity as it actualizes a project.

The Three Key Steps:

Understand the Relationship to Place: Integral assessment – a whole-systems (cultural, economic, geographic, climatic, and ecological) assessment of

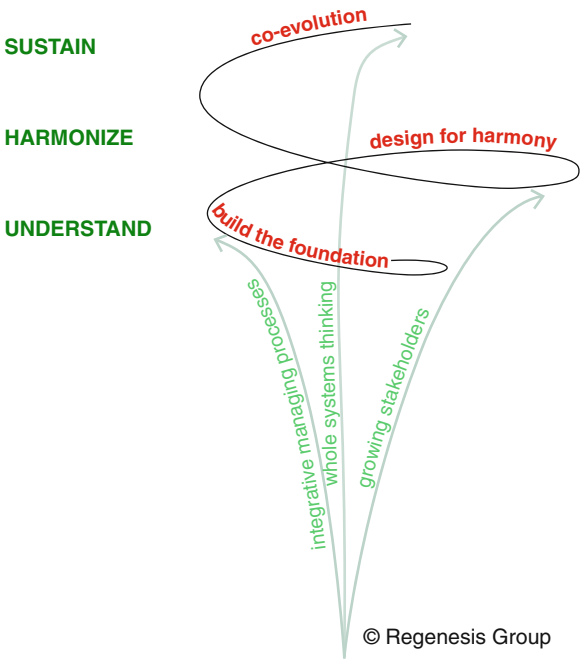

Regenerative Development and Design. Figure 4 Regenerative practice methodology framework. © Regenesis Group. Reprinted with permission

site and place as living systems lays the foundational understanding and thinking required to see how humans can enable the health and continuing evolution of the place and themselves as a part of it. A Story of Place® is codeveloped with the client and/or community. It uses the power of storytelling to articulate the essence of a place, how it fits in the world, and what the role of those who inhabit it can be as collaborators in its evolution.

Designing for Harmony with Place: Translates this understanding into design principles and systemic, integrated plans, designs and construction processes that optimize the presence of people in a landscape by harmonizing with the larger pattern of place. Buildings and infrastructure improve land and ecosystems, and the unique attributes of the land improve the built environment and those who inhabit it. Synergy with the land and ecosystems leverages the effectiveness of green design features and technologies and lowers costs while improving ecosystem health and productivity.

Co-Evolution: "*. . .sustainability means maintaining the dynamic potential for further evolution. Living systems survive by maintaining a condition of dynamic equilibrium with the environment through constant change and adaptation. In the game of evolution, equilibrium is death*" *Urban Sustainability Learning Group* [56]. This phase unfolds from the work of the previous two phases. If they have succeeded in creating a culture of coevolution in and around the project, and not just a physical product, its effect can be seen even before final build out. The role of designer becomes one of resource, providing processes and methods for sustaining the connection to place as a context that enables owners, managers and maintenance contractors, and community stakeholders to recognize and incorporate new social, economic, and ecological opportunities as their place evolves.

The Three Key Determining Factors: Success in the above three steps is determined by how one thinks, how one identifies harmonies and harmonizes the human role, and how one engages stakeholders *throughout* the planning and development process. Specifically, whether one:

- *Applies whole-systems thinking* to the design, planning, and decision making processes.
- *Manages integration and harmonization* across disciplines, between phases and team members and local stakeholders.
- *Grows stakeholders* understanding and appreciation of the place and the new potential offered and their capacity to be increasingly effective partners with the whole system of evolving life.

The following are examples of the thinking and practice frameworks and methodologies applied within the three phases and processes, some developed by Regenesis, some drawn from other ecological design systems.

Understand the Relationship to Place Principles from permaculture and Biomimicry are helpful in developing specific land use, building, and infrastructure design strategies.

Permaculture: *As* a design system rooted in the ability to discern the patterns that are structuring both natural and human systems and to generate new patterns that weave the human and natural together into a dynamic whole, permaculture assessment methodologies provide a source for developing holistic site assessments. *Pattern as Process*, an article by Regenesis principal Tim Murphy and Vickie Marvick, provides a detailed description of their method for understanding and interpreting the patterning of a site and its place [43].

Assessment Scope Framework for Pattern Understanding (Fig. 5): The challenge in any assessment process is to ensure that the scope being assessed is whole enough to encompass the interweaving of human and natural systems, dynamics and flows that shaped the distinct character of a place. Regenesis developed the following framework as a means of illuminating the core patterns structuring a place as the basis for "mapping" their dynamic and evolving interrelationships. These include:

- The ecological, social, and cultural systems creating and managing the conditions that shape how life expresses itself in a place.
- The value-adding processes life engages in within the context of those conditions and how they influence and are influenced by them.

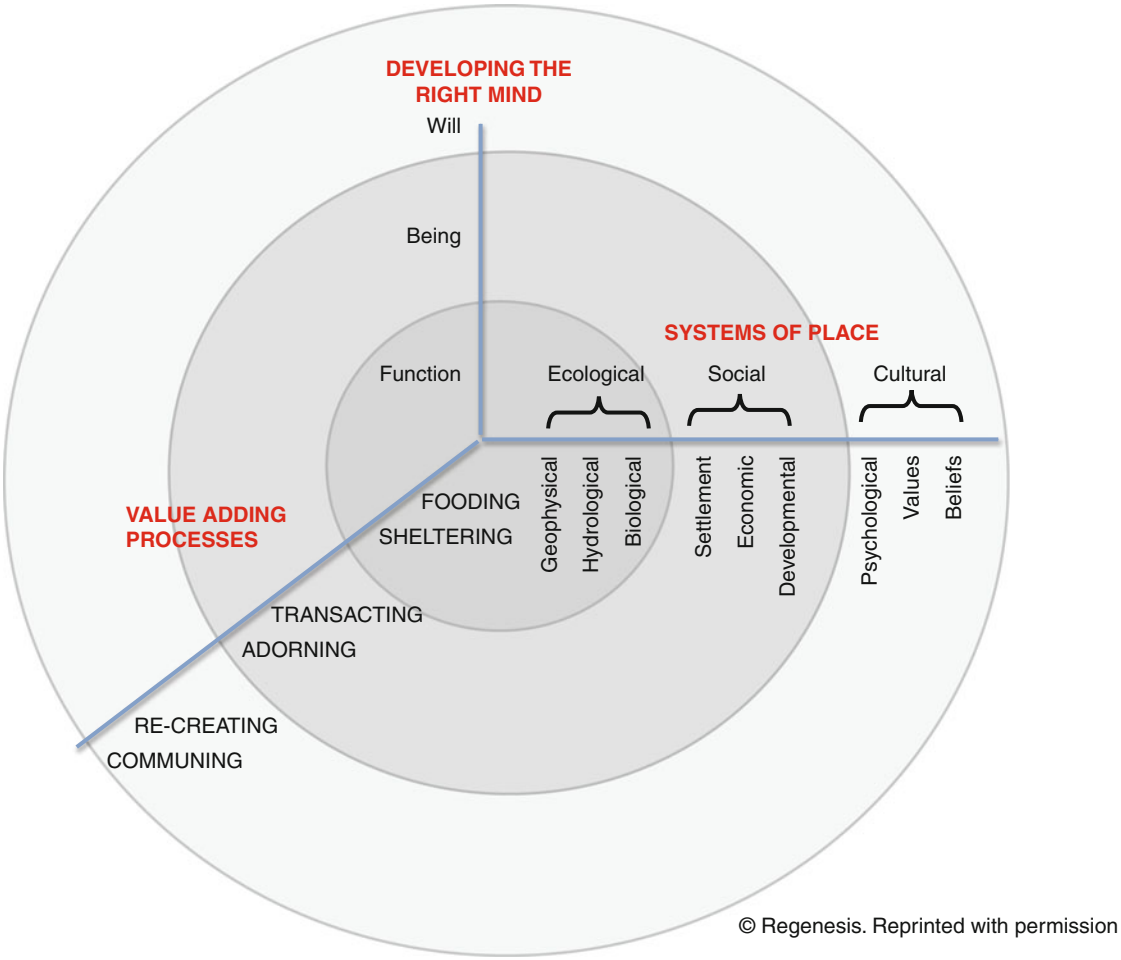

Regenerative Development and Design. Figure 5
Integral Assessment Scope framework. Used as a means of illuminating the core patterns structuring a place as the basis for "mapping" their dynamic and evolving interrelationships. © Regenesis Group. Reprinted with permission

- The developmental implications and opportunities for how individuals (people and buildings) can enable the health and continuing evolution of the place and themselves through how they function, the qualitative state of being they seek and enable, and what they value and express will toward (Adapted from a framework developed by Charles Krone as part of his thinking technology [8]).

Essence Understanding: The essence understanding that conveys "who" a place is as a living being emerges from the whole-systems assessment. Questions used to reveal the essence include: What is at the core of a system, around which it is organized? What is the web or larger context of reciprocal relationships within which it is embedded since all systems are comprised of smaller systems and part of larger systems? And what is the potential inherent in a living system that it is attempting to live out since this is the fuel for regeneration – this constant reaching toward being more whole, being more alive?

▸ Simple example of patterns and the essence of a system: [51]

Mahogany Ridge, Idaho, USA: *A reductionist approach or an approach that abstracts life into a checklist might state that nothing should be built on existing farmland. This might be a good principle if the*

agriculture system was truly symbiotic with nature. In this case, farming had nearly destroyed three distinct ecological systems. An integral assessment looked for possible patterns of life that allowed for high levels of relationship between species and ecological niches.

The aerial photo in Fig. 6 depicts approximately 3,500 acres of current farmland along the eastern edge of the Big Hole Mountains (just west of the Grand Tetons) that was being considered for development. Originally, these mountain watercourses and alluvial fan supported beaver, otter, native cutthroat trout, salmon, turkeys, grouse, and mega-fauna, such as deer, elk, moose, and bears. These animals were all responsible for carrying nutrients back upstream into the mountains to feed the forest and diversify the terrestrial and riparian ecosystem. Pioneers of European descent arrived in this place 100 years ago and used row-crop agriculture techniques to farm on this alluvial fan. As a result, ninety percent of the water from the Big Hole Mountains (in picture) was being used for agricultural purposes (spray irrigation), the salmon were no longer breeding in the river, the Yellow Tail cutthroat trout were in species decline, the river was polluted from overloads of nitrogen, and the upstream forests were in decline.

The area farmers were going out of business or bankrupt due to the short growing season. The farms, in the past, had been used to support local needs. Twenty to forty acre-per-home zoning is planned as the alternative to large farms.

Looked at closely, this photo in Fig. 6 reveals that farming was superimposed on top of this alluvial fan between the stream in the mountain valley (top center of the photograph) and the river. The soils mapping indicated in Fig. 7 reveals the pattern more clearly.

Before farming took place here, these radiating streams and drainage ways served as additional corridors of cover for wildlife moving back and forth between the mountains and the river. When farmers settled the land, they diverted this perennial stream along the highest possible course (in elevation) to irrigate fields that were gridded over a highly productive and robust prairie ecosystem. This action severely simplified and destabilized the ecosystem that once was there. The farming pattern did not preserve the integrity of the pattern that contained it; rather, this larger healthy pattern was obliterated. The ecological function of this alluvial fan, and one of the *core patterns* of the ecosystem in this place, is that of a *"living bridge"* between the mountains to the west and the Teton River.

The pattern of a living nutrient bridge between the mountains and the valley that had been revealed in the assessment indicated that a higher level of potential

Regenerative Development and Design. Figure 6
Aerial photo of Mahogany Ridge Resort Community site

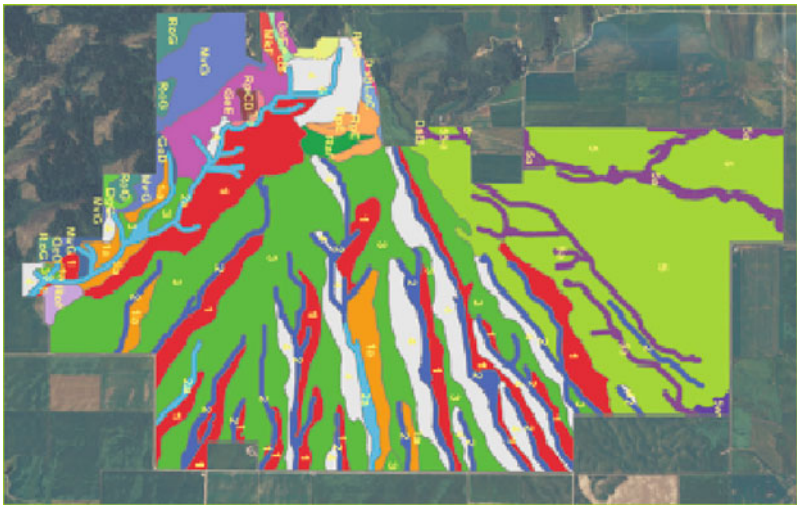

Regenerative Development and Design. Figure 7
Soil map of Mahogany Ridge site showing alluvial fan patterns

health can be reestablished in this mountain, alluvial fan, and River system. The development of homes in tight clusters could be used to pay for the restoration of the stream and habitat corridors that originally connected the Teton River and the mountains and provide wildlife corridors as well as many ecosystem services for community residents. To support the reestablishment of wildlife corridors, no fences would be allowed, native grasses would be planted (minimal turf grass), no off-leash dogs to disrupt nesting, and territory establishment by new wildlife.

By integrating the community into the development and management of these systems, they could produce food (through diversified agriculture and wild harvesting), timber, and other products, as well as the development of a diversified economy while insuring the provision of ecosystem services for their community. The human involvement in these patterns and processes is key to the ongoing regeneration and development of potential of the site.

Designing for Harmony with Place *Biomimicry*: The Biomimicry Guild's Life's Principles and their Genius of Place program provide guidance and models for establishing locally attuned strategies for building design through looking at how local species live out universal ecological principles within the conditions of a particular site and its surroundings, and how they have adapted to thrive within it (web link: www.biomimicryguild.com/).

Permaculture principles, which draw both on an understanding of ecology and of how indigenous people engaged with their place provide a lens for developing design strategies for responding to site conditions and opportunities in a way that is mutually beneficial (http://permacultureprinciples.com/; www.tagari.com/).

Two other useful frameworks that can be utilized as a part of the designing for harmony phase include:

A Regeneration-Based Checklist for Design and Construction (SBSE).
Malcolm Wells' Environmental Checklist.
www.sbse.org/resources/docs/wells_checklist_explanation.pdf

Essential Living Processes Framework: This framework was developed by Regenesis for setting overarching project aims to guide the design and construction process. It is based on the six critical processes that enable living systems to support the evolution of life. They include the ability to provide the material structuring that forms the basis for life processes – nourishment, shelter (habitat), and the generation and exchange of resources for growing and evolving more life. Because humans cannot be separated out from any living system, the factors go beyond the material

factors – the outer landscape of a place. They also include the "inner landscape" that sources one's spirit and will and drives one to cherish and protect the places one inhabits. They include the ability of a living system to create a sense of identity and foster belonging through its culture, to support meaningful and contributory lives, and to invoke the spirit and inspiration that sustains caring. The framework enables setting aims and goals (and later developing indicators and measuring systems) for how the processes generated by the project support ecological, economic, and social health in each of the six areas. The interrelationship of these processes and how they cross ecological, societal, and economic arenas is graphically represented in Fig. 8:

An example of ecological aims for nourishing:
Capacity of soil, water, and air to nourish life –
Aims:

- Invest water in increasingly higher order life processes through storing and cycling (vs. hoarding) so water becomes the driver for improving soil and air quality.
- Products and processes used in construction and operations are investments in growing the capacity of soil, water, and air to store, transform, and transport nutrients for optimal accessibility and utilization.

Future Directions

While regenerative development and design still occupies a relatively small niche in the larger world of sustainability efforts, interest in regenerative approaches to the built environment is on the rise. Beyond the USA itself, this growing interest has been particularly marked in Australia and New Zealand, including a government-commissioned research report that recommended the latter adopt regenerative development as a national policy [10].

A number of interrelated factors, working as a system, are creating a favorable climate that is likely to continue to feed such interest, among them: more practitioners encountering the limits of green building to address the global crises, shifting market dynamics and public awareness, the growing influence of the ecological perspective and the ecosystem concept, the movement toward integrative design with its reliance on interdisciplinary teams, and the growing recognition of the need for community

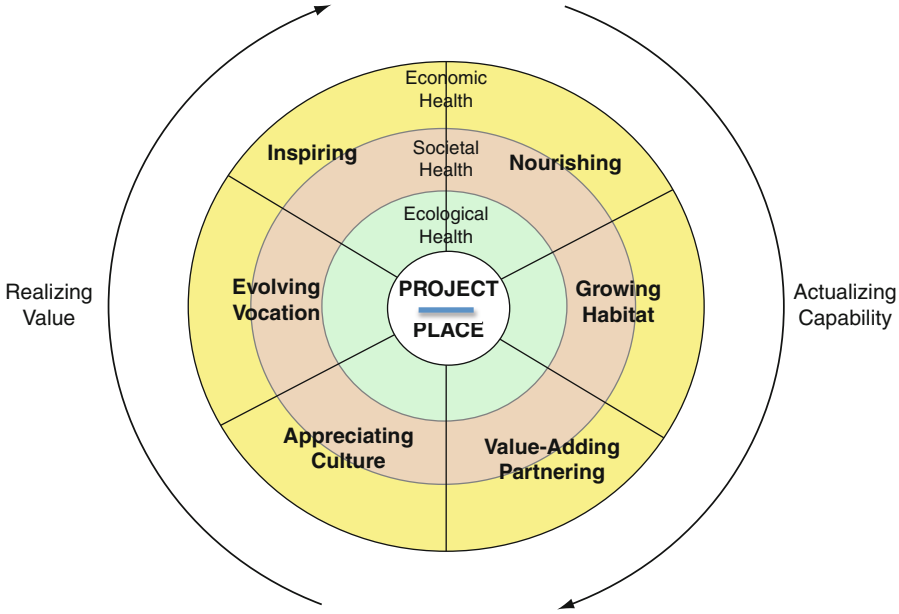

Regenerative Development and Design. Figure 8
Framework showing interrelationship of the 6 essential living processes and how they cross ecological, societal, and economic arenas. Used to set holistic, integrative goals and indicators. © Regenesis Group. Reprinted with permission

engagement and participation to support the behavior changes required for enduring sustainability.

In the 1990s, the most discussed issue for aspiring green designers was how to convince clients to incorporate sustainability features. By 2010, the discussions increasingly were about how to meet clients' demands for making their project "the greenest" of their kind. Over the same period, appreciation and understanding of ecological sustainability and the ecosystem perspective as it applies to human settlements and institutions has been significantly reshaping thinking in such fields as public health, education, economic and community development, and urban planning, as well as design of the built environment. Its core concepts, especially the concept of seeing communities as ecosystems in which nature and culture, human and natural designed features are interwoven and interdependent, are driving a move toward increasingly systemic and comprehensive goals. These comprehensive goals are, in turn, defining new standards of sustainability. Projects seeking to be "the greenest" now include social, economic, educational, and esthetic goals as well as goals around energy efficiency and pollution. More comprehensive goals affecting multiple fields are necessarily stimulating more integrative and interdisciplinary approaches. They are also adding the need to build community support and stewardship to the list of essential design issues. The ecological and ecosystem perspectives are providing a common "language" or set of frameworks across those fields that is facilitating integrative and participatory approaches across disciplines and between design teams and the public and in the process, further reinforcing an ecological worldview.

One effect of this system of factors has been the extension of explicitly regenerative approaches across a wider spectrum of fields and the integration of these fields with regenerative development of the built environment as part of regenerative community development. Regenerative development had already begun to shift the old, building-centric definition of the built environment to include the relationships between and among buildings, infrastructure, and natural systems, as well as the culture, economy, and politics of communities. Its concept of place-sourced design is providing a means of engaging the will of a community around aligning human and natural communities around shared purposes. Given its holistic and integrative character, it could be anticipated that these more comprehensive applications will be a continuing trend.

Regenerative Development makes possible a new and critically needed role for developers and developments, the full potential of which is still unfolding. Development projects already exist that, by the way they are built and occupy land, serve as instruments for reversing ecological damage, and as economic forces for constructing sustainable livelihoods. Still other projects offer glimpses of how, through weaving the many stories of Place into a mutually appreciating whole, a Regenerative Development becomes a harmonizing force within communities and among different stakeholders, inspiring new standards of appropriate relationship to Place. It is possible to envision how, by introducing larger systemic vision and potential, development can become a catalyst for the creation of self-evolving bioregional infrastructures and cultures of regeneration.

While this new role is beginning to emerge in small scales and at scattered locations, it is largely unrecognized as being part of a larger evolution. What is needed now is to bring consciousness and intention to its emergence as the new pattern shaping the field of development.

Bibliography

Primary Literature

1. Benyus J (1997) Biomimicry. Harper Collins, New York
2. McDonough W, Braungart M (2003) Cradle-to-cradle design and the principles of green design. www.mcdonough.com/writings/c2c_design.htm. Accessed 18 Oct 2011
3. McDonough W, Braungart M (2002) Cradle to cradle: remaking the way we make things. Northpoint, New York
4. Orr D (1992) Ecological literacy: education and the transition to a post-modern world. State University of New York Press, Albany
5. Capra F (1996) The web of life: a new scientific understanding of living systems. Anchor Books, New York
6. Tansley AG (1935) The use and abuse of vegetational concepts and terms. Ecology 16:284–307. doi:10.2307/1930070
7. Van der Ryn S, Cowan S (1996) Ecological design. Island Press, Washington, DC
8. Krone C (2001) West coast resource development: session notes. Unpublished transcription of dialogue by members of the Institute for Developmental Processes, Carmel
9. Mollison B (1988) Permaculture: a designers' manual. Tagari, Australia

10. Jenkin S, Zari MP (2009) Rethinking our built environments: towards a sustainable future. Ministry for the Environment, Manatu Mo Te Taiao, Wellington
11. Lyle JT (1994) Regenerative design for sustainable development. Wiley, Hoboken
12. Howard SE (2011) Encyclopædia Britannica. http://www.britannica.com/EBchecked/topic/273428/Sir-Ebenezer-Howard. Accessed 18 Oct 2011
13. Geddes P (1915) Cities in evolution. Williams & Norgate, London
14. Marcotullio PJ, Boyle G (eds) (2003) Defining an ecosystem approach to urban management and policy development. United Nations University Institute of Advanced Studies (UNU/IAS), Yokohama
15. Pickett STA, Grove JM (2009) Urban ecosystems: what would Tansley do? Urban Ecosyst 12:1–8. Published online: Springer Science + Business Media, LLC
16. Odum HT (1971) Environment society and power. Wiley Interscience, New York
17. Mitsch WJ, Jørgensen SE (1989) Ecological engineering: an introduction to ecotechnology. Wiley, New York
18. Von Bertalanffy L (1968) General system theory: foundations, development, applications. George Braziller, New York
19. Lyle JT (1993) Urban ecosystems. In context 35, p 43
20. SBSE/Wells (1999) www.sbse.org/resources/docs/wells_checklist_explanation.pdf. Accessed 18 Oct 2011
21. Sanford C (2011) The responsible corporation: reimagining sustainability and sustainability and success. Josey-Bass, San Francisco
22. McHarg IL (1969) Design with nature. Doubleday, Garden City
23. Rodale R (1988) Whole Earth Review, interview. http://findarticles.com/p/articles/mi_m1510/is_n61//ai_6896856/. Accessed 18 Oct 2011
24. Medard G, Pahl E, Shegda R, Rodale R (1985) Regenerating America: meeting the challenge of building local economies. Rodale, Emmaus
25. Lyle JT (1984) Designing human ecosystems. Wiley, Hoboken
26. Pliny F http://cmpbs.org. Accessed 18 Oct 2011
27. Haggard B, Reed B, Mang P (2006) Regenerative development. Revitalization, Mar/Apr 2006
28. Mang N (2009) Toward a regenerative psychology of urban planning, Saybrook Graduate School and Research Center, San Francisco. http://gradworks.umi.com/33/68/3368975.html. http://powersofplace.com/papers.htm. Accessed 18 Oct 2011
29. Haggard B (2002) Green to the power of three. Environ Des Constr, 24–31 Mar/Apr 2002
30. Orr D (1994) Earth in mind. Island Press, Washington, DC
31. Zari MP, Storey J (2007) An ecosystem based biomimetic theory for a regenerative built environment. In: Lisbon Sustainable Building Conference, Lisbon
32. Wilson EO (1984) Biophilia. Harvard University Press, Cambridge
33. Heerwagen J (2007) Biophilia and design. Handout for Portland lectures, Aug 2007
34. Kellert S (2004) Beyond LEED: From low environmental impact to restorative environmental design. Keynote address, greening rooftops for sustainable communities conference. Sponsored by Green Roofs for Healthy Cities, Toronto, and City of Portland, Portland, 4 June 2004
35. Anderson MK (2005) Tending the wild: native American knowledge and the management of California's natural resources. University of California Press, Berkeley
36. Cole RJ, Charest S, Schroeder S (2006) Beyond green: drawing on nature (for the Royal Architectural Institute of Canada's "Beyond green: adaptive, restorative and regenerative design" course – SDCB 305). The University of British Columbia
37. Reed B (2007) A livings systems approach to design. AIA National Convention May – Theme Keynote address
38. Cole R (2010) New context, new responsibilities: building capability. https://members.weforum.org/. . ./Ray%20Cole%20-%20Building%20Capability.pdf; http://www.google.com/url?sa=t&source=web&cd=1&ved=0CCIQxQEwAA&url=http%3A%2F%2Fdocs.google.com%2Fviewer%3Fa%3Dv%26q%3Dcache%3AaiaZ4YMGb0IJ%3Ahttps%3A%2F%2Fmembers.weforum.org%2Fpdf%2Fip%2Fec%2Fbreakthroughideas%2FRay%252520Cole%252520-%252520Building%252520Capability.pdf%2Bray%2Bcole%2BNew%2BContext%2C%2BNew%2BResponsibilities%3A%2BBuilding%2BCapability%26hl%3Den%26gl%3Dus%26pid%3Dbl%26srcid%3DADGEEShGS-VECswRMKKDehwApC-PqrSXfEB7LVbS2FGYn7eF7SuydqGa-76EwFbOdRXXa05jSlcKwPy13JevQLvd_Z3wD4lhOQVCZTjzJ63T-D9tcJXvvlDYO0OocQhRaJu3rlgk09fT0%26sig%3DAHIEtbRfn0IrDnH7Bqa2piU7yKiuWbpfzw&ei=4OadTtTNDPPaiQLjwZ3MCQ&usg=AFQjCNGXqaLa9z0t0FrfdQxeNvdHTia2ng&sig2=6x71Tx9WJSSjx5IjeDikLw. Accessed 18 Oct 2011
39. Williams D (2007) Sustainable design: ecology, architecture, and planning. Wiley, Hoboken
40. Bailey RG (2002) Ecoregion-based design for sustainability. Springer, New York
41. Mang N (2006) The rediscovery of place and our human role within it, Saybrook Graduate School and Research Center, San Francisco. http://powersofplace.com/papers.htm. Accessed 18 Oct 2011
42. Ramo J (2009) Age of the unthinkable: why the new world disorder constantly surprises us and what we can do about it. Little Brown and Company, New York
43. Marvick V, Murphy T (1998) Patterning as process. Permaculture Activist, Jul 1998
44. Lerner J (2005) Acupuntura Urbana. Institute for Advanced Architecture of Catalonia
45. Gabel M (2009) Regenerative development: going beyond sustainability. Design Science Lab, New York
46. Mang P (2001) Regenerative design: sustainable design's coming revolution. Design Intelligence. http://www.di.net/articles/archive/2043/. Accessed 18 Oct 2011
47. Orr D (2001) Architecture, ecological design, and human ecology. In: Proceedings of the 89th ACSA annual meeting. ACSA, Washington, DC, pp 23–32

48. von Hayek F (1974) The Pretence of Knowledge. Nobel Prize acceptance speech
49. Pickett STA, Cadenasso ML (2002) Ecosystem as a multidimensional concept: meaning, model and metaphor. Ecosystems 5:1–10. doi:10.1007/s10021-001-0051-y
50. Sanford C (2006) Building intelligence: a living systems view. Springhill, Battleground
51. 7 Group, Reed B (2009) The integrative design guide to green building: redefining the practice of sustainability. Wiley, Hoboken
52. Alexander C (1997) A pattern language: towns, buildings construction, Center for Environmental Structure Series. Oxford University Press, New York
53. Berry W (1981) Solving for pattern in gift of good land. Counterpoint, Berkeley
54. Kauffman S (2008) Reinventing the sacred: a new view of science, reason, and religion. Basic Books, New York
55. Prigogine I (1997) End of certainty. Free Press, New York
56. Urban Sustainability Learning Group (1996) Staying in the game: exploring options for urban sustainability, Tides Foundation Project

Books and Reviews

Aberley D (1994) Futures by design: the practice of ecological planning. New Society, Gabriola Island

Alexander C (2001) The nature of order. The Center for Environmental Structure, Berkeley

Bartuska T (1981) Values, architecture and context: the emergence of an ecological approach to architecture and the built environment. In: ACSA annual conference proceedings, San Francisco, Mar 1981

Bartuska T, Young G (1994) The built environment definition and scope. In: Bartuska TJ, Young GL (eds) The built environment: a creative inquiry into design and planning. Crisp, Menlo Park

Beatley T, Manning K (1997) The ecology of place: planning for environment, economy, and community. Island Press, Washington, DC

Birkeland J (2010) Positive development: from vicious circles to virtuous cycles through built environment design. Earthscan, London

Bossel H (2001) Assessing viability and sustainability: a systems-based approach for deriving comprehensive indicator sets. Conserv Ecol 5(2):12. (Online) URL: http://www.consecol.org/vol5/iss2/art12/

Charles J, Kibert J (1999) Reshaping the built environment: ecology, ethics, and economics. Island Press, Washington, DC

Cowan S (2004) Evaluating wholeness. Resurgence 225:56

Crowe N (1997) Nature and the idea of a man-made world: an investigation into the evolutionary roots of form and order in the built environment. MIT Press, Cambridge, MA

Cunningham S (2008) reWealth! McGraw Hill, New York

Edwards A (2010) Thriving beyond sustainability: pathways to a resilient society. New Society, Gabriola Island

France RL (ed) (2008) Handbook of regenerative landscape design. CRC Press, Boca Raton

Franklin C (1997) Fostering living landscapes. In: Thompson G, Steiner F (eds) Ecological design and planning. Wiley, New York

Golley FB (1993) A history of the ecosystem concept in ecology: more than the sum of the parts. Yale University Press, New Haven

Graham R (1993) Restorative design: an interview with Bob Berkebile. Designing a Sustainable Future, in context 35, p 9

Gross M (2010) Ignorance and surprise: science, society, and ecological design. MIT Press, Cambridge

Haggard B (2001) The next step: transforming the building industry to model nature. Hope Dance Nov/Dec 2001

Hawley AH (1950) Human ecology: a theory of community structure. Ronald, New York

Holling CS (1994) New science and new investments for a sustainable biosphere. In: Jansson A (ed) Investing in natural capital: the ecological economics approach to sustainability. Island, Washington, pp 57–97

Holmgren D (2002) Permaculture: principles and pathways beyond sustainability. Holmgren Design Services, Hepburn

International Federation of Landscape Architects (2003) Definition of the profession of landscape architecture. IFLA News, No. 48

Kingsland SE (2005) The evolution of American ecology, 1890–2000. Johns Hopkins University Press, Baltimore

Lemons J, Westra L, Goodland R (eds) (1998) Ecological sustainability and integrity: concepts and approaches. Kluwer, Dordrecht

Likens GE (1992) The ecosystem approach: its use and abuse. Ecology Institute, Oldendorf/Luhe

Mang P (2002) Evolving the new role of development: healing places to heal a planet. Regenesis Collaborative Development Group, Santa Fe. http://www.regenesisgroup.com/articles.php. Accessed 18 Oct 2011

Mang P (2010) Tapping the power of place: stories, cities, and sustainability. Sustainable Santa Fe

McDaniel CN (2006) Design on the edge review. Ann Earth XXIV(3). http://docs.google.com/viewer?a=v&q=cache:UWlG1Y4-I-4J:homepages.rpi.edu/~mcdanc/opEdsAndCommentary/OrrDesignOnEdgeAnnalsPublished.pdf+McDaniel+design+on+the+edge&hl=en&gl=us&pid=bl&srcid=ADGEESjHnEXiHa3cb5RUjKNPOy8VMLejauMjSBdsBFF1-4tIbMLaTle2nl1dRTOGNGrccAeno516J2ThGMhEFvHR4Jf62blSmA_ZZzTOnRkea0J2QENYjOJfKgI1fb7bkun5jsLZJHMl&sig=AHIEtbR7aGogSklQAB0h7uZbSGzBGJYVrg. Accessed 18 Oct 2011

McIntosh R (1985) The background of ecology: concept and theory. Cambridge University Press, New York

McMurry A (2006) Community health and wellness: a socio-ecological approach. Elsevier, Chatswood

Melby P, Cathcart T (2002) Regenerative design techniques: practical applications in landscape design. Wiley, Hoboken

Murphy T, Reed B (2003) Brattleboro food co-op: preparing the ground for a regenerative market and marketplace:

preliminary report prepared for the Brattleboro Food Co-op. Unpublished regenesis report. http://www.regenesisgroup.com/articles.php. Accessed 18 Oct 2011
Nabhan G (1997) Cultures of habitat. Counterpoint, Washington, DC
Naess A (1989) Ecology, community and lifestyle: outline of an ecosophy. Cambridge University Press, Cambridge
Newman P, Jennings I (2009) Cities as sustainable ecosystems: principles and practices. Island Press, London
Orr D (2002) The nature of design: ecology, culture, and human intention. Oxford University Press, New York
Orr D (2006) Design on the edge: the making of a high-performance building. MIT Press, Cambridge
Reed B (2006) Shifting our mental model – "sustainability" to regeneration. Paper submitted for the conference: rethinking sustainable construction 2006: next generation green buildings, Sarasota, 19–21 Sept 2006
Reed B (2007) Shifting from 'sustainability' to regeneration. Build Res Inf 35:674–680
Regenesis Collaborative Development Group (2006) Bibliography: introduction to thinking behind regenerative design/development. http://www.regenesisgroup.com/pdf/Regenesis_Bibliography.pdf. Accessed 18 Oct 2011
Todd NJ, Todd J (1993) From eco-cities to living machines: principles of ecological design. North Atlantic Books, Berkeley
Wann D (1996) Deep design. Island Press, Washington, DC
Zari MP (2007) Biomimetic approaches to architectural design for increased sustainability. Paper number: 033, School of Architecture, Victoria University, Wellington
Zimmerman M (2004) Being nature's mind: indigenous ways of knowing and planetary consciousness. ReVision 26(4):8, Heldref Publications/Gale Group, Farmington Hills

Regional Air Quality

Erika von Schneidemesser, Paul S. Monks
Department of Chemistry, University of Leicester, Leicester, UK

Article Outline

Glossary
Definition of the Subject and Its Importance
Introduction
Air Quality Measurements
Health Effects, Ecosystem Effects, and Air Quality Modeling
Current Air Quality Legislation and Metrics
Regional Context
Future Directions
Bibliography

Glossary

Anthropogenic Caused by humans; man-made.

Biogenic Produced by biological processes.

Cohort study A long-term study of the same group of people (the cohort) over time, typically used in medicine social science, and ecology.

Diurnal Relating to the 24 h/day time period.

Dry deposition The deposition of gaseous or particulate species from the atmosphere to a surface without the involvement of precipitation.

Exceedance The amount by which something (in this case an air quality pollutant) exceeds the permissible standard or limit value.

Feedback An internal climate process that amplifies or dampens the climate response to an initial forcing, e.g., the release of methane into the atmosphere due to warmer temperatures, the atmospheric methane increase furthers warming, which causes the release of more methane into the atmosphere, etc.

Megacity City with a population of greater than ten million inhabitants.

Metrics A set of measurements used to quantitatively gauge efficiency, progress, or performance. In this case, as applied to air quality.

Mobile sources Any object that releases pollution that is not stationary, e.g., vehicles, planes, trains, ships, etc.

Radiative forcing A change imposed on the Earth's radiation balance in units of heat flux as watts per square meter ($W\,m^{-2}$).

Smog A term derived from smoke and fog applied to extensive contamination by aerosols.

Stationary sources Any object that releases pollution from one set location, e.g., power plants, industrial factories, etc.

Temperature inversion The temperature of the troposphere normally decreases with increasing altitude; however, a temperature inversion results when warm air lies above cool air, which is an extremely stable condition, also known as an inversion layer.

Temporal Pertaining to time.

Wet deposition The deposition of gaseous or particulate species from the atmosphere to a surface during precipitation events (e.g., rain, snow, fog, dew).

Definition of the Subject and Its Importance

What is Regional Air Quality?

- Clean air is considered to be a basic requirement of human health and well-being. However, air pollution continues to pose a significant threat to health worldwide [1].

Air pollution can be defined as "when gases or aerosol particles emitted anthropogenically build up in concentrations sufficiently high to cause direct or indirect damage to plants, animals, other life forms, ecosystems, structures, or works of art" [2]. The state of air pollution is often expressed as air quality (AQ). Air quality is a measure of the concentrations of gaseous pollutants and size, number or mass of particulate matter (PM). Air quality is typically measured using in situ monitors that monitor species such as ozone (O_3), particulate matter, nitrogen oxides, and/or sulfur dioxide.

Why is Regional Air Quality Important?

An awareness of the detrimental effects of air pollution came to the forefront because of the catastrophic effects of the "London Smog" episode of 1952 where more than 4,000 people died [3]. Shortly after this, the Clean Air Act was passed by the UK Parliament in 1956 to limit smoke/sulfur dioxide emissions and improve air quality in the cities. Air quality legislation evolved from there, mainly in Europe and the USA, to what it is today. Current air quality legislation is discussed in more detail in section Current Air Quality Legislation and Metrics. Air quality remains an important topic because of its impact on human health, ecosystems, and its interactions with climate change (CC).

Introduction

The Development of Regional Air Quality Monitoring and Legislation

The state of air pollution is often expressed as air quality (AQ). Air quality is a measure of the concentrations of gaseous and aerosol pollutants in the atmosphere. Human health, ecosystems, national heritage (e.g., buildings, monuments), and regional climate are all impacted by air pollution. The implications for human health and ecosystem impacts can range from superficial surface discoloration of buildings to serious adverse health effects, such as loss of months to years of life. These effects are discussed in further detail in section Health Effects, Ecosystem Effects, and Air Quality. Air pollution and air quality control measures have implications for climate change, owing to feedbacks between composition and climate as well as wider atmospheric interactions. Policies to improve air quality may not always have positive effects on climate change and vice versa. Therefore, as we move forward with air quality and climate regulation, interactions and feedbacks from air quality and climate change trade-offs need to be taken into consideration. Some of these trade-offs are shown in Fig. 1. The topic as a whole is addressed in section Regional Context.

Air pollution has a history far longer than the development of contemporary air quality policies. Ozone, a current air quality problem and significant contributor to urban pollution, was discovered in 1839 by a German chemist, Christian Fredrich Schönbein. Air pollution from copper smelting from as far back as Roman times has been detected in ice-core measurements [2]. The plentiful use of fossil fuels in industry and home heating starting in the Middle Ages, latterly in trains, was the main progenitor of degraded air quality through to modern times. A number of extreme air pollution events starting in the late 1800s provided the motivation for modern air quality regulation. A number of smog episodes in London from 1878 to 1962 resulted in excess deaths of hundreds to thousands of people, with the most extreme and well known of these events being the "Big Smoke" of early December 1952 that killed upward of 4,000 people [2–4]. Similar episodes were also recorded in the Meuse Valley, Belgium in 1930, and Donora, Pennsylvania, USA in 1948 where smog events resulted in tens of excess deaths and the illness of thousands of residents [2]. Around the same time, Los Angeles was suffering from a different type of smog, this one photochemical in origin, that arose from the mixture of ozone, nitrogen oxides, and volatile organic compounds (VOCs) produced from a combination of large amounts of vehicle traffic, sunny weather, and persistent temperature inversions [4].

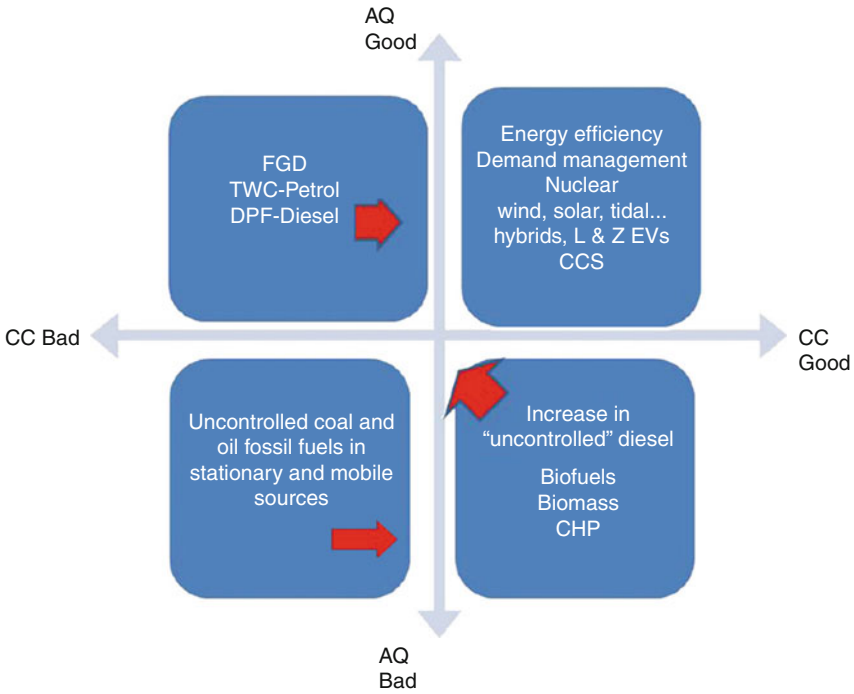

Regional Air Quality. Figure 1
The synergies and trade-offs between policies to improve air quality (AQ) and to reduce greenhouse gas emissions/improve climate change (CC) (Monks et al. [36])

These "smog" events, among others, spurred the development of air quality regulation in the USA and Europe. The US Air Pollution Control Act was first passed in 1955, identifying air pollution as a national problem. Further air pollution legislation followed with the Clean Air Act in 1963 which set emission standards for stationary sources (e.g., power plants). This was followed by a number of amendments in the 1960s that set standards for motor vehicle emissions. In 1970, the Clean Air Act was passed, which established the National Ambient Air Quality Standards (NAAQS), set new limits on stationary and mobile sources emissions, and allowed states to set their own stricter standards [4]. Catalytic convertors for vehicles in the USA were introduced in 1975, developed in response to the 1970 Clean Air Act, significantly reducing hydrocarbon (HC) and carbon monoxide emissions. Further incarnations of the Clean Air Act and amendments were passed in the years since then, reducing standards for stationary and mobile sources, and mandating control technology. In the USA, California has frequently been ahead of the curve with more stringent air quality standards and tighter standards for vehicles emissions. In 2002, California passed legislation that required automakers to reduce greenhouse gas emissions from vehicles [4].

Just after the first US Air Pollution Control Act, the UK Clean Air Act was passed in 1956, setting controls for household and industrial emissions of smoke. In 1968, the UK Clean Air Act was passed which required tall smoke stacks for industries using fossil fuels to improve dispersal of emissions and avoid local deposition [2]. As of 1972, the UK joined the EU and the majority of air quality policy has been determined by EC directives applicable across Europe. In 1979, the International Convention on Long-Range Transboundary Pollution was adopted to limit emissions of acidifying pollutants. The first directive on ambient air quality was adopted in 1980 and assigned limits to sulfur dioxide and particles [3]. Subsequent directives in 1982 and 1985 put limits on ambient air concentrations of lead and nitrogen dioxide, and in 1989 a directive required all new cars in the EU to run on unleaded fuel [3]. A 1993 directive required the use

of catalytic convertors on all new petrol vehicles. In 1996, an EC directive was established to provide a new framework to control levels of sulfur dioxide, nitrogen dioxide, particulate matter, lead, ozone, benzene, carbon monoxide, and hydrocarbons. This included establishing common methods and criteria for assessment of air quality, and setting concentration limits for the pollutants. These limits were then tightened by a following directive in 1999. Current legislation and regulations are outlined in more detail in section Current Air Quality Legislation and Metrics.

Air Quality Pollutants

Air pollution has many different components that differ in concentration depending on the superimposition of local, regional, and global emission sources. These emissions are frequently separated into anthropogenic ("man-made") and biogenic ("natural") sources. The components of air pollution can be roughly separated into gaseous and particulate (or aerosol) fractions. Within both gas and particulate pollution there can be primary and secondary pollutants, organic and inorganic compounds. Primary pollutants are those emitted directly into the atmosphere from a source, such as sulfur dioxide or black carbon (BC) (a significant light absorbing component of soot). Secondary pollutants are those formed in the atmosphere from chemical and/or physical transformations of primary pollutants, such as ozone (O_3) and secondary organic aerosol (SOA).

Regional air pollution results from the combination of emissions, which vary both spatially and temporally and meteorological factors (that allow the pollutants to build up in an area or transport pollutants into an area where they can mix with local emissions) causing poor regional air quality. Figure 2 shows different emissions sources and meteorological components that have an impact on regional air quality. In addition to wind transporting pollutants, sunlight plays an important role in photochemical reactions in the atmosphere that create some of the secondary pollutants. Air pollutants are then removed from the atmosphere through dry deposition (e.g., settling) or wet deposition (e.g., rain scavenging). The following two sections will discuss the two main components of air pollution – gaseous pollutants and particulate pollutants in terms of their sources, sinks, atmospheric transport, and transformations.

Gaseous Pollutants

There are myriad different gaseous species that are emitted into the atmosphere from various air pollution sources. Some of the major gaseous pollutants are carbon monoxide (CO), nitrogen compounds (e.g., NO, NO_2, HNO_3), sulfur compounds (e.g., SO_2), hydrocarbons (HCs) including methane and non-methane hydrocarbons (NMHCs), and photochemical oxidants (e.g., O_3). Other gaseous pollutants, such as carbon dioxide (CO_2) and methane (CH_4), will not be addressed here because they are not a major focus for regional air quality concerns because their longer lifetimes qualify them as global pollutants.

Carbon monoxide's primary source is from incomplete combustion. In addition to being an important primary pollutant, it is also an important precursor compound for the formation of ozone, as well as a secondary pollutant itself, formed from the oxidation of methane and other NMHCs by the OH radical [5]. It has a lifetime of a couple months which makes it a regional and global scale pollutant that can be transported significant distances from its emission source. Carbon monoxide is primarily removed from the atmosphere by reaction with OH, a small amount being removed by deposition. Ambient levels of 0.15–10 ppmV are common in urban areas mainly owing to road transport–related sources [6, 7]. In the USA, mobile sources (including non-road mobile sources) make up 80% of national CO emissions, while in the UK 47% of CO emissions are attributed to road transport sources. Figure 3 shows how CO emissions largely follow the road network in the UK, with the highest emissions in urban areas [8]. Furthermore, the high correlation of CO with population density in Asia is shown in Fig. 4 [9]. Carbon monoxide emissions have shown significant reductions over the past 2 decades [7]. These emission reductions are largely credited to the increased use of catalytic convertors in cars. Total CO emissions in the USA have decreased 68% since the 1990s until 2008, and currently all monitoring stations in the USA show that no areas are in non-attainment for the 8-h CO standard of 9 ppmV [10]. Similarly, CO emissions in the UK have been reduced by 71% from 1990 to 2005 in the UK. Elevated levels of CO observed in rural/remote areas are possible because of agricultural or biomass burning and forest fires.

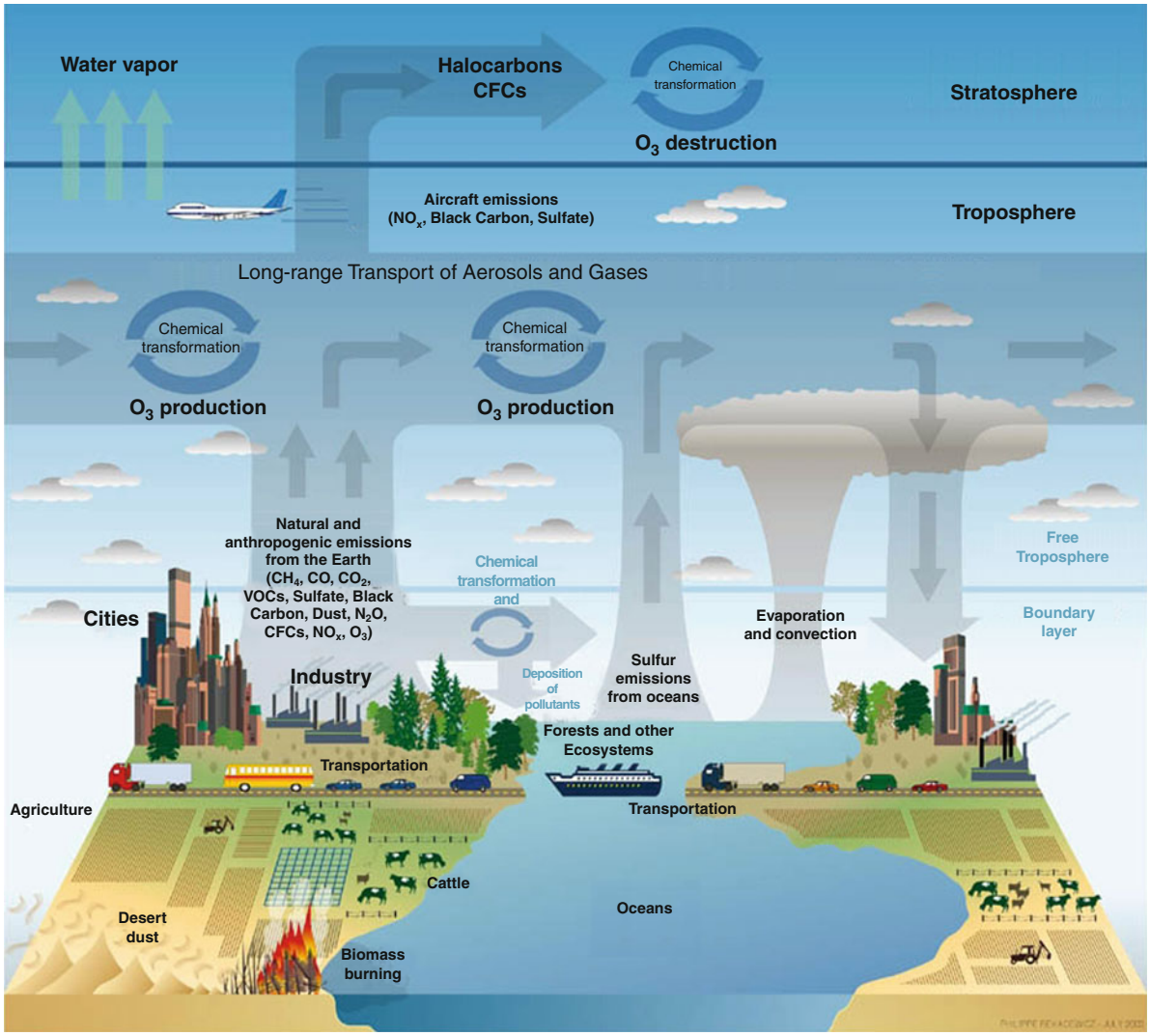

Regional Air Quality. Figure 2
Summary of emissions, emissions sources, and atmospheric processing of air pollutants

Sulfur dioxide emissions originate primarily from coal-fired power plants. Once in the atmosphere SO_2 is oxidized to sulfuric acid (H_2SO_4) both homogeneously and heterogeneously in the liquid and gas phases [11]. The resultant sulfuric acid can be deposited in the gas phase or can condense with water vapor onto aerosol particles or cloud drops to produce aqueous phase sulfuric acid which can then be deposited through rain or fog. Acid deposition came to the forefront of environmental issues in the 1950s and 1960s when the acidification of Scandinavian lakes was linked to sulfur emissions in Europe. A Swedish study in 1972 connected sulfur dioxide emissions with negative environmental impacts which led to an international effort to reduce acidification [2, 3]. It was later also determined that emissions other than SO_2 were also contributing to the acid deposition, such as direct emissions of HCl and nitric acid formed from nitrogen oxides emission and chemical transformation. Efforts to reduce acid deposition spawned international agreements such as the Convention on Long-Range Transboundary Air Pollution (LRTAP), which was the first such agreement to deal with international air pollution issues. Measures in the USA to reduce and

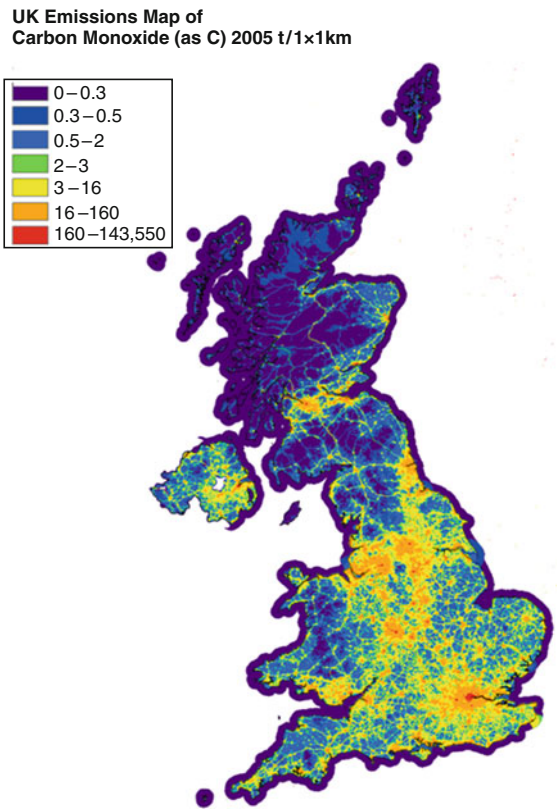

© Crown copyright. All rights reserved defra Licence number 100018880 2007.

Regional Air Quality. Figure 3
Spatially disaggregated emissions of carbon monoxide in the UK from 2008 (Murrells et al. [8])

monitor sulfur emissions included amendments to the Clean Air Act of 1970, as well as the creation of the National Atmospheric Deposition Program of 1977 [2]. Significant reductions in SO_2 emissions were achieved in North America and Europe, resulting in some regeneration and recovery of many forests and water bodies in these areas. The current guideline set by the World Health Organization (WHO) for SO_2 is 20 μg m^{-3} (24-h average). A study looking at annual average SO_2 concentrations for the late 1990s of various megacities (cities with populations greater than ten million) worldwide found that a number of cities, such as Dhaka, Bangladesh, Beijing, China, and Shanghai, China were still above this guideline; most other cited megacities in the study had annual average concentrations of just under 25 μg m^{-3} [12]. Additionally, SO_2 emissions from megacities in Asia accounted for 30% of the ambient concentrations measured

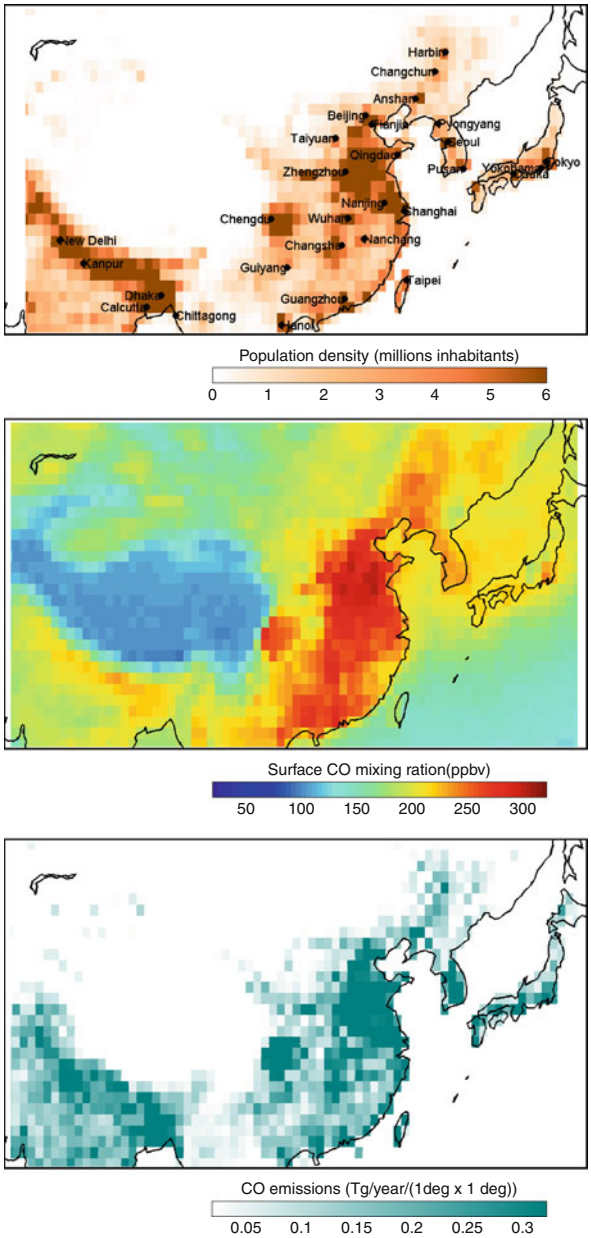

Regional Air Quality. Figure 4
(*top*) Population density over China and surroundings. All cities with more than two million inhabitants are indicated. (*middle*) MOPITT carbon monoxide mixing ratios at the surface level; average measurements from March 2000 to June 2007. (*bottom*) The EDGAR carbon monoxide emission inventory for the year 2000. All data are on a 1°×1° grid (Clerbaux et al. [9])

regionally, including areas hundreds of kilometers from the urban centers [13]. Levels of SO_2 measured in the USA declined by 59% from 1990 to 2008, and are currently well below the 0.03 ppmV (~80 μg m^{-3}) national standard. The majority of the monitoring sites in the USA report SO_2 annual average levels between approximately 0.002 and 0.008 ppmV for 2008 [10].

Similar to SO_2, power plants are a significant emissions source for nitrogen oxides (NO_x). However, NO_x has many other important emission sources including mobile sources, which make up the majority of global NO_x emissions, as well as biomass burning, and natural emissions from soils and lightning [2, 5]. NO_x is the collective term for NO and NO_2 as the photolysis of NO_2 to NO and the subsequent regeneration of NO_2 *via* reaction of NO with ozone is sufficiently fast, in the moderately polluted environment, for these species to be in dynamic equilibrium, namely,

$$NO_2 + h\nu \rightarrow NO + O \quad (1)$$

$$O + O_2 + M \rightarrow O_3 + M \quad (2)$$

$$O_3 + NO \rightarrow NO_2 + O_2 \quad (3)$$

Therefore, at suitable concentrations, ambient NO, NO_2, and O_3 can be said to be in a photochemical steady state or photostationary state (PSS) [14], provided that they are isolated from local sources of NO_x and that sunlight intensity is relatively constant.

The majority of NO_x emissions are initially emitted as NO. For example, the majority of NO_x from power stations is released from the stack as NO. Also, a study of vehicle emissions in Europe (for Euro-II emission standards) showed that for passenger cars, only 5% of NO_x is emitted as NO_2 on average [15]. Since the Euro-II emission standards were introduced NO_x standards have been reduced through the introduction of Euro-III, IV, and V. This has resulted in an increase in the fraction of NO_x emitted as primary NO_2, likely due in large part to particle filters fit to diesel vehicles [16]. In urban environments, NO_x emissions typically show diurnal cycles, peaking during rush hours, owing to the dominant source from the transportation sector. The data in Fig. 5 show typical source time profiles from Mexico City [17]. The adverse health effects of NO_x stem from NO_2 which can be inhaled and passed into the pulmonary region causing tissue damage; NO is believed to be largely nontoxic at ambient levels [18]. The greater impact, in terms of health effects and air quality, results from the role that NO_x plays in ozone formation. NO_x along with volatile organic compounds (VOCs) and CO are the important precursor compounds for the formation of ozone (see later).

The main anthropogenic sources of VOCs are from mobile sources, evaporation from liquid fuels, and industrial sources. VOCs such as isoprene and monoterpenes also have a significant biogenic source from vegetation [19]. VOCs are defined as non-methane hydrocarbons plus heavy hydrocarbons plus carbonyls plus halocarbons, typically $<C_{20}$ [20]. VOCs include alkanes, alkenes, alkynes, and aromatics, as well as oxygenated organics that have low boiling points (50–260°C). Certain VOCs such as the highly reactive "BTEX" compounds (benzene, toluene, ethylbenzene, and xylenes) and 1,3-butadiene that are often prevalent at significant concentrations are frequently monitored even if other VOCs are not [21–24]. Highly reactive aromatics, as well as some other VOCs, are important precursor compounds to secondary organic aerosol (SOA) formation (see discussion in the particulate matter/aerosol pollutants section). Methane is also a VOC, but those discussed here are limited to non-methane VOCs (NMVOCs). Methane has very different sources and because of its lifetime is a global pollutant; it also has very important effects on climate. A study of NMHCs in 28 US cities reported mean mixing ratios of individual HCs of 9 pptV–8740 pptV, with Los Angeles typically reporting among the highest mixing ratios [21]. A similar study measuring NMHCs in 43 cities in China reported a range of minimum and maximum mixing ratios from 40 pptV to 58,300 pptV for the same set of compounds [25]. On the other end of the spectrum, measurements at a remote, high altitude observatory at Izana, Tenerife, reported mean values for a similar set of individual NMHCs ranging from 1 pptV to 501 pptV [26]. A comparison of NMHC (and CO) measurements from global cities found that, in agreement with the small sampling of measurements discussed here, the highest mixing ratios were found in Asian and Latin American cities [7]. While ambient air quality standards do not include VOCs, many vehicular emissions standards do, such as the European emissions standards for passenger cars or the US "Tier" regulations. The standards set for VOCs are formulated

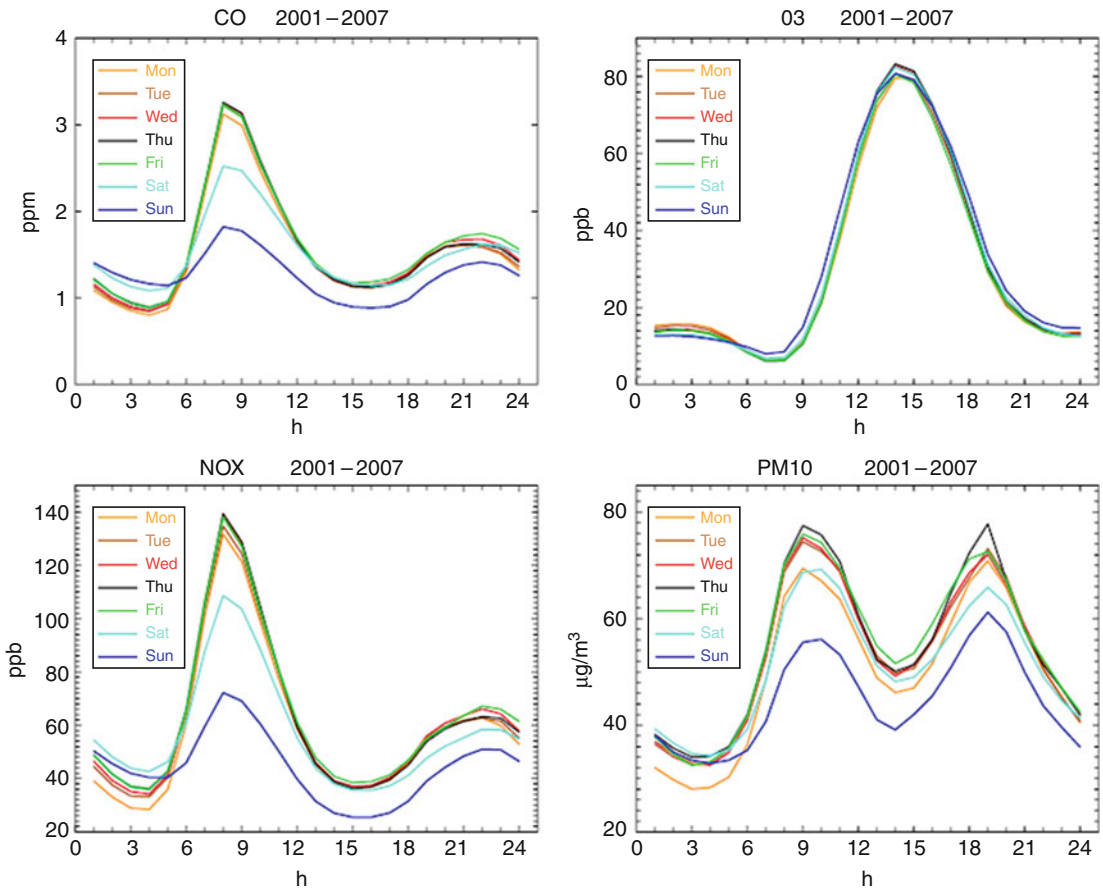

Regional Air Quality. Figure 5
Diurnal cycle of carbon monoxide, nitrogen oxides, ozone, and PM_{10} in Mexico City, averaged for 39 monitoring stations throughout the city over the 2001–2007 period (Stephens et al. [17])

to achieve ozone standards, as the many of the VOCs themselves pose relatively low health risks owing to minimal exposures. Some VOCs, such as 1,3-butadiene and benzene are genotoxic carcinogens and have significant health risks for any amount of exposure. These compounds along with some semi-volatile organic compounds, such as polycyclic aromatic hydrocarbons (PAHs) frequently have specific air quality standards because of their carcinogenic properties [2, 18, 24].

Ozone is currently a problematic regional air quality issue for many locations. Ozone is formed in the atmosphere from the photochemically driven reactions of NO_x, VOCs, and CO. The atmospheric cycle of reactions that form ozone are shown in Fig. 6, where RH represents the VOCs/hydrocarbons. High levels of ozone can be found in urban areas, as well as in rural

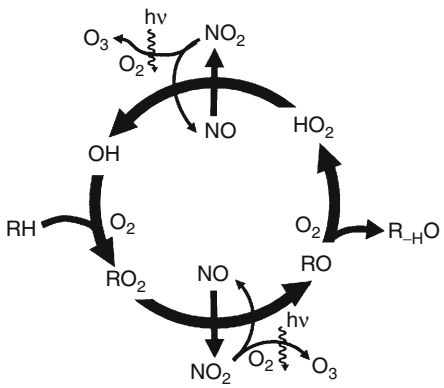

Regional Air Quality. Figure 6
Atmospheric cycle for the production of ozone. RH are hydrocarbons/non-oxygenated volatile organic compounds (VOCs) (Reproduced from Fowler et al. [32])

areas. Ozone is a secondary pollutant and takes time to form in the atmosphere, during that time can be transported away from the emission source. The time necessary for ozone formation depends on factors such as sunlight and the availability of the precursor compounds, and is typically on the order of hours. Modern day average background O_3 mixing ratios in the Northern Hemisphere range from 20 to 45 ppbV (~39–88 μg m^{-3}). Background in this case is defined as the fraction of ozone that is not attributed to anthropogenic sources of local origin and is therefore resulting from stratospheric ozone transport to the troposphere, ozone production from natural sources of NO_x and VOCs (e.g., lightning, biogenic emissions), or long-range transport of ozone from distant pollutant sources [27]. The contribution of background ozone, specifically that from long-term transport, is a concern for many locations that are in exceedance of air quality standards, as the background contribution can make the difference between being in attainment and not. This is of particular concern in the Western US where influence from Asian emissions may be making it more difficult to achieve current regulatory air quality standards [28]. Many urban areas, beyond those in the Western US, are often in exceedance of their respective air quality standards for ozone, such as cities in the USA, Canada, Europe, and China [29–34]. These exceedances often affect rural areas as well [35]. Ozone has adverse impacts on human health, as well as vegetation. Surface ozone is associated with respiratory problems and premature human mortality. In addition, it can damage plants, reduce photosynthesis and growth, leading to reduced crop yields [36].

Many of the pollutants discussed above, including carbon monoxide, sulfur oxides, nitrogen oxides, and ozone, as well as particulate matter (see below), are classified as "criteria pollutants" by the US EPA. These criteria pollutants are among the most common air pollutants and are used as indicators of air quality [37].

Particulate Matter/Aerosol Pollutants

Particulate matter is an air quality concern because of its adverse health effects, as well as its contribution to reductions in visibility. Particulate matter is currently monitored, in the air quality area, based on size-resolved fractions. These are typically PM_{10} (particles with an aerodynamic diameter of 10 μm or smaller) and $PM_{2.5}$ (particles with an aerodynamic diameter of 2.5 μm or smaller). This size fractionation is also typically referred to as the coarse mode (the fraction between PM_{10} and $PM_{2.5}$) and the fine mode (equivalent to $PM_{2.5}$). Particles in the fine mode are a more significant health concern than those in the coarse mode because of their ability to penetrate deeper into the lungs than particles in the coarse mode, remain in the air longer, transport over longer distances, and penetrate more easily into indoor environments [38]. The scale of the possible impact of adverse health effects from particulate matter is shown in Fig. 7 which depicts the estimated loss of life expectancy attributable to $PM_{2.5}$ from anthropogenic emissions in 2000 and 2020 in Europe [39].

Particulate matter (PM) is composed of many different species, including carbonaceous aerosols, inorganic species (sulfate, nitrate, ammonium, chloride), trace metals, and crustal elements from dust and water [5]. The relative contribution of aerosol components to the total aerosol burden for the present atmosphere, based on a model simulation for 1990 using emission estimates from 1990 and later, is shown in Fig. 8 [40]. Aerosols technically refer to the suspension of fine solid or liquid particles in a gas; however, the term aerosols is more commonly used to refer to just the particulate/nongaseous component, which is how it will be used here [5]. There are anthropogenic and natural sources of particulate matter. Natural sources of PM include volcanic eruptions, sea spray, biological debris, and dust. These types of PM emissions tend to fall into the coarse mode (PM_{10}–$PM_{2.5}$) and are emitted owing to mechanical processes [5]. Anthropogenic particulate matter is emitted primarily from combustion sources and falls largely into the fine mode ($PM_{2.5}$) [38]. In many locations the majority of these anthropogenic emissions stem from fossil fuel combustion use by the transportation sector [18, 41], but other sources include stationary fuel combustion (e.g., power plants), industry, and biomass burning. The schematic representation in Fig. 9 summarizes aerosol sources, sinks, and transformations in the atmosphere, by particle size [5, 42].

In addition to primary aerosols, secondary aerosols, i.e., those formed in the atmosphere by gas-to-particle

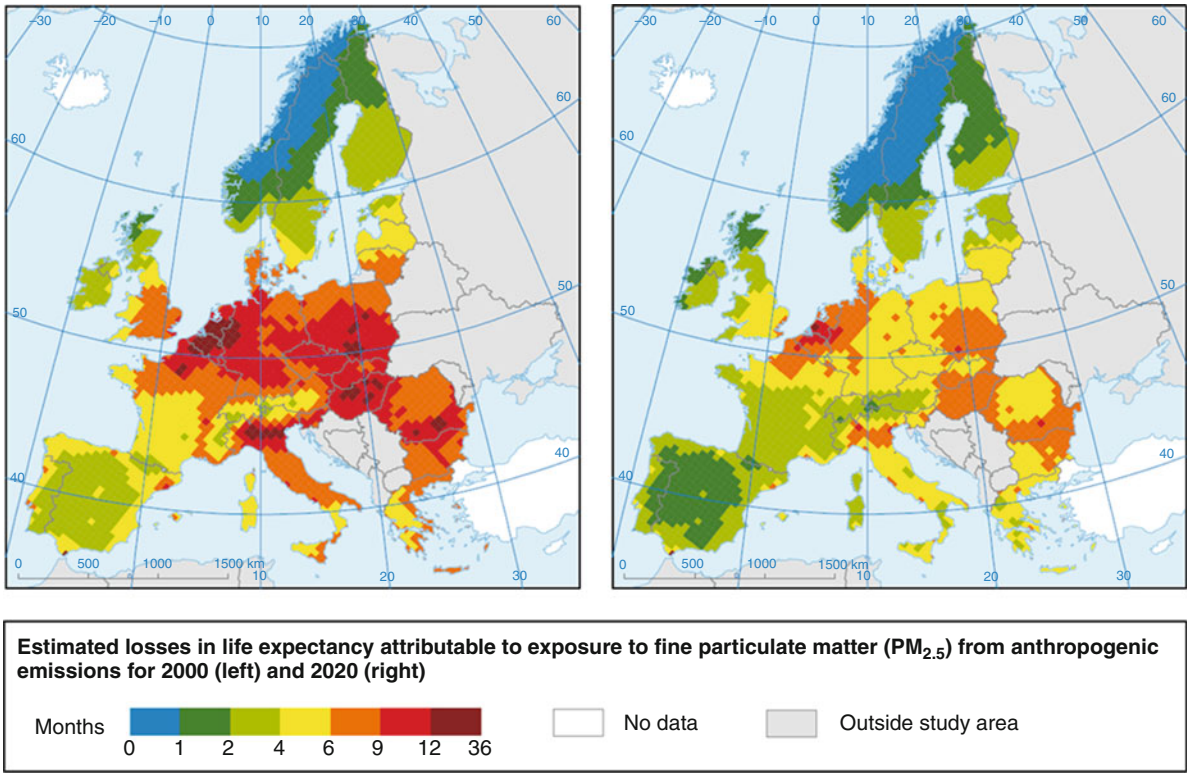

Regional Air Quality. Figure 7

Health impact of particulate matter (PM) mass concentrations (μg m^{-3}). Loss in statistical life expectancy (months) that can be attributed to anthropogenic contributions to $PM_{2.5}$ for the year 2000 (*left*) and for 2020 (*right*) for the Clean Air for Europe (CAFE) baseline scenario, which takes into account changes in air quality standards and reductions in emissions (IIASA; EEA [39])

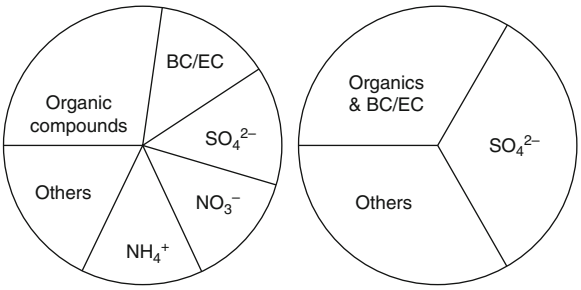

Regional Air Quality. Figure 8

Relative contribution of aerosol components to the total aerosol burden (28.9 Tg) for the present atmosphere, based on a model simulation from 1990 using emission estimates from 1990 and later. Secondary organic aerosol (SOA) produced from anthropogenic sources (SOAa), secondary organic aerosol from biogenic VOC oxidation (SOAb), primary organic aerosol (POA), black carbon (BC), and methane sulfonic acid (MSA) (Tsigaridis et al. [40])

conversion and/or condensation of gaseous compounds onto preexisting aerosol particles can be a significant fraction of the PM. Secondary aerosols can be organic or inorganic, formed primarily from (photo)chemical reaction of VOC precursor emissions or the oxidation of NO_x and SO_2 [43]. Secondary organic aerosols (SOAs) are formed in a two-step process: (1) the production of the organic aerosol compound from the reaction of parent organic gases, (2) the partitioning of the organic compound between the gas and particulate phases forming SOA [5]. Secondary organic aerosol concentrations tend to be higher during periods of greater photochemical reactivity (e.g., summer months), but can be significant year-round depending on the location, meteorology (e.g., humidity and temperature), solar radiation, the existing aerosols and availability, abundance, and reactivity of gas-phase precursors and oxidants [44–47]. The atmospheric processes

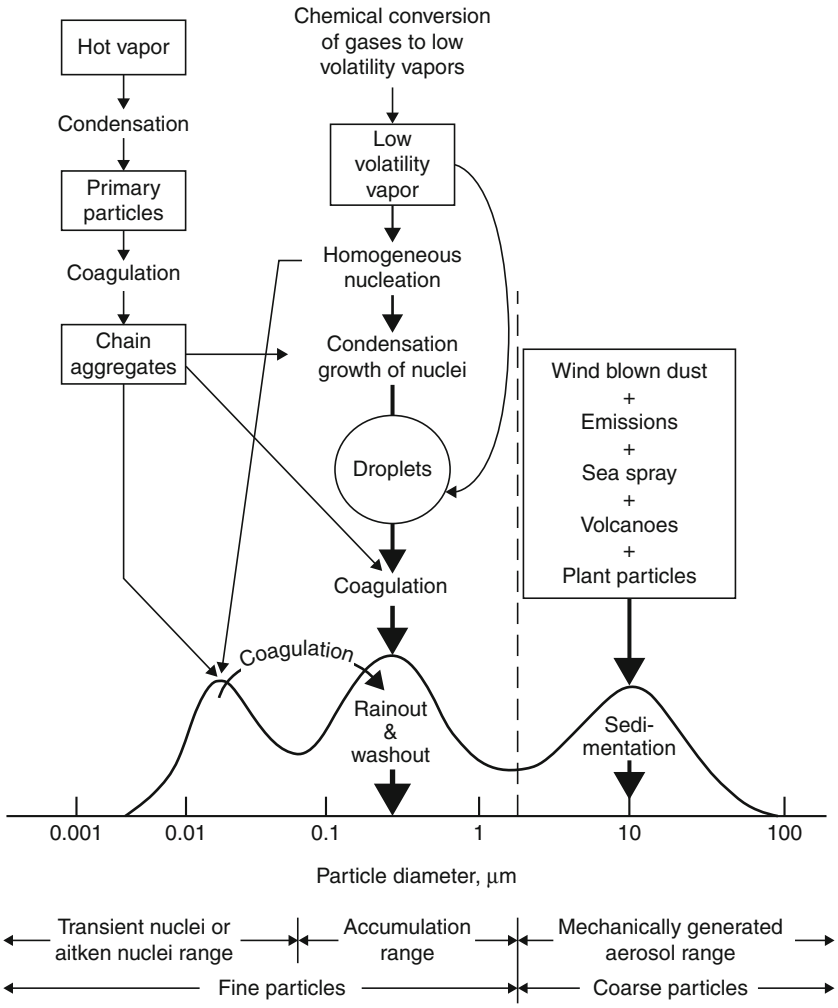

Regional Air Quality. Figure 9
Schematic of the distribution of atmospheric aerosols, showing principal modes, sources, and particle formation and removal mechanisms (Whitby and Cantrell [79])

undergone by aerosols after emission or formation in the atmosphere are detailed in Fig. 10 [44, 48].

Concentrations of reported PM range from less than 1 μg m^{-3} (PM_{10}) in a remote location such as the Antarctic to 340 μg m^{-3} (PM_{10}) and 194 μg m^{-3} ($PM_{2.5}$) annual average concentrations for Lahore, Pakistan in 2007, which is extremely polluted and has some of the highest PM concentrations recorded [49–51]. The WHO annual average guideline for PM_{10} is 20 μg m^{-3} and 10 μg m^{-3} for $PM_{2.5}$. Annual average concentrations in 2001 of $PM_{2.5}$ and PM_{10} from three European cities ranged from 7.8 to 28.0 μg m^{-3} to 15.7–41.0 μg m^{-3}, respectively [52].

Various types of modeling have been established that are able to determine the contributions of different types of aerosol sources to ambient particulate matter samples, including factor analysis and chemical mass balance (CMB) modeling. More information about these types of models can be found in section Modeling.

Air Quality Measurements

Networks of air pollution monitoring stations have been set up across many areas of the globe, especially in developed countries. In the USA, for example,

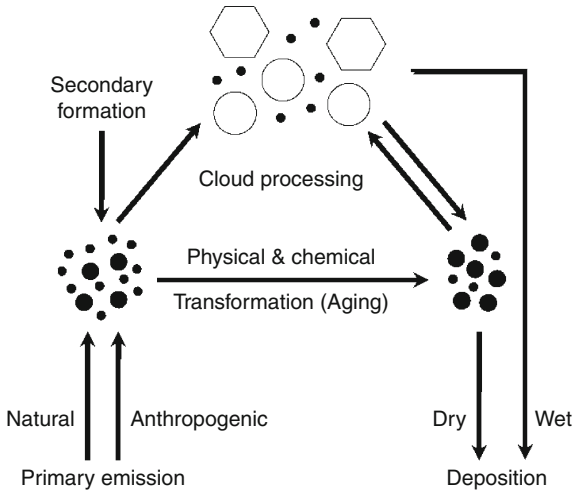

Regional Air Quality. Figure 10
Primary emissions, secondary formation, and atmospheric processing of natural and anthropogenic aerosols (Fuzzi et al. [48]; Poeschl [44]; Monks et al. [36])

ambient air quality monitoring programs are required of states by the US EPA to assess and determine compliance with the national ambient air quality standards. The air quality monitors and monitoring programs must comply with design and quality assurance requirements, as well as using monitoring techniques based on federal reference methods. The results from these monitoring networks are then reported to the US EPA annually [18]. There are different levels of monitoring networks in the USA, including the National Air Monitoring Stations (NAMS), the State and Local Air Monitoring Stations (SLAMS), and the Photochemical Assessment Monitoring Stations (PAMS). The national network is for long-term monitoring to provide a systematic, consistent database for comparison with other air quality data and trend analysis. The state and local network is for determining compliance with air quality standards, while the PAMS network is designed for monitoring ozone in areas of persistently high ozone concentrations [18]. More information on monitoring and the federal reference methods used in the US air quality networks is available on the US EPA Web site and in Godish (2004) [18].

The overarching air monitoring network for all of Europe, which focuses on transboundary air pollution, was established as part of the Convention on Long-Range Transboundary Air Pollution (LRTAP). Within that convention, the EMEP programme (Co-operative Programme for Monitoring and Evaluation of the Long-range Transmission of Air Pollutants in Europe) was tasked to "regularly provide governments and subsidiary bodies under the LRTAP Convention with qualified scientific information to support the development and further evaluation of the international protocols on emission reductions negotiated within the Convention" [53]. At this point, data are collected for the following areas of interest: acidification and eutrophication, ground-level ozone, persistent organic pollutants (POPs), heavy metals, and particulate matter. These are monitored using air and precipitation sampling methods. In addition to measurements (monitoring), EMEP also collects emissions data, and uses modeling to look at atmospheric transport and deposition of air pollutants [53]. The focus here will be on the established monitoring network. There are over 300 sites in the monitoring network in 37 countries, and more than 20 participating institutions. There are three different levels of monitoring stations within the EMEP network depending on the number and type of measurements being conducted, but all EMEP stations are located in areas classified as measuring regional or global background. Many of the EMEP stations are also part of or working in cooperation with other European monitoring framework initiatives, such as the World Meteorological Organization-Global Atmospheric Watch programme (WMO-GAW), national monitoring networks that report to the European Commission under the European Union Air Quality Directives, and other national and local monitoring networks [54]. The European Air Quality Directives focus on regional air pollution.

In addition to the EMEP network, many countries also have monitoring networks that have been established in urban areas to monitor roadside pollution levels, and urban background levels. For example, the UK has an extensive air quality network, across the country (UK Automatic Urban and Rural Network, AURN) and in the major urban areas, such as London (London Air Quality Network, LAQN). The UK AURN has over 100 monitoring stations located across the country for NO_x, $PM_{2.5}$, PM_{10}, SO_2, CO, and/or O_3. A map showing the distribution of monitoring stations and station types, given by monitoring in compliance with AQ legislation, is shown in Fig. 11.

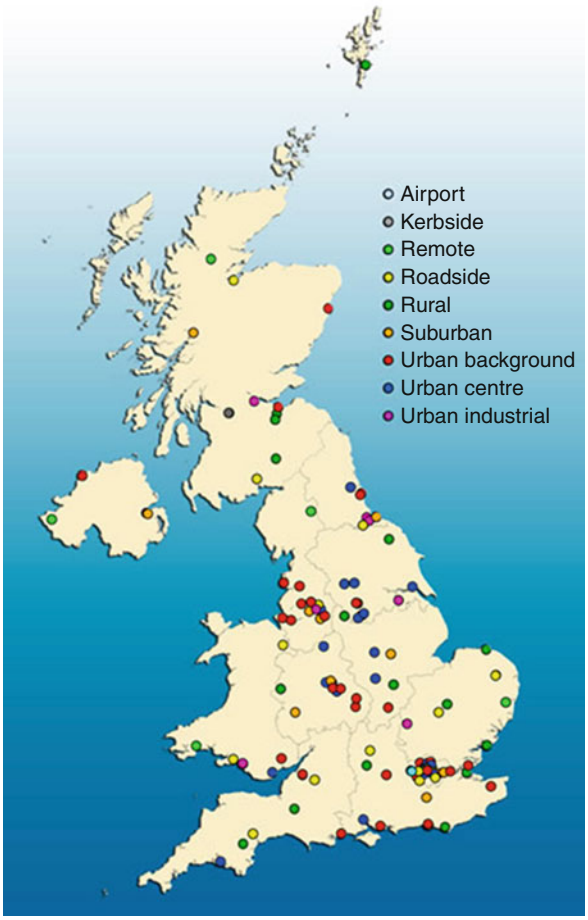

Regional Air Quality. Figure 11
Monitoring stations in the UK, shown by station classification (http://www.airquality.co.uk/monitoring_networks.php?n=aurn)

Health Effects, Ecosystem Effects, and Air Quality

Air pollution was not always associated with negative connotations. Before the Second World War, air pollution (e.g., car exhaust, plumes from smoke stacks) were associated to a certain degree with growth and prosperity [55]. Going back as far as 1873 London was affected by smogs, the most infamous of which was the London smog of December 1952 [18]. The word smog originates from the combination of the words smoke and fog. The smogs of London were caused by extremely high concentrations of smoke and sulfur dioxide emissions largely from coal burning. During the 1940s, it became clear that cities like Los Angeles had severe air quality problems owing to a different kind of smog – a photochemical smog. This type of smog stems from high concentrations of oxidants (e.g., ozone) and peroxide compounds that are produced through photochemical reactions. The basic reaction scheme for the formation of ozone, the primary ingredient in photochemical smog is

$$\mathrm{VOC} + \mathrm{OH} \xrightarrow{[O_2]} \mathrm{RO_2} + \mathrm{H_2O} \tag{4}$$

$$\mathrm{CO} + \mathrm{OH} \xrightarrow{[O_2]} \mathrm{HO_2} + \mathrm{CO_2} \tag{5}$$

$$\mathrm{RO_2} + \mathrm{NO} \xrightarrow{[O_2]} \text{secondary VOC} + \mathrm{H_2O} + \mathrm{NO_2} \tag{6}$$

$$\mathrm{H_2O} + \mathrm{NO} \rightarrow \mathrm{OH} + \mathrm{NO_2} \tag{7}$$

$$\mathrm{NO_2} + hv \rightarrow \mathrm{NO} + \mathrm{O} \tag{8}$$

$$\mathrm{O} + \mathrm{O_2} + \mathrm{M} \rightarrow \mathrm{O_3} + \mathrm{M} \tag{9}$$

where RO_2 represents a chain organic with an attached O_2. The OH radical is formed from photolysis of ozone, formaldehyde, and other secondary VOCs [56]. Since these early smogs which documented a connection between exposure to elevated pollution levels and acute illness in the affected population, a number of epidemiological, toxicological, and occupational exposure studies have documented the association between aerosols and adverse health effects [18, 38, 57]. Health effects can range from eye irritation to cardiovascular system related mortality. The Harvard Six Cities study was a cohort study which estimated the effects of air pollution on mortality, while also controlling for other individual risk factors, such as smoking [58]. Over 8,000 adults in six US cities were included in the study that lasted approximately 15 years. Statistically significant associations were found between air pollution and mortality with positive associations between air pollution and death from lung cancer, as well as air pollution and cardiopulmonary disease. The air pollutants most associated with the mortality were fine particulates and sulfate [58]. A later cohort study from 1982 to 1989 using data from 151 US cities and over 550,000 adults found that increased mortality was associated with sulfate and fine-particulate air pollution and that particulate air pollution was linked with cardiopulmonary and lung cancer mortality, very similar to the Six City study findings [59]. Later studies and reanalysis of the data found that there was no consistent toxicological evidence to suggest that long-term

exposure to sulfates had significant effects on the cardiovascular system [60]. The association of sulfate with adverse health effects remains under debate. Figure 12 shows life expectancies versus $PM_{2.5}$ concentrations from a study looking at fine-particulate air pollution and life expectancy throughout the USA [61]. Additional studies in Canada, Germany, Finland, and the Czech Republic also reported comparable results for particulate pollution and adverse health effects, such as respiratory symptoms and hospitalizations and mortality [38]. For more detailed information on air pollution and health effects, a number of books and review articles are recommended in the Further Reading section of the Bibliography.

In addition to adverse human health effects, air pollution can damage vegetation, buildings, and cause loss of revenue due to impaired visibility. Vegetation effects include reduction in yields, leaf damage, loss of sensitive species, and subsequent reduction in plant diversity and sensitivity to other environmental stresses [62]. Buildings and other outdoor structures can be damaged by air pollution as well. The blackened walls of historical monuments and other buildings, such as cathedrals, are because of high levels of aerosols depositing on the surface. Physical erosion owing to windblown dust can impact buildings, and some building materials (mainly certain kinds of stone, such as limestone or marble) can also be chemically eroded by acid aerosols [18].

Modeling

The fate of any chemical species (C_i) in the atmosphere can be represented as a continuity or mass balance equation such as

$$\frac{dC_i}{dt} = \frac{duC_i}{dx} - \frac{dvC_i}{dy} - \frac{dwC_i}{dz} + K_z\frac{dC_i}{dz} + P_i - L_i + S_i + \left(\frac{dC_i}{dt}\right)_{\text{clouds}} \tag{10}$$

where t is the time, u, v, and w are the components of the wind vector in x, y, and z accounting for the horizontal and vertical large-scale transport. Small-scale turbulence can be accounted for using K_z, the turbulent diffusion coefficient, P_i and L_i are the chemical production and loss terms, and S_i are the sources owing to emissions. Cloud processes (vertical transport, washout, and aqueous phase chemistry) are represented in

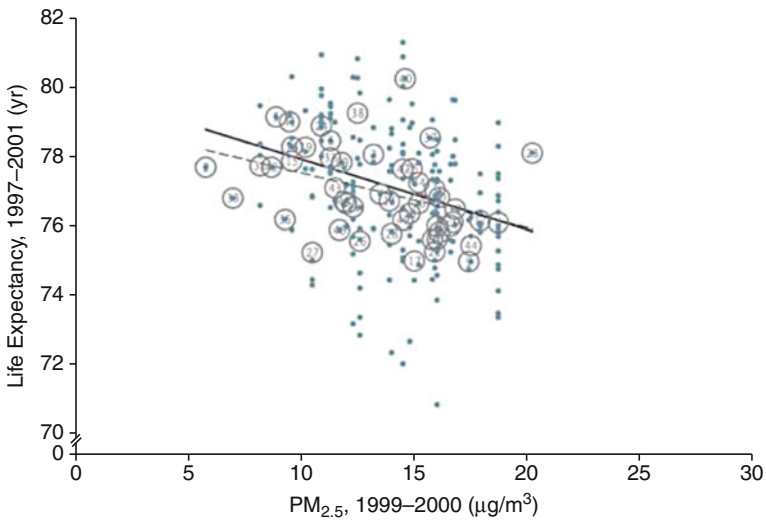

Regional Air Quality. Figure 12
Cross-sectional life expectancies for 1997–2001, plotted against PM2.5 concentrations for 1999–2000 for the USA. Dots and circles labeled with numbers represent population-weighted mean life expectancies at the county level and the metropolitan-area level, respectively. The solid and broken lines represent regression lines with the use of county-level and metropolitan-area-level observations, respectively (Pope et al. [59])

a cloud processing term. The application of this type of equation is the basis of chemical modeling. There are two main types of modeling that deal with air pollution and air quality objectives, atmospheric (chemical) transport models and statistical models [5].

Atmospheric Models

Atmospheric (chemistry) transport models are based on the fundamental description of atmospheric physical and chemical properties [5]. The reason for the "chemical" term in parentheses is that there are a number of models which model only transport and do not necessarily always include chemical transformations, but the general principles behind the models are the same. There are two basic kinds of atmospheric models – Lagrangian and Eulerian. Lagrangian models track the path of a given air parcel (and the concentrations of the chemical components therein) as it is advected in the atmosphere, while Eulerian models describe the concentrations in an array of fixed (nonmoving) computational cells [5]. The concentration of any chemical species in the atmosphere are controlled by four types of processes, namely emissions, chemistry, transport, and deposition (see Eq. 10) that are taken into account in the atmospheric models [19]. Atmospheric models can be run on different scales from local and regional to global. The regional or local models are most applicable to regional air quality and are frequently used as predictors for possible future scenarios, including prediction of air quality, cost-benefit, and environmental impact analyses of pollutant increases or reductions. An example is shown in Fig. 13 where the model has been used to predict ozone concentrations for two different scenarios, emissions from a base case scenario and then projected emissions based on the technology and regulations that will be or are currently being implemented (in this case for 2000 and 2010). The model data show the expected impact of various

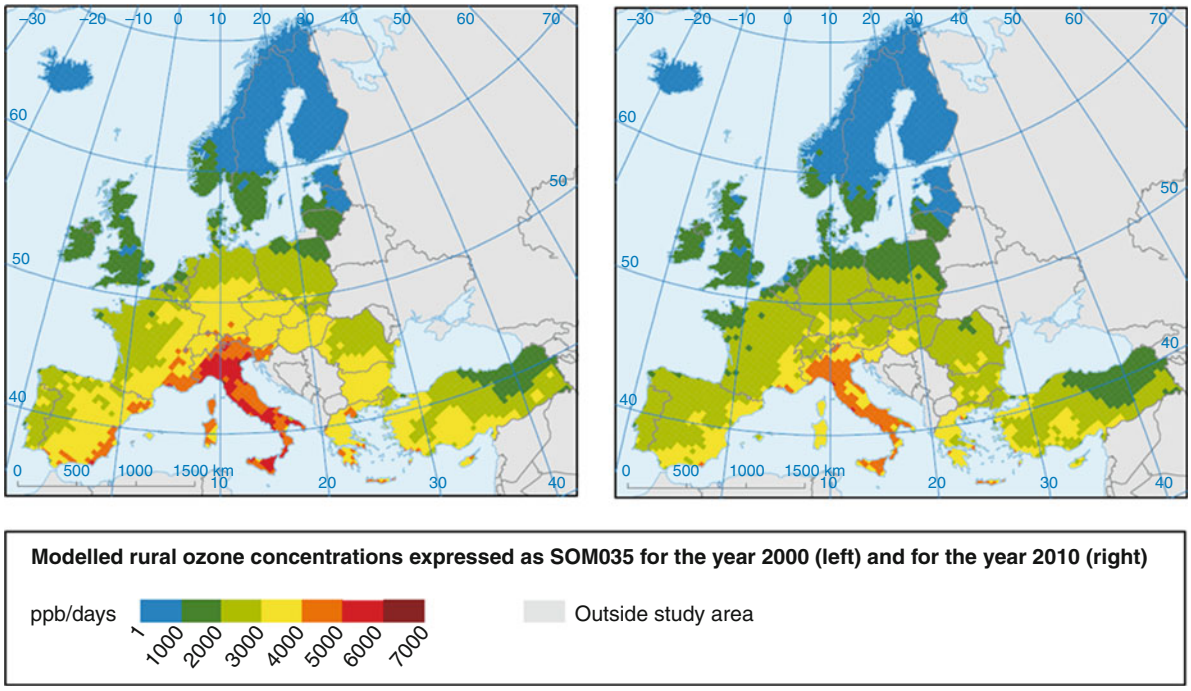

Regional Air Quality. Figure 13
Modeled ozone concentrations expressed as the sum of means over 35ppbV (SOMO35) for the year 2000 (*left*) and for the year 2010 (*right*) for the Air for Europe (CAFE) baseline scenario, which takes into account changes in air quality standards and reductions in emissions (IIASA; EEA [39])

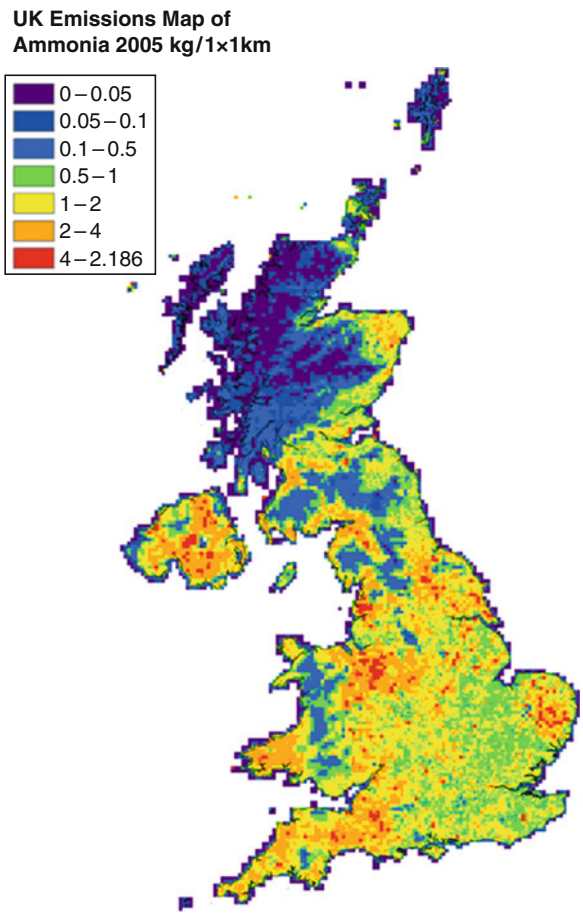

© Crown copyright. All rights reserved Defra, Licence number 100018880 2007.

Regional Air Quality. Figure 14
Spatially disaggregated emissions of ammonia in the UK from 2008 (Murrells et al. [8])

emission legislation measures, including legislation regarding combustion plants, the Euro standards for vehicles and non-road machinery, as well as International Panel on Climate Change (IPCC) and national legislation. As is visible in Fig. 13, the model predicts the largest impacts in ozone reduction will occur in the Mediterranean region [39].

The input data for many models are based on emission inventories. Emission inventories, like models, exist for different scales, i.e., local, regional, and global and resolutions, ranging from 1 km × 1 km to 1° × 1° (which is approximately 110 km × 110 km at the largest, depending on latitude). The species included in many emission inventories are greenhouse gases, nitrogen oxides, carbon monoxide, methane, non-methane volatile organic compounds, sulfur dioxide, ammonia, particulate matter, and recently black carbon and organic carbon [36]. Emission sources in inventories include anthropogenic emissions from fuel production, industrial and domestic combustion, transportation, waste disposal, industrial processes, solvent production and use, and agriculture, and biogenic emissions from vegetation and dust, and biomass burning emissions, which can be natural or anthropogenic [36]. Anthropogenic, natural, and biomass burning emissions are typically compiled in separate inventories. Examples of emission inventory data are given in Fig. 3 for carbon monoxide and Fig. 14 for ammonia [8].

Statistical Models

Statistical models are empirical or semiempirical models based on the statistical analysis of measured data. Instead of following the evolution of emissions in the atmosphere, statistical models work backward, from measured data collected at a given location, a receptor site, and work out the responsible emission sources. These models are also frequently referred to as receptor models. There are a number of different approaches that are used based on the understanding of source–receptor relationships including the chemical mass balance (CMB) model, which requires complete knowledge of sources and results in a quantitative output of source contributions and uncertainties, and factor analysis methods, such as Principal Component Analysis (PCA), which require no a priori source information. The different types of receptor models and the amount of knowledge required for model use is summarized in Fig. 15 [63, 64].

Chemical mass balance models are frequently used to support air quality decision-making for policy, such as was the case for CMB studies in Los Angeles, CA, and Las Vegas, NV which were used for the creation of State Implementation Plans to attain PM_{10} requirements [65]. In addition, CMB can be used to assess the success of implemented control technologies, and which sources are potentials for reduction controls. Such applications are possible in that CMB results yield quantitative source contributions to the measured metric, i.e., $PM_{2.5}$, organic carbon, or total mass. From such results the sources with the largest contributions

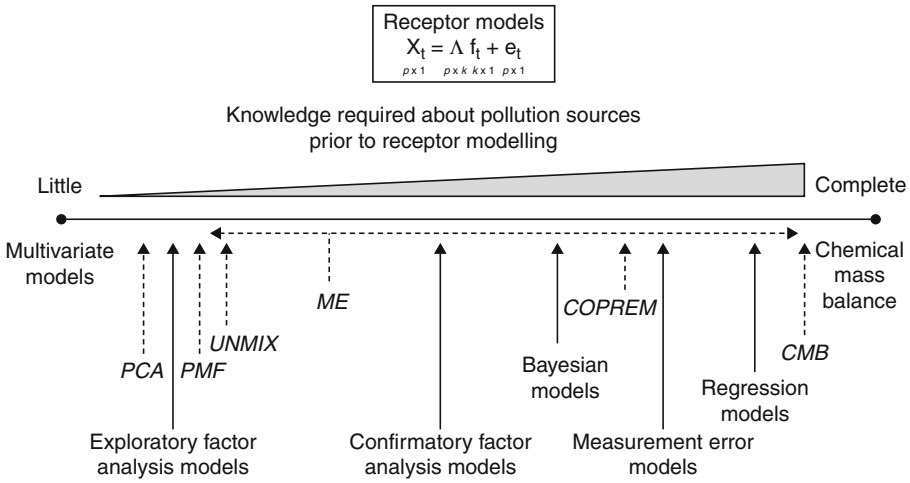

Regional Air Quality. Figure 15

Approaches for estimating pollution source contributions using receptor models. Specific models are shown in italics and with dotted arrows (Schauer et al. [63]; Viana et al. [64])

can be targeted for reduction, or changes in specific source contributions assessed. Recent reviews of CMB and other receptor models found that for the studies analyzed (the majority of which were from measurements in the USA and Europe), fossil fuel combustion is an important contributor to PM concentrations, with the primary contributions stemming from gasoline and diesel vehicle exhaust [64, 65]. Stationary sources, such as power stations, have only minimal source contributions when the facilities have effective pollution controls in place, but can be large contributors without such control technologies [65]. An example of the type of result produced by CMB modeling where fine-particulate matter organic carbon mass is apportioned is shown in Fig. 16 for West Jerusalem in 2007 [66].

In addition to receptor models, other types of statistical models are also frequently used in atmospheric chemistry, such as simple regression analysis, land use regression models, and neural network models. Land use regression models have been used in atmospheric chemistry to characterize air pollution exposure and health effects for people residing in urban areas, integrating traffic and geographic information into the models [67]. To learn about neural network models and their uses in the air pollution modeling field the reader is referred to Boznar and Mlakar, 2002 [68].

Current Air Quality Legislation and Metrics

Air quality guidelines are established to protect human health and the environment. The World Health Organization (WHO) has established air quality guidelines for use worldwide that are focused on protecting human health. Air quality guidelines in the USA and Europe are intended to protect human health, including sensitive populations (e.g., elderly, asthmatics), with secondary limits set for the protection of public welfare (e.g., visibility, animals, crops, buildings) [37]. The standards are set based on the extensive amount of research available concerning air pollution and health effects at the time of regulation.

The guidelines set by the WHO exist for the most common air pollutants: size-resolved particulate matter, ozone, nitrogen dioxide, and sulfur dioxide [1]. These were most recently updated in 2005. While the WHO has set guidelines for all countries to use as a basis for regulation if they choose to do so, most national air monitoring authorities have a list of "air quality pollutants" that are monitored and regulated. In the USA, these are the "criteria pollutants" that are regulated under the National Ambient Air Quality Standards (NAAQS) by the US Environmental Protection Agency (EPA) and include carbon monoxide, lead, nitrogen dioxide, particulate matter of two-size fraction, ozone,

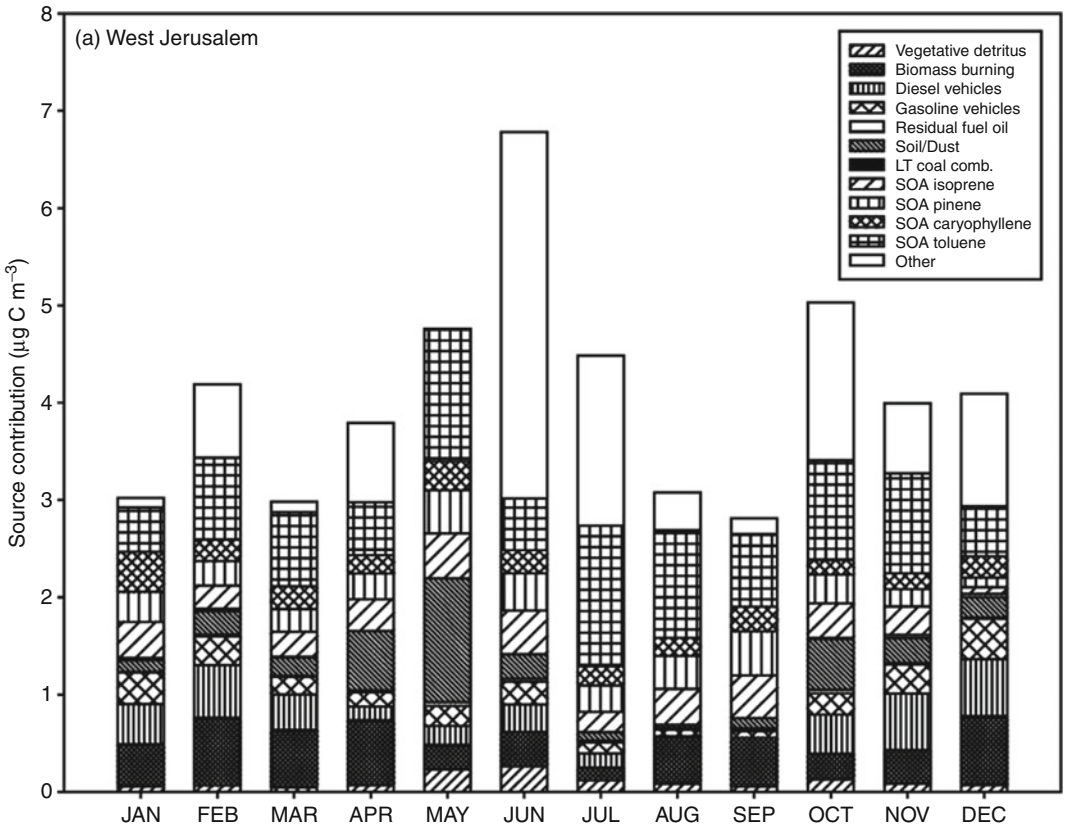

Regional Air Quality. Figure 16

Source apportionment by chemical mass balance (CMB) modeling of monthly averaged ambient fine organic aerosol mass concentrations for West Jerusalem for 2007. LT Coal Comb = low-temperature coal combustion; SOA = secondary organic aerosol from the named precursor compound (e.g., isoprene) (von Schneidemesser et al. [66])

and sulfur dioxide, similar to those pollutants for which the WHO has established guidelines [37]. European Union air quality pollutants include particulate matter, sulfur dioxide, nitrogen dioxide, lead, carbon monoxide, benzene, ozone, arsenic, cadmium, nickel, and PAHs and are regulated under the air quality standards which were simplified in 2008 by combining all existing legislation on air quality under one directive known as the ambient air quality and Clean Air for Europe (CAFE) directive [69]. As is apparent here, all air quality pollutant regulation tends to contain a similar set of air pollutants with some countries/regulating bodies selecting additional species, such as trace metals, to be included. Regulatory standards and WHO guidelines are listed in Table 1.

Metrics also exist to quantify health or environmental effects of air pollutants, with different metrics established for human health and the environment. For example, AOT40 is the accumulated exposure over a threshold of 40 ppbV during daylight hours for a relevant period. SOMO35 is the sum of the daily maximum of running 8-h means over 35 ppbV. Both the AOT40 and SOMO35 are ozone metrics. Metrics such as AOT40 and SOMO35 are frequently considered to be more appropriate measures of the effects of ozone on crops and vegetation than those metrics designed to protect human health. A sample of environmental and health metrics are given in Table 2 [70].

Regional Context

There are a variety of spatial scales that both influence air quality and that air quality impact, such as the local, regional, and global. It is clear that these scales are not

Regional Air Quality. Table 1 Annual mean (unless noted otherwise) air quality guidelines as established by the World Health Organization (WHO), the United States Environmental Protection Agency (US EPA), and the European Union (Euro Directives)

	WHO	US EPA	Euro directive
Particulate matter (PM_{10})	20 μg m^{-3}	150 μg m^{-3} (24 h)	40 μg m^{-3}
Particulate matter ($PM_{2.5}$)	10 μg m^{-3}	15.0 μg m^{-3}	25 μg m^{-3}
Nitrogen dioxide	40 μg m^{-3}	53 ppb (~100 μg m^{-3})	40 μg m^{-3}
Sulfur dioxide	20 μg m^{-3} (24 h)	0.03 ppm (~80 μg m^{-3})	125 μg m^{-3}
Carbon monoxide		10 mg m^{-3} (8 h)	10 mg m^{-3} (8 h)
Lead		1.5 μg m^{-3} (quarterly average)	0.5 μg m^{-3}
Benzene			5 μg m^{-3}
Arsenic			6 ng m^{-3}
Cadmium			5 ng m^{-3}
Nickel			20 ng m^{-3}
Polycyclic aromatic hydrocarbons			1 ng m^{-3}

independent and definitions are loose. The local scale tends to the anthropogenic emission/human influence scale encompassing a city or a smaller area within a city, while regional scales are typically larger, encompassing an entire metropolitan region and the surrounding area or even greater. An example of a regional scale could be London and southeast England, or it could also be as large as all of Europe, depending on how the user defines it. When considering air quality on any regional scale, secondary pollutants from atmospheric processing and the transport of pollutants become much more important and primary emissions less so.

For example, as discussed earlier, ozone is an important secondary pollutant, which because of atmospheric processing time, has significant implications for regional air quality. Plume transport for urban areas into the surrounding region can have a significant influence on the air quality in the surrounding region [71]. In many cases, ozone concentrations have been observed to be higher in rural areas than urban areas [72, 73]. Furthermore, since regional air quality frequently includes rural areas, and thereby areas with fewer primary anthropogenic emissions, natural emissions can play a more significant role. For example, biogenic VOCs, such as isoprene, can contribute to ozone and other secondary pollutant formation, and wind erosion can add soil and/or dust to the existing aerosol loading. While these factors can and do also exist on a local scale, their relative importance on a local or regional scale varies depending on the location and size of the areas chosen.

Future Directions

Air Quality and Climate

Air quality and climate change are important issues with complex interactions (see Figs. 1 and 17). Both are environmental issues that are and will continue to be addressed by environmental policies in the coming years. Much of the current focus is on trade-offs between different scenarios. While there are win-win situations where policy will improve both air quality and reduce greenhouse gas emissions, many measures may not result in such co-benefits. As stated in the IPCC Fourth Assessment Report "Future climate change may cause significant air quality degradation by changing the dispersion rate of pollutants, the chemical environment for ozone and aerosol generation and the strength of emissions from the biosphere, fires, and dust. The sign and magnitude of these effects are highly uncertain and will vary regionally" [74]. Ozone and aerosols are the two air pollutants of

Regional Air Quality. Table 2 A sample of ozone metrics of relevance to human health (Reproduced from AQEG 2009)

Metric	Relevance	Key influences on the values of this metric at urban locations
Annual average	Basic metric used to show long-term trends	Includes all of the hours in the year. Strongly influenced by the magnitude of local NO_x emissions and by topography through nocturnal depletion
Annual average of the daily maximum of the running 8-h mean	Used as "basic metric" for many of the health metrics.	Strongly influenced by the magnitude of local NO_x emissions
Annual average of the daily maximum of the running 8-h mean with a 70 $\mu g\ m^{-3}$ cutoff	Health impact, related to SOMO35	Influenced by the magnitude of local NO_x emissions and by photochemical episodes
Annual average of the daily maximum of the running 8-h mean with a 100 $\mu g\ m^{-3}$ cutoff	Health impact	Strongly influenced by photochemical episodes and to a lesser extent by the magnitude of local NO_x emissions
Maximum 1-h average (peak hour in the year)	Used as the basis for some epidemiological studies, although it has been suggested that the 8-h metric is more representative. Also an indicator of short-term peaks, but note low statistical power, since it is the value for one single hour	The metric most sensitive to the magnitude of regionally generated photochemical episodes and thus likely to show a response to reductions in relevant precursor emissions
Number of days with daily maximum of running 8-h mean exceeding 100 $\mu g\ m^{-3}$	Equates to the number of exceedences of the UK ozone standard (the Air Quality Strategy objective is no more than 10 exceedences per year)	Strongly influenced by photochemical episodes and to a lesser extent by the magnitude of local NO_x emissions
Number of days with daily maximum of running 8-h mean exceeding 120 $\mu g\ m^{-3}$	Equates to the number of exceedences of the EU Target Value (no more than 25 days, averaged over 3 years) and Long-Term Objective (no exceedences) from the third Daughter Directive	Strongly influenced by photochemical episodes and to a lesser extent by the magnitude of local NO_x emissions
SOMO35 (sum of means over 35 ppb)	Used as a metric by IIASA, for Clean Air for Europe (CAFE) and NECD revision, related to annual average of the daily maximum of the running 8-h mean with a 70 $\mu g\ m^{-3}$ cutoff	Influenced by the magnitude of local NO_x emissions and by photochemical episodes

greatest concern for public health [75], while being key players in climate change and feedbacks [36, 76].

Air pollution and greenhouse gases often have common sources of emission. In addition to the common sources, there are some gases which are both air pollutants and act as greenhouse gases, such as ozone [77]. To best address both issues, a significant effort will need to be made to understand the impact of a changing climate on air quality and vice versa. Current work with global and regional models that couple chemical transport and general circulation simulations have found that climate change alone could increase summertime ozone concentrations and the severity of summer smogs over the coming decades, with the largest effects in polluted, urban areas [75–77]. The potential impact of climate change on PM is much less certain. Important factors in changes in PM owing to climate change include precipitation frequency and mixing depth, as

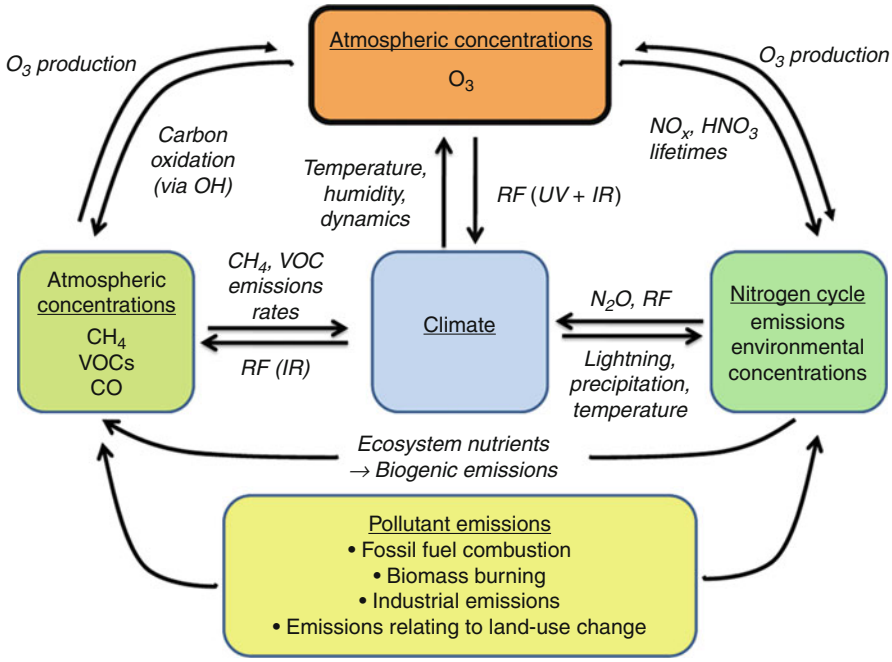

Regional Air Quality. Figure 17
Schematic representation of the multiple interactions between tropospheric chemical processes, biogeochemical cycles, and the climate system. *RF* radiative forcing, *UV* ultraviolet radiation, *IR* infrared radiation (IPCC, 2007; EPA [76])

well as wildfire frequencies [75, 76]. In addition to the uncertainty of the impact of climate change on PM emissions, the uncertainty of the reverse, the impact of PM on climate change, is also large. Part of this uncertainty arises from the differences in aerosol types and their climate properties. Sulfates and nitrates have an overall cooling (negative radiative forcing) effect, whereas black carbon has an overall warming effect [36]. Therefore, while the reduction of PM improves air quality, it may result in further atmospheric warming in terms of climate change. In addition to direct forcing, aerosols can also act as cloud condensation nuclei (CCN) and exert an indirect effect on climate. The abundance of CCN affects cloud formation and cloud lifetime, which in turn affects the scattering and absorption of radiation and therefore climate. Preliminary model results show a range of increases and decreases in PM concentrations for different regions in response to climate change [75, 76].

While controls of CO_2 emissions should remain a priority for mitigation of global climate change, reductions in emissions of air pollutants could have a faster impact on slowing warming trends in the short term (10–30 years). Raes and Seinfeld [78] have pointed out that we maybe on a "bumpy road" to recovery with larger short-term increases in temperature, owing partly to the fact that significant amounts of long-lived GHGs are already in the atmosphere but also because reductions in atmospheric aerosols in the next decade or so will add to the positive radiative forcing of the Earth's climate.

Mitigation of short-lived agents with high radiative forcing may reduce the possibility of catastrophic climate change in particularly sensitive regions such as the Arctic. However, mitigation decisions must be based on sound science and would benefit from a sector-based approach accounting for benefits for health, ecosystems, climate, and mitigation costs. While the ideal goal is to achieve win-win solutions for air pollution and climate, in some cases health improvements via reductions in pollutant emissions may greatly outweigh possible negative effects on climate. This is particularly true of the developing world where improving health and ensuring food security currently have immediate priority over the benefits of slowing the rate of climate change. Nevertheless, the

development of emission reduction strategies or cleaner energy alternatives for both CO_2 and short-lived climate forcers (SLCFs) are needed. There are clearly many challenges in the area of air quality and climate and a need for sound underpinning science across the spatial and temporal scales that air quality and climate act on.

Bibliography

Primary Literature

1. WHO (2005) WHO Air quality guidelines for particulate matter, ozone, nitrogen dioxide and sulfur dioxide. World Health Organization Regional Office for Europe, Copenhagen
2. Jacobson MZ (2002) Atmospheric pollution history, science, and regulation. Cambridge University Press, Cambridge
3. Fenger J (2009) Air pollution in the last 50 years – from local to global. Atmos Environ 43:13–22
4. Seinfeld JH (2004) Air pollution: a half century of progress. Environ Energy Eng 50(6):1096–1108
5. Seinfeld JH, Pandis SN (2006) Atmospheric chemistry and physics: from air pollution to climate change, 2nd edn. Wiley, New York
6. Bradley KS, Stedman DH, Bishop GA (1999) A global inventory of carbon monoxide emissions from motor vehicles. Chemosphere Glob Change Sci 1:65–72
7. von Schneidemesser E, Monks PS, Duelmer PC (2010) Global comparison of VOC and CO observations in urban areas. Atmos Environ 44(37):4772–4816
8. Murrells T, Passant N, Thistlethwaite G, Wagner A, Li Y, Bush T, Norris J, Walker C, Stewart R, Tsagatakis I, Whiting R, Conolly C, Okamura S, Peirce M, Sneddon S, Webb J, Thomas J, MacCarthy J, Choudrie S, Brophy N (2010) UK Emissions of Air Pollutants 1970 to 2008. AEA
9. Clerbaux C, Edwards DP, Deeter M, Emmons L, Lamarque J-F, Tie XX, Massie ST, Gille J (2008) Carbon monoxide pollution from cities and urban areas observed by the Terra/MOPITT mission. Geophys Res Lett 35:L03817. doi:10.1029/2007GL032300
10. EPA U (2010) Our Nation's air, status and trends through 2008. United States Environmental Protection Agency
11. Finlayson-Pitts BJ, Pitts JN Jr (2000) Chemistry of the upper and lower atmosphere: theory, experiments, and applications. Academic, San Diego/London
12. Gurjar BR, Butler TM, Lawrence MG, Lelieveld J (2008) Evaluation of emissions and air quality in megacities. Atmos Environ 42:1593–1606
13. Guttikunda SK, Tang Y, Charmichael GR, Kurata G, Pan L, Streets DG, Woo J-H, Thongboonchoo N, Fried A (2005) Impacts of Asian megacity emissions on regional air quality during spring 2001. J Geophys Res 110:D20301
14. Leighton PA (1961) The photochemistry of air pollution. Academic, New York
15. Soltic P, Weilenmann M (2003) NO2/NO emissions of gasoline passenger cars and light-duty trucks with Euro-2 emission standard. Atmos Environ 37:5207–5216
16. Carslaw DC (2005) Evidence of an increasing NO2/NOx emissions ratio from road traffic emissions. Atmos Environ 39:4793–4802
17. Stephens S, Madronich S, Wu F, Olson JB, Ramos R, Retama A, Munoz R (2008) Weekly patterns of Mexico City's surface concentrations of CO, NOx, PM10 and O3 during 1986–2007. Atmos Chem Phys 8:5313–5325
18. Godish T (2004) Air quality, 4th edn. Lewis, Boca Raton
19. Jacob DJ (1999) Introduction to atmospheric chemistry. Princeton University Press, Princeton
20. Watson JG, Chow JC, Fujita EM (2001) Review of volatile organic compound source apportionment by chemical mass balance. Atmos Environ 35:1567–1584
21. Baker AK, Beyersdorf AJ, Doezema LA, Katzenstein A, Meinardi S, Simpson IJ, Blake DR, Rowland FS (2008) Measurements of nonmethane hydrocarbons in 28 United States cities. Atmos Environ 42:170–182
22. Borbon A, Locoge N, Veillerot M, Galloo JC, Guillermo R (2002) Characterisation of NMHCs in a French urban atmosphere: overview of the main sources. Sci Total Environ 292:177–191
23. Bower J, Broughton G, Connolly C, Cook A, Grice S, Kent A, Loader A, Stedman J, Targa J, Telling S, Tsagatakis I, Vincent K, Willis P, F-w Y, Yardley R (2009) Air pollution in the UK: 2008. AEA, Didcot
24. Dollard GJ, Dore CJ, Jenkin ME (2001) Ambient concentrations of 1, 3-butadiene in the UK. Chem-Biol Interact 135–136:177–206
25. Barletta B, Meinardi S, Roland FS, Chan C-Y, Wang X, Zou S, Chan LY, Blake DR (2005) Volatile organic compounds in 43 Chinese cities. Atmos Environ 39:5979–5990
26. Fischer H, Nikitas C, Parchatka U, Zenker T, Harris GW, Matuska P, Schmitt R, Mihelcic D, Muesgen P, Paetz HW, Schultz M, Thomas VA (1998) Trace gas measurements during the oxidizing capacity of the tropospheric atmosphere campaign 1993 at Izana. J Geophys Res 103(D11):13505–513518
27. Vingarzan R (2004) A review of surface ozone background levels and trends. Atmos Environ 38:3431–3442
28. Oltmans SJ, Lefohn AS, Harris JM, Shadwick DS (2008) Background ozone levels of air entering the west coast of the US and assessment of longer-term changes. Atmos Environ 42(24):6020–6038. doi:10.1016/j.atmosenv.2008.03.034
29. Chan CK, Yao X (2008) Air pollution in mega cities in China. Atmos Environ 42(1):1–42. doi:10.1016/j.atmosenv.2007.09.003
30. de Leeuw F, Bogman F (2001) Air pollution by ozone in Europe in summer 2001. European Environment Agency, Copenhagen
31. de Leeuw FAAM, de Paus TA (2000) Exceedance of EC Ozone threshold values in Europe in 1997. Water Air Soil Pollut 128:255–281
32. Fowler D, Coyle M, Anderson R, Ashmore MR, Bower JS, Burgess RA, Cape JN, Cox RA, Derwent RG, Dollard GJ, Grennfelt P, Harrison RM, Hewitt CN, Hov O, Jenkin ME, Lee DS,

Maynard RL, Penkett SA, Smith RI, Stedman JR, Weston KJ, Williams ML, Woods PJ (1997) Ozone in the United Kingdom. Air and Environment Quality Division, Department of the Environment, Transport and the Regions, London, UK
33. Geddes JA, Murphy JG, Wang DK (2009) Long term changes in nitrogen oxides and volatile organic compounds in Toronto and the challenges facing local ozone control. Atmos Environ 43:3407–3415
34. Sather ME, Cavender K (2007) Trends analysis of ambient 8 hour ozone and precursor monitoring data in the south central US. J Environ Monit 9(2):143–150. doi:10.1039/b617603h
35. Carvalho A, Monteiro A, Ribeiro I, Tchepel O, Miranda AI, Borrego C, Saavedra S, Souto JA, Casares JJ (2010) High ozone levels in the northeast of Portugal: analysis and characterization. Atmos Environ 44:1020–1031
36. Monks PS, Granier C, Fuzzi S, Stohl A, Williams ML, Akimoto H, Amann M, Baklanov A, Baltensperger U, Bey I, Blake N, Blake RS, Carslaw K, Cooper OR, Dentener F, Fowler D, Fragkou E, Frost GJ, Generoso S, Ginoux P, Grewe V, Guenther A, Hansson HC, Henne S, Hjorth J, Hofzumahaus A, Huntrieser H, Isaksen ISA, Jenkin ME, Kaiser J, Kanakidou M, Klimont Z, Kulmala M, Laj P, Lawrence MG, Lee JD, Liousse C, Maione M, McFiggans G, Metzger A, Mieville A, Moussiopoulos N, Orlando JJ, O'Dowd CD, Palmer PI, Parrish DD, Petzold A, Platt U, Poschl U, Prevot ASH, Reeves CE, Reimann S, Rudich Y, Sellegri K, Steinbrecher R, Simpson D, ten Brink H, Theloke J, van der Werf GR, Vautard R, Vestreng V, Vlachokostas C, von Glasow R (2009) Atmospheric composition change – global and regional air quality. Atmos Environ 43(33):5268–5350. doi:10.1016/j.atmosenv.2009.08.021
37. EPA U (2010) United States Environmental Protection Agency National Ambient Air Quality Standards. http://epa.gov/air/criteria.html
38. Pope CAI, Dockery DW (2006) Health effects of fine particulate air pollution: lines that connect. J Air Waste Manage Assoc 56:709–742
39. EEA (2007) Air pollution in Europe 1990–2004. EEA Report No2/2007. European Environment Agency, Copenhagen
40. Tsigaridis K, Krol M, Dentener F, Balkanski Y, Lathiere J, Metzger S, Hauglustaine D, Kanakidou M (2006) Change in global aerosol composition since preindustrial times. Atmos Chem Phys 6:5143–5162
41. Colvile R, Hutchinson E, Mindell J, Warren R (2001) The transport sector as a source of air pollution. Atmos Environ 35:1537–1565
42. Hewitt CN, Jackson AV (eds) (2009) Atmospheric science for environmental scientists. Blackwell, Chichester
43. Williams PI, Baltensperger U (2009) Particulate matter in the atmosphere. In: Hewitt CN, Jackson AV (eds) Atmospheric science for environmental scientists. Blackwell, Chichester
44. Poeschl U (2005) Atmospheric aerosols: composition, transformation, climate and health effects. Angew Chem Int Ed 44:7520–7540
45. Stone EA, Hedman CJ, Zhou JB, Mieritz M, Schauer JJ (2010) Insights into the nature of secondary organic aerosol in Mexico City during the MILAGRO experiment 2006. Atmos Environ 44(3):312–319. doi:10.1016/j.atmosenv.2009.10.036
46. Stone EA, Zhou JB, Snyder DC, Rutter AP, Mieritz M, Schauer JJ (2009) A comparison of summertime secondary organic aerosol source contributions at contrasting urban locations. Environ Sci Technol 43(10):3448–3454. doi:10.1021/es8025209
47. von Schneidemesser E, Zhou JB, Stone EA, Schauer JJ, Qasrawi R, Abdeen Z, Shpund J, Vanger A, Sharf G, Moise T, Brenner S, Nassar K, Saleh R, Al-Mahasneh QM, Sarnat JA (2010) Seasonal and spatial trends in the sources of fine particulate organic carbon in Israel, Jordan, and Palestine. Atm Environ 44:3669–3678
48. Fuzzi S, Andreae MO, Huebert BJ, Kulmala M, Bond TC, Boy M, Doherty SJ, Guenther A, Kanakidou M, Kawamura K, Kerminen VM, Lohmann U, Russell LM, Poschl U (2006) Critical assessment of the current state of scientific knowledge, terminology, and research needs concerning the role of organic aerosols in the atmosphere, climate, and global change. Atmos Chem Phys 6:2017–2038
49. Stone E, Schauer J, Quraishi TA, Mahmood A (2010) Chemical characterization and source apportionment of fine and coarse particulate matter in Lahore, Pakistan. Atmos Environ 44:1062–1070
50. Toscano G, Gambaro A, Moret I, Capodaglio G, Turetta C, Cescon P (2005) Trace metals in aerosol at Terra Nova Bay, Antarctica. J Environ Monit 7:1275–1280
51. von Schneidemesser E, Stone EA, Quraishi TA, Shafer MM, Schauer JJ (2010) Toxic metals in the atmosphere in Lahore, Pakistan. Sci Total Environ 408(7):1640–1648. doi:10.1016/j.scitotenv.2009.12.022
52. Sillanpaa M, Frey A, Hillamo R, Pennanen AS, Salonen RO (2005) Organic, elemental and inorganic carbon in particulate matter of six urban environments in Europe. Atmos Chem Phys 5:2869–2879
53. European Monitoring and Evaluation Programme (2010) EMEP Convention on long-range transboundary air pollution. http://www.emep.int/. Accessed July 2010
54. EMEP (2009) Progress in activities in 2009 and future work: measurements and modelling (acidifications, eutrophication, photo-oxidants, heavy metals, particulate matter and persistant organic pollutants). Geneva
55. Fenger J (2009) Urban air pollution. In: Hewitt CN, Jackson AV (eds) Atmospheric science for environmental scientists. Blackwell, Chichester
56. Sillman S (1999) The relation between ozone, NOx and hydrocarbons in urban and polluted rural environments. Atmos Environ 33:1821–1845
57. Brunekreef B, Holgate ST (2002) Air pollution and health. Lancet 360:1233–1242
58. Dockery DW, Pope CA III, Xu X, Spengler JD, Ware JH, Fay ME Jr, Ferris BG, Speizer FE (1993) An association between air pollution and mortality in six US Cities. N Eng J Med 329(24):1753–1759
59. Pope CAI, Thun MJ, Namboodiri MM, Dockery DW, Evans JS, Speizer FE, Heath JCW (1995) Particulate air pollution as a predictor of mortality in a prospective study of U.S. adults. Am J Respir Crit Care Med 151:669–674
60. COMEAP (2009) Long-term exposure to air pollution: effect on mortality. Health Protection Agency for the Committee on

the Medical Effects of Air Pollutants, Chilton, Didcot, Oxfordshire, UK
61. Pope CAI, Ezzati M, Dockery DW (2009) Fine-particulate air pollution and life expectancy in the United States. N Engl J Med 360(4):376–386
62. Harrison RM (ed) (1999) Understanding our environment. The Royal Society of Chemistry, Cambridge
63. Schauer JJ, Lough GC, Shafer MM, Christensen WF, Arndt MF, DeMinter JT, Park J-S (2006) Characterization of metals emitted from motor vehicles. HEI Research Report, vol 133. Health Effects Institute, Boston
64. Viana M, Kuhlbusch TAJ, Querol X, Alastuey A, Harrison RM, Hopke PK, Winiwarter W, Vallius A, Szidat S, Prevot ASH, Hueglin C, Bloemen H, Wahlin P, Vecchi R, Miranda AI, Kasper-Giebl A, Maenhaut W, Hitzenberger R (2008) Source apportionment of particulate matter in Europe: a review of methods and results. J Aerosol Sci 39(10):827–849. doi:10.1016/j.jaerosci.2008.05.007
65. Chow JC, Watson JG (2002) Review of PM2.5 and PM10 apportionment for fossil fuel combustion and other sources by the chemical mass balance receptor model. Energy Fuels 16(2):222–260. doi:10.1021/ef0101715
66. von Schneidemesser E, Zhou JB, Stone EA, Schauer JJ, Shpund J, Brenner S, Qasrawi R, Abdeen Z, Sarnat JA (2010) Spatial variability of carbonaceous aerosol concentrations in East and West Jerusalem. Environ Sci Technol 44:1911–1917
67. Ryan PH, LeMasters GK (2007) A review of land-use regression models for characterizing intraurban air pollution exposure. Inhal Toxicol 19(Suppl 1):127–133
68. Boznar MZ, Mlakar P (2002) Use of neural networks in the field of air pollution modelling. In: Borrego C, Shayes G (eds) Air pollution modelling and its application XV. Kluwer, Secaucus
69. EC (2010) European commission environment air quality standards. http://ec.europa.eu/environment/air/quality/standards.htm
70. AQEG (2009) Ozone in the United Kingdom. Department for the Environment, Food and Rural Affairs, London
71. Penkett S, Clemitshaw K, Savage N, Burgess R, Cardenas L, Carpenter L, McFadyen G, Cape J (1999) Studies of oxidant production at the weybourne atmospheric observatory in summer and winter conditions. J Atmos Chem 33:111–128
72. Jenkin ME (2008) Trends in ozone concentration distributions in the UK since 1990: local, regional and global influences. Atmos Environ 42:5434–5445
73. EEA (2001) Air pollution by ozone in Europe in summer 2001. European Environment Agency, Copenhagen
74. Denman KL, Brasseur G, Chidthaisong A, Ciais P, Cox PM, Dickinson RE, Hauglustaine D, Heinze C, Holland E, Jacob D, Lohmann U, Ramachandran S, da Silva Dias PL, Wofsy SC, Zhang X (2007) Couplings between changes in the climate system and biogeochemistry. climate change 2007: the physical science basis. Contribution of Working Group I to the Fourth Assessment Report of the Intergovernmental Panel on Climate Change. Cambridge University Press, Cambridge/New York
75. Jacob DJ, Winner DA (2009) Effect of climate change on air quality. Atmos Environ 43:51–63
76. EPA U (2009) Assessment of the impacts of global change on regional U.S. air quality: a synthesis of climate change impacts on ground-level ozone. National Center for Environmental Assessment, Washington DC
77. AQEG (2010) Air pollution: action in a changing climate. Department for Environment Food and Rural Affairs, London
78. Raes F, Seinfeld JH (2009) New directions: climate change and air pollution abatement: a bumpy road. Atmos Environ 43:5132–5133
79. Whitby KT, Cantrell BK (1976) Atmospheric Aerosols: Characteristics and Measurement. International Conference on Environmental Sensing and Assessment (ICESA), Institute of Electrical and Electronic Engineers (IEEE). Las Vegas, NV. September 14–19, 1975

Books and Reviews

Brasseur GP, Orlando JJ, Tyndall GS (1999) Atmospheric chemistry and global change. Oxford University Press, Oxford

Brimblecombe P, Hara H, Houle D, Novak M (2007) Acid rain-deposition to recovery. Springer, Dordrecht

IPCC (2007) Climate change 2007 – The physical science basis; Contribution of working group I to the fourth assessment report of the IPCC, Cambridge University Press, Cambridge

Finlayson-Pitts BJ, Pitts JN (2000) Chemistry of the upper and lower atmosphere. Academic, San Diego/London

Hewitt CN, Jackson AV (2003) Handbook of atmospheric science: principles and applications. Blackwell, Oxford

Holloway AM, Wayne RP (2010) Atmospheric chemistry. The Royal Society of Chemistry, Cambridge

Houghton JT (2002) The physics of atmospheres, 3rd edn. Cambridge University Press, Cambridge

Jacobson MZ (2005) Fundamentals of atmospheric modeling, 2nd edn. Cambridge University Press, New York

Seinfeld JH, Pandis SN (2006) Atmospheric chemistry and physics: from air pollution to climate change, 2nd edn. Wiley, New York

Wallace JM, Hobbs PV (2006) Atmospheric science: an introductory survey, 2nd edn. Academic, London/San Diego

Regional Climate Models

L. Ruby Leung
Atmospheric Sciences and Global Change Division, Pacific Northwest National Laboratory, Richland, WA, USA

Article Outline

Glossary
Definition of the Subject and Its Importance

Introduction
Modeling Approach
Evaluating Regional Climate Models
Application of Regional Climate Models
Future Directions
Acknowledgments
Bibliography

Glossary

Downscaling Development of climate information at local or regional scale from coarse resolution data or model outputs; both statistical and dynamical methods can be used.

GCM Global climate model, a climate model based on the general circulation of the atmosphere, often coupled with models of ocean circulation and sea ice.

Mesoscale In the atmosphere, mesoscale generally refers to horizontal scales that lie between the scale height of the atmosphere (about 10 km) and the Rossby radius of deformation (tens to hundreds of kilometers).

Nudging Method to reduce the differences between the simulated and observed or imposed states by applying corrections, usually in the form of tendencies to the prognostic equations, based on the differences.

RCM Regional climate model (also called nested regional climate model), a climate model applied over a limited area with boundary conditions provided by global models or analyses.

Definition of the Subject and Its Importance

Regional climate models are numerical models that simulate the climate of geographic regions typically covering a few thousand square kilometers to a continent. Most regional climate models include models that describe the atmosphere and the underlying land surface, but a few also include models of ocean and sea ice and atmospheric aerosols and chemistry. Given the atmospheric state at the lateral boundaries, regional climate models simulate regional climate in the context of the evolving global climate. Because regional domains cover only a fraction of the globe, it is computationally more feasible to apply regional climate models at higher grid resolution compared to global climate models to better resolve atmospheric and terrestrial processes and how they respond to regional forcings such as topography and land cover/land use. While global climate models are generally applied at grid resolution of a few hundred kilometers, regional climate models have been more commonly applied at grid resolution of a few tens of kilometers. Therefore, a common application of regional climate models is the dynamical downscaling of global climate simulations to provide regional climate information related to climate change projections or climate predictions. As such, regional climate models have served an important function of providing regional climate scenarios needed to assess a wide range of societal relevant climate impacts such as climate change effects on water resources and ecosystems. Regional climate models are also used to study regional climate processes, particularly those that are related to the water cycle that is inherently multi-scale; so explicitly representing finer scale processes is important to simulate its variations at multiple time and space scales.

Introduction

Regional climate models were first developed in the late 1980s to provide a means to simulate climate features that were not well captured by global climate models (GCMs) because of their coarse spatial resolution. Figure 1 shows the representation of surface elevation and land cover/land use in climate models of different horizontal resolutions. At 400 km resolution, which was typical for GCMs in the early 1990s, climate models can only resolve very crude topographic variations and land surface heterogeneities to simulate their effects on large-scale and mesoscale circulation. At 50 km resolution, which is a common resolution used in regional climate models even today, models can begin to realistically capture topographic and land cover features important for regional climate.

The first regional climate model (RCM) was developed and applied to the western USA where regional climate is significantly influenced by the complex terrain not well resolved by GCMs [13,17]. The RCM was adapted from a mesoscale or limited-area atmospheric model that was designed for weather forecasting or short-term simulation of a few days. The model was enhanced for climate simulation by improving the physics representations for processes such as radiative transfer and biosphere-atmosphere exchange at the land surface that governs the energy and water budgets

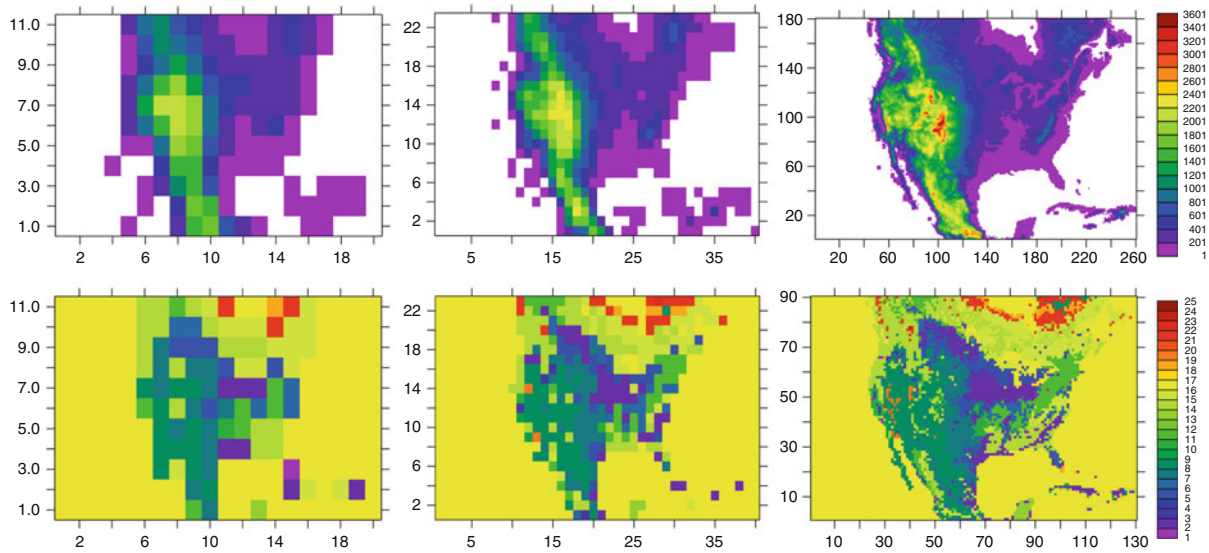

Regional Climate Models. Figure 1

Surface elevation (in meters) (*top row*) and land cover/land use (type) (*bottom row*) represented at 400 km (*left*), 200 km (*middle*), and 50 km (*right*) horizontal resolution in climate models. The land cover/land use types are: *1* urban, *2* dryland crop, *3* irrigated crop, *4* mixed crop, *5* crop/grass, *6* crop/woodland, *7* grass, *8* shrub, *9* mixed shrub/grass, *10* savanna, *11* deciduous broadleaf, *12* deciduous needleleaf, *13* evergreen broadleaf, *14* evergreen needleleaf, *15* mixed forest, *16* water bodies, *17* herbaceous wetland, *18* wooded wetland, *19* barren/sparsely vegetated, *20* herbaceous tundra, *21* wooded tundra, *22* mixed tundra, *23* bare ground tundra, *24* snow/ice, *25* playa. The x- and y-axes show the number of grid points in the domain at the three spatial resolutions

of the climate system. This was achieved by adopting the physics parameterizations used in a GCM. The RCM was driven at the lateral boundaries by atmospheric analysis [17] that provides an observationally constrained and dynamically balanced atmospheric state and global climate simulations [13].

Giorgi and Bates [17] showed, for the first time, that limited-area models could be used to produce long-term (more than a month) continuous simulations, as opposed to prior applications that use limited-area models to simulate weather for just a few days. By comparing the regional simulations with observations and the GCM simulations, it was demonstrated that a mesoscale weather model, with appropriate modifications, could be used for regional climate simulations. Following these pioneering studies, Giorgi et al. [19] further enhanced their RCM by updating the physics parameterizations with newer options available from the GCM, and explored model sensitivity to physics parameterizations and methods of assimilating the lateral boundary conditions. Giorgi and Mearns [16] showed that errors (e.g., measured by the deviation of the model solution from the driving large-scale fields) in limited-area models grow initially during model spin up, but reach an asymptotic value after a few days. At this stage, the climate simulated by the models is defined by the large-scale driving conditions and the model internal physics and dynamics, as well as the regional forcings within the model domain.

Subsequent to the early studies by Giorgi and his colleagues, more regional climate models have been developed following a similar approach and development path. These models have been applied to many regions around the world to assess their simulation skill under different climate regimes such as the monsoon, arid and semiarid deserts, mid-latitude regimes influenced by synoptic systems, and the high latitudes where cryospheric processes are important. As regional climate models became more widely used, questions have been raised about the validity and usefulness of the approach that prompted a series of studies to vigorously assess the various assumptions, and proposed

practical or more mathematically well-posed solutions to regional climate modeling (section "Modeling Approach"). Different datasets and approaches have been used to evaluate RCMs, and large model intercomparison projects have been organized to evaluate and intercompare simulations produced by different RCMs (section "Evaluating Regional Climate Models"). At the same time, many studies have applied RCMs to simulate regional climate change that provided insights on climate change impacts. Regional climate models have also been used to study regional climate processes such as the role of land-atmosphere feedbacks on droughts and monsoon precipitation, effects of aerosols and land use on regional climate and the hydrological cycle, and processes leading to extreme climate events. The following sections provide a synopsis of these topics, and discuss the future directions in regional climate modeling. Examples of RCM applications are given in section "Application of Regional Climate Models."

Modeling Approach

How Do Regional Climate Models Work

Regional climate models are numerical models that simulate the climate of a specific region. Although some regional climate models, or regional earth system models, are beginning to include models of ocean, sea ice, and atmospheric aerosol and chemistry coupled to the atmosphere and land components, this review focuses mainly on regional climate models that traditionally include only atmosphere and land components with prescribed sea surface temperature and sea ice.

Similar to global atmospheric models, regional climate models numerically and simultaneously solve the equations of the conservation of energy, momentum, and water vapor that govern the atmospheric state. These equations are based on the Navier-Stokes equations for fluid flow (conservation of momentum) with approximations that apply to the atmosphere, the thermodynamic energy equation (conservation of energy), the continuity equation (conservation of mass), and the equation of state (ideal gas law). These partial differential equations are cast in various forms for different conservative properties and integrated forward in time using dynamical solvers. The solvers are applied to three-dimensional computational domains that are divided horizontally with grid spacing of a few to tens of kilometers and vertically into tens of vertical layers with a model top near 10–50 hPa. In regional climate models, solving these equations on limited-area domains require lateral boundary conditions, which can be derived from global climate simulations or global analyses to describe the large-scale atmospheric states. This method of simulating regional climate using limited-area models with prescribed lateral boundary conditions is called nesting (Fig. 2), so regional climate models are also called nested regional climate models to distinguish them

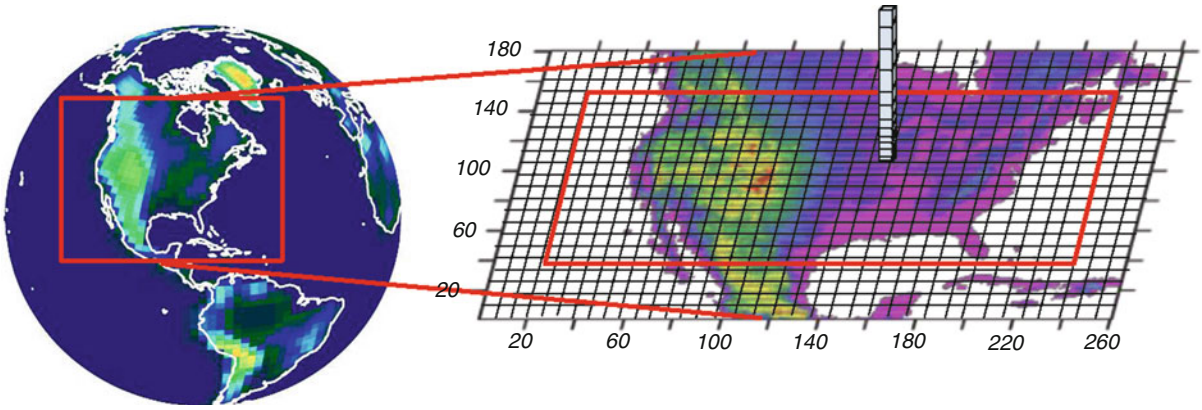

Regional Climate Models. Figure 2
A schematic showing the nesting of a regional climate model within a global climate model. The *right hand* figure shows the regional domain over North America with the horizontal grid (*black lines*), boundary of the buffer zone (*red box*), and a vertical column indicating the atmospheric layers represented by the model

from other dynamical frameworks such as global variable resolution or global stretched-grid models that simulate regional climate for specific regions through regional refinement within the global domain.

The most commonly used lateral boundary treatment in nested regional climate models involves the relaxation of the interior flow in the vicinity of the boundary, called the lateral boundary buffer zone, to the prescribed flow [8]. In most models, the same treatment is also applied to the thermodynamics variables. When applied to RCMs, increasing the width of the lateral boundary buffer zone allows stronger control of the lateral boundary conditions to keep the simulated large scales closer to the global simulations or analyses that provide the lateral boundary conditions. Some RCMs have the capability to use nesting to further zoom into smaller regions with increasing grid resolutions. As computational resources increased over time, more RCMs are now formulated using non-hydrostatic dynamics, as the mean vertical motion of the air column within a model grid cell can no longer be assumed negligible at higher grid resolution. In contrast, most GCMs use hydrostatic solvers because the hydrostatic assumption is valid in coarser grids.

Besides numerically solving the momentum, thermodynamics, and continuity equations, climate models, global or regional, include parameterizations of physical processes such as radiative transfer, convection, cloud microphysics, land surface and biosphere-atmosphere exchange, and boundary layer turbulence. These parameterizations calculate the diabatic heating, moistening, and momentum changes due to the various processes. The resulting tendencies or rates of change are included as sources and sinks in the equations of energy, momentum, and water vapor to drive the atmospheric circulation.

Traditionally, GCMs use more sophisticated parameterizations of slow physical processes such as radiation and land surface for more accurate simulations of the global energy budgets, while limited-area models that are developed mainly for weather forecasting and short-term simulations emphasize detailed parameterizations of fast physical processes such as cloud microphysics and turbulence transfer. To simulate regional climate, both fast and slow physical processes are important because of the short spatial scale and long time scale of interest. Therefore many RCMs have adapted parameterizations of slow processes from GCMs, while maintaining the suite of the relatively detailed parameterizations of fast processes used in weather forecasting. Sharing of physics parameterizations between the global and regional models is considered desirable to reduce inconsistency between the simulated and driving large-scale conditions (see section "Modeling Issues" for a discussion of potential issues caused by mismatch of GCM and RCM solutions) and facilitate interpretation of differences simulated by the RCMs and GCMs. Since the first RCM (section "Introduction"), most RCMs developed and in use today still include subsets of physics parameterizations that are adapted from their host GCMs. Driven by high performance computing and the need to improve accuracy, both global and regional climate models are including more and more sophisticated parameterizations for all physical processes, which together with increasing model resolution, demand significant advances in high performance computing to support climate modeling research.

Modeling Issues

The climate of a region is determined by the large-scale atmospheric circulation as well as regional forcings such as topography within the region, and how they interact through various physical and dynamical processes. For example, the regional climate of the US Great Plains is strongly influenced by atmospheric circulation that brings moisture from the Gulf of Mexico during summer. How much precipitation is produced over land depends on moisture convergence, which is influenced not only by large-scale circulation patterns, but mesoscale features such as the Great Plain Low Level Jet, propagating disturbance from the Rocky Mountain, and local moisture sources from the land surface also play an important role. Therefore in the nested regional climate modeling approach, regional climate simulations depend on both the lateral boundary conditions that control the large-scale circulation, regional topography and land cover/land use features being resolved by the model, as well as physics parameterizations that ultimately determine the local changes in the energy, moisture, and momentum as influenced by the large-scale circulation and regional forcings.

Because of the dependence on large-scale circulation, large biases in global climate simulations used to provide lateral boundary conditions could have detrimental effects on the regional climate simulations under the nesting approach. Even if the global climate simulations were perfect, the lateral boundary conditions do not uniquely define the regional climate because the associated boundary value problem (i.e., solving the hyperbolic equations) is ill posed. Relaxation methods such as proposed by Davies [8] convert the hyperbolic equations to the well-posed parabolic form. However, mismatches between the large-scale circulation simulated by the regional models and the imposed atmospheric states at the lateral boundaries that may result from differences in grid resolution, physics, and dynamical formulations between the global and regional models can induce errors that propagate to the interior of the domains and contaminate the regional simulations [56]. This issue also leads to the sensitivity of the simulated regional climate to the domain size and locations of the lateral boundaries – an undesirable feature as it introduces uncertainties to the simulation results.

To address the validity of the nested regional climate modeling approach, a series of idealized numerical experiments have been designed and performed to assess the various assumptions used in regional climate modeling. The idealized experimental framework, known as "Big Brother Experiments (BBE)" [10], addresses modeling issues specifically related to the nested regional climate modeling approach. The Big Brother Experiment protocol consists of performing a high-resolution global climate simulation, referred as the Big Brother, BB, that serves as reference against which a regional climate simulation, referred as the Little Brother, LB, would be compared (Fig. 3). The BB, with proper spatial filtering to remove the fine scales to emulate coarse resolution global climate simulations, provides lateral boundary conditions for driving the LB. The differences between the climate simulated by the LB and the reference BB could be attributed to the nesting approach of the

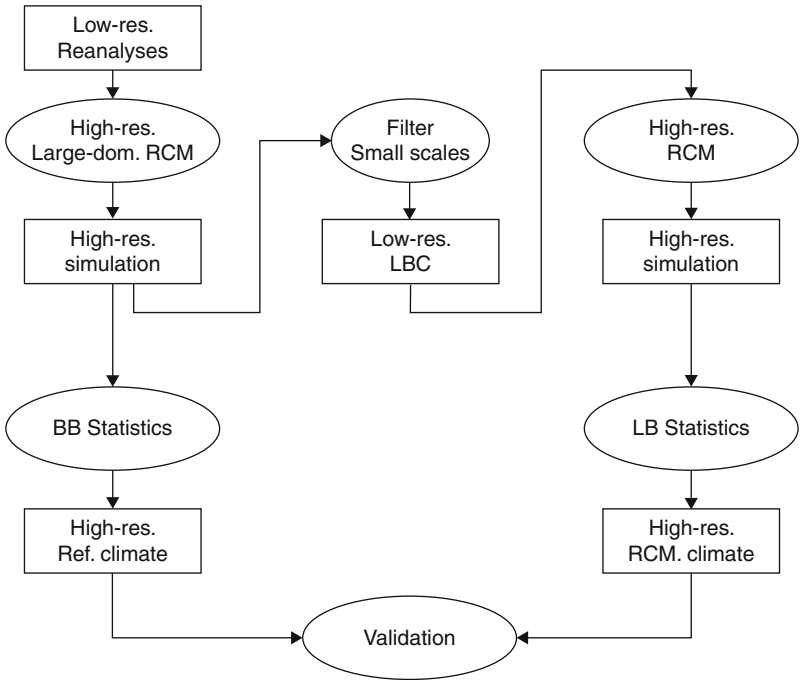

Regional Climate Models. Figure 3
Flow chart of the Big Brother Experiment (BBE). The high-resolution large domain RCM simulation is used as a virtual reality to evaluate the high-resolution simulation generated by the same RCM for a smaller domain achieved through nesting (Source Laprise et al. [31] © 2008 *Meteor. Atmos. Phys.*)

limited-area model. Unlike the evaluation of real-world simulations that depends on the fidelity of model physics and availability of observational data, the idealized BBE framework allows different nesting-specific issues (e.g., the relaxation treatment and width of the buffer zone, frequency of LBC update) to be evaluated regardless of limitations of model physics and data because deficiencies of the nesting approach can be identified and quantified based on the comparison of the LB and BB alone.

A series of studies using the BBE protocol has been performed, focusing on different modeling issues specific to the nested regional modeling approach. As summarized by Laprise et al. [31], the BBE shows that the LB is capable of generating small-scale features absent from the lateral boundary conditions, and the small-scale features are consistent with the BB. These results demonstrate that the nested regional climate modeling approach does work as designed. That is, given large-scale conditions provided by the GCMs at the lateral boundaries, the RCMs can downscale to produce finer scale features absent from the GCMs. Moreover, the fine scales produced by the RCMs are consistent with what the GCMs would generate if they were applied at similar spatial resolution as the regional models. However, the small scales are not uniquely defined by the lateral boundary conditions and the domain-specific regional forcings, as the interactions between the two can be sensitive to small perturbations in the initial conditions that alter the time evolution of the small scales. The variations produced in regional simulations by perturbations in the initial conditions have been called "internal variability," as they relate to internal processes rather than external or LBC forcings. This issue has also been investigated by others (e.g., [3, 9, 21, 27]) who found that model internal variability depends on factors such as seasons, atmospheric flow regimes, and domain size. This puts a caveat on using single member short (seasonal and sub-seasonal) RCM simulations for model evaluation or hypothesis testing, as internal variability may overwhelm the signals (e.g., model errors or model response to external perturbations) being sought.

To address the issue of internal variability, ensemble modeling with perturbed initial conditions can be performed to quantify the internal variability and its impacts on model errors or model response. Alternatively, different techniques have been developed to constrain the large scales simulated by the regional models by the global climate simulations or global analyses throughout the regional domains. Spectral nudging [2, 28, 44, 54] is one example of such techniques. With spectral nudging, both the regional climate simulation and the global analyses or global climate simulations that provide lateral boundary conditions are decomposed into different spectral components in space. The simulated large-scale spectral components are nudged toward that of the global data using relaxation to provide stronger large-scale constraints on the regional climate simulations than that imposed by the lateral boundary conditions alone. These methods reduce the mismatch between the simulated large scales and the imposed lateral boundary conditions that contaminate the regional simulations. They also reduce internal variability, so simulation with a single initial atmospheric condition may be sufficient to assess model errors or estimate model response to external forcings. On the other hand, the degree of nudging to be applied to constrain the large scales can be rather arbitrary. Also, one may argue that by nudging the large scales of the regional climate simulations toward the global climate simulations, these methods increase the dependence of the regional simulations on the skill of the global models and eliminate the potential for the regional models to improve the large scales through upscaling of mesoscale features that are better resolved by the regional models [43].

Besides some form of large-scale nudging applied throughout the regional model domain, some studies have proposed a different mode of simulating regional climate by applying regional climate models with frequent initialization of the atmosphere to simulate short time segments that are then concatenated to compose the long-term regional climate simulations [45, 47]. This method takes advantage of the time period of limited error growth shortly after model initialization so the mismatch between the simulated and imposed large scale is small even without additional constraints on the large scale in the interior of the model domain. Two-way nesting of global and regional models has also been proposed as an approach to reduce large-scale inconsistency that may develop in one-way nested regional climate models because the upscaled influences of the regional models are included in the global

models through feedbacks [40]. Such an approach has only been evaluated in a few studies [26, 41], and the results have been encouraging.

In summary, although the limited-area or nested modeling approach upon which regional climate models are based is an ill-posed boundary value problem, practical solutions such as the relaxation boundary treatment and spectral nudging of the large scale throughout the regional climate model domain have been developed and found to work well for a large number of cases. Furthermore, idealized experiments have confirmed most of the assumptions used in regional climate modeling [31]. However, uncertainty in regional climate simulations remain, owing in part to issues such as physics parameterizations, model resolutions, and initial conditions that are common to both global and regional climate models, and issues such as dependence on the lateral boundary condition, boundary treatment, regional domain size and location, and use of interior nudging that are specific to the nested regional modeling. Reviews and discussions of these issues can be found in Giorgi and Mearns [16], Laprise et al. [31], Leung et al. [35], and Wang et al. [55]. More research is needed to better understand the sensitivity of regional climate simulations to different factors and develop ways to reduce the uncertainty introduced by the nested modeling framework.

Evaluating Regional Climate Models

Model evaluation is important for assessing and documenting model skill and how it may evolve over time as changes and improvements are added to the models. It also provides information needed to understand model behaviors and diagnose model biases, and to assess uncertainties associated with the regional climate simulations. Model evaluation is achieved primarily by comparing model simulations with observations. The most common observation data used in evaluating regional climate simulations are atmospheric data such as 500 hPa height and upper level winds from global analyses, and surface temperature and precipitation from surface meteorological stations (e.g., Climatic Research Unit (CRU) and University of Delaware (UD) datasets), satellite-derived data (e.g., Tropical Rainfall Measurement Mission (TRMM)), and integrated station/satellite products (e.g., Global Precipitation Climatology Project (GPCP) [24] and Climate Prediction Center (CPC) Merged Analysis of Precipitation CMAP) [59]. These data are typically spatially interpolated to uniform latitude/longitude grids.

Both surface temperature and precipitation have high spatial variability due to surface topography and other factors. The effect of topography is relatively easy to account for in surface temperature as it varies with altitude more or less according to the standard temperature lapse rate, but its influence on precipitation is more spatially variable depending on a number of factors such as wind direction and surface slope and aspect. Statistical methods such as Parameter-elevation Regressions on Independent Slopes Model (PRISM) [7] have been developed to account for surface topographical effects in gridded precipitation data. There is a continuing need to develop high temporal and spatial resolution datasets for evaluating regional climate models. Recent efforts in Europe [22] and Asia [60] have made great strides in providing high resolution (0.1° and 25/50 km resolution for Europe and 0.25° and 0.5° for Asia) gridded daily precipitation data for model evaluation and analysis, although differences among datasets can still be substantial in mountain areas due to measurement methods, retrieval algorithms, grid resolutions, and whether topographic effects are explicitly accounted for.

By comparing observed and simulated surface temperature, precipitation, and atmospheric fields, model biases can be identified. However, determining the sources of model errors and thereby providing guidance on reducing model biases requires more information. Observations that can be used to diagnose model errors are more limited. For example, to understand model biases in surface temperature, it is useful to know which components (e.g., net shortwave and longwave radiation and sensible and latent heat fluxes) of the surface energy budgets may be in error. Ground-based measurements of the surface energy fluxes are limited both spatially and temporally. However, some flux data are available from a global network (FLUXNET) of about 400 micrometeorological tower sites that provide continuous measurements, some dating back to 1996. There is a challenge in relating point measurements of surface fluxes with model simulations that represent grid box averages. Satellite retrievals of

radiation fluxes are available globally for recent decades, but large differences exist among different datasets such as Clouds and the Earth's Radiant Energy System (CERES) and International Satellite Cloud Climatology Project (ISCCP).

Diagnosing errors in precipitation is even more challenging because precipitation is the end product of many interactive processes. Although precipitation is more directly related to clouds, measurements of cloud macrophysical and microphysical properties are limited. Cloud climatologies are available from ISCCP and CERES, but the grid resolution is relatively coarse (280 km for ISCCP and 1° for CERES) compared to regional models. Furthermore, errors in simulating clouds may be reflecting other problems because myriads of processes can influence the formation and evolution of clouds. Higher temporal and spatial resolution precipitation can provide a means to evaluate temporal variability from diurnal to seasonal, and probability distribution of precipitation rates, which can provide important clues to processes that may not be well represented in models. Some surface hydrological variables such as river runoff and snowpack may also be used to infer model biases in precipitation or combinations of precipitation and temperature biases.

Besides advances in the development of datasets for model evaluation, the methods used to evaluate models have also become more sophisticated. In the 1990s, comparisons of observations and model simulations were mostly limited to seasonal/annual and regional averages, but more studies now also compare observed and simulated temporal and spatial variability such as interannual variability and spatial distributions. With more studies producing longer regional climate simulations, more aspects of the simulations such as diurnal variability, extreme statistics, regime-specific features, frequency distributions, co-variability of different variables (e.g., between temperature and precipitation), and parameters that reflect the strengths of feedback processes have been evaluated (e.g., comparing land-atmosphere coupling strengths between models).

Although model evaluation studies are broadly aimed at understanding and quantifying model biases so model improvements can be made, some efforts also evaluate specific aspects such as precipitation and runoff [32], wind resources [57] of the regional simulations to provide practical guidance on their usefulness to provide climate information for impact assessments and resource management or planning. To support more detailed analyses, the requirements on model outputs have significantly increased as higher temporal frequency model outputs (e.g., hourly and daily) and more simulated state variables and tendencies are becoming more commonly archived.

Besides comparing model simulations with observations, model intercomparison can add significant information to understand and characterize model differences and uncertainties. The Atmospheric Model Intercomparison (AMIP) project [15] was initiated in the early 1990s to determine the systematic errors of global atmospheric models used to simulate long-term climate. Since the first AMIP project, many intercomparison projects have been developed to evaluate climate models used in different simulation modes. Similar coordinated projects have also been initiated to intercompare regional climate simulations since the mid-1990s. The first of such projects is the Project to Intercompare Regional Climate Simulations (PIRCS) [53]. PIRCS includes two phases, with the first phase focusing on simulations of two anomalous years, the 1988 drought and 1993 flood in the US Great Plains, and the second phase comparing multiyear simulations over North America. All simulations were driven by global reanalysis data and observed sea surface temperature. Besides regional climate models, one global stretched-grid model also participated in PIRCS for comparison between two dynamical frameworks for regional climate modeling. Following PIRCS, several intercomparison projects were developed to compare regional climate simulations over the Arctic (ARCMIP) (http://curry.eas.gatech.edu/ARCMIP/) and East Asia (RMIP) [14]. More discussions of intercomparison projects that focus on climate change simulations are provided in section "Dynamical Downscaling."

Applications of Regional Climate Models

Climate Process Studies

An important application of regional climate models is to advance the understanding of regional climate processes. In this context, regional climate models are often used to test hypotheses of how different regional

forcings or feedback mechanisms play a role in regional climate variability and change.

For example, Leung et al. [34] used long-term simulations of the western USA to investigate the role of topography on precipitation spatial distribution during El-Nino and La-Nina events. Comparing precipitation during El-Nino years with the 20-year simulated climatology, they found a positive-negative-positive anomaly pattern in the Olympic Mountains and the west side and east side of the Cascades Mountains in the US Pacific Northwest. The pattern was found to be a result of the interactions between the large-scale atmospheric circulation that are influenced by the ENSO conditions and the orientation of the mountains. With atmospheric flow assuming a more southwesterly rather than a westerly direction during El-Nino years, the rain shadow created by the north-south oriented Cascades Mountains is reduced, resulting in more precipitation reaching the lee side of the mountains. Such regional anomaly patterns are generally not found in global reanalyses or global climate simulations because of their coarser resolution, but are consistent with observed precipitation and streamflow anomalies in the region.

Hughes and Hall [25] performed regional climate simulations for the western USA to investigate large-scale and local controls on Santa Ana winds in Southern California. Using a simulation at 6 km resolution, their analysis showed that both large-scale anomaly corresponding to a high pressure over the Great Basins, and local thermodynamic forcing due to surface temperature gradient between the cold desert (Mojave Desert) and warm ocean create pressure gradients that drive offshore winds. The latter was found to be particularly important in determining the timing of Santa Ana winds, which occur more frequently during December when the temperature gradient between the desert and Pacific coast is the largest.

The role of soot on mountain snowpack and hydrology was investigated by Qian et al. [48] using regional climate simulations with and without soot deposition in western USA. Their study shows that soot-induced snow-albedo perturbations increase the surface net solar radiation flux during late winter to early spring. This increases the surface air temperature and reduces snow accumulation and spring snowmelt, causing a trend toward earlier snowmelt. Snow-albedo feedback was found to play an important role in amplifying the soot effects in the mountains.

Riddle and Cook [50] used regional climate simulations to study the mechanism of abrupt rainfall transition in the Greater Horn of Africa. The yearly monsoon jump of about 20° latitude during April and May was found to coincide with abrupt circulation changes associated with the Somali jet that develops during that time. The cross-equatorial branch of the Somali jet brings moisture to the southern slopes of the Ethiopian plateau, which then produces the abrupt rainfall transition in the region.

To investigate why temperature in the central USA has cooled by 0.2–0.8°C in the late twentieth century, instead of warmed as in most continental regions, Pan et al. [46] used a regional climate model and found that under a global warming scenario, increased moisture from the Gulf of Mexico due to warming and increasing occurrence of the Great Plain Low Level Jet (LLJ) in the south and decreasing occurrence in the north enhances atmospheric moisture convergence and cloudiness and precipitation in the central USA. These changes replenish soil moisture during summer, which increases late-summer evapotranspiration and suppresses daytime maximum temperature, and hence the "warming hole." Because of coarse resolution, most GCMs cannot simulate the observed "warming hole" in the late twentieth century.

Regional climate models also offer great potentials to understand the mechanisms of extreme events and their projected changes in the future. For example, Seneviratne et al. (2006) performed two regional climate simulations with and without land-atmosphere interactions to investigate the role of land-atmosphere feedbacks on heat waves in Europe. They showed that soil moisture – temperature and soil moisture – precipitation feedbacks increase summer temperature variability in central and eastern Europe. Under climate change, the region of stronger land-atmosphere coupling shifts northward in response to greenhouse warming to central and eastern Europe, and enhances summer temperature variability and increases the potential for more frequent heat waves in that region.

In the above examples, high resolution is important for the model to reproduce the observed climatology of temperature, precipitation, wind, or snowpack, which in the western USA, Europe, and the Greater Horn of

Africa depend strongly on regional orography. High resolution is also important for simulating soot deposition caused by anthropogenic emissions in cities being carried to the mountains downwind, or LLJ and its effects on cloudiness and precipitation. Successful simulations of the base states and model ability to simulate regional forcings and feedback mechanisms (e.g., snow-albedo, soil moisture – temperature feedbacks, LLJ – precipitation coupling) are critical for assessing their role in the observed regional climate phenomena.

Dynamical Downscaling

Dynamical downscaling is an important application of regional climate models, which aims to provide more spatially resolved climate predictions or projections provided by GCMs. Most of the downscaling applications to date are related to climate change projections. Early efforts described the use of an individual RCM to dynamically downscale climate change projections by a specific GCM. Typically only a single emission scenario such as the business-as-usual scenario (1% increase of CO_2 per decade) was used. Although GCMs generally produce simulations that cover preindustrial to 2100, RCM simulations are usually performed only for two time segments of 10–30 years corresponding to a current and a future time period.

Giorgi et al. [18] reported the first set of studies on using a regional climate model to dynamical downscale climate change scenario for Europe and the western Mediterranean basin. The GCM and RCM they used had a spatial resolution of R15 (about 400 km) and 70 km, respectively. The current and future climate corresponds to the equilibrium conditions simulated by the GCM using $1 \times CO_2$ (preindustrial level) and $2 \times CO_2$ (doubling of preindustrial level), respectively. Although the GCM generally reproduced the basic seasonal migration patterns of storm tracks, significant biases were also found in large-scale features such as the location and strength of the North Atlantic jet, cold tropospheric temperature and low tropospheric relative humidity, and underprediction of summer precipitation. Overall, the RCM was found to inherit most of the large-scale biases from the GCM, but the spatial distribution of temperature and precipitation was better simulated due to topographic effects. In addition, the RCM produced more spatially refined temperature and precipitation change scenarios. The RCM also simulated significant sub-GCM-scale changes in surface hydrological variables such as snow depth and runoff.

Following a similar approach, Leung and Ghan [36] used a regional climate model driven by GCM $1 \times CO_2$ and $2 \times CO_2$ simulations to produce climate change scenarios for the western USA. However, much more spatially resolved simulations of temperature and precipitation were produced by using a subgrid parameterization of orographic precipitation and vegetation [38,39]. This method divides a model grid cell into subgrid surface elevation and vegetation classes based on high resolution (1 km) DEM and vegetation data. The influence of topography and vegetation on atmospheric and land surface processes is represented through a parameterization that accounts for orographic effects on clouds, which then affect precipitation and surface hydrology. During postprocessing, surface temperature and precipitation, among other variables, simulated for each subgrid class are mapped geographically to 1 km resolution based on the DEM and vegetation data. This approach greatly improves the simulation of surface temperature, precipitation, and snowpack compared to the GCMs. Their results show that snowpack will potentially be reduced by up to 50% under a $2 \times CO_2$ scenario. They also found a strong elevation dependence of climate change signals in temperature, precipitation (amount and phase), snow cover, and runoff (see also [1,20] for a discussion of elevation dependence of climate change signals in mountainous regions).

In the 2000s, as more GCM transient simulations became available and the regional modeling community has grown, more studies have been published that investigated the potential effects of climate change in different climatic regimes or geographical locations. Figure 4 shows an example of cold season heavy precipitation (95th percentile) simulated by a GCM and an RCM driven by the GCM boundary conditions, using the same models described by Leung et al. [32], except for a change in the regional domain to cover the conterminous USA. Comparison of the simulated and observed heavy precipitation shows that the RCM reproduced the observed spatial distribution of heavy precipitation better than the GCM primarily because of the increased spatial resolution. As regional climate

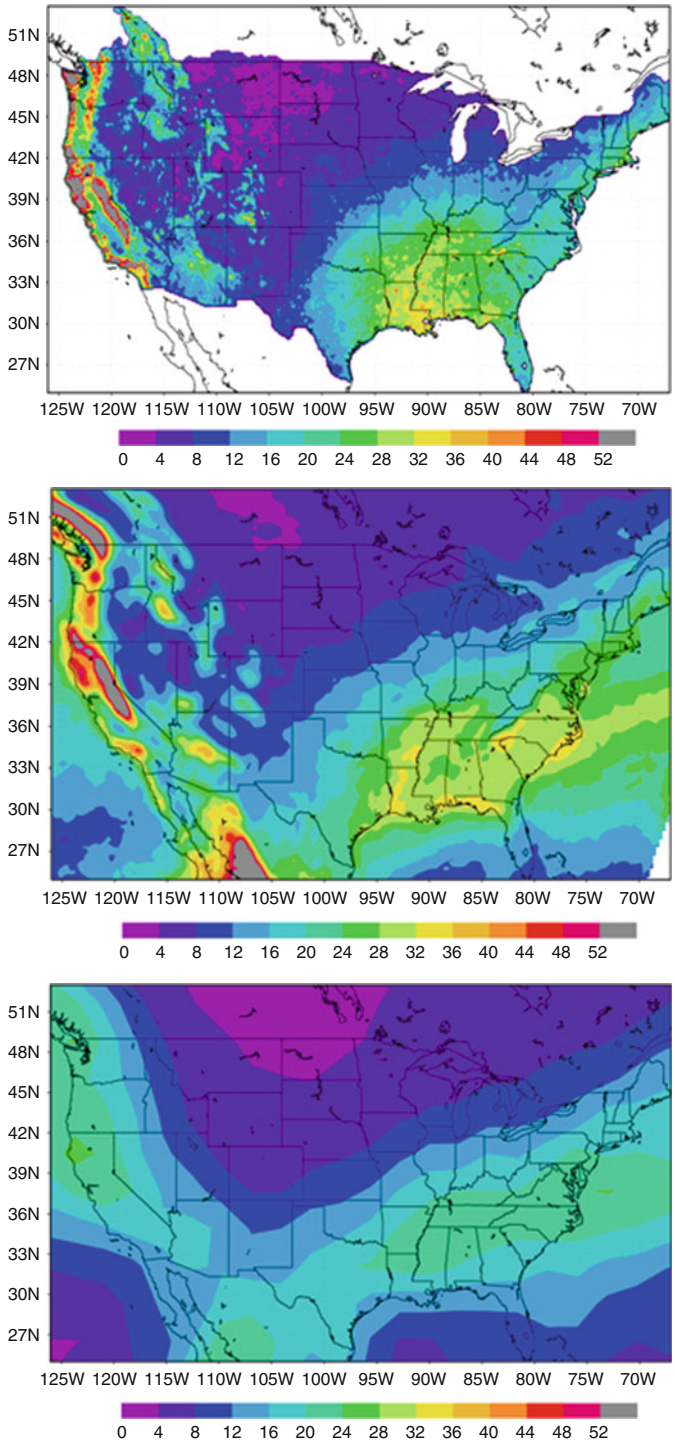

Regional Climate Models. Figure 4

An example of cold season heavy (95th percentile) precipitation simulated by a GCM (*Top*) and an RCM (*middle*) and comparison with observation (*Bottom*) over the USA. The prominent effects of topography are well captured by the RCM at 36 km grid resolution compared to the GCM, which was applied at roughly 250 km resolution

information is useful for assessing climate impacts and addressing climate adaptation, many studies that involve the use of regional climate models for producing regional climate change scenarios included scientists and stakeholders of the specific regions being studied to focus on subjects both scientifically interesting and societally relevant. The regional human resources and knowledge base that have been tapped have proven beneficial and contributed to more diverse analyses and applications of the climate change results. More examples of these efforts have been summarized in Christensen et al. [5].

Besides individual efforts of using a particular RCM to downscale climate predictions or projections from a particular GCM, larger efforts have also been coordinated to develop ensembles of dynamically downscaled simulations. Common to these coordinated efforts is the objective to fill the gap in providing regional climate change scenarios for different geographic regions and to improve the characterization of uncertainty of the scenarios. To this end, an ensemble modeling approach is used in which multiple RCMs are nested within multiple GCMs to generate a matrix of regional climate change scenarios to facilitate the interpretation and characterization of uncertainty of regional climate change. These efforts also enable large, multi-model datasets to be archived following common protocols similar to the AMIP and CMIP efforts adopted by the GCM community over the last two decades.

In Europe, two large coordinated projects, PRUDENCE [5] and ENSEMBLES [23], intercompared regional climate models driven by global reanalysis as well as global climate simulations for the current and future climate. PRUDENCE designed, executed, analyzed, and synthesized regional climate scenario development for Europe. In brief, four GCMs and ten RCMs were involved to produce regional climate scenarios at 50 km resolution, but a few scenarios at 20 km resolution were also produced. Two time slices were simulated by each RCM, corresponding to 30 years of control and future (2071–2100) conditions. Two emission scenarios, A2 and B2, were considered, and some GCMs and RCMs provided multiple ensemble members (using different initial conditions) for assessing internal variability. Although only 28 combinations out of the full matrix of GCM, RCM, and scenario combinations were performed, PRUDENCE provided sufficient model outputs to evaluate the variance due to the four sources of uncertainty: GCM, RCM, scenario, and sampling. Figure 5 summarizes the surface temperature and precipitation changes simulated by the regional models for Europe.

One of the main conclusions of PRUDENCE is that the largest source of uncertainty resides in the GCM boundary conditions applied to the RCM [11]. The choice of RCM becomes more important, however, for certain subregions or seasons (summer in particular). Furthermore, many local features and aspects of extremes can vary substantially between RCMs [30] to alter the climate change signal from that simulated by the driving GCM. For example, RCM simulations performed at higher resolution (12 km vs 25 km) reduced the magnitude of future summer drying over southern Europe [4]. This effect could be attributed to the diminished control of the LBCs on RCM simulations during summer, and the general tendency of RCM to produce more precipitation at higher resolutions (e.g., [33,49]).

Building on the foundation of PRUDENCE, ENSEMBLES is the largest and most comprehensive RCM comparison project conducted to date. Focusing again on Europe, ENSEMBLES utilized 15 GCMs and 11 RCMs to create a large GCM-RCM matrix for a single emission scenario (A1B). Simulations were also performed with reanalysis boundary conditions at 25 km and 50 km horizontal resolution. Interestingly, higher resolution (25 km vs 50 km) did not improve the simulation of large-scale weather types [51] or seasonal precipitation [49] by many RCMs, suggesting that physics and/or downscaling approach (i.e., dynamical framework) may be more important than resolution. The most novel aspect of the ENSEMBLES project is the construction and use of a set of metrics to weight models according to their performance to construct an ensemble mean [6]. However, application of the weights to the GCM-forced RCM simulations for the twentieth century did not substantially improve the performance of the multi-model temperature or precipitation mean over the unweighted multi-model mean when averaged over Europe. This suggests that more research is needed to further explore the productive use of ensembles of climate change scenarios to reduce uncertainty.

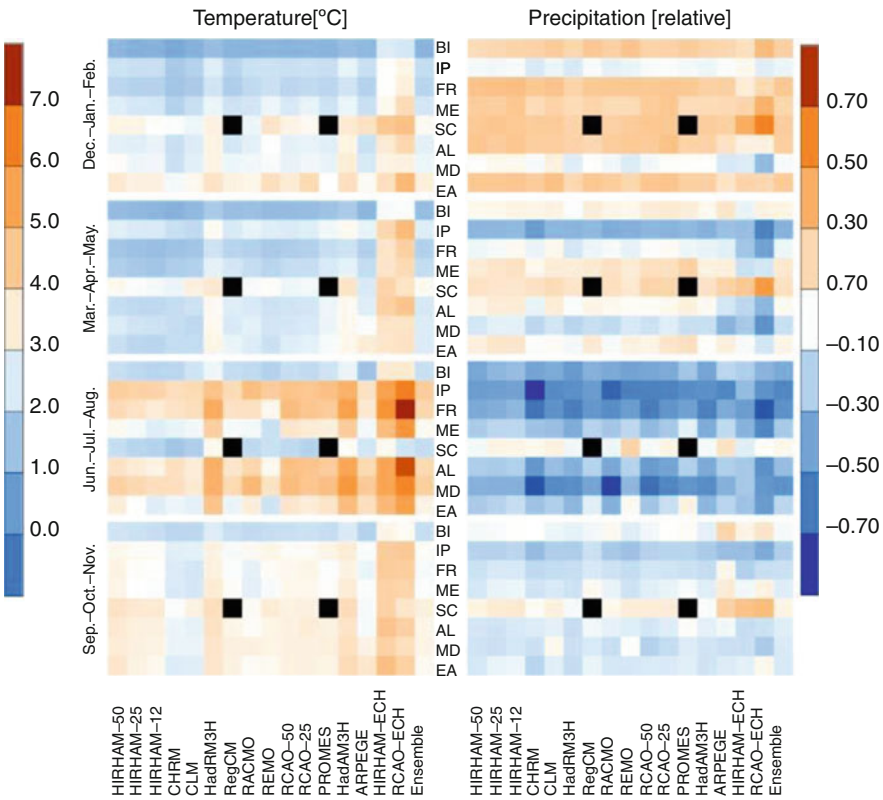

Regional Climate Models. Figure 5

An overview of seasonal changes in surface temperature (degree C) (*left*) and precipitation (relative change) (*right*) simulated by the PRUDENCE regional climate models for different analysis areas (row) and models (column). The analysis areas are: *BI* British Isles, *IP* Iberian Peninsula, *FR* France, *ME* Mid-Europe, *SC* Scandinavia, *AL* Alps, *MD* Mediterranean, *EA* Eastern Europe. Results from 17 regional simulations (some are produced by the same model at different resolutions) are shown, but some simulations did not cover certain geographical areas (shown by the *black squares*) (Source Christensen and Christensen [4] © 2007 *Climatic Change*)

The North American Regional Climate Change Assessment Program (NARCCAP) [42] is another coordinated project similar to PRUDENCE and ENSEMBLES, but with a geographic focus on North America. The NARCCAP GCM-RCM matrix includes mapping 4 GCMs with 6 RCMs statistically for a more balanced design for uncertainty analysis. In addition, two high-resolution time-slice global simulations are included for comparison with the RCM simulations over North America. More recently, CORDEX (a COordinated Regional Downscaling EXperiment) has been developed to coordinate regional climate change scenario development for all continents around the world, and to foster international collaborations and promote interactions and communications between the various communities involved in scenario development and applications. The CORDEX design is similar to the multi-GCM/RCM matrix used in PRUDENCE, ENSEMBLES, and NARCCAP, but an additional level of uncertainty being assessed is model dependence on climate regimes and/or geographic locations. Therefore, an important CORDEX effort is to develop and compare climate simulations across different continents. Additionally, CORDEX encourages the development of Regional Analysis and Evaluation Teams to develop a set of regionally specific metrics for model evaluation, collect observational data, design experiments to investigate the added value of RCMs, and evaluate the ensemble of simulations from CORDEX.

Besides climate change, dynamical downscaling has also been applied to the area of seasonal climate predictions, but to a much lesser extent compared to downscaling of climate change simulations. The Multi-Regional Ensemble Downscaling (MRED) is a coordinated project in which multiple RCMs were used to downscale global seasonal climate forecasts for the USA (http://ecpc.ucsd.edu/projects/MRED/). Dynamical downscaling has also been used to develop regional analysis for studying climate variability and trends. Unlike regional analysis such as the North American Regional Reanalysis that assimilates observation data in regional models driven by global analysis, the dynamical downscaling approach assimilates only global analysis, but no additional observational data within the regional model domains to generate regional climate information. As examples, Sotillo et al. [52] used a regional model to downscale global reanalysis to generate a high-resolution 44-year atmospheric analysis for the Mediterranean Basin. Kanamitsu and Kanamaru [29] used a regional climate model at 10 km resolution driven by a global reanalysis in the California Reanalysis Downscaling at 10 km (CaRD10) project to produce 57 years of regional analysis for California.

Although numerous studies that evaluated different aspects of regional climate simulations using observations have demonstrated some skill in simulating regional temperature and precipitation, the skill depends very much on the large-scale data used to drive the model, the model physics, and how the models were configured. More recently, besides asking what ability RCMs have in reproducing observed climate features, the question of whether dynamical downscaling adds values to global climate simulations has become an important topic. Essentially, this begs the question of whether the additional step of running regional climate models as a means to dynamically downscale global climate simulations indeed provides additional (useful) information not available from the global climate simulations. One way to address this question is to define and apply various metrics to quantitatively measure the added skill or added information provided by the regional models. For example, spatial filters can be used to partition the model-simulated variability to a larger scale that is resolved by the global simulation and a smaller scale that is beyond the limit resolved by the global simulation. The amount of finer scale variability generated by the regional models is considered value added since it provides climate information beyond what the global simulations provide (e.g., [12]). Similarly, spectral decomposition can be applied to simulated quantities such as different components of the surface water budgets and forecast skill to determine the added value of regional modeling.

Another aspect of evaluating the value added by RCMs is to compare dynamical downscaling with statistical downscaling, which is computationally a much cheaper method to produce regional climate information. To date, comparison of dynamical and statistical downscaling methods is limited to a few studies. Wood et al. [58] represent an early effort to apply a simple statistical downscaling method called Bias Correction Spatial Disaggregation (BCSD) to not only global simulations, but also regional climate simulations. The latter is a hybrid approach that combines dynamical and statistical downscaling. Comparing statistically downscaled simulations driven by global and regional simulations with the global and regional simulations, this study showed that hydrologic response to climate change can be enhanced using the hybrid approach compared to applying statistical downscaling directly to the GCM outputs because the RCM simulated larger warming in mountainous areas as a result of snow-albedo feedbacks, which are not captured by GCM or statistical downscaling.

Future Directions

In summary, both idealized experiments and real case applications have demonstrated that nested regional climate modeling is a viable approach for regional climate simulations. However, applications of regional climate models must be exercised with care because many factors can introduce uncertainty in the simulated results. These factors, which include domain size and location, physics parameterization, model resolution, lateral boundary condition and treatment, and use of interior nudging, must be carefully assessed before proceeding to long-term climate simulations. More research is also needed to better understand the sensitivity of regional climate simulations to those factors and develop ways to characterize and reduce

uncertainty introduced by the nested modeling framework. As computing resources allow global models to be applied at higher and higher spatial resolution, and alternative approaches such as global variable resolution models become feasible, more research is needed to evaluate and compare different approaches to modeling regional climate to establish their validity and usefulness in addressing different aspects of climate research and applications.

Acknowledgments

I would like to thank my colleagues at the Pacific Northwest National Laboratory and my collaborators over the years, whose research has inspired me. I also thank them for sharing their ideas, knowledge, and results with me.

Bibliography

1. Beniston M, Diaz HF, Bradley RS (1997) Climatic change at high elevation sites: an overview. Clim Chang 36:233–251
2. Castro CL, Pielke RA Sr, Leoncini G (2005) Dynamical downscaling: an assessment of value added using a regional climate model. J Geophys Res 110. doi:10.1029/2004JD004721, D05108
3. Caya D, Biner S (2004) Internal variability of RCM simulations over an annual cycle. Clim Dyn 22(1):33–46
4. Christensen JH, Christensen OB (2007) A summary of the PRUDENCE model projections of changes in European climate by the end of this century. Clim Chang 81:7–30. doi:10.1007/s10584-006-9210-7
5. Christensen JH, et al (2007) Regional climate projections. In: Solomon S, Qin D, Manning M, Chen Z, Marquis M, Avery KB, Tignor M, Miller HL (eds) Climate change 2007: the physical science basis, contribution of Working Group I to the Fourth Assessment Report of the intergovernmental panel on climate change. Cambridge University Press, Cambridge, UK/New York
6. Christensen JH, Rummukainen M, Lenderink G (2009) Formulation of very high-resolution regional climate model ensembles for Europe, chapter 5. In: van der Linden P, Mitchell JFB (eds) ENSEMBLES: climate change and its impacts: summary of research and results from the ENSEMBLES project. Met Office Hadley Centre, Exeter, 160pp
7. Daly C, Neilson RP, Phillips DL (1994) A statistical-topographic model for mapping climatological precipitation over mountanious terrain. J Appl Meteor 33:140–158
8. Davies HC (1976) A lateral boundary formulation for multi-level prediction models. Quart J Roy Meteor Soc 102:405–418
9. de Elía R, Laprise R, Denis B (2002) Forecasting skill limits of nested, limited-area models: a perfect-model approach. Mon Weather Rev 130:2006–2023
10. Denis B, Laprise R, Caya D, Côté J (2002) Downscaling ability of one-way-nested regional climate models: the Big-brother experiment. Clim Dyn 18:627–646
11. Déqué M, Rowell DP, Lüthi D, Giorgi F, Christensen JH, Rockel B, Jacob D, Kjellström E, Castro M, van den Hurk B (2007) An intercomparison of regional climate simulations for Europe: assessing uncertainties in model projections. Clim Chang 81:53–70
12. Di Luca A, de Elía R, Laprise R (2011) Assessment of the potential added value in multi-RCM simulated precipitation. Clim Dyn. doi:10.1007/s00382-011-1068-3
13. Dickinson RE, Errico RM, Giorgi F, Bates GT (1989) A regional climate model for the western United States. Clim Chang 15:383–422
14. Fu C, Wang S, Xiong Z, Gutowski WJ, Lee D-K, McGregor JL, Sato Y, Kato Hi, Kim J-W, Suh M-S (2005) Regional climate model intercomparison project for Asia. Bull Amer Meteorol Soc 86. doi:10.1175/BAMS-86-2-257
15. Gates WL (1992) AMIP: the atmospheric model intercomparison project. Bull Amer Meteorol Soc 73:1962–1970
16. Giorgi F, Mearns LO (1999) Introduction to special section – regional climate modeling revisited. J Geophys Res 104(D6):6335–6352
17. Giorgi F, Bates GT (1989) On the climatological skill of a regional model over complex terrain. Mon Weather Rev 117:2325–2347
18. Giorgi F, Marinucci MR, Visconti G (1990) Use of a limited area model nested in a general circulation model for region climate simulation over Europe. J Geohys Res 95:18,413–18,431
19. Giorgi F, Marinucci MR, DeCanio G, Bates GT (1993) Development of a second generation regional climate model (REGCM2): cumulus cloud and assimilation of lateral boundary conditions. Mon Weather Rev 121:2814–2832
20. Giorgi F, Hurrell JW, Marinucci MR, Beniston M (1997) Elevation signal in surface climate change: a model study. J Clim 10:288–296
21. Giorgi F, Bi X (2000) A study of internal variability of a regional climate model. J Geophys Res 105:29503–29521
22. Haylock MR, Hofstra N, Klein Tank AMG, Klok EJ, Jones PD, New M (2008) A European daily high-resolution gridded dataset of surface temperature and precipitation. J Geophys Res (Atmos) 113(D20119). doi:10.1029/2008JD10201
23. Hewitt CD, Griggs DJ (2004) Ensembles-based predictions of climate changes and their impacts. EOS 85:566
24. Huffman GJ, Adler RF, Morrissey M, Bolvin DT, Curtis S, Joyce R, McGavock B, Susskind J (2001) Global precipitation at one-degree daily resolution from multisatellite observations. J Hydrometeor 2:36–50
25. Hughes M, Hall A (2010) Local and synoptic mechanisms causing Southern California's Santa Ana winds. Clim Dyn 34. doi:10.1007/s00382-009-0650-4
26. Inatsu M, Kimoto M (2009) A scale interaction study on East Asian cyclogenesis using a general circulation model coupled with an interactively nested regional model. Mon Weather Rev 137. doi:10.1175/2009MWR2825.1

27. Ji YM, Vernekar AD (1997) Simulation of the Asian summer monsoons of 1987 and 1988 with a regional model nested in a global GCM. J Climate 10:1965–1979
28. Kanamaru H, Kanamitsu M (2007) Scale-selective bias correction in a downscaling of global analysis using a regional model. Mon Weather Rev 135:334–350
29. Kanamitsu M, Kanamaru H (2007) 57-Year California reanalysis downscaling at 10 km (CaRD10) part 1. System detail and validation with observations. J Climate 20:5527–5552
30. Kjellström E, Bärring L, Jacob D, Jones R, Lenderink G, Schär C (2007) Modelling daily temperature extremes: recent climate and future changes over Europe. Clim Chang 81:249–265
31. Laprise R, de Elía R, Caya D, Biner S, Lucas-Picher Ph, Diaconescu EP, Leduc M, Alexandru A and Separovic L (2008) Challenging some tenets of regional climate modelling. Meteor. Atmos Phys 100, Special Issue on Regional Climate Studies, 3–22. doi:10.1007/s00703-008-0292-9
32. Leung LR, Qian Y, Bian X, Washington WM, Han J, Roads JO (2004) Mid-century ensemble regional climate change scenarios for the western United States. Clim Chang 62(1–3):75–113
33. Leung LR, Qian Y (2003) The sensitivity of precipitation and snowpack simulations to model resolution via nesting in regions of complex terrain. J Hydrometeorol 4(6):1025–1043
34. Leung LR, Qian Y, Bian X, Hunt A (2003) Hydroclimate of the western United States based on observations and regional climate simulation of 1981–2000. Part II: mesoscale ENSO anomalies. J Clim 16(12):1912–1928
35. Leung LR, Mearns LO, Giorgi F, Wilby R (2003) Workshop on regional climate research: needs and opportunities. Bull Amer Meteorol Soc 84(1):89–95
36. Leung LR, Ghan SJ (1999) Pacific northwest climate sensitivity simulated by a regional climate model driven by a GCM. Part I: control simulations. J Clim 12(7):2010–2030
37. Leung LR, Ghan SJ (1999b) Pacific Northwest climate sensitivity simulated by a regional climate model driven by a GCM. Part II: 2xCO2 simulations. J Clim 12(7):2031–2053
38. Leung LR, Ghan SJ (1998) Parameterizing subgrid orographic precipitation and surface cover in climate models. Mon Weather Rev 126(12):3271–3291
39. Leung LR, Ghan SJ (1995) A subgrid parameterization of orographic precipitation. Theor Appl Climatol 52:95–118
40. Leung LR, Kuo Y-H, Tribbia J (2006) Research needs and directions of regional climate modeling using WRF and CCSM. Bull Am Meteorol Soc 87(12):1747–1751
41. Lorenz P, Jacob D (2005) Influence of regional scale information on the global circulation: a two-way nesting climate simulation. Geophys Res Lett 32:L18706. doi:10.1029/2005GL023351
42. Mearns LO, Gutowski W, Jones R, Leung R, McGinnis S, Nunes A, Qian Y (2009) A regional climate change program for North America. Eos Trans AGU 90:311–312
43. Mesinger F, Brill K, Chuang H, DiMego G, Rogers E (2002) Limited area predictability: can upscaling also take place? Research activities in atmospheric and oceanic modelling. Report No. 32, WMO/TD – No. 1105, 5.30–5.31
44. Miguez-Macho G, Stenchikov GL, Robock A (2004) Spectral nudging to eliminate the effects of domain position and geometry in regional climate model simulations. J Geophys Res 109(D13):D13104. doi:10.1029/2003JD004495
45. Pan Z, Takle E, Gutowski W, Turner R (1999) Long simulation of regional climate as a sequence of short segments. Mon Weather Rev 127:308–327
46. Pan Z, Arritt RW, Takle ES, Gutowski WJ Jr, Anderson CJ, Segal M (2004) Altered hydrologic feedback in a warming climate introduces a "warming hole". Geophys Res Lett 31: L17109. doi:10.1029/2004GL020528
47. Qian J-H, Seth A, Zebiak S (2003) Reinitialized versus continuous simulations for regional climate downscaling. Mon Weather Rev 131:2857–2874
48. Qian Y, Gustafson WI Jr, Leung LR, Ghan SJ (2009) Effects of soot-induced snow albedo change on snowpack and hydrological cycle in Western U.S. based on WRF chemistry and regional climate simulations. J Geophys Res 114:D03108. doi:10.1029/2008JD011039
49. Rauscher SA, Coppola E, Piani C, Giorgi F (2009) Resolution effects on regional climate model simulations of seasonal precipitation over Europe. Clim Dyn. doi:10.1007/s00382-009-0607-7. 28
50. Riddle EE, Cook KH (2008) Abrupt rainfall transitions over the Greater Horn of Africa: Observations and regional model simulations. J Geophys Res 113:D15109
51. Sanchez-Gomez E, Somot S, Déqué M (2008) Ability of an ensemble of regional climate models to reproduce weather regimes over Europe-Atlantic during the period 1961–2000. Clim Dyn 33(5):723–736. doi:10.1007/s00382-008-0502-7
52. Sotillo M, Ratsimandresy A, Carretero J, Bentamy A, Valero F, Gonzalez-Rouco F (2005) A high-resolution 44-year atmospheric hind-cast for the Mediterranean basin: contribution to the regional improvement of global reanalysis. Clim Dyn 25:219–236
53. Takle ES, Gutowski WJ Jr, Arritt RW, Pan Z, Anderson CJ, Silva R, Caya D, Chen S-C, Christensen JH, Hong S-Y, Juang H-MH, Katzfey JJ, Lapenta WM, Laprise R, Lopez P, McGregor J, Roads JO (1999) Project to intercompare regional climate simulations (PIRCS): description and initial results. J Geophys Res 104:19,443–19,462
54. von Storch H, Langenberg H, Feser F (2000) A spectral nudging technique for dynamical downscaling purposes. Mon Weather Rev 128:3664–3673
55. Wang Y, Leung LR, McGregor JL, Lee D-K, Wang W-C, Ding Y, Kimura F (2004) Regional climate modeling: progress, challenges, and prospects. J Meteor Soc Jpn 82(6):1599–1628
56. Warner TT, Peterson RA, Treadon RE (1997) A tutorial on lateral conditions as a basic and potentially serious limitation to regional numerical weather prediction. Bull Amer Meteor Soc 78(11):2599–2617
57. Winterfeldt J, Weisse R (2009) Assessment of value added for surface marine wind speed obtained from two regional climate models. Mon Weather Rev 137:2955–2965
58. Wood AW, Leung LR, Sridhar V, Lettenmaier DP (2004) Hydrologic implications of dynamical and statistical

approaches to downscaling climate model outputs. Clim Chang 62(1–3):189–216
59. Xie P, Yatagai A, Chen M, Hayasaka T, Fukushima Y, Liu C Yang S (2007) A gauge-based analysis of daily precipitation over East Asia. J Hydrometeor 8:607–626
60. Yatagai A, Arakawa O, Kamiguchi K, Kawamoto H, Nodzu MI, Hamada A (2009) A 44-year daily gridded precipitation dataset for Asia based on a dense network of rain gauges. SOLA 5:137–140. doi:10.2151/sola.2009-035

Remote Sensing Applications to Ocean and Human Health

Frank E. Muller-Karger
College of Marine Science, University of South Florida, St. Petersburg, FL, USA

Article Outline

Glossary
Definition of the Subject and Its Importance
Introduction
Future Directions
Bibliography

Glossary

Attenuation depth Attenuation depth is a measure of how far electromagnetic radiation including light can penetrate into a substance. It is the depth at which the intensity of the radiation falls to 1/e (~37%) of its original value immediately below the surface.

Diffuse attenuation coefficient The irradiance at a wavelength λ propagates over a distance (z) as determined by the diffuse attenuation coefficient. In aquatic environments, the diffuse attenuation coefficient is an indicator of the turbidity of the water.

Hyperspectral Hyperspectral data are collected by instruments called imaging spectrometers. These sensors are able to collect information from across the electromagnetic spectrum at a fine resolution of bands as narrow as 0.001 or smaller μm over a wide wavelength range, typically at least 0.4–2.4 μm.

Irradiance Irradiance is a radiometry term for the power of electromagnetic radiation per unit area at a surface. Irradiance is used when the electromagnetic radiation is incident on the surface, and it has units of watts per square meter (W/m^2).

Ocean color Ocean color is a general term used in the study of the biological and biogeochemical properties of ocean waters through remote sensing of the reflected and transmitted visible radiation. The "color" of the ocean comes from the interaction between light, water, and substances in the water, particularly phytoplankton (microscopic, free-floating photosynthetic organisms), detritus and inorganic particulates, and colored dissolved matter.

Radiance Radiance is a radiometric measure that describes the amount of light that passes through or is emitted from a particular surface area, contained within a given solid angle in a specified direction. It is used to characterize both emission and reflection from surfaces. The SI unit of radiance is watts per steradian per square meter ($W \cdot sr^{-1} \cdot m^{-2}$).

Thermal infrared radiation (TIR) Thermal infrared radiation refers to electromagnetic waves with a wavelength of between 3.5 and 20 μm. These waves are used to estimate the temperature of the surface of targets. This is a radiation typically emitted by objects as opposed to visible and short-wave infrared radiation which is part of the spectrum of sunlight reflected by objects.

Turbidity Turbidity is the relative clarity of a liquid and is an expression of the optical properties of water that causes light to be scattered and absorbed by particles and molecules rather than transmitted in a straight line through a water sample. It is a function of the concentration of suspended matter or impurities that interfere with the clarity of the water. Turbidity is a common index of water quality.

Visible, near infrared, and short-wave infrared (VIS, NIR, and SWIR) This broad band of electromagnetic radiation is used in remote sensing of the reflectance of the Earth. Light that is visible to the human eye is visible radiation (VIS) and encompasses a wavelength range from about 380–400 nm to about 760–780 nm. Near-infrared (NIR) radiation encompasses 0.75–1.4 μm in wavelength. The short-wave infrared (SWIR) is the wavelength range 1.4–3 μm. Together, this region of the spectrum is sometimes known as VSWIR.

Definition of the Subject and Its Importance

Remote sensing is defined here as the acquisition of information about an object without physical contact by way of recording or sensing devices mounted on aircraft, satellites, or simply sited on a high hill or bluff overlooking an area of interest. Ocean and human health is the general field that assesses conditions in the marine environment including estuaries that are relevant to the well-being of living resources and to the use of these resources and seawater by humans for amenities or the sustenance of life.

Remote sensing of environmental conditions in coastal and marine waters using space-based sensors has made great progress since the deployment of the Coastal Zone Color Scanner on the Nimbus 7 satellite in 1978. Remote sensing is an important complement to observations collected from field programs, because satellites provide estimates of a number of environmental parameters over large geographic areas (hundreds of square kilometers to globally) rapidly (in minutes), frequently, and periodically (often near-daily or better), and over the long term (in some cases, now upward of two decades). These observations support research, monitoring, and public outreach, providing a cost-effective complement to traditional monitoring efforts. Yet much work remains to be done to refine the technology to address the growing challenges to the health of marine ecosystems, including humans living within them, due to marine pollution, urban sprawl, overuse of resources, and changes in climate. This entry very briefly outlines the technologies used to conduct water quality assessments, including phytoplankton standing stock, turbidity, suspended sediment load, colored dissolved organic material (CDOM), diffuse light attenuation coefficients, temperature, salinity, wind stress, wave direction, amplitude and wavelength, and current speed and direction. The student and reader are encouraged to look for further detail on how to use these observations in the scientific and technical literature. A large number of international Earth-observing satellite missions are planned for the 2010–2025 time frame to monitor the marine environment. As part of this effort, a solid scientific base for remote sensing methods of marine pollution needs to be established, and multidisciplinary, international training programs need to be developed so that operational agencies can make effective use of these technologies. It is capable human resources that we are currently lacking the most.

Introduction

Satellite remote sensing of the Earth's environment has advanced significantly every decade since the late 1950s, when the first reconnaissance satellites were launched. There continue to be leaps toward more powerful personal computing, faster and more accessible global communication networks and media, standardization of a number of file formats, large and open-access databases, widely available photo-processing software, and online mapping and data visualization software including geographical information systems. These advances, combined with the growing computer literacy of broader segments of the world's population, permit the regular observation and application of several key terrestrial, atmospheric, and oceanic variables to understand how the environment changes at regional to global scales. Satellite-based sensors now routinely provide data that help interpret local environmental measurements in the context of large spatial scales, longer time frames, and of complex interactions between different processes. Satellite data facilitate the study of connectivity between ecosystems and human communities, of change against baseline environmental conditions over both small and larger geographic areas, and of possible natural or human-caused drivers of point and nonpoint sources of pollution and other threatening conditions.

This entry gives a brief overview of remote sensing applications in marine pollution, focusing on satellite instrumentation of singular interest, recent advances, and expectations for future directions. It is an update to the summary presented by Muller-Karger [1]. Only a few aspects of remote sensing can be presented here. For more detail on the history of the technology, the reader is referred to the references provided in that publication. While atmospheric pollutants are also relevant, here the focus is on detection of water properties or constituents in coastal regions.

Many relevant research efforts that provide a framework for analysis of the ocean's role in human health are coordinated by the International Geosphere-Biosphere Program (IGBP) and the World Climate

Research Program (WCRP). The Group on Earth Observations (GEO) has a 10-year plan (2005–2015) to implement a Global Earth Observation System of Systems (GEOSS) to connect remote sensing and users, fostering a global infrastructure to assess environmental change and its impacts on ecosystems including humans. A number of countries maintain space-based programs to map Earth resources and assess changes in the environment (Argentina, Brazil, China, several European countries as well as the European community, India, Israel, Japan, Russia, South Korea, the United States, and others). The Committee on Earth Observation Satellites (CEOS), which coordinates civil spaceborne observations of the Earth provides a useful online database on relevant missions, instruments, and measurements (http://database.eohandbook.com/). This database includes tables detailing mission dates, data characteristics, and applications.

Several national and international programs are also developing interfaces to facilitate merging of satellite data with other information to assist resource managers, policymakers, educators, and scientists. For example, NASA's SERVIR initiative integrates satellite observations, ground-based data, and forecast models to monitor and forecast environmental changes and to improve response to natural disasters. In 2006, the United Nations General Assembly agreed to establish the "United Nations Platform for Space-based Information for Disaster Management and Emergency Response Space-based Information for Disaster Management and Emergency Response" (UN-SPIDER), which seeks to further broaden access to space-based information to support disaster mitigation and response. Several other programs are being developed around the world, both by focused research efforts in academic institutions as well as by national and international government agencies. The reader is encouraged to follow the development of these global networks.

Measurable Variables

Remote sensing of the Earth's properties is based on the measurement of electromagnetic radiation reflected or emitted by a target. In terms of human health, all ocean waters are ultimately relevant as trends in global and regional ocean productivity and temperature are more than simply of academic interest. These tendencies, which can be assessed from space, may indicate large-scale changes related to climate variability [2–4]. They affect the pH of the upper ocean [5], affect lower trophic levels [6], and have impacts on higher trophic levels including fish [7, 8].

Estuarine, coastal, and continental shelf waters are directly relevant to human health. This is where much of the effort is concentrated on collecting resources from the ocean or to input our discharges. These waters support commercial and recreational boating, tourism, fisheries, and other industries and activities, and they receive materials from land either through rivers that drain inland areas, effluents from coastal cities, and from atmospheric deposition. There is a need to understand processes that change any factor in these waters that affect these uses, over both short and long time frames, as well as over short to synoptic space scales, including climate-scale changes.

While there had been some important attempts to apply remote sensing to coastal waters in the 1970s and 1980s, most of the research on coastal and estuarine waters conducted to date has been done more recently in the 1990s and the first decade of the new millennium. This research has focused on refining quantitative estimates of sediment load, turbidity or water clarity, algal concentration as a measure of eutrophication, detection of hydrocarbon slicks, and measuring temperature, bathymetry, and types of benthos. Studies by Epstein [9] highlighted the importance of remote sensing in addressing large-scale factors, including climate change, that promote the spread of disease in the coastal ocean.

Yet progress in the application of remote sensing to marine pollution, spreading of disease, or assessing the linkages between human and ocean health has been slow because few environmental parameters lend themselves to remote sensing. Often, these parameters are not easily measurable at the appropriate space and time scales. Pollution and disease vectors are time and again introduced to the marine environment at relatively small scales, and they disperse following complicated pathways. Limitations exist in observing these patterns using available satellite sensors, and the electromagnetic signal of the variables of interest is often masked or contaminated by other environmental factors. Clearly, the potential benefits of remote sensing

are large, considering the high costs of monitoring using only traditional methods, but much work is needed to refine the technology to address even basic marine pollution problems.

Progress in this field has been made through interdisciplinary studies of indicator parameters designed to detect pollution or conditions that promote pathogen growth or their vectors by proxy or through studies of dispersal processes. Such inferences are best made when measurements are based on physical principles and when users are aware of technological limitations. For example, present state-of-the-art technologies and methods still do not permit direct estimates of nutrient, heavy metal concentrations, or pH, despite some early reports suggesting that this is possible (cf. [10, 11], and numerous unpublished reports). In many cases, any correlation between remotely sensed parameters and these variables is site specific, ephemeral, and may be coincidental, necessitating statistical validation on a site-specific, image-per-image basis.

Phytoplankton standing stock, estimated in terms of chlorophyll or "pigment" concentration, is an important indicator of water quality. Among other relevant variables that may be sensed remotely are diffuse light attenuation coefficients, suspended sediment load, "turbidity," dissolved organic material (yellow substance), temperature, salinity, wind stress, wave direction, amplitude and wavelength, and current speed and direction. This entry provides a very brief overview of methods used to detect these variables.

Approaches

The most successful approach to remote sensing combines a variety of measurement platforms and data types, including automated in situ and shipboard observations for detailed ground truth and remote sensors to cover a range of spatial and temporal scales. Satellite and airborne remote sensing is typically limited to signals originating from the surface or "skin" of the ocean (microwave and infrared radiance) or, at most, a few attenuation depths from the surface of the sea (for visible light, the attenuation depth is the distance over which radiance decays by a factor of 1/e; c.f. [12]). It is therefore very important to obtain complementary measurements at greater depths to resolve one of the most important dimensions in the aquatic environments, namely the vertical. Similarly, since remote sensing only provides direct estimates of a few parameters, it is critical to establish the empirical or deterministic relationship with any proxy that may be used to asses ocean health.

Advances in telemetering of data from remote sampling sites and platforms (e.g., [13–15]) promise solutions to a range of environmental monitoring problems, including in situ measurement of chemical processes [16], contaminants [138], nutrient concentrations [17–19], precipitation [20, 21], bioluminescence [22–24], zooplankton and larger animals [25–27], light (c.f. [28–30]), and primary productivity, and other variables (see [31], and references therein). This is an area of active development that will provide important calibration and supporting data for remote sensing work, thus facilitating ground truth efforts.

The advantage of satellites is that they augment the scope of oceanographic studies by providing frequent and repetitive coverage of large spatial scales, and that the user is rarely involved in the complicated process of collecting the raw data [32]. Many of these synoptic time series now extend for many years, and decadal datasets are now available. This permits evaluation of anomalies relative to a specific time frame and comprehensive comparative studies. However, satellite data is voluminous, and processing is computationally intensive, which leads to trade-offs between spatial and temporal resolution. Spatial resolution is also sacrificed to improve radiometric sensitivity, which is critical because many signals are weak and because target identification is usually based on narrow features in reflectance spectra.

Aircraft, including helicopters and balloons, are platforms on which prototype satellite instruments are frequently tested. Instruments flown on aircraft provide finer spatial and temporal resolution than their satellite counterparts, flexible flight patterns and altitude, and short deployment times. These features frequently make aircraft the platform of choice during catastrophic pollution events (see, e.g., [33, 34]). However, aircraft fitted for remote sensing are expensive and often are not readily available, a situation that may be at least partially remedied by drone planes and helicopters. Also, while merging observations with navigation data has become easier, sunglint, surface wave patterns,

and contamination by unmeasured factors (e.g., cloud shadows, electronic aircraft system noise, calibration drift, etc.) are common.

Applications and Sensors

Since the 1970s, there have been significant advances in the development of sensors flown on international satellite missions and on aircraft to measure coastal, estuarine, and marine parameters of interest to ocean and human health. Extremely sensitive sensors are required to measure the visible sunlight reflected by materials suspended in the surface layers of the ocean or lying on the bottom in coastal waters shallower than about 20 m. Sensors finely tuned to specific infrared wavebands to which the atmosphere is relatively transparent are used routinely by many sensors to measure the temperature of lakes, coastal waters, and the world's oceans several times per day, both during daytime and nighttime. A number of microwave sensors are used to estimate wind and surface current speed and direction, temperature, ice cover, and even salinity. The satellite sensors therefore afford rapid, repeated, and synoptic assessment of a number of environmental parameters concurrently anywhere on the planet, at pixel resolutions that typically range between a few meters to hundreds of kilometers and at particular times of the day, at a relatively low or no cost to the user. Airborne sensors provide much higher spatial resolution spanning centimeters to meters and the ability to sample a particular time of the day, but logistics are expensive, and obtaining good data quality in aquatic environments is challenging.

Remote sensing data have been tested in a number of applications over the years. Many attempts have been made to link various observable parameters to factors that affect ocean and human health. Much work remains to be done with both historical datasets as well as observations from new sensors and combining data from various sensors and automated or discrete ground observation platforms. Today, the most significant application in coastal and marine observation remains the use of various sensors to characterize a number of environmental parameters concurrently over synoptic scales rapidly and repeatedly and within the context of long time series. This allows detection of change and anomalous conditions relative to some previous condition or arbitrarily constructed "climatology." Some applications are extremely useful but still as of yet mostly underutilized by the public, resource management officials, and the public health community. Some other applications have great potential, but as of yet they have not been proven and have been oversold. A few of these applications are described in the next few paragraphs under the headings of specific technologies.

Ocean Color Among the most useful indicators of water quality is ocean color. The color of the ocean is the result of the interaction between visible solar irradiance, water, and substances like phytoplankton, suspended sediment, colored dissolved organic matter, or with the bottom of the ocean. The color contains much information about the condition and health of water bodies [141].

Ocean color studies fall broadly under the category of aquatic bio-optics, and their objective is to gain insight on processes such as the distribution and dispersal of dissolved organic carbon, changes in oceanic primary productivity, targeting and identifying coastal phytoplankton blooms, conducting regional and global biogeochemical assessments, understanding changes in benthic communities in clear, shallow tropical coral reefs, and monitoring coastal water quality. Sensors with high, medium, and low spatial resolution have been used to develop and test applications to assess various parameters relevant to ocean and human health. Most attempts at using high spatial resolution sensors have not led to accurate assessments nor developed into widely used operational tools. At this stage, the best promise for remote sensing of biogeochemical processes in the coastal ocean remains with sensors that have high sensitivity and high dynamic range and frequent coverage. This restricts the type of sensors to those having narrow spectral bands, medium spatial and spectral resolution, repeat orbits that provide daily or near-daily observations, and well-calibrated visible radiance data, i.e., those that are commonly known as "ocean color" instruments.

An important issue that requires significant attention is the estimation of the atmospheric radiance seen by an ocean color sensor [35, 36]. Over 80–90% of the total visible radiance received by a satellite sensor looking at the ocean is due to atmospheric scattering

of solar radiation or specular reflection of light by the ocean's surface. These sources of radiance need to be estimated with high precision and accuracy exceeding 1% since an error of this order will lead errors that can exceed 10% in the water-leaving radiance. The water-leaving radiance is light backscattered by the water column, not by the surface, which is detected by a downward-looking sensor just above the surface. In addition, marine waters are dark compared to land, and coastal and estuarine waters are especially dark since materials suspended or dissolved in them typically absorb visible light strongly across the spectrum. Therefore, ocean color sensors have to be extremely well calibrated and have signal-to-noise ratios exceeding 500 to over 1,000 the typical radiance values observed over the ocean. Among the most used ocean color sensors are the following:

Satellite sensors (see CEOS; http://database.eohandbook.com/ for a complete list):

- Coastal Zone Color Scanner (CZCS; 1978–1986; NASA/USA).
- Sea-viewing Wide-Field-of-view Sensor (SeaWiFS; 1997–2010; NASA and Orbimage/GeoEye; USA).
- Moderate Resolution Imaging Spectrometer (MODIS on the NASA Terra and Aqua satellites; 1999 and 2000 launches and continuing in 2011).
- Medium Resolution Imaging Spectrometer (MERIS on the ESA ENVISAT satellite; 2002 launch and continuing in 2011).
- Ocean Color Monitor (OCM; on several ISRO Oceansat satellites; from 1999 and continuing in 2011).
- Visible/Infrared Imager/Radiometer Suite (VIIRS, planned for launch in late 2011 on the US National Polar-Orbiting Operational Environmental Satellite System Preparatory Mission/NPP and on the future Joint Polar Satellite System/JPSS with a planned launch date of 2015).
- Hyperion (on the NASA EO-1 satellite; launched in 2000 and continuing in 2011).
- Several other international missions.

Aircraft sensors:

- Airborne Visible/Infrared Imaging Spectrometer (AVIRIS).
- Compact Airborne Spectrographic Imager (CASI).
- Airborne Oceanographic Lidar (AOL).
- Several other research and commercial sensors.

Applications of Ocean Color Data Ocean color data permit a wide range of observations relevant to ocean and human health applications. Ocean color observations are of particular interest because of their ultimate utility in estimating the spatial distribution of stocks and rate of change of various organic carbon pools in the ocean, including those associated with living and detrital particulate materials and with colored dissolved organic matter. In addition, these data are useful for coastal applications including monitoring of suspended particulate and dissolved materials associated with river discharge and resuspension from the bottom and, in general, for assessing coastal water quality. This is accomplished primarily by retrieving chlorophyll concentration and absorption and backscattering properties of the water from spectral measurements of the surface reflectance of the ocean.

Attempts to quantify chlorophyll concentration, colored dissolved organic matter (CDOM) absorption, suspended sediment load, "turbidity," and the diffuse attenuation coefficient of light as an index of water clarity have been made using a variety of satellite sensors. Geographically, of particular interest are coastal and estuarine waters, where so many human activities are focused. River plumes often lack an infrared (IR) signature that distinguishes them from marine waters, especially as distance from the estuary increases. However, plumes are strongly colored relative to sea water. Ocean color sensors are characterized by their narrow spectral bands, very sensitive sensors, and spatial resolution of between ca. 250×250 m^2 and 1×1 km^2 pixels. The advantage of these sensors is that they cover areas $>10^6$ km^2 in only 2–3 min, with revisit times of 1–3 days.

The CZCS [37] proved the value of using ocean color satellite images for tracing plumes over long distances. CZCS bands were centered at 443, 520, 550, 670, 750, and 11,500 nm and sought to match chlorophyll absorption maxima and minima. The red channels allowed atmospheric correction. Since the CZCS was an experimental sensor, data coverage was not continuous, the instrument was less sensitive than required for coastal observations, and the calibration was hard to establish. In effect, the technology was extremely useful

to visualize, for the first time, global ocean phytoplankton biomass and river plume dispersal in the open ocean; the CZCS did not allow accurate estimates of coastal water colors, coastal chlorophyll concentrations, or turbidity. The CZCS ceased operating in 1986, leaving behind a very large data set [38].

Among the most relevant ocean and human health studies were the pioneering studies of Barale et al. [39]. They used the CZCS to help calibrate numerical simulations of the circulation of the Adriatic Sea and the Po River plume to provide information on seasonal dispersal of contaminants in the region [40, 41]. Maynard et al. (1987) then used the CZCS to map the dispersal of Yukon River water and that of smaller rivers in Norton Sound (Alaska) to determine the area of impact of potential pollutants on the northern Bering Sea. Holligan et al. [42] compiled an atlas of CZCS and AVHRR images to document advection and mixing processes in the North Sea, where human impact is intense.

In an attempt to outline seasonal circulation patterns of the tropical western Atlantic, the Caribbean Sea, and the Gulf of Mexico, and to evaluate the effect of nutrient inputs via rivers into these oligotrophic seas, Muller-Karger et al. [43, 44] illustrated the seasonal dispersal of the Amazon, Orinoco, and Mississippi river plumes. CZCS imagery showed the marked seasonal variability of these plumes. These papers illustrated the connectivity between distant locations in ocean basins, with river plumes often extending hundreds to over 1,000 km from their source. Müller-Karger et al. [45] also combined ocean color and infrared imagery (from the AVHRR) to trace eddies and other oceanic circulation features in the Gulf of Mexico. Müller-Karger et al. [45] and del Castillo et al. [46] used CZCS and SeaWiFS images to demonstrate that the Mississippi plume does not always disperse to the west of the Mississippi Delta but that it also disperses to the east and south in the Gulf of Mexico and that it can reach the Florida Keys and disperse along the eastern seaboard of the USA. The significant river influence over shelf areas can be appreciated in satellite images of many river deltas and river plumes. These studies laid some of the groundwork for analyses of potential dispersion pathways of contaminants like oil.

There effectively was a 10-year gap between the end of the CZCS mission in 1986 and the resumption of ocean color observations with the Japanese OCTS on the ADEOS-I mission. The field of ocean color research and applications moved forward significantly with the launch of the SeaWiFS sensor in 1997 shortly after the failure of the ADEOS-I satellite, and the MODIS and MERIS sensors in 1999 and 2000 as the twenty-first century began. Oceanic remote sensing moved toward complex and multidisciplinary studies of environmental change over a wide range of time and space scales. These studies merged observations from various satellites. A concerted effort was initiated to understand coastal and turbid waters [47].

The differences between sensors and missions are considerable, ranging from orbit and ground revisit time to swath width, spectral and spatial resolution, sensitivity, accuracy, and so on. Examining each is beyond the scope of this review. For the purposes of illustrating applications, NASA's Moderate Resolution Imaging Spectroradiometer (MODIS, [139]) and Orbimage's SeaWiFS [144] are focused on because of their multiyear time series, global coverage, and their high-quality observations. The SeaWiFS sensor ceased operations in 2010. MODIS sensors continue data collections, and all data from the CZCS, SeaWiFS, and MODIS satellite sensors are public. The MODIS model is of particular interest because it is the prototype for the Visible/Infrared Imager/Radiometer Suite (VIIRS), which will fly on the US National Polar-Orbiting Operational Environmental Satellite System Preparatory Mission (NPP) and the future Joint Polar Satellite System (JPSS).

The overall accuracy of retrieved geophysical parameters (water leaving radiance, CDOM absorption, chlorophyll concentration, etc.) depends on the performance of the atmospheric correction and in-water algorithms. Of primary concern are sensor calibration and characterization. Errors in water-leaving radiance estimates can easily by exacerbated or exaggerated in coastal and estuarine waters because the blue water-leaving radiance is often much smaller than that in clear ocean waters. Significant research has focused on improving the traditional multiband chlorophyll retrievals. The MODIS and MERIS sensors are also equipped with spectral bands specifically designed for measuring chlorophyll fluorescence relative to a baseline (chlorophyll fluorescence line height algorithm; [48]). The chlorophyll fluorescence efficiency

varies in time and space, which is an area of research. Aggregating such data with those from other bio-optical algorithms helps address high-chlorophyll coastal waters (e.g., [49–51]). Unfortunately, the VIIRS sensor lacks the capability to detect this solar-stimulated fluorescence, limiting its capability for coastal observations relative to MODIS and MERIS.

Water constituents are estimates based on the water-leaving radiance. Algorithms related to biological oceanographic properties are referred to as "bio-optical" algorithms. For Case I waters, where one variable (phytoplankton) dominates color, a band-ratio (blue/green) bio-optical algorithm is often effective to estimate chlorophyll-a concentration because phytoplankton absorbs more blue light than green. Robust band-ratio algorithms have been used for CZCS [52], SeaWiFS, and MODIS [53]. In turbid coastal waters where constituents do not co-vary and phytoplankton does not dominate water color, band-ratio algorithms often fail (e.g., [50]). Semi-analytical algorithms may help in these cases [54–57]. The objective is to differentiate between various constituents, namely chlorophyll, colored dissolved organic matter (CDOM), and total suspended solids (TSS). While some progress has been made over time (e.g., [50]), assumptions need to be fine-tuned regionally, as Case II waters vary in space and time. Examples of parameters that are difficult to estimate but that are required in these optical models are the spectral slope of CDOM absorption, particle backscattering, bottom reflectance, and depth.

There has been significant progress in estimating and mapping the distribution of colored dissolved organic matter in the oceans (see [58–60], and references therein) and in coastal waters. The work of the SWFDOG group [49] illustrates the importance of using time series of satellite images to detect and track anomalies in coastal water quality. They detected an event off western Florida, USA, which the media called a "black water" event and which caused significant anxiety among local coastal residents, divers, and fishermen. Daily SeaWiFS data collected between September 1997 and August 2002 showed this unique event that lasted over 4 months. The "black water" was advected into the Florida Keys National Marine Sanctuary, where it led to the death of corals and sponges. By tracking the event, it was possible to determine that the extensive dark water patch evolved from a senescent bloom that was stimulated into activity again by local river input. The dark color of the water was due to high concentrations of CDOM and decreased backscattering. A field survey showed chlorophyll concentration was 5–10 mg m^{-3} due to a nontoxic diatom (Rhizosolenia) bloom.

While chlorophyll is a parameter desired by many coastal managers, it remains very difficult to estimate with sufficient accuracy in coastal and estuarine waters. A small error in CDOM assessment significantly affects blue absorption estimates and causes large errors in chlorophyll retrievals. For example, the CDOM absorption coefficient at 443 nm in an estuarine area may be $0.3-0.4\ m^{-1}$ or larger, while a chlorophyll concentration $\sim$1 mg m^{-3} effects an absorption coefficient of 0.03–0.04 m^{-1} at 443 nm. Thus, a 10% error in CDOM estimates leads to 100% errors in chlorophyll estimates. Throughout the "black water" and other similar events off western Florida, it was possible to differentiate between coastal plumes that contained a phytoplankton bloom and those that were dominated by CDOM by examining both the blue and green water-leaving radiance bands of SeaWiFS and MODIS and the fluorescence line height (FLH) images from MODIS [50].

Satellite ocean color sensors have shown great advantage over traditional means to monitor the spatial extent and duration of harmful algal blooms (HAB) or red tides. The state-of-the-art primary indicator of a bloom (toxic or not) is high chlorophyll concentration. At present, there is still no reliable algorithm to discriminate between red tides and other blooms, such as one dominated by diatoms or by other nontoxic phytoplankton. For example, during Alexandrium blooms which occur in the Gulf of Maine off the northeastern United States, these organisms co-occur with significant quantities of other phytoplankton, and therefore, waters do not seem to have a particular spectral signature that would allow identification of this HAB.

Chlorophyll concentration has been used as a proxy to build a crude operational monitoring tool for Karenia blooms off Florida (e.g., [61]). However, reliable estimates of chlorophyll concentration in these coastal waters have not been achieved, and bio-optical algorithms are still the focus of intense research [62–64]. A fundamental difficulty is the presence of CDOM since a small error in CDOM estimates

generates large errors in computed chlorophyll values. A positive chlorophyll concentration anomaly also does not represent proof positive of a red tide bloom. Therefore, false positives are inevitable, particularly during periods of higher river discharge or when other blooms occur. At this stage, the capability to detect an anomalous chlorophyll concentration provides an important advantage in planning proper field surveys and other responses by resource managers.

Great expectations revolve around identification of phytoplankton species by spectral analyses combined with other environmental observations [65, 140]. A recent study, for example, found that the backscattering to chlorophyll ratio is generally lower in *Karenia brevis* blooms relative to other blooms [66]. The proposed explanation is that this species experiences less grazing. How to take this scientific discovery to an algorithm and into an operational system is being investigated.

A useful and important application of remote sensing data is the assessment of suspended solids in aquatic environments. High concentration of suspended matter is an indication of erosion, resuspension of benthic sediments that may have contaminants, or of eutrophication due to a variety of causes. This condition also blocks sunlight from reaching benthic algae and sea grass, negatively affecting the health of coastal and estuarine waters. Turbidity is an index of light attenuation and water quality commonly used in estuarine and coastal areas. Several studies have demonstrated the utility of remote sensing to estimate turbidity in coastal, turbid waters. Miller and McKee [67] used MODIS 250 m data to assess total suspended matter in Lake Ponchartrain and adjacent waters in Mississippi, USA. Chen et al. [68, 69] and Moreno et al. [70] examined time series of 250 m MODIS images of Tampa Bay and showed that the synoptic satellite observations, collected every 1–3 days, are an important complement to the monthly water quality sampling program carried out in the bay. They illustrated rapid changes in spatial and temporal water clarity and turbidity conditions that were missed by the in situ surveys and were able to explain turbidity changes related to tidal, wind-driven, and discharge events. Rodríguez-Guzmán and Gilbes-Santaella [145] used 250 m MODIS data to estimate suspended matter concentrations in Mayaguez Bay, Puerto Rico. Similar studies have been conducted in France by Doxaran et al. [71].

An interesting conceptual framework for coastal ocean and human health applications was defined by Lobitz et al. [72] and Colwell [73], who identified a need for synoptic observations of phytoplankton blooms and sea surface temperature to help assess the potential for cholera outbreak conditions in coastal and estuarine waters. Colwell [73] and Hu et al. [74] further made the case that climate change affects the distribution and frequency of diseases, many of which spread along coastal zones with biological carriers. Colwell [73] found that the spread of the phytoplankton blooms and associated cholera outbreaks throughout the tropical and subtropical Pacific Ocean coasts of South America were associated with El Niño-Southern oscillation events. Hu et al. [74] found a linkage between climate variability, as quantified by the Southern Oscillation Index (SOI), and dengue fever epidemics in Queensland, Australia. They found an increase in the numbers of dengue fever cases 3–12 months after a decrease in the average SOI (i.e., warmer conditions).

Several attempts have been made to use the Advanced Very High Resolution Radiometer (AVHRR) on the NOAA Polar Orbiters to estimate coastal and oceanic water quality parameters [75–77, 146, 147]. The AVHRR (see [78]) has a nominal pixel resolution of 1×1 km and near-infrared bands that are sensitive to reflected sunlight and which have a dynamic range that accommodates the high reflectance of land and coastal waters. Since it is an operational facility, data are available several times a day, worldwide. Stumpf et al. found that when calibrated with concurrent in situ observations, individual AVHRR images provided information on sediment load and phytoplankton concentration in estuaries. They point out that the technique can be improved by correcting for atmospheric effects.

While the moderate-resolution class of ocean color and near-infrared sensors (historically, the CZCS, SeaWiFS, MODIS and MERIS, and AVHRR) allow observation of large-scale phenomena, there is a need for high spatial resolution data to address local marine pollution problems. Landsat data from the Thematic Mapper class of sensors are available for many areas around the globe since the mid-1980s and are now free

to the public and distributed by the United States Geological Survey (USGS). Attempts to map coastal and oceanic water quality parameters have been made since the 1970s, initially using Landsat sensors ([79–85]; and others). Use of Landsat and the French SPOT sensors has grown rapidly because they provide pixel resolutions of 30–80 m in spectral mode. They have been used to map suspended sediment and variations in water color in the nearshore environment [81, 84, 86–89, 143].

Since the late 1990s, higher spatial resolution imagery from several commercial satellites has become available, although at considerable cost to the user. These data are used extensively to map general land features, for urban and land-use planning, resource assessment, and disaster response efforts. Hellweger et al. [90] provide an example of the utility of high-resolution (1 m IKONOS) multispectral satellite imagery for estimating water quality patterns in the lower Charles River (Boston, USA), with limited results. Single image applications do not satisfy coastal and ocean health studies or applications. These important applications will continue to be limited as long as the data remain costly because building any time series and/or climatology against which to assess change is prohibitively expensive.

However, compared to the ocean color sensors mentioned above, past Landsat-class sensors have broad bands; for example, the "blue" channel on Landsat TM and ETM + (0.45–0.52 μm) spans the blue chlorophyll absorption peak and blue-green shoulder, the "green" band (0.52–0.60 μm) spans part of the blue-green shoulder, the green absorption minimum, and the green-yellow shoulder. SPOT lacks blue bands. The Landsat Data Continuity Mission (LDCM), planned for launch in late 2012 or 2013, includes a new Coastal/Aerosol band spanning 0.433–0.453 μm. This will be a very important tool in coastal resource assessment.

Most attempts to evaluate concentrations of in-water constituents with Landsat or SPOT have been based on scene-specific, concurrent in situ observations to provide a statistical base. In general, good qualitative information may be obtained in the immediate nearshore environment (e.g., [91]). At best, they may provide similar information to that derived from the AVHRR in highly turbid environments using red and near-IR bands but with much better spatial resolution [92]. The high cost of these data and the long revisit times (8–17 days due to orbital characteristics and narrow swaths) precludes detailed time series analyses or even use as monitoring tools.

Two significant advantages of Landsat-class data are that historical data are available since the mid-1980s and this allows comparison of a number of parameters including shoreline location and that Landsat data are now free of cost. However, Landsat and most other high spatial resolution sensors data provide only a limited capability to conduct systematic studies of waterborne constituents such as phytoplankton or sediment concentration either in coastal zones or elsewhere because of the limited radiometric, geometric, and revisit characteristics of the sensors. They are not well suited for quantification of aquatic chlorophyll in open waters and much less in areas of high chlorophyll because of the problems listed above. An important issue is the very high-cost per square kilometer of data for data from most of the commercial high-resolution sensors. These data are of great interest to the science community, but research using these data has been hampered by their cost.

One of the most exciting developments of the last decade is the availability of data from a series of proof-of concept hyperspectral satellite sensors. Hyperspectral data provide a significant improvement over the traditional multispectral sensors that provide between four and ten bands in the visible to differentiate between various optically active constituents present in coastal and estuarine waters [93]. The most widely accessible sensor is the NASA Hyperion sensor, launched in 2000 aboard the EO-1 proof-of-technology satellite. Hyperion collects images in 220 spectral bands at 30 m resolution, compared to the ten multispectral bands flown on traditional Landsat missions. The instrument collects images spanning 7.5 km by 100 km. The Hyperion data are new to coastal water quality assessments. Brando and Dekker [94] tested the Hyperion data and found that the sensor sensitivity is sufficient to estimate colored dissolved organic matter, chlorophyll, and suspended matter in Moreton Bay, an estuary in Australia. The Hyperspectral Imager for the Coastal Ocean (HREP-HICO; [95]), installed aboard the International Space Station since 2009, operates a visible and near-infrared (VNIR) Maritime

Hyperspectral Imaging (MHSI) system. The goal is to detect, identify, and quantify coastal geophysical features and to test algorithms for water clarity, chlorophyll content, water depth, and ocean or sea floor composition for civilian and naval purposes.

Aircraft Sensors Aircraft instruments play an important role in monitoring aquatic pollution at small scales. The AVIRIS, flown on NASA's ER-2 high-altitude aircraft (a U2), provides 224 bands of visible/infrared data at ~20 m resolution [96–98]. Its sensitivity for detecting variations in water-leaving radiance is relatively low but adequate where highly reflective constituents occur. Karaska et al. [99] used AVIRIS images of the Neuse estuary in North Carolina to estimate the concentrations of chlorophyll, suspended matter, CDOM, and turbidity and created an index of eutrophication for these waters. Bagheri and Yu [100] applied similar techniques to map water quality in the Hudson/Raritan estuary.

Another aircraft instrument is the FLI, also called the Programmable Multispectral Imager (PMI), of Moniteq Inc., Canada [101]. Dekker et al. [102] examined variations in eutrophication of the Loosdrecht Lakes in the Netherlands with the PMI and concluded that this instrument was ideally suited to examine distribution of pigments because of its high spatial resolution and sensitivity at long wavelength bands (ratios of bands between 600 and 720 nm were needed).

Among popular aircraft instruments used for water quality monitoring is the CASI of Moniteq Inc., Canada [103, 104]. Unlike others, this instrument is well calibrated, small (about the size of a personal computer), and may be used in an "imaging" mode with a few selectable bands or in a "spectral" mode in which a few pixels are collected for 288 bands between 450 and 950 nm for limited "look directions." The applicability of the CASI to marine pollution problems still needs to be better documented.

Active sensors, namely those which illuminate a target and measure electromagnetic radiation returned to the system, also show promise in water quality studies [105]. Among the most prominent is the NASA AOL. The AOL can be operated in a LIDAR mode (time gated) or as a multispectral analyzer with or without a fixed time (depth) delay [32]. This laser sensor presents many advantages, among which are specificity of response, relative simplicity of signal interpretation, low-altitude operation (including below cloud ceiling), and the potential of providing depth distribution of relevant variables by time-gating laser pulses [32]. Hoge and Swift [106] demonstrate the high correlation between fluorescent return and chlorophyll. This instrument is also useful for mapping horizontal and vertical turbidity variations [107].

Other Measurable Variables

Oil Spills, Surface Organic Slicks, Surfactants, and Yellow Substance Traditional remote sensing techniques to address oil spills in aquatic environments include optical (passive visible and infrared, laser fluorosensors), and passive and active microwave (e.g., Synthetic Aperture Radar, SAR) using aircraft or satellites (see [108, 109, 148, 149]). Most of the satellite SAR sensors and the various airborne sensors used to detect oil at the surface of the ocean are expensive and do not provide the required high-frequency coverage. The MODIS sensors include bands that generate images at 250 and 500 m spatial resolution. These have great unexploited potential for coastal monitoring because they can be used to study small-scale features. One application is in assessments of oil spills and water quality where 1-km satellite data are often inadequate. One example was illustrated by Hu et al. [51]. The medium-resolution (250- and 500-m) MODIS Level-1 total radiance imagery from 1 December 2002 to 9 March 2003 was examined, and patterns were found within Maracaibo Lake that is suspected to be extensive spill patches; the presence of oil was confirmed by the ground surveys.

This experience was important as it helped to rapidly implement the use of MODIS and MERIS data to map surface oil features during the British Petroleum Deepwater Horizon (BP DWH) disaster in 2010. Satellite remote sensing was essential in mapping and tracking surface oil dispersal during this event (Muller-Karger, 20 May 2010, testimony before the House Subcommittee on Energy and Environment, US Congress). Exploring the promise of this technology is important to understand the potential of the VIIRS imaging bands on the NPP and JPSS satellite platforms.

Organic films on the ocean surface can be detected and mapped by laser light [110]. In 1978–1979, a series

of oil spills were made off Sandy Hook, New Jersey, in waters >40 m depth. These spills were treated with helicopter-deployed dispersants containing surfactants soon after deployment and overflights with the NASA AOL were used to map the spills [111]. The results show that Raman backscatter strength can be related to oil-film thickness after removal of background and oil fluorescence contributions [111, 112]. Laser light can also be used to determine the spatial distribution of dissolved organic material in marine and estuarine environments [113, 114].

Infrared imagery such as that of the AVHRR has also proved useful to trace very large oil spills. During the Persian Gulf War of January–March 1991, oil slicks could be traced off the coast of Kuwait as sea surface temperature (SST) anomalies in the nighttime imagery. Such patterns were undetectable in the daytime AVHRR imagery (O. Brown, U. Miami, personal communication 1991).

Oil contamination of the Persian Gulf could also be traced in handheld photography collected by Space Shuttle astronauts [115]. During the Iran-Iraq war, oil slicks emanating from burning oil tankers and drilling platforms along the Iranian coast could be seen in the photography. Similarly, oil released from Kuwaiti loading facilities and oil fields during the 1991 Gulf war could be seen spreading along the Kuwait and Saudi Arabia shorelines in sunglint photography.

Microwave sensors also have an application in monitoring oil pollution in the ocean. In particular, the SURSAT (Surveillance Satellite) program, implemented in 1977 by the Canadian government, proved the utility of microwave sensors in monitoring ocean traffic, ice coverage, weather, and ocean pollution [116]. SURSAT provided the basis for participation by Canada in the US SEASAT program. The NASA SEASAT satellite, which operated between 26 June 1978 and 10 October 1978, was a test-bed for a variety of ocean-looking instrumentation. Among the most successful instruments was a Synthetic Aperture Radar (SAR), with 25 m resolution, which seemed able to detect oil spills. However, the subtle distinctions between oil slicks and natural phenomena resembling oil slicks require further work [116, 117].

Temperature Satellite instruments designed to measure sea surface temperature (SST) are among the most successful for both research and operational applications. Several instruments now provide routine, daily coverage of the world's coastal and marine environments, including the NOAA and MetOP AVHRR, and NASA MODIS. They provide observations that facilitate tracing of circulation features of spatial scales ranging from 10 to 1,000 km (c.f. [45]). These sensors are also used to track weather patterns and map land vegetation indices [118, 119].

An important application of satellite SST is detection of temperature extremes in coastal environments [120, 121]. Temperature variability can both enhance the resilience of coastal and marine organisms, but both cold and warm extremes can be fatal. Soto [122], for example, documented larger benthic coral reef cover in coastal areas of the Florida Keys, USA, where SST variability was larger than where SST was more stable. Satellite images are now also routinely used to assess areas around the world at risk of coral reef stress due to high-temperature anomalies [123].

Temperature contamination frequently occurs at smaller scales (<<100 km) as a result of industrial discharge, and the sensors with 1 km spatial resolution such as the AVHRR and MODIS are generally inadequate to resolve these scales. The Landsat TM and ETM + sensors provide a useful tool to assess surface temperature of aquatic environments at such scales, with Thermal Infrared (TIR) data at 60 m pixel resolution. For example, Thomas et al. [124] and Fisher and Mustard [125] used Landsat data to study sea surface temperature patterns off the coast of New England, USA. These studies demonstrated that it is possible to assess the dominant seasonal patterns in cross-shelf SST gradients at scales of small embayments and estuaries in coastal zones around the world. A limitation remains the repeat cycle of the Landsat-class satellites, i.e., every 16 days.

An instrument that provides higher resolution is the Precision Radiometric Thermometer Model 5 (PRT-5), deployed from aircraft or even ships. This sensor provides an operational capability to map along-track SST.

Salinity Remote sensing of sea surface salinity from aircraft and satellites, using microwave radiometers tuned to frequencies of order of 1 GHz, has been limited primarily by the poor spatial resolutions obtained with conventional microwave antennas

(i.e., >500 km from satellites). Proven aircraft capabilities are accuracies <10 practical salinity units and 0.2 units in resolution. Lagerloef et al. [126] discuss synthetic aperture antenna technology that would allow resolutions of ca. 10 km from space and higher resolutions from aircraft altitude.

Two missions are now poised to provide global satellite observations of sea surface salinity. The European Soil Moisture and Ocean Salinity Satellite (SMOS), launched in November 2009, is part of ESA's Living Planet Programme and was designed to facilitate the study of the Earth's water cycle and climate. The Aquarius/SAC-D mission, launched in June 2011, is a focused satellite mission to measure global sea surface salinity. The Aquarius/SAC-D mission was developed by NASA and the Space Agency of Argentina (Comisión Nacional de Actividades Espaciales, CONAE). These instruments are expected to have accuracies of 0.5–1.0 psu and be unaffected by cloud cover. The limited spatial resolution and accuracy, however, will be of limited use in pollution monitoring work.

Ocean Currents, Wave Height and Direction An important capability afforded by satellites is the ability to map sea surface topography (sea level variations in space), sea level changes, and the roughness of the ocean's surface over large to global scales, repeatedly and over long periods of time. This is possible with a number of active microwave sensors (radar). Most of the radar sensors that fall under the category of "altimeters" and "scatterometers" have relatively low spatial resolution (tens of kilometers), which limits direct application to examine physical oceanographic conditions within estuaries and most coastlines. Synthetic aperture radars (SAR) on the other hand have very high spatial resolution (order of meters) and are helpful to map larger waves, including internal waves. SAR data are also very useful to map characteristics of the texture of the sea surface that may be a telltale of pollution or other conditions relevant to ocean and human health. As mentioned above, SAR data have been instrumental in mapping surface slicks, oil spills, and natural oil seeps in the ocean.

Altimeter radar sensors can today accurately measure changes in sea surface topography in the order of 1–2 cm over areas spanning from several tens of square kilometers to global. Among the most important applications of altimeters are measuring sea level and the variability in sea surface height in an ocean basin ([127, 128, 142]). The importance of understanding regional and global trends in sea level over short and longer periods cannot be overemphasized. Altimeter observations show that sea level around the turn of the millennium rose at an accelerated rate of about 3.1 mm per year. This is significantly higher than the average rate for the twentieth century and is now considered a major threat to coastal communities by the Intergovernmental Panel on Climate Change (IPCC, [129]). Sea surface height variability also provides a means to measure regional circulation in the interior of the ocean over large scales, but these measurements have very large uncertainties near the coast and over continental shelves because of limitations in the technology and in the ability that the altimeter data has to be corrected for gravitational factors. A summary of coastal applications may be found in Emery et al. [130].

Radar altimeters are also useful to help characterize waves in the ocean [131–133]. Knowledge of ocean currents and waves is important to ocean and human health in a number of ways. For example, they affect ship routing in the ocean, they are relevant in search and rescue efforts, they are useful to fishermen or recreational boaters, and they help understand coastal erosion and flooding patterns.

Wind Speed Wind is relevant to marine pollution because of its role in the generation of currents, waves, and the direct dispersal of contaminants. Passive remote sensing of wind is possible using visible, infrared, or microwave imagery of the ocean. Using series of visible and infrared images, wind fields may be derived by tracking identifiable clouds. However, extrapolation of such winds to the surface and lack of coverage can render these techniques unsatisfactory.

Instead, microwave emissions by the sea surface have been empirically related to surface wind speed, and several experiments were conducted with Scanning Multichannel Microwave Radiometers (SMMR) carried aboard the SEASAT and Nimbus-7 satellites to refine this relationship. The understanding of the relationship between emissivity of the ocean and wind characteristics has grown substantially since the late 1970s. Unfortunately, large uncertainties in the results

occur due to sensor calibration drifts. Somewhat better accuracies are possible with the Special Sensor Microwave/Imager (SSM/I), presently operational on the Defense Meteorological Satellite Program (DMSP) satellites. Swift [134] summarizes the physical basis for passive remote sensing of wind speed, and Abbott and Chelton [135] review literature in this field.

Active painting of the sea surface with radar can provide important information on winds. Using microwave scattering techniques, it is possible to estimate near-surface wind velocity under all weather conditions [136]. In particular, the Seasat-A Satellite Scatterometer (SASS) was designed to provide an accuracy of $\pm$ 2 m/s and $\pm$ 20° direction over a range of 4–26 m/s wind speed. The underlying principle is that very short gravity waves, which affect the strength of Bragg scattering, are in equilibrium with near-surface wind speed. Several wind scatterometers have now been flown in space by NASA, ESA, and NASDA. The first scatterometer was the Seasat Scatterometer (SASS), launched in 1978, but again Seasat had a very short life. The ESA European Remote-Sensing Satellite ERS-1, launched in 1991, carried a scatterometer named the Advanced Microwave Instrument (AMI) scatterometer. This was followed by the ERS-2 AMI scatterometer, launched in 1995. In 1996, NASA launched the NASA Scatterometer (NSCAT), which unfortunately also had a short lifespan. NASA then launched the first scanning scatterometer, "SeaWinds," on QuikSCAT in 1999. A second SeaWinds instrument was flown on the NASDA ADEOS-2 satellite in 1993. The only sensor of this class still operating by mid-2011 was the ASCAT sensor, launched by ESA in 2007.

Future Directions

Historical oceanographic satellite sensors have limited utility in studying or monitoring coastal zones, in part because of their coarse ground resolution and limited spectral resolution and range. Refining ground resolution, expanding the spectral resolution and range, and addressing significant absorbing aerosol contamination issues together create an enormous challenge for accurately distinguish coastal ocean components and characteristics from remote sensing imagery. The limited spectral measurements from the current suite of ocean color sensors are clearly inadequate for coastal zone remote sensing research. Coastal remote sensing presents significant technological challenges. A range of space-based observations, suborbital systems, and models need to be developed over the next 25 years to advance the understanding of coastal habitats. Foremost is the requirement to obtain frequent and synoptic observations of small-scale phenomena in both aquatic and adjacent land environments. The effective discrimination of biogeochemical constituents of the water and seafloor (e.g., colored dissolved organic matter, phytoplankton concentration and composition, suspended sediments, bottom type) and physical properties (e.g., temperature, salinity, wind, circulation, bathymetry, light attenuation) must be achieved over long-term and short-term (daily to weekly) periods, at medium spatial resolution (10–100 m), and within the topographic and bathymetric regime of coastal habitats (watershed to about 20 m depth). Model development must proceed in parallel and at equivalent scales to the new observations. Together these advanced capabilities will lead to new understandings on linkages between lower and higher trophic levels and assessing coastal and estuarine waters for safe ocean resource use and for recreation and cultural purposes. Developing a workforce capable of processing and using these advanced observing technologies and products is also critical. Significant progress can be made by establishing effective links between research and decision-support tools for coastal managers and policymakers.

The next two decades, between 2010 and 2030, will bring a new series of advanced sensors. In the USA, a series of missions is planned. The operational JPSS missions will carry a number of ocean-observing systems, with the precursor NPP satellite scheduled for launch in 2011. The NPP and JPSS will carry the Visible/Infrared Imager/Radiometer Suite (VIIRS). The VIIRS features 22 channels, based primarily on the heritage from three instruments, the NOAA AVHRR, the NASA MODIS, and the Defense Meteorological Satellite Program (DMSP) Operational Linescan System (OLS). VIIRS effectively provides some of the MODIS and SeaWiFS 1-km resolution bands and adds a number of ~300 m resolution "imaging" channels. Unfortunately, the VIIRS suite of channels, however, does not include the red bands required to estimate solar-stimulated fluorescence that are present

on the MODIS and MERIS sensor. As mentioned earlier, these bands are essential to differentiate between phytoplankton blooms and CDOM patches in the coastal ocean.

The Landsat Data Continuity Mission (LDCM), planned for launch in late 2012 or 2013, continues the nearly 40-year legacy of the Landsat satellite series. The LDCM, however, includes a new band, centered at 443 nm, with a lower band edge at 433 nm and an upper band edge at 453 nm, and 30 m resolution. This band will revolutionize coastal water quality applications of the Landsat series. Nevertheless, Landsat-class sensors (NASA's Landsat, France's SPOT, Space Imaging, Inc.'s Ikonos, GEOEye's Quikbird, etc.) provide higher spatial resolution but have limited sensitivity and are unable to detect the subtle changes in reflectance linked to the geophysical properties of interest.

Designing decision-support systems that include synoptic and frequent high-resolution satellite observations to assess coastal and ocean human health is a tractable problem. This will require scientific advances in coastal aquatic environments, innovative techniques, and diverse approaches. An effective strategy must incorporate active and multispectral passive observations and both global and local measurement capabilities. Advanced sensors require expanded capabilities beyond the JPSS and NPP missions, with an aim toward high quality, high spatial, temporal, and spectral observation. Coastal observing capabilities require sensors that can dwell on dark targets or illuminate them with advanced Lidar. Observations need to be consistent and calibrated, accessible, and well-documented.

A series of relevant US missions that provide a solution is being planned following the recommendations of the National Research Council "Decadal Survey" [137]. The HyspIRI, GEO-CAPE, and ACE are a highly complementary set of missions that will provide a wide range of opportunities for multidisciplinary, international collaboration aimed at detecting and monitoring marine pollution. Each of these hyperspectral mission offers an important complementary set of capabilities. Specifically, HyspIRI will have relatively high spatial resolution (60 m), ACE will feature global coverage at medium spatial resolution, and NASA is considering the development of a Pre-ACE mission with similar characteristics, to be launched before 2020, to minimize the potential impacts of a gap in global ocean color observations. GEO-CAPE will afford high temporal coverage from a geostationary orbit. More specifically:

HyspIRI: The NASA HyspIRI (Hyperspectral Infrared Imager) is planned as a polar-orbiter mission with a mid-morning equatorial crossing time and which includes two instruments mounted on a satellite in low Earth orbit. There is an imaging spectrometer measuring from the visible to short-wave infrared (VSWIR) and a multispectral thermal infrared (TIR) imager. The VSWIR and TIR instruments will both have a spatial resolution of 60 m at nadir. The VSWIR will have a temporal revisit of approximately 3 weeks, and the TIR will have a temporal revisit of approximately 1 week. HyspIRI is designed to address issues on both land and in aquatic environments including inland water bodies and shallow coastal environments. The science team helping design this mission seeks to use HyspIRI to examine changes in ecosystem functioning due to many factors including pests, diseases, invasive species, disturbance, climate change, and land management that can alter water quality and food services to humans.

ACE and PACE: The NASA Aerosol-Cloud-Ecology (ACE) Mission and its precursor (the pre-ACE or PACE mission) also are planned polar-orbiter missions with mid-morning equatorial crossing time. These are aerosol-cloud and ocean ecosystem research missions designed to reduce the uncertainty in climate forcing in aerosol-cloud interactions and ocean ecosystem CO_2 uptake. The marine ecosystem goals are to characterize and quantify changes in the ocean biosphere and quantify the amount of dissolved organic matter, carbon, and other biogeochemical species to define the role of the oceans in the carbon cycle (e.g., uptake and storage). The present concepts for the ACE mission includes a wide array of sensors, including Lidars, cloud radars, a multi-angle swath polarimeter for imaging aerosols and clouds, and an ocean color radiometer.

GEO-CAPE: The NASA Geostationary Coastal and Air Pollution Events (GEO-CAPE) mission was recommended to gather science that identifies

human versus natural sources of aerosols and ozone precursors, tracks air pollution transport, and studies the dynamics of coastal ecosystems, river plumes, and tidal fronts. The geostationary vantage point would provide a tool with which to examine coastal events in high spatial, (~300 m), high spectral, and high temporal resolution.

The NRC [137] Decadal Survey placed the HyspIRI, GEO-CAPE, and ACE missions in a tier 2 (or phase 2) category, delayed until after a series of other missions deemed prioritary in the report are launched by the US government. Launch for these tier 2 missions is now slated for the second half of the 2010 decade or in the early 2020 decade. It is important to find ways to accelerate this timetable to implement a robust set of tools to monitor and help bridle problems in marine pollution.

It is imperative that the scientific base is strengthened to maximize the application of this technology. As part of this effort, it is important to invest in the training of scientists in the understanding of remote sensing and large multidisciplinary databases. Such scientists will contribute significantly to advances and conscious policymaking regarding marine pollution.

Bibliography

1. Muller-Karger FE (1992) Remote sensing of marine pollution: a challenge for the 1990s. Mar Pollut Bull 25(1–4):54–60
2. Boyce DG, Lewis MR, Worm B (2010) Global phytoplankton decline over the past century. Nature 466:591–596. doi:10.1038/nature09268
3. Polovina JJ, Howell EA, Abecassis M (2008) Ocean's least productive waters are expanding. Geophys Res Lett 35: L03618. doi:10.1029/2007GL031745
4. Behrenfeld MJ, O'Malley RT, Siegel DA, McClain CR, Sarmiento JL, Feldman GC, Milligan AJ, Falkowski PG, Letelier RM, Boss ES (2006) Climate-driven trends in contemporary ocean productivity. Nature 444:752–755 (7 Dec 2006). doi:10.1038/nature05317
5. Gledhill DK, Wanninkhof R, Eakin CM (2009) Observing ocean acidification from space. Oceanography 22(4):48–59
6. Orr JC et al (2005) Anthropogenic ocean acidification over the twenty-first century and its impact on calcifying organisms. Nature 437(7059):681–686
7. Chavez FP, Ryan J, Lluch-Cota SE, Miguel ÑC (2003) From anchovies to sardines and back: multidecadal change in the Pacific ocean. Science 299:217
8. Polovina JJ (2005) Climate variation, regime shifts, and implications for sustainable fisheries. Bull Mar Sci 76(2): 233–244
9. Epstein PR (1999) Climate and health. Perspective. Science 285(5426):347–348. doi:10.1126/science.285.5426.347
10. Zirino A, Fiedler PC, Keir RS (1988) Surface pH, satellite imagery, and vertical models in the tropical ocean. Sci Total Environ 75:285–300
11. Dube C, Lamarche A, Alfoldi T (1989) Resultats preliminaires d'une methode d'evaluation de la dispersion des rejets des eaux usees dans le Fleuve Saint-Laurent par teledetection. In: IGARSS proceedings: quantitative remote sensing: an economic tool for the nineties, 12th Canadian symposium on remote sensing, IEEE, Vancouver, Canada, vol 5: pp2820–2824
12. Gordon HR, McCluney WR (1975) Estimation of the depth of sunlight penetration in the sea for remote sensing. Appl Opt 14:413–416
13. Boyd JD, Myrick RK, Linzell RS (1991) Isis: a portable system for near real time oceanographic analysis. In: Abstract, EOS Supplement, AGU 1992 Ocean sciences meeting, New Orleans 72(51):28
14. Frye DE, Fougere A, Kery S (1991) Prototype expendable surface mooring with inductive telemetry. In: Abstract, EOS Supplement, AGU 1992 Ocean sciences meeting, New Orleans 72(51):29
15. OSB (Ocean Studies Board) (2003) Enabling ocean research in the 21st century: implementation of a network of ocean observatories. National Research Council. The National Academies Press, Washington, DC, 221p
16. Walt D, Urban E (1991) Chemical measurement technologies for ocean science. In: Abstract, EOS Supplement, AGU 1992 Ocean sciences meeting, New Orleans 72(51):28
17. Whitledge TE, Liljestrand HM (1991) In situ nitrate analyzer: design, development and field results. In: Abstract, EOS Supplement, AGU 1992 Ocean sciences meeting, New Orleans 72(51):27
18. Johnson KS, Needoba JA, Riser SC, Showers WJ (2007) Chemical sensor networks for the aquatic environment. Am Chem Soc. doi:10.1021/cr050354e
19. Honda MC, Watanabe S (2007) Utility of an automatic water sampler to observe seasonal variability in nutrients and DIC in the northwestern North Pacific. J Oceanogr 63:349–362
20. McPhaden MJ, Milburn HB (1991) Moored precipitation measurements. In: Abstract, EOS Supplement, AGU 1992 Ocean sciences meeting, New Orleans 72(51):27
21. Serra YL, McPhaden MJ (2004) In situ observations of diurnal variability in rainfall over the tropical Pacific and Atlantic oceans. J Climate 17:3496–3509
22. Case JF, Widder EA (1991) HIDEX-type bioluminescence detectors: modifications for moored and towed use. In: Abstract, EOS Supplement, AGU 1992 Ocean sciences meeting, New Orleans 72(51):30
23. Lapota D, Geiger ML, Lavoie DM, Bernstein SH, Case JF (1991) Measurements of planktonic bioluminescence in Vestfjord, Norway using HIDEX, a new rapid profiling bathyphotometer. In: Abstract, EOS Supplement, AGU 1992 Ocean sciences meeting, New Orleans 72(51):30
24. Widder EA (2010) Bioluminescence in the ocean: origins of biological, chemical, and ecological diversity. Science 328(5979):704–708

25. Jaffe JS (1991) Three dimensional sonar sensing of underwater animals. In: Abstract, EOS Supplement, AGU 1992 Ocean sciences meeting, New Orleans 72(51):28
26. Macaulay MC (1991) Applications of hydroacoustic technology to the study of zooplankton and micronekton in open ocean and shallow water environments. In: Abstract, EOS Supplement, AGU 1992 Ocean sciences meeting, New Orleans 72(51):28
27. Remsen AW (2008) Evolution and field application of a plankton imaging system. Ph.D. dissertation, University of South Florida, 145p
28. Smith RC, Waters KJ, Baker KS (1991) Optical variability and pigment biomass in the Sargasso Sea as determined using deep-sea optical mooring data. J Geophys Res 96(C5): 8665–8686
29. Dickey T, Marra J, Granata T, Langdon C, Hamilton M, Wiggert J, Siegel D, Bratkovich A (1991) Concurrent high resolution bio-optical and physical time series observations in the Sargasso Sea during the spring of 1987. J Geophys Res 96(C5):8643–8663
30. Boss E, Behrenfeld M (2010) In situ evaluation of the initiation of the North Atlantic phytoplankton bloom. Geophys Res Lett 37(L18603):5
31. Dickey TD, Itsweire EC, Moline MA, Perry MJ (2008) Introduction to the limnology and oceanography special issue on autonomous and lagrangian platforms and sensors (ALPS). Limnol Oceanogr 53(5, part 2):2057–2061
32. Esaias WE (1980) Remote sensing of oceanic phytoplankton: present capabilities and future goals. In: Falkowski PG (ed) Primary productivity in the sea. Plenum, New York, pp 321–337
33. Freilich MH (2010) NASA Earth science activities related to the deepwater horizon oil spill. American Geophysical Union, Fall Meeting 2010, Abstract #U14A-02
34. Zielinski O, Busch JA, Cembella AD, Daly KL, Engelbrektsson J, Hannides AK, Schmidt H (2009) Detecting marine hazardous substances and organisms: sensors for pollutants, toxins, and pathogens. Ocean Sci Discuss 6:953–1005. www.ocean-sci-discuss.net/6/953/2009/
35. Chomko RM, Gordon HR (2001) Atmospheric correction of ocean color imagery: test of the spectral optimization algorithm with the sea-viewing wide field-of-view sensor. Appl Opt 40:2973–2984
36. Chomko RM, Gordon HR, Maritorena S, Siegel DA (2003) Simultaneous retrieval of oceanic and atmospheric parameters for ocean color imagery by spectral optimization: a validation. Remote Sens Environ 84:208–220
37. Hovis WA, Clark DK, Anderson F, Austin RW, Wilson WH, Baker ET, Ball D, Gordon HR, Mueller JL, El-Sayed SZ, Sturm B, Wrigley RC, Yentsch CS (1980) Nimbus-7 coastal zone color scanner: system description and initial imagery. Science 210:60–63
38. Feldman G, Kuring N, Ng C, Esaias WE, McClain C, Elrod J, Maynard N, Endres D, Evans R, Brown J, Walsh S, Carle M, Podesta G (1989) Ocean color, availability of the global data set. The oceanography report. EOS 70(23):634
39. Barale V, Rizzoli PM, Hendershott MC (1984) Remotely sensing the surface dynamics of the Adriatic Sea. Deep Sea Res 31(12):1433–1459
40. Barale V, McClain CR, Rizzoli PM (1986) Space and time variability of the surface color field in the northern Adriatic Sea. J Geophys Res 91(C11):12957–12974
41. Bergamasco A, Barale V (1988) Comparison between coastal runoffs patterns from CZCS imagery and from a general circulation model. In: Marani A (ed) Advances in environmental modelling. Elsevier, Amsterdam, pp 395–404
42. Holligan PM, Aarup T, Groom SB (1989) The North Sea satellite colour atlas. Cont Shelf Res 9(8):667–765
43. Muller-Karger FE, McClain CR, Richardson PL (1988) The dispersal of the Amazon's water. Nature 333:56–59
44. Muller-Karger FE, McClain CR, Fisher TR, Esaias WE, Varela R (1989) Pigment distribution in the Caribbean Sea: observations from space. Prog Oceanogr 23:23–69
45. Müller-Karger FE, Walsh JJ, Evans RH, Meyers MB (1991) On the seasonal phytoplankton concentration and sea surface temperature cycles of the Gulf of Mexico as determined by satellites. J Geophys Res 96(C7):12645–12665
46. Del Castillo C, Gilbes F, Coble P, Muller-Karger FE (2000) On the dispersal of riverine colored dissolved organic matter over the West Florida Shelf. Limnol Oceanogr 45(6):1425–1432
47. IOCCG (2000) Remote sensing of ocean colour in coastal, and other optically-complex waters. In: Sathyendranath S (ed) International Ocean-Colour Coordinating Group, No.3: general introduction. International Ocean-Colour Coordinating Group (IOCCG) Report, pp 5–22
48. Abbott M, Letelier R (1999) Chlorophyll fluorescence (MODIS Product No. 20). Algorithm theoretical basis document. http://modis.gsfc.nasa.gov/data/atbd/atbd_mod22.pdf. Accessed 11 October 2011
49. SWFDOG (2002) Satellite images track 'black water' event off Florida coast. EOS Trans AGU 83(281):285
50. Hu C, Hackett KE, Callahan MK, Andréfouët S, Wheaton JL, Porter JW, Muller-Karger FE (2003) The 2002 ocean color anomaly in the Florida Bight: a cause of local coral reef decline? Geophys Res Lett 30(3):1151. doi:10.1029/2002GL016479
51. Hu C, Muller-Karger FE, Taylor C, Myhre D, Murch B, Odriozola AL, Godoy G (2003) MODIS detects oil spills in Lake Maracaibo, Venezuela. Eos Trans Am Geophys Union 84(33):313–319
52. Gordon HR, Clark DK, Brown JW, Brown OB, Evans RH, Broenkow WW (1983) Phytoplankton concentrations in the Middle Atlantic Bight: comparison ship determinations and CZCS estimates. Appl Opt 22:20–35
53. O'Reilly JE et al (2000) Ocean chlorophyll-a algorithms for SeaWiFS, OC2 and OC4: Version 4. In: Hooker SB, Firestone ER (eds) SeaWiFS postlaunch calibration and validation analyses, Part 3. NASA Tech. Memo. 2000–206892, vol 11. NASA Goddard Space Flight Center, Greenbelt, pp 9–23
54. Carder KL, Chen FR, Lee ZP, Hawes S, Kamykowski D (1999) Semi-analytic MODIS algorithms for chlorophyll a and absorption with bio-optical domains based on nitrate-depletion temperatures. J Geophys Res 104(C3):5403–5421

55. Hu C, Lee ZP, Muller-Karger FE, Carder KL (2002) Application of an optimization algorithm to satellite ocean color imagery: a case study in Southwest Florida coastal waters. In: Frouin RJ, Yuan Y, Kawamura H (eds) Ocean remote sensing and applications: SPIE proceedings, Washington, USA, vol 4892, pp 70–79
56. Maritorena S, Siegel DA, Peterson AR (2002) Optimization of a semianalytical ocean color model for global-scale applications. Appl Opt 41:2705–2714
57. Lee Z, Carder KL, Arnone RA (2002) Deriving inherent optical properties from water color: a multiband quasi-analytical algorithm for optically deep waters. Appl Opt 41:5755–5772
58. Morel A, Gentili B (2009) A simple band ratio technique to quantify the colored dissolved and detrital organic material from ocean color remotely sensed data. Remote Sens Environ 113:998–1011
59. Siegel DA, Maritorena S, Nelson NB, Behrenfeld MJ (2005) Independence and interdependencies of global ocean color properties: re-assessing the bio-optical assumption. J Geophys Res 110:C07011. doi:10.1029/2004JC002527
60. Chen Z, Muller-Karger FE, Hu C (2007) Remote sensing of water clarity in Tampa Bay. Remote Sens Environ. doi:10.1016/j.rse.2007.01.002
61. Stumpf RP (2001) Applications of satellite ocean color sensors for monitoring and predicting harmful algal blooms. Hum Ecol Risk Assess 7:1363–1368
62. Hu C, Muller-Karger FE, Taylor C, Carder KL, Kelble C, Johns E, Heil CA (2005) Red tide detection and tracing using MODIS fluorescence data: a regional example in SW Florida coastal waters. Remote Sens Environ 97:311–321
63. Hu C, Cannizzaro J, Carder KL, Muller-Karger FE, Hardy R (2010) Remote detection of Trichodesmium blooms in optically complex coastal waters: examples with MODIS full-spectral data. Remote Sens Environ 114(9):2048–2058. doi:10.1016/j.rse.2010.04.011
64. Hu C, Li D, Chen C, Ge J, Muller-Karger FE, Liu J, Yu F, He M-X (2010) On the recurrent Ulva prolifera blooms in the Yellow Sea and East China Sea. J Geophys Res 115(C5). doi:10.1029/2009JC005561
65. Zhang H (2002) Detecting red tides on the West Florida shelf by classification of SeaWiFS satellite imagery. Master's thesis, Department of Computer Science and Engineering, University of South Florida
66. Cannizzaro et al (2004) Bio-optical signatures of red tides on the west Florida shelf. Cont Shelf Res 28(1):137–158
67. Miller RL, McKee BA (2004) Using MODIS Terra 250 m imagery to map concentrations of total suspended matter in coastal waters. Remote Sens Environ 93(2004):259–266
68. Chen Z, Hu C, Conmy RN, Swarzenski P, Muller-Karger F (2007) Colored dissolved organic matter in Tampa Bay, Florida. Mar Chem 104:98–109
69. Chen Z, Hu C, Muller-Karger FE (2007) Monitoring turbidity in Tampa Bay using MODIS 250 M imagery. Remote Sens Environ. doi:10.1016/j.rse.2006.12.019
70. Moreno MJ, Al-Hamdan M, Rickman D, Muller-Karger FE (2010) Using the surface reflectance MODIS terra product to estimate turbidity in Tampa Bay, Florida. Remote Sens 2(12):2713–2728. doi:10.3390/rs2122713
71. Doxaran D, Froidefond J-M, Castaing P, Babin M (2009) Dynamics of the turbidity maximum zone in a macrotidal estuary (the Gironde, France): observations from field and MODIS satellite data. Estuar Coast Shelf Sci 81:321–332
72. Lobitz B, Beck L, Huq A, Wood B, Fuchs G, Faruque ASG, Colwell R (2000) Climate and infectious disease: use of remote sensing for detection of *Vibrio cholerae* by indirect measurement. Proc Natl Acad Sci USA 97(4):1438–1443
73. Colwell RR (2005) Global climate and infectious disease: the cholera paradigm. Science 274:2025–2031
74. Hu W, Clements A, Williams G, Tong S (2010) Dengue fever and El Niño/Southern Oscillation in Queensland, Australia: a time series predictive model. Occup Environ Med 67:307–311. doi:10.1136/oem.2008.044966
75. Gagliardini DA, Karszenbaum H, Legeckis R, Klemas V (1984) Application of LANDSAT MSS, NOAA/TIROS AVHRR, and Nimbus CZCS to study the La Plata River and its interaction with the ocean. Remote Sens Environ 15:21–36
76. Stumpf RP, Tyler MA (1988) Satellite detection of bloom and pigment distributions in estuaries. Remote Sens Environ 24:385–404
77. Froidefond JM, Castaing P, Jouanneau JM, Prud'Homme R, Dinet A (1993) Method for the quantification of suspended sediments from AVHRR NOAA-11 satellite data. Int J Remote Sens 14(5):885–894
78. Maul GA (1985) Introduction to satellite oceanography. Martinus Nijhoff, Dordrecht/Boston, 606p
79. Maul GA, Gordon HR (1975) On the use of the Earth resources technology satellite (LANDSAT-1) in optical oceanography. Remote Sens Environ 4:95–128
80. Amos CL, Alfoldi TT (1979) The determination of suspended sediment concentration in a macrotidal system using Landsat data. J Sediment Petrol 49:159–174
81. Khorram S (1981) Water quality mapping from Landsat digital data. Int J Rem Sens 2(2):145–153
82. Dwivedi RM, Narain A (1987) Remote sensing of phytoplankton: An attempt from the landsat thematic mapper. Int J Remote Sens 8(10):1563–1569
83. Braga CZF, Setzer AW, Drude de Lacerda L (1993) Water quality assessment with simultaneous Landsat-5 TM data at Guanabara Bay, Rio de Janeiro, Brazil. Remote Sens Environ 45:95–106
84. Tassan S (1987) Evaluation of the potential of the tematic mapper for marine application. Int J Remote Sens 8(10): 1455–1478
85. Tassan S (1993) An improved in-water algorithm for the determination of chlorophyll and suspended sediment concentration from thematic mapper data in coastal waters. Int J Remote Sens 14(6):1221–1229
86. Khorram S, Cheshire H, Geraci AL, La Rosa G (1989) IGARSS proceedings: quantitative remote sensing: an economic tool for the nineties, 12th Canadian symposium on remote sensing, IEEE, Vancouver, Canada, vol 1, pp 335–338

87. Catts GP, Khorram S, Cloern JE, Knight AW, DeGloria SD (1985) Remote sensing of tidal chlorophyll a variations in estuaries. Int J Remote Sens 6(11):1685–1706
88. Munday JC, Fedosh MS (1981) Chesapeake Bay plume dynamics from Landsat. In: Campbell JW, Thomas JP (eds) Superflux: Chesapeake Bay plume study, NASA Conference Publ 2188. NASA, Greenbelt
89. Munday JC, Alfoldi TT (1979) Landsat test of diffuse reflectance models for aquatic suspended solids measurement. Remote Sens Environ 8:169–183
90. Hellweger FL, Miller W, Oshodi KS (2007) Mapping turbidity in the Charles River, Boston using a high-resolution satellite. Environ Monit Assess 132(1–3):311–320, Epub 14 Dec 2006
91. Sorensen K, Nilsen J, Saebo HV, Holbaek-Hanssen E (1989a) Use of thematic mapper data for mapping of water quality. In: IGARSS proceedings: quantitative remote sensing: an economic tool for the nineties, 12th Canadian symposium on remote sensing, IEEE, Vancouver, Canada, vol 2, p 696
92. Sorensen K, Lindell T, Nisell J (1989b) The information content of AVHRR, MSS, TM, and SPOT data in the Skagerrak Sea. In: IGARSS proceedings: quantitative remote sensing: an economic tool for the nineties, 12th Canadian symposium on remote sensing, IEEE, Vancouver, Canada, vol 4, pp 2439–2442
93. Lee Z, Carder KL, Mobley CD, Steward RG, Patch JS (1999) Hyperspectral remote sensing for shallow waters. II. Deriving bottom depths and water properties by optimization. Appl Opt 38:3831–3843
94. Brando VE, Dekker AG (2003) Satellite hyperspectral remote sensing for estimating estuarine and coastal water quality. IEEE Trans Geosci Remote Sens 41(6):1378–1387
95. Corson MR, Korwan DR, Lucke RL, Snyder WA, Davis CO (2008) The hyperspectral imager for the coastal ocean (HICO) on the international space station. In: IEEE proceedings of the international geoscience and remote sensing symposium, Boston, USA, 978-1-4244-2808-3/08
96. Vane G, Chrisp M, Enmark H, Macenka S, Solomon J (1984a) Airborne visible/infrared imaging spectrometer: an advanced tool for earth remote sensing. In: IGARSS '84, Strasbourg, France, SP215, p 751
97. Vane G, Goetz AFH, Wellman JB (1984) Airborne imaging spectrometer: a new tool for remote sensing. IEEE Trans Geosci Remote Sens GE-22:546
98. Goetz AF (1987) High-resolution imaging spectrometer: science opportunities for the 1990s. NASA Earth observing system report: instrument panel report, vol IIc, 74p
99. Karaska MA, Huguenin RL, Beacham JL, Wang Mo-Hwa, Jensen JR, Kaufmann RS (2004) AVIRIS measurements of chlorophyll, suspended minerals, dissolved organic carbon, and turbidity in the Neuse River, North Carolina. Photogramm Eng Remote Sensing 70(1):125–133
100. Bagheri S, Yu T (2008) Hyperspectral sensing for assessing nearshore water quality conditions of Hudson/Raritan estuary. J Environ Inf 11(2):123–130. doi:10.3808/jei.200800116
101. Gower JFR, Buxton RAH, Borstad GA (1989) The FLI airborne imaging spectrometer: experience with land and water targets. In: IGARSS proceedings: quantitative remote sensing: an economic tool for the nineties, 12th Canadian symposium on remote sensing, IEEE, Vancouver, Canada, vol 2, pp 1024–102
102. Dekker AG, Malthus TJ, Seyhan E (2002) Quantitative modelling of inland water quality for high resolution MSS-systems. Geosci Remote Sens IEEE Trans 29(1):89–95
103. Babey SK, Anger CD (1989) A compact airborne spectrographic imager (CASI). In: IGARSS proceedings: quantitative remote sensing: an economic tool for the nineties, 12th Canadian symposium on remote sensing, IEEE, Vancouver, Canada, vol 2, p 1028–1031
104. Ammenberg P, Flink P, Lindell T, Pierson D, Strombeck N (2002) Bio-optical modelling combined with remote sensing to assess water quality. Int J Remote Sens 23(8): 1621–1638
105. Hengstermann T, Reuter R (1990) Lidar fluorosensing of mineral oil spills on the sea surface. Appl Opt 29(22):3218–3227
106. Hoge FE, Swift RN (1980) Application of the NASA airborne oceanographic lidar to the mapping of chlorophyll and other organic pigments. In: Campbell JW, Thomas JP (eds) Superflux: Chesapeake Bay Plume Study, Conference Publ. 2188. NASA, Greenbelt, pp 349–374
107. Hoge FE, Swift RN (1983) Airborne detection of oceanic turbidity cell structure using depth-resolved laser-induced water Raman backscatter. Appl Opt 23:3778–3786
108. Brekke C, Solberg AHS (2005) Oil spill detection by satellite remote sensing. Remote Sens Environ 95:1–13
109. Garcia-Pineda O, MacDonald I, Zimmer B, Shedd B, Roberts H (2010) Remote-sensing evaluation of geophysical anomaly sites in the outer continental slope, northern Gulf of Mexico. Deep Sea Res Part 2 Top Stud Oceanogr 57:1859–1869
110. Korenowski GM, Frysinger GS, Asher WE, Barger WR, Klusty MA (1989) Laser based optical measurement of organic surfactant concentration variations a te air/sea interface. In: IGARSS proceedings: quantitative remote sensing: an economic tool for the nineties, 12th Canadian symposium on remote sensing, IEEE, Vancouver, Canada, vol 3, pp 1506–1509
111. Hoge FE, Swift RN (1980) Oil film thickness measurement using airborne laser-induced water Raman backscatter. Appl Opt 19(19):3269–3281
112. Hoge FE, Swift RN (1983) Experimental feasibility of the airborne measurement of absolute oil fluorescence spectral conversion efficiency. Appl Opt 22(1):37–47
113. Hoge F, Swift RN (1982) Delineation of estuarine fronts in the German Bight using airborne laser-induced water Raman backscatter and fluorescence of water column constituents. Int J Remote Sens 3:475–495
114. Vodacek A (1989) Synchronous fluorescence spectroscopy of dissolved organic matter to optimize lidar detection parameters. In: IGARSS proceedings: quantitative remote sensing: an economic tool for the nineties, 12th Canadian symposium on remote sensing, IEEE, Vancouver, Canada, vol 2, pp 1046–1049

115. Duncan ME, Ackleson SG (1991) A summary of hand-held photography of the Persian Gulf area taken during space shuttle missions: 1981–1991. In: Abstract, EOS Supplement, AGU 1992 Ocean sciences meeting, New Orleans 72(51):40
116. Raney RK (1983) The Canadian SAR experience, Chapter 13. In: Allan TD (ed) Satellite microwave sensing. Wiley, Tornoto, pp 223–234
117. Wadsworth A, Robertson C, De Staerke D (1983) Use of SEASAT-SAR data in oceanography at the IFP, Chapter 14. In: Allan TD (ed) Satellite microwave sensing. Ellis Horwood Ltd , Chichester pp 235–245
118. Tucker C, Holben B, Elgin J, McMurtrey J (1989) Relationship of spectral data to grain yield variation. Photogramm Eng Remote Sensing 46(5):657–666
119. Tucker CJ, Sellers PJ (1986) Satellite remote sensing of primary production. Int J Remote Sens 7:1395–1416
120. Hu C, Muller-Karger F, Murch B, Myhre D, Taylor J, Luerssen R, Moses C, Zhang C, Gramer L, Hendee J (2009) Building an automated integrated observing system to detect sea surface temperature anomaly events in the Florida Keys. IEEE Trans Geosci Remote Sens 47(6):1607–1620
121. Barnes BB, Chuanmin Hu, Muller-Karger F (2011) An improved high-resolution SST climatology to assess cold water events off Florida. Geosci Remote Sens Lett 8:769, (Accepted Jan 2011)
122. Soto I (2006) Environmental variability in the Florida keys: impacts on coral reef health. Master's thesis, University of South Florida, College of Marine Science
123. Eakin CM, Nim CJ, Brainard RE, Aubrecht C, Elvidge C, Gledhill DK, Muller-Karger F, Mumby PJ, Skirving WJ, Strong AE, Wang M, Weeks S, Wentz F, Ziskin D (2010) Monitoring coral reefs from space. Oceanogr Soc Mag, special volume: The future of oceanography from space, Dec 2010, pp 119–133
124. Thomas A, Byrne D, Weatherbee R (2002) Coastal sea surface temperature variability from Landsat infrared data. Remote Sens Environ 81:262–272
125. Fisher JI, Mustard JF (2004) High spatial resolution sea surface climatology from Landsat thermal infrared data. Remote Sens Environ 90:293–307
126. Lagerloef GSE, Swift CT, Levine DM (1991) Remote sensing of sea surface salinity: airborne and satellite concepts. In: Abstract, EOS Supplement, AGU 1992 Ocean sciences meeting, New Orleans 72(51):29
127. Wagner CA, Cheney RE (1992) Global sea level change from satellite altimetry. J Geophys Res 97(C10):15607–15615. doi:10.1029/92JC01641
128. Merrifield MA, Merrifield ST, Mitchum GT (2010) Evidence for anomalous recent acceleration of global sea level rise. J Climate 22:5772–5781
129. Bindoff NL, Willebrand J, Artale V, Cazenave A, Gregory J, Gulev S, Hanawa K, Le Quéré C, Levitus S, Nojiri Y, Shum CK, Talley LD, Unnikrishnan A (2007) Observations: oceanic climate change and sea level. In: Solomon S, Qin D, Manning M, Chen Z, Marquis M, Averyt KB, Tignor M, Miller HL (eds) Climate change 2007: the physical science basis. Contribution of working group I to the fourth assessment report of the intergovernmental panel on climate change. Cambridge University Press, Cambridge/New York
130. Emery WJ, Strub T, Leben R, Foreman M, McWilliams JC, Han G, Ladd C, Ueno H (2010) Satellite altimetry applications off the coasts of North America. In: Vignudelli S, Kostianoy A, Cipollini P, Benveniste J (eds) Coastal altimetry. Springer Verlag, Germany, pp 417–451. doi:10.1007/978-3-642-12796-0_16
131. Hwang PA, Teague WJ, Jacobs GA, Wang DW (1998) A statistical comparison of wind speed, wave height and wave period derived from satellite altimeters and ocean buoys in the Gulf of Mexico Region. J Geophys Res 103:10451–10468
132. Hwang PA, Walsh EJ, Krabill WB, Swift RN, Manizade SS, Scott JF, Earle MD (1998) Airborne remote sensing applications to coastal wave research. J Geophys Res 103:18791–18800
133. Bidlot J-R, Holmes DJ, Wittmann PA, Lalbeharry R, Chen HS (2002) Intercomparison of the performance of operational ocean wave forecasting systems with buoy data. Weather Forecasting 17:287–310. doi:10.1175/1520-0434(2002)017<0287:IOTPOO>2.0.CO;2
134. Swift CT (1990) Passive microwave remote sensing of ocean surface wind speed. In: Geernaert GL, Plant WJ (eds) Surface waves and fluxes, vol 2. Kluwer Academic, Dordrecht, pp 265–292
135. Abbott MR, Chelton DB (1991) Advances in passive remote sensing of the ocean. Contributions in Oceanography. U.S. National Report to International Union of Geodesy and Gophysics 1987–1990. American Geophysical Union, p 571–589
136. Guymer TH (1983) Validation and applications of SASS over JASIN, Chapter 5. In: Allan TD (ed) Satellite microwave sensing. Wiley, Toronto, pp 87–104
137. NRC (2007) Earth science and applications from space: national imperatives for the next decade and beyond. Committee on Earth science and applications from space: a community assessment and strategy for the future. National Research Council, p 456. ISBN: 978-0-309-10387-9
138. Chadwick DB, Lieberman SH, Reimers CE (1991) In-situ release rate measurements of contaminants from marine sediments. In: Abstract, EOS Supplement, AGU 1992 Ocean sciences meeting, New Orleans 72(51):29
139. Esaias W (1986) MODIS – moderate resolution imaging spectrometer. NASA Earth observing system instrument panel report, vol IIb, 59p
140. Huang WG, Lou XL (2003) AVHRR detection of red tides with neural networks. Int J Remote Sens 24:1991–1996
141. Muller-Karger FE, Hu C, Andréfouët S, Varela R (2005) The color of the coastal ocean and applications in the solution of research and management problems. In: Miller RL, Del Castillo CE, McKee BA (eds) Remote sensing of coastal aquatic environments: technologies, techniques and application. Springer, Dordrecht, pp 101–127
142. Nerem RS, Leuliette E, Cazenave A (2006) Present-day sea-level change: a review. Comptes Rendus Geoscience 338:1077–1083

143. Stumpf RP (1988) Sediment transport in chesapeake bay during floods: analysis using satellite and surface observations. J Coast Res 4(1):1–15
144. McClain, Charles R, Cleave ML, Feldman GC, Gregg WW, Hooker SB, Kuring N (1998) Science quality seaWiFS data for global biosphere research. Sea Technology. September 1998, pages 10–16
145. Rodríguez-Guzmán V, Gilbes F (2009) Estimating total suspended sediments in tropical open bay conditions using MODIS. In: Proceedings of the 8th WSEAS International Conference on Instrumentation, Measurement, Circuits and Systems, Hangzhou, China, May 20–22, 2009, pp 83–86
146. Gallegos SC, Gray TI, Crawford MM (1989) A study into the responses of the NOAA-n AVHRR reflective channels over water targets. In: Proceedings of the 1989 IEEE IGARSS Meeting, Vancouver, BC
147. Stumpf RP, Pennock JR (1991) Remote estimation of the diffuse attenuaton coefficient in a moderately turbid estuary. Rem. Sens. Environ. 38:183–191
148. Fingas MF, Brown CE (1997) Airborne oil spill remote sensors - do they have a future. In: Proceedings of the Third International Airborne Remote Sensing Conference and Exhibition, Environmental Research Institute of Michigan (ERIM), Ann Arbor, MI, pp I 715–722
149. Fingas MF, Brown CE (2000) Review of oil spill remote sensing. In: proceedings of the Sixth International Conference on Remote Sensing for Marine and Coastal Environments, Veridian ERIM International, Ann Arbor, MI, pp I211–218
150. Stumpf RP, Pennock JR (1989) Calibration of a general optical equation for remote sensing of suspended sediments in a moderately turbid estuary. J Geophys Res 94 (C10):14363–14371

Remote Sensing of Natural Disasters

Steve Chien[1], Veerachai Tanpipat[2]
[1]Jet Propulsion Laboratory, California Institute of Technology, Pasadena, CA, USA
[2]Forest Fire Control Division, National Park, Wildlife and Plant Conservation Department of Thailand, Chatuchak, Bangkok, Thailand

Article Outline

Glossary
Definition: Remote Sensing of Natural Disasters
Introduction
Remote Sensing for the Study of Volcanic Activity
Flooding Applications of Remote Sensing
Fire Applications of Remote Sensing
Other Applications of Remote Sensing to Natural Disasters
Future Directions
Conclusions
Acknowledgments
Bibliography

Glossary

MODIS The MODerate resolution Imaging Spectrometer is a general purpose instrument flying on the Terra and Aqua spacecraft that can sense both visible and thermal infrared information on the earth's surface and atmosphere.

GOES The Geostationary Operational Environmental Satellite system is a set of satellites that continuously cover fixed regions of Earth. For example, GOES-East provides continuous coverage of North and South America.

AVHRR Advanced Very High Resolution Radiometer is a sensor carried on the National Oceanic and Atmospheric Administration (NOAA) family of polar orbiting platforms (POES). AVHRR has five wide spectral bands that sense principally the near-infrared and thermal infrared spectrum.

ASTER Advanced Spaceborne Thermal Emission and Reflection Radiometer is an instrument on the Terra satellite that senses visible, near-infrared, short infrared, and long-wave/thermal infrared spectrum.

Earth Observing One (EO-1) An Earth orbiting, pointable spacecraft that has been used to demonstrate a wide range of automation and autonomic technologies including onboard mission replanning and sensorwebs.

Hyperion The Hyperspectral instrument on EO-1 used onboard to detect flooding, volcanic activity, and cryosphere change. Hyperion is able to measure in the Very Near to Short Wave infrared spectrum.

Synthetic aperture radar (SAR) A radar remote sensing technique in which motion of the radar is used to synthesize a large array through radar processing. SAR can be used to distinguish between various surface types such as water, land, vegetation cover type and density, and others.

Interferometric synthetic aperture radar (InSAR) A remote sensing technique which enables detailed

topography, change detection, and motion tracking with great precision. InSAR has applications to deriving digital elevation maps (DEMs) as well as tracking land motion (e.g., after earthquakes), ice sheet motion, and change detection after major disturbances such as landslides, fires, flooding, and other natural disasters.

Lahar A mud or debris flow–caused volcanic activity combined with water, snow, or ice.

Definition: Remote Sensing of Natural Disasters

Remote sensing involves the use of instruments to study phenomena from a distance. Natural disasters derive from natural hazards such as volcanoes, flooding, fires, and weather. Practically speaking, "remote sensing of natural disasters" principally refers to the use of airborne or spaceborne sensors to study natural disasters for detecting, modeling, predicting, analyzing, and mitigating effects on human populations and activities.

Remote sensing can be further characterized by the sensitivity of the instrument. Passive sensors rely either on reflected sunlight to illuminate the target or by radiation emitted from the target. Typical passive sensors might include the visible spectrum (~1 μm wavelength) or very near and short wave infrared (up to 2.5 μm wavelength). These spectra tend to be useful for distinguishing various vegetation and surface types. Applications for monitoring of natural hazards include detection of urban areas, plants, surface water, ice, snow, lava, lahar, and roads. Typical passive sensors for emissive targets would include sensitivity in the Thermal Infrared (TIR) spectrum (8–12 μm wavelength). Applications of TIR to natural hazards include measurement of volcanic activity, and active fire mapping.

Active sensors such as radar produce a signal to illuminate the surface of interest and rely on the surface impact on the reflected energy to distinguish different surface characteristics. For example, Synthetic Aperture Radar (SAR) emits a signal with specific polarizations (e.g., HH, VV) and measures the returned energy at various polarizations to distinguish surface characteristics. These radars are useful in that they are less affected by weather such as cloud cover and thus have unique capabilities in flooding and fire applications where clouds and smoke may obscure areas of interest.

In this entry we focus on spaceborne applications. However, all of the sensing modalities described (e.g., visible, near-infrared, very near-infrared, thermal infrared, radar, SAR, etc.) are also often provided via airborne platforms. Thus, all of the same applications of space-based remote sensing are relevant to airborne remote sensing.

Introduction

Remote sensing can provide valuable data to aid in the study and mitigation of natural disasters. Satellite instruments can provide imagery of large areas of Earth's surface and overflights can often easily provide data for hard to access locations (either due to terrain, weather, or causes of the disaster itself). Airborne instruments can also provide much of the same utility from remote sensing with the potential advantages of greater loiter or dwell time and rapid response. While in the remainder of this entry we focus on spaceborne remote sensing, generally speaking, any of the applications of remote sensing described can be deployed as airborne instruments as well.

In this entry, we provide an overview of the wide range of methods used to apply remote sensing to the study and mitigation of natural disasters. We first describe the use of remote sensing to study volcanic activity – including measurement of thermal emissions, mapping of lava flows, measurement of plumes and ash, and gas. We next describe the use of remote sensing to study flooding. MODIS is the workhorse of remote sensing of flooding; however, a range of other multispectral sensors and synthetic aperture radar (SAR) have also been used for this application. We then describe the use of remote sensing in the study of forest fires – including active fire monitoring, risk area mapping, burn scars estimation, burn severity measurement, fuel load estimation, smog and haze monitoring, and fire management. Finally we describe the use of remote sensing in change-based measurements in which before and after imagery of natural disasters can provide valuable information relating to earthquakes, tsunami, landslides, tornadoes, blowdown/tropical storms, and typhoons/hurricanes. Digital elevation maps (DEMs) are a cross-cutting

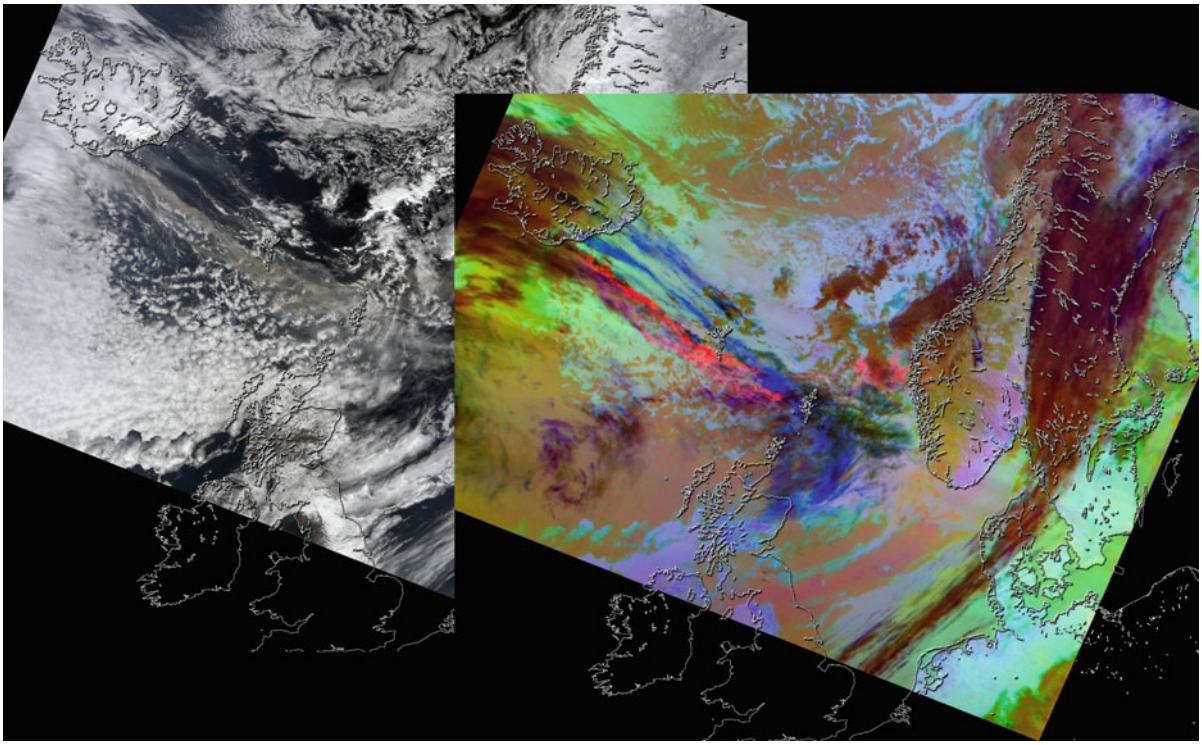

Remote Sensing of Natural Disasters. Figure 1
MODIS imagery of the Eyjafjallajökull eruption (Image courtesy: NASA GSFC/JPL/Caltech)

application of remote sensing. These detailed topographical maps are generally created using remote sensing data and have a wide range of applications relating to natural disasters such as prediction of lava flow movement and lahar flows for volcanoes, flooding, tsunami risk areas, landslide risk areas, fire movement modeling, and others.

Remote Sensing for the Study of Volcanic Activity

Remote sensing has many applications to volcanology. A wide range of instruments have been used to study the thermal emissions of volcanic activity. Measurement of thermal emissions can then drive models to estimate surface lava, effusion rates, and other key physical parameters of volcanic activity. GOES and AVHRR [1] have been used to detect thermal signatures of volcanic activity from space. MODVOLC uses the MODIS sensor (flying on both Terra and Aqua) to detect volcanic thermal signatures [2, 3]. These methods use the multispectral capability of the instrument to fit the thermal emissions to blackbody radiation curves to estimate the surface area emitting at a specific temperature. However, all of these methods are restricted by the low spatial resolution (and corresponding lower thermal sensitivity) of these instruments. While site-specific algorithm parameterization for background thermal signatures can increase sensitivity, higher spatial resolution instruments (typically pointable) can provide more information. In this approach, many other pointable sensors including ASTER [4] and Hyperion [5, 6] have been used to study the thermal emission of volcanic activity.

Remote sensing can also be used to study volcanic plumes. ASTER and MODIS have been used to track such activity [7, 8]. In these applications the plumes and gas emissions of volcanoes can be distinguished from the normal atmosphere due to difference in spectral response from both ash and SO_2 constituents. The AVHRR sensor has also been used in conjunction with ground measurements to study volcanic plumes [9].

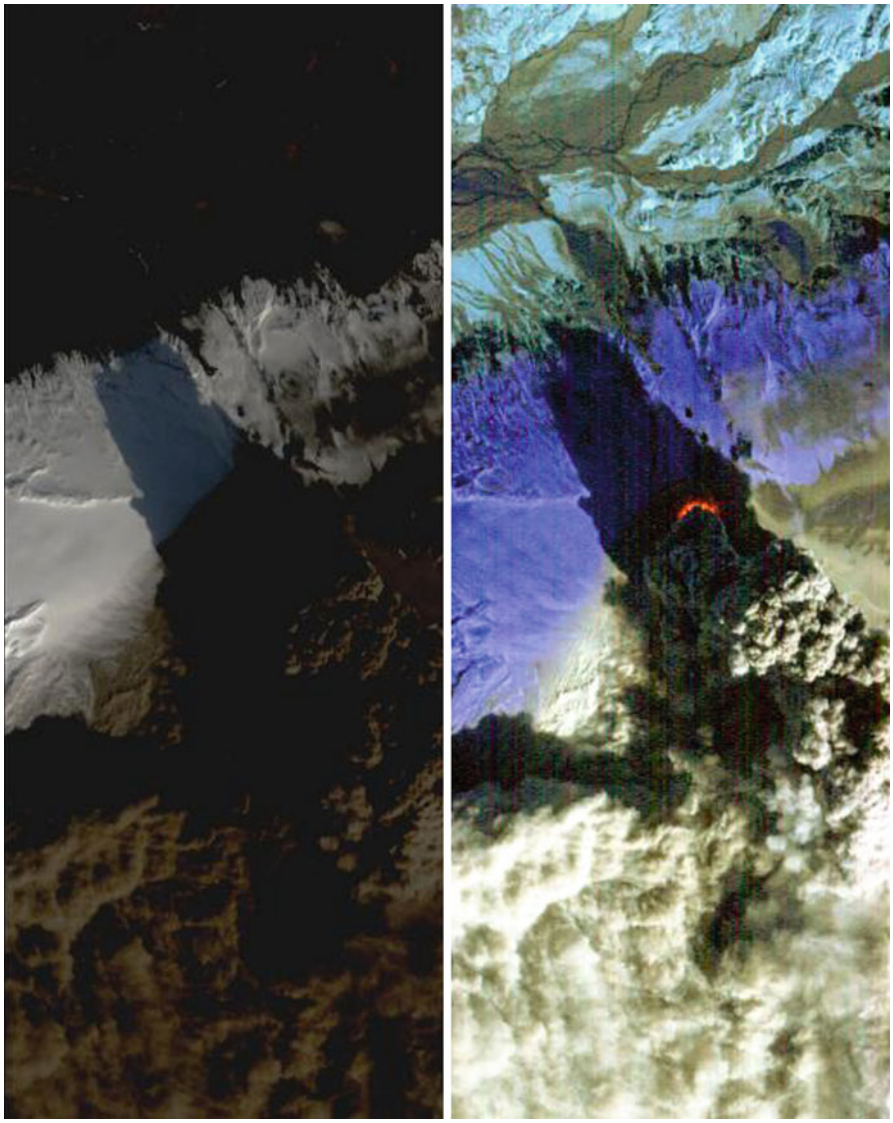

Remote Sensing of Natural Disasters. Figure 2
EO-1/ALI true color (*left*) thermal enhanced (*right*) imagery acquired April 17, 2010 (Images courtesy: NASA/JPL/Caltech/EO-1 mission/GSFC/Ashley Davies)

Synthetic aperture radar (SAR) can also be used in an interferometric fashion to study inflation in volcanoes as both a precursor and during eruptions [10].

Tracking of lahar from volcanoes is another application of remote sensing. Visible, Near-Infrared, Synthetic Aperture Radar, and Light Detection And Ranging (LIDAR) sensors have all been used to map lahar flows (see [11] for a comparison of these methods). Note that digital elevation maps, also typically derived by remote sensing, can be used to model (predict) where lahar flows are likely.

The 2010 eruption of the Eyjafjallajökull Volcano in Iceland represents an excellent example of the use of remote sensing in volcanic study. In the weeks immediately following this eruption, data from many space-based sensors, such as MODIS, AIRS, MISR, ASTER, and ALI, were all used in the analysis of the eruption.

The MODIS instrument provides broad swath (2,000+ km wide) moderate spatial resolution (250–1,000 m/pixel) imagery of Earth in visible to thermal infrared spectra. This workhorse of remote sensing has numerous applications to natural hazards including volcanology. MODIS thermal infrared channels can distinguish ash from other atmospheric conditions as shown in this April 15, 2010, imagery of the Eyjafjallajökull eruption (Fig. 1).

The Advanced Land Imager (ALI) on EO-1 is a targetable instrument sensitive in the visible, short wave infrared, and very near infrared spectra. Figure 2 shows true color (left) and false color to highlight thermal features (right) to highlight the Eyjafjallajökull volcanic activity on April 17, 2010.

The Multi-angle Imaging SpectroRadiometer (MISR) aboard NASA's Terra satellite collected data on ash height when it passed just east of the Eyjafjallajökull Volcano mid-morning on May 7. MISR uses nine different cameras with each camera viewing the event from a different angle to enable hyper-stereo reconstruction of the distance of viewed substances from the instrument. In this application of MISR, the nine angle views are used to reconstruct the distance of the plume from the MISR instrument. Because the altitude of the satellite orbit is known the height of the volcanic plume can then be calculated as shown below in Fig. 3.

Flooding Applications of Remote Sensing

Remote sensing is frequently used in tracking flooding worldwide. The MODIS sensor has been used to study long-term impacts from flooding, with products

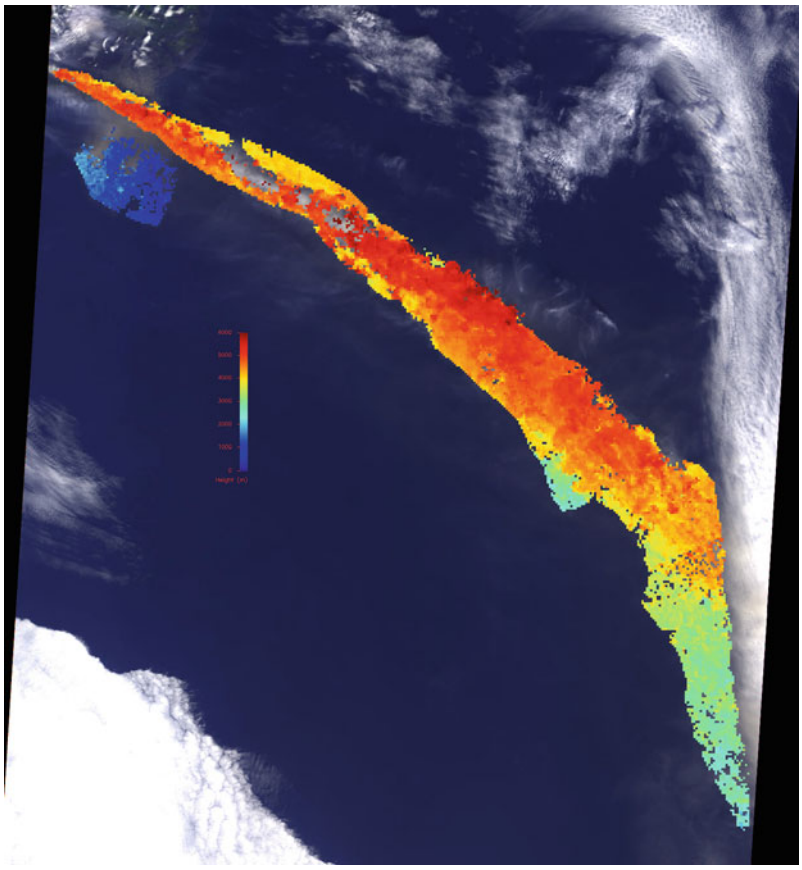

Remote Sensing of Natural Disasters. Figure 3
MISR extracted plume height from the Eyjafjallajökull Volcano May 7, 2010 (NASA image courtesy: GSFC/LaRC/JPL/Caltech MISR team)

spanning decades by the Dartmouth Flood Observatory [12, 13] and the University of Maryland [14]. These methods leverage the fact that surface water from flooded areas is very dark and thus can be distinguished spectrally from other substances. For a reliable product cloud shadow areas are removed by looking at multiple images in sequence as MODIS provides at least two daylight overflights per 24 h period. Figure 4 shows a MODIS-derived product developed by the University of Maryland highlighting flooding in Myanmar in 2008.

Hyperion [15] and ALI [16] have also been used to study flooding by using spectral analysis methods to automatically derive surface water extent.

Use of multispectral remote sensing to track flooding suffers from the drawback that flooding often occurs in conjunction with cloud cover. Use of radar to track flooding does not suffer from this limitation. QuikSCAT (Quick Scatterometer) has been used to study flooding worldwide [17] providing global coverage maps of flooding. Figure 5 shows QuikSCAT-derived mapping of flooding in China in September 2003.

On a regional scale many SARs including Radarsat-1 SAR [18] and ASAR on Envisat [19] have been used in a targeted mode to track flooding. In these applications, changes in the radar returns allow discrimination between flooded areas and other types of land surfaces such as sand, soil, and vegetation. Below Fig. 6a, b shows the formed SAR image and a derived surface water extent classification. The surface water can be distinguished because water has dielectric properties that differ from most land types resulting in a change in the radar returns. However, in cases where weather (e.g., wind) causes a significant change in the water surface roughness it can become more difficult to distinguish between water and land surfaces.

Fire Applications of Remote Sensing

Forest fire is one of the most significant and natural causes of terrestrial biomass change. Forest fires play a major and vital role in the deforestation of the tropical and subtropical regions, especially in the developing and underdeveloped countries. Since it is

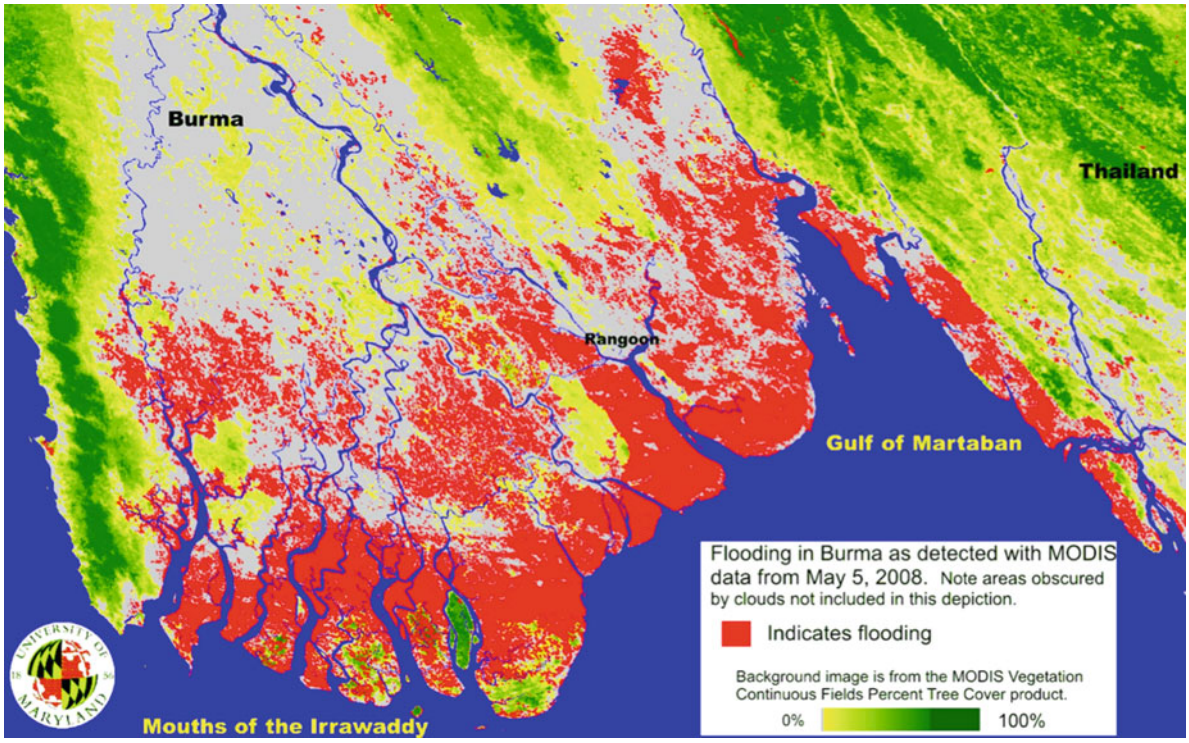

Remote Sensing of Natural Disasters. Figure 4
Flooding in Myanmar May 2008 as derived from MODIS imagery (Images courtesy: University of Maryland)

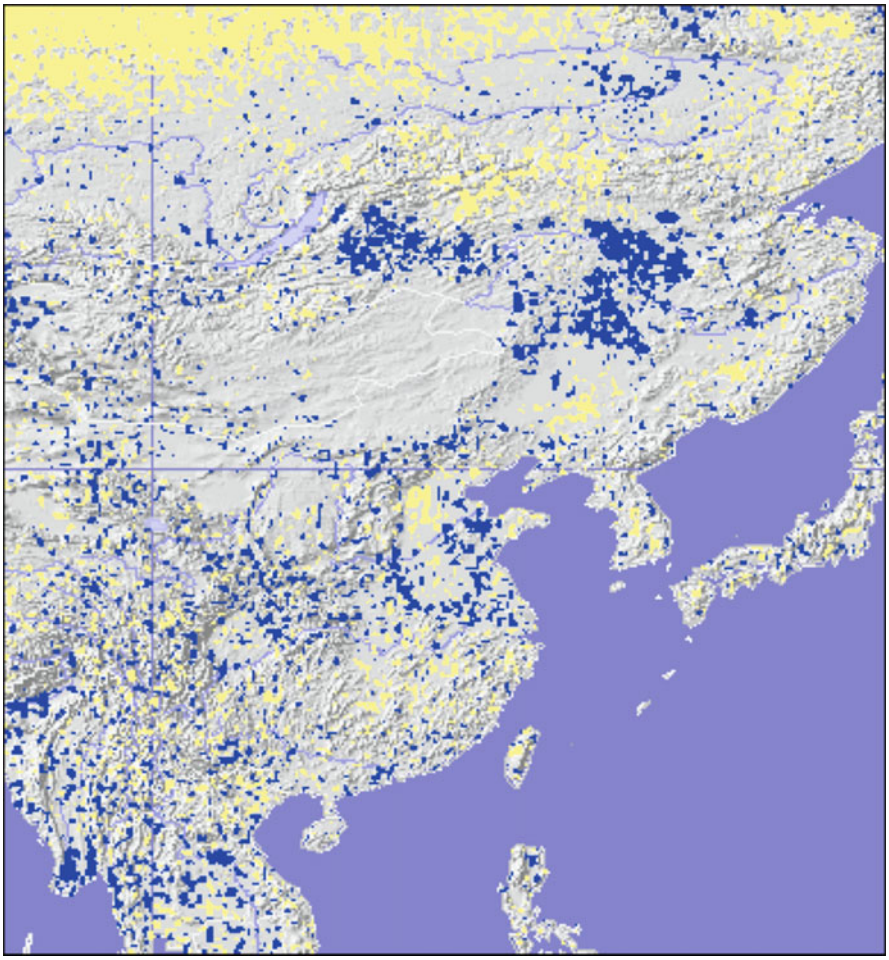

Remote Sensing of Natural Disasters. Figure 5
QuikSCAT-derived flood map for September 2003. Blue indicates flooded areas (Product courtesy: R. Brakenridge/ Dartmouth flood observatory & S. Nghiem/Jet propulsion laboratory)

impossible to monitor forest fires of a large area at a ground level, satellite remote sensing is critical. In addition, routine monitoring via satellite remote sensing technology offers the most efficient and cost-effective means for forest fire management over larger areas [20].

An early space system used to study fires is the Advanced Very High Resolution Radiometer (AVHRR) of the National Oceanic and Atmospheric Administration (NOAA) polar orbiting platforms (POES) family. It was originally used for weather monitoring, and then employed as the main sensor in the detection of active fires, or "hotspots," on a global scale and with relatively high temporal frequency. Other sensors include those in the Geostationary Operational Environmental Satellite (GOES) such as the Visible Infrared Spin Scan Radiometer Atmospheric Sounder (VAS) [21] and the GOES Imager [22]. In addition to their main functions, the Defense Meteorological Satellite Program Operational Linescan System (DMSP-OLS) [23, 24] the Along Track Scanning Radiometer (ATSR) [25], the Tropical Rainfall Measuring Mission Visible and Infrared Scanner (TRMM-VIRS) [26] are also used in the forest fire monitoring. However, MODIS is the first sensor specifically designed and developed for the forest fires detection [27, 28].

Figure 7 shows MODIS imagery of Nepal acquired in March 2009. In the image active fire detections are

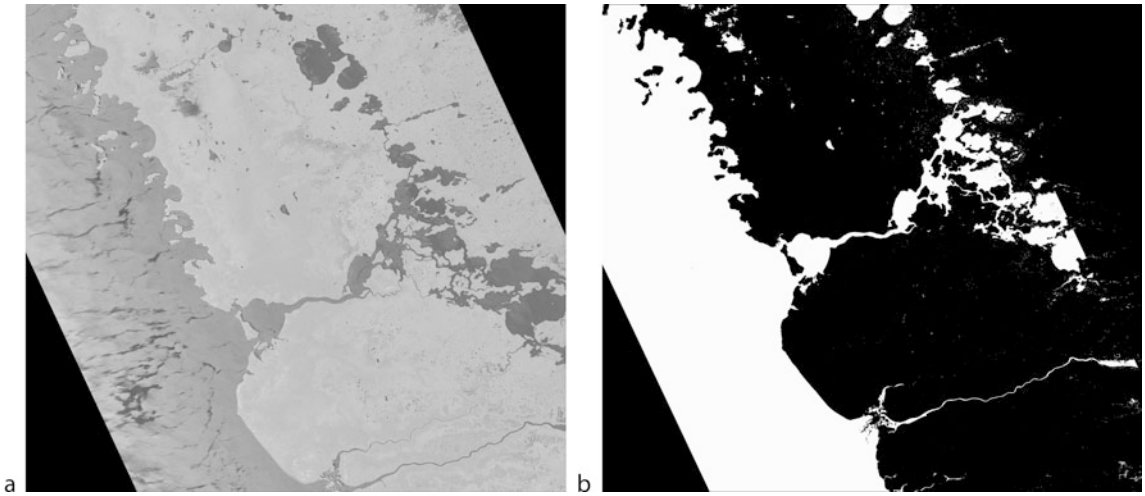

Remote Sensing of Natural Disasters. Figure 6
(**a**) Synthetic aperture radar imagery from the Florida Everglades acquired by the unpiloted aerial vehicle SAR (UAVSAR) L-band SAR in 2009 (Image courtesy: UAVSAR team). (**b**) Surface water classification derived from UAVSAR L-band SAR imagery of Florida Everglades (Image courtesy: UAVSAR team and J. Doubleday/JPL/Caltech)

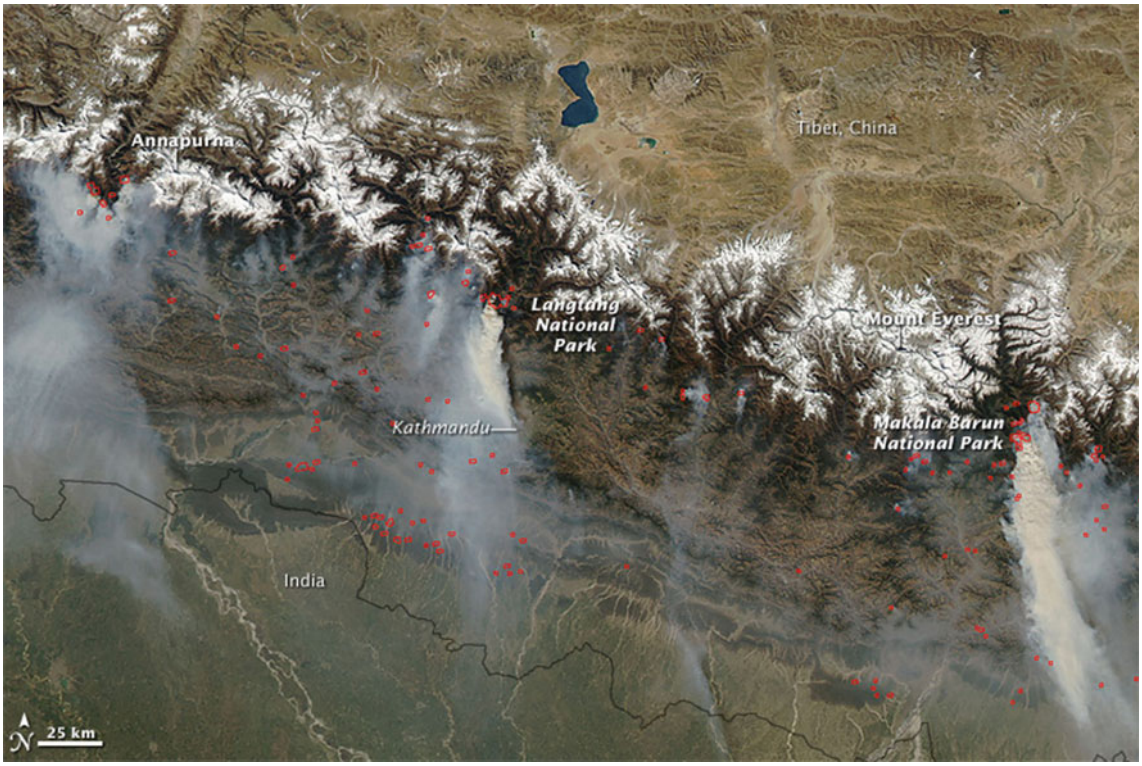

Remote Sensing of Natural Disasters. Figure 7
MODIS imagery showing 2009 fires in Nepal, *red* boxes indicate active fire detections (Image courtesy: NASA and MODIS rapid response team)

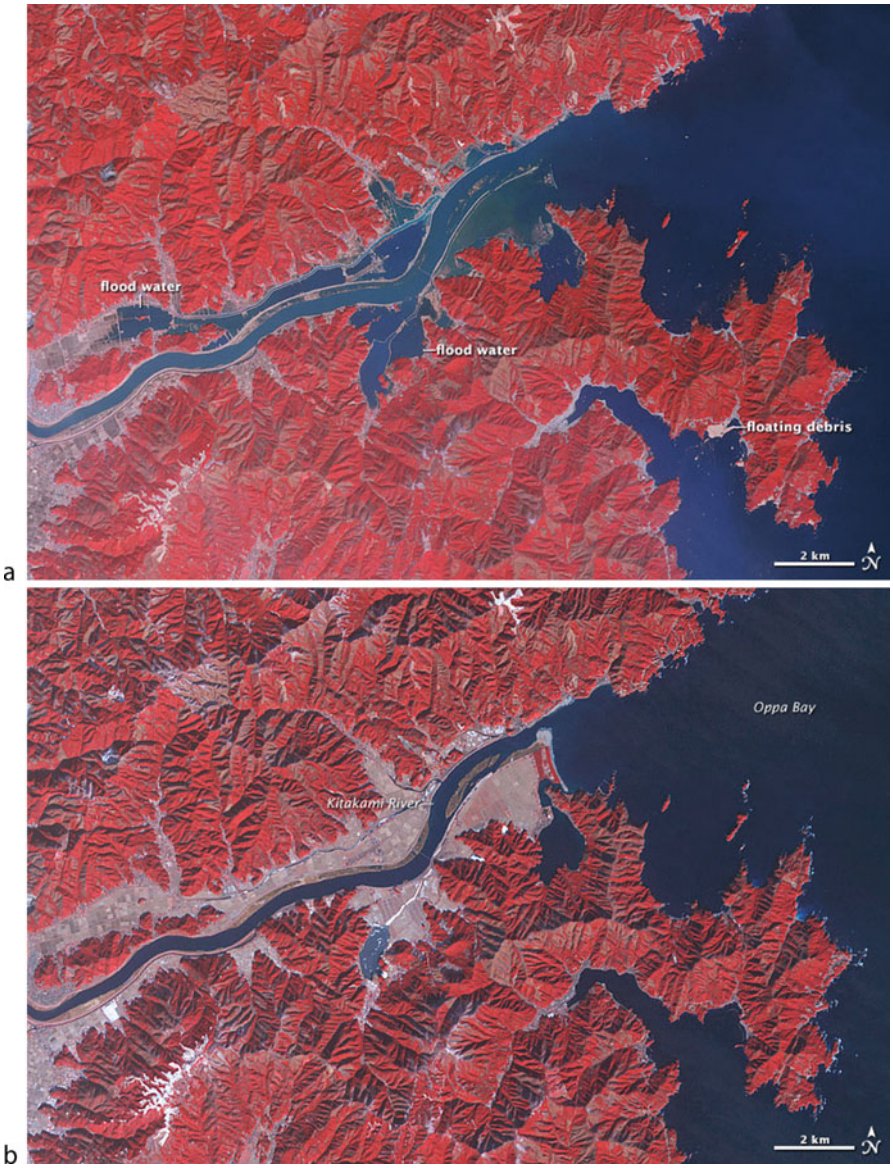

Remote Sensing of Natural Disasters. Figure 8
(**a**) ASTER imagery showing the extent of Tsunami-induced flooding at the Kitakami river, March 2011 (NASA earth observatory image by Robert Simmon and Jesse Allen, using data from the GSFC/METI/ERSDAC/JAROS, and USA/Japan ASTER science team). (**b**) ASTER imagery from January 2011 showing pre-tsunami shoreline of the Kitakami river, Japan, January 2011 (NASA earth observatory image by Robert Simmon and Jesse Allen, using data from the GSFC/METI/ERSDAC/JAROS, and USA/Japan ASTER science team)

indicated and the large smoke plumes caused by the fire are quite evident.

An array of technologies used in the satellite remote sensing of forest fires includes spaceborne system/sensors in a variety of tasks which are active fire monitoring [29–32], risk area mapping and assessment [33–36], burn scar estimation and monitoring [37–40], burn severity measurement [41–43], fuel moisture content estimation [44, 45], smog and haze monitoring [46–48], fire behavior [49], and fire management [50].

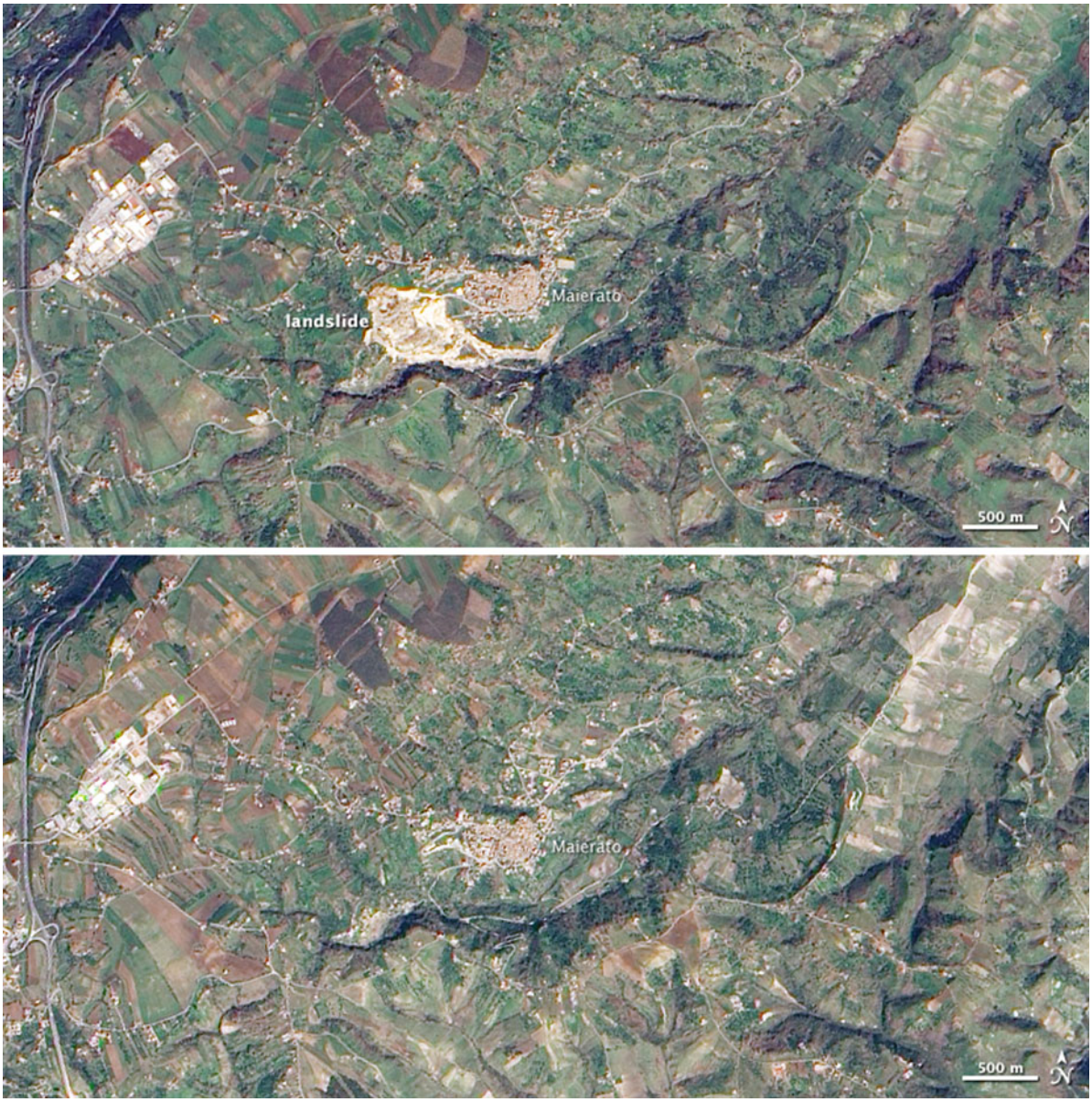

Remote Sensing of Natural Disasters. Figure 9
"After" (*top*) and "before" (*bottom*) imagery of a landslide in Maierato, Italy (Image courtesy of NASA earth observatory and NASA EO-1 team)

One emphasis of current work is to increase the sensitivity of fire detection systems – MODIS capabilities can only detect moderate-sized fires. Another emphasis of current work is to allow for faster delivery of data to enable rapid response to fires before they grow in size and are harder to contain.

Other Applications of Remote Sensing to Natural Disasters

Another major application of remote sensing is the use of "before" and "after" images to assess damage from natural disasters. This type of analysis is relevant to a wide range of natural disasters including tsunamis,

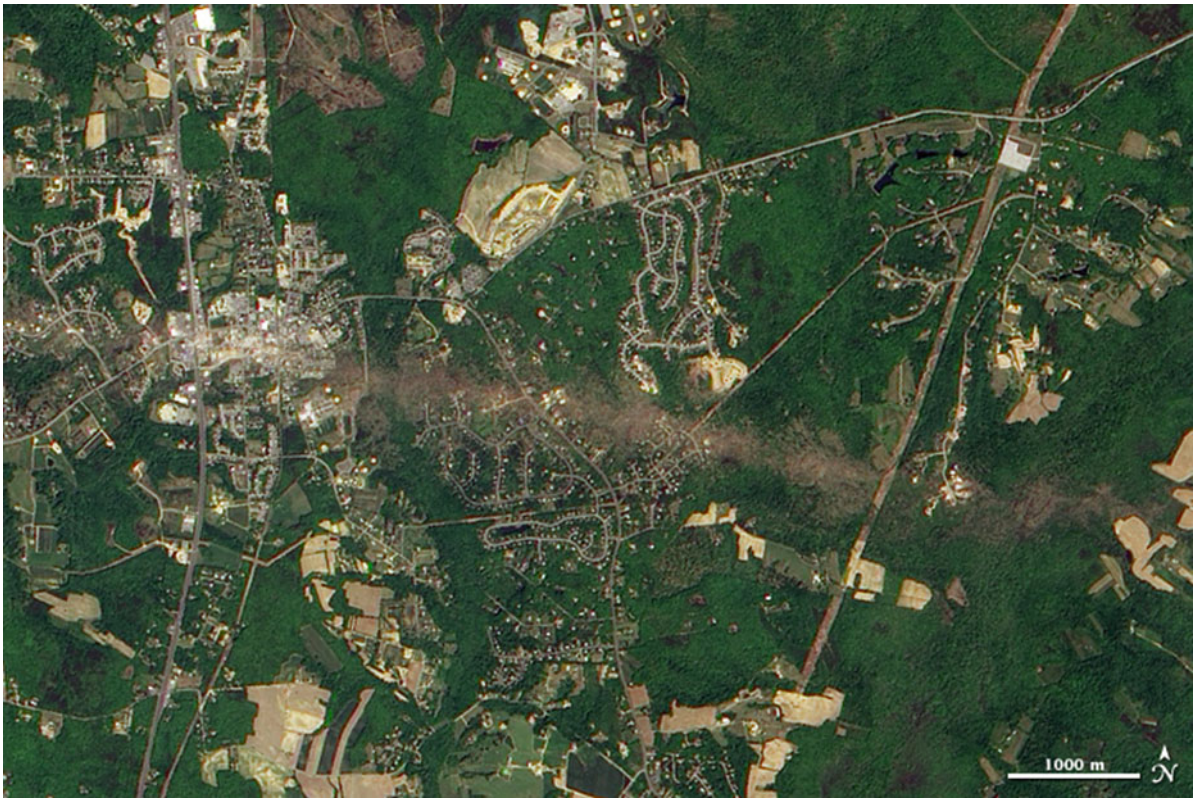

Remote Sensing of Natural Disasters. Figure 10
EO-1 advanced land imager imagery of La Plata, Maryland following tornado in May 2002 (Image courtesy of NASA earth observatory and NASA EO-1 team)

earthquakes, flooding, and tornadoes. For example, Fig. 8 shows the extent of the tsunami-induced flooding in northern Japan following the earthquake–tsunami disaster of March 2011. Figure 8a shows the "after" and Fig. 8b "before." The pair of images clearly indicates the large amount of flood damage and resultant inundation along the Kitakami river.

Another before/after application of satellite imagery for natural disasters is tracking landslide damage. Figure 9 highlights the progression of a landslide in Southern Italy near the town of Maierato using Advanced Land Imager (ALI) data from the EO-1 mission.

Figure 10 shows the devastation caused by a tornado in La Plata, Maryland in April 2002 (imagery from May 2002). In this EO-1 Advanced Land Imager (ALI) imagery, the devastation along the tornado's path is clearly shown in the image as a linear area following the tornadoes path from left to right in the image.

Future Directions

There are many areas of current work aimed at enhancing the utility of remote sensing for assessment, response, and mitigation of natural disasters. Central areas of improvement in remote sensing are directly relevant: improving the resolution of remote sensing, reducing the time lag from acquisition of data to delivery to users, increasing the temporal frequency of coverage, and improving the ability to correct data from degradation due to atmospheric, environmental, or man-made factors.

A major area of improvement is the integration of remote sensing data with environmental models. Increasingly, sensor data are automatically processed and fed into models that perform hindcasting, nowcasting, and forecasting. These models allow for key physical parameters to be estimated even if not directly measureable, for past or ongoing events, as well as the more typical forecasting of how events will progress. These capabilities have dramatic

ramifications for natural disasters. For example, such models can be used to estimate whether volcanic activity is increasing or decreasing. Or such capabilities can combine surface water data, topographical and terrain data, and weather forecasts to estimate areas likely at risk for flooding. Active fire mapping, terrain, vegetation, and weather data can be used to estimate likely progressions for active forest fires as a third example. In all of these cases, key data (much of it being remote sensing data) combined with modeling can provide important capabilities for disaster response and mitigation.

An additional exciting new area is the use of "sensorwebs" for environmental monitoring and specifically in the use of sensing for natural disasters. In a sensorweb, data are processed "on the fly" and used to actively reconfigure other portions of the sensorweb to better acquire data and track an evolving phenomena [51]. For example, detections of volcanic activity by one satellite might trigger observations by other satellites [52]. Or weather reports in concert with satellite rainfall observations might trigger observations of likely flood areas [16]. These techniques, in concert with modeling, will enhance future sensing of natural disasters.

Conclusions

Remote sensing has a wide range of applications to risk assessment, tracking, response, and mitigation of natural disasters. In this entry, we have outlined only a few of the applications to several categories of natural disasters focusing volcanoes, flooding, and fires. Remote sensing also provides secondary products such as topographical maps that are widely used in modeling natural disaster phenomena. Topographical maps can be used to estimate risk (to tsunamis, flooding, landslide, etc.) as well as provide inputs to model and predict flood progression, and lava and lahar flows. All of these areas and many more are the subject of active research with new applications and techniques being developed continuously.

Acknowledgments

Portions of the research described in this entry were carried out at the Jet Propulsion Laboratory, California Institute of Technology, under a contract with the National Aeronautics and Space Administration.

Bibliography

1. Harris AJ, Flynn LP, Dean K, Wooster EM, Okubo C, Mouginis-Mark P et al (2000) Real-time satellite monitoring of volcanic hot spots. Geophys Monogr 116:139–159
2. Wright R, Flynn LP, Garbeil H, Harris A, Piler E (2003) Automated volcanic eruption detection using MODIS. Remote Sens Environ 82:135–155
3. Wright R, Flynn LP, Garbeil H, Harris A, Piler E (2004) MODVOLC: near-real-time thermal monitoring of global volcanism. J Volcanol Geoth Res 135:29–49
4. Pieri D, Abrams M (2004) ASTER watches the world's volcanoes: a new paradigm for volcanological observations from orbit. J Volcanol Geoth Res 135(1–2):13–28
5. Davies AG, Chien S, Baker V, Doggett T, Dohm J, Greeley R, Ip F, Castano R, Cichy B, Rabideau G, Tran D, Sherwood R (2006) Monitoring active volcanism with the autonomous sciencecraft, experiment on EO-1. Remote Sens Environ 101:427–446
6. Davies AG, Calkins J, Scharenbroich L, Vaughan G, Wright R, Kyle P, Castano R, Chien S, Tran D (2008) Multi-instrument remote and in situ observations of the erebus volcano (Antarctica) lava lake in 2005: a comparison with the Pele lava lake on the Jovian moon Io. J Volcanol Geoth Res 177(3): 705–724
7. Pieri D, Gubbels T, Hufford G, Olsson G, Realmuto V (2006) Assessing mesoscale volcanic aviation hazards using ASTER. Eos Trans AGU 87(52). Fall meet. Suppl, Abstract H33E-1554
8. Novak MA, Watson IM, Delgado-Granados H, Rose WI, Cardenas-Gonzalez L, Realmuto VJ (2008) Volcanic emissions from Popocatépetl volcano, Mexico, quantified using moderate resolution imaging spectroradiometer (MODIS) infrared data: a case study of the December 2000–January 2001 emissions. J Volcanol Geoth Res 170:76–85
9. Andronico D, Spinetti C, Cristaldi A, Buongiorno MF (2009) Observations of Mt. Etna volcanic ash plumes in 2006: an integrated approach from ground-based and polar satellite NOAA–AVHRR monitoring system. J Volcanol Geoth Res 180(2–4):135–147
10. Tralli DM, Blom RG, Zlotnicki V, Donnellan A, Evans DL (2005) Satellite remote sensing of earthquake, volcano, flood, landslide and coastal inundation hazards. ISPRS J Photogramm 59(4):185–198
11. Joyce K, Samsonov S, Manville V, Jongens R, Graettiner A, Cronin S (2009). Remote sensing data types and techniques for lahar path detection: a case study at Mt Ruapehu, New Zealand. Remote Sens Environ113(8) 1778–1786; Wright R, Flynn L, Garbeil H, Harris A, Piler E (2002). Automated volcanic eruption detection using MODIS. Remote Sens Environ 82(1) 135–155
12. Brakenridge GR, Anderson E (2005) MODIS-based flood detection, mapping, and measurement: the potential for operational hydrological applications. In: Transboundary floods, proceeding of NATO advanced research workshop, Baile Felix – Oradea, 4–8 May 2005

13. Brakenridge G R (2010). DFO MODIS flood retrieval algorithm. http://floodobservatory.colorado.edu/Tech.html. Accessed 21 Mar 2011
14. Carroll M, Townshend J, Noojipady P, DiMiceli C, Sohlberg R (2009). Surface water dynamics derived from the MODIS data record. Spring AGU
15. Ip F, Dohm J, Baker V, Doggett T, Davies A, Castano R, Chien S, Cichy B, Greeley R, Sherwood R, Tran D, Rabideau G (2006) Flood detection and monitoring with the autonomous sciencecraft experiment onboard EO-1. Remote Sens Environ 101(4):463–481
16. Chien S, Doubleday J, Mclaren D, Tran D, Khunboa C, Leelapatra W, Plergamon V, Tanpipat V, Raghavendra C, Mandl D (2011). Using multiple space assets with In-situ measurements to track flooding in Thailand. In: 34th international symposium on remote sensing of environment, Sydney
17. Brakenridge GR, Nghiem SV, Anderson E, Chien S (2005) Space-based measurement of river runoff. Eos Trans AGU 86(19):185. doi:10.1029/2005EO190001
18. Townsend P (2001) Mapping seasonal flooding in forested wetlands using multi-temporal Radar- sat SAR. Photogramm Eng Remote Sens 67:3055–3074
19. Marti-Cardona B, Lopez-Martinez C, Dolz-Ripolles J, Blade-Castellet E (2010) ASAR polarimetric, multi-incidence angle and multitemporal characterization of Doñana wetlands for flood extent monitoring. Remote Sens Environ 114(11):2802–2815
20. Justice CO, Malingreau JP, Seltzer A (1993) Satellite remote sensing of fires: potential and limitations. In: Crutzen P, Goldammer J (eds) Fire in the environment: the ecological, atmospheric, and climatic importance of vegetation fires. Wiley, New York, pp 77–88
21. Prins EM, Menzel WP (1992) Geostationary satellite detection of biomass burning in South America. Int Remote Sens 13:2783–2799
22. Menzel WP, Prins EM (1996). Monitoring fire activity in western hemisphere with the new generation of geostationary satellites. In: 22nd conference on agricultural and forest meteorology with symposium on fire and forest meteorology, Atlanta, 28 Jan–2 Feb, 1996, pp 272–275
23. Elvidge C, Kroehl HW, Kihn EA, Baugh KE, Davis ER, Hao WM (1996) Algorithm for the retrieval of fire pixels from DMSP operational linescan system data. In: Levine JS (ed) Biomass burning and global change, vol 1. The MIT Press, Cambridge, MA, pp 73–85
24. Elvidge C, Dee WP, Elaine P, Eric AK, Jackie K, Kimberly EB (1998) Remote sensing change detection: environmental monitoring methods and applications, wildfire detection with meteorological satellite data: results from New Mexico during June of 1996 using GOES, AVHRR, and DMSP-OLS. CRC Press, Boca Raton, FL, pp 103–121
25. Arino O, Rosaz J (1999). 1997 and 1998 world ASTR fire atlas using ERS-2 ATSR-2 data. In: Neuenschwander LF, Tyan KC, Golberg GE (eds) Proceedings of the joint fire science conference, Boise, Idaho, 15–17 June 1999. University of Idaho and the International Association of Wildland Fire, Boise, pp 177–182
26. Giglio L, Kendall JD, Tucker CJ (2000) Remote Sensing of fires with TRMM VIRS. Int J Remote Sens 21:203–207
27. Giglio L, Descloitres J, Justice CO, Kaufman YJ (2003) An enhanced contextual fire detection algorithms for MODIS. Remote Sens Environ 87:273–282
28. Justice CO, Giglio L, Korontzi S, Owens J, Morisette JT, Roy D, Descloitres J, Alleaume S, Petitcolin F, Kaufman Y (2002) The MODIS fire products. Remote Sens Environ 83:244–262
29. Roy DP, Boschetti L, Justice CO, Ju J (2008) The collection 5 MODIS burned area product – Global evaluation by comparison with the MODIS active fire product. Remote Sens Environ 112(9):3690–3707. doi:10.1016/j.rse.2008.05.013, ISSN 0034-4257
30. Ressl R, Lopez G, Cruz I, Colditz RR, Schmidt M, Ressl S, Jimenez R (2009) Operational active fire mapping and burnt area identification applicable to Mexican nature protection areas using MODIS and NOAA-AVHRR direct readout data. Remote Sens Environ 113(6):1113–1126. doi:10.1016/j.rse.2008.10.016, ISSN 0034-4257
31. Amraoui M, DaCamara CC, Pereira JMC (2010) Detection and monitoring of African vegetation fires using MSG-SEVIRI imagery. Remote Sens Environ 114(5):1038–1052. doi:10.1016/j.rse.2009.12.019, ISSN 0034-4257
32. Tanpipat V, Honda K, Nuchaiya P (2009) MODIS hotspot validation over Thailand. Remote Sens 1:1043–1054. doi:10.3390/rs1041043, ISSN 2072-4292
33. Chuvieco E, Aguado I, Yebra M, Nieto H, Salas J, Martin MP, Vilar L, Martinez J, Martin S, Ibarra P, Riva JDL, Baeza J, Rodriguez F, Molina JR, Herrera MA, Zamora R (2010). Development of a framework for fire risk assessment using remote sensing and geographic information system technologies. Ecol Model 221(1 Special issue on spatial and temporal patterns of wildfires: models, theory, and reality) 46–58, doi:10.1016/j.ecolmodel.2008.11.017, ISSN 0304–3800
34. Maeda EE, Arcoverde GFB, Pellikka PKE, Shimabukuro YE (2011) Fire risk assessment in the Brazilian Amazon using MODIS imagery and change vector analysis. Applied Geography 31(1):76–84. doi:10.1016/j.apgeog.2010.02.004, ISSN 0143-6228
35. Schneider P, Roberts DA, Kyriakidis PC (2008) A VARI-based relative greenness from MODIS data for computing the Fire Potential Index. Remote Sens Environ 112(3):1151–1167. doi:10.1016/j.rse.2007.07.010, ISSN 0034-4257
36. Huesca M, Litago J, Palacios-Orueta A, Montes F, Sebastian-Lopez A, Escribano P(2009). Assessment of forest fire seasonality using MODIS fire potential: a time series approach. Agr Forest Meteorol 149(11 Special section on water and carbon dynamics in selected ecosystems in China) 1946–1955, doi:10.1016/j.agrformet.2009.06.022, ISSN 0168–1923
37. Giglio L, Loboda T, Roy DP, Quayle B, Justice CO (2009) An active-fire based burned area mapping algorithm for the MODIS sensor. Remote Sens Environ 113(2):408–420. doi:10.1016/j.rse.2008.10.006, ISSN 0034-4257

38. Libonati R, DaCamara CC, Pereira JMC, Peres LF (2010) Retrieving middle-infrared reflectance for burned area mapping in tropical environments using MODIS. Remote Sens Environ 114(4):831–843. doi:10.1016/j.rse.2009.11.018, ISSN 0034-4257
39. Dubinin M, Potapov P, Lushchekina A, Radeloff VC (2010) Reconstructing long time series of burned areas in arid grasslands of southern Russia by satellite remote sensing. Remote Sens Environ 114(8):1638–1648. doi:10.1016/j.rse.2010.02.010, ISSN 0034-4257
40. Zhang X, Kondragunta S (2008) Temporal and spatial variability in biomass burned areas across the USA derived from the GOES fire product. Remote Sens Environ 112(6):2886–2897. doi:10.1016/j.rse.2008.02.006, ISSN 0034-4257
41. Veraverbeke S, Lhermitte S, Verstraeten WW, Goossens R (2011) A time-integrated MODIS burn severity assessment using the multi-temporal differenced normalized burn ratio (dNBRMT). Int J Appl Earth Obs Geoinformation 13(1):52–58. doi:10.1016/j.jag.2010.06.006, ISSN 0303–2434
42. Santis AD, Asner GP, Vaughan PJ, Knapp DE (2010) Mapping burn severity and burning efficiency in California using simulation models and landsat imagery. Remote Sens Environ 114(7):1535–1545. doi:10.1016/j.rse.2010.02.008, ISSN 0034–4257
43. Fox DM, Maselli F, Carrega P (2008) Using SPOT images and field sampling to map burn severity and vegetation factors affecting post forest fire erosion risk. CATENA 75(3):326–335. doi:10.1016/j.catena.2008.08.001, ISSN 0341–8162
44. Yebra M, Chuvieco E, Riano D (2008) Estimation of live fuel moisture content from MODIS images for fire risk assessment. Agr Forest Meteorol 148(4):523–536. doi:10.1016/j.agrformet.2007.12.005, ISSN 0168–1923
45. Peterson HS, Roberts DA, Dennison PE (2008) Mapping live fuel moisture with MODIS data: A multiple regression approach. Remote Sens Environ 112(12):4272–4284. doi:10.1016/j.rse.2008.07.012, ISSN 0034–4257
46. Hyer EJ, Chew BN (2010) Aerosol transport model evaluation of an extreme smoke episode in Southeast Asia. Atmos Environ 44(11):1422–1427. doi:10.1016/j.atmosenv.2010.01.043, ISSN 1352–2310
47. Henderson SB, Burkholder B, Jackson PL, Brauer M, Ichoku C (2008) Use of MODIS products to simplify and evaluate a forest fire plume dispersion model for PM10 exposure assessment. Atmos Environ 42(36):8524–8532. doi:10.1016/j.atmosenv.2008.05.008, ISSN 1352–2310
48. Zhang X, Kondragunta S, Schmidt C, Kogan F (2008) Near real time monitoring of biomass burning particulate emissions (PM2.5) across contiguous United States using multiple satellite instruments. Atmos Environ 42(29):6959–6972. doi:10.1016/j.atmosenv.2008.04.060, ISSN 1352–2310
49. Balch JK, Nepstad DC, Curran LM, Brando PM, Portela O, Guilherme P, Reuning-Scherer JD Jr, Carvalho OD (2011) Size, species, and fire behavior predict tree and liana mortality from experimental burns in the Brazilian Amazon. Forest Ecol Manage 261(1):68–77. doi:10.1016/j.foreco.2010.09.029, ISSN 0378–1127
50. Bonazountas M, Kallidromitou D, Kassomenos P, Passas N (2006) A decision support system for managing forest fire casualities. Environ Manage. doi:10.1016/j.jenvman.2006.06.016
51. Chien S, Cichy B, Davies A, Tran D, Rabideau G, Castano R, Sherwood R, Mandl D, Frye S, Shulman S, Jones J, Grosvenor S (2005) An autonomous earth observing sensorweb. IEEE Intell Syst 20:16–24
52. Chien S, Davies A, Doubleday J, Tran D, Jones S, Kjartansson E, Vogfjord K, Gudmundsson M, Thordarson T, Mandl D (2011). Integrating multiple space and ground sensors to track volcanic activity. In: 34th international symposium on remote sensing of environment, Sydney

Remote Sensing of Ocean Color

Heidi M. Dierssen, Kaylan Randolph
Department of Marine Sciences, University of Connecticut, Groton, CT, USA

Article Outline

Glossary
Definition of the Subject, Relevance, Motivation
Introduction
Optical Properties of the Water Column
Basics of Ocean Color Remote Sensing
Ocean Color Algorithms
Applications for Oceanography
Applications for Environmental Monitoring
Future Directions
Bibliography

Glossary

Absorption, $a(\lambda)$ The fraction of a collimated beam of photons in a particular wavelength (λ), which is absorbed or scattered per unit distance within the medium (units 1/length or m^{-1}). Photons which are absorbed by ocean water alter the spectral distribution of light that can be observed remotely.

Apparent optical properties (AOP) Optical properties which depend primarily on the medium itself but have a small dependence on the ambient light field. Typically, AOPs are derived from measurements of the ambient light field, particularly upwelling and downwelling radiance and irradiance. Principal AOPs include irradiance reflectance,

remote sensing reflectance, and the diffuse attenuation coefficients.

Backscattering, $b_b(\lambda)$ Light of a particular wavelength (λ) that is scattered in a direction 90–180° away from its original path (i.e., backward hemisphere). Backscattered light is what is measured as ocean color in remote sensing, namely, downward propagating sunlight that has been redirected back toward the sea surface and out into the atmosphere. For natural waters, only a few percent of the light entering the ocean is backscattered out.

Colored or chromophoric dissolved organic material (CDOM) CDOM is yellow-brown in color and absorbs primarily ultraviolet and blue light decreasing exponentially with increasing wavelength. Produced from the decay of plant material, it consists mainly of humic and fulvic acids and is operationally defined as substances that pass though a 0.2 μm filter.

Diffraction Light which propagates or bends along the boundary of two different mediums with different indices of refraction.

Diffuse attenuation coefficient, K(λ) A normalized depth derivative that describes the rate of change of light, plane incident irradiance, with depth. Sunlight underwater typically decreases exponentially with depth.

Index of refraction (real), n The speed of light in a medium, c_{med}, relative to the speed of light in a vacuum, c_v expressed as $n = c_v/c_{med}$. The real index of refraction determines the scattering of light at the boundary between two different mediums and within the medium from thermal and molecular fluctuations. The relative refractive index, n', is the ratio of the speed of light within the medium, c_m, to the speed of light within a particle, c_p. As n' deviates from 1, the scattering caused by the particle increases for a general size and shape particle (e.g., minerals and bubbles).

Inherent optical properties (IOP) Optical properties which depend on the medium itself and are independent of the ambient light field. IOPs are defined from a parallel beam of light incident on a thin layer of the medium. Two fundamental IOPs are the absorption (a) and the volume scattering coefficient (β), which describe how light is either absorbed or directionally scattered by ocean water.

Irradiance (downward planar), $E_d(\lambda)$ The incremental amount of radiant energy per unit time (W) incident on the sensor area (m^{-2}) from all solid angles contained in the upper hemisphere, expressed per unit wavelength of light (λ, nm^{-1}). This is used to measure the amount of spectral energy from the sun reaching the sea surface.

Irradiance reflectance, R(λ) The ratio of the upwelling irradiance, $E_u(\lambda)$, to the plane downwelling irradiance, $E_d(\lambda)$, in different wavelengths (λ).

Optical depth, ζ A measure of how opaque a medium is to radiation. The optical depth is a function of the geometric depth and the vertical attenuation coefficient.

Optically shallow waters An aquatic system where the spectral reflectance off the bottom contributes to radiance measured above the sea surface and is defined by the water clarity, bottom depth, and bottom composition.

Photosynthetically available radiation (PAR) The integrated photon flux (photons per second per square meter) within the 400–700 nm wavelength range at the ocean surface. PAR is the total energy available to phytoplankton for photosynthesis and is reported in units of Q m^{-2} s^{-1}, where Q is quanta, or in μE m^{-2} s^{-1}, where E is Einsteins.

Radiance, $L(\lambda)$ The incremental amount of radiant energy per unit time (in Watts) incident on the sensor area (m^{-2}) in a solid angle view (sr^{-1}) per unit wavelength (λ) of light (nm^{-1}). A satellite measures radiance.

Reflection At the boundary of two different mediums with different indices of refraction, a certain amount of radiation is returned at an angle equal to the angle of incidence.

Refraction The direction of light propagation changes, or is bent, at the boundary between two mediums with different indices of refraction. The refracted light bends toward the normal boundary when the index of refraction increases from one medium to another and away from the normal boundary when the index of refraction decreases from one medium to another.

Remote sensing reflectance, $R_{rs}(\lambda)$ A specialized ratio used for remote sensing purposes formulated as the ratio of the spectral water-leaving radiance, $L_w(\lambda)$, to the plane irradiance incident on the water, $E_d(\lambda)$.

It represents the spectral distribution of sunlight penetrating the sea surface that is backscattered out again and potentially measured remotely. Theoretically, it is proportional to spectral backscattering $b_b(\lambda)$ and inversely proportional to absorption $a(\lambda)$ of the surface water column.

Water-leaving radiance, $L_w(\lambda)$ The component of the radiance signal measured above the water consisting of photons that have penetrated the water column and been backscattered out through the air-sea interface. It does not include photons reflected off the sea surface, also called sun glint.

Definition of the Subject, Relevance, Motivation

The oceans cover over 70% of the earth's surface and the life inhabiting the oceans play an important role in shaping the earth's climate. Phytoplankton, the microscopic organisms in the surface ocean, are responsible for half of the photosynthesis on the planet. These organisms at the base of the food web take up light and carbon dioxide and fix carbon into biological structures releasing oxygen. Estimating the amount of microscopic phytoplankton and their associated primary productivity over the vast expanses of the ocean is extremely challenging from ships. However, as phytoplankton take up light for photosynthesis, they change the color of the surface ocean from blue to green. Such shifts in ocean color can be measured from sensors placed high above the sea on satellites or aircraft and is called "ocean color remote sensing." In open ocean waters, the ocean color is predominantly driven by the phytoplankton concentration and ocean color remote sensing has been used to estimate the amount of chlorophyll *a*, the primary light-absorbing pigment in all phytoplankton. For the last few decades, satellite data have been used to estimate large-scale patterns of chlorophyll and to model primary productivity across the global ocean from daily to interannual timescales. Such global estimates of chlorophyll and primary productivity have been integrated into climate models and illustrate the important feedbacks between ocean life and global climate processes. In coastal and estuarine systems, ocean color is significantly influenced by other light-absorbing and light-scattering components besides phytoplankton. New approaches have been developed to evaluate the ocean color in relationship to colored dissolved organic matter, suspended sediments, and even to characterize the bathymetry and composition of the seafloor in optically shallow waters. Ocean color measurements are increasingly being used for environmental monitoring of harmful algal blooms, critical coastal habitats (e.g., seagrasses, kelps), eutrophication processes, oil spills, and a variety of hazards in the coastal zone.

Introduction

Remote sensing of ocean color allows for the estimation of phytoplankton biomass and carbon fixation over the global ocean. From these data, approximately half of the global carbon fixation is estimated to occur by ocean phytoplankton, accounting for roughly 50 Gt C year^{-1} [1, 2]. Phytoplankton are the base of the marine food web, responsible for producing organic carbon from carbon dioxide. The premise behind ocean color remote sensing is to relate the intensity and spectral distribution of visible light reflected out of the water ("ocean color") to the biological and biogeochemical processes that influence the optical properties of the water column ("bio-optical properties") [3]. The distribution, abundance, and temporal variation in various biological, physical, and chemical processes can be observed synoptically from local and regional to global spatial scales from sensors placed on satellites or aircraft. Ocean color remote sensing provides the long-term, continuous time series of phytoplankton biomass and productivity data necessary for global carbon cycle and climate research [4–6], but the uses of ocean color data are increasingly diverse from military to environmental monitoring applications [7].

Phytoplankton have a marked influence on the subsurface and emergent light field [8]. The light harvesting systems of phytoplankton, including the chlorophyll *a* pigment which is ubiquitous among phytoplankton species, absorb light across the visible spectrum and influence the color of the near-surface ocean [9]. An increase in absorption, or reduction in reflectance, in the blue relative to the green portion of the spectrum can be empirically related to chlorophyll *a* concentration [10]. In other words, as phytoplankton are added to the water column, more blue light is absorbed and the reflected color changes from blue to green. The advent of space-based ocean color sensors in

1978 with NASA's Coastal Zone Color Scanner (CZCS) and the follow on Sea-viewing Wide Field of View Sensor (SeaWiFS) in 1997 greatly enhanced the understanding of phytoplankton distribution and concentration in the ocean [11]. Satellite ocean color imagery provides estimates of phytoplankton abundance across all ocean basins (Atlantic, Pacific, Indian, Arctic, and Southern Oceans) and quantifies the variability from seasonal to interannual timescales.

Over the last several decades, ocean color has expanded beyond chlorophyll and a whole field has emerged to study how the nature of the upwelling light field changes as a function of the quantity and composition of a variety of constituents in the near-surface ocean, including biogenic and nonbiogenic inorganic material, nonliving and living organic material (i.e., phytoplankton, bacteria and viruses), dissolved substances, and benthic habitats. Ocean color research has sought to define the fundamental relationship between the inherent optical properties of the ocean, or the absorption and scattering properties of the constituents, and water-leaving radiance. With improved technology, including radiometers with better spectral resolution, calibration, and a high signal-to-noise ratio, and in situ optical instrumentation, which provided a description of the optical properties of oceanic constituents, biogeochemical parameters are being estimated with greater accuracy and precision. Ocean color remote sensing has moved beyond estimations of chlorophyll alone and is now used to measure total suspended sediment, colored dissolved organic material, particulate inorganic carbon, and phytoplankton functional groups, as well as critical habitats and hazards influencing pelagic and coastal waters.

Optical Properties of the Water Column

Scattering and absorption of photons, the basic unit of light energy, in the surface ocean determines the intensity and spectral shape of the water-leaving light signal measured at an ocean color sensor. Photons that propagate into the ocean interact with water molecules, dissolved and particulate matter and are either absorbed or scattered. Because most of the light is propagated downward into the water column, only a small amount of the signal is scattered back out of the water column and measured remotely. The bulk optical properties of water are used to describe how the spectral and directional distribution of photons is altered within the natural water body.

Inherent Optical Properties

The absorption and scattering properties of water molecules and the dissolved and particulate constituents within the water are called inherent optical properties (IOPs). IOPs do not depend on the ambient light conditions, but are a function of the medium alone. The two IOPs commonly used for remote sensing purposes include the *absorption* (a) and scattering (b) coefficients, which refer to the fraction of incident light, a single, narrow, collimated beam of photons, which is absorbed or scattered per unit distance within the medium (units 1/length or m^{-1}). The scattering coefficient stems from the volume scattering function (β), which is the differential scattering cross section per unit volume per solid angle, and is calculated as the integral over all directions (0–180°). The attenuation coefficient (c) accounts for the reduction in light intensity due to absorption and scattering processes combined.

Both absorption and scattering processes can change the color of the ocean as observed from a satellite. Oceanic constituents that are primarily responsible for absorption of photons include water molecules, phytoplankton pigments, particulate detritus, and *colored or chromophoric dissolved organic material* (CDOM) (Fig. 1). Pure water is increasingly effective at absorbing light at wavelengths greater than 550 nm and absorbs minimally in the blue and green portion of the visible spectrum. Conversely, CDOM, operationally defined as all of the colored material that passes through a 0.2 μm filter, absorbs maximally in the ultraviolet and blue portion of the spectrum, decreasing exponentially with wavelength at a rate which is related to the composition, or degradation state, of the material. CDOM is generally comprised of humic and fulvic acids and small colloidal material released through the degradation of plant tissue, whether in soils or in water [12, 13]. Commonly, CDOM is modeled with an exponential function, but a hyperbolic model may be more accurate [14]. Nonliving particulate material, called detritus or tripton, absorbs in a manner similar to CDOM and the two components are difficult to differentiate spectrally.

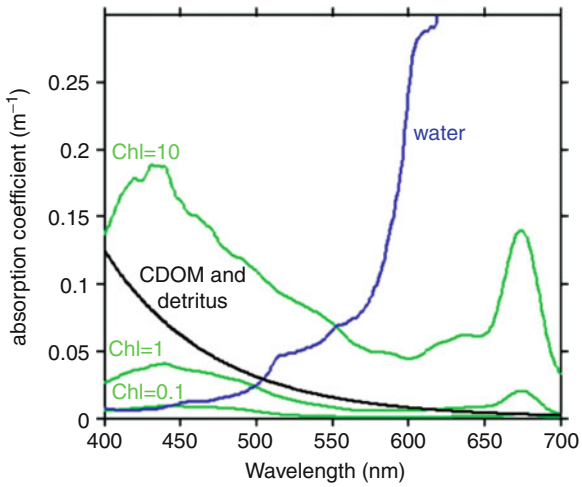

Remote Sensing of Ocean Color. Figure 1
Absorption spectrum for different constituents in seawater including water molecules, chromophoric dissolved organic matter and detritus, and phytoplankton contributions bio-optically modeled for chlorophyll at 0.1, 1 and 10 mg m^{-3} [16]

Phytoplankton absorb light in a complex manner related to the composition and quantity of their photosynthetic pigments, molecules structured to absorb photons within the visible range of 400–700 nm, dubbed *photosynthetically available radiation* or PAR. There are three distinct classes of pigments, namely, chlorophylls, carotenoids, and biliproteins [101]. All phytoplankton contain chlorophyll *a* and most contain chlorophylls *b* and/or *c*. Chlorophylls *a*, *b*, and *c* have two strong absorption bands in the red and blue portions of the spectrum. Chlorophyll *a* absorption is low in the green (450–650 nm) portion of the spectrum. The presence of chlorophylls *b* and *c* extend the range of light available for photosynthesis further into both the short- and regions. Carotenoids, of which there are many types, have both light harvesting and photoprotective functions. Finally, some phytoplankton contain red or blue pigments called biliproteins, which are divided into classes based on the position of their absorption peaks. The phytoplankton absorption coefficient describes the spectral absorption for natural waters comprised of mixtures of phytoplankton and has been commonly parameterized by chlorophyll concentration and dominant cell size [15, 16].

Scattering processes, which include *refraction*, *reflection* and *diffraction*, occur at the boundary of a particle with a different *index of refraction*, the ratio of the speed of light in the surrounding medium to the speed of light within the particle, than the surrounding medium. Scattering is predominantly elastic, the energy of the photon is conserved, but the direction of propagation is altered. Rather than reducing light, scattering works to inhibit the straight-path vertical penetration of light. The total scattering coefficient (b) can be subdivided into light which scatters in the forward direction (b_f) (0–90°) and the backward direction (b_b) (90–180°) relative to the unattenuated beam. The backscattered light is the radiance that is scattered out of the water column and measured by a sensor as "ocean color." The magnitude of b_b is a function of the concentration, composition (i.e., index of refraction), shape, and size of particles [17].

Water molecules, salts, organic and inorganic particles, and bubbles provide strong contributions to light scattering in the ocean. Scattering by pure water is the result of density fluctuations from the random motion of water molecules and has a wavelength dependence of λ^{-4} [18]. The presence of salt increases scattering, where pure seawater, with a salinity of 35–38‰, scatters 30% more light than pure water devoid of salt. When particles are present, as in natural waters, scattering increases markedly [19]. The scattering coefficient for the clearest surface waters is an order of magnitude greater than that of pure seawater. Particles that are large relative to the wavelength of light scatter mainly in the forward direction via diffraction, where photons propagating along the particle boundary change their direction in response to the boundary in a manner proportional to the cross-sectional area of the particle. Photons entering large particles are likely absorbed. Conversely, small particles mainly reflect and refract light in a manner proportional to the volume of the particle. Small particles with an index of refraction that deviates markedly from 1, including micron (10^{-6} m)-sized calcium carbonate plates or coccoliths generated by coccolithophorid phytoplankton ($n' = 1.25$) or bubbles ($n' = 0.75$), are highly efficient at scattering light in the backward direction [17].

The processes of absorption and scattering are considered additive, therefore the sum of the contribution of each constituent determines the magnitude of the

total coefficients a_t and b_t. As such, IOPs are separated into operationally defined components which comprise a and b_b:

$$a_t = a_w + a_{ph} + a_d + a_g, \text{ and}$$
$$b_{bt} = b_{bw} + b_{bp}$$

where the subscripts correspond to water (w), algal or phytoplanktonic (ph), non-algal or detrital (d) matter, and dissolved material, originally termed "gelbstoff" (g). Dissolved material does not scatter light and the contributions of both algal and non-algal matter are generally consolidated into backscattering from particulate (p) material. Recent advances in optical instrumentation have allowed for the measurement of absorption and scattering properties in situ and contributed to advances in ocean color remote sensing [20].

Apparent Optical Properties

Measurements of how light of different wavelengths attenuates with depth in the water column have been the historical basis of optical oceanography [21] following from the use of white Secchi disks to estimate water clarity. The properties that can be derived from measurements of ambient light in the water column are generally termed "apparent" optical properties (AOP) because they operate as optical properties describing the fundamental properties of the medium with only a slight dependence on the angular distribution of the light field. Spectral radiance, L, is the fundamental radiometric quantity which describes the spatial, temporal, directional, and wavelength-dependent structure of the light field in units of radiant flux per area per wavelength per solid angle (W m^{-2} nm^{-1} sr^{-1}) [18]. Planar downwelling irradiance, E_d, is a measure of the radiant energy flux incident on the surface from all directions or solid angles contained in the upper hemisphere, with units of radiant flux per unit area per unit wavelength (W m^{-2} nm^{-1}). The same concept, applied to the lower hemisphere, describes upwelling irradiance, E_u. The ratio of the upwelling to downwelling irradiance yields *irradiance reflectance*, R, a measure of how much light of a certain wavelength entering the ocean is scattered backward by ocean molecules and particles.

For remote sensing purposes, only the radiance from a specific direction is measured by a sensor, not the entire upwelling irradiance. Hence, the color is parameterized as *remote sensing reflectance* (R_{rs}, sr^{-1}), which is the ratio of water-leaving radiance to downwelling irradiance. The term "water-leaving radiance" represents the radiance signal emerging from the water column in a nadir direction and specifically excludes those upward-directed photons that have only reflected off the sea surface and not penetrated the water column (i.e., sun glint). The term R_{rs} represents the proportion of the downwelling light incident on the water surface that is returned through the air-water interface in the nadir direction due to differential absorption and scattering processes. The parameter R_{rs} is proportional to backscattering coefficient and inversely proportional to absorption coefficient and can be approximated as:

$$R_{rs} = \frac{f}{Q}\frac{b_b}{(a + b_b)}$$

where the ratio f/Q is related to the bidirectionality of the light field and varies from 0.09 to 0.11 for most remote sensing applications [22].

The rate of change of radiance and irradiance with depth, known as the vertical diffuse attenuation coefficient (K; m^{-1}), is another principle AOP. Irradiance and radiance decrease approximately exponentially with depth. The downward diffuse attenuation coefficient, K_d, the rate of decrease in downwelling irradiance, $E_d(0)$, with depth (z),

$$E_d(z) = E_d(0)e^{-K_d z}$$

is commonly used in biological studies and is closely linked to the absorption coefficient of the medium specifically. The optical depth, ζ, corresponding to any given physical depth is defined below:

$$\zeta = K_d z$$

Optical depths frequently used by biologists include 2.3 and 4.6, corresponding to the 10% and 1% light levels, respectively. Also, the portion of the surface water column contributing 90% of the water-leaving radiance has a depth, z, described by $z = 1/K_d$ [12]. The radiative transfer equation is the mathematical formulation that defines the relationship between the apparent and inherent optical properties of natural water bodies [18] and is the basis for the semi-analytical models used in ocean remote sensing.

Basics of Ocean Color Remote Sensing

Many challenges are inherent to remote sensing of ocean color. In comparison to land, the ocean target is dark, with an albedo of only a few percent. This means that most of the light that enters the water is propagated downward into the water column and only a few percent is scattered back out again. This is quite different from land and ice surfaces which have a much higher albedo. Most ocean color sensors are passive in that they measure only the radiation that originates from the sun, as opposed to active sensors that produce and sense their own stream of light (e.g., Light Detection and Ranging or LIDAR). Viewed from space, moreover, the ocean is observed through a thick atmosphere which reflects sunlight back to the sensor and is significantly brighter in the visible wavelengths than the water itself. In technical terms, this is quantified as a low signal-to-noise ratio where the "signal" is the light reflected from within the ocean and the "noise" is light reflected from the atmosphere and sea surface. This section outlines the platforms, calibration, atmospheric correction, and levels of data processing critical for successful ocean color remote sensing.

Sensors and Platforms

Ocean color sensors can be mounted on space-based satellites or on suborbital platforms like aircraft or unmanned aerial vehicles. The spatial and temporal sampling and the questions that can be addressed with the data depend on the type of platform employed. Most current ocean color sensors have a wide field of view, which translates to a wide sampling swath, and are mounted on sun synchronous polar-orbiting satellites (e.g., CZCS, SeaWiFS, MODIS Aqua and Terra). These sensors have the potential to provide global coverage of the earth roughly every 3 days at the equator and more frequently at the poles. However, clouds obscure the ability of the sensor to view the ocean color and, in reality, temporal sampling for any given region is much less. Data are frequently averaged over longer time periods to produce weekly, monthly, and seasonal composite images of the global ocean (Fig. 2). The spatial resolution is also limited nominally to 1 km pixel widths (and down to 250 m for select channels) in these polar-orbiting sensors in part because of limitations in signal-to-noise inherent to the dark ocean surfaces (see atmosphere correction below). Global datasets are often aggregated to 4-km

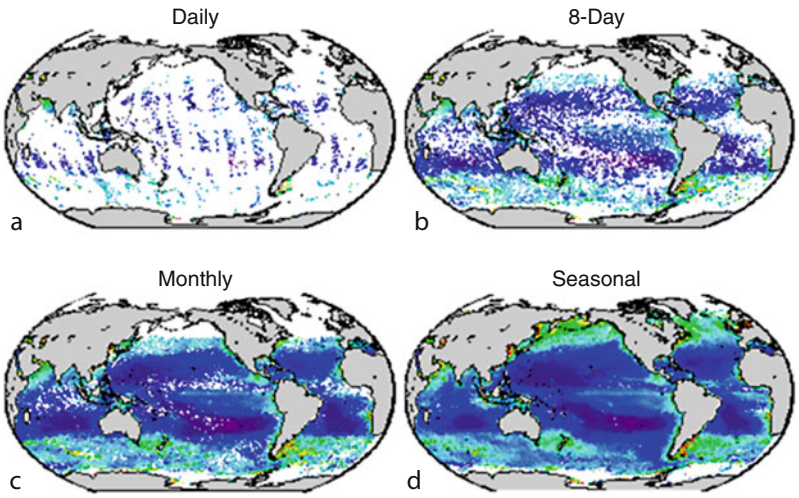

Remote Sensing of Ocean Color. Figure 2
Global maps of satellite-derived chlorophyll showing increasing levels of temporal resolution from daily to seasonal. Imagery from MODIS Aqua satellite from 2006: (**a**) 17 December; (**b**) 11–17 December; (**c**) 1–31 December; (**d**) Autumn. White spacing in imagery represents gaps in orbital coverage (daily image), as well as clouds and ice cover. Merging of imagery from different sensors can provide enhanced daily coverage [100]

or 9-km pixels. However, higher spatial resolution on the scale of meters can be obtained from some space-based platforms and from ocean color sensors placed on aircraft (Fig. 3).

The current suite of ocean color sensors has nominally six to seven spectral bands spanning the visible wavelengths (400–700 nm). These bands are not spread uniformly across the visible spectrum, but have been selected to correspond to reflectance characteristics of open ocean waters, particularly those related to phytoplankton pigment absorption features. Three bands are generally found in the "blue" (near 410, 440, and 490 nm), one to two bands in the "green" (510 or 530, 560 nm), and one to two channels in the

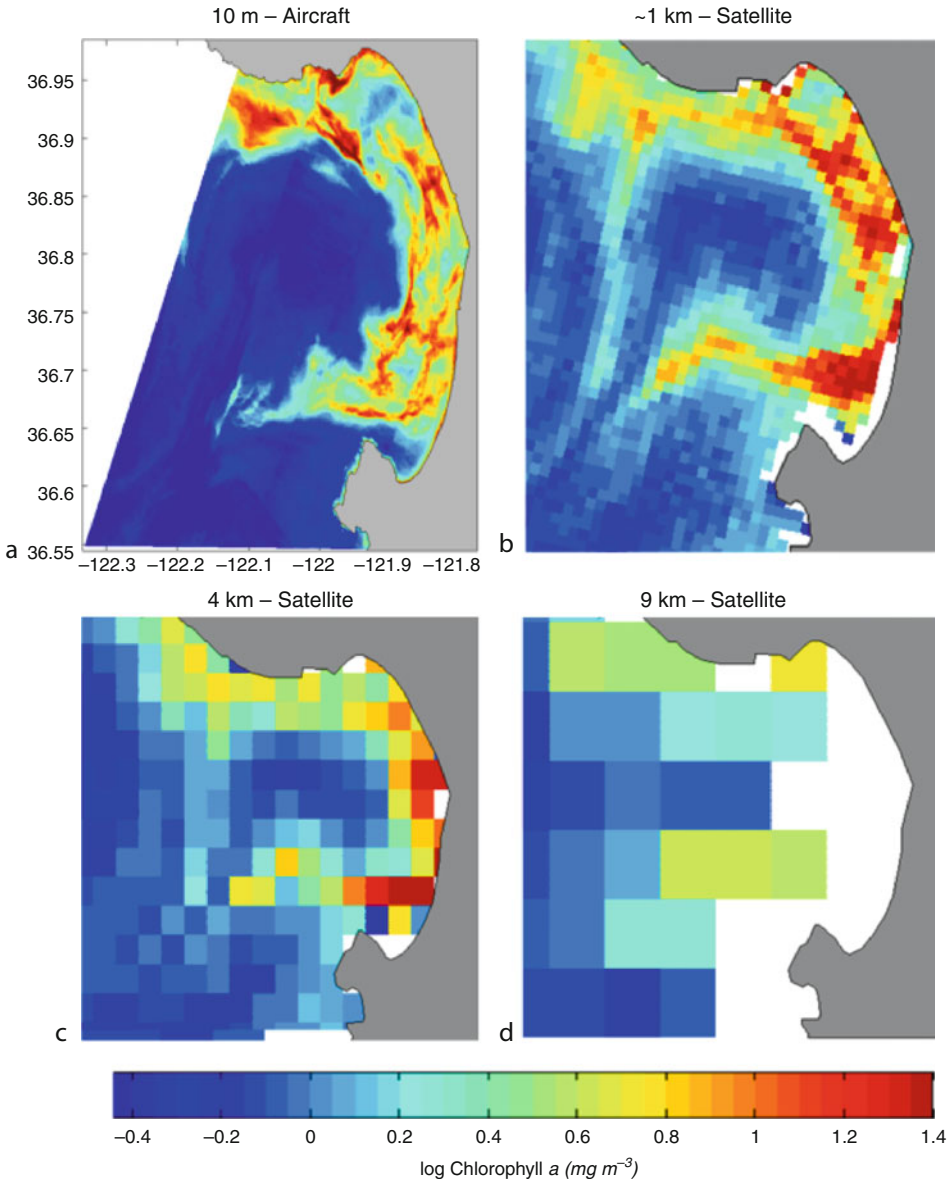

Remote Sensing of Ocean Color. Figure 3

Ocean color remote sensing imagery of Monterey Bay, California, illustrates different spatial resolutions available: (**a**) AVIRIS sensor flown on an aircraft, 10 m pixels [25]; (**b**) SeaWiFS satellite Level 2 data, 1 km pixels; (**c**) SeaWiFS satellite gridded to 4-km pixels; (**d**) SeaWiFS satellite Level 3 9-km standard product

"red" (670, 680 nm). In addition, channels are also incorporated in the near infrared (NIR) to short-wave infrared (SWIR) for purposes of atmospheric correction (see section "Atmospheric Correction"). Most of the visible channels were selected to match absorption features of phytoplankton and other constituents. Additional channels are also needed to bridge the large 100 nm gap between 560 and 670 nm, where absorption features are dominated by water, to better constrain backscattering in complex coastal waters [23, 24]. New technology has allowed for the development of sensors that span the full range of visible and near infrared (NIR) spectrum or "hyperpsectral," also referred to as imaging spectrometers.

No single platform is ideal for addressing all of the temporal and spatial variability in the oceans. A constellation of ocean color imagers with complementary capabilities and specifications is ultimately required to adequately address the diverse requirements of the coastal research and applied user communities. For example, the Hyperspectral Imager for the Coastal Ocean (HICO) was recently installed on the International Space Station for the study of the coastal ocean and adjacent lands. This imaging spectrometer is intended to provide hyperspectral imagery at 100-m resolution sampling at different angles and times of the day for selected regions. Sensors are also being considered for placement on geostationary satellites, similar to the international constellation of meteorological satellites. Such sensors would look at the same regional location on earth for extended periods of time and be able to provide better temporal resolution of ocean processes and episodic hazards. Regional efforts such as the Geostationary Ocean Color Imager (GOCI) on the COMS-1 platform from South Korea are already planned for launch. In addition, higher spatial and spectral resolution polar orbiting sensors are proposed to address questions related to seasonal variability in global coastal habitats and polar ice cover.

Portable sensors flown on aircraft or unmanned aerial vehicles (UAV's) provide a critical sampling niche distinct from satellite-borne sensors that is particularly well suited for coastal applications and ice research (Fig. 3a) [25]. Airborne sensors can sample at finer spatial scales (meters), can operate under clouds and with nearly unlimited repeat coverage, and are effective platforms for high-resolution active sensors (e.g., LIDAR). Flight lines and scanning geometries can also be oriented to avoid sun glint and their range can be greatly expanded by launching from ships. The technology required to build portable sensors for coastal applications is developing with wide field of views, minimum polarization dependence, high response uniformity, and optimized signal-to-noise ratio for low-light channels [26, 27]. These sensors are becoming more popular for use in the environmental management of coral reefs, seagrasses, kelps, and other coastal targets, and have the potential to monitor episodic events such as harmful algal blooms and runoff and flooding from storms.

Ocean color sensors in space have traditionally been "whisk broom" in design where a single detector collects data one pixel at a time as the telescope rotates to build up pixels along a scan line. Some satellites and most of the suborbital sensors are "pushbroom" where the entire scan line is imaged synoptically by a line of sensors arranged perpendicularly to the flight direction. In order to achieve high-quality data that can track climatological trends in ocean color, sensors are required to have very high radiometric accuracy and stability. Detectors are calibrated pre- and post-launch and degradation over time is carefully quantified with vicarious calibrations from field measurements and ideally lunar imaging. Periodic reprocessing of the satellite data is considered critical to obtaining high-quality datasets and continuity over multiple missions [5, 28].

Atmospheric Correction

One of the most challenging aspects of ocean color remote sensing is successfully removing the atmospheric signal from the water column signal. Aerosols and gas molecules are the primary contributors to the radiance measured at the top of the atmosphere. Approximately 80–85% of the radiance measured at the sensor is the result of Rayleigh scattering by molecules in the atmosphere that are small relative to the wavelength of light. Photons reaching the sensor (L_u) are a combination of those scattered by the atmosphere (L_p), reflected at the air-water interface (L_r), known as specular reflection, or have been backscattered from within the water column, dubbed water leaving radiance, or L_w (Fig. 4). The water-leaving radiance, used for most ocean color applications, is only a small portion of the signal retrieved at a satellite and must be

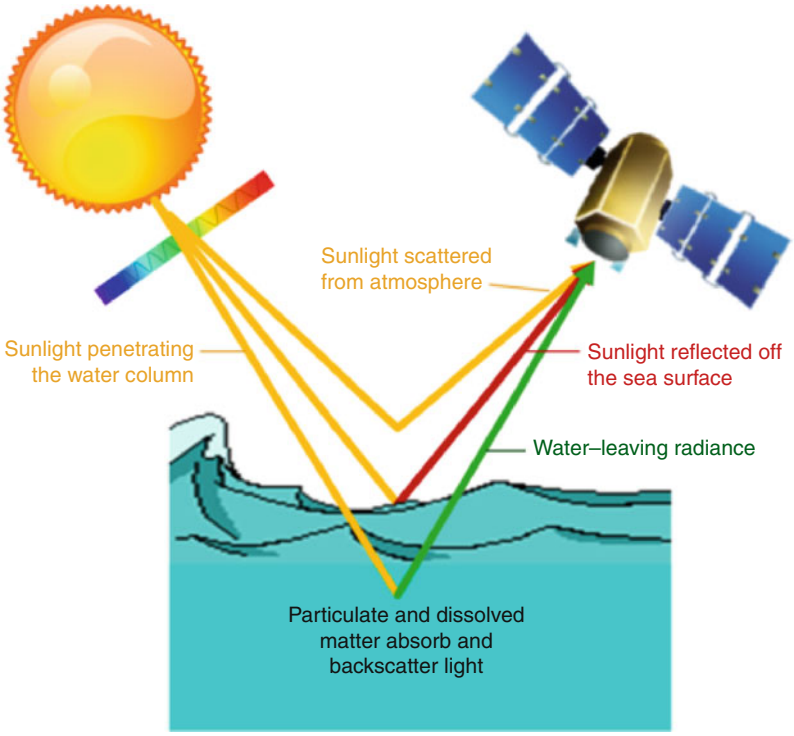

Remote Sensing of Ocean Color. Figure 4
Radiance measured by a satellite includes light scattered by the atmosphere and reflected off the sea surface (i.e., glint). In a process called "atmospheric correction," these signals are removed leaving the "water-leaving radiance" or the light that has penetrated the water column and been backscattered out to the satellite – a measure of ocean color

differentiated from the photons scattered within the atmosphere and specularly from the sea surface in a process called "atmospheric correction."

Rayleigh scattering, which decreases with wavelength (λ) following λ^{-4}, can be estimated using a single-scattering radiative transfer equation using the atmospheric pressure and appropriate viewing geometry [29]. An additional 0–10% of the radiance signal is due to aerosols (i.e., haze, dust, and pollution), particles with sizes comparable to the wavelength of light which absorb and scatter as a complex function of their type, size, and concentration. The type and concentrations of aerosols overlying the ocean are quite variable in space and time, particularly in coastal regions subject to urban pollution and terrestrial dust [30].

Atmospheric correction of aerosols remains a challenge for accurately deriving water-leaving radiance from satellites and aircraft. Approaches generally focus on channels in the NIR and even in the short wave infrared (SWIR) [29, 31, 32]. Because water absorbs so heavily in the infrared, very few photons are reflected out of water in this part of the electromagnetic spectrum and the signal is dominated by reflection from atmospheric gases and aerosols. Various types of models are used, including coupled models and multi-scattering models, to infer the contribution of aerosol reflectance in the visible portion of the spectrum from the infrared. Aerosol reflectance is not spectrally flat, but varies with wavelength, and at least two channels are necessary to determine the spectral shape of aerosol reflectance and extrapolate from the NIR to visible wavelengths [29, 33].

Dust, particularly from desert storms, can also impact the optical properties of the atmosphere and most atmospheric correction algorithms for ocean color sensors are not capable of handling absorbing mineral dust (i.e., colored dust) [34]. For example, airborne plumes of Saharan dust are observable all year on satellite images over the Tropical Atlantic and

may be increasing in areas like the Mediterranean Sea [35]. If colored dusts are not properly corrected for in the atmospheric correction schemes, then the color of the ocean is not accurately estimated resulting in errors in chlorophyll and other biogeochemical properties retrieved from the satellite data [36]. In addition to its radiative impact, it has been suggested that this mineral dust has a substantial influence on the marine productivity and may also carry pollutants to the oceans [37, 38].

Whitecaps breaking on the sea surface must also be corrected from derivations of water-leaving radiance. Whitecap reflectance is often modeled using an empirical cubic relationship to wind speed and an approximate reflectance value for an individual whitecap [39], but such models often overcorrected the imagery, and a fixed whitecap correction is applied when wind speeds exceed a threshold (e.g., 8 m s^{-1} for SeaWiFS). At high winds, some of the signal attributable to whitecaps is removed by the aerosol corrections.

Levels of Processing

Standards for ocean color data processing, developed at US National Aeronautics and Space Administration (NASA) for the SeaWiFS mission [40], are widely followed by the international community of ocean color users and involve four levels of processing (Table 1).

Remote Sensing of Ocean Color. Table 1 Levels of data processing products from ocean color satellites

Level	Processing	Spatial qualities
0	Raw data as measured directly from the spacecraft	Satellite coordinates at highest spatial resolution
1	Converted to radiance using calibrations and sensor characterization information	Satellite coordinates at highest spatial resolution
2	Atmospherically corrected to water-leaving radiance and derived products	Satellite coordinates at highest spatial resolution
3	Derived products have been mapped onto a two-dimensional grid at known spatial resolution and can be averaged over timescales (weekly, monthly)	Regular gridded data at lower spatial resolution (e.g., 4 or 9 km)
4	Products that have been merged or assimilated with data from other sensors, in situ observations, or model outputs	Regular gridded data at lower spatial resolution

Ocean Color Algorithms

This section presents the classification of the global ocean into two optical classes: Case 1 and Case 2. The general approaches for two of the main products from ocean color imagery, chlorophyll and primary productivity, for Case 1 waters and a description of the semi-analytical algorithms used for both Case 1 and Case 2 waters are presented.

Optical Classification of Aquatic Systems

Ocean waters have long been classified based on their color properties [41]. A classification system introduced in 1977 differentiates phytoplankton-dominated waters from those where inorganic particles are dominant, known as Case 1 and Case 2, respectively [42]. These cases have evolved from their original forms into the categories used today: Case 1 waters are those waters where optical properties are determined primarily by phytoplankton and related colored dissolved organic matter (CDOM) and detritus degradation products; Case 2 waters are waters where optical properties are significantly influenced by other constituents such as mineral particles, CDOM, or microbubbles that do not covary with the phytoplankton concentration [8, 43]. In today's world, approximately 97% of the surface ocean falls toward the optically simple, deep water, Case 1 classification. When inorganic, organic, particulate, and dissolved material all vary independently of one another, such as in coastal ecosystems with considerable riverine influence, bottom resuspension, or optically shallow regions, the system falls toward the Case 2 classification, also called "optically complex."

This binary classification scheme has been prevalent in bio-optical modeling of ocean waters and development of ocean color algorithms. However, many problems exist with use of such simplified schemes in modeling natural systems. For example, there is no sharp dividing line between the cases and each investigation tends to use as different criteria for defining Case 1 and Case 2. Commonly the two cases are defined by the relationship between chlorophyll and remote sensing reflectance or scattering. Even in the global ocean considered to be Case 1, CDOM concentrations do not covary with the instantaneous chlorophyll concentration [44], but can vary from 30% to 60% of the total non-water light absorption [45] and result from differences in water mass ventilation, water column oxidative remineralization, and photobleaching [46].

In *optically shallow waters*, in addition to the water column and its constituents (i.e., dissolved and particulate material), the bottom contributes to the water leaving radiance in a way that depends on the bottom composition and roughness. Periodic measurements of bottom types using passive remote sensing in coastal systems are valuable for describing and monitoring habitats [47]. The magnitude and spectral quality of light reflected off of the bottom material can allow separation of bottom reflectance from the water column signal, where different bottom types will have a different effect on reflectance. Shallow, clear water will yield the most information about bottom material, more readily allowing spectral discrimination of bottom type. However, as depth and the diffuse attenuation coefficient, K_d, increase, the bottom signal becomes difficult to differentiate.

Empirical Chlorophyll Algorithms

Standard calculation of chlorophyll from ocean color imagery involves an empirical relationship developed from field observations collected throughout the global ocean [10]. Algorithms are typically not developed from the remotely sensing imagery itself, because this would incorporate any biases in calibration and atmospheric correction procedures used to derive reflectance, as well as any spatial inhomogeneity in parameters over pixel scales, and would require new algorithms for every new calibration, reprocessing, and sensor. Empirical solutions are used because an analytical solution to the problem requires an assessment of the entire radiance distribution and depth derivative and such measurements are not possible with remote sensing [48]. Only the upward flux incident upon the water-air interface at angles less than 48°, the angle at

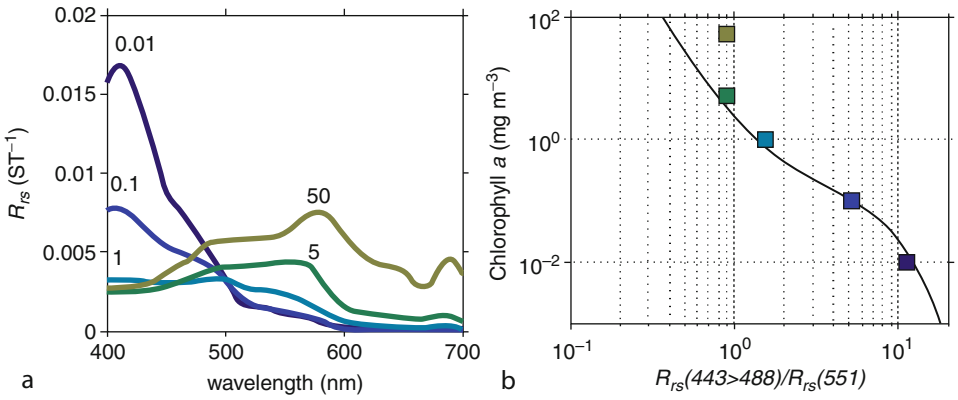

Remote Sensing of Ocean Color. Figure 5
(**a**) Remote sensing reflectance (R_{rs}) spectra modeled for different concentrations of chlorophyll *a* (Chl) from 0.01 to 50 mg m^{-3}. The color of each line represents the modeled ocean color a human might observe following [61]. (**b**) The empirical OC3M model for deriving Chl from R_{rs} for the MODIS Aqua sensor. The model uses the "blue" channel with the highest R_{rs} value (443 or 488 nm) divided by the "green" channel at 551 nm. Each *square* represents the modeled Chl for the corresponding R_{rs} spectra in panel A and demonstrates how the model becomes less accurate at high Chl

which complete internal reflection occurs, is measurable from above the sea surface [6] and generally only the flux emitted in a single viewing angle is remotely sensed.

The current empirical algorithms use the shift in ocean color from "blue" at low Chl, where R_{rs} peaks at 400 nm, to "green" at high chlorophyll, where R_{rs} peaks at 555 nm (Fig. 5a). Empirical ocean color algorithms have been applied to the vast majority of the global ocean considered Case 1 and use multiple ocean color bands typically log-transformed and in a ratio formulation to minimize problems with atmospheric correction and differential scattering in the ocean. The coefficients for the algorithms are regularly adjusted to account for different sets of wavebands in various sensors and as new field data becomes available (Table 2). The OC3M algorithm developed for MODIS, for example, uses a 4th order polynomial derived from a large global dataset of field measurements of chlorophyll and R_{rs}. It uses a logarithmic ratio of blue light (either 443 and 488 nm depending on which is greater) to green light (555 nm) and follows an inverse relationship such that low Chl is retrieved or high ratios when the ocean color is blue and high Chl when more green light is reflected (Fig. 5b). These types of algorithms tend to work best at lower Chl (<1 mg m^{-3}), found in most of the world ocean, where the algorithm has a flatter slope [49].

For much of the open ocean where chlorophyll concentrations are low, the empirical algorithms work well and relative error is estimated to under 35% [50]. However, empirical derivations of chlorophyll in Case 1 waters can be in error by a factor of 5 or more, particularly at higher Chl [49]. Such variability is due to differences in absorption and backscattering properties of phytoplankton and related concentrations of colored dissolved organic matter (CDOM) and minerals. The empirical algorithms have built-in assumptions that follow the basic precept of biological oceanography; i.e., oligotrophic regions with low phytoplankton biomass are populated with small phytoplankton while more productive regions contain larger bloom-forming phytoplankton. With a changing world ocean, phytoplankton composition may shift in response to altered environmental forcing and CDOM and mineral concentrations may become uncoupled from phytoplankton stocks creating further uncertainty and error in the empirical approaches [49].

The empirical approach is not widely applicable in Case 2 waters, generally found near the coasts. Such waters are influenced by freshwater plumes with CDOM and minerals that significantly impact the

Remote Sensing of Ocean Color. Table 2 Empirical chlorophyll algorithms for a variety of ocean color sensors

Name[a]	Sensor	Channels[b]		Coefficients[c]				
		Blue	Green	a0[c]	a1	a2	a3	a4
OC4	SeaWiFS	443 > 490 > 510	555	0.366	−3.067	1.93	0.649	−1.532
OC3S	SeaWiFS	443 > 490	555	0.2409	−2.4768	1.5296	0.1061	−1.1077
OC2S	SeaWiFS	490	555	0.2372	−2.4541	1.7114	−0.3399	−2.788
OC3M	MODIS	443 > 488	551	0.283	−2.753	1.457	0.659	−1.403
OC2M	HMODIS	469	555	0.1543	−1.9764	1.0704	−0.2327	−1.1404
OC4O	OCTS	443 > 490 > 520	565	0.4006	−3.1247	3.1041	−1.4179	−0.3654
OC3O	OCTS	443 > 490	565	0.2836	−2.1982	1.0541	0.186	−0.717
OC2O	OCTS	490	565	0.2805	−2.167	1.1789	−0.1597	−1.5591
OC3C	CZCS	443 > 520	550	0.3012	−4.4988	9.0983	−9.9821	3.235

[a]Name of ocean color (OC) algorithm incorporates the number of wavebands (2–4) used in the formulation and the initial for the sensor used (S = SeaWiFS; M = MODIS; O = OCTS; C = CZCS)

[b]The algorithms use a log-transformed ratio of "Blue" (443–520 nm) to "Green" (550–565 nm) remote sensing reflectance (R_{rs}). When more than one "Blue" channel is provided, only the channel with the highest R_{rs} is used. x = log10(R_{rs}(Blue)/R_{rs}(Green))

[c]Chlorophyll *a* is modeled as a fourth polynomial fit to the field data such that: $\mathrm{Chl} = 10\hat{}(a0 + a1^{*}x + a2^{*}x^{2} + a3^{*}x^{3} + a4^{*}x^{4})$

optical properties, as well as resuspension of bottom sediments [51]. Phytoplankton assemblages can also be diverse in coastal regimes and light absorption per unit of Chl is difficult to constrain. Melting and runoff of glacial sources can increase particle concentrations in the nearshore and change phytoplankton assemblages. In order to use remote sensing in coastal waters, semi-analytical models are employed that are able to decompose the reflected color into the many absorbing and scattering constituents in the water column (see section "Semi-analytical Algorithms").

Primary Productivity Algorithms

Net primary production is a key parameter derived from ocean color data that provides a measure of how much carbon dioxide is taken up and incorporated into ocean phytoplankton during photosynthesis. Export of fixed carbon to the ocean interior, while only a fraction of the total biomass produced, provides a long-term sink for atmospheric carbon dioxide [52]. While satellite-derived Chl is not a direct measure of carbon fixation in phytoplankton, such estimates are typically derived from correlates of Chl and rates of carbon fixation [53]. Net primary productivity varies with phytoplankton species assemblages and their physiological state related to light, temperature, nutrients, and other environmental factors.

A variety of formulations have been developed for ocean color remote sensing and parameterized for the global ocean or specific regions. Models are generally restricted to parameters that can also be globally derived from remote sensing imagery, such as sea surface temperature and photosynthetically available radiation (PAR). Moving from a standing stock of phytoplankton biomass to photosynthetic rate requires a time-dependent variable. Solar radiation in the form of PAR is commonly used in formulations to convert biomass to primary productivity. The physiological response of the measured chlorophyll to light, nutrients, temperature, and other environmental variables must also be incorporated in the model. Primary productivity models can be differentiated by the degree of explicit resolution in depth and irradiance [53].

Round robin experiments have been conducted to compare the performance of models for assessing global productivity from ocean color imagery, as well as the output from ecosystem-based general circulation models [1, 54]. The third such effort found that global average primary productivity varied by a factor of two between models and the global mean productivity for the different model groups ranged from 44 to 57 Gt C year^{-1} with an average of 50.7 Gt C year^{-1}. The models diverged the most in the high-nutrient low chlorophyll waters of the Southern Ocean. Primary productivity algorithms have also been formulated from remote sensing estimates of the inherent optical properties (such as light absorption and backscattering) directly [55, 56], without incorporating Chl and the associated uncertainties inherent in that parameter.

Semi-analytical Algorithms

The empirical algorithms used for deriving chlorophyll have been likened to a "black box" that provides no mechanistic understanding of ocean optics and are particularly challenging to apply in a changing ocean, when the water properties are different from the empirical data used to develop the formulation [57]. Analytical solutions to deriving IOPs from water-leaving radiance are not possible because the radiance can only be measured from a few angles. Semi-analytical algorithms (or "quasi-analytical") are based on a fundamental understanding of the propagation of light in the ocean and provide a more mechanistic approach to ocean color. These algorithms incorporate some empirical approximations, but do not rely on fixed predetermined relationships between the absorption and backscattering components of the water column.

In semi-analytic models, the ocean color signal is inverted to obtain estimates of the various absorbing and backscattering constituents directly. Parameterization of how water, phytoplankton, and dissolved and detrital material inherently absorb and backscatter light across the visible spectrum (i.e., their spectral shape) is used in these models. The spectral reflectance measured at the satellite is often inverted to retrieve the amounts of each individual component contributing to the absorption and backscattering of light. Such algorithms are the primary methods for obtaining CDOM distributions across the ocean surface [58]. In semi-analytical models, the biogeochemical parameters, such as Chl and total suspended matter, are derived

secondarily from the IOPs. Semi-analytical formulations vary in terms of their architecture and statistical methods employed to retrieve the inherent optical properties from the remote sensing signal and the empirical parameterizations within the models [57].

Applications for Oceanography

Ocean color remote sensing is an important tool for many branches of oceanography, including biological, physical, and chemical oceanography. The section below summarizes only some of the main applications of ocean color remote sensing with the understanding that the uses of ocean color are continuously expanding. A recent monograph from the International Ocean Color Coordinating Group (IOCCG) entitled "Why Ocean Colour?: The Societal Benefits of Ocean-Colour Technology" extensively documents the many uses of ocean color remote sensing from scientists to environmental managers to the general public [7]. Web-based software has also been developed, see, e.g., Giovanni [59], which allows the public to freely map and analyze ocean color imagery over time and space. Figure 6 provides an example of various types of figures that can be easily generated from remotely sensed chlorophyll using that software.

Biological Oceanography

Apart from estimating chlorophyll and primary productivity, ocean color remote sensing has many biological applications that range from phytoplankton physiology to assessing distributions of migrating whales. Phytoplankton physiology, particularly the efficiency of light capture and utilization, has been modeled from the natural fluorescence signature provided by ocean color remote sensing [60]. Even though the spectral resolution available in most current ocean color satellite is limited to six to eight available spectral channels [61], a variety of phytoplankton taxa and groups have also been distinguished from satellite imagery based on their unique optical properties and/or regional tuning of algorithms using knowledge of the local phytoplankton composition. Phytoplankton taxa can have unique sets of accessory pigments that differentiate them from one another and can result in unique absorbance spectra. In addition, phytoplankton can have cell walls or exterior plates comprised of different materials (e.g., silica, calcium carbonate) that can make them more or less reflective. Various approaches have been developed to map size classes (from pico- to microplankton) or major groups of phytoplankton in the global ocean [62]. Other algorithms have targeted particular phytoplankton taxa such as coccolithophores, nitrogen-fixing *Trichodesmium* [63], toxic dinoflagellates [64], and nuisance cyanobacteria [65].

Satellite-derived chlorophyll and primary productivity provide a key metric to assess marine ecosystems temporally on a global scale and have been used extensively to monitor conditions that impact other biological organisms in the sea. The relationship between satellite-derived chlorophyll data and organisms at higher trophic levels depends upon the number of linkages in the food web. For species like anchovies and sardines, which eat phytoplankton in their life cycle, the linkage can be direct [66]; whereas, many trophic levels can exist for other species and the relationship can be quite nonlinear [7]. The distribution, movement, and migration of whales, dolphins, pinnipeds, penguins, and sea turtles has been related, either directly or indirectly, to remotely sensed patterns of Chl (reviewed in [7]). Most fish have planktonic larval stages that are strongly influenced by ocean circulation and recruitment success has been found to be related to the degree of timing between spawning and the seasonal phytoplankton bloom, as observed from satellites [67]. Ocean color remote sensing has also been used to study invertebrates in the global ocean, such as shrimp in the Newfoundland-Labrador Shelf [68] and pteropods and pelagic mollusks in the Ross Sea [69]. Mean net primary productivity, determined from ocean color satellite imagery, elucidates species richness in biogeographical studies of cephalopods [70].

New techniques have also been developed to use ocean color remote sensing in optically shallow water systems to deduce changes in benthic habitats [71]. Optically shallow water occurs when the seafloor contributes to the reflectance signal observed remotely by a satellite (Fig. 7a) and is defined by a combination of water clarity, water depth, and bottom composition.

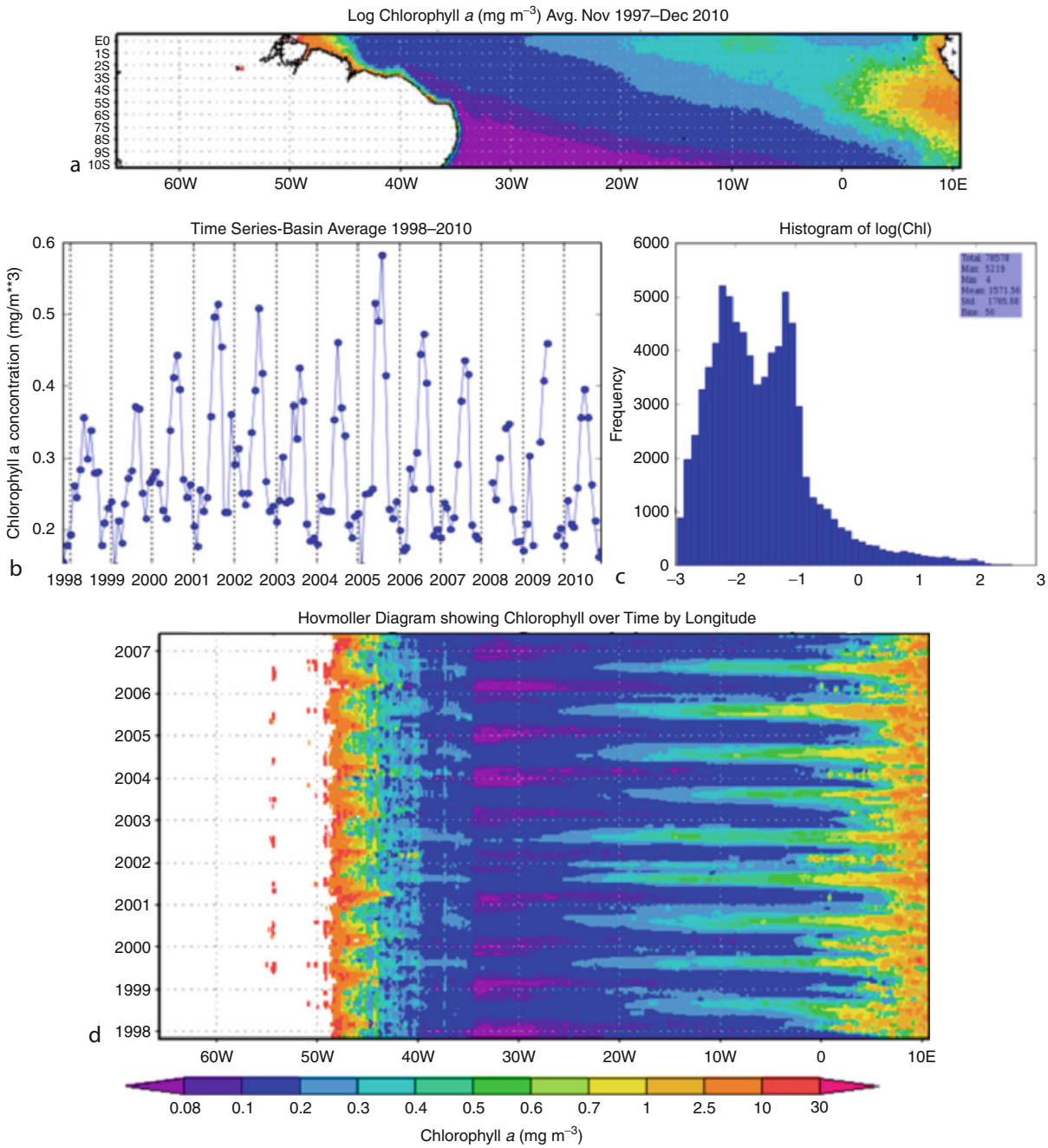

Remote Sensing of Ocean Color. Figure 6

Various times series analyses that can be conducted with standard Level 3 chlorophyll imagery including (**a**) Temporally averaged spatial distributions; (**b**) time series of interannual variability; (**c**) histograms showing the statistical distributions; (**d**) Hovmoller plots presenting both spatial (x-axis) and temporal (y-axis) variability. Such plots can be easily generated by the public with the Giovanni interface [59]

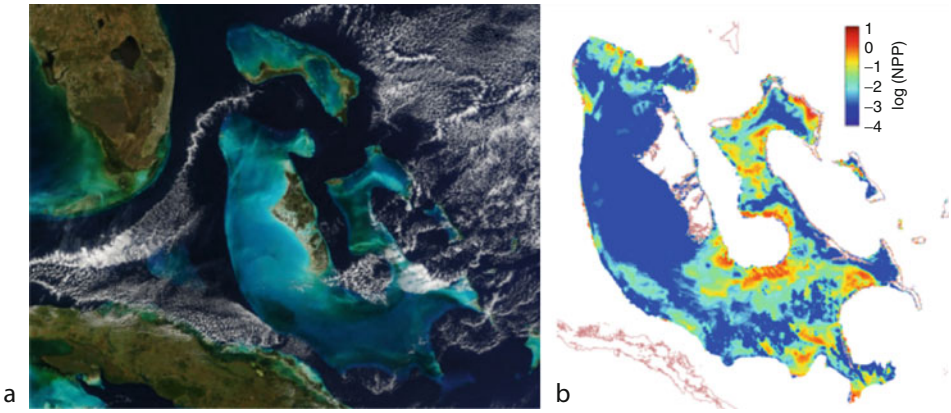

Remote Sensing of Ocean Color. Figure 7
The Great Bahama Bank is an example of optically shallow water where the seafloor color can be observed from space. (**a**) Pseudo-true color image from MODIS Aqua showing the bright Bahamas Banks with Florida, USA, to the West and Cuba to the Southwest. White wispy clouds can obscure the ocean color. (**b**) Net primary productivity (mgC m^{-2} d^{-1}) of seagrass and benthic algae estimated from ocean color imagery over the Great Bahama Bank [47]

Satellite estimates of biomass and net productivity of seagrasses, kelps, and other benthic producers have been conducted over regional scales [47, 72] (Fig. 7b). Ocean color imagery from aircraft can map fine-scale distributions of seagrasses, coral reefs, and other coastal habitats at local scales [73, 74]. Changes in ocean color signals over time can also be used to assess contributions of coastal carbon to the global carbon cycle [75, 76]. Responses of coastal regions linked to terrestrial changes can also be observed with ocean color imagery. Warming of the Eurasian landmass, for example, has led to enhanced productivity in the water column [77]. Agricultural runoff from fields in Mexico was shown to stimulate large phytoplankton blooms in the Gulf of California that alter water clarity and potentially lead to anoxic conditions [78].

Ocean Physics

Ocean color data is well suited to the detection of convergence zones and oceanic fronts, sometimes better than thermal sensors which penetrate only the skin layer, or the first 10 μm, of the water column. Interestingly, a sequence of ocean-color-derived chlorophyll images may help predict the formation of eddies days before they appear. The increased penetration of visible radiation reveals more frontal features and with greater detail than those retrieved with sea surface temperature data alone [79]. Likewise, upwelling regions, which bring cold, nutrient-rich waters up to the surface can be readily identified in ocean color images as areas with an enhanced chlorophyll concentration. The intensity of upwelling from year-to-year can be tracked through the time series of chlorophyll abundance. Chlorophyll is an effective indicator for detecting anomalous activity in the oceanic environment. Evidence of an El Niño event beginning in November of 1997, during which phytoplankton pigment concentrations appeared anomalously low in the Equatorial Upwelling Zone, was obvious in the continuous coverage supplied by SeaWiFS. The onset of restored upwelling was likewise evident with the increased chlorophyll concentrations during the months of June and July 1998 [80].

Ocean water clarity also affects the distribution of shortwave heating in the water column. Both chlorophyll and CDOM concentrations have been linked to changes in heating of surface waters [81, 82]. Increased clarity would be expected to cool the surface and heat subsurface depths as shortwave radiation penetrates deeper into the water column. Recent studies show that water clarity, as determined from ocean color remote sensing, is an important feature in atmospheric circulation (the Hadley cells), oceanic circulation (Walker Circulation), and formation of mode water [83]. Importantly, ocean color imagery is also critical

to predicting tropical cyclone activity. The presence of light-absorbing constituents (like Chl and CDOM) shapes the path of Pacific tropical cyclones and propagation to higher latitudes [84].

Chemical Oceanography

A major contributor to the ocean carbon system is colored dissolved organic material (CDOM), a mixture of compounds produced primarily by decomposition of plant matter. CDOM, when present in high enough concentrations, produces a yellow or brownish color and is highly reactive in the presence of sunlight. When CDOM undergoes photodegradation, organic compounds essential to phytoplankton and bacterial growth are released [85]. Satellite measurements collected using SeaWiFS, MODIS, and MERIS produce daily estimates of CDOM at 1 km resolution. High temporal resolution CDOM maps can be used to identify and track water masses at timescales close to the processes determining its distribution. CDOM dynamics play an important role in ocean biogeochemistry, regulating the absorption of blue and UV radiation in the surface ocean and therefore altering the depth of the euphotic zone [58] and heating surface waters [82]. Although CDOM is difficult to analyze chemically, its distribution and abundance, identifiable using ocean color remote sensing, is highly relevant to understanding carbon cycling in the ocean.

The particulate inorganic carbon (PIC) pool, calcium carbonate ($CaCO_3$), contributes substantially to the ocean carbon cycle and ocean color reflectance. Calcification reduces surface carbonate, decreasing alkalinity. Organic carbon production via photosynthesis counterbalances this effect. Coccolithophores, haptophyte algae, are responsible for the majority of the biogenic particulate inorganic carbon production. Coccolithophores generate and shed tiny white plates of calcium carbonate called coccoliths, which are highly efficient at reflecting light, ultimately producing large turquoise patches in the ocean readily visible in ocean color imagery [86]. Ocean color remote sensing algorithms have been formulated for generating quantitative estimates of particulate inorganic carbon and calcification rates on regional and global scales [87, 88]. A continued, long-term assessment of coccolithophore and particulate inorganic carbon abundance from satellite imagery will aid in understanding the impact of ocean acidification on marine organisms reliant on carbonate for the formation of shells [89].

Ocean color imagery provides the ability to expand small-scale biogeochemical studies to regional or global scales. For example, the marine inorganic carbon cycle has been shown to be not only influenced by marine plankton but also by fish that precipitate carbonates into the surface waters. Extrapolations from satellite-derived net primary productivity up several trophic levels to marine fish [90] reveal that fish may contribute 3–15% of the total oceanic carbon production [91].

Applications for Environmental Monitoring

Ocean color remote sensing plays a major role in monitoring and sustaining the health and resilience of marine ecosystems, including fisheries and endangered species [40]. Ocean color products are helping to address how environmental variability influences annual recruitment of fish stock [92] and to locate and manage fisheries [7]. Ocean color imagery coupled with other remote sensing products such as sea surface temperature is a fundamental tool in ecosystem-based management of marine resources [93].

Ocean color remote sensing can monitor a variety of acute and chronic hazards influencing the oceans including: harmful algal blooms, oil spills, coastal flooding, icebergs and marine debris [7]. A combination of ocean color, field, and meteorological datasets have been critical in identifying the onset of harmful algal blooms (HABs), which can produce toxins and create hypoxic conditions. While toxins cannot be directly observed from ocean color, the onset of potential harmful blooms can be identified using a chlorophyll anomaly method [94] in concert with other forecasting tools such as field and meteorological datasets. This information can then be passed on to coastal managers and state agencies to put strategies in place to deal with an impending bloom. A long-term time series of ocean color products can aid in elucidating forcing and transport mechanisms of these harmful blooms and help improve predictability.

New techniques are being developed for early detection, containment, and clean up of oil spills. Remote sensing can be used to detect oil spills that can change surface reflectance properties and the color of the

ocean [95]. Coarse spatial and temporal resolution, limited spectral bands, cloud-cover issues and high sunlight requirements have generally restricted the usefulness of ocean color imagery for oil-spill detection from polar orbiting satellites [96]. Moreover, current processing methods may not allow data availability within hours of data capture. The spatial, temporal, and spectral resolution needed for oil spill recovery planning requires high-resolution, hyperspectral ocean color radiometers deployed in geostationary orbit [40].

Ocean color imagery has also been used to track marine debris on the ocean surface which can entangle a variety of pelagic species, such as endangered sea turtles, seals, and whales. The nets also become ensnared on coral reefs and damage the reef structure and associated organisms that require a healthy reef ecosystem [97, 98]. Satellite ocean color data are part of the methods being developed to locate and identify potential locations of marine debris to aid their removal from these ecosystems.

Ocean color imagery is also useful in monitoring water quality in inland aquatic water bodies. Nuisance algal blooms, such as cyanobacteria, cause aesthetic degradation to lakes and reservoirs resulting in surface scum, unpleasant taste and odor in drinking water (from the production of metabolites such as methyl isoborneol and geosmin), and possible adverse effects to human health from blue-green algal toxins. Predicting the locations and timing of blue-green algal bloom using traditional sampling techniques is difficult and hyperspectral remote sensing can be an important tool in such monitoring efforts [99].

Future Directions

Within a few decades, the ability to view the global ocean color regularly through remote sensing has revolutionized the perceptions about ocean processes and feedbacks to the earth's climate. The decade of continuous ocean color imagery has provided a foundation for assessing change in the earth's systems and long-term averages or "climatologies" of products, such as chlorophyll, CDOM, and PIC, have been produced to provide a baseline of ocean biogeochemistry (Fig. 8). The products obtained from ocean color are now incorporated into all domains of oceanography, global climate forecasts, military applications, and environmental monitoring across the expansive global ocean and the vulnerable coastal regions where most of the human population resides [11]. While successful, the technology and processing of ocean color remote sensing is still in its infancy in terms of monitoring the ocean from immediate to climatological timescales.

The relationships between climatological forcing and biological carbon storage in the ocean are complex and not readily incorporated in models. Ocean color imagery can provide assessments of potential changes to ocean processes including primary productivity, surface heating, sediment plumes, altered food webs, harmful algal blooms, changing acidity, and alterations of benthic habitats in response to shifts in winds and upwelling, clouds and radiative forcing, and storm intensity and frequency. Recent observed changes in chlorophyll, primary production, and the size of the oligotrophic gyres from ocean color satellites are compelling evidence of significant changes in the global ocean. A recent study demonstrates that a time series of at least 40 years in length is needed to unequivocally distinguish a global warming trend from natural variability [6] and sustained long-term observations of ocean color are in jeopardy [40].

In addition to sustained imagery, there is a need for integrating ocean color imagery from different platforms to monitor the oceans and aquatic habitats at a variety of desired spectral, spatial, and temporal resolutions. Integration of satellite sensors with suborbital platforms will allow for better assessment of vulnerable marine and aquatic habitats, as well as responses to hazards such as harmful algal blooms, oil spills, and storms that cause coastal flooding and erosion. Active sensors, such as Light Detection and Ranging (LIDAR), will allow us to probe into the depths of the oceans. Moreover, integrating surface ocean color measurements with three-dimensional measurements and models of the ocean will be increasingly important in discerning a changing ocean [49].

Finally, the approaches or algorithms for conducting ocean color remote sensing will be augmented as more spectral channels become routinely available and as ocean properties change. Purely statistical or empirical models are only accurate when conditions are similar to past conditions. When considering a changing ocean, the cause of the color

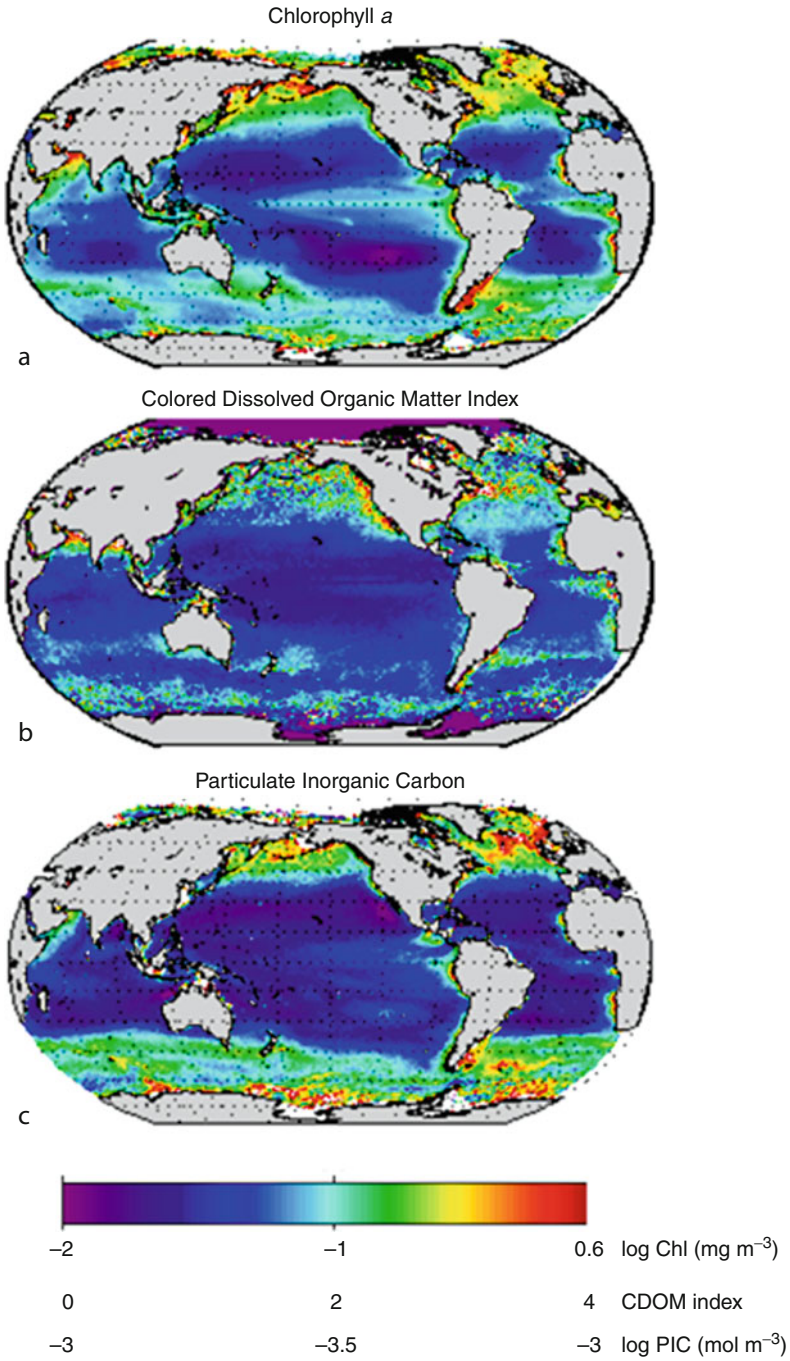

Remote Sensing of Ocean Color. Figure 8
Global climatologies or long-term averages of products derived from the Ocean Color SeaWiFS sensor from 1998–2011. (**a**) Chlorophyll *a* (mg m^{-3}); (**b**) colored dissolved organic matter (CDOM) index; (**c**) particulate inorganic carbon (PIC) (mol m^{-3})

change must be carefully assessed to separate the spectral variability due to phytoplankton from other sources of variability, such as sediments, CDOM, and even atmospheric aerosols. Considerable growth is also expected in approaches and technology for remote sensing of coastal habitats and assessing acute and chronic hazards. Comprehensive and consistent field observations from ships to autonomous vehicles and floats are required to assess the accuracy of satellite-derived products, build improved algorithms, and provide better linkages between surface measurements made from space and the processes within the water column [49]. Future effort will also be directed at assimilation of ocean color imagery into global circulation and climate models. As outlined above, remote sensing of ocean color is a complex discipline requiring radiometrically accurate and calibrated sensors, advanced techniques for atmospheric correction of aerosols and dust, and approaches that can deduce the source of variability in the color signal measured by a sensor. With the many important applications of ocean color remote sensing, from climate forecasting to environmental monitoring, a consistent and coordinated international investment in education, research, and technology is required to maintain and advance this dynamic field.

Bibliography

Primary Literature

1. Carr ME et al (2006) A comparison of global estimates of marine primary production from ocean color. Deep Sea Res Part II: Top Stud Oceanogr 53:741–770
2. Field CB, Behrenfeld MJ, Randerson JT, Falkowski P (1998) Primary production of the biosphere: integrating terrestrial and oceanic components. Science 281:237–240
3. Smith RC, Baker KS (1978) Optical classification of natural waters. Limnol Oceanogr 23:260–267
4. Martinez E, Antoine D, D'Ortenzio F, Gentili B (2009) Climate-driven basin-scale decadal oscillations of oceanic phytoplankton. Science 326:1253–1256
5. Siegel DA, Franz BA (2010) Century of phytoplankton change. Nature 466:569–570
6. Henson SA et al (2010) Detection of anthropogenic climate change in satellite records of ocean chlorophyll and productivity. Biogeosciences 7:621–640
7. IOCCG (2008) Why ocean colour? the societal benefits of ocean-colour technology. In: Platt T, Hoepffner N, Stuart V, Brown C (eds) Reports of the International Ocean-Colour Coordinating Group, Dartmouth, Canada
8. Morel A (1988) Optical modeling of the upper ocean in relation to its biogenous matter content (case I waters). J Geophys Res 93:10749–10768
9. Gordon HR, Morel AY (1983) Remote assessment of ocean color for interpretation of satellite visible imagery: a review. Springer, New York
10. O'Reilly JE, Maritorena S, Mitchell BG, Siegel DA (1998) Ocean color chlorophyll algorithms for SeaWiFS. J Geophys Res 103:24937–24953
11. McClain CR (2009) A decade of satellite ocean color observations*. Annu Rev Mar Sci 1:19–42
12. Kirk JTO (1994) Light and photosynthesis in aquatic ecosystems. Cambridge University Press, Cambridge
13. Blough NV, Del Vecchio R (2002) Chromophoric DOM in the coastal environment. In: Hansell DA, Carlson CA (eds) Biogeochemistry of marine dissolved organic matter. Academic, San Diego, pp 509–546
14. Twardowski MS, Boss E, Sullivan JM, Donaghay PL (2004) Modeling the spectral shape of absorption by chromophoric dissolved organic matter. Mar Chem 89:69–88
15. Ciotti AM, Cullen JJ, Lewis MR (2002) Assessment of the relationships between dominant cell size in natural phytoplankton communities and the spectral shape of the absorption coefficient. Limnol Oceanogr 47:404–417
16. Bricaud A, Claustre H, Ras J, Oubelkheir K (2004) Natural variability of phytoplanktonic absorption in oceanic waters: influence of the size structure of algal populations. J Geophys Res 109:C11010
17. Stramski D, Boss E, Bogucki D, Voss KJ (2004) The role of seawater constituents in light backscattering in the ocean. Prog Oceanogr 61:27–56
18. Mobley CD (1994) Light and water: radiative transfer in natural waters. Academic, San Diego
19. Gordon HR et al (2009) Spectra of particulate backscattering in natural waters. Opt Express 17:16192–16208
20. Twardowski MS, Lewis M, Barnard A, Zaneveld JRV (2005) In-water instrumentation and platforms for ocean color remote sensing applications. In: Miller R, Del-Castillo C, McKeee D (eds) Remote sensing of coastal aquatic waters. Springer, Dordrecht
21. Smith RC, Baker K (1978) The bio-optical state of ocean waters and remote sensing. Limnol Oceanogr 23:247–259
22. Morel A, Gentilli B (1993) Diffuse reflectance of oceanic waters. II. Bidirectional aspects. Appl Opt 32:6864–6879
23. Lee ZP, Carder KL, Arnone RA (2002) Deriving inherent optical properties from water color: a multiband quasi-analytical algorithm for optically deep water. Appl Opt 41: 5755–5772
24. Aurin DA (2010) Developing ocean color remote sensing algorithms for retrieving optical properties and biogeochemical parameters in the optically complex waters of Long Island Sound. Ph.D. Thesis. University of Connecticut
25. Ryan JP et al (2005) Coastal ocean physics and red tides: an example from Monterey Bay, California. Oceanography 18:246–255

26. Mouroulis P, Green RO, Wilson DW (2008) Optical design of a coastal ocean imaging spectrometer. Opt Express 16:9087–9096
27. Davis CO et al (2002) Ocean PHILLS hyperspectral imager: design, characterization, and calibration. Opt Express 10(4):210–221
28. McClain CR, Cleave ML, Feldman GC, Gregg WW (1998) Science quality SeaWiFS data for global biosphere research. Sea Technol 39:10–16
29. Gordon HR (1997) Atmospheric correction of ocean color imagery in the Earth Observing System era. J Geophys Res 102:17081–17106
30. Antoine D, Morel A (1999) A multiple scattering algorithm for atmospheric correction of remotely sensed ocean color (MERIS instrument): principle and implementation for atmospheres carrying various aerosols including absorbing ones. Int J Remote Sens 20:1875–1916
31. Gao BC, Montes MJ, Ahmad Z, Davis CO (2000) Atmospheric correction algorithm for hyperspectral remote sensing of ocean color from space. Appl Opt 39:887–896
32. Wang M, Son SH, Shi W (2009) Evaluation of MODIS SWIR and NIR-SWIR atmospheric correction algorithms using SeaBASS data. Remote Sens Environ 113:635–644
33. Yan B et al (2002) Pitfalls in atmospheric correction of ocean color imagery: how should aerosol optical properties be computed? Appl Opt 41:412–423
34. Fukushima H, Toratani M (1997) Asian dust aerosol: optical effect on satellite ocean color signal and a scheme of its correction. J Geophys Res 102:17119–17130
35. Antoine D, Nobileau D (2006) Recent increase of Saharan dust transport over the Mediterranean Sea, as revealed from ocean color satellite (SeaWiFS) observations. J Geophys Res 111: D12214
36. Claustre H et al (2002) Is desert dust making oligotrophic waters greener? Geophys Res lett 29:107–1
37. Paytan A et al (2009) Toxicity of atmospheric aerosols on marine phytoplankton. Proc Natl Acad Sci 106:4601
38. Garrison VH et al (2003) African and Asian dust: from desert soils to coral reefs. Bioscience 53:469–480
39. Monahan EC, O'Muircheartaigh I (1981) Improved statement of the relationship between surface wind speed and oceanic whitecap coverage as required for the interpretation of satellite data. In: Gower JFR (ed) Oceanography from space. Plenum, New York, pp 751–755
40. National Research Council Committee on Assessing Requirements for Sustained Ocean Color Research and Operations (2011) Assessing requirements for sustained ocean color research and operations. National Academies Press, Washington DC
41. Jerlov NG (1974) Optical aspects of oceanography. Academic, London, pp 77–94
42. Morel A, Prieur L (1977) Analysis of variations in ocean color. Limnol Oceanogr 22:709–721
43. Mobley CD, Stramski D, Bissett WP, Boss E (2004) Optical modeling of ocean water: is the case 1 – case 2 classification still useful? Oceanography 17:60–67
44. Morel A, Bricaud A (1981) Theoretical results concerning light absorption in a discrete medium and application to the specific absorption of phytoplankton. Deep-Sea Res 28:1357–1393
45. Siegel DA, Maritorena S, Nelson NB, Behrenfeld MJ (2005) Independence and interdependencies among global ocean color properties: reassessing the bio-optical assumption. J Geophys Res 110:C07011
46. Swan CM, Siegel DA, Nelson NB, Carlson CA, Nasir E (2009) Biogeochemical and hydrographic controls on chromophoric dissolved organic matter distribution in the Pacific Ocean. Deep Sea Res Part I: Oceanogr Res Pap 56:2175–2192
47. Dierssen HM (2010) Benthic ecology from space: optics and net primary production in seagrass and benthic algae across the Great Bahama Bank. Mar Ecol Progress Ser 411:1–15
48. Zaneveld JRV (1989) An asymptotic closure theory for irradiance in the sea and its inversion to obtain the inherent optical properties. Limnol Oceanogr 34:1442–1452
49. Dierssen HM (2010) Perspectives on empirical approaches for ocean color remote sensing of chlorophyll in a changing climate. Proc Natl Acad Sci 107:17073
50. Moore TS, Campbell JW, Dowell MD (2009) A class-based approach to characterizing and mapping the uncertainty of the MODIS ocean chlorophyll product. Remote Sens Environ 113:2424–2430
51. Schofield O et al (2004) Watercolors in the coastal zone: what can we see? Oceanography 17:25–31
52. Falkowski P et al (2000) The global carbon cycle: a test of our knowledge of earth as a system. Science 290:291
53. Behrenfeld MJ, Falkowski PG (1997) Consumers guide to phytoplankton primary productivity models. Limnol Oceanogr 42:1479–1491
54. Campbell J et al (2002) Comparison of algorithms for estimating ocean primary production from surface chlorophyll, temperature, and irradiance. Glob Biogeochem Cycle 16:1035
55. Westberry T, Behrenfeld MJ, Siegel DA, Boss E (2008) Carbon-based primary productivity modeling with vertically resolved photoacclimation. Glob Biogeochem Cycle 22:GB2024
56. Mouw CB, Yoder JA (2005) Primary production calculations in the Mid-Atlantic Bight, including effects of phytoplankton community size structure. Limnol oceanogr 50(4):1232–1243
57. IOCCG (2006) Remote sensing of inherent optical properties: fundamentals, tests of algorithms, and applications. In: Lee ZP (ed) Reports of the International Ocean-Colour Coordinating Group, Dartmouth
58. Siegel DA, Maritorena S, Nelson NB, Hansell DA, Lorenzi-Kayser M (2002) Global distribution and dynamics of colored dissolved and detrital organic materials. J Geophys Res 107:3228
59. U.S. National Aeronautics and Space Administration, Goddard Earth Sciences, Data and Information Services Center (2011) *Giovanni*. http://disc.sci.gsfc.nasa.gov/giovanni/

60. Behrenfeld MJ et al (2009) Satellite-detected fluorescence reveals global physiology of ocean phytoplankton. Biogeosciences 6:779–794
61. Dierssen HM, Kudela RM, Ryan JP, Zimmerman RC (2006) Red and black tides: quantitative analysis of water-leaving radiance and perceived color for phytoplankton, colored dissolved organic matter, and suspended sediments. Limnol oceanogr 51:2646–2659
62. Brewin RJW et al (2011) An intercomparison of bio-optical techniques for detecting dominant phytoplankton size class from satellite remote sensing. Remote Sens Environ 115:325–339
63. Balch WM, Kilpatrick KA, Trees CC (1996) The 1991 coccolithophore bloom in the central North Atlantic. 1. Optical properties and factors affecting their distribution. Limnol Oceanogr 41:1669–1683
64. Tomlinson MC, Wynne TT, Stumpf RP (2009) An evaluation of remote sensing techniques for enhanced detection of the toxic dinoflagellate, Karenia brevis. Remote Sens Environ 113:598–609
65. Simis SGH, Peters SWM, Gons HJ (2005) Remote sensing of the cyanobacterial pigment phycocyanin in turbid inland water. Limnol Oceanogr 50:237–245
66. Chavez FP, Ryan J, Lluch-Cota SE, Niquen CM (2003) From anchovies to sardines and back: multidecadal change in the Pacific Ocean. Science 299:217–221
67. Platt T, Csar Fuentes-Yaco KTF (2003) Marine ecology: spring algal bloom and larval fish survival. Nature 423:398–399
68. Fuentes-Yaco C, Koeller PA, Sathyendranath S, Platt T (2007) Shrimp (Pandalus borealis) growth and timing of the spring phytoplankton bloom on the Newfoundland–Labrador Shelf. Fish Oceanogr 16:116–129
69. Seibel BA, Dierssen HM (2003) Cascading trophic impacts of reduced biomass in the Ross Sea, Antarctica: just the tip of the iceberg? Biol Bull 205:93–97
70. Rosa R, Dierssen HM, Gonzalez L, Seibel BA (2008) Large-scale diversity patterns of cephalopods in the Atlantic open ocean and deep sea. Ecology 89:3449–3461
71. Dekker A et al (2005) Remote sensing of seagrass ecosystems: use of spaceborne and airborne sensors. In: Larkum AWD, Orth RJ, Duarte CM (eds) Seagrasses: biology, ecology, and conservation. Springer, Dordrecht, pp 347–359
72. Cavanaugh KC, Siegel DA, Kinlan BP, Reed DC (2010) Scaling giant kelp field measurements to regional scales using satellite observations. Mar Ecol Prog Ser 403:13–27
73. Phinn S, Roelfsema C, Dekker A, Brando V, Anstee J (2008) Mapping seagrass species, cover and biomass in shallow waters: an assessment of satellite multi-spectral and airborne hyper-spectral imaging systems in Moreton Bay (Australia). Remote sens Environ 112:3413–3425
74. Lesser MP, Mobley CD (2007) Bathymetry, water optical properties, and benthic classification of coral reefs using hyperspectral remote sensing imagery. Coral Reefs 26:819–829
75. Dierssen HM, Zimmerman RC, Drake LA, Burdige DJ (2009) Potential export of unattached benthic macroalgae to the deep sea through wind-driven Langmuir circulation. Geophys Res Lett 36:L04602
76. Burdige DJ, Hu X, Zimmerman RC (2010) The widespread occurrence of coupled carbonate dissolution/reprecipitation in surface sediments on the Bahamas Bank. Am J Sci 310(6):492–521. doi:10.2475/06.2010.03
77. Goes JI, Thoppil PG, Gomes HR, Fasullo JT (2005) Warming of the Eurasian landmass is making the Arabian Sea more productive. Science 308:545–547
78. Beman JM, Arrigo KR, Matson PA (2005) Agricultural runoff fuels large phytoplankton blooms in vulnerable areas of the ocean. Nature 434:211–214
79. Dwivedi RM, Solanki HU, Nayak SR, Gulati D, Somvanshi VS (2005) Exploration of fishery resources through integration of ocean colour with sea surface temperature: Indian experience. IJMS 34:430–440
80. Chavez FP, Strutton PG, McPhaden MJ (1998) Biological-physical coupling in the Central Equatorial Pacific during the onset of the 1997–98 El Nino. Geophys Res Lett 25:3543–3546
81. Lewis MR, Platt TC (1987) Remote observation of ocean colour for prediction of upper ocean heating rates. Adv Space Res 7:127–130
82. Hill VJ (2008) Impacts of chromophoric dissolved organic material on surface ocean heating in the Chukchi Sea. J Geophys Res 113:C07024
83. Gnanadesikan A, Anderson WG (2009) Ocean water clarity and the ocean general circulation in a coupled climate model. J Phys Oceanogr 39:314–332
84. Gnanadesikan A, Emanuel K, Vecchi GA, Anderson WG, Hallberg R (2010) How ocean color can steer Pacific tropical cyclones. Geophys Res Lett 37:L18802
85. Miller WL, Moran MA (1997) Interaction of photochemical and microbial processes in the degradation of refractory dissolved organic matter from a coastal marine environment. Limnol Oceanogr 42:1317–1324
86. Ackleson SG, Balch WM, Holligan PM (1994) Response of water-leaving radiance to particulate calcite and chlorophyll a concentrations: a model for Gulf of Maine coccolithophore blooms. J Geophys Res 99:7483–7499
87. Gordon HR et al (2001) Retrieval of coccolithophore calcite concentration from SeaWiFS imagery. Geophys Res Lett 28:1587–1590
88. Balch W, Drapeau D, Bowler B, Booth E (2007) Prediction of pelagic calcification rates using satellite measurements. Deep Sea Res Part II: Top Stud Oceanogr 54:478–495
89. Balch WM, Fabry VJ (2008) Ocean acidification: documenting its impact on calcifying phytoplankton at basin scales. Mar Ecol Prog Ser 373:239–247
90. Ryther JH (1969) Photosynthesis and fish production in the sea. Science 166:72–76
91. Wilson RW et al (2009) Contribution of fish to the marine inorganic carbon cycle. Science 323:359–362

92. Platt T, Sathyendranath S, Fuentes-Yaco C (2007) Biological oceanography and fisheries management: perspective after 10 years. ICES J Marine Sci 64:863
93. Platt T, Sathyendranath S (2008) Ecological indicators for the pelagic zone of the ocean from remote sensing. Remote Sens Environ 112:3426–3436
94. Stumpf RP et al (2003) Monitoring Karenia brevis blooms in the Gulf of Mexico using satellite ocean color imagery and other data. Harmful Algae 2:147–160
95. Hu C et al (2003) MODIS detects oil spills in Lake Maracaibo, Venezuela. Eos AGU Trans 84:313–319
96. Fingas M, Brown C (2000) A review of the status of advanced technologies for the detection of oil in and with ice. Spill Sci Technol Bull 6:295–302
97. Boland RC, Donohue MJ (2003) Marine debris accumulation in the nearshore marine habitat of the endangered Hawaiian monk seal, Monachus schauinslandi 1999–2001. Mar Pollut Bull 46:1385–1394
98. Donohue MJ, Boland RC, Sramek CM, Antonelis GA (2001) Derelict fishing gear in the Northwestern Hawaiian Islands: diving surveys and debris removal in 1999 confirm threat to coral reef ecosystems. Mar Pollut Bull 42:1301–1312
99. Randolph K et al (2008) Hyperspectral remote sensing of cyanobacteria in turbid productive water using optically active pigments, chlorophyll a and phycocyanin. Remote Sens Environ 112:4009–4019
100. IOCCG (2007) Ocean-colour data merging In: Gregg W (ed) Reports of the International Ocean-Colour Coordinating Group, Dartmouth
101. Roy S, Llewellyn C, Egeland ES, Johnsen G (2011) Phytoplankton pigments: updates on characterization, chemotaxonomy and applications in oceanography. Cambridge University Press. Cambridge Environmental Chemistry Series. Cambridge, UK. pp 845. ISBN: 978110700066-7

Books and Reviews

Campbell J, Antoine D, Armstrong R, Arrigo K, Balch W, Barber R, Behrenfeld M, Bidigare R, Bishop J, Carr ME et al (2002) Comparison of algorithms for estimating ocean primary production from surface chlorophyll, temperature, and irradiance. Glob Biogeochem Cycle 16:1035

Carr ME, Friedrichs MAM, Schmeltz M, Noguchi Aita M, Antoine D, Arrigo KR, Asanuma I, Aumont O, Barber R, Behrenfeld M et al (2006) A comparison of global estimates of marine primary production from ocean color. Deep Sea ResPart II: Top Stud Oceanogr 53:741–770

GlobCOLOUR: An EO based service supporting global ocean carbon cycle research. European Space Agency. http://www.globcolour.info/

IOCCG. Reports of the International Ocean-Colour Coordinating Group No. 1–10. Dartmouth. http://www.ioccg.org/reports_ioccg.html

Jerlov NG, Nielsen ES (eds) (1974) Optical aspects of oceanography. Academic, London

Miller R, Del-Castillo C, McKee BA (eds) (2005) Remote sensing of coastal aquatic waters. Springer, Dordrecht

Morel A (1991) Optics of marine particles and marine optics. In: Demers S (ed) Particle analysis in oceanography. Springer, Berlin, pp 141–188

Morel A, Bricaud A (1986) Inherent optical properties of algal cells including picoplankton: theoretical and experimental results. Can Bull Fish Aquat Sci 214:521–559

National Aeronautics and Space Administration (NASA) Ocean optics protocols for satellite ocean color sensor validation, vol I–VI. http://oceancolor.gsfc.nasa.gov/DOCS/

National Aeronautics and Space Administration (NASA) Ocean color web. http://oceancolor.gsfc.nasa.gov/

Platt T, Nayak S (eds) (2005). Special issue on: ocean colour remote sensing. Indian J Marine Sci 34(4):341–355

Siegel D (2004) Views of ocean processes from the sea-viewing wide field- of-view sensor mission: introduction to the first special issue. Deep Sea Res Part II Top Stud Oceanogr 51(1–3):1–3. http://dx.doi.org/10.1016/j.dsr2.2003.12.001

The Oceanography Society (2004) Special issue: coastal ocean optics and dynamics. Oceanography 17(2):1–95

Thomas A, Siegel D, Marra J (2004) Views of ocean processes from the sea-viewing wide field- of-view sensor (SeaWiFS) mission: introduction to the second special issue. Deep Sea Res Part II Top Stud Oceanogr 51(10–11):911–912. http://dx.doi.org/10.1016/j.dsr2.2004.06.003

Renewable Energy from Biomass, Introduction

Martin Kaltschmitt
German Biomass Research Centre, Leipzig, Germany
Institute of Environmental Technology and Energy Economics, Hamburg University of Technology, Hamburg, Germany

Biomass has been a major energy source for humans since the mastering of the fire in ancient days. In addition, for a very long time in the history of humankind, bioenergy has been basically the one and only energy source for cooking, heating, and lighting. Beside this, biomass has been used as a horse or cattle feed for the provision of power and transportation duties and thus in an indirect way for energy provision. Therefore, the development of the human culture would have not been possible without the extensive use of biomass for energy.

During the last two centuries, the relative contribution of bioenergy within the overall energy system has been decreased due to an increasingly extensive use of, first, coal and, later, crude oil and natural gas. Nevertheless, on a global scale, biomass contributes still with roughly 10% to cover the overall primary energy consumption. Thus, bioenergy is still today the most important renewable source of energy used by humanity. It contributes in energy terms more within the global energy system as nuclear or hydropower. Moreover, this is true for developing as well as for industrialized countries. Biomass is not only the fuel for the poor people as it is often called in some developing countries.

In the years to come, the fossil fuel resources technically and economically easily accessible will decrease. Consequently, the prices for these commodities – and thus the overall energy price level – will increase due to the expected shortage resulting from the strongly growing energy demand especially from the emerging economies like China, India, and Brazil. Additionally, the international environmental politics will increase its efforts to reduce the greenhouse gas emissions for stabilizing the climate on a certain level (i.e., 2°C goal). Both developments will contribute to the fact that the importance of biomass for energy will continue to grow significantly in the future.

Biomass as a domestic energy carrier is stored solar energy; for this reason, it can be used depending on the actual given energy demand and can help to equalize the strong fluctuations of an energy provision from wind and solar likely to be used to a much higher extent in the years to come. Biomass is the most important carbon source available to humans beside the limited resources of fossil fuels (i.e., crude oil, natural gas, hard coal, and lignite). This is one of the reasons why additionally the combined provision of energy and raw materials (e.g., for the chemical industry) from biomass will gain more and more importance in the future (i.e., biorefinery approach). Moreover, biomass as an energy carrier can be used for the provision of heat and of electricity and for transportation purpose with existing technology available on the market ready for commercial applications. This makes organic material so valuable within a future energy system based compulsory to a much higher degree on renewable sources of energy compared to today for reasons outlined above.

Against this background, the goal of this section is to discuss various aspects associated with the energetic use of organic material. Therefore, first, biomass as a renewable source of energy is disputed in detail. Then, various possibilities to convert organic matter for the provision of heat, electricity, and fuels are presented under different frame conditions considering technical, economic, environmental, and social aspects.

To understand the possibilities and constraints of biomass for energy currently discussed very emotionally within politics and society, the *principles and prospects of biomass production* need to be understood from a biological point of view. Among other aspects, this makes it obvious how the overall efficiencies are between the solar radiation affecting the plant leaf and the energy content of the plant material synthesized from this solar energy. Based on this knowledge of the – from a biological point of view – possible plant productivity, the *worldwide biomass resources* are assessed to give an overview of the biomass potential available to humankind under various frame conditions. This shows that even if additionally to purely biological aspects other constraints (e.g., water and nutrient availability, appropriate production schemes, ecological criteria) are taken into consideration (which has to be the case without any doubts), the biomass potential available for the energy markets without affecting the markets for food and fodder and for raw materials is still huge. This is true even against the background of the enormous global primary energy consumption as well as the potentials of other renewable sources of energy. Nevertheless, due to the food vs. fuel discussion, an intensive search for "new" or alternative biomass resources, which cannot be used within the food and fodder markets, is ongoing, promising much higher area specific yields and/or a much better use of the solar insulation. This is especially true for the assessment of the *possibilities and constraints of algae as a "new" biomass resource* discussed currently as the big white hope especially for the provision of fuels for transportation purpose.

However, the biomass potential available to fuel the world population is already used to certain extents. Although it is impossible for fundamental reasons to assess accurately the overall current use (e.g., due to insufficient data), the *biomass use on a global scale*

can be roughly estimated based on robust assumptions and approximate calculations. This allows making valuations on how the use of biomass as an energy carrier can be expanded on a global scale. Additionally, it shows very clearly that biomass contributes today to all important energy markets (i.e., heat, electricity, fuels). Beside this, it becomes obvious that the contribution of biomass within the global energy system is strongly increasing in absolute terms. This is especially true for a modern use of biomass realized in industrialized countries and with an increasing share also in developing nations. Additionally, biomass is used in a "traditional" way in developing countries mainly for the provision of energy for cooking and heating. However, the assessment of the potentials and the use shows that partly biomass use exceeds production. This means that a nonsustainable situation is given in some parts of this world, as it is, for example, the case in some densely populated and very poor areas in selected developing countries. Therefore, *sustainability aspects of a biomass provision and use* are gaining more and more attention in energy politics and economy on a global as well as on a national scale. Consequently, some governments have implemented already quite strict sustainability criteria to be fulfilled if biomass-derived fuels should be used within the energy system especially under the viewpoint of climate protection. Thus, the production, provision, and use of biomass as a sustainable energy carrier (i.e., fulfilling the given sustainability demands) become more and more complex and demanding. Therefore, *possible conversion routes for biomass as an energy source* are analyzed and discussed to give an idea about the huge variety of the given possibilities.

Based on this overview of various provision routes and their determinants, different biomass resources available for energy purpose are discussed in detail. First of all, this is true for the *production and provision of woody energy crops* from "classical" forests as well as from short rotation plantations (i.e., agricultural production of wood). These wood resources are usually used for the provision of solid fuels. Based on this, *solid biofuels and their characteristics* as well as *upgraded new solid biofuels (like pellets, torrefied wood, etc.)* are presented in detail. This discussion makes it obvious that wood logs and wood chips are still dominating the local wood fuel markets. However, wood pellets as a globally traded commodity gain more and more market importance in recent years, and this development is likely to continue in the years to come. Beside these wood-based biofuels used mainly in combustion devices, substrates for biogas production are used in an increasing manner in recent years among others due to effective subsidy schemes in industrialized countries as well as in emerging economies. Therefore, the *provision of biogas substrates from municipalities and from industry* as well as *production and provision of energy crops for biogas production* is tackled in detail, showing the fuel characteristics as well as the production and provision options including the determining parameters.

The biomass resources discussed above are used traditionally to a large extent within the heat market (i.e., for the provision of thermal energy mainly for cooking and space heating). This application field can be subdivided in several subareas. Depending on the thermal capacity installed within the combustion device, *heat provision in modern small-scale systems* and *heat provision in modern large-scale systems* can be distinguished. Both options are characterized by very advanced conversion technologies, minimizing the environmental burden and maximizing the overall conversion efficiency between the fuel energy and the provided useful energy. Thus, it becomes obvious that today combustion of solid biofuels is realized in high-tech devices, taking the latest findings from numerous research activities into consideration. The fact that one can smell if the neighbor is heating his house based on wood fuels is history. Additionally, *small-scale heat and power (CHP) systems* are gaining more and more importance for the provision of heat and power to cover the local demand of both energy carrier and to maximize the exergetic conversion efficiencies in parallel. However, most of these small-scale CHP options are still in a developing phase. They have gained only very limited market relevance yet. For developing countries with a lack of access to modern, high-tech conversion devices for solid biofuels, *heat provision for cooking and heating* is realized still with traditional technologies (like the three-stone oven) characterized by rather low conversion efficiencies as well as high environmental impacts especially of emissions with a toxic impact on humans. One option to overcome the manifold problems resulting from the use of solid biofuels (e.g., dried dung) in such primitive devices in

these poor regions could be *biogas production in developing countries for small-scale heat and cooking applications*. This possibility is characterized by various advantages if it is implemented locally in an intelligent way (which is unfortunately often not the case in reality).

During the last century, more and more biomass is used for electricity generation, helping to cover the strongly increasing demand for electrical energy in developing as well as in industrialized countries. Therefore, the various options converting organic material into electricity to be fed into the local and supraregional electricity grids are discussed in detail. This is especially true for the "classical" and most widely used option – *biomass combustion for electricity generation*. Within such combustion devices coupled to a conventional power plant cycle or maybe an Organic Rankine Cycle (ORC), basically, only solid biofuels – like wood chips, wood logs, wood pellets, and sometimes even straw – are used with installed electrical capacities varying between a couple of megawatts up to some 100 MW. Especially in countries with cold winter months and thus a high space heating demand, these plants are often operated in a CHP mode to enhance the overall efficiency and thus to reduce the costs of these systems. Beside such an electrification or combined heat and power generation based exclusively on solid biofuels, *biomass cofiring in large-scale coal-fired power plants* is realized with an increasing importance. This option of burning solid biofuels together with coal in existing power plants allows to reduce the investment costs, to increase the overall conversion efficiencies, and to contribute to greenhouse gas mitigation. Due to these reasons, this option has gained more and more importance for electricity generation partly coupled with heat provision especially in industrialized countries.

Nevertheless, due to an increasing lack of cheap solid biomass on the local and global markets, the overall development aim is to provide electricity from such feedstock with a much higher overall electrical efficiency resp. an increased exergetic conversion rate. The key technology promising to allow for significantly improved efficiencies compared to the "classical" combustion with a steam cycle coupled to a combustion device is the gasification of solid biofuels to a gaseous energy carrier to be used in an engine, a gas turbine, a fuel cell, or even an IGCC (i.e., integrated gasification combined cycle). Therefore, the *large-scale biomass gasification for the provision of electricity and fuels* is discussed, showing that the technology is on the borderline to market introduction even due the fact that some technological challenges have to be met in the future. Additionally, the *small-scale biomass gasification for rural electrification* allows in principle to provide electricity with high efficiencies for small-scale, local, and decentralized applications (e.g., electricity generation for stand-alone application). Therefore, this option is tackled in detail, showing that the technology is fundamentally available but much too expensive for the time being. Nevertheless, it becomes obvious that on the shorter or longer term, gasification will play a much more important role within the conversion of solid biofuels into electricity due to fundamental thermodynamic and technological advantages compared to combustion.

Beside solid biofuels dominating the markets for biomass feedstock for electricity generation so far, also liquid and gaseous bioenergy carrier are more and more widely used for the conversion to electrical energy partly coupled with the provision of thermal energy. Therefore, the *possibilities and constraints of liquid biofuels for combined heat and power* (*CHP*) as well as *biogas provision* (*high-tech applications*) for electricity generation are discussed in detail. These two contributions show that for certain niche markets and/or specific applications, these options are very promising according to technical, economic, and especially environmental aspects.

In accordance with the development of the markets for heat and electricity, also the use of biomass-derived liquid and gaseous fuels to be used within the transportation sector has gained more and more market relevance in recent years. For example, liquid biofuels (i.e., bioethanol and biodiesel) contributed in 2010 with 0.5% to cover the overall global primary energy consumption. One main driver for this development is the fact that biomass is the one and only renewable source of energy which can be used with available and market-ready technology within the existing transportation system. For these reasons, the production and provision of *biodiesel* is discussed, showing that the processes to provide a fuel with similar characteristics compared to fossil diesel fuel are rather simple.

Therefore, such conversion processes can be implemented also in rural areas of developing countries; this is one reason why countries with a strong vegetable oil production industry are promoting this provision route with administrative measures. The same is true – maybe to a minor extent – also for bioethanol. However, the globally existing ethanol production can be subdivided in roughly two different markets representing two slightly varying technologies based on two differing types of biomass feedstock: bioethanol from sugar and from starch. The former is realized primarily in Brazil (and other tropical countries) and the latter in the US (and other countries in temperate zones). Both countries provide together more than 85% of the globally produced bioethanol. To cover these two different provision chains in an adequate way, firstly, the production and provision of *bioethanol from sugar – the Brazilian experience* – is discussed in detail. Secondly, aspects related to *principles and available experiences for bioethanol manufacturing from starch* are presented. Both essays as well as the development of the global bioethanol markets show clearly that the technology is market ready. Nevertheless, there are manifold ways to improve the processes to maximize the overall conversion efficiency and to minimize the waste products. Anyhow, due to fundamental biological and physical reasons, the overall conversion efficiency from biomass to bioethanol is limited, and the overall energy demand for the production of dehydrated ethanol ready to be used within a flex-fuel vehicle is high in bioethanol factories realized today. Therefore, globally enormous research money is currently spent to develop better and more integrated processes (i.e., biorefinery approach) and to expand the resource basis to increase the hectare-specific bioethanol yield. One option for the latter is the production of *bioethanol from celluloses*. Therefore, this option is discussed in detail with a special focus on the presentation of the ongoing developments of principles and processes for a most efficient use of lignocellulosic biomass.

Such processes for the conversion of lignocellulosic biomass via fermentation to bioethanol compete with other options for the provision of liquid and gaseous fuel based on solid biomass. On the one hand side, this is true for the thermochemical conversion of biomass, e.g., Fischer–Tropsch diesel, to be used as a liquid fuel in existing diesel engines. Therefore, *biomass to liquid* (*BtL*)concepts are presented and assessed, showing that based on a thermochemical gasification of solid biomass and an upgrading of the provided gas, basically all fuels currently used within the transportation sector can be provided. The same is true for *biomass pyrolysis* promising also the provision of liquid biofuels for a possible use as a transportation fuel. On the other hand, also gaseous fuels can be provided based on thermochemical processes, allowing for relatively high conversion efficiencies. For these reasons, the provision chains for *bio-synthetic natural gas* (*Bio-SNG*) as well as *biohydrogen* are outlined and discussed in detail. Additionally, *biomethane from anaerobic processes* can also be used as a substitute for natural gas in CNG vehicles. Thus, the experiences and perspectives available so far are also debated in detail for this biochemical conversion route. Finally, a *technical, economic, and environmental comparison of the different biofuels* is carried out, indicating that there is no silver bullet for the provision of biofuels available so far.

All over, this section gives a broad overview on biomass as an energy carrier for the provision of heat, electricity, and transportation fuel considering technical, economic, environmental, and social aspects.

Renewable Generation, Integration of

Bri-Mathias Hodge[1], Erik Ela[1], Paul Denholm[2]
[1]Transmission and Grid Integration Group, National Renewable Energy Laboratory, Golden, CO, USA
[2]Energy Forecasting and Modeling Group, National Renewable Energy Laboratory, Golden, CO, USA

Article Outline

Glossary
Definition of the Subject and Its Importance
Introduction
Electricity System Background
Characteristics of Renewable Resources
Generator Modeling and Interconnection

Operating Impacts
Market Considerations
Transmission Planning
Enabling Greater Renewable Penetration
Future Directions
Bibliography

Glossary

Ancillary services All of the actions necessary for supporting the transmission of power from the generator to the consumer and ensuring reliable system operations. Some examples of these services include: voltage and frequency control, generation scheduling, load following, and system protection.

Balancing area An area in which electricity supply and demand are locally matched and over which a balancing authority maintains system frequency and provides operating reserve.

Independent system operator The organization that is charged with controlling the operation of the electrical power transmission system in a certain geographic area.

Operating reserve Extra generating capacity available at short notice to replace scheduled capacity that is currently unavailable due to some sort of system disruption.

Unit commitment and economic dispatch The process by which generators are scheduled by the grid operator in order to meet expected demand at all timeframes. Commitment refers to deciding which generators will be turned on far in advance of the time period under consideration. Dispatch refers to the decision of how much power each generator will supply during a timeframe that is closer to realization than the commitment period.

Variable generation Generation from units that cannot be well controlled and thus are not perfectly dispatchable. This term is often applied to generation from weather-driven units, such as wind and solar.

Definition of the Subject and Its Importance

The integration of renewable generation consists of all of the changes in power system operations that are required in order to allow renewable generation sources to play a significant role in the electricity system. The impacts are mostly due to variable generation (VG), like wind and solar power. Historically these technologies have been labeled as intermittent generation, but recent trends prefer the label variable generation [1]. Variable generators have a maximum available generation limit that changes with time (variability) and this limit is not known with perfect accuracy (uncertainty). This uncertainty and variability is in addition to that of the existing system and can therefore create additional challenges for grid operators to maintain their current levels of reliability.

Introduction

Renewable electricity generation encompasses a number of distinct technology types, often classified by their power source, such as geothermal, hydroelectric, marine, biomass, solar, and wind power. Within each of these groupings there are a number of different technologies for harnessing the energy of the power source. However, when discussing renewable integration wind, marine, run of river hydro, and solar generation tend to garner most of the interest. This is due to the fact that the output of these plants is variable and uncertain. Other types of renewable generation are more similar to traditional power sources, such as fossil fuels and nuclear power, in that they are dispatchable. This means that they can be reliably scheduled in advance to provide power when desired, and do not need to rely on the current weather conditions. This is the result of the fact that the availability of their energy source can be controlled. While no generator can guarantee availability at a scheduled time, every generator has the possibility of being unavailable. The unplanned outage rates for dispatchable generators are low enough for the system to treat them as if they will produce at the desired level in the scheduled timeframe, while holding contingency reserves should an outage occur. While other renewable generating units can occasionally have uncertain output, for example, hydroelectric units cannot operate below certain reservoir levels, they are normally treated similarly to conventional units. For this reason the integration of these generating technologies is not normally considered an issue for electrical system operation. Another way of demonstrating the difference between variable generation and dispatchable generation is to examine some of

the factors used to describe their patterns of usage. One common metrics is the capacity factor. A capacity factor is the amount of electricity a unit would be physically able to generate divided by the theoretical maximum that the unit would produce if it ran at full capacity over a certain time period. Therefore times when the unit would be down or at a reduced capacity due to forced and unforced outages count against the capacity factor. Baseload power plants typically have capacity factors on the order of 90% or higher. Wind power plants sited in good onshore locations have capacity factors of around 30%, while solar PV plants, even in very good locations, tend to have capacity factors under 20%. However, capacity factor alone does not tell the whole story. For example, a natural gas turbine that is used only for peaking may have a capacity factor under 5%. Even though the turbine is available for a greater percentage of the time, it is not always chosen in the unit commitment and dispatch process due its higher operating costs than baseload plants. For this reason other metrics such as forced and unforced outage rates are also used to characterize unit usage. These metrics however do not apply as well to variable generators and therefore metrics such as capacity value and effective load-carrying capability are often utilized when discussing the availability of wind and solar generators. When the integration of renewable generation is considered, wind and solar generation are usually the focus due to their variable and uncertain nature and their current presence in relatively large quantities in the system.

Worldwide wind power output grew sevenfold and solar photovoltaic (PV) production grew 16-fold from 2000 to 2008 [2]. Wind power has been the fastest growing source of electrical generation capacity in the United States for the last several years [3]. In 2009, there were over 34 GW of wind capacity operating in the United States and over 600 MW of solar PV [3]. These trends have transformed variable generation from a minor component in the electricity system to a contributor whose effects on the overall system must be thoroughly considered. As the future electricity system is expected to contain even larger quantities of variable generation, it is important that means of integrating variable generation are well researched before the higher penetration rates are achieved.

Electricity System Background

The current electricity system is the product of over 100 years of evolution and growth. A central pillar of the system is dispatchable generation, generally from fossil fuels, hydroelectricity, and nuclear power. As most large-scale power systems have relatively small amounts of electricity storage, electrical supply must always meet electrical demand. The instantaneous matching of supply and demand is needed in order to maintain a nominal electrical frequency. When supply does not equal demand, the frequency can change from its scheduled value (60 Hz in the North America, 50 Hz in many other locations). Frequency that deviates too far from its scheduled value can trigger under-frequency load shedding or over-frequency relays disconnecting machines to prevent damage. If this is not controlled, cascading events can lead to blackouts. This need for supply–demand balance coupled with the fact that the vast majority of demand is noncontrollable necessitates the current structure of system operation. Electricity system operation is a complex process where demand must be forecast and generation scheduled in advance, but numerous types of reserves must also be kept waiting in order to ensure system reliability, should forecast demand errors occur or scheduled generation units become unavailable.

Electricity demand follows strong seasonal and daily patterns. Seasonal demand patterns are highly correlated with seasonal weather patterns. Most systems in the United States tend to have their highest demand during the summer due to the large additional loads attributable to air conditioning. European systems generally tend to reach peak levels during the winter due to the demand from electric space heating. Figure 1 demonstrates both the seasonal and daily patterns that occur in the Electric Reliability Council of Texas (ERCOT) system. As may be observed, the summer peaks can be as much as double the spring minimum loads. The daily differences can also be very large during the summer months. Figure 1 shows an instance where total system load varies between 40 and 60 GW in the course of a single day. In order to meet these vastly different conditions, utilities build generating units with very different production characteristics.

Baseload power plants are utilized to cover the large amounts of demand for electricity that fall below the

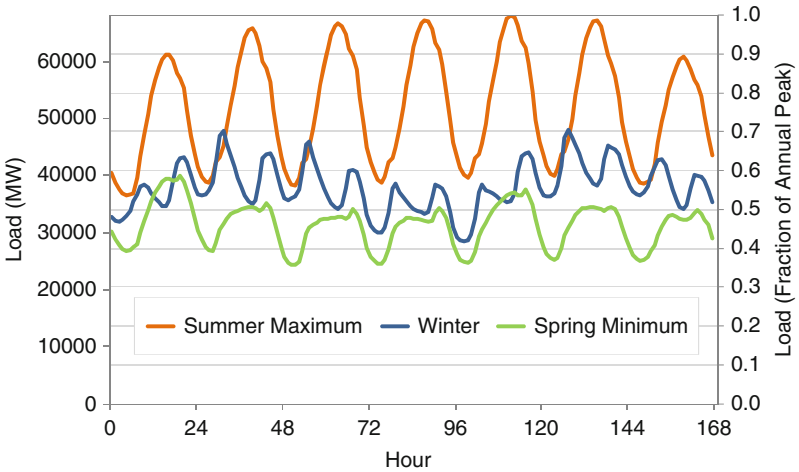

Renewable Generation, Integration of. Figure 1
Hourly loads from ERCOT 2005 [4]

minimum daily demand level. Coal-fired and nuclear plants are the two most typical types of baseload plants. They are often very high capacity plants that have very large capital costs, and relatively low operating costs. Baseload plants also typically require long start-up times and cannot ramp rapidly to follow changes in load. For these reasons utilities prefer to run the plants as close to maximum output as possible the majority of the time they are in service. Variations in load are usually met through the use of another type of generating unit, the load following plant. These units can be further subdivided into intermediate load plants and peaking plants. Intermediate plants are typically used to meet the daily variability in demand and are often hydroelectric or combined cycle plants fueled by natural gas. Peaking plants usually have a very high marginal cost of production, and as such are only utilized during periods of extremely high demand, often less than a few hundred hours per year. These plants are often natural gas or oil-fired simple cycle turbines. The normal usage patterns of baseload, intermediate, and peaking units can be observed in Fig. 2.

The generating units that will meet the expected load are usually scheduled 1 day beforehand in what is known as a security-constrained unit commitment. This optimization of total system costs schedules the start-up of units based on forecasted loads for the next day. Because system load cannot be perfectly forecast, there is the need for another assignment process closer to the actual time point. This process is known as security-constrained economic dispatch and it changes the level of output of units already online in order to ensure that supply meets demand. The amount of time ahead that this process occurs varies by system operator. Advances in telecommunications have allowed some systems to operate at smaller dispatch timings, down to 5 min ahead. Both of these processes should ensure that the commitment and dispatch are secure considering the generator constraints, transmission network constraints, and n-1 contingency constraints. The n-1 criterion states that a system must be secure following any credible single outage, be that a generator, or other system component (e.g., a transmission line).

In addition to advanced scheduling that needs to occur to balance the generation, system operators often schedule capacity as operating reserve to be used in case of unexpected changes from schedules or for variability occurring within a scheduling interval. Operating reserves can be classified according to the type of situation that triggers their deployment, the timescale of the response, and the direction of deployment. Figure 3 illustrates the different types of reserves based upon the event type and the speed of response. The most commonly utilized reserves are those that are required during normal operating conditions. Generating units must be kept in reserve in order to respond to continuous differences between forecasted and actual conditions. This function falls under the category of reserves

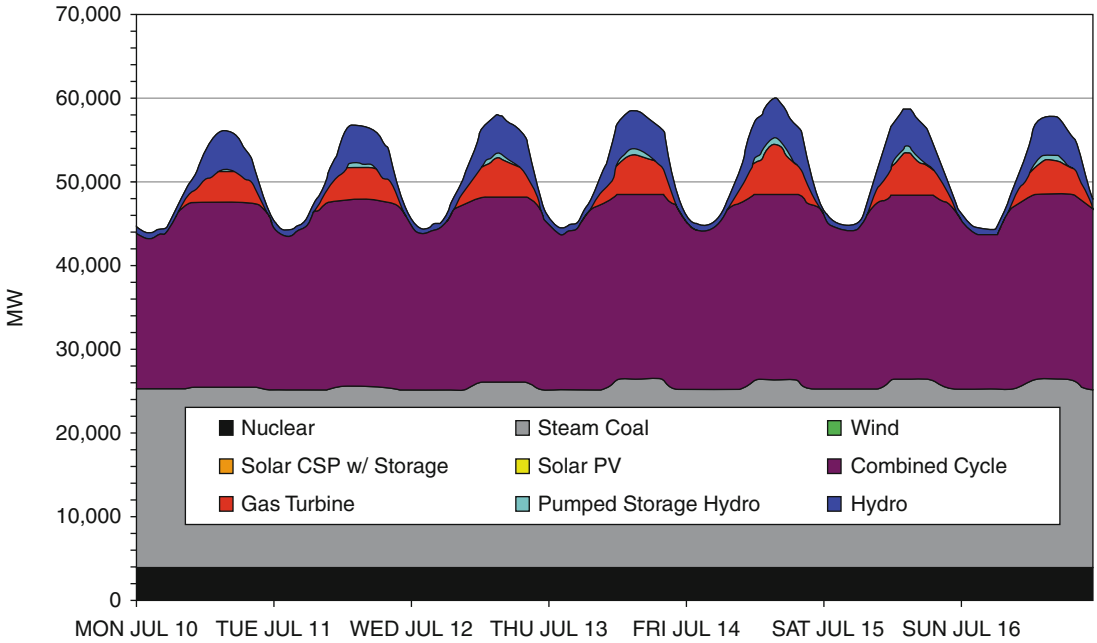

Renewable Generation, Integration of. Figure 2
Normal unit commitment and dispatch patterns in the western United States with a very low renewable generation penetration rate [5]

known as regulation reserve. It is employed to respond to the minor random fluctuations that occur around normal load in order to maintain system frequency. Regulation reserves are required in both the up and down directions, in other words, regulation reserve must be able to both increase and decrease output to match the fluctuating conditions. Regulation reserves are generally employed on the sub-minute timescale. More sustained trends over the timescale of minutes are handled through following reserve (often called load following reserve in practice).

In addition, reserves must be kept on hand should a generating plant or transmission line currently importing power suddenly become unavailable. Contingency reserves are those in place for unexpected events that change the instantaneous availability of generators or transmission. Primary reserve, that is, frequency responsive reserves, responds within seconds in order to stabilize the system frequency after a major disturbance. Secondary reserve is then used to restore the frequency back to its scheduled setting. Tertiary reserve is then used to replace the reserve used during the event so that the system is secure toward a subsequent event. Ramping reserve is utilized in order to respond to events that occur over a longer duration, such as variable generation forecast errors or ramping events. Ramping reserve also requires frequency or control error to return to its nominal setting and for it to be replaced in case of a secondary event. However, due to the slow time it takes for these events to occur it is usually not necessary to stabilize the quickly changing frequency. Reserves are also often classified according to their synchronization status. Reserves provided by units that are already running and synchronized to the system are known as spinning reserves, while non-spinning reserves are not synchronized and thus take longer to respond. Fast response reserve, such as regulating reserve and primary or frequency response reserve, require spinning reserve exclusively while slower reserve categories usually contain mixtures of both spinning and non-spinning reserves in different proportions.

Characteristics of Renewable Resources

As described in the Introduction, the discussion of renewable resource characteristics is generally limited

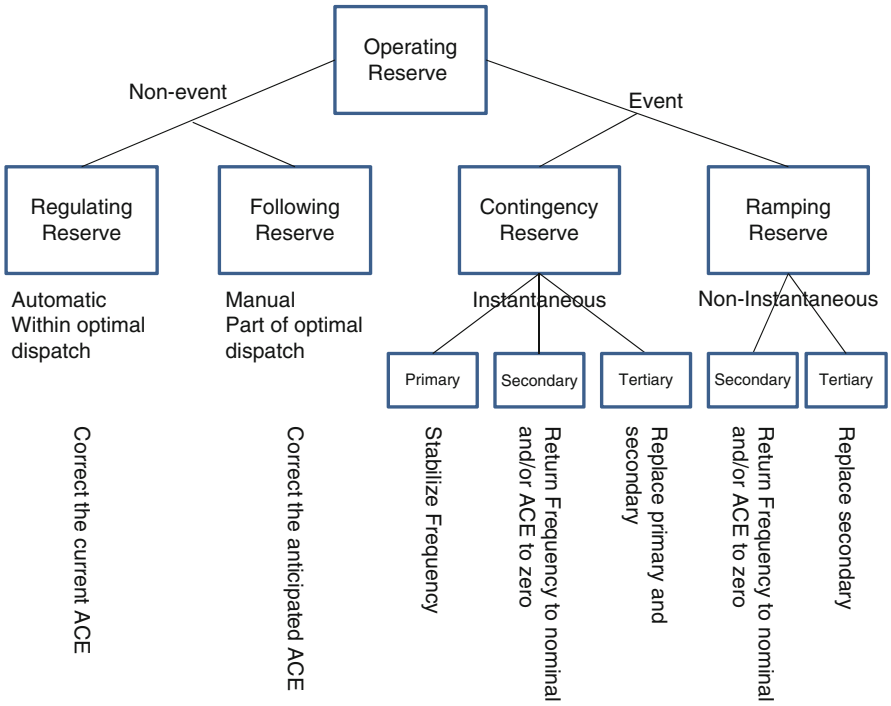

Renewable Generation, Integration of. Figure 3
Illustration of reserve types [6]

to wind and solar generation, since they operate quite differently from other types of generation. While both are considered variable resources, wind and solar generation have distinct characteristics that need to be considered when attempting to integrate them into the electricity system. Perhaps the most important difference is in their diurnal patterns. Solar generation output follows the daily cycle of the sun in its particular location on earth, and thus is limited to daylight hours. Wind power output may occur during both daylight and night hours, but in most locations output has a tendency to be higher and more consistent during the night hours. This is demonstrated in the plot of average wind power output over the course of a day for the year 2004 in the MISO system seen in Fig. 4. Plotted on the same graph are the average locational marginal prices (LMPs) for the MISO system over the course of a day. As may be observed, the wind output tends to be highest when energy prices are lowest, corresponding to times of low demand, and dips during the daily peak when prices are highest.

Solar generation can be subdivided into two different categories: concentrating solar thermal and solar PV. From an operational perspective the biggest difference between the two is that concentrating solar thermal plants can have thermal storage capabilities. This allows them to store energy that can later be used to provide electricity during periods where output would be diminished if relying solely on immediate solar irradiation. Solar PV on the other hand is completely reliant on the immediate solar irradiation and thus has reduced output in cloudy weather, and no output at night. The difference in daily profiles for concentrating solar thermal plants with storage versus PV plants can be seen in the July portion of Fig. 5. Another major difference between the two technologies is the locations in which they can be deployed. Concentrating solar thermal plants require larger areas for installation and the high capital costs dictate that they be deployed in only very high quality resource areas with high direct normal irradiance. Solar energy contains both a direct and a diffuse component. The direct component is the light from the solar beam and the diffuse component consists of light that has

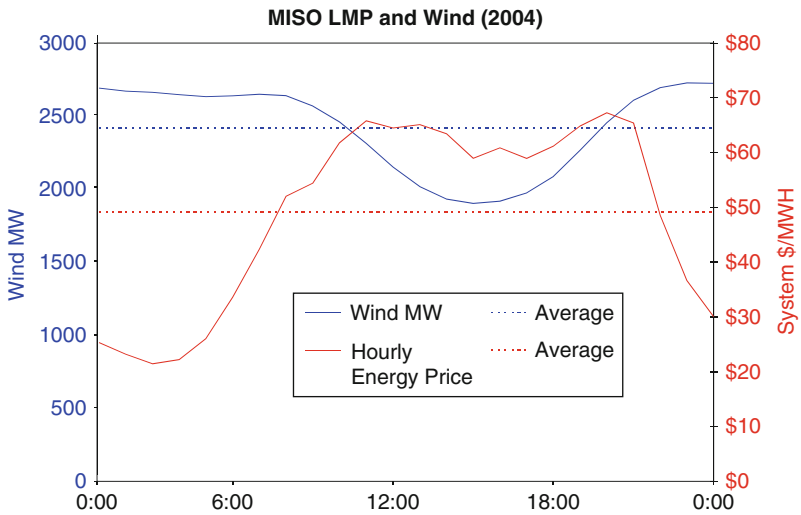

Renewable Generation, Integration of. Figure 4
Average energy prices and wind power output over the course of the day in the MISO system [7]

been scattered by the atmosphere. The direct component can be focused using mirrors or lenses and accounts for 60–80% of total solar insolation in clear sky conditions, but decreases with high levels of humidity, cloud cover, and atmospheric aerosols. This limits their construction to arid regions, such as those in the southwestern United States. PV on the other hand can be deployed in nonutility scale system sizes and thus can be present in large plant configurations or distributed over a number of locations, such as rooftops. This can be an important distinction in the case of very high levels of distributed PV penetration as the output from these locations only appears to the system operator as reduced load.

Wind generation is also subdivided into two categories, though usually based on the location of the wind plant, not the technology being used. Onshore locations have been the dominant choice thus far as wind power capacity has grown. However, offshore locations generally have more consistent output and the accompanying higher capacity factors are attractive. Offshore locations tend to involve the construction of larger turbines, and are usually more expensive due to the difficulties associated with their construction in large bodies of water. While onshore locations can require building new transmission, the additional transmission demands of offshore locations are more extensive, but conversely have the advantage that they are generally located closer to load centers.

One very important positive aspect of both wind and solar is the large size of the resource base. For example, while global electricity consumption in 2005 was estimated to be 16.6 PWh, the resource base of global onshore wind power, restricted to locations with a minimum 20% turbine capacity factor, is approximately 700 PWh [8]. The global offshore resource base, while not as large, is still considerable. Even after restricting the locations to those within 50 nautical miles of the coast and water depth of 50 m or less, the potential energy production is still approximately 80 PWh [8]. The total potential capacity of offshore wind power in the United States is over 4,000 GW, based on locations within 50 nautical miles of the coast with average annual wind speeds at 90 m greater than 7 m/s [9]. Solar PV power has an even larger potential resource base, with the technical potential estimated to be approximately 4,100 PWh per year by 2050 [10], while concentrating solar thermal potential is estimated to be between 630 and 4,700 GW of capacity [11]. As a point of comparison, small and micro hydroelectric plants have an estimated global technical potential of 150–200 GW of capacity [11]. These enormous resource bases, combined with the current low utilization of the potential energy from these sources, make renewable resources attractive options for long-term planning of energy supply sources.

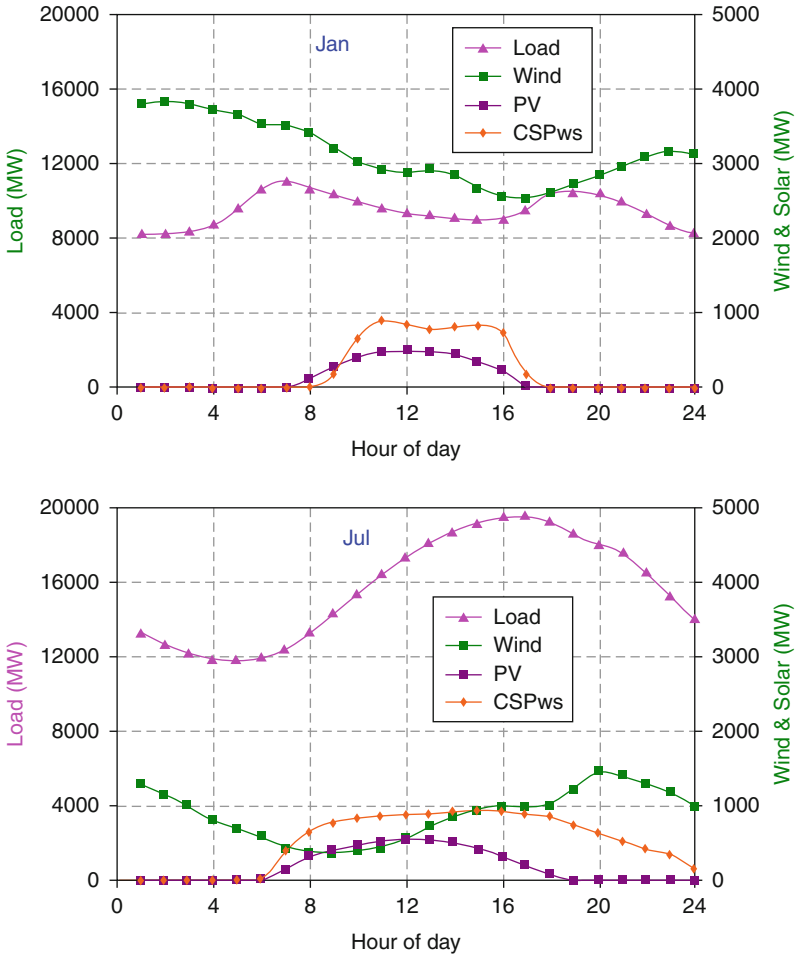

Renewable Generation, Integration of. Figure 5

Load, wind, solar pv, and concentrating solar thermal (with storage) daily profiles for both January and July in Arizona in a high renewable penetration scenario [5]

Because these variable generation sources are not dispatchable, they present new issues for integration into the electricity grid. One major difference is that they are often considered to be a negative load, instead of a generation source. Essentially, any variable generation that is being produced at the current time is accepted and reduces the total load that must be met by conventional generators. This residual load is equal to normal demand minus electricity from renewable generators, and has greater variability than load alone. While this is a suitable representation for low levels of variable generation penetration, it will need to change in order to accommodate higher levels. In fact this is already starting to change as wind is being used to alleviate transmission constraints.

Generator Modeling and Interconnection

There are many technical aspects that concern the physical connection of renewable plants to the electricity grid, and their contributions to stable system operation. As renewable power becomes a larger contributor to the electricity system, it must also take on the responsibilities of maintaining system security. We focus mostly on wind in this section due to the currently higher market share. The requirements of

wind turbines connected to the electricity system are prescribed through grid codes that detail the turbine contributions to ensure power system stability. The interactions that occur between the grid and the wind plant are heavily influenced by the type of machine in use and the stiffness of the grid. There are four different types of wind turbine machines commonly in use (Types 1–4), differing in their ability to control output power and reactive power and the type of generator utilized. The creation of accurate models of the physical representation of these different turbines can aid in the understanding of the effects that wind plant interconnection will have on the system. Small wind plants may be connected at low or medium voltage distribution networks. In a larger plant many turbines are connected together through a collector system and then connect to the substation where a transformer steps up the voltage from the distribution level to the transmission level.

Fault Ride Through

One common requirement made of wind turbines is fault ride through in the case of a system fault. Early wind plants would simply disconnect from the system when a system fault occurred. In systems with larger amounts of wind power this disconnection would exacerbate the problem [12]. This requirement specifies that the generator must stay online during faults with a duration and voltage variation under certain thresholds that vary by system. Further advances in wind turbine technology will allow for the post-fault recovery characteristics of turbines to be better than those of conventional generators. While wind turbines must comply with the requirements for normal network operation, they must also have system protection that prevents damage to the turbine during events that take the system out of its normal operating ranges. Plants typically are required to have protection from over- and under-frequency, current and voltage events. Additionally, the type of power electronics utilized by any renewable generation can significantly enhance its response to events.

Frequency Control

Frequency fluctuations in the power system result from an instantaneous difference between the amount of power being generated and the demand, including system losses. Wind plants can contribute to the stabilization of frequency in over-frequency events by decreasing output, either through blade feathering or shutting down individual turbines. Under-frequency events are more challenging because they require additional generating capacity. Since the wind speed cannot be increased to produce more generation when desired, this requires holding a portion of possibly generating capacity free, despite the lost revenue incurred. If decreases in the wind power output can be forecast, the turbines can reduce their output slowly in advance reducing the impact of the negative ramp rate.

Voltage Control

In order for a power system to operate as designed, the voltage throughout the system should be kept within the normal operating range (0.95–1.05 of the set point), though transients are allowed a wider range (0.9–1.1). The impedance of a power line causes a change in voltage between the two ends when a current is flowing. The introduction of renewable generators changes the power flow in the system, and hence the local voltages. Unlike frequency, voltage is a local phenomenon that cannot be controlled system-wide. Thus voltage must be kept within its specified range locally by generators in the area, or by power electronics, such as tap-changing transformers. Voltage control in transmission lines is normally adjusted through the consumption or supply of reactive power by generators, or through capacitor banks or flexible AC transmission system (FACTS) devices.

Reactive Power

Wind turbines with induction generators consume reactive power, which can lead to voltage collapse, if not properly compensated, and increased system losses from voltage drops and reactive current, respectively. To mitigate the effects, reactive power can be supplied through the inverter on variable speed turbines, or through capacitors in fixed speed turbines.

Interconnection Queue Process

The process by which a new generator receives the requisite permissions from the local grid operator to

connect into the transmission system is known as the interconnection queue process. This process enables the system operator to conduct feasibility, system impact, and facility studies to ensure that the new generator will not have negative effects on system operation. The process also includes the planning steps necessary for generator participation in local markets and the acquisition of necessary transmission rights.

Operating Impacts

With the increasing amounts of wind power being added into electricity systems in recent years, a number of studies have been conducted in order to assess the impacts on the system incurred by integrating these large amounts of wind power. These studies typically examine two cases, one with wind and one without, and compare the results of statistical and production cost simulation analysis in order to determine the cost differences in system operation that may be attributed to wind power. A common assumption is that system reliability must be held at a constant level, which may necessitate the inclusion of additional operating reserves in the with wind case to remedy the increased system variability and uncertainty introduced by the wind plants.

Regulation

The goal of regulation is to compensate for the system variability at small timescales. The majority of this variability is due to normal load fluctuations, with an additional component of variability attributable to conventional generators minor deviations from their set points. The addition of renewable generation to the system adds another source of variability that must be accounted for. However, the impacts of wind generation on regulation services have been found to be relatively minor. For example, the addition of 3300 MW of wind into a system with approximately 30 GW of system peak load required only 36 MW of additional regulation [13]. This is due to the fact that the variability of a large number of wind turbines aggregated together is fairly small at the regulation timescale. Additionally, load and wind power are uncorrelated on the small timescales considered for regulation and thus their fluctuations are rarely amplified and often cancel each other out. However, studies are continuing to use different methods to determine the impact to regulation reserve, and the requirements differ sometimes substantially.

Load Following

One of the areas where the integration of renewable generation sources can have a major impact on grid operations is in the load following domain. In the minutes to hours time frame in which load following operates, there can be large ramps in renewable generation output. The addition of variable generation to load increases the overall system variability within this timeframe. For example, these effects occur when wind power output starts to ramp down following its diurnal pattern, just as the morning load starts to ramp up. This case marks extremely poor timing for the system operator as they must not only be able to handle the increase in load, but must simultaneously replace power that was being generated.

Wind Uncertainty Costs

The main costs of wind uncertainty are the result of having a suboptimal generation mix online due to an inaccurate forecast. One example of a commitment cost can be seen in the case of wind over-forecasting. If the wind output is forecast to be high, but is actually much lower in real time, a unit must be ready to serve the load that the wind was scheduled to serve. If this amount is significant it is possible that a slow starting baseload unit should have been made available at this time. In this case the wind overestimation causes an expensive fast starting unit to produce when a cheaper, but slow starting, unit would have been chosen if the forecast was more accurate. On the other hand, if the wind is under-forecast there may be more plants online than is necessary, causing higher start-up and fuel costs and leading to the possibility of wind curtailment.

It is important to note that since individual wind and solar plants are currently always smaller than the largest generator in the system, additional contingency reserves are not required by traditional metrics, such as the n-1 criteria. This could change in the future at higher renewable penetration rates if very large renewable generation plants are installed, or in the case of number plants being routed through a single large transmission line. However, at very high renewable

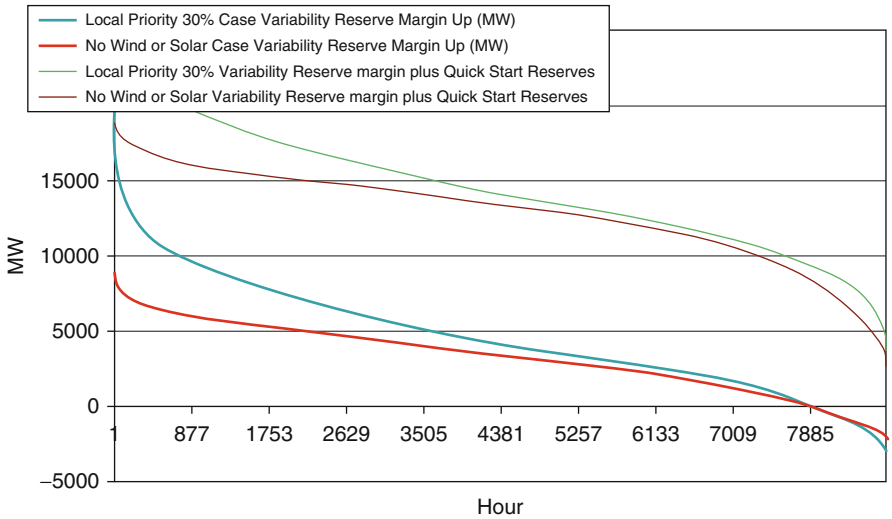

Renewable Generation, Integration of. Figure 6
Increase in available spinning reserves for a base case and a high renewable penetration rate case [5]

penetration rates it can be expected that very large renewable forecast errors could lead to situations where even contingency reserves are not sufficient to cover the error, as has been seen in a study of the western United States [5]. In the Western Wind and Solar Integration Study (WWSIS) it was found that these errors occur in approximately 1% of operating hours. While additional spinning reserves could be added to the system to handle these extreme events, it was proposed that some form of demand response would be more economic. While additional reserves of up to one to one backup have been proposed, this ignores the fact that the addition of renewable generation increases the amount of up-reserves available in the system. The incorporation of increased renewable sources causes the backing down of traditional generators, creating larger amounts of spinning reserve available to the system, as was shown in the WWSIS. One example of this result is shown in the up-reserve duration curve in Fig. 6. The amount of down spinning reserve is also increased as wind curtailment provides a very simple option.

Thermal Unit Cycling

At very high penetrations of renewable generation it is not only peaking and intermediate units that are displaced.

Figure 7 shows an instance where baseload power is forced to produce at levels below maximum generation because of the large amounts of renewable power provided in a 30% renewable penetration scenario. When baseload generation must frequently change its level of output it is referred to as cycling, and it imposes additional wear and tear costs on units that were designed for near constant output. This particular instance is a case where a combination of low demand and high wind output combine to produce results that are far from normal system operation. The most damaging cycling events for thermal units are those where large changes in temperature cause material fatigue, decreasing the normal life of generator components. For this reason unit start-ups are the most damaging due to the large temperature differences between the operating mode and the shutdown mode. The length of the shutdown period is also important with hot-starts and warm-starts being preferred to cold-starts. Though less damaging than shutting down, bringing the generator down to its minimum output level, and then back up to maximum output, also creates large temperature changes that increase wear and tear on the unit.

Market Considerations

While it has been shown that low levels of renewable generation can be incorporated into the electricity

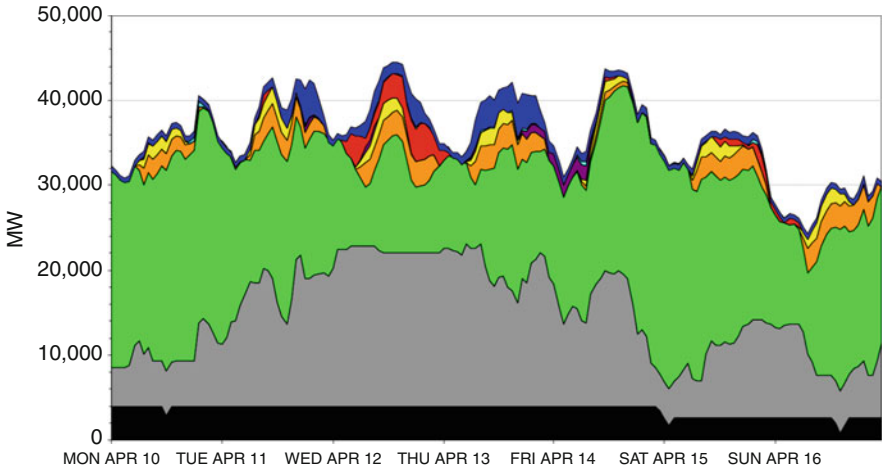

Renewable Generation, Integration of. Figure 7
An example of unit commitment and dispatch in the western United States with 30% renewable generation penetration [5]

system, with few or no changes to current system operations, the variable and uncertain nature of wind and solar power do create limitations on the penetration rates that are reasonably achievable within the context of the existing system. The effects of the uncertainty and variability are mitigated by large day-ahead and hour-ahead markets that provide many options for the balancing of supply and demand.

Balancing Area Cooperation

In 2010, there were over 100 balancing areas in the United States and Canada. Recent trends favor balancing area consolidation and the number of balancing areas is expected to continue to decrease. This is a positive development for the integration of renewable generation. Small balancing areas suffer larger consequences from routine variability. This is true for both supply and demand. For example, in a system with 100 MW total demand, an increase in demand of 10 MW is very significant, while in a system of 10,000 MW the 10 MW change is much more easily accommodated. Aggregated demand is also less variable for larger systems due to the larger number of individuals, and hence the smaller roles of the individuals in the aggregated system load. The variability of renewable generation also decreases with the aggregation of multiple generators in different locations. This geographical diversity of variable generation is due to the fact that the further the two generators are apart, the less likely they are to be affected by the same weather patterns, and hence the correlation of their power output is lower.

Figure 8 shows how the wind speed correlations decrease between geographically distant locations. Larger balancing areas will increase the potential area from which renewable generation can be drawn, and therefore lower the overall variability of total renewable output.

Reserve Sharing

Balancing areas may also choose to cooperate through other mechanisms besides full consolidation. One way that they may reduce the costs of variable generation integration is through reserve sharing agreements. Under these conditions the balancing areas independently schedule and dispatch generation to meet their own loads. However, since certain types of reserves, such as contingency reserves, are utilized only infrequently they may serve as backup to multiple balancing areas, should sufficient transmission capacity be available.

Dispatch Intervals

Another means by which markets may reduce the effects of system variability is through the use of more

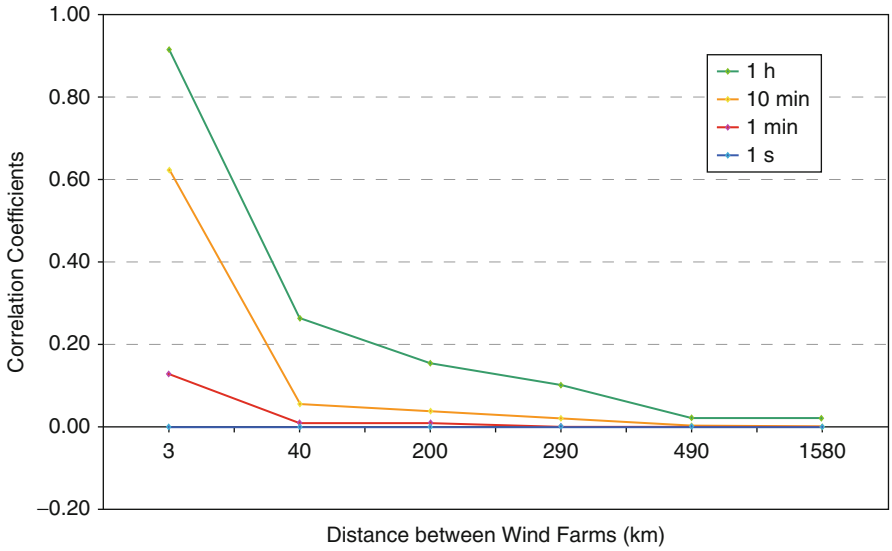

Renewable Generation, Integration of. Figure 8
Wind speed correlations with distances between locations in the United States [14]

frequent market operations than the typical 1-h period for dispatch. Sub-hourly balancing markets aid in the integration of renewable generators by enabling the utilization of existing flexibility in the system and reducing the requirements for ancillary services. In addition, they allow the renewable generators to revise their production forecasts closer to the operating period to minimize forecast errors and thus imbalances.

Ancillary Service Markets

Ancillary service markets will play a key role in the integration of high levels of renewable energy resources. However, the current services offered may not be sufficient and new services should be created based on power system reliability requirements. For example, load following is an important system function with large amounts of renewable generators due to the increased system variability. While this is currently supplied through other units in the energy market, at high renewable penetration rates a market for fast ramping resources may prove to be advantageous. Another key consideration is the adoption of varying ancillary service requirements in response to current renewable generation conditions. When the amount of wind power currently being produced is high, the securing of large amounts of load following reserves would be wise, should a significant decrease in wind power output occur. However, when the wind power output is at a low level, the need for load following reserves is significantly decreased. By co-optimizing not only the choice of ancillary service providers with energy providers, but also the amount of ancillary services, the cost of variable generation integration can be reduced.

Capacity Markets

Well functioning electricity markets are required not only to supply the necessary amount of energy to meet demand at each point in time, but also to supply the generating capacity necessary. The calculation of the capacity credit for variable generation is one of the most contentious issues related to renewable integration, with many different methods being utilized in different systems [15]. Since a capacity credit is normally based on a system reliability measure, such as loss of load probability, it is effectively a measure of a units contribution to system reliability. Since the need for reserve capacity is highest at times of high system stress, when a loss of load is most likely to occur, capacity credit measures value available capacity at these times as more valuable than at times with a low probability of unserved

load. Variable generators have a lower capacity credit than all but the most unreliable of conventional generators due to their high effective forced outage rate. These high effective forced outage rates are the result of weather-induced unavailability and not generator failures. Since the correlation between wind power output and peak load is weak in most locations wind generators tend to have fairly low capacity credit, as the timing of the capacity availability is so critical in the credit determination. On the other hand, solar generators tend to have relatively higher capacity credits, despite their generally lower overall capacity factors. This is due to the fact that the most regular instances of high solar output correspond to the same times as peak demand.

Locational Marginal Prices

Variable generators generally have high capital costs, but low variable costs when compared with conventional generators. The practical implication is that variable generation units will have lower marginal costs of production (often bid as zero) that they may submit as bids into energy markets. When the amount of variable generation is sufficient to remove the highest bidding unit that would otherwise be producing, the market cost of energy at that point in time is reduced. This reduces the total revenue collected by all generators and thus total system costs. Transmission system congestion leads to different prices at different nodes in the system, known as locational marginal pricing (LMP). When government policies for renewable energy production, such as production tax credits, are combined with very high renewable output at a particular point in the transmission system, the possibility of negative LMPs arises. In this case the production incentives offered make it economically efficient for units to pay to produce electricity. This situation is not sustainable in the long-term, neither for the variable generator nor for conventional units in the same area. If this situation occurs at a high enough frequency it could lead to the decommissioning of conventional units in the area, to the detriment of system reliability that relies on those units for reserve capacity [16].

Transmission Planning

The sites that offer renewable generation sources the highest capacity factors are often located far from load centers. This dictates that new transmission must be built in order to utilize these areas with high renewable resources. While the need for new transmission is easily identified the process times for permitting and construction of the transmission often exceed those for the siting and construction of renewable generation. This can lead to situations where large amounts of renewable generation cannot be utilized because of transmission bottlenecks.

Transmission planning is not only important for gaining access to renewable resources, it can also be important in helping to integrate large amounts of renewable generation into the electricity system. Additional transmission between balancing areas or interconnects can allow for better utilization of renewable generation by providing alternative outlets for generation above what can be utilized within the local area. Having strong transmission ties between areas is a critical element in taking advantage of the geographic diversity of renewable resources. When the current renewable generation is low in one area but high in another additional transmission allows this energy to be utilized instead of curtailed. One proposed project in the United States that plans on utilizing increased transmission to aid renewable integration is the Tres Amigas project [17]. The North American electricity grid is split into three essentially independent interconnections: the Western, the Eastern, and Texas. The Tres Amigas project aims to provide expanded transmission links through the addition of 5 GW DC superconducting lines between each of the interconnections. The proposed site on the border of New Mexico and Texas is located close to areas of excellent wind and solar resources.

An even more ambition project for the integration of vast renewable resources over a large geographic footprint is the DESERTEC project [18]. This project aims to create a supergrid throughout Europe, the Middle East, and North Africa. This supergrid would open access to a larger number of renewable resources, including concentrating solar electricity from the Middle East and North Africa and wind power from Northern Europe. The enormous footprint of the project would ensure a smoothing of the renewable generation sources and demand sinks.

Enabling Greater Renewable Penetration

Just as there are currently a number of generation technologies utilized to fulfill electricity supply, there

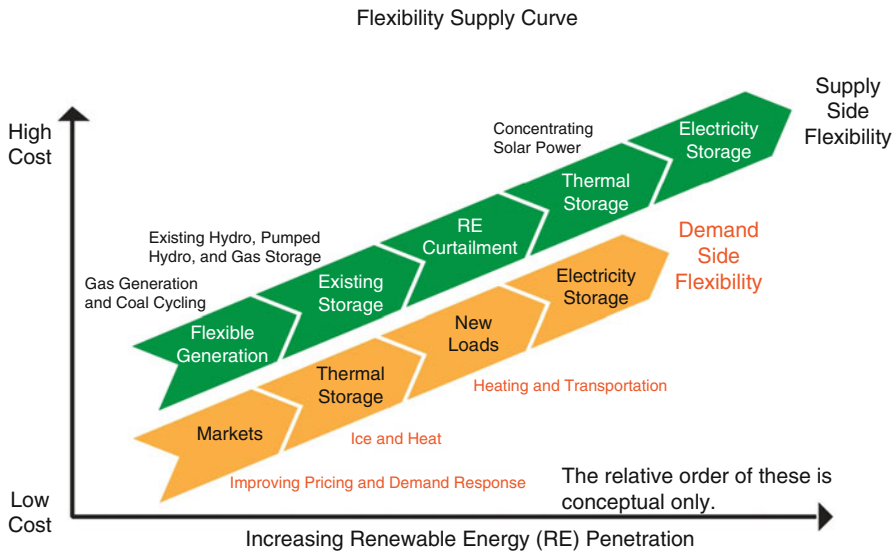

Renewable Generation, Integration of. Figure 9
The flexibility supply curve shows a number of different methods of providing system flexibility that may be useful in integrating renewable generation sources [19]

will be a number of technologies and strategies needed in order to enable the inclusion of larger amounts of renewable generation into the electricity system. Figure 9 shows a conceptual cost ranking of different demand and supply side technologies and systems that provide the electricity system with additional flexibility, and thus can help in the integration of variable generation. The inclusion of a number of different renewable generation technologies, with complementary generation characteristics, in future capacity expansion will also help to facilitate operating a high renewable electricity system. Dispatchable renewable sources, such as geothermal, biomass-fired thermal and hydroelectric plants, are able to contribute to renewable generation goals without significantly altering system operations. Geothermal and biomass-fired plants can serve as baseload units that reduce the amount of variable generation necessary at all times. Hydroelectric units can also serve this function, but may better serve the system by providing load following capabilities for variable generation due to their quick response times. However, the limited geographic potential and/or economic costs of these plants dictate that large capacities from variable sources will also be required to meet high renewable penetration goals. A number of different strategies for mitigating the effects of these plants' variability and uncertainty are described in what follows.

Variable Generation Forecasting

Renewable generation is both variable and uncertain; however, the uncertainty is a much more critical factor than the variability. If the variable output of renewable generation was known in advance the impact would be considerably reduced. The variable output could still be scheduled in a normal unit commitment and dispatch system, and would in fact be dispatchable. It is the uncertainty associated with renewable output that is most troubling. Thankfully, the future output of a variable generator is not completely random at smaller timescales, due to the fact that it is weather-driven. Forecasting techniques can be used to estimate the future output and this information can be incorporated into future generation plans. However, forecasting results tend to improve with reduced lead times between making the forecast and the time of realization. The inaccuracies associated with forecasting at longer timescales, in conjunction with the long start-up times of baseload units, diminishes the practical impacts of wind forecasting in particular. Numerical weather prediction models are commonly used to make

wind forecasts for the day-ahead unit commitment process. Further improvements to these models, and their use at smaller geographic distances, has the potential to improve the utilization of variable generation through better forecasting.

Stochastic Planning and Operating Tools

One way in which variable generation forecasting can be better utilized is through the use of stochastic unit commitment and economic dispatch models. Instead of a simple point forecast these models incorporate a number of different scenarios of variable generation power output, with associated probabilities, during the future time frames under consideration. Through their explicit consideration of the stochastic nature of the variable generation these models are able to produce more robust schedules that can respond more easily to the different possible variable generation scenarios. The more robust schedules produced tend to produce lower average system costs than those that utilize only a point forecast [20]. Improved forecasting that considers not only the most likely value for the next time point, but also a consideration of the range and likelihood of possible values will increase the impact of stochastic operating tools. For this reason the consideration of the distribution of forecasting errors for variable generation production is important as it can inform the creation of more realistic forecasting scenarios. Improved stochastic programming algorithms that reduce the computational time necessary to solve for an optimal schedule will also increase the effect of these tools by allowing for the consideration of a larger number of scenarios and their application at smaller timescales.

Faster Markets

As the time between the forecast of variable generation and the actual production time decreases, so does the average error of the forecast. For this reason the implementation of faster dispatch markets can help lead to further renewable generation penetration as it decreases the costs associated with variable generation uncertainty. By having less time between the time of forecast and the actual time of output, more current information can be utilized in deciding the forecast. Since day-ahead markets followed by 1-h dispatch market tend to be the normal historical system of market operation, sub-hourly markets are necessary for further improvements. These sub-hourly balancing markets also provide another means by which the regulation and load following reserve impacts of variable generation may be reduced.

Demand Response

Another possible approach to incorporating larger fractions of renewable generation into the electricity system is known as demand response. This approach is based upon changing one of the main tenets of traditional electricity system operation: varying generation to match an uncontrollable load. Demand response gives the system operator control over the timing of some portion of load by allowing blocks of load to be delayed. This approach has traditionally been used by system operators as a last resource during times of very high peak loads. Large industrial loads often structure their contracts with utilities so that they receive either payments or lower base rates for allowing the utility the privilege of interrupting their service periodically, up to a maximum number of occurrences. Industrial customers are preferable from the utilities' perspective because they allow a large reduction in load through a single customer interruption. Large commercial installations also have the possibility of participating in demand response programs, as the heating or cooling of a large commercial building could be a significant resource.

The adoption of "SmartGrid" technologies has the promise of allowing residential customers to also participate in demand response programs. Unlike industrial loads, individual residential customers are a very small percentage of the total system load. However, if the utility can simultaneously control a large number of large-load distributed residential appliances, such as air conditioners, the aggregated effect can be comparable to the response provided by a large load industrial customer. It is important to note that demand response programs do not significantly reduce total electricity usage, instead the load is shifted from times of high demand, when additional generation may be unavailable, to periods of lower demand. Household

demand response is limited by cost to large appliances, and by consumer acceptance to appliances whose usage patterns are somewhat time insensitive. For example, a refrigerator's load can be postponed, but only for very short timescales, so that the contents do not spoil. On the other hand, a dishwasher turning on can presumably be delayed until the total demand levels fall at night, with far less negative effects to the consumer. In the extreme case one can imagine the linking of certain appliances' usage to the current level of variable generation output. A related idea is the use of time of use pricing for residential electricity, as opposed to the flat-rate (or limited peak/off-peak split) rate structure that currently prevails. The most troublesome aspect of time of use pricing is the limited ability or desire of residential customers to react to different prices. For extensive changes in residential usage patterns the time of use pricing scheme would need to be paired with meters that can be programmed to adjust appliance usage patterns based on the current price of electricity.

Electricity Storage

A commonly proposed solution to mitigate the effects of renewable generation variability is the use of electricity storage. There are a number of different technologies that could be used for such purposes, with each technology operating most efficiently over a range of timescales and power and energy levels. An illustration of the effective ranges for different technologies can be seen in Fig. 10. There are three basic timescales on which electricity storage is needed, based on response duration: very short duration, short duration, and long duration. Generally speaking, the longer the timeframe is, the higher the associated energy requirements are. These types of storage can also be classified according to their application, where power quality, bridging power, and energy management correspond well to very short, short, and long duration timeframes, respectively [21]. Very short duration storage is needed to respond on the millisecond timescale and provide large amounts of power for a matter of seconds. This type of power is important for power quality and frequency regulation applications. Requiring a response on the multiple second to minute timescale is short duration storage, used for bridging power. This type of storage is useful in the role of generation reserve, and similar applications, to provide power in the event of a system contingency. Very long duration storage can respond on the multiple minute timescale and is used to provide power over long durations, such as those needed for load leveling applications.

While both bridging power and power quality applications are important considerations in integrating variable generation, storage technologies with large rated power output and long discharge times will be the most important for large penetration rates of renewable generation due to their ability to shift energy from times when variable output exceeds demand to those where demand is greater than variable output. Pumped hydroelectricity is one large-scale technology that is applicable for long timescales. During times of excess generation the pumped hydro facility can transfer water from a lower reservoir to a higher reservoir and utilize the potential energy gained during times of high demand. Pumped hydroelectricity storage is somewhat limited by geographic considerations; there must be a fairly large height difference between the two reservoirs, ruling out very flat locations. Compressed air electricity storage is also limited by geographic considerations, particularly for systems with long discharge times. This is due to the fact that very large systems rely on caverns as the compressed air storage vessel. In these systems excess power is used to compress air into a storage area, where it can later be expanded to produce electricity when desired. Current systems use natural gas combustion to supplement the storage compressed air, but designs for future systems need to include this option. Chemical storage in the form of batteries is another possible solution. Lead acid batteries are currently a cost-effective solution, but are also a very mature technology that have relatively low roundtrip efficiency and are limited in grid applications due to their relatively short lifetimes. Sodium-sulfur (NaS) batteries have long cycle life, relatively high efficiency, and are used primarily for grid applications due to the high operating temperatures. A number of other battery chemistries are also available, from those such as lithium-ion that are seen in many other applications where portability is essential, to technologies such as redox flow batteries that are exclusive to large-scale power applications.

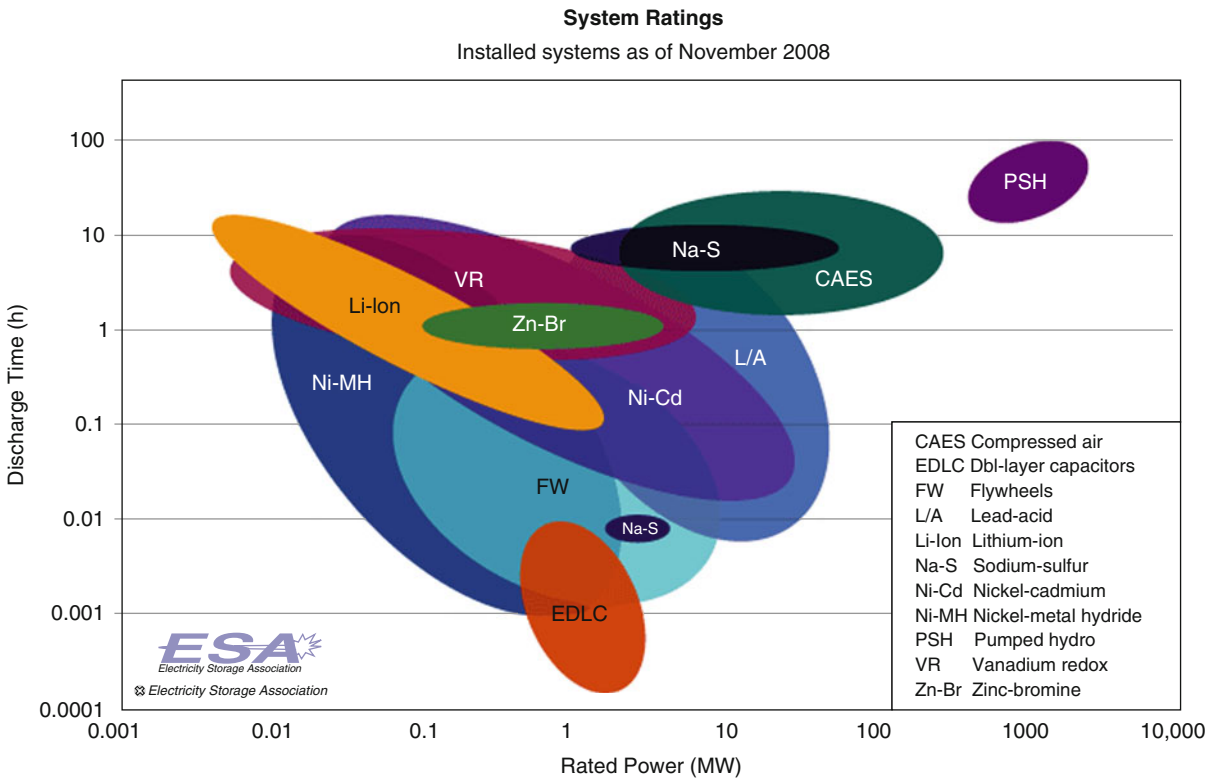

Renewable Generation, Integration of. Figure 10

The range of power and energy combinations available for different storage technologies

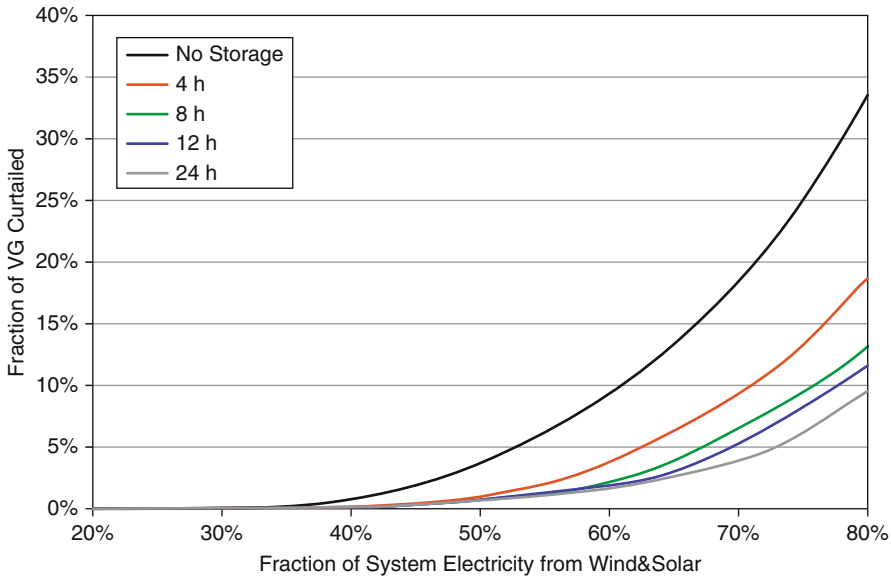

Renewable Generation, Integration of. Figure 11

Total curtailment as a function of VG energy penetration for different amounts of energy storage. Assumes 30/70 solar/wind mix, 12 h of storage, and a 100% flexible system. Each hour of storage represents 1 h of average system demand [19]

Figure 11 shows the effect that electricity storage can have on efficient system operation, in terms of reduced wind curtailment, in a theoretical completely flexible system. As may be seen, even a relatively small amount of storage can greatly increase the potential renewable penetration rate by reducing the amount of variable generation that must be curtailed, thus improving the economic viability of additional variable generation capacity. Additional amounts of energy storage can aid in the integration of renewable generation, but provide diminishing marginal returns. Currently electricity storage options are fairly expensive, limiting their potential applications. Even if significant cost improvements in storage technologies are realized, electricity storage should be viewed as but one tool to aid in renewable generation integration.

Renewable Generation Curtailment

Another solution that is occasionally used, even at the current low levels of renewable generation penetration, is production curtailment or spilling. If the production from variable generation is so large that it affects the operation of other units, such as putting baseload production below minimum generation levels, or reaches physical constraints, such as transmission line capacities, then the production can be temporarily halted. While this is a simple solution for small amounts of variable generation, it has its limits of applicability. These are often economic, in that excess variable capacity can be built that will only produce energy at a very small number of needed time points, and will be curtailed during the rest of its possible production times. This would significantly affect the economics of the variable generation plant at very high levels of curtailment, making it economically inefficient to build further capacity unless the load production schedule is expected to be anti-correlated with other variable generation locations.

New Loads

The peak and trough cycle of daily electricity usage requires the use of different types of generation in order to maintain system flexibility. However, the system would be able to operate more efficiently if the daily usage profile was more flat and baseload generators could provide a larger fraction of total energy. This would require sources of new load whose usage patterns coincided with the current nightly trough. In the same vein, since wind power output is generally higher at night, new nighttime loads would allow for less wind curtailment as there would be fewer situations where wind plus minimum baseload generation exceeded the current demand. The most commonly named source of a new load that can serve these purposes is the electric vehicle. Most vehicle usage occurs during the day, leaving vehicles idle during the night. For electric vehicles this provides the opportunity to charge and have their full range capabilities in time for the owner's use in the morning. The charging pattern that the vehicles follow is very important in ensuring that they flatten the load profile, instead of increasing peak loads [22]. To this end, policies must be put in place that can benefit the electricity system without disturbing the benefits that consumers derive from the vehicles, and thus blunting the rate of adoption. One extreme example of a policy intended to derive the most system benefits from the vehicles is the idea of utility controlled charging. In this case the utility would be able to use the vehicles as a form of demand response, perhaps providing an outlet for variable generation that might otherwise be curtailed.

Flexible Generation

The current electricity generation portfolio was not designed with the incorporation of variable generation resources in mind. Very high levels of variable generation penetration will most likely require more flexible accompanying generation, in order to help compensate for the non-dispatchable output. Generator flexibility includes the ability to both start and ramp quickly. For example, current inflexible nuclear and coal plants can require hours to ramp up from a cold start to full capacity. On the other hand, simple cycle natural gas turbines are an example of a unit that can start quickly and ramp from minimum generation levels to full capacity quickly enough to be used to compensate for generator outages. While these flexible units provide the system operator with more dynamic options for meeting the load, they also tend to be more expensive than inflexible baseload plants. However, the current level of system flexibility is not fixed. As older inflexible units reach the end of their operating lives and are

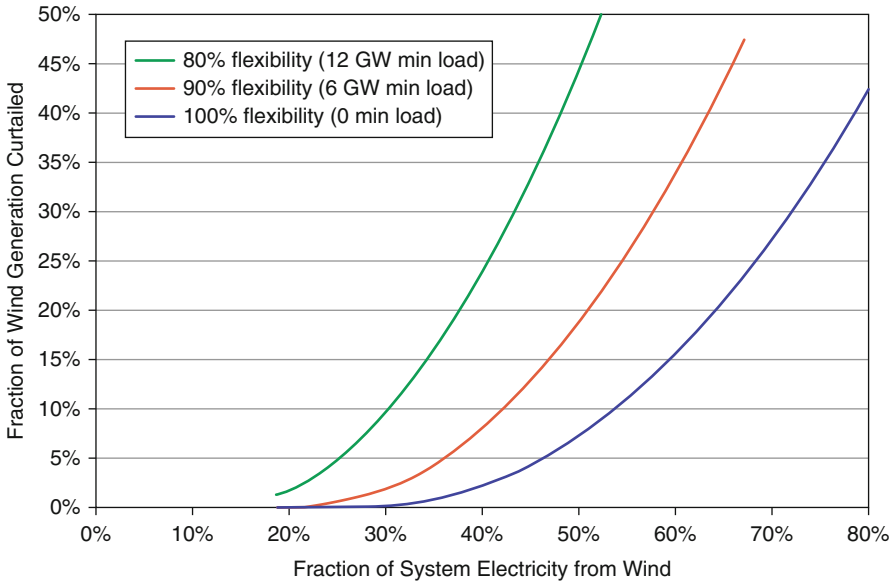

Renewable Generation, Integration of. Figure 12
Total curtailment as a function of usable wind energy penetration for different system flexibilities [19]

retired, new more flexible units can be brought online to replace them. The impact of system flexibility on the integration of variable generation is shown in Fig. 12. Here flexibility is represented solely by the combined minimum load levels of all generation units in the system. The ability to integrate variable generation is represented by the amount of available wind generation that must be curtailed as a percentage of the fraction of the total system energy provided by wind power. As may be observed, increased system flexibility causes the amount of wind generation curtailment to drop significantly.

Future Directions

Variable generation penetration rates are still relatively low (below 10% by energy) in most large systems. At these lower levels variable generation can be fairly easily incorporated into existing electricity system operations. However, if global trends persist very significant penetration rates will soon be reached. At high penetrations of variable generation significant restructuring of current system operations could be necessary to accommodate the additional system variability and uncertainty. As many electricity systems reach penetration rates of between 15% and 30%, methods of economically and reliably integrating variable generation sources will start to be tested on a daily basis. This will quickly bring attention to issues that were not properly considered in previous integration studies. Potential operating issues at higher levels of variable generation must be anticipated before these higher levels of renewable penetration are realized in order to maintain system reliability. The electricity system is such a vital part of daily life that even small changes in the reliability of the system would have far-reaching economic and societal consequences. Further work is required in many areas of renewable generation integration. Resource assessment of wind and solar resources can lead to better decisions on where to site new generation capacity to maximize not only power output, but the benefit to the system. Technological development of generators can both reduce system costs and allow for variable generators to interact more smoothly with the traditional system operation paradigm. Further work on the characterization of variable generators is necessary to understand how systems with large penetration rates will behave. Finally, extensive work is necessary in the area of system operations. Understanding the ability of both supply and demand technologies to increase system flexibility will be critical, as will new ideas on the structure of systems with large amounts of variable generation.

Bibliography

Primary Literature

1. NERC (2009) Accommodating high levels of variable generation. North American Electric Reliability Corporation. The North American Electric Reliability Corporation is the publisher. The report may be found at: http://www.nerc.com/files/IVGTF_Report_041609.pdf
2. IEA (2010) World energy outlook 2010. International Energy Agency, Paris
3. EIA (2011) Electric power annual 2009. Energy Information Administration, Washington, DC
4. Denholm P, Ela E, Kirby B, Milligan M (2010) The role of energy storage with renewable electricity generation. National Renewable Energy Laboratory, Golden
5. GE (2010) Western wind and solar integration study. National Renewable Energy Laboratory, Golden, 536pp
6. Milligan M et al (2010) Operating reserves and wind power integration: an international comparison. The 9th Annual International Workshop on Large-Scale Integration of Wind Power into Power Systems, Quebec, Canada
7. Milligan M, Kirby B (2009) Calculating wind integration costs: separating wind energy value from integration cost impacts. National Renewable Energy Laboratory, Golden
8. Lu X, McElroy M, Kiviluoma J (2009) Global potential for wind-generated electricity. Proc Natl Acad Sci USA 106:10933–10938
9. Schwartz M, Heimiller D, Haymes S, Musial W (2010) Assessment of offshore wind energy resources for the United States. National Renewable Energy Laboratory, Golden
10. de Vries B, van Vuren D, Hoogwijk M (2007) Renewable energy sources: their global potential for the first-half of the 21st century at a global level: an integrated approach. Energ Policy 35:2590–2610
11. Sims R et al (2007) Energy supply. In: Metz B, Davidson O, Bosch P, Dave R, Meyer L (eds) Contribution of working group III to the fourth assessment report of the intergovernmental panel on climate change. Cambridge University Press, Cambridge
12. Chen Z (2005) Issues of connecting wind farms into power systems. In: IEEE/PES transmission and distribution conference and exhibition: Asia and Pacific, Dalian
13. GE (2005) The effects of integrating wind power on transmission system planning, reliability, and operations: phase 2: system performance evaluation. The New York State Energy Research and Development Authority, Albany
14. Wan Y-H (2005) A primer on wind power for utility applications. National Renewable Energy Laboratory, Golden
15. Milligan M, Porter K (2006) The capacity value of wind in the United States: methods and implementation. Electr J 19:91–99
16. Smith JC et al (2010) Impact of variable renewable energy on US electricity markets. In: IEEE power and energy society general meeting, Minneapolis
17. Z-Global (2010) Study of the economic impact of Tres Amigas. Western Electricity Coordinating Council – Transmission Expansion Planning Committee. The Western Electricity Coordinating Council is the publisher. The report may be found at: http://www.wecc.biz/committees/BOD/TEPPC/TAS/MWG/Shared%20Documents/Tres%20Amigas%20Modeling/Z-Global%20Analysis.pdf
18. DESERTEC (2007) Clean power from deserts – the DESERTEC concept for energy, water and climate security. Protext, Bonn
19. Denholm P, Hand M (2011) Grid flexibility and storage required to achieve very high penetration of variable renewable electricity. Energy Policy 39(3):1817–1830
20. Tuohy A, Meibom P, Denny E, O'Malley M (2009) Unit commitment for systems with significant wind penetration. IEEE Trans Power Syst 24(2):592–601
21. Nourai A (2002) Large-scale electricity storage technologies for energy management. In: IEEE power engineering society summer meeting, Chicago
22. Hodge B-M, Shukla A, Huang S, Reklaitis G, Venkatasubramanian V, Pekny J (2011) A multi-paradigm modeling simulation of the effects of PHEV adoption on electric utility usage levels and emissions. Ind Eng Chem Res 50(9):5191–5203

Books and Review

Ackermann T (ed) (2005) Wind power in power systems. Wiley, Chichester

Anaya-Lara O, Jenkins N, Ekanayake J, Cartwright P, Hughes M (2009) Wind energy generation: modeling and control. Wiley, Chichester

Blume S (2007) Electric power system basics: for the nonelectrical professional. IEEE/Wiley, Hoboken

Brinkman G, Denholm P, Drury E, Margolis R, Mowers M (2011) Toward a solar-powered grid: operational impacts of solar electricity generation. IEEE Power Energy Mag 9–3:24–32

Burton T, Sharpe D, Jenkins N, Bossanyi E (2001) Wind energy handbook. Wiley, Chichester

Carrasco JM, Garcia Franquelo L, Bialasiewicz J, Galvan E, Portillo Guisado RC, Martin Prats MA, Leo JI, Moreno-Alfonso N (2006) Power-electronic systems for the grid integration of renewable energy sources: a survey. IEEE Trans Ind Electron 53:1002–1016

Corbus D, Lew D, Jordan G, Winters W, Van Hull F, Manobianco J, Zavadil B (2009) Up with wind: studying the integration and transmission of higher levels of wind power. IEEE Power Energy Mag 7–6:36–46

Freris L, Infield D (2008) Renewable energy in power systems. Wiley, Chichester

Grant W, Edelson D, Dumas J, Zack J, Ahlstrom M, Kehler J, Storck P, Lerner J, Parks K, Finley C (2009) Change in the air: operational challenges in wind-power production and prediction. IEEE Power Energy Mag 7–6:47–58

Grubb MJ (1991) The integration of renewable electricity sources. Energ Policy 19:670–688

von Meier A (2006) Electric power systems: a conceptual introduction. IEEE/Wiley, Hoboken
Miller R, Malinowski J (1993) Power system operation. McGraw Hill, Boston
Mills A, Ahlstrom M, Brower M, Ellis A, George R, Hoff T, Kroposki B, Leox C, Miller N, Milligan M, Stein J, Wan Y (2011) Dark shadows: understanding variability and uncertainty of photovoltaics for integration with the electric power system. IEEE Power Energy Mag 9–3:33–41
Shahidehpour M, Yamin H, Li Z (2002) Market operations in electric power systems. IEEE/Wiley, New York
Smith JC, Milligan MR, DeMeo EA, Parsons B (2007) Utility wind integration and operating impact state of the art. IEEE Trans Power Syst 22:900–908
Soder L, Hofmann L, Orths A, Holttinen H, Wan Y, Tuohy A (2007) Experience from wind integration in some high penetration areas. IEEE Trans Energy Convers 22:4–12

Reservoir Engineering in Geothermal Fields

Enrique Lima, Hiroyuki Tokita, Hideki Hatanaka
West Japan Engineering Consultants, Inc, Chuou-ku, Fukuoka, Japan

Article Outline

Glossary
Definition of the Subject and Its Importance
Introduction
Purposes of Reservoir Engineering in Geothermal Fields
Information and Processing Required for Geothermal Reservoir Evaluation
Numerical Simulation
Resource Evaluation
Future Directions
Bibliography

Glossary

Aquifer A geological formation (or formations) which contains water or geothermal fluid and will allow fluid movement.

Baseline Data set acquired before exploitation begins, against which any future measurements are compared.

Deep liquid zone Region of single-phase liquid conditions below a two-phase (liquid and vapor) zone.

Deep liquid level Boundary between the two-phase and deep liquid zones.

Energy Conversion technology Term that refers to the thermodynamic cycle used to convert the heat energy from geothermal fluids into electricity, there are several of these technologies. Binary in which the heat of the geothermal fluids is transferred to a low-vaporization-temperature fluid (usually isopentane, ammonia, or a combination of water–ammonia) that is the working fluid driving the turbine generator. The heat source for the binary technology could be the separated geothermal brine or the steam or both exchanging energy in separated exchangers. When the steam is used directly, it can be used in single-flash or double-flash cycles, depending on the number of times the geothermal brine is flashed into steam or a combination of binary and steam technologies in the conversion cycle.

Geothermal system A body of hot water and rock within the Earth.

Groundwater Water, generally cold and of meteoric origin, which resides in near-surface aquifers and is often used for domestic and industrial purposes.

Injection zone The formation into which injected fluid is put. Generally, this has high porosity and permeability.

High-temperature system A geothermal system, or part thereof, containing fluid having a temperature greater than 150°C. c.f. *Low-temperature system* in which the temperature is less than 150°C. Note, however, that this temperature value is arbitrary and that different authorities adopt different values or divide the range into low, intermediate, and high temperature.

Makeup well Well drilled to replace production lost from an existing production well due to decreases in fluid temperature or pressure or permeability of the production zone, or drilled to replace reinjection lost from an existing reinjection well because of a decrease of permeability in the injection zone(s) or excessive rise of water level within the well.

Model In the reservoir engineering terminology, there are two kinds of models: one is called the *conceptual*

model that is an integration of all the physical features of a reservoir such as size, geological structure, geochemical features, temperature and pressure, underground fluid flow patterns, etc., that is estimated through the integration of all available surface and underground geoscientific information. The other kind of model is called the *numerical model*, and it is the conceptual model itself presented in terms of elements that can be manipulated using numerical tools in order to extrapolate, from known information and following strict physical–mathematical rules, features of the underground that cannot be directly measured, such as volume, recharge and discharge zones, pressure and temperature distribution, energy content, etc., with the objective to mathematically forecast the response of the reservoir when subjected to different exploitation scenarios. Numerical models are constructed in three dimensions (x, y, and z) this is the common denomination of 3D numerical model. These numerical exercises of reservoir modeling will lead to crucial decisions such as to develop or not to develop the geothermal field and if decision to develop is made, then what would be the size of facilities that, in terms of economy, will produce an acceptable return to the country and investors.

Permeability A measure of the capacity of a geological rock formation to transmit a fluid.

Production zone That region (depth) of the geothermal reservoir from which most of the production of fluid occurs.

PT Pressure and temperature wellbore surveys could be static (not flowing conditions) or dynamic (flowing conditions). When a spinner tool is added in the dynamic surveys, the activity is called PTS wellbore survey.

Reservoir The region of a geothermal system from which geothermal fluid is withdrawn or is capable of being withdrawn.

Residual (liquid) saturation The amount of liquid that remains in the pores (as % of pore volume) and which decreases in pressure will not vaporize. The liquid saturation level below which vaporization of liquid will not occur.

Steam zone A region of the reservoir in which steam (vapor) is the pressure-controlling phase.

Two (2)-phase zone A region where the liquid and vapor (steam) phases of water coexist in pores or fractures.

Definition of the Subject and Its Importance

Reservoir engineering is the comprehensive integration of all available surface and underground information regarding the geology, geophysics, geochemistry, well drilling-testing, exploitation data, and information concerning the developer objectives, such as market targets, costs, and finance becoming the most power tool to evaluate the feasibility of a geothermal development. As in any scientific or engineering activity, results derived from reservoir engineering depend upon the quantity and quality of information and in the ability (experience) in handling all this information. Reservoir engineering is not limited to the final numerical tool but to the information acquisition, too. The present description encompasses both acquisition and processing of information to guarantee high-quality results.

Introduction

Among all forms of primary energies, renewable and nonrenewable geothermal energy is the only one that, from the perspective of a country together, offers values, such as energy source reliability, energy independence, contribution to improved commercial balance, clean energy, and local socioeconomic development due to multipurpose utilization possibilities. Again, from the point of view of energy mix, it is necessary to evaluate the potential available of the geothermal resource to plan where and when geothermal energy has to be deployed in order to produce the best effects of its inherent values. Planning should consider the risk and long lead time required to develop geothermal resources. Reducing lead time and eliminating or at least mitigating risks are among the aims of geothermal engineering. The development of geothermal energy is carried out in several steps until its utilization is possible: (1) national reconnaissance, (2) prefeasibility studies, (3) resource feasibility studies including exploration and appraisal drilling, (4) facilities < technical-economic/financial > feasibility studies, (5) financing acquisitions, (6) field development and facilities construction, and (7) facilities operation. Each of these steps is concatenated to

the success of the preceding one, and each of them depends on the quantity and quality of the acquired data and its processing. The ultimate tool for the evaluation of the geothermal potential and the definition of the feasibility of its exploitation is reservoir engineering. The application of this tool is most relevant in steps 3 and 4 and is the basis for the success of step 5. The tool continues to be applied in step 6 and during all the exploitation period, step 7.

Purposes of Reservoir Engineering in Geothermal Fields

Reservoir engineering will be used for the following purposes:

1. Data acquisition
   (a) Wellbore pressure–temperature and mass flow surveys
   (b) Completion tests
      - Pressure transient tests
      - Injectivity tests
   (c) Well production test
      - Mass flow
      - Enthalpy
      - Chemical characteristics
   (d) Well interference test
   (e) Tracer tests
2. Data processing
   (a) Wellbore data analysis to obtain:
      - Static pressure–temperature profiles to determine stabilization temperature and reservoir pressure
      - Dynamic pressure–temperature profiles to determine production characteristics of the permeable zones
      - Position of permeable zones and evaluation of their thermal–hydraulic characteristics
      - Construction of the conceptual model
      - Calibration of the numerical model
   (b) Analysis of well completion data
      - Pressure transient data to determine permeability, storativity, and skin effect of formation around the permeable zones
      - Injection capacity of the well
      - Construction of the conceptual model
      - Data for the numerical model
   (c) Analysis of well production data
      - Construction of the production characteristics curve to determine production characteristics and chemistry at different well pressures and, in turn, to help to determine optimum well exploitation pressure and sizing of facilities
      - Calibration of the numerical model
   (d) Reservoir simulation
      - Estimation of the spatial pressure, temperature, and vapor saturation distribution within the reservoir volume
      - Estimation of the geothermal potential of the reservoir
      - Estimation of the strength and location of recharge, discharge, and heat source areas
      - Estimation of the location of promising permeable areas for production and reinjection
      - Estimation of the optimum sustainable exploitation capacity of the reservoir
      - Contribute to the optimal positioning of geothermal facilities (well pads and pipelines for both production and reinjection, and energy conversion facilities)
      - Contribution in the selection of energy conversion technology
      - Estimation of the optimum wellhead pressure for exploitation of the reservoir
      - Targeting and optimization of the number of initial production and reinjection wells
      - Targeting and optimization of the number of makeup production and reinjection wells
      - Estimation of development and construction costs
      - Contribution to the economic and financial study
3. Financing acquisition
   - Bankable report
4. Reservoir monitoring
   - Updating of reservoir analysis and forecasting of future performance as experience and new data are gained during exploitation of the field

Information and Processing Required for Geothermal Reservoir Evaluation

To assess the capability of reservoir fluids to produce electricity or to be used in other applications, it is

necessary to gather and analyze information on the thermodynamics of the fluids, hydrogeological characteristics of the reservoir, and connectivity of the formation through which geothermal fluids are migrating. Thus, information on the temperature, pressure, enthalpy, and chemistry of the geothermal fluids and information on the location of permeable zones and permeability of the geological formations shall be collected and analyzed.

Temperature

Since the measure of the heat content in geothermal fluids is temperature, this parameter is of paramount importance in geothermal developments. The higher temperature fluid is, so will be the heat content. In terms of electricity generation, there is an appropriate range of temperatures of geothermal fluids at which energy conversion using a determined technology (from water-binary to double-flash cycles). At current commercial energy conversion technologies, the range of reservoir temperature in use is from around 90°C to over 300°C.

Reservoir temperature, therefore, becomes a parameter of importance to be measured. When deep wells are available, this is done by lowering instruments into the wellbore (Temperature Wellbore Survey), or when wells are not available, temperature is indirectly estimated using geochemical methods. Downhole temperature measurements are done at several times during and after drilling to estimate the thermal conditions around the surveyed well at undisturbed conditions (static surveys) and, most importantly, to determine the position of permeable zones along the open portion of the wellbore. The spatial distribution of the measurements in different wells is a guide to understanding the position of the heat source and flow patterns within the reservoir. When these measurements are done during drilling, the information serves to make important decisions regarding drilling operations. Nevertheless, suspension of drilling operations to collect downhole temperature represents costs such as the one to keep the rig in standby; thus, a compromise between the importance of data and cost should be attained. Other temperature measurements which are necessary to evaluate the reservoir are those done within the wellbore while the well is in production (dynamic surveys). These measurements help to understand the variations of enthalpy when the well is subject to mass production at different conditions of wellhead pressure. Temperature measurements are continuously done in the several wells of the development and during the life of the geothermal exploitation because the spatial control of temperature is an excellent measure of the form in which the reservoir is responding to exploitation.

Pressure

It is almost a standard that together with temperature, wellbore pressure measurements are also done. The combination of temperature and pressure profiles along the well (static and dynamic) provides information about the thermodynamic state of the geothermal fluid, which in turn renders information regarding the deep liquid zone (static), flashing point (dynamic), and flow patterns within the wellbore. Pressure information can be also utilized in combination with the discharge data for the further understanding of the flow mechanism and productivity of the well.

Pressure of geothermal reservoir is one of the factors that control the productivity of the well. The higher the reservoir pressure is, the shallower the static water level within the well will be. This translates into a higher productivity of the well because as the water level is at shallow depths, the distance of the reservoir fluids to the ground surface is shorter, thus requiring less energy for geothermal fluid to reach (ascend) to the ground surface.

Wellbore pressure and temperature are measured as shown in Fig. 1. Since the pressure is the cumulative weight of liquid inside the wellbore per unit area, the static pressure profiles are quasi-straight lines, as shown (Fig. 2). The slope of the pressure profile shows variations due to variations in fluid density caused by the temperature gradient within the wellbore. Static pressure profiles during the heating up of the well are useful to estimate the position of permeable zones. The pressure profile measured at long standing time that assures stabilization of the temperature profile is used to estimate reservoir pressure. The stabilized pressure and temperature profiles are in turn used to calibrate the 3D numerical model.

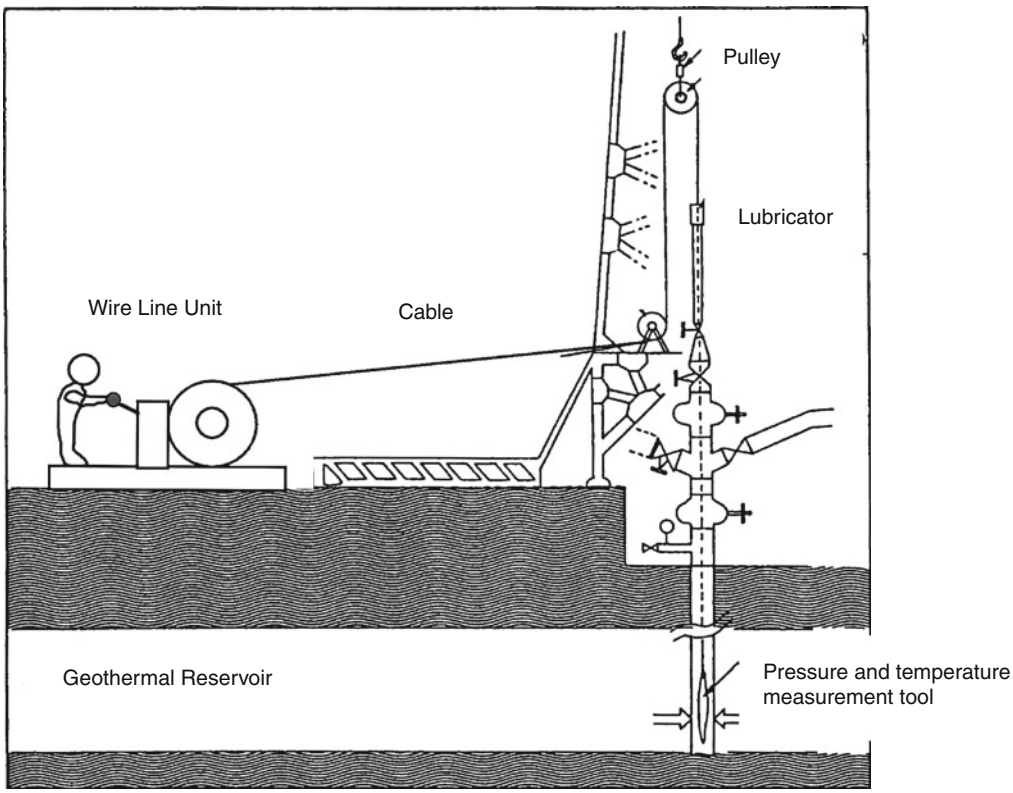

Reservoir Engineering in Geothermal Fields. Figure 1
Schematic of pressure and temperature logging

When pressure profiles of several wells are available, a spatial pressure distribution map of the field at different elevation levels can be created. Since the fluid basically moves from the high- to low-pressure environment, the pressure distribution map, together with the geological structure map and geochemistry information, can be used to estimate flow patterns of the fluid within the reservoir. Flow patterns information is of extreme importance during the calibration of the numerical model.

Wellbore pressure profiles in dynamic (flowing) conditions show lower values compared to those taken at static condition because of the frictional pressure drop within the wellbore and because of the appearance of a pressure drop between the reservoir and the production zone caused by the flow of the fluid within the geological formations. The degree decrease of pressure values is a good indicator of the "permeability" of the well. Variations in gradient of the pressure profile in dynamic conditions also are an indicator of the position of permeable zones and whether the fluids enter the wellbore in liquid, two-phase, or steam conditions. If the fluids enter the wellbore in liquid state, the position of the flashing zone can also be estimated from the dynamic pressure profile and calculated using information of the temperature profile (dynamic).

Although dynamic pressure and temperature profiles are not directly used in 3D numerical simulation, the value of this information is when it is analyzed using wellbore simulators. This wellbore simulation helps to further understand the flow mechanism within the wellbore and within the producing formations, which in turn provides the knowledge of the number of production zones and their individual productivities in terms of mass flow and enthalpy at the different wellhead pressures at which the well was flowing when the P/T tools were inside the wellbore. This information is also crucial when doing the evaluation of the pressure at which the different wells shall be operated to draw the maximum of energy at sustainable levels.

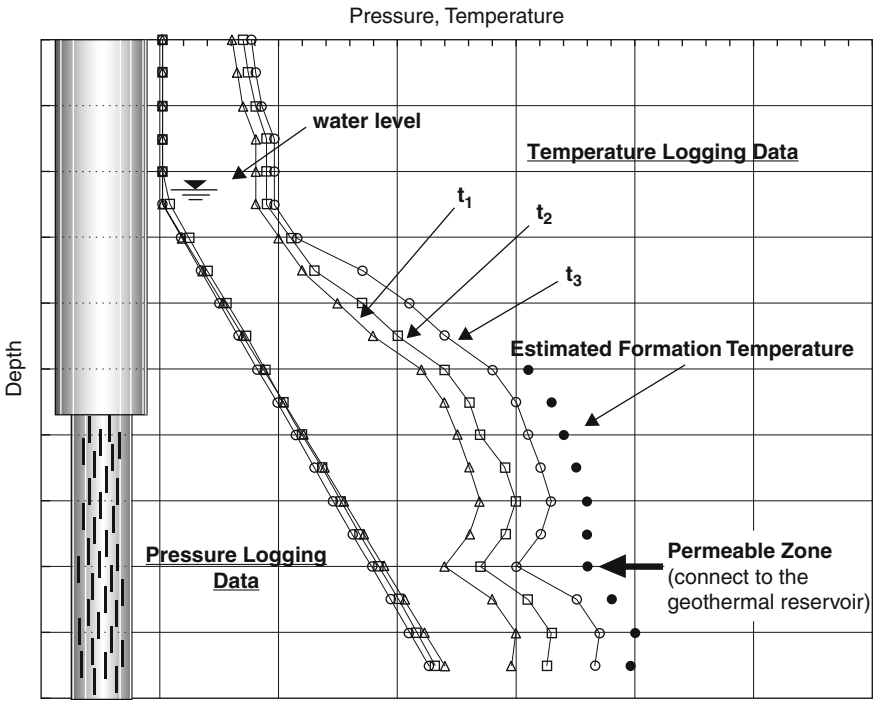

Reservoir Engineering in Geothermal Fields. Figure 2
Example of pressure and temperature logging results

Permeable Zone

To identify the permeable zone(s) in a well, it is necessary not only to characterize the well itself, but also, it is important in the construction of the distribution of the permeable zones within the reservoir. Generally, permeable zones appear when wells encounter fault structures and/or fracture zones associated to fault structures or contact between formation and intrusive rocks or appear when the well taps permeable formations (even not related to fault structures) or when striking a zone of contact between different formations. After the completion of drilling works, PTS (Pressure, Temperature, and Spinner) surveys are carried out to detect the location (depth) of the permeable zones more precisely. PTS surveys are carried out by injecting water into the well; the spinning element of the tool rotates proportionally to the amount of injected water. When the injected water reaches permeable zones, part of the mass flow is lost to the pay zone; therefore, the rotation of the spinning tool changes. The depths at which spinning values change are recorded, thus providing number and depth location of permeable zones. The relative spinning between wellbore locations prior and after the permeable zone is an indicator of the proportional amount of mass lost to the permeable zone (Fig. 3) (please also refer to Permeability).

The spatial positioning of permeable zones in wells contributes to the construction of the geothermal conceptual model, which in turn will be the base of the 3D numerical model. In the 3D numerical model, relatively higher permeability values are given to the elements where permeable zones were identified by either surface exploration (faults, tectonic structure, etc.) or wellbore surveys to represent the distribution of permeability within the geothermal reservoir. Since the simulated fluid flow tends to happen through the permeable elements of the 3D numerical model, the distribution of the permeable zone and the value of permeability are crucial for the modeling work so as to reproduce pressures, temperatures, and flow patterns, as defined in the conceptual model.

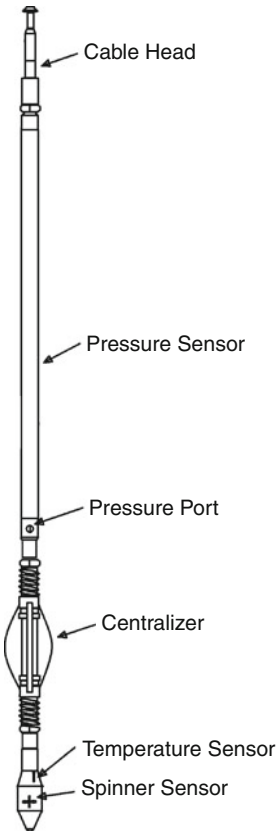

Reservoir Engineering in Geothermal Fields. Figure 3 PTS logging tool

Permeability

The permeability is a measure of the ability of the underground formations to permit the flow of fluids. A well tapping a permeable zone will also benefit of the capacity of the formation to produce geothermal fluids and the ability of the reservoir to sustain production; therefore, to evaluate the well's permeability is an important factor. In terms of the parameter to be obtained from direct measurements when carrying injection tests, the parameter to be estimated is the permeability–thickness product (the so-called kh value) and not permeability itself. Injection tests generally consist of three tests: multirate injection test, water loss test, and pressure falloff test. The necessary tool for this test is a PT or a PTS downhole tool. The procedure for the multirate injection test is to lower the tool at the depth of the main permeable zone as it was identified during the drilling records or through wellbore PT surveys. Then, water is injected into the well at three or four different injection rates. The injections are sequentially done, and each of the flow rates is maintained during a time in which pressure reading in the PT tool stabilizes. (When only mechanical tools are available, it is advisable to inject each of the rates at the longest time permitted by the water storage, and it is recommendable to use the longest time clock to permit running all injections and other tests in one operation. Refer to Fig. 4.) After the last injection rate, the tool will be run up and down to obtain PT(S) profiles vs. depth during injection (water loss test) which will help to define other permeable zones. After completing the water lost test, the PT(S) tool is left at the depth of the known most important permeable zone, and water pumping is stopped to start the recording the pressure falloff. If mechanical tool is used, the instrument is left for several hours (depending on the clock in use) to assure stabilization of pressure readings upon which the tool will be retrieved from the well. This operation is called pressure falloff test. Using the results of the multirate injection test, the "injectivity index" will be calculated, as shown in Fig. 5. This index expresses the rate of mass the well is able to accept per unit pressure buildup. This value is the simplest crude gauge of the total permeability of the well. The results of the falloff test will be used to estimate the flow capacity such as permeability–thickness products (kh value) of permeable formations surrounding the well. Injectivity index and kh value are very important reservoir parameters to evaluate the productivity and/or injectivity of the well. Figure 6 shows the example of results of the analysis of pressure falloff test. An example of the results of water loss test is shown in Fig. 7.

Discharge Characteristics

The records of the discharged mass flow of all production wells and reinjection mass flow of all reinjection wells are necessary as input data for dynamic numerical simulation. To measure the discharge mass flow rate, adequate equipment should be prepared. The type and size of equipment needed for a "production test" depend on the type of well and reservoir being tested and on the expected maximum flow rate and discharge

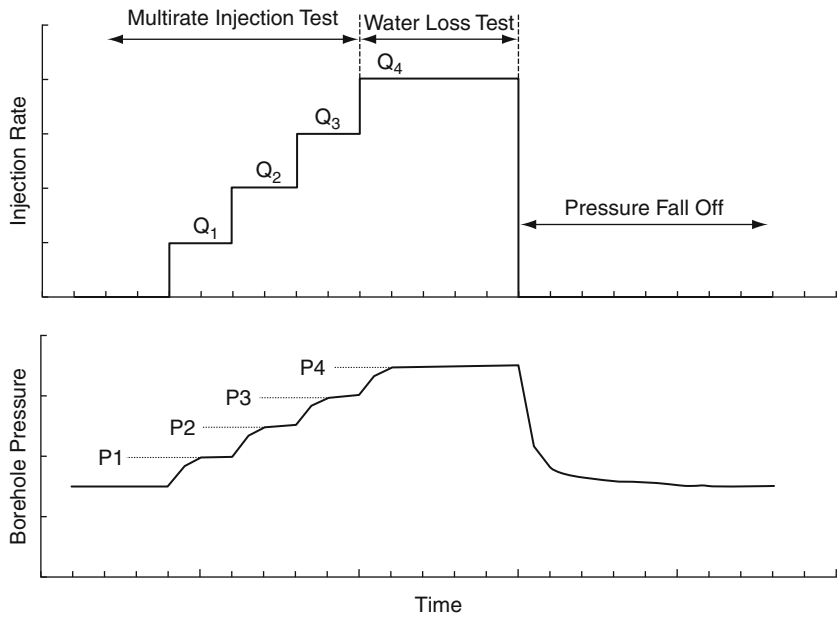

Reservoir Engineering in Geothermal Fields. Figure 4
Injection test procedure

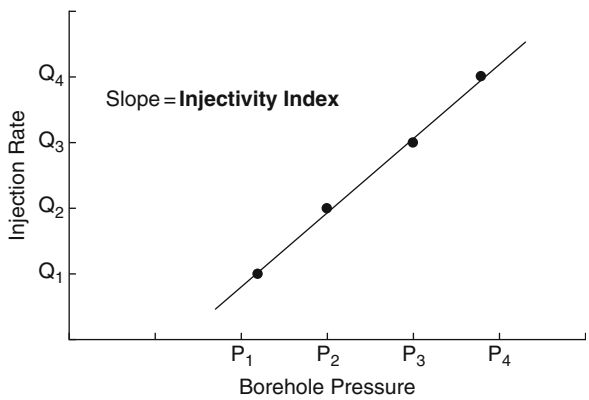

Reservoir Engineering in Geothermal Fields. Figure 5
Injectivity index

enthalpy. In general, one of two kinds of test methods is selected for production test. One is the "separator method," and another is the "lip pressure method."

In the separator method, the discharged fluid, which is, in most case, the mixture of vapor phase and liquid phase, is separated into steam (vapor phase) and brine (liquid phase) at the separator. The separated steam mass flow rate is measured using an orifice plate which is installed in the steam pipeline. The flow rate can be calculated from the differential pressure measured at upstream and downstream of the orifice plate. The brine mass flow rate can be calculated by measuring the water height at the weir and applying the general equation of triangular or rectangular weir.

Figure 8 shows the equipment setting used for the lip pressure method. The empirical equation used by this method relates the enthalpy of the two-phase fluid and the mass flow rate to the lip pressure measured at the end of the discharge pipe, where mass flow and enthalpy are usually unknown parameters. However, using an atmospheric separator and a weir, the mass flow of the water separated at atmospheric conditions can be calculated by measuring the water level in the weir. Considering an isenthalpic expansion and a numerical root-finding procedure, the production enthalpy and the total mass flow (combined steam and water, exclusive of noncondensable gas, at wellhead conditions) can be calculated. The input values are weir height, size of discharge pipe, and thermodynamic properties of water.

To obtain the discharge characteristics of a well, production tests are carried out. The discharge flow rate is continuously measured at least at three or four different wellhead pressures so as to allow enough data

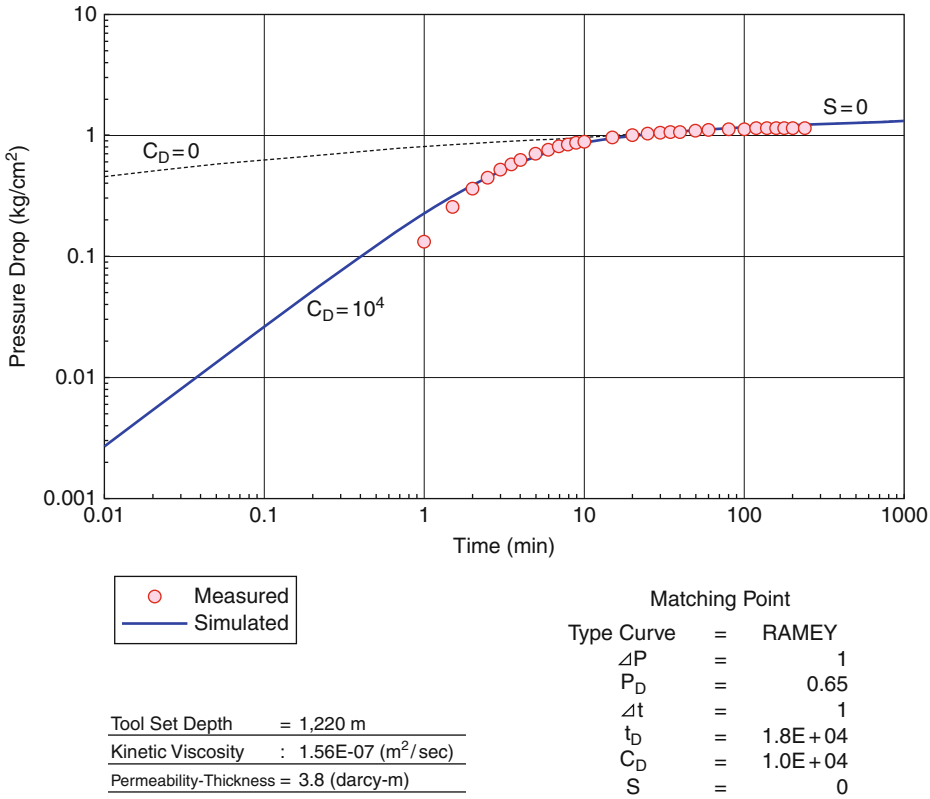

Reservoir Engineering in Geothermal Fields. Figure 6
Example of analysis result of falloff test (curve matching method)

to plot the discharge characteristic curve. To modulate the amount of mass discharge and the wellhead pressure that will permit to plot the discharge characteristics curve (enthalpy, steam, hot water mass flow vs. wellhead pressure), the side valve is opened or throttled. An example of discharge characteristic curve is shown in Fig. 9.

Wellbore Simulation

The objective of wellbore simulation is to analyze production data to determine reservoir parameters by repetitive calculation at each of the simulation result to the measured discharge characteristic curve and pressure/temperature profiles. The productivity of the well is mainly controlled by the reservoir pressure and temperature around the well and its permeability. The wellbore simulator has been developed to calculate the relationship between wellhead pressure and steam mass flow rate, water mass flow rate with enthalpy. The main input parameters are feed point depth, well configuration (casing program), reservoir pressure, reservoir temperature (or fluid enthalpy), and permeability–thickness products (kh value). Figure 10 shows wellbore model with the surrounding formation. The reservoir parameters can be estimated by matching the simulation result to the measured discharge characteristic curve. The example of the matching result to the discharge characteristic curve is shown in Fig. 11. The wellbore simulator can also calculate the pressure and temperature profiles vs. depth, and the calculated profiles will be compared to the measured dynamic surveys so as to confirm the enthalpy of the fluid at the point where the permeable area was identified. An example is shown in Fig. 12.

When the 3D numerical simulation is done using a reservoir simulator coupled to a wellbore simulator, the temperature and pressure of each of the element of

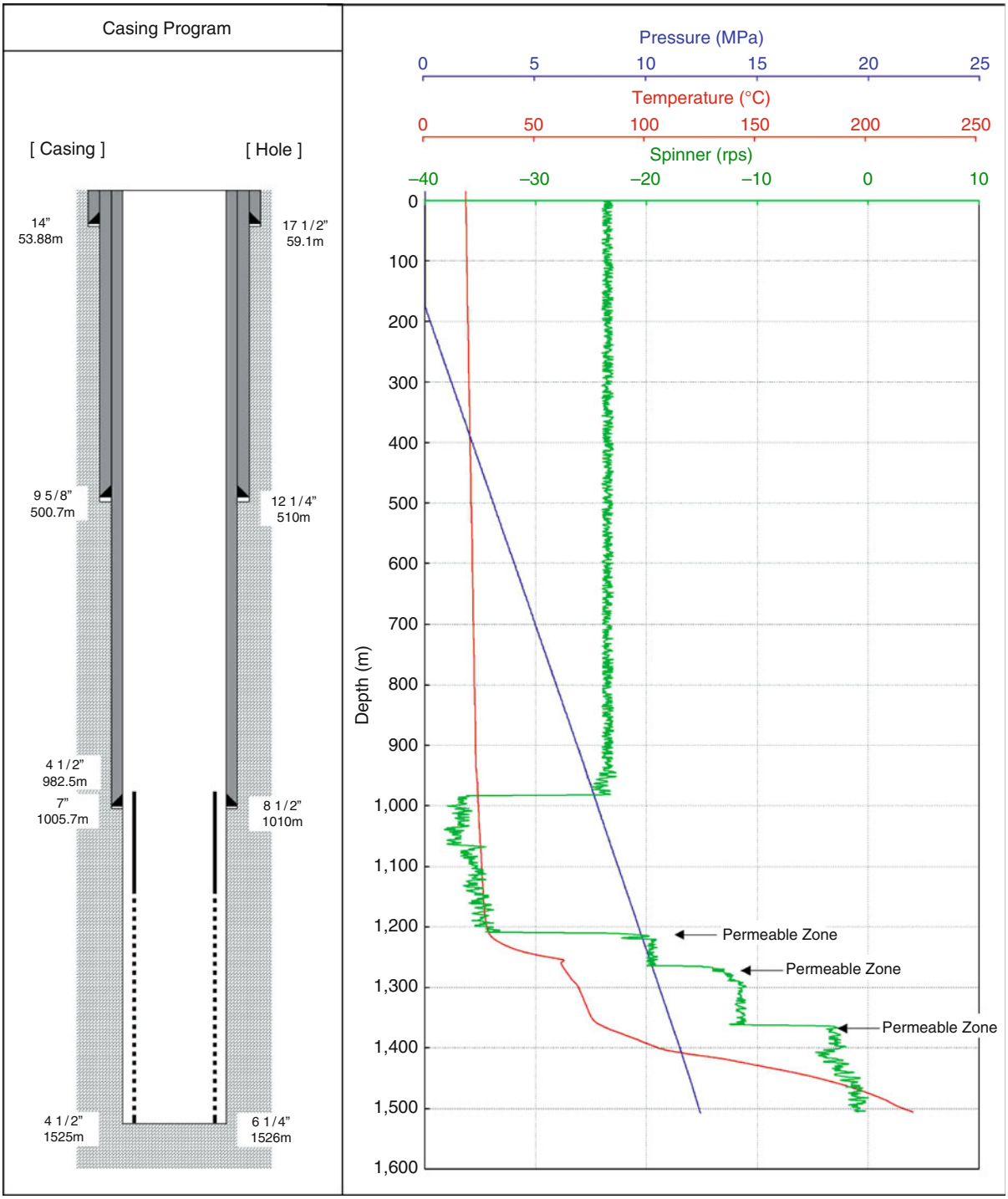

Reservoir Engineering in Geothermal Fields. Figure 7
Example of water loss test using PTS tool

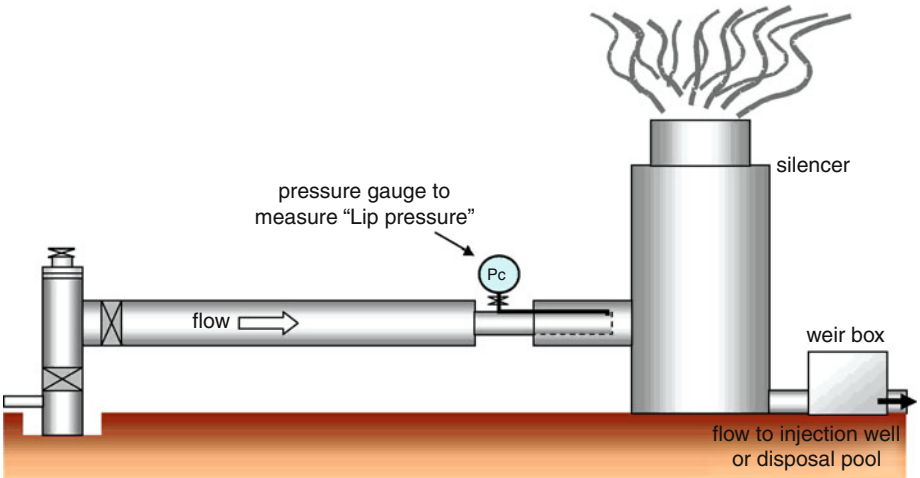

Reservoir Engineering in Geothermal Fields. Figure 8
Schematic equipment setting for the lip pressure method

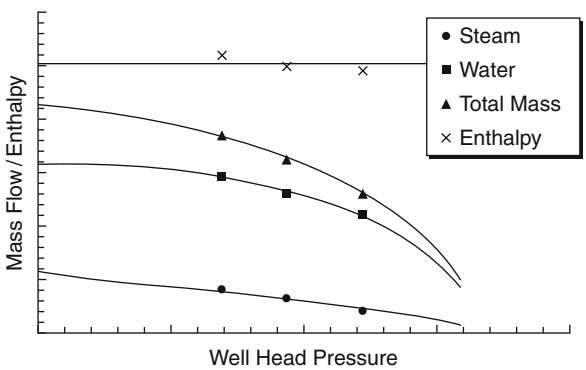

Reservoir Engineering in Geothermal Fields. Figure 9
Example of discharge characteristic curve

the numerical model that corresponds to a permeable zone identified in a well should match the temperature and pressure calculated by the wellbore simulation analysis after match is attained between calculated and measured production characteristics curves. Once the numerical model of the reservoir is calibrated (definition of the permeability characteristics of the well), the future change of discharge characteristics can be calculated from the values of pressure, temperature, and/or enthalpy predicted by the 3D numerical simulation for the elements containing the permeable zone of the wells. Nevertheless, in this calculation, the kh value is assumed constant during all the time of simulation period. Actually, kh values increase due to the continuous discharge or can decrease due to scale deposition. This is an issue necessary to be challenged for a more realistic forecasting simulation.

Interference Among Wells

During the discharge test, the reservoir pressure (and sometimes temperature also) is monitored at the observation well. The objective is to verify whether the monitoring pressure changes are not due to the production and/or reinjection of the geothermal fluid. For the monitoring, in general, capillary tubing system is used as pressure monitoring tool. The capillary tubing system consists of pressure chamber, capillary tube, helium gas vessel, and transducer with data recording system. The pressure chamber is set at the depth where it is detected as permeable zone and then filled with helium gas. The change in helium gas pressure in the pressure chamber with capillary tube, which indicates reservoir pressure, is transferred to a data recording system through the transducer. It is necessary to start pressure monitoring before the discharge test because there might be some natural trend of the pressure change which is not related to the testing activity. Sometimes tidal fluctuation in pressure can be observed.

The observed pressure data is examined considering the actual discharge and reinjection record. If there is a relationship between the mass extraction/injection and the change in monitoring pressure, it indicates the

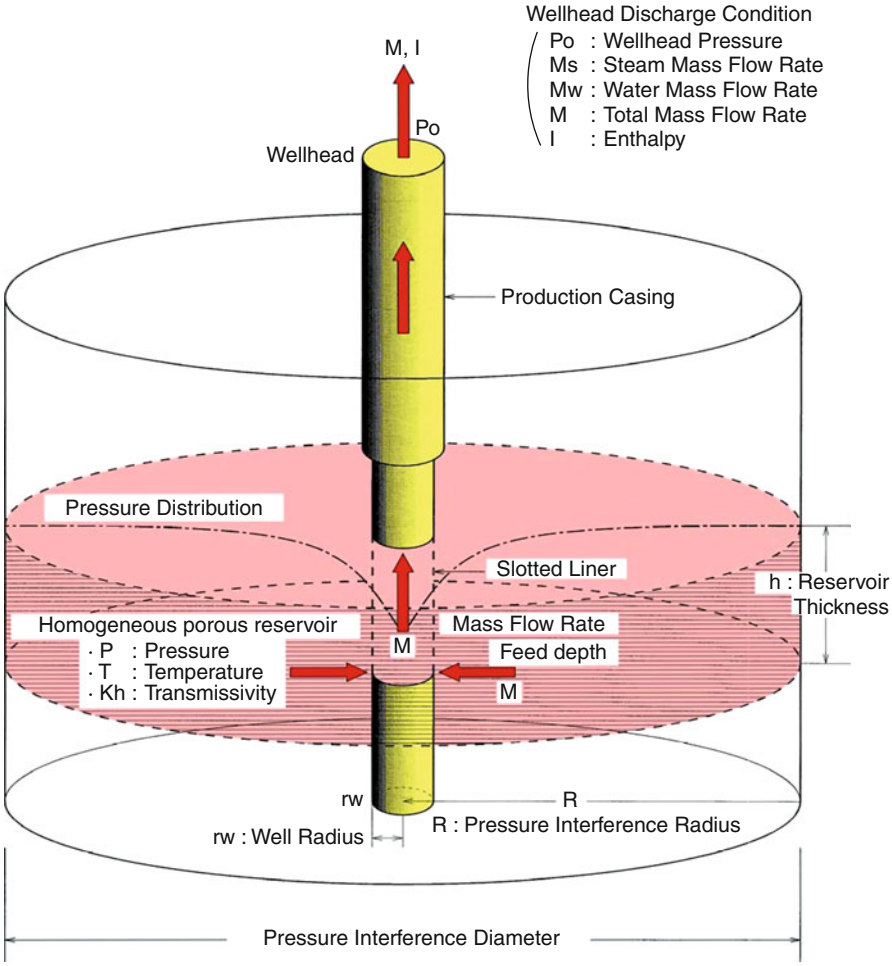

Reservoir Engineering in Geothermal Fields. Figure 10
Wellbore simulation model with the surrounding formation

hydraulic connectivity and mutual interference between the wells. The analysis of this data provides reservoir properties, such as the permeability–thickness products (kh) and reservoir boundary. This information is very useful to construct the 3D numerical model, and also the observed pressure change should be one of the guidance to calibrate the numerical model.

Tracer Test

Tracer testing, which is used to study flow paths and quantify fluid flow in hydrological systems, is probably the most efficient tool to evaluate the direct communication between reinjection well and production well. Tracer tests involve injecting a chemical tracer into a hydrological system and monitoring its recovery through time at various observation points. The results are, consequently, used to study flow paths and quantify fluid flow.

When designing a tracer test, the following aspects must be considered carefully:

1. What tracer to select
2. The amount of tracer to inject
3. The sampling plan to follow (sampling points and frequency)

The tracer selected needs to meet a few criteria: (1) It should not be present in the reservoir (or at a constant concentration much lower than the expected tracer concentration). (2) It should not react with or

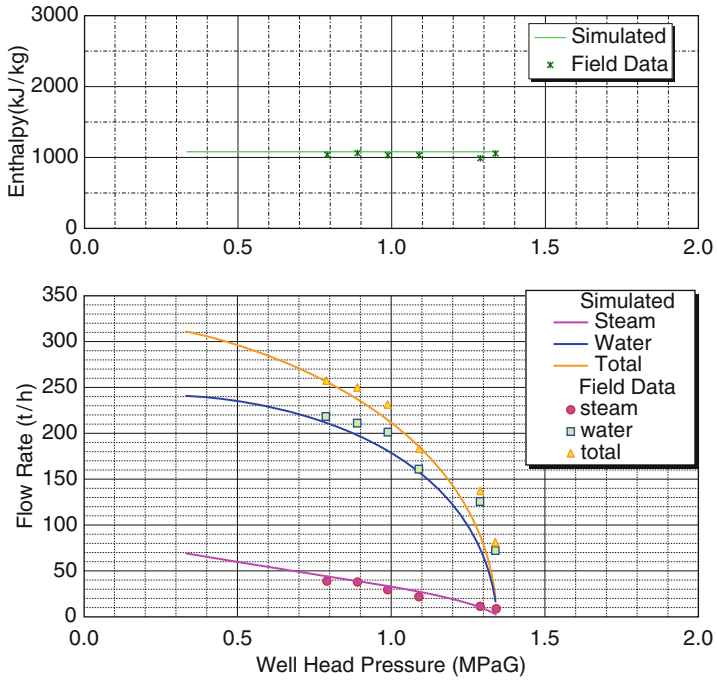

Well Name : Example-1

Input Data

Reservoir Pressure	=	6.86 (MPaA)
Reservoir Temperature	=	250.58 (°C)
Permeability-Thickness (kh)	=	100.00 (darcy-m)
Production Casing Depth	=	617.00 (m)
Feed Point Depth	=	1400.00 (m)
Production Casing Diameter	=	0.2240 (m)
Liner Diameter	=	0.2160 (m)
Skin Factor	=	0.00

Reservoir Engineering in Geothermal Fields. Figure 11
Example of the matching result to the production characteristic curve

absorb to the reservoir rocks. (3) It should be easy (fast/inexpensive) to analyze. The following are the tracers most commonly used in geothermal applications:

1. Radioactive tracers like iodide-125 (^{125}I), iodide-131 (^{131}I), tritium (^{3}H), etc.
2. Fluorescent dyes such as sodium fluorescein
3. Chemical tracers such as iodide, bromide, etc.

Sodium fluorescein has been used successfully in numerous geothermal fields. Fluorescein has the advantage of being absent in natural hydrological systems. It may also be detected at very low levels of concentration. Furthermore, the concentration of fluorescein is measured very easily, it being a fluorescent dye. The main disadvantage in using fluorescein is that it decays at high temperatures.

After a suitable tracer has been selected, the mass of tracer to inject needs to be determined. This is always difficult to determine beforehand but depends on several factors:

1. Detection limit
2. Tracer background (if any)
3. Injection rate
4. Production rate and how many wells are involved
5. Distances involved
6. Return rate anticipated (slow/fast)

The length of a tracer test depends on local reservoir conditions and distances between wells involved, which control the fluid flow pattern in the reservoir (Fig. 13). They usually last from a few weeks to months or even years. When distances are long and/or fluid flow is slow, tracer tests must be expected to be quite long. The length is preferably not determined beforehand, however, since the rate of return is hard to forecast. Once a sufficiently good data set has been obtained, a tracer test may be terminated.

An example of analysis of tracer test data is shown in Fig. 14. Three separate flow channels were used in the analysis, which are assumed to connect the different feed zones of the injection and production wells. The properties of the channels are different from each other. This kind of information can contribute to the construction of 3D numerical model, although such

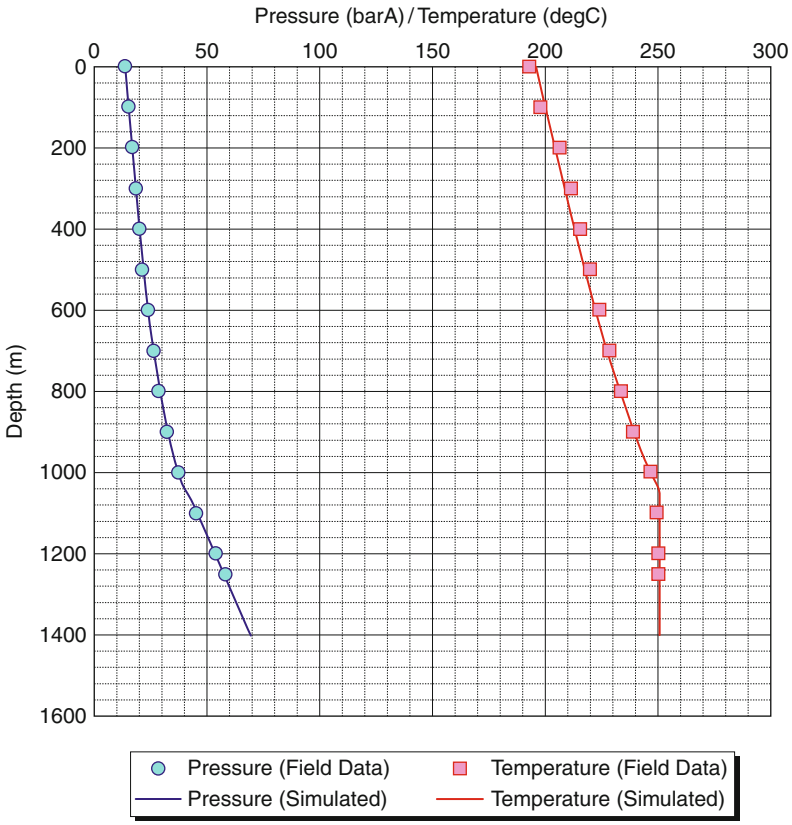

Reservoir Engineering in Geothermal Fields. Figure 12
Example of the matching result to the pressure and temperature profiles

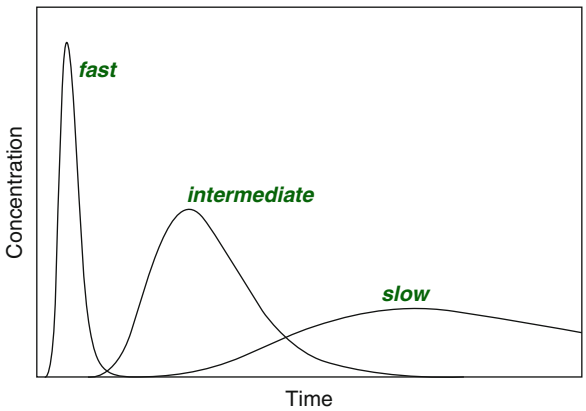

Reservoir Engineering in Geothermal Fields. Figure 13
Typical fast, intermediate, and slow tracer return profiles [1]

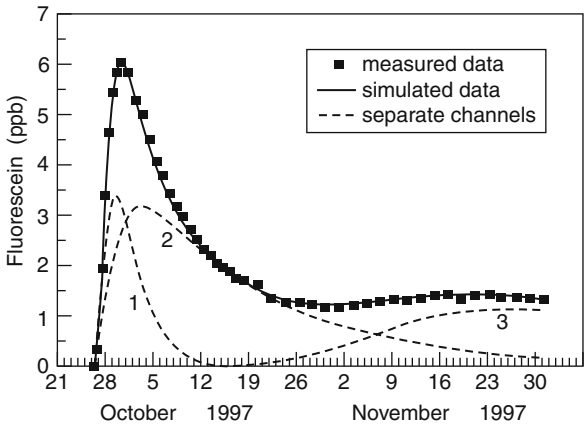

Reservoir Engineering in Geothermal Fields. Figure 14
An example of analysis of tracer test data [1]

detailed path setting and reproduction is not easy. However, the trial to reproduce the tracer return in 3D numerical simulation has already been carried out.

Historical Data

After the development of the geothermal power plant, the reservoir condition changes with time because of the extraction and reinjection of geothermal fluid. Thus, the historical data of following parameters is required for the 3D reservoir simulation.

Mass Production and Reinjection The historical data of mass production and reinjection is absolutely imperative for the reservoir management. It is the most basic data to evaluate the reservoir condition and behavior and also to maintain the output of the geothermal power plant. For example, if the mass flow from a production well declines, study for the possible reason (pressure decline, scaling problem, impact of cold reinjection, etc.) is required, and proper countermeasures should be applied. In any case, the historical data of mass production and reinjection is absolutely important. In the 3D numerical simulation, this data is used as input to the simulator to calculate the change of reservoir conditions.

Enthalpy of Each Well Similarly, fluid enthalpy produced from each well should be monitored. If the fluid enthalpy tends to decline, it indicates the cooling of the reservoir, and thus, the negative impact by the cold reinjection should be suspected. On the other hand, if the fluid enthalpy tends to increase, the reservoir might be drying, and the reservoir pressure drawdown might be serious. In this case, overextraction of the geothermal fluid is suspected. Thus, it is necessary to monitor the fluid enthalpy of each well for the stable operation of the reservoir. The historical enthalpy data can be used as matching target for the dynamic calibration of the 3D numerical model.

Pressure and Temperature If the well out of use is available, it can be used as monitoring well. Pressure and temperature monitoring system (please refer to Interference Among Wells) can be installed to the well. This information is very useful to observe the reservoir behavior and can be a good matching target for the dynamic calibration of the 3D numerical model.

Numerical Simulation

Work Flow

Numerical simulation is a computational work on the reservoir numerical model, which is the most popular technology to quantitatively evaluate geothermal resource potential and also optimize the strategic plan of the steam field development and/or its management. In general, the work of numerical simulation consists of three steps: model establishment, model calibrations, and forecasting (Fig. 15).

Establishment of Reservoir Numerical Model

Once the reservoir conceptual model is made, the next step is to establish the reservoir numerical model. The most important thing for establishing the numerical model is that it should coincide with the conceptual model in terms of the structures, heat source(s), and fluid flows in the reservoir. For example, even if the numerical model reasonably explains distributions of the pressure and temperature in the reservoir, ignoring the reservoir conceptual model, it should be revised until the numerical model is harmonized with the conceptual model because the conceptual model is the base of the numerical model. After careful considerations of the conceptual model, a grid is generated to discretize the geothermal system in three dimensions (Fig. 16). The simulation area should cover all the geothermal reservoirs and also their surrounding areas where are, as it were, buffer zones to mitigate impacts of boundary conditions on insides of the numerical model. The boundary conditions define the calculation conditions at all the boundaries at top, lateral sides, and bottom of the numerical model. The boundary conditions are unique concept of the numerical model and necessary to solve equations of mass and energy balances in the numerical model. In areas where reservoir information is available or where the well density is high, the grid blocks should be small. Conversely, in areas where no reservoir information is readily available or where the well density is low, the grid blocks are larger (Fig. 17). In general, the area of the numerical model will range from several square kilometers to several 10 km^2, depending on the reservoir conceptual model. In the vertical dimension, the model should extend to the basement rocks or to the

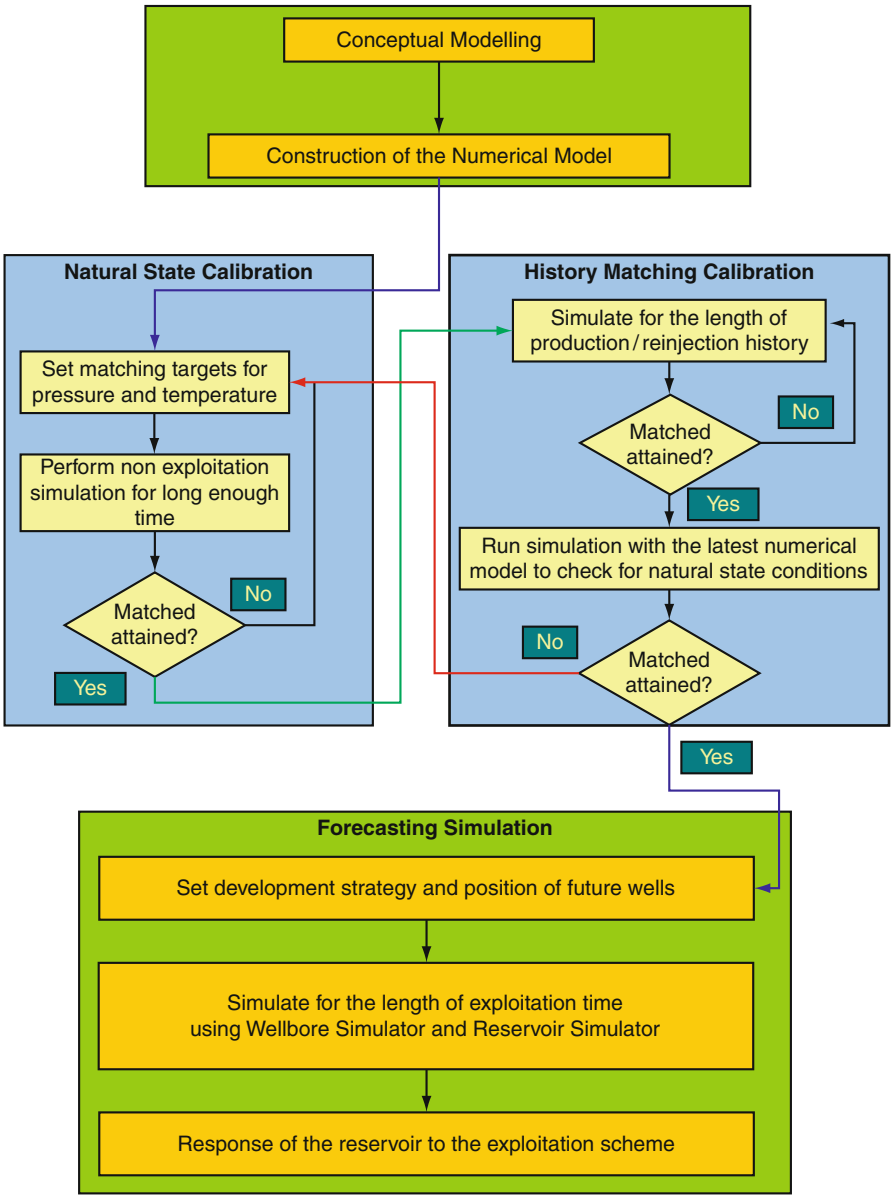

Reservoir Engineering in Geothermal Fields. Figure 15
Flowchart of reservoir simulation works

depth that is deep enough to mitigate the impacts of boundary conditions at the bottom of the model on the reservoir depths. Therefore, in many cases, the overall thickness of the numerical model will be a few kilometers and is subdivided into the number of layers, depending on the sectional information such as distributions of the geological formations, cap rocks, reservoirs, and basement rocks. For example, the thickness of each layer will be a few 100 m. Some grid blocks corresponding to the elevations close to the top of the model are eliminated, depending on the topographic elevation.

Once the grid system is constructed, the required grid block parameters are entered. Rock properties required for the reservoir simulation are density, porosity, permeability, specific heat, and thermal

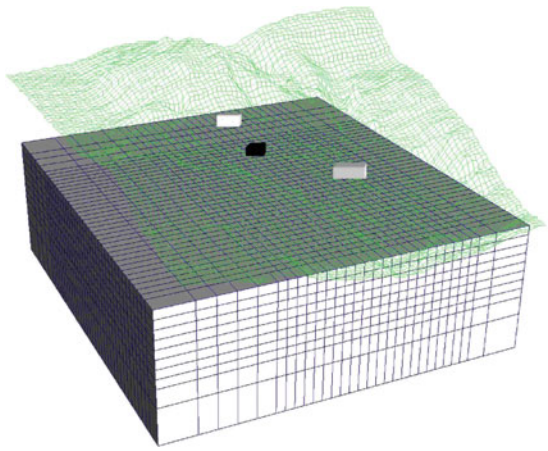

Reservoir Engineering in Geothermal Fields. Figure 16 Three-dimensional view of a reservoir simulation grid model

conductivity of each rock. The rock properties should be set for all grid blocks (Fig. 18). The most important parameter is permeability because permeability of the rocks usually has a wide range, depending on the rock type and structure and depending also on the control flow direction and mass flow rate of the fluids in the reservoirs. In order to estimate the permeability distribution, resistivity distributions are good reference because low-resistivity regions are considered to be low-permeability regions that play the role of cap rocks. Cap rocks limit the reservoir extent by preventing high-temperature fluids from flowing out into the surroundings. Thus, reservoirs with high-temperature fluids will be formed beneath the cap rocks, meaning that the distribution of low resistivity that is correlated with cap rocks may represent the reservoir distribution. The basic distributions of rock properties were examined, with a consideration of the resistivity distribution, geological formations, and fault structures in the geothermal field. Then both rock properties and their distribution were repeatedly modified by trial and error until the numerical model could reasonably explain the natural-state conditions in the reservoirs.

Calibration of the Reservoir Numerical Model

In order to make the reservoir numerical model reliable and available for predictions of reservoir performance under exploitation, a two-step calibration of the reservoir numerical model should be made. The first-step calibration is a natural-state simulation in which the reservoir numerical model should represent the steady state conditions of the reservoir under preproduction. The next step calibration is a history matching in which the reservoir numerical model satisfactorily representing the natural-state conditions should also represent the dynamic conditions of the reservoir during the exploitation. In these calibrations, the judgment of appropriateness of the numerical model should be done by comparison between the measured values and the corresponding computed values of each step simulation. When the reservoir numerical satisfies the two-step calibration, it is judged that the model can be applied to the forecasting simulation.

Natural-State Simulation Geothermal systems evolve over geologic time, during which the thermodynamic and hydrodynamic conditions in the system move toward a dynamic equilibrium. The rate of this change is exceedingly small compared to the changes induced during the exploitation of such a system. Therefore, for all practical purposes, undeveloped geothermal systems are considered to be in a quasi-steady state. The main objective of the natural-state calibration is to verify the distributions of temperature, pressure, and steam faction in the reservoir and the heat/mass flow aspects of the model. Therefore, more detailed distributions are needed to be specified for the permeability and thermal conductivity of the rock in order to match the subsurface temperature and pressure distribution. Once the natural-state calculation starts, high-temperature fluids will begin to flow upward due to buoyancy along the higher permeable structures or formations from the zones where the boundary conditions are set as upflow zones or heat sources at the bottom of the model. The fluids will decrease temperature and buoyancy due to contamination with the surrounding fluids with lower temperature and then begin to flow downward after reaching the depth of cap rocks where the fluid flow is constraint due to small permeability. The fluids will flow down to the basement rocks and recover temperature and buoyancy again at the depth, and then the natural convection will eventually occur (Fig. 19). A set of initial values for the petrophysical properties of the materials is selected,

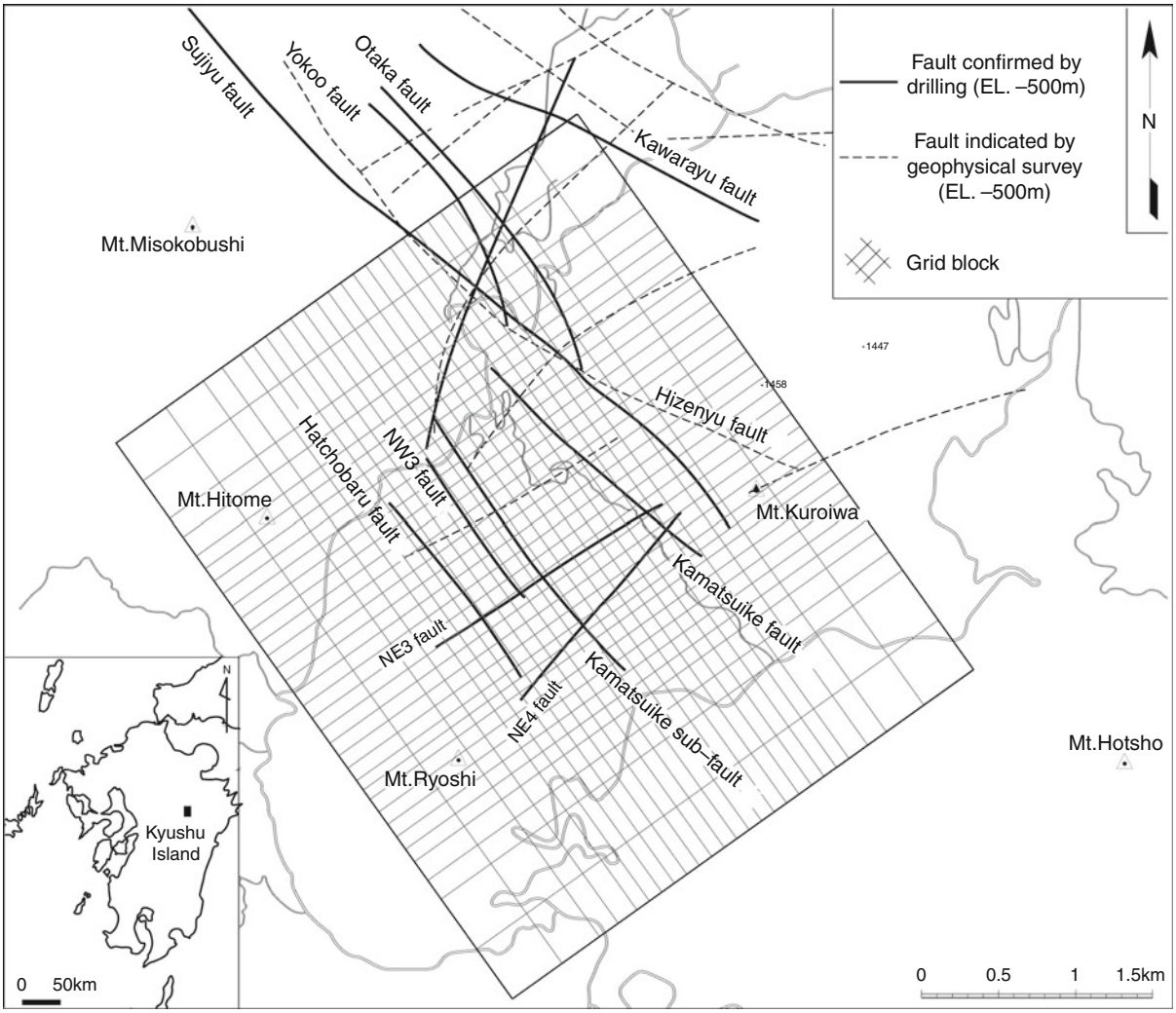

Reservoir Engineering in Geothermal Fields. Figure 17
Plan view of the grid used to model the Hatchobaru geothermal field [4]

and the model is allowed to run to a quasi-steady state condition, which takes, in simulated time terms, an order of more than 10^5 years. When the model fails to reach a quasi-steady state, it is because the numerical model is unstable or not realistic, and the input parameters have to be modified accordingly. After a lot of iteration, a temperature and pressure match between measured and simulated will be obtained (Figs. 20 and 21).

History Matching When historical data of mass flow rates of production and injection wells is available and also when there is availability of pressure and temperature changes over time during the production monitored by observation wells, the history matching can be done as the second calibration step of the numerical model following the natural-state simulation. It is a basic rule of the reservoir simulation that the numerical model always employs the same distributions of rock properties and boundary conditions which were imposed in the preceding the natural-state simulation. In the history matching, the simulator is provided with the mass extraction history as input data and reservoir response history such as pressure and temperature changes over time as reference data. The accuracy of the numerical model depends on the results

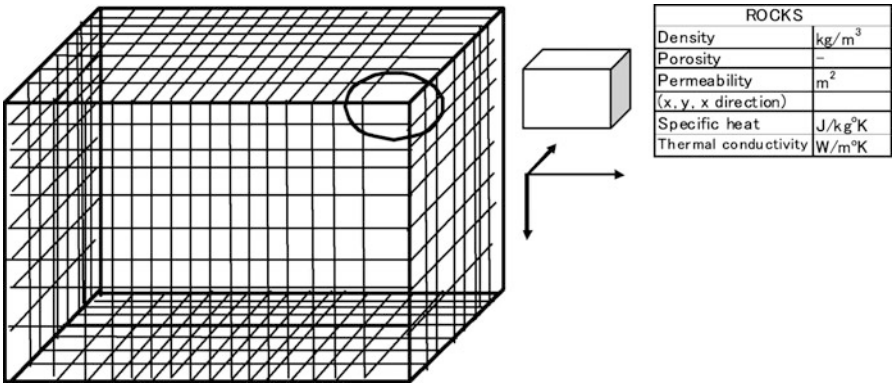

Reservoir Engineering in Geothermal Fields. Figure 18
Rock properties assigned to an element of the reservoir numerical model

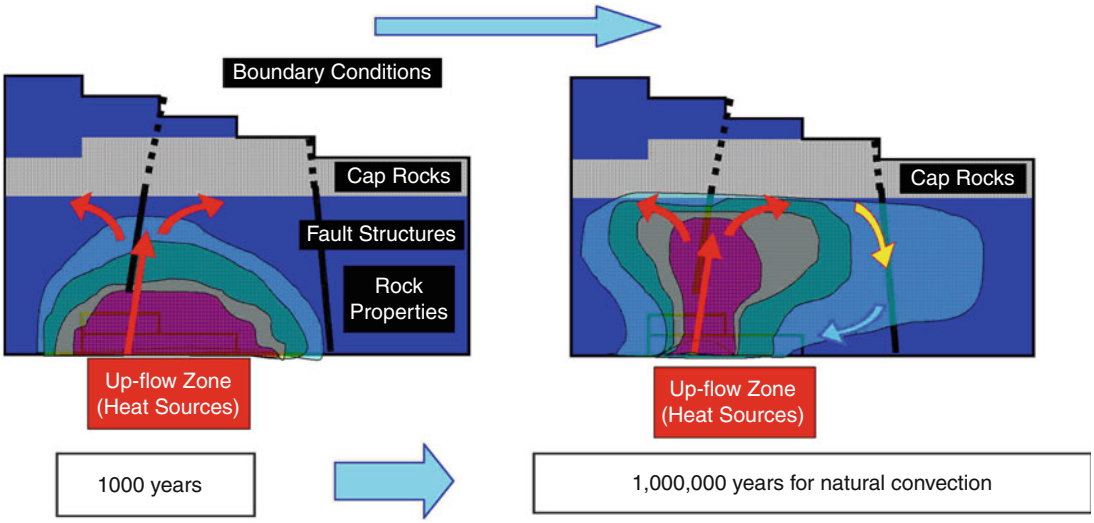

Reservoir Engineering in Geothermal Fields. Figure 19
Simulated natural convection of geothermal fluids in natural state

of both natural-state simulation and history matching. Therefore, quality and quantity of the measured data for the reference of the matching is very important. The longer and much more the term and items of reservoir monitoring during exploitation or plant operation are, the higher the accuracy of the numerical model is. For example, it is possible to use as reference the monitoring data of pressure, temperature, and gravity changes over time, and also the result of tracer return during plant operation [2]. In the Hatchobaru geothermal field, Japan, partial success in satisfactorily matching results with monitoring data of pressure, temperature, gravity changes, and tracer behavior was obtained (Fig. 22). In the history matching, satisfied matches to such various kinds of measured data will increase confidence of the numerical model because a lot of measured data to be referenced takes a role of providing considerable constraint to the numerical model. If significant disagreement exists between the computed results and field observations, appropriate adjustments should be made in the parameters in the numerical model, such as permeability distribution

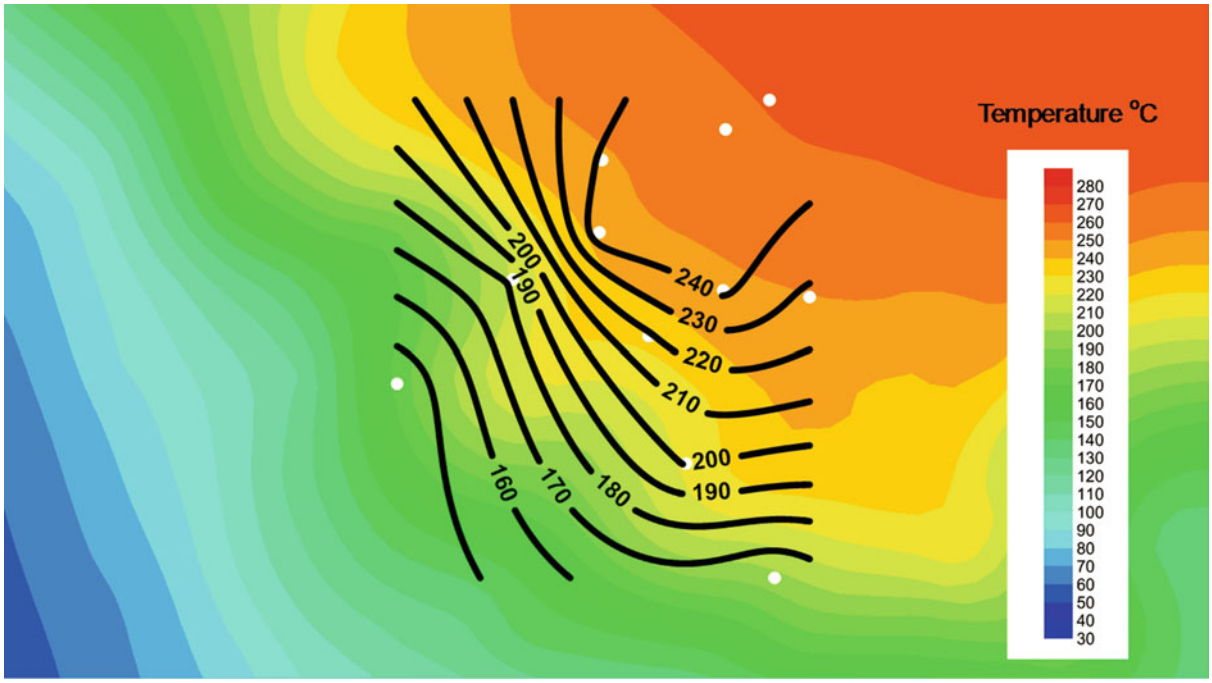

Reservoir Engineering in Geothermal Fields. Figure 20
Matching of temperature distributions in the natural-state simulation (black: derived from measured values; colored: calculated values)

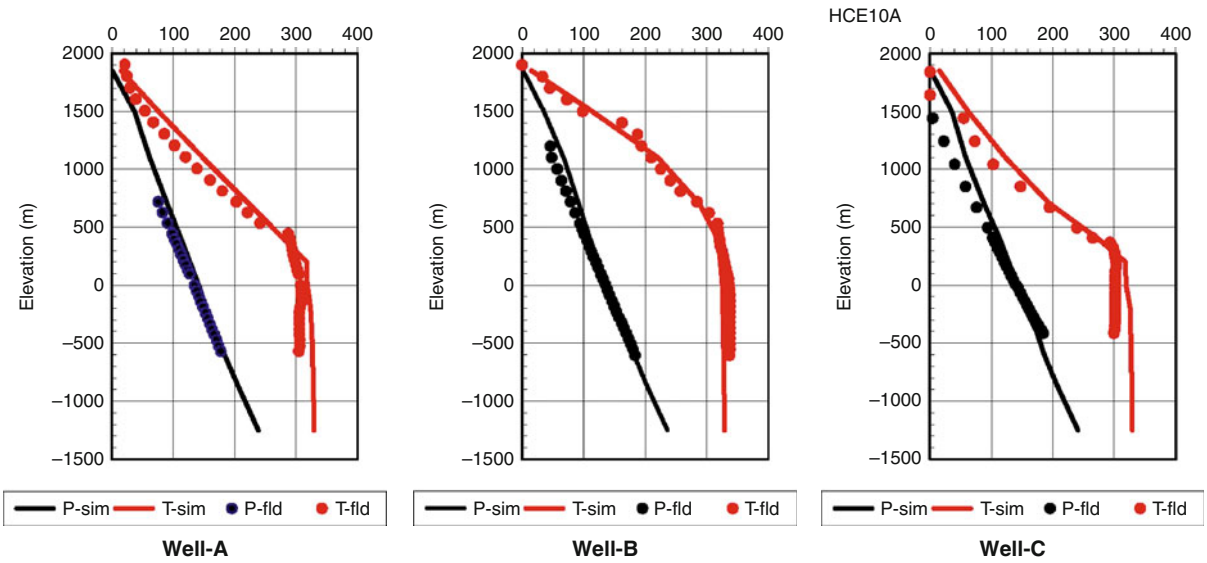

Reservoir Engineering in Geothermal Fields. Figure 21
Matching of wellbore static temperature and pressure profiles in natural-state simulation

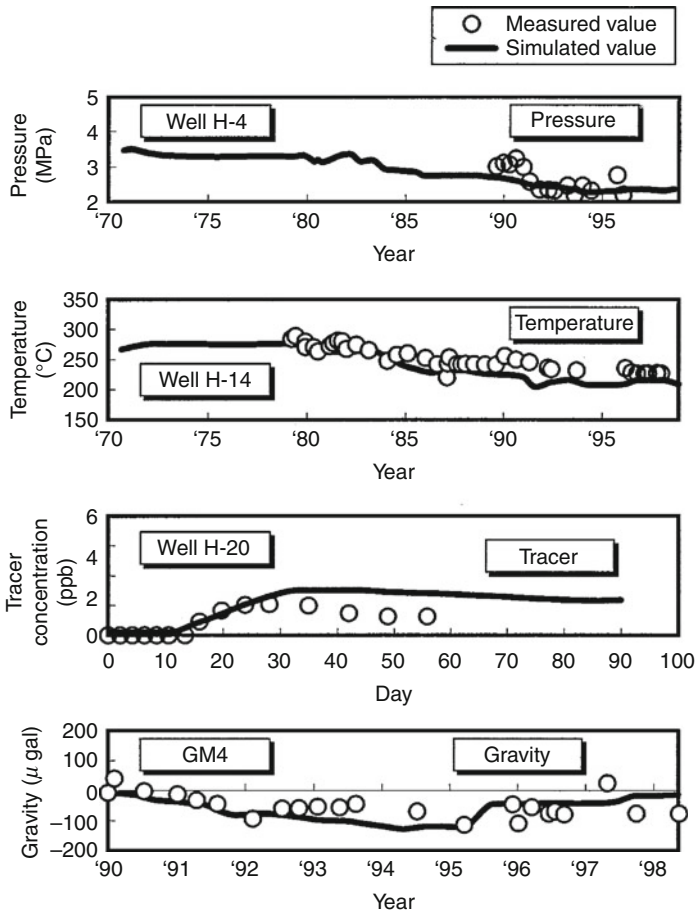

Reservoir Engineering in Geothermal Fields. Figure 22
Matching to reservoir monitoring data during the operation of the Hatchobaru power plant, Japan

and boundary conditions, and the entire process should be repeated, starting with the recalculation of the natural state, until satisfied history matching can be obtained. Accordingly, the entire matching process for the model calibration usually needs to be repeated numerous times to achieve satisfactory agreement between the computed results and the available field measurements.

Forecast Simulation

Once the history matching process is complete, the calibrated model can be used to make predictions of the future behavior of the geothermal field under the hypothetical development scenarios. Results of the forecast simulation will clarify degree of sustainable power development in the geothermal field, which can be defined as a geothermal resource potential.

In the forecast simulation, the development scenarios, including type and capacity of power plant (required steam and water production rate), location of both production and reinjection wells, and future well drilling plan, have to be assumed. Along the hypothetical scenario(s), the reservoir response will be calculated for long-term operation period (30 years, for example). The forecast simulation is recommended to be conducted by directly coupling the reservoir simulator with the wellbore simulator to have more accurate future performance of the production wells [3, 4]. The wellbore simulator calculates the mass flow rate and power output of each production well at the given wellhead pressure on the basis of the reservoir

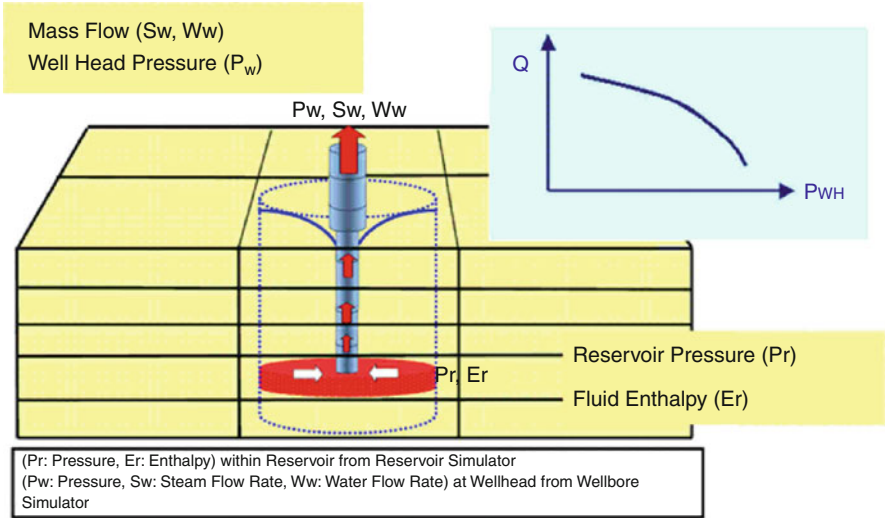

Reservoir Engineering in Geothermal Fields. Figure 23
Concept of coupling reservoir simulator and wellbore simulator

conditions that are calculated by the reservoir simulator (Fig. 23) [5–9]. Accordingly, the direct coupling method of a reservoir simulator and a wellbore simulator provides the predictions of the changes of power output over time of not only each production well but also the power plant.

In many geothermal fields in the world, it is reported that decline of the power output of geothermal power plant occurred, more or less, after commissioning the plant operation. The reasons of the power decline are case-by-case and field-by-field; however, they are generally classified into three categories below:

1. Pressure drawdown in the production zones due to interferences between wells or overproduction
2. Cooling in the production zones due to migration of injected brine or local water
3. Decrease of the permeability in the production zones or decrease of useful diameter of pipelines due to scale deposition

The above reasons can be avoided or mitigated by optimizing well allocation in the field or optimizing wellhead pressure. These optimizations can be done through the forecast simulation, by employing the best scenario among the hypothetical scenarios relating to well allocation and wellhead pressure. For example, the pressure drawdown and cooling in the production zones will be avoided or mitigated by keeping enough space between production wells and also between production and reinjection zones [10]. In addition, the scaling problem may be mitigated by setting higher wellhead pressure of production wells, although their productivity may decrease in accordance with higher wellhead pressure. Therefore, optimum wellhead pressure should be discussed in terms of the well productivity and mitigation of the scaling.

In order to maintain the rated output of the power plant through the plant operation life, additional drilling of makeup wells will be required at appropriate timing. The forecast simulation clarifies the number of wells required and appropriate timing of its drilling (Fig. 24). After running the several different scenarios and comparing the results, the most optimum development scenario can be decided.

Sensitivity Study

Sensitivity studies are methods to validate the certainty and uniqueness of the reservoir numerical model and compensate its uncertainty. Sensitivity studies are done by changing the parameters set in the model and then comparing their forecasted results with those of the base model to check how some of the parameters set in the model affect the prediction results. A simple procedure of the sensitivity studies is to change the parameters of the

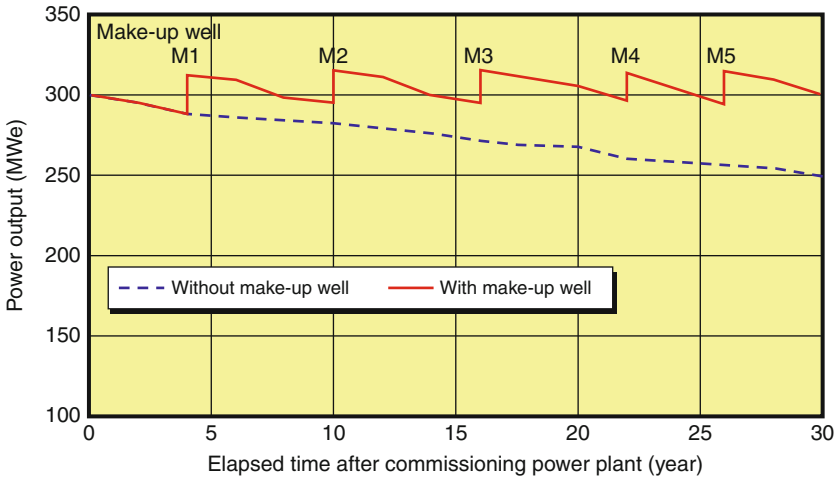

Reservoir Engineering in Geothermal Fields. Figure 24
Forecast simulation to predict the number and timing of commissioning of makeup production wells

numerical model selected and then conduct the forecast simulation to check their influences on the predicted results. For example, if the permeability values of the main productive faults in the numerical model change by 10%, the results forecasted will be changed compared to those of the base model. If they are drastically changed, it suggests that the permeability of the main productive faults is a key factor to determine the model accuracy as well as results of predictions. More complex procedure of the sensitivity study is to try to find other reasonable combination of the parameter settings of the numerical model and then compare the forecasting results to those of the base model. Even if the parameters of the base model are changed, some cases may satisfy the results of both natural-state simulation and history matching. Especially in the early exploitation stage, it will be very difficult to establish a unique numerical model due to poor measured data for the reservoir. In such cases, all the models that indicate fairly good matching in the natural-state simulation and history matching are available for the forecast simulation. Therefore, these models may show some range for the predictions of the decline of power output and/or number of makeup wells required from the conservative to optimistic values. This range can be made small when data of the reservoir is accumulated, which means that the reservoir model becomes more precise and the forecasts becomes more accurate as new data becomes available.

Resource Evaluation

As a general concept, a power plant should maintain its rated power output throughout the plant operation life of around 30 years. The power output of the geothermal power plant should be designed based on its resource potential that sustains continuous provision of the geothermal fluids required to the power plant from the geothermal reservoir(s) through production wells during the plant operation. Taking a balance of fluid production and provision in the reservoir is most important in terms of mass and energy. If the balance is successfully taken, the rated power output will be easily kept throughout the plant operation life. In such case, no or only a small number of makeup wells may be required. On the contrary, if mass or energy is produced significantly beyond the resource potential of the geothermal reservoir, it will be difficult to maintain the rated power output, even if makeup wells are added, and then the power output will be eventually declined (Fig. 25). Therefore, evaluation of resource potential is indispensable for optimizing not only the design of geothermal development but also the reservoir management plan for the stable power plant operation. As an effective method, a case study

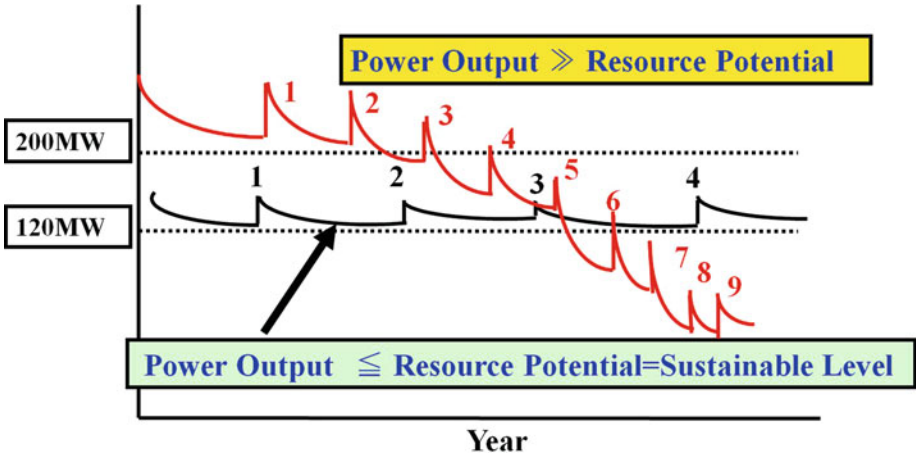

Reservoir Engineering in Geothermal Fields. Figure 25
Forecast simulation to estimate sustainability of the resource exploitation

that predicts the decline of power output over time-assuming several scenarios of the development is commonly used to evaluate resource potential.

For example, in the case of the Hatchobaru geothermal power plant (110 MW), three scenarios were considered in which a total of 17, 26, and 31 makeup production wells were assumed to produce from the productive faults in the field. Both the number of wells and the spacing between them (100–200 m) were specified regardless of the actual number of wells that could be drilled from the existing drilling pads. These scenarios showed that the simulated total power output temporally reached 190–265 MW, depending on the number of assumed makeup wells; however, in all three scenarios, a power decline was experienced until it stabilized at around 120 MW (Fig. 26). The prediction period is 9 years, which may not be sufficient to determine the sustainable potential. Since a smaller number of makeup wells than assumed in this case study are required to maintain around 120 MW from beginning of the calculation, it will be easy to sustain around 120 MW over 9 years. Therefore, it is suggested that the sustainable power potential of the Hatchobaru reservoirs is approximately 120 MW. It will also be possible to maintain the rated power output of 110 MW if the targets for production makeup wells were selected in such a way as not to overproduce the faults beyond their sustainable power potential [2, 4, 11].

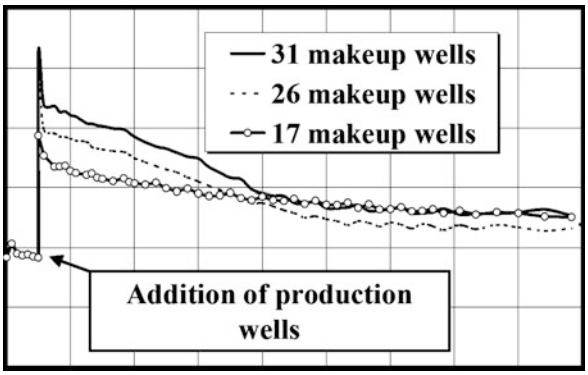

Reservoir Engineering in Geothermal Fields. Figure 26
Prediction of sustainable power output of the Hatchobaru reservoirs [2, 4]

Future Directions

Reservoir simulation will become a common technology to evaluate the resource potential and optimize the development scenario in the geothermal fields in the world [12–14]. In accordance with significant increase of computer capability, the reservoir simulator has been also improving and increasing its capability to perform more accurate reservoir simulation [15]. Three kinds of technical improvement and development have been currently endeavored. One is to enhance the simulation capabilities to calculate the transportation of a number of fluids; those

are, for example, not only pure water but also brine, noncondensable gas, chemical species, volatile organic, and so on [16, 17]. In addition, the module of calculating chemical reactions between rocks and fluids has been developed [18–21]. Another one is to facilitate an inverse modeling application that enables to do an automatic history matching and parameter estimation based on data obtained during testing and exploitation of geothermal fields [22, 23]. The other one is a speedup of calculation for the entire reservoir simulation by adopting a parallel computing technology that enables multicomputers to be used simultaneously. Since the source program of the reservoir simulator includes subroutines that can be calculated in parallel, it is possible to reduce the calculation time by modifying the source program of those routines so that multicomputers can share the corresponding calculations. The above-mentioned capability improvement and expansion for the reservoir simulation will contribute to accelerate geothermal power development and reduce the entire costs, because accuracy of resource potential evaluation will increase, and therefore, the output of geothermal power plant will be successfully maintained.

Bibliography

Primary Literature

1. Axelsson G, Björnsson G, Montalvo F (2005) Quantitative interpretation of tracer test data. In: Proceedings of the World Geothermal Congress 2005, Antalya
2. Tokita H, Haruguchi K, Kamenosono H (2000) Maintaining the rated power output of the Hatchobaru geothermal field through an integrated reservoir management. In: Proceedings of World Geothermal Congress 2000, Kyushu – Tohoku, pp 2263–2268
3. Lima E, Tokita H, Tsukamoto S (2004) Operation of the Hatchobaru geothermal field based upon a coupled reservoir-well and piping network numerical simulator. In: Proceedings of the KenGen geothermal conference, Nairobi Kenya, CD-ROM
4. Tokita H, Lima E, Itoi R, Akiyoshi M, Senjyu T (2006) Application of coupled numerical reservoir simulation to design a sustainable exploitation of the Hatchobaru geothermal field. In: Proceedings of renewable energy 2006, Makuhari Messe, CD-ROM
5. Aunzo ZP, Bjornsson G, Bodvarsson GS (1991) Wellbore models GWELL, GWNACL, and HOLA user's guide. Lawrence Berkeley laboratory Report LBL-31428, DE92 009494, Oct 1991
6. Gunn C, Freeston D (1991) An integrated steady-state wellbore simulation and analysis package. In: Proceedings of the 13th New Zealand geothermal workshop 1991, Auckland, pp 161–166
7. Itoi R, Kakihara Y, Fukuda M, Koga A (1988) Numerical simulation of well characteristics coupled with steady radial flow in a geothermal reservoir. In: International symposium on geothermal energy, exploration and development of geothermal resources, Kumamoto and Beppu, Japan, pp 201–204
8. Takahashi M (1988) A wellbore flow model in the presence of CO_2 gas. In: Proceedings of the 13th workshop on geothermal reservoir engineering. Stanford University, Stanford, pp 151–157
9. Tokita H, Itoi R (2004) Development of MULFEWS a multi-feed wellbore simulator. In: Proceedings of 29th workshop on geothermal reservoir engineering, Stanford University, California, CD-ROM
10. Tokita H, Yahara T, Kitakoga I (1995) Cooling effect and fluid behavior due to reinjected hot water in the Hatchobaru geothermal field, Japan. In: Proceedings of the World Geothermal Congress 1995, vol 3, Florence, pp 1869–1874
11. Yahara T, Tokita H (2010) Sustainability of the Hatchobaru geothermal field, Japan. Geothermics 39:382–390
12. Pruess K (1991) TOUGH2 – A general-purpose numerical simulator for multiphase fluid and heat flow. Report LBL-29400, UC-251, pp 1–102
13. Pruess K, Oldenburg C, Moridis G (1999) TOUGH2 user's guide, version 2.0. Lawrence Berkeley National Laboratory, Berkeley, LBNL-43134
14. Prichett JW (1995) STAR: a geothermal reservoir simulation system. In: Proceedings of the World geothermal congress 1995, Florence, Italy, pp 2959–2963
15. Antunez E, Morids G, Pruess K (1995) Large-scale three-dimensional geothermal reservoir simulation on small computer system. In: World Geothermal Congress 1995, vol 4, Florence, pp 2977–2980
16. Battistelli A, Calore C, Pruess K (1997) The simulator TOUGH2/EWASG for modeling geothermal reservoirs with brines and non-condensable gas. Geothermics 26(4):437–464
17. Pruess K, Finsterle S, Moridis G, Oldenburg C, Wu Y (1997) General-purpose reservoir simulators: the TOUGH2 family. Geotherm Resour Council Bull 26:53–57
18. Kim J, Schwartz FW, Shi J, Xu T (2003) Modeling the coupling between flow and transport developed by chemical reactions and density differences using TOUGHREACT. In: Proceedings of the TOUGH symposium 2003, Berkeley
19. Sato T, Ohsato K, Shiga T, Sato M, White SP, Kissling WM (2003) A study of reservoir estimation for a deep-seated geothermal reservoir using TOUGH2 and CHEMITOUGH2. In: Proceedings of the TOUGH symposium 2003, Berkeley
20. Xu T, Sonnenthal E, Spycher N, Pruess K (2003) TOUGHREACT: A new code of the TOUGH family for non-isothermal multiphase reactive geothermal transport in variable saturated geologic media. Lawrence Berkeley National Laboratory, Berkeley, LBNL-52342

21. Xu T, Sonnenthal E, Spycher N, Pruess K (2003) Using toughreact to model reactive fluid flow and geochemical transport in hydrothermal system. In: GRC 2003 Annual meeting, Morelia
22. Finsterle S, Pruess K, Bullivant DP, O'Sullivan MJ (1997) Application of inverse modeling to geothermal reservoir simulation. In: Proceedings of the 22nd workshop on geothermal reservoir engineering, Stanford University, Stanford
23. Finsterle S (2007) iTOUGH2 user's guide. Lawrence Berkeley National Laboratory, Berkeley, CA94720

Books and Reviews

Grant MA, Bixley PF (2011) Geothermal reservoir engineering, 2nd edn. Academic, Burlington, 349 pp. ISBN 978-0-12-383880-3

Resource Repletion, Role of Buildings

Katja Hansen[1,2], Michael Braungart[1,2], Douglas Mulhall[1,2]
[1]EPEA Internationale Umweltforschung GmbH, Hamburg, Germany
[2]Academic Chair Cradle to Cradle for Innovation and Quality, Rotterdam School of Management, Erasmus University, Rotterdam, The Netherlands

Article Outline

Glossary
Definition of the Subject
Introduction
Unintended Consequences of Traditional Sustainability
Materials Repletion for an Abundant Healthy Footprint
Application Tools for Implementing Beneficial Resource Repletion
Redefining Recycling
Introducing Nutrient Certificates
Conclusions
Acknowledgments
Bibliography

Glossary

Improving the approach to materials and products sometimes requires revising traditional terminology. In the approach described here, usage of certain terms differs from traditional definitions, to account for innovative features of materials and products.

Biobased vs. biodegradable Many biobased products such as, for example, biopolymers are not necessarily safely biodegradable because they contain additives such as heavy metals or are combined with nonbiodegradable materials. As well, petroleum-based products that are not biobased can be biodegradable. So it is important to distinguish these features to develop an effective defined-use pathway for materials. Especially, it is important to evaluate biobased and biodegradable in the context of the intended use of the material, e.g., if it is intended for a biosphere or technosphere pathway. For example, many materials designed for single use before disposal in a biosphere pathway and defined as biodegradable, such as cups, do not biodegrade in the processing time frame used in an industrial composting facility and, as a result, end up being incompletely decomposed and incinerated, or degrade the quality of compost. Because of this, the definition of "biodegradable" includes that the material is shown to degrade completely in an industrial composting facility within a prescribed time frame.

Counter-footprint Calculation showing activities that can be used to counterbalance a negative "environmental footprint." Example, producing renewable energy instead of just consuming energy. Counter-footprinting is still at an early stage and often, for example, does not calculate defined material content, defined-use pathways, or beneficial functions of materials such as, for example, cleaning the air. For example, Coto-Millan et al. [1] list construction materials as resource consumption, but not as a material resource on the counter-footprint side of the equation. The part of land "consumed" for structures is regarded only on the negative side of the footprint equation, rather than as a productive contributor to the ecology. In general, when materials are used for constructing a building, their impacts are frequently still considered only on the negative side of the environmental footprint and no longer considered as beneficial resources. See also "offset."

Cradle to Cradle® An innovation platform to improve the beneficial qualities of products and services in biosphere and technosphere metabolisms as a step beyond the traditional sustainability approach of reducing negative impacts. The term *Cradle to Cradle®* is a registered mark for quality assurance purposes, similar to how the broadly accepted International Standards Organization governs use of its marks and standards. However, the philosophy, principles, and many application tools of the Cradle to Cradle® approach are widely published. The founders of the C2C approach encourage governments, companies, and NGOs to use the philosophy and principles. The right to use the Cradle to Cradle Design Protocol® for certification is assigned to an independent nonprofit organization, and certification criteria are also broadly published.

Defined use Materials and products that are designed according to their intended use in biosphere or technosphere metabolisms.

Depletion Loss of nonrenewable resources and destruction of renewable resources.

Ecological footprint Usually a calculation of negative environmental impacts of human activity. Many definitions are used, but an example in relation to the built environment is "Corporate ecological footprint is defined as the environmental impact (in hectares) of any organisation, caused by: (a) the purchase of any kind of product and service clearly reflected in their financial accounts; (b) the sale of products deriving from the primary production of food and other forestry or biotic resources, or in other words when vegetables, fruit and meat enter the market chain for the first time; (c) occupation of space; and (d) generation of waste clearly reflected in their environmental report. Moreover, this impact measured in hectares can be transformed to obtain a result in tons of CO_2 emitted (the carbon footprint)…" [1]. See also Counter-footprint and Offset.

Intelligent materials pooling (IMP) Sharing of defined material streams among partners to achieve economy of scale and accelerate the use of C2C-defined materials.

Materials bank Database-supported pool of defined materials.

Materials security Security of supply for strategically important materials such as rare metals or phosphate.

Nutrient certificates Set of data describing defined characteristics of materials in products that give them value for recovery and reuse. Nutrient Certificates are a marketplace mechanism to encourage product designs, material recovery systems, and chain of possession partnerships that improve the quality, value, and security of supply for materials so they can be reused in continuous loops or closed loops or beneficially returned to biological systems. This is done by adding a new value dimension to materials quality. This new dimension is based on the suitability of materials for recovery and reuse as resources in other products and processes.

Offset Assessment of activities that compensate for negative environmental impacts. As opposed to counter-footprints, offsets are often used to describe remotely located activities, such as growing trees in another location to replace trees lost due to development. However, counter-footprint and offsets can also overlap.

Recycled vs. recyclable Products can be beneficial if they have defined recyclable content regardless if it is recycled or not. Defined recyclable content is an enabler for recycled content. If virgin content is not recyclable then it will pollute recycling streams, so recyclable is just as important as being recycled. Recycled content that is also recyclable at a similar level of quality is the end goal of product design for Nutrient Certificates.

Recycling There are many definitions of recycling, but for these purposes, recycling is defined as recovering and reusing materials at a similar level of quality by defining their content, as compared to "downcycling" where materials are recovered and reused at a lower quality level. For example, the term "recycling" is often applied to materials such as paper, but in reality, paper is almost always downcycled due to shortening of its fibers. Many current definitions of recycled content do not define what is in the material, with the result that it is not possible to recycle the materials at a similar level of quality. The important distinguishing factor is "defined" content, which can be indicated as defined to 100 ppm.

Repletion Replenishing the supply of biosphere and technosphere materials for use in products and processes.

Scarcity Geographically, politically, or commercially limited supply of strategic materials.

Upcycling Improving the existing quality of a material for its next reuse. A material can be defined as upcycled under various conditions:

(1) When its current downcycling is improved so the material is recycled at a similar level of quality instead of lower level. For example, high-grade steel is separated from motors containing copper contaminants so the steel can be resmelted at the same level instead of downcycled
(2) When a degraded material is repaired for effective reuse, e.g., an additive is added to a plastic to repair its damaged molecular strings so the material can be reused for a high quality purpose

Definition of the Subject

Raw materials scarcity, rising raw materials extraction costs, and biodiversity loss are apparent globally. Recycling of materials is cited as one solution to those problems. However, maintaining the consistent quality of materials is excluded from most traditional sustainability assessments, and current regimes of carbon, emissions, and energy trading are not well designed to account for the quality or value of materials, or the processes for achieving materials recovery and reuse.

The building industry is a large consumer of scarce resources, and because of this, it is regarded as a leading cause of resource depletion. However, at the same time, materials contained in and moving through buildings have been extensively evaluated for their recovery potential [2], and as a result, could be used in a new model where buildings are resource repleters instead of depleters. Materials repletion is a value-based business model that defines new dimensions of quality to generate quantifiable benefits for builders, suppliers, building occupants, operators, and owners. For this model, the inherent conservatism of the industry could work in favor of a new approach due to the emphasis on value, reliability, and documentation. This would introduce a new type of beneficial agenda into the supply chain of the construction, operations, maintenance, decommissioning, and recycling industries.

To support this beneficial paradigm, a framework for resource repletion and security is described where materials are defined according to qualities that enhance their bankable and tradable value. The concept of *Nutrient Certificates* is introduced as a counterpart to emissions certificates to account for the value of defined high-quality material flows. The focus is distinct from mechanisms such as environmental product declarations, material safety data sheets (MSDS), or emissions trading. For this approach, new criteria are introduced for materials and for "recycled content." Financial enabling innovations are described, and early adopters are identified among governments and companies, including participants in Cradle to Cradle® networks.

Introduction

► Our economy will run out of materials before it runs out of energy.

(Michael Braungart 2009)

► China. . .has now quietly halted some shipments of (rare earth metals) to the United States and Europe. . . industry and government are joining forces by appealing to the European Commission and the World Trade Organization to intervene. . .

(*New York Times* October 19, 2010 [3, 4])

The globalized depletion of material resources is well documented quantitatively and qualitatively [5]. Skeptics argue that such claims are exaggerated [6] and that scarcity has a positive side effect of driving innovation. Despite those arguments, scarcity is still disrupting economies. This scarcity is generated more by geopolitical distribution inequity than geological availability. For example, Europe depends on just two countries, China and Morocco, to support most of its agricultural system with the fertilizer phosphate. In 2008, China puts export tariffs on its phosphate supplies, disrupting phosphate pricing [7]. China also has a near-monopoly on producing certain rare metals, not because of geographic distribution but because other countries let their rare metal processing capacities dwindle [8, 9] via outsourcing. The city of Barcelona once had to import water in ships due to a water shortage, resulting in prioritization conflicts with other regions of Spain [10]. As well, Central and Southern Europe suffered when Russia interrupted gas supplies.

In addition to distribution disruptions, the costs of extracting material resources are accelerating as supplies become more remote and difficult to access. Biodiversity losses are accelerating as species habitats are put under greater pressure by expanding incursion for urbanization and resource extraction [11].

Together, those factors pose economic security risks to regions such as Europe, USA, and Japan, along with suppliers such as China who come under pressure to solve shortages by exporting their own limited supplies. Materials security is taking the stage alongside energy security as an economic and military consideration. This is generating an economic, social, and ecological imperative for materials repletion instead of depletion.

A first step to establishing a materials repletion paradigm is to recognize the unintended consequences of traditional approaches to "sustainability," which pose barriers to repletion. The step after that is to describe solutions for those unintended consequences.

Unintended Consequences of Traditional Sustainability

The Unintended Consequences of Eco-Efficiency

The traditional approach to materials sustainability in buildings is exemplified by the draft topical outline provided to the authors for this article:

- Green sustainable building is the practice of increasing the efficiency with which buildings and their sites use and harvest energy, water, and material, while at the same time reducing impact on the local and global natural environment. [12]

An unintended consequence of this approach has been that greater efficiency often has the opposite effect by accelerating instead of reducing impacts. This is self-evident, for example, with accelerated material and energy throughputs for personal electronic devices. Here, efficiency improvements in the use of materials and energy have been exceptional over past decades. Miniaturization resulted in devices that require only a fraction of the energy and the materials compared to earlier devices to perform the same function, while at the same time adding functional features. However, this resulted in price drops that made the technology accessible to billions of customers, generating exponential increases in materials and energy throughputs due to collective demand [13]. By increasing the efficiency of individual devices, the industry accelerated collective materials and energy throughputs, including flows of materials for products to waste from product disposal.

The same occurred with buildings, as efficiencies have improved and economic activity expands globally, real growth in the collective "ecological footprint" of buildings (see Glossary) has accelerated in developing economies of Eurasia, Africa, the Middle East, and South America, while still expanding in developed economies of Europe, North America, and elsewhere. The results are marginal reductions in the footprints of individual buildings negated by the collective expansion of land use, materials, and energy. In many cases, individual building footprints are increasing as well to house diverse technologies and the lifestyles they suggest. Electronic technologies and networking services in particular are growing rapidly, resulting in increasing demands for space, materials and energy.

This collective expansion of impacts due to economic and technological development is also described in recent studies finding that wealth, not poverty, is the main driver of environmental impacts [14]. As collective wealth improves globally, consumption of energy and resources is accelerating.

Due to the phenomenon of efficiency accelerating throughputs, the "reduction" approach to resources on its own is unlikely to significantly mitigate environmental impacts in buildings or of products that move through them, and instead is likely to accelerate those impacts.

Disregarding Beneficial Footprints

- Minimization vs. Benefits. Green assessment methods focus more on minimizing use of materials and energy instead of focusing on the intended benefits of materials and energy in a system. As a result, the value of some beneficial aspects is underemphasized in green building standards. By contrast, natural processes often maximize their own footprint, and an example of this is the largest living thing on Earth, the giant sequoia. See following sections for example.
- Measurement Criteria. To accurately assess the benefits of some materials, it is important to

evaluate factors such as their "defined use" in ecosystems, the active benefits they generate, and the time frame and rate of reuse, as discussed under Section III. Current measurement systems often disregard those.

- Assessing Impacts vs. Calculating Resources. Most green rating systems for buildings do not award many points for designing materials as resources for the future. Instead, those materials are often considered as part of a negative "consumption" footprint. Until now, this has been justifiable because many building products today are not designed with next use in mind, so they are not considered beneficial resources. But the unintended consequence is that when green rating systems do not encourage the transformation from minimizing impacts to maximizing future resources, they become part of the problem instead of the solution. An example of this can be found with "recycled content."

Unintended Consequences of "Recycled Content"

Part of the approach of green rating systems to materials depletion includes "recycled content" and "reuse of materials." However, those rating systems do not distinguish, for example, materials downcycled from high to low quality from materials with recycled or "virgin" content that is defined, easily separated, and recyclable at a similar level of quality. For example, LEED 2009 for existing buildings does not require "postconsumer recycled content" to be defined or to be recyclable at a similar level of quality [15]. Also BREEAM 2010 standards for real estate specify materials with a "high recycled content" and "reuse of materials," and although these also specify "nontoxic" materials, the standards do not specify defined or recyclable at a similar level of quality [16].

As a result, companies that invest in important quality aspects such as design for materials recovery are sometimes penalized for focusing on those investments. For example, well-defined virgin material for ongoing use would not receive credit, whereas undefined downcycled material would. Nor are actively beneficial functions of materials considered. So, a building containing materials defined to 100 ppm and consisting of surfaces that clean the air would not qualify under many green building evaluation systems because those materials do not contain "recycled" content. The defined content for ongoing use and the functional qualities of materials might be more beneficial for the building than undefined recycled content, but those benefits are underemphasized in Green building scoring systems and regulations.

This is especially problematic if contract tendering documents require contractors to maximize the amount of materials recycled or reused from an existing building into new construction or renovation. By mandating maximal on-site reuse or recycling, contracts can inadvertently penalize contractors who use well-defined materials wherein the next intended use as agricultural or industrial resource is known. Tenders can also discourage other innovative off-site reuse or recycling of materials that might be more suitable, including the reuse of those materials unsuitable for human exposure in a building.

> This is not to say recycled content is a bad requirement, but rather that the traditional definition could be improved to reward other properties and promote the use of defined and truly recyclable materials.

Likewise, material safety data sheets (MSDS) for products contain a list of aspects defined as hazardous and how to handle those, but are not designed to show the beneficial qualities or whether a product is sufficiently "defined" to be recycled at a similar level of quality. Nor are MSDS intended to evaluate the suitability of materials content for recycling after their first installation. Indeed, a material might be contaminated with an additive that makes it unsuitable for recycling, but this would not be described in the MSDS. Nor do MSDS keep up with science effectively. They are based on regulatory definitions that usually take many years to recognize hazards in products, long after the hazard has been established through scientific analysis. The effect of this is to increase contingent liabilities for companies because something that might not be listed on an MSDS today might suddenly appear when legislation changes. So MSDS provide no early warning system to prepare companies and owners for new findings.

Consequences of Traditional Assessment Boundaries

Beyond the confines of product selection, very little attention is paid to what happens to the products and materials that flow through buildings. Over the lifetime of a building, flow through might equal or exceed the mass of its construction materials. Often, no score is assigned to the quality of material in office equipment, furniture, and finishes that flows through the building, including food, paper products, and other biogenic materials, as illustrated in Fig. 1 in a following section.

The emphasis of assessment language on being "less bad" is endemic throughout the literature. For example, the terms "minimize" and "reduce" are used throughout LEED design innovation credit documents [17]. Terms such as "offset" are used to signify compensation for negative impacts, and reference is also made to habitat conservation, but those approaches are rarely used in reference to materials quality. Nor are they intended to transform buildings into net positive generators of biodiversity, energy, or defined materials. Instead they are largely directed at reducing or compensating for the negative impacts of a building.

The effect of this language is that most attention and funding is spent on minimizing the negative impacts of building materials, and less attention is paid to evaluating or improving the benefits of material quality.

> Such examples are not intended to discredit green building ratings as a mechanism, but instead, to show that limiting boundaries and emphasis can skew the focus of investment and limit the capacity to be truly beneficial. When boundaries are too limited, innovation is limited.

Unintended Consequences of Biomass Energy

The value of biological materials in buildings is usually considered in terms of how much wood and other

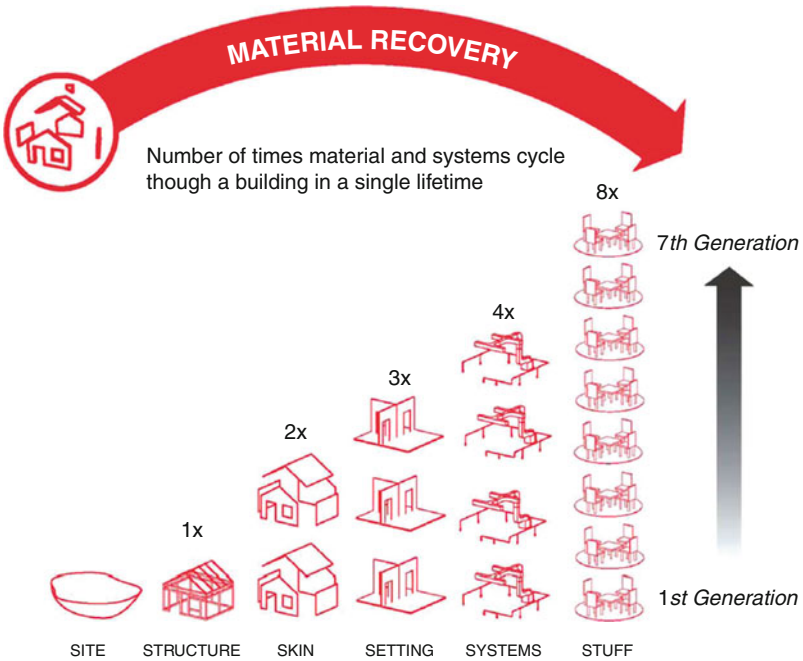

Resource Repletion, Role of Buildings. Figure 1
Number of times materials and systems cycle through a building in a single lifetime. It can be seen here that buildings are effective mechanisms for tracking materials with relatively short turnover periods as well as those with extended turnover periods, and that the shorter-term innovation potential is with products that have shorter generations for optimization (Source: Redrawn from a William Mc Donough & Partners drawing adapted from Brand 1994 [44])

agricultural products are used during construction. However, one of the largest components of biomass use for buildings, and one of the fastest growing in terms of investment, is biomass for energy [18]. It is noteworthy that technology has progressed over the centuries toward increasingly intensive embodied-energy fuel sources, from biomass to coal to oil to uranium, but now seems to be regressing to biomass. The widespread burning of virgin wood and other biomass is now sanctioned as "sustainable" and is given government incentives. However, the impacts of that burning whether in Africa or Europe are quickly becoming apparent in resource depletion. For example, a FAO study estimates that despite uncertainties over data, an approximately 400 million cubic meter shortfall by 2020 can be projected for wood availability in Europe [19]. This forecast was already manifested in 2010 when some biomass incineration facilities had to start limiting operations due to supply shortages. Europe would have to cut down many of its forests and use much of its farmland to meet this shortfall, so instead, it is importing wood from the Americas, Russia, South-East Asia, and Africa to meet demand [20]. Moreover, the fertilizer requirement for growing such large amounts of biomass is usually not considered in forecasting e.g, the capacities of soils to continually produce biomass that is not returned to the soil. The costs and materials flows involved in replacing humus, NPK, and trace elements are often absent from biomass supply chain estimates.

> This is not to say biomass energy is inherently impractical for meeting a minor portion of energy demand, but rather that current strategies are already leading to shortages and have not adequately considered nutrient flows required to meet production requirements. Nor do they consider the unintended consequences for the wood construction, pulp and paper, and furniture manufacturing industries that find themselves adversely affected by subsidized biomass burning [21].

Confusion Over Biobased Materials

Large investments are being directed into biobased materials, but at the same time, there is much confusion in the marketplace over what biobased materials are and under what conditions they are eco-friendly. "Biobased" is often confused with "biodegradable." Biobased materials are often not safely biodegradable due to the additives they contain. Nor are biobased materials necessarily eco-friendly. They can compete with food supplies and lead to topsoil depletion. To solve this, a systematic implementation regime is required that can define conditions under which biobased materials are beneficial along their intended pathway of production, use, and disposal.

Impracticality of "Local Materials" Criteria

In a globalized economy, sustainability criteria that reward local sourcing of materials do not adequately address regional materials imbalances. For example:

- Rare-earth metals required for industry are found in just a few countries.
- "Fair trade" regimes often involve transport of goods long distances to locations where similar resources are impractical to produce, e.g., coffee grown in Africa would require vast greenhouse complexes in Alaska.
- Innovative materials such as, e.g., Nanogels® that improve the performance of buildings are only manufactured in a few locations. Green building assessment systems such as BREEAM give preference to "local materials" [16]. Under those rules, innovative materials could be penalized.

While sourcing local materials, components, and labor can sometimes ensure reduced transportation costs, enhanced employment, and industrial durability in a region, and may source more climatically appropriate materials, those goals need to be modified to recognize where local sourcing is not the most practical alternative.

Deficiencies of Emissions Trading Schemes

Because emissions trading schemes and habitat offset schemes are usually characterized in terms of energy and wildlife, these are usually not referred to in relation to materials quality. However, those schemes are largely materials dependent. For example, fuels are materials. Energy systems in and for buildings are made of materials. Substances that make up habitats are materials. Greenhouse gases are made of chemicals that can be reused. Those examples suggest that emissions trading

schemes are as much materials depletion and repletion questions as they are climate change or energy questions.

Emissions trading schemes are inadequately designed to promote conditions necessary for regenerating materials resources. For example, there are few if any emission credits for directly regenerating our primary carbon-sequestering systems, such as topsoil which is the upper 1–2 m of soil required by most plants to grow. Soil organic carbon is the biggest carbon pool of the planet after the oceans and far greater than what is found in the atmosphere [22]. Soil is a forgotten climate solution. Aside from the oceans, top soil is the leading repository of carbon in the biosphere. Much of the productive topsoil globally has been lost in the past century due to industrialized farming, soil compaction, erosion, and urbanization [23]. This loss has been a leading contributor to carbon release into the atmosphere. Conversely, soil conservation is shown to sequester atmospheric carbon [24]. Emissions trading schemes can be used to support soil conservation, which is distinct from soil manufacturing, but they do not account for the nitrogen, phosphorous, potassium (NPK) fertilizer cycle in topsoil, or soil quality degradation from rock phosphate fertilizer that is contaminated with uranium mined with the rock phosphate [25].

Topsoil is often not considered as a significant factor in buildings, but actually, buildings and topsoil have substantial interactions. Buildings usually occupy space where topsoil used to be. Runoff from buildings has substantial impacts on topsoil. Landscaping for buildings makes extensive use of topsoil. Products used in buildings are often made from biomass grown in soil. So it can be said that buildings rely heavily on topsoil. Because of this, converting buildings from materials depleters to materials repleters also involves a basic revision in the approach to soil.

Due to those various factors, emissions trading schemes are ill-equipped to support or quantify materials flows that are essential for the continued development of our industrial society. However, it is not the intention here to describe all the pros and cons of such trading schemes, as these are described elsewhere [26].

Instead, the main purpose here is to point out that those systems often do not recognize the role of materials. They often do not quantify the contribution of materials to carbon sequestration, biodiversity, nutrient recycling, and other beneficial aspects. They do not distinguish between high quality and low quality recycling.

Materials Repletion for an Abundant Healthy Footprint

How might it be possible to solve the unintended consequences of traditional sustainability approaches? Practical lessons can be taken from natural systems.

Big Footprints Can Be Beneficial

One example of a big, healthy footprint is the largest living thing on Earth, the giant sequoia [27]. Like many buildings, it reaches heights of more than 90 m, weighs thousands of tons, and uses thousands of liters of water and large amounts of energy daily. As the fastest growing tree in the world, it consumes large amounts of energy to pump nutrients and relies on the massive transport of water from hundreds of kilometers away to provide the marine layer that feeds the forest canopy. Its outer skin is far from minimal; it is thicker than the outer skin of many buildings and can be more than a meter thick. Its root system extends farther underground and laterally than the foundations of many buildings. The total throughput of energy and materials of a forest containing giant sequoia and similar giant tree species can rival that of small human settlements. In total, the giant sequoia has a giant footprint.

The sequoia also depends on destructive processes. It depends for its early existence on fires that pollute the environment and kill other trees, clearing the forest floor so sequoia species can compete and get established. To protect itself, it uses the toxic material tannin which can be harmful to insects and other wildlife. At the same time though, the sequoia has a maximal beneficial footprint, which can be described as an "offset" or "counter-footprint" [28] (see Glossary) that maximizes the positive use and reuse of resources. It provides a habitat for hundreds of species, generates oxygen, beneficially uses CO_2, filters the air, is an exceptionally long-term carbon sink, and sheds biomass that is converted into soil. Its cellular capacities allow it to use large amounts of water while returning it to the environment in a state beneficial for

other biosystems. Its immune system resists disease, letting it live more than 3,000 years. The species is so genetically successful, it has outlived the dinosaurs.

Maximizing Benefits is More than Just Semantics

While the distinction between "maximizing benefits" and "minimizing impacts" might seem like semantics, it extends far beyond terminology. Natural design principles are increasingly recognized by architects and designers and applied to building and product designs through techniques such as biomimicry and calculation of offsets or counter-footprints. When innovation is directed at maximizing benefits instead of minimizing damage, different outcomes occur. For example, instead of minimizing the amounts of rare metals in devices to a level where it might not be economic to recover them, the designer focuses on design for disassembly to recover those rare metals so they can be used again. This approach might in some cases increase the amounts of rare metals used, but also enables their recovery. In this way the materials can be used as resources for other industrial processes.

This different approach can be seen in the Cradle to Cradle® approach to resource reutilization.

Cradle to Cradle® for Achieving Resource Repletion and Beneficial Footprints

The Cradle to Cradle® (C2C) [29] approach emphasizes those beneficial factors. The "Cradle to Cradle" Design Protocol® has taken an approach that generates benefits for stakeholders by going beyond the "cradle to grave" and beyond traditional interpretations of "environment."

Cradle to Cradle® is a paradigm-changing, quality-enhancing innovation platform developed in the 1990s by Michael Braungart, William McDonough, and others based on research at the Environmental Protection Encouragement Agency [30] in Hamburg Germany, for designing beneficial economic, social, and environmental features into products, processes, and systems. Cradle to Cradle® is primarily an entrepreneurial and innovation approach that starts by determining the intended benefits of a product or service instead of focusing on minimizing negative environmental impacts.

C2C philosophy, principles, and many of its application tools are broadly published, and the philosophy and principles are available for anybody to use with attribution.

The C2C Design Protocol described here, as well as the *Cradle to Cradle® Criteria for the Built Environment* are further described in other publications and are only partially excerpted here [31].

To enhance quality and add value for stakeholders, C2C promotes innovation partnerships along the entire chain of a product, including manufacturing, distribution, use, disassembly, recovery, and reuse.

By characterizing hundreds of products and thousands of materials for their human and environmental health attributes, as well as defining systems to safely and fully cycle materials into new products, C2C has already provided a practical yet inspirational scientific and business model for improving quality.

This innovation and value model makes C2C potentially attractive to planners, builders, and manufacturers for integration into products, processes, buildings, materials recovery systems, and purchasing.

Extensive books, cover stories, and documentary films have been published and broadcasted about C2C since the 1990s. The book *Cradle to Cradle* [32] is well known and translated into at least a dozen languages. However, many planners are not yet familiar with how to integrate into the built environment C2C features such as beneficial materials. There is a tendency when encountering well-known phrases such as "safe materials" and "species diversity," to respond with "yes we do that already." But most buildings and area plans do not incorporate defined-use pathways for materials. Methods are still not well established for designing sites so they contain "defined" materials, or are species-positive.

Various guidelines for C2C in the built environment were integral to published declarations such as the Hannover principles [33] and more recently in The Netherlands, the Almere principles [34].

Those extensive documents are only effective if they can be translated into measurable results. The first step is to understand the overall C2C framework, then study

and implement the three defining Cradle to Cradle® principles encompassed in that framework.

C2C Framework
Cradle to Cradle® can be divided into these categories that together make up the C2C Framework;
(1) Philosophy e.g., a quality-based innovation platform for benefitting the economy, ecology and social equity.
(2) Principles that are translated into measurable criteria.
(3) Application tools.

C2C Principles
Waste = Food. Everything is a Nutrient for Something Else.
Use Current Solar Income. Energy that can be Renewed as it is Used.
Celebrate Diversity. Species, Cultural, and Innovation Diversity.

These principles define and support two types of metabolism for every product and process; biosphere metabolisms for products designed to support biological processes, and technosphere metabolisms for products designed to provide a technical service and whose materials are continuously recycled. See Fig. 2.

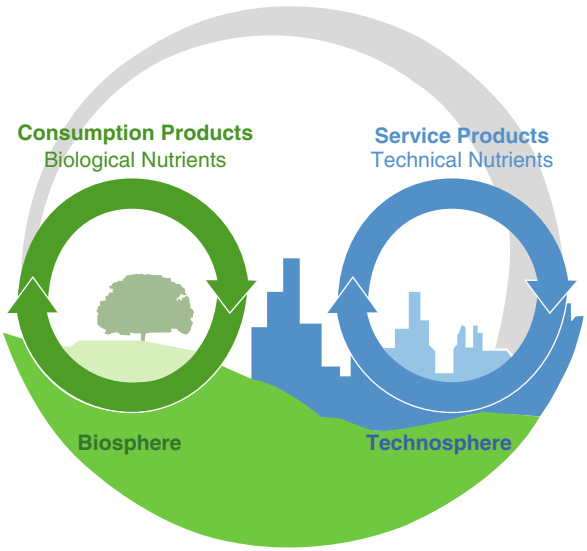

Resource Repletion, Role of Buildings. Figure 2
Cradle to Cradle® metabolisms and product types

Using the C2C principles as a basis, a Cradle to Cradle® building can be defined this way:

A Cradle to Cradle® building contains defined elements that add value and celebrate innovation and enjoyment by measurably enhancing the quality of materials, biodiversity, air, and water, using current solar income, being deconstructable and recyclable, and performing diverse practical and life-enhancing functions for its stakeholders.

The definition also applies to materials and products such as furnishings, cleaning materials, and office equipment that move through buildings because, often, things that move through buildings have equal or greater impacts on the economy, environment, and users than the structures themselves. This "moveables" factor is often underemphasized in various "green" guidelines for buildings, but it is a central feature of the Cradle to Cradle® approach.

Ten Criteria for Applying and Quantifying C2C Principles in Buildings

Broad principles are a prerequisite for eco-effectiveness. However, measurable criteria are also important for practical implementation. The following ten criteria for applying C2C principles have been organized to facilitate implementation.

Through these criteria, materials in buildings can be defined to constitute a new value chain (1) themselves, (2) through the services they provide in a building, such as cleaning air. For example, defined materials often have a greater recovery value than undefined ones due to their enhanced qualities, but it can also result in cleaner air and water flowing through a building. The quality of air, water, biological nutrients, and biodiversity each constitute value streams that make buildings beneficial contributors. Integrating those aspects also enhances the overall value of a building because the whole is often greater than the sum of its parts. For example, a building whose materials clean the air and water reduces the costs of conventional purification systems.

The ten criteria constitute a guide for achieving those value streams.

State Your Intentions Design is the first signal of human intention. To achieve truly eco-effective solution sets, it is important to design so that; every material can be a nutrient for the next design, every element is generated within our solar income, and the design embraces human- and bio-diversity.

Examples of those design intentions: Do you want the building to contribute air and water that are cleaner than when they were taken from the outdoor environment? Do you want the building to be deconstructable? Do you want to demonstrate that the ingredients in building materials are defined and safe?

Define Materials and Their Intended Use Pathways

(a) Use materials whose quality and contents are measurably defined in technical or biological pathways from manufacturing through use and recovery.
(b) Use materials whose impacts are measurably beneficial for human health and the environment.

For example, a defined product would be a chair whose component parts come from known renewable or recycled materials and energy sources, whose composition is known to 100 parts per million, whose materials are safe for contact with human skin and lungs and can be disassembled into materials that each can be recycled for use in other products or decomposed as beneficial nutrients for biological systems. A "beneficial" ingredient would be an ingredient added to coatings that allows them to actively clean the air.

Integrate Biological Nutrients Measurably recycle biological nutrients and water by integrating biomass production into buildings, landscaping, and spatial plans to generate more biomass, soil, and clean water than before development of the site.

For example, biological nutrients from gray water, biodigestion, and interior and exterior landscaping can be recaptured. Air-cleaning vegetative walls can be designed to metabolize pollutants, and "green roofs" can be designed to retain moisture, capture CO_2, metabolize particulates, and provide oxygen. "Topsoil manufacturing" can be integrated into projects to use biodigestion and composting to produce humus and capture CO_2.

Enhance Air and Climate Quality

(a) Measurably make air quality healthier for biological metabolisms than before it enters a building and provide a comfortable climate for occupants.
(b) Measurably contribute to enhancing outdoor climate by contributing air that is healthier for biosphere metabolisms than before it enters a building and using climate change gases as resources through carbon management.

For example, (a) Air quality can be enhanced by integrating C2C materials across products such as exposed window frames, floors, wall materials, HVAC systems, wall and floor coverings, indoor plants and green walls, furnishings, office equipment, and mold inhibitors. (b) Active carbon management is achieved with vegetation and renewable energy. Climate change gases such as methane and CO_2 are resources that can be used to produce biomass, to be further discussed in later sections.

Enhance Water Quality Measurably improve water quality so the water is healthier for biological metabolisms than before it entered the building.

For example, water quality improvement can be achieved by integrating water recycling systems with nutrient recycling, rainfall capture and storage, indoor plants, and green walls.

Integrate Renewable Energy Integrate renewable energy (current solar, wind, and gravitational income) into buildings and area plans so that the building and site generate more energy than they use. Use exergy as a way to guide energy effectiveness.

For example, integrate "threshold" energy efficiency used in high-efficiency LED lighting with direct current from photovoltaic cells, daylight, ventilation, solar heating, and cooling as renewable energy sources.

Actively Support Biodiversity Integrate measurable species diversity so the area supports more diversity than before development.

For example, species diversity applies to plants, animals, and insects and is quantified by counting numbers and varieties supported by a building. The concept of "natural" or "native" species has to be evaluated in each

case because in many regions, the natural environment has been transformed by humans, and returning it to an earlier "natural" state might be impractical.

Support Diversity with Innovation Pursue diversity innovations by focusing on special beneficial features of a building and integrating innovative components that are beneficial for the well-being of occupants and the environment.

For example, diversity gains can be quantified by the variety and prevalence of materials designed as nutrients in a building, the percentage of energy used that is truly renewable, and the amount of beneficial air, water, topsoil, and biodiversity contributed to the outside environment. "Buildings like trees" is a guiding C2C innovative approach. Some innovation can be achieved through biomimicry, e.g., coatings that metabolize pollutants, while others require a level of systems integration that rival the giant sequoia.

Add Value and Enhance Quality for Stakeholders In addition to generating value for the general environment and population, describe what the C2C features of a building do practically for the building owners, operators, and occupants.

For example, cleaner indoor air enhances productivity; recycling water reduces water fees; building integrated photovoltaics can be less expensive than other claddings while providing energy security in regions with irregular power supply; design for disassembly of HVAC systems supports inexpensive replacement during the life of the building; natural lighting cuts energy costs and can enhance human health.

Enhance quality of life for diverse stakeholders Enhance quality of life by designing C2C materials and integrated systems to support sociocultural richness.

For example, innovations can meet C2C principles and make areas safe for children, enhance accessibility, and provide ready access to outdoors and fresh air.

Application Tools for Implementing Beneficial Resource Repletion

Context for C2C Application Tools

C2C principles are primarily qualitative. The criteria related to those principles described earlier are designed to allow quantification of those qualities in buildings.

To implement the criteria and to solve many of the unintended consequences associated with conventional green building criteria, a number of application tools have been developed. These are described more completely in the publication *Cradle to Cradle® Criteria for the Built Environment* [31].

Those application tools are guided closely by C2C principles and criteria. This link distinguishes their use in C2C from how they might be used under conventional sustainability approaches.

For example, C2C approaches CO_2 and energy as *materials opportunities* rather than problems to be "capped and traded" or "captured and stored." Instead of focusing on cap and trade or carbon capture and storage (CCS), C2C application tools would focus on carbon capture and reuse (CCR).

A brief explanation of the C2C approach to energy and CO_2 is an appropriate example, to demonstrate how C2C application tools are applied differently from conventional sustainability approaches;

Cradle to Cradle® (C2C) energy is energy that is generated and applied effectively, using current solar or gravitational income, and material media that are defined as biological or technical nutrients. The definition is qualified and quantified by the following criteria together:

- *Energy sources.* Use current solar or gravitational income, or other defined C2C sources. Primary examples of current solar income use, conversion, and storage include natural light, solar thermal, photovoltaic, photochemical, wave and wind energy, thermal mass storage, and heat exchange. Secondary solar uses include, currently renewable biomass-derived energy from composting, biodigestion, thermolysis, hydrothermolysis, pyrolosis, gasification, and fuel cells. Gravitational income examples, kinetic energy from inertia or weight, e.g., descending waterways. Each of those energy sources is also evaluated under C2C according to the defined use of the material media.
- *Material media.* For generating, converting, and using energy, use materials that contain defined biological or technical nutrients at each stage, converted to energy in the final stage of the material cascade.

- *Energy effectiveness*. Generate and use energy in definably effective ways, using exergy as a way of measuring effectiveness.

From the C2C perspective, carbon dioxide and related gases are a resource. Surprisingly, many methods used to calculate "carbon footprint" of buildings do not include the beneficial use of carbon by, for example, vegetation. Although some carbon footprint methods are beginning to include "counter-footprint" calculations, the concept that buildings themselves could be beneficial users of carbon has not made its way into methodologies.

Primary Application Tools

Because materials and nutrients are the basis for energy generation as well as product manufacturing, the following sections describe three material-related application tools for achieving beneficial resource repletion in buildings including the products and energy devices that are used in buildings:

- Redefining recycling to include defined content and intended use.
- Introducing Nutrient Certificates to quantify the contents and benefits of materials.
- Quantifying and applying economic benefits from those improvements.

Redefining Recycling

The definition of "recycled content" could be improved by including these factors that describe the quality of a product:

Content

What is in the recycled content? For example, are all contents known, especially additives that give materials such as paper, plastic, and metals added functional qualities?

- The material description distinguishes "recycled" from "recyclable" content and "biobased" from "biodegradable" content (see Glossary).
- In the case of recyclable content, the material has infrastructures in place for recovering content.
- For biodegradable content, the material can decompose in available biodegradation facilities. For example, many biodegradable materials do not decompose fast enough in industrial composting facilities and are incinerated. To solve this, the material is defined for industrial composting.

Intended Use

What the material is intended to do and the pathway it is defined for. Intended use is described later in Cradle to Cradle® biosphere and technosphere metabolisms. For example:

- The material is used once then discarded into biological pathways, or is used repeatedly in technological pathways.
- The material can contain toxic materials that perform a function but only if they are safely locked into the material and can be recovered safely for reuse.
- The material performs a beneficial function such as cleaning the air or generating renewable energy.

Material Integrity

- The material can be recycled at a similar level of quality as distinguished from downcycled into lower quality products. If the quality cannot be maintained, e.g., with paper, can the material be downcycled in a controlled "cascade" so its uses are maximized? See *Nutrient Certificates* and *Material Cascades*, as well as Glossary for clarifications on recycling terminology.
- The materials are assembled into the product in such a way that their integrity can be recovered when the product is disassembled.
- If the material is made from recyclable virgin content, then it has a designated pathway for recycling at a similar level of quality.

Distinguishing between Renewable and Recoverable

Sometimes recycling information includes a statement that the material comes from "renewable" resources. However, it is more important whether and how the materials can be recovered and reused as nutrients. This avoids the "renewability" designation being undermined by increasing demand vs. supply of a given material. For example, some natural fibers that only grow in certain regions might be renewable the first year then unsustainable the next when billions of people use them

in their products. Wood is renewable until governments subsidize burning it for energy, at which point, it becomes rapidly unsustainable, as occurred in Europe recently. By contrast, "nonrenewable" elements such as silver and gold can satisfy the requirements of billions of users if they are recovered and recycled effectively.

Introducing Nutrient Certificates

The concept of Nutrient Certificates as a counterpart to emissions, energy, and carbon trading was first proposed by Katja Hansen as part of her investigations as senior researcher at The Cradle to Cradle Chair, Erasmus University and is further defined here.

Definition. Nutrient Certificates are sets of data describing defined characteristics of materials in products that give them value for recovery and reuse. The certificates are a marketplace mechanism to encourage product designs, material recovery systems, and chain of possession partnerships that improve the quality, value, and security of supply for materials so they can be reused in continuous loops or closed loops or beneficially returned to biological systems. This is done by adding a new value dimension to materials quality. This new dimension is based on the suitability of materials for recovery and reuse as resources in other products and processes.

Nutrient Certificates have a focus distinct from, for example, Environmental Product Declarations (EPD) [35], whose main aim is to catalog the environmental impacts of a product. EPDs are often based on Life Cycle Assessment (LCA) and as a result, face the boundary and scoping uncertainties as well as methodological variations inherent to LCA methods since their inception. Factors such as embodied-energy, transport distances, and "consumption" of resources play a primary role in EPDs. By comparison, Nutrient Certificates focus on describing what is in the product, especially its suitability for reuse in continuous loops or cascade chains and materials pooling.

Nutrient Certificates are also distinct from, but related to, recyclability indexes [36]. However, those indexes focus more on volumes and weights instead of detailed contents. For example, factors such as coatings and additives are often not considered in recycling indexes, and interpretations of "thermal recycling" differ from the Cradle to Cradle® interpretation.

Why the Term "Nutrient Certificate"?

The term "Nutrient Certificate" is used here to signify the fundamental importance of materials as nutrients for other processes. Instead of ending as unusable undefined waste and poor or unusable nutrients as many materials end today, materials would be defined for continuous reuse as nutrients for other processes.

In this case, the term "nutrient" extends beyond the conventional definition applied to a biological nutrient and includes for example rare metals that are "nutrients" for electronics products.

The term "resource certificate" or "materials certificate" could just as easily be applied, but those terms do not recognize the role of resources and materials as nutrients for continuous processes.

Who Could Use Nutrient Certificates?

Various users will benefit from Nutrient Certificates, for example:

- Chemical manufacturers who want to gain access to new markets based on the suitability of their products for use in recyclable materials.
- Materials manufacturers.
- Complex products manufacturers.
- Designers who want to add value to the products they are designing.
- Retailers who want to include recyclability and materials recovery in their purchasing criteria for products they buy.
- Governments who want to provide the marketplace with certainty about how to define materials recycled content and recyclability.
- Recyclers who have to know what is in a product and how it comes apart.
- Builders, building owners, and managers aspiring to go beyond the confines of traditional sustainability.

Intended Applications of Nutrient Certificates

Enhance Quality, Value, and Security in the Chain of Possession

- Value Chain Enhancement.
  Nutrient Certificates would enhance and reinforce the value chain among producers, users, and

reprocessors of materials. Those materials used in buildings already have a commercial value when they are sold to contractors and installed in buildings. They also have a residual value as "waste" or used products when they are removed from buildings. Nutrient Certificates provide a mechanism to convert that "waste" into a more defined marketable resource whose residual value is enhanced compared to what it might be today. By so doing, Nutrient Certificates also eliminate the cost of "waste" disposal because there is no waste anymore and instead only resources. For further descriptions of value refer to subsection *Quantifying Economic Value*.

- Authentication.
  Nutrient Certificates when combined with "chain of possession" authentication can protect businesses from industrial counterfeiting, adulteration, and diversion, which cost industry large financial losses annually. In this way, the certificates pay for themselves quickly.
- Security of Supply.
  The continuing supply volatility supply crisis for rare-earth metals suggests that security of supply will be increasingly important to companies. Nutrient Certificates provide a basis for reliable material recovery and pooling in defined pathways that guarantee supplies for manufacturers.
- Transition Mechanism.
  The transformation from low-quality waste to high-quality resources will not occur immediately due to the time frame required for industry to adapt to this new paradigm. Nutrient Certificates can support this transition by identifying materials in a product that can be easily extracted as resources, compared to other portions that might have to be disposed of conventionally. This approach can be described as a "roadmap to improvement" where the percentage of reusable material in a product increases over time. This roadmap can be used along the whole pathway of a material by chemicals manufacturers to improve the recyclability of a virgin material and by manufacturers of complex products to make sure the recycled materials contained in those products are themselves recyclable.
- Value Partnerships.
  A value chain for Nutrient Certificates could be established in a partnership between "waste management" companies, who are already transforming their role into that of "materials managers," and product manufacturers who have a direct relationship with materials suppliers. It is in the financial interests of materials managers to work with product manufacturers to upgrade the recoverability of materials because this improves the value of the materials they reprocess and trade. As well, materials managers have expertise that product manufacturers do not; they know what is required to take apart a product so its contents can be recovered, and they work daily in the materials marketplace with logistics and brokering. It is in the interests of product manufacturers to collaborate with materials managers to redesign products because in this way manufacturers know the chain of possession and in many cases offer greater opportunities to retrieve their materials at a higher level of quality and lower cost through greater ease of disassembly and recovery. Some examples of these are already occurring in the marketplace, for example, with glass, metals, and plastics.

Improve Quality Assurance and Risk Management Standards A quality assurance standard lets companies participate in materials pooling while assuring customers of materials quality. Companies increasingly rely on pools of recycled materials for raw materials, but undefined recycled materials carry inherent risks that limit companies' participation in pooling. In addition, toxic product scandals arising from undefined "virgin" materials have demonstrated that quality assurance is required to manage liability risk. Nutrient Certificates can enhance the quality assurance system by defining conditions for intelligent materials pooling or smart pools. This carefully defined type of materials pooling is known as "intelligent" or "smart," because it is based on information networks that let companies participate in the same way they are beginning to participate in smart energy grids, where multiple input and output points are managed with sophisticated information technologies. Nutrient Certificates could also play a supporting role in other quality assurance systems that require transparency. Cradle to Cradle Certification®, Green building standards, and REACH are examples.

Improve Resource Tracking Between Regions Nutrient Certificates could allow for resources to be tracked as

they move between regions, for example, the tracking of phosphate in animal feed flowing from South America to Europe, or rare metals in computer parts flowing from China to assemblers in Japan to customers in Africa. Tracking could serve as a basis for nutrient banking and trading to measure nutrient surpluses and deficits, incentives to restore topsoil used for agricultural production, and mechanisms to compare carbon storage and reuse with carbon depletion.

Nutrient Certificates could provide a basis for a globalized system for more accurately determining available stocks especially of rare materials. A globalized database of Nutrient Certificates would be one way to achieve this. However, such a database is not a prerequisite for starting with Nutrient Certificates. In worst case scenarios, inability to reach accurate estimates of the global circulation of some materials would not discredit the Nutrient Certificate scheme, because unlike emissions mechanisms these are not issued by governments on the basis of estimates, but instead, are issued based on defined materials. In that context, the main shorter-term benefits of Nutrient Certificates are to improve value and reliability in the chain of possession.

Examples of the Contents of Certificates

Many of the parameters prescribed here for Nutrient Certificates are not new, although some, such as *Preferred Ingredients,* were developed as part of Cradle to Cradle® application tools. The critical value of Nutrient Certificates is to provide a way of quantifying and valuing the nutrients each material or product contains. In the following sections, an emerging list of material attributes important for Nutrient Certificates are discussed to stimulate further development.

Material Composition

- *Recycled and/or recyclable content* and the chain by which the material can support recycling or reuse at a high level of quality. This includes a description of *recoverable content,* i.e., what portions are recoverable in a defined recovery pathway and accompanied by disassembly or recovery instructions. In the case of complex products, the disassembly instructions are the more important feature, whereas in the case of component materials the recovery instructions are most important. For example, depolymerizing and repolymerizing of plastics.
- *Defined ingredients* in the material. Aspects such as:
  - Physical properties
  - Element composition
  - Beneficial and harmful off-gassing, leaching, or wearing
  - Elution
  - Stable components
  - Contaminants
  - Thermal degradation products
  - Aging of products where they are transformed over their use period
- *Preferred Ingredients.* Has the material been assessed to determine if it contains preferred safe ingredients? This is a fundamentally different approach than only declaring hazardous ingredients or being "free of" hazardous ingredients.
- Defined Nutrient Classes
  - *Material Classes.* Products are comprised of various classes of biosphere and technosphere nutrients; from basic elements such as copper and silver, to basic materials such as glass and paper, and to the hundreds of thousands of additives that give those materials their functional qualities. Those classes can be defined as follows, but it is emphasized that these provisional definitions are primarily for the purpose of establishing the basis for further definitions rather than core to the Nutrient Certificate quantification or valuation methods. For example, defining a substance as a "chemical" or "compound" will not alter its intrinsic value for Nutrient Certificates.
  - *Base Elements.* Base elements in the periodic table, e.g., copper.
  - *Chemicals.* Basic chemicals used in the manufacture of more sophisticated compounds and materials.
  - *Complex compounds.* Complex combinations, e.g., glucose, of basic chemicals.
  - *Basic Materials.* A basic material can contain multiple elements and compounds, but in this definition, it is normally limited to commodity materials that are broadly used in manufacturing, e.g., plastic, wood, biomass, glass, and cotton, which form components of more complex products.

- *Additives.* Additives are referred to here as chemicals that are added to basic materials to give them functional qualities, e.g., fire retardants in plastics. This can also be applied in the case of, for example, coatings.
- *Products, Complex Products.* This is often a confusing category because a product for one industry is often a chemical or material for another. For example, the chemical industry produces base chemicals as products that are then used in other more sophisticated materials and products. However, for these purposes here, a "product" is defined as something that contains multiple complex chemicals or materials, e.g., specialty concrete, carpet, and furniture. A "complex product" would be a product containing hundreds or thousands of materials, e.g., a computer or vehicle.
- *Grade of Material.* Many national and international grading systems already exist to establish material grades at national and international levels for substances ranging from steel and plastics to topsoil. Those systems can be incorporated into certificates if they provide added valuable information. Nutrient Certificates do not have to reinvent quality standards if they are already available.
- *Biobased, Biodegradable, or Both.* A description of whether the whole material including additives is biobased, and if the material and additives together can be safely biodegraded according to their defined pathways or are to be kept in technical cycles.

Material Functions

Actively Beneficial Functions If a material actively performs an enhancing function such as metabolizing pollutants as some synthetic coatings and natural plants do, or producing electric current via conversion of photovoltaic or kinetic energy. It is important to include such features in a Nutrient Certificate to determine if recycling can maintain such properties.

Material-Defined Pathways

- *Material Pools.* Description of the type of material pools where the material can be used after it is recovered at end of use, and the defined material pools the materials is sourced from, if any.
- *Preferred Defined Use.* "Defined use" establishes if the use of the material in a technological or biological cycle has been defined, and if a preferred pathway in that cycle has been identified. This includes the *Cascade Function.* See the later description of cascades.
- *Chain of Possession.* If the materials come from identifiable sources such as a pool of recycled materials, and how far back along the chain of possession they can be traced.
- *Roadmap to Improvement.* Description of roadmap to improving the product or material over time, if any.
- *Authentication.* If the declaration is authenticated by an outside auditor.

Proprietary Information Although proprietary formulas are sometimes seen as a barrier to transparency, mechanisms still exist for validation, for example, a statement that an independent agency has verified the formulas, and a source where the ingredient information can be obtained. Also, in the case of broadly used materials such as grades of plastics, glass, and steel, there are few if any proprietary barriers for larger volumes.

Industry Labeling Compared to Retail Labeling Nutrient Certificates described here are designed for use by industry and government rather than as consumer product labeling. In the future, certain aspects might enhance product labeling for retail customers, but this is not the intention of Nutrient Certificates.

Certificate Categories There are two distinct categories for Nutrient Certificates, differentiating the biosphere and technosphere metabolisms of materials:

Biosphere Nutrient Certificates Because topsoil and biomass are among the leading terrestrial surface repositories for carbon and have direct interface with atmospheric carbon in a cycle that is essential for agriculture, livestock, and forestry, Biosphere Nutrient Certificates (BNC) could provide a quantifiable and beneficial basis for tracking and trading carbon and other important nutrients. BNC would be applied in cases where materials are intended to be

returned to the biosphere during or after use. BNC would apply to products derived from agro-industry and forestry sources, or resulting from post-use bio-recovery processes such as biodegradation, biogas generation, topsoil manufacturing, recycled phosphate, and ash recovered from burning of biomass, digestate, or compost.

For example, biosphere Nutrient Certificates could be issued for:

- Food and agro-industry biogenic byproducts
- Digestate from biodigesters
- Manure
- Swill and food from restaurants, households, and other sources
- Fuels
- Paper and paper sludge
- Forestry products
- Biodegradable polymers
- Landscape maintenance clippings
- Ash from biomass incineration
- Sludge from sewage, subject to legislative restrictions
- Phosphate extracted from nutrient streams

Technosphere Nutrient Certificates Technosphere Nutrient Certificates (TNC) provide a quantifiable basis for recovering materials in technical systems, where materials are designed for being used in continuous loops at a similar level of quality.

Technosphere Nutrient Certificates (TNC) could be issued for bulk and commonly used materials such as plastics, steel, aluminum, concrete, and glass, including defined "virgin" as well as "recycled" content, or for more rare materials. For example, TNC could be issued for:

- Base metals, e.g., copper, zinc, silver and rare metals, e.g., gallium
- Defined grades of alloys such as steel
- Defined grades of plastics such as PP, PET
- High quality reusable additives for plastics and metals
- Chemical compounds designed for recovery and reuse

Integrated Nutrient Certificates A complex product containing biosphere and technosphere materials could be accompanied by an integrated certificate describing how biosphere and technosphere components can be separated to become material resources.

Modeling Nutrient Calculations It is not the intention here to describe a detailed model for nutrient calculations. This requires further research into the capacity to quantify each type of nutrient in each type of material. However, as a rule, it is far easier to calculate the actual carbon or nitrogen, phosphorous, potassium, or rare metal content of materials than it is to estimate the "implied" carbon value of many processes, as is the practice with emissions trading today.

Some precedents exist in the C2C methodology for assigning value to nutrients. For example, the textiles company Backhausen in cooperation with Trevira and EPEA has a "Returnity®" certificate [37] that accompanies its products and gives customers a guarantee of 100% recyclability as well as a discount on future purchases if they bring back the product to the manufacturer. The term "Returnity®" embodies the intentions of Nutrient Certificates, returning for eternity.

As well, under C2C certification, a system of "nutrient reutilization scoring" was established as part of a rating system for products [38]. That system, based on an earlier system developed by Braungart et al. and known as the *Intelligent Product System (IPS)* takes into account factors such as Defined Appropriate Cycle, e.g., as technical or biological resources, a documented recovery plan, and "actively closing the loop."

However, the IPS system and C2C certification system are not designed to provide defined information to users and recyclers about features such as material pooling or methods for recovery of nutrients such as phosphate, *in a format that can be attached to materials and tracked along the chain of possession*. Nor are they designed to provide a basis for evaluating the financial recovery value of nutrients in materials.

So, a different type of valuation, authentication, and labeling is required and is further described in the following sections.

Future Directions. Applying and Quantifying Economic Value

Material Cascades In the early sections of this chapter, the unintended economic and nutrient consequences of biomass burning for energy were

described. One way to avoid such misguided approaches is to establish "cascades" of material use and reuse.

Cascades can solve various challenges. (1) With many products such as wood or paper, it is not possible to recycle materials at the same level of quality due to deterioration of components during use and recycling. For example, with paper, fibers are damaged and shortened in each reuse until eventually they become unusable. (2) Biomass for paper takes a long time to grow, so if the paper is only used once, then it is incinerated or composted or downgraded quickly, e.g., toilet paper, then the use period quickly exceeds the growth period required for replacement. (3) Immediate incineration of biomass without using it first in products, or after only one use in a product, releases carbon far more quickly than if the materials is reused in products repeatedly.

In material cascades, the goal is to extend the use of the material for as long as practicable instead of using the product once and then burning or composting it [39]. In a cascade, a material can enter technical loops for multiple uses, then return to biological systems as a nutrient or be incinerated with the ash recovered as a nutrient. Alternatively, if a material such as paper or wood cannot be kept in similar quality technical loops, then its downcycling can be extended in a controlled way by recovering high-quality fibers for use in products for as long as possible (see Fig. 3). This type of controlled downcycling is not to be confused with present downcycling where undefined materials are downcycled with minimal knowledge of their content or pathways.

There are quantifiable economic benefits to material cascades. J. Jokinen calculates that when total employment creation is analyzed, the ratio of reusing wood for pulp and paper industry (PPI) products instead of immediately burning it for energy is 13:1 in favor of the PPI alternative [40].

Due to factors like that, the German Federal Ministry of Food, Agriculture, and Consumer Protection has recommended using products/components within the economic system for as long as possible, from a high level of value stepwise to lower levels [41].

One problem with material cascades is the difficulty of tracing the material as it moves from one use to another. This is especially important to assure that cascades are not misused for downcycling. Nutrient Certificates could be introduced in the cascade process, identifying the cascade supply chain and which stages in the cascade the material has already participated.

Chain of Possession-Tracking Mechanisms It might seem impractical to trace nutrients from bulk materials such as plastics and agro-industry products into more sophisticated complex materials and then into the complex products that may enter a cascade process. However, this form of tracking is already being done to some extent for authenticating mechanisms used to guard against industrial diversion, counterfeiting, and brand abuse [42]. Many companies now offer globalized authentication for a variety of materials ranging from pharmaceuticals to fuel and currencies, with different authentication solutions for different types of materials. Although there is yet no "one size fits all" mechanism to track chain of possession in such a range of materials, the tracking technologies themselves are sufficiently varied and making rapid advances in accuracy as well as affordability to meet this challenge.

Chemical and DNA fingerprinting are advancing quickly as are nano-tagging and electronic micro-tagging, e.g., RFID. These are becoming so sophisticated that they are being used to monitor everything from the origin of oil spills from ships to the origin of uranium in a weapon. Recently, various frameworks have been developed for the management of tagging and tracking systems to support reverse logistics and other chain of possession methods [43]. Large retail chains and manufacturers have sophisticated mechanisms for tracking inventories of component materials used in their products. As well, systems such as Underwriters Laboratory (UL) certifications have been used for years to label and track components in millions of devices. It might be possible to optimize such systems to include Nutrient Certificate-related data.

Building on these systems, a primary implementation path for Nutrient Certificates could be to embed data records in micro-tags that describe "defined-use" standards for recycled and "cascading" raw materials. The data records would complement, not replace, material data safety sheets.

The Potential Role of Buildings for Implementing Nutrient Certificates Nutrient Certificates could be

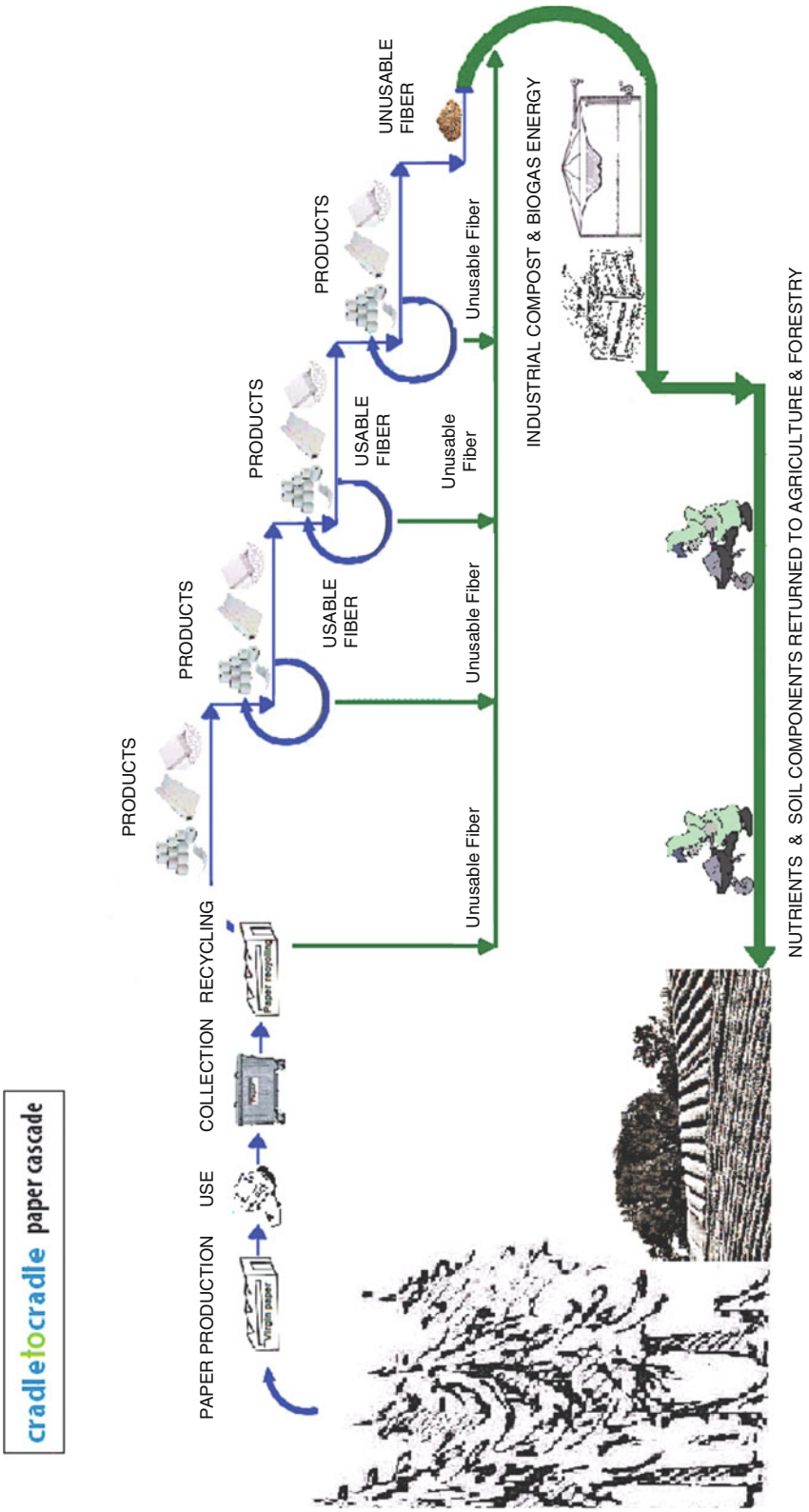

Resource Repletion, Role of Buildings. Figure 3
Diagram of the potential for using paper in a product cascade (Source: Redrawn from an EPEA drawing [39])

effective mechanisms for transforming buildings and products that move through them to a materials repletion value chain.

Buildings are early candidates for the transition to Nutrient Certificates due to:

- *Value*. Nutrient Certificates represent a way of enhancing the value of buildings for their owners and managers. Instead of materials becoming waste that is expensive to get rid of, they become part of the value chain of the building. This can also enhance property lease and resale value.
- *Tracking*. Buildings involve large material flows that are already quantified in terms of volumes, location, and other specifications. Frequently, inventories are kept of materials used to build, maintain, and operate buildings. These would be transition mechanisms for defining Nutrient Certificate parameters.
- *Chain of Possession*. Institutions such as hospitals, educational institutions, government buildings, large corporations, and airports have extended ownership of their buildings and have a vested interest in maintaining value. They also provide continuity of record-keeping.
- *Volumes*. Building structures use large volumes of materials in one place so it is more convenient to inventory those volumes in one location than trace consumer products that are purchased in small quantities and are transient.
- *Local Material Sourcing*. Many high-volume building materials tend to be locally sourced so it is relatively easy to identify the chain of possession and to go back to the supplier to verify what is in the materials.

Time frame for Recovery of Value from Materials in Buildings Although buildings are perceived as largely longer-term repositories for materials, in reality, many materials used in the construction and operation of buildings have a shorter use period. For example, packaging for construction materials, topsoil removed to make way for new buildings and replaced in the form of landscaping, cleaning products, maintenance equipment, floor coverings, and office equipment all have shorter life cycles. Because of this, Nutrient Certificates can offer economic benefits for building owners and operators early into the process, when materials are transformed from their use in a product to resources for reuse. The resource recovery can occur relatively quickly or may require decades as further discussed below.

Early Candidate Products for Nutrient Certificates in Buildings The "low hanging fruit" for Nutrient Certificates consists of business-to-business materials in buildings that involve a chain of possession where the players are relatively well defined. For example, on the technosphere side, heating, ventilation, and air conditioning (HVAC) equipment and other systems that represent close to half the value of many buildings have defined chains of possession for their component materials, from manufacture through to transport, sales, use, and disposal. Their components are well cataloged for maintenance purposes. "Moveable" office equipments such as photocopiers also have defined chains of possession because they are leased as part of service agreements. On the biosphere side, office paper in large institutions offers chain of possession opportunities because it is collected and reprocessed in large volumes. Interior and exterior landscaping is often maintained as part of service agreements, and these provide a mechanism for quantifying the nutrient contribution of plants and soil. The important characteristic of many of those inventory systems is that they already exist, with accounting systems that can be modified to track and quantify materials. In some cases, individual companies already have a form of Nutrient Certificates for materials used in building interiors, such as the previously discussed Backhausen Returnity® certificates. Less well-defined, but still traceable in large institutions, food waste and sewage can be tracked for organic nutrients.

Early Adopters for Nutrient Certificates in Buildings Because regulatory regimes typically lag behind the science, governments might not be leaders at proactively defining materials. However, governments will be important for advancing recovery of materials as nutrients because they are:

- Good at inventorying what is in their buildings
- Long-term players in the property marketplace
- The owners and occupants of substantial numbers of buildings

Hospitals, educational institutions, large corporations, and airports also are potential early adopters because they have extended ownership of their

buildings and a vested interest in maintaining value. One ready-made network of companies exists that is accustomed to the principles and practices underlying a Nutrient Certification system. That is the network of the hundreds of companies working on Cradle to Cradle®-defined products and infrastructures. Nutrient Certificates could be introduced into the supply chain of those companies, involving the thousands of suppliers of those companies as well as millions of customers at the receiving end. In particular, "waste management" companies who are transforming themselves to materials providers are well equipped to implement Nutrient Certificates. For example, in The Netherlands, companies such as Van Gansewinkel Groep have declared their intentions to use C2C application tools in partnerships with customers [45], an important step in bridging the economic intentions of industry with the environmental intentions of customers.

Establishing Bankable and Trading Value Nutrient Certificates do not have to be legislated into existence. Their parameters already provide the marketplace with the motivations, guarantees of content, recyclability, residual value, risk management, and authentication. Governments can accelerate adoption of Nutrient Certificates by specifying them for purchasing, but this is not a prerequisite for their existence.

Nutrient Certificates vs. *Emissions Mechanisms.* One advantage of Nutrient Certificates over emissions trading mechanisms is their connection to traceable materials. When connecting to traceable materials, it is more difficult to distort the marketplace by issuing extra certificates, as occurs with emissions trading. In addition, Nutrient Certificates often quantify what is already given value by the marketplace, so there is no need to match supplies of certificates with, for example, emissions because marketplace mechanisms are already in place to establish value.

Calculating Loss of Value Nutrient Certificates can also be used to calculate *loss of value*. If a material is destroyed, for example through incineration, the certificate is invalidated or modified to reflect the residual value of remaining ash. This procedure is an effective way to measure the true cost of incineration because, presently, the loss of value of millions of tons of materials is not calculated when they are incinerated.

Risk Management Features Nutrient Certificates might on the surface seem to add bureaucracy and costs for the building industry, but in reality, they can do the opposite. By improving the quality of materials, industry can use Nutrient Certificates to:

- Gain added protection from the substantial health liabilities that are arising related to indoor air quality and groundwater pollution. Costs of indoor air pollution to human health have the potential to cripple industries financially.
- Add new value to buildings by enhancing the secondary value of the component materials, which today are often regarded as low value or toxic waste. This "value" can produce benefits only a few years into the operation of a building, when maintenance requirements result in the replacement of damaged and worn out products such as carpeting, lighting, and HVAC components.
- Add new revenue streams from short-term flows of materials through a building. For example, food "waste" from cafeterias and restaurants can be part of materials pooling for industrial composting and biodigestion.
- Add new value to buildings through beneficial functions such as topsoil manufacturing, oxygen manufacturing, CO_2 reuse, energy generation, and recovery of scarce materials.
- More rapidly, amortize the cost of generating electricity by replacing traditional cladding materials with energy-generating materials whose qualities for recycling are defined.
- Cut capital and operating costs through service agreements with companies who lease instead of sell materials and products ranging from office equipment to carpets and power generators.
- Gain emissions credit by defining the greenhouse gas "counter-footprint" of a building more precisely and expanding that counter-footprint to include innovative materials such as cladding materials to generate renewable energy.
- Reducing Risks of Market Distortions. Unlike emissions trading, Nutrient Certificates will make it

more difficult to distort markets. When someone acquires a Nutrient Certificate, they will usually be able to check that the material comes along with it, and vice versa.

DBFMO Risk Management New lifecycle costing financial instruments are conducive to the materials-banking approach. For example, in The Netherlands, government buildings are being financed according to a design-build-finance-maintain-operate (DBFMO) approach where a consortium performs each of those functions and is involved in the building for 15–25 years. This provides an extended planning perspective for designing and recovering materials that move through buildings, and an alternative to the typical DBFMO approach of building-in a financial "cushion" to their bids to guard against future unknown cost overruns. Defined materials and related revenue streams can reduce this uncertainty by providing extra value cushions. For example, if the consortium knows it will not have toxic or other waste management costs and has a lower risk of liability from indoor air pollution, this provides a greater level of certainty. If cladding materials are producing revenues from energy generation, the energy benefits will protect against uncontrolled energy price fluctuations.

In those ways, defined materials provide reliability and predictability in the marketplace.

Conclusions

Innovative quality-based approaches including "defined" materials, cascades, and Nutrient Certificates can be used to overcome unintended consequences of traditional approaches to sustainability such as loss of rare materials due to minimization, undefined recycled content, confusion between biobased and biodegradable, depletion from burning virgin biomass, and distortion of markets due to poorly designed emissions credits schemes. The conservatism of the building industry can be advantageous in applying a quality-based approach due to the industry's emphasis on inventorying and value generation. Buildings can thus transcend the current paradigm of materials depletion to become beneficial materials repletion contributors.

Acknowledgments

Portions of this article regarding criteria for the built environment are excerpted from *Cradle to Cradle® Criteria for the Built Environment*, Mulhall & Braungart, CEO Media 2010, Rotterdam, The Netherlands. Reprinted by permission. http://www.duurzaamgebouwd.nl/bookstore. The authors' appreciation goes to Yael Steinberg and other EPEA scientists for their input.

Bibliography

Primary Literature

1. Coto-Millan P, Mateo-Mantecón I, Domenech Quesada JL, Carballo Panela A, Pesquera MA (2010) Evaluation of port externalities: the ecological footprint of port authorities. In: Coto-Millan P et al (eds) Essays on port economics, contributions to economics. Springer, Berlin/Heidelberg, pp 323–340. doi:10.1007/978-3-7908-2425-4_20, Table 1
2. Chini A (2003) Deconstruction and materials reuse. CIB publication 287. In: Proceedings of the 11th Rinker international conference, Gainesville, 7–10 May 2003
3. Bradsher K (2010) China said to widen its embargo of minerals. *New York Times*, 19 Oct 2010
4. Dempsey J (2010) Decline in rare-earth exports rattles Germany. *New York Times*, 19 Oct 2010
5. European Commission Ad-hoc Working Group on Defining Critical Raw Materials (2010) Critical raw materials for the EU. Report of the Ad-hoc working group on defining critical raw materials, European Commission Enterprise & Industry, Brussels, June 2010
6. Greimel H (2009) Enough lithium for hybrid boom? Most say yes. Automotive News, 21 Sept 2009
7. Pannekoek G, de Bruijne G, Smit B (2010) Phosphorus depletion: the invisible crisis. DPRN Phase II report no. 18
8. Richardson M (2010) China's chokehold on rare-earth minerals. *International Herald Tribune*: 9, 11 Oct 2010
9. Doggett T (2010) U.S. aims to end China's rare earth metals monopoly. Reuters, 30 Sept 2010. http://www.reuters.com/article/idUSTRE68T68T20100930. Accessed 20 Oct 2011
10. Keeley G (2008) Barcelona forced to import emergency water. *The Guardian*, 14 May 2008. http://www.guardian.co.uk/world/2008/may/14/spain.water. Accessed 20 Oct 2010
11. Ahrends A, Burgess ND, Milledge SAH, Bulling MT, Fisher B, Smart JCR, Clarke GP, Mhorok BE, Lewis SL (2010) Predictable waves of sequential forest degradation and biodiversity loss spreading from an African city. Proc Natl Acad Sci USA 107:14556–14561
12. Draft topical outline science and technology of the sustainable built environment. Email from Springer Encyclopedia to Prof. Michael Braungart, 30 Nov 2009

13. Cohen D (2007) Earth's natural wealth: an audit. New Scientist 2605:34–41 (23 May 2007)
14. Bradshaw CJA, Giam X, Sodhi NS (2010) Evaluating the relative environmental impact of countries. PLoS One 5(5):e10440. doi:10.1371/journal.pone.0010440
15. USGBC (2008) LEED 2009 for existing buildings and operations maintenance. United States Green Building Council member approved, Nov 2008
16. DGBC (2010) BREEAM-Nl 2010 label for sustainable real estate, assessor manual new buildings. Dutch Green Building Council Version 2.0, Sept 2010
17. An example of this approach can be seen in USGBC (2008) Innovation in design credit catalog. USGBC, Washington, DC, Mar 2008
18. KPMG (2010) Biomass set to overtake wind as renewable energy champion. In: Powering Ahead: 2010 – an outlook for renewable energy M&A, KPMG survey of global renewable energy mergers & acquisitions, KPMG Cooperative, Switzerland
19. Mantau U, Steierer F, Hetsch S, Prins K (2007) Wood resources availability and demands – implications of renewable energy policies. UNECE, FAO, University of Hamburg, 19 Oct 2007
20. Olsson O (2009) European bioenergy markets: integration and price convergence. Licentiate thesis, Swedish University of Agricultural Sciences, Uppsala
21. United Nations, Economic Commission for Europe (2010) Forest products annual market review 2009–2010. Geneva timber and forest study papers no. 25
22. European Commission (2008) Climate change – can soil make a difference? Report on the conference, Brussels, 12 June 2008
23. Pimentel D, Harvey C, Resosudarmo P, Sinclair K, Kurz D, McNair M, Crist S, Shpritz L, Fitton L, Saffouri R, Blair R (1995) Environmental and economic costs of soil erosion and conservation benefits. Science 267:1117–1123, Estimates of topsoil loss vary but the severity has been well accepted for decades.
24. Brenner J, Paustian K, Bluhm G, Cipra J, Easter M, Elliott T, Kautza T, Killian K, Schuler J, Williams S (2001) Quantifying the change in greenhouse gas emissions due to natural resource conservation practice application in Iowa. The Iowa carbon storage project. Final report to the Iowa conservation partnership, Mar 2001. USDA Natural Resources Conservation Service and Colorado State University, Natural Resource Ecology Laboratory, Fort Collins
25. Kratz S, Schnug E (2006) Rock phosphates and P fertilizers as sources of U contamination in agricultural soils. In: Uranium in the environment. Springer, Berlin/Heidelberg, pp 57–67. doi:10.1007/3-540-28367-6_5
26. Gilbertson T, Reyes O (2009) Carbon trading how it works and why it fails, Critical currents, Dag Hammarskjöld foundation occasional paper series no. 7, Nov 2009
27. Hartesveldt RJ, Harvey HT, Shellhammer HS, Stecker RE (1975) The giant sequoia of the sierra nevada. U.S. Department of the Interior National Park Service, Washington, DC
28. Herva M, Hernando R, Carrasco EF, Roca E (2010) The term "offset" has frequently been applied to emissions or habitat and usually refers to the purchase of offset credits for energy or greenhouse gasses. The term "counter-footprint" to describe some positive impacts of activities is used for example in: Methodological advances in ecological footprinting. In: Bastianoni S (ed) The State of the art in ecological footprint theory and applications, short communications, pp 61–62
29. Cradle to Cradle is a registered wordmark of McDonough Braungart Design Chemistry www.mbdc.com. Accessed 21 Nov 2011
30. www.epea.com. Accessed 20 Oct 2010
31. Mulhall D, Braungart M (2010) Cradle to cradle criteria for the built environment, CEO Media, Rotterdam, Oct 2010
32. McDonough W, Braungart M (2002) Cradle to cradle. Remaking the way we make things. North Point Press, New York
33. McDonough W, Braungart M et al (1992) The hannover principles: design for sustainability. W. McDonough Architects, Charlottesville
34. Duivesteijn A (2008) The Almere principles; for an ecologically, socially and economically sustainable future of Almere 2030, Nieuwe 's-Gravelandseweg 3. Thoth Press, Bussum. ISBN 10; 9068684841
35. Magerholm Fet A, Skaar C, Michelsen O (2009) Product category rules and environmental product declarations as tools to promote sustainable products: experiences from a case study of furniture production. Clean Technol Environ Policy 11(2):201–207. doi:10.1007/s10098-008-0163-6
36. Villalba G, Segarra M, Chimenos JM, Espiell F (2004) Using the recyclability index of materials as a tool for design for disassembly. Ecol Econ 50:195–200
37. Global innovation: RETURNITY® The fabric of many lives. http://www.backhausen.com. Accessed 20 Oct 2010. See also Backhausen Returnity Factsheet and Returnity Info Folder downloadable at same website.
38. Cradle to Cradle® Certification Program, Version 2.1.1, MBDC updated Jan 2010
39. CO2-Speicherung und Wertschöpfung – Holznutzung in einer Kaskade (2009) EPEA Internationale Umweltforschung GmbH, Hamburg, May 2009
40. Jokinen J (2006) Value added and employment in PPI and energy alternative. Study prepared for CEPI by Pöyry Forest Industry Consulting Oy & Foreco Oy, November 2006
41. Bekanntmachung ueber die Förderung der angewandten Forschung auf dem Gebiet der nachwachsenden Rohstoffe im Rahmen des Förderprogramms "Nachwachsende Rohstoffe" der Bundesregierung zum Schwerpunkt "Innovative Mehrfachnutzung von nachwachsenden Rohstoffen, Bioraffinerien" (2008) Bundesministerium fuer Ernährung, Landwirtschaft und Verbraucherschutz, 24 Apr 2008
42. A glossary of industry authentication terms can be found for example at http://www.authentix.com/faqs_terms.asp. Accessed 15 Oct 2010
43. Hans C, Hribernik KA, Thoben K-D (2010) Improving reverse logistics processes using item-level product lifecycle management. Int J Prod Lifecycle Manag 4(4):338–359, 22

44. Brand Stewart (1994) How buildings learn: what happens after they're built. Stewart Brand Viking, New York. This diagram courtesy William McDonough & Partners is a rendition of an earlier published description.
45. Cradle to cradle roadmap, Van Gansewinkel Groep annual report for the year 2009

River Fate and Transport

Zhen-Gang Ji
Minerals Management Service, Herndon, VA, USA

Article Outline

Glossary
Definition of the Subject and Its Importance
Introduction
Fate and Decay
Transport in a River
River Modeling
Future Directions
Bibliography

Glossary

Advection The horizontal transport by flows that move patches of material around but do not significantly distort or dilute them.

Biodegradation The breakdown of a compound by enzyme-mediated transformation primarily due to bacteria, and to a lesser extent, fungi.

Dispersion The mixing of water properties in rivers.

Henry's law A law which states that at a given temperature, the solubility of a gas is proportional to the pressure of the gas directly above the water.

Hydrograph A graph showing time variation in flow rate or stage (depth) of water in a river.

Hydrolysis The reaction of a chemical with water in which splitting of a molecular bond occurs in the chemical and there is formation of a new bond with either the hydrogen component (H^+) or the hydroxyl component (OH^-) of a water molecule.

Manning equation An empirical formulation relating velocity (or flow rate) depth, slope, and a channel roughness coefficient in a river.

Mineralization The process by which a dissolved organic substance is converted to dissolved inorganic form.

Nonpoint SOURCE A pollution source that cannot be traced to a specific spot.

Photolysis The transformation of a compound that results directly from the adsorption of light energy.

Point source A pollution source that comes from a specific identifiable source such as a pipe.

Residence time The time required by a particle to cross a river reach.

River A naturally flowing waterbody.

Volatilization The process representing a chemical substance entering the atmosphere by evaporation from water.

Definition of the Subject and Its Importance

Rivers are naturally flowing waterbodies. Small rivers are also called streams or brooks. Rivers are a watershed's self-formed gutter system and usually empty into an ocean, lake, or another river. This chapter describes the characteristics of rivers and the fate and transport in rivers. The mathematical description of river processes and the modeling of rivers are also described here.

Rivers are complex and dynamic. A river often acts as a sink for contaminants discharged along the river, such as effluents from wastewater treatment plants that discharge nutrients, heavy metals, and/or pathogens into the river. Rivers may also act as sources of contaminants in the watershed, depending on the time of the year or the section of the river. The health of a river is directly linked to the health of the surrounding watershed. The water quality in a river will deteriorate, if the watershed condition deteriorates. Via rivers, pollutants can travel hundreds or even thousands of kilometers and cause environmental problems in a waterbody that is located far away from the sources. The common designated uses of a river include aquatic life support, water supply, and recreation activities (such as swimming, fishing, and boating).

Introduction

The rivers and their tributaries, normally occupying less than a few percent of the total drainage basin, are the conduits of the river basin. They are like a gutter system and transport water, nutrients, sediment, and toxicants downstream (often to an estuary or a large lake).

Compared with lakes and estuaries, the most distinct characteristic of a river is its natural downstream flow. Lakes typically have much smaller flow velocities than rivers. Flow velocities in estuaries, though their magnitudes can be comparable to the ones in rivers, are tidally driven and can be in either direction (downstream or upstream).

The origins of contaminants can be divided into point and nonpoint sources. Point source pollution comes from a specific, identifiable source such as a pipe. Nonpoint source pollution cannot be traced to a specific spot. Point sources include wastewater treatment plants, overflows from combined sanitary and storm sewers, and industry discharges. Nonpoint sources include runoffs from urban, agriculture, and mining areas. Point and nonpoint sources have caused a wide range of water quality problems and the deterioration of the ecological state in rivers. Leading pollutants and stressors in the USA include [1]:

1. Pathogens (bacteria)
2. Siltation
3. Habitat alterations
4. Oxygen-depleting substances
5. Nutrients
6. Thermal modifications
7. Toxic metals
8. Flow alterations

Pathogens are the most common pollutant affecting rivers and streams in the USA. Pathogen pollution is a major public health problem especially in the use of river water for water supply and the consumption of fish and shellfish harvested in rivers and estuaries. Bacteria commonly enter surface waters in inadequately treated sewage, fecal material from wildlife, and runoff from pastures, feedlots, and urban areas.

Sediment siltation is one of the leading environmental problems in rivers. The filling of river channels, harbors, and estuaries by sediments brings a high cost to society. The condition of a river's watershed greatly affects the amount of sediment delivered into the river. The sediment sources vary among rivers, and even within a particular river, from year to year. Extreme events, such as hurricanes, can produce dramatic changes in the amounts and types of sediments that are delivered into a river. The vulnerability of a river to sediments and contamination reflects a complex combination of upstream flows, land use, and land-management practices. The vast majority of river sediments is discharged during only 10% of the year (36 days), and 90% of the year represents a very small amount of the sediment load [2]. Low flow rates usually result in net deposition conditions. High flow rates may cause net erosion in upstream reaches and net deposition in downstream reaches or in the estuary into which the river flows.

Often water quality is defined in terms of concentrations of the various dissolved and suspended substances in the water, for example, temperature, salinity, dissolved oxygen, nutrients, phytoplankton, bacteria, heavy metals, etc. The distribution of these substances can be calculated by a mathematical model. Based on the principle of conservation of mass, the concentration change can be represented simply in a one-dimensional form [3]:

$$\frac{\partial C}{\partial t} = -U\frac{\partial C}{\partial x} + \frac{\partial}{\partial x}\left(D\frac{\partial C}{\partial x}\right) + S + R + Q \qquad (1)$$

where C = substance concentration
t = time
x = distance
U = advection velocity in x direction
D = mixing and dispersion coefficient
S = sources and sinks due to settling and resuspension
R = reactivity of chemical and biological processes
Q = external loadings to the aquatic system from point and nonpoint sources

The changes of concentration C in Eq. 1 are determined by the following:

1. The hydrodynamic processes control the water depth (D), the advection (represented by the U term), and mixing (represented by the D term).
2. The size and properties of sediment (or particular organic matter) affect the settling and resuspension (represented by the S term).
3. The chemical and biological reactions of pathogens, toxics, and/or nutrients are represented by the R term.
4. External loadings from point and nonpoint sources are included by the Q term.

Fate and Decay

Contaminants in rivers include nutrients, organic toxicants, heavy metals, and pathogens. If no degradation reactions occurred in Nature, every single contaminant

discharged in the past would still be polluting the environment. Fortunately, natural purification processes dilute, transport, remove, and degrade contaminants. It is essential to understand the kinetics of reactants and to describe them mathematically. This section summarizes the fate and decay of contaminants and their mathematical formulations.

The fate and transport of contaminants are controlled by two factors: their reactivity and their hydrodynamic transport. Reactivity includes:

1. Chemical processes
2. Biological processes
3. Bio-uptakes

Transport in a river, which will be discussed in the next section, includes three mass transport processes:

1. Advection of water current
2. Diffusion and turbulent mixing within the water column
3. Deposition and resuspension on the water-sediment bed interface

Mathematical Formulations

How long contaminants remain in a waterbody depends on the nature of the compound. Most chemicals undergo chemical or biological decay. Some chemicals are conservative and do not undergo these types of reactions, even though it is very difficult to find a truly conservative chemical in Nature. The fate and decay of a contaminant represent the gradual decrease in the amount of a substance in a river, as the result of various sink processes, including chemical and biological transformation, or dissipation/deposition to other environmental systems.

Although reaction kinetics in aquatic systems can be described in numerous ways, the form for a single reactant is generally expressed as:

$$\frac{dC}{dt} = R = -kC^m \tag{2}$$

where m = the order of reaction

k = rate constant of the m-order reaction

In natural waters, the commonly used forms of Eq. 2 are with m = 0, 1, and 2.

Zero-order reactions: A zero-order reaction (m = 0) represents irreversible degradation of a reactant that is independent of the reactant concentration. The solution to Eq. 2 is:

$$C = C_0 - kt \tag{3}$$

where C_0 = the initial concentration at t = 0. In this case, a plot of concentration versus time should yield a straight line with a slope of k, as shown in the left panel of Fig. 1. Zero-order reactions have their reaction rates determined by some factor other than the concentration of the reacting materials.

First-order reactions: First-order reactions (m = 1) have their reaction rates proportional to the concentration of the reactant and are most commonly used in describing chemical and biological reactions. For first-order reactions, the solution to Eq. 2 is:

$$C = C_0 e^{-kt} \tag{4}$$

Equation 4 indicates that for first-order reactions, reactant concentration decreases exponentially with

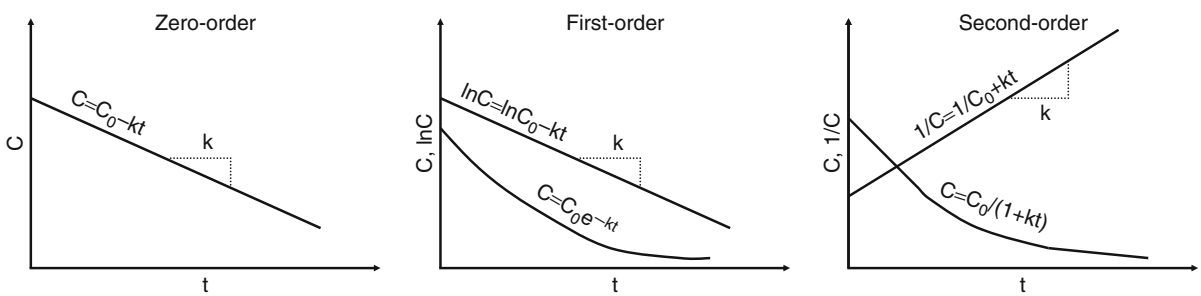

River Fate and Transport. Figure 1
Left panel: concentration versus time for zero-order reaction. *Middle panel*: concentration and logarithm concentration versus time for first-order reaction. *Right panel*: concentration and inverse concentration versus time for second-order reaction

time. In this case, a plot of logarithm concentration versus time should yield a straight line with a slope of k, as shown in the middle panel of Fig. 1. Most of the reactions found in the environment can be conveniently expressed by a first-order approximation without much error. Examples of first-order reactions include biochemical oxygen demand in surface waters, death and respiration rates for bacteria, and production reaction of algae.

Second-order reactions: For second-order reactions (m = 2), the solution to Eq. 2 is:

$$\frac{1}{C} = \frac{1}{C_0} + kt \tag{5}$$

Therefore, if a reaction is indeed second-order, a plot of inverse concentration of C (1/C) with time should yield a straight line with a slope of k (the right panel of Fig. 1). Equation 5 can also be expressed as

$$C = \frac{C_0}{1 + kC_0t} \tag{6}$$

which reveals that, similar to the first-order reaction, the resulting concentration of a second-order reaction also decreases and approaches zero as time increases.

Processes Affecting Fate and Decay

The fate and decay of contaminants can result from physical, chemical, and/or biological reactions. In addition to sorption and desorption, processes that can significantly affect the fate and decay processes include:

1. Mineralization and decomposition
2. Hydrolysis
3. Photolysis
4. Biodegradation
5. Bioconcentration
6. Volatilization

Most decay processes are expressed as first-order reactions. The first-order decay coefficients for individual processes are additive and can be linearly superimposed to form a net decay coefficient:

$$k_d = k_m + k_h + k_p + k_{bd} + k_{bc} + k_v \tag{7}$$

where k_d = net decay coefficient
k_m = mineralization coefficient
k_h = hydrolysis coefficient
k_p = photolysis coefficient
k_{bd} = biodegradation coefficient
k_{bc} = bioconcentration coefficient
k_v = volatilization coefficient

In modeling studies, either the net degradation coefficient or the individual coefficients can be specified.

Mineralization and Decomposition Mineralization is the process by which a dissolved organic substance is converted to dissolved inorganic form. Mineralization makes nutrients, such as nitrogen and phosphorus, available for a fresh cycle of plant growth. Bacteria decompose organic material to obtain energy for growth. Plant residue is broken down into glucose that is then converted to energy:

$$C_6H_{12}O_6 + O_2 \xrightarrow{\textit{energy released}} CO_2 + H_2O \tag{8}$$

In water quality models, the term "mineralization" often represents the process by which dissolved organic matter is converted to dissolved inorganic form, and thus includes both heterotrophic respiration of dissolved organic carbon and mineralization of dissolved organic phosphorus and nitrogen.

Hydrolysis Hydrolysis is the reaction of a chemical with water, in which splitting of a molecular bond occurs in the chemical and there is formation of a new bond with either the hydrogen component (H^+) or the hydroxyl component (OH^-) of a water molecule. This involves ionization of the water as well as splitting of the compound hydrolyzed:

$$RX + H_2O \rightarrow ROH + HX \tag{9}$$

Essentially, water enters a polar location on a molecule and inserts itself, with an H^+ component going to one part of the parent molecule and an OH^- component going to the other. The two components then separate. The concentration of hydrogen and hydroxide ions, and therefore pH, is often an important factor in assessing the rate of a hydrolysis reaction. Hydrolysis is a major pathway for the degradation of many toxic organics.

Photolysis Photolysis is the transformation of a compound that results directly from the adsorption of light energy. Compounds that absorb sunlight may gain sufficient energy to initiate a chemical reaction. Some of these photochemical reactions result in the decomposition or transformation of a substance.

The energy of light varies inversely with its wavelength. Longwave light lacks sufficient energy to break chemical bonds. Short wave light (x-rays and gamma rays) is very destructive. Fortunately for life on earth, this type of radiation largely is removed by the upper atmosphere. Light near the visible spectrum reaches the earth's surface and can break the bonds of many organic compounds, which can be important in the decay of organic chemicals in a water system.

The basic characteristics of photolysis are:

1. Photolysis has two types of energy absorption: direct photolysis and indirect photolysis. The direct photolysis is the result of direct absorption of sunlight by the toxic chemical molecule. Indirect photolysis is the result of energy transfer to the toxic chemical from some other molecule that has absorbed the sunlight.
2. Photolysis is the destruction of a compound activated by the light energy and is an irreversible decay process.
3. Products of photolysis may remain toxic and the photolysis process does not necessarily lead to detoxification of the system.
4. The photolysis coefficient in Eq. 7 is usually a function of the quantity and wavelength distribution of incident light, the light adsorption characteristics of the compound, and the efficiency at which absorbed light produces a chemical reaction.

Biodegradation Biodegradation is the breakdown of a compound by enzyme-mediated transformation, primarily due to bacteria, and to a lesser extent, fungi. Although these types of microbial transformations can detoxify and mineralize toxics, they can also activate potential toxics. The rate of biodegradation can be very rapid, which means that biodegradation is often one of the most important transformation processes in rivers.

Even though the biodegradation process is largely mediated by bacteria, the growth kinetics of the bacteria is complicated and is not well understood. As a result, toxic models often assume constant decay rates rather than modeling the bacteria activity directly. The first-order decay rate is commonly used. Biodegradation rate is influenced by water temperature and can be represented by an Arrhenius function:

$$k_b = k_{b20}\theta^{(T-20)} \tag{10}$$

where k_b = biodegradation rate
k_{b20} = biodegradation rate at 20°C
T = water temperature in °C
θ = temperature correction factor

The effect of the Arrhenius function is that a higher temperature will cause a faster chemical reaction rate. It gives a quantitative relationship between the reaction rate and its temperature.

Biodegradation rate is also related to the contaminant concentration and can be expressed by a typical Michaelis–Menten formulation:

$$k_b = k_{bmax}\frac{c}{c + c_{1/2}} \tag{11}$$

where k_{bmax} = the maximum biodegradation rate
c = the contaminant concentration
$c_{1/2}$ = half saturation (Michaelis) constant.

The combination of the above two formulations yields

$$k_b = k_{max}\theta^{(T-20)}\frac{c}{c + c_{1/2}} \tag{12}$$

where k_{max} = maximum decay rate due to biodegradation. Equation 12 combines the effects of contaminant concentration and water temperature on the biodegradation process.

Volatilization Volatilization represents a chemical substance entering the atmosphere by evaporation from water. Volatilization is often treated as an irreversible decay process, because of its mathematical similarities to these decay processes. However, volatilization is actually a reversible transfer, in which the dissolved concentration in water attempts to equilibrate with the gas phase concentration in the overlying atmosphere. Equilibrium occurs when the partial pressure exerted by the chemical in water equals the partial pressure of the chemical in the atmosphere.

Henry's law states that, at a given temperature, the solubility of a gas is proportional to the pressure of the gas directly above the water. Volatilization is often

treated similarly to surface oxygen exchange, where the volatilization flux is proportional to the difference between the chemical concentration in water and the saturation concentration, as:

$$F_v = k_v(c_w - c_{ws}) \tag{13}$$

where F_v = volatilization flux
k_v = transfer rate
c_w = dissolved concentration of the chemical in water
c_{ws} = saturation dissolved concentration of the chemical in water

Equation 13 indicates that the chemical enters the water when the chemical in the water is unsaturated ($c_w < c_{ws}$) and the chemical leaves (volatizes from) the water when the chemical in the water is oversaturated ($c_w > c_{ws}$). The saturation dissolved concentration is dependent upon the atmospheric partial pressure and Henry's law constant for the chemical. The transfer rate, k_v, depends on the properties of the chemical as well as the characteristics of the waterbody and the atmosphere, including the molecular diffusion coefficient of the chemical in the water and in the atmosphere, the temperature, the wind speed, the current velocity, and the water depth.

Transport in a River

Rivers have distinct hydrodynamic characteristics that are different from those of lakes or estuaries. This section focuses on the following:

1. River flow and the Manning equation
2. Advection and dispersion processes in rivers

River Flow and the Manning Equation

The flow rate of a river is the volume of water that passes a cross section of the river in a unit of time, which is usually expressed in cubic meters per second (cms) or cubic feet per second (cfs) and is calculated as:

$$Q = A\,V \tag{14}$$

where Q = Flow rate in cms or cfs
A = Area through which the water is flowing in m^2 or ft^2
V = Average velocity in the downstream direction in m/s or ft/s

The river flow can generally be separated into two components:

1. Base flow
2. Storm flow

Base flow is composed largely of groundwater effluent and sustains river flow during dry weather periods. Storm flow is from the runoff during or shortly after a precipitation event. The water from base flow is the precipitation that percolates into the ground and flows slowly through a long path before reaching the river, whereas the water from storm flow is the precipitation that reaches the river shortly after precipitation through runoff. In addition to base flow from the groundwater and the storm flow from the runoff, point sources, such as wastewater treatment plant discharges and tributaries to the river, also contribute to a river flow.

A hydrograph is a graph showing time variation in flow rate or stage (depth) of water in a river. As sketched in Fig. 2, the river flow is composed of the storm flow and the base flow. After the beginning of a rainfall, the storm flow from runoff starts to increase and reaches its peak some time after the peak rainfall. There is a time lag between the two peaks. The rising limb is the portion of the hydrograph to the left of the peak of the storm flow, which shows how long the river takes to reach its peak flow rate after a rainfall event. The receding limb is the portion of the hydrograph to the right of the peak, which shows how long the river takes to return to the base flow.

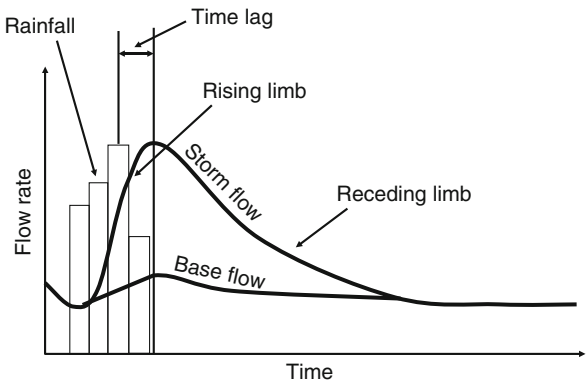

River Fate and Transport. Figure 2
A storm hydrograph of a river

In addition to flood events, low flow conditions are also important characteristics of a river. When there is no precipitation contributing to the storm flow, and the base flow from groundwater is low, the river experiences low flow conditions. Low flow results in less water available for dilution of pollutants from point sources, causing high pollutant concentrations in the river. Therefore, point source discharges during low flow conditions have the most significant impact on the river's water quality, since the discharge may constitute a larger percentage of river flow. For instance, wastewater discharges to the Blackstone River can account for up to 80% of the total river flow in summer [4].

A hydrodynamic model based on momentum and continuity equations is often used to calculate flow velocity, flow rate, and water depth in a waterbody. A simpler approach to calculate these parameters is to use the Manning equation, which is an empirical formulation relating velocity (or flow rate), depth, slope, and a channel roughness coefficient in a river. The Manning equation was derived by curve-fitting data measured in rivers and channels. The equation is:

$$V = \frac{Q}{A} = \frac{R^{\frac{2}{3}} S^{\frac{1}{2}}}{n} \tag{15}$$

where V = mean flow velocity in m/s
Q = flow rate in m^3/s
A = cross-sectional area in m^2
R = hydraulic radius in m
S = slope of the channel bed in m/m
n = Manning roughness coefficient
The hydraulic radius is defined as:

$$R = \frac{A}{P} \tag{16}$$

where P is the wetted perimeter in m, which is the length of contact of the water with the channel in m, measured in a direction normal to the flow. The Manning roughness coefficient, n, represents the channel roughness that contributes to the dissipation of flow energy. Table 1 shows a range of n values for various channels and rivers.

Originally developed in the 1880s, the Manning equation is still widely used in hydraulic calculations with reasonable accuracy today. In hydrodynamic modeling, the Manning equation may serve the purpose of giving a quick estimation of flow conditions in a river. However, the Manning equation is an empirical formulation that may not reflect actual conditions of a river.

River Fate and Transport. Table 1 Values of the Manning roughness coefficient, n, for various channels and rivers [5]

Type of channel	Manning roughness coefficient (n)
Smooth concrete	0.012
Ordinary concrete lining	0.013
Earth channels in best condition	0.017
Straight unlined earth canals in good condition	0.020
Natural rivers and canals	0.020–0.035
Mountain streams with rocky beds and rivers with variable sections and some vegetation along banks	0.040–0.050
Alluvial channels without vegetation	0.011–0.035

Advection and Dispersion in Rivers

Advection refers to horizontal transport by flows that move patches of material around but do not significantly distort or dilute them. In rivers, advection often represents the primary transport process of pollutant in the longitudinal direction. Dispersion is the mixing of water properties. In rivers, a prominent feature is the longitudinal dispersion: the transport and spreading of pollutants downstream from a point source. When a tracer is released into a river, two distinct processes control the tracer transport:

1. Flow advection carries the tracer away from the releasing point.
2. Turbulence dispersion spreads out and dilutes the tracer concentration.

Mathematically, the above two processes are represented by the first and second terms on the right-hand side of Eq. 1, respectively. Advection results in the pollutant's moving downstream, while longitudinal mixing leads to spreading or smearing in the longitudinal dimension. Lateral and vertical mixing processes

determine how long it takes for a pollutant to be completely mixed across a river. The dominant transport process in rivers is the advection due to river flow. Flow velocity controls a river's residence time, the time required by a particle to cross a river reach. The dispersion process in rivers is often less important in the transport of pollutants. The effect of dispersion may be ignored in analyzing a continuous pollutant load to a river. Figure 3 is a velocity vertical profile in a channel. In small rivers, however, the turbulence generated by bed friction is strong, and the depth is generally small, resulting in rivers that are often well mixed vertically.

To illustrate the longitudinal dispersion in a river, an idealized dye release experiment is shown in Fig. 4, in which Panel A gives the plain view of the dye transport in the river and Panel B presents the lateral-averaged dye concentration along the river. In the river, a line source of constant concentration is instantaneously released at time t = 0, and the longitudinal velocity has parabolic variation across the river. As shown in Panel A, the advection process transports the dye downstream, and the dispersion process spreads the dye and reduces the maximum concentration. Dye travels downstream faster in the middle of the river than near the banks. As a result, the line source released at t = 0 becomes approximately a parabolic shape at $t = t_1$ and $t = t_2$. The concentration profiles at t_1 and t_2 in Panel A also reflect the random fluctuations of turbulence activities in the river. Because of variations in flow velocity across the river, dye spreads both along and across the river by dispersion. The laterally averaged dye concentration in Panel B also indicates that the velocity shear and turbulent dispersion contribute to the concentration spreading along the river.

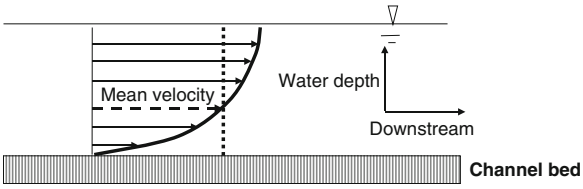

River Fate and Transport. Figure 3
Velocity vertical profile in a channel

Impacts of River Flow on Water Quality

Water quality processes can be highly dependent on river flow conditions. The time that a pollutant remains

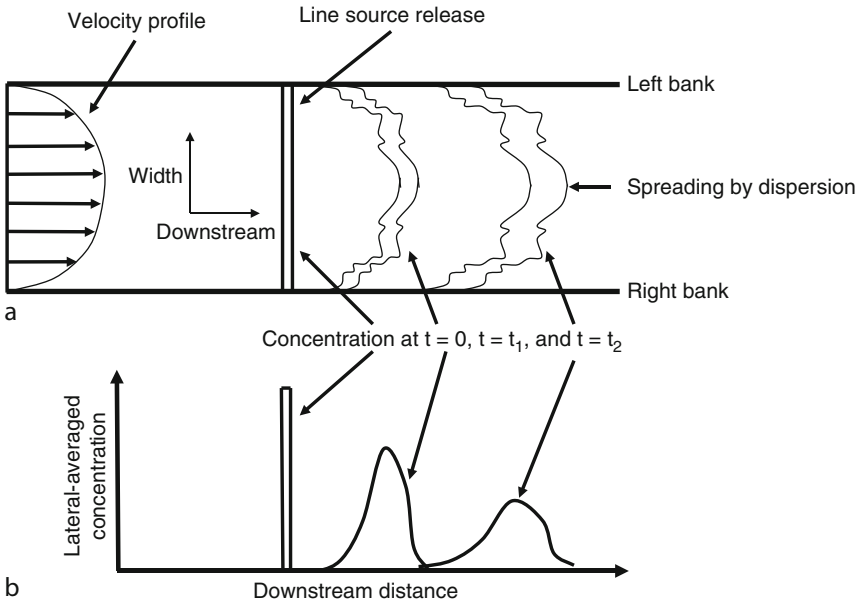

River Fate and Transport. Figure 4
Advection and dispersion processes in a river. *Panel A* gives the plain view of dye transport in the river. *Panel B* presents the lateral-averaged dye concentration along the river

within a section of a river is called residence time. The flow velocity and the length of the river section determine the residence time. River flow affects water quality in a river in several ways:

1. *Dilution.* A large volume of flow dilutes concentrations of pollutants that are discharged into the river.
2. *Residence time.* High flow velocity reduces the residence time and affects the amount of material that can be produced or degraded in the river section.
3. *Mixing.* High flow velocity increases mixing in the river, enhances the assimilative capability of the river, and reduces pollutant concentration gradients.
4. *Erosion.* High flow can erode bed material and destabilize the benthic environment.

The impact of pollutant loadings to a river is largely determined by the magnitudes of the loadings and the flow rate. Rapid transport of pollutants by high flow results in a short residence time and often causes minimal water quality problems. Conversely, slow transport of pollutants by low flow results in a long residence time and can lead to water quality problems, such as oxygen depletion and eutrophication. Channel alteration and watershed disturbance can lead to abnormally high flow rates for a given amount of rain and amplify the impact of floods. Watershed disturbance can also increase sedimentation and harm aquatic biota in a river.

In temperate regions, seasonally high flow typically occurs during the periods of snowmelt in early spring and spring rains, whereas seasonally low flow normally occurs in summer and early fall. The river flow affects the concentration and distribution of water quality variables. Generally, point sources have a larger impact on a river during low flow (dry weather) conditions due to less water diluting the pollutants. Low DO concentrations and high algal growth in a river often occur during low flow periods and hot weather conditions. The combination of low flow, minimum dilution, and high temperature often makes summer and early fall the critical periods for evaluating the impact of point sources (such as wastewater treatment plants).

In contrast, nonpoint sources can bring large amounts of pollutants from the watershed into a river during high flow (wet weather) conditions. It is important to examine both point and nonpoint sources in both high and low flow conditions. Point sources of nutrients often cause algal blooms in rivers during low flow conditions, while nonpoint sources may increase nutrient concentrations and turbidity following periods of wet weather events. Municipal discharges, agriculture runoff, and urban runoff are among the most common sources of impairment to rivers.

In the study of the Blackstone River, for example, Ji et al. [2] reported that a discharge from a wastewater treatment plant was the dominant point source of contaminants and had significant impact on the sediment contamination in the river. However, this point source alone is still insufficient to account for the total metal concentrations in the river. Nonpoint sources and the processes of sediment deposition and resuspension are also important factors that control the concentrations of sediment and toxic metals.

Dissolved oxygen is essential to river ecosystems. Processes controlling DO spatial distribution in a river include:

1. Oxidation of the biochemical oxygen demand (BOD): BOD is used to represent all sinks of dissolved oxygen, such as the oxidation of carbonaceous and nitrogenous organic matter, the benthic oxygen demand, and the oxygen utilized by algal respiration.
2. Reaeration of DO from the atmosphere: In addition to atmospheric reaeration, DO produced by photosynthesis and DO contained in incoming flows are also major oxygen sources.
3. Transport due to the river flow: Advection and diffusion processes enhance DO mixing and reaeration within a river.

The pioneering work by Streeter and Phelps [6], who developed the first water quality model to describe the oxygen depletion in the Ohio River, is useful for understanding DO processes in a river. It can be described in a first-order reaction equation:

$$U\frac{dC}{dx} = -k_d B + k_a(C_s - C) \tag{17}$$

where x = distance
U = advection velocity in x direction
C = DO concentration

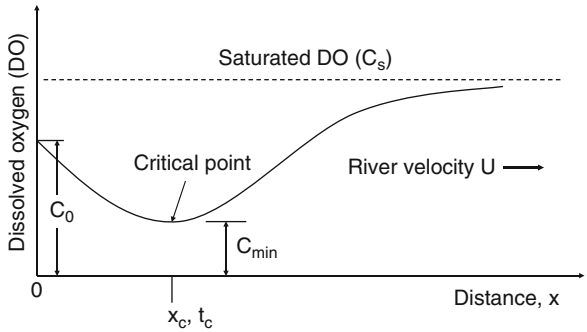

River Fate and Transport. Figure 5
DO sag curve in a river

B = BOD concentration
C_s = saturated dissolved oxygen concentration
k_d = deoxygenation rate constant of BOD
k_a = first-order reaeration rate constant of DO

By assuming that BOD has a first-order degradation reaction with a decay rate constant of k_r, the solution to Eq. 17 is the famous Streeter-Phelps equation:

$$C = C_s - \frac{k_d L_0}{k_a - k_r}\left(e^{-k_r x/U} - e^{-k_a x/U}\right) - (C_s - C_0)e^{-k_a x/U} \tag{18}$$

A schematic representation of the Streeter-Phelps equation is shown in Fig. 5, describing a DO sag curve in a river. The DO sag curve gives DO longitudinal variation as the result of oxygen depletion and recovery, after a BOD load is discharged into a receiving river. Between the discharge point ($x = 0$) and the critical distance ($x = x_c$), oxidation exceeds reaeration (i.e., $k_d B > k_a(C_s - C)$ in Eq. 17) because of high BOD concentrations and a small DO deficit ($= C_s - C$). Oxygen in the river is consumed faster than it is resupplied. The DO concentration decreases to a minimum C_{min} at a critical distance x_c (or critical time $t_c = x_c/U$). This position is the critical location where the lowest DO concentration occurs, and the oxidation rate and reaeration rate are equal. After passing the critical location, reaeration exceeds oxidation (i.e., $k_d B < k_a(C_s - C)$ in Eq. 17) because of a low BOD concentration and a high DO deficit. Thus, oxygen in a river increases gradually. Further downstream, the rate of supply exceeds the utilization rate, resulting in a full recovery of the DO concentration.

River Modeling

The two primary reasons to conduct river modeling are:

1. To better understand physical, chemical, and biological processes
2. To develop models capable of realistically representing rivers, so that the models can be used to support water quality management and decision making

Water quality management needs to understand key processes affecting environmental problems in order to evaluate management alternatives. Examples of such environmental problems are:

1. Thermal pollution due to power plant discharges
2. Sedimentation in harbors causing siltation and high dredging costs
3. Eutrophication due to excessive nutrient loadings
4. Low dissolved oxygen conditions caused by wastewater discharges
5. Accumulation of toxic materials in the sediment bed

Models play a critical role in advancing the state-of-the-art of hydrodynamics, sediment transport, and water quality, and of water resources management. Because of their requirements for precise and accurate data, models also ultimately contribute to the design of field data collection and serve to identify data gaps in characterizing waterbodies. Models are used to analyze the impact of different management alternatives and to select the ones that result in the least adverse impact to the environment.

Models are often used to improve the scientific basis for theory development, to make and test predictions, and to clarify cause-and-effect relationships between pollutant loadings and the receiving waterbody. Models are often used to evaluate and test potentially expensive water quality management alternatives prior to their implementation. The cost of a hydrodynamic and water quality modeling study is usually a small fraction of the implementation cost. Models can simulate changes in an ecosystem due to changes in internal and/or external conditions, such as water elevation variations or increased external pollutants. These simulations predict positive or negative changes within the river ecosystem due to the management actions, such as improved sewage treatment or reduced agricultural runoff. These simulations are obviously far more

cost-effective than testing expensive management actions on a trial-and-error basis, thus making models a useful tool for water quality management.

In the past decades, hydrodynamic and water quality models have evolved from simplified one-dimensional, steady-state models, such as the legendary QUAL2E model [7], to complex three-dimensional, time-dependant models of hydrodynamics, sediment, toxics, and eutrophication. Three-dimensional modeling has matured from a research subject to a practical engineering tool. Over this same period, computational requirements for realistic three-dimensional modeling have changed from supercomputers, to high-end workstations, and then to personal computers.

These advanced three-dimensional and time-dependant models, which can also be readily applied for one- and two-dimensional problem settings, provide a powerful computational tool for sediment transport, water quality, eutrophication, and toxic chemical fate and transport modeling studies. These advanced models often include several coupled submodels for different physical, chemical, biological processes in surface waters, such as:

1. Hydrodynamic model
2. Wind wave model
3. Sediment model
4. Toxic model
5. Eutrophication model
6. Sediment diagenesis model
7. Submerged aquatic vegetation (SAV) model

As an example, Fig. 6 illustrates the major components of the Environmental Fluid Dynamics Code (EFDC) model [8]. In addition to computational modules, these advanced models tend to evolve into complex software systems, comprising many tools and sources of information. They may contain components for grid generation, data analysis, preprocessing, postprocessing, statistical analysis, graphics, and other utilities.

Transport in rivers is often dominated by the processes of advection and dispersion. One-, two-, and three-dimensional models have been developed to describe these processes. Study objectives, river characteristics, and data availability are key factors determining model applicability. In river studies, 1D and steady-state models are commonly used, such as the QUAL2E model [7]. If a river is wide enough to have significant lateral variations or deep enough to develop vertical stratifications, 2D (and even 3D) models may be needed to simulate sediment and toxicant transport in the river. For instance, sediment transport within a meandering river is very complex. The velocities are faster at the outer bank and slower at the inner bank. The lateral velocity difference directly influences the sediment transport. There might be erosion occurring along the outer bank and deposition occurring on the inner bank. Using a 1D model to represent the river is equivalent to treating sediment transport as being uniform across the river, eliminating the effect of river meandering on sediment transport and vertical stratifications. A 1D model represents the entire cross section of the river as being either net depositional or net erosional.

One-dimensional models, such as the widely used QUAL2E model [7], are traditionally applied to river modeling. For most small and shallow rivers, these 1D models are often adequate to simulate hydrodynamic and water quality processes. In 1D models, water surface elevation, velocity, and discharge vary only in the longitudinal (along-the-river) direction and are constants in the lateral (across-the-river) direction. This approach provides a simplified mathematical description of river flows.

Rivers with a steep bottom slope often have a relatively high velocity and a shallow water depth, and are characterized by gravel, cobbles, and rocks in the riverbed. Coarse sands and finer particles are washed out by the high velocity. The dominant gradient of water quality constituents is along the river in the direction of flow. A 1D laterally and verticallyaveraged model is thus appropriate for describing water flow and the transport of sediment and toxic chemicals. Rivers with a moderate bottom slope result in a low-velocity waterway, often characterized by a sediment bed consisting of a mixture of fine-grained cohesive particles and fine sands. The dominant gradient of water quality constituents in this kind of river is in the direction of the flow and a 1D model may still be adequate. One-dimensional models are limited in their ability to capture the complexity of natural rivers. The assumption that the characteristics of the river are uniform both vertically and laterally may

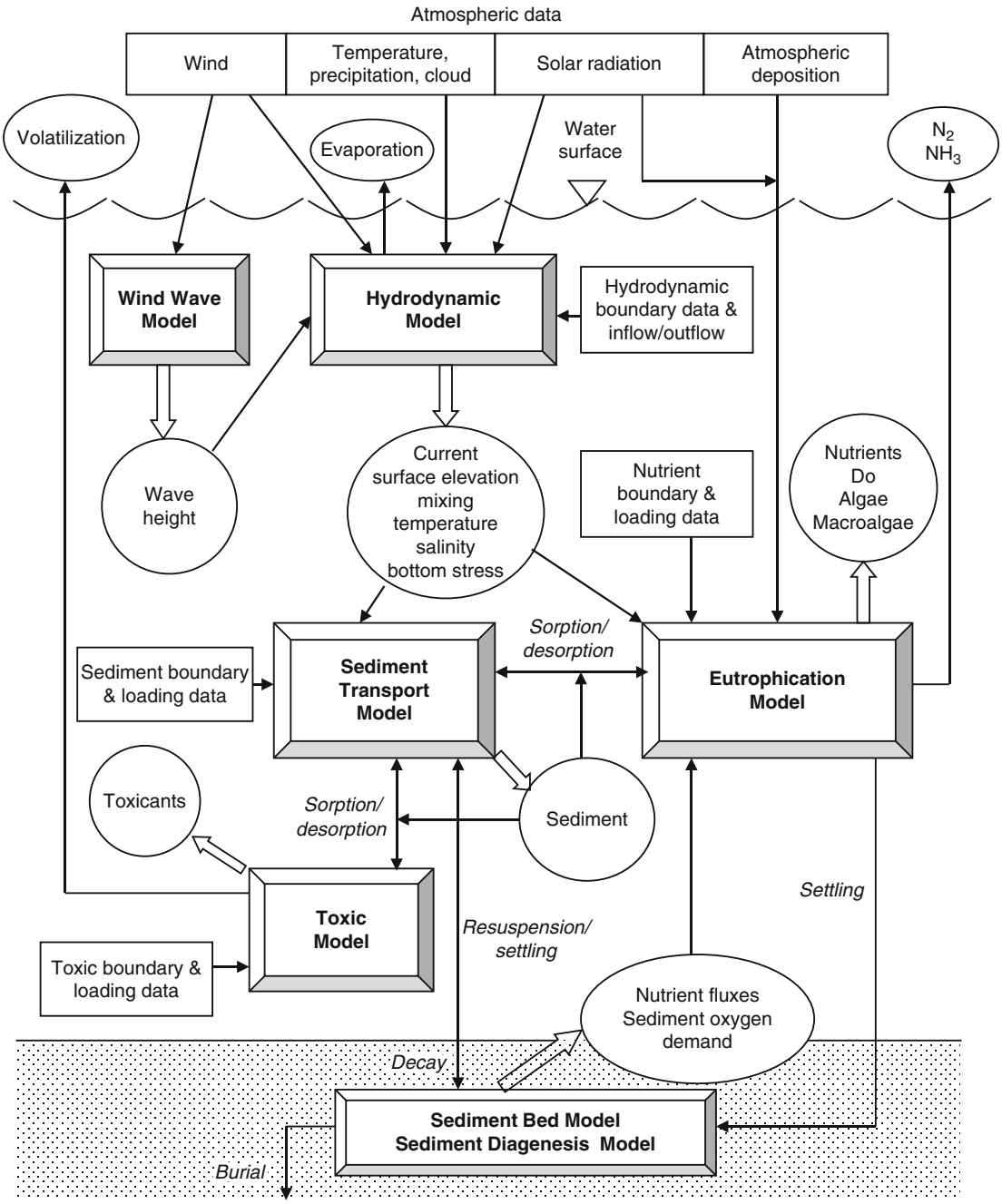

River Fate and Transport. Figure 6
Major components (submodels) of the EFDC model

not be valid for wide, deep rivers. In this case, the 1D approach may fall short of describing the river processes. Transport in these rivers can have significant gradients either laterally or vertically. In this case, a 2D or 3D model is needed to provide a better representation of the river. Ji et al. [4] gave an example of modeling hydrodynamics, sediment transport, and toxics in a small, shallow river.

Future Directions

The fate and transport of contaminants in rivers are complicated processes that include physical transport and chemical and biological kinetics. Contaminants in a river may be the result of either past or present disposal practices. Shutting off the sources does not always solve the problem (e.g., DDT persists many years). Consequently, it is essential that mathematical models for assessing contaminants are accurate and reliable. In the past decades, significant progress has been made in numerical model development, data collection, and computer software and hardware. These developments have helped mathematical models to become reliable tools for environmental management and engineering applications.

"Modeling is a little like art in the words of Pablo Picasso. It is never completely realistic; it is never the truth. But it contains enough of the truth, hopefully, and enough realism to gain understanding about environment systems" [9]. Water quality management increasingly depends upon accurate modeling. This dependency is further amplified by the adoption of the watershed-based approach to pollution control. Models enable decision-makers to select better, more scientifically defensible choices among alternatives for river water quality management.

In many cases, the models are used to evaluate which alternative will be most effective in solving a long-term water quality problem. The management decisions require the consideration of existing conditions, as well as the projection of anticipated future changes of the water system. In these applications, the river models not only need to represent the existing conditions, but also have to be predictive and give conditions which do not yet exist. Models are also used to provide a basis for economic analysis, so that decision makers can use the model results to evaluate the environmental significance of a project as well as the cost-benefit ratio.

Three key factors have contributed to the great progress in the modeling of rivers:

1. Better understanding and mathematical descriptions of physical, chemical, and biological processes in rivers
2. Availability of fast and efficient numerical schemes
3. Progress in computer technology

The powerful, yet affordable computers in combination with fast numerical algorithms have enabled the development of sophisticated 3D hydrodynamic and water quality models. These advanced models contain very few simplifying approximations to the governing equations. Personal computers (PCs) have evolved rapidly to become the standard platform for most engineering applications (with the exception of very large scale problems). PCs represent the most widely used computer platform today. Models developed on a PC can be transformed to other PCs without much difficulty. The relatively low prices of PCs also make modeling more cost-effective. Due to the rapid advances in computer technology, PCs are now widely used in river modeling studies.

Bibliography

Primary Literature

1. USEPA (2000) National water quality inventory: 1998 report to Congress. EPA 841-R-00-001. US Environmental Protection Agency, Office of Water, Washington, DC
2. CSCRMDE (1987) Sedimentation control to reduce maintenance dredging of navigational facilities in estuaries. Report and symposium proceedings. Committee on sedimentation control to reduce maintenance dredging in estuaries, National Academy Press, Washington, DC
3. Ji Z-G (2008) Hydrodynamics and water quality: modeling rivers, lakes, and estuaries. Wiley, Hoboken, 676 pp
4. Ji Z-G, Hamrick JH, Pagenkopf J (2002) Sediment and metals modeling in shallow river. J Environ Eng 128:105–119
5. Chow V (1964) Handbook of applied hydrology, a comparison of water-resources technology. McGraw Hill, New York
6. Streeter HW, Phelps EB (1925) A study of the pollution and natural purification of the Ohio river. III: factors concerned in the phenomena of oxidation and reaeration. Bulletin Number 146, US Public Health Service
7. Brown LC, Barnwell TO (1987) The enhanced stream water quality models QUAL2E and QUAL2E-UNCAS: documentation and user manual. EPA/600/3-87-007. US Environmental Protection Agency, Athens, Georgia
8. Hamrick JM (1992) A three-dimensional environmental fluid dynamics computer code: theoretical and computational aspects. The College of William and Mary, Virginia Institute of Marine Science, Special Report 317, p 63
9. Schnoor JL (1996) Environmental modeling: fate and transport of pollutants in water, air, and soil. Wiley, New York

Books and Reviews

Blumberg AF, Mellor GL (1987) A description of a three-dimensional coastal ocean circulation model. In: Heaps NS (ed)

Three-dimensional coastal ocean models, coastal and estuarine science, vol 4. American Geophysical Union, Washington, DC, pp 1–19
Bowie GL, Mills WB, Porcella DB, Campbell CL, Pagenkopf JR, Rupp GL, Johnson KM, Chan PWH, Gherini SA (1985) Rates, constants, and kinetics formulations in surface water quality modeling, 2nd edn. USEPA, Environmental Research Laboratory, Athens. EPA/600/3-85/040
Casulli V, Cheng RT (1992) Semi-implicit finite difference methods for three-dimensional shallow water flow. Int J Numer Meth Fl 15:629–648
Cerco CF (1999) Eutrophication models of the future. J Environ Eng 125(3):209–210
Chapra SC (1997) Surface water-quality modeling. McGraw-Hill, New York, 844 pp
Chapra SC, Canale RP (1998) Numerical methods for engineers, with programming and scientific applications. McGraw-Hill, New York, 839 pp
Di Toro DM (2001) Sediment flux modeling. Wiley, New York
Fischer HB, List EJ, Imberger J, Brooks NH (1979) Mixing in inland and coastal waters. Academic, New York, 483 pp
Gill AE (1982) Atmosphere-ocean dynamics. Academic, New York, 662 pp
Hutchinson GE (1957) A treatise on Limnology. In: Geography, physics and chemistry, vol I. Wiley, New York, p 1015
Ji Z-G (2004) Use of physical sciences in support of environmental management. Environ Manage 34(2):159–169
Ji Z-G (2005) Water quality models: chemical principles. In: Water encyclopedia, vol 2, Water quality and resources development. Wiley, New Jersey, pp 269–273
Ji Z-G (2005) Water quality modeling-case studies. In: Water encyclopedia, vol 2, Water quality and resources development. Wiley, New Jersey, pp 255–263
Martin JL, McCutcheon SC (1999) Hydrodynamics and transport for water quality modeling. Lewis, Boca Raton
Morel F (1983) Principles of aquatic chemistry. Wiley, New York, 446 pp
Park K, Kuo AY, Shen J, Hamrick JM (1995) A three-dimensional hydrodynamic-eutrophication model (HEM3D): description of water quality and sediment processes submodels. The College of William and Mary, Virginia Institute of Marine Science. Special Report 327, 113 pp
Schumm SA (1977) The fluvial system. Wiley, New York
Thomann RV, Mueller JA (1987) Principles of surface water quality modeling and control. Harper and Row, New York
USEPA (1994) Water quality standards handbook, 2nd edn. US Environmental Protection Agency, Office of Water, Washington, DC, EPA-823-B-94-005b
USEPA (1998) Bacteria water quality standard status report. US Environmental Protection Agency, Office of Water, Washington, DC
USEPA (2000) Nutrient criteria technical guidance manual: rivers and streams. EPA-822-B-00-002. Office of Water, Office of Science and Technology, Washington, DC
Wezernak CT, Gannon JJ (1968) Evaluation of nitrification in streams. J Sanit Eng Div ASCE 94(SA5):883–895
Wool AT, Ambrose RB, Martin JL, Corner EA (2003) Water quality analysis simulation program (WASP), Version 6: Draft users manual. Available at: http://www.epa.gov/athens/wwqtsc/html/wasp.html
Ziegler CK, Nesbitt B (1994) Fine-grained sediment transport in Pawtuxet river, Rhode Island. J Hydraul Eng 120:561–576
Ziegler CK, Nesbitt B (1995) Long-term simulation of fine-grained sediment transport in large reservoir. J Hydraul Eng 121:773–781

Roots and Uptake of Water and Nutrients

Carvalho P., M. J. Foulkes
Division of Plant and Crop Sciences, School of Biosciences, University of Nottingham, Loughborough, UK

Article Outline

Glossary
Definition of the Subject and Its Importance
Introduction
Root System Morphology and Anatomy
Effects of Abiotic Stress and Root Development
Root Traits and Resource Capture
Application of Rooting Traits in Breeding for Tolerance of Abiotic Stresses
Future Directions
Bibliography

Glossary

Fibrous root system Root system formed by various root axis of similar size, typical of cereals.

Lateral roots Lateral roots are the roots formed from the pericycle cells of other roots. The first-order laterals refer to the roots emerging from the primary and secondary root axes. Second-order laterals emerge from the first-order laterals, and third-order laterals from the second-order lateral, and so on. Usually, lateral branching is limited to the fifth-order laterals.

Primary roots Often called seminal roots, these are the first root axes to develop arising from the coleorhizae of the seed.

Rhizosphere Volume of soil immediately adjacent to plant roots (usually between 10 and 20 mm), which is affected by their growth, secretions, respiration, nutrient and water, and associated soil microorganisms.

Root architecture Describes the spatial configuration of the root system as a whole. Since it describes multiple root axes it subsumes both topology and distribution.

Root cap Root cap is the tissue that covers the apex of the root. It protects the apical meristem, acts as gravisensor tissue, and facilitates the passage of the growing roots by producing root mucilage.

Root distribution Root distribution refers to the distribution of different root traits, often morphologic ones (e.g., weight, length, volume), as a function of several factors, the most common being soil depth.

Root hair Specialized projection formed by a modified epidermal root cell. It augments the total surface area of a root system, dramatically increasing its absorption capacity.

Root morphology Root morphology refers to the surface features of a single root axes as an organ. It includes the characteristics of the epidermis such as root hairs, root cap, pattern of appearance of lateral roots, cortical senescence, and diameter. Weight, volume, and area are also part of the morphology.

Secondary roots Secondary roots are the roots that grow from the hypocotyl, the coleoptile, stem, and tillers; they are also called crown, nodal, or adventitious roots. This term is also used to describe the roots emerging from the primary roots; however, first-order laterals is a better term to describe those roots.

Taproot In many gymnosperms and dicotyledons, the primary root axis to arise from the seed, greatly enlarges to become the most prominent root axis of the plant, and is usually referred to as a taproot.

Taproot system Taproot system refers to the root systems formed from a central and usually relatively large root axis, the taproot.

Topology Describes the branching pattern of the individual root axes.

The main quantitative root traits and resource capture variables discussed in this entry are summarized in Table 1.

Definition of the Subject and Its Importance

The UN forecasts that the world population will reach 9.4 billion by 2050. The world must therefore develop the capacity to feed 10 billion within the next 40–50 years [1, 2]. The increase in production has to come from greater yields on existing cropland; but also without proportionate increases in the use of water or fertilizer, and within the context of climate change [3, 4]. A substantial increase in the effectiveness with which available water and nutrients are used is therefore required to ensure food security and environmental protection in future decades. Water is recognized as the most limiting factor in crop production worldwide, though nutrient shortages may often be as important as water scarcity and worldwide recovery of nitrogen (N) fertilizer in cereal systems worldwide is on average low at ca. 30–50% [5], with implications for potential environmental impacts. Crop improvement under these conditions seems likely to be increasingly dependent on breeding for deeper or denser root systems, which promote soil moisture and nutrient capture and high dry matter production in cultivars subjected to water and/or nutrient stresses. In this entry, information is set out on the current understanding of the structure and functions of crop root systems. The avenues for the optimization of root anatomy and morphology traits that could be applied to the genetic and agronomic improvement of crop root systems for more effective below-ground resource capture are considered. Specifically, the determinants of effectiveness of capture by root systems of two key resources, water and nitrogen, according to their structure and function are considered.

Introduction

All higher plants have roots and the root fraction of the plant's total dry weight varies widely, both between and within species [6]. Although roots encounter many environmental fluctuations that affect their growth, they have a capacity to adjust to these as a whole system that makes them strongly dynamic in their spatial and temporal expansion. Understanding of these modifications in the form and function of the root system and their relationships with resource capture, whether due to environmental response or genetic control, is of importance for sustainable crop production.

Roots and Uptake of Water and Nutrients. Table 1 List of physiological variables, their definitions and units

Physiological variable (symbol)	Definition	Units
Nitrogen-use efficiency (NUE)	Grain DM at harvest (kg) per N available (soil + fertilizer) (kg)	Dimensionless
Nitrogen-uptake efficiency (UPE)	Above-ground N (kg) at harvest per N available (soil + fertilizer) (kg).	Dimensionless
Water-use efficiency (WUE)	Above-ground DM per water used (soil evaporation + crop transpiration).	$g\ l^{-1}$
Transpiration efficiency (TE)	Above-ground DM (g) per water used (l) through crop transpiration.	$g\ l^{-1}$
Radiation-use efficiency (RUE)	Above-ground dry mass (g) per intercepted global radiation (MJ).	$g\ MJ^{-1}$
Root to shoot ratio (R:S)	Ratio between the root and above-ground shoot dry mass.	Dimensionless ($g\ g^{-1}$)
Root mass ratio (RMR)	Ratio between the root dry mass (g) and total plant dry mass (g).	Dimensionless ($g\ g^{-1}$)
Root mass (RM)	Dry mass (g) of the total root system.	g
Root length (RL)	Total length (cm) of all roots present.	cm
Root length density (RLD)	Root length (cm) per unit of soil volume (cm^3).	$cm\ cm^{-3}$
Root volume (RV)	Total volume of the root system (cm^3).	cm^3
Root diameter	Average diameter (mm) of an individual root; commonly assumed to be a cylinder.	mm
Root fineness (RL:RV)	Ratio of the total root length (mm) to total root volume (mm^3).	$mm\ mm^{-3}$
Root depth	Maximum depth reached by a plant root system (m)	m
β Parameter	Describes the cumulative root distribution with depth. Estimated from: $p = 1 - \beta^d$, where p is the proportion of roots accumulated from the surface to a depth, d.	Dimensionless
k Parameter	Resource capture coefficient. Estimated from $\Phi = 1 - e^{-k.RLD}$, where Φ is the proportional resource captured (resource captured/ available resource).	m^2
Specific root length (SRL)	Ratio between root length (m) and root weight (g).	$m\ g^{-1}$
Root tissue density (RM:RV)	Ratio between root dry mass (mg) and root volume (mm^3).	$mg\ mm^{-3}$
Root front velocity (RFV)	Downward extension rate of the root front (mm) per day.	$mm\ day^{-1}$
Root longevity	Length of time of which an individual root is present in the soil.	days

Although the influence of canopy characteristics on above-ground productivity of crops is now relatively well understood, due to the difficulty of access and complexity of environment interactions, understanding the role of the root system is less complete. There is no doubt of the importance of the form and function of root systems to water and nutrient capture, and information has increased in the last decades on the role of

crop root systems in maintaining yields under abiotic stress [7–9]. Root traits are a relatively new target in crop improvement programs aimed at improving tolerance of abiotic stress (water and nutrients). There are reports that particular root morphology and/or anatomical traits help plants maintain higher grain yields under low resource availability, for example, relatively deeper distribution of roots increasing water uptake under drought in wheat [10] and rice [11], longer root hairs increasing P acquisition under low P availability in barley [12], and narrower root xylem vessels in wheat were associated with increased water uptake during grain filling [13]. Nevertheless, the genetic control of root characteristics is poorly understood in most major staple crops, especially in bread wheat. Future improvement will depend on a better understanding of the morphological and anatomical traits determining below-ground resource capture, as well as the development and application of phenotypic screens to characterize genetic variation in the key traits. In this entry, the prospects for manipulating roots systems for improved resource capture and yield (drought and low nutrient availability) are considered, with a particular emphasis on cereal crops. The root traits that are focused on are principally morphological relating to root proliferation, root biomass and root length density, and their distribution with depth; although some consideration is given to anatomical features, for example, xylem root frequency and diameter. Roots and the uptake of water and nutrients are considered with regard to: (1) root morphology, (2) responses of root systems to water and nutrient stress, (3) the capacity of root systems for resource capture, and (4) prospects for breeding crops with optimized root systems for resilience to abiotic stresses.

Root System Morphology and Anatomy

Due to the difficulty of access and complexity of environmental interactions, roots are still one of the most challenging subjects in plant investigations, but their importance is unquestionable. Anchorage, support, and water and nutrient uptake are the main functions of the plant root system. With regard to crop root systems, the terms morphology and architecture are frequently used. The root system may be characterized according to four main categories of morphology/architecture [14, 15]. "Root morphology" refers to the surface features of a single root axes as an organ. It includes the characteristics of the epidermis such as root hairs, root cap, pattern of appearance of lateral roots, cortical senescence, and diameter. Root weight, volume, and area are also part of the morphology. "Root topology" describes the branching pattern of the individual root axes. "Root distribution" refers to the distribution of root traits, often morphologic ones (e.g., biomass length, biomass, etc.) as a function of several factors, the most common being soil depth. Finally, "root architecture" relates to the spatial configuration of the root system as a whole.

The root morphology of monocotyledons differs from that of dicotyledons in several important respects. In the monocotyledons, for example, small grain cereals, two types of roots constitute the root system: the primary and the secondary roots [7, 16]. The primary roots (often called seminal roots; usually between three and eight axes) develop first arising from the coleorhizae of the seed [17, 18] and are active throughout all the crop life cycle [18]. Their extension is mainly downward allowing them to occupy the deeper layers of the soil profile [17]. The secondary (often called crown, nodal, or adventitious roots) are the roots that grow from the nodes of the coleoptile, main shoot, and tillers. The onset of tillering is the starting point of the growth of the secondary roots, and their formation is intimately related to tiller formation [19], so that factors favoring tillering will increase secondary root production. In dicotyledons, for example, oilseed rape, for most species the primary root consists of a taproot from which lateral roots and their branches arise. In both monocotyledons and dicotyledons, lateral roots are initiated in the pericycle and grow through the cortex to emerge at the surface of the parent root.

Rooting depth is affected by root-penetration rate and phenology. Generally, the longer a crop is growing, the deeper it roots [20]. Rooting depth (maximum depth reached by the roots) determines the amount of the soil that a plant can explore. Maximum rooting depth is typically 140–200 cm in winter cereals [18, 21] and 80–120 cm in spring cereals [22]. Rooting depth also strongly depends on the soil type and depth as well as below-ground resource availability, but generally the longer a crop grows the deeper the root system. Root growth and rooting depth of crop plants can be restricted because of physical and chemical impediments. Where physical and chemical soil

constraints are absent, the maximum depth of rooting on deep soils is genetically determined and differs not only between vegetation types but also between crop species grown under identical conditions [8]. Much of within season variation in maximum rooting depth can be explained by temperature [23].

In monocotyledons, immediately after sowing root growth is favored, followed by a gradual decrease in assimilate partitioning to the root in favor of shoot growth after emergence. After flowering, the above-ground growth (fruit and grain formation) is favored, whereas root weight usually remains constant or decreases [24, 25]. Thus, root biomass and total length production generally follow a sigmoidal pattern from sowing to flowering in cereals, at which point further increases are not usually observed [18, 21].The root dry mass ratio (root DM/total DM; RMR) is ca. 0.3 in wheat and barley during early growth, decreasing to ca. 0.1 at harvest [18, 22]. Another important trait influencing the crop's capacity to capture resources per unit soil volume is the root length density (RLD), which describes the total root length per unit of soil volume. Typical values of RLD in the upper 0.1 m of soil are about 20 cm cm^{-3} in grasses, 5–10 cm cm^{-3} in temperate cereal crops and 1–2 cm cm^{-3} in other crops [8]. The distribution of the RLD through the soil profile typically follows an exponential decrease with depth [26]. The cumulative distribution of RLD with depth (β) can be approximated by the equation described by Gale and Grigal [27] as:

$$Y = 1 - \beta^d \quad (1)$$

where Y is the fraction of the root system accumulated from the soil surface to depth, d, and β is a parameter that describes the shape of the cumulative distribution with depth.

This equation has been widely adopted since (e.g., [28–30]). The distribution of roots of many crops (e.g., cauliflower and winter wheat) is well described by the relationship, but in others (e.g., oilseed rape and sugar beet), this relation is found in the surface layers, but there is a tendency for values of RLD in deeper soil layers to be almost constant [8]. Differences in the distribution of RLD with depth may be associated with the velocity at which roots elongate to depth (root front velocity [RFV]) and the proliferation rate at each soil layer [31]. Root front velocity is closely related with the water and N extracted by the crop [31–33]. Another important trait influencing the potential for water and nutrient acquisition by roots is the mean root diameter (see Root traits and resource capture below).

Specific root length (root length per unit root DM - SRL; km g^{-1}) strongly influences the RLD. Theoretically, a high SRL (thinner roots) would be beneficial especially in resource-deficit situations. Specific root length is also positively correlated with root extension rate [34]. Specific root length varies considerably in the field and is strongly affected by environment; typical values are 130–250 m g^{-1} for cereals [35–37]. Root tissue density (root weight (RW): root volume (RV)) is highly correlated with root life span but inversely correlated with root expansion [38, 39]. So low RW: RV will may be one strategy to increase SRL of crop root systems [40] and potentially resource acquisition. Specific root length is a complex parameter that is determined by root length, tissue density, and diameter. It influences plant investment in potential resource acquisition (RLD) but also reflects root longevity and root growth rate, and therefore it is of potential interest as a selection criteria in breeding programs for optimized root systems. Maximizing SRL seems to be an advantage particularly in water- and nutrient-limited conditions [39, 41] and is associated with higher RLD. Intuitively, thinner roots would be advantageous for acquiring soil resources, though there may be trade-offs with other root functions such as anchorage, support, and transport [42]. The interrelationships between these root traits and their relations with resource capture are summarized in Fig. 1. Additionally, there are reported effects of root diameter on resource capture, which has been shown to be highly correlated with plant dry mass [43, 44] and the diameter of conducting vessels. The principal root traits described above may be influenced by abiotic stresses during the rapid phase of root growth and expansion in the pre-flowering period with implications for resource capture during later seed filling, and these effects are now considered in the following section of this entry.

Effects of Abiotic Stress and Root Development

Drought and Root Development

Drought overall usually reduces the size of root systems. Water deficits decrease carbon assimilation by the

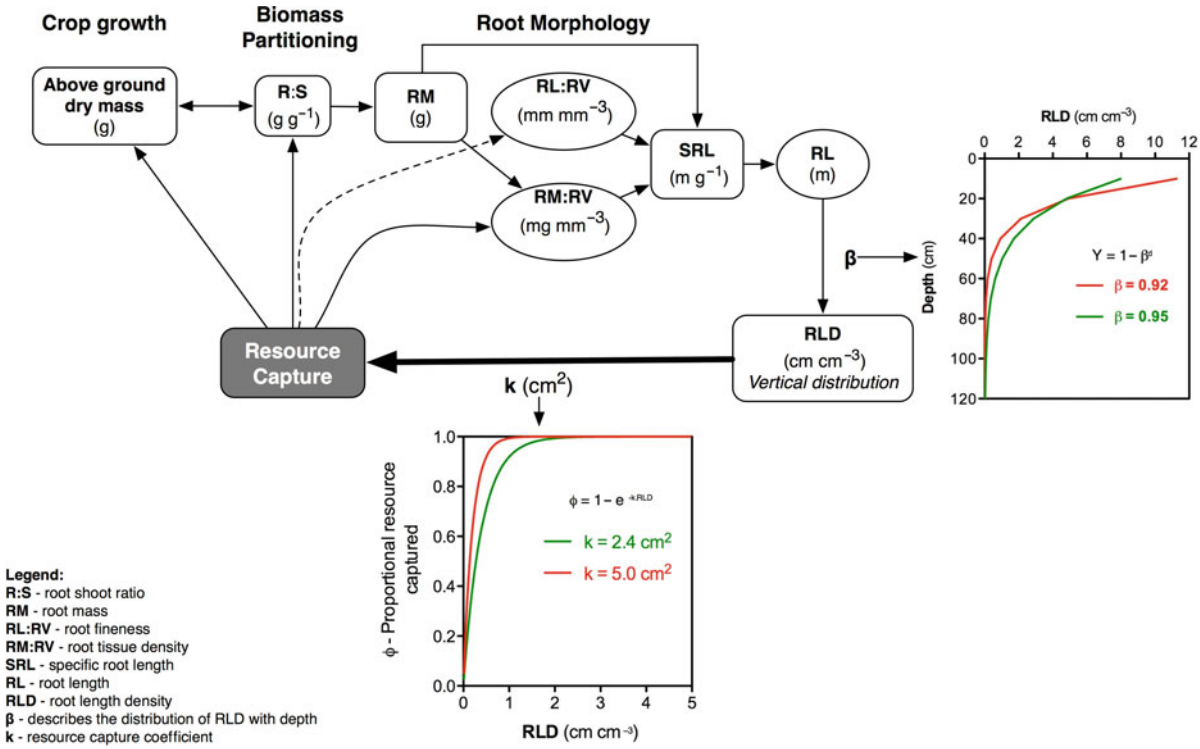

Roots and Uptake of Water and Nutrients. Figure 1
Interrelationships between these root traits and their relations with resource capture

plant due to a reduction of green leaf area, but also due to a decline in net photosynthetic rate. Nevertheless, under drought plants tend to increase the proportion of total carbon allocated to the roots [25, 45]. For example, plants responded to water deficits by increasing the proportion of assimilate allocated to roots in wheat [46, 47] and barley [48]. Experiments using pulse-labeled 13C in wheat have shown that water deficits increase the allocation of assimilated C to the roots due to a greater reduction of growth in the above-ground than below-ground plant components [49]. Although the relative root dry mass tends to increase with water deficits the absolute weight of both roots and shoots tends to decrease. As the soil dries, there are changes in its physical condition such as increases in soil strength [50]. Shoots are generally more affected by drought than roots, associated with more severe water deficits developing and persisting longer in the transpiring shoots [49, 51, 52]. Thus, roots are typically prioritized during drought to facilitate access to water while decreasing transpiration. The relationship between these two systems is often described as a competition where both roots and shoots compete for carbohydrates, minerals, and water, the most successful being the one nearer the source [24]. Therefore, the growth of the root and shoot systems is an integrative process working in a functional equilibrium [53, 54]. So when light is limited, root growth will be more restricted than shoots and the opposite happens when soil resources are in deficit; this functional balance hypothesis is elegantly explained by Brouwer [24]. In addition, under water-limiting conditions, solutes may accumulate in the root tip attracting the movement of water by diffusion, allowing the cells in the root tip to maintain their turgor and growth [55].

Although water deficits typically increase the percentage of carbon allocated to the roots, there are some reports of contrasting responses of root partitioning to drought amongst cultivars, for example, in glasshouse- [52] and field-grown wheat [56]. Therefore, the root growth response under drought is not simple, since drought not only affects plant and root growth but

also the soil structure and N availability [57]. For example, water deficits may have a neutral effect on root weight, but still influence root length and its distribution with depth in wheat [47]; or increase SRL with drought in bread wheat [58] and durum wheat and barley [59]. There is some evidence that thinner roots may themselves be more vulnerable to drought [44, 60]. Therefore, the relatively high diameters reported for irrigated compared to droughted plants [58, 61] might relate to the necessity of the root system to support a larger plant and facilitate faster and greater water uptake and transport in well-watered conditions.

Leaf expansion and senescence are particularly susceptible to water deficiency [62]. The causes for restricted leaf expansion with drought have been discussed extensively, and there are mainly two views on the underlying mechanisms involved. Some authors attribute the cause to water relations (water potential and cell turgor) in the leaf [63, 64], while others attribute it to root chemical signals, such as abscisic acid (ABA), transmitted to the leaves, in response to water depletion in the soil [65–67]. ABA concentration increases in shoots, leaves, and roots in plants grown under water deficits and its exogenous application on well-watered plants mimics many of the drought effects on the plant [68, 69]. The chemical mechanism involves the synthesis of the plant hormone ABA by the roots when sensing the drying of the soil, and the transfer of ABA in the xylem to shoots and leaves inducing stomatal closure hence reducing water uptake and shoot and leaf growth [68, 70–72].

Evidence for water relations as the main cause of the decrease in leaf expansion was described by Boedt & Hensley (1987 in [63]) where leaves of field-grown maize showed visual symptoms of water stress in soil near field capacity. Tazaki et al. (1980 in [63]) in Japan reported similar effects for rice leaves, even though plants were rooted in wet soil. Furthermore, seedling experiments in maize plants using the pressure-pump technique [64] showed that an increase in the water pressure in the roots was quickly and fully transmitted to the base of the leaf increasing the leaf elongation. In contrast with these findings, Passioura [66] growing wheat seedlings in drying soil but maintaining leaf turgidity using the pressure-chamber method, showed a decrease in the relative expansion rate of leaves. Additional evidence for the root chemical signal was given by Gollan et al. [73] where wheat and sunflower plants showed a decrease in stomatal conductance with an increase of water deficits while the pressure in the plant was maintained. Using partial root-zone drying (PRD) techniques where half of the root system is droughted while the other half is irrigated, to maintain the same leaf water status as control plants (full irrigation), results showed a decrease of 65% of leaf area and 70% of water loss in apple plant seedlings subjected to PRD [67].

A more recent hypothesis is that both hydraulic and chemical signals interact and that the importance of one or the other will depend on the timescale considered [74]. Experiments in maize and barley showed that sudden changes in leaf water status by light, humidity, or salinity greatly affect leaf-elongation rate, and that those effects vanished when their roots were placed in a pressure chamber to maintain the xylem and air pressures in equilibrium, showing that hydraulic relations dominated in this response [75]. If the saline or water stress was prolonged, water relations were overridden by chemical signals and pressurization failed to maintain leaf elongation rates [75]. The combination of hydraulic and chemical factors was also demonstrated by differences in the sensitivity of different maize lines under drought to xylem ABA [76].

Nutrients and Root Development

It is well established that plants respond to N and P deficiencies by increasing RMR due to the functional equilibrium between the growth of the root and shoot [24, 77–81]. Crop root systems are plastic and respond by proliferating roots to exploit patches of nutrients where the distribution within the soil is uneven [82]. For example, responses to aqueous fertilizer in wheat have been observed within 24 h of application [83]. Frequently there is a strong association between root length and P uptake. Root proliferation in P-rich patches is, therefore, relatively straightforward to interpret in terms of a "foraging" response. The responses of roots to N- and P-rich patches of soil include proliferation of laterals and stimulation of nutrient inflow (uptake rate per unit root length) within the patch [81]. Nitrate uptake from a N-rich patch may compensate for an uneven supply of nitrate to the whole root system. Localized N application on barley seminal

root systems promoted the number and extension rate of both first- and second-order lateral roots [84]. The potential magnitude of the responses to N and P has been demonstrated in barley by Drew and Saker [85, 86]. With regard to genetic effects, Zhang and Forde [87] demonstrated that, in Arabidopsis, the extension of lateral roots in nitrate-rich patches is partly under genetic control. Since irrigation and N fertilizer can cause root proliferation in the surface soil [47, 88], the distribution of the availability of these resources earlier in the crop's growth may alter the relative distribution of roots with depth (β) at anthesis.

For two barley varieties grown in Mediterranean field conditions, RMR increased under low N and P fertilizer supply compared to a control treatment with ample N and P supply [89]. Herrera et al. [90] in wheat showed that high N supply increased the number of roots, and when N was limited root formation ceased earlier. Barraclough et al. [47] observed an increase in RMR with low N supply in N x drought field experiments in winter wheat in the UK. N application effects on SRL are inconsistent, and increases, decreases, or neutral effects are reported for different species [44, 91]. Field experiments on spring barley and durum wheat in Jordan showed no consistent response for SRL for three different levels of N fertilizer [59]. SRL increased with N application under rain-fed conditions for durum wheat, but the opposite was found for spring barley. There appear to be few previous investigations regarding the effects of N fertilization on SRL and its components in cereals in field conditions. N application has been observed to increase mean root diameter in cereals but to decrease RW:RV [44, 91].

Root Traits and Resource Capture

The primary root traits for improved below-ground resource capture would appear to be root morphology (root axis number, rooting depth, rooting length density), root extension rates, root longevity, and root function along the length of the root system [9, 92, 93].

Water Capture

The importance of water for plants is unquestionable; it performs a varied number of physiological and structural functions. Water constitutes on average 80–90% of the fresh weight of herbaceous plants providing a continuous liquid phase in which gases, minerals, and other solutes enter the cells and move from one cell to another and within the different plant organs [94]. Water is a reactant or substrate in most of the plant's biochemical reactions (e.g., photosynthesis) and it maintains the plant turgor essential for cell growth, enlargement, form and movement of various plant structures, like the stomata opening [8, 94].

Crop production is closely related to water transpired; therefore, maintaining an uninterrupted supply of water to leaves is essential to maximize yields. Water capture is intimately related with root size, usually measured, as surface area, volume, or length. According to the theoretical model of van Noordwijk [95], the rate of water uptake by the plant is mainly limited by the transport in the soil toward the root (soil–root interface). Therefore, the density of roots, measured as length per unit soil volume (root length density – RLD, cm cm^{-3}), is the most suitable parameter to describe water uptake by plant roots. Prolific root systems are more effective at capturing water than sparse systems, but inter-root competition sets a natural ceiling on optimum RLD in cereals, above which further increases require excessive roots which do not have measurable effects on water uptake [95]. Theoretical calculations predict a critical root length density (C_{RLD}) of about 1 cm cm^{-3} for water uptake. This figure broadly concurs with the values reported for water uptake of Gregory and Brown [96] and Barraclough et al. [47] who showed that a RLD of 1 cm cm^{-3} was associated with the abstraction of all of the available water by both spring barley and winter wheat, respectively. However, for upland rice, values of C_{RLD} between 1.5 and 1.6 cm cm^{-3} have been reported [97, 98] and in controlled environment conditions values as low as 0.30 cm cm^{-3} [99].

RLD distribution with depth is principally determined by time for growth (residence times are greater in the topsoil than the subsoil), soil porosity and strength, and water availability [20]. Root length density in wheat is typically below the C_{RLD} of ca. 1 cm cm^{-3} at soil depths below ca. 80 cm [18, 21, 36, 100]. A modeling study concluded that distributing roots relatively deeper in the soil profile and decreasing SRL would confer greater water capture and yield under low water availability in wheat [30]. Experimental evidence also supports the strategy of distributing roots

relatively deeper to improve water capture under drought. Synthetic derivative wheat lines showed increased water uptake associated with a root system that was distributed relatively deeper in the soil compared with recurrent parents [10], and the drought tolerance of spring wheat SeriM82 was related to its relatively deep root system compared to the check cultivar Hartog [101]. Further root traits which could be beneficial in boosting water capture include enhanced post-anthesis root longevity and root penetration ability [102], although there is relatively little information on genetic variation in these traits in cereals.

In rice under flooded conditions, attempts to optimize the root system through plant breeding methods must additionally allow for the complicated interplay between adaptations for internal aeration and those for efficient nutrient acquisition. A recent model developed by Kirk [103] provides a coherent representation of the rice root system in submerged soil and predicted that a system of coarse, aerenchmymatous primary roots with gas-impermeable walls conducting O_2 down to short, fine, gas-permeable laterals provided the best compromise between the need for internal aeration and the need for the largest possible absorbing surface per unit root mass.

Nutrient Capture

Water and nutrient uptake should really be considered together since nutrients become less available as the soil dries. Nitrate is readily leached down the soil profile and consequently rooting depth is an important attribute for soil N acquisition. For a long time, due to its high mobility in soil, N supply was considered independent of the root system characteristics, assuming that only mass flow and diffusion were the relevant mechanisms for the uptake of N by the plant [90]. The role of crop root systems in capturing N is still a topic of debate. Findings of Robinson et al. [104] indicated only 4–11% of the total root length is involved in N uptake. On the other hand, Palta and Watt [9] demonstrated through 15N labeling experiments on wheat that vigorous root systems captured ca. 60% more N in the top 0.2 m of the soil profile than non-vigorous root systems. Furthermore, a positive correlation was found between nitrate and water uptake and root length density in maize [105–107] and in several catch crop species [108]. These studies indicated that greater root length densities are generally more effective in N acquisition. However, root length is probably more important for the uptake of relatively immobile ions such as phosphates [109, 110]. However, some investigations have found uptake rates of phosphate, calcium, and potassium from solution are poorly related to root length [111, 112], possibly because root length is only significant if the uptake of these nutrients is limiting [7]. In addition, several investigations have shown that nitrate capture depends on the ability of the root system to respond to spatial and temporal nitrogen supply [81, 113].

The ability to capture N depends mainly on the amount of nitrate present in the soil relative to the morphology of the root system. Nitrate is supplied to the root system by mass flow (ions carried along in the transpiration stream) and diffusion (ions moving down a concentration gradient, either through bulk soil water or along water films surrounding particles). About 50% of the N taken up by wheat crops may be transported by mass flow [16]. As for water uptake, inter-root competition sets a natural ceiling on optimum RLD in cereals of about 1 cm cm^{-3} [95]. RLD distribution with depth is principally determined by time for growth (residence times are greater in the topsoil than the subsoil), soil porosity and strength, and nutrient and water availability [20]. The modeling study of King et al. [30] concluded that distributing roots relatively deeper in the soil profile and increasing SRL would confer greater N capture and yield under low N availability. The particular properties of each nutrient in the soil impose different RLD requirements for effective uptake. For example, due the low mobility of phosphorous (P) in the soil, a higher RLD of ca. 10 cm cm^{-3} is required for effective P uptake compared to water and/or nitrogen [114, 115]. Similar to water uptake, root traits that could be beneficial in boosting N capture include enhanced root longevity post-anthesis and root penetration ability [102], although there is relatively little information on genetic variation in these traits in wheat. Barraclough et al. [47] in N × drought field experiments in winter wheat in the UK found that water uptake increased with N due to a higher RLD and higher ground cover reducing soil evaporation. Positive correlations between nitrogen

capture and RLD have also been found in maize [106, 107] and durum wheat and barley [59]. Although higher N supply tends to increases total RLD and N uptake by the crop, this generally results in a decrease in N uptake efficiency (crop N uptake/N available) [116, 117] leading to potentially greater losses of nitrate to the environment. A recent modeling exercise suggested that higher RLD and deeper rooting depths would reduce residual nitrate in high leaching soils [118]. Forde & Clarkson [119] concluded that there was no strong evidence for significant age-dependent changes in capacity of roots to absorb nitrate or ammonium ions.

Nutrient uptake may also be influenced by root membrane transporter systems. With regard to N uptake, recent work in *Arabidopsis* indicates nitrate is actively transported across the plasma membranes of plant cells, but net uptake is a balance between active influx and passive efflux. Two distinct gene families of nitrate transporters, *NRT1* and *NRT2*, have been identified [119–122] in the *Arabidopsis* genome. Some members of both *NRT1* and *NRT2* gene families are nitrate inducible, and are expressed in the root epidermis and in root hairs, and are likely to be responsible for the uptake of nitrate from the soil (e.g., [123–126]). There are prospects for transferring this information to wheat for improving efficiency of N uptake in the long term if the root screens used for *Arabidopsis* could be adapted to the larger and structurally different root system of wheat. An extensive review of this area is beyond the scope of this entry. Fortunately, excellent reviews are recently available in this topic area [127, 128].

With regard to the carbon costs of roots, it seems there is likely only a limited capacity to reduce root partitioning below current values of ca. 10% at anthesis in cereals in high yield potential ideotypes, due to the trade-off with water and N capture required for future biomass gains. However, a deeper relative distribution of roots while maintaining RMR could comprise part of an ideotype to maximize yield in future breeding programs.

Application of Rooting Traits in Breeding for Tolerance of Abiotic Stresses

Genetic variation in root system size has been widely reported in grain crops (e.g., [6, 45, 129]), but root distribution varies strongly with soil characteristics such as water and nutrient availability and mechanical impedance [54]. The RMR of wheat or barley is typically ca. 30% during early vegetative growth decreasing to ca. 10% by anthesis [18, 96, 130]. Effects of increasing plant height on root partitioning have been studied using isolines and are generally either neutral or negative in wheat [22, 130–132].

Breeding cultivars better adapted to particular conditions of drought and/or low nutrient availability will play a major role for the future of crop production for adaptation to climate change. Breeding for more effective use of water or nutrients while maintaining, or ideally, increasing yield potential is a difficult task. It will be important in the most efficient crop systems to combine optimized agronomy and new cultivars efficient at acquiring below-ground resources. To date there are relatively few examples of root morphological or anatomical traits that have been successfully selected for crop breeding programs to result in improved performance. In a recent review on this topic, Palta and Watt [9] cited five examples of rooting traits directly related to below-ground resource capture in breeding, including long root hairs for increased P uptake in barley [12], reduced xylem vessel diameter in seminal roots of wheat [13], and increased root density at depth through faster root extension rate in wheat [133]. In addition, improved resource capture has been achieved by alleviating other stresses on roots, for example, resistance to cereal cyst nematode in wheat [134]. Another encouraging example of introgression of rooting traits in crop breeding can be found in rice. When near isogenic lines (NILs) obtained through marker-assisted backcrossing for four QTLs for root length were field-tested, they outperformed the recurrent parent for yield and biomass [135]. In order to introgress rooting traits into elite genotypes, it will be necessary to identify genetic diversity for the key traits as well as developing methods for rapid high-throughput screening of lines in breeders trials.

Field phenotyping methods for roots in cereals were reviewed by Manske et al. [136] and Polomski and Kuhn [137], including the use of rhizotrons and assessments of root parameters from soil cores (root washing and root counts/image analysis). Although several screening tests have been designed to generate accurate and robust data from seedling plants grown under

artificial conditions, these phenotypes can rarely be extrapolated to field conditions because of the pronounced plasticity of root growth and development processes [138]. Field phenotyping for root traits in breeding programs is currently infeasible, so genetic progress will depend on the development of high-throughput controlled-environment screens or molecular markers for root traits for marker-assisted selection (MAS). The use of root-observation chambers and a nondestructive digital imaging technique offers some promise [139], but may be less suitable for screening of root traits that are expressed at later stages of crop development.

Future Directions

The existence of significant genetic variation for rooting traits has not resulted to date, except for a few exceptions as mentioned above, in the incorporation of rooting traits in conventional breeding. Nevertheless, future genetic progress for resistance to abiotic stresses should be accelerated by the fact that the genetic control of rooting traits can now be revealed through the application of rapidly emerging genetic resources facilitating the fine mapping of root QTL. Indeed, the cloning of the first root QTL is ongoing. However, successful exploitation of genomics tools and strategies in plant breeding requires extensive and precise phenotyping of agronomic traits for breeding materials and mapping populations. The capacity for precise phenotyping under reliable conditions probably represents the most limiting factor for the progress of genomic studies on root traits underlying resilience to abiotic stresses. There is a need for a high precision because the differences may be small, and detailed physiological measurements (e.g., of growth rate) are difficult when a large numbers of genotypes are involved.

Physiological perspectives that require more attention are analyses to measure the full carbon costs of the turnover of root material (and therefore of the root system), which are presently poorly quantified especially in environments where soil stresses are common. The role of organic substances in the rhizosphere secreted by the root that are able to modify the environment to secure improved water uptake requires more attention. Future research should focus on the importance of root plasticity for nutrient capture rather than simply measuring the size of the response. More studies at the plant community level rather than on single plants are required to translate fundamental studies on root growth and function to the improved water and nutrient capture at the crop scale.

Additionally, future work should aim to address the potential use of marker-assisted backcrossing for root QTLs and to exploit findings in *Arabidopsis* where root screens for mutants have identified genes such as AUX1 and LAX3 that regulate important root architectural traits such as lateral root development [140]. There is a continuing need to integrate "omics" technologies with plant physiology, agronomy, breeding, and disciplines related to the rhizosphere. In the future to meet the challenge of raising biomass and yield potential as well as improving resilience to abiotic stresses it will be crucial that new root research fosters collaborations between breeders, geneticists, physiologists, crop physiologists, and soil scientists (among others) to translate the genetic data generated from the new genomics resources into improved crop performance.

Bibliography

Primary Literature

1. Lutz W, Sanderson W, Scherbov S (2001) The end of world population growth. Nature 412(6846):543–545
2. Hamilton R (2009) Agriculture's sustainable future: breeding better Crops. In: Scientific American: http://www.scientificamerican.com/article.cfm?id=agricultures-sustainable-future
3. Hirel B, Le Gouis J, Ney B, Gallais A (2007) The challenge of improving nitrogen use efficiency in crop plants: towards a more central role for genetic variability and quantitative genetics within integrated approaches. J Exp Bot 58(9):2369–2387
4. Cattivelli L, Rizza F, Badeck FW, Mazzucotelli E, Mastrangelo AM, Francia E, Marë C, Tondelli A, Stanca AM (2008) Drought tolerance improvement in crop plants: an integrated view from breeding to genomics. Field Crops Res 105(1–2):1–14
5. Raun WR, Solie JB, Johnson GV, Stone ML, Mullen RW, Freeman KW, Thomason WE, Lukina EV (2002) Improving nitrogen use efficiency in cereal grain production with optical sensing and variable rate application. Agron J 94:815–820
6. O'toole JC, Bland WL (1987) Genotypic variation in crop plant-root systems. Adv Agron 41:91–145
7. Hoad SP, Russell G, Lucas ME, Bingham IJ (2001) The management of wheat, barley and oat root systems. Adv Agron 74:193–246
8. Gregory PJ (2006) Plant roots: growth, activity, and interaction with soils. Blackwell, Oxford

9. Palta J, Watt M (2009) Vigorous crop root systems: form and function for improving the capture of water and nutrients. In: Crop Physiology – Applications for genetic improvement and agronomy, Elsevier, San Diego
10. Reynolds M, Dreccer F, Trethowan R (2007) Drought-adaptive traits derived from wheat wild relatives and landraces. J Exp Bot 58(2):177–186
11. Yoshida S, Hasegawa S (1982) The rice root system its development and function. In: O'Toole JC (ed) Drought resistance in crops with emphasis on rice. IRRI, Manila
12. Gahoonia TS, Nielsen NE (2004) Barley genotypes with long root hairs sustain high grain yields in low-P field. Plant Soil 262(1):55–62
13. Richards RA, Passioura JB (1989) A breeding program to reduce the diameter of the major xylem vessel in the seminal roots of wheat and its effect on grain yield in rain-fed environments. Aust J Agric Res 40(5):943–950
14. Fitter AH (1985) Functional significance of root morphology and root system architecture. In: Fitter AH, Atkinson D, Read DJ, Usher MB (eds) Ecological interactions in soil, plants, microbes and animals. Blackwell, Oxford, pp 87–106
15. Lynch J (1995) Root architecture and plant productivity. Plant Physiol 109:7–13
16. Gregory PJ, Crawford DV, Mcgowan M (1979) Nutrient relations of winter wheat. 2. Movement of nutrients to the root and their uptake. J Agri Sci 93:495–504
17. Key JM (1973) The wheat root. In: Sears ER, Sears LMS (eds) 4th International wheat genetics symposium pp 827–842. Agricultural Experiment Station, College of Agriculture, University of Missouri, Columbia, Missouri, Columbia
18. Gregory PJ, Mcgowan M, Biscoe PV, Hunter B (1978) Water relations of winter wheat.1. Growth of root system. J Agric Sci 91:91–102
19. Klepper B, Belford RK, Rickman RW (1984) Root and shoot development in winter wheat. Agron J 76(1):117–122
20. Barraclough PB, Weir AH, Kuhlmann H (1991) Factors affecting the growth and distribution of winter wheat roots under UK field conditions. Dev Agr Manag For Ecol 24:410–441
21. Barraclough PB, Weir AH (1988) Effects of compacted subsoil layer on root and shoot growth, water use and nutrient uptake of winter wheat. J Agric Sci 110:207–216
22. Siddique KHM, Belford RK, Tennant D (1990) Root:shoot ratios of old and modern, tall and semidwarf wheats in a mediterranean environment. Plant Soil 121(1):89–98
23. Barraclough PB (1984) The growth and activity of winter-wheat roots in the field – root-growth of high-yielding crops in relation to shoot growth. J Agri Sci 103:439–442
24. Brouwer R (1983) Functional equilibrium: sense or nonsense? Neth J Agric Sci 31(4):335–348
25. Gregory PJ, Palta JA, Batts GR (1997) Root systems and root: mass ratio – carbon allocation under current and projected atmospheric conditions in arable crops. Plant Soil 187(2): 221–228
26. Gerwitz A, Page ER (1974) An empirical mathematical model to describe plant root systems. J Appl Ecol 11(2):773–781
27. Gale MR, Grigal DF (1987) Vertical root distributions of northern tree species in relation to successional status. Can J For Res 17(8):829–834
28. Robertson MJ, Fukai S, Hammer GL, Ludlow MM (1993) Modelling root growth of grain sorghum using the CERES approach. Field Crops Res 33:113–130
29. Zhuang J, Yu GR, Nakayama K (2001) Scaling of root length density of maize in the field profile. Plant Soil 235:135–142
30. King J, Gay A, Sylvester-Bradley R, Bingham I, Foulkes J, Gregory P, Robinson D (2003) Modelling ceral root systems for water and nitrogen capture: towards an economic optimum. Ann Bot 91:383–390
31. Thomas Fukai S, Hammer GL (1995) Growth and yield response of barley and chickpea to water stress under three environments in Southeast Queensland. II* Root growth and soil wate extraction pattern. Aust J Agric Res 46:35–48
32. Monteith JL (1986) How do crops manipulate water-supply and demand. Philos Trans R Soc Lond Ser Math Phys Eng Sci 316(1537):245–259
33. Robertson MJ, Fukai S, Ludlow MM, Hammer GL (1993) Water extraction by grain sorghum in a sub-humid environment. II. Extraction relation root growth. Field Crops Res 33:99–112
34. Eissenstat DM (1991) On the relationship between specific root length and the rate of root proliferation - a field-study using citrus rootstocks. New Phytol 118(1):63–68
35. Welbank PJ, Gibb MJ, Taylor PJ, Williams ED (1974) Root growth of cereal crops. In: Rothamsted Experimental Station Report, 1973, Part 2 pp 26–66
36. Barraclough PB, Leigh RA (1984) The growth and activity of winter wheat roots in the field: the effect of sowing date and soil type on root growth of high yielding crops. J Agric Sci 103:59–74
37. Van Noordwijk M, Brouwer G (1991) Review of quantitative root length data in agriculture. Elsevier, Amsterdam, Pays-Bas
38. Ryser P (1996) The importance of tissue density for growth and life span of leaves and roots: A comparison of five ecologically contrasting grasses. Funct Ecol 10(6):717–723
39. Wahl S, Ryser P (2000) Root tissue structure is linked to ecological strategies of grasses. New Phytol 148:459–471
40. Valenzuela-Estrada LR, Vera-Caraballo V, Ruth LE, Eissenstat DM (2008) Root anatomy, morphology, and longevity among root orders in *Vaccinium corymbosum* (*Ericaceae*). Am J Bot 95(12):1506–1514
41. Eissenstat DM (1992) Costs and benefits of constructing roots of small diameter. J Plant Nutr 15(6–7):763–782
42. Fitter AH (1996) Characteristics and functions of root systems. In: Waisel Y, Eshel A, Kafkafi U (eds) Plant roots: the hidden half. Marcel Dekker, New York, pp 1–20
43. Hetrick BAD, Leslie JF, Wilson GT, Kitt DG (1988) Physical and topological assessment of effects of a vesicular-arbuscular mycorrhizal fungus on root architecture of big bluestem. New Phytol 110(1):85–96
44. Ryser P (1998) Intra- and interspecific variation in root length, root turnover and the underlying parameters. In: Lambers H, Poorter H, van Vuuren MMI (eds) Inherent variation in plant

growth. Physiological mechanisms and ecological consequences. Backhuys, Leiden
45. Ehdaie B, Waines JG (2003) 1RS translocation increases root biomass in Veery-type wheat isogenic lines and associates with grain yield. In: Pogna NE, Romano M, Pogna EA, Galterio G (eds) Proceedings of the 10th International wheat genetics symposium, ISC Paestum, Italy, Rome, pp 693–695
46. Hamblin A, Tennant D, Perry MW (1990) The cost of stress - dry-matter partitioning changes with seasonal supply of water and nitrogen to dryland wheat. Plant Soil 122(1):47–58
47. Barraclough PB, Kuhlmann H, Weir AH (1989) The effects of prolonged drought and nitrogen-fertilizer on root and shoot growth and water-uptake by winter-wheat. J Agron Crop Sci 163(5):352–360
48. Zenisceva L (1990) The importance of the root-system in adaptation of spring barley genotypes to the conditions of environment. Rost Vyroba 36:937–945
49. Palta JA, Gregory PJ (1997) Drought affects the fluxes of carbon to roots and soil in C-13 pulse-labelled plants of wheat. Soil Biol Biochem 29(9–10):1395–1403
50. Martino DL, Shaykewich CF (1994) Root penetration profiles of wheat and barley as affected by soil penetration resistance in field conditions. Can J Soil Sci 74:193–200
51. Kramer PJ (1983) Water relations of plants. Academic, London
52. Karrou M, Maranville JW (1994) Response of wheat cultivars to different soil nitrogen and moisture regimes: I. Dry matter partitioning root growth. J Plant Nutr 17(5):729–744
53. Davidson RL (1969) Effect of root/leaf temperature differentials on root/shoot ratios in some pasture grasses and clover. Ann Bot 33(3):561–569
54. Gregory PJ (1994) Root growth and activity. In: Boote KJ, Bennett JM, Sinclair TR, Paulsen GM (eds) Physiology and determination of crop yield. Soil Science Soc America, Madison, pp 65–93
55. Sharp RE, Davies WJ (1979) Solute regulation and growth by roots and shoots of water-stressed maize plants. Planta 147(1):43–49
56. Li FM, Yan X, Li FR, Guo AH (2001) Effects of different water supply regimes on water use and yield performance of spring wheat in a simulated semi-arid environment. Agric Water Manage 47(1):25–35
57. Robinson D (1994) Resource capture by single roots. In: Monteith JL, Scott RK, Unsworth MH (eds) Resource capture by crops. Nottingham University Press, Nottingham, pp 53–76
58. Baburai Nagesh AK (2006) The physiological and genetic bases of water-use efficiency in winter wheat. Ph.D. thesis, University of Nottingham
59. Ebrahim NM (2008) Responses of root and shoot growth of durum wheat (Triticum turgidum L. var durum) and barley (Hordeum vulgare L.) plants to different water and nitrogen levels. PhD Thesis University of Jordan, Jordan, 284 pp
60. Fitter AH (1987) An architectural approach to the comparative ecology of plant root systems. New Phytol 106:61–77
61. Li FM, Liu XL, Li SQ (2001) Effects of early soil water distribution on the dry matter partition between roots and shoots of winter wheat. Agric Water Manage 49(3):163–171
62. Turner NC, Begg JE (1981) Plant-water relations and adaptation to stress. Plant Soil 58(1–3):97–131
63. Kramer PJ (1988) Changing concepts regarding plant water relations. Plant Cell Environ 11(7):565–568
64. Hsiao TC, Frensch J, Rojas-Lara BAR (1998) The pressure-jump technique shows maize leaf growth to be enhanced by increases in turgor only when water status is not too high. Plant Cell Environ 21(1):33–42
65. Passioura JB (1988) Changing concepts regarding plant water relations - response. Plant Cell Environ 11(7):569–571
66. Passioura JB (1988) Root signals control leaf expansion in wheat seedlings growing in drying soil. Aust J Plant Physiol 15(5):687–693
67. Gowing DJG, Davies WJ, Jones HG (1990) A positive root-sourced signal as an indicator of soil drying in Apple, *Malus x domestica* Borkh. J Exp Bot 41(233):1535–1540
68. Davies WJ, Tardieu F, Trejo CL (1994) How do chemical signals work in plants that grow in drying soil? Plant Physiol 104(2):309–314
69. Taylor IB, Burbidge A, Thompson AJ (2000) Control of abscisic acid synthesis. J Exp Bot 51(350):1563–1574
70. Zhang J, Davies WJ (1990) Changes in the concentration of aba in xylem sap as a function of changing soil-water status can account for changes in leaf conductance and growth. Plant Cell Environ 13(3):277–285
71. Davies WJ, Zhang J (1991) Root signals and the regulation of growth and development of plants in drying soil. Annu Rev Plant Physiol Plant Mol Biol 42(1):55–76
72. Hartung W, Jeschke WD (1999) Abscisic acid: a long-distance stress signal in salt-stressed plants. In: Lerner HR (ed) Plant responses to environmental stresses. Marcel Dekker, New York, pp 333–348
73. Gollan T, Passioura JB, Munns R (1986) Soil water status affects the stomatal conductance of fully turgid wheat and sunflower leaves. Aust J Plant Physiol 13(4):459–464
74. Aphale SL (2004) Role of root to shoot signalling in coordinating responses to nitrogen deficiency. Ph.D. thesis, University of Nottingham
75. Munns R, Passioura JB, Guo JM, Chazen O, Ramer GR (2000) Water relations and leaf expansion: importance of time scale. J Exp Bot 51(350):1495–1504
76. Stikić R, Davies WJ (2000) Stomatal reactions of two different maize lines to osmotically induced drought stress. Biol Plant 43(3):399–405
77. Novoa R, Loomis RS (1981) Nitrogen and plant production. Plant Soil 58(1–3):177–204
78. Dreccer M, Schapendonk A, Slafer G, Rabbinge R (2000) Comparative response of wheat and oilseed rape to nitrogen supply: absorption and utilisation efficiency of radiation and nitrogen during the reproductive stages determining yield. Plant Soil 220(1):189–205

79. Mengel K, Kirkby EA (2001) Principles of plant nutrition. Kluwer, London
80. Reich PB (2002) Root-shoot relations: optimality in acclimation and adaptation or the: "Emperor's new clothes"? In: Waisel Y, Eshel A, Kafkafi U (eds) Plant roots: the hidden half. Marcel Dekker, New York, pp 205–220
81. Robinson D (2001) Root proliferation, nitrate inflow and their carbon costs during nitrogen capture by competing plants in patchy soil. Plant Soil 232(1–2):41–50
82. Robinson D, Hodge A, Griffiths BS, Fitter AH (1999) Plant root proliferation in nitrogen-rich patches confers competitive advantage. Proc R Soc Lond B Biol Sci 266(1418):431–435
83. Jackson RB, Caldwell MM (1989) The timing and degree of root proliferation in fertile-soil microsites for 3 cold-desert perennials. Oecologia 81(2):149–153
84. Drew MC, Saker LR, Ashley TW (1973) Nutrient supply and the growth of the seminal root system in barley: I. Effect nitrate concentration growth axes laterals. J Exp Bot 24(6): 1189–1202
85. Drew MC, Saker LR (1975) Nutrient supply and the growth of the seminal root system in barley. II. Localized, compensatory increases in lateral root growth and rates op nitrate uptake when nitrate supply is restricted to only part of the root system. J Exp Bot 26(1):79–90
86. Drew MC, Saker LR (1978) Nutrient supply and the growth of the seminal root system in barley. III. Compensatory increases in growth of lateral roots, and in rates of phosphate uptake, in response to a localized supply of phosphate. J Exp Bot 29(2):435–451
87. Zhang HM, Forde BG (1998) An Arabidopsis MADS box gene that controls nutrient-induced changes in root architecture. Science 279(5349):407–409
88. Robinson D (1994) The responses of plants to non-uniform supplies of nutrients. New Phytol 127(4):635–674
89. Brown SC, Keatinge JDH, Gregory PJ, Cooper PJM (1987) Effects of fertilizer, variety and location on barley production under rainfed conditions in northern syria 1root shoot growth. Field Crops Res 16:53–66
90. Herrera JM, Stamp P, Liedgens M (2005) Dynamics of root development of spring wheat genotypes varying in nitrogen use efficiency. In: Foulkes J, Russel G, Hawkesford M, Gooding M, Sparkes D, Stockdale E (eds) Roots and the soil environment II. Association of Applied Biologists, Warwick, pp 197–201
91. Ryser P, Lambers H (1995) Root and leaf attributes accounting for the performance of fast- and slow-growing grasses at different nutrient supply. Plant Soil 170:251–265
92. Foulkes MJ, Hawkesford MJ, Barraclough PB, Holdsworth MJ, Kerr S, Kightley S, Shewry PR (2009) Identifying traits to improve the nitrogen economy of wheat: recent advances and future prospects. Field Crops Res 114:329–342
93. Doussan C, Pages L, Pierret A (2003) Soil exploration and resource acquisition by plant roots: an architectural and modelling point of view. Agronomie 23(5–6):419–431
94. Kramer PJ, Boyer JS (1995) Water relations of plants and soils. Academic, San Diego
95. Van Noordwijk M (1983) Functional interpretation of root densities in the field for nutrient and water uptake. In: Böhm W, Kutschera L, Lichtenegger E (eds) Root ecology and its practical application, Interantinal Symposium. Gumpenstein 1982, Irdning, Bundesanstalt Gumpenstein, pp 207–226
96. Gregory PJ, Brown SC (1989) Root growth, water use and yield of crops in dry environments: what characteristics are desirable? Aspects Appl Biol 22:235–243
97. Pantuwan G, Fukai S, Cooper M, O'toole JC, Sarkarung S (1997) Root traits to increase drought resistance in rainfed lowland rice. In: Fukai S, Cooper M, Salisbury J (eds) Proceedings of Breeding Strategies for Rainfed Lowland Rice in Drought-Prone Environments, vol 77, Canberra, pp 170–179
98. Lilley JM, Fukai S (1994) Effect of timing and severity of water deficit on four diverse rice cultivars I. rooting pattern soil water extraction. Field Crops Res 37(3):205–213
99. Siopongco J, Yamauchi A, Salekdeh H, Bennett J, Wade LJ (2005) Root growth and water extraction response of doubled-haploid rice lines to drought and rewatering during the vegetative stage. Plant Prod Sci 8(5):497–508
100. Ford KE, Gregory PJ, Gooding MJ, Pepler S (2006) Genotype and fungicide effects on late-season root growth of winter wheat. Plant Soil 284(1–2):33–44
101. Christopher JT, Manschadi AM, Hammer GL, Borrell AK (2008) Developmental and physiological traits associated with high yield and stay-green phenotype in wheat. Aust J Agric Res 59(4):354–364
102. Bengough AG, Bransby MF, Hans J, Mckenna SJ, Roberts TJ, Valentine TA (2006) Root responses to soil physical conditions; growth dynamics from field to cell. J Exp Bot 57(2): 437–447
103. Kirk GJD (2003) Rice root properties for internal aeration and efficient nutrient acquisition in submerged soil. New Phytol 159(1):185–194
104. Robinson D, Linehan DJ, Caul S (1991) What limits nitrate uptake from soil. Plant Cell Environ 14(1):77–85
105. Cooper PJM, Gregory PJ, Keatinge JDH, Brown SC (1987) Effects of fertilizer, variety and location on barley production under rainfed conditions in Northern Syria. 2: Soil water dyamics and crop water use. Field Crops Res 16:67–84
106. Wiesler F, Horst WJ (1993) Differences among maize cultivars in the utilization of soil nitrate and the related losses of nitrate through leaching. Plant Soil 151:193–203
107. Wiesler F, Horst WJ (1994) Root growth and nitrate utilization of maize cultivars under field conditions. Plant Soil 163: 267–277
108. Thorup-Kristensen K (1993) Root development of nitrogen catch crops and of a succeeding crop of broccoli. Acta Agriculturae Scaninavica B Soil Plant Sci 43:58–64

109. Gregory PJ (1994) Resource capture by root networks. In: Monteith JL, Scoot RK, Unsworth MH (eds) Resource capture by crops. Nottingham University Press, Nottingham, pp 77–97
110. Nielsen NE, Schjorring JK (1983) Efficiency and kinetics of phosphorus uptake from soil by various barley genotypes. Plant Soil 72(2–3):225–230
111. Gregory PJ (1994) Resource capture by root networks. In: Monteith JL, Scott RK, Unsworth MH (eds) Resource capture by crops. Nottingham University Press, pp 77–97
112. Gao S, Pan WL, Koenig RT (1998) Wheat root growth responses to enhanced ammonium supply. Soil Sci Soc America J 62:1736–1740
113. Fitter AH, Stickland TR (1991) Architectural analysis of plant-root systems. 2. Influence of nutrient supply on architecture in contrasting plant-species. New Phytol 118(3):383–389
114. López-Bucio J, Hernández-Abreu E, Sánchez-Calderón L, Nieto-Jacobo MF, Simpson J, Herrera-Estrella L (2002) Phosphate availability alters architecture and causes changes in hormone sensitivity in the arabidopsis root system. Plant Physiol 129(1):244–256
115. Poirier Y, Bucher M (2002) Phosphate transport and homeostasis in Arabidopsis. American Society of Plant Biologists, Rockville
116. Cabrera-Bosquet L, Molero G, Bort J, Nogués S, Araus JL (2007) The combined effect of constant water deficit and nitrogen supply on WUE, NUE and D13C in durum wheat potted plants. Ann Appl Biol 151(3):277–289
117. Pask A (2009) Optimising nitrogen storage in wheat canopies for genetic reduction in fertiliser nitrogen inputs. Ph.D. thesis, University of Nottingham
118. Dunbabin V, Diggle A, Rengel Z (2003) Is there an optimal root architecture for nitrate capture in leaching environments? Plant Cell Environ 26:835–844
119. Forde BG, Clarkson DT (1999) Nitrate and ammonium nutrition of plants: physiological and molecular perspectives. In: Ellow JA (ed) Advances in botanical research incorporating advances in plant pathology, vol 30. Academic, San Diego, pp 1–90
120. Crawford NM, Glass ADM (1998) Molecular and physiological aspects of nitrate uptake in plants. Trends Plant Sci 3(10):389–395
121. Williams LE, Miller AJ (2001) Transporters responsible for the uptake and partitioning of nitrogenous solutes. Annu Rev Plant Physiol Plant Mol Biol 52:659–688
122. Hawkesford MJ, Miller AJ (2004) Ion-coupled transport of inorganic solutes. In: Blatt MR (ed) Membrane transport in plants annual reviews 15. Blackwell/CRC Press, Oxford, pp 105–134
123. Lauter FR, Ninnemann O, Bucher M, Riesmeier JW, Frommer WB (1996) Preferential expression of an ammonium transporter and of two putative nitrate transporters in root hairs of tomato. Proc Natl Acad Sci USA 93(15):8139–8144
124. Zhuo DG, Okamoto M, Vidmar JJ, Glass ADM (1999) Regulation of a putative high-affinity nitrate transporter (Nrt2;1At) in roots of Arabidopsis thaliana. Plant J 17(5): 563–568
125. Ono F, Frommer WB, Von Wiren N (2000) Coordinated diurnal regulation of low- and high-affinity nitrate transporters in tomato. Plant Biol 2(1):17–23
126. Orsel M, Krapp A, Daniel-Vedele F (2002) Analysis of the NRT2 nitrate transporter family in Arabidopsis. structuer and gene expression. Plant Physiol 129(2):886–896
127. Bucher M (2007) Functional biology of plant phosphate uptake at root and mycorrhiza interfaces. New Phytol 173(1):11–26
128. Miller AJ, Shen Q, Xu G (2009) Freeways in the plant: transporters for N, P and S and their regulation. Curr Opin Plant Biol 12(3):284–290
129. Waines JG, Ehdaie B (2007) Domestication and crop physiology: roots of green-revolution wheat. Ann Bot 100(5): 991–998
130. Miralles DJ, Slafer GA, Lynch V (1997) Rooting patterns in near-isogenic lines of spring wheat for dwarfism. Plant Soil 197(1):79–86
131. Bush MG, Evans LT (1988) Growth and development in tall and dwarf isogenic lines of spring wheat. Field Crops Res 18(4):243–270
132. Mccaig TN, Morgan JA (1993) Root and shoot dry-matter partitioning in near-isogenic wheat lines differing in height. Can J Plant Sci 73(3):679–689
133. Hurd EA (1974) Phenotype and drought tolerance in wheat. Agric Meteorol 14(1–2):39–55
134. Ogbonnaya FC, Seah S, Delibes A, Jahier J, Lopez-Brana I, Eastwood RF, Lagudah ES (2001) Molecular-genetic characterisation of a new nematode resistance gene in wheat. Theor Appl Genet 102(4):623–629
135. Steele KA, Price AH, Shashidhar HE, Witcombe JR (2006) Marker-assisted selection to introgress rice QTLs controlling root traits into an Indian upland rice variety. Theor Appl Genet 112(2):208–221
136. Manske GGB, Ortiz-Monasterio JI, Vlek PLD (2001) Thecniques for measuring genetic diversity in roots. In: Reynods MP, Ortiz-Monasterio JI, McNab A (eds) Application of physiology in wheat breeding. Mexico, Cimmiyt
137. Polomski J, Kuhn N (2002) Root research methods. In: Waisel Y, Eshel A, Kafkafi U (eds) Plant roots: the hidden half. Marcel Dekker, New York, pp 295–321
138. De Dorlodot S, Forster B, Pages L, Price A, Tuberosa R, Draye X (2007) Root system architecture: opportunities and constraints for genetic improvement of crops. Trends Plant Sci 12:474–481
139. Manschadi A, Hammer G, Christopher J, Devoil P (2008) Genotypic variation in seedling root architectural traits and implications for drought adaptation in wheat (Triticum aestivum L). Plant Soil 303(1):115–129

140. Swarup K, Benkova E, Swarup R, Casimiro I, Peret B, Yang Y, Parry G, Nielsen E, De Smet I, Vanneste S, Levesque MP, Carrier D, James N, Calvo V, Ljung K, Kramer E, Roberts R, Graham N, Marillonnet S, Patel K, Jones JDG, Taylor CG, Schachtman DP, May S, Sandberg G, Benfey P, Friml J, Kerr I, Beeckman T, Laplaze L, Bennett MJ (2008) The auxin influx carrier LAX3 promotes lateral root emergence. Nat Cell Biol 10(8):946–954

Books and Reviews

Bassirirad H (2000) Kinetics of nutrient uptake by roots: responses to global change. New Phytol 147(1):155–169

Beeckman T (ed) (2010) Root development. Blackwell, Chichester

Bingham IJ (2001) Soil-root-canopy interactions. Ann Appl Biol 138(2):243–251

Bingham IJ, Hoad SP (2000) Towards below ground management In: HGCA conference: crop management into the millennium, Homerton College, Conference Centre, HGCA, Cambridge, pp 7.1–7.8

Bingham IJ, Foulkes MJ, Gay AP, Gregory PJ, King JA, Robinson D, Bradley RS (2002) Balancing root and canopy growth. In: HGCA (ed) R & D conference: agronomic intelligence: the basis for profitable production, pp 6.1–6.14

Blum A (ed) (2009) Plant stress http://plantstress.com/

Dakora FD, Phillips DA (2002) Root exudates as mediators of mineral acquisition in low-nutrient environments. Plant Soil 245(1):35–47

Lynch JP (2007) Roots of the second green revolution. Aust J Bot 55(5):493–512

Lynch J, Brown KM (eds) (2009) Root research methods. http://roots.psu.edu/en/methods

Schachtman DP, Goodger JQD (2008) Chemical root to shoot signaling under drought. Trends Plant Sci 13(6):281–287

Smit AL, Bengough AG, Engels C, Noordwijk MV, Pllerin S, Geijn SCVD (eds) (2000) Root methods. A handbook. Springer, Berlin

Van Noordwijk M, Martikainen P, Bottner P, Cuevas E, Rouland C, Dhillion SS (1998) Global change and root function. Glob change Biol 4:759–772

Waisel Y, Eshel A, Kafkafi U (eds) (2002) Plant roots: the hidden half. Marcel Dekker, New York

Wang E, Smith CJ (2004) Modelling the growth and water uptake function of plant root systems: a review. Aust J Agric Res 55:501–523

S

Science, Policy, and Risk Management: Case of Seafood Safety

Damaris A. F. Meujo[1], Mark T. Hamann[1,2,3,4]
[1]Department of Pharmacognosy, The University of Mississippi, University, MS, USA
[2]Department of Chemistry and Biochemistry, The University of Mississippi, University, MS, USA
[3]Department of Pharmacology, The University of Mississippi, University, MS, USA
[4]Institute of Marine and Environmental Technology, University of Maryland Center for Environmental Science, Baltimore, MD, USA

Article Outline

Glossary
Definition of the Subject
Introduction
"Food Safety Hazards" Associated with Seafood
What Are the Approaches Used to Assure Public Safety?
Future Directions and Conclusions
Acknowledgments
Bibliography

Glossary

Action levels "Action levels and tolerances represent limits at or above which the FDA will take legal action to remove products from the market" – FDA.

An outbreak Involves two or more ill people – CSPI.

Biological contaminants In the context of this document, these are pathogenic microorganisms (bacteria, viruses, and parasites) found in seafood.

Chemical contaminants In the context of this entry, are regrouped under this denomination, all nonbiological contaminants (deleterious chemicals) traceable to seafood.

Environmental pollutants Seafood-associated deleterious substances traceable to the environment such as heavy metals and persistent organic pollutants.

Etiological agent A microorganism responsible for a given disease.

Food safety hazards According to the Seafood HACCP Regulation, a "food safety hazard" is "any biological, chemical, or physical property that may cause food to be unsafe for human consumption."

Seafood Edible marine plants and animals (fish and shellfish) are usually grouped under the denomination of seafood in some contexts, these are referred to as "fish and fishery products" [1]. This same term is often given a broader meaning: all edible aquatic plants and animals.

Seafood-associated toxins Harmful chemical substances produced either by seafood-associated bacterial contaminants, cyanobacteria, or toxic microscopic algae (dinoflagellates and diatoms) on which seafood feed.

Tolerance threshold Maximum allowable amount of ubiquitous deleterious substance in seafood.

Definition of the Subject

In order to function properly, the human body needs a wide range of essential nutrients, which it gets from food that is ingested on a daily basis. Unfortunately, food also represents a vector for harmful creatures (bacterial, viral, protozoan pathogens) and chemical substances (organic toxins as well as toxic metals and various environmental contaminants). According to the most recent surveys of the Center for Science for Public Interest (CSPI), for more than a decade now, seafood has ranked first as the most likely source of foodborne disease outbreaks of established origin [2, 3]. Based on these surveys, seafood-associated hazards that have caused the largest number of outbreaks are toxins (especially scombrotoxin and ciguatera), followed by bacteria, the most problematic of which

Robert A. Meyers (ed.), *Encyclopedia of Sustainability Science and Technology*, DOI 10.1007/978-1-4419-0851-3,
© Springer Science+Business Media, LLC 2012

are *Vibrio* spp, and finally viruses (especially norovirus). Though food safety is primarily the responsibility of regulatory agencies, several other groups are involved. These include industries, consumers, and the scientific community upon which rests the responsibility of developing cutting-edge technologies capable of eliminating seafood-associated biological and chemical contaminants. The international community also relies on science for the development of revolutionary technologies for a faster, cheaper, easier, and more accurate detection of seafood-associated health hazards; tools without which enforcing laws and regulations set forth by regulatory agencies is virtually impossible. In this entry, different categories of seafood-associated health hazards as well as a few relevant regulatory and scientific efforts dedicated to reduce the incidence of seafood-borne illnesses are reviewed.

Introduction

Seafood constitutes a significant portion of the world's food supply and is renowned for its delightful taste. It is a critical component of the human diet because of its unique nutritional properties. Fish, for instance, is a good source of protein as its major components are proteins and lipids. All essential amino acids can be derived from fish consumption. Approximately 40% of the lipids found in fish are comprised of highly unsaturated long-chain fatty acids. Other outstanding nutritional qualities are reduced saturated fats and carbohydrates and plentiful essential nutrients. Some fish species are a valuable source of important nutrients such as vitamins A and D, phosphorus, iron, calcium, magnesium, selenium, and iodine [4, 5].

There are numerous reports of health benefits associated with the consumption of seafood. Several of these health benefits have been attributed to seafood's high content of vital nutrients, such as *n*-3 polyunsaturated fatty acids (PUFAs), specifically eicosapentaenoic acid (EPA), and docosahexaenoic (DHA). These health benefits include a reduced risk of developing serious diseases such as depression, [6] myocardial infarction, Alzheimer's [7], dementia [8], and weight loss [9]. A number of reports have associated seafood consumption with a reduced risk of mortality among individuals suffering from coronary heart disease [10] and a reduced risk of developing diseases such as ischemic and thrombotic strokes, colon and intestinal cancers, as well as others [9, 11–13]. These positive effects are counted among the factors that have driven current market trends. There has been a steady increase in the world's per capita fish and fishery products consumption for several decades now [14]. According to the December 2009 Food Outlook Report of the Food and Agriculture Organization (FAO), the annual per capita fish consumption in the world during the years 2007–2009 was estimated at ~17.1 kg. It is important to note that in the 1970s, 1980s, and 1990s, these values were 11.5, 12.8, and 16.4 kg per capita, respectively [15, 16].

As indicated by recent estimates, there has been a net increase in the demand for seafood in countries around the world [17]. In the UK for instance, the seafood retail market has experienced a considerable increase between the years 2003 and 2007, increasing from £2.4 billion (retail price) to an estimated £3.25 billion in 2007 [14]. A significant increase in seafood demand in developing countries has been observed, as well [16]. Millions of tons of seafood are caught each year worldwide to sustain the current demand. There has been a steady increase in the total world fish production since the 1950s, from 19.3 million tons to about 134 million tons in 2002 [18]. According to a 2009 FAO report, the current world production (capture fisheries plus aquaculture) is estimated at 144.1 million tons, divided into 98.8 million from capture fisheries and 54.3 million from aquaculture [15, 16].

Unfortunately, seafood consumption is not without risks and food is an important vector of a wide range of health hazards (Fig. 1). Foodborne illnesses are a serious public health concern and according to the Centers for Disease Control and Prevention (CDC) roughly 76 million foodborne illnesses corresponding to about 325,000 hospitalizations and 5,000 deaths are recorded in the USA each year [19]. A recent survey conducted by the Center for Science for Public Interest (CSPI) [2] revealed that the food categories that were associated with the largest number of outbreaks in the USA during the period 1990–2006 were seafood, produce, poultry, beef, and eggs. Seafood was responsible for 1,140 out of 5,778 outbreaks and therefore was the most problematic food (Fig. 2). Also reported was an increase in the

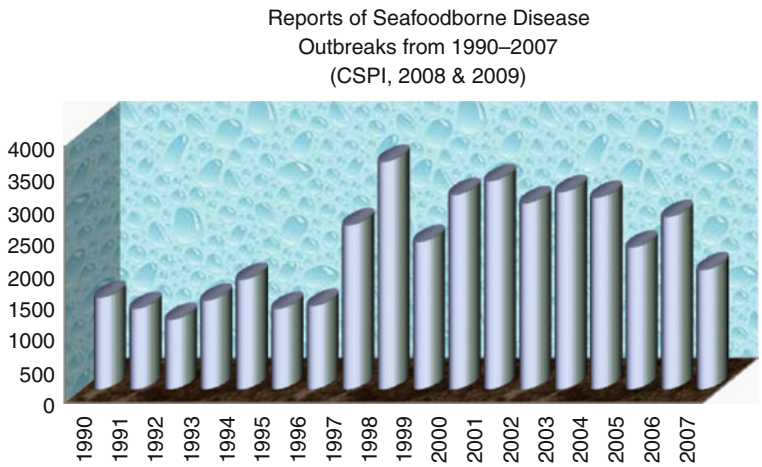

Science, Policy, and Risk Management: Case of Seafood Safety. Figure 1
Variation in the number of reported seafood-borne disease outbreaks since the 1990s in the USA

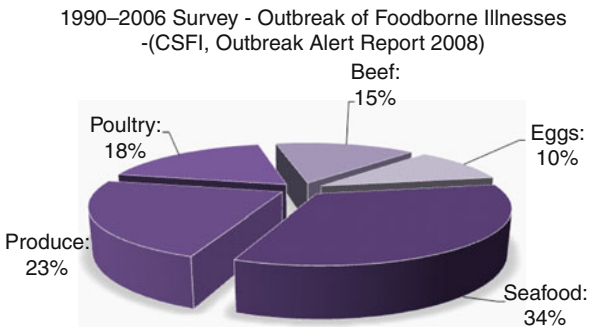

Science, Policy, and Risk Management: Case of Seafood Safety. Figure 2
Foodborne outbreaks reported during the years 1998–2007 by category of food in the USA

number of seafood-related outbreaks compared to the early 1990s (Fig. 1). It is important to mention that the number of reported cases of seafood-borne illness has remained constant over the years. Though it ranked second as far as number of outbreaks, produce caused the largest number of cases of illness during that same time frame [2].

"Food Safety Hazards" Associated with Seafood

Seafood-associated health hazards can be classified into two main categories: (1) biological contaminants (includes a long list of bacteria, viruses, parasites) and (2) chemical contaminants such as environmental pollutants (pesticides, heavy metals, approved or unapproved drug substances) and finally natural toxins from a variety of structural classes. According to the CSPI's 2008 report, the latter category was associated with the largest number of seafood-borne outbreaks from 1990 through 2006 (Fig. 3) [2]. Currently known health hazards associated with seafood are either naturally occurring or from various anthropogenic activities. Seafood becomes contaminated either as a result of feeding on poisonous phytoplankton species or in sewage-contaminated marine environments. Seafood contamination can also arise from inappropriate storage or accidental exposures during handling. Certain types of seafood are more likely vehicles of dangerous substances and pathogenic microorganisms than others.

Categories of seafood that have been associated with greater public safety risks are considered a high priority in sampling and surveillance efforts by the Food and Drug Administration (FDA) [20]. At the top of the FDA's seafood watch list are products such as molluskan shellfish from uncertified sources, refrigerated reduced oxygen packaged products, ready-to-eat seafood, seafood mixes containing cooked, raw, or partially cooked seafood components, as well as, scombrotoxin (histamine)-forming fish, aquaculture-derived seafood, and finally salt-cured or dried uneviscerated finfish [20]. According to the 2008 CSPI report, based on the number of reported outbreaks, finfish (such as tuna and grouper) was the

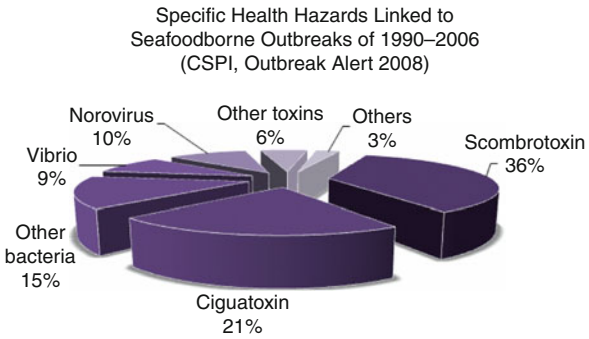

Science, Policy, and Risk Management: Case of Seafood Safety. Figure 3
Specific health hazards that caused seafood-borne outbreaks reported during the years 1990–2006 in the USA

most dangerous type of seafood between the years 1990 and 2006. Finfish was responsible for 61% of all reported seafood-borne outbreaks during this period, followed by molluskan shellfish (15%) (Fig. 4a). The largest number of cases of seafood-borne illness was attributable to mollukcan shellfish (Fig. 4b) [2].

Seafood-Associated Toxins

Seafood-associated toxins, especially scombrotoxin and ciguatoxin, have been linked to the majority of seafood-borne outbreaks that occurred during the last decade and as such, could be viewed as the most dangerous seafood-associated "food safety hazard" [2, 3]. Scombrotoxin and ciguatoxin alone were responsible

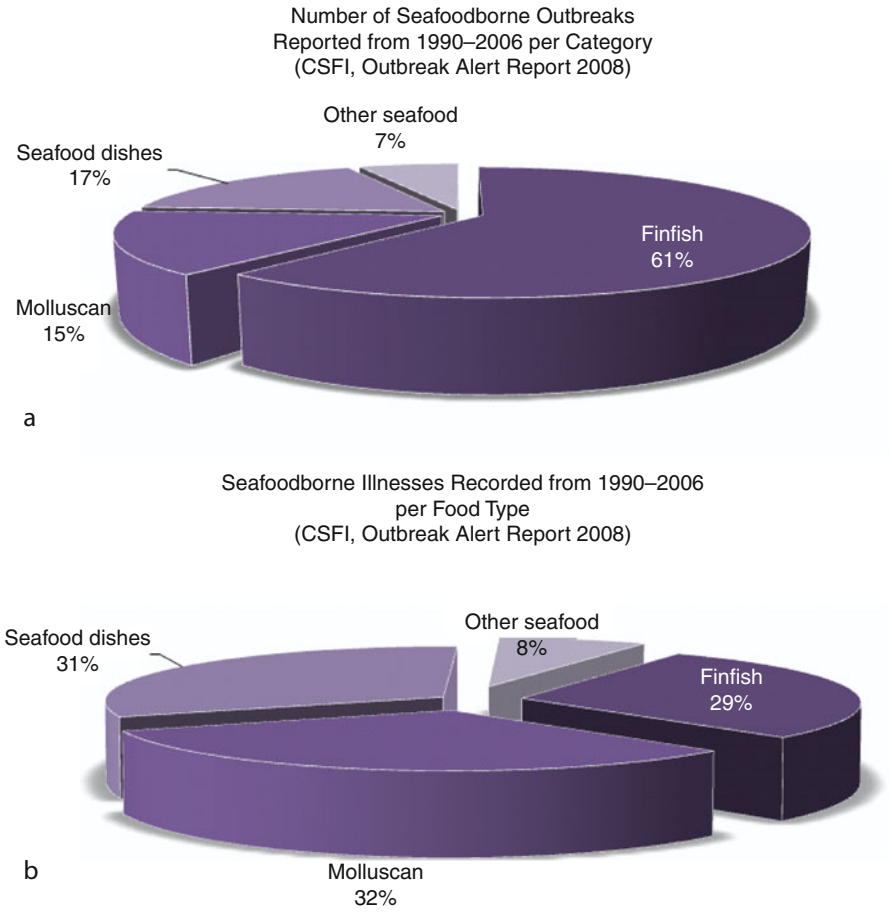

Science, Policy, and Risk Management: Case of Seafood Safety. Figure 4
Seafood-borne, outbreaks (**a**) and cases of illnesses (**b**) reported in the USA during the years 1990–2006 (by category of seafood)

for 57% of all seafood-related outbreaks in the USA reported from 1990 to 2006 [2].

Seafood-associated toxins have been linked to a wide variety of intoxications. These include, poisoning associated with shellfish consumption, namely diarrheic shellfish poisoning (DSP), paralytic shellfish poisoning (PSP), amnesic shellfish poisoning (ASP), neurologic shellfish poisoning (NSP), aZaspiracid shellfish poisoning (AZP), and poisonings associated with fish consumption. The latter include ciguatera fish poisoning (CFP) and puffer fish poisoning [21]. It is necessary to point out that some seafood-associated biotoxins, namely ciguatoxin and toxins responsible for PSP, NSP, and ASP, can be lethal [22]. Seafood-associated toxins are generated either by bacterial contaminants that freely proliferate when seafood is improperly stored or by cyanobacteria and toxic microscopic algae (dinoflagellates and diatoms) on which the seafood feed. The blooms of these latter organisms, which occur from season to season, forming red tides (Harmful Algae Blooms [HAB]) are a subject of public health and environmental concerns, affecting the tourism and fishing industries [23].

Ciguatera Fish Poisoning Ciguatera fish poisoning has been reported in countries around the world (Europe, Africa, America, Asia, and Oceania). This form of poisoning is frequent between the months of April through August and has been linked to the consumption of certain fish. Some examples are shark, barracuda, snapper, hogfish, horse-eye jack, red grouper, gray triggerfish, Spanish mackerel, narrowhead gray mullet, chinamanfish, swordfish, and amberjack. Ciguatera fish poisoning is caused by a set of heat-resistant polyether toxins known as ciguatoxins (Fig. 5), which are the product of in situ gambiertoxin biotransformation [23, 24]. Ciguatoxin, maitotoxin, palytoxin, and scaritoxin are members of this group. These toxins are produced by a variety of organisms; these include *Gambierdiscus toxicus*, *Gymnodinium sangieneum, G. polyedra, Ostreopsis lenticularis, Prorocentrum concavum, P. mexicanum,* and *P. rhathytum*, among others [21, 25]. Symptoms of ciguatera fish poisoning are mainly gastrointestinal and neurological. A few therapeutic approaches in case of poisoning include, but are not limited to, antihistamines, antiemetics (droperidol, prochlorperazin, metoclopramide), atropine, as well as intravenous hydration [23].

Scombrotoxic Fish Poisoning Scombroid fish poisoning differs from other types of toxin-mediated seafood poisonings because the responsible toxin is not produced by a microalgae. Instead, it is generated under improper storage conditions (temperature $> 20°C$). This toxin is the result of a catalytic reaction involving the conversion of in situ histidine into histamine (Fig. 5). The enzyme responsible for this conversion, histidine decarboxylase, can be produced by several types of bacteria. These include various *Vibrio* sp. *Clostridium, Enterobacteriaceae* (such as *Morganella morganii* and *Klebsiella pneumoniae* and *Hafnia alvei*) and *Lactobacillus* sp. [26]. Scombrotoxin is stable to both heat and cold conditions. Scombroid fish (fish containing a high level of free histidine) and non-scombroid fish have been implicated in this form of poisoning. These include fish such as amberjack, abalone, tunas, sardines, mackerel, bonito, and bluefish, just to name a few [25]; associated symptoms rank from mild and self-limiting to severe. Groups at risk for developing the severe form of this disease are people with respiratory and cardiac conditions or those on medication such as isoniazid and doxycycline that slow histamine degradation [23, 25, 27]. Symptoms of scombrotoxic fish poisoning include headache, abdominal cramps, nausea, diarrhea, and palpitations, among others. As far as pathophysiology, bioamines other than histamine are believed to play a critical role; a few examples are spermine, cadaverine, agmatine, and putrescine [25, 28]. There are several therapeutic approaches for this type of food poisoning. These include administration of activated charcoal, diphenhydramine, cimetidine, and famodine [27].

Other Major Seafood-Borne Poisonings *Paralytic shellfish poisoning* (PSP) can be caused by a wide range of tetrahydropurine type toxins (carbamate, *N*-sulfo-carbamoyl, decarbamoyl, and deoxydecarbamoyl) [24] collectively called saxitoxins (Fig. 5). These are neurotoxins that act by blocking sodium channels, causing symptoms like numbness, paralysis, and disorientation. Saxitoxins are produced by dinoflagellates and blue-green algae. Dinoflagellates

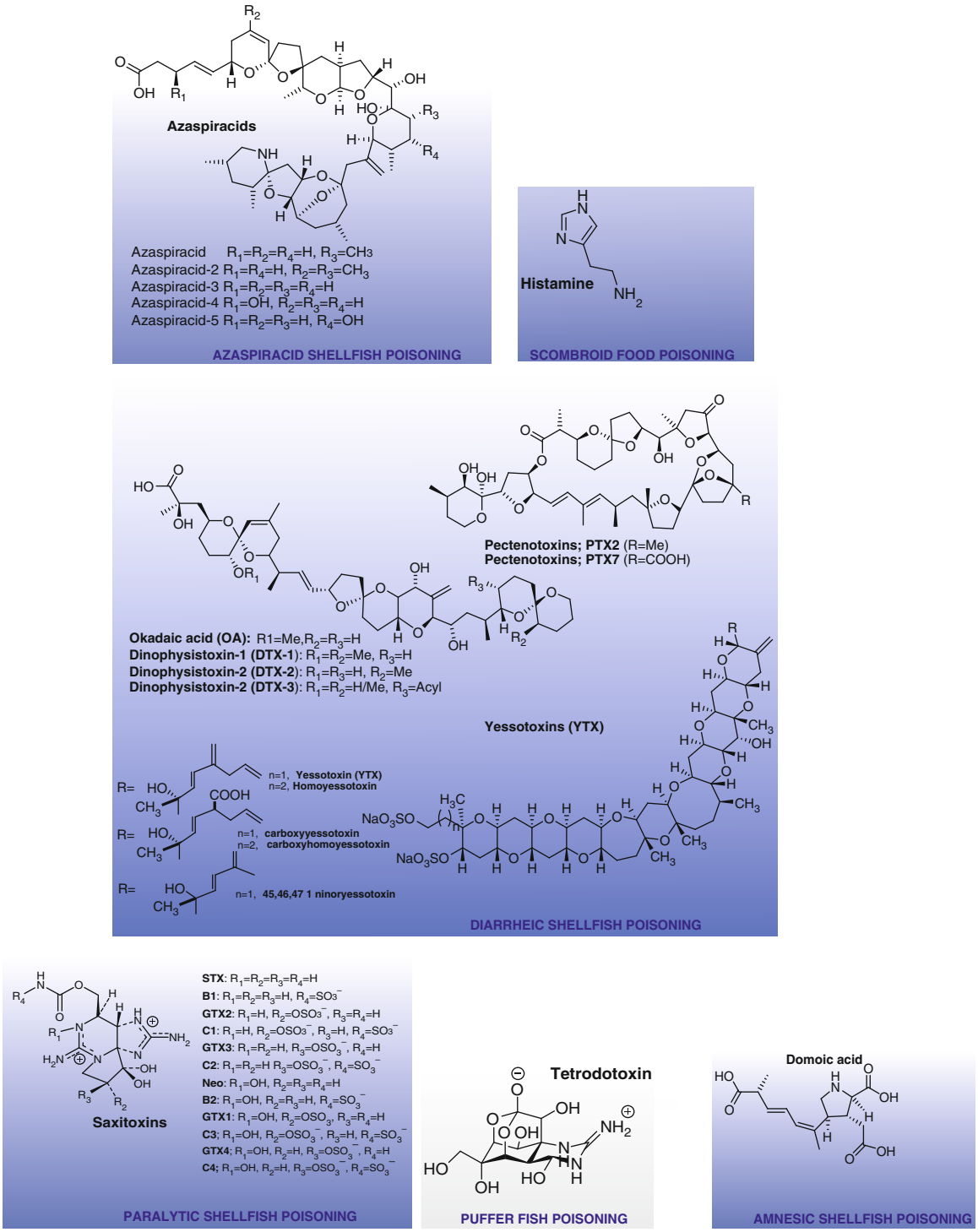

Science, Policy, and Risk Management: Case of Seafood Safety. Figure 5 (Continued)

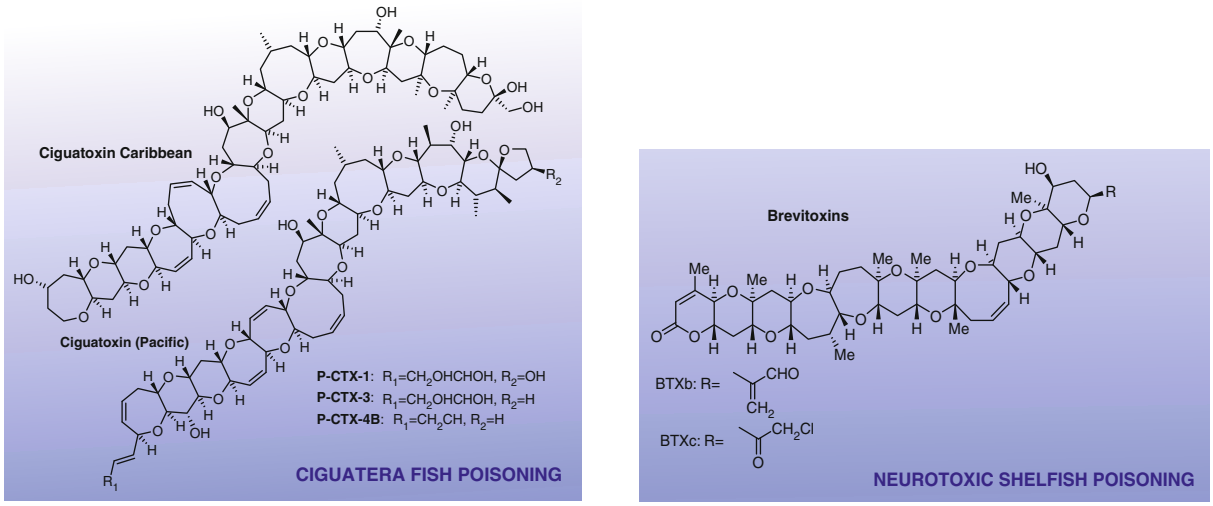

Science, Policy, and Risk Management: Case of Seafood Safety. Figure 5
Toxins involved in seafood-borne intoxications

that have been linked to this form of poisoning include *Pyrodinium bahamense, Gymnodinium catenatum,* as well as several organisms belonging to the genus *Alexandrium* [21, 24, 29]. Various types of seafood can serve as vectors; these include clam, crabs, cockles, oysters, salmon, mackerels, scallops, and whales to name a few [21, 23]. PSP has been reported on all continents. Regrettably, there is no antidote for PSP, and therapeutic approaches are mostly supportive and include respiratory support in a life-threatening situation, gastric emptying, dialysis and enhancing renal clearance [23].

Diarrheic shellfish poisoning (DSP) has also been reported worldwide. Diarrhea, nausea, cramps, and vomiting are common signs of DSP. It is usually associated with consumption of contaminated clams, mussels, oysters, and scallops. This syndrome is caused by a group of acidic (okadaic acid and related dinophysistoxins) and neutral toxins (pectenotoxin). Yessotoxins have also been reported to cause this form of poisoning (Fig. 5) [24, 30]. These toxins are produced by a variety of marine dinoflagellates including *Dinophysis* spp. (*D. acuta, D. acuminate, D. caudate, D. mitra, D. norvegica*) as well as *Protoceratium* spp., *Prorocentrum* spp., *Gonyaulax* spp., and *Phalacroma* spp [21].

Amnesic shellfish poisoning (ASP) has been reported in various areas around the world including Europe, North, Central, and South America, Asia, and Oceania. Several types of seafood, including anchovies, clams, crabs, oysters, mussels, mackerels, lobsters, scallops, and gastropods are potential vectors. ASP is caused by a marine biotoxin called domoic acid (Fig. 5). This toxin is produced by a red-brown marine diatom called *Pseudo-nitzschia pungens.* Diarrhea, nausea, and abdominal pain are examples of symptoms that indicate amnesic shellfish poisoning [21].

Neurotoxic shellfish poisoning (NSP) is caused by brevetoxins and its analogs (Fig. 5). Occurrences have been reported in countries around the world. This form of poisoning has been associated with the consumption of contaminated clams, mullets, mussels, oysters, tunas, and whelks. *Fibrocapsa japonica, Gymnodinium breve* (*Karenia brevis*), *Raphidophyceae* sp., and *Chattonella marina,* among others, are examples of organisms that produce these toxins [21, 24].

Puffer fish poisoning has been linked to the most potent and lethal marine neurotoxin: tedrodotoxin (Fig. 5). It is produced by a variety of animals including the California newt, trumpet shell, the blue ringed octopus, and puffer fish, especially a species known as fugu (present in the liver). Puffer fish is a delicacy in Japan and is the main vector for this form of poisoning. Once again, there is no antidote. The first case in Europe occurred in 2009 and involved an individual that had consumed trumpet shellfish (*Charonia sauliae*)

harvested from the Atlantic Ocean in Southern Europe [31]. The main therapeutic approach upon poisoning is supportive and includes respiratory support (life-threatening circumstances). Activated charcoal, atropine, anticholinesterase agents, and alpha agonists, among others, are also recommended [32].

AZaspiracid shellfish poisoning (AZP). Mussels and oysters are known vectors of toxins responsible for azaspiracid shellfish poisoning. AZP has been reported in countries around Europe, namely Norway, Portugal, the UK, and Ireland. AZP is caused by marine toxins known as azaspiracids (Fig. 5), which are produced by *Protoceratum crassipes* and *Protoperidinium*. Nausea, vomiting, and diarrhea are a few symptoms of azaspiracid shellfish poisoning [21, 24].

Several other marine biotoxins not listed above have been reported. A few examples able to impair human health are gymnodimine, neosurugatoxin, prosurugatoxin, polycavernoside, and debromoaplysiatoxin [21]. It is also important to note that a number of biotoxin producers (dinoflagellates) have been associated with massive fish mortality and thus represent a major issue to the seafood and tourism industry worldwide. Examples in this case are *Pfiesteria piscicida* and *Karlodinium veneficum*; however, there is growing evidence that *P. piscicida* associated fish kills in the past may indeed have been *K. veneficum* derived. Blooms of *K. veneficum* have been linked to various episodes of massive fish kill around the world. In this particular case, a set of toxins believed to be the etiological agents and regrouped under the denomination karlotoxins or KmTxs has been isolated [33, 34]. Examples of such toxins include the karlotoxin-1 (KmTx-1), the 10-*O*-sulfo-KmTx-1, the KmTx-3, the 64-*E*-chloro-KmTx-3, the 10-*O*-sulfo-KmTx-3, the 65-*E*-chloro-KmTx-1, and, finally, the KmTx-2 (Fig. 6) [35], for which the relative and absolute configurations were assigned only recently [36]. Ongoing work in this area actually began with research by Abbott and Ballantine in the 1940s and 1950s [37]. Karlotoxins kill fish by osmotic cell lysis, a result of the alteration of the ion transport system of the cell membrane. The fish dies as a result of damage to its vital gill epithelial tissues. These toxins are environmental pollutants and detectable in water during fish kill episodes. The ecological role of these toxins was investigated recently and because the toxins possess an allelopathic inhibitory effect on competitors as well as a prey immobilization it was established that the organism produce these toxins in order to facilitate feeding and control of competition during a bloom [38, 39].

Microbial Pathogens

Following chemical toxins, pathogenic microorganisms were the most likely cause of seafood-borne disease outbreaks throughout 1990–2006 (Fig. 3). The CSPI's survey associated bacteria to 24% of reported outbreaks during this period, trailed by norovirus (10%) [2].

Pathogenic Bacteria Seafood's bacterial pathogens can be found either in their GI system (bivalve mollusks) or on their surface (crustaceans). These bacteria have been linked to various infections and intoxications. Pathogens accumulate in the digestive track of bivalve mollusks (cockles, mussels, oysters, clams) as a result of filter feeding in heavily contaminated water. Seafood-associated bacterial pathogens are either indigenous to the marine environment (case of *Vibrionaceae,* a source of greater concern) or nonindigenous (resulting from fecal contamination). Members of the first category are pathogenic *Vibrio* spp. such as *V. cholerae, V. parahaemolyticus, V. vulnificus, Clostridium botulinum* (non-proteolytic types B, E, F), *Aeromonas hydrophila, Plesiomonas shigelloides,* and *Listeria monocytogenes*, just to name a few [22, 26, 40]. Diarrhea is a common symptom of infection caused by several of these microorganisms. *V. parahaemolyticus, V. vulnificus, V. hollisae,* and *V. cholera* non O–1 have been also associated with more serious conditions such as septicemia. These microorganisms are most prolific during summer months as the water temperature rises. The second category includes bacteria such as *Salmonella* (nontyphoidal), *Shigella, Campylobacter, Staphylococcus aureus,* and *Escherichia coli* [26].

Proper seafood storage is sufficient to protect against diseases caused by several of these bacteria. It has been established that their concentration in seafood is normally low (below the minimum infective dose) and will remain so providing that the seafood is stored in conditions that are not conducive to bacterial growth, multiplication, or toxin production

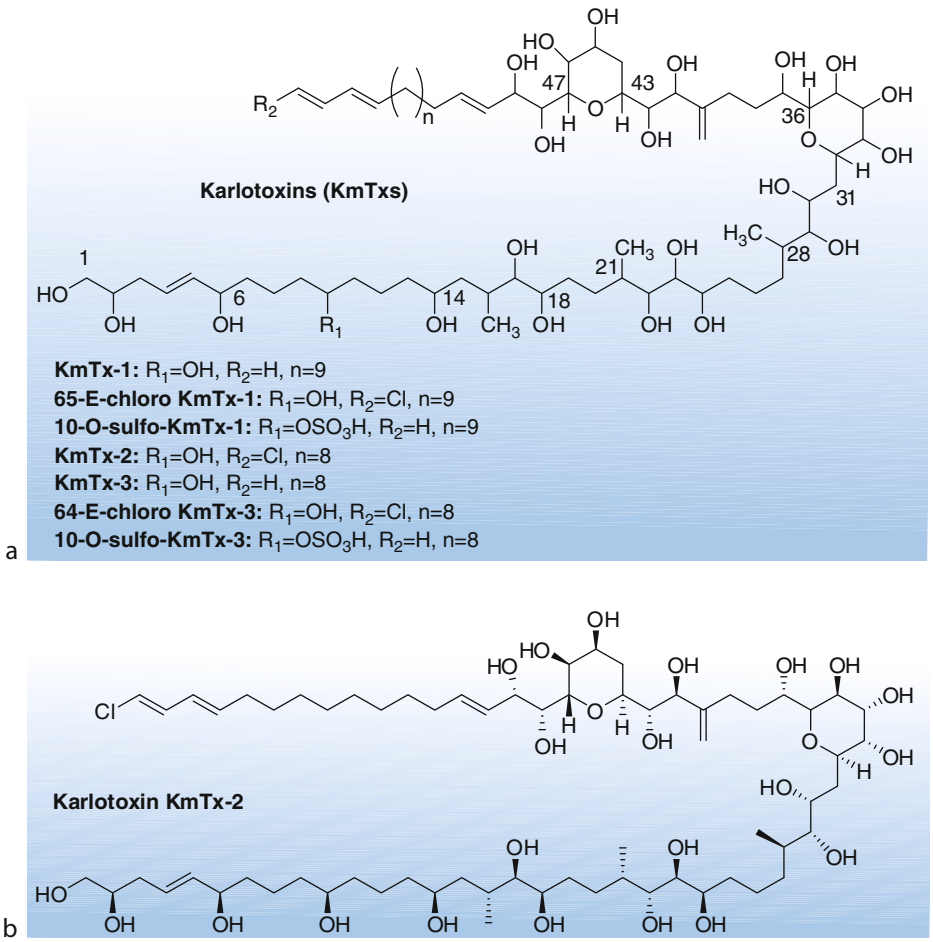

Science, Policy, and Risk Management: Case of Seafood Safety. Figure 6
(**a**) Structure of biotoxins produced by *Karlodinium veneficum*. (**b**) The absolute configuration of KmTx-2

(refrigerated (4°C) and frozen (−18°C)). It is important to note that this does not apply to mollusks and their predators [28, 41]. While, in several cases, a low concentration in seafood is tolerated, FDA regulations become more stringent when it comes to bacteria such as *L. monocytogenes, V. vulnificus, Salmonella, C. botulinum*, and toxigenic 01 *V. cholera*. Current regulations require that these be undetectable in seafood requiring minimal cooking before consumption, for instance [1].

Vibrio spp *Vibrio* spp., especially *V. parahaemolyticus* and *V. vulnificus*, are a cause of significant concern in the USA and several Asian countries (Japan, Taiwan, India, and China). *V. parahaemolyticus* (Vp), for instance, has been associated to the vast majority of seafood-borne gastroenteritis in the USA. This bacterium has been associated with fewer outbreaks in Europe [40, 41]. The pathophysiology of Vp is centered on several virulence factors; a few examples in this case are the thermostable direct hemolysin (TDH) and TDH-related hemolysin (TRH), which are encoded by tdh and trh genes, respectively [40]. Healthy individuals are also at risk of developing Vp associated infection [25]. The FDA can take legal action when seafood products are found to contain a Vp count $\geq 1 \times 10^4$/g [1]. Raw or improperly cooked fish and shellfish are potential vectors [25]. The minimal infective dose for this pathogen is $>10^6$/g [26]. *V. vulnificus* (Vv) infections can also result from consumption of raw or undercooked seafood. In addition, transmission can occur via wound infection.

Though Vv is not a major issue in healthy individuals, in certain groups, Vv can cause serious infections or death. People suffering from alcoholic cirrhosis, hemochromatosis/cirrhosis, chronic hepatitis, postnecrotic cirrhosis, as well as diabetics and alcoholics are at higher risk. *V. vulnificus* is the second leading cause of seafood-related fatality in the USA [42–44]. Vv infections that occur as a result of consumption of contaminated seafood (especially raw oysters) are primarily septicemia and gastroenteritis. One therapeutic approach is the use of antimicrobial agents (tetracycline and intravenous doxycycline with ceftazidime) [43].

Other Seafood-Associated Bacteria Clostridium botulinum – This bacterium is responsible for a condition known as botulism, the responsible agent being a toxin. Lightly preserved, semi-preserved, and fully preserved smoked, fermented, salted, and pickled fish products are likely vectors. Cold-smoked and fermented fish products are of greater risk. Chilling, autoclaving, and salting are approaches used to prevent botulism [26, 28]. *Listeria monocytogenes* – Infections caused by this other bacterium can, at worst, result in septicemia spreading to several organs and even, in the case of pregnant women, to the fetus. This type of infection can be fatal. Groups most at risk are pregnant women, neonates, fetuses, and immunocompromised patients. Shrimp is an important vector [26, 28, 45]. *S. aureus* has also been isolated from seafood. This bacterium is, as *C. botulinum*, a toxinogenic species. It produces toxins that are resistant both to enzymes degradation and heat. It is introduced in seafood as a result of environmental contamination or transferred from an infected worker involved in seafood handling [26, 28]. *Enterobacteriaceae* such as *Salmonella, Shigella*, and *E. coli* have also been reported in seafood. *Enterobacteriaceae* usually occurs in seafood as a result of fecal contamination. *Salmonella* is responsible for salmonellosis and is especially problematic for the shrimp industry [45]. Compared to other food categories, seafood is a less likely vector of *Salmonella* [25, 26]. The minimum infective dose for *Salmonella* sp has been estimated to be in the range of $<10^2$–$>10^6$. Non-bloody diarrhea, fever, abdominal pain and nausea, just to name a few, are indicators of infection by this pathogen. Symptoms of a *Shigella* infection, on the other hand, are bloody stools, severe abdominal cramps, fever, and dehydration. The minimum infective dose in this case has been estimated at 10^1–10^2. This is similar to what has been reported for *E. coli*, for which the minimal infective dose is 10^1–10^3 (Table 1) [26, 28].

Seafood-Associated Viruses Seafood can also serve as a vector of viruses. Non-A, non-B enteral hepatitis

Science, Policy, and Risk Management: Case of Seafood Safety. Table 1 Safety levels set by FDA for several seafood-associated bacteria

Hazards	FDA & EPA thresholds	Analytical approach	Targeted seafood	Higher risk populations
Salmonella sp.	Presence of organism[a]	Conventional culture methods	All fish	Severe in the elderly, infants, AIDS patients
E. coli	MPN of 230/100 g[b]	Hemorrhagic colitis agar – direct plating method	Imported fresh and frozen clams and oysters	All people – most susceptible are young children and the elderly
	APC – 500,000/g			
S. aureus	Presence of staphylococcal enterotoxin, or a load $\geq 10^4$/g (MPN)[c]	Specific precipitation with antiserum	All fish	All people
C. botulinum	Presence of viable spores or vegetative cells or toxin[c]	Mouse neutralization test	All fish	All people

Compliance policy/programs
[a]Sec 555.300 Compliance Policy Guide
[b]Sec 560.600 Compliance Policy Guide
[c]Compliance Program 7303.842

viruses, hepatitis A virus (HAV), poliovirus, and norovirus, among others, have been associated with seafood-borne outbreaks [25, 26, 46, 47]. Viruses end up in seafood as a result of fecal contamination of the marine environment or when handled by an infected worker. Viruses are one of the most serious seafood-associated threats. So far, reports of seafood-borne infection outbreaks linked to viruses have emerged from countries around the world. HAV was associated with the largest seafood outbreak ever reported. This outbreak, which occurred in 1998, in the Chinese city of Shanghai, was linked to the consumption of contaminated clams and *over 292,000 cases were reported* [47, 48]. Another virus, namely norovirus, a single-stranded nonenveloped RNA virus, is currently responsible for roughly 50% of all foodborne outbreaks of gastroenteritis according to the CDC [49]. Norovirus was reported by CSPI as the most problematic seafood-associated virus during the period 1990–2006 (Fig. 3), as it caused 10% of all reported seafood outbreaks during that time [2]. It is important to point out that of the five genogroups of norovirus, GII has been linked to the majority of infections. Filter-feeding bivalve shellfish are important vectors [43]. Norovirus gastroenteritis-associated symptoms are vomiting, watery stools, non-bloody diarrhea with abdominal cramps, and nausea. It is a fairly resistant virus that can survive harsh conditions such as chlorine treatments (10 ppm), heating to 60°C (4 h), or freezing [49].

Seafood-Associated Parasites Seafood (raw or undercooked) can also serve as a vector of pathogenic parasites. These include nematodes, cestodes, and trematodes. *Anisakis simplex, Pseudoterranova dicipiens, Gnathostoma* sp., *Capillaria* sp., and *Angiostrongylus* sp. are examples of seafood-associated nematodes. Examples of tapeworms that can be isolated from seafood include *Diphyllobothrium latum* and *D. pacificum; Clonorchis* sp., *Opisthorchis* sp., *Metagonimus yokagawai, Heterophyes* sp., *Paragonimus* sp., and *Echinostoma* sp., on the other hand, are a few examples of seafood-associated trematodes [26].

Several parasite-infected seafood dishes such as sushi, crab, sashimi, herring roe, and undercooked grilled fish have been associated with illnesses [1]. Compared to bacteria and viruses, however, parasites are of lesser concern. Trematodes (such as *Paragonimus westermani)*, cestodes (such as *Diphyllobothrium latum, D. pacificum*), and nematodes (such as *Angiostrongylus cantonensis, Contraceacum osculatum)* have been associated with domestic fish and shellfish. Several other organisms have been associated with imported products instead. These include *Clonorchis sinensis, Heterophyes heterophyes, Metagonimus yokogawai, Opisthorchis felineus*, and *Gnathostoma spinigerum* [49]. Some nematodes, cestodes, and trematodes are of greatest concern as far as seafood safety. These include *Anisakis simplex*, *Pseudoterranova* spp., *Eustrongylides* spp., *Gnathostoma* spp., *Opisthorchis* spp., *Chlonorchis sinensis, and Paragonimus* spp., just to name a few [1, 49].

Toxic Heavy Metals

Heavy metals are a threat to the environment and public health and are problematic in regard to their long-term persistence. A variety of heavy metal contaminants has been reported in seafood. These elements originate from natural occurrences (marine volcanism, and geological and geothermal events) and anthropogenic activities. Several categories of anthropogenic activities threaten the marine environment. These include, activities that take place in tanneries, steel plants, battery industries, thermal power plants, and farms, especially those farms using heavy metal containing fertilizers and pesticides. Runoff from roadways has also been recently cited as an important source of contamination [4, 50, 51].

Heavy metals found in seafood include antimony, arsenic, cadmium, chromium, lead, mercury, nickel, copper, iron, manganese, selenium, zinc, aluminum, silver, strontium, thallium, and tin. Of these heavy metal contaminants, those of greatest concern are antimony, arsenic, cadmium, chromium, lead, mercury, and nickel. It is important to note that elements such as copper, selenium, iron, and zinc (known essential micronutrients) are toxic only at high concentrations [4].

Arsenic can be present under a variety of forms: toxic (inorganic) and nontoxic (organic). Arsenic is an extremely potent poison in its trivalent form and can cause a wide range of acute and chronic illnesses. A few examples include cancer, nephritis, hepatomegaly, peripheral symmetrical neuropathy, and palmar

hyperkeratosis, among others. In seafood, arsenic is mainly present in a nonpoisonous form known as arsenobetaine or arsenocholine [46]. A compilation of data (about 100,000 results) received from 15 European countries revealed that seafood is among the food commodities with the highest arsenic levels [52].

Methyl mercury is a neurotoxic contaminant. Due to its potential effects on the fetus, it is one of the most regulated seafood-associated toxic metals. There are several related FDA recommendations to nursing/pregnant women, women of childbearing age, or children when it comes to seafood consumption. CH_3Hg^+ is present in nearly all seafood, but some types of fish such as shark, swordfish, king mackerel, and tilefish are believed to have a higher content. The FDA and the US Environmental Protection Agency (US EPA) have recommended being very selective of the type of fish consumed, limiting uptake to ~12 oz/week as a healthy approach for groups at risk [5]. This has been supported by scientific data [12, 53, 54]. Several reports have shown that moderate to high consumption of fish species containing only a low amount of CH_3Hg^+ during pregnancy has a positive effect on fetal brain development. However, it is also important to note that several other studies, Myers et al. (2003) for instance, did not support the fact that exposure of pregnant women to methyl mercury through fish consumption could have deleterious effects on fetal development [13, 55].

Other toxic heavy metals include nickel, chromium, cadmium, selenium, and lead. Cadmium tends to be bioaccumulated by crustacea and bivalves. Clinical signs of cadmium poisoning include osteoporotic and osteomalacic disease, as well as kidney damage. Lead poisoning, on the other hand, has been associated with anemia, convulsions, paralysis, and proteinuria. This metal tends to accumulate in cortical and trabecular bone, kidney, lung, as well as the CNS. Edema, hepatitis, and hemorrhage are conditions that can result from selenium poisoning, which is also known, to result in congenital malformations and infertility. Arsenic (As), nickel (Ni), and chromium (Cr) are carcinogens [46].

Other Chemical Environmental Contaminants

Organochlorine compounds. Until recently, organochlorine compounds were widely used. A wide range of polychlorinated substances can be found in seafood. These include various insecticides, agrochemicals, industrial chemicals, and by-products. Examples of pesticides traceable to seafood include endrin, heptachlor, dieldrin, benzene hexachloride (BHC), chlordane, dichlorodiphenyltrichloroethane (DDT) and lindane. Polychlorinated biphenyls (PCBs) and dioxins, such as 2,3,7,8-tetrachlorodibenzo-*p*-dioxin, are example of industrial chemicals that contaminate seafood. Prior to 1970, PCBs were widely used industrially [56]. Because they are non-biodegradable, toxic in nature, and tend to bioaccumulate in seafood, organochlorine compounds now constitute a major environmental and public health concern. Several of these substances are known carcinogens (dioxins and polychlorinated biphenyls); but because seafood-associated health benefits outweigh potential risks, seafood consumption is recommended [13]. The level of these substances in fish is truly minimal. However, it is important to note that people whose diet is predominantly made of seafood are still at risk [56]. Reports on farm raised salmon (especially European farms) containing higher levels of these contaminants compared to wild-type salmon is believed to have had a serious impact on the consumer acceptance of this type of seafood [57, 58].

Antimicrobial drug contaminants of seafood. This is a problem mainly associated with aquaculture, as farmers rely more and more on various drugs and antimicrobial agents to deal with specific seafood diseases (bacterial, fungal, viral), to improve the quality of water, and to manage pest-related issues.

There are quite a few reasons why there are concerns over drug residues being present in seafood. Several antimicrobial agents used in aquaculture have been linked to various adverse health effects, such as hypersensitivity reactions. In vivo studies, in animals, have established several others as carcinogens; these include nitrofuran, malachite green, gentian violet, and fluoroquinolones. Fluoroquinolones have been also associated with antibiotic resistance. There are several drugs used to this end in the USA that have been approved by the Center for Veterinary Medicine (CVM) (Table 2). Substances such as ciprofloxacin, erythromycin, tetracyclines, chloramphenicol, nitrofurans, malachite green, gentian (crystal) violet, and fluoroquinolones have been frequently reported in seafood imported into the USA in recent years [20]. A short, recent survey by the FDA has shown that

Science, Policy, and Risk Management: Case of Seafood Safety. Table 2 Aquaculture drugs approved in the USA and action levels

FDA-approved aquaculture drugs			
Drug name	Tolerance level in the flesh	Type of seafood	Purpose
Unapproved drugs	No trace tolerated[a]	All fish	–
Chorionic gonadotropin[b]		Brood finfish	Reproductive
Formalin solution[c]		Salmon trout, catfish, largemouth bass, and bluegill	Antiparasitic and fungicidal/static
Tricaine methanesulfonate[d]		Catfish, salmon, and trout, pike and perch	–
Oxytetracycline	2.0 ppm[e]	Salmonids, catfish, and lobster	Disease control
Sulfamerazine[f]	Undetectable[g]	Trout	–
Sulfadimethoxine/Ormetoprim combination[h]	0.1 ppm[i]	Salmonids and catfish.	–

Compliance policy/programs
[a]Sec 615.200 Compliance Policy Guide
[b]21 CFR 522.1081
[c]21 CFR 529.1030
[d]21 CFR 529.2503
[e]21 CFR 556.500
[f]21 CFR 558.582
[g]21 CFR 556.660
[h]21 CFR 558.575
[i]21 CFR 556.640

imports from China test positive for the presence of a variety of unapproved substances, such as gentian violet, malachite green, nitrofuran, and fluoroquinolones. Consequently, these products are the subject of great concern and the focus of regulatory surveillance [59].

Similar issues have been reported in Europe. In fact, during the years 1999–2002, the presence of residues of antimicrobial drugs, mainly nitrofuran and chloramphenicol, was one of the main reasons for detention or rejection of seafood imports into Europe (Fig. 7) [28]. A handful of aquaculture drugs approved in Europe are presented in Table 3.

What Are the Approaches Used to Assure Public Safety?

Regulatory authorities and the scientific community are two groups with complementary goals that play a key role in ensuring public safety against seafood-associated health hazards.

Regulatory Agencies

Seafood regulatory agencies, via promulgation and enforcement of various laws and regulations, guidance, and recommendations, are usually at the heart of protecting the public from seafood-associated hazards. Numerous programs have been designed over the years to this end. In the USA, the primary responsibility of assuring seafood safety falls to the FDA, which is in charge of setting the maximum safe levels of unavoidable toxic substances in seafood [59]. The FDA has the authority to detain and even refuse import entries into the USA. A recent related event was the June 28, 2007, decision of the FDA to detain Chinese farm-raised catfish, basa, shrimp, and dace until they were cleared from containing unapproved drug substances [59]. As for domestic seafood, the FDA can recommend legal sanctions, which include "warning letters, seizure of products, injunction against further non-compliant practices, or prosecution of an individual or establishment" [20]. There are a few other regulatory agencies;

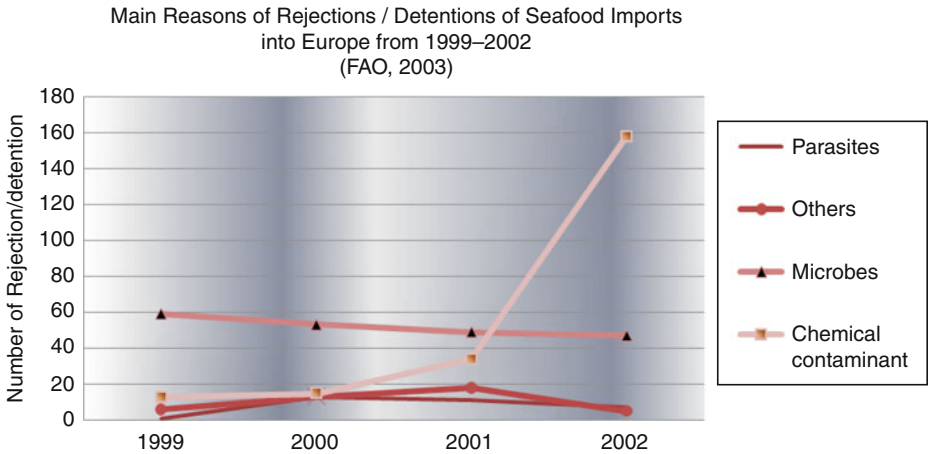

Science, Policy, and Risk Management: Case of Seafood Safety. Figure 7
Main causes of rejection or detention of seafood imports into Europe during the years 1999–2002

Science, Policy, and Risk Management: Case of Seafood Safety. Table 3 Aquaculture drugs approved in Europe and action levels

The Council of the European Communities approved aquaculture drugs		
Drug name	Maximum Residue Limit (MRL) – muscle and skin in natural portion	Type of seafood
Trimethoprim	50 μg/kg[a]	Finfish
Flumequine	600 μg/kg[a]	Finfish
Oxolinic acid	100 μg/kg[a]	Finfish
Sarafloxacin	30 μg/kg[a]	Salmonidae
Tylosin A	100 μg/kg[a]	Finfish
Thiamphenicol	50 μg/kg[a]	Finfish
Colistin	150 μg/kg[a]	Finfish
Deltamethrin	10 μg/kg[a]	Finfish
Emamectin B1a	100 μg/kg[a]	Finfish
Oxolinic acid	300 μg/kg[a]	Finfish
Florfenicol	1000 μg/kg[a]	Fish
Thiamphenicol	50 μg/kg[a]	Finfish
Deltamethrin	10 μg/kg[a]	Finfish

Compliance policy/programs
[a]Council Regulation (EEC) No 2377/90 of 26 June 1990

these include the EPA (Environmental Protection Agency) in charge of chemical contaminants such as pesticides and the National Marine Fisheries Service for instance. In Europe, the EU parliament is at the heart of food safety control. This organization promulgates food safety-related laws, regulations, and directives, which are mandatory in all states of the European Union. The EU parliament works in close collaboration with the European Food Safety Authority, which was established by regulation (EC) No.178/2002. This latter organization, more science oriented, is in charge of risk assessment.

There is a long list of guidance and regulations, mostly to seafood industries that protect the public from dangers associated with seafood consumption. Several of these are preventive measures. A few examples in the USA are the National Shellfish Sanitation Program, the Salmon Control Plan, the Low-Acid Canned Food (LACF) Program, the Hazard Analysis & Critical Control Points (HACCP) Program, and the Good Manufacturing Practice regulation. The latter is intended to assure that recommended processing conditions were used. The Salmon Control Program, on the other hand, was designed to assure the safety of salmon consumers and is a cooperative approach involving the FDA, industries, and various associations. As part of the Shellfish Sanitation Program in the USA, the level of various pollutants in coastal water is to be

monitored in order to classify each given area as suitable or unsuitable for shellfish harvest. As for the HACCP, it applies to domestic as well as imported seafood. HACCP requires both domestic and foreign processors of fish and fishery products to understand all concepts behind food safety hazards and through a system of precautionary control measures to prevent hazards from occurring [20, 59]. The EU parliaments, as well as regulatory agencies of countries around the world, have issued several similar regulations and directives that apply to domestic and imported seafood. A few examples of seafood-related regulations promulgated by the European Parliament include regulations (EC) No. 852/2004 and No. 853/2004, which established some key hygienic rules for food (including seafood) business operators and regulation (EC) No. 854/2004 in which key exigencies related to the organization of seafood official control programs are determined. Several of these regulations elaborate on the "tolerance threshold" for contaminants present in seafood. Examples of "tolerance threshold" for seafood-associated health hazards, set by regulatory agencies around the world are presented in Tables 4, 5, and 6.

The Scientific Community's Contribution in Ensuring Seafood Safety

Through the development of cutting-edge technologies to solve problems at hand, science has also played a critical role in ensuring public safety against dangers associated with seafood. A simple literature search with a keyword such as "seafood safety" in ScienceDirect shows a significant and steady increase in seafood safety-related research effort since 1991 (Fig. 8). The international community relies on science to develop cutting-edge technologies and techniques that can rid seafood from associated biological and chemical contaminants in order to bring a safer product to the market. The development of cutting-edge technologies for faster, cheaper, easier, and more accurate detection methods of seafood-associated health hazards is another way scientists have contributed in the protection of consumers against these dangers.

Detection Tools for Seafood-Associated Health Hazards *Detection of biotoxins.* Years of effort have yielded a wide range of approaches for toxin detection in seafood. These include various bioassays (in vivo and in vitro assays), biochemical techniques (immunoassays), and chemical techniques including fluorometric and colorimetric techniques, chromatographic techniques, electrophoretic techniques, mass spectrometry, and finally biosensor-based techniques (Table 7). In countries around the world, the mouse bioassay, despite its numerous shortcomings, and liquid chromatography are the two official methods recommended for biotoxin detection in seafood (Table 4).

Chromatographic techniques are at the heart of several effective analytical approaches to biotoxin separation and detection. Compared to animal assays, analytical techniques present the advantages of higher accuracy and sensitivity. While with animal bioassays, it is impossible to clearly determine the nature of contaminants, these techniques, coupled with the appropriate detection methods, will permit not only separation and accurate identification of incriminated toxins, but also, using a standard curve, their quantification. A variety of analytical approaches is currently available for the detection of marine toxins. These include Gas Chromatography (GC), Thin-Layer Chromatography (TLC), Liquid Chromatography (LC), Liquid Chromatography–Mass Spectrometry (LC-MS), and Capillary electrophoresis [21, 59]. In addition to advantages listed above, with chromatography-based detection methods, several toxins can be monitored simultaneously. A new liquid chromatography–tandem mass spectrometry method was developed recently [60]. With this method, up to 28 marine lipophilic toxins can be monitored at the same time. In this case, toxins are separated using a gradient of acetonitrile/water at alkaline pH on a new type of C18 column proven stable under these conditions: a Waters X-Bridge C_{18} (150 mm × 3 mm, 5 μm) [60].

Biosensor-based detection methods have also been investigated for application in seafood safety programs. They are not only economical, straightforward, and easy to use, but also offer the advantages of high sensitivities/low limit of detection, plus, these technologies are portable [21]. An example of a recent development in this field is a new planar interdigital sensor-based sensing system developed by Syaifudin et al. (2009). This approach involves simple monitoring of variations of reactive impedance of the planar interdigital

Science, Policy, and Risk Management: Case of Seafood Safety. Table 4 Seafood-associated marine biotoxins and action level set by regulatory agencies around the world

Hazards	Detection method (analytical methods for regulatory purposes)	Tolerated thresholds	Targeted seafood
Paralytic shellfish poison	USA – mouse bioassay	0.8 ppm (80 μg/100 g) saxitoxin equivalent[a]	All fish
		800 ug/kg (live bivalve mollusks)	
	EU – mouse bioassay[b]	80 mg STX eq/100 g of meat[c,d]	Bivalve mollusks
	Africa – mouse bioassay[b]	80 μg STX eq/100 g	mollusks
	Canada – mouse bioassay[b]	<80 mg STX eq/100 g	Mollusks
	Asia – mouse bioassay[b]	400 MU/100 g	Shellfish
	Australia – mouse assay[b]	80 mg STX eq/100 g	Shellfish meat
Amnesic shellfish poison	USA – LC method	20 ppm domoic acid (in general)[a]	All fish
		30 ppm (in viscera of dungeness crab)[a]	
	Europe – LC method	20 mg/kg of domoic acid[c]	Live bivalve mollusks
	Canada – LC method	20 mg DA/kg	Mussel
	New Zealand – LC method	20 mg DA/kg	Shellfish
Neurotoxic shellfish poison		0.8 ppm (20 mouse units/100 g) (USA)	Clams, mussels, and oysters, fresh, frozen, or canned
Diarrheic shellfish poison	EU – mouse bioassay[b]	160 ug of okadaic acid/kg[c]	Mollusks, echinoderms, tunicates and marine gastropods
	Asia (Japan) mouse bioassay	5 MU/100 g whole meat	Shellfish
	Australia	16–20 μg OA eq/100 g	Shellfish
Azaspiracids	USA – mouse or rat bioassay	160 ug azaspiracid equivalents/kg[c]	Bivalve mollusks, echinoderms, tunicates, and marine gastropods
	Europe – mouse or rat bioassay	160 μg/kg	Live bivalves
Ciguatoxin		Presence[c]	Fishery products
Histamine	USA – extraction coupled to fluorescence spectroscopy	50 ppm	Tuna, mahi mahi, and related fish
	Europe	<200 ppm[e]	Scombridae,clupeidae, engraulidae, and coryphaenidae

Compliance policy/programs

[a]Compliance Program 7303.842 or Sec 540.250 Compliance Policy Guide

[b]FAO (2004) Marine Biotoxins Food and Agriculture Organization of the United Nations Rome, 2004 http://www.fao.org/docrep/007/y5486e/y5486e00.HTM available online, retrieved December 30, 2009

[c]Regulation (EC) No 853/2004 (European standards)

[d]EU Directive 91/492/EEC

[e]Council directives 91/493/EEC

Science, Policy, and Risk Management: Case of Seafood Safety. Table 5 Seafood-associated toxic heavy metals and action level set by the FDA

Seafood Health Hazard	Tolerance threshold	Targeted seafood
Methyl mercury	1.0 ppm[a]	All fish
Arsenic	86 ppm (76 ppm for crustacea)[b]	Clams, oysters, and mussels
Cadmium	4 ppm (3 ppm for crustacean)[b]	Clams, oysters, and mussels
Chromium	13 ppm (12 ppm for crustacea)[b]	Clams, oysters, and mussels
Lead	1.7 ppm (1.5 ppm for crustacea)[b]	Clams, oysters, and mussels
Nickel	80 ppm (70 ppm for crustacean)[b]	Clams, oysters, and mussels

Compliance Policy/program
[a]Sec 540.600 Compliance Policy Guide
[b]Appendix 5 – FDA & EPA Safety Levels in Regulations and Guidance

Science, Policy, and Risk Management: Case of Seafood Safety. Table 6 Seafood-associated environmental pollutants and action level set by the FDA

Seafood health hazard	Tolerance threshold	Targeted seafood
Polychlorinated biphenyls (PCBs)	2.0 ppm (edible portion)[a]	All fish
DDT, TDE and DDE	5.0 ppm (edible portion)[b]	All fish
Chlordane –	0.3 ppm (edible portion)[b]	All fish
Chlordecone –	0.3 ppm (0.4 ppm in crabmeat)[b]	All fish
Mirex	0.1 ppm[b]	All fish
Diquat	0.1 ppm[c]	All fish
Heptachlor and heptachlor epoxide	0.3 ppm[b]	All fish
Glyphosate	0.25 ppm[d] 3.0 ppm (for Shellfish)	Fin fish
Fluridone	0.5 ppm[e]	Fin fish and crayfish
Simazine	12 ppm[f]	Fin fish
Aldrin and dieldrin –	0.3 ppm[b]	Fin fish and shellfish

Compliance Policy/program
[a]21 CFR 109.30
[b]Sec 575.100 Compliance Policy Guide
[c]40 CFR 180.226
[d]40 CFR 180.364
[e]40 CFR 180.420
[f]40 CFR 180.213

sensors. Using this approach, as little as 12.6 μg/g of domoic acid in mussel meat, for instance, can be successfully detected [61].

ELISA has also been investigated widely for application in seafood biotoxin detection. An example of a recent development in this field was made by Zhou et al. (2010), who reported a reliable ELISA-based approach to monitor brevitoxin in mollusks with reduced interference from the matrices. Oysters and cockles were used in this experiment. With such a method, the limit of detection of brevitoxin is improved. The main advantage of immunoassays, which are based on antibody–antigen interactions, is high specificity [62].

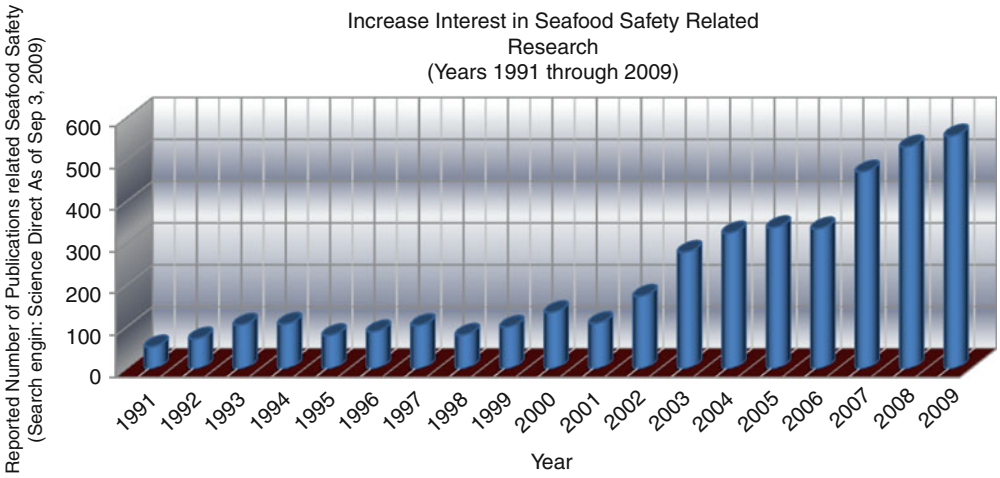

Science, Policy, and Risk Management: Case of Seafood Safety. Figure 8
Increased interest in seafood safety related research

Drug residues in seafood. With the rise in demand of fish and shellfish, a large portion of seafood found in market places around the world comes from aquaculture, especially from China. As it is the case with any animal husbandry, veterinary drugs are often heavily used in aquaculture to control pests, infections, or to increase production. Unfortunately, drug residues, often molecules that have proven harmful to humans, are found in edible seafood tissues. As previously mentioned, lately in the USA as in Europe, there have been a significant number of alerts regarding seafood imports contaminated with unapproved drug residues (Fig. 7). Over the years, through the dedication of the scientific community, better and more improved detection methods have been made available. An example in this case is liquid chromatography (LC) coupled with triple-quadrupole mass-spectrometry (LC–QqQ-MS). Until recently, in a single run, this sort of method could only analyze related molecular entities. An upgraded and more robust version, a multicomponent quantitative HRLC–ToF-MS, was reported recently. This new approach has proven effective at simultaneously monitoring a wide range of unrelated drugs generally used in aquaculture or found in seafood tissues [64]. Smith et al. (2009) also developed an LC-ion trap mass spectrometry approach, effective at detecting several types of veterinary drugs in fish samples. In this case, the extraction of drug residues from seafood matrixes is completed in acetonitrile and hexane followed by HPLC separation on a phenyl column. In certain cases, imidazoles, macrolides, fluoroquinolones for instance, very low concentrations (0.01 ppm) could be detected using this technique. Other drugs involved in these studies included ionophores, macrolides, nitroimidazoles, benzimidazoles, anthelmintics, penicillins, quinolones, sulfonamides, tetracyclines, amphenicols, and tranquilizers, among others [64, 65].

Detection of microbial pathogens in seafood. The best approaches for the detection of microbes in seafood are usually a combination of culture-based and molecular-based techniques; the latter being often used to assist in bacterial strain identification, while culture is required for enrichment purpose. The kind of medium used to this end is dictated by the type of microorganisms targeted. Over the years, a tremendous amount of effort has been dedicated to the conception of superior media. Recommended Standard Operating Protocols for use in microorganism detection, in seafood, are described in detail in the FDA's 1998 Bacteriological Analytical Manual (BAM) [63]. Targets of quality control programs are numerous. These include various pathogenic bacteria such as *Vibrio*, *Salmonella*, *S. aureus*, *L. monocytogenes*, and *E. coli* as well as indicators of fecal contamination [26].

Several molecular and culture-based methods have been developed to assist in the detection of *V. parahaemolyticus* (Vp) and *V. vulnificus* (Vv), which are major issues as far as seafood safety is concerned. Commonly used culture-based approaches, which present the main disadvantages of being time

Science, Policy, and Risk Management: Case of Seafood Safety. Table 7 Proposed methods for biotoxin detection in seafood [21, 24, 63]

	PSP	DSP	ASP	Ciguatera	NSP	SFP
Bioassays						
In vivo assays	Mouse bioassay	Mouse bioassay	Mouse bioassay	Mouse bioassay	Mouse bioassay	
		Suckling mouse assay		Chicken assay	Fish bioassay	
		Rat bioassay		Mongoose and cat assay		
		Daphnia magna assay		Brine shrimp assay		
		Intestinal loop assays		Mosquito assay		
				Diptera larvae assay		
In vitro assays	In vitro hippocampal slice assay	Cytotoxicity assays (rat hepatocytes, KB cells, fibroblasts)	Receptor binding assays	Sodium channel binding assays for ciguatoxins	Neuroblastoma cell assay	
	Sodium channel blocking assay		Hippocampal slice preparations		Synaptosome binding assay	
					Hippocampal slice assay	
Biochemical techniques	Immunoassay (ELISA)	Immunoassay (RIA or ELISA)	Immunoassay (ELISA)	Immunoassay (Radioimmunoassay	Immunoassay (ELISA)	
		Acid phosphatase assay		Enzyme-linked immunosorbent assay (ELISA)		
				Stick tests		
				Immunoassays based on monoclonal antibodies		
				Solid-phase immunobead assay)		

Science, Policy, and Risk Management: Case of Seafood Safety. Table 7 (Continued)

	PSP	DSP	ASP	Ciguatera	NSP	SFP
Chemical/ analytical techniques	Fluorometric and colorimetric technique, MS	TLC,GC, LC	Amino acid analysis	Chromatographic detection	Micellar electrokinetic capillary chromatography detection	Chromatography coupled with fluorimetric detection or derivatization techniques
	Chromatographic and Electrophoretic techniques	MEKC, MS	TLC, LC, CE, MS	Nuclear magnetic resonance (NMR)/mass spectrometry (MS)	Electrospray LC/MS	(TLC, GC,CE, HPLC)
					Ionspray LC/MS	
				Mass spectrometry	LC/MS/MS	
				Capillary zone electrophoresis		
Biosensors based techniques	Sodium channels based biosensors	Immuno sensors	Optical immuno sensors			
		Enzyme inhibition based biosensors	Molecularly imprinted polymer based biosensors			

consuming, laborious, and inaccurate, are the MPN and the ISO cultural methods [40]. Quite a few *Vibrio*-specific media has been developed to assist in the isolation of these bacteria from seafood matrixes; these include TCBS agar (for *V. cholera* and *V. parahaemolyticus)* and modified cellobiose polymyxin colistin (mCPC) and CC agar for *V. vulnificus* [66]. The MPN method, coupled with various techniques to assist in the identification of suspect isolates, is recommended for detection of Vv and Vp in seafood. Examples of approaches used for these identifications are the establishment of a biochemical profile, DNA probes, or PCR. In the case of PCR for instance, DNA primers targeting tdh and *trh* genes are used to detect virulent strains of *V. parahaemolyticus.*

Until the advent of real-time PCR, this approach presented the main drawback of being limited to qualitative evaluation of food samples. Today, faster and quantitative assessment of *Vibrio*'s presence in food samples is possible [40] More sophisticated methods have been introduced. In 2009 for instance, Espiñeira et al. introduced a sequential multiplex PCR system for the detection of *Vibrio* sp. that have been involved in fish and shellfish poisoning, namely *V. cholerae*, *V. parahaemolyticus, V. vulnificus, V. alginoliticus*, and *V. mimicus*. This method, which has been validated, is not only able to detect problematic *Vibrio* species, but it can also, using a fragment analysis, confirm the viable/dead status of these microorganisms and most importantly, probe for the presence of important serogroups and virulence factors [67]. Genetic markers, a precious tool for PCR, have been identified for several other seafood-borne pathogens. These include cytotoxin-hemolysin (*V. vulnificus*), *ctxAB* (*V. cholerae*), *oriC*, chromosomal origin of replication (*Salmonella* spp.), listeriolysin O (*hly*), and the 16 S rRNA (*L. monocytogenes*), polymerase gene (hepatitis A virus), and polymerase gene for norovirus, just to name a few [66].

Examples of Recent Technological Breakthroughs in Efforts to Free Seafood from Associated Contaminants In recent years, outstanding breakthrough techniques and cutting-edge technologies to aid in freeing seafood from associated contaminants have been developed. Molluskan shellfish and associated pathogens (especially *V. vulnificus* and *V. parahaemolyticus*), scombrotoxin, fish safety (especially of cold-smoked salmon), and bio-preservation of seafood are a few examples of highly investigated topics.

Molluskan shellfish and associated pathogens. Nowadays, seafood regulatory authorities face major issues with molluskan shellfish. For years now, molluskan shellfish has been classified as "high-risk" seafood by the FDA. They were responsible for the largest number of seafood-borne illnesses during 1990–2006 (Fig. 4). Because of their filter-feeding habits, they tend to accumulate a wide range of etiological agents (pathogenic bacteria, parasites, and viruses) as well as biotoxins. The emergence of innovative FDA-approved Post-Harvest Processing (PHP) technologies such as Individual Quick Freezing (IQF), Heat-Cool Pasteurization (HCP), and High Hydrostatic Pressure (HHP) has revolutionized the industry of seafood, particularly in regard to oysters. These technologies, which are currently commercially available, have made it possible to bring raw and healthy products to consumers. An end product of high quality (fresh taste and superior appearance) is the major advantage of IQF, HCP, and HHP. These processing techniques reduce the level of *Vibrio* bacteria to undetectable levels [67]. Though HHP is already approved by the FDA, several attempts to perfect this technology are currently on the way. In 2008 for instance, using a pressure-resistant strain of Vp (MLT 403) to picture the worst-case scenario, Kural et al. proposed better pasteurizing conditions. Under such conditions, a 5-log reduction in the load of the pressure-resistant Vp in live oysters could be achieved. These conditions were as follows: a 2-min treatment at pressure $\geq$350 MPa (1–35°C) and a 2-min treatment at 40°C (pressure $\geq$300 MPa) [68].

As far as seafood safety is concerned, HHP processing is an especially promising technology. Its inactivating effect on a variety of pathogenic agents isolable from seafood has been documented. These agents include viruses, parasites, and several other types of seafood-associated bacterial pathogens. The ability of HHP to inactivate oyster-associated viruses has been extensively studied [69–72]. A 5-min HHP treatment at pressure 400-MPa and 0°C was established as an effective approach to bring murine norovirus-1 to undetectable levels in oysters [71]. HAV can also be

effectively inactivated from oyster tissues using HHP. Calci et al. (2005) could achieve a PFU reduction >3 $\log_{10}$ with a 1-min treatment at 400 MPa [69]. It is important to note that temperature, matrices' pH, and salinity have a great effect on the efficiency of pressure-mediated HAV inactivation [70].

Another recent development in the field of molluskan shellfish safety is the application of super critical CO_2 ($scCO_2$), a known antibacterial substance widely used in the food industry to reduce the load of oyster-associated bacteria. Two conditions, 100 bar and 37°C for 30 min and at 172 bar and 60°C for 60 min, were reported as able to induce 2-log and 3-log reductions in the oysters' aerobic plate count, respectively. No significant change in the physical appearance, smell, or texture was recorded (Fig. 9) [73].

As previously stated, *V. vulnificus* and *V. parahaemolyticus* are major seafood-associated health concerns. In recent years, there has been a tremendous amount of effort to design approaches to reduce their load, especially in molluskan shellfish. One of the latest innovations in this field is the introduction of a "weak acidic electrolyzed water"-based approach [74]. Quan et al. (2010) have demonstrated that weak acidic electrolyzed water possesses outstanding antibacterial potency against Vv and Vp, especially when compared to sodium hypochlorite (NaClO), a commercial sanitizer [74].

A chlorine dioxide (ClO_2)-based approach was also recently introduced. According to Wang et al. (2010), a 6-h treatment with 20 mg/L of ClO_2 is enough to disinfect oyster tissues contaminated with Vp.

Science, Policy, and Risk Management: Case of Seafood Safety. Figure 9
Appearance of oysters before and after a 40-min exposure to $scCO_2$

These authors particularly recommend this method because it is cost effective; it also has the potential of increasing seafood's shelf life (~12 days) [75]. In addition, *E. coli* O157:H7, *S. typhimurium*, and *L. monocytogenes*, other pathogens of importance regarding seafood safety, have proven sensitive to this type of treatment.

Scombrotoxin. Because of the large number of associated outbreaks, scombrotoxin can be viewed as the most dangerous seafood-associated health hazard [2, 3]. To store fish at low temperatures is generally considered sufficient to prevent the growth of causative bacteria. Unfortunately, such conditions cannot always be respected, especially during retail processes. Phuvasate and Su (2010) proposed an alternative to low temperature storage applicable under these circumstances, namely the use of Electrolyzed Oxidizing (EO) water and ice. According to these authors, the load of several histamine-producing bacteria on food surfaces and fish skin can be significantly reduced simply by using electrolyzed oxidizing water and ice. Conditions reported as effective using salmon and tuna's skin were, for EO water, 100 ppm chlorine for 120 min, and for EO ice, 100 ppm chlorine for 24 h, respectively. Experts now agree that electrolyzed oxidizing water possesses a great potential as far as seafood safety. Its use is recommended not only because it is environmentally friendly, safe, and cost effective, but also because its application is quite straightforward. Its antibacterial effects against several other seafood-associated bacteria have been reported. A few examples are *E. coli* O157:H7, *L. monocytogenes*, as well as *Salmonella enteritidis*, *Campylobacter jejuni*, *Enterobacter aerogenes*, and *S. aureus* [76].

Bio-preservation of seafood. To add various chemicals to seafood in order to reduce its bacterial load or inhibit the growth of unwanted bacteria is an option that many have proposed as a solution to some seafood safety issues. Regrettably, consumer acceptance of these products is not always guaranteed. As chemical/preservative-free, ready-to-eat seafood products are gaining in popularity alternatives to the use of chemicals have emerged, and an example is bio-preservation. Recently, there have been a few innovations in this field. An example in this case is the proposed use of *Carnobacterium divergens* M35 and divergicin M35 in an effort to rid seafood from one of its most persistent bacterial contaminants, namely *L. monocytogenes* [77]. Matamoros et al. (2009) characterized several strains of lactic acid bacteria that can be used to this end as well. These bacteria (*Lactobacillus fuchuensis, Leuconostoc gelidum, Lactococcus piscium,* and *Carnobacterium alterfunditum*) showed inhibitory potential against seafood spoiling and pathogenic bacteria [78]. Pinto et al. (2009) also reported two bacteriocins produced by lactic acid bacteria (*Enterococcus faecium* and *Pediococcus pentosaceus*) that can be used to this end [79].

Irradiation and other recent breakthroughs. Several other cutting-edge technologies designed to help deal with seafood-associated health issues have been introduced in recent years. A few examples are X-ray, gamma ray, and electron beam irradiation-based technologies. Gamma irradiation (0.5, 1, 2, and 5 kGy) and electron beam irradiation have recently proven an effective non thermal approach to reduce the load of *V. parahaemolyticus* as well as several other seafood-associated contaminants, namely *L. monocytogenes* and *S. aureus*, in a raw seafood dish (oyster *Jeotkal*). Organoleptic properties were not negatively affected by the irradiation. In this particular case, gamma irradiation appears a better alternative to electron beam irradiation [80].

The beneficial antibacterial effects of electron-beam irradiation applied to another seafood dish (salted and seasoned short-necked clam) were reported in 2009 by Kim et al. It is important to note that, in this case, no change in sensory qualities was observed. A significant microbial inactivation (coliform bacteria, aerobic bacteria, yeast and mold) was reported [81]. Similar results were achieved with cold-smoked salmon [82]. This technique appears to be a better alternative to HHP in regards to sanitization of cold-smoked salmon. In fact, while both approaches (irradiation at 2 kGy and HPP: 450 MPa for 5 min) yielded a safer final product, the visual aspect of HHP-treated, not irradiation-treated, salmon was negatively affected. The microbial load of both products did not exceed 6 $\log_{10}$ cfu/g after 35 days storage at 5°C [82].

X-ray irradiation has also been investigated for use in improving seafood microbiological quality. Several recent publications have demonstrated its beneficial effects on *V. parahaemolyticus*, *V. vulnificus* (shrimp contaminants). It is important to note that several

other shrimp-associated bacterial contaminants, namely *E. coli*, *Salmonella enterica*, and *Shigella flexneri*, were inactivated as well [83, 84].

High Hydrostatic Pressure (HHP) was also reported as an excellent alternative to reduce the level of *Listeria* in fish. According to Gudbjornsdottir et al. (2010), a 700–900 MPa treatment of 10 s is sufficient to reduce the load of *L. innocua* to undetectable levels. This experiment was completed with cold-smoked salmon. In this case, though there was no lipid oxidation, some variations in color and microstructure of the final product were noted [85]. The potential of HHP to rid mackerel from parasites, such as the nematode *Anisakis simplex*, was also recently reported. In this particular case, a complete inactivation of the larvae in the fish tissue was achieved at 300 MPa after a 5-min exposure [86].

Another recent report has proposed using CO_2 in packaging fish. Schirmer et al. (2009) proposed using CO_2 combined with various organic acids: citric acid (3% w/w, pH 5) and acetic acid (1% w/w, pH 5) in packaging fresh fish, as an effective way to improve its quality and shelf life. This combination has proven efficient at completely inhibiting bacterial growth in naturally contaminated salmon stored at 4°C for 14 days. Monitored bacteria were *Enterobacteriaceae*, lactic acid bacteria, and sulphur reducing bacteria. Sensory analysis was not completed by these authors [87].

A better alternative to rid shrimp from *V. parahaemolyticus* was recently introduced. The use of chlorine is the current approach to reduce the level of shrimp-associated pathogenic bacteria. Unfortunately, health issues such as bronchitis and pulmonary edema in workers have been reported. Norhana et al. (2009) proposed an even simpler approach to deal with shrimp-associated acterial pathogens. These authors show that washing shrimp with acidic fruit juice, namely bilimbi (*Averrhoa bilimbi*) or tamarind (*Tamarindus indica* L.) was also an effective way to significantly reduce its load of bacteria [88]. In 2007, Chaiyakosa et al. reported another safer alternative to reducing the load of *V. parahaemolyticus* in shrimp, namely the use of Chitosan [89]. Another author reported this same substance as an effective means of bringing safer salmon to consumers. Packing cold-smoked salmon in chitosan-coated plastic films containing 4.5 mg/cm^2 sodium lactate or either a combination of 4.5 mg/cm^2 sodium lactate plus 0.6 mg/cm^2 potassium sorbate or 2.3 mg/cm^2 sodium lactate plus 500 IU/cm^2 nisin was found to be beneficial. It was established that for seafood conditioned using this approach and stored at low temperature (~4°C), *L. monocytogenes*' growth was inhibited for at least 6 weeks [90].

Future Directions and Conclusions

From pathogenic bacteria, parasites, and viruses of all sorts, to life threatening biotoxins, the range of chemical and biological contaminants present in seafood is broad in scope and challenging to manage. Despite years of efforts from regulatory authorities and the scientific community, the public at large is still at risk of dangers associated with seafood consumption. For several years now, seafood has ranked foremost as the most significant source of food-borne disease outbreaks of known origin. Contributing factors are numerous and represent key points upon which urgent action, from regulatory authorities and the scientific community is required. Special attention should be paid to deleterious agents that have been associated with the largest number of outbreaks in the past years. In the USA for instance, major threats were scombrotoxin, responsible for 36% of all reported seafood-borne outbreaks from 1990 to 2006, followed by ciguatera (responsible for 21% of outbreaks), bacteria (especially *Vibrio* spp) responsible for 24% and finally noroviruses, which cause about 10% of all outbreaks reported during this same period [2]. It is important to note that these same agents pose serious problems in other parts of the world, as well. Scombroid fish poisoning, for instance, is also a serious problem in countries like Japan and the UK [28] *Vibrio* spp, especially *V. parahaemolyticus,* have been reported as a major problem in several Asian countries [40]. A recent study, a 2005–2008 survey of shellfish (mussels, clams and oysters), showed that norovirus is a problem in Italy, as well [91].

The task of ensuring consumers protection against the dangers of seafood is shared by several groups. These include (1) regulatory authorities, which depend heavily on the scientific community, and are in charge of the promulgation and enforcement of laws and regulations, (2) establishments involved in the harvest,

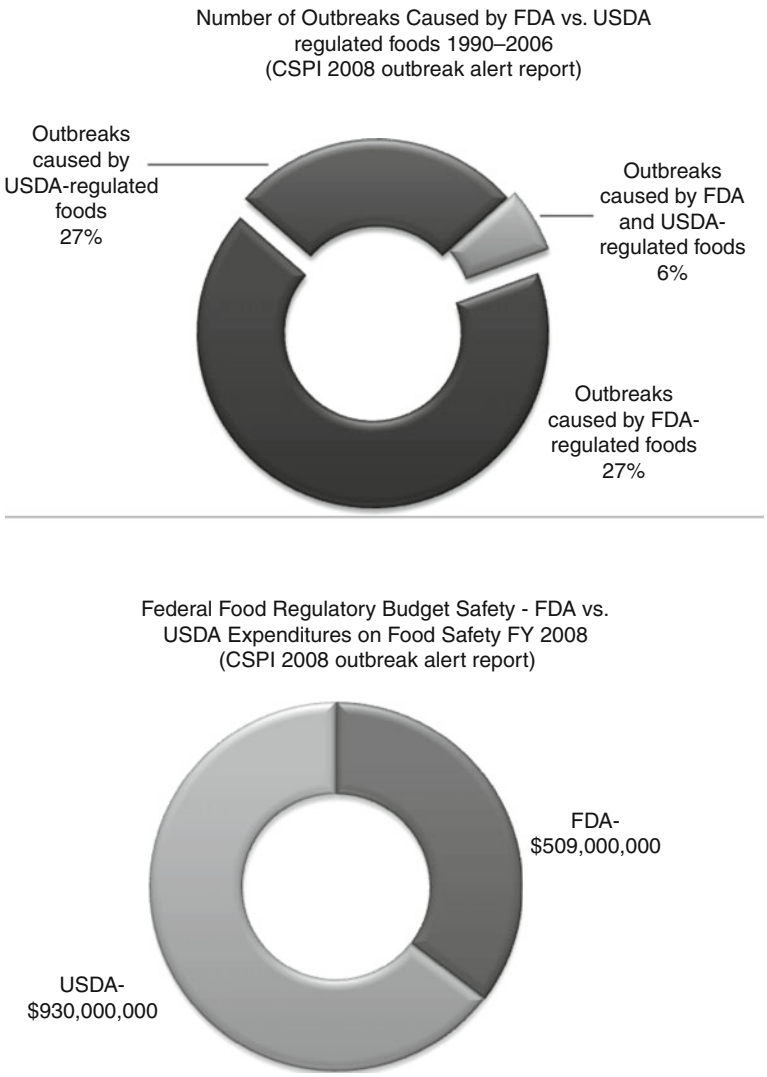

Science, Policy, and Risk Management: Case of Seafood Safety. Figure 10
Graphical representation of some limitations in the current federal food safety regulatory system with significant impact on seafood safety

processing, storage, and retail of seafood, and (3) consumers themselves. Failures and flaws at various levels of the current safety management system explain why seafood has been a persistent issue for the past few years. A certain number of defects in the seafood regulatory system of the USA for instance are presented in a 2008 report of the Center for Science in the Public Interest (CSPI). Mentioned shortcomings are the "voluntary recall" approach currently in place, added to financial issues. CSPI sees in the limited budget allocated to the FDA (Fig. 10), a serious hindrance to its efficiency. This can be a serious hindrance, for instance, when it comes to law enforcement. CSPI reports an extremely low inspection rate of food processing companies by the FDA, a rate that is insignificant compared to the USDA's [2]. Currently, in the USA, there are approximately 13,400 seafood-processing establishments. The FDA reports having inspected only 3,066, 2,830, and 2,456 during the fiscal years 2004, 2005, and 2006 respectively.

Financial limitations are not the only obstacle to full efficiency of regulatory agencies. The unavailability of effective technological tools that could either help rid seafood from hazardous entities/substances, or assist regulatory authorities in effective risk assessment and management during various control programs is also critical. Without effectual detection methods, efficient law enforcement is nearly impossible. Though numerous approaches applicable to virtually all seafood-associated health hazards have been proposed so far, several gaps remain.

This is the case of biotoxins for instance, which alone were responsible for 63% of all reported seafood-borne diseases from 1990 to 2006. Because they are extremely resistant to various post-harvest processing techniques, as far as assuring seafood safety, preventive measures are a better option. More effective detection tools are thus critically needed in order to reduce the current incidence of biotoxin-linked seafood-borne illnesses. Presently, in this field, there is still a need for cost-effective, rapid, sensitive, specific, and straightforward methods that can be operated by untrained personnel on a routine basis.

Though several approaches to toxin detection in seafood have been proposed so far, and even significant progress made recently (Table 7), animal-based assays and liquid chromatography, techniques that have their share of shortcomings, are still the official methods (Table 4). Animal bioassays for instance, are fit to assess the overall toxicity of a sample but cannot give insight on the nature of the toxin(s) involved. Moreover, these assays are time consuming, of limited accuracy and controversial (ethics). As stated previously, liquid chromatography, on the other hand, when coupled with effectual detection methods, is valuable at accurately identifying the nature and concentration of the incriminated toxin(s). However, it is important to note that, chromatography-based methods are lengthy and not cost-effective; heavy equipments and trained specialists are needed. Better methods have been proposed, but, none has so far been approved by regulatory authorities for routine use. Though these new methods present some clear advantages, it is important to point out that they also possess some weaknesses. Among these are difficulty of application on a routine basis, the necessity for heavy equipment, and the complexity of protocols and generated data, just to name a few.

There are flaws in current approaches to control scombroid fish poisoning and ciguatera. In the case of scombroid fish poisoning for instance, there is still a need for more effective alternatives to control Histamine-Producing Bacteria (HPB). Current recommendations of the FDA involve rapid cooling ($\leq$40°F) after visceration (for larger fish) upon death. Unfortunately, this approach possesses a few shortcomings. It is important to note that not all HPB are mesophiles. Several studies showed that histamine can be produced even at low temperature by physchrophilic HPB [28, 92]. Ciguatera was second to scombrotoxin as the most likely cause of seafood-borne disease outbreak from 1990 to 2006. Though ciguatera is such an issue in the USA, "there are neither standards, nor an official method" that applies to Ciguatera Fish Poisoning (CFP) in this country [24]. Innovations, regulation-wise, in this regard are obviously critical. Current efforts with respect to CFP prevention involve various toxin-monitoring programs, education, alongside with bans on the sale and capture of fish most likely to cause poisoning (Europe, Australia).

Bacteria were next to toxins as the most prevalent cause of seafood-borne illnesses during the past decade. Fortunately, in this case, there are currently several approved Post-Harvest-Processing (PHP) approaches aimed at reducing their load in seafood. These included IQF (Individually Quick Frozen), HCP (Heat Cold Pasteurization), and HHP (High Hydrostatic Pressure). Though these techniques have revolutionized the industry of oysters, for instance, there is still room for improvement, especially because oysters do not survive such processing [93]. In terms of shelf life, this can be an issue. To store, HHP-, IQF- and HCP-treated oysters at low temperatures is, unfortunately, not enough to solve the issue. Prapaiwong et al. [94], studying variations in the bacterial load (total aerobic bacterial counts) of HHP-treated oysters stored at 4°C for instance, determined that the bacterial count of processed products can rise quickly during storage and can even reach $\sim 10^7$ CFU/g in just 7 days [94]. Moreover, long-term storage presents the disadvantage of increasing the final production cost. Post-harvest-processing techniques non lethal to oysters would be, without the shadow of a doubt, a better alternative. Mahmoud and Burrage (2009c) reported X-ray irradiation as a better approach for reducing the load of

oysters-associated *V. parahaemolyticus* because oysters are able to survive even extremely high X-ray doses [95]. Oysters have also been shown to be able to survive $scCO_2$ exposure, making it an attractive tool for further exploration [73].

Norovirus is another major seafood-associated health hazard. Major gaps in the current system are regulatory and scientific. Despite the clear threat posed by this virus, not much effort has apparently being exerted regulation-wise. As mentioned by Terio et al. [91], "there is no virological standard for bivalve shellfish in European legislation" [91]. Though several approaches to the detection of norovirus in seafood have been proposed so far, much still needs to be done; an area in need of improvement is the development of more efficient methods of viral RNA extraction. RNA extraction is a critical step in several virus detection protocols. RNeasy Kit was recently presented by Husman et al. (2009) as a most useful alternative for viral RNA extraction after comparing five such approaches side by side. A modified paramagnetic silica-based guanidium extraction based technique was also developed recently [96, 97].

Other challenges faced in norovirus detection are related to the virus' genetic variability and scarcity in samples. Interferences of seafood matrix, mainly, the presence of inhibitory substances, also represents a serious obstruction [97]. An effective TaqMan RT-PCR based approach for quantification of genogroups I and II norovirus, which presents the advantage of overcoming background inhibitory effects, was introduced recently by Gentry et al. (2009) [98]. An effective and more sensitive multiplex RT–PCR-based approach to norovirus and rotavirus detection in oysters was also introduced recently [99].

There is no doubt that the development of effective technologies able to surmount each and every one of these challenges will aid efforts to reduce outbreak incidents of seafood-borne infections attributable to viruses.

Compliance Policy/Regulation Related Citations

Compliance Program 7303.842
Sec 560.600 Compliance Policy Guide
Sec 555.300 Compliance Policy Guide
21 CFR 522.1081
21 CFR 529.1030
21 CFR 529.2503
21 CFR 556.500
21 CFR 558.450
21 CFR 558.582
21 CFR 556.660
21 CFR 558.575
21 CFR 556.640
Council Regulation (EEC) No 2377/90 of 26 June 1990
Sec 615.200 Compliance Policy Guide
21 CFR 556.660
Compliance Program 7303.842 or Sec 540.250 Compliance Policy Guide
Sec 540.600 Compliance Policy Guide
21 CFR 109.30
Sec 575.100 Compliance Policy Guide
40 CFR 180.226
Sec 615.200 Compliance Policy Guide
21 CFR 556.660
40 CFR 180.364
40 CFR 180.420
40 CFR 180.213
Sec 540.525
Regulation (EC) No 853/2004 (European standards)
EU Directive 91/492/EEC
Council directives 91/493/EEC

Acknowledgments

We thank the NOAA (Mississippi-Alabama Sea Grant consortium, NIUST) Kraft Foods, CDC, and the NIH for financial support. We also thank Carol-Scott Defore, Mark Guy, and Derrick Donald for the precious assistance. Damaris A.F. Meujo is supported by a fellowship from the Medicines for Malaria Venture.

Bibliography

Primary Literature

1. Appendix 5 – FDA & EPA Safety Levels in Regulations and Guidance Fish and Fisheries Products Hazards and Controls Guidance
2. Outbreak Alert 2008, http://www.cspinet.org/new/pdf/outbreak_alert_2008_report_final.pdf
3. Outbreak Alert 2009, http://cspinet.org/new/pdf/outbreakalertreport09.pdf
4. Fish and Seafood Utilization, http://www.fao.org/fishery/topic/424/en
5. What You Need to Know About Mercury in Fish and Shellfish March 2004, EPA-823-R-04-005, http://www.fda.gov/food/resourcesforyou/consumers/ucm110591.htm

6. Naliwaiko K, Araújo RL, da Fonseca RV, Castilho JC, Andreatini R, Bellissimo MI, Oliveira BH, Martins EF, Curi R, Fernandes LC, Ferraz AC (2004) Effects of fish oil on the central nervous system: a new potential antidepressant. Nutr Neurosci 7:91–99
7. Morris MC, Evans DA, Bienias JL, Tangney CC, Bennett DA, Wilson RS, Aggarwal N, Schneider J (2003) Consumption of fish and n-3 fatty acids and risk of incident Alzheimer disease. Arch Neurol 60:940–946
8. Barberger-Gateau P, Letenneur L, Deschamps V, Pérès K, Dartigues JF, Renaud S (2002) Fish, meat, and risk of dementia: cohort study. BMJ 325:932–933
9. Food is getting healthier and better, thanks to EU research, http://europa.eu/rapid/pressReleasesAction.do?reference=IP/06/1759&format=HTML&aged=0&language=EN&guiLanguage=en
10. Yokoyama M, Origasa H, Matsuzaki M, Matsuzawa Y, Saito Y, Ishikawa Y, Oikawa S, Sasaki J, Hishida H, Itakura H et al (2007) Effects of eicosapentaenoic acid on major coronary events in hypercholesterolaemic patients (JELIS): a randomized open-label, blinded endpoint analysis. Lancet 369:1090–1098
11. Cohen JT, Bellinger DC, Connor WE, Kris-Etherton PM, Lawrence RS (2005) A quantitative risk-benefit analysis of changes in population fish consumption. Am J Prev Med 29:325–334
12. Mozaffarian D, Longstreth WTJ, Lemaitre RN, Manolio TA, Kuller LH, Burke GL, Siscovick DS (2005) Fish consumption and stroke risk in elderly individuals: the cardiovascular health study. Arch Intern Med 165:200–206
13. Mozaffarian D, Rimm EB (2006) Fish intake, contaminants, and human health: evaluating the risks and the benefits. JAMA 296:1885–1899
14. Fish & Fish Products Market Report 2008, http://www.researchandmarkets.com/reportinfo.asp?cat_id=0&report_id=597257&q=seafood market&p=1
15. Food Outlook – Global Market Analysis – Global Information and Early Warning System on Food and Agriculture, http://www.fao.org/docrep/012/ak341e/ak341e00.htm
16. Food Outlook – Global Market Analysis, http://www.fao.org/docrep/010/ai466e/ai466e00.HTM
17. Delgado CL, Wada N, Rosegrant MW, Meijer S, Ahmed M (2003) Outlook for fish to 2020: meeting global demand. International Food Policy Research Institute and The WorldFish Center, Washington, DC
18. Review of the State of World Marine Fishery Resources Food and Agriculture Organization of the United Nations, FAO FISHERIES TECHNICAL PAPER 457, http://www.fao.org/docrep/009/y5852e/Y5852E00.htm#TOC
19. Food-Related Illness and Death in the United States, http://www.cdc.gov/ncidod/EID/vol5no5/mead.htm
20. Report to Congress Food and Drug Administration Amendments Act of 2007 Public Law 110-85 Section 1006 – Enhanced Aquaculture and Seafood Inspection. Enhanced Aquaculture and Seafood Inspection – Report to Congress, http://www.fda.gov/Food/FoodSafety/Product-SpecificInformation/Seafood/SeafoodRegulatoryProgram/ucm150954.htm
21. Campas M, Beatriz PS, Jean-Louis M (2007) Biosensors to detect marine toxins: assessing seafood safety. Talanta 72:884–895
22. Fleming LE, Broad K, Clement A, Dewailly E, Elmir S, Knap A, Pomponi SA, Smith S, Gabriele HS, Walsh P (2006) Oceans and human health: emerging public health risks n the marine environment. Mar Pollut Bull 53:545–560
23. Marine Toxins, http://www.cdc.gov/ncidod/dbmd/diseaseinfo/marinetoxins_g.htm
24. Marine Biotoxins, http://www.fao.org/docrep/007/y5486e/y5486e00.HTM
25. BBB – Various Shellfish-Associated Toxins-Bad Bug Book: Foodborne Pathogenic Microorganisms and Natural Toxins Handbook Various Shellfish-Associated Toxins, http://www.fda.gov/Food/FoodSafety/FoodborneIllness/FoodborneIllnessFoodbornePathogensNaturalToxins/BadBugBook/ucm070008.htm
26. Assurance of Seafood Quality, http://www.fao.org/docrep/003/t1768e/T1768E00.htm#TOC
27. Clark RF, Williams SR, Nordt SP, Manoguerra AS (1999) A review of selected seafood poisonings. Undersea Hyperb Med 26:175–184
28. Assessment and Management of Seafood Safety and Quality, http://www.fao.org/docrep/006/y4743e/y4743e00.htm#Contents
29. Brief review of natural nonprotein neurotoxins, Applied science and analysis Inc., http://www.asanltr.com/newsletter/02-2/articles/Neurotoxins.htm
30. García C, Pereira P, Valle L, Lagos N (2003) Quantitation of diarrhetic shellfish poisoning toxins in Chilean Mussel using pyrenyldiazomethane as fluorescent labeling reagent. Biol Res 36:171–183
31. Fernández-Ortega JF, Morales-de los Santos JM, Herrera-Gutiérrez ME, Fernández-Sánchez V, Loureo PR, Rancaño AA, Téllez-Andrade A (2010) Seafood intoxication by tetrodotoxin: first case in Europe. J Emerg Med 39(5):612–617
32. Hwang DF, Noguchi T (2007) Tetrodotoxin poisoning. Adv Food Nutr Res 52:141–236
33. Bachvaroff TR, Adolf JE, Squier AH, Harvey HR, Place AR (2008) Characterization and quantification of karlotoxins by liquid chromatography-mass spectrometry. Harmful Algae 7:473–484
34. Van Wagoner RM, Deeds JR, Satake M, Ribeiro AA, Place AR, Wright JLC (2008) Isolation and characterization of karlotoxin 1, a new amphipathic toxin from *Karlodinium veneficum*. Tetrahedron Lett 49:6457–6461
35. Van Wagoner RM, Deeds JR, Tatters AO, Place AR, Tomas CR, Wright JLC (2010) Structure and relative potency of several Karlotoxins from *Karlodinium veneficum*. J Nat Prod 73(8):1360–1365
36. Peng J, Place AR, Yoshida W, Anklin C, Hamann MT (2010) Structure and absolute configuration of Karlotoxin-2, an Ichthyotoxin from the marine Dinoflagellate Karlodinium veneficum. J Am Chem Soc 132:3277–3279

37. Abbott BC, Ballantine D (1957) The toxin from *Gymnodinium veneflcum* Ballantine. J Mar Biol Assoc UK 36
38. Adolf JE, Bachvaroff TR, Krupatkina DN, Nonogaki H, Brown PJP, Lewitus AJ, Harvey HR, Place AR (2006) Species specificity and potential roles of Karlodinium micrum toxinAfr. J Mar Sci XI HAB Proc 28:177–180
39. Sheng J, Malkiel E, Katz J, Adolf JE, Place AR (2010) A dinoflagellate exploits toxins to immobilize prey prior to ingestion. PNAS 107:2082–2087
40. Su YC, Liu C (2007) *Vibrio parahaemolyticus*: a concern of seafood safety. Food Microbiol 24:549–558
41. Feldhusen F (2000) The role of seafood in bacterial foodborne diseases. Microb Infect 2:1651–1660
42. Andrews LS, DeBlanc S, Veal CD, Park DL (2003) Response of *Vibrio parahaemolyticus* O3: K6 to a hot water/cold shock pasteurization process. Food Add Contam 20:331–334
43. Interstate Shellfish Sanitation Conference Vibrio vulnificus fact sheet- Health care providers, http://www.issc.org/client_resources/Education/VvFactSheet.pdf
44. Samir M, Haq BS, Hari HD (2005) Chronic liver disease and consumption of raw oysters: a potentially lethal combination – a review of *Vibrio vulnificus* septicemia. Am J Gastroenterol 100:1195–1199
45. Norhana MNW, Poole SE, Deeth HC, Dykes GA (2010) Prevalence, persistence and control of *Salmonella* and *Listeria* in shrimp and shrimp products: a review. Food Control 21:343–361
46. Committee on Evaluation of the Safety of Fishery Products. Seafood Safety (1991) Institute of Medicine (IOM). Food and Nutrition Board Institute of Medicine, http://www.nap.edu/openbook.php?record_id=1612&page=30
47. Potasman I, Paz A, Odeh M (2002) Infectious outbreaks associated with bivalve shellfish consumption: a worldwide perspective. Clin Infect Dis 35:921–928
48. Halliday ML, Kang LY, Zhou TK, Hu MD, Pan QC, Fu TY, Huang YS, Hu SLI (1991) An epidemic of hepatitis A attributable to the ingestion of raw clams in Shanghai, China. J Infect Dis 164:852–859
49. Norovirus: Technical Fact Sheet, http://www.cdc.gov/ncidod/dvrd/revb/gastro/norovirus-factsheet.htm
50. Kar D, Sur P, Mandal SK, Saha T, Kole RK (2008) Assessment of heavy metal pollution in surface water. Int J Environ Sci Tech 5:119–124
51. Heavy Metal Pollution – Heavy Metal Pollution is More Common Than You Think, http://www.fairfaxcounty.gov/nvswcd/newsletter/heavymetal.htm
52. Scientific Opinion on Arsenic in Food Question number: EFSA-Q 2008-425, http://www.efsa.europa.eu/EFSA/efsa_locale-1178620753812_1211902959840.htm
53. Daniels JL, Longnecker MP, Rowland AS, Golding J (2004) Fish intake during pregnancy and early cognitive development of offspring. Epidemiology 15:394–402
54. Oken E, Wright RO, Kleinman KP, Bellinger D, Amarasiriwardena CJ, Hu H, Rich-Edwards JW, Gillman MW (2005) Maternal fish consumption, hair mercury, and infant cognition in a U.S. Cohort. Environ Health Perspect 113:1376–1380
55. Myers GJ, Davidson PW, Cox C, Shamlaye CF, Palumbo D, Cernichiari E, Sloane-Reeves JW GE, Kost J, Huang LS, Clarkson TW (2003) Prenatal methylmercury exposure from ocean fish consumption in the Seychelles child development study. Lancet 361:1686–1692
56. Smith AG, Gangolli SD (2002) Organochlorine chemicals in seafood: occurrence and health concerns. Food Chem Tox 40:767–779
57. Hites RA, Foran JA, Carpenter DO, Hamilton MC, Knuth BA, Schwager SJ (2004) Global assessment of organic contaminants in farmed salmon. Science 303:226–229
58. Willett WC (2005) Fish: balancing health risks and benefits. Am J Prev Med 29:320–321
59. How FDA Regulates Seafood: FDA Detains Imports of Farm-Raised Chinese Seafood, http://www.fda.gov/ForConsumers/ConsumerUpdates/ucm094558.htm
60. Gerssen A, Mulder PPJ, McElhinney MA, de Boer J (2009) Liquid chromatography-tandem mass spectrometry method for the detection of marine lipophilic toxins under alkaline conditions. J Chromatogr A 1216:1421–1430
61. Syaifudin ARM, Jayasundera KP, Mukhopadhyay SC (2009) A low cost novel sensing system for detection of dangerous marine biotoxins in seafood. Sens Actuators B 137:67–75
62. Zhou Y, Li YS, Pan FG, Zhang YY, Lu SY, Ren HL, Li ZH, Liu ZS, Zhang JH (2010) Development of a new monoclonal antibody based direct competitive enzyme-linked immunosorbent assay for detection of brevetoxins in food samples. Food Chem 118:467–471
63. Önal A (2007) Analytical, nutritional and clinical methods a review: current analytical methods for the determination of biogenic amines in foods. Food Chem 103:1475–1486
64. BY PRJB, Rutgers P, Stolker AAM, Nielen MWF (2009) Multi-residue screening of veterinary drugs in egg, fish and meat using high-resolution liquid chromatography accurate mass time-of-flight mass spectrometry. J Chromat A 1216:8206–8216
65. Smith SGC, Reimschuessel R, Decker C-S, Carson MC (2009) Simultaneous screening and confirmation of multiple classes of drug residues in fish by liquid chromatography-ion trap mass spectrometry. J Chromat A 1216:8224–8232
66. Bacteriological Analytical Manual (BAM) Bacteriological Analytical Manual – Revision A. Last Updated: 05/14/2009, http://www.fda.gov/Food/ScienceResearch/LaboratoryMethods/BacteriologicalAnalyticalManualBAM/default.htm
67. Espiñeira M, Atanassova M, Vieites JM, Santaclara FJ (2010) Validation of a method for the detection of five species, serogroups, biotypes and virulence factors of Vibrio by multiplex PCR in fish and seafood. Food Microbiol 27: 122–131
68. Kural AG, Shearer AE, Kingsley DH, Chen H (2008) Conditions for high pressure inactivation of Vibrio parahaemolyticus in oysters. Int J Food Microbiol 127:1–5

69. Calci KR, Meade GK, Tezloff RC, Kingsley DH (2005) High-pressure inactivation of hepatitis A virus within oysters. Appl Environ Microbiol 71:339–343
70. Kingsley DH, Chen H (2009) Influence of pH, salt, and temperature on pressure inactivation of hepatitis A virus. Int J Food Microbiol 130:61–64
71. Li D, Tang Q, Wang J, Wang Y, Zhao Q, Xue C (2009) Effects of high-pressure processing on murine norovirus-1 in oysters (Crassostrea gigas) in situ. Food Control 20:992–996
72. Murchie LW, Kelly AL, Wiley M, Adair BM, Patterson M (2007) Inactivation of a calicivirus and enterovirus in shellfish by high pressure. Innovative Food Sci Emerg Technol 8:213–217
73. Meujo DAF, Kevin D, Peng J, Bowling JJ, Liu J, Hamann MT (2010) Reducing oyster-associated bacteria levels using supercritical fluid CO_2 as an agent of warm pasteurization. Int J Food Microbiol 138:63–70
74. Quan Y, Choi KD, Chung D, Shin IS (2010) Evaluation of bactericidal activity of weakly acidic electrolyzed water (WAEW) against *Vibrio vulnificus* and *Vibrio parahaemolyticus*. Int J Food Microbiol 136:255–260
75. Wang D, Zhang D, Chen W, Yu S, Shi X (2010) Retention of Vibrio parahaemolyticus in oyster tissues after chlorine dioxide treatment. Int J Food Microbiol 137:76–80
76. Huang YR, Hung YC, Hsu SY, Huang YW, Hwang DF (2008) Application of electrolyzed water in the food industry. Food Control 19:329–345
77. Tahiri I, Desbiens M, Kheadr E, Lacroix C, Fliss I (2009) Comparison of different application strategies of divergicin M35 for inactivation of Listeria monocytogenes in cold-smoked wild salmon. Food Microbiol 26:783–793
78. Matamoros S, Pilet MF, Gigout F, Prévost H, Leroi F (2009) Selection and evaluation of seafoodborne psychrotrophic lactic acid bacteria as inhibitors of pathogenic and spoilage bacteria. Food Microbiol 26:638–644
79. Pinto AL, Fernandes M, Pinto C, Albano H, Castilho F, Teixeira P, Gibbs PA (2009) Characterization of anti-*Listeria* bacteriocins isolated from shellfish: potential antimicrobials to control non-fermented seafood. Int J Food Microbiol 129:50–58
80. Song HP, Kim B, Jung S, Choe JH, Yun H, Kim YJ, Jo C (2009) Effect of gamma and electron beam irradiation on the survival of pathogens inoculated into salted, seasoned, and fermented oyster. LWT Food Sci Technol 42:1320–1324
81. Kim B, Song HP, Choe JH, Jung S, Jang A, Kim YJ, Jo C (2009) Application of electron-beam irradiation on the production of salted and seasoned short-necked clam, Tapes Pilippinarum, for safe distribution. Rad Phys Chem 78:585–587
82. Medina M, Cabeza MC, Bravo D, Cambero I, Montiel R, OrdóñezNuñez JAM, Hoz LA (2009) comparison between E-beam irradiation and high pressure treatment for cold-smoked salmon sanitation: microbiological aspects. Food Microbiol 26:224–227
83. Mahmoud BSM (2009) Effect of X-ray treatments on inoculated *Escherichia coli* O157: H7, *Salmonella enterica*, *Shigella flexneri* and *Vibrio parahaemolyticus* in ready-to-eat shrimp. Food Microbiol 26:860–864
84. Mahmoud BSM (2009) Reduction of *Vibrio vulnificus* in pure culture, half shell and whole shell oysters (*Crassostrea virginica*) by X-ray. Int J Food Microbiol 130:135–139
85. Gudbjornsdottir B, Jonsson A, Hafsteinsson H, Heinz V (2010) Effect of high-pressure processing on Listeria spp. and on the textural and microstructural properties of cold smoked salmon. LWT Food Sci Technol 43:366–374
86. Brutti A, Rovere P, Cavallero S, D'Amelio S, Danesi P, Arcangeli G (2010) Inactivation of Anisakis simplex larvae in raw fish using high hydrostatic pressure treatments. Food Control 21:331–333
87. Schirmer BC, Heiberg R, Eie T, Møretrø T, Maugesten T, Carlehøg M, Langsrud S (2009) A novel packaging method with a dissolving CO_2 headspace combined with organic acids prolongs the shelf life of fresh salmon. Int J Food Microbiol 133:154–160
88. Norhana MNW, Azman AMN, Poole SE, Deeth HC, Dykes GA (2009) Effects of bilimbi (*Averrhoa bilimbi* L.) and tamarind (*Tamarindus indica* L.) juice on *Listeria monocytogenes* Scott A and *Salmonella typhimurium* ATCC 14028 and the and the sensory properties of raw shrimps. Int J Food Microbiol 136:88–94
89. Chaiyakosa S, Charernjiratragul W, Umsakul K, Vuddhakul V (2007) Comparing the efficiency of chitosan with chlorine for reducing *Vibrio parahaemolyticus* in shrimp. Food Control 18:1031–1035
90. Ye M, Neetoo H, Chen H (2008) Effectiveness of chitosan-coated plastic films incorporating antimicrobials in inhibition of *Listeria monocytogenes* on cold-smoked salmon. Int J Food Microbiol 127:235–240
91. Terio V, Martella V, Moschidou P, Di Pinto P, Tantillo G, Buonavoglia C (2010) Food norovirus in retail shellfish microbiology. Food Microbiol 27:29–32
92. Bakar J, Yassoralipour A, Bakar FA, Rahman RA (2010) Biogenic amine changes in barramundi (*Lates calcarifer*) slices stored at 0°C and 4°C. Food Chem 119:467–470
93. Post-harvest Oyster Processing Technologies – Fact Sheet for Seafood Dealers and Processors, http://www.dmr.state.ms.us/Fisheries/Seafood-Technology/pdfs/fact-sheet-postharvest-oyster-processing.pdf
94. Prapaiwong N, Wallace RK, Arias CR (2009) Bacterial loads and microbial composition in high pressure treated oysters during storage. Int J Food Microbiol 131:145–150
95. Mahmoud BS, Burrage DD (2009) Inactivation of *Vibrio parahaemolyticus* in pure culture, whole live and half shell oysters (*Crassostrea virginica*) by X-ray. Lett Appl Microbiol 48:572–578
96. De Roda Husman AM, Lodder-Verschoor F, van den Berg HH, Le Guyader FS, van Pelt H, van der Poel WH, Rutjes SA (2007) Rapid virus detection procedure for molecular tracing of shellfish associated with disease outbreaks. J Food Prot 70:967–974
97. Le Guyader FS, Parnaudeau S, Schaeffer J, Bosch A, Loisy F, Pommepuy M, Atmar RL (2009) Detection and quantification of noroviruses in shellfish. Appl Environ Microbiol 75:618–624

98. Gentry J, Vinjé J, Lipp EK (2009) A rapid and efficient method for quantitation of genogroups I and II norovirus from oysters and application in other complex environmental samples. J Virol Meth 156:59–65
99. Xiaoxia K, Qingping W, Dapeng W, Jumei Z (2008) Simultaneous detection of norovirus and rotavirus in oysters by multiplex RT-PCR. Food Control 19:722–726

Books and Reviews

Balaban M, Odabaşi A, Damar S, Oliveira A (2007) Quality evaluation of seafood. In: Da-Wen Sun (ed) Computer vision technology for food quality evaluation. Academic, San Diego, pp 189–209

Ciminiello P, Dell' Aversano C, Fattorusso E, Forino M (2009) Recent developments in mediterranean harmful algal events. In: Fishbein JC (ed) Advances in molecular toxicology. Elsevier, New York, pp 1–41

Fung D (2009) Food spoilage, preservation and quality control. In: Encyclopedia of microbiology. 3rd edn. Elsevier, New York, pp 54–79

Halvorson H, Smolowitz R (2009) Aquaculture. In: Encyclopedia of microbiology, 3rd edn. Elsevier, New York, pp 17–22

Hwang D-F, Noguchi T (2007) Tetrodotoxin poisoning. In: Advances in food and nutrition research, vol 52. Elsevier, New York, pp 141–236

Jong E (2008) Toxic syndromes the travel and tropical medicine manual. In: Fish and shellfish poisoning, 4th edn. Saunders, Philadelphia, pp 474–480

Keener K (2007) Food regulations. In: Handbook of farm, dairy, and food machinery. William Andrew, Norwich, pp 15–43

Landrigan P, Kotelchuck D, Grandjean P (2007) Principles for prevention of the toxic effects of metals. In: Handbook on the toxicology of metals, 3rd edn, Academic, San Diego, pp 319–337

Le Guyader F, Atmar R (2007) Viruses in shellfish. In: Perspectives in Medical Virology, vol 17. Elsevier, Barcelona, pp 205–226

Ling KH, Nichols P, But P-H (2009) Fish-induced keriorrhea. In: Advances in food and nutrition research, vol 57. Elsevier, New York, pp 1–52

Niemira B, Zhang Q (2009) Advanced technologies for detection and elimination of pathogens. In: The produce contamination problem. Elsevier, New York, pp 425–443

Paulsen P, Luf W, Smulders F (2006) Different legislations on toxicants in foodstuffs. In: Food toxicants analysis. Elsevier, New York, pp 11–31

Rzeżutka A, Cook N (2009) Review of currently applied methodologies used for detection and typing of foodborne viruses. In: Global issues in food science and technology. Academic, San Diego, pp 229–246

Still K, Mohapatra A (2009) Biotoxins. In: Information resources in toxicology, 4th edn. Academic, San Diego, pp 91–102

Taylor S (2008) Molluscan shellfish allergy. In: Advances in food and nutrition research, vol 54. pp 139–177

Seaweed Aquaculture for Human Foods in Land-Based and IMTA Systems

Rui Pereira[1], Charles Yarish[2], Alan T. Critchley[3]
[1]CIMAR/CIIMAR – Centre for Marine and Environmental Research, University of Porto, Porto, Portugal
[2]Departments of Ecology & Evolutionary Biology and Marine Sciences, University of Connecticut, Stamford, CT, USA
[3]Acadian Seaplants Limited, Dartmouth, NS, Canada

Article Outline

Glossary
Definition of the Subject and Its Importance
Introduction
Past and Present Uses of Seaweeds
Seaweed Aquaculture
Introduction of the IMTA Concept
Physiological Considerations for the Production of Seaweeds in Land-Based Cultivation Systems
Examples of Successful On-Land Cultivation Enterprises
Future Directions
Acknowledgments
Bibliography

Glossary

Algae A group of autotrophic organisms, containing chlorophyll a and sometimes other accessory pigments, which are able to convert solar energy into chemical energy via photosynthesis.

Aquaculture The farming of autotrophic and heterotrophic organisms in aquatic systems.

Bioextraction An environmental management strategy by which nutrients are removed from an aquatic ecosystem through the harvest of enhanced biological production, including the aquaculture of suspension-feeding shellfish and/or marine macroalgae.

Ecosystem Is the grouping of all living organisms occupying a particular unit of space and interacting with each other and their environment.

EPA Eicosapentaenoic acid is an omega-3 polyunsaturated fatty acid, sometimes presented with the chemical notation 20:5(n-3).

HDL High-density lipoprotein; composed of a high proportion of protein and relatively little cholesterol; high levels of HDL are thought to be associated with a decreased risk of coronary heart disease and atherosclerosis.

Heteromorphic life histories Life histories in which there are clear morphological differences between the different stages of the life cycle, i.e., individuals of the sporophyte and gametophyte stages are morphologically different and distinguishable. In some cases, such as the genus *Porphyra* and members of the kelps, there are macroscopic and microscopic stages alternating life cycle phases.

IMTA Integrated Multi-Trophic Aquaculture is a form of aquaculture in which organisms from different trophic levels, with complementary resource needs, are produced in the same system. Typically, these aquaculture systems integrate the production of a fed organism, such as fish or shrimp, with that of extractive organic aquaculture such as shellfish and the extractive inorganic aquaculture of seaweed.

Isomorphic life histories Life histories in which there are no distinguishing morphological differences between the different stages of the life cycle, i.e., the individuals of the sporophyte (diploid, 2n) and gametophyte (haploid, n) stages are morphologically identical and can be distinguished only when their respective, characteristic reproductive structures are present, e.g., *Chondrus crispus* and *Palmaria palmata*.

LDL Low-density lipoprotein; a lipoprotein that transports cholesterol in the blood, composed of a moderate amount of protein and a large amount of cholesterol; high levels of LDL are thought to be associated with an increased risk of coronary heart disease and atherosclerosis.

Macroalgae A group of macroscopic algae of which at least one part of their life history is multicellular and visible with unaided eye.

Mariculture Farming of autotrophic and heterotrophic organisms in marine systems, i.e., using seawater.

Polysaccharides Complex structural polymers. They have a structural function in the alga but may be extracted industrially to provide a range of polysaccharides used for their rheological properties, e.g., agar, carrageenan, and alginic acid.

Seaweed A group of macroscopic, marine autotrophic algae.

Sea-vegetables A group of macroscopic, marine autotrophic algae, also called seaweeds, seaplants, or macroalgae; they may be used as vegetables for human consumption or raw materials for a range of industrial, commercially important extracts such as bioactives or polysaccharides.

Definition of the Subject and Its Importance

The production of seaweeds for human foods in land-based aquaculture, is an activity poorly presented by the scientific community. Of the thousands of seaweed species identified, a remarkably small subset is actually farmed in the marine environment (i.e., open water) and even fewer are grown in land-based aquaculture systems. Of those that are used in land-based systems, most are monocultures grown for specific high value uses. For instance, *C. crispus, P. palmata*, and *Saccharina latissima* are grown for human consumption; *Chondrocanthus* and the "*Trailiella*" stage of *Bonnemaisonia/Asparagopsis* for the cosmetic industry; and *Gracilaria* spp., *Palmaria* and *Ulva* spp. as feed for abalone). Given the many centuries history of terrestrial production of land plants for human and animal feed crops and the tremendous efforts given over to the selection and crossbreeding of these plants, by contrast, selection and improvement of seaweed crops is very much in its infancy. Even more so, of all the relatively small number of seaweeds which are domesticated for open water cultivation, even fewer species have actually been tested in land-based culture systems. This is in part due to the lack of reliable, domesticated species and their selected strains suitable for the rigors of on-land cultivation, and in part due to the complexities of life histories and the lack of understanding of the environmental regulation of growth. There is, therefore, a need to test other species since open water systems may not be appropriate for niche cultivation applications. The historical development of open water cultivation and multi-species pond cultivation may have originated in Asia (for discussion and references see later section); however, modern land-based

aquaculture of seaweeds began with the work of John Ryther at Woods Hole Oceanographic Institute (WHOI) in the late 1960s through the mid-1970s [1]. Land-based Integrated Multi-Trophic Aquaculture systems (IMTA) may contribute to the development of sustainable fed aquaculture systems by minimizing environmental impacts (i.e., removing excess dissolved inorganic nutrients, *d*issolved *o*rganic *m*atter (DOM), and *p*articulate *o*rganic *m*atter (POM). Furthermore, while the systems may yet have to be optimized geographically and in relation to the species utilized, the controlled production of seaweed biomass in these systems may offer a reliable and safe source of food or ingredients for human consumption, fish feeds, as well as a source of valuable compounds for biotechnological applications. As a special focus, this entry will discuss the importance of land-based seaweed aquaculture systems and their global utilization.

Introduction

Seaweed is a popular term used to collectively describe marine macroalgae. Among this large and diverse assemblage of photosynthetic marine organisms are a number of species with a varied array of uses; when used for human consumption, they are more popularly known as "sea-vegetables." This collective of convenience includes the macroscopic, multicellular, red, green, and brown algae [2]. Seaweeds are often abundant and predominantly found in the near-shore marine ecosystems in all the oceans of the world. As a result of their diverse intercellular compounds including alginic acid, carrageenans, and agar, seaweeds have very important industrial applications [3, 4]. Being important primary producers in marine ecosystems, macroalgae are an integral component of near-shore environment and form a fundamental part of the basis of the photosynthetic food chains, playing a role similar to that of terrestrial plants [5]. In these natural environments, seaweeds often perform a large number of ecosystem services [6] (e.g., nurseries, nutrient cycling, and reduction of coastal erosion among others), which are neither fully costed nor often appreciated by the public or users of the marine environment. Humans have wild harvested (sometimes called "wild crafting") and cultivated seaweeds for several centuries for animal and human consumption as well as other applications including valuable sources of phycocolloids and most recently, researched as feedstock for biofuels and carbon sequestration [7–11].

Some seaweeds may attain lengths exceeding 90 m or more (e.g., the kelp *Macrocystis pyrifera*), while others may grow only a few centimeters per year. Many seaweeds have isomorphic life cycles (e.g., *C. crispus, P. palmata*, where the gametophyte and sporophyte generations are morphologically similar), while others have heteromorphic life histories (e.g., the genus *Porphyra* and many species of brown algae including the kelps, where the generations are morphologically distinct). The morphology of various seaweeds may include multicellular, highly differentiated kelp with their organs such as blades, complex stipes, and their anchoring structure referred to as haptera. Other multicellular seaweeds may be small and bushy with flat or cylindrical axes (*Gracilaria*), while others may form sheet-like specimens of one or two layers of cells thickness (*Porphyra*, *Ulva*, *Monostroma*). Some macroalgae may be encrusting forms, while yet others may have the ability to precipitate calcium carbonate to varying degrees and be lightly calcified yet remain flexible (e.g., *Padina*) or fully calcareous and occur as prostrate crusts (e.g., *Lithothamnion*, *Phymatolithon*) or fully articulated, e.g., many coralline species such as *Corallina* and *Jania*.

This entry will discuss the advantages for land-based aquaculture of seaweeds for human foods and animal consumption. The first section gives a brief introduction to seaweed uses, both past and present, followed by an introduction as to how seaweed aquaculture has been practiced more recently. Section "Introduction of the IMTA Concept" briefly explains the concept of integrated multi-trophic aquaculture (IMTA), since this can also be an integral component of land-based seaweed aquaculture systems. Section "Physiological Considerations for the Production of Seaweeds in Land-Based Cultivation Systems" presents some of the particularities of intensive, land-based seaweed production, which make it different from the more common extensive, open water seaweed mariculture. Section "Examples of Successful On-Land Cultivation Enterprises" presents success stories of land-based seaweed aquaculture. The entry concludes with

a discussion of the potential impacts of the development of land-based seaweed aquaculture as well as future directions and perspectives of research in this area.

Past and Present Uses of Seaweeds

Seaweeds have been used in the human diet since ancient times. Although Asian food culture has seen the most prominent use of seaweed for direct human consumption, there is also recent evidence of the use of seaweeds by prehistoric humans, in other parts of the world. Dillehay et al. [12], in an archeological study conducted in Monte Verde, southern Chile, identified remains of nine species of marine algae, including *Durvillaea antarctica* ("cochayuyo"), *Porphyra* sp. ("luche"), *Gracilaria* sp. ("pelillo"), and *Sargassum* sp. These authors also suggest that some algae may have been burned, suggesting that they had been dried to facilitate transportation and/or storage, or were even cooked and could have been used for their medicinal properties as well. Erlandson et al. [13] discussed the cold water, coastal fringing kelp beds on the Pacific Coast of the Americas as being a route, or a "highway," by which early travelers made their way in northerly and southerly migrations. In Asian and Pacific Island countries, the tradition is to consume seaweeds as raw or cooked sea vegetables [14–16]. In Western countries, the principal use of seaweeds has been as a source of phycocolloids (alginate, carrageenan, and agar) which are structural, thickening, and gelling agents for various industrial applications, including uses in textile, paper, food, toothpastes, shampoos, cosmetics, and pharmaceutical industries [3, 4].

There is presently an increasing interest by the general public regarding the impacts of the human diet in general health and the potential health benefits in the consumption of selective seaweeds in a varied human diet. In fact, the physiological or pharmacological functions of food factors were classified as the third function of food in addition to the nutritional and sensory roles as the primary and secondary function, respectively [17, 18]. Among the bioactive compounds known to have an impact in the human health, there are those described as prebiotic functional ingredients. These are defined as nondigestible, selectively fermented compounds that stimulate the growth and/or activity of beneficial gut microbiota which, in turn, confer health benefits on the host [19].

Due to their varied nutritional properties, seaweeds are the subject of research seeking new, natural sources of functional ingredients for food. Table 1 presents a summary of that information [20–22]. *Porphyra*, for instance, contains high levels of protein (25–50%), vitamins (higher vitamin C than in oranges), trace minerals, and dietary fibers [23]. This alga contains nearly 17 types of free amino acids, including taurine which controls blood cholesterol levels and is thought to prevent obesity [24, 25]. Several reviews have been published outlining the nutritional properties of seaweeds (e.g., [21, 22, 26]), the most recent of which include the comprehensive review of Holdt and Kraan [27] and another on antioxidants from macroalgae by Cornish and Garbary [28]. The review of Holdt and Kraan [27] is particularly valuable since it also details the regulatory environment affecting marketing and use of active compounds from seaweeds in human applications. On the other hand, Cornish and Garbary [28] consider the application of seaweed antioxidants in foods, food supplements, nutraceuticals, and medicine from the perspective of benefits to human health. The review provides examples not only from laboratory studies but also from clinical trials where antioxidants derived from seaweeds may provide major health benefits that warrant subsequent investigative studies and possible utilization. Furthermore, those authors advocate that the direct consumption of seaweed products for their antioxidant composition alone provides a useful alternative to nonnatural substances, while simultaneously providing worthwhile nutritional benefits. Finally, the review by Cornish and Garbay [28] includes a comprehensive listing of algal species evaluated for antioxidant activity and potential applications of detected compounds.

Burtin [26] elaborates upon the nutritional value of seaweeds as they are rich in polysaccharides and dietary fibers, minerals, proteins and amino acids, lipids and fatty acids, and micronutrients such as vitamins (vitamin B_{12}, C, and E) and polyphenols (phlorotannins). This author concludes that from a nutritional standpoint, the main beneficial properties of seaweeds are their high mineral (iodine, calcium) and soluble dietary fiber contents, the occurrence of vitamin B_{12} and specific components such as fucoxanthin, fucosterol,

Seaweed Aquaculture for Human Foods in Land-Based and IMTA Systems. Table 1 Some examples of seaweeds with their functional ingredients and possible effects on human health (Adapted from Plaza et al. [20]; Kumar et al. [21], Bocanegra et al. [22])

Seaweed	Functional ingredient	Possible health benefits
Sargassum vulgare (B)	Alginic acid, xylofucans	Antiviral activity
Himanthalia elongata (B)	PUFAs	Reduce risk of certain heart diseases
	α-Tocoferol	Antioxidant activity
	Sterols	Reduce total and LDL cholesterol
	Soluble fiber	Reduce total and LDL cholesterol
U. pinnatifida (B)	PUFAs	Reduce risk of certain heart diseases
	Sterols	Reduce total and LDL cholesterol
	Soluble fiber	Reduce total and LDL cholesterol
	Folates	Reduce risk of certain types of cancer
	Sulfated polysaccharides	Antiviral activity
	Fucoxanthin	Preventive effect on cerebrovascular diseases; Increase the metabolism
Porphyra spp. (R)	PUFAs	Reduce risk of certain heart diseases
	Sterols	Reduce total and LDL cholesterol
	Soluble fiber	Reduce total and LDL cholesterol
C. crispus (B)	PUFAs (n-3) fatty acids	Reduce risk of certain heart diseases
	Sterols	Reduce total and LDL cholesterol
	Soluble fiber	Reduce total and LDL cholesterol
Cystoseira spp. (B)	Terpenes	Valuable curative properties
	Sterols	Reduce total and LDL cholesterol
	Sulfated polysaccharides	Regulate the bioactivity of growth factors and cytokines
Ulva spp. (G)	Sterols	Reduce total and LDL cholesterol
Grateloupia filicina (R)	"methanolic extract"	Antioxidant activity
Brown algae (non specified)	Phlorotannins	Detoxification of heavy metals; antibacterial effects
	Fucoidan	Anti-inflammatory, anticoagulant
Colpomenia sinuosa (B)	Fatty acid profile (ω-3)	Increase HDL cholesterol
Hypnea charoides (R)	Fatty acid profile (ω-3)	Decreased LDL cholesterol
A. nodosum (B)	Sodium-binding fiber	Antihypertensive effects

R red, *B* brown, *G* green seaweed

and phlorotannins. Burtin also states that seaweeds can be regarded as an underexploited source of health-promoting molecules for food processing and the increasingly important nutraceutical industries [26].

Kumar et al. [21] reviewed the presence and value of various bioactive substances which may be derived from certain seaweeds, namely, polysaccharides and related compounds; proteins and related substances; lipids and related compounds; minerals; vitamins and antioxidant compounds. These authors concluded that seaweeds are a low calorie food source, particularly from the nutritional point of view, since they have

high concentrations of certain minerals, vitamins, proteins, and indigestible carbohydrates. Seaweeds also have low lipid content, but the lipids present are of a high quality in terms of their nutritional value. In fact, Blouin et al. [29] suggested that native, Atlantic species of *Porphyra* such as *Porphyra amplissima* and *Porphyra umbilicalis* have potential in foods for North American consumers. They analyzed the fatty acid content of freshly collected *P. umbilicalis* and reported that eicosapentaenoic acid [EPA; 20:5 (n-3)] and palmitic acid were the most common fatty acids. Those authors reported that the concentration of fatty acids found in wild collected *P. umbilicalis* (i.e., 3.2 mg EPA g dry wt^{-1} or 74 mg EPA 100 g fresh wt^{-1}) was not high enough to make this a primary source of daily omega-3 fatty acids, but the favorable n-3/n-6 ratio (2–3:1) in these species constituted an interesting nutritional value. In their review, Kumar et al. [21] concluded that the quality of protein and lipids in seaweeds generally is as acceptable as those present in other dietary vegetables due to high content of essential amino acids and relatively higher levels of unsaturated fatty acids. Furthermore, all of these authors suggested that seaweeds exhibit antioxidant, antimutagenic, anticoagulant, anticancer, and antitumor activity. In many cases, these properties were actually tested and proved in vivo and in vitro, as follows. Zhang et al. [30] showed that a sulfated polysaccharide fraction from *Porphyra haitanensis* could be used to compensate the decline in total antioxidant capacity and activities of antioxidant enzymes. The implications of these findings are that seaweeds and their extracts might play a role in retarding the aging process. In addition, unprocessed powder from the brown seaweed *Fucus vesiculosus* has proven to have strong antioxidant capacities [31]. The authors concluded that the polyphenol (phlorotannin) content of *F. vesiculosus* seemed to provide the main antioxidant properties. Other research using polysaccharides extracted from *Porphyra yezoensis* demonstrated anticoagulant [32] and immune-stimulating activities [33, 34]. Saito et al. [34] showed that *Porphyra* peptides induced a significant reduction in the blood pressure of hypertensive human patients. Various fucoidans, common sulfated polysaccharides of various commercially important brown algae, have been tested in several studies in rats and in humans, showing beneficial effects as an anticoagulant, antithrombotic, antiviral, and anticancer agent ([35, 36]; see also www.marinova.com). Anticancer properties of seaweeds are also reported in the studies of Teas et al. [37] and Yang et al. [38] among others. In particular, the results of Teas et al. [37] suggested that a diet containing 5% brown seaweed (i.e., *Laminaria*) was effective in delaying the time for chemically induced tumor development in rats. In turn, Yang et al. [38] investigated the association between the intake of *Porphyra* (red seaweed) and *Undaria* (brown seaweed) and the risk of breast cancer, in a case-control study. The authors concluded that the consumption of *Undaria pinnatifida* did not have any significant associations with the disease but the results also suggested that high intake of *Porphyra* may decrease the risk of breast cancer.

Bocanegra et al. [22] reviewed the major physicochemical properties of seaweed fiber, the nutritional properties of the seaweed, and their value as functional foods. In terms of physicochemical properties of the fiber, the authors highlighted the hydration properties and viscosity, the oil retention and fat absorption, the fermentability, and binding capacity (cation-exchange capacity responsible for heavy metal biosorption). As for the nutritional properties of the seaweed, Bocanegra et al. [22] pointed to numerous studies that demonstrated the chemical and nutritional importance of the seaweed, namely in relation to bioavailability, effect on growth and body weight, effects on digestion, excretion and gastrointestinal functions, effects on lowering cholesterol and blood pressure, antioxidant activities and effects on glucose metabolism. Those authors concluded, however, that although some antioxidant compounds are present in algae, other compounds that are also present, such as the arsenic (As), can induce a poor endogenous antioxidant status. Therefore, the use of marine algae in herbal medications or excessive consumption of some of these organisms requires some caution. As with all things, seaweeds should be consumed in moderation as part of a well-balanced diet. Bocanegra et al. [22] also highlighted that, at that point there were no data available on the changes that cooking (e.g., microwave oven, traditional oven, frying, boiling, etc.) might impact on the properties of algal constituents. It is clear that much more work remains to fully realize the full nutritional and health-promoting potential of the consumption of

seaweeds. These authors also illustrated that although numerous beneficial health properties can be attributed to seaweed components and extracts, robust studies of potential functional foods containing seaweeds have yet to be carried out, namely, the determination of different matrices affecting their technological and nutritional properties. The points raised by Holdt and Kraan [27], regarding the requirements of various food regulatory agencies, particularly with regard to novel foods and ingredients, should also be carefully considered.

As marine organisms with unique structural and biochemical compositions, seaweeds could be responsibly exploited for their multifunctional properties in the form of food, energy, medicine and cosmetics, and as biotechnological tools. In recent times, the use of seaweeds in a wide variety of biotechnological applications has become more common. Sahoo et al. [39] and Gantt et al. [40] pointed out the advantages of the use of *Porphyra* as a model organism for both applied and basic research. In fact, part of the genome of *P. umbilicalis* and the transcriptome of *Porphyra purpurea* have been recently released by the Joint Genome Institute (U.S. Department of Energy, www.jgi.doe.gov/genome-projects/ Program CSP2008; see also www.porphyra.org) and made available to the public. The aforementioned authors specifically point to the possibility of establishing several pure lines. In particular, the small genome size, which is estimated to be 2.6×10^8 base pairs consisting of three chromosomes and also the short generation time (1–3 months) of the alga are suitable traits for genetic analysis. The "*Porphyra* Genome" project, currently underway, will be one of the first to sequence the full genome of a multicellular red seaweed species and provide valuable information for biotechnological applications [40]. Other macroalgal genome projects include that of *C. crispus*, likely to be published in early 2011 (Jonas Collén, personal communication) and *Ectocarpus* [102]. As has been experienced with microalgal research (see [41, 42] and references therein), such major advances allow for rapid implementation of genetic engineering techniques that may modify seaweeds, thereby increasing their biotechnology applications. Some caution however needs to be applied to applications of such techniques. Should these "modified" seaweeds be destined for food or food products, then the necessity to label them as GMO (*g*enetically *m*odified *o*rganisms) sources would actually reduce their market acceptance, particularly in Europe and even increasingly in North America.

Seaweed Aquaculture

The largest database reference for seaweed taxonomy (www.algaebase.org) currently has over 10,000 macroalgal species listed, the majority being seaweeds [43]. Despite the variety of life forms and the many thousands of seaweed species, seaweed aquaculture is presently based upon a relatively very small group of less than 100 species worldwide [7]. In fact, only five to seven genera alone (i.e., *Laminaria/Saccharina, Undaria, Porphyra, Eucheuma/Kappaphycus* and *Gracilaria*) account for about 83% of the world seaweed production (Table 2). The basic cultivation techniques of these genera are described in Yarish and

Seaweed Aquaculture for Human Foods in Land-Based and IMTA Systems. Table 2 Main seaweed aquaculture production and value in 2008, according to FAO 2010 [45]

Genera	Production (metric tons)	Value	
		(*1,000 USD)	USD/ton
Laminaria (=*Saccharina*)	4,765,076	2,835,558	595
Eucheuma/Kappaphycus	3,551,273	563,146	159
Undaria	1,755,913	749,213	427
Porphyra	1,389,360	1,345,414	968
Gracilaria	1,418,986	600,223	423
Others	2,661,054	1,262,018	474

Pereira [7] and Pereira and Yarish [44] and the references therein.

The use of seaweeds for food has strong roots in Asian countries such as China, Japan, and the Republic of Korea. For that reason, these are the primary areas where seaweed aquaculture was first developed and, furthermore, the species of seaweed most cultivated are the ones commonly found from those shores. Tseng [46] defined the commercial cultivation of seaweeds as: "the large scale production of macroscopic marine algae for commercial purposes." Doty [47] applied the term "marine agronomy" to define seaweed cultivation as a type of agricultural practice carried out in the sea.

Despite this analogy, marine agronomy is an activity in its infancy, when compared to the traditional terrestrial agronomy, with obvious differences when we compare the developmental status of both activities. While the origin of marine agronomy can be traced back to approximately 200 years ago, the birth of agriculture is still subject of debate among anthropologists but is thought to have happened approximately 10,000–12,000 years ago [48, 49]. In fact, the presently cultivated seaweeds were selected from local flora (i.e., from the wild) and limited "selection and breeding" techniques have been applied to develop domesticated strains, especially when compared to the efforts placed on staple terrestrial crops such as rice, potatoes, wheat, etc. For the latter, agronomic institutions have developed on various continents, which have specialized in their breeding, selection, and improvement, sometimes even using genetic manipulation.

In China, more than 200 years ago, the first methods to manage a seaweed crop, a species of the red marine alga *Porphyra*, consisted of simply cleaning rocky areas in early autumn. This was done just before the mass liberation of algal reproductive spores, so that they had more surface area for attachment and growth [50]. In Japan, a similar approach consisted of inserting bundles of bamboo twigs into sandy/muddy substrata before the spore release season. Net cultivation methods for mass production of "laver" were only introduced in the 1920s, resulting in some increase in productivity but still reliant on the collection of spores released from natural populations [46]. However, the substantive development of the aquaculture of this genus came with the description of the life cycle of *P. umbilicalis* by Katherine Drew (Baker), in 1949 [51]. Drew established that the filamentous red alga, "*Conchocelis rosea*," until then considered as a completely separate entity, was in fact the sporophyte phase of the life cycle *Porphyra*. This finding, together with subsequent research [51–54], allowed for the development of methods which could control the life cycle and also the artificial production and collection of spores. These were monumental findings allowing the aquaculture of *Porphyra* to move into a completely different phase of technological developments. Modern commercial cultivation methods were established in the 1960s which led to the very pronounced expansion of cultivation activities and economic development. China is currently the largest global producer of *Porphyra*, with more than 800,000 t, fresh weight, produced in 2008, followed by Japan – 337,000 t and the Republic of Korea – 224,000 t [45].

The brown, kelp species, *Saccharina japonica* (formerly known as *Laminaria japonica*), is presently the largest single species produced in aquaculture. It is grown as a monoculture and the volumes of production exceed any other marine species, including fish, crustacea, and molluscs. More than three million tons fresh weight (FW) are reported to be cultivated on ropes in open coastal waters. The cultivation of *Saccharina* was developed mainly during the second half of the twentieth century, initially using a stone planting technique. Since 1968, a method called "forced cultivation" led to a reduction of the previous 2-year cycle of production to 1 year; the shift to modern methods allowed for a tremendous increase in productivity and commercialization of the kelp and its products [46, 55].

The commercial cultivation of all other seaweed species is even more recent than that of *Porphyra* and *Saccharina*. For instance, the cultivation of the red alga *Gracilaria* probably began as recently as 1967 in Taiwan [46]. Seaweed aquaculture or marine agronomy is, therefore, an activity still in its relative infancy, especially when compared to traditional, terrestrial agriculture.

Despite being a recently developed activity, when compared with the traditional land agriculture sector, seaweed aquaculture has been developing steadily. According to the latest production data from FAO [45], in 2008, total seaweed aquaculture production

was more than 15 million tons FW (fresh weight), valued at more than seven billion USD. This corresponds to 23% of the world's aquaculture production and approximately 7% of its global value. Besides the undeniable economic value of the biomass, seaweed aquaculture is nowadays also increasingly recognized for the significant ecosystems services it provides, namely through its extractive process of nutrient removal [56–58]. Chopin et al. [59] argued that evolving aquaculture practices will require a conceptual shift toward understanding the working of food production networks as opposed to simplistic and narrow focus on technological solutions. One of the innovative solutions promoted for environmental sustainability, as well as for economic stability and societal acceptability, is the system coined "IMTA" (or **I**ntegrated **M**ulti-**T**rophic **A**quaculture), which will be discussed in more detail in the next section.

Introduction of the IMTA Concept

In western countries, an interest in integrated aquaculture began toward the end of the twentieth century. After the initial work of Ryther et al. [1], interest in using algae as nutrient scrubbers in an integrated aquaculture system was renewed by a group of like-minded scientists including: Fujita et al. [60], Kautsky and Folke [61], Neori et al. [62], Krom et al. [63], Buschmann [64], Sphigel and Neori [65], Troell et al. [66], Chopin and Yarish [67], Neori and Shpigel [68], Yarish et al. [69], Chopin et al. [70] and Neori et al. [71], among others. In the last decade particularly, numerous papers continued to establish that the concept and implementation of Integrated Multi-Trophic Aquaculture (*sensu* [56, 71–73]) was and will increasingly be of paramount importance for the sustainable development of aquaculture. The advantages are not just important for a sustainable environment, as evidenced by Matos et al. [74], Msuya and Neori [75] and Abreu et al. [76], but also economic, as shown by Troell et al. [77], Whitmarsh et al. [78], Robertson-Andersson [79], Robertson-Andersson et al. [80], and Nobre et al. [58].

The over-riding principle is that in IMTA systems the "wastes" or by-products of animal (fed) aquaculture are used as nutrient source for growth and development of the other trophic component of the system, such as macroalgae or other extractive, filter or detrital feeding organisms (e.g., bivalves, sea cucumbers, marine worms). The practical result is an added production of biomass which may have a direct economic value in addition to the ecosystem services which are provided by the extractive organisms. At the same time, the concentric alignment of the trophic levels provides substantial reduction of the load of inorganic nutrients in the effluents from intensive aquaculture systems, which in themselves can constitute a potential ecological problem leading to coastal eutrophication and harmful algal blooms (HABs).

Integrated mariculture has been practiced traditionally, although not necessarily intentionally, in China, Japan, and South Korea, where farms of fish net pens, shellfish, and seaweed have been situated in close proximity to one another [71, 81]. The arrangements and ultimate optimal integration of the trophic elements were largely achieved through trial and error and, as a consequence, traditional information regarding quantification and design has seldom been published (e.g., [82–84]). Nevertheless, in Asian countries, macroalgae are naturally considered as nutrient removers. For instance, the production of *S. japonica* (the Japanese kelp) was estimated as 4.765 million tons in 2008 [45]. Considering a very conservative N content of 2.79% DW (dry weight) and a wet to dry ratio of 5:1 [85], it can be estimated that approximately 5.58 kg of N are removed from the water with every ton FW of *Saccharina* produced. Therefore, the annual production of *S. japonica* removed approximately 26,588 metric tons of N from the surrounding seawater in 2008. In contrast, production of *Porphyra* and *Gracilaria*, while lower biomass volumes were produced, their N tissue content can exceed 7% DW for *Porphyra* [86] and 8% DW for *Gracilaria* [76].

On a global scale, the aquaculture of extractive organisms (e.g., seaweeds and shellfish) already removes a significant fraction of nutrients from the oceans [87]. According to Troell et al. [88], the harvests of those organisms already extract roughly 150,000 metric tons of N. However, as those authors also note, extractive and fed aquaculture are very often separated geographically, rarely balancing each other on a regional or local scale. An environmentally sustainable, balanced integrated aquaculture operation creates a mini-ecosystem in which the plant autotrophy

balances the animal and microbial heterotrophy, not only in terms of nutrient removal (particularly C, N, and P) but also with respect to oxygen, pH, and carbon dioxide [87, 89]. It is unfortunate that, to date, there are only a few demonstration IMTA systems, in part due to the seasonality of the extractive seaweeds and the lack of "seed-stock." For instance, kelps for extraction of nutrients are only present for part of the cycle. The efficiency of dissolved nutrient removal will improve as alternation of extractive crop species is more clearly understood and refined.

As mentioned in the previous section, seaweed production is presently also recognized for its "ecosystem services" (see http://www.longislandsoundstudy.net/issues-actions/water-quality/nutrient-bioextraction/). Among these ecosystems services, the bioextraction capacity (through which the removal of biomass removes nutrients from the ecosystem) can be key for urban waterways that are not degraded by industrial pollution or don't have restrictions because they are away from sewage treatment facilities. However, as pointed out by Chopin et al. [59], these ecosystems services [90] have an economic benefit that is often ignored both by the industry and the regulators. A recent book sponsored by the World Conservation Monitoring Centre, in its chapter about Marine Systems, says very little about the role and direct economic value of algae in Marine Ecosystems [91]. Chopin et al. [59] argued that to improve the sustainability of anthropogenically derived nutrient-loading practices such as aquaculture, incentives such as nutrient trading credits (NTCs) are required. This would promote nutrient load reduction or nutrient recovery via a "polluter must pay" principle. The question can be posed that if carbon credits are now part of the internalized costs of some industries, why can the same process not be applied to nitrogen (N) and phosphorus (P), released through fed aquaculture, or point source pollution in the coastal marine environment. Neglecting the release of such nutrients in the marine environment can have quite striking consequences such as recently, when N released was associated with eutrophication of coastal waters resulting in massive algal blooms or "green tides" (see [92]). Also P has been discussed as "the next chemical element in global short supply"; therefore, its recovery makes considerable economic and ecological sense [93]. The land-based cultivation of seaweeds, particularly as part of an IMTA system, may also play an important role on the future recovery of these nutrient wastes.

A particularly interesting initiative, regarding the promotion of IMTA at a national level, was reported by the Australian government under the auspices of the Rural Industries Research and Development Corporation (RIRDC; [94]). The objective of that report was to clearly identify the potential for seaweeds to be cultured in Australia for domestic and export markets. The report identified an enormous potential for growth and development of this activity and defined that targeted markets should include the food and nutritional sectors. The associated health benefits of human consumption of a variety of seaweeds were also indicated in the report.

Following this initiative, the Australian RIRDC moved to support the formation of "Seaweed Australia" – a new organization for the emerging cultivated seaweed industry in that country. Under that context, a new report was prepared [95] to assist all industry and research groups involved in the production, processing, and marketing of seaweed products in a broad range of industries including health and nutrition, aquaculture, animal feeds, nutraceuticals, and pharmaceuticals. The report is the result not just of desktop research but of a series of meetings, workshops, and other forms of extensive consultation of the different stakeholders (for instance, industry and researchers). The conclusions include a clear identification of the priorities for the development of the cultivated seaweed industry in Australia in terms of: market focus; market research; higher value products; regulatory issues, and industry research.

Physiological Considerations for the Production of Seaweeds in Land-Based Cultivation Systems

The physicochemical parameters that affect seaweed physiology in land-based systems are essentially the same as those that affect these organisms in natural populations and in open water aquaculture systems. Factors such as temperature, light and nutrient availability, pH and salinity are always critical for seaweed growth. The work of Craigie and Shacklock in

particular was essential for the development of the cultivation of the red seaweed, Irish Moss (*C. crispus*) and that information is a primer for any land-based seaweed aquaculture facility [96]. These authors described the importance of appropriate site selection as a fundamental requirement for the success of any aquaculture undertaking. Craigie and Shacklock [96] confirmed that seawater in the vicinity of the potential site must be of the highest quality, i.e., low sediment and particulate matter, free of agricultural runoff and pollutants from other activities such as industrial, mining, and urban sources. The authors also briefly presented the requirements of the target cultivated species in terms of temperature, pH, salinity, nutrient requirements (i.e., carbon and nitrogen supply), seawater exchange, plant agitation, and interactions with other species. All of this information was the result of integrated basic research conducted for each one of those factors.

The traditional phycological literature, from the past 3–4 decades, contains considerable fundamental research on the physiology of seaweeds in general. However, this research was mainly conducted under laboratory conditions and much less practical work was undertaken in tank systems at scales relevant for economically viable commercial purposes. As with many other organisms, different algal species have different physiological requirements and optima [97]. As pointed out by Troell et al. [88], after reviewing 28 studies on various IMTA systems, where the majority included tank systems, there is a need to:

1. Understand in detail the important biological/biochemical processes in closed recirculating and open seaweed culture systems
2. Conduct research into these advanced aquaculture technologies at scales relevant to commercial implementation or suitable for extrapolation
3. Broaden the focus to include factors affecting seaweed growth and uptake capacity
4. Improve experimental design for statistical calculations
5. Understand the temporal variability in seaweed-filtered mariculture systems
6. Define numerical design parameters critical for engineers in designing commercial recirculation systems with seaweed filters
7. Study the influences of location-specific parameters, such as latitude, climate, and local seaweed strains/species, on seaweed filter performance
8. Include economic components, considering the added value of seaweeds, their products, and feasibility aspects
9. Analyze the role and function of integrated aquaculture practices for improved environmental, economic, and social acceptability within the broader perspective of integrated coastal management initiatives
10. Develop educational, training, and financial incentive approaches to transfer these novel and somewhat complex technologies of integrated mariculture from the scientists to an industrial scale

Despite the potential benefits for seaweed aquaculture as part of land-based IMTA systems, little progress has been made during the most recent decades, in terms of solving the needs as raised by Troell et al. [88]. The only published and, therefore, known exceptions are the work by Abreu et al. [76] taking into account an appropriate experimental design and scale (Figs. 1 and 2), and the research of Robertson-Anderson [79], Robertson-Anderson et al. [80] and Nobre et al. [58]. The differentiating factor is that Robertsson-Anderson and Nobre et al. performed

Seaweed Aquaculture for Human Foods in Land-Based and IMTA Systems. Figure 1
Aspect of the seaweed tank system as part of a pilot scale IMTA in a land-based intensive fish aquaculture. A. Coelho e Castro Lda, Póvoa de Varzim, Portugal

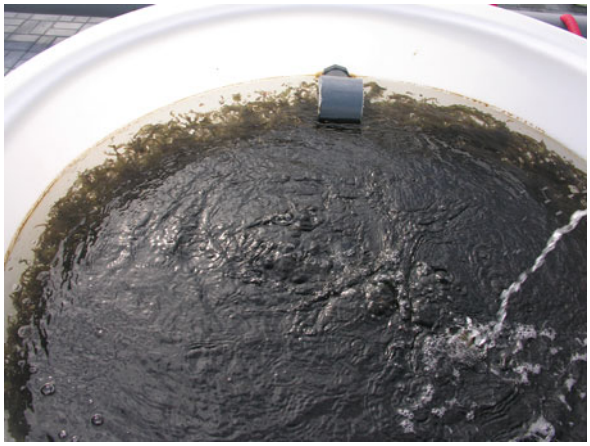

Seaweed Aquaculture for Human Foods in Land-Based and IMTA Systems. Figure 2
Detail of a seaweed production tank (1,200 L) as part of a pilot scale IMTA system in a land-based intensive fish aquaculture. A. Coelho e Castro Lda, Póvoa de Varzim, Portugal

economic and ecological assessments of a commercial, abalone-seaweed farm in South Africa.

Another less commonly applied method of land-based seaweed production is that of spray cultivation. This method has not been tested extensively on many species, but *Ascophyllum nodosum* [98] and *Gracilaria chilensis* [99] have been grown in such systems with some success. In the spray method, the seaweeds are not fully immersed in seawater but instead are held in adequate containers (often inside a modified greenhouse) and seawater is sprayed continuously or periodically over the target seaweeds. As referred to by Msuya and Neori [75], the documented benefits of seaweed spray culture included: construction and pumping costs, temperature control, gas (CO_2 and O_2) exchange, irradiance, nutrient uptake, and control of pests and epiphytes. Although the reported growth rates for these systems were usually low, Msuya and Neori [75] showed that the performance of *Ulva lactuca* in a spray system was in fact close to that of a standard, air-agitated tank culture system. In that work, *U. lactuca* was spray cultured in a "mattress-like layer," held in air on slanted boards by plastic netting. Fish mariculture effluents were applied by being sprayed onto the algal mattresses. The growth rate, yield, and ammonia-N removal rates were 11.8% day^{-1}, 171 g fresh weight (FW) m^2 day^{-1}, and 5 g N m^2 day^{-1}, respectively, by the spray cultured *U. lactuca*, and 16.9% day^{-1}, 283 g fresh weight (FW) m^2 day^{-1}, and 7 g N m^2 day^{-1}, respectively, by traditional tank, immersed cultivated materials.

Examples of Successful On-Land Cultivation Enterprises

Acadian Seaplants Limited (www.acadianseaplants.com) is a Canadian company founded in 1981 and is probably the foremost example of an economically successful, land-based seaweed aquaculture enterprise. The company initially began with the collection of wild harvested *C. crispus* (Irish Moss) and progressed to the manual harvesting and processing of Rockweed (*Ascophyllum nodosum*). In particular, harvesting of the rockweed can be regarded as a positive case study for stewardship and successful, sustainable management of a wild resource (see [100, 101]). With respect to *C. crispus*, the company continues to successfully manage wild harvested materials in South West Nova Scotia and Prince Edward Island and also progressed to the land-based production of a specific strain of *Chondrus*.

While the *Chondrus* cultivation enterprise was initially planned to be a source of high-grade carrageenan, the production of *C. crispus* became more sophisticated to produce a value-added, salad product for the Japanese food market. Over the years, this enterprise has grown to become the world's largest, land-based seaweed cultivation system for the production of human food (Fig. 3). The production operation occupies a large site in south-western Nova Scotia, and the seaweeds are grown for the Asian food market and to conduct fundamental and applied research on seaweed extracts.

Spurred on by the needs created by design and construction of the land-based cultivation tanks and the challenges of cultivation of carragenophytes, the company was able to succeed and expand production facilities. The basis for this success was a strong R&D and market development strategies to diversify the company and its products. Presently, the company exports its diversified products to over 70 countries. More than 95% of its products are exported. According to the company managers, the cultivation division of

Seaweed Aquaculture for Human Foods in Land-Based and IMTA Systems. Figure 3
Aerial view of Acadian Seaplants Limited seaweed production facilities, south-western Nova Scotia (2010) (Photo courtesy of ASL)

the company has been gaining momentum and future plans include domestication of new species for additional target markets, plus enhancements to the existing edible seaweed product line, new product formats, and additional colors (Fig. 4).

Another example of a land-based seaweed production company is the Sylter Algenfarm GmbH & Co.KG (SAF), founded in 2006 by the marine botanist, Prof. Dr. Klaus Lüning. He spent most of his professional life unraveling the complexities of the environmental and internal control of seaweed growth and reproduction [2]. SAF cultivates seaweeds in a land-based seaweed farm at the North Sea island of Sylt, using a seawater source flowing from the oyster tanks of Dittmeyer's Austern-Compagnie. The two main seaweed species cultivated by SAF are young sporophytes of the brown alga *S. latissima* (formerly known as *Laminaria saccharina*) harvested in May, at a blade length of approximately 0.8 m, for the human food sector (Fig. 5) and the red alga *P. palmata* for the cosmetics industry. The niche in the *Laminaria* market occupied by SAF is a result of an opportunity due to the fact that the iodine content of imported *Laminaria* (kombu) from the Far East or from France, with concentrations of 3,000–6,000 mg iodine/kg algal dry weight, is considered too high for safe consumption. In contrast to the imported red alga *Porpyhra* (nori) for European

Seaweed Aquaculture for Human Foods in Land-Based and IMTA Systems. Figure 4
Hana Tsunomata™ (*C. crispus*) commercial product from Acadian Seaplants Limited. Hana = "flower"; Tsunomata = *Chondrus* (Photo courtesy of ASL)

Sushi restaurants, which contains very little iodine, imported kombu from Asia cannot pass the German "veterinary barrier" for human food, while the "young *Laminaria*" produced by SAF contains only 600 mg iodine/kg algal dry weight, probably because of the young age of the thin blades: This has enabled SAF to

Seaweed Aquaculture for Human Foods in Land-Based and IMTA Systems. Figure 5
S. latissima seeded by Sylter Algenfarm on 8-mm diameter rope, grown out to harvesting size by Danish cooperator Rasmus Bjerregaard, holding up the harvested kelp (Photo, courtesy of Dr. Klaus Lüning)

occupy that niche market and gives *Laminaria* the position as an innovative, marine vegetable in German restaurants.

In order to meet the growing demands for "young *Laminaria*" in Germany, in 2008, SAF began a cooperation with two sea farms in the Northern Baltic Sea (Kattegat Sea area), where *S. latissima* is grown on ropes, in the sea, either together with blue mussels (*Mytilus edulis*), or fish (rainbow trout). Harvesting of the young, thin kelp blades in May secures the low iodine content. Moreover, this co-cultivation of kelp with marine animals provides a further example of integrated multi-trophic aquaculture (IMTA). For the fish cultivators in Denmark, this is important since the Danish state urges them to employ countermeasures against the uncontrolled release of ammonium, nitrate, and phosphate from the fish cages into coastal waters. The total N of 6% kelp dry weight assists the fish cultivators to demonstrate that for each ton of fresh harvested kelp (dry weight is $\approx$ 10% of fresh weight), 6 kg of N are removed from the system. This is yet another advantage of the local production of the kelp. Naturally, this ecosystem service (nutrient removal) would not be performed in the direct vicinity of Danish fish farms if the *Laminaria* or *Saccharina* was imported from Asia. On the other hand, for SAF, the harvested kelp biomass in the Kattegat provides the sufficient biomass for the German food market.

Another example, although not producing seaweeds directly for human food, is the Big Island Abalone Company, in Hawai. This company cultivates a proprietary strain of *Palmaria mollis* on a significant scale as feed for abalone cultivation. More details are available at their Web site (www.bigislandabalone.com).

Future Directions

Land-based cultivation of seaweeds reduces the pressure on wild harvest of seaplants, particularly those which are difficult to access in time or space or their harvest would be unsustainable and perhaps ecologically damaging. Furthermore, land-based seaweed production allows for the evaluation of numerous species that, due to their size, morphology, and/or particular physiological needs might not necessarily be good candidates for traditional, open water systems, such as those routinely used for *Porphyra*, kelp, and the major phycocolloid-producing seaweeds (i.e., *Kappaphycus* and *Eucheuma*). Another important feature of seaweed production in land-based systems is that they allow for much greater environmental and input controls than would ever be possible in open water seaweed aquaculture. Such high levels of control, or intensive production, is critical to provide the necessary traceability, security of supply, high-quality standards and safety, not just for human consumption as food but especially for nutraceutical and pharmacological applications. Furthermore, the control of some environmental parameters (as well as controlling growth and quality) can also be used to promote the expression of desirable characteristics of the seaweeds, such characteristics may be morphological or biochemical. Further advantages of land-based seaweed production are the possibilities to quarantine foreign species, if grown on land with approved effluent water treatment systems. This feature is definitely not possible in open water cultivation systems, and can allow a land-based facility to work with more species than just those locally available. However, the environmental stewardship responsibilities for the introduction of nonnative species cannot be minimized nor lightly undertaken.

One promising avenue of future research associated with on-land cultivation of seaweeds would be to find the most appropriate culture conditions that maximize the production of particular, valuable biochemical constituents. This would be important for the promotion of a variety of seaweeds as functional foods or food-ingredients. More research is required into the genetics and responses of new target species which, in turn, could provide insight to achieve the high level of control. Unlike terrestrial plants and even microalgae, genetic transformation in seaweeds remains at a very low level. The first fully sequenced genome of a seaweed species are that of *P. umbilicalis*, *P. purpurea*, and *Ectocarpus siliculosus* and were concluded only recently ([40, 102]; the genome of *C. crispus* to follow shortly thereafter). Not forgetting the huge potential that remains in specific, selection of seaweed strains, the genomic and molecular tools now available for seaweeds could provide further insights into algal physiology and metabolism. Even taking into account the caveat of lack of public acceptance of GMO food, just as occurred with their terrestrial counterparts, this knowledge might be used in seaweed research to improve productivity, biofiltration efficiency, disease resistance, and to direct metabolic pathways to produce higher concentrations of desirable metabolites and secondary compounds (these might even play a role in biofuel production from seaweed feed stocks). Overall, these activities and discoveries could contribute to an improved market value of the target seaweeds, including new insights into human nutrition.

In addition, future research should focus on the evaluation and selection of more seaweed species suitable for land-based aquaculture that may be used as the extractive inorganic nutrient component in IMTA systems. In fact, we believe that IMTA systems will play an important role in the overall development of land-based seaweed production in the future. Several factors may account for this:

(a) The availability of water and its quality
(b) The size and morphological characteristics of seaweeds making them suitable candidates for tank cultivation
(c) The diversity of products derived from various target species produced in the same system

The water requirements of intensive animal aquaculture ensure a plentiful supply of water available for seaweed cultivation. In terms of synergies and efficiencies, particularly in engineering, the use of the same water stream allows for sharing of the energetic costs associated with water pumping. On the other hand, since water quality is also important for animal production and health, the seaweed component should have access to high-quality water, free of toxins, heavy metals, and other pollutants. Finally, but equally very important, and the essence of the IMTA concept, the extractive, seaweed production system would have access to nutrient-enriched seawater derived from the animal (fed aquaculture) component of the system. As an example, Burri [103] tested the inclusion of the IMTA-produced red seaweed (*G. vermiculophylla*) in a new form of vegetarian sausages for children. This author verified that the chemical composition of the seaweed chemical was below the permitted values for children consumption in terms of mercury (Hg), lead (Pb), and cadmium (Cd). Even when the initial wild collected stocking biomass had metal values close to or above the limits, these values decreased after 4 weeks in the IMTA conditions. In conclusion, pollutant-free seawater, nutrient-rich and at a free or shared cost, would be available for the seaweed production system when associated with an IMTA system.

As mentioned previously, intensive, land-based seaweed production allows for exploitation of seaweeds which are not necessarily suited to open water techniques such as those applied to various kelps or *Porphyra*. For obvious reasons, open water seaweed production is not the most suited, for instance, for free-floating techniques and vegetative propagation for seaweed cultivation. The free-floating method of tank or pond production can, however, be highly suited to land-based systems, allowing for optimization of water volume in the tanks as well as stocking density, thereby ensuring access to light and nutrient supply. Furthermore, on-land production methods are also highly suited to seaweeds where vegetative, or clonal, propagation is possible, in as much as the seaweed production system guaranties the homogeneity of the biomass (provided that the environmental conditions do not overly influence it). This feature can also decrease the operational costs associated with the production of seaweeds with a complex life cycle.

In terms of the production diversity, land-based systems could be planned to include several independent production units. Even considering the increase in the operation costs, these production units, managed independently from one other but sharing common parts of the infrastructure, could have two main advantages:

1. Produce different species/varieties of seaweed
2. Allow for an easier control of the environmental parameters that can influence the quality of the biomass

Depending on the applications of the biomass, the production units could be scaled to produce either a few kilograms or a few tons per year instead of the thousands of tons required for seaweed such as those used as raw materials for polysaccharide extraction. Such relatively small volumes might be more appropriate for the biomass required for some direct human consumption products or for application as ingredients of functional foods and cosmetic products. In turn, this smaller scale would allow a better control of production parameters and the biomass can be tailored more closely to the needs of the final consumer.

In conclusion, land-based seaweed aquaculture can provide for the production of biomass required for human food and other advanced applications. Rather than focusing on biomass production in the order of thousands of tons, this form of seaweed production can specialize in niche markets, which requires highly specific and tailored biomass. By doing this, land-based seaweed production can contribute to the development of more seaweed or seaweed-based products for human food and health. Finally, when used as part of an IMTA system approach, land-based seaweed production can contribute to the sustainable development of intensive fed aquaculture in an economical and ecological perspective.

Acknowledgments

R. Pereira is sponsored by a fellowship from the Portuguese Foundation for Science and Technology (FCT) through program POCI 2010, with the support of FEDER and FSE(SFRH/BPD/36451/2007). Support to C. Yarish was provided by the Connecticut Sea Grant (DOC/NOAA/Ocean & Atmospheric Research Contract No. NA10OAR4170095); the Department of Energy's NETL Program, FOA# 0000015 to Gas Technology Institute; NOAA-SBIR Phase I (Ocean Approved, LLC, DOC/National Oceanic and Atmospheric Administration Award/Contract #: AG100206); and National Fish and Wildlife Foundation (contract ##24266).

Bibliography

Primary Literature

1. Ryther JH, Goldman JC, Gifford JE, Huguenin JE, Wing AS, Clarner JP, Williams LD, Lapointe BE (1975) Physical models of integrated waste recycling marine polyculture systems. Aquaculture 5:163–177
2. Lüning K (1990) Seaweeds: their environment, biogeography, and ecophysiology. Wiley, New York, p 527
3. McHugh DJ (2003) A guide to the seaweed industry. FAO Fisheries Technical Paper 441. FAO, Rome, Italy
4. Bixler HJ, Porse H (2010) A decade of change in the seaweed hydrocolloids industry. J Appl Phycol. doi:10.1007/s10811-010-9529-3
5. Graham L, Graham J, Wilcox L (2009) Algae, 2nd edn. Benjamin Cummings (Pearson), San Francisco, p 720
6. Levin SA, Lubchenco J (2008) Resilience, robustness, and marine ecosystem-based management. Biosciences 58(1):27–32
7. Yarish C, Pereira R (2008) Mass production of marine macroalgae. In: Jørgensen SE, Fath BD (eds) Ecological engineering, vol 3 of encyclopedia of ecology, 5 vols. Elsevier, Oxford, pp 2236–2247
8. Goh CS, Lee KT (2009) A visionary and conceptual macroalgae-based third generation bioethanol (TGB) biorefinery in Sabah, Malaysia as an underlay for renewable and sustainable development. Renewable Sustainable Energy Rev 14:842–848
9. Chung IK, Beardall J, Mehta S, Sahoo D, Stojkovic S (2010) Using marine macroalgae for carbon sequestration: a critical appraisal. J Appl Phycol. doi:10.1007/s10811-010-9604-9
10. Kumar P (2010) Biofuels set for a sea-change. Biospectrum November 2010:48–50
11. Notoya M (2010) Production of biofuel by macroalgae with preservation of marine resources and environment. In: Israel A, Einav R, Seckbach J (eds) Seaweeds and their role in globally changing environments, vol 15, Cellular origin, life in extreme habitats and astrobiology. Springer Science+Business Media BV, Dordrecht, pp 217–228
12. Dillehay TD, Ramírez C, Pino M, Collins MB, Rossen J, Pino-Navarro JD (2008) Monte Verde: seaweed, food, medicine, and the peopling of South America. Science 320:784–786
13. Erlandson JM, Graham MH, Bourque BJ, Corbett D, Estes JA, Steneck RS (2007) The kelp highway hypothesis: marine ecology, the coastal migration theory, and the peopling of the Americas. J Isl Coast Archaeol 2:161–174

14. Mumford TF, Miura A (1988) *Porphyra* as food: cultivation and economics. In: Lemby CA, Walland JR (eds) Algae and human affairs. Cambridge University Press, Cambridge, pp 87–117
15. Abbott IA (1996a) Ethnobotany of seaweeds: clues to uses of seaweeds. International Seaweed Symposium XV. Hydrobiologia 326/327:15–20
16. Abbott IA (1996) Limu: an ethnobotanical study of some Hawaiian seaweeds, 4th edn. National Tropical Botanical Garden, Lawai, p 39
17. Konishi T (2008) Integrated functions of diet in anti-aging and cancer prevention. Papers from the 4th international Niigata symposium on diet and health, Niigata, Japan, 20–30 Nov 2008. BioFactors 34(4):261–342
18. Parrot MD, Greenwood CE (2008) Dietary influences on cognitive function with aging: from high-fat diets to healthful eating. Ann NY Acad Sci 1114:389–397
19. O'Sullivan L, Murphy B, McLoughlin P, Duggan P, Lawlor PG, Hughes H, Gardiner GE (2010) Prebiotics from marine macroalgae for human and animal health applications. Mar Drugs 8:2038–2064. doi:10.3390/md8072038
20. Plaza M, Cifuentes A, Ibañez E (2008) In the search of new functional food ingredients from algae. Trends Food Sci Technol 19:31–39
21. Kumar CS, Ganesan P, Suresh SV, Bhaskar N (2008) Seaweeds as a source of nutritionally beneficial compounds. J Food Sci Technol 45(1):1–13
22. Bocanegra A, Bastida S, Benedí J, Ródenas S, Sánchez-Muniz FJ (2009) Characteristics and nutritional and cardiovascular-health properties of seaweeds. J Med Food 12(2):236–258
23. Noda H (1993) Health benefits and nutritional properties of nori. J Appl Phycol 5:255–258
24. Nisizawa K, Noda H, Kikuchi R, Watanabe T (1987) The main seaweed foods in Japan. Hydrobiologia 151/152:5–29
25. Tsuboyama-Kasaoka N, Shozawa C, Sano K, Kamei Y, Kasaoka S, Hosokawa Y, Ezaki O (2006) Taurine (2-aminoethanesulfonic acid) deficiency creates vicious circle promoting obesity. Endocrinology 147(7):3276–3284
26. Burtin P (2003) Nutritional value of seaweeds. Electron J Environ Agric Food Chem 2(4):498–503
27. Holdt S, Kraan S (2011) Bioactive compounds in seaweed: functional food applications and legislation. J Appl Phycol. doi:10.1007/s10811-010-9632-5
28. Cornish ML, Garbary DJ (2010) Antioxidants from macroalgae: potential applications in human health and nutrition. Algae 25(4). doi:10.4490/algae.2010.25.4.000
29. Blouin N, Calder BL, Perkins B, Brawley SH (2006) Sensory and fatty acid analysis of two Atlantic species of *Porphyra*. J Appl Phycol 18:79–85
30. Zhang Q, Li N, Zhou G, Lu X, Xu Z, Li Z (2003) In vivo antioxidant activity of polysaccharide fraction from *Porphyra haitanesis* (Rhodophyta) in aging mice. Pharmacol Res 48:151–155
31. Díaz-Rubio ME, Pérez-Jiménez J, Saura-Calixto F (2009) Dietary fiber and antioxidant capacity in *Fucus vesiculosus* products. Int J Food Sci Nutr 60(S2):23–34
32. Zhou HP, Chen QH (1990) Anticoagulant and antihyperlipedemic effects of polysaccharide from *Porphyra yezoensis*. J China Pharm Univ 21:358–360
33. Yashizawa Y, Ametani A, Tsunehiro J, Numera K, Itoh M, Fukui F, Kaminogawa S (1995) Macrophage stimulation activity of the polysaccharide fraction from a marine alga (*Porphyra yezoensis*): structure-function relationships and improved solubility. Biosci Biotechnol Biochem 59: 1933–1937
34. Saito M, Kawai M, Hagino H, Okada J, Yamamoto K, Hayashida M, Ikeda T (2002) Antihypertensive effect of nori-peptides derived from red alga *Porphyra yezoensis* in hypertensive patients. Am J Hypertens 5(4, Part 2):210A (Published by Elsevier Science Inc)
35. Béress A, Wassermann O, Bruhn T, Béress L, Kraiselburd EN, González LU, De Motta GE, Chávez PI (1993) A new procedure for the isolation of anti-HIV compounds (polysaccharides and polyphenols) from the marine alga *Fucus vesiculosus*. J Nat Prod 56:478–488
36. Aisa Y, Miyakawa Y, Nakazato T, Shibata H, Saito K, Ikeda Y, Kizami M (2005) Fucoidan induces apoptosis of human HS-sultan cells accompanied by activation of caspase-3 and down-regulation of ERK pathways. Am J Hematol 78:7–14
37. Teas J, Harbison ML, Gelman RS (1984) Dietary seaweed (*Laminaria*) and mammary carcinogenesis in rats. Cancer Res 44:2758–2761
38. Yang YJ, Nam SJ, Kong G, Kim MK (2010) A case–control study on seaweed consumption and the risk of breast cancer. Br J Nutr 103:1345–1353
39. Sahoo D, Tang X, Yarish C (2002) *Porphyra* – the economic seaweed as a new experimental system. Curr Sci 83(11):1313–1316
40. Gantt E, Berg GM, Bhattacharya D, Blouin NA, Brodie JA, Chan CX, Collén J, Cunninghan FX Jr, Gross J, Grossman AR, Karpowicz S, Kitade Y, Klein AS, Levine IA, Lin S, Lu S, Lynch M, Minocha SC, Müller K, Neefus CD, de Oliveira CM, Rymarquis L, Smith A, Stiller JW, Wu W-K, Yarish C, Zhuang YY, Brawley SH (2010) Porphyra: complex life histories in a harsh environment. P. umbilicalis, an intertidal red alga for genomic analysis. In: Seckbach J, Chapman DJ (eds) Red algae in the genomic age, vol 13, Cellular origin, life in extreme habitats and astrobiology. Springer, Dordrecht, pp 129–148
41. Grossman AR (2007) In the grip of algal genomics. In: León R, Galvin A, Fernandez E (eds) Transgenic microalgae as green cell factories. Landers bioscience Publishers and Springer Science+Business Media, Austin, TX, pp 54–76
42. Grossman AR, Karpowicz SJ, Heinnickel M, Dewez D, Hamel B, Dent R, Niyogi KK, Johnson X, Alric J, Wollman F-A, Li H, Merchant SS (2010) Phylogenomic analysis of the *Chlamydomonas* genome unmasks proteins potentially involved in photosynthetic function and regulation. Photosynth Res 106:3–17
43. Guiry MD, Guiry GM (2010) AlgaeBase. World-wide electronic publication. National University of Ireland, Galway, http://www.algaebase.org; searched on 30 May 2010

44. Pereira R, Yarish C (2010) The role of Porphyra in sustainable culture systems: physiology and applications. In: Israel A, Einav R, Seckbach J (eds) Seaweeds and their role in globally changing environments, vol 15, Cellular Origin, Life in Extreme Habitats and Astrobiology. Springer, Dordrecht, pp 339–353. ISBN 978-90-481-8568-9
45. FAO (2010) FAO fisheries and aquaculture information and statistics service (2010) Aquaculture production 1950–2008, Rome, Italy
46. Tseng CK (1981) Commercial cultivation. In: Lobban CS, Wynne MJ (eds) The biology of seaweeds, vol 17, Botanical Monographs. Blackwell, Oxford, pp 680–725
47. Doty MS (1977) Eucheuma – current marine agronomy. In: Krauss RW (ed) The marine plant biomass of the Pacific Northwest Coast. A potential economic resource. Oregon State University Press, Corvallis, pp 203–214
48. Houyuan L, Zhang J, Liu K, Wu N, Li Y, Zhou K, Ye M, Zhang T, Zhang H, Yang X, Shen L, Xu D, Li Q (2009) Earliest domestication of common millet (Panicum miliaceum) in East Asia extended to 10, 000 years ago. PNAS 106(18): 7367–7372
49. Munro ND, Grosman L (2009) Early evidence (ca. 12,000 B.P.) for feasting at a burial cave in Israel. PNAS 107(35): 15362–15366
50. Tseng CK, Chang CF (1956) On China's Porphyra and its cultivation. Shengwuxue Tongbao 3:29–33 Tseng CK (1981) Commercial cultivation. In: Lobban CS, Wynne MJ (eds) The biology of seaweeds. Botanical monographs, Vol 17. Blackwell Scientific Publications, University of California Press, Berkeley and Los Angeles, pp 680–725
51. Drew KM (1949) *Conchocelis*–phase in the life history of *Porphyra umbilicalis* (L.) Kütz. Nature 164:748–749
52. Kurogi M (1953) Study of the life-history of *Porphyra* I. The germination and development of carpospores. Bull Tohoku Reg Fish Lab 2:67–103
53. Kurogi M (1953) On the liberation of monospores from the filamentous thallus (*Conchocelis*-stage) of *Porphyra tenera* Kjellm. Bull Tohoku Reg Fish Lab 2:104–108
54. Kurogi M, Sato S (1962) Influence of light on the growth and maturation of Conchocelis-thallus of Porphyra II. Effect of different photoperiods on the growth and maturation of Conchocelis-thallus of *P. tenera Kjellm*. Bull Tohoku Reg Fish Lab 20:127–137
55. Brinkhuis BH, Levine HG, Schlenk CG, Tobin S (1987) *Laminaria* cultivation in the far east and North America. In: Bird KT, Benson PH (eds) Seaweed cultivation for renewable resources. Elsevier, Amsterdam, pp 107–146
56. Chopin T, Robinson SMC, Troell M, Neori A, Buschmann AH, Fang J (2008) Multitrophic integration for sustainable marine aquaculture. In: Sven EJ, Fath BD (eds) Ecological engineering, vol 3 of encyclopedia of ecology, 5 vols. Elsevier, Oxford, pp 2463–2475
57. Neori A (2008) Essential role of seaweed cultivation in integrated multi-trophic aquaculture farms for global expansion of mariculture: an analysis. J Appl Phycol 20:567–570
58. Nobre AM, Robertson-Andersson D, Neori A, Sankar K (2010) Ecological-economic assessment of aquaculture options: comparison between abalone monoculture and integrated multi-trophic aquaculture of abalone and seaweeds. Aquaculture 306:116–126
59. Chopin T, Troell M, Reid GK, Knowler D, Robinson SMC, Neori A, Buschmann AH, Pang SJ (2010) Integrated multi-trophic aquaculture. Part I. Responsible practice provides diversified products, biomitigation. Glob Aquac Advocate September/October 2010:38–39
60. Fujita RM, Wheeler PA, Edwards RL (1989) Assessment of macroalgal limitation in a seasonal upwelling region. Mar Ecol Prog Ser 53:293–303
61. Kautsky N, Folke C (1991) Integrating open system aquaculture: ecological engineering for increased production and environmental improvement through nutrient recycling. In: Etnier C, Guterstam B (eds) Ecological engineering for wastewater treatment. Bokskogen, Gothenburg, pp 320–334
62. Neori A, Cohen I, Gordin H (1991) *Ulva lactuca* biofilters for marine fish-pond effluents. II. Growth rate, yield and C:N ratio. Bot Mar 34:483–489
63. Krom MD, Ellner S, van Rijn J, Neori A (1995) Nitrogen and phosphorus cycling and transformations in a prototype "non-polluting" integrated mariculture system, Eilat, Israel. Mar Ecol Prog Ser 118:25–36
64. Buschmann AH (1996) An introduction to integrated farming and the use of seaweeds as biofilters. Hydrobiologia 326/327:59–60
65. Shpigel M, Neori A (1996) Abalone and seaweeds intensive cultivation in integrated land-based mariculture system. I. Proposed design and cost analyses. Aquacult Eng 15:313–326
66. Troell M, Halling C, Nilsson A, Buschmann AH, Kautsky N, Kautsky L (1997) Integrated marine cultivation of *Gracilaria chilensis* (Gracilariales, Rhodophyta) and salmon cages for reduced environmental impact and increased economic output. Aquaculture 156:45–61
67. Chopin T, Yarish C (1998) Nutrients or not nutrients? World Aquac Mag 29:31–33, 60–61
68. Neori A, Shpigel M (1999) Using algae to treat effluents and feed invertebrates in sustainable integrated mariculture. World Aquac 30(2):46–51
69. Yarish C, Chopin T, Wilkes R, Mathieson AC, Fei XG, Lu S (1999) Domestication of nori for Northeast America: the Asian experience. Bull Aquacult Assoc Can 99:11–17
70. Chopin T, Buschmann AH, Halling C, Troell M, Kautsky N, Neori A, Kraemer GP, Zertuche-González JA, Yarish C, Neefus C (2001) Integrating seaweeds into marine aquaculture systems: a key towards sustainability. J Phycol 37:975–986
71. Neori A, Chopin T, Troell M, Buschmann AH, Kraemer GP, Halling C, Shpigel M, Yarish C (2004) Integrated aquaculture: rationale, evolution and state of the art emphasizing seaweed biofiltration in modern mariculture. Aquaculture 231:361–391
72. Kraemer GP, Yarish C (1999) A preliminary comparison of the mariculture potential of *Porphyra purpurea* and *Porphyra umbilicalis*. J Appl Phycol 11:473–477

73. Chopin T (2006) Integrated multi-trophic aquaculture. What it is and why you should care. Northern Aquac July/August 2006:4
74. Matos J, Costa S, Rodrigues A, Pereira R, Sousa Pinto I (2006) Experimental integrated aquaculture of fish and red seaweeds in Northern Portugal. Aquaculture 252:31–42
75. Msuya FE, Neori A (2010) The performance and chemical composition of spray irrigated seaweed *Ulva lactuca* as a crop and as a biofilter of fishpond effluents. J Phycol. doi:10.1111/j.1529-8817.2010.00843.x
76. Abreu MH, Pereira R, Yarish C, Buschmann AH, Sousa-Pinto I. IMTA with *Gracilaria vermiculophylla*: productivity and nutrient removal performance of the seaweed in a land-based pilot-scale system. Aquaculture (in press). doi:10.1016/j.aquaculture.2010.12.036
77. Troell M, Robertson-Andersson D, Anderson RJ, Bolton JJ, Maneveldt G, Halling C, Probyn T (2006) Abalone farming in South Africa: an overview with perspectives on kelp resources, abalone feed, potential for on-farm seaweed production and socio-economic importance. Aquaculture 257:266–281
78. Whitmarsh DJ, Cook EJ, Black KD (2006) Searching for sustainability in aquaculture: an investigation into the economic prospects for an integrated salmon-mussel production system. Mar Policy 30:293–298
79. Robertson-Andersson DV (2007) Biological and economical feasibility studies of using *Ulva lactuca* (Chlorophyta) in recirculating systems in abalone farming. Doctoral dissertation, University of Cape Town, South Africa
80. Robertson-Andersson DV, Potgieter M, Hansen J, Bolton JJ, Troell M, Anderson RJ, Halling C, Probyn T (2008) Integrated seaweed cultivation on an abalone farm in South Africa. J Appl Phycol 20:579–595
81. Rawson MV, Chen C, Ji R, Zhu M, Wang A, Wang L, Yarish C, Sullivan JB, Chopin T, Carmona R (2002) Understanding the interaction of extractive and fed aquaculture using ecosystem modelling. In: Stickney RR, McVey JP (eds) Responsible marine aquaculture. CABI, London, pp 263–296
82. Fang J, Kuang S, Sun H, Li F, Zhang A, Wang X, Tang T (1996) Status and optimising measurements for the culture of scallop *Chlamys farreri* and kelp *Laminaria japonica* in Sanggou Bay. Mar Fish Res (Haiyang Shuichan Yanjiu) 17:95–102 (in Chinese)
83. Sohn CH (1996) Historical review on seaweed cultivation of Korea. Algae 11:357–364
84. Fei XG (2004) Solving the coastal eutrophication problem by large scale seaweed cultivation. Hydrobiologia 512:145–151
85. Egan B, Yarish C (1990) Productivity and life history of *Laminaria ongicruris* at its southern limit in the western Atlantic Ocean. Mar Ecol Prog Ser 67(3):263–273
86. Chopin T, Yarish C, Wilkes R, Belyea E, Lu S, Mathieson A (1999) Developing *Porphyra*/salmon integrated aquaculture for bioremediation and diversification of the aquaculture industry. J Appl Phycol 11:463–472
87. McVey JP, Stickney RR, Yarish C, Chopin T (2002) Aquatic polyculture and balanced ecosystem management: new paradigms for seafood production. In: Stickney RR, McVey JP (eds) Responsible marine aquaculture. CABI, London, pp 91–104
88. Troell M, Halling A, Neori A, Buschmann A, Kautsky N, Yarish C (2003) Integrated mariculture: asking the right questions. Aquaculture 226:69–90
89. Rai LC, Kumar HD, Mohn FH, Soeder CJ (2000) Services of algae to the environmemt. J Microbiol Biotechnol 10:119–136
90. Lubchenco J, Petes LW (2010) The interconnected biosphere: science at the ocean's tipping points. Oceanography 23(2):115–129
91. Ash N, Blanco H, Brown C, Garcia K, Tomich T, Vira B, Zurek M (eds) (2010) Ecosystems and human well-being: a manual for assessment practitioners. Island Press, Washington, DC, p 288
92. Pang SJ, Liu F, Shan TF, Xu N, Zhang ZH, Gao SQ, Chopin T, Sun S (2010) Tracking the algal origin of the *Ulva* bloom in the Yellow Sea by a combination of molecular, morphological and physiological analyses. Mar Environ Res 69: 207–215
93. Vaccari DA (2009) Phosphorus: a looming crisis. Sci Am 300(6):54–59
94. Winberg P, Ghosh D, Tapsell L (2009) Seaweed culture in integrated multi-trophic aquaculture: nutritional benefits and systems for Australia. Rural Industries Research and Development Corporation, RIRDC Publication No 09/005
95. Lee B (2010) Cultivated seaweed and seaweed industry development in Australia. Rural Industries Research and Development Corporation – RIRDC. Publication No. 10/164, Project No. PRJ-004681, p 39. ISBN 978-1-74254-131-0
96. Craigie JS, Shacklock PF (1995) Culture of Irish Moss. In: Boghen AD (ed) Cold water aquaculture in Atlantic Canada. The Canadian Institute for Research on Regional Development, Moncton, pp 365–390
97. Lobban CS, Harrison PJ (1994) Seaweed ecology and physiology. Cambridge University Press, Cambridge, p 366
98. Rheault RB, Ryther JH (1983) Growth, yield and morphology of *Ascophyllum nodosum* (Phaeophyta) under continuous and intermittent seawater spray culture regimes. J Phycol 19:252–254
99. Pickering TD, Gordon ME, Tong LJ (1995) A preliminary trial of a spray culture technique from growing the agarophyte *Gracilaria chilensis* (Gracilariales, Rhodophyta). Aquaculture 130:43–49
100. Ugarte RA, Craigie JS, Critchley AT (2010) Fucoid flora of the rocky intertidal of the Canadian Maritimes: implications for the future with rapid climate change. In: Israel A, Einav R, Seckbach J (eds) Seaweeds and their role in globally changing environments, vol 15, Cellular Origin, Life in Extreme Habitats and Astrobiology. Springer, Dordrecht, pp 73–90. ISBN 978-90-481-8568-9
101. Ugarte R (2010) An evaluation of the mortality of the brown seaweed *Ascophyllum nodosum* (L.) Le Jol. produced by cutter rake harvests in southern New Brunswick, Canada. J Appl Phycol. doi:10.1007/s10811-010-9574-y
102. Cock MJ, Sterck L, Rouzé P, Scornet D, Allen AE, Amoutzias G, Anthouard V, Artiguenave F, Aury J-M, Badger JH, Beszteri B,

Billiau K, Bonnet E, Bothwell JH, Bowler C, Boyen C, Brownlee C, Carrano CJ, Charrier B, Cho GY, Coelho SM, Collén J, Corre E, Da Silva C, Delage L, Delaroque N, Dittami SM, Doulbeau S, Elias M, Farnham G, Gachon CMM, Gschloessl B, Heesch S, Jabbari K, Jubin C, Kawai H, Kimura K, Kloareg B, Küpper FC, Lang D, Le Bail A, Leblanc C, Lerouge P, Lohr M, Lopez PJ, Martens C, Maumus F, Michel G, Miranda-Saavedra D, Morales J, Moreau H, Motomura T, Nagasato C, Napoli CA, Nelson DR, Nyvall-Collén P, Peters AF, Pommier C, Potin P, Poulain J, Quesneville H, Read B, Rensing SA, Ritter A, Rousvoal S, Samanta M, Samson S, Schroeder DC, Ségurens B, Strittmatter M, Tonon T, Tregear JW, Valentin K, von Dassow P, Yamagishi T, Van de Peer Y, Wincker P (2010) The *Ectocarpus* genome and the independent evolution of multicellularity in brown algae. Nature 465:617–621

103. Burri S (2009) Concepção de um alimento funcional à base de legumes e algas para consumo infantil. Master thesis, Universidade Católica Portuguesa. Escola Superior de Biotecnologia. Porto, Portugal, p 83 (in portuguese)

Phang SW, Critchley AT, Ang PO (eds) (2006) Advances in seaweed cultivation and utilisation in Asia. University of Malaya Maritime Research Centre, Kuala Lumpur, p 177

Sahoo D, Yarish C (2005) Mariculture of seaweeds. In: Andersen R (ed) Phycological methods: algal culturing techniques, chapter 15. Academic, New York, pp 219–237

Seckbach J, Chapman DJ (eds) (2010) Red algae in the genomic age, vol 13, Cellular origin, life in extreme habitats and astrobiology. Springer, New York, p 486

Sun S, Wang F, Li CL, Qin S, Zhou MJ, Ding LP, Pang SJ, Duan DL, Wang GC, Yin BS, Yu RC, Jiang P, Liu ZL, Zhang GT, Fei XG, Zhou M (2008) Emerging challenges: massive green algal blooms in the Yellow Sea. Nature Precedings hdl:10101/npre.2008.2266.1

Titlyanov EA, Titlyanova TV (2010) Seaweed cultivation: methods and problems. Russ J Mar Biol 36:227–242

Yuan YV, Bone DE, Carrington MF (2005) Antioxidant activity of dulse (*Palmaria palmata*) extract evaluated *in vitro*. Food Chem 91:485–494

Books and Reviews

Barrington K, Chopin T, Robinson S (2009) Integrated multi-trophic aquaculture (IMTA) in marine temperate waters. In: Soto D (ed) Integrated aquaculture: a global review. FAO Fisheries and Aquaculture Technical Paper. No. 529. FAO, Rome, pp 7–46

Buschmann AH, Hernández-González MC, Aranda C, Chopin T, Neori A, Halling C, Troell M (2008) Mariculture waste management. In: Jørgensen SE, Fath BD (eds) Ecological engineering, vol 3 of encyclopedia of ecology, 5 vols. Elsevier, Oxford, pp 2211–2217

Critchley AT, Ohno M (eds) (1997/2001). Interactive, computer-based, CD-ROM "Cultivation and farming of marine plants". Expert Centre for Taxonomic Identification (ETI), University of Amsterdam Netherlands. ISBN: 90-75000-31-6, http://www.eti.uva.nl

Critchley AT, Ohno M, Largo D (2006) World seaweed resources: an authoritative reference system, A multimedia, interactive DVD ROM. ETI Bioinformatics Publishers, Univ, Amsterdam. ISBN: 90-75000-80-4

Fei XG, Lu S, Bao Y, Wilkes R, Yarish C (1998) Seaweed cultivation in China. World Aquac 29(4):22–24

Fleurence J (1999) Seaweed proteins: biochemical, nutritional aspects and potential uses. Trends Food Sci Technol 10:25–28

Friedlander M (2008) Israeli R&D activities in seaweed cultivation. Isr J Plant Sci 56:15–28

He P, Xu S, Zhang H, Wen S, Dai Y, Lin S, Yarish C (2008) Bioremediation efficiency in the removal of dissolved inorganic nutrients by the red seaweed, *Porphyra yezoensis*, cultivated in the open sea. Water Res 42:1281–1289

Lembi CA, Waaland R Jr (eds) (1988) Algae and human affairs. Cambridge University Press, London, p 590

Nisizawa L (2002) Seaweeds Kaiso: bountiful harvests from the sea. Japan Seaweed Association, Kochi, p 106

Sediment–Water Interfaces, Chemical Flux at

Louis J. Thibodeaux[1], Joseph Germano[2]
[1]Cain Department Chemical Engineering, Louisiana State University, Baton Rouge, LA, USA
[2]Germano & Associates, Inc., Bellevue, WA, USA

Article Outline

Glossary
Definition of the Subject
Introduction
Transport Process Theories
Theories and Model Development
Simulation Methods and Results
Significance to Aquatic Environments
Future Directions
Bibliography

Glossary

Benthic boundary layer A slow moving water layer above the sediment.

Bioturbation transport A chemical mobility process driven by the presence of macrofauna and macroflora residing near the interface.

Chemical flux The basic term that quantifies chemical mobility across an interface with units of mass per area per time (kg/m^2/s)

Chemical mobility A general term used to denote the idea that chemicals do move from place to place.

Interface A real or imaginary plane which separates water from sediment.

Mass transfer rate The chemical flux times the area perpendicular to its direction of movement (kg/s).

Sediment surface layers A series of distinctive mud layers occupying thickness of several centimeters depth.

Transport model One of several concepts for describing a chemical mobility process, and the associated formula or algorithm needed to describe it mathematically (a.k.a., the flux expression).

Definition of the Subject

Numerous individual transport processes which mobilize chemicals on either side of the interface have been studied. However, a consistent theoretical framework connecting the processes across the interface that correctly quantifies the overall flux remains elusive. This occurs because two fundamentally different individual flux relationships are needed to represent the two very different transport mechanisms needed for quantifying the numerous chemical, biological, and physical processes ongoing at this unique locale. The two basic types of transport processes are the chemical potential driven and the media advection driven. Several theoretical modeling approaches exist for combining these, but all have problematic conceptual features, which will be reviewed. By generalizing flux continuity across the interface, which is the fundamental basis for arriving at the well-known and accepted two-resistance theory, the "interface compartment model" is presented and offered as a unifying theory describing advection-driven and potential-driven transport across the sediment–water interface.

Introduction

All theories for chemical transport across the interface originate from the nineteenth century with the Ohm–Kirchhoff laws of electrical currents and potentials. Lewis and Whitman [1] used an analogous electrical flux approach for deriving the chemical potential–driven flux across a gas–liquid interface. It is presumed that most of the significant, individual chemical transport processes on both sides of the sediment–water interface, which influence the flux of geochemicals as well as the anthropogenic ones, have been discovered. Many have been reported and are the subject of several reviews. They are the result of biological, chemical, and geophysical processes, and most have been verified based on observations in the field and/or in the laboratory. Some have been thoroughly studied while others have not. As a consequence, there are well-developed descriptions for several processes as well as many theoretical equations for the flux. A unified theory is proposed for connecting flux across the interface.

Photographs taken of the interface region, obtained using a sediment profile camera [2, 3] are displayed in Figs. 1–4. (Figures 1–4 A collection of color images of the sediment–water interface. These are selected photos taken by Joseph Germano over a time period of 28 years. Four categories are presented.) Fig. 1 contains images of the interface and a small sampling of the wide range of effects caused by various macrofauna. Figure 2 shows images of the interface being acted upon by submerged aquatic plants with leafy parts in the water column above and holdfasts below. Figure 3 has images which indicate an interface under the influence of low oxygen and/or chemical pollutant stresses. Finally, Figure 4 shows the particle advection process. These are but a few glimpses of the character and forms of this important global environmental interface which occupies the largest plane area on Earth. It separates the fluid water–dominated media above and the underlying solid, fluid water–saturated zone below. Figure 5 is a conceptual illustration of the interface and its adjoining regions, modified from the original by Santschi et al. [4]. It is an idealized model of the previous images showing the location of the interface plane and some of the processes occurring in the adjoining bulk media phases or compartments.

At any interface locale, it is expected that a combination of individual processes on either side may control the net flux. There may be a dozen or more individual processes, identifying the key ones on either side and coupling them in a logical fashion so as to understand the overall process and quantify the effective flux is an ongoing challenge. As the photographs show, each sediment–water interface has unique

a Deep-sea octocoral (Kophobolemnon) suspension feeding in benthic boundary layer. San Francisco Deep Ocean Disposal Site, 2850 meters.

b Mound of clam fecal pellets effectively changing sediment grain-size and transport properties. Elliott Bay Disposal Site, Puget Sound, 102 meters.

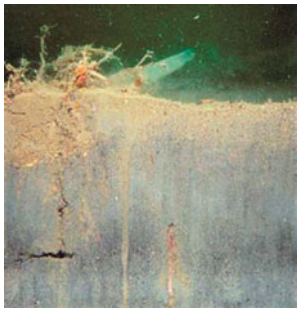

c Bryozoans, polychaetes and a clam siphon can be seen projecting above the sediment-water interface. San Diego Harbor, 10 meters.

d Infaunal deposit-feeding polychaetes aerating sediment to depth. Puget Sound, 70 meters.

e Deep sea colonial foram colony with commensal amphipods. Mid-Atlantic continental slope off Virginia, USA,1600 meters.

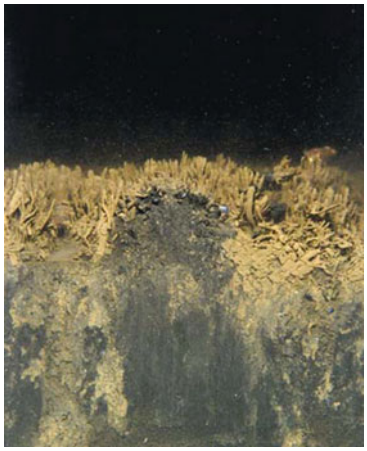

f Dense assemblage of *Ampelisca abdita* tubes. Jamaica Bay, Long Island, 5 meters.

g Subsurface excavations caused by ghost shrimp (*Calianassa)* visible at sediment surface. Pearl Harbor, Hawaii, 12 meters.

h Deposit-feeding polychaetes are visible in the sediments below the nudibranch at the surface. Nearshore embayment in Unalaska, Aleutian Islands, 36 meters.

i Transected polychaete burrow at depth demonstrates how animals in the "anoxic subsurface sediments" create their own oxygenated mileu. Peconic Estuary, Long Island, NY, 6 meters.

Sediment–Water Interfaces, Chemical Flux at. Figure 1
Animal–sediment–fluid relationships (9 photos)

a Subsurface infaunal burrows can be seen beneath the fronds of *Caulerpa prolifera* on the sediment surface. Coastal embayment off Sicily, 14 meters.

b These sandy clays support a dense assemblage of the invasive *Caulerpa racemosa*. Coastal embayment off Sicily, 8 meters.

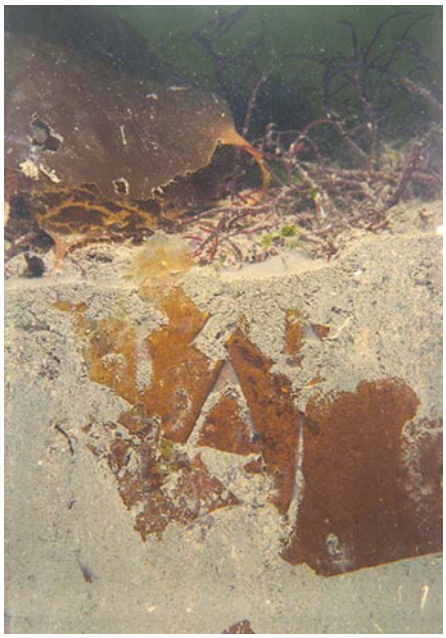

c Mixed assemblage of red algae with a frond of *Laminaria* pushed below the sediment surface by the camera prism. Sinclair Inlet, Puget Sound, 5 meters.

d Fronds of seagrass can be seen above these silty fine sands. Sinclair Inlet, Puget Sound, 4 meters.

Sediment–Water Interfaces, Chemical Flux at. Figure 2
Submerged aquatic vegetation (4 photos)

a Records of past anoxic events are preserved in the layers of these clays. Caspian Sea, 750 meters.

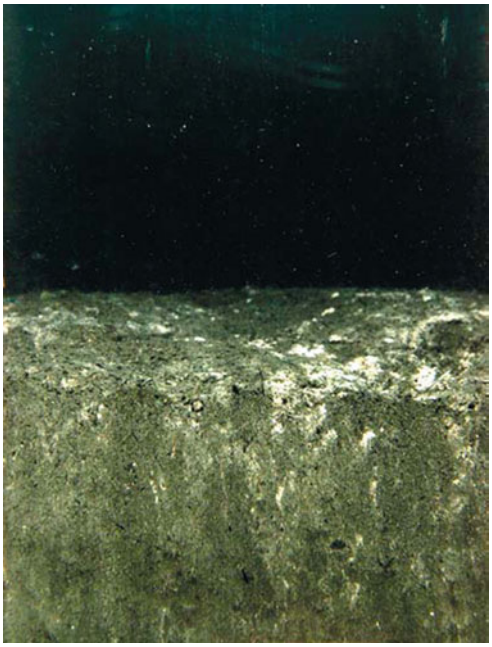

b White aggregations of *Beggiatoa* colonies can be seen on the surface of these anoxic sediments. Nearshore embayment in Unalaska, Aleutian Islands, 32 meters.

c No visible RPD can be seen in these organically enriched sediments. Hackensack River, New Jersey, 3 meters.

d A diffusional layer of oxidized sediment can be seen on the surface of these riverine sediments. Hackensack River, New Jersey, 4.5 meters.

Sediment–Water Interfaces, Chemical Flux at. Figure 3
Polluted sediments (4 photos)

a Deposit-feeding infaunal taxa such as maldanid polychaetes can loosen sediment fabric and eject particles into the benthic boundary layer. Long Island Sound, 15 meters.

b Subsurface methanogenesis can also periodically release gas and sediment particles into the overlying water. Saginaw River , 3 meters.

Sediment–Water Interfaces, Chemical Flux at. Figure 4
Examples of particle advection (2 photos)

characteristics so that the flux is expected to be highly variable from locale to locale. One goal of this chapter is to develop a unified theory for combining the individual processes on the water-side to those on the sediment-side and to obtain the appropriate algorithm for the across-media or interphase flux. The substances of concern are geochemicals such as nitrogen, silica, carbon, and lead and anthropogenic chemicals such as polychlorinated biphenyls, naphthalene, ibuprofen, and caffeine. The development also is applicable to aquasols, nanoparticles, and other identifiable particles moving across the sediment–water interface.

This chapter will first review the available transport processes theories. Several significant individual processes will be listed and summarized. Based on the mechanisms that drive the transport, each will be placed into one of two categories of flux equation types. The theoretical arguments supporting the use of two categories will be covered. Then, a model development section will begin with a literature review and summary of the various theoretical approaches proposed for combining the individual processes arriving at the net flux across the interface. The algebraic forms of the flux equations will be given. Finally, the concepts behind the proposed interface compartment (IC) theory will be presented and the flux equation derived. Included will be a discussion of the IC theory in relation to the existing ad hoc protocols in use.

The methods section will describe the modeling approach, the chemicals used in numerical simulations, and the individual processes selected for performing the flux calculations. Including flux calculations in the theoretical section is necessary because it extends and amplifies the IC model theory by providing a layer of reality to accompany the mathematical formulas. In addition, it provides a quantitative means of comparing it to the approaches being used.

Transport Process Theories

There are numerous individual chemical transport processes operating on both sides of the sediment–water interface, and they have been the subject of literature reviews [4–6] and monographs [7–12].

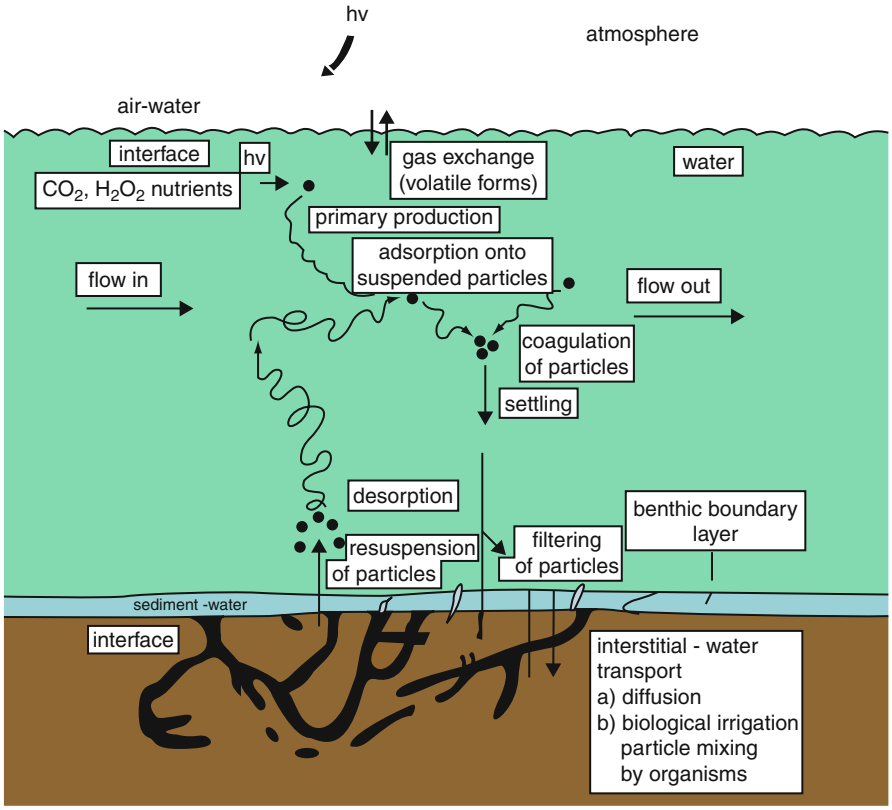

Sediment–Water Interfaces, Chemical Flux at. Figure 5
Transport processes near the sediment–water interface. This figure is a slightly modified version of the original produced by Santschi et al. [4]. It is a classical graphical illustration of the interface plane. It is an idealized model of the interface region showing some of the processes occurring in the water column and the bed surface layers

Two types of equations are commonly used that reflect process mechanisms. They are the chemical potential and media advection; one or the other type will be applicable to each process as they are presented and discussed. The chemical potential type will be considered first.

The molecular diffusive transport process derived from Fick's first law of diffusion is the most basic and ubiquitous process [13–15]. The integrated equation is a chemical potential–type process. It contains a concentration difference term that reflects the chemical potential between two locations in space. It also contains an effective diffusion coefficient for the porous medium and the path length. It is applicable to the transport of all solutes and to Brownian particles in bed sediment as well as on the water-side of the interface. On the water-side of the interface, the mass transfer coefficient often replaces the diffusion coefficient and path length quotient [14].

At this juncture, it is well appreciated by the reader that chemical flux, such as molecular diffusion, is a function of the concentration difference or gradient and a kinetic transport parameter. Chemical reactions and phase partitioning can and do occur in the layers on either side of the interface, which affects the magnitude of the respective concentrations and hence the flux. However, applying the transient, reactive-diffusion equation to the chemical species of interest in each layer is beyond the scope of this article. For the sake of clarity, the tactical analytical approach taken in this manuscript portrays the sediment–water interface region so as to isolate and focus only on the transport processes. Therefore, the reader should note that the two layers of interest are assumed to be very thin, void

of chemical reactions within (i.e., degradation, oxidation/reduction, polymerization, etc.), and have constant concentration differences across them. In other words, the chemical species are conserved, and a steady-state flux is occurring in the defined sediment–water interface region.

The term Brownian diffusion is conventionally applied to very small particles that respond to the kinetic motions of the surrounding solvent molecules. The transport of colloids, also termed aquasols, in the water on either side of the interface is quantified by a chemical potential–type transport process. These are present in the form of dissolved organic carbon (DOC) particles or inorganic particles with sorbed chemical fractions. The bioturbation transport process of particles in the bed as well as in the adjoining porewater is driven by the presence of macrofauna. It is consistent with the chemical potential–type transport mechanism in that the randomness of a collection of macrofauna-driven particle and fluid motions mimics the molecular kinetic mechanism of diffusion on a larger physical scale. For this reason, it is termed a biodiffusion process and is treated as such mathematically [9, 14, 16–19]. Bioturbation has also been depicted as a convective transport process. This typically involves use of bed turnover rate and nonlocal particle movement rates. However, the potential-based biodiffusion also has theoretical merit in that the range of macrofauna sizes and transport lengths tends to approach a Gaussian distribution, indicating that the process can be described by a diffusion type of equation. In addition, the biodiffusion model has an extensive database of field- and laboratory-measured biodiffusion transport coefficients that convective transport lacks for this process [19].

The two generic forms of the chemical potential–type flux equations are

$$F = (D/h)(C_s - C_i) \tag{1}$$

and

$$F = K(C_i - C_w), \tag{2}$$

where F (kg/m^2/s) is the flux, D is the diffusion coefficient (m^2/s), h is the path length (m), K is the convective mass transfer coefficient (m/s), and C (kg/m^3) represents the concentration in water for the sediment bed (s), the interface (i), and the water column (w) beyond the benthic boundary layer, respectively.

The media convective–type rate equation for chemical flux reflects a transport mechanism driven by the directed motion of a bulk media. Several types operate across the interface region. In-bed porewater convection moves solutes and fine particles in both directions. The porewater flow direction responds to hydraulic pressure differences across the bed layers. These can be long-range pressure differences such as in-bank and water column head differences or localized pressure differences generated by the flowing water column as it encounters local bottom roughness such as sand waves, mounds, etc. [20]. In either case, the chemical flux is the product of the effective Darcian porewater velocity and its aqueous concentration.

Solid particles moving through the water-side benthic boundary layer are also a media convective–type flux. The primary ones are particle deposition onto the bed from the water column and resuspension from the bed surface. These transport mechanisms are initiated and maintained by the action of the flowing water. The fluid-generated shear stress at the bed surface drives particle movements into suspension as well as change the particle deposition probability [21, 22]. However, particles and so-called marine snow are also formed in the water column [23], and others originate as wind-blown dust on the sea surface, etc.; all types are deposited onto the bed. The physics of cohesive and noncohesive sediment transport employs complex algorithms for their estimation [24, 25]. For the purpose of this manuscript, a deposition velocity and a resuspension velocity will be used to characterize the respective processes. In each case, the flux is equal to a velocity–concentration product so the generic forms of the media convective–type equation are

$$F = v_w C_w \tag{3}$$

and

$$F = v_p C_p, \tag{4}$$

where v_w and v_p (m/s) are the effective media velocities of water and particles perpendicular to the interface plane, and C_w and C_p are the media concentrations.

The above review covers the most well-known, characterized, and quantified individual processes.

Several other processes have been observed and described. One termed the "benthic cannon" is dramatic and appears in Fig. 4. As shown, the organism responsible for this phenomenon (a maldanid polychaete) is seen injecting a spray of fine particles from its burrow into the lower portion of the water column. In a similar mechanism, gas bubbles generated within the bed can also move to the interface and emerge, likewise injecting fine particles into the water-side boundary layer (Fig. 4). The role of the nepheloid layer, made up of submerged aquatic vegetation and other macrofauna activities that enhance and attenuate chemical transport processes, remains to be studied and quantified. Due to the lack of sufficient information on these and other individual processes, they cannot be included in numerical simulations at this time.

Several computational studies have been performed aimed at comparing aspects of various individual processes. The most comprehensive of these is a study of trichlorobiphenyl (TCP) for nine in-bed transport mechanisms [26]. Individual processes were ranked by characteristic times-of-recovery of TCP in freshwater riverine bed sediment. It was concluded that in high-energy environments, sediment transport was likely the dominant sediment-side TCP transport process, while in low-energy environments, bioturbation was likely to dominate the movement rate of TCP in the upper layer of the bed. Singh et al. [21] developed a framework for a comprehensive mathematical model for fine and cohesive sediment transport to be combined with contaminant transport models in rivers, lakes, and estuaries; they observed that much research needs to be done before truly realistic chemical exchange models for the sediment–water interface will be available for practical use. They further noted that sediment transport and chemical transport must be meshed in development of a comprehensive model. In assessing the soluble release process of polychlorinated biphenyls (PCBs) from bed sediment in three North American rivers, Thibodeaux et al. [27] evaluated five individual transport processes by comparing the magnitudes of the mass transfer coefficients. However, such individual process studies do not completely address the interconnections that result in across-media transport at the sediment–water interface. Comprehensive studies of the interconnections of transport processes are lacking. A study limited to solute transport of polychlorinated biphenyls in the Hudson River highlights the importance of connecting processes across the interface plane [28, 29]. It was found that during active in-bed bioturbation, the transport resistance on the water-side benthic boundary layer is significant and that both of these processes regulate the PCB flux from the bed.

The number and complexity of the biological, chemical, and geophysical processes cooperating to drive chemical flux across the interface is daunting, and sorting out the cause-and-effect factors is confusing without the aid of theoretical guidance. Ad hoc approaches are in use, but all have theoretical shortcomings and may not, therefore, extend into areas outside of the data set. A robust theory that can accommodate the types of various individual chemical transport processes on either side of the interface and connect them in a logical and transparent procedure is needed for several reasons. In the first place, there appear to be none available. Second, having one will lead to much better understanding of the overall situation related to transport and will provide a hypothesis for interpretation of flux data from both laboratory and field measurements. Third, modelers of aquatic chemodynamic processes need a theory-based procedure for connecting chemical movement between the adjoining bulk-phase compartments based on first principles.

Theories and Model Development

G. S. Ohm (1787–1854) found that the electric current (I) is directly proportional to the difference in voltaic potential between the ends of a conductor (V) and the proportionality constant is R^{-1}, where R is the resistance. G. R. Kirchhoff (1824–1887) extended Ohm's law. By analogy, the Ohm–Kirchhoff laws were applied by Whitman [30] and Lewis and Whitman [1] to chemical flux (F) across a gas–liquid interface plane. The emf potential, V, was replaced by chemical concentration potential such as $(C_s - C_i)$, and the result is the well-known resistance-in-series (RIS) law for chemical mass transfer. When applied to the solute at the sediment–water interface the flux equation is

$$F = (C_s - C_w) / \left[\frac{1}{B} + \frac{1}{D}\right], \tag{5}$$

where B and D (m/s) are the water-side and sediment-side mass transport coefficients, respectively. Because of chemical-to-water partitioning, with coefficient K_d (L/kg), the $C_s = w_s/K_d$, where w_s (g/kg) is chemical loading on sediment solids and $D = D_b\ \rho\ K_d/h$, where D_b (m^2/s) is the biodiffusion transport coefficient, ρ (kg/L) particle density, and h (m) bed depth. This result has been verified using field data [29, 31].

Resistance-in-series is applicable only to potential-driven processes. It is often time referred to as Ohm's law [32, 33] and has become a shortcut modeling approach. Misapplication occurs, for example, when media velocity is treated as a potential-type transport coefficient and likewise added in the resistance fashion to obtain the overall resistance. It has been misapplied for atmospheric deposition of gases and particles where both potential and convective processes resistances are summed [34, 35]. Hybrid applications that involve converting the chemical potential resistance to an equivalent media convective type for use with the adjoining bulk-phase concentrations appear in multimedia compartment (MMC) models [33, 36] for the sediment–water interface. As presented in the next section, a return to first principles embodied in the Ohm–Kirchhoff and Lewis–Whitman laws will mend the problem and produce a unified theoretical construct that accommodates both types individually and in unison.

Environmental models contain multiple phases so interfaces are necessary. The sediment–water interface is depicted as an idealized concept in Fig. 5. It is an imaginary plane within the complex transition zones separating bulk water phase from bulk sediment phase as depicted in the Figs. 1 to 4. The "interfacial compartment" is defined based on the following assumptions and concepts: (a) it is a two-dimensional surface containing no mass that separates the adjoining bulk phases, (b) the chemical flux direction is perpendicular to the surface plane, (c) the net entering and departing fluxes are equal, (d) a hypothetical aqueous chemical concentrations with mass per volume units (mg/m^3) is assumed, and (e) because solid (i.e., particle) phases exist on one side, chemical equilibrium is assumed to exist at the interface plane for estimating the equivalent aqueous concentration. A mass balance on the interface plane is performed. Because of assumption, a steady-state equation results and yields a simple algebraic relationship for the interface compartment concentration. It in turn yields a single flux equation containing the individual process mass transfer coefficients and the bulk chemical concentrations in the adjoining media compartments.

Although there are many individual processes occurring in the region of the interface, for demonstration purpose, only four will be used in the following derivation of the interfacial compartment model. This approach simplifies the mathematics of the theoretical procedure while maintaining the essence of the concept. The combination of chemical potential–type and media convective–type transport mechanisms used is shown in Fig. 6. The double-tipped arrows on either side of the interface are the chemical potential type.

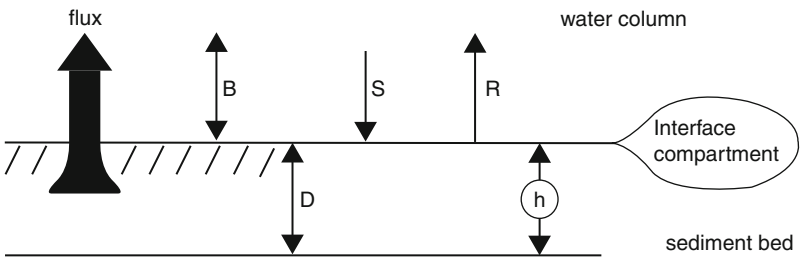

Sediment–Water Interfaces, Chemical Flux at. Figure 6
The essence of the interface compartment. The bubble indicates the location of the IC. It is a plane surface so the line depicts one edge. The large arrow to the left depicts the chemical flux and direction. Transport begins in the sediment bed, crosses the interface, and emerges into the water column. This net flux is a result of four individual processes. The B process is solute transport through the water-side benthic boundary layer. The S process is particle deposition (i.e., settling) onto the bed surface and R is particle resuspension from the bed surface. On the sediment side, the D denotes a diffusive process across a distance h. This illustration is used in deriving the IC model equation (i.e., Eq. 8)

They represent respectively the solute transport across the benthic boundary layer with coefficient B (m/s) and diffusive transport within the upper sediment layers with coefficient D/h (m/s), where the layer thickness is h (m). The single-tipped arrows depict the media convective–type flux equations. They represent particle deposition or settling with coefficient S (m/s) and particle resuspension with transport coefficient R (m/s). The assumed chemical movement pathway and direction of flux F (kg/m^2/s) is depicted by the large arrow. The sediment bed porewater concentration, C_S (kg/m^3), in equilibrium with the bed load fraction, w_a (mg/kg), is at position h, and the bulk water column concentration is C_W (kg/m^3) and is located at the edge of the benthic boundary layer. The overall chemical potential driving force is the concentration difference, $C_S - C_W$.

A steady-state Lavoisier mass balance for the interface compartment requires that the flux from the sediment-side to the interface, F_{si}, equals that departing the interface on the water-side, F_{iw}. It is

$$F_{si} = (D/h)(C_s - C_i) = B(C_i - C_w) + RC_i - SC_w = F_{iw} \tag{6}$$

This result yields the concentration in the interface compartment:

$$C_i = ((D/h)C_s + (S+B)C_w)/(D/h + B + R) \tag{7}$$

Combining the two equations yields flux between the compartments in terms of the bulk-phase concentrations:

$$F_{IC} = \frac{C_s(1 + R/B) - C_W(1 + S/B)}{h/D + 1/B + Rh/BD} \tag{8}$$

This result is the interface compartment model (IC) flux; it is consistent with the traditional potential flux in that it takes the form of Eq. 5 when the convective parameters S and R are set to zero. It is the opinion of the authors that the above procedure is the correct one. However, alternative flux relationships have been proposed for the across-interface flux based on various assumptions and methodologies. Two commonly used approaches appear below.

Invoking the RIS concept directly by mimicking the form of Equation 5 is one approach used [32]. In its derivation, the water-side conductances are summed and then inverted to obtain the overall water-side resistance which is then added to the sediment-side resistance. This procedure yields

$$F_{RIS} = \frac{C_s - C_w}{h/D + 1/(B + R - S)} \tag{9}$$

for the RIS flux equation. The multimedia compartment or box model approach is a hybrid [33]. Its derivation starts by decomposing chemical potential flux into two individual convective-type flux components. It then uses the Lavoisier mass balance for summing the individual fluxes but assumes all are driven by the bulk compartment concentrations. The multimedia compartment (MMC) flux equation is

$$F_{MC} = \frac{C_s - C_w}{h/D + 1/B} + (RC_s - SC_w) \tag{10}$$

The flux equation for the RIS and MMC models reduce to Eq. 5 when S and R are set to zero.

At this juncture, it is clear that three very different algebraic algorithms based on as many approaches are available for estimating the flux across the sediment–water interface. In all cases, the fluxes are linear in relation to the bulk media concentrations and contain the appropriate conductance. Only in the case of the RIS model must the bulk media concentrations be equal for a zero flux. For both the IC model and the MMC model equations, a simple algebraic proof shows that positive, nonzero bulk media concentrations can yield a zero flux. This is a more realistic outcome because in nature it is possible to have a situation where a mix of conductance produces a zero net flux and the bulk media concentration is unequal. Numerical simulations using the theoretical models in flux calculations provide a realistic and quantitative means demonstrating these and other outcomes. The methods used and the results of the numerical flux calculations are presented and discussed in the next section.

Simulation Methods and Results

Although only four individual transport processes were used in the development of the three theoretical models presented in the previous section, nine individual transport processes will be used in the numerical simulation. This is done in order to realistically mimic and

highlight the most significant process typically present in the sediment–water interface region. The four on the water-side include solute transport in the benthic boundary layer, particle resuspension from the bed surface, particle deposition from the water column onto the surface, and colloid Brownian transport through the benthic boundary layer. The five on the bed-side are colloid Brownian diffusion in the porous bed, Darcian water advection into and out the bed, solute molecular diffusion in porewater, particle biodiffusion, and porewater biodiffusion. Altogether, there are five chemical potential–type flux expressions and five media advection type. The types and categories of the processes plus the base case numerical values of the parameters are summarized in Table 1. The top four lines represent the water-side transport coefficients and the remaining six represent the bed-side transport coefficients. The large numerical difference in the PCB versus BZ transport coefficients are due to partitioning for the particle-associated processes. For details on how the bed and water column transport coefficients are calculated, see Chapters 10 through 13 in the *Handbook of Chemical Mass Transport in the Environment* [37].

Data available in the literature on several North American rivers and lakes with bed sediment and water column contaminated with organic chemicals were used. Several studies [27, 29, 38–41] provide the necessary physical, chemical, and biological data and information needed for estimating the bed and water column transport coefficients used in the calculations. Typical bed and water column characteristics at 25°C and 3 m water column depth were used. These characteristics were bed porosity, 75%; bulk density, 572 kg/m^3; sediment layer thickness for active transport, 0.05 m; fraction organic carbon in bed solids, 50 g/kg; dissolved organic carbon (DOC) in the porewater, 50 g/m^3; particle biodiffusion coefficient, 2E-6 m^2/day; porewater biodiffusion coefficient, 2E-5 m^2/day; colloid Brownian diffusivity, 1.61E-5 m^2/day; Darcian water convection into bed, 4E-4 m/day, and out, 1.1E-3 m/day; Peclet number = 1; water column suspended particle concentration, 0.005 kg/m^3; particle deposition velocity, 4E-4 m/day; particle resuspension velocity, 1E-4 m/day; and colloid benthic boundary layer transport coefficient, 2.3E-4 m/day.

The porewater chemical concentrations are separated into dissolved and particle-bound DOC fractions and the fractions transported separately, the dissolved as solute molecular diffusion and the DOC as Brownian particle diffusion. The chemical equilibrium phase distribution partition coefficient is used to relate the solute and DOC-bound concentrations. For characterizing the physical properties of the bed, the New Bedford Harbor estuary site was used [41]. The chemical 2,4,2',4'-tetrachlorobiphenyl was used as the PCB. Its partition coefficient was 21.6 m^3/kg and that used

Sediment–Water Interfaces, Chemical Flux at. Table 1 Transport coefficients (m/day)

Name, location, and type[a]	Benzene	PCB
Solute, water-side mass transfer coefficient, cp.	0.32	0.30
Particle resuspension, ma.	5.72E-5	1.24
Particle deposition, ma.	2.0E-9	4.32E-5
Colloid, water-side, ma.	2.31E-7	4.99E-3
Colloid, bed-side, cp.	2.31E-4	2.31E-4
Darcian velocity into bed (−), ma.	4.35E-4	3.99E-4
Darcian velocity from bed (+), ma.	1.18E-3	1.08E-3
Solute diffusion in bed, cp.	7.48E-4	6.85E-4
Particle biodiffusion, cp.	1.14E-5	0.25
Porewater biodiffusion, cp.	2.0E-4	2.0E-4

[a]*cp* chemical potential, *ma* media advection–type flux

for benzene (BZ) was 0.001 m^3/kg. The tabulated molecular diffusivity in water for each was used [14]. For the benthic boundary layer, solute transport coefficients were based on those from the Hudson River; they were 0.32 and 0.30 m/day for BZ and PCB, respectively. These two chemicals represent the extremes of hydrophobic properties typically encountered in contaminated bed sediments. In addition, they also represent the extremes of numerous soluble and particle-phase geochemicals.

The data appearing above were used with the appropriate algorithms and formulations to estimate the numerical values of the nine transport coefficients [14]. Water (porewater in the bed and in the column above) is the continuous phase across the interface. The transport coefficients use chemical concentrations in water for flux calculations with both the chemical potential–type and media advection–type equations. A summary of typical numerical values of the nine transport coefficients appear in Table 1 for BZ and PCB. Several of the base-case transport parameters were perturbed in doing numerical simulations to cover their expected range of variation.

The results of the first numerical study appear in Table 2. Calculated fluxes for the PCB using the three theoretical models, the interface compartment (IC) model, resistance-in-series (RIS) model, and multimedia compartment (MMC) model, appear. In addition, the IC model interface concentration, C_i (g/m^3), is given. This simulation uses a porewater concentration of 0.065 g/m^3 and water column 0.020 for a chemical potential gradient driving the PCB flux from the bed to the water column for positive flux values with unit g/m^2·d. The negative values denote fluxes directed into the bed. The first numerical study was to assess the role of transport aggressiveness or intensity on the flux.

The first three simulations (i.e., 1, 2, and 3) represent molecular diffusion and in-bed water advection. The flux varies from low positive to negative. Low bed porosity will produce a low flux; all models have essentially the same values for simulation 2. Porewater advection in the opposite direction is sufficient to reverse flux direction as shown in simulation 3. This reverse in flux behavior is present in all three models, but flux numbers are different for each. This is expected because the algebraic forms are different (see Eqs. 8, 9, and 10).

These IC model simulations reveal an interconnection between the media convective–type erosion process on the water-side and the chemical potential–type diffusive process in the bed (see simulations 4, 5, and 6). In the absence of biodiffusion, which is the case for these three simulations, the flux for the IC and RIS models remains unchanged with increasing particle resuspension aggressiveness. This occurs because the in-bed transport processes are slow; they are combined porewater advection and molecular diffusion. The resistance-in-series law is operating properly in the IC and RIS models, where the slowest

Sediment–Water Interfaces, Chemical Flux at. Table 2 PCB flux (g/m^2·d) increasingly active processes

Active processes C_s =.065, C_w =.020	C_i(g/m^3)	IC	RIS	MMC
1. Mol. diff., bed porosity 0.1%	.020	4.3E-9	4.3E-9	5.0E-8
2. Mol. diff., bed 78% porosity	.021	3.1E-5	3.1E-5	3.18-5
3. Water advection into bed, Pe = −10	.0196	−1.3E-4	−2.8E-3	−4.1E-4
4. Mild resuspension, Pe = +10, DOC on.	.0195	4.5E-4	3.3E-4	2.4E-3
5. Aggressive resuspension	.00418	4.5E-4	3.4E-4	8.1E-2
6. "Storm event" resuspension	.00013	4.5E-4	3.4E-4	3.2
7. Mild resusp., mild in-bed biodiff.	.0468	9.4E-3	9.0E-3	1.1E-2
8. Mild resusp., aggressive biodiff.	.0648	1.5E-2	1.5E-2	1.6E-2
9. "Storm" resusp., aggressive biodiff.	.0413	2.1	1.4	3.2

process controls. However, an equivalent resistance-in-series functionality is absent in the MMC model, and the flux tracks particle resuspension directly, resulting in substantially higher fluxes. The generally higher MMC model flux values are due to the porewater solute concentration because it, rather than the interface concentration, is the driver and is always numerically larger.

More interesting process interconnections are revealed in simulations 7, 8, and 9. In these cases, in-bed particle and porewater biodiffusion are active as well as particle resuspension. The flux increases for both the IC and RIS model simulations as they track the level of biodiffusion; however, the MMC model does not change much because it is already high. This behavior by the IC and RIS models shows that an active bed-side process must be present to provide chemical mass readily available and in the upmost layer in order for erosion to be an effective transport process. The rapid biodiffusion provides the mass while the slower molecular diffusion and water advection processes cannot. Finally, all three models give high and approximately equal flux for the most aggressive resuspension and biodiffusion transport coefficients (see simulation 9).

To summarize, the simulation study starts with mild in-bed passive molecular diffusion and a very low-porosity sediment layer. The flux is very low. As one moves down the table, level of transport aggressiveness increases. The final one is for aggressive particle biodiffusion and hydraulic flows that result in aggressive particle resuspension. The flux is very high in this case. The variation in flux from low and high is approximately 10^9. The flux numbers for the IC and RIS models are similar in magnitude while the MMC is consistently higher and, in some cases, much higher. Its flux behavior seems to track the particle resuspension process in aggressiveness. Clearly, Eq. 10 supports this behavior.

The flux behavior of BZ is somewhat different; no tabular data are provided. The behavior for simulations 1, 2, and 3 are similar to the PCB ones. Low porosity yields low flux, and into bed water advection can reverse the weak diffusion-driven flux. Being less hydrophobic, BZ displays limited sorption to their surfaces. For this reason the in-bed particle transport is not a significant chemical mobilization process for BZ. For simulations 2 through 9, all three models give essentially the same numerical flux values. All models reflect no particle process dependence, and all display only chemical potential flux–driven behavior patterns. Theoretically, in the absence of particle processes, all three models are equal and become identical to Eq. 5.

The second numerical study was on the in-bed concentration gradient difference polarity and the effect on the direction of the flux. Equations 8, 9, and 10 show each model has a different mathematical dependence on the porewater and water column concentration. In the above simulations, the concentration difference was set to simulate chemical transport from the bed, so for PCB, the concentration differences as C_s were =.065 and 0.02 g/m^3, and for BZ, they were 20 and 2.0 g/m^3. So as to further test the models for realistic flux behavior characteristics, the chemical potential gradient range and the direction were reversed; the flux results for reversing the gradient direction appear in Figs. 7 and 8. In each figure, the flux is on the vertical axis and the imposed concentration difference on the horizontal axis. Each line in Fig. 7 represents a model from top to bottom; they are MMC, IC, and RIS.

Figure 7 presents aspects of the flux behavior. The vertical axis displays the flux. Positive numbers represent the PCB moving from the bed to the water column. Negative numbers represent the PCB moving from the water column to the bed. The zero flux indicates no net chemical movement in either direction. The horizontal axis displays chemical concentrations in the water column and the porewater. It is an unusual axis in that it has zero on each end and maximum in the center. The horizontal axis consists of two sections divided vertically by a dotted line. The concentration is a maximum at the position of the dotted line. To the left side of the vertical line, the porewater concentration in the bed, C_S, is held constant at a value of 0.065 g/m^3 and the water column concentration, C_W, is varied from 0.0 to 0.065 g/m^3 as shown. Under these conditions, the concentration difference tends to move the PCB from the bed to the water column and produce a positive flux. It does for all three models. Only for the RIS model does the flux equal zero for the condition where $C_S = C_W = 0.065$. Due to the particle resuspension process, the PCB flux result for both the IC and MMC models remain positive and nonzero when moving from the bed to the water column. In the next simulation, concentration

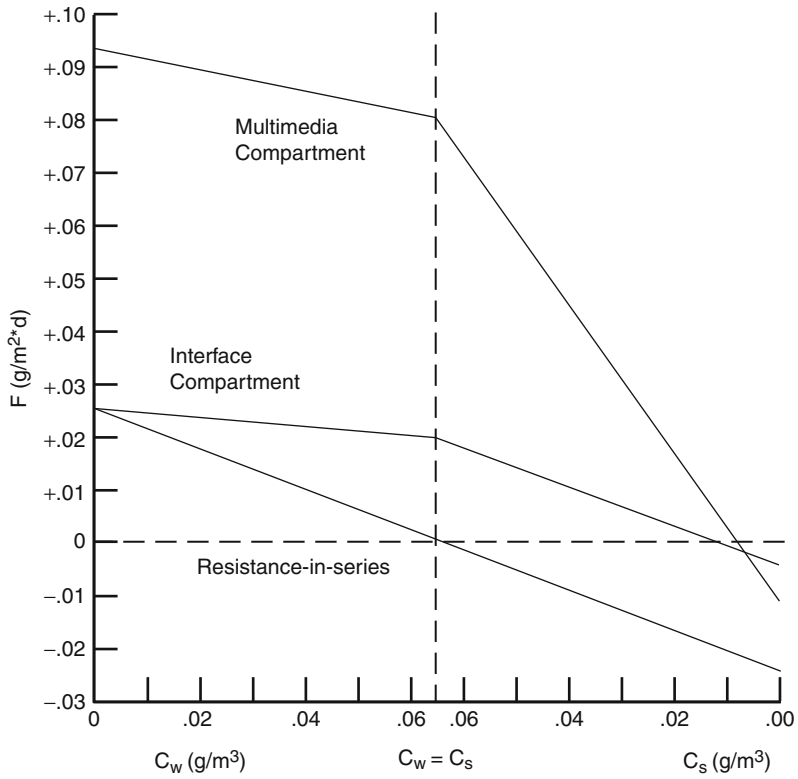

Sediment–Water Interfaces, Chemical Flux at. Figure 7

PCB flux across the sediment–water interface. A positive flux, F, is from the bed to the water column and negative is from water to the bed. The concentration differences between bed and water column used in the calculations are displayed on the ordinate. The progression of concentration difference values was devised to force the chemical potential out the bed, on the left, and into the bed on the right so as to drive the flux accordingly. At the vertical dotted line, bed and water concentrations are equal. Only for the RIS model is the flux zero. The three lines depict the theoretical behavior of the PCB flux for the three models: IC, RIS, and MMC

levels in bed porewater versus the water column concentration will be reversed.

Consider concentration conditions to the right of the dotted line in Fig. 7. As shown on the horizontal axis, the water column concentration, C_W, is held constant at 0.065 g/m^3 and the porewater concentration, C_S, is reduced from 0.065 down to 0.0 g/m^3. The flux for the RIS model starts at zero and goes negative as the PCB moves into the bed. The other model results display a positive flux at the start and both trends downward. The MMC model shows a steep decline and reaches zero flux at C_S of about 0.01 g/m^3. The IC flux declines to the same value as well, and this occurs because the imposed concentration gradient encourages PCB movement from the water column to bed.

The point of the above flux versus concentration study for PCBs was to show the different behavior patterns produced by the three models. The horizontal concentration axis was contrived to force the flux to range in magnitude from positive to negative and therefore cover all possible conditions to be encountered in nature. The IC model is theory-based, and so it characterizes the correct PCB flux behavior. Hopefully, future experiments will be able to verify or refute this behavior. The RIS model predicts lower flux values while those for the MMC model are much higher. All three models behave according to the algebraic forms of 8, 9, and Eqs. 10 for the IC, RIS, and MMC, respectively. Both the IC and the MMC models have a flux inflection; this suggests they are better quantitative

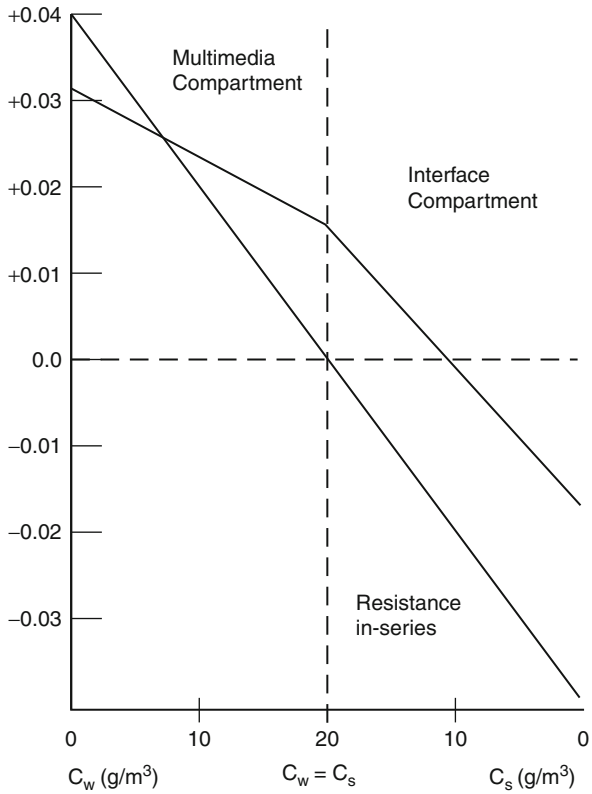

Sediment–Water Interfaces, Chemical Flux at. Figure 8 Benzene flux across the sediment–water interface. A positive flux, F, is from the bed to the water column and negative is from water into the bed. The concentration differences between bed and water column used in the calculations are displayed on the ordinate. The progression of concentration values were devised to force the chemical potential out the bed, on the left, and into the bed on the right, so as to drive the flux accordingly. The two lines depict the theoretical behavior of the BZ flux for the three models: IC, RIS, and MMC. The IC and MMC flux values overlap

representations of the overall flux process. Crossing the $C_w = C_s$ line and interchanging concentration represents a switching of processes; it is in the algebra (see Eqs. 8 and 10).

A somewhat different behavior occurs for BZ. The results are displayed in Fig. 8 where the graph is constructed similar to that for PCB. The RIS and MMC flux values are identical and appear as a single diagonal line that starts positive, goes to zero, and then ends negative. The IC model starts at a slightly lower positive flux. It decreases then goes through a slope change at $C_S = C_W$. This is an algebra-driven inflection point in the IC model; it occurs at $C_S = C_W = 20$ g/m^3 (see Eq. 8). As C_S decreases toward zero, the flux goes into a steep decline with increasing negative values. It parallels the behavior of the RIS and MC models but with slightly higher flux values. Beyond the IC model, flux is higher than the others. The particle transport process is low, and the MMC model takes the same algebraic form as the RIS. However, the IC model reflects the correct theoretical approach and displays a very different behavior pattern. Being water soluble, BZ has minimal particle association. However, the particle processes enter as ratios (see Eq. 8). This has the effect of delaying the zero flux. It occurs at C_S of 11.0 g/m^3.

The flux results for the IC versus RIS and MMC models using this specific simulation with BZ and PCB are different numerically. They also display different behavior patterns as the imposed concentration gradient condition is changed to encourage chemical movement from the bed to a condition of chemical movement into the bed. Presumably, the IC model result is the correct one since it is theory-based. However, at this juncture, it is a hypothesis in need of testing against laboratory and field experimental measurements.

Significance for Aquatic Environments

There are numerous individual transport processes on both sides of the interface that are driven by biological, chemical and geophysical phenomena. Some processes work in parallel while others work in series, forming a connected network of processes moving anthropogenic substances and geochemicals across the interface. The interface compartment (IC) concept and associated mathematical model is developed and presented as the appropriate theoretical approach for understanding the overall process and quantifying the resulting net flux. For aquatic researchers, it is a tool with several uses. It provides a testable hypothesis and a means of interpreting rate data based from measurements in the laboratory or field. It provides a mathematical rate equation for individuals making numerical flux estimates. Finally, the derivation provides a protocol for

obtaining one additional model equation for use by chemical fate modeler's connecting mobility across the interface that separates the adjoining bulk sediment and water compartments.

Future Directions

The sediment–water interface is the largest plane surface on Earth. Understanding and quantifying chemical and particle mobility across this semipermeable interface is relevant to the work of a broad community of aquatic researchers. The interface compartment model provides the basic theory for connecting chemical flux across the sediment–water interface. Correctly quantifying the net chemical, particle, and aquasol exchange rates across this plane is a key factor for understanding the fate of numerous natural and anthropogenic substances on Earth and aid in assessing the ecological significance. The potential impact of the IC model's further development and use in the environmental and geosciences fields may be a key contributing factor. Life-forms residing on both sides, in the water column or the surface sediment layers, depend on oxygen and nutrient fluxes. The bed is a source or a sink of soluble and particulate carbon compounds depending on the chemodynamics of the specific locale. The bed is a sink for chemical pollutants entering the aquatic system but, later as conditions improve in the water column, it becomes the source. These are just a few examples of the types of possible uses which require theoretically sound and verified science-based tools. As outlined above, further work is needed on the interface compartment concept before it is accepted as a unified theory and modeling protocol.

Bibliography

1. Lewis WK, Whitman WG (1924) Principles of gas absorption. Indust Eng Chem 16:1215–1220
2. Rhoads DC, Germano JD (1982) Characterization of benthic processes using sediment profile imaging: An efficient method of remote ecological monitoring of the seafloor (REMOTS™ System). Mar Ecol Prog Ser 8:115–128
3. Rhoads DC, Germano JD (1986) Interpreting long-term changes in benthic community structure: a new protocol. Hydrobiologia 142:291–308
4. Santschi P, Hohener P, Benoit G, Brink MB (1990) Chemical processes at the sediment-water interface. Mar Chem 30:269–315
5. Duursma EK, Smies M (1982) Sediments and transfer at and in the bottom interfacial layer. In: Kullenberg G (ed) Pollutant transfer and transport in the sea, vol II. CRC Press, Boca Raton, pp 101–137
6. Krantzberg G (1985) The influence of bioturbation on physical, chemical and biological parameters in aquatic environment – a review. Environ Pollut (Ser A) 39:99–122
7. DiToro DM (2001) Sediment flux modeling. Wiley, New York
8. Kullenberg G (ed) (1976) Pollutant transfer and transport in the Sea-II. CRC Press, Boca Raton
9. Boudreau BP, Jorgensen BB (eds) (2001) The benthic boundary layer. Oxford University Press, New York
10. McCave IN (ed) (1976) The benthic boundary layer. Plenum, New York
11. Windom HL, Duce RA (1976) Marine pollutant transport. Lexington, Lexington
12. Tenore KR, Coull BC (eds) (1980) Marine benthic dynamics. University of South Carolina Press, Columbia
13. Fanning KA, Manheim FT (eds) (1982) The dynamic environment of the ocean floor. Lexington Books, Lexington
14. Thibodeaux LJ (1996) Environmental chemodynamics. Wiley, New York
15. Lerman A (1979) Geochemical processes water and sediment environments. Wiley, New York
16. Boudreau BP (1997) Diagenetic models and their implementation. Springer, Berlin
17. Schink DR, Guinasso NL Jr (1975) Modeling the influence of bioturbation and other processes of $CaCO_3$ dissolution at the sea floor. In: Andersen NR, Malahoff A (eds) The fate of fossil fuel CO_2 in the oceans. Plenum, New York, pp 375–399
18. Berner RA (1980) Early diagenesis. Princeton University Press, Princeton
19. Thibodeaux LJ, Matisoff G, Reible DD (2010) Bioturbation and other sorbed-phase transport processes in surface soils and sediment. In: Thibodeaux LJ, Mackay D (eds) Handbook of chemical mass transport in the environment. CRC Press, Boca Raton (Chap 13)
20. Thibodeaux LJ, Wolfe JR, Dekker TJ (2010) Advective porewater flux and chemical transport in bed-sediment. In: Thibodeaux LJ, Mackay D (eds) Handbook of chemical mass transport in the environment. CRC Press, Boca Raton (Chap 11)
21. Singh VP, Reible DD, Thibodeaux LJ (1988) Mathematical modeling of fine sediment transport. Hydrol J IAH 11:1–3
22. Lick W (2009) Sediment and contaminant transport in surface waters. CRC Press, Boca Raton
23. Lohmann R, Dachs J (2010) Deposition of dissolved and particle-bound chemicals from surface ocean. In: Thibodeaux LJ, Mackay D (eds) Handbook of chemical mass transport in the environment. CRC Press, Boca Raton (Chap 17)
24. Yang CT (2003) Sediment transport. Krieger, Malabar
25. DePinto JV, McCulloch RD, Redder TM, Wolfe JR, Dekker TJ (2010) Deposition and resuspension of particles and associated chemical transport across the sediment-water interface.

In: Thibodeaux LJ, Mackay D (eds) Handbook of chemical mass transport in the environment. CRC Press, Boca Raton (Chap 10)
26. Reible DD, Valsaraj KT, Thibodeaux LJ (1991) Chemodynamic models for transport of contaminants from sediment beds. In: Hutzinger O (ed) The handbook of environmental chemistry, part F, vol 2. Springer, Berlin, pp 186–228
27. Thibodeaux LJ, Reible DD, Valsaraj KT (2002) Non-particle resuspension chemical transport from stream beds. In: Lipnick RL, Mason RP, Phillips ML, Pittman CU Jr (eds) Chemicals in the environment, vol 806, ACS symposium series. American Chemical Society, Washington, DC, pp 130–149
28. Thibodeaux LJ, Valsaraj KT, Reible DD (2001) Bioturbation–driven transport of hydrophobic organic contaminants from bed sediment. Environ Eng Sci 18:215–223
29. Erickson MJ, Turner CL, Thibodeaux LJ (2005) Field observation and modeling of dissolved fraction-sediment-water exchange coefficients for PCBs in the Hudson River. Environ Sci Technol 39:549–555
30. Whitman WG (1923) The two-film theory of gas absorption. Chem Metall Eng 29:146–148
31. Thibodeaux LJ, Bierman VJ (2003) The bioturbation-driven chemical release process. Environ Sci Technol 1:253A–258A
32. Monteith JL, Unsworth M (1990) Principles of environmental physics. Butterworth-Heinemann, Oxford
33. Mackay D (2001) Multimedia environmental models. Lewis, Boca Raton
34. Slinn WGN (1978) 4-Wet and dry removal processes. In: NRC (ed) The tropospheric transport of pollutants and other substances to the oceans. National Academy of Sciences, National Academy Press, Washington, DC
35. Trapp S, Matthies M (1998) Chemodynamics and environmental modeling. Springer, Berlin
36. Van de Meent D (1993) Simple box: a generic multimedia fate evaluation model. RIVM Report No. 6727200001. Bilthoven
37. Thibodeaux LJ, Mackay D (eds) (2010) Chapters 10,11,12,13 &17. In: Handbook of chemical mass transport in the environment. CRC Press, Boca Raton
38. Thoma GJ, Koulermos AC, Valsaraj KT, Reible DD, Thibodeaux LJ (1991) The effect of pore-water colloids on the transport of hydrophobic organic compounds from bed sediments. In: Baker RA (ed) Organic substances in water, vol 1, Humics and soils. Lewis, Boca Raton
39. Valsaraj KT, Thibodeaux LJ, Reible DD (1997) A quasi-steady-state pollutant flux methodology for determining sediment quality criteria. Environ Toxicol Chem 16:391–396
40. Savant SA, Reible DD, Thibodeaux LJ (1987) Convective transport within stable river sediments. Water Resour Res 23:1763–1768
41. Thibodeaux LJ, Reible DD, Bosworth WS, Sarapas LC (1990) A theoretical evaluation of the effectiveness of capping PCB contaminated New Bedford Harbor bed sediments. Final Report. HSRC. Middelton Library, Louisiana State University, Baton Rouge

Seed Dormancy and Agriculture, Physiology

Roberto L. Benech-Arnold[1], M. Verónica Rodriguez[2], Diego Batlla[3]
[1]IFEVA – Cátedra de Cultivos Industriales/CONICET-Universidad de Buenos Aires, Buenos Aires, Argentina
[2]IFEVA – Cátedra de Fisiología Vegetal/CONICET-Universidad de Buenos Aires, Buenos Aires, Argentina
[3]IFEVA – Cátedra de Cerealicultura/CONICET-Universidad de Buenos Aires, Buenos Aires, Argentina

Article Outline

Glossary
Definition of the Subject
Introduction
Dormancy (Classifications and Definitions)
Dormancy and Its Implications in Agriculture
Future Directions
Bibliography

Glossary

Dormancy Internal inadequacy of a seed that impedes its germination under, otherwise, favorable thermal, hydric, and gaseous conditions.

Abscisic acid Plant growth regulator that, among other processes, inhibits seed germination and is involved in dormancy imposition.

ROS Reactive oxygen species implicated in tissue aging and, more recently, in seed dormancy relief.

Preharvest sprouting Untimely grain germination in the mother plant due to a combination of low dormancy and damp conditions prior to crop harvest.

Stratification thermal time index An index calculated by summing thermal time below a threshold temperature, which is used to estimate dormancy release as a function of stratification temperature and time.

Definition of the Subject

Dormancy is a common attribute of temperate species. Its adaptive significance is quite evident for species living in

the wild: dormancy is a mean for restricting germination to the season when environmental conditions are suitable for plant establishment. From an agricultural perspective, dormancy represents a problem, both when it is long lasting and when it is too short. For that reason, selection against dormancy has been always behind any domestication effort. In some cases, the aim of removing dormancy has not been achieved, and in others, it has gone too far resulting in susceptibility to preharvest sprouting. In addition, the fight against weeds is frequently impaired by the existence of long-lasting seed banks as a result of seed dormancy.

Introduction

A seed can be declared to be dormant when it fails to germinate despite it is given all the "proper" conditions (i.e., enough water and appropriate temperature) for germination to happen. Assuming that there is a living seed (a dead seed would not germinate either), then why does it not germinate? Will it ever germinate? These types of questions were probably first asked in despair by farmers about 10,000 years ago, while staring at their useless recently harvested grains that would not give way to a new crop or allow malting for beer (a process that also relies on germination).

Despite historical human concerns with dormancy, this "internal block to germination" has been positively selected throughout millions of years of evolution in most temperate species, and has obvious ecological benefits in the wild. The main apparent role of seed dormancy is to delay germination until a proper environment is encountered, for example, by keeping track with seasonal changes in temperature to avoid unfavorable conditions for plant establishment [1]. Within the life of most plants, the only chance to travel is as a seed. After separating from the mother plant, the seed is moved by different means (wind, gravity, water, animals) until it is randomly located in a new microenvironment that may prove adequate or not for completing its life cycle. Once germination happens, the small plant will most probably remain attached to that spot until its death. As a consequence of plants being sessile organisms, seeds have developed sophisticated mechanisms to collect information from the environment, and the resulting output is a vital decision: to germinate right away, or not (at least not this time, this place) until new environmental conditions that are good enough are finally met with.

Seed dormancy has been a subject of intensive research during the last decades. Physiological and environmental control of dormancy has been studied deeply and, more recently, its molecular and genetic bases have started to be elucidated. As in other areas of plant science, knowledge on the molecular bases of dormancy has been attained through the use of model organisms. Indeed, work with *Arabidopsis thaliana,* a small winter annual weed preferred by most plant scientists, has revealed the involvement of multiple genes controlling seed dormancy, which is a continuous and complex character. Cultivated species also display different degrees of dormancy, and either the presence or the absence of dormancy can have strong consequences on the utilization of the seeds, and this will be discussed in more detail in this entry. Different strategies exist that are directed to control dormancy through genetic changes (as a result of classical breeding or transgenic events) or to cope with varying degrees of dormancy, such as the development of predictive models. As the level of dormancy a seed will effectively display is the result of its genotype interacting deeply with a changing environment, predictive models have been developed for some species (e.g., malting barley or some weeds). Most of these strategies require a thorough knowledge on the biology of dormancy at different levels.

In this entry, the focus is on what is termed as physiological dormancy, or the lack thereof. The most important challenges facing agriculture, in relation to the presence or the absence of dormancy in both cultivated and weedy species, are also pointed out. Some examples of each type of problem are presented, illustrating on the physiological mechanisms responsible for the expression of the character and commenting how the molecular information coming from studies on *Arabidopsis* and other model species, have started to be used to attain the final aim of solving these dormancy problems.

Dormancy (Classifications and Definitions)

Dormancy is the result of mechanisms operating within the seed that impede germination even when the seed is exposed to an environment known to be friendly for that species (i.e., in which water, oxygen and adequate temperature are available). This

impediment or block to seed germination can be determined by both morphological and/or physiological properties of the seed [2]. On the basis of this fact, Baskin and Baskin [3] developed a classification system which includes five classes of seed dormancy: physiological, morphological, morphophysiological, physical, and a combination of physical and physiological. In this entry, mainly physiological dormancy which is the most prevalent dormancy type in temperate seed banks and is also the major form of dormancy in most laboratory model species is referred to [4]. This type of dormancy is caused by a physiological inhibiting mechanism of the embryo that prevents radicle emergence, although other seed structures that cover the embryo can be involved as well [1]. From a physiological point of view, there is enough evidence showing that the mechanism of seed dormancy is mainly regulated by the phytohormones abscisic acid and gibberellins [4, 5].

Dormancy can be also classified in primary and secondary dormancy. Primary dormancy refers to the innate dormancy possessed by seeds upon dispersal from the mother plant. Secondary dormancy refers to a dormant state that is induced in nondormant seeds by unfavorable conditions for germination, or reinduced in once-dormant seeds after a sufficiently low dormancy had been attained.

Primary dormancy is acquired during seed development, and, in most species, is gradually lost after natural seed dispersal (in wild species) or harvest, during post-maturation or after-ripening period. As pointed out before, both the primary dormancy level that seeds present at dispersal or harvest (maturity) and the rate of release from primary dormancy (which determines the time lapse required by a seed population to lose dormancy) are dependent on the genotype, the environment, and the interaction between them. Therefore, although different species or genotypes (i.e., cultivars, inbred lines, etc.) can present more dormant or less dormant seeds at maturity, and faster or slower rates of dormancy release, those traits can be modulated by the environment perceived by the seed during their development-maturation phase (parental environment) and their post-maturation period, respectively. In relation to the parental environment, for example, there is evidence indicating that there are certain environmental factors tending to have similar effects on different species [6]. For example, low dormancy at seed maturity is generally associated with high temperatures, short days, drought, and nutrient availability during seed development and maturation [7–11]. For the post-maturation period, storage temperature and moisture are the most relevant factors regulating dormancy loss rate in cultivated species, while in natural wild conditions a diverse number of factors can be affecting seed dormancy loss. In wild species (i.e., weeds), the post-maturation process usually takes place in the soil because, after dispersal, seeds usually become part of the soil seed bank [12]. Under these conditions, primary dormancy loss can be affected by many naturally occurring factors, as soil temperature and soil water regime (through changes in seed moisture content), temperature fluctuations, light, etc. [13–15]. Although many factors can be affecting the dormancy level of seeds from cultivated and wild species, there is evidence showing that temperature appears to be primarily responsible for year-to-year variation in dormancy level at maturity [6] and for differences in the dormancy loss rate during post-maturation, though the latter can be modulated by seed moisture content [15, 16].

In many species, nondormant seeds can be reinduced into secondary dormancy after dispersal. There are many factors that can be responsible for induction into secondary dormancy, as specific temperature ranges, changes in light quality and quantity, the gaseous environment, etc. Although induction into secondary dormancy is an uncommon phenomenon in most seeds of cultivated species, it is very common under field conditions for seeds of many wild species, particularly those forming persistence seed banks. Indeed, under natural field conditions, the release from primary dormancy followed by subsequent entrance into secondary dormancy (whenever conditions are given for this entrance) may lead to dormancy cycling. Evidence for dormancy cycling in natural seed soil banks has been obtained for many species.

Dormancy and Its Implications in Agriculture

Seeds in their natural form are still the best way to preserve and propagate most crop species, and their capacity to germinate at the right moment (either in the field or under controlled conditions) is a most important

feature. Therefore, any factors (internal or external) affecting the germination capacity of seeds and ultimately their agronomical performance should be understood in order to improve seed quality through breeding and/or crop management strategies. Among the factors that may affect germination, dormancy is probably the most important, as it is a heritable trait that can inhibit germination of a viable seed. Indeed, beyond the fact that dormancy is a highly intriguing biological process and consequently moves the curiosity of scientists, the study of dormancy has strong practical implications. Both farmers and seed companies encounter problems associated either to an anticipated dormancy loss or to a long-lasting dormancy. In the same way, industrial processes like malting, which depends on seed germination, can be largely hampered by the existence of dormancy or, alternatively, face important reductions in the quality of the received lots due to a precocious dormancy termination and pre-germination in the field.

Since dormancy is highly undesirable for agricultural purposes, selection pressure against this trait must have been important throughout the domestication process, particularly in species with temperate origin. In some cases, this pressure must have gone too far, as in the case of cereals, leading to an anticipated dormancy loss which makes some crops susceptible to preharvest sprouting or pre-germination. Nevertheless, intraspecific variability for dormancy exists and "dormancy genes" are still present in some genotypes, although their positive selection through breeding has been difficult due to strong linkage to other undesired traits. In some other cases, selection pressure might have not succeeded in eliminating dormancy, so seeds are not germinable by the time of the next sowing or by the time they need to be "ready" by the malting industry. In any case, dormancy release should take place within a precise "time window." This rarely can be achieved without a solid knowledge of the mechanisms on which dormancy relies in each species.

Dormancy in Cultivated Species

Problems Associated with the *Excess of Dormancy* (Dormancy Persistence)

Sunflower Sunflower is a good example of a crop species with prolonged dormancy. Dormancy persistence in different sunflower genotypes can vary from several weeks up to almost a year. Also, important variation has been reported on this trait for the same genotype under different environments, indicating a strong interaction with the environment. Sunflower is cultivated in many areas around the globe, and is a summer crop. At harvest time, sunflower seeds are dormant and germinate poorly [17–19]. This dormancy is the result of true embryo dormancy [17, 18] and the inhibitory action of the envelopes [17, 18, 20] including the seed coat and the pericarp, since sunflower "seeds" are achenes. In the case of freshly harvested sunflower seeds, dormancy is expressed at temperatures lower and higher than 25° C [17]. Dormancy expression at low temperatures is attributed to embryo dormancy which is not expressed at high temperatures [17]; conversely, dormancy expressed at high temperatures results from coat-imposed dormancy [17]. The deep dormancy that sunflower grains present at harvest results from the coexistence of coat-imposed dormancy and some remnant embryo dormancy [17]. Embryo dormancy is lost shortly after harvest if the seed is subjected to dry after-ripening, but coat-imposed dormancy persists for longer and may require several weeks of dry after-ripening to be overcome. Consequently, few weeks of dry after-ripening allow seed germination at low temperatures due to termination of embryo dormancy; the acquisition of the capacity to germinate at high temperatures, in contrast, may take several weeks of dry after-ripening [17].

The plant growth regulator ABA appears to be involved in the imposition of embryo dormancy. The inclusion of fluridone (an inhibitor of ABA biosynthesis) in culture media for sunflower embryo development prevents the induction of embryo dormancy [21, 22]. Nevertheless, the pattern of accumulation of ABA in the developing embryo does not coincide with the embryo physiological behavior: during seed development, embryos germinate well at the time when the endogenous ABA level is at its highest (7–12 DAP); thereafter, ABA decreases to a low value when embryo dormancy becomes established [21]. It seems, then, that the ABA peak at early stages is responsible for the imposition of the dormant state that is established immediately after that peak has taken place. Moreover, it appears that ABA needs to be present during a critical time period to induce dormancy. Le Page-Degivry and

Garello [22] showed that when young (7 DAP), non-dormant embryos were cultured in the presence of ABA, the hormone produced a temporary inhibition of germination but did not induce dormancy (i.e., embryos were able to germinate when transferred to a basal medium). In contrast, exogenous ABA became effective if applied immediately prior to the natural induction of dormancy. For example, 5 days culture on a medium containing 5×10^{-5} M ABA resulted in partial dormancy in 13 DAP embryos while total induction of dormancy occurred in 17 DAP embryos.

As mentioned before, embryo dormancy can be terminated by dry storage. To identify the process by which dormancy is broken during after-ripening, Oracz et al. [23] focused on the role of reactive oxygen species (ROS) in this phenomenon. After-ripening entailed a progressive accumulation of ROS, namely, superoxide anions and hydrogen peroxide, in cells of embryonic axes. This accumulation, which was investigated at the cellular level by electron microscopy, occurred concomitantly with lipid peroxidation and oxidation (carbonylation) of specific embryo proteins. Incubation of dormant seeds for 3 h in the presence of hydrogen cyanide (a compound that breaks dormancy) or methyl viologen (a ROS-generating compound) also released dormancy and caused the oxidation of a specific set of embryo proteins. In summary, the mechanism proposed by the authors involves ROS production and targeted changes in protein carbonylation patterns [23].

As with other cultivated species such as *Lactuca sativa* [24] and *Arachis hypogea* [25], ethylene (C_2H_4) and etephon strongly stimulate the germination of dormant sunflower seeds [17, 18, 26]. In contrast, gibberellic acid and cold stratification do not overcome dormancy in this species [27] though it was shown that 1 mM GA_3 is effective for overcoming dormancy in some wild sunflowers [28]. Corbineau, Bagniol, and Côme [17] showed that ethylene and its immediate precursor (1-aminocyclopropane-1-carboxylic acid) strongly stimulated germination of primary dormant sunflower seeds; on the contrary, inhibitors of ethylene (i.e., amino-oxyacetic acid and $CoCl_2$) or ethylene action (silver thiosulfate and 2.5 norbomadiene) inhibited germination of nondormant seeds.

Oracz et al. [29] assessed the possible role of cyanide, which is produced by the conversion of 1-aminocyclopropane 1-carboxylic acid to ethylene, in dormancy release. The beneficial HCN effect on germination of dormant embryos was found to be associated with a marked increase in hydrogen peroxide and superoxide anion generation in the embryonic axes [29].

Malting Barley In addition to impairing a rapid and simultaneous germination after sowing, a persistent dormancy would prevent the utilization of a seed lot for industrial purposes when the process requires germination. This is the case of the malting process which uses barley as the main grain. The malting process itself requires grain germination, so a low dormancy level at harvest is a desirable characteristic because the grain can be malted immediately after crop harvest, thus avoiding costs and deterioration resulting from grain storage until dormancy is terminated. Therefore, breeders have to solve the compromise between obtaining genotypes with low dormancy at harvest, but not with such an anticipated termination of dormancy that leads to sprouting risks (a phenomenon which is referred to in the next section). Dormancy of the barley grain is typically imposed by the seed-covering structures (lemma and palea, pericarp plus seed coat). Indeed, embryos can germinate well from the very early stages of development if they are isolated from the rest of the grain and incubated in water [30]. Limitation of oxygen supply to the embryo by oxygen fixation as a result of oxidation of phenolic compounds in the lemma and palea (hereafter referred to as the glumellae or the hull) has been suggested to be responsible for the dormancy of dressed caryopses of cereals such as barley [31] and oat [32]. In dormant grains of barley, for example, whole intact caryopses germinated with difficulty, even in the air, while de-hulled caryopses were all able to germinate under oxygen tensions of at least 10%, suggesting that oxygen concentration under the covering structures might be less than 10% [31].

Dormancy of the barley grain also appears to be under ABA control: termination of glumellae-imposed dormancy during grain development was shown to be correlated with a sharp decline both in ABA embryonic content and sensitivity [30]. A role for ABA in

dormancy maintenance of the barley grain has also been suggested: ABA embryonic content declines during the first hours of incubation of nondormant seeds, whereas it remains at high levels in embryos of dormant grains [33]. In recent years, Benech-Arnold et al. [34] confirmed this role of ABA in dormancy maintenance. The ABA level of the embryo largely decreased during the first hours of incubation and prior to any visible germination in both dormant and nondormant grains at 20° C, the temperature at which dormancy is not expressed, and in nondormant grains incubated at 30° C, suggesting that ABA catabolism and/or conjugation exceeds ABA biosynthesis. By contrast, at 30° C dormancy expression was associated with a maintenance of ABA at high levels: after an initial increase, ABA content decreased very smoothly and was always between two- and fourfold higher than in embryos from grains in which dormancy was not expressed (Fig. 1).

Both the removal of the glumellae and the incubation of de-hulled grains under low oxygen concentrations modified grain germination behavior and ABA content evolution throughout incubation at 30° C [34]. These results indicate that the presence of the glumellae is instrumental for dormancy maintenance because it imposes oxygen deprivation to the embryo which, in turn, promotes ABA synthesis and/or inhibits ABA inactivation. Indeed, removal of the glumellae in dormant grains incubated at 30° C under 21% oxygen suppressed the initial increase in ABA content that was observed in dressed dormant grains incubated at the same temperature. By contrast, incubation under hypoxia (5% oxygen) of de-hulled grains restored it and inhibited germination [34].

Artificially imposed hypoxia also enhanced embryo sensitivity to ABA by several fold [34]. These results suggest that, in addition to interference with ABA metabolism, the presence of the glumellae increases embryo responsiveness to the phytohormone. To explore this possibility, Mendiondo et al. [35] measured the expression of several components of the ABA signaling pathway during incubation of entire and de-hulled grains: the presence of the glumellae enhanced the expression of most of the investigated genes, suggesting that the hull increases the sensitivity to ABA of the enclosed embryos and that this enhancement is effected at the level of gene expression. Again, artificially imposed hypoxia was not able to mimic the effect of the glumellae on the expression of ABA signaling components, indicating that the apparent enhancement of embryo sensitivity to ABA under low oxygen tensions was in fact due to over-accumulation of ABA as a result of malfunctioning of the enzyme committed to ABA inactivation [34].

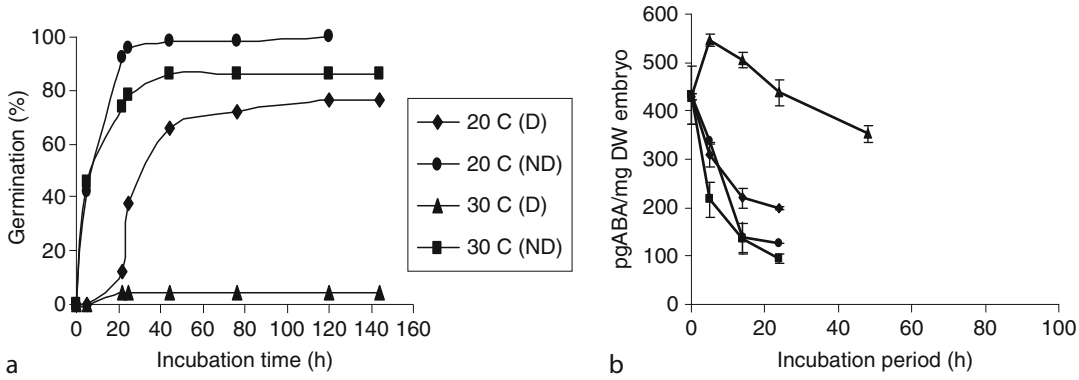

Seed Dormancy and Agriculture, Physiology. Figure 1

Germination (**a**) and embryo ABA content evolution (**b**) during incubation at 20° C (circles, diamonds) and 30° C (triangles, squares) of dormant (circles, triangles) and nondormant (diamonds, squares) grains. Freshly harvested (dormant, *D*) grains and grains stored dry for at least 3 months at 25° C (nondormant, *ND*). Means of two measurements ± arithmetical spread (germination) and of three measurements ± SD (ABA content) (Redrawn with data originally published in [34])

Problems Associated with *the Lack of Dormancy* (Preharvest Sprouting in Cereals)

The advantages of having a freshly harvested seed lot with the capacity to germinate rapidly and uniformly under a wide range of environmental conditions are related to the possibility of immediate sowing or malting, thus avoiding financial costs derived from delays and/or storage until germination capacity is good enough. Nevertheless, genotypes that produce nondormant seeds at harvest may already be able to germinate to some degree even before harvest. The main problem related to an early loss of dormancy in crop species is preharvest sprouting (PHS). This phenomenon is characteristic of cereal species like rice, barley, wheat, and sorghum. As these species all exhibit intraspecific variability for the rate of dormancy loss and PHS behavior, genotypes with contrasting sprouting behavior have proved useful for many comparative studies [36–39], in addition to QTL analysis that leads to the identification of several loci related to dormancy [40–43]. When low levels of dormancy during late grain maturation period are combined with rainy or damp conditions in the field, the process of germination is activated while the seeds are still attached to the mother plant, and the resulting emergence of the radicle from the seed coats is called preharvest sprouting (PHS). Depending on the intended purpose for the seeds after harvest, PHS can have serious negative consequences on their quality and this is economically penalized by the industry. Direct economic losses caused by PHS to producers occur in several ways: Desiccation of a sprouted grain leads to its subsequent loss of viability because, together with the activation of metabolism implicated in embryo growth, tolerance to dehydration is lost rendering the sprouted grains useless for sowing or malting. Sprouting also promotes carbohydrate respiration that not only reduces grain yield, but also creates a favorable environment for the attack of saprophytic fungi and bacteria that produce toxins.

Depending on the level of dormancy and environmental cues such as water availability for imbibition and temperature, the germination process can advance to different extents, and not always reaches completion of germination and sprouting (i.e., germination is complete when embryo growth begins, and post-germinative growth leads to visible radicle and/or coleoptile emergence through the seed-covering structures). Even when desiccation occurs before germination is complete, starch degradation may have advanced partially. This phenomenon is known as pregermination. Pregerminated grains cannot be distinguished visually, but the level of starch degradation is correlated with a decrease in FN values [36] and a reduction in seed lot longevity [44]. Industrial processes based on wheat and barley (flour and malting) are particularly sensitive to sprouting and pregermination. Seed lots are commonly assessed with the falling number (FN) test, with smaller FN values indicating a greater degree of starch degradation. Wheat and barley seed lots can be penalized or even rejected if FN values show moderate incidence of pregermination and sprouting.

The phenomena of PHS and pregermination are closely related with the process of domestication. Cereal crops have a brief period of dormancy as compared to their wild ancestors. Throughout many years, farmers have pressed toward selection of low levels of dormancy along with other traits such as non-shattering, increased grain size, and less pigmentation. The occurrence of PHS depends not only on morphological and physiological traits genetically controlled (such as infructescence structure and permeability of structures surrounding the seeds, and seed dormancy) but also on environmental factors (water availability and temperature). A single genotype may express PHS when grown in some areas but not in others. Seed dormancy is the main heritable factor that contributes to PHS resistance, but the many attempts to control it through breeding programs have shown that dormancy is tightly linked to other interesting traits. Breeding programs that attempted to separate characters associated with seed color, dormancy, and longevity suggest that these characteristics may not always be separable and are referred to as domestication block [45]. For example, in rice, both loci sh-h (for shattering) and Rc (conferring red pericarp) are tightly linked together with a QTL qSDs-7-1 for seed dormancy, implying that this region might represent a domestication block in the evolutionary pathway of rice [46]. A mutation in the *R*-gene in white wheat is required for low tannin content (higher flour quality) but is also responsible for lower levels of dormancy (low PHS resistance).

However, grain dormancy is a complex trait that relies on numerous genes, and other QTLs contributing to dormancy that are not linked to seed color have been identified and are being considered in breeding for PHS tolerance in white wheat [47].

In addition to classical breeding techniques, elucidation of the mechanisms involved in the control of dormancy may open other possibilities for manipulation of dormancy through genetic engineering techniques. Cereal species like barley and sorghum have served as model systems to study the mechanisms behind dormancy with the objective to understand the hormonal metabolic and signaling steps involved in the repression of germination (*Barley*: 31, 30, 34, 48; *Sorghum*: 37, 38, 39).

Dormancy in Natural Seed Banks and Its Implications in Weed Control

Dormancy is a common attribute of many weed species, and is probably the most important of a series of processes that determine the seasonal annual pattern of weed emergence from soil seed banks under field conditions [49, 50]. Although there are many environmental factors that can be affecting the dormancy status of seeds composing the soil bank (i.e., alternating temperature, soil water status, light, etc.), seasonal dormancy changes are mainly regulated by soil temperature [4, 51]. For example, in summer annual species, dormancy relief is produced by the low temperatures experienced during winter, while high temperatures enhance their dormancy level during summer. Most winter annual species show the reverse dormancy pattern. Hence, high temperatures during summer produce dormancy relief, while low temperatures during winter induce secondary dormancy. Although much experimental data support the main role of soil temperature as regulator of seed dormancy, there is evidence indicating that the effect of temperature on dormancy may be modulated by soil moisture conditions [16, 52].

Changes in dormancy status of weed seed populations are associated with changes in the range of temperatures and water potentials permissive for seed germination [15]. As dormancy is relieved, the range of temperatures and water potentials permissive for germination widens until it is maximal; on the contrary, as dormancy is induced, the range of temperatures and water potentials over which germination can proceed narrows until germination is no longer possible at any temperature or water potential. Germination in the field is therefore restricted to the period when the field temperature and soil water potential, and the temperature and water potential range over which germination can proceed, overlap [14, 53].

However, in many weed species, once environmental temperature and water potential are within the permissive range, dormancy must be terminated by the effect of additional environmental factors for germination to proceed. In these cases, changes in the degree of dormancy not only comprise changes in temperature and water potential requirements for germination, but also in the sensitivity of the seed population to the effect of those dormancy terminating factors [51]. Fluctuating temperatures and light are two critical environmental factors that can trigger dormancy termination in seeds of many weed species. An ecological interpretation of this requirement to complete exit from dormancy has been related to the possibility of detecting canopy gaps as well as depth of burial under field situations [51, 54, 55].

Agronomic practices can alter the physical environment to which weed seed banks are exposed, and thus, their dormancy status. Knowledge about the ways in which agronomic practices affect the dormancy status of weed seeds could be used to develop and improve weed management strategies [56, 57]. For example, many weed seeds require light to terminate dormancy and give way to the germination process; consequently, the light environment could be managed in order to impede seed germination. Light signals are perceived by seeds through the phytochrome system. Generally, low red/far-red wavelengths ratios inhibit seed germination, while high red/far-red ratios promote seed germination. Light filtered by green leaves are rich in far-red wavelengths and explains the low red/far-red ratios measured under plant canopies [58]. Therefore, plant cover could be managed to reduce some weed problems. For example, changing plant architecture, crop-sowing densities, and crop plant spacing may have a high potential for improving weed management by preventing the exit of weed seeds from dormancy and reducing germination under field situations [59].

The brief light pulse received during soil cultivation can promote seed germination of buried weed seeds. Many weed seeds buried in the soil acquire an extremely high light sensitivity that permits them to detect sub-milliseconds of sunlight when the soil is disturbed. This is reflected in the high weed emergence rates usually observed following tillage operations, and suggests that germination of light-requiring seeds would be impeded if a non-tillage crop production system is implemented or if cultivation is performed at night [60]. Indeed, Scopel et al. [61] observed a significant reduction in weed emergence (between 70% and 400%) when plots were cultivated at night in comparison to emergence levels obtained under daytime cultivation.

Other environmental factor that usually terminates dormancy in many weed seeds under field conditions is temperature fluctuation. Generally, large temperature fluctuation regimes determine dormancy breakage of a higher proportion of the seed bank population than that observed under small temperature fluctuation regimes. Thus, changing the amplitude of temperature fluctuation regimes in the field environment through management of plant cover or crop residues would lead to a reduction in weed emergence [57, 59]. This is the case of Johnson grass (*Sorghum halepense*), in which seeds do not germinate if they are under a dense plant cover due to the lack of temperature fluctuations stimuli required to terminate seed dormancy [54].

Weed emergence models that predict the proportion and timing of seed bank emergence would be useful tools for determining the most suitable time for seedling control and, consequently, should result in a higher efficacy of controls methods. In the last decade, many models able to predict seed dormancy changes in relation to environmental factors for different weed species have been developed [14, 15]. For example, Batlla et al. [62] and Batlla and Benech-Arnold [63] developed models to account for the effect of fluctuating temperatures and light on *Polygonum aviculare* (a worldwide distributed spring emerging weed) seed dormancy level based on a stratification thermal time index (S_{tt}). This index allow the prediction of changes in seeds sensitivity to increasing doses of cycles of fluctuating temperatures or different light treatments for seeds stratified at different temperatures in relation to the accumulation of degree days units below a ceiling temperature of 17° C. Using these models, for example, the progressive increase in *P. aviculare* seed bank sensitivity to light during winter and early spring can be predicted based on soil temperature records (Fig. 2). Due to the fact that, for example, the acquisition of a very low fluence response (VLFR) phytochrome action mode would permit buried seeds to germinate in response to the light flash perceived during soil disturbance [64], this model could be used to predict the proportion of the seed bank that will germinate in response to tillage operations after the accumulation of a certain amount of S_{tt} during winter burial [63].

Another example of how knowledge in relation to regulation of seed bank dormancy by environmental factors could be used to forecast weed emergence is the WeedCast model developed by Forcella [65] at the US Department of Agriculture. This model can be used to predict the "emergence potential" of several summer annual weeds. In the model, the "emergence potential" indicates which fraction of the weed seed bank would be nondormant and available for germination at a given time during the season. The possibility of predicting the "emergence potential" of the different

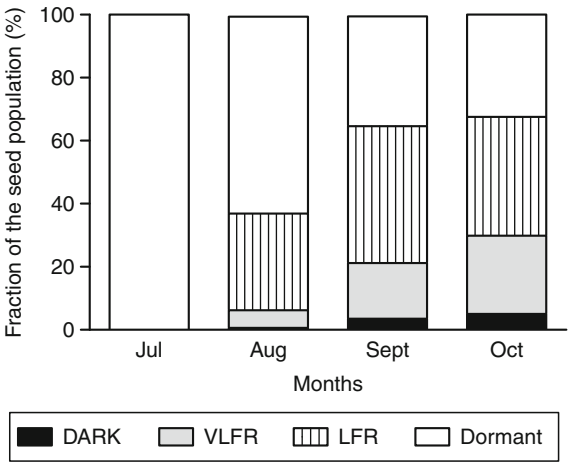

Seed Dormancy and Agriculture, Physiology. Figure 2 Simulated proportions of a *Polygonum aviculare* seed bank showing different action modes of phytochrome (low fluence response [*LFR*] and very low fluence response [*VLF*]), seeds not requiring light for germination (darkness) and the non-germinating fraction (dormant) at the beginning of different months. Simulations were done using year 2000 soil temperature and equations published in [63] (Redrawn from [14])

weed species allows farmers to make more rationale decisions regarding the degree and type of weed management required [65].

With increased pressure to reduce pesticide inputs in agricultural systems, optimal timing and rates of chemical products as well as finding sustainable nonchemical options for weed control will be of paramount importance. A better understanding of how environmental factors and agronomic practices affect the dormancy status of weed seed banks could be used to develop and improve weed control strategies in order to meet this challenge.

Future Directions

Seed dormancy has enormous implications in agriculture. Its importance is related both to its persistence and to its lack. Dormancy persistence affects crop establishment as well as grain industrialization whenever this process requires seed germination (i.e., malting), but also the design of weed management practices. The lack of dormancy can lead to untimely germination in the mother plant (i.e., preharvest sprouting) with severe consequences to grain quality. The possibility of assessing the very many aspects of the agricultural activity that could be interfered by the presence or absence of dormancy requires a thorough knowledge of the phenomenon, not only at a fundamental level (i.e., physiological and/or molecular) but also in terms of its control by environmental factors. In this entry, the attempt was to illustrate with examples the way in which these different aspects can be assessed. Only a detailed knowledge of how the dormancy mechanisms are controlled at a physiological, molecular, and environmental level would eventually lead to attain our ultimate aim: to adjust the timing of dormancy release to our convenience from an agricultural point of view.

Bibliography

1. Baskin CC, Baskin JM (1998) Seeds: ecology biogeography and evolution of dormancy and germination. Academic, San Diego
2. Nikolaeva MG (1967) Physiology of deep dormancy in seeds. Leningrad, Russia: Izdatel'stvo 'Nauka' (in Russian). [Trans from Shapiro Z (1969), National Science Foundation, Washington, DC, p 219]
3. Baskin JM, Baskin CC (2004) A classification system for dormancy. Seed Sci Res 14:1–16
4. Finch-Savage WE, Leubner-Metzger G (2006) Seed dormancy and the control of germination. New Phytol 171:501–523
5. Hilhorst HWM (1995) A critical update on seed dormancy. I. Primary dormancy. Seed Sci Res 5:61–73
6. Benech-Arnold RL (2004) Inception, maintenance and termination of dormancy in grain crops. Physiology, genetics and environmental control. In: Benech-Arnold R, Sánchez RA (eds) Handbook of seed physiology: applications to agriculture. Food Product Press, New York, pp 169–198
7. Walker-Simmons MK, Sesing J (1990) Temperature effects on embryonic abscisic acid levels during development of wheat grain dormancy. J Plant Growth Regul 9:51–56
8. Fenner M (1991) The effects of the parent environment on seed germinability. Seed Sci Res 1:75–84
9. Benech-Arnold RL, Fenner M, Edwards PJ (1991) Changes in germinability, ABA levels and ABA embryonic sensitivity in developing seeds of *Sorghum bicolor* induced by water stress during grain filling. New Phytol 118:339–347
10. Benech-Arnold RL, Fenner M, Edwards PJ (1995) Influence of potassium nutrition on germinability, ABA content and embryonic sensitivity to ABA of developing seeds of *Sorghum bicolor* (L.) Moench. New Phytol 130:207–216
11. Gate P (1995) Ecophysiologie de la germination sur pied. Perspect Agri 204:22–29
12. Fenner M, Thompson K (2005) The ecology of seeds. Cambridge University Press, Cambridge, pp 250
13. Allen PS, Benech-Arnold RL, Batlla D, Bradford KJ (2007) Modeling of seed dormancy. In: Bradford K, Nonogaki H (eds) Seed development, dormancy and germination, vol 27. Blackwell, Oxford, pp 72–112
14. Batlla D, Benech-Arnold RL (2007) Predicting changes in dormancy level in weed seed soil banks: implications for weed management. Crop Prot 26:189–197
15. Batlla D, Benech-Arnold RL (2010) Predicting changes in dormancy level in natural seed soil banks. Plant Mol Biol 73:3–13
16. Batlla D, Benech-Arnold RL (2006) The role of fluctuations in soil water content on the regulation of dormancy changes in buried seeds of *Polygonum aviculare* L. Seed Sci Res 16:47–59
17. Corbineau F, Bagniol S, Côme D (1990) Sunflower (*Helianthus annuus* L.) seed dormancy and its regulation by ethylene. Israel J Bot 39:313–325
18. Corbineau F, Côme D (1987) Regulation de las semences de tournesol par l'éthylene. In: Annales ANPP (ed) 2ème Colloque sur les substances de croissance et leurs utilisations en agriculture, vol 1. Association Nationale de Protection des Plantes, Paris, pp 271–282
19. Cseresnyes Z (1979) Studies on the duration of dormancy and methods of determining the germination of dormant seeds of *Helianthus annuus*. Seed Sci Technol 7:179–188
20. Corbineau F (1987) La germination des semences de tournesol et sa regulation par l´éthylene. CR Acad Sci Agr Fr 266:477–479
21. Le Page-Degivry MT, Barthe P, Garello G (1990) Involvement of endogenous abscisic acid in onset and release of *Helianthus annuus* embryo dormancy. Plant Physiol 92:1164–1168
22. Le Page-Degivry MT, Garello G (1992) In situ abscisic acid synthesis. A requirement for induction of embryo dormancy in *Helianthus annuus*. Plant Physiol 98:1386–1390

23. Oracz K, El-Maarouf BH, Farrant JM, Cooper K, Belghazi M, Job C, Job D, Corbineau F, Bailly C (2007) ROS production and protein oxidation as a novel mechanism of seed dormancy alleviation. Plant J 50:452–465
24. Abeles FB (1986) Role of ethylene in *Lactuca sativa* cv. Grand Rapids seed germination. Plant Physiol 81:780–787
25. Ketring DL (1977) Ethylene and seed germination. In: Khan AA (ed) The physiology and biochemistry of seed dormancy and germination. Elsevier/North Holland Biomedical Press, Amsterdam, pp 157–178
26. Srivastava AK, Dey SC (1982) Physiology of seed dormancy in sunflower. Acta Agron Hung 31:70–80
27. Bagniol S (1987) Mise en évidence de l´intervention de l'ethylene dans la germination et la dormance des semences de tournesol (*Helianthus annuus* L.). Diplôme d'Ëtudes Approfondies, Université Pierre et Marie Curie, Paris
28. Seiler GJ (1998) Seed maturity, storage time and temperature, and media treatment effects on germination of two wild sunflowers. Agron J 90:221–226
29. Oracz K, El Maarouf-Bouteau H, Bogatek R, Corbineau F, Bailly C (2008) Release of sunflower seed dormancy by cyanide: crosstalk with ethylene signaling pathway. J Exp Bot 59:2241–2251
30. Benech-Arnold RL, Giallorenzi MC, Frank J, Rodriguez V (1999) Termination of hull-imposed dormancy in barley is correlated with changes in embryonic ABA content and sensitivity. Seed Sci Res 9:39–47
31. Lenoir C, Corbineau F, Come D (1986) Barley (*Hordeum vulgare*) seed dormancy as related to glumella characteristics. Physiol Plant 68:301–307
32. Corbineau F, Poljakoff-Mayber A, Côme D (1991) Responsiveness to abscisic acid of embryos of dormant oat (*Avena sativa*) seeds. Involvement of ABA-inducible proteins. Physiol Plant 83:1–6
33. Wang M, van der Meulen RM, Visser K, Van Schaik H-P, Van Duijn B, de Boer AH (1998) Effects of dormancy-breaking chemicals on ABA levels in barley grain embryos. Seed Sci Res 8:129–137
34. Benech-Arnold RL, Gualano NA, Leymarie J, Come D, Corbineau F (2006) Hypoxia interferes with ABA metabolism and increases ABA sensitivity in embryos of dormant barley grains. J Exp Bot 57:1423–1430
35. Mendiondo GM, Leymarie J, Farrant J, Corbineau F, Benech-Arnold RL (2010) Differential expression of abscisic acid metabolism and signaling genes induced by seed covering structures or hypoxia in barley (*Hordeum vulgare* L.) grains. Seed Sci Res 20:69–77
36. Biddulph TB, Plummer JA, Setter TL, Mares DJ (2008) Seasonal conditions influence dormancy and preharvest sprouting tolerance of wheat (*Triticum aestivum* L.) in the field. Field Crop Res 107:116–128
37. Steinbach HS, Benech-Arnold RL, Kristof G, Sánchez RA, Marcucci-Poltri S (1995) Physiological basis of pre-harvest sprouting resistance in *Sorghum bicolor* (L.) Moench. ABA levels and sensitivity in developing embryos of sprouting-resistant and sprouting-susceptible varieties. J Exp Bot 46:701–709
38. Steinbach HS, Benech-Arnold RL, Sánchez RA (1997) Hormonal regulation of dormancy in developing sorghum seeds. Plant Physiol 113:149–154
39. Rodríguez MV, Mendiondo GM, Maskin L, Gudesblat GE, Iusem ND, Benech-Arnold RL (2009) Expression of ABA signalling genes and ABI5 protein levels in imbibed *Sorghum bicolor* caryopses with contrasting dormancy and at different developmental stages. Ann Bot 104:975–985
40. Gao FY, Ren GJ, Lu XJ, Sun SX, Li HJ, Gao YM, Luo H, Yan WG, Zhang YZ (2008) QTL analysis for resistance to preharvest sprouting in rice (*Oryza sativa*). Plant Breed 127:268–273
41. Kumar A, Kumar J, Singh E, Garg T, Chhuneja P, Balyan HS, Gupta PK (2009) QTL analysis for grain colour and pre-harvest sprouting in bread wheat. Plant Sci 177:114–122
42. Lohwasser U, Roder MS, Borner A (2005) QTL mapping of the domestication traits pre-harvest sprouting and dormancy in wheat (*Triticum aestivum* L.). Euphytica 143:247–249
43. Zanetti S, Winzeler M, Keller M, Keller B, Messmer M (2000) Genetic analysis of pre-harvest sprouting resistance in a wheat x spelt cross. Crop Sci 40:1406–1417
44. Del Fueyo P, Sánchez RA, Benech-Arnold RL (2003) Seed longevity in two sorghum varieties with contrasting dormancy level prior to harvest. Seed Sci Technol 31:639–650
45. Finkelstein RR, Reeves W, Ariizumi T, Steber C (2008) Molecular aspects of seed dormancy. Annu Rev Plant Biol 59:387–415
46. Ji HS, Chu SH, Jiang W, Cho YI, Hahn JH, Eun MY, McCouch SR, Koh HJ (2006) Characterization and mapping of a shattering mutant in rice that corresponds to a block of domestication genes. Genetics 173:995–1005
47. Mares DJ, Mrva K, Cheong J et al (2005) A QTL located on chromosome 4A associated with dormancy in white- and red-grained wheats of diverse origin. Theor Appl Genet 111:1357–1364
48. Barrero JM, Talbot MJ, White RG, Jacobsen JV, Gubler F (2009) Anatomical and transcriptomic studies of the coleorhiza reveal the importance of this tissue in regulating dormancy in barley. Plant Physiol 150:1006–1021
49. Buhler DD, Hartzler RG, Forcella F (1997) Implications of weed seedbank dynamics to weed management. Weed Sci 45:329–336
50. Forcella F, Benech-Arnold RL, Sánchez RA, Ghersa CM (2000) Modelling seedling emergence. Field Crop Res 67:123–139
51. Benech-Arnold RL, Sánchez RA, Forcella F, Kruk BC, Ghersa CM (2000) Environmental control of dormancy in weed seed banks in soil. Field Crop Res 67:105–122
52. Bair NB, Meyer SE, Allen PS (2006) A hydrothermal after-ripening time model for seed dormancy loss in *Bromus tectorum* L. Seed Sci Res 16:17–28
53. Karssen CM (1982) Seasonal patterns of dormancy in weed seeds. In: Khan AA (ed) The physiology and biochemistry of seed development, dormancy and germination. Elsevier, Amsterdam, pp 243–270

54. Benech-Arnold R, Ghersa C, Sánchez R, García Fernandez A (1988) The role of fluctuating temperatures in the germination and establishment of *Sorghum halepense* (L.) Pers. Regulation of germination under leaf canopies. Funct Ecol 2:311–318
55. Ghersa CM, Benech-Arnold RL, Martinez Ghersa MA (1992) The role of fluctuating temperatures in germination and establishment of *Sorghum halepense* (L.) Pers. II. Regulation of germination at increasing depths. Funct Ecol 6:460–468
56. Dyer WE (1995) Exploiting weed seed dormancy and germination requirements through agronomic practices. Weed Sci 43:498–503
57. Ghersa CM, Martinez-Ghersa MA, Benech-Arnold RL (1997) The use of seed dormancy to improve grain production. J Prod Agric 10:111–117
58. Smith H (1982) Light quality, photoperception, and plant strategy. Annu Rev Plant Phys 33:481–518
59. Kruk B, Insausti P, Razul A, Benech-Arnold RL (2006) Light and thermal environments as modified by a wheat crop: effects on weed seed germination. J Appl Ecol 43:227–236
60. Juroszek P, Gerhards R (2004) Photocontrol of weeds. J Agron Crop Sci 190:402–415
61. Scopel AL, Ballaré CL, Sánchez RA (1991) Induction of extreme light sensitivity in buried weed seeds and its role in the perception of soil cultivations. Plant Cell Environ 14:501–508
62. Batlla D, Verges V, Benech-Arnold RL (2003) A quantitative analysis of seed responses to cycle-doses of fluctuating temperatures in relation to dormancy level. Development of a thermal-time model for *Polygonum aviculare* L. seeds. Seed Sci Res 13:197–207
63. Batlla D, Benech-Arnold RL (2005) Changes in the light sensitivity of buried *Polygonum aviculare* seeds in relation to cold-induced dormancy loss: development of a predictive model. New Phytol 165:445–452
64. Casal JJ, Sánchez RA (1998) Phytochromes and seed germination. Seed Sci Res 8:317–329
65. Forcella F (1998) Real-time assessment of seed dormancy and seedling growth for weed management. Seed Sci Res 8:201–209

Sentinel Species in Oceans and Human Health

Lori H. Schwacke[1], Frances M. Gulland[2], Susan White[1]
[1]NOAA Center for Excellence in Oceans and Human Health, National Oceanic and Atmospheric Administration's Hollings Marine Laboratory, Charleston, SC, USA
[2]The Marine Mammal Center, Sausalito, CA, USA

Article Outline

Glossary
Definition of the Subject and Its Importance
Introduction
Desirable Characteristics for Marine Sentinels
Sentinel Applications for Monitoring Exposure
Sentinels for Establishing Pathogenicity and Elucidating Mechanisms for Toxicity
Sentinel Habitats
Future Directions
Bibliography

Glossary

Bioaccumulation The accumulation of a substance in an organism. Bioaccumulation occurs when a substance is absorbed by an organism at a more rapid rate than it is metabolized and/or excreted by the organism.

Bioavailable Being in a state that can be readily absorbed by an animal.

Biomagnification The increase in concentration of a chemical or toxin that occurs as it is passed up the food chain.

Confounding factor A factor that correlates with both the exposure and response (i.e., independent and dependent variables in statistical terminology) so that it masks an actual association or falsely indicates an apparent association.

Epidemiology The study of the distribution and determinants of health-related states in populations.

Exposure Disease-causing factors, including infectious, toxic, nutritional, traumatic, genetic, degenerative, physiological, social, and behavioral.

HAB Harmful algal bloom, a proliferation or aggregation of algae forming dense patches which are harmful to the environment, plants, or animals. The harmful algae may produce hazardous toxins or may harm other marine organisms by depleting oxygen and blocking sunlight.

Hazardous agent Any chemical contaminant, biological toxin, or pathogen which presents a threat to human or animal health.

PAH Polycyclic aromatic hydrocarbon, a class of environmental pollutants that occur in oil and coal and are produced as byproducts of fuel burning. The toxicity of PAHs depends on the structure of the specific compound but many are carcinogens and/or have been linked to congenital defects.

Pathogenicity The ability of an agent to cause disease.

PCBs Polychlorinated biphenyls, a class of persistent chemicals with a broad range of toxic effects. PCBs were widely used in industrial applications until the late 1970s when their manufacture was banned in the USA.

POPs Persistent organic pollutants, organic compounds that persist in the environment because they are resistant to degradation and tend to bioaccumulate in animal tissues.

Zoonotic pathogen A pathogen that can be transmitted between animals and humans.

Definition of the Subject and Its Importance

A sentinel marine species is one which can provide early warning of existing or emerging health hazards from the ocean environment. Sentinel species are generally considered in two categories: (1) those which are sensitive indicators of a chemical contaminant, biological toxin, or pathogen due to their ability to concentrate or integrate exposures within a food web or ecosystem, and (2) marine organisms with physiology and/or diet similar enough to humans such that they may provide early indication of potential adverse health effects and provide insight into toxic mechanisms of a given hazardous agent.

The sentinel concept has been extended to include marine habitats as well as species. Sentinel habitats generally encompass key ecosystem components (such as nursery grounds) and are particularly sensitive to exposure to a given hazardous agent or to other environmental perturbations which may increase or alter the distribution of a hazardous agent, thereby increasing the likelihood for human exposure.

Introduction

- "The concept of the combined health of people and wildlife – one health – when combined with the concept of the ocean as an essential modulator/caregiver of all life on Earth, inexorably leads to the prime tenet that the health of the "one ocean" is essential to the "one health" of all life on earth, including that of humans." NOAA Science Advisory Board Report (2010).

Few would argue the close connections among human health, animal health, and the health of the ecosystems of which they are a part. Recognizing these linkages, there has been a growing movement to expand collaborations among the medical community, veterinary and wildlife researchers, and environmental scientists to improve the understanding of how the environment, and changes in the environment, can affect human health. This holistic approach may be even more apropos when applied to the world's ocean, which is so critical for the elements and processes that sustain life on Earth. Oceans cover more than 70% of the Earth's surface, play an essential role in climate, support the life of nearly half the world's species, and provide a large portion of the protein necessary to support the Earth's human population. The recognition of the ocean's importance and the inextricable linkages between the health of people and the health of animals and ecosystems has led to the "One Ocean-One Health" research paradigm.

A natural component of the "One Ocean-One Health" paradigm is the use of marine animals as sentinels of potential emerging hazards. A sentinel by definition is one who is assigned to warn of danger, and the concept of using animals as sentinels to warn of environmental health hazards has long been recognized. As early as the 1960s, studies of Baltic fish and birds warned of the presence of polychlorinated biphenyls (PCBs) in the marine food chain [1], and in 1971, California sea lions alerted the scientific community to extraordinarily high levels of DDT off the coast of California and Baja California, Mexico [2]. A committee organized by the National Research Council described how animal sentinel systems, i.e., "systems in which data on animals exposed to contaminants in the environment are regularly and systematically collected and analyzed" could be used for identifying potential health hazards to other animals or humans [3]. Since that time, the use of sentinel animals has been promoted [4] and debated in the literature [5, 6] but has primarily been viewed in the context of chemical contaminant risk assessment.

Under the NOAA's Oceans and Human Health Initiative, the idea of using animal sentinels has been expanded to a more broad application to include marine toxins, particularly those associated with harmful algal blooms (HABs). HABs appear to be increasing in frequency and expanding in geographic distribution [7], heightening concerns for the human health

impacts of HAB toxins which may include neurological, respiratory, or digestive distress or even death. While technology is advancing for the detection and prediction of HAB events, the degree to which a harmful algal bloom may represent a hazard for human health will depend not only on the occurrence of the bloom itself but also upon the physical processes and food web dynamics that drive the transport and persistence of the toxin, as well as the availability of potential vectors for human exposure. Monitoring of appropriate sentinels may assist not only in detecting the presence of hazardous toxins but also in elucidating the complex processes which drive toxin availability and the mechanisms by which the toxins exert their harmful effects. In fact, it has often been an increase in mortality or morbidity of marine wildlife that has signaled that a HAB toxin hazard is present [8, 9].

Sentinel marine species can also provide an early warning of threats from disease-causing pathogens which can affect seafood consumers, as well as for people who swim or recreate at beaches or in other coastal waters. Concern for infectious pathogens from the marine environment is perhaps greatest for food- or water-borne pathogens [10], and recurring human outbreaks of bacterial food poisoning resulting from contamination of shellfish with fecal microorganisms provide clear evidence that pathogens in marine ecosystems can impact human health [11]. However, nonfood marine wildlife may also act as an indicator or even reservoirs for zoonotic pathogens [12]. Some of these zoonotic pathogens may occur naturally in the marine environment, but others are being pumped into coastal waters through sewage or stormwater runoff. The potential for "spillover" across the marine animal–human interface increases as coastal development expands and a growing human population moves to our coast.

Regardless of the agent, whether chemical or biological, marine sentinels can signal presence in the environment and help differentiate between strict presence versus a presence in which humans are likely to be exposed. Additionally, a sentinel can provide indication of potential harmful effects, and if physiologically similar enough to humans, can offer insight into mechanisms of toxicity. The chapter starts by outlining the criteria that determine a good sentinel. The application of sentinels for surveillance or monitoring for potential exposures is discussed next; applications for chemical contaminants, marine toxins, and pathogens are discussed. The alternative use of sentinels for elucidating pathogenicity and to understand toxic pathways and modes of action is then presented. Finally, the concept of how a sentinel can be expanded to include sentinel habitats which can provide an early warning of ecosystem or community level effects that may increase or alter the distribution of hazardous agents, increasing the likelihood for human exposure, are discussed.

Desirable Characteristics for Marine Sentinels

In the ocean environment, sentinels to provide early warning of hazards may be even more critical in that many of the processes that drive the emergence of a hazard are complex and difficult to observe. Marine animals, which inhabit ocean waters 24/7 and/or consume a 100% seafood diet, receive the most intense and sustained exposures when ocean hazards are present. However, sentinel species and populations should be chosen carefully to ensure sensitivity to the exposure or associated health effect, as well as to ensure that the interpretation of data is meaningful and unambiguous. While the selection of an appropriate sentinel species will depend on the agent of concern and the desired region for surveillance, in general, the appropriateness of a given species as a sentinel can be judged based on the following criteria:

1. *Ease of sampling.* Tissue samples can be obtained with minimal effort and individuals can be randomly sampled from the population.
2. *Appropriate distribution.* The species should have a broad distribution to allow for analysis of geographic trends, or for localized studies have a distribution that overlaps with the agent of concern. The appropriate distribution will depend upon the agent of concern and the specific purpose of monitoring.
3. *Sensitivity for bioaccumulation and/or biomagnification.* The species should be particularly sensitive to accumulation of the agent in tissues or be sufficiently high on the food chain to be susceptible to biomagnification.
4. *Similar trophic position as humans or as a food animal.* Animals at a similar trophic position as humans and which have prey similar to those consumed by humans can provide an integrated index for potential exposures. Alternatively, animals

consumed by humans provide a direct indication of potential dose.

5. *Indicator on appropriate spatial scale.* Some species will be better indicators of the immediate local environment while others may integrate across a geographic region. The sentinel should be chosen based on its ability to represent the appropriate spatial scale.
6. *Existing infrastructure and protocols for consistent collection, analysis, and data archiving.* Consistent sample collection and processing will ensure spatial and temporal comparability and is essential for long-term surveillance.

Meeting as many of these criteria as possible will aid in the design of statistically robust studies, facilitate the interpretation of results, and provide the best opportunity to obtain information relevant for human health. However, meeting all criteria is generally not possible, and certainly, the importance of meeting a given criterion must be weighed against the other benefits that a species may offer. For example, marine mammals are commonly selected sentinels despite the logistical difficulties in sampling (Table 1) and the legal and ethical constraints against experimental study and lethal sampling. However, physiological similarities to humans and high trophic position with diets that include many of the same types of seafood consumed by humans provide unique benefits that have prompted the inclusion of many marine mammal species as key elements of marine sentinel research. Due to the protected status of marine mammals in the USA [13], researchers rely heavily on epidemiological approaches for studying associations between exposures and disease, similar to approaches applied for human populations. In this case, it is often beneficial to supplement the research with experimental studies of other species (e.g., invertebrates, fish, rodents) to provide additional weight of evidence for establishing cause–effect relationships.

In addition to the above criteria for species selection, it is important to have existing infrastructure and protocols in place for consistent collection, analysis, and data archiving. This is imperative for consistent sample collection and processing which will ensure spatial and temporal comparability necessary for long-term surveillance.

Sentinel Applications for Monitoring Exposure

Chemical Contaminants

Traditionally, the use of sentinels has focused on chemical contaminants, and monitoring of sentinel animals as indicators of potential exposure offers several advantages over direct measurement in water, sediment, or other substrate. A primary advantage is that a measurement in a marine animal implies that the agent is bioavailable; that is, it is in a state that can be readily absorbed by an animal and, thus, is more likely to represent a human hazard.

Sentinels also may provide greater sensitivity for detection of an agent. For example, bivalves such as mussels and oysters filter and accumulate particles to concentrations much higher than in the ambient water and with little metabolic transformation, making them suitable sentinels for many chemical contaminants. Bivalves are sessile organisms and have been shown to be responsive to changes in ambient environmental levels of contaminants, making them particularly good indicators for local contamination [14]. In the USA, the Mussel Watch Program, sponsored by NOAA since 1986, monitors an array of legacy and emerging chemical contaminants in bivalves across the US coast [15]. No single species is common across all coastal regions, so the program samples a variety of bivalves: mussels (*Mytilus* spp.) from the North Atlantic and Pacific coasts, oysters (*Crassostrea virginica*) from the mid-Atlantic southward and in the Gulf of Mexico, and zebra mussels (*Dreissena* spp.) in the Great Lakes in order to provide a national perspective on chemical contaminant status and trends in estuarine and coastal waters.

Higher level marine predators may offer the greatest sensitivity for detection of lipophilic compounds such as polychlorinated biphenyls (PCBs), organochlorine pesticides, and polybrominated flame retardants. These persistent organic pollutants (POPs) accumulate in an animal's fatty tissues and biomagnify up the food chain. Upper trophic marine mammals, such as toothed whales, sea lions, some seal species, and polar bears are particularly susceptible to the biomagnification of POPs, often having tissue concentrations that are six to seven orders of magnitude higher than those found in water, sediments, or lower trophic biota. Some of the highest concentrations of polybrominated

Sentinel Species in Oceans and Human Health. Table 1 Examples of key sentinel species used in Oceans and Human Health Research and advantages and disadvantages of their use

Family/ Species	General		Chemical contaminants		Biological toxins		Zoonotic pathogens	
	Advantages	Disadvantages	Advantages	Disadvantages	Advantages	Disadvantages	Advantages	Disadvantages
Tursiops truncatus	Mammal; physiologically similar to humans so appropriate for examining pathogenicity	Ethical considerations of sampling; protected species under Marine Mammal Protection Act (MMPA); studies require permits	Integrator across food web	Some stocks may range across estuaries or even migrate across regions; requires understanding of stock structure	Integrator across food web	Difficult to obtain appropriate samples (e.g., urine, feces, stomach contents) from free-ranging animals	As a mammal, able to host many of the same pathogens as humans	Implications for human exposure potential not well understood
		Logistical considerations of sampling very large animals in water; adults generally range from 200 to 300 kg	Apex predator susceptible to biomagnification	Compounds may be preferentially metabolized, altering chemical profiles	Network in place for stranding response & mortality/ morbidity investigation in U.S.			
		Long lifespan and reproductive cycle makes longitudinal studies difficult	Samples can be obtained via remote biopsy	Females offload lipophilic contaminants to young; tissue contaminants not representative of cumulative exposure				
		Spend entire life in water making it difficult to observe endpoints such as birth and reproduction	Broad coastal and oceanic distribution with discrete spatial stock structure allows for geographic comparisons					

Zalophus californianus	Mammal; physiologically similar to humans so appropriate for examining pathogenicity	Ethical considerations of sampling; protected species under Marine Mammal Protection Act (MMPA); studies require permits	Distribution along U.S. Pacific coast		Distribution along U.S. Pacific coast and oceanic waters, overlapping with many algae of concern (e.g., *Pseudonitzchia* sp.)		As a mammal, able to host many of the same pathogens as humans	Implications for human exposure potential not well understood
	Periodically haul-out on shore, providing opportunity for sampling and census of births	Logistical considerations of sampling; age- and sex-classes are generally segregated	High trophic predator susceptible to biomagnificaiton	Compounds may be preferentially metabolized, altering chemical profiles	Integrator across food web			
				Females offload lipophilic contaminants to young; tissue contaminants not representative of cumulative exposure	Network in place for stranding response and mortality/ morbidity investigation in U.S.			
Bivalves	Ease of sampling; not covered by Animal Welfare Act; greater social acceptance of use		Sessile, so good indicator of local environment	May not detect compunds which are transported via pathways other than water/ sediments	Food source, so direct indication of potential dose for humans	Does not detect toxins that enter or persist in other parts of food web (e.g., through planktivorous or benthic fish)	Accumulates and concentrates many microbial pathogens	Not suitable host for many of human infectious pathogens

Sentinel Species in Oceans and Human Health. Table 1 (Continued)

Family/ Species	General		Chemical contaminants		Biological toxins		Zoonotic pathogens	
	Advantages	Disadvantages	Advantages	Disadvantages	Advantages	Disadvantages	Advantages	Disadvantages
	High fecundity allows experiments on reproductin in reasonable time scale		Compounds generally not metabolically altered		Accumulates and concentrations toxins		Food source, so direct indication of potential dose for humans via ingestion route	
	Coastal distribution appropriate for monitoring pollutants being input from terrestrial sources		Accumulates and concentrates many chemical contaminants					
Salmonids	Not covered by Animal Welfare Act; greater social acceptance of use; can be lethally sampled	Non-mammal, so less similarity to human physiology	Internal organs/ tissue (e.g., liver, bile) can be sampled to detect chemicals such as PAHs that do not persist in other tissues	Migrate during some life stages; requires an understanding of life history and range		Due to differences in physiology, mechanistic pathways may be dissimilar and many species are less sensitive to toxic effects		Not suitable host for many of human infectious pathogens
	Recreational and commercial fisheries offer opportunity to obtain samples		Food source, so direct indication of potential dose for humans if contaminants measured in edible tissue					
			High trophic position; susceptible to biomagnification					

flame retardants, an emerging contaminant class of concern, have been reported in killer whales (*Orcinus orca*) which feed on other marine mammals and occupy an apex position in the Pacific marine food chain [16, 17]. Bottlenose dolphins (*Tursiops truncatus*) provided the first warning that legacy PCBs from a point source on the U.S. Atlantic coast had entered the coastal food web and spread far beyond the previously established source footprint [18]. In this case, the geographic extent of the contamination had not been recognized from monitoring of sediments and bivalves [19] because the contaminants were not elevated in these localized, less-mobile components of the ecosystem. This illustrates the utility of top predators as sentinels, not only because of their sensitivity to biomagnification, but as an integrative indicator across the broader coastal food web.

Historically, marine mammals were not considered useful species for biomonitoring due to the difficulty in obtaining tissue samples. However, after several large-scale mortality events of marine mammals, concern from the scientific community and the public prompted the establishment of a biomonitoring program to collect data to help elucidate temporal and geographic trends [20]. The National Marine Mammal Tissue Bank (NMMTB) was formally established in 1992 under the Marine Mammal Health and Stranding Response Act (Public Law 102–587) as a collaboration between NOAA Fisheries and the National Institute of Standards and Technology (NIST). Similar to NIST's Environmental Specimen Bank Program which has banked samples from Mussel Watch Program, the NMMTB focused on standardized collection, banking, and analysis of marine mammal tissues. Initially, samples were collected opportunistically from stranded and bycaught marine mammals, or those taken as part of authorized subsistence hunts. The reliance on stranded animals and carcasses somewhat hindered the interpretation of chemical analyses, as these animals may not be representative of the general population. The cause of stranding is often disease, and a diseased marine mammal is likely to carry abnormal levels of chemical contaminants [21]. Improved remote sampling techniques, including systems which use a crossbow, rifle or polespear with a dart to collect skin and blubber, now allow sampling of tissues from live marine mammals and have been applied for a variety of both pinniped and cetacean species [16, 22, 23]. The remote techniques allow for more robust sampling design, allowing studies to obtain a random sample of the free-ranging population. Methods for capture–release studies of some free-ranging marine mammals have also matured, and these types of studies, which allow sampling and banking of multiple tissue types, are conducted quite frequently across much of the US coast (e.g., [24–26]). Improved sampling techniques and standardization of protocols across studies have allowed for the synthesis of data to obtain an understanding of chemical contaminant trends in one common marine mammal species, the bottlenose dolphin, across the US southeast coast (Kucklick et al., submitted). The bottlenose dolphin is broadly distributed, and estuarine stocks generally maintain limited movements within a given region; therefore, monitoring of this species can offer a national perspective on chemical contamination of coastal waters.

Harmful Algal Bloom (HAB) Toxins

Sentinel species can warn of potential for exposure to known hazardous chemical agents but also can warn of previously unrecognized emerging hazards from algal toxins. While forecast systems using satellite data have been developed to detect and track some HABs, the forecast systems do not necessarily detect toxins which persist after a bloom or which accumulate in fish or invertebrate tissues, allowing the toxin to be transported through the food web. Because shellfish can accumulate algal toxins and are also harvested for human consumption, levels of algal toxins in shellfish are regularly monitored by states. However, upper trophic marine animals can often provide a broader perspective for detection of toxins in the marine food web. As an example, California sea lions (*Zalophus californianus)* are high-level predators that range from Baja California in the south to British Columbia in the north, feeding on species that often enter the human seafood market, such as anchovies, sardines, hake, rockfish, salmon, and market squid. The detection of domoic acid, an algal toxin produced by the marine diatom *Pseudo-nitzschia* spp., in California sea lions dying off the California coast in 1998 [9] raised public awareness of the presence of this algal toxin in a variety of seafood species.

Similarly, bottlenose dolphins in the Northern Gulf of Mexico provided the first indication that brevetoxin, a potent neurotoxin produced by the "red tide" dinoflagellate *Karenia brevis*, can accumulate in fish and remain in the food web long after a bloom has dissipated. An unusual mortality event, in which at least 107 bottlenose dolphins died, occurred on the coast of the Florida Panhandle in 2004 [8]. Although extensive sampling of water found only low levels of *K. brevis*, stomach contents of the dolphin carcasses showed high levels of brevetoxin and recent ingestion of menhaden, a planktivorous fish. Prior to this event, the common assumption, based on fish kills which occur during red tides, was that even low concentrations of brevetoxin would be lethal to fish and the toxin would therefore not accumulate in their tissues. However, sampling of fish that followed the dolphin mortalities showed high levels of brevetoxin that remained for several weeks. The event prompted long-term fish sampling and feeding studies which determined that because brevetoxins are sequestered in fish food, the fish may remain healthy while the toxin concentrations increase in their tissue, including the edible muscle tissue [27]. Brevetoxin accumulated to the highest levels in the liver and stomach of the fish and did not reach dangerous levels in the edible tissues. However, the findings raise awareness of the potential for brevetoxin exposure through consumption of fish and provide a warning of associated toxic effects in mammals. A follow-up capture–release health assessment of dolphins in the same region led to the finding that another marine toxin, domoic acid, was also present [25]. The low levels of domoic acid detected in urine and feces of dolphins during two separate capture–release sampling events and during one of the previous unusual mortality events, combined with the fact that domoic acid is rapidly eliminated from the body [28, 29], suggest that exposure to the toxin for dolphins in this area may be chronic.

Zoonotic Pathogens

Coastal waters have been historically monitored for presence of fecal indicator bacteria and advances in molecular technologies now allow for direct detection of some pathogens from environmental samples. However, despite technological advances, the difficulty in concentrating cells in order to extract the appropriate molecular markers generally limits the sensitivity of assays using environmental samples [30]. In some cases, marine animals may be more sensitive indicators for potential pathogenic hazards as they concentrate microbial pathogens in their tissues and may even act as pathogen reservoirs. Specifically, bivalves have been shown to accumulate bacterial as well as protozoan pathogens [31, 32]. Furthermore, a broad survey of seabirds and marine mammals along the northeast US coast revealed a number of human pathogens, most considered typically terrestrial, including *Giardia* spp., *Cryptosporidium* spp., influenza A, and avian influenza H3N8 virus [12]. A range of bacteria were isolated in the same study, and over 70% of these showed some level of antibiotic resistance. Similar reports of typically terrestrial pathogens occurring in free-ranging marine mammals have come from the Pacific US coast [33]. Many of the bacteria in marine mammals demonstrate resistance to multiple antibiotics, suggesting that their introduction to marine systems may be through human sewage or agricultural runoff [34]. The associated risk for human health is yet to be determined, but the presence and prevalence of these resistant pathogens in the coastal waters is a growing concern [35].

In some cases, surveillance of pathogens in marine mammals has demonstrated apparent shifts in distribution, potentially signaling an ecological response to climate change. An infection of a harbor porpoise (*Phocoena phocoena*) with *Cryptoccocus gatti* was the first of a cluster of human and animal cases that occurred on southern Vancouver Island, British Columbia between 1999 and 2002 [36]. Prior to this event, *C. gatti* was not recognized as a variant associated with disease in North America and was considered a tropical or semitropical pathogen. The emergence into more northern latitudes was potentially encouraged by a complex interaction of climatic variation, host susceptibility, and a creation of an ecological niche for the fungal pathogen [37, 38]. The range of the fungi may still be expanding as the first case in Hawaiian waters was recently reported in a spinner dolphin (*Stenella longirostris*) [39].

Another fungi, *Lacazia loboi*, also associated with tropical and semitropical climates, has emerged into more northern latitudes of North America where it was also first detected through surveillance of marine

mammals. *L. loboi* infections have been reported in humans [40, 41] and multiple dolphin species [42, 43] and present as dermal and subcutaneous granulomas (wart-like lesions). While previously reported on the US coast in transitional tropical regions of the central Florida and Texas coasts [43, 44], a recent study reported the emergence as far north as the US mid-Atlantic coast [45].

Sentinels for Establishing Pathogenicity and Elucidating Mechanisms for Toxicity

Biological systems have the advantage that along with indicating potential for exposure, they can help to establish pathogenicity, provide insight into mechanisms of action, and contribute to the weight of evidence to establish causality of specific agents. In addition, the response of in situ sentinels to broad environmental changes provides insight to potential impacts on human populations. The mechanism of action of specific agents can be difficult to identify in natural systems due to the complex interactions among different exposures, as well as natural variability in response associated with different life history stages. Confirming that one specific factor is responsible for a physiological, anatomical, or health change in an animal or person can be difficult for logistical, ethical, or economical reasons. The careful selection of sentinel species can sometimes circumvent these constraints. Selection of a sentinel for understanding a mechanism of action of a hazard or establishing causality usually results in choice of an invertebrate or lower vertebrate such as a fish, so that lethal sampling and controlled exposures can be used. In contrast, use of sentinels to detect impacts of natural exposures, mixtures, and broad-scale ecological changes, such as those in response to changing ocean temperature or acidity, may focus on marine wildlife epidemiological studies. Below are examples of sentinel species that have increased the understanding of mode of action for chemical hazards, algal toxins, or pathogenic organisms.

Invertebrates

Invertebrates are useful sentinels for investigating the effects of pollutants and toxins on enzyme pathways, as these animals can be readily sampled and analyzed in laboratory situations. The phenomenon of "green oysters" was first documented in the late eighteenth century [46]; the intense green coloration was later demonstrated to be correlated with highly elevated copper concentrations [47]. Oysters and other bivalves detoxify accumulated copper and other metals by inducible metal-binding proteins (metallothioneins) and by sequestration in metal-rich granules, resulting in bioaccumulation [48]. Direct measurements of the effects of hazards on invertebrate enzyme pathways allow accumulation of evidence for harmful effects of an environmental hazard on animal systems that can contribute to risk assessments, despite the great difference between invertebrate and human physiology.

Amphibian, Fish, and Reptiles

Amphibians and reptiles are well-recognized sentinels of freshwater aquatic systems with the presence of developmental abnormalities in frogs and reproductive abnormalities in alligators associated epidemiologically with exposure to organochlorines and endocrine-disrupting chemicals in the environment [49]. Although their distribution is mostly limited to coastal and estuarine habitats, factors influencing health of freshwater systems, such as toxins like atrazine and PCBs, will ultimately make their way to marine waters.

Fish have become increasingly popular as sentinels of toxic effects as they contain most of the vertebrate genes of interest to human health but have fewer introns (sequences between genes) making sequencing studies more efficient. Although early studies using fish as sentinels focused on protein biomarkers of exposure, more recent studies have focused on alterations in genes that can be sequenced [50]. Fish are useful sentinels for estrogenic compounds in the environment, as the yolk protein precursor, vitellogenin (Vtg), is induced after exposure to estrogens and can be readily measured in individual fish [51]. Relationships have been demonstrated between Vtg or Vtg mRNA and skewed sex ratios, prevalence of intersexuality, and reduced fertilizing capacity of gametes, indicating that biochemical effects in an individual are likely to have population level impact on wildlife [52–54].

Evidence implicating environmental contaminants as causative agents of neoplasia in fish has accrued over the past five decades, with early reports focusing on

epidemiological associations between contaminants and high prevalence of neoplasia and later reports showing direct induction of neoplasia following exposure of fish to certain compounds. In the 1960s, high incidences of papillomas in white croakers (*Genyonemus lineatus*) and Dover sole (*Paropyrys vetulus)* were observed at several sites in Southern California, while hepatic neoplasms were observed in white suckers (*Catostomus commersoni*) in Maryland [55] [56]. Studies of English sole, Pacific tomcod (*Microgadus proximus*), and rock sole (*Lepidopsetta bilineata*) in the heavily industrialized Puget Sound (Washington state) showed a tumor incidence that appeared to correlate with PCB levels [57, 58]. There was also a correlation between sediment polycyclic aromatic hydrocarbon (PAH) concentrations or bile fluorescent aromatic hydrocarbon concentrations and hepatic lesions. Laboratory studies confirming these observations were conducted by injecting English sole with an extract from either the contaminated or reference sediment or the model hepatocarcinogen benzo [a]pyrene [59]. The results demonstrated that injections with benzo[a]pyrene or the contaminated sediment extract increased the incidence of hepatotoxic lesions and preneoplastic lesions. The investigators formulated a model to determine prevalence associated with species of fish, type of exposure, location of capture, age, and gender. For example, an English sole from Elliot Bay, Washington, was 734 times more likely to have a neoplasm than a fish from a reference site, after controlling for both age and gender.

Effects and mechanisms of algal toxins have also been examined in fish, but fish generally have been found to be less sensitive to toxicity, particularly neurotoxicity, as compared to mammalian species [60]. Dosing studies of coho salmon (*Oncorhynchus kisutch*) with domoic acid showed that although the toxin was absorbed in the gut, the toxin was excreted via the kidneys and bile and did not reach sensitive nervous tissue [61].

Although not a true environmental sentinel, one freshwater fish species has been widely employed by marine researchers as an important model organism for understanding the effects of marine contaminants and toxins, particularly on embryonic development. The zebrafish (*Danio rerio*) is an ideal model species for understanding developmental processes and the potential impacts of toxins in that its embryos develop outside of the mother, and the egg as well as the embryo itself are transparent [62]. This feature allows for full observation of the developing organ systems. In addition, the species can be easily maintained, and there are now thousands of well-characterized mutant forms and behaviors which can be easily observed and tested. Zebrafish were initially used as a model to understand the health effects of PAHs, which derive from fossil fuels and were of concern following the Exxon Valdez oil spill, on marine fish. Additional sources of PAHs include vehicle exhaust and other forms of air pollution, which creates significant exposure potential for human populations in many areas. Research using the zebrafish model determined that PAHs can interrupt cardiac rhythm and contractility [63, 64], and this research may provide insight into the potential for PAH exposure to contribute to the incidence of cardiac disease in some human cohorts. The zebrafish model has also been applied to examine toxic mechanisms for algal toxins and microbial pathogens [64–66].

Marine Mammals

Domestic mammals have acted serendipitously as sentinels of human health when outbreaks of disease have been traced to an environmental factor that could impact humans. In Japan in the 1950s, domestic cats developed "dancing cat fever," which was eventually traced to high mercury concentrations in fish and shellfish in Minamata Bay [67]. The high concentrations were caused by effluents from a nearby factory using mercuric chloride in the production of vinyl chloride. More recently, attention has focused on marine mammals as sentinels of ocean change as they are charismatic and mortality events attract considerable public attention. Marine mammals have similar mammalian physiology to humans and are long lived so they may be effective indicators for chronic, latent, or slow-developing pathologies that are more difficult to detect in human populations exposed to lower levels of the same hazard (if it is in shared prey items or habitat). A variety of diseases and lesions have been observed in marine mammals worldwide that have heightened public awareness of their risk of environmental exposure to contaminants, biotoxins, and pathogens.

Since 1998, domoic acid producing algal blooms have become increasingly common along the California coast within the foraging range of sea lions. Accompanying this increase, there has been an increase in sea lions with epilepsy characterized by hippocampal atrophy, as well as cardiac lesions and reproductive failure [68–70]. Clinical examination, histology, and molecular diagnostics ruled out infectious causes for these health changes in sea lions, and epidemiological evidence indicated exposure to domoic acid was the factor most strongly associated with these problems. Thus sea lions have acted as sentinels for sublethal effects of domoic acid on mammalian health that can be further investigated using laboratory models such as rodents. A recent paper in the medical literature drew the public health community's attention to this potent marine toxin, hypothesizing that dietary exposure to doses of domoic acid that are subclinical in pregnant women may be sufficient to damage the fetal hippocampus and initiate epileptogenesis [71].

California sea lions have also drawn attention to the potential health impacts from high levels of POPs in the food chain off coastal California, as these compounds in sea lion blubber are associated with a high prevalence of cancer: 17% of stranded adult sea lions examined at necropsy have urogenital cancer [72]. This cancer is associated with a novel herpes virus and exposure to anthropogenic contaminants (such as PCBs and DDTs) [73]. More genetically inbred sea lions, and those with a specific major histocompatibility complex genotype, are more likely to develop cancer [74]. These data suggest that interactions among genes, toxic chemicals, and viruses result in cancer in this ubiquitous marine mammal that shares its coastal California environment with humans.

High levels of contaminants and cancer have also been documented in cetaceans, again raising concerns for health impacts of feeding in polluted waters [75]. A population of 450–500 belugas (*Delphinapterus leucas*) resides in the polluted estuary of the St. Lawrence River, Canada. Cancer has been identified in 50% of these belugas in a recent survey, and high concentrations of organochlorines, heavy metals, and benzo [a]pyrene (BaP) have been measured in tissues, which could act directly or indirectly to increase risk of cancer development [76]. Furthermore, lesions suggestive of endocrine disruption are common in this population of whales, including hyperplastic and degenerative changes of the adrenal gland, "adenomas" of the thyroid gland, hermaphroditism, and pseudohermaphroditism [77, 78]. Most recently, a high prevalence of thyroid hyperplasia was identified in these animals [79]. Polychlorinated biphenyls are one of the major recognized contaminants causing hyperplastic and neoplastic lesions of the thyroid gland [79]. Some polycyclic aromatic hydrocarbons, such as BaP, are among the most potent carcinogens, acting as initiators. Other compounds, such as PCBs, are recognized promoters for the induction of tumors from initiated cells. Thus, although the direct causal relationship between environmental contaminant exposure and either cancer or glandular lesions in the belugas is unknown, the existence of these lesions in wild marine mammals draws attention to the need for concern over increased risk to human health.

Marine mammals thus act as sentinels by attracting attention to naturally occurring diseases potentially linked to environmental exposure to chemical contaminants and other toxins. A limitation to their use as sentinels, however, is that experiments to confirm causality are usually ethically, legally, and logistically impossible. Thus teasing apart confounding variables in disease pathogenesis is difficult, unlike in fish (see above). For example, although California sea lions with cancer have higher levels of organochlorine compounds in blubber than control, non cancer animals, they are also thinner. Blubber contaminant residues are highly mobile, and two studies, one monitoring changes in blubber organochlorine levels during weight loss [80], the other using regression analyses to investigate relationships among blubber and plasma organochlorine levels [81] have demonstrated that weight loss resulting in thinner blubber levels must be considered as a confounding factor when investigating the relationship between cancer and blubber contaminants in sea lions.

Sentinel Habitats

The application of sentinels for early warning of health hazards in the marine environment cannot only be applied to marine organisms but also more broadly to marine habitats. Combining these two approaches to examine and monitor potential environmental

impairments, particularly in the coastal environment, can provide a strong foundation investigating linkages among coastal land use, ecosystem condition, and risks to human and marine animal health. Certain sensitive coastal and marine habitats may exhibit ecological decline in quality and quantity that may be more rapidly detected prior to observable changes in the broader ecosystem. Monitoring of habitat level change often provides an early signal to researchers to look more closely at specific marine organisms for further understanding of any observed declining conditions and potential causality. Links between ecosystem condition and public health and well-being are poorly understood; however, working to better understand these linkages may provide additional insights into potential impacts on human health and well-being in the coastal environment.

National reports on the condition of coastal ecosystems within the United States note measurably diminished conditions [82, 83]. Major sources of impairment identified included chemical and microbial contamination, changes in freshwater inflows, nutrient enrichment, hypoxia, habitat modification and land use changes, wetland loss, increases in nonnative species, and overharvesting of fisheries. The cumulative and potentially synergistic effect of multiple stressors significantly contributes to diminished habitat quality and quantity. One of the earliest symptoms of broad-scale coastal ecosystem impairment has, historically, been decline in the amount and condition of habitats that are particularly sensitive to fluctuations in environmental conditions. The use of sentinel habitats, or first responders, for capturing the ecosystem level impacts of changing coastal conditions is growing.

Marine habitats that are strong candidates as sentinels often have the following attributes:

1. *Shallow water habitats with close proximity to land.* Shallow, nearshore habitats are immediate endpoints to terrestrial inputs and do not benefit from the dilution that occurs in deeper water offshore habitats. Terrestrial pollutants and/or changes in freshwater inflow volume directly impact these habitats and generally produce high cumulative exposure over time.
2. *Easily, and often, observed habitats.* Declining environmental conditions in marine habitats that the public regularly enjoy, due to their easy access, provide unambiguous signals that both the public and scientists understand such as a reduction in the extent or quality of that habitat.
3. *Habitats with multiple roles in sustaining overall ecosystem function.* Habitats that provide multiple key roles in marine environments (e.g., nurseries, refuges, feeding grounds, high biological productivity) provide a complexity of functions that can be assessed as healthy or in good ecological condition.
4. *Habitats with environmentally sensitive structural components.* Key organism sensitivities (e.g., narrow tolerances to environmental fluctuations in temperature, salinity, or light availability) to fluctuations in the natural range of environmental conditions provide indicators of impaired ecosystem condition rapidly.

Coral reefs, submerged aquatic vegetation (e.g., sea grass beds), oyster reefs, tidal creeks, and the estuarine wetlands associated with them are examples of sentinel habitats which generally decline in extent and condition years before system-wide impairment is documented by routine environmental monitoring [84–86]. Linking declines in environmental condition to specific causes (or multiple causes) is challenging but research continues to progress in this arena [87–90]. Coral reef and tidal creek habitats are highlighted below as examples of sentinels for broad-scale changes in environmental condition.

Coral Reefs

Tropical coral reefs exist within narrow ranges of environmental conditions (e.g., temperature and light) and tolerate only limited fluctuations in these conditions. Coral communities experiencing persistent environmental disturbances (e.g., coastal development, land-based pollution, warming temperatures) are one of the first coastal ocean ecosystem components to signal impairment including loss of diversity, increased incidence of disease, reduced growth, reduced reproduction, and mass mortality. These habitats are experiencing rapid declines from changing environmental conditions across the globe. Recent reports indicate that 58–70% of coral reefs worldwide are directly threatened by human-associated activities [88, 91, 92]. Coral reefs are accepted sentinels for the

adverse effects of rapid global warming as they exhibit extreme sensitivity to episodes of prolonged thermal stress [93]; temperatures of just a few degrees above mean summer highs can cause bleaching involving significant losses of mutualistic symbiotic dinoflagellates (microalgae) from the tissues of corals. Such episodes of mass bleaching and mortality adversely affect the health, growth, and fitness of coral communities throughout the world, highlighting the global effects of climate change on ocean health. However, our understanding of the ecological and evolutionary response of corals to episodes of thermal stress remains inadequate, and studies on the mechanisms involved in coral death are few.

Tidal Creeks

Tidal creeks and estuarine salt marshes are the interface between the landscape and estuaries where freshwater from the land mixes with saline water, resulting in complex environments that are renowned for their ecological complexity, biological productivity, and seafood production [19, 86, 94–98]. Most of the US population lives in watersheds that drain into estuaries; as a result, estuaries are a repository for much of the pollution released into the environment [99–101]. The amount and timing of rainfall affects freshwater inflows into estuaries and the pollutants it contains. These processes are increasingly being affected by humans who in turn impact the health of both ecosystems and people. Billions of dollars have been spent to reduce anthropogenic impacts upon estuarine ecosystems with mixed results [99, 102, 103]. These shallow ecosystems can provide early warnings of ensuing harm for both marine organisms and human health [19].

Future Directions

Sentinel species data can be useful as additional weight of evidence in a risk assessment, in providing early warning of situations requiring further study, or for monitoring the course of remedial activities. The risks to aquatic organisms resulting from changes in the ocean serve as an early warning signal for humans because of the close linkage between human and animal health. Approximately 60% of all emerging infectious diseases in humans are zoonotic [104], and the molecular and metabolic processes of higher animals, including man, are very similar, so that aquatic organisms serve as effective sentinels for how ocean anomalies can affect human health. This underlying linkage is the basis for the "One Health" approach in which scientists have recognized that human health and animal health are inextricably linked (www.onehealthinitiative.com). The One Health initiative seeks to promote the health of all species by enhancing cooperation and collaboration among physicians, veterinarians, and other scientific health professionals. This paradigm of interdependence among human, wildlife, and ecosystem health has been well accepted for the terrestrial biosphere and now is being applied to the water-based biosphere, creating the "One Ocean-One Health" perspective. However, despite the increasing number of examples of health changes in sentinel marine species and habitats, the public health community is less engaged in concern for ocean "One Health" than the veterinary and ecological communities. There is now a real need to integrate findings from sentinel studies into the main stream public health community. Just as translational medicine grew from the need to effectively move basic research into medical practice and pharmaceutical applications, a call for "translational ecology" has been made to connect the outcomes of environmental research with public health experts and policy makers who can utilize the results and take appropriate action [105]. Soliciting the input from potential end users and connecting these end users with major funders of environmental research has been proposed as a mechanism to promote translational ecology, and this would be particularly appropriate for marine sentinel research. Funding opportunities geared toward joint eco-epidemiologic and human epidemiologic surveys so that data can be simultaneously collected and compared would go a long way toward promoting the appropriate interactions between ecological and human health researchers.

The data obtained from sentinel species need to be more readily available to the public health community. This could be achieved by use of tumor registries and reportable disease-tracking systems for animals so that geographic trends in disease prevalence and incidence can be detected and related to changes in human health. There is also a need for consistent surveillance and rapid-response teams of experts to investigate disease epidemics and morbidity and mortality in

wildlife to determine if the cause was related to environmental changes. Making data on chemical and biological toxins measured in marine wildlife readily available to epidemiologists and other public health researchers would facilitate their use for generating hypotheses for human cohort studies. The Mussel Watch Program (http://ccma.nos.noaa.gov/about/coast/nsandt/musselwatch.aspx) provides a model for web-based data presentation.

Although the use of aquatic sentinel species is expanding, there are several areas of activity that need further attention. Specifically, there is a need to improve veterinary diagnostics and develop biomarkers of exposure and toxic effects that reflect similar biological events in both humans and sentinel species. In order for a sentinel to provide a true "early warning," diagnostics that observe early, potentially subclinical responses that occur shortly after exposure to a hazardous agent are required. These might include changes in hematologic or serum biochemical parameters but improved diagnostics that involve the use of novel "omics" approaches–genomics, proteinomics, and metabolomics – are needed. These techniques are being developed for clinical use in humans, but their development has been limited in the veterinary and ecological communities. Such techniques could help overcome some of the logistical difficulties facing researchers using species such as marine mammals as sentinels.

A further future direction for the field of sentinel species is the improvement of communication among government agencies, researchers, and public health officials regarding the availability, interpretation, and application of animal sentinel data and methods. Regulators need to be informed about the existence of sentinel animal databases, such as the Marine Mammal Health and Stranding Program in the USA (http://www.nmfs.noaa.gov/pr/health/) and reportable disease-tracking systems for domestic animals (http://www.oie.int/) and animal tumor registries.

Bibliography

Primary Literature

1. Jensen S (1966) Report of a new chemical hazard. New Science 32:612
2. Le Boeuf BJ, Bonnell ML (1971) DDT in California sea lions. Nature 234(5324):108–110
3. NRC (1991) Animals as sentinels of environmental health hazards. National Academy Press, Washington, DC
4. van der Schalie WH, Gardner HS Jr, Bantle JA, De Rosa CT, Finch RA, Reif JS, Reuter RH, Backer LC, Burger J, Folmar LC et al (1999) Animals as sentinels of human health hazards of environmental chemicals. Environ Health Perspect 107(4):309–315
5. Burkhart J, Gardner H (1997) Non-mammalian and environmental sentinels in human health: "back to the future?". Hum Ecol Risk Assess 3(3):309–328
6. Stahl R (1997) Can mammalian and non-mammalian "sentinel species" data be used to evaluate the human health implications of environmental contaminants? Hum Ecol Risk Assess 3(3):329–335
7. Van Dolah FM (2000) Marine algal toxins: origins, health effects, and their increased occurrence. Environ Health Perspect 108(Suppl 1):133–141
8. Flewelling LJ, Naar JP, Abbott JP, Baden DG, Barros NB, Bossart GD, Bottein MYD, Hammond DG, Haubold EM, Heil CA et al (2005) Red tides and marine mammal mortalities. Nature 435(7043):755–756
9. Scholin CA, Gulland F, Doucette GJ, Benson S, Busman M, Chavez FP, Cordaro J, DeLong R, De Vogelaere A, Harvey J et al (2000) Mortality of sea lions along the central California coast linked to a toxic diatom bloom. Nature 403(6765):80–84
10. Lipp EK, Rose JB (1997) The role of seafood in foodborne diseases in the United States of America. Rev Sci Tech 16(2):620–640
11. Potasman I, Paz A, Odeh M (2002) Infectious outbreaks associated with bivalve shellfish consumption: a worldwide perspective. Clin Infect Dis 35(8):921–928
12. Bogomolni AL, Gast RJ, Ellis JC, Dennett M, Pugliares KR, Lentell BJ, Moore MJ (2008) Victims or vectors: a survey of marine vertebrate zoonoses from coastal waters of the Northwest Atlantic. Dis Aquat Organ 81(1):13–38
13. Marine Mammal Protection Act (1972) 16 USC Chapter 31, vol 16, USC Chapter31, MMPA 1972
14. Roesijadi G, Young J, Drum A, Gurtisen J (1987) Behavior of trace metals in *Mytilus edulis* during a reciprocal transplant field experiment. Mar Ecol Prog Ser 15:155–170
15. Kimbrough K, Johnson W, Lauenstein G, Christensen J, Apeti D (2008) An assessment of two decades of contaminant monitoring in the Nation's Coastal Zone, NOAA Technical Memorandum NOS NCCOS 74. National Oceanic and Atmospheric Administration, National Ocean Service, National Centers for Coastal Ocean Science, Center for Coastal Monitoring and Assessment, Silver Spring, p 105
16. Ross PS, Ellis GM, Ikonomou MG, Barrett-Lennard LG, Addison RF (2000) High PCB concentrations in free-ranging Pacific killer whales, *Orcinus orca*: effects of age, sex and dietary preference. Mar Pollut Bull 40(6):504–515
17. Krahn MM, Hanson MB, Schorr GS, Emmons CK, Burrows DG, Bolton JL, Baird RW, Ylitalo GM (2009) Effects of age, sex and reproductive status on persistent organic pollutant concentrations in "southern resident" killer whales. Mar Pollut Bull 58(10):1522–1529

18. Balmer B (2011) Patterns of persistent organochlorine contaminants in relation to sighting patterns of bottlenose dolphins from coastal Georgia, USA. Sci Total Environ 409(11): 2094–2101
19. Sanger D, Blair A, DiDonato G, Washburn T, Jones S, Chapman R, Bergquist D, Riekerk G, Wirth E, Stewart J et al (2008) Support for integrated ecosystem assessments of NOAA's National Estuarine Research Reserves System (NERRS), Volume 1: the impacts of coastal development on the ecology and human well-being of tidal creek ecosystems of the US Southeast, NOAA Technical Memorandum NOS NCCOS 82. National Oceanic and Atmospheric Administration, National Ocean Service, National Centers for Coastal Ocean Science, Hollings Marine Laboratory, Charleston, p 76
20. Pugh RS, Becker PR, Porter BJ, Ellisor MB, Moors AJ, Wise SA (2008) Design and applications of the National Institute of Standards and Technology's (NIST's) environmental specimen banking programs. Cell Preserv Technol 6(1):59–72
21. Aguilar A, Borrell A, Pastor T (1999) Biological factors affecting variability of persistent pollutant levels in cetaceans. In: Reijnders P, Aguilar A, Donavan G (eds) Chemical pollutants and cetaceans, vol Special Issue 1. International Whaling Commission, Cambridge, pp 83–116
22. Hansen LJ, Schwacke LH, Mitchum GB, Hohn AA, Wells RS, Zolman ES, Fair PA (2004) Geographic variation in polychorinated biphenyl and organochlorine pesticide concentrations in the blubber of bottlenose dolphins from the US Atlantic coast. Sci Total Environ 319(1–3):147–172
23. Whitehead H, Gordon J, Mathews E, Richard K (1990) Obtaining skin samples fromliving sperm whales. Mar Mamm Sci 6(4):316–326
24. Greig DJ, Gulland FM, Rios CA, Hall AJ (2010) Hematology and serum chemistry in stranded and wild-caught harbor seals in central California: reference intervals, predictors of survival, and parameters affecting blood variables. J Wildl Dis 46(4):1172–1184
25. Schwacke LH, Twiner MJ, De Guise S, Balmer BC, Wells RS, Townsend FI, Rotstein DC, Varela RA, Hansen LJ, Zolman ES et al (2010) Eosinophilia and biotoxin exposure in bottlenose dolphins (*Tursiops truncatus*) from a coastal area impacted by repeated mortality events. Environ Res 110(6):548–555
26. Wells RS, Rhinehart HL, Hansen LJ, Sweeney JC, Townsend FI, Stone R, Casper D, Scott MD, Hohn AA, Rowles TK (2004) Bottlenose dolphins as marine ecosystem sentinels: developing a health monitoring system. EcoHealth 1:246–254
27. Naar JP, Flewelling LJ, Lenzi A, Abbott JP, Granholm A, Jacocks HM, Gannon D, Henry M, Pierce R, Baden DG et al (2007) Brevetoxins, like ciguatoxins, are potent ichthyotoxic neurotoxins that accumulate in fish. Toxicon 50(5):707–723
28. Truelove J, Iverson F (1994) Serum domoic acid clearance and clinical observations in the cynomolgus monkey and Sprague-Dawley rat following a single i.v. dose. Bull Environ Contam Toxicol 52(4):479–486
29. Suzuki CA, Hierlihy SL (1993) Renal clearance of domoic acid in the rat. Food Chem Toxicol 31(10):701–706
30. Stewart JR, Gast RJ, Fujioka RS, Solo-Gabriele HM, Meschke JS, Amaral-Zettler LA, Del Castillo E, Polz MF, Collier TK, Strom MS et al (2008) The coastal environment and human health: microbial indicators, pathogens, sentinels and reservoirs. Environ Health 7(Suppl 2):S3
31. Kueh CS, Chan KY (1985) Bacteria in bivalve shellfish with special reference to the oyster. J Appl Bacteriol 59(1):41–47
32. Miller WA, Atwill ER, Gardner IA, Miller MA, Fritz HM, Hedrick RP, Melli AC, Barnes NM, Conrad PA (2005) Clams (*Corbicula fluminea*) as bioindicators of fecal contamination with *Cryptosporidium* and *Giardia* spp. in freshwater ecosystems in California. Int J Parasitol 35(6):673–684
33. Thornton SM, Nolan S, Gulland FM (1998) Bacterial isolates from California sea lions (*Zalophus californianus*), harbor seals (*Phoca vitulina*), and northern elephant seals (*Mirounga angustirostris*) admitted to a rehabilitation center along the central California coast, 1994–1995. J Zoo Wildl Med 29(2):171–176
34. Johnson SP, Nolan S, Gulland FM (1998) Antimicrobial susceptibility of bacteria isolated from pinnipeds stranded in central and northern California. J Zoo Wildl Med 29(3):288–294
35. Miranda CD, Zemelman R (2001) Antibiotic resistant bacteria in fish from the Concepcion Bay, Chile. Mar Pollut Bull 42(11):1096–1102
36. Stephen C, Lester S, Black W, Fyfe M, Raverty S (2002) Multispecies outbreak of cryptococcosis on southern Vancouver Island, British Columbia. Can Vet J 43(10):792–794
37. Datta K, Bartlett KH, Baer R, Byrnes E, Galanis E, Heitman J, Hoang L, Leslie MJ, MacDougall L, Magill SS et al (2009) Spread of *Cryptococcus gattii* into Pacific Northwest region of the United States. Emerg Infect Dis 15(8):1185–1191
38. Datta K, Bartlett KH, Marr KA (2009) *Cryptococcus gattii*: emergence in Western North America: exploitation of a Novel Ecological Niche. Interdiscip Perspect Infect Dis 2009:176532
39. Rotstein DS, West K, Levine G, Lockhart SR, Raverty S, Morshed MG, Rowles T (2010) *Cryptococcus gattiivgi* in a spinner dolphin (*Stenella longirostris*) from Hawaii. J Zoo Wildl Med 41(1):181–183
40. Rodriguez-Toro G (1993) Lobomycosis. Int J Dermatol 32(5):324–332
41. Rodriguez-Toro G, Tellez N (1992) Lobomycosis in Colombian Amer Indian patients. Mycopathologia 120(1):5–9
42. Van Bressem M, Van Waerebeek K, Reyes J, Felix F, Echegaray M, Siciliano S, Beneditto AD, Flach L, Viddi F, Avila I et al (2007) A preliminary overview of skin and skeletal diseases and traumata in small cetaceans from South American waters. Lat Am J Aquat Mamm 6(1):7–42
43. Cowan D (1993) Lobo's disease in a bottlenose dolphin (*Tursiops truncatus*) from Matagorda Bay, Texas. J Wildl Dis 29:488–489
44. Reif JS, Mazzoil MS, McCulloch SD, Varela RA, Goldstein JD, Fair PA, Bossart GD (2006) Lobomycosis in Atlantic bottlenose dolphins from the Indian River Lagoon, Florida. J Am Vet Med Assoc 228(1):104–108

45. Rotstein DS, Burdett LG, McLellan W, Schwacke L, Rowles T, Terio KA, Schultz S, Pabst A (2009) Lobomycosis in offshore bottlenose dolphins (*Tursiops truncatus*), North Carolina. Emerg Infect Dis 15(4):588–590
46. O'Shaughnessy A (1866) On green oysters. Annual Magazine of Natural History 18:221–228
47. Orton J (1923) Summary of an account of investigations into the cause or causes of the unusual mortality among oyster in English oyster beds during 1920 and 1921. J Mar Biol Assoc UK 13:1–23
48. Langston W, Bebianno M, Burt G (1998) Metal handling strategies in molluscs. In: Langston W, Bebianno M (eds) Metal matabolism in aquatic environments. Chapman and Hall, London, pp 219–283
49. Crain DA, Guillette LJ Jr (1998) Reptiles as models of contaminant-induced endocrine disruption. Anim Reprod Sci 53(1–4):77–86
50. Cossins AR, Crawford DL (2005) Fish as models for environmental genomics. Nat Rev Genet 6(4):324–333
51. Sumpter JP, Jobling S (1995) Vitellogenesis as a biomarker for estrogenic contamination of the aquatic environment. Environ Health Perspect 103(Suppl 7):173–178
52. Jobling S, Coey S, Whitmore JG, Kime DE, Van Look KJ, McAllister BG, Beresford N, Henshaw AC, Brighty G, Tyler CR et al (2002) Wild intersex roach (*Rutilus rutilus*) have reduced fertility. Biol Reprod 67(2):515–524
53. Jobling S, Nolan M, Tyler C (1998) Widespread sexual distribution in wild fish. Environ Sci Technol 32(2):498–506
54. Grosell M, Walsh P (2006) Sentinel species and animal models of human health. Oceanography 19:126–133
55. Black JJ, Baumann PC (1991) Carcinogens and cancers in freshwater fishes. Environ Health Perspect 90:27–33
56. Mix M (1986) Cancerous diseases in aquatic animals and their association with environmental pollutants: a critical review of the literature. Mar Environ Res 20:1–141
57. McCain BB, Pierce KV, Wellings SR, Miller BS (1977) Hepatomas in marine fish from an urban estuary. Bull Environ Contam Toxicol 18(1):1–2
58. Pierce KV, McCain BB, Wellings SR (1978) Pathology of hepatomas and other liver abnormalities in English sole (*Parophrys vetulus*) from the Duwamish River estuary, Seattle, Washington. J Natl Cancer Inst 60(6):1445–1453
59. Schwiewe M, Weber D, Myers M, Jacques F, Reichert W, Krone C, Malins D, McCain B, Chan S, Varanasi U (1991) Induction of cellular alteration and other hepatic lesions in English sole (*Parophrys vetulus*) exposed to an extract of an urban marine sediment. Can J Fish Aquat Sci 48:1750–1760
60. Nogueira I, Lobo-da-Cunha A, Afonso A, Rivera S, Azevedo J, Monteiro R, Cervantes R, Gago-Martinez A, Vasconcelos V (2010) Toxic effects of domoic acid in the Seabream *Sparus aurata*. Mar Drugs 8(10):2721–2732
61. Lefebvre KA, Noren DP, Schultz IR, Bogard SM, Wilson J, Eberhart BT (2007) Uptake, tissue distribution and excretion of domoic acid after oral exposure in coho salmon (*Oncorhynchus kisutch*). Aquat Toxicol 81(3):266–274
62. Dahm R (2006) The zebrafish exposed: 'see-through' mutants may hold the key to unraveling the mysteries of embryonic development. Am Sci 94:446–453
63. Incardona JP, Day HL, Collier TK, Scholz NL (2006) Developmental toxicity of 4-ring polycyclic aromatic hydrocarbons in zebrafish is differentially dependent on AH receptor isoforms and hepatic cytochrome P4501A metabolism. Toxicol Appl Pharmacol 217(3):308–321
64. Billiard SM, Timme-Laragy AR, Wassenberg DM, Cockman C, Di Giulio RT (2006) The role of the aryl hydrocarbon receptor pathway in mediating synergistic developmental toxicity of polycyclic aromatic hydrocarbons to zebrafish. Toxicol Sci 92(2):526–536
65. Saslowsky DE, Cho JA, Chinnapen H, Massol RH, Chinnapen DJ, Wagner JS, De Luca HE, Kam W, Paw BH, Lencer WI (2010) Intoxication of zebrafish and mammalian cells by cholera toxin depends on the flotillin/reggie proteins but not Derlin-1 or −2. J Clin Invest 120:4399–4409
66. Lefebvre KA, Tilton SC, Bammler TK, Beyer RP, Srinouanprachan S, Stapleton PL, Farin FM, Gallagher EP (2009) Gene expression profiles in zebrafish brain after acute exposure to domoic acid at symptomatic and asymptomatic doses. Toxicol Sci 107(1):65–77
67. Eto K (1997) Pathology of minamata disease. Toxicol Pathol 25(6):614–623
68. Goldstein T, Zabka TS, Delong RL, Wheeler EA, Ylitalo G, Bargu S, Silver M, Leighfield T, Van Dolah F, Langlois G et al (2009) The role of domoic acid in abortion and premature parturition of California sea lions (*Zalophus californianus*) on San Miguel Island, California. J Wildl Dis 45(1):91–108
69. Zabka TS, Goldstein T, Cross C, Mueller RW, Kreuder-Johnson C, Gill S, Gulland FM (2009) Characterization of a degenerative cardiomyopathy associated with domoic acid toxicity in California sea lions (*Zalophus californianus*). Vet Pathol 46(1):105–119
70. Goldstein T, Mazet JA, Zabka TS, Langlois G, Colegrove KM, Silver M, Bargu S, Van Dolah F, Leighfield T, Conrad PA et al (2008) Novel symptomatology and changing epidemiology of domoic acid toxicosis in California sea lions (*Zalophus californianus*): an increasing risk to marine mammal health. Proc Biol Sci 275(1632):267–276
71. Stewart I (2010) Environmental risk factors for temporal lobe epilepsy–is prenatal exposure to the marine algal neurotoxin domoic acid a potentially preventable cause? Med Hypotheses 74(3):466–481
72. Gulland FM, Trupkiewicz JG, Spraker TR, Lowenstine LJ (1996) Metastatic carcinoma of probable transitional cell origin in 66 free-living California sea lions (*Zalophus californianus*), 1979 to 1994. J Wildl Dis 32(2):250–258
73. Ylitalo GM, Stein JE, Hom T, Johnson LL, Tilbury KL, Hall AJ, Rowles T, Greig D, Lowenstine LJ, Gulland FM (2005) The role of organochlorines in cancer-associated mortality in California sea lions (*Zalophus californianus*). Mar Pollut Bull 50(1):30–39

74. Acevedo-Whitehouse K, Gulland F, Greig D, Amos W (2003) Inbreeding: disease susceptibility in California sea lions. Nature 422(6927):35
75. Martineau D, Lagace A, Beland P, Higgins R, Armstrong D, Shugart LR (1988) Pathology of stranded beluga whales (*Delphinapterus leucas*) from the St. Lawrence Estuary, Quebec, Canada. J Comp Pathol 98(3):287–311
76. De Guise S, Lagace A, Beland P (1994) Tumors in St. Lawrence beluga whales (*Delphinapterus leucas*). Vet Pathol 31(4):444–449
77. Girard C, Lagace A, Higgins R, Beland P (1991) Adenocarcinoma of the salivary gland in a beluga whale (*Delphinapterus leucas*). J Vet Diagn Invest 3(3):264–265
78. De Guise S, Lagace A, Beland P (1994) True hermaphroditism in a St. Lawrence beluga whale (*Delphinapterus leucas*). J Wildl Dis 30(2):287–290
79. Mikaelian I, Labelle P, Kopal M, De Guise S, Martineau D (2003) Adenomatous hyperplasia of the thyroid gland in beluga whales (*Delphinapterus leucas*) from the St. Lawrence Estuary and Hudson Bay, Quebec, Canada. Vet Pathol 40(6):698–703
80. Hall AJ, Gulland FM, Ylitalo GM, Greig DJ, Lowenstine L (2008) Changes in blubber contaminant concentrations in California sea lions (*Zalophus californianus*) associated with weight loss and gain during rehabilitation. Environ Sci Technol 42(11):4181–4187
81. Yordy JE, Wells RS, Balmer BC, Schwacke LH, Rowles TK, Kucklick JR (2010) Partitioning of persistent organic pollutants between blubber and blood of wild bottlenose dolphins: implications for biomonitoring and health. Environ Sci Technol 44(12):4789–4795
82. Pew Oceans Commission (2003) America's living oceans: charting a course for sea change. A report to the nation, May 2003. Pew Oceans Commission, Arlington
83. US Commission on Ocean Policy (2004) An ocean blueprint for the 21st Century. Final report, Washington, DC. ISBN#0-9759462-0-X
84. Bayley S, Stotts VD, Springer PF (1978) Changes in submerged aquatic macrophyte populations at the head of Chesapeake Bay, 1958–1975. Estuaries 1(3):171–182
85. Dustan P, Halas JC (1987) Changes in the reef-coral community of Carysfort Reef, Key Largo, Florida: 1974–1982. Coral Reefs 6:91–106
86. Holland AF, Sanger DM, Gawle CP, Lerberg SB, Santiago MS, Riekerk GHM, Zimmerman LE, Scott GI (2004) Linkages between tidal creek ecosystems and the landscape and demographic attributes of their watersheds. J Exp Mar Biol Ecol 298:151–178
87. Kemp WM, Twilley RR, Stevenson JC, Boynton WR, Means JC (1983) The decline of submerged vascular plants in upper Chesapeake Bay: summary of results concerning possible causes. Mar Technol Soc J 17:78–89
88. Hoegh-Guldberg O (1999) Coral bleaching, climate change and the future of the world's coral reefs. Review. Mar Freshw Res 50:839–866
89. Porter JW, Tougas JI (2001) Reef ecosystems: threats to their biodiversity. In: Levin S (ed) Encyclopedia of biodiversity, vol 5. Academic, New York, pp 73–95
90. Turgeon DD et al (2002) The state of coral reef ecosystems of the United States and Pacific Freely Associated States: 2002. National Oceanic and Atmospheric Administration/National Ocean Service/National Centers for Coastal Ocean Science, Silver Spring, p 265
91. Goreau T, McClanahan T, Hayes R, Strong A (2000) Conservation of coral reefs after the 1998 Global Bleaching Event. Conserv Biol 14(1):5–15
92. Knowlton N (2001) The future of coral reefs. Proc Natl Acad Sci USA 98(10):5419–5425
93. Coles SL, Brown BE (2003) Coral bleaching–capacity for acclimatization and adaptation. Adv Mar Biol 46:183–223
94. Kneib RT (1997) The role of tidal marshes in the ecology of estuarine nekton. Oceanogr Mar Biol Ann Rev 35:163–220
95. Mallin MA, Burkholder JM, Cahoon LB, Posey MH (2000) North and South Carolina coasts. Mar Pollut Bull 41:56–75
96. Lerberg SB, Holland AF, Sanger DM (2000) Responses of tidal creek macrobenthic communities to the effects of watershed development. Estuaries 23(6):838–853
97. Sanger DM, Holland AF, Scott GI (1999) Tidal creek and salt marsh sediments in South Carolina coastal estuaries: I. Distribution of trace metals. Arch Environ Contam Toxicol 37:445–457
98. Sanger DM, Holland AF, Scott GI (1999) Tidal creek and salt marsh sediments in South Carolina coastal estuaries: II. Distribution of organic contaminants. Arch Environ Contam Toxicol 37:458–471
99. Boesch DF, Brinsfield RB, Magnien RE (2001) Chesapeake Bay eutrophication: scientific understanding, ecosystem restoration, and challenges for agriculture. J Environ Qual 30(2):303–320
100. Beach D (2002) Coastal sprawl: the effects of urban design on aquatic ecosystems in the United States. Pew Oceans Commission, Arlington
101. DiDonato GT, Stewart JR, Sanger DM, Robinson BJ, Thompson BC, Holland AF, Van Dolah RF (2009) Effects of changing land use on the microbial water quality of tidal creeks. Mar Pollut Bull 58(1):97–106
102. U S Environmental Protection Agency (2001) National coastal condition report, EPA-620/R-01/005. Office of Research and Development, Office of Water, Washington, DC
103. H. John Heinz III Center for Science EatE (2008) The state of the nation's ecosystems: measuring the lands, waters, and living resources of the United States. Island, Washington, DC
104. Jones KE, Patel NG, Levy MA, Storeygard A, Balk D, Gittleman JL, Daszak P (2008) Global trends in emerging infectious diseases. Nature 451(7181):990–993
105. Schlesinger WH (2010) Translational ecology. Science 329(5992):609

Books and Reviews

Bossart G (2006) Marine mammals as sentinel species for oceans and human health. Oceanography 19:134–137

Boyd IL, Bowen WD, Iverson SJ (eds) (2010) Marine mammal ecology and conservation, a handbook of techniques. Oxford University Press, New York

Gulland FM (1999) Stranded seals: important sentinels. J Am Vet Med Assoc 214:1191

Scotch ML, Odofin PR (2009) Linkages between animal and human health sentinel data. BMC Vet Res 5:15

Shellfish Aquaculture, Methods of Sustainable

Francis X. O'Beirn[1], Christopher W. McKindsey[2], Thomas Landry[3], Barry A. Costa-Pierce[4]

[1]Marine Institute, Galway, Ireland

[2]Ocean and Environmental Sciences Division, Fisheries and Oceans Canada, Institut Maurice-Lamontagne Fisheries and Oceans Canada, Mont-Joli, Québec, Canada

[3]Fisheries and Oceans Canada, Gulf Fisheries Centre, Moncton, NB, Canada

[4]Graduate School of Oceanography, Rhode Island Sea, Grant College Program, University of Rhode Island, URI Bay Campus, Narragansett, RI, USA

Article Outline

Glossary
Definition of the Subject
Introduction
Interactions of Shellfish Culture
Evolution of Sustainability for Shellfish Culture
Measuring Sustainability: The Development of Indicators
Progressing Sustainability in Shellfish Aquaculture
Future Directions
Bibliography

Glossary

Azoic conditions Conditions that prevail when no organisms or their remains are found in a system as a consequence of stress on a system.

Biodeposition Organic matter deriving from (shellfish) species that falls to the seafloor. The matter can take the form of feces, pseudofeces, or the shellfish themselves.

Far-field effects The effects of impacts of activities measured at a predefined distance or time from the location of the pressure. The effects may or may not be distinguishable from other effects in the system leading to cumulative impacts.

Ecological aquaculture The implementation of aquaculture practices whose design and implementation result in economically viable and socially responsible aquaculture systems.

Integrated coastal zone management (ICZM) The management of activities in marine environments in a coherent and practical fashion so as to result in the most efficient use of resources and avoid conflicting claims on space and missed opportunities for more sustainable coastal development.

Performance standards Defined expectations represented by some measurable variable which reflects the impact an activity will have on the marine environment.

Best management practices A series of operating procedures, schedules of activities, and other management practices that aquaculture operations can use to prevent or reduce impact on the marine environment while retaining an economically viable operation.

Definition of the Subject

Worldwide aquaculture production of finfish and shellfish species is an ever-increasing sector of food production and now represents nearly half (48%) of all aquatic species intended for human consumption [1]. It is thought that the increased aquaculture production is driven primarily by the vacuum created as a consequence of the static (or declining) status of wild capture fisheries allied to an overall greater demand for fishfood products [1]. This generalization is broadly accepted as the primary driver for increased aquaculture production; however, more specific drivers may be, increased profit as a consequence of targeted marketing allied with development of new species in developing countries and as a means of providing more self-sufficient mechanisms to grow fishfood and provide a regular income in developing countries. Typically, aquaculture production has been dominated by the culture of

finfish species; however, shellfish production has shown a steady increase in production over the last number of decades [1] and represents 27% by weight and 15% by value of worldwide aquaculture production. The culture of shellfish in aquaculture is comprised primarily of species of crustaceans (e.g., shrimp and crab) and molluscs (e.g., oysters, clams, mussels). A major distinction between the crustaceans and molluscs is that crustaceans, as omnivores, typically require the input into their culture system of feed, usually derived from external sources (e.g., fish protein or oils). Consequently, issues surrounding the sustainability of crustacean culture as activities are more akin to those encountered with finfish aquaculture. Molluscs, particularly those identified above, are filter feeders. Filter-feeding organisms, for the most part, feed at the lowest trophic level, usually relying primarily on ingestion of phytoplankton. The process in extractive in that it does not rely on the input of feedstuffs in order to produce growth.

The steady increase in world aquaculture production over the last number of decades allied with greater environmental awareness has resulted in an increased level of scrutiny of these activities in relation to their interactions with the environment. The increased focus on environmental issues in the marine environment (driven by consumer demands and/or regulatory requirements) has resulted in a concomitant increase in efforts to identify methods to culture shellfish that are considered sustainable. Consequently, there is a move toward rearing aquatic shellfish species in the marine environment such that negative interactions are minimized. In addition, it has also become apparent that there are considerable marketing benefits that will accrue as a consequence of food being reared in an environmentally acceptable fashion. These efforts (to identify and activate more sustainable method of culture) have been driven both by industry and environmental nongovernmental organisations (e.g., Pacific Shellfish Growers Association and World Wildlife Fund) as well as regulatory drivers (e.g., Natura 2000 Legislation in the European Union). Notwithstanding the efforts to carry out shellfish aquaculture activities in a more sustainable fashion, there is still some confusion relating to the definition of sustainability and how an activity might be carried out in a sustainable fashion. At first, identifying if an activity and its consequences in the marine environment is acceptable or not will help define whether the activity is sustainable. Clarifying or clearing defining some of the terms utilized in this subject area will lend itself to a clearer and understandable of how the culture of shellfish can be managed to achieve sustainability goals.

Introduction

Worldwide aquaculture production has increased steadily since 1980 [1]. Production of aquatic products in 1980 accounted for 7% of food fish supply (five million tons), in 2007 this quantity had risen to 50 million tons. Based upon current trends, it is apparent that production of shellfish will continue to increase at a stable rate (6.5% per annum since 2002). This increase is fueled by an increase in market demand, adoption of more efficient and effective culture methods, and the financial rewards associated with the production of value-added products to higher end markets. Notwithstanding the important differences between finfish production and the majority of shellfish production methods, i.e., the introduction of feedstuffs into the environment, which has led to well-documented resource demands and impacts on the marine environment, shellfish aquaculture also has the potential to impact on the marine environment in a negative fashion if not carried out in a responsible manner. This is underpinned by a background of greater environmental awareness and increased legislative drivers toward maintaining biodiversity and minimizing negative interactions between a range of conservation goals and development activities. Some authors [2] correctly highlight that aquaculture cannot be considered as one single "monolith," which can be tarnished with the single level of criticism, as it reflects a diverse array of species, methods, and potential interactions. In addition to the differences highlighted above between those culture methods reliant on input of feedstuffs necessary for the culture of some species (finfish and crustaceans), the degree of structural input and environmental alteration is also highly varied among the different species cultured and the method employed. In short, this entry will identify some of the issues associated with sustainability of shellfish aquaculture and whether or not the efforts directed to date are considered to be on a trajectory toward sustainability [3].

Interactions of Shellfish Culture

Early incarnations of shellfish culture are considered not far removed from wild fisheries in that the activities were broadly extensive with only small-scale manipulation of stocks (e.g., movement of wild seed to production areas; an activity still practiced today with on-bottom mussel and oyster culture). Over time, the industry has evolved with the development of more contained systems. With such intensification, the risk of detrimental environmental interactions increased, e.g., disease risks or greater deposition of organic matter beneath structures, as a consequence of higher holding densities of culture organisms. Notwithstanding density-related issues, in many instances, it is not the presence of the culture organisms that result in largely negative interactions but the activities associated with the culture mechanisms, e.g., dredging extensive culture systems, pesticides, or chemotheraputents in pond systems.

The culture of shellfish (bivalve molluscs) as distinct from finfish and crustaceans, for the most part, requires no input of feed to the culture process. Given this difference, this entry will focus primarily on the culture of molluscan shellfish (primarily bivalves). Under certain circumstances, e.g., hatchery production of shellfish, the input of feed in the form of phytoplankton is required to produce seed [4]. Thereafter, for the majority of their life cycle, shellfish consume at the lowest trophic level, feeding largely as herbivores and relying on ambient seston [5]. This distinction is important in that it highlights the fact the culture of shellfish, upon harvest, is considered a process that facilitates the net export of carbon (and other nutrients) from marine systems. While this may be considered an exploitation of a resource and detrimental to the system, there are situations where this is also inherently beneficial to the ecosystem. The impacts of shellfish culture have been well documented in research literature where specific interactions are described and quantified (Table 1). In addition, this topic has been a subject of numerous reviews highlighting similarities and differences inherent in culture methods and considers the factors governing any differences observed.

The extent of the interactions between shellfish culture and the environment are primarily a function of the type of species being cultured, the system of culture, and the properties of the receiving environment. Table 1 provides a summary of the interactions identified between shellfish culture practices and the environment. The interactions are summarised as the mechanism which acts on the system. For example, the dredging associated with the collection of mussel seed for aquaculture practices can have the effect of physically disturbing the seafloor and the organisms therein (the impact indicator). It has been demonstrated empirically that this activity can have an impact at the community level of marine ecosystems. The culture of shellfish species using structures presents a number of likely interactions. The use of structures, i.e., bags and trestles, longlines with droppers will increase the density of culture organisms above the seafloor, thus influencing the flux of material and nutrients to the seafloor and into suspension. This higher density can also modify water flow in and around the culture system. These and other more general interactions are discussed below.

Nutrients

Bivalve shellfish can function in the ecosystem by filtering seston and releasing nutrients in solid or dissolved forms. They are responsible for deposition onto the seafloor of particulate matter (as either feces or pseudofeces), thus influencing benthic-pelagic coupling of organic matter and nutrients. The deposition of organic matter by molluscs has been demonstrated to impact on the infauna organisms and communities found in sedimentary environments. The changes have broadly reflected the Pearson–Rosenberg [6] pattern of community development whereby moderate increases in organic matter stimulate species' richness and abundance. Further increases in organic matter could result in a reduction in species richness and abundance such that excesses result in azoic conditions as a consequence of protracted anoxic conditions. The effects of biodeposition are exacerbated by the increase in density of culture organisms above the seafloor. The use of bags on trestles (e.g., oyster culture) and longlines (with mussels) will increase the density of culture organisms over a particular point and increase the risk of impact due to biodeposition. While effects of organic loading have been demonstrated with shellfish

Shellfish Aquaculture, Methods of Sustainable. Table 1 Interactions between shellfish culture methods and the environment identifying the interaction route and indicator

Culture type (species)	Interactions	Indicator	References
Off-bottom – Suspended culture (e.g., mussels, oysters) using longlines, rafts, floating bags	Water flow alteration	Sediment particle size analysis (PSA) – increase in fine sediment composition due increased sediment deposition or increase in coarse sediment complement due to scouring	[7, 79–85, 163]
		Benthic infauna – adjustment in species composition and abundance; community composition	[86–89]
	Depostion of organic matter (feces and pseudofeces)	Increase in sulfide reduction, Decrease in REDOX depth; Sediment biogeochemistry changes	[84, 88, 90–93]
		Benthic infauna	[81, 86, 87, 94, 95]
	Shading	Condition of light-sensitive species (macroalgae, maerl, eel grass)	[96, 97]
	Habitat creation/fouling	Secondary production on culture organisms or structures. Increased nekton species	[22, 98–103]
	Seston filtration	Alteration of phytoplankton communities, impact on production/ecological carrying capacity; changes in zooplankton assemblages	[80, 104–107]
	Nutrient exchange	Ammonium, DIN – increased primary production, N2 removal via harvest or denitrification	[93, 108–111]
	Introduction of exotic species with culture organisms	Presence of non-endemic or exotic species	[22, 112, 151]
On-bottom (Mussels, oysters, clams)	Physical alteration, dredging, intertidal picking	Benthic infauna	[86, 114, 115]
	Monoculture	Epifuana community alteration: PSA alteration	[52, 86, 89, 91, 96, 115–118]
	Depostion of organic matter (feces and pseudofeces)	Increase sulfide reduction, Decrease in REDOX depth; sediment biogeochemistry changes	[119–126]
		Benthic infauna	[8, 127]
	Shading	Condition of light-sensitive species (macroalgae, maerl, eel grass)	[11]
	Habitat creation/fouling	Secondary production on culture organisms or structures	[78, 79, 89, 115, 127–129]
	Seston filtration	Alteration of phytoplankton communities, impact on production/ecological carrying capacity; increased light penetration	[11, 91, 106, 107, 109, 130–141]
	Nutrient exchange	Increased primary production, N_2 removal via harvest or denitrification; alteration of N:P ratios	[109, 110, 142–150]
	Introduction of exotic species with culture organisms	Presence of non-endemic of exotic species	[112, 113]

culture activities, the impacts are considered relatively small when compared with other culture systems where externally derived organic matter, i.e., food, is inputted directly to the system, e.g., finfish culture. A number of factors mediate the level of impact on the seafloor. In addition to density of culture organisms, the hydrography of the system including residence time, tidal range, and residual flow will all dictate the likely influence the extent of an impact on the seafloor. The greater the residual flow and/or tidal regime, the risk of accumulation of organic material is reduced [7, 8] due to the dispersive regime. Similarly, the high density of structures can result in the impediment of water flow (baffling effect), slow it down, and cause localized deposition of suspended material on the seafloor. Depending on the extent of the structures, the effect can be localized or extensive [9] with concomitant impacts on sedimentary infauna.

Organic deposition by shellfish on the seabed can also influence the remineralization of nutrients in marine systems. This process as well as normal excretion (of ammonium NH_4^+) demonstrates that shellfish in both their natural state and in culture can influence nutrient dynamics in marine systems. In fact, in a coastal bay in France it has been estimated that between 15% and 40% of nitrogen in the system is derived from oysters in culture [10]. Notwithstanding the factors that govern extent of impacts on systems, molluscs are considered net consumers of particulate and dissolved nutrients, and, by virtue of the movement of product to market the nutrients are exported from the system. The area required to assimilate material is generally confined to the production area and as such the area required to assimilate material is less with culture than without.

Filtration

Bivalve shellfish (oysters and mussels) have a high filtration capacity and can respond rapidly to changes in phytoplankton abundance (as a result of eutrophication) in marine systems. In nearshore marine environments, the presence of large numbers of bivalve shellfish has provided the system with the ability to buffer the effects of large phytoplankton blooms. This phenomenon applies equally to shellfish in culture which likewise provides the system with resilience against natural or anthropogenically derived fluctuations in phytoplankton numbers (blooms) [11–14]. As a consequence of this phenomenon, the subsequent removal of natural bivalve populations from marine systems (e.g., by fishing) has resulted in well-documented ecological shifts in system processes. The dramatic reduction of oyster numbers in the Chesapeake Bay (USA) has coincided with a deterioration in water quality of the Bay; this situation was exacerbated by increased athropogenic pressures [15–17]. Shellfish in culture while having demonstrable localized effects do also appear to have the ability to moderate the effects of nutrients more broadly in marine systems [9, 18].

Exotic Species

The importance of aquaculture as a vector for the introduction and spread of exotic species has been well documented [19–23]. There are two broad classes of introductions that may result from bivalve aquaculture.

First, there is the establishment and spread of non-endemic species that have been intentionally introduced into an area for aquaculture purposes, the "target" species. Classic examples of this include the establishment of the Pacific oyster (*Crassostrea gigas*) on the Pacific coast of North America [24] and in various countries throughout Europe [25–27] and of the Mediterranean mussel (*Mytilus galloprovincialis*) in South Africa [28]. More recently, the large expansion of *C. gigas* in the Oosterschelde and the Dutch and German Wadden Sea have been a cause of concern in both countries from a fisheries, ecological, and human health perspective. Wild populations of the Pacific oysters have expanded from 15 ha in 1980 to 750 ha in 2005 in the Oosterschelde [29]. They have become a competitor (for space and food) with the commercially important mussel industry [25, 30]. In addition, they have become an increasing health risk associated with human encounters given the sharp nature of the shell [31]. Efforts to remove wild Pacific oysters from the Oosterschelde in the Netherlands are ongoing (Aad Smaal, IMARES, NL personnel communication). It is important to note that in the Netherlands, Pacific oysters were first introduced by broadcast spreading in an uncontained fashion on the seabed under the assumption that the summer temperatures were such that they

would not successfully complete gametogenesis, spawn, and most importantly recruit.

Second, there is the establishment and spread of species that are associated with the introduced bivalves [32, 33]. These species may include both "hitchhiking" species – animals, plants that grow associated with the bivalves and diseases or parasites that may cause outbreaks in the same or other species [34]. This acts at two spatial scales: at an interregional or international scale with respect to the initial introduction of hitchhiking species and also at a regional scale, where the transfer of stock among sites may be very important to the spread of established exotic species locally [35]. The provision of novel habitat by the species being cultured may also allow for the establishment or amplification of exotic species that may be introduced through other vectors or of native species that thrive in the novel habitat [36–38].

Introductions of the *C. gigas*, and to a lesser extent *C. virginica* and other oyster species, outside of their native range for aquaculture have been suggested to be one of the greatest single modes of introduction of exotic species worldwide [19, 39]. For example, transfer of organisms with bivalves has been suggested to be the most important source of exotic species in northern Europe [17, 40] and among the most important vectors elsewhere in that continent [17, 41, 42]. In the northeast Pacific, some authors suggest that oyster (*C. gigas*) introductions have even been the major source of introduction of exotic molluscs [14] and invertebrates in general [43], historically contributing at least as many of the exotic species in that area as has international shipping.

The slipper limpet (*Crepidula fornicata*), originally introduced into England with *C. virginica*, has had great impacts on some benthic communities in Europe, particularly in France [44] and the UK [45]. It has displaced important commercial bivalves, such as the great scallop (*Pecten maximus*) in some areas and native oysters beds in Normandy [46] and the south coast of England [39]; however, in other areas where it has not proliferated as much, it appears to have had little effect on overall macrobenthic community diversity [47].

Introductions have not just been confined to macrofaunal species. Oyster introductions have also been strongly implicated in the introduction of parasitic organisms and macroalgal species into novel regions [48–50]. Notwithstanding the records of aquaculture-mediated introductions of nonnative species into marine systems, there still appears to be a paucity of information and experimental evidence quantifying the impacts of nonnative oyster introductions on the receiving environment [13]. The structures associated with shellfish culture (e.g., ropes, bags, floats) in some areas provide novel habitat for the colonization and proliferation of exotic species [18]. In addition to the likely effects on system function, the colonization of structures associated with shellfish culture also presents practical problems for the aquaculturists from a husbandry perspective.

Biodiversity

The physical presence of large numbers of shellfish in culture can result in a monoculture which has a finite period of time in the system as a consequence of husbandry practices, e.g., thinning or harvesting. Given this constraint, the development of communities associated with the cultured shellfish will be restricted and hence biodiversity is likely to be reduced. This is particularly true if the culture period is short (i.e., approximately 1 year). The activities associated with shellfish culture can also be impacting. For example, dredging associated with on-bottom culture of mussels and oysters can cause damage to seabed (and organisms therein) and cause sediment plumes to be distributed beyond the culture environs [51, 52].

Structures

The culture of shellfish species using structures presents a number of likely interactions with the environment. The use of structures, i.e., bags and trestles, longlines with droppers will increase the density of culture organisms above the seafloor, thus influencing the flux of materials and nutrients to the seafloor and into suspension. The physical presence of the structures can also modify water flow in and around the culture system resulting in increased deposition of material or scouring in areas of higher flow. Either way there is a potential to impact on the sediment structure and associated communities. As stated above, shellfish aquaculture can also provide structures that can provide for the proliferation of individual (fouling)

organisms in a system. Some of which might be new to the system. Finally, the physical presence of the structures and culture animals can have the effect of shading the seafloor and thus potentially impacting on species reliant on light (e.g., maerl or seagrasses).

The interaction of shellfish culture activities with the marine environment can be considered from the perspective of near-field and far-field impacts. While near-field effects are more easily measured (using many standard near-field impact indicators identified in Table 1) and mitigated, the measurement of far-field effects is more difficult to achieve, although some of the impacts might be lessened if near-field activities are reduced or mitigated. Other far-field effects may not be as easily measured and assigned to a specific causative activity (as there may be multiple causative factors) yet they all must be considered when managing marine systems. To this end, a number of authors (e.g., Tucker and Hargraves [163]; Costa-Pierce and Page [3]) have provided a good contextual presentation on the issues surrounding sustainability of aquaculture activities. They acknowledge that sustainability solutions can extend from ecological, technical, and socioeconomic and cover very small spatial scales to adjusting broader societal values.

It is important to appreciate that in order to manage activities in marine systems, it is imperative that there is a good understanding linking the culture practice to a specific environmental response. These interactions are important in order to coordinate management responses between regulatory agents and aquaculture operators, in order to minimize negative environmental effects while maintaining production returns and hence, profits.

Evolution of Sustainability for Shellfish Culture

It is widely accepted that most human activities in the marine environment will have some effect on marine species and habitats. The scale of these impacts depends on the nature of the activity, its intensity, and the sensitivity of the receiving environment. The degree of change that is considered permissible depends on a number of factors, not the least of which is public perception. Empirical data demonstrating change or impact is the most obvious basis on which to justify management actions or inactions. Equally important is linking the change observed directly to the process under consideration (e.g., bivalve molluscan mariculture). Best management practices (BMPs) and performance standards have been adopted as means of mitigating against unacceptable environmental interactions. The major categories of practices and standards include the following:

- Regulatory standards governing molluscan mariculture
- BMPs (or design standards or specifications) for bivalve growers, mariculture regulators, and managers
- Certification standards for molluscan products (e.g., organic, sustainable, fair trade, domestically or even locally grown)
- Other innovations, Integrated Multi-Trophic Aquaculture (IMTA)

Legislative Drivers Toward Sustainable Practices

As in many countries there is much national and internationally derived legislation governing the production and placement of aquaculture-derived food products on the market. These regulations consider the product primarily from a food safety perspective with the goal of protecting the consumer. In European Union member states, Regulation (EC) No 854/2004 [53] of the European Parliament and of the Council of 29 April 2004 laying down specific rules for the organization of official controls on products of animal origin intended for human consumption was implemented to ensure that consumers of shellfish products are not exposed to toxins that might have accumulated in shellfish flesh as a consequence of filtering phytoplankton species responsible for producing these toxins. Shellfish are effective bioaccumulators. Such regulation requires continual monitoring of shellfish products derived from marine waters. In the event of an excess of defined thresholds, the product is not placed on the market and monitoring continues. The broader environmental benefits of this legislation are that it can identify areas of risk (for harmful algal blooms) and has spawned research to identify factors governing the causes of bloom events including anthropogenic sources. How this impacts on sustainability of shellfish aquaculture? The persistence of HAB and toxic events can dictate the

feasibility of locating or developing shellfish culture these areas. If areas are subject to prolonged closures, the product is generally restricted from being removed and can result in overload and subsequent impact on system processes.

The Water Framework Directive [54] is a legislative driver designed to improve surface and groundwater quality throughout the European Union. Allied with a full-risk assessment, each waterbody will be assessed for its condition in terms of ecological quality elements. This monitoring program focuses on a range of ecological quality elements (e.g., benthic invertebrates, phytoplankton, macroalgae, fish in transitional waters) for which a series of standards have been developed. The waterbodies included in the monitoring program were selected on the basis of no obvious pressures and site for which some pressure has been identified, e.g., aquaculture activities. The goal of the WFD is to ensure that all waterbodies achieve good ecological status by 2015.

The Habitats and Birds Directive [55] in EU member states is considered the cornerstone of Europe's nature conservation policy. The Directive requires that certain areas are designated as conservation sites (Natura sites) and that the conservation features therein managed such that they are preserved in a natural state. In many EU member states, licensed aquaculture activities take place in Natura sites. The designation does not preclude licensing activities in Natura sites but the licensing process must ensure that the proposed activities do not pose a significant risk to the conservation objectives of the site. In this regard, the licensing authority must be seen to carry out and appropriate assessment on the likelihood of these activities significantly impacting on the conservation features. If the activity is considered impacting, then the licensing authority or the applicant can mitigate with a view to reducing the significance of the impacts and still fulfill both conservation and aquaculture objectives. Similarly, in the USA, the Magnuson-Stevenson Fishery Conservation and Management Act, provides for the protection of essential fish habitat and the restoration of coastal habitats. Both objectives can cause the relocation of shellfish aquaculture operations to less ecologically sensitive areas (e.g., away from seagrass beds). However, the act also provides some opportunity for shellfish aquaculturists from the perspective of the benefits shellfish aquaculture can provide specifically as it relates to habitat restoration goals. The worldwide depletion of natural populations of shellfish in nearshore coastal areas has been well documented (reviewed in National Research Council [18]). The ability of aquaculture to fill the ecological niche previously provided by native populations has been postulated. At a minimum aquaculture has provided stock for the implementation of restoration projects in Chesapeake Bay in Virginia and Maryland [56].

The International Council Exploration of the Sea Code of Practice on the Introductions and Transfers of Marine Organisms [57] is not legislation per se; however, it is cited in legislation and is considered a good example of a guide/code of practice developed in response to particular pressures or risks identified with human activities including, *inter alia*, shellfish aquaculture. The ICES Code of Practice recommends a series of protocols with a view to mitigating any negative risks associated with intentional introductions and transfers of marine organisms and is targeted at individuals or organization that engages in such activities. As an example of specific legislation citing the ICES Code is the European Union regulation concerning use of alien and locally absent species in aquaculture (708/2007/EC). Specifically, the legislation is designed to avoid alterations to ecosystems, prevent negative biological interactions (including genetic change) with indigenous populations, and restrict the spread of nontarget species and detrimental impacts on natural habitats. This legislation directs member states to ensure that a full-risk assessment is carried out prior to the introduction of a nonnative species for aquaculture purposes. In order to facilitate any introduction, the regulator must ensure that the operator mitigate fully any negative interactions identified as a consequence of the risk assessment. The protocols identified in the ICES Code can provide an avenue toward this mitigation.

The Code is aimed at a broad audience since it applies to both public (commercial and governmental) and private (including scientific) interests. In short, any persons engaged in activities that could lead to the intentional or accidental release of exotic species should be aware of the procedures covered by the Code of Practice.

Notwithstanding the potential for regulation to positively guide the development and practice of shellfish aquaculture activities, there is also the risk that regulation can result in constraint of bivalve aquaculture development. This has been demonstrated in the USA where a range of local, state, and federal ordinances govern the licensing of activities in nearshore waters (i.e., areas conducive to bivalve aquaculture). For example, while some coordination has occurred between state and federal agencies in the USA, it still requires up to 30 permits to establish a shellfish culture operation (National Research Council [18]). The complexity can result in a protracted and expensive application process on the part of the aquaculturist that can end with the permit application being refused. The conflict inherent in the regulatory processes is also reflected by conflicts of users in the coastal areas, e.g., wild fishery and aquaculture interests. As a solution to such conflicts, some jurisdictions have implemented zoning of activities where certain activities are only permitted. For example, in an effort to mitigate the conflicts between shellfish culturists and fisherman, some states (Massachusetts and North Carolina) allow shellfish culture in areas where bivalves do not naturally grow. While this offers a somewhat artificial solution to user conflicts, it would appear to favor fishermen, as shellfish typically grow best where they are found naturally in the wild and the availability of approved growing areas might be hard to locate if shellfish are ubiquitous.

Industry Solutions Toward Sustainable Practices

There have been a number of industry-led initiatives that have directly or indirectly led to the implementation of more sustainable practices relating to shellfish culture. As already stated, an important realization among promoters of aquaculture and/or regulatory bodies is that a good understanding of the likely interactions between culture practices and environmental concerns is paramount in order to structure management responses. From the industry perspective, these responses are structured with a view to minimizing the negative environmental interactions while maximizing profits.

Integrated Multi-Trophic Aquaculture

Integrated Multi-Trophic Aquaculture (IMTA) is based upon the principle that the coculture of aquaculture products in carried out in sequence and that one species production is dependent upon the outputs of another [58]. Integration at larger scales may address the optimization of shared resources among various aquaculture users (e.g., shellfish or seaweed culture near fish farms), but assumes that the integrated components (species) are situated within the influence of the system component upon which it directly depends for waste/energy transfer and utilization. In a well-balanced system this relationship provides the environmental benefits associated with polyculture, and is the basis of definitions such as sustainable, or ecological, aquaculture.

Initiatives on the east coast of Canada (New Brunswick) have recently evaluated the performance of mussels (*Mytilus trossulus*) and large macrophytes (*Laminaria*) cultured within the infrastructure of an open net-cage salmon (*Salmo salar*) aquaculture facility (see IMTA chapter) [58]. To date, there have been mixed results in terms of performance of secondary species, i.e., shellfish species in demonstration projects for IMTA; however, there are a number of other perceived benefits of location shellfish operations in the influence of finfish farms. Most notably is the effect of the shellfish on diseases and parasites of the fish species. Concern has been raised about the ability of the shellfish species of retaining and/or transmitting disease-causing organisms to fish species. The counterargument to these concerns is that the shellfish species is likely endemic to the area and may form part of fouling community on structures such that the risk is not magnified by the presence of the species in culture. In addition, a demonstrated benefit is that the blue mussel (*Mytilus edulis*) has been shown to destroy the virus for infectious salmon anemia (ISA) [59]. Furthermore, the blue mussel has also been demonstrated to eat copepodids (the larval stage of the sea louse, a parasite of salmon) [60] and represents a potential alternative control mechanism to sea lice to chemical treatment which have limited efficacy due to a buildup of resistance in the louse.

The environmental benefits of MTA are not constrained solely to the direct assimilation of waste constituents among the cocultured species, but will also be achieved indirectly through the physical design/configuration and orientation of such a system with respect to adjacent, and potentially sensitive marine

habitats. Furthermore, there are a number of perceived social benefits associated with the development of marine integrated aquaculture including: (1) optimizing culture opportunities where space is constrained; (2) the provision of development opportunities in remote coastal regions; and/or (3) improving public awareness of aquaculture or aquaculture subsequent environmental accountability. To this end, in the European Union, the Common Agriculture Policy and Common Fishery Policy requires primary users of the natural resources (e.g., agriculturists, fishermen, aquaculturists) to implement an ecosystem approach in the management and conservation of the environment and landscape. It considers polyculture (MTA) as a viable utilization approach for these areas that could provide restoration at a lower cost for society.

Certification Schemes

The increasing demand from consumers for information pertaining to the products they are consuming has been the primary driver for the development of aquaculture certification schemes. The schemes operate on the principal that aquaculture products are produced in fashion that considers a range of factors including, *inter alia*:

- Social responsibility and comply with laws such that they are produced in a legal, safe, and fair manner
- Environmentally responsible manner such that any negative impacts on the system are minimized
- That all food safety and quality standards are complied with in the member states
- That all animal health issues are considered and managed consistent with legislative requirements

To date, the most prominent schemes are overseen by the Global Aquaculture Alliance (GAA) [61], which is responsible for the development of best aquaculture standards for mostly "fed" aquaculture products, including shrimp hatchery and farm standards. It would appear that there are currently no plans for the GAA to develop standards for bivalve shellfish culture. The Aquaculture Stewardship Council is an association founded jointly by the WWF and Dutch Sustainable Trade Initiative with a view to ensuring aquaculture is carried out in an environmentally and socially sustainable fashion. The ASC has developed standards for the culture of bivalve shellfish products (on foot of the Bivalve Aquaculture Dialogues [62]). The standards are governed by a range of broad principles for addressing the environmental and social issues associated with bivalve aquaculture. These principles are consistent with those identified above. The principles provided the framework for developing the criteria, indicators, and standards applicable to bivalve farming. The standards attempt to provide quantitative performance levels that determine whether a principle is achieved or not. The ultimate goal of ASC is to have comprehensive participation in the certification scheme by shellfish aquaculturists, which is planned to be certified by a third party. In addition to bivalves (clams, oysters, mussels, and scallops) standards have also been established for abalone. In summary, certification standards have been developed by buyers, public agencies, nongovernmental organizations, or marketing groups as a means of providing consumers with information about a product. The ultimate goal of certification schemes is to persuade growers to modify culture practices by influencing consumer choice and market forces. However, pursuit of certification is voluntary for growers.

Best Management Practices

The origin of Best Management Practices (BMPs) dealing specifically with environmental interactions is primarily from broader land-based agricultural practices used to mitigate the effects of soil erosion and nutrient loading. Similarly, mariculture BMPs have been developed with a view to minimizing effects resulting from aquaculture culture practices (see Table 2). Best management practices often are developed or strongly supported by the industry group (e.g., oyster growers) to which they apply and as such, adoption of and adherence to these codes is usually voluntary. As with other practices (cited above) the adoption of BMPs tend to have multiple objectives including, for example, reducing the likelihood that shellfish farming will have unacceptable ecological effects. These effects relate primarily to changes in the ecology of the system and interactions with other stakeholders in the system. As highlighted in Table 2, some examples of BMPs relating to shellfish culture consist of outreach brochures on

Shellfish Aquaculture, Methods of Sustainable. Table 2 Examples of best management practices and environmental standards for the farming of bivalve molluscs produced by a range of organizations, demonstrating the range of topics and the variety of subjects covered. Ecosystem Concepts for Sustainable Bivalve Mariculture by Committee on Best Practices for Shellfish Mariculture and the Effects of Commercial Activities in Drakes Estero, Pt. Reyes National Seashore, California Reproduced with permission of National Academies Press

Author	Affiliation	Scope	Scale	References
U.S. Agency for International Development	Regulator, nongovernmental organization, and academia	Generic guidelines and environmental interactions	International	[151]
World Wildlife Fund	Nongovernmental organization	Environmental interactions	International	[72]
U.S. Department of Agriculture	Regulator	Policy on organic certification and environmental interactions	National	[152]
State of Virginia	Advisory agency, regulator, and industry	Environmental interactions and permitting	State	[153]
Pacific Coast Shellfish Growers Association	Industry	Policy and environmental interactions	Regional	[154]
Seafish (UK)	Regulator, industry, and advisory agency	Alien species interactions	National	[155]
State of Massachusetts	Industry, regulatory, and advisory agency	Environmental interactions, permitting, and husbandry	State (local)	[156]
Maryland Aquaculture Coordinating Council	Industry, regulatory, and advisory agency	Environmental interactions, permitting, and husbandry advice	State	[157]
Ireland	Industry and advisory agency	Generic environmental interactions	National	[158]
Florida Department of Agriculture and Consumer Services	Regulator	Permitting and environmental interactions	State	[159]
International Council for the Exploration of the Sea	International convention	Alien species Interactions	International	[56]
Maine Aquaculture Association	Industry	Environmental interactions and permitting	State	[160]
National Oceanic and Atmospheric Administration	Regulatory	Environmental interactions and policy	National	[161]
Creswell and McNevin (2008)	Academia	Generic guidelines, environmental interactions, and husbandry	International	[162]

Source: From National Research Council [18]

husbandry techniques (e.g., Washington Sea Grant, 2002; Alaska Sea Grant, 2009; University of Maryland, 2009) to identify the optimal ways to culture bivalve molluscs. While these publications focus on methodologies to maximize production, they can still be considered as rudimentary BMPs, in that they require, of the culturists or advisors, a good understanding of the likely interactions between the specific

culture methods and the environment (e.g., performance in light of productivity).

The development of BMPs with a view to managing environmental interactions should be considered a fluid or transitory process that should allow for feedback and subsequent modification of culture practices to mitigate negative effects associated with the shellfish culture.

Some BMPs are usually nontechnical wherein they identify a range of issues and present a framework of general principles and solutions and as such, are unlikely to address the range of detailed and local in aspect, issues that present to regulatory agencies and the producers. Other BMPs do deal with more regional issues, and yet others specifically consider the day-to-day operations at farms and their interactions. These guidelines can provide important advice on pertinent laws and ordinances and focus on important local issues (e.g., environmental interactions, stakeholder interactions, community relationships). In addition, they can identify solutions that range from farm- or small-scale measures to broader societal solutions focusing upon competing uses and values. Toward this end, there are a number of general principles that have applied to the development of BMPs that have directed the practice of shellfish aquaculture toward producing molluscs under the broader umbrella of sustainability. These principles can be broadly categorized under the following headings [50, 63]:

1. Promote a good understanding of environmental and ecological processes, with the broader view of generating carrying capacity models for production areas. This can be further expanded including important socioeconomic considerations also (i.e., ecological and socioeconomic sustainability).
2. Utilize the BMP as a means of promoting the product, i.e., a marketing tool to target a niche market and/or premium price (i.e., economic sustainability).
3. Allow a staged increase in production and reduce uncertainty in terms of environmental interactions (i.e., ecological sustainability).
4. Provide an important communication tool to highlight issues and benefits of shellfish culture to relevant regulatory authorities as well other stakeholders (e.g., nongovernmental organizations) (i.e., social sustainability).

While a goal of implementing BMPs will undoubtedly be the improvement of environmental conditions or mitigation of negative effects caused by the aquaculture activity, there still remains a question of how the effects of the BMP are measured. There can be a sharp distinction between BMPs and performance standards. On the face of it, both schemes are broadly designed to limit risk of undesirable environmental impacts. Some authors [15, 64] correctly note, however, that BMPs are not a proxy for performance and that they may have little or no impact in terms of measurable environmental improvements. Typically there are no measures associated with BMPs to validate the claims about mitigating environmental effects. BMPs, in effect, are akin to design standards, whereby procedures and practices are strictly defined (e.g., number of longlines per hectare) which are relatively easily verified. BMPs, therefore, will have a lower administrative burden for demonstrating compliance by identifying easily measured metrics, but have the drawback that there is no guarantee of environmental benefit. Performance standards, on the other hand, measure specific environmental objectives, i.e., the effect on the activity on some aspect of the environment (e.g., free sulfide concentration in sediments). Performance standards relate more specifically to objectives focusing upon ecological integrity of a system [15]. However, performance standards have resource implications in terms of monitoring and enforcement; they are likely more expensive to administer and implement that BMPs.

Notwithstanding with distinction highlighted between BMPs and performance standards, it is still possible for managers to align husbandry practices with some measure of performance. For example, it is possible for managers to identify the carrying capacity of a system and subsequently advise on the design of husbandry systems. The process must be fluid and allow for changes in practices and standards as more information on effects is gathered and uncertainty is reduced. It also should allow for stakeholder participation to inform management decisions. In this regard, the science underpinning management actions is communicated concisely to all with an interest in the subject matter and that the views and experience of stakeholders are brought to bear on the process.

Measuring Sustainability: The Development of Indicators

Indicators are important management and communication tools used in order to

1. Inform and raise public awareness on environmental issues
2. Provide information linking driving forces and impacts
3. Develop policy responses. To this end, the indicators can be used:
   a. To supply information on environmental problems in order to enable policy makers to value their seriousness
   b. To support policy development and priority setting by identifying key factors that cause pressure on the environment
   c. To monitor the effects of policy decisions

Communication is a primary function of indicators – they should enable or promote information exchange regarding the issue they address. Communication, however, demands simplicity and therefore indicators should always simplify complex realities. Sustainability indicators are different from "impact" indicators in that they tend to be more inclusive and consider not only environmental issues but also social and economic features [3]. Based upon these broad criteria, sustainability indicators represent an amalgam of the Integrated Coastal Area Management (ICAM) guidance of the United Nations Educational, Scientific, and Cultural Organisation (UNESCO) recommends three basic categories of indicators:

1. Environmental: Reflect trends in the state of the environment; are descriptive in nature; and become performance indicators if they compare actual conditions to desired conditions expressed in terms of environmental targets.
2. Socioeconomic: Represent the demographics of humans in the coastal zone and measure quality of life issues.
3. Governance: Measure the performance of the state of implementation, measuring the progress and quality of interventions of the governance process in relation to program goals set at the outset.

To this end, sustainability indices (SIs) are needed by aquaculture resource managers who must sort through large amounts of information and make numerous decisions relating to environmental management and policy implementation. SIs, therefore, offer a means to prioritize those aquaculture systems most in need of immediate management attention and allow scarce management assets to be applied in the most cost-effective manner. The development and subsequent utilization of SIs are also valuable to owners of seafood businesses who wish to procure or develop "sustainable seafoods," i.e., as a marketing tool.

Well-developed and scientifically credible SIs are important tools which can make a range of ventures including monitoring, baseline data collection, research enterprises, and communications efforts better organized and targeted, and thereby, more cost effective. Therefore, indicators must be selected or developed and cover the three components of sustainability. It has been argued that indicators should be as quantitative as possible. While this is a practical goal, some descriptors do not lend themselves as easily to quantitative measurements and therefore qualitative descriptions may be more appropriate for describing, say, for example, the social aspects of sustainability [3].

Indicators must be measurable objects that can be simplified by aggregation and calculation. Outcomes from theoretical models cannot be considered as indicators. Nevertheless, models may help to indicate the most relevant factors to be monitored. Ideally, indicators might address the following issues:

- Continuity of supply (environmental, economic, and social services)
- Social, economic, and environmental costs to provide this continuity of supply
- Long-term aspects
- Financial viability
- Social and ecological impacts
- Global efficiency

Environmental Indicators

While there is considerable effort directed toward the development of indicators for coastal areas throughout the world, the focus primarily remains on environmental

indicators that link specific pressures with impacts. The development in European Union Member States of indicators relating to the implementation of the Water Framework Directive [52, 65] is a clear example of one such endeavor. Indicators developed in response to this legislation, for the most part, are responsive to a range of pressures. The development of sustainability indicators (particularly those targeted at shellfish aquaculture) is at a more nascent stage. It is broadly accepted that sustainability indicators for shellfish aquaculture (and aquaculture generally) should encompass the criteria outlined previously, i.e., track aquaculture's (positive and negative) impacts on the environment and be able to monitor economic, social, and cultural externalities, as well as evaluate governance impacts of policies and regulatory measures on aquaculture. Once accepted as practical tools, SIs need to be ultimately included in codes of best practices, decision support systems, and should be used by managers to steer aquaculture development and how it might interact with other activities and features in the marine environment.

Composite Sustainability Indices

While it is possible to assess sustainability with several indicators [66], it may sometimes be difficult to make decisions and comparisons among sectors, production systems, or companies based on a large number of performance measurements. To help decision makers in this respect, it may be useful to use composite sustainable development index, linking many sustainability issues and so reducing the number of decision-making criteria that need to be considered.

In recent years, research has focused on the development of composite indices mostly for cross-national comparisons of economic, societal, environmental, and/or sustainable progress of nations in a quantitative fashion [67]. Care must be taken in the development of composite indicators as, for example, weighting of constituent indicators can be applied subjectively without any clear quantitative basis. However, this may be corrected by the application of sensitivity analysis whereby weightings are adjusted to reflect the true influences of indicators (and by association, pressures). In addition, the selection of the indicators to be used in a composite indicator is crucial to the utility of a sustainability indicator. A solution to this is it requires a transparent and inclusive process to determine how and who will select the most appropriate indicators [50]. Such a process should avoid risks associated with too much complexity as well as concerns about the costs associated with monitoring multiple indicators that could be irrelevant to managers and the public. Usable indicators must be more than just a description of state and should have diagnostic properties that lead to some insights into processes taking place (i.e., provide a specific link to the pressure under consideration).

As previously stated, SIs for environmental and aquaculture management are still in the early stages of development. However, some investigators [68] have recommended a simple set of easily quantifiable indicators for sustainability in aquaculture (generally) and which broadly reflect the criteria outlined previously describing sustainability indicators:

- Biological: domestication, trophic level, nutrient/energy conversion
- Ecological: footprint, emissions, escapes
- Intersectoral: water sharing, diversity, cycling, stability, and capacity

The development of tool-box approach toward assessing sustainability for aquaculture has been proposed [60]. This approach has been taken further with the utilization of indicators specifically to shellfish culture operations [69] with the production of guidance for effective site selection and targeted approach to conducting environmental impact assessments and establishing monitoring standards. Furthermore, the incorporation of a stakeholder consultation process in order to identify the most pertinent indicators has also been incorporated into a variety of initiatives.

Notwithstanding the relatively slow progress toward the development of specific indicators of sustainability for shellfish aquaculture, there are still a number of clear criteria proposed that can help define and direct future development efforts. These are best elucidated by the International Council for the Exploration of the Sea [70] which has addressed the issue of sustainability in aquaculture over the last number of years. They offer some general principles on sustainability indices and how they relate to aquaculture activities (including shellfish culture). The basic points

below summarize much of the previous discussion and are as follows:

1. It is important to discern the differences between "sustainability" indicators and "impact" indicators which are narrow in their focus. Sustainability indicators should be able to track more than aquaculture's impacts on the environment and be able to monitor economic, social, and cultural externalities, as well as evaluate governance impacts (e.g., policies and regulatory measures) on aquaculture and the environment broadly.
2. Once accepted, SIs should be ultimately included in codes of best practices (BMPs), decision support systems, and should be used to inform aquaculture development by the authorities (e.g., integrated coastal zone management systems, see below).
3. Sustainability indices must be of the highest scientific credibility and be accepted only after peer review of the chosen index, and analyses of precision, accuracy, reliability, and consistency are completed. It may be contrary to the criteria outlined above but the SIs must also be cost-effective and be applicable across a range of environments, habitat types, and activities.
4. SIs must be flexible enough to be adapted to the local environment in which they will be used. There is no chance that a single set of "generic" indicators may be universally applicable and used in all the situations in the aquaculture sector. In addition, SIs may be of use to address the interactions with other users of marine resources, locally or internationally because of the opening of global markets.
5. In the development of SIs for aquaculture it is important to develop them collaboratively and consider SIs from a managers' and other stakeholders' perspective. Managers are a critical link between the science community and the public. Collaborations between managers, scientists, and the public should be formalized to facilitate rapid decision-making and communication. It is important that levels that exceed those which are accepted by the society are scientifically credible so that managers can determine causative agents and what remediation actions are necessary.
6. SIs must be able to detect the linkages between the 3Ps – people, profit, planet – which suggests a development of a "sustainability indicator matrix." Such a matrix approach could allow flexibility and be able to address the sustainability factors more comprehensively for any given situation. Regular evaluation of SIs may be necessary among the various actors assessing aquaculture developments, e.g., producers, policy makers, consumers, NGOs, suppliers, since aquaculture technologies and site locations are constantly evolving.
7. To this end it is important to emphasize that SIs must be sustainable themselves. The production of information must be practicable at a low cost for the government, public, and the aquaculture sectors. Data from SIs must provide meaningful long-term data series. These time series will need to be housed in data management frameworks at the institutional level, but be universally accessible.

Progressing Sustainability in Shellfish Aquaculture

Heretofore, the difficulty in developing a single (composite) indicator relating to shellfish aquaculture remains and one has yet to be definitively proposed. This is borne out by the general conclusion that the majority of exercises examining the sustainability of aquaculture operations recommend only specific and localized "sustainability" (or impact) indicators, without fully addressing the sustainability of aquaculture from an interactive perspective. It is generally accepted that the main goal of these programs is to determine an acceptable aquaculture production capacity for a defined area. It is also accepted that aquaculture activities should be managed while fully cognizant of other activities in a particular area. Consequently, the likely impacts of aquaculture will, therefore, have to be assessed individually, cumulatively (with other aquaculture operations), and in combination with other activities, on the environment, ecosystem, and function of a system. The interactions and impacts of aquaculture have been well documented; it has been this information that has provided the framework for many monitoring programs for aquaculture operations. The notion of acceptability is critical to fully determining the sustainability of an activity in the marine environment. The term "acceptable" is governed primarily by

social values, starting from a global to local perspectives. The social carrying capacity of aquaculture should be the basis of a sustainability program to assess the sum of activities, such as aquaculture, within a defined area. The principles of these programs could flow from global vision, with regionally based criteria. For example, no net loss or biodiversity may be a global vision.

Considering the goal of ensuring sustainable levels of activities in the marine environment, the application of Integrated Coastal Zone Management (ICZM) is likely to be an important tool toward achieving this objective. As already highlighted, the importance of linking social, economic, and environmental aspects into the management of marine systems is critical as well as the need to have broad sectoral cooperation and input into the development of these practices.

ICZM facilitates a shift from management and regulation of activities in the marine environment in isolation to a system where all activities can be considered and the resource use is optimized with a view to maintaining the health and productivity of coastal ecosystems so that they can continue to supply resources that sustain different forms of activity, including mariculture. While these goals are lofty, the implementation will be challenging. Benthic and pelagic effects of shellfish culture are well documented in the literature (from both modeled and empirical studies). The risk posed by practices associated with aquaculture (both finfish and shellfish) have also been well documented and evaluated in the areas of disease transmission and introductions of exotic species to areas. The *in-depth* knowledge relating to these impacts and interactions have placed the pressures posed by mariculture to the forefront in terms of public awareness and criticism. Ironically the lack of information pertaining to other pressures may be a reason they have not been the focus of scrutiny or criticism (e.g., static gear fisheries, sewage effluent discharges over broad spatial scales). ICZM can be supported by the development of appropriate decision support systems (DSS), i.e., in the form of conceptual models allied with the presentation of geospatial data in geographic information systems (GIS) can be used to identify what would seem to be the most appropriate use of marine ecosystems. The term "use" also includes nonexploitive activities particularly in areas that have high intrinsic natural value or have some protection conferred by legislation (e.g., national parks).

The social science dimension is an important component on the issue of ICZM [50, 65]. Application of social science principles will facilitate a better understanding of the expectations of different stakeholders competing for space and resources in coastal areas and help establish a consensus among relevant users. More specifically, a recent initiative in France [71] called EVAD (ÉVAluation de la Durabilité des systemés aquacole) addressed the issue of aquaculture sustainability by examining the contribution that aquaculture systems make to the sustainability at regional levels. The first component of this approach much merit and could be an important component into an Integrated Coastal Zone Management program. Similarly an ecosystem approach to aquaculture management that is comprehensive and based on the best available scientific knowledge of the ecosystem and its dynamics is also proposed by numerous fora [72, 73]. Actions are designed to be taken on the influences of aquaculture developments that are critical to the health of ecosystems, thereby achieving sustainable uses of ecosystem goods and services and maintenance of ecosystem integrity. In these instances, the aim is to assess the sustainability of all the activities in an area where aquaculture is fully and fairly integrated rather than the sustainability of aquaculture in isolation. At that point, indicators can be developed, negotiated, and used to evaluate the effect or impact (positive or negative) of aquaculture and other activities (drivers) on the sustainable utilization of resources in a region, based upon the global principals and the regional-territorial criteria. Sustainability would thereby no longer be assessed by indicators of impacts, but mainly criteria based on objectives instead of thresholds. The sustainability of all activities within a region would thereby be evaluated on the merit of criteria developed under an Integrated Coastal Zone Management (ICZM) approach. It is important to note that assessment of sustainability at the activity level can lead to the establishment of thresholds that can be ineffective or even detrimental to the activity which may only contribute marginally to one or several criterion. In addition, smaller aquaculture operations would not be constrained by the responsibility of monitoring the sustainability of an area, because they are the newer addition to the coastal zone territory, already affected by numerous players.

Future Directions

Sustainability by definition and in application must include consideration of planning for multiple impacts and identifying the likely challenges posed by existing and future development and conservation (general sense) needs. To this end, sustainability therefore refers to the ability of a society to continue functioning in the future without being forced into decline through exhaustion or overloading of key resources upon which society's systems rely [74]. Proponents of shellfish aquaculture [75] propose that the accelerated development of aquaculture in a sustainable fashion is a realistic goal going forward. Consistent with the broad view offered above, the focus for aquaculture development should be to manage existing activities and proposed expansions in coincidence with other activities in marine systems such that the management actions are fully integrated, and that any impacts will be at a minimum, neutral on both natural and social ecosystems [76]. It is appreciated that some codes of conduct and guidelines for certifying sustainability are sometimes too complex and narrowly focused. Therefore, there would be an imperative on the part of managers to see to it that inclusive yet simple and scientifically credible sustainability indices for mariculture activities are developed and are considered a cost-effective complement to any codes employed. This would be driven by the need of regulatory or licensing agents to have systems with which to take defendable decisions relating to management of marine issues. Furthermore, the need to communicate in a transparent, concise, and credible fashion the likely issues relating to shellfish culture activities to consumers is another important justification toward the development of sustainability indices for shellfish culture.

In summary, a SI applicable to shellfish aquaculture should be able to incorporate all information in a system, identify what the goals (global vision) for the system are, and evaluate both positive and negative aspects of any proposed development. It should be able to determine if the positive aspects outweigh the negative ones such that a decision to permit the activity can be taken. In other words, will the mitigation of eutrophication effects afforded by the filtration of shellfish outweigh the increased biodeposition beneath the culture structures? While these considerations apply generally to all activities and how they interact with the natural environment (both terrestrial and aquatic), they also provide a framework with which to focus more clearly on specific activities in the marine environment and how these activities interact with features therein. However, it has become clear that the application of these concepts have not been fully implemented because it is apparent that such generalities apply at the level of the (eco)system and are difficult to apply at the level of specific activities and/or environmental features. It is apparent that in order to fully implement these definitions and take a total view of sustainability in the marine environment, it is the job of managers to apply a system-wide view of sustainability. Such an initiative would have to take into account a broad range of pressures and would have to define clearly what might be permissible and acceptable (i.e., social carrying capacity guided by legislative or policy drivers). Such an initiative would have to consider both spatial and temporal considerations of pressures (activities) and sensitivities. Of considerable importance, however, is that the development of management systems must be informed by a clear notion of an acceptable endpoint that would be either defined as the level that a particularly activity (or range of activities) might be carried out in the marine environment or the maintenance of a specific condition of an environmental feature (environmental standard). It is important to point out that, to date, sustainability has been a much used word with abundant pedagogy but little practice [77] (this article is a case in point). It would appear that progression toward truly sustainable practices is hampered when there is a clear need for interdisciplinary actions but there is little scientific knowledge to inform these actions. This contribution highlights, we hope, that the mechanism toward identifying sustainable activities in the marine environment will be progressed when clear policies are elucidated and an inclusive approach is adopted reflecting fully legislative requirements and the views of all stakeholders.

Bibliography

Primary Literature

1. Food and Agriculture Organization of the United Nation (2009) The state of world fisheries and aquaculture 2008. Food and Agriculture Organization of the United Nation, Rome

2. Tucker CS, Hargreaves JA, Boyd CE (2008) Aquaculture and the environment in the United States. In: Tucker CS, Hargreaves JA (eds) Environmental best management practices for aquaculture. Blackwell, Ames, pp 3–54
3. Costa-Pierce BA, Page GG (2011) Sustainability science in aquaculture. In: Meyers RA (ed) Encyclopedia of sustainability science and technology. Springer, New York
4. Helm M, Bourne N (2004) Hatchery culture of bivalves: a practical manual. Food and Agriculture Organization of the United Nations, Rome
5. Duarte CM, Holmer M, Olsen Y, Soto D, Marba N, Guiu J, Black J, Karakassis I (2009) Will the oceans help feed humanity? Bioscience 59:967–976
6. Pearson T, Rosenberg R (1978) Macrobenthic succession in relation to organic enrichment and pollution of the marine environment. Oceanogr Mar Biol Ann Rev 16:229–311
7. Chamberlain J, Fernandes TF, Read P, Nickell TD, Davies IM (2001) Impacts of biodeposits from suspended mussel (*Mytilus edulis* L.) culture on the surrounding surficial sediments. ICES J Mar Sci 58:411–416
8. Weise AM, Cromey CJ, Callier MD, Archambault P, Chamberlain J, McKindsey CW (2009) Shellfish-DEPOMOD: modelling the biodeposition from suspended shellfish aquaculture and assessing benthic effects. Aquaculture 288: 239–253
9. Nugues MM, Kaiser MJ, Spencer BE, Edwards DB (1996) Benthic community changes associated with intertidal oyster cultivation. Aquac Res 27:913–924
10. Dame RF (1996) Ecology of marine bivalves: an ecosystem approach. CRC Press, Boca Raton
11. Jackson JBD, Kirby MX, Berger WH, Bjorndal KA, Botsford LW, Bourque BJ, Bradbury RH, Cooke R, Erlandson J, Estes JA, Hughes TP, Kidwell S, Lange CB, Lenihan HS, Pandolfi JM, Peterson CH, Steneck RS, Tegner MJ, Warner RR (2001) Historical overfishing and the recent collapse of coastal ecosystems. Science 295:629–637
12. Newell RIE, Koch EW (2004) Modeling seagrass density and distribution in response to changes to turbidity stemming from bivalve filtration and seagrass sediment stabilization. Estuaries 27:793–806
13. DeAngelis DL, Post WM, Travis CC (1986) Positive feedback in natural systems. Springer, Berlin
14. Lotze HK, Lenihan HS, Bourque BJ, Bradbury RH, Cooke RG, Kay MC, Kidwell SM, Kirby MX, Peterson CH, Jackson JBC (2006) Depletion, degradation, and recovery potential of estuaries and coastal seas. Science 312:1806–1809
15. Newell RIE, Fisher TR, Holyoke RR, Cornwell JC (2005) Influence of eastern oysters on N and P regeneration in Chesapeake Bay, USA. In: Dame R, Olenin S (eds) The comparative roles of suspension-feeders in ecosystems: proceedings of the NATO advanced research workshop on the comparative roles of suspension-feeders in ecosystems, Nida, 4–9 Oct 2003. Springer, Dordrecht
16. Newell RIE, Kemp WM, Hagy JD, Cerco CF, Testa JM, Boynton WR (2007) Top-down control of phytoplankton by oysters in Chesapeake Bay, USA: comment on Pomeroy et al. (2006). Mar Ecol Prog Ser 341:293–298
17. Pomeroy LR, D'Elia CF, Schaffner LC (2006) Limits to top-down control of phytoplankton by oysters in Chesapeake Bay. Mar Ecol Prog Ser 325:301–309
18. National Research Council (2010) Ecosystems concepts for sustainable bivalve culture. Academic, Washington, DC
19. Carlton JT (1992) Introduced marine and estuarine mollusks of North America: an end-of-the-20th-century perspective. J Shellfish Res 11:489–505
20. Carlton JT (1992) Dispersal of living organisms into aquatic ecosystems as mediated by aquaculture and fisheries activities. In: Rosenfield A, Mann R (eds) Dispersal of living organisms into aquatic ecosystems. Maryland Sea Grant, College Park, pp 13–46
21. Naylor RL, Williams SL, Strong DR (2001) Aquaculture – a gateway for exotic species. Science 294:1655–1656
22. Streftaris N, Zenetos A, Papathanassiou E (2005) Globalisation in marine ecosystems: the story of non-indigenous marine species across European seas. Oceanogr Mar Biol Ann Rev 43:419–453
23. McKindsey CW, Landry T, O'Beirn FX, Davies IM (2007) Bivalve aquaculture and exotic species: a review of ecological considerations and management issues. J Shellfish Res 26:281–294
24. Ruesink JL, Lenihan HS, Trimble AC, Heiman KW, Micheli F, Byers JE, Kay MC (2005) Introduction of non-native oysters: ecosystem effects and restoration implications. Annu Rev Ecol Syst 36:643–689
25. Grizel H, Heral M (1991) Introductions into France of the Japanese oyster (*Crassostrea gigas*). ICES J Mar Sci 47:339–403
26. Reise K (1998) Pacific oysters invade mussel beds in the European Wadden. Senckenbergiana maritima 28:167–175
27. Drinkwaard AC (1999) Introductions and developments of oysters in the North Sea area: a review. Helgolander Meeresun 52:301–308
28. Branch GM, Steffani CN (2004) Can we predict the effects of alien species? A case-history of the invasion of South Africa by *Mytilus galloprovincialis* (Lamarck). J Exp Mar Biol Ecol 300:189–215
29. Smaal AC, van Stralen M, Craeymeersch J (2005) Does the introduction of the pacific oyster Crassostrea gigas lead to species shifts in the Wadden sea? pp 277-289. In: Dame R, Olenin S (eds). The comparative roles of suspension-feeders in ecosystems. Proceedings NATO ARW, Nida. Kluwer Academic, Dordrecht, NL
30. Diederich S (2005) Differential recruitment of introduced Pacific oysters and native mussels at the North Sea coast: coexistence possible? J Sea Res 53:269–281
31. Smaal A, Wijsman J, Poelman M (2006) Proliferation of the pacific oyster, *Crassostrea gigas* in Dutch coastal waters and its consequence for human use. In: ICES annual science conference, Maastricht
32. Carlton JT (1989) Man's role in changing the face of the ocean: biological invasions and implications for conservation of near-shore environments. Conserv Biol 3:265–273

33. Carlton JT (1999) Molluscan invasions in marine and estuarine communities. Malacologia 41:439–454
34. Barber BJ (1996) Impacts of Shellfish introductions on local communities. In: Pedersen J (ed) Exotic species workshop: issues relating to aquaculture and biodiversity. MIT Sea Grant College Program (MITSG 96–15), Cambridge, pp 18–21
35. Bourque D, Landry T, Davidson J, McNair N (2003) Impact of an invasive tunicate in Atlantic Canada: recruitment and competition. J Shellfish Res 22:320
36. Carver CE, Chisholm A, Mallet A (2003) Strategies to mitigate the impact of *Ciona intestinalis* (L.) biofouling on shellfish production. J Shellfish Res 22:621–631
37. Rodriguez LF (2005) Novel habitats created by non-indigenous species: the role of oysters and ascidians as biological substrata for fouling communities. In: Carman M (ed) International invasive sea squirt conference, Woods Hole Oceanographic Institution, 21–22 Apr 2005, pp 17/59
38. Locke A, Hanson JM, Ellis KM, Thompson J, Rochette R (2007) Invasion of the southern Gulf of St. Lawrence by the clubbed tunicate (*Styela clava* Herdman): potential mechanisms for invasions of Prince Edward Island estuaries. J Exp Mar Biol Ecol 342(1):69–77
39. Wasson K, Zabin CJ, Bedinger L, Diaz MC, Pearse JS (2001) Biological invasions of estuaries without international shipping: the importance of intraregional transport. Biol Conserv 102:143–153
40. Minchin D (1996) Management of the introduction and transfer of marine molluscs. Aquat Conserv Mar Freshwater Ecosyst 4:229–244
41. Ribera-Siguan MA (2003) Pathways of biological invasions of marine plants. In: Ruiz GM, Carlton JT (eds) Invasive species: vectors and management strategies. Island Press, Washington, DC, pp 183–226
42. Gollasch S (2006) Overview on introduced aquatic species in European navigational and adjacent waters. Helgol Mar Res 60:84–89
43. Wonham MJ, Carlton JT (2005) Trends in marine biological invasions at local and regional scales: the Northeast Pacific Ocean as a model system. Biol Invasions 7:369–392
44. Goulletquer P, Bachelet G, Sauriau PG, Noel P (2002) Open Atlantic coasts of Europe – a century of introduced species into French waters. In: Leppäkoski E, Gollasch S, Olenin S (eds) Invasive aquatic species of Europe: distribution, impacts and management. Kluwer, Dordrecht, pp 276–290
45. Barton E, Heard J (2005) Alien, non-native and invasive marine species. The marine biological association of the United Kingdom and the marine life information network for Britain and Ireland. http://www.marlin.ac.uk/PDF/MLTN_alien_non_natives.pdfs. Accessed Aug 2011
46. Blanchard M (1997) Spread of the slipper limpet *Crepidula fornicata* (L.1758) in Europe. Current state and consequences. Sci Mar 61(Suppl 9):109–118
47. De Montaudouin X, Labarraque D, Giraud K, Bachelet G (2001) Why does the introduced gastropod *Crepidula fornicata* fail to invade Arcachon Bay (France)? J Mar Biol Assoc UK 81:97–104
48. Critchley AT, Dijkema R (1984) On the presence of the introduced brown alga *Sargassum muticum*, attached to commercially imported *Ostrea edulis* in the S. W. Netherlands. Bot Mar 27:211–216
49. Maggs CA, Stegenga H (1999) Red algal exotics on North Sea coasts. Helgolander Meeresun 52:243–258
50. Verlaque M (2001) Checklist of the macroalgae of Thau Lagoon (Herault, France), a hot spot of marine species introduction in Europe. Oceanol Acta 24:29–49
51. Beadman HA, Kaiser MJ, Galanidi M, Shucksmith R, Willows RI (2004) Changes n species richness with stocking density of marine bivalves. J Appl Ecol 41:464–475
52. Kaiser MJ (2001) Ecological effects of shellfish cultivation. In: Black KD (ed) Environmental impacts of aquaculture. CRC Press, Boca Raton
53. Regulation 854/2004/EC of the European Parliament and of the Council of 29 April 2004 laying down specific rules for the organisation of official controls on products of animal origin intended for human consumption. http://eur-lex.europa.eu/LexUriServ/LexUriServ.do?uri=CELEX:32004R0854:EN:NOT
54. Directive 2000/60/EC of the European Parliament and of the Council of 23 October 2000 establishing a framework for community action in the field of water policy. http://ec.europa.eu/environment/water/water-framework/index_en.html. Accessed Aug 2011
55. Directive 92/43/EEC of 21 May 1992 on the conservation of natural habitats and of wild fauna and flora. online: http://eur-lex.europa.eu/LexUriServ/LexUriServ.do?uri=CELEX:31992L0043:EN:NOT. Accessed Oct 2011
56. Luckenbach MW, Mann R, Wesson JA (eds) (1999) Oyster reef habitat restoration. A synopsis and synthesis of approaches. Virginia Institute of Marine Science, Gloucester Point, p 358
57. ICES (2005) International council for the exploration of the sea code of practice on the introductions and transfers of marine organisms, 30 pp
58. Chopin T (2011) Integrated multi-trophic aquaculture (IMTA). In: Meyers RA (ed) Encyclopedia of sustainability science and technology. Springer, New York
59. Skar CK, Mortensen S (2007) Fate of infectious salmon anaemia virus (ISAV) in experimentally challenged blue mussels *Mytilus edulis*. Dis Aquat Organ 74:1–6
60. Molloy SD, Pietrak MR, Bouchard DA, Bricknell I (2011) Ingestion of *Lepeophtheirus salmonis* by the blue mussel *Mytilus edulis*. Aquaculture 311:61–64
61. Global Aquaculture Alliance (2011) Best Aquaculture Practices Program. online http://www.gaalliance.org/bap/. Accessed Oct 2011
62. World Wildlife Fund (2010) Bivalve aquaculture dialogue standards, 50 pp. http://www.worldwildlife.org/what/globalmarkets/aquaculture/WWFBinaryitem17872.pdf. Accessed Aug 2011
63. McKindsey CW, Thetmeyer H, Landry T, Silvert W (2006) Review of recent carrying capacity models for bivalve culture and recommendations for research and management. Aquaculture 261(2):451–462

64. Clay JW (2008) The role of better management practices in environmental management. In: Tucker CS, Hargreaves JA (eds) Environmental best management practices for aquaculture. Wiley, Hoboken
65. Carletti A, Heiskanen A-S (eds) (2009) Water framework directive intercalibration technical report part 3: coastal and transitional waters. JRC scientific and technical reports no. 51341, 244 pp. http://publications.jrc.ec.europa.eu/repository/bitstream/111111111/10473/1/3010_08-volumecoast.pdf. Accessed Oct 2011
66. Caffey RH, Kazmierczak RF, Avault Jr JW (2001) Developing consensus indicators for sustainability for southeastern United States aquaculture. LSU Agriculture Center Bulletin Number 879, Baton Rouge
67. Krajnc D, Glavic P (2005) A model for integrated assessment of sustainable development. Resour Conserv Recy 43:189–208
68. Pullin R, Froese R, Pauly D (2001) Indicators for the sustainability of aquaculture. In: Bert T (ed) Ecological and genetic implications of aquaculture activities. Kluwer, Dordrecht
69. Scottish Association for Marine Science, Oban, Scoltland (2004) ECASA- An Ecosystem Approach for Sustainable aquaculture. EU Framework 6 RTD project. (www.ecasa.org.uk). Accessed Oct 2011
70. ICES (2005) Report of the Working Group on Environmental Interactions of Mariculture (WGEIM), 11–15 Apr 2005, Ottawa. CM 2005/F:04, 112 pp
71. Rey-Valette H, Clément O, Aubin J, Mathé S, Chia E, Legendre M, Caruso D, Mikolasek O, Blancheton J-P, Slembrouck J, Baruthio A, René F, Levang P, Morissens P, Lazard J (2008) Guide to the co-construction of sustainable development indicators in aquaculture, 144 pp. © Cirad, Ifremer, Inra, IRD, Université Montpellier 1; Diffusion: Cirad-Montpellier
72. ICES (2009) Report of the Working Group for Marine Shellfish Culture (WGMASC). 7–9 Apr 2009, Bremerhaven, ICES CM 2009/MCC:02
73. Soto D, Aguilar-Manjarrez J, Bermúdez J, Brugère C, Angel D, Bailey C, Black K, Edwards P, Costa-Pierce B, Chopin T, Deudero S, Freeman S, Hambrey J, Hishamunda N, Knowler D, Silvert W, Marba N, Mathe S, Norambuena R, Simard F, Tett P, Troell M, Wainberg A (2008) Applying an ecosystem-based approach to aquaculture: principles, scales and some management measures. In: Soto D, Hishamunda N (eds) Building an ecosystem approach to aquaculture. Food and Agriculture Organization of the United Nations, Rome
74. Frankic A, Hershner C (2003) Sustainable aquaculture: developing the promise of aquaculture. Aquacult Int 11: 517–530
75. Costa-Pierce BA (2002) Ecological aquaculture. Blackwell, Oxford, UK
76. Byron C, Bengtson D, Costa-Pierce B, Calanni J (2011) (2011) Integrating science into management: ecological carrying capacity of bivalve shellfish aquaculture. Marine Policy 35:363–370
77. Ecological Aquaculture (2011) online: http://ecologicalaquaculture.org/welcome/the-future-of-the-blue-revolution/sustainable-aquatic-foods. Accessed Oct 2011
78. Mallet AL, Carver CE, Landry T (2006) Impact of suspended and off-bottom Eastern oyster culture on the benthic environment in eastern Canada. Aquaculture 255:362–373
79. Mallet AL, Carver CE, Hardy M (2009) The effect of floating bag management strategies on biofouling, oyster growth and biodeposition levels. Aquaculture 287:315–323
80. Rodhouse PG, Roden CM (1987) Carbon budget for a coastal inlet in relation to intensive cultivation of suspension-feeding bivalve molluscs. Mar Ecol Prog Ser 36:225–236
81. Christensen PB, Glud RN, Dalsgaard T, Gillespie P (2003) Impacts of longline mussel farming on oxygen and nitrogen dynamics and biological communities of coastal sediments. Aquaculture 218:567–588
82. Mesnage V, Ogier S, Bally G, Disnar JR, Lottier N, Dedieu K, Rabouille C, Copard Y (2007) Nutrient dynamics at the sediment–water interface in a Mediterranean lagoon (Thau, France): influence of biodeposition by shellfish farming activities. Mar Environ Res 63:257–277
83. Richard M, Archambault P, Thozeau G, McKindsey CW, Desrosiers G (2007) Influence of suspended scallop cages and mussel lines on pelagic and benthic biogeochemical fluxes in havre-aux-Maisons lagoon, Iles-de-la-Madelaine (Quebec, Canada). Can J Fish Aquat Sci 64:1491–1505
84. Hargrave BT, Doucette LI, Cranford PJ, Law BA, Milligan TG (2008) Influence of mussel aquaculture on sediment organic enrichment in a nutrient-rich coastal embayment. Mar Ecol Prog Ser 365:137–149
85. De Grave S, Moore SJ, Burnell G (1998) Changes in benthic macrofauna associated with intertidal oyster, *Crassostrea gigas* (Thunberg) culture. J Shellfish Res 17:1137–1142
86. Ysebaert T, Hart M, Herman PMJ (2009) Impacts of bottom and suspended cultures of mussels *Mytilus* spp. on the surrounding sedimentary environment and macrobenthic biodiversity. Helgoland Mar Res 63:59–74
87. Callier MD, McKindsey CW, Desrosiers G (2008) Evaluation of indicators used to detect mussel farm influence on the benthos: two case studies in the Magdalen Islands, Eastern Canada. Aquaculture 278:77–88
88. Grant J, Hatcher A, Scott DB, Pocklington P, Schafer CT, Winters GV (1995) A multidisciplinary approach to evaluating impacts of shellfish aquaculture on benthic communities. Estuaries 18:124–144
89. Murray LG, Newell CR, Seed R (2007) Changes in the biodiversity of mussel assemblages induced by two methods of cultivation. J Shellfish Res 26:153–162
90. Dahlbäck B, Gunnarsson LAH (1981) Sedimentation and sulfate reduction under mussel culture. Mar Biol 63: 269–275
91. Tenore KR, Boyer LF, Cal RM, Corral J, García-Fernández C, González N, González-Gurriaran E, Hanson RB, Iglesias J, Krom M, López-Jamar E, McClain J, Pamatmat MM, Pérez A, Rhoads DC, deSantiago G, Tietjen J, Westrich J, Windom HL (1982) Coastal upwelling in the Rias Bajas, N.W. Spain: contrasting the benthic regimes of the Rias de Arosa and de Muros. J Mar Res 40:701–772

92. Kautsky N, Evans S (1987) Role of biodeposition by *Mytilus edulis* in the circulation of matter and nutrients in a Baltic coastal ecosystem. Mar Ecol Prog Ser 38:201–212
93. Giles H, Pilditch CA (2006) Effects of mussel (*Perna canaliculus*) biodeposit decomposition on benthic respiration and nutrient fluxes. Mar Biol 150:261–271
94. Mattsson J, Linden O (1983) Benthic macrofauna succession under mussels, *Mytilus edulis* L. (Bivalvia), cultured on hanging long-lines. Sarsia 68:97–102
95. Hartstein ND, Rowden AA (2004) Effect of biodeposits from mussel culture on macroinvertebrate assemblages at sites of different hydrodynamic regime. Mar Environ Res 57:339–357
96. Dumbauld BR, Ruesink JL, Rumrill SS (2009) The ecological role of bivalve shellfish aquaculture in the estuarine environment: a review with application to oyster and clam culture in West Coast (USA) estuaries. Aquaculture 290:96–223
97. Tallis HM, Ruesink JL, Dumbauld BR, Hacker SD, Wisehart LM (2009) Oysters and aquaculture practices affect eelgrass density and productivity in a Pacific Northwest estuary. J Shellfish Res 28:251–261
98. Brooks KM (2004) The fouling community found in association with the intensive raft culture of *Mytilus edulis galloprovincialis* in Totten Inlet, Washington. Report to the national oceanic and atmospheric administration, Seattle
99. Switzer SE, Barnes PA, McKinley RS (2008) Invertebrate fouling community composition and succession associated with Pacific oyster *Crassostrea gigas* deep-water suspended tray culture. Abstract. J Shellfish Res 27:1055
100. McKindsey CW, Lecuona M, Huot M, Weise AM (2009) Biodeposit production and benthic loading by farmed mussels and associated tunicate epifauna in Prince Edward Island. Aquaculture 295:44–51
101. Lambert G (2007) Invasive sea squirts: a growing global problem. J Exp Mar Biol Ecol 342:3–4
102. Grant J, Stenton-Dozey JME, Monteiro P, Pitcher G, Heasman K (1998) Shellfish culture in the Benguela System: a carbon budget of Saldanha Bay for raft culture of *Mytilus galloprovincialis*. J Shellfish Res 17:41–49
103. Ramsay A, Davidson J, Landry T, Arsenault G (2008) Process of invasiveness among exotic tunicates in Prince Edward Island. Canada. Biol Invasions 10:1311–1316
104. Comeau LA, Drapeau A, Landry T, Davidson J (2008) Development of longline mussel farming and the influence of sleeve spacing in Prince Edward Island Canada. Aquaculture 281:56–62
105. Heral M (1993) Why carrying capacity models are useful tools for management of bivalve molluscs culture. In: Dame RF (ed) Bivalve filter feeders in estuarine and coastal ecosystem processes. Springer, Berlin/Heidelberg, pp 455–477
106. Lam-Hoai T, Rougier C (2001) Zooplankton assemblages and biomass during a 4-period survey in a northern Mediterranean coastal lagoon. Water Res 35:271–283
107. Lam Hoai T, Rougier C, Lasserre G (1997) Tintinnids and rotifers in a northern Mediterranean coastal lagoon. Structural diversity and function through biomass estimations. Mar Ecol Prog Ser 152:13–25
108. Lindahl O, Hart R, Hernroth B, Kollberg SS, Lars-Ove L, Olrog L, Rehnstrom-Holm A, Svensson J, Svensson S, Syversen U (2005) Improving marine water quality by mussel farming: a profitable solution for Swedish society. Ambio 34:131–138
109. Newell RIE (2004) Ecosystem influences of natural and cultivated populations of suspension-feeding bivalve molluscs: a review. J Shellfish Res 23:51–62
110. Kaspar HF, Gillespie PA, Boyer IC, MacKenzie AL (1985) Effects of mussel aquaculture on the nitrogen cycle and benthic communities in Kenerupu Sound, Marlborough Sounds, New Zealand. Mar Biol 85:127–136
111. Hatcher A, Grant J, Schofield B (1994) Effects of suspended mussel culture (*Mytilus* spp.) on sedimentation, benthic respiration and sediment nutrient dynamics in a coastal bay. Mar Ecol Prog Ser 115:219–235
112. Minchin D (2007) Aquaculture and transport in a changing environment: overlap and links in the spread of alien biota. Mar Pollut Bull 55:302–313
113. Carlton JT, Mann R (1996) Transfers and world-wide introductions. In: Kennedy VS, Newell RIE, Eble AF (eds) The eastern oyster C*rassostrea virginica*. Maryland Sea Grant, College Park, pp 691–706
114. Kaiser MJ, Laing I, Utting SD, Burnell GM (1998) Environmental impacts of bivalve mariculture. J Shellfish Res 17:59–66
115. Dolmer P (2002) Mussel dredging: impact on epifauna in Limfjorden, Denmark. J Shellfish Res 21:529–537
116. Dittmann S (1990) Mussel beds – amensalism or amelioration for intertidal fauna? Helgoländer Meeresun 44:335–352
117. Commito JA, Boncavage EM (1989) Suspension-feeders and co-existing infauna: an enhancement example. J Exp Mar Biol Ecol 125:33–42
118. Coen LD, Luckenbach MW, Breitberg DL (1999) The role of oyster reefs as essential fish habitat: a review of current knowledge and some new perspectives. In: Benaka LR (ed) Fish habitat: essential fish habitat and rehabilitation. American Fisheries Society, Bethesda, pp 438–454
119. Graf G, Rosenberg R (1997) Bioresuspension and biodeposition: a review. J Mar Syst 11:269–278
120. Norkko A, Hewitt JE, Thrush SF, Funnell GA (2001) Benthic–pelagic coupling and suspension-feeding bivalves: linking site specific sediment flux and biodeposition to benthic community structure. Limnol Oceanogr 46: 2067–2072
121. Sorokin II, Giovanardi O, Pranovi F, Sorokin PI (1999) Need for restricting bivalve culture in the southern basin of the Lagoon of Venice. Hydrobiologia 400:141–148
122. Stenton-Dozey JME, Probyn T, Busby AJ (2001) Impact of mussel (*Mytilus galloprovincialis*) raft-culture on benthic macrofauna, in-situ oxygen uptake, and nutrient fluxes in

Saldanha Bay, South Africa. Can J Fish Aquat Sci 58: 1021–1031
123. Holmer M, Wildish D, Hargrave BT (2005) Organic enrichment from marine finfish aquaculture and effects on sediment processes. Environmental effects of marine finfish aquaculture, Chapter 9. In: The handbook of environmental chemistry, vol 5. Springer, Berlin, pp 181–206
124. Vinther HF, Holmer M (2008) Experimental test of biodeposition and ammonium excretion from blue mussels (*Mytilus edulis*) on eelgrass (*Zostera marina*) performance. J Exp Mar Biol Ecol 364:72–79
125. Vinther HF, Laursen JS, Holmer M (2008) Negative effects of blue mussel (*Mytilus edulis*) presence in eelgrass (*Zostera marina*) beds in Flensborg fjord, Denmark Estuarine. Coast Shelf Sci 77:91–103
126. Castel J, Labourg PJ, Escaravage V, Auby I, Garcia ME (1989) Influence of seagrass beds and oyster parks on the abundance and biomass patterns of meiobenthos and macrobenthos in tidal flats. Estuar Coast Shelf Sci 28:71–85
127. Gutierrez JL, Jones CG, Strayer DL, Iribarne OO (2003) Mollusks as ecosystem engineers: the role of shell production in aquatic habitats. Oikos 1001:79–90
128. Asmus H (1987) Secondary production of an intertidal mussel bed community related to its storage and turnover compartments. Mar Ecol Prog Ser 39:251–266
129. Crooks JA (2002) Characterizing ecosystem-level consequences of biological invasions: the role of ecosystem engineers. Oikos 97:153–166
130. Souchu P, Vaquer A, Collos Y, Landrein S, Deslous-Paoli JM, Bibent B (2001) Influence of shellfish farming activities on the biogeochemical composition of the water column in Thau lagoon. Mar Ecol Prog Ser 218:141–152
131. Prins TC, Escaravage V, Smaal AC, Peeters JCH (1995) Nutrient cycling and phytoplankton dynamics in relation to mussel grazing in a mesocosm experiment. Ophelia 41: 289–315
132. Prins TC, Smaal AC, Dame RF (1998) A review of the feedbacks between bivalve grazing and ecosystem processes. Aquat Ecol 31:349–359
133. Cranford PJ, Anderson R, Archambault P, Balch T, Bates SS, Bugden G, Callier MD, Carver C, Comeau L, Hargrave B, Harrison WG, Horne E, Kepkay PE, Li W, Mallet A, Ouellette M, Strain P (2006) Indicators and thresholds for use in assessing shellfish aquaculture impacts on fish habitat. Can Sci Advis Sec Res Doc 2006/034, Can Dept Fish Oceans, Ottawa, 126 pp
134. Bougrier S, Hawkins AJS, Heral M (1997) Preingestive selection of differential microalgal mixtures in *Crassostrea gigas* and *Mytilus edulis*, analysed by flow cytometry. Aquaculture 150:123–134
135. Cranford PJ, Hill PS (1999) Seasonal variation in food utilization by the suspension-feeding bivalve molluscs *Mytilus edulis* and *Placopecten magellanicus*. Mar Ecol Prog Ser 190:223–239
136. Wetz MS, Lewitus AJ, Koepfler ET, Hayes KC (2002) Impact of the Eastern oyster *Crassostrea virginica* on microbial community structure in a salt marsh estuary. Aquat Microb Ecol 28:87–97
137. Sfriso A, Pavoni B (1994) Macroalgae and phytoplankton competition in the central Venice lagoon. Environ Technol 15:1–14
138. Phelps HL (1994) The Asiatic clam (*Corbicula fluminea*) invasion and system-level ecological change in the Potomac River estuary near Washington, DC. Estuaries 17:614–621
139. Wall CC, Peterson BJ, Gobler CJ (2008) Facilitation of seagrass *Zostera marina* productivity by suspension-feeding bivalves. Mar Ecol Prog Ser 357:165–174
140. Ulanowicz RE, Tuttle JH (1992) The trophic consequences of oyster stock rehabilitation in Chesapeake Bay. Estuaries 15:298–306
141. Miller DC, Geider RJ, Macintyre HL (1996) Microphytobenthos: The ecological role of the "secret garden" of unvegetated, shallow-water marine habitats. II. Role in sediment stability and shallow-water food webs. Estuaries 19:202–212
142. Reusch TBH, Chapman ARO, Groger JP (1994) Blue mussels *Mytilus edulis* do not interfere with eelgrass *Zostera marina* but fertilize shoot growth through biodeposition. Mar Ecol Prog Ser 108:265–282
143. Reusch TBH, Williams SL (1998) Variable responses of native eelgrass *Zostera marina* to a non-indigenous bivalve *Musculista senhousia*. Oecologia 113:428–441
144. Peterson BJ, Heck KL Jr (1999) The potential for suspension feeding bivalves to increase seagrass productivity. J Exp Mar Biol Ecol 240:37–52
145. Peterson BJ, Heck KL Jr (2001) An experimental test of the mechanism by which suspension feeding bivalves elevate seagrass productivity. Mar Ecol Prog Ser 218:115–125
146. Peterson BJ, Heck KL Jr (2001) Positive interactions between suspension-feeding bivalves and seagrass – a facultative mutualism. Mar Ecol Prog Ser 213:143–155
147. Swanberg IL (1991) The influence of the filter-feeding bivalve *Cerastoderme edule* L. on microphytobenthos, a laboratory study. J Exp Mar Biol Ecol 151:93–111
148. Mazouni N (2004) Influence of suspended oyster cultures on nitrogen regeneration in a coastal lagoon (Thau, France). Mar Ecol Prog Ser 276:103–113
149. Asmus H, Asmus RM (2005) Significance of suspension-feeders systems on different spatial scales. In: Dame RF, Olenin S (eds) The comparative roles of suspension- feeders in ecosystems. Springer, Berlin, pp 199–219
150. Sara G (2007) A meta-analysis on the ecological effects of aquaculture on the water column: dissolved nutrients. Mar Environ Res 63:390–408
151. Boyd CE, Lim C, Queiroz J, Salie K, de Wet L, McNevin A (2008) Best management practices for responsible aquaculture [Online]. http://pdacrsp.oregonstate.edu/pubs/featured_titles/boyd.pdf

152. Belle S, Bullis RA, Elston R, Goldburg R, Hardy RW, Hargreaves JA, Lockwood GS, Mayo RA, Nelson CL, Reid B, Tacon AGJ, Quagrainie KK (2008) Revisions to the supplemental to interim final report (Bivalve molluscs) of the Aquaculture Working Group. In: Response to public comments. National Organic Program, U.S. Department of Agriculture, Washington, DC
153. Oesterling M, Luckenbach M (2008) Best management practices for the Virginia Shellfish culture industry [Online]. http://web.vims.edu/adv/aqua/MRR%202008_10.pdf?svr=www
154. Pacific Coast Shellfish Growers Association (2005) *Shellfish production on the West Coast* [Online] http://www.pcsga.org/pub/uploads/production.pdf. Accessed Aug 2009
155. Syvret M, Fitzgerald A, Hoare P (2008) Development of a pacific oyster aquaculture protocol for the UK—technical report. Sea Fish Industry Authority, Edinburgh
156. Leavitt DF (ed) (2004) Best management practices for the shellfish culture industry in Southeastern Massachusetts [Online]. http://www.mass.gov/agr/aquaculture/docs/Shellfish_BMPs_v09-04a.pdf. Accessed Sep 2009
157. Maryland Aquaculture Coordinating Council (2007) Best management practices: a manual for Maryland aquaculture [Online]. http://www.marylandseafood.org/pdf/best_management_practices_manual.pdf. Accessed Sep 2009
158. Irish Sea Fisheries Board (2003) ECOPACT: environmental code of practice for irish aquaculture companies and traders. Irish Sea Fisheries Board, Dublin
159. Bronson C (2007) Aquaculture best management practices rule. Division of Aquaculture, Florida Department of Agriculture and Consumer Affairs, Tallahassee
160. Maine Aquaculture Association (2006) Recommended code of practice for aquaculture in maine. In: Howell L, Belle S (eds) Maine aquaculture association. Hallowell, Maine
161. National Oceanic and Atmospheric Administration (1998) NOAA's aquaculture policy. National Oceanic and Atmospheric Administration, Silver Spring
162. Creswell RL, McNevin AA (2008) Better management practices for bivalve molluscan aquaculture. In: Tucker CS, Hargreaves JA (eds) Environmental best management practices for aquaculture. Blackwell, Oxford, UK
163. Tucker CS, Hargreaves JA (eds) (2008) Environmental best management practices for aquaculture. Blackwell, Oxford, p 592

Books and Reviews

Costa-Pierce BA (2010) Sustainable ecological aquaculture systems: the need for a new social contract for aquaculture development. Mar Technol Soc J 44(3):88–112

Soto D, Hishamunda N (eds) (2008) Building an ecosystem approach to aquaculture. Food and Agriculture Organization of the United Nations, Rome, p 231

Silicon Solar Cells, Crystalline

Santo Martinuzzi[1], Abdelillah Slaoui[2], Jean-Paul Kleider[3], Mustapha Lemiti[4], Christian Trassy[5], Claude Levy-Clement[6], Sébastien Dubois[7], Remi Monna[7], Yves Veschetti[7], Isabelle Périchaud[8], Nam Le Quang[9], Jed Kraiem[10]

[1]Formerly University of Marseilles, Marseilles, France
[2]CNRS-INESS, Strasbourg, France
[3]LGEP, Paris, France
[4]INL-INSA, Lyon, France
[5]CNRS, Grenoble, France
[6]CNRS, Thiais, France
[7]INES-CEA, Le Bourget du Lac, France
[8]University of Marseilles, Marseilles, France
[9]Photowatt International S.A, Bourgoin Jailleu, France
[10]Apollon Solar, Lyon, France

Article Outline

Glossary
Definition
Introduction
The Silicon Feedstock (Polysilicon)
Silicon Single Crystals, Multicrystals, Ribbons, and Sheet Growth Techniques
Future Directions
Abbreviations
Bibliography

Glossary

Antireflection coating layer (ARC) Layer deposited on the illuminated surface of a cell which reduces the reflection of the light.

Dislocations Lack or additional line of atoms in the crystal.

Gettering process Extraction of unwanted impurities and trapping in a region of a wafer which does not contribute to the photocurrent.

Grain boundary (GB) Border zone of two adjacent crystalline grains.

Homojunction (heterojunction) Part of a semiconductor diode which separates a p-type region from an n-type one made with the same material (in a heterojunction, the materials are different).

Minority carrier lifetime τ and diffusion length L Duration and distance run by an electron in excess

(generated by the sunlight) in p-type silicon or by a hole in excess in n-type silicon.

Minority carrier diffusion length L Distance run by carriers in excess.

Multicrystalline silicon Large grained polycrystalline material, a few mm to 1 cm in size.

Passivation Mechanism which reduces the electrical activity of crystallographic defects, of surfaces, of interfaces, and of unwanted impurities.

Precipitates Agglomeration of impurity atoms within the crystal.

Solar cell conversion efficiency η Ratio of the electrical power output to the sunlight power input.

Texturization Chemical or physical technique which increases the roughness of the surface in order to reduce the light reflection and the diffusion.

Wafer Trench of silicon cut out from an ingot, ~200 μm in thickness.

Definition

Solar cells are sources of electrical energy when they are illuminated by solar radiations. They deliver to a load a photocurrent and a photovoltage. First used for space applications, solar cells were progressively taken into account for terrestrial applications. The main problems to solve are, today, the photovoltaic energy cost which is too high and the conversion efficiency which is limited. Most of the cells are based on a p–n junction made with a p-type semiconductor and an n-type semiconductor. When both materials are the same, the cell is based on a homojunction. When the materials are different, the cell is based on a heterojunction. One silicon cell, 15.6 × 15.6 cm^2, can deliver 7–9 A under ~0.6 V only, and for this reason, the cells are connected in modules in order to provide a substantial electrical power (about 100–250 W). The semiconductor silicon is known as an extremely pure material; 9 N purity level is required for electronic components. However, for solar cells, a 6 N purity level could suffice, and the use of polycrystalline materials is acceptable. Wafers were initially cut out from monocrystalline and also of multicrystalline ingots grown from electronic-grade feedstock, but progressively, solar-grade feedstocks could be used. The physical, the chemical, and the electrical properties of such wafers must be investigated in order to be qualified for cell production. The structure of the solar cells can be very basic, i.e., one p–n junction with simple metallization and antireflection coating. However, in order to increase the conversion efficiency, which tend to reduce the cost of the produced electrical energy, advanced concepts must be used in industrial production like selective emitters, new metallization techniques, and new cell structures like interdigitated back contact and back junction cells and heterojunction cells.

Introduction

Silicon solar cells were used, for the first time, as electrical energy sources for satellites. The first one was Vanguard launched 52 years ago. The technical success of the photovoltaic panels was so clear that their use in terrestrial applications was proposed at the end of the 1960s. Several solutions have been considered to decrease the cost of the photovoltaic systems and energy. Thin film cells, like CdS–Cu_2S or CdTe–Cu_2 Te structures, were investigated at the end of the 1960s, but they were not convincing. Silicon solar cells based on monocrystalline, on multicrystalline wafers, and on hydrogenated amorphous silicon thin films appear, during the 1980s, as a possible solution. Indeed, although new thin films cells have been developed during the last 20 years, at the end of 2010, crystalline silicon solar cells share ~87% of the worldwide photovoltaic market. This success is due to the stability of the photovoltaic silicon structures, to the lack of toxicity of this element, and, last but not the least, to its very high abundance in the Earth's crust. Moreover, the huge knowledge accumulated in the electronic device research and industrial production is a source of continuous progress.

However, the cost is always a problem, and a lot of efforts in the field of research and engineering are devoted to reduce the cost of the peak watt W_p, i.e., the cost of the electrical power produced when the cells are illuminated by the sun under optimal conditions. Such a cost depends on the cost of materials, of the cell processing steps, and of the module fabrication, but it depends also markedly on the cell conversion efficiency. Therefore, there was a competition between monocrystalline and multicrystalline solar cells during the last 20 years,

and today, both type of cells share approximately the same part of the worldwide market. The conversion efficiency of commercial monocrystalline cells achieve ~18–24%, while that of multicrystalline cells, which increases continuously, is by 2–3% absolute less higher. Although multicrystalline wafers contain large densities of imperfections like grain boundaries, dislocations, and impurities, they lead to acceptable solar cells because the processing steps needed to make the devices (phosphorus diffusion, aluminum–silicon alloying, deposition of a hydrogen-rich antireflection coating) improve the electrical properties of the wafers, enhancing the minority carrier lifetime and diffusion length, unless the cost of the cells be increased. An intense research activity was developed in the field of impurity gettering and passivation, which contributes to a clear understanding of the influence of metallic elements, distinguishing the role of fast and slow diffusers in silicon. It was clearly shown that the extended crystallographic defects, by themselves, are not very detrimental to the electrical properties of the wafers, and it is the interaction between impurities and crystallographic defects which impair the electrical properties.

From a material point of view, R&D efforts must lead to a very abundant production of a low-cost solar-grade silicon feedstock which can be used in the monocrystalline ingots pullers, as well as in the casting of multicrystalline ingots. The crystalline and the electrical quality of the ingots, as well as that of the wafers, must be improved and controlled. In order to save a pure and crystallized material, the thickness of the wafers must be reduced to less than 120 μm. To avoid the sawing of ingots, maybe ribbons or sheets could replace the wafers cut out from a crystalline ingot.

Solar cell structures are still improving at an industrial production level because well-investigated concepts are included in the processing steps. Such concepts like the selective emitter, the back contact, and back junction cells, the use of heterojunctions in place of homojunctions, present definite advantages which contribute to reach conversion efficiencies higher than 20% at an industrial level and 24% at a laboratory scale.

Such results are close to the theoretical limits of silicon solar cells based on single junction, and the way is open for new cell structures, like tandem cells and new silicon-based materials (nanomaterials, intermediate band materials, nanowires, quantum dots).

Crystalline silicon solar cells are made with wafers that are cut out from monocrystalline or multicrystalline ingots after some processing steps. Ingot growth requires very pure silicon feedstock, although the purity level is lower than that needed for electronic devices. The following chapters describe successively the feedstock production, the ingot growth and properties, the conventional and advanced cell structures.

The Silicon Feedstock (Polysilicon)

The Metallurgical Silicon

Metallurgical-grade silicon (MG-Si) is produced by the carbothermic reduction of pure quartz and quartzite rocks (silica), as indicated by the overall reaction:

$$SiO_2(s) + 2C(s) \rightarrow Si(l) + 2CO(g) \quad (1)$$

The reaction occurs in an electric arc furnace and requires a huge amount of electrical energy.

MG-Si is ~99% pure (2N), and major impurities are Al, Fe, and C. MG-Si is mainly used in the aluminium and iron industries (~60%) and for the production of silicones (~25%). Only a few part (~15%) is highly purified in order to reach the electronic-grade (EG-Si), at least 9 N pure, required by the semiconductor industry, or 6–7 N needed for solar cells.

The Purification of MG-Si

The required purification results from two different ways: the chemical or liquid routes and the direct metallurgical routes.

The Chemical Route The requirements of the semiconductor industry appear extremely hard to be satisfied but, fortunately, chlorine when purchased as HCl and MG-Si are inexpensive, and that open the way for the use of trichlorosilane $SiHCl_3$ (TCS). TCS is a very pure precursor for the deposition of EG polysilicon by the chemical vapor deposition technique (CVD). Indeed, MG-Si is transformed mainly (90%) into trichlorosilane $SiHCl_3$ (TCS) by the

reaction with HCl at 575 K, as indicated by the overall reaction:

$$Si(s) + 3HCl(g) \rightarrow SiHCl_3(g) + H_2(g) \quad (2)$$

Obviously, other chlorides are also produced, like $SiCl_4$.

Trichlorosilane is generally transported to polysilicon production plants where it can be purified to a very high level by fractional distillation because its boiling point is higher than those of other chlorides [1]. Boron, phosphorus, and metallic atom concentrations are reduced to less than 1 ppba (9 N level).

(Notice that a large par of $SiCl_4$ can be converted into $SiHCl_3$ by simple processes.)

A lot of extraction techniques have been proposed in the past [2]; however, today, the Siemens process is dominant [3]. It is based on the bell-jar reactor system and on elaborated techniques to recover the chemical by-products from the reactors. Inside the reactor chamber, gaseous trichlorosilane is dissociated at 575°C in elemental silicon thanks to resistance-heated filaments. Several hundreds of reactors are located in one silicon plant in order to produce several thousands of metric tons a year. A schema of the Siemens-type bell-jar reactor is given by Fig. 1. TCS is carried by hydrogen, comes in contact with filaments heated at 1,100°C, and then, silicon is deposited in form of rods. The sizes of a 40-metric tons/year capacity reactor are ~1.2 m in diameter and ~2.5 m in height. The reactors can dissipate thousands of kilowatt of heat, accept and exhaust thousands of cubic meters of hydrogen per hour, use corrosive HCl, and may produce ~1,000 kg of silicon in a single run. The electrical energy consumption is 120–160 kWh/kg.

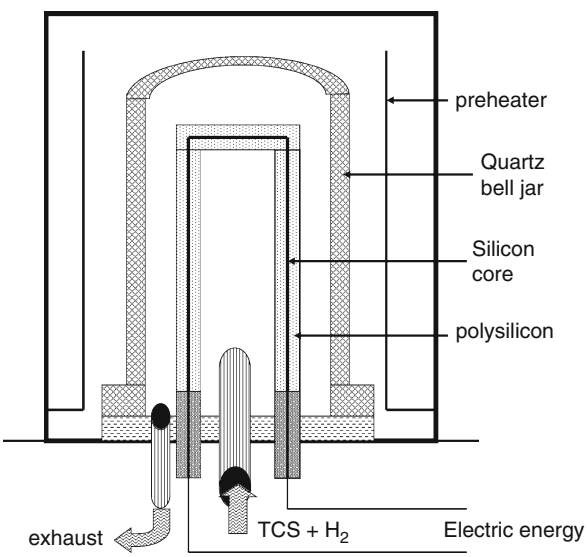

Silicon Solar Cells, Crystalline. Figure 1
The Siemens bell-jar reactor

The Siemens process is very efficient; however, the plants are very expensive and need huge investment as a 1,000 t/y production plant requires ~100 M€. Moreover, the chemical products are hazardous ($SiHCl_3$; SiH_4) or explosive (SiH_2Cl_2), and a lot of cautions must be taken. These plants are in fact more suited to the silicon production for the electronic device industry than for a mass production devoted to solar cells.

Other techniques to produce polysilicon have been investigated like the fluidized bed reactor (FBR), the vapor to liquid deposition process, or the free-space reactor. The more efficient is FBR, investigated by REC and Wacker Chemie [4]. In this technique, silicon fluoride instead of MG-Si is converted to monosilane SiH_4, and then, a silicon seed is dropped into the reactor in a flow of monosilane and hydrogen gases, as shown by Fig. 2. At the heated zones of the reactor, the gaseous flow dissociates to solid silicon in form of pellets. The theoretical advantages of this process are the possible continuous operation as well as lower capital and electricity costs. The produced polysilicon is less pure than that given by the Siemens process and could be a good candidate for photovoltaic devices.

Polysilicon could also be obtained through decomposition of silane (SiH_4), as indicated by the overall reaction:

$$SiH_4(g) \Rightarrow Si(l) + 2H_2(g) \quad (3)$$

The advantages are that the temperature needed for decomposition is lower than for TCS, the conversion efficiency is higher, and corrosive compounds are not formed [5].

It is difficult to give the amount of polysilicon produced in 2010 because all the production plants have increased their capacity in order to satisfy the requirements of the photovoltaic industry. For instance, Wacker Chemie is contributing to polysilicon

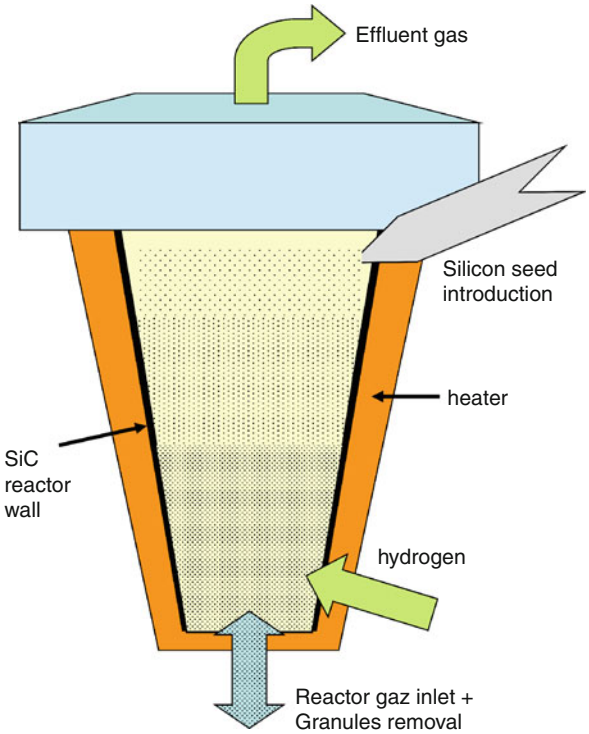

Silicon Solar Cells, Crystalline. Figure 2
Schema of the fluidized bed reactor

supply by expanding its annual capacity to more than 25,000 metric tons [6]. Probably, the worldwide amount will be larger than 150,000 metric tons in 2010.

The Metallurgical Route For solar cells, a solar-grade silicon (SoG-Si), less pure than EG-Si, could be acceptable at a 6–7 N level. Downgrading the Siemens process to make it less energy consuming was proposed, but such a technique does not enable to reach the capacity production for GWp installation of solar cells.

Another approach is to upgrade MG-Si more cheaply with metallurgical methods, e.g., slagging, leaching, or impurity segregation combined with directional solidification, as proposed by Crystal Systems Inc. [7], leading to the so-called upgraded metallurgical silicon (UMG-Si). Investment cost and energy consumption are drastically reduced; the material could be very abundant, but the degree of impurity is higher, and refining processes are needed, especially to reduce the concentrations of phosphorous and boron (n- and p-type dopants) which are difficult to eliminate, in order to avoid a compensation of silicon and a reduction of minority carrier lifetime.

The metallurgical refining techniques include raw material selection, segregation, leaching, and slag treatment. However, the most critical point remains the dopant concentration.

High-purity precursors have been used in the frame of the Sintef Solsilc project [8]. Ultrapure silica is obtained by selection of high-purity quartz or by oxidation of gaseous silicon chloride. This silica is reduced by black carbon obtained by gaseous route in an arc furnace. However, the high-purity silicon obtained is polluted by SiC, which has to be removed by several solidification steps.

The choice of pure quartz and pure reducer, generally charcoal, is the first step to obtain MG-Si with a low content of boron and phosphorus. At this stage, metallic pollutants are not the most critical because they can be reduced afterward by segregation or acid leaching, what is not the case of boron and, to a lower extent, of phosphorus. Slag treatment can be used to reduce boron [9]; it is the route developed by Elkem.

Another way to remove boron or phosphorus is to use plasma treatment or electron beam evaporation under low pressure. The first studies on plasma treatment have been carried out at laboratory scale by a French research group [10]. But it is the Kawasaki research group, in the frame of a NEDO project, which has developed a four-stage process. This process used electron beam for phosphorus removal, arc plasma with steam added argon for boron removal, and two segregation steps [11–13]. The boron and phosphorus concentrations were reduced to 0.2 ppma.

Alemany et al. have developed, at laboratory scale, a process involving an inductive plasma torch with the electromagnetic stirring of the molten silicon [14, 15]. The reactive gas was hydrogen and oxygen.

This process has been implemented by FerroPem in the frame of the Photosil project [16].

Several companies and academic laboratories [6, 17] are currently involved with the development of solar-grade silicon by different approaches. For instances, Elkem Solar uses in house production of MG-Si followed by three sequential purification steps to reduce impurity level of critical elements. Promising results have been obtained with the Elkem

Solar Silicon (ESS) [18, 19] as well as with the Sintef Solsilc silicon [8] when the material is blended with EG polysilicon (ESS results from the reaction between highly pure raw materials like carbon black and high-purity quartz).

Several other techniques of refining MG-Si have been proposed, such as slagging or segregation steps. However, the dopant concentrations, especially boron, are generally too high (above 5×10^{17} cm^{-3}). The mixing of EG and UMG feedstock was used successfully and more recently by IBM [20]. Details of the processes are generally missing, and information may only come from the laboratory scale about plasma torch process [16] used by FerroPem. In such a process, the feedstock is introduced and melted in a crucible, and an argon plasma gas, containing other reactive species, is created by induction. The plasma is blown onto the surface of liquid silicon, which is continuously renewed by electromagnetic stirring. Impurities like B, C, Al, and Ca are partly removed and volatilized. It is less easy to remove phosphorus atoms, even by evaporation, and the best solution is to lower the phosphorus content at the beginning of the entire process. After the plasma treatment, the concentration of boron is reduced by a factor 2–3. Following such treatment, the boron concentration can be adjusted to less than 2 ppma. Figure 3 shows a picture of the plasma torch in operation.

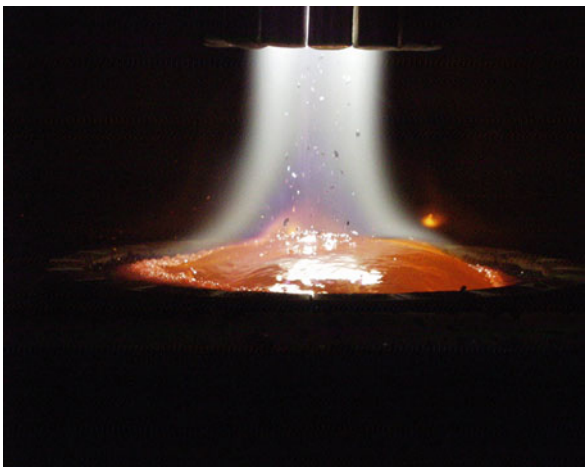

Silicon Solar Cells, Crystalline. Figure 3
Purification of melted UMG-Si by the plasma torch

Additional problems in the material come from light elements like C and O, as well as from slow diffusers like Ti or Al.

Researches have been carried out recently in Europe and Japan to develop cleaning and crystallization processes for metallurgical silicon feedstock and wafers. Due to confidential restrictions, only few results are known.

Notice that a marked advantage for refined UMG-Si is that the processes for producing solar cells are similar to those used for current silicon material but with different parameters to be applied, as will be shown later.

Silicon Single Crystals, Multicrystals, Ribbons, and Sheet Growth Techniques

Crystalline silicon wafers used for solar cells are cut from monocrystalline float zone (FZ), from Czochralski grown (Cz), from multicrystalline (mc-Si) ingots, or from ribbons. Such crystals are grown from a melt contained in various crucibles, except for FZ crystals.

Cz silicon is mainly used for manufacturing highly integrated low-power devices, especially memories, whereas FZ silicon is mainly used for power devices and photo detectors. Both crystals can be used for high-efficiency solar cells, especially FZ silicon. In 2009, ~37% of the photovoltaic market was shared by single-crystalline cell modules, ~45% by multicrystalline cell modules, and ~2% by ribbon-based cell modules.

The crystalline ingots are cut into thin wafers ($\leq$180 μm) by means of a diamond blade or a wire saw, while from ribbons wafers, crystalline ingots are cut out by means of a laser.

In the following paragraphs, a few basic properties of single crystals are given (they are well known and described in Ref. [1]), while the properties of multicrystalline silicon will be detailed in section "Physical, Chemical and Electrical Properties of mc-Si Wafers".

Float-Zone-Grown Monocrystals (FZ)

The FZ pulling method, described in details by Dietze et al. [21], has the great advantage to be crucible free. A rod of polysilicon, containing a monocrystalline seed at its bottom, experiences a local fusion by means of an RF coil. The molten zone is moved from the bottom to

the top of the rod, and the rod is rotated in order to reduce the inhomogeneities. Figure 4 shows a diagram of the pulling process.

During the growth process, two basic effects are operating, crystallization and purification. Indeed, impurities, with higher solubility in the liquid compared to that in the solid phase, are transported with the molten zone and can be accumulated at the extremities of the grown crystal, as a consequence of the impurity segregation phenomena, resulting of their distribution coefficients between the solid and the liquid silicon phases, given in Table 1.

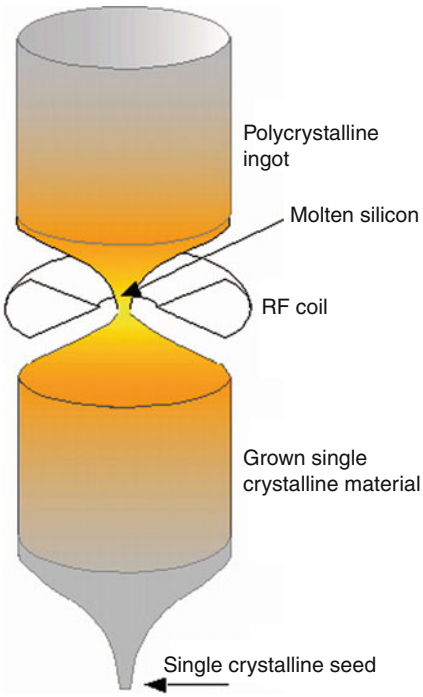

Silicon Solar Cells, Crystalline. Figure 4 Diagram of the FZ growth process (Courtesy of UNSW)

The repeatability of the process, the lack of crucible, and the use of a neutral atmosphere lead to a quasi-perfect single crystal (practically without dislocations) of extreme high purity, provided the silicon rod is itself of high purity. These basic steps have not changed since they were first established in the 1950s [22–24], and if FZ silicon crystal sizes have considerably increased, such crystals are always the best from a crystallographic as well as from a purity level point of view. Indeed, today, commercial FZ silicon ingots achieve ~15 cm in diameter, ~60 cm in height, and the purity level is higher than 10 N (less than 1 ppba, except for oxygen and carbon). In FZ single crystals, the minority carrier diffusion length and lifetime can reach a few mm and a few ms, respectively.

Czochralski-Grown Monocrystals (Cz-Si)

Invented in 1918, the crucible pulling of single crystals according to the Czochralski (Cz) technique [25] was applied first to germanium crystals and later to silicon [26]. As shown in Fig. 5, polysilicon is melted in a pure quartz crucible, and a seed crystal just touches the top of the liquid before it is then slowly retired in order that

Silicon Solar Cells, Crystalline. Table 1 Distribution coefficients *k* between liquid and solid phases of some impurities in silicon (From Ref. [1])

Impurity	Distribution coefficient	Impurity	Distribution coefficient	Impurity	Distribution coefficient
Lithium	10^{-2}	Indium	4×10^{-4}	Bismuth	7×10^{-4}
Copper	4×10^{-4}	Thallium	1.7×10^{-4}	Oxygen	1.25
Silver	10^{-6}	Carbon	6×10^{-2}	Sulfur	10^{-5}
Gold	2.5×10^{-5}	Germanium	3.3×10^{-1}	Manganese	$10 \times {}^{-5}$
Zinc	10^{-5}	Tin	1.6×10^{-2}	Iron	8×10^{-6}
Cadmium	10^{-6}	Nitrogen	7×10^{-4}	Cobalt	8×10^{-6}
Boron	8×10^{-3}	Phosphorus	3.5×10^{-1}	Nickel	3×10^{-5}
Aluminium	2×10^{-3}	Arsenic	3×10^{-1}	Tantalum	10^{-7}
Gallium	8×10^{-3}	Antimony	2.3×10^{-2}		

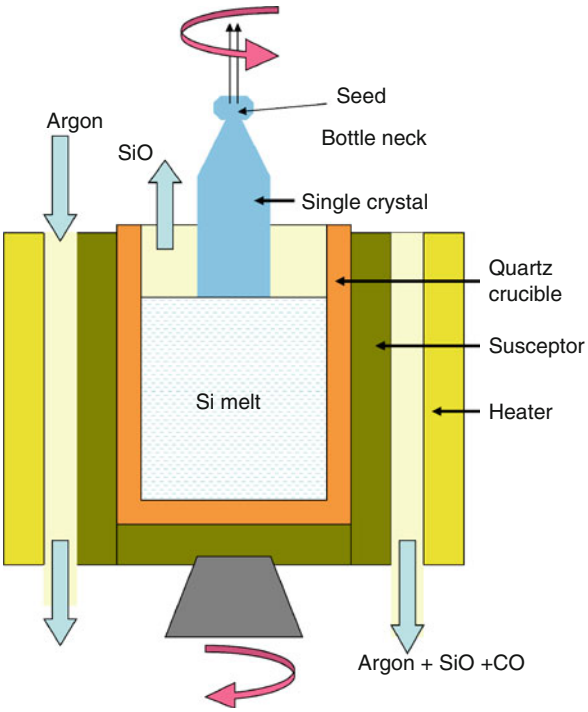

Silicon Solar Cells, Crystalline. Figure 5
Diagram of a Cz single-crystal growth puller. Notice the counter rotation of the pulled single crystal and of the crucible

liquid silicon solidifies close to the seed. The slow vertical ascent of the solidified silicon gives rise to a single-crystalline ingot, which emerge from the melt. To obtain a dislocation-free material, a crystal neck must be grown which becomes dislocation-free after few cm because dislocations grow laterally out of the crystal. Then, the diameter is enlarged, and the crystal growth is finished without dislocations by reducing the diameter to zero at the bottom of the crystal.

Like for FZ pulling, the Cz process is a crystallization and a purification step, and a large part of the impurities contained in the polysilicon and coming from the silica crucible remains in the melt, except oxygen which the distribution coefficient, given in Table 1, is higher than 1.

Fortunately, silicon monoxide evaporates easily from the melt. Nevertheless, oxygen concentration can achieve up to 20 ppma in the crystals, which, in fact, are supersaturated at room temperature. To enhance the removal of SiO and to prevent a contamination by CO, the furnace is purged by a strong argon stream. Today very large commercial single-crystalline ingots are produced by the Cz techniques up to 30 cm in diameter and 1.5–2.5 m in height. Ingots, 45 cm in diameter, are announced. The properties of these single crystals have been widely investigated, and it is impossible to give an exhaustive bibliography in this chapter. For detailed information, the reader could consult the chapters 6–8 in Handbook of Semiconductor Silicon Technology [1].

Albeit they are close to perfection, FZ and Cz crystals contain imperfections like swirl defects. Such defects are more concentrated in Cz crystals due to oxygen-related defects coming from an oxygen super saturation and a slightly higher metallic impurity level. Nevertheless, such crystals are used to make integrated circuits for electronic device thanks to internal gettering effects [27] and to the formation of a precipitate-denuded zone in the region where the components are realized. Large-area efficient solar cells can also be obtained, provided that the material does not experience high-temperature anneals (above 900°C) which could lead to the formation of oxygen-related precipitates and stacking faults.

In Cz single crystals, minority carrier diffusion lengths and lifetime are higher than 400 and 200 μs, respectively.

However, in p-type Cz wafers, the high concentration of oxygen led to the formation of boron–oxygen complexes under sunlight, and this will be a drawback for the high-efficiency cells as will be shown later.

Topsil in Denmark, MEMC in USA and in Italy, as well as Siltronic in Germany and France are the more important producers.

Multicrystalline Silicon (mc-Si) Ingot Growth

For a massive production of large-size cells, mc-Si cast ingots are the material of choice. In 2007, more than 4 GWp of mc-Si modules have been installed. In 2010, mc-Si modules shared more than 45% of the 24 GWp produced.

If single-crystalline silicon wafers are a very mature product, which the properties are well controlled, mc-Si ingots suffer from a large variation of basic properties like crystalline defect and impurity concentrations. Each ingot may have various properties,

depending on the growth techniques, and in a given ingot, the basic properties of the wafers are depending on their position in the ingot. This is why the crystalline, the chemical, and the electrical properties of mc-Si wafers will be detailed in section Physical, Chemical and Electrical Properties of mc-Si Wafers.

In order to decrease the cost of the material and to increase the size of solar cells, a lot of researches were devoted to the production of large grain size (few mm to few cm) crystalline silicon in which the concentration of impurities could be below the 0.01 ppma. Square cells, up to 21 × 21 cm^2, could be realized. Such a material was frequently labeled "solar-grade silicon" because its utilization is restricted to the production of solar cells. In addition to metallic impurities of carbon and, at a lesser extent, of oxygen and nitrogen, mc-Si wafers contain extended crystallographic defects like grain boundaries (GBs), dislocations, and twin boundaries. Moreover, metallic precipitates are frequently formed at extended defects and within the grains. When the carbon and oxygen concentrations are both higher than 10 ppma, a severe crystallographic degradation occurs with the formation of grit structures. In these grit structures, it is found with high concentrations of C, O, and SiC, and the grain size becomes very small. Such regions cannot contribute to the photocurrent of solar cells, but today, such bad regions are practically eliminated by a better control of the growth conditions.

The first material produced at an industrial level was the so-called "Silso," developed by Wacker/Heliotronics [28] in Germany at the end of the 1970s. It was followed by other companies like Photowatt in France with the "Polix" in USA and in Japan. More than 220 bibliographic references of papers and patents can be found in Ref. [30], for a period going from 1970 to 1980 only. Today, mc-Si is a quasi-standard product produced worldwide, especially in China and Taiwan, which the growth is based on the directional solidification, and most of the research and development activities are concentrated in Germany, Japan, and more recently in China.

The basic principle is the following. In a quartz crucible, heated by graphite heaters and coated with Si_3N_4, silicon (EG-Si or silicon waste coming from the microelectronic industry) is melted. Then, a vertical temperature gradient between the bottom and the top of the melt is established in order that the bottom solidifies first and the top solidifies last. Crystallization begins at the contact of the crucible bottom when its temperature decreases below the fusion point. After a few cm from the bottom of the crucible, quasi-columnar grains grow more or less vertically. Larger blocks can be obtained up to 650 kg in weight and up to 35 cm in height [29, 30].

The temperature gradient results from a mobile heating RF core or, more simply, by the so-called heat exchange method [29], in which the bottom of the crucible is cooled by a gas flow. Other methods of cooling use a natural cooling down due to the removing of the thermal insulation of the crucible bottom or, more originally, the action of an infrared radiation transparent bottom [31]. The process time for one cycle, from loading the crucible to unloading, is usually around 48 h. Figure 6 summarizes the directional solidification process.

The dominant (in concentration) impurities in mc-Si are carbon, oxygen, and nitrogen due to the

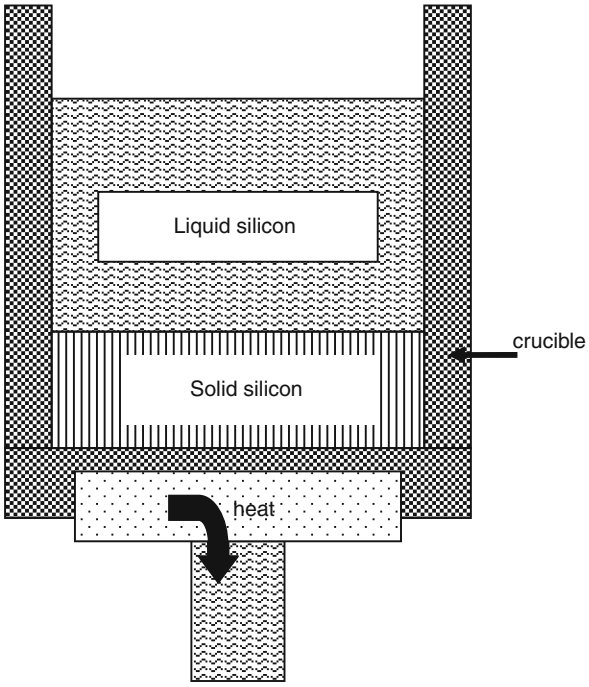

Silicon Solar Cells, Crystalline. Figure 6
Directional solidification of multicrystalline silicon ingot. A temperature gradient results from heat extraction through the crucible *bottom*

contact with the crucible followed, at a lesser extent, by metallic atoms.

Notice that larger ingots can be produced by the electromagnetic continuous casting into a cooled crucible. This technique was first developed by Sumco in Japan, formerly Sumitomo-Sitix [32], and then in France by EMIX [33, 34]. The principle of the electromagnetic continuous casting is to feed continuously a copper cold crucible in which alternative electric current is flowing. This current creates an induced current in the silicon, and the Joule effect heats the material up to the melting point. Simultaneously, the induced magnetic field and current create a Lorentz force close to the surface of the melt that prevents contact with the cold crucible wall (a gap of some hundreds of μm exists). The process begins by heating a graphite piece which is pulled down when the Si melt is large enough. The pulling rate is typically 50 μm s^{-1}.

The blocks are cut into columnar bricks, which are wire-sawed into thin wafers (≤200 μm), then cleaned and texturized.

Notice that a new product will be proposed which combines the advantage of mono- and multicrystals: it is the quasi-monocrystal or the monocast silicon. This point will be developed at the end of the chapter in "Future Directions."

Wafer Sawing Wafers are commonly cut out of the ingots or of the bricks by means of wire saws using a SiC loose abrasive, which enables the production of ~200 μm thick slices. This technique possesses a high throughput, but up to 50% of the crystallized and purified silicon is lost during process. In order to reduce this waste, 100 μm diameter wires can be used with fine SiC particles in the slurry [35]. The sawing can also be improved, employing diamond grains fixed onto the surface of the wires by means of a resin [36], because the sawing speed is increased by 2.5 while the thickness variation is decreased by 3. Moreover, after sawing, the slurry could be reused because it does not contain SiC particles like in the conventional process. Obviously, kerf-loss-free techniques are also of a great interest, as that proposed recently by IMEC group [37].

Ribbons The sawing of the ingots wastes at least 40% of an expensive, pure, and crystalline material (the subproduct powder is too much contaminated to be reused). To avoid this wasting, the growth of shaped crystalline ribbons from silicon melt, which has been already investigated in the 1970s, became of interest during the last 20 years [38–40].

Ribbons have been prepared mainly by various techniques such as edge-defined film-fed growth (EFG), edge-supported pulling called also String Ribbon (SRT), ribbon on graphite substrate (RGS), and ribbon on sacrificial carbon template (RST). EFG and SRT techniques have, today, reached the production level. Such techniques are recognized to enable the direct production of flat wafers after laser cutting.

The EFG ribbons, which the growth technique is described in Fig. 7, can be pulled in a multiple ribbon growth furnace, for instance, in shape of nonagon tubes with a side width of 156 mm or in form of 12-face tubes with a side width of 125 mm. The length of the tube can be as long as 6.5 m [41, 42]. The EFG ribbon is developed by RWE Schott Solar.

In the STR ribbon [43–46], two high-temperature resistant wires (strings) are pulled vertically through

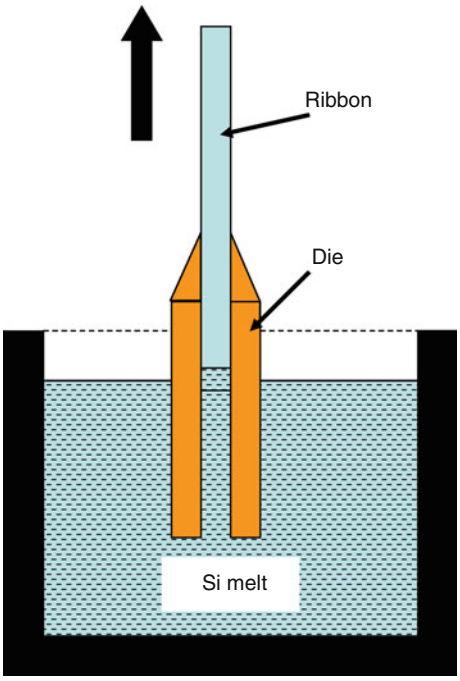

Silicon Solar Cells, Crystalline. Figure 7
Schema of the growth of an edge-defined film-fed (EFG) ribbon

a shallow silicon melt, and the molten silicon spans and freezes between the strings, as shown by Fig. 8.

The process is continuous: long strings are used, the melt is replenished, and the silicon ribbon is cut to length for further processing, without interrupting growth. The STR ribbon was developed by Evergreen Solar.

RGS ribbons that consist mainly in melting of silicon powders possess the advantage of a higher throughput production, but it remains to a pilot line production due to contamination problems [47]. These horizontal growth processes, described by Fig. 9 which was developed at ECN, the Netherlands, have the highest throughput rate. However, these processes appear to be bound to the production of thick wafers, typically over 400 μm, with a poor crystalline texture, and, in turn, lower cell conversion efficiencies. Moreover, extended chemical treatments are necessary to eliminate surface corrugations and backside contamination of the sheets.

The RST ribbon growth process [48] is based upon the crystallization of two opposite silicon films drawn along by a carbon ribbon substrate, which is pulled upward through a silicon melt (see Fig. 10). The carbon ribbon is passed vertically through a slot at the bottom of a crucible (silica or carbon), which contains the melt. As it emerges from the melt upper surface, this ribbon shapes the freestanding silicon meniscus and is coated on both sides with silicon layers.

After growth, the carbon ribbon is burnt in an oxygen-containing gas at high temperature, upon which the self-supported silicon sheets are released and ready for the fabrication of the solar cells. The substrate participates in the elimination of the latent heat of crystallization, which allows relatively high pull rates. It shapes the freestanding freezing meniscus, which ultimately yields essentially flat silicon sheets free of grooves. However, thermoelastic stresses, generated by the difference in thermal expansion coefficients between the silicon films and the carbon substrate, set

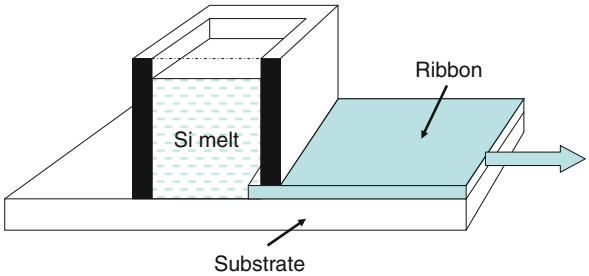

Silicon Solar Cells, Crystalline. Figure 9
Schema of the growth of a ribbon on graphite substrate (RGS)

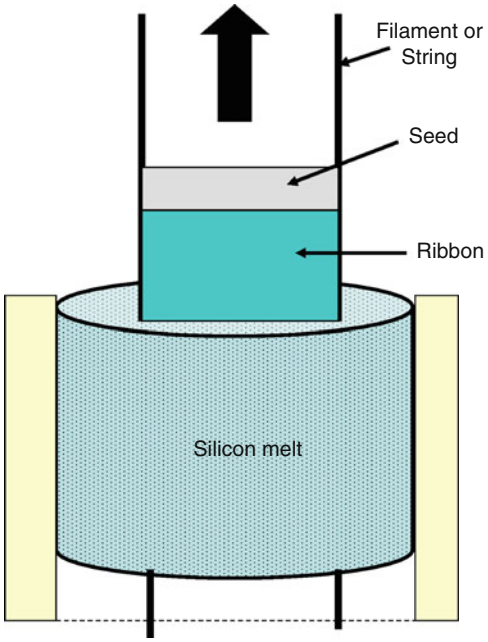

Silicon Solar Cells, Crystalline. Figure 8
Schema of the growth of a string (STR) ribbon

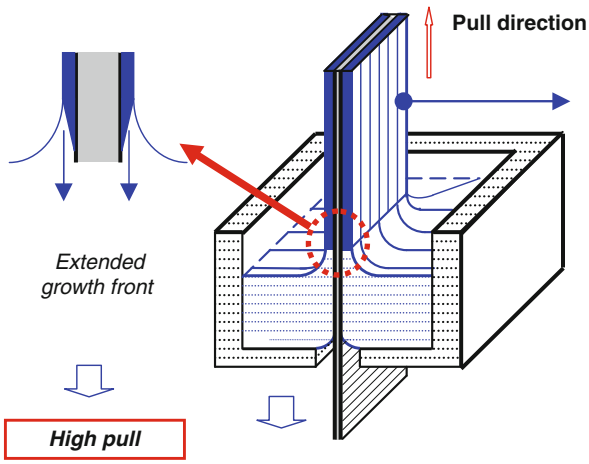

Silicon Solar Cells, Crystalline. Figure 10
Schema of the RST ribbon growth process

Silicon Solar Cells, Crystalline. Table 2 Throughput rate and actual thickness for vertical ribbon growth processes

Process	RST	EFG	STR
Throughput (cm^2/min)	>300	165	55 (4 ribbons)
Thickness (μm)	≤80	≈300	≈280

a limit to the minimal thickness of the silicon films at around 40–50 μm.

Table 2 gives the throughput rate (cm^2/min) and compares the actual thickness for vertical ribbon growth. Although not in production yet, the RST process, developed by Solar Force in France, is the only ribbon process which can simultaneously achieve thin silicon films with relatively flat and smooth surfaces and a high throughput rate. Typically, at a pull rate of 10 cm/min, the thickness of the silicon films is 80 μm (or below).

In all ribbon technologies, there is a very high-temperature gradient at the solid–liquid interface related to the high growth speed. Wafers cut out of ribbons are multicrystalline and contain large amounts of carbon and also of metallic impurities coming from the dies. There are also large densities of intragrain defects like dislocations and twins. Dislocations are detrimental, but the minority carrier lifetime is higher in twin lamellae lying parallel to the growth direction.

The main impurity is carbon, with a substitutional concentration of $\sim 10^{18}$ cm^{-3}, exceeding the solubility limit at the melting temperature.

In addition to the material saving (there is no kerf-loss), ribbons posses another advantage: the energy pay back of the cells is lower than that of other crystalline cells because the pulling processes are less energy consuming.

Silicon Sheets Another technique to produce directly large-size flat wafers proposed by the Sharp group in 1997 is the crystallization on dipped substrate (CDS). The basic principle of CDS technology consists of to dip a cold refractory substrate into molten silicon. The silicon crystallizes uniformly; then, the substrate is pulled out of the molten silicon; a multicrystalline silicon sheet is detached from the substrate and cut by a laser to 15.6 × 15.6 cm^2 size. The main advantage of the CDS is a high production throughput which achieves 1,825 cm^2/min [49].

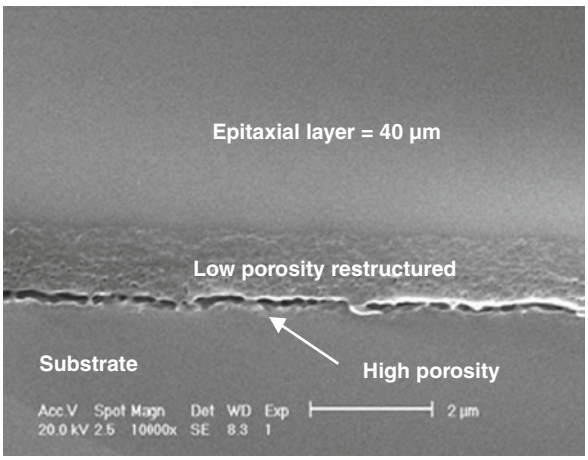

Silicon Solar Cells, Crystalline. Figure 11 Microphotography of an epitaxial layer before detachment

The wafer molding has also been studied by some laboratories, and the molded wafers have been realized on graphite mold coated with SiC or Si_3N_4.

The research efforts are focused today on the improvement of molded wafer's photovoltaic quality and on the reduction of their thickness. Moreover, directional crystallization is obtained by means of a reusable oriented seed.

Transfer Layer To produce thin substrates of monocrystalline silicon, less than 50 μm, a new technological route has been considered: the transfer of thin film [50–53]. It is based on the use of a sacrificial layer of porous silicon on which grows by epitaxy, the active layer of silicon, as described by Fig. 11. Then, the thin film is transferred on a low-cost substrate and depends on the architecture of the cell considered. The starting silicon substrate can then be reused after cleaning its surface. This avoids the sawing step.

Porous silicon (PS) is formed using a specific anodization cell. Indeed, in order to simplify the further transfer step, porous silicon is formed on the whole surface. Electrochemical anodization of (100) silicon wafers in HF solution is realized on the entire surface. A double-phase etching process generates two superposed PS layers: a top layer with low porosity (20–23%) allowing high-quality crystal growth and a buried layer with high porosity (65–70%) for the further detachment of the epilayer [54, 55].

Physical, Chemical, and Electrical Properties of mc-Si Wafers

The huge number of publications and conferences dedicated to the properties of mc-Si wafers is so high that it is impossible to respect an exhaustive list in the references. Moreover, progresses are so fast that only some "historical" and recent results will be given (233 references can be found in Ref. [30] covering the results up to 1980).

Extended Crystallographic Defects and Impurities

In addition to the whole defects found in single crystals, multicrystalline silicon wafers contain grain boundaries (GBs) and intragrain defects like subgrain boundaries, dislocations, and twin boundaries, as shown by Fig. 12. Due to a higher impurity concentration, precipitates could be formed within the grains or at extended defects.

Notice that the grain growth is columnar, and this is a great advantage because in the wafers cut perpendicularly to the ingot growth direction, there is only one grain between the front and the back surface. Consequently, the photogenerated carriers do not have to cross grain boundaries before to be collected by a junction.

The large grains have various orientations; the dominant one is (111). GB types vary from one grain to another, and one can distinguish small-angle GBs with a misorientation level from 0° to 10° from large-angle GBs with larger misorientation angles [56, 57]. In these large grained materials, dislocations are the more harmful intragrain defects. Dislocations are more or less homogeneously distributed or agglomerated in clusters, which frequently induce metallic atom precipitation [58].

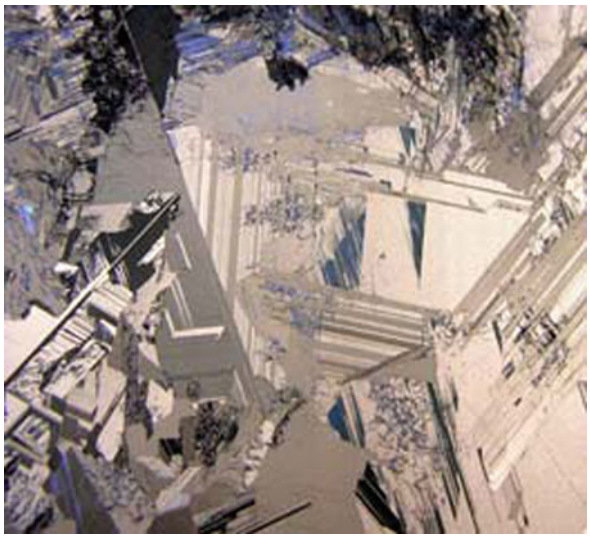

Silicon Solar Cells, Crystalline. Figure 12
Photography of a "polix" mc-Si wafer after alkaline etching

Crystallographic defects are harmful to the electrical properties of the material, mainly in terms of minority carrier lifetime τ or diffusion length L. However, by themselves (without any decoration by impurities), their influence is weak, and it is the interaction between the crystallographic defects and segregated or precipitated impurities (light elements; metallic atoms), which generates the more harmful recombination centers.

The effect of twin boundaries has also been extensively studied. Exact twinning (the $\Sigma 3$ twin) has no electrical effect because all bonds are saturated and there is no distortion of the bond angles across the twin boundary. More deviated twins show distorted "reconstructed" bonds and a dislocation structure, and they have an electrical effect, as was shown for $\Sigma 9$ twins. Subgrain boundaries formed essentially by dislocations [59] are very detrimental in terms of minority carrier lifetime reduction.

From an electrical point of view, rain boundaries (GBs) are characterized both by an electrical potential barrier which reduces the mobility of the majority carriers and energy levels in the band gap which reduce the lifetime τ (or diffusion length L) of the minority carriers. However, electron beam induced current (EBIC), as well as light beam induced current (LBIC), scan maps indicate that this electrical activity is inhomogeneous from 1 GB to another one and also along a given GB [60–62]. In fact, this activity depends strongly on the segregation of metallic atoms or of light elements. In large grained wafers, the electrical influence of GBs is limited, while that of subgrain boundaries and of dislocations is dominant, especially when they are decorated by impurities. This was very well demonstrated first by Sopori [63] by means of diffusion length measurements as a function of dislocation density determined by etch pit counting, later confirmed by El Ghitani [64, 65], and more recently by Warta [66, 67]. Nevertheless, the role of

transition metallic impurities is dominant [68]. An illustration of the impurity defect interaction at GBs is given by the lifetime scan map around GBs in a raw wafer cut out from the top of a polix ingot [69]. As shown by Fig. 13, there is an increase of τ at the vicinity of GBs which could be explained by the trapping of impurities (metal; oxygen) by these defects.

The electrical activity of extended crystallographic defects is related to the presence of shallow or deep energy levels in the silicon band gap. A simple distinction could be made by cooling the wafer and investigating their electrical activity by electron or light beam induced current (LBIC) contrast. If the contrast increases when T decreases, deep energy levels have to be considered, generally related to metallic impurities. If the contrast is irrespective of the variations of T, shallow levels are dominant [70–72]. Figure 14a, b gives an example of such variation. Low-temperature scan maps reveal the presence of extended defects in raw samples which are poorly recombining in the initial material. Such defects are "sleeping defects" which are activated after an annealing at $T > 500°C$ and become recombining after processing steps.

Like in the FZ and Cz growth processes, liquid and solid phases are present during the solidification of the multicrystalline ingots, and in addition to the crystallization, a marked purification by impurity segregation occurs. Impurities which are contained in the silicon melt or which have been introduced by contact with the crucible walls are progressively accumulated at the very top of the future ingot. The segregation efficiency is directly related to the distribution coefficient k_0 given in Table 1. Metallic impurities which the k_0 value is below 10^{-3} tend to remain in the liquid phase, while oxygen accumulates preferentially in the solid phase which solidifies first. Nevertheless, metallic impurities

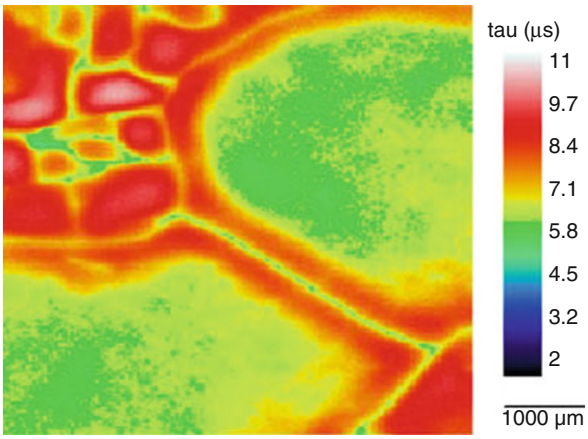

Silicon Solar Cells, Crystalline. Figure 13
Minority carrier lifetime scan map around a GB in a wafer cut out from the top of a large polix ingot: segregation of impurities improves the grains near the grain boundary

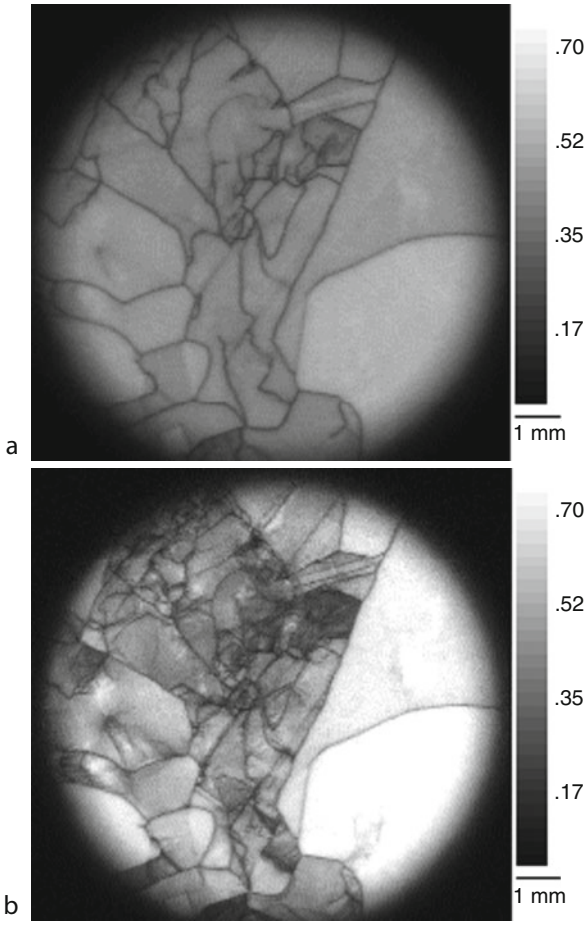

Silicon Solar Cells, Crystalline. Figure 14
(**a**) Light beam induced current contrast scan map at 300 K of a typical raw polix sample. Few intragrain defects appear in the picture because the contrast is weak. (**b**) Same picture at 100 K of the sample scanned in **a**. Due to the presence of deep levels in the gap, probably associated to metallic impurities, both grains in the *right* of the picture appear in *white*. Due to the presence of shallow levels, a marked contrast appears at the extended defects in the *left* part of the picture

and light elements are present in the crystallized ingot in which they can be dissolved and precipitated in the homogeneous regions of the grains like at extended defects. As a consequence of all these imperfections, mc-Si ingots and wafers are characterized by a pronounced in homogeneity, and along a given ingot, the macroscopic and microscopic electrical properties of the wafers are not the same. It was found that the very bottom and the very top of the ingots must be discarded; the mean values of lifetime τ and diffusion length L increase from the bottom to the middle of the ingot and then decrease to the top [73]. Figure 15 shows the variation of L as a function of the height in a typical brick cut out of a large polix ingot. In virgin p-type wafers, the minority carrier properties vary very widely, diffusion lengths are found between 50 and 200 μm, and the lifetimes are in the range 3–20 μs. All materials need improvements before to be used to make efficient solar cells; fortunately, improvements come from the solar cell processing steps.

Material Improvement Techniques The electrical quality of the wafers, evaluated by the measurement of lifetime τ or diffusion length L, could be improved by two basic treatments: hydrogenation and impurity gettering.

Hydrogen is able to in-diffuse rapidly as an atomic species H^+, at T ∼ 450°C, and can interact with dangling bonds and impurities [74–76]. It was verified that deep-level transient spectroscopy (DLTS) signal of some impurities disappears after a hydrogen in-diffusion and reappears after a short anneal at T ∼ 500°C. However, H^+ ions tend to recombine to form hydrogen molecules which diffuse slowly, and the passivation depth is limited to a few tens of micrometer below the surface.

Hydrogenation can be carried out by different techniques such as the immersion in direct or remote plasma, or by low-energy ion implantation, using a Kaufmann source. All these techniques have been described by M. Stavola [76]. However, the best solution for mc-Si wafers was proposed by the Kyocera group. It results from the deposition of a hydrogen-rich silicon nitride by plasma enhanced CVD (PECVD at ∼450°C. This layer, which is antireflection coating (ARC), can release hydrogen during a further annealing, giving rise to a marked passivation of the defects in the material.

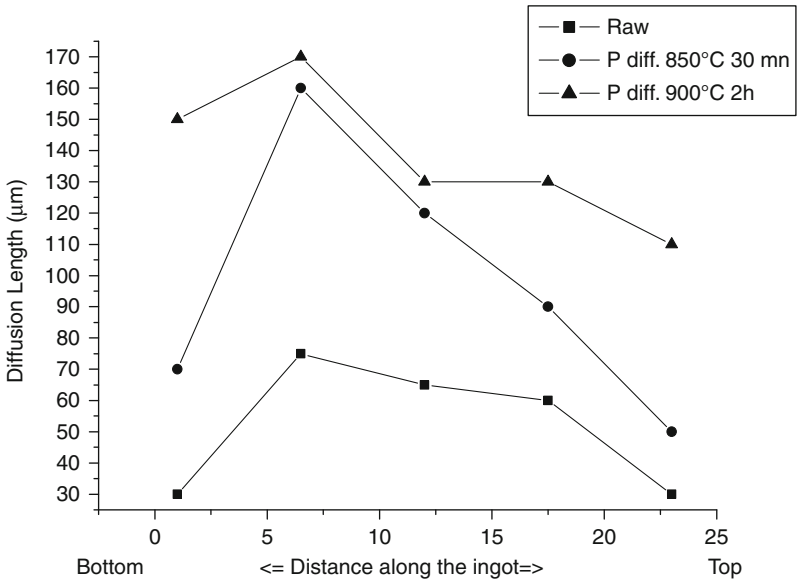

Silicon Solar Cells, Crystalline. Figure 15
Typical variation of minority carrier diffusion length vs the height (in cm) in a polix ingot for raw and phosphorus diffused wafers (Phosphorus diffusion at 900°C for 2 h is in fact a gettering treatment)

Very stable improvement results from impurity gettering treatments [77–80]. They consist in extracting impurities (mainly fast diffusers) from the bulk of the wafers and to accumulate them in a region where they are not harmful for minority carriers. A very efficient gettering technique results from the phosphorus diffusion near the surface at temperatures in the range of 800–900°C for ~30 min to some hours. For short-time treatment, phosphorus diffusion creates an n^+ layer (~0.3 μm thick). In this layer, the solubility of metallic impurities is enhanced and that produces a segregation gettering. In addition, when the in-diffusion of phosphorus is carried out by $POCl_3$, the phosphorus concentration at the surface exceeds the solubility limit ($>10^{22}$ cm^{-3}), and orthorhombic precipitates of SiP are formed near the surface. Dislocations are formed at the interface between the precipitates and the cubic silicon matrix, leading to a relaxation gettering in the n^+ layer. Moreover, due to the molar volume expansion developed by these precipitates, self-interstitials are injected in the bulk in which they interact with dissolved and precipitated impurities. Substitutional metallic impurities are transferred in interstitials sites, oxygen-related precipitates are shrunken, and, provided they are fast diffusers, metallic atoms diffuse through the wafer and can be trapped in the n^+ layer.

On the other hand, a thermal treatment at T ~ 850°C for at least 30 min of a mc-Si wafer covered with a thick Al layer (~1 μm thick) can lead to an efficient gettering as well. Indeed, at T > 570°C a liquid eutectic alloy is formed and vacancies are injected in the bulk. In the liquid alloy, the solubility of most metallic impurities is ten to thousand times higher than in the solid silicon [81], and fast metallic diffusers can be trapped easily. This is a pure segregation gettering with an efficiency which depends on the diffusion coefficient of impurities at the annealing temperature. The best results are obtained for T in the range 700–900°C.

After each preceding treatments, τ and L substantially increase, and such improvements are observed, irrespectively of the position of the wafers along the ingots, as shown by Fig. 15.

If the gettering treatment can extract fast diffusers, it is practically ineffective toward slow diffusers which remain in the wafers and limit the increase of L. From the values of τ_0 (initial bulk lifetime) and of τ_{dif} (after phosphorus diffusion at 850°C for 30 min), it is possible to deduce a lifetime τ_{Mi} related to the interstitial metallic atoms (M_i) which are extracted by gettering during the phosphorus diffusion, according to the expression:

$$\frac{1}{\tau_{Mi}} = \frac{1}{\tau_0} - \frac{1}{\tau_{dif}} \tag{5}$$

Assuming that the captured cross-section of the recombination centers related to these interstitial metal atoms is $\sim 10^{-15}$ cm^2 and that SRH statistics could be used, it is possible to evaluate approximately their concentration [M_i]. The variation of [M_i] along the height of the ingot is given by Fig. 16. In wafers cut out of large (310 kg) polix ingot [73], it is found, after phosphorus diffusion, that [M_i] $\sim 10^{13}$ cm^{-3} in the bottom, $\sim 10^{12}$ cm^{-3} in the central part of ingots, and $\sim 5 \times 10^{12}$ cm^{-3} in the top. Half of these impurity amounts are due to iron, which the identification and the evaluation of the concentration as interstitial atoms [Fe_i] in p-type mc-Si are possible by means of the dissociation of the Fe–B complexes.

It is important to evaluate also the concentration variations of recombination centers due to impurities precipitated or segregated by extended defects and also to slow diffusers. This variation could be given by that of the reverse of τ_{get} (after phosphorus diffusion at 900°C for 2 h) because it could be reasonably assumed that most of fast diffusers are removed whatever is their

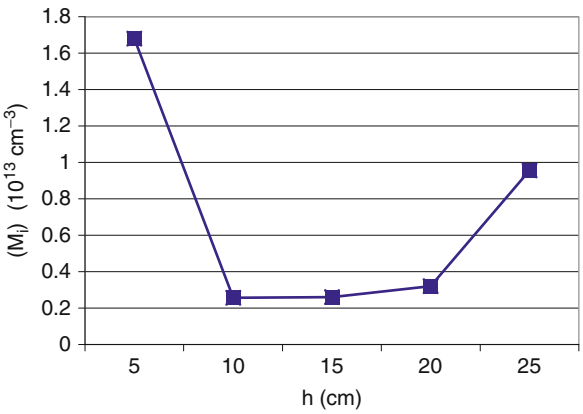

Silicon Solar Cells, Crystalline. Figure 16
Computed variation of the concentration of interstitial metallic atoms [M_i] along a polix ingot

position in the wafer (interstitial atoms, easily dissolved precipitates in grains and at GBs). It is observed that the concentration of such recombination centers is more marked in the bottom and in the top than in the central part of the ingot. This is a consequence of the precipitation and segregation at extended defects of impurities coming from the crucible floor and of the accumulation of impurities in the top, linked to the duration of the solidification process.

Figure 15 illustrates also the increases of the diffusion length after a long phosphorus diffusion, which is a gettering step, and shows that the gettering is very efficient in the lower middle of the brick because this part is protected from the back diffusion of impurities coming from the top and sufficiently far from the crucible floor.

Due to the growth conditions of the mc-Si ingots, oxygen atoms are also present at concentration levels larger than those deduced from infrared spectroscopy. Indeed, with such a technique, interstitial oxygen atoms are detected while precipitated or aggregated ones are not. Oxygen precipitation occurs certainly at dislocation cores, at dislocation clusters, and at GBs. These precipitates can, in turn, trap metallic impurities and become recombining. This is probably why the wafer properties are degraded after anneals at temperatures higher than 900°C.

The improvement of the wafers is enhanced when phosphorus gettering, aluminium gettering, and hydrogenation are applied successively or combined, provided that phosphorus diffusion is applied first [82–88]. Certainly, they induce complementary effects on the different defects and impurities contained in mc-Si wafers. For instance, the diffusion length scan map of a multicrystalline sample which experienced long phosphorus diffusion and then long aluminium gettering is given by Fig. 17. Very high values are found, indicating that the material has been strongly improved due to the extraction of impurities.

Fortunately, the preceding treatments are processing steps which are included anyway in most of the preparation techniques leading to industrial mc-Si solar cells. For instance, for cells made with wafers of Fig. 12, diffusion length L_n values reached up to 300 μm [73]. These strong improvements explain while conversion efficiencies higher than 16% can be achieved, despite that the initial material properties were very poor compared to those of single crystals. Probably, it seems today that the major part of the improvement is due, after the phosphorus diffusion,

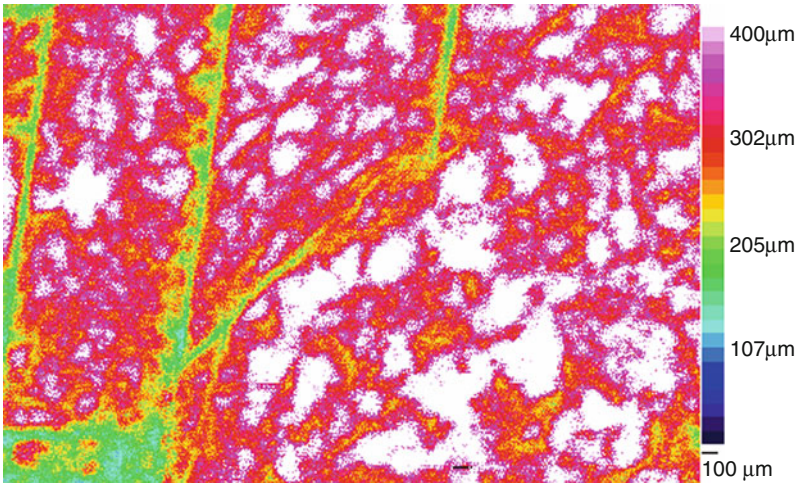

Silicon Solar Cells, Crystalline. Figure 17
Minority carrier diffusion length L_n scan map of a sample which experienced first a phosphorus gettering and then an aluminium gettering; both treatments were carried out at 900°C for 2 h. Notice the high values of L_n in the grains and also at the grain and twin boundaries

to the aluminium gettering developed during the rapid thermal anneal at ~700°C which gives rise to the ohmic back contact [89] and to the back surface field effect, as will be shown in section "Single Junction p-type Silicon Based Solar Cells (n^+-p-p^+ Structure)".

n-Type mc-Si Although the first solar cells have been made with n-type single-crystalline silicon, most of the industrial production is based on p-type material, essentially because the processing steps are simple and relatively not expensive. However, n-type material possesses some remarkable advantages. First, there are little or no boron–oxygen complexes and no light-induced degradation. Secondly, the minority carrier capture cross-sections of metallic impurities, frequently found in processed silicon, are markedly smaller for holes than for electrons. This property of n-type silicon was clearly explained [90] on the basis of the formation of donor trap levels in the gap which are positively charged or neutral and can be strongly attractive for electrons or poorly attractive for holes. Experimental results have reported exceptional values of lifetime in raw n-type wafers cut from ingots made by Italsolar and then by Deutsche Solar or from ribbons. Indeed, Cuevas et al. [91] and Libal et al. [92] have found lifetime values of several hundreds of μs in raw materials and values in the range of ms in wafers gettered by weak phosphorus diffusion. A lot of papers have investigated the role of impurities and have confirmed the interest of n-type material [93–95]. For example, interstitial iron which is one of the more harmful contaminant in mc-Si wafers is a good example because the capture cross-sections for electrons and for holes, reported by Istratov [96], are $\sigma_n = 5 \times 10^{-14}$ cm^2 and $\sigma_p = 7 \times 10^{-17}$ cm^2, respectively. Assuming that Schockley-Read-Hall (SRH) recombinations occur and that interstitial iron is the dominant impurity, high lifetime values are expected for holes in n-type iron-contaminated silicon. The same tendency is observed for several other metallic impurities except for chromium for which the capture cross-sections are closed in both n- and p-type silicon, but this impurity cannot be present in sufficiently large concentrations in the wafers after the end of the crystallization and after a gettering treatment [97]. Although the diffusion coefficient of electrons is three times higher than that of holes, it is expected that diffusion lengths of minority carriers, in such a simple configuration, are neatly higher in n-type than in p-type silicon (provided the nature and the concentration of impurities is the same in both types of wafers). Oxygen precipitates are also less harmful in n-type silicon because their surfaces are expected to have a hole repelling positive charge [98]. Obviously, there are other sources of recombination centers, like precipitates, and the reality is more complex.

Another remarkable advantage of n-type silicon results from the lifetime of minority carrier variation with the injection level: it does not decrease too much with this level, suggesting that n-type base cells will be more efficient at low illumination levels than p-type base cells.

As an example of the typical high electrical quality of the n-type wafers, Fig. 17 shows a light beam induced current scan map (LBIC) at λ = 960 nm, with local values of the hole diffusion length L_p, of a region which contains GBs and dislocations, especially in the center of the picture (Fig. 18).

Such interesting properties can be useful for solar cells, as will be described later.

Refined UMG-mc-Si To open the way to the huge production of silicon solar cells which could be predicted for 2013 [99], another approach is to cast refined upgraded metallurgical silicon

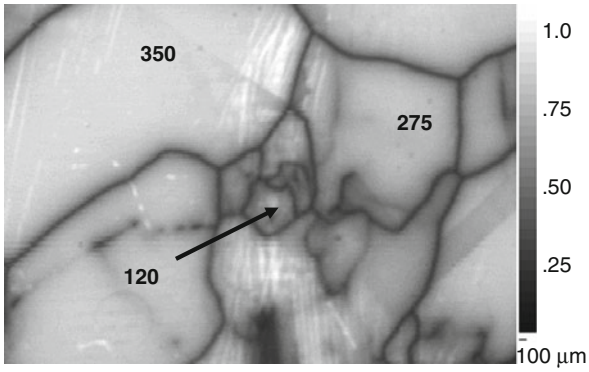

Silicon Solar Cells, Crystalline. Figure 18
Light beam induced current contrast scan map of a raw n-type silicon wafer. Some local values (in μm) of minority carrier diffusion length L_p are indicated. Notice the high values of L_p, even in the central zone where the density of extended defects are high

feedstock (UMG-Si). After crystallization by directional solidification, the wafers look like the conventional ones (large grains, same intragrain defects). Problems come from the high concentrations of dopant and of light elements, mainly carbon. The dopant concentrations are close to 2 ppma, and due to the distinct distribution coefficients of boron and phosphorus atoms, the material is compensated, and in the top of the ingot, the conduction type changes from p- to n-type. Concentrations of carbon are close to 20 ppma in the top of the ingots, as a consequence of the carbothermic reduction and process contamination. Precipitation of SiC filaments occurs frequently in the upper part of the silicon block [100] as shown by Fig. 19.

These filaments can be detrimental because they cause damage during the sawing and can form ohmic shunts [101, 102]. Blends of electronic grade (EG) and of upgrade metallurgical (UMG) feedstock have given unexpected good results because L values are found higher than 100 μm in raw wafers [18–21]. However, such results cannot be generalized; they are depending on where UMG feedstock was obtained and on its impurity concentrations as well as on the nature of these impurities. This is why we give more details on the results obtained for ingots made with plasma torch refined UMG-Si [103, 104].

The wafers cut out from the bottom and the middle of the ingots are p-type and contain high concentrations of Al, Cu, and Zn (other impurities are below the detection limit of the high resolution glow discharge mass spectroscopy). Interstitial oxygen and substitutional carbon atom concentrations detected by Fourier transformed infrared spectroscopy (FTIR) are about 5×10^{17} cm^{-3} and 7×10^{17} cm^{-3}, respectively. In these wafers, electron diffusion length L_n values are in the range 30–60 μm because, probably, B, P, and also Al concentrations [105, 106] are too high. Obviously, other impurities, like Ti, are present.

In the top of the ingot, wafers are n-type. The advantage of n-type silicon is again very clear: the light beam induced current (LBIC) contrast is more marked than for p-type wafers, and the mean values of electron diffusion length L_p reach 100 μm in the raw wafers, as shown by the scan map of Fig. 20.

When n-type wafers experimented phosphorus diffusion and aluminium alloying, the mean values of L_p achieve 180 μm. Light beam induced current (LBIC) scan maps of n-type wafers look like those of conventional p-type mc-Si wafers; the grain boundary contrast is marked while intragrain defects are weakly active.

However, a difference with conventional mc-Si could be noted: there is a weak improvement of L_p after short phosphorus diffusion. Probably, that is due to the presence of slow diffusers like Al and Zn and

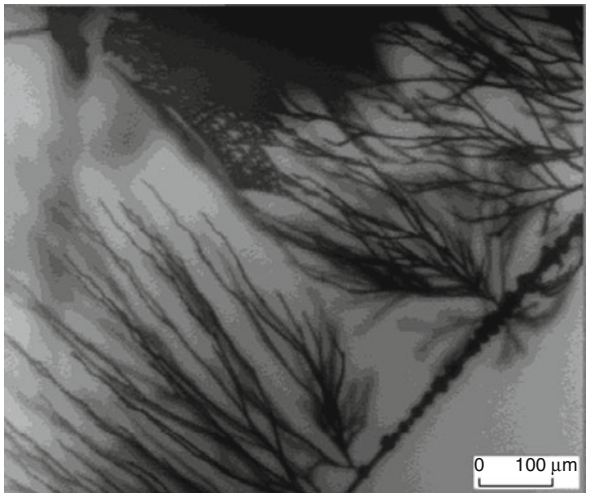

Silicon Solar Cells, Crystalline. Figure 19
SiC filaments observed in UMG-Si wafers (Courtesy of Dr Möller-TU-Freiberg)

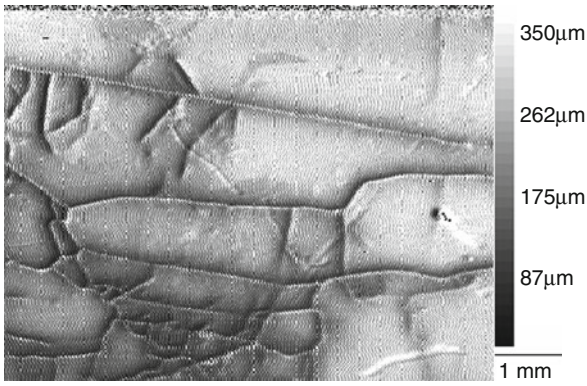

Silicon Solar Cells, Crystalline. Figure 20
Hole diffusion length scan map L_p in a raw n-type refined UMG-Si wafer

other ones which have not been detected by HR-GDMS but which are certainly contained in the material.

Notice that the preceding results could be impaired when the concentrations of oxygen and carbon are higher than 8×10^{17} cm^{-3}, as frequently observed in the top of the ingots. As reported by Pizzini [107], a detrimental coprecipitation of these elements could occur.

Single-Junction p-Type Silicon-Based Solar Cells (n^+-p-p^+ Structure)

Solar cells made with crystalline silicon wafers have been investigated for a long time, and in 2010, they share at least 83% of the total photovoltaic market (~45% for mc-Si cells), although the part of thin film cells is increasing. This success is explained by the relative low cost and/or by the high conversion efficiency of these devices.

The conversion efficiency of solar cells depends on the quality of silicon wafer, i.e., on the values of the minority carrier lifetime τ and diffusion length L, and on the cell structure design. Particularly, the passivation of the surface, the surface texturization, the antireflection coatings, as well as the metallization techniques are also of a paramount importance because they strongly influence the short circuit photocurrent density J_{sc}, the open circuit photovoltage V_{oc}, and the fill factor FF.

Notice that the conversion efficiency η of a solar cell is given by:

$$\eta = \frac{J_{sc} \times V_{oc} \times FF}{P} \tag{6}$$

where P is the incident sunlight power per cm^2 (W/cm^2).

The Basic Structure Figure 21 shows the schema of a very basic solar cell structure made on p-type silicon. Most of such conventional cells used an n^{++}-p or an n^+-p junction which results most often from the in-diffusion of phosphorus at ~850°C from $POCl_3$ through the front surface. The depth of the n^+ layer is typically ~0.3–0.5 μm; its sheet resistance is in the range 40–90 Ω/square; phosphorus surface concentration can exceed 10^{21} cm^{-3} in the case of an n^{++}-p junction. A dead layer is thus formed at the emitter surface, which does not contribute to the photocurrent.

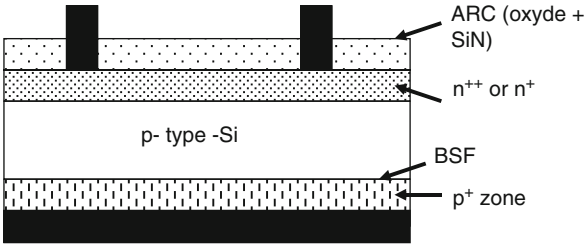

Silicon Solar Cells, Crystalline. Figure 21
Diagram of the very basic structure of a p-type silicon cell. Metallization are drawn in black (Figure is not drawn to scale)

Recombination in this heavily doped region causes a high dark current which impairs the photovoltage. This very high doping level makes easier the formation of a good ohmic contact with the metallic front grid used as top electrode; however, it is not easy to reduce the carrier recombination at such a surface although a silicon oxide or a silicon nitride layer is deposited or grown on it.

The back surface is also a source of recombination. To reduce this recombination activity, the back surface doping level is enhanced (p^+-type), totally or locally, by means of aluminium–silicon alloying or boron diffusion in order to develop a repulsive back surface field (BSF) for electrons. The edges of the cell must be discarded in order to eliminate parasitic shunting paths, and a single or a double antireflection coating (ARC) layer is deposited on the front surface before or after the metallization step.

Notice that the processing steps used to make the cells, e.g., phosphorus diffusion, aluminium–silicon alloying, deposition of a hydrogen-rich silicon nitride layer always improve the performances of the cells, especially when the base is made with multicrystalline silicon.

Antireflection Coating and Texturization The optical properties of silicon play a major role in the design and operation of solar cells; the light absorption and the reflectance of the front surface must be taken into account. The reflectance is ~30% for wavelengths $\lambda < 1.1$ μm and increases to ~60% for $\lambda \leq 0.4$ μm [108]. Thus, to minimize the optical losses, deposition of an antireflective coating or/and texturization of the silicon surface are essential.

Antireflection Coatings Reflectance is reduced by employing an antireflective coating (ARC) on the silicon front surface. Predominantly, single-layered ARCs are generally used industrially. The optical thickness of the ARC should be equal to a quarter of the wavelength λ_{min} at which zero reflectance occurs (i.e., reflected waves must be out of phase by π) [109]:

$$n_{ARC} d_{ARC} = \frac{\lambda_{min}}{4} \quad (7)$$

The refractive index of the layer, n_{ARC}, has to be equal to $\sqrt{n_{c-Si}}$ for the crystalline silicon (c-Si) cell in air. As $n_{c\text{-}Si}$ varies from 4.28 to 3.76 between 0.5 and 0.7 μm, the refractive index of an optimized ARC should be, for instance, equal to 1.9 at 600 nm. For a glass-encapsulated cell, the refractive index of the glass being n_{glass} = 1.5 instead of 1 for air; the optimal index value for the ARC will be 2.3. Such ARC reduces the sunlight lost by reflectance on polished silicon from 30% down to 10% and from 20% to 5% in air and under a protecting glass, respectively.

Antireflection coatings used in the industry are dielectric materials such as TiO_2 (n = 2.3) [110] and SiN_x:H (whose refractive index varies between 1.9 and 2.3) [111]. For laboratory cells, two complementary dielectric layers are sometimes applied to broaden the spectral band reduction of the reflectance.

TiO_2 was first introduced in the early 1970s [112, 113] and presents numerous advantages such as high chemical stability, insulating properties when stoichiometric, good mechanical properties. TiO_2 thin films can be deposited at low temperatures (~400°C) by atmospheric pressure chemical vapor deposition (APCVD) or by spray pyrolysis [114]. Nontoxic and noncorrosive liquid precursors, such as tetraisopropyl titanate (TPT), are used as a deposition source. At such temperatures, the metastable anatase crystalline phase is formed which exhibits an optimal refractive index for glass-encapsulated silicon solar cells, as well as excellent transmittance. A thin silicon dioxide (SiO_2) layer could be grown before deposition of TiO_2 in order to provide passivation of the front silicon surface.

SiN_x:H deposition by PECVD was invented in 1965 [115]. The amorphous a-SiNx:H films are typically deposited using plasma-enhanced chemical vapor deposition (PECVD), at temperatures of less than 450°C with deposition rates as high as 1.7 nm/s.

The properties of a-SiNx:H films are extremely dependent on the deposition system, process conditions, and gas composition. Thus, when using dilute silane and ammonia reactant gases, the best surface passivation results (see Surface Passivation. The Selective Emitter Concept) from stoichiometric a-SiNx:H films that have a refractive index of 1.95, while the Si-rich films deposited from pure silane and ammonia possess a refractive index of 2.3 [114]. Effective reflectance of ~11% is observed on a planar silicon surface, as shown by Fig. 22.

SiN_x:H coating is presently widely used in the industry as the efficiency of the solar cells is strongly increased.

Notice that porous silicon exhibiting a refractive index intermediate between those of silicon and air has been widely investigated as an AR coating in the 1990s [116, 117].

Silicon Surface Texturization Light incident normally to the silicon is transmitted to an amount of ~70% into silicon while ~30% is reflected away from the flat surface as shown by Fig. 23a. Texturing the front surface of a solar cell increases the short-circuit current due to three distinct mechanisms. All of which are related to the fact that the incident photons strike the cell surface at a specific angle [108, 118]. Firstly, some light rays will be reflected from one angled surface

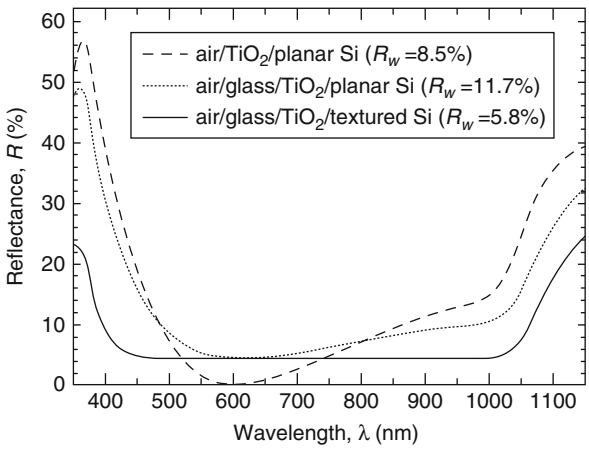

Silicon Solar Cells, Crystalline. Figure 22
Effective reflectance of planar and textured emitter surfaces with TiO_2 single-layer antireflection coating (From [114], courtesy of Dr. BS Richards)

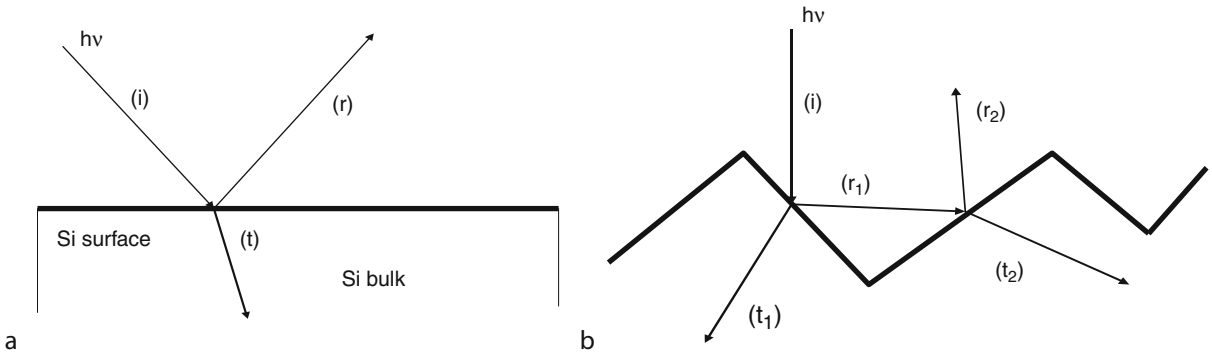

Silicon Solar Cells, Crystalline. Figure 23
The influence of surface texture on light reflection: (**a**) planar surface; (**b**) textured surface. (1) incident light, (r_1) and (r_2) reflected lights, (t_1) and (t_2) absorbed lights

merely to strike another as shown by Fig. 23b, resulting in an increased probability of absorption, and therefore reduced reflection. Minimal facet angles of 30° and 54° are required for double- and triple-bounce reflectance, respectively. For the double bounce case shown in Fig. 23b, the light reflected away from the silicon is lost. However, if the silicon is encapsulated under glass, it is possible to totally reflect the light arriving at the glass–air interface, above the critical angle of 42°, whereby it will be redirected toward silicon yet again for possible re-incidence. Critical angles for total internal reflectance at silicon–air interface are 16–17°. Secondly, photons refracted into the silicon will propagate at an angle causing them to be absorbed closer to the junction than would occur with a planar surface. This is especially relevant in material with minority carrier diffusion lengths comparable to or less than the cell thickness. Thirdly, long-wavelength photons which are reflected from the rear surface will encounter an angled silicon front surface, improving their chance of being internally reflected [119]. This process is referred to as light trapping and gives an improved response to infrared light, especially for thin Si substrates.

There are two types of texturization. When the etching rate varies with crystallographic direction, the texturing is anisotropic, while when the material etches in all directions at same rate, the texturing is isotropic.

Anisotropic Alkaline Etching A geometrical texture (V-shaped grooves texture, random pyramidal structures) at the front surface of silicon can be done mechanically, for instance using specially developed dicing saws or (electro)chemically, by etching the silicon in an alkaline or acidic solution [120]. The first solar cell using the alkaline etching process was reported in 1974 [121]. It is a well-established texturing method for single-crystal silicon solar cell. The wet etching process can be globally represented by the overall reaction:

$$Si + 2H_2O + 2OH^- \rightarrow \left[Si(OH)_2O_2\right]^{2-} + 2H_2 \quad (8)$$

Etching rates in NaOH or KOH depend on the crystallographic orientations; the (100) planes being etched more rapidly than (111) planes, which are thus revealed. (111)-oriented surfaces are flat etched, with some triangular features due to the presence of terraces, while (100)-oriented surfaces exhibit random square-shaped pyramids [122] made of (111) facets, as shown by Fig. 24.

An anisotropic etched on (100) plane forms a facet angle of 54.7° on a (100)-oriented surface [123]. This angle satisfies the requirements for both external reflection control and total internal reflections.

The reflectivity decreases from 34% for a mirror-polished silicon surface to 11% for an alkaline-textured silicon wafer [126], as shown in Fig. 24.

A promising alternative solution is quaternary ammonium hydroxide etchings, typically tetramethylammonium hydroxide (TMAH) [124, 125]. This solution is clean (room compatible, nontoxic, and easy to handle). A low weighted reflectance of 2.7% can be

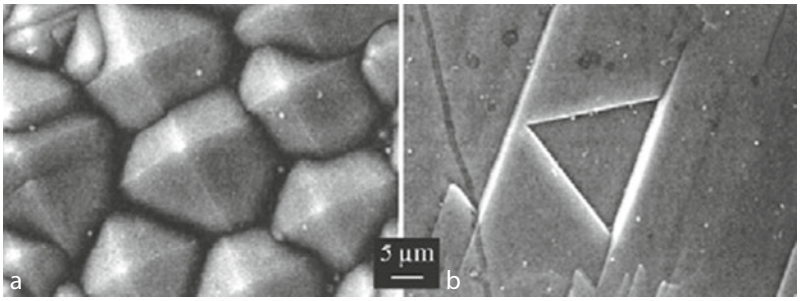

Silicon Solar Cells, Crystalline. Figure 24
SEM images in plane view of NaOH-textured silicon: (**a**) (100)- and (**b**) (111)-oriented crystals

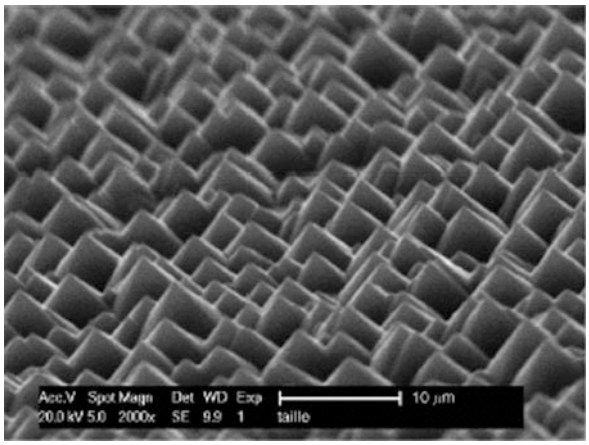

Silicon Solar Cells, Crystalline. Figure 25
SEM picture of a typical texturized silicon surface using TMAH texturization

obtained with a combination of TMAH pyramidal texture and SiNx:H AR coating, as shown in Figs. 25 and 26 [126].

Anisotropic alkaline texturing does not work very well on multicrystalline substrates due to the different crystallographic grain orientations. A number of different surface geometries will determine the interaction of incident light with the surface and will contribute to the overall reflectance of the multicrystalline wafer. The bare saw etched wafers have reflectance in air equivalent to polished silicon because the tilt angles of the dominant etch facets exposed are lower than the 30° required for double-bounce reflection. The (111)-oriented surfaces are flat etched, with triangular plateaus as predicted by Sopori [109], while (100)-oriented surfaces exhibit the upright random pyramids. By measuring the reflectivity of individual grains, it was found that (100) and (111) grains exhibit minimum and maximum effective reflectivity between 400 and 1,100 nm of 11.7% and 34.2%, respectively, while grains with other orientations exhibit intermediate values [127]. However, the anisotropic texturization is still currently used in multicrystalline silicon industry because under encapsulation, both saw damage and textured etched multicrystalline wafers couple light more effectively into the silicon.

Isotropic Texturization Numerous methods such as chemical, electrochemical, defect etching, or based on more sophisticated techniques (e.g., reactive ion etching (RIE), lithography, laser scribing, and mechanical grooving) have been investigated.

Among these methods, the acid texturization method has been the most developed and is currently used in industry. The RIE method is very attractive because it allows a better automatized solar cell processing, avoiding the use of wet techniques.

In search of a simple method with high throughput, low-cost investment, and compatible with thin wafers, Sarti et al. proposed the wet acidic texturing that tends to etch isotropically the multicrystalline silicon wafers, resulting in features with rounded surfaces [128]. The acidic water solution consists of a mixture of nitric acid, hydrofluoric acid ($HF–HNO_3$), water, and eventually some additives. The overall reaction is the following:

$$3Si + 4HNO_3 + 18HF \rightarrow 3H_2SiF_6 + 8H_2O + 4NO \quad (9)$$

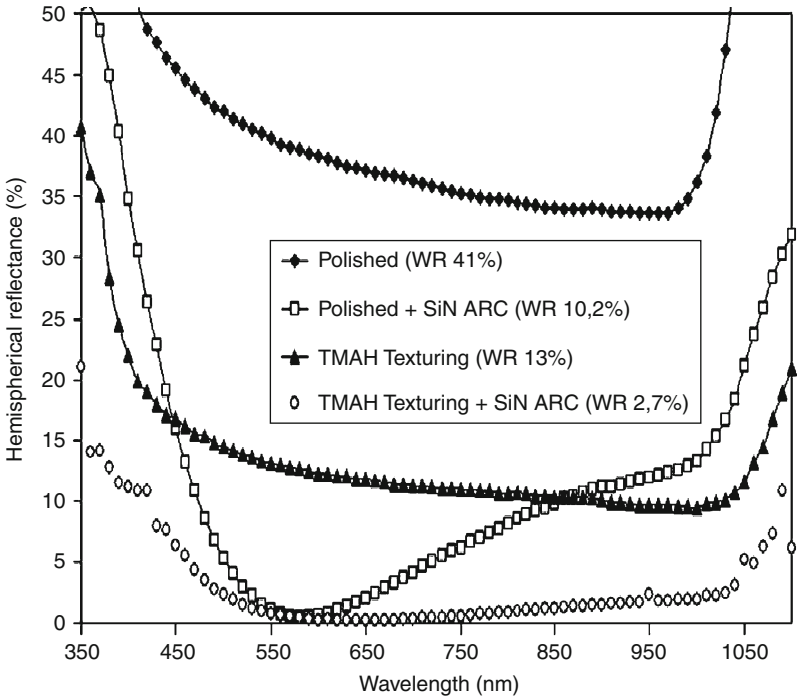

Silicon Solar Cells, Crystalline. Figure 26
Weighted reflectance of different silicon surface morphologies, with or without ARC and TMAH texturing

The etching rate as well as the surface morphology depends strongly on the chemical composition of the texturization bath but not on the crystallographic orientation. Etch textures vary between rough, concave-shaped "tub" structures, and smooth surfaces. The rough texture is of interest for solar cell industry [129, 130].

The texturing process starts on "as-cut" multi-Si wafers. The saw damages trigger the etching process. Thus, the removal of saw damage and the surface texturing are being done simultaneously in one short single chemical step. The resulting etch pits of 1–10 μm in diameter are uniformly distributed over the wafer surface irrespective of crystallographic orientation, giving a homogenous reflectance over the surface of the wafer and the absence of steps between grains, as shown in Fig. 27.

The acidic isotexturing results in lower reflection than traditional anisotropic etching on multicrystalline material, as shown in Fig. 28, and better conversion efficiency [130–132]. Short-circuit current density increases of up to 1.5 mA/cm^2 have been measured.

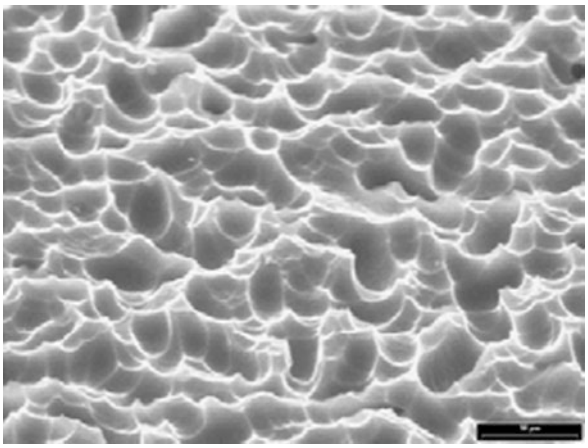

Silicon Solar Cells, Crystalline. Figure 27
SEM plan view image of multicrystalline silicon surface after isotropic acid etching (From [130], Courtesy of Dr. R Einhaus)

In laboratory, the masked acidic etching has been developed to produce hexagonally symmetric "honeycomb" surface texture. This texture reduces reflection loss as well as substantially increasing the cell effective

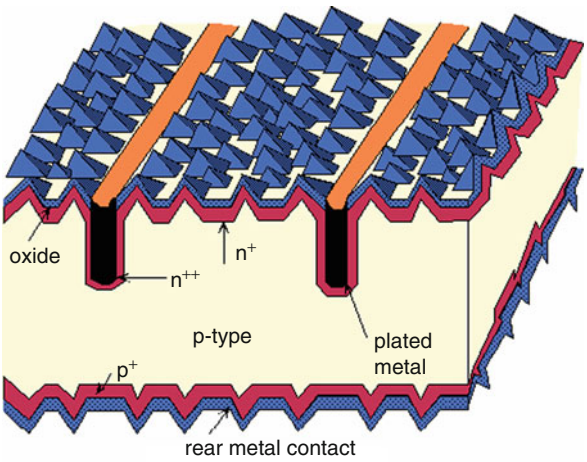

Silicon Solar Cells, Crystalline. Figure 28
Passivated emitter and buried front contact solar cell (Courtesy of UNSW)

optical thickness by causing light to be trapped within the cell by total internal reflection. Multicrystalline solar cells with record efficiency of 19.8% have been obtained [130, 131].

Plasma-enhanced dry chemical etching at atmospheric pressure is a promising alternative to isotropic wet etching, especially when combined with similar process technologies, to provide a continuous in-line processing steps. Plasma texturing is particularly appropriate for advanced solar cell structures, for wafers produced without surface damage such as Si ribbons and epitaxial layers on low-cost Si substrates. It allows decoupling the properties of the front and rear surfaces which are both texturized with the wet etching. A nontextured rear surface appears to be needed to reach low effective recombination in advanced solar cells.

First report on reactive ion etching (RIE) texturization of Si in chlorine plasma was published by Gittlemen et al. [132]. In the plasma technology, a plasma discharge is created, and molecules are partially dissociated into radicals (typically halogens) upon electron impact. Those radicals, with or without the assistance of ions, etch the silicon. RIE technique has proved to yield uniform and low reflectance [133–135], but the defects induced by the ion bombardment are a drawback.

Surface Passivation. The Selective Emitter Concept
The surface recombination activity could be characterized by means of an effective surface recombination velocity S_{eff} evaluated by:

$$S_{eff} = \sigma \times v_{th} \times N_{ts} \tag{10}$$

with σ the minority carrier cross-section, v_{th} their thermal velocity, and N_{ts} the density of surface states.

Such recombination activity at the front like at the rear surface of the wafers is detrimental because it implies an effective lifetime τ_{eff} for minority carrier in place of the true bulk lifetime τ_b. τ_{eff} could be expressed by:

$$\frac{1}{\tau_{eff}} = \frac{1}{\tau_b} + \frac{2S_{eff}}{W} \tag{11}$$

with W the wafer thickness.

For an n^{++} emitter, S_{eff} is about 10^5 cm·s^{-1} due to a high N_{ts} value, and as a consequence, the quantum efficiency of the cell for wavelengths below 500 μm is lowered.

Like in microelectronics, S_{eff} can be strongly reduced by surface oxidation at high temperatures (~1,000°C). As the silicon oxide grows, the interface between silicon and oxide moves deeper into the bulk that induces a strong decrease of the surface state density below 10^{10} cm^{-2}, and S_{eff} values could be lowered below 20 cm·s^{-1} [136]. However, such a strong reduction only occurs provided that the material at the surface is lightly doped. Moreover, it is more easy to passivate n-type surfaces than p-type ones [137] due to the high-electron capture cross-sections and to electrostatic effect of positive fixed charges in the native oxide which tends to accumulate n-type surfaces and to deplete p-type ones.

The main reason why a thermal oxidation step was not always included in the industrial processes is the sensitivity of the bulk lifetime τ_b to high-temperature processes, especially for mc-Si cells. Therefore, low-temperature passivation techniques are preferred, and the solution came from the use of a double passivation layer: a very thin oxide film covered by a silicon nitride layer. The use of a hydrogen-rich silicon nitride layer (SiN-H) deposited by plasma-enhanced chemical vapor deposition (PECVD) at ~450°C was successfully proposed in the 1990s. Such a layer, which was first used as an antireflection coating, can introduce hydrogen in the emitter, in the space charge region, and in the base of the cell after a very short annealing step at

~700°C. Probably, hydrogen satisfies dangling bonds and passivates the dislocations formed in the n^{++} emitter, as well as around the orthorhombic SiP precipitates.

Recently remarkable results in passivation of n-type and p-type surfaces have been obtained by means of the deposition of an Al_2O_3 layer by atomic layer deposition (ALD) [138] and also by the deposition of a very thin (<10 nm) intrinsic amorphous silicon (a-Si-i). Both processes can be carried out at low temperatures. Al_2O_3 passivation works very well on lightly doped p- and n-type silicon surfaces as well as on highly boron-doped p^+ emitters.

Surface recombination comes also from the contact between the emitter surface and the metallic grid due to the formation of a potential barrier opposed to the flow of majority carriers. To minimize this contact resistance, two solutions have been proposed. Either a thin oxide layer is inserted between the metal and the semiconductor and the oxide thickness is chosen so thin that the current can flow across it by tunnel effect, or the grid metal is deposited on a heavily doped n^{++} or p^{+} $^{+}$ region. The second solution is preferred in industrial production due its simplicity in achieving a high fill factor. But, in this case, S_{eff} cannot be reduced enough, and the precipitate containing region formed just below the emitter surface behaves like a dead zone, e.g., a zone in which the recombination of holes is so high that no photocurrent results from the illumination of the cells by short wavelengths.

A compromise was proposed: the selective emitter concept. It consists to preserve the high doping level beneath the metallic grid contacts and to reduce the phosphorus concentration below 10^{19} cm^{-3} in the open area of the cell. Different techniques have been proposed. Two phosphorus diffusions at different temperatures have been used by Green [136]. The first one is carried out at the higher temperature (~900°C) and then, a chemical etch through a mask, removes the n^{++} layer except where the future metallic contacts will be located. Then, the second phosphorus diffusion is carried out at a lower temperature and forms a less doped n^+ emitter between the n^{++} lines. Such lightly doped surface is more easily passivated. The grid fingers are then deposited on the highly doped regions. This is the principle of the PESC (passivated emitter solar cell) developed first by Green [136]. An improved version using buried front contacts and is described in Fig. 28.

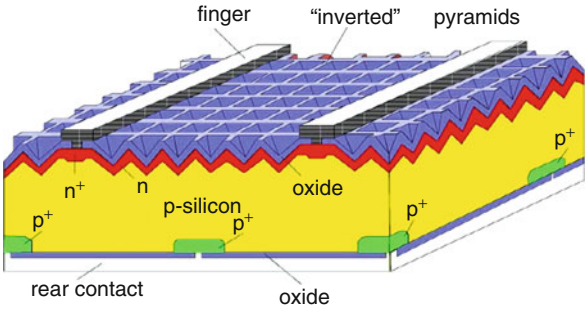

Silicon Solar Cells, Crystalline. Figure 29
Structure of the PERL solar cell (Courtesy of UNSW)

On the backside, a full area aluminium layer could be successfully used because the formation of a silicon–aluminium alloy develops a p^+-p region, giving rise to a back surface field (BSF), and a gettering effect. Another version is given by Fig. 29 in which buried back aluminium contacts are used, the passivation of the back surface resulting from a dielectric layer covered by an aluminium film which locally contacts the silicon. This is the PERL structure proposed first by Green [136]. At the back surface, S_{eff} is lower than that resulting from the Al–Si BSF; there is no bending of the silicon wafer, but there is no gettering effect.

Notice that front and back surface recombination affects the photovoltage of the cells when the base is below 120 μm, because V_{oc} must be expressed by:

$$V_{oc} = \frac{kT}{q}\ln\left(\frac{J_{sc}}{Jo} + 1\right) \tag{12}$$

and J_0 includes the contributions of the emitter and of the back contact.

Conventional and Advanced Metallization Techniques (IBC; MWT; EWT) The front grid is designed in order to reduce the internal resistance of the device and to minimize the shadowing of the cell area. The fingers of the grid are made by thermal evaporation or by screen printing of silver; this last technique being more suited to a high production throughput. Figure 30 shows the application of the silk screening technique in industrial production. The finger width is limited to less than 100 μm, and to

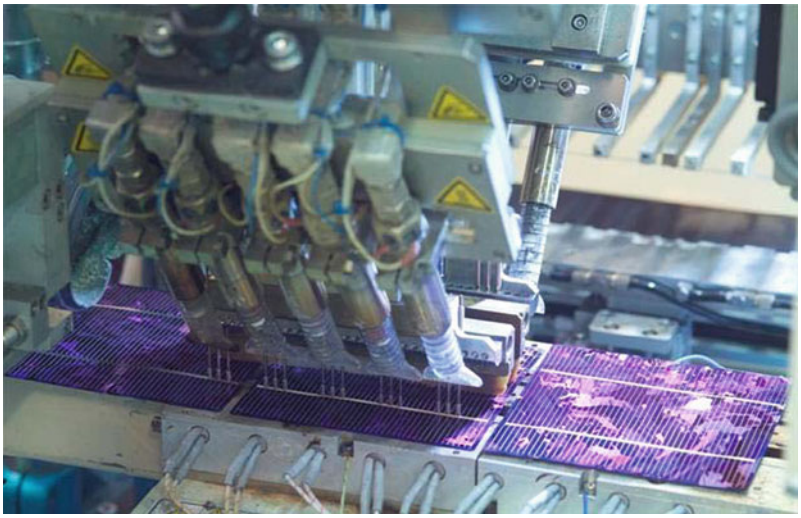

Silicon Solar Cells, Crystalline. Figure 30
Front metallization in the production line of Photowatt Intl. SAS

collect photocurrent intensities of about 7–9 A per 15×15 cm^2 cells, two or three larger fingers are used, called bus bars. On industrial cells, the total shadowing due to the front metallization represents about 7% of the total area (2.5% are due to the bus bars).

On the backside, the metallic contact could be a full area layer of aluminium, or a grid or an array of buried point contacts.

Other metallization concepts have been proposed, so-called interdigitated back contacts (IBC), emitter wrap through (EWT), and metallization wrap through (MWT).

Interdigitated Back Contact (IBC) Solar Cells: Structure and Principle The IBC cells have been initially conceived [139] to work upon concentrated sunlight. They are back contacts and back junction cells. All the metallization is on the backside, and there is no shadowing.

Such cells required high quality n- or p-type silicon substrate, with a diffusion length larger than the substrate thickness, and an excellent front surface passivation generally achieved by a front surface field (FSF) due to the formation of an n^+/n or p^+/p junction [140, 141]. The p–n junctions and the ohmic contacts are made in the form of interpenetrating combs on the non-illuminated backside, as shown by the schema of Figs. 31 and 32.

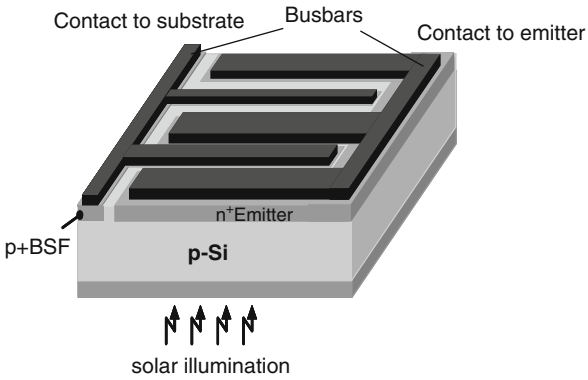

Silicon Solar Cells, Crystalline. Figure 31
Interpenetrating back contacts of an IBC cell

A BSF is created at the p contact; the front of the cell is texturized and then covered by a passivation–antireflection layer. The generated electrons diffuse to the emitter and the holes to the BSF.

The contacts can be large, thereby reducing the serial resistance of the cell, and may be used as back reflector. The dark current of the cell (J_0) is reduced, as the surface of the p–n junction is smaller. The recombination in the non-illuminated emitter is lowered, and the emitter can be highly doped, increasing the open-circuit voltage. The connection of IBC cells in a module is simplified because all contacts are located on one side.

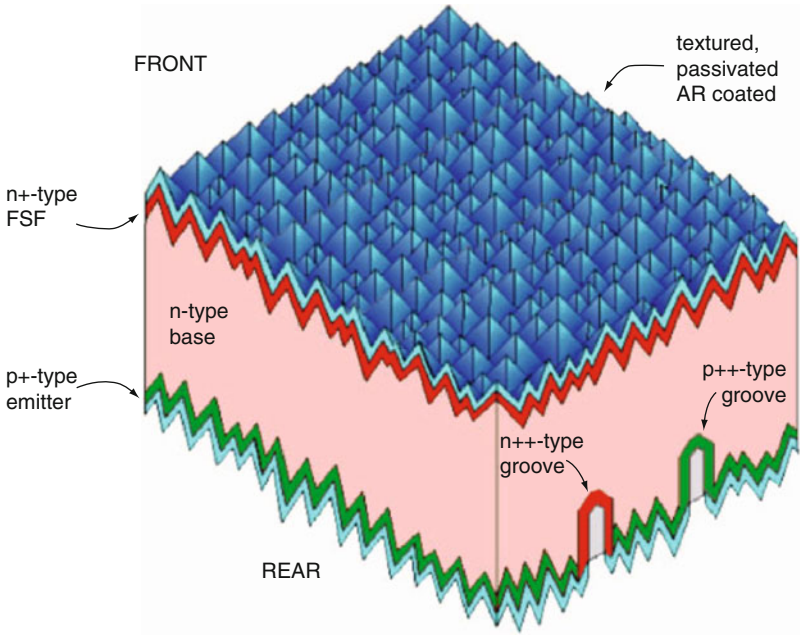

Silicon Solar Cells, Crystalline. Figure 32
Schema of an interdigitated back contact cell (Courtesy of UNSW). Note the texturization of the surfaces

The Emitter Wrap Through (EWT) Technique The concept was proposed first by Gee [142] in 1993. As shown in Fig. 33, the emitter covers the front surface and thanks to a dense array of laser-drilled small vias (<20 μm) and continues on a part of the backside. As for IBC cells, all the metallic contacts are on the backside, but lower electrical silicon quality can be used due to the fact that minority carriers are closer to the p–n junction than in classical cells.

The Metallization Wrap Through Technique (MWT) The MWT cells are also back contact cells in which the current collected from the front side is transported to a backside contact through metallized vias that have been laser drilled in the cell, as shown in Fig. 34. Because of the absence of bus bar ribbons on the front side, the EWT and also MWT modules look uniform. MWT technique is relatively simple and can be applied on both medium and high-quality material.

Both techniques simplify the connections of the cells in the modules. However, they tend to degrade the fill factor, and attention must be paid to minimize this drawback.

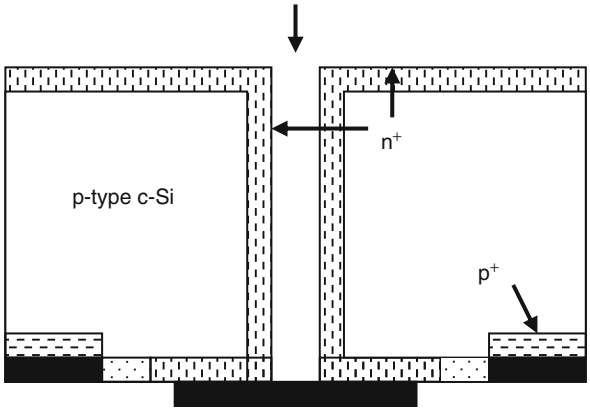

Silicon Solar Cells, Crystalline. Figure 33
Diagram of the EWT cell: all the contacts are at the rear side (metallization is drawn in *black*)

Monocrystalline Cells High-efficiency solar cells ($\eta \geq 20\%$) are made with p-type FZ or Cz monocrystalline wafers, and their structures include at least one of the advanced techniques described in sections "Antireflection Coating and Texturization" to "Conventional and Advanced Metallization Techniques (IBC; MWT; EWT)".

The first non-concentrating silicon cell to exceed 20% conversion efficiency was obtained by Green in 1985 with the microgrooved PESC (passivated emitter solar cell) [136]. A simplified version used the buried contact on the front side, a selective emitter formed by double phosphorus diffusion, and an Al–Si alloy BSF on the back surface. An improved version is the PERL cell (passivated emitter and rear contact locally diffused) with localized buried Al–Si alloyed point contacts on the backside. As shown in Fig. 35, a large part of the rear side is passivated by a transparent layer of SiO_2, and this last structure can be illuminated by the front side and also by diffused light entering through the backside. This is a bifacial cell structure.

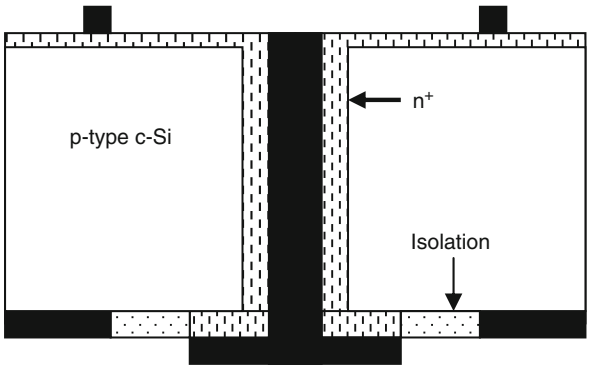

Silicon Solar Cells, Crystalline. Figure 34
Structure of the MWT cell: the bus bars are on the backside; only fingers are on the front side. Metallization is in *black*

Beginning 2000, the trend was to increase the size of the cell up to 15 × 15 cm^2, to reduce the width of the front metallic contacts, and also to minimize the metallic grid finger resistance by covering them with copper. Thanks to the new metallization concepts EWT or MWT, to the progress in the passivation of both front and back surfaces, and to the use of back junction and back contact cells, the conversion efficiency continues to increase slowly (~24.7% have been achieved by Martin Green's group at UNSW, approaching the theoretical limit of silicon cells).

High-efficiency interdigitated back contact cells have been proposed for terrestrial use under direct sunlight like PEGASUS and A 300 modules commercialized by SunPower Co. which the conversion efficiency achieves 22.5% and 21.5%, respectively [4]. Several other simplified versions have been proposed [143–148], like the self-aligned contact cell [149].

The cell A 300 has an FSF junction n^+-n performed on the front of the cell to reduce the surface recombination. To reduce the recombination at the contacts, openings are made in the passivating oxide to limit the

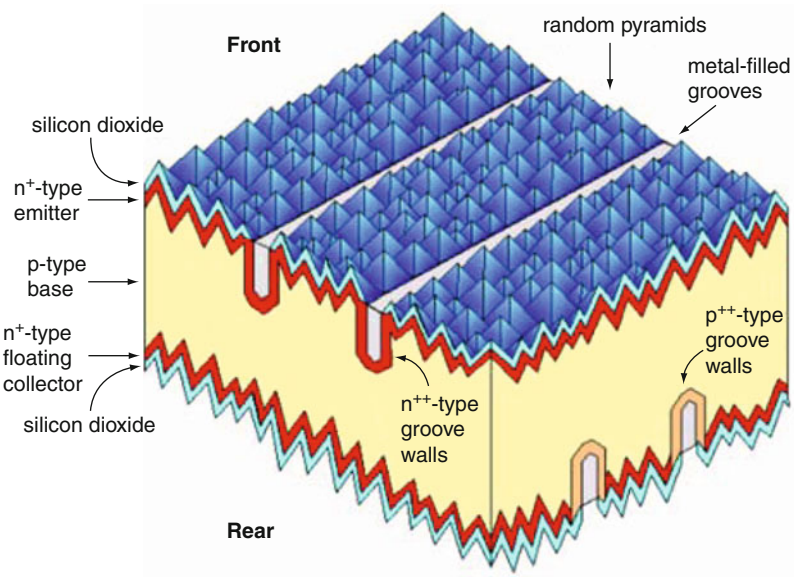

Silicon Solar Cells, Crystalline. Figure 35
Passivated emitter, buried front and rear contact cell, resulting in a bifacial solar cell (Courtesy of UNSW)

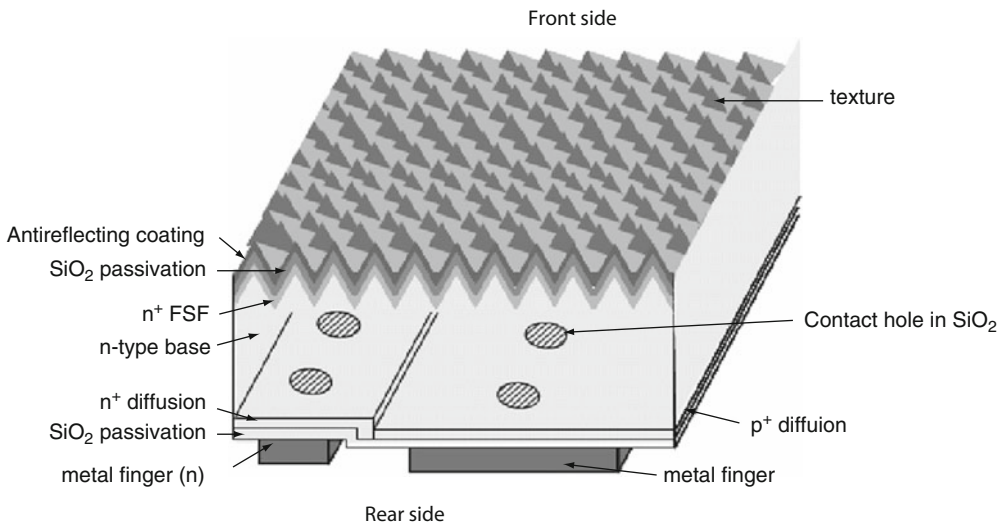

Silicon Solar Cells, Crystalline. Figure 36
Schema of the A300 IBC solar cell of SunPower

size of the contacts (point contacts), as shown in Fig. 36. Multiple photolithography steps are needed to make such cells. PEGASSUS and A300 have the highest efficiencies among the silicon cells without concentration, but the use of FZ substrates with $\tau_b > 1$ ms and the need of multiple photolithography steps explain the high cost of the module. (Such cells reach today the highest conversion efficiency for industrial products: 24.2% have been published by the SunPower-Philippines plant.)

Notice that for high-efficiency p-type-based cells made with boron-doped Cz monocrystal, a problem appears during the sun exposure of the cells; it is the light-induced degradation [150] of the conversion efficiency. Such degradation is due to the formation of recombination-active boron–oxygen complexes. This LID effect induces decrease of the efficiency of about 1–2% absolute, depending on both the boron and the oxygen concentrations. This problem has been introduced within the section "Czochralski Grown Monocrystals (Cz-Si)", and some solutions to solve this problem have been proposed, which concerned mainly the ingot growth. It is also possible to suppress or attenuate this problem by modifying the cell process. For instance, Bothe proposed to anneal the wafer at 450°C to agglomerate the O dimers, responsible for this effect, under the form of thermal donors [151]. The amplitude of this deleterious effect could also be reduced by using rapid thermal annealing [152], high-temperature oxidation steps [153], and optimized temperature ramps for the phosphorus diffusion [151]. Finally, Lim showed that the light-induced regeneration process, briefly described in section "Czochralski Grown Monocrystals (Cz-Si)", which completely suppresses the LID effects could be successfully transposed to high-efficiency Cz solar cells [154] (nevertheless, the stability of this "regenerated" state has to be studied for time comparable with the lifetime of a solar panel).

mc-Si-Based Solar Cells Due to a huge amount of academic and industrial researches and publications since 1980, the performances of mc-Si cells, as well as the production throughput, have continuously increased, accompanied by a constant decrease of the Wp cost. Their size which begun with 10×10 cm^2, currently achieve 15.6×15.6 cm^2, and some cells with 21×21 cm^2 size have been made. Today, the conversion efficiencies η of commercial cells are in the range 16–18%, while at a laboratory scale, η reaches 20.4% [155, 156]. The main interest of mc-Si cells is due to the flexibility in the cell size, the lower energy consumption, and the low cost of the ingots compared to the Cz and FZ monocrystalline ingots. Figure 37

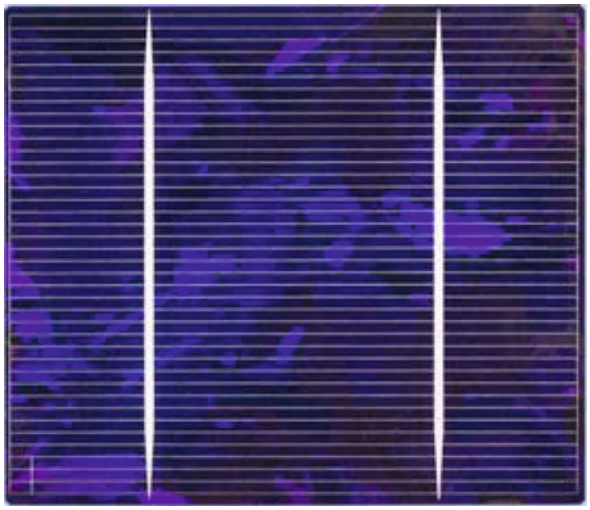

Silicon Solar Cells, Crystalline. Figure 37
Picture of a mc-Si cells, 180 μm thick and 15.6 × 15.6 cm^2 in size, made with polix multicrystalline silicon

shows a picture of a mc-Si cell covered by a blue antireflection coating.

Such cells suffer from the presence of a lot of extended crystallographic defects and of residual metallic impurities which limit the diffusion length or the lifetime of minority carriers. The conversion efficiency is always 2–2.5% absolute lower than that of monocrystalline cells. Nevertheless, as described in section "Extended Crystallographic Defects and Impurities", the crystallization of the wafers and the associated segregation phenomena like the processing steps used to make the cells (which include gettering treatments and hydrogenation) minimize the metallic impurity concentrations which are currently below 20 ppba in the central part of ingots. For instance, a marked attention was paid to the influence of iron, but it was demonstrated clearly that the influence of Fe is often negligible in the finished solar cells by Dubois et al. [62]. The oxygen, carbon, and nitrogen concentrations are relatively low, generally below the solubility limit: $[O] \leq 5 \times 10^{17}$ cm^{-3}, $[C] \leq 6 \times 10^{17}$ cm^{-3}, and $[N] \leq 10^{16}$ cm^{-3} and that avoid the formation of precipitates or coprecipitation. Problems can come from species with high segregation coefficients and from slow diffuser metallic atoms like Al, Ti, V, or W which cannot be entirely removed during crystallization and processing steps. Dislocations are

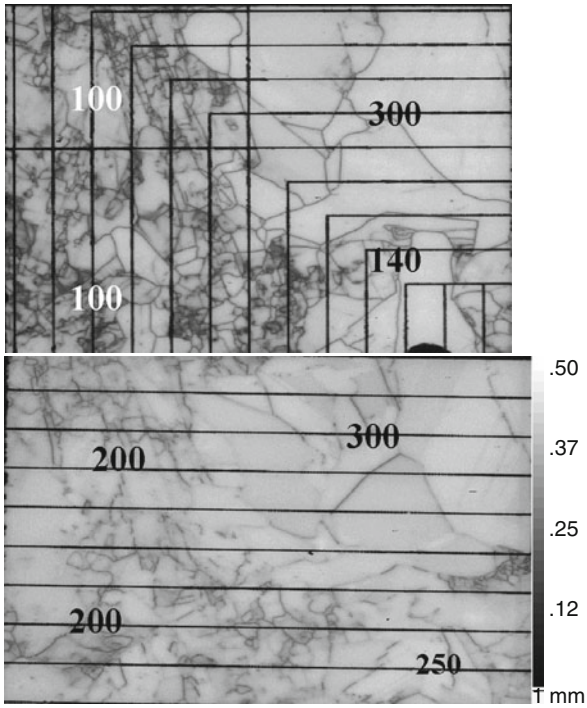

Silicon Solar Cells, Crystalline. Figure 38
LBIC contrast scan map at λ = 940 nm of two mc-Si cells made with companion wafers: the upper cell was covered with TiO_2 ARC, and the back contact is an aluminium grid, while the other cell was covered with the SiN_x–H ARC on the front side and with a plane Al layer on the backside and then annealed at ~700°C for few minutes. The beneficial effects of the second processing steps are very clear

the more harmful extended crystallographic defects when there are concentrated in tangles or in clusters. At these very large defects, impurities are trapped and tend to form silicates [41] which are not entirely dissolved during phosphorus diffusion or Al–Si alloying. Even the extension of these gettering treatments for several hours cannot suppress their recombination activity.

All the processing steps applied to monocrystalline cells, except high-temperature treatments (above 920°C), can be applied to the production of mc-Si cells. Moreover, the processing steps, particularly the phosphorus diffusion, the Al–Si alloying, and the hydrogenation through a SiN_x-H layer, improve the base and the emitter electrical properties. That explains their success. An example of such improvements is described in Fig. 38 by means of

light beam induced current contrast (LBIC). Two solar cells made with companion samples cut adjacently from the same ingot and presenting the same features and density of extended defects are transformed in solar cells. The first one is made with a rear Al grid and a TiO_2 antireflection coating (ARC), the second with a plane, ~15 μm thick, Al layer and a SiN_x-H ARC, then annealed at ~700°C for few minutes. The improvement is clearly demonstrated by the reduction of the LBIC contrast at the extended defects and by the strong increase of the minority carrier diffusion length in the grains.

The structure of the cells will not change too much because back junction cells cannot work efficiently when such materials are used.

The recent tendency is the use of selective emitters and of MWT [157, 158] as well as EWT [159] metallization techniques. The most impressive recent results come from Japan and from China. A conversion efficiency of 19.1% was obtained by Mitsubishi Electric Co. for 217.6 cm^2 cell made with a selective emitter, a honeycomb textured surface, a backside reflector, and small width grid fingers [160]. A commercialized mass production is expected from Suntech Power Holding Co. with the so-called PLUTO technology [161] which includes a selective emitter and very narrow metal lines. Conversion efficiency of such cells over 17% has been achieved while that of the module is over 15%.

For ribbon solar cells, the worldwide market share was ~2% in 2009. The edge-defined film fed growth (EFG) ribbon [162] and string ribbon (SRT) [163] lead also to n^+-p-p^+ cells with production efficiencies about 14–15%, while at the laboratory scale, they arrive at 17.8% and 18.2%, respectively for SRT and EFG ribbons [164, 165]. Such materials have high concentration of vacancies which are introduced into the bulk during the ribbon growth or cell processing steps. Such vacancies can enhance hydrogen in-diffusion and defect passivation by providing an additional driving force for diffusion or by dissociation H_2 molecules. For these reasons, the cells are very sensitive to hydrogenation.

Despite the excellence of the technology, the production of STR ribbons is stopped in 2011 because they do not reach the standard wafer size (>125 × 125 mm^2) and cannot compete with the low-cost products coming from Asia.

p-Type UMG-mc-Si-Based Solar Cells Solar cells can be made with upgraded multicrystalline silicon resulting from a blend of solar or electronic-grade silicon and of purified metallurgical feedstock. Results of Elkem and Sintef [10, 13] indicate that medium-efficiency cells are obtained thanks to the usual processing steps with conversion efficiencies ~15–16%. These results have been confirmed by Bronsveld [166], by Prettyman [20], and by Braun [167].

Plasma torch refined UMG-Si is also of interest, as efficiencies up to 15.9% have been obtained on 12.5 × 12.5 cm solar cells prepared at INES laboratory, Chambery. Notice that these cells are made with genuine refined and upgraded metallurgical silicon, without any blending with another high-purity silicon feedstock. The minority carrier diffusion lengths are limited to about 60 μm in the raw wafers and do not increase too much after phosphorus diffusion, but the base material seems to be very sensitive to the combination of hydrogenation and Al–Si alloying because in cells which the structure is that described in section "The Basic Structure", values of L exceeding 180 μm are measured.

A disadvantage of the UMG-mc-Si cells is the high concentrations of oxygen and carbon, which can induce coprecipitates or SiC filaments. The SiC precipitates are found to be conductive and form shunts which can impair the cell properties, especially at low illumination. The base material is generally highly doped by boron and by phosphorus. The effects of the resulting compensation on the electrical properties of the silicon wafers and solar cells have been poorly studied, and a gain of interest has grown around compensated silicon these last years. Dopant compensation poses one major problem which is due to the different partition coefficients between boron and phosphorus. The marked segregation of phosphorus during the ingot growth induces strong variations of the resistivity along the ingot height and across the surface of the wafer particularly if the shape of the solid/liquid interface is not well controlled. In some cases, a change in the type of conductivity can be observed which is detrimental since only the p-type wafers can be processed to solar cells. Nevertheless, solutions have been proposed to solve this main drawback regarding dopant compensation, which are mainly based on the introduction in the feedstocks of other doping species

(gallium for instance), with partition coefficients much lower than those of boron and phosphorus [168]. Dopant compensation could also be detrimental regarding carrier mobility. Indeed, additional carrier scattering mechanisms, other than usual scattering by ionized charge impurities, could occur in the most compensated zone of the ingot [169]. This mechanism is always under study at the moment. Nevertheless, dopant compensation offers also some remarkable advantages. Indeed, for a given boron concentration, increases in the phosphorus concentration are related with increases in the carrier lifetime limited by defects introducing shallow levels in the silicon band gap (dopants, FeB, and CrB pairs) [170]. In addition, the amount of boron–oxygen recombination-active complexes formed under illumination decreases when the phosphorus concentration increases [171].

Notice that n-type UMG-mc-Si, which is more tolerant toward impurities than the p-type material, could be the best material to prepare medium conversion efficiency solar cells at a huge industrial production level.

N-Type Silicon-Based Cells (p^+-n-n^+ and n^+-n-p^+ Structures)

These cells make the most of the advantages of n-type silicon wafers, described in section "n-type mc-Si". It could be noticed that the highest conversion efficiencies have been always obtained with n-type monocrystalline FZ silicon. However, low-cost solar cells are also required to achieve the grid parity for the electrical energy, and n-type Cz or mc-Si wafers are of interest.

IBC, Back Contact, and Back Junction HIT High-Efficiency Solar Cells Made with n-Type FZ and Cz c-Si After the success of the IBC solar cells conceived for concentrated sunlight ($\eta \sim 27\%$ under 96 suns), a new progress, at the production scale, was achieved in 2007 by the SunPower group [172] with the improved A300 interdigitated back contact 155 cm^2 solar cell, which the conversion efficiency mode reaches in 2009 ~22.4%, under one-sun illumination (this type of cell is conceived for a terrestrial use). The total area efficiency of the 96-cell modules of SunPower was also increased to ~20%, by the reduction of the inactive areas and by the deposition of an antireflection coating on the protecting front glass. This is the most impressive result in the field of commercial high-efficiency cells because such modules were in production at a level of 300 MW a year in 2009 (SunPower has recently announced 24.2% efficiency using industrial processes).

Sharp group [173] has also obtained remarkable results in pilot line production employing high-quality Cz single crystals. With screen-printed contacts, their cells achieved in 2008, a conversion efficiency of 20% for 12.6×12.6 cm^2 and 120 μm thick cells.

At a laboratory scale, remarkable results have been obtained with efficiencies around 21.3% [174] and 21.8% with Cz wafers [175].

Another high-efficiency structure was proposed by the Sanyo group: the so-called HIT silicon cells (heterojunction with intrinsic tunnel intermediate layer). Such cell structure was inspired by the results of Okuda [176].

The silicon heterojunction solar cells are obtained through very thin hydrogenated amorphous silicon (a-Si:H) layers deposited on both sides of a monocrystalline Si wafer (CZ or FZ) in order to form both the front emitter and the back surface field. Low processing temperatures (<250°C) and use of plasma-enhanced chemical vapor deposition (PECVD) techniques allow one to produce cells at low thermal budget and high throughput. A schematic view of this type of structure is shown in Fig. 39.

The thickness of the a-Si:H layers is kept very thin in particular at the top side (typically <20 nm) in order to minimize absorption in these layers that contain a lot of defects. Since the room temperature conductivity of highly doped a-Si:H (of the order of 10^{-2} S cm^{-1} for n-type and less for p-type) is orders of magnitude lower compared to that of highly doped c-Si, it is necessary to introduce a transparent conductive oxide (TCO) layer below the metal grid in order to minimize lateral conduction losses. Indium tin oxide or zinc oxide (doped with aluminium) has been used. This layer also acts as an antireflection coating layer that, in addition to conventional surface texturing, improves light penetration in the cell and thus helps to increase the short-circuit current.

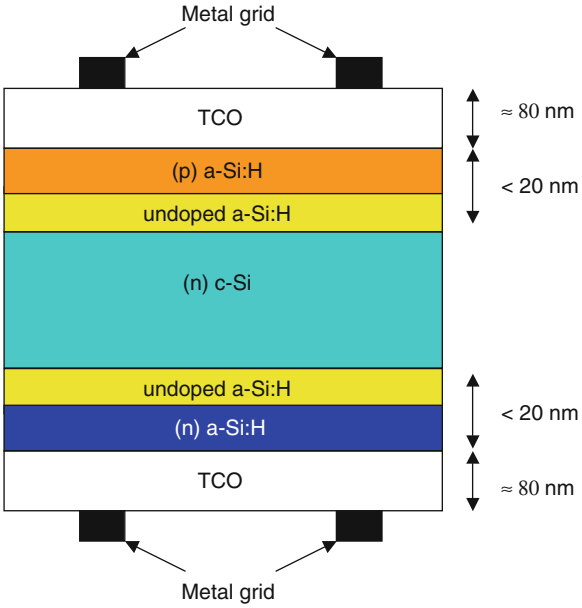

Silicon Solar Cells, Crystalline. Figure 39
Schematic view of a double-side silicon heterojunction solar cell on n-type c-Si with p-type a-Si:H front emitter and n-type a-Si:H BSF. Also indicated are typical thickness values

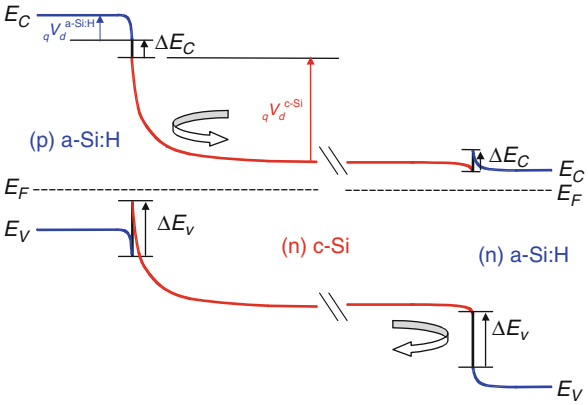

Silicon Solar Cells, Crystalline. Figure 40
Schematic energy band diagram at equilibrium of a (p) a-Si:H/(n) c-Si/(n) a-Si:H heterostructure. The *top* and *bottom solid lines* show the conduction band and valence band edges, respectively, while the dashed line shows the equilibrium Fermi level

The first relevant study on transport properties of structures with hydrogenated amorphous silicon deposited onto c-Si was performed by Fuhs et al. [177], who observed a well diode rectifying behavior. Application of such heterostructures to solar cells was successfully lead by researchers from Sanyo Electric Co. [178] in 1991. At that time, efficiencies of 18.1% were already obtained on 1 cm^2 textured cells, and the solar cell performance of such HIT structures has been steadily improved [179, 180, 181] until nowadays, where values of 23% have been announced on large areas for 200 μm thick cells and 22.8% for 98 μm thick cells, with open-circuit voltage values up to 743 mV [182]. The high open-circuit voltage values achieved in such structures are due to the presence of heterojunctions. Hydrogenated amorphous silicon has a larger bandgap (1.7–1.9 eV) compared to c-Si (1.12 eV), leading to both conduction and valence band offsets. These, in turn, induce strong band bending at the c-Si surface, acting as field effect passivation, and contributing to minimize recombination losses. Contradictory results have been published in literature regarding the relative amplitude of conduction band versus valence band offsets. However, there is now a significant agreement on a relatively low conduction band offset, ΔE_C, compared to a relatively large valence band offset, ΔE_V. Recently, values of ΔE_C and ΔE_V of 0.15 eV and 0.45 eV were obtained from independent measurement techniques: (1) from planar conductance measurements [183] and (2) from UV-photoelectron spectroscopy [184].

Figure 40 shows a schematic band diagram of the (p) a-Si:H/(n) c-Si/(n) a-Si:H structure at equilibrium. There is a large band bending at the (p) a-Si:H/(n) c-Si emitter interface that is related to the large difference in work functions and thus to the valence band offset. The main part of this band bending occurs in the c-Si due to the high charge density in the depleted region in a-Si:H, originating from the high density of gap states in the amorphous semiconductor. In other words, there is a large diffusion potential in the c-Si, $qV_d^{c\text{-}Si}$. This implies a strongly inverted region at the c-Si surface, where the high concentration of holes can form a lateral conduction channel, as revealed from planar conductance measurements [185]. The strong band bending at the emitter junction can help electrons be reflected rather than recombined at the emitter interface. Additionally, the large valence band offset also prevents holes being recombined at the (n) c-Si/(n) a-Si:H back

interface, reinforcing the back surface field effect. While the relatively low conduction band offset does not provide a significant hint to the collection of photogenerated electrons at the back interface, the large valence band offset could be a drawback for the collection of photogenerated holes at the emitter interface. This is evidenced in numerical simulations that yield I(V) characteristics exhibiting a pronounced S-shape at room temperature when the valence band offset value is larger than 0.5 eV. Fortunately, the high density of states in the band gap of amorphous silicon (and in particular, in the valence band tail) can favor tunneling of holes through the valence band spike.

Another key feature in explaining the outstanding performance of silicon heterojunction solar cells is the high quality of surface passivation at the a-Si:H/c-Si interfaces that allow to decrease recombination losses of the carriers photogenerated in c-Si. It is well known that a high density of defects (mainly silicon dangling bonds) can exist at the c-Si surface. Such defects act as recombination centers for photogenerated carriers. Therefore, it is necessary to decrease the density of surface states in order to increase the open-circuit voltage of the solar cells. In order to have a well-passivated silicon surface prior to a-Si:H deposition, one generally uses wet chemical treatments for surface etching (in order to remove the native oxide layer) and cleaning [186]. Note that a route for the future technology is to replace the wet chemical treatments by dry plasma treatments (some interesting results were obtained recently [187] which would simplify the fabrication process and provide an all-plasma process from cleaning to a-Si:H deposition). Also, the deposition conditions of the a-Si:H layer have to be tailored in order to avoid surface damaging from the plasma during deposition. Fortunately, a-Si:H can passivate the c-Si surface very well, which is partly due to the passivation of dangling bonds by hydrogen. Very large effective lifetimes ($\tau_{eff} > 1$ ms) and very low surface recombination velocities (<20 cm/s) have been reported from quasi-steady-state photoconductance measurements performed on c-Si wafers passivated by a-Si:H [188, 189]. Such low values are comparable to that obtained with insulating passivation layers like silicon oxide or silicon nitride, with the advantage of a low-temperature deposition process ($T < 250°C$). The challenge is to obtain a very good passivation with also a very thin a-Si:H layer, in order to minimize absorption in the a-Si:H layers. It has been suggested by Sanyo's group that inserting a very thin undoped a-Si:H layer between the c-Si wafer and the doped a-Si:H layer helps reducing interface recombination and leading to the so-called "HIT" concept (heterojunction with intrinsic thin layer) [178]. One can understand the benefit of such an undoped buffer layer since the defect density in a-Si:H is known to increase with doping [190]. Arguments based on the formation of dangling bonds from Si–H bond breaking in relation with the Fermi energy have also been proposed recently [191, 192]. In order to avoid plasma surface damaging during a-Si:H deposition, the deposition conditions of a-Si:H have to be properly tailored. Thus, it has been suggested that the formation of an epitaxial silicon layer or a mixed-phase layer at the early stage of a-Si:H deposition [193] must be avoided. Good passivation properties have been reported for a-Si:H layers obtained from either conventional radio-frequency plasma-enhanced chemical vapor deposition (RF-PECVD) or very high frequency (VHF-PECVD) or hot wire CVD from various groups. Several institutes have fabricated silicon heterojunction solar cells with certified efficiencies between 19% and 20% on n-type c-Si [194–196] or p-type c-Si [197]. However, these results have been obtained so far on small-size cells (between 0.3 and 1 cm^2). It is worth mentioning the recent performance obtained at INES, France, on very large areas (19.5% efficiency on 148 cm^2) [198].

Following the success of the "HIT" solar cells, several departures from the historical 1D front side emitter silicon heterojunction solar cell have been proposed, from inverted heterojunction cells [199] to interdigitated back contact heterojunction cells (IBC-HJ) [200]. The latter combine the rear contact cell concept, which has proved to be able to provide high efficiencies in c-Si [201] with silicon heterojunctions. A simplified sketch of such a cell is presented in Fig. 41, and several different architectures based on the IBC-HJ concept have been proposed: RECASH (rear emitter back contact amorphous/crystalline silicon heterojunction) [202], PRECASH (planar rear emitter back contact amorphous/crystalline silicon heterojunction) [203], BEHIND (back-enhanced heterostructure with interdigitated back contacts). However, the present performance of

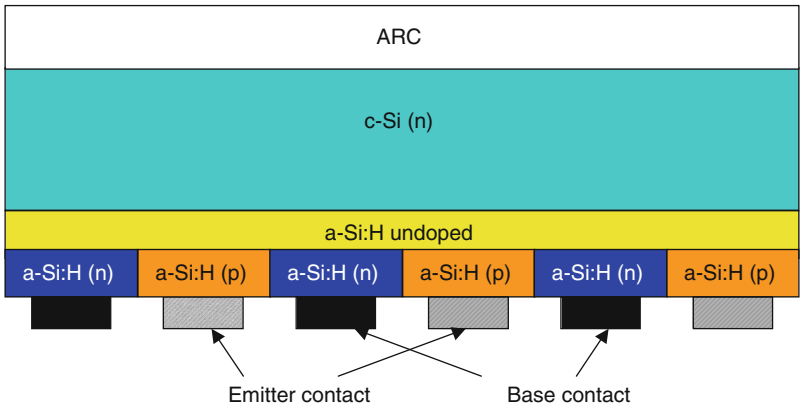

Silicon Solar Cells, Crystalline. Figure 41
Schematic sketch of an interdigitated back contact silicon heterojunction solar cell with a top antireflection coating (ARC) layer

IBC-HJ cells is still far from being optimized. The best performance so far has been achieved with the BEHIND cell, with 15% efficiency obtained on p-type c-Si [204].

Nevertheless, such silicon heterojunctions can be used in the field of nanowire radial junction cells to passivate their front surface [205–208].

However, the present performance of IBC-HJ cells is still far from being optimized, and more technological work is necessary for further improvement.

n-Type Solar Cells Made with Cz-Si or mc-Si Compared o p-type Si substrate, n-type substrates generally present higher carriers' lifetime, and solar cells fabricated on n-type substrates show no LID. The cell processes are very close to those of p-type-based ones, and the first results obtained with n-type base were very encouraging as they have demonstrated that substantial conversion efficiencies are more easily achievable with n-type silicon than with p-type. The main difficulties with such cells come from the formation of a front side p-type emitter by boron in-diffusion and the passivation of its highly doped p^+-type surface. Indeed, boron diffusion requires higher temperatures than phosphorus diffusion, and the SiN-H (or SiOx/SiN-H) passivation is not effective because of the positive fixed charges contained in the layers.

This is why two structures are proposed for low-cost solar cell mass production. The first is based on a rear junction formed by Al–Si alloying at relatively low temperatures. The second is based on front side or backside boron diffusion with new surface passivation techniques. The first structure is very attractive because thermal evaporation or screen-printing can be used to deposit the aluminium layer and gettering of impurities occur during the alloying.

Aluminium Alloyed Rear Emitter Cells (n^+-n-p^+ Structure) The very high minority carrier diffusion lengths of the n-type monocrystals allow prepare rear junction by means of a very simple technique: the aluminium–silicon alloying, and Fig. 42 shows that their structure is very close to that Fig. 21 except that the junction is on the rear side due to p^+ Al-doped region created above the Al–Si alloy. Front phosphorus diffusion forms the front surface field and induces a gettering effect.

After that, some encouraging results have been obtained with small samples [64, 209, 210], efficiencies higher than 17% have been reported with 100 cm^2 cells, and a decisive progress resulted from the emitter passivation by means of a 30 nm Al_2O_3 layer covered by a 150 nm PECVD SiOx layer: the photovoltage reaches 650 mV, and the efficiency increases to 20.1% [211] at a laboratory scale. With low-cost industrial processes (phosphorus FSF, Al–Si alloyed emitter, and SiN-H antireflection coating), Weeber et al. [212] have prepared Cz solar cells (thickness 200 μm and area 140 cm^2) which the efficiency reaches 17.4%,

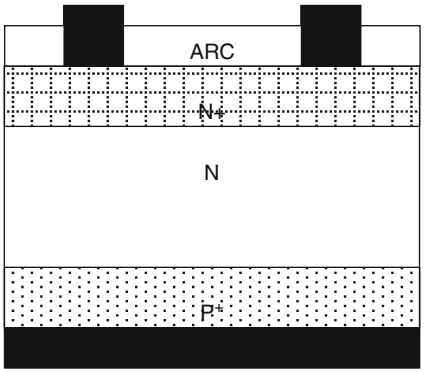

Silicon Solar Cells, Crystalline. Figure 42
Structure of rear junction solar cell made by Al–Si alloying. The structure is very close to that of the very basic cell of Fig. 21

while Schmiga et al. achieved 18.2% with 148.5 cm^2 cells [213].

Since the emitter is at the rear, only high-quality base material can be applied, and the preceding results have been obtained with monocrystalline wafers. However, very thin mc-Si wafers (~100 μm thick) could also be acceptable candidates because L_p, at the end of the processes, is up to three times higher than such thicknesses.

The comparison under low-illumination conditions of the performances of n-type and p-type solar cells made using identical processes reveals another advantage of n-type-based cells. It was demonstrated by Cong et al. [214] that n-type cells outperform p-type cells (and amorphous silicon single-junction cells) as a conversion efficiency of 12.7% is measured at 0.01 sun illumination.

Notice that the Ebara group has prepared rear junction cells with n-type monocrystalline dendritic WEB ribbons (a ribbon technique close to the string ribbon one) and has achieved a conversion efficiency ~14.5% [215].

Boron-Diffused Front Emitter (p^+-n-n^+ Structure) Contrary to the rear junction cells, front junction cells could be made with high- and low-quality material. For a 4 cm^2 PERL cell with a front boron diffused and passivated emitter, Benick et al. have achieved 23.2% cell efficiency [216]. One of the key successes was the excellent passivation of the front p^+ surface by atomic layer deposition (ALD) of Al_2O_3 [87]. With a rear totally diffused back contact, Zhao et al. have obtained 22.7% for 1.5 Ωcm FZ wafers and 20.8% for 5 Ωcm Cz wafers [217]. In 2009, Benick et al. [218] reported mean conversion efficiencies of 22.5% with a maximum value of 23.4% thanks to a PERL structure with a front Al_2O_3 passivating layer and a SiO_2 passivation layer on the backside.

Using low-cost industrial processes (boron and phosphorus are co-diffused to form the emitter and the BSF), Weeber et al. [219] have reached conversion efficiencies ~18.5% for 156 and 243 cm^2 cells made with Cz wafers and 16.7% with mc-Si wafers. The front surface was passivated by a wet chemical oxidation process covered by a SiN-H layer.

For n-type UMG-mc-Si cells, first results on large area were presented by Veschetti et al. over an entire compensated ingot. Efficiencies between 12.8% and 14.2% were obtained with a nonoptimized process depending on the wafer position along the ingot [220, 221].

Remark on n-type mc-Si cells. The preceding results have been rapidly obtained with Cz wafers, demonstrating the interest of n-type silicon, and new progresses are expected thanks to improved metallization and texturization technologies. However, taking into account the high values of L_p in these wafers, the conversion efficiency of front junction mc-Si solar cells is disappointing. That may be due to the boron diffusion which the required temperature is too high and which the associated gettering effect is less pronounced than that resulting of phosphorus diffusion and aluminium–silicon alloying [80, 81]. In addition, the gettered impurities are located after the diffusion within a p-type region in which they are very detrimental in terms of carrier recombination.

Future Directions

Undoubtedly, the production at an industrial scale of crystalline silicon solar cells is a success, and this success is mainly due to the exceptional material quality of silicon wafers. Improvements should come again from "monocast" ingots as developed by BP Solar [222]. This is a new technique to produce single-crystalline large ingots using a standard "cast-in-place" process, where the ingot is directionally solidified inside

a crucible. A crystalline seed orients the growth which is enhanced by a thermal gradient. The material associates the advantages of a single crystal (chosen orientation; low crystalline extended defect density) with that of multicrystalline ingots (large size, relatively low-oxygen concentration). High efficiencies are expected for solar cells.

Conversion efficiencies as high as 22–24.5% are reached today with monocrystalline cells and 18–21% with multicrystalline cells. Recently, Q-Cells announced for the industrial mc-Si quantum solar cell (243 cm^2) efficiencies higher than 19% and for 1.49 m^2 module efficiencies about 17.8%, respectively [223].

At the laboratory scale or in pilot line production, the results are a little bit better, only. Moreover, the cells are very stable, and their lifetime could be about 30 years, provided that they are interconnected and encapsulated in well-protected modules. This is a clear indication that the limit of what it is practically possible to get with a single-junction silicon solar cell is not very far (the theoretical limit for a single-junction solar cell is 28–29%). Nevertheless, some progresses are again expected in industry when the mass production will include the selective emitter, the advanced metallization, and ultra-efficient surface texturization and passivation techniques.

Attention must be paid to n-type silicon, especially to refined metallurgical multicrystalline material. Such a material possesses the advantage to combine a high tolerance toward metallic impurities, a low cost and a very large abundance. Recent results have shown that conversion efficiencies higher than 20% have been obtained at a laboratory scale with boron-diffused junctions as well as with Al-diffused back side emitter [224, 225]. At an industrial scale, Weeber et al. [226] and Veschetti et al. [226] achieved 19.3% for 156 cm^2 cells. The production has begun with Yingli in China [226].

The main problem will be the cost of the peak-watt, which is, at least today, two times higher than that of CdTe thin film solar cells and which is always far from the grid parity. Such a cost could be decreased significantly when huge production plants are at work.

This is not good news for research laboratories because the production throughput and the peak-watt cost will become the driving force to the detriment of innovation.

If the photovoltaic production continues to grow by 30% a year, the problem of the material stock availability must be taken into account. For silicon cells, it will be certainly essential to use silicon feedstock produced by the metallurgical route and to avoid the sawing of the ingots by wire saws which destroys a highly pure and well-crystallized material. Thin texturized wafers and probably ribbons and sheets will be also of interest.

To achieve conversion efficiencies exceeding 30% in the next future, new cell structures must be employed like tandem junctions made with nanomaterials eventually illuminated by weakly concentrated sunlight. This will be a hard challenge, but it opens the way to new R&D developments.

Abbreviations

EUPVSEC	European Photovoltaic Solar Energy Conferences
IEEE-PVSC	Photovoltaic Specialist Conferences
SOLMAT	Solar Energy Materials and Solar Cells

Bibliography

Primary Literature

1. Hunt LP (1990) Silicon precursors: their manufacture and properties. In: O'Mara WC, Herring RB, Hunt LP (eds) Handbook of semiconductor silicon technology. William Andrew/Noyes, Park Ridge, pp 1–32
2. Rogers LC (1990) Polysilicon preparation. In: O'Mara WC, Herring RB, Hunt LP (eds) Handbook of semiconductor silicon technology. William Andrew Publishing/Noyes, Park Ridge, pp 33–933
3. Bischoff F (1954) German Patents n° 1102117 and 1140549, filed May 18, USP 3146123
4. Weihaus D, Schlimbeck E, Hesse K, Dornberger E (2005) Pilot production of granular polysilicon from trichlorosilane using a fluidized bed reactor. In: 20th EUPVSEC, Barcelona, Spain, pp 564–568
5. Cecarolli B, Lohne O (2003) Solar grade silicon feedstock. In: Luque A, Hegedus S (eds) Handbook of photovoltaic science and engineering. Wiley, Sussex, pp 153–204
6. Hesse K, Schindlbeck E, Dornberger E, Fischer M (2009) Status and development of solar grade silicon feedstock. In: 24th EUPVSEC, Hamburg, Germany, p 883
7. Joyce DB, Khattak CP, Schmid F (2001) Segregation steps applied to the purification of metallurgical silicon. In: 11th NREL workshop on crystalline silicon solar cell materials and processes, Estes Park (CO), USA, p 177

8. Di Sabatino M, Øvrelid EJ, Kopecek R, Binetti S, Mihailetchi VD, Geerligs L, Vaenes AN (2009) FoXy-development of solar grade silicon feedstock for crystalline wafers and cells by purification and crystallisation. In: 3rd international workshop on crystalline silicon solar cells, Trondheim, Norway
9. Enebakk E, Tranell GM, Tronstad R (2003) Calcium-silicate based slag for phosphorus and boron removal from molten silicon, patent PCT/NO03/00091
10. Amouroux J, Morvan D (1981) Production of high-purity silicon ingot. US Patent 4399116
11. Yuge N, Baba H, Sakaguchi Y, Nishikawa K, Terashima H, Aratami F (1994) Purification of metallurgical silicon up to solar grade. Sol Energ Mat Sol Cells 34:243–250
12. Naomichi N, Misamichi A, Kazuhiro H, Hiroyuki B, Kenkichi Y, Yasuhiko S, Yoshihide K (1998) Purification of silicon for solar battery and apparatus, Japanese patent JP10273311
13. Nakamura N, Baba H, Sakaguchi S, Kato Y (2004) Boron removal in molten silicon by a steam-added plasma melting method. Mater Trans 45:858–864
14. Alemany C, Trassy C, Pateyron B, Li KI, Delannoy Y (2002) Refining of metallurgical-grade silicon by inductive plasma. Sol Energ Mat Sol Cells 72:41–48
15. Delannoy Y, Alemany C, Li KI, Proulx P, Trassy C (2002) Plasma-refining process to provide solar-grade silicon. Sol Energ Mat Sol Cells 72:69–75
16. Einhaus R, Kraiem J, Cocco F, Caratini Y, Bernou D, Sarti D, Rey G, Monna R, Trassy C, Degoulange J, Delannoy Y, Martinuzzi S, Périchaud I (2006) PHOTOSIL-simplified production of solar silicon from metallurgical silicon. In: 21st EUPVSEC, Dresden, Germany, p 580
17. Pizzini S, Acciari M, Binetti S (2005) From electronic grade to solar grade silicon: chances and challenges in photovoltaics. Phys Stat Sol (a) 15:1928–1942
18. Peter K, Kopecek R, Soiland A, Enebakk E (2008) Future potential for SoG-Si feedstock from the metallurgical route. In: 23 rd EUPVSEC, Valencia, Spain, Sept 2008, pp 947–950
19. Hoffman V, Petter K, Djordjevic-Reiss J, Häckedal JT, Tronstad R, Vlasenko T, Buchovskaja I, Beringov S, Bauer M (2008) First results on industrialization of ELKEM solar silicon at Pillar JSC and Q-Cells. In: 23 rd EUPVSEC, Valencia, Spain, p 1117
20. Prettyman K, Pfeiffer G, Krause R, Hovel H (2009) Solar cell production using UMG silicon. In: 24th EUPVSEC, Hamburg, Germany, p 1333
21. Dietze W, Keller K, Mühlbauer A (1981) Float zone silicon in crystals. In: Grabmaier J (ed) Crystals, growth, properties, and applications. Springer, Berlin/Heidelbreg, pp 1–42
22. Pfann WG (1952) Principle of zone melting. Trans AIME 194:747
23. Theuerer H (1952) USP 3060123 filed Dec 17
24. Emeis RZ (1954) Tiegelfreies ziehen von silicium einkristallen, Naturforsch. 9a, 67
25. Czochralski JZ (1918) Phys Chem 92:219
26. Teal GT, Little JB (1950) Phys Rev 78:657
27. O' Mara WC (1990) Oxygen, carbon and nitrogen in silicon. In: O'Mara WC, Herring RB, Hunt LP (eds) Handbook of semiconductor silicon technology. William Andrew Publishing/Noyes, Park Ridge, pp 451–537
28. Dietl J, Helmreich D, Sirtl E (1981) Solar silicon. In: Grabmaier J (ed) Crystals, growth, properties, and applications. Springer, Berlin, pp 43–107
29. Schmid F, Basaran M, Khattak CP (1980) Purification of metallurgical silicon by slagging and segregation. In: 3rd EUPVSEC, Berlin, Germany, p 252
30. Le Quang N, Gauthier M, Pihan E, Nichiporuk O, Madon F, Goaer G (2007) 22nd EUPVSEC Milan, p 943–947
31. Kraiem J, Einhaus R, Lissalde F, Dubois S, Enjalbert N, Drevet B, Servant F, Camel D (2008) Innovative crystallisation on mc-Si ingots from different types of silicon feedstock. In: 23rd EUPVSEC, Valencia, Spain, p1071
32. Kawamura R, Sasatani K, Onizuka T, Kaneko K (1994) Continuous growth of mc-Si ingots by cold crucible technique. In: 24th IEEE PVSC, vol 2, Waikola, Hawai, USA, pp 1652–55
33. Landaud D (2006) Continuous growth of mc-Si ingot in a cold crucible. Photon Int 12:38
34. Dour G, Erhet H, Laugier A, Sarti D, Garnier M, Durand F (1998) Continuous solidification of mc-Si from an inductive cold crucible. J Cryst Growth 193(1–2):230
35. Weber B, Bierwisch C, Kübler R, Kleer G (2008) Investigation on the sawing of solar silicon by application of wires of 100 μm diameter. In: 23rd EUPVSEC, Valencia, p 1285
36. Kondo Y, Watanabe N, Ide D, Matsuki T, Takato H, Sakata I (2008) Characterization of mc-Si wafers for solar cell applications sliced with a fixed abrasive wire. In: 23rd EUPVSEC, Valencia, p 1297
37. Dross F, Milhe A, Robbelein J, Gordon I, Bouchard PO, Beaucarne G, Poortsmans J (2008) SLIM-CUT a kerf-loss free method for wafering 50 μm thick crystalline Si wafers based on stress-induced lift-off. In: 23rd EUPVSEC, Valencia, Spain, p 127
38. Ciszek J (1985) Crystallographic growth forms of Si on a free melt surface. J Electrochem Soc 132:422
39. Wald F (1981) Crystal growth of silicon ribbons for terrestrial solar cells by the EFG method. In: Grabmaier J (ed) Silicon. Springer, Berlin, p 147
40. Kalejs JP (2002) Silicon ribbons and foils-state of the art. Sol Energ Mat Sol Cells 72:139
41. Mosel F, Birkmann B, Müller M, Westram I, Seidl A (2009) Growth conditions and material properties of EFG ribbon silicon. In: 3rd international workshop on crystalline silicon solar cells, SINTEF/NTU, Trondheim
42. Ciszek TF, Hurd LL, Schietzelt MJ (1982) Filament materials for edge-supported pulling of silicon sheet crystals. J Electrochem Soc 19:2838
43. Ro A, Kim DS, Nakayashiki K, Yelundur V, Rounsainville B (2004) High efficiency solar cells on edge defined film def grown 18.2% and string ribbon 17.8% by rapid thermal processing. Appl Phys Lett 84:145
44. Hayes JR, Zhang X, Meier DL, Maahjan S (2001) Origins of defect structures in dendritic web silicon. J Cryst Growth 233:451

45. Nakayashiki K, Rounsainville B, Yelundur V, Kim DS, Rohatgi A, Clarkphelps R, Hanoka JJ (2006) Fabrication and analysis of high-efficiency string ribbon Si solar cells. Solid-State Electron 50:1406
46. Wallace R, Hanoka JJ, Rohatgi A, Grotty G, SOLMAT 48: 179
47. Seren H, Kaes M, Hahn G, Gutjahr A, Burgers AR, Schönecker A (2007) Efficiency potential of RGS Si from current R&D production. In: 22nd EUPVSEC, Milan, Italy, p 854
48. Focsa A, Slaoui A, Schmitt SB, Jolivet E, Belouet C (2009) Gettering effect and FG annealing on thin RST Si solar cells. In: 24th EUPVSEC, Hamburg, Germany, p 1887
49. Yamatsugu H, Goma S, Kidoguchi S, Oishi R, Yoshida K, Yano K, Taniguchi H (2008) Characteristics of CDS silicon wafers. In: 23rd EUPVSEC, Valencia, Spain
50. Eltran YY (2000) SOI-epi and SCLIPS by epitaxial layer transfer from porous Si. In: Parthulik V, Canham L (eds) Proceedings of the 2nd international conference on porous semiconductors – science and technology, Technical University of Valencia, Valencia
51. Bergmann RB, Werner JH (2002) The future of crystalline silicon films on foreign substrates. Thin Solid Films 403–404:162
52. Brendel R (2004) Thin-film crystalline silicon mini-modules using porous Si for layer transfer. Solar Energy 77:969
53. Solanki CS, Bilyalov RR, Poortmans J (2004) Porous silicon layer transfer processes for solar cells. Sol Energ Mat Sol Cells 83:101
54. Fave A, Quoizola S, Kraiem J, Kaminski A, Lemiti M, Laugier A (2004) Comparative study of LPE and VPE silicon thin film on porous sacrificial layer. Thin Solid Films 451–452:308
55. Kraiem J, Papet P, Nichiporuk O, Amtablian S, Lelievre J-F, Quoizola S, Fave A, Kaminski A, Ribeyron P-J, Jaussaud C, Lemiti M (2006) ELIT Process: epitaxial layers for interdigitated back contacts solar cells transferred. In: 4th World conference on photovoltaic energy conversion, Waikoloa, Hawaii, USA, p 1126
56. Duffar Th (2010) Comprehensive review on grain boundary and twin structures in bulk photovoltaic silicon. Recent Res Dev Cryst Growth 5:61–11
57. Chen J, Sekikuchi T, Ito S, Yang D (2008) Carrier recombination activity and structural properties of small angle grain boundaries in mc-Si. Solid State Phenomena 131–133:9
58. Scott McHugo A, Thompson AC, Mohammed A, Lamble G, Périchaud I, Martinuzzi S, Werne M, Koch W (2001) Nanometer scale metal precipitates in mc-Si solar cells. J Appl Phys 89:4282
59. Arafume K, Sasaki T, Wakabayashi F, Terada Y, Oshida Y, Yamaguchi M (2006) Study on defects and impurities in cast-grown polycrystalline silicon substrates for dollar cells. Physica B 376–377:236
60. Dubois S, Palais O, Pasquinelli M, Martinuzzi S, Ribeyron P-J, Enjalbert N (2007) Effect of intentional iron contamination on multicrystalline silicon solar cell properties. J Appl Phys 102:083525
61. Martinuzzi S, Pizzini S (1994) Large grain polysilicon substrates for solar cells. In: Nijs J (ed) Advanced silicon and semiconducting silicon alloy based materials and devices. IOP, Bristol, pp 323–357
62. Kaminski A, Breitenstein O, Boyeaux JP, Rakotaniaina P, Laugier A (2004) J Phys Condens Matter 16:S9
63. Sopori B, Nilson T, Mclure M (1981) Diodes arrays for photovoltaic characterization of silicon substrates. J Electrochem Soc 128:215
64. El Ghitani H, Martinuzzi S (1989) Influence of dislocations on electrical properties of polycrystalline silicon. J Appl Phys 66:1717
65. El Ghitani H, Martinuzzi S (1989) Influence of dislocations on electrical properties of polycrystalline silicon experimental. J Appl Phys 66:1723
66. Kieliba T, Riepe S, Warta W (2006) Effect of dislocations on minority carrier diffusion length in practical solar cells. J Appl Phys 100:063706
67. Kieliba T, Riepe S, Warta W (2006) Effect of dislocations on open circuit voltage in crystalline silicon solar cells. J Appl Phys 100:093708
68. Mcdonald D, Cuevas A, Kinomura NY, Geerligs LJ (2005) Transition-metal profiles in a multicrystalline silicon ingot. J Appl Phys 97:033523
69. Martinuzzi S, Palais O, Perichaud I (2007) Segregation phenomena in large-size cast multicrystalline ingots. Sol Ener Mat Sol Cells 91:1172
70. Hanoka J (1986) Hydrogen passivation of polycrystalline silicon. In: Bowman RC (ed) Hydrogen in disordered and amorphous solids. Plenum, New York, p 81
71. Seifert W, Morgenstern G, Kittler M (1993) Influence of dislocation density on recombination at grain boundaries in mc-Si. Semicond Sci Technol 9:1687
72. Périchaud I, Martinuzzi S (1998) Recombination strength at intra and intergrain defects in mc-Si investigated by low temperature LBIC scan maps. In: Proceedings of MRS spring meeting, vol 510, San Francisco USA, p 633
73. Martinuzzi S, Gauthier M, Barakel D, Périchaud I, Le Quang N, Palais O, Goaer G (2007) Minority carrier bulk lifetimes through a large multicrystalline silicon ingot and related solar cell properties. Eur Phys J Appl Phys 40:83
74. Dube C, Hanoka J (1984) Hydrogen passivation of defects in silicon. Appl Phys Lett 45:1135
75. Hahn G, Sontag D, Seren S, Schönecker A, Burgers A, Stavola M (2004) Hydrogenation of mc-Si: the story continues. In: 19th EPVSEC, Paris, p 861
76. Pearton SJ, Corbett JW, Stavola M (1992) Hydrogen in crystalline semiconductors. Springer, Berlin
77. Narayan S, Wenham SR, Green MA (1986) High efficiency polycrystalline silicon solar cells using phosphorus pre-treatment. Appl Phys Lett 48:873
78. Périchaud I, Martinuzzi S, Stemmer M (1991) Additivity of phosphorus gettering and hydrogenation improvements in multicrystalline silicon cells. In: 22nd IEEE-PVSC, Las Vegas, p 877
79. Périchaud I, Martinuzzi S (1992) Effet Getter dans des plaquettes de silicium multicristallin par diffusion de phosphore : J de Phys III, 2:313

80. Périchaud I (2002) Gettering of impurities in solar silicon. Sol Energ Mat Sol Cells 72:315
81. Joshi SM, Ulrich M, Gösele UM, Tan TY (2001) Extended high temperature Al gettering for improvement and homogenisation of minority carriers in mc-Si. Sol Energ Mat Sol Cells 70:231
82. Boudaden J, Monna R, Loghmarti M, Muller JC (2002) Comparison of phosphorus gettering for different mc-Si. Sol Energ Mat Sol Cells 72:381
83. Estreicher SK, Hastings JL, Fedders L (1999) Hydrogen-defects interactions in Si. Mat Sci Eng B 58:130
84. Martinuzzi S, Périchaud I, Warchol F (2003) Hydrogen passivation of defects in mc-Si solar cells. Sol Energ Mat Sol Cells 80:343
85. Geerligs LJ, Komatsu Y, Röver I, Wambach K, Yamaga I, Saitoh T (2007) Precipitates and hydrogen passivation at crystal defects in n and p-type mc-Si. J Appl Phys 102:093702
86. Seibt M, Sattler A, Rudolf C, Vos O, Kveder V, Schröter W (2006) Gettering in silicon photovoltaics: current state and future perspectives. Phys Stat Sol (a) 4:696
87. Sheoran M, Upadhyaya A, Rohatgi A (2008) Bulk lifetime efficiency enhancement due to gettering and hydrogenation of defects during cast mc-Si solar cell fabrication. Solid State Electron 52:612
88. Tan J, Macdonald D, Bennet N, Kong D, Cuevas A, Romijn I (2007) Dissolution of metal precipitates in mc-Si during annealing and the protective effect of phosphorus emitters. Appl Phys Lett 91:043505
89. Dubois S, Enjalbert N, Warchol F, Martinuzzi S (2009) Is hydrogen or aluminium gettering the improvement key of mc-Si wafers? Mat Sci Eng B 151:239
90. Macdonald D, Geerligs LJ (2004) Recombination activity of interstitial iron and other transition metal point defects in n and p-type crystalline silicon. Appl Phys Lett 85:4061
91. Cuevas A, Kerr MJ, Samundsell C, Ferrazza F, Coletti G (2002) Millisecond minority carrier lifetime in n type multicrystalline silicon. Appl Phys Lett 81(26):4952
92. Libal J, Buck T, Kopecek R, Fath P, Wambach K, Acciari A, Binetti S, Geerligs L (2004) Properties of n-type mc-Si: lifetime, gettering and H-passivation. In: 19th EUPVSEC, Paris, France, p 1013
93. Schmiga C, Schmidt J, Gosh M, Metz A, Hezel R (2004) Gettering and passivation of recombination centres in n-type mc-Si. In: 19th EPUVSEC Paris, p 439
94. Cotter JE, Guo JH, Cousins PJ, Abbott MD, Chen FW, Fisher KC (2005) p-type vs. n-type silicon wafers. In: 15th Workshop on crystalline silicon solar cells, Vail, CO, (NREL), Golden, CO, pp 3–10
95. Martinuzzi S, Palais O, Ferrazza M (2005) N-type mc-Si wafers and rear junction solar cells. Eur Phys J Appl Phys 32:187–192
96. Istratov AA, Hieslmair H, Weber EW (1999) Iron and its complexes in silicon. Appl Phys A 69:13
97. Martinuzzi S, Warchol F, Dubois S, Enjalbert N (2009) Influence of chromium on minority carrier properties in intentionally contaminated n-type mc-Si wafers. Mat Sci Eng B 151:239
98. Kang JS, Schroder DK (1982) Gettering in silicon. J Appl Phys 65:2974
99. Woditsch P, Koch W (2002) Solar grade silicon feedstock supply for PV industry. Sol Energ Mat Sol Cells 72:11
100. Möller HJ, Funke C, Würzner S (2009) Melt growth of SiC and Si3N4 precipitates during crystallization of multicrystalline silicon for solar cells. In: 3rd international workshop on crystalline silicon solar cells, SINTEF/NTU, Trondheim Norway
101. Liu L, Nakano S, Kakimoto K (2008) Carbon concentration and particle precipitation during directional solidification of mc-Si for solar cells. J Cryst Growth 310:2192
102. Bauer J, Breitenstein O, Rakotoniaina JP (2007) Electronic activity of SiC precipitates in mc-solar silicon. Phys Stat Sol A 204:2190
103. Degoulange J, Périchaud I, Trassy C, Martinuzzi S (2008) Multicrystalline silicon wafers prepared from upgraded metallurgical feedstock. Sol Energ Mat Sol Cells 92:1269–1273
104. Martinuzzi S, Périchaud I, Trassy C, Degoulange J (2009) n-type multicrystalline silicon wafers prepared from plasma torch refined upgraded metallurgical feedstock. Prog Photovolt Res Appl 17:297–305
105. Rodot M, Bourrée JE, Mesli A, Revel G, Kishore R, Pizzini S (1987) Al-related recombination centre in polycrystalline Si. J Appl Phys 62:2556
106. Rosenith O, Roth T, Glunz SW (2007) Determining the defect parameters of the deep aluminium related defect centre in silicon. Appl Phys Lett 91:122109
107. Pizzini S, Borsani F, Acciari M (1989) Effect of oxygen and carbon on the electrical properties of grain boundaries in silicon. Mat Sci Eng B4:353
108. Green MA (1995) Silicon solar cells, advanced principle and practice, centre for photovoltaic devices and systems. Bridge, Sydney
109. Sopori BL, Pryor RA (1983) Design of anti-reflection coatings for textured silicon solar-cells. Solar Cells 8:249
110. Duerinckx F, Noppe A, Choulat P, Szlufcik J, Nijs J, Habbraken B (2000) Advanced industrial process for large area screen printed mc-Si solar cells. In: 16th EU PVSEC, Glasgow, p 1301
111. Revesz AG (1973) Vitreous oxide antireflection films in high-efficiency solar cells. In: 10th IEEE PVSEC, Lisbon, p 180
112. Kern W, Tracy E (1980) Titanium dioxide antireflection coating for silicon solar cells by spray deposition. RCA Rev 41:19
113. Zhao J, Green MA (1991) Optimized antireflection coatings for high-efficiency silicon solar cells. IEEE Trans Electron Devices 38(8):1925–1934
114. Richards BS (2004) Comparison of TiO_2 and other dielectric coatings for buried contact solar cells: a review. Prog Photovolt Res Appl 12:253–281
115. Streling HF, Swann RCG (1965) Chemical vapour deposition promoted by RF discharge. Solid State Electron 8:653
116. Bilyalov RR, Stalmans L, Schirone L, Lévy-Clément C (1999) Use of porous silicon antireflection coating in multicrystalline silicon solar cells. IEEE Trans Electron Devices 46(10): 2035–2040

117. Strehlke S, Bastide S, Guillet J, Lévy-Clément C (2000) Design of porous silicon antireflection coatings for silicon solar cells. Mat Sci Eng B69–70:81–86
118. Green MA (1982) Solar cells, operating principles, technology and system applications. Prentice Hall, Englewood Cliffs. ISBN 0-13-82270
119. Hylton JD, Burgers AR, Sinke WC (2004) Alkaline etching for reflectance reduction in multicrystalline silicon solar cells. J Electrochem Soc 151(6):G408–G427
120. Nunoi T (1990) Cast polycrystalline silicon solar cell with grooved surface. In: 21st IEEE –PVSC, p 664
121. Seidel H, Csepregi L, Heuberger A, Baumgärtel H (1990) Anisotropic etching of crystalline silicon in alkaline solutions – I – orientation dependence and behavior of passivation layers. J Electrochem Soc 137(11):3612
122. Bastide S, Lévy-Clément C (2006) Electrochemical macroporous texturization of multicrystalline silicon. J New Mater Electrochem Syst 9(3):269
123. Luque A (1988) Solar cells and optics for photovoltaic concentration. Adam Hilger, Bristol, Chapter 14
124. Campbell P (1993) Enhancement of light absorption from randomising and geometric textures. J Opt Soc Am B 10:2410–2415
125. Hylton JD, Kinderman K, Burgers AR, Sinke WC, Bressers PMMC (1996) Uniform pyramid formation on alkaline-etched polished monocrystalline (100) silicon wafers. Prog Photovol Res Appl 4:435–438
126. Papet P, Nichiporuk O, Kaminski A, Roz Y, Kraiem J, Lelievre JF, Chaumart A, Fave A, Lemiti M (2006) Pyramidal texturing of silicon solar cell with TMAH chemical anisotropic etching. Sol Energ Mat Sol Cells 90:2319
127. Hylton JD (2006) Light coupling and light trapping in alkaline textured multicrystalline silicon wafers for solar cells, PhD thesis, Utrecht. ISBN-10- 90-810463-1-4, ISBN—13-978-90-810463-1-2
128. Sarti D, Le QN, Bastide S, Goaer G, Ferry D (1995) Thin industrial mc-Si solar cells and improved optical absorption. In: 13th EUPVSEC, Nice, France, p 25
129. Einhaus R, Vazsonyi E, Szlufcik J, Nijs J, Mertens R (1997) In: 26th IEEE PV SC, Anaheim, CA, USA, p 170
130. Stocks MJ, Carr AJ, Blakers AW (1996) Texturing of polycrystalline silicon. Sol Energ Mat Sol Cells 40:33–42
131. Zhao J, Wan A, Green MA (1998) 19.8% Efficient multicrystalline silicon solar cells with "honeycomb" textured front surface. In: The 2nd World conference and exhibition on photovoltaic solar energy conversion, Vienna, Austria, July 1998, p 516
132. Gittlemen JM, Sichel EK, Lehman HW, Widner R (1979) Textured silicon – selective absorber for solar thermal conversion. Appl Phys Lett 35:742
133. Winderbaum S, Reinhold O, Yun F (1997) Reactive ion etching (RIE) as a method for texturing polycrystalline silicon solar cells. Sol Energ Mat Sol Cells 46:239
134. Inomata Y, Fukui K, Shirasawa K (1997) Surface texturing of large area multicrystalline silicon solar cells using reactive ion etching method. Sol Energ Mat Sol Cells 48:237, Part II
135. Koynov S, Brandt MS, Stutzmann M (2007) Black multi-crystalline silicon solar cells. Phys Stat Sol A 1(2):R53
136. Green MA (1987) High efficiency silicon solar cells. Trans Tech, Aedermannsdorf. ISBN 0-87849-537-1
137. Eades WD, Swanson RM (1985) Calculation of surface generation and recombination velocities at the Si-SiO_2 interface. J Appl Phys 58:4267
138. Hoex B, Schmidt J, Bock R, Altermatt PP, Van de Sanden MM, Kessels MM (2007) Excellent passivation of highly doped p-type Si surfaces by the negatively charged dielectric Al_2O_3. Appl Phys Lett 91:112107
139. Lammert MD, Schwartz RJ (1997) The interdigitated back contact solar cell: a silicon solar cell for use in concentrated sunlight. IEEE Trans Electron Dev ED-24:337
140. Swanson RM, Beckwith SK, Crane RA, Eades WD, Sinton RA, Swirhun SE (1984) Interdigitated back contact solar cells. Trans Electron Devices ED-31:661
141. Van Kerschaver E, Beaucarne G (2006) Back-contact solar cells: a review. Prog Photovolt Res Appl 14:107
142. Gee J (1993) Emitter wrap through solar cells. In: 23rd IEEE PVSC, Louisville, p 265
143. Dicke J Jr, Schumacher O, Warta W, Glunz SW (2002) Analysis of one-sun monocrystalline rear-contacted silicon solar cells with efficiencies of 22.1%. J Appl Phys 91:4335
144. Hezel R, Meyer R, Metz A (2001) A new generation of crystalline silicon solar cells: Simple processing and record efficiencies for industrial-size devices. Sol Energ Mat Sol Cells 65:311
145. Sinton RA, Swanson RM (1990) Simplified backside-contact solar cells. IEEE Trans Electron Devices 37:348
146. Verlinden P (1991) High-efficiency backside contact solar cells with a self-aligned process and new texturization technique for silicon. In: 10th EUPVSEC, Lisbon, Portugal, p 246
147. Papet P, Kaminski A, Fourmond E, Calmon F, Lemiti M, Jozwik J (2008) Interdigitated back contact solar cells with SiO_2 and SiN back surface passivation. J Non Cryst Solids 354(35–39):4341
148. Swanson RM (2006) A vision for crystalline silicon solar cells. Prog Photovolt Res Appl 14:443
149. Papet P, Nychyporuk O, Kaminski A, Lemiti M (2008) Realization of self-aligned back-contact solar cells. Electrochem Solid State Lett 11:H114
150. Bothe K, Schmidt J, Hezel R (2002) Effective reduction of the metastable defect concentration in boron-doped Czochralski silicon for solar cells. In: 29th IEEE-PVSC, New Orleans LA, USA, p 194
151. Lee JY, Peters S, Rein S, Glunz SW (2001) Improvement of charge minority-carrier lifetime in p(boron)-type Czochralski silicon by rapid thermal annealing. Prog Photovol Res Appl 9:417
152. Glunz SW, Rein S, Warta W, Knobloch J, Wettling W (2001) Degradation of carrier lifetime in Cz silicon solar cells. Sol Energ Mat Sol Cells 65:219
153. Lim B, Liu A, Macdonald D, Bothe K, Schmidt J (2009) Appl Phys Lett 95:232109
154. Shultz O, Glunz SW, Willeke GP (2004) mc-Si solar cells exceeding 20% in efficiency. Prog Photovol Res Appl 12:553

155. Inoue S, Sakamoto T, Komoda H, Ohwada H, Fukui K, Shirasawa K (2008) High efficiency mc-Si back contact solar cells. In: 23rd EUPVSEC, Valencia, p 988
156. Romijn IG, Mewe AA, Lamers M, Kossen E, Bende EE, Weeber AW (2008) An overview of MWT cells and evolution to the aspire concept : a new integrated mc-Si cell and module design for high efficiencies. In: 23rd EUPVSEC, Valencia, Spain, p 1000
157. Van der Heide A, Gribenski D, Szlufcik J (2009) Industrial fabrication of multicrystalline silicon MWT cells with interconnection flexibility. In: 24th EUPVSEC, Hamburg, Germany, p 942
158. Peters C, Engelhart P, Wade R, Jesswein R, Rychtarik D, Müller JW (2008) Alba-development for high efficiency mc-Si solar for industrial fabrication at Q-Cells. In: 23rd EUPVSEC, Valencia, Spain, p 1010
159. Hamamoto S, Ishihara T, Sato T, Fujikawa M, Morikawa H, Matsuno S, Fujioka H Arimoto Investigation for 19% at mc-Si solar cell by industrial probable approach. In: 24th EUVSEC, Hamburg, Germany, p 1410
160. Shi Z, Wenham S, Ji J (2009) Mass production of new high efficiency mc-Si solar cells with selective emitter. In: 24th EUPVSEC, Hamburg, Germany, p 1090
161. Kaes M, Hahn G, Metz A, Agostinelli G, Ma Y, Junge J, Zuschlag A, Groetschel D (2007) Progress in high efficiency processing of EFG silicon solar cells. In: 22rd EUPVSEC, Milan, Italy, p 897
162. Oberholtzner F, Dubé CM (2007) Efficiency improvements of string ribbon silicon solar cells. In: 22rd EUPVSEC, Milan, Italy, p 916
163. Seren S, Kaes M, Hahn G, Gutjahr A, Burgers AR, Schoneker A (2007) Efficiency potential of RGS Si from current R&D production. In: 22rd EUPVSEC, Milan, Italy, p 854
164. Kim DS, Yelundur V, Nakayashiki K, Rousaville B, Rohatgi A (2006) Ribbon Silicon solar cells with efficiencies over 18% by hydrogenation of defects. Sol Energ Mat Sol Cells 9(23):1227
165. Bronsveld PCP, Naber RCG, Geerligs LJ, Pozigun S, Syvertsen M, Knopf C, Kvande R (2009) p and n-type mono and mc-Si solar cells using blended upgraded metallurgical grade silicon. In: 24th EUPVSEC, Hamburg, Germany, p 1137
166. Braun S, Raab B, Kohler D, Seren S, Hahn G (2009) Comparison of buried contacts and screen printed 100% UMG solar cells resulting in 16.2% efficiency. In: 24th EPVSEC, Hamburg, Germany, p 1736
167. Kraiem J, Einhaus R, Lauvray H (2009) Method for producing photovoltaic-grade crystalline silicon by addition of doping impurities and photovoltaic cell, WO Patent number WO/2009/130,409
168. Veirman J, Dubois S, Enjalbert N, Garandet JP, Lemiti M, Heslinga DR (2010) Hall mobility reduction in single-crystalline silicon gradually compensated by thermal donor activation. Solid State Electron 54:671
169. Dubois S, Enjalbert N, Garandet JP (2008) Effects of the compensation level on the carrier lifetime of crystalline silicon. Appl Phys Lett 93:032114
170. Macdonald D, Rougieux F, Cuevas A, Lim B, Schmidt J, Di Sabatino M, Geerligs LJ (2009) Light-induced boron-oxygen defect generation in compensated p-type Czochralski silicon. J Appl Phys 105:093705
171. De Ceuster D, Cousins P, Rose D, Vicente, Tipones P, Mulligan W (2007) Low cost, high volume production of $>$22% efficiency silicon solar cells. In: 22nd EUPVSEC, Milan, Italy, p 816
172. Nakamura K, Kohira M, Abiko, Isaka Y, Funakoshi Y, Machida T (2008) Development of back contact solar cells and modules in production line. In: 23rd EUPVSEC Valencia, Spain, p 1006
173. Granek F, Hermle M, Reichel C, Schlutz-Wittmann O, Glunz SW (2008) High efficiency back contact back junction silicon solar cell. In: 23rd EUPVSEC,Valencia, Spain, p 991
174. Mertens V, Bordihn S, Larionova Y, Harder NP, Brendel R (2009) The buried emitter solar cell concept: interdigitated back-junction structure. In: 24th EUPVSEC Hamburg, Germany, p 934
175. Okuda K, Okamoto H, Yamakawa H (1983) Amorphous Si-polycrystalline Si stacked solar cells having more than 12% conversion efficiency. Jpn J Appl Phys 22:L605
176. Fuhs W, Niemann K, Stuke J (1974) Heterojunctions of amorphous silicon and silicon single crystals. Bull Am Phys Soc 19:345
177. Wakisaka K, Taguchi M, Sawada T, Tanaka M, Matsuyama T, Matsuoka T, Tsuda S, Nakano S, Kishi Y, Kuwano Y (1991) More than 16% solar cells with a new "HIT" (doped a-Si/nondoped a-Si/crystalline Si) structure. In: Conference record of the 22nd IEEE-PVSC, Washington DC, p 887
178. Tanaka M, Taguchi M, Matsuyama T, Sawada T, Tsuda S, Nakano S, Hanafusa H, Kuwano Y (1992) Development of new a-Si/c-Si heterojunction solar cells, ACJ-HIT (artificially constructed junction–heterojunction with intrinsic thin layer). Jpn J Appl Phys 31:3518
179. Taguchi M, Kawamoto K, Tsuge S, Baba T, Sakata T, Morizane M, Uchihashi K, Nakamura N, Kiyama S, Oota O (2000) HITTM cells – high-efficiency crystalline Si cells with novel structure. Prog Photovolt Res Appl 8:503
180. Taguchi M, Terakawa A, Maruyama E, Tanaka M (2005) Obtaining a higher V_{oc} in HIT cells. Prog Photovolt Res Appl 13:481
181. Taira S, Yoshimine Y, Baba T, Taguchi M, Kanno H, Kinoshita T, Sakata H, Maruyama E, Tanaka M (2007) Our approaches for achieving HIT solar cells with more than 23% efficiencies. In: 22nd EUPVSEC, Milan, Italy, p 932
182. Taguchi M, Tsunomura Y, Inoue H, Taira S, Nakashima T, Baba T, Sakata H, Maruyama E (2009) High-efficiency hit solar cell on thin ($<$100 μm) silicon wafer. In: 24th EUPVSEC, Hamburg, Germany, p 1690
183. Kleider JP, Gudovskikh AS, Roca Cabarrocas P (2008) Determination of the conduction band offset between hydrogenated amorphous silicon and crystalline silicon from surface inversion layer conductance measurements. Appl Phys Lett 92:162101

184. Schmidt M, Korte L, Laades A, Stangl R, Schubert Ch, Angermann H, Conrad E, Kv M (2007) Physical aspects of a-Si:H/c-Si hetero-junction solar cells. Thin Solid Films 515:7475
185. Favre W, Labrune M, Dadouche F, Gudovskikh AS, Roca i Cabarrocas P, Kleider JP (2010) Study of the interfacial properties of amorphous silicon/n-type crystalline silicon heterojunction through static coplanar conductance measurements. Phys Stat Sol (c) 7:1037
186. Angermann H, Rappich J, Korte L, Sieber I, Conrad E, Schmidt M, Hübener K, Polte J, Hauschild J (2008) Wet-chemical passivation of atomically flat and structured silicon substrates for solar cell application. Appl Surf Sci 254: 3615–3625
187. Moreno M, Labrune M, Roca i Cabarrocas P (2010) Dry fabrication process for heterojunction solar cells through in-situ plasma cleaning and passivation. Sol En Mat Sol Cells 94:402
188. Das UK, Burrows MZ, Lu M, Bowden S, Birkmire RW (2008) Surface passivation and heterojunction cells on Si (100) and (111) wafers using dc and rf plasma deposited Si:H thin films. Appl Phys Lett 92: 063504.1
189. Fesquet L, Olibet S, Vallat-Sauvain E, Shah A, Ballif C (2007) High quality surface passivation and heterojunction fabrication by VHF-PECVD deposition of amorphous silicon on crystalline Si: theory and experiment. In: 22nd EUPVSEC, Milan, Italy, p 1678
190. Schmidt M, Schoepke A, Korte L, Milch O, Fuhs W (2004) Density distribution of gap states in extremely thin a-Si:H layers on crystalline silicon wafers. J Non Cryst Solids 338–340:211
191. De Wolf S, Kondo M (2009) Nature of doped a-Si:H/c-Si interface recombination. J Appl Phys 105: 103707–1
192. Fujiwara H, Kondo M (2007) Impact of epitaxial growth at the heterointerface of a-Si: H/c-Si solar cells. Appl Phys Lett 90:013503–1
193. Korte L, Conrad E, Angermann H, Stangl R, Schmidt M (2007) Overview on a-Si:H/c-Si heterojunction solar cells – physics and technology. In: 22nd EUPVSEC, Milan, Italy, p 859
194. Mueller T, Schwertheim S, Meusinger K, Wdowiak B, Fahrner WR (2009) Application of plasma deposited nanocomposite silicon suboxides and microcrystalline silicon alloys to heterojunction solar cells. In: 34th IEEE-PVSC, Philadelphia, PA, USA, p 002378
195. Fesquet L, Olibet S, Vallat-Sauvain E, Shah A, Ballif C (2007) High quality surface passivation and heterojunction fabrication by VHF-PECVD deposition of amorphous silicon on crystalline Si: theory and experiment. In: Proceedings of the 22nd EUPVSEC, Milan, Italy, p 1678
196. Wang Q, Page MR, Iwaniczko E, Xu Y, Roybal L, Bauer R, To B, Yuan HC, Duda A, Hasoon F, Yan YF, Levi D, Meier D, Branz HM, Wang TH (2010) Efficient heterojunction solar cells on p-type crystal silicon wafers. Appl Phys Lett 96: 01350.1
197. Muñoz D, Ozanne AS, Harrison S, Danel A, Souche F, Denis C, Favier A, Nguyen N, Hickel PE, Mur P, Salvetat T, Ribeyron PJ (2010). Towards high efficiency on full wafer a-Si:H/c-Si heterojunction solar cells: 19.5% on 148 cm^2. In: 35th IEEE – PVSC, Hawaï, to be published
198. Wünsch F, Citarella G, Abdallah O, Kunst M (2006) An inverted a-Si:H/c-Si hetero-junction for solar energy conversion. J Non Cryst Sol 352:1962
199. Lu M, Bowden S, Das UK, Birkmire RW (2007) A-Si/c-Si heterojunction for interdigitated back contact solar cell. In: 22nd EPVSEC, Milan, Italy, pp 924–927
200. Dicker J, Schumacher JO, Warta W, Glunz SW (2002) Analysis of one-sun monocrystalline rear-contacted silicon solar cells with efficiencies of 22.1%. J Appl Phys 91:4335
201. Stangl R, Bivour M, Conrad E, Didschuns I, Korte L, Lips K, Schmidt M (2007) RECASH a novel high efficiency buried grid rear contact amorphous/crystalline silicon heterojunction solar cell concept. In: 22nd EUPVSEC, Milan, Italy, p 870
202. Stangl R, Haschke J, Bivour M, Korte L, Schmidt M, Lips K, Rech B (2009) Planar rear emitter back contact silicon heterojunction solar cells. Sol Energ Mat Sol Cells 93:1900
203. Tucci M, Serenelli L, Salza E, De Luliis S, Geerligs LJ, Caputo D, Ceccarelli M, de Cesare G (2008) Back contacted a-Si:H/c-Si heterostructure solar cells. J Non Cryst Solids 354:2386
204. Swanson RM (2005) Approaching the 29% limit efficiency of silicon solar cells. In: 31st IEEE-PVSC, Orlando, Florida, USA, pp 889–894
205. Diouf D, Kleider JP, Desrues T, Ribeyron PJ (2009) Study of interdigitated back contact silicon heterojunctions solar cells by two-dimensional numerical simulations. Mat Sci Eng B 159–160:291
206. Desrues T, Ribeyron PJ, Vandeneynde A, Ozanne AS, Souche F, Muñoz D, Denis C, Diouf D, Kleider JP (2010) B-doped a-Si:H contact improvement on silicon heterojunction solar cells and interdigitated back contact structure. Phys Stat Sol (c) 7:1011–1015
207. Stelzner Th, Pietsch M, Andrä G, Falk F, Ose E, Christiansen S (2008) Silicon nanowire-based solar cells. Nanotechnology 19:295203
208. Guao JH, Tjahjono BS, Cotter JE (2005) In: 31st IEEE-PVSC, Orlando, Florida, USA, p 983
209. Schmiga C, Nagel H, Schmidt J (2006) Czochraslki silicon solar cells with screen printed Al alloyed rear emitter. Prog Photovolt Res Appl 14:533–539
210. Schmiga C, Hermle M, Glunz SW (2008) Towards 20% efficient n-type Si solar cells with screen printed Al-alloyed rear emitter. In: 23rd EUPVSEC, Valencia, Spain, p 982
211. Weeber A, Naber R, Guillevin N, Barton P, Carr A, Saynova D, Burgers T, Geerligs B (2009) Status of n-type solar cells for low cost industrial production. In: 24th EUPVSEC, Hamburg, Germany, p 891
212. Schmiga C, Hörteis M, Rauer M, Meyer K, Lossen J, Hermle M, Glunz J (2009) Large area n-type silicon solar cells with printed contacts and aluminium-alloyed rear emitter. In: 24th EUPVSEC, Hamburg, Germany, p 1167
213. Cong C, Posthuma N, Dross F, Giovanni F, Van Kerschaver, Beaucarne G, Poortmans J (2008) Comparison of n and p-type

high efficiency silicon solar cell performance under low illumination conditions. In: 23rd EUPVSEC, Valencia, Spain, p 1360
214. Meier DL, Davis HP, Garcia RA, Salami J, Rohatgi A, Ebing A, Doshi P (2001) Aluminium alloy back p-n junction dendritic web silicon cell. Sol Energ Mat Sol Cells 65:621
215. Benick J, Hoex B, van de Sanden MCM, Kessels W, Schultz O, Glunz SW (2008) High efficiency n-type solar cells on Al_2O_3 passivated boron emitter. Appl Phys Lett 92:253504–253504-3
216. Mihailetchi VD, Komatsu K, Geerligs LJ (2008) Nitric acid pretreatment for the passivation of boron emitter for n-type base silicon solar cells. Appl Phys Lett 92:063510
217. Zhao J, Wang A (2006) Rear emitter n-type passivated emitter, rear totally diffused silicon solar cell structure. Appl Phys Lett 88:242102
218. Benick J, Hoex B, Dingemans G, Kessels W, Richter A, Hermle A, Glunz SW (2009) High efficiency n-type silicon solar cells with front side boron emitter. In: 24th EUPVSEC, Hamburg, Germany, p 863
219. Schutz-Kuchly T, Veschetti Y, Cabal R, Sanzone V, Heslinga D (2009) High efficiency on inversed emitter n-type Si solar cells. In: 24th EUPVSEC, Hamburg, Germany, p 955
220. Veschetti Y, Schutz-Kuchly T, Sanzone V, Heslinga D (2009) Electrical properties of n-type solar grade silicon – fabrication of solar cells and investigation of LID effect. In: 24th EUPVSEC, Hamburg, Germany, p 2209
221. Stoddard N, Wu B, Witting L, Wagener M, Park Y, Rozgonyi GA, Clark RF (2008) Casting single crystal silicon: novel defect profiles form BP Solar's Mono 2TM wafers. Solid State Phenomena 131(1):8
222. Engelhart P, Zimmermann G, Klenke C, Wendt J, Kaden T, Junghänel M, Barkenfelt B, Petter K, Herman S, Schmidt S, Rychtarik D, Fischer M, Müller JW, Wawer P (2011) In: 37th IEEE- PVSC, Seattle, USA
223. Woehl R, Keding R, Rüdiger M, Gentischer H, Clement F, Wilde J, Biro D (2001) 20% efficient screen-printed and aluminium-alloyed back contact back junction and interconnection scheme of point-shaped metalized cells. In: 37th PVSC, Seattle, USA
224. Kiefer F, Ulzhofer C, Bendenmühl T, Harder NP, Brendel R, Mertens V, Bordihn S, Peters C, Müller JW (2011) In: 37th IEEE-PVSC, Seattle, USA
225. Weeber AW, Burgers AR, Guillevin N, Carr AJ, Barton PC, Geerligs LJ, Jingfeng X, Gaofer L, Weipeng S, Haijiao A, Zhiyan H, Venema PR, Vlooswijk AHG (2010) Recent developments of low cost industrial processing of n-type silicon solar cells. In: Proceedings of crystalline silicon solar cells 4, Taipei
226. Veschetti Y, Cabal R, Brand P, Sanzone V, Raymond G, Betinelli A (2011) High efficiency on boron emitter n-type Cz silicon solar cells with industrial process. In: 37th IEEE-PVSC, Seattle, USA

Silicon Solar Cells, Thin-film

Christopher R. Wronski[1], Nicolas Wyrsch[2]
[1]Electrical Engineering Department, Center for Thin Film Devices, Pennsylvania State University, University Park, PA, USA
[2]Photovoltaics and Thin-film Electronics Laboratory, Institute of Microengineering (IMT), Ecole Polytechnique Fédérale de Lausanne (EPFL), Neuchâtel, Switzerland

Article Outline

Glossary
Definition of Subject and Its Importance
Introduction
Growth and Microstructure
Optoelectronic Properties
Light-Induced Degradation
Solar Cells
Future Directions
Bibliography

Glossary

Amorphous A material with no long-range order and crystalline structure.

Gap states Defect-related states in the forbidden gap of semiconductor materials affecting their optical and electrical properties.

Metastability The creation of light-induced defects and corresponding gap states that can be annealed out (in the case of hydrogenated amorphous silicon and related alloys) at temperatures around or above 150°C.

Microcrystalline Structure of a material composed of 1 μm sized crystallites. Term used for silicon thin-film layers composed of a micron or sub-micrometer sized crystallites. See also *nanocrystalline*.

Microstructure Structure of a material on a scale of a micrometer or less.

Nanocrystalline Structure of a material composed of nanometer (more generally sub-micrometer) sized crystallites.

n-i-p solar cell n-type - intrinsic – p-type Si thin-film solar cell structures where the n-type layer is deposited first onto a (usually opaque) substrate.

Optical enhancement Enhancement of absorption of sunlight in a thin-film solar cells in particular at the longer wavelengths with use of textured and reflective layers.

p-i-n solar cell p-type – intrinsic – n-type Si thin-film solar cell structures where the p-type layer is deposited first onto a (transparent) substrate.

Plasma-enhanced chemical vapor deposition (PECVD) Deposition processes in which materials are deposited onto a substrate by the decomposition of gases with a plasma discharge.

Protocrystalline silicon Amorphous hydrogenated silicon deposited under conditions where the amorphous microstructure changes with thickness.

Stabilized efficiency Steady-state efficiency value attained after light-induced degradation of a solar cell.

Transparent conductive oxide (TCO) Transparent thin films, typically made of tin or zinc oxide, which serve as electrical contacts to the solar cells.

Definition of Subject and Its Importance

Terrestrial photovoltaics, in which electricity is generated directly from sunlight, is one of the technologies in renewable energy which is actively pursued. There are several approaches that have been developed and are now in mass production with currently the ones based on crystalline silicon wafers being dominant. However, the ones based on thin films have a high potential for significantly lower cost below that of these well-established technologies. An attractive alternative for such a sustainable energy supply is the silicon thin-film solar cell technology. Because of the large differences between these and the well-understood crystalline solar cells, it is important to understand their nature and limitations on performance. It is also essential to understand the advantages that they offer for lowering the cost in mass production of solar panels.

In the last several years the rapid expansion in terrestrial photovoltaics has included both the increase in production as well as in installation capacity which in 2010 exceeded 16,000 MW_p per year. The International Energy Agency Technology Roadmap estimates that by 2050 photovoltaic energy will provide around 11% of global electricity (4,500 TWh/year) [1]. This forecast is probably rather conservative as growth rates of 17% till 2020 and 11% after 2020 have been assumed while the average growth rate of the industry has been over 40% between 2000 and 2010. By 2030, >100 GW_p of PV modules should be installed yearly. The technology based on thin-film silicon solar cells has played an important role where not only have the manufacturers expanded their production but also numerous turnkey factories have come on line throughout the world.

Introduction

The first investigation of hydrogenated amorphous silicon (a-Si:H) deposited from a silane discharge was performed by Chittik et al. in 1969 [2]. Subsequent work carried out on this material showed that it had a much lower density of defects than evaporated or sputtered amorphous silicon. The ability to dope this material both n- and p-type was independently discovered by Carlson [3] in 1974 and Spear and LeComber [4] in 1975. Carlson and Wronski [5] showed that a-Si:H had useful optoelectronic properties when they reported the first results on a-Si solar cells with a conversion efficiency of 2% in 1976, and the efficiency was increased to 5% shortly afterward [6]. These results sparked a worldwide interest not only in a-Si:H solar cells but also in other applications and it soon became evident [7] that glow discharge-deposited a-Si is actually an alloy of hydrogen and silicon or hydrogenated amorphous silicon (a-Si:H). In 1977, Staebler and Wronski [8] discovered large changes in the photoconductivity and dark conductivity of a-Si:H when the material was exposed to sunlight. These metastable changes are reversible upon annealing for several hours at or above 150°C [8]. This early discovery of what is known as the Staebler–Wronski Effect (SWE) had a critical effect on the development of a-Si:H solar cell technology by having a key impact on the design of the solar cells and the optimizing of the a-Si:H alloys [9].

Hydrogenated microcrystalline silicon (μc-Si:H), also called hydrogenated nanocrystalline silicon (nc-Si:H), was first reported by Vepřek and Mareček [10] in 1968. During the following years Vepřek and coworkers extensively studied μc-Si:H (deposited by

chemical transport in hydrogen plasma at 600°C) and were able to produce material with relatively low defect density [11–13]. In 1979, μc-Si:H deposited with plasma-enhanced chemical vapor deposition (PECVD) was first reported [14]. The material was grown at considerably lower temperature from silane strongly diluted in hydrogen. In the 1980s several groups investigated μc-Si:H properties and growth and its applications in devices [15]. Despite this pioneering work, μc-Si:H was never envisaged for use as an active layer of thin-film silicon solar cells and its application remained limited to highly conductive thin-film silicon layers (e.g., in a-Si:H solar cells). The reason can be found in the facts that most early undoped μc-Si:H materials exhibited rather large defect densities and a strong n-type character. The latter was generally attributed to the presence of native defects in the material [16]. The μc-Si:H layers were in most cases deposited by PECVD from silane highly diluted in hydrogen.

Development of high-performance solar cells and their technology advanced along several fronts with continuous improvements in a-Si:H materials and solar cell structures. It was found in the early 1990s that the plasma-assisted decomposition of silane diluted with hydrogen improved the properties of both the initial as well as the light-induced degraded states of a-Si:H materials and solar cells [17–21]. Subsequently, in the late 1990s, researchers at The Pennsylvania State University showed that the thin-film Si:H prepared under moderate-to-high H_2 dilution conditions exhibits a higher degree of ordering than materials deposited under similar conditions without H_2. The thin-film materials, which have been called "protocrystalline" evolve with the accumulated thickness of the layer from the amorphous phase to a mixed amorphous + nano/microcrystalline phase [(a + n/μc)-Si:H] and then predominantly microcrystalline phase [22–24]. Furthermore, they showed that the phase evolution with thickness and, the phase transitions depend not only on the H_2-dilution ratio but also on the substrate material. With high hydrogen dilution, it is possible to minimize the thickness of both the amorphous layer and the mixed phase region so that nano/microcrystalline growth can occur almost instantly. With such an optimum control of the growth and material optimization, in the early 1990s, R. Flückiger, J. Meier et al. of the University of Neuchâtel were able to fabricate an entirely microcrystalline thin-film silicon p-i-n solar cell with an efficiency close to 5% [25, 26]. With this innovation, this material gained a renewed worldwide interest. The two key advantages of μc-Si:H (compared to a-Si:H) for its use in photovoltaic devices are: on one hand the enhanced infrared light absorption and on the other hand the near total absence of light-induced degradation.

Already, in the early 1980s, it was found that the bandgap of a-Si:H can be changed by varying the incorporation of hydrogen [27] as well as alloying with carbon or germanium [28]. The development of narrow bandgap a-SiGe:H alloys led to both tandem and triple junction cells [29–31]. However the incorporation of Ge into the materials created additional defects, as well as increasing their light induced degradation, which limited the bandgap and thicknesses of the alloy layers that could be used. In this context μc-Si:H or nc-Si:H offers an interesting alternative as these materials exhibit the same bandgap of 1.1 eV as crystalline silicon (c-Si). Shortly after the demonstration of entirely μc-Si:H p-i-n cells, a-Si:H/μc-Si:H tandem devices, also called micromorph or hybrid solar cells, were fabricated [32]. These structures offer several advantages such as an optimum combination of material bandgap values (for a solar cell tandem structure) [33] and a μc-Si:H bottom cell almost immune to light-induced degradation. However, due to the fact that almost 2/3 of the power is generated by the top a-Si:H cell, light-induced degradation of the latter still remains a critical issue.

The use of such multi-junction solar cell structures allowed not only the solar spectrum to be utilized more efficiently but also the use of thinner component cells, which in turn helps to reduce the degradation resulting from SWE [8]. However, the practical constraints imposed on the reduction in thicknesses still seriously limited the absorption of sunlight. This difficulty was addressed in the early 1980s by the development of efficient optical enhancement obtained by introducing and developing textured rather than smooth optical reflectors or substrates [34, 35]. Such optical enhancement, which was first successfully applied to a-Si:H-based solar cells, is now extensively used in all the different types of thin-film solar cells.

There has also been continuous progress in developing large-scale processing for Si:H-based PV modules. All the commercial PV modules are fabricated using PECVD to deposit layers since excellent uniformity can be obtained over substrates more than 1 m^2 in area [36]. This is also a result of the early work at RCA Laboratories, which led to the development of a laser scribing process that patterned the a-Si:H on insulating substrates (such as glass) so that the resulting product is a large-area, monolithic PV module of solar cells connected in series [37]. Such large area processing technologies can also be applied to flexible substrates, and several production lines are fabricating thin-film silicon solar cells on stainless steel or plastic substrates using roll-to-roll facilities. Current solar module production (on rigid and flexible substrates) comprises of single-junction (a-Si:H cells), tandem (a-Si:H/a-Si:H, a-Si:H/a-SiGe:H, and a-Si:H/μc-Si:H), as well as triple-junction devices (a-Si:H/a-SiGe:H/a-SiGe:H). Also the development of triple-junction devices with a μc-Si:H cell component is a promising way for increasing further the device efficiency that is being pursued [38, 39].

Growth and Microstructure

Introduction/Background

The Si:H-based materials used in solar cells are deposited using PECVD with a wide range of deposition conditions. While the early depositions were performed using primarily DC and RF PECVD [3], subsequent studies showed that good quality a-Si:H alloys could also be deposited using VHF (~30–240 MHz) [40–42] and microwave (~2.45 GHz) PECVD [43, 44]. Somewhat surprisingly, it was possible to obtain similar materials with all these techniques even though the materials produced by the PECVD process depend on a variety of deposition parameters. These include not only the frequency but also parameters such as: the substrate temperature, the pressure, the flow rate of the source gases, the plasma power, the electrode spacing, the source gases, as well as the geometry of the reactors.

The temperature of the substrate plays an important role in controlling the surface and subsurface reactions, which are important in determining the quality of the material [45–47]. The gas pressure determines the mean free path for the collisions of the gas molecules and influences whether the reactions are at the growing surface or in the gas. The flow rate of the source gases is an important deposition parameter since it determines the residence time of the gas species in the plasma and hence affects the growth kinetics. The power controls the rate of dissociation of the gas and therefore also the film growth rate. The frequency used also affects the nature of the plasmas, and in particular the ion bombardment, which becomes less significant at VHF and microwave frequencies. It has been found that the best Si:H materials are deposited at relatively slow deposition rates from about 0.1–0.5 nm/s. Because of the complex interactions between the species that are created in the plasma and the surface and subsurface, it has been difficult to systematically improve the deposition rate of these high quality materials. Nevertheless, there has been progress made particularity with the introduction of depositions carried out with VHF and high pressure depletion regimes [48].

In addition to such deposition parameters, properties of the Si:H materials can be adversely affected by impurities such as oxygen, carbon, and nitrogen, which can be introduced by air leaks, residual water vapor, and pump oil contamination [49–53], also, not surprisingly, by the introduction of a-Si:H alloy forming gases such as GeH_4 and CH_4, as well as the n-type or p-type doping gases PH_3 and B_2H_6 and Trimethyl Boron (TMB).

In all the different PECVD depositions, hydrogen plays a key role in determining the microstructure, reducing defects and improving the quality of the materials. Because of the large number of variables in deposition that are *interdependent*, PECVD deposition is a very complex process thus making it difficult to improve the microstructure and optoelectronic properties of these materials in systematic way. However, the beneficial effects of the hydrogen available from the feedstock gases have been very successfully augmented by diluting them with hydrogen. This was first utilized in the deposition of a-Si:H alloys [46] and in the fabrication of intrinsic a-Si:H [54]. It turned out hydrogen dilution not only had beneficial effects on the quality of amorphous films but also high quality nano/microcrystalline materials [55]. An understanding of the role that hydrogen dilution has in the growth and microstructure of Si:H films was obtained from optical in situ characterization of the materials in real time

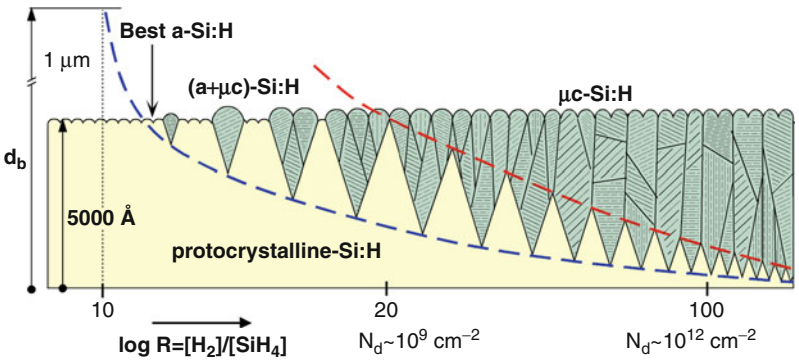

Silicon Solar Cells, Thin-film. Figure 1
Schematic of the structure of Si:H films prepared as a function of R. The *lower* and *upper dashed lines* identify the a→(a+µc), and (a+µc)→µc transitions, respectively. N_d is the density of nucleating centers initiating microcrystalline growth. For the case illustrated here, the protocrystalline a-Si:H would no longer be obtained with R lower than about 10

during their deposition, which is illustrated in Fig. 1 with a schematic representation of how the microstructure evolves with thickness d_b in a Si:H film as a function of hydrogen dilution of the silane, R [24]. The origin and nature of the protocrystalline a-Si:H: the amorphous + nano/microcrystalline mixed phase (a + µc)-Si:H and the microcrystalline phase (µc-Si:H) are discussed below.

At this point, it is important to stress that silane concentration $c = [SiH_4]/([SiH_4] + [H_2])$ (or hydrogen dilution $R = [H_2]/[SiH_4]$) does not solely determine the structure of the deposited material. For almost any value of c or R, various microstructures can be obtained as illustrated by the fact that µc-Si:H can be obtained from pure silane plasma discharge [56, 57]. As was demonstrated experimentally and supported by a simple plasma chemistry model, it is not the silane concentration in the gas feed, c, which is controlling the growth but the silane concentration in the plasma c_p [58]. These two concentration values are related to each other by the silane depletion factor D defined as $c_p = c(1\text{-}D)$. The relation between silane concentration and silane depletion and the growth regimes is illustrated in Fig. 2.

Increasing deposition rate when depositing a-Si:H by PECVD can lead to the formation of polysilane radicals in the plasma. Such radicals may aggregate and form particle or powder that can be incorporated in the growing film. Such occurrence is in most cases very detrimental for the quality of the deposited material. Nevertheless, transitional materials of high quality have been obtained at the onset of powder formation. This material, also called *polymorphous silicon*, comprises very small nanocrystals embedded in an amorphous tissue. It exhibits similar properties as amorphous or protocrystalline materials [59].

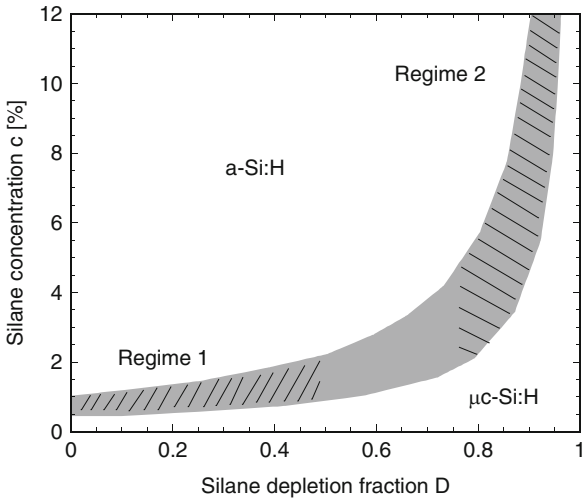

Silicon Solar Cells, Thin-film. Figure 2
a-Si:H, µc-Si:H and transition growth regime as a function of silane concentration c and silane depletion fraction D. Transition to µc-Si:H regime (and µc-Si:H growth) can be achieved either at low c (regime 1) or at considerable higher c (regime 2). For both regimes crystallinity along the growth axis will evolve according to the behavior described in Fig. 1

Protocrystalline Si:H Materials

Using real-time spectroscopic ellipsometry (RTSE), first developed by Collins et al. [23, 24, 60] to characterize thin-film growth and microstructure, researchers at Pennsylvania State University have shown that the thin-film Si:H prepared under moderate-to-high H_2-dilution conditions evolves from the amorphous phase to a mixed amorphous + microcrystalline phase [(a+μc)-Si:H] with the accumulated thickness of the layer. The thin-film material in the amorphous regime of growth has been called protocrystalline Si:H and exhibits a higher degree of ordering than materials deposited under similar conditions without H_2-dilution [61]. Furthermore, they showed that the phase evolution of this material with thickness and, in particular, the transition to the mixed-phase (a+μc)-Si:H material depends, not only on the H_2-dilution ratio, $R = [H_2]/[SiH_4]$, but also on the substrate material.

A key capability of RTSE is the ability to generate deposition phase diagrams for different hydrogen dilution ratios, R, different substrate materials, as well as different deposition conditions. Such diagrams identify the ranges of thickness over which it is possible to obtain the pure a-Si:H protocrystalline phase as well as the ranges corresponding to the mixed-phase deposition. Despite the evolutionary nature of the Si:H materials prepared with moderate H_2-dilution, they exhibit relatively uniform bulk properties over certain extended regions of thickness. Using such phase diagrams as a guide, it is possible to identify and control this evolutionary nature in both films as well as in solar cell structures. Using RTSE, deposition phase diagrams have been developed that describe how the microstructure and phase evolve during the growth of Si:H films as a function of film thickness and hydrogen dilution on different substrates. The hydrogen-dilution gas flow ratio is most often used as the key parameter in these phase diagrams since it provides the most direct control over the phase.

Figure 3 shows an example of an oxide-covered crystalline silicon substrate where the shaded area indicates the regime where the amorphous protocrystalline Si:H is being deposited [62]. When smooth crystalline silicon substrates are used (as in Fig. 4), a roughening transition in the a-Si:H film growth regime can be

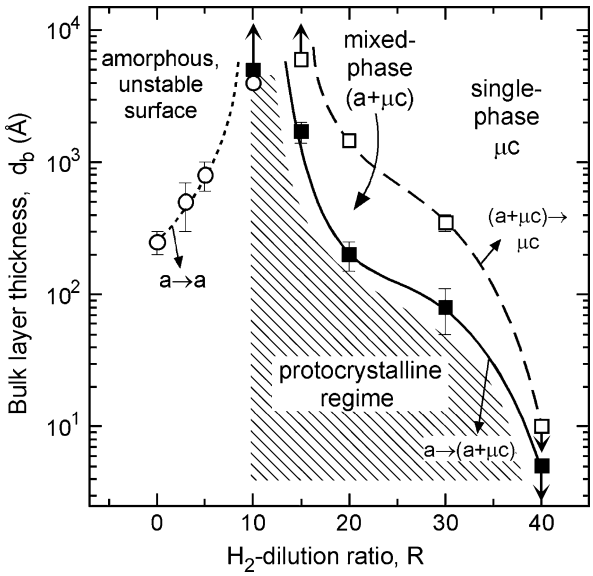

Silicon Solar Cells, Thin-film. Figure 3
Film thickness, d_b, at which the different phase transitions occur during Si:H film growth plotted as a function of the H_2 dilution ratio R using a c-Si substrate with a native oxide. In the figure the *protocrystalline* Si:H growth regime is *shaded* [62]

detected with high sensitivity and precision, thus allowing to identify when the film exhibits a stable surface (or smoothens) below the transition but roughens continuously above the transition. To the left of the protocrystalline regime, with no or low dilution, because the film is amorphous on both sides of this roughening transition it is designated "a→a" in Fig. 3. The thickness at which the a→a transition occurs provides insight into the deposited a-Si:H material quality. In the protocrystalline regime, the transition from a-Si:H to mixed phase (a+μc)-Si:H is designated "a→(a+μc)"; and the transition from (a+μc)-Si:H to single-phase μc-Si:H is designated "(a+μc)→μc." It can be noted here, for the chosen deposition conditions, that at the high hydrogen dilutions, $R > 40$, there is almost instantaneous nucleation of the nano/microcrystalline phase even on a smooth crystalline silicon surface. The phase diagram in Fig. 3 is for a given set of deposition conditions, such as power, pressure, and flow rates, which result in a certain deposition rate which can be most readily increased by raising the input power. Such an increase

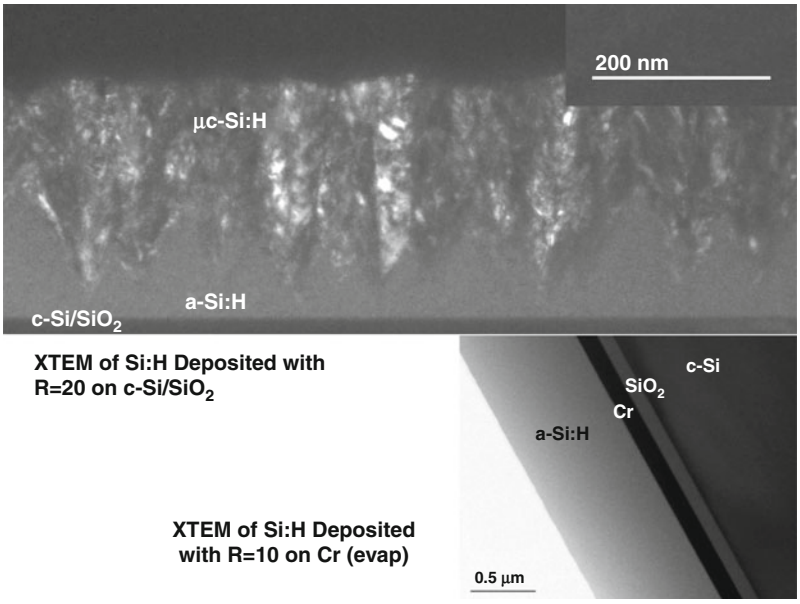

Silicon Solar Cells, Thin-film. Figure 4
Cross-sectional TEM images of an R = 20 Si:H film deposited onto c-Si with a native oxide and a R = 10 a-Si:H film on an evaporated Cr substrate deposited under the same conditions as those in Fig. 3 (Image courtesy of M.M. Al-Jassim and K.M. Jones, NREL)

in power modifies somewhat the overall shape of the phase diagram in Fig. 3 but the largest effect is lateral shift of the transition regions to higher values of R [63, 64].

Figure 4 illustrates how the phase diagrams, such as shown in Fig. 3, relate to the resultant microstructure of a film deposited with a given hydrogen dilution. It shows a cross-sectional transmission electron microscope (TEM) image of a R = 20 film on a c-Si substrate with a native oxide, as well as a R = 10 film on a Cr substrate film deposited onto c-Si. It can be seen in the figure that indeed in the case of the R = 20 there is, at around 200 Å, a phase transition from amorphous to an amorphous + nano/microcrystalline phase whereas in the case of R = 10 the film remains amorphous even to a thickness of 1 μm.

There are three important characteristics of the protocrystalline Si:H regime.

1. As its name implies, the protocrystalline growth regime is one in which predominantly a-Si:H is deposited, but the film will ultimately evolve – given sufficient thickness – first to mixed-phase (a+μc)-Si:H and finally to a single-phase μc-Si:H. Obviously, once the a→(a+μc) transition is present, the accumulating material is no longer considered protocrystalline.
2. A second characteristic of the protocrystalline growth regime is the extreme substrate dependence of the phase of the growing material. In many cases, if the Si:H film is growing in the protocrystalline regime on a freshly deposited amorphous film substrate, the same deposition conditions would lead to single-phase microcrystalline silicon growth on a freshly deposited μc-Si:H substrate film. Thus, under protocrystalline growth conditions, local epitaxy is favored on a c-Si substrate; however, crystallite nucleation is suppressed on an amorphous substrate. For this reason, it is difficult, if not impossible, to grow protocrystalline Si:H i-layers directly on μc-Si:H p and n layers in p-i-n and n-i-p solar cells, respectively, without a conventional amorphous interlayer.
3. A third characteristic of the protocrystalline growth regime is the observed enhanced degree of nuclei

coalescence, which yields smoother surfaces than conventional a-Si:H films. Thus an additional comment should be made, however, regarding protocrystalline materials and the so-called "edge" materials optimized with maximal H_2 dilution, just within the amorphous side of the a→(a+μc) transition. First, it should be noted that such optimization of fixed thickness i-layers using the concept of maximal H_2-dilution, that is, deposition just before the a→(a+μc) phase boundary, was first proposed in 1994 by Lu et al. [65] for the a-$Si_{1-x}C_x$:H i-layers of wide bandgap solar cells. The term "edge" was used later to describe a similar concept for optimization of pure a-Si:H i-layers for solar cells. In fact, this term was coined before it was recognized that the a→(a+μc) transition was strongly thickness dependent (and substrate dependent), and this led to some erroneous conclusions in the early work [66, 67]. The term "edge" becomes even more ambiguous in view of the recent demonstration that μc-Si:H i-layers are optimized for solar cells at the minimal H_2-dilution level just above the onset of the (a+μc)→μc transition [55].

Studies carried out on films of different thickness in which the contributions from a mixed-phase transition layer were avoided showed that despite the evolutionary nature of the Si:H materials prepared with moderate H_2-dilution, they exhibit relatively uniform bulk properties over certain extended regions of thickness, in particular within the initial protocrystalline growth regime. Results have been obtained that are independent of thickness indicating clearly that the film properties are sufficiently uniform as to allow the nature of such film materials and intrinsic layers in solar cells to be characterized with confidence. This has been found in the thickness independence of carrier transport and the light-induced changes in thin films and from the thickness dependence in solar cell structures [68–70]. In addition to the unique evolutionary growth behavior exhibited under the protocrystalline Si:H growth conditions, the protocrystalline material itself exhibits not only improved but also some unique optoelectronic properties. Consequently, by taking into account the evolutionary nature, it is possible to maximize the bandgap for different thickness layers while maintaining their excellent properties as protocrystalline a-Si:H [71]. It also allows doped protocrystalline a-Si:H deposited with high R to be successfully applied in forming the p-contacts in n-i-p solar cells [72].

In situ real-time spectroscopic ellipsometry has also been recently applied to study hydrogenated silicon germanium alloys (a-SiGe:H) for use as narrower bandgap absorbing layers in amorphous silicon-based photovoltaic devices [73]. The microstructural transitions observed in Si:H have also been observed in thin-film a-SiGe:H [74]. This includes the amorphous to amorphous roughening transition [a → a], amorphous to mixed-phase amorphous plus microcrystalline transition [a → (a + μc)], mixed-phase to single-phase microcrystalline transitions [(a + μc) → μc)], as well as the characteristics of protocrystallinity. Differences in the microstructural evolution with the addition of germanium indicate that a greater degree of disorder is present in these materials. Specifically, with increasing germanium incorporation, the maximum [a → a] transition is shifted to much lower bulk layer thickness than for a-Si:H, and significantly more hydrogen dilution is required in order to nucleate microcrystallites from the amorphous matrix [75]. In addition, the hydrogen dilution conditions for the optimum amorphous material to be produced must increase monotonically with germanium content [76, 77].

Although the a-Si:H and its alloy materials in solar cells and thin films were for a long time being deposited from undiluted feedstock gases, because of the importance of hydrogen in determining the quality of the a-Si:H, attention was given to its concentration and bonding in the thin-film materials. Attention was also given to the corresponding densities of microvoids [78], the sharpening of valence band tail gap states and associated disorder, and the densities of silicon dangling bonds as measured with ESR, NMR [79, 80] and sub-bandgap absorption [81]. However, the improvements in the microstructure of thin-film materials were characterized primarily by the changes in the infrared absorption [82–84].

Despite the extensive research activities on obtaining an understanding of the disordered network, having been carried out for the last 3 decades, there has been a lack of a detailed and consistent understanding of the amorphous network on the short- and

medium-range length scales. One of the reasons for this is that the microstructural view of the a-Si:H network has been limited to its treatment as a continuously random network (CRN). In this view, isolated dangling bonds and the randomly distributed isolated hydrogen are the only entities considered as defect sites and hydrogen emission sites, respectively. Recently however, the Eindhoven Technical University group has reported on a self-consistent model for hydrogen incorporation in a-Si:H based on infrared, IR, absorption spectroscopy [85–87], which has enabled highly significant progress to be made in the insight into the microstructure of a-Si:H films. The infrared analysis that was developed reveals the configurations of incorporated hydrogen, like the predominance of hydrogenated vacancies in a dense a-Si:H network and the predominance of hydrogenated nano-sized voids in less dense a-Si:H. The clear distinction between these two microstructural ranges has been identified by using the relation between the film mass density and the hydrogen concentration [85]. In their approach it was possible to self-consistently explain the configurations of incorporated hydrogen responsible for the IR hydride stretching modes; the relation of their densities to the mass deficiency of a-Si:H network; the oscillator strength of dipole vibrations of the hydrides; the frequency shift of hydride vibrations in the bulk relative to their unscreened frequencies in molecules; and the screening mechanism of the hydrides by their environment using only *three* parameters [86, 87]. Based on their assignments, it was found that the fully hydrogen passivated divacancy is the dominant hydrogen complex in dense (current device-grade) a-Si:H material. The results are in agreement with studies based on nuclear magnetic resonance (NMR) [79, 88], positron annihilation (PA) [89–91], and film density analysis [85, 92, 93]. Furthermore, the case was made that an amorphous network controlled by hydrogenated vacancies leads to a more consistent view for the properties of plasma-processed hydrogenated amorphous silicon, compared to the extensively held views based on CRN. A summary of possible configurations for incorporated hydrogen in hydrogenated silicon matrix is illustrated in Fig. 5. The latter shows the frequency position of the stretching monohydride mode versus the nanostructure parameter K, which represents the

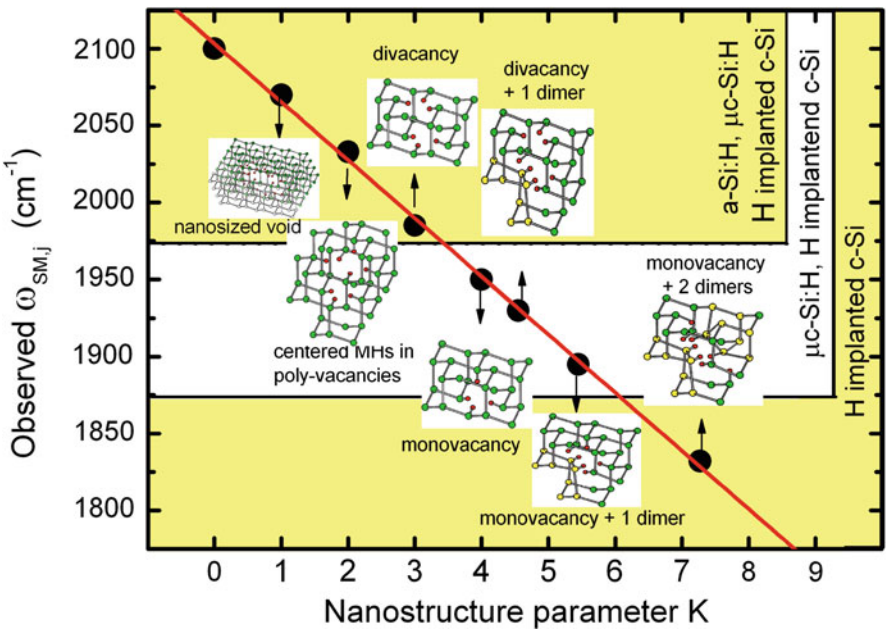

Silicon Solar Cells, Thin-film. Figure 5

The relation between the frequency positions of the stretching mode of monohydrides incorporated in various Si:H networks [94]

local hydrogen density in the configuration of incorporated hydrogen. It is defined as the number of hydrogen atoms present in the volume equal to that of one missing silicon atom in the network. Also the figure includes schematics of the types of amorphous microstructures including those that are associated with K values between 1 and 3.

It can be seen that undiluted materials, falling into the category of K = 1 or 2, have microstructures which include large numbers of nano-voids and poly-voids. On the other hand, in the dense (current device-grade) a-Si:H material, such as protocrystalline a-Si:H' which corresponds to K = 3, the microstructure is dominated by hydrogen complexes associated with hydrogen passivated divacancies.

Their work has clearly shown that the fully hydrogen passivated divacancy is the dominant hydrogen complex in the current device-grade a-Si:H material. This dense network, exhibiting predominantly fully hydrogen passivated divacancies, offers an alternative explanation for the amorphous nature of a-Si:H, its phase transition from amorphous-to-microcrystalline, and the characteristics of its electronic structure like the bandgap, the a symmetric widths of the gap tails and the various defect states in the gap.

Transition to Microcrystalline Material Deposition and Microstructure

As can be seen in Fig. 1, the onset of the mixed phase and the transition into the microcrystalline phase is greatly accelerated when high hydrogen dilution is used. From Fig. 2, it is also evident that the width of this transition regime, in terms of H dilution or of silane concentration, will depends on the silane depletion factor. For low depletion, the transition is rather sharp, resulting in a narrower process window for material deposited at the edge of the transition regime [95].

As ellipsometry is not always available or is difficult to use (in case of rough substrates), the crystalline phase and the crystalline fraction in the materials are commonly characterized using Raman spectroscopy. As seen in Fig. 6, the presence of a peak at around 520 cm^{-1} is the signature of the crystalline fraction while the broad peak at 480 cm^{-1} is attributed to the amorphous phase. An additional peak at 500 cm^{-1} is generally attributed to some different forms of the crystalline phase. The Raman crystalline fraction is determined by integrating the three components (one is amorphous I_a and the other two crystalline I_c) given by [96]:

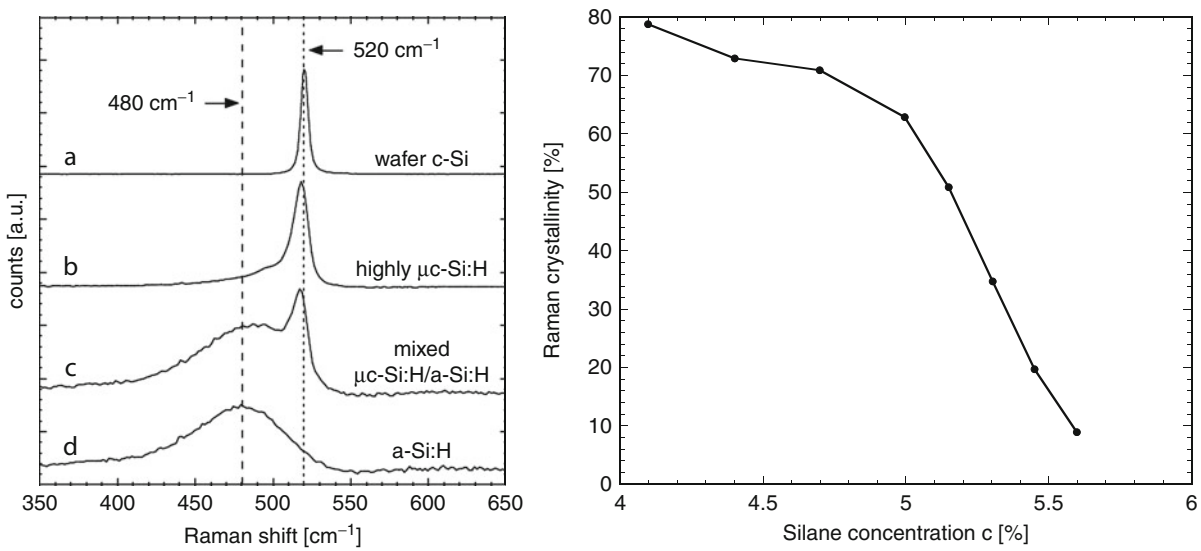

Silicon Solar Cells, Thin-film. Figure 6
Typical Raman spectra (*left*, From [97]) for various thin-film Si and (*right*) an example of the evolution of the Raman crystalline fraction as a function of silane concentration c

$$\chi_c^{RS} = \frac{I_c}{(I_a + I_c)}$$

The crystalline fraction, as determined by Raman spectroscopy or "Raman crystallinity," does not represent the real crystalline fraction which is much more difficult to quantify. However, it is very convenient for describing the evolution of the crystalline fraction in thin-film silicon.

Crystallite size and orientation are usually determined by X-ray diffraction (XRD) spectroscopy. An example of the evolution in the diffraction spectra as a function of the silane concentration c is shown in Fig. 7. Comparison of the peak intensity relative to that of a c-Si powder XRD spectrum allows the prominent orientation of the film to be determined, whereas the analysis of the peak width, using the Debye-Scherrer formula, allows the crystallite size to be determined. It should be noted that the latter tends to be underestimated due to the XRD being predominantly controlled by the smaller grains. Typical state-of-the-art materials for solar cell application exhibit a preferential <220> orientation but <111> is also very often observed and the necessity or benefit of a given orientation for solar cell application is still controversial.

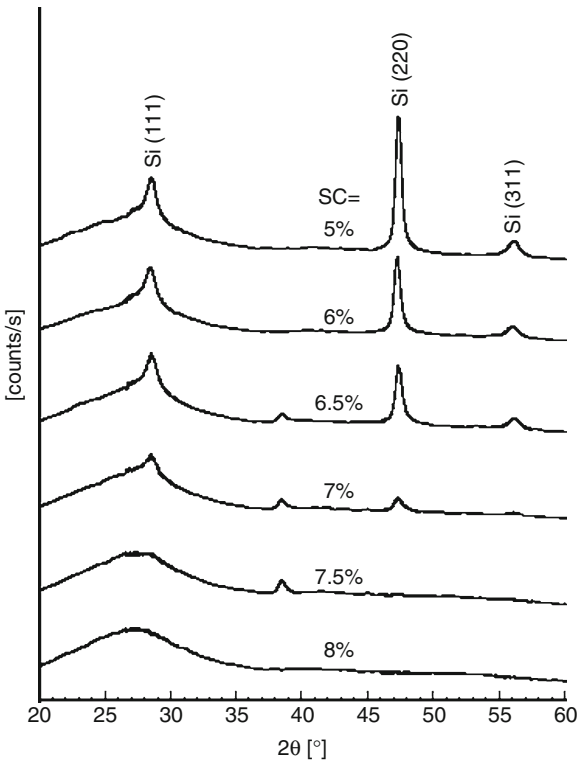

Silicon Solar Cells, Thin-film. Figure 7
Typical XRD spectra of thin-film Si as a function of silane concentration (From [97])

As shown in Fig. 8, nucleation usually takes place after an a-Si:H incubation layer has been deposited. After the onset of nucleation, the crystalline phase grows conically until the nanocrystal conglomerates coalesce and result in a mainly crystalline material. Such μc-Si:H can be described as a mixture of grains (or nanocrystals) embedded in a disordered material which includes an amorphous tissue, grain boundaries, as well as voids (cf. Fig. 9). The nanocrystal sizes are typically in the order of few tens of nanometers while the conglomerate sizes are several hundreds of nanometers. An increase in the Raman crystallinity corresponds to an increase in the crystallite size δ and a decrease in the conglomerate size Δ (as defined in Fig. 8) [98]. The surface of the material on the other hand exhibits a cauliflower-like morphology, with large features given by the nanocrystals conglomerates and small features due the nanocrystals themselves. The surface roughness is also found to increase with increasing silane dilution and crystalline fraction [99]. Due to the evolution of the material with thickness, under fixed deposition conditions, the crystalline fraction is thickness dependent for materials grown at the transition regime or close to it. Furthermore, the nucleation as given by the nuclei density depends on the substrate composition [100, 101]. For example, the nuclei density on Si coated with a native oxide is found to be a factor of 2 higher than the one on sputtered ZnO or Cr substrate. It can also be noted here that the conical shape of the start of the crystalline phase growth is independent of the deposition conditions as well as the nature of the substrate.

Besides the evolution of crystallinity with silane concentration c (shown in Fig. 1), the microstructure is also found to evolve considerably with thickness as sketched in Fig. 10 [99, 101]. At the onset of crystalline growth, very small crystallites embedded in an amorphous tissue are formed. As c is reduced, or R increased, the conical shape of the μc-Si:H crystalline regions appear and the amorphous phase is limited to an incubation layer on the substrate. As c is further

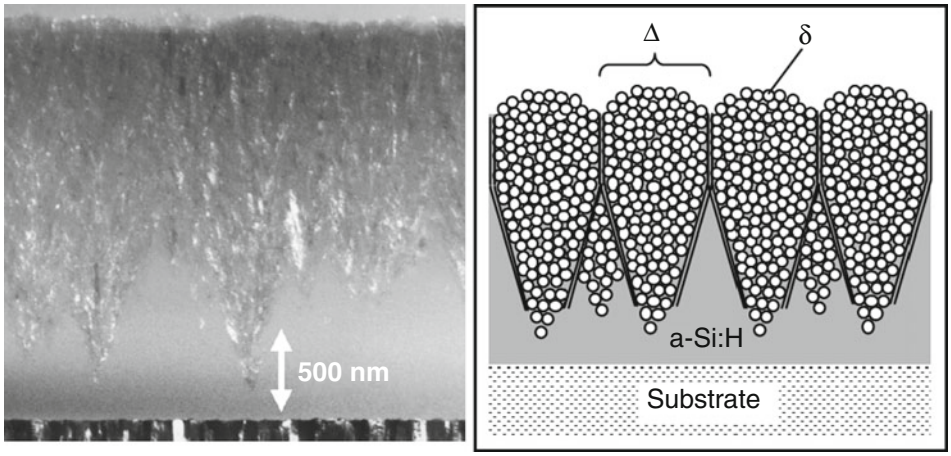

Silicon Solar Cells, Thin-film. Figure 8
Typical microstructure observed in the transition regimes during growth of a μc-Si:H layer. An a-Si:H incubation layer is clearly visible (From [97])

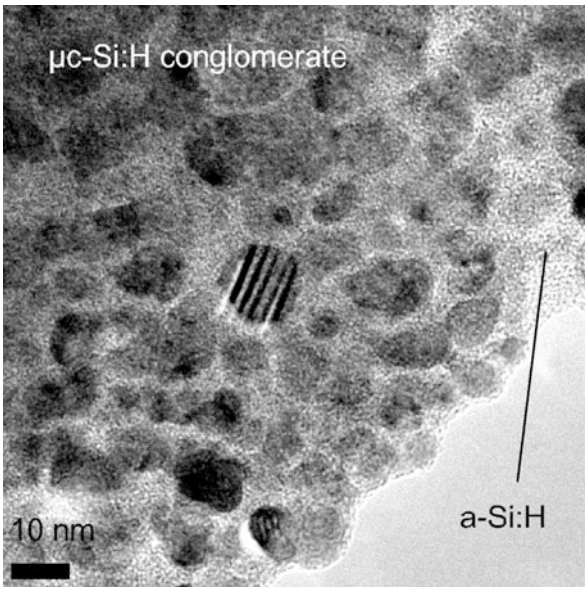

Silicon Solar Cells, Thin-film. Figure 9
High resolution transmission electron microscopy micrograph of a plane view taken within a microcrystalline conglomerate. Spherical nanocrystals embedded in amorphous tissue constitute the microcrystalline phase itself (From [97])

reduced, the a-Si:H incubation layer is further reduced, and the shape of the conglomerates becomes more columnar with the grain size increasing. At very low c, crystalline growth can start without the formation of an incubation layer, and a marked columnar structure with relatively large grain is obtained.

Several models have been proposed to describe the growth of μc-Si:H including those based on surface diffusion [57], etching of the amorphous tissue [102], or chemical annealing of the growing layer [103]. A comprehensive discussion of the growth of a-Si:H and μc-Si:H can be found in [58, 104]. All three models show that the relevant parameter for obtaining high crystalline fraction is the atomic hydrogen flux striking the surface with a high ratio of hydrogen flux relative to that of silane being needed. A simple model based on plasma chemistry has also been proposed to explain how the silane concentration in the plasma controls the crystallinity of the deposited films [58].

Optoelectronic Properties

Bandgaps and Optical Properties

Amorphous Si:H A key property of any solar cell material is its bandgap and optical absorption since they determine the possible currents and voltages that can be generated by sunlight. The absence of long-range order broadens the distribution of states compared to crystalline Si, forming bandtails and a continuous distribution of localized states in the gap that reduces carrier scattering lengths to atomic distances. The localized states that lie in the bandgap are a result of the disorder and structural defects such as

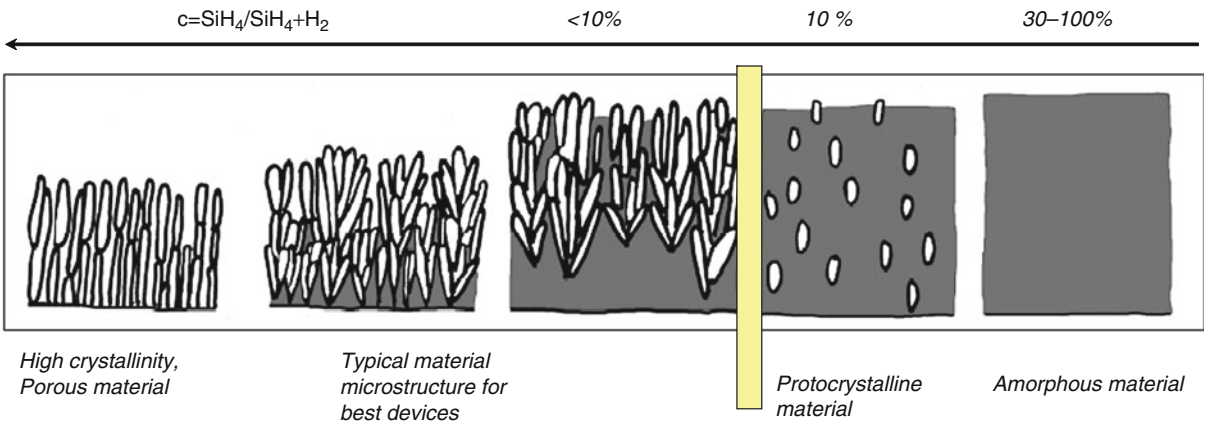

Silicon Solar Cells, Thin-film. Figure 10
Typical microstructure observed for various thin-film Si material deposited under various hydrogen dilution of silane. Nanocrystallites are drawn in *white* while the amorphous tissue is in *gray* (After [101])

broken bonds, nano-voids and poly-vacancies [86]. These gap states determine many of the electronic properties since they cause carrier trapping and also can act as recombination centers [105]. Amorphous a-Si:H and its alloys have very high absorption coefficients due to the random nature of the atomic ordering so that they become similar to those in direct bandgap semiconductors [106]. The electron densities of states are still a function of energy, but there is now a continuous distribution of localized states which results in two types of bandgaps. One is the mobility gap associated with free carrier transport and corresponds to a separation between regions of nonlocalized, extended states in which electrons and holes can move as free carriers. The other is an optical gap which characterizes optical absorption and is different from the mobility gap because of the continuous transition from the nonlocalized to localized states.

The bandgap that is most often referred to in a-Si:H and its alloys is the optical gap obtained from optical absorption. The most often reported values are those for the Tauc's gap which is derived on the assumption that, as in the case of crystalline silicon, the optical transitions between the extended states have constant matrix elements [107]. Unfortunately, these values rely on the extrapolations of experimental data that has a very limited range and thus results in large uncertainties. There is also the Cody-Collins gap [108], which is based on constant dipole elements and actually gives much longer extrapolation regions, thus increasing its accuracy. However, in general, it is the Tauc's gaps, which are about 50–80 mV wider than the Collins-Cody gaps that are quoted in the literature as the gaps of a-Si:H and its alloys. The information about the mobility gaps of these materials is much more limited with their values being estimated from transport measurements. They have also been measured directly in a-Si:H with the internal photoemission of electrons and holes and found to be around 60 mV larger than the Cody-Collins optical gap [109].

Both the strong light absorption and the values of the mobility gaps, which are adjustable by alloying, make a-Si:H attractive for solar cell technology, since it offers the possibility of very thin cells as compared to crystalline silicon cells. The bandgaps and optical absorption, α, of the a-Si:H-based materials can be changed by the extent to which hydrogen, germanium, and carbon are incorporated to form a-Si:H, a-SiGe:H, and a-SiC:H alloys [27–29]. In Fig. 11 the optical absorption characteristics are shown of an a-SiC;H, a-Si:H, and a-SiGe:H film having bandgaps of 2.0, 1.7, and 1.4 eV, respectively.

The changes in the gaps can be clearly seen from the systematic horizontal shifts of the absorption spectra whose regions of $\alpha \sim 10^3$ cm^{-1} correspond to the optical transitions between the valence and conduction bands. The regions of α between about 10^3 and 10 cm^{-1}, which are exponential in nature, arise from the absorption in valence band tail states which are due to gap states introduced by the disorder in these

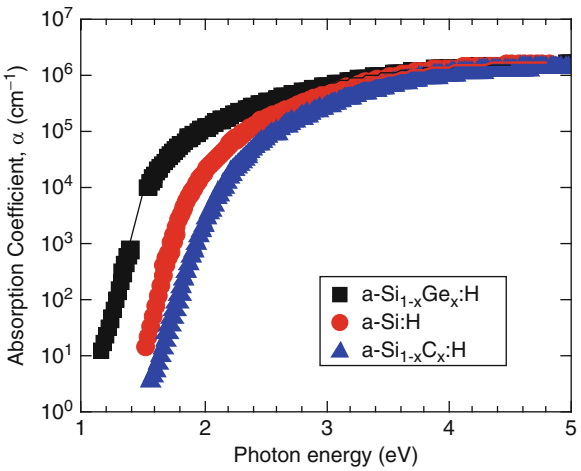

Silicon Solar Cells, Thin-film. Figure 11
The optical absorption of an a-SiGe:H, a-Si:H, and an a-SiC;H film versus photon energy. Their respective bandgaps are 1.4, 1.7, and 2.0 eV

amorphous materials [110]. These exponential regions are also known as the *Urbach tails*. The densities of the valence band tail states are significantly higher than those of the conduction band tails [111], even in the recently developed materials with a highly ordered network [68]. Although not shown in the figure, at values of α below ~1–10 cm^{-1}, shoulders set in the absorption spectra that are due to the optical transitions originating from defect states outside the band tails. This absorption depends on the densities and nature of these states [111, 112], and for a-Si:H materials the absorption coefficient at 1.2 eV is commonly used to determine the defect density (i.e., dangling bond density) in the materials [113].

Incorporation of hydrogen into the a-Si:H network not only removes defects and their states in the gap, but also widens the gap. Using hydrogen dilution of silane, it is possible to obtain bandgaps of around 1.8 eV without deteriorating the microstructure and electronic properties [70, 71]. However, the rapid transition in the microstructure with high hydrogen dilution limits the protocrystalline a-SiH regime to very thin layers, which does not allow such materials to be used as intrinsic absorber layers. As in the case of a-Si:H, hydrogen dilution allows one to deposit a-SiGe:H and a-SiC:H alloys with better microstructure, and hence lower defect densities. However, the electronic properties of a-SiGe:H and a-SiC:H alloys are not as good as that of a-Si:H, and because these deteriorate with the increase of either germanium or carbon there are limits on the range of bandgaps that can be used in efficient solar cells [114, 115].

The absorption that is useful in creating free carriers in the thin solar cells is at values of α greater than about 10^3 cm^{-1}, which corresponds to photons energies that are greater than the bandgap of the materials. The phase transitions in protocrystalline a-Si:H (discussed in the previous section) set an upper limit of ~1.8 eV for the bandgap of a-Si:H, while the increase in defects with the incorporation of germanium has currently set the lower limit at ~1.3 eV for the bandgap of a-SiGe:H [116]. These bandgaps, however, cover a sufficiently wide range to offer the flexibility required for constructing efficient single-junction, as well as multi-junction solar cells.

Microcrystalline μc-Si:H Infrared light absorption in μc-Si:H is mainly controlled by the crystalline phase; so, as the crystallinity increases, the bandgap of the material approaches that of c-Si (cf Fig. 12). For materials with high crystalline fraction, the absorption coefficients for all photon energies are found to be higher than those of c-Si. This apparent lower bandgap value for μc-Si:H is however due to a light scattering effect which enhances the light absorption at photon energies below 1.8 eV [118]. The presence of grain boundaries in the material leads to bulk light scattering effect and the rough surface morphology created by the grain conglomerates leads to even stronger surface scattering of light. The effect of surface scattering could be demonstrated by eliminating it by polishing the surface whereupon the optical absorption approaches that of c-Si [118] (cf. Fig. 13). The bandgap found for highly crystalline μc-Si:H is very similar to that of c-Si having a value ~1.1 eV. However, because of the presence of a residual a-Si:H tissue and the grain boundaries the optical absorption is higher than that of c-Si for photon energies greater than the bandgap of a-Si:H [118]. At photon energies smaller than the bandgap there is an exponential fall-off in the absorption, similar to that observed in a-Si:H (*Urbach edge*), then a shoulder in the absorption at lower energies resulting from the disorder at the grain boundaries and defects such as dangling bonds. In the case of

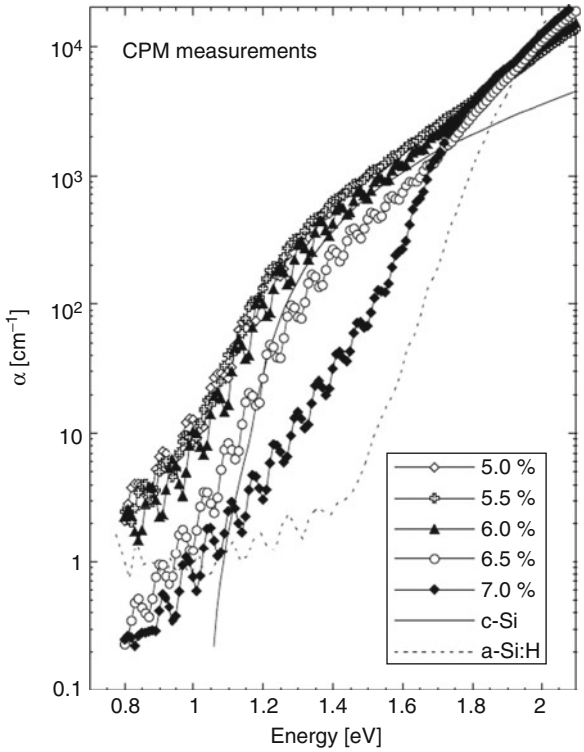

Silicon Solar Cells, Thin-film. Figure 12
Apparent optical absorption coefficient measured by Constant Photocurrent Measurement CPM [117] on series of Si samples deposited at various silane concentration values (From [97])

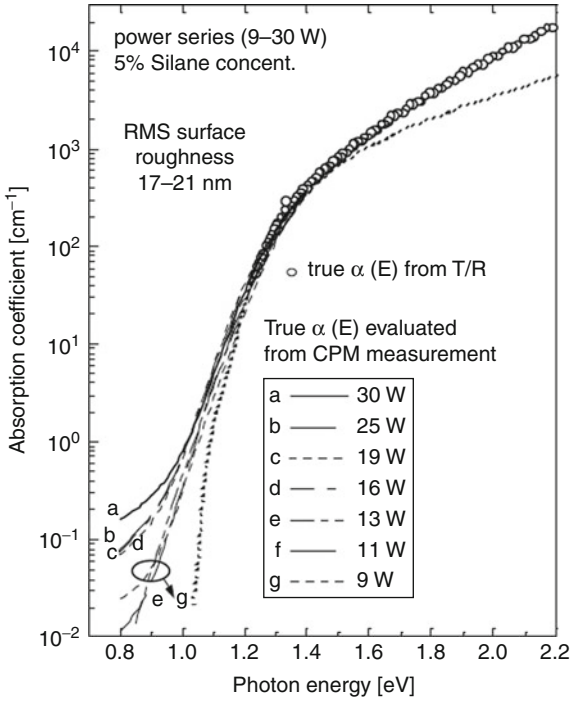

Silicon Solar Cells, Thin-film. Figure 13
Real (with scattering component removed, or "true") absorption coefficient for a series of μc-Si:H samples deposited at silane concentration c = 5% as measured by CPM and optical transmission/reflection T/R [121]

μc-Si:H such a sub-bandgap absorption spectra can be conveniently measured using Fourier Transform Photocurrent Spectroscopy [119].

For reliable comparison between different materials, the scattering component in the absorption must be eliminated so that the "true" absorption can be obtained either by polishing the layer [118] or relying on optical modeling to determine accurate absorption coefficients. Comparisons of μc-Si:H materials (with relatively large crystalline fractions) differ mainly in their sub-bandgap absorption regions and in particular for photon energies below about 0.9 eV where the defect absorption plays a major role. Therefore, the magnitude of the absorption at 0.8 eV is usually considered a reliable measure of the defect density in μc-Si:H as long as there are no significant changes in the bandgap [120]. This is illustrated in Fig. 13 with the effect of the deposition rate indicated by the increase in the input power in the plasma discharge, on the increase of the absorption coefficient at 0.8 eV [121].

Semiconductor Properties

Intrinsic Material Properties

Amorphous Si:H Because Si:H materials do not have a unique structure like crystalline silicon, they have a very wide range of optical and semiconductor properties. However, it has been well established that the semiconductor properties and stability of a-Si:H depend on the mechanisms which determine the growth processes, the incorporation of hydrogen, and the resultant microstructure [54, 86, 122, 123]. By improving the growth conditions, which included the incorporation of ~10% hydrogen, it was possible to obtain a-Si:H materials with properties which were outstanding for an amorphous semiconductor. These intrinsic (undoped) materials

have Fermi levels near the middle of the gap, free carrier transport that occurs in the extended states of the conduction and valence bands, and the hole and electron lifetimes in the range of 10^{-8}–10^{-6} s, respectively. However, because of the lack of long-range order, the free carrier mobilities in these bands are significantly lower than those in c-Si, being only about 10 and 1 cm^2V^{-1} s^{-1} for electrons and holes, respectively [111].

Such properties were already obtained with a-Si:H materials that were prepared from undiluted feedstock and were far less dense than the current hydrogen diluted and protocrystalline materials. However, because of such good properties, it was proposed and generally accepted that their microstructure could be explained in terms of a continuous random network [124]. As a consequence, the defects dominating the semiconductor properties were considered to be isolated dangling bonds that were not passivated by hydrogen and could be identified with a specific ESR signal [80]. The increase in this ESR signal with light-induced degradation was taken as a further confirmation that such dangling bond defects were the source of the defect states around the middle of the gap [125]. The energy band diagrams that are used to represent intrinsic, undoped a-Si:H and its alloys are significantly different from that for c-Si. This is illustrated in Fig. 14 where it can be seen that in both cases there is a bandgap separating the extended states where free carrier transport occurs, which are represented as the conduction and valence bands.

In the case of undoped c-Si, there is only a small density of discrete states in the gap. In the case of a-Si:H, on the other hand, there is a continues distribution of gap states near both the band edges with very large densities of tail states that fall of exponentially with energy toward the middle of the gap. The exponents of these distributions in dense a-Si:H are around 25 meV and 45 meV for the conduction and valence band tails, respectively. In the regions around midgap, there is still a continuous distribution, generally represented in the form of Gaussians that are associated with defects in the microstructure. In general, states that would be associated with impurities such as O, N, C are not included, since for low levels that are generally less than several times 10^{18} cm^{-3}, there is little effect on the electronic properties of the materials [126]. The defect states that are important in the operation of solar cells lie in the regions ~0.5 eV above and below midgap, since they are the ones that act as recombination centers for the carriers that are photogenerated under 1 sun illumination. Despite their importance, there is as yet no general consensus about their nature or the exact energy location of the defect states in the gap. This is in part because it is very difficult to characterize different states when they are

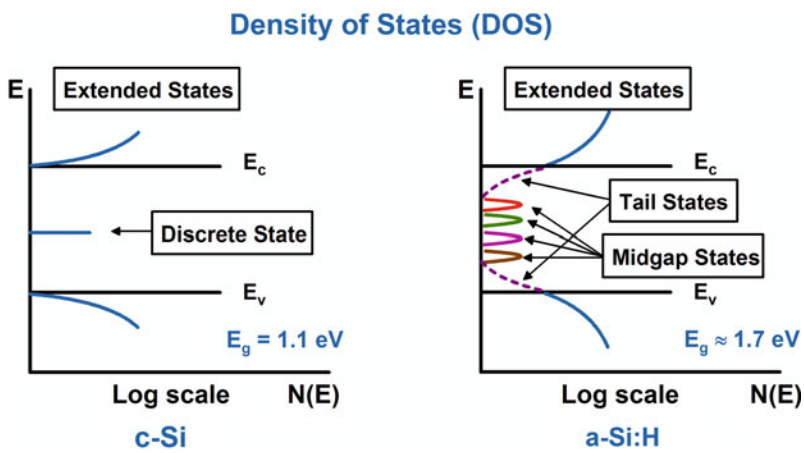

Silicon Solar Cells, Thin-film. Figure 14
On the *left* is an energy band diagram for c-Si with a discrete energy level in the gap. On the *right* is an energy band diagram of a-Si:H with continuous distributions of tail and defect states in the gap

part of a continuous distribution. It also in part due to the absence of a unique form of a-Si:H so that different conclusions could be reached from results on the materials that have been most extensively studied. These are materials which, although claimed to be "device quality," were deposited without hydrogen dilution of the feedstock gases with a microstructure that contains a significant number of nano-voids and poly-vacancies.

From early on, because the microstructure of a-Si:H was viewed in terms of a CRN, isolated dangling bonds were considered the principal defects so that the gap states near the middle of the gap were associated solely with these defects. Since there are three charged states of the dangling bonds (D^0 neutral, D^- negative, D^+ positive), there would be three possible distributions of gap states. Initially, only those associated with D^0 and D^- were considered with their respective locations at and above midgap. However, most emphasis was placed on the importance of just the D^0 states, in part because an ESR signal was identified as corresponding to the neutral dangling bond and thus allowed their densities to be measured directly [127]. In a-Si:H materials with hydrogen content of ~10 at%, the densities of such ESR signals were around 10^{16} cm^{-3} before light-induced degradation. The emphasis on such D^0 gap states led to them being considered solely responsible for subgap optical absorption. This led to the assumption that in order to obtain the gap state densities around midcap it was necessary only to measure the magnitude of the subgap absorption spectra, and not as would be the case for multiple defect states, their derivative with respect to photon energy [128]. Attempts to self-consistently model photoconductive and subgap absorption results on the same a-Si:H films with just two distributions of states met with very limited success, but nevertheless two Gaussian gap state distributions representing dangling bond defect states were extensively used in modeling solar cells. Self-consistent fittings of experimental results of photoconductivities and subgap absorption spectra could be obtained with three Gaussian distributions of states [129, 130]. Such distributions were similar to those proposed for the three charge states of dangling bonds, except in these configurations the D^- states would be below and the D^+ states above midgap. The three charge states of the dangling bond were found to be useful in the studies of photoconductivity in different Si:H films [131], as described in the next section, as well as in explaining the differences in solar cell properties and their improvement [131, 132].

Additional models have been proposed for the nature, energy in the gap, and densities of states (DOS) with each having distinctly different distributions of states near the middle of the gap [133–135]. Consequently, different distributions of states were applied in the analysis of the optoelectronic properties of different a-Si:H materials. Recently, however, results have been obtained for the distribution of states in dense, high quality protocrystalline a-Si:H materials whose microstructure has been shown to consist predominantly of hydrogen passivated divacancies. In these studies, the gap states were investigated on both thin a-Si:H films as well as on corresponding solar cells. The self-consistent results obtained between the photoconductive electron recombination in the films and the Shockley Reed Hall (SRH) [136] hole electron recombination in the cells clearly indicated the presence of both midgap and non-midgap states [137]. The distributions of these states were characterized directly with sub-bandgap absorption measurements measured with Dual Beam Photoconductivity (DBP) [128] and where the analysis of the spectra took into account the presence of multiple defect states by taking the derivatives of the absorption spectra. Example of the absorption spectrum after differentiation of the subgap absorption is shown in Fig. 15a, and b illustrates the distributions of the gap states after deconvolution of this result into three Gaussians.

In Fig. 15a the density of states, obtained after normalizing the derivatives to the density of states at the band edge, is shown versus the separation energy from the valence band and clearly indicates the presence of different distributions of gap states. The spectra, such as in Fig. 15a, can be deconvoluted into Gaussian distributions of A, B, and C states lying outside the exponential tail states as is shown in Fig. 15b. The A states are 0.05 eV above midgap, the B states 0.19 eV, and the C states 0.39 eV below midgap. It can be pointed out that the gap state distributions found here for this dense a-Si:H, has a similar energy distribution to that found for the divacancies in c-Si, which is consistent with its microstructure that consists predominantly of hydrogen passivated divacancies. The nature of these states is covered in greater detail in

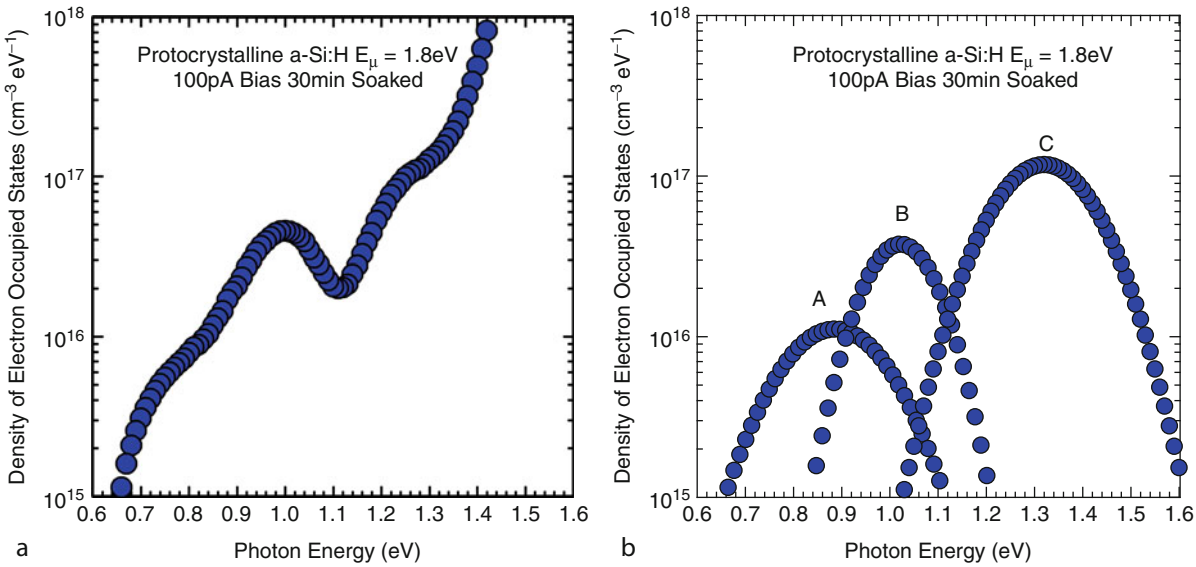

Silicon Solar Cells, Thin-film. Figure 15

In (**a**) is the derivative of a subgap absorption spectrum, after Fast Fourier Transform to eliminate interference fringes, for an a-Si:H film. In (**b**) are the distributions of gap states after deconvolution of the spectrum in (**a**) into three Gaussians

section "Light-Induced Degradation." It should be pointed out here that the A and B states act as recombination centers even at low illumination levels, whereas the C states contribute to carrier recombination only when they are embraced by the Quasi Fermi level splitting that occurs at illumination intensities approaching 1 sun [138]. Although evidence has been reported from capacitance and DLTS measurements on Schottky barrier structures for a distribution of states about 0.6 eV from the conduction band [139, 140], such states could not be identified in the studies described here.

Incorporation of Ge in forming a-SiGe:H alloys not only introduces additional defects which increase the densities of gap states but also make their characterization even more difficult. However, whatever the exact nature and distributions of the deep lying gap states are in the currently used solar cell materials, in the initial state the densities of the midgap states are of the order of 10^{16} cm^{-3}, which allows the hole and electron lifetimes to be from 10^{-8} to 10^{-6} s. They also enable the space charge densities to be sufficiently low as to allow the junction electric fields to extend over the entire thickness of efficient solar cells. Such conditions are satisfied by a variety of materials, but what distinguishes them from a-Si:H as solar cell materials is their significantly larger light-induced degradation.

Amorphous to microcrystalline Si:H properties Extensive characterization of μc-Si:H has been carried out with electron spin resonance (ESR) to obtain insight into the defects in μc-Si:H [120, 141]. The main resonance, with a spin density of $\geq 10^{16}$ cm^{-3} that is observed, is very similar to that associated with the dangling bonds of a-Si:H. This resonance is observed to shift the signal from a g-value of 2.0055 for a-Si:H to values of 2.0052–2.0045 in μc-Si:H. Annealing of the material at temperatures above 400°C (above the threshold for hydrogen exodiffusion) leads to the creation of an addition defect with a g-value of 2.0030 while at the same time increasing the signal of the main defect at ~2.0055 (assumed to correspond to dangling bonds). In contrast to a-Si:H, the relationship between the spin density of μc-Si:H and the sub-bandgap absorption measured at 0.8 or 0.9 eV is more ambiguous, especially if the crystallinity is changed [141, 142].

Transport properties of thin-film Si layers are commonly characterized by steady state dark and photoconductivity measurements. Compared to a-Si:H, the heterogeneity and microstructure of μc-Si:H have

a large effect on the optoelectronic properties of the material. The electronic properties are usually found to change as a function of the crystalline fraction with a dependence on the layer thickness. This is especially true for μc-Si:H materials deposited at or close to the transition regime between amorphous and microcrystalline growth. Dark conductivity σ_d increases exponentially from 10^{-10} to 10^{-12} Ω^{-1} cm^{-1}, values for intrinsic a-Si:H, to values of $\sim 10^{-6}$ Ω^{-1} cm^{-1} intrinsic μc-Si:H having a high fraction of the crystallinity and the reduction in bandgap from ~1.75 to 1.1 eV. Photoconductivity is also observed to increase weakly with increasing crystalline fraction [143]. Photoconductivity is given by

$$\sigma_{ph} = Ge\left(\mu_n^0\tau_n^R + \mu_p^0\tau_p^R\right)$$

where G is the generation rate, e is the elementary charge, and $\mu_n^0\tau_n^R$ and $\mu_p^0\tau_p^R$ are the band mobility – recombination lifetime products of the electrons and holes, respectively. Due to the increase in σ_d and decrease of σ_{ph} with increasing crystallinity, the photosensitivity (ratio of σ_{ph} to σ_d) is also reduced [143].

When the Fermi level in the material shifts from midgap toward the conduction band or the valence band, electrons or holes (the majority carriers) start dominating photoconductivity, and the other carriers (the minority carriers) can be neglected. Photoconductivity therefore can be used to characterize the transport of the majority carriers (as given by their mobility-lifetime product $\mu^0\tau^R$) while the minority carrier transport properties can be obtained, for example, from the ambipolar diffusion length L_{amb} measured by steady-state photo-carrier grating (SSPG) [144]. Both σ_{ph} and L_{amb} also depend strongly on the Fermi level position E_F. For accurate comparison of different films, it is therefore necessary to compare either intrinsic materials or to take into account the position of E_F. This requirement is particularly important for μc-Si:H as the layers tend to exhibit a n-type character due to the incorporation (during growth or after deposition) of contaminants such as O which shift E_F [51, 145, 146]. In order to characterize the transport properties (of both majority and minority carries) in Si:H thin films, and avoid as much as possible the effect of E_F, an aggregated mobility lifetime product $\mu^0\tau^0$ has been proposed [132].

Figure 16 shows $\mu^0\tau^R$ for both electrons and holes as a function of E_F for various undoped (nonintentionally doped) or slightly doped a-Si:H films in the annealed and degraded states as well as μc-Si:H layers. An increase in the majority carrier $\mu^0\tau^R$ can be observed as the material becomes more n-type or p-type while the minority carrier $\mu^0\tau^R$ becomes smaller. Transport characteristics for μc-Si:H are found to be quite similar, and even slightly better [97] than the ones for annealed a-Si:H. The values for $\mu^0\tau^R$ in the degraded a-Si:H films are however roughly one order of magnitude lower due to the reduced lifetime of the carriers.

In general, almost all the electron and hole transport properties in μc-Si:H are found to be very similar to those of a-Si:H, both for parallel and transverse carrier transport [97, 148]. This suggests that the amorphous tissue between the nanocrystals is controlling the carrier transport. This is also supported by the fact that carrier transport is not affected by changes in the size of the nanocrystallites, where even when their size increases their $\mu^0\tau^0$ remains unchanged [98]. However, the transport in the plane of the film, as characterized by the ambipolar diffusion length L_{amb}, follows the same trend as the decrease in the conglomerate size Δ, thus suggesting that the conglomerate boundaries limit the in-plane transport [98]. Further evidence for the role of crystallite grain boundaries in carrier transport is the absence of a percolation threshold, which should be present at a certain crystallinity fraction due to the coalescence of the nanocrystals. Such a threshold has never been clearly demonstrated [149] even though, in general, the transport properties in μc-Si:H are found to be isotropic. Anisotropy in materials deposited at low rate is sometimes observed with carrier transport along the growth axis being better than the transport parallel to the surface [147, 150]. The only transport characteristic which is found to change considerably in μc-Si:H, as compared to a-Si:H, is the drift mobility of holes. This hole mobility is found to be significantly higher than in a-Si:H due to a sharpening of the valence band tails [151, 152].

The presence of grain boundaries in μc-Si:H, and especially the conglomerate boundaries, is generally associated with the presence of voids and cracks in the material. These voids can favor the diffusion of impurities into the material, such as oxygen or water vapor, that can greatly affect the transport properties

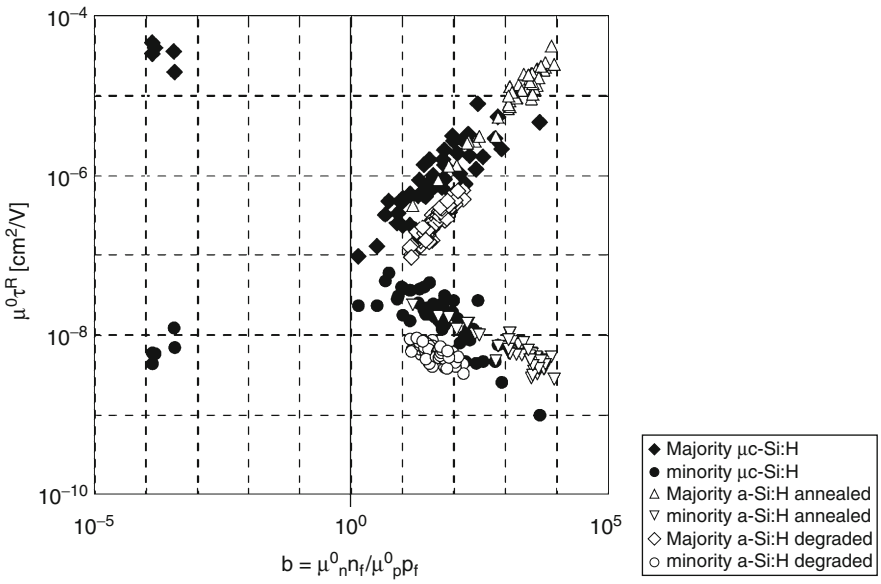

Silicon Solar Cells, Thin-film. Figure 16
Mobility-recombination time for electrons and holes as a function of Fermi level position (as given by the parameter *b*) for various annealed and degraded a-Si:H as well as for μc-Si:H layers deposited at various silane concentration values. The parameter $b = \left(\mu_n^0 n_f \middle/ \mu_p^0 p_f\right)$ is the ratio of the carrier band mobility times the ratio of free electrons to free holes [132, 147]. $b = 1$ in case of a fully intrinsic layer; samples with $b < 50$ may be considered intrinsic (From [97])

due to their doping efficiency of μc-Si:H being much higher than for a-Si:H. The effect of the so called "post-oxidation" leads to shifts of the Fermi level toward the conduction band thus giving a strong n-type character to the material [146]. In general the changes can be annealed out by heating the sample in vacuum to temperatures close the deposition temperature. The reversal of this "post-oxidation" process has time constants varying between hours and weeks and is a function of both crystallinity and the deposition conditions; materials deposited at high deposition rates tend to be more susceptible to such post-oxidation [146, 153]. Generally, bare layers are affected more than solar cells (sealed by the cell contacts), which makes comparison between different materials more difficult. This is discussed in section "Solar Cells."

Doped Material Properties The undoped a-Si:H materials currently used in high performance cells have their Fermi levels at midgap or displaced toward the conduction band so as to make them very slightly n type. Although such intrinsic nature was not always the case, good undoped a-Si:H is always highly resistive even though somewhat n type. One of the outstanding properties of a-Si:H as an amorphous material is that it can be doped both n- and p-type. As in the case of crystalline silicon, this can be achieved with phosphorous and boron as donors and acceptors, be it with their doping efficiency lower than in crystalline silicon. However, because a-Si:H-based materials have such low densities of midgap defect states, their introduction can readily move its Fermi level away from midgap toward the conduction or the valence band, respectively [4]. This is achieved by introducing phosphine, diborane or trimethyl boron into the silane being used in depositing the a-Si:H. As in the case of crystalline silicon, n-type doping is achieved by incorporating the phosphorous into the materials, and p-type doping by incorporating the boron. However, since their doping efficiencies in a-Si:H are much lower than in the case of crystalline silicon, in order to achieve high conductivities it is necessary to incorporate large densities of these dopants into the material requiring silane dilution of around 1–2% in order to achieve the highest conductivities.

The upper limits in the doping and corresponding conductivities are reached, not only because of the low

efficiency of the dopants, but also for two other reasons. One is that the introduction of the dopants is accompanied by a corresponding creation of defect states around midgap, which then act to form a compensation effect that limits the progress of the Fermi levels to ward the conduction or valence band. The other is the presence of the tail states, whose densities increase rapidly with energy away from midgap, so that once the Fermi levels enter these regions it becomes more and more difficult for them to move toward the conduction and valence bands. As a consequence, the much higher density of states in the tail at the valence than the conduction band is one of the contributing factors to the maximum p-type conductivities being smaller than the n-type conductivities. Doping of the a-SiC:H alloys has also been carried out, where by introducing either diborane or trimethyl boron into the deposition gases, this wider bandgap material could be made p-type and thus be used as a heterojunction contact in a-Si:H solar cells [28]. The creation of the large densities of gap states accompanying the incorporation of the dopants not only inhibits the efficiency of the doping but also drastically reduces the free carrier lifetimes [154, 155]. As a result, because of the very short carrier lifetimes, the doped materials cannot be used as active absorber layers in solar cells.

Instead, in a-Si:H-based solar cells, thin films of either p-type a-SiC:H [28] or p-type protocrystalline Si:H, which have in the past been mistakenly called microcrystalline [72], are used as the p contacts and n-type a-Si:H as the Ohmic contacts. Both the p-type a-SiC:H and the protocrystalline Si:H materials result in excellent window contacts in such cell since both their quasi Fermi levels are located at about the same energies that are close to the valence band of a-Si-H. Part of the reason why the Fermi level in the wider bandgap a-SiC:H is not significantly closer to the a-Si:H valence band is due to its very wide valence band tail which limit its closest position to 0.4–0.5 eV from the valence band. The n-type a-Si: H provides excellent Ohmic contacts to the i-layers since its Fermi level is about 0.2 eV from their conduction band. By incorporating such p-type and n-type materials into p-i-n and n-i-p cells, it is possible to obtain built-in voltages well over 1 volt [156].The use of these thin amorphous p- and n-type contacts, with absorber i layers that have adjustable bandgaps and low densities of deep gap states, offers great flexibility in the efficient absorption and utilization of the different parts of the solar spectrum.

It is also possible to dope μc-Si:H to both n and p by introducing phosphine, diborane, or trimethyl boron into the silane highly diluted with hydrogen. Not surprisingly, because of its predominant crystallinity, the μc-Si:H materials can be doped much more efficiently than amorphous Si:H and its alloys. In the case of n-type doping, the Fermi level can be as close as 50 meV from the conduction band. As a consequence, even though the μc-Si:H bandgap is smaller than that of a-Si:H, the Fermi level is sufficiently close to the conduction band of the a-Si:H so as to form a good Ohmic contact, so it can be used not only in microcrystalline but also in amorphous Si:H solar cells. Unlike doped a-Si:H, the conductivity of doped μc-Si:H material usually increases as a function of the layer thickness while the activation energy of the conductivity decreases. Both values saturate for thickness of typically $\geq$100 nm with activation energies close to 10 meV for n- and p-doped materials being obtained [25].

Light-Induced Degradation

Background and Effect in a-Si:H

The light-induced changes in a-Si:H-based materials, known as the Staebler–Wronski effect (SWE), are still not only of great scientific interest but also of great technological importance because of their effect on the long-term stability of a-Si:H-based solar cells and panels. In the extensively used Si:H tandem solar cells, the top a-Si:H cells produce two thirds of the power. SWE was first observed as the changes due to sunlight in the carrier transport in thin films which were found to be reversible after annealing the materials for a few hours at temperatures at or above ~150°C [8]. These changes were attributed to the introduction of metastable defects whose rate of creation and densities depend on both the intensity of illumination as well as temperature. The reversible changes that occur between an annealed initial state A and a "light soaked" state B have become one of the most investigated phenomena in a-Si:H-based materials and solar cells [157–159]. However, although progress has been made

in obtaining more stable a-Si:H materials, it has been relatively slow as it is the result of primarily empirical approaches which in large part are due to the absence of a definitive understanding of SWE. An example of the light-induced changes observed under illumination with 100 mW/cm^2 of sun light in an a-Si:H film and a cell prepared from undiluted feedstock are shown in Figs. 17 and 18.

Figure 17 shows the now well-known decrease in photoconductivity, which here is generated by the white light, as well as the decrease in the dark conductivity in this slightly n-type a-Si:H film. These were clear indications that light-induced defect states are being created around midgap which increase the recombination of photo-generated electrons and pull the Fermi level down away from the conduction band. Figure 18 shows the large reversible decrease in efficiency, reflecting an increase in the recombination of the photo-generated carriers due to the creation of additional defect states. It should be pointed out here that under 1 sun illumination the gap states that act as recombination centers are not just those around midgap but as much as ~0.5 eV on either side of it.

Though progress has been made in the understanding of SWE, as yet there is still no *general consensus on the exact nature* of the light-induced defect states in a-Si:H or the *mechanism responsible for their creation.* This, to a large part, is due to the complexity associated with the nature of the defects and their gap states, as well as the differences in microstructure of the a-Si:H materials prepared under a wide range of growth conditions. However, there is general agreement that hydrogen, which is critical to the passivation of dangling bonds and determining microstructure, also plays an important role in the creation of the light-induced defects [160, 161].

Because of the widely held view that the gap states due to isolated dangling bonds were the dominant carrier recombination centers in a-Si:H, it was generally accepted that the creation of dangling bonds by light was the principal mechanism responsible for SWE. Furthermore, such a view agreed with the observed increases of the ESR signal associated with the neutral dangling bond, D^o, observed by the Marburg group [125]. So it became generally accepted that the only important light-induced gap states are those associated with this defect [158, 162, 163]. Significant progress was made over the years not only in improving the initial properties of a-Si:H-based materials and cells but also in reducing their light-induced degradation. This was achieved by optimizing the growth conditions for improving the microstructure of the materials as well as optimizing the cell structures.

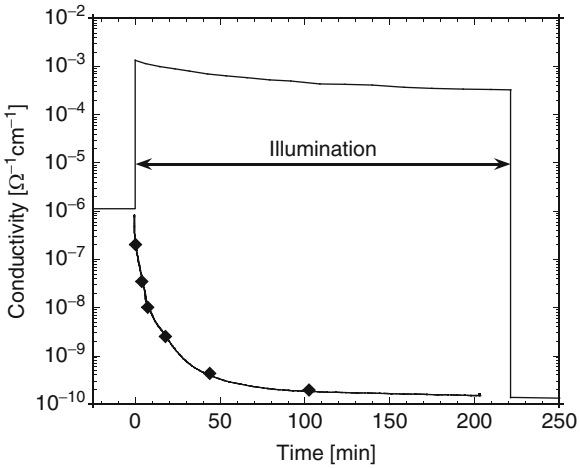

Silicon Solar Cells, Thin-film. Figure 17
Dark conductivity and photoconductivity of an a-Si:H thin film shown as a function of 1 sun illumination time

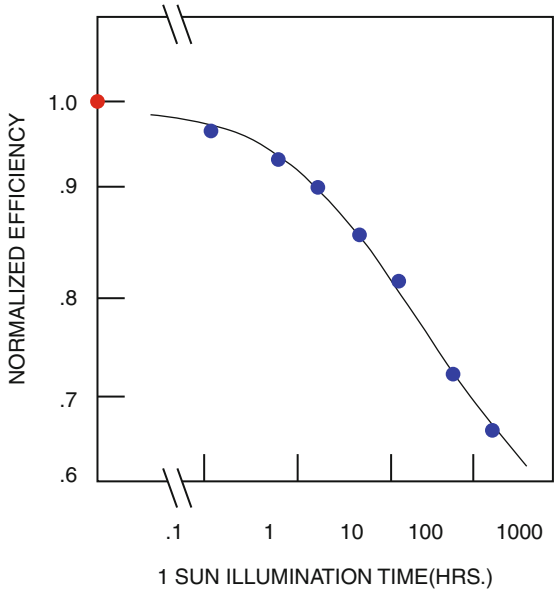

Silicon Solar Cells, Thin-film. Figure 18
Degradation of normalized efficiency in a-Si:H solar cell shown as a function 1 sun illumination time

The development of the dense hydrogen diluted protocrystalline a-Si:H materials, discussed in section "Growth and Microstructure," resulted in solar cells with significantly better performance in the degraded steady state (DSS). In addition, these materials and their solar cells required drastically shorter times to reach a DSS, where under 1 sun illumination at room temperature the DSS was reached in about a hundred hours, as compared to the previous times that were in excess of more than a thousand hours [160, 164]. The significant changes in the degradation of solar cells and films obtained with these new a-Si:H materials is illustrated in Fig. 19. The figure shows the changes in fill factors (FF) of two p-i-n solar cells with 4,000 Å thick i-layers under 1 sun illumination at 25°C. One is with a protocrystalline R = 10 a-Si:H i-layer and the other a cell deposited under the same conditions but with an undiluted R = 0 intrinsic layer. It is noteworthy that despite the large difference in the microstructure of the i layers it is possible to obtain in their initial state the same FF which are excellent for such thickness of the i-layers. This difference in microstructure however is clearly reflected in their degradation kinetics and their DSS resulting from the light-induced changes in their i layers. Not only are the changes in the dense protocrystalline a-Si:H cell much smaller than in the undiluted material but, as indicated earlier the DSS, is reached much more rapidly.

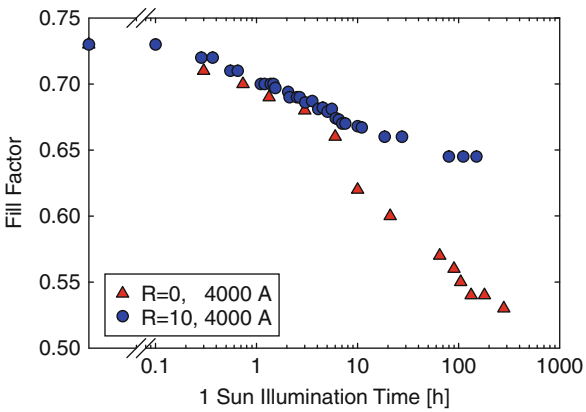

Silicon Solar Cells, Thin-film. Figure 19
Fill factors of 4,000 Å thick p-i-n solar cells with a protocrystalline (R = 10) and an undiluted (R = 0) intrinsic layers under AM.1.5 illumination

The extensive studies characterizing light-induced changes and on understanding the mechanisms responsible for SWE were carried out on thin films. Unfortunately, not only was the vast majority of them carried out on undiluted a-Si:H materials, but this was also accompanied by a striking absence of correlations made between the results on films and those on solar cells. A contributing factor to this was that for these materials the 1 sun DSS at room temperature, which was generally characterized for cells by industry, took around 1,000 h. Because this took such a long time, in the fundamental studies carried out primarily in universities and research laboratories, the experiments were carried out with high illumination intensities in order to achieve the DSS in a reasonable time. This however overlooked the fact that at these high intensities not only were the kinetics different but also the nature of the light-induced defect states were different from those under 1 sun illumination [165]. This absence of correlations between the results of these extensive fundamental studies on films and results on cells also contributed to the absence of systematic approaches being developed for improving the performance and stability of a-Si:H solar cells.

The most widely held view on the origin of metastable defect states is that they are a result of light-induced dangling bonds even though serious questions were raised about them being the sole light-induced states [166]. Nevertheless, the vast majority of the studies on SWE interpreted the results based on the model by Stutzmann, Jackson, and Tsai [162], which is based on the light-induced breaking of weak bonds to create dangling bonds. The $t^{1/3}$ time dependence found for the overall increases in the densities of dangling bonds was key prediction of this model and interestingly enough such a $t^{1/3}$ time dependence was found in a variety of other light-induced changes. However, as in reference [162], the overall increases in the densities of the defects were mistakenly taken to represent the actual creation rate of the light-induced defects and their gap states. There were no such kinetics observed for the changes in solar cells, but this was not too surprising, since those were generally in terms of fill factors, which cannot be directly correlated with the creation of defect states. There were, however, interesting results reported on solar cells, which indicated the presence of at least two types of defect states having

distinctly different creation and annealing kinetics [166, 167]. Similar conclusion was also reached from concurrent results on photoconductivity and subgap absorption [68, 168].

As indicated earlier, there has been a striking absence of correlations between results on films and those on corresponding cells. This has limited the extent to which light-induced gap states could be characterized by not allowing the electron recombination in films to be correlated with the electron and hole recombination in solar cells. In part, this was due to the fact that the light-induced changes in solar cells were primarily characterized with those in FF or efficiencies that cannot be directly related to carrier recombination. However, the recent studies on dense protocrystalline a-Si:H films and corresponding solar cells established direct correlations between the light-induced changes in gap states in films with those in corresponding solar cells. This was obtained from the concurrent correlation of the changes in carrier recombination in films with those of the SRH recombination in solar cells, as well as the direct characterization of the light-induced states with sub-bandgap absorption [128, 137]. In these studies also, the presence of the fast processes in protocrystalline a-Si:H was taken into account in the measurements on both the films and cells. The light-induced changes in the three states described in the previous section were identified from the changes in the recombination kinetics through states in different regions in the gap which was monitored by varying the Quasi Fermi splitting. In the case of the film photocurrents this was carried out by varying the illumination intensity, while in the case of SRH recombination in the cells by applying different forward biases. The changes under 1 sun illumination in the SRH recombination for different Quasi Fermi splitting in a p-i-n cell with a 4.000 Å i-layer are illustrated in Fig. 20 with the changes in the dark forward bias current characteristics that are dominated by the recombination in the bulk of the cell.

It can be seen in Fig. 20 that the rates at which the SRH recombination increases depend on the bias voltage which determines the Quasi Fermi level splitting, thus clearly indicating that the rate at which the gap states increase depends on their location in the gap. It is found that all the three distributions of states, identified from sub-bandgap absorption measurements

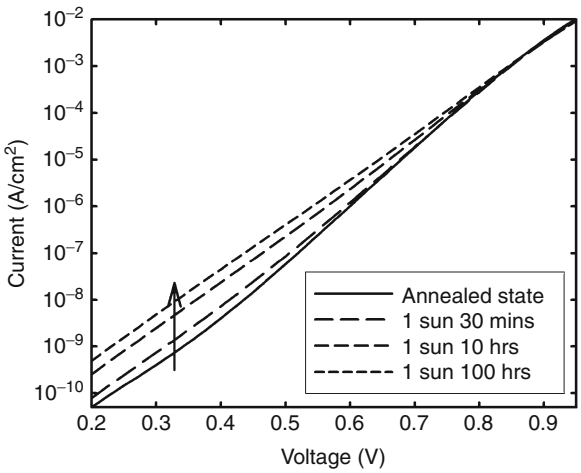

Silicon Solar Cells, Thin-film. Figure 20
The change in the dark forward bias current – voltage characteristics for a protocrystalline p-i-n solar cell with a 4,000 Å i-layer under 1 sun illumination

[128] and discussed in the previous section, exhibit two distinct regimes in their light-induced changes with a transition in the kinetics after 1–2 h of 1 sun illumination. In the case of the A and B midgap states, their densities increase with the extensively reported $t^{1/3}$ relation covering the limited period of 1–2 h before a transition into kinetics that lead to the DSS. In the case of the B states, there is a significant reduction in the rate of their increase, while in the case A states there is virtually no longer any increase. This absence of any further increase in the density of the A states points to them as being the so called "fast" states that anneal out rapidly even at room temperature [167]. The light-induced change in the non-midgap C states, obtained from both SRH and subgap absorption, is distinctly different from that of the A and B states. In contrast to the rapid increase in the midgap states during the first 1–2 h there is no change in the density of the C states before increasing at a slow rate very similar to that of the B states. From the results on the recombination kinetics, it is found that the A and B states are efficient electron and poor hole recombination centers, thus having a large effect on the photoconductivities of the films over a wide range of illuminations. On the other hand, the C like non midgap states are inefficient electron recombination centers. However, more importantly, they become very efficient hole recombination

centers under Quasi Fermi level splitting, such as occurs with 1 sun illumination [169].

Since the performance of the a-Si:H solar cells is limited by hole transport, these C like non midgap states, and not the midgap states, are key to solar cell operation under 1 sun illumination. That this is indeed the case is clearly illustrated in Fig. 21 where the change under 1 sun illumination is shown for the 1 sun fill factor, together with the changes in the SRH recombination currents for just the midgap as well when the C like states act as recombination centers.

Figure 21 shows that in the first hour or so there is a rapid fivefold increase in the SRH recombination through the A and B states enclosed by a Quasi Fermi splitting of 0.4 eV. When the C states are also included as recombination centers with a Quasi Fermi splitting of 0.6 eV, the overall recombination current remains unchanged during this time. It can be seen also that during this period the fill factor changes very little which is consistent with the A and B states not being efficient hole recombination centers. However, on the other hand, the fill factor begins to seriously degrade with the onset of the increase in recombination resulting from the C like non midgap states clearly reflecting their key role in the degradation of the solar cell. The inability to identify and characterize these *non-midgap states with their large hole capture cross sections* has been a serious impediment to the understanding not only of SWE but also its contribution to solar cell degradation.

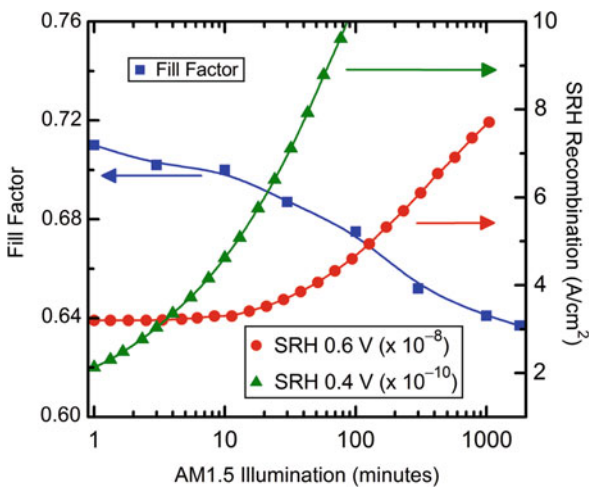

Silicon Solar Cells, Thin-film. Figure 21
Changes under 1 sun illumination in the 1 sun fill factor together with the corresponding SRH recombination currents with 0.4 and 0.6 V forward bias (Quasi Fermi splitting)

In these studies, it was also shown that, as has generally been done, it is not valid to take the $t^{1/3}$ time dependence of the increases in gap states to also represent creation kinetics of just the light-induced states. It was conclusively shown that when the contribution of the initial states is taken into account, the rate at which the light-induced midgap states are being created actually has a $t^{1/2}$ time dependence [170]. Another recent important finding has been that in the protocrystalline a-Si:H, whose microstructure is dominated by hydrogen passivated divacancies, the position in the gap of the three identified distributions of states is similar to that of the gap states associated with divacancies in crystalline silicon [94, 169].

In view of these important experimental facts described here, it may be concluded that even the most advanced models describing SWE [162, 171] do not reveal the correct kinetics for the fast A states but also exclude the presence of more than one metastable defect state. One should note that this kinetics may vary considerably between samples deposited by different deposition techniques or under distinct deposition regimes. One of the reasons for this is that the microstructural view of a-Si:H network has been limited to its treatment as a CRN. In this treatment the isolated dangling bond and the randomly distributed isolated hydrogen are the only entities considered as defect sites and hydrogen emission sites, respectively. However, it has been shown recently that hydrogen passivated divacancies are the dominant entities in dense a-Si:H. Since it is believed that the origin of the SWE is related to a redistribution of a small fraction of bonded hydrogen in the material, the entity of a not fully hydrogenated divacancy in a disordered network is an interesting configuration to be considered as possible native or metastable defect site. This and the $t^{1/2}$ time dependence for the creation of the midgap states are new and powerful insights into identifying the mechanisms for the creation of metastable defects [94].

Light-Induced Degradation in μc-Si:H Materials

From the early work on intrinsic μc-Si:H layers for solar cells, the material was assumed to be rather stable

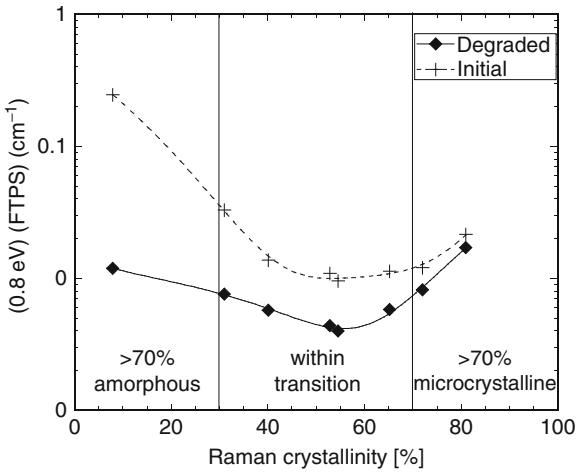

Silicon Solar Cells, Thin-film. Figure 22
Absorption coefficient at 0.8 eV in the annealed and degraded (light-soaked) state as measured by FTPS for a series of μc-Si:H p-i-n cells with various Raman crystalline fractions (After [174])

upon light soaking [172]. In fact, as seen in Fig. 22, small increases in the absorption coefficient at 0.8 eV (which is used to monitor defect density in μc-Si:H as discussed in section "Optoelectronic Properties") correspond to increases in the deep defect state densities by a factor of about ~2. As the amorphous phase faction is increased, the degradation of the material become more and more important as it approaches that of pure a-Si:H [173, 174]. Light-induced degradation kinetics as well as the defect annealing is found to be similar to those of a-Si:H. These observations suggest that the light-induced degradation of μc-Si:H is completely due to the metastability of the amorphous tissue. As best μc-Si:H solar cells are obtained with devices in which there is a significant fraction of amorphous phase present, light-induced degradation still remains an important issue even though its effect is considerably less than that in a-Si:H.

Solar Cells

Principles of Cell Operation

The operation of all solar cells is based on common physical principles. However, efficient a-Si:H-based solar cells rely on material properties that are different from those of crystalline Si, the mechanisms which determine and limit their energy conversion have to be briefly reviewed. There are two important differences between a-Si:H and crystalline silicon solar cell operation. The first, which is a serious disadvantage, is that the diffusion lengths of both carriers in a-Si:H are much shorter than in crystalline silicon so that the efficient collection of the photo-generated carriers now relies on their drift in the presence of an electric field. The other, which is an important advantage, is the high optical absorption a-Si:H that is similar to that found in semiconductors with a direct bandgap. This optical absorption, resulting from the absence of conservation of momentum requirement due to its disordered nature, is in contrast to that of crystalline silicon which has the low optical absorption associated with its indirect bandgap. Such high optical absorption is key in helping to overcome the limitations on the collection of photo-generated carriers, imposed by their low mobilities and lifetimes, by allowing less than a micron thick solar cell structures to be used. In order to take advantage of the superior properties of the intrinsic (undoped) a-Si:H and a-SiGe:H materials, p-i-n and n-i-p heterojunction cell structures are used rather than the classic n/p structures in crystalline silicon. Normally, the p-i-n cell structures are TCO-p (a-SiC:H) – i(a-Si:H, a-SiGe:H) – n(a-Si:H, *μc*-Si:H) [175] and the n-i-p cells are n(a-Si:H, μc-Si:H) – i(a-Si:H, a-SiGe:H) – p(protocrystalline -Si:H)-TCO [176] where TCO is a transmitting oxide like tin or zinc oxide. In both these cases, the built in potentials in excess of 1 volt are obtained across the cell with heavily doped *n* and *p*-layers serving as an Ohmic and a window p contact, respectively. Because of the low densities of midgap states the space charge densities in the junction are sufficiently low as to allow the electric fields across the *i*-layers of the cells to be uniform and in excess of $\sim 10^4$ V/cm. In Fig. 23 energy band diagrams are presented for a p(a-SiC:H) – i(a-Si:H) – n(a-Si:H) solar cell with an 0.32 mm thick i-layer which is schematically illustrated in Fig. 23a. These energy band diagrams are simulated using the numerical model AMPS 1-D [177] with a gap state distribution in the i-layer similar to that in Fig. 15b. Figure 23b shows the cell in thermodynamic equilibrium (no illumination and zero bias). Figure 23c shows the band diagram for the cell at the "*maximum power point*" on its light I-V characteristic under AM1.5 illumination as well as

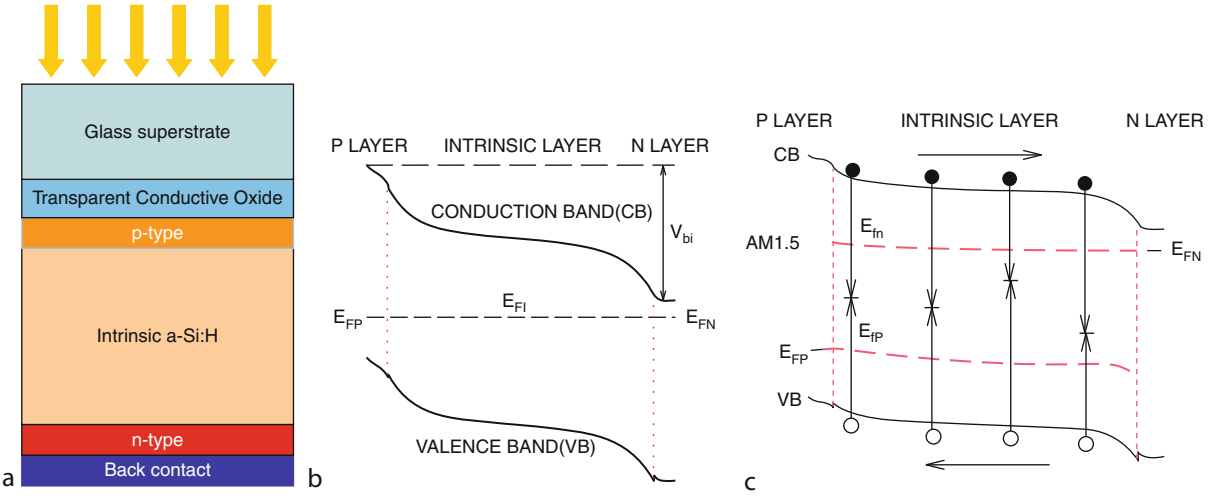

Silicon Solar Cells, Thin-film. Figure 23

(**a**) Schematic view of a p-i-n solar cell with a 320 nm thick p(a-SiC:H)-i(a-Si:H)-n(μc-SI:H) cell (**b**) Energy band diagram of cell in the dark and under zero bias with the built-in potential, V_{bi}, being indicated (**c**) Energy band diagram of cell under AM1.5 illumination under load at maximum power point. Also included are the different recombination paths for volume absorbed photo-generated carriers

the corresponding recombination paths for the photo-generated carriers. The diagrams in Fig. 23 were calculated for an a-Si:H i-layer with a mobility gap of 1.76 eV, and 10^{16} cm^{-3} density of midgap states contributing to the space charge in the i layer.

The built-in potential, which is determined by the separation of Fermi levels E_{FP} in the *p* and E_{FN} in *n* contacts, is in this case 1.3 V. This is reflected in Fig. 23b as the band bending across the i-layer and the electric field is clearly large as indicated by the gradient of this band bending. Built-in potentials like this not only allow high values of V_{oc} to be obtained but also result in built-in electric fields greater than 10^4 V/cm across cells with *i*-layers less than 1 μm thick. It should be pointed out here that the band diagrams in Fig. 23 represent solar cells with *i*-layers composed of high-quality materials such protocrystalline a-Si:H in an optimized cell structures where p/i interface recombination has been minimized. Only in such cell structures is it possible to directly relate carrier recombination under forward bias both in the dark as and under illumination, as well as other cell characteristics, to bulk properties of the *i*-layers [178].

Unfortunately, for one reason or another, over the years the majority of studies investigating a-Si:H solar cell operation and cell properties were carried out on cell structures that at the time were seriously limited by having high p\i carrier recombination; as well as by the complex defects present in undiluted materials with significant numbers of nano-voids and poly-vacancies. Consequently, in such cases, attempting to relate cell operation to the properties of the bulk *i*-layers could easily lead to erroneous conclusions about the operation of a-Si:H solar cells [179, 180]. Rather than relying on examples with numerical modeling to explain a-Si:H solar cell operation, as is often done, even though it relies on many adjustable parameters [175], the short circuit current(J_{sc}); the open circuit voltage (V_{oc}); and the fill factor (FF) are addressed here in a manner that can be related to the operation and characteristics of the well-understood cell parameters in crystalline solar cells [181].

As is well known, J_{sc} is determined by the number of free carriers generated in the cell by sunlight and the efficiency in collecting both the electrons and holes. In the case of the a-Si:H cells, this corresponds to the number of photo-generated carriers in the *i*-layers, which depends on the number of photons absorbed in these layers. This number is equal to $N_o[1-\exp(-\alpha(\lambda)d)]$ where N_o is the flux of photons entering

the i layer, $\alpha(\lambda)$ is the optical absorption at a wavelength λ, and d is the thickness of the i layer. In order to maximize N_o for illumination incident onto the p layer with a TCO contact, it is desirable to have low reflection at the TCO/p interface where this is obtained with the two oxides that are generally used, To minimize the absorption in the p contacts because they are "dead" layers from which no photo-generated carriers can be collected, their thickness is limited to about 100 to 200 Å, as well as in the case of a-SiC:H taking advantage of its wider bandgap material.

It can be seen from the relation for absorption in the i layer that the absorbed fraction of the incident photons increases with $\alpha(\lambda)$ and d, so these are made as large as possible within the constraints that are imposed by the material properties on the different cell parameters. The $\alpha(\lambda)$ can be increased by decreasing the bandgap of the a-Si:H but this leads to a tradeoff which lowers maximum open circuit voltage that can be achieved with the a narrower bandgaps. The other approach is to increase the thickness of i-layers. However, such increase is seriously limited by the ability to generate an electric field across the i-layers that is necessary to collect the photo-generated carriers having the low electron, and in particular hole mobilities and carrier lifetimes. Since the efficient collection of photo-generated carriers depends on their drift in an electric field, it is necessary for their average transit time across the i-layers, t, be shorter than their recombination lifetimes [181]. Such field-assisted carrier collection, however, is very sensitive to the thickness of the *i*-layer, d, being approximately proportional to $1/d^2$ rather than 1/d. This makes it difficult to maintain efficient carrier collection in i-layers that are made thicker in order to increase the amount of sunlight absorbed in a cell, The decrease in electric field and carrier collection has an effect not only on J_{sc} but even more so on the FF, since under load (forward bias) the fields are significantly reduced.

A major breakthrough in achieving thin, high-efficiency cells was obtained with the development of optical enhancement based on textured substrates and reflectors [35, 36]. Such large optical enhancements arise from the large angle scattering caused by the texture that results in multiple, internal reflections, which allow weakly absorbed light to undergo many passes through the i-layer. This, in effect, greatly increases the optical absorption at longer wavelengths so that correspondingly higher quantum efficiencies can be obtained without any increase in the cell thickness. An example of improvements that can be obtained in the spectral response at the long wavelengths using different reflector on p(a-SiC:H) – i(a-Si:H) – n(a-Si:H) cells is shown in Fig. 24 for the two (Cr, Ag) flat metal and the two textured (detached, tuned) reflectors from the original work by Deckman, Wronski, and Yablonovitch in 1984 [35].

It is important to note that in the example shown here for an a-Si:H i-layer it is possible to increase the quantum efficiency at a wavelength of 0.7 μm from about 10% to 60% of the maximum value at 0.55 μm. Using textured substrates, it is now possible to obtain short circuit currents of up to 18 mA/cm^2 with a-Si:H cells having a bandgap of ~1.8 eV and *i*-layers that are of only between 2,000 and 3,000 Å thick [182].

In a discussion of J_{sc}, the losses in the photo-generated carriers in the p/i interface regions should also be included. They are sensitive to the nature of these regions and result primarily in reducing quantum efficiencies at the short wavelengths. Accordingly, the p/i interface regions have to be optimized by reducing their carrier recombination, which has beneficial effects not only on J_{sc} but more importantly on V_{oc}.

In the crystalline solar cells, the 1 sun open circuit voltage is viewed as the Quasi Femi level splitting achieved with the illumination or alternatively when the forward bias current becomes equal to J_{sc} [181]. In both cases, the bandgap and the built-in potential play a key role as well as the carrier recombination in the dark and under illumination. When the V_{oc} is addressed in terms quasi Fermi level splitting it is much more difficult to quantify and this does not yield any information about the contributions of p/i interface recombination which can be a significant factor in limiting V_{oc}. This was recognized early on and led to an approach for improving the p/i interface regions which was based on the introduction of a wide variety of empirically derived "buffer" layers [183–185]. In those cases, however, no systematic optimization of V_{oc} was possible, as the real reasons for the improvements were not identified nor the changes in the recombination in the p/i regions quantified. More recently, Lee et al. [186] showed that significant improvement in V_{oc} could be obtained in

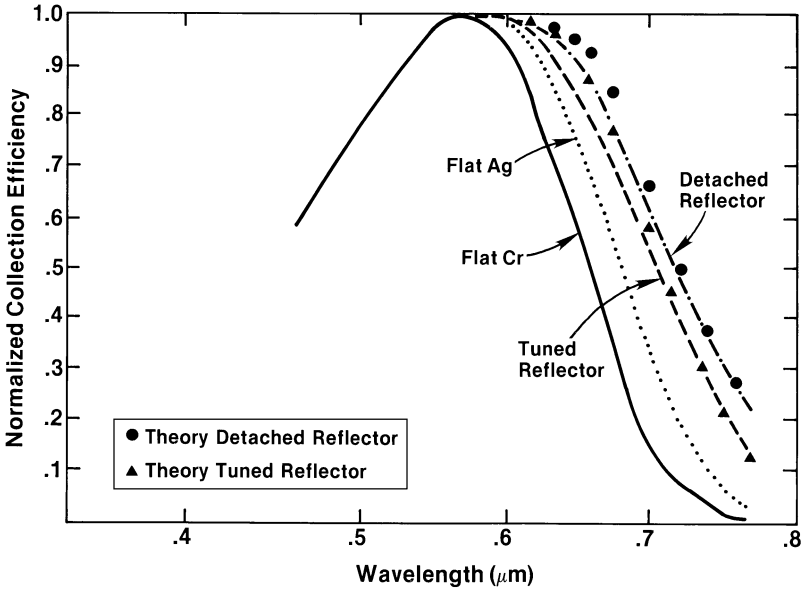

Silicon Solar Cells, Thin-film. Figure 24
The experimental results for the collection efficiency as a function of wavelength for an a-Si:H p-i-n solar cell with flat Cr and Ag reflectors. The results are normalized to the peak quantum efficiency at 0.55 μm. Also shown as symbols are the theoretical results for a tuned and a detached reflectors

protocrystalline p-i-n cells with just the introduction of more highly diluted a-Si:H thin layers as the p/i interface regions.

Although the contributions of p/i interface recombination to the dark J_D-V characteristics and 1 sun open circuit voltages were identified [187], initially its adequate separation and characterization was limited by the current understanding of the dark forward J_D-V characteristics. At the time J_D-V was characterized in terms of a bias independent diode quality factor, n, rather than the bias dependent, n(V), which can have values between 1 and 2. Taking this into account, a clear separation was subsequently obtained between the bulk and interface recombination in cell structures, which was based on theoretical considerations by Deng and Wronski [178]. Example of this is illustrated in Fig. 25 with the results on cell structures in which the protocrystalline i-layers were deposited in a two-step process [188]. In the figure, the J_D-V characteristics are shown for two p(a-SiC:H)-i-n cell structures with a 4,000 Å R = $[H_2]/[SiH_4]$ = 10 i- layer and 200 Å p/i interface layers of R = 40 and undiluted R = 0. In these cell structures the R = 40 layer thickness was thin enough as not to have a transition into the (a + μc) mixed phase, which would significantly increases the p/i interface recombination.

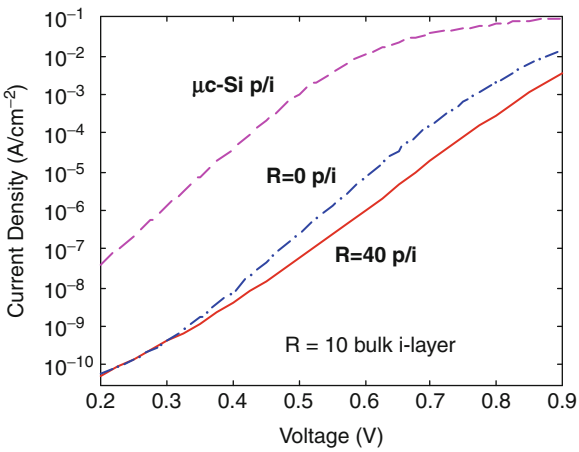

Silicon Solar Cells, Thin-film. Figure 25
Dark J_D-V characteristics for cells with the same 4,000 Å bulk R = 10 i-layers but with 200 Å p/i interface layers which are R = 40 and R = 0 in p-i-n cells and microcrystalline in corresponding n-i-p cell

In the case of the cell with R = 40 p/interface, very low recombination is present in the p/i interface region

because of the wider bandgap, high quality protocrystalline R = 40 a-Si:H region. In this case, the currents are dominated by bulk recombination over almost the entire voltage regime, which is reflected in their low current densities. In the cell with the R = 0 p/i interface, on the other hand, there is significantly higher recombination in this interface region due to the narrower bandgap and inferior quality of the R = 0 layer. As a consequence this recombination can supersede that of the bulk and results in the higher currents seen in Fig. 25. This increase in recombination at the p/i interface reduces the 1 sun V_{oc} from 0.93 V in the R = 40 cell to 0.84 V in the R = 0 cell. It is important to note in Fig. 25 that the higher currents in the R = 0 cell are present only for forward biases larger than ~0.3 V at which point the contributions from the R = 0 p/i interface recombination dominate the predicted bias dependence of n(V) that is different to that of the bulk [178]. The excellence of such R = 40 p/i interfaces was further confirmed by including them in p(a-SiC:H) – i - n cells with R = 0 i-layers. In that case, the interface recombination was sufficiently low, relative to that of the bulk; therefore, as is the case with crystalline Si solar cells, it was possible to obtain a thickness dependence of the 1 sun V_{oc}.

Also shown in the Fig. 25 is the J_D-V characteristic, for a corresponding n-i-p(a-SiC:H) cell in which now a 200 Å microcrystalline layer was inserted as the p/i interface layer. In this case, the carrier recombination is dominated by that p/i interface recombination over the entire voltage regime exhibiting the predicted n(V) as a bias independent value close to 1. In this cell, the microcrystalline p/i interface recombination reduces the 1 sun V_{oc} from the 0.93 V of a R = 40 p/i interface to ~0.6 V. In this case, not only are the currents much larger right from the beginning but also exhibit a very rapid increase with voltage which corresponds to the expected constant n(V) equal to 1.

It was important to include the results for the microcrystalline p/i interface layer here not only as it has a direct bearing on microcrystalline solar cells but also because the result runs counter to the claims that the very high 1 sun V_{oc} in a-Si:H n–i-p cells is obtained with microcrystalline silicon p-layers [189–191]. This apparent contradiction was however clarified in the studies on (a-Si:H) n-i-p solar cell structures with highly diluted p-Si:H layers that were characterized with in situ spectroscopic ellipsometry [176]. In these studies, where the contributions of the recombination at the p/i interfaces to the forward bias dark current characteristics were identified and quantified for the different p-Si:H layers, it was found that the lowest p/i interface recombination is obtained with protocrystalline p-Si:H layers having no microcrystalline component. The high V_{oc} results with p-Si:H layers is attributed not only to its protocrystalline nature but also to a beneficial subsurface modification of the p/i interface regions resulting from the high hydrogen dilution and power used in the deposition of these p-layers. The investigations by Guha et al. [189] were handicapped in that they were not aware of protocrystallinity in hydrogen diluted a-Si:H films and the evolution of their microstructure. It appears that the wrong conclusion was reached due the difference in thickness of the very thin p-layers used in the solar cell evaluation where the layers were still amorphous as compared to the much thicker layers used to characterize the microstructure layers that had evolved, so as to contain the microcrystalline phase. This evolutionary nature of the hydrogen diluted Si:H becomes even more critical for a-Si:H p-i-n cells since any transition into an (a-μc) phase occurs at the p/i interfaces thus introducing large carrier recombination that can seriously limit the 1 sun $V_{oc.}$

Another misconception that was recently clarified about the nature of a-Si:H solar cells is the assertion that it is not possible to relate carrier recombination in the dark with that under illumination. This conclusion was based on the absence of superposition between the dark forward bias current (J_D-V) and the short circuit current versus open circuit voltage, (J_{sc}–V_{oc}), characteristics found for a variety of cell structures [179]. A possible reason for this could be that unlike in crystalline solar cells, there is a difference between the diffusive carrier transport in the dark as compared to the drift transport of photo-generated carriers. However, in the studies carried out on solar cell structures, where bulk properties were clearly identified, superposition of the forward bias dark current – voltage and the short circuit current – and open circuit voltage characteristics was obtained over wide range of illumination intensities. This is illustrated in Fig. 26 with the results of J_D-V and J_{sc}–V_{oc} characteristics obtained with p-i-n

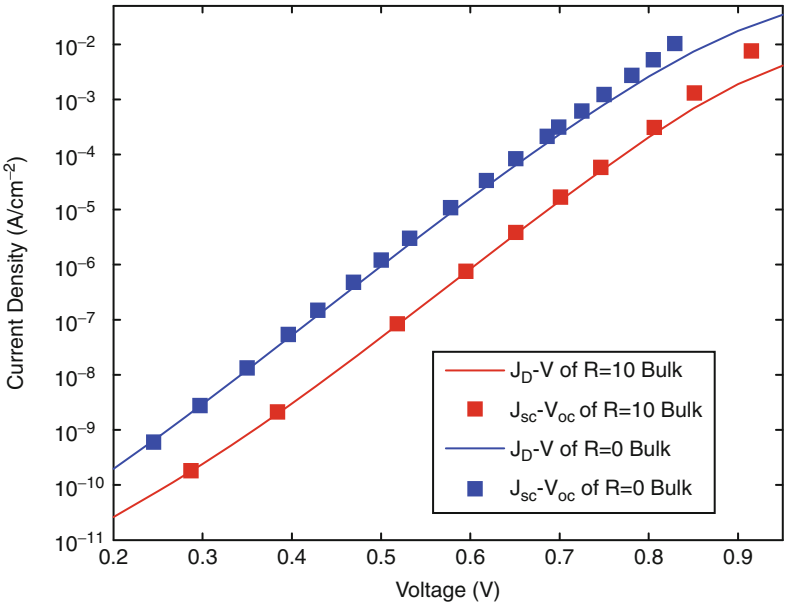

Silicon Solar Cells, Thin-film. Figure 26
J_D-V and J_{sc}–V_{oc} characteristics of p-i-n cells with R = 0 and R = 10 4000 Å i-layers

cells where one has an undiluted R = 0 and the other a protocrystalline R = 10 4,000 Å i-layer.

The results in Fig. 26 show the superposition of these characteristics over extended current voltage regimes. The superposition and the observed separation between the two characteristics at the high voltages are due to the potential barriers at the contacts V_n and V_p which are consistent with arguments that were based on first principles for explaining the J_D–V characteristics such as in Fig. 25. It should be pointed out here that superposition of the two characteristics occurs even after the introduction of light-induced defect states. In this case, however, the separation occurs at lower biases because of the higher potential barriers at the contacts due to the higher densities of defect states, particularly of those away from midgap The presence of very large values in V_n and V_p can move the separation to such low values of bias as not to allow superposition to be observed which would then explain the misconception [179].

The most difficult cell parameter to quantify in terms of the junction and material properties is the FF. This is because unlike J_{sc}, where the electric field, E, is at its maximum value across the cell, the light I-V is generated under forward bias. Such an ever decreasing E is reduced to quite small values at the maximum power point as can be seen from the small band bending across the bulk of the i-layer in Fig. 23. It is also important to realize that in order to obtain the high FFs discussed in section "Light-Induced Degradation," it is necessary to collect the photo-generated carriers efficiently even when E decreases to these small values. As a consequence, the FF is the cell parameter which is most sensitive to the cell thickness as well as the densities and types of states in the gap, since they determine the carrier lifetimes and their space charge the uniformity of the electric fields across the bulk *i*-layers. In addition, E depends on both the built-in potential V_{BI} and the potential barriers V_n and V_p, even though the latter are relatively small, since E across the bulk is $V_I = (V_{BI}–V_p–V_n)/d$ where d is essentially the thickness of the i-layer.

As indicated in the discussion of J_{sc}, collecting the photo-generated carriers is very sensitive to increases in the cell thickness, which makes the FF even more sensitive to the thickness d. This is illustrated in Fig. 27 which shows the measured light I-V's for p(a-SiC:H) – i(a-Si:H) – n(μc-Si:H) cells with protocrystalline i-layer thicknesses of 5,000 and 3,000 Å. It is interesting to note that in the case here, the carrier collection under short circuit conditions remains efficient for both thicknesses, as in these cells which did not rely on

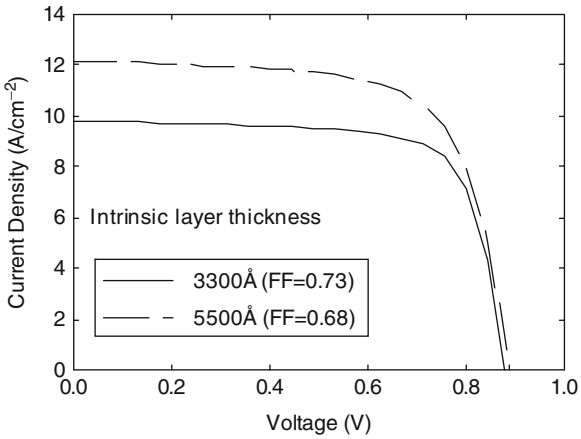

Silicon Solar Cells, Thin-film. Figure 27
Current–voltage characteristics under AM1.5 illumination for a-Si:H p-i-n solar cells with 5,000 and 3,000 Å i-layers

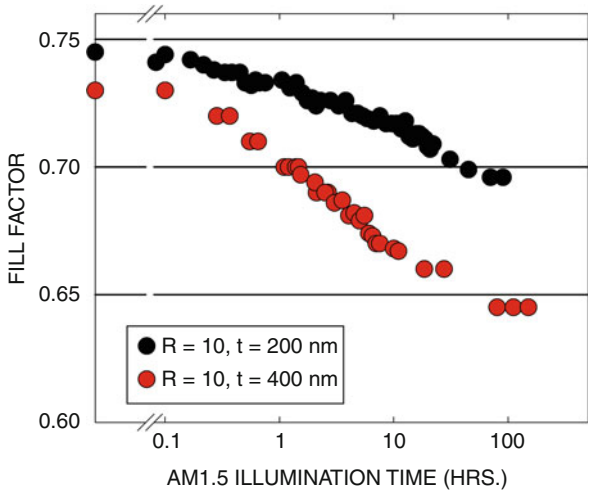

Silicon Solar Cells, Thin-film. Figure 28
1 sun degradation to a degraded steady state at 25°C of two protocrystalline p-i-n solar cells with 4,000 Å and 2,000 Å i-layers having virtually the same excellent initial fill factors

optical enhancement there is a corresponding increase of J_{sc} with thickness. However, the increased thickness lowers significantly the effective collection under load (forward bias) so as to reduce the FF from 0.73 to 0.68.

As was pointed out in section "Light-Induced Degradation," the important values of FFs are not in the initial state but in the DSS. Unfortunately, as was seen in that section, unlike in the case of J_{sc} and V_{oc}, there is significant degradation in the FFs under 1 sun illumination. This is even in the case of the dense protocrystalline cells which results in corresponding losses in the efficiencies of the cells. This degradation of FF is of course due to the introduction of the light-induced states whose effect is not only to reduce the carrier lifetimes but also to increase the space charge that distorts the uniformity of the electric field across the i-layer. There is also an increase in both V_n and V_p, due to the light-induced states away from midgap which then reduces the field across the bulk of the i-layer. Because of these effects, there are large differences in the FF attained in the DSS with changes in thickness, even in cells that initially have virtually the same excellent FFs. This is illustrated in Fig. 28 with the results on two protocrystalline p-i-n cells, one with a 4,000 Å and the other with a 2,000 Å i-layer, that are degraded with 1 sun illumination. Whereas, the initial FF of the 4,000 Å cell is 0.735 and of the 2,000 Å cell 0.745, after degradation to a DSS they exhibit the very large difference of being 0.65 and 0.70, respectively.

In summary, the limitations on the operation of a-Si:H solar cells imposed by the low nobilities of the free carriers are compensated to a large degree by the high optical absorption and the low space charge densities in the i-layers that allow the electric fields to sweep out the carriers before they recombine. However, both the recombination lifetimes and the electric fields depend strongly on the densities and types of the defect states. The introduction of light-induced gap states associated with SWE still remains a serious problem since this limits the thicknesses of the cells in which the photo-generated carriers can be collected sufficiently well so as to yield high fill factor values. The application of optical enhancement has been very helpful in addressing this problem and it is highly desirable to continue further developing this approach.

The main advantage of μc-Si:H for solar cell is the much better light-induced stability as observed in Fig. 29 [172]. Even under very high illumination levels, stable operation of the solar cell without any light-induced degradation can be obtained. Compared to a-Si:H, the lower gap of μc-Si:H leads to both a smaller open circuit voltage and higher short circuit current. μc-Si:H device structure is similar to those of a-Si:H using p-i-n diode configurations. However, the much lower absorption coefficient of μc-Si:H

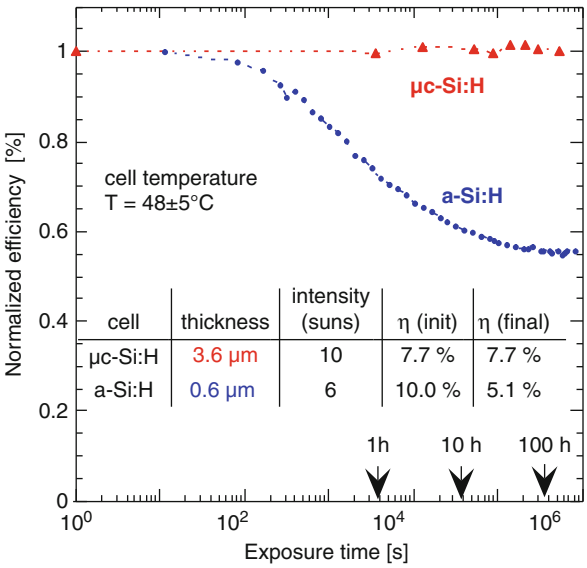

Silicon Solar Cells, Thin-film. Figure 29
Single-junction a-Si:H and μc-Si:H cell normalized efficiency as a function of time upon light soaking with high pressure sodium lamp illumination of 6 and 10 suns, respectively (After [172])

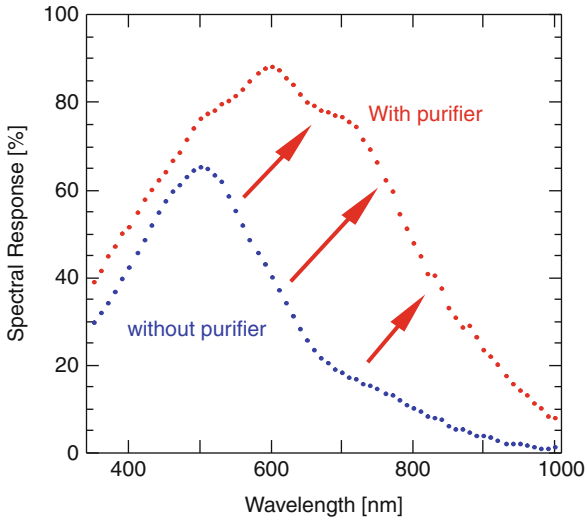

Silicon Solar Cells, Thin-film. Figure 30
External quantum efficiency (at a bias voltage of 0 V) as a function of wavelength for two similar single-junction p-i-n solar cells with the intrinsic layer deposited with or without a process gas purifier (After [51])

compared to a-Si:H (cf. Fig. 12), due to the indirect bandgap of crystalline silicon, requires a much thicker intrinsic layer in order to absorb most of the incoming sunlight. Therefore, light-trapping schemes have to be implemented to keep the device thickness as thin as possible and achieve optimum carrier collection. In μc-Si:H cells, the FFs are usually found to decrease linearly with increasing cell thickness which leads to a broad optimum of efficiency as a function of cell thicknesses between 1 and 3 μm [192]. While carrier collection in a-Si:H p-i-n device relies only on drift processes, in the case of μc-Si:H cells diffusion process also have a role [193]. In μc-Si:H cells, the internal electric field is considered to be localized at the grain boundaries, thus requiring diffusion driven transport within the grains for the collection of the photo-generated carriers.

As discussed in section "Optoelectronic Properties," oxygen (as incorporated during growth or from post-deposition oxidation) has a detrimental effect on the material transport properties. It shifts the Fermi level much closer to the conduction band and significantly reduces the carrier collection. This effect is illustrated in Fig. 30 by the fact that a μc-Si:H cell deposited without a gas purifier, and therefore with significantly higher oxygen impurities incorporated into its intrinsic layer, exhibits much lower external quantum efficiencies for wavelengths above 600 nm [51, 172]. Studies have shown that oxygen concentrations above 2×10^{19} cm^{-3} contribute to very large reductions in μc-Si:H cell performance [52]. A similar effect of impurities is also present in the case of a-Si:H cells but to a much smaller degree. Other impurities coming from the reactor cleaning/etching gas are also found to affect μc-Si:H cell performance [53].

Defects in the μc-Si:H material also play an important role in carrier collection and cell efficiency. Relatively good correlation has been found between the transport properties as given by $\mu^0\tau^0$ (see section "Optoelectronic Properties") and the efficiencies of both a-Si:H [132] and μc-Si:H cells [150]. In the case of the latter, a clear correlation is also found between the open circuit voltages and the defect densities (cf. Fig. 31) for both p-i-n and n-i-p cells [194].

As expected from a comparison between Figs. 28 and 29, the stability of μc-Si:H cells depends on the crystalline volume fraction. Results are shown in

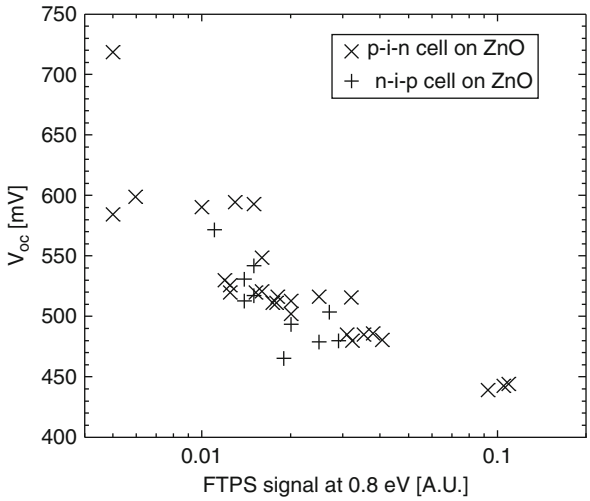

Silicon Solar Cells, Thin-film. Figure 31
Open circuit voltage V_{oc} for various single-junction p-i-n solar cells in both p-i-n and n-i-p configuration as a function of absorption coefficient at 0.8 eV (in arbitrary units, as measured by FTPS). These cells also exhibit a wide range of crystalline volume fraction f; with high V_{oc} obtained in cells having a large amorphous material fraction (After [194])

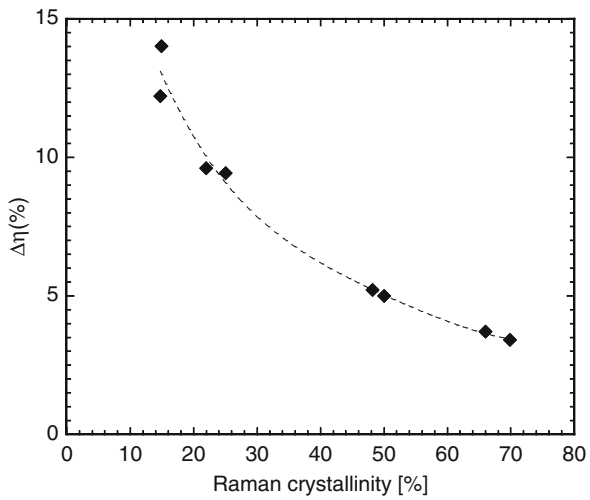

Silicon Solar Cells, Thin-film. Figure 32
Relative efficiency degradation of μc-Si:H solar cells upon light soaking as a function of Raman crystallinity factor (After [195])

Fig. 32, which illustrate how there is a systematic decrease in the light-induced degradation of the solar cell with the increase in the crystalline volume fraction of the intrinsic layer [195].

Cell Optimization and Optical Enhancement

As was seen in the first part of this section, the photogenerated current of a cell increases with an increase of the intrinsic layer thickness. At the same time, however, such an increase leads to a larger light-induced degradation of the cell efficiency (driven mainly by a loss in short circuit current and fill factor). In order to maximize the efficiency, a cell should be electrically thin (to minimize light-induced degradation) and optically thick (to maximize photon conversion). This is obtained by the introduction of light trapping or optical enhancement schemes in the thin film solar cells which allow increases in the optical paths while still maintaining a thin intrinsic layer. In the case of p-i-n cells, such schemes involve the use of rough TCO and back contact optical reflector. The structure of such a device is shown in Fig. 33. In the case of μc-Si:H cells, the need for an electrically thin device is much less important than in the case of a-Si:H cells due to the higher stability of the material, which in principle should compensate for the low optical absorption coefficient of the μc-Si:H relative to a-Si:H. However, there is a constraint on the thickness of the μc-Si:H layer placed by the deposition time acceptable (for economical reasons), which still makes light trapping for this type of cell of paramount importance. Theoretically, for the sun light spectrum, an optical thickness increase by a factor of 10 results in a current gain of 52% for a 300 nm thick a-Si:H cell and by 90% for a 1 μm thick μc-Si:H cell [196]. Such optical thickness increases can be achieved in practice for state-of-the-art device.

Typical examples of rough TCO, as used in thin-film Si solar cells, are shown in Fig. 34. Roughness of the films is obtained either directly with the deposition process or can be obtained by subsequent processing of the deposited layers. Most commercially available solar cells are deposited on SnO_2-coated glass. The process is carried out by atmospheric pressure CVD either inline during the float glass fabrication or off-line. Recent advances in TCO development include ZnO deposited

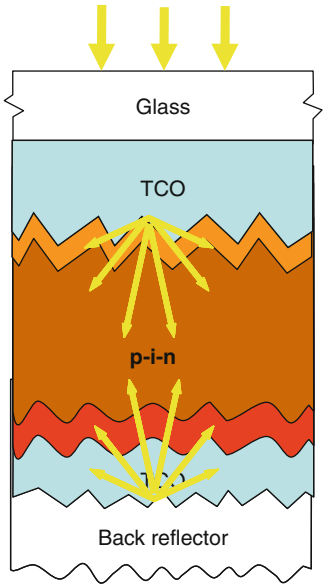

Silicon Solar Cells, Thin-film. Figure 33
Schematic view of the light trapping scheme in p-i-n solar cells with a rough front TCO layer that diffuses the light in the absorber intrinsic layer, and a back reflector for infrared light

by low-pressure CVD (LP-CVD), which leads to a pyramidal shaped surface morphology [197] as well as texture etched sputtered ZnO [198]. In the latter case, texturization of the surface is obtained by a wet chemical etching of the layer which creates a crater like morphology. Alternative rough substrates for p-i-n cells are obtained by the deposition of flat TCO layers on textured glass. For this approach, textured surfaces can also be implemented on flat glass by the texturing (using replication techniques) of optical glue deposited on the glass [199]. In the case of the n-i-p devices, where there is no need for optically transparent substrates, the range of possibilities is much broader since there is no need for optically transparent substrates, so a larger variety of other choices is possible. Possible solutions include the use of rough Ag layers deposited on a flat substrate [200] as well as hot embossed plastic substrates [201].

Optimization of the front TCO layer which allows the illumination enter the device is a nontrivial task. This layer should be optically transparent for the spectral sensitivity range of the device, highly conductive to limit serial resistance and exhibit large surface roughness for high optical enhancement. Sufficiently high conductivity is obtained by doping the layers with fluor in the case of SnO_2 or with aluminum or boron in the case of ZnO. However, high doping increases the free carrier absorption which then limits the optical transmission. Independent of any constrain imposed by the thickness or cost for obtaining the best cell performance, it is thus preferable to limit doping and to increase the TCO layer thickness [202, 203]. In addition to the total optical transmission, a high diffuse component in the transmitted light, as characterized by the Haze factor, is extremely important for light trapping: The Haze factor is defined by the ratio of the diffuse to specular transmission at a given wavelength or as an average over a certain wavelength region. However, the measurement of Haze is usually carried out in air (on a TCO coated glass samples) and a priori this does not correspond to the situation in a solar cell [204]. Furthermore, because the angular diffusion of the transmitted light is also very important, a function such as a Lambertian is required for optimum light trapping [205].

It has been found that surface roughness has a strong influence on the growth of μc-Si:H thin-film materials, that is, the growth of the p-i-n thin-film silicon device. Growth of Si:H by PE-CVD is normal on a rough surface. Thus a V-shaped morphology of a substrate, such as the one shown in Fig. 34a or c, leads to the collision of two growing fronts, thus creating defective regions, microvoids, or cracks [206] (cf. Fig. 35). Any rough substrate will create such defects, however, the importance and effect of these "cracks" depends on the opening angle and shape of the "valleys" [207] as well as on the deposition conditions [208]. A smoother surface morphology such as the one found in sputtered etched ZnO (Fig. 34b) may reduce considerably the occurrence and severity of theses defects. Even though the latter can also be observed in the case of a-Si:H, they have a major effect on limiting the performance of μc-Si:H cells and a strong correlation has been found between loss in FF and V_{oc} with the density of cracks [207]. To mitigate the problem of cracks, TCOs have been treated by plasma to modify the surface morphology. Such a treatment has been proven quite effective in the case of LP-CVD deposited ZnO [209], even though

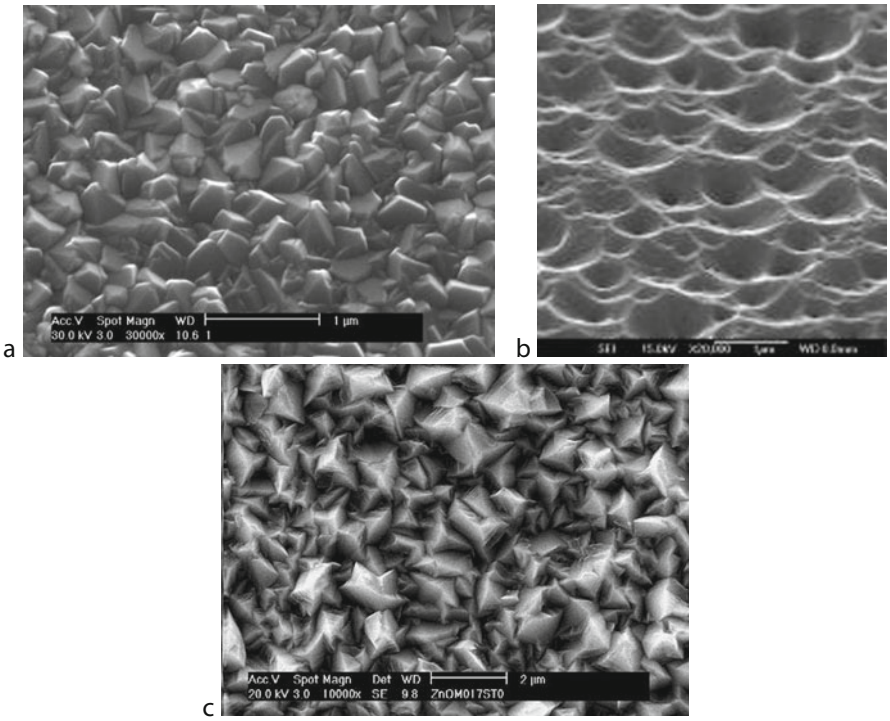

Silicon Solar Cells, Thin-film. Figure 34
Examples of rough TCOs deposited on glass: (**a**) SnO_2 deposited by atmospheric CVD, (**b**) textured etched ZnO deposited by sputtering, (**c**) ZnO deposited by low pressure CVD (LP-CVD)

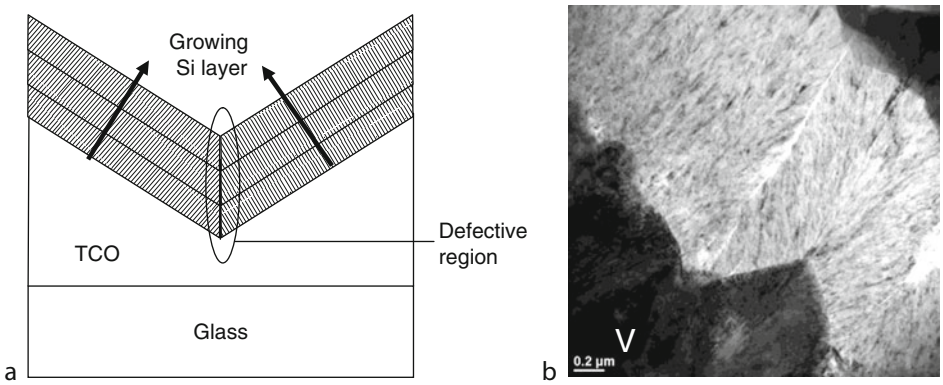

Silicon Solar Cells, Thin-film. Figure 35
(**a**) Cartoon of thin-film Si growth on rough TCO. (**b**) SEM micrograph of µc-Si:H layer deposited on rough LP-CVD ZnO. The columnar structure of the layer growing perpendicular to the substrate and leading to the formation of a crack is clearly visible

it also reduced the Haze factor and modified the angular diffusion function [209, 210]. A critical optimization is therefore required for optimum cell performance [211]. The cracks and microvoids induced by the Si:H growth can also influence impurity diffusion in the material as well as well as the post-deposition oxidation (as discussed in section "Optoelectronic Properties").

In order to keep the benefit of highly textured TCOs and to mitigate the effect of cracks on the cell performance, the incorporation of a resistive layer between the cell and its contacts [212] or the modification of the doped layer have been proposed. A remarkable improvement of the cell performances is obtained when a n-doped SiO_x layer is inserted in addition of or in place of the standard n-doped μc-Si:H layer of a-Si:H [213–215] or μc-Si:H [214, 215] cells deposited on rough TCOs. A further improvement is also observed when the p-doped μc-Si:H layer is replaced by a p-doped SiO_x layer [214, 215]. The quenching of the detrimental effect of cracks or shunts can be explained by a relatively simple electrical modeling involving the addition of a local serial resistance (given by the resistive layer, e.g., the SiO_x layer) added to the (local) cell equivalent electrical circuit [212, 214]. In this context, n-doped SiO_x layers can also replace the TCO back layers of the back ZnO/Ag light reflector [216]. In this case, such SiO_x layer act as both doped layer and diffusion barrier for the Ag back reflector, and eliminate the need for an ex situ deposition of ZnO.

Back reflectors in thin-film solar cells usually consist either of a thin ZnO layer, (as an antidiffusion barrier) combined with a metallic Ag layer (as an electrical contact and mirror) or a thick ZnO layer (as electrical contact) and a white dielectric (as light reflector). Both of these two approaches offer suitable back contacts and back reflectors [217]. An a-Si:H single-junction solar cell (1 cm^2) with a stabilized efficiency of 10.1% (I_{SC} = 18.1 mA/cm^2, V_{oc} = 877 mV and FF = 66.7%) has been recently fabricated using LP-CVD front and back TCO layers together with a white dielectric reflector [182]. Similar efficiency values are also obtained for μc-Si:H single-junction solar cells [209, 218–220].

Multi-junction Cells

The large interest in the improvement of not only the initial but particularly the *end of life* efficiencies initiated early on the development of multi-junction cells along a two track approach. In the first approach, the improved *end of life* efficiency was sought by replacing one thick a-Si:H cell by two thinner ones. In such an a-Si:H/a-Si:H tandem cell, the smaller thickness of the individual cells leads to less stringent requirements on carrier transport for efficient operation of the component cells. This in turn results in reduced carrier recombination and thus smaller light-induced degradation. The thickness of the bottom cell required to achieve equal J_{sc}s from the two cells was not that large since the optical enhancement, such as discussed earlier, is more efficient for the bottom cell. This approach was successfully implemented in both cells and modules to obtain initial efficiencies greater than 10% and *end of life* efficiencies greater than 9% [221].

The second approach is a more traditional one where, to more efficiently generate power from the different parts of the solar spectrum, the stacked cells have different bandgaps. Since the a-Si:H-based materials cover a wide range of bandgaps, solar modules having even three junction stacked cells are considered to be practical. Thus, not only a-Si:H/a-SiGe:H tandem cells but also a-Si:H/a-SiGe:H/a-SiGe:H triple junction cells were developed. The optimization of such cells centers around the ability to split the absorption of sunlight in the component cells in such a way as to maximize their carrier collection efficiencies, while at the same time generating equal currents in the component cells. Due to the flexibility provided by the available bandgaps, there are a number of different combinations for the absorber layer bandgaps which lead to high-efficiency a-Si:H alloy junction cells.

Extensive work has been carried out on the a-Si:H/a-SiGe:H tandem cells, but despite continuous progress, their performance thus far has been limited by the quality of the narrow bandgap a-SiGe:H materials which are markedly inferior to a-Si:H. To overcome this limitation, special cell designs were developed for optimizing cell performance while at the same time minimizing its light-induced degradation. This includes constructing cells whose initial performance is not optimized, but rather taking account of their subsequent degradation for achieving maximum stabilized overall performance [222, 223].

The characteristics of an a-Si:H/a-SiGe:H tandem solar cell are presented in Fig. 36 where the a-Si:H has a bandgap of 1.75 eV and the a-SiGe:H a bandgap of 1.41 eV. Figure 36a shows the stabilized current–voltage characteristic under AM1.5 illumination after it has been degraded with AM1.5 for 600 h at 50°C to an efficiency of 11.16%. In this case: J_{sc} of 10.61 mA/cm^2 is limited by the smaller of the two currents generated in

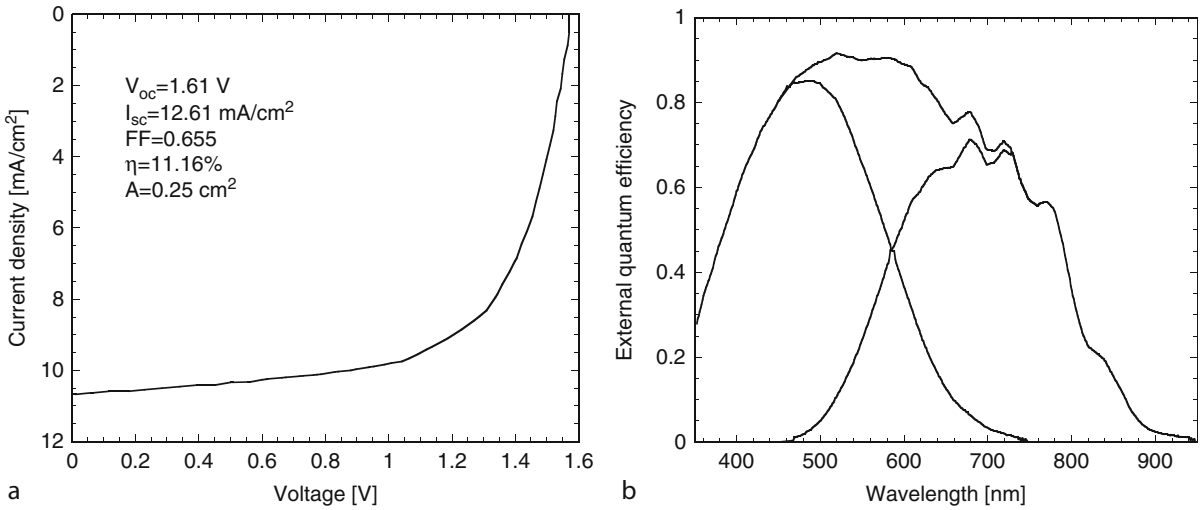

Silicon Solar Cells, Thin-film. Figure 36

(**a**) The current–voltage characteristic of an a-Si:H/a-SiGe:H tandem solar cell in the AM1.5 degraded state and (**b**) its quantum efficiency as a function of wavelength (After Yang and Guha [222])

the individual cells; the V_{oc} of 1.61 V is the sum of the voltage in the two individual cells; and the FF of 0.655 is determined by the degree of current matching between the two cells, their ability to collect carriers, and the quality of the interconnect between the two cells. Figure 36b shows the quantum efficiency as a function of wavelength for the cell in the degraded state, where the quantum efficiencies on the left of the figure are for a-Si:H and on the right for a-Ge:H, and illustrates how the currents in the two cells are generated by the different parts of the solar spectrum. The change in the cell efficiency between the initial and the degraded state is due to the decrease in: V_{oc} from 1.65 to 1.61 V; FF from 0.716 to 0.655; J_{sc} from 10.67 to 10.61 mA/cm^2; and efficiency from 12.61% to 11.16%.

Triple junction stacked cells offer a more efficient utilization of the solar spectrum by using thin component cells to absorb and collect the blue, green, and red photons in cells with correspondingly decreasing bandgap i-layer materials [224]. The highest efficiencies have been obtained using cell combinations in which the top cell that captures the blue photons has an a-Si:H i-layer with a gap of ~1.8 eV; the middle cell, ideally suited for absorbing the green photons, has an *i*-a-SiGe:H layer with 10–15 at.% Ge, and a gap of ~1.6 eV; and the bottom cell, capturing the red and the infrared photons, has an i-layer of a-SiG:H with 40–50 at.% Ge and a gap of ~1.4 eV. In the highest efficiency cells, the electrical and optical losses in the interconnects between adjacent cells have been minimized by developing thin, highly doped *n-p* tunnel/recombination junctions. Also, in these cells, the currents in the bottom a-SiGe:H cells were optimized by highly efficient optical enhancement with textured detached reflectors. Efficiency of such an a-SiGe:H/a-SiGe:H/a-Si:H *n-i-p* stacked cell on stainless steel, fabricated by Uni-Solar, reached a 1 sun degraded steady state at 50°C of 13.1% [224]. The efficiency of this 0.25 cm^2 cell in the initial state is 15.2%, as compared with the 12.61% for the tandem cell in Fig. 36. The introduction of the third cell increases the open circuit voltage but lowers the short circuit current relative to the tandem structures: The voltage of 2.34 V obtained from the three cells in series is much higher than the 1.65 V in Fig. 36a. Similarly, the J_{sc} of 8.99 mA/cm^2 is significantly lower than the 12.6 mA/cm^2 being generated in the tandem cell since now each component cell absorbs a smaller fraction of the solar spectrum.

However, the total current of 27.16 mA/cm^2 being generated here is higher than that in the tandem cell. It is important to note here that these currents are generated in component cells that are *thinner* than those of other cell structures. This *minimizes the requirements*

on carrier transport for efficient operation and high fill factors as well as reducing the deleterious effects of SWE. Large area cells with comparable efficiencies have not yet been achieved, but the recent insights into the growth and microstructure of a-SiGe:H alloys discussed in section "Optoelectronic Properties" point to possible new approaches for further progress.

μc-Si:H offers a very attractive alternative low bandgap material to a-SiGe:H alloys for multi-junction solar cells. As seen in previous sections, μc-Si:H is more stable than a-Si:H (and in particular a-SiGe:H) upon light soaking. Furthermore, the combination of bangaps of a-Si:H and μc-Si:H for a tandem device is close to the optimum for maximum conversion efficiency [33]. Despite the better stability of μc-Si:H, the stability of a-Si:H remains an important issue, as the top a-Si:H is roughly delivering 2/3 of the output power of the tandem device.

In order to reduce the top cell thickness and improve the device stability, the introduction of an optical intermediate reflector (IR) between the component cell has been proposed [225] (cf. Fig. 37). The effect of such an IR is to reflect some of the light back to the a-Si:H top cell, increasing the current in the top cell and reducing the current in the bottom cell. The gain in the top and the loss in the bottom cell depend on the IR index of refraction, thickness, and roughness [210]. Due to the absorption of the IR itself, the net gain in the current is always negative. The benefit of its introduction however is that the increase in the efficiency of the top cell should ultimately lead to an improved stabilized tandem efficiency, even with an increase in the thickness of the bottom cell necessary to compensate for the reflection into the top cell.

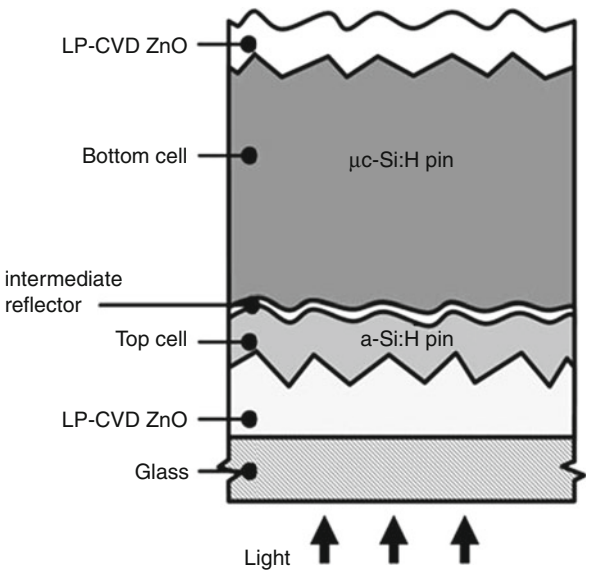

Silicon Solar Cells, Thin-film. Figure 37
Schematic structure of a a-Si:H/μc-Si:H tandem structure with intermediate reflector

IR was first implemented using ZnO as an optically transparent layer with a low index of refraction (compared to Si:H) [225–227] but this solution requires an ex situ deposition of ZnO (between the two Si:H cells). To overcome this limitation, IR based on SiO_x was proposed by Yamamoto et al. [228] and subsequently adopted by other laboratories [229, 230]. Optimization of IR in general is rather complicated as the currents in the two cells depend critically on the IR roughness and therefore on the underlying TCO surface morphology [210]. Best a-Si:H/μc-Si:H tandem device with or without IR exhibit stabilized efficiency values in excess of 11% [231–233] with a record (confirmed) efficiency of 11.7% for a 14.2 cm^2 sub-module [234] and 11.9% for a 1 cm^2 cell [235].

In order to further improve the efficiency of thin-film silicon devices a triple junction solar cell has been developed with a μc-Si:H component cell. The possible device configurations comprise a-Si:H/a-Si:H/μc-Si:H, a-Si:H/μc-Si:H/μc-Si:H or a-Si:H/a-SiGe:H/μc-Si:H. As in the case of other multi-junction devices, the current generation in each of the component cells must be matched for maximum efficiency. Current matching with high stabilized currents is difficult to achieve in the case of the a-Si:H/a-Si:H/μc-Si:H multi-junction structures. The a-Si:H/a-SiGe:H/μc-Si:H configuration has however led to a solar cell with the highest initial efficiency value, for a thin-film Si-based device, with an initial efficiency of 15.4% [236] and even 16.3% [237]. The light current–voltage and quantum efficiency curve characteristics of the record cell are shown in Fig. 38. Meanwhile, the best stabilized efficiencies have been obtained using an 0.25 cm^2 a-Si:H/μc-Si:H/μc-Si:H cell which had a confirmed value of 12.5%; using a similar structure an unconfirmed stabilized value of 13.5% was reported [238]. Table 1 summarizes the best confirmed and notable efficiencies of thin-film silicon solar cells.

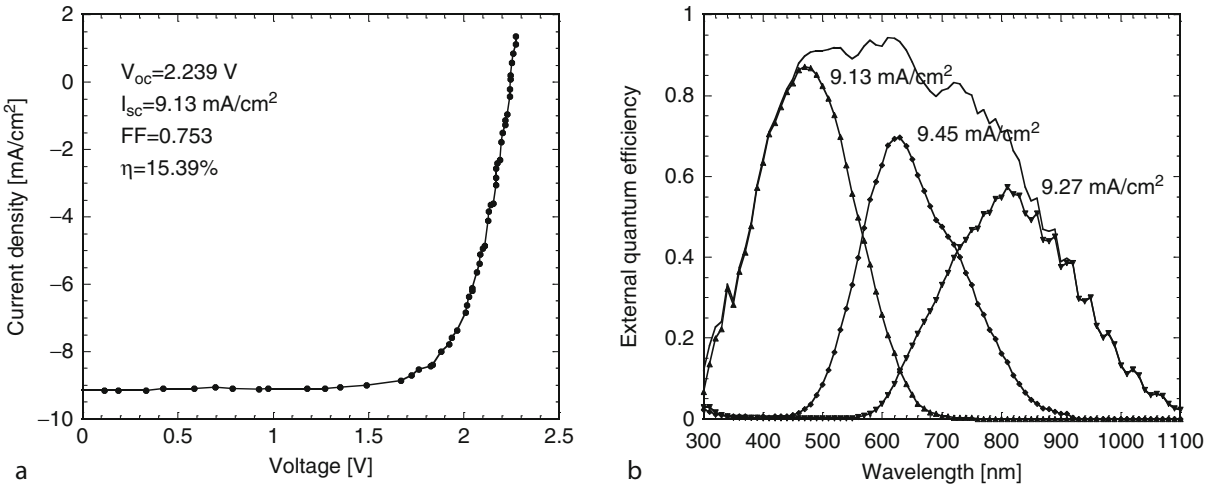

Silicon Solar Cells, Thin-film. Figure 38
(**a**) The current–voltage and (**b**) the quantum efficiency as a function of wavelength of an a-Si:H/a-SiGe:H/μc-Si:H triple junction n-i-p cell with an efficiency of 15.4%. The short circuit currents generated in the individual cells are indicated in (**b**) as is the total J_{sc} of 27.85 mA/cm^2 (After Yan et al. [237])

Silicon Solar Cells, Thin-film. Table 1 Best efficiencies obtained on thin-film silicon-based solar cells. Cell state (initial or stabilized) is indicated in the remark column is given. Confirmed efficiency data are indicated in the upper part of the table followed by other notable (initial efficiency) values from the literature

Material and device structure	Efficiency (%)	Area (cm^2)	V_{oc} (V)	J_{sc} (mA)	FF (%)	Group, remark	Refs.
Confirmed stabilized efficiencies							
a-Si single p-i-n junction	10.09	1.047	0.876	17.28	0.665	Oerlikon, stabilized	[235]
μc-Si single n-i-p junction	10.1	1.199	0539	24.4	76.6	Kaneka	[234]
a-Si/μc-Si p-i-n tandem	11.9	1.227	1.346	12.92	68.5	Oerlikon, stabilized	[235]
a-Si/a-Si/a-SiGe n-i-p triple	12.1	0.27	2.297	7.56	69.7	USSC, stabilized	[239]
a-Si/μc-Si/μc-Si n-i-p triple	12.5	0.27	2.010	9.11	68.4	USSC, stabilized	[238]
Notable efficiencies (unconfirmed values)							
μc-Si single p-i-n junction	10.8	0.25	0.535	27.47	74.2	EPFL, 2 μm, initial	[220]
a-Si/μc-Si p-i-n tandem	14.7	1	1.41	14.4	72.8	Kaneka, initial	[39]
a a-Si/a-SiGe/μc-Si n-i-p triple	15.39	0.27	2.24	9.4	75.3	USSC, initial	[236]
a a-Si/a-SiGe/μc-Si n-i-p triple	16.3	0.27	2.242	9.43	77	USSC, initial	[237]
a-Si/μc-Si/μc-Si n-i-p triple	13.5	0.27	1.964	9.37	73.3	USSC, stabilized	[238]

The optimization of these multi-junction solar cells is a nontrivial task since the current generated in each of the component cells depends not only on the operating conditions (solar spectrum and temperature) but also on the overall DSS. In practice, such optimization should be carried out with the maximum energy output of the device in mind for the installed conditions. In the case of a-Si:H/μc-Si:H tandem device, it is preferable to have bottom cell limited devices in the initial state in order to achieve a lower degradation factor.

However, it has been shown that slightly top limited devices are more efficient in outdoor conditions and lead to a higher overall energy output [240, 241].

Cell Structures, Modules, and Performance Issues

One of the main advantages of thin-film solar cells, and Si:H in particular, is the ability to monolithically interconnect individual cells on a common substrate. This interconnection allows for a low current, high voltage output of the solar modules for a reduction of the power loss in the serial resistance. In addition, it allows the fabrication of very large modules with flexible designs (in terms of shape, voltage, and current output). Such monolithic interconnection requires an insulating substrate and is usually made with three consecutive laser scribing steps: The first after the TCO deposition, the second after the deposition of the active layers, and the third after back contact deposition [37, 242, 243]. A schematic view of such interconnects and a picture of a corresponding module is shown in Fig. 39. The Si:H modules consist of stripe-like individual cells connected in series, and groups of such cells can also be connected in parallel for increased current output. The optimum width of a cell (width of the stripes in the modules) is given by the trade-off between the electrical loss in the TCO layer (the wider the stripe the higher the serial resistance) and the loss of module active area. The dead area is proportional to the number of cells on the module and to the width of the interconnects [242, 243]. In the case of large area modules, additional scribing lines are sometimes introduced to minimize the effect of local shunts on the module performance [244].

Si:H solar cells are being developed in both p-i-n and n-i-p configurations. The choice of the configuration is basically determined by the choice of the substrate and the need for a flexible (or rigid) solar module. Historically, a-Si:H cells have been deposited in the p-i-n configuration on glass substrates to take advantage of a rigid, flat, chemically, and thermally stable substrate as well their use as part of the encapsulation for the solar module. Such module configuration simplifies the encapsulation as there is no need for a transparent additional encapsulant on the front side. On the back side of the module, a second glass plate is usually used as it provides a very good barrier against moisture and offer high electrical isolation. Glass substrates are also well adapted for the laser patterning process used for the series interconnects. Even though such modules are quite heavy and fragile, they are very appropriate for building integration.

Development of Si:H modules on polymer substrates is very attractive as it allows the fabrication of light weight and unbreakable solar modules. However, it requires the use of the n-i-p configuration, due to the insufficient transparency of suitable polymers, as well as the introduction of different processing steps. The handling of a flexible substrate requires the use of a roll-to-roll deposition technology in which the laser patterning steps for fabricating the interconnects are more difficult as they now have to avoid damaging the substrate. A large variety of substrates are suitable as long as they are sufficiently stable at the deposition temperatures of the Si:H layers (at least 170°C) and are relatively smooth. The most commonly used polymers are the polyimides (PI) and polyethylene-naphthalate (PEN). The best stabilized efficiency for

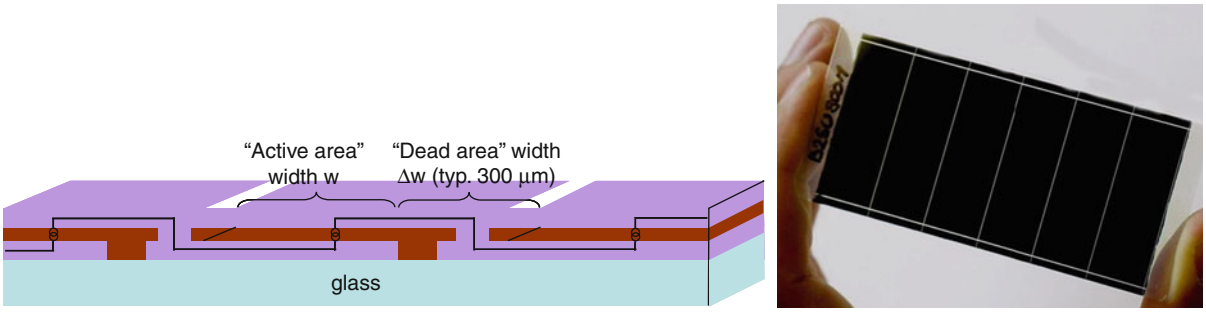

Silicon Solar Cells, Thin-film. Figure 39
Schematic view of monolithic interconnection of an a Si:H module and a picture of a corresponding finished mini-module

a Si:H cell deposited on a polymer film (PEN) substrate is 9.8% obtained with an a-Si:H/μc-Si:H tandem cell structure [245]. Studies have also been carried out on polyethylene-terephtalate (PET) as a substrate, but its low glass transition temperature has made device processing quite difficult [246]. In the case of the n-i-p cell structures used on this type of non-transparent substrates, it is necessary to have a transparent encapsulation material.

As an alternative to flexible polymer substrates, metallic substrates are being used. Triple junction devices discussed in this section are, for example, developed on stainless steel foils. The latter offers better thermal stability and easier handling compared to polymer films but does not allow the implementation of a monolithic series interconnects. An alternative technology has been recently employed in order to keep the p-i-n deposition sequence (which is easier to master) and at the same time allow the use of a flexible substrate. This approach consists of depositing the entire p-i-n cell layer stack on a temporary Al substrate from which it is then removed after lamination to a polymer foil which then becomes the permanent substrate [247]. This results in a product which is similar to the one fabricated in the n-i-p configuration, but with the advantage that the permanent substrate in this case does not need to be compatible with the deposition conditions of the cell.

The n-i-p cell structure offers some advantages in achieving higher cell efficiencies. In the Si:H technology, the p-layer deposition with the resultant p/i interface is one of the most critical steps in the fabrication of efficient solar cells. In this context, the deposition of the p-layer as the last layer of the cell structure may be advantageous for obtaining an interface with the best properties. It also avoids some potentially damaging diffusion of boron impurities into the i-layer. In the case of μc-Si:H, the n-i-p configuration allows for a growth of the μc-Si:H on a substrate with a small degree of roughness that avoids as much as possible void and crack formation, and then the introduction of more rough interfaces (for efficient optical enhancement) after the growth of the μc-Si:H n-i-p cell structure [248]. Despite the few advantages mentioned here, there is no inherent reason for there being a substantial difference in the efficiency limits for n-i-p cells as compared to p-i-n solar cells.

Production of Si:H modules is currently being carried out with three type of cell structures: a-Si:H single-junctions, a-Si:H/a-Si:H, and a-Si:H/μc-Si:H tandems as well as a-Si:H/a-SiGe:H/a-SiGe:H triple junctions. Advances in the development of Si:H technology have led to a number of companies manufacturing glass modules from 1.4 m^2 up to 5.7 m^2. Roll-to-roll manufacturing on flexible substrates of up to 60 cm^2 wide and 1.6 km long has also been achieved. The main issue facing all these technologies is the production of the modules in a very cost-effective way that requires very fast and uniform deposition of layers on theses large area substrates. Increasing the deposition rate however, in general, leads to a reduction of the material quality affecting both the material stability and the device performance. The best materials are usually obtained at relatively low deposition rates (below 0.5 nm/s), rates that have to be considerably increased in the future for ensuring the long-term success of the Si:H technology.

As the plants get larger, the material costs become the substantial cost component [249] where, for example, in the case of a-Si:H/a-SiGe:H tandem modules, more than 60% of the material costs are associated with the glass, frames, and packaging, While it will be difficult to reduce most of the other material costs (such as glass), the cost of the modules (in $\$/W_P$) can be reduced by increasing the efficiency of the modules. Increasing the module efficiency also helps to reduce the total cost of a PV system by reducing area-related balance of system costs (such as mounting structures and land). Another way to significantly reduce the cost of PV systems is to integrate the thin-film PV structure into building materials such as roofs or windows.

Future Directions

Materials and Light-Induced Degradation

Advantages offered by the low temperature PECVD process employed should be utilized in the further development of Si:H materials and cells. This applies not only to the improvement of the quality of these materials and cells but also to the concurrent increase in their deposition rates. This is a major undertaking since this has been attempted with a variety of different approaches which have led to only modest improvements. In order to rectify this, it will be necessary to

further address and improve the understanding in several key areas. One of these is still the issues related to the role that the different deposition parameters, and in particular hydrogen, play in the growth of materials and the processing of their solar cells. A better understanding of this, and in particular in the evolution of the microstructure in both amorphous as well as nano/microcrystalline Si:H, will be required. In order to guide the approaches to be taken for improving the materials and cells it will also be important to carry out concurrent characterization of their optoelectronic properties relevant to solar cell operation. In this way, it will then be possible to take advantage offered by the PECVD deposition process in controlling the changes in composition with high precision related to p/i interfaces in both p-i-n and n-i-p cell structures, grading of the microstructure in Si:H cells, and bandgap profiling. Although it has been shown that the PECVD processes can be scaled up to large panel areas, it will be very important to continuously assess the scalability of the processing changes being made.

Regarding the semiconductor properties, a more thorough investigation of the gap states in the dense protocrystalline a-Si:H that is currently being used in the high performance solar cells is needed. It is important to better understand how the microstructure, dominated by hydrogen passivated divacancies, affects the gap states that determine the performance of the solar cells.

Improving the stability of a-Si:H cells has to be vigorously addressed as it still remains a serious limitation on the performance of not only single-junction but also tandem and multi-junction cells. Further progress is needed in understanding the nature of the light-induced gap states that are keys in determining the instability of solar cells. The recent results on the creation kinetics of light-induced defect states underscore the necessity of developing new approaches for establishing the mechanisms responsible for SWE. Only a clear understanding of the origin of the light-induced defect states will enable a systematic approach to be carried out on their control and possible elimination. Since it is believed that the origin of the SWE is related to a redistribution of a small fraction of the bonded hydrogen in the material, the entity of a not fully hydrogenated divacancy in a disordered network is an interesting configuration to be considered as possible native or metastable defect site.

Devices

Even though material stability can be improved by careful optimization of the material growth, optical enhancement is the most effective way of addressing the effect of light-induced degradation in solar cells. New cell designs have been recently proposed for very thin intrinsic (absorbing) layers, which at the same time have a very long optical absorption length. These new devices are usually based on 3D structures which are determined by the substrate or the TCO, thus resulting in rather thick devices relative to the intrinsic layer thickness. For efficient coupling of light into the cells, such cells consist of ZnO pillar arrays or arrays of holes in thick ZnO substrates [250] as well as "nanocoax-based solar cells" [251]. Also being actively investigated are new light diffusion structures fabricated by nano-imprinting [199, 252], nano-moulding [253], or by incorporating grating structures [254] as well as those based on photonic crystals [255]. While the optical aspects of these new structures are relatively easy to investigate and simulate, the development of efficient thin-film solar cells on such substrates, which sometimes have very complicated surface morphologies, is very challenging. The effect of the surface morphology, as discussed in the previous section, can be magnified with these approaches in some cases so as make it impossible to fabricate improved devices. What is required is the development of a comprehensive understanding of not only the potential improvements but also the practical limitations that accompany the different approaches being proposed. In this context, comparisons of solar cells deposited on textured TCOs and corresponding devices deposited on substrates obtained from a replication of the same TCO light-trapping structures by nano-imprinting UV lithography [2455] enable the separation of the light-scattering and TCO free carrier absorption effects. Replication of light-trapping structures combined with low optical absorption TCO layers is an attractive strategy for further efficiency improvement [255].

A very important factor in the Si:H device performance is the quality of the TCO. For enhanced cell performances, high mobility TCO is required in order to achieve both a high transparency and a high conductivity that is necessary to reduce the series resistance losses in solar modules. Extensive work is being carried

out on optimizing the growth of TCO layers, on their post-deposition treatments as well as investigating new materials. Such an extensive effort is necessary if further improvements in cell performance are to be achieved.

In order to achieve the highest efficiencies it will be necessary to use triple junction cells where, in all probability, μc-Si:H will be the bottom cell intrinsic material in order to minimize cell degradation. The full potential of such cell structures is not yet known and it depends critically on the type of optical enhancement scheme that would be successfully implemented. For the long-term however, new thin-film materials should be developed and used to achieve even higher efficiencies.

Production Technology

Success of any technology is obtained only if it can be industrialized using cost-effective solutions. The cost of thin-film technology is, in general, mainly given by the equipment cost and is therefore very much driven by the processing speed. For the current Si:H technology, the deposition of quality layers at high rates over large areas is one of the main issues that has to be addressed. In this regard, further development of improved or new plasma sources for the PECVD deposition of Si:H solar cells over large areas has to be continued. However, it has to be along paths that are distinct from those developed for the thin-film transistors for the flat panel technology. Even though both deposition approaches are for large areas and include a-Si:H as one of the key materials, the similarity ends there. Not only are the device structures (thickness, component layers, substrates, etc.) drastically different in the two cases, but also the requirements on the intrinsic material properties since the thin-film transistors are unipolar and the solar cells ambipolar devices.

The reliability of a-Si:H PV modules has improved over the last 20 years with the development of new processes for electrically isolating and encapsulating the modules. However, more research and development is required to assure that all thin-film PV modules can survive for extended periods (>20 years) in hostile environments, such as high-voltage arrays operating in hot humid climates. However, the module fabrication technology, including their encapsulation, has so far not received the attention that is required in order to achieve the high product reliability for a very long lifetime. For example, the possible effects of different encapsulants on cell performance have not been thoroughly investigated and, as a consequence, are not well understood. Since such issues are of key importance not only to Si:H panels, they should be addressed in collaboration with those in other thin-film PV technologies. In addition, even though Si:H thin-film modules do not contain any toxic materials, the entire process of mining and refining the raw materials, manufacturing PV modules, and disposing of obsolete modules must be developed not only for low cost, but also to be environmentally friendly.

The cost of Si:H modules is expected to decrease significantly as the size of the manufacturing plants increases above 100 MW_p per year. The issue of Si:H thin-film module cost will become more and more important as the cost of competing PV technologies, c-Si and in particular thin-film CdTe, continue to decrease. The cost of Si:H thin-film modules has been decreasing but other technologies also exhibit important cost reductions. However, there is now a real possibility of major cost reductions being achieved with the introduction of a number of manufacturing plants having capabilities well in excess of 100 MW_p per year. For very large production volumes, the Si:H technology combines the advantages of the *short energy payback time* of a thin-film technology with the *unlimited availability of the semiconductor material.*

In conclusion, while amorphous microcrystalline Si:H as well as its alloy materials are complex and still understood to a limited extent, there are a large number of talented scientists and engineers in laboratories around the world who are working to make the promise of low-cost photovoltaic electricity a reality. It is this large pool of experienced and talented people that makes it highly probable that this goal will be achieved in part with Si:H thin-film technology.

Bibliography

Primary Literature

1. International Energy Agency (2010) Technology roadmap: solar photovoltaic energy. http://www.iea-pvps.org
2. Chittik RC, Alexander JH, Sterling HE (1969) The preparation and properties of amorphous silicon. J Electrochem Soc 116:77

3. Carlson DE (1977) Semiconductor device having a body of amorphous silicon. US Patent 4,064,521
4. Spear WE, LeComber PG (1975) Substitutional doping of amorphous silicon. Solid State Commun 17:1193
5. Carlson DE, Wronski CR (1976) Amorphous silicon solar cells. Appl Phys Lett 28:671
6. Carlson DE, Wronski CR, Triano A, Daniel RE (1976) Solar cells using Schottky barriers on amorphous silicon. In: Proceedings of 12th IEEE photovoltaic specialists conference, Baton Rouge, LA, p 893
7. Brodsky MH, Frisch MA, Ziegler JF, Lanfard WA (1977) Quantitative analysis of hydrogen in glow discharge amorphous silicon. Appl Phys Lett 30:561
8. Staebler DL, Wronski CR (1977) Reversible conductivity change in discharge produced amorphous silicon. Appl Phys Lett 31:292
9. Hanak JJ, Korsun V (1982) Optical stability studies of a-Si:H solar cells. In: Proceeding of the 16th IEEE photovoltaic specialists conference, San Diego, CA, p 1381
10. Vepřek S, Mareček V (1968) The preparation of thin layers of Ge and Si by chemical hydrogen plasma transport. Solid-State Electron 11:683–684
11. Vepřek S, Iqbal Z, Oswald HR, Webb AP (1981) Properties of polycrystalline silicon prepared by chemical transport in hydrogen plasma at temperatures between 80 and 400 degrees C. J Phys C 14:295–308
12. Vepřek S, Iqbal Z, Kühne RO, Capezzuto P, Sarott F-A, Gimzewski JK (1983) Properties of microcrystalline silicon: IV: electrical conductivity, electron spin resonance and the effect of gas adsorption. J Phys C 16:6241–6262
13. Vepřek S, Heintze M, Sarott F-A, Jurcik-Rajman M, Willmott P (1988) Mechanisms of plasma induced silicon deposition and the control of the properties of the deposit. Mater Res Soc Symp Proc 118:3–17
14. Usui S, Kikuchi M (1979) Properties of heavily doped GD-Si with low resistivity. J Non-Cryst Solids 34:1–11
15. Spear WE, Willeke G, Le Comber PG, Fitzgerald AG (1981) Electronic properties of microcrystalline silicon films prepared in a glow discharge plasma. J Phys Colloq 42(C4):257–260
16. Wang C, Lukovsky G (1990) Intrinsic microcrystalline silicon deposited by remote PECVD: a new thin-film photovoltaic material. In: Proceedings of the 21st IEEE photovoltaic specialist conference, Kissimmee, FL, pp 1614–1618
17. Tanaka K, Matsuda A (1987) Glow-discharge amorphous silicon: growth process and structure. Mater Sci Rep 2:139
18. Yang L, Chen LF (1994) The effect of H_2 dilution on the stability of a-Si:H based solar cells. Mater Res Soc Symp Proc 336:669
19. Yang J, Xu X, Guha S (1994) Stability studies of hydrogenated amorphous silicon alloy solar cells prepared with hydrogen dilution. Mater Res Soc Symp Proc 336:687
20. Bennett M, Rajan K, Kritikson K (1993) Amorphous silicon based solar cells deposited from H_2-diluted SiH_4 at low temperatures. In: Proceedings of 23rd IEEE photovoltaic specialists conference, Louisville, KY, p 845
21. Lee Y, Jiao L, Liu H, Lu Z, Collins RW, Wronski CR (1996) Stability of a-Si:H solar cells and corresponding intrinsic materials fabricated using hydrogen diluted silane. In: Proceedings of 25th IEEE photovoltaic specialists conference, Washington, DC, p 1165
22. Lu Z, Jiao H, Koval K, Collins RW, Wronski CR (1999) Characteristics of different thickness a-Si:H/metal Schottky barrier cell structures-results and analysis. Mater Res Soc Symp Proc 557:785
23. Collins RW, Koh J, Lu Y, Kim S, Burnham YS, Wronski CR (1996) Characterization of amorphous silicon solar cell preparation processes by real time spectroscopic ellipsometry. In: Proceedings of 25th IEEE photovoltaic specialists conference, Washington, DC, p 1035
24. Collins RW, Koh J, Ferlauto A, Rovira P, Lee Y, Koval R, Wronski CR (2000) Real time analysis of amorphous and microcrystalline silicon film growth by multichannel ellipsometry. Thin Solid Films 364:129
25. Flückiger R, Meier J, Keppner H, Götz M, Shah A (1993) Preparation of undoped and doped microcrystalline silicon (μc-Si:H) by VHF-GD for p-i-n solar cells. In: Proceedings of the 23th IEEE photovoltaic specialists conference, Louisville, KY, pp 839–844
26. Meier J, Flückiger R, Keppner H, Shah A (1994) Complete microcrystalline p-i-n solar cell-crystalline or amorphous cell behavior? Appl Phys Lett 65:860–862
27. Zanzucchi P, Wronski CR, Carlson DE (1977) Optical and photoconductivity properties of discharge produced a-Si. J Appl Phys 48:5227
28. Tawada Y, Okamoto H, Hamakawa Y (1981) a-SiC:H/a-Si:H heterojunction solar cell having more than 7.1% conversion efficiency. Appl Phys Lett 39:237
29. Nakamura G, Sato K, Ishihara T, Usui M, Okaniwa K, Yukimoto Y (1983) Tandem type amorphous solar cells. J Non-Cryst Solids 59–60:1111
30. Ishihara T, Terazono K, Sasaki H, Kawabata K, Itagaki T, Morikawa H, Deguchi M, Sato K, Usui M, Okaniwa K, Aiga M, Otsubo M, Fujikawa K (1987) High efficiency triple-junction amorphous solar cells. In: Proceedings of the 19th IEEE photovoltaic specialists conference, New Orleans, LA, p 749
31. Yang J, Banerjee A, Lord K, Guha S (1998) Correlation of component cells with high efficiency amorphous silicon alloy triple junction solar cells and modules. In: Proceedings of the 2nd world conference on photovoltaic solar energy conversion, Osaka, Japan, p 387
32. Meier J, Dubail S, Fischer D, Anna Selvan JA, Pellaton Vaucher N, Platz R, Hof C, Flückiger R, Kroll U, Wyrsch N, Torres P, Keppner H, Shah A, Ufert K (1995) The 'Micromorph' solar cells: a new way to high efficiency thin film silicon solar cells. In: Proceedings of the 13th European photovoltaic solar energy conference, Nice, France, pp 1445–1450
33. Shah A, Vanecek M, Meier J, Meillaud F, Guillet J, Fischer D, Droz C, Niquille X, Faÿ S, Vallat-Sauvain E, Terrazzoni-Daudrix V, Bailat J (2004) Basic efficiency limits, recent experimental results and novel light-trapping schemes in a-Si:H, μc-Si:H

and "micromorph tandem" solar cells. J Non-Cryst Solids 338–340:639–645
34. Yablonovitch E, Cody GD (1982) Intensity enhancement in textured optical sheets for solar cells. IEEE Trans Electron Dev 29:300
35. Deckman H, Wronski CR, Yablonovitch E (1984) Optical enhancement of solar cells. In: Proceedings of the 17th IEEE photovoltaic specialists conference, Kissimmee, FL, p 995
36. Arya RR, Carlson DE (2002) Amorphous silicon PV module manufacturing at BP solar. Prog Photovoltaics 10:69
37. Hanak JJ (1981) Laser processing technique for fabricating series connected and tandem junction series-connected solar cells into a solar battery. US Patent 4,292,092
38. Yan B, Yue G, Xu X, Yang J, Guha S (2010) High efficiency amorphous and nanocrystalline silicon solar cells. Phys Status Solidi A 207:671–677
39. Yamamoto K, Nakajima A, Yoshimi M, Sawada T, Fukuda S, Suezaki T, Ichikawa M, Koi Y, Goto M, Tanaka H, Sasaki T, Tawada Y (2003) Novel hybrid thin film silicon solar cell and module. In: Proceedings of the 3rd world conference on photovoltaic energy conversion, Osaka, Japan, pp 2789–2792
40. Curtins H, Wyrsch N, Favre M, Shah AV (1987) Influence of plasma excitation frequency for a-Si:H thin film deposition. Plasma Chem Plasma Process 7:267–273
41. Finger F, Kroll U, Viret V, Shah A, Beyer W, Tang X-M, Weber J, Howling A, Hollenstein C (1992) Influences of high exitation frequency (70 MHz) in the glow discharge technique on the process plasma and the properties of hydrogenated amorphous silicon. J Appl Phys 71:5665–5674
42. Zedlitz R, Heintze M, Bauer GH (1999) Analysis of VHF glow discharge of a Si:H over a wide frequency range. Mater Res Soc Symp Proc 258:147–152
43. Watanabe T, Azuma K, Nakatani M, Suzuki K, Sonobe T, Shimada T (1986) Chemical vapor deposition of a-Si:H films utilising a microwave excited Ar plasma stream Japanese. J Appl Phys 25:1805
44. Saito K, Sano M, Ogawa K, Kajita I (1993) High efficiency a-Si:H alloy cell deposited at high deposition rate. J Non-Cryst Solids 164–166:689
45. Tsai CC, Knights JC, Chang G, Wacker B (1986) Film formation mechanisms in the plasma deposition of hydrogenated amorphous silicon. J Appl Phys 59:2998
46. Shimizu T, Zhang Q, Nishino T, Takashima H, Kumeda M (1996) Influence of hydrogen content and Si-H bond structure on photocreated dangling bonds in hydrogenated amorphous silicon films. Jpn J Appl Phys 35:4409
47. Ganguly G, Matsuda A (1996) Role of hydrogen dilution in improvement of a-SiGe:H alloys. J Non-Cryst Solids 198–200:559
48. Smets AHM, Matsui T, Kondo M (2008) High-rate deposition of microcrystalline silicon p-i-n solar cells in the high pressure depletion regime. J Appl Phys 104:034508
49. Carlson DE, Gleaton M, Ganguly G (2000) Effects of oil and dopant contaminants on the performance of amorphous silicon solar cells. In: Proceedings of the 16th European photovoltaic solar energy conference, Glasgow, UK, pp 502–505
50. Kinoshita T, Isomura M, Hishikawa Y, Tsuda S (1996) Influence of oxygen and nitrogen in the intrinsic layer of a-Si solar cells. Jpn J Appl Phys 35:3819
51. Torres P, Meier J, Flückiger R, Kroll U, AnnaSelvan J, Keppner H, Shah A, Littlewood SD, Kelly IE, Giannoulès P (1996) Device grade microcrystalline silicon owing to reduced oxygen contamination. Appl Phys Lett 69:1373–1375
52. Kilper T, van den Donker MN, Grunsky D, Mück A, Schmitz R, Zastrow U, Rech B, Bräuer G, Klein S, Repmann T (2006) Quantification of the influence of oxygen and nitrogen contamination on the performance of microcrystalline silicon solar cells. In: Proceeding of the 21st European photovoltaic solar energy conference, pp 1738–1743
53. Hrunski D, Rech B, Schmitz R, Mück A, Pinçon O, Breuer U, Beyer W (2008) Influence of contaminations on the performance of thin-film silicon solar cells prepared after in situ reactor plasma cleaning. Thin Solid Films 516:4639–4644
54. Collins RW (1994) Real time spectroscopic ellipsometry studies of the nucleation, growth and optical functions of thin films Part 1: tetrahedrally bonded materials. Physics of thin films. Academic Press, New York, pp 49–125
55. Shah AV, Meier J, Vallat-Sauvain E, Wyrsch N, Kroll U, Droz C, Graf U (2003) Material and solar cell research in microcrystalline silicon. Sol Energ Mat Sol C 78:469–491
56. Feitknecht L, Meier J, Torres P, Zürcher J, Shah A (2002) Plasma deposition of thin film silicon: kinetics monitored by optical emission spectroscopy. Sol Energ Mat Sol C 74:539–545
57. Matsuda A (1983) Formation kinetics and control of microcrystallite in μc-Si:H from glow discharge plasma. J Non-Cryst Solids 59&60:767–774
58. Strahm B, Howling AA, Sansonnens L, Hollenstein C (2007) Plasma silane concentration as a determining factor for the transition from amorphous to microcrystalline silicon in SiH_4/H_2 discharges. Plasma Sources Sci Technol 16:80–89
59. Roca i Cabarrocas P, Fontcuberta i Morral A, Poissant Y (2002) Growth and optoelectronic properties of polymorphous silicon thin films. Thin Solid Films 403:39–46
60. Koh J, Fujiwara H, Lu Y, Wronski CR, Collins RW (1998) Real time spectroscopic ellipsometry for characterization and optimization of amorphous silicon-based solar cell structures. Thin Solid Films 313–314:469
61. Fujiwara H, Koh J, Wronski CR, Collins RW, Burnham JS (1998) Optical depth profiling of band gap engineered interfaces in amorphous silicon solar cells at monolayer resolution. Appl Phys Lett 72:2993
62. Ferlauto AS, Ferreira GM, Koval RJ, Pearce JM, Wronski CR, Collins RW, Al-Jassim MM, Jones KM (2002) Thickness evolution of the microstructural and optical properties of Si:H films in the amorphous-to-microcrystalline phase transition region. In: Proceedings of 29th IEEE photovoltaic specialists conference, New Orleans, LA, p 1076
63. Ferlauto AS, Koval RJ, Wronski CR, Collins RW (2001) Phase diagrams for the optimization of rf plasma enhanced chemical

vapor deposition of a-Si:H: variations in plasma power and substrate temperature. Mater Res Soc Symp Proc 664:A5.4.1
64. Ferreira GM, Ferlauto AS, Pearce JM, Wronski CR, Ross C, Collins RW (2004) Comparison of phase diagrams for vhf and rf plasma-enhanced chemical vapor deposition of Si:H films. Mater Res Soc Symp Proc 808:A5.2
65. Lu Y, Kim S, Gunes M, Lee Y, Wronski CR, Collins RW (1994) Process-property relationships for a-$Si_{1-x}C_x$:H deposition: excursions in parameter space guided by real time spectroellipsometry. Mater Res Soc Symp Proc 336:595
66. Tsu DV, Chao BS, Ovshinsky SR, Guha S, Yang J (1998) Effect of hydrogen dilution on the structure of amorphous silicon alloys. Appl Phys Lett 71:1317
67. Guha S, Yang J, Williamson DL, Lubianiker Y, Cohen JD, Mahan AH (1999) Structural, defect, and device behavior of hydrogenated amorphous Si near and above the onset of microcrystallinity. Appl Phys Lett 74:1860
68. Wronski CR, Pearce JM, Koval RK, Niu X, Ferlauto AS, Koh J, Collins RW (2002) Light induced defect creation kinetics in thin film protocrystalline silicon materials and their solar cells. Mater Res Soc Symp Proc 715:A13.4
69. Deng J, Pearce JM, Koval RJ, Vlahos V, Collins RW, Wronski CR (2003) Absence of carrier recombination associated with the defect pool model in intrinsic amorphous silicon layers: evidence from current–voltage characteristics on p-i-n and n-i-p solar cells. Appl Phys Lett 82:3023
70. Koval RJ, Koh J, Lu Z, Jiao L, Wronski CR, Collins RW (1999) Performance and stability of Si:H p-i-n solar cells with i-layers prepared at the thickness-dependent amorphous-to-microcrystalline phase boundary. Appl Phys Lett 75:1553
71. Koval RJ, Pearce JM, Ferlauto AS, Collins RW, Wronski CR (2001) Evolution of the mobility gap with thickness in hydrogen-diluted intrinsic Si:H materials in the phase transition region and its effect on p-i-n solar cell characteristics. Mater Res Soc Symp Proc 664:A16.4
72. Koval RJ, Pearce JM, Chen C, Ferreira GM, Ferlauto AS, Collins RW, Wronski CR (2002) Microstructurally engineered p-layers for obtaining high open-circuit voltages in a-Si:H n-i-p solar cells. In: Proceedings of the 29th IEEE photovoltaic specialists conference, New Orleans, LA, p 1090
73. Podraza NJ, Ferreira GM, Wronski CR, Collins RW (2005) Development of deposition phase diagrams for thin film Si:H and $Si_{1-x}Ge_x$:H using real time spectroscopic ellipsometry. Mater Res Soc Symp Proc 862: A.16.3.1
74. Podraza NJ, Wronski CR, Horn MW, Collins RW (2006) Roughness and phase evolution in $Si_{1-x}Ge_x$:H: guidance for multijunction photovoltaics. In: Proceedings 4th world conference on photovoltaic solar energy conversion, Waikoloa, HI, p 1657
75. Podraza NJ, Wronski CR, Collins RW (2006) Deposition phase diagrams for $Si_{1-x}Ge_x$:H from real time spectroscopic ellipsometry. J Non-Cryst Solids 352:1263
76. Stoke JA, Dahal LR, Li J, Podraza NJ, Cao X, Deng X, Collins RW (2008) Optimization of Si:H multijunction n-i-p solar cells through the development of deposition phase diagrams. In: Proceedings of the 33rd photovoltaics specialists conference, San Diego, CA, p 762
77. Stoke JA, Podraza NJ, Li J, Cao X, Deng X, Collins RW (2008) Advanced deposition phase diagrams for guiding Si:H-based multijunction solar cells. J Non-Cryst Solids 354:2435
78. Acco S, Williamson DL, Stolk PA, Saris FW, van den Boogaard MJ, Sinke WC, van der Weg WF, Roorda S, Zalm PC (1996) Hydrogen solubility and network stability in amorphous silicon. Phys Rev B 53:4415
79. Baum J, Gleason KK, Pines A, Garroway AN, Reimer JA (1986) Multiple-quantum NMR study of clustering in hydrogenated amorphous silicon. Phys Rev Lett 56:1377
80. Carlos WE, Taylor PC (1980) Hydrogen-associated disorder modes in amorphous Si:H films. Phys Rev Lett 45:358
81. Fejfar A, Poruba A, Vaněček M, Kočka J (1996) Precise measurement of the deep defects and surface states in a-Si:H films by absolute CPM. J Non-Cryst Solids 198–200:304
82. Beyer W, Abo Ghazala MS (1998) Absorption strengths of Si-H vibrational modes in hydrogenated silicon. Mater Res Soc Symp Proc 507:601
83. Langford AA, Fleet MI, Nelson BP, Lanford WA, Maley N (1992) Infrared absorption strength and hydrogen content of hydrogenated amorphous silicon. Phys Rev B 45:13367
84. Fang CJ, Gruntz CJ, Ley L, Cardona M (1980) The hydrogen content of a-Ge:H and a-Si:H as determined by IR spectroscopy, gas evolution, and nuclear reaction techniques. J Non-Cryst Solids 35–36:255
85. Smets AHM, Kessels WMM, van de Sanden MCM (2003) Vacancies and voids in hydrogenated amorphous silicon. Appl Phys Lett 82:1547
86. Smets AHM, van de Sanden MCM (2007) Relation of the Si-H stretching frequency to the nanostructural Si-H bulk environment. Phys Rev B 76:073202
87. Smets AHM, Wronski CR, van de Sanden MCM (2010) Hydrogen incorporation in hydrogenated amorphous silicon. To be published in Sol Energ Mat Sol
88. Stephen JT, Rutland JM, Han D, Wu Y (1997) An NMR investigation of H cluster configurations in a-Si:H. Mater Res Soc Symp Proc 467:159
89. Bhide VG, Dusane RO, Rajarshi SV, Shaligram AD, David SK (1987) Positron-lifetime studies of hydrogenated amorphous silicon. J Appl Phys 62:108
90. Suzuki R, Kobayashi Y, Mikado T, Matsuda A, McElheny PJ, Mashima S, Ohgaki H, Chiwaki M, Yamazaki T, Tomimasu T (1991) Characterization of hydrogenated amorphous silicon films by a pulsed positron beam. Jpn J Appl Phys 30:2438
91. Gordo PM, Ferreira Marques MF, Lopes Gil C, de Lima AP, Lavareda G, Nunes de Carvalho C, Amaral A, Kajcsos Z (2007) Positron annihilation and constant photocurrent method measurements on a-Si:H films: a comparative approach to defect identification. Radiat Phys Chem 76:220
92. Remeš Z, Vaněček M, Mahan AH, Crandall RS (1997) Silicon network relaxation in amorphous hydrogenated silicon. Phys Rev B 56:12710

93. Remeš Z, Vaněček M, Torres P, Kroll U, Mahan AH, Crandall RS (1998) Optical determination of the mass density of amorphous and microcrystalline silicon layers with different hydrogen contents. J Non-Cryst Solids 227–230:876
94. Smets AHM, Wronski CR, Zeman M, van de Sanden MCM (2010) The Staebler-Wronski effect: new physical approaches and insights as a route to reveal its origin. Mater Res Soc Symp Proc 1245:A.14.02
95. Feltrin A, Strahm B, Bugnon G, Sculati-Meillaud F, Ballif C, Howling AA, Hollenstein C (2010) Input silane concentration effect on the a-Si:H to μc-Si:H transition width. Sol Energ Mat Sol C 94:432–435
96. Houben L, Luysberg M, Hapke P, Carius R, Finger F, Wagner H (1998) Structural properties of microcrystalline silicon in the transition from highly crystalline to amorphous growth. Philos Mag A 77:1447–1460
97. Droz C (2003) Thin film microcrystalline silicon layers and solar cells: microstructure and electrical performances. PhD Thesis, University of Neuchâtel
98. Droz C, Vallat-Sauvain E, Bailat J, Feitknecht L, Meier J, Niquille X, Shah A (2003) Electrical and microstructural characterisation of microcrystalline silicon layers and solar cells. In: Proceedings of the 3rd world conference on photovoltaic energy conversion, Osaka, Japan, pp 1544–1547
99. Vallat-Sauvain E, Kroll U, Meier J, Wyrsch N, Shah A (2000) Microstructure and surface and roughness of microcrystalline silicon prepared by VHF-GD using hydrogen dilution. J Non-Cryst Solids 266–269:125–130
100. Bailat J, Vallat-Sauvain E, Feitknecht L, Droz C, Shah A (2002) Influence of substrate on the microstructure of microcrystalline silicon layers and cells. J Non-Cryst Solids 299–302:1219–1223
101. Vallat-Sauvain E, Shah A, Bailat J (2006) Advances in microcrystalline silicon solar cell technologies. Wiley series in materials for electronic and optoelectronic applications, John Wiley & Sons, Ltd, Chichester, pp 133–165
102. Tsai CC, Anderson GB, Thompson R, Wacker B (1989) Control of silicon network structure in plasma deposition. J Non-Cryst Solids 114:151–153
103. Nakamura K, Yoshida K, Takeoka S, Shimizu I (1995) Roles of atomic hydrogen in chemical annealing. Jpn J Appl Phys 34:442–449
104. Matsuda A (2004) Microcrystalline silicon growth and device application. J Non-Cryst Solids 338:1–12
105. Collins RW, Vedam K (1995) Optical properties of solids. In: Trigg GL (ed) Encyclopedia of applied physics. VCH Publishers, New York, pp 285–336
106. Luft W (1988) Characteristics of hydrogenated amorphous silicon-germanium alloys. In: Proceedings of 20th IEEE photovoltaic specialists conference, Las Vegas, NV, p 218
107. Grigorovici R, Vancu A (1966) Optical properties and electronic structure of amorphous germanium. Phys Status Sol 15:627
108. Cody GD, Tiedje T, Brooks BG, Goldstein Y (1982) Disorder and the optical-absorption edge of hydrogenated amorphous silicon. Phys Rev Lett 47:1480
109. Wronski CR, Lee S, Hicks M, Kumar S (1989) Internal photoemission of holes and the mobility gap of hydrogenated amorphous silicon. Phys Rev Lett 63:1420
110. Roxlo CB, Abeles B, Wronski CR, Cody GD, Tiedje T (1983) Comment on optical absorption edge in a-Si:H. Solid State Commun 47:985
111. Tiedje T (1984) Information about band-tail states from time-of-flight experiments. In: Pankove JI (ed) Semiconductors and semimetals, vol 21C. Academic Press, New York, pp 207–238
112. Jackson WB, Biegelsen DK, Nemanich RJ, Kinghts JC (1983) Optical absorption spectra of surface or interface states in hydrogenated amorphous silicon. Appl Phys Lett 42:105
113. Wyrsch N, Finger F, McMahon TJ, Vaněček M (1991) How to reach more precise interpretation of subgap absorption spectra in terms of deep defect density in a-Si:H. J Non-Cryst Solids 137&138:347–351
114. Lu Y, Kim S, Gunes M, Wronski CR, Collins RW (1994) Process-property relationships for a-Si1-xCx:H deposition: excursions in parameter space guided by real time spectroellipsometry. Mater Res Soc Symp Proc 336:595
115. Ganguly G, Matsuda A (1996) Role of hydrogen dilution in improvement of a-SiGe:H alloys. J Non-Cryst Solids 198–200:559
116. Guha S, Yang J, Pawliklewicz T, Glatfelter T, Ross R, Ovshinsky SR (1989) Band-gap profiling for improving the efficiency of amorphous silicon alloy solar cells. Appl Phys Lett 54:2330
117. Vaněček M, Kočka J, Poruba A, Fejfar A (1995) Direct measurement of the deep defect density in thin amorphous silicon films with the "absolute" constant photocurrent method. J Appl Phys 78:360566
118. Poruba A, Fejfar A, Remeš Z, Špringer J, Vaněček M, Kočka J, Meier J, Torres P, Shah A (2000) Optical absorption and light scattering in microcrystalline silicon thin films and solar cells. J Appl Phys 88:148–160
119. Poruba A, Vaněček M, Meier J, Shah A (2002) Fourier transform infrared photocurrent spectroscopy in microcrystalline silicon. J Non-Cryst Solids 299–302:536–540
120. Vaněček M, Poruba A, Remeš Z, Rosa J, Kamba S, Vorlíček V, Meier J, Shah A (2000) Electron spin resonance and optical characterization of defects in microcrystalline silicon. J Non-Cryst Solids 266–269:519–523
121. Wyrsch N, Torres P, Goerlitzer M, Vallat E, Kroll U, Shah A, Poruba A, Vaněček M (1999) Hydrogenated microcrystalline silicon for photovoltaic applications. Solid State Phenom 67–68:89–100, Polycrystalline semiconductors V – bulk materials thin films, and devices
122. Tanaka K, Matsuda A (1987) Glow-discharge amorphous silicon: growth process and structure. Mater Sci Rep 2:139
123. Collins RW, Fujiwara H (1997) Growth of hydrogenated amorphous and its alloys. Curr Opin Solid State Mater Sci 2:417–424

124. Street RA, Winer K (1989) Defect equilibrium in undoped a-Si:H. Phys Rev B 40:6236
125. Dersch H, Stuke J, Beichler J (1981) Light-induced dangling bonds in hydrogenated amorphous silicon. Appl Phys Lett 38:456
126. Kamei T, Hata N, Matsuda A, Uchiyama T, Amano S, Tsukamoto K, Yoshioa Y, Hirao T (1996) Deposition and extensive light soaking of highly pure hydrogenated amorphous silicon. Appl Phys Lett 68:2380
127. Taylor C (1984) Magnetic resonance in a-Si:H. In: Pankove JI (ed) Semiconductors and semimetals, vol 21C. Academic Press, New York, pp 99–154
128. Niu X (2006) Nature and evolution of light induced defects in hydrogenated amorphous silicon. PhD Thesis, Pennsylvania State University
129. Siebke S, Stiebig H, Abo-Arais A, Wagner H (1994) Charged and neutral dangling defect states in a-Si:H determined from improved analysis of constant photocurrent method. In: Proceedings of the 1st world conference on photovoltaic energy conversion, Waikoloa, HI, p 543
130. Günes M, Wronski CR (1997) Differences in the densities of charged defect states and the kinetics of Staebler-Wronski effect in undoped hydrogenated amorphous silicon thin films. J Appl Phys 81:3526
131. Wyrsch N, Beck N, Pipoz P, Goerlitzer M, Beck H, Shah A (1995) Recent progress in the interpretation of a-Si:H transport properties: lifetimes mobilities and mobility-lifetime products. Solid State Phenom 44–46:525–534
132. Beck N, Wyrsch N, Hof C, Shah A (1996) Mobility lifetime product – a tool for correlating a-Si:H film properties and solar cell performances. J Appl Phys 79:9361–9368
133. Schumm G, Bauer GH (1991) Equilibrium and non-equilibrium gap state distribution in undoped a-Si:H. Philos Mag B 64:515
134. Branz HM, Silver M (1990) Potential fluctuation due to inhomogeneity in hydrogenated amorphous silicon and the resulting charged dangling bond defects. Phys Rev B 42:7420
135. Powell MJ, Dean DC (1993) Improved defect-pool model for charged defects in amorphous silicon. Phys Rev B 48:10815
136. Shockley W, Read WT (1952) Statistics of the recombination of holes and electrons. Phys Rev 87:835
137. Deng J, Ross B, Albert M, Collins RW, Wronski CR (2006) Evolution of metastable defects in intrinsic layers of a-Si:H solar cells and corresponding thin film materials characterized by carrier recombination through midgap states. In: Proceedings of the 4th world conference on photovoltaic solar energy conversion, Waikoloa, HI, p 1576
138. Rose A (1962) Concepts in photoconductivity and allied problems. Interscience, New York
139. Nadazdy V, Zeman M (2004) Origin of charged gap states in a-Si:H and their evolution during light soaking. Phys Rev B 69:165213
140. Zhong F, Cohen JD (1993) Measured and calculated distributions of deep defect states in hydrogenated amorphous silicon: verification of deep defect relaxation dynamics. Phys Rev Lett 71:597
141. Finger F, Müller J, Malten C, Wagner H (1998) Electronic states in hydrogenated microcrystalline silicon. Philos Mag A 77:805–830
142. Astakhov O, Carius R, Finger F, Petrusenko Y, Borysenko V, Barankov D (2009) Relationship between defect density and charge carrier transport in amorphous and microcrystalline silicon. Phys Rev B 79:104205
143. Vetterl O, Groß A, Jana T, Ray S, Lambertz A, Carius R, Finger F (2002) Changes in electric and optical properties of intrinsic microcrystalline silicon upon variation of the structural composition. J Non-Cryst Solids 299–302:772–777
144. Ritter D, Weiser K, Zeldov E (1987) Steady-state photocarrier grating technique for diffusion length measurement in semiconductors: theory and experimental results for amorphous silicon and semi-insulating GaAs. J Appl Phys 62:4563–4570
145. Kroll U, Meier J, Keppner H, Littlewood SD, Kelly IE, Giannoulès P, Shah A (1995) Origin and incorporation mechanism for oxygen contaminants in a-Si:H and μc-Si:H films prepared by the very high frequency (70 MHz) glow discharge technique. Mater Res Soc Symp Proc 377:39–44
146. Goerlitzer M, Torres P, Beck N, Wyrsch N, Keppner H, Pohl J, Shah A (1998) Structural properties and electronic transport in intrinsic microcrystalline silicon deposited by the VHF-GD technique. J Non-Cryst Solids 227–230:996–1000
147. Švrček V, Pelant I, Kočka J, Fojtík P, Rezek B, Stuchlíkova H, Fejfar A, Stuchlík J, Poruba A, Toušek J (2001) Transport anisotropy in microcrystalline silicon studied by measurement of ambipolar diffusion length. J Appl Phys 89: 1800–1805
148. Wyrsch N, Droz C, Feitknecht L, Goerlitzer M, Kroll U, Meier J, Torres P, Vallat-Sauvain E, Shah A, Vaněček M (2000) Hydrogenated microcrystalline silicon: from material to solar cells. Mater Res Soc Symp Proc 609:A15.1.1–A15.1.11
149. Wyrsch N, Droz C, Feitknecht L, Spitznagel J, Shah A (2002) Transport path in hydrogenated microcrystalline silicon. Mater Res Soc Symp Proc 715:363–368
150. Wyrsch N, Droz C, Feitknecht L, Goerlitzer M, Kroll U, Meier J, Torres P, Vallat-Sauvain E, Shah A, Vaněček M (2000) Hydrogenated microcrystalline silicon: how to correlate layer properties and solar cell performance. J Non-Cryst Solids 266–269:1099–1103
151. Wyrsch N, Goerlitzer M, Beck N, Meier J, Shah A (1996) Transport properties of compensated μc-Si:H. Mater Res Soc Symp Proc 420:801–806
152. Dylla T, Reynolds S, Carius R, Finger F (2006) Electron and hole transport in microcrystalline silicon solar cells studied by time-of-flight photocurrent spectroscopy. J Non-Cryst Solids 352:1093–1096
153. Matsui T, Matsuda A, Kondo M (2004) High efficiency and high-deposition-rate microcrystalline silicon p-i-n solar cells. In: Proceedings of the 19th European photovoltaic solar energy conference, New Orleans, LA, pp 1407–1410

154. Luft W, Tsuo Y (1993) Hydrogenated amorphous silicon alloy deposition processes. Marcel Dekker, New York
155. Wronski CR, Abeles B, Tiedje T, Cody GD (1982) Recombination centers in phosphorous doped hydrogenated amorphous silicon. Solid State Commun 44:1423
156. Lee Y, Ferlauto A, Wronski CR (1997) Contributions of bulk, interface and built-in potential to the open circuit voltage of a-Si solar cells. In: Proceedings of the 26th IEEE photovoltaic specialists conference, Anaheim, CA, p 683
157. Wronski CR (1984) The Staebler-Wronski effect. In: Pankove JI (ed) Semiconductors and semimetals, vol 21C. Academic Press, New York, pp 347–373
158. Fritzsche H (1997) Search for explaining the Staebler-Wronski effect. Mater Res Soc Symp Proc 467:19
159. Wronski CR (1997) The light-induced changes in a-Si:H materials and solar cells-where we are now. Mater Res Soc Symp Proc 467:7
160. Yang L, Chen LF (1994) The effect of H_2 dilution on the stability of a-Si:H based solar cells. Mater Res Soc Symp Proc 336:669
161. Sakata I, Yamanaka M, Namase S, Hayash Y (1992) Deep defect states in hydrogenated amorphous silicon studied by a constant photocurrent method. J Appl Phys 71:4344
162. Stutzmann M, Jackson WB, Tsai CC (1985) Light-induced metastable defects in hydrogenated amorphous silicon: a systematic study. Phys Rev B 32:23
163. Stradins P, Fritzsche H (1994) Photo-induced creation of metastable defects in a-Si:H at low temperature and their effect on photoconductivity. Philos Mag B 69:121
164. Lee Y, Jiao L, Liu H, Lu Z, Collins RW, Wronski CR (1996) Stability of a-Si solar cells and corresponding intrinsic materials fabricated using hydrogen diluted silane. In: Proceedings of the 25th IEEE photovoltaic specialists conference, Washington, DC, p 1165
165. Young L, Chen L, Catalano A (1991) Intensity and temperature dependence of photodegradation of amorphous silicon solar cells under intense illumination. Appl Phys Lett 59:840
166. Yang L, Chen L (1993) Fast and slow metastable defects in hydrogenated amorphous silicon. Appl Phys Lett 63:400
167. Albert A, Deng JD, Pearce JM, Niu X, Collins RW, Wronski CR (2005) The creation and annealing kinetics of fast light induced defect states created by 1 sun illumination in a-Si:H. Mater Res Soc Symp Proc 862:457
168. Jiao L, Liu H, Semoushikina S, Lee Y, Wronski CR (1996) Initial, rapid light induced changes in hydrogenated amorphous silicon materials and solar cell structures: the effect of charged defects. Appl Phys Lett 69:3713
169. Wronski C, Deng J, Niu X, Smets A (2010) Dependence of carrier recombination in protocrystalline a-Si:H films and cells on their different light induced gap states. In: Proceedings of the 35th IEEE photovoltaic specialists conference, Honolulu, HI, pp 146–151
170. Deng JD, Ross B, Albert M, Collins RW, Wronski CR (2006) Characterization of the evolution in metastable defects created by recombination of carriers generated by photo-generation and injection in p-i-n a-Si:H solar cells. Mater Res Soc Symp Proc 910:A02–02
171. Branz HM (2003) Hydrogen collision model of metastablity after 5 years: experimental tests and theoretical extensions. Sol Energ Mat Sol C 78:425
172. Meier J, Torres P, Platz R, Dubail S, Kroll U, Anna Selvan JA, Pellaton-Vaucher N, Hof C, Fischer D, Keppner H, ShahA UK-D, Giannoulès P, Köhler J (1996) On the way towards high-efficiency thin film silicon solar cells by the 'micromorph' concept. Mater Res Soc Symp Proc 420:3–14
173. Meillaud F, Vallat-Sauvain E, Niquille X, Dubey M, Bailat J, Shah A, Ballif C (2005) Light-induced degradation of thin film amorphous and microcrystalline silicon solar cells. In: Proceedings of the 31st IEEE photovoltaic specialist conference, Lake Buena Vista, FL, pp 1412–1415
174. Meillaud F, Feltrin A, Dominé D, Buehlmann M, Python P, Bugnon G, Billet A, Parascandolo G, Bailat J, Faÿ S, Wyrsch N, Ballif C, Shah A (2009) Limiting factors in the fabrication of microcrystalline silicon solar cells and microcrystalline/amorphous ('micromorph') tandems. Philos Mag 89:2599–2621
175. Deng X, Schiff EA (2007) Amorphous silicon–based solar cells, Chapter 12. In: Hegedus S, Luque A (eds) Handbook of photovoltaic science and engineering. Wiley, Somersat
176. Pearce JM, Podraza N, Collins RW, Al-Jassim MM, Jones KM, Deng J, Wronski CR (2007) Optimization of open-circuit voltage in amorphous silicon solar cells with mixed phase amorphous-nanocrystalline p-contacts. J Appl Phys 101:114301
177. Zhu H, Fonash SJ (1998) Computer simulation for solar cell applications: understanding and design. Mater Res Soc Symp Proc 507:395
178. Deng J, Wronski CR (2005) Carrier recombination and differential diode quality factors in the dark forward bias current–voltage characteristics of a-Si:H solar cells. J Appl Phys 98:24509
179. Hegedus S, Salzman N, Fagen E (1998) The relation of dark and illuminated diode parameters to the open-circuit voltage of amorphous silicon p-i-n solar cells. J Appl Phys 63:5126
180. Crandall RS, Branz HM (1990) Band bending due to charged dangling bonds in amorphous silicon p-i-n solar cells. In: Proceedings of 21th IEEE photovoltaic specialists conference, Kissimmee, FL, p 1630
181. Hovel HJ (1976) Solar cells semiconductors and semimetals, vol II, 1st edn. Academic Press, New York
182. Benagli S, Borrello D, Vallat-Sauvain E, Meier J, Kroll U, Hoetzel J, Bailat J, Steinhauser J, Marmelo M, Monteduro G, Castens L (2009) In: Proceedings of the 24th European photovoltaic solar energy conference, Hamburg, Germany, pp 2293–2298
183. Yamamoto Y, Nomoto K, Okuno T, Moriuchi S, Nakata Y, Inoguchi T (1987) A role of composition graded layer in p/i interface of amorphous silicon solar cell. In: Proceedings of the 19th IEEE photovoltaic specialists conference, New Orleans, LA, p 981

184. Sakai H, Yoshida T, Fujikake S, Hama T, Ichikawa Y (1980) Effect of p/i interface layer on dark J-V characteristics and Voc in p-i-n a-Si solar cells. J Appl Phys 67:2494
185. von Roedern B (1994) Innovative optimization procedures for solar cells based on a unique model for junction optimization. In: Proceedings of 12th European photovoltaic solar energy conference, Amsterdam, The Netherlands, p 1354
186. Lee Y, Ferlauto A, Wronski CR (1997) Contributions of bulk, interface and built-in potential to the open circuit voltage of a-Si:H solar cells. In: Proceedings of the 26th IEEE photovoltaic specialists conference, p 683
187. Pearce JM, Koval RJ, Ferlauto AS, Collins RW, Wronski CR, Yang J, Guha S (2000) Dependence of open-circuit voltage in hydrogenated protocrystalline silicon solar cells on carrier recombination in p/i interface and bulk regions. Appl Phys Lett 77:3093
188. Koh J, Lee Y, Fujiwara H, Wronski CR, Collins RW (1998) Optimization of hydrogenated amorphous silicon p-i-n solar cells with two-step i layers guided by real-time spectroscopic ellipsometry. Appl Phys Lett 73:1526
189. Guha S, Yang J, Nath P, Hack M (1986) Enhancement of open circuit voltage in high efficiency amorphous silicon alloy solar cells. Appl Phys Lett 49:218
190. Banerjee A (1995) Study of top contact/p-layer junction for the optimization of large-area amorphous silicon multijunction cells. Sol Energ Mat Sol C 36:295
191. Deng X, Jones SJ, Liu T, Izu M, Ovshinsky SR, Hoffman K (1997) VHF plasma deposition of mc-Si p-layer materials. Mater Res Soc Symp Proc 467:795
192. Vetterl O, Lambertz A, Dasgupta A, Finger F, Rech B, Kluth O, Wagner H (2001) Thickness dependence of microcrystalline silicon solar cell properties. Sol Energ Mat Sol C 66:345–351
193. Wyrsch N, Torres P, Meier J, Shah A (1998) Microcrystalline p-i-n cells: a drift controlled device? J Non-Cryst Solids 227–230:1272–1276
194. Bailat J, Vallat-Sauvain E, Dubey M, Meillaud F, Niquille X, Guillet J, Shah A, Poruba A, Mullerova L, Springer J, Vaněček M (2004) Active layer quality and open-circuit voltage of nip and pin microcrystalline solar cells. In: Proceedings of the 19th European photovoltaic solar energy conference, Paris, France, pp 1541–1544
195. Meillaud F, Vallat-Sauvain E, Niquille X, Dominé D, Shah A, Ballif C (2006) Annealing behaviour and nature of defects of light-soaked microcrystalline silicon solar cells. In: Proceedings of the 21st European photovoltaic solar energy conference, Dresden, Germany, pp 1729–1732
196. Zeman M, Isabella O, Jaeger K, Santbergen R, Liang R, Solntsev S, Krc J (2010) Advanced light trapping in thin-film silicon solar cells. Mater Res Soc Symp Proc 1245: A03–03
197. Faÿ S, Feitknecht L, Schlüchter R, Kroll U, Vallat-Sauvain E, Shah A (2006) Rough ZnO layers by LP-CVD process and their effect in improving performances of amorphous and microcrystalline silicon solar cells. Sol Energ Mat Sol C 90:2960–2967
198. Kluth O, Rech B, Houben L, Wieder S, Schöpe G, Beneking C, Wagner H, Löffl A, Schock HW (1999) Texture etched ZnO:Al coated glass substrates for silicon based thin film solar cells. Thin Solid Films 351:247–253
199. Battaglia C, Söderström K, Escarré J, Haug F-H, Dominé D, Cuony P, Boccard M, Bugnon G, Denizot C, Despeisse M, Feltrin A, Ballif C (2010) Efficient light management scheme for thin film silicon solar cells via transparent random nanostructures fabricated by nanoimprinting. Appl Phys Lett 96:213504
200. Deng X, Narasimhan KL (1994) New evaluation technique for thin-film solar cell back reflector using photothermal deflection spectroscopy. In: Proceeding of the 1st world conference on photovoltaic energy conversion, Waikoloa, HI, pp 555–558
201. Bailat J, Terrazzoni-Daudrix V, Guillet J, Freitas F, Niquille X, Shah A, Ballif C, Scharf T, Morf R, Hansen A, Fischer D, Ziegler Y, Closset A (2005) Recent development of solar cells on low-cost plastic substrates. In: Proceedings of the 20th European photovoltaic solar energy conference, Barcelona, Spain, pp 1529–1532
202. Faÿ S, Steinhauser J, Oliveira N, Vallat-Sauvain E, Ballif C (2007) Opto-electronic properties of rough LP-CVD ZnO:B for use as TCO in thin-film silicon solar cells. Thin Solid Films 515:8558–8561
203. Agashe C, Kluth O, Schöpe G, Siekmann H, Hüpkes J, Rech B (2003) Optimization of the electrical properties of magnetron sputtered aluminum-doped zinc oxide films for opto-electronic applications. Thin Solid Films 442:167–172
204. Dominé D, Haug F-J, Battaglia C, Ballif C (2010) Modeling of light scattering from micro- and nanotextured surfaces. J Appl Phys 107:044504
205. Berginski M, Hüpkes J, Gordijn A, Reetz W, Wätjen T, Rech B, Wuttig M (2008) Experimental studies and limitations of the light trapping and optical losses in microcrystalline silicon solar cells. Sol Energ Mat Sol C 92:1037–1042
206. Python M, Vallat-Sauvain E, Bailat J, Dominé D, Fesquet L, Shah A, Ballif C (2008) Relation between substrate surface morphology and microcrystalline silicon solar cell performance. J Non-Cryst Solids 354:2258–2262
207. Python M, Madani O, Dominé D, Meillaud F, Vallat-Sauvain E, Ballif C (2009) Influence of the substrate geometrical parameters on microcrystalline silicon growth for thin-film solar cells. Sol Energ Mat Sol C 93:1714–1720
208. Python M, Dominé D, Söderström T, Meillaud F, Ballif C (2010) Microcrystalline silicon solar cells: effect of substrate temperature on cracks and their role in post-oxidation. Prog Photovoltaics: Res Appl 18:491–499
209. Bailat J, Dominé D, Schlüchter R, Steinhauser J, Faÿ S, Freitas F, Bücher C, Feitknecht L, Niquille X, Tscharner R, Shah A, Ballif C (2006) High-efficiency p-i-n microcrystalline and micromorph thin film silicon solar cells deposited on LPCV ZnO coated glass substrates. In: Proceedings of the 4th world conference on photovoltaic energy conversion, Waikoloa, HI, p 1533

210. Dominé D, Buehlmann P, Bailat J, Billet A, Feltrin A, Ballif C (2008) Optical management in high-efficiency thin-film silicon micromorph solar cells with a silicon oxide based intermediate reflector. Phys Status Solidi RRL 2:163–165
211. Boccard M, Cuony P, Despeisse M, Dominé D, Feltrin A, Wyrsch N, Ballif C (2011) Substrate dependent stability and interplay between optical and electrical properties in μc-Si:H single junction solar cells. Sol Energ Mat Sol C 95:195–198
212. Grabitz PO, Rau U, Werner JH (2005) Modeling of spatially inhomogeneous solar cells by a multi-diode approach. Phys Status Solidi A 202:2920–2927
213. Despeisse M, Bugnon G, Feltrin A, Stueckelberger M, Cuony P, Meillaud F, Billet A, Ballif C (2010) Resistive interlayer for improved performance of thin film silicon solar cells on highly textured substrate. Appl Phys Lett 96:073507
214. Despeisse M, Boccard M, Bugnon G, Cuony P, Söderström T, Parascandolo G, Stuckelberger M, Charrière M, Lofgren L, Battaglia C, Hänni S, Billet A, Ding L, Nicolay S, Meillaud F, Wyrsch N, Ballif C (2010) Low-conductivity doped layers for improved performance of thin film silicon solar cells on highly textured substrates. In: Proceedings of the 25th European photovoltaic solar energy conference, Valencia, Spain, pp 2793–2797
215. Despeisse M, Battaglia C, Boccard M, Bugnon G, Charrière M, Cuony P, Hänni S, Löfgren L, Meillaud F, Parascandolo G, Söderström T, Ballif C (2011) Optimization of thin film silicon solar cells on highly textured substrates. Phys Status Solidi A 208:1863–1868
216. Delli Veneri P, Mercaldo LV, Usatii I (2010) Silicon oxide based n-doped layer for improved performance of thin film silicon solar cells. Appl Phys Lett 97:023512
217. Lipovšek B, Krč J, Isabella O, Zeman M, Topič M (2010) Analysis of thin-film silicon solar cells with white paint back reflectors. Phys Status Solidi C7:1041–1044
218. Yamamoto K, Toshimi M, Suzuki T, Tawada Y, Okamoto T, Nakajima A (1998) Thin film poly-Si solar cell on glass substrate fabricated at low temperature. Mater Res Soc Symp Proc 507:131–138
219. Mai Y, Klein S, Carius R, Stiebig H, Houben L, Geng X, Finger F (2006) Improvement of open circuit voltage in microcrystalline silicon solar cells using hot wire buffer layers. J Non-Cryst Solids 352:1859–1862
220. Ballif C, Barraud L, Battaglia C, Benkhaira M, Billet A, Biron R, Boccard M, Bugnon G, Charrière M, Cuony P, Despeisse M, Ding L, Escarré J, Haug F-H, Hänni S, Löfgren L, Meillaud F, Nicolay S, Pahud C, Parascandolo G, Perruche B, De Wolf S, Söderström K, Stückelberger M (2011) Novel materials and superstrates for high-efficiency micromorph solar cells. In: Proceedings of the 26th European photovoltaic solar energy conference, pp 2384–2391
221. Ichikawa Y, Fujikake S, Takayama T, Saito S, Ota H, Yoshida T, Ihara T, Sakai H (1993) Large-area amorphous silicon solar cells with high stabilized efficiency and their fabrication technology. In: Proceedings of the 23rd IEEE photovoltaic specialists conference, Louisville, KY, pp 27–33
222. Yang J, Guha S (1992) Double-junction amorphous silicon-based solar cells with 11% stable efficiency. Appl Phys Lett 61:2917–2919
223. Guha S, Yang J, Pawliklewicz T, Glatfelter T, Ross R, Ovshinsky SR (1989) Band-gap profiling for improving the efficiency of amorphous silicon alloy solar cells. Appl Phys Lett 54:2330–2332
224. Yang J, Banerjee A, Lord K, Guha S (1998) Correlation of component cells with high efficiency amorphous silicon alloy triple-junction solar cells and modules. In: Proceedings of the 2nd world conference on photovoltaic energy conference, Vienna, Austria, pp 387–390
225. Fischer D, Dubail S, Anna Selvan JA, Pellaton Vaucher N, Platz R, Hof C, Kroll U, Meier J, Torres P, Keppner H, Wyrsch N, Goetz M, Shah A, Ufert KD (1996) The micromorph solar cell: extending a-Si:H technology towards thin film crystalline silicon. In: Proceedings of the 25th IEEE photovoltaic specialists conference, Washington, DC, pp 1053–1056
226. Dominé D, Bailat J, Steinhauser J, Shah A, Ballif C (2006) Micromorph solar cell optimization using a ZnO layer as intermediate reflector. In: Proceedings of the 4th world conference on photovoltaic energy conference, Waikoloa, HI, pp 1465–1468
227. Myong SY, Sriprapha K, Miyajima S, Konagai M (2007) High efficiency protocrystalline silicon/microcrystalline silicon tandem cell with zinc oxide intermediate layer. Appl Phys Lett 90:263509
228. Yamamoto K, Nakajima A, Yoshimi M, Sawada T, Fukuda S, Suezaki T, Ichikawa M, Koi Y, Goto M, Meguro T, Matsuda T, Kondo M, Sasaki T, Tawada Y (2005) A thin-film silicon solar cell and module. Prog Photovoltaics 13:489–494
229. Lambertz A, Dasgupta A, Reetz W, Gordijn A, Carius R, Finger F (2007) Microcrystalline silicon oxide as intermediate reflector for thin film silicon solar cells. In: Proceedings of the 22nd European photovoltaic solar energy conference, Milano, Italy, pp 1839–1842
230. Buehlmann P, Bailat J, Dominé D, Billet A, Meillaud F, Feltrin A, Ballif C (2007) In situ silicon oxide based intermediate reflector for thin-film silicon micromorph solar cells. Appl Phys Lett 91:143505
231. Feltrin A, Buehlmann P, Dominé D, Despeisse M, Meillaud F, Bugnon G, Parascandolo G, Ballif C (2009) Latest developments on micromorph tandem cells at IMT. In: Technical digest of the 18th international photovoltaic science and engineering conference, Kolkata, India, pp 209–210
232. Meier J, Bailat J, Castens L, Benagli S, Kroll U, Hötzel J, Borrello D, Djeridane Y, Steinhauser J, Vallat-Sauvain E, Orhan J-B, Ufert K, Henz J (2009) High efficiency micromorph tandem developments in KAI-M PECVD reactors. In: Proceedings of the 24th European photovoltaic solar energy conference, Hamburg, Germany, pp 2398–2401
233. Rech B, Repmann T, Wieder S, Ruske M, Stephan U (2006) A new concept for mass production of large area thin-film silicon solar cells on glass. Thin Solid Films 502:300–30

234. Green MA, Emery K, Hishikawa Y, Warta W (2011) Solar cell efficiency tables (version 37). Prog Photovoltaics: Res Appl 19:84–92
235. Bailat J, Fesquet L, Orhan J-B, Djeridane Y, Wolf B, Madliger P, Steinhauser J, Benagli S, Borrello D, Castens L, Monteduro G, Marmelo M, Dehbozorghi B, Vallat-Sauvain E, Multone X, Romang D, Boucher J-F, Meier J, Kroll U, Despeisse M, Bugnon G, Ballif C, Marjanovic S, Kohnke G, Borrelli N, Koch K, Liu J, Modavis R, Thelen D, Vallon S, Zakharian A, Weidman D (2010) Recent developments of high-efficiency micromorph® tandem solar cells in KAI-M PECVD reactors. In: Proceedings of the 25th European photovoltaic solar energy conference, Valencia, Spain, pp 2720–2723
236. Yan B, Yue G, Xu X, Yang J, Guha S (2008) Correlation of current mismatch and fill factor in amorphous and nanocrystalline silicon based high efficiency multi-junction solar cells. In: Proceedings of the 33rd IEEE photovoltaic specialists conference, San Diego, CA, pp 257–262
237. Yan B, Yue G, Sivec L, Yang J, Guha S (2011) Innovative dual function nc-SiOx:H leayer leading to a $>$16% efficient multi-junction thin-fil silicon solar cell. Appl Phys Lett 99:113512
238. Yue G, Sivec L, Yan B, Yang J, Guha S (2010) High efficiency hydrogenated nanocrystalline silicon solar cells deposited at high rates. Mater Res Soc Symp Proc 1245:A21–01
239. Green MA, Emery K, King DL, Hishikawa Y, Warta W (206) Solar cell efficiency tables (version 28). Prog Photovoltaics: Res Appl 14:455–461
240. Nakajima A, Ichikawa M, Sawada T, Yoshimi M, Yamamoto K (2004) Optimization of device design for thin-film stacked tandem solar modules in terms of outdoor performance. Jpn J Appl Phys 43:L1162–L1165
241. Yamamoto K, Nakajima A, Yoshimi M, Sawada T, Fukuda S, Suezaki T, Ichikawa M, Koi Y, Goto M, Miguro T, Matsuda T, Kondo M, Sasaki T, Tawada Y (2005) Thin film silicon solar cell and module. In: Proceedings of the 31st IEEE photovoltaic specialists conference, Lake Buena Vista, FL, pp 1468–1471
242. Hanak JJ (1979) Monolithic solar cell panel of amorphous silicon. Solar Energy 23:145–147
243. Brecl K, Topič M, Smole F (2005) A detailed study of monolithic contacts and electrical losses in a large-area thin-film module. Prog Photovoltaics: Res Appl 13: 297–310
244. Frei M, Wang D (2009) Performance and yield calculations for large-area thin-film modules through distributed modeling. In: Proceedings of the 34th IEEE photovoltaic specialists conference, Philadelphia, PA, pp 1708–1712
245. Söderström T, Haug F-J, Terrazzoni-Daudrix V, Ballif C (2010) Flexible micromorph tandem a-Si/μc-Si:H solar cells. J Appl Phys 107:014507
246. Koch C, Ito M, Schubert M (2001) Low-temperature deposition of amorphous silicon solar cells. Sol Energ Mat Sol C 68:227–236
247. Hamers EAG, van den Donker MN, Stannowski B, Schlatmann R, Jongerden GJ (2007) Helianthos: roll-to-roll deposition of flexible solar cell modules. Plasma Process Polymers 4:275–281
248. Söderström T, Haug F-J, Terrazzoni-Daudrix V, Ballif C (2010) Flexible micromorph tandem a-Si/μc-Si solar cells. J Appl Phys 107:014507
249. Woodcock JM, Schade H, Maurus H, Dimmler B, Springer J, Ricaud A (1997) A study of the upscalingof thin film solar cell manufacture towards 500 MWP per annum. In: Proceedings of the 14th European photovoltaic solar energy conference, Barcelona, Spain, pp 857–860
250. Vanecek M, Poruba A, Remes Z, Holovsky J, Purkrt A, Babchenko O, Hruska K, Meier J, Kroll U (2009) Five roads towards increased optical absorption and high stable efficiency for thin film silicon solar cells. In: Proceedings of the 24th European photovoltaic solar energy conference, Hamburg, Germany, pp 2286–2289
251. Naughton MJ, Kempa K, Ren ZF, Gao Y, Rybczynski J, Argenti N, Gao W, Wang Y, Peng Y, Naughton JR, McMahon G, Burns MJ, Shepard A, Clary M, Ballif C, Haug F-J, Söderström T, Cubero O, Eminian C (2010) Efficient nanocoax-based solar cells. Phys Status Solidi RRL 4:181–183
252. Battaglia C, Escarre J, Söderström K, Erni L, Ding L, Bugnon G, Billet A, Boccard M, Barraud L, De Wolf S, Haug F-J, Despeisse M, Ballif C (2011) Nanoimprint lithography for high-efficiency thin-film silicon solar cells. Nano Lett 11:661–665
253. Battaglia C, Escarre J, Söderström K, Charrière M, Despeisse M, Haug F-J, Ballif C (2011) Nanomoulding of transparent zinc oxide electrodes for efficient light trapping in solar cells. Nat Photon 5:535–538
254. Haase C, Stiebig H (2006) Optical properties of thin-film silicon solar cells with grating couplers. Prog Photovoltaics: Res Appl 14:629–641
255. Zhou D, Biswas R (2008) Photonic crystal enhanced light-trapping in thin film solar cells. J Appl Phys 103:093102

Books and Reviews

Hamakawa Y (2004) Thin-film solar cells: next generation photovoltaics and its applications, Springer series in photonics. Springer, Berlin

Poortmans J, Arkhipov V (2006) Thin film solar cells: fabrication, characterization and applications, Wiley series in materials for electronic and optoelectronic applications. Wiley, New York

Schropp REI, Zeman M (1998) Amorphous and microcrystalline silicon solar cells: modeling, materials and device technology, Electronic materials: science and technology. Springer, Berlin

Shah AV (2010) Thin-film silicon solar cells. EPFL Press, Lausanne

Street RA (1991) Hydrogenated amorphous silicon. Cambridge University Press, Cambridge

Wronski CW, Carlson DE (2001) Amorphous silicon solar cells, clean energy from photovoltaics, vol 1, Series on photoconversion of solar energy. Imperial College Press, Singapore

Silicon-Based Anodes for Li-Ion Batteries

Ji-Guang Zhang, Wei Wang, Jie Xiao, Wu Xu, Gordon L. Graff, Gary Yang, Daiwon Choi, Deyu Wang, Xiaolin Li, Jun Liu
Pacific Northwest National Laboratory, Richland, WA, USA

Article Outline

Glossary
Definition of the Subject
Introduction
Strategies to Improve the Cycle Life of Silicon-Based Anodes
Full Cells Containing Silicon-Based Anodes
Future Directions
Bibliography

Glossary

Li-ion battery A family of rechargeable batteries in which lithium ions move from the negative electrode to the positive electrode during discharge, and back to the anode when charging.

Electric vehicle Vehicle propelled by an electric motor (or motors) powered by rechargeable battery packs.

PHEV Plug-in hybrid electrical vehicle. This is a hybrid vehicle with rechargeable batteries that can be restored to full charge by connecting a plug to an external electric power source.

Nanowire A nanowire is a nanostructure, with the diameter of the order of a nanometer and aspect ratio greater than 10:1.

CVD Chemical vapor deposition.

HEMM High-energy mechanical milling.

Coulombic efficiency The efficiency with which charge (electrons) is transferred in a system facilitating an electrochemical reaction.

Specific capacity Capacity per unit weight of a battery (Ah/kg or mAh/g).

Specific energy Energy per unit weight of a battery (Wh/kg).

Energy density Energy per unit volume of a battery (Wh/l).

Definition of the Subject

Silicon is environmentally benign and ubiquitous. Because of its high specific capacity, it is considered one of the most promising candidates to replace the conventional graphite negative electrode used in today's Li-ion batteries. The theoretical specific capacity of silicon is 4,212 mAh/g ($Li_{22}Si_5$) [1], which is 10 times greater than the specific capacity of graphite (LiC_6, 372 mAh/g). However, the high specific capacity of silicon is associated with large volume changes (more than 300%) when alloyed with lithium. These extreme volume changes can cause severe cracking and disintegration of the electrode and lead to significant capacity loss. Significant scientific research has been conducted to circumvent the deterioration of silicon-based anode materials during cycling. Various strategies, such as reduction of particle size, generation of active/inactive composites, fabrication of silicon-based thin films, use of alternative binders, and the synthesis of one-dimensional silicon nanostructures, have been implemented by a number of research groups. Fundamental mechanistic research also has been performed to better understand the electrochemical lithiation and delithiation processes during cycling in terms of crystal structure, phase transitions, morphological changes, and reaction kinetics. Although efforts to date have not attained a commercially viable silicon anode, further development is expected to produce anodes with three to five times the capacity of graphite. In this entry, an overview of research on silicon-based anodes used for lithium-ion battery applications is presented. The overview covers electrochemical alloying of the silicon with lithium, mechanisms responsible for capacity fade, and methodologies adapted to overcome capacity degradation observed during cycling. The recent development of silicon nanowires and nanoparticles with significantly improved electrochemical performance also is discussed relative to the mechanistic understanding. Finally, future directions on the development of silicon-based anodes are considered.

Introduction

Energy-storage technologies, particularly lithium-ion batteries, have been a focal point for development of advanced, fuel-efficient vehicles, especially plug-in hybrid electric vehicles (PHEVs). Although significant

progress has been made during the last 20 years in various battery systems, existing systems do not satisfy all of the energy-storage needs for PHEV applications. More improvements are required with respect to energy density, power density, cycle life, safety, and cost. Commercial lithium-ion batteries primarily use graphite-based anodes, which have a theoretical specific capacity of 372 mAh/g (LiC_6). Continuous efforts have been made to find alternative anode materials, such as elemental metals, to replace graphite-based anodes since the early 1960s [2], when Dey first reported that lithium could be electrochemically alloyed with a number of metals at room temperature. Many elements such as aluminum (Al), silicon (Si), tin (Sn), antimony (Sb), bismuth (Bi), magnesium (Mg), and zinc (Zn) are known to react with lithium to form alloys (see Eq. 1) by undergoing partially reversible electrochemical reactions that result in high specific and volumetric capacities.

$$Li_xM \leftrightarrow xLi^+ + xe^- + M \quad (1)$$

Among possible alternative alloying elements, silicon is the most attractive and widely investigated [3, 4] because of its high gravimetric and volumetric capacities and abundance in the natural environment. Silicon in the fully lithiated form of $Li_{4.4}Si$ provides a theoretical specific capacity of 4,212 mAh/g which is 10 times more than the capacity of graphite. The specific capacities and volume changes of the different electrochemically active elements are shown in Table 1.

Silicon-Based Anodes for Li-Ion Batteries. Table 1
Specific capacities and molar volume changes exhibited by different candidate elements during cycling [5]

Elements	C	Al	Si	Sn	Bi
Lithiated phase	LiC_6	Li_9Al_3	$Li_{21}Si_5$	$Li_{17}Sn_4$	Li_3Bi
Theoretical specific capacity (Ah/kg)	372	2235	4012	959	385
Theoretical volumetric capacity (Ah/l)	833	6035	9340	7000	3773
Molar volume change (%)	12	238	297	257	115

Although the silicon-based anode has great potential, the alloying and subsequent de-alloying reactions during lithium insertion and lithium de-insertion result in severe crystallographic volume changes (~300% for silicon as shown in Table 1) because of various phase transitions. The mechanical strain generated during these phase transformations leads to cracking and disintegration of the electrode that, in turn, leads to failure of the anode after only a few cycles from loss of electrical contact between particles and the current collector. More details on the electrochemical alloying/de-alloying processes between lithium and silicon and the related failure mechanisms are discussed below. To prevent confusion, the following conventions are used in this chapter: discharge of silicon means lithium is inserted into silicon (lithiation or alloying of lithium with silicon); charge of silicon means lithium is de-inserted from silicon (delithiation or de-alloying of silicon).

Electrochemical Alloys of Lithium with Silicon

Studies of electrochemical alloys of lithium and silicon began with elemental lithium electrodes in high-temperature lithium/metal-sulfide secondary batteries [1, 6–8]. Lithium-silicon alloys with different stoichiometry were reported during the electrochemical lithiation of silicon at elevated temperatures (~400–500°C). The formation of $Li_{12}Si_7$, $Li_{14}Si_6$, $Li_{13}Si_4$, and $Li_{22}Si_5$ alloys was identified at distinct voltage plateaus according to each two-phase region, which follows the equilibrium lithium-silicon phase diagram as shown in Fig. 1. However, the electrochemical alloying process of lithium with silicon at room temperature was not readily understood because only one voltage plateau was observed for the silicon anode cycled between 0.0 V and ~1.2 V. Additionally, only ~3,500 mAh/g of capacity was obtained during the first discharge of a silicon anode at room temperature. Very few reports describing fundamental research on room-temperature electrochemical lithiation and delithiation of the silicon anode were published prior to the year 2000. Between 2000 and 2003, several groups observed that crystalline silicon undergoes electrochemical solid-state amorphization upon reacting with lithium at room temperature to form a metastable, lithium-silicon-based, amorphous phase where

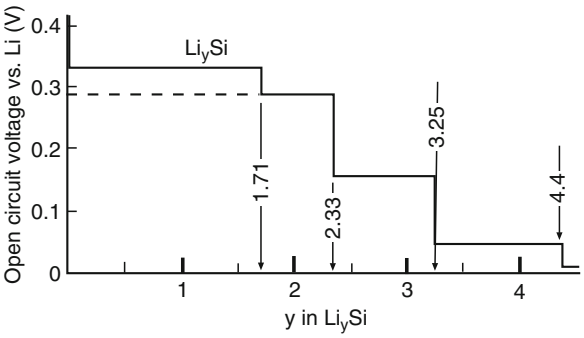

Silicon-Based Anodes for Li-Ion Batteries. Figure 1 Silicon lithiation showing two-phase plateaus at 415°C. (Reprinted with permission from Boukamp et al. [1]. Copyright 1981 The Electrochemical Society)

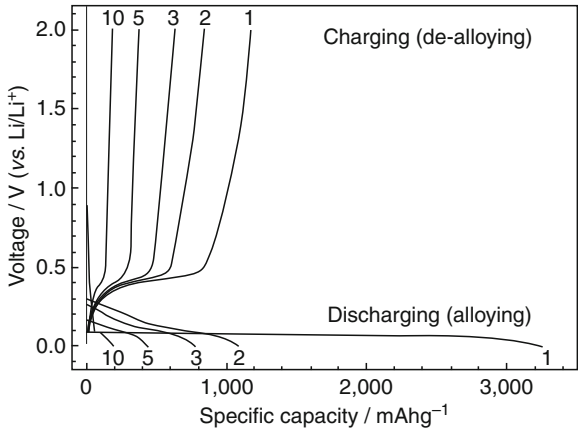

Silicon-Based Anodes for Li-Ion Batteries. Figure 2 Galvanostatic charge/discharge profiles for micro-silicon (10 μm) cycling at a current density of 100 mA/g in the voltage window of 0.0–2.0 V (versus Li/Li^+) (Reprinted with permission from Ryu et al. [13]. Copyright 2004 The Electrochemical Society)

crystallization of the equilibrium intermetallic phases is kinetically suppressed [9–12]. The thermodynamically favored, high-temperature intermetallics do not easily crystallize at room temperature because of the sluggish kinetics.

Figure 2 shows the typical cycling performance of a pure crystalline silicon anode [13]. This sample has a discharge capacity of ~3,260 mAh/g, and a charge capacity of 1,170 mAh/g, which gives an irreversible loss of ~64%. Such a large irreversible capacity loss in the first cycle is commonly observed for silicon-based anodes when discharged to near-zero potential. The coexistence of an amorphous lithium-silicon phase with the unreacted crystalline silicon leads to a single voltage plateau that is long and flat. This finding is consistent with results reported by several researchers who observed similar single, long, flat plateaus at ~0.1 V during electrochemical lithiation of crystalline silicon [3, 7, 9]. Though contrary to the equilibrium lithium-silicon phase diagram that shows multiple lithium-silicon phases [10, 14, 15], both ex situ and in situ X-ray diffraction (XRD) studies revealed a decrease and disappearance of the crystalline silicon peaks during the first lithium insertion, while no peaks corresponding to the equilibrium lithium-silicon phases were detected [10, 14, 15]. High-resolution transmission electron microscopy (HR-TEM) results confirmed that the lithiated silicon is formed primarily as an amorphous phase [10]. A change in the slope of the cell potential profile has been observed toward the end of the first discharge if the silicon anode is lithiated at an extremely low rate (~C/100), indicating formation of a new lithium-silicon phase. Obrovac and Christensen first reported the formation of a new crystalline phase when the highly lithiated amorphous silicon was electrochemically driven to ~50 mV versus Li/Li^+. Using XRD analysis, this new phase was identified as $Li_{15}Si_4$ [15]. Dahn et al. also confirmed the formation of $Li_{15}Si_4$ in both crystalline and amorphous silicon thin-film anodes when discharged below ~50 mV using in situ XRD analysis [14, 16]. Therefore, rather than forming the equilibrium $Li_{22}Si_5$ phase, $Li_{15}Si_4$ is the terminal phase that is achieved when the silicon anode is discharged to near-zero potential at ambient temperature. This phase renders a theoretical capacity of 3,579 mAh/g, a value that is in good agreement with most published reports on the silicon anode. It is worth noting that the formation of the $Li_{15}Si_4$ phase is observed only when the silicon anode is discharged at an extremely low rate (C/100). When the electrode is cycled at a moderate current rate (~C/10), the change of slope toward the end of the discharge is not observed. This characteristic provides further evidence of kinetically suppressed crystallization of lithium-silicon phases at low temperatures [17, 18].

Upon charge, the $Li_{15}Si_4$ phase delithiates to form an amorphous Li_ySi phase. The coexistence of these

phases leads to a narrow potential window between ~0.3 V and 0.4 V, as shown in Fig. 2, which corresponds to the potential range of the de-alloying reaction. The in situ XRD study of the charge process and the XRD results from the chemical delithiation of the $Li_{12}Si_7$ phase have confirmed that the lithiated silicon becomes amorphous after charging [14, 15]. During the first discharge/charge process of the silicon-based anode, it is important to note that the formation of the $Li_{15}Si_4$ phase occurs only when the potential is driven below ~50 mV. Control of the cycling voltage above this value will bypass the formation of the $Li_{15}Si_4$ phase, leading to a different potential profile. For example, Obrovac [15] showed that a cell discharged to 0 V showed a change of slope at the end of the first discharge and a two-phase region during charging, both of which can be attributed to the formation of $Li_{15}Si_4$ phase. These two features are not present in the voltage profile of the cell cycled above 50 mV.

Amorphous silicon demonstrates different features than those of crystalline silicon when subjected to lithiation at room temperature. Studies on an amorphous silicon thin-film anode prepared by magnetron sputtering and an amorphous silicon anode obtained through chemical delithiation of $Li_{12}Si_7$ phase show two distinctive, slightly sloping plateaus during the first discharge. These plateaus correspond to the two peaks observed in the dQ/dV curves [12, 15, 16]. The first peak is observed at ~0.2 V, which is about 0.1 V higher than the starting potential of lithiation observed in crystalline silicon. The second sloping plateau appears at ~0.1 V. The formation of the $Li_{15}Si_4$ phase also was identified in the amorphous silicon anode at a voltage ~30 mV. However, Dahn et al. reported that the crystalline phase only forms when the amorphous silicon thin films have a thickness greater than 2 μm. During the first lithiation, the amorphous silicon thin film that was cycled at a very low rate of C/48 exhibited a flat plateau at ~0.4 V, which may correspond to the conversion of the crystalline $Li_{15}Si_4$ phase to the amorphous Li_xSi. In comparison, the amorphous silicon thin-film anode cycled at a higher rate generally produced two broad humps at 0.3 V and 0.5 V, respectively. The phase formation of amorphous silicon during the first discharge/charge is not entirely understood. It generally is believed that the different peaks measured on the dQ/dV curves are related to the transition between different amorphous Li_xSi phases [17]. Because of the solid-state amorphorization discussed above, the voltage profile of the crystalline silicon anode and amorphous silicon anode exhibit similar features after the first charge/discharge cycle. The potential window in which silicon anodes operate is low enough to be useful in high-energy-density Li-ion batteries; however, Fig. 2 also reveals a large irreversible loss and rapid capacity fade during the lithium alloying/de-alloying process with silicon. These two problems have been reported by many researchers and are discussed in more detail below.

Failure Mechanisms of Bulk Silicon Anodes

The main challenge with the bulk silicon anode is the poor cycling stability as shown in Fig. 2. The reversible capacity decreases to less than 500 mAh/g by the fifth cycle. Several observations can be made concerning the rapid capacity fade from the charge/discharge profile. First, the irreversible loss is observed in every cycle, in contrast to conventional graphite anodes, where the irreversible losses cease after the initial one to two cycles. Second, although capacity fade occurs with every charge (i.e., de-alloying) cycle, upon re-discharging (alloying), the capacity recovers to approximately the same value measured in the previous charge cycle. This observation suggests that the degradation of the silicon anode is much more severe in the de-alloying cycle than in the alloying cycle.

There is strong evidence that failure of the silicon anode is caused by massive volume variations during lithiation and delithiation of the lithium-silicon alloys because the intermetallics formed have greater molar volume than the parent pure silicon phase. For example, $Li_{22}Si_5$ has a ~300% volume expansion over pure silicon, which causes substantial internal stress during lithiation or alloying. The fully lithiated phase of $Li_{15}Si_4$ exhibits a capacity of 3,579 mAh/g and has a density of 1.179 g/cm^3 calculated from XRD data, which represents a volume expansion of 280% [19]. The amorphous Li_ySi alloy formed during discharging progressively undergoes volume expansion until formation of a final $Li_{15}Si_4$ intermetallic, which has nearly three times the volume per atom than the parent silicon. During the

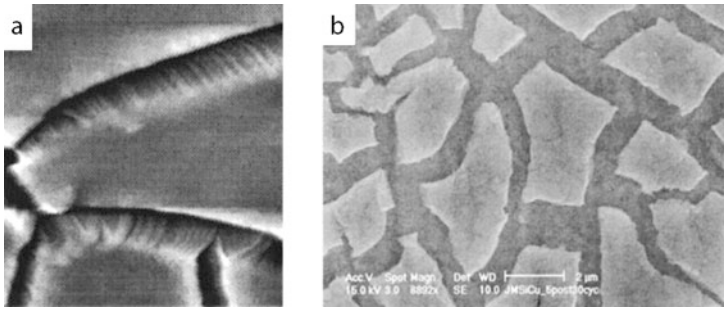

Silicon-Based Anodes for Li-Ion Batteries. Figure 3
(**a**) In situ AFM image showing the cracks of a silicon thin-film anode during cycling. (Reprinted with permission from Beaulieu et al. [20]. Copyright 2001 The Electrochemical Society) (**b**) SEM morphology of a 250-nm silicon thin film after 30 charges at a C/2.5 rate. (Reprinted with permission from Maranchi et al. [12]. Copyright 2003 The Electrochemical Society)

subsequent delithiation (de-alloying) process, the volume then contracts as lithium is extracted from the lithium-silicon intermetallic and amorphous phases [17, 20]. Crack formation and disintegration caused by the repetitive volume expansion and contraction are evident from the in situ atomic force microscopy (AFM) and scanning electron microscopy (SEM) images shown in Fig. 3 [12, 20]. The repeated volume expansion/contraction results in mechanical cracking and disintegration of the electrode, loss of electronic contact between active materials, and between active materials and current collector, thus rapid capacity fading.

A galvanostatic intermittent titration (GITT) study of the silicon anode shed more light on the poor cycling stability of the bulk silicon anode by measuring the variation in internal resistance during charge/discharge cycling [13]. In that study, a current of 100 mA/g was applied for 10 min, and then turned off for 20 min. A closed-circuit voltage (CCV) was measured while the current was on. A quasi-open-circuit voltage (QOCV) was obtained while the current was off. The internal resistance was then calculated from the difference between QOCV and CCV for each voltage transient. Figure 4 shows that, upon discharge, the internal resistance decreases, which is attributed to better electronic contact between the silicon particles resulting from the volume expansion during formation of Li_xSi alloys. One also could argue that the Li_xSi alloys have a slightly higher electronic conductivity than the pure silicon [19]. A drop in the internal resistance is observed below 0.3 V, which suggests that the alloying process primarily occurs below that voltage. During charge, the internal resistance increases because of increased contact resistance resulting from contraction of silicon particles/grains. Loss of electrical contact between particles leaves lithium ions trapped inside the anode (incomplete de-alloying) as the charge cycle is prematurely terminated when the electrode potential exceeds the cycling potential window. Upon charge, an abrupt increase in internal resistance is seen above 0.4 V, which suggests that the de-alloying reaction occurs primarily above that voltage. These results confirm that failure of silicon anodes is caused by breakdown of the electronically conductive network resulting from the large volume changes and cracking of the native anode structures.

Strategies to Improve the Cycle Life of Silicon-Based Anodes

In recent years, tremendous research efforts have been made to improve the electrochemical performance of silicon-based materials. One strategy is to create a fine composite microstructure comprising an active lithium alloy phase uniformly dispersed in an inert host matrix, such as silicon/carbon, Si/TiB_2, or Si/TiN composite materials [22, 23]. Composites of silicon and carbonaceous materials have been reported to have enhanced cycle life. These can be made by chemical vapor deposition (CVD), pyrolysis of silicon-containing organic compounds, or by

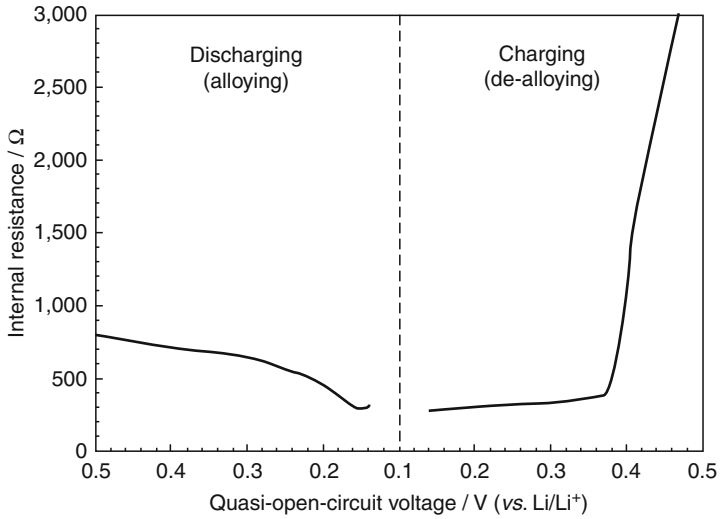

Silicon-Based Anodes for Li-Ion Batteries. Figure 4
Variation of internal resistance in a silicon anode (Reprinted with permission from Ryu et al. [13]. Copyright 2004 The Electrochemical Society)

mechanochemical methods. The carbon increases the electrical conduction and also may accommodate the volume change of silicon and buffer the mechanical stress, thereby improving the cycle life. Another strategy is to develop various nanoscale silicon or silicon/carbon architectures, including one-dimensional nanowires, two-dimensional thin films, and three-dimensional composite architectures. This section will provide a brief review of various approaches used to improve the capacity and cycling stability of silicon-based anodes [24–26].

Active/Inactive Nanocomposites

Although nanostructured materials are known to exhibit superplastic behavior, it is difficult to envisage that even nanostructured silicon would survive mechanical degradation (cracking) after long-term cycling because of the large volume expansion/contraction. A concept that has been developed to capitalize on the attributes of nanostructured materials is the generation of electrochemically active/inactive composites [4, 27–29] in which the material reactive to lithium (termed "active") is dispersed within materials that are nonreactive or less reactive to lithium (termed "inactive"). To generate a successful nanocomposite, both the active and inactive components need to be carefully selected to satisfy the requirement of low irreversible loss (20–30%), high capacity (>500 mAh/g), and good cyclability (~0.01% loss/cycle). Large volume changes are expected during the lithiation of silicon; therefore, the selection of matrix materials is of paramount importance to maintain the structural integrity.

The inactive components acting as the matrix usually consist of soft and ductile materials that play a very important role as "buffers" to alleviate the mechanical stresses arising from the large volumetric change of the active components. Increasing the inactive components in the electrode also was reported to suppress the aggregation of the active components upon cycling [30]. In this regard, inactive matrix components act as a skeleton or a network to form a microstructure that not only accommodates the volume changes, but also provides reaction sites for the active elements. Matrix materials also must exhibit good electronic and lithium-ion conductivity. Furthermore, the inactive matrix elements should be lightweight so that high gravimetric capacity can be achieved. Finally, the matrix materials should be inert to the active components because any reaction between matrix materials and active components will greatly reduce the useable capacity. The ratio between the active and inactive components is important to achieve

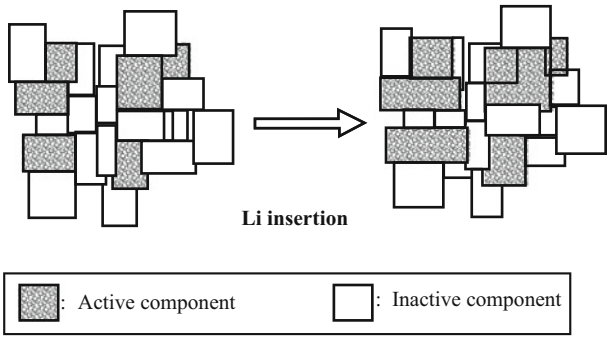

Silicon-Based Anodes for Li-Ion Batteries. Figure 5
Schematic model of the active/inactive nanocomposite and the morphological change occurring during lithium insertion Wang et al. [32]

the desirable cyclability and capacity. Previous reports show TiO_2 and ZrO_2 nanoparticles exhibit superplastic deformation [31], suggesting that other nanometer-size particles/phases may behave similarly and function as matrix components that accommodate structural changes upon cycling.

A schematic model of the "active/inactive" nanocomposite is shown in Fig. 5 [32]. Fuji Photo Film Celltec Company reported a tin-based amorphous composite oxide (TCO) [33] in 1997, which is the first demonstration of the "active/inactive" nanocomposite concept. In their results, the tin compound is the only active component reacting with lithium. The volume expansion of tin during cycling is reduced by the presence of other electrochemically inert oxide components including B_2O_3, P_2O_5, and Al_2O_3, which leads to good reversibility at a specific capacity of 800 mAh/g. The limitation of TCO is the large irreversible loss of >50% resulting from the electrochemical reaction depicted below.

$$SnO_2 + 8.4Li \rightarrow Li_{4.4}Sn + 2Li_2O \quad (2)$$

The Li_2O formed in situ helps to bond the $Li_{4.4}Sn$ species but does cause a large irreversible loss of Li. Efforts have subsequently been made to synthesize composites containing the pure active phase (such as tin) in the electrochemically inactive phase, thus eliminating or minimizing the irreversible loss. Over the years, many different combinations of active and inactive systems have been investigated using two general approaches: (1) in situ nanocomposites and (2) ex situ nanocomposites. In the in situ approach, alloys or compounds such as Mg_2Si and SiAg are used as starting materials, and upon lithium insertion, the active phases (lithium-silicon alloys) are formed in situ with the less active phases or compounds [34, 35]. XRD and atomic emission spectroscopy (AES) studies showed that the lithium-silicon and lithium-magnesium alloys were formed during the first insertion [35]. The in situ approach relies on phase instability of the parent phases Mg_2Si and SiAg upon lithium insertion. Because magnesium and silver are high-density elements with large atomic masses, the net specific capacity that can be attained is only moderate. The availability of suitable compounds and the ability to synthesize such nanocomposites in the case of silicon also are very limited.

Like SnO_2, SiO was also investigated as a lithium-ion battery anode through the reduction of SiO in the first-discharge process to form, in situ, a silicon active phase and the compound Li_2O as the matrix, possibly according to the following reaction.

$$5SiO + 6Li \rightarrow 4Si + Li_2O + Li_4SiO_4 \quad (3)$$

Electrodes produced using this approach typically deliver a capacity of ~600 mAh/g with stable cycling, and could become an effective and low-cost route for preparing silicon-based anodes.

The ex situ approach relies on generation of active and inactive phases that are known to be thermodynamically stable. Thus, the lithium-ion reactions are confined to the active elements while the inactive phase(s) act as buffering agents to prevent electrode cracking/crumbling. The ex situ approach typically

uses mechanical milling to form nanocomposites through mechanical alloying. The ex situ approach is attractive because of the ease of sample preparation and the lack of chemical reactions between active and matrix components, even upon cycling. A number of systems studied as inactive materials have demonstrated limited improvements in the performance of the silicon anode [5]. Hard materials such as SiC have been used as the inactive material to curtail volume expansion during cycling. Kim et al. successfully achieved stable reversible capacities up to ~600 mAh/g by ex situ generation of amorphous silicon particles embedded within nanocrystalline matrices of SiC, TiN, TiB_2, and C [36–38].

Both inactive and active forms of carbon have been investigated as possible host matrices with finely divided silicon [36–38]. As with the inactive phases, active matrices must accommodate the volume changes in silicon and provide good mechanical strength and facile transport for both electrons and lithium ions. Of the various materials investigated in this approach, graphite is a good candidate as an active matrix material because of its good electronic conductivity and lubrication characteristics. In recent years, active/inactive and active/active silicon/carbon composites have attracted considerable interest and the electrochemical performance reported appears quite promising. The graphite matrix acts as a buffer to accommodate the large volume expansions of silicon while the silicon contributes to the overall capacity because of its large gravimetric and volumetric capacity. Various synthesis methods have been reported to prepare silicon/carbon composites and nanocomposites, ranging from high-energy mechanical milling (HEMM), pyrolysis, and physical mixing. The raw materials used include a variety of phases, such as crystalline and amorphous silicon, graphite, disordered carbon, mesoporous carbon, carbon nanotubes, and fullerenes. The following sections provide more detail on the various approaches used to produce silicon/carbon electrodes.

Silicon/Carbon Composites Prepared through Ball Milling Mechanical milling can readily generate alloy systems with desirable compositions, structures, and particle sizes; therefore, HEMM has become a common approach for the synthesis of silicon/carbon composites. Results from different starting carbon materials such as graphite and disordered carbon [39] show a high first discharge and charge capacity (~800–1,400 mAh/g). However, the cycling stability is not as good as silicon/carbon composites derived from thermal pyrolysis of silicon-containing polymers. Gross et al. [40] reported a first-lithiation capacity of ~800 mAh/g with a fading rate of ~1.25% for a composite made by 15-min mechanical milling of graphite and a pre-milled silicon powder. The poor capacity retention is likely caused by the large silicon particles (>1 μm) in the composite. These particles disintegrate because of volume changes during lithium alloying and de-alloying processes, as discussed above. This hypothesis suggests that extended milling may improve the cycling stability by decreasing the silicon particle size and homogeneously distributing silicon particles in the graphite matrix. However, extended milling leads to formation of electrochemically inactive SiC because of mechanochemical reactions between silicon and carbon [37]. In addition to the formation of SiC, amorphization of graphite during prolonged milling also prevents stable high-capacity cycling of the silicon/carbon composite. Several polymer additives have been identified that serve as effective diffusion barriers to circumvent the formation of SiC and preserve the graphite structure during prolonged milling. Kim et al. [41] reported nanocomposites of silicon/carbon with a capacity as high as ~850 mAh/g and reasonable capacity retention (~1.1% loss/cycle). These nanocomposites were synthesized from silicon and polystyrene (PA resin) using HEMM. Datta et al. [22] recently reported methods to stabilize a composite using silicon, graphite, and polyacrylonitrile-based disordered carbon through HEMM, followed by subsequent heat treatment.

Si/C Composites Prepared Through High-Temperature Pyrolysis and CVD Processes In addition to the selection of appropriate starting materials to form active/inactive or active/active composites, the synthesis method must be carefully chosen to generate materials with desired properties. Recently, several novel methods including CVD, physical vapor deposition (PVD), and templated growth have been developed to generate nanoscale and nanostructured silicon-based materials. Control of structure, particle size, and

composition of silicon/carbon composites using CVD or pyrolysis reactions is difficult. In addition, maintaining a homogeneous distribution of silicon throughout the sample, which is a critical attribute for good cycling performance, is particularly challenging. In general, the chosen method should synthesize composites containing discrete phases without any chemical interaction to prevent loss of the active component and minimizing subsequent loss of electrochemical capacity.

Decomposition of organic precursors is one of the most common approaches investigated. Dahn et al. [42] systematically studied the pyrolysis of different silicon-containing polymers during the mid-1990s. More recent results include thermal pyrolysis of polyvinyl chloride dispersed with nanosized silicon and fine graphite particles to achieve a reversible capacity of ~700 mAh/g as reported by Yang et al. [43]. The same group also reported similar results from pyrolysis of pitch embedded with graphite and silicon powders [43]. However, silicon/carbon composites synthesized by pyrolysis of silicon-containing polymers suffer from a large irreversible loss (~50–60%) in the first cycle mainly because of the presence of disordered carbon and sulfur/oxygen/hydrogen impurities generated during high-temperature decomposition.

Another high-temperature approach for generating silicon/carbon composites is to deposit silicon particles on carbon or vice versa using CVD. Xie et al. [44] reported the deposition of silicon on mesocarbon microbeads (MCMB) by CVD of silane at 450°C and 500°C, but only a very small amount of silicon actually deposited on the MCMB. The material also demonstrated a very high (55%) irreversible loss. Vacuum deposition of nanometer-sized silicon particles on graphite surfaces has also been reported [45, 46]. The as-prepared anode showed an irreversible capacity loss of 26% with a capacity fade rate of less than 1% over 100 cycles. This cycling performance probably is one of the best reported for a silicon/carbon composite, and is attributed to the nanoscale silicon particle size (~50 nm) and strong adhesion of the silicon particles with the graphite matrix. In an attempt to reduce irreversible loss, carbon also has been deposited on pure silicon powders [47, 48]. However, the electrochemical performance of these materials was inferior to the silicon/carbon composite generated by depositing silicon on the carbon surface.

Silicon/Carbon Nanotube Composites Recently, carbon nanotubes (CNTs) also were investigated as candidate matrix materials. CNTs possess certain unparalleled characteristics that could be valuable in producing stable silicon/carbon composite anodes. The diameter of single-wall nanotubes (SWNTs) is in the range of 1–10 nm, while that of multiwall nanotubes (MWNTs) is in the range of ~100 nm. CNTs can be several microns in length, resulting in aspect ratios greater than ~1,000. Their specific surface area (SSA) is usually greater than 500 m^2/g. Strong C=C bonding to three adjacent neighboring atoms results in excellent mechanical properties in CNTs. The Young's modulus of SWNTs is approximately 1 TPa, and the maximum tensile strength is ~30 GPa [49]. Treacy et al. [50] reported an elastic modulus as high as 1.25 TPa. These values compare well with the modulus of MWNTs (1.28 TPa) measured by Wong et al. [51]. High tensile strengths up to ~63 GPa have been reported for MWNTs [52], which is an order of magnitude higher than that of carbon fibers and stainless steel (~5 GPa and ~3 GPa, respectively). The unique bonding structure also enables exceptional flexibility. The theoretical maximum elongation of an SWNT is almost 20% [53]. CNTs also are highly resistant to damage from external forces. Application of force to a nanotube typically results in bending, but not permanent damage. When the force is removed, the tube returns to its original state [54]. With respect to electrical conductivity, both MWNTs and SWNTs are excellent electrical conductors. The resistivity of SWNT ropes is approximately 10^{-4} Ω-cm at 300 K or roughly on the same order of magnitude as graphite [55]. MWNTs can carry extremely high current densities that exceed 107 Acm^{-2}, while a current density of 109 Acm^{-2} has been reported in SWNTs [56, 57]. These values clearly exceed the electrical property requirement of lithium-ion anodes. All of these attributes suggest that CNTs would be good candidates for matrix materials. The high-aspect-ratio, one-dimensional structures can form entangled three-dimensional networks that maintain electrical contact with silicon particles during cycling. The unusual flexibility and elongation could further facilitate stability, particularly after the active materials undergo cracking and disintegration. Finally, the high electrical conductivity and current density, combined with the low material density, could produce unprecedented matrix properties.

Although promising, in practice, the high irreversible loss and large voltage hysteresis during electrochemical cycling greatly limit the use of CNTs as active anode materials in lithium-ion batteries. Shu et al. [58] reported the synthesis of CNT-based silicon/carbon composites by decomposition of acetylene at 800°C using a nickel-phosphorus catalyst deposited on the silicon particles to seed nanotube growth. This silicon/carbon composite anode demonstrated a first cycle discharge capacity of 1,120 mAh/g and an irreversible loss of 20%. Wang et al. [59] achieved a capacity of ~1,000 mAh/g by homogenously dispersing a pre-milled silicon/graphite powder into a single-wall carbon nanotube matrix using ultrasonication. Si et al. [60] reported that the direct mixing of carbon nanofibers with carbon-coated silicon nanoparticles helped to maintain a stable cycling for the silicon-based anode. When carbon nanofibers are used as the current collector, superior overall capacity, cyclability, and rate capability have been demonstrated [61]. Lee et al. [62] also reported the use of wet ball milling to thoroughly mix silicon starting materials with different carbon sources, including single-walled and multiwalled CNTs. Although a high first-discharge capacity of ~2,000 mAh/g was achieved, rapid capacity fade was observed after 15 cycles [62]. Generally, anodes generated from simple mixtures of silicon particles and CNTs show poor capacity retention, but significant improvements were observed when silicon was directly deposited, using silane-based CVD, onto the CNTs or carbon nanofibers. The performance improvements were attributed to the formation of strong bonding layers between the silicon cluster and the CNT surface, which helped facilitate transport of lithium ions and electrons, in addition to the relaxation of stresses generated from the repetitive volume changes [18, 63].

Nanoscale Architectures

Several research groups have reported that reduction of the particle size leads to better accommodation of the strain generated during lithium insertion/de-insertion, therefore resulting in improved cycling performance. Although this work initiated with tin-based anode materials, the same strategy soon was applied to silicon-based systems by Yang et al. [64–66]. Huggins et al. [67] also suggested that decrepitation leads to a critical particle size more tolerant to mechanical stress. Researchers have reported superior electrochemical performance of nanoscale, over bulk, silicon, and attributed the performance to better strain accommodation in the smaller particles [68].

Generation of nanosized particles (~1–100 nm) results in a relatively low number of atoms per grain, less volume change upon cycling, and therefore, reduced mechanical stresses within the particles. In addition, the large number of grain boundaries existing in nanosized materials may help stabilize the particles and also act as channels for lithium insertion and de-insertion [69]. Other advantages include increased contact area between particles, within the electrode, and between the electrode and electrolyte, all leading to higher charge/discharge rates. Nanosized systems also provide a shorter diffusion path for the transport of both electrons and lithium ions, which improves performance for materials exhibiting poor electronic or lithium-ion conductivity. Another possible benefit of nanostructured materials is the potential to undergo superplastic deformation during cycling to better accommodate strain generated by large volumetric changes. Equation 4 describes the relationship between applied stress (σ), temperature (T), grain size (d), and the resulting strain rate ($\dot{\epsilon}$) [31].

$$\dot{\epsilon} = A\sigma^{n}d^{-p}D_0 \exp(-Q/RT) \tag{4}$$

where A is a constant, n is the stress exponent ($n \approx 2$), p is the grain size exponent ($p \approx 2$–3), Q is the activation energy, and R is the gas constant. An examination of Eq. 4 reveals that the strain rate for nanocrystalline materials will be several orders of magnitude higher than that of conventional-sized (i.e., micron-sized) materials at the same temperature. Therefore, nanostructured materials could possibly achieve appreciable superplastic strain at room temperature and are more suitable for use as anode materials. Nanocrystalline materials can be either single-phase or multiphase materials, which are in the size range of about 1 nm to 100 nm. Compared to materials containing larger grain sizes, the nanocrystalline materials generally exhibit improved mechanical hardness, fracture toughness, and ductility because of the large fraction of the atoms located at surfaces or grain boundaries [70]. Therefore, using nanocrystalline materials as anodes

will enhance not only the diffusion rates because of higher grain-boundary diffusion, but also the overall mechanical strength of the anode. Recently, this nanoscale synthesis approach has expanded into the growth of one-dimensional silicon nanowires and silicon nanoparticles with demonstrated superior electrochemical cycling performance, as will be discussed in a later section.

Two-Dimensional Silicon Thin-Film Anodes

Inspired by the improved performance of nanoscale-sized silicon particles over bulk silicon particles, many groups have tested silicon thin films deposited on metallic substrates (e.g., copper or nickel), in which the thin-film silicon contains nanometer-sized silicon features. In general, thin-film silicon anodes can be classified into nanocrystalline thin-film anodes and amorphous thin-film anodes. Graetz et al. [71] prepared nanocrystalline silicon thin-film anodes using PVD. These anodes exhibited specific capacities of approximately 1,100 $mAhg^{-1}$ with a 50% capacity retention after 50 cycles. The improved electrochemical performance of the thin-film anode was linked to good adhesion between deposited silicon particles and the substrate current collector.

Because of isotropic expansion of the particles/grains, amorphous thin-film silicon anodes typically perform better than crystalline thin films. Maranchi et al. [12, 72] demonstrated that 250-nm-thick amorphous silicon thin films deposited by radio-frequency magnetron sputtering on copper substrates achieved near theoretical capacity for a limited number of cycles. The authors stated that growth of a lithium-copper-silicon phase at the interface between silicon and copper, and the incremental plastic strain in the copper substrate upon cycling, resulted in a reduction of adhesion between the silicon film and the current collector, and progressive failure of the silicon film. Good electrochemical cycling performance also has been reported for multicomponent thin films, such as submicron-sized iron/silicon multilayer films and alternating cobalt/silicon layers [73, 74].

Surface roughness of the substrate can significantly influence the performance of silicon thin films [75, 76]. Yonezu et al. [77] reported that an amorphous silicon (a-silicon) film sputtered on a moderately roughened copper foil achieved virtually 100% reversibility with a corresponding capacity greater than 3,000 mAh/g. The as-deposited a-silicon film (5-μm thick) grew to a thickness of 17 μm during the first full charge. After the first cycle, the silicon thin film divided into micro-columns.

Figure 6a, b show that the micro-columns of lithium-silicon predominantly expand/contract along the column diameter. This preferential expansion may directly relate to minimization of surface tension and surface energy in the given structures. Although these sputtered a-silicon thin films show excellent capacity and cycle performance, materials prepared by sputtering are not economical for large-scale, high-volume applications. Another serious limitation is that the practical electrode thickness attainable using vacuum deposition is not useful for anodes in large-scale applications such as PHEVs. If silicon nanorods can be prepared, using scalable synthesis routes, and that retain the high aspect ratio (similar to those shown in Fig. 6), it is reasonable to expect that the lithium-silicon nanorod would expand/contract preferentially along its diameter and maintain mechanical integrity during lithium insertion/de-insertion. Anodes with

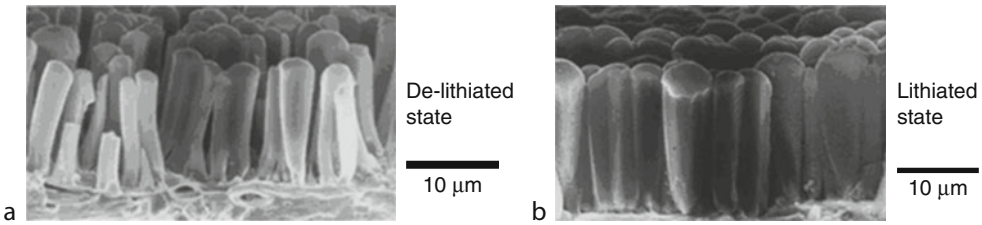

Silicon-Based Anodes for Li-Ion Batteries. Figure 6
Cross-sectional SEM images of an a-silicon thin-film electrode in the (**a**) de-lithiated and (**b**) lithiated states (Reprinted with permission from Yonezu et al. [77]. Copyright 2004 The Electrochemical Society)

capacities >600 mAh/g and improved mechanical/structural stability over silicon thin films or bulk powders would be possible. Such developments could enable the use of silicon nanorod anodes in large-scale applications such as PHEVs and other commercial applications.

Another approach involves dispersing silicon nanoparticles with graphene sheets to form another class of two-dimensional, silicon-based nanostructures in which the silicon particles are in intimate contact with the graphene. In this method, regions of graphene restack to form a graphite network that anchors the more flexible graphene and provides a highly electronically conductive matrix. The highly dispersed graphene/graphite matrix then buffers the volume expansion/contraction of silicon particles during repeated alloying and de-alloying with lithium [78, 79]. Specific capacities exceeding 1,500 mAh/g after 200 cycles with a capacity fading rate of less than 0.5% per cycle have been achieved using this approach.

One-Dimensional Silicon Nanowires The previous section clearly established that the morphology, size, and structure of the silicon phase can have a dramatic effect on the ultimate performance and stability of a silicon-based anode. Figure 7 graphically depicts observed morphological changes that occur in thin-film silicon during electrochemical cycling when different starting morphologies are used. The rod-like microstructures formed during initial charge processes of silicon films (Fig. 6) suggest that one-dimensional geometries (such as silicon nanowires [SiNWs]) may provide a stable structure that could be synthesized from a more viable manufacturing route. In 2008, Chan et al. [80] prepared SiNWs (diameter < 100 nm) using a CVD method based on the vapor-liquid-solid mechanism using silane gas as the silicon source, gold as the catalyst with stainless steel substrates. The one-dimensional SiNWs grown directly on the stainless steel current collector had a measured capacity of 4,277 mAh/g (based on the weight of silicon) during the first discharging process; this capacity is essentially the theoretical value for silicon within the experimental error. In subsequent cycles, the SiNWs maintained a charge/discharge capacity of 75% of the initial capacity, with little fading during cycling. The shortened lithium transport distances in the silicon

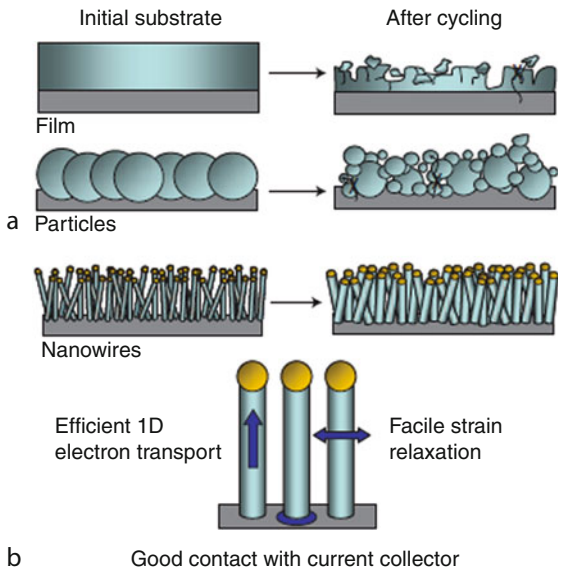

Silicon-Based Anodes for Li-Ion Batteries. Figure 7 Schematic of morphological changes of silicon during cycling. (**a**) The volume of silicon anodes changes by about 400% during cycling. (**b**) SiNWs do not disintegrate or break into smaller particles after cycling. This SiNW anode design has each nanowire connecting with the current collector (Reprinted with permission from Chan et al. [80]. Copyright 2008)

nanostructure and the low-resistance electrical connection to the current collector also led to an excellent rate capability (>2,100 mAh/g at 1C). While sufficient for concept demonstration and material design, the large-scale application of SiNWs grown directly on a current collector (foil) is still limited by the high production cost of SiNWs and the small weight ratio of active material to inactive material in the complete anode (which includes the substrate/current collector).

Several other approaches have been used to grow silicon-based nanowires. For example, Yu et al. [81] prepared SiNWs on silicon wafers using the solid-liquid-solid (SLS) mechanism. Kolb et al. [82] prepared silicon-based nanowires by evaporating silicon monoxide (SiO) in an inert gas atmosphere using a gold-coated silicon wafer as a substrate. Chang et al. [83] reported growth of silicon-based nanowires by heat treatment of an iron-catalyst–coated silicon nanopowder at 980°C. However, no electrochemical performances of these silicon-based nanowires were reported. Recently,

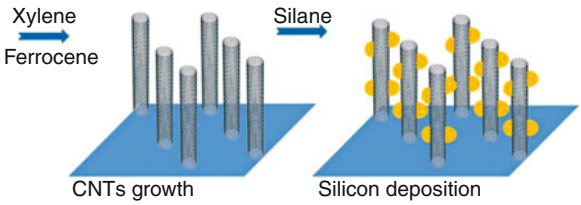

Silicon-Based Anodes for Li-Ion Batteries. Figure 8 Schematic diagram depicting the fabrication of silicon/carbon hybrid nanostructures using a liquid-injection CVD process to grow the initial vertically aligned CNTs, followed by the subsequent deposition of silicon (Reprinted with permission from Wang and Kumta [18]. Copyright 2010 American Chemical Society)

Zhang et al. [84] prepared free-standing silicon-based nanowires from commercial silicon powders in a three-dimensional manner rather than on the surface of the substrate (i.e., two-dimensional growth). A vapor-induced SLS mechanism was proposed to explain the observed growth of the resulting multicomponent nanowires from solid-powder sources. The composition, morphology, crystal structure, and electrochemical performance of the nanowires also were investigated.

In addition to growth of SiNWs, one-dimensional composite structures prepared by vacuum deposition of silicon clusters on CNTs also have been investigated. Hybrid silicon/carbon nanotube one-dimensional nanostructures were synthesized using a two-step CVD process (see Fig. 8) [18]. The spaces between the CNTs, formed through controlled nucleation in the first deposition step, allow for subsequent penetration of silane gas and a homogenous deposition of silicon clusters on the surfaces of the CNTs during the second CVD deposition step. The hybrid silicon/CNTs exhibit a high reversible capacity of 2,000 mAh/g with a 0.15% capacity loss per cycle over 25 cycles. When compared with commercially available silicon particles, in situ prepared silicon by CVD always has a smaller irreversible capacity loss in the first cycle. This may be related to the reduced amount of SiO_x on the surface of the silicon particles which usually traps lithium in the form of Li_2O and silicon in the first cycle. Coating silicon clusters on graphite nanofibers may also provide promising improvements in the cycling performance of silicon-based anodes.

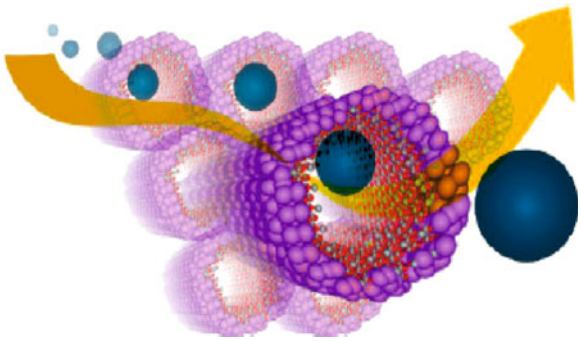

Silicon-Based Anodes for Li-Ion Batteries. Figure 9 Schematic diagram of the lithium-ion pathway in silicon nanotubes (Reprinted with permission from Park et al. [21]. Copyright 2009 American Chemical Society)

Three-Dimensional Nanostructured Silicon Anodes

In addition to one-dimensional and two-dimensional silicon anodes, several forms of three-dimensional nanostructured silicon have been explored. For example, silicon nanotubes (Fig. 9) were investigated by Cho et al. [21] as an anode material for lithium-ion batteries. Both interior and exterior surfaces of the nanotubes are accessible to the electrolyte and lithium ions. Through carbon coating, a stable solid electrolyte interface (SEI) was generated on the inner and outer surfaces of the silicon nanotubes. These silicon/carbon assemblies showed a reversible capacity as high as 3,247 mAh/g (based on the weight of silicon) and good capacity retention.

Three-dimensional porous silicon was recently investigated as a high-performance anode material for lithium-ion batteries [85]. The three-dimensional porous silicon particles with in situ coated carbon on the surface contained many "octopus foot"-like voids as shown in Fig. 10. This highly porous, interconnected structure not only facilitates the transport of lithium ions but also significantly alleviates the detrimental effects of volume expansion and shrinkage. At a 3C rate (1C rate = 2,000 mA/g or 40 mA/cm^2), a discharge capacity of 2,158 mAh/g (based on the weight of silicon) with a 72% capacity retention was obtained after 100 cycles. Earlier reports on nanoporous silicon/carbon composites showed similar cycling stability [86]. A reversible capacity of 700 mAh/g based on the total weight of nanoporous silicon/graphite/carbon electrode was obtained with negligible capacity loss

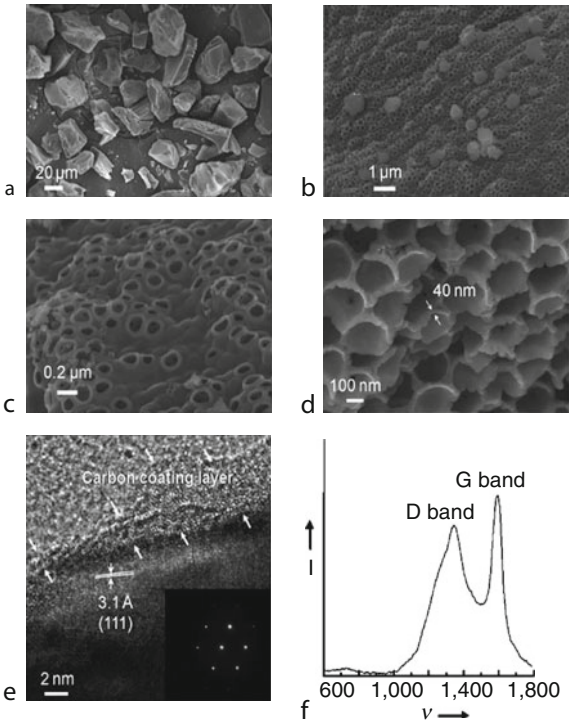

Silicon-Based Anodes for Li-Ion Batteries. Figure 10 (**a**), (**b**), (**c**), (**d**) SEM images of the three-dimensional porous c-silicon particles after etching ([**d**] is the cross-sectioned image of [**e**]). (**e**) TEM image of the cross-sectioned, three-dimensional porous c-silicon particle (the inset shows a selected area diffraction pattern. (**f**) Raman spectrum of three-dimensional porous c-silicon particles after etching. I = intensity (Reproduced with permission from Kim et al. [85]. Copyright Wiley-VCH Verlag GmbH & Co. KGaA)

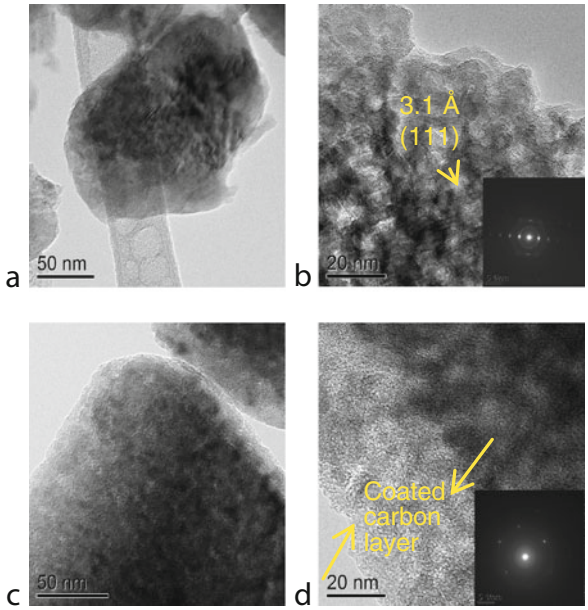

Silicon-Based Anodes for Li-Ion Batteries. Figure 11 (**a**) and (**b**) TEM images of porous silicon at different magnifications before carbon coating. (**c**) and (**d**) TEM images of silicon at different magnifications after carbon coating using CVD [1] (Reprinted with permission from Xiao et al. [87]. Copyright 2010 The Electrochemical Society)

up to 120 cycles. Commercially available micrometer-sized silicon particles with nanoporous surface structures (Fig. 11) have also been investigated. Stable cycling behavior could be achieved if CVD carbon coatings were applied to individual silicon particles and an elastic carbon additive was used to improve interparticle contact in the anode [87]. Nest-like silicon structures also are reported to have better electrochemical performance than that of coil-like silicon nanospheres, probably through a mechanism similar to that used to form three-dimensional nanostructured silicon [88].

To further improve the mechanical and electrical stability of silicon-based anodes, a hierarchical bottom-up approach (Fig. 12) was successfully utilized to develop a three-dimensional nanostructured silicon/carbon porous composite [89]. The existence of pores in the composite granules provides sufficient space to accommodate silicon expansion during lithium insertion. CVD deposition of silicon clusters (Fig. 12b) avoids formation of SiO_x, thus reducing the first cycle, irreversible capacity. A high specific capacity of ~1,950 mAh/g (C/20 rate) based on the total weight of the silicon/carbon composite was reported. In addition, the composite anodes had negligible capacity fade after 100 cycles at 1C rate and excellent rate capability (870 mAh/g at 8C rate).

Effect of Binder on the Performance of Silicon-Based Anodes

Sodium Carboxylmethylcellulose–Based Binder Polyvinylidenedifluoride (PVDF) has been used widely as the binder for graphite-based anodes in lithium-ion batteries. However, silicon-based anodes with

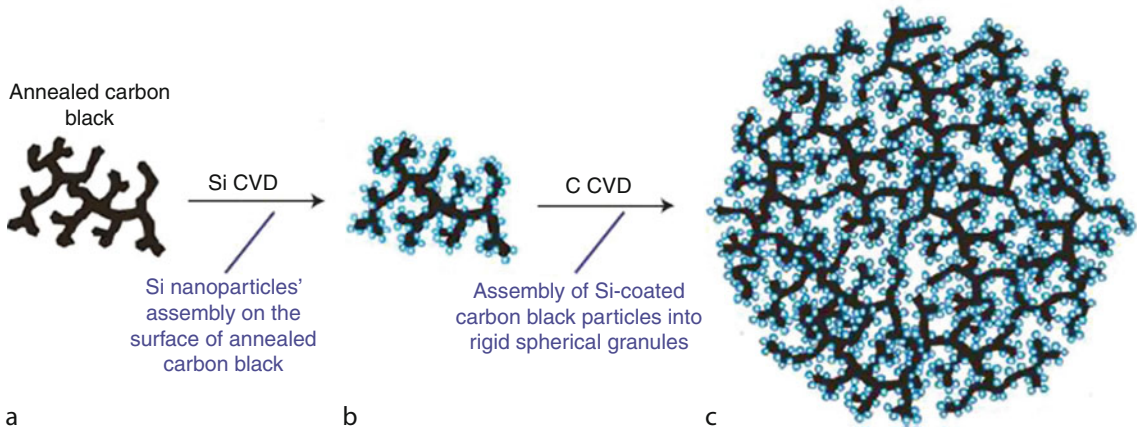

Silicon-Based Anodes for Li-Ion Batteries. Figure 12
Schematic of silicon/carbon nanocomposite granule formation through hierarchical bottom-up assembly. (**a**–**c**). Annealed carbon-black dendritic particles (**a**) are coated by silicon nanoparticles (**b**) and then assembled into rigid spheres with open interconnected internal channels during C deposition (**c**) (Reprinted with permission from Magasinski et al. [89]. Copyright 2010)

a PVDF-based binder exhibit poor cyclability. Therefore, significant efforts have been made during the last 10 years to develop new binders that can improve the performance of silicon-based anodes. Chen et al. [90] first reported that a poly(vinylidene fluoride–tetrafluoroethylene–propylene)-based elastomeric binder system kept the capacity of the amorphous $Si_{0.6}Sn_{0.4}$ alloy at around 800 mAh/g for 40 cycles, while the PVDF binder only showed ~490 mAh/g at the thirtieth cycle. Considering the fact that breakage elongation of the new elastomeric binder is much larger than that for PVDF [91, 92], the elastomeric binder could improve the cycling performance of a silicon-based alloy electrode.

In recent years, several new materials have been developed as effective binders for silicon-based anodes. Liu et al. [93] reported that the cycle life of silicon-based electrodes (either with or without carbon coating) was significantly improved by using a modified elastomeric binder containing styrene-butadiene-rubber (SBR) and sodium carboxylmethylcellulose (SCMC). When an SBR-SCMC mixture binder was used, the anodes with bare silicon and carbon-coated silicon exhibited a capacity of 600 mAh/g and 1,000 mAh/g, respectively at >50 cycles. In comparison, the capacity of a silicon electrode with a PVDF binder quickly decreased to several mAh/g after eight cycles. This is because the SBR-SCMC binder has a lower elastic modulus, a larger maximum elongation, better adhesion to the copper current collector, and much less solvent absorption in organic carbonate electrolytes. Several other research groups [46, 94–97] also have reported improved performance on silicon/carbon composite electrodes using an SBR-SCMC mixture binder over PVDF binder (sometimes combined with SBR [98]). Although a recent report shows that a thermally annealed PVDF can reconstruct the compact morphology of the electrode, the long-term cycling stability of a silicon electrode using an annealed PVDF binder is still inferior to that using CMC as the binder [99]. Li et al. [94] showed that the cycling performance of the crystalline silicon-powder electrode was improved further by using only SCMC as the binder over the SBR-SCMC mixture binder. Li et al. suggests that the stiff SCMC polymer might restrict the volume change of the silicon particles to only about 100% and also might modify the silicon particle surface. Thus, the binding mechanism of SCMC for a silicon electrode should be different from that of PVDF.

Hochgatterer et al. [100] reported that the improved long-term cycling behavior in an anode with an SCMC binder can be attributed to the formation of a covalent chemical bond between the SCMC

binder and the silicon particles. SCMC exhibits a porous scaffold structure with cavities or pores that allow the silicon particles to expand without severe deformation of the electrode. Therefore, the cycle stability can be improved. Lestrie et al. [96] suggested that the efficiency of SCMC was likely attributed to the formation of an efficient conductive silicon/carbon-SCMC network because of its extended conformation in solution. Moreover, the silicon/carbon-SCMC electrode prepared at pH 3 showed prolonged cyclability improvement, which probably resulted from the physical cross-linking of the SCMC chains in the acid solution. Guo and Wang [101] recently reported a polymer scaffold structure based on an SCMC binder for a silicon electrode. The SCMC scaffold-based silicon electrode had much higher surface area and total pore volume but a reduced mean pore diameter than the SCMC-based silicon electrode prepared using a conventional method. Therefore, silicon nanoparticle electrodes with a SCMC scaffold binder structure could accommodate greater volume changes from the silicon, enhance lithium-ion transport in the electrodes, and improve the electrochemical reaction kinetics. In addition, high energy and power densities and superb cycle stability were achieved for porous SCMC, scaffold-based silicon electrodes. After 150 cycles at a rate of 250 mA/g, the anode capacity remained at 1,685 mAh/g based on the weight of silicon. The improved rate performance of silicon is attributed to the SCMC scaffold, which facilitates lithium-ion transport in the porous electrode and accelerates the charge transfer reaction kinetics [101].

Although the binding mechanism of SCMC in silicon electrodes is unclear, the significant performance improvements observed drives efforts to optimize SCMC/silicon-based electrodes. In fact, some researchers believe that the binder plays a more important role than the nanostructure of the silicon particles on the performance of silicon-based anodes. Beattie et al. [102] reported that silicon-based electrodes with a relatively low silicon content (20–34 wt.%) and a high SCMC content (33–56 wt.%) had large capacities (660 mAh/g) for hundreds of cycles. They believed that, if an appropriate binder was used with silicon electrodes, no special electrode processing or cycling procedures were required to achieve high capacities with good cyclability.

Other Binders In addition to SCMC, several other polymeric binders have been developed for silicon-based anodes in recent years. Zheng et al. [103] reported that a nanoporous silicon/graphite/carbon composite electrode containing polyacrylic latex LA132 binder (10 wt.%) exhibited a reversible capacity of 650 mAh/g after 200 cycles with negligible capacity loss. Chen et al. [104] reported a significant cycling-performance enhancement for silicon/carbon composite electrodes using an acrylic adhesive (polyacrylic latex, LA132) and a modified acrylic adhesive with SCMC. The capacity retentions of the silicon/carbon composite electrodes were 79% and 90% after 50 cycles, respectively, while the silicon/carbon composite electrode with PVDF retained only 67% of its initial capacity. This was ascribed to improved adhesion between the coating and the copper current collector, as well as reduced solvent absorption of the electrolyte solvent than with PVDF. Polyamide imide (PAI) also can significantly improve the initial coulombic efficiency of a silicon-based anode because of PAI's excellent mechanical properties and ease of processing, which maintains the stability of the electrical-conducting network during charge/discharge processes [105].

Recently, Liu et al. [106] reported on conductive polymers used as both the binder and the conductive matrix. The electronic conductivity of the reported binder increases during the lithium-insertion process. Stable cycling above ~1,200 mAh/g (based on silicon) was reported for the silicon-based anode using these binders. The cycling stability of silicon improved significantly, especially within the reduced electrochemical window (0.17–0.9 V) [107]. However, the initial irreversible capacity loss in these anodes still requires further improvement (i.e., reduction) before these silicon-based anodes can be used in a full cell. Cámer et al. [108] reported that silicon-composite electrodes with very good electrochemical performance could be prepared by simply mixing appropriate amounts of nanosized silicon and cellulose fibers without including conductive carbon and other binders. A silicon/carbon cellulose composite electrode at a weight ratio of 34:66 exhibited very good cycling performance. A specific capacity of ~1,400 mAh/g after 50 cycles was obtained, compared to only 400 mAh/g for an electrode made from pure silicon. Cámer et al. believe that the improved performance

resulted from mitigation of the large volume changes of silicon particles during lithium insertion and de-insertion and the retention of connectivity between particles by the binder-like fibers.

Effect of Electrolytes on the Performance of Silicon-Based Anodes

The effect of nonaqueous electrolytes and additives on the performance of silicon electrodes has not been systematically investigated. The electrolytes used in the investigation of silicon-based electrodes were mainly adopted from electrolytes for graphite-based lithium-ion batteries (i.e., $LiPF_6$ in carbonate mixtures of EC and DMC, ethyl methyl carbonate [EMC] or diethyl carbonate [DEC]). Alternative electrolytes used in the study of silicon-based anodes include (1) adding SEI formation additives into the regular electrolytes of $LiPF_6$ in carbonates, (2) using different lithium salts, (3) using different solvent systems, (4) using ionic-liquid-based electrolytes, (5) using polymer electrolytes, and (6) using solid-state electrolytes. The effects of these electrolytes on the performance of a silicon-based electrode are reviewed in this section.

SEI Formation Additives Formation of the SEI layer plays an important role on the cycling stability of silicon-based anodes. Kulova and Skundin [109] reported a method used to preform the SEI layer on an electrode surface (prior to initial cathodic polarization) by direct contact of silicon and lithium metal in the electrolyte. The electrolyte was 1-M $LiClO_4$ in a mixture of propylene carbonate (PC) and dimethoxyethane. This method effectively reduced the irreversible capacity of the amorphous silicon electrode. Pretreatment of nanometer-sized silicon in ethanol also can form functionalized surfaces on the silicon particles that improve adhesion of silicon-based electrodes. A stable capacity of 2,500 mAh/g after 25 cycles has been reported for ethanol-treated silicon electrodes [110].

Several electrolyte additives have been used to form stable SEI layers and improve cyclability of silicon anodes. Doh et al. [111] used 5% 4-fluoroethylene carbonate (FEC) in the electrolyte of 1.0-M $LiPF_6$ in EC/DMC/EMC/PC at a volume ratio of 4:3:3:1 when investigating silicon/carbon composites formed by polyaniline carbonization. They found that the addition of FEC to the electrolyte increased the initial discharge capacity of the silicon/carbon composites when compared with the electrolyte without FEC. Choi et al. [112] reported that the discharge capacity retention and coulombic efficiency of a silicon thin-film electrode could be significantly improved by adding 3% of FEC into the electrolyte of 1.3-M $LiPF_6$ in EC/DEC (3:7 by volume). They used SEM and X-ray photoelectron spectroscopy (XPS) to investigate the surface morphology and chemical composition of the SEI layers formed on the surface of the silicon thin-film electrode after cycling. The SEI layer structure formed in the FEC-containing electrolyte was much smoother and more stable than those formed in electrolytes that did not contain the FEC additive. Chen et al. [113] investigated the effect of vinylene carbonate (VC) as an electrolyte additive on the electrochemical performance of a silicon thin-film anode. They found that the cycle performance and efficiency of the silicon thin-film anode were significantly enhanced with the addition of 1% VC into the electrolyte of 1-M $LiPF_6$ in EC/DMC. The capacity of the silicon thin film shows minimal fade after 500 cycles, which was attributed to the advanced properties of the SEI layer formed during the initial cycles. Actually, in both VC-containing and VC-free electrolytes, the major components of the SEI layer on the silicon thin-film anode were quite similar and primarily consist of lithium salts (e.g., $ROCO_2Li$, Li_2CO_3, LiF), polycarbonates, and silicon oxide formed through the reaction of lithiated silicon with permeated electrolyte. However, the morphology of the SEI layer was smoother and more uniform in VC-containing electrolytes than in VC-free electrolytes. The impedance of the SEI layer in VC-containing electrolytes did not change significantly upon cycling because of the presence of VC-reduced products and less LiF content in the SEI layer, which led to better properties of the SEI layer. However, the impedance of the SEI layer in a VC-free electrolyte increased constantly upon cycling because of the increasing thickness and high LiF content in the SEI layer, resulting in increased electrode polarization and degradation in the cycling performance of the silicon thin-film anode.

Han et al. [114] studied the effect of succinic anhydride (SA) as an electrolyte additive on the

electrochemical performances of a silicon thin-film electrode. They found that addition of a small amount (3 wt.%) of SA into the electrolyte of 1-M $LiPF_6$ in EC/DEC could significantly enhance the capacity retention and coulombic efficiency of the silicon electrode. SA also prevented decomposition of the $LiPF_6$ salt, and the SEI layer contained higher levels of hydrocarbon and Li_2CO_3 on the silicon surface. Modification to the SEI layer by SA was probably the primary factor for the enhanced performance of the silicon thin-film electrode. Baggetto et al. [115] used a poly-silicon thin film as the active anode material and cycled the poly-silicon anodes in one solid and two liquid electrolytes to investigate the thermodynamic and kinetic properties of the anodes and the growth of SEI layers on top of poly-silicon anodes. They studied the electrochemical and material characteristics of a potential planar anode stack (active anode material/barrier layer/silicon substrate) for all-solid-state, three-dimensional, integrated batteries. The solid-state electrolyte was amorphous lithium phosphorus oxynitride (LiPON), and the two liquid electrolytes were 1-M $LiPF_6$ in EC/DEC and 1-M $LiClO_4$ in PC. The silicon electrodes cycled in the two liquid electrolytes showed stable storage capacities up to about 30 or 40 cycles, respectively, then the capacities decreased sharply. When the inorganic solid-state electrolyte LiPON was used to overcoat the silicon, no degradation in capacity was observed for 60 cycles. Cross-sectional SEM analysis revealed thick, porous SEI layer formation in the case of $LiPF_6$ and $LiClO_4$ based electrolytes. The silicon layer was almost invisible, and it seemed to be "dissolved" within the SEI layer, implying that the active silicon clusters slowly became electronically isolated resulting in the loss of reversible capacity. In contrast, the silicon covered by a LiPON layer had no visible SEI layer formation and improved cycle life over cells that were LiPON-free.

Arie et al. [116] investigated the electrochemical characteristics of phosphorus- and boron-doped silicon thin-film (n-type and p-type silicon) anodes integrated with a solid polymer electrolyte in lithium-polymer batteries. The doped silicon electrodes showed enhanced discharge capacity and coulombic efficiency over the un-doped silicon electrode, and the phosphorus-doped, n-type silicon electrode showed the most stable cyclic performance after 40 cycles with a reversible specific capacity of about 2,500 mAh/g. The improved electrochemical performance of the doped silicon electrode was mainly due to enhancement of its electrical and lithium-ion conductivities and stable SEI layer formation on the surface of the electrode. In the case of the un-doped silicon electrode, an unstable surface layer formed on the electrode surface, and the interfacial impedance was relatively high, resulting in high electrode polarization and poor cycling performance.

Alternative Solvents and Salts Inose et al. [117] studied the influence of glyme-based electrolyte solutions on charge-discharge properties of two silicon-based anodes prepared from (1) a silicon/carbon mixture and (2) a mixture of a silicon-SiO_2-carbon composite and carbon (Si-C/C). After glymes of poly(ethylene glycol) dimethyl ethers [$(CH_3O(CH_2CH_2O)_nCH_3$, $n = 1, 2, 3$ and 4)] were added into an electrolyte solution of 1 M $LiPF_6$ in EC and EMC (3:7 by vol), the discharge capacity tended to increase relative to electrolytes without glyme additions. Carbon coating of the silicon particles in the Si-C/C electrode improved cycle life when compared to the silicon/carbon electrode. Physical breakdown of the electrode was suppressed by the thin carbon surface layer, and reactivity of electrolyte toward lithium metal also was reduced. They also found that the discharge capacity of the silicon/carbon electrode was dependent on the reduction potential of the glymes, while the discharge capacity of the Si-C/C electrode depended on electrolyte conductivity.

Choi et al. [118] compared the effect of two different lithium salts on the cycling performance of a 200-nm silicon thin-film electrode. The electrolytes tested were 1.3-M $LiPF_6$ in EC/DEC (3:7 by vol) and 0.7-M lithium bis(oxalato) borate (LiBOB) in the same solvent mixture. They found that the LiBOB-based electrolyte markedly improved the discharge capacity retention of the lithium-silicon half-cell, over the $LiPF_6$-based electrolyte. The surface layer on the silicon electrode in the LiBOB-based electrolyte was less porous and effectively limited the formation of electrochemically inactive silicon phases. The capacity fading of the lithium-silicon half-cell was strongly related to the physical

morphology of the silicon surface and also to the formation of inactive silicon phases in the surface layer.

Ionic liquids have also been studied as possible electrolytes in silicon-based anode cells. Lux et al. [119] evaluated the use of N-butyl-N-methylpyrrolidinium bis(trifluoromethylsulfonyl)imide (PYR14TFSI) as a solvent for silicon electrodes at room temperature. The electrolyte contained 0.3-M lithium bis(trifluoromethylsulfonyl)imide ($LiN(SO_2CF_3)_2$, LiTFSI) in PYR14TFSI+5 wt.% VC. The performance of silicon electrodes in PYR14TFSI-based electrolytes was comparable with that of the same electrodes in more conventional organic solvent-based electrolytes. The degree of affinity between ionic liquids and active materials was suggested as an important parameter for the selection and use of ionic liquids in lithium batteries.

Full Cells Containing Silicon-Based Anodes

To fully evaluate the efficacy of silicon-based anodes, testing in a full-cell configuration against a lithium intercalation cathode, such as $LiCoO_2$, is required because of possible detrimental interactions between the cathode and anode (through electrolyte as the media), as was discovered in the case of graphite/$LiMn_2O_4$. In addition, the management of volume change in the complete cells is not a trivial challenge for silicon-based cells where the anode exhibits large volume variations during cycling. Nonetheless, studies of electrochemical performance for silicon-anode-based full batteries are rare, possibly because of the poor cycling performance of these anodes, which remains a hurdle to practical application of the technology.

Cui et al. [120] reported a full-cell test using a $LiCoO_2$ cathode and carbon-silicon core-shell nanowire anode. This anode has about 10 times the specific capacity of the cathode and, therefore, a mass loading approximately 10 times lower than that of the cathode. The full cell operated at ~3.3 V with a sloping voltage profile and a fast fade of ~0.7% per cycle. The same group also reported full battery performance of the silicon nanowire anode and sulfur-based cathode pair [121]. Although the voltage profile of the full-cell test revealed large over-potentials because of poor electrical conductivity of the Li_2S cathode, the specific energy density of the battery was reported to be approximately four times higher than the current $LiCoO_2$/graphite-based, lithium-ion battery mostly because of the high specific capacity of the sulfur cathode. High-voltage $LiNi_{0.5}Mn_{1.5}O_4$ also has been paired with silicon nanoparticles to form a full-cell battery [122]. The cycling performance at increased operating voltage resulted in higher specific capacity than a conventional $LiCoO_2$/graphite-based commercial battery. However, the cycling stability of this battery is still problematic. There also are reports of thin-film batteries using amorphous silicon anodes paired with $LiMn_2O_4$ [123] or $LiCoO_2$ cathodes [124–126] with better cyclability than the similar bulk batteries, but large-scale manufacturing of thin-film batteries is hindered by the high manufacturing cost of these materials.

Future Directions

Although the silicon-based anode has great potential to significantly improve the capacity of lithium-ion batteries, there are still many obstacles that prevent its practical application. Long-term cycling stability remains the foremost challenge facing the battery research community. The cyclability of full cells using silicon-based anodes is complicated by multiple factors, such as diffusion-induced stress and fracture [127], loss of electrical contact among silicon particles and between silicon and current collector, and the breakdown of SEI layers during volume expansion/contraction processes. A detailed study of the design and engineering of a full cell with a silicon-based anode still needs to be conducted after a stable silicon-based anode structure is developed. Critical research remaining in this area includes, but is not limited to, the following:

- Further understanding of the effect of SEI formation on the cyclability of silicon-based anodes. Electrolytes and additives that can produce a stable SEI layer need to be developed. In situ SEM of working electrochemical test cells could be a very useful tool to directly observe the formation and evolution of SEI layers.
- The effect of particle size and the mechanical stability of silicon particles need to be understood.

A theoretical model needs to be developed to find the critical dimension at which silicon particles are stable under long-term expansion/shrinking cycles.

- A good binder and conductive matrix (such as carbon) need to be developed. They should provide flexible but stable electrical contacts among silicon particles and between particles and the current collector under repeated volume changes during charge/discharge processes. The specific capacity of the complete anode (including the silicon, binder, and conductive matrix) needs further optimization. An acceptable balance between the specific capacity and the long-term stability of the anode also is needed. Considering the fact that the specific capacity of state-of-the-art cathodes is between ~140 mAh/g and 200 mAh/g, Kasavajjula et al. [24] suggest that improvement in the total capacity of an 18,650 cell is negligible after the anode specific capacity reaches more than 1,200 mAh/g if other components of the batteries remain unchanged. Based on this analysis, a specific capacity of ~1,200 mAh/g for the complete anode with a loading of 5–10 mg/cm^2 would be a reasonable technical target. Improvement in cycling stability remains the primary challenge for silicon-based anodes.
- The performance of full cells needs to be studied and optimized. Parameters to be optimized include cell geometry, anode and cathode balancing, accommodation of volume expansion, and electrolyte/additive selection.

Last, it should be recognized that the overall effect of the high-capacity anode on the performance of lithium-ion batteries is limited primarily because the anode only occupies a relatively small portion of the total weight (15–20%) and volume of the lithium-ion battery [128]. An anode with infinite specific capacity (or zero weight) could only lead to less than a 20% reduction in the total weight of the system, if other components of the battery remain the same. Many factors affect the total specific capacity and weight/volume of a full battery, such as the specific capacities of the anode and cathode, electrolyte, separator, current collectors, and case. Therefore, significant improvements in both the anode and the cathode, as well as other battery components, must be achieved to realize the goal of producing widely applied, high-energy batteries.

Bibliography

1. Boukamp BA, Lesh GC, Huggins RA (1981) All-solid lithium electrodes with mixed-conductor matrix. J Electrochem Soc 128:725–729
2. Dey AN (1971) Electrochemical, alloying of lithium in organic electrolytes. J Electrochem Soc 118:1547–1549
3. Tirado JL (2003) Inorganic, materials for the negative electrode of lithium-ion batteries: state-of-the-art and future prospects. Mater Sci Eng R Rep 40:103–136
4. Winter M, Besenhard JO (1999) Electrochemical lithiation of tin and tin-based intermetallics and composites. Electrochim Acta 45:31–50
5. Kim I-S (2003) Synthesis, structure and properties of electrochemically active nanocomposites. Ph.D thesis, Carnegie Mellon University
6. Sharma RA, Seefurth RN (1976) Thermodynamic properties of the lithium-silicon system. J Electrochem Soc 123:1763–1768
7. van der Marel C, Vinke GJB, van der Lugt W (1985) The phase diagram of the system lithium-silicon. Solid State Commun 54:917–919
8. Lai S-C (1976) Solid lithium-silicon electrode. J Electrochem Soc 123:1196–1197
9. Li H et al (2000) The crystal structural evolution of nano-Si anode caused by lithium insertion and extraction at room temperature. Solid State Ionics 135:181–191
10. Limthongkul P, Jang Y-I, Dudney NJ, Chiang Y-M (2003) Electrochemically-driven solid-state amorphization in lithium-silicon alloys and implications for lithium storage. Acta Mater 51:1103–1113
11. Limthongkul P, Jang Y-I, Dudney NJ, Chiang Y-M (2003) Electrochemically-driven solid-state amorphization in lithium-metal anodes. J Power Sources 119–121:604–609
12. Maranchi JP, Hepp AF, Kumta PN (2003) High capacity reversible silicon thin film anodes lithium ion batteries. Electrochem Solid-State Lett 6:A198–A201
13. Ryu JH, Kim JW, Sung Y-E, Oh SM (2004) Failure modes of silicon powder negative electrode in lithium secondary batteries. Electrochem Solid-State Lett 7:A306–A309
14. Li J, Dahn JR (2007) An in situ x-ray diffraction study of the reaction of Li with crystalline Si. J Electrochem Soc 154: A156–A161
15. Obrovac MN, Christensen L (2004) Structural changes in silicon anodes during lithium insertion/extraction. Electrochem Solid-State Lett 7:A93–A96
16. Hatchard TD, Dahn JR (2004) In situ XRD and electrochemical study of the reaction of lithium with amorphous silicon. J Electrochem Soc 151:A838–A842
17. Datta MK, Kumta PN (2009) In situ electrochemical synthesis of lithiated silicon-carbon based composites anode materials for lithium ion batteries. J Power Sources 194:1043–1052
18. Wang W, Kumta PN (2010) Nanostructured hybrid silicon/carbon nanotube heterostructures: reversible high-capacity lithium-ion anodes. ACS Nano 4:2233–2241

19. Obrovac MN, Krause LJ (2007) Reversible cycling of crystalline silicon powder. J Electrochem Soc 154:A103–A108
20. Beaulieu LY, Eberman KW, Turner RL, Krause LJ, Dahn JR (2001) Colossal reversible volume changes in lithium alloys. Electrochem Solid-State Lett 4:A137–A140
21. Park MH et al (2009) Silicon nanotube battery anodes. Nano Lett 9:3844–3847
22. Datta MK, Kumta PN (2006) Silicon and carbon based composite anodes for lithium ion batteries. J Power Sources 158: 557–563
23. Sandia National Laboratories. Sandia National Laboratories News Releases. Sandia National Laboratories, Livermore, CA, 6 March 2003
24. Kasavajjula U, Wang C, Appleby AJ (2007) Nano- and bulk-silicon-based insertion anodes for lithium-ion secondary cells. J Power Sources 163:1003–1039
25. Larcher D et al (2007) Recent findings and prospects in the field of pure metals as negative electrodes for Li-ion batteries. J Mater Chem 17:3759–3772
26. Timmons A et al (2007) Studies of Si[sub 1 – x]C[sub x] electrode materials prepared by high-energy mechanical milling and combinatorial sputter deposition. J Electrochem Soc 154: A865–A874
27. Huggins RA (1999) Lithium, alloy negative electrodes. J Power Sources 81–82:13–19
28. Mao O et al (1999) Active/inactive nanocomposites as anodes for Li-ion batteries. Electrochem Solid-State Lett 2:3–5
29. Weydanz WJ, Wohlfahrt-Mehrens M, Huggins RA (1999) A room temperature study of the binary lithium-silicon and the ternary lithium-chromium-silicon system for use in rechargeable lithium batteries. J Power Sources 81–82: 237–242
30. Courtney IA, McKinnon WR, Dahn JR (1999) On the aggregation of tin in SnO composite glasses caused by the reversible reaction with lithium. J Electrochem Soc 146:59–68
31. Mayo MJ (1997) High, and low temperature superplasticity in nanocrystalline materials. Nanostruct Mater 9:717–726
32. Wang W (2009) Silicon Based Nanocomposites as Lithium-ion Battery Anodes. PhD dissertation, Carnegie Mellon University
33. Idota Y, Kubota T, Matsufuji A, Maekawa Y, Miyasaka T (1997) Tin-based amorphous oxide: a high-capacity lithium-ion-storage material. Science 276:1395–1397
34. Hwang S-M et al (2001) Lithium insertion in SiAg powders produced by mechanical alloying. Electrochem Solid-State Lett 4:A97–A100
35. Kim H, Choi J, Sohn H-J, Kang T (1999) The insertion mechanism of lithium into Mg[sub 2]Si anode material for Li-ion batteries. J Electrochem Soc 146:4401–4405
36. Kim I-S, Kumta PN, Blomgren GE (2000) Si/TiN nanocomposites novel anode materials for Li-ion batteries. Electrochem Solid-State Lett 3:493–496
37. Kim I-S, Blomgren GE, Kumta PN (2004) Si-SiC nanocomposite anodes synthesized using high-energy mechanical milling. J Power Sources 130:275–280
38. Kim I-S, Blomgren GE, Kumta PN (2003) Nanostructured Si/TiB_2 composite anodes for Li-ion batteries. Electrochem Solid-State Lett 6:A157–A161
39. Wang CS, Wu GT, Zhang XB, Qi ZF, Li WZ (1998) Lithium insertion in carbon-silicon composite materials produced by mechanical milling. J Electrochem Soc 145:2751–2758
40. Gross KJ, Wang JCF, Roberts GA (2004) Synthesis of carbon/silicon composites. US Patent 2004/137,327 (2004)
41. Kim I-S, Kumta PN (2004) High capacity Si/C nanocomposite anodes for Li-ion batteries. J Power Sources 136:145–149
42. Wilson AM, Reimers JN, Fuller EW, Dahn JR (1994) Lithium insertion in pyrolyzed siloxane polymers. Solid State Ionics 74:249–254
43. Yang J et al (2003) Si/C composites for high capacity lithium storage materials. Electrochem Solid-State Lett 6: A154–A156
44. Xie J, Cao GS, Zhao XB (2004) Electrochemical performances of Si-coated MCMB as anode material in lithium-ion cells. Mater Chem Phys 88:295–299
45. Holzapfel M et al (2005) Chemical vapor deposited silicon/graphite compound material as negative electrode for lithium-ion batteries. Electrochem Solid-State Lett 8:A516–A520
46. Holzapfel M, Buqa H, Scheifele W, Novak P, Petrat F-M (2005) A new type of nano-sized silicon/carbon composite electrode for reversible lithium insertion. Chem Commun 1566–1568
47. Dimov N, Fukuda K, Umeno T, Kugino S, Yoshio M (2003) Characterization of carbon-coated silicon: structural evolution and possible limitations. J Power Sources 114:88–95
48. Liu W-R et al (2005) Electrochemical characterizations on Si and C-coated Si particle electrodes for lithium-ion batteries. J Electrochem Soc 152:A1719–A1725
49. Yu M-F, Files BS, Arepalli S, Ruoff RS (2000) Tensile loading of ropes of single wall carbon nanotubes and their mechanical properties. Phys Rev Lett 84:5552
50. Krishnan A, Dujardin E, Ebbesen TW, Yianilos PN, Treacy MMJ (1998) Young's modulus of single-walled nanotubes. Phys Rev B 58:14013
51. Wong EW, Sheehan PE, Lieber CM (1997) Nanobeam mechanics: elasticity, strength, and toughness of nanorods and nanotubes. Science 277:1971–1975
52. Roche S (2000) Carbon nanotubes: exceptional mechanical and electronic properties. Ann Chim Sci Matériaux 25:529–532
53. Zhao Q, Nardelli MB, Bernholc J (2002) Ultimate strength of carbon nanotubes: a theoretical study. Phys Rev B 65:144105
54. Demczyk BG et al (2002) Direct mechanical measurement of the tensile strength and elastic modulus of multiwalled carbon nanotubes. Mater Sci Eng A 334:173–178
55. Thess A et al (1996) Crystalline ropes of metallic carbon nanotubes. Science 273:483–487
56. Yao Z, Kane CL, Dekker C (2000) High-field electrical transport in single-wall carbon nanotubes. Phys Rev Lett 84:2941
57. Frank S et al (1998) Carbon nanotube quantum resistors. Science 280:1744–1746

58. Shu J, Li H, Yang R, Shi Y, Huang X (2006) Cage-like carbon nanotubes/Si composite as anode material for lithium ion batteries. Electrochem Commun 8:51–54
59. Wang W, Kumta PN (2007) Reversible high capacity nanocomposite anodes of Si/C/SWNTs for rechargeable Li-ion batteries. J Power Sources 172:650–658
60. Si Q et al (2010) A high performance silicon/carbon composite anode with carbon nanofiber for lithium-ion batteries. J Power Sources 195:1720–1725
61. Guo JC, Sun A, Wang CS (2010) A porous silicon-carbon anode with high overall capacity on carbon fiber current collector. Electrochem Commun 12:981–984
62. Lee J et al (2009) Effect of randomly networked carbon nanotubes in silicon-based anodes for lithium-ion batteries. J Electrochem Soc 156:A905–A910
63. Jang S-M, Miyawaki J, Tsuji M, Mochida I, Yoon S-H (2009) The preparation of a novel Si-CNF composite as an effective anodic material for lithium-ion batteries. Carbon 47:3383–3391
64. Yang J, Winter M, Besenhard JO (1996) Small particle size multiphase Li-alloy anodes for lithium-ionbatteries. Solid State Ionics 90:281–287
65. Yang J, Takeda Y, Imanishi N, Ichikawa T, Yamamoto O (2000) SnSbx-based composite electrodes for lithium ion cells. Solid State Ionics 135:175–180
66. Yang J, Takeda Y, Imanishi N, Yamamoto O (1999) Ultrafine Sn and $SnSb_{0.14}$ Powders for lithium storage matrices in lithium-ion batteries. J Electrochem Society 146:4009–4013
67. Huggins R, Nix W (2000) Decrepitation model for capacity loss during cycling of alloys in rechargeable electrochemical systems. Solid State Ionics 6:57–63
68. Li H, Huang X, Chen L, Wu Z, Liang Y (1999) A high capacity nano-Si composite anode material for lithium rechargeable batteries. Electrochem Solid-State Lett 2:547–549
69. Beaulieu LY, Dahn JR (2000) The reaction of lithium with Sn-Mn-C intermetallics prepared by mechanical alloying. J Electrochem Soc 147:3237–3241
70. Gleiter H (1989) Nanocrystalline materials. Prog Mater Sci 33:223–315
71. Graetz J, Ahn CC, Yazami R, Fultz B (2003) Highly reversible lithium storage in nanostructured silicon. Electrochem Solid-State Lett 6:A194–A197
72. Maranchi JP, Hepp AF, Evans AG, Nuhfer NT, Kumta PN (2006) Interfacial properties of the a-Si/Cu:active–inactive thin-film anode system for lithium-ion batteries. J Electrochem Soc 153:A1246–A1253
73. Kim J-B, Lee H-Y, Lee K-S, Lim S-H, Lee S-M (2003) Fe/Si multilayer thin film anodes for lithium rechargeable thin film batteries. Electrochem Commun 5:544–548
74. Kim Y-L et al (2003) Electrochemical characteristics of Co-Si alloy and multilayer films as anodes for lithium ion microbatteries. Electrochim Acta 48:2593–2597
75. Lee KL, Jung JY, Lee SW, Moon HS, Park JW (2004) Electrochemical characteristics of a-Si thin film anode for Li-ion rechargeable batteries. J Power Sources 129:270–274
76. Kim YL, Sun YK, Lee SM (2008) Enhanced electrochemical performance of silicon-based anode material by using current collector with modified surface morphology. Electrochim Acta 53:4500–4504
77. Yonezu I, Tarui H, Yoshimura S, Fujitani S, Nohma T (2004) Abstracts of the 12th International Meeting on Lithium Batteries, vol 58. Electrochemical Society, Nara, Japan, 2004
78. Lee JK, Smith KB, Hayner CM, Kung HH (2010) Silicon nanoparticles-graphene paper composites for Li ion battery anodes. Chem Commun 46:2025–2027
79. Chou SL et al (2010) Enhanced reversible lithium storage in a nanosize silicon/graphene composite. Electrochem Commun 2:303–306
80. Chan CK et al (2008) High-performance lithium battery anodes using silicon nanowires. Nat Nanotechnol 3:31–35
81. Yu DP et al (2001) Controlled growth of oriented amorphous silicon nanowires via a solid-liquid-solid (SLS) mechanism. Physica E 9:305–309
82. Kolb FM et al (2004) Analysis of silicon nanowires grown by combining SiO evaporation with the VLS mechanism. J Electrochem Soc 151:G472–G475
83. Chang JB et al (2006) Ultrafast growth of single-crystalline Si nanowires. Mater Lett 60:2125–2128
84. Zhang JG et al (2010) Vapor-induced solid–liquid–solid process for silicon-based nanowire growth. J Power Sources 195:1691–1697
85. Kim H, Han B, Choo J, Cho J (2008) Three-dimensional porous silicon particles for use in high-performance lithium secondary batteries. Angew Chem Int Ed 47:10151–10154
86. Zheng Y, Yang J, Wang JL, NuLi YN (2007) Nano-porous Si/C composites for anode material of lithium-ion batteries. Electrochim Acta 52:5863–5867
87. Xiao J et al (2010) Stabilization of silicon anode for Li-ion batteries. J Electrochem Soc 157:A1047–A1051
88. Ma H et al (2007) Nest-like silicon nanospheres for high-capacity lithium storage. Adv Mater 19:4067–4070
89. Magasinski A et al (2010) High-performance lithium-ion anodes using a hierarchical bottom-up approach. Nat Mat 9:353–358
90. Chen ZH, Christensen L, Dahn JR (2003) Large-volume-change electrodes for Li-ion batteries of amorphous alloy particles held by elastomeric tethers. Electrochem Commun 5:919–923
91. Chen ZH, Christensen L, Dahn JR (2003) Comparison of PVDF and PVDF-TFE-P as binders for electrode materials showing large volume changes in lithium-ion batteries. J Electrochem Soc 150:A1073–A1078
92. Chen ZH, Christensen L, Dahn JR (2004) Mechanical and electrical properties of poly(vinylidene fluoride-tetrafluoroethylene-propylene)/super-S carbon black swelled in liquid solvent as an electrode binder for lithium-ion batteries. J Appl Polym Sci 91:2958–2965
93. Liu WR, Yang MH, Wu HC, Chiao SM, Wu NL (2005) Enhanced cycle life of Si anode for Li-ion batteries by using modified elastomeric binder. Electrochem Solid-State Lett 8:A100–A103
94. Li J, Lewis RB, Dahn JR (2007) Sodium carboxymethyl cellulose – a potential binder for Si negative electrodes for Li-ion batteries. Electrochem Solid-State Lett 10:A17–A20

95. Dimov N, Xia Y, Yoshio M (2007) Practical silicon-based composite anodes for lithium-ion batteries: Fundamental and technological features. J Power Sources 171:886–893
96. Lestrie B, Bahri S, Sandu I, Roue L, Guyomard D (2007) On the binding mechanism of CMC in Si negative electrodes for Li-ion batteries. Electrochem Commun 9:2801–2806
97. Key B et al (2009) Real-time NMR investigations of structural changes in silicon electrodes for lithium-ion batteries. J Am Chem Soc 131:9239–9249
98. Buqa H, Holzapfel M, Krumeich F, Veit C, Novak P (2006) Study of styrene butadiene rubber and sodium methyl cellulose as binder for negative electrodes in lithium-ion batteries. J Power Sources 161:617–622
99. Xu YH, Yin GP, Ma YL, Zuo PJ, Cheng XQ (2010) Simple annealing process for performance improvement of silicon anode based on polyvinylidene fluoride binder. J Power Sources 195:2069–2073
100. Hochgatterer NS et al (2008) Silicon/graphite composite electrodes for high-capacity anodes: Influence of binder chemistry on cycling stability. Electrochem Solid-State Lett 11: A76–A80
101. Guo JC, Wang CS (2010) A polymer scaffold binder structure for high capacity silicon anode of lithium-ion battery. Chem Commun 46:1428–1430
102. Beattie SD, Larcher D, Morcrette M, Simon B, Tarascon JM (2008) Si electrodes for Li-ion batteries – a new way to look at an old problem. J Electrochem Soc 155:A158–A163
103. Zheng Y, Yang J, Tao L, Nuli YN, Wang JL (2007) Study of nano-porous Si/Graphite/C composite anode materials for Li-ion batteries. Chin J Inorg Chem 23:1882–1886
104. Chen LB, Xie XH, Xie JY, Wang K, Yang J (2006) Binder effect on cycling performance of silicon/carbon composite anodes for lithium ion batteries. J Appl Electrochem 36:1099–1104
105. Choi NS, Yew KH, Choi WU, Kim SS (2008) Enhanced electrochemical properties of a Si-based anode using an electrochemically active polyamide imide binder. J Power Sources 177:590–594
106. Liu G (2010) DOE hydrogen program and vehicle technologies program annual merit review and peer evaluation meeting. Department of Energy, Office of Energy Efficiency & Renewable Energy, Washington DC, 2010
107. Zhang JG, Liu J (2010) DOE hydrogen program and vehicle technologies program annual merit review and peer evaluation meeting. Department of Energy, Office of Energy Efficiency & Renewable Energy, Washington DC, 2010
108. Carmer JLG, Morales J, Sanchez L (2008) Nano-Si/cellulose composites as anode materials for lithium-ion batteries. Electrochem Solid-State Lett 11:A101–A104
109. Kulova TL, Skundin AM (2010) Elimination of irreversible capacity of amorphous silicon: direct contact of the silicon and lithium metal. Rus J Electrochem 46:470–475
110. Urbonaite S, Baglien I, Ensling D, Edstrom K (2010) Effect of ethanol-assisted electrode fabrication on the performance of silicon anodes. J Power Sources 195:5370–5373
111. Doh CH et al (2006) Synthesis of silicon-carbon by polyaniline coating and electrochemical properties of the Si-C vertical bar Li cell. Bull Korean Chem Soc 27:1175–1180
112. Choi NS et al (2006) Effect of fluoroethylene carbonate additive on interfacial properties of silicon thin-film electrode. J Power Sources 161:1254–1259
113. Chen LB, Wang K, Xie XH, Xie JY (2007) Effect of vinylene carbonate (VC) as electrolyte additive on electrochemical performance of Si film anode for lithium ion batteries. J Power Sources 174:538–543
114. Han GB, Ryou MH, Cho KY, Lee YM, Park JK (2010) Effect of succinic anhydride as an electrolyte additive on electrochemical characteristics of silicon thin-film electrode. J Power Sources 195:3709–3714
115. Baggetto L et al (2009) On the electrochemistry of an anode stack for all-solid-state 3D-integrated batteries. J Power Sources 189:402–410
116. Arie AA, Chang W, Lee JK (2010) Electrochemical characteristics of semi conductive silicon anode for lithium polymer batteries. J Electroceramics 24:308–312
117. Inose T, Watanabe D, Morimoto H, Tobishima SI (2006) Influence of glyme-based nonaqueous electrolyte solutions on electrochemical properties of Si-based anodes for rechargeable lithium cells. J Power Sources 162:1297–1303
118. Choi NS, Yew KH, Kim H, Kim SS, Choi WU (2007) Surface layer formed on silicon thin-film electrode in lithium bis(oxalato) borate-based electrolyte. J Power Sources 172:404–409
119. Lux SF et al (2010) Li-ion anodes in air-stable and hydrophobic ionic liquid-based electrolyte for safer and greener batteries. Int J Energy Res 34:97–106
120. Cui LF, Yang Y, Hsu CM, Cui Y (2009) Carbon – silicon core – shell nanowires as high capacity electrode for lithium ion batteries. Nano Lett 9:3370–3374
121. Yang Y et al (2010) New nanostructured Li2S/silicon rechargeable battery with high specific energy. Nano Lett 10:1486–1491
122. Arrebola JC et al (2009) Combining 5 V LiNi0.5Mn1.5O4 spinel and Si nanoparticles for advanced Li-ion batteries. Electrochem Commun 11:1061–1064
123. Lee K-L, Jung J-Y, Lee S-W, Moon H-S, Park J-W (2004) Electrochemical characteristics and cycle performance of LiMn2O4/a-Si microbattery. J Power Sources 130:241–246
124. Yin J et al (2006) Micrometer-scale amorphous Si thin-film electrodes fabricated by electron-beam deposition for Li-ion batteries. J Electrochem Soc 153:A472–A477
125. Baranchugov V, Markevich E, Pollak E, Salitra G, Aurbach D (2007) Amorphous silicon thin films as a high capacity anodes for Li-ion batteries in ionic liquid electrolytes. Electrochem Commun 9:796–800
126. Yang H et al (2007) Amorphous Si film anode coupled with $LiCoO_2$ cathode in Li-ion cell. J Power Sources 174:533–537
127. Christensen J (2010) Modeling diffusion-induced stress in Li-Ion cells with porous electrodes. J Electrochem Soc 157: A366–A380
128. Gaines L, a.C., Roy in http://www.transportation.anl.gov/pdfs/TA/149.pdf

Simulation Models as Tools for Crop Management

Herman van Keulen
Chairgroup Plant Production Systems, Wageningen University, Wageningen, The Netherlands
Business Unit Agrosystems Research, Plant Research International, Wageningen University and Research Centre, Wageningen, The Netherlands

Article Outline

Glossary
Definition of the Subject
Introduction
Simulation Models in Support of Crop Management
Future Directions
Bibliography

Glossary

Strategic crop management Decisions with respect to agro-ecosystems on the basis of the expected long-term performance of these systems, as influenced by the natural resource base and the socioeconomic boundary conditions, independent of the current state of the system.

Tactical crop management Seasonal decision-making in reaction to the variable and unpredictable environment, with a time horizon of the order of 1 year, independent of the current state of the system.

Operational crop management Decisions concerned with daily activities of the farm, in response to the current state of the system and the (anticipated) environment.

Simulation Building a model and studying its dynamic behavior.

Model Simplified description of a system.

System A limited part of reality with well-defined boundaries, containing related elements.

Decision support system (DSS) A class of information systems (including but not limited to computerized systems) that support business and organizational decision-making activities. A properly designed DSS is an interactive software-based system, intended to help decision makers compile useful information from a combination of raw data, documents, personal knowledge, or business models to identify and solve problems and make decisions.

Farming system The particular mix of agricultural activities in which a farm household engages.

Definition of the Subject

Agricultural production can be defined as the transformation of sun energy in useful organic material in the form of food, feed, and fiber. The transformation requires in principle only limited resources: a piece of land, some seeds from a wanted plant species, some sun and rain, and some human labor. However, the transformation takes place under erratic and unpredictable conditions, as especially the availability and timing of the sun and the rain are extremely difficult, if not impossible to predict, while their effects are modified by the qualities of the land and the interventions of the farmer. Any methodology that would improve the predictability of the availability of the resources and their impact on the performance of the production system could in principle improve that performance and reduce the level of uncertainty. Crop growth simulation models that were developed from the late 1960s onward and that allowed exploration of the performance of plant production systems as governed by the properties of the plant species/variety in interaction with the environmental conditions, promised to be excellent tools for the reduction of this uncertainty. Following 40 years of experience in this realm of the application of crop growth simulation models in support of the management of plant production systems, the current situation is still highly ambiguous. On the one hand, some of the modelers still advocate the use of these tools in crop management, while many others have become disenchanted and emphasize their limited impact on crop performance. Although definitely the last word has not been said about their advantages and disadvantages, in this contribution an attempt will be made to summarize the past experiences and the current state of affairs, and to make an effort to identify their possible contribution in the future. As mentioned, there appear large differences among agricultural and systems-analytical specialists in judging the contribution and the possibilities for application of crop growth models in

support of crop management, and thus this contribution will not lead to unequivocal judgments and recommendations, but it should serve as a starting point for those interested in the subject.

Introduction

Crop Management

Performance of agricultural production systems at any given location is determined on the one hand by the agro-technical possibilities and constraints and on the other by the socio-economic conditions under which the farmer and his customers operate. The agro-technical possibilities are largely determined by the quality of the natural resources, most importantly, soil characteristics and the prevailing climatic conditions. Agricultural systems that have developed in various regions are therefore strongly linked to these characteristics of the environment. However, within comparable natural environments, the viability of various agricultural systems is dependent on the socio-economic environment, which can broadly be characterized by the prevailing price ratios of crop products and inputs, modified by other factors, such as the risk that can be accepted, access to credit facilities, and the relative importance attached to other objectives than purely economic, for example, environmental considerations. In agricultural production systems, decision making can be schematically subdivided in three hierarchical levels [1]. The first level is that of *strategic management*, that is, strategic decisions with respect to agro-ecosystems, made on the basis of expected long-term performance of these systems, determined by the (quality of the) natural resource base and the socio-economic boundary conditions, but independent of the current state of the system and its expected short-term performance. Strategic management is mainly oriented toward long-term planning and deals with the selection of farming systems, that is, the particular mix of agricultural activities in which the farm household engages (e.g., arable farming, horticulture, animal husbandry), and the associated investment decisions. The time horizon for such decisions varies therefore from more than 1 year up to 10 or 20 years, that is, the time it takes, for instance, for machinery to become technically obsolete, or for farmers to become acquainted with new production techniques.

Once the strategic decisions have led to the selection of a certain cropping system, the farmer, in actual practice, is faced with the task of implementing a certain number of crop systems. A conspicuous characteristic of agricultural production systems is that they operate in highly variable and hardly predictable natural environments [2]. Although climate for a given region may be characterized on the basis of long-term records, that hardly helps the farmer in his actual decision-making, as year-to-year variability is generally large and the actual performance of the system is dependent on weather conditions rather than on climate. Therefore, in most agricultural production systems, the quality of the *tactical decision-making process*, that is, the reaction to this variable and unpredictable environment, is a major factor in determining their success. The time horizon of tactical management, that is, seasonal decision making, is therefore in the order of 1 year, dealing with such issues as the selection of a specific crop (and/or variety) mix to be cultivated and the allocation of land, both in terms of how much and where, to the various crops.

Finally, decisions at the *operational level* are mainly concerned with daily activities on the farm, such as selection of sowing dates, water (irrigation), nutrient (fertilizer), and pest and disease management, and time horizons varying from days to, sometimes, hours in relation to decisions on spraying and harvesting.

Crop Modeling

Crop modeling as a scientific activity has been in existence now for almost 50 years, following among others, the pioneering work of De Wit (cf. [3–5]). Its history and its position within current agricultural research have been dealt with extensively in the last two decades from various angles [6–10]. An interesting analysis is that of Sinclair and Seligman [6], who draw parallels between the growth and development of crop simulation models and human development. Their overview ranges from *birth* and *infancy* of the discipline with the appearance of mainframe computers in the 1960s, via a *juvenile* stage in the 1970s, and an *adolescent* stage in the 1980s, to a *maturity* stage in the 1990s. The *infancy* and *juvenile* stages were characterized by the expectation that crop modeling would provide the answers to questions in many areas of crop science, which led to

the development of detailed "comprehensive" models, aiming mainly at increasing understanding of the interactions between the crop and its environment.

These development stages of the models were subsequently translated into functional categories [9], that is, in the 1960s and 1970s, the main aim of these modeling activities was to generate understanding at the crop scale, on the basis of the underlying processes and to test hypotheses on crop-physiological functioning, as illustrated among others in the series Simulation Monographs (cf. [11]). In the 1980s, major efforts were directed to obtaining full understanding of crop performance under a wide range of environmental conditions. In the 1990s, the focus shifted toward applications in agronomic practice and policy making. In the 1990s, crop models also found their application in studies at higher levels of integration, that is, farm and regional scale. In these studies, crop models were used to quantify a broad range of land use systems; subsequently, these land use systems were aggregated to farm or regional scale using various techniques (e.g., linear programing) or procedures. Studies on designing environmentally friendly systems for arable, dairy, and flower bulb farms were conducted, also enabling analysis of trade-offs between economic and environmental objectives.

Land use studies were carried out with a focus on interactive exploration of different strategies for the European Union, Mali, Costa Rica, and Southeast Asia. Finally, crop models were used to explore limits for food production capabilities at global scale.

In the beginning of the twenty-first century, all of the functions of crop growth models continued to be performed and improved, but the development efforts shifted to reuse of models and to their applications for policy support [12].

Crop simulation models were thus originally developed as research tools and have had their greatest usefulness and impact so far as part of the research process. The advantages of integrating simulation modeling approaches into a research program have adequately been summarized [13]: (1) identification of knowledge gaps; (2) generation and testing of hypotheses, as an aid to the design of experiments; (3) determination of the most influential parameters of a system (sensitivity analysis); (4) provision of a medium for better communication between researchers in different disciplines; and (5) bringing researchers, experimenters, and producers together to solve common problems.

In addition to their use as tools in research, almost from the beginning of their development, crop models have been advocated as tools to help in decision-making processes of practitioners, with the development of so-called decision support systems (DSSs) for crop management. DSSs have evolved over the years from rudimentary single-decision rules to multiple-criteria optimization software. In its simplest form, a DSS can be a pest management threshold, calculated using empirical relations and field data on a calculator. In a sophisticated form, it can be an interactive computer system that utilizes simulation models, databases, and decision algorithms in an integrative manner. DSSs typically have quantitative output (as opposed to an expert system with qualitative reasoning) and place emphasis on the end user for final problem solving and decision-making. There is often no clear-cut boundary between models used in research and those used in DSS, that is, in the literature, models used in research are promoted in terms of their potential to aid in decision-making, although there is not always evidence that they have been or are being used for this purpose!

Simulation Models in Support of Crop Management

Crop modeling has helped in finding improved ways to manage crops, fields, and farms in practice, but the pathway has been problematic. Early expectations of computerized decision support systems as the connecting vehicle between crop models and management practice have, to a large extent, been unrealized. Nonetheless, some lessons have emerged from the attempts. It has been argued that the most significant contribution of these attempts at decision support has not been the actual production of decision support systems, but rather the bringing together of researchers and farmers to improve farm management [14]. Alternatively, it has been argued that for successful development and adoption of simulation approaches: (1) issues to be addressed must be neither trivial nor obvious, (2) a modeling approach must reduce complexity rather than proliferate choices in order to aid

the decision-making process, and (3) the cropping systems must be sufficiently flexible to allow management interventions based on insights gained from models [15]. Despite the limited application of operational decision support systems in actual commercial farming at the moment, a wide variety of such systems have been described. Without trying to be exhaustive, a number of illustrative examples are given here, following the classification of strategic, tactical, and operational decisions, as explained earlier.

Strategic Management

Strategic management support does not aim at generating answers for management to practitioners, but focuses on facilitating and supporting the dialogue with various stakeholders. This has led to the development of "discussion" support software [16], systems designed to facilitate dialogue about management practice that is relevant and significant to the decision maker. There exist significant opportunities for current capabilities in cropping systems analysis and modeling to contribute better to discussions about long-term economic and ecological issues associated with agricultural production systems. A number of these opportunities have been explored during the 1990s and cropping system simulation tools, such as APSIM (Agricultural Production system SIMulator; [17, 18]), CropSyst [19, 20], STICS [21], and DSSAT (Decision Support System for Agrotechnology Transfer; [22]), were designed with these targets in mind.

Increasingly over the last decade, crop models have been used to explore and design options for farm and regional land use systems. Studies at farm and regional scale require proper coverage of the system's physical conditions and the agroecological production options. Once sufficient information on soils and climate of an agricultural production system is available, crop models are useful tools for assessing their performance, that is, quantifying the inputs and outputs of (new) production systems. Two ways of using crop-soil models for farm and regional scale studies have been developed and elaborated. In the first method, crop yields are simulated for a range of well-defined (by soil and climate) points in a region and a geographical information system (GIS) is used to interpolate input data and aggregate results for the entire region. This method is generally suited to analyze or evaluate a limited number of land uses with little or no spatial interaction, but if necessary, with significant physiological detail. Examples of such approaches are an agroecological zonation for potato production at global scale [23] and an assessment of potential global food supply for a number of scenarios with respect to food demand, using low and high external input production systems [24]. In the second approach, crop models, supplemented with empirical relations and expert knowledge, are incorporated in so-called technical coefficient generators (TCGs) for production activities (e.g., [25, 26]). In this approach, crop models are used to quantify a broad range of land use systems in terms of inputs and outputs, which are subsequently aggregated to farm or regional scale using bio-economic optimization models (e.g., [27–34]). Examples of such TCGs are PASTOR and LUCTOR [35] and TechnoGIN [36]. The use of TCGs in combination with optimization models is particularly helpful in situations where many alternative crops and production technologies must be evaluated concurrently, and where spatial or temporal interactions are limited or less relevant for the type of questions to be addressed. The approach has proven to facilitate effective cooperation between agro-ecological and economic disciplines, and enables analysis of trade-offs between economic and environmental objectives at farm and regional scales.

Tactical Management

Tactical management basically refers to the medium term and deals with decisions that are taken once during the growing season, with respect to such issues as crop/variety selection, allocation of land to various crops, and identification of the most appropriate sowing or planting date.

An early example of a tactical decision support system is the program TACT, targeted at farm advisers and consultants but as the authors assure, readily useable by farmers [37]. It includes a simulation model of wheat performance (development, biomass accumulation, and yield) with a user-friendly interface. It calculates probability distributions of yield and gross margin, using data on location, soil type, wheat variety, sowing time, and weather conditions to date, and

historical rainfall records. In addition to calculating expected crop performance, TACT can also be used for climatological analyses which have an impact on 'break of season' decisions, using criteria defined by the program user in combination with historical daily rainfall and temperature records to investigate, for example, the incidence of frost. Other suggested applications at the time were calculating the probabilities of sowing opportunities, given a sowing rule and the probability of a dry period after a given date. This kind of information aids tactical decisions by estimating the risks of replanting if crops are sown early and the penalties for missing an early sowing opportunity. Most of the analyses generate a distribution of expected outcomes, for example, yield, which is used to derive probabilities.

TACT could be tailored to individual circumstances in two ways. Users could select from a wide range of parameters from TACT program menus, such as location, soil type, and sowing rule. These parameters tailor either the simulation model or climatic analyses to the user's specifications. Users could also adopt a probability level in the output, consistent with their attitude to risk.

In the last decade, computer-aided support for tactical decision making has received substantial attention, especially since it appeared possible to generate a characterization of in-season rainfall in (semi-)arid regions on the basis of, for instance, the El Niño/Southern Oscillation (ENSO) phenomenon [38]. Especially in (northeast) Australia this procedure has been relatively successful, because of three factors: a highly variable environment, which heightened riskiness of crop production decisions [39]; some ability to anticipate risks by utilizing seasonal climate forecasting [40, 41]; and a research culture that fostered close linkages between researchers and decision makers [42]. To facilitate crop management discussions in farmer-driven workshops, using analyses of management options based on crop simulation and seasonal climate forecasts, the Whopper Cropper software tool was designed [43]. As an example of using Whopper Cropper in relation to an issue involving seasonal climate forecasting, consider farmers in the Callide valley of Central Queensland, Australia, planning summer cropping options. For this scenario, it is November and the SOI phase [40] for September–October was positive. The farmers have heard that a positive SOI at this time of year means an improved chance of a better-than-usual season in terms of rainfall, and are considering sowing sorghum earlier than usual. The clay soil on properties in this area has a plant available water-holding capacity (PAWC) of about 170 mm, and is two-thirds full of moisture after good spring rain. To start with, it was assumed that a medium-maturing hybrid of sorghum was sown at a density of 10 plants m^{-2} on November 15 and that total nitrogen available to the crop (the amount in the soil plus the amount applied) is 100 kg ha^{-1}. By conducting a simulation of this scenario with the 100-year historical climate record for the location, a 100-year time series of yield outcomes was generated, with each year differing only in the seasonal climate realized. Time series analysis showed the year-to-year variability in yield for this scenario, compared to the long-term median, and then compared to those years in which the September–October SOI phase was positive. For this scenario, a positive SOI phase is often, but not always, associated with higher-than-median yields. Similar graphs can be produced for each SOI phase. The value of seasonal climate forecasting based on SOI phases in crop management stems from the shift in the expected yield distribution associated with each of the five phases [44]. For the sorghum cropping scenario, the distribution of yield associated with years having a positive SOI phase at the end of September–October has higher median yield and reduced risk of low yield compared to the distributions associated with years in the other phase categories. Products such as Whopper Cropper can be used for discussions about tactical decision-making, but can also be used to encourage debate on the design of planned and flexible rotations.

The El Niño-Southern Oscillation (ENSO) also contributes to the vulnerability of crop production to climate variability in the Pampas region of Argentina. Predictability of regional climate anomalies associated with ENSO provides opportunities to tailor decisions to expected climate, either to mitigate expected adverse conditions or to take advantage of favorable conditions. Model analysis was used to explore the potential for tailoring land allocation among crops to ENSO phases at the farm scale in two subregions of the Pampas [45]. The model identifies, as a function of risk preferences and initial wealth, the crop mix that maximizes expected utility of wealth at the end of a 1-year decision period, based on current costs and prices, and

crop yields simulated for each year of historical weather. The model reproduced recent land allocation patterns at the district scale under moderate risk aversion, and predicted increasing diversification with increasing risk aversion. Differences in land allocation among ENSO phases were consistent with known climate response to ENSO, and crop response to water availability. The relationship between the potential value of ENSO information and risk aversion was not monotonic, and differed between locations. Crop mix and information value also varied with crop prices and initial soil moisture. There are potential financial benefits of applying this approach to tailoring decisions to ENSO phases.

It was also shown that a similar procedure yielded relevant results for Kenya [46], thus increasing confidence in the use of seasonal weather forecasts for tactical crop management.

Water Management Crop growth simulation models have been used extensively to analyze the effects of tactical crop water (irrigation) management. In most instances, various water management regimes are being tested under local conditions, sometimes with the aim of exploring the scope for improvements in actual management practices, sometimes with the aim of contributing to the discussion on water management. Without trying to be exhaustive, a few typical examples are given.

The ORYZA W model [47] was used [48] to evaluate alternative management options for rice production in the light of farmers' attitudes toward risk. The model was used to generate probability distributions of rainfed lowland rice yields under different management scenarios which included water management (bund height, puddled soil depth, planting density, seedling age at transplanting). Stochastic dominance analysis was applied to identify risk-efficient management options. It appeared not possible to evaluate to what extent farmers (or extension officers) actually (have) apply(ied) the methodology in decision-making in commercial farming.

The interactive computer program WIRROPT7, a modification of the CERES-Wheat model, was applied [49] to explore the possibilities for the intra-seasonal irrigation regime that maximizes total gross margin for particular soil, weather, and crop management combinations, within the constraints of land and water availability. The use of the system was demonstrated for two soils near Harare in Zimbabwe and for two strategies – maximizing gross margin per unit area with a frequent irrigation schedule, or maximizing overall profits by reducing the application per unit area by irrigating less frequently but growing a larger area. As the variability of yields and gross margins are higher with the second strategy, the farmer's attitude to risk will determine which strategy he or she adopts. The authors recommend that the model should be seen only as a guide to irrigation management due to its limitations such as lack of routines describing nutrients and pests and the need to use mean historical weather data. The actual irrigation strategy should take into account real-time estimates of water use as well. It is not stated if the system is actually being used by farmers or extension staff.

The Environmental Policy Integrated Climate (EPIC) model was used to evaluate its application as a decision support tool for irrigation management of cotton and maize under South Texas conditions [50]. Simulation of the model was performed to determine crop yield, crop water use, and the relationships between the yield and crop water use parameters such as crop evapotranspiration (ETc) and water use efficiency (WUE). On-farm simulation results in this study demonstrated that the EPIC model can be used as a decision support tool for crops under full and deficit irrigation conditions in South Texas. EPIC specifically appears to be effective in long-term (strategic) and preseason (tactical) decision making for irrigation management of crops. However, more studies are needed to employ the model as a decision support tool addressing other irrigation issues such as operational management, dealing with irrigation allocation and scheduling.

Within the Australian cotton industry, the imperative to reduce water use and optimize irrigation management through the understanding of risk, using information generated by computerized decision aids was identified and subsequently developed into the HydroLOGIC irrigation management software [51]. On-farm experiments throughout the development period allowed the validation of internal software logic, irrigator decision processes, and the OZCOT cotton growth model [52]. The software demonstrated

the ability to improve yield and water use efficiency by optimizing strategic and tactical irrigation decisions in the Australian furrow irrigation cotton production system. In 7 of the 11 on-farm experiments conducted, the use of HydroLOGIC helped improve overall field water use efficiency by optimizing the timing of irrigation events or by indicating further irrigations would not provide yield or maturity benefits. Using concise reports, users can easily assess the risk of different irrigation management options at any crop stage, from land preparation through to postharvest benchmarking. HydroLOGIC may also be used within an integrated whole farm water management planning process to provide information on the impact of water allocations and subsequent evaluation of water security, water cost, and risk.

Nutrient Management As a basis for formulation of crop nitrogen requirements for rice, the ORYZA 0 model was developed and tested [53, 54], a "parsimonious" model based on incident solar radiation, bulk leaf nitrogen, and a site calibration factor. The model was subsequently applied [55] to classify some irrigated rice soils in India into those in which the soil N supply was sufficient to meet crop demand up to the onset of flowering and those that required a basal dressing of N fertilizer. The results were then used to generate fertilizer N recommendation curves that identified different optimal timing of N application for the different soil N supply regimes. The model was also used in a similar exercise in China, where it was found that significantly higher yields were obtained by following the recommendations produced by the model compared to the local recommendations [56]. Whether the model is able to make significant improvements over local recommendations in a wider range of environments remains to be seen. A limitation of ORYZA 0 is that it must be calibrated for each site, in this case by measuring the seasonal pattern of crop N uptake, which, because of year-to-year variation, makes it difficult to use the model in a predictive way. Also, no account is taken of the ability of the soil to act as a reservoir or "bank" of nitrogen – that is, nitrogen applied earlier in the season can remain in the soil for uptake by the crop later, so that it is not critical when the fertilizer is applied. The model only indicates how much nitrogen must have been applied by a specific crop age, and not when and how (i.e., as a single dressing or as split doses) it should be applied.

In a study for Walbundrie in Southeast Australia, the Agricultural Production System Simulator (APSIM) was used to simulate crop production and drainage passing the crop root zone of wheat and canola crops in response to nitrogen application rates from 0 to 300 kg N ha^{-1} $year^{-1}$, using historical climate records from 1889 to 2002 and variable values of stored soil water at sowing time (SSMS) [57]. The capability of the Southern Oscillation Index (SOI) phases to forecast growing season rainfall and crop yield was analyzed. The results showed that the optimal N rates were 100, 150, and 200 kg N ha^{-1} $year^{-1}$ in the years when April/May SOI phases were falling/negative, near zero, and rising/positive, respectively. Combining April/May SOI phases and SSMS to manage N application increased wheat gross margin, and reduced deep drainage for wheat, compared with N management based on historical climate data only. Similar results were obtained for a continuous canola cropping system.

Pest Management InfoCrop, a generic crop growth simulation model [58] was applied to simulate rice planthopper damage on Pusa Basmati 1 rice [59]. The model was used to simulate economic injury levels (EILs) of planthoppers and iso-loss curves, depicting combinations of crop age and planthopper populations that resulted in similar yield losses. Combinations of EILs and iso-loss curves can be used in monitoring planthopper populations and promoting judicious pesticide applications to avoid unwarranted control expenditure and environmental contamination. The simulation models, based on detailed crop ecological and physiological processes and pest damage mechanism can thus aid in the development of location-specific decision support tools and ensure precision in pest management decisions.

Operational Management

Operational management refers to day-to-day management of agricultural production systems, and deals with decisions by individual farmers on timing and intensity of interventions in their crops. From the very beginning of the development of crop growth simulation models, their capabilities for support in

operational management have been recognized. In hindsight, it must be concluded that in actual practice, at the moment, only a very limited number of such operational support systems are actually being applied at large scale. The scope for the use of crop growth simulation models as part of operational decision support systems has been expanded in the last decade through integration of mechanistic crop growth simulation models with earth observation techniques. Both, simulation modeling and remote sensing have been shown to be valuable tools in separate applications in agriculture. Integration of both techniques can lead to improvements in the dynamic simulation of the crop-soil system and thus contribute to improvements in management decision support systems for environmentally sound agricultural production [60–63].

In this section, a number of the decision support systems for operational management are illustrated that have been proposed, subdivided in the categories derived from the production situations [25], that is, water management (including irrigation), nutrient management (including fertilizer application), and crop protection management (including weed control and pest and disease control).

Water Management In many agricultural production systems, availability of water is the yield-determining factor, and therefore water management is an important aspect of crop management. The objective generally is to supply supplementary water to the crop in such a way that the water constraint is alleviated, the applied water is used as efficiently as possible, and, in some cases, specific water quality criteria are met.

Irrigation scheduling is an area in which models have been used extensively as decision support systems. It has been claimed [64] that there are at least 140 models based on the use of the water production functions developed by FAO [65]. However, he cautions that such models do not correctly forecast the effect of water stress on crop growth, as they do not take into account the dynamic processes. In mechanistic crop growth models such as CERES–Maize [66], EPIC [67], and CROPSYST [20], the effects of soil water depletion in the course of the crop growth cycle are simulated. They can, therefore, be used as effective tools for forecasting the water content of the soil and the crop response to it [64].

As an early example, the use of the real-time crop growth model EPIC-PHASE is illustrated [68], functioning at a daily time step, as a new method that might support the irrigator in answering questions such as "how much" and "when" to irrigate. Their results showed the potential progress that the irrigator could make by scheduling irrigation according to the predictions of water stress intensities. However, the efficiency of this schedule is dependent on the accuracy of weather forecasts. The study noted that the simulations gave a large difference in the choice of operational irrigation, depending on whether weather forecasts or actual weather data were used. From an agronomic standpoint, it is necessary to test other methods such as updating the weather forecasts every 24 h, or determining, in terms of risk on yields, the weight of possible climatic errors according to the crop phase, thus allowing the irrigator to take his decision to irrigate or not with a full knowledge of the facts.

A pilot irrigation scheduling project was established in Northern Zululand in South Africa on a commercial estate [69]. Meteorological variables were measured with an Automatic Weather Station (AWS) and the data transmitted electronically to the experimental station every week. A model was used to estimate the soil water content on a daily basis. A report on the current soil water status was then generated and advice on when next to irrigate was sent to the irrigator.

In Denmark, irrigation scheduling based on local experience and rules of thumb proved inadequate to deal with the increasing complexity of water management. A PC-based DSS (MARKVAND) was developed in response to a need to find more efficient forms of irrigation due to increasing water demands in different sectors of society in Denmark [70]. It is being used to give daily information on the timing, amount, and economic net return of irrigation for a wide group of agricultural crops. The model includes conceptual and empirical sub-models for crop development, water balance, and crop yield.

In the United Kingdom, Irrigation Management Services (IMS) provided a consultancy service that gave farmers weekly advice on which fields to irrigate, when and how, based on the results of computer simulation [71, 72]. IMS employs a simple water balance model with crop evapotranspiration estimated on the basis of soil, crop, and weather factors. It was used

between 1984 and 1989 to provide an irrigation scheduling service to farmers and growers in eastern England in conjunction with in-field monitoring of soil water and crop cover [72]. When the service began in 1984, it operated on a bureau basis with communication by phone combined with farm visits. Farmers saw this personal touch as beneficial, since it gave them confidence in the service and enabled them to discuss broader issues with the adviser. However, by 1990, the use of microcomputers had become more common and farmers began to demand the scheduling packages themselves as this was greatly cheaper than paying for a consultancy service [72]. In time, some farmers eventually felt experienced enough in estimating when to irrigate such that they no longer needed to use the model. Despite the technological advancements in irrigation scheduling, most irrigators do not use the real-time procedures that have been developed by scientists. However, it has been argued [73] that if the efficiency of irrigation is to improve in order to help meet the increased demands for water from all sectors of society, such tools must be adopted. The challenge to researchers is to develop economically viable technology that is readily adaptable for use by farmers. This requires more interactive communication between researchers, extension staff, and farmers for improving the transferability and applicability of irrigation scheduling techniques [73].

Recently [74], an approach was presented to explore water management options in irrigated agriculture, combining remote sensing, crop growth modeling, and optimization, taking into account the constraints of water availability and the heterogeneity of irrigation system properties. The method contains two components: (i) system characterization using a stochastic data assimilation procedure where the irrigation system properties and operational management practices are estimated using remote sensing (RS) data; and (ii) water management optimization, exploring water management options under various levels of water availability. A soil–water–atmosphere–plant model (SWAP) is applied in a deterministic–stochastic mode for regional modeling. The distributed data, for example, sowing dates, irrigation practices, soil properties, depth to groundwater, and water quality, required as inputs for the regional modeling is estimated by minimizing the residuals between the distributions of field-scale evapotranspiration (ET) simulated by the regional application of SWAP, and a surface energy balance algorithm for land (SEBAL; [75]) using two Landsat7 ETM+ images. The derived distributed data were used as inputs in exploring water management options. A generic algorithm was used in data assimilation and water management optimizations.

The results showed that regional crop productivity can be improved by considering water and crop management practices as one, not as independent entities under limited water conditions. Adjusting sowing dates and their distributions in the irrigated area were found to impact positively the regional yield. This management option could complement the practice of deficit irrigation. On average, the farmers could allow their crops to experience water stress of about 27% before irrigation, with the current conditions in the study area. This could result in an increase of about 8.5% in the expected regional wheat yield and a regional water productivity of 1.6 kg m^{-3}. When water supply is very limited, high equity in water distribution could result in better performance of the irrigation system, and this should be also complemented by an earlier date of sowing in the growing season with wider distribution. This is also true when water is non-limiting but the farmers have higher degrees of freedom in their planting activities. There is an optimum point where the benefit would justify additional use of water for irrigation, beyond this point, water should be saved.

In a more proactive mode, if a seasonal climate forecast is available, the approach can be applied to explore water management decisions before the wheat-growing season [76].

Nutrient Management In the Netherlands, in an interdisciplinary project, nitrogen-fertilizer recommendations were formulated on the basis of results of a simulation model [77]. The model was initialized in early spring on the basis of field measurements of crop biomass and soil mineral nitrogen contents. Anticipated wheat yields were calculated on a weekly basis using measured weather data until the day of simulation and historical weather data for a 20-year period prior to the season of prediction. Expected yield and its range were then calculated from the simulated yields for the 20-year period. Fertilizer recommendations

were derived from these values on the basis of simulated N deficiencies in the crop. The results, following 3 years of testing on a number of experimental and commercial fields in the Netherlands, were rather disappointing, as final yield appeared strongly dependent on the actual weather conditions (temperature, determining the length of the grain filling period and radiation, determining the rate of grain growth) after flowering of the wheat crop. At that point in the crop's phenology, total crop nitrogen content can hardly be changed anymore (uptake takes place essentially before flowering), so that no adjustment was possible. The recommendations were therefore not better than those based on measured mineral nitrogen content in the soil profile in early spring, the common method at that time in the Netherlands.

AmaizeN [78] is a decision support system to help maize growers schedule nitrogen (N)-fertilizer applications for site-specific maize crops. It forecasts crop yields and N-fertilizer application rates for potential yield and best economic returns, and predicts the consequences of user management decisions. It takes into account both crop production and environmental impact. In an evaluation study with 16 field trials, covering a wide range of weather and soil conditions, AmaizeN-predicted maize yields (for both silage and grain) matched field measurements well, and gave a reasonably good indication of silage crude protein content and silage harvest date. The system was also capable of estimating N-leaching during the cropping season and predicting residual soil mineral-N at the end of the season, but more effort is needed to improve the accuracy of some predictions. In all instances, the AmaizeN-recommended N-fertilizer strategy was more efficient than the growers' practice. Recommended N-fertilizer rates were on average 85 kg ha^{-1} less than conventional application rates across ten crops, with no yield reduction. Its recommended higher-than-conventional application rate at another crop brought about a significant yield increase. System development was guided by an industry user group who requested the decision support system interface to be 'simple and easy to use'. To ensure user adoption of the system, some compromises in system prediction accuracy were required. Local agricultural production conditions were also incorporated.

Pest and Disease Management Because of the complex relationships between crops and their pests and diseases, and because populations of pests and diseases are dynamic in nature, a systems analysis approach is required to understand how pest and disease problems arise and how they may be tackled. In the case of pest and disease populations themselves, the approach bridges the gap between knowledge at the individual level and understanding at the population level.

The EPIPRE (EPIdemic PREvention) system was developed between 1977 and 1981 in the Netherlands as a system for supervised control of diseases and pests in winter wheat [79] and was intended to reduce the use of chemical crop protection agents. A major advantage of the system was that the farmers, recruited from Wheat Study Clubs, were able to learn as they went along and were always aware of how the system worked. They were trained to recognize disease symptoms, carrying out their own disease and pest monitoring, and sending their field observations to a central team who entered them on a daily basis into a computerized data bank. The system produced recommendations for treatment by optimizing financial returns for crop protection. There were three major decision options: (1) treat, (2) do not treat, and (3) make another field observation. When the season was over, every farmer received a record of his actions and the recommendations, as well as a financial account of the crop protection activities. The results were discussed with farmers in regional meetings. The farmers listened critically and often expressed appreciation of their improved expertise. Eighty-five percent of farmers participating in 1 year participated in the next. Complete adherence varied between 20% and 80%. Partial adherence was far greater than full adherence [79]. In 1981, 6% of Dutch winter wheat was covered by the system [80] saving on average £15 ha^{-1} [79]. In Belgium, the system functioned under the auspices of the National Soil Service, and in 1992, EPIPRE was used to advise on disease control in 500 fields in Belgium and northern France [81]. The research in Sweden (from 1982 to 1985) found that although EPIPRE was an interesting and useful system, it would require alteration if it were to be introduced to farmers for routine use. There was a need to incorporate meteorological parameters into the model and to adjust the plant growth model to suit Swedish conditions, as the model was still

recommending unnecessary spraying [82]. Experience in Switzerland found that EPIPRE-treated fields yielded 3% less than traditionally treated fields (0.5% with corrected gross return), but that farmers were able to reduce the spray frequency by 20–100%. The conclusion was that although the farmers did not make more profit, the new practice was ecologically beneficial and helped to reduce selection pressure for pesticide resistance [83]. It was calculated that in 1981, if all Dutch winter wheat would have been treated with the EPIPRE recommendations, the pollution load would have been reduced by 12 Mg [79]. Characteristic for the EPIPRE system was that there was an initial steady increase in membership, which resulted in an improvement in pest management. However, subsequently membership declined, as the growers felt that they had learned what the model would predict and therefore did not need it any more [6]. The system was successful in that it contributed to improved pest management by developing farmers' understanding and by helping them to interpret their own field observations more effectively.

A comparable system was developed in Australia, that is, SIRATAC, a dial-up crop management system to assist cotton growers in making good tactical decisions about the use of insecticides in irrigated cotton on a day-to-day basis [84]. It was run by SIRATAC Ltd., a nonprofit commercial company formed in 1981 to market the system to the cotton industry. SIRATAC aimed to reduce the risk associated with pesticide use by adopting Integrated Pest Management principles. It consisted of several simulation models and a decision model helping the grower decide whether or not to spray pesticide and which pesticide. The area managed using SIRATAC increased steadily during the early 1980s. In 1981–1982, there was demand for a tenfold expansion [14]. However, by 1985, it had reached a ceiling in adoption at 25% (by area) of the industry and its use declined after 1987 [85]. In 1989, SIRATAC Ltd. went into voluntary liquidation due to a predicted declining market share and cash flow problems, despite the fact that the area managed by SIRATAC was at a historical high [14]. It was replaced by an informal user group (SUG) that continued the program for a few more seasons, but by 1993 the group had ceased operation and the field-support system was no longer available. A moratorium on SIRATAC development meant that only minor changes were made to the program. Attempts to achieve similar functionality on a microcomputer failed. An in-depth participatory analysis found that many of the reasons for the poor adoption of SIRATAC were based on organizational issues rather than on problems with the model itself [84]. The important themes that emerged from their survey were:

- Widely held negative views against SIRATAC and SIRATAC Ltd. by nonusers.
- Many growers did not consider SIRATAC's intangible benefits to be worth paying for. They wanted to see tangible cost-saving benefits.
- Many people based their opinions on hearsay and did not really know what SIRATAC was or what it could do.
- Many felt that they were often overriding the system and so abandoned it. They felt uncomfortable with the recommendations of the system (e.g., expensive sprays when cheaper ones would do, not enough spraying – they felt it may put crops at risk).
- Practical limitations: no office or computer or reliable telephone service.
- Growers felt threatened – they saw it as a man versus machine issue and felt that their own experience and knowledge was being undervalued.

Hence, in both, the SIRATAC and EPIPRE cases, there was an initial steady increase in membership, which resulted in an improvement in pest management. However, both organizations then experienced a decline in membership as the growers felt that they had learned what the models would predict and therefore did not need them any more [6]. Both systems were successful in that they contributed to improved pest management by developing farmers' understanding and by helping them to interpret their own field observations more effectively.

Future Directions

Since the beginning of the development of crop growth simulation models, attention has been paid to application of these models in crop and farm management. The possibility to quantitatively address, in an integrated fashion, many different aspects of decision-making and the expected consequences on crop and

agricultural system performance, made such models attractive tools for such analyses.

With respect to *strategic management*, substantial progress has been made in methodological development in the last decade, and tools have been developed that (can) play a role as discussion and decision support systems in such areas as agricultural land use planning [86–88]. However, in a recent review on quantitative assessment of agricultural production systems, the remark was made: "The probably biggest challenge is to transfer the methodologies developed in land use studies to the unruly practice of land use policy formulation and implementation" [89]. "That requires close cooperation with the ultimate users of the methodologies, the various stakeholders, through the development of discussion and negotiation platforms" [90].

In the same sphere, it was concluded that the combination of the boundary arrangement perspective with critical leverage points presents a basis to design an institutional pathway for enhancing impact of modeling research in the policy sphere [91]. For researchers functioning in a science-domain-oriented environment, more options appear available than the frequently proposed 'more participation' for increasing the likelihood that their policy-oriented work is used. These include establishing contacts with research groups or institutes that are in a position to function as "stepping stones," or engaging with others to develop social networks in the policy sphere.

Following a critical evaluation of development and application of the Land Use Planning and Analysis System (LUPAS), it was concluded that its successful use is only possible if there is sufficient, shared awareness of problems and the need for solutions among the stakeholders [88]. Once a prototype of LUPAS was operational (preferably with a user-friendly interface) and stakeholders had the proper level of comprehension, LUPAS served as a vehicle to demonstrate potential conflicts, reveal strategic resource use options, and stimulate discussion among different stakeholder groups. However, presumably the project would have benefited from a more complete identification of problems and information needs as perceived by stakeholders and policy makers. A better contextualization (cf. [92]) would have been an asset in bridging the gap between the information supply of LUPAS and the needs of the stakeholders (cf. [93, 94]).

All of these experiences thus point in the direction of the fact that cooperation with the stakeholders, that is to say with the clients of the information, is critical in creating impact of the modeling work in the policy arena. This interaction with stakeholders should start at the beginning of the modeling work, so that problem identification and the associated design of the modeling tool should also be carried out jointly. The transition from the research field to the application field thus requires more attention than at the moment in general is being accorded.

In the area of *tactical management*, an extensive analysis of a long-term effort to develop in a multi-stakeholder setting an operational system was analyzed by the FARMSCAPE project team in Australia [95]. Their self-evaluation, supported by external evaluations, shows mixed feelings with respect to their success. Near the end of the first round of training and accrediting commercial agronomists in the application of FARMSCAPE tools, with the main focus on facilitating the agronomists involved in the application of these new skills and tools within their business systems, the team states "their success is our primary goal and our evaluation of how system monitoring and simulation is perceived and adopted within agribusiness and their clientele will continue as a key learning objective."

Looking ahead, they state that they are in serious negotiations with a consortium of agribusiness companies who wish to invest in a national delivery system for APSIM simulations targeted at farmer clients. This initiative was first mooted and is now being designed, promoted, and will be financed and implemented by the agribusiness consortium. APSRU (Agricultural Production System Research Unit)'s role will be to provide and support the APSIM software and train accredited users. The commercial system being proposed is well aligned with the FARMSCAPE approach to decision support, with emphasis on the need for simulations to be contextualized to the requests and circumstances of individual farmers. If established, this commercial delivery system could be an important market test for the applicability of computerized decision support to the industry.

While the operational focus is on facilitating development of delivery systems through commercial agronomic service providers, research continues to focus on learning about the market for decision support and its

viable delivery, through (i) continued efforts at assessing the internet as a delivery vehicle [96] and (ii) addressing a market barrier to wide adoption of decision support. As pointed out [97], a major challenge to the delivery of DSSs is gaining the attention of farmers beyond "Innovator"/"Early Adopter" types to those who comprise the majority. Accordingly, research has been initiated aimed at penetrating the "Early Majority" market for improved risk management, by creating reference groups of satisfied adopters among the pragmatist category of farmers who are crucial to the diffusion process required for viable market volume. This new project is to be based on case studies built around farmer groups involving both innovative and pragmatist farmers, consultant agronomists, and key researchers.

FARMSCAPE has developed into a successful approach to systems research, specifically in the exploration of a role for computerized decision support. Its focus has been on dryland farming systems of northeast Australia with participant interest concentrating on decisions that impact on the economics of alternative cropping options. There is now interest, both within APSRU and from collaborating researchers, to expand and replicate the FARMSCAPE approach in other regions, and to address a broader range of issues. Research projects implementing the FARMSCAPE approach have already commenced elsewhere in Australia, as well as internationally. Collaborative projects have commenced to assess the role for APSIM in improving management practices in smallholder agriculture, such as a WifAD session successfully held with smallholder farmers in Zimbabwe [98]. Expanding the systems view to incorporate natural resource management, weed management and agroforestry systems are all new project initiatives being undertaken by the FARMSCAPE team.

When leaning backward, and trying to identify systems that at the moment actually are used in *operational farm management*, the results are on the whole disappointing.

Although crop-soil simulation models dealing with soil water balances and crop water used have proliferated and in general, the relevant processes are well understood, there are very few examples where these models are being applied at the individual plot level to guide irrigation scheduling. One of the reasons is no doubt the fact that there is always a substantial degree of uncertainty, because rainfall cannot be predicted with great accuracy, neither in timing nor in amount, an uncertainty that propagates into predictions of future irrigation requirements. An additional constraint on the use of these models is that individual farmers are often dependent on irrigation system management, that determines when and how much water is available.

Application of operational nutrient management systems (fertilizer recommendations) is hampered by a number of difficulties. As mentioned in the description of the wheat nitrogen-fertilizer recommendation system in the Netherlands, the "final" demand for nitrogen, governed by the realized yield level, is determined at a point in the crop's life cycle when uptake by the crop cannot any more be affected by management. An additional problem is that the fertilizer is added to the soil and that it is impossible to predict when and how much of the fertilizer nutrient is actually being taken up by the crop, because that depends, among others, again on the soil and crop water balance, almost impossible to accurately predict. The uncertainty associated with simulation of the nutrient supply from natural sources, particularly that from soil organic matter, in general the largest source, adds uncertainty to the accuracy of estimating fertilizer requirements, both in timing and in rate.

Crop protection systems in the field of pest and disease management have had substantial success in the past, in a combination of farmers' monitoring and simulation models. However, these systems have largely disappeared again, mainly as farmers indicated, because the learning associated with application of these systems made them redundant. Farmers felt that after a number of years, interpretation of the monitoring data did not require model results, but could be done by the farmers themselves. Whether crop growth simulation models can really provide added value in this area is difficult to foresee, although they could play a role in quantitative assessment of damage levels on the basis of famer-supplied incidence levels at different stages of crop development, with or without control measures. The farmer could then decide, taking into account the level of risk that he is prepared to take, whether to implement control measures or not, very much in line with the original EPIPRE and SIRATAC decision support systems.

At present, there is an increasing demand for weed management systems with reduced use and reliance on herbicides, and the ecophysiological competition models have great potential for contributing to the design of such alternative weed management systems. In the near future, more attention should be given in these models to the accuracy with which growth, morphological development, and seed production of weed species are being simulated, as the long-term development of weed populations becomes increasingly important. In this way, a functional link can be established between crop-weed competition research and research on weed population dynamics. Continuous interaction between modeling and experimental research should support determination of the required level of detail in crop-weed competition models and will provide leads for focusing future weed ecological research.

In conclusion, the great expectations that originally existed with respect to the use of crop growth simulation models in crop management (cf. [6]) unfortunately have not materialized. There are a number of reasons for this disappointing development. One is doubtless the fact that crop production takes place in an uncertain environment and that meteorological sciences have as yet, not been able to predict weather conditions in the near future with any great accuracy. The performance of crops is to a large extent governed by these weather conditions and thus it remains difficult to recommend actual actions when the future weather conditions are uncertain. Another problem is that most simulation models have been developed, tested, and validated against data from experimental stations and commercial crops often perform differently from those in experimental stations. When sufficient time and capacity is available, this problem can to a large extent be overcome, as reported for the Australian situation [99], but such extended programs for the development of crop management systems are seldom if ever available.

In contrast, there appears to be ample scope for application of crop growth simulation models in strategic and tactical management, in which such models are part of so-called discussion support systems that can be used by farmers to explore "what-if" questions, based on explicit quantitative information [100]. It has been shown convincingly that the success of such discussion support systems is greatly enhanced when the relevant stakeholders ("clients") are from the very beginning involved in the design and development of these systems, so that the relevant questions and the available information can be dovetailed in the most efficient way [101].

Therefore, although substantial progress has been made in the last 3 years, the situation has not basically changed and that in order to effectively make use of crop growth simulation models in crop management, the biggest challenge is to transfer the methodologies developed in land use studies to the unruly practice of land use policy formulation and implementation. That requires close cooperation with the ultimate users of the methodologies, the various stakeholders, through the development of discussion and negotiation platforms [89, 91, 101].

Bibliography

Primary Literature

1. Lentz W (1998) Model applications in horticulture: a review. Sci Hortic 74:151–174
2. Van Keulen H (1987) Forecasting and estimating effects of weather on yield. In: Wisiol K, Hesketh D (eds) Plant growth modeling for resource management. CRC Press, Boca Raton, pp 105–124
3. Brouwer R, De Wit CT (1968) A simulation model of plant growth, with special attention to root growth and its consequences. In: Whittington WJ (ed) Root growth. Butterworths, London, pp 224–244
4. De Wit CT (1970) Dynamic concepts in biology. In: Setlik I (ed) Prediction and measurement of photosynthetic productivity. Proceedings of IBP/PP Technical Meeting, Trebon, Pudoc, Wageningen, The Netherlands, pp 17–23
5. De Wit CT, Brouwer R, Penning de Vries FWT (1970) The simulation of photosynthetic systems. In: Setlik I (ed) Prediction and measurement of photosynthetic productivity. Proceedings of IBP/PP Technical Meeting, Trebon, Pudoc, Wageningen, The Netherlands, pp 47–70
6. Sinclair TR, Seligman NG (1996) Crop modelling: from infancy to maturity. Agron J 88:698–703
7. Bouman BAM, Van Keulen H, Van Laar HH, Rabbinge R (1996) The 'School of de Wit' crop growth simulation models: a pedigree and historical overview. Agr Syst 52:171–198
8. Boote KJ, Jones JW, Pickering NB (1996) Potential uses and limitations of crop models. Agron J 88:704–716
9. Van Ittersum MK, Leffelaar PA, Van Keulen H, Kropff MJ, Bastiaans L, Goudriaan J (2003) On approaches and applications of the Wageningen crop models. Eur J Agron 18:201–234

10. Hammer GL, Kropff MJ, Sinclair TR, Porter JR (2002) Future contributions of crop modelling-from heuristics and supporting decision making to understanding genetic regulation and aiding crop improvement. Eur J Agron 18: 15–31
11. Rabbinge R, Goudriaan J, Van Keulen H, de Vries Penning FWT, Van Laar HH (eds) (1990) Theoretical production ecology: reflection and prospects. Simulation Monographs. Pudoc, Wageningen, The Netherlands
12. Van Ittersum MK, Ewert F, Heckelei T, Wery J, Alkan Olsson J, Andersen E, Bezlepkina I, Brouwer F, Donatelli M, Flichman G, Olsson L, Rizzoli AE, Van der Wal T, Wien JE, Wolf J (2007) Integrated assessment of agricultural systems – a component-based framework for the European Union (SEAMLESS). Agr Syst 96:150–165
13. Seligman NG (1990) The crop model record: promise or poor show? In: Rabbinge R, Goudriaan J, Van Keulen H, Penning de Vries FWT, Van Laar HH (eds) Theoretical production ecology: reflection and prospects. Simulation Monographs. Pudoc, Wageningen, The Netherlands, pp 249–263
14. Cox P (1996) Some issues in the design of agricultural decision support systems. Agr Syst 52:355–381
15. Meinke H, Baethgen WE, Carberry PS, Donatelli M, Hammer GL, Selvaraju R, Stőckle CO (2001) Increasing profits and reducing risks in crop production using participatory systems simulation approaches. Agr Syst 70:493–513
16. Nelson RA, Holzworth DP, Hammer GL, Hayman PT (2003) Infusing the use of seasonal climate forecasting into crop management in North East Australia using discussion support software. Agr Syst 74:393–414
17. McCown RL, Hammer GL, Hargreaves JNG, Holzworth DP, Freebairn DM (1996) APSIM: a novel software system for model development, model testing and simulation in agricultural systems research. Agr Syst 50:255–271
18. Keating BA, Carberry PS, Hammer GL, Probert ME, Robertson MJ, Holzworth D, Huth NI, Hargreaves JNG, Meinke H, Hochman Z, McLean G, Verburg K, Snow V, Dimes JP, Silburn M, Wang E, Brown D, Bristow KL, Asseng S, Chapman S, McCown RL, Freebairn DM, Smith CJ (2003) An overview of APSIM, a model designed for farming analysis simulation. Eur J Agron 18:267–288
19. Stöckle CO, Donatelli M (1997) The CropSyst model: a brief description. In: Plentinger MC, Penning de Vries FWT (eds) Rotation models for ecological farming, pp 35–43 (Quantitative Approaches in Systems Analysis No. 10, AB-DLO). Wageningen, The Netherlands
20. Stöckle CO, Donatelli M, Nelson R (2003) CropSyst, a cropping systems simulation model. Eur J Agron 18:289–307
21. Brisson N, Gary C, Justes E, Roche R, Mary B, Ripoche D, Zimmer D, Sierra J, Bertuzzi P, Burger P, Bussière F, Cabidoche YM, Cellier P, Debaeke P, Gaudillère JP, Hénault C, Maraux F, Seguin B, Sinoquet H (2003) An overview of the crop model STICS. Eur J Agron 18:309–332
22. Jones JW, Hoogenboom G, Porter CH, Boote KJ, Batchelor WD, Hunt WA, Wilkens PW, Singh U, Gijsman AJ, Ritchie JT (2003) The DSSAT cropping system model. Eur J Agron 18:235–265
23. Van Keulen H, Stol W (1995) Agro-ecological zonation for potato production. In: Haverkort AJ, MacKerron DKL (eds) Potato ecology and modelling of crops under conditions limiting growth. Kluwer, Dordrecht, The Netherlands, pp 357–371
24. Penning de Vries FWT, Van Keulen H, Rabbinge R (1995) Natural resources and limits of food production in 2040. In: Bouma J, Kuyvenhoven A, Bouman BAM, Luyten J, Zandstra HG (eds) Eco-regional approaches for sustainable land use and food production. Kluwer, Dordrecht, The Netherlands, pp 65–87
25. Van Ittersum MK, Rabbinge R (1997) Concepts in production ecology for analysis and quantification of agricultural input-output combinations. Field Crops Res 52:197–208
26. Hengsdijk H, Van Ittersum MK (2002) A goal-oriented approach to identify and engineer land use systems. Agr Syst 71:231–247
27. Rabbinge R, Van Latesteijn HC (1992) Long term options for land use in the European Community. Agr Syst 40:195–210
28. Ten Berge HFM, Van Ittersum MK, Rossing WAH, Van de Ven GWJ, Schans J, Van de Sanden PACM (2000) Farming options for the Netherlands explored by multi-objective modelling. Eur J Agron 13:263–277
29. Roetter R, Van Keulen H, Van Laar HH (2000) Synthesis of methodology development and case studies, vol 3, Sysnet Research Paper Series. International Rice Research Institute, Los Banos, Philippines, p 94
30. Dogliotti S, Rossing WAH, Van Ittersum MK (2004) Systematic design and evaluation of crop rotations enhancing soil conservation, soil fertility and farm income: a case study for vegetable farms in South Uruguay. Agr Syst 80:277–302
31. Dogliotti S, Van Ittersum MK, Rossing WAH (2005) A method for exploring sustainable development options at farm scale: a case study for vegetable farms in South Uruguay. Agr Syst 86:29–51
32. Van de Ven GWJ, Van Keulen H (2007) A mathematical approach to comparing environmental and economic goals in dairy farming: identifying strategic development options. Agr Syst 94:231–246
33. Hengsdijk H, Bouman BAM, Nieuwenhuyse A, Jansen HGP (1999) Quantification of land use systems using technical coefficient generators: a case study for the northern Atlantic zone of Costa Rica. Agr Syst 61:109–121
34. Laborte AG, Schipper RA, Van Ittersum MK, Van Den Berg MM, Van Keulen H, Prins AG, Hossain M (2009) Farmers' welfare, food production and the environment: a model-based assessment of the effects of new technologies in the northern Philippines. NJAS Wageningen J Life Sci 6:345–373
35. Hengsdijk H, Guanghuo W, Van den Berg MM, Jiangdi W, Wolf J, Changhe L, Roetter RR, Van Keulen H (2007) Poverty and biodiversity trade-offs in rural development: a case study for Pujiang county, China. Agr Syst 94:851–861
36. Ponsioen TC, Hengsdijk H, Wolf J, Van Ittersum MK, Rötter RP, Son TT, Laborte AG (2006) TechnoGIN, a tool for exploring and

evaluating resource use efficiemcy of cropping systems in East and Southeast Asia. Agr Syst 87:80–100
37. Abrecht DG, Robinson SD (1996) TACT: a tactical decision aid using a CERES based wheat simulation model. Ecol Model 86:241–244
38. Stone RC, Meinke H (2005) Operational seasonal forecasting of crop performance. Philos Trans Roy Soc B 360:2109–2124
39. Muchow RC, Bellamy JA (eds) (1991) Climatic risk in crop production: models and management for the semiarid tropics and subtropics. CAB International, Wallingford, UK, p 548
40. Stone RC, Hammer GL, Marcussen T (1996) Prediction of global rainfall probabilities using phases of the Southern Oscillation Index. Nature 384:252–255
41. Hammer GL, Nicholls N, Mitchell C (eds) (2000) Applications of seasonal climate forecasting in agricultural and natural ecosystems – the Australian experience. Kluwer, Dordrecht, The Netherlands, p 469
42. Carberry PS (2001) Are science rigour and industry relevance both achievable in participatory action research? Proceedings Australian Agronomy Conference, Hobart, January 2001. Available from http://www.regional.org.au/papers/agronomy/2001/plenery/5/Carberry,Peter.htm
43. Nelson RA, Hammer GL, Holzworth DP, McLean G, Pinington GK, Frederiks AN (1999) User's Guide for Whopper Cropper (CD-ROM) Version 2.1. QZ99013. Department of Primary Industries, Queensland, Brisbane, Australia
44. Hammer GL (2000) Applying seasonal climate forecasts in agricultural and natural ecosystems – a synthesis. In: Hammer GL, Nicholls N, Mitchell C (eds) Applications of seasonal climate forecasting in agricultural and natural ecosystems – the Australian experience. Kluwer, Dordrecht, The Netherlands, pp 453–462
45. Messina CD, Hansen JW, Hall AJ (1999) Land allocation conditioned on El Niño-Southern Oscillation phases in the Pampas of Argentina. Agr Syst 60:197–212
46. Hansen JW, Indeje M (2004) Linking dynamic seasonal climate forecasts with crop simulation for maize yield prediction in semi-arid Kenya. Agr Forest Meteorol 125:143–157
47. Wopereis MCS, Bouman BAM, Tuong TP, Ten Berge HFM, Kropff MJ (1996) ORYZA_W: Rice growth model for irrigated and rainfed environments. SARP Research Proceedings, AB-DLO, Wageningen, The Netherlands, p 159
48. Lansigan FP, Pandey S, Bouman BAM (1997) Combining crop modelling with economic risk-analysis for the evaluation of crop management strategies. Field Crops Res 51:133–145
49. MacRobert JF, Savage MJ (1998) The use of a crop simulation model for planning wheat irrigation in Zimbabwe. In: Tsuji GY, Hoogenboom G, Thornton PK (eds) Understanding options for agricultural production. Systems approaches for sustainable agricultural development. Kluwer, Dordrecht, The Netherlands, pp 205–220
50. Ko J, Piccinni G, Steglich E (2009) Using EPIC model to manage irrigated cotton and maize. Agr Water Manage 96:1323–1331
51. Richards QD, Bange MP, Johnston SB (2008) HydroLOGIC: an irrigation management system for Australian cotton. Agr Syst 98:40–49
52. Hearn AB (1994) OZCOT: a simulation model for cotton crop management. Agr Syst 44:257–299
53. Ten Berge HFM, Shi Q, Zheng Z, Rao KS, Riethoven JJM, Zhong X (1997) Numerical optimisation of nitrogen application to rice. II. Field evaluations. Field Crops Res 51:43–54
54. Ten Berge HFM, Thiyagarajan TM, Shi Q, Wopereis MCS, Drenth H, Jansen MJW (1997) Numerical optimisation of nitrogen application to rice. I. Description of MANAGE-N. Field Crops Res 51:29–42
55. Thiyagarajan TM, Stalin P, Dobermann A, Cassman KG, Ten Berge HFM (1997) Soil N supply and plant N uptake by irrigated rice in Tamil Nadu. Field Crops Res 51:55–64
56. ZhiMing Z, LiJiao Y, ZhaoQian W, Zheng Z, Yan L, Wang Z (1997) Evaluation of a model recommended for N fertilizer application in irrigated rice. Chin Rice Res Newslett 5:7–8
57. Wang E, Xu JH, Smith CJ (2008) Value of historical climate knowledge, SOI-based seasonal climate forecasting and stored soil moisture at sowing in crop nitrogen management in south eastern Australia. Agr Forest Meteorol 148:1743–1753
58. Aggarwal PK, Kalra N, Chander S, Pathak H (2006) InfoCrop: a dynamic simulation model for the assessment of crop yields, losses due to pests, and environmental impact of agro-ecosystems in tropical environments. I. Model description. Agr Syst 89:1–25
59. Yadav DS, Chander S (2009) Simulation of rice planthopper damage for developing pest management decision support tools. Crop Prot 29:67–76
60. Fischer A, Kergoat L, Dedieu G (1997) Coupling satellite data with vegetation functional models: review of different approaches and perspectives suggested by the assimilation strategy. Remote Sens Rev 15:283–303
61. Moulin S, Bondeau A, Delecolle R (1998) Combining agricultural crop models and satellite observations: from field to regional scales. Int J Remote Sens 19:1021–1036
62. Jongschaap REE, Quiroz RA (2000) Integrating remote sensing with process-based simulation models to assess primary production capacity for grazing lands in The Andes. Proceedings of the 5th seminar on GIS and developing countries: GISDECO 2000, Los Baños, Philippines, 2–3 November 2000
63. Clevers JPGW, Vonder OW, Jongschaap REE, Desprats DF, King C, Prévot L, Bruguier N (2002) Using SPOT data for calibrating a wheat growth model under Mediterranean conditions. Agronomie 22:687–694
64. Cabelguenne M (1996) Tactical irrigation management using real time EPIC-phase model and weather forecast: experiment on maize. In: ICD-CIID F (ed) Irrigation scheduling from theory to practice (Water Reports). FAO, Rome, Italy, pp 185–193
65. Doorenbos J, Kassam AH (1979) Yield response to water. Irrigation and Drainage Paper No. 33, Food and Agricultural Organisation, Rome, Italy

66. Jones CA, Kiniry JR (1986) CERES-Maize: a simulation model of maize growth and development. Texas A&M University Press, College Station, TX, USA
67. Williams JR, Jones CA, Dyke PT (1984) A modelling approach to determining the relationship between erosion and soil productivity. Trans Am Soc Eng 27:129–144
68. Cabelguenne M, Debaeke Ph, Puech J, Bose N (I997) Real time irrigation management using the EPIC-PHASE model and weather forecasts. Agr Water Manage 32:227–238
69. McGlinchey MG, Inman-Bamber N, Culverwell TL, Els M (1995) An irrigation scheduling method based on a crop model and an automatic weather station. Proceedings of the Annual congress of the South African Sugar Technologists' Association, vol 69, pp 69–73
70. Plauborg F, Heidmann T (1996) MARKVAND: an irrigation scheduling system for use under limited irrigation capacity in a temperate humid climate. In: ICD-CIID F (ed) Irrigation scheduling from theory to practice (Water Reports). FAO, Rome, pp 177–184
71. Hess TM (1990) Practical experiences of operating a farm irrigation scheduling service in England. Acta Hortic 278:871–878
72. Hess TM (1996) A microcomputer scheduling program for supplementary irrigation. Comput Electron Agr 15:233–243
73. Tollefson L (1996) Requirements for improved interactive communication between researchers, managers, extensionists and farmers. In: ICD-CIID F (ed) Irrigation scheduling from theory to practice (Water Reports). FAO, Rome, pp 217–226
74. Ines AVM, Honda K, Das Gupta A, Droogers P, Clemente RS (2006) Combining remote sensing-simulation modeling and genetic algorithm optimization to explore water management options in irrigated agriculture. Agr Water Manage 83:221–232
75. Bastiaanssen WGM, Menenti M, Feddes RA, Holtslag AAM (1998) A remote sensing surface energy balance algorithm for land (SEBAL). 1. Formulation. J Hydrol 212–213:198–212
76. Hansen JW, Ines AVM (2005) Stochastic disaggregation of monthly rainfall data for crop simulation studies. Agr Forest Meteorol 131:233–246
77. Groot JJR, Van Keulen H (1990) Prospects for improvement of nitrogen fertilizer recommendations for cereals: a simulation study. In: Van Beusichem ML (ed) Plant nutrition: physiology and applications. Developments in Plant and Soil Sciences, vol 41. Kluwer, Dordrecht, The Netherlands, pp 685–692
78. Li FY, Johnstone PR, Pearson A, Fletcher A, Jamieson PD, Brown HE, Zyskowskia RF (2009) AmaizeN: a decision support system for optimizing nitrogen management of maize. NJAS Wageningen J Life Sci 57:93–100
79. Zadoks JC (1981) EPIPRE: a disease and pest management system for winter wheat developed in The Netherlands. EPPO Bull 11:365–369
80. Rabbinge R, Rijsdijk FH (1983) EPIPRE: a disease and pest management system for winter wheat, taking account of micrometeorological factors. EPPO Bull 13:297–305
81. Smeets E, Vandenriessche H, Hendrickx G, De Wijngaert K, Geypens M (1992) Photosanitary balance of winter wheat in 1992 by the EPIPRE advice system. Parasitica 48:139–148
82. Djurle J (1988) Experience and results from the use of EPIPRE in Sweden. SROP Bulletin. In: Pest and disease models in forecasting crop loss appraisal and decision supported crop protection systems, vol 11, pp 94–95
83. Forrer HR (1988) Experience and current status of EPIPRE in Switzerland. SROP Bulletin. In: Pest and disease models in forecasting crop loss appraisal and decision supported crop protection systems, vol 11, pp 91–93
84. Macadam R, Britton I, Russell D, Potts W, Baillie B, Shaw A (1990) The use of soft systems methodology to improve the adoption by Australian cotton growers of the Siratac computer-based crop management system. Agr Syst 34:1–14
85. Hamilton WD, Woodruff DR, Jamieson AM (1991) Role of computer-based decision aids in farm decision-making and in agricultural extension. In: Muchow RD, Bellamy JA (eds) Climatic risk in crop production-models and management for the semi-arid tropics and subtropics. CAB International, Wallingford, UK, pp 411–423
86. Roetter RP, Hoanh CT, Laborte AG, Van Keulen H, Van Ittersum MK, Dreiser C, Van Diepen CA, De Ridder N, Van Laar HH (2005) Integration of Systems Network (SysNet) tools for regional land use scenario analysis in Asia. Environ Model Softw 20:291–307
87. Roetter RP, Laborte AG, Van Keulen H (2000) Using SysNet tools to quantify the trade-off between food production and environmental quality. International Rice Research Newsletter, December 2000:4–9
88. Van Ittersum MK, Roetter RP, Van Keulen H, De Ridder N, Hoanh CT, Laborte AG, Aggarwal PK, Ismail AB, Tawang A (2004) A systems network (SysNet) approach for interactively evaluating strategic land use options at sub-national scale in South and South-east Asia. Land Use Policy 21:101–113
89. Van Keulen H (2007) Quantitative analyses of natural resource management options at different scales. Agr Syst 94:768–783
90. Van Paassen A, Roetter RP, Van Keulen H, Hoanh CT (2007) Can computer models stimulate learning about sustainable land use? Experience with LUPAS in the humid (sub-) tropics of Asia. Agr Syst 94:874–887
91. Sterk B, Carberry P, Leeuwis C, Van Ittersum MK, Howden M, Meinke H, Van Keulen H, Rossingh WAH (2009) The interface between land use systems research and policy: multiple arrangements and leverages. Land Use Policy 26:434–442
92. David A (2001) Models implementation: a state of the art. Eur J Oper Res 134:459–480
93. Rykiel EJ Jr, Berkson J, Brown VA, Krewitt W, Peters I, Schwartz M, Shogren J, Van der Molen D, Blok R, Borsuk M, Bruins R, Cover K, Dale V, Dew J, Etnier C, Fanning L, Felix R, Nordin Hasan M, Hong H, King AW, Krauchi N, Lubinsky K, Olson J, Onigkeit J, Patterson G, Rajan KS, Reichert P, Sharma K, Smith V, Sonnenschein M, St-Louis R, Stuart D, Supalla R, Van Latesteijn H (2002) Science and decision making. In: Costanza R, Jörgensen SE (eds) Understanding and solving environmental problems in the 21st century. Toward a new, integrated hard problem science. Elsevier, Amsterdam, The Netherlands, pp 153–166

94. Walker DH (2002) Decision support, learning and rural resource management. Agr Syst 73:113–127
95. Carberry PS, Hochman Z, McCown RL, Dalgliesh NP, Foale MA, Poulton PL, Hargreaves JNG, Hargreaves DMG, Cawthray S, Hillcoat N, Robertson MJ (2002) The FARMSCAPE approach to decision support: farmers', advisers', researchers' monitoring, simulation, communication and performance evaluation. Agr Syst 74:141–177
96. Hargreaves DMG, Hochman Z, Dalgliesh N, Poulton P (2001) FARMSCAPE online – developing a method for interactive Internet support for farmers situated learning and planning. In: Proceedings of the Tenth Australian Agronomy Conference, Hobart, Australia. www.regional.org.au/au/asa/2001/5/a/hargreaves.htm)
97. McCown RL (2002) Changing systems for supporting farmers' decisions: problems, paradigms, and prospects. Agr Syst 74:179–220
98. Twomlow S (2001) Linking Logics II: taking simulation models to the farmers. British Society of Soil Science Newsletter, December 2001 (40):12–14
99. Carberry PS, Hochman Z, Hunt JR, Dalgliesh NP, McCown RL, Whish PM, Robertson MJ, Foale MA, Poulton MA, van Rees H (2009) Re-inventing model-based decision support with Australian dryland farmers. 3. Relevance of APSIM to commercial crops. Crop Pasture Sci 60: 1044–1056
100. Dalgliesh NP, Foale MA, McCown RL (2009) Re-inventing model-based decision support with Australian dryland farmers. 2. Pragmatic provision of soil information for paddock-specific simulation and farmer decision making. Crop Pasture Sci 60:1031–1043
101. McCown RL, Carberry PS, Hochman Z, Dalgliesh NP, Foale MA (2009) Re-inventing model-based decision support with Australian dryland farmers. 1. Changing intervention concepts during 17 years of action research. Crop Pasture Sci 60:1017–1030

Books and Reviews

European Journal of Agronomy (2003) Volume 18, Issues 3–4, special issue Modelling Cropping Systems: Science, Software and Applications. pp 187–393

Gary C, Heuvelink E (1998) Advances and bottlenecks in modelling crop growth: summary of a group discussion. Acta Hortic (ISHS) 456:101–104

Goudriaan J, Van Laar HH (1994) Modelling potential crop growth processes, textbook with exercises. Current Issues in Production Ecology, vol 2. Kluwer, Dordrecht, The Netherlands, p 238

Jongschaap REE (2006) Integrating crop growth simulation and remote sensing to improve resource use efficiency in farming systems. Ph.D. thesis, Wageningen University, Wageningen, The Netherlands

Leffelaar PA (ed) (1993) On system analysis and simulation of ecological processes, with examples in CSMP and FORTRAN. Current Issues in Production Ecology, vol 1. Kluwer, Dordrecht, The Netherlands, p 294

Matthews RB, Stephens W (2002) Crop-soil simulation models: applications in developing countries. CAB International, Wallingford, UK

Roetter RP, Van Keulen H, Kuiper M, Verhagen J, Van Laar HH (eds) (2007) Science for agriculture and rural development in low-income countries. Springer, Dordrecht, The Netherlands, p 222

Willocquet L, Savary S, Fernandez L, Elazegui FA, Castilla N, Zhu D, Tang Q, Huang S, Lin X, Singh HM, Srivastava KA (2002) Structure and validation of RICEPEST, a production situation-driven, crop growth model simulating rice yield response to multiple pest injuries for tropical Asia. Ecol Model 153:247–268

Wolf J, Van Ittersum MK (2009) Crop models: main developments, their use in CGMS and integrated modeling. Agro-Informatica 22:15–18

Smart Grids, Distributed Control for

Frank Kreikebaum[1], Deepak Divan[2]
[1]Georgia Institute of Technology, Atlanta, GA, USA
[2]School of Electrical and Computer Engineering, Georgia Institute of Technology, Atlanta, GA, USA

Article Outline

Glossary
Definition of Distributed Control for Smart Grids
Introduction
Emerging Challenges
Distributed Control Techniques
Existing Distributed Control Technologies
Emerging Technologies
Power Flow Control as an Enabler for Improved Energy Markets
Conclusions and Future Directions
Bibliography

Glossary

Flexible AC transmission system (FACTS) A system deployed on the electrical network to control one or more parameters of the network. FACTS is typically realized with solid-state or mechanical switches.

Optimal power flow (OPF) A method to control generation and transmission assets to minimize cost of

operation, operate assets at or below rated values, and meet reliability requirements.

Reactive power One of the two forms of power in AC power transmission, reactive power is the energy stored in magnetic and capacitive devices that is returned to the system every cycle. Reactive power is required to maintain grid functionality and is measured in (volt-ampere reactive) VARs. By definition, capacitors generate reactive power, and inductors consume reactive power.

Definition of Distributed Control for Smart Grids

Distributed control for smart grids is the use of distributed grid assets to achieve desired outcomes such as increased utilization of transmission assets, reduced cost of energy, and increased reliability. Distributed control is a key enabler to meet emerging challenges such as load growth and renewable generation mandates.

Introduction

The utility grid is a massive system with tens of thousands of generators, hundreds of thousands of miles of high-voltage transmission lines and millions of assets such as transformers and capacitors, all working with split-second precision to deliver reliable electrical energy to hundreds of millions of customers. The grid was designed at a time when electromechanical controls and generator excitation control were the only available control handles to keep the system operating. In addition, the inability to guide electricity flows and to store electricity inexpensively forced the adoption of rules that distorted market operation, and created inefficient use of assets. The decision of the US government to make electricity a universal right of the people and a regulated industry, further removed drivers that moved the industry toward effective and competitive operation. The result of these technology limitations and policy structures that were created, with the best of intentions, is that the electricity markets work ineffectively at best.

The electricity industry asset base in the USA is worth an estimated $2.2 trillion in terms of replacement value. Global and US electrical demands are expected to rise 80% and 24%, respectively over the next 20–25 years. In the USA, if grid-enabled vehicles (GEVs) are widely adopted, total electrical demand could be 45% higher in 2035 than 2008. Mandates for renewable energy are expected to require a doubling in annual transmission investment yet will lower utilization of the transmission system. A ubiquitous roll-out of smart grid functionality would provide better utilization of the transmission and distribution system, reduce the investment required to meet renewable mandates, and raise reliability. However, there is no economic basis for implementing such a far-reaching transformation. It is however possible, with correctly defined priorities, to implement an upgrade of selected portions of the grid, to achieve a large part of the important gains. Selective introduction of newer technologies that allow dynamic granular control (DGC) of voltage and power flows on the grid can enable a much more efficient use of grid assets, minimizing the need to build new transmission lines to accommodate variable generation resources such as wind and solar.

Such control capability will transform the electricity market, allowing transactions between willing generators and users, along pathways that have the capacity to handle more power. It will directly mitigate problems of cost allocation that have plagued transmission-line building. It will reduce the cost of absorbing more wind and solar energy, and of adopting GEVs to improve energy security and to reduce carbon emissions. This control cannot be implemented at the traditional generation excitation controls, but has to be implemented at various points on the grid, so that the utilization of diverse grid assets can be improved substantially. Such control will necessarily be distributed in nature, and points to a future vision of grid control.

Distributed control is a key enabler to meet emerging challenges in the electric power sector. This entry begins by surveying the emerging challenges. It then discusses general methods for two types of distributed control, namely VAR control and power flow control. Next, the technologies currently available to realize VAR control and power flow control are discussed. It then surveys emerging technologies and methods before concluding.

Emerging Challenges

Load Growth

Globally, electrical energy demand is expected to grow 2.5% per year from 2006 to 2030 with total demand

rising from 15,665 TWh in 2006 to 28,141 TWh in 2030 [1]. Worldwide generation capacity is expected to grow 2.3% per year from 2006 to 2030, rising from 4,344 to 7,484 GW [1]. The DOE Energy Information Agency (EIA) expects US electrical load to increase 1% annually to 2035, a 24% increase in annual demand relative to 2010 demand [2]. These projections include negligible amounts of GEVs with electricity supplying less than 3% of global transport energy and 0.2% of US light-duty transit sector energy in 2030 and 2035, respectively [1, 3]. Historically, load growth has required investment in generation as well as the transmission and distribution systems. Utilities are facing pressure to meet this load growth at low cost to consumers, a challenge given high costs for fuel and materials.

Challenges Permitting Urban Generation and Transmission

The need for distributed control can be mitigated through the installation of generation in load centers or new transmission connecting distant generation with load centers. Siting generation in load centers is difficult due to noise, emissions, viewshed concerns, land acquisition cost, and the limited capacity of the urban fuel delivery system. In addition, generator cooling water availability is projected to be limited in many load centers [4]. A study in the USA shows that 19 of the 22 counties identified as most at risk for water shortage due to electricity generation are located in the 20 fastest growing metropolitan statistical areas.

Construction of new transmission to supply load centers is also difficult. Concerns include viewshed, land acquisition cost, and electromagnetic radiation. High-voltage transmission lines require more than a decade to build. Also, the allocation of cost is problematic, especially for lines that cross state and utility boundaries. Finally, the construction of new lines increases the MW-miles of line serving a given amount of load, decreasing rather than increasing utilization of the existing system, leading to cost increases and inefficiencies.

Policy Drivers for Renewable Generation

Policies are driving the adoption of renewable generation around the world. China aims to increase renewable energy from 7.1% of total electrical energy in 2005 to 20% in 2020 with the installed wind capacity rising from 1,260 MW in 2005 to 30,000 MW in 2020 [5]. Grid operators in China are required to accommodate renewable energy, with prices for wind decided in an auction in which only wind plants participate [5]. In the USA, 29 states plus the District of Columbia have enacted binding renewable portfolio standards (RPSs), and 7 states have voluntary goals [6]. RPSs require a certain percentage of annual electrical energy demand to be met with renewable generation by a specified year. In addition, the US federal government incents the development of renewable generation through the Production Tax Credit (PTC) and the US Treasury Section 1603 Investment Tax Credit.

The renewable mandates stress the transmission system and require additional investment. One metric of this stress is the ratio of peak generation capacity to average power demanded. In 2008, the US ratio was 2.18. In the EIA 2035 reference scenario, which sources 5% of national electricity from nonhydro renewables resources, the ratio improves to 2.03. All things being equal, this reduction shows increased utilization of the generation fleet in 2035 relative to 2008 and lower unit cost of energy. If a 20% RPS is mandated, the ratio rises to 2.29, a degradation resulting in lower utilization in 2035 relative to 2008. So, while the 2035 nonrenewable case shows a 7% increase in utilization, the RPS case shows a 5% degradation. To avoid curtailment of renewables, transmission must be built to accommodate the peak power output of the renewable fleet.

Globally, both wind and solar photovoltaic generation have grown exponentially over the last fifteen years, as seen in Fig. 1. As seen in Fig. 2, the highest quality wind and solar resources in the USA are remote from load centers. Siting generation at these high-quality resources maximizes the plant owner's return on investment if the transmission network can accommodate the generated energy. A number of integration studies have been performed around the globe to assess the transmission and system operation impacts of wind and solar energy on the system [7–22]. Two studies covering large, multistate regions of the USA are the Eastern Wind Integration and Transmission Study (EWITS) and the Western Wind and Solar Integration Study (WWSIS). In EWITS, the design of the transmission build-out was iterated using a committee of

stakeholders. Undiscounted transmission costs were $33–59 billion (2009$) higher than the reference case, which had minimal additional wind capacity. This amounted to $300–447 of added cost per kW of installed wind capacity. With the transmission build-out, wind curtailment averaged 7–11%, higher than current levels in the USA. In the WWSIS, Wyoming, Colorado, Montana, Arizona, and Nevada were supplied with up to 35% renewables. A simplified transmission build-out was developed to trade renewable energy among these states. The cost was $11B with a benefit-to-cost ratio of 0.9.

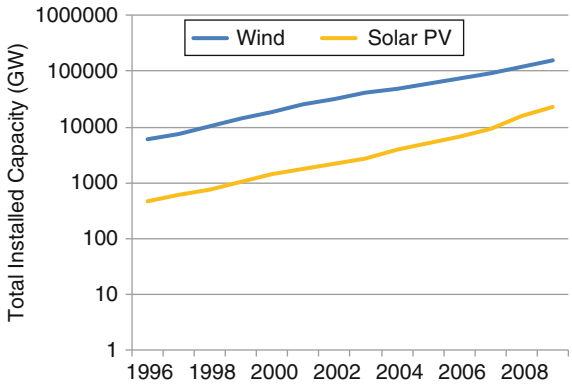

Smart Grids, Distributed Control for. Figure 1
Logarithmic plot of global cumulative wind and solar PV capacity installed [23]

For a scenario in which 20% of US demand is met with renewable energy, the estimated transmission cost is $360 billion over 25 years, or $14 billion per year. This assumes the average distance between renewable generation and load is 1,000 miles, a reasonable scenario if renewable generation is installed in high resource areas in the Midwest and Southwest. Currently, total transmission investment, including long-distance and local transmission, is $9 billion per year. If renewable energy transmission investment substitutes for 50% of the current investment, total annual investment would be $18.5 billion per year, a 105% increase

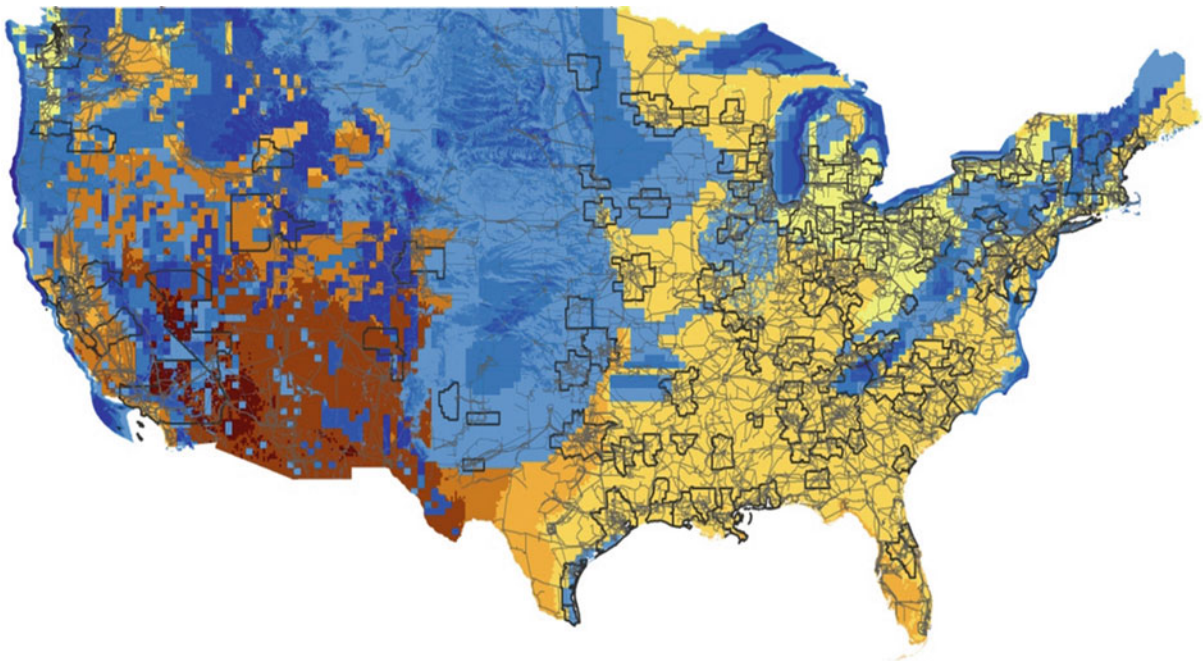

Smart Grids, Distributed Control for. Figure 2
Map of US wind and solar resources and major metropolitan areas. Solar resources are shown from *light yellow* to *brown*, with the highest resource sites in *brown*. Wind resources are shown from *light blue* to *dark blue*, with darker being more attractive. Only wind sites viable with current technology are shown. Major metropolitan areas are outlined in *black*. *Gray lines* in the background show the high-voltage transmission system

over current investment levels. This increased level of investment would need to be sustained for 25 years to supply 20% of projected US demand with renewable energy.

Policy Drivers for GEVs

Grid-enabled vehicles (GEVs) are experiencing a renaissance following their last resurgence in the 1990s. Mainstream manufacturers and new entrants offer or plan to offer GEVs spanning a broad price range. In the USA, GEVs are currently supported through federal and state tax credits. Proposals have been developed to electrify 75% of the miles traveled by the light-duty fleet by 2040 [24]. In Europe, high fuel taxes and a requirement that fleet average emissions drop from 160 to 95 g CO_2/km are likely to foster GEV development [24]. The Chinese government recognizes the ability of GEVs to improve energy security and has implemented a program to build charging infrastructure in the 13 largest cities. It also offers a tax incentive program for vehicles and buses on the order of $8,000 and $70,000 per vehicle, respectively [24]. The impact of GEVs on the power system is dependent on the level of GEV adoption, the charging model, and the level of coordination between the time of charging and the power system state. If 80% of the miles traveled by the US light-duty fleet are electrified by 2035, annual electrical demand is projected to increase 45% relative to 2008, compared to a 24% increase without GEVs. Uncoordinated charging will lead to overloading and accelerated aging of distribution assets [64]. The monitoring system for distribution assets is less developed than for transmission assets, making it difficult to proactively upgrade strained distribution assets. Without coordination of vehicle charging, significant new transmission and distribution investment will likely be required.

Differences Between the Electrical Network and Other Commodity Delivery Networks

In the USA, natural gas and petroleum pipelines have become less regulated over the last two decades. Before the 1990s, pipeline developers submitted plans for new pipelines to FERC. FERC selected which pipelines would be built based on its assessment of societal needs. It was assumed that FERC could not allow competition among pipelines. Following PUC CA v. CA 1990, FERC allowed more competition in the pipeline industry. Different rates could be charged to anchor customers, who supported pipeline construction at an early stage, and other customers who requested pipeline access after construction.

In petroleum pipelines, product differentiation is possible by separating shipments via a marker liquid called transmix. As of 2005, most shipment of oil was regulated by FERC, but refined products based on petroleum used market-based rates [25, 26]. However, market-based rates are the fastest growing rate type [25]. FERC permits the use of market rates on a case by case basis after ensuring that the pipeline does not have an unreasonable level of market power.

Due to deregulation, by 2000, the natural gas pipelines were no longer guaranteed a rate of return [27]. Users who reserved capacity were given firm transmission rights. Tariffs for firm capacity were regulated [28]. Remaining capacity was sold in bulletin boards at market rates. Owners of capacity can resell their capacity to realize arbitrage opportunities.

The electric network is considered a natural monopoly due to the inability of transmission line owners to control the flow of power through their lines. This lack of control means owners cannot take bids for the use of their lines, as is done in natural gas pipelines. The lack of control creates free-rider effects whereby entities benefit from investments made by others. Collectively, this creates a disincentive for transmission owners to upgrade their assets.

Reliability Challenges in Emerging Economies

A country-wide overview of reliability statistics was not identified for the emerging economies. Statistics for 1997–2008 were found for five utilities in Brazil, serving a combined electrified population of 389 million [29]. Statistics were also found for two power companies in India, the North Delhi Power Limited (NDPL) and the Bangalore Electricity Supply Company (BESCOM) [30]. Compared to the USA, the Brazilian utilities had eight times the annual outage duration and 14 times the annual outage frequency. The BESCOM system had 20 times the US outage duration. It is anticipated that continued economic growth will require more reliable supply of electricity, necessitating investment in emerging economies.

Distributed Control Techniques

Distributed control has been used to operate the electrical system since its inception. The initial subsection of this section will describe optimal power flow (OPF), which traces its history back to the earliest days of power system operation. Today's power system relies primarily on OPF to realize control. As discussed in the previous section, numerous challenges are emerging for power system investment and operation. Accommodating renewable energy and GEVs will likely require a response time not possible with traditional control techniques such as OPF. This section will introduce VAR control and power flow control. Realized with appropriate technologies, VAR control and power flow control can provide fast-responding control, called dynamic granular control (DGC), to meet the emerging challenges.

The techniques described in this section can be applied to both the transmission and distribution systems. Controllability of the distribution system has lagged behind that of the transmission system. This is in part due to the large number of distribution assets, relative to transmission assets. The number of assets increases the complexity and cost of controlling the distribution system. Unlike the transmission system, the distribution system has traditionally been operated as a radial network rather than a meshed network. This simplifies control but leads to lower reliability. Smart grid activities to date have been largely aimed at improving control of the distribution system to improve efficiency, increase capacity without new asset construction, and accommodate distributed generation.

Optimal Power Flow

Optimal power flow (OPF) is used by system operators and planners to minimize the total cost of system operation. OPF is the primary control technique in today's grid. The main control handles, or control actions, are adjustments of the real and reactive power injections of the generators. However, OPF can include other control handles, such as the settings of a phase-shifting transformer (PST). Although control decisions are typically made centrally, OPF is considered distributed control because the control actuators, such as generators and PSTs, are distributed throughout the system. OPF set points are not typically changed more frequently than every 5 min. OPF is configured to provide sufficient safety margins to accommodate unexpected events such as load forecast error, renewable generation forecast error, and contingencies. A contingency is when any one or more grid assets, such as a power line or transformer, suddenly go offline.

The realization of OPF is different in vertically integrated and market environments. In both, power flows are changed by directly changing the output power of the generators. In the absence of other power flow control technologies, OPF does not allow the control of flow in individual lines.

In a vertically integrated environment, a single utility is responsible for generation, transmission, and distribution in a given region. This utility owns all of the assets in the region and knows the costs and technical limitations of its assets. The inputs to the OPF are as follows:

- Generator parameters – For each generator, the maximum power output, minimum power output, bus to which the generator is connected, and a cost curve are provided to the OPF. Each cost curve describes the variable cost of operating the unit at each potential operating point between minimum power and maximum power. Variable cost includes fuel and variable O&M costs.
- Transmission line parameters – For each transmission line, the line impedance values, nominal voltage, current rating, and terminal locations are specified.
- Transformer parameters – For each transformer, the transformer impedance values, nominal voltages, current rating, and terminal locations are specified.
- Load data – The expected demand at each bus is forecasted for each time step over which the OPF will be run.
- Contingency list – Normally, the OPF is run for a set of potential contingencies rather than all possible contingencies to reduce the solution time.
- Stability limits – The OPF does not typically compute the stability of the network endogenously. Rather, rules are provided to the OPF in the form of a nomogram or lookup table to ensure that unstable solutions are avoided.

- Reserve margin – The amount of surplus generation capacity that must be available to meet uncertainties in load and renewable forecasts as well as generator outages.

In a market area, an independent system operator (ISO) or regional transmission operator (RTO) runs the OPF to decide which generators will be used and at what level. The transmission network is typically owned by regulated entities, which may also own the distribution networks. Generators are independent of the owners of the transmission and distribution networks. Rather than cost curves, the generator owners submit bid curves to the ISO or RTO. The bid curves designate the minimum price generation owners are willing to accept to generate energy over the whole range of the generator output. In the simplest scheme, owners of the distribution network designate how much power their customers will require, and consumers are price takers. The other inputs to the OPF are the same as those used by the vertically integrated utility. Using the generator bids and forecasted demand, the ISO or RTO runs the OPF to compute the least cost dispatch of generators to serve the load and meet security requirements.

The economic impact of the lack of power flow control is visible in Fig. 3. In the figure, generators, each indicated by a circle with the letter "G" inside, are connected to bus 1 and bus 3. Load is connected at bus 3. Three transmission lines connect the three buses. Each line has a thermal rating of 1,000 MW. All transmission lines have the same impedance X. G1 is the cheapest generator. To minimize cost, G1 should serve the entire load at bus 3. However, due to transmission network constraints, G1 can only supply 1,500 MW. One thousand megawatts flows from bus 1 to bus 3 through line 1–3, and 500 MW flows from bus 1 to bus 3 via line 1–2 and line 2–3. The flow is less in line 1–2 and line 2–3 compared to line 1–3 because of the increased impedance. Because of this impedance difference, the flow through line 1–2 reaches the limit of 1,000 MW when the total power transfer is 1,500 MW. This sets the maximum amount of power G1 can supply to bus 3 even though 500 MW of unused capacity exists on line 1–2 and line 2–3.

OPF alone is limited to adjustments of generator output and is not able to resolve numerous challenges, including those described above. While the following sections will describe some power flow control capabilities beyond generation control that are currently implemented, the majority of power today is controlled, inefficiently, through OPF control of generator set points.

VAR Control

VAR control provides a number of benefits to the system. First, it can be used to control the voltage

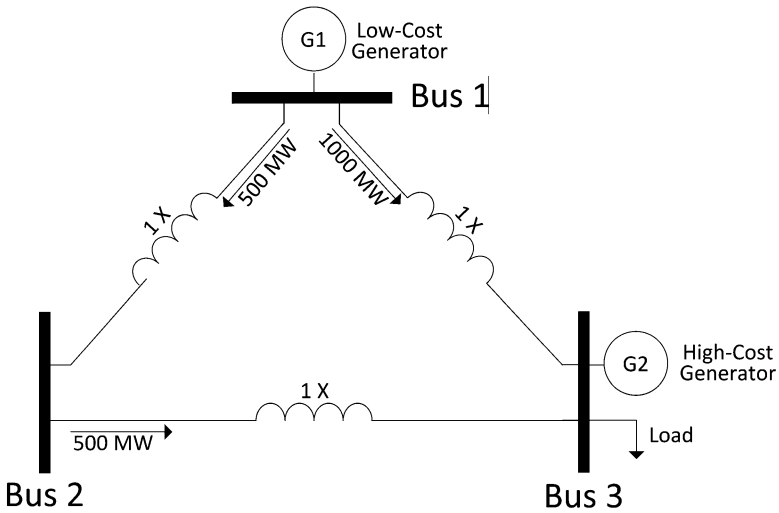

Smart Grids, Distributed Control for. Figure 3
Three-bus system showing power flows resulting from OPF control of generation

profile along a transmission line, thereby increasing the maximum amount of power which can be transmitted in the line. It can also be used to decrease the reactive power which must be sourced at the endpoints of a line and reduce line losses. VAR control can also be used to improve voltage stability if the end of a power line does not have sufficient generation. VAR control, if appropriately fast, can improve transient stability. Improvement of transient stability also increases the power which can be transferred on the line. Finally, VAR control can be used to damp power system oscillations, averting damage to rotating machinery, increasing power transfer capability, and potentially improving stability.

Power Flow Control

Under certain simplifying assumption, the power flow between two buses of an electrical network is determined by Eq. 1. The power flow can be modified by modifying any of the parameters of the equation:

- V_1 and V_2 are the voltage magnitudes of the endpoints of the transmission line.
- δ is the angle difference between the voltage phasors at the endpoints of the transmission line.
- X is the reactance of the transmission line.
- P is the power transmitted over the transmission line.

Voltage changes alone cannot impact power flow in a large way, since the voltage is typically maintained within ±5% of a nominal value to avoid damaging generators, the transmission network, the distribution network, or customer equipment.

The following sections will detail the methods used to change power flows:

Power flow between two AC buses.

$$P = \frac{V_1 V_2 sin\delta}{X}. \quad (1)$$

Impedance Control Impedance control of power flow aims to directly change the impedance, represented by the value X, as seen in Eq. 1. Technologies able to change impedance include the series mechanically switched capacitor (series MSC), the series mechanically switched reactor (series MSR), the thyristor-controlled series capacitor (TCSC), the static synchronous series compensator (SSSC), and the unified power flow controller (UPFC). These technologies will be discussed in more detail in section "Existing Distributed Control Technologies."

The benefit of impedance control is shown in Fig. 4, a modification of the three-bus system previously shown in Fig. 3. Here, a power flow controller able to change line impedance has been installed on line 2–3. Through an appropriate modification of the

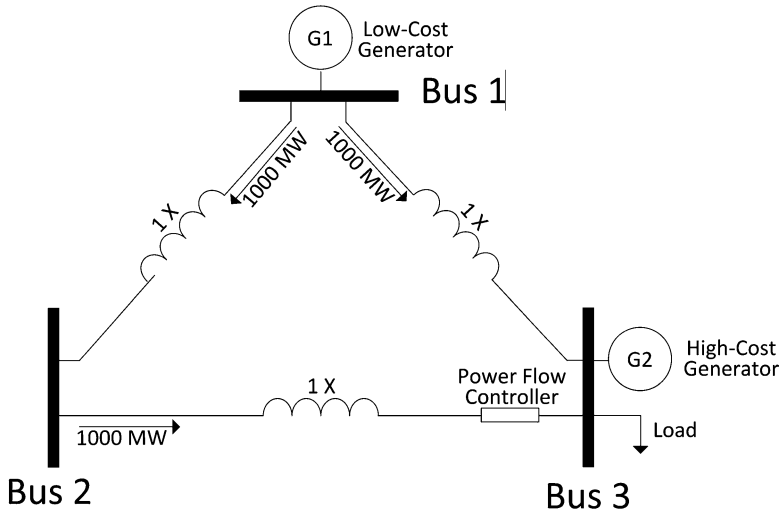

Smart Grids, Distributed Control for. Figure 4
Three-bus system with power flow controller installed on line 2–3. The OPF determines the optimal settings for the generator and power flow controller

impedance, the power flow in all lines can be equalized, allowing up to 2,000 MW to be transferred between bus 1 and bus 3, compared to the 1,500 MW using generator control alone. This allows the entire load at bus 3 to be served by the low-cost generator, resulting in a reduction in the cost of energy.

Angle Control Angle control aims to change power flows through the parameter δ as seen in Eq. 1. Technologies able to control the angle include the phase-shifting transformer (PST), also known as phase angle regulator (PAR), the variable frequency transformer™ (VFT), and the solid-state transformer. The power flow control of Fig. 4 can also be realized using angle control. The PST and VFT will be discussed in more detail in section "Existing Distributed Control Technologies." The solid-state transformer will not be discussed as it is not commercially available and is expected to have high cost.

Voltage Control Angle control aims to change power flows through the parameter V_1 or V_2 as seen in Eq. 1. Technologies able to control voltage include the static VAR compensator (SVC) and the static synchronous compensator (STATCOM). The power flow control of Fig. 4 cannot be realized via voltage control although voltage control can be used for limited power flow control in more complicated networks.

DC Control It is also possible to control AC power flows by converting from AC to DC and then back to DC. Two technologies include the high-voltage DC transmission (HVDC) and the back-to-back converter (B2B). Both will be discussed in more detail in section "Existing Distributed Control Technologies."

Existing Distributed Control Technologies

This section will discuss existing distributed control technologies for VAR control and power flow control. These technologies provide various levels of dynamic granular control (DGC). These technologies can be actuated through OPF for response times on the order of minutes or through separate control algorithms for response times on the order of microseconds.

VAR Control

Shunt Mechanically Switched Capacitor (shunt MSC) A mechanically switched capacitor (MSC), when connected in shunt at a bus, can provide VAR control by delivering capacitive VARs. A typical installation is shown in Fig. 5. Switching causes deterioration of the mechanical switch. Thus, MSCs are typically not actuated frequently. MSCs are ubiquitous. The cost for an MSC was $8–10/kVAR in the mid-1990s [31].

Shunt Mechanically Switched Reactor (shunt MSR) A mechanically switched reactor (MSR), when connected in shunt at a bus, can provide VAR control by delivering inductive VARs. A typical installation is shown in Fig. 6. A circuit breaker is typically used to connect and disconnect the MSR due to the inductive load. As with MSCs, frequent actuation deteriorates the mechanical switching element. MSRs are widely used.

Thyristor-Switched Capacitor (TSC) A thyristor-switched capacitor (TSC), shown in Fig. 7, is a shunt capacitor which is switched in and out using a thyristor

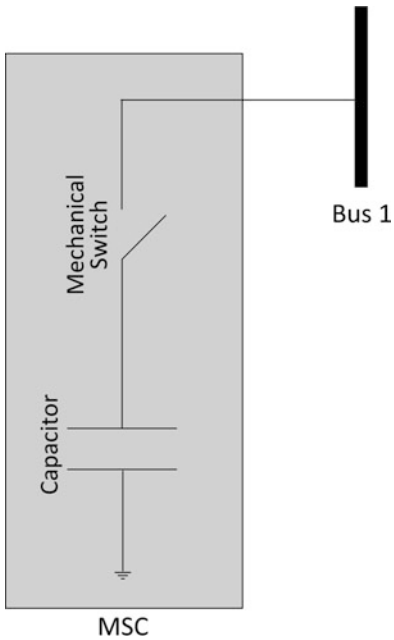

Smart Grids, Distributed Control for. Figure 5 Shunt mechanically switched capacitor (MSC) connected to bus 1

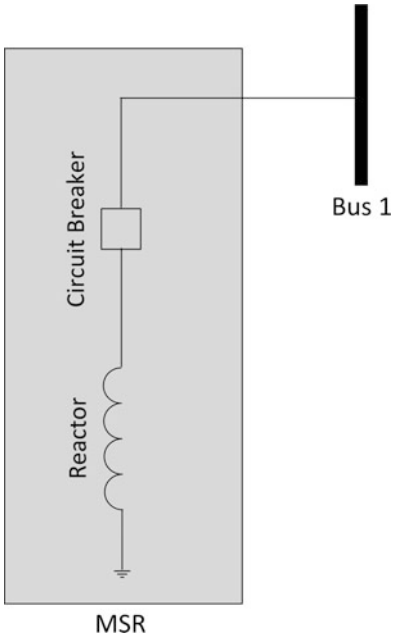

Smart Grids, Distributed Control for. Figure 6
Shunt mechanically switched reactor (MSR) connected to bus 1

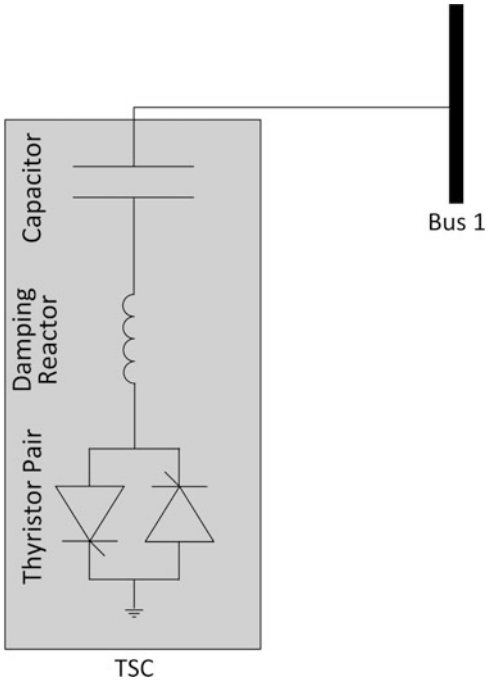

Smart Grids, Distributed Control for. Figure 7
Thyristor-switched capacitor (TSC) connected to bus 1

pair. The use of a thyristor pair, rather than a mechanical switch as in the MSC, allows for longer life. Also, a TSC can respond faster than an MSC, allowing for an injection of VARs following a system transient.

Static VAR Compensator (SVC) The static VAR compensator (SVC) is comprised of a combination of shunt MSCs, TSCs, and thyristor-controlled reactors (TCRs) to control grid parameters by changing the reactive admittance of the SVC. A typical SVC configuration is shown in Fig. 8. The maximum level of reactive current changes linearly with the bus voltage, and maximum VAR output varies as the square of the bus voltage. An SVC cannot increase VAR generation during a transient. However, since an SVC is typically implemented in a single-phase, line-to-ground manner, it can provide support during unbalanced faults. Mechanically switched capacitors are preferred for applications consistently requiring capacitive injection, as they have lower losses than TSCs. However, an MSC is limited to 2,000–5,000 switching cycles before the switch must be replaced, limiting the use of the MSC unless the required level of VAR compensation changes slowly [32]. In addition, an MSC has a slower response time than a TSC. The configuration in Fig. 8 combines an MSC for steady-state capacitive injection with a TCR for transient performance. The TCR generates harmonics which are removed with the shunt filters.

Worldwide, ABB has installed 499 SVCs totaling 73.3 GVAR, 54% of the global total [33]. Of these, 228 units, with a total capacity of 49 GVAR, are for utility customers. The remaining units are for industrial customers. Siemens has installed at least 45 utility SVCs representing almost 10 GVAR of capacity [34]. AMSC, formerly known as American Superconductor, has installed 130 SVCs and STATCOMs, although the breakdown between the two types is unknown [35]. An SVC cost $50/KVAR in the mid-1990s and is expected to cost roughly $80/KVAR now [31].

Static Synchronous Compensator (STATCOM) A STATCOM uses solid-state gate turnoff devices to mimic the operation of a synchronous condenser, an electrical machine configured to only produce reactive power. The most common type of STATCOM, shown in Fig. 9, uses a single three-phase voltage source converter. The STATCOM maximum reactive output

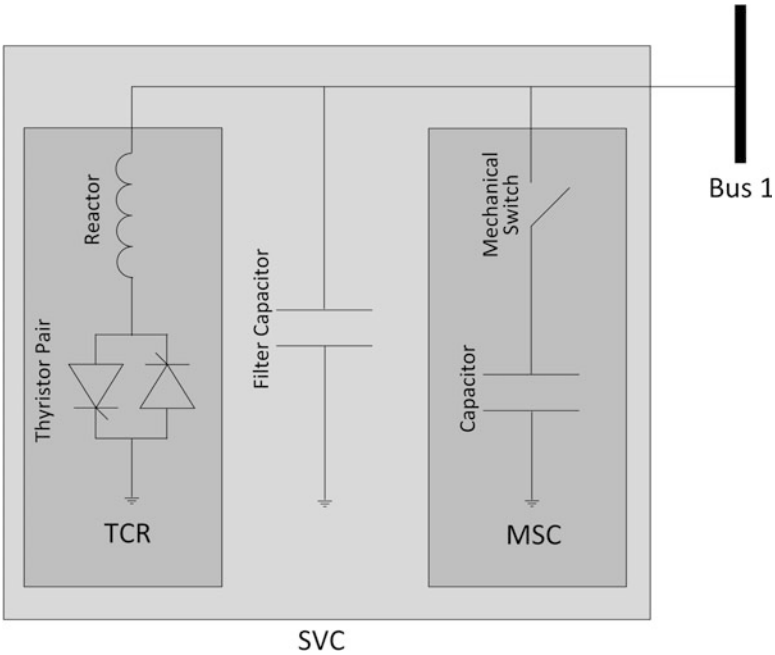

Smart Grids, Distributed Control for. Figure 8
Static VAR compensator (SVC) connected to bus 1

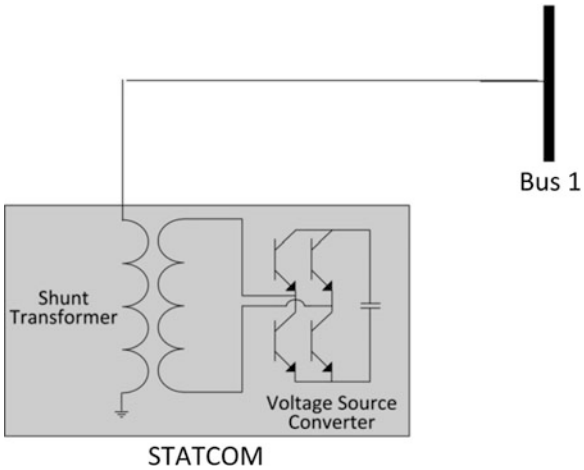

Smart Grids, Distributed Control for. Figure 9
One-line diagram of a static synchronous compensator installed at bus 1

current is nearly constant over a wide voltage range, so reactive power output is nearly linear over a wide bus voltage range. Bus voltages are typically depressed during faults and portions of transients, allowing the STATCOM to provide additional VARs during periods with depressed bus voltages compared to an SVC of the same rating. The STATCOM response is an order of magnitude faster than an SVC, and its footprint is 30–40% smaller than an SVC [32].

A STATCOM can also be configured to provide a temporary increase in reactive current during transients. Use of a STATCOM for three-phase fault and transient mitigation allows the use of a lower rating for the STATCOM than the SVC. However, the three-phase converter implementation limits the STATCOM's ability to provide VARs during unbalanced faults unless the DC capacitor is significantly overrated relative to steady-state operation. This is a significant disadvantage compared to an SVC since an SVC can typically support unbalanced faults. However, AREVA has implemented a STATCOM able to support unbalanced faults through the use of separate converters for each phase.

A single, three-phase STATCOM was estimated to cost $55/kVAR in the 1990s [31] and $150/kVAR now. A system comprised of three single-phase STATCOMs is estimated to cost $200/kVAR.

Siemens has installed at least 14 STATCOMs [46], and ABB has installed an unspecified number of STATCOMs. AMSC has installed 130 SVCs and STATCOMs, although the breakdown between the two types is unknown [35].

Hybrid VAR Systems Some installations use an SVC-STATCOM configuration, replacing the TCR of the SVC with a STATCOM. This allows for the use of an MSC, offering lower losses than a TSC, while retaining the quick response of the STATCOM. This also allows for smaller filters since TCRs generate harmonics [32]. The cost and performance characteristics lie between the SVC and STATCOM and depend on the relative rating of the components.

Comparison of Technologies Table 1 provides a comparison of the VAR controllers discussed above.

Power Flow Control

Series Mechanically Switched Reactor (series MSR) A mechanically switched reactor (MSR) can modify line impedance if installed in series with the line as shown in Fig. 10 [36, 37]. Appropriately designed, a series MSR can be installed on an overloaded, low-impedance line within a meshed

Smart Grids, Distributed Control for. Table 1 Comparison of salient elements of VAR controllers

Technology	Cost ($/kVAR)	Dependency of VARs on bus voltage	Temporary overload capability	Support during unbalanced faults	Response time
MSC	<50	Quadratic	No	Yes	Slow
MSR	<50	Quadratic	No	Yes	Slow
TSC	<50	Quadratic	No	Yes	Medium
SVC	80	Quadratic	No	Yes	Medium
STATCOM – Three phase	150	Linear	Yes	Limited without additional cost	Fast
STATCOM – Single phase	200	Linear	Yes	Yes	Fast
Hybrid	Depends	Depends	Yes	Depends	Depends

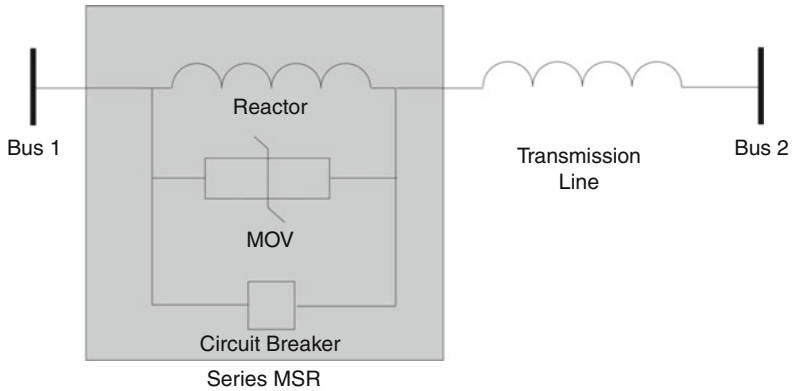

Smart Grids, Distributed Control for. Figure 10
Series mechanically switched reactor (MSR) installed on a transmission line between bus 1 and bus 2

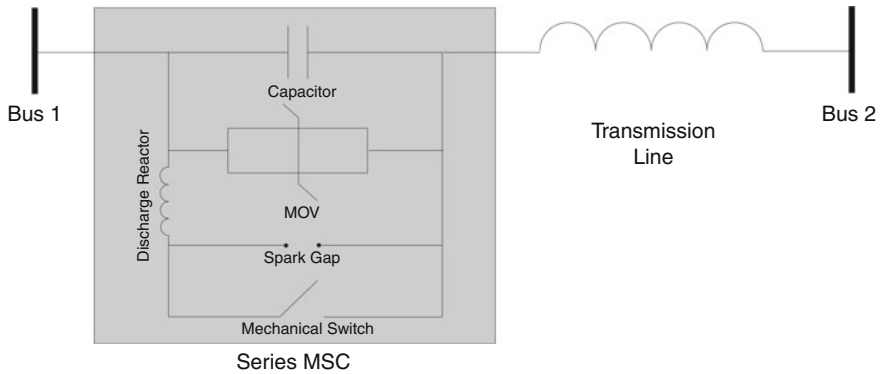

Smart Grids, Distributed Control for. Figure 11
Series mechanically switched capacitor (MSC) installed on a transmission line between bus 1 and bus 2 [45]

system to push power flow onto less utilized paths, to prevent frequent tripping of the line under system transients and contingencies, and to limit fault currents. It is possible to design the series MSR to be switched out, although that is not frequently done. Further, the speed at which the reactors are switched out is slow, designed mainly for a planned change in system/line impedances, and is not sufficient for the rapid response required to mitigate transients.

A series MSR has a number of advantages and disadvantages relative to other methods to control or increase power flow. It is quicker to install than a new transmission line, with historical projects requiring 6–8 months for construction [38]. In addition, given that the MSR does not require new right of way, it requires significantly less time to plan and permit. However, it imposes an additional footprint requirement somewhere along the line, typically at one of the substations, which may require permitting and add cost. A 230 kV MSR solution in California required an additional 5,000 ft^2 of substation area [37]. To reduce cost, manage mechanical stresses, and avoid core saturation during faults, air core reactors are typically used which leads to increased noise and magnetic fields. The magnetic fields are sufficiently high that care must be taken to mitigate unintentional heating of metallic equipment in the substation and hazards to workers in the substation. Finally, a series MSR is heavy and cannot be supported by the line. This requires that they be ground mounted with the requisite, and costly, isolation between ground and line potential. In the early 2000s, a series MSR cost \$11–22/KVAR, although these figures are dated and the current cost is expected to be closer to \$50/KVAR [36, 39].

Series Mechanically Switched Capacitor (series MSC) A mechanically switched capacitor (MSC), when inserted in series with a transmission line, can control power flow by lowering the impedance of lightly loaded lines, thereby drawing power away from heavily loaded lines. A typical installation is shown in Fig. 11. Like a series MSR, a series MSC is not designed to be switched in or out rapidly and can thus not be used to mitigate transients. Since an MSC is not typically built to endure the high currents of a fault, protection methods are used to bypass the MSC during the fault and reengage it soon thereafter to increase system stability [40]. While early series capacitors were protected from fault currents using a maintenance intensive spark gap, more recent designs utilize an MOV or thyristor protection [41]. Like a series MSR, a series MSC imposes a footprint requirement along the line. As with a series MSR, a series MSC is sufficiently heavy that it cannot be supported by the line and requires an isolated, elevated platform. Finally, an MSC can lead to subsynchronous resonance with the rotating elements of a generator which can cause generator failure and power system instability [42]. This results in siting limitations. The cost for an MSC is \$30–50/KVAR [43, 44].

Thyristor-Controlled Series Capacitor (TCSC) A TCSC, shown in Fig. 12, is a series capacitor augmented with an additional shunt path comprised of an

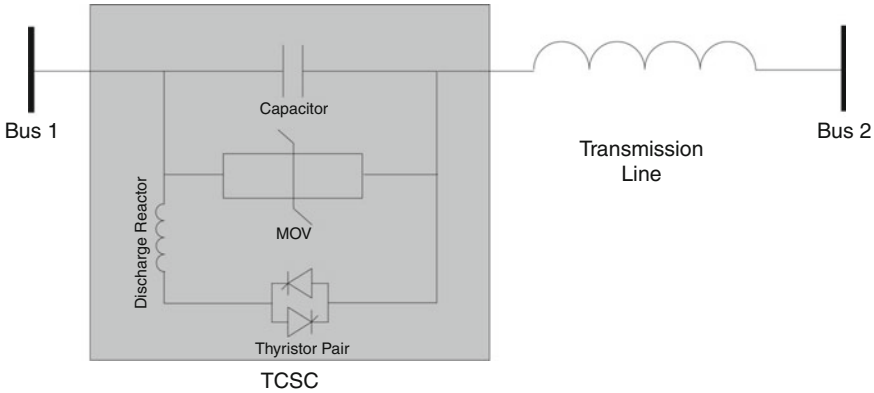

Smart Grids, Distributed Control for. Figure 12
Thyristor-controlled series capacitor (TCSC) installed on a transmission line between bus 1 and bus 2

inductor and thyristor pair. A TCSC is able to inject a capacitance higher than the nameplate capacitance of the capacitor. However, like the series MSC, this solution is plagued by the need for an isolation platform, which increases cost and requires additional space at the substation. Unlike a series MSC, a TCSC can avert subsynchronous resonance challenges and is fast enough to improve transient stability.

Multiple manufacturers produce TCSCs. Siemens alone has installed five TCSCs as of late 2009 [46], with the first installation conducted for WAPA in 1992. BPA's 500 kV TCSC project was commissioned in 1993 [47]. Typically, the TCSC solution requires a construction period of 12–18 months. The typical cost for a TCSC is $150/kVAR [48].

Phase-Shifting Transformer (PST) A phase-shifting transformer (PST), also known as phase angle regulator (PAR), controls power flow between two electrical buses by changing the δ term of Eq. 1. Numerous PST topologies exist. The simplest type has a fixed phase angle. In more complicated topologies, mechanical load tap-changers (LTCs) or solid-state switches are used to vary the phase angle. The most common type of PST uses a single core as seen in Fig. 13. While previous figures have been one-line diagrams, the PST figures show all three phases due to the cross-coupled nature of the PST. Winding 1 induces a voltage on windings 1′ and 1″, which are connected in series with phase A of the transmission line. Since winding 1 is connected between phase B and phase C, the voltages injected into phase A by windings 1′ and 1″ are in quadrature to the phase A voltage. The tap changers connected to windings 1′ and 1″ allow for the level of the injected quadrature voltage to be varied, regulating the phase shift. A symmetric structure allows a variable quadrature voltage to be injected into phases B and C as well.

This single-core design requires the full line current to pass through the LTCs, exacerbating fault current management and increasing the cost of the LTCs [49]. A more expensive PST relieves some of the drawbacks of a single-core PST through the use of shunt and series transformers, as shown in Fig. 14. This version couples a series connected transformer and a delta-connected exciting transformer. The voltages of windings Y′ and Z′ drive winding A′. The resulting winding A′ voltage is in quadrature to the phase A voltage. Winding A′ impresses a voltage upon phase A of the line, changing the angle. Like the single-core PST, LTCs are used to vary the level of quadrature injection. Another type of PST replaces the mechanical LTCs with pairs of thyristors. Finally, a fifth type of PST uses voltage source converters to synthesize the quadrature injection voltages. Although the PST is frequently used to alter power flows, only the versions using thyristors or voltage source converters are sufficiently fast to mitigate transients. Minimum cost for the single-core PST is estimated to be $150/kVA. Only a fraction of a PST's rating will be controllable, so the actual cost per controlled kVA will be much higher.

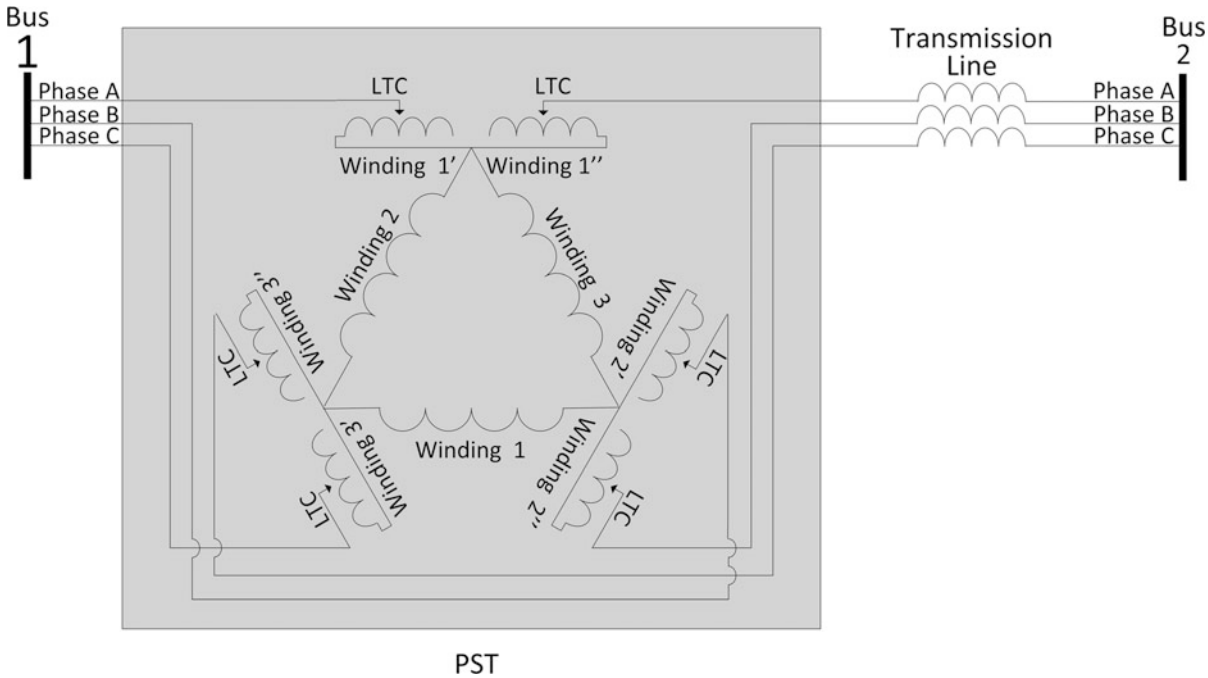

Smart Grids, Distributed Control for. Figure 13
Three-phase diagram of a single-core phase-shifting transformer (PST) installed on a transmission line between bus 1 and bus 2, inspired by [52]

PSTs have been identified with ratings up to 500 MW and 230 kV [50]. PSTs have been used in WECC for at least 35 years [51]. Most PSTs deployed in the USA can respond to operator commands or take automatic action to maintain preset power flows in a matter of minutes [50]. The Montana Alberta Tie Limited (MATL), believed to be the first AC merchant project in the USA, is slated to have a PST. In the USA, there are at least 20 PSTs in WECC, at least 36 PSTs in the Eastern Interconnection, and at least 3 in ERCOT.

High-Voltage DC Transmission (HVDC) and Back-to-Back Converter (B2B) The high-voltage DC transmission system (HVDC) and the back-to-back converter (B2B) transform power from AC to DC and then back to AC. Both can be used to interconnect synchronous or asynchronous networks.

HVDC transports the power in DC form over a distance of up to thousands of miles between the two terminals of the line. HVDC provides full control of the line power. If HVDC is used to connect distant generation to a load pocket, the generation is assigned the same capacity benefits as if it was located in the load pocket [53]. Controllability and capacity benefits have incented the use of HVDC for merchant transmission projects in the USA. In addition, the HVDC line can be configured to limit maximum system fault current levels, an advantage over new AC lines which tend to increase fault current. The most popular type of HVDC system is the bipole, as shown in Fig. 15. In the figure, bus 1 and bus 2 are AC, and conversion from DC to AC occurs in the HVDC terminals. Each HVDC terminal includes a converter, a power factor correction system, and a harmonic filter. Power factor correction is required due to the reactive power requirements of the converter. Harmonic filtration is required due to the harmonics generated by the converter. A bipole uses two conductors and does not use the earth return under balanced operation. If one of the poles or conductors is offline, the system can continue to operate at a fraction of rated power. When a pole or conductor is offline, current is returned through the earth. A two-terminal, 3,000 MW bipole HVDC system costs \$70/kW for each terminal and \$1 M/km [54].

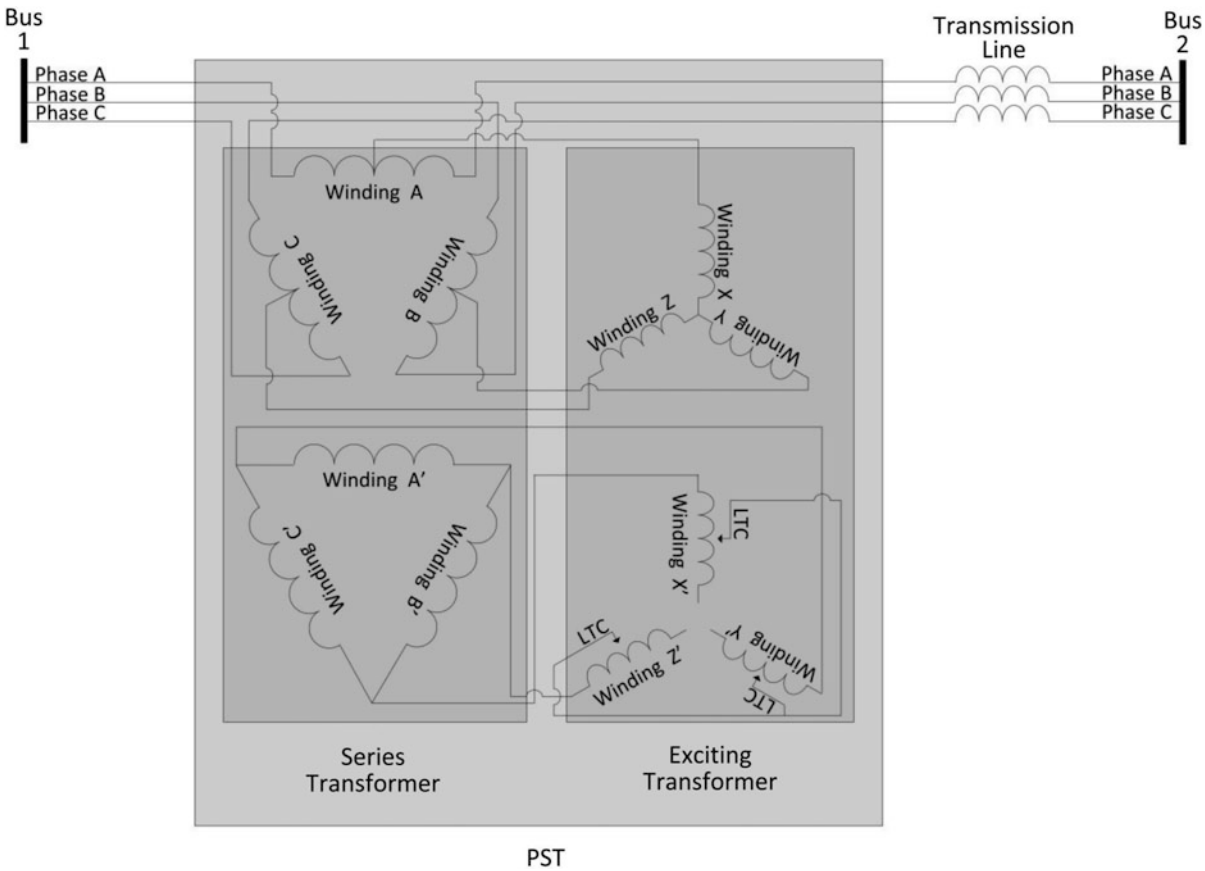

Smart Grids, Distributed Control for. Figure 14
Three-phase diagram of a two-core phase-shifting transformer (PST) installed on a transmission line between bus 1 and bus 2, inspired by [52]

A B2B is an HVDC system with the two terminals directly connected, as shown in Fig. 16. The B2B consists of the same components of an HVDC, less the DC transmission line. Like a PST, the B2B allows for the control of the power flow. Unlike a PST, it is not limited by the phase shift and fault current limitations of the PST. Also, while a B2B can be used to interconnect asynchronous systems, a PST cannot. However, the B2B cost of $100–300/kW is higher than the PST [55]. Also, the availability of the B2B is around 97%, lower than the 99.9% availability of a transformer [56]. For additional cost, B2B can be used to support black start after a blackout.

HVDC and B2B systems are realized using thyristors or gate turnoff devices. Gate turnoff devices are used for smaller power/voltage levels, but the power/voltage capability of HVDC and B2B systems using gate turnoff devices are increasing. Currently, thyristor-based systems dominate the HVDC and B2B markets.

In total, nearly 140 GW of HVDC and B2B capacity is installed or planned worldwide. There are numerous B2B systems installed globally. B2Bs are installed at the seams of the three US interconnections as well as interfaces between the US eastern interconnection and the Hydro-Quebec system. ABB alone has completed 30 HVDC projects and 13 B2B projects using thyristors [57] as well as 13 HVDC projects and 1 B2B project using gate turnoff devices. Siemens has installed 13 HVDC projects and 8 B2B projects using thyristor technology [58] as well as one HVDC system with gate turnoff devices [59].

Variable Frequency Transformer™ (VFT) A variable frequency transformer™ (VFT), as shown in Fig. 17, provides functionality similar to a B2B without

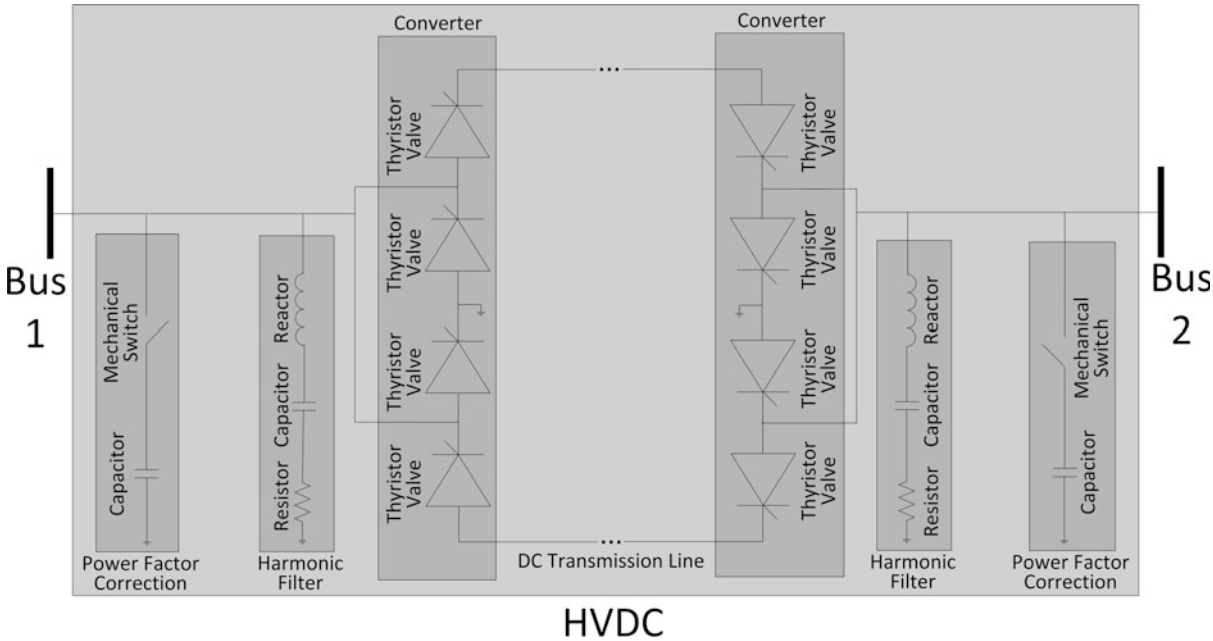

Smart Grids, Distributed Control for. Figure 15
Bipole high-voltage DC transmission system (HVDC) installed between bus 1 and bus 2

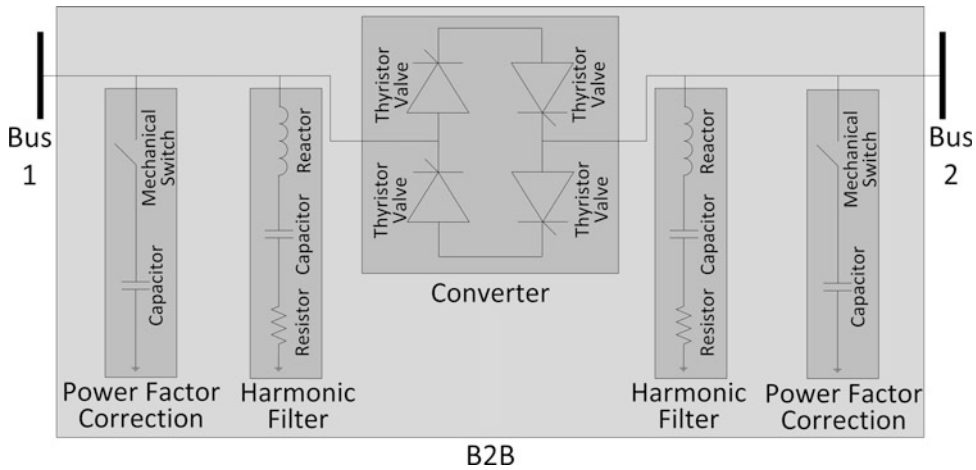

Smart Grids, Distributed Control for. Figure 16
Back-to-back converter (B2B) placed between two AC buses

conversion to DC. The VFT is a large doubly fed induction motor developed by GE for power flow control applications. Power flow from the rotor to stator is varied by changing the torque on the rotor. Torque is applied using a drive motor and variable speed drive. The VFT is able to change power flow from full-rated output in one direction to full-rated output in the other direction in roughly half a second [60]. Each VFT is rated for steady state of 100 MW, but short-term overload power can exceed 150 MW [61]. GE specifies an efficiency of 99% [62] at full power. GE also claims that the area required for a 200 MW VFT station is 47% less than a 200 MW HVDC station [62]. The VFT cost is unknown.

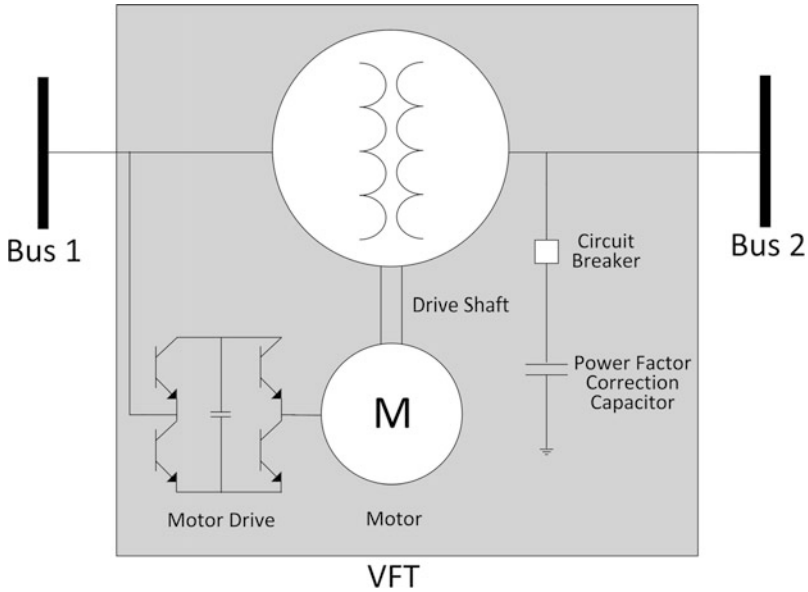

Smart Grids, Distributed Control for. Figure 17
Variable frequency transformer (VFT) connected between two AC buses

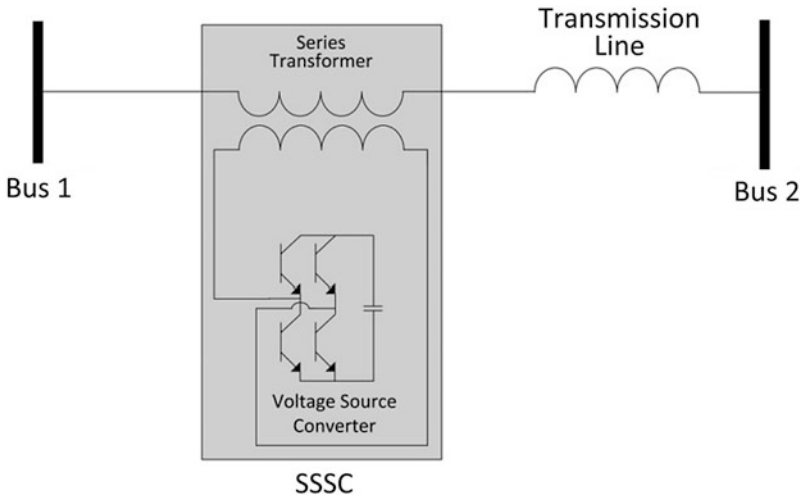

Smart Grids, Distributed Control for. Figure 18
Static synchronous series compensator (SSSC) installed on a transmission line between bus 1 and bus 2

GE has installed 5 VFTs at three locations. The first VFT was used to interconnect the Hydro-Quebec and New York networks. The next three were installed in parallel in Laredo, Texas. The most recent is the Linden VFT, between New York City and New Jersey.

Static Synchronous Series Compensator (SSSC) The SSSC, shown in Fig. 18, improves upon the functionality of a combined series MSR and series MSC through the use of inverters using gate turnoff power electronic devices. Unlike the MSR/MSC combo, the

SSSC can provide subcycle response times and actively mitigate transients. Using a voltage source inverter, a voltage is injected into the line in quadrature with the line voltage. Whether this voltage leads or lags the line current determines if the injected VARs are inductive or capacitive. The risk of subsynchronous resonance is mitigated. While no evidence of SSSC installations could be found, it seems the SSSC is designed to be ground mounted and connected to the line via a series transformer. This eliminates the need for the elevated platform used in the MSR, MSC, and TCSC. However, it still requires additional substation space. Also, the series transformer is expensive as it has to be designed to handle high basic insulation levels and high fault currents. The SSSC solution is also plagued by very high costs which are further exacerbated by series protection requirements and customizations. No evidence of global stand-alone SSSC installations was found. The Marcy convertible static compensator (CSC) can be configured to provide SSSC functionality on two lines simultaneously. Cost is unknown but expected to exceed $200/kVAR [63].

Unified Power Flow Controller (UPFC) A UPFC, as shown in Fig. 19, combines a STATCOM and SSSC. The STATCOM and SSSC share a common DC bus, allowing for the injection of real and reactive power into the line. UPFC devices are able to regulate line voltage using shunt VAR control and real and reactive power flow control using series voltage injection. UPFC devices are able to meet the technical performance requirements for power flow control, but are expensive. Cost estimates range from $190/kVA up to $300/kVA [48].

There is at least one dedicated UPFC in the USA, located in Inez, Kentucky. It has a 40 MVA series converter and a 40 MVA shunt converter. There is also a UPFC in Kanjin, Korea. The Marcy convertible static compensator (CSC) can be configured to provide UPFC functionality.

Comparison of Technologies Table 2 provides a brief comparison of the technologies. It is important to recognize that the cost of some technologies is priced in terms of $/kVAR and others in $/kVA. The PST is priced in terms of total throughput power, and the price per KVA controlled will be significantly higher than the value listed. The B2B is also priced in terms of throughput power, but the full-rated power of the B2B is controllable. The UPFC cost is given in terms of dollars per unit control effort.

Emerging Technologies

The following section reviews three emerging technologies which may resolve the limitations of the power flow and VAR controllers described above. All three are thin AC converters (TACC).

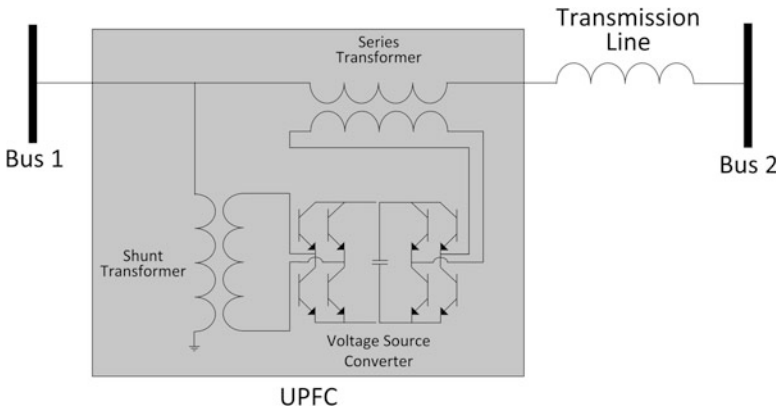

Smart Grids, Distributed Control for. Figure 19
Unified power flow controller (UPFC) with shunt element installed at bus 1 and series element installed between bus 1 and bus 2

Smart Grids, Distributed Control for. Table 2 Comparison of salient elements of power flow controllers

Technology	Cost	Level of usage	Response time
Series MSR	$50/kVAR	Unknown	Slow, multiple cycles
Series MSC	$30–50/kVAR	Unknown	Slow, multiple cycles
TCSC	$150/kVAR	Minimal	Medium, able to improve transient stability
PST	$150/kVA (single core)	Moderate	Depends on design, the most widely deployed version is very slow with a response in seconds to minutes
	Unknown (double core)		
HVDC	Depends on distance	Moderate	Medium
B2B	$150/kVA (thyristor based)	Moderate	Medium (thyristor)
			Fast (gate turnoff)
VFT	Unknown	Minimal	Slow, multiple cycles
SSSC	Unknown, likely >$200/kVAr	Assumed to be nonexistent as a stand-alone technology	Fast
UPFC	$190–300/kVA	Minimal	Fast

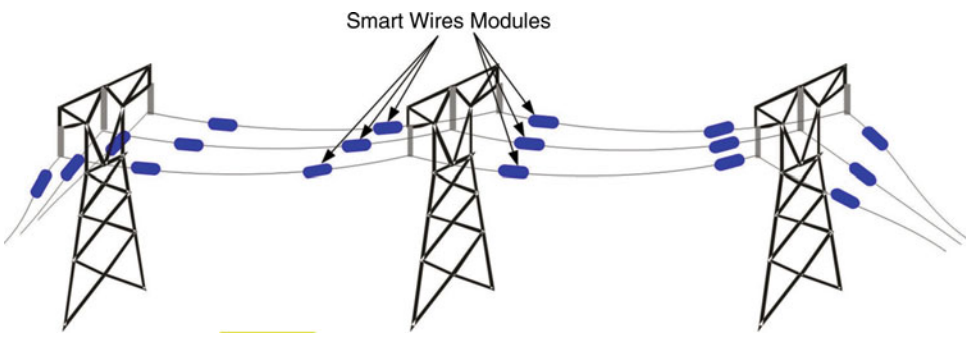

Smart Grids, Distributed Control for. Figure 20
Overview of how smart wires modules will be installed in a transmission line

Thin AC Converters

To increase the cost effectiveness and reliability of power electronic-based control technologies, the concept of a thin AC converter (TACCs) has been proposed. The TACC augments a passive grid asset, like a power line, shunt capacitor, or transformer, with a fractionally rated converter. In the process, the asset is transformed into a dynamically controllable asset that performs similarly to traditional FACTS devices. In addition, reliability is improved relative to traditional FACTS because the TACC can be bypassed if it fails, leaving the passive asset in service. This is called fail-normal operation. Three TACCs are presented below: smart wires, the controllable network transformer (CNT), and the dynamic capacitor (D-CAP). The technologies have been demonstrated in the lab and are currently being scaled to utility voltage and power levels.

Smart Wires (SW) A family of distributed impedance control technologies has been proposed to control power flow. The simplest version of the technology, SW, is comprised of modules hung on the individual conductors of the transmission line as seen in Fig. 20.

Each module monitors the line current. If line current crosses a preset threshold, the module autonomously takes action by injecting inductive impedance into the line. Other modules inject impedance at different current levels. The heart of each module, as shown in Fig. 21, is a single-turn transformer which when operated with the secondary open injects inductive impedance. The SW modules are self-powered using the line current and do not require communications among the modules or with a central control center. The modules operate at line potential and do not connect to the ground, eliminating the cost of isolation and substation footprint requirements. The target retail price for smart wires is $100/kVAR injected. Figure 22 shows the line utilization levels for a system with and without smart wires.

Controllable Network Transformer (CNT) The CNT provides simultaneous control of bus voltage magnitudes and phase angles by augmenting an existing multitap transformer with a fractionally rated converter, as shown in Fig. 23. Since power flow control typically requires small changes to system parameters, the converter can be fractionally rated with respect to the transformer and achieve meaningful, independent control of real and reactive power through the transformer. Any real and reactive power combination within the control range of the CNT, shown in Fig. 24, is possible. The CNT provides the functionality of both a PST and an LTC transformer. An LTC transformer is often used to adjust output voltage or VARs, but it cannot adjust phase angle. The CNT response is significantly faster than the typical LTC or PST, allowing it to help mitigate transients.

Dynamic Capacitor (D-CAP) The D-CAP, shown in Fig. 25, combines a traditional shunt capacitor with a pair of AC switches and small filtering elements. The switches operate with a duty cycle to effectively change the total capacitance seen by at the bus. Like an SVC, the D-CAP is able to dynamically vary the amount of capacitance. However, unlike an SVC, the D-CAP can

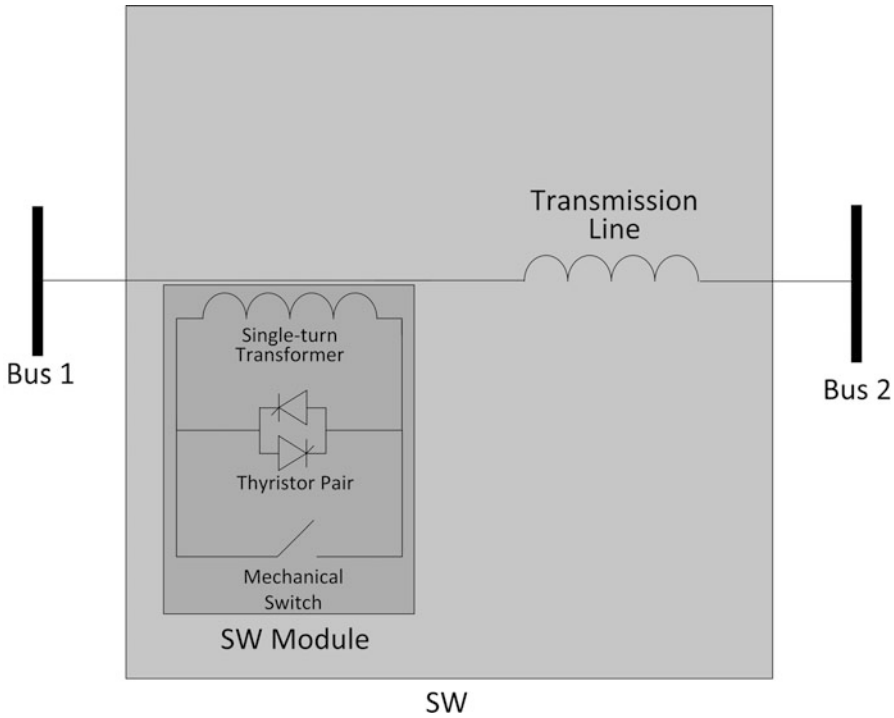

Smart Grids, Distributed Control for. Figure 21
A smart wire (SW) module, installed on a transmission line between bus 1 and bus 2, converts a traditional transmission line into a smart wire (SW)

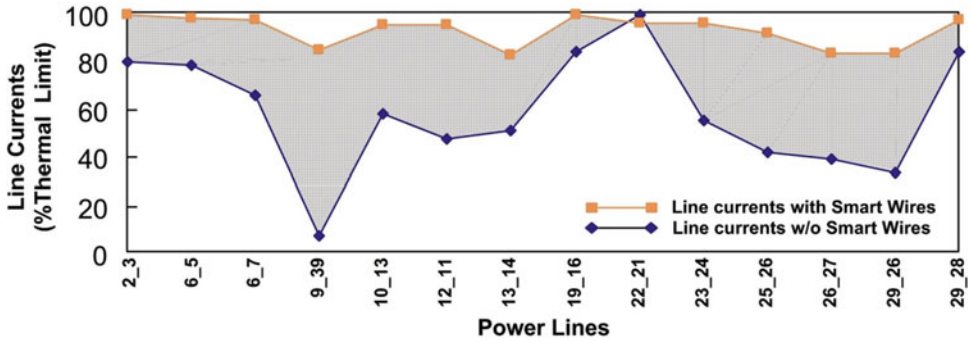

Smart Grids, Distributed Control for. Figure 22
Line utilization of a test system with and without installation of smart wires

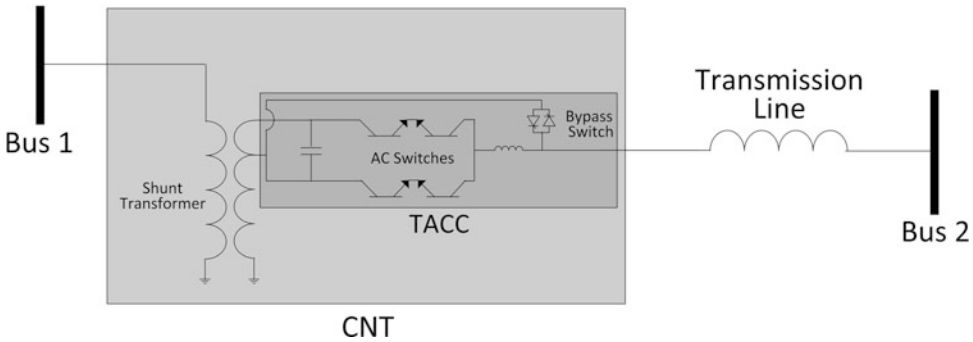

Smart Grids, Distributed Control for. Figure 23
Controllable network transformer (CNT) installed on transmission line between bus 1 and bus 2

react within a fraction of a cycle. The D-CAP configured in a "boost" configuration as shown, also can maintain the VARs delivered to the line, even as the voltage sags under a grid fault. An SVC is unable to deliver this level of grid voltage support. In addition, the D-CAP is able to remove unwanted harmonics caused by other loads connected to the power system, as seen in Fig. 26. The ability to remove harmonics is in sharp contrast to the SVC, which creates harmonics. Costly and space-intensive filters must be used to remove the harmonic content generated by the SVC.

Power Flow Control as an Enabler for Improved Energy Markets

Due to the lack of power flow control, contentious cost allocation methods have been developed to ensure transmission owners recover their costs. Because transmission owners have little incentive to invest in new lines, RTOs/ISOs mandate the construction of transmission lines deemed necessary to relieve pending reliability problems or severe economic congestion. The thresholds to judge proposed transmission projects to relieve economic congestion are conservative, resulting in less investment than would occur if the power flow was more controllable. This leads to higher cost of energy for consumers.

Every merchant transmission project built in the USA thus far has included some form of power flow control. Widespread power flow control would allow the types of market transactions seen in the petroleum and natural gas pipeline industries. Examples include bidding, bilateral transactions, and bulletin boards to match transmission owners with prospective transmission users. With control, a transmission user urgently needing to use a line to deliver to market, such as

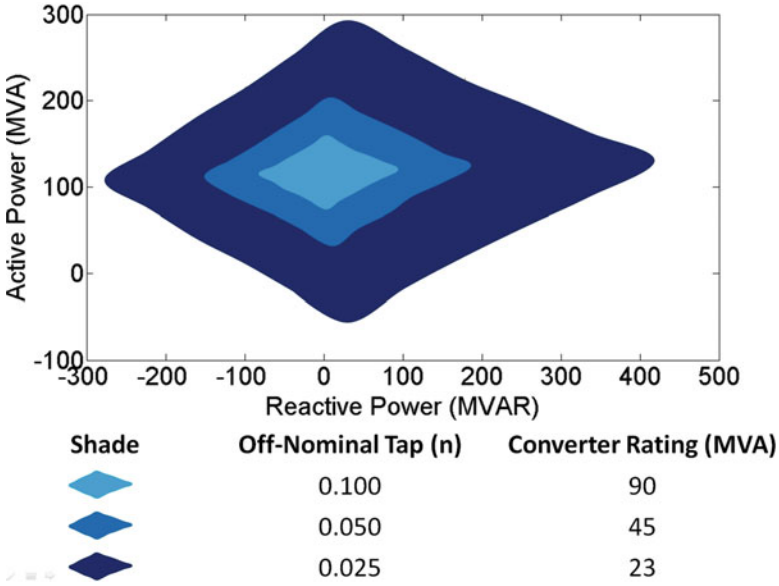

Smart Grids, Distributed Control for. Figure 24
CNT control range as a function of the transformer tap range. 0.10 means up to 10% of the transformer voltage is connected to the converter

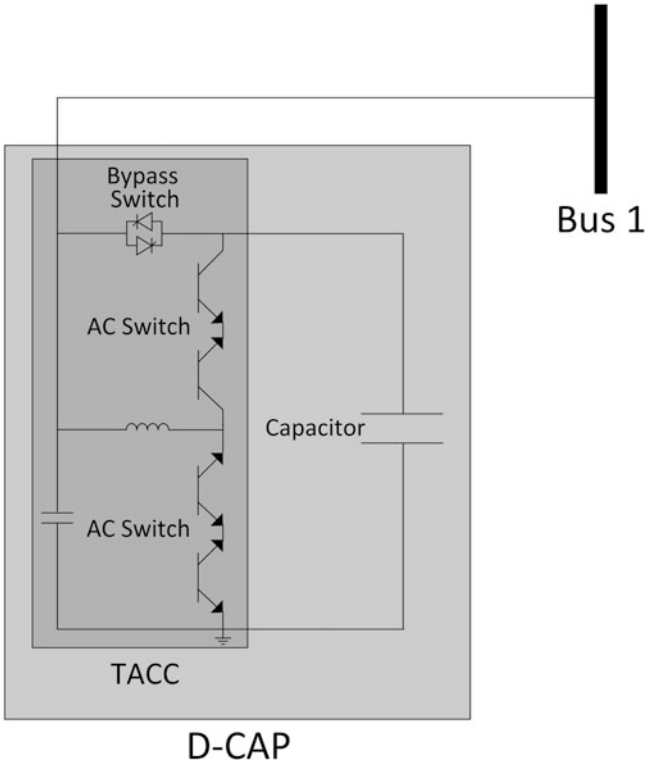

Smart Grids, Distributed Control for. Figure 25
Dynamic capacitor (D-CAP) connected to bus 1

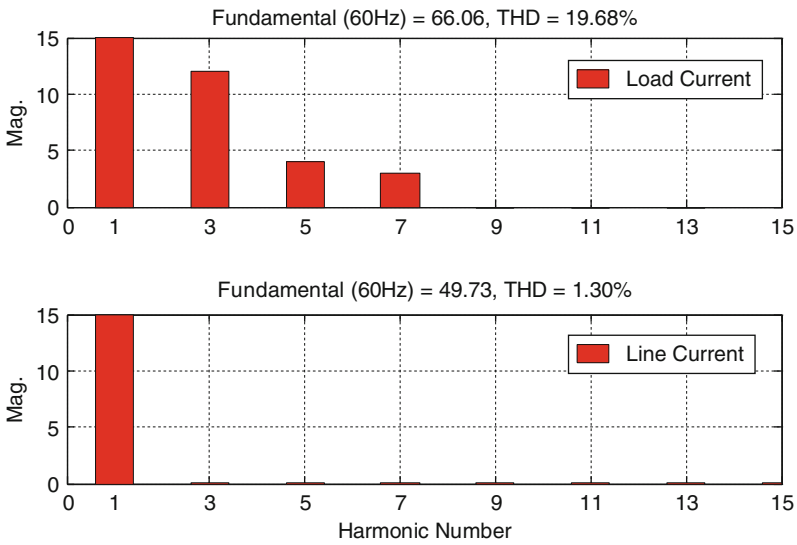

Smart Grids, Distributed Control for. Figure 26
Plot of fundamental and harmonic magnitudes in load current (top) and line current (bottom) with D-CAP installed. Without the D-CAP, the load current harmonics would appear in the line current

a wind generator which cannot cheaply store its energy, can pay a premium during windy periods to outbid other would-be users of the line. In this case, a user willing to defer generation, such as coal plant able to store energy by leaving coal unburned, would benefit from lower transmission costs when the renewable resource is unavailable. In contrast, under current transmission operation rules, transmission users of all types are often backed down pro rata based on the amount of long-term transmission capacity reserved. This leads to economic inefficiencies and higher costs.

The ability to inexpensively control power flows along specific paths can lead to significant benefits at the system and market level. The need for new transmission line build to accommodate renewable portfolio standards can be dramatically reduced. Loop flows, that reduce the capacity of the line available for use by the line owner, can be controlled. Improved interarea support during contingencies can improve the reliability and stability of the network. Costs associated with grid build-out and operation can be allocated more fairly. Owners of generation assets can sell energy to interested customers, finding uncongested pathways for power delivery. Overall, the smart and controllable grid is a critical element in realizing a greener and more economically efficient energy market.

Conclusions and Future Directions

This entry has discussed the emerging challenges which will place additional stress on the transmission system and some of the potential methods to relieve these stresses. A number of methods already exist to provide VAR control and power flow control. All of these methods are expensive and have disadvantages, which have limited their adoption. Emerging technologies that use fractionally rated control elements, and are inherently more distributed in nature, may overcome the significant disadvantages, allowing widespread adoption of VAR control and power flow control. These capabilities could transform the operation of the transmission system, enabling the delivery of low cost and renewable energy, and allowing efficient operation of a competitive energy market.

Bibliography

1. IEA (2008) World energy outlook 2008. http://www.iea.org/textbase/nppdf/free/2008/weo2008.pdf. Accessed 30 Mar 2011
2. EIA (2010) Table 8: electricity supply, disposition, prices, and emissions. Annual energy outlook 2011. http://www.eia.doe.gov/forecasts/aeo/excel/aeotab_8.xls. Accessed 16 Mar 2011
3. EIA (2010) Table 46: transportation sector energy use by fuel type within mode. Annual energy outlook

2011. http://www.eia.gov/oiaf/aeo/supplement/suptab_46.xls. Accessed 24 Apr 2011
4. Sovacool B, Sovacool K (2009) Identifying future electricity–water tradeoffs in the United States. Energy Policy 37(7):2763–2773
5. Wang F, Yin H, Li S (2010) China's renewable energy policy: commitments and challenges. Energy Policy 38(4):1872–1878
6. DOE (2011) RPS data spreadsheet. http://www.dsireusa.org/rpsdata/RPSspread010211.xlsx. Accessed 30 Mar 2011
7. NYSERDA (2004) The effects of integrating wind power on transmission system planning, reliability, and operations: report on phase I
8. Xcel Energy, Minnesota Department of Commerce (2004) Wind integration study – Final report
9. NYSERDA (2005) The effects of integrating wind power on transmission system planning, reliability, and operations, report on phase 2: system performance evaluation
10. Minnesota Public Utilities Commission (2006) Final report – 2006 Minnesota Wind Integration Study, vol I
11. CEC (2007) Intermittency analysis project: final report, CEC-500-2007-081
12. Arizona Public Service Company (2007) Final report: Arizona Public Service wind integration cost impact study
13. CA ISO (2007) Integration of renewable resources. http://www.caiso.com/1ca5/1ca5a7a026270.pdf. Accessed 27 Oct 2010
14. ERCOT (2008) Analysis of wind generation impact on ERCOT Ancillary Services requirements – final report
15. Xcel Energy (2008) Final report: wind integration study for Public Service of Colorado
16. SPP (2010) SPP WITF wind integration study
17. NREL (2010) Eastern wind integration and transmission study. Subcontract report NREL/SR-550-47078
18. NREL (2010) Nebraska statewide wind integration study, Apr 2008–Jan 2010. NREL/SR-550-47519
19. NREL (2010) Western wind and solar integration study. Subcontract No. AAM-8-77557-01
20. NYISO (2010) Growing wind: final report of the NYISO 2010 wind generation study
21. NREL (2010) Oahu wind integration and transmission study: summary report. TP-5500-48632
22. GE Energy (2010) Final report: new england wind integration study – executive summary. Prepared for ISO New England
23. BP (2010) BP statistical review of world energy. http://www.bp.com/liveassets/bp_internet/globalbp/globalbp_uk_english/reports_and_publications/statistical_energy_review_2008/STAGING/local_assets/2010_downloads/Statistical_Review_of_World_Energy_2010.xls. Accessed 24 Apr 2011
24. Electrification Coalition (2009) Electrification roadmap, Revolutionizing Transportation and Achieving Energy Security. http://www.electrificationcoalition.org/reports/EC-Roadmap-screen.pdf. Accessed 7 Mar 2011
25. Allegro Energy (2001) How pipelines make the oil market work their networks, operation and regulation – a memorandum prepared for the association of oil pipe lines and the American Petroleum Institute's Pipeline Committee. http://www.pipeline101.com/reports/Notes.pdf. Accessed 25 May 2009
26. Hull B (2005) Oil pipeline markets and operations. J Transp Res Forum 44(2):111–125
27. Brown S, Yücel M (2008) Deliverability and regional pricing in U.S. Natural Gas Markets. Energy Econ 30(5):2441–2453
28. Cremer H, Gasmi F, Laffont J (2003) Access to pipelines in competitive gas markets. J Regul Econ 24(1):5–33
29. Silvestre B, Hall J, Matos S, Figueira L (2010) Privatization of electricity distribution in the Northeast of Brazil: the good, the bad, the ugly or the naïve? Energy Policy 38(11): 7001–7013
30. Balijepalli V, Khaparde S, Gupta R (2009) Towards Indian smart grids. In: IEEE region 10 TENCON, pp 1–7
31. ORNL (1997) Ancillary service details: voltage control. ORNL/CON-453
32. Hingorani N, Gyugyi L (1999) Understanding FACTS: concepts and technology of flexible AC transmission systems. IEEE Press, New York
33. ABB (2010) ABB SVC and SVC light projects worldwide. http://search-ext.abb.com/library/Download.aspx?DocumentID=SVC_U%20Ref&LanguageCode=en&DocumentPartID=&Action=Launch. Accessed 1 Apr 2011
34. Siemens (2010) FACTS – flexible AC transmission systems: static VAR compensators. http://www.energy.siemens.com/hq/pool/hq/power-transmission/FACTS/FACTS_References_SVC.pdf. Accessed 1 Apr 2011
35. American Superconductor (2010) AMSC™ SVC static VAR compensator. http://www.amsc.com/pdf/PESSVC_BRO_0810_lores.pdf. Accessed 2 Apr 2011
36. Wolf G, Skliutas J et al. (2003) Alternative method of power flow control: using air core series reactors. In: Proceedings of the IEEE Power Engineering Society General Meeting, Vol. 2
37. Bonheimer D, Lim E, Dudley R, Castanheira A (1991) A modern alternative for power flow control. In: Proceedings of the IEEE Power Engineering Society transmission and distribution conference, Dallas, 22–27 Sep 1991, pp 586–591
38. Papp K, Christiner G, Popelka H, Schwan M (2004) High voltage series reactors for load flow control. e&i Elektrotechnik und Informationstechnik 121:455–460
39. Surapongpun L, Phuyodying P, Pimjaipong W (2002) New alternative of power control for transmission line investment in Thailand. In: Proceedings of the IEEE PES transmission and distribution conference and exhibition, Yokohama, pp 1596–1600
40. Courts A, Hingorani N, Stemler G (1978) A new series capacitor protection scheme using nonlinear resistors. IEEE Trans Power Appar Syst 97:1042–1052
41. Bhargava B, Haas R (2002) Thyristor protected series capacitors project at Southern California Edison Co. IEEE Power Eng Soc Summer Meet 1:241–246
42. Elfayoumy M, Moran C (2003) A comprehensive approach for subsynchronous resonance screening analysis using frequency scanning technique. In: IEEE power tech conference proceedings, Bologna

43. Agrawal B (2009) Reactors, capacitors, SVC, PSS: long term transmission planning seminar. Arizona Public Service Co, Long term transmission planning seminar
44. Acharya N (2004) Facts and figures about FACTS. Presented at: AIT training workshop on FACTS application, Asian Institute of Technology, December 16, 2004
45. Altuve H, Mooney J, Alexander G (2009) Advances in series-compensated line protection. In: Proceedings of the 62nd Annual Conference for Protective Relay Engineers, pp 263–275
46. Retzmann D (2009) Tutorial on VSC in transmission systems HVDC & FACTS. http://www.ptd.siemens.de/Siemens2_VS_Application_Prospects_V1.pdf. Accessed 1 Apr 2011
47. Urbanek J, Piwko R, Larsen E, Damnsky B, Furumasu B, Mittlestadt W, Eden J (1993) Thyristor controlled series compensation prototype installation at the slatt 500 kV substation. IEEE Trans Power Deliv 8(3):1460–1469
48. Cai L, Erlich I, Stamtsis G (2004) Optimal choice and allocation of FACTS devices in deregulated electricity market using genetic algorithms. In: Proceedings of the 2004 IEEE PES Power Systems Conference and Exposition, pp 201–207
49. IEEE (2010) IEEE draft guide for the application, specification and testing of phase shifting transformers. IEEE PC57.135, Draft revision 8, Nov 2010, pp 1–53
50. Bladow J, Montoya A (1991) Experiences with parallel EHV phase shifting transformers. IEEE Trans Power Deliv 6(3): 1096–1100
51. WECC (2009) Unscheduled Flow (USF) FAQ. http://www.wecc.biz/committees/StandingCommittees/OC/UFAS/Shared%20Documents/USF%20FAQ.doc. Accessed 20 Mar 2011
52. IEEE (2010) IEEE draft guide for the application, specification and testing of phase shifting transformers. IEEE PC57.135_D8, pp 1–53
53. O'Neill R (2010) Merchant transmission: a new approach to transmission expansion. In: Proceedings of the 2010 IEEE Power and Energy Society general meeting, pp 1–5
54. Bahrman M, Johnson B (2007) The ABCs of HVDC transmission technologies. IEEE Power Energ Mag 5(2):32–44
55. Hingorani N (1996) High-voltage DC transmission: a power electronics workhorse. IEEE Spectr 33(4):63–72
56. ABB (2011) HVDC classic reliability and availability. http://www.abb.com/industries/ap/db0003db004333/eb8b4075fb41252ec12574aa00409424.aspx. Accessed 5 May 2011
57. ABB (2010) HVDC classic – reference list. http://www05.abb.com/global/scot/scot221.nsf/veritydisplay/a0f3c70bc17b846fc12577a8004da670/$file/pow-0013%20rev10%20lr.pdf. Accessed 1 Apr 2011
58. Siemens (2011) References. http://www.energy.siemens.com/hq/en/power-transmission/hvdc/hvdc-classic/references.htm. Accessed 1 Apr 2011
59. Siemens (2011) HVDC plus (VSC Technology). http://www.energy.siemens.com/hq/en/power-transmission/hvdc/hvdc-plus/#content=References. Accessed 1 Apr 2011
60. Larsen E, Piwko R, McLaren D, McNabb D, Granger M, Dusseault M, Rollin L, Primeau J (2004) Variable frequency transformer – a new alternative for asynchronous power transfer. http://www.gepower.com/prod_serv/products/transformers_vft/en/downloads/overview_vftmarketing.pdf. Accessed 6 Apr 2011
61. Miller N, Clark K, Piwko R, Larsen E (2006) Variable frequency transformer: applications for secure inter-regional power exchange. Presented at PowerGen Middle East 2006. http://www.gepower.com/prod_serv/products/transformers_vft/en/downloads/vftfor_pgmev9.pdf. Accessed 4 Apr 2011
62. GE (2004) Variable frequency transformer™: fact sheet. http://www.gepower.com/prod_serv/products/transformers_vft/en/downloads/vft_factsheet.pdf. Accessed 1 Apr 2011
63. Song W, Bhattacharya S, Huang A (2008) Fault-tolerant transformerless power flow controller based on ETO light converter. In: Proceedings of the 2008 IEEE Industry Applications Society annual meeting, pp 1–5
64. Moghe R, Kreikebaum F, Hernandez J, Kandula R, Divan D (2011) Mitigating distribution transformer lifetime degradation caused by grid-enabled vehicle (GEV) charging. In: Proceedings of the IEEE Energy Conversion Congress & Expo, Phoenix, 17–22 Sep 2011, pp 835–842

Socially Affected Traits, Inheritance and Genetic Improvement

Piter Bijma
Animal Breeding and Genomics Centre, Wageningen University, Wageningen, The Netherlands

Article Outline

Glossary
Definition of the Subject
Introduction
Quantitative Genetics of Socially Affected Traits
Estimation of Genetic Parameters
Future Directions
Bibliography

Glossary

Animal breeding The process of selection and mating of parents to produce the next generation of a population, aiming to genetically improve populations of livestock and fish.

Associative effect Heritable effect of an individual on the phenotypic of another individual.

BLUP (best linear unbiased prediction) a method to estimate breeding values of individuals, making use of their pedigree and observed phenotypes.

Breeding value Expected phenotypic trait value of an individual given its genes

Genetic parameters Genetic component of the variances and covariances of traits in a population. Also encompasses derived parameters such as heritability.

Heritability Magnitude of the heritable variation in a population, expressed as a proportion of the observed variation among individuals.

Phenotype Observable trait value of an individual.

Response to selection Change in mean value of a phenotypic trait due to genetic selection.

Selection The choice of individuals to become parents of the next generation. The selection determines which genes are passed on to the next generation.

Social interactions The social process between individuals, which may affect the phenotypic trait values of those individuals.

Definition of the Subject

Livestock genetic improvement, also known as animal breeding, refers to the selection and mating of parents to produce the next generation of a population. The aim is to genetically improve populations of livestock and fish so that they better meet the future needs of markets and societies. Genetic improvement programs gradually change the genetic composition of populations and may create large changes over time. The social environment that individuals experience profoundly affects their productivity, health, and welfare, but has largely been overlooked in animal breeding. There is, however, increasing evidence that traits of individuals are affected not only by the genes carried by those individuals, but also by genes in the individuals present in their social environment. Thus there is a need to generalize the classical theory of inheritance and response to selection to make optimum use of the genetic variation present in the social environment. This involves both the basic mathematical description of the inheritance of socially affected traits, and methods for statistical genetic analysis of populations and designs of breeding schemes.

Introduction

Classical breeding has been very successful [1]. In many species, yields have increased dramatically, particularly in species with short generation intervals in which the focus has been on traits of moderate to high heritability recordable on the selection candidate, such as growth rate in broiler chickens [2, 3]. In many cases, however, there has been a trend for aspects of fitness to decline. Balanced genetic improvement in multiple traits is hampered by trade-offs between those traits, which are observed as unfavorable genetic correlations. Typical examples are trade-offs between yield and fertility in dairy cattle, between litter size and piglet survival in pigs, egg size and egg number in laying hens, and between growth rates and female fertility in broilers. Particularly the widespread trade-off between production and reproduction traits appears to be a systematic biological phenomenon [4].

Genetic improvement in the presence of trade-offs has compromised animal welfare, at least in some livestock species. This has partly been due to a lack of tools to efficiently breed for health-related traits. In many cases, production traits have been most easy to record, have higher heritabilities than reproduction or health-related traits, and are available earlier in life. Breeding for longevity in dairy cattle, for example, has long been hampered by the lack of suitable statistical tools to account for censored records [5]. Moreover, in cases where yield related traits have greater heritability and better or earlier available phenotypic information, selection for the economically optimal index tends to yield negative responses in traits related to fitness. In addition, there has been a difficulty to market traits related to health and welfare of livestock. Profit margins in livestock production are often narrow, so that there is a strong emphasis on the economics of production. Genomic selection [6] is a very promising tool for a more balanced genetic improvement of productivity versus health and welfare, mainly because it provides estimated breeding values early in life for all recordable traits. However, though genomic selection largely removes trade-offs related to breeding scheme design, it does not remove the biological trade-offs between traits. In the absence of genetic engineering, traditional genetic parameters, such as the genetic correlation, remain the key parameters reflecting the prospects for genetic improvement.

There are different levels of modeling the causal mechanisms underlying the observed trade-offs. From a physiological perspective, for example, trade-offs can

be understood from a resource allocation point of view. When resource intake becomes increasingly limiting, traits sharing the same resources will show an increasingly negative relationship [7, 8]. This perspective suggests that breeding for increased efficiency, which should be the overall goal of livestock genetic improvement [9], will lead to increasingly negative relationships between traits. From a genetic perspective, systematic trade-offs are the result of unfavorable pleiotropic effects of segregating genes. Sustained multitrait selection will increase such trade-offs because genes with favorable pleiotropic effects will become fixed by selection, while genes with unfavorable pleiotropic effects will remain segregating for much longer. There is no contradiction between the physiological and the genetic perspective; they merely represent different levels of causality. The evolutionary history of a population represents the ultimate level of causality because millions of years of evolution have shaped the biology of current livestock species. Hence, an evolutionary perspective may help to identify new opportunities for genetic improvement because it provides some understanding of the forces that have shaped the current livestock populations.

Denison et al. [10] consider opportunities for genetic improvement of agricultural populations from an evolutionary perspective. They argue that breeders cannot compete with the natural selection that has occurred in the evolutionary history of livestock populations because of the difference in time scales, being years for breeders and millions of years for natural selection. Consequently, it is unlikely that breeders can improve traits that have always been a target of natural selection. Typical examples are general disease resistance and basic efficiencies of metabolic processes. Hence, rather than trying to mimic natural selection, breeders should investigate other directions for genetic improvement.

A second reason why breeders should not try to mimic natural selection is that they have a fundamentally different objective. While natural selection acts on individual fitness, breeders are interested in the average performance of groups of animals or entire populations. Because natural selection acts on individual fitness, it has the intrinsic tendency to increase competition among population members. Thus natural selection may result in selfish individuals that are successful at the expense of others, rather than in maximization of output on the population, flock, or herd level. A clear example comes from the difference between wild wheat and rice versus modern cultivars. In natural populations, individual plants compete for sunlight. Natural varieties and traditional cultivars, therefore, have long stems making them sensitive to lodging (falling over). Modern wheat and rice cultivars, however, owe their high-yield potential largely to their short stature, relative to traditional cultivars. Short stature reduces lodging and increases growth of grain at the expense of stems, but artificial selection for these traits has resulted in decreased individual competitiveness. Forced to compete with traditional, low-yielding cultivars, modern high-yield rice cultivars completely disappear within as few as three generations [10]. This result clearly demonstrates that natural populations do not provide a useful blueprint for agriculture. Moreover, it illustrates the relevance of competition among individuals in natural populations, which may also be relevant for livestock genetic improvement.

Denison et al. [10], therefore, conclude that breeders should investigate directions of human interest that are not already exhausted by natural selection. They identify two such directions. First, since domestication has greatly changed the environment to which populations are exposed, certain traits that are essential in nature may no longer be useful in domestic populations. Thus this change in environment releases usable genetic variation. Most modern agricultural species do, e.g., not need the capacity to escape from predators, or to deal with seasonal starvation. Hence, to achieve progress in traits of human interest, breeders should provide good environments and accept sacrificing traits that are essential in natural populations, rather than trying to breed robust individuals that can deal with very challenging environments. This direction has already been exhausted to a great deal in livestock. Improvement of genetics, husbandry, and feeding have gone together ever since domestication, and classical selection strategies implicitly utilize the genetic variance released by improvement of the environment. This approach, however, is gradually reaching limits. Concerns about animal welfare are on the increase in Western societies, and producers sometimes have difficulty providing the environment allowing animals to express their full genetic potential

(personal communication Egbert Knol (IPG) and Frans van Sambeek (ISA)). Hence, breeders already utilize opportunities arising from improved environments, and it seems unlikely that current rates of genetic improvement can be accelerated by further improvement of the environment.

Second, Denison et al. [10] argue that breeders should target traits beneficial to the population but not to the individual expressing the trait. This is because natural selection acts on individual fitness and does, therefore, not exhaust the genetic variance in the social effect that individuals have on each other. Hence, they suggest breeding for decreased competition among population members. Thus the quantity of interest here is the heritable effect of an individual on the trait values of its group mates, known as the associative or indirect genetic [11, 12], rather than on its own trait value. Most livestock populations are kept in groups, ranging from cages of four laying hens, groups of moderate size in pigs and beef cattle in feed lots, to large flocks of broilers, sheep or beef cattle. In those systems, performance of individuals may depend on (social) characteristics of the other individuals present in the same group. Well-known examples are mortality due to cannibalistic behaviors in non-beak-trimmed laying hens [13], and tail biting and aggression at mixing in swine [14]. Results in pigs, moreover, indicate that growth rate is affected by heritable social effects, even in ad libitum feeding [15]. Also aquaculture species provide a typical example of social effects, where variation among individuals is often considerably increased due to competition for feed [16].

When trait values depend on social interactions among individuals, selection of the best individuals may cause the average performance of a population to decline, rather than increase. In non-beak-trimmed laying hens, for example, selection of the survivors has decreased survival in the next generation because the survivors had a negative heritable effect on survival of their cage mates [17]. Results in plant breeding, however, illustrate that selection for increased yield in the presence of social interactions can be successful. Properties of modern crops show that plant breeders have successfully improved yields by decreasing competition (see above). Reasons for this success may be that plant breeders are more aware of competition among individuals, and that breeding for reduced competition is much easier in plants. (Theory shows that selection between clonal plots exploits the full heritable variance in traits, including the component due to competition; see below and in [18]). In livestock breeding, in contrast, relatively little is known of the magnitude of associative effects. With the exception of maternal genetic effects, breeders have hardly attempted to utilize associative effects for genetic improvement (But see Muir's selection experiments; [17, 19–21]). Hence, there is a need for further research on the magnitude of associative effects in livestock populations.

At first glance, breeding for improved social effects may seem difficult to apply in practice because social effects will often be the result of certain behaviors that may be difficult to record. Breeding for improved behavior is rarely applied in modern breeding practice because recording behaviors is usually very labor intensive. [22], however, showed that heritable social effects can be estimated in a similar way as maternal genetic effects [23] without the need to record the behaviors underlying the associative effects. At present, flexible tools are available to estimate social genetic effects without the need to observe the traits underlying them (See section on "Estimation of Genetic Parameters" below). Hence, nowadays breeders have the opportunity to address improvement of social interactions in their improvement programs.

Whether or not social interactions are of interest to breeders will depend on the trait considered and on the environment in which individuals are kept. Selection experiments on mortality in non-beak-trimmed layers kept in cages illustrate the relevance of social genetic effects in that situation [17, 20, 21]. For non-beak-trimmed laying hens, Ellen et al. [24] found that more than half of the total heritable variation in survival days originated from social effects. Bergsma et al. [15] found that social genetic effects contribute to heritable variation in growth rate and feed intake in pigs. In contrast, results of Arango et al. [25] in growing pigs indicate that social genetic effects may be difficult to estimate and not deviate significantly from zero. At present, knowledge of the importance of social genetic effects in populations of livestock and fish is still limited. In aquaculture, the large size differences among individual fish indicate that competition is important and that it affects uniformity [16], but the heritable

effects underlying such competition are largely unknown. It would be interesting to see whether fish breeders can achieve something similar as plant breeders, who have effectively reduced competition among individuals in wheat [10]. Though social genetic effects may not always be important and may be difficult to utilize in some cases, the promising results observed in layer chickens should be sufficient incentive for further research in this area. Moreover, genetic improvement of productivity resulting from improved social interactions may cause less trade-offs in health and welfare traits because it may reduce energy waste rather than shifting resources from fitness traits toward production traits [17]. This chapter summarizes the quantitative genetic theory of socially affected traits, covering the basic models, expressions for response to selection, and estimation of genetic parameters.

Quantitative Genetics of Socially Affected Traits

Quantitative Genetic Model

Classical Model In classical quantitative genetics and animal breeding theory, individual phenotypic values, P, are modeled as the sum of a heritable component, A, known as breeding value, and a residual, E, known as environment (Table 1) [26, 27],

$$P = A + E \tag{1}$$

The breeding value is the sum of the so-called average effects of the genes of the individual on its phenotype [28, 29]. It represents the heritable

Socially Affected Traits, Inheritance and Genetic Improvement. Table 1 Notation key

Symbol	Meaning
P, A, h^2	Phenotypic value, breeding value, heritability
i, j, n	Focal individual, group mate of focal individual, group size
$P_{D,i}$, $P_{S,i}$	Direct effect of i, (full) associative effect of i
$A_{D,i}$, $A_{S,i}$	Direct genetic effect of i, associative genetic effect of i
$E_{D,i}$, $E_{S,i}$	Direct non-genetic effect of i, associative non-genetic effect of i
$A_{T,i}$, T^2	Total breeding value of i, relative heritable variance
$A_{M,i}$, $E_{M,i}$	Breeding value for maternal effect of i, non-genetic maternal effect of i
R	Response to selection
ρ, ρ_T	Traditional accuracy of selection, total accuracy of selection
ρ_D, ρ_S	Direct and social accuracy of selection
g, r	Degree of between-group selection, relatedness between group mates
r_f, τ	relatedness between candidate and relatives, intraclass correlation between relatives
$\sigma^2_{A_D}$, $\sigma^2_{A_S}$	Direct genetic variance, associative genetic variance
$\sigma_{A_{DS}}$, r_g	Covariance and correlation between direct and associative genetic effects
$\sigma_{E_{DS}}$, r_E	Covariance and correlation between direct and non-genetic associative effects
σ^2_P, $\sigma_{P_{DS}}$	Phenotypic variance, full covariance between direct and associative effects
$\sigma^2_{A_T}$	Total heritable variance
σ^2_g, σ^2_e	Between-group non-genetic variance, residual variance
d	Degree of dilution of associative effects with group size
N_f, m	Number of families, effective number of records per family
σ^2_z, σ^2_f, σ^2_e	Full variance of records, between-family variance, residual variance
SE, $n_{opt,x}$	Standard error, optimum family size for parameter x

component of an individual's phenotype, whereas the "environment" comprises all non-heritable effects, including the non-heritable genetic effects arising from dominance and epistasis.

The absolute magnitude of the heritable effects is measured by the variance of the breeding values, σ_A^2, known as the additive genetic variance. The relative magnitude of the heritable effects is measured by the heritability, the ratio of heritable variance over phenotypic variance [26, 27],

$$h^2 = \sigma_A^2/\sigma_P^2 \tag{2}$$

Heritability expresses the relative contribution of heritable effects to phenotypic variance among individuals, taking values from 0 through 1. In the classical model, heritability also has the natural interpretation as the regression coefficient of offspring phenotype on mean phenotype of the parents; it is the proportion of phenotypic superiority in the parents that is recovered in the offspring. In the context of selection experiments, this quantity is known as the realized heritability [26].

Social Model As summarized in the Introduction, individuals may affect each other's phenotypes. The "environmental" component of the phenotype, therefore, also includes effects of the social environment provided by other individuals that interact with the focal individual. In contrast to the physical environment, however, the social environment is biological in origin and may therefore contain a heritable component. Hence, the E-term in Eq. 1 may contain heritable components due to other individuals. Such heritable effects on trait values of others are known as indirect genetic effects in the evolutionary genetic literature [12, 30], and as associative effects or social effects in the animal breeding literature [11, 17, 31]. Associative effects are of interest to animal breeders because they are heritable and thus can contribute to response to selection. Hence, for socially affected traits, the classical model in Eq. 1 needs to be modified because it treats associative effects as part of the non-heritable environment [11]. Also the definition of heritable variance may be modified because the classical additive genetic variance excludes the contribution of associative effects.

In most livestock and aquaculture populations, individuals are kept in groups, and interactions among individuals occur within group. In a population consisting of groups of n individuals each, the phenotype of an individual can be expressed as the sum of a direct effect rooted in the individual itself, and the associative effects of each of its $n-1$ group mates [11],

$$P_i = P_{D,i} + \sum_{i \neq j}^{n-1} P_{S,j}, \tag{3}$$

where $P_{D,i}$ denotes the direct effect due to the focal individual i, $P_{S,j}$ the associative effect of its group mate j, and the summation is over the $n-1$ group mates of the focal individual. Both the direct and associative effect may be decomposed into a heritable component, A, and a non-heritable component, E. The phenotype, therefore, is the sum of the direct breeding value and direct environmental effect of the focal individual, and the summed associative breeding values and associative environmental effects of each of its $n-1$ group mates [11, Fig. 1a],

$$P_i = A_{D,i} + E_{D,i} + \sum_{i \neq j}^{n-1} A_{S,j} + \sum_{i \neq j}^{n-1} E_{S,j} \tag{4}$$

In this expression, $A_{D,i}$ is the direct breeding value (DBV) of individual i, and $A_{S,j}$ the associative breeding value (SBV) of its group mate j. The DBV corresponds to the classical (direct) breeding value, whereas the SBV is a generalization of a breeding value for maternal effect (See section on "A Special Case: Maternal Genetic Effects" below). An individual's DBV is the sum of the direct average effects of its genes, whereas its SBV is the sum of the associative effects of its genes. In total, the $A_{D,i} + \sum_{i \neq j}^{n-1} A_{S,j}$ is the best predictor of the phenotype of the focal individual from the average effects of its own genes and those in its group mates, obtained using the method of least squares [27–29, 32]. The $E_{D,i}$ and $E_{S,i}$ are the corresponding non-heritable effects ("environment").

At first glance, it seems that the summation in Eq. 4 implies additivity of associative effects, whereas, in reality, an individual's associative effect may depend on the individual it interacts with. For example, an individual may interact in a positive manner with a certain group mate, but have adverse effects on

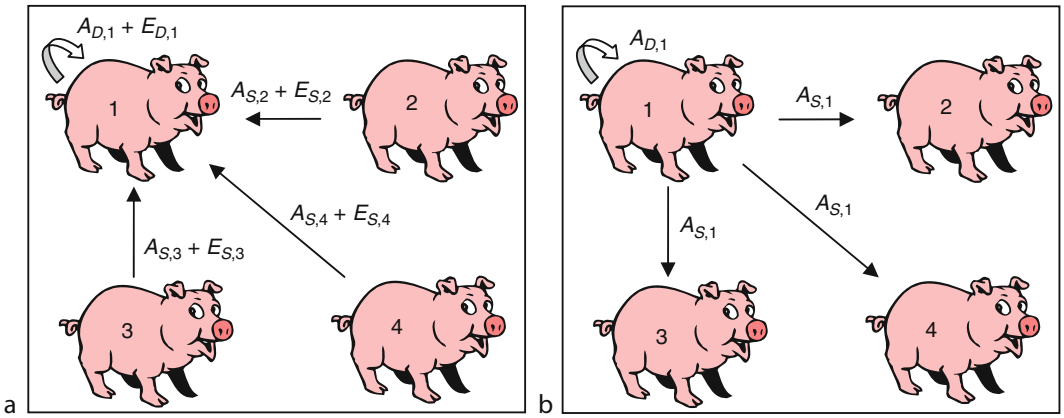

Socially Affected Traits, Inheritance and Genetic Improvement. Figure 1
(**a**) The phenotype of individual 1 is the sum of its own direct effect plus the associative effects of its group mates, $P_1 = A_{D,1} + E_{D,1} + \sum_{j=2,3,4}\left(A_{S,j} + E_{S,j}\right)$. (**b**) The total breeding value of individual 1 is the sum of its heritable effects on all group members, including itself, $A_{T,1} = A_{D,1} + 3A_{S,1}$

other group mates. Equation 4, however, considers the average associative effect of a genotype, which is additive by definition. This is an analogy of the average effect of an allele in, e.g., a single locus model [26, 29]. In the presence of dominance, the effect of an allele depends on the other allele at the locus. Nevertheless, one can still define the average effect of an allele, which is the effect relative for heritable variance and response to selection (at least in the short term). Hence, Eq. 4 does not assume additivity of the social interactions, but focuses on the heritable component of these interactions.

Breeding Value The objective of livestock genetic improvement is to generate response to selection, that is, to genetically change the mean trait values of the population. For this purpose, an individual's quality is measured by its heritable effect on the mean trait value of the population. In the classical model, an individual's heritable effect on the population mean simply equals the classical breeding value, A, as defined in Eq. 1. With associative effects, an individual's full heritable effect on the mean trait value of the population is the sum of its direct heritable effect on its own phenotype, plus its social heritable effect on the phenotypes of its group mates. Hence, an individual's total breeding value may be defined as [31; Fig. 1b]

$$A_{T,i} = A_{D,i} + (n-1)A_{S,i} \tag{5}$$

In contrast to an individual's phenotype, its total breeding value is entirely a property of its own genes (Fig. 1a vs 1b). The total breeding value is a generalization of the classical breeding value and is the heritable property relevant for response to selection in socially affected traits. Taking the average phenotype of the population shows that response to selection equals the change in mean total breeding value,

$$R = \Delta\bar{A}_T \tag{6}$$

In contrast to the classical breeding value, however, the total breeding value contains a part that is not expressed in the individual's own phenotype, nor in the phenotypes of its offspring, but in the group mates of the individual and of its offspring.

Heritable Variance In the classical model, heritable variance equals the variance of the breeding values among individuals. By analogy, for socially affected traits, the total heritable variance may be defined as the variance in total breeding values among individuals [31],

$$\sigma^2_{A_T} = \sigma^2_{A_D} + 2(n-1)\sigma_{A_{DS}} + (n-1)^2\sigma^2_{A_S}, \tag{7}$$

where $\sigma^2_{A_D}$ is the variance in direct breeding values, $\sigma^2_{A_S}$ the variance in associative breeding values, and $\sigma_{A_{DS}}$ the covariance. The total heritable variance reflects the magnitude of the heritable differences among

individuals that determine the potential of the population to respond to selection (See section "Response to Selection" below). The $(n-1)^2\sigma^2_{A_S}$ term represents the heritable variance present in the social environment. This term shows that even small associative effects can substantially increase the total heritable variance, particularly when groups are large. (But see the section "The Effect of Group Size on Heritable Variance" below.) This may explain the rapid response to group selection observed by Muir [19, 21]. The term $2(n-1)\sigma_{A_{DS}}$ shows that a negative genetic covariance between direct and associative breeding values reduces the total heritable variance. With negative $\sigma_{A_{DS}}$, individuals with positive breeding values for their own phenotype have on average negative associative effects on the phenotypes of their group mates, and vice versa. Thus a negative $\sigma_{A_{DS}}$ may be interpreted as "heritable competition." Heritable competition, therefore, reduces total heritable variance and thus the potential of the population to respond to selection. Heritable cooperation ($\sigma_{A_{DS}} > 0$), in contrast, increases total heritable variance.

The $\sigma^2_{A_T}$ expresses heritable variance in absolute units. The interpretation of the magnitude of the heritable variation is facilitated by expressing heritable variance relative to phenotypic variance, analogous to classical heritability (Eq. 2). By analogy, for socially affected traits, the ratio of total heritable variance over phenotypic variance equals [15],

$$T^2 = \frac{\sigma^2_{A_T}}{\sigma^2_P} \tag{8}$$

A comparison of h^2 and T^2 reveals the proportional contribution of associative to heritable variance. When group members are unrelated, phenotypic variance equals

$$\sigma^2_{P_{r=0}} = \sigma^2_{A_D} + \sigma^2_{E_D} + (n-1)\left(\sigma^2_{A_S} + \sigma^2_{E_S}\right) \tag{9}$$

With associative effects, phenotypic variance depends on relatedness between group members [15, 33]. As a consequence, T^2 depends on relatedness between group members when using the realized phenotypic variance in Eq. 8, which is inconvenient for a standardized parameter. Hence, to achieve standardization, it is preferable to scale total heritable variance by the phenotypic variance for populations with unrelated group members, using $T^2 = \sigma^2_{A_T}/\sigma^2_{P_{r=0}}$, rather than using the realized phenotypic variance in Eq. 8.

Comparison of Eqs. 7 and 9 shows that total heritable variance, $\sigma^2_{A_T}$, is not a component of phenotypic variance, illustrating that an individual's total breeding value is not a component of its trait value (Eq. 4 vs Eq. 5). Because an individual's total breeding value is dispersed over multiple individuals, it is hidden to direct observation. As a consequence, total heritable variance may exceed phenotypic variance, and T^2 may take values greater than one, whereas classical heritability has an upper limit of one. When group members are unrelated, the difference between the genetic component of phenotypic variance and total heritable variance equals (personal communication J. Bruce Walsh)

$$\sigma^2_{A_T} - \sigma^2_P = (n-1)\left[2\sigma_{A_{DS}} + (n-2)\sigma^2_{A_S}\right], \tag{10}$$

illustrating that heritable variance may substantially exceed phenotypic variance particularly when groups are large. (But see the following section on "The Effect of Group Size".) Social interactions, therefore, result in hidden heritable variation. Empirical results indeed indicate that T^2 may considerably exceed h^2, but values greater than one have not been found so far (See Table 3 below). Note, however, that greater heritable variance than phenotypic variance does not necessarily imply that associative effects increase response to selection. Whether or not the available heritable variance translates into response to selection depends on selection criterion and on relatedness between group members [11, 18, 33] (See section on "Response to Selection" below).

The Effect of Group Size on Heritable Variance The careful reader will have noted that total heritable variance approaches infinity when groups become large (Eq. 7), which is unrealistic. Indeed, when $\sigma^2_{A_S}$ remains constant while group size increases, the $\sigma^2_{A_T}$ in Eq. 7 increases continuously. The magnitude of the associative genetic variance, $\sigma^2_{A_S}$, however, will probably also depend on group size because interactions between a specific pair of individuals are likely to be less intense in large groups [25]. The relationship between the magnitude of associative effects and group size is

relevant because it affects the dynamics of response to selection, heritable variance, and group size. It determines, for example, whether or not selection is more efficient with larger groups.

Models accounting for the relationship between group size and associative effects have been provided in Refs. [25, 42, 43]. In [43], the relationship between associative effects and group size is modeled as

$$A_{S,i,n} = \left(\frac{\bar{n}-1}{n-1}\right)^{d} A_{S,i,\bar{n}}, \tag{11}$$

where $A_{S,i,n}$ is the associative effect of individual i when it would be expressed in a group of n members, $A_{S,i,\bar{n}}$ the associative effect of i when expressed in a group of the average size, $\bar{n}$, and d the degree of dilution. The degree of dilution measures the decrease of an individual's associative effect when group size increases.

With no dilution, $d = 0$, an individual's associative effect is the same for all group sizes, $A_{S,i,n} = A_{S,i,\bar{n}}$, so that its total associative effect summed over all group mates is proportional to the number of group mates, $(n-1)A_{S,i,n} = (n-1)A_{S,i,\bar{n}}$. This may occur, for example, in trees, where a large tree's associative effect may result from shading all individuals under its canopy, the effect on each individual being independent of the total number of individuals under the canopy (personal communication J. Bruce Walsh). With full dilution, $d = 1$, in contrast, an individual's total associative effect summed over all group mates is independent of group size, $(n-1)A_{S,i,n} = (\bar{n}-1)A_{S,i,\bar{n}}$, while its associative effect on each individual group mate is inversely proportional to the number of group mates, $A_{S,i,n} = [(\bar{n}-1)/(n-1)]\ A_{S,i,\bar{n}}$. This may occur, for example, with restricted feeding on group level, where an individual consuming 1 kg of feed has a total associative effect of -1 kg, and an average associative effect of $A_{S,i,n} = -1/(n-1)$ kg on each of its group mates. More generally, the magnitude of associative effects may be modeled as a function of the intensity of the interaction. In trees, for example, the associative effect of one tree on another may be modeled inversely proportional to the distance between both trees [17]. The degree of dilution of associative effects is an empirical issue, which may be trait and population specific, and needs to be estimated for the population of interest (See section on "Estimation of Genetic Parameters" below).

Dilution of associative effects alters the relationship between genetic variances and group size. The associative genetic variance for groups of $n$members equals,

$$\sigma^2_{A_S,n} = \left(\frac{\bar{n}-1}{n-1}\right)^{2d} \sigma^2_{A_S,\bar{n}}, \tag{12}$$

which decreases with group size for $d > 0$. The total heritable variance for groups of n members equals

$$\begin{aligned}\sigma^2_{A_T,n} = \sigma^2_{A_D} + 2(\bar{n}-1)^{d}(n-1)^{1-d}\sigma_{A_{DS},\bar{n}} \\ +(\bar{n}-1)^{2d}(n-1)^{2-2d}\sigma^2_{A_S,\bar{n}}\end{aligned} \tag{13}$$

(This expression may seem complex, but note that $\bar{n}$ is a constant for any particular population). Hence, for $\sigma_{A_{DS}} = 0$, total heritable variance increases with group size as long as dilution is incomplete ($d < 1$), and total heritable variance is independent of group size with full dilution ($d = 1$). Since total heritable variance depends on group size and on the degree of dilution, response to selection will also depend on those factors. To account for the effect of dilution on response to selection, the $\sigma^2_{A_S}$ and $\sigma^2_{A_T}$ should be substituted by Eqs. 12 and 13 in the expressions for response to selection provided below.

When genetic and non-genetic associative effects show the same dilution with group size, the phenotypic variance in populations of groups of $n$unrelated members equals

$$\sigma^2_{P,n} = \sigma^2_{P_D} + (\bar{n}-1)^{2d}(n-1)^{1-2d}\sigma^2_{P_S,\bar{n}} \tag{14}$$

showing that phenotypic variance increases with group size for $d < 0.5$, is independent of group size for $d = 0.5$, and decreases with group size for $d > 0.5$. Hence, the relationship between phenotypic variance and group size provides an approximate impression of the degree of dilution.

Response to Selection

In a series of papers, Griffing [11, 33, 44–46] showed theoretically that associative effects on trait values alter response to genetic selection, not only in magnitude but potentially also in direction, and demonstrated that response depends strongly on relatedness among interacting individuals and on the selection criterion. Results of Griffing, however, do not fit easily in the common animal breeding framework for response to

selection and have largely been overlooked. Griffing [44] summarized his results into a more common theoretical framework, but this work was published in a conference proceeding and was also largely overlooked. Muir [17] and Bijma et al. [31] rediscovered those results and expressed them in terms familiar to animal breeders. This section summarizes the resulting expressions for response to artificial selection, accounting for associative effects, genetic relatedness among interacting individuals, and selection acting on multiple levels, such as individual or group, or on an (optimum) index of both.

General Expression for Response to Selection In classical animal breeding theory, i.e., in the absence of associative effects, response to selection is commonly expressed as the product of the intensity of selection, $\imath$, the accuracy of selection, ρ, and the additive genetic standard deviation in the trait, σ_A [e.g., 47],

$$R = \imath\rho\sigma_A \tag{15}$$

In this expression, R is the genetic change in mean trait value from one generation to the next. The selection intensity expresses the phenotypic superiority of the selected parents in standard deviation units, $i = S/\sigma$, where S is the superiority of the selected parents for the selection criterion and σ is the standard deviation of the selection criterion among the candidates for selection. The accuracy is the correlation between the value of the selection criterion (SC) and the additive genetic merit for the trait (the breeding value) in the candidates for selection,

$$\rho = \mathrm{corr}(A, \mathrm{SC}) \tag{16}$$

Equation 15 partitions response to selection into three clearly distinct components; a scale-free measure of the strength of selection, $\imath$, a scale-free measure of how accurately the selection criterion resembles an individual's true breeding value for the trait of interest, ρ, and a measure of the magnitude of the heritable differences in the population, σ_A. The intensity of selection is largely determined by the reproductive potential of the species and the availability of reproductive technologies such as artificial insemination. The accuracy reflects the quality of the selection criterion, which depends on the type and amount of information collected. The genetic standard deviation is an intrinsic biological property of the population, reflecting its potential to respond to selection, and is outside human control. (Equation 15 can easily be extended to account for two sexes [26]).

The classical expression for response can be generalized to account for associative effects [48]. From the trait model (Eq. 4), it follows that response to selection equals the increase in mean direct breeding value plus the increase in mean associative breeding value weighted by the number of group mates, $R = \Delta[\bar{A}_D + (n-1)\bar{A}_S]$, which is the change in mean total breeding value, $\Delta\bar{A}_T$ (Eq. 5). The change in mean total breeding value equals the mean total breeding value of the selected parents expressed as a deviation from the overall mean and follows from regression of the total breeding value on the selection criterion, $R = b_{A_T,\mathrm{SC}}(\mathrm{SC} - \overline{\mathrm{SC}})$. From the definitions of regression and correlation coefficients, and using $\mathrm{SC} - \overline{\mathrm{SC}} = \imath\sigma_{\mathrm{SC}}$, it follows that

$$R = \imath\rho_T\sigma_{A_T}, \tag{17}$$

where the total accuracy of selection, ρ_T, is the correlation between the selection criterion and the total breeding value in the candidates for selection, and σ_{A_T} is the total genetic standard deviation in the trait (Eq. 7). Equation 17 applies to any selection strategy and inheritance model, as long as the total breeding value represents the average effects of an individual's genes on the mean trait value of the population. (See [49] for an application to maternal effects, and [49] for an application to both associative and maternal effects). Equation 17 corresponds to the first term of Price's Theorem [50] and represents the change in trait value due to change in allele frequency, keeping average effects of alleles constant for all elements of the inheritance model. Because intensity and accuracy are scale-free parameters depending on the breeding design, the total genetic standard deviation reflects the intrinsic potential of a population to respond to selection. Thus the total heritable variance defined in Eq. 7 bears a direct relationship to response to selection. In theory, σ_{A_T} may exceed σ_P (see above), suggesting that response in socially affected traits can be very large relative to phenotypic standard deviation. While this agrees with the very large response observed by Muir [19, 21] in cannibalistic laying hens, it is unlikely that

this phenomenon is widespread in livestock. Nevertheless, the potential for genetic improvement of socially affected traits may be larger than suggested by classical theory (see Table 3 below).

Accuracies of Selection Traditional selection methods include mass selection, selection based on information recorded on relatives, mostly full sibs, half sibs, or progeny, index selection [51, 52], and selection on estimated breeding values (EBV) obtained using Best Linear Unbiased Prediction (BLUP, [53]). Those methods are aimed at the classical (direct) breeding value and do therefore not fully utilize the available heritable variation when trait values are affected by associative effects. Efficient improvement of socially affected traits, therefore, requires modification of classical selection methods. Research in the field of evolutionary biology [12, 18, 30, 54–57] and early work on associative effects [11, 33] indicates that genetic relatedness among interacting individuals and selection acting on the group rather than the individual level strongly affect response to selection. Relatedness between group members and selection between groups are, therefore, important factors in response to selection for socially affected traits.

The following summarizes the accuracies for direct, associative, and total breeding value for a number of selection strategies (Table 2). In all cases, the individuals that provide the information for selection are kept in groups of n members, but the selection criterion may differ. For any parameter, response to selection is the product of intensity ($\imath$), accuracy (ρ), and genetic standard deviation (σ_A) for the parameter of interest,

$$R_D = \imath \rho_D \sigma_{A_D} \tag{18a}$$

$$R_S = \imath \rho_S \sigma_{A_S} \tag{18b}$$

$$R = R_D + (n-1)R_S = \imath \rho_T \sigma_{A_T} \tag{18c}$$

Individual Selection (IS) With individual selection (also known as "mass selection"), the individuals with the best phenotypes are selected as parents of the next generation. The total accuracy of individual selection equals (Ellen et al. 2007),

$$\rho_{T,\mathrm{IS}} = \frac{r\,\sigma^2_{A_T} + (1-r)[\sigma^2_{A_D} + (n-1)\sigma_{A_{DS}}]}{\sigma_{A_T}\sigma_P} \tag{19}$$

In the numerator of Eq. 19, relatedness acts as a weighting factor; greater relatedness increases the $\sigma^2_{A_T}$ term, while decreasing the $\sigma^2_{A_D} + (n-1)\sigma_{A_{DS}}$ term (Fig. 2a).

When group members are unrelated, IS does not directly target the associative breeding value, as illustrated by the accuracy of associative effects, $\rho_{S,\mathrm{IS}}(r=0) = \sigma_{A_{DS}}/(\sigma_{A_S}\sigma_P)$ (Table 2). Hence, when group member are unrelated, response in associative effects is entirely dependent on the covariance between direct and associative effects (Fig. 2b). When this covariance is negative, IS yields a negative response in associative effects, meaning that competition among individuals increases. Moreover, with unrelated group members, the negative response in associative effects may exceed the positive response in direct effect, $-(n-1)R_S > R_D$, yielding a negative net response and a negative total accuracy. This occurs when $\sigma^2_{A_D} + (n-1)\sigma_{A_{DS}} < 0$. The risk of negative response is not merely a theoretical possibility, but has been observed for egg number in cannibalistic laying hens by Muir [17].

When relatedness between group members increases, components in the numerator shift away from a potentially negative term, $\sigma^2_{A_D} + (n-1)\sigma_{A_{DS}}$, toward a positive term, $\sigma^2_{A_T}$, which increases the accuracy (Fig. 2a). In the extreme case with fully related group members (clones), $\rho_{T,\mathrm{IS}}(r=1) = \sigma_{A_T}/\sigma_P$, which is an analogy of the classical accuracy of individual selection, $\rho_{\mathrm{mass}} = h = \sigma_A/\sigma_P$ [26]. This illustrates that a population consisting of clone groups is genetically equivalent to a population consisting of noninteracting individuals with heritability $h^2 = \sigma^2_{A_T}/\sigma^2_P$. In other words, the "group becomes an individual" when group members are fully related. In summary, with individual selection, relatedness between group members can prevent negative accuracies.

Group Selection (GS) With group selection, selection is based solely on mean trait values of the groups, so that parents are selected from the best groups [33, 58, 59]. The accuracy of group selection equals [48]

$$\rho_{T,\mathrm{GS}} = \frac{[1+(n-1)r]\sigma_{A_T}}{n\sigma_{\bar{P}}}, \tag{20a}$$

where $\sigma_{\bar{P}}$ is the standard deviation of the group means,

Socially Affected Traits, Inheritance and Genetic Improvement. Table 2 Accuracies of selection

		Total	Direct	Associative
IS[a]	$r = 0$	$\frac{\sigma^2_{A_D} + (n-1)\sigma_{A_{DS}}}{\sigma_P \sigma_{A_T}}$	$\frac{\sigma_{A_D}}{\sigma_P}$	$\frac{\sigma_{A_{DS}}}{\sigma_P \sigma_{A_S}}$
	$r \neq 0$	$\frac{r\,\sigma^2_{A_T} + (1-r)[\sigma^2_{A_D} + (n-1)\sigma_{A_{DS}}]}{\sigma_{A_T}\sigma_P}$	$\frac{\sigma^2_{A_D} + r(n-1)\sigma_{A_{DS}}}{\sigma_{A_D}\sigma_P}$	$\frac{\sigma_{A_{DS}} + r(n-1)\sigma^2_{A_S}}{\sigma_{A_S}\sigma_P}$
GS[b]	$r = 0$	$\frac{\sigma_{A_T}}{n\sigma_{\bar{P}}}$	$\frac{\sigma^2_{A_D} + (n-1)\sigma_{A_{DS}}}{n\sigma_{A_D}\sigma_{\bar{P}}}$	$\frac{\sigma_{A_{DS}} + (n-1)\sigma^2_{A_S}}{n\sigma_{A_S}\sigma_{\bar{P}}}$
	$r \neq 0$	$\frac{[1+(n-1)r]\sigma_{A_T}}{n\sigma_{\bar{P}}}$	$\frac{[1+(n-1)r]\,[\sigma^2_{A_D} + (n-1)\sigma_{A_{DS}}]}{n\sigma_{A_D}\sigma_{\bar{P}}}$	$\frac{[1+(n-1)r]\,[\sigma_{A_{DS}} + (n-1)\sigma^2_{A_S}]}{n\sigma_{A_S}\sigma_{\bar{P}}}$
Indx[c]	$r = 0$	$\frac{g\,\sigma^2_{A_T} + (1-g)[\sigma^2_{A_D} + (n-1)\sigma_{A_{DS}}]}{\sigma_{A_T}\sigma_I}$	$\frac{g[\,\sigma^2_{A_D} + (n-1)\sigma_{A_{DS}}] + (1-g)\sigma^2_{A_D}}{\sigma_{A_D}\sigma_I}$	$\frac{g[\,\sigma_{A_{DS}} + (n-1)\sigma^2_{A_S}] + (1-g)\sigma_{A_{DS}}}{\sigma_{A_S}\sigma_I}$
	$r \neq 0$	$\left\{[g + r + (n-2)gr]\,\sigma^2_{A_T} + (1-g)(1-r)[\sigma^2_{A_D} + (n-1)\sigma_{A_{DS}}]\right\}/(\sigma_{A_T}\sigma_I)$	$\left\{[g + r + (n-2)gr][\sigma^2_{A_D} + (n-1)\sigma_{A_{DS}}] + (1-g)(1-r)\sigma^2_{A_D}\right\}/(\sigma_{A_D}\sigma_I)$	$\left\{[g + r + (n-2)gr][\sigma_{A_{DS}} + (n-1)\sigma^2_{A_S}] + (1-g)(1-r)\sigma_{A_{DS}}\right\}/(\sigma_{A_D}\sigma_I)$
Rel's[d]	$r = 0$[e]	$\frac{r_f[\sigma^2_{A_D} + (n-1)\sigma_{A_{DS}}]}{\sigma_{\bar{P}_f}\sigma_{A_T}}$	$\frac{r_f\sigma_{A_D}}{\sigma_{\bar{P}_f}}$	$\frac{r_f\sigma_{A_{DS}}}{\sigma_{\bar{P}_f}\sigma_{A_S}}$
	$r = r_w$[f]	$\frac{r\sigma_{A_T}}{\sigma_{\bar{P}_f}} = \frac{r_f\eta}{\sqrt{\tau + (1-\tau)/mn}}$	$\frac{r_f[\sigma^2_{A_D} + (n-1)\sigma_{A_{DS}}]}{\sigma_{A_D}\sigma_{\bar{P}_f}}$	$\frac{r_f[\sigma_{A_{DS}} + (n-1)\sigma^2_{A_S}]}{\sigma_{A_S}\sigma_{\bar{P}_f}}$

[a]Individual selection.
[b]Group selection; $\sigma_{\bar{P}}$ is the standard deviation of the group means (Eq. 20b).
[c]Index selection, $I_i = P_i + g\sum_{n-1} P_j$, g represents the degree of group selection, σ_I is the standard deviation of the index.
[d]Selection based on phenotypes of relatives; r_f is the additive genetic relatedness between the candidate and the relatives providing information, which equals 0.25 for half sibs, and 0.5 for full sibs and progeny; $\sigma_{\bar{P}_f}$ is the standard deviation of the family mean.
[e]The relatives of the selection candidate are mixed at random over groups, so that group members are on average unrelated.
[f]The relatives of selection candidates are kept together in groups, so that relatedness within groups equals within-family relatedness (r_w), which equals 0.25 for half sib families and 0.5 for full sib families. The m is the number of groups of relatives per candidate, so that mn is the total number of relatives per candidates. See Eq. 35 for η and τ.

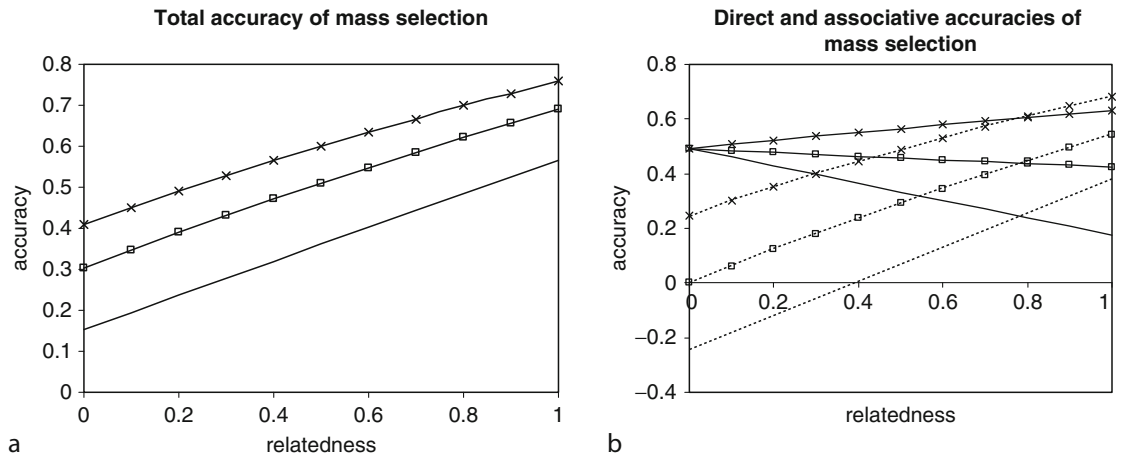

Socially Affected Traits, Inheritance and Genetic Improvement. Figure 2
Accuracies of mass selection. (**a**) Total accuracy. *No symbols*: $r_{A_{DS}} = -0.5$; *boxes*: $r_{A_{DS}} = 0$; *crosses*: $r_{A_{DS}} = +0.5$. (**b**) Direct and associative accuracies. *Solid lines*: direct accuracy; *dotted lines*: associative accuracy. Symbols as in panel **a**. Other genetic parameters are $n = 8$, $\sigma^2_{A_D} = 1.5$, $\sigma^2_{A_S} = 0.05$, $h^2_D = h^2_S = 0.3$ and $r_{E_{DS}} = r_{A_{DS}}$. These parameters yield a phenotypic variance of $\sigma^2_P = 6.17$ when relatedness equals zero, and total heritable variances of $\sigma^2_{A_T} = 2.03$ for $r_{A_{DS}} = -0.5$, $\sigma^2_{A_T} = 3.95$ for $r_{A_{DS}} = 0$, and $\sigma^2_{A_T} = 5.87$ for $r_{A_{DS}} = +0.5$, respectively

$$\sigma^2_{\bar{P}} = \frac{1}{n}\left[\sigma^2_P + (n-1)\mathrm{Cov}(P_i, P_j)\right] \tag{20b}$$

in which $\mathrm{Cov}(P_i, P_j)$ is the covariance between the phenotypes of two group members,

$$\begin{aligned}\mathrm{Cov}(P_i, P_j) = {} & 2\sigma_{P_{DS}} + (n-2)\sigma^2_{P_S} \\ & + r\left[\sigma^2_{A_D} + 2(n-2)\sigma_{A_{DS}}\right. \\ & \left. + (n^2 - 3n + 3)\sigma^2_{A_S}\right].\end{aligned} \tag{20c}$$

Because both the numerator and denominator of Eq. 20a are nonnegative, accuracy of group selection is nonnegative, irrespective of relatedness. Accuracy of GS has lower limit of zero, which occurs when all groups are composed in exactly the same manner; for example, when 10 clones are allocated to 10 groups, each group containing precisely one individual of each clone. In that case, $r = -1/(n-1)$ and accuracy is zero [60]. In this case, there is no between-group genetic variance, so that group selection cannot create response. In all other cases, GS directly targets the total breeding value, as illustrated by the σ_{A_T} in the numerator of Eq. 20a. This is because an individual's total breeding value surfaces in the group mean; the direct breeding value via its own phenotype and the associative breeding value via the phenotypes of each of its $(n-1)$ group mates. Group selection, therefore, also directly targets both direct and associative breeding values, as illustrated by the $\sigma^2_{A_D}$ and $\sigma^2_{A_S}$ in the numerator of the direct and associative accuracy, respectively (Table 2).

When group members are unrelated, however, the n in the denominator causes accuracy to be low particularly when groups are large. This is because the between-group genetic variance is proportional to $1/n$ when group members are unrelated. Hence, with unrelated group members, the genetic variance that can be utilized by group selection decreases with group size, and approaches zero for large groups. Relatedness between group members considerably increases the accuracy of group selection because it increases the between-group genetic variance. In the extreme case of fully related group members (clones), $\rho_{T,\mathrm{GS}}(r = 1) = \sigma_{A_T}/\sigma_{\bar{P}}$, which may be interpreted as the square root of the group heritability, $\sigma^2_{A_T}/\sigma^2_{\bar{P}}$. Note that GS outperforms IS when group members are fully related because $\sigma_{A_T}/\sigma_{\bar{P}} > \sigma_{A_T}/\sigma_P$. This occurs because GS does not waste effort on within-group selection, which is useless when group members are genetically identical. In summary, group selection prevents negative accuracy, but is efficient only when group members are sufficiently related.

Multilevel Selection Rather than selecting solely on individual or mean group phenotype, one may select on a linear combination of phenotypes of group mates and individual phenotype. In terminology used in evolutionary biology, this is an application of multilevel selection, where the levels of selection are the individual and the group. In natural populations, multilevel selection occurs when individual fitness depends on both properties of the individual itself and on properties of its groups. Multilevel selection is widespread in nature [61], but can also be applied as a breeding strategy in livestock and aquaculture [17, 31, 44].

Multilevel selection may be described by the following index [17, 31, 44]

$$I_i = P_i + g\sum_{n-1} P_j \tag{21}$$

where g represents the weight on the summed phenotypes of the $(n-1)$ group mates. A $g = 0$ corresponds to individual selection, whereas a $g = 1$ corresponds to selection on $I_{i,g=1} = \sum_n P_j$, where the summation is over all $n$group members, including the individual of interest. Hence, a $g = 1$ corresponds to between-group selection. Thus the $g$may be interpreted as a measure of the degree of group versus individual selection. A $g = -1/(n-1)$ corresponds to within-group selection, where individuals are selected based on the deviation of their phenotype from the mean phenotype of their group. (Interestingly, the value of $-1/(n-1)$ is also the lower bound for relatedness between group members, indicating a symmetry between $g$and r; [60]).

The accuracy of multilevel selection equals [62]

$$\rho_{T,I} = \frac{[g + r + (n-2)gr]\,\sigma^2_{A_T} + (1-g)(1-r)[\sigma^2_{A_D} + (n-1)\sigma_{A_{DS}}]}{\sigma_{A_T}\sigma_I} \tag{22}$$

Note that the numerator of this expression is fully symmetric in the degree of group selection, g, and relatedness, r, indicating that group selection and relatedness have precisely the same effect on the covariance between the index value and the total breeding value of selection candidates. The first term in the numerator, $[g + r + (n-2)gr]\,\sigma^2_{A_T}$, shows that group selection and relatedness cause selection to target the total breeding value. The second term, $(1-g)(1-r)[\sigma^2_{A_D} + (n-1)\sigma_{A_{DS}}]$, shows that the complement of group selection and relatedness acts on a term that is potentially negative. The $[\sigma^2_{A_D} + (n-1)\sigma_{A_{DS}}]$ is the numerator of the accuracy of individual selection with unrelated group members, which may indeed give negative response (See section on "Individual Selection" above). Hence, group selection and relatedness shift selection away from a potentially negative term toward the total genetic variance, thereby preventing negative response due to increased competition. Figure 3a illustrates this effect, showing that the combination of multilevel selection and relatedness may strongly increase accuracy. When group members are unrelated, the effect of multilevel selection on accuracy may be only moderate, and an intermediate value of $g$may be optimal. Figure 3b shows that multilevel selection and relatedness increase the accuracy of the associative effect, which may be at the expense of the direct effect when the direct-associative genetic correlation is negative.

Optimum Index Selection If the genetic parameters of direct and associative effects are known, then the degree of between-group selection, g, can be optimized using selection index theory [17, 44, 48, 51]. For this purpose, it is convenient to rescale the index to

$$I_i = b_1 P_i + b_2 \sum_{n-1} P_j \tag{23}$$

This index is equivalent to $I_i = P_i + (b_2/b_1)\sum_{n-1} P_j$, so that the optimum degree of group selection is

$$g_{\text{opt}} = \frac{b_{2,\text{opt}}}{b_{1,\text{opt}}} \tag{24}$$

From selection index theory, optimum index weights are [52]

$$\mathbf{b}_{\text{opt}} = \mathbf{P}^{-1}\mathbf{G}\mathbf{v}, \tag{25}$$

where $\mathbf{b}_{\text{opt}}$ is a column-vector of optimum index weights, $\mathbf{b}'_{\text{opt}} = [\,b_{1,\text{opt}} \quad b_{2,\text{opt}}\,]$, $\mathbf{P}$ is the symmetric matrix of covariances between the information sources in the index,

$$\mathbf{P} = \begin{bmatrix} \text{Var}(P_i) & \text{Cov}\left(P_i, \sum_{n-1} P_j\right) \\ \text{Cov}\left(P_i, \sum_{n-1} P_j\right) & \text{Var}\left(\sum_{n-1} P_j\right) \end{bmatrix},$$

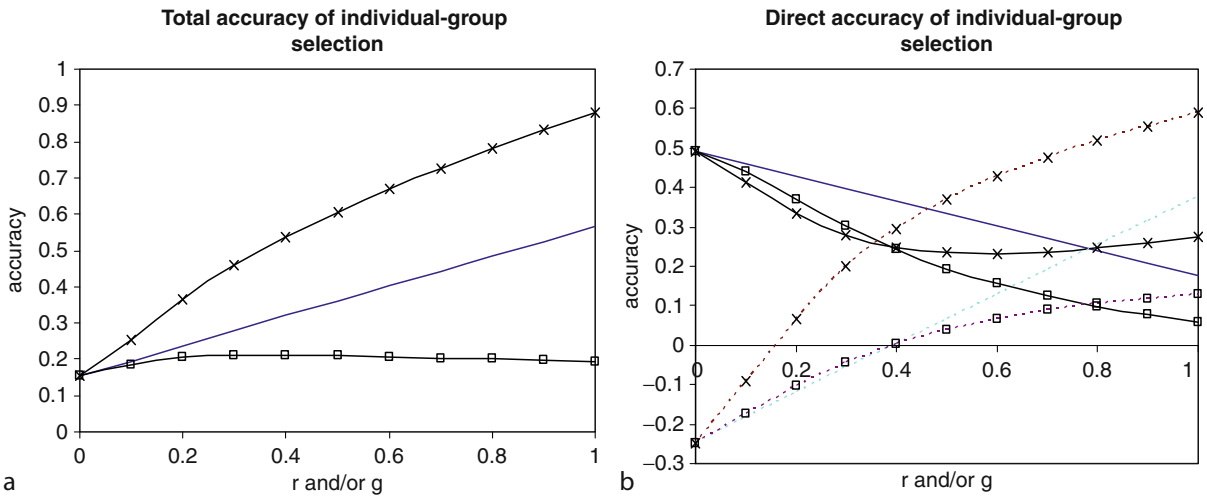

Socially Affected Traits, Inheritance and Genetic Improvement. Figure 3
Accuracy of multilevel selection, $I_i = P_i + g\sum_{n-1} P_j$. (**a**) Total accuracy. *No symbols*: $g = 0$, $r \in [0, 1]$; *boxes*: $r = 0$, $g \in [0, 1]$; crosses: $r = g \in [0, 1]$. (**b**) Direct and associative accuracies. *Solid lines*: direct accuracy; *dotted lines*: associative accuracy. Symbols as in panel **a**. Other genetic parameters are $n = 8$, $\sigma^2_{A_D} = 1.5$, $\sigma^2_{A_S} = 0.05$, $r_{A_{DS}} = -0.5$, $h^2_D = h^2_S = 0.3$ and $r_{E_{DS}} = r_{A_{DS}}$. These parameters yield a phenotypic variance of $\sigma^2_P = 6.17$ when relatedness equals zero, and a total heritable variance of $\sigma^2_{A_T} = 2.03$

G is the matrix of covariances between the information sources in the index (rows of **G**) and the true direct and associative breeding values of the individual of interest (columns of **G**),

$$\mathbf{G} = \begin{bmatrix} \mathrm{Cov}(P_i, A_{D,i}) & \mathrm{Cov}(P_i, A_{S,i}) \\ \mathrm{Cov}\left(\sum_{n-1} P_j, A_{D,i}\right) & \mathrm{Cov}\left(\sum_{n-1} P_j, A_{S,i}\right) \end{bmatrix},$$

and **v** is a vector of weights on direct and associative breeding values (also known as "economic values"). Because response equals $R = \Delta[A_D + (n-1)A_S]$, the weights required to optimize response to selection are given by $\mathbf{v}' = [1 n - 1]$.

Elements of **P** are

$$P_{11} = \sigma^2_P \tag{26a}$$

$$P_{12} = P_{21} = (n-1)\mathrm{Cov}(P_i, P_j) \tag{26b}$$

$$P_{22} = (n-1)\mathrm{Var}(P_i) + (n-1)(n-2)\mathrm{Cov}(P_i, P_j), \tag{26c}$$

where $\mathrm{Cov}(P_i, P_j)$ is the covariance between the phenotypes of two group members, which equals

$$\mathrm{Cov}(P_i, P_j) = 2\sigma_{P_{DS}} + (n-2)\sigma^2_{P_S} + r\left[\sigma^2_{A_D} + 2(n-2)\sigma_{A_{DS}} + (n^2 - 3n + 3)\sigma^2_{A_S}\right]. \tag{27}$$

The first two terms of this expression can be obtained from mixed model analysis using, $2\sigma_{P_{DS}} + (n-2)\sigma^2_{P_S} = 2\sigma_{A_{DS}} + (n-2)\sigma^2_{A_S} + \sigma^2_g$, where σ^2_g is the between-group non-genetic variance (See section "Estimation of Genetic Parameters" below). Elements of **G** are

$$G_{11} = \sigma^2_{A_D} + (n-1)r\sigma_{A_{DS}} \tag{28a}$$

$$G_{12} = \sigma_{A_{DS}} + (n-1)r\sigma^2_{A_S} \tag{28b}$$

$$G_{21} = (n-1)\left[r\sigma^2_{A_D} + \sigma_{A_{DS}} + (n-2)r\sigma_{A_{DS}}\right] \tag{28c}$$

$$G_{22} = (n-1)\left[r\sigma_{A_{DS}} + \sigma^2_{A_S} + (n-2)r\sigma^2_{A_S}\right] \tag{28d}$$

Using those **P** and **G**, the optimum weight on group versus individual, g_{opt}, follows from Eqs. 25 and 24. Note that g_{opt} may fall outside the 0–1 range. For

example, when associative effects are large, g_{opt} may exceed one, indicating that the individual phenotype is weighted negatively relative to the overall group mean.

The accuracy of the optimum index can be obtained either by substituting g_{opt} into Eq. 22, or from

$$\rho_{T,I_{opt}} = \sigma_I / \sigma_{A_T}, \tag{29}$$

where σ_I is the standard deviation of the index,

$$\sigma_I = \sqrt{\mathbf{b}'\mathbf{P}\mathbf{b}} \tag{30}$$

For any index, i.e., for any combination of weights on the phenotype of the individual versus the summed phenotypes of its group mates, accuracy is given by

$$\rho_T(\mathbf{b}) = \frac{\mathbf{b}'\mathbf{G}\mathbf{v}}{\sigma_I \sigma_{A_T}} \tag{31}$$

This expression is equivalent to Eq. 22, where $g = b_2/b_1$. Total response to selection follows from Eq. 17, and responses in direct and associative effects are given by

$$\begin{bmatrix} \Delta\bar{A}_D \\ \Delta\bar{A}_S \end{bmatrix} = \mathbf{b}'\mathbf{G}\frac{\imath}{\sigma_I}, \tag{32}$$

where $\imath$ is the intensity of selection [26].

Figure 4 illustrates the accuracy of index selection, showing that accuracy is always positive and increases considerably with relatedness among group members. Hence, also when index weights are optimized, there is still a clear benefit of using groups composed of related group members. This result extends to selection on estimated breeding values using best linear unbiased prediction (see below).

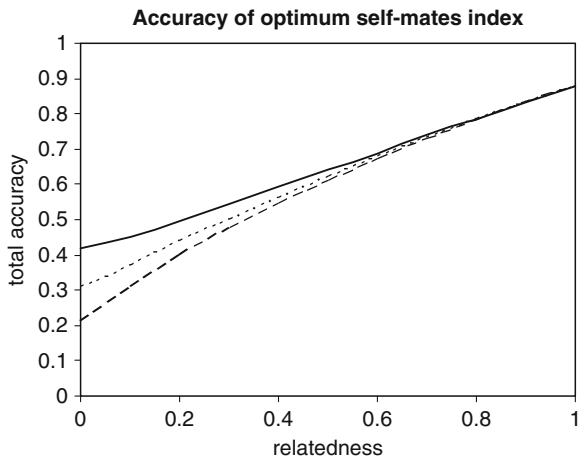

Socially Affected Traits, Inheritance and Genetic Improvement. Figure 4
Accuracy of an optimum index of own performance and group mates, $I = b_1 P_i + b_2 \sum_{n-1} P_j$, as a function of relatedness among group members. For three genetic correlations between direct and associative effects; *dashed line* $r_{A_{DS}} = -0.5$, *dotted line* $r_{A_{DS}} = 0$, *solid line* $r_{A_{DS}} = +0.5$. Other genetic parameters are $n = 8$, $\sigma^2_{A_D} = 1.5$, $\sigma^2_{A_S} = 0.05$, $h^2_D = h^2_S = 0.3$ and $r_{E_{DS}} = r_{A_{DS}}$. These parameters yield a phenotypic variance of $\sigma^2_P = 6.17$ when relatedness equals zero, and total heritable variances of $\sigma^2_{A_T} = 2.03$ for $r_{A_{DS}} = -0.5$, $\sigma^2_{A_T} = 3.95$ for $r_{A_{DS}} = 0$, and $\sigma^2_{A_T} = 5.87$ for $r_{A_{DS}} = +0.5$, respectively

Selection Based in Information of Relatives The above-mentioned selection methods rely on phenotypic information collected on the selection candidates themselves, which requires that the selection candidates are kept in groups (When selection candidates are housed individually, their phenotypes provide no information on their associative effect). Keeping selection candidates in groups, however, is often undesirable or difficult to apply in practice, particularly in laying hens and broilers. This is because group housing may interfere with recording data on an individual basis for important traits such as egg number or individual feed intake. Moreover, for behavioral traits such as cannibalism, group housing may increase loss of selection candidates which is costly and reduces the intensity of selection. Also for veterinary reasons, it is often required that selection candidates are kept in clean conditions, such as Specific Pathogen Free environments, which are very different from the average production environment. Hence, response to selection based on information collected on the candidates themselves may be sensitive to genotype by environment interaction. Finally, recording of certain traits, such as carcass quality, may require sacrificing the individual, in which case selection cannot be based on own performance information.

For those reasons, selection decisions are often based on phenotypic information collected on relatives

of the selection candidates, particularly sibs or progeny. Ideally, those relatives are kept in environments resembling commercial production environments, such as group housing and increased levels of disease. The following provides expressions for response to selection in socially affected traits when selection decisions are based on phenotypes of relatives kept in groups [48].

Consider selection on the average phenotype of relatives of the selection candidate, $\bar{P}_{\text{rels}}$. The phenotypic value of a relative j consists of the direct effect of j, and the summed associative effects of its group mates, $P_j = P_{D_j} + \sum_{n-1} P_{S_k}$, k denoting a group mate. When the group mates of the relative are unrelated to the candidate ($r_{ik} = 0$, $i$denoting the candidate), then the phenotype of the relative provides information only on the direct effect of the candidate, so that response in associative effect is entirely dependent on the genetic correlation between direct and associative effects. This is illustrated by the covariance between the total breeding value of the selection candidate and the phenotype of its relative, of which the component $\text{Cov}(A_{T,i}, \sum_{n-1} P_{S_k}) = 0$, so that $\text{Cov}(A_{T,i}, P_j) = r_{ij}[\sigma^2_{A_D} + (n-1)\sigma_{A_{DS}}]$ (Beware of a typo in this expression in [48]). In this case, accuracy is simply a scaled version of that with mass selection and unrelated group members,

$$\rho_{T,\text{rels}} = \frac{r_{\text{rels}}[\sigma^2_{A_D} + (n-1)\sigma_{A_{DS}}]}{\sigma_{A_T}\sigma_{\bar{P}_{\text{rels}}}}, \tag{33}$$

where r_{rels} is relatedness between the candidate and its relatives providing the information for selection. Hence, just as with mass selection, when using information recorded on sibs kept in groups with unrelated members, there is a risk of negative accuracy and thus negative response.

To capture the entire total breeding value of the selection candidates, relatedness between a candidate and the group mates of its relatives needs to be equal to relatedness between the candidate and its relatives, $r_{ik} = r_{ij}$, i denoting the candidate, j its relative, and k a group mate of j. In that case, $\text{Cov}(A_{T,i}, P_j) = \text{Cov}(A_{T,i}, A_{D,j} + \sum_{n-1} A_{S,k}) = r_{\text{rels}}\sigma^2_{A_T}$, showing that the phenotype of the relative captures the total breeding value of the candidate. This can be achieved by keeping relatives in family groups. For example, when selection is based on sib information, groups may be composed of full sibs of the candidate, so that $r_{ik} = r_{ij} = 0.5$. The following, therefore, describes the accuracy of selection based on relatives when they are kept in family groups.

The accuracy of selection based on the mean phenotypic value of relatives kept in family groups is an analogy of the classical expression for traits not affected by social interactions [48]. In the absence of social interactions, the accuracy of selection based on relatives is commonly expressed in terms of relatedness between the candidate and its relatives, r_{rels}, the square root of heritability, h, and the intraclass correlation t between the relatives (e.g., [63]),

$$\rho = \frac{r_{\text{rels}}h}{\sqrt{t + (1-t)/N}}, \tag{34}$$

where $t = r_w h^2$, being the product of mutual relatedness between the relatives, i.e., the within-family relatedness r_w, and heritability, and N is the number of records of relatives for each selection candidate. Note that there may be a difference between relatedness between the candidate and its relatives, r_{rels}, and mutual relatedness r_w within the group of relatives. For example, for half-sib progeny of the candidate, $r_{\text{rels}} = \frac{1}{2}$, whereas $r_w = \frac{1}{4}$. For full sibs of the candidate, $r_{\text{rels}} = r_w = \frac{1}{2}$, and for half sibs of the candidate, $r_{\text{rels}} = r_w = \frac{1}{4}$. When relatives are kept in family groups, with m groups per candidate each containing n members, yielding a total of mn records of relatives per candidate, the accuracy for socially affected traits equals,

$$\rho_{\text{rel}} = \frac{r_{\text{rels}}\eta}{\sqrt{\tau + (1-\tau)/mn}}, \tag{35a}$$

which is an analogy of Eq. 34 [48]. The Greek symbols in Eq. 35 are analogies of the "heritability" and the intraclass correlation;

$$\eta = \frac{\sigma_{\text{TBV}}}{\sigma_{\text{TPV}}} \tag{35b}$$

is an analogy of the square root of heritability, $h = \sigma_A/\sigma_P$, and

$$\tau = r_w\eta^2 \tag{35c}$$

is an analogy of the intraclass correlation between relatives $t = r_w h^2$. The η and τ account for interactions

among individuals, and, therefore, depend on the total breeding value (TBV) and on the total phenotypic value (TPV) contributed by an individual. The TPV is the phenotypic analogy of the TBV (Eq. 5). It is not the observed phenotype of the individual, but represents an individual's effect on all phenotypes in the population, which is the sum of its direct phenotypic effect and $n-1$ times its associative phenotypic effect, $P_{T,i} = P_{D,i} + (n-1)P_{S,i}$, so that,

$$\sigma^2_{P_T} = \sigma^2_{P_D} + 2(n-1)\sigma_{P_{DS}} + (n-1)^2\sigma^2_{P_S} \qquad (35d)$$

Thus, the TPV measures the total effect of an individual on performance of its group, the total breeding value is the heritable component of the TPV, and $\eta^2 = \sigma^2_{A_T}/\sigma^2_{P_T}$ is the proportion of the variance of the TPV which is heritable, analogous to the classical heritability. The intraclass correlation τ equals the correlation between TPVs of relatives, analogous to the classical intraclass correlation t, which equals the correlation between phenotypes of relatives for traits not affected by interactions [26]. In the absence of interactions, η reduces to h, τ reduces to t, and σ_{TBV} reduces to σ_A, so that Eq. 35a reduces to Eq. 34.

Hence, Eq. 35a shows that response to selection based on relatives kept in family groups can be obtained from the classical expression for response to selection based on relatives (Equation 34), when replacing heritability by $\sigma^2_{A_T}/\sigma^2_{P_T}$ and the intraclass correlation between relatives by $r_w\sigma^2_{A_T}/\sigma^2_{P_T}$. The key issue is that the sibs need to be kept in family groups. For example, when 16 half sibs are available and groups consist of 4 individuals, 4 groups of 4 individuals each should be used; the 16 half sibs should not be distributed over 16 groups each also containing 3 unrelated individuals.

Figure 5 illustrates the accuracy of selection based on relatives as a function of the number of groups of relatives per candidate. With many groups of relatives per candidate, $m \to \infty$, accuracy approaches

$$\max(\rho_{T,\text{rels}}) = \frac{r_{\text{rels}}}{\sqrt{r_w}}, \qquad (36)$$

which is 0.5 for half sib information, $\sqrt{0.5}$ for full sib information, and 1 for information on half-sib progeny

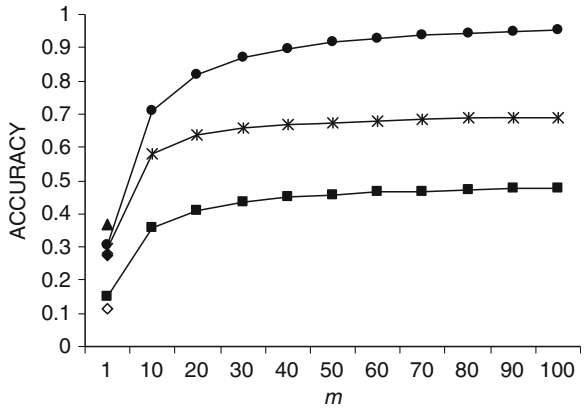

Socially Affected Traits, Inheritance and Genetic Improvement. Figure 5
Accuracy of selection methods. The accuracy is shown for individual selection when the animals in a group are either full sibs (♦) or unrelated (◇), for group selection with groups of full sibs (▲), and for selection based on relatives kept in family groups, as a function of the number of groups per candidate (m), where relatives can be either half sibs (■), full sibs (⁎) or half-sib progeny (●). (For $n = 4$; $\sigma^2_{P_D} = 1$; $\sigma^2_{P_S} = 0.33$; $h^2_D = 0.10$; $h^2_S = 0.10$; $r_A = r_E = 0$; Taken from Ellen et al. 2007)

of the candidate [26]. Those values are the same as for classical selection based on relatives. Hence, with selection based on phenotypes of relatives, limiting accuracies for socially affected traits are the same as those for classical traits. For example, it is possible to obtain an accuracy approaching unity by using information on a large number of half-sib progeny kept in groups consisting of half sibs.

Selection on Estimated Breeding Values (EBVs) In animal breeding practice, breeding values are usually estimated using the so-called BLUP-procedure (Best Linear Unbiased Prediction; [53]. In the traditional BLUP approach, phenotypes of individuals are analyzed using a mixed "animal model" containing fixed correction factors, such as herd, sex, or age of the individual, and a random genetic effect of the animal [27, 53, 64],

$$\mathbf{y} = \mathbf{Xb} + \mathbf{Za} + \mathbf{e}, \qquad (37)$$

where **y** is a vector of phenotypes, **b** a vector of fixed correction factors with incidence matrix **X, a** a vector of random additive genetic effects ("breeding values") of individuals with incidence matrix **Z,** and **e** a vector of residuals (Note that elements of **y** in Eq. 37 correspond to P_i in Eq. 4.). In animal breeding, interest is in the vector of estimated breeding values, $\hat{\mathbf{a}}$. Estimates for fixed effects and breeding values are obtained from the so-called Mixed Model Equations (MME). When residuals are independent and identically distributed, the MME are [27, 53, 64]

$$\begin{bmatrix} \mathbf{X}'\mathbf{X} & \mathbf{X}'\mathbf{Z} \\ \mathbf{Z}'\mathbf{X} & \mathbf{Z}'\mathbf{Z} + \alpha\mathbf{A}^{-1} \end{bmatrix} \begin{bmatrix} \mathbf{b} \\ \mathbf{a} \end{bmatrix} = \begin{bmatrix} \mathbf{X}'\mathbf{y} \\ \mathbf{Z}'\mathbf{y} \end{bmatrix}, \tag{38a}$$

so that the estimates follow from

$$\begin{bmatrix} \hat{\mathbf{b}} \\ \hat{\mathbf{a}} \end{bmatrix} = \begin{bmatrix} \mathbf{X}'\mathbf{X} & \mathbf{X}'\mathbf{Z} \\ \mathbf{Z}'\mathbf{X} & \mathbf{Z}'\mathbf{Z} + \alpha\mathbf{A}^{-1} \end{bmatrix}^{-1} \begin{bmatrix} \mathbf{X}'\mathbf{y} \\ \mathbf{Z}'\mathbf{y} \end{bmatrix}, \tag{38b}$$

where **A** is a matrix of relatedness coefficients between all individuals in **a**, and $\alpha = \sigma_E^2/\sigma_A^2$. The use of BLUP requires knowledge of heritability of the trait to calculate the $\alpha = (1 - h^2)/h^2$. Further details and extensions are in [27, 64].

In contrast to selection index theory, BLUP is extremely flexible. It utilizes all available information, it allows correction for systematic non-genetic effects such as herd, sex or age, it allows for any degree of relatedness among individuals, any number of relatives, it provides also estimated breeding values for individuals without records, and it accounts for selection (under certain conditions).

Deterministic prediction of the accuracy of selection on BLUP-EBV is possible with selection index theory [65, 66], but is tedious, particularly when the model contains additional random effects such as maternal or associative effects. For this reason, consequences of selection on BLUP-EBV are often investigated using stochastic simulations. The following discusses the consequences of selection on BLUP-EBV when trait values are affected by associative effects, first when the mixed model ignores the associative effects, and afterward when accounting for associative effects.

BLUP Ignoring Associative Effects When only direct breeding values are modeled (i.e., when using Eq. 37), the consequences of selection on BLUP-EBV will depend critically on relatedness among group members [67]. When group members are unrelated, the EBV captures only the direct genetic effect of individuals, so that response in associative effects depends entirely on the genetic correlation between direct and associative effects. The accuracy derived from the MME, therefore, refers to the direct breeding value, not to the total breeding value. The actually achieved accuracy for the total breeding value is given by

$$\rho_{T,\mathrm{BLUP}}(r = 0) \approx \hat{\rho}_{\mathrm{MME}} \left[\frac{\sigma_{A_D}^2 + (n-1)\sigma_{A_{DS}}}{\sigma_{A_D}\sigma_{A_T}} \right] \tag{39}$$

The $\hat{\rho}_{\mathrm{MME}}$ is the ordinary accuracy of BLUP-EBV derived from the diagonal elements of the inverse of the coefficient matrix of the MME [64], and the term in square brackets is the correlation between the direct and total breeding value (Note that this result reduces to $\rho_{T,\mathrm{BLUP}}(r = 0) \approx \hat{\rho}_{\mathrm{MME}}$ when associative effects are absent). This result shows that BLUP selection with unrelated group member yields a negative accuracy when $\sigma_{A_D}^2 + (n-1)\sigma_{A_{DS}} < 0$, which is the same condition as for mass selection with unrelated group members (Table 2). When $\sigma_{A_D}^2 + (n-1)\sigma_{A_{DS}} < 0$, the correlated response in associative effects is negative and greater in absolute magnitude than the direct response, yielding a negative net response. Results of Muir [17] in cannibalistic quail illustrate that this is not merely a theoretical possibility, but may indeed occur in practice. (See section "Results of Social Selection Experiments" below.)

When groups are composed of families, the EBV of the traditional BLUP model implicitly captures the total breeding value of individuals, even though the associative component of trait values is not explicitly included in the model (Eq. 37; [67]). The reason is that the covariance between family members equals $r\sigma_{A_T}^2$, where $r = 0.5$ for full sibs and 0.25 for half sibs, when groups consist of family members (When groups are composed at random with respect to family, the covariance between sibs equals $r\sigma_{A_D}^2$). Consequently, the

accuracy of BLUP-EBV obtained from data containing groups of family members is approximately equal to the ordinary accuracy derived from the MME,

$$\rho_{T,\mathrm{BLUP,fam}} \approx \hat{\rho}_{\mathrm{MME}} \tag{40}$$

Moreover, the estimated additive genetic variance from an ordinary mixed model as in Eq. 37 will yield an estimate of $\sigma^2_{A_T}$ rather than $\sigma^2_{A_D}$. This occurs because the covariance between relatives equals $r\sigma^2_{A_T}$ rather than $r\sigma^2_{A_D}$ when groups consist of family members. Hence, the accuracy of BLUP-EBVs will always be positive when it is obtained from data consisting of family groups. This theoretical prediction agrees with results of Muir et al. [67] in quail, who found a negative response with BLUP selection and unrelated group members, but a positive response to BLUP selection when group members were related (referred to as Kin-BLUP in [67]).

BLUP Including Associative Effects Muir and coworkers [17, 22] extended the traditional mixed animal model to include Griffing's associative effects. In this model, the phenotype of each individual contains two separate components: a direct breeding value of the individual itself and the summed associative breeding values of its group mates,

$$\mathbf{y} = \mathbf{Xb} + \mathbf{Z}_D\mathbf{a}_D + \mathbf{Z}_S\mathbf{a}_S + \mathbf{e}, \tag{41}$$

where $\mathbf{y}$ is the usual vector of observations, $\mathbf{b}$ a vector of fixed effects with incidence matrix $\mathbf{X}$, $\mathbf{a}_D$ a vector of direct additive genetic effects with incidence matrix $\mathbf{Z}_D$ linking phenotypes of individuals to their own direct genetic effect, and $\mathbf{e}$ a vector of residuals. (Note that elements of $\mathbf{y}$ in Eq. 41 correspond to P_i in Eq. 4.) The $\mathbf{Z}_S\mathbf{a}_S$ represents the associative additive genetic effects, where $\mathbf{a}_S$ is a vector of associative effect, with incidence matrix $\mathbf{Z}_S$ linking phenotypes of individuals to the associative effects of their group mates. For example, for a population of 8 individuals kept in two groups of 4 individuals, individuals 1 through 4 in the first group and 5 through 8 in the second group, where individuals 2, 5, and 8 are female and the rest is male, a mixed model with a separate mean for both sexes and direct and associative effects for all records is

$$\begin{bmatrix} y_1 \\ y_2 \\ y_3 \\ y_4 \\ y_5 \\ y_6 \\ y_7 \\ y_8 \end{bmatrix} = \begin{bmatrix} 1 & 0 \\ 0 & 1 \\ 1 & 0 \\ 1 & 0 \\ 0 & 1 \\ 1 & 0 \\ 1 & 0 \\ 0 & 1 \end{bmatrix} \begin{bmatrix} \mu_m \\ \mu_f \end{bmatrix}$$
$$+ \begin{bmatrix} 1 & 0 & 0 & 0 & 0 & 0 & 0 & 0 \\ 0 & 1 & 0 & 0 & 0 & 0 & 0 & 0 \\ 0 & 0 & 1 & 0 & 0 & 0 & 0 & 0 \\ 0 & 0 & 0 & 1 & 0 & 0 & 0 & 0 \\ 0 & 0 & 0 & 0 & 1 & 0 & 0 & 0 \\ 0 & 0 & 0 & 0 & 0 & 1 & 0 & 0 \\ 0 & 0 & 0 & 0 & 0 & 0 & 1 & 0 \\ 0 & 0 & 0 & 0 & 0 & 0 & 0 & 1 \end{bmatrix} \begin{bmatrix} a_{D,1} \\ a_{D,2} \\ a_{D,3} \\ a_{D,4} \\ a_{D,5} \\ a_{D,6} \\ a_{D,7} \\ a_{D,8} \end{bmatrix}$$
$$+ \begin{bmatrix} 0 & 1 & 1 & 1 & 0 & 0 & 0 & 0 \\ 1 & 0 & 1 & 1 & 0 & 0 & 0 & 0 \\ 1 & 1 & 0 & 1 & 0 & 0 & 0 & 0 \\ 1 & 1 & 1 & 0 & 0 & 0 & 0 & 0 \\ 0 & 0 & 0 & 0 & 0 & 1 & 1 & 1 \\ 0 & 0 & 0 & 0 & 1 & 0 & 1 & 1 \\ 0 & 0 & 0 & 0 & 1 & 1 & 0 & 1 \\ 0 & 0 & 0 & 0 & 1 & 1 & 1 & 0 \end{bmatrix} \begin{bmatrix} a_{S,1} \\ a_{S,2} \\ a_{S,3} \\ a_{S,4} \\ a_{S,5} \\ a_{S,6} \\ a_{S,7} \\ a_{S,8} \end{bmatrix}$$
$$+ \begin{bmatrix} e_1 \\ e_2 \\ e_3 \\ e_4 \\ e_5 \\ e_6 \\ e_7 \\ e_8 \end{bmatrix}$$

The covariance structure of the random genetic terms is: $\mathrm{Var}\begin{bmatrix} \mathbf{a}_D \\ \mathbf{a}_S \end{bmatrix} = \mathbf{C} \otimes \mathbf{A}$, where $\mathbf{C} = \begin{bmatrix} \sigma^2_{A_D} & \sigma_{A_{DS}} \\ \sigma_{A_{DS}} & \sigma^2_{A_S} \end{bmatrix}$, $\mathbf{A}$ is a matrix of relatedness coefficients between individuals, and $\otimes$ denotes the Kronecker product of matrices. Thus, Eq. 41 is involves three genetic variance components, $\sigma^2_{A_D}$, $\sigma_{A_{DS}}$ and $\sigma^2_{A_S}$. (See section "Estimation of Genetic Parameters" below

for more details, such as the residual variance structure.)

The estimated breeding values for the direct and associative effects follow from the solution of the mixed model equations,

$$\begin{bmatrix} \hat{\mathbf{b}} \\ \hat{\mathbf{a}}_D \\ \hat{\mathbf{a}}_S \end{bmatrix} = \begin{bmatrix} \mathbf{X}'\mathbf{R}^{-1}\mathbf{X} & \mathbf{X}'\mathbf{R}^{-1}\mathbf{Z}_D & \mathbf{X}'\mathbf{R}^{-1}\mathbf{Z}_S \\ \mathbf{Z}_D'\mathbf{R}^{-1}\mathbf{X} & \mathbf{Z}_D'\mathbf{R}^{-1}\mathbf{Z}_D + g^{11}\mathbf{A}^{-1} & \mathbf{Z}_D'\mathbf{R}^{-1}\mathbf{Z}_S + g^{12}\mathbf{A}^{-1} \\ \mathbf{Z}_S'\mathbf{R}^{-1}\mathbf{X} & \mathbf{Z}_S'\mathbf{R}^{-1}\mathbf{Z}_D + g^{21}\mathbf{A}^{-1} & \mathbf{Z}_S'\mathbf{R}^{-1}\mathbf{Z}_S + g^{22}\mathbf{A}^{-1} \end{bmatrix}^{-1} \times \begin{bmatrix} \mathbf{X}'\mathbf{R}^{-1}\mathbf{y} \\ \mathbf{Z}_D'\mathbf{R}^{-1}\mathbf{y} \\ \mathbf{Z}_S'\mathbf{R}^{-1}\mathbf{y} \end{bmatrix} \tag{42}$$

where $\mathbf{R}$ is the covariance matrix of the residuals, $\mathbf{R} = \mathrm{Var}(\mathbf{e})$, and the g^{ij} denote elements of the inverse of the genetic covariance matrix, $\begin{bmatrix} g^{11} & g^{12} \\ g^{21} & g^{22} \end{bmatrix} = \begin{bmatrix} \sigma^2_{A_D} & \sigma_{A_{DS}} \\ \sigma_{A_{DS}} & \sigma^2_{A_S} \end{bmatrix}^{-1}$. The elements of $\mathbf{R}$ are given in the section on "Estimation of Genetic Parameters" below.

When fitting Eq. 41, fixed effects and potential additional random effects must be chosen carefully because not only an individual's direct effect but also its associative effect may be affected by fixed and random factors. Hence, in addition to the ordinary fixed effects, which refer to effects on the individual producing the record, one may need to fit fixed effects for its group mates. For example, when groups consist of mixed breeds, one may fit a fixed associative effect for the breed of each group mate. When associative breed effects are omitted, they may inflate the estimated associative effects and their variance. Similarly, when groups consist of mixed sexes, one may fit a fixed associative effect for the sex of each group mate. Moreover, when common-litter effects play a role, one may fit a random common-litter associative effect [41]. An example is given in the section on "Estimation of Genetic Parameters" below.

Deterministic prediction of the accuracy of selection on BLUB-EBV obtained from Model 41 is very tedious. In principle, selection index theory can be used to derive that accuracy, using the pseudo-BLUP selection index methodology suggested by [66]. However, for a population consisting of full and half sib families, a pseudo-BLUP selection index for a single trait contains 24 distinct sources of information. Hence, the variance matrix of the index contains 24^2 elements. Thus the use of stochastic simulation is more practical.

Some insight in the factors determining accuracy of BLUP selection can be obtained from a simplified index. The selection index of Muir et al. [67] shows that relatedness between group members may have greater impact on accuracy than extension of the mixed model to account for associative effects. They compared Kin-BLUP, in which the mixed model contained direct effects only (Eq. 37) and group members were related, to C-BLUP, in which the mixed model contained both direct and associative effects (Eq. 41), but group members were unrelated. The accuracy of Kin_BLUP exceeded that of C_BLUP, and the correlation of the true associative BV with the EBV of Kin_BLUP was greater than that with the associative EBV of C_BLUP. Hence, though Kin_BLUP does not explicitly account for associative effects, it can have greater accuracy for associative effects than C_BLUP. This result agrees with the empirical observations of Muir et al. [67] who observed greater response with Kin-BLUP than with C-BLUP in cannibalistic quail. Kin_BLUP picks up associative effects because they are hidden in the own performance and FS-performance when group members are related.

In conclusion, both empirical and theoretical results indicate that relatedness within groups is the key factor for response to selection; the use of C_BLUP does not make relatedness superfluous. C_BLUP, however, will always outperform Kin_BLUP when applied to the same breeding structure because it explicitly models the associative effects. When both methods are applied to data with full-sib groups, for example, C_BLUP will outperform Kin_BLUP [67].

A Special Case: Maternal Genetic Effects Maternal genetic effects are a common case of social interactions among individuals, where the mother affects the trait values of her offspring. Maternally affected traits usually depend on both the genes for maternal effect in the mother and genes for direct effect in the offspring [23, 27, 68, 69]. Preweaning growth rate and survival of piglets, for example, will depend on maternal milk yield and behavior of the sow, but also on the direct effect of the piglets for growth rate. Other examples are calving ease in dairy cattle [70], and preweaning survival in sheep [71].

Maternal effects should not be confused with the genes for direct effect that the offspring inherits from its mother, but refers to the effect of the mother on her offspring that arises through the environment, for example, due to maternal care. Hence, direct and maternal effects are genetically distinct traits. For growth rate in piglets, for example, genes for direct effect will relate to juvenile growth rate, whereas genes for maternal effect may relate to milk yield or behavior of sows.

Maternal effects may be modeled as [68, 69]

$$P_i = A_{D,i} + E_{D,i} + A_{M,j} + E_{M,j}, \tag{43}$$

where i is the offspring, j the mother, P_i is the phenotype of the offspring, A_D and A_M the direct and maternal breeding values, and E_D and E_M the non-heritable direct and maternal effects, respectively. From Eq. 43, response to selection equals the sum of the changes in mean direct and mean maternal breeding value [68, 69],

$$R = \Delta\bar{A}_D + \bar{\Delta}A_M, \tag{44}$$

Based on Eq. 44, Eaglen and Bijma [49] defined a total breeding value for maternally affected traits, being the sum of an individual's breeding values for direct and maternal effect,

$$A_T = A_{D,i} + A_{M,i}, \tag{45}$$

so that response to selection equals $R = \Delta\bar{A}_T$. In contrast to the phenotypic value, the total breeding value includes the individual's own breeding value for maternal effect, rather than that of its mother. This is because an individual transmits its own genes for maternal effects to its offspring, not those of its mother. The total heritable variance that can be used to generate response to selection in maternally affected traits equals the variance in total breeding values among individuals,

$$\sigma^2_{A_T} = \sigma^2_{A_D} + 2\sigma_{A_{DM}} + \sigma^2_{A_M} \tag{46}$$

From Eq. 17, response to selection equals [49]

$$R = \imath\rho_M\sigma_{A_T}, \tag{47}$$

where ρ_M is the accuracy of selection for maternally affected traits, which is the correlation between the selection criterion and the total breeding value of an individual.

A number of studies have referred to a "total heritability" [72, 73], citing Willham [69],

$$h^2_r = \frac{\sigma^2_{A_D} + 1\frac{1}{2}\sigma_{A_{DM}} + \frac{1}{2}\sigma^2_{A_M}}{\sigma^2_P} \tag{48}$$

Willham [23, 69] referred to h^2_r as the "fraction of the selection differential realized if selection were on P_x" (P_x being the offspring phenotype). Hence, h^2_r represents the realized heritability for mass selection, $h^2_r = R/S$, the ratio of response over the selection differential, rather than the ratio of heritable variance over phenotypic variance [68]. Thus response to mass selection can be predicted as $R = h^2_r S$. Equation 47 yields the same result for mass selection, but applies to any selection strategy.

Maternal genetic effects can be estimated using mixed models that include both a direct and maternal genetic effect [64]. Issues related to the estimation of maternal genetic effects are discussed in [23, 64, 74–78].

Results of Social Selection Experiments Only a few social selection experiments have been applied in livestock. Muir [19] selected laying hens, housed in half-sib groups, based on total egg production per group. Hence, this experiment combined group selection with relatedness. In six generations, mortality decreased from 67% to 8%. Most of the response occurred within the first few generations of selection. Eggs per hen housed increased from 91 to 237 eggs, mainly as a result of increased survival. In the seventh generation, the group selected and control lines were compared to the commercial line from which the group selected line was derived [20, 79, 80]. In single-bird cages, egg production was significantly greater for the commercial line. In 12-bird cages, however, the reverse was seen. The most remarkable difference was for mortality at 58 weeks of age, which was 89% for the commercial line, 20% for the group selected line and 54% for the control. These results confirm the theoretical expectation that group selection with related group members yields large response to selection when associative effects are important.

The changes in mortality were accompanied by changes in behavior, stress physiology, and

immunology [81, 82].Under conditions of social stress, birds from the low mortality population were more hesitant to attack other birds, showed less feather pecking, had a lower H/L ratio and had lower dopamine and corticosterone blood concentrations, indicating lower stress levels [83, 84]. Cheng and Muir [82] suggested that these changes in birds from the low mortality population may reflect a greater ability to cope with novel environments and to have a greater resistance to stressors than birds from the high mortality population.

Muir and coworkers [17, 22, 67] presented results of 25 cycles of selection for body weight in quail housed in groups of 16 birds. Three selection programs were compared. First, selection on conventional animal model BLUP EBV considering direct effects only (AM_BLUP, Eq. 37). Second, selection on estimated total breeding values derived from a mixed model, including both direct and associative effects (C_BLUP, Eq. 41). Group members were unrelated in those selection programs. The third selection program used groups consisting of half-sibs families, and selection on conventional animal model BLUP EBV considering direct effects only (Kin_BLUP). Results showed that the AM_BLUP program decreased body weight and increased mortality, whereas the Kin_BLUP program increased body weight and decreased mortality. The C_BLUP program was intermediate. Those results agree with expectations based on the theory presented above.

At Wageningen University, Ellen and coworkers initiated a selection experiment in laying hens, combining individual selection for egg number and group selection for low mortality in non-beak-trimmed kin-groups, based on the method of [48]. Selection candidates were housed individually, allowing recording of individual egg number. Non-beak-trimmed full sibs of these selection candidates were housed in family groups in which mortality was recorded. Selection was for a combination of egg number and mortality. Rodenburg et al. [85, 86] and Bolhuis et al. [87] investigated the behavioral and physiological consequences of this selection program in the second generation. Animals of the selected line were less fearful and less sensitive to stressors in a range of behavioral tests. Consistent results were found both in young chicks [87] and in adult birds [88] in two environments (cages and floor pens).

A number of group selection experiments have been performed in laboratory species, particularly in flour beetles (*Tribolium castaneum*). Wade [58, 59] was the first to demonstrate the power of group selection experimentally. Goodnight [89] reviewed 12 group selection experiments. Without exception, all group selection experiments showed a significant response to selection both in animals, plants, and microbial communities. Similar results have been found in bacteria [90]. Again, those results demonstrate that selection between groups and use of related group members increases response to selection in traits affected by social interactions, which agrees with theoretical expectations (see above).

Estimation of Genetic Parameters

Statistical Methodology

Some of the selection methods described above can be applied without knowledge of the genetic parameters, such as mass and group selection. Without knowledge of the genetic parameters, however, it is unclear whether associative effects are present and whether those selection strategies are needed and/or efficient. Moreover, most applied breeding programs make use of Best Linear Unbiased Prediction [53] for estimating breeding values, e.g., to correct for systematic environmental effects, which requires knowledge of the genetic parameters. Knowledge of the genetic parameters is also needed to quantify the expected response to selection, which may be required to make decisions on investment in breeding programs. Moreover, there is a wider biological interest in the heritable components affecting individual trait values and responses to selection, both in agriculture and in other fields of biology such as evolutionary genetics [30, 62]. Thus there is a need to estimate the genetic parameters for socially affected traits, which are the additive genetic variances of direct genetic effects, $\sigma^2_{A_D}$, the additive genetic variances of associative effects, $\sigma^2_{A_S}$, and the additive genetic covariance of direct and associative effects, $\sigma_{A_{DS}}$. This section addresses the estimation of those parameters, starting with a review of existing results.

Empirical Estimates of the Associative Variance Table 3 summarizes estimates of direct and associative heritabilities. Brichette et al. [37] were the first to publish estimates of the associative genetic variance. They analyzed growth in mussel cultures and found strongly significant direct and associative effects. Their model is somewhat different from the mixed models discussed in this chapter, and estimates may not be directly comparable. In each group, they tested a single focal family against a mixed reference set containing members of all families. In this design, the effect of the focal family on the mean phenotype of the reference group represents the associative effect of that family. Hence, in this setup, the associative effect is defined for a set of family members, rather than for a single individual, and the factors $(n-1)$ and $(n-1)^2$ in the total genetic variance do not apply (Eq. 7). Brichette et al. [37] obtained direct heritabilities of 0.104 and 0.232 for length measures, and 0.097 and 0.234 for area measures. Corresponding estimates for associative heritability were 0.010 and 0.087 for length and 0.220 and 0.082 for area. Direct-associative genetic correlations were negative, averaging −0.2. These results suggest that $\sigma^2_{A_t}/\sigma^2_P \approx 0.24$, and that associative effect contributed ∼1/3 of heritable variance in growth of mussel cultures.

Socially Affected Traits, Inheritance and Genetic Improvement. Table 3 Genetic parameter estimates from agriculture and aquaculture populations

	$\hat{h}^2_D$	$\hat{h}^2_S$	$\hat{T}^2$	$\hat{r}_{A_{DS}}$
Beef cattle (*Bos taurus*)[a]				
Feed lot growth rate	0.06	0.003	2.01	0.69
Cod (*Gadus morhua*)[b]				
Condition factor	0.05	NR	0.21	NR
Dorsal fin erosion	0.83	NR	1.32	NR
Caudal fin erosion	0.08	NR	0.47	NR
Growth rate	0.11	NR	0.12	NR
Body weight	0.37	NR	0.57	NR
Laying hens (*Gallus gallus*)				
Survival time, Line W1[c]	0.07	0.010	0.19	0.18 (n.s.)
Survival time, Line WB[c]	0.10	0.014	0.15	−0.31
Survival time, Line WF[c]	0.02 (n.s.)	0.004 (n.s.)	0.06 (n.s.)	0.11 (n.s.)
Survival time, Cross W1×WB[d]	0.03	0.033	0.26	−0.37
Survival time, Cross WB×W1[d]	0.05	0.036	0.17	−0.83
Mussel cultures (*Mytilus galloprovincialis*)[e]				
Length	0.17	0.049[f]	0.21	−0.09 (n.s.)
Area	0.17	0.151[f]	0.27	−0.30 (n.s.)
Pigs (*Sus scrofa*)				
Growth rate fattening[g]	0.21	0.007	0.71	0.20 (n.s.)
Growth rate fattening[h]	0.13	0.002	0.23	0.11 (n.s.)
Growth rate fattening[i]	0.20	0.001	0.61	0.24
Body weight[j]	0.39	0.001 (n.s.)	0.47	0.07 (n.s.)
FI fattening[g]	0.17	0.006	0.70	0.38 (n.s.)

Socially Affected Traits, Inheritance and Genetic Improvement. Table 3 (Continued)

	$\hat{h}^2_D$	$\hat{h}^2_S$	$\hat{T}^2$	$\hat{r}_{A_{DS}}$
Back fat[g]	0.35	0.001 (n.s.)	0.41	−0.02 (n.s.)
Back fat[j]	0.45	0.001 (n.s.)	0.47	0.07 (n.s.)
Muscle depth[g]	0.21	<0.001 (n.s.)	0.32	0.33 (n.s.)
Muscle area[j]	0.29	0.001 (n.s.)	0.31	−0.63 (n.s.)
Growth suckling piglets[k]	0.07	0.001 (n.s.)	0.15	−0.27 (n.s.)
Quail (*Coturnix coturnix japonica*)				
Body weight[l]	0.17	0.014	2.56	−0.56

$\hat{h}^2_D = \hat{\sigma}^2_{A_D}/\hat{\sigma}^2_P$, $\hat{h}^2_S = \hat{\sigma}^2_{A_S}/\hat{\sigma}^2_P$, $\hat{T}^2 = \hat{\sigma}^2_{A_T}/\hat{\sigma}^2_P$, $\hat{r}_{A_{DS}} = \hat{\sigma}_{A_{DS}}/(\sigma_{A_D}\sigma_{A_D})$, see Eqs. 4–9 for further information.
[a][34], first 28 days of growth period, no evidence for associative effects found in other periods.
[b][35], significance levels not reported.
[c][24], individuals were not beak-trimmed.
[d][36], individuals were not beak-trimmed.
[e][37].
[f]The h^2_S is defined somewhat different here, see text.
[g][15].
[h][38], for d= 1.
[i][39], model 2.
[j]H [40], model 2, significance levels tested against model 6.
[k][41], model 4.
[l] [17], non-genetic associative effects not accounted for, thus $\hat{\sigma}^2_{A_S}$ and $\hat{T}^2$may be inflated; significance levels not reported. NR: not reported. n.s. not significantly different from zero.

Later studies focused primarily on laying hens and pigs. Particularly in pigs and beef cattle, it has proven difficult to reliably estimate the associative genetic variance. Often the estimates suggested a considerable contribution of associative effects to total heritable variance ($T^2 >> h^2_D$), but the estimated associative genetic variance was nevertheless not significantly different from zero (Table 3). This occurred particularly when group sizes were relatively large, so that the number of groups was fairly small [25]. These observations agree with theoretical predictions, which indicate that the number of groups is the major determinant of statistical power, and that designs with small groups are often superior ([32]; see section on "Power and Optimum Designs" below). Hence, in large groups, even small values of the associative heritability can make a major contribution to total heritable variation (Eq. 7), but this contribution is difficult to estimate accurately, as reflected by the large standard errors of $\hat{\sigma}^2_{A_T}$. Estimates in laying hens, which come from data containing groups of four individuals, have been more accurate [24, 36].

Several studies have shown that the estimated associative genetic variance is very sensitive to the choice of the statistical model. Models not accounting for non-genetic associative effects, i.e., models that fit neither environmental associative effects nor pen effects or correlated residuals, generally yielded strongly inflated estimates [34, 40, 91, 92]. Hence, the choice of the statistical model requires careful consideration. To properly estimate the genetic variance components, additional fixed and random associative effects may be required to account for other sources of variation, such as litter environment or group size (see below).

QTL: There appears to be only a single QTL-study involving associative effects. Biscarini et al. [93] performed an association study to map direct and associative QTL for feather damage across nine different genetic lines of laying hens. A total population of 662 hens were genotyped for 1022 SNPs. Eleven significant SNPs were detected for direct effect and 81 for associative effect. From the significant associative SNPs, six were located at the sex chromosome. The SNPs identified suggest a relationship between

behavior and immunology, and a role of the serotonergic system in feather pecking.

Mixed Models Muir and coworkers [17, 22] extended the traditional mixed animal model to include Griffing's associative effects (See Eq. 41 above). The following describes an extension of their model, taking the basic model as a starting point. In the basic model (Eq. 3), observed trait values are the sum of direct and associative effects, $P_i = P_{D,i} + \sum_{j=1}^{n-1} P_{S,j}$. The full direct and associative effects are not solely genetic, but may depend also on fixed effects, random genetic effects, and other random effects such as permanent or litter effects,

$$P_{D,i} = \text{fixed}_D + A_{D,i} + E_{D_P,i} + E_{D_C,i} + E_{D,i} \quad (49a)$$

$$P_{S,i} = \text{fixed}_S + A_{S,i} + E_{S_P,i} + E_{S_C,i} + E_{S,i}, \quad (49b)$$

where subscripts P and C indicate permanent and common-litter effects, respectively. (Note that Eqs. 49a and b are not exhaustive; they may be extended with, e.g., maternal genetic effects.) Just as in classical mixed models, omission of associative permanent effects or associative common-litter effects may lead to overestimation of $\sigma^2_{A_S}$. In pigs, for example, two full sibs may develop similar social skills because they experienced the same litter environment. In the fattening period, this similarity in social skills will create a covariance between the pen mates of both full sibs. When not accounted for, this covariance will largely be attributed to the associative genetic variance because the mixed model implies that $\text{Cov}(\bar{P}_{\text{pen mates}(FS1)}, \bar{P}_{\text{pen mates}(FS2)}) = \frac{1}{2}\sigma^2_{A_S}$ when associative litter effects are not included. A similar reasoning applies to permanent effects. For example, when an individual has been member of two distinct groups, the covariance between the phenotypes of two group mates, one taken from each group, equals $\sigma^2_{A_S} + \sigma^2_{E_S}$. When permanent associative effects are omitted from the mixed model, this covariance will be fully attributed to associative genetic effects, leading to overestimation of $\sigma^2_{A_S}$.

In general, therefore, the mixed model for socially affected traits is given by

$$\mathbf{y} = \{\mathbf{X}_D\mathbf{b}_D + \mathbf{Z}_D\mathbf{a}_D + \mathbf{Z}_{D_P}\mathbf{e}_{D_P} + \mathbf{Z}_{D_C}\mathbf{e}_{D_C} + \cdots + \mathbf{e}_D\} + \{\mathbf{X}_S\mathbf{b}_S + \mathbf{Z}_S\mathbf{a}_S + \mathbf{Z}_{S_P}\mathbf{e}_{S_P} + \mathbf{Z}_{S_C}\mathbf{e}_{S_C} + \cdots + \mathbf{e}_S\} \quad (50)$$

where subscripts D and S indicate direct and associative effects, P and C indicate permanent and common-litter effects, $\mathbf{X}$ and $\mathbf{Z}$ denote incidence matrices, and $\mathbf{e}$ the residual. Whether or not a specific model component needs to be included will depend on the data structure. Direct and associative fixed effects may often be fully confounded, so that fitting a single effect is sufficient. For example, group members will usually be in the same herd at the same time. Hence, the direct and associative herd-year effects will be fully confounded, so that fitting a single herd-year effect suffices. In some cases, therefore, the simplest model, $\mathbf{y} = \mathbf{Xb} + \mathbf{Z}_D\mathbf{a}_D + \mathbf{Z}_S\mathbf{a}_S + \mathbf{e}$, may be appropriate. (But see the section on "Non-Genetic Associative Effects" below.)

In other cases, however, additional fixed or random associative effects may be required. Consider, for example, a pen of four beef cows, the first individual being a Hereford, and individuals two through four being Charolais. In this situation, fitting both a direct and an associative fixed breed-effect may be appropriate,

$$\mathbf{y} = \mathbf{X}_D\mathbf{b}_D + \mathbf{X}_S\mathbf{b}_S + \mathbf{Z}_D\mathbf{a}_D + \mathbf{Z}_S\mathbf{a}_S + \mathbf{e}$$

$$\begin{bmatrix} y_1 \\ y_2 \\ y_3 \\ y_4 \end{bmatrix} = \begin{bmatrix} 1 & 0 \\ 0 & 1 \\ 0 & 1 \\ 0 & 1 \end{bmatrix} \begin{bmatrix} H_D \\ C_D \end{bmatrix} + \begin{bmatrix} 0 & 3 \\ 1 & 2 \\ 1 & 2 \\ 1 & 2 \end{bmatrix} \begin{bmatrix} H_S \\ C_S \end{bmatrix} + \mathbf{Z}_D\mathbf{a}_D + \mathbf{Z}_S\mathbf{a}_S + \mathbf{e}$$

where H_D and C_D are the fixed direct breed effect of Hereford and Charolais, respectively, and H_S and C_S are the fixed associative breed effect of Hereford and Charolais, respectively. The record of individual 1, for example, contains three fixed Charolais associative effects, because its three pen mates are all of the Charolais breed. When associative breed effects are omitted, they may partly end up in the estimated associative genetic variance. Moreover, when groups consist of mixed sexes, fitting a fixed associative effect for sex of the group mates may be appropriate.

As a second example, consider social interactions in fattening pigs. Because litter-mates may develop

similar social skills, fitting a common-litter associative effect is of interest in this case [15]. Consider a pen of 8 individuals originating from three distinct litters; individuals 1 through 3 are born in litter 1, individual 4 is born in litter 2, and individuals 5 through 8 are born in the third litter. The mixed model for this pen is

$$\mathbf{y} = \mathbf{Xb} + \mathbf{Z}_D\mathbf{a}_D + \mathbf{Z}_S\mathbf{a}_S + \mathbf{Z}_{C_D}\mathbf{e}_{C_D} + \mathbf{Z}_{C_S}\mathbf{e}_{C_S} + \mathbf{e} \tag{51}$$

$$\begin{bmatrix} y_1 \\ y_2 \\ y_3 \\ y_4 \\ y_5 \\ y_6 \\ y_7 \\ y_8 \end{bmatrix} = \mathbf{Xb} + \begin{bmatrix} 1 & 0 & 0 & 0 & 0 & 0 & 0 & 0 \\ 0 & 1 & 0 & 0 & 0 & 0 & 0 & 0 \\ 0 & 0 & 1 & 0 & 0 & 0 & 0 & 0 \\ 0 & 0 & 0 & 1 & 0 & 0 & 0 & 0 \\ 0 & 0 & 0 & 0 & 1 & 0 & 0 & 0 \\ 0 & 0 & 0 & 0 & 0 & 1 & 0 & 0 \\ 0 & 0 & 0 & 0 & 0 & 0 & 1 & 0 \\ 0 & 0 & 0 & 0 & 0 & 0 & 0 & 1 \end{bmatrix} \begin{bmatrix} a_{D,1} \\ a_{D,2} \\ a_{D,3} \\ a_{D,4} \\ a_{D,5} \\ a_{D,6} \\ a_{D,7} \\ a_{D,8} \end{bmatrix}$$

$$+ \begin{bmatrix} 0 & 1 & 1 & 1 & 1 & 1 & 1 & 1 \\ 1 & 0 & 1 & 1 & 1 & 1 & 1 & 1 \\ 1 & 1 & 0 & 1 & 1 & 1 & 1 & 1 \\ 1 & 1 & 1 & 0 & 1 & 1 & 1 & 1 \\ 1 & 1 & 1 & 1 & 0 & 1 & 1 & 1 \\ 1 & 1 & 1 & 1 & 1 & 0 & 1 & 1 \\ 1 & 1 & 1 & 1 & 1 & 1 & 0 & 1 \\ 1 & 1 & 1 & 1 & 1 & 1 & 1 & 0 \end{bmatrix} \begin{bmatrix} a_{S,1} \\ a_{S,2} \\ a_{S,3} \\ a_{S,4} \\ a_{S,5} \\ a_{S,6} \\ a_{S,7} \\ a_{S,8} \end{bmatrix}$$

$$+ \begin{bmatrix} 1 & 0 & 0 \\ 1 & 0 & 0 \\ 1 & 0 & 0 \\ 0 & 1 & 0 \\ 0 & 0 & 1 \\ 0 & 0 & 1 \\ 0 & 0 & 1 \\ 0 & 0 & 1 \end{bmatrix} \begin{bmatrix} e_{C_D,1} \\ e_{C_D,2} \\ e_{C_D,3} \end{bmatrix}$$

$$+ \begin{bmatrix} 2 & 1 & 4 \\ 2 & 1 & 4 \\ 2 & 1 & 4 \\ 3 & 0 & 4 \\ 3 & 1 & 3 \\ 3 & 1 & 3 \\ 3 & 1 & 3 \\ 3 & 1 & 3 \end{bmatrix} \begin{bmatrix} e_{C_S,1} \\ e_{C_S,2} \\ e_{C_S,3} \end{bmatrix} + \begin{bmatrix} e_1 \\ e_2 \\ e_3 \\ e_4 \\ e_5 \\ e_6 \\ e_7 \\ e_8 \end{bmatrix}$$

The $\mathbf{Z}_S$ links the record of each individual to the associative genetic effect of its group mates, whereas $\mathbf{Z}_{C_S}$ links the record of each individual to the litter of its group mates. Hence, with groups of 8 individuals, each row of both $\mathbf{Z}_S$ and $\mathbf{Z}_{C_S}$ has a sum of 7, because each individual has 7 group mates. For this model, the variance structures for genetic effects is $\mathrm{Var}\begin{bmatrix} \mathbf{a}_D \\ \mathbf{a}_S \end{bmatrix} = \mathbf{G} \otimes \mathbf{A}$, where $\mathbf{G} = \begin{bmatrix} \sigma^2_{A_D} & \sigma_{A_{DS}} \\ \sigma_{A_{DS}} & \sigma^2_{A_S} \end{bmatrix}$, $\mathbf{A}$ is the usual numerator relationship matrix [27], and $\otimes$ denotes the Kronecker product of matrices. The variance structure of the common-litter effects is $\mathrm{Var}\begin{bmatrix} \mathbf{e}_{C_D} \\ \mathbf{e}_{C_S} \end{bmatrix} = \mathbf{C} \otimes \mathbf{I}$, where $\mathbf{C} = \begin{bmatrix} \sigma^2_{E_{C_D}} & \sigma(E_{C_D}, E_{C_S}) \\ \sigma(E_{C_D}, E_{C_S}) & \sigma^2_{E_{C_S}} \end{bmatrix}$, and $\mathbf{I}$ is an identity matrix of dimension equal to the number of litters. The $\sigma^2_{E_{C_D}}$ is the variance of the (usual) direct litter effects, $\sigma^2_{E_{C_S}}$ the variance of the associative litter effects, and $\sigma(E_{C_D}, E_{C_S})$ the covariance between the direct and associative effect of a litter. Hence, Eq. 51 involves the estimation of six variance components and the residual variance. (See below for the variance structure of the residual). Canario et al. [38] showed that an associative common-litter effect may be required to prevent overestimation of the associative genetic variance in fattening pigs.

Non-Genetic Associative Effects In both above examples, the direct residual effect of the focal individual and the associative residual effects of its group mates have been summarized into a single residual, $e_i = E_{D,i} + \sum_{j=1}^{n-1} E_{S,j}$. This is because the non-genetic parameters $\sigma^2_{E_D}$, $\sigma_{E_{DS}}$ and $\sigma^2_{E_S}$ are not uniquely identifiable when group size is constant [39, 40, 92]. Hence, a model including both E_S and a (direct) residual is overspecified. Nevertheless, non-genetic associative effects have consequences for the variance structure of the residuals. First, the residual variance becomes dependent on group size [39, 92],

$$\sigma^2_e = \sigma^2_{E_D} + (n-1)\,\sigma^2_{E_S}, \tag{52}$$

Hence, when group size varies in the data, it may be appropriate to fit a separate residual variance for each group size. Second, the residuals of group mates become correlated [39, 92],

$$\mathrm{Cov}(e_i, e_j) = 2\sigma_{E_{DS}} + (n-2)\sigma^2_{E_S}, \tag{53}$$

where i and j are group mates. Equations 52 and 53 illustrate that the non-genetic variance components are non-identifiable because there are only two observable (co)variances in the data, but three unknowns. In other words, there is an infinite number of combinations of $\sigma^2_{E_D}$, $\sigma_{E_{DS}}$ and $\sigma^2_{E_S}$ that yield the same values of σ^2_e and $\mathrm{Cov}(e_i, e_j)$ [15, 39, 92]. (This becomes different when group sizes vary; see below).

Equation 53 shows that the residual covariance may take negative values, particularly when groups are small. In that case, it may be required to allow for correlated residuals within group in the mixed model, using [92] $\mathrm{Var}(\mathbf{e}) = \mathbf{R}\sigma^2_e$, with

$$R_{ii} = 1, \tag{54}$$

$R_{ij} = \rho_e$ when i and j are group mates, and $R_{ij} = 0$ when i and j are in different groups.

This results in a block-diagonal structure for the correlation matrix of residuals, $\mathbf{R}$. For two groups of four individuals, for example, the correlation matrix of residuals equals

$$\mathbf{R} = \begin{bmatrix} 1 & \rho_e & \rho_e & \rho_e & 0 & 0 & 0 & 0 \\ \rho_e & 1 & \rho_e & \rho_e & 0 & 0 & 0 & 0 \\ \rho_e & \rho_e & 1 & \rho_e & 0 & 0 & 0 & 0 \\ \rho_e & \rho_e & \rho_e & 1 & 0 & 0 & 0 & 0 \\ 0 & 0 & 0 & 0 & 1 & \rho_e & \rho_e & \rho_e \\ 0 & 0 & 0 & 0 & \rho_e & 1 & \rho_e & \rho_e \\ 0 & 0 & 0 & 0 & \rho_e & \rho_e & 1 & \rho_e \\ 0 & 0 & 0 & 0 & \rho_e & \rho_e & \rho_e & 1 \end{bmatrix}$$

The correlation between residuals of group mates equals $\rho_e = \left[2\sigma_{E_{DS}} + (n-2)\sigma^2_{E_S}\right] / \left[\sigma^2_{E_D} + (n-1)\sigma^2_{E_S}\right]$. This structure can be fitted in ASREML using the CORU statement in the description of the R-structure [94].

When groups are reasonably large, the residual correlation is likely to be positive because the $(n-2)\sigma^2_{E_S}$ becomes the dominant term in Eq. 53. In that case, one can account for residual correlations by adding a random group effect to the model and fitting independent residuals [15, 34, 39]. Fitting a random group effect is computationally easier than fitting correlated residuals and is therefore preferable when the correlation between residuals of group mates is positive. This leads to the model

$$\mathbf{y} = \mathbf{Xb} + \mathbf{Z}_D\mathbf{a}_D + \mathbf{Z}_S\mathbf{a}_S + \mathbf{Z}_g\mathbf{g} + \mathbf{e}, \tag{55}$$

where $\mathbf{g}$ is a vector of random group effects, with incidence matrix $\mathbf{Z}_g$ linking phenotypes of individuals to their group, $\mathrm{Var}(\mathbf{g}) = \mathbf{I}\sigma^2_g$, $\mathrm{Var}(\mathbf{e}) = \mathbf{I}\sigma^2_e$, $\mathbf{I}$ denoting an identity matrix, σ^2_g the between-group non-genetic variance and σ^2_e the residual variance. With Eq. 55,

$$\sigma^2_g = 2\sigma_{E_{DS}} + (n-2)\sigma^2_{E_S}, \textit{ and} \tag{56a}$$

$$\sigma^2_e = \sigma^2_{E_D} - 2\sigma_{E_{DS}} + \sigma^2_{E_S} \tag{56b}$$

Note that, in contrast to Eq. 41, the residual variance of Eq. 55 is independent of group size, whereas the between-group variance depends on group size. Hence, when group size varies in the data, it may be appropriate to fit a different group variance for each group size. (But see the section "Accounting for Variation in Group Size" below.)

Ignoring non-genetic associative effects, e.g., by omitting a group effect and fitting a simple residual, may inflate the estimated genetic variance components by as much as 200–300% [39, 40, 92]. In this case, the covariance between trait values of group mates, which equals $2\sigma_{P_{DS}} + (n-2)\sigma^2_{P_S}$, is attributed entirely to the genetic components because the model implies that $\mathrm{Cov}_{\text{group mates}} = 2\sigma_{A_{DS}} + (n-2)\sigma^2_{A_S}$.

Accounting for Variation in Group Size The above has ignored variation in group size within a population, which will be very common in practice. When group sizes vary in the population, merely fitting a fixed effect for group size may not be sufficient because variance components may also differ between group sizes. For example, interactions among individuals may be less intense in large groups, meaning that the associative genetic variance decreases with group size.

When the underlying parameters, $\sigma^2_{A_D}$, $\sigma_{A_{DS}}$, $\sigma^2_{A_S}$, $\sigma^2_{E_D}$,$\sigma_{E_{DS}}$ and $\sigma^2_{E_S}$ are assumed to remain constant, variation in group size requires only modifying the variance structure of the non-genetic part of the model. In the genetic part of the model (Eq. 51), $\mathbf{Z}_D\mathbf{a}_D + \mathbf{Z}_S\mathbf{a}_S$, variation in group size is automatically accounted for in $\mathbf{Z}_S$. Consequences for the non-genetic part of the model will depend on the model. When fitting a model with correlated residuals, both the residual variance and the residual within-group correlation will vary among group sizes (Eqs. 52–54). When fitting a model with random group effects, the group

variance will be heterogeneous among group sizes while the residual variance is homogeneous (56 and Eqs. 57). Hence, when the underlying variance components are assumed constant, a model including a random group effect is more easily adapted to account for varying group size.

However, assuming that the underlying parameters remain constant with varying group size is a strong a priori assumption. In many cases, associative effects may become smaller in larger groups because they are distributed over more group mates, a phenomenon known as "dilution" [25, 42, 43]. In principle, one could estimate separate genetic parameters for each group size. However, this would be a waste of information, and require large data sets for each group size. A simpler solution is to scale the magnitude of associative effects by a factor depending on the inverse of the number of group mates (Eq. 11),

$$A_{S,i,n} = \left(\frac{\bar{n}-1}{n-1}\right)^d A_{S,i,\bar{n}},$$

where $A_{S,i,n}$ represents the associative effect of individual i when expressed in a group of n members, $A_{S,i,\bar{n}}$ the associative effect when expressed in a group of the average size, and d the degree of dilution. Further details on dilution of associative effects are summarized above in the section "The Effect of Group Size on Heritable Variance".

The degree of dilution can be estimated from data containing variation in group size by using a mixed model with Restricted Maximum Likelihood and evaluating the likelihood for different fixed values of d [25, 38]. Estimates of A_S, $\sigma^2_{A_S}$ and $\sigma_{A_{DS}}$ referring to the average group size may be obtained from the following mixed model [38, 43],

$$\mathbf{y} = \mathbf{Xb} + \mathbf{Z}_D\mathbf{a}_D + \mathbf{Z}_{S(d)}\mathbf{a}_{S,\bar{n}} + \mathbf{Z}_g\mathbf{g} + \mathbf{e}, \tag{57}$$

where $\mathbf{y}$ is the vector of observations, $\mathbf{Xb}$ are the usual fixed effects, $\mathbf{Z}_D\mathbf{a}_D$ are the direct genetic effects, $\mathbf{Z}_g\mathbf{g}$ are random group-effects, and $\mathbf{e}$ is a vector of residuals. The $\mathbf{a}_{S,\bar{n}}$ is a vector of associative effects referring to the average group size, and $\mathbf{Z}_{S(d)}$ is the incidence matrix for associative effects, which depends on the degree of dilution. Elements of $\mathbf{Z}_{S(d)}$ are

$$\mathbf{Z}_{S(d)}(i,j) = \left(\frac{\bar{n}-1}{n_i-1}\right)^d \text{ when } j \text{ is a group member of } i,$$
$$\mathbf{Z}_{S(d)}(i,j) = 0 \text{ otherwise,} \tag{58}$$

where $\bar{n}$ denotes the average group size, and n_i the size of the group of individual i. This model yields estimates of genetic parameters and breeding values referring to the average group size because the $[(\bar{n}-1)/(n_i-1)]^d = 1$ when $n_i = \bar{n}$.

When non-genetic associative effects depend on group size in the same manner, also the group and residual variance for the model in Eq. 57 will depend on group size [43],

$$\sigma^2_{g,n} = 2\left(\frac{\bar{n}-1}{n-1}\right)^d \sigma_{E_{DS},\bar{n}} + (n-2)\left(\frac{\bar{n}-1}{n-1}\right)^{2d} \sigma^2_{E_S,\bar{n}} \tag{59a}$$

$$\sigma^2_{e,n} = \sigma^2_{E_D} - 2\left(\frac{\bar{n}-1}{n-1}\right)^d \sigma_{E_{DS},\bar{n}} + \left(\frac{\bar{n}-1}{n-1}\right)^{2d} \sigma^2_{E_S,\bar{n}} \tag{59b}$$

Hence, to obtain unbiased estimates of the genetic parameters and d, it may be required to fit a separate group and residual variance for each group size. An alternative solution is to explicitly model E_S. When group size is constant, the non-genetic parameters cannot be estimated, and a model including both E_S and a residual is overspecified (See below Eq. 53). When group size varies, however, $\sigma^2_{E_D}$, $\sigma_{E_{DS}}$ and $\sigma^2_{E_S}$ may be identifiable (unless $d = 1$), and it may be possible to fit the model

$$\mathbf{y} = \mathbf{Xb} + \mathbf{Z}_D\mathbf{a}_D + \mathbf{Z}_{S(d)}\mathbf{a}_{S,\bar{n}} + \mathbf{Z}_{S(d)}\mathbf{e}_{S,\bar{n}} + \mathbf{e},$$

with $\mathrm{Var}\begin{bmatrix}\mathbf{e}_{S,\bar{n}}\\ \mathbf{e}\end{bmatrix} = \mathbf{E}\otimes\mathbf{I}$, where $\mathbf{E} = \begin{bmatrix}\sigma^2_{E_{S,\bar{n}}} & \sigma(E_D, E_{S,\bar{n}})\\ \sigma(E_D, E_{S,\bar{n}}) & \sigma^2_{E_D}\end{bmatrix}$.

However, it may not be possible to implement the nonzero $\mathrm{Cov}(\mathbf{e}_{S,\bar{n}}, \mathbf{e})$ of this model in standard software.

Canario et al. [38] present estimates for the degree of dilution of both associative genetic effects and associative common-litter effects in fattening pigs, with group sizes varying from 5 through 15 individuals. Their results suggest that both effects are fully diluted with group size ($\hat{d} = 1$). Their results also indicate that

the estimate of the associative variance may depend on whether or not the analysis accounts for dilution.

Hadfield and Wilson [42] presented an alternative approach to account for the relationship between associative effects and group size. They fit an additional associative genetic effect that is proportional to the inverse of the number of group mates. Bijma [43] compares their model to Eq. 57, and concludes that it has greater flexibility, but is also less tractable.

Identifiability of the Associative Genetic Variance Not all data structures are equally suited for estimating the genetic variance of associative effects. A particularly critical aspect is group composition. When groups are composed of equally related individuals, for example, full or half-sib families, then direct and associative effects are fully confounded and cannot be estimated [34, 92, 95]. Also the use of specific distributions of families over groups may cause non-identifiability of the associative genetic variance [92]. Genetic parameters are identifiable when groups are composed at random with respect to family, but the standard error of $\hat{\sigma}^2_{A_S}$ may be large. Groups composed of members of two distinct families yield more precise estimates of $\sigma^2_{A_S}$ (See section "Statistical Power and Optimum Designs" below).

Moreover, the associative genetic variance is not identifiable when a fixed group-effect is fitted [96]. When fitting group as a random effect, however, $\sigma^2_{A_S}$ is identifiable and simulations with normally distributed group effects indicate that estimates are unbiased [92]. Nevertheless, the non-identifiability of $\sigma^2_{A_S}$ when using fixed group effects indicates that the information for estimating $\sigma^2_{A_S}$ is closely linked to variation in the group means, suggesting that estimates may be sensitive to the distribution of group effects. The importance of the group agrees with the observation of Bijma [97], who found that number of groups, rather than number of individuals, is the main determinant of the standard error of $\hat{\sigma}^2_{A_S}$. Cantet and Cappa [96] present methods to investigate whether variance components are identifiable from a particular data set.

Statistical Power and Optimum Designs

Standard Errors of Estimated Variance Components Optimization of experimental designs and evaluation of the power of experiments aiming to estimate genetic parameters for socially affected traits requires knowledge of the factors determining the standard errors (SE) of estimated parameters. Accurate prediction equations for those SEs are available for balanced designs containing N_f families with n_f members each, yielding a total of $N_t = N_f\, n_f$ individuals in the experiment [97]. Two group compositions have been investigated; groups composed at random with respect to family, and groups composed of two families. In the latter design, each group is composed of members of two distinct families, each family contributing ½n individuals. This design leads to a block structure (Table 4), where each of the families within a block is combined with each of the other families in that same block, each combination occurring precisely once.

For both designs, the SEs of estimated genetic variances follows from

$$\mathrm{SE}(\hat{\sigma}^2_A) \approx \frac{1}{r}\sqrt{\frac{2}{N_f-1}\left[\sigma^4_f + \frac{2\sigma^2_f\sigma^2_e}{m} + \frac{\sigma^4_e}{m(m-1)}\right]}, \tag{60}$$

where N_f is the number of families, m the effective number of records per family, σ^2_f the between-family variance, and σ^2_e the residual variance,

$$\sigma^2_e = \sigma^2_z - \sigma^2_f, \tag{61}$$

Socially Affected Traits, Inheritance and Genetic Improvement. Table 4 Example of the design with groups composed of two distinct families

	Family B				
Fam. A	2	3	4	5	6
1	2/2	2/2	2/2	2/2	2/2
2		2/2	2/2	2/2	2/2
3			2/2	2/2	2/2
4				2/2	2/2
5					2/2

Group size equals n= 4. Each group consists of members of two distinct families, each family contributing two individuals. Family size equals n_f = 10, so that each family can be combined with 10/(½ × 4) = 5 other families. Thus a block consists of six families, each being combined with each of the five other families in that block. Hence, there are 5*6/2 = 15 groups per block, 15*4 = 60 individuals per block, and $N_t/60$ blocks, N_t denoting the total number of individuals in the experiment.

where σ_z^2 is the variance of an "effective record" [97]. Equations 60 and 61 allow prediction of $\mathrm{SE}(\hat{\sigma}^2_{A_D})$, $\mathrm{SE}(\hat{\sigma}^2_{A_S})$ and $\mathrm{SE}(\hat{\sigma}^2_{A_T})$. Application of those Equations requires knowledge of m, σ_z^2 and σ_f^2, which depend on the parameter and experimental design of interest, and are given in Table 5 for schemes with groups composed at random, and in Table 6 for schemes with groups composed of two distinct families.

The SE of the estimated genetic covariance, $\mathrm{SE}(\hat{\sigma}_{A_{DS}})$ follows from

$$\mathrm{SE}(\hat{\sigma}_{A_{DS}}) = \sqrt{\frac{\mathrm{SE}(\hat{\sigma}^2_{A_D})\ \mathrm{SE}(\hat{\sigma}^2_{A_S})}{2} + \frac{\sigma^2_{A_{DS}}}{N_f - 1}}, \quad (62)$$

where $\mathrm{SE}(\hat{\sigma}^2_{A_D})$ and $\mathrm{SE}(\hat{\sigma}^2_{A_S})$ follow from Eq. 60.

The SE of the ratio of total heritable variance over phenotypic variance follows from

$$\mathrm{SE}(\hat{T}^2) \approx \frac{\mathrm{SE}(\hat{\sigma}^2_{A_T})}{\sigma^2_P}, \quad (63)$$

where $\mathrm{SE}(\hat{\sigma}^2_{A_T})$ follows from Eq. 60. An accurate prediction equation for the SE of the estimated genetic correlation between direct and associative effects is available only for cases where the true value of this correlation is near zero. Designs with two families per group yield lower $\mathrm{SE}(\hat{\sigma}^2_{A_S})$ than schemes with groups composed at random with respect to family, except when group size equals two individuals, in which case both designs are nearly equivalent [97].

Socially Affected Traits, Inheritance and Genetic Improvement. Table 5 Components of SEs[a] with random group composition

Parameter	Expression	
All VC	$m = n_f$	
	$\sigma^2_P = \sigma^2_{P_D} + (n-1)\,\sigma^2_{P_S}$	
	$\mathrm{Cov}_\omega = 2\sigma_{P_{DS}} + (n-2)\,\sigma^2_{P_S}$	
$\hat{\sigma}^2_{A_D}$	$\sigma^2_z = \sigma^2_P$	$\sigma^2_f = r\sigma^2_{A_D}$
$\hat{\sigma}^2_{A_S}$	$\sigma^2_z = \frac{\sigma^2_P + (n-2)\mathrm{Cov}_\omega}{n-1}$	$\sigma^2_f = r\sigma^2_{A_S}$
$\hat{\sigma}^2_{A_T}$	$\sigma^2_z = n\left[\sigma^2_P + (n-1)\mathrm{Cov}_\omega\right]$	$\sigma^2_f = r\sigma^2_{A_T}$

[a]SEs for the estimated genetic variance of interest follow from substituting σ^2_z and σ^2_f for that parameter into Eq. 60.

Socially Affected Traits, Inheritance and Genetic Improvement. Table 6 Components of SEs[a] with group composed of two distinct families (See Table 4)

Parameter	Expression	
All VC	$m = 2n_f/n$	
	$\sigma^2_P = \sigma^2_{P_D} + (n-1)\sigma^2_{P_S} + 2r\left(\frac{1}{2}n - 1\right)\left[\sigma_{A_{DS}} + \left(\frac{1}{2}n - 1\right)\sigma^2_{A_S}\right]$	
	$\mathrm{Cov}_{\omega,\mathrm{fam}} = 2\sigma_{P_{DS}} + (n-2)\sigma^2_{P_S} + r\left[\sigma^2_{A_D} + 2(\frac{1}{2}n - 2)\sigma_{A_{DS}} + (\frac{1}{2}n^2 - 2n + 3)\sigma^2_{A_S}\right]$	
	$\mathrm{Cov}_{\omega,\mathrm{nonfam}} = 2\sigma_{P_{DS}} + (n-2)\sigma^2_{P_S} + 2r(\frac{1}{2}n - 1)\left[\sigma_{A_{DS}} + (\frac{1}{2}n - 1)\sigma^2_{A_S}\right]$	
	$\mathrm{Var}(\bar{P}_{\mathrm{fam}}) = \dfrac{\sigma^2_P + (\frac{1}{2}n - 1)\mathrm{Cov}_{\omega,\mathrm{fam}}}{\frac{1}{2}n}$	
$\hat{\sigma}^2_{A_D}$	$\sigma^2_z = (1 + \varphi^2)\,\mathrm{Var}(\bar{P}_{\mathrm{fam}}) - 2\varphi\,\mathrm{Cov}_{\omega,\mathrm{nonfam}}\varphi = \dfrac{\frac{1}{2}n - 1}{\frac{1}{2}n}$	$\sigma^2_f = r\sigma^2_{A_D}$
$\hat{\sigma}^2_{A_S}$	$\sigma^2_z = \frac{4\,\mathrm{Var}(\bar{P}_{\mathrm{fam}})}{n^2}$	$\sigma^2_f = r\sigma^2_{A_S}$
$\hat{\sigma}^2_{A_T}$	$\sigma^2_z = \frac{4}{n}\left[\sigma^2_P + (\frac{1}{2}n - 1)\mathrm{Cov}_{\omega,\mathrm{fam}} + \frac{1}{2}n\mathrm{Cov}_{\omega,\mathrm{nonfam}}\right]$	$\sigma^2_f = r\sigma^2_{A_T}$

[a] SEs for the estimated genetic variance of interest follow from substituting σ^2_z and σ^2_f for that parameter into Eq. 60.

For designs with group composed at random, the optimum family size for estimating a genetic variance is

$$n_{f\,\mathrm{opt},\sigma^2,\mathrm{random}} \approx \sigma_z^2/\sigma_f^2 \tag{64a}$$

For designs with group composed of two families, the optimum family size for estimating a genetic variance is

$$n_{f\,\mathrm{opt},\sigma^2,2\mathrm{fam}} \approx \frac{1}{2}\,n\,\sigma_z^2/\sigma_f^2 \tag{64b}$$

These expressions can be applied for the genetic variance of interest by using the appropriate σ_z^2 and σ_f^2 from Tables 5 or 6. Results of Eqs. 64a and b show that optimum family size for estimating $\sigma_{A_S}^2$ may be very large when group are composed at random and may differ considerably from optimum family size for estimating $\sigma_{A_D}^2$. When groups are composed of two families, optimum family size for estimating $\sigma_{A_S}^2$ is smaller, and more similar to that for $\sigma_{A_D}^2$. Thus the scheme with two families per group may be a good compromise to estimate both the direct and associative genetic variance [97].

Expressions for optimum group sizes for estimating $\sigma_{A_S}^2$ are not available. Numerically obtained results in [97] indicate that optimum group sizes are small ($\leq$3–4) in most cases. Optimum group sizes are large only for designs with two families per group, and only when the number of groups, rather than the number of individuals, is the limiting factor in the experiment. An R-package named SE.IGE is available, which calculates SEs and optimum family and group sizes, and can be downloaded from the repository of R-packages, CRAN, at http://cran.r-project.org/package=SE.IGE, following the usual method to install R-packages.

Future Directions

This chapter has summarized the quantitative genetic theory of traits affected by social interactions among individuals and reviewed the existing empirical evidence for such effects. The theoretical framework is now well developed, both in the field of artificial selection and in evolutionary biology [18, 56, 57]. The theory of genetic variance, inheritance, and response to selection has been developed [17, 31], and statistical methodology to estimate associative variance components has become available [17, 22, 25, 39, 92, 98]. Selection experiments and data analysis provide convincing evidence of substantial associative effects on survival time in cannibalistic laying hens and quail [17, 19, 21, 24, 36, 67, 93]. The evidence is less strong for other livestock species, such as pigs and beef cattle, where some studies have found large effects [15], but others none or only small effects [25, 95]. Further research is required on those species. Associative effects appear to be very relevant for aquaculture populations as well (see below), but estimates of the associative genetic variance are almost completely lacking at present.

Genetic improvement of associative effects has the potential to contribute significantly to animal welfare because a significant proportion of welfare issues is related to mutual behaviors [99]. Well-known examples are feather pecking and cannibalism in laying hens [100], and fighting after mixing and tail biting in pigs [14]. In the past, genetic improvement of behaviors has been hampered by the cost and labor involved in routine collection of behavioral data. As a consequence, breeding for improved behavior is rare in livestock genetic improvement. The use of associative-effect models offers the potential to solve this problem because they estimate the associative effect from the resulting phenotype without the need to observe the causative behavior. Biscarini et al. [93], for example, identified 81 QTL for associative effect on plumage condition, without observing feather pecking behavior.

Not all welfare problems are related to behavioral interactions among animals. Welfare is also threatened by metabolic stress related to high efficiency of production [4]. Results in quail [17] and in Medaka [101, 102] suggest that a genetic reduction of agonistic behaviors may produce strains that waste less resources on competitive behaviors. This suggests that genetic improvement of associative effects may have the potential to increase the efficiency of production without increasing metabolic stress. Whether this phenomenon is widespread awaits further empirical testing.

Though the statistical methodology to estimate associative variance components is available, application is practice has many pitfalls, particularly in pigs, and careful model comparison is required to assess the stability of the estimates [15, 34, 39, 91]. The omission of random group effects from the statistical model, for example, may yield a strongly overestimated associative

genetic variance. Interpretation of early results has been hampered by the lack of a proper theoretical framework to judge the relevance of the estimated associative genetic variance, which is often very small compared to phenotypic variance, but can nevertheless contribute substantially to heritable variance. The definition of a total heritable variance facilitates interpreting the relevance of associative effects for livestock genetic improvement [31]. If current estimates of the associative genetic variance in pigs and laying hens reflect the true parameters, then selection for associative effects can increase rates of genetic improvement considerably. Particularly in pigs and aquaculture, there is a need for validation by means of selection experiments.

A challenging problem is the improvement of associative effects when populations are kept in large groups, which is increasingly the case. When groups are large, the number of groups is usually small, which hampers the estimation of genetic parameters. Investigation of optimum designs to estimate genetic parameters shows that the number of groups, rather than the number of individuals, is the primary determinant of statistical power [97]. Moreover, in large groups, the intensity of the interactions is probably less, as found in pigs [38], which reduces the accuracy of estimated genetic parameters and breeding values. This issue requires further investigation.

Optimum designs for maximizing response to selection suggest a trade-off between improvement of associative effects and rates of inbreeding. The key factor to increase response to selection is the use of related group members (see above). However, such designs will probably increase the correlation between EBVs of relatives, which in turn increases rates of inbreeding when selection is based on EBVs. Rates of inbreeding can be restricted by using flexible selection algorithms, such as optimum contribution selection [103–105]. Hence, high rates of inbreeding can be avoided, but this may be at the expense of response to selection. This issue has not yet been investigated; it probably becomes less relevant when breeders start using genomic selection (see below and in [106]).

Particularly interesting is the relationship between competition and variability. Breeders have long been interested in increasing uniformity. However, though animal breeders have successfully increased the average performance of livestock, genetic improvement of uniformity has proven difficult. In the classical model, where $P = A + E$, opportunities for genetic changes in variability are very limited [107]. At best, breeders can achieve $\sigma_A^2 \approx 0$, which reduces phenotypic standard deviation by only ~16% when heritability equals 0.3. There is, however, increasing evidence that the environmental variance is under direct genetic control [e.g., 108, 109], and theoretical models for inherited variability have been developed [110–112]. Results suggest a substantial genetic coefficient of variation in the environmental variance, but also a difficulty to obtain reliable estimated breeding values for environmental variance [112].

The mechanisms underlying such inherited variability are largely unknown at present. In aquaculture, competition for feed is believed to inflate size variation among individuals. In carp, for example, Moav and Wohlfarth [16] found greater variability in ponds of mixed genetic strains than in ponds of a single genetic strain. Results in Medaka [101, 102] suggest that behavioral consequences of selection for growth depend on whether or not there is competition for feed in the selection environment. To limit size variation among individuals, regular grading of fish is common practice in aquaculture. Because group selection has the potential to reduce competition among individuals (see above), it seems to be a promising tool for reduction of variability in aquaculture. At present, however, there appear to be no studies on the consequences of group selection for variability in aquaculture. Current models of associative effects (see above) cannot explain a relationship between competition and variability because the phenotypic variance is independent of the average social breeding value. Hence, extension of current models is required to theoretically link variability and competition. The link between competition and variability may, however, largely be an empirical, rather than theoretical, issue.

At present, the use of genome wide marker information is rapidly increasing in livestock genetic improvement. A method know as Genomic Selection [6], which estimates effects of markers covering the entire genome, has become a routine tool in dairy cattle breeding and will soon be adapted by breeders of other livestock species. Genomic selection extends readily to socially affected traits, which seems particularly useful

for crossbreeding schemes. A comparison of estimated genetic parameters for direct and associative effects for survival in cannibalistic laying hens shows large differences between purebred parental lines [24] and their crossbred offspring [36]. The genetic correlation between direct and social effects appears to be strongly negative in crossbreds, while around zero in purebreds. Moreover, estimated parameters differ between reciprocal crosses. Those results indicate considerable "GxE-interaction" between purebreds and crossbreds. Genomic selection based on phenotypes recorded on crossbreds can be used to predict breeding values of nucleus individuals for direct and social effects referring to crossbred performance. Hence, combining genomic selection with associative-effect models seems promising to reduce mortality due to cannibalism in commercial crossbred herds.

Bibliography

1. Hill WG (2008) Estimation, effectiveness and opportunities of long term genetic improvement in animals and maize. Lohmann Inf 43(1):3–20
2. Havenstein GB, Ferket PR, Qureshi MA (2003a) Growth, liveability, and feed conversion of 1957 versus 2001 broilers when fed representative 1957 and 2001 broiler diets. Poult Sci 82:1500–1508
3. Havenstein GB, Ferket PR, Qureshi MA (2003b) Carcass composition and yield of 1957 versus 2001 broilers when fed representative 1957 and 2001 broiler diets. Poult Sci 82:1509–1518
4. Rauw WM, Kanis E, Noordhuizen-Stassen EN, Grommers FJ (1998) Undesirable side effects of selection for high production efficiency in farm animals: a review. Livest Prod Sci 56:15–33
5. Ducrocq V, Sölkner J (1994) "The Survival Kit", a Fortran package for the analysis of survival data. In: Proceedings of the 5th world congress on genetics applied to livestock production, University of Guelph, Guelph, Canada, vol 22, pp 51–52
6. Meuwissen THE, Hayes BJ, Goddard ME (2001) Prediction of total genetic value using genome-wide dense marker maps. Genet Sel Evol 157(4):1819–1829
7. De Jong G (1993) Covariances between traits deriving from successive allocation of resources. Funct Ecol 7:75–83
8. Van der Waaij EH (2004) A resource allocation model describing consequences of artificial selection under metabolic stress. J Anim Sci 82:973–981
9. Smith C, James JW, Brascamp EW (1986) On the derivation of economic weights in livestock improvement. Anim Prod 43:545–551
10. Denison RF, Kiers ET, West SA (2003) Darwinian agriculture: when can humans find solutions beyond the reach of natural selection. Q Rev Biol 78:145–167
11. Griffing B (1967) Selection in reference to biological groups. I. Individual and group selection applied to populations of unordered groups. Aust J Biol Sci 20:127–142
12. Moore AJ, Brodie ED III, Wolf JB (1997) Interacting phenotypes and the evolutionary process: I. Direct and indirect genetic effects of social interactions. Evolution 51:1352–1362
13. Muir WM, Aggrey SE (2003) Poultry genetics, breeding and biotechnology. CABI, Wallingford
14. Turner SP, D'Eath RB, Roehe R, Lawrence AB (2010) Selection against aggressiveness in pigs at re-grouping: Practical application and implications for long-term behavioural patterns. Anim Welfare 19(suppl 1):123–132
15. Bergsma R, Kanis E, Knol EF, Bijma P (2008) The contribution of social effects to heritable variation in finishing traits of domestic pigs (*Sus scrofa*). Genetics 178:1559–1570
16. Moav R, Wohlfarth GW (1974) Magnification through competition of genetic differences in yield capacity in carp. Heredity 33:181–202
17. Muir WM (2005) Incorporation of competitive effects in forest tree or animal breeding programs. Genetics 170:1247–1259
18. Bijma P, Wade MJ (2008) The joint effects of kin, multilevel selection and indirect genetic effects on response to genetic selection. J Evol Biol 21:1175–1188
19. Muir WM (1996) Group selection for adaptation to multiple-hen cages: selection program and direct responses. Poult Sci 75:447–458
20. Craig JV, Muir WM (1996) Group selection for adaptation to multiple-hen cages: behavioral responses. Poult Sci 75(10):1145–1155
21. Craig JV, Muir WM (1996) Group selection for adaptation to multiple-hen cages: beak-related mortality, feathering, and body weight responses. Poult Sci 75:294–302
22. Muir WM, Schinkel A (2002) Incorporation of competitive effects in breeding programs to improve productivity and animal well being. In: Proceedings of the 7th world congress on genetics applied to livestock production, Montpellier, France, communication no. 14–07
23. Willham RL (1972) The role of maternal effects in animal breeding III. Biometrical aspects of maternal effects in animal. J Anim Sci 35:1288–1292
24. Ellen ED, Visscher J, Van Arendonk JAM, Bijma P (2008) Survival of laying hens: genetic parameters for direct and associative effects in three purebred layer Lines. Poult Sci 87:233–239
25. Arango J, Misztal I, Tsuruta S, Cubertson M, Herring W (2005) Estimation of variance components including competitive effects of Large White growing gilts. J Anim Sci 83:1241–1246
26. Falconer DS, Mackay TFC (1996) Introduction to quantitative genetics. Pearson Education, Harlow
27. Lynch M, Walsh B (1998) Genetics and analysis of quantitative traits. Sinauer Associates, Sunderland
28. Fisher RA (1918) The correlation between relatives on the supposition of Mendelian inheritance. Trans R Soc Edinb 52:399–433
29. Fisher RA (1941) Average excess and average effect of a gene substitution. Ann Eugen 11:53–63

30. Wolf JB, Brodie ED III, Cheverud AJ, Moore AJ, Wade MJ (1998) Evolutionary consequences of indirect genetic effects. Trends Ecol Evol 13:64–69
31. Bijma P, Muir WM, Van Arendonk JAM (2007a) Multilevel selection 1: Quantitative genetics of inheritance and response to selection. Genetics 175:277–288
32. Bijma P (2010) Fisher's fundamental theorem of inclusive fitness and the change in fitness due to natural selection when conspecifics interact. J Evol Biol 23:194–206
33. Griffing B (1976) Selection in reference to biological groups. VI. Analysis of full sib groups. Genetics 82:723–731
34. Van Vleck LD, Cundiff LV, Koch RM (2007) Effect of competition on gain in feedlot bulls from Hereford selection lines. J Anim Sci 85:1625–1633. doi:10.2527/jas.2007-0067
35. Monsen BB, Ødegård J, Nielsen HM, Arnesen KR, Toften H, Damsgård B, Bijma P, Olesen I (2010) Genetics of social interactions in Atlantic cod (*Gadus morhua*). In: Proceedings of the 9th world congress on genetics applied to livestock production, Leipzig, August 2010. Book of Abstracts page 100; Paper ID 910
36. Peeters K, Eppink T, Ellen E, Visscher J, Bijma P (2010) Survival in laying hens: Genetic parameters for direct and associative effects in the reciprocal crosses of two purebred layer lines. In: Proceedings of the 9th world congress on genetics applied to livestock production, Leipzig, August 2010. Book of Abstracts page 54; Paper ID 575
37. Brichette I, Reyero MI, Garcı'a C (2001) A genetic analysis of intraspecific competition for growth in mussel cultures. Aquaculture 192:155–169
38. Canario L, Lundeheim N, Bijma P (2010) Pig growth is affected by social genetic effects and social litter effects that depend on group size. In: Proceedings of the 9th world congress on genetics applied to livestock production, Leipzig, August 2010 (in press). Book of Abstracts page 87; Paper ID 170
39. Chen CY, Kachman SD, Johnson RK, Newman S, Van Vleck LD (2008) Estimation of genetic parameters for average daily gain using models with competition effects. J Anim Sci 86:2525–2530
40. Hsu WL, Johnson RK, VanVleck LD (2010) Effect of pen mates on growth, backfat depth, and longissimus muscle area of swine. J Anim Sci 88:895–902
41. Bouwman AC, Bergsma R, Duijvesteijn N, Bijma P (2010) Maternal and social genetic effects on average daily gain of piglets from birth till weaning. J Anim Sci 88:2883–2892. doi:10.2527/jas.2009-2494
42. Hadfield JD, Wilson AJ (2007) Multilevel Selection 3: Modeling the effects of interacting individuals as a function of group size. Genetics 177:667–668
43. Bijma P (2010) Multilevel selection 4: Modeling the relationship of indirect genetic effects and group size. Genetics 186:1029–1031
44. Griffing B (1977) Selection for populations of interacting genotypes. In: Proceedings of the international conference on quantitative genetics, Iowa State University Press, Ames, pp 413–434
45. Griffing B (1981a) A theory of natural-selection incorporating interaction among individuals. 1. The modeling process. J Theor Biol 89:635–658
46. Griffing B (1981b) A theory of natural-selection incorporating interaction among individuals. 2. Use of related groups. J Theor Biol 89:659–677
47. Bourdon RM (2000) Understanding animal breeding, 2nd edn. Prentice Hall, Upper Saddle River
48. Ellen ED, Muir WM, Teuscher F, Bijma P (2007) Genetic improvement of traits affected by interactions among individuals: Sib selection schemes. Genetics 176:489–499
49. Eaglen SAE, Bijma P (2009) Genetic parameters of direct and maternal effects for calving ease in Dutch Holstein-Friesian cattle. J Dairy Sci 92:2229–2237
50. Price GR (1970) Selection and covariance. Nature 227:529–531
51. Hazel LN (1943) The genetic basis for constructing selection indexes. Genetics 28:476–490
52. Hazel LN, Dickerson GE, Freeman AE (1994) The selection index – Then, now and for the future. J Dairy Sci 77:3236–3251
53. Henderson CR (1975) Best linear unbiased estimation and prediction under a selection model. Biometrics 31: 423–447
54. Hamilton WD (1964) The genetical evolution of social behavior. J Theor Biol 7:1–52
55. Wade MJ (1985) Hard selection, soft selection, kin selection, and group selection. Am Nat 125:61–73
56. McGlothlin JW, Brodie ED III (2009) How to measure indirect genetic effects: the congruence of trait-based and variance-partitioning approaches. Evolution 63:1785–1795
57. McGlothlin JW, Moore AJ, Wolf JB, Brodie ED III (2010) Interacting phenotypes and the evolutionary process. III. Social evolution. Evolution 64(9):2558–2574
58. Wade MJ (1976) Group selection among laboratory populations of Tribolium. Proc Natl Acad Sci USA 73: 4604–4607
59. Wade MJ (1977) An experimental study of group selection. Evolution 31:134–153
60. Bijma P, Aanen DK (2010) Assortment, Hamilton's rule and multilevel selection. Proc R Soc B 2010(277):673–675. doi:10.1098/rspb.2009.1093
61. Frank SA (2007) All of life is social. Curr Biol 17(16):R650
62. Wade MJ, Bijma P, Ellen ED, Muir WM (2010) Group selection and social evolution in domesticated animals. Evol Appl 3:453–465. doi:10.1111/j.1752-4571.2010.00147.x, ISSN 1752-4571
63. Cameron ND (1997) Selection indices and prediction of genetic merit in animal breeding. CABI, Wallingford
64. Mrode RA, Thompson R (2005) Linear models for the prediction of animal breeding values. CABI, Wallingford
65. Wray NR, Hill WG (1989) Asymptotic rates of response from index selection. Anim Prod 49:217–227
66. Villanueva B, Wray NR, Thompson R (1993) Prediction of asymptotic rates of response from selection on multiple traits using univariate and multivariate best linear unbiased predictors. Anim Prod 57:1–13

67. Muir WM, Bijma P, Chen CY, Misztal I, Wade MJ (2010) Advances in selection theory including experimental demonstrations: The theory of selection with social competition. In: Proceedings of the 9th world congress on genetics applied to livestock production, Leipzig, August 2010. Book of Abstracts page 141; Paper ID 16
68. Dickerson GE (1947) Composition of hog carcasses as influenced by heritable differences in rate and economy of gain. Iowa Agric Exp Stn Res Bull 354:492–524
69. Willham RL (1963) The covariance between relatives for characters composed of components contributed by related individuals. Biometrics 19:18–27
70. Manfredi E, Ducrocq V, Foulley JL (1991) Genetic analysis of calving ease in dairy cattle. J Dairy Sci 74:1715–1723
71. Sawalha RM, Conington J, Brotherstone S, Villanueva B (2007) Analyses of lamb survival of Scottish Blackface sheep. Animal 1:151–157
72. Koch RM, Cundiff LV, Gregory KE (1994) Cumulative selection and genetic change for weaning or yearling weight or for yearling weight plus muscle score in Hereford cattle. J Anim Sci 72:864–885
73. Luo MF, Boettcher PJ, Schaeffer LR, Dekkers JCM (2002) Estimation of genetic parameters of calving ease in first and second parities of Canadian Holsteins using Bayesian methods. Livest Prod Sci 74:175–184
74. Meyer K (1992) Bias and sampling covariances of estimates of variance components due to maternal effects. Genet Sel Evol 24:487–509
75. Robinson DL (1996) Model which might explain negative correlation between direct and maternal genetic effects. Livest Prod Sci 45:111–122
76. Koerhuis ANM, Thompson R (1997) Models to estimate maternal effects for juvenile body weight in broiler chickens. Genet Sel Evol 29:225–249
77. Quaas RL, Pollak EJ (1980) Mixed model methodology for farm and ranch beef cattle testing programs. J Anim Sci 51:1277–1287
78. Bijma P (2006) Estimating maternal genetic effects in livestock. J Anim Sci 84:800–806
79. Muir WM, Liggett DL (1995) Group selection for adaptation to multiple-hen cages comparisons with a control and commercial lines. Poult Sci 74(suppl 1):101, Abstr
80. Muir WM, Craig JV (1998) Improving animal well-being through genetic selection. Poult Sci 77:1781–1788
81. Cheng HW, Freire R, Pajor EA (2004) Endotoxin stress responses in chickens from different genetic lines 1. sickness, behavioral, and physical responses. Poult Sci 83:707–715
82. Cheng HW, Muir WM (2005) The effects of genetic selection for survivability and productivity on chicken physiological homeostasis. World's Poult Sci J 61:383–397
83. Cheng HW, Freire R, Pajor EA, Chen Y, Muir WM (2001) Different regulation of physiological and behavioral response to social stress in two genetically selected lines of laying hens. In: Garner JP, Mench JA, Heekin SP (eds) Proceedings of the 35th international congress of the ISAE, Davis, pp 128
84. Cheng HW, Muir WM (2004) Chronic social stress differentially regulates neuroendocrine responses in laying hens II. Genetic basis of adrenal responses under three different social conditions. Psychoneuroendocrinology 29:961–971
85. Rodenburg TB, Komen H, Ellen ED, Uitdehaag KA, van Arendonk JAM (2008) Selection method and early-life history affect behavioural development, feather pecking and cannibalism in laying hens: A review. Appl Anim Behav Sci 110:217–228
86. Rodenburg TB, Bolhuis JE, Koopmanschap RE, Ellen ED, Decuypere E (2009a) Maternal care and selection for low mortality affect post-stress corticosterone and peripheral serotonin in laying hens. Physiol Behav 98:519–523
87. Rodenburg TB, Uitdehaag KA, Ellen ED, Komen J (2009b) The effects of selection on low mortality and brooding by a mother hen on open-field response, feather pecking and cannibalism in laying hens. Anim Welf 18:427–432
88. Bolhuis JE, Ellen ED, Van Reenen CG, De Groot J, Ten Napel J, Koopmanschap R, De Vries GR, Uitdehaag KA, Kemp B, Rodenburg TB (2009) Effects of genetic group selection against mortality on behaviour and peripheral serotonin in domestic laying hens with trimmed and intact beaks. Physiol Behav 97:470–475
89. Goodnight CJ (2005) Multilevel selection: the evolution of cooperation in non-kin groups. Popul Ecol 47:3–12. doi:10.1007/s10144-005-0207-2
90. Griffin AS, West SA, Buckling A (2004) Cooperation and competition in pathogenic bacteria. Nature 430:1024–1027
91. Van Vleck LD, Cassady JP (2005) Unexpected estimates of variance components with a true model containing genetic competition effects. J Anim Sci 83:68–74
92. Bijma P, Muir WM, Ellen ED, Wolf JB, Van Arendonk JAM (2007b) Multilevel selection 2: Estimating the genetic parameters determining inheritance and response to selection. Genetics 175:289–299
93. Biscarini F, Bovenhuis H, van Arendonk JAM, Parmentier HK, Jungerius AP, Van Der Poel JJ (2010) Across-line SNP association study of innate and adaptive immune response in laying hens. Anim Genet 41:26–38
94. Gilmour AR, Gogel BJ, Cullis BR, Thompson R (2006) ASReml User Guide, Release 2.0. VSN International Ltd, Hemel Hempstead
95. Cheng J, Janssens S, Buys N (2009) Full sib pens of pigs are not suitable to identify variance component of associative effect: a simulation study using Gibbs Sampling. BMC Genet 10:9
96. Cantet RJC, Cappa EP (2008) On identifiability of (co)variance components in animal models with competition effects. J Anim Breed Genet 125:371–381
97. Bijma P (2010) Estimating indirect genetic effects: precision of estimates and optimum designs. Genetics 186:1013–1028
98. Cappa EP, Cantet RJC (2008) Direct and competition additive effects in tree breeding: Bayesian estimation from an individual mixed tree model. Silvae Genet 57:45–57
99. Rodenburg TB, Bijma P, Ellen ED, Bergsma R, de Vries S, Bolhuis JE, Kemp B, van Arendonk JAM (2010) Breeding amiable animals? Improving farm animal welfare by including social effects in breeding programmes. Anim Welf 19:S77–S82

100. Kjaer JB, Sørensen P (1997) Feather pecking behaviour in White Leghorns, a genetic study. Br Poult Sci 38:333–341
101. Ruzzante DE, Doyle RW (1991) Rapid behavioural changes in Medaka (*Oryzias latipes*) caused by selection for competitive and noncompetitive growth. Evolution 45:1936–1946
102. Ruzzante DE, Doyle RW (1993) Evolution of social behaviour in a resource-rich, structured environment: selection experiments with Medaka (*Oryzias latipes*). Evolution 47:456–470
103. Wray NR, Goddard MG (1994) Increasing long-term response to selection. Genet Sel Evol 26:431–451
104. Meuwissen THE (1997) Maximizing response of selection at a predefined rate of inbreeding. J Anim Sci 75:934–940
105. Grundy B, Villaneuva B, Woolliams JA (1998) Dynamic selection procedures for constrained inbreeding and their consequences for pedigree development. Genet Res Camb 72:159–168
106. Daetwyler HD, Villanueva B, Bijma P, Woolliams JA (2007) Inbreeding in genome-wide selection. J Anim Breed Genet 124(6):369–376
107. Hohenboken WD (1985) The manipulation of variation in quantitative traits: a review of possible genetic strategies. J Anim Sci 60:101–110
108. Rowe SJ, White IMS, Avendano S, Hill WG (2006) Genetic heterogeneity of residual variance in broiler chickens. Genet Sel Evol 38:617–635
109. Ibanez-Escriche N, Sorensen D, Waagepetersen R, Blasco A (2008) Selection for environmental variation: a statistical analysis and power calculations to detect response. Genetics 180:2209–2226
110. Sancristobal-Gaudy M, Elsen JM, Bodin L, Chevalet C (1998) Prediction of the response to a selection for canalisation of a continuous trait in animal breeding. Genet Sel Evol 30:423–451
111. Hill WG, Zhang XS (2004) Effects of phenotypic variability of directional selection arising through genetic differences in residual variability. Genet Res Camb 83:121–132
112. Mulder HA, Bijma P, Hill WG (2007) Prediction of breeding values and selection responses with genetic heterogeneity of environmental variance. Genetics 175:1895–1910

Solar Cells, Chalcopyrite-Based Thin Film

Hans-Werner Schock
Institut Technologie, Solar Forschung Division, Helmholtz Zentrum für Materialien und Energie, Berlin, Germany

Article Outline

Glossary
Definition of Subject
Introduction
Multinary Chalcopyrite Compounds as Photovoltaic Materials
Survey of Absorber Fabrication Processes
Status of Large-Scale Production
Present Limitations
Perspectives
Future Directions
Bibliography

Glossary

Chalcopyrite compounds These compounds originate from the mineral $CuFeS_2$ and are composed of elements with valence states I–III–VI_2. Due to ordering of the different cations, the unit cell is a doubled zinc blende unit cell.

Defects Disorders of the crystal lattice either intrinsically (vacancies, interstitials, antisites) or by extrinsic impurities. Photovoltaic quality of the material depends on the concentration of defects.

Grain boundaries Interfaces between different grains.

Heterojunctions In contrast to pn junctions formed by doping a homogeneous semiconductor, heterojunctions use to two different semiconductors.

High efficiency Present high-efficiency PV modules reach efficiencies 15% to over 20% in production.

Polycrystalline thin films The films consist of single grain with a size in the order of the thickness of the film or smaller. Typical grain sizes are in the 0.1–5 μm range.

Thin-film solar cells Solar cells that are produced by technologies that allow deposition of materials on very large areas. Depending on the absorber material, thicknesses are in the range of 0.1–20 μm.

Definition of Subject

Developments in photovoltaics technologies aim for solutions that allow manufacturing of efficient photovoltaic modules at low cost. The chalcopyrite-type compounds $Cu(In,Ga)(S,Se)_2$ (CIGS) or (CIS) are semiconductors which could significantly contribute as thin-film materials to the future share of photovoltaics in the supply of electrical power. In a long-lasting

process of understanding the specific properties, CIGS became one of the most attractive materials for efficient thin-film photovoltaic modules. The remarkable attention received by CIGS as a future material for thin-film solar cells results from the specific properties of this fascinating semiconductor:

- Lab cell efficiencies beyond 20%
- Very high flexibility for manufacturing
- Free choice of substrates (glass or flexible foils)

The high-efficiency potential makes it one of the most important materials for thin-film photovoltaic technologies.

Introduction

The history of CIGS began in the early 1950s when the ternary compound $CuInSe_2$ was first synthesized and semiconducting properties were identified by Hahn et al. [1]. At that time, photovoltaics was still limited to Se-based photodetector applications until the first Si- and CdS-based solar cells reached notable conversion efficiencies in the mid-1950s. In parallel to the development of crystalline, Si solar cells, the first chalcogenide-based thin-film solar cells, in particular, Cu_2S–CdS, were considered as promising technology approaching efficiencies of 10% in the late 1970s. Further development of this technology was hampered by stability problems of the ionic conductor Cu_2S under photovoltaic operation. Adding indium to the binary copper chalcogenide compound created an intrinsically stable compound. The publication of a 12% efficient photovoltaic device based on a $CuInSe_2$ single crystalline in 1974 by Shay and Wagner [2] draws first attention to this material. In the first attempts to produce thin-film solar cells, the $CuInSe_2$ absorber layers were prepared by evaporation of the ternary compound $CuInSe_2$ from a single source. Kazmerski et al. [3] were able to demonstrate the first thin-film solar cells. Later, coevaporation of the single elements yielded devices with efficiencies approaching 10% [4]. A first review of the chances and obstacles of CIS-based solar cells was given by Kazmerski [5] in 1983. The concerns regarding the performance of this kind of solar cells have been largely overcome:

- Device efficiency can compete with polycrystalline Si solar cells.
- Stability has been proven in outdoor operation and accelerated testing.

The Cu-chalcopyrite compound $CuInSe_2$ and its alloys $Cu(In,Ga)(Se,S)_2$ provide the absorber material for the to date most efficient thin-film solar cells. The high optical absorption coefficient of the chalcopyrite compounds allow absorber layers with a thickness <1 μm well suited for thin flm solar cells.

A high-power conversion efficiency of more than 20% obtained with an alloy $Cu(In,Ga)Se_2$ (with a Ga/(Ga+In)-ratio $\sim$0.3) reaches the performance of conventional wafer-based polycrystalline silicon solar cell technology. Even though the first results of the development were very promising, it took a decade until the first commercial CIGS modules were produced. Only after some important modifications of the growth and composition of the absorber film the material reached its full potential. The addition of Ga stabilized p-type conductivity and increased the bandgap. The key for control of film growth and free-carrier concentration is the use of sodium-containing glass or the deliberate addition of Na to the growth process. These developments were mostly empirical and sometimes serendipitous. In the meantime, advanced techniques for microanalysis and calculation of defects by density functional theory led to a deeper understanding of the properties of these complex materials. The involvement of more research teams worldwide has improved basic understanding as a prerequisite for reproducible manufacturing processes.

The generic CIGS device in Fig. 1 is based upon a so-called substrate structure. In contrary to the superstrate design of most CdTe and thin-film silicon-based modules, the CIGS solar cell structure can be built on opaque substrates. The present design of a CIGS cell is the result of a historic development based upon empirical optimization. Improved knowledge about the material and devices now allows systematic developments. Even though there is no significant difference between the structure of devices in laboratory dimensions and in large-area modules, the difference between maximum large-area module efficiencies of about 14% and record laboratory efficiency exceeding 20% [6] is remarkable.

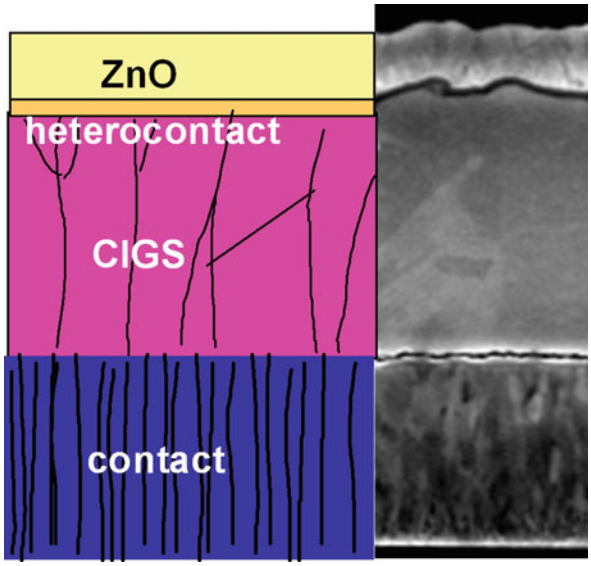

Solar Cells, Chalcopyrite-Based Thin Film. Figure 1 Generic structure of a multinary CIGS thin-film solar cell together with the corresponding SEM picture of the cross section

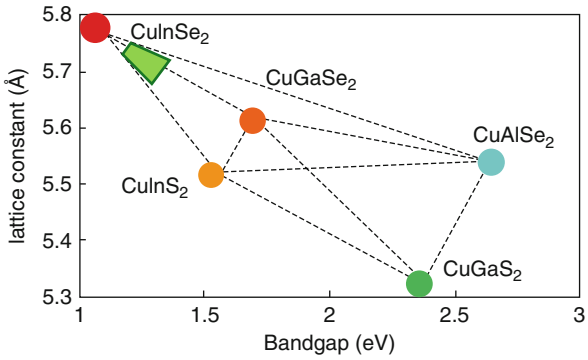

Solar Cells, Chalcopyrite-Based Thin Film. Figure 2 Lattice constant vs energy gap of Cu-chalcopyrites for thin-film solar cells

Multinary Chalcopyrite Compounds as Photovoltaic Materials

From the beginning of the development, CIS turned out to be a very efficient PV material. However, the complexity of the material impeded a systematic development. Hence, early progress and success were driven by empirical development connected to lucky circumstances such as the success of chemically deposited CdS buffer layers in connection with ZnO transparent contacts. The tolerance of the material at moderate efficiency levels was long-time misleading with respect to the necessary control of deposition processes. An important discovery was the impact of Na on the quality of absorber films. The controlled introduction of Na during growth leads to real breakthrough in device performance.

The ternary compound $CuInSe_2$ has an 80-mV lower bandgap than silicon and therefore below the optimum for efficient conversion of the solar radiation. Besides the technologically advantageous features including the outstanding radiation hardness of $CuInSe_2$ and its alloys [7], the Cu-chalcopyrites attract also considerable scientific interest because of their unusual defect physics: for example, the ability to form electronically inactive defect complexes explains the great tolerance of these materials to deviation from stoichiometry and to foreign impurities.

The success of the chalcopyrite compounds, in particular, $CuIn(Ga)Se_2$, results from their very beneficial material properties. Besides the high optical absorption, electronic properties are very well suited for solar cells. Synthesis of thin films at moderate temperatures on cheap substrates complies with the requirements for large-scale production.

Possibilities for the design of efficient photovoltaic thin-film devices are significantly extended by alloys of multinary chalcogenide compounds. Since the bandgap can easily be increased by adding Ga and S, the $Cu(In_{1-x}Gax)(Se_{1-y}S_y)_2$ alloy system provides wide design options for processing and properties for the development of high-efficiency solar cells with high-open-circuit-voltage solar cells as the bandgap energy E_g of $CuInSe_2$ increases upon alloying with Ga. The range of bandgaps which are covered by the Cu-chalcopyrite is displayed in Fig. 2. Typical CIGS cells have a bandgap of 1.15–1.2 eV as highlighted in the figure.

Structure and Defects

The chalcopyrite semiconductors belong to the adamantine structure derived from the diamond lattice. There, lattice elements are tetrahedrally coordinated like in all adamantine (diamond-like) semiconductors. The tetragonal chalcopyrite structure of, for example, $CuInSe_2$ is derived from the cubic zinc blende structure

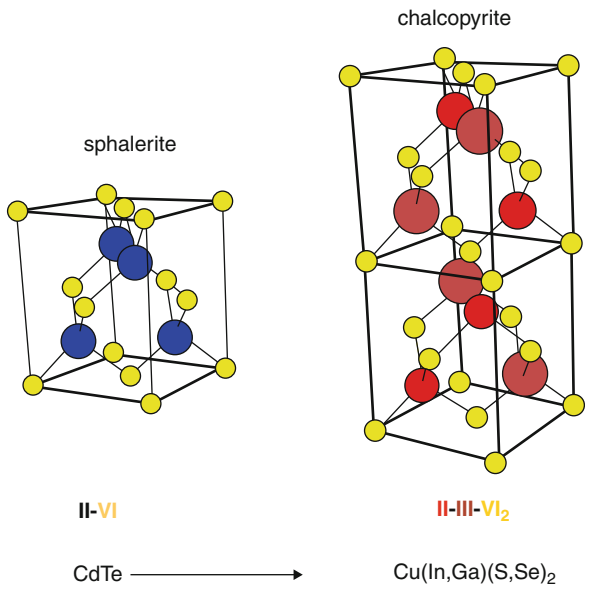

Solar Cells, Chalcopyrite-Based Thin Film. Figure 3 Structure of zinc blende (*cubic*) and chalcopyrite (*tetragonal*) compounds

of II–VI materials like ZnSe by occupying the Zn sites alternately with Cu and In atoms. In the chalcopyrite structure, each I (Cu) or III (In) atom has four bonds to the VI atom (Se). In turn, each Se atom has two bonds to Cu and two to In. The crystal structure of the I–III–VI_2 compounds of CIS is shown in Fig. 3.

With the chalcogen sublattice being unchanged (with the exception that positions of the anions are slightly distorted), the cation lattice sites are occupied by different group I and group III elements. Because the strengths of the I–VI and III–VI bonds are different, the ratio of the lattice constants c/a is not exactly 2, i.e., it varies from 2.01 in $CuInSe_2$ to 1.96 in $CuGaSe_2$. Due to the multitude of elements and compounds involved in the formation of $Cu(In_{1-x}Gax)(Se_{1-y}Sy)_2$ films, the resulting defect structure is quite complex.

Phase Diagram The phase diagrams have been extensively investigated by Goedecke et al. [8]. These investigations had a special focus on temperatures and compositions relevant for the preparation of thin films. On the Cu-rich side of the $CuInSe_2$ single-phase region of the phase diagram, Cu_2Se segregates as a secondary phase. In thin films, Cu_2Se can be easily removed by dissolving in potassium cyanide (KCN) solution leaving behind a $CuInSe_2$ or $Cu(In,Ga)Se_2$ film which is slightly Cu poor. Films prepared with an originally Cu-rich composition exhibit good electronic quality (e.g., from photoluminescence) [9, 10]. However, solar cells with absorber films grown in such a way are far less efficient than those with a slightly Cu-deficient absorber.

The related compound $CuInS_2$ - gained some attention as absorber material for thin-film solar cells [11]. In this case, growth processes rely on the Cu-rich growth of the films in connection with subsequently removing excess CuS by dissolving in KCN solution. Cu-poor growth immediately leads to deterioration of the film quality by the segregation of spinel type phase $CuIn_5Se_8$.

The ternary phase diagram can be reduced to a simpler pseudobinary phase diagram along the tie line between Cu_2Se and In_2Se_3. By combining these two compounds, $CuInSe_2$ is formed:

$$x\,(Cu_2Se) + (1 - x)\,In_2Se_3 \qquad 0 < x < 1.$$

There are three different phases which have been found to be adjacent to the chalcopyrite: α-phase ($CuInSe_2$), the β-phase ($CuIn_3Se_5$), and the δ-phase (the high-temperature sphalerite phase, $Cu_{2-y}Se$). An interesting point is that the phases adjacent to the α-phase have a similar structure. The β-phase is actually a defect chalcopyrite phase built by ordered arrays of defect pairs (Cu vacancies V_{Cu} and In–Cu antisites In_{Cu}). Similarly, $Cu_{2-y}Se$ can be derived from the chalcopyrite by using Cu–In antisites Cu_{In} and Cu interstitials Cu_i. Disordering the cation (Cu, In), sublattice causes the transition to the sphalerite phase and leads back to the zinc blende structure. Neutron or anomalous X-ray diffraction allows detailed insight in the defect structure because site occupancy is reflected by variation of diffraction peak intensities [12].

The existence range of the chalcopyrite phase in pure $CuInSe_2$ at room temperature extends from a Cu content of 24–24.5% on the quasi-binary Cu_2Se–In_2Se_3 tie line [8]. Thus, the existence range of single-phase $CuInSe_2$ is small and does even not include the stoichiometric composition of 25% Cu. The Cu content of absorbers for efficient thin-film solar cells typically varies between 22 and 24 at.% Cu. At the growth temperature of 500–550°C, this region

lies within the single-phase region of the α-phase. However, at room temperature, it lies outside this region of the equilibrium phase diagram in [8]. Hence, there is a tendency for phase separation in $CuInSe_2$ after deposition. Fortunately, it turns out that partial replacement of In with Ga, as well as the use of Na-containing substrates, considerably widens the single-phase region in terms of ratios (In + Ga)/(In + Ga + Cu) >0.5 [15]. Thus, the studies of the phase diagram, especially in connection with the addition of Ga and Na, explain the substantial improvements actually achieved in recent years by adding Na to the growth process either from Na-containing substrates or from Na-containing precursor layers, as well as by using $Cu(In,Ga)Se_2$ alloys. First, in these films, about 20–30% of the In is replaced by Ga, and second, these films grow on Na-containing glass and, consequently, contain around 0.1 atom % Na that diffuses out of the glass during deposition. The incorporation of both Ga and Na inhibits the ordering of the defect complexes and, hence, the formation of secondary Cu-poor phases in the bulk of the thin film [13].

Further important properties for the collection of photocurrent in solar cells are charge-carrier mobilities. Electron mobilities in single crystals reach more than 900 cm^2/Vs [14]. In connection with lifetimes of several ns, the electron diffusion length is in the order of a few μm. Diffusion length and minority carrier lifetimes depend very much on the preparation conditions of the thin films. With an absorption length for the solar radiation with an energy above the bandgap below 1 μm in combination with a sufficient diffusion length of photogenerated carriers, CIGS-based solar cells could reach very high efficiencies with a thickness of less than a μm.

Defects The semiconductor compound $CuIn(Ga)Se_2$ is extremely tolerant to defects (i.e., deviations from stoichiometry, crystallographic imperfections, and grain boundaries due to fortunate circumstances) [15, 16] (note: this is only true for $CuIn(Ga)Se_2$ and, in part, for $CuInS_2$):

- Secondary phases have commensurate structures, i.e., phase segregations do not cause severe distortion during growth.
- Cu vacancies are not electrically active defects but just reduce the density of states in the valence band. Therefore, deviations from stoichiometry, in particular, Cu/In+Ga ratios, form neutral defect complexes.
- Other relevant defects like Cu_{In} are energetically positioned in the conduction band.

The complex defect structure of ternary or multinary semiconductor makes control of electronic properties by extrinsic doping mostly impossible. On the one hand, simply considering valence states of dopants is not leading to reliable results, because foreign elements could occupy any lattice site and act as donor or acceptor. On the other hand, a high level of impurities can be tolerated, in particular, at moderate efficiencies (<15%).

There is much room for device design and the need for working around limitations by processing the material in a way where defects are minimized. It is important to note that device optimization is not possible by simple engineering based on textbook solutions but requires understanding of the complex material science of a system with numerous components. Reconstruction of surfaces leads to the formation of defect structures that are not electrically active in terms of surface recombination. These very lucky circumstances make surface and grain boundaries self-passivating [15]. The tendency of the compound to stabilize in a state with a minimum of electrically active defects allows for flexibility in film preparation. If the film is slightly Cu poor and the processing ends with a high-temperature step (>400–600°C), reasonable device efficiencies can be reached.

The role of defects in the ternary compound $CuInSe_2$, and even more in $Cu(In,Ga)Se_2$, is of special importance because of the large number of possible intrinsic defects [17] and the role of deep recombination centers in the performance of the solar cells [18]. The defect physics in $Cu(In,Ga)Se_2$ explains:

- Doping of $Cu(In,Ga)Se_2$ has to rely on native defects
- Extrinsic doping by foreign impurities is not possible
- The tolerance of electrical properties to large off-stoichiometries

– The electrically neutral nature of the structural defects

Efficiency limitations might arise only from minor potential fluctuations due to local modulation of energy bands. It is obvious that the understanding of these effects significantly contributes to the explanation of the photovoltaic performance of this material. Intrinsic defects control doping of $CuInSe_2$. Samples are *p*-type conductive if the material is grown Cu poor and under high Se vapor pressure, whereas Cu-rich material with Se deficiency tends to be *n*-type [19, 20]. The Se vacancy V_{Se} is considered to be the dominant donor in *n*-type material (and also the compensating donor in *p*-type material), and the Cu vacancy V_{Cu}, the dominant acceptor in Cu-poor *p*-type material.

In contrast to the binary compounds where small deviations from stoichiometry cause drastic changes of the electronic properties, the ternary compounds, in particular, $CuInSe_2$, are much more tolerant, at least with respect to the composition of the group 1 or group III metals. The Cu content of device-quality $CuInSe_2$ or $Cu(In,Ga)Se_2$ absorbers varies typically between 22at.% and 24 at.% Cu. Even though these films strongly deviate from the 25:25:50% composition, they maintain favorable optoelectronic properties which make them well suited for photovoltaic devices. A nonstoichiometry of 1% would correspond to a defect concentration of roughly 10^{21} cm^{-3}. This concentration is far beyond the net doping concentration in films of about 10^{17} cm^{-3} in the photovoltaic active part of a solar cell.

The concentration of defects resulting from off-stoichiometry of the group I and III metals has to be compatible with the good electronic quality that is required for a photovoltaic device. Deviations of the valence stoichiometry, i.e., the proper Se/metals ratio according to the pseudobinary Cu_2Se–In_2Se_3 tie line, cause significant changes of the electronic properties. If the material is grown under Se saturation, the Se content in the film is self-adjusting, i.e., excess Se reevaporates and the selenium vacancy concentration adjusts according to the thermodynamic equilibrium.

There are two possibilities that could lead to a material with good electronic properties at high stoichiometry deviations: either the nonstoichiometry is accommodated in a secondary phase that is not harmful to the photovoltaic performance or the off-stoichiometry-related defects are electronically inactive. In $CuInSe_2$, both mechanisms are realized. The two point defects which are related to an overall Cu-poor composition are the Cu vacancy V_{Cu} (a shallow acceptor) and the In–Cu antisite In_{Cu} (a deep double donor). According to first-principle calculations, these two defects form a defect complex ($2V_{Cu}$, In_{Cu}) which is electronically neutral and has no energy levels within the energy gap of $CuInSe_2$ [21]. Therefore, these complexes are not electronically active defects. Ordered arrays of the ($2V_{Cu}$, In_{Cu}) complex can be considered as the building blocks of a series of Cu–In–Se compounds like $CuIn_3Se_5$ and $CuIn_5Se_8$ [22], i.e., the secondary phases that delimit the single-phase region of $CuInSe_2$ toward the Cu-poor side. Due to the lower Cu concentration, these compounds have a lower valence band energy and, hence, a wider bandgap. Segregations of these phases occur in thin films and Cu-poor single crystals [23]. For the metal-related defects in $CuInSe_2$ and $CuGaSe_2$, the defect formation energies for some intrinsic defects are low and depend on the chemical potential of the components (i.e., by the composition of the compound) as well as by the electrochemical potential of the electrons (i.e., the energetic position of Fermi level). For V_{Cu} in Cu-poor and stoichiometric material, a negative formation energy implies the spontaneous formation of those defects if the Fermi level changes. Low (but positive) formation energies are also found for the Cu-on-In antisite Cu_{In} in Cu-rich material (this defect is a shallow acceptor which could be responsible for the p-type conductivity of Cu-rich, non-Se-deficient $CuInSe_2$). The dependence of the defect formation energies on the electron Fermi level could explain the strong tendency of $CuInSe_2$ to self-compensation and the difficulties of achieving extrinsic doping. The work of [22] provides a theoretical basis for the calculation of defect formation energies and defect transition energies, which exhibit good agreement with experimentally obtained data. The formation energies of some defect complexes such as the combination of antisite defects with vacancies ($2V_{Cu}$, In_{Cu}), (Cu_{In}, In_{Cu}) and interstitials ($2Cu_i$, Cu_{In}) are even lower than those of corresponding isolated defects [23].

As the ($2V_{Cu}$, In_{Cu}) complex is most likely to occur in In-rich material, it can accommodate a large amount of excess In (or likewise Cu deficiency). Since ($2V_{cu}$, In_{Cu}) does not exhibit defect levels within the forbidden gap, off-stoichiometry does not significantly influence the electrical performance of the material. Furthermore, ordered arrays of this complex can be thought as the building blocks of the In-rich Cu–In–Se compounds such as $CuIn_3Se_5$ and $CuIn_5Se_8$ [12]. Defects and related clusters have been verified by structural analysis with Rietveld refinement of neutron and anomalous X-ray scattering spectra [12].

Surface Properties The surface of In-rich films as measured by photoelectron spectroscopy (XPS) exhibits the 1–3–5 composition of the $Cu(In,Ga)_3Se_5$ defect phase [24, 25], i.e., the surface is always more Cu poor than the bulk of the material. The surface reconstruction is accompanied by Cu depletion of the uppermost atomic layers of the CIGS surface. Most likely, the Cu-poor surface of these thin films is not the consequence of the segregation of a secondary bulk phase but rather the result from the accumulation of Cu-deficiency-related defects and defect complexes. The precise properties of this surface defect layer are not yet known and still under discussion. However, it is of major importance that the bandgap at the surface of the $Cu(In,Ga)Se_2$ thin films is somewhat larger than the bandgap in the bulk of the material accompanied by a barrier for holes [26].

There is still no clear picture of the defect structure of the surface [26]. However, it is an accepted fact that grain boundaries and the heterojunction cause only small recombination losses. Due to the importance of the interface, the interaction with buffer layers is a key problem for device optimization. Here, CdS is still the standard for the high-efficiency devices. Careful optimization of the junction formation is needed for other compounds like InS and ZnS as buffer layers.

Grain Boundaries A further important feature of the material is the role of the grain boundaries [15]. Even in high-efficiency cells, grain size does not seem to play an important role for device performance [27]. A similar reconstruction in the grain boundary as assumed on the surface could also reduce recombination. Recent studies of the microstructure reveal a structural confinement at the grain boundary extending less than 1 nm. Even though substantial progress has been made with analytics on the atomic scale, detailed understanding of grain boundary properties is still lacking.

The Role of Sodium A very important impurity and the key to high efficiencies of CIGS-based devices is Na. The presence of Na either during film growth or in an annealing step afterward increases carrier concentration [28–30] or affects the crystallinity of the films. Soda lime glass is not only a very cheap substrate but also a very efficient source for Na. If other substrates like metal or polymer foils are used, methods for introducing Na by other sources like precursor layers are essential. The early thin-film devices were fabricated on alumina or on Na-free glass substrates. The influence of Na on the growth of $Cu(In,Ga)Se_2$ films was found some years ago [31]. When soda lime glass is used, Na from the glass substrate diffuses into the absorber. In order to better control sodium content, it is also deliberately incorporated in the film by the use of Na-containing precursors such as Na_2Se [32], Na_2O_2 [26], and NaF [33]. Among different alkali precursors, Na-containing precursors yielded the best cell efficiencies. The most obvious effects of Na incorporation are a reduced defect concentration and a higher conductivity of the films [29, 34]. Furthermore, the incorporation of Na affects the growth of the absorber films, for example, grain size and interdiffusion of In and Ga.

The explanations for the effect of Na are manifold, and it is most likely that the interaction of Na with the growing film has a variety of consequences. A basic process appears to be the reaction of Na with Se and the formation of intermediate compounds. During film growth, the incorporation of Na leads to the formation of $NaSe_x$ compounds. This slows down the growth of $CuInSe_2$ and could, at the same time, facilitate the incorporation of Se into the film [35]. The widening of the existence range of the α-($CuInSe_2$) phase in the phase diagram as discussed above, as well as the reported larger tolerance to the Cu/(In + Ga) ratio of Na-containing thin films, could be explained in this picture. Furthermore, the higher conductivity of Na-containing films could result from the diminished number of compensating Vse donors. The presence of Na has a significant influence on the kinetics during

formation of $CuInSe_2$ films from stacked elemental layers. Thin-film calorimetry [36] revealed that Na inhibits the growth of $CuInSe_2$ at temperatures below 380°C. The retarded phase formation due to stabilization of the intermediate binary Cu compounds is responsible for the better morphology in the case of Na-containing samples.

The amount of Na found in device-quality polycrystalline $Cu(In,Ga)Se_2$ films is of the order 0.1 at.%, which is a concentration of 10^{20} cm^{-3} [37]. Sodium is detected in grain boundaries or on the surface of the film. The effective doping resulting from Na incorporation leads to concentrations of $\sim 10^{16}$ cm^{-3}, four orders of magnitude below the absolute Na content. The main part of Na is incorporated on the film surface and the grain boundaries, as confirmed by various high resolution methods like secondary ion mass spectrometry, scanning Auger electron spectroscopy, or atom probe microscopy.

A further effect of Na is passivation of grain boundaries by oxygenation [38]. Reducing positive charge at the grain boundaries could lead to an enhancement of the net film doping by Na incorporation. Diffusion of Na into epitaxial $Cu(In,Ga)Se_2$ films at a temperature of 550°C decreases the degree of compensation by several orders of magnitude [39]. This effect could be attributed to a Na-enhanced reorganization of the defects, which allows them to build electrically passive clusters. Despite of the importance of Na for CIGS film formation and properties, the benefit is far from being explained in terms of simple models. In view of the amounts of Na (~0.1 at.%) necessary for preparation of films with optimum properties, the effect on film growth and control of defect formation are the most likely mechanisms. However, posttreatment of absorber films with Na significantly improves the performance of solar cells [40]. Most recent success in growing film at low substrate temperatures revealed the beneficial effect of Na when it is introduced at the end of the growth of the film [41].

Multinary Alloys Alloys of multinary chalcopyrite compounds allow all kinds of bandgap variations in the absorber film. The system of copper chalcopyrites covers the visible spectrum with a wide range of bandgap energies from 1.04 eV in $Cu(In,Ga)Se_2$ up to 2.7 eV in $CuAlSe_2$. Pioneering work on single crystals was performed by [42]. Varying composition during growth opens the possibility of bandgap engineering and the design of wide-bandgap devices in the $Cu(In,Ga,Al)(S,Se)_2$ system.

The energy gap of Cu chalcogenides as displayed above in Fig. 2 allows to produce any desired alloys between the compounds as there is no miscibility gap in the entire system. For efficient solar cells, $Cu(Ga,In)Se_2$ alloys provide design options for the absorber layer. Even though there is a significant change of the lattice constants upon alloying, there is no significant increase in the concentration of electrically active defects, even if strong gradients of composition exist. There is much room for device design and the need for working around limitations by processing the material in a way where defects are minimized.

In spite of the structural similarities, the different compounds have different electronic properties. In particular, the phase diagram of all chalcopyrite compounds is not necessarily as favorable for the electronic properties as $CuInSe_2$ [43, 44].

Survey of Absorber Fabrication Processes

Development of CIGS thin films has diversified in various directions already in the beginning. Not only coevaporation technology was brought to pilot production, but also various other deposition processes like sputtering, stacked layer annealing, screen printing, and electrodeposition were developed [45]. Main parameters for the growth of high-quality CIGS thin films are the proper supply of the metals in combination with the controlled interaction with the chalcogens either from the gas phase or from elemental layers.

Photovoltaic-grade $Cu(In,Ga)Se_2$ films have a slightly In-rich overall composition. The allowed stoichiometry deviations are astonishingly large, yielding a wide process window with respect to composition. This great tolerance of CIS to deviations to the stoichiometry is a prerequisite for the success of CIGS solar cell production. Devices with efficiencies above 18% are obtained from absorbers with ((In + Ga)/Cu) ratios between 0.95 and 0.8 provided the sample contains Na. Cu-rich $Cu(In,Ga)Se_2$ shows the segregation of a secondary $Cu_{2-y}Se$ phase preferentially at the surface of the absorber film. The metallic nature of this phase does not allow the formation of

efficient heterojunctions. Even after *removal* of the secondary phase from the surface by dissolving in KCN, the performance of Cu-rich material for photovoltaic applications is limited, probably due to the high doping density of 10^{18} cm^{-3} in the bulk and the surface defects. However, Cu-rich composition is important during film growth. Cu-rich films have grain sizes in excess of 1 μm, whereas In-rich films have much smaller grains. A model for the film growth under Cu-rich compositions comprises the role of $Cu_{2-y}Se$ as a flux agent during the growth process of coevaporated films [46]. This model for the growth of $Cu(In,Ga)Se_2$ in the presence of a quasi-liquid surface film of Cu_ySe assumes that the presence of Cu_xSe crystal growth is determined by this quasi-liquid surface phase which helps to incorporate In and Se in a liquid–solid growth mechanism. Because of the unique properties of the material connected with the necessity to control composition over large areas, many different processing options have been investigated [47]. Besides selenization and coevaporation, other deposition methods have been studied, either to obtain films with very high quality or to reduce cost of film deposition on large areas.

Coevaporation of the elements from single sources became a well-established process due to advances in source developments and process control. Besides the improvement of evaporation processes, other methods that use precursor-based technologies, i.e., conversion of metal films or printed particles including atmospheric pressure deposition also yield high-quality absorber material. This diversification is characteristic for CIGS technology. There are numerous companies worldwide, each with a different approach for CIGS fabrication.

Since absorber deposition is the limiting step for the throughput of the production line, tact time for in-line processes or the capacity of batch processing is an important parameter of production processes. Till now, both approaches are used in high production lines with capacities of 100 MW–1 GW. Figure 4 gives a schematic overview of deposition processes for CIGS films.

Growth of Single Crystals and Epitaxial Layers

The first photovoltaic device based on $CuInSe_2$ was a heterojunction with evaporated CdSon, a CIS single crystal [2]; high-efficiency single-crystal devices have never been reproduced. Various attempts to produce epitaxial films as a reference contribute to the basic understanding of the material [48] but did not result in the development of very high-efficiency devices. Epitaxial III–V compound films, grown by molecular beam epitaxy (MBE) [49] or metal organic chemical vapor deposition (MOCVD) [50], have revealed interesting features for fundamental studies, such as phase segregation and defect formation, but cannot be used to form the base material for high-efficiency solar cells.

Vacuum Evaporation Methods

The first thin-film cells were produced by evaporation of $CuInSe_2$ as a compound together with elemental selenium [51]. After the historic start with single-source evaporation and additional Se, coevaporation of the single elements became a viable method. First devices close to 10% efficiency have been fabricated with separate sources for the metals in connection with suitable control of vapor fluxes by electron impact emission spectroscopy (EEIS). Evaporation became a reliable method for absorber deposition due to the development of advanced evaporation sources for in-line deposition. Progress of process control allows very high yield of large-area modules at high throughput. Control of the fluxes of the elements in the vapor by atomic absorption spectroscopy, temperature control with pyrometers, and fluorescence allow deposition of films at high yield. For scalable production processes, a good control of film growth is essential.

Coevaporation Processes The absorber material yielding the highest efficiencies is $Cu(In,Ga)Se_2$ with a Ga/(Ga + In) ratio of ~30%, prepared by coevaporation from elemental sources. The process requires a substrate temperature of ~550 C for a certain time during film growth, preferably toward the end of growth. One advantage of the evaporation route is that material deposition and film growth take place during one processing step. A high reproducibility of the film properties is obtained if the evaporation rates and substrate temperatures are well controlled. A feedback control based on electron impact emission spectroscopy (EEIS), a quadrupole mass spectrometer (QMA), or an atomic absorption spectrometer (AAS) controls the rate of each source. The composition of the

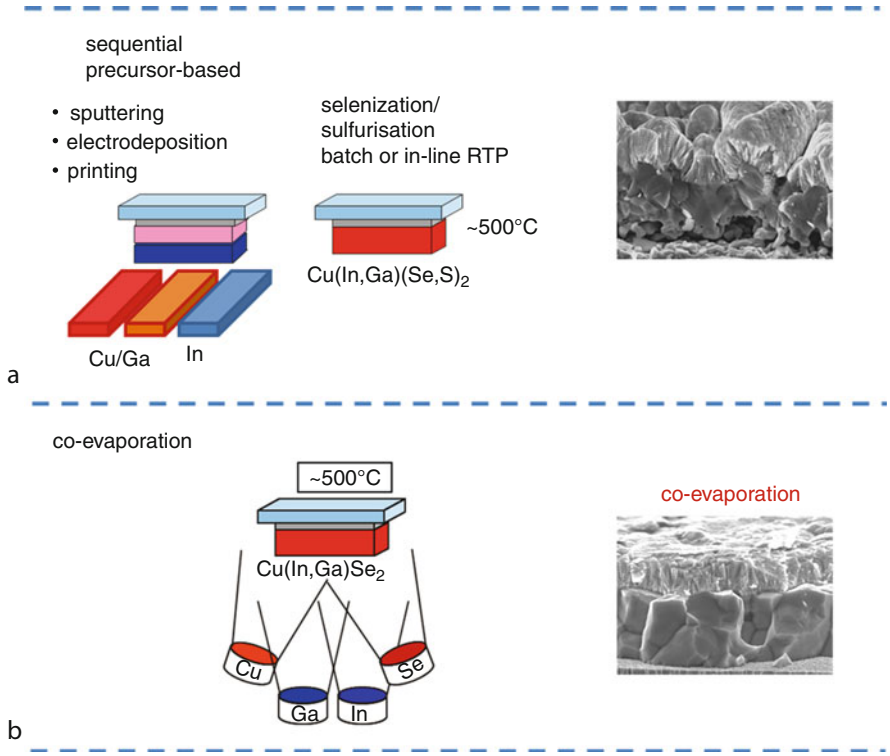

Solar Cells, Chalcopyrite-Based Thin Film. Figure 4
Schematic view of deposition processes of the (**a**) sequential processes. Stacked metal layers are selenized and converted into $CuInSe_2$ in H_2Se atmosphere or Se is provided by a solid layer, and reaction kinetics is controlled by the annealing temperature and temperature profile. (**b**) In-line coevaporation

deposited material with regard to the metals corresponds to their evaporation rates, whereas Se is always evaporated in excess. An additional possibility to control the composition is to monitor the emissivity [52] or the optical reflectivity [53] of the films. At the transition between In-rich and Cu-rich composition, the thermal emission and optical reflection changes resulting in a change of substrate temperature at constant heating power or a change of heating power for keeping a constant substrate temperature. This behavior allows to adjust the process precisely because it can be used as an end point detection in the process sequence.

This precise control over the deposition rates allows for a wide range of variations and optimizations with different substeps or stages for film deposition and growth. In the most simple single-step process, all rates as well as the substrate temperature are kept constant during the whole process.

Advanced preparation sequences always include a Cu-rich stage during the growth process and end up with an overall In-rich composition in order to combine the large grains of the Cu-rich stage with the otherwise more favorable electronic properties of the In-rich composition [47]. The so-called Boeing or *bilayer process* [54, 55] starts with the deposition of Cu-rich $Cu(In,Ga)Se_2$ and ends with an excess In rate and a Cu-poor composition of the film. Another possibility is the *inverted process* where first $(In,Ga)_2Se_3$ (likewise In, Ga, and Se from elemental sources to form that compound) is deposited at a lower temperatures (typically around 300 C). Then Cu and Se are evaporated at an elevated temperature until an overall composition close to stoichiometry is reached [56]. This process leads to smoother film morphology as compared to processes starting Cu rich. The most successful modification of the inverted process is the so-called *three-stage process* [57]. In this process, In, Ga, and Se

are again evaporated at the end of an inverted process to ensure the overall In-rich composition of the film even if the material is Cu-rich during the second stage. The three-stage process currently leads to the best solar cells. In general, variations of the Ga/In ratio during deposition allow the design of graded bandgap structures. [58, 59]. However, the distribution of Ga in the depth of the film depends on various parameters such as substrate temperature, Na content, and deposition rate [60].

Reactive Film Formation The complexity of the equipment for coevaporation processes is reduced if the layer can be formed from elemental or compound precursor films. These precursor films can be formed by any method for thin-film deposition. For Cu(In,Ga)Se_2 prepared by selenization, the role of $Cu_{2-y}Se$ is similar to the coevaporation process [61], where Cu_xSe mediates the growth of the crystallites, during the selenization from solid Se films (RTP) or elemental evaporation from the gas phase, or therefore, growth processes for high quality have to go through a copper-rich stage and end in In-rich stage.

Selenization from Se Vapor The second class of absorber preparation routes separates of deposition and compound formation into two different processing steps. High efficiencies are obtained from absorber prepared by selenization of metal precursors in H_2Se [62–64] and by rapid thermal processing of stacked elemental layers in a Se atmosphere. These sequential processes have the advantage that approved large-area deposition techniques such as sputtering for the deposition of the precursor layers are applicable. The Cu(In,Ga)Se_2 film formation then requires selenization as a second step. This selenization step is crucial for the quality of the film.

The very first large-area modules were prepared by the selenization of metal precursors in the presence of H_2Se in the late 1980s, years ago [65]. Today, a modification of this process is the basis of a gigawatt scale production line [66]. First, a precursor stack of Cu, In, and Ga is sputter deposited on the Mo-coated glass substrate. Then selenization takes place under $H_2Se/H_2/Ar$ atmosphere. To improve device performance, a second thermal process under H_2S is added, resulting in an absorber that contains a Cu(In,Ga)$(S,Se)_2$ surface layer with a wider bandgap.

Annealing of Stacked Elemental Layers A variation of reactive film formation that avoids the use of the toxic H_2Se during selenization is the rapid thermal processing of stacked elemental layers. Here, the precursor stack includes a layer of elemental Se. The stack is then reacted by a rapid thermal process (RTP) in either an inert or a Se atmosphere. The highest efficiencies are obtained if the RTP is performed in an S-containing atmosphere (either elemental S or H_2S).

On the laboratory scale, the efficiencies of cells made by these preparation routes are smaller as compared with the record values obtained with coevaporated CIGS absorber layers. However, on the module level, coevaporated and sequentially prepared absorbers have about the same efficiency. Sequential processes need two or even three stages for absorber completion, often in different pieces of equipment. These additional processing steps may counterbalance the advantage of easier deposition of the metal layers by sputtering. The detailed and sophisticated control over composition and growth achieved during coevaporation is not possible for the selenization process. The reaction kinetics is controlled by the time and temperature of the annealing process. Fortunately, the distribution of the elements within the film grown during the selenization process turns out to be close to a certain optimum, especially if the process includes the sulphurization stage. Since the reaction for the formation of $CuInSe_2$ is much faster than that of $CuGaSe_2$, and because the formation of the ternary chalcopyrite phase starts at the reaction front with the Se at the surface, Ga is concentrated toward the back surface of the film. An increasing Ga content implies an increase in bandgap energy. The Ga gradient introduces a so-called back-surface field, improving carrier collection at the same time as minimizing back-surface recombination. In turn, S from the sulphurization step is incorporated at the front surface of the film, where it reduces recombination losses and also increases the absorber bandgap in the space-charge region of the heterojunction.

Nonvacuum Processing Developments of so-called low-cost processes include electrodeposition, [67–69] screen printing, and particle deposition [70, 71]. Electrodeposition is carried out in either one or two steps. Codeposition of all elements requires adjustment of

concentrations and complexing agents. The crucial step in all cases is final film formation in a high-temperature annealing process in Se-containing atmosphere. The recrystallization process competes with decomposition of the compound; therefore, process optimization is quite difficult. Cells with good efficiencies were obtained by a hybrid process combining electrodeposition of a Cu-rich $CuInSe_2$ film and subsequent conditioning by a vacuum evaporation step of In(Se) [72, 73]. Again, annealing of the films at elevated temperature in a suitable atmosphere is an important add-on to the low-cost deposition processes of the precursor film.

Large-Scale Processing

The advantages of thin-film technologies are related to high throughput processing in connection with a minimum usage of material. Analyzing the many approaches with "proprietary" methods for CIGS deposition, a convergence to a certain standard should be expected. None of the methods solves all the problems of CIGS technology and fulfills all the expectation. Present production lines which supply modules to the market look back to a very long history of R&D.

In the beginning of CIGS development, coevaporation was realized only for relatively small areas. Great efforts have been invested in the development of large-area in-line coating system that allows continuous coating of substrates with a width of 0.6 m. High-volume production by coevaporation has been already demonstrated in the 30–100 MW range. Figure 5 shows the schematic view of such a deposition system, where the substrates can be continuously processed in an air to air load-lock system [74]. An important component of this deposition system are linear evaporation sources that allow homgeneous deposition on wide substrates.

Several production lines use coevaporation. However, the ambitious plans of a 1 GW/a production are based on the technology with the longest experience for module production, namely, sputtered precursors and selenizaton/sulfurization processes [75]. The success of CIGS deposition techniques for high-quality material proofs the maturity of the equipment for handling complex multicomponent systems [76]. Furthermore, production lines with "nonvacuum processing" which use sputtering, electrodeposition, printing of precursor particles followed by a selenization/annealing step at high or even atmospheric pressure are put into operation. Most of these production lines use flexible foils for role-to-role processing, for example, Al foils [77]. They reached a remarkable efficiency of 17.1% [78]. Table 1 gives an overview about the different processes and the actual production capacities. Until now, even on the level of more than 100 MW/a production, the process of the future is not yet known. This diversification seems to be a specific feature of CIGS technology.

Substrates

Production lines for CIS technology use the substrate configuration. In this case, no transparent substrate is needed, and therefore wider choices for substrate materials are possible. Even though most production lines use glass substrates, many new lines are based on role-to-role deposition of either metal or polymer (polyimide foils). These foils are either integrated as single cells in a glass/glass module or laminated with foils to maintain

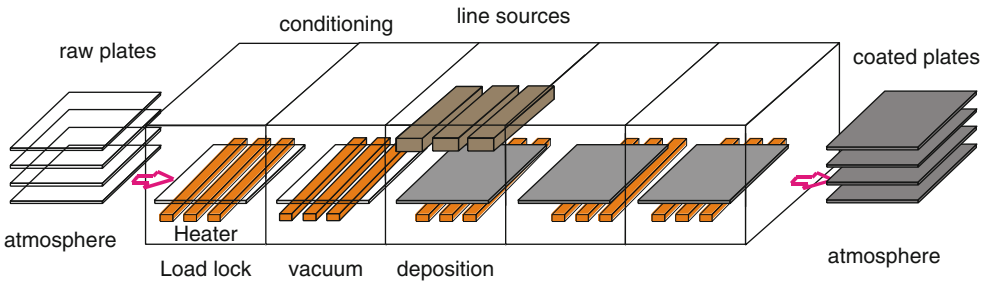

Solar Cells, Chalcopyrite-Based Thin Film. Figure 5
In-line co-evaporation processes with line sources for large-area substrates

Solar Cells, Chalcopyrite-Based Thin Film. Table 1 Processes and estimated actual production capacities (projections in brackets)

Process	Steps, precursors, or films	Complexity of equipment	Film quality and control
Multistage coevaporation	Binary chalcogenide compounds	High	Very high
Reactive annealing pure metal films	Sputtered metal or alloy films	Medium–high	High
Reactive annealing Se/S-containing precursors	Electrodeposited compound films	Low–medium	Low–medium
Reactive annealing particle precursors	Printed particles	Low–medium	Medium–low

flexibility. Fully integrated flexible modules are under development. Either metal foils with isolation barrier layers or nonconductive polymer films are used as substrate materials. A key issue for the substrates is the supply of Na during growth. For monolithic integration of cells, precise patterning of the films is necessary. Interconnection is selective patterning of the layers in the solar cell. Recent announcements claim outdoor stability of these flexible modules.

Junction Formation

Since pn junctions cannot be realized by simple extrinsic doping, solar cells have to be realized as heterojunctions. The band diagram of a typical CIGS-based solar cell is depicted in Fig. 6.

The highly conductive n-type window layer serves as transparent front electrode. Criteria for the quality of this layer are high transparency and conductivity. Furthermore, band alignment of the conduction band is essential for device performance, in particular, open-circuit voltage. Mismatch to the absorber layer is moderated by a suitable buffer layer. Due to the importance of the interface, the interaction absorber surface with buffer layers is a key problem for device optimization. Here, CdS is still the standard for the high-efficiency devices. Therefore, many production lines rely on chemical deposition of CdS. However, replacement of CdS is a major objective of actual developments. Improved understanding of the junction allows to use other compounds like InS and ZnS. The choices are Zn(OH,S) or InS(OH), mostly formed by chemical bath deposition. Partial replacement of ZnO in the window layer by (Zn,Mg)O helps to adapt these buffer materials [79]. Common observation with non-CdS buffer layers is an increased

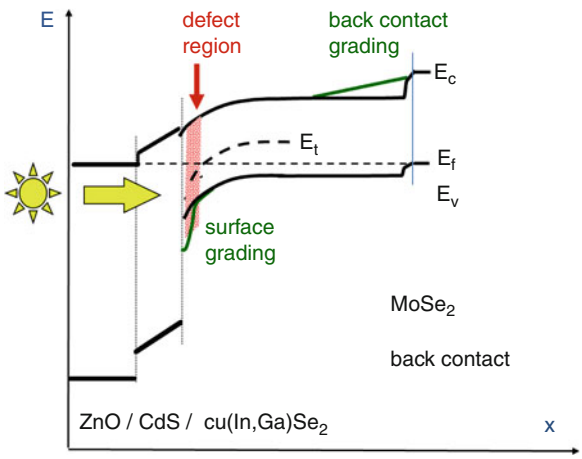

Solar Cells, Chalcopyrite-Based Thin Film. Figure 6 Band diagram of a Cu(In,Ga)Se_2-based solar cell with ZnO window layer

tendency to light soaking effects, i.e., the efficiency increases during illumination.

Status of Large-Scale Production

CIGS is the only thin-film material that has the potential to compete with wafer-based multicrystalline silicon modules. In the production lines for CIGS, a continuous improvement of module efficiency is achieved. Large-area (0.8–1.5 m^2) standard modules approach 14% efficiency. Prototype modules with an area of about 900 cm^2 reach efficiencies of more than 17% [80]. Several production lines produce modules by different processes [81, 82]. The biggest manufacturing line for CIGS is operated by Solar Frontier in Japan [83].

Present Limitations

Limitations due to Material Properties

In principle, efficiency should not be limited by the material because of high radiative lifetimes and high mobilities. In present efforts, there is still room for improving material quality by better control of extrinsic impurities, quality of substrates and back contacts and growth processes. One major issue is the control of defects at wider bandgaps.

Limitations due to Availability and Environmental Issues

The availability of the elements indium and gallium topic is discussed quite intensely [84]. In principle, there is no real limitation by the natural resources, but there is the issue of production cost if the raw material prices rise. Since the thickness of absorber layers of present modules is redundant with respect to optical absorption, there is still room for saving material. However, reducing thickness may affect yield of the production so that only careful process optimization could lead to a benefit for the module cost [85, 86].

Perspectives

Due to the complexity of the material, great challenges cannot be met by simple engineering approaches but need disruptive solutions. On the one hand, CIGS offers many opportunities for future high-efficiency PV module development; on the other hand, one should be aware of the limitations implied by the self-organizing nature and flexibility of the material. There is still lack of understanding of major issues of material science, for example, the role of Na, the role of Cu in the metastable behavior of the devices and the properties of the heterojunction. Furthermore, limitations of wide-bandgap compounds still need investigation.

Efficiency

The possibility to adjust the bandgap to the optimum position in the solar spectrum at operating conditions and the favorable properties of the material should, in principle, allow efficiencies very close to the theoretical limit. A careful analysis of loss processes shows that losses occur in various parts of the heterojunction [87]. However, intrinsic properties of the multinary semiconductor may impose losses which have to be minimized by the proper choice of alloys and preparation methods. Since there is no ideal single-crystal reference available, it is very difficult to identify the relevant defects. Due to the low energy of formation of some defects, the defect concentration under equilibrium conditions depends on deviation from stoichiometry and will always remain on a certain level. The phase boundaries between chalcopyrite and the neighboring Cu-poor or Cu-rich phases according to the phase diagram are still not known precisely (in terms of doping concentrations). Compositional fluctuations on different scales in the film require to keep distance of the composition from the Cu-rich phase boundary to guarantee single-phase material. Therefore, one has to tolerate a higher density of Cu vacancy–related defects.

An efficiency >19% is reached on small area in several laboratories worldwide. Recently, 20% efficiency has been exceeded [6]. This progress is based on incremental improvements in the last 10 years when the efficiency has been increased from about 19% to 20.3% today. The actual parameters of the record device are still not optimum. Defect concentrations and, hence, efficiencies depend on many process parameters during device fabrication which are not yet completely understood. For exploring efficiency limits, it is important to understand more about defects and impurities in high-efficiency devices. Table 2 lists the IV data of high-efficiency devices fabricated in different laboratories.

A further remarkable achievement is the fabrication of an 18.7% efficient flexible solar cell on a polyimide foil substrate by the group at EMPA [42]. This solar cell was grown at low substrate temperature and optimized Ga grading together with well-controlled incorporation of Na.

Solar Cells, Chalcopyrite-Based Thin Film. Table 2 Summary of confirmed IV data of high-efficiency devices

Performance	ZSW [6]	NREL [88]	HZB [89]	Best values
V_{OC} (mV)	740	691.8	702.5	740
J_{SC} (mA)	35.4	35.74	35.63	35.5
FF (%)	77.5	81.03	77.52	81.0
η (%)	20.3	20.0	19.4	21.3

The big challenge is to develop a thin-film technology that combines all advantages of thin films with the performance potential of photovoltaics already demonstrated with high-quality crystalline materials. To some extent, this has been demonstrated for $Cu(In,Ga)Se_2$ laboratory scale devices. Taking the best values achieved by the different laboratories, an efficiency of more than 21% would be achieved. This simple calculation should be justified in view of the high fill factor expected at increased open-circuit voltage.

A major step forward would be the realization of monolithic tandem structures. The major issue is development of the high-efficiency wide-bandgap part of such a device. The alloy system with the elements Ag, Cu, In, Ga, Al, Se, and S, in principle, enables design of optimum combinations of bandgaps. However, in all development with varying alloy compositions, the efficiency of wide-bandgap cells drops at bandgaps beyond 1.3 eV, regardless of the compositions of the multinary alloy with the possible combination of the elements [90]. In contrary to thin-film amorphous silicon, deposition temperatures are too high for the straightforward fabrication of monolithic stacks. Continued research is important to develop solutions to this important problem. Following the rules for the fabrication of high-efficiency $Cu(Ga,In)Se_2$, efficiency could reach 18% at 1.3 eV [91]. Best efficiencies of wide gap devices with Eg> 1.5 eV $Cu(In,Ga)S_2$ reach close to 13% at an open-circuit voltage of 800–900 mV [92].

Modification of the Material System

$Cu(In,Ga)(Se,S)_2$ (CIGS) based solar cells reach efficiencies of >20% but might suffer from high material cost of In and Ga. Replacing these elements by abundant low-cost elements like tin and zinc without sacrificing performance would be an important step toward sustainability of this technology. Even though no shortage of raw materials (in particular, In and Ga) for CIGS technology is expected in the near and midterm future, replacing indium and gallium by abundant elements like tin and zinc would allow a sustainable development of thin-film solar cell technology also on the terawatt scale. New analytical methods and reliable equipment for thin-film processing and control facilitate control of thin-film processes for these new and complex materials [93]. Due to the similarity of most material properties, $Cu_2ZnSn(Se,S)_4$ (CZTS), in principle, could be handled in actual production lines with device structures similar to the state of the art CIGS modules [94]. It took 10 years to reach efficiencies close to 10% [95–98]. Recently, efforts for the development of this material significantly increased, and devices with efficiencies close to 10% were fabricated [99]. However, the complexity of the compound needs significant efforts in the design of processes for large-scale production and provides challenging tasks for the design of deposition systems and process control.

Future Directions

CIGS has proven to be the high-efficiency option among the thin-film photovoltaic technologies. The variety of material, device, and process designs opens many different ways for future developments. The future mainstream technology for the manufacturing of CIGS modules is not yet decided even though a 1 GW production is in operation based on the selenization of sputtered metal precursor films. The potential for large-scale manufacturing of other processes like coevaporation, electrodeposition, sputtering, or printing is also quite high, in particular, if role-to-role processing is considered.

Concerning efficiency of laboratory devices, there should be no reason for not getting close to the theoretical limit. Depending on the adjustment of the bandgap, 25% efficiency could be exceeded. In the midterm, module efficiencies of 17% should be reached; in the long term, a performance exceeding 18% on the production level is expected [100]. Further improvements beyond 20% efficiency are expected with multijunction devices.

Bibliography

Primary Literature

1. Hahn H, Frank G, Klingler W, Meyer A, Störger G (1953) Untersuchungen über ternäre Chalkogenide. V. Über einige ternäre Chalkogenide mit Chalkopyritstruktur Z Anorg. u Allg Chem 271:153–170
2. Wagner S, Shay JL, Migliorato P, Kasper HM (1974) $CuInSe_2$/Cd Shetero junction photovoltaic detectors. Appl Phys Lett 25:434–435

3. Kazmerski LL, Ayyagari MS, Juang YJ, Patterson RP (1977) Growth and characterisation of thin film compound semiconductor heterojunctions. J Vac Sci Technol 13:65
4. Mickelsen RA, Chen WS, Hsiao YR, Lowe VE (1984) Polycrystalline thin-film CUINSE2/CDZNS solar-cells. IEEET Trans Electron Devices 31(5):542–546
5. Kazmerski LL (1983) Ternary-compound thin-film solar cells. Il Nuovo Cimento 2D:2013
6. Jackson P, Hariskos D, Lotter E, Paetel S, Wuerz R, Menner R, Wischmann W, Powalla M (2011) New world record efficiency for Cu(In,Ga)Se_2 thin-film solar cells beyond 20%. Prog Photovolt Res Appl. doi:10.1002/pip.1078
7. Jasenek A, Schock HW, Werner JH, Rau U (2001) Defect annealing in Cu(In, Ga)Se_2 heterojunction solar cells after high-energy electron irradiation. Appl Phys Lett 79(18):2922–2924
8. Gödecke T, Haalboom T, Ernst F (2000) Phase equilibria of Cu–In–Se. Zeitschriftfür Metallkunde 91:622–662
9. Zott S, Leo K, Ruckh M, Schock HW (1997) Radiative recombination in $CuInSe_2$ thin films. J Appl Phys 82(1):356–367
10. Dirnstorfer I, Wagner MT, Hofmann DM, Lampert MD, Karg F, Meyer BK (1998) Physica characterization of CuIn(Ga)Se_2 thin films. Stat Sol A 168:163–175
11. Klaer J, Klenk R, Schock HW (2007) Progress in the development of CuInS2 based mini-modules. Thin Solid Films 515(15):5929–5933
12. Stephan C, Schorr S, Tovar M, Schock HW (2011) Comprehensive insights into point defect and defect cluster formation in $CuInSe_2$. Appl Phys Lett 98:091906
13. Herberholz R, Rau U, Schock HW, Haalboom T, Gödecke T, Ernst F, Beilharz C, Benz KW, Cahen D (1999) Phase segregation, Cu migration and junction formation in Cu(In, Ga)Se_2. Eur Phys J Appl Phys 6(2):131–139
14. Endo S, Irie T, Nakanishi H (1986) Preparation and some properties of $CuInSe_2$ single crystals. Sol Cells 16:1–15
15. Schock HW, Rau U (2001) The role of structural properties and defects for the performance of Cu-chalcopyrite-based thin-film solar cells. Physica B 308:1081–1085
16. Siebentritt S, Igalson M, Persson C, Lany S (2010) The electronic structure of chalcopyrites: bands, point defects and grain boundaries. Prog Photovolt 18:390–410
17. Cahen D (1987) Some thoughts about defect chemistry in ternaries. In: Proceedings of the 7th international conference on ternary and multinary compounds. Mat Res Soc, Pittsburgh, pp 433–442
18. Burgelman M, Engelhardt F, Guillemoles J-F, Herberholz R, Igalson M, Klenk R, Lampert M, Meyer T, Nadenau V, Niemegeers A, Parisi J, Rau U, Schock H-W, Schmitt M, Seifert O, Walter T, Zott S (1997) Defects in Cu(In, Ga)Se_2 semiconductors and their role in the device performance of thin-film solar cells. Prog Photovoltaic Res Appl 5:121–130
19. Migliorato P, Shay JL, Kasper HM, Wagner S (1975) Analysis of the electrical and luminescent properties of $CuInSe_2$. J Appl Phys 46:1777–1782
20. Noufi R, Axton R, Herrington C, Deb SK (1984) Electronic properties versus composition of thin films of $CuInSe_2$. Appl Phys Lett 45:668–670
21. Zhang SB, Wei SH, Zunger A, Katayama-Yoshida H (1998) Defect physics of the $CuInSe_2$ chalcopyrite semiconductor. Phys Rev B 57:9642
22. Zhang SB, Wei SH, Zunger A (1997) Stabilization of ternary via ordered arrays of defect pairs. Phys Rev Lett 78:4059–4062
23. Hornung M, Benz KW, Margulis L, Schmid D, Hornung M, Benz KW, Margulis L, Schmid D, Schock HW (1995) Growth of Bulk $Cu0_{.85}In_{1.05}Se_2$ and characterization on a micro scale. J Cryst Growth 154:315
24. Schmid D, Ruckh M, Grunwald F, Schock HW (1993) Chalcopyrite/defect chalcopyrite heterojunctions on the basis of $CuInSe_2$. J Appl Phys 73:2902
25. Schmid D, Ruckh M, Schock HW (1996) Photoemission studies on Cu(In, Ga)Se-2 thin films and related binary selenides. Appl Surf Sci 103(4):409–429
26. Mönig H, Fischer Ch-H, Caballero R, Kaufmann CA, Allsop N, Gorgoi M, Klenk R, Schock H-W, Lehmann S, Lux-Steiner MC, Lauermann I (2009) Surface Cu depletion of Cu(In, Ga)Se_2 films: an investigation by hard X-ray photoelectron spectroscopy. Acta Mater 57:3645–3651
27. Nichterwitz M, Abou-Ras D, Sakurai K, Bundesmann J, Unold T et al (2009) Influence of grain boundaries on current collection in Cu(In, Ga)Se_2 thin-film solar cells. Thin Solid Films 517:2554–2557
28. Ruckh M, Schmid D, Kaiser M, Schäffler R, Walter T, Schock HW (1996) Influence of substrates on the electrical properties of Cu(In,Ga)Se_2 thin films. Solar Energy Mater Solar Cells 41/42:335
29. Holz J, Karg F, Phillipsborn HV (1994) The effect of substrate impurities on the electronic conductivity in CIGS thin films. In: Stephens HS, Associates Proceedings of the 12th European photovoltaic solar energy, conference. Bedford, Amsterdam, pp 1592–1595
30. Hedström J, Ohlsen H, Bodegard M, Kylner A, Stolt L, Hariskos D, Ruckh M, Schock H-W (1993) ZnO/CdS/Cu(In,Ga)Se_2 thin film solar cells with improved performance. In: Conference record 23 rd. IEEE photovoltaic specialists conference. IEEE Press Piscataway, Louisville, pp 364–371
31. Stolt L, Hedström J, Kessler J, Ruckh M, Velthaus KO, Schock HW (1993) ZnO/CdS/$CuInSe_2$thin-film solar cells with improved performance. Appl Phys Lett 62:597–599
32. Nakada T, Iga D, Ohbo H, Kunioka A (1997) Effects of sodium on Cu(In, Ga)Se_2-based thin films and solar cells. Jpn J Appl Phys 36:732–737
33. Contreras MA, Egaas B, Dippo P, Webb J, Granata J, Ramanathan K, Asher S, Swartzlander A, Noufi R (1997) On the role of Na and modifications to Cu(In,Ga)Se absorber materials using thin MF (M = Na, K, Cs) precursor layers. In: Conference record: 26th. IEEE photovoltaic specialists conference. IEEE Press, Piscataway, Anaheim, pp 359–362
34. Schäffler R, Hariskos D, Kaiser M, Ruckh M, Rühle U, Schock HW (1996) Electrical characterization of Cu(In, Ga)Se_2 chalcopyrite thin films: methods of influencing the effective doping. Cryst Res Technol 31:543

35. Braunger D, Hariskos D, Bilger G, Rau U, Schock HW (2000) Influence of sodium on the growth of polycrystalline Cu(In, Ga)Se_2 thin films. Thin Solid Films 361–362:161–166
36. Wolf D (1998) Technologienahe in-situ Analyse der Bildung von $CuInSe_2$ zurAnwendung in Dünnschicht-Solarzellen. Dissertation Universität Erlangen-Nürnberg
37. Niles DW, Ramanathan K, Haason F, Noufi R, Tielsh BJ, Fulghum JE (1997) Na impurity chemistry in photovoltaic CIGS thin films: Investigation with X-ray photoelectron spectroscopy. J Vac Sci Technol A 15:3044–3049
38. Kronik L, Cahen D, Schock HW (1998) Effects of sodium on polycrystalline Cu(In, Ga)Se_2 and its solar cell performance. Adv Mater 10:31–36
39. Schroeder DJ, Rockett AA (1997) 'Electronic effects of sodium in epitaxial $CuIn_{1-x}Ga_xSe_2$. J Appl Phys 82:5982–5985
40. Rudmann D, da Cunha AF, Kaelin M, Kurdesau F, Zogg H, Tiwari AN, Bilger G (2004) Efficiency enhancement of Cu(In, Ga)Se_2 solar cells due to post-deposition Na incorporation. Appl Phys Lett 84:1129
41. Chirilă A, Buecheler S, Pianezzi F, Bloesch P, Gretener C, Uhl AR, Fella C, Kranz L, Perrenoud J, Seyrling S, Verma R, Nishiwaki S, Romanyuk YE, Bilger G, Tiwari AN (2011) Highly efficient Cu (In, Ga)Se_2 solar cells grown on flexible polymer films. Nat Mater 10:857–861
42. Paoricia C, Zanottia L, Romeo N, Sberveglierib G, Tarricone L (1979) Crystal growth and properties of $CuGa_xIn_{1-x}Se_2$ chalcopyrite compound. Solar Energy Mater 1:3–9
43. Kötschau IM, Turcu M, Rau U, Schock HW (2001) Structural and electronic properties of Cu(In,Ga)$(Se,S)_2$ alloys. Mat Res Symp Proc 668:H4.5
44. Turcu M, Koetschau IM, Rau U (2002) Composition dependence of defect energies and band alignments in the Cu In_{1-x} Ga_xSe_{1-y} S_y alloy system. J Appl Phys 91:1391
45. Schock HW (1994) Solar cells based on $CuInSe_2$ and related compounds: recent progress in Europe. Sol Energy Mater Sol Cell 34(1–4):19–26
46. Klenk R, Walter T, Schock HW, Cahen D (1993) A model for the successful growth of polycrystalline films of $CuInSe_2$ by multisource physical vacuum evaporation. Adv Mat 5:114–119
47. Niki S, Contreras M, Repins I, Powalla M, Kushiya K, Ishizuka S, Matsubara K (2010) CIGS absorbers and processes. Prog Photovolt: Res Appl 18:453–466
48. Niki S, Fons PJ, Yamada A, Suzuki R, Ohdaira T, Ishibashi S, Oyanagai H (1994) High quality $CuInSe_2$ epitaxial films – molecular beam epitaxial growth and intrinsic properties. Inst Phys Conf Ser 152E:221–227
49. Tiwari AN, Blunier S, Zogg H, Filzmoser M, Schmid D, Schock HW (1994) Characterization of heteroepitaxial CuIn3Se5 and $CuInSe_2$ layers on Si substrates. Appl Phys Lett 65(26):3347
50. Rega N, Siebentritt S, Beckers IE, Beckmann J, Albert J, Lux-Steiner M (2003) Defect spectra in epitaxial $CuInSe_2$ grown by MOVPE. Thin Solid Films 431–432:186–189
51. Kazmerski LL, Ayyagari MS, White FR, Sanborn GA (1976) Growth and properties of vacuum deposited $CuInSe_2$ thin films. J Vac Sci Technol 13:139
52. Wada T, Nishikawa S, Hashimoto Y, Negami T (2001) Physical vapour deposition of Cu(In,Ga)Se_2 films for industrial applications. Mater Res Symp Proc 668:2.1.1
53. Sakurai K, Hunger R, Scheer R, Kaufmann CA, Yamada A, Baba T, Kimura Y, Matsubara K, Fons P, Nakanishi H, Niki S (2004) In situ diagnostic methods for thin-film fabrication: utilization of heat radiation and light scattering. Prog Photovolt: Res Appl 12:219–234
54. Mickelsen RA, Chen WS (1980) High photocurrent polycrystalline thin-film CdS/$CuInSe_2$ solar cell. Appl Phys Lett 36:371–373
55. Mickelsen RA, Chen WS (1982) Polycrystalline thin-film $CuInSe_2$ solar cells. In: Conference record 16th. IEEE photovoltaic specialists conference. IEEE Press, Piscataway, San Diego, pp 781–785
56. Kessler J, Schmid D, Dittrich H, Schock HW (1994) $CuInSe_2$ film formation from sequential deposition of In(Se):Cu:Se. In: Proceedings of the 12th European photovoltaic solar energy conference, Amsterdam, p. 648
57. Gabor AM, Tuttle JR, Albin DS, Contreras MA, Noufi R, Hermann AM (1994) High-efficiency CuInxGa1−xSe_2 solar cells from (InxGa1−x)2 Se3 precursors. Appl Phys Lett 65:198–200
58. Gabor AM, Tuttle JR, Bode MH, Franz A, Tennant AL, Contreras MA, Noufi R, Jensen DG, Hermann AM (1996) Band-gap engineering in Cu(In, Ga)Se_2 thin films grown from (In, Ga)2Se3 precursors. Solar Energy Mater Solar Cells 41:247–260
59. Dullweber T, Hanna G, Rau U, Schock HW (2001) A new approach to high efficiency solar cells by band gap grading in Cu(In, Ga)Se_2 chalcopyrite semiconductors. Solar Energy Mater Solar Cells 67:145–150
60. Kaufmann CA, Caballero R, Unold T, Hesse R, Klenk R, Schorr S, Nichterwitz M, Schock H-W (2009) Depth profiling of Cu(In, Ga) Se_2 thin films grown at low temperatures. Solar Energy Mater Solar Cells 93:859–863
61. Probst V, Karg F, Rimmasch J, Riedl W, Stetter W, Harms H, Eibl O (1996) Advanced stacked elemental layer progress for Cu(InGa)Se_2 thin film photovoltaic devices. Mater Res Soc Symp Proc 426:165–176
62. Binsma JJM, Van der Linden HA (1982) Preparation of thin $CuInS_2$ films via a two-stage process. Thin Solid Films 97:237–243
63. Chu TL, Chu SC, Lin SC, Yue J (1984) Large grain copper indium diselenide films. J Electrochem Soc 131:2182–2184
64. Kapur VK, Basol BM, Tseng ES (1987) Low-cost methods for the production of semiconductor films for $CuInSe_2$/CdS solar cells. Solar Cells 21:65–72
65. Mitchell KCE, Ermer J, Pier D (1988) Single and tandem junction $CuInSe_2$ cell and module technology. In: Conference record 20th IEEE photovoltaic specialists conference. IEEE Press, Piscataway, Las Vegas, pp 1384–1389
66. Solar frontier press release 2011. http://www.solar-frontier.com
67. Thouin L, Vedel J (1995) Electrodeposition and characterization of $CuInSe_2$ thin films. J Electrochem Soc 142:2996–3001

68. Abken A, Heinemann F, Kampmann A, Leinkühler G, Rechid J, Sittinger V, Wietler T, Reineke-Koch R (1998) Large area electrodeposition of Cu(In,Ga)Se_2 precursors for the fabrication of thin film solar cells. In: Proceedings of the 2nd world conference on photovoltaic solar energy conversion. European Commission, Vienna, pp 1133–1136
69. Guillien C, Herrero J (2001) Recrystallization and components redistribution processes in electrodeposited $CuInSe_2$ thin films. Thin Solid Film 387:57–59
70. Eberspacher C, Pauls KL, Fredric CV (1998) Improved processes for forming $CuInSe_2$ films. In: Proceedings of the 2nd world conference on photovoltaic solar energy conversion. European Commission, Vienna, pp 303–306
71. Kapur VK, Fisher M, Roe R (2001) Nanoparticel oxide precursor inks from thin film copper gallium indium selenide (CIGS) solar cells. Mater Res Symp Proc 668:H2.6
72. Ramanathan K, Bhattacharya RN, Granata J, Webb J, Niles D, Contreras MA, Wiesner H, Haason FS, Noufi R (1998) Advances in CIGS solar cell research at NREL. In: Conference. record 26th IEEE photovoltaic specifications conference. IEEE Press, Piscataway, Anaheim, pp 319–325
73. Battacharya RN, Fernandez AM (2001) $CuIn_{1-x}GaxSe_2$ based photovoltaic cells from electrodeposited precursor films. Mater Res Symp Proc 668:H 8.10
74. Dimmler B, Schock HW (1996) Scaling-up of CIS technology for thin-film solar modules. Prog Photovolt Res Appl 4:425
75. Solar Frontier (2011) Japan's largest solar panel factory reaches full commercial operations, announces solar frontier. http://www.solar-frontier.com/news/143. Accessed 29 July 2011
76. Dimmler B, Powalla M, Schock H (2002) CIS-based thin-film photovoltaic modules: potential and prospects. Prog Photovolt: Res Appl 10:149–157
77. (2011) http://en.wikipedia.org/wiki/Nanosolar
78. Nanosolar Communications (2011) Nanosolar achieves 17.1% aperture efficiency through printed CIGS process. http://www.nanosolar.com. Accessed 5 Oct 2011
79. Naghavi N, Abou-Ras D, Allsop N, Barreau N, Buecheler S, Ennaoui A, Fischer C-H, Guillen C, Hariskos D, Herrero J, Klenk R, Kushiya K, Lincot D, Menner R, Nakada T, Platzer-Bjoerkman C, Spiering S, Tiwari AN, Toerndahl T (2010) Buffer layers and transparent conducting oxides for chalcopyrite Cu(In,Ga)(S,Se)$_2$ based thin film photovoltaics: present status and current developments. Prog Photovolt 18:411–433
80. Dalibor T, Jost S, Vogt H, Heiß A, Visbeck S, Happ T, Palm J, Avellán A, Niesen T, Karg F (2011) Towards module efficiencies of 16% with an improved CIGSSe device design. In: 26th EU PVSEC, Hamburg
81. Powalla M, Cemernjak M, Eberhardt J, Kessler F, Kniese R, Mohring HD, Dimmler B (2006) Large-area CIGS modules: pilot line production and new developments. Solar Energy Mater Solar Cells 90(18–19):3158–3164
82. Britt JS, Wiedeman S, Schoop U, Verebelyi D (2008) High-volume manufacturing of flexible and lightweight CIGS solar cells. In: Proceedings of the 33rd IEEE photovoltaic specifications conference, San Diego
83. Sugimoto H, Kawaguchi Y, Yasaki Y, Aramoto T, Tanaka Y, Hakuma H, Kuriyagawa S, Kushiya K (2011) Challenge to 18% efficiency with 30 x 30cm^2-sized Cu(InGa)(SeS)$_2$ submodules. In: Proceedings of the 26th EU photovoltaics solar energy conference, Hamburg, pp 2307–2310
84. Unold T, Schock HW (2011) Nonconventional (non-silicon-based) photovoltaic materials. Annu Rev Mater Res 41:297–321
85. Edoff M, Schleussner S, Wallin E, Lundberg O (2011) Technological and economical aspects on the influence of reduced Cu(In, Ga)Se_2 thickness and Ga grading for co-evaporated Cu(In, Ga)Se_2 modules. Thin Solid Films 519:7530–7753
86. Orgassa K, Schock HW, Werner JH (2003) Alternative back contact materials for thin film Cu(In,Ga)Se_2 solar cells. Thin Solid Film 431–432:387
87. Siebentritt S (2011) What limits the efficiency of chalcopyrite solar cells? Solar Energy Mater Solar Cells 95:1471–1476
88. Repins I, Contreras MA, Egaas B, DeHart C, Scharf J, Perkins CL, To B, Noufi R (2008) 19·9%-efficient ZnO/CdS/$CuInGaSe_2$ solar cell with 81·2% fill factor. Prog Photovolt 16(3):235–239
89. Haarstrich J, Metzner H, Oertel M, Ronning C, Rissom T, Kaufmann CA, Unold T, Schock HW, Windeln J, Mannstadt W, Rudigier-Voigt E (2011) Increased homogeneity and open-circuit voltage of Cu(In, Ga)Se_2 solar cells due to higher deposition temperature. Solar Energy Mater Solar Cells 95:1028
90. Hanket GM, Boyle JH, Shafarman WN (2009) Characterization and device performance of (Ag,Cu)(In,Ga)Se_2 absorber layers. In: Proceedings of the 35th IEEE photovoltaics specialists conference, Hawaii, pp 1240
91. Contreras MA, Mansfield LM, Egaas B, Li J, Romero1 M, Noufi R, Rudigier-Voigt E, Mannstadt W (2011) Improved energy conversion efficiency in wide bandgap Cu(In,Ga)Se_2 solar cells. In: Proceedings of 35th IEEE photovoltaic specialists conference, Seattle
92. Merdes S, Mainz R, Klaer J, Meeder A, Rodriguez-Alvarez H, Schock HW, Lux-Steiner MCh, Klenk R (2011) 12.6% efficient CdS/Cu(In, Ga)S2-based solar cell with an open circuit voltage of 879 mV prepared by a rapid thermal process. Solar Energy Mater Solar Cells 95:864–869
93. Schubert B-A, Marsen B, Cinque S, Unold T, Klenk R, Schorr S, Schock HW (2011) Cu_2ZnSnS_4 thin film solar cells by fast coevaporation. Prog Photovolt 19:93–96
94. Weber A, Mainz R, Unold T, Schorr S, Schock HW (2009) In-situ XRD on formation reactions of Cu_2ZnSnS_4 thin films. Phys Stat Sol C 6(5):1245–1248
95. Ito K, Nakazawa T (1989) In: Proceedings 4th international conference on PVSEC, pp 341–346
96. Friedlmeier TM, Dittrich H, Schock HW (1998) Growth and characterization of Cu_2ZnSnS_4 and $Cu_2ZnSnSe_4$ thin films for photovoltaic applications. Inst Phys Conf Ser 152:345–348, IOP Publ Ltd
97. Katagiri H, Jimbo K, Yamada S et al (2008) Enhanced conversion efficiencies of Cu_2ZnSnS_4-based thin film solar cells by using preferential etching technique. Appl Phys Express 1:041201–041202

Solar Cells: Very High Efficiencies Approaches

Jean-François Guillemoles
Institut de Recherche et Developpement sur l'Energie Photovoltaique, Chatou, France

Article Outline

Glossary
Definition of the Subject and Its Importance
Introduction
The Shockley–Queisser Limit and Other Thermodynamic Limits
Main Paths
New Concepts
Future Directions
Acknowledgments
Bibliography

Glossary

Blackbody (BB) radiation Radiation in equilibrium with a perfectly absorbing (black) body at a given temperature T. The spectrum and intensity of the radiation is completely determined by T.

Detailed balance principe that imposes a relationship between any forward and backward reaction rates.

Epitaxy mode of crystal growth on a cristalline substrate, where crystal orderind is continued in the growing phase.

Impact ionization interband electron-electron interaction whereby the excess energy of a carrier is given off to another carrier in a low lying state to promote it in a higher band of states.

Multijunction Photovoltaic device composed of several sub cells. Most of the time, these are series connected and have semiconductor with different band gaps to address different parts of the solar spectrum.

Photon cutting process by which a given photon gives two photons of lower energies (obeying of course energy conservation).

Recombination process by which a (photogenerated) electron-hole pair is anihilated (the excited electron returns to its fundamental state).

Shockley–Queisser limit (SQ limit) fundamental limit on the photovoltaic conversion efficiency imposed on a single junction solar cell by the laws of physics.

Tandem synonyme of multijunction

Thermalization processes by which a system returns to thermal equilibrium

Upconversion process by which two photons are converted in a photon of higher energy

Definition of the Subject and Its Importance

The issue of photovoltaic conversion efficiency of solar energy has always been on top of priorities and might still be at this place for a while. First, devices had to display some efficiency to convince. Early in the XXth century devices using elemental Se were below one efficiency point. Only when devices' efficiencies exceeded 10% (in the 60') could PV start to develop as a credible energy generation route.

Since then, and till today with commercial device efficiencies in the 30% range, increasing solar cell efficiency remained an important way of reducing the cost of solar electricity (LCOE), albeit, not the only one.

And finally, the discussion around efficiency of solar energy conversion is fascinating because it delves with the principles of solar energy conversion and it tells us how long the road in front of us is and how bright the perspectives could be.

Introduction

Historically, PV developed in several stages. In early times, the problem was to find a system with reasonable efficiency. The photovoltaic effect was discovered in 1839 by Edmond Becquerel in a photoelectrochemical device [5]. It took several decades before solid-state systems were discovered. The first such system is based on elemental selenium and was discovered by D. Day (A.D. 1870) and developed by C. Fritts (A.D. 1883) with Se° wafers whose efficiency was probably below 1%.

Applications for electricity production did not take off before Chapin, Fuller, and Pearson demonstrated photovoltaic cells based on Si with efficiencies close to 5% (by Chapin, Pearson and Fuller, 1954). This was soon followed by the discovery of two other

material systems with similar efficiencies: AsGa at RCA (1956) and Cu2S/CdS by USAF (1955).

Achievement of significant efficiencies at the moment when satellites required powering prompted more research and led to a rapid development through the 1960s with eventually 14% efficient cells at the end of the decade. The oil crisis in early 1970s then prompted a renewed interest in terrestrial applications, with Si wafers and thin film–based technologies (a-Si, CdTe, etc.). A general historical account of PV can be found in [61].

In the 1980s, crystalline Si cells passed the 20% efficiency barrier. Importantly, this is also the decade when III–V cells demonstrated high efficiencies (>20%) and when tandem cells (devices using several junctions in series) were demonstrated. Cells under concentration passed the 25% barrier. Progress was continuous in this domain, and today, multijunctions achieved 43.5% under concentration and terrestrial applications are growing rapidly, nearing 100 MWp installed.

In terms of devices, it has been proposed to distinguish three steps or three "generations" of devices, providing a useful framework to discuss the various options to reduce the cost of photovoltaics [31].

Yet, albeit semiconductor devices enabled to make the first reasonably efficient systems, their fundamental limitation in converting efficiently a broad spectrum of radiation was evidenced early on [73]. The question of the limiting efficiency of solar energy has been debated at length since early times. We will give the main conclusions of these studies in a first part.

It was quickly realized that there are two ways to increase the efficiency:

- Concentration of solar power
- Use of an optimized semiconductor for each spectral band

The second part of this chapter deals with these two pathways. Combined, these have been extremely successful at demonstrating very high efficiencies, currently above 40% [78]. These high efficiencies are obtained at the cost of complex, technologically demanding, and in the end rather costly, devices.

It could be asked whether it is possible to achieve similar results, using different photovoltaic conversion principles, with simpler, and possibly cheaper, devices.

These are the questions we then turn to discuss by describing a series of proposed concepts (up and down conversions, intermediate levels or bands, multiple exciton generation, hot carriers, etc.).

The Shockley–Queisser Limit and Other Thermodynamic Limits

Thermodynamic Limits

Thermodynamics is the best framework to make general statements about energy conversion: actually, it was developed for that precise purpose.

One of its main achievements was to find that there is nothing like a free lunch and to quantify to minimal cost for energy conversion in terms of entropy production.

Now, although it is pretty clear what a thermodynamic cycle is for a motor, it is not so for photovoltaic conversion: does light have thermodynamic properties like temperature and pressure?

Indeed, and the realization of that marked the passage into the twentieth-century physics, from the classical to the quantum world.

An excellent discussion can be found in [31].

Carnot

Does this limit apply to photovoltaic conversion? Carnot process deals with heat exchange, and a solar cell is very different from a heat engine, or so it seems, and proceeds via transformation of radiation into electrical work. But the sun radiation is very close to a blackbody spectrum, with a temperature $T_s \sim 6{,}000$ K, and the electrical work is delivered at ambient temperature (around $T_s = 300$ K). Carnot limit (95% = $1-T/T_s$) has to apply to photovoltaics, otherwise it would be possible to beat the Carnot limit for any thermal source using thermal radiation. This 5% loss originates from the unavoidable heat flow and subsequent entropy production when work is produced using heat sources and sink. As we will see below, a lower limit is to be found.

Blackbody Limit

A more reasonable limit (the endoreversible limit, or thermal limit) is given by

$$\eta_{\text{therm}} = \left(1 - \frac{T_a^4}{T_s^4}\right)\left(1 - \frac{T}{T_a}\right) \quad (1)$$

where solar flux heats up an absorber (at temperature Ta, which can also reemit blackbody radiation), and a Carnot engine operates between Ta and the cold sink (at T ~ 300 K).

The maximum efficiency is ~85%, obtained for Ta ~2,500 K (Landsberg, De Vos, etc.).

The difference with the above Carnot limit is that in the former, the sun's surface was included in the thermodynamic device and the Carnot engine works reversibly with the Sun, a quite preposterous assumption.

Multicolor Limit

It is also possible to build (as a thought experiment) a device doing even better than the previous one in converting radiation into electrical work. This can be obtained by separating the light in its different components and having each wavelength drive a solar cell whose gap E_g matches perfectly the energy of the incident photons [31]. This way, all the solar spectrums can be absorbed while thermalization losses (originating essentially from the excess energy between that of the incident photon and the energy that can be harvested, lower than E_g) are minimized. A slightly better efficiency than with the blackbody limit, ~87% (the "multicolor limit"), is then obtained under maximal concentration, and ~68% can be obtained without concentration. This is at the origin of the multijunction approach (see below). The losses here originate from recombination and, in the best case, from radiative recombination that are unavoidable: light has to be reemitted toward the sun as part of the conversion process.

Landsberg Limit and Time Reversibility

A higher limiting efficiency of 93.3% can in principle be achieved, using non-time-reciprocal optics to convert most of the light reemitted by the absorbers [31]. This limit is given by:

$$\eta_{\text{Landsberg}} = 1 - \frac{4}{3}\left(\frac{T_{\text{ambient}}}{T_{\text{sun}}}\right) + \frac{1}{3}\left(\frac{T_{\text{ambient}}}{T_{\text{sun}}}\right)^4 \quad (2)$$

Classification of Losses in Semiconductor-Based Devices

Intrinsic: Losses that Cannot be Avoided, Even in Principle

- Net Absorption Losses (Absorption and Luminescence Losses) In semiconductors (organic or inorganic), there is an absorption threshold, or band gap (E_g): photons below E_g are not absorbed while those above can be absorbed. Ideally, they could all be absorbed. Conversely, those of energy below E_g are lost for photovoltaic conversion as they cannot be absorbed. Unless $E_g = 0$, some photons will be lost, but with $E_g = 0$, a semiconductor yields no power (remember that the energy harvested per photon is smaller than E_g).

  If photons are reflected or emitted by the device, their energy is also lost. While reflection losses can be, in principle at least, reduced to nothing, this is not so with luminescence. Because photons can be absorbed to produce an electron and a hole, due to the microreversibility principle, there is a finite probability that an electron and a hole can recombine and produce a photon that escapes the device. It turns out that this is not a negligible quantity, and especially in very efficient devices, operating close to the radiative limit. This characteristic is the core of the detailed balance model (see below).
- Relaxation/Thermalization Photogenerated carriers have generally a kinetic energy much larger than the average kinetic energy of carriers of the same type present in the absorber (~kT) just after absorption. They will lose this excess kinetic energy by collision with other carriers or with atoms. The energy lost by this process per photon absorbed is essentially given by the difference between the average energy of an absorbed photon and E_g (–3 kT, the equilibrium kinetic energy of an electron–hole pair).
- Collection Losses Almost each and every electron–hole pair photogenerated can in principle be collected at the contact in good devices (provided for instance that the mobility and the carrier lifetimes are large enough). But while each electron–hole pair photogenerated has a total energy of about the bandgap after thermalization, only a fraction of that, the device voltage (i.e., the free energy of the pair), can be recovered as electrical power. The difference is

related to the entropy of the electron–hole pair times the carrier temperature. Moving the carriers from the absorber to the contacts (i.e., collection) involves an entropy change that has to be accounted for. The smaller the carrier concentration in the absorber, the larger the change and the smaller the output voltage.

Extrinsic: Losses that Could, in Principle, Be Made Vanishingly Small

- Optical Losses Encompass parasitic absorption (e.g., in parts of device where it is immediately dissipated, as in metal contacts) and reflection. They result primarily in a current loss.

  Reflection losses can be made near zero using efficient antireflection coatings. While parasitic absorption can, in principle at least, be vanishingly small.

  Moreover, if a fraction of the photons of a given energy is not used to create an electron–hole pair, this is clearly suboptimal; therefore, absorptivity of the active material should ideally be either 0 (under the absorption threshold) or 1 (above). This situation can be approached with adequate light trapping.
- Nonradiative Recombination Losses originate from nonradiative processes, where an electron and a hole recombine without emitting a photon, yield primarily a voltage loss but also a current loss. They result in additional losses as compared to pure radiative recombination (mandatory for consistency: detailed balance rule, and has to be accounted for, as discussed above). They can be made very small in some systems such as molecular systems or in very high-quality semiconductors of the III–V family. Such recombinations contribute to heat dissipation, and are therefore also nonoptimal.

  In the following, we will most of the time consider only radiative processes. Other processes only serve to get faster to equilibrium and therefore produce additional entropy. As we are here interested in conversion limits, we will not consider them here.
- Electrical Losses Occur because current flow in a conductor goes with and ohmic drop, which is a voltage loss. Charge transport can be made with negligible ohmic losses in devices with a high enough carrier mobility.

  Parasitic electrical path usually exists in devices and can create short circuiting between the electrodes.

  Different parts of a device act as if they were connected in parallel. If the device is heterogeneous, this may result in an impedance mismatch between its different parts and therefore in a suboptimal working point, as compared to what could be achieved with a homogeneous device.
- Thermal Losses Occur because of the dissipation of power (*thermalization*), photovoltaic devices become warmer under operation, and this is detrimental to the conversion efficiency. Yet, in principle, the device could be efficiently coupled to a thermostat and its temperature uniform and fixed at a given value, so variations in temperature are often ignored. These could be of importance in solar cells working under high solar flux (as in CPV or concentrated solar power).

The SQ Limit

The fraction of energy that can effectively be converted by an absorbed photon, qV/hν, is therefore much smaller than its maximum value because the free energy obtained from each photon is independent of its energy (the remainder goes to the atomic lattice heat in less than a few picoseconds, during carrier thermalization). Including the fraction of the photons that is not absorbed, the efficiency is limited to ~30% for the optimal gap E_g under standard conditions of illumination [73]. In short, this limit can be derived provided some idealizations are made so as to focus on intrinsic losses and neglect extrinsic losses (those that can, in principle, be made vanishingly small):

- Negligible ohmic losses: a high carrier mobility is assumed.
- Optical losses such as reflection or parasitic absorption are very small. Moreover, absorptivity of the active material is either 0 (under the absorption threshold) or 1 (above).
- The quantum efficiency of the device is equal to the absorber's absorptivity (perfect collection).
- Losses from nonradiative processes are neglected.
- The device is efficiently coupled to a thermostat.

The system studied entails some intrinsic losses:

- Below gap photons are not absorbed.
- Some photons are absorbed, leading to the reverse process of photon emission and therefore radiative

losses. Losses are incurred by establishing an equilibrium between the generated photocarriers (whose average kinetic energy is generally significantly larger than $\frac{3}{2}kT$) and the lattice. This is generally called "thermalization losses."

- The free energy collected per electron–hole pair (the cell voltage) is lower than the bandgap of the semiconductor (i.e., the energy of the pair). This is called "collection losses" and is ultimately due to the finiteentropy loss associated with carrier collection.

When these simplifying (but physically consistent) assumptions are taken into account, one obtains the so-called Shockley–Queisser limit [73], that is, the maximum value of the electrical power that a p–n junction can generate under solar illumination, depicted Fig. 1.

Detailed Balance. The principle of detailed balance has been stated in many different forms (e.g., by Onsager). In essence, it stems from the fact that no work can be extracted from equilibrium: it follows that, at equilibrium, each microscopic process has to be compensated. This compensation could be global (say, optical generation of an exciton compensated by nonradiative recombination). The detailed balance principle states that each process is compensated at equilibrium by its reverse process.

A consequence is that if an elementary process leading to energy flow between states is possible, then its exact reverse is also possible and occurs with the same probability: the rates of a process and its time reverse are therefore related (the transition matrix elements are equal). If then radiative recombination

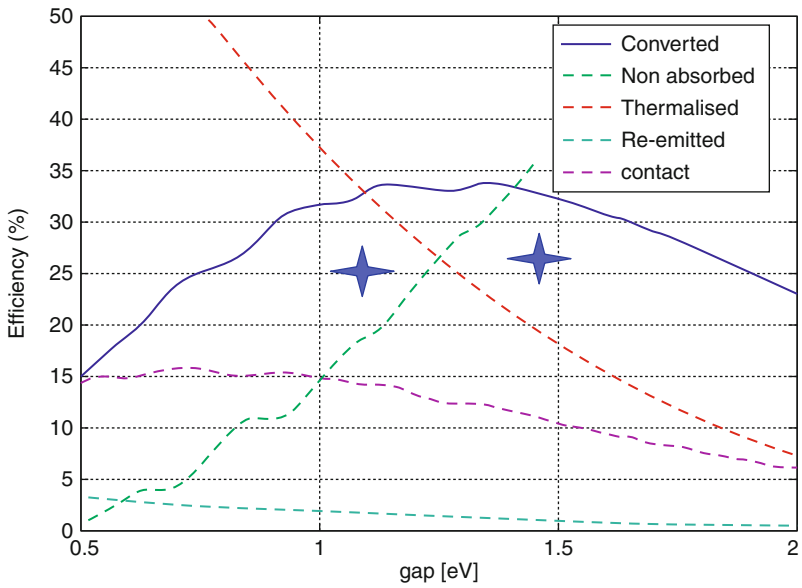

Solar Cells: Very High Efficiencies Approaches. Figure 1
Limiting efficiency of p–n junction solar cells as a function of the bandgap of the absorbing material, taking into account only unavoidable losses, under AM 1.5 illumination at 300 K. The crosses mark the efficiencies achieved for Si and GaAs cells. The blue continuous line is the Shockley–Queisser limit, that is, the maximum fraction of the incident (here, AM 1.5) flux that can be converted. The *green dashed line* gives the fraction of the incident power that is not absorbed by the photoactive material. The *red dashed line* gives the fraction of the incident power that is thermalized as a result of the excess initial energy of the electron–hole pair formed after photon absorption versus its equilibrium value (i.e., hv- E_g-3kT). *The blue dashed line* gives the fraction of the incident power that is lost through radiative recombination. The purple dashed line gives the fraction of the incident power that is lost during the process of carrier collection in the photoactive material or in the contacts (i.e., E_g + 3kT-qV, where E_g + 3 kT is the average energy, potential and kinetic, of electron–hole pairs after thermalization and qV is the work effectively extracted). These collection losses are sometimes divided into "Carnot" and "Boltzman" losses (Hirst 2010); they depend on the illumination level of the solar cell

processes only are considered, the balance on photons gives the balance on charge carriers as:

$$I = q(\Phi_{\text{abs}} - \Phi_{\text{em}}) \tag{3a}$$

$$I = q(\Phi_{abs} - \Phi_{em})$$

$$\Phi_{abs} = \int A(E).\ \dot{N}_{inc}\ (E).dE$$

$$\Phi_{em} = \int \epsilon(E).\ \dot{N}_{em}\ (E).dE$$

$\dot{N}_{inc}\ \dot{N}_{em}$ are, respectively, the incident and emitted photon flux densities, and A(E) is the photoactive materials' absorptive. It actually follows from detailed balance that A(E) = ε(E). This is also called Kirchhoff's law.

Equation 3a shows that the electron flux I is simply equal to the difference between the fluxes of photons absorbed, Φ_{abs}, and photons emitted, Φ_{em}. When the electron population of the absorber (which is also an emitter by virtue of the detailed balance principle) is in thermal equilibrium, Φ_{em} expresses the *law of black-body radiation*. When it is not, but the electron and holes populations can be ascribed to a quasi Fermi level each, $\dot{N}^{em}$ is given by [88]:

$$\dot{N}^{em}(E) = 2\pi h^3 c^2 \frac{E^2}{e^{(E-\mu)kT} - 1} \tag{3b}$$

where $\mu = E_{fn} - E_{fp} = qV$.

The electrical power extracted from a photovoltaic device is

$$P = I.V = \mu.(\Phi_{abs} - \Phi_{em}(\mu)) \tag{4}$$

From Eqs. 3 and 4, using the AM 1.5 spectrum for incident photon spectrum, one can recover the Shockley–Queisser limiting curve as in Fig. 1.

Another situation of interest is that of a monochromatic incident photon flux incident on a two-level system tuned to absorb it (see scheme Fig. 2), as it is of general and fundamental significance because it enables the calculation of the maximum value of free energy that can be extracted for each absorbed photon, μ_{opt} (Fig. 2), independently of the conversion system [31]. This free energy depends solely on the energy of the photon and the incident flux, and it can be computed using Eqs. 3a and 4 applied to a two-level system [19]. The conversion efficiency of a two-level system under monochromatic light can be read from Fig. 2; it is simply $\mu_{\text{opt}}(E)/E$ per collected electron hole pair and $\mu o/E^{*}1/(1+kT/\mu o)$ per absorbed photon.

With the help of Fig. 2, it can be calculated that the maximum efficiency ("multicolor limit") of a photovoltaic device is 67% under standard solar illumination and ~87% under maximum concentration

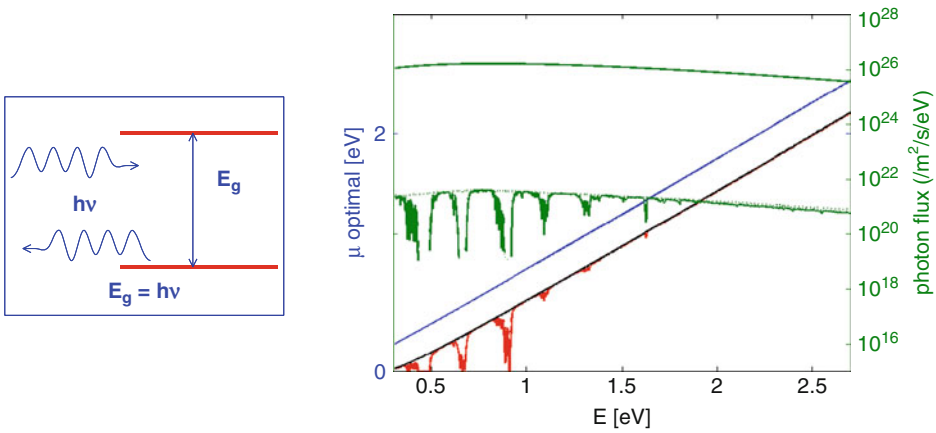

Solar Cells: Very High Efficiencies Approaches. Figure 2
(**a**) Scheme of the two-level systems considered. (**b**) Recoverable optimal free energy μ by an absorbed photon, that is, at the maximum electric power extraction (ordinate, *left axis*), according to both the photon energy (abscissa axis) and the incident photon flux (different *curves*). *The blue curve* corresponds to a 6,000 K blackbody spectrum, the *red curve* to the terrestrial solar intensity, and *the black curve* with that of solar flux above the atmosphere. *Green curves*: the photons fluxes on a log scale (*right axis*) for the same spectra (From Guillemoles 2009)

as the weighted (by the photon flux) average of μ_{opt} divided by incident power. The fact that no such efficiencies have been approached yet is because the materials and technologies were not ready to meet the severe specifications necessary (as described in the assumption list above). Clearly, following the way suggested by the method used in deriving the result to realize a device would be very difficult in practice.

Main Paths

Impressive progress, at an average rate of 0.4% per year, has been made on the efficiency of solar cells. Record efficiencies above 43.5% have been obtained by Solar Junction recently, but many Labs and Companies now make solar cells working under high concentration with efficiencies above 40%, using a variety of approaches, with multijunction solar cells based on III-V semiconductors. This makes III-V multijunction the path with the fastest progress at the moment. It shows how successfully the knowledge gathered on these materials and on similar devices for other applications (LED and Lasers notably) could be put to use in the photovoltaic context.

It should be stressed that this progress is due to two factors: the ability to use concentration to increase efficiency and the use of several semiconductors to make a better use of the solar power, reducing thermalization and non absorption losses as compared to single junctions. Indeed, the best triple junction under one sun illumination (presented by Sharp Corp.) has a confirmed efficiency of 36.9% (as compared to 28.2% for the best single junction under one sun [72]). Thus, about as much is gained going from one to three junctions as is gained between one and 400 suns.

Concentration

Solar concentration is a primary driver towards high efficiency. Indeed photovoltaic efficiency is not a constant, but rather depends on the incoming light flux intensity. This is reflected in Fig. 2, where it can be seen that the maximum recoverable work per photon (μopt) increases when the photon flux increases. This can also be seen from Eqs. 3a, b: since the recombination current increases exponentially with the electron–hole gas chemical potential μ, the μ value needed to cancel a given fraction of the photocurrent increases logarithmically with the photocurrent (which itself is proportional to the flux).

The cell voltage can be identified with the difference in chemical potential of electrons in the conduction band (CB) and of the electrons in the valence band (VB). These chemical potential difference, μ, increases with the incoming flux as the CB is populated (increasing Efn: the chemical potential increases with the concentration) and the VB depopulated (decreasing Efp). This increases amounts typically to +2 efficiency points per concentration decade.

Concentration is about increasing the inflow of radiative power in the device. In a certain sense it is akin to increasing the source temperature, and, taking an analogy with a Carnot engine (as e.g., in Eqs. 1 and 2), this results in an increased conversion efficiency.

But increasing power inflow means that the power outflow also needs to be increased. It occurs as electrical power and waste heat, and both extraction need to be efficient. An inefficient electric power extraction results in series resistance losses as Joule heat and a reduced electromotive force of the device. It manifests itself as an inflexion, then a plateau and finally a drop on the efficiency versus solar concentration curves (Fig. 3).

Limits of extraction of waste heat results in an increase of the device temperature. Taking again the Carnot engine analogy, this should result in an efficiency loss. It manifests itself on Fig. 6 as an accelerated drop of efficiency when the temperature start to increase.

Practical limits to concentration are set by heat and electrical power extraction, as explained above. Nevertheless, there is a fundamental limit to solar concentration set by thermodynamics: the energy density at the focal point of the concentrator cannot exceed that of a blackbody at sun's surface temperature (otherwise we could have heat to flow from the colder sun to the hotter focal spot). This limit is achieved at a concentration 46,200 times the standard if the focal point is in air.

There are several types of concentrators, based on lenses or/and mirrors. Most systems are based on Fresnel lenses (Fig. 4) that enable to reduce the cost: these can be easily molded and require much less material than traditional lenses. For high concentration (> x100), they are used as a primary optical

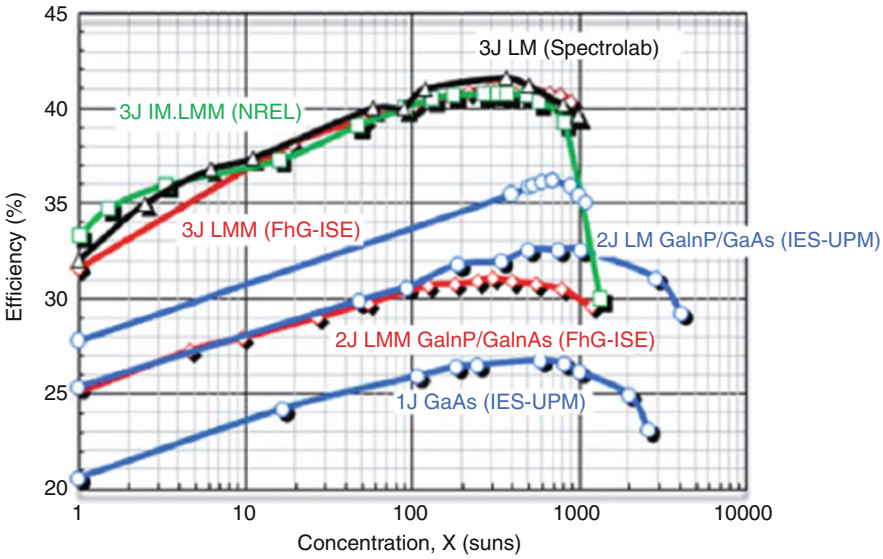

Solar Cells: Very High Efficiencies Approaches. Figure 3
Efficiency-concentration data of champion certified cells in the world (From [54])

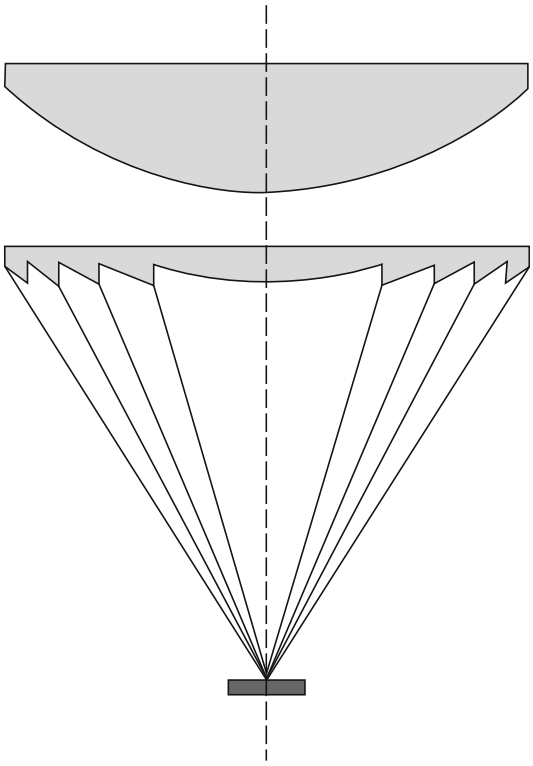

Solar Cells: Very High Efficiencies Approaches. Figure 4
Schematic of the Fresnel lens showing the teeth (From G. Sala and I. Anton, in handbook of photovoltaic science and engineering, 2nd edition (2011), Wiley)

element (POE) and associated to a secondary optical element (SOE) to improve uniformity and tolerance to tracking errors (Fig. 5).

Modules for concentrated photovoltaics (CPV) have to be precisely aligned optically. They are then mounted on sun trackers (Fig. 6) to ensure that the solar flux is focused on the solar cells at any moment.

It should be noted that this approach only works with the direct component of the solar radiation, and misses out the diffuse part (due to cloudiness of the sky, or emanating from the blue part of the sky). On the nice side, CPV modules being at all times normal to the sun's rays, produces close to their nominal capacity from sunrise to sunset, yielding 30% more power than fixed, flat plate, modules.

Multijunctions

Principles and Achievements In a traditional device, the photons whose energy conversion is most effective are those whose energy is just above the threshold of absorption (bandgap energy E_g). For those photons, efficiencies of about 60% are reached in experiments, rather close to expectations (Fig. 2). The use of several different cell materials, each one with a bandgap optimized for a part different from the solar spectrum, makes it possible to increase the output power using several configurations.

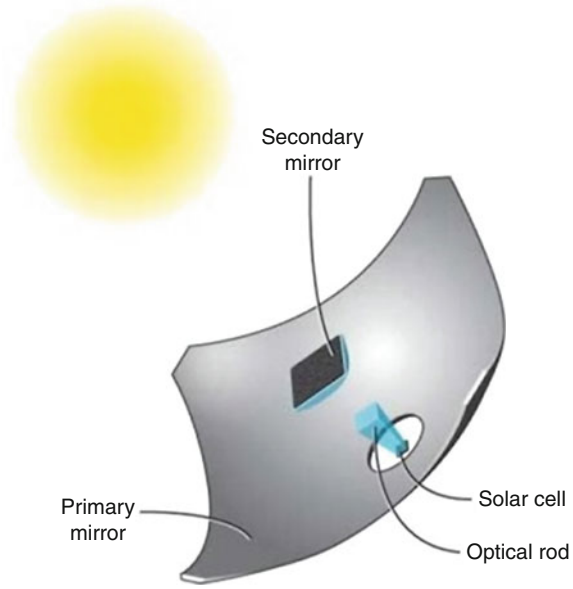

Solar Cells: Very High Efficiencies Approaches. Figure 5 Scheme of the principle of a concentrator with secondary optics with mirrors in a Cassegrain configuration (The Solfocus design). The Glass rod further increases the concentration and the homogeneity of the beam

Several configurations are possible (Fig. 7): (a) An optical device separates sunlight by means of filters in three beams "blue," "green," and "red," which are converted by three cells whose bandgaps were adapted for these three spectral bands. One can simplify the device as indicated in (b), noticing that the "blue" cell does not absorb the wavelengths higher than its threshold of absorption. It can thus be used as filter for "green" and "red" cells. In the same way, the "green" cell lets the "red" beam pass. It is necessary, of course, that the substrates of the first two cells are transparent. Finally, in (c), a transparent electrical contact between the cells is realized. One can achieve this stack by deposition of the various cells on the same substrate. To avoid creation of a reverse diode at the interface between two cells (a diode p–n if diodes n–p are piled up), one connects them by a tunnel junction. In case (c), the cells are connected in series, whereas in case (a) or (b) one remains free to use the electricity produced in the most effective way.

For a given number of cells and an incident spectrum, there is an optimal choice for the gaps that give the highest output [31]: For example, for three cells under maximum concentration, the maximum theoretical yield is 63% (49% without concentration). As a general rule, stack efficiency goes as (see also [7]):

$$\eta(N) = \frac{\eta^{\infty}}{1 + \frac{a}{N}} \tag{3}$$

where a ≈ 1 and depends slightly on solar concentration. This formula expresses that, for a multijunction device composed of N junctions to operate optimally, the incident spectrum should be partitioned into $N + 1$ portions containing about the same fraction of photons, with the upper limits of the N first regions giving the optimal gaps of the absorber materials to be chosen for the junctions.

Moreover, in the tandem, the current is lower (for a given number of photons of incident) and the tension higher than for a simple junction device. This is favorable to the use of the concentration, which even allows a reduction of the costs.

This pathway to high efficiency is based on what exists and is already understood rather well.

It takes advantage of a large body of knowledge that has been developed for III–V optoelectronics, as well as for this purpose. There are several pathways to achieve an optimal current matching while keeping the very high material quality required for very high conversion efficiencies.

Highest material quality and best optoelectronic properties are obtained in extremely pure and well crystallized III-V semiconductors, and these are prepared using epitaxial growth: a technique where the grown material continues the crystallographic arrangement of the substrate. This imposes that substrate and grown compounds have very similar crystallographic systems and lattice parameters. It therefore restricts considerably the possibilities of growth.

Figure 8 presents the combinations of band gaps and lattice parameters for main III–V semiconductors. The bandgap determines how the solar spectrum is split between the cells in a multijunction (see Fig. 7 for a triple junction). The lattice parameters should be equal to within a fraction of a % if high quality material is to be obtained. A non optimal splitting and/or a non optimal lattice match can result in large losses, finding the best material combination has been the main

Solar Cells: Very High Efficiencies Approaches. Figure 6
Installations from Soitec-concentrix (*top*) and Solfocus (*bottom*) showing the modules and traking dimensions and installations

problem in the field to obtain the highest efficiencies possible (that is 50% under one sun for a triple junction). Sticking to possibilities offered by Fig. 8 restricted the efficiencies to little better than 35%. New strategies involve metamorphic growth (growth of a buffer layer with a continuously varying lattice parameter that accommodates the crystallographic changes between active materials), or the inverted metamorphic variant, lift off (where active materials are grown on lattice matched substrates, and then lifted-off and reported on the final structure), use of meta-materials made from quantum wells or quantum dots or development of new materials (such as dilute nitrides). The challenges are well known:

- The cost of production has to be reduced (reduce substrate cost, lower cost processing, etc.).
- Reduce electric and optical interconnection losses.
- Improve intercompatibility of the growth methods for stacks.
- Improve the efficiency via a better match with solar spectrum (keeping a high crystalline quality).
- Achieve higher concentration.

Why Beyond Multijunctions? It must be realized from Eq. 3 that the incremental gain in power from the addition of a cell in a stack including N junctions varies as $1/N$. If one takes into account the induced losses (electrical and optical), the expected net gain from another cell is close to zero after the fourth cell (i.e., the practical limit on N is 4).

$$\eta(N) = \frac{\eta^{\infty}}{1 + \frac{a}{N}}$$

Another point is that the tandems "stack" series-connected, which have the best prospects for the reduction for the costs become very sensitive to spectral variations (the complete structure must be optimized precisely according to the incidental spectrum), and this more especially as the number of cells is important.

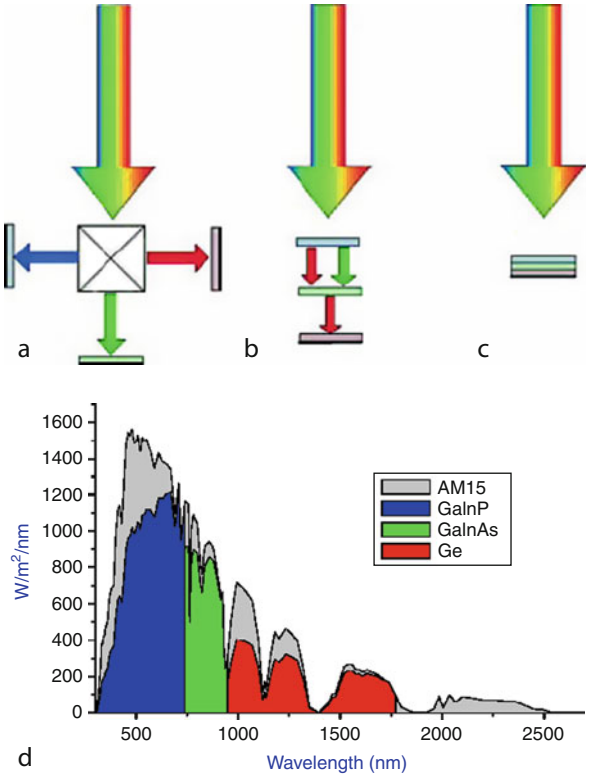

Solar Cells: Very High Efficiencies Approaches. Figure 7

Principle of multijunction conversion (specifically for a triple junction) and possible practical configurations thereof: (**a**) An optical device separates sunlight by means of filters into three beams, denoted *blue*, *green*, and *red*, which are converted by three cells whose bandgaps were adapted for these three spectral bands. One can simplify the device as indicated in (**b**), noticing that the *blue cell* does not absorb the wavelengths higher than its threshold of absorption. It can thus be used as filter for the *green* and *red cells*. In the same way, the *green cell* lets the *red beam* pass. It is necessary, of course, that the substrates of the first two cells be transparent. Finally, in (**c**), a transparent electrical contact between the cells is realized. One can achieve this stack by deposition of the various cell materials on the same substrate. To avoid creation of a reverse diode at the interface between two cells (a p–n diode if n–p diodes are piled up), one connects them by a tunnel junction. In case (**c**), the cells are connected in series, whereas in cases (**a**) and (**b**), one remains free to use the electricity produced in the most effective way (From EPN 2009 (**d**) The solar spectrum and its partition between three junctions as in present-day highly efficient devices. A typical such structure is a stack of about 20 layers, epitaxially grown on a crystalline substrate (e.g., Ge, from which the bottom junction is made) forming p–n junctions of adjusted bandgaps for photon conversion (generally GaAs and $GaInP_2$) and tunnel junctions to connect them

New Concepts

Classification of New Concepts

There are many possible strategies to achieving very high-efficiency solar devices, many of which have ultimate conversion efficiencies close to 85%. All concepts essentially fall in three main groups (below) according to the assumption of the SQ analysis that is relaxed (Fig. 9):

1. Several electrons collected per photon
2. Subgap photons can produce collectable electron–hole pairs
3. Nonisothermal devices

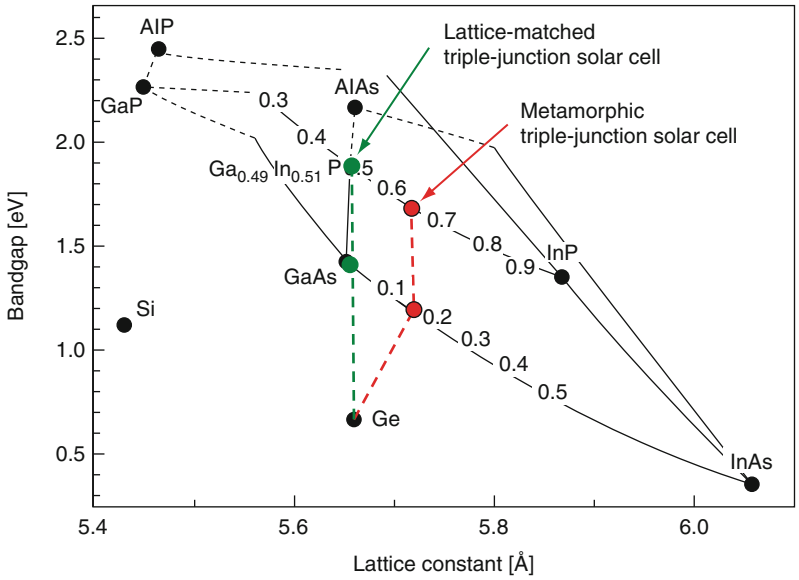

Solar Cells: Very High Efficiencies Approaches. Figure 8
Combinations of bandgap and lattice constant for various materials used in III–V solar cells. The potential substrate materials silicon (Si) and germanium (Ge) are also indicated. As an example, the bandgap combinations of the lattice-matched triple-junction solar cell on Ge as well as of a metamorphic triple-junction solar cell developed at FhG-ISE are indicated. The *upper cells* of the metamorphic solar cells have a lattice-mis-match of 1.2% compared to the Ge substrate. In order to achieve sufficient material quality, a buffer layer is intregrated into the structure (From [54])

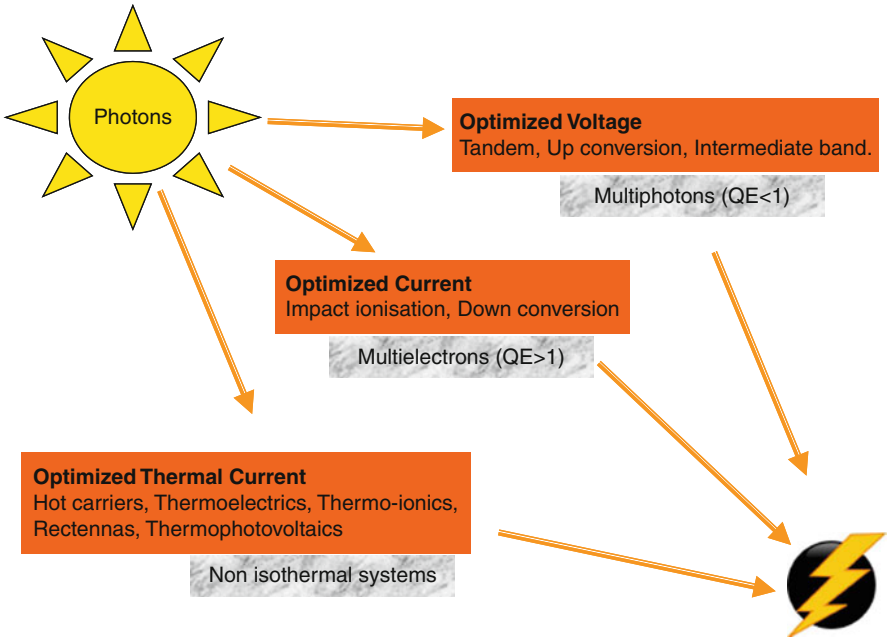

Solar Cells: Very High Efficiencies Approaches. Figure 9
Scheme illustrating the relationships between main conversion concepts and relaxed assumptions in the SQ analysis

Multiphoton Conversion (QE < 1)

Intermediate-Level Materials

Proposals have been made to better utilize the low energy part of the incident solar spectrum by using Intermediate Level Semiconductors (ILSC) either with localized states [41] or delocalized ones [43, 55]. It has been shown that such concepts have efficiency expectations up to 49% in an optimal device [31], comparable to those of triple junction devices (51%) under Air Mass 1.5 (AM 1.5) standard terrestrial solar radiation [31]. Indeed, these intermediate-level materials also have three possible optical transitions that may be adjusted to optimally use the solar spectrum. Contrary to multijunction devices, only one absorber material is needed, a fact which limits optical losses, tunnel junction losses and would help to design simpler, possibly cheaper, elaboration schemes. However, approaching those values would require rather low nonradiative recombination rates as compared to the radiative ones [41], a fact which has so far impeded the development of ILSC devices: without a specific mechanism to prevent them, nonradiative processes are far more efficient than radiative ones, especially those that involve the intermediate levels.

At this stage, intermediate level or bands that have been tried experimentally suffer both from a low absorption of the transitions involving the intermediate levels and a high rate of nonradiative recombination they induce so that in the end the losses they cause outweigh largely the small gain in photocurrent that is at best measured Fig. 10.

Upconversion Fig. 11

In the "upconversion" or "photon addition" approaches, the photons whose energy is too weak to be used directly by a photodiode could be converted by nonlinear processes into a lower number of photons of larger energy.

Early attempts were done [25, 26, 71], proving feasibility of the concept but with a limited success in terms of absolute efficiency gains: approximately 3% of the IR photons in the narrow band of absorption of proposed rare earths, under an illumination equivalent to 250 suns, were actually converted into photons of higher energy. Recently, power efficiency of upconversion from 15 to 1 μm have been demonstrated using CaF2:Er material [62]. Also, using plasmonic resonators, a large enhecement factor was demonstrated on YF3:Er [1].

Most of the research on the subject is done using systems containing rare earths and taking advantage of the processes of transfer of energies between rare earths. Molecular systems have also been considered.

Nonlinear optical systems taking advantage of polarizabilities of the second or third order have capabilities of conversion of broader frequency bands but are not very effective unless unrealistic intensities of illumination would be used (not achieved with a solar source).

A last category of process is represented by the phenomena of absorption of excited state which one can meet in the solids [80] but also in many molecular species [3, 21, 39, 85]. In particular, systems presenting

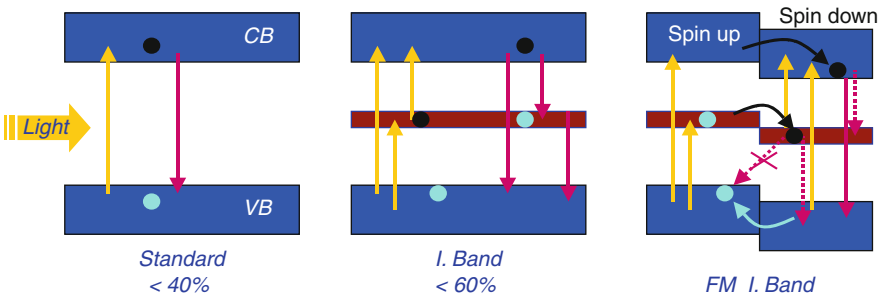

Solar Cells: Very High Efficiencies Approaches. Figure 10
Schematic representation of generation recombination processes in a standard semiconductor (*left*), a semiconductor comprising an intermediate band through which additional generation and recombination can occur (*middle*) and a spin polarized semiconductor where some of the recombination processes are blocked due to spin selection rules (*right*)

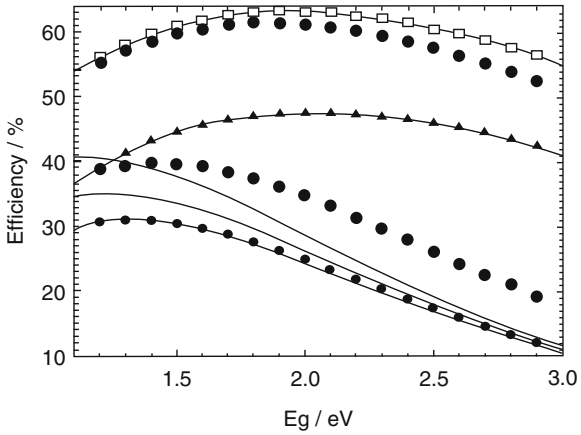

Solar Cells: Very High Efficiencies Approaches. Figure 11 Higher limits of conversion efficiency for upconversion systems as a function of the gap of the solar cell in the case of the angular restriction of emission (*squares*), and various concentration factors (1, 100, 46,200 times, *round blacks*). For comparison, the limits of outputs for a simple junction within the limit of Shockley for the same concentrations (*lines*) are also given (From [79])

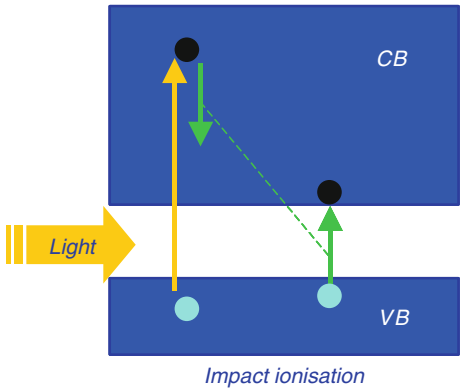

Solar Cells: Very High Efficiencies Approaches. Figure 12 The excess energy of a photogenerated carrier (*yellow arrow*) is given off to a carrier in the valence band, creating a second electron hole pair

a small relaxation of the first excited state, such as, for example, the passage to triplet state, which sometimes makes it possible to increase its lifetime considerably and thus the probability of the excited state absorption, are particularly interesting. Yet, upconversion in organic systems was found to have issues related to molecular stability.

In the case of certain organic molecules, absorption cross sections of excited state as large as 10^{-16} cm^2 and μs lifetimes were measured. One thus expects an efficient conversion of IR photons for photons' fluxes of about 10^{22} cm^{-2} s^{-1}, which is approximately what is achievable with the maximal concentration of solar radiation.

To summarize, upconversion has a strong potential for efficiency increase of single junction devices, and this improvement can be implemented as a supplementary layer with minimal interference with the photovoltaic p–n junction. Yet systems that have demonstrated any efficiency suffer from either narrow band absorption or from large internal dissipation (so that the upconverted photon has hardly more energy than the source photons).

These systems see their efficiency increase rapidly with illumination intensity (power delivered increases at least as square of intensity, and sometimes as cube or more for 3 photon processes and more) before saturation or degradation, so that high incident flux is preferred.

Finally, optimizing the coupling to the cell, a domain with potential large losses, has hardly been done [62].

Multicarrier Generation (QE > 1)

Multiple Exciton Generation

The absorption of photons having energy more than twice that of the gap makes it possible to consider other mechanisms, where the excess energy can be used to create a second electron–hole pair. This phenomenon is called "impact ionization" (Fig. 12). The outputs of devices with impact ionization can have practical interest, provided that the process is effective in the vicinity of the physical threshold (~2 E_g). Work at the Max Planck Institute of Stuttgart predicted that the alloys Si-Ge could show a measurable effect. But this was found to be lower than 1% of the output power of cells made of this material. High values of impact ionization have so far been observed only for energies of photons higher than 3 E_g [46, 68, 86] (Fig. 13).

Recently [70], a working device based on PbSe quantum dots demonstrated a photocurrent increase

that could be traced back to multicarrier generation (peak external quantum efficiencies of 114% were measured). The device efficiency did not exceed 5%.

Photon Cutting

Another principle, "photon cutting" consists, conversely, in absorbing photons of high energy in a luminescent converter to emit several photons of lower energy, to increase the current output of the photodiode (Fig. 14).

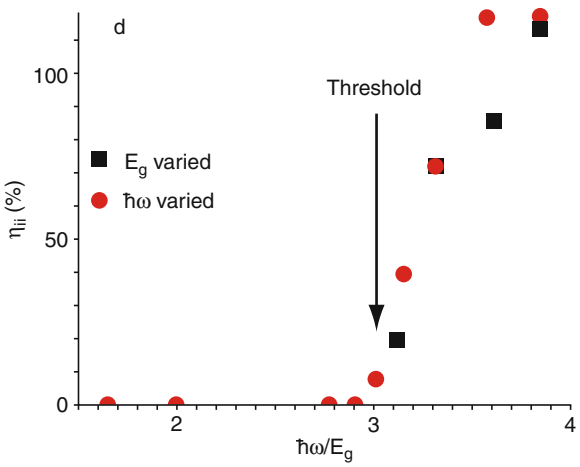

Solar Cells: Very High Efficiencies Approaches. Figure 13 Impact ionization efficiency in PbSe nanocristals. The threshold for the formation of the second electron-hole pair is relatively abrupt at 3 times the gap E_g and is larger than 100 % for photon energies lower than 4 times E_g

Fluorescent converters with quantum yield <1 already made it possible to show an improvement of the performances of the solar cells while shifting toward the red of the photons slightly used by these cells [57]. In addition, of fluorescent materials with quantum yield >1 were discovered in the recent years:

- YF3:Pr with QE = 1.4 [75]
- LiGdF4 with QE = 2 [83]. The measured quantum yield corresponds to the quantum yield of internal energy transfer but not to a real output of photons.
- Nanocrystals of PbSe with QE > 2 for hv > 3.E_g [68].

However, although high quantum yields (close to 2) were reached, it should be noted that the energetic efficiency is not very good: less than 70% at best of the total energy of the source photon is recovered in the emitted photon due to internal relaxation processes. There are numerous challenges to this approach, notwithstanding the process efficiency itself (powerwise). Firstly, the converter is placed in front of the cell, and can easily interfere with the device quantum efficiency in all spectral ranges. The converter will absorb light at the photon energies where it emits (that is where photon cutting occurs). The optical coupling with the cell

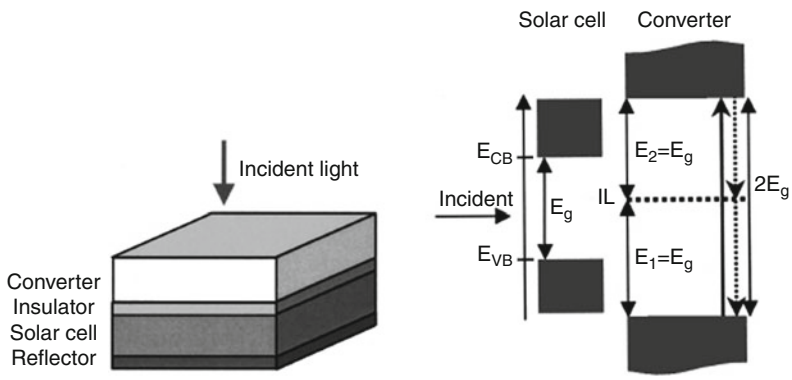

Solar Cells: Very High Efficiencies Approaches. Figure 14
Schematic representation of a down conversion system. The converter can be in front of the solar cell (*left*) or on its rear face (*right*). In the latter case, the cell has a limited absorption range towards the high energy side. Optimally, the gap of the converter is twice that of the solar cell

is non trivial as well, if most photons emitted by the converter are to be harvested by the cell.

Finally, no materials are known with significant efficiencies in a range relevant for solar cells.

Multitemperature Generation (QE = 1)

Hot Carrier Solar Cells

The carriers generated in the absorber are not thermalized instantaneously with the network at temperature T_A, but form in a transitory way a hot gas of electrons and holes: their distribution corresponds to a temperature $T_H > T_A$. If these carriers can be collected quickly via selective energy levels (Fig. 15), the heat flow through the contacts is minimal and the kinetic energy conversion of hot gas into electrical potential energy is optimal [90]. Calculations of the limit of output give values very close to those obtained with a multijunction device containing an infinite number of cells, each one adapted to a fraction of the spectrum, and this for a system of a much simpler concept: it thus acts, to some extent, as the ultimate device of solar transformation energy. No cell with hot carriers was built yet; however, experiments showed that hot carriers' thermalization rates can be reduced under strong excitation in nanostructures to the point that conversion efficiencies above 50% under concentration are possible [13]. The efficiency is sensitive to the energy width of the contacts beyond some meV because the latter introduce a thermal loss by transfer of heat. But more than decreasing the thermalization rate, the practical realization of selective contacts is likely to be the delicate point in the fabrication of these devices.

At this stage, only thermalization rates have been measured both in bulk materials and in MQW. Those have been measured from time resolved PL as well as from CW techniques. They have yielded thermalization rates compatible with a significant gain under maximum concentration [49].

It has been shown also that reducing the thickness of the absorber is important to reduce thermalisation rates. Therefore a very efficient light confinement will be required. Thermalization rate reduction can also be achieved by phononic engineering, i.e., by preventing complete dissipation of the electron excess energy [12]. Finally, extraction of hot carrier may prove the most

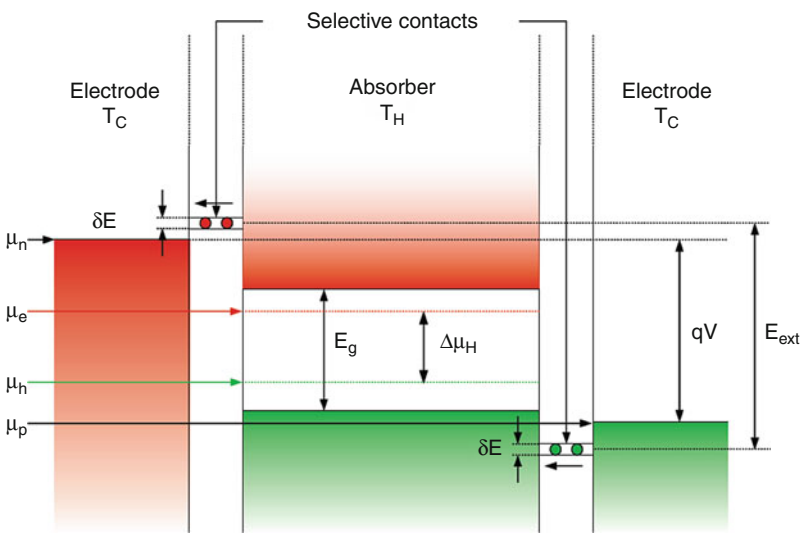

Solar Cells: Very High Efficiencies Approaches. Figure 15
Energy band diagram of a hot carrier solar cell. Photons are absorbed in the absorber where electron-hole pairs are generated, forming a hot electron-hole gaz. Photogenerated carriers can be collected in electrodes, ideally using energy selective contacts

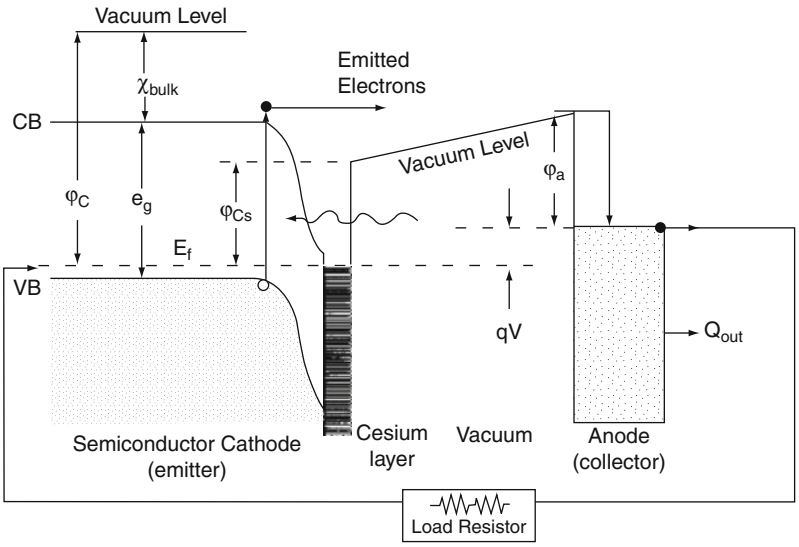

Solar Cells: Very High Efficiencies Approaches. Figure 16
Energy band diagram of a cesiated semiconductor photocathode and a metalic anode. Here, the energy of the emitted electron can be above the vacuum level. This is a configuration used in photodetectors (from Smestad 2005)

delicate challenge. There, a possible solution has recently been proposed to replace selective contacts by semiselective contacts [48].

Another mode of realization of the hot carrier solar cell is base on thermoionic conversion (Fig. 16), whereby hot carriers (or carriers from a hot cathode) are emitted in vacuum and collected at the anode.

There are numerous issues with this approach, on which a lot of work was carried out in the 50's [36], and namely, material stability at the high temperatures needed for significant thermoionic emission, creation of the space charge at large current. Recently, it was proposed to use semiconductor cathodes such as cesiated GaN, that could operate at much lower temperature [69]. This may enable to revisit the question.

TPV

In the thermophotovoltaïc configuration, solar energy heats a radiator at relatively high temperatures (>1,000 K typically). The energy radiated by the radiator is then converted by a photovoltaic cell whose gap is adapted to radiated energy. This system can be used to convert heat into electricity [22]. In the thermophotonic configuration [28], the radiator, an online polarized junction p–n, is what makes it possible to increase the quantity of radiation emitted. It is actually not so easy to find a selective emitter being effective at radiating the power in a relatively narrow band.

The thermal management of this device is particularly difficult, and, as the current density should be large, then it is also required to pay attention to possible Joule losses.

Rectennas

If the solar radiation is seen like an electromagnetic wave, it is in theory possible to collect it with an antenna and to rectify the induced current. Of course, one would need micron-scale antennas and especially high-speed diodes (> THz), beyond the state of current technology (Fig. 17).

Very important efficiencies were announced (70%) with the possibility of using molecular systems (at low prices thus). A company under contract with the US army would have started a few years ago (Lumeloid). Another company (ITN) under contract with the NREL explores the systems resulting from microelectronics (diodes MIM) and predicted outputs of

96% [6]. It is the Rectenna concept (network of antennas and rectifiers) illustrated below.

An effect (very weak) has been highlighted in experiments [53]. A deeper analysis raises some questions nevertheless: the antennas would function well with a monochromatic and coherent radiation, how would they perform with natural light? It thus seems that the estimates are to be strongly reexamined with the fall.

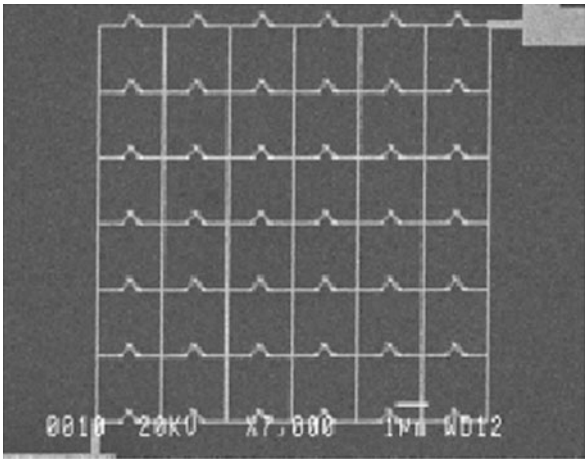

Solar Cells: Very High Efficiencies Approaches. Figure 17 SEM image of a network of antennas for the Rectenna concept [6]

It is impossible to rectify noise, but it is on the other hand it is possible to extract some energy from noise if this noise has a larger temperature than that of the diode. The limit of output for a system using a broad band antenna is 48% [74]. The problem of the antennas is well discussed by [14, 15].

Future Directions

Two well established paths to high efficiency have been identified: concentration and multijunctions. Both should make progress. For instance, advanced optical management, as implemented in the recent nanophotonic approaches are very promising and have a strong potential to contribute to further efficiency progress [2]. By increasing the energy density per unit volume, plasmonic and other nanophotonic approaches contribute to the concentration impact on efficiency. Multijunctions approaches will certainly flourish in the near term as many successful

Solar Cells: Very High Efficiencies Approaches. Table 1 Maximum theoretical performance expectancy (thermodynamic limit) of the various approaches. The possible gains are given for the range of concentration 1× to 46,000× (maximum of possible concentration). In *italics*, in the third column, the systems for which one expects a particularly important impact of solar concentration in real systems

Type of cell (ideal limits)	Range of output AM 1.5 to ×46,000	Remarks
Tandem N > 100	68–87%	Extremely complex
Hot carriers	67–86%	*Not shown in practice*
Impact ionizations (ts multiple E_g)	44–86%	Extremely complex, 5% in practice
Thermionic, thermal, TPV	54–85%	*In practice **23%** carried out*
Intermediate levels (N > 10)	62–85%	Extremely complex
N = 3 tandem	49–64%	In practice **39%** carried out
Upconversion	48–63%	*Small gain shown in practice*
Intermediate level (N = 1)	48–63%	*Not shown in practice*
N = 2 tandem	43–56%	In practice **32%** carried out
Down conversion	39–52%	Not shown in practice
Impact ionization (2 E_g)	38–52%	Small profit shown in practice
Rectennas	?–48%	*Not shown in practice*
Simple junction p–n	31–41%	In practice **28%** carried out

innovations on the processing (metamorphic and inverted metamorphic growth) and on the device architecture (integration of quantum dots and quantum wells) have been implemented. Yet it will become increasingly difficult to add more junctions, for an ever decreasing return, and at some point, one of the other concepts exposed above may take the relay to enable further efficiency increase (the potential of the various concepts is presented in Table 1).

Bibliography

1. Andriamiadamanana C, Ferrier A, Lombez L, Joudrier A-L, Naghavi N, Ghenuche P, Bardou N, Pelouard J-L, Collin S, Pellé F, Guillemoles J-F (2012) Plasmonic enhancement of up-conversion in ultrathin layers. SPIE 2012 (in press)
2. Atwater HA, Polman A (2010) Plasmonics for improved photovoltaic devices. Nat Mater 9:205
3. Baluschev S, Miteva T, Yakutkin V, Nelles G, Yasuda A, Wegner G (2006) Up-conversion fluorescence: noncoherent excitation by sunlight. PRL 97:143903
4. Barnham KWJ, Duggan G (1990) J Appl Phys 67:3490
5. Becquerel E (1839) Mémoire sur les effets électriques produits sous l'influence des rayons solaires. Comptes Rendus de l'Académie des Sciences, novembre 1839
6. Berland B (2001) Optical rectenna for direct conversion of sunlight to electricity. In: Proceedings of the national center for photovoltaics program review meeting (NREL 2001), Seattle, p 323
7. Brown A (2003) Thèse UNSW
8. Carminati R, Greffet J-J (1999) Phys Rev Lett 82:1660
9. Cinco RM (1999) J Phys Chem B 102:8248–8256
10. Clifano M, Zunger A et al (2004) Appl Phys Lett 84
11. Conibeer GJ, Guillemoles JF et al (2005) In: Proceedings of the 20th EPVSEC, Barcelona
12. Conibeer G, Konig D, Green MA, Guillemoles JF (2008) Slowing of carrier cooling in hot carrier solar cells. Thin Sol Films 516:6948–6953
13. Corkish R, Green MA (1993) In: Proceedings of the 23rd IEEE photovoltaic specialists conference, Louisville, p 675
14. Corkish R, Green MA, Puzzer T (2002) Solar energy collection by antennas. Sol Energy 73:395
15. Corkish R, Green MA, Humphrey T, Puzzer T (2003) Efficiency of antenna solar collection. Presented at the 3rd world PV conference, Osaka
16. Coutts TJ (2001) Clean electricity from PV. Imperial College Press, London
17. Cuadra LR, Marti A, Luque A (2002) Physica E 14
18. Cuadra L, Martí A, Luque A (2004) IEEE Trans Electron Device 51(6)
19. De Vos A (1992) Endoreversible thermodynamics of solar energy conversion. Oxford University Press, Oxford
20. De Vos A et al (1998) Solar Energy Mater Solar Cells 51:413–424
21. Dini D, Hanack M, Meneghetti M (2005) Nonlinear optical properties of tetrapyrazinoporphyrazinato indium chloride complexes due to excited-state absorption processes. J Phys Chem B
22. Fortini A (1962) L'Onde Electrique 442:530
23. Freundlich A (2005) In: Proceedings of the photovotaic solar energy conference, Shanghai
24. Chen G et al (2004) Superlattices Microstruct 35:161–172
25. Gibart P, Auzel F, Guillaume JC, Zahraman K (1995) In: Proceedings of the 13th European photovoltaic solar energy conference (13th EU PVSEC), Nice, France, p 85
26. Gibart P, Auzel F, Guillaume JC, Zahraman K (1996) Below band-gap IR response of substrate-free GaAs solar cells using two-photon up- conversion. Jpn J Appl Phys 35(Part 1):4401–4403. doi:10.1143/JJAP
27. Goetzberger A, Hebling C, Schock H-W (2003) Mater Sci Eng R 40:1–46
28. Green MA (2000) In: Proceedings of the 16th EC photovoltaic solar energy conference. James & James, p 51
29. Green MA (2001) Prog Photovoltaics 9:137
30. Green M (2002) Physica E 14:65
31. Green MA (2003) Third generation photovoltaics: advanced solar electricity generation. Springer, Berlin
32. Guillemoles JF (2003) In: Proceedings of the 3rd workshop on high efficiency solar energy conversion. JRC, Ispra
33. Güttler G, Queisser H (1970) Impurity photovoltaic effect in silicon. Energy Conver 10:51–55
34. Harder N (2003) Theoretical limits of thermophotovoltaic solar energy conversion. Semicond Sci Technol 18:S151–S157
35. Harder N-P, Green MA (2003) Thermophotonics. Semicond Sci Technol 18:S270–S278
36. Hatsopoulos GN, Kaye J (1958) Measured thermal efficiencies of a diode configuration of a thermo electron engine. J Appl Phys 29:1124–1125
37. Henry CH (1980) J Appl Phys 51:4494
38. Hofler H, Wurfel P, Ruppel W (1983) Sol Cells 10:257
39. Islangulov RR, Kozlov DV, Castellano FN (2005) Low power upconversion using MLCT sensitizers. Chem Commun 30:3776–3778
40. Kammerer C, Cassabois G, Voisin C, Delalande C, Roussignol P, Gerard JM (2001) Phys Rev Lett 87:207401
41. Keevers MJ, Green MA (1994) Efficiency improvements of silicon solar cells by the impurity photovoltaic effect. J Appl Phys 75:4022–4031
42. Keevers MJ, Green MA (1996) Extended infrared response of silicon solar cells and the impurity photovoltaic effect. Solar Energy Mater Solar Cells 41–42:195–204
43. Kettemann S, Guillemoles JF (1995) In: Proceedings of the 13th photovoltaics solar energy conference, Nice
44. Kettemann S, Guillemoles JF (2002) Physica E 14
45. Koeck FAM et al (2004) On the thermionic emission from nitrogen-doped diamond films with respect to energy conversion. Diamond Relat Mater 13:2052–2055
46. Kolodinski S, Werner J, Wittchen T, Queisser H (1993) Appl Phys Lett 63:2405

47. Laroche F (2005) Thèse Ecole Centrale Paris
48. Le Bris A, Guillemoles J-F (2010) Hot carrier solar cells: achievable efficiencies accounting for main thermalization paths. Appl Phys Lett 97:113506
49. Le Bris A, Lombez L, Laribi S, Boissier G, Christol P, Guillemoles J-F (2012) Thermalization rate study of GaSb-based heterostructures by continuous wave photoluminescence and their potential as hot carrier solar cell absorbers. Energy Environ Sci. doi:10.1039/C2EE02843C
50. Lewis (2005) Basic needs for solar energy utilisation. Rapport DOE, http://www.sc.doe.gov/bes/reports/files/SEU_rpt.pdf
51. Li J, Chong M, Zhu J, Li Y, Xu J, Wang P, Shang Z, Yang Z, Zhu R, Cao X (1992) 35% efficient nonconcentrating novel silicon solar cell. Appl Phys Lett 60:2240–2242
52. Licht S (2005) Solar water splitting to generate hydrogen fuel – a photothermal electrochemical analysis. Int J Hydrogen Energy 30:459–470
53. Lin GH, Abdu R, Bockris JOM (1996) Investigation of resonance light absorption and rectification by subnanostructures. J Appl Phys 80:565
54. Luque A (2011) Will we exceed 50% efficiency in photovoltaics? J Appl Phys 110:031301
55. Luque A, Marti A (1997) Phys Rev Lett 78:5014
56. Matsuura D (2002) Appl Phys Lett 81:4526
57. Maruyama T, Kitamura R (2001) Transformations of the wavelength of the light incident upon solar cells. Solar Energy Mater Solar Cells 69:207–216
58. Nelson J, Barnes J, Ekins-Daukes N, Kluftinger B, Tsui E, Barnham K (1998) J Appl Phys 82:6240
59. Nield J et al (2000) Nature 7:44–47
60. Olson JM, Kurtz SR, Kibbler KE (1990) Appl Phys Lett 56:623
61. Palz W (ed) (2010) Power for the world: the emergence of electricity from the sun. Pan Stanford publishing
62. Pellé F, Ivanova S, Guillemoles J-F (2011) Improved c-Si solar cell efficiency by upconversion in Er^{3+} doped fluoride-based materials. EPJ Photovolt 2:20601. http://dx.doi.org/10.1051/epjpv/2011002
63. Raulot JM, Domain C, Guillemoles JF (2005) Phys Rev B 71:35203
64. Roosmalen JAM (2004) Molecular-based concepts in PV towards full spectrum utilization. Semiconductors 38(8): 970–975
65. Rosenwaks Y et al (1993) Phys Rev B 48:14675
66. Ross RT, Nozik AJ (1982) J Appl Phys 53:3813
67. Sariciftci NS (2004) Mater Today 7:36–40
68. Schaller RD, Klimov VI (2004) High efficiency carrier multiplication in PbSe nanocrystals: implications for solar energy conversion. Phys Rev Lett 92:186601
69. Schwede JW, Bargatin I, Riley DC, Hardin BE, Rosenthal SJ, Sun Y, Schmitt F, Pianetta P, Howe RT, Shen Z-X, Melosh NA (2010) Photon-enhanced thermionic emission for solar concentrator systems. Nat Mat 9:762. doi:10.1038/NMAT2814
70. Semonin OE, Luther JM, Choi S, Chen H-Y, Gao J, Nozik AJ, Beard MC (2011) Peak external photocurrent quantum efficiency exceeding 100% via MEG in a quantum dot solar cell. Science 334:1530
71. Shalav A, Richards BS, Trupke T, Corkish RP, Krämer KW, Güdel HU, Green MA (2003) Presented at the 3rd world PV conference, Osaka
72. Sheldon MT, Eisler CN, Atwater HA (2012) GaAs passivation with trioctylphosphine sulfide for enhanced solar cell efficiency and durability. Adv Energy Mater. Article first published online: 7 Feb 2012, doi:10.1002/aenm.201100666
73. Shockley W, Queisser HJ (1961) J Appl Phys 32:510
74. Sokolov IM (1998) On the energetics of a nonlinear system rectifying thermal fluctuations. Europhys Lett 44:278
75. Sommerdijik JL, Bril A, deJager Lumin AWJ (1974) 8,341
76. Spirkl W et al (1995) Phys Rev B 52:11319
77. Tablero C, Garcia AJ, Fernandez JJ, Palacios P, Wahnon P (2003) First principles characterization of direct transitions for high efficiency new photovoltaic materials. Comput Mater Sci 27:58
78. Tables PV (2011) Solar cell efficiency tables (version 38). Prog Photovolt Res Appl 19:565–572
79. Trupke T, Green MA, Wurfel P (2002) J Appl Phys 92:4117
80. Ullrich B, Schroeder R (2002) Two-photon-excited green emission and its dichroic shift of oriented thin-film CdS on glass formed by laser deposition. Appl Phys Lett 80:356
81. VanMaeckelberg D (2003) In: Proceedings of the 3rd workshop on high efficiency solar energy conversion. JRC, Ispra
82. Venkatasubramanian R, Siivola E, Colpitts T, O'Quinn B (2001) Nature 413(6856):597
83. Wegh RT, Donker H, Donker KD, Meijerink A, Lumin J (1999) 82:93
84. Wegh RT, Donker H, Oskam KD, Meijerink A (1999) Science 283:663
85. Wenseleers W et al (2002) J Phys Chem B 106:6853–6863
86. Werner JH, Kolodinski S, Queisser HJ (1994) Phys Rev Lett 72:3851
87. Wolf M, Brendel R (1998) J Appl Phys 83:4213
88. Wurfel P (1982) The chemical potential of radiation. J Phys C: Solid State Phys 15:3967
89. Wurfel P (1993) Limiting efficiency for solar cells with defects from a three-level model. Solar Energy Mater Solar Cells 29:403–413
90. Wurfel P (1997) Solar energy conversion with hot electrons from impact ionisation. Solar Energy Mater Solar Cells 46: 43–52
91. Wurfel P (2003) Theoretical limits of thermophotovoltaic solar energy conversion. Semicond Sci Technol 18:S151–S157
92. Wurfel P et al (2005) Prog Photovolt
93. Yamaguchi M (2001) Clean electricity from PV. Imperial College Press, London
94. Yu KM, Walukiewicz W, Wu J, Shan W, Beeman JW, Scarpulla MA, Dubon OD, Becla P (2003) Diluted II–VI oxide semiconductors with multiple band gaps. Phys Rev Lett 91:246403–246411

Solar Cells: Energy Payback Times and Environmental Issues

Vasilis Fthenakis
National Photovoltaic Environmental Research Center, Brookhaven National Laboratory, Upton, NY, USA
Center of Life Cycle Analysis, Columbia University, New York, NY, USA

Article Outline

Glossary
Definition of the Subject
Introduction
Material and Energy Inventories in the Life Cycle of Photovoltaics
Energy Payback Times and Greenhouse Gas Emissions: Methodology
Energy Payback Times and Greenhouse Gas Emissions: Results
Conclusion
R and D Needs
Acknowledgment
Bibliography

Glossary

a-Si Amorphous silicon
AC Alternate current
BOS Balance of system (includes all system parts except modules, i.e., inverters, transformers, wiring, mounting structure tracking if applicable, foundations)
c-Si Crystalline silicon
CdS Cadmium sulfide
CdTe Cadmium telluride
CIGS Copper indium gallium diselenide
CIS Copper indium diselenide
DC Direct current
DNI Direct normal irradiance
EPBT Energy payback time
ESP Electrostatic precipitators
FBR Fluidized bed reactor
GaAs Gallium arsenide
GHG Greenhouse gas
GWP Global warming potential
HCPV High-concentration PV
LCA Life cycle analysis (or assessment)
LCI Life cycle inventory
mc-Si Multicrystalline silicon
mono-Si Monocrystalline silicon
PR Performance ratio
PV Photovoltaics
SiH_4 Silane
$SiHCl_3$ Trichlorosilane
SOx Sulfur oxide
TeO_2 Tellurium dioxide
UCTE Union for the Coordination of Transmission of Electricity
VTD Vapor transport deposition

Definition of the Subject

Assessments of the environmental impacts of energy-generation technologies are essential in evaluating their sustainability. Common metrics for evaluations of renewable energy systems include energy payback times greenhouse gas emissions, and toxic emissions in their cradle-to-grave life cycles. This chapter discusses the energy payback times (EPBTs) and environmental profiles of major commercial types of photovoltaics, i.e., monocrystalline silicon, multicrystalline silicon, and cadmium telluride, mounted on fixed-tilt ground-mount systems, and GaInP/GaInAs/Ge high-concentration solar tracking systems.

Introduction

Life cycle assessment (LCA) is a tool for measuring the indicators of environmental sustainability of products and technologies, including the generation of

Author Biosketch
Vasilis Fthenakis is a Senior Chemical Engineer, Senior Scientist, and the Head of the Photovoltaics Environmental Research Center at Brookhaven National Laboratory in a joint appointment with Columbia University where he is a Professor of Earth and Environmental Engineering and the Founder and Director of the Center for Life Cycle Analysis. He is the author of 250 publications, member of the Editorial Boards of Progress in Photovoltaics and the Journal of Loss Prevention. He is also a Fellow of the American Institute of Chemical Engineers, a Fellow of the International Energy Foundation, and member of several energy- and sustainability expert panels.

electricity through solar PV devices. Recent LCA studies show that PV technologies have very low environmental impacts compared to those of conventional electricity generation [1]. However, a broad review of the literature reveals several PV LCA studies with widely differing estimates. For example, the reported life cycle greenhouse gas (GHG) emissions of thin-film amorphous silicon (a-Si) PV systems range from 11- to 226-g CO_2-eq. per kWh of electricity produced [2]. Such divergence reflects different assumptions about key parameters, like product design, solar irradiation, performance ratio (PR), and lifetime. The estimates also deviate because of the different types of installation used, such as ground-mounts, rooftops, and façades. Most importantly, the assessments often are made from outdated information in the literature collected from antiquated PV systems, and are used for guiding policy analyses.

This chapter summarizes the results of PV life cycle analyses using as the main indicators energy payback times (EPBTs), greenhouse gas (GHG) emissions, and toxic emissions, based on actual data from the present-day commercial production of silicon-, thin-film-, and high-concentration photovoltaic systems. These indicators are crucial in assuring the public's acceptance of energy technologies because climate change arguably is the most significant threat facing our planet.

Material and Energy Inventories in the Life Cycle of Photovoltaics

The life cycle stages of photovoltaics involve (1) the production of raw materials, (2) their processing and purification, (3) the manufacture of solar cells, modules, and the balance of system (BOS) components, (4) the installation and operation of the systems, and, (5) their decommissioning, disposal, or recycling (Fig. 1). Typically, separate life cycle assessments (LCAs) are undertaken for the modules and the BOS components (inverters, transformers, mounting, supports, wiring), as the module's technologies evolve more rapidly and entail more options than do the BOS structures. The latter were considered herein for both ground-mount and rooftop installations; façade systems are not described as they are very much site specific. Processes in the life cycle stages of PV systems include the following:

1. Upstream Processes
   - Raw-material acquisition: e.g., mining the ores, extracting the fossil fuel, and growing trees
   - Materials production: e.g., metal smelting, purification, alloying, polymerization, wafer production)
   - Solar-cell production or thin-film deposition: e.g., wafer cutting, sputtering, chemical vapor deposition, vapor transport deposition

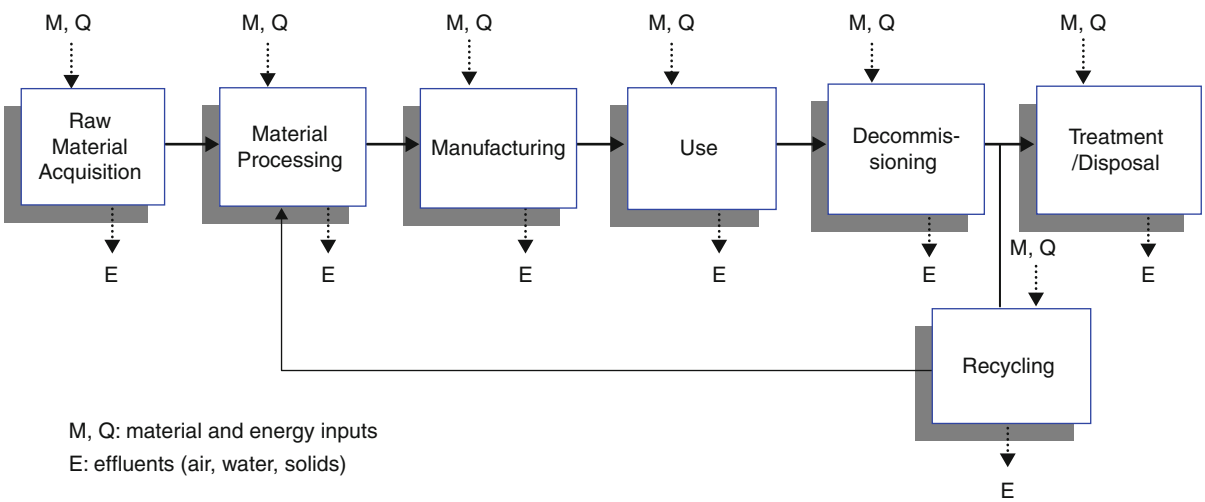

Solar Cells: Energy Payback Times and Environmental Issues. Figure 1
Flow of the life cycle stages, energy, materials, and wastes for PV systems

- Module production: e.g., contact formation, encapsulation, wiring, and assembly
- Module and BOS installation: e.g., installing module, inverter, and support structures

2. Operation and Maintenance: e.g., tracker operation, if applicable, rinsing if applicable, other scheduled maintenance, and office use for utility-scale plant
3. Downstream Processes
   - Decommissioning and disposal: demolition and transportation
   - Recycling: collection, disassembly, shredding, and material separation

Crystalline Si-PV Modules

A life cycle analysis starts with mining the raw materials (i.e., quartz sand for silicon PV; Zn- and Cu-ores for CdTe PV and the metals used in the balance of systems – BOS), and continues with their processing and purification (Fig. 2). The silica in the quartz sand is reduced in an arc furnace to metallurgical-grade silicon, which is purified into solar-grade polysilicon by either a silane (SiH_4)- or a trichlorosilane ($SiHCl_3$)-based process. The energy requirement for purification is the largest expense for making crystalline Si-PV modules, accounting for 45% of the primary energy used in fabricating multi-Si modules. Two technologies are

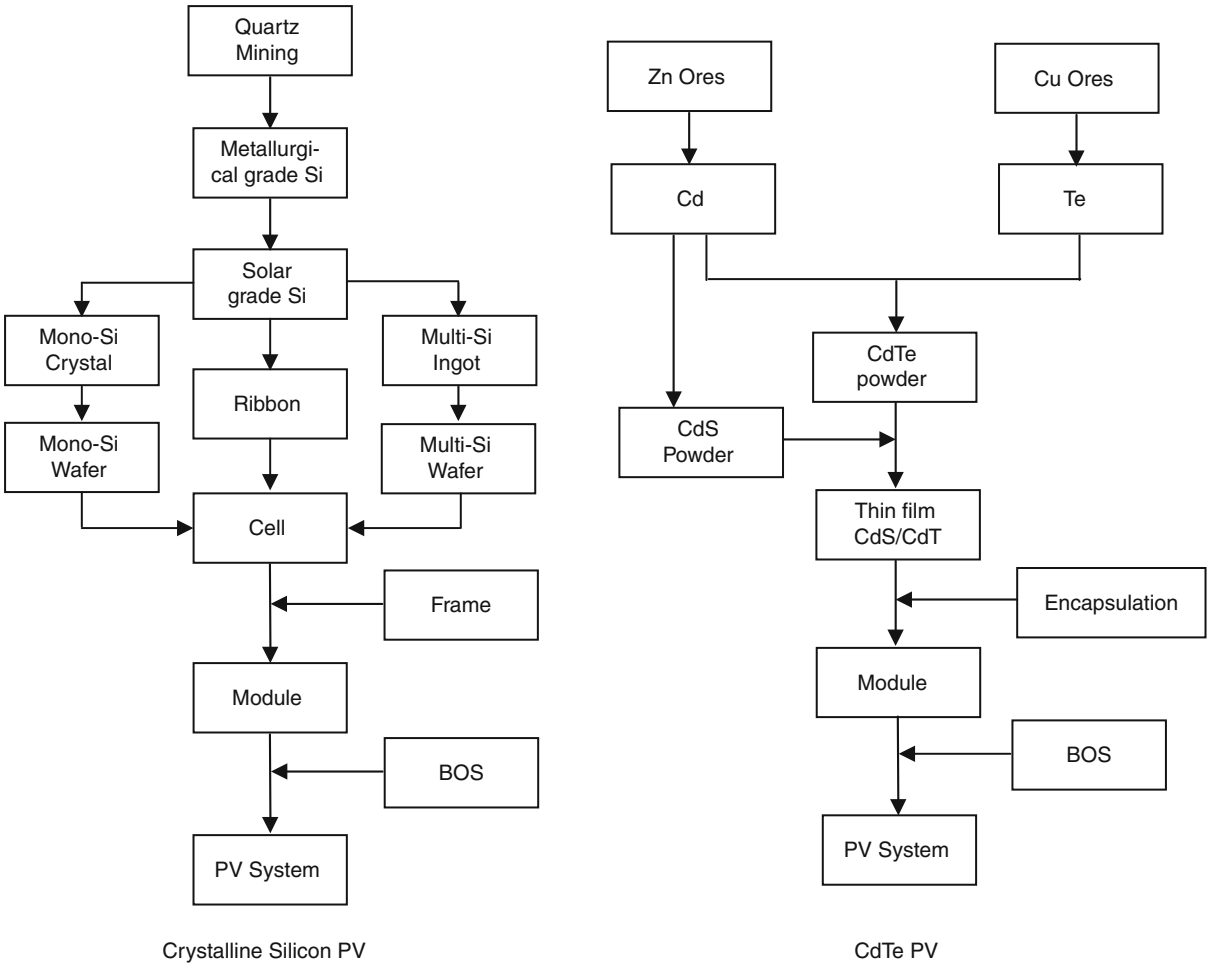

Solar Cells: Energy Payback Times and Environmental Issues. Figure 2
Detailed flow diagram for PV from the acquisition of raw material to its manufacturing stage

employed for producing polysilicon from silicon gases: the Siemens reactor method, and the fluidized bed reactor (FBR) method. In the former, which accounts for the majority (~90% in 2004) of solar-grade silicon production in the United States, silane or trichlorosilane is introduced into a thermal-decomposition reactor with high-temperature (~1,100–1,200°C) polysilicon rods [3, 4]. The silicon rods grow as silicon atoms from the gas phase deposited on them [3]. In 1987, MEMC Electronic Materials commercialized the FBR method on a small scale; recent developments show promise for scaling up production to meet the needs of the emerging solar industry. In this approach, granular polysilicon is produced by decomposing silane around seed particles in a mixture of silane/hydrogen fed into the reactor. This continuous production process offers inherent advantages over the Siemens batch-process, requiring lower energy consumption while enabling higher throughput. However, such advantages have not been quantified in life cycle analyses [5]. The life cycle inventory (LCI) data used in the studies reviewed here correspond to polysilicon production via the Siemens method, and were gathered in the European "Crystal Clear" project [3, 4]. Table 1 presents the aggregated life cycle inventories (LCIs), compiled from data from 11 European and a US plant [6–8]. Data on ribbon-silicon technologies are not presented herein, because these were found to be insufficiently documented. Detailed LCIs appear in a forthcoming IEA PVPS Task 12 report [9].

CdTe PV Modules

Fthenakis and Kim reported the LCI data for CdTe thin-film technology gleaned from the 2005 production data from First Solar's plants, Perrysburg, United States in 2005, and from Frankfurt-Oder, Germany data in 2008 [10, 11]. Held [12, 13] and Raugei [14, 15] used the same data in their independent investigations.

The life cycle inventories of the minor metals used in thin-film CdTe PVs (e.g., Cd and Te) are related closely to the production cycle of the respective base metals, Zn and Cu [16]. Cadmium is obtained from the waste streams in zinc smelting, mainly in the slimes from the Zn-electrolyte purification stages, and the particulates collected in baghouses, electrostatic precipitators, and cyclones in the thermal-oxidation units; thereafter, it is processed further and purified to the 99.999% purity required for synthesizing CdTe. Te is recovered after treating with dilute sulfuric acid the slimes produced during electrolytic copper refining; these slimes also contain Cu and other metals. After its cementation with copper, CuTe is leached out with caustic soda to produce a sodium-telluride solution that is used as the feed for Te and TeO_2. Additional leaching and vacuum-distillation produces Te- and TeO_2-powders of 99.999% purity required for

Solar Cells: Energy Payback Times and Environmental Issues. Table 1 Materials and energy inputs in the production of Si and CdTe PV modules –per square meters of module (excluding frames, commonly used for Si modules) [8]

Category	Inputs	Multi-Si	Mono-Si	CdTe
Components (kg)	Cell materials	1.6	1.5	0.065
	Glass	9.1	9.1	19.2
	Ethylene vinyl acetate	1.0	1.0	0.6
	Others	1.8	1.8	2.0
Consumables (kg)	Gases	2.2	7.8	0.001
	Liquid	6.8	6.6	0.67
	Others	4.3	4.3	0.4
Energy	Electricity (kWh)	248	242	59
	Oil (liter)	0.05	0.05	0.05
	Natural gas (MJ/)	308	361	–

synthesizing pure CdTe. This same route is followed in generating solar-grade CdS, used as a window layer in CdTe PV. Both the CdTe- and CdS-layers are placed by vapor-transport deposition, based on subliming the powders and condensing the vapors on glass substrates. A stream of inert carrier gas guides the cloud of sublimed dense vapor to deposit the films on glass substrates at 500–600°C at a line speed of up to 8 ft/min [17], followed by depositing layers of metals. Thereafter, a series of scribing and heat treatments form interconnections and back contacts. Currently (4Q2010), First Solar produces CdTe PV modules with an efficiency of 11.6%.

Glass is the heaviest part of PV module, particularly in frameless CdTe modules where two panes of glass ensure their structural toughness. The double-glass design eliminates the need for an aluminum frame that accounts for a significant fraction of emissions from making silicon modules. The use of thin-film layers per unit area of thin-film CdTe, CIGS, and a-SiGe is minimal compared with silicon modules since the thickness of cell materials in the former is 1–3 μm compared with ~200 μm for the latter. Thin-film modules also require lesser amounts of consumables than do silicon modules, as fewer process steps are involved (Table 1).

CIGS PV Modules

Currently, CIGS PV are available in several major layer configurations depending on the substrate and encapsulation materials, including glass/glass, glass/polymer, and polymer/polymer. Reported module efficiencies range from 9.4% to 13.1%. In double-glass configuration, manufacturers offer frameless modules as the two glass sheets provide sufficient structural integrity.

The European Commission's project ECLIPSE (Environmental and Ecological Life Cycle Inventories for present and future Power Systems in Europe) was the first major research on the life cycle inventory of commercial CIGS PV. This project compiled life cycle inventories of emerging options for power generation, including PV, wind, and biomass. The PV technologies investigated were single- and multicrystalline silicon modules, and thin-film modules, such as amorphous silicon (a-Si), copper indium gallium diselenide (CIGS), and cadmium telluride (CdTe). This study reported the usage of mass of metals, glass, encapsulating polymer, and a frame, along with electricity requirement during manufacturing based on data from the literature [14].

Raugei et al. [15] collected the first life cycle inventory from an actual production line of CIGS PV, from a pilot-scale manufacturing process of Würth Solar, Germany [14]. The SENSE report [18] gave information on the production of CIGS solar modules by Würth Solar; Lazonovski and Held [19] summarize it. The sputtering of molybdenum aims at coating the "back contact." The substrates are structured by laser techniques. Targets of copper, indium, gallium, and selenium are coevaporated, and substrates carry the vapors under an inert-gas-flow process. A buffering layer of CdS (cadmium sulfide) is put on to the substrates by dip coating. The front electrode is deposited by the sputtering of zinc oxide, doped with Al_2O_3. Laser scribing follows the deposition of each layer. A functional test identifies the defective products. The addition of interconnects and front glass completes the module production. Section "Energy Payback Times and Greenhouse Gas Emissions: Results" shows the results of the SENSE report; however, the corresponding LCI data are not available.

Amorphous Si and Microcrystalline Silicon PV Modules

Uni-Solar, the biggest US producer of amorphous silicon PV products, manufactures triple junction a-SiGe photovoltaics on rolls of stainless steel that are cut to different sizes, varying from solar shingles to large laminates that follow the curvature of any roof. Keoleian and Lewis [20] modeled the environmental performance of a-Si BIPV roofing shingles. Since then, the company generated large laminates that are suitable for a variety of applications, while further developing their a-SiGe production line; recently, they announced their transition to TF-Si-based laminates. Kim and Fthenakis [21] conducted a life cycle analysis of replacing the intrinsic a-Si layer with a nano-crystalline Si layer. The investigators modeled a triple junction a-Si module, a-Si:H/a-SiGe:H/a-SiGe:H, while for nanotechnology, they assessed three prospective combinations of hybrid amorphous- and crystalline silicon cells (Fig. 3). The first configuration is a tandem

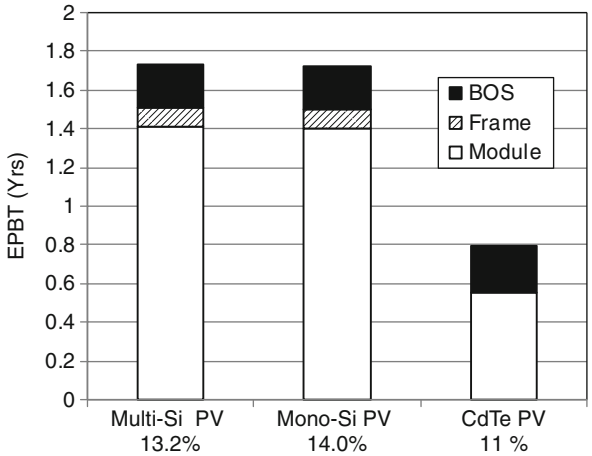

Solar Cells: Energy Payback Times and Environmental Issues. Figure 3
EPBT of PV systems: Rooftop installed module with insolation =1,700 kWh/m^2/year and performance ratio = 0.75; European production

junction that consists of a-Si top layer and nc-Si bottom layer, i.e., a-Si:H/nc-Si:H; the second configuration is a triple junction with nc-Si as the bottom layer, i.e., a-Si:H/a-SiGe:H/nc-Si:H; and, lastly, a triple junction with two layers of nc-Si, i.e., a-Si:H/nc-Si:H/nc-Si:H. Oerlikon Solar developed a design called "Micromorph" that employs a glass substrate on which it laid out a TCO layer (transparent conductive oxide), followed by a-Si- and nc-Si-films. The life cycle energy demand of this design was compared with the above triple junction designs [21].

Major companies in producing thin-film silicon (TF-Si) equipment include Oerlikon and Applied Materials, both of which use NF_3, a potent greenhouse gas for cleaning the reactor in glass-based TF-Si; presently Uni-Solar does not do so. Fthenakis et al. [22] completed a comprehensive study on NF_3 emissions, from its production by Air Products and its use by Applied Materials.

High-Concentration Photovoltaics

High-concentration PV systems are equipped with GaInP/GaInAs/Ge triple junction cells produced by Spectrolab Inc. The cells have a nominal aperture-area efficiency of 37% under 500 kW/m^2, 25°C, and AM1.5

Solar Cells: Energy Payback Times and Environmental Issues. Table 2 Materials and energy inputs for processing 1,000 wafers, corresponding to 915 kWp[a] of GaInP/GaInAs/Ge terrestrial concentrator solar cell [2]

Inputs	Amount
Materials for components (kg)	
Wafer/precursors	21.7
Contact metals	3.4
Anti-reflection coating	0.02
Materials use for process (kg)	
Hydrogen	57.2
Nitrogen	0.2
Photoresist	2.3
Solvents	1073.4
Acids	255.8
Bases	161.3
Electricity (kWh)	
MOVPE	2,365
Others[b] (gas scrubbing and cell processing)	470

[a]At 37% rated efficiency
[b]Estimated from literature [3]

conditions. The semiconductor layers are grown on a germanium substrate via metal-organic vapor-phase epitaxy (MOVPE). Spectrolab Inc. provided the data on materials and energy input for the cell processing that are and summarized in Table 2. A 10% loss of inputs was assumed during the solar-cell production/dicing and assembly. The inventories are scaled for processing 1,000 wafers into 50,000 cells, corresponding to 915 kWp of capacity [23].

Fthenakis and Kim [24] reported an LCA of the Amonix 7700 high-concentration PV system employing these cells. This consists of seven concentrating module units, the MegaModules, mounted on a two-axis tracker. Sunlight is concentrated on to 7,560 focal spots at a rate of 500:1. This system uses multijunction GaInP/GaInAs/Ge cells, grown on a germanium substrate rated at 37% efficiency, under the test condition of 50 W/cm^2, 25°C, and AM1.5D conditions. With an aperture area of 267 m^2, the capacity of this unit corresponds to 53 kW$_p$ AC power.

Solar Cells: Energy Payback Times and Environmental Issues. Table 3 Material breakdown of the Amonix 7700

Sub module	Components	Materials	Mass (kg)	Fraction (%)
MegaModules	Cell	Semiconductor	0.2	0.001
	Frame	Steel	6,566	23.0
	Fresnel lenses	Acrylic	1,143	4.0
	Heat sink	Aluminum	3,086	10.8
Tracker	Foundation	Concrete	3,126	10.9
	Hydraulic drive	Steel	2,724	9.5
	Pedestal and torque tube	Steel	11,260	39.4
	Motor	Various	16	0.1
Electrical	Inverter	Various	500	1.7
	Transformer	Various	100	0.3
	Cables	Copper/PVC	35	0.1
Other	Controller	Various	18	0.1
	Sensor	Various	1.4	0.005
	Anemometer	Various	0.1	0.0003

Table 3 shows the materials composition and mass balance of the Amonix 7700 system. While the measurements of the mass of manufactured parts were taken directly from the assembly line, the quantity of concrete used was calculated from the foundation's dimensions, i.e., 5.5 m deep, and 1.1 m diameter. The detailed material compositions of electrical parts, i.e., motor, transformer, and inverter, were estimated from Mason et al. [25]. The LCI includes the materials used in scheduled maintenance over an expected life time of 30 years; they include changing the hydraulic- and bearing-oils, cleaning the lens, and changing the air- and oil-filters. The MegaModules (36%) and tracker (58%) account for most of the components, while steel (75%), concrete (11%), and aluminum (11%) dominate the material usages.

Balance of System (BOS)

Photovoltaic modules are either rooftop- or ground-mounted. Silicon modules need an aluminum frame for structural robustness, while a second glass back-sheet performs the same function for thin-film CdTe PV. For a rooftop PV application, the BOS typically includes inverters, mounting structures, cables, and connectors. Large-scale ground-mounted PV installations require additional equipment and facilities, such as transformers for grid connections, office facilities, and, in some cases, concrete for installations.

De Wild-Scholten et al. [26] report the material inventories for two types of rooftop-mounting systems: on-roof mounting wherein the system is built on existing roofing material, and in-roof mounting where the modules replace the roof tiles. Table 4 shows the material life cycle inventory (LCI) of common rooftop-mounting systems, cabling, inverters, and transformers, including two sizes (500 W and 2,500 W) of small inverters adequate for rooftop PV designs.

Data on materials- and energy use for a ground-mounted BOS were obtained from the 5-MW_p PV plant at the Springerville, Arizona facility operated by Tucson Electric Power (TEP) (Table 5) [25]. The inverters are utility-scale models with a wide-open frame, allowing the facile replacement of failed parts. Thus, inverters and transformers are expected to last 30 years, with parts amounting to 10% of their total

Solar Cells: Energy Payback Times and Environmental Issues. Table 4 LCI of balance of system (BOS) [19, 20]

(a) Mounting system (kg/m^2 module)				
	On-roof		*In-roof*	
	Phönix, TectoSun	Schletter Eco05 + EcoG	Schletter, Plandach 5	Schweizer, Solrif
Low alloy steel	0	0	0	0
Stainless steel	0.49	0.72	0.28	0.08
Aluminum	0.54	0.97	1.21	1.71
Concrete	0	0	0	0
Frame	3.04	0	0	0
(b) Cabling (g/m^2)				
	Helukabel, Solarflex 101, 4 mm^2, DC		*Helukabel, NYM-J, 6 mm^2, AC*	
Copper	83.0		19.9	
Thermoplastic elastomer (TPE)	64.0		0.0	
PVC	0.0		16.9	
(c) Inverters (g)				
	Philips PSI 500 (500 W)		*Mastervolt SunMaster 2,500 (2,500 W)*	
Steel	78		9,800	
Aluminum	682		1,400	
Copper	2			
Polycarbonate	68			
ABS	148			
Other plastics	5.4			
Printed circuit board	100		1,800[a]	
Connector	50			
Transformers, wire-wound	310		5,500	
Coils	74			
Transistor diode	10			
Capacitor, film	72			
Capacitor, electrolytic	54			
Other electric components	20			

[a]Including electric components (e.g., connectors, transistors)

mass, being replaced every 10 years. The life cycle inventory includes the office facility's materials- and energy use for administrative-, maintenance-, and security staff, as well as for running the maintenance vehicles. Detailed LCIs are shown in a forthcoming IEA PVPS Task 12 report [9].

Energy Payback Times and Greenhouse Gas Emissions: Methodology

The methodology employed in PV LCA studies conforms to the ISO standards 14040 and 14044. Furthermore, the basic assumptions employed for

Solar Cells: Energy Payback Times and Environmental Issues. Table 5 Mass balance of major components for the 3.5 MW Tucson Electric Power Generating plant in Springerville, AZ, based on 30 years of operation

	Balance of system	Mass (kg/MW_p)	% of total
BOS	PV support structure	16,821	10.3
	Module interconnections	453	0.3
	Junction boxes	1,385	0.8
	Conduits and fittings	6,561	4.0
	Wire and grounding devices	5,648	3.4
	Inverters[a] and transformers	28,320	17.3
	Grid connections	1,726	1.1
	Office facilities	20,697	12.6
	Concrete	76,417	46.6
	Miscellaneous	5,806	3.5
	Total	163,834	100.0
Frame[a]		18,141	

Based on 12.2% rated efficiency for mc-Si module
[a]Xantrec PV-150 inverter type

photovoltaics-specific parameters are those agreed within the International Energy Agency (IEA) Task 12 [27]; they are summarized below:

Life expectancy
- Modules: 30 years
- Inverters: 15 years for small plants (residential PV); 30 years with 10% of replacement of parts every 10 year for large plants
- Structure: 30 years for rooftop- and façade-installations and 60 years for ground-mounted ones
- Cabling: 30 years

Performance ratio
- The performance ratio (PR) accounts for the losses from dc to ac conversion, thermal losses, and wire losses, and depends on the kind of installation. In general, the ratio increases with a decline in temperature build-up and monitoring the PV systems for early detection of defects; this means that well-ventilated and large-scale systems have a high performance ratio. A PR of 75% was assumed for rooftop and 80% for ground-mount utility-scale installations.

Degradation
- The degradation of the modules lowers efficiency over the life time. For mature module technologies, a linear degradation of 80% of the initial efficiency was assumed at the end of the 30 years life.

Energy Payback Time

The energy payback time (EPBT) is defined as the period required for a renewable energy system to generate the same amount of energy as that used by the system from cradle to grave. For a PV system, it is quantified as follows:

$$\text{Energy Payback Time(EPBT)} = \frac{E_{comp} + E_{man} + E_{inst} + E_{EOL}}{E_{a.gen.:} + E_{a.oper}}$$

where,

$E_{comp.}$: Primary-energy demand to manufacture the components (includes the energy to produce materials comprising each component)

E_{man}: Primary-energy demand to manufacture the modules (includes electricity as primary-energy equivalent)

$E_{inst.}$: Primary-energy demand to assemble and install the system

E_{EOL}: Primary-energy demand for end-of-life management

$E_{a.gen.}$: Annual electricity generation (primary-energy equivalent)

$E_{a.oper.}$: Annual energy demand for operation and maintenance (primary-energy equivalent)

Calculating the primary-energy equivalent requires knowing the country-specific, energy mixture used to generate electricity and produce materials. The annual electricity generation (E_{agen}) is represented as primary energy based on the efficiency of electricity conversion at the demand side. The electricity is converted to the primary-energy term by dividing it by the average conversion efficiency of 0.29 for the United States and 0.31 for Western Europe [28, 29].

Greenhouse Gas Emissions

Greenhouse gas (GHG) emissions during the life cycle stages of a PV system are estimated as equivalents of CO_2 using an integrated time-horizon of 100 years; the major emissions included in GHG emissions are CO_2 (GWP = 1), CH_4 (GWP = 23), N_2O (GWP = 296) and chlorofluorocarbons (GWP = 4,600–10,600) [30]. (Global Warming Potential is an indicator of the relative radiative effect of a substance compared to CO_2, integrated over a chosen time-horizon; the GWP_{100} corresponding to a 100 year horizon is used here.) Electricity- and fuel use during the production of the PV materials and modules are the main sources of the GHG emissions for PV cycles. Methods of generating the upstream electricity also play an important role in determining the total GHG emissions, as the higher the mixture of fossil fuels is in the grid, the higher are the GHG- and toxic- emissions. Thus, the GHG emission factor of the average US electricity grid is higher than that of the average Western European (UCTE) grid; that of China is higher than both of them. During 1999–2002, the US average CO_2 emissions inventory from electricity production and transmission was 676 g CO_2/kWh, while, in Germany, it was 539 g CO_2/kWh, and in China, it was 839 g CO_2/kWh [31]. These differences correspond to an estimated increase of 20% in the GHG emissions for producing modules and BOS components in China versus in the United States. Furthermore, transporting the modules and BOS components from China to either the United States or Europe could add an additional 15% to the GHG emissions.

Energy Payback Times and Greenhouse Gas Emissions: Results

EPBT

The latest (2010) estimates of the primary-energy used in the life cycle of complete rooftop Si-PV systems are 2,700 and 2,900 MJ/m^2, respectively, for multi-, and monocrystalline Si modules, down from 5,000 to 2,700 in 2006 [11]. The EPBT of these systems is 1.8 years for module efficiencies of 13.2% and 14% correspondingly, in rooftop installations under Southern European insolation of 1,700 kWh/m^2/year and a performance ratio (ratio between the dc-rated and actual ac electricity output) (PR) of 0.75 (Fig. 3). In these estimates, the BOS for rooftop application accounts for 0.3 years of EPBT, but there are different types of rooftop-mounting systems with different energy burdens.

For CdTe PV, the energy consumption is 850 MJ/m^2 and 970 MJ/m^2, correspondingly based on actual production from First Solar's plant in Frankfurt-Oder, Germany and Perrysburg, Ohio, United States. The energy burden at the US plant is higher than that in Germany because the former includes R&D and additional administrative functions. For insolation levels of 1,700 kWh/m^2/year, the EPBT for the European production is 0.8 year and for the US production is 0.9 year.

The EPBT decreases as the solar irradiation levels increases; for example, in Phoenix, Arizona, US Southwest, (latitude optimal irradiation of 2,370 kWh/m^2/year), the EPBTs of crystalline silicon- and cadmium telluride-PV in fixed-tilt ground-mount utility installations, respectively, are 1.3 and 0.6 years. At the same location, the two-axis Amonix HCPV would have an EPBT of 0.9 years (Table 6).

Greenhouse Gas Emissions

Brookhaven National Laboratory (BNL) in collaboration with the National Renewable Energy Laboratory (NREL) recently undertook a harmonization study of greenhouse estimates from the hundreds of reported

Solar Cells: Energy Payback Times and Environmental Issues. Table 6 Comparison of life cycle parameters and performances across PV technologies (normalized for Phoenix insolation)

PV system	Amonix HCPV, 7700 current	Multi c-Si ground-mount	Mono c-Si ground-mount[a]	CdTe ground-mount[b]
Module DC efficiency (%)	37 (cell)	13.2	14	10.9
Insolation (kWh/m^2/year)	2480[c]	2370[d]	2370[d]	2370[d]
EPBT (years)	0.9		1.8	0.7

[a]Adapted from [2, 12]
[b]Adapted from [13]
[c]Direct normal insolation with 2-axis tracker
[d]Longitude optimal insolation for flat-plate collectors
[e]100 years of integrated time-horizon

life cycle assessments. It consisted of systematically gathering nearly all publicly available life cycle assessments (LCAs) that referred to photovoltaics, screening them to ensure minimum standards of quality and relevance, and then reconciling several key performance characteristics (e.g., irradiation, system lifetime, module efficiency, and performance ratio) with standard values following the IEA Task 12 Guidelines [27].

Four crystalline Si-PV 400 studies were screened; before matching them, the median life cycle GHG emissions reported in the c-Si LCAs passing screens was 57 g CO_2e/kWh, with an interquartile range (IQR) of 44–73. After harmonization, the median estimate declined to 32–57 g CO_2e/kWh and IQR tightened to 27–35 [32]. The median GHG decreased because of higher irradiation, and a longer system lifetime. Standardizing irradiation and system lifetime were the most effective parameters reducing variability. The most valid LCAs for crystalline silicon modules are those based on data obtained from the CrystalClear Project. The GHG emissions of Si modules are ~29 g CO_2-eq./kWh range, for a rooftop application under Southern European insolation of 1,700 kWh/m^2/year, and a performance ratio (ratio between the dc-rated and actual ac electricity output) (PR) of 0.75 (Fig. 4). Notably, under these estimates, the BOS for rooftop applications accounts for ~5 g CO_2-eq./kWh of GHG emissions. These calculations were based on the electricity mixture for the current (2009) production of Si that is powered by hydroelectricity.

The harmonization process of thin-film photovoltaics involved 109 LCA studies [33]. As with the work

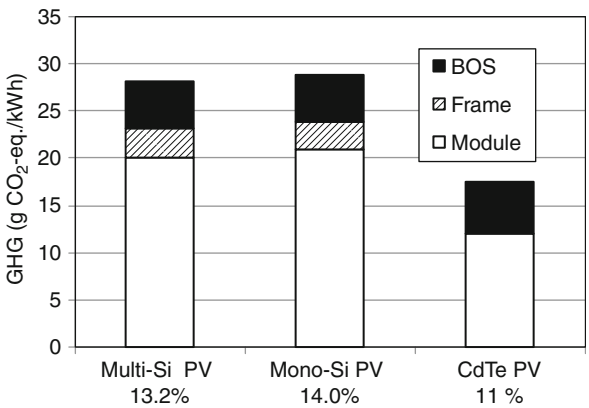

Solar Cells: Energy Payback Times and Environmental Issues. Figure 4
GHG emissions of PV systems: rooftop installed module with insolation =1,700 kWh/m^2/year and performance ratio = 0.75; European production

on c-Si activity, the initial screening eliminated abstracts, short conference papers, presentations without supporting documentation, and unrelated analyses; 90 studies passed this screening. In the primary screening, rigorous criteria were applied to assure the completeness of reporting, the validity of LCA methods, and the relevance to present times of the PV system studied. Additionally, it was determined whether the product is a commercial one, whether the production line still exists, and whether the study's core data is original or secondary. These screenings identified four studies as the best representations of the carbon footprint of the modern thin-film PV

technologies: Pacca et al. [34] for a-Si; Fthenakis et al. [1, 11] for CdTe; Raugei et al. [15, 35]; and SENSE for CIGS[18, 19]. The corresponding GHG emissions are 28, 17, 55, and 35 g CO_2-eq./kWh for irradiation levels of 1,700 kWh/m^2/year. The wide difference in the CIGS estimates highlights the need for more complete analyses of these technologies.

For assessing BOS, estimates were used of GHG emissions from rooftop systems, based on the Crystal Clear project [36, 37]; they correspond to 5 g CO_2-eq./kWh under 1,700 kWh of insolation, with 14% module efficiency, and performance ratio of 0.75. For ground-mounted BOS, data were employed corresponding to the Tucson Electric Power (TEP) power plant in Springerville, Arizona [25]. They are 5.4 g CO_2-eq./kWh, harmonized for the same conditions as the rooftop application. Emissions from the structural part of the BOS were adjusted according to the conversion efficiency of PV, whereas emissions from the inverter portion of the BOS that depend on power output were unchanged. Thin-film CdTe PV modules have no frames, and the same was assumed for CIGS modules. A triple junction a-Si module deposited on a stainless-steel substrate, manufactured by Uni-Solar, uses as a frame one with a very thin aluminum profile, specifically, 15 g of anodized extruded aluminum per m^2 of module, except for building-integrated applications [34]. Crystalline silicon modules employ a single glass sheet, and have an aluminum frame for structural stability, weighting ~3 kg per m^2 of module.

Both the as published- and harmonized-LCA results suggest that the carbon footprint of thin-film PV technologies fall significantly as production capacity increases, reflecting the technological advances in process- and device designs. For example, between 2005 and 2010, First Solar's annual production capacity of CdTe PV jumped from 25- to 1,100-MW_p, and, during the same period, the module efficiency of CdTe PV increased from 9% to 11.6% while the life cycle GHG estimates fell by ~30% [1, 11, 37]. Scaling up a CIGS PV prototype to a 15 MW_p commercial line for Würth Solar also likely will result in significant, but yet to be accurately determined, reductions in GHG emissions [15, 19].

Figure 5 compares GHG emissions from the life cycle of PV with those of conventional fuel-burning power plants, revealing the environmental advantage of using PV technologies. The majority of GHG emissions come from the operational stage for the coal-, natural gas-, and oil fuel cycles, while the material and device production accounts for nearly all the emissions for the PV cycles. With over 50% contributions, the GHG emissions from the electricity demand in the life cycle of PV are the most impactful input. Therefore, the LCA results strongly depend on the available electricity mix. The GHG emissions from the nuclear fuel cycle mainly are related to the fuel production, i.e., mining, milling, fabrication, conversion, and the enrichment of uranium fuel. The details of the US nuclear fuel cycle are described elsewhere [38].

Other comparisons between the life cycles of photovoltaics and conventional power generation cover land use [39] and water use [40]. Accounting for the land occupation in coal mining, it is shown that the life cycles of PV in the US-SW occupy about the same or less land, and orders of magnitude less water, on an electricity produced (GWh) basis, than the average coal-based power generation.

Toxic Gas Emissions

The emissions of toxic gases (e.g., SO_2, NO_x) and heavy metals (e.g., As, Cd, Hg, Cr, Ni, Pb) during the life cycle of a PV system are largely proportional to the amount of fossil fuel consumed during its various phases, in particular, processing and manufacturing PV materials. Figure 6 shows estimates of SO_2 and NO_x emissions. Heavy metals may be emitted directly from material processing and PV manufacturing, and indirectly from generating the energy used at both stages. For the most part, they originate as trace metals in the coal used.

Direct emissions of cadmium in the life cycle of CdTe PV were assessed in detail [41]. They total 0.016 g per GWh of PV-produced energy under an irradiation of 1,700 kWh/m^2/year (Table 7); this includes emissions during fires on rooftop residential systems, quantified in experiments at Brookhaven National Laboratory that simulated actual fires [42]. These experiments were designed to replicate average conditions, and the estimated emissions were calculated by accounting for US fire-statistics pointing to 1/10,000 houses catching fire over the course of a year in the United States where most houses have wood-frames, by assuming that all fires involve the roof. The indirect

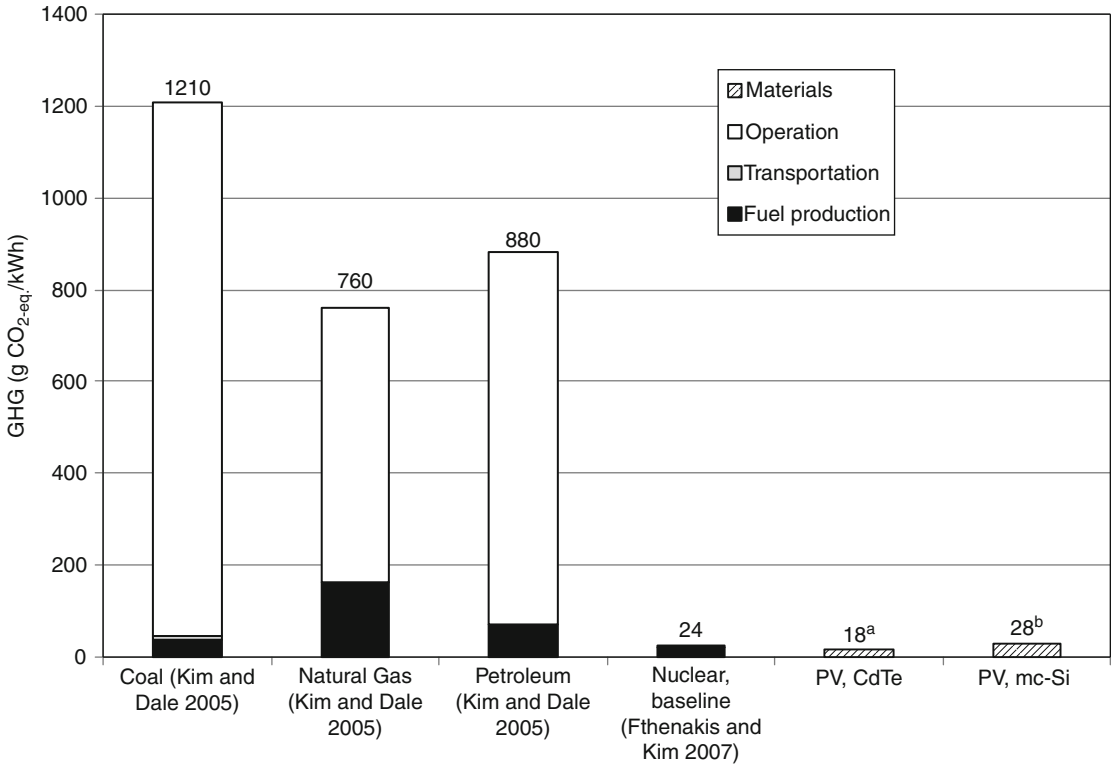

Solar Cells: Energy Payback Times and Environmental Issues. Figure 5
Comparison of emissions from PV with those from conventional power plants (Insolation of 1,700 kWh/m^2/year, performance ratio of 0.75)

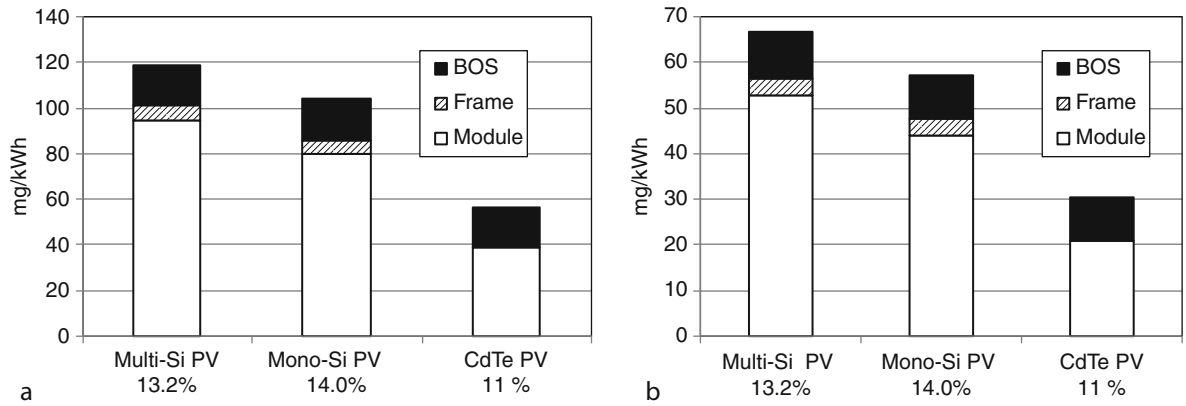

Solar Cells: Energy Payback Times and Environmental Issues. Figure 6
Life cycle emissions of (**a**) SO_2, and (**b**) NO_x emissions from silicon and CdTe PV modules. BOS includes module supports, cabling, and power conditioning. The estimates are based on rooftop-mount installation, insolation of 1,700 kWh/m^2/year, performance ratio of 0.75, lifetime of 30 years, and European production with electricity supply from the UCTE grid

Solar Cells: Energy Payback Times and Environmental Issues. Table 7 Direct, atmospheric Cd emissions during the life cycle of the CdTe PV module (Allocation of emissions to coproduction of Zn, Cd, Ge, and In)

	Air emissions (g Cd/tonne Cd[a])	Allocation (%)[b]	Air emissions (g Cd/ton Cd[a])	mg Cd/GWh[c]
Mining of Zn ores	2.7	0.58	0.016	0.02
Zn smelting/refining	40	0.58	0.23	0.3
Cd purification	6	100	5.97	7.79
CdTe production	6	100	5.97	7.79
PV manufacturing	3	100	0.40	0.52
Operation	0.3	100	0.05	0.06
Disposal/recycling	0	100	0.10	0.13
Total			12.74	16.61

[a]Ton of Cd produced

[b]Emissions are allocated between coproducts (Zn, Cd and other) based on mass and cost proportioning, according to ISO 14040 guidelines

[c]Energy produced assuming average Southern European insolation (i.e., 1,700 kWh/m^2/year), 9% electrical conversion efficiency, and a 30-year life for the modules

Cd emissions from electricity usage during the life cycle of CdTe PV modules (i.e., 0.24 g/GWh) are an order-of-magnitude greater than the direct ones (routine and accidental) (i.e., 0.016 g/GWh) [1, 10]. (Indirect emissions of heavy metals result mainly from the trace elements in coal and oil. According to the US Electric Power Research Institute's (EPRI's) data, under the best/optimized operational- and maintenance conditions, burning coal for electricity releases into the air between 2- and 7-g of Cd/GWh [43]. In addition, 140 g/GWh of Cd inevitably collects as fine dust in boilers, baghouses, and electrostatic precipitators (ESPs). Furthermore, a typical US coal-powered plant emits per GWh about 1,000 t of CO_2, 8 t of SO_2, 3 t of NO_x, and 0.4 t of particulates. The emissions of Cd from heavy oil burning power plants are 12–14 times higher than those from coal plants, even though heavy oil contains much less Cd than coal (~0.1 ppm); this is because these plants do not have particulate-control equipment [41].) Cadmium emissions from the electricity demand for each module were assigned, assuming that the life cycle electricity for the silicon and CdTe PV modules was supplied by the Union for the Coordination of Transmission of Energy's (European) grid. The complete life cycle atmospheric Cd emissions, estimated by adding those from the usage of electricity and fuel in manufacturing and producing materials for various PV modules and Balance of System (BOS), were compared with the emissions from other electricity-generating technologies (Fig. 7) [1]. Undoubtedly, displacing others with Cd PV markedly lowers the amount of Cd released into the air. Thus, every GWh of electricity generated by CdTe PV modules can prevent around 5 g of Cd air emissions if they are used instead of, or as a supplement to, the UCTE electricity grid. In addition, the direct emissions of Cd during the life cycle of CdTe PV are ten times lower than the indirect ones due to use of electricity and fuel in the same life cycle, and about 30 times less than those indirect emissions from crystalline photovoltaics. Furthermore, examining the indirect heavy metal emissions in the life cycle of the three silicon technologies discussed earlier revealed that, among the PV technologies, CdTe PV had the lowest energy burden and, consequently, the fewest heavy metal emissions (Fig. 8) [1]. Regardless of the particular PV technology, these emissions are extremely small compared to the emissions from the fossil fuel–based plants that PV will replace.

Ongoing LCA studies include evaluating replacing building materials with PV in building-integrated photovoltaics (BIPV) [44], and recycling of PV modules at the end of their useful life [45–47].

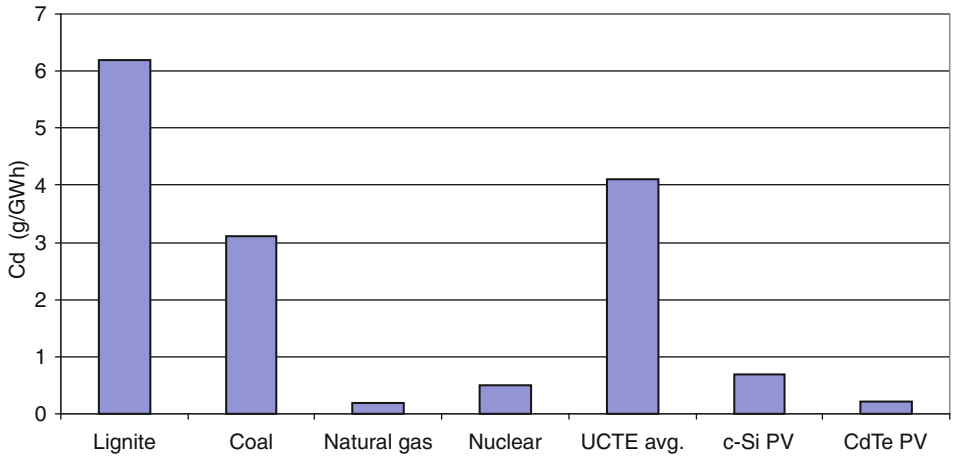

Solar Cells: Energy Payback Times and Environmental Issues. Figure 7
Life cycle atmospheric Cd emissions for PV systems from electricity and fuel consumption, normalized for a Southern Europe average insolation of 1,700 kWh/m^2/year, performance ratio of 0.75, and lifetime of 30 year

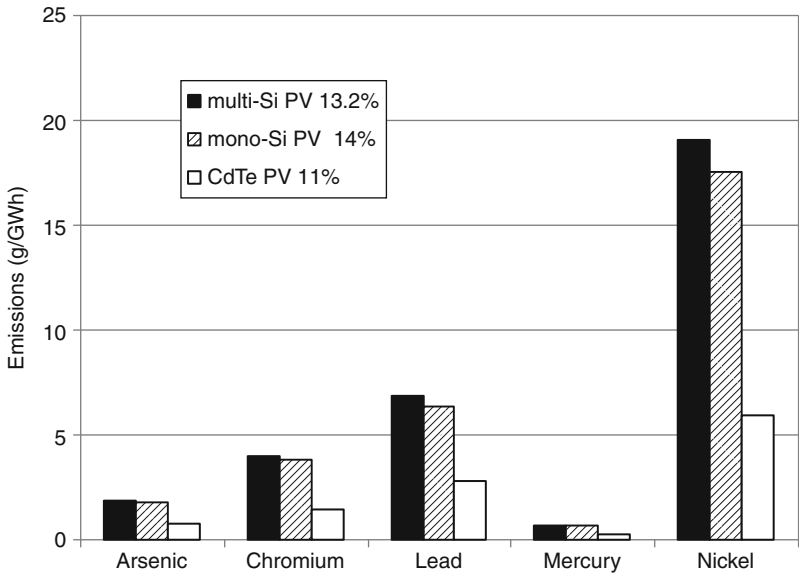

Solar Cells: Energy Payback Times and Environmental Issues. Figure 8
Emissions of heavy metals due to electricity use, based on European UTCE averages (Ecoinvent database). Emissions are normalized for Southern European average insolation of 1,700 kWh/m^2/year, performance ratio of 0.75, and lifetime of 30 year

Conclusion

This chapter gives an overview of the life cycle environmental performance of photovoltaic (PV) technologies. Energy payback time (EPBT) is a basic metric of this performance: The lower the EPBT, that is the time it takes for a PV system to generate energy equal to the amount used in its production, the lower will be the emissions to the environment because emissions

mainly occur from using fossil fuel–based energy in producing materials, solar cells, modules, and systems. These emissions differ in different countries, depending on that country's mixture in the electricity grid, and the varying methods of material/fuel processing. Under average US and Southern European conditions (e.g., 1,700 kWh/m^2/year), the EPBT of crystalline Si-, and CdTe-rooftop PV systems were estimated respectively to be 1.8 and 0.8 years. Ground-mount installations entail a greater amount of BOS and, therefore, have a longer EPBT. Under US SW irradiation (e.g., Phoenix, AZ, 2,370 kWh/m^2/year at a fixed latitude tilt), the EPBT of ground-mount installations is estimated to be 1.3 years and 0.6 years, respectively, for crystalline silicon- and cadmium telluride-PV. At the same location, the EPBT of the Amonix 2-axis HCPV is assessed as 0.9 years.

The environmental impacts of the life cycle of photovoltaics as assessed by the common metrics of GHG emissions, toxic emissions, and heavy metal emissions are very small in comparison to those of the power generation technologies they replace.

R and D Needs

The EPBT and GHG emissions of photovoltaics will keep decreasing as the efficiencies of modules, inverters, and material utilization all increase. Such improvements and new products entering the market necessitate frequent updates of the environmental performance of PV.

New LCAs are needed for CIGS and a-Si as the published estimates are uncertain and outdated, correspondingly.

The environmental issues related to the installation and operation phases of very large (e.g., thousands of acres) PV facilities have not, so far, been addressed comprehensively in the literature; these need to be evaluated in a comparative context as PV are displacing fossil fuel life cycles.

Acknowledgment

The author gratefully acknowledges multiyear support from the US DOE Office of Energy Efficiency and Renewable Energy, under contract DE-AC02-76CH000016 to Brookhaven National Laboratory.

Bibliography

Primary Literature

1. Fthenakis VM, Kim HC, Alsema E (2008) Emissions from photovoltaic life cycles. Environ Sci Technol 42:2168–2174
2. Kim HC, Fthenakis VM, Choi J-k, Turney DE (2011) Life cycle GHG emissions of thin-film photovoltaic electricity generation: systematic review and harmonization. J Ind Ecol (in press)
3. Aulich HA, Schulze F-W (2002) Crystalline silicon feedstock for solar cells. Prog Photovoltaics Res Appl 10:141–147
4. Woditsch P, Koch W (2002) Solar grade silicon feedstock supply for PV industry. Solar Energ Mater Solar Cells 72:11–26
5. Williams E (2000) Global production chains and sustainability: the case of high-purity silicon and its applications in IT and renewable energy. Institute of Advanced Studies/The United Nations University, Tokyo
6. Alsema E, de Wild-Scholten M (2005) Environmental impact of crystalline silicon photovoltaic module production. In: Material Research Society fall meeting, symposium G: life cycle analysis tools for "green" materials and process selection, Boston, MA
7. de Wild-Scholten M, Alsema E (2005) Environmental life cycle inventory of crystalline silicon photovoltaic module production. In: Material Research Society fall meeting, symposium G: life cycle analysis tools for "green" materials and process selection, Boston, MA
8. Fthenakis V, Alsema E (2006) Photovoltaics energy payback times, greenhouse gas emissions and external costs: 2004-early 2005 status. Prog Photovoltaics Res Appl 14:275–280
9. Fthenakis V et al LCI and LCA overview, IEA PVPS task 12 (in press)
10. Fthenakis VM, Kim HC (2007) CdTe photovoltaics: life cycle environmental profile and comparisons. Thin Solid Films 515:5961–5963
11. Fthenakis V, Kim HC, Held M, Raugei M, Krones J (2009) Update of PV energy payback times and life-cycle greenhouse gas emissions. In: 24th European photovoltaic solar energy conference, Hamburg, 21–25 Sep 2009
12. Held M (2009) Life cycle assessment of CdTe module recycling. Presented at 24th European photovoltaic solar energy conference and exhibition, Hamburg, Sep 2009
13. Held M, Ilg R (2010) Update of environmental indicators and energy payback time of CdTe PV systems in Europe. Prog Photovolt Res Appl (2011) Published online in *Wiley Online Library* (wileyonlinelibrary.com). doi: 10.1002/pip.1068.
14. Raugei M (2010) Material intensity analysis of CdTe PV vs. conventional electricity. In: 25th EU PV-SEC, Valencia, 6–10 Sep 2010
15. Raugei M, Bargigli S, Ulgiati S (2007) Life cycle assessment and energy pay-back time of advanced photovoltaic modules. CdTe and CIS compared to poly-Si. Energy 32(8):1310–1318
16. Fthenakis V, Wang W, Kim HC (2009) Life cycle inventory analysis of the production of metals used in photovoltaics. Renew Sust Energ Rev 13:493–517

17. Powell RC, Jayamaha U, Dorer GL, McMaster H (1999) Scaling and quantifying CdTe/CdS module production. In: AIP Conference Proceeding, 5 Mar 1999, 462, pp 31–36
18. SENSE: Sustainability Evaluation of Solar Energy Systems (2006). Summary report on LCA. http://www.sense-eu.net
19. Lozanovski A, Held M (2010) Update of the environmental indicators and energy payback time (EPBT) of CIS modules in Europe and scenario analysis of solar cell printing. In: Proceedings 25th European PVSC, 6–10 Sep 2010, Valencia
20. Keoleian GA, Lewis GM (2003) Modeling the life cycle energy and environmental performance of amorphous silicon BIPV roofing in the US. Renew Energ 28(2):271–293
21. Kim HC, Fthenakis VM (2010) Prospective life cycle assessment of nanotechnology: multi-junction a-Si photovoltaics. Prog Photovoltaics Res Appl 18(1–13):2010
22. Fthenakis V, Clark DO, Moalem M, Chandler P, Ridgeway RG, Hulbert FE, Cooper DB, Maroulis PJ (2010) Life-cycle nitrogen trifluoride emissions from photovoltaics. Environ Sci Technol 44(22):8750–8757
23. Kim HC, Knight KG, Krishnan N, Fthenakis VM (2008) Life cycle analysis of two new concentrator PV systems. In:23 rd European photovoltaic solar energy conference, Valencia, pp 909–913
24. Fthenakis V, Kim HC Life cycle assessment of high-concentration PV systems. Prog Photovoltaics Res Appl (in press)
25. Mason JE et al (2006) Energy payback and life-cycle CO_2 emissions of the BOS in an optimized 3.5 MW PV installation. Progr Photovoltaics Res Appl 14:179–190
26. de Wild-Scholten MJ (2007) Environmental life cycle inventory of crystalline silicon photovoltaic system production – status 2005/2006. ECN Solar Energy, Petten
27. Fthenakis VM (Operating Agent), Alsema E, Fraile D, Frischknecht R, Held M, Kim HC, Polz W, Raugei M, de Wild–Scholten MJ (2009) Methodology guidelines on life cycle assessment of photovoltaic electricity. International Energy Agency Report IEA-PVPS T12-01:2009 http://www.iea-pvps-task12.org/fileadmin/IEA-PVPS_Docs/Images/LCA_guidelines-8-2-10.pdf
28. Dones R et al (2003) Sachbilanzen von energiesystemen. Final report ecoinvent 2000, vol 6. Swiss Centre for LCI, PSI, Dubendorf and villigen
29. Franklin Associates (1998) USA LCI database documentation, Prairie Village, Kansas
30. Intergovernmental Panel on Climate Change (2001) Climate change 2001: the scientific basis. Cambridge University Press, Cambridge, UK
31. US Department of Energy, Energy Information Administration, Form EIA-1605 (2007) OMB No. 1905–0194 voluntary reporting of greenhouse gases; appendix F. Electricity emission factors
32. Chu D, Donahue P, Fthenakis V, Kim CH C, Choi J-K, Turney D (2011) Life cycle GHG emissions of crystalline-Si photovoltaic electricity generation: systematic review and harmonization. J Ind Ecol (in press)
33. Fthenakis V, Heath G, Kim CH (2011) Harmonization of PV Life-cycle GHG estimated emissions. In: 26th European photovoltaic solar energy conference and exhibition, Hamburg
34. Pacca S, Sivaraman D, Keoleian G (2006) Life cycle assessment of the 33 kW photovoltaic system on the Dana Building at the University of Michigan: thin film laminates, multi-crystalline modules, and balance of system components. CSS05-09. University of Michigan, Ann Arbor
35. Raugei M, Fthenakis V (2010) Cadmium flows and emissions from CdTe PV: future expectations. Energ Policy 38(9):5223–5228
36. de Wild-Scholten MJ, Alsema E, ter Horst EW, Bachler M, Fthenakis VM (2006) A cost and environmental impact comparison of grid-connected rooftop and ground-based PV systems. In: Proceedings of 21st European photovoltaic solar energy conference, Dresden, 4–8 Sep 2006, pp 3167–3172
37. de Wild-Scholten MJ et al (2006) A cost and environmental impact comparison of grid-connected rooftop and ground-based PV systems. In: 21st European photovoltaic solar energy conference, Dresden
38. Fthenakis VM, Kim HC (2007) Greenhouse-gas emissions from solar electric- and nuclear power: a life-cycle study. Energ Policy 35:2549–2557
39. Fthenakis V, Kim HC (2009) Land use and electricity generation: a life-cycle analysis. Renew Sust Energ Rev 13:1465–1474
40. Fthenakis VM, Kim HC (2010) Life cycle uses of water in U.S. electricity generation. Renew Sust Energ Reviews 14:2039–2048; Renew Sust Energ Reviews 13(6–7):1465–1474
41. Fthenakis VM (2004) Life cycle impact analysis of cadmium in CdTe PV production. Renew Sust Energ Rev 8(4):303–334
42. Fthenakis VM et al (2005) Emissions and encapsulation of cadmium in CdTe PV modules during fires. Prog Photovoltaics Res Appl 13:713–723
43. Electric Power Research Institute (EPRI) (2002) PISCES data base for US power plants and US coal, 2002
44. Perez M, Fthenakis V, Kim HC, Pereira A Façade-integrated photovoltaics: a lifecycle and performance assessment case study. Prog Photovoltaics Res Appl (in press)
45. Fthenakis VM (2000) End-of-life management and recycling of PV modules. Energy Policy 28(14):1051–1058
46. Fthenakis VM, Wang W (2006) Extraction and separation of Cd and Te from cadmium telluride photovoltaic manufacturing scrap. Prog Photovoltaics Res Appl 14:363–371
47. Fthenakis V (2009) Sustainability of photovoltaics: the case for thin-film solar cells. Renew Sust Energ Rev 13(9): 2746–2750

Books and Reviews

Fthenakis V, Mason JE, Zweibel K (2009) The technical, geographical, and economic feasibility for solar energy to supply the energy needs of the US. Energ Policy 37(2):387–399

Zweibel K, Mason J, Fthenakis V (2008) A solar grand plan. Sci Am 298(1):64–73

Solar Collectors, Non-concentrating

Stefan Fortuin, Gerhard Stryi-Hipp
Division Solar Thermal and Optics,
Fraunhofer-Institut für Solare Energiesysteme ISE,
Freiburg, Germany

Article Outline

Glossary
Definition of the Subject
Introduction
Functioning of a Solar Collector
Construction of Solar Thermal Collectors
Collector Types
Future Directions
Bibliography

Glossary

Absorptivity or absorptance (α) The fraction of the incoming radiation which is absorbed at a specified wavelength (absorptivity) or summed over a specified spectrum range (absorptance). Absorptivity and absorptance are dimensionless quantities.

Collector area: Aperture, absorber, and gross area Net area (of a flat surface) through which the collector receives solar radiation. The gross collector area, the aperture area, or the absorber area can be used. Usually, the performance of the collector is referred to the aperture area. For nonflat areas, a projected area is used for the aperture area, but the full surface area is taken for absorber areas.

Collector mean temperature (T_m) Defined, in operating terms, as the average value of the inlet and outlet temperatures of the collector (fluid) medium:

$$T_m = \frac{T_{outlet} + T_{inlet}}{2}.$$

Emissivity (ε) Ratio of energy radiated by a particular material at a certain temperature to energy radiated by a blackbody at the same temperature. For a true blackbody, $\varepsilon = 1$, while any real object would have $\varepsilon < 1$.

Emittance (M) Quantitative ability of a material to release radiative heat per area (W/m^2).

Evacuated tube collector (ETC) Solar collector with many parallel glass tubes each covering an individual long and slim absorber. The glass tubes maintain a vacuum insulation cavity around the absorber.

Flat plate collector (FPC) Solar collector with a large flat absorber. Optionally, a flat cover (covered flat plate collector) and conventional thermal insulation can be added to reduce thermal losses.

Heat pipe Heat transfer construction enabling heat transfer through (closed) convective mass flow. Usually, a critical fluid-gas material is used where gas rises when a fluid is heated below and flows down again when cooled at the top (liquid), thus transferring some sensible but also large amounts of latent heat. Very high heat transfer rates can be sustained through a single, small channel.

Incident angle modifier (IAM) Dependence of the collector efficiency on the angle between the solar beam radiation incident on a surface and the normal to the collector surface. With increasing incidence angle, reflections of the cover usually increase and the performance of the covered collector drops.

Operating temperature difference Difference between the collector mean temperature (T_m) and the ambient temperature (T_a). Usually, the collector performance curve is shown dependent on the operating temperature difference.

(Solar) Irradiance (G) Irradiated power density (in W/m^2) of (solar) radiation. An example is the solar constant, that is, the solar irradiance measured just outside the earth's atmosphere, which is roughly 1,361 W/m^2.

Spectral-selective coating Multilayer surface coating with high absorptivity in the wavelength range of solar radiation and low emissivity in the infrared thermal radiation range so that radiative thermal losses of the solar absorber are reduced.

Solar fraction (F_{sav}) Ratio of solar energy to total energy used by a heating system. Calculated from the auxiliary energy still needed when using solar energy, divided by the energy needed by a comparable reference system that does not use solar energy:

$$F_{sav} = 1 - \frac{Q_{aux}}{Q_{ref}}.$$

Solar spectrum AM 1.5 Typical spectral distribution of the solar radiation intensity on the earth resulting from transmission through an air mass of 1.5 times (AM 1.5) the thickness of the atmosphere of the earth, which corresponds with incoming solar radiation at an (solar zenith) angle of roughly 45° (to the vertical axis).

Definition of the Subject

The purpose of a solar thermal collector is to capture solar radiation, convert it into heat, and make the heat available, for example for use in a solar-heating or solar-cooling system. At the heart of the solar thermal collector is the absorber where the conversion from radiation into useful heat happens.

The simplest collector consists only of an absorber. But usually, the efficiency of the collector and the temperature of the heat produced are improved by reducing the temperature losses from the absorber by adding a collector housing or by increasing the intensity of the solar radiation with concentrating mirrors before it strikes the absorber. Concentrating solar collectors are used to produce medium- or high-temperature process heat above 100°C/212°F, to run thermal cooling machines, or to produce electricity by using steam generators. Non-concentrating solar thermal collectors are used for swimming pool heating, domestic hot water (DHW) heating, space heating, and heating of water for industrial and other processes and to run thermal cooling machines.

Engineered solar thermal systems were first used as far back as the nineteenth century (Fig. 1). In 1891, American Clarence Kemp received a patent for a solar heater device which combined the use of a black-colored water storage tank and the principle of the "hot box," a (wooden) insulated box with a glass front to capture and store solar radiation [1]. In the following decades, further design improvements were made. In 1909, William J. Bailey patented a new design. He reduced the heat losses by placing an insulated storage tank inside the house and exposed the solar collector to the sun outside. The two separate components were connected with thin pipes. At any time, little water was present in the collector; thus the collector heated the present water fast and to sufficiently high temperatures.

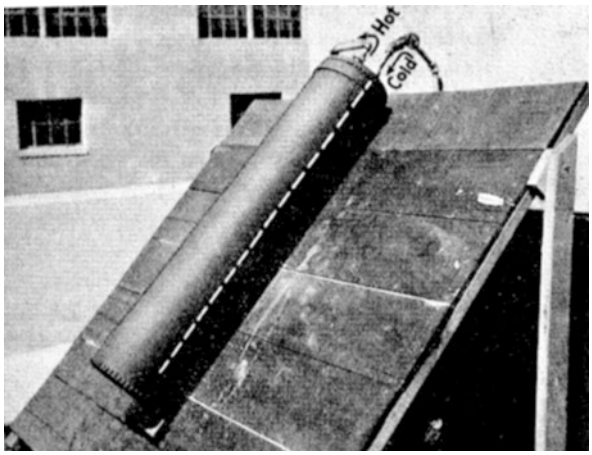

Solar Collectors, Non-concentrating. Figure 1
A bare-tank solar water heater used throughout rural America in the nineteenth century (John Perlin Solar Archives)

This design enabled the heated water to be stored overnight with reduced thermal losses and allowed the heated water to be used the next day.

Non-concentrating collectors are able to use direct (beam) solar radiation under various angles as well as diffuse radiation scattered by atmospheric influences. They do not need to track the sun's position and can be installed in a fixed orientation. In contrast, concentrating collectors can only use direct radiation and a very small fraction of the diffuse radiation available. Therefore, they need to be tracked to the sun's position.

Non-concentrating solar thermal collectors can reach temperatures of up to 250°C/482°F, but since the efficiency decreases with increasing operating temperature, they usually operate and deliver heat at acceptable efficiencies at temperatures up to 100°C/212°F, with special high-efficiency non-concentrating collectors delivering heat up to 150°C/302°F.

This document only discusses non-concentrating solar thermal collectors, here referred to only by "solar collectors" or "collectors."

Introduction

Heating of domestic water became simple and cheap using fossil fuels and interest in solar thermal heating disappeared, until the 1970s when the oil crises led to

a growing interest in alternative energy sources. The development of solar thermal systems boomed in most European countries in the 1970s but dropped again at the beginning of the 1980s due to quality problems and because fossil fuel prices dropped again. A relevant market for solar thermal systems remained only in Israel, Cyprus, and Greece due to the obligation to use solar thermal systems for hot water production (Israel) or a high inflation rate (Greece). In general, in these countries, cheap and simple solar thermal systems were used. The solar thermal markets in Austria and Germany grew again since the end of the 1980s due to growing environmental awareness, technical improvements, and subsidy programs. Other European countries followed this trend in the first decade of the twenty-first century, mainly stimulated by subsidy programs. Europe was the leading solar thermal market in the twentieth and at the beginning of the twenty-first century, but today, the world's largest solar thermal market is in China, with a global share of more than 80% (Fig. 2), where mainly simple thermosiphon solar thermal systems equipped with evacuated tubes for heating domestic hot water are used.

In Europe, growing concerns about climate change, scarcity of fossil energy sources, and the increasing dependency on imported fossil fuels have led to a fast-growing interest in local renewable energy options. About 50% of the final energy demand is caused by heating and cooling needs in European countries, and renewable heating and cooling technologies are seen as an important pillar of a sustainable energy system. Solar thermal is the renewable energy technology with the largest potential among them. According to the European Solar Thermal Technology Platform (ESTTP), solar thermal is able to cover 50% of the heat demand in Europe by 2030 [3].

In contrast, the huge solar thermal market in China is driven by the growing demand for comfort and by the fact that solar thermal is often the cheapest option to heat domestic hot water in China.

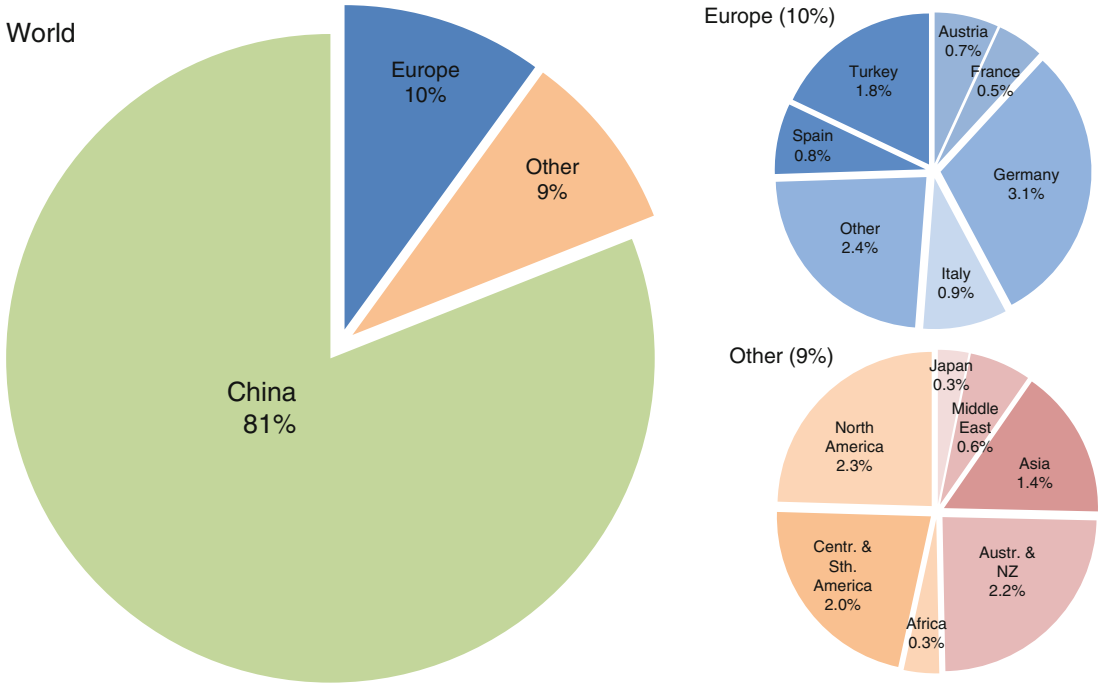

Solar Collectors, Non-concentrating. Figure 2
Share of the newly installed capacity (glazed and unglazed water and air collectors) by economic regions in 2009 [2].

Functioning of a Solar Collector

The task of solar collectors is to convert solar radiation into thermal energy and make it useable at a suitable temperature for a specific application with a high efficiency. In this chapter, the functionality of solar collectors is explained principally for flat plate collectors with a fluid as heat transfer medium, which are usually used in Europe for domestic hot water–heating and space-heating applications. The differences to other types of collectors are described in the following chapters.

The principal energy gain and loss mechanisms for a solar collector are shown in Fig. 3. Its power losses can be divided into optical losses (G_{loss}), occurring until absorption of the radiation, and thermal losses, occurring after absorption of the solar radiation. The power absorbed (useful thermal power $\dot{Q}_U$) is either removed by the heat transfer fluid as useable heat ($\dot{Q}_{\mathrm{out}}$) or is lost to the environment ($\dot{Q}_{loss}$). The radiation (G) and the thermal power ($\dot{Q} = \frac{Q}{\Delta t}$), with thermal energy Q and time difference Δt, are power units and describe an energy flow, which means energy per time unit.

To reduce thermal losses, most of the non-concentrating solar thermal collectors are insulated to the back and the side and covered with a transparent cover at the front. The transparent cover reduces the amount of solar radiation that reaches the absorber due to reflections of both sides of the cover as well as due to absorption of a small part of the radiation by the cover. The transmitted radiation reaches the absorber, where a small part is reflected and the remaining is absorbed and converted into thermal power. Using the share of radiation that is transmitted through the cover (transmittance τ_{cov}) and the share of radiation that is absorbed (absorption $\alpha_{\mathrm{abs}} = 1 -$ reflection), the thermal power ($\dot{Q}_{\mathrm{u}}$) converted from the absorbed radiation can be determined as follows:

$$\dot{Q}_U = \tau_{cov}\alpha_{abs}G_{tot}$$

The absorbed radiation heats up the absorber plate. If the heat transfer fluid, which is flowing through tubes connected on the back of the absorber, is cooler than the absorber, it is heated up and can remove the thermal power from the collector to the heat storage or a heat exchanger for direct usage. Therefore, the thermal energy must flow from every point of the absorber to the heat transfer fluid within the tubes. The thermal resistance between the point of absorption and the heat transfer fluid composed of the thermal resistance within the absorber sheet, at the connection point of the absorber sheet and the tube, within the tube material, and from the tube material to the fluid, is reducing the efficiency of the collector in addition. This is reflected by the collector efficiency factor F′ in the following equation:

$$\dot{Q}_{out} = F'\tau_{cov}\alpha_{abs}G_{tot} - \dot{Q}_{loss}$$

There are three physical mechanisms, which contribute to the heat losses ($\dot{Q}_{loss}$): conduction, convection, and (infrared) radiation, which are shown for a flat plate collector in Fig. 4.

Convection losses are reduced significantly by adding the casing, especially when operating in windy or cold surroundings. With the casing, convection is separated between convection between the heated absorber and the cover and the outside airflow (wind) over the cover.

Conduction losses mainly occur through the insulation material and through the transparent cover.

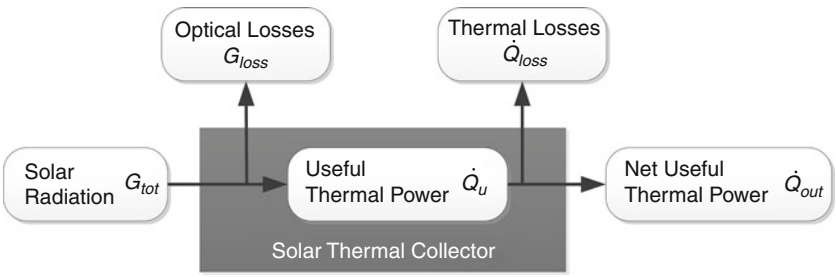

Solar Collectors, Non-concentrating. Figure 3
Principle energy flow in a solar thermal collector

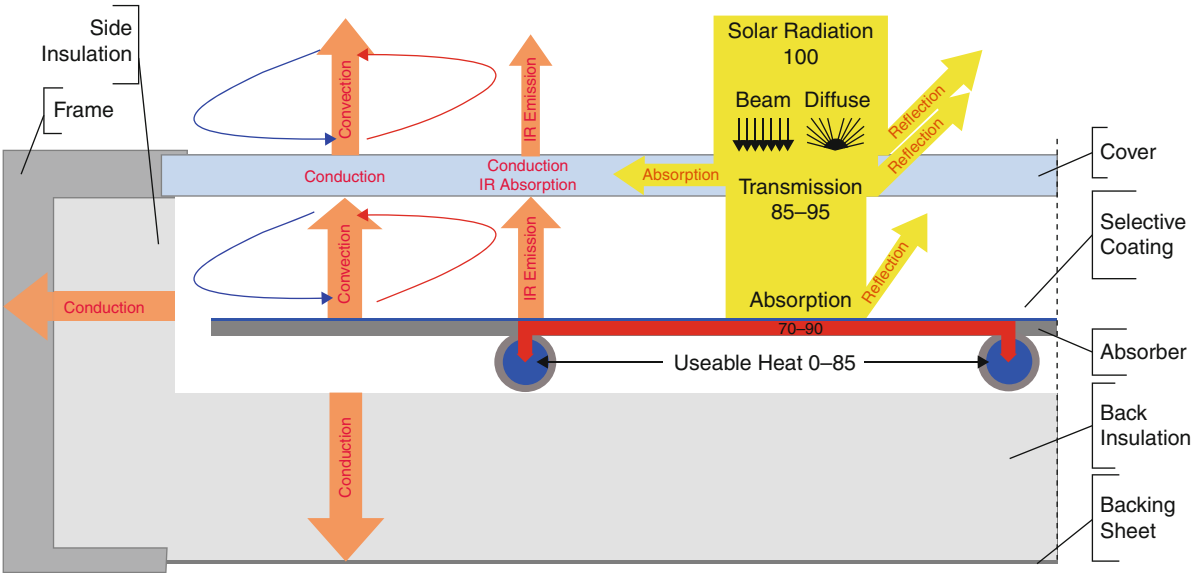

Solar Collectors, Non-concentrating. Figure 4
Gain and loss mechanisms in a flat plate collector, with typical values relative to the incident solar radiation (in percentage of the incoming radiation)

Convection and conduction losses can be minimized by optimizing the distance between the absorber and the transparent cover [4]. The largest reduction of conduction and convection losses can be achieved by evacuating the gap between cover and absorber (i.e., by evacuated tube).

All thermal losses increase with increasing difference between the absorber temperature ($T_{absorber}$) and the ambient temperature (T_a). Since we are interested in the net useful thermal power ($\dot{Q}_{out}$), which is calculated from the temperature difference between inlet and outlet of the heat transfer fluid, the thermal losses are usually related to the difference between the mean collector temperature (T_m), defined as the average between the inlet and the outlet temperature of the heat transfer fluid, and the ambient temperature. Therefore, the thermal losses can be characterized quantitatively using the "operational" temperature difference ($T_m - T_a$) and a heat loss factor U_L:

$$\dot{Q}_{loss} = F' U_L (T_m - T_a)$$

The efficiency of a solar collector is defined as:

$$\eta = \frac{\dot{Q}_{out}}{G_{tot}}$$

Therefore, the linear efficiency curve of a solar collector can be described by [4]:

$$\eta = F'\tau\alpha - \frac{F' U_L (T_m - T_a)}{G}$$

with $\tau = \tau_{cov}$ (cover transmittance), $\alpha = \alpha_{abs}$ (absorber absorption), and $G = G_{tot}$ (solar irradiation).

Since the thermal losses are not exactly proportional to the operational temperature difference ($T_m - T_a$), often, the more precise quadratic collector efficiency curve is used:

$$\eta = \eta_0 - a_1 \frac{(T_m - T_a)}{G} - a_2 \frac{(T_m - T_a)^2}{G}$$

Therefore, the collector is typically characterized with the three parameters: maximum efficiency ($\eta_0 = F'\tau\alpha$), linear (a_1), and quadratic loss factor (a_2). The efficiency of a collector at a specific operating point is also called "instantaneous efficiency."

To compare the performance of solar collectors, their efficiency curves are usually presented as a function of the main influencing factors: the operational temperature difference ($T_m - T_a$) and the solar radiation (G) as shown in Fig. 5.

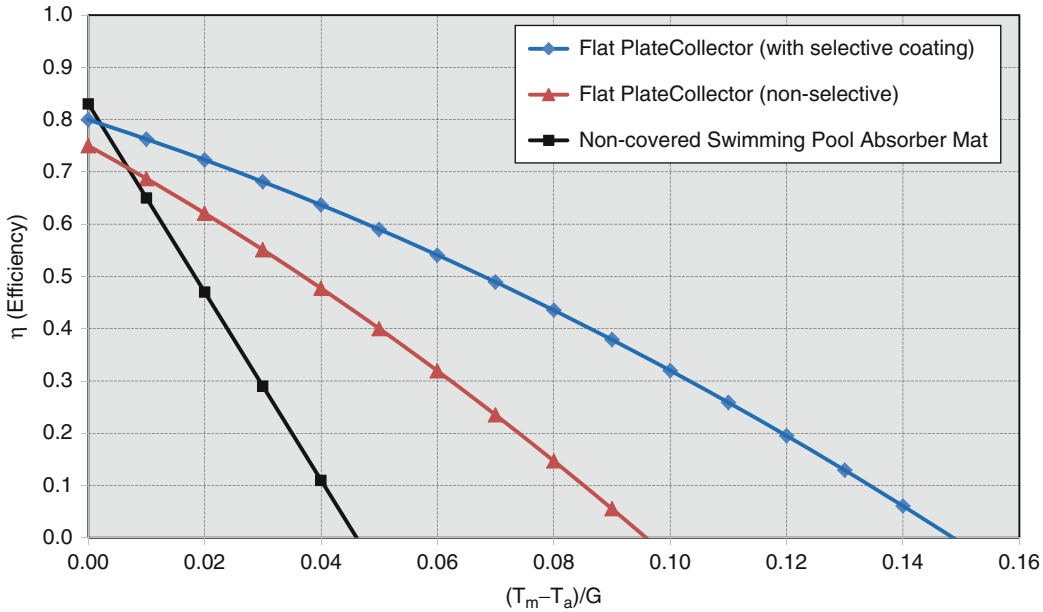

Solar Collectors, Non-concentrating. Figure 5
Typical efficiency curves of two covered and one noncovered flat plate collector (η = efficiency, T_m = mean collector temperature, T_a = ambient temperature, G = irradiation; the efficiency is related to the aperture area and is shown for an irradiation level of 1,000 W/m^2)

Figure 5 shows the efficiency curves of two covered flat plate collectors and one noncovered collector. A standard covered flat plate collector with a black-painted absorber shows typically a maximum efficiency of about 75%. Since the thermal losses increase with increasing operational temperature difference, the efficiency always curves downward starting from the maximum efficiency (η_0) where the temperature difference is zero. The highest collector temperature occurs when the heat transfer fluid is not circulating and the collector is in so-called stagnation mode; this is where the efficiency, and therefore net useful thermal power ($\dot{Q}_{out}$), is zero. In this case, the thermal losses are equal to the absorbed radiation. For a standard, covered, black-painted flat plate collector, the stagnation temperature is at around 150°C/302°F. An improved flat plate collector with a selective absorber coating and improved insulation, which is typically used in central Europe, shows a higher maximum efficiency of about 80% and lower loss coefficients a_1 and a_2. With improved heat loss reduction, the efficiency curve drops slower. A much higher stagnation temperature, of about 220°C/428°F, is achieved. In contrary, a noncovered swimming pool absorber has a slightly higher maximum efficiency point, since there are less radiation losses without a cover, but the efficiency curve drops much faster due to high-temperature-dependent losses (high values for loss coefficients a_1 and a_2) as a result, and the stagnation temperature is below 100°C/212°F.

To make efficiency curves comparable, two parameters must be stated: the referring collector area and the irradiation level. The relevant collector area must be referenced when presenting an efficiency curve since the total irradiation used in the efficiency is proportional to it. There are three options: the gross collector area, corresponding with the overall dimensions of the collector including the frame; the aperture area, through which the radiation can enter the collector; and the absorber area, which is the dimension of the absorber. The reference dimensions of collectors for the areas are shown in Fig. 6. The difference between the gross collector area and the absorber area is much smaller for a flat plate collector than for evacuated tube collectors.

The collector efficiency curve is usually shown as a function of $(T_m - T_a)/G$, which implies that the

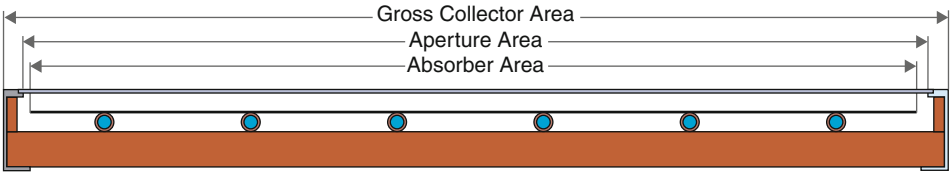

Solar Collectors, Non-concentrating. Figure 6
Different dimensions of reference areas to calculate the efficiency of a flat plate collector

efficiency curve of a collector is always the same for the same value of $(T_m - T_a)/G$. But the quadratic efficiency equation shows an additional factor "G" in the quadratic term:

$$\eta = \eta_0 - a_1\left(\frac{T_m - T_a}{G}\right) - a_2 G\left(\frac{T_m - T_a}{G}\right)^2$$

This means that it is necessary to state for which irradiation the efficiency curve is shown as the efficiency for a given value of $(T_m - T_a)/G$ is similar only within a limited range of the irradiation (G). This second order effect is higher for larger values of $(T_m - T_a)/G$. According to the European standard EN 12975, the collector efficiency must be tested at irradiation values between 800 and 1,000 W/m^2 and the efficiency curve must be shown for the irradiation of 1,000 W/m^2.

To present the collector curve as a function of $(T_m - T_a)/G$ helps with understanding the efficiency dependency of the collector. Generally, with increased irradiation (G), the operation point on the x-axis moves to the left, toward higher efficiencies. However, with increasing irradiation, the mean temperature increases as well; therefore, the movement along the x-axes is smaller than the change in the value of 1/G. In the first order, the efficiency is proportional to the temperature difference $(T_m - T_a)$. The lower the ambient temperature (T_a) (a shift to the right), the lower is the efficiency of the collector. Therefore, in winter, the collector efficiency is not only lower due to lower irradiation values but also due to a larger operating temperature difference.

On the other hand, the lower the mean temperature (T_m) (a shift to the left), the higher the efficiency. This shows the importance of low inlet temperatures (T_{in}), since the mean temperature strongly depends on it $(T_m = \frac{1}{2}(T_{in} + T_{out}))$.

To calculate the operational efficiency of a collector means to identify the mean temperature (T_m), since the irradiation (G) and the ambient temperature (T_a) are given in a specific operational situation. To identify the mean temperature (T_m), it is helpful to see what is happening if the sun is shining on the collector. Then, the net useful thermal power $(\dot{Q}_{out})$ is increasing with the mean temperature for a given inlet temperature (T_{in}) as follows:

$$\dot{Q}_{out} = \dot{m}c(T_{out} - T_{in}) = 2\dot{m}c(T_m - T_{in})$$

Further factors of the equation are the mass flow $(\dot{m})$ and the specific heat capacity (c) of the heat transfer fluid.

On the other hand, with the increasing mean temperature (T_m), the thermal losses $(\dot{Q}_{loss})$ increase and the net useful thermal power $(\dot{Q}_{out})$ decreases:

$$\dot{Q}_{out} = G - G_{loss} - \dot{Q}_{loss}$$

Therefore, it can be followed that the resulting mean temperature (T_m) is the temperature for which both equations for the net thermal power $(\dot{Q}_{out})$ are true; this means:

$$2\dot{m}c(T_m - T_{in}) = G\left(\eta_0 - a_1\frac{(T_m - T_a)}{G} - a_2\frac{(T_m - T_a)^2}{G}\right)$$

This equation shows that the mean temperature (T_m) depends not only on the outside conditions of the collector, the irradiation (G), and the ambient temperature (T_a) but also on the inlet temperature (T_{in}), the mass flow $(\dot{m})$, and the thermal capacity (c) of the heat transfer fluid and, thus, on parameters which are provided by the solar thermal system.

The conclusion is that the efficiency curve of a solar collector with the collector parameters (η_0, a_1, a_2) is helpful to make solar collectors comparable. However, the operational efficiency of a solar collector at

a specific operation point not only depends on the outside conditions (G, T_a), but is also strongly influenced by some parameters of the solar thermal system (T_{in}, $\dot{m}$, c), which are influenced by the design and the operation mode of the system as well as the real load profile. This makes it very difficult to determine the mean temperature and therefore the efficiency of the collector at a specific time of operation. Since the outside conditions and the status of the solar system are changing continuously, the energy gains of a collector in a real solar system can only be calculated with a simulation program.

Construction of Solar Thermal Collectors

The central component of a solar collector is the absorber, which absorbs the solar radiation and converts it into thermal energy. The absorber is connected with a heat removal construction, which allows for the useful removal of heat by means of a heat transfer medium.

In order to reduce heat losses, the absorber can be embedded into a collector casing. For flat plate collectors, this includes a flat transparent cover and insulation material at the back and sides or, as is the case for evacuated tube collectors, the absorber can be covered entirely by a glass tube using vacuum as insulation.

Figure 7 shows cut sections of common collector constructions and their main components, from top to bottom: a noncovered (pool) collector mat, a covered flat plate collector, an air collector, and an evacuated tube collector (Sidney type). The header channels and manifolds of the evacuated tube collector, which collect the heated medium from the heat transfer tubes, are not shown. Many other variants exist especially of the evacuated tube collector type.

Absorber

The function of the absorber is to absorb the solar radiation, convert it into heat, and allow for the removal of the thermal energy for usage or storage. Different absorber constructions are used. In covered flat plate collectors, a thin metal absorber made from

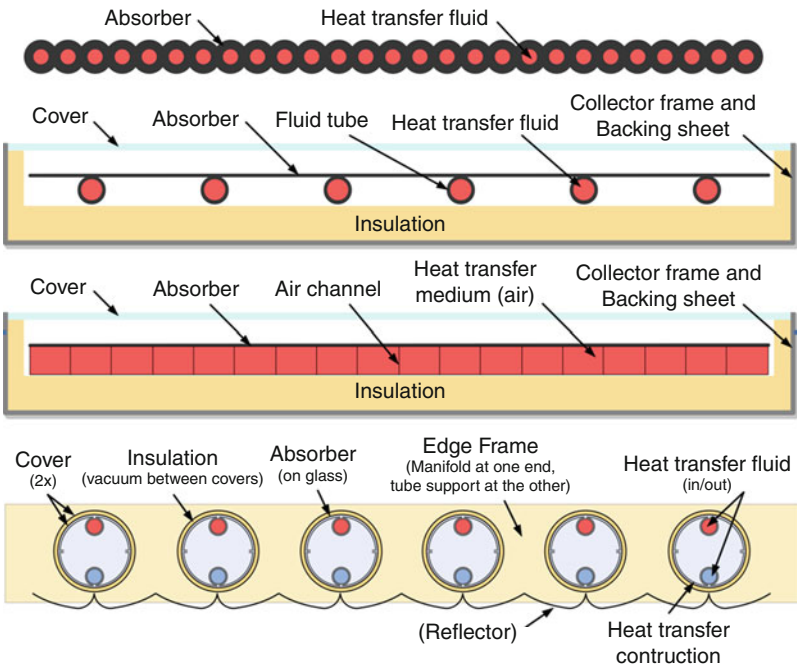

Solar Collectors, Non-concentrating. Figure 7
Cut sections of common non-concentrating solar collectors showing their main components. From top to bottom: non-covered (pool) collector mat, covered liquid-heating flat plate collector ('sheet & tube'), covered air-heating collector (with air channels), evacuated tube collector (Sidney type)

a full sheet or a series of parallel fin-and-tube strips with heat removal tubing attached underneath is used.

Absorber Coating The solar radiation striking the absorber is either reflected or absorbed. Absorptivity (α) and reflectivity (ρ) are defined by:

$$\alpha = \frac{\textit{absorbed radiation}}{\textit{incident radiation}} = 1 - \rho$$

Absorptivity represents the share of solar energy that is converted into heat. The absorptivity of an ideal blackbody has the value 1. Solar absorbers are painted black or coated otherwise, for example, by applying a galvanic or a vacuum sputter process. Their absorptivity is usually between 0.9 and 0.95.

Like any object, the absorber emits infrared (thermal) radiation and exchanges this radiation with objects in its surroundings. The net radiative heat flow from the hot absorber to its surroundings, for example, a glass cover, increases with increasing temperature difference. The rate at which an object emits thermal radiation is characterized by the emissivity (ε) of its surface. The emissivity (ε) is defined as the ratio between the emissions of the object and the emissions of an ideal blackbody at the same temperature.

Ideally, a solar absorber should combine high absorptivity with low emissivity. Spectral-selective absorber coatings were developed which combine a high absorption in the solar spectrum with low emission in the infrared spectrum. Figure 8 shows the solar radiation spectrum, which occurs mainly at wavelengths between 0.3 and 2.5 μm, and the infrared emissions of a body with 100°C/212°F, which occurs mainly above 4 μm.

Figure 8 shows also the wavelength-dependent reflectivity of a high-quality spectral-selective absorber coating. Below 2 μm, its reflectivity is low and thus the absorptivity is high. In the infrared part of the spectrum above 4 μm, its reflectivity is high and therefore the emissivity is low.

The total absorptance (α) of good spectral-selective coatings is typically in the range of 0.90–0.95 for the AM 1.5 solar spectrum. This means that 90–95% of the radiation in this solar spectrum is absorbed. The emissivity (ε) of good spectral-selective coatings is between 0.05 and 0.10. This means that the absorber emits 5–10% of the infrared radiation of an ideal blackbody at the same temperature (e.g., 100°C/212°F in Fig. 8).

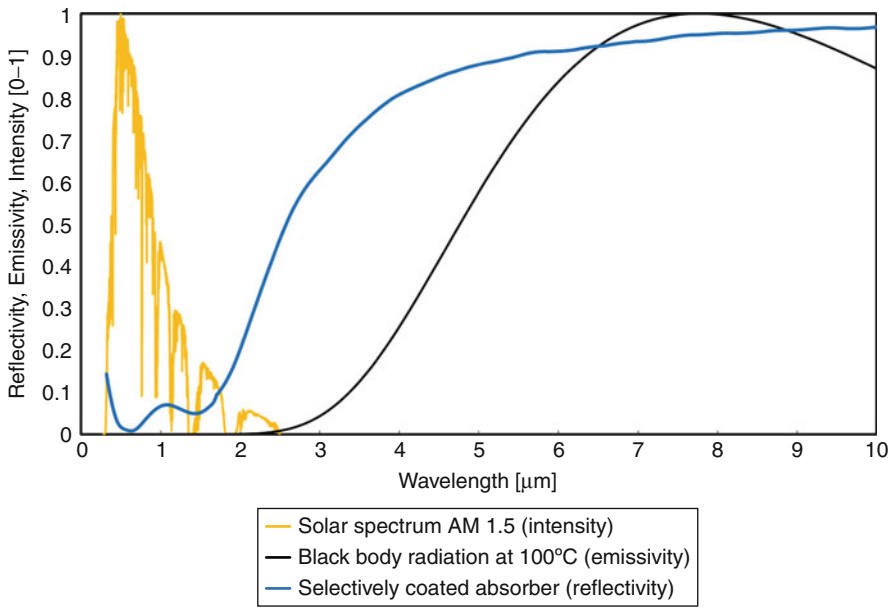

Solar Collectors, Non-concentrating. Figure 8
Intensity spectrum of solar radiation AM 1.5, emissivity of a blackbody radiation at 100°C/212°F and reflectivity of a selective absorber coating (all values normalized)

The spectral-selective coatings are made up of multiple layers containing compounds such as ceramic-metal structures (applied by PVD or physical vapor deposition), titanium-nitride-oxide (also applied by PVD), a selective lacquer (applied by coil coating), or black chrome (applied by electroplating). PVD usually leads to thin coatings which do not need to be removed before recycling; galvanic coatings (thickness 5–10 μm) and lacquer are thicker and one should consider removing these before recycling [5].

Absorber Material An absorber should be resistant to atmospheric conditions, since the collector is usually not hermetically sealed, and it must be resistant to it's stagnation temperature. Good collector performance requires high thermal conductance of the absorber; therefore, mainly well-conducting metals are used as absorber material.

In the past, mainly copper was used for absorbers due to its excellent heat conductivity (λ) (380–400 W/mK). Since the copper price increased dramatically and the ability of the collector manufacturers to reliably connect aluminum sheets with copper tubes has improved, the use of aluminum absorbers is steadily growing and has exceeded a 50% share in the European flat plate collector market. To compensate for the lower heat conductivity (200–240 W/mK), the aluminum absorber sheet typically has a thickness of 0.4 mm in comparison to copper absorber sheets with a typical thickness of 0.2 mm. To further decrease material costs, some manufacturers are also trying to replace copper heat removal pipes by improved and special corrosion-protected aluminum pipes. Stainless steel is very resistant against corrosion; however, it is very expensive and has a much lower heat conductivity (about 20 W/mK) and is therefore seldom used, for example, for noncovered stainless steel preheat absorbers.

Noncovered absorbers for swimming pool heating typically use cheaper polymer absorbers. These are usually made from EPDM (ethylene propylene diene monomer, an M-class rubber). Their heat conductivity is very low, only about 0.3 W/mK, but this is compensated for by placing many heat transfer channels closely side by side, which provides for short conduction distances between place of absorption and the heat transfer fluid. Polymer absorbers are extruded in one production step which includes the heat transfer fluid channels.

Some research is focused on reducing costs by replacing the metal sheet absorber by a polymer absorber for use in covered flat plate collectors. Since these collectors usually show a stagnation temperature between 200°C/392°F and 250°C/482°F, new heat-resistant polymers must be found or the stagnation temperature must be limited. Several experts, working together in Task 39 of the IEA Solar Heating and Cooling program, are working on new polymer concepts for solar absorbers [6].

Heat Removal Construction Only solar thermal energy, which is removed by the heat transfer medium, is usable. Therefore, the heat transfer medium must be in close contact with the absorber sheet. In the case of flat plate collectors, the heat removal construction mostly consists of pipes for a liquid heat transfer medium connected to the back of the absorber sheet or of air channels for air-heating collectors. In the case of evacuated tube collectors, the liquid sometimes flows through metal pipes as well, although in typical evacuated tube thermosiphon systems for the Chinese market, the heat transfer fluid is contained by the inner glass tube itself.

Up to now, in flat plate collectors, almost always copper heat removal tubes are used because of its good corrosion resistance. Copper is also used in other parts of the solar circuit, for example, the piping between the collector and the hot water storage tank and the heat exchanger in the tank. In Europe, the coated copper or aluminum absorber sheet and the heat removal tubes are usually welded together by laser or ultrasonically. In the past, the absorber sheet and pipes were connected by soldering, but due to the growing efficiency of the collectors, the stagnation temperature increased up to 250°C/482°F. Since this is a critical temperature for soldered absorbers, most of the European manufacturers of flat plate collectors abandoned this in their production method. But flat plate collectors with lower efficiency are still soldered. Rather seldom, the heat removal tubes are clamped to the absorber.

Another production method for absorbers is roll bonding, where two aluminum sheets are laminated by means of a high-pressure rolling process. The bonding of the two inner surfaces is a kind of autogenous weld formed by temperature (preheating) and pressure (rolling). The desired pattern of the flow channels are obtained by printing a nonwelding medium onto the

inside surface of one of the sheets. The nonwelded areas are expanded by applying pressurized air, thus forming the heat transfer fluid flow channels. These panel constructions have already been used for a long time for heat exchangers in refrigerators and freezers [7]. Roll bonding can be a cost-effective production method when volumes are large, and it has the advantage that it allows for very flexible designs for flow patterns to be created across the absorber surface. In the 1980s, solar equipment manufacturers experienced serious corrosion issues with aluminum components and roll bonding was no longer used. Nowadays, improvements have been made in understanding of and protection against corrosion so that some manufacturers are evaluating again the use of roll-bonding production methods.

The different ways to connect the heat transfer fluid tube to the absorber are shown in Fig. 9.

The coverage of the heat removal tubes across the absorber influences the efficiency of the collector directly through the collector efficiency factor F′ introduced in chapter "Functioning of a Solar Collector". With decreasing distance between the tubes, the collector efficiency factor F′ increases. At the same time, the number of tubes needed and thus production costs increase as well. Therefore, an optimum can be found. Currently, relative high values of F′, around 0.90–0.95, are common for most flat plate collectors in central Europe.

For fin-and-tube constructions, two patterns of the heat removal tubes are most common: harp and meander. In the harp pattern, the parallel tubes are connected at the bottom and the top with a header pipe. In the meander pattern, a single tube meanders across the absorber. Figure 10 shows the common patterns of the heat removal tubes for flat plate collectors. The advantage of the harp pattern is a lower hydraulic pressure drop, but there is a risk of unequal flow across the absorber. In the meander pattern, the fluid flows through a single tube, which leads to an equal flow across the absorber, but it has a higher pressure drop.

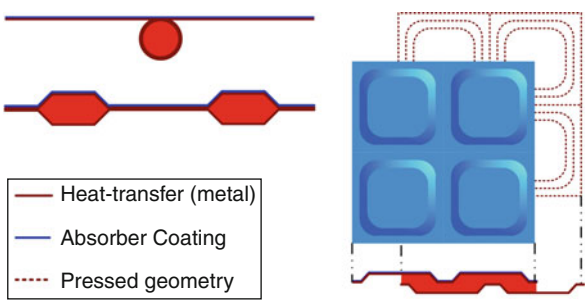

Solar Collectors, Non-concentrating. Figure 9
Cut sections of different constructions for flat plate absorber-tube connections. *Left*: absorber and tube laser or ultrasonically welded or soldered; *center*: roll-bonded sheets; *right*: pressed sheets

The main considerations for the heat transfer construction are good collector efficiency factor F′, low material usage, and low production costs. Influence factors are the required specific mass flow [kg/m^{2}h], the allowed pressure loss [Pa] which affects the pump power and energy needed, and an equal flow across each part of the collector. The heat removal of the absorber construction also has an influence on how several collectors can be connected to each other in a collector field.

Transparent Cover

Noncovered collectors cannot sustain acceptable efficiencies at absorber temperatures much above the ambient temperature. To reduce heat losses and allow higher temperatures, the absorber is usually built into a casing with a transparent cover at the top and insulation on the back and sides (for flat plate collectors) or encased in an evacuated glass tube (for evacuated tube collectors). The casing also provides protection to the absorber from environmental influences (e.g., rain, hail, dirt, and insects).

The cover should have high transmittance for solar radiation; else, it would reduce the radiation that reaches the absorber. The transmittance (τ) of a transparent cover is defined as the ratio between the transmitted and the incident radiation, measured at a right angle (90°) to the cover. It is reduced through reflections (ρ_{in} and ρ_{out}) on both sides of the cover and by absorption (α) within the cover material. Transmittance is thus determined by:

$$\begin{aligned} \textit{Transmittance}\ \tau &= \frac{\textit{transmitted radiation}}{\textit{incident radiation}} \\ &= 1 - \rho_{in} - \alpha - \rho_{out} \end{aligned}$$

The transmittance of "solar glass," with reduced iron content, is typically in the range of 0.89–0.91, compared to 0.84–0.88 for normal "float" glass. The higher iron content in float glass increases the

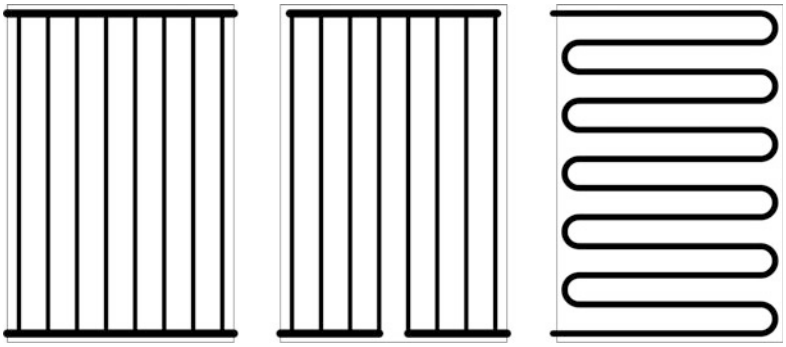

Solar Collectors, Non-concentrating. Figure 10
Various pattern of the heat removal tubes in flat plate collectors. From left to right: harp, double harp, and meander

absorption and typically causing the glass to appear green at the edges. For solar glass, transmittance can be enhanced to 0.94–0.96 by using antireflective (AR) coatings. The glass of vacuum tubes has similar values as solar glass, but no AR coatings are applied [8–10].

In a flat plate collector, heat losses through the cover can be further reduced by using a double cover. But adding another transparent cover also has the drawback of further reducing the radiation that reaches the absorber due to reflection and transmission losses by the second cover. With antireflective coatings becoming cheaper there is a growing interest in double covered flat plate collectors.

Flat plate collectors mainly use hardened (tempered or "safety") solar glass with common thicknesses of 3.2 or 4 mm. Hardened glass will shatter in many small pieces when damaged. This is a safety requirement reducing the danger caused by large pieces of falling glass. Hardened glass may not be accepted at recycling facilities because it melts at a higher temperature than normal bottle glass. Medium- and high-quality flat plate collectors use solar glass; only very simple and cheap collectors for regions with abundant insolation use float glass.

Evacuated tube collectors are usually made of blown borosilicate glass, which has a very low coefficient of expansion ($\sim 3 \times 10^{-6}/°C$ at 20°C). Just like tempered glass, borosilicate glass melts at a higher temperature than ordinary bottle glass and should thus not be recycled together with ordinary glass.

Other Collector Housing Elements

The collector needs to withstand augmented local wind and accumulated snow loads and must be tight to prevent water ingress. However, a fully hermetically sealed flat plate collector is very difficult to achieve due to high temperature differences between day and night, summer and winter, as well as absorber and ambient which leads to fluctuating positive and negative pressures in the collector. Therefore, flat plate collectors, in almost all cases, are allowed to "breathe."

The edge frame is the part of the absorber housing of flat plate collectors that not only allows the collector to be fixed to a supporting structure but also provides the necessary mechanical strength of the collector, maintains the distance between cover and absorber, and also protects the absorber and the insulation against environmental influences. The back is usually protected by a backing sheet, which protects the insulation from damaging, water ingress, and animal intrusion. The backing sheet is usually clamped, screwed, riveted, or glued to the frame. Figure 11 shows some different edge frame constructions for flat plate collectors.

The edge frame is usually made of extruded aluminum profiles, the back sheet of aluminum or sheet metal. Sometimes, the collector is integrated in the roof and replaces other roof cover material like tiles. The collector edge frame can also be made of wood when integrated into the roof or façade. The wood frame needs to be protected against environmental influences. This type of collector is mainly used in Austria. Sometimes, the collector housing parts are made from one piece; this could be from deep-drawn stainless steel sheet, from polycarbonate, or from fiberglass.

A main environmental consideration is the ability to replace, reuse, or recycle components. Frame, cover,

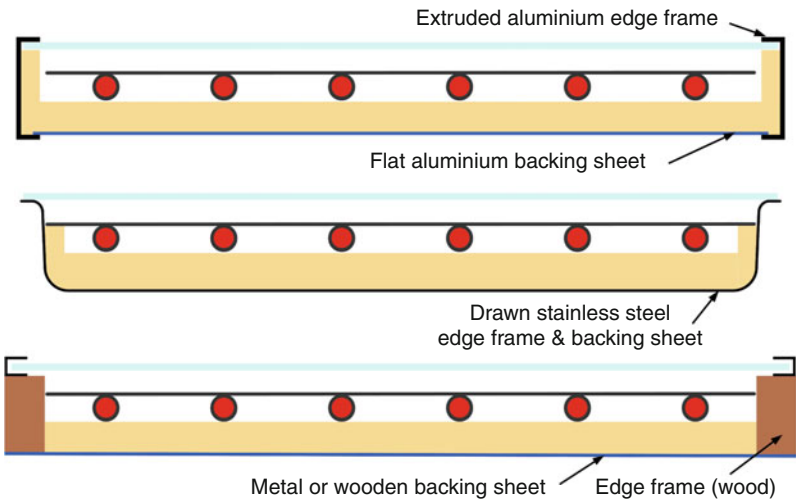

Solar Collectors, Non-concentrating. Figure 11
Different edge frame configurations for flat plate collectors

absorber, insulation, and backing sheet may be replaced, recycled, or even reused when they can easily be disassembled. From this point of view, components should thus not be irreplaceably connected to each other. The design of the edge frame plays a key role in facilitating this.

Insulation

In flat plate collectors, the edge and the back are usually insulated with mineral wool and sometimes with polyurethane foam. The insulation provides for low heat conductivity, temperature protection of some components, and in some cases, mechanical strength. The thickness of the back insulation depends on insulation material applied and is determined by the required efficiency of the collector. High-efficiency collectors for central Europe often use mineral wool with a thickness of 60 mm. In warmer climates, the insulation thickness is lower. Sometimes, different insulation materials are combined. Figure 12 shows a drawing of a cut section of a typical flat plate collector with side and back insulation.

Insulation material must be resistant against the stagnation temperature of the collector. For highly efficient flat plate collectors with stagnation temperatures reaching up to 250°C/482°F, special mineral wool is used to avoid outgassing of the binding agent in the mineral wool.

The tubes of evacuated tube collectors are sufficiently insulated by the vacuum and do not require additional insulation, but the manifold where the heat transfer tubes come together is usually insulated with mineral wool or polyurethane foam.

Reflector

Some evacuated tube collectors use a glossy sheet behind the tubes as a reflector. The sheet is usually corrugated showing a compound parabolic curved (CPC) profile, reflecting the radiation which passed between the tubes, back toward the absorber. This works as well as for beam as for diffuse radiation. The sheet, made from aluminum or from a polymer, has typically a polished and coated reflecting surface (Fig. 13).

Collector Types

Most of the solar thermal collectors used worldwide are evacuated tube collectors, since China has by far the largest solar thermal market and almost all collectors used in China are of the type evacuated tube. In contrast, about 90% of the solar collectors used in Europe are flat plate collectors. Up to now, almost all collectors use a liquid heat transfer medium, but air-heating collector use is increasing. Based on these characteristics, a general classification of non-concentrating solar thermal collectors is given in Fig. 14.

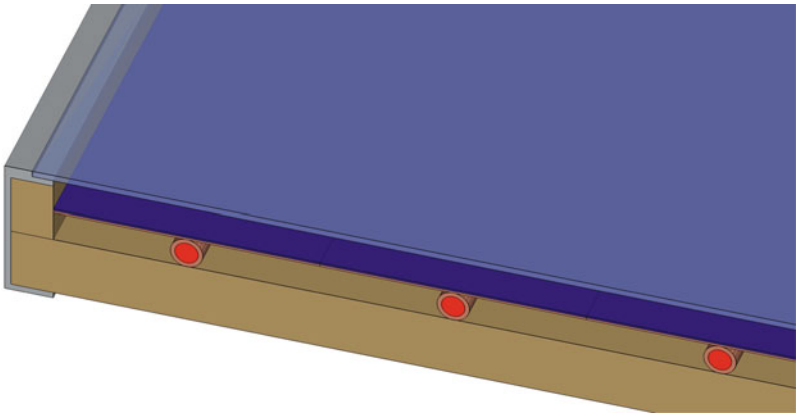

Solar Collectors, Non-concentrating. Figure 12
Cut section drawing of a typical flat plate collector with insulating material in the back and the side (*brown*)

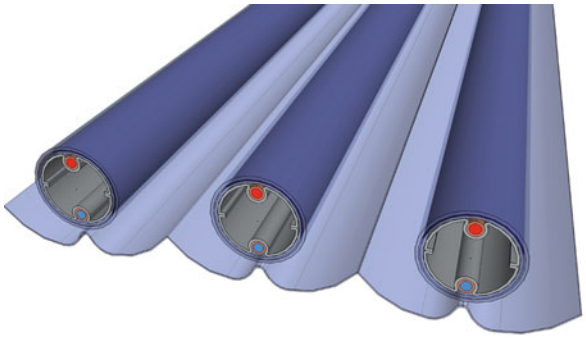

Solar Collectors, Non-concentrating. Figure 13
Cut section drawing of an evacuated tube (Sidney tube type) collector with back reflector

Which type of collector "is best" depends on the intended application, location of use, required performance and operating temperatures, the typical ambient temperature range, the type of heating system in which the collector is to be integrated, as well as on mounting and aesthetic requirements, and of course the available budget.

However, the most important factor for choosing a solar collector type is the required operating temperature range. The application areas with their typical temperature ranges and the related collector types with their typical outlet temperatures are shown in Fig. 15.

Figure 16 shows a sample of efficiency curves of four different collector types. Typically, the efficiency at higher operating temperature differences increases for noncovered to covered flat plate collectors, without and with spectral-selective absorber coating, up to evacuated tube collectors.

In the following chapters, the most common collector types are described.

Noncovered Flat Plate Collectors

The simplest solar thermal collector consists only of an absorber with channels for the heat transfer fluid integrated into the absorber. The absorber is made of a dark material for high absorption of solar radiation. Since its heat losses increase strongly with the temperature difference between the absorber and the ambient, the usable operational temperature range of noncovered collectors is typically between 10 and 20 K above the ambient temperature. In the example shown in Fig. 16, the efficiency is 55% at an operating temperature difference of 10 K and an irradiation of 500 W/m^2 and of 20 K at 1,000 W/m^2. Therefore, noncovered solar collectors are used for swimming pool heating, preheating, and in combination with heat pumps only or as air-heating collectors for direct space-heating purposes.

The most common application of noncovered collectors is for pool heating. They are generally made of heavy-duty rubber or plastic treated with an ultraviolet (UV) light inhibitor to extend the life of the panels. The absorber consists either of many joined parallel polymer pipes or of extruded mats with channels made of

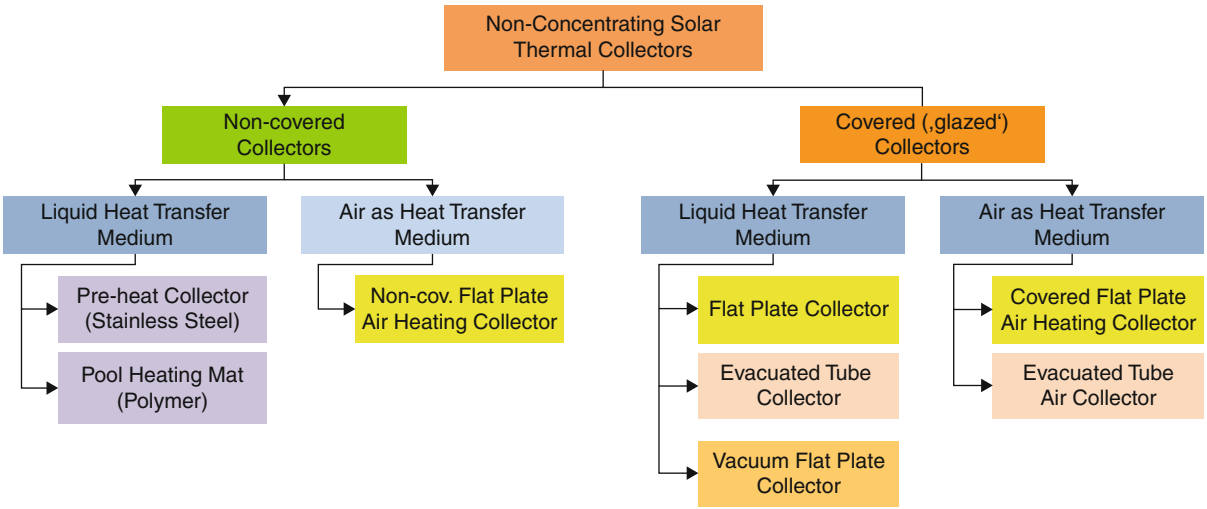

Solar Collectors, Non-concentrating. Figure 14
Breakdown of different types of non-concentrating solar thermal collectors

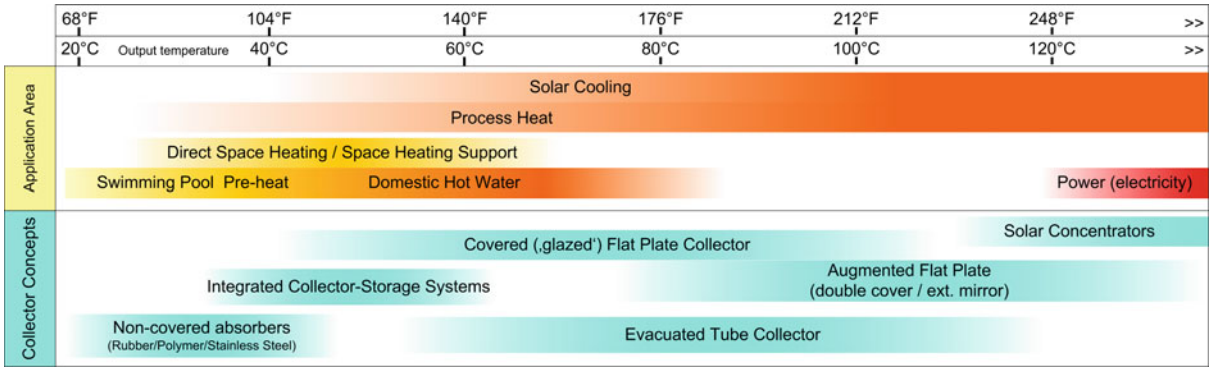

Solar Collectors, Non-concentrating. Figure 15
Indicative overview of solar thermal applications (based on temperature requirements) and a rough classification of solar thermal collector technologies, which can be used for these applications (based on typical output temperature of the collector)

a rubber compound. The joined pipes or mats are cut to length, and a manifold is added which connects the ends into a supply and removal header pipe.

Often, swimming pool water flows directly through the channels, picks up heat from the mat, and flows back into the pool. Figure 17 shows a drawing of a cut section of a typical polymer swimming pool absorber.

In some cases, noncovered collectors are made of stainless steel. Here, two sheets are bonded together, with the heat transfer fluid flowing between them through expanded or impressed structures (see Fig. 18).

Another type of noncovered metal absorber is from zinc plates, which is sometimes used as roof material. In this case, the heat removal pipes are connected on the back side of the zinc plates. Noncovered metal collectors can be used with the compression fluid of a heat pump which allows for lower operating temperatures. In some cases, the collector can function as the roof cover material at the same time.

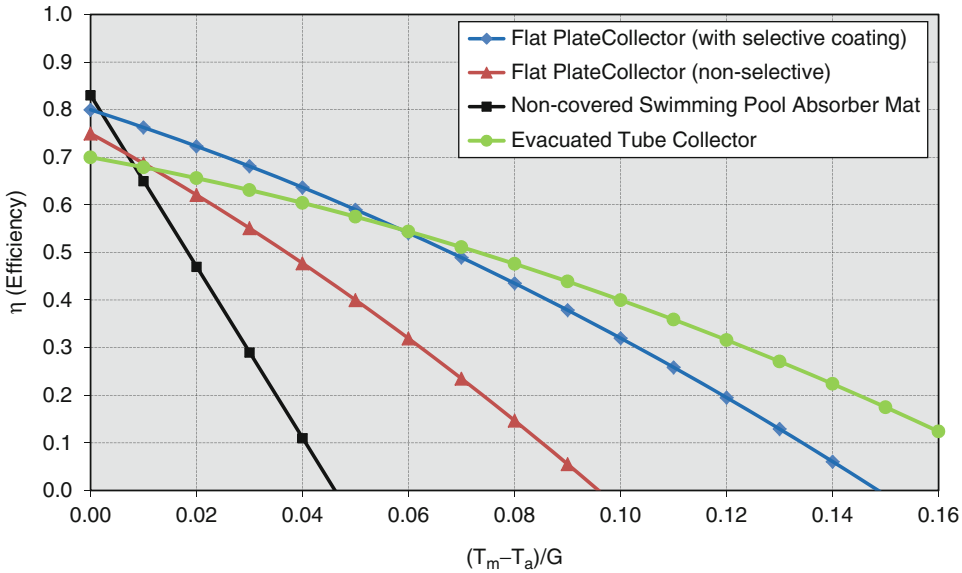

Solar Collectors, Non-concentrating. Figure 16
Typical efficiency curves of various collector types (performances of actual collectors may differ significantly from this sample)

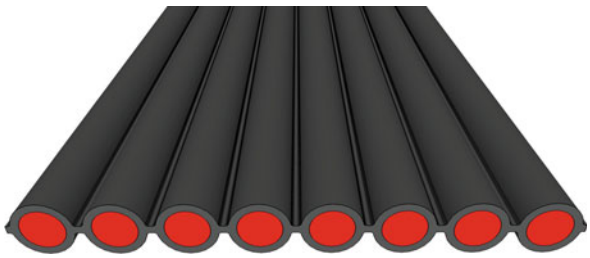

Solar Collectors, Non-concentrating. Figure 17
Cut section drawing of (part of) a noncovered EPDM swimming pool mat with extruded channels

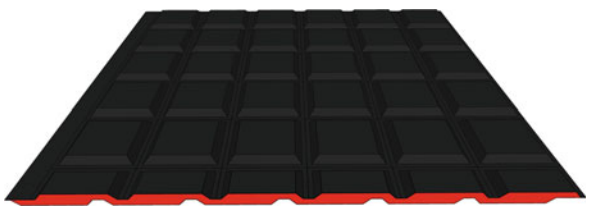

Solar Collectors, Non-concentrating. Figure 18
Cut section drawing of a stainless steel noncovered absorber, a so-called pillow absorber

Covered Liquid-Heating Flat-Plate Collectors

To reduce convection and radiative heat losses in covered flat plate collectors, the absorber is built into an insulated casing of metal, wood, or plastics to the back and the side and covered by a transparent cover at the top. The cover and the casing also provide protection to the absorber (coating) from environmental influences such as rain, hail, dirt, etc.

Flat-plate collectors are most common in Europe, with a market share of about 90%. Their main application area is domestic hot water–heating and space-heating support. The typical gross area of a flat plate collector is 2–2.5 m^2. Larger collectors of 6–12 m^2 are built as well, especially for use in large collector systems; however, a crane is needed for their installation.

In central and northern Europe, almost all flat plate collectors for domestic hot water and space heating have a spectral-selective coating of the absorber. Partly in southern Europe and mostly in northern Africa, absorbers are only painted (nonselective) black, since the irradiation and the ambient temperatures are higher. Therefore, the same solar gains can be achieved with a lower collector efficiency.

The distance between absorber and transparent cover must be optimized to significantly reduce the conductive and convective heat losses between absorber and cover. Since the absorber may curve due to the thermal expansion of the absorber cover, distance is typically a little more than the theoretical optimum, thus around 2 cm.

One option to further reduce heat losses through the cover of a flat plate collector is the use of a double cover. In a few cases, vacuum or low-pressure inert gas is maintained between the absorber and the transparent cover or in the entire collector because this is often not cost effective.

Evacuated Tube Collectors

Convection and conduction heat losses through the cover can very well be reduced without significantly affecting the transmission by using vacuum as insulation. For flat plate collectors, the air pressure differences cause large forces on the cover and casing, and to guarantee the tightness over 2 decades is a huge challenge. However, circular glass tubes are resistant to the pressure due to their edgeless shape, and for glass-glass-sealed tubes, the vacuum tightness is very high and reliable over time. The evacuated tube collector is therefore made-up of many parallel glass tubes each covering an absorber strip.

Two constructions of evacuated tube collectors are on the market. In single-walled tubes, the vacuum exists within the entire tube, and the absorber fin sits in the vacuum space; this construction requires a glass-metal seal to be able to effectively remove the heat; here, it is a challenge to maintain the vacuum reliable under varying operating conditions. In double-walled tubes, a second glass tube is located within the outer one and the vacuum exists only between these double walls; here, a glass-glass seal can be used since the heat removal construction is not placed in the vacuum space. In the so-called Sidney tube, the inner glass tube is selectively coated and works as the absorber. Within the inner glass tube, a metal heat removal construction is placed. There are different methods to transfer heat from the absorber in a single glass tube to the header of the collector. Either the heat transfer fluid flows through the pipe in the tube or a "heat pipe" is used.

A heat pipe is a sealed pipe filled with a liquid, for example, water or ethanol under low pressure, used for heat transfer. The heat of the absorber evaporates the liquid, which rises to the header where it condenses and thereby transferring the heat to the solar circuit. By using the latent heat of this evaporating/condensing mechanism, a large heat transfer capacity in a narrow connection is possible. For so-called dry connected heat pipes, the condenser is connected conductively with the metal of the heat transfer circuit; for wet connections, the condensing end is immersed into the fluid of the heat transfer circuit. The dry connection allows for easier replacement. The different types are shown in Fig. 19. At the top end of the collector, the so-called header, the heat removal fluid flows through the solar circuit (i.e., collector loop).

Because a glass cylinder may break, for example, due to hail or its vacuum may fail over time, the vacuum glass tubes are usually removable. Often, evacuated tubes contain a "barium getter" which helps to achieve high vacuum through barium reacting with common gasses. A resulting white area around the getter indicates when the vacuum is lost.

The evacuated tube collector's performance can be enhanced through the use of compound parabolic

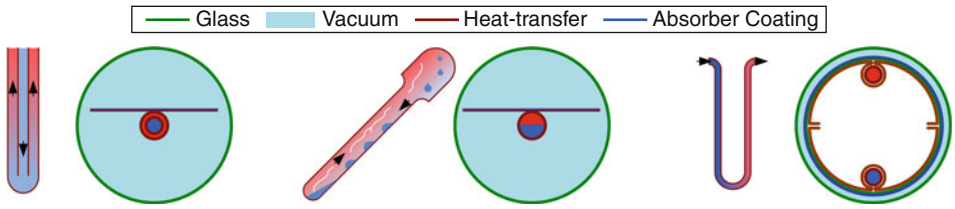

Solar Collectors, Non-concentrating. Figure 19
Sectional views of the heat removal construction and the glass tubes of different types of evacuated tube collectors: left, single glass tube with coaxial heat removal tube; center, single glass tube with heat pipe; right, double glass tube (Sidney tube type) with vacuum between the two glass tubes

curved (CPC) reflectors located behind the tubes. This shaped mirror will reflect the solar radiation that passes between each evacuated tube back to the underside of the cylindrical absorber in the collector tubes (see Fig. 13).

Air-Heating Collectors

The use of air as heat transfer medium has some advantages: air does not cause problems when temperatures drop below 0°C/32°F or reach above 100°C/212°F; therefore, no frost nor overheat protection is needed. In addition, tightness requirements are much lower for air-heating collectors. On the other hand, other, less favorable, characteristics of air lead to some drawbacks: lower heat capacity and lower heat transfer capacity. Larger volume flows are needed for the same heat transfer due to the lower heat capacity of air; heat transfer from the absorber to the air is worse due to lower heat conductivity; in addition, storage of heated air is not practical. In general, air ducts are more voluminous than with liquid heat removal channels, but air collector constructions can also be simpler due to lower pressure and reduced leakage requirements.

The physical properties of air as a heat transfer medium differ significantly from those of water. In Table 1, the main relevant properties are listed.

Air-heating collector development focuses on improvements in the heat transfer construction due to its lower thermal capacity and the much lower heat transfer coefficient between absorber and air. An improved heat transfer coefficient can be achieved by increasing the surface area that is in direct contact with the air or by improving the contact itself, for example, by letting the air flow through holes in a sheet absorber, so-called perforated absorber.

Solar Collectors, Non-concentrating. Table 1 Comparison of relevant properties of air and water as heat transfer fluid at 25°C/77°F and 1 bar

Property	Units	Air	Water	Factor
Density	kg/m^3	1.18	998.20	~842
Specific heat capacity c (by weight)	kJ/(kgK)	1.00	4.18	~4
Specific heat capacity c (by volume)	kJ/(m^{3}K)	1.18	4,171.48	~3,500
Heat conductivity λ	W/mK	0.026	0.6	~23

Air as heat transfer medium allows for higher flexibility in the collector construction, such as the position of the absorber. Many different absorber geometries and collector flow designs can be realized. Figure 20 shows different absorber flow designs of air-heating collectors. Examples A1 to A3 and B1 to B3 are covered; A4 and B4 are noncovered constructions. Row "A" shows a perforated transparent cover or perforated absorbers, through which the air is passed and the transfer of heat is improved. A1 and A4 configurations take in fresh outside air through the perforated cover or absorber and are sometimes called "transpired." Row "B" shows covered and noncovered air collectors where the air flows between the cover and the absorber, behind the absorber, or on both sides of the absorber. A possible channel or fin structure attached to the absorber, which increases the absorber-air contact area, is not shown here.

The absorbers are usually made of metal (aluminum, copper, steel) or polymer sheets. Since they operate only at low temperatures, nonselective absorber coatings or just dark materials are used. Sometimes, a fleece made from polymers is used as absorber.

Air-heating collectors are most efficient and cost effective if the heated air is used directly for space heating within air-heating systems or other applications using hot air like drying of agricultural products or drying of sorption wheels of thermal cooling machines. The latter requires high operating temperatures.

Generally, two types of collector loop constructions can be distinguished: closed and open. For closed collector loops, the air is circulating through a closed solar air collector circuit and the heat produced is transferred to the point of usage by a heat exchanger. For open collector loop systems, the air coming in the collector is outside air, through holes in the perforated transparent cover or absorber or even a porous back, or a manifold supplying the outside air. The heated air in this "open loop" type is then used directly for heating or, for example, drying. Transpired collectors can only be part of open loop systems.

Covered air-heating collectors are mainly used in closed loop systems. These collectors are often installed

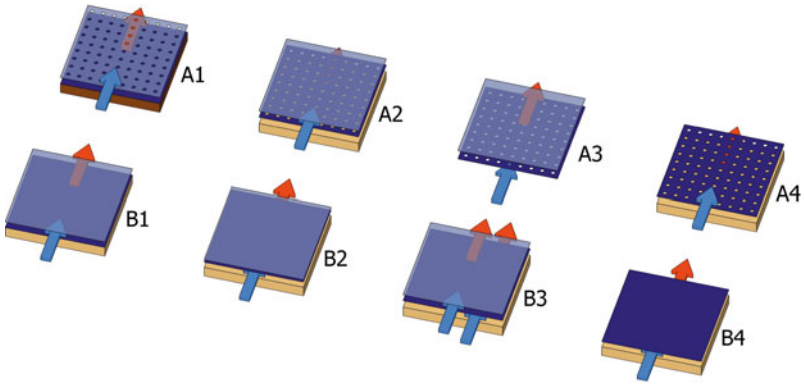

Solar Collectors, Non-concentrating. Figure 20
Different construction types of air-heating collectors

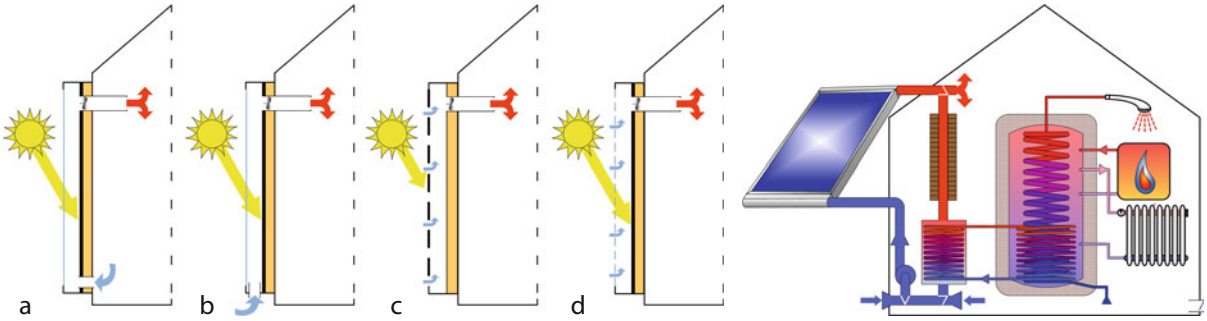

Solar Collectors, Non-concentrating. Figure 21
Schemes of solar air-heating collector systems: left, façade integrated; right, closed loop system with a covered flat plate collector

on the roof of a commercial building, and the heat is transferred into the ventilation system of the building by heat exchanger. The close loop can also be used to heat up water for use or storage. A scheme of such a system is shown in Fig. 21. For high-efficiency and high-temperature applications, a relatively new evacuated tube air-heating collector for temperatures up to 120°C has been developed [11].

Some air collector units operate independently of the electricity grid using a small PV panel integrated into the collector area to power a fan in the collector. These systems are often used in remote areas or to heat and ventilate holiday homes.

A common construction is to integrate air-heating collectors into the façade of a building. Covered as well as noncovered transpired air-heating collectors are used. The absorber then functions as the façade cover. Typically, the heated air is directly used for space heating in the rooms behind the façade, as shown in Fig. 21.

Noncovered air collectors can heat ventilation air and are used in places with high solar radiation during the heating season and buildings with large south-oriented façades. In North America, many solar air collector façades are realized for commercial, industrial, or institutional buildings.

The air-heating solar collector can also be used to heat a water store. However, with any air-water heat exchanger, there is a temperature drop between the supplying primary circuit and the receiving secondary circuit, and therefore, the efficiency is lower than in a liquid-heating collector system.

Another way to store the thermal energy from heated air is to lead it through a solid storage, for example, a pebble bed, which then stores the heat. Discharging is done in a similar way, again by leading air through the maze, picking up heat. Also, the structure of a building itself can be used as storage; in so-called hypocaust systems, the heated air is led through channels in walls, roofs, or floors, which store the heat. The heat is then slowly released through the building material into the building space.

An important difference to liquid-heating collectors is the strong dependency of the efficiency of solar air-heating collectors on the flow rate of the heat transfer medium. With increasing mass flow rate the efficiency of a air-heating collector increases, however, the pressure drop and therefore the electricity consumption of the blower significantly increases as well. It is thus important to take the electricity consumption of the blowers into account in the overall efficiency of the solar air-heating system.

Future Directions

Solar thermal collector technologies in the first phase are relatively mature. Well-performing, affordable, standard collectors for hot water heating are on the market with an efficiency close to the physical limits and which are durable and of high quality. However, since research and development in the solar thermal technology was rather small over the last decades, there is large room for further improvements for specific application areas and new concepts. The European Solar Thermal Technology Panel (ESTTP) within the European Technology Platform for Renewable Heating and Cooling (RHC-platform) showed in its vision of solar thermal technologies the potential for further developments [3]. For solar thermal collectors, the following developments are expected:

- Reduction of costs by introducing new materials and production methods into the collector
- Extension of the collector technology to other temperature ranges like process heat up to 250°C
- Integration of the collectors into the building envelope
- Adaptation of the collectors to the type of application, for example, cheaper collectors for lower temperature applications
- Development of multifunctional collectors like photovoltaic-thermal (PV-T) hybrid collectors for the production of electricity and thermal energy simultaneously on an irradiated area
- Further development of air-heating collectors for the optimization and integration into air-heating and ventilation systems
- Development of multifunctional solar thermal façade elements which can also be used for the refurbishment of existing buildings and which provide adjusted daylighting, insulation, ventilation, and active solar thermal collection
- Further development of large-area collectors to cover entire roofs of residential buildings and for very large collector fields for commercial applications and solar district-heating systems

Due to their potentially high efficiency, albeit at low temperature, non-concentrating solar thermal collectors are a very efficient path to harvesting the energy from the sun. The new challenge is to combine structural and functional building elements into one new construction as this often harbors contradicting requirements. New, cheaper materials and constructions are required, which are stagnation proof in addition to weather resistant over the long required lifetime of the element, to realize the high potential of solar thermal collectors.

Bibliography

1. Butti K, Perlin J (1980) A golden thread: 2500 years of solar architecture and technology. Cheshire Books, Van Nostrand Reinhold Company, New York/London
2. Weiss W, Mauthner F (2011) Solar heat worldwide. Solar heating & cooling program, IEA
3. European Solar Thermal Technology Platform (2008) Solar heating and cooling for a sustainable energy future in Europe. www.rhc-platform.org/cms/index.php?id=11. Accessed 10 Mar 2011
4. Duffie J, Beckmann W (2006) Solar engineering of thermal processes, 3rd edn. Wiley, Hoboken
5. BINE (1999) Informationsdienst Projektinfo 5/99: Selektive Absorberbeschichtungen in Solarkollektoren
6. IEA-SHC Task 39: Polymeric materials in solar thermal applications. www.iea-shc.org. Accessed 23 Mar 2011
7. Website of C.G.A. Compagnia Generale Alluminio S.p.A. http://www.cgaspa.it/eng/evaporators.htm. Accessed 5 Apr 2011
8. IEA-SHC Task 18: Solar materials R&D. www.iea-shc.org. Accessed 1 Apr 2011

9. IGDB, International Glazing Database, Lawrence Berkeley National Laboratory, http://windows.lbl.gov/materials/IGDB/. Accessed 15 Mar 2011
10. SPF, Solartechnik Prüfung Forschung, Rapperswil, Swiss. http://www.solarenergy.ch/Test_Reports-Glasses. Accessed 10 Jan 2011
11. Schüle K, Siems T, (2009) Vakuumröhren-Luftkollektor für hohe solare Deckungsgrade, Erneuerbare Energie 2009-01, AEE Intec, Austria

Solar Constant and Total Solar Irradiance Variations

Claus Fröhlich
PMOD/WRC, Davos, Switzerland

Article Outline

Glossary
Definition of the Subject
Introduction
Radiometry from Space, the Basis for Total Solar Irradiance Observations
Construction of a Composite of Total Solar Irradiance for the Last Three Solar Cycles
What is the Origin of the Variability of Solar Irradiance?
Future Directions
Bibliography

Glossary

Sun A so-called main-sequence star – converting He to H – with an age of 4.6 billion years. It rotates with a period of 27.28 days (seen from Earth) around its axis which is inclined to the ecliptic by 7.09° with an ascending node around 7–8 July.

Photosphere Visible surface of the Sun with $T_{\mathrm{eff}} \approx$ 6,050 K. It is defined as $\tau = 1$ at 500 nm which means that the "surface" at optical depth one is seen at the maximum of sensitivity of the human eye.

Solar cycle It is the main source of periodic solar variation and is observed by counting the number of sunspots visible on the Sun. It has an average period of about 11 years, and the last cycle with the number 23 started in August 1996 and ended November 2008.

Sunspot number The sunspot number R is defined as $R = k(10g + f)$ with the number of groups g, the number of spots f and a calibration factor k which accounts for instrumental and seeing condition of the observation. R is also a rough estimate of the total magnetic field penetrating the visible hemisphere.

Open magnetic field This is the radial component of the magnetic field in the heliosphere. It is measured at the orbit of Earth, that is at 1 AU (astronomical unit = 1.49598×10^{11} m) and varies with the solar cycle and on secular timescales.

Active region Complex of sunspots and faculae clustered together, starting at the beginning of a solar cycle at latitudes of about ±40° and migrating toward the equator during the cycle.

Ephemeral region Small bipolar region with sizes typically less than 20,000 km along their long axis, lifetimes of a few hours, and no sunspots. Their numbers vary only weakly with the solar cycle. Unlike active regions, ephemeral regions occur over the entire solar surface.

Sunspot Dark magnetic feature on the solar surface with diameters of 3,000–70,000 km. Spots larger than about 10,000 km have besides the dark umbra ($T_{\mathrm{eff}} \approx$ 4,240 K) a less dark penumbra ($T_{\mathrm{eff}} \approx$ 5,680 K). Normally, they exist in pairs with the leading (in the sense of rotation) spot having the opposite magnetic polarity of the cycle (after reversal of the polarity at solar maximum).

Facula Bright magnetic feature on the solar surface, mainly in active regions with similar sizes as sunspots. In contrast to sunspots with lifetimes of the order of a month, faculae can live for several rotations, even after the accompanying spot of the active complex has disappeared.

Plage The same as faculae but observed in the chromosphere in, e.g., CaK-II at 393.36 nm. They are larger in size because of the fan out of the magnetic field with height in the solar atmosphere, and can be used as a proxy for faculae with appropriate scaling.

Network Besides faculae and plages, there are small magnetic features summarized by the term network. They are mainly from decaying active region magnetic fields and are migrating poleward during a solar cycle.

Solar constant The amount of total solar energy of all wavelengths received by unit time and unit area at the mean Sun–Earth distance in the absence of the Earth's atmosphere. The term "Solar Constant" is somewhat misleading, because the irradiance is varying with the 11-year solar activity cycle and possibly over centennial timescales and hence "Total Solar Irradiance" or TSI is used. An irradiance of 1,365 W m^{-2} correspond to an effective temperature of the Sun of 5,777 K.

Definition of the Subject

Solar radiation received by the Earth, the "Solar Constant" is the main energy source and hence changes may influence the Earth's climate. Its value is between 1,361 and 1,365 W m^{-2}, a rather large range which reflects the uncertainty of the measurements in absolute terms. Decreases of total solar irradiance (TSI) over the solar-rotation timescale (27-day period) can be as large as 0.5% during the passage of large sunspots over the visible disk. The number of sunspots varies with the 11-year activity cycle and TSI shows an increase of about 0.1% or about 1.3 W m^{-2} during high activity, although more sunspots should result in lower TSI. This increase is due to faculae and network which enhance TSI. Although the absolute accuracy is the order or less than the cycle amplitude, these variations can be reliably observed due to the fact that the relative precision of the radiometers over an 11-year period is much higher, namely <0.001% or 0.5 mW m^{-2} per year. Reliable measurements from space started in November 1978 with the launch of NIMBUS7 and together with overlapping missions provide now a more than 30-year-long record for the study of solar variability. Understanding TSI variability is not only important for the advancement of solar physics, but also to understand its influence of the climate of Earth.

Introduction

The radiative output of the Sun was termed "Solar Constant" until the start of solar monitoring by satellite experiments revealed that it varies continuously and exhibits variations on all timescales – from minutes to decades, accessed thus far. Prior to the advent of space-based observations, astronomers and solar physicists argued that the radiative output of the Sun as a star changed in a substantial way only on evolutionary timescales of millions of years. While it was recognized that the occurrence of sunspots might change the irradiance at the Earth, their effect was considered negligible because they cover at most a few tenths of a percent of the visible solar disk. As well, the results of a half-century of ground-based program from 1902 to 1957 of the "Solar Constant" by the Smithsonian Institution inferred changes associated with the Sun's activity cycle for both the short-term decrease due to sunspots [1] and the 11-year cycle, shown as a positive correlation between sunspot numbers and the solar constant especially during the strong solar cycle 19 [2, 3]. However, the determined amplitudes were nearly an order of magnitude higher than evident from the space-based record shown in Fig. 1 and the results obviously were influenced by the highly varying terrestrial atmosphere. As a result, the view that the total radiative output was a constant quantity prevailed until the late 1970s, when space-based records became available. The first unequivocal evidence of solar irradiance variability on timescales from minutes to days and months was published by Willson et al. [4] from measurements by the ACRIM (Active Cavity Radiometer for Irradiance Monitoring) experiment on SMM (Solar Maximum Mission of NASA) during 1980 (see Fig. 1). The radiometer detected fluctuations that sometimes reached a few tenths of a percent and were associated with the movement of sunspots across the face of the solar disk visible at Earth as the Sun rotated on its axis. Such observations have been continued with overlapping missions until present and confirm TSI variability on all timescales. The understanding of these variations will not only improve the knowledge of the responsible mechanisms on the Sun, but also allow to reconstruct TSI back in time, possibly back to the Maunder Minimum in seventeenth century during which solar activity was very low with essentially no spots over a few decades and the temperature in Europe was low, it was the time of the so-called Little Ice Age.

Radiometry from Space, the Basis for Total Solar Irradiance Observations

Observations of TSI use radiometers which are based on the comparison of the absorbed solar radiation with electrical power; hence, they are called "Electrically

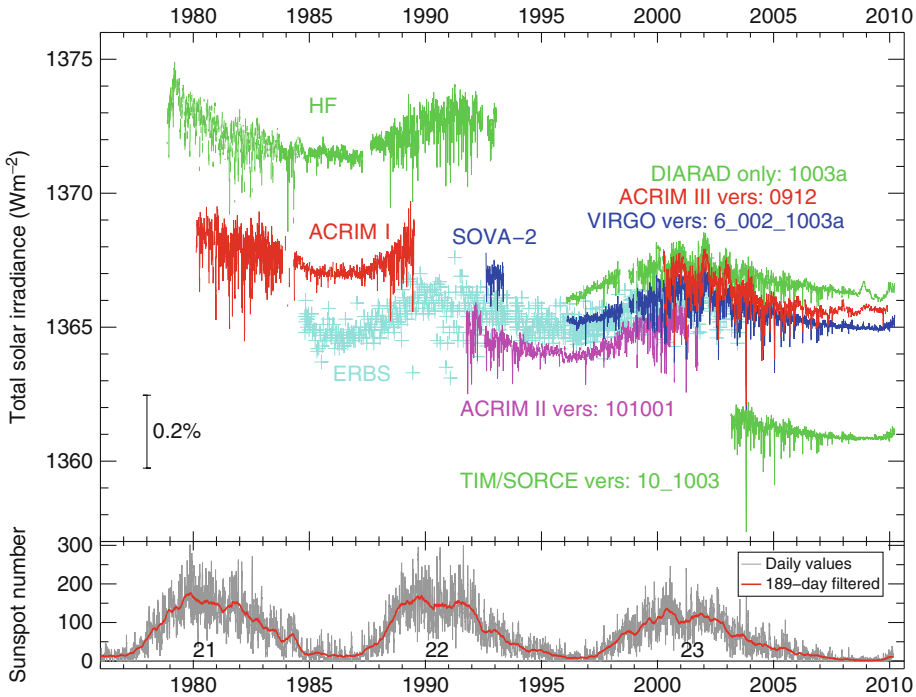

Solar Constant and Total Solar Irradiance Variations. Figure 1

Top panel: Compared are daily averaged values of the Sun's total irradiance from radiometers on different space platforms as published by the instrument teams since November 1978. Note that the VIRGO TSI is determined from both VIRGO radiometers (PMO6V and DIARAD), whereas the DIARAD TSI is only based on this one alone. *Bottom panel*: Sunspot number to illustrate the variability of solar activity for cycles 21, 22, and 23

Calibrated Radiometers" or ECR. Cavities replace a flat black-painted receiver to enhance the absorptivity of solar radiation to more than 99.99%. Moreover, the radiometers have a shutter which opens and closes periodically for a calibration of the heat flux meter without radiation. Most radiometers are operated in a so-called active mode which maintains the heat flux constant by controlling the electrical power in the receiver – hence the term "Active Cavity Radiometer" or ACR. The difference between the electrical power during closed and open phases determines the solar radiative power and, with the knowledge of the area of the precision aperture, the irradiance in W m^{-2}. A detailed description of the radiometers presently used in space and their operation can be found in Fröhlich [5].

Since late 1978 TSI measurements were made by different radiometers in space, namely HF (developed by Hickey and Frieden, Hoyt et al. [6]) within the Earth Radiation Budget (ERB) experiment on NIMBUS 7 (NOAA/NASA), ACRIM I [7] on SMM, ERBE (Earth Radiation Budget Experiment, Luther et al. [8]) on ERBS (Earth Radiation Budget Satellite) and other NOAA satellites, ACRIM II [9] on the UARS (Upper Atmosphere Research Satellite of NASA). SOVA (Solar Variability, Crommelynck et al. [10]) on EURECA (European Retrievable Carrier of ESA). VIRGO (Variability of Irradiance and Gravity Oscillations, Fröhlich et al. [11]) on SOHO, ACRIM III [12] on ACRIMSat and since 2003 TIM (Total Irradiance Monitor, Kopp and Lawrence [13]) on SORCE (Solar Radiation and Climate Experiment of NASA). Figure 1 shows these original time series, and it is clear that not only the absolute values are quite different, especially at the beginning of the period shown, but also early ACRIM I and HF data show differences which are due to the lack of a less exposed backup radiometer in the latter experiment. The ACRIM, VIRGO, and TIM experiments have such backup radiometers, which are only rarely exposed to the Sun, and by periodic comparison

with the operational one, the exposure-dependent degradation can be determined in situ.

Construction of a Composite of Total Solar Irradiance for the Last Three Solar Cycles

The time series from the HF, ACRIM I, II, and III, and VIRGO radiometers can be used for the construction of a TSI composite by shifting each series to a common level and merging them together. Presently, there are three composites available, the first one was presented in 1997 at the IAU General Assembly in Kyoto by Fröhlich and Lean [14] and is now called PMOD composite (for its construction see [15]). A few months later the ACRIM composite was published by Willson [16] which has been updated in 2003 by Willson and Mordvinov [17]. Somewhat later, a third composite, called IRMB, was presented by Dewitte et al. [18] (The composites are shown in Fig. 2 and available from: PMOD: http://www.pmodwrc.ch/pmod.php?topic=tsi/composite/SolarConstant, ACRIM: http://www.acrim.com/Data/%20Products.htm and IRMB: http://remotesensing.oma.be/en/3377935-TSI+composite.html). The ACRIM and IRMB composite use the data as published, whereas the PMOD composite introduces corrections of effects not considered in the original data analysis. Already in the early versions of the PMOD composite corrections for the HF degradation were applied [14, 19]. Similarly, the degradation of ACRIM I during first years was corrected for the effect of the rather short exposure time during the spin mode which was not taken into account in the original treatment by Willson and Hudson [20]. The corrected HF time series was used for the period before ACRIM started and during the spin mode of SMM and the corrected ACRIM I for the rest of time (1980 and 1984–1989) as basis for the composite of Fröhlich and Lean [19]. Fröhlich [15] included a further correction

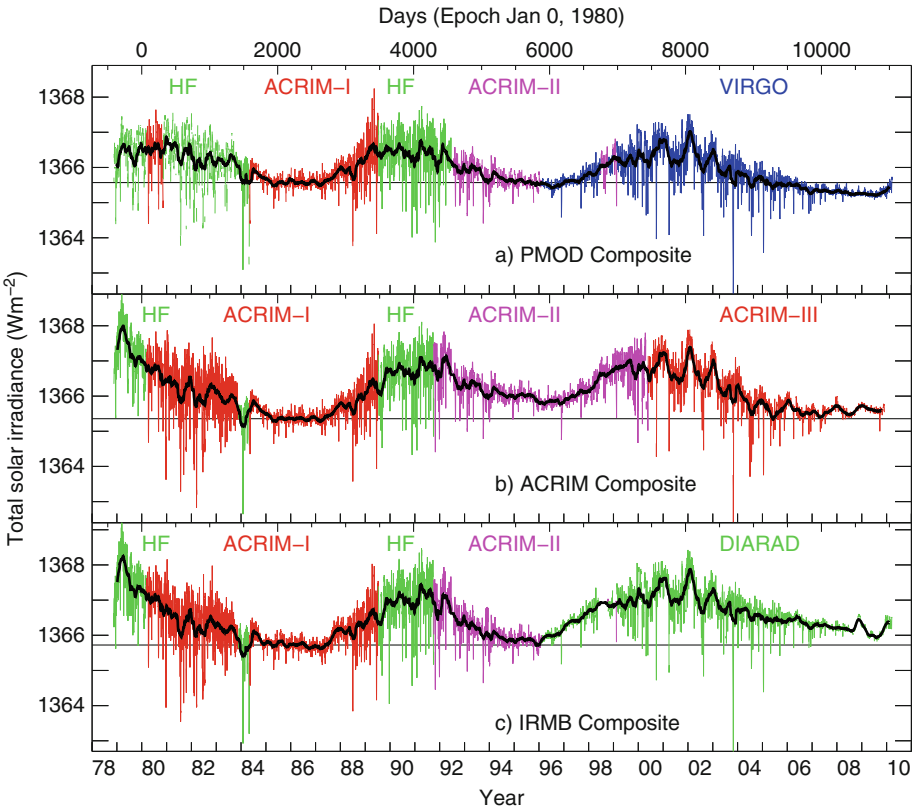

Solar Constant and Total Solar Irradiance Variations. Figure 2
Shown are the three composites: (**a**) PMOD [14, 15], (**b**) ACRIM [16, 17], and (**c**) IRMB [18]

of ACRIM I for the early increase which was first observed in the PMO6-V measurements of VIRGO/SOHO and seems to be an inherent effect of most classical radiometers. Moreover, the substantially lower exposure time during the spin mode operation of SMM 1981–1984 imposed to take the effective dose into account which changes the rate of degradation substantially (see Figs. 3 and 4 of [15]). During the first 15 months of HF, no other radiometer is available as reference and a proxy model was used. This is the only period when a model is involved as reference. It is, however, calibrated to the corrected ACRIM I data over the period from 1980 to 1988 and is thus quite reliable for the period of a few years before 1980. For HF, all glitches throughout the mission are removed first and then the corrections for the early increase, the degradation and the long-term sensitivity increase were determined over the full period from November 1978 until January 1993, which yields an internally consistent time series (see Figs. 6 and 7 of [15]). In a last step, the absolute value of the PMOD composite is shifted to represent the SARR reference (SARR: Space Absolute Radiometric Reference as defined by Crommelynck et al. [21]).

Another problem for the composite constructions is how to bridge the so-called ACRIM gap between the end of ACRIM I and the start of ACRIM II (June 1989 to October 1991). During this period, daily values from HF and some 70 data points from ERBE with a sampling every 14 days are available. Already Lee III et al. [22] revealed two slips in the HF data resulting in a total change of -0.68 W m^{-2} over this period which was confirmed by comparison with a model derived from solar disk observations by the San Fernando group [23]. Fröhlich [24] re-analyzed this period and the overall change was again confirmed, but with a slightly different value of -0.58 W m^{-2}. Such changes no longer need to be corrected individually, because the HF time series, consistently corrected over the full period, can now be used directly for bridging the ACRIM gap.

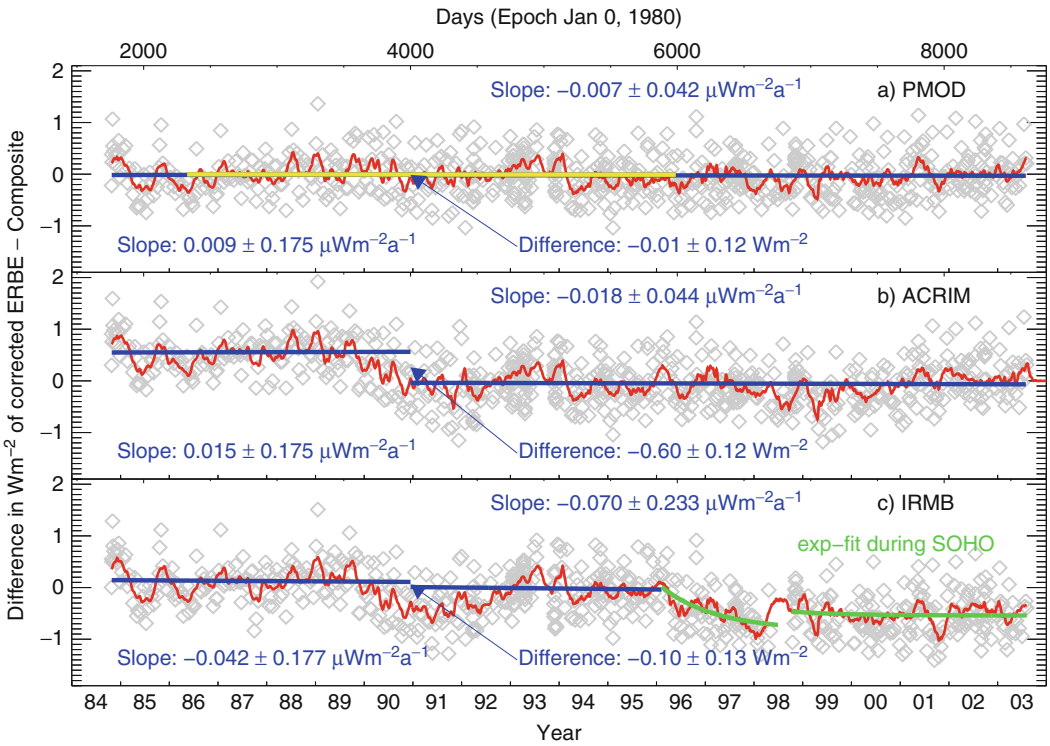

Solar Constant and Total Solar Irradiance Variations. Figure 3

Shown are comparison of the three composites with the 18-year record of ERBS from 1985 to 2003: (**a**) PMOD [14, 15], (**b**) ACRIM [16, 17], and (**c**) IRMB [18]. The *yellow line* in (**a**) is the result of the linear fit to the difference over solar cycle 23

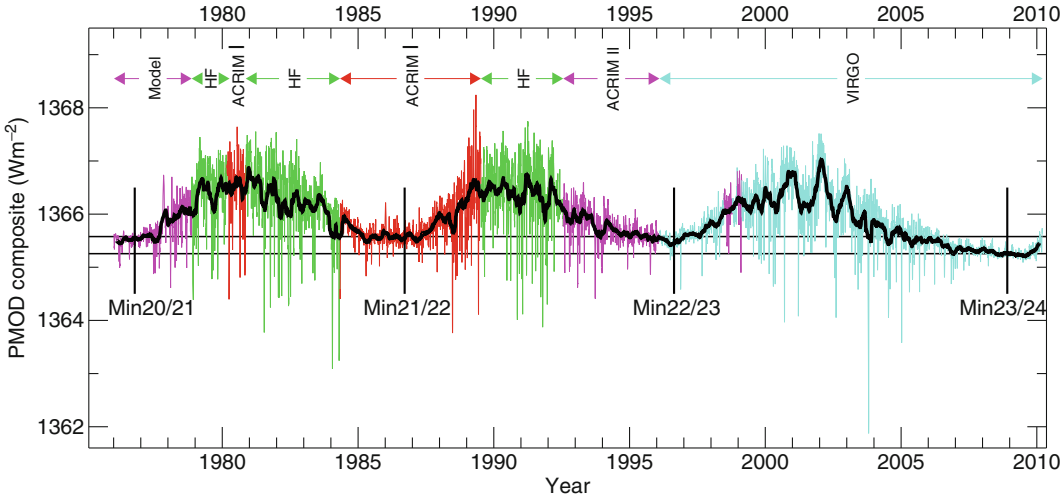

Solar Constant and Total Solar Irradiance Variations. Figure 4
Daily TSI of the PMOD composite (updated until end of March 2010 Version 41_62_1003a) and extrapolated with a proxy model back to 1976. The amplitudes of the three cycles decrease first and then increase again. The two *horizontal lines* indicate the value of the minima in 1986 and 2008, respectively. Note the low value of the 2008/2009 minimum, which is 0.22 W m^{-2} lower than the previous one, or 25% in terms of the mean cycle amplitude

The ERBE data set covers the period from 1985 to 2003 and more specifically the controversial time of the ACRIM gap. Although the record is quite noisy – mainly because of a low rate of sampling every 14 days – it can be used to illustrate the differences between the three composites as shown in Fig. 3. The ACRIM composite neglects the corrections of the HF during the ACRIM gap and thus shows a significant upward trend of TSI between 1985 and 1995 [16, 17, 25]. The IRMB composite traces ACRIM II to I via ERBE which results in an insignificant difference between the two minima in 1985 and 1995 similar to the PMOD composite. However, the IRMB time series during the ACRIM gap shows a strange variation which comes from the fact that it is normalized to the average of ERBE and HF, both referred to SARR. During the period of SOHO the IRMB composite is based on DIARAD data alone, which means that it is corrected for degradation by comparison with its backup, but misses the effect of non-exposure-dependent sensitivity increase. This latter effect can only be determined by comparison with another radiometer – in the case of VIRGO with PMO6-V – and its omission is the main reason for the increase of TSI during solar cycle 23 in contrast to the PMOD and ACRIM composites (see also Fig. 3). The deviation from ERBE can be fitted with an exponential function similar to the one which is used in the evaluation of the VIRGO data [26]. Furthermore, both the ACRIM and IRMB composite use the original data for the early part of the NIMBUS-7 mission which is – as explained above – strongly influenced by instrumental changes and is not representing solar variability.

Recently Scafetta and Willson [25], Scafetta [27] insinuated again that the PMOD composite is incorrect, because the corrections applied to the original ACRIM I and HF time series have no basis at all and are only applied to get agreement with a proxy model originally proposed by Foukal and Lean [28, 29]. As explained in detail in Fröhlich [15] and summarized above, the corrections are based on an improved understanding of the long-term behavior of radiometers in space, the results of which were not available to the teams evaluating ACRIM and HF. This was made possible by the detailed analysis of the almost 14-year-long solar irradiance record from the two VIRGO radiometers (PMO6V and DIARAD) on a thermally very quiet spacecraft SOHO (see, e.g., [26], and references therein). Besides the excellent agreement with the ERBE record, the PMOD composite agrees also much

better with proxy (e.g., [30, 31]) and other models Wenzler [32], Wenzler et al. [33], Krivova et al. [34], which demonstrates the consistency of the applied corrections. Thus, the PMOD composite is a reliable representation of TSI back to November 1978. From the experience gained by extrapolating ACRIM I back to the beginning of HF, the PMOD composite can be further extended back to the beginning of 1976 in order to cover cycle 21 from its minimum as shown in Fig. 4.

What is the Origin of the Variability of Solar Irradiance?

Figure 4 shows clearly that the TSI is variable on all timescales from days to decades. There are obvious changes on the solar-rotation (27-day) timescale during the passage of active regions with dips due to sunspots and rises due to faculae. Moreover, there is also a modulation with the 11-year period which may change in amplitude from cycle to cycle. The fact that TSI is higher during high activity contradicts the conjecture that more sunspots should make a darker Sun, but it supports the solar-terrestrial relationship that low TSI may lower the Earth's temperature as during the little ice age in Europe in the seventeenth century when the Sun showed very low activity with essentially no visible sunspots, a coincidence first noted by Eddy [35], who called this "Grand Minimum" Maunder Minimum. During the most recent cycle, the number of sunspots was less than during the two cycles before (see lower panel of Fig. 1) and there were even periods with essentially no spots which made the TSI amplitude during this cycle of the same order as during the ones before. The amplitude is defined here as an equivalent of a sine square (twice the average between the minima of the considered quantity). This may not ideally represent the detailed behavior of a solar cycle, which shows a much faster increase during the ascending phase compared to the rather slow decrease during the descending phase (see, e.g., Fig. 4). Besides the fact that this definition can be applied to any other quantity considered, it is for TSI relevant for the solar-terrestrial influence on the global climate with its rather long response time. Also an independent definition of the "time of minimum" is needed and the first appearance of an important sunspot group of the new cycle (at high latitude and of opposite polarity) is used. This method is illustrated by the butterfly diagram of PSI shown on Fig. 8, and the dates of the last four minima are 10 October 1976, 19 September 1986, 21 August 1996, and 29 November 2008.

Solar activity is driven by the magnetic fields produced periodically by a dynamo at the base of the convection zone at about 0.71 $R_\odot$ (for a review see, e.g., [36], and references therein). Magnetic fields threading the visible solar surface, the photosphere, produce features like sunspots and faculae related to active regions and bright network in and outside active regions. Figure 5 shows time series for solar cycles 20–23 of typical measures of solar activity. The sunspot number (SSN, Fig. 5a) is certainly the most widely used index mainly because it is available since the seventeenth century, but also because its cycle amplitude represents a measure for the varying amount of bipolar regions reaching the surface and hence the strength of solar activity during a cycle. The next parameter is the solar radio flux at 10.7 cm (F10.7, Fig. 5b) which is an absolute physical measurement available since 1947 (solar flux units $\equiv 10^{-22}$ W m^{-2} Hz^{-1}) which similar to the SSN represents a measure of the strength of solar activity. Figure 5c shows daily values of the Ly-α composite (starting with the measurements by AE-E from Woods et al. [37]) which is representative to the changes in solar chromosphere due to the magnetic fields on the surface. A similar behavior shows the CaII K and MgII indices (Fig. 5d, e) which also represent changes of the chromosphere due to the surface magnetism. None of these quantities show a significant decrease during the recent minimum as TSI. The observed trends between minima are at least a factor of 5–6 smaller than for TSI, summarized in Table 1.

For SSN, such a behavior is expected as the number cannot be negative, but all the other parameters of Fig. 5 have no lower limit of their values and thus could show a similar change as TSI. For F10.7, there is no significant change of the values at minima back to the start of the measurements in 1947. The CaII K index deduced from the Mt Wilson and Kodaikanal observations [39] back to around 1910 shows also no change in the minima to within ±4%. As the chromospheric indices are highly correlated with the UV and EUV irradiance and as shown by the Ly-record, secular changes of the spectral irradiance below about 300 nm

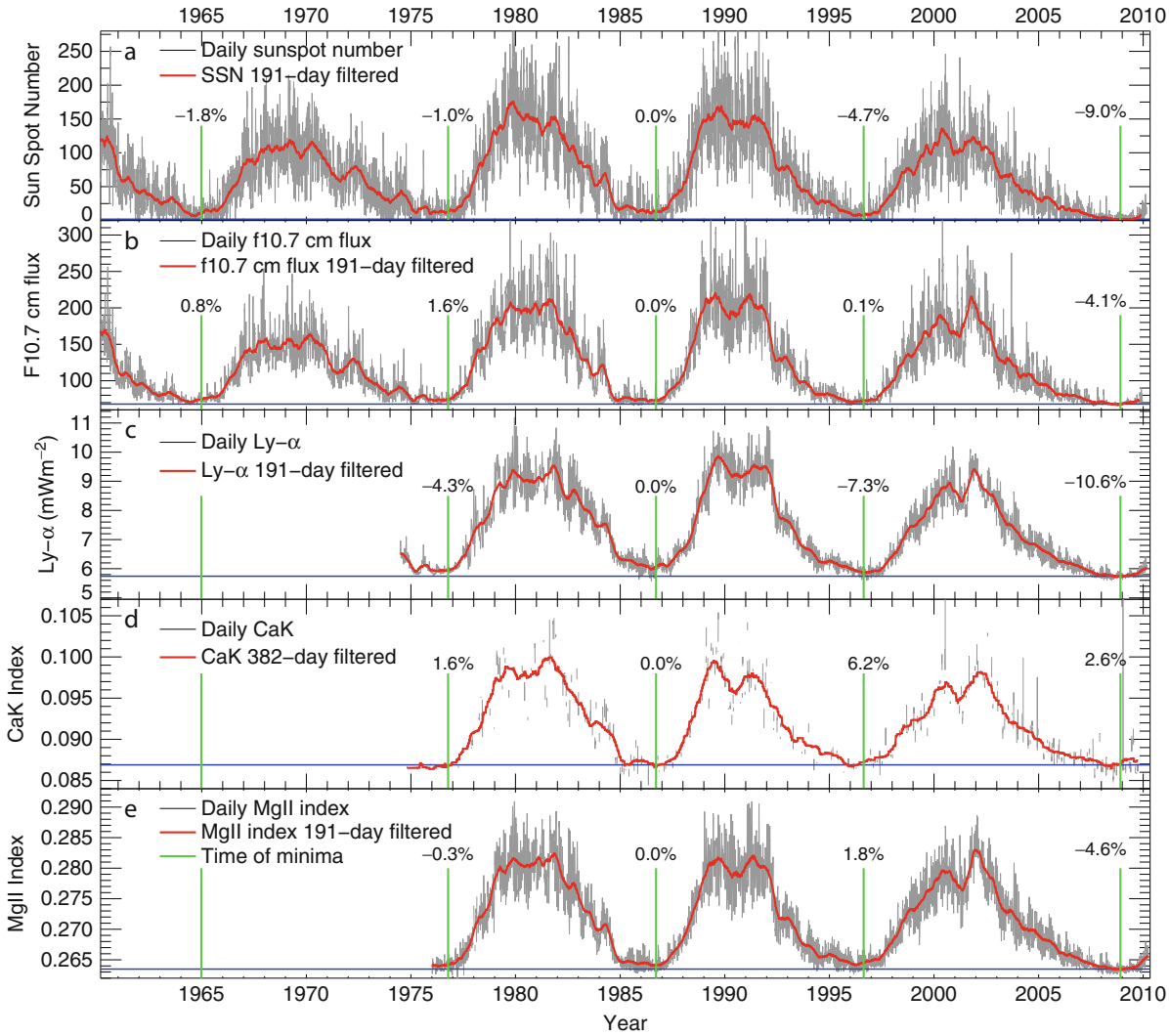

Solar Constant and Total Solar Irradiance Variations. Figure 5

Daily values of the time series of (**a**) SSN, (**b**) F10.7, (**c**) Ly-α irradiance, (**d**) Call K, and (**e**) MgII indices. The values indicated at solar minima (above the *vertical lines*) are the percent changes relative to the amplitude of cycle 22 and normalized to the value between cycles 21 and 22 indicated by the *horizontal blue line*. In contrast to TSI of Fig. 4, none of these records show the large decrease during the present minimum

are hence unlikely. All these observations show that the chromospheric temperatures during minima and hence the "quiet" magnetic Sun do not seem to change on secular timescales (see also [40]). This observation contradicts the assumption that the long-term changes of solar irradiance – spectral or total – are also caused by the same mechanism as the intra-cycle variation, namely by manifestations of the surface magnetic fields, that is sunspots, faculae and network, including ephemeral regions for a description (see, e.g., [41]).

As shown in Fig. 6 and Table 1, the only parameter that does exhibit inter-cycle changes similar to TSI is the open magnetic field. B_R, as observed at 1 AU by satellites since the 1960s (Fig. 6b). B_R is determined by taking the absolute value of the daily mean of B_X from the OMNI2 dataset (available from ftp://nssdcftp.gsfc.nasa.gov/spacecraft_data/omni/omni_m_daily.dat). Recently, Lockwood et al. [42, 43] have shown that a kinematic correction is needed to determine the open field of the Sun at the source region (at 2.5 $R_\odot$)

Solar Constant and Total Solar Irradiance Variations. Table 1 Cycle amplitudes and relative changes of minima in percent of the amplitude during cycle 22. The amplitudes are equivalent sine-squared with the trend during each cycle removed. The units are: TSI (W m^{-2}), the open field at 1 AU B_R (nT), SSN (number), F10.7 (sfu $\equiv 10^{-22}$ W m^{-2} Hz^{-1}), Ly-α (mW m^{-2}), CaII K and MgII indices (core-to-wing ratio). Updated from Fröhlich [38]

Parameter	Cycle 20	Cycle 21	Cycle 22	Cycle 23
Corrected cycle amplitude				
TSI	...	0.9244	0.8489	0.8427
B_R	...	1.361	1.482	1.161
SSN	95.1	139.8	132.9	98.1
F10.7	76.7	125.5	121.3	94.3
Ly-α	...	3.48	3.15	2.63
Call K	...	0.01270	0.00992	0.00810
MgII	...	0.0175	0.0151	0.0137
Change of minima over each cycle in percent				
TSI	...	6.0	−12.9	**−25.0**
B_R	...	5.0	−17.4	**−45.8**
SSN	0.8	1.0	−4.7	−4.3
F10.7	0.8	−1.6	0.1	−4.0
Ly-α	...	4.3	−7.3	−3.4
Call K	...	−1.6	−2.7	−1.5
MgII	...	0.3	1.8	−2.8

from the measurements at 1 AU. This correction, however, is not needed because B_R is more directly related to the interplanetary field (IMF) than the true open field and the IMF is what can be inferred from, e.g., the concentration of cosmogenic isotopes in ice cores produced by the galactic cosmic rays (GCR) or from magnetic measurements on Earth like the aa index. B_R has an intra-cycle variation quite different from TSI, because B_R changes sign around the maximum of the cycle (during periods of the reddish areas in Fig. 6b), and since the northern and southern hemisphere may change at different times, it is a prolonged period during which the behavior of the B_R variability is dominated by this reversal. This reversal happens during each cycle and produces the 22-year magnetic Hale cycle with the solar polar field having the same polarity as Earth's field. B_R during minima is mainly determined by polar field of the Sun and thus is more representative of the strength of activity during the solar cycle before and after than to the amount of surface magnetism which is due the non-axisymmetric fields.

Figure 6c shows the correlation between TSI and B_R as determined by linear regression. It is interesting that the line is very close to the points – much closer than one would expect from the error bars. This is also true for the point of the 1976 minimum, which is not used in the regression, indicating that its value – although based on a proxy model – is indeed quite reliable. The result of this correlation can be now used to calculate TSI at minima whenever B_R is known. An example of such a reconstruction of TSI during the Holocene is based on the record of the cosmogenic isotope ^{10}Be [44]. It is important to note that this correlation does not mean a direct physical relationship between TSI and B_R. As already suggested by Tapping et al. [45] and Fröhlich [38], the long-term trend may be due to global temperature change of the Sun with a magnitude related to the strength of the activity and hence to B_R

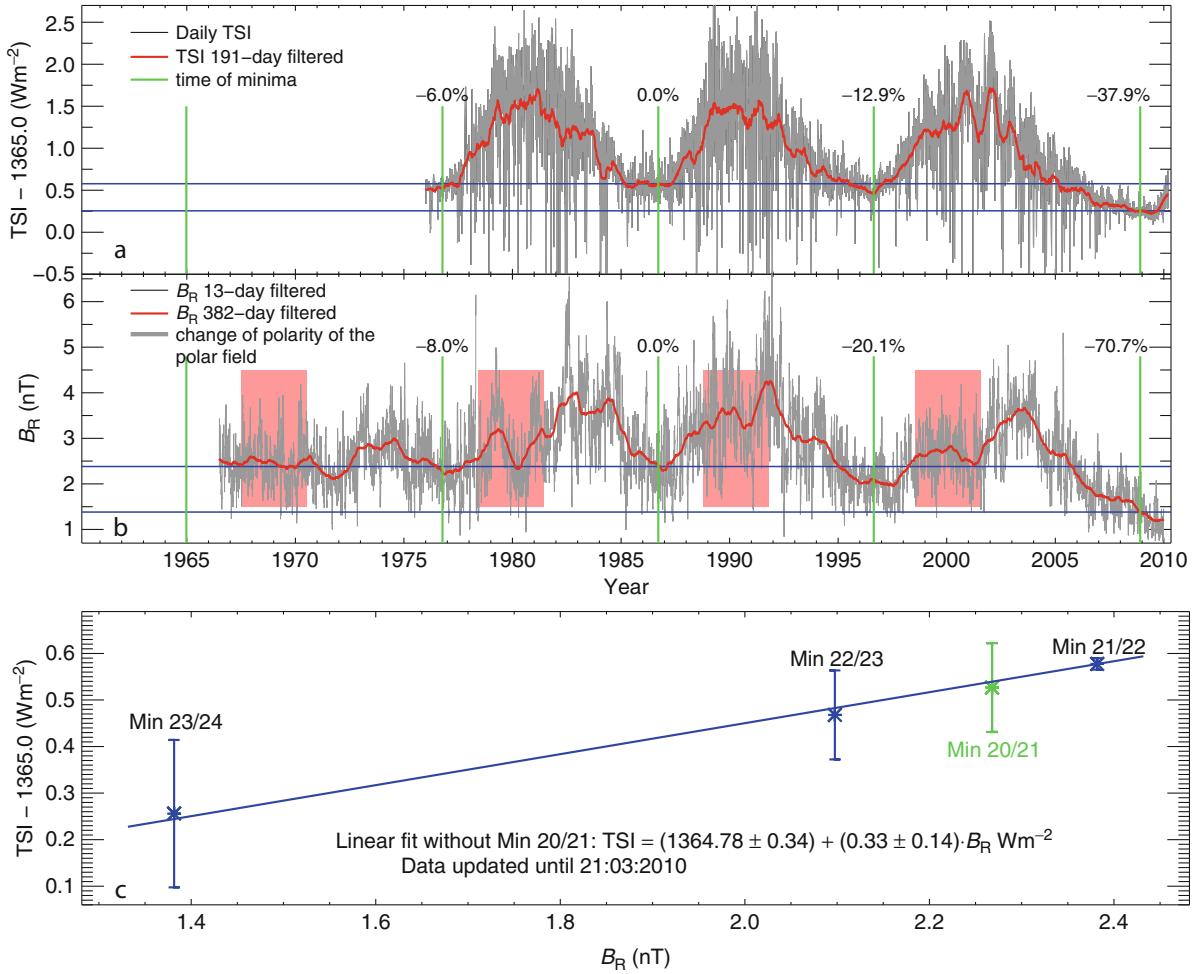

Solar Constant and Total Solar Irradiance Variations. Figure 6

Comparison of TSI and the open solar magnetic field. (**a**) Daily values of TSI (as Fig. 1) and (**b**) those of the open magnetic field B_R at 1 AU. The correlation between the minimum values of TSI and those of B_R (*blue points* and the *blue line*) is shown on (**c**). The *green point* is the extrapolated value not used in the regression. The error bars are from a detailed analysis as described in Fröhlich [38] and the errors of regression coefficients include these uncertainties, and hence are quite large

during minima. The temperature change needed to explain the difference between the last two minims is of the order of 0.25 K.

Extension of the Three-Component Proxy Model for Total Solar Irradiance

Proxy models of TSI are based on daily indices representing the darkening of sunspots and the brightening by faculae and network as illustrated in Fig. 7. A two-component model uses information on sunspots, ΔS_S from daily observations of their position and area, and one index for the brightening features ΔS_F, from, e.g., Mgll index. A three-component model uses two different indices for the brightening: ΔS_F and ΔS_N (for a review, see, e.g., [30], and references therein). But, as all three components do not show substantial changes between minima, a fourth component is needed to model the trends of TSI between the minima as already shown by Fröhlich [31]. The fourth

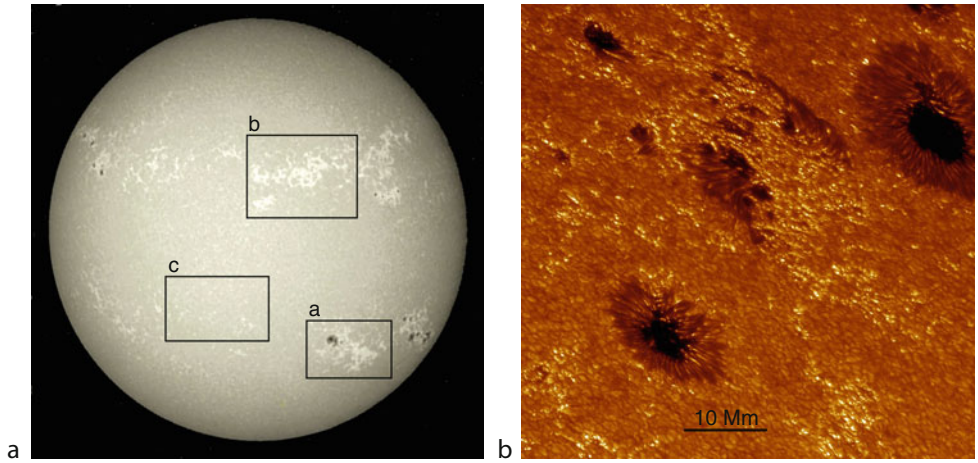

Solar Constant and Total Solar Irradiance Variations. Figure 7
(**a**) Sunspots and faculae in active regions (a, b), and network (c) imaged in the chromospheric Call K line where faculae and network are enhanced over their contrast in broad-band light and seen as so-called plages and bright network (Image taken by the National Solar Observatory on 28 August 1988). (**b**) A detailed image of the active region on the left limb as seen in the g-band (430.5 nm). The granules, covering most of the area, are the convective flows transporting the energy from the interior which contribute the steady component of the solar radiation. The magnetic features in an active region are the sunspots with the dark umbra and somewhat brighter penumbra and the faculae which are a dense carpet of bright points. (Image taken with the Swedish 1-m Solar Telescope by Dan Kiselman on 29 June 2003)

component can now be constructed from the values of B_R at the minima, connected by linear trends and providing ΔS_T. Since sunspots and faculae typically occur on the Sun together, a competition of their relative strengths determines the short-term solar irradiance variability. The solar cycle amplitude seems to be determined by magnetic features with smaller sizes than sunspots and faculae and distributed all over the Sun as network and the small bipolar ephemeral regions (see, e.g., [46]). The part coming from the latter are in the following included in what is called network. So, the four-component proxy model of TSI can be constructed as

$$S(t) = S_Q + a_F P_F(t) + a_N P_N(t) + a_S P_S(t) + a_T P_T(t), \quad (1)$$

with the value of the quiet Sun, S_Q, and $a_{F,N,S,T}$ the four coefficients for the influence of faculae, network, sunspots, and the trend from ΔS_T.

Sunspot Darkening

Sunspot darkening, the fractional change in TSI caused by sunspots, is calculated explicitly as

$$P_S = \sum \Delta S / S_Q = \sum \mu A_s \alpha_S \frac{R(\mu)}{\int_0^1 R(\mu)\mu d\mu} \quad (2)$$

where ΔS is the reduction in irradiance relative to the quiet Sun, S_Q, for a sunspot of area A_s (in fractions of the solar hemisphere) at location μ in heliocentric coordinates. $R(\mu)$ is the center-to-limb variation function which is assumed to be the same for the quiet photosphere and the spot and α_s is the bolometric contrast. The summation is over all spots on the solar disk at a specific time, and utilizes bolometric contrast and center-to-limb functions (Eddington limb darkening $R(\mu) = (3\mu + 2)/5$) or more elaborate functions of μ as, e.g., from Pierce [47] appropriate for modelling total or also spectral solar irradiance variations. Ground-based white light images made from 1882 to 1976 by the Greenwich Observatory, and most recently by the U.S. Air Force at the operational Solar Observation Optical Network (SOON) sites. Observations of the sunspot regions are available from the National Geophysical Data Center (NGDC) operated by the National Oceanographic and Atmospheric Administration (NOAA) at Boulder, Colorado, from ftp://ftp.ngdc.noaa.gov/STP/SOLAR_DATA/SUNSPOT_REGIONS,

and supply the basic time-dependent information about sunspot areas and locations. Greenwich sunspot areas are reported to be 20–40% larger than SOON sunspot areas [48, 49]. The differences between these two data sets were determined by Balmaceda et al. [49] and have been confirmed for the period after January 1977 when the USAF/NOAA data started [50]. Hence, they are corrected to agree with the Greenwich data, mainly to get a consistent record for the period from 1882 until present.

Sunspots comprise a very dark central umbra and a less dark surrounding penumbra (see also Fig. 7b), but present versions of P_S do not include this distinction because the SOON data lack the information about the relative areas of umbra and penumbra. The bolometric contrast α is obviously different for the two parts and they depend on the temperature of the umbra T_u, penumbra T_p, the quiet Sun T_0, and the respective areas A_u and $A_s = A_u + A_p$. The combined contrast of a spot α_s is

$$\alpha_s = \frac{A_u}{A_s}\left(1 - \left(\frac{T_u}{T_0}\right)^4\right) + \frac{A_p}{A_s}\left(1 - \left(\frac{T_p}{T_0}\right)^4\right). \quad (3)$$

Equation 3 yields with T_u = 4,240 K, T_p = 5,680 K T_0 = 6,050 K and A_u/A_p = 0.22 a value of 0.32 which was first proposed by Hudson et al. [51]. Figure 8 shows the time-latitude appearance of sunspots, the typical butterfly diagram. From detailed observations of sunspots with the Vacuum Tower Telescope (VTT) of the Kiepenheuer Institute in Tenerife, Steinegger et al. [52] and later Steinegger et al. [53] deduced a size-dependent α according to

$$\alpha_s = (0.223 \pm 0.010) + (0.024 \pm 0.005)\log A_s \quad (4)$$

$$\alpha_s = (0.125 \pm 0.019) + (0.048 \pm 0.010)\log A_s. \quad (5)$$

Equation 4 was generally adopted (see, e.g., [30, 49, 54, 55]). A comparison of the relation of Eq. 5 with results from sunspot data observed by MDI/SOHO [56] shows that this relation is indeed more appropriate [50]. The calculation of P_S presented here is based on Eq. 5 with the average coefficients between their original coefficients and those determined from Mathew et al. [56], α_s = (0.127 ± 0.011) + (0.050 ± 0.006) log A_s. The sunspot data from January 1975 to February 2010 are used to determine P_S and are shown in Fig. 9a (on the plots, P_S is identified as PSI, and they are given in parts per million, ppm).

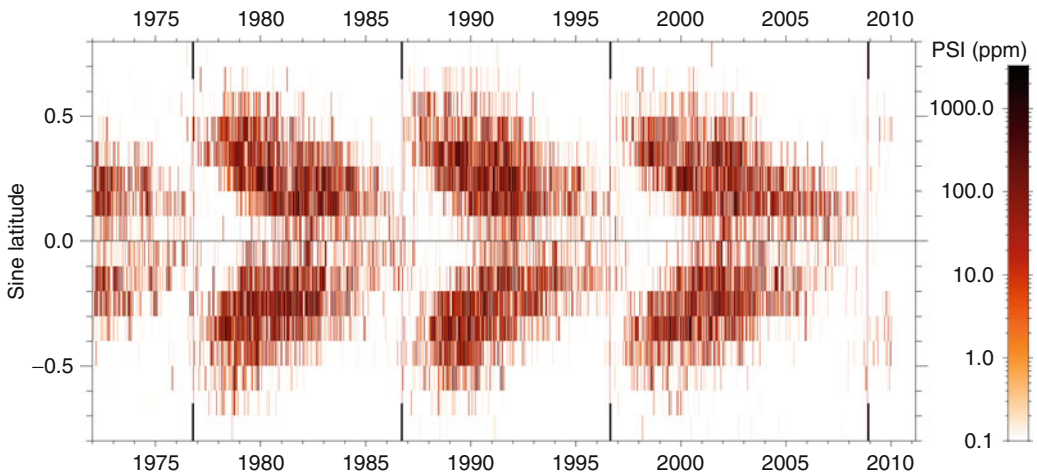

Solar Constant and Total Solar Irradiance Variations. Figure 8
Daily values of PSI as function of the latitude providing the famous butterfly diagram of sunspots. At the beginning of a cycle, they start at latitudes around ±40° and then migrate down toward the equator. The vertical lines indicate the time of the minima and it becomes also clear that they are determined by the first important sunspots emerging at high latitudes

Brightening by Faculae and Network

Images like Fig. 7a can provide areas covered by plages and bright network in the upper solar atmosphere which in turn can be used to determine the effect of photospheric faculae and network on TSI. Such images are called spectroheliograms because they are observed in a narrow wavelength band in the resonance line of CaII K at 393.37 nm, which is the strongest solar spectral line observable from the ground. Archives of daily spectroheliograms maintained at Kodaikanal Observatory (KKO), India, since 1907, and at Mt. Willson Observatory (MWO), USA, since 1915, provide the longest available record of the daily changing structure of magnetic plages and network (see, e.g., [39], and references therein). Spectroheliograms compiled since 1965 (as Fig. 7a) at the National Solar Observatory (NSO) provide supplementary information. The MWO record was discontinued in 1985 and the ones of KKO and NSO in 1999. These spectroheliograms can be analyzed individually to determine the area and position of the faculae and bright points [39, 57, 58], as it is done from images in magnetograms for the SATIRE model (e.g., [59, 60]).

At Kitt-Peak Observatory, monthly observations of disk-integrated CaII K line fluxes started in 1975 and proved to be a good surrogate for the plage and

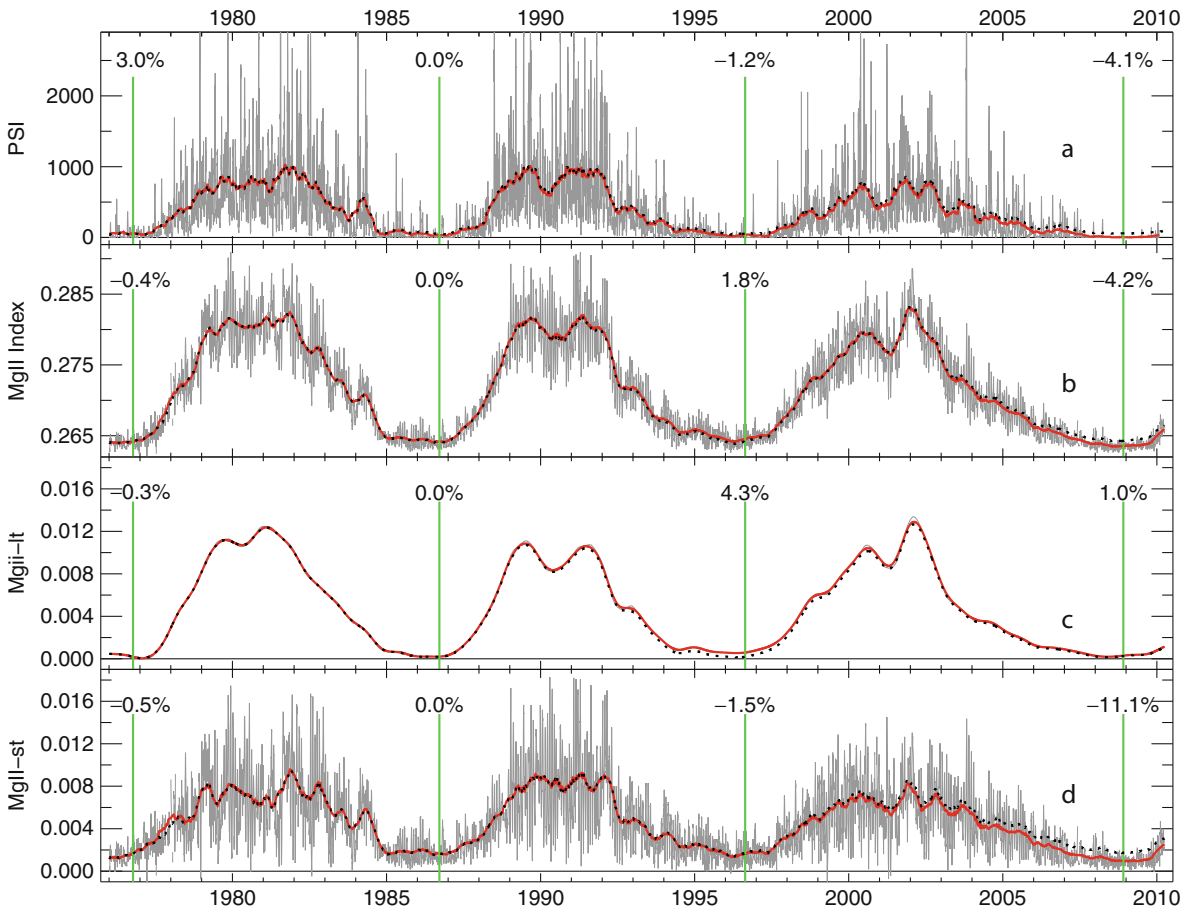

Solar Constant and Total Solar Irradiance Variations. Figure 9

Daily PSI (**a**), MgII index as observed (**b**) and decomposed in a long- (MgII-lt: **c**) and short-term (MgII-st: **d**) part. Times of the minima are given as *vertical green lines* and are labelled with the percentage deviation of that minimum from the value of the minimum around 1986 relative to the mean amplitude of the parameter. The *dotted lines* correspond to the parameter if a linear trend between minima is removed

network area covering the Sun. With the start of NIMBUS7, observations of the core-to-wing ratio of the MgII H & K lines, called MgII index [61], became available. Now there is a continuous daily record since November 1978, which is updated weekly with SOLSTICE/SORCE data [62]. The time series of the MgII index used here is shown in Fig. 9b and is separated into a short- and long-term part, MgII-st and MgII-lt. This separation is performed by calculating a running average of the standard deviation over 217 days (eight solar rotations) which is then used – multiplied by an appropriate factor – to define the lower limit of the short-term variations of the MgII index. The values above this limit are the short-term part of Fig. 9d and the values below the long-term part of Fig. 9c. The reason for calling the short-term part the facular contribution is quite clear – it is related to the passage of active regions on rotational timescale. As shown below, the long-term part gets a much higher coefficient from the multi-linear regression analysis. This can be interpreted as coming from small magnetic features, called here the network, which have a higher specific contrast for TSI than larger ones [63]. So the daily MgII-lt values are used for $P_N(t)$ and those of MgII-st $P_F(t)$ in Eq. 1, providing the second and third components of the proxy model. Figure 9c and d illustrate the influence of faculae and network during the recent minimum and show that its value is determined by the small number of faculae and not by the network. This is in further support of the fact that the chromospheric indices do not show a secular trend and confirming the conclusions of a recent study of the long-term behavior of solar-like stars by Judge and Saar [64].

Calibration of the Four Components by Multi-Linear Regression

The value of the quiet Sun, S_Q, and coefficients $a_{F,N,S,T}$ are determined by a multi-linear regression according to Eq. 1 with the extended PMOD composite for $S(t)$. The results are shown in Table 2(a) and Fig. 10.

Earlier results of the two- and three-component models (e.g., [30]) showed that 77.2% and 78.6% of the variance are explained. The four-component model shown here explains 84.4%, which is an important improvement over the three-component model. The use of Eq. 5 instead of Eq. 4 (still used in most calculations of PSI) does not improve the correlation (from 84.3% to 84.4%), but changes the coefficients as shown in Table 2(b) significantly (up to 10-σ of the uncertainty). It is interesting that the PSI uncertainty decreases, whereas those for Mgll-st, Mgll-lt, and the trend increase, the latter substantially. This may indicate that Eq. 5 represents better the change of the contrast during cycle 23 as observed by Livingston and Penn [65]. This is, however, probably more due to a change in size as suggested by Mathew et al. [56] than a real change of contrast.

The trend is well represented by the model with a slope of the TSI–B_R relation of 0.3466 ± 0.0032 which is close to the result of direct correlation with 0.3357 ± 0.1426 (including the minimum value at 1977). That is, within the correlation uncertainty and within 3-σ of the model coefficient uncertainty, they agree. This confirms the need for the fourth component which is related to the strength of the activity, and not to the manifestations of the surface magnetism.

Solar Constant and Total Solar Irradiance Variations. Table 2 Coefficients of the four-component model. Note that the coefficient for the trend agrees within the uncertainty with the result found from the direct regression of the TSI and B_R values at the minima as shown in Fig. 6c

S_Q	a_F	a_N	a_S	a_T	r^2
(a): α according to Eq. 5					
1,364.66	76.17	122.91	−0.7997	0.3466	0.8444
Standard error	1.02	0.73	0.0048	0.0032	
(b): α according to Eq. 4					
1,364.66	78.85	125.39	−0.7515	0.3470	0.8429
Standard error	1.03	0.74	0.0046	0.0033	

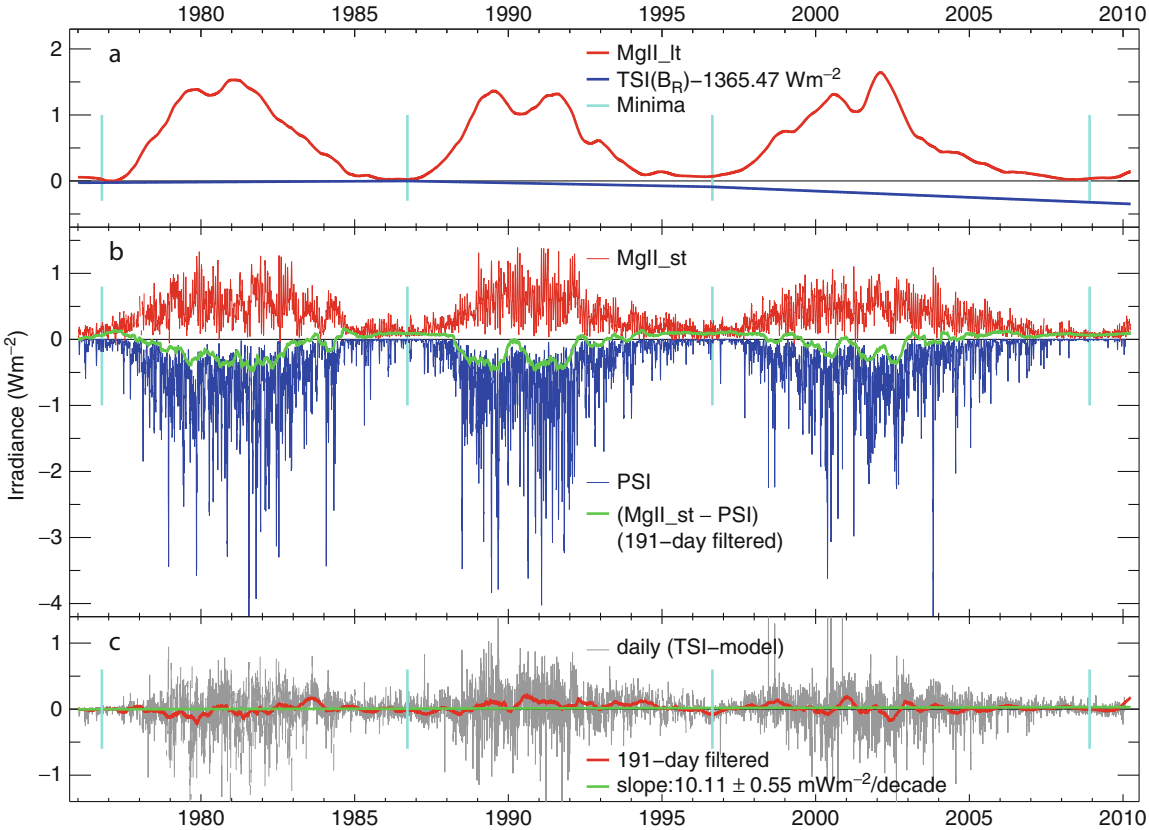

Solar Constant and Total Solar Irradiance Variations. Figure 10
Panel (**a**) shows the calibrated long-term MgII-lt (*red*) together with the corresponding trend (*blue*) of the "quiet Sun," and panel (**b**) the calibrated short-term MgII-st (*red*) and PSI (*blue*). Note that all three panels have the same scale. The green curve of (b) shows the 191-day filtered difference between facular and sunspot influence. The net effect of active regions increases TSI during minima by ≈0.08 W m^{-2}, whereas during maxima, TSI is dominated by sunspots and a decrease by ≈0.25 W m^{-2} is observed

This is obviously in contradiction to the vastly accepted assumption that *all* the changes of TSI and SSI are due to surface magnetism. This means that the UV radiation has probably no long-term trend even back to the Maunder Minimum, only changes of the cycle amplitude. On the other hand, TSI shows a long-term trend which could be due to a change of the temperature of the photosphere, which changes TSI but the UV radiation only by a very small amount [38, 45]. As the strength of activity may also be represented by the total number of sunspots during a cycle, this can also be used to determine the long-term trend of TSI (see, e.g., [66, 67]). So, a long-term trend for TSI on top of the amplitude changes of the individual cycles is highly probable. But the same long-term trend cannot be applied to the UV irradiance, which then shows only the important variation of the cycle amplitude.

Future Directions

Observations of TSI during the last three solar cycles have revealed very interesting and partly unexpected variations which challenges the solar physics community. The differences between the behavior of TSI during each cycle are an important test bed for proposed explanations, and at present, the variability can be explained to a high degree (nearly 85% of the variance during the last three cycles), although the understanding of the underlying mechanisms is still incomplete. The success of the four-component proxy model proposed by

Fröhlich [50] and the results presented here suggest two different mechanisms producing irradiance variability, which are both related to the strength of solar activity: (1) related to the manifestations of the surface magnetism during a cycle and (2) related to a global temperature change on longer timescales. This contradicts the assumption that *all* irradiance changes (total and spectral) are due to surface magnetism on solar cycle and secular timescales (e.g., [68–70]), which provokes interesting discussions about the physical mechanisms on the Sun. This controversy has fundamental consequences on the long-term behavior of the UV radiation and needs certainly more analysis. Data from the ascending phase of the just-started solar cycle 24 will certainly deepen the understanding and provide new insights.

Although the understanding of TSI has well advanced during the last decades, there is a need to continue the observations with overlapping missions. This is not only to continue the present TSI record, but also to learn more about the reliability of the understanding, which is "only" based on three solar cycles. As for cycle 23, the next one may be different again and the understanding may have to be revised – a great opportunity for the advancement of understanding the solar engine.

Bibliography

Primary Literature

1. Abbot CG (1963) Solar variation and weather. Smithson Misc Collect 146(3):1–62
2. Abbot CG (1952) Periodicities in the solar-constant measures. Smithson Misc Collect 117(10):1–31
3. Aldrich LB, Hoover WH (1954) Annals of the Astrophysical Observatory of the Smithsonian Institution, vol 7. Chapter 7: statistical studies of the solar-constant record. Smithsonian Institution, Washington, DC, pp 165–168
4. Willson RC, Gulkis S, Janssen M, Hudson HS, Chapman GA (1981) Observations of solar irradiance variability. Science 211:700–702
5. Fröhlich C (2010) Solar radiometry. In: Huber MCE, Culhane JL, Pauluhn A, Timothy JG, Wilhelm K, Zehnder A (eds) Observing photons in space. ISSI Scientific Reports SR-009, chapter 32. ESA Communications, Noordwijk, pp 525–540
6. Hoyt DV, Kyle HL, Hickey JR, Maschhoff RH (1992) The NIMBUS-7 solar total irradiance: a new algorithm for its derivation. J Geophys Res 97:51–63
7. Willson RC, Hudson HS (1981) Solar maximum mission: initial observations by the active cavity radiometer. Adv Space Res 1:285–288
8. Luther MR, Lee RB III, Barkstrom BR, Cooper JE, Cess RD, Duncan CH (1986) Solar calibration results from two earth radiation budget experiment nonscanner instruments. Appl Opt 25:540–545
9. Willson RC (1994) Irradiance observations from SMM, UARS and ATLAS experiments. In: Pap J, Fröhlich C, Hudson HS, Solanki S (eds) IAU colloquium 143: the sun as a variable star: solar and stellar irradiance variations. Cambridge University Press, Cambridge, UK, pp 54–62
10. Crommelynck D, Domingo V, Fichot A, Fröhlich C, Penelle B, Romero J, Wehrli Ch (1993) Preliminary results from the SOVA experiment on board the European Retrievable Carrier (EURECA). Metrologia 30:375–380
11. Fröhlich C, Crommelynck D, Wehrli C, Anklin M, Dewitte S, Fichot A, Finsterle W, Jiménez A, Chevalier A, Roth HJ (1997) In-flight performances of VIRGO solar irradiance instruments on SOHO. Sol Phys 175:267–286
12. Willson RC (2001) The ACRIMSAT/ACRIM III experiment: extending the precision, long-term total solar irradiance climate database. Earth Obs 13:14–17
13. Kopp G, Lawrence G (2005) The Total Irradiance Monitor (TIM): instrument design. Sol Phys 230:91–109. doi:10.1007/s11207-005-7446-4
14. Fröhlich C, Lean J (1998) Total solar irradiance variations: the construction of a composite and its comparison with models. In: Deubner FL, Christensen-Dalsgaard J, Kurtz D (eds) IAU Symposium 185: new eyes to see inside the sun and stars. Kluwer Academic, Dordrecht, pp 89–102
15. Fröhlich C (2006) Solar irradiance variability since 1978: revision of the PMOD composite during solar cycle 21. Space Sci Rev 125:53–65. doi:10.1007/s11214-006-9046-5
16. Willson RC (1997) Total solar irradiance trend during solar cycles 21 and 22. Science 277:1963–1965, see also comment by R. Kerr on page 1923 of the same issue of Science
17. Willson RC, Mordvinov AV (2003) Secular Total Solar Irradiance trend during solar cycles 21–23. Geophys Res Lett 30:1199. doi:10.1029/2002GL016038
18. Dewitte S, Crommelynck D, Mekaoui S, Joukoff A (2004) Measurement and Uncertainty of the Long-Term Total Solar Irradiance Trend. Sol Phys 224:209–216. doi:10.1007/s11207-005-5698-7
19. Fröhlich C, Lean J (1998) The sun's total irradiance: cycles and trends in the past two decades and associated climate change uncertainties. Geophys Res Lett 25:4377–4380
20. Willson RC, Hudson HS (1991) The Sun's luminosity over a complete solar cycle. Nature 351:42–44
21. Crommelynck D, Fichot A, Lee RB III, Romero J (1995) First realisation of the Space Absolute Radiometric Reference (SARR) during the ATLAS 2 flight period. Adv Space Res 16(8):17–23
22. Lee RB III, Gibson MA, Wilson RS, Thomas S (1995) Long-term total solar irradiance variability during sunspot cycle 22. J Geophys Res 100:1667–1675
23. Chapman GA, Cookson AM, Dobias JJ (1996) Variations in total solar irradiance during solar cycle 22. J Geophys Res 101:13541–13548

24. Fröhlich C (2000) Observations of irradiance variability. Space Sci Rev 94:15–24
25. Scafetta N, Willson RC (2009) ACRIM-gap and TSI trend issue resolved using a surface magnetic flux TSI proxy model. Geophys Res Lett 36:L05701. doi:10.1029/2008GL036307
26. Fröhlich C (2003) Long-term behaviour of space radiometers. Metrologia 40:60–65
27. Scafetta N (2010) Climate change and its causes, a discussion about some key issues. In: SPPI original paper. Science and Public Policy Institute, Haymarket, pp 1–56. http://scienceandpublicpolicy.org/images/stories/papers/originals/climate_change_cause.pdf. Accessed 18 March 2010
28. Foukal PV, Lean J (1988) Magnetic modulation of solar luminosity by photospheric activity. Astrophys J 328:347–357
29. Foukal PV, Lean J (1990) An empirical model of total solar irradiance variation between, 1874 and 1988. Science 247:556–558
30. Fröhlich C, Lean J (2004) Solar radiative output and its variability: evidence and mechanisms. Astron Astrophys Rev 12:273–320. doi:10.1007/s00159-004-0024-1
31. Fröhlich C (2009) Total solar irradiance variability: what have we learned about its variability from the record of the last three solar cycles? In: Tsuda T, Fujii R, Shibata K, Geller MA (eds) Climate and weather of the Sun-Earth System(CAWSES): selected papers from the 2007 Kyoto symposium. Terra, Setagaya-ku, pp 217–230. http://www.terrapub.co.jp/onlineproceedings/ste/CAWSES2007/index.html
32. Wenzler T (2005) Reconstruction of solar irradiance variations in cycles 21–23 based on surface magnetic fields. PhD thesis, ETH Nr 16199, Eidgenössische Technische Hochschule, Zürich
33. Wenzler T, Solanki SK, Krivova NA (2009) Reconstructed and measured total solar irradiance: is there a secular trend between 1978 and 2003? Geophys Res Lett 36:L11102. doi:10.1029/2009GL037519
34. Krivova NA, Solanki SK, Wenzler T (2009) ACRIM-gap and total solar irradiance revisited: is there a secular trend between 1986 and 1996? Geophys Res Lett 36:L20101. doi:10.1029/2009GL040707
35. Eddy JA (1976) The maunder minimum. Science 192:1189–1202
36. Charbonneau P (2005) Dynamo Models of the Solar Cycle. Living Rev Sol Phys 2:2–83
37. Woods TN, Tobiska WK, Rottman GJ, Worden JR (2000) Improved solar Lyman α irradiance modeling from 1947 through 1999 based on UARS observations. J Geophys Res 105:27195–27216. doi:10.1029/2000JA000051
38. Fröhlich C (2009) Evidence of a long-term trend in total solar irradiance. Astron Astrophys 501:L27–L30. doi:10.1051/0004-6361/200912318
39. Foukal P, Bertello L, Livingston W, Pevtsov A, Singh J, Tlatov A, Ulrich R (2009) A century of solar ca II k measurements and their implications for solar UV driving of climate. Sol Phys 255:229–238. doi:10.1007/s11207-009-9330-0
40. Livingston W, Wallace L (2003) The Sun's immutable basal quiet atmosphere. Sol Phys 212:227–237
41. Harvey K (2000) Solar Active Regions: Ephemeral. In: Murdin P (ed) Encyclopedia of astronomy and astrophysics. Institute of Physics, Bristol, pp 1–5. doi:10.1888/0333750888/2275, Article 2275
42. Lockwood M, Owens M, Rouillard AP (2009) Excess open solar magnetic flux from satellite data: 1. Analysis of the third perihelion Ulysses pass. J Geophys Res 114:A11103. doi:10.1029/2009JA014449
43. Lockwood M, Owens M, Rouillard AP (2009) Excess open solar magnetic flux from satellite data: 2. A survey of kinematic effects. J Geophys Res 114:A11104. doi:10.1029/2009JA014450
44. Steinhilber F, Beer J, Fröhlich C (2009) Total solar irradiance during the holocene. Geophys Res Lett 36:L19704. doi:10.1029/2009GL040142
45. Tapping KF, Boteler D, Charbonneau P, Crouch A, Manson A, Paquette H (2007) Solar Magnetic Activity and Total Irradiance Since the Maunder Minimum. Sol Phys 246:309–326. doi:10.1007/s11207-007-9047-x
46. Harvey K (1994) Irradiance models based on solar magnetic field observations. In: Pap JM, Fröhlich C, Hudson HS, Solanki SK (eds) The sun as a variable star: solar and stellar irradiance variations. Cambridge University Press, Cambridge, UK, pp 217–225
47. Pierce AK (2000) Limb darkening, chapter 14.7. In: Cox AN (ed) Allen's astrophysical quantities, 4th edn. Althone Press, London, pp 355–357
48. Fligge M, Solanki SK (1997) Inter-cycle variations of solar irradiance: sunspot areas as a pointer. Sol Phys 173:427–439
49. Balmaceda LA, Solanki SK, Krivova NA, Foster S (2009) A homogeneous database of sunspot areas covering more than 130 years. J Geophys Res 114:A07104. doi:10.1029/2009JA014299
50. Fröhlich C (2011) A four-component proxy model for total solar irradiance calibrated during solar cycles 21–23. Contrib Astron Obs Skalnate Pleso 41:113–132
51. Hudson HS, Silva S, Woodard M, Willson RC (1982) The effects of sunspots on solar irradiance. Sol Phys 76:211–218
52. Steinegger M, Brandt PN, Pap J, Schmidt W (1990) Sunspot photometry and the total solar irradiance deficit measured in, 1980 by ACRIM. Astrophys Space Sci 170: 127–133
53. Steinegger M, Vazquez M, Bonet JA, Brandt PN (1996) On the Energy Balance of Solar Active Regions. Astrophys J 461: 478–498. doi:10.1086/177075
54. Brandt PN, Stix M, Weinhardt H (1994) Modeling solar irradiance variations with an area dependent photometric sunspot index. Sol Phys 152:119–124. doi:10.1007/BF01473193
55. Fröhlich C, Pap JM, Hudson HS (1994) Improvement of the photometric sunspot index and changes of disk-integrated sunspot contrast with time. Sol Phys 152:111–118
56. Mathew SK, Martínez Pillet V, Solanki SK, Krivova NA (2007) Properties of sunspots in cycle 23. I. Dependence of brightness on sunspot size and cycle phase. Astron Astrophys 465:291–304. doi:10.1051/0004-6361:20066356

57. Tlatov AG, Pevtsov AA, Singh J (2009) A New Method of Calibration of Photographic Plates from Three Historic Data Sets. Sol Phys 255:239–251. doi:10.1007/s11207-009-9326-9
58. Ermolli I, Solanki SK, Tlatov AG, Krivova NA, Ulrich RK, Singh J (2009) Comparison amoung Ca II K Spectroheliogram Time Series with an Application to Solar Activity Studies. Astrophys J 698:1000–1009. doi:10.1088/0004-637X/698/2/1000
59. Unruh YC, Solanki SK, Fligge M (2000) Modelling solar irradiance variations: comparison with observations, including line-ratio variations. Space Sci Rev 94:145–152
60. Krivova NA, Solanki SK, Fligge M, Unruh YC (2003) Reconstruction of solar total and spectral irradiance variations in cycle 23: is solar surface magnetism the cause? Astron Astrophys 399:L1–L4
61. Heath DF, Schlesinger BM (1986) The Mg-280nm doublet as a monitor of changes in solar ultraviolet irradiance. J Geophys Res 91:8672–8682
62. Viereck RA, Snow M (2008) Update of the composite Mg II index, personal communication, a weekly updated version is available from http://lasp.colorado.edu/lisird/mgii/mgii.html
63. Ortiz A (2005) Solar cycle evolution of the contrast of small photospheric magnetic elements. Adv Space Res 35:350–360. doi:10.1016/j.asr.2005.03.014
64. Judge PG, Saar SH (2007) The outer solar atmosphere during the maunder minimum: a stellar perspective. Astrophys J 663:643–656. doi:10.1086/513004
65. Livingston W, Penn M (2009) Are Sunspots Different During This Solar Minimum? EOS Trans 90:257–258. doi:10.1029/2009EO300001
66. Lean J, Beer J, Bradley R (1995) Reconstruction of solar irradiance since 1610: implications for climate change. Geophys Res Lett 22:3195–3198
67. Wang Y-M, Lean JL, Sheeley NR (2005) Modeling the Sun's Magnetic Field and Irradiance since 1713. Astrophys J 625:522–538. doi:10.1086/429689
68. Solanki SK, Krivova NA, Wenzler T (2005) Irradiance models. Adv Space Res 35:376–383. doi:10.1016/j.asr.2004.12.077
69. Krivova NA, Balmaceda L, Solanki SK (2007) Reconstruction of solar total irradiance since 1700 from the surface magnetic flux. Astron Astrophys 467:335–346. doi:10.1051/0004-6361:20066725
70. Lockwood M (2010) Solar change and climate: an update in the light of the current exceptional solar minimum. Proc R Soc A 466:303–329. doi:10.1098/rspa.2009.0519

Books and Reviews

Haigh JD, Lockwood M, Giampapa MS (2005) The sun, solar analogs and the climate, Saas-Fee advanced course 34, Swiss Society for Astrophysics and Astronomy. Springer, Berlin

Lang KR (2000) The sun from space (Astronomy and Astrophysics Library). Springer, Berlin

Michael Stix (2002) The sun: an introduction (Astronomy and Astrophysics Library). Springer, Berlin

Tsuda T, Fujii R, Shibata K, Geller MA (eds) (2009) Climate and weather of the Sun-Earth system: selected papers from the 2007 Kyoto symposium. Terrapub, Setagaya-ku

Solar Cookers and Dryers to Conserve Human and Planet Health

Shyam S. Nandwani
Laboratorio de Energia Solar, Department of Physics, Universidad Nacional, Heredia, Costa Rica

Article Outline

Glossary
Definition of the Subject
Introduction
Solar Driers
Cooking of Food
Energy and Temperature Required for Cooking
History of Solar Cooking
Different Types of Cookers
Author's Work: Personal Interest in Solar Cooking
Some Models of Other Authors
Advantages
Other Uses of Solar Cooker
Number of Solar Cookers Globally
What Can Be Done to Extend the Use of Solar Cookers
Conclusions
Future Directions
Acknowledgments
Bibliography

Glossary

Electric storage cookers Solar cooker with the short-term storage of electricity for cooking during cloudy period.

Global warming Heating of the planet due to the use of fossil fuels and other unplanned human and agricultural activities.

Heat storage cookers Solar cooker with the short-term storage of heat for cooking during cloudy period.

Hybrid solar cookers To cook, bake, and fry meals using clean and free solar energy plus conventional-fuel-like electricity or gas during night and cloudy period.

Indoor solar cooking Cooking inside the house using solar energy.

Multipurpose cookers Modified solar cooker to cook, bake, and fry meals and heat water, purify water, and dry agricultural products.

Multivoltage solar-electric cooker Solar cum electric cooker with 12-VDC electricity (direct current) and 110-VAC electricity (alternating current) cooker.

Solar cookers To cook, bake, and fry meals using free and clean solar energy.

Solar dryer Dehydrate agricultural and marine products using solar energy for long-term storage.

Definition of the Subject

Based on the 31 years of experience, the author in this entry will like to inform the use of different types of cookers and some driers to cook, bake, and fry meals and dehydrate agricultural products using solar energy. These simple and practical devices and use of clean fuel will not only save conventional fuels but will also help in the reduction of pollutants and thus global warming.

Introduction

Food processing is the integration of various processes to get the required product of given quality at the right time, using the minimum fuels and minimizing the adverse impact on the environment. Conventional fuels like oil, coal, and biomass are used to achieve this, spending expensive budget and creating deforestation, air pollution, and global warming.

There is no simple solution to revert this global warming; however, as mentioned by Al Gore 2007, shared Nobel Prize Winner for peace, some possible steps are conservation of energy, recycling of materials, use of renewable sources of energy, etc. The use of solar energy – clean, abundant, and free fuel – to reduce the consumption of firewood or fossil fuels is one of the possible solutions.

During last 30 years, the author has studied many solar thermal devices for different processes like heating water, drying, and cooking meal at domestic level. The details of these devices are published in technical journals and conference proceedings [1, 2]. Depending on the need, one or more of these devices can be used. We will be mentioning only cookers and dryers, mainly for domestic uses.

Solar Driers

All the agricultural and marine products contain a lot of water (60–90%) which cannot be stored at the ambient temperature for a longer period, even for a week, because of the microorganism and internal humidity. The purpose of drying is to separate the water contained in solids. When products are dried (dehydrated) to 14–20%, it significantly decreases respiratory activity and controls associated microorganisms, which allows storage of the products in the closed environment for a period of 6–12 months, without losing its nutritional and organoleptic properties.

Drying is one of the oldest applications of solar energy for preserving the food and meat. Egyptians were using direct sun radiation for drying fish 4,000 years ago.

Basically, there are two types of driers [3, 4].

Direct Solar Dryer

It consists of a metal box whose bottom is insulated and has a sloping single glass cover, which is arranged on the box to receive/transmit solar radiation (Fig. 1). At the bottom of this box, a metal sheet painted black is kept. The materials to be dried are placed in a metal tray with mesh placed over the plate. The front or bottom of the dryer has various holes for the entrance

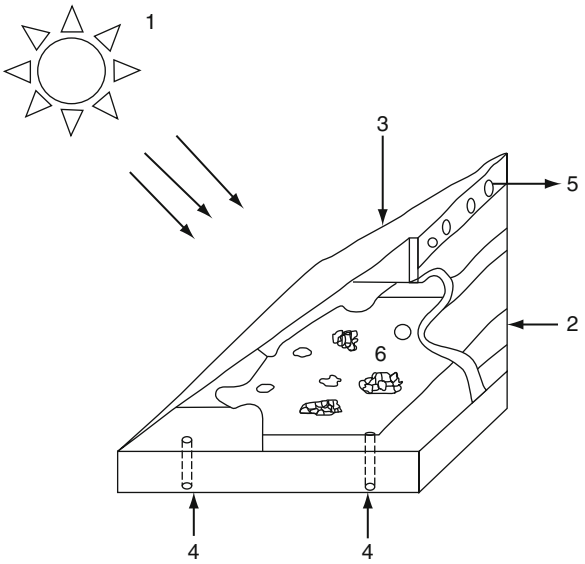

Solar Cookers and Dryers to Conserve Human and Planet Health. Figure 1
Concept of passive solar dryer: *1* Sun, *2* outer box, *3* transparent glass, *4* entrance of ambient air, *5* tray with products, and *6* exit of humid air

Solar Cookers and Dryers to Conserve Human and Planet Health. Figure 2
Direct solar dryer made for the community to dry cashew nuts fruit

of ambient and humid air. The back of this dryer has also various holes (at a level higher than entrance) for the exit of humid air coming from the products to be dried.

The direct dryer, although simple to make, has some inconvenience, like exposure from direct sunlight which can be harmful to food in terms of quality (natural color loss, destruction of vitamins, and nutritional value). Therefore, it is not recommended for drying light-sensitive products like coriander and other herbs.

Many driers have been made [3, 4], but to explain the concept, Fig. 2 shows one constructed (4 m^2) for local community (Puriscal) to dry cashew nut fruit. This cashew nut has many uses: fruit, nuts, as well as to make alcohol.

In 1998, a model similar to this was designed and constructed for a rural community (Costa Pajaros, Puntarenas). Since then, it is being used for drying and selling herbs (medicinal plants) for tourists and thus serves as an income generation.

Indirect Solar Drier

In order to minimize the effect of direct sun rays on the products, one can use the indirect solar drier. It has basically two components, air heater (similar to water collector) to heat air to reduce its water content and a drying chamber where the products to be dried are kept in different trays.

The ambient humid air enters the air collector; it is heated, and hot dry air leaves the collector and enters in a chamber. Inside the chamber, there are various trays separated from each other to place the product to dry, especially those sensitive to direct sunlight. In this case, warm air from the air heater passes through the trays and removes the moisture from the product, which goes through a hole at the top of the chamber. In order to increase the flow of air and, hence, performance of the dryer, one can use either chimney or a small fan [4].

Figure 3a shows the concept of indirect solar dryer, and Fig. 3b shows a solar drying plant of 600 m^2 for coffee designed and partially financed by Canadian Ministry of Energy and installed at Coopeldos, Guanacaste, Costa Rica. This is a hybrid plant and uses biomass (coffee waste) as backup.

Combined Solar Dryer

In this case, dryer includes both concepts for drying. This dryer can be used for standard products and other highly sensitive with regard to light. Figures 4a and b show one dryer designed and studied by author in 2007 [4, 5].

Here, the circulation of air through the products is via natural circulation using chimney, whose height could be varied (0.8–1.4 m). Increase in air temperature of 40–60°C was observed in the solar dryer. Also, the initial humidity of ambient air (60–80%) was

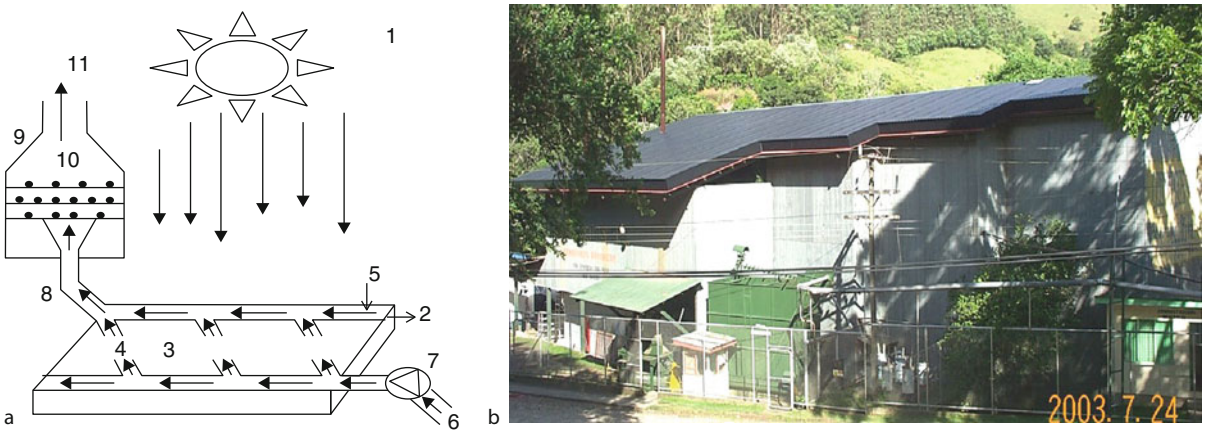

Solar Cookers and Dryers to Conserve Human and Planet Health. Figure 3
(**a**) Concept of an active (forced) solar dryer: *1* Sun, *2* air collector, *3* absorbing plate, *4* metallic tubes, *5* transparent glass, *6* entrance of humid air, *7* blower (optional), *8* exit of hot air, *9* drying chamber, *10* trays with products, and *11* exit of humid air (chimney). (**b**) Solar coffee drying plant in Costa Rica

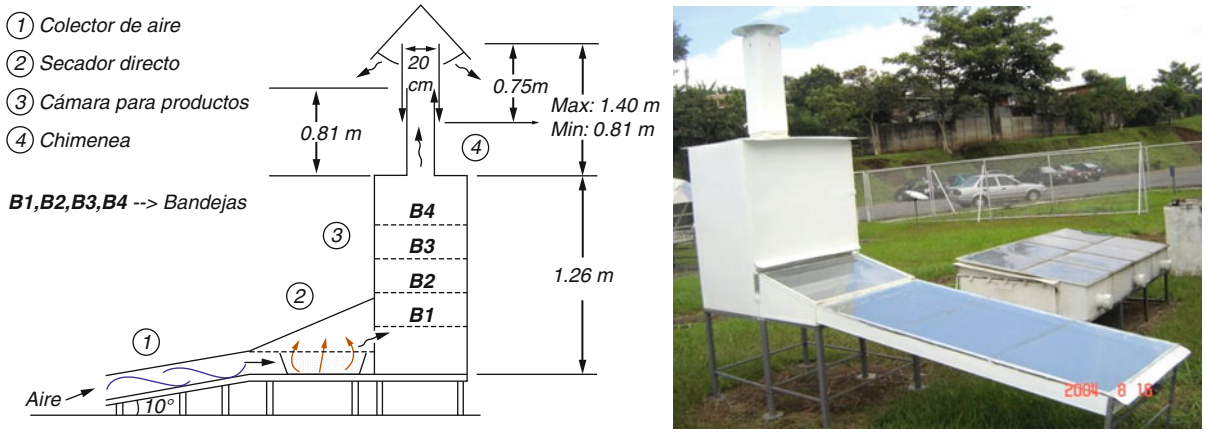

Solar Cookers and Dryers to Conserve Human and Planet Health. Figure 4
(**a**) Schematic drawing of solar dryer under study: *1* air collector, *2* direct solar dryer, *3* chamber for light-sensitive products, *4* chimney to increase the heat flow rate. B1, B2, B3, and B4 are drying trays. (**b**) Direct and indirect solar dryer, designed and studied by author (2007)

reduced to 11–14% at the exit of air collector and to 10% inside the solar dryer. In the more recent model [4], a small fan run with solar panel and automatic control was added.

Now, we pass on to the cooking.

Cooking of Food

Eating is one of the habits/processess which is very much required as it provides fuel to run one's body – rich or poor. Food supplies the body with nutrients for growth and energy. Thus, we are what we eat. Therefore, if we improve the quality of cooking capability, we improve the quality of life.

Somebody once correctly said:

- We can't sleep well,
  We can't think well,
  We can't love well, if
  We don't dine well.

I would add to this: "We can't dine well if it is not cooked well." In order to have food cooked well, we need to have good cookers: it has to be the solar cooker – an excellent device based on personal experience of research, dissemination, and use in the family.

Energy and Temperature Required for Cooking

Cooking needs good quantity of energy especially in developing countries – may be from 10% (urban area) to 80% (rural area) of the domestic energy need.

Half of the world's population cooks their food over firewood. According to the United Nations, one in every four people on earth suffers from fuel wood shortages. Increased use of firewood causes the spread of deforestation, resulting in soil erosion, flooding, famine and loss of wildlife, more CO_2 emissions, and finally climate change. Table 1 shows the various temperatures required for different processes related to cooking.

It can be seen that the temperature required for cooking is not high, about 80–100°C. Thus, solar energy – free, clean, and abundant fuel – can be used for this purpose. Higher temperatures than this only reduce the cooking time and also quality of food.

History of Solar Cooking

In general, concentrators and hot boxes are used for cooking and other applications. The concept of the solar concentrator is about 4,000 years old when the Greek philosopher Archimedes used some reflecting material to burn the Roman fleet in 2300 BC. The concept later on was used for other purposes and also for cooking. On the other hand, concept of the hot box is over 230 years. In 1776, Benedict de Saussure, a Swiss alpinist using a simple box with various glasses on the top and solar energy, could attain temperature of around 90–100°C. There are some indications of baking of fruits by him. In 1780, Ducarla, a French scientist using hot box and five glasses could cook meat in 1 h (Fig. 5).

In the year around 1889, US patent was issued to W. Calver on solar stove. Both types of cookers, concentrating and hot box, have been studied for the last 100 years, and many governments have been encouraging their promotion since oil crisis in 1973.

Different Types of Cookers

Although there are over 100 models around the world – made, distributed, taught, and even sold commercially – they all can be divided into three main categories: the hot box type, the concentrating type, and vapor type [6].

Hot-Box-Type Cookers

As the name implies and shown in Fig. 6, it is made of a wooden/metallic box, with galvanized iron metal sheet painted black on top to absorb maximum solar radiation, glass wool as heat insulation, and single or double window glass to allow low-wavelength solar radiation and, at the same time, impede the exit of higher-wavelength radiations emitted from hot plate.

Solar Cookers and Dryers to Conserve Human and Planet Health. Table 1 Temperatures required for various cooking processes

Process	Temperature required, °C (°F)
Room temperature	22 (72)
Most germs cannot grow	49 (120)
Water pasteurization	65 (150)
Food pasteurization	71 (160)
Food cooks	82 (180)
Water boils (at sea level)	100 (212)

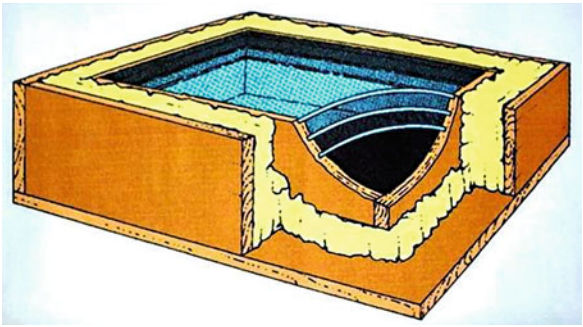

Solar Cookers and Dryers to Conserve Human and Planet Health. Figure 5
Concept of hot box to cook and bake food in 1776–1780

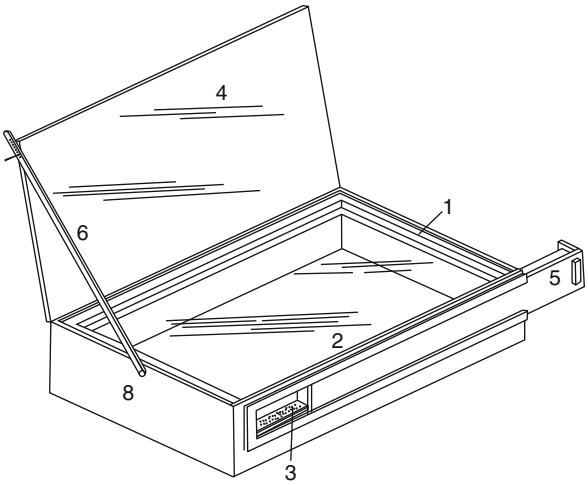

Solar Cookers and Dryers to Conserve Human and Planet Health. Figure 6
Hot-box-type cooker: *1* two transparent window glasses, *2* metallic plate, *3* heat-insulating material, *4* reflecting sheet, *5* door to keep and take out cooking pots, *6* rod with some holes to adjust reflector angle, and *8* outer box

The air in the box is thus heated through the greenhouse effect and is used for cooking meals. The box can have one or more reflectors to increase the amount of solar radiation. This model can be used for cooking and baking.

Concentrating-Type Cookers

This is another type of cooker also used worldwide, mainly for frying meals. As shown in Fig. 7, here, solar radiation is received by a shining parabolic surface and is reflected at the focal point where the food to be cooked is kept. The simple equation to make proper parabola so that the direct solar radiation is reflected to focal point (or cooking pot) is:

$$Y = X^2/4F,$$

where F is the focal length required. X and Y are the coordinates in axis X and Y, respectively.

Depending on the requirements, ease for users, the focal point could be either inside or outside the parabola. In addition, the parabola can be fixed and the focal point movable, or the focal point can be kept fixed while the parabola is movable. These models although produce higher temperatures as compared to box types; however,

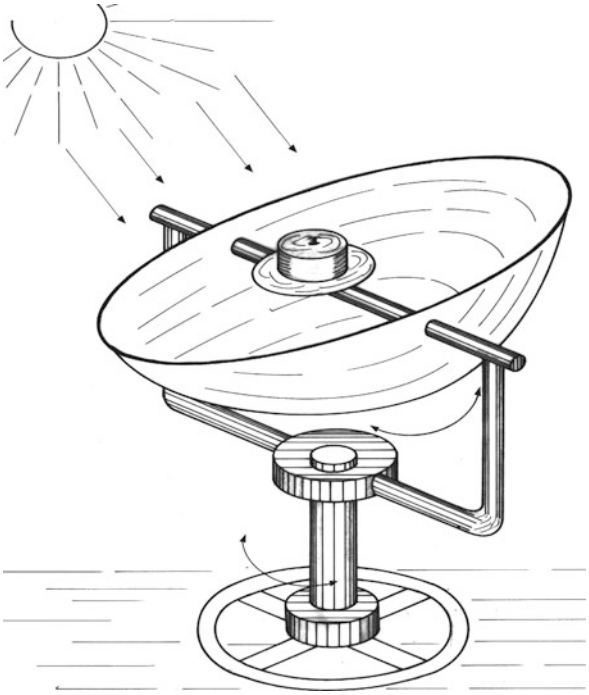

Solar Cookers and Dryers to Conserve Human and Planet Health. Figure 7
Concentrating-type cooker

for its working, one needs clear sky as well some manual or continuous tracking of concentrator.

Vapor-Type Cookers

This type is designed to cook inside a house. As shown in the Fig. 8, here, a flat plate water collector (or concentrator) is used with either water or oil heated in tubes. This hot fluid rises through a thermal syphon to another insulated box (with cooking pot) kept inside the house. After the hot liquid or vapor transfers heat to the food kept in the box, it is condensed and returned to the collector for further heating.

Figure 9 shows a design by Augustin Mouchot of France in 1870, which uses all three concepts to cook, bake, grill, and fry food by just changing the position.

In order to enable these solar cookers to be used during cloudy periods or at night, two additional types of cooker have been developed.

Hybrid Cookers

In hybrid cookers, solar energy is integrated with conventional energy sources, such as electricity, gas, or

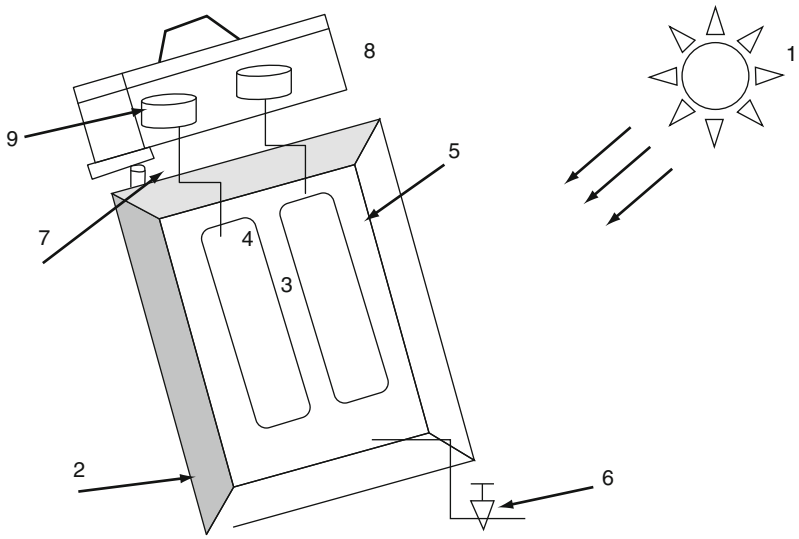

Solar Cookers and Dryers to Conserve Human and Planet Health. Figure 8
Solar cooker based on vapor for cooking inside: *1* Sun, *2* water heater, *3* metallic plate, *4* metallic tubes, *5* transparent glass, *6* inlet of water, *7* exit of vapor, *8* cooking chamber, and *9* cooking pots

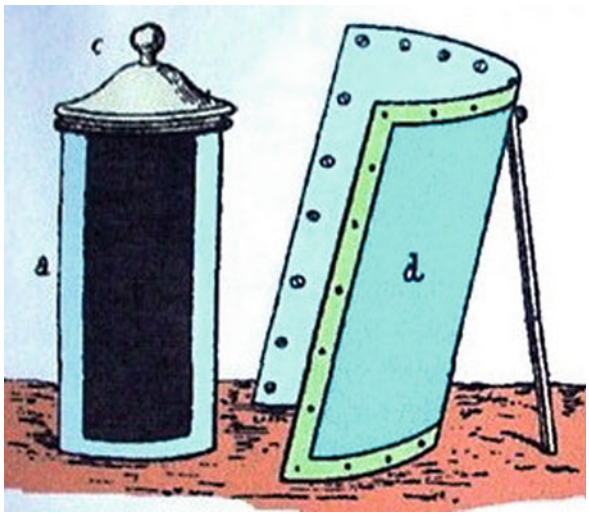

Solar Cookers and Dryers to Conserve Human and Planet Health. Figure 9
La Marmite Solaire by French Augustin Mouchot in 1870 for cooking, baking, and frying meals

firewood. The switching between two fuels could be manual or automatic. One example of this type of cooker is an electric/solar oven, which was designed by the author in 1986 and will be explained later on [7].

Energy Storage Cookers

Storage cookers store solar energy in the form of:

- Heat (sensible or latent) – Using different solids, liquids, or salts [8, 9].
- Electricity – Here, the DC electricity generated from solar cells is stored in a battery, which can be used for cooking directly [10] or can be converted in AC to be used with a conventional AC device including microwave oven [11].
- Hydrogen – The electricity from the solar panel is used to electrolyze water to produce oxygen and hydrogen. Hydrogen is stored in a tank and can be used for cooking at any time. This system, designed by Fraunhofer Solar Energy Institute was installed in 1994 at the self-sufficient solar house at Freiburg, Germany [12].

Author's Work: Personal Interest in Solar Cooking

For the last 32 years, the author has designed, constructed, studied, published, promoted in many countries and even used at home various types of cookers – hot box types, hybrid solar-electric (110 VAC and 12 VDC), solar-electric microwave oven, cooker with dryer, with water heater/pasteurizer, etc.

Although the details of various cookers can be seen in various articles, we can mention in brief some of our cookers with corresponding references.

Food Warmer

The main source of electricity in this country was, and still is, hydropower. Like most people, I was using an electric range for cooking at my house. At the start of 1979, due to high solar radiation, there was a shortage of water in rivers; this resulted in a shortage of electricity generation. Due to this, national electricity utility, Instituto Costarricense de Electricidad (ICE), decided to ration electricity for 2 days a week, from 7 am to 5 pm. Thus, we made a simple solar hot box at house to warm food cooked the previous night. As shown in Fig. 10, basically, it is an insulated wooden box and a galvanized iron metal sheet painted black, glass wool as heat insulation and one window glass on top to reduce the heat losses (Fig. 10). The solar radiation (low wavelength) passes through transparent glass and is absorbed by black paint. With this, the metallic plate is heated. Now, the metallic hot plate also emits the radiation but in higher-wavelength region (heat). To reduce the heat losses at four sides and at bottom of the box, heat-insulating material like glass wool is used. The same window glass on the top of the box impedes the transmission of heat radiation, with the result: the air in the box is heated and can be used for warming food.

The maximum air temperature in solar oven reached up to 80–90°C, and three to four meals could be heated during midday in 40–60 min [13]. Material's cost was approximately US$ 10–15.

Solar Cookers and Dryers to Conserve Human and Planet Health. Figure 10
Simple low-cost solar food warmer (March, 1979)

Simple Hot Box Oven

After observing the success with food warmer, it was decided to improve the box and convert into a solar food cooker. Two changes were made in the solar food warmer mentioned already. Firstly, we added another window glass on the top of the box to reduce heat losses, and secondly, we used a reflector to increase the solar radiation during the day. Reflector can be adjusted (recommended) every hour or two. Figures 11a and b show the improved solar oven constructed in 1982 and still in use [14] at author's house.

This reflector also acts as an insulator to keep the food hot. With these two changes, the maximum plate temperature was increased to 150°C with no food inside and 110–130°C during cooking.

This has been used for cooking, baking, roasting food (rice, beans, vegetables, lentils, meat, deserts, etc.), and also for purifying tap/river water from microbiological point of view (pasteurization). This model cannot be used for frying meals which requires the temperature of oil as 180–200°C. On an average sunny day, three to four meals can be cooked in 2–4 h. Once convinced with its working, another cooker was made with stainless steel as an outer box for family use (Fig. 11b). Figure 12 shows some of the meals cooked [15].

In 1984, we got the national patent on this solar cooker/oven. (*No. 2367*). This type is the most common type of solar cooker used worldwide.

Concentrating Cooker

Figure 13 shows one of our parabolic cooker assembled based on model developed by a nonprofit organization, EG Solar in Germany [16]. This model produces higher temperature (about 350–400°C); however, for its proper working, it needs the direct radiation, perfect shape, and some frequent (15–45 min) tracking.

Some Problems Although it is expected that one will keep the items to be cooked in solar cooker when it is sunny, however, there are few days when sky looked clear in the morning when you put the food, but the

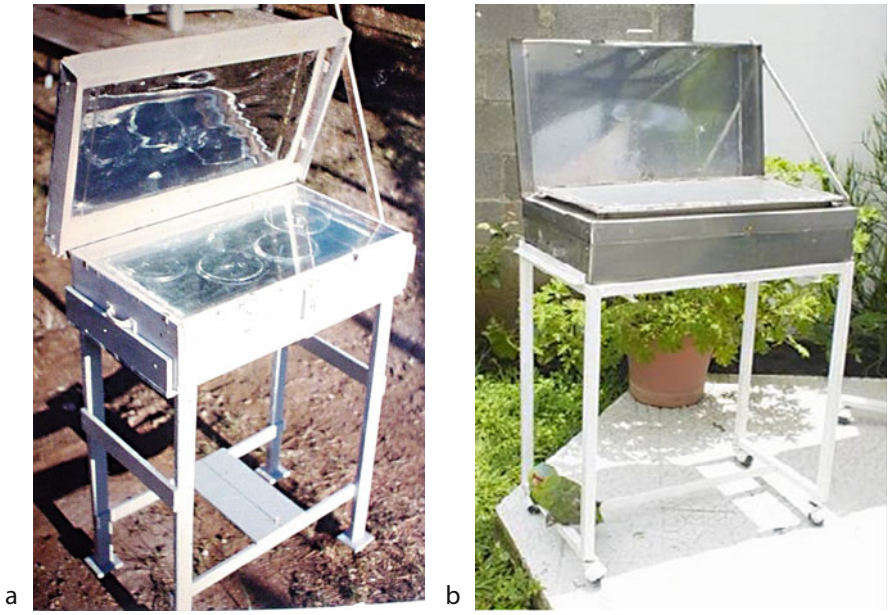

Solar Cookers and Dryers to Conserve Human and Planet Health. Figure 11
(**a**) and (**b**) Solar ovens constructed in 1980

Solar Cookers and Dryers to Conserve Human and Planet Health. Figure 12
Some meals cooked and baked with solar cooker/oven

climate changes after 1 h or 2, especially in central American region, due to sea on both East and West coasts. Depending on the quantity of food and the climate, the food may or may not be cooked properly. Although this could happen only 15–30 days a year, some aggressive promoters will say no problem and will suggest the user to take the partially cooked food on conventional stove and finish the cooking. However, within few days of using solar cooker, practically, no housewife will love this idea, and this could be sufficient reason to get frustrated. Fortunately, this happened with my wife, and it compelled me to look for a solution. Thus, hybrid cooker was made in 1986.

Solar Cookers and Dryers to Conserve Human and Planet Health. Figure 13
Solar concentrating cooker in use

Hybrid Cookers (Sun – AC Electricity)

In hybrid cookers, solar energy is integrated with conventional energy sources, such as electricity, firewood, or other fossil fuels (as backup fuel).

Designed in 1986 and as shown in Figs. 14a and b, it is similar to a hot box oven, but the black metallic plate has an electrical resistance beneath and a thermostat to regulate the temperature [7]. The hybrid cooker is connected with electricity, and the thermostat is fixed at 90–100°C. If solar radiation alone enables the system to reach this temperature, electricity will not be consumed. If the solar intensity falls below this, and plate temperature does not attain the required temperature, electricity is connected automatically to the electric plate to raise the temperature and is disconnected if the solar intensity is increased.

With these types of devices, your meal is cooked at the right time with the reduced consumption of conventional fuel, as electricity in this case.

To see really the effectiveness of the device, consumption of electric energy during cooking could be measured with the simple electronic timer or watt-hour meter.

Although it looks strange to convert electricity (high-quality energy) into heat (low-quality energy) and use it for cooking, it is worth mentioning that it could be justified, to some extent, in countries where good percentage of electricity is generated from renewable sources. In Costa Rica, 85–90% of electricity is generated from water, wind, and geothermal.

Hybrid Cooker (Sun – Gas)

This model was made in Honduras as a collaboration project. As shown in Figs. 15a and b, in this case, beneath the metallic plate, various tubes are soldered for passing the LPG gas. Rest is the same as the conventional model. Here, both fuels – solar (first choice) and gas (backup) – are used [17]. It is worth mentioning that model works fine with minimum quantity of gas.

Electric Storage Models

In the hybrid model mentioned already, the electricity from the conventional source (110 VAC) was used; thus, it could be used only at places connected to the electric grid. There are many families/places (like farm house, ecological cabins) which are not connected to electric grid. Thus, we designed other models using electricity generated from photovoltaic panels and solar energy. Comparatively, high cost of the new cooker is not first concern for some environment-conscious people.

Here, photovoltaic panels are used to convert solar energy in DC electricity. This is then stored in deep-cycle batteries. The stored electricity in 12-V battery is used directly for cooking or converted in 110 (or 220) VAC through an inverter, which can be used efficiently for running conventional 110-VAC microwave oven. This could make sense for the remote places for rich and/or nature-conserving persons.

Solar-Electric Microwave Oven Figures 16a and b show the setup for a microwave oven (700–800 W) using solar panel, battery (12 V, 100 Ah), and an invertor (1,500 W). Cooking with microwave oven [11] is fast and efficient. It heats the food internally and to temperatures higher (in general) than conventional solar ovens.

For a mostly clear day with insulation of 5.0 kWh/m^2/day, about 300 Wh of energy is collected and as the overall efficiency of the battery and inverter used is about 65%; thus, 200 Wh is available for microwave cooking. This is sufficient for 20 min of cooking with the 700 W microwave oven. If more microwave cooking time is routinely required, another PV panel and battery could be added to increase collected and stored energy each day.

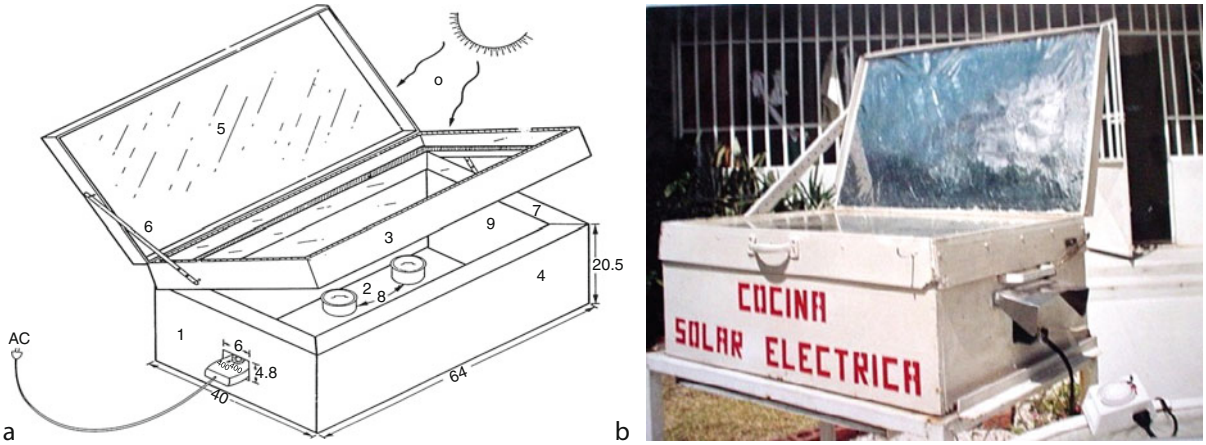

Solar Cookers and Dryers to Conserve Human and Planet Health. Figure 14
(**a**) Hybrid solar oven combined with 110-VAC electricity: *0* solar radiation, *1* thermostat, *2* metallic electric plate, *3* transparent window glasses, *4* outer case, *5* reflecting sheet, *6* rod with some holes or adjusting angle of reflector, *7* heat-insulating material, *8* cooking pots, and *9* aluminum-reflecting paper. (**b**) Hybrid solar oven combined with 110-VAC electricity (1986)

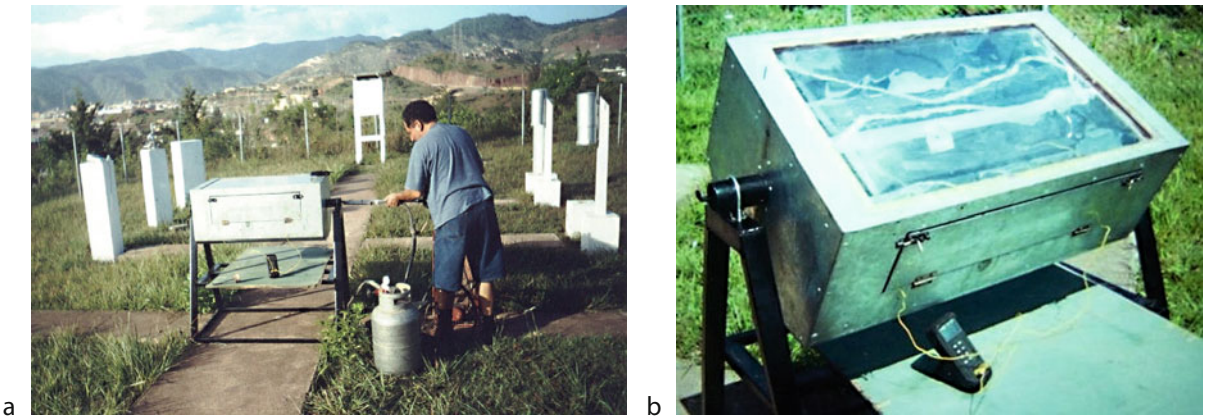

Solar Cookers and Dryers to Conserve Human and Planet Health. Figure 15
(**a**) and (**b**) Hybrid solar oven with LPG as an additional fuel in Honduras (2000)

Real cooking has been done; however, this is used mostly in our solar house daily by four to six colleagues for warming their lunch.

Portable 12-VDC Cooker In this case, no inverter (device to convert DC electricity into AC electricity) is used. One commercial 12-VDC portable cooker, which runs mainly with car cigarette lighter, was bought in USA and converted so that it could be used with electricity produced from solar energy. Although 12-V battery was used, no inverter was required. Figures 17a and b show the model. The power of the cooker was found in the range of 100–190 W [18]. The real cooking has been done.

Solar Multivoltage Cooker Based on the previous experience, another model was designed, constructed, and studied. The basic model is the same as conventional hybrid (sun electric) model (Fig. 14b). Here, the electric plate was not bought, but rather designed and constructed by us. Here, we have used eight electric resistances in the form of rods and riveted them firmly

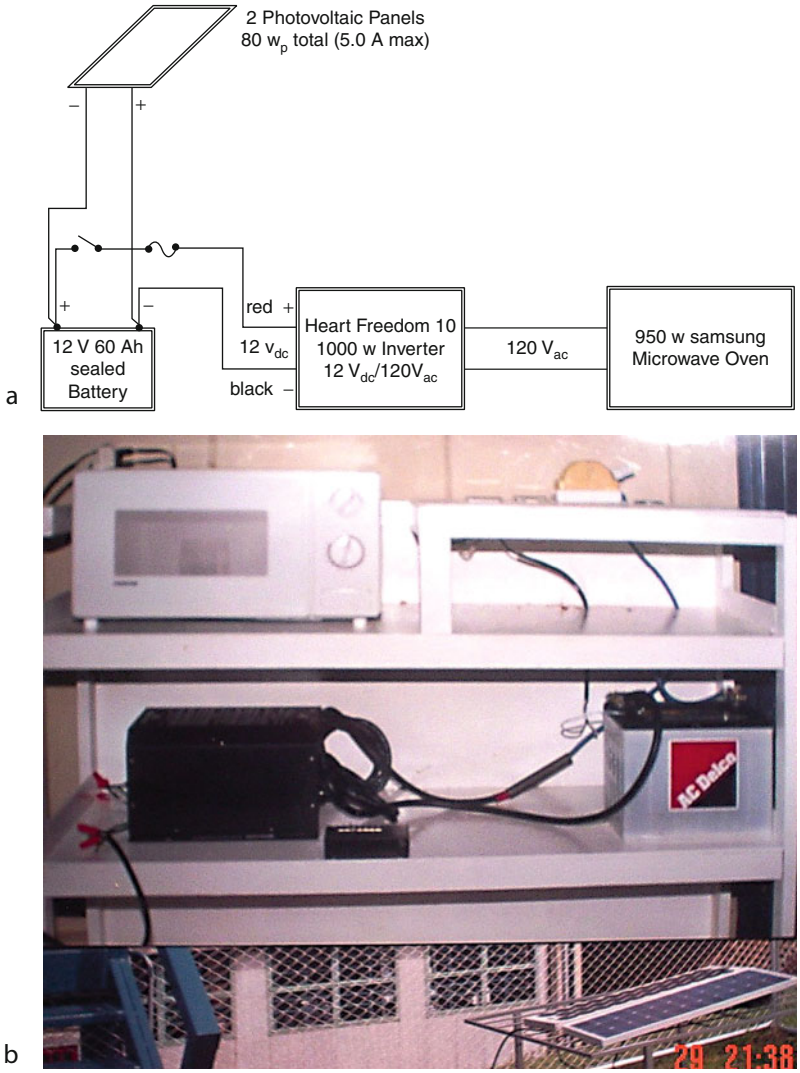

Solar Cookers and Dryers to Conserve Human and Planet Health. Figure 16
(**a**) and (**b**) Solar-electric microwave oven at our solar house (1994)

underneath a metallic aluminum plate. To operate them with 12 VDC, we connected these resistances in parallel (maximum power, 190 W), and for 110 VAC, we connected them in series (maximum power = 336 W). Finally, we have two sockets outside the box.

There is a thermostat which is used for the regulation of temperature. Figure 18 shows the final model. In other words, depending on the connections, the cooker could be used with 12 VDC or 110 VAC [10].

Again, this is studied directly with solar energy and/or with stored electricity. Some of the important results are, with charged battery (90 Ah), 500–600 g of food could be cooked in 2–2.5 h. The time is reduced when additional solar energy is used. Also, this battery could be charged in 1 day with one 100-Wp panel.

This hybrid solar-electric, dual-voltage (12 VDC/110 VAC) oven can be used in electrified as well in nonelectrified regions.

Multipurpose Device

Cooking needs higher temperature thus requires high solar radiation. Thus, depending on the climate/solar radiation at a given place, solar cooker can be used for

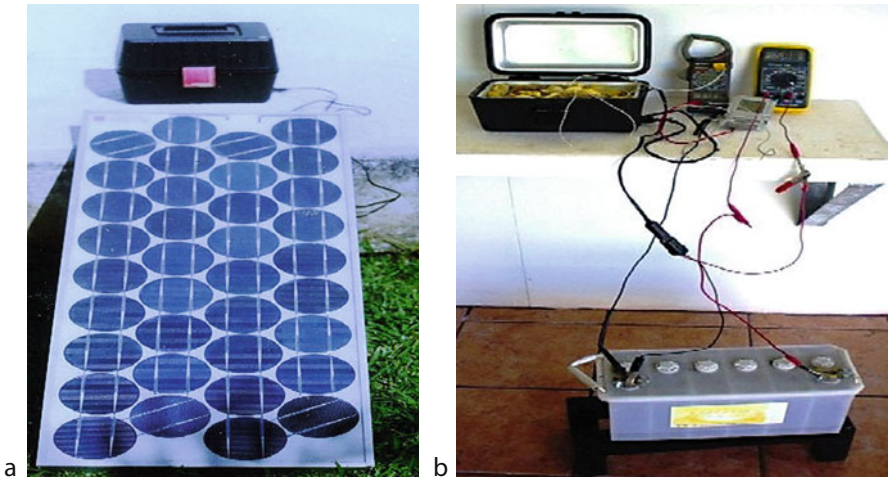

Solar Cookers and Dryers to Conserve Human and Planet Health. Figure 17
(**a**) and (**b**) Solar/electric 12-VDC cooker (2004)

Solar Cookers and Dryers to Conserve Human and Planet Health. Figure 18
Multivoltage sun electric oven (2008)

6–9 months in a year. On the other hand, water heating (and drying) needs less temperature and thus low solar radiation. It means that if the same cooker (with some modification) can be used for both purposes – cooking and water heating (or drying) – it can be used for more period (8–10 months). With this objective, multipurpose device was designed, made, and studied.

Solar Cooker cum Water Heater

As shown in Fig. 19a, this is similar to conventional hot box solar oven except that the flat absorbing plate is replaced by an aluminum U-shaped tank. The dimensions of this tank are such that total capacity is 50 l maximum. The tank has an inlet for cold water (at the bottom) and an outlet for taking hot water at the top of the tank.

The top surface of this tank (0.5 m^2), exposed to solar radiations, is painted black to absorb the maximum sun rays. This complete tank with a flat base like a valley with a capacity of four to five cooking pots is enclosed in another metal box with glass wool as a heat insulation on four sides and at the bottom (Fig. 19b). On top of this box, there are two normal window glasses as covers and one reflector. The reflector can be adjusted at different angles through a metallic bar with different holes [19].

For cooking purpose, no water is filled in the tank and the pots with food are kept in the valley space. The maximum plate temperature could reach up to 137°C (without any load) and 108–100°C (when 2–3 kg of food was used for cooking purpose).

To heat water, 30–50 l of water can be filled in the tank. Forty liters of water in the tank could be heated to 40–42°C. In another experiment after cooking 2 kg of

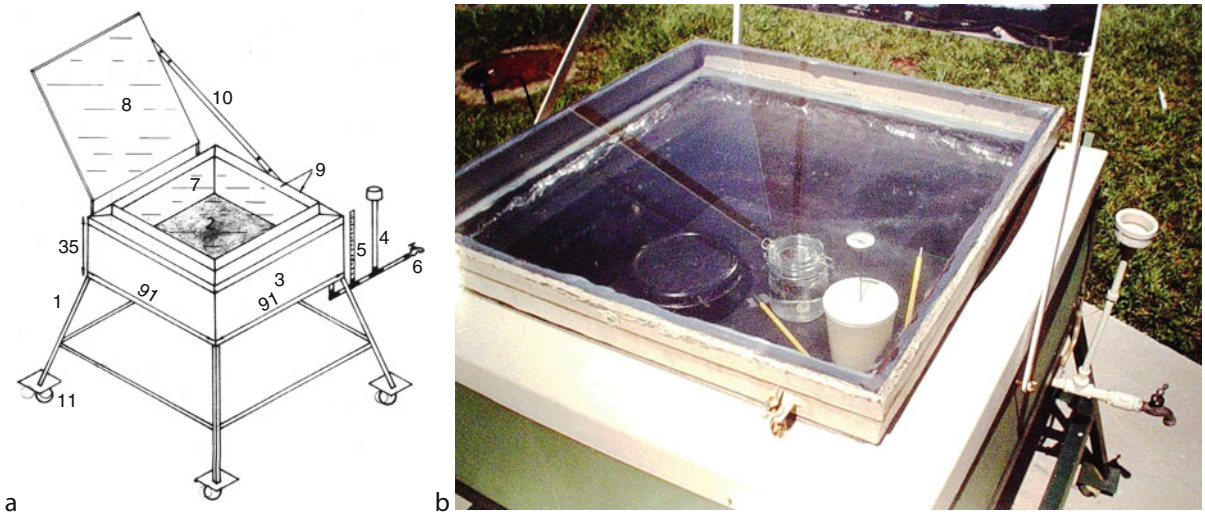

Solar Cookers and Dryers to Conserve Human and Planet Health. Figure 19
(**a**) and (**b**) Solar cooker cum water heater at our solar park (1993):*1* base for solar device, *2* metallic plate, *3* outer case, *4* inlet for cold water, *5* glass tube to see water level, *6* water for final use, *7* metallic plate, *8* reflecting sheet, *9* transparent glasses, *10* rod with various holes, and *11* wheels to rotate the device

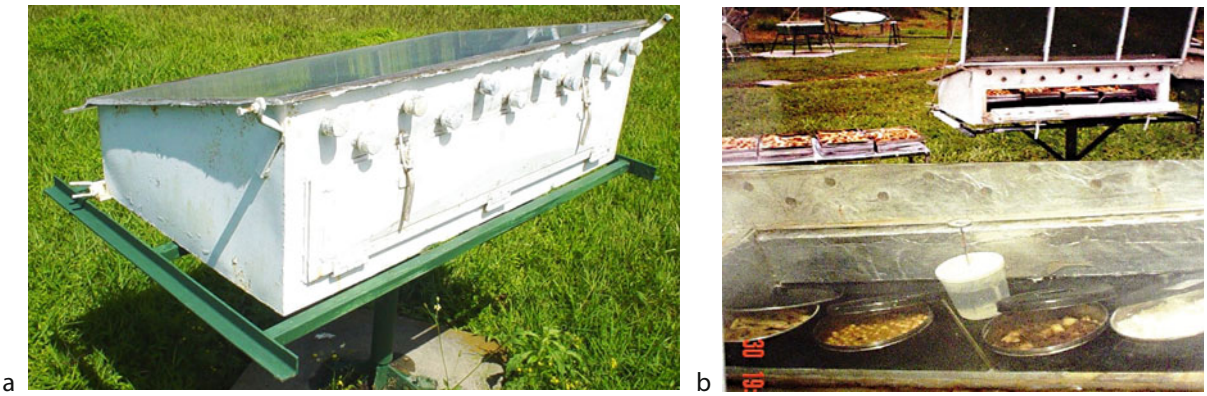

Solar Cookers and Dryers to Conserve Human and Planet Health. Figure 20
(**a**) and (**b**) Solar cooker cum dryer in our solar park (1993)

food, 10 l of water was added in the tank at 13 h and 30 min, it could be heated to 39°C.

The objective of the present system is not to heat the large quantity of water for bathing but to heat little quantity of water for dish washing, making coffee, and other uses, either after the cooking is finished (sunny days) or instead of cooking, during cloudy period. [19].

Solar Cooker cum Dryer

As shown in Figs. 20a and b, it has a conventional hot box oven with galvanized iron plate painted black, as an absorbing surface and two normal inclined window glasses (separated by a distance of 2 cm) as covers and one reflector. In addition, it has various holes in front of the oven for entrance of ambient air and holes at the back of the oven for the exit of hot humid air. To introduce the food to be cooked or products to be dried, there is a door at the back of the device. The whole box has glass wool insulation on the four sides and under the metallic plate.

Again, the objective is not to use the device for the both purposes at the same time [19, 20].

The maximum plate temperature without load (food or drying products) reached to 140°C.

For cooking purpose, all the holes are closed and the food is kept in normal metallic utensils. In addition to cook normal meals, it has been used for drying onion, meat, turmeric, and cauliflower.

To use as drier, instead of cooking utensils, some perforated trays with products to be dried are kept on the top of the absorbing sheet. To control quantity of air flow, any number of holes could be closed on both sides and the rest remained opened. In one particular case of cauliflower (April 1993), during 3 days of experiments (partially sunny climate) 2,329 g of cauliflower (bought at cheaper rate), cut into small pieces, could be dried to 247 g. Thus, the quantity of water evaporated was around 89%. This could be stored in plastic bag. When cooking of this was required, cauliflower was rehydrated (by soaking in water) for 15–30 min, removed water, and then it was used for cooking.

Multipurpose and Hybrid Food Processor (Solar-Electric 110-VAC Cooker/Water, Pasteurizer/Still, and Dryer)

Many devices mentioned already were combined to design and construct a single device – hybrid food processor – to cook, pasteurize water, dry different products, demineralize water, etc. As can be seen in Figs. 21a and b, the model is conceptually similar to a conventional solar oven and is made of inclined stainless steel box with an outer dimension of 0.54 × 0.35 m and 0.20-m high in front and 0.25-m high at the back side. It has an electric black plate as an absorbing surface with an area of 0.13 m^2 (0.45 × 0.28 m) and two normal window glasses on the top separated by a distance of 2 cm. It also has one reflector made of bright stainless sheet. Again, an electric plate has a resistance as well a thermostat to regulate the plate temperature. To introduce the food to be cooked or products to be dried, frame with two glasses can be lifted. To use as a dryer, the box also has two holes in front of the oven for the entrance of ambient air as well as another three holes at the back of the oven for the exit of hot humid air. The metallic tray(s) with the products to be dried are kept at the top of the absorbing plate. The holes could be closed for cooking and pasteurizing or opened for drying.

Again, as many processes (like drying, distillation, etc.) need less temperature and thus less solar intensity, as compared to cooking, the device can be used for more number of days.

On a sunny day and without any load, the plate temperature, only with solar radiation, can reach to about 130–150°C. It works fine. During the partial cloudy days, absorbing plate is connected with electrical energy, in addition to solar, to realize the process required [21].

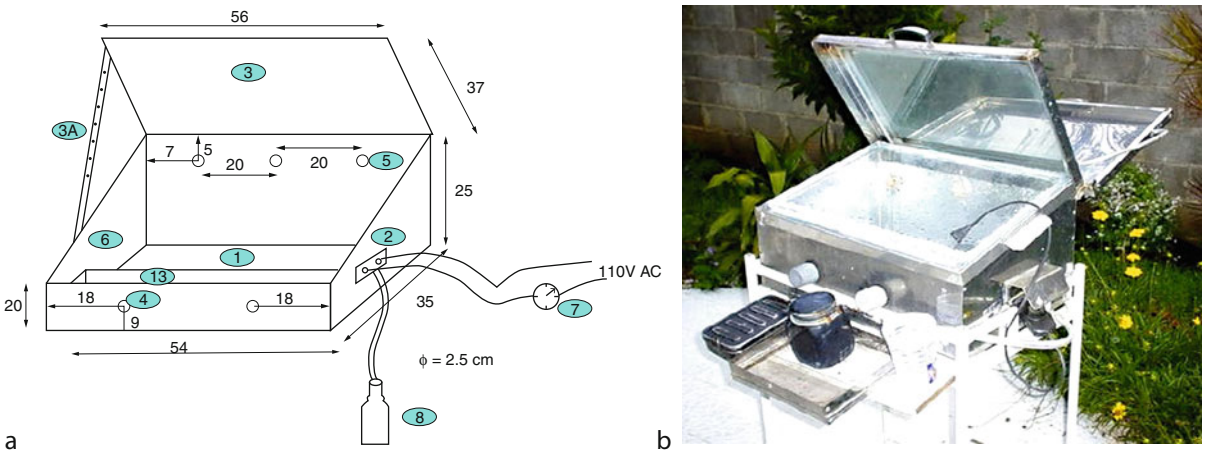

Solar Cookers and Dryers to Conserve Human and Planet Health. Figure 21
(**a**) and (**b**) Hybrid fuel food processor (2005): *1* electric plate, *2* electric power and thermostat, *3* reflector, *3A* rod to adjust reflector, *4* holes for air entrance, *5* holes for the exit of humid air, *6* outer box, *7* electric timer, *8* bottle for final distilled water, and *13* trough/gutter for distilled water

Food is cooked with only solar and/or combined with electric energy, consuming the minimum quantity of electric energy if required. Cooking time is between 2 and 4 h depending on the climate and the quantity of food. Real cooking is done many times (Fig. 22a).

On one particular day to cook 2,156 g of meal (additional weight of pots, 835 g), 410 Wh of solar and 400 Wh of electric energy (worth US$ 0.025) was used. Total input energy is 810 Wh or 696.6 kCal.

Effective Efficiency,

$$\eta = \frac{\text{Useful energy gained by food (vegetables and cake)}}{\text{Total input (solar + electrical) energy}} = \frac{M_F * C_F * \Delta T}{A_P \int Hi\ dt_S + P_E * \int dt_E} = 158.8\text{kCal}/696.6\text{kCal} = 22.8\%.$$

Where

M_F mass of food (kg)
C_F specific heat of food (kcal/kg°C)
ΔT rise in temperature (°C)
A_P area of the absorbing plate (m^2)
P_E power of the electric plate (W)
H_I solar intensity on horizontal surface (W/m^2)
dt_S and dt_E time of solar and electric consumption.
Here, we have taken specific heat of food as that of water, 1 kCal/kg°C.

It has been known that heat can deactivate pathogenic (disease-causing) microbes. Although it is recommended that contaminated water can be made safe by boiling, it is also true that same water can be pasteurized (drinkable) at temperatures well below boiling, at 67–70°C, depending on the time.

To use the device as a dryer (Fig. 22b), holes in front and at the back are opened during the sunny (drying) period and are closed after sunset or during rainy period. The metallic tray(s) with the products to be dried are kept at the top of the absorbing plate. The real solar drying has been done with various domestic products (like tomatoes, coriander, onions, pineapple, etc.).

To minimize the color loss, in case of green coriander, it was covered with a perforated metallic tray to reduce the direct solar radiation.

Two Compartments Oven

Mainly for research purpose, double-compartment solar oven was designed, constructed, and studied by author and other collaborators [22] at Fraunhofer Solar Energy Institute, Freiburg, Germany, in 1996. As shown in Fig. 23, it is similar to conventional oven explained already, except that it has two identical compartments, so that two different comparative studies can be made under the similar climatic conditions. This box has been used for (a) comparing the performance of a metallic slab filled with a phase change material for short-term heat storage, with a conventional absorbing sheet, (b) the use of selectively coated, as compared to a normal black-painted cooking pots, (c) pasteurization of water in glass jar and metallic pot, and (d) for finding the overall heat coefficient and thermal capacity of the box [22].

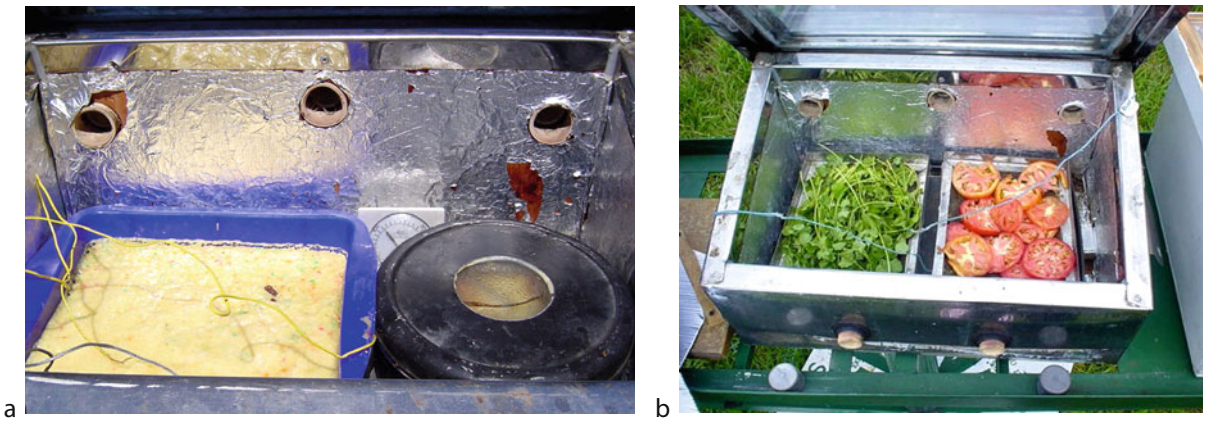

Solar Cookers and Dryers to Conserve Human and Planet Health. Figure 22
(**a**) and (**b**) Food processor in the mode of cooking and drying mode

Solar Cookers and Dryers to Conserve Human and Planet Health. Figure 23
Double-compartment solar oven mainly for research purpose (1996)

Using some phase change materials, 30–40 min of heat storage was possible for cooking during partially cloudy period. Also, in addition to cooking, it was used to pasteurize (65–67°C) 14–16 l of water, inactivating most of the pathogenic germs [22].

Some Models of Other Authors

Not all users have the time, tools, or skills to make even a simple solar cooker, but they require one. They can either buy in the local market or import. Fortunately, there are many commercial models of hot box and concentrating-type cookers, ranging from $15 (Cook Kit for single family) to $10,000 (large hybrid cooker for multimeals), available in many countries [23]. Figure 24 shows an exhibit of solar cookers at Granada, Spain, in 2006.

Using the various concepts described above, solar cookers have been made in both developed and developing countries. We will just describe in brief two models: cheapest and expensive one.

Cook Kit Model

One of the simplest cooker was designed by Solar Cookers International, nonprofit organization, to promote solar cooking worldwide and based at Sacramento, CA, USA [6]. Designed and constructed in 1998, using cardboard and aluminum foil, in such a way that when faced towards sun, the solar radiations are reflected at the focal point where cooking pot (or heating jar) is placed (Fig. 25a). In order to reduce the heat losses, the cooking/heating pot is covered with one plastic bag. The device is light with its own advantages (carrying/transporting) and limitations (gone with the wind). Fifteen to twenty thousand of these Cook Kits have used for cooking and water heating mainly in refugee's camp in Kenya for refugees from Somalia, Sudan, and Ethiopia.

In another model (Hot Pot) designed and promoted by another nonprofit organization, Solar Household Energy (SHE), the cardboard is replaced by thin, shining reflecting sheet (Fig. 25b) and the metallic cooking pot is covered with inverted Pyrex container to reduce the heat losses [24].

Hybrid Concentrating Model

Mr. Wolfgang Scheffler [25], designer from Germany, and Deepak Gadhia [26], developer and manufacturer from India, are promoting solar cookers on large scale for schools, temples, and meditation centers in India

Solar Cookers and Dryers to Conserve Human and Planet Health. Figure 24
One of the exhibit of solar cookers at Granada, Spain (2006)

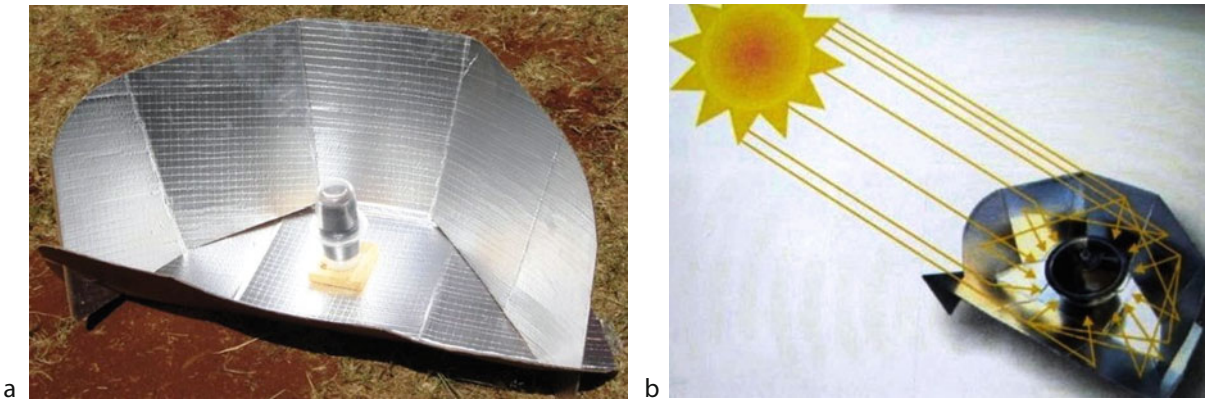

Solar Cookers and Dryers to Conserve Human and Planet Health. Figure 25
(**a**) and (**b**) Simple and cheap solar cookers – Cook Kit by Solar Cookers International (1998) and Hot Pot by SHE (2002)

and other countries. It is based on a parabolic concentrator (single or multiple, each 3–10 m^2) which focuses the solar radiation at the focal point for cooking inside the kitchen. In this case, the focal point is fixed, whereas the concentrator is tracked automatically with chain, pulley, motor, timer, etc. Figure 26 shows the cooker at Valsad, Gujarat, in India to cook for 30–50 persons. Similar system is also installed by Dr. Luis Saravia and collaborators in 2005, from University of Salta, in Northern Argentina [27]. It does cooking and baking for 50 students.

Figure 27 shows the world's largest solar steam cooking system with 106 solar concentrators of 9.4 m^2 each installed at Tirumala Tirupati Devasthanams to cook for 15,000 persons (30,000 meals). These concentrators are tracked automatically and heat water in cylindrical pipes (kept at focal line) to produce high-pressure steam which is transported inside the kitchen, and food is cooked in big vessels [26]. Also, the system uses propane gas, whenever required.

Advantages

Solar cookers have many advantages like energy, economy, health, social, and for the planet [15, 23, 28]. We will mention in brief.

Solar Cookers and Dryers to Conserve Human and Planet Health. Figure 26
Solar cooker at Valsad, India, for cooking 40–50 meals (1995)

Solar Cookers and Dryers to Conserve Human and Planet Health. Figure 27
Big solar cooker using steam at Tirupati Temple, India (2009)

Energy Saving

With an average solar intensity of 3.5 kWh/m^2/day, the maximum plate/air temperature in hot box oven can reach to about 150°C without any food or load inside and between 100°C and 120°C while cooking. In the case of concentrating cookers, the temperature will be in the range of 300–400°C. Normally, three to four meals can be cooked in 3–4 h. As an example, based on these data and knowledge of climatic conditions, a single family in Costa Rica (4–6 kWh/m^2/day) can use solar oven for 7–9 months in a year. This can save 1,000 kWh of electricity, 240 l of propane gas, or 725 kg of firewood per year.

Cash Saving

Depending on the cost of the fuel, including transportation cost, one can calculate the amount of money saving using solar cooker. Payback period could be between 8 (rural area) and 24 (urban area) months.

Human Health

Food being cooked with no or less water and at low temperature (less than 100°C) retains most of the nutrients as proteins and vitamins [29].

Studies have also shown that women who cook over indoor firewood are more likely to have active tuberculosis. Children exposed to indoor smoke are two or three times likely have higher respiratory infection. Indoor air pollution from the burning of solid fuels kills over 1.6 million people, predominately women and children, each year. This is more than three people per minute. Solar cookers (smokeless stove) will definitely help in keeping the health better.

Social Aspects

There are at least 2,500 million persons (500 million families) in developing countries that cook with firewood. Children and women in many developing countries have to walk 4–8 h a day to look for firewood.

Free firewood is no longer available to many families since most of the forests have been destroyed by improper uses, for cattle feeding, timber, cooking, and years of drought. Even where sticks, branches, or bushes can be collected from the fields, the chance of being injured, attacked, or even raped are well reported/documented in the literature.

People, combining solar cooker with conventional fuel stove, will need less conventional fuel (especially firewood) and have not to walk daily, could be once every third or fourth day to look for firewood. Reduced use of firewood for cooking will lead to less deforestation.

Environmental Aspects

One of the main greenhouse gas, CO_2, is emitted if cooking is done using firewood stoves or from electric range when the electricity is generated from thermal (coal or oil) plants.

As most of the rural people use firewood for cooking, we can make some approximate numbers from the saving through the use of solar cookers.

One family solar cooker (0.20–0.25 m^2 of absorbing area), using 7–8 months in a year, can save about 750 kg of firewood per year. Knowing the carbon content of the firewood and through the chemical reaction ($C + O_2 \rightarrow CO_2$), one can find the emission of CO_2 from direct burning. On the other hand, cutting of trees for getting firewood also avoids the absorption of CO_2. Adding these, one can show [28] that one family solar cooker can reduce the emission of about 1.6 t of CO_2 per year. Assuming that only 5% of the families cooking with firewood (500 million) use solar oven, this can prevent roughly the emission of 40 million tons of carbon dioxide per year.

Other Uses of Solar Cooker

Solar cookers, in addition to cook food, can be used for many other purposes [30]. One of the most important of these is the pasteurization of water (Fig. 23b). As shown in Table 1, if water is heated to 67–70°C, almost all of the microbes affecting the quality of the water are eliminated; the water is pasteurized and can be drunk safely. The automatic water pasteurization indicator (WAPI) promoted by Solar Cookers International of the USA is used to conveniently check the portability of water [6, 30].

In recent years, directors of the some schools and colleges are asking for solar cookers for warming lunch of the students during midday. The objective is to reduce the buying of more microwave ovens and consumption of electricity. Figure 28 shows just one of the solar oven (1.5 m^2) designed by us and installed in 2005

Solar Cookers and Dryers to Conserve Human and Planet Health. Figure 28
Use of solar ovens for warming lunch at educational centers, Costa Rica (2005)

at Claretiano College in Heredia, Costa Rica. More have been installed at different places including at our university.

Also, in many communities, it has been used to dry/toast herbs and maize and even melt paraffin to make candles, etc.

Number of Solar Cookers Globally

According to a survey carried out by the author few years ago, about 1.7–2 million solar cookers of all types have been manufactured, sold, and distributed freely or at subsidized price around the world including 1.1 million just in China and India in the last 30 years. The number is very low if we compare with other cooking devices used only by rural people:

- Firewood stoves – over 800 million
- Improved firewood stoves – over 140 million
- Biogas stoves – 3.3 millions only in India

Thus, in spite of the fact that solar energy is a pollution-free fuel, that solar cookers have many other advantages, it is not used on a massive scale. Just another comparison, only in the last 15–20 years, more than 3,000 million mobile phones are used worldwide.

There are many reasons (limitations) for this, including the fact that even now, not many people have heard or seen a working example of a solar cooker, and other reasons are unstable climate, not having proper backyard and balcony, not available on the market, more time to cook, cannot be cooked at night and in cloudy period, no post service, comparatively high initial cost, cultural and social aspects, etc. [31, 32].

What Can Be Done to Extend the Use of Solar Cookers

There is no doubt that solar cooking has many advantages; however, we cannot forget that it has some limitations too. On the other hand, conventional fuels like firewood and gas, although haves limitations as deforestation and global warming, however for the most of the users it is not the primary concern. On the other hand security/avalability of the fuel in any quantity and at any time is most important. Thus, one should not expect massive use of solar cookers. It does not mean that nothing should be done to preserve the planet.

Although there is no magical answer, there are various steps that could be undertaken to increase the awareness and use of solar cookers. Some of these could be [31, 32]:

- Use of different medium of communications to inform, show, and convince people about the use of solar cookers.
- The designs of the solar cookers should be appropriate for the needs of the people and communities for which they are intended.
- The buyers should be taught the proper uses of the solar cookers.
- The users should be informed of both the benefits and limitations of solar cookers – including very clearly that the device is intended to save and not to substitute conventional fuels.

Thus, with the combined efforts of designers, manufacturers, promoters, government, users, etc., its use could be increased.

Conclusions

There are more than 200 varieties of solar cookers for different requirements – cheap (US$ 5–10), expensive (US$ 500–10,000), small (cook for three to four

persons), bigger size to cook for 30,000 persons, etc. However:

1. Weak benefits like deforestation, soil erosion, global warming, and national foreign debt are not the primary worry for most of the users (except talking collectively at the national and international meetings), as compared to their daily problems.
2. For most of the users, the convenience, assurance, and necessity of the fuels even at slightly higher price (paid each month) are much more important than another fuel not completely reliable and inconvenient to use even at lower price.
3. Use of solar cookers cannot be expected on a mass scale neither in rural area due to high initial cost nor in urban due to other priorities and the availability of convenient fuels.
4. However there are many places (a) where the solar radiation is high and constant for more than 6 months, (b) where there is real shortage of fuel, (c) like ecological lodges and (d) still some energy/environment concious people exist etc. Here the solar cookers can play an important role.
5. They (solar cookers) should be available in different varieties, subsidized properly, but, more than that, taught to use properly and informed advantages without exaggeration and also informed limitations in advance.

Solar energy is free, abundant, and pollution-free fuel. If on the earth, instead of receiving the solar radiation which just heats the environment, some simple boxes (solar cookers) are placed, the food will be cooked and the environment will be more comfortable.

Even if only 5% of the population facing fuel shortage (25 million families) use solar ovens, roughly, the emission of 40 million tons of carbon dioxide per year will be prevented. Moreover, saving conventional fuels reduces the emissions of other pollutants.

Solar ovens are thus economically and ecologically viable.

Future Directions

In order to promote the use of solar energy and, in particular, solar cookers, various steps should be considered like:

- The design of the solar cooker should be appropriate for the needs of the people considering their cultural and local food habits.
- Both commercial and DIY models should be available.
- The buyers should be taught the proper uses of the solar cookers.
- The users should be informed clearly that the device is intended to save and not to substitute the conventional fuels, etc.

If taken into account these aspects, definitely, more persons both in rural and urban areas will use these devices for their personal benefit and for the planet.

Acknowledgments

The author is thankful to Solar Cookers International, Sacramento, CA, USA; the Abdus Salam International Center for Theoretical Physics, Trieste, Italy; Red Iberoamericana de Coccion Solar de Alimentos, Salta, Argentina; and Network on South South Cooperation on Renewable Energy Technology, Italy/England, for the invitation at their meetings, where good information was exchanged from participants of different countries for research and dissemination. The author is also thankful to Tec. Carlos Delgado for constructing some of these cookers.

Bibliography

Primary Literature

1. Nandwani SS (2008) Thirty years of experience with solar cookers and cooking – to reduce global warming. In: Conference WREC X, realize at Glasgow, Scotland, 14–19 Jul 2008, published in the CD
2. DeLong D (1979) How to dry foods. HP Books, Tucson, p 160
3. Espinoza R, Saravia L (eds) (2010) Book Secado solar de Productos Agroalimentarios en Iberoamericana. Red Iberoamericana de Secado Solar de Productos Agroalimentarios (RISSPA), Argentina and Ciencia y Tecnología para el Desarrollo (CYTED), Spain, p 376
4. Nandwani SS (2010) Design, construction and study of direct and indirect natural circulation solar dryer in Costa Rica-II. Presented at XI World conference on renewable energy, held at Abu Dhabi, UAE, during 25 Sept–2 Oct 2010. Article to be published in Science and Technology Vision, Official journal of ISESCO (Islamic Educational Scientific and cultural Organization), Rabat, Kingdom of Morocco, May 2011, vol. 7, No. 11, pp 43–47

5. Nandwani SS (2009) Solar food processing- authors experience with cooking and drying in Costa Rica. Presented at international solar food conference, held at Indore, India, 14–16 Jan 2009, published in CD Rom
6. Nongovernmental organization, Solar Cookers International, Sacramento, CA, USA. www.solarcooking.org and www.solarcookers.org
7. Nandwani SS (1989) Design, construction and experimental study of electric cum solar oven. Sol Wind Technol 6(2): 149–158, Pergamon Press
8. Matthias R, Stahl W, Wittwer V (1986) A solar cooker based on a flat plate collector with oil storage. Sun at Work in Europe, April, No. 1, pp 3–5
9. Klemens S, Vieira de Silva ME (2003) Solar cooking system with or without heat storage for families and institutions. Sol Energy 75:35–41
10. Nandwani SS (2008) Design, construction and study of a hybrid and dual voltage solar cooker in the climate of Costa Rica, renewable energy, Annual edition. Sovereign Publications, London, UK, pp 103–105
11. Currin C, Nandwani SS, Alpizar M (1994) Preliminary study of solar microwave oven. In: Nandwani SS, Pejack E, Blum B (eds) Proceedings of the second world conference on solar cookers' use and technology, Universidad Nacional, Costa Rica, 12–15 Jul 1994, pp 149–158
12. Goetzberger A, Luther J (1993) Living in the Freiburg self sufficient solar house, Germany. SunWorld 17(4):17–19, Pergamon Press
13. Nandwani SS (1979) Sunny visións – getting a charge from Old SUN. Report on this Solar Food warmer. The TICO TIMES (Central American News Paper, www.ticotimes.net), Costa Rica, 4 May 1979, p 21
14. Nandwani SS (1988) Experimental and theoretical analysis of simple solar oven in the climate of Costa Rica-I. Sol Wind Technol 5(2):159–170, Pergamon Press
15. Nandwani SS (1993) La Cocina/Horno Solar, Hagala Usted mismo, Editorial Fundación. Universidad Nacional, Costa Rica, Second revised edition, 2004, p 120
16. Jobst G (1994) SK 12 production and solar cooking promotion in South America. In: Proceedings of the second world conference on solar cookers – use and technology, Heredia, Costa Rica, 12–15 Jul 1994, pp 197–201. Also manual for the Solar Cooker, SK 14. EG Solar, Altotting, Germany, Sept 1995
17. Flores MA, Flores AE, Nandwani SS (2002) Diseño, Construcción y Funcionamiento de un Horno Solar Híbrido CPC. Presented at XI Congreso Iberico e VI Congresso Ibero- Americano de Energía Solar, held at Vilamoura (Algarve), Portugal, 29 Sept–2 Oct 2002, pp 128–137, published in the CD Rom
18. Nandwani SS (2006) Estudio de una Estufa Solar Portatil y Hibrida-I. HIDRORED (Spanish Journal, Peru) 2:1–6
19. Nandwani SS, Gomez OF (1994) Experimental study of solar oven cum water heater and solar oven cum drier-II. In: Nandwani SS, Pejack E, Blum B (eds) Proceedings of the second world conference on solar cookers – use and technology, Universidad Nacional, Costa Rica, 12–15 Jul 1994, pp 273–284
20. Nandwani SS, Fernandez O (1994) Design, construction and experimental study of a domestic solar oven cum drier in the climate of Costa Rica. Presented at 1993 solar world congress, Budapest, Hungary, 23–27 Aug 1993, published in the proceedings, vol 8, pp 91–96, 1994
21. Nandwani SS (2007) Design, construction and study of a hybrid solar food processor in the climate of Costa Rica. Renewable Energy Int J 32(3):427–441
22. Nandwani SS, Jose Steinfart HM, Henning MR, Rommel M, Wittwer W (1997) Experimental study of multipurpose solar hot box at Freiburg, Germany. Renewable Energy Int J 12:1–20
23. Nandwani SS (2006) Varieties of solar cooker devices and uses. Presented at solar cookers and food processing – an international conference, Granada, Spain, 11–16 Jul 2006, published in CD Rom
24. Solar Household Energy (SHE) (2003) Solar Hot Pot, USA. www.she-inc.org
25. Ulrich O, Scheffler W (1994) The use of indigenous materials for solar conversion. Sol Energy Mater Sol Cells 33:379–389
26. Gadhia D (2009) Solar concentrator technology and successful uses of for various applications– from cooking to process food, Indian experience. Talk given at Seminario/Taller Las Aplicaciones Practicas de la Energia Solar, Universidad Nacional, Costa Rica, during 21–24 Jul 2009, also www.gadhiasolar.net
27. Judith F, Cadena C, Saravia L (2004) Multiple use communal solar cookers. Sol Energy 77:217–223
28. Nandwani SS (1996) Solar cookers-cheap technology with high ecological benefits. Ecol Econ 17:73–81
29. Devadas RP (1994) Nutritive value of food cooked in solar box cooker. In: Nandwani SS, Pejack E, Blum B (eds) Proceedings of the second world conference on solar cookers – use and technology, Universidad Nacional, Costa Rica, 12–15 Jul 1994, pp 112–118
30. Robert M (1994) Solar water pasteurization and other non cooking applications of solar cookers. In: Nandwani SS, Pejack E, Blum B (eds) Proceedings of the second world conference on solar cookers – use and technology, Universidad Nacional, Costa Rica, 12–15 Jul 1994, pp 44–50
31. Nandwani SS (1994) From cheap/simple three stones to expensive advanced convective cookers. In: Nandwani SS, Pejack E, Blum B (eds) Proceedings of the second world conference on solar cookers – use and technology, Universidad Nacional, Costa Rica, 12–15 Jul 1994, pp 17–26
32. Nandwani SS (2003) Solar cookers – what we are looking for. Paper presented at ISES solar world congress 2003, Goteborg, Sweden, during 14–19 June 2003, published in the proceedings

Books and Reviews

Bremm-Gerhards U (1991) Chancen Solarer Kochkisten als angepaβte Technologie in Entwicklungslandern, Social science studies on international problems, Book No. 165. Verlag Breitenbach, Saarbrücken, Germany, p 145

Centro de Estudios de la Energia Solar (2004) Cocinas Solares: Manual de uso y Construccion. PROGENSA, Sevilla, pp 1–75
Grotti S, Pieri A (eds) (1999) Proceedings on international world solar cooking and food processing, Varese, Italia, 3–6 Oct 1999, p 418, published by FAST, Milano, Italy
Grupp M (1991) New prospects in solar cooking, SYNOPSIS, France, May 1991, p 110
Herliyani S, Sayigh AM, Nasser SH (2005) Sun cooking is the best practice in Indonesia. ISESCO Sci Technol Vis 1:69–75
Kuhnke K, Reuber M, Schwefel D (1990) Solar cookers in the Third World. Friedr. Vieweg and Sohn, Braunsachweig/Wiesbaden, p 228
Pejack E (ed) (1992) Advances in solar cooking: proceedings of the first world conference on solar cooking, University of the Pacific, Stockton, California, USA, 19–20 June 1992, p 158
Proceedings of solar cookers and food processing, international conference, held at Granada, Spain, 11–16 Jul 2006, Organized by Marta Pahissa, Fundacion Al Terra, Spain, and Bev Blum, Solar Cookers International, USA, published in CD Rom
Proceedings of the second world conference on solar cookers held at Coimbatore, India 6–10 Jan 1997, pp 143–152. Organised by Rajammal Devdass, Avinashilingam Institute for Home Science and Higher Education for Women, Coimbatore, India, and Bev Blum, Solar Cookers International, USA – use and technology, Universidad Nacional, Costa Rica, 12–15 Jul 1994, pp 357
Radabaugh J (1991) Heavens flame: a guide book to solar cookers. Home Power, Ashland, p 79
Rajammal D. Proceedings, third international conference on solar cookers, held at Coimbatore, India, during 6–10 Jan 1997, pp 143–152
Rodriguez PS (2000) Cocinas y Hornos Solares, Book, Fundacion Nicaraguense para la Promocion y Desarrollo de Tecnologia Alternativa (FUNPROTECA), Leon, Nicaragua, p 138
Telkes M (1959) Solar cooking ovens. Sol Energy III(1):1–11

Solar Cooling Systems

Hans-Martin Henning
Department of Thermal Systems and Buildings, Fraunhofer Institute for Solar Energy Systems ISE, Freiburg, Germany

Article Outline

Glossary
Definition of the Subject and Its Importance
Introduction
Physical Principles
Common System Designs
Energy and Cost Performance
System Experiences
Future Directions
Bibliography

Glossary

Air-conditioning Temperature and humidity control in buildings of each typology.

Coefficient of performance (COP) Factor which describes the ratio between useful and supplied energy.

Cooling Removing of heat.

Cost of saved primary energy Theoretical cost for 1 kWh of primary energy which is saved using an alternative system (e.g., driven by renewable energy sources) instead of a conventional one (only driven by fossil fuels or electricity from grid).

Demonstration project Organized implementation of a novel approach which aims at assessing the merits of widespread use of the approach and at gaining practical experience.

Primary energy saving Difference between the annual primary energy consumption of a conventional system which uses fossil fuels or electricity from grid and the annual primary energy consumption of a comparable system driven (partly) by renewable energy sources.

Sorption Exothermic process which comprises adsorption (a liquid or gaseous substance is attached to the surface of a solid, porous material) and absorption (a liquid or gaseous substance is taken in by a liquid volume).

Definition of the Subject and Its Importance

Cooling is needed for two main fields of application. On the one hand, it is needed in buildings and other closed spaces, for example, vehicles, which are occupied by human beings. Cooling assures that occupants feel comfortable. On the other hand, in industrial and commercial applications, cooling is needed to cool commodities or processes. In a wider sense, cooling in buildings refers to both control of temperature and control of humidity. In the following, it is referred to as *air-conditioning*. Cooling of commodities or processes is referred to as *refrigeration*. Cooling in a thermodynamic sense means to withdraw heat. Any heat flux is always directed from a source of high

temperature to a sink of lower temperature. Unless a natural heat sink is available – such as the ground or outside air – a thermodynamic cycle has to be employed in order to provide a low-temperature heat sink. *Solar cooling* means that a major part of the driving energy to operate such thermodynamic cycle is originating from the terrestrial solar radiation.

The first solar cooling installation has been developed by Augustin Mouchot and was presented at the World Exhibition in Paris in 1878 [39]. This system consisted of a concentrating solar collector in which solar radiation was converted into heat. The heat was used in an absorption cycle to produce ice. However, this process did not receive any economic importance for almost 100 years due to the development of electrically driven vapor compression systems and the increasing availability of cheap electricity to operate such systems. In the 1980s of the last century, similar processes – solar heat–driven cooling – received new attention mainly in the USA and in Japan [30]. Increasing energy prices after the oil price shocks led to a recollection of the possibility to make use of the sun's energy to provide cooling. Today, various heat-driven cooling technologies can be used in combination with heat which is generated in solar collectors. An alternative approach is to convert solar radiation into electricity by the application of photovoltaic modules and then to use this electricity to operate a vapor compression machine.

Introduction

Solar cooling has achieved more and more attention in particular in the twenty-first century. The main reasons were the rising prices of conventional, finite energies, an increasing awareness of environmental problems due to energy consumption and due to use of conventional refrigerants employed in vapor compression cycles, and a growing wish to use clean technologies for covering the energy demand in buildings. In the first decade of the twenty-first century, numerous pilot solar cooling installations have been built worldwide, particularly in Europe. Also, thermally driven cooling technologies were further developed to increase their efficiency, reduce their costs, and make them available in small capacity ranges.

This chapter starts with a brief overview on the physical principles which underlie the conversion of solar radiation into useful cooling. The discussion of the thermodynamic limits leads to a classification of different types of thermally driven cooling cycles in relation to the corresponding solar collector technology section ("Physical Principles"). Dominating technologies and system components are described technically and economically in more detail in sections "Common System Designs" and "Energy and Cost Performance." The section "System Experiences" presents overall systems including a few examples of existing installations. Finally, section "Future Directions" provides an outlook and outlines the perspectives and limits of solar cooling technologies.

Despite the fact that common cooling technologies and solar or solar-assisted systems, which are described in sections "Physical Principles" and "Common System Designs," are worth considering for several applications, for example, food conservation or industrial processes, this chapter mainly focuses on comfort cooling in buildings.

Physical Principles

This section covers physical principles of the conversion of solar radiation energy into useful cooling. After a brief presentation of the different conversion chains, a thermodynamic analysis is carried out which helps to classify different solar cooling systems in terms of efficiency and temperature.

Conversion Chains

Figure 1 shows the different conversion chains for the conversion of solar radiation energy into useful cooling.

A general distinction has to be made between systems driven by electric energy and systems driven by thermal energy (heat).

Photovoltaic modules (PV modules) are used to convert solar radiation into electric energy. In principle, any kind of electrically driven cooling devices can be used to produce useful cooling. The two main important systems are:

- Vapor compression cycle: mechanical vapor compression is the most common way of cold production. Electric engines are used to convert electricity into mechanical energy (mainly rotation) and for the compression of the refrigerant in the gas phase. Many different types of compressors are used for

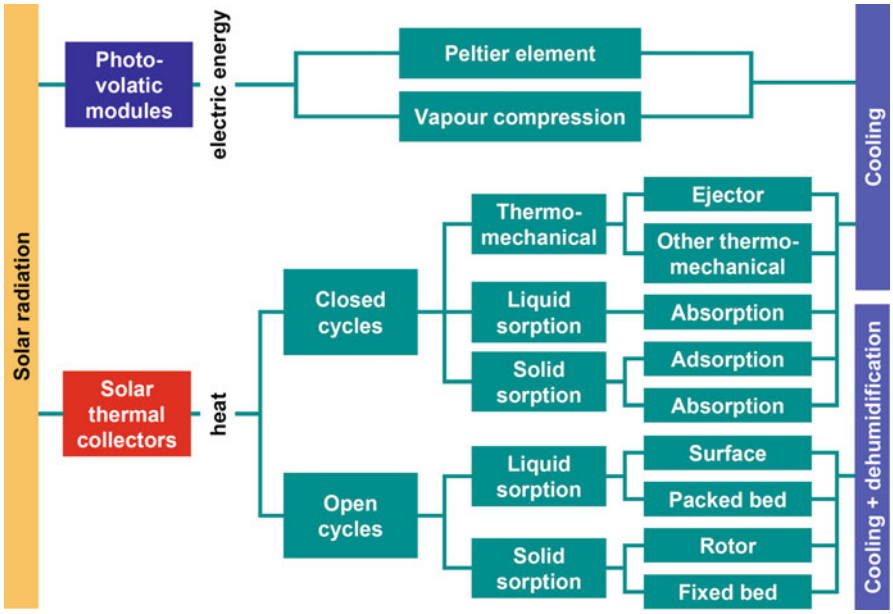

Solar Cooling Systems. Figure 1
Conversion chains for the conversion of solar radiation energy into useful cooling

different technical applications. To employ photovoltaic modules for operation of a vapor compression cycle, an inverter normally has to be employed which converts the DC (direct current) electricity of the PV module into AC (alternating current) electricity which is needed by the electric engine. Today, PV-coupled vapor compression systems are mainly used in small-scale cooling devices such as refrigerators to conserve medicine or food in remote areas. In the future, cooling systems using PV modules connected to vapor compression chillers may play an important role even in other applications for refrigeration and air-conditioning. However, as long as the PV modules are connected to a public grid and feed the produced electricity into this grid, this combination should not be called solar cooling system because no direct coupling between PV modules and cooling device exists.

- Peltier cooling: the Peltier effect is a thermoelectric phenomenon which occurs when two materials with a different electric conductivity are connected. This principle can be used to produce cooling at the contact surface between two materials by inducing an electric current in the closed circuit. The efficiency is relatively low (approximately 3–8%). Therefore, this concept plays only a minor role in technical application, for instance in small transportable cooling devices for medicine.

Solar collectors are used to convert solar radiation energy into heat. The achievable temperature level depends on the type of used solar collector. For a detailed description of existing collectors and solar thermal systems, please see the chapters "► Solar Collectors, Non-concentrating," "► Linear Fresnel Collectors," and "► Parabolic Trough Solar Technology." Solar heat can be used to operate thermally driven cooling devices. A main distinction can be made between closed thermodynamic cycles which produce cooling and open cycles which are typically used for cooling and dehumidification of ventilation air. In machines using closed cycles the cold is typically transferred to the load using water as heat transfer fluid as long as temperatures above the freezing point of water are sufficient. Water-glycol mixtures are in use (antifreeze) when temperatures below 0°C are needed.

Today, the most dominating thermally driven cooling techniques are based on sorption technology using either liquid or solid sorption materials in open or closed cycles.

Therefore, the physical principles of the underlying processes are briefly described here. A detailed description of existing technical systems follows in section "Common System Designs."

Sorption refers to either absorption or adsorption. Absorption means the mixing of two substances, namely liquid absorbent and another liquid or vaporous material, without chemical reaction. Adsorption is the physical addition of a liquid or gas onto the surface of a solid material mainly by van der Waals forces and capillary condensation.

Absorption describes the incorporation or solving of a liquid or gas by the volume of another liquid material without chemical reaction. The two materials have an affinity for each other. Mixing of two materials with an affinity for each other is normally an exothermic process because heat of solution is released. Liquid or vaporous atoms or molecules "migrate" into the absorbent material by diffusion. The migration stops as soon as the solubility of the migrating material in the absorbent material is reached. This state is a dynamic equilibrium depending on the temperature level. Absorbent and absorbed material can be dissolved by heat treatment.

Adsorption describes a two-step energy conversion. In the first step, a volatile compound is bound by a solid adsorbent after diffusing in the pores of the solid material. This is an exothermic process. In the second step, the bound compound is driven off by heat. The binding of the molecules to the adsorbent is achieved by means of several forces but has to be fully reversible for technical applications. To optimize the adsorptive effect and the amount of adsorbed particles per volume of adsorbent, adsorbents should be of highly porous materials with a large internal surface. During the adsorption process, first, a monomolecular layer is formed on this surface by the molecules of the vaporous material due to van der Waals forces and electrostatic attraction [43]. After the monolayer is completed within the pores of the adsorbent, a liquefaction of the vapor takes place, and the liquid is further adsorbed by capillary condensation.

Beside techniques based on sorption, various other phenomena can be used for the transformation of heat into cooling. The most important one is the ejector technology. In an ejector cycle, the low-pressure refrigerant (e.g., water) is driven by fluid kinetic or thermal energy. The driving heat is utilized to convert water to superheated steam and this steam is accelerated in a nozzle. The produced steam is utilized by a steady-stream ejector to compress a secondary water stream. This secondary water stream evaporates in the evaporator and thereby produces the cooling effect. Also other fluids can be employed as refrigerants but using water allows a direct connection to the hydraulic network. Various other thermomechanical systems for thermally driven cold production are possible. Most straightforward is the operation of a Rankine cycle to produce mechanical energy from heat and to convert this mechanical energy (mainly rotation) into cooling using vapor compression systems. Such approach involves many different machines and is therefore only viable in large capacity systems. Since typically the level of temperature of the solar field is limited, organic Rankine cycles have to be used. Another thermodynamic machine which allows a directly heat-driven cooling is the Vuilleumier cycle which consists basically of an integrated direct coupling of two Stirling cycles operating in different directions.

Thermodynamic Analysis of Thermally Driven Chillers

A basic figure to describe the quality of the conversion of heat into cold is the thermal Coefficient of Performance COP, defined as the useful cold Q_{cold} per unit of invested driving heat Q_{heat}, see Eq. 1:

$$COP = \frac{Q_{cold}}{Q_{heat}} \tag{1}$$

The first and second law of thermodynamics applied to the basic process of a thermally driven chiller, according to the scheme shown in Fig. 2, lead to an equation for the upper limit of the Coefficient of Performance, COP_{ideal}, in which the COP is only dependent of the three governing temperature levels (all temperatures in Kelvin, K), see Eq. 2:

$$COP_{ideal} = \left(\frac{Q_{cold}}{Q_{heat}}\right)_{ideal} = \frac{T_c}{T_h} \cdot \frac{T_h - T_m}{T_m - T_c} \tag{2}$$

where T_c is the temperature of the cold source (useful cooling), T_h is the temperature of the driving heat source, and T_m is the intermediate temperature level at which the heat is rejected to a heat sink (in most

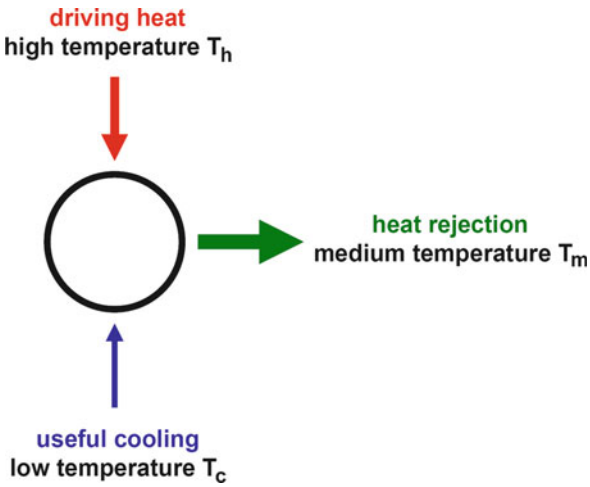

Solar Cooling Systems. Figure 2
Basic scheme of a thermally driven cooling cycle with the three dominating temperature levels

cases, this heat sink is environmental air using either a wet cooling tower or a dry air cooling tower; see also section "Subsystems and Further Equipment Components"), see Fig. 2.

The COP_{ideal} calculated according to Eq. 2 gives the upper thermodynamic limit which can never be achieved in practice. Real COP values of thermally driven chillers range between 0.6 for systems which work with low driving temperatures starting at about 60°C and 2.0 for a recently newly developed machine [53] which operates with driving temperatures above 200°C. Common systems, which will be described in more detail in section "Common System Designs," are characterized by COP values of 0.7 up to 1.2.

The fraction between real COP, COP_{real}, and maximum COP, COP_{ideal}, at the same conditions, is called Carnot Efficiency Factor ξ_{Carnot} and is given by Eq. 3:

$$\xi_{Carnot} = \frac{COP_{real}}{COP_{ideal}} \tag{3}$$

The Carnot Efficiency Factor can never exceed 1 and has a value which lies significantly below 1 for any real technical system. This factor is a single number that expresses all irreversibility within a thermodynamic machine. Its value lies in the range of 0.25–0.35 for common thermally driven cooling systems available on the market. The ξ_{Carnot} can be increased by different measures which lead to a reduction of entropy production such as improved heat recovery in the internal cycle, increased heat exchanger areas, measures for enhanced mass transfer, and others.

The task for any cooling process is to create a temperature difference between the heat flux entering the thermodynamic machine at low temperature T_c and a heat flux leaving the thermodynamic machine at medium temperature T_m. This temperature difference is called temperature lift Δ:

$$\Delta = T_m - T_c \tag{4}$$

The higher the temperature lift, the higher the thermodynamic effort.

Combination of Eqs. 2, 3 and 4 leads to an equation for the needed driving temperature $T_{h,needed}$ as a function of the temperature lift Δ, including given Carnot Efficiency Factor ξ_{Carnot} and given COP_{real} of the machine:

$$T_{h,needed} = \frac{T_c + \Delta}{1 - \frac{COP_{real} \cdot \Delta}{\xi_{Carnot} \cdot T_c}} \tag{5}$$

Figure 3 highlights the dependence of the needed driving heat temperature on the COP, ξ_{Carnot}, and the temperature lift. Four different lines show exemplary COP values of 0.75 and 1.2 combined with Carnot Efficiency Factors of 0.3 and 0.4. The typical operation temperature ranges of different solar collector technologies are marked, and different ranges of the temperature lift Δ are characterized. Several types of fixed and tracking solar collectors which can be used as driving source of cooling systems are described in other chapters; see "▶ Solar Collectors, non-concentrating," "▶ Linear Fresnel Collectors," and "▶ Parabolic Trough Solar Technology."

The required temperature lift is a basic value in the design phase of a (solar or solar-assisted) cooling system. In Table 1 various possible system examples are shown and the temperature levels for cooling and heat rejection using different technical solutions are described. Together with the analysis of Fig. 3, Table 1 allows a rough selection of a possible solar collector technology which is suitable for a specific system.

Typical applications and examples of systems are:

- In case of a low-energy cooling system, that is a system which can be operated with a low

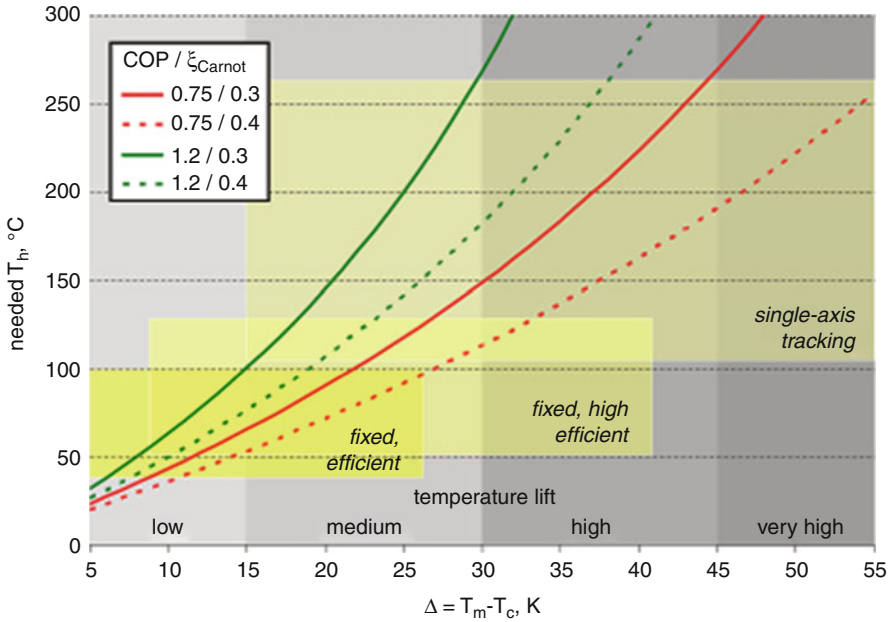

Solar Cooling Systems. Figure 3
Needed heat source temperature as a function of the temperature lift for different COP/ξ_{Carnot} combinations

Solar Cooling Systems. Table 1 Overview on different solar cooling systems characterized by the required temperature lift; only configurations for which market available solutions exist are shown

	Temperature lift	Low (10–15 K)	Medium (15–30 K)		High (30–45 K)	Very high (>45 K)
	Supply temperature (room system in case of comfort A/C)	15–20°C, e.g., chilled ceiling, floor cooling, radiative cooling	15–20°C, e.g., chilled ceiling, floor cooling, radiative cooling	6–12°C, e.g., fan coil, AHU with dehumidification	6–12°C, e.g., fan coil, AHU with dehumidification	<0°C, e.g., ice production, ice storage
	Reject temperature, reject system	25–30°C wet cooling tower; ground	35–45°C dry cooling tower	25–30°C wet cooling tower; ground	35–45°C dry cooling tower	35–50°C dry cooling tower
Low COP technology	**Driving temperature range**	70–85°C	85–110°C	85–110°C	100–130°C	180–250°C
	Possible solar collector types	Efficient, fixed	Efficient to highly efficient, fixed	Efficient to highly efficient, fixed	Highly efficient, fixed; single-axis tracking	Single-axis tracking
High COP technology	**Driving temperature range**	*No market available cooling system for this configuration*	130–200°C	130–200°C	200–300°C	*No market available cooling system for this configuration*
	Possible solar collector types		Single-axis tracking	Single-axis tracking	Single-axis tracking	

temperature difference between room temperature and temperature of cold water such as a chilled ceiling (or more generally radiative cooling), a low temperature lift in the range of 15 K is sufficient, at least in moderate climates and when a wet cooling tower is used. Such systems can be operated using cooling machines (see section "Common System Designs") driven by heat at moderate temperatures which is generated in normal efficient, fixed solar collectors, that is solar collectors that do not have to be tracked to the sun's direct radiation.

- The same system as described above but using a dry cooling tower works with a higher temperature lift in the range of 15–30 K because the temperature level for heat rejection is higher. In this case, there are also cooling machines which can be operated at a higher thermal COP (double-effect chillers; see section "Common System Designs"). Correspondingly, another solar collector technology has to be employed in order to provide the needed higher driving temperature.
- A common fan-coil system in which dehumidification is realized by cooling the air below the dew point needs chilled water in the range of 6–8°C. With a temperature for heat rejection in the range of 25–35°C a temperature lift of about 20–30 K is necessary. For such a system, very highly efficient flat-plate collectors or evacuated tube collectors are necessary in case cooling machines with low COP value are used. For cooling machines with high COP values, high-efficiency evacuated tube collectors can possibly be employed but in most cases solar collector systems with optical concentration which are tracking the sun are necessary.
- Under conditions of high ambient air temperatures (>35°C) and when wet cooling towers cannot be employed (e.g., due to high wet-bulb temperatures or no availability of water), a high temperature lift above 30 K will be necessary. This is even more valid if a low temperature on the cold side is needed, for example in case of ice production or using an ice storage to overcome mismatches between cooling load and solar gains because then the temperature lift can even exceed 45°C. In this latter case, only a machine with low COP value can be used if driving temperatures up to 300°C are available. Therefore a solar collector system with optical concentration will be necessary. These conditions correspond to the needs in hot, arid regions in which fresh water is costly or a scarce commodity.

Figure 3 also indicates that, in principle, two tracks are possible in order to improve the efficiency of solar cooling systems. On the one hand, using a highly efficient solar collector allows higher driving temperatures and thus an increased COP. On the other hand, an increase in the Carnot Efficiency Factor allows operation of a thermally driven chiller at lower operation temperatures. Both tracks are subject of ongoing R&D activities.

An overview on the COP values of most common closed cycle heat-driven chillers is given in Fig. 4.

Common System Designs

One of the main reasons for the application of solar cooling is to replace common compression chillers for which electrical energy is required to drive the compressor by technologies using renewable energies. Solar cooling systems are based on different technical designs. Therefore, it makes sense to divide the mainly applied technologies into closed systems: mainly absorption chiller and adsorption chiller, and open systems: desiccant evaporative cooling (DEC) systems and liquid desiccant air-conditioning (LDAC) systems. Absorption and adsorption chillers are used for cooling; desiccant systems are used for air-conditioning: cooling and dehumidification. Absorption chillers are the most widespread-used solar-driven chillers with a current share in realized installations of about 71%. The corresponding share of solar-driven adsorption chillers is 13%, of DEC systems 14%, and of LDAC systems 2% [21].

A diagram of a common vapor compression system is shown in Fig. 5, with the main components evaporator, condenser, and compressor. The simplified principle of the cold production can be explained as follows: liquid refrigerant evaporates under low pressure and low temperature, extracting heat from the system to be cooled. Refrigerant vapor is compressed to higher pressure, condenses at a higher temperature, and thereby releases heat which needs to be rejected. Subsequently, the pressure of the liquid refrigerant is reduced by expansion through a throttle valve, and the cycle is repeated [15].

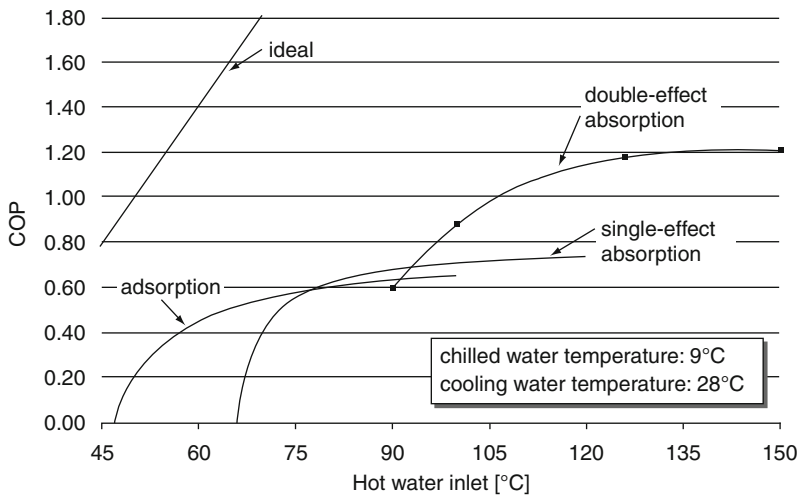

Solar Cooling Systems. Figure 4
Typical COP curves of sorption chillers and the upper thermodynamic limit (ideal) according to Eq. 5

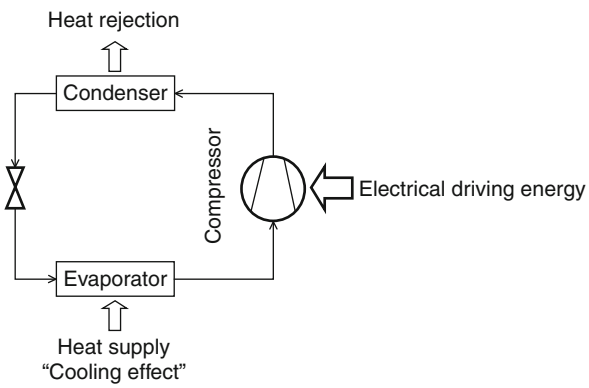

Solar Cooling Systems. Figure 5
Scheme of a vapor compression system in which an electrically driven compressor is used

Closed Absorption Systems

The development of absorption processes for applications in refrigeration dates back to the eighteenth century. In 1777, G. Nairne observed the absorptivity of concentrated sulfuric acid in water which is considered as the starting point of absorption technology [52]. Another father of absorption technology is F. Carré. He presented a patent of the first absorption cooling machine based on the working pair ammonia/water in 1859. At the same time, W. Thomson (better known as Lord Kelvin) presented the concept of a heat pump to make use of the waste heat of a refrigerator for heating purposes [34, 49, 53]. In his work, he described different combinations of compression and expansion cylinders for heating and cooling applications.

In absorption systems, the mechanical compressor is replaced by a "thermal compressor" existing of absorber, desorber (generator) and solution pump, see Fig. 6. In contrast to mechanical compression, the main driving power to the generator is not provided by mechanical energy (or electrical energy in combination with an electric engine, respectively) but by heat using a low-temperature heat source, for example solar collector, district heating, or waste heat. The solution pump needs only little mechanical (electrical) energy since it has only to increase the pressure of a liquid and not of a gas like in a vapor compression cycle. Further, main components are the evaporator, the condenser and the throttle valves used for expansion.

Absorption chillers can be divided into different types. They are continuously working closed cycle systems but occur as single-effect, double-effect, triple-effect, or double-lift systems or as systems combining different designs, for example single-effect/double-lift (SE/DL) systems. More detailed descriptions of the different systems follow later in this section. Installation differences lie furthermore in the utilized heat source for the generator.

The operating media determines the operating temperature level. The medium used as refrigerant depends on the needed temperature of the useful cooling.

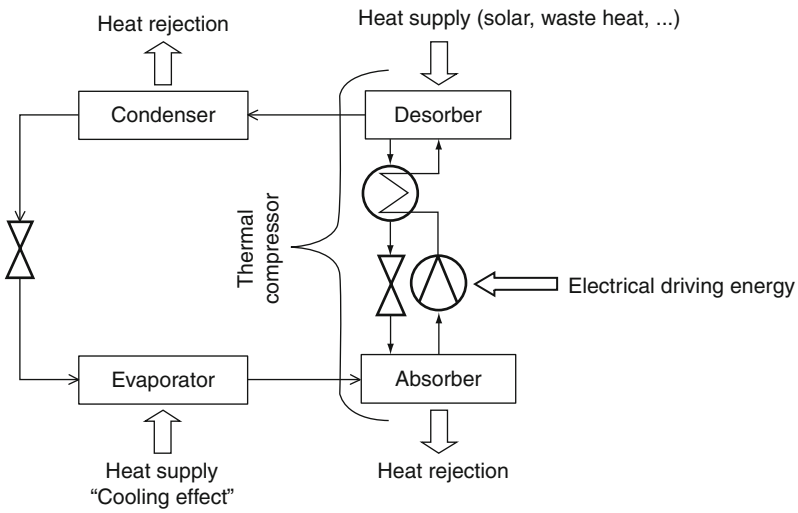

Solar Cooling Systems. Figure 6
Scheme of an absorption system for cooling

For cooling applications with a temperature level above the freezing point of water (273.16 K/0°C), often water (H_2O) is used as refrigerant, and a solution of water and lithium bromide (LiBr) is used as sorbent. For cooling applications with a temperature level below the freezing point of water, in most cases ammonia/water (NH_3/H_2O) is used as working pair; here, ammonia is the refrigerant and water the sorbent. For comfort air-conditioning temperatures above 0°C are sufficient [53].

The refrigerant/absorbent working pair H_2O/LiBr was first developed by the Carrier Company which constructed a laboratory prototype in 1942 which was first distributed in 1944 in the USA [49].

Process and system technology can be explained best by showing a standard single-effect system. Such a system consists of the following main components: evaporator, absorber, desorber, and condenser.

Since the *evaporator* is responsible for the cold production, the process cycle is explained by starting from this point. The working point at this place is determined by the saturation line of the pure refrigerant. Consequently, the less pressure exists, the less temperature is necessary to evaporate the liquid refrigerant. The refrigerant (e.g., water) which is fed in the low-pressure evaporator is evaporated at low temperature by extracting heat from the heat source which thereby cools down. This step represents the desired cooling effect.

The refrigerant vapor migrates to the *absorber* which operates also at low pressure and is continuously absorbed by a suitable liquid solvent (e.g., LiBr) and condenses. This results in a liquid solution with heat release (exothermic process). The heat produced in this process step has to be withdrawn continuously (by an external circuit) in order to extract the heat of condensation and binding and thus to keep the absorption process ongoing. The lower-boiling component functions as refrigerant (water), the high-boiling component functions as absorbent (LiBr solution). The advantage is that not the pressure of gas but of liquid has to be increased, and the driving power is significantly lower than that of compression systems [37]. The weak solution which is pumped to the desorber flows through a heat exchanger device and is preheated; as a consequence, both pressure and temperature rise. A solution heat exchanger is not necessarily needed for an absorption system but helps to reduce the required desorption heat due to preheating the weak solution. For this purpose, the heat is taken from the back-flowing rich solution (LiBr), which passes the heat exchanger from its way back from desorber to absorber.

In the *desorber* the weak solution is heated further and the refrigerant evaporates at a higher pressure level. Nonmechanical work serves as driving energy of the chiller but heat at a temperature level of about 80–200°C depending on the thermodynamic design.

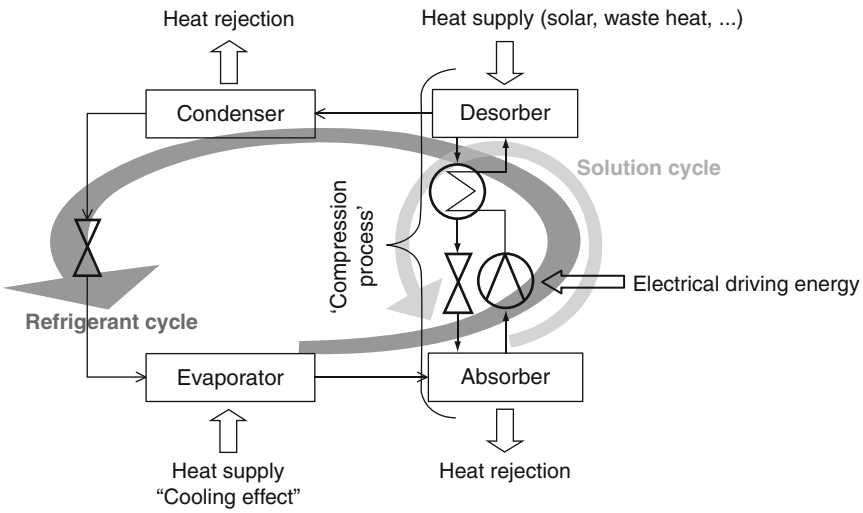

Solar Cooling Systems. Figure 7
Schematic picture of an absorption system for cooling depicting solution with refrigerant cycle and solution heat exchanger

Driving heat is supplied by an external heat source such as waste heat of an industrial process or a cogeneration unit or heat from a solar thermal collector. The refrigerant vapor migrates to the condenser. The reconcentrated rich solution is led back to the absorber and thereby passes the other side of the solution heat exchanger. Heat is transferred to the counterflowing weak solution, and the temperature of the rich solution decreases. The liquid absorbent is expanded through a throttle valve from high to low pressure. The solution cycle is closed when the rich solution reenters the absorber.

Following up the refrigerant cycle the refrigerant (e.g., water) vapor flows to the *condenser* and condenses through the application of cooling water at the same pressure level as the desorber. Liquid refrigerant circulates back into the *evaporator*. Being expanded by a throttle valve the liquefied cooling agent cools down on its way back to the evaporator. The cycle restarts at a low pressure and temperature level [8, 15, 49].

For a better understanding, see Fig. 7 which shows schematically refrigerant and solvent cycle, Fig. 8 which shows schematically the pressure and temperature levels of the corresponding single-effect absorption process (with E as evaporator, A as absorber, D as desorber, and C as condenser) and Fig. 9 which shows the corresponding ln p-x and ln p-(1/t)-diagram of a single-effect absorption with water/LiBr.

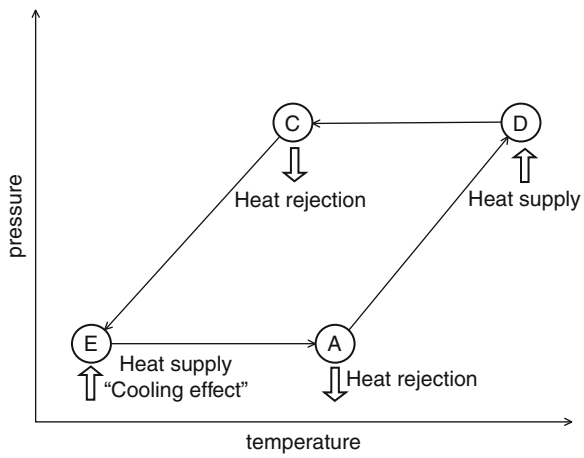

Solar Cooling Systems. Figure 8
Scheme of pressure and temperature levels of a single-effect absorption process

An essential part of the system is the source of driving heat (for the desorber). Possible heat sources are, for example, industrial waste heat, heat supplied by a thermal power station or district heating system, gas or oil firing and exhaust gas of motors, fuel cells, and turbines (cogeneration). Solar cooling systems are – completely or predominantly – driven by heat provided by solar collectors [6]. For details on solar collectors, please have a look at the following chapters in this

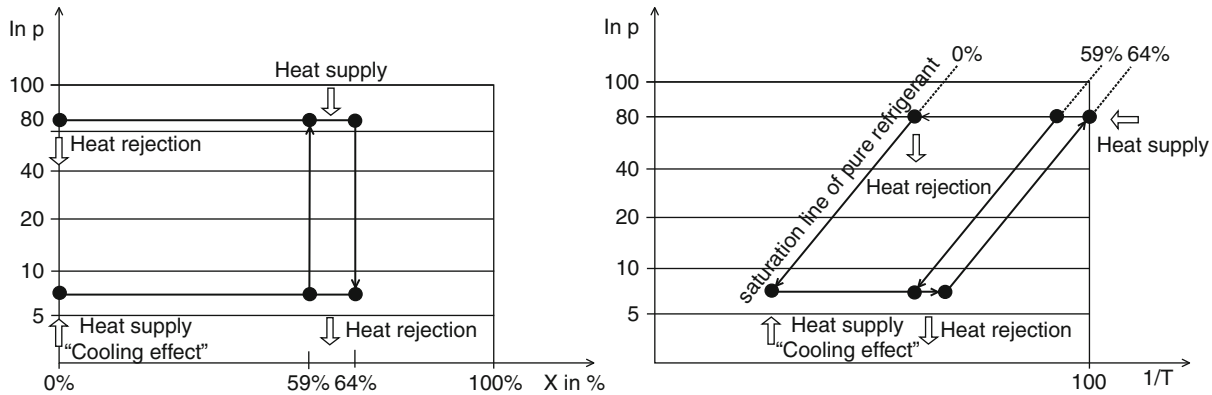

Solar Cooling Systems. Figure 9
ln p-x and ln p-(1/T)-diagram of a single-effect absorption process with water/LiBr

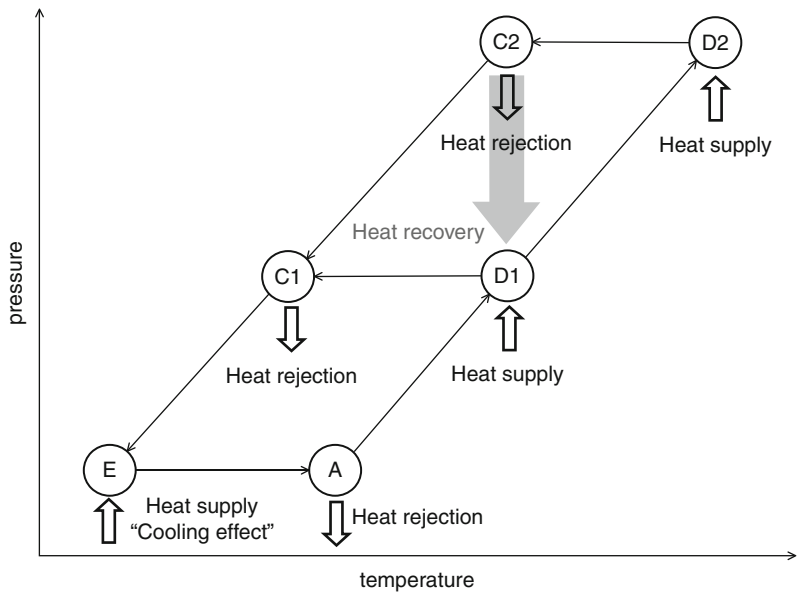

Solar Cooling Systems. Figure 10
Scheme of pressure and temperature levels of a double-effect absorption cooling process

book: "► Solar Collectors, non-concentrating," "► Linear Fresnel Collectors," and "► Parabolic Trough Solar Technology."

A double-effect machine has a second desorber (generator) and a second condenser which works at a higher pressure and temperature level, see Fig. 10. The rejected heat of the condenser working at high pressure and temperature drives the desorber at the first stage. Generally, the second desorber is driven either directly by a natural gas or oil burner or indirectly by supplying steam or pressurized water at high temperature level. If solar energy shall be used to drive such systems, solar collectors working at high operation temperatures have to be used. Heat is added to the generator of the top cycle (primary generator) which generates refrigerant vapor at a higher temperature and pressure relatively to the bottom cycle. The vapor is then condensed at this higher temperature and pressure and the heat of condensation is used to drive the generator of the lower cycle (secondary generator) which is at a lower temperature. Double-effect cycles have a higher COP than single-effect cycles but need

higher driving temperatures for their operation. The COP can be up to one, two [10], or slightly above, and typical driving temperatures lie in the range of 140–160°C. Current research is concentrating on three and four effect systems, which present an attractive potential for improved cooling performance, with a COP of 1.7–2.2, but these systems require a distinctly higher temperature of driving heat [15].

Single-effect and double-effect cycles as described above are the most common designs of liquid absorption systems. However, various other design options exist which aim at adjustment of the cycle to special boundary conditions. Double-lift cycles are for instance used to allow lower driving temperatures. For double-lift systems NH_3/H_2O solutions are typically used [10]. A double-lift machine has a second absorber and a second desorber, see Fig. 11. Compared to a single-effect machine a lower driving temperature is needed. The second absorber is used to absorb the refrigerant vapor generated in the first generator and the second generator produces pure refrigerant vapor which condenses in the condenser. Overall, more heat at lower temperature level is needed compared to a single-effect cycle and thus lower COP results. A combination of a single-effect and a double-lift cycle is called single-effect/double-lift (SE-DL), see Fig. 12 [10]. It requires a driving heat temperature similar to a single-effect system but allows a large temperature spread along the driving heat circuit. This is an advantage for many driving heat sources which need a sufficiently high-temperature spread such as for instance combined heat and power systems. A detailed description of these cycles and discussion of alternative working pairs can be found in [35].

Table 2 provides a short overview on the COP values of the different types of absorption system designs. The COP values reported in literature differ and the ranges given in Table 2 correspond to the lowest and highest values reported.

Typical chilling capacities of absorption chillers are above 100 kW up to MWs. Since a few years, several single-effect absorption chillers with capacities below 50 kW are available. For instance, a water/LiBr chiller which has been newly developed for small capacities (nominal capacity 10 kW) enables part-load operation with reduced chilling power at a heat source temperature of 65°C and a COP of still approximately 0.7. This is very promising in combination with a solar

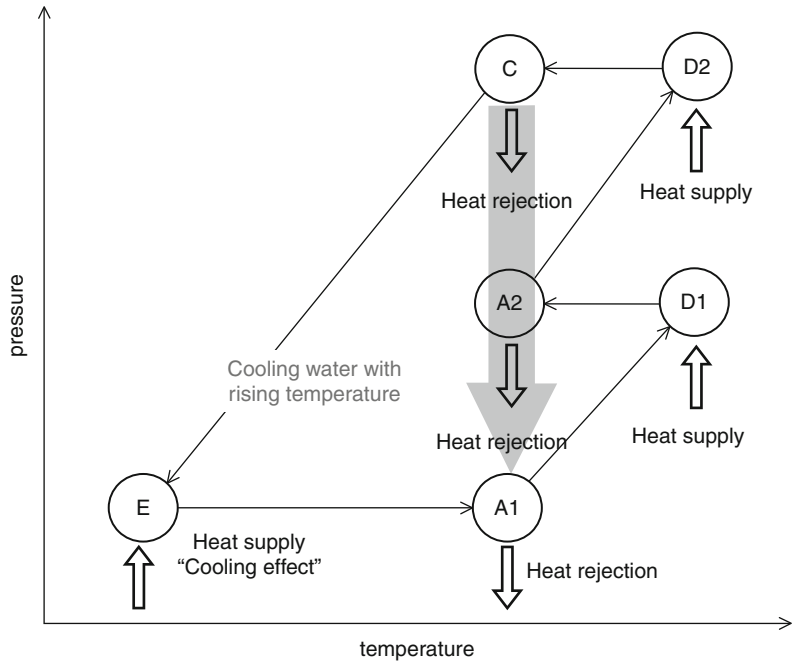

Solar Cooling Systems. Figure 11
Scheme of pressure and temperature levels of a double-lift absorption cooling process [10]

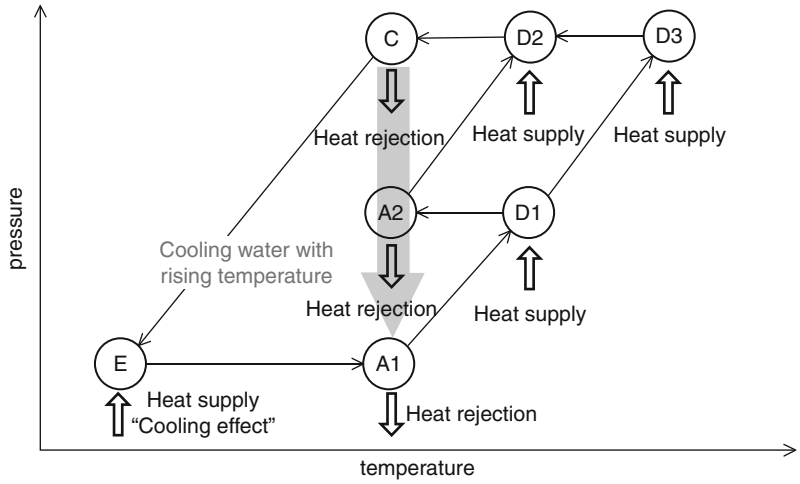

Solar Cooling Systems. Figure 12
Scheme of the pressure and temperature levels of a single-effect/double-lift absorption cooling process [12]

Solar Cooling Systems. Table 2 Overview on typical temperature levels of closed cycle absorption chillers, values from [18, 29, 42, 46]

Closed cycle system	Single effect (H_2O/LiBr)	Double effect (H_2O/LiBr)	Single effect/Double lift (H_2O/LiBr)	Double lift (NH_3/H_2O)
Cold temperature [°C]	6. . .20	6. . .20	6. . .20	−50. . .20
Heating temperature [°C]	70. . .110	130. . .160	65. . .100	55. . .65
Cooling water temperature [°C]	26. . .35	26. . .35	30. . .35	30. . .35
COP [−]	0.5. . .0.8	0.9. . .1.3	0.4. . .0.7	0.4

heat source and shows the high potential for performance improvements of absorption chillers. The new medium-sized and small-sized developments have been designed recently by European and Asian manufacturers, convenient to cover the cooling loads of small buildings with floor areas in the range from 150 to 500 m^2. The European manufacturers are located in various countries and many of the new developments are still being tested in pilot installations.

In Germany, in 2000, only 10% up to 30% of absorption chillers were estimated to be double-effect systems [41]. The reason may be that the system cannot work with low-temperature heat and hence is inappropriate for combined heating, cooling and power (CHPC) applications, comes along with high invest costs, and needs high driving temperature. The need for higher driving temperatures also makes double-effect chillers less suitable for solar-assisted air-conditioning systems using common solar collectors. However, it is possible to use high-temperature solar collectors such as single-axis tracking concentrating solar collectors. These systems need a high fraction of direct solar radiation since optical concentration with mirror or lens systems requires direct radiation while the diffuse radiation cannot be used [15].

Closed Adsorption Systems

Process and system technology of adsorptive cooling is similar to that of absorptive cooling regarding main components and the production of the useful cooling effect but differ in respect of its system design. Adsorption systems combine the system components evaporator, condenser and "compression technology": sorption,

desorption and heat source. The sorption process is performed under vacuum by an adsorber with solid adsorbent which hence cannot be circulated through the system. Adsorption is a quasi-static batch process. By making use of more than one adsorber, a periodic, quasi-continuous operation is possible. Typically, two adsorbers are used and operated in an alternating way. The four resulting components are arranged as a four chamber system linked by valves, see Fig. 13.

Like in absorption systems the main driving power is not provided by electrical energy but is replaced by a heat source and the refrigerant compression is performed by an ad- and desorption process. The medium used as refrigerant is often water. Typical working pairs are water/silica gel and water/zeolite. Also, ammonia/activated carbon, ammonia/zeolite, or methanol/activated carbon are possible working pairs. For applications in the field of cooling only machines using silica gel or zeolite as adsorbent and water as refrigerant are currently available on the market [15]. Silica gel is highly porous and hydrophilic and possesses an extensive surface in its interior.

Since the evaporator is responsible for the cold production and is therefore the main part of the system, the process cycle is explained starting from here.

The less pressure exists, the less temperature is necessary to evaporate liquid. The refrigerant (e.g., water) which is fed in the *evaporator* evaporates at low temperature and extracts heat from a warmer source which thereby cools down. This is the useful cooling effect.

The refrigerant vapor migrates to one of the *adsorber* chambers, namely the one which is cooled and has a low refrigerant loading. The refrigerant vapor is adsorbed on the inner surface in the pores of the solid adsorbent. The heat produced in this process step by condensation and binding of the refrigerant has to be removed by the cooling water system. The colder the adsorbent the more refrigerant (water) can be adsorbed.

At the same time, the refrigerant (water) is driven off the adsorbent by the use of heat in the other chamber which now function as *desorber* (generator). Heat is supplied by an external hydraulic circuit and is transferred to the sorption material by a heat exchanger. The vaporous refrigerant migrates to the condenser and condenses through rejecting heat to the cooling water system. Liquefied refrigerant is led back to the evaporator through a throttle (e.g. formed as a U-pipe).

The adsorption process in the adsorption chamber is operated until a refrigerant loading close to the

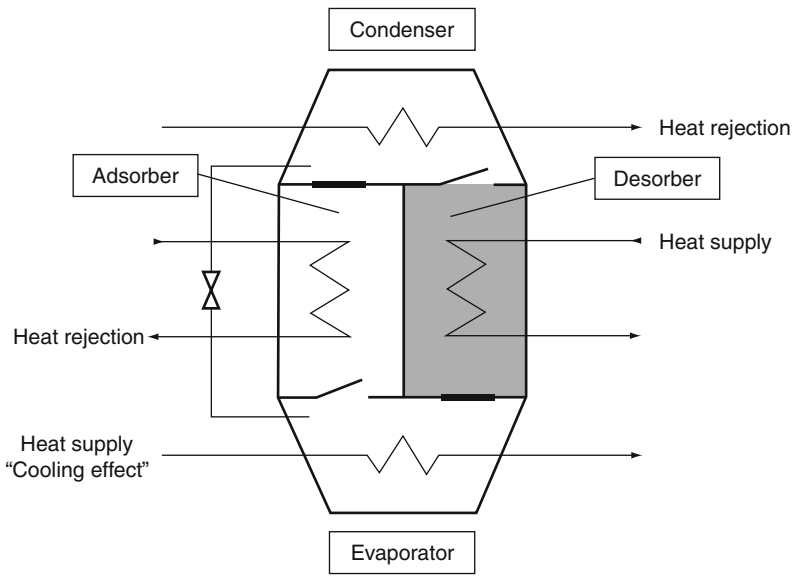

Solar Cooling Systems. Figure 13
Scheme of an adsorption system for cooling

equilibrium at given temperature conditions is achieved. Similarly, the desorption process in the desorption chamber is operated until almost no more refrigerant is released at given temperature conditions. Now, the functions of the chambers interchange. This interchange phase can be realized with heat recovery. Heat recovery enables preheating of the chamber which is switched from adsorption to desorption and vice versa precooling of the other chamber.

The second period starts: the regenerated adsorbent in the previous desorption chamber – which now functions as adsorption chamber – adsorbs vaporous refrigerant and the previous adsorption chamber functions as desorption chamber; the refrigerant is driven off the adsorbent [1, 45]. Figure 14 depicts schematically the whole adsorption process in four stages which allow a quasi-continuous operation.

For further understanding, the pressure and temperature profiles of an ideal adsorption process for one chamber is explained in detail in the following, see also Fig. 15.

There are two pressure levels: that of the evaporator and that of the condenser whereby that of the evaporator is lower. Before the adsorption process starts, the adsorption chamber, with both valves closed, is cooled down until the pressure level of the evaporator is reached. At the beginning of the adsorption process, the valve to the evaporator opens. This valve could be controlled either mechanically and based on an external control or can be an automatic valve which simply follows the pressure difference that is created by the temperature conditions. The low-temperature refrigerant (e.g., water vapor) enters the adsorption chamber and is adsorbed by the adsorbent (e.g., silica gel). Since

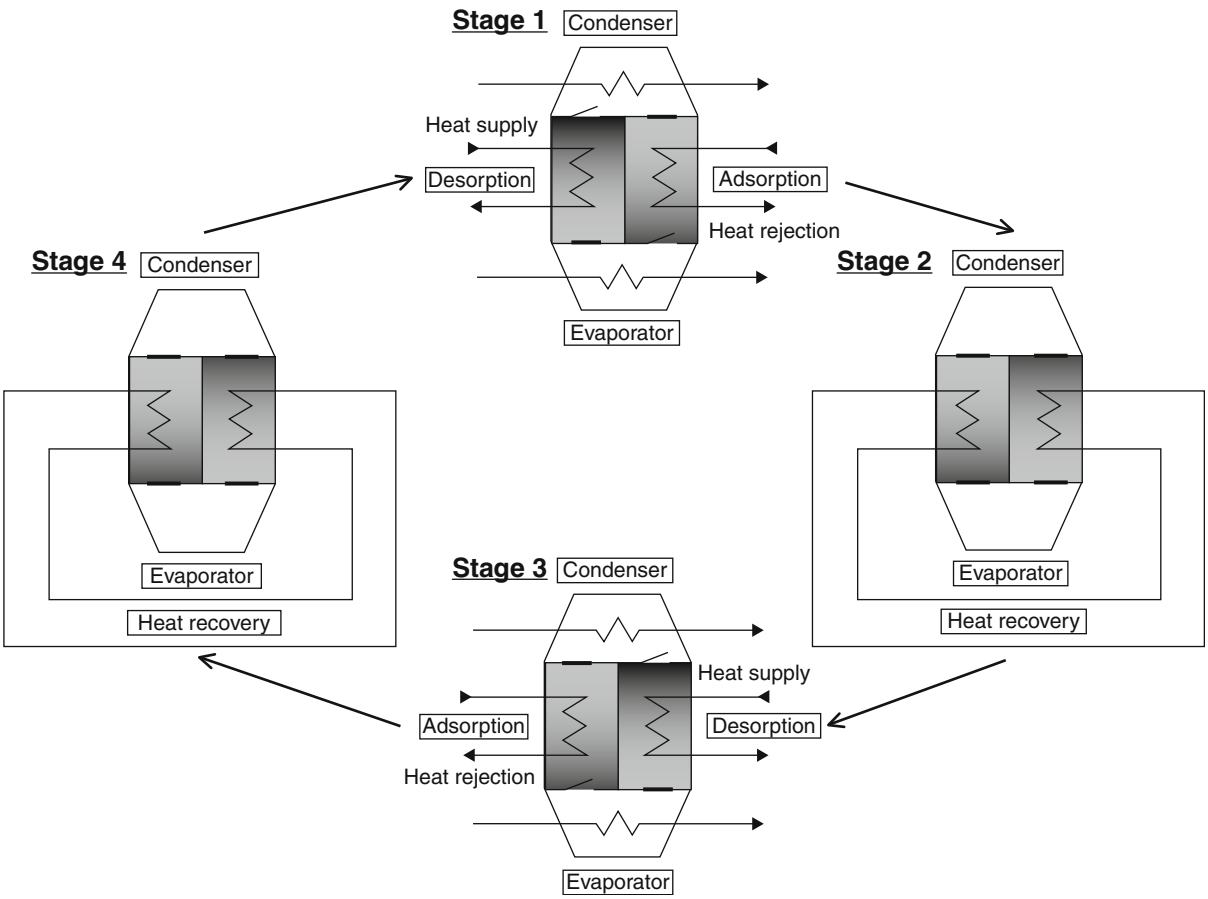

Solar Cooling Systems. Figure 14
Scheme of an adsorption process in four stages which allows a quasi-continuous operation

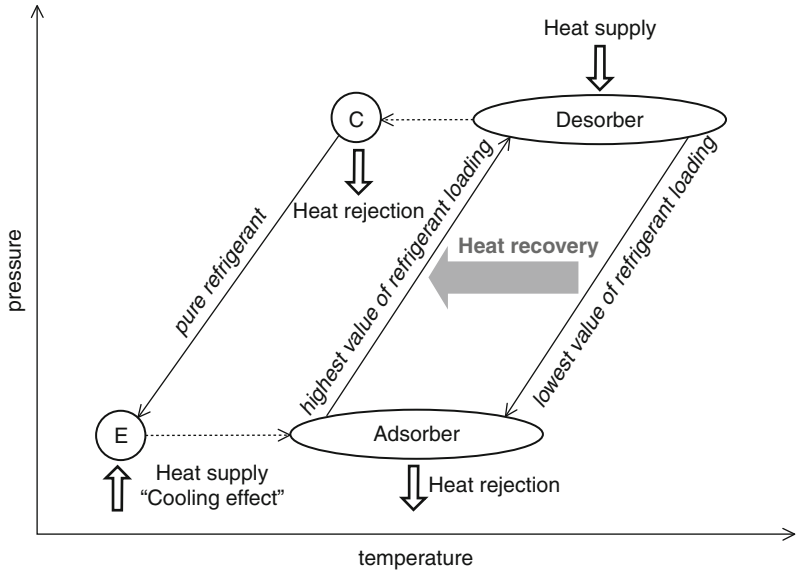

Solar Cooling Systems. Figure 15
Scheme of pressure and temperature cycle of an adsorption system for cooling

this process is exothermal, heat has to be removed continuously. As soon as the refrigerant loading of the adsorbent is close to the equilibrium loading at given temperatures, further adsorption and evaporation diminishes. The valve to the evaporator closes, and heating of the chamber begins. The pressure rises to the pressure of the condenser. The valve to the condenser opens and under constant pressure and rising temperature the refrigerant is driven off. The desorption process ends at desorption end temperature, namely the highest temperature that occurs in the cycle which is defined by the available temperature of the external heat source. The valve to the condenser closes and the adsorption chamber is cooled down again [4, 11, 18].

The driving heat to the process is typically supplied by waste heat from industrial processes or a combined heat and power system, district heating, or solar energy. As adsorption systems already start working at temperatures of about 55°C. Different solar collectors can be used, such as vacuum tube solar collectors or flat-plate collectors [51]. Solar collectors are explained in detail in the following chapters: "► Solar Collectors, non-concentrating," "► Linear Fresnel Collectors," and "► Parabolic Trough Solar Technology."

Adsorption cooling systems are produced by few manufacturers in Asia and, recently, Europe. The simple mechanical construction and robustness of adsorption chillers is an advantage. Further positive facts are the minimized electricity demand, the possibility to work at low driving temperatures and that there is no risk of crystallization as is in the case of using water/LiBr absorption chillers. Adsorption chillers show two main disadvantages: the periodic nature of the process reduces the potential for heat recovery in comparison to system employing liquid sorption materials, and the used sorption materials usually have very low thermal conductivity. As a result, adsorption systems have somewhat lower COP values and a larger volume compared to absorption systems [17, 18].

Another disadvantage is that the periodic process leads to temperature fluctuations on all temperature levels and, in particular, on the driving heat side, see Fig. 16. The figure shows an excerpt of monitoring data of an installed plant. These fluctuations have to be taken into consideration in the hydraulic design of a cooling system using adsorption technology. One possibility to reduce the impact of the fluctuations is the in-series installation of a small buffer on the return line of the heating cycle of the adsorption chiller.

Recent research work focuses on overcoming the disadvantages of the adsorber's large needed volume and weight by developing advanced heat exchanger

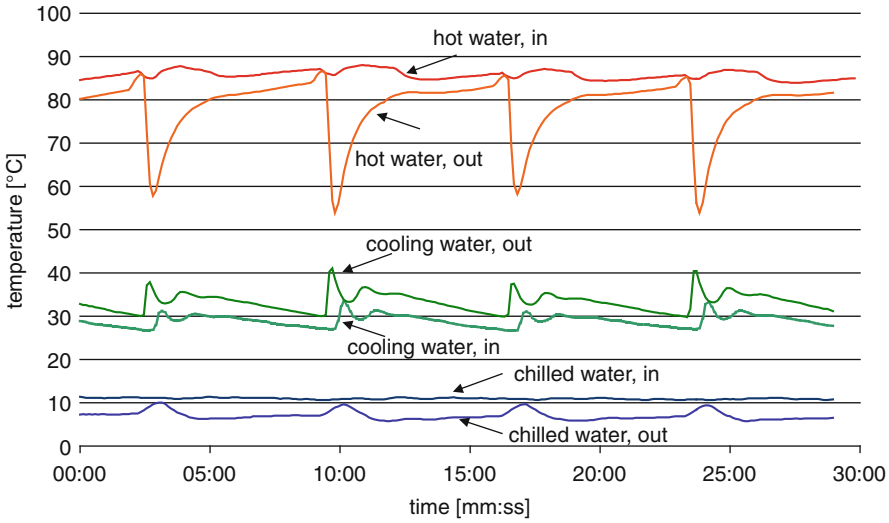

Solar Cooling Systems. Figure 16
Excerpt of monitoring data of an installed adsorption chiller plant

constructions with enhanced heat and mass transfer and thus reduced volume and weight.

Open Solid Desiccant Systems

Desiccant systems cannot only serve for cooling but also for control of humidity and are thus air-conditioning systems. The aim is to provide rooms and other closed spaces with dehumidified and cool air and thereby to ensure comfortable indoor climate conditions.

In desiccant systems, air is treated in an open sorptive cooling cycle where the sensible and latent functions are separated. In principle, warm and moist fresh air is dehumidified by a desiccant and then cooled by sensible heat exchange. If the humidity ratio behind the desiccant component is low enough, direct evaporative cooling may be used for lowering the temperature of the air. A desiccant is a material with a strong attraction for water vapor, classified as either solid or liquid depending on its normal physical state. In desiccant air-conditioning systems silica gel and lithium chloride (LiCl) are typically used desiccants. LiCl can absorb water vapor both either as a solid, hydrated salt, or as an aqueous solution. Further desiccants which might be employed in desiccant air-conditioning are calcium chloride ($CaCl_2$), activated carbon, zeolites, and LiBr.

Although all common desiccant cooling systems include at least the three major components sorption device, evaporative cooler (indirect, direct, or both), and sensible heat exchanger, many different configurations and technical designs exist.

Differences depend on various aspects:

- For the sorption process, solid or liquid desiccants can be used.
- The sorptive dehumidification can be realized as an adiabatic or nonadiabatic process.
- Depending on climatic conditions and desired supply air conditions, a desiccant process can be designed in combination with a conventional air-handling process using vapor compression cooling devices.
- Evaporative cooling may be used in a direct way, in an indirect way, or in both direct and indirect way. This depends on climatic conditions [17].

To explain the DEC process in detail, a typical standard installation using a rotor type desiccant wheel for applications in temperate climate zones is described. Main components are air filter, desiccant component, heat recovery device, evaporation humidifier, fans, and air heater [40]. The desiccant is regenerated by heat. This can for instance be achieved with solar energy. A schematic representation of a typical DEC installation is shown in Fig. 17. The technical design includes two interacting airstreams (Fig. 17: bottom: fresh/supply air and top: return/exhaust air), flowing in opposite directions.

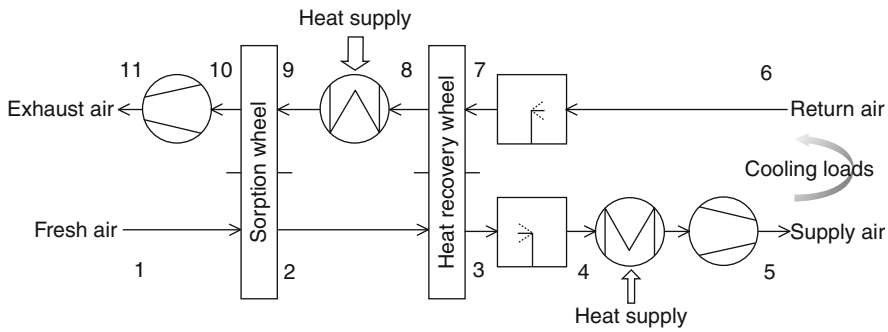

Solar Cooling Systems. Figure 17
Scheme of a DEC system for air-conditioning in temperate climate conditions; the lower heat supply is only used for heating conditions

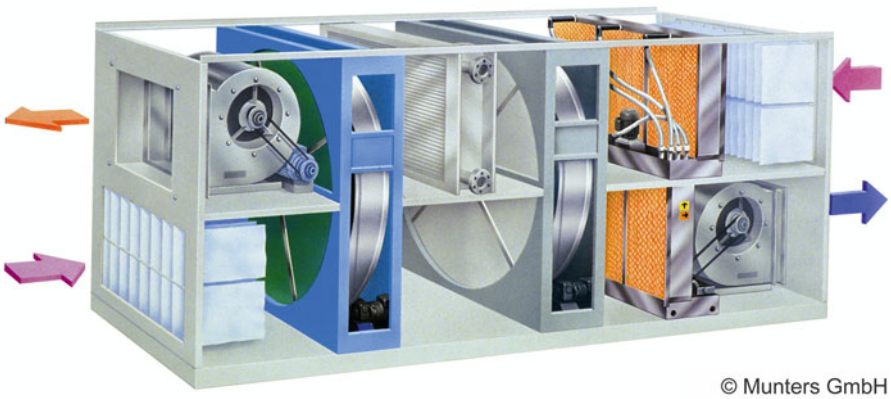

Solar Cooling Systems. Figure 18
Picture of a standard solid desiccant cooling system for applications in temperate climate zones (Source: Munters GmbH)

As solid desiccant component serves a rotating sorption wheel equipped with sorption material (in most cases silica gel or LiCl). Figure 18 shows a picture of a DEC installation, named DesiCool, of the company Munters GmbH.

The steps to describe the DEC process are explained in detail in the following; additionally, please see the T-x-diagram in Fig. 19.

Process steps on supply air side [9, 15, 20]:

(1) Fresh, warm and moist air enters the system from outside and first flows through a filter. Temperature and humidity at this state are equal to outside air conditions.
(1) ➔ (2) The sorption wheel rotates slowly (typically 8–12 rotations per hour). The air passes into the wheel and is dehumidified by the desiccant because the water vapor is adsorbed by the desiccant material. The temperature of the dehumidified air rises through the adsorption and by being heated from the hot thermal mass of the desiccant wheel. The process is almost adiabatic.
(2) ➔ (3) Warm and dehumidified air passes into the heat recovery unit (heat recovery wheel or plate heat exchanger) and heat is transferred to the colder air on the return air side.
(3) ➔ (4) The supply air, precooled and dehumidified, enters the humidifier. Incoming water evaporates and the needed heat is taken from the supply air which effects evaporative cooling. Different types of direct evaporative cooling devices can be employed such as air washers, spray nozzle humidifiers

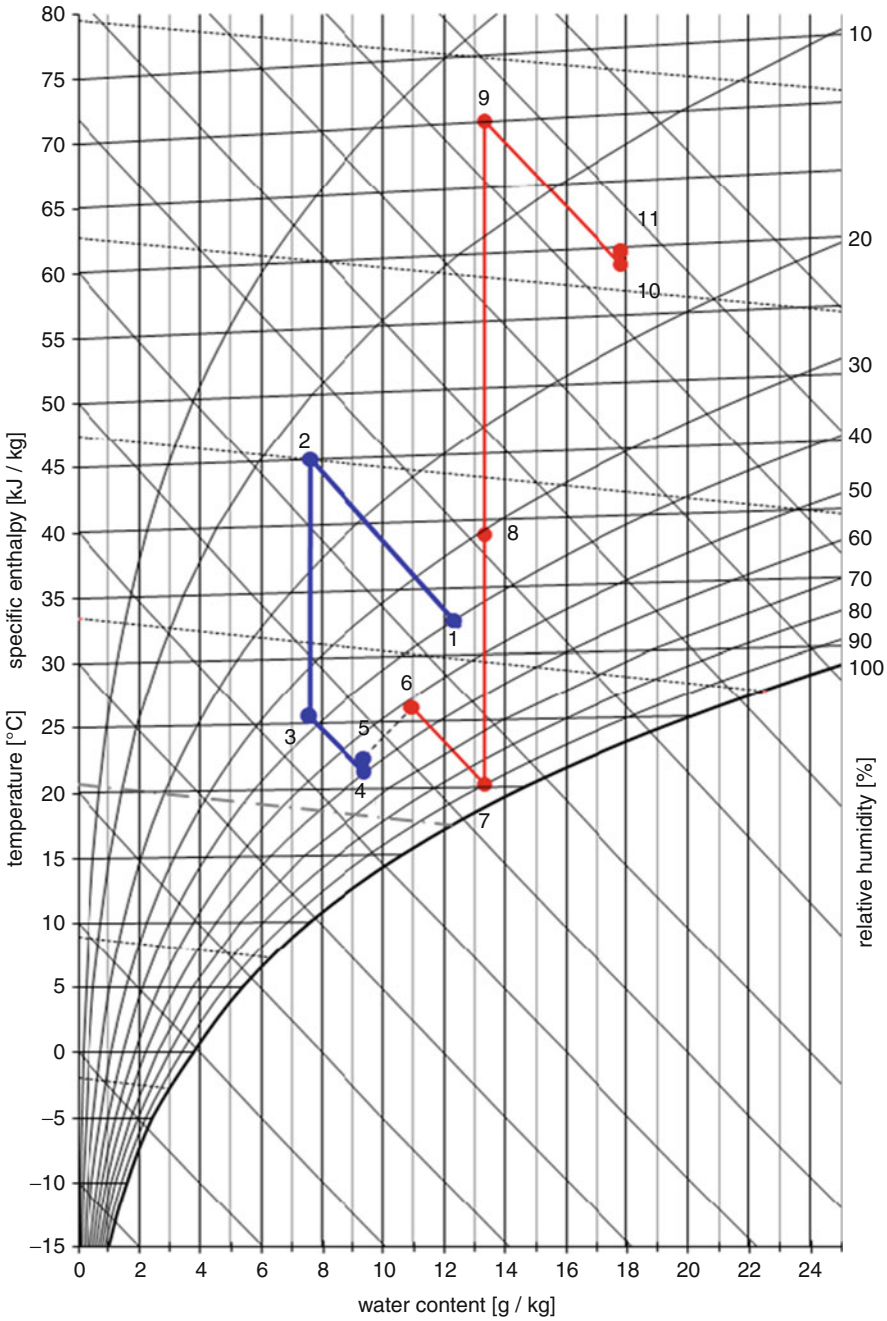

Solar Cooling Systems. Figure 19

T-x-diagram of a DEC process in cooling operation for applications in moderate climate zones

(low or high pressure) or ultra-sonic devices. This component would not be employed in case of humid climatic conditions since the humidity at this position would not allow for the use of direct evaporative cooling.

(4) ➔ (5) In summer/cooling season: a small temperature increase caused by the fan leads to desired supply air conditions. In winter/heating season: the heating coil is operated for heating of the supply air to the desired room air conditions. Again a small

temperature increase occurs due to the fan's waste heat.

(5) ➔ (6) Air temperature and humidity are increased by means of internal loads.

Process steps on return air side:

(6) Return air leaves the conditioned space. Temperature and humidity depend on the place where the air is sucked from the room. If the air is taken from a level of building occupants, temperature and humidity correspond to the comfort room air conditions.

(6) ➔ (7) The air is cooled using evaporative cooling close to the saturation line intending to get close to the lowest possible temperature (wet-bulb temperature) and thereby to maximize the precooling of the supply air in the heat recovery unit.

(7) ➔ (8) In counterflow to the supply air the exhaust air is preheated, see process step (2) ➔ (3).

(8) ➔ (9) The exhaust air, humidified and preheated, flows through a heat exchanger device to be further heated by means of an external heat source. The heat can be provided by waste heat, a cogeneration plant, a combined heat and power (CHP) cycle, or solar energy. Either flat-plate collectors or solar air collectors are employed in case of solar energy-driven systems.

(9) ➔ (10) The hot air passes into the sorption wheel and regenerates the desiccant, see process step (1) ➔ (2), thereby the temperature of the exhaust air falls and the humidity ratio increases.

(10) ➔ (11) The exhaust air is blown to the environment by means of an air fan.

To adapt such a standard model to other climate conditions, several measures can be taken, for example adding a cooling coil behind the heat recovery wheel on the supply side, adding two cooling coils (one before the sorption wheel and a second behind the humidifier), or implementation of a second sorption wheel with a cooling coil before and a second cooling coil behind the heat recovery wheel [17]. Also, combinations of sorption wheels and enthalpy wheels can be used to obtain an increased reduction of the humidity ratio of ambient air.

One of the disadvantages of conventional evaporative sorptive cooling systems which use sorptive wheels to dehumidify the fresh air is that the air is not only dehumidified but also heats up. The released sorption heat leads to a temperature increase of the desiccant material which leads to a reduced dehumidification potential. This is due to the adiabatic characteristic of the sorption process and the fact that the sorption process is not cooled. Recent developments aim at cooling the sorption process in desiccant systems using solid sorptive materials. An example is the so-called ECOS process which has been developed at the Fraunhofer-Institute for Solar Energy Systems ISE in Freiburg/Germany. The acronym stands for indirect Evaporative COoling counterflow heat exchanger with Sorption. This system is particularly intended for climates with high ambient air humidity (e.g., tropical climates). The design of the ECOS process results in a far higher dehumidification potential in comparison to conventional systems [16].

The ECOS system bases on crossflow or counterflow air-to-air heat exchanger technology; see scheme in Fig. 20.

Process steps on supply air side:

(1) Fresh, warm, and moist air enters the system from outside.

(1) ➔ (2) The air flows through a heat exchanger to be cooled down and is dehumidified simultaneously by means of sorptive coated heat exchanger channels (green line in Fig. 20, top).

(2) ➔ (3) The supply air stream can optionally be further cooled down to meet specific load demands.

(3) ➔ (4) Air temperature and humidity of the air increase due to internal loads.

Process steps on return air side:

(4) ➔ (5) The return air is humidified and cools down.

(5) ➔ (6) The cool and humidified return air flows through the cooling channels (orange line in Fig. 20, top) at return air side of the heat exchanger which are physically separated but in close thermal contact to the supply side channels. In the cooling channels, the indirect evaporative cooling is obtained by a continuous humidification process ensuring a high heat exchange potential. The return air stream is humidified to close-to-saturated conditions during this process.

As soon as the sorptive material is enriched with water, the process is stopped. The heat exchanger is

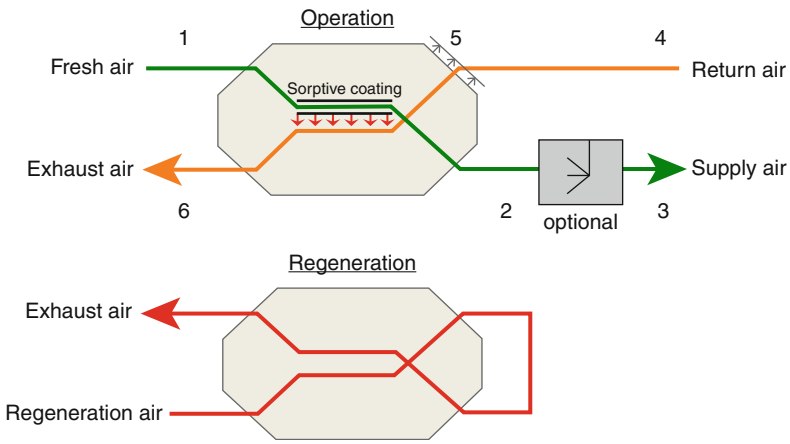

Solar Cooling Systems. Figure 20
Scheme of the ECOS (Evaporative COoling counterflow heat exchanger with Sorption) system and process steps; the lower part shows one possible flow pattern for regeneration

regenerated (possible flow pattern shown in the red line in Fig. 20, bottom). In the regeneration phase, the water vapor load of the sorbent material is released to the environment by means of a hot air stream (60–95°C). Thereby, the heat exchanger heats up. After the regeneration, a precooling phase is performed to lower the temperature of the heat exchanger before it is again used for conditioning of fresh air.

Figure 21 shows the corresponding T-x-diagram of the ECOS process.

A complete air-conditioning system consists of two sorptive heat exchangers which operate periodically creating a quasi-continuous air-conditioning process. While one heat exchanger is used in air-conditioning operation mode, the other one is regenerated and precooled. After one operation phase, the functions are changed. Optionally, a humidifier can be installed on the supply air side in order to exploit the potential for direct evaporative cooling [16, 37, 38].

Open Liquid Desiccant Systems

Though liquid desiccants have been successfully working since a long time, there are only a few installations nowadays. Dr. Russell Bichowsky from Frigidaire Division of General Motors had used solutions of lithium chloride to dry air in the 1930s and sold the technology to Surface Combustion Corporation (SCC). A residential liquid-desiccant dehumidifier was developed by SCC, but no market introduction followed. Simultaneously, the Niagara Blower Company introduced a liquid desiccant technology that used glycol solutions to prevent frost formation on low-temperature evaporators. However, the development of air-conditioning systems went in another direction due to low prices for electricity and because, at those times, sustainability was not an issue. Nevertheless, in recent years, some liquid desiccant systems for comfort air-conditioning have been developed, have been tested in pilot installations and are now available on the market [31].

The design, process and utilized working fluids of open desiccative air-conditioning systems based on liquid sorbents (LDAC) differ from DEC systems. A schematic drawing of a possible general type of a desiccant system using liquid desiccant is shown in Fig. 22. Liquid desiccant technology uses absorption to dehumidify an air stream. The absorption process can be either cooled or operated adiabatic.

Desiccants have to be nonvolatile if they are used in air-conditioning systems. For example, halide salt solutions meet this requirement but, at the same time, are corrosive. The corrosiveness can be managed by either working with very low desiccant flow rates or using noncorrosive materials (e.g., based on polymers). In current systems typically hygroscopic aqueous salt solutions, for example calcium chloride/water, lithium bromide/water, or lithium chloride/water are used. A great advantage of such liquid desiccants is the

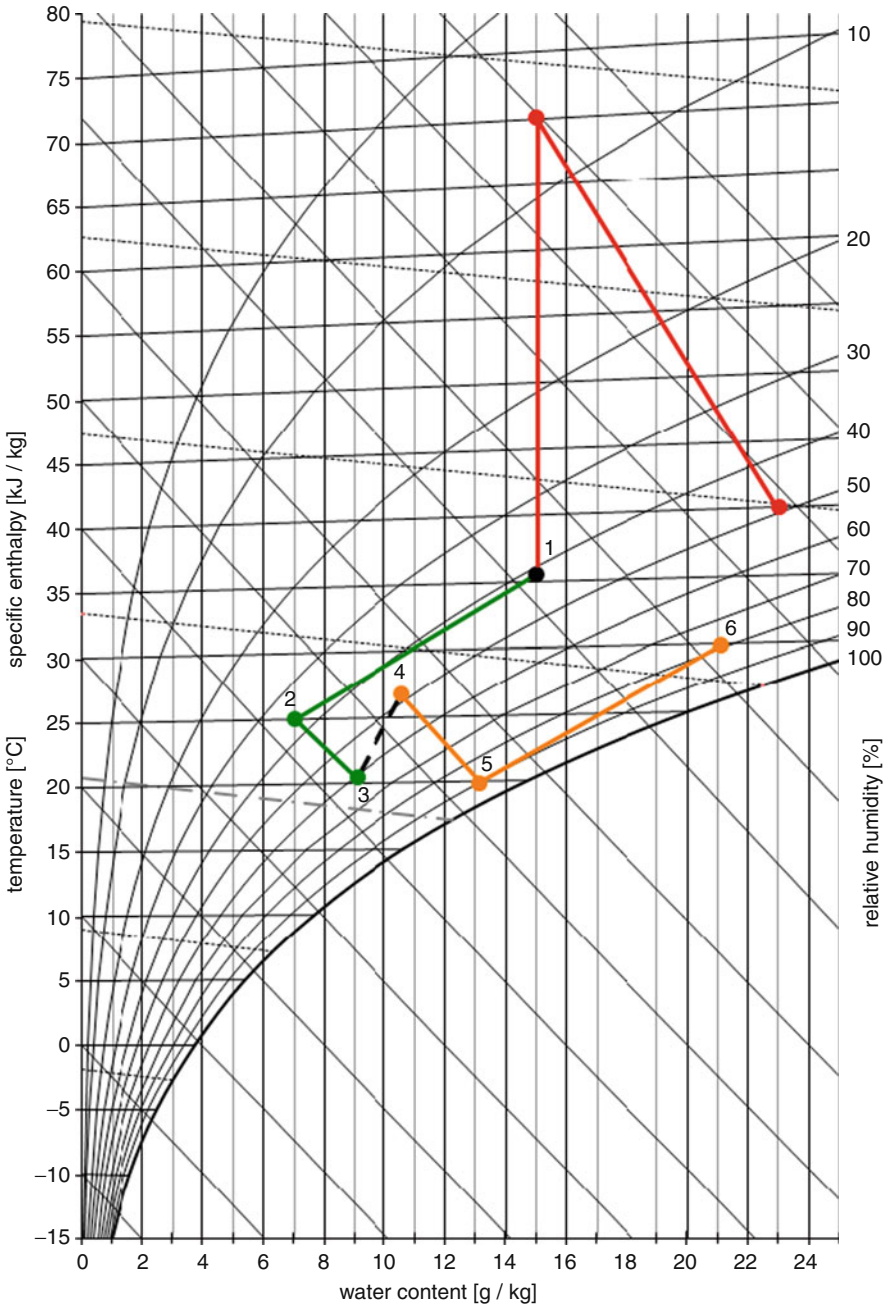

Solar Cooling Systems. Figure 21
T-x-diagram of the ECOS (Evaporative COoling counter-flow heat exchanger with Sorption) process

much higher energy storage capacity compared to solid materials.

The (warm and humid) fresh air enters the *absorption* chamber. The chamber in which the absorption process of LDAC systems takes places is realized either in a packed bed absorber filled with structured material (similar to the corrugated filling that might be used in a cooling tower), in other enhanced mass transfer surface or packing units, or in plate heat exchangers with a falling film regime of the liquid desiccant. Important

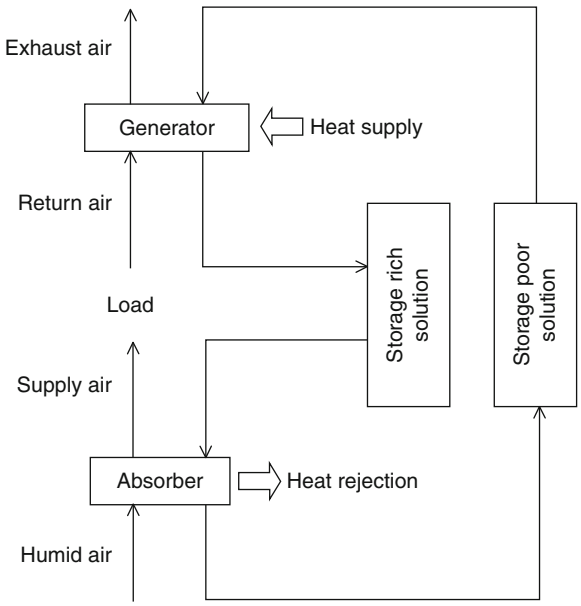

Solar Cooling Systems. Figure 22
Scheme of a desiccant air-conditioning system using liquid desiccant

is to ensure optimal heat and mass transfer between desiccant solution and air. The liquid desiccant is usually sprayed into the absorber chamber. The flow rate of the desiccant must be high enough to ensure complete wetting of the fill's surface [32]. The fresh air flows over the wet surface of the fill. When the desiccant absorbs water vapor from the air, heat will be released and the desiccant's temperature increases. The released heat includes the chemical heat of mixing between the desiccant and water, in addition to the vapor–liquid latent heat for the water vapor [33]. The dehumidification capacity depends both on the temperature of the absorption process and the concentration ratio of the desiccant solution which is sprayed in. In adiabatic systems a high flow rate of the desiccant limits its temperature rise to a few degrees. Cooled systems comprise a heat exchanger device to control the temperature of the process and therefore can be operated with a much lower flow rate of desiccant. The air leaves the absorption chamber, dehumidified and cooled, and can directly be used to condition an indoor space (e.g., rooms or production halls) [9].

In the desorber (generator) the water is driven off the desiccant, for example by means of an external hot water circuit. Because liquid desiccants can be regenerated at temperatures below 80°C [22], LDAC is suitable for using solar energy in combination with flat-plate solar thermal collectors as driving source. The desiccant may first be heated to raise its equilibrium vapor pressure. The desiccant is then sprayed over a bed of random fill (e.g., Raschig rings) or enters the distribution manifold to flow along microstructured plates in a plate exchanger design. Flow rates have again to be sufficient high to ensure complete wetting of the media when using filled bed design, but may be lower in a plate exchanger design in order to achieve a large concentration spread in a single step. The hot desiccant desorbs water to air that flows through the bed. Meaningfully, this air might be the return air of the air-conditioning. The moisture-laden air is typically exhausted to the ambient atmosphere. The reconcentrated rich solution functions as thermochemical storage and thus allows operation of regeneration and air-conditioning at different times.

Since the 1980s several studies on LDAC systems have been launched. In the context of these developments, the Bavarian Center of Applied Energy Research (ZAE Bayern e.V.) developed an open desiccant system aiming at a highly efficient air dehumidification in which the desiccant, 40%-concentrated LiCl/water-solution, is used not only as working fluid but also as high-capacity energy storage. In the following these developments and important thermodynamic backgrounds are explained exemplarily in brief. For more detailed descriptions, please see [22] and [23].

The main component of this development was an absorptive air dehumidifier performing a cooled absorption process to guarantee a low water vapor pressure of the desiccant and to be capable of distributing the solution flow as low as 0.2 liters per hour and m^2 (lh^{-1} m^{-2}). The higher the mass ratio between to-be-treated fresh air and aqueous desiccant solution, the higher is the concentration difference between the solution entering and leaving the absorption chamber and the higher is the achievable storage capacity. The small needed amount of desiccant solution leads to the necessary concentration difference because of its significant dilution.

The storage capacity for dehumidification enthalpy per volume diluted salt is given by Eq. 6:

$$SC = \frac{M_{air} \cdot \Delta Y \cdot \Delta h_{ev}}{V_{dil.sol}} = \Delta X \cdot \Delta h_{ev} \cdot C_{dil.sol.} \cdot \rho_{dil.sol.} \quad (6)$$

with the mass of air M_{air} [kg], the air dehumidification ΔY as the difference of the humidity ratio at the air inlet and outlet [kg/kg], the enthalpy of evaporation/condensation of pure water at T_o, Δh_{ev} [kJ/kg], the volume of the diluted solution $V_{dil.sol}$, the difference of the water content at the solution outlet and inlet of the absorption chamber ΔX, the density of the diluted solution $\rho_{dil.sol}$, and the concentration of the diluted solution $C_{dil.sol.}$.

The low solution flow and the need to spread it uniformly across the surface challenge the design of the exchanger. The air dehumidifier was designed as a flat-plate exchanger with a hydrophobic polypropylene surface to prevent corrosion. Its surface was covered by a fleece to spread the solution by capillary forces. To strengthen this effect, extra spacers between the exchanger plates caused turbulence within the through-flowing air stream.

Though a satisfactory air dehumidification and a high storage capacity could be achieved the target values were not achieved. One problem was the exchanger surface which was not managed to be wetted uniformly completely and which showed defects in its material and design. Therefore, the developments were launched with respect to alternative surfaces and solution distribution systems [22].

Recent work on advanced liquid desiccant cooling systems has been performed by various research teams in the world, for example University of Adelaide in Australia, Queens University in Canada, and Kassel University in Germany. However, only few pilot installations have been put into operation, many of them using technology from the German manufacturer Menerga or the US company AIL Research. Please see [2, 24–27, 36] for further information.

In the near future, liquid desiccant systems may play an important role in air-conditioning due to several promising advantages. LDAC is well suited for latent cooling, its electrical demand is low, and it works with low temperature–driving heat which, for example, can be supplied by low-cost solar collectors. A solar LDAC system can "operate at night" as the concentrated desiccant serves as cold storage. Also, in CHPC systems in which heat is available at a lower temperature, LDAC is worth considering [32].

Subsystems and Further Equipment Components

Besides the indicative components a solar or solar-assisted cooling system comprises further equipment components, for example the heat source and heat rejection systems. These subsystems contribute essentially to the energy performance, see the following section "Energy and Cost Performance", and for this reason are described briefly here.

The overall efficiency of a solar-assisted cooling system depends on the efficiency of each of its subcomponents and their interaction. A major component is the solar collector which yields the main part of the needed driving heat of the thermally driven cooling/air-conditioning system. Several different types of solar collectors can be used in solar cooling and air-conditioning systems. These will not be discussed here but are described in detail in the specific chapters, "▶ Solar Collectors, non-concentrating," "▶ Linear Fresnel Collectors," and "▶ Parabolic Trough Solar Technology." Further introductive and useful information is given in the section "Physical Principles" where the relation between different solar collector technologies and performance of the cooling system is discussed.

All cooling processes produce heat, for example sorption heat and heat released by the condensation process. This heat has to be rejected by heat rejection equipment. Generally, the lower the temperature of heat rejection, the lower is the needed driving temperature (see section "Physical Principles"). Lower driving temperatures lead to a higher efficiency of the solar collector and thus lead to overall lower cost per produced unit of cold. Especially for thermally driven systems, the effectiveness of the heat rejection plant is of high importance since it has a large influence on the effectiveness of the thermally driven system.

Any recooling unit needs a heat sink where the heat can be rejected. This heat sink can be either ambient air, the ground, natural water resources, or another process which is able to make use of the low-temperature heat. The majority of recooling units in practical applications make use of the ambient air; the most important technical solutions for systems using ambient air are described first and are summarized in Table 3.

Solar Cooling Systems. Table 3 Overview on common cooling towers [19]

System	Wet cooling tower	Dry cooling tower	Dry cooling tower with optional evaporative cooling	Hybrid cooling tower
Principle	Direct or indirect evaporative cooling of the refrigerant	Indirect sensible cooling by heat transfer to ambient air	Dry cooling tower with optional spraying humidification at the air side	Wet cooling tower which enables dry recooling operation in case the ambient air is at low temperature level
Water consumption	High	None	Low to medium	Medium
Advantages	High thermal efficiency, low temperatures, comparatively low electricity consumption	No problems with hygiene issues	Possible controlling of recooling temperature, reduced water consumption compared to wet cooling tower	Prevents high recooling temperature in case the ambient air is at high temperature level
Disadvantages	High maintenance requirements, high effort to avoid formation of legionellae	Comparative high electricity consumption, large construction volume	Higher complexity and maintenance compared to dry cooling towers	Higher electricity consumption compared to wet cooling towers

Wet Recooling (Open and Closed) Wet recooling includes open and closed cooling towers. The process bases on evaporative cooling, whereby in open systems the cooling water comes in direct contact with the cooling agent (air), while in closed systems the cooling water does not come in contact with the cooling agent but flows through a closed heat exchanger which is sprayed by means of a secondary circuit.

In principle, an open wet cooling tower works as follows: water exits spray manifolds, falls under the influence of gravity and takes outside air with it. While in direct contact with the air, some of the water evaporates and dissipates evaporation heat. The heat is extracted from the water stream by the air, thereby cooling it. As this design is ineffective for larger heat rejection rates, often *mechanical draft* towers are utilized which use fans or blowers to cause air to flow upward against the falling water. Towers which use an external centrifugal fan to realize the counterflow are called *forced-draft* cooling towers. The major problem in this application is that humid air can be drawn back through the cooling tower which results in a reduced performance. Another problem is the possible fan blade freezing, therefore forced draft towers are not often used under northern climate conditions. Besides forced-draft towers, there are *induced-draft* towers which use a fan to draw air through a tower fill. The back-drawing of humid air (short-circuiting) is avoided since the exit velocities are higher and the exit air plume does not mix with the air at the fan inlet. The freezing is avoided since the fan is located in the warm exit airstream. As result of the cooling tower operation, the enthalpy of the water stream decreases due to heat transfer to the cooler air and, to a minor part, due to the evaporation of water.

To design an appropriate cooling tower, the following parameters have to be considered: the heat rejection rate which is set by the condenser load of the chiller system at design cooling load conditions. The tower size (volume) increases proportionally with the load. The water-flow rate is determined by the condenser specifications and its temperature range is determined by the heat rejection rate and the tower size. The tower water outlet temperature is mostly given by recommendation of the chiller manufacturers [28].

Closed systems comprise an external and internal fluid circuit. In the external circuit, water is sprayed on tubes of a coil bundle and is exposed to the atmosphere. In the internal circuit the fluid to be cooled flows inside the tubes. Heat is transferred from the fluid flowing in the tubes to the water (drops) and to the air (by an evaporative cooling process). The air is released to the atmosphere. Compared to open cooling towers, closed ones show less efficient operation, increased electricity consumption and higher investment costs. However, some chillers require a closed recooling water loop and in such cases closed cooling towers are required. In a closed cooling tower transfer of oxygen or pollutants in the recooling cycle is avoided.

Dry Recooling (Closed) Dry air coolers transfer sensible heat to ambient air: the refrigerant to be cooled flows through a water/air heat exchanger device, but the heat exchange happens by means of convection and without evaporation. The heat is released to the ambient air.

Some dry cooling towers provide optional spraying humidification at the air side which results in cooling of the incoming air. This option can be employed for instance in cases of too high dry-bulb temperature of the ambient air for a direct operation of the recooling cycle.

Hybrid Recooling Hybrid recooling is a combination of wet and dry recooling. This provides a possible switch between latent and sensible cooling according to actual recooling power needs and temperature conditions.

Geothermal Recooling Geothermal recooling is realized by geothermal probes (vertical heat exchangers) or ground collectors (horizontal heat exchangers), whereby normally brine is used to transfer heat. In temperate climates the same system can be used as low-temperature heat source of a heat pump for heating application.

Recooling by Natural Water Resources Recooling by means of natural water resources like ground-, sea-, or river water is restricted by a limited heating permitted by law. Of course, this only works if natural water resources are geographically conveniently situated.

Recooling by a Process Which Uses Low-Temperature Heat The heat which has to be removed from the cooling system can be further used for any other process which is able to make use of low-temperature heat. An example is the heating of swimming pools or preheating of hot water, for example for showers in a swimming pool or a hotel. However, such solution depends on a suitable coincidence in terms of power and availability of waste heat from the cooling system and corresponding heating loads of the potential processes.

Further components which may be part of solar-assisted cooling/air-conditioning systems are backup devices for cold and/or heat, storage devices, several water and coolant supply subsystems, hydraulics and regulation devices, pumps, fans, filter systems, noise attenuators, and safety devices. For wider explanations please see [15, 24]. If integrated, these components also have an impact on the energy performance. For example, a buffer storage device which is added at hot water side stores surplus heat of the solar system and allows higher solar fraction. The buffer storage device can be used to support the heating or domestic water supply in phases without cooling demand. On the other hand, integration of a storage device leads to increased thermal losses. Therefore, a careful dimensioning is necessary in order to identify the best solution, that is, the solution which leads to highest energy savings compared to standard solutions. A buffer storage which is implemented at cold water side improves the operation of the cooling units. At sites with low- and high-load phases, such cold buffer storage allows continuous operation of the cold production. On the other hand, fluctuating temperatures of the cold water caused by varying solar driving energy are compensated which otherwise might lead to control problems.

An overall solar-assisted cooling/air-conditioning system is shown in Fig. 23. This scheme comprises an overall system with all possible components including a closed cycle thermally driven chiller and an open sorptive system. In reality, most systems will be composed only by parts of this comprehensive overall system.

Energy and Cost Performance

For an overall energetic and economic assessment of solar cooling/air-conditioning systems, several aspects

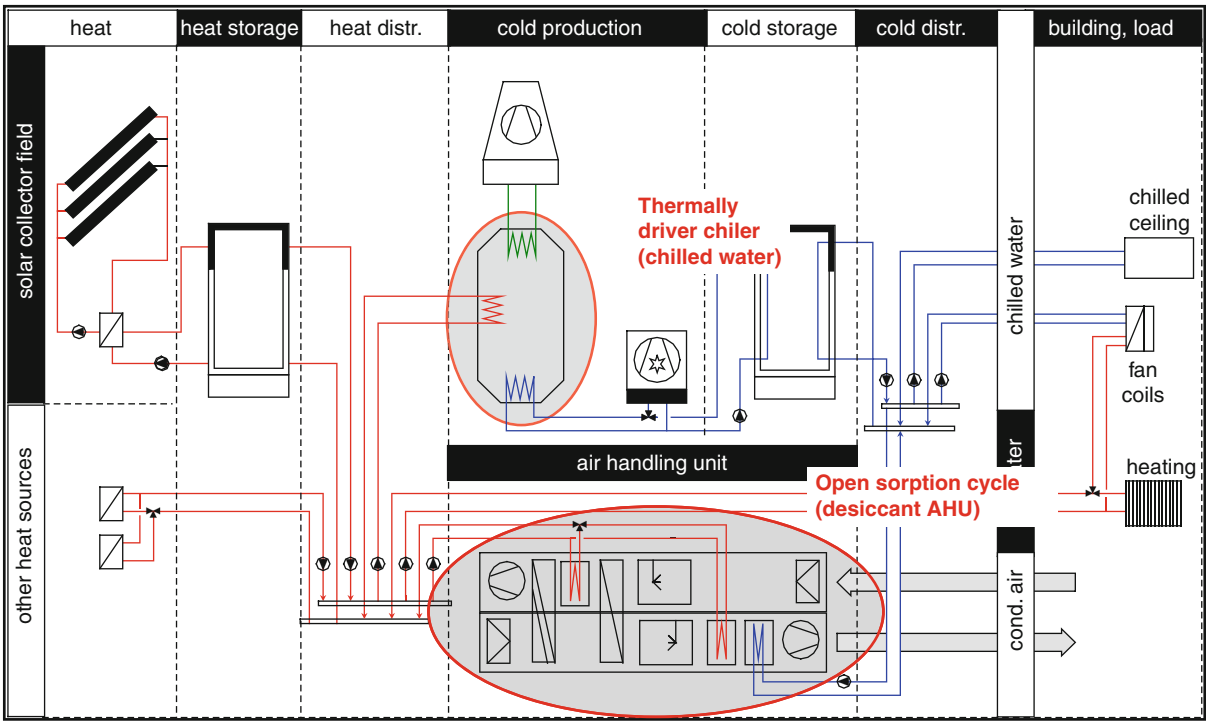

Solar Cooling Systems. Figure 23

Overall solar-assisted air-conditioning system with all possible components including a closed cycle thermally driven chiller and an open sorptive system

have to be taken into account: the energy saving in comparison to a conventional reference system, the first cost of the installation, and the cost difference in comparison to the conventional system. For the latter, different cost functions can be defined. However, a fair comparison has to include the complete life cycle of either system in order to provide a full picture.

Overall, there is no balance equation or value which describes a cooling system comprising all possible parameters and providing the "best" solution for a certain application "all-in-one" or "at the touch of a button." One possible approach in a design study is to begin with a sensitivity analysis based on a simulation of an annual system performance which covers an entire "performance period." Sometimes, these annual figures are called seasonal figures, for example, cooling periods do not cover a whole year but only few months (the longer the summer months of a site, the longer this cooling period lasts). The impact of the variation of important system variables on goal functions such as energy saving or life cycle costs are assessed and linked. The results can form a useful basis for further considerations and appraisals [7].

In the first part of the section "Energy and Cost Performance," the primary energy efficiency of a typical solar-assisted cooling system is investigated by performing a sensitivity analysis. In this section, also basic equations are introduced which are used to describe the energy performance of solar cooling systems. In the second part, an economic performance is taken into consideration, and results of a recent simulation study are presented.

Energy Balance

To analyze the energy balance of a solar-assisted cooling system, a scheme as shown in Fig. 24 is assumed which consists of a thermally driven chiller that receives its driving heat either from the solar collector/storage system or from the backup heat source.

The energy which is provided by the installed solar collector system and which is used for cooling purposes

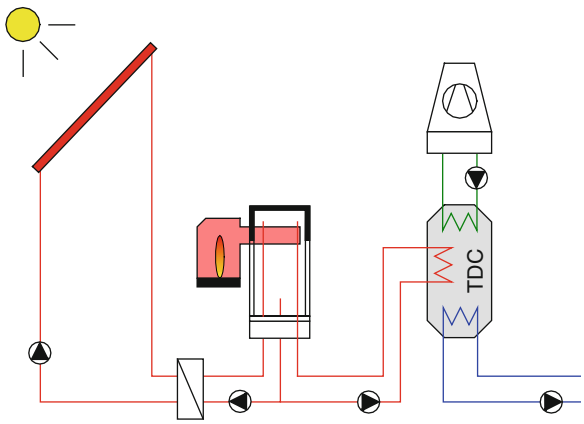

Solar Cooling Systems. Figure 24
Scheme of a solar thermally driven cooling system with a fossil-fuelled backup heat source (TDC = thermally driven chiller)

is the so-called useful solar heat of a cooling system. It depends on several parameters like weather and climatic conditions, tilt angles, control concept, or failure rate during operation and construction of the solar collector. The annual solar useful heat, $Q_{sol,use}$, for a cooling application with integrated secondary heat source is given by Eq. 7:

$$Q_{sol,use} = Q_{total} - Q_{backup} \tag{7}$$

whereby Q_{total} is the total annual heat invested in the thermally driven cooling system, and Q_{backup} is the annual heat from a secondary heat source, also called backup heat source.

The solar fraction SF_{cool} is the amount of heat requirements for cooling that can be met by a solar energy source, see Eq. 8:

$$SF_{cool} = 1 - \frac{Q_{backup}}{Q_{total}}. \tag{8}$$

The solar fraction thus ranges from zero for no solar energy utilization to 1 for all energy provided by solar.

Saving (fossil) primary energy is the main reason for the application of solar or solar-assisted cooling systems.

The total primary energy consumed by a solar-driven system PE_{sol} is the sum of the primary energy demand of all fossil-fuelled sources of the system PE_{fuel} and the primary energy demand of all components that consume electricity PE_{el}, see Eq. 9:

$$PE_{sol} = PE_{fuel} + PE_{el} = \frac{E_{fuel}}{\eta_{PE,fuel}} + \frac{E_{el}}{\eta_{el,grid}}. \tag{9}$$

E_{fuel} is the secondary energy provided by fuel. $\eta_{PE,fuel}$ describes the primary energy efficiency of the fuel used to operate the backup heat source. As example, for natural gas the primary energy factor is less than 1 because of grid losses and the embodied primary energy for keeping the pressure of the natural gas network. E_{el} is the electricity needed to operate the system, for example, the electricity needed to operate circulation pumps, the recooling system and the system control. $\eta_{el,grid}$ is the efficiency of the electric network system which depends on the structure of the electricity production and network of each country (for instance, for the EU, the average value of $\eta_{el,grid}$ is about 40%).

When looking at the system energy performance in detail, all the auxiliary energy consumers such as pumps, fans, control units, etc., have to be taken into consideration. The main subsystems which consume primary energy are the backup heat system (e.g., gas boiler), the solar subsystem, the thermally driven chiller itself and the heat rejection subsystem. Electricity is mainly consumed for the collector cycle, the thermally driven cooling machine itself (e.g., refrigerant pump, control unit) and the heat rejection device (cooling tower, cooling cycle pump). The corresponding equations of these subsystems are introduced in the following.

The primary energy demand of the fossil-fuelled backup heat source is given by Eq. 10:

$$PE_{backup} = \frac{Q_{cold}}{COP_{annual}} \cdot \frac{1 - SF_{cool}}{\eta_{backup} \cdot \eta_{PE,fuel}} \tag{10}$$

where COP_{annual} describes the average thermal COP of the system considered over a 1-year period, and η_{backup} is the energy efficiency of the backup heat system.

The primary energy of the electricity consumption of the solar collector subsystem, mainly pumps, is given by Eq. 11:

$$PE_{coll} = \frac{Q_{cold}}{COP_{annual}} \cdot \frac{SF_{cool} \cdot f_{el,sol}}{\eta_{PE,grid}}, \tag{11}$$

with the electric efficiency factor of solar heat generation

$$f_{el,sol} = \frac{E_{el,sol}}{Q_{sol}}. \tag{12}$$

$E_{el,sol}$ is the annual electricity consumption to operate the solar system and Q_{sol} denotes the annual useful solar gains for cooling.

The primary energy consumption of the thermally driven chiller includes also the electricity to operate the pump of the driving heat cycle and is defined by Eq. 13:

$$PE_{TDC} = \frac{Q_{cold} \cdot f_{el,TDC}}{\eta_{PE,grid}}, \tag{13}$$

with the electric efficiency factor for the thermally driven chiller

$$f_{el,TDC} = \frac{E_{el,TDC}}{Q_{cold}}. \tag{14}$$

$E_{el,TDC}$ is the annual electricity consumption to operate the thermally driven chiller (for instance, the solution and refrigerant pump in an absorption chiller).

The primary energy consumption of the heat rejection subsystem, including the cooling cycle pump, is given by Eq. 15:

$$PE_{reject} = \frac{Q_{cold}}{COP_{annual}} \cdot \frac{f_{el,reject} \cdot \left(1 + \frac{1}{COP_{annual}}\right)}{\eta_{PE,grid}}, \tag{15}$$

with the annual electric efficiency factor for the heat rejection device

$$f_{el,reject} = \frac{E_{el,reject}}{Q_{reject}}. \tag{16}$$

$E_{el,reject}$ is the annual electricity consumption to operate the heat rejection device and Q_{reject} is the annual rejected heat given by the sum of the driving heat of the thermally driven chiller, Q_{heat}, and the produced cold, Q_{cold}, see Eq. 17:

$$Q_{reject} = Q_{heat} + Q_{cold} = Q_{heat} \cdot (1 + COP_{annual}) \tag{17}$$

The summation of the equations for the different subsystems leads to a formula for PE_{sol}, see Eq. 18:

$$PE_{sol} = \frac{Q_{cold}}{COP_{annual}} \cdot \left(\frac{1 - SF_{cool}}{\eta_{backup} \cdot \eta_{PE,fuel}} + \frac{SF_{cool} \cdot f_{el,sol}}{\eta_{PE,grid}} + \frac{COP_{annual} \cdot f_{el,TDC}}{\eta_{PE,grid}} + \frac{f_{el,reject} \cdot (1 + COP_{annual})}{\eta_{PE,grid}} \right) \tag{18}$$

Implementation of a solar or solar-assisted cooling installation only makes sense if there is a considerable lowering of primary energy consumption compared to a conventional system. To this aim, it is suitable to calculate both a conventional system which is able to accomplish the same task as the solar cooling system but with no use of solar energy [13] and a solar system of which the primary energy savings and cost for saved primary energy shall be determined.

The efficiency of a conventional system, for example an electric chiller based on vapor compression, is described with the Energy Efficiency Ratio EER, defined as the useful cold Q_{cold} per supply energy W (in most cases, W is in form of electricity, and the chiller is composed of both the compressor cycle and the electric motor to run the compressor), see Eq. 19:

$$EER = \frac{Q_{cold}}{W} \tag{19}$$

The primary energy consumption of the reference system, PE_{ref}, which is completely based on electricity operation, is given by Eq. 20:

$$PE_{ref} = \frac{Q_{cold}}{EER_{annual} \cdot \eta_{el,grid}} \tag{20}$$

with EER_{annual} describing the average EER of the conventional driven chiller of an overall considered cooling period.

The annual primary energy savings PE_{sav} are given by:

$$PE_{sav} = PE_{ref} - PE_{sol} \tag{21}$$

and the fractional primary energy savings are defined as:

$$f_{PE,sav} = 1 - \frac{PE_{sol}}{PE_{ref}} = \frac{PE_{sav}}{PE_{ref}} \tag{22}$$

In the following, the above defined equations are used to derive some basic insights in the primary energy performance of solar thermally driven cooling systems. For this purpose, a sensitivity analysis is carried out for which a set of standard parameters is used, see the values given in Table 4.

The main results which are provided by such an analysis are displayed graphically, see Figs. 25, 26 and 27.

As Fig. 25 shows, the solar fraction for cooling has a strong influence on the fractional primary energy

Solar Cooling Systems. Table 4 Set of standard values for the various parameters in a sensitivity analysis

Parameter	Meaning	Standard value
$\eta_{PE,fuel}$	Primary energy efficiency of the fuel at application site	0.95
η_{backup}	Energy efficiency of backup heat source	0.9
SF_{cool}	Solar fraction for cooling (i.e., for driving heat of the TDC)	0.9
$\eta_{PE,grid}$	Primary energy efficiency of electric grid	0.4
EER_{annual}	Annual efficiency of the reference cooling system, here: air-cooled compression chiller	3.0
COP_{annual}	Annual thermal COP of the thermally driven chiller	0.7
$f_{el,sol}$	Electric efficiency factor of the solar subsystem, kWh_{el}/kWh_{th}	0.02
$f_{el,TDC}$	Electric efficiency factor of the TDC subsystem, kWh_{el}/kWh_{cold}	0.02
$f_{el,reject}$	Electric efficiency factor of the heat rejection subsystem, kWh_{el}/kWh_{reject}	0.03

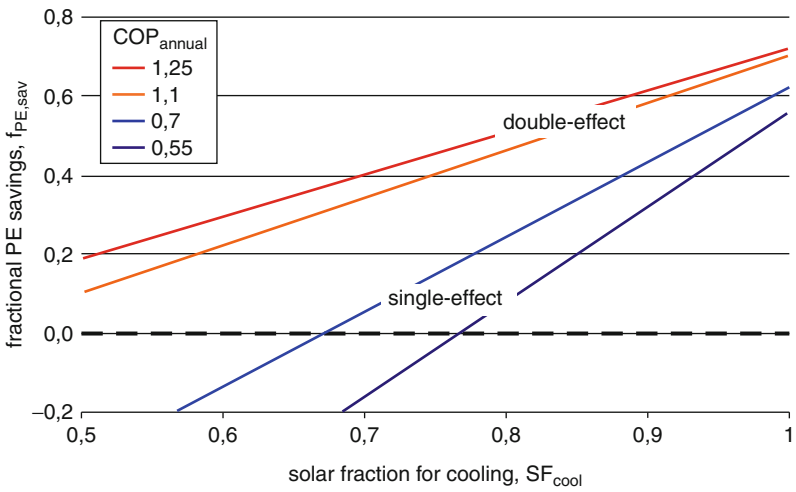

Solar Cooling Systems. Figure 25
Fractional primary energy savings as a function of the solar fraction for cooling for different values of the COP of the thermally driven chiller

savings of solar cooling systems. Positive values on the y-axis indicate a positive fractional primary energy saving and thus a lower primary energy consumption of the solar-driven system when compared to a reference solution. In particular, for systems with a low seasonal COP of the thermally driven chiller, the effect is significant and a too low solar fraction can even lead to higher primary energy consumption than for the conventional reference, negative values of the $f_{PE,sav}$. The reason is that a significant amount of cooling is produced by converting primary energy of a fossil fuel into cold with a low COP of the thermally driven cooling device and thus with a low overall conversion rate. Figure 25 also shows that an operation of the thermally driven cooling system which is completely driven by solar energy, that means SF_{cool} = 1, leads to significant primary energy savings. This corresponds either to a system where cooling is only provided if sufficient solar energy (or energy from a solar-driven heat buffer) is available or to a system

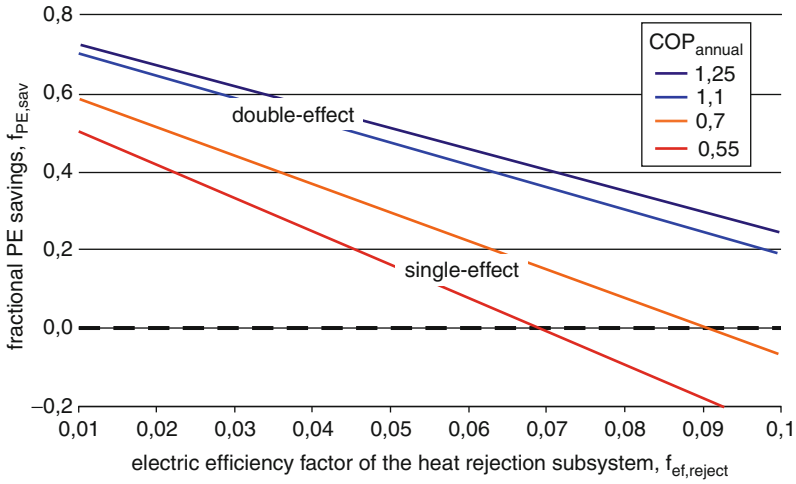

Solar Cooling Systems. Figure 26
Fractional primary energy savings as a function of the electric efficiency factor of the heat rejection subsystem for different values of the COP of the thermally driven chiller

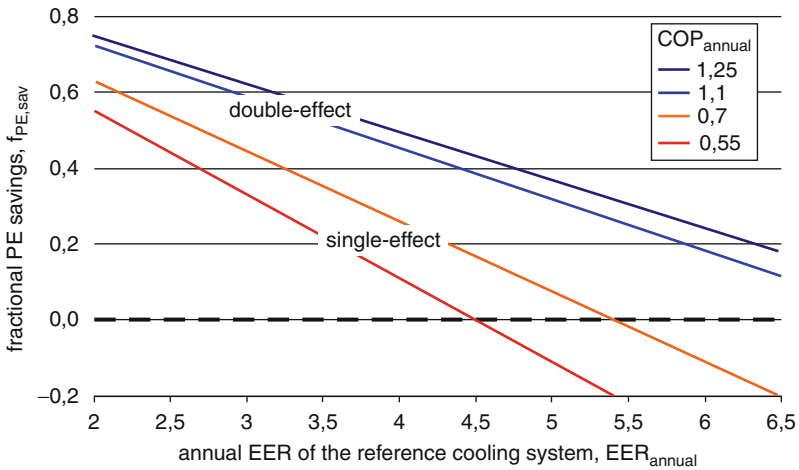

Solar Cooling Systems. Figure 27
Fractional primary energy savings as a function of the COP of the reference chiller for different values of the COP of the thermally driven chiller

with a conventional backup compression chiller that provides cooling in case of absence of solar thermally driven cooling. However, such system requires that an electrically driven compression system is installed beside the thermally driven cooling device.

Another important influence is due to the efficiency of the heat rejection system, as can be seen from Fig. 26. The amount of electricity needed for heat rejection depends strongly on the heat rejection technology which is used. The amount of electricity for heat rejection can be kept low by using highly efficient components, for example highly efficient pumps and fans, and by employing speed-controlled components which can be operated at reduced capacity under part-load conditions.

Finally, the fractional primary energy savings of course depend on the EER of the conventional reference system. Values of decentralized small room

air-conditioners typically range from 2 to 2.5. Values of large centralized compression water chillers using wet cooling towers can be up to 5. The influence of this parameter and the fractional primary energy savings are depicted in Fig. 27.

Economical Assessment

One of the most important and interesting questions is the one of the cost effectiveness of any optional system. A cost calculation bases on the annual energy balance of a solar system, see section "Energy Balance." The calculation has to complete the balancing of the whole system with an economical consideration and aims especially at the cost of saved primary energy. As in the case of the primary energy balancing, this cost calculation is performed for both a solar system and a conventional reference system which covers the same loads. Obtained results are compared to each other.

The cost of saved primary energy $C_{PE,sav}$ is defined by Eq. 23:

$$C_{PE,sav} = \frac{C_{annual,sol} - C_{annual,ref}}{PE_{sav}}. \tag{23}$$

$C_{annual,\ sol}$ corresponds to the sum of all annual costs of the solar system; $C_{annual,\ ref}$ relates to the sum of all annual costs of the conventional reference system. A negative value of $C_{PE,sav}$ means that the system amortizes within its lifetime, at least as long as PE_{sav} is positive, that is, the solar-driven system consumes less primary energy as the conventional reference. The $C_{PE,sav}$ turns out as a very useful figure of merit as it combines energy and cost performance and allows comparison of different systems on the basis of a single parameter. But it makes only sense as long as the total annual cost of an alternative solution leads to higher total annual cost than the conventional reference. Only in such case the relation between expenditure – higher annual cost – can be related to a benefit – saving of primary energy. Then minimizing of $C_{PE,sav}$ can contribute to make a decision between different possible solutions.

In case the solar solution leads to lower total annual cost and saves primary energy, a goal function, F, which combines economic- and energy-related parameters has to be introduced. A possible, of course arbitrary, goal function would be the sum of the fractional cost saving $f_{cost,sav}$, defined as

$$f_{\cos t,sav} = \frac{C_{annual,ref} - C_{annual,sol}}{C_{annual,ref}} \tag{24}$$

and the fractional primary energy saving $f_{PE,sav}$, called F_1:

$$F_1 = \frac{C_{annual,ref} - C_{annual,sol}}{C_{annual,ref}} + \frac{PE_{annual,ref} - PE_{annual,sol}}{PE_{annual,ref}} = f_{cost,sav} + f_{PE,sav} \tag{25}$$

Another way to describe more distinctly the difference between several solutions is achieved by replacing the summation of Eq. 25 through a multiplication of the fractional cost saving and fractional primary energy saving. This goal function F_2 is defined as:

$$F_2 = \frac{C_{annual,ref} - C_{annual,sol}}{C_{annual,ref}} * \frac{PE_{annual,ref} - PE_{annual,sol}}{PE_{annual,ref}} = f_{\cos t,sav} * f_{PE,sav} \tag{26}$$

Although, at first sight, Eqs. 23, 24, 25 and 26 seem to be simple, they are based on a complex interaction of many different aspects. All costs of a system's design, construction and operation phase for the whole life cycle have to be involved and put in an annualized way. This includes, for example, the total investment costs, financing costs, costs of the energy consumption of supporting systems like pumps or cooling towers, and other costs such as for maintenance. For the energy and cost calculation, also a total annual energy balance has to be made including cooling, heating and hot water production (depending on all purposes and functions of the specific system) since the solar collector field can be used for all these applications.

Due to its complexity, the calculation of the annual energy balance is usually done by a computational simulation program, for example TRNSYS [47]. The different programs may differ but operate on similar principles. To get an idea of the considerations and conditions which are behind such a simulation program, a short overview of its sequences is given below. The applied methodology was developed within the SACE project. To gain a more detailed insight, [15] and [44] are recommended.

At the very beginning of the calculation, two site-specific time series are generated with each series covering a period of a year; typically, hourly average values for all variables are used.

The first time series includes the hourly values of total irradiation on the solar collector of the solar system which is under consideration and ambient air temperatures. These values influence the solar gains of a certain system with specific conditions. They can, for instance, be obtained by the national weather services.

The second time series displays the cooling and heating demand of the building which loads have to be covered and are the same for solar and reference system. Such time series can be computed by use of dynamic (multizone) building simulation.

These data series form the application-specific basis of the calculation performance and have to be created for each individual project. Combined with the balance equations introduced in section "Energy Balance," the simulation program generates the corresponding results. Table 5 shows an energy analysis spreadsheet and Table 6 an economic assessment spreadsheet. Both are commonly used approaches to display the results of a cost calculation and to determine the cost of saved primary energy.

The section "General Data" contains data of the dimensions of the system components such as the solar collector, the buffer tank, the chiller, and the air-handling unit. These values have to be inserted by the user for both the reference system and the solar system.

Solar Cooling Systems. Table 5 Energy analysis spreadsheet to compare a solar thermal system with a reference system (example values from a simulation study; for more details see [15])

Energy analysis spreadsheet	Unit	Reference system (R)	Solar system (S)
0. General data			
Solar collector type	–	–	–
Solar collector area (aperture)	m^2		
Volume of heat buffer storage	m^3	0	18
Heating capacity backup heater	kW	18.8	17.9
Nominal chiller power, compression chiller	kW	29.4	0
Nominal chiller power, thermally driven chiller	kW	0	29.4
Nominal power of cooling tower	kW		
1. Results of system design with annual balance (e.g., achieved with simulation program)			
Annual total electricity consumption (including pumps, fans, control)	kWh	24811	10997
Total annual heat needs	kWh	14395	117724
Annual heat from second heat source (fossil fuel)	kWh	15152	14113
Maximum electricity demand (maximum hourly value)	kW	10.0	2.9
Total annual water consumption	m^3	0	368.3
2. Energy-related evaluation (computed from design results)			
Annual gross solar collector efficiency	%	–	38%
Annual net solar collector efficiency	%	–	30%
Annual primary energy consumption	kWh	84 868	45402
Annual primary energy saving	kWh	–	39466
Fractional primary energy saving	%	–	47%

Solar Cooling Systems. Table 6 Economic assessment spreadsheet to compare a solar thermal system with a reference system (example values from a simulation study; for more details see [15])

Economic assessment spreadsheet	Unit	Reference system (R)	Solar system (S)
1. Investment costs			
Solar collector system including supporting structure	€	0	50000
Heat storage	€	0	9000
(additional) Heat source (e.g., gas burner)	€	7520	7160
Installation costs (including piping, pumps, . . .)	€	10000	10000
Compression chiller	€	11760	0
Thermally driven chiller	€	0	11760
Cooling tower	€	–	2611
Pumps	€	750	750
Control system	€	8000	8000
Planning cost	€	3803	9928
Total investment cost without funding	€	41833	109209
Final total investment cost	**€**	**41833**	**84209**
2. Annual costs			
Annuity factor conventional equipment	%	6.7	6.7
Annuity factor solar system (solar collector, storage)	%	–	5.1
Capital cost	€	2811	4675
Cost for maintenance, inspection	€	837	1594
Annual electricity cost (consumption)	€	4962	2199
Annual electricity cost (peak)	€	1000	290
Annual heat cost (fossil fuel)	€	606	565
Annual water cost	€	0	1105
Total annual cost	**€**	**10216**	**10428**
Annual extra cost of solar system	€	–	212
Annual operation cost	€	7405	5753
Cost of saved primary energy	**€/kWh**	**–**	**0.005**

The section "Results of System Design" contains the main results of an annual energy balance which can be derived using a simulation program, a design tool, or any other calculation method. To allow comparison of the solar system performance with a reference system, comparable figures of a reference system have to be entered.

The "energy-related evaluation" provides energy-related performance figures which are calculated based on the annual simulation results from section "Definition of the Subject and Its Importance" of the work sheet, that is, results of system design. The following figures are not self-explaining and thus described.

The annual gross collector efficiency, η_{gross}, is defined by Eq. 27:

$$\eta_{gross} = \frac{Q_{coll}}{A_{coll} \cdot I_{coll}} \tag{27}$$

where Q_{coll} is the annual heat production of the solar system including unused excess heat, A_{coll} is the solar collector's aperture area, and I_{coll} is the annual

global (total) solar radiation incident on the solar collector plane.

The net collector efficiency, η_{net}, is defined by Eq. 28:

$$\eta_{net} = \frac{Q_{use}}{A_{coll} \cdot I_{coll}} \tag{28}$$

The net collector efficiency can be compared to the annual gross collector efficiency. The difference indicates the amount of solar energy that cannot be used because there is no actual demand for the available solar energy, and the available heat buffer is fully charged.

In the following, items of the economic assessment spreadsheet which are not self-explanatory are briefly described.

The total annual cost, C_{annual}, of a system is composed of the investment and maintenance and operation costs, see Eq. 29. The respective costs are explained later in this chapter.

$$C_{annual} = C_{investment,annual} + C_{maintenance,annual} + C_{operation,annual} \tag{29}$$

Firstly, the initial investment costs have to be carefully calculated. Main cost items to be considered are given in the list below:
Direct on-site costs are:

- Purchased equipment cost, which is dominated by costs for the chiller system and the solar collector. For both components, the specific cost (cost per unit) decreases with the installed size (typically expressed kW of cooling capacity for chillers and m^2 of aperture area for the solar collector field).
- Purchased equipment installation
- Piping
- Instrumentation and controls
- Electrical equipments and materials

Direct off-site costs are caused by:

- Land
- Civil, structural, and architectural costs
- Service facilities

Indirect costs include:

- Engineering and supervision
- Contractor's profits
- Contingency

Other depending costs are:

- Start-up costs
- Licensing, research and development
- Allowances for funds used during construction [5]

To calculate the investment cost, an annual basis accounting for the value of money over time has to be taken into consideration. This can, for instance, be made by spreading the initial investment, C_{inv}, over the lifetime of the system in years in constant annual quantities, called annuities, according to Eq. 30:

$$C_{investment,annual} = C_{inv} \cdot \frac{i_{eff}}{1 - (1 + i_{eff})^{-n}} \tag{30}$$

Here, i_{eff} is the effective rate of return, which can be estimated as the difference between the average interest rate offered by the banks and the inflation rate and n denotes the considered lifetime period.

Operating costs are due to fuel, electricity, wages, supplies and water. Maintenance costs are due to maintenance parts and services. Energy consumption is an important part of operating cost and the amount of consumed energy depends on the efficiency of the system. Electricity rates are usually more complex than those of gas or water. For instance, the price may be different according to the season and the time of the day, or can increase when a consumption threshold is overcome [3].

Once the annual maintenance costs, $C_{maintenance,annual}$, and the annual operating costs, $C_{operation,annual}$, have been calculated, combination of Eqs. 29 and 30 allows calculation of the total annual cost of either system. Together with the calculated annual amount of saved primary energy, PE_{sav}, this allows calculation of the cost of saved primary energy according to Eq. 23.

In the following, results of a simulation study are presented in which different systems were compared including solutions using photovoltaic installations.

Methodology of Economical Assessment – An Exemplary Simulation Study

The goal of the study presented below is to assess the energy saving potential and related economic results of different solar energy solutions for a given load. As an example, a (virtual) hotel in Madrid was chosen. The study is based on dynamic building simulation to

produce a load file and includes subsequent modeling of different solar-assisted systems to cover this load. The load is characterized by hourly values for heating load, cooling load, heat demand for preparation of sanitary hot water SHW (e.g., for showers) and electricity demand for artificial lighting and appliances.

Different systems were simulated to cover this load:

- A conventional reference system consisting of a natural gas-fuelled condensation boiler to cover the energy demand for heating and SHW and a vapor compression chiller to cover cooling. Electricity demand is completely covered by the public grid.
- A system using a solar thermal collector to partly cover the heating and SHW demand and a natural gas-fuelled condensation boiler to cover the rest of heating and SHW. A vapor compression chiller is used to cover the cooling demand. The electricity demand is completely covered by the public grid.
- A system using a solar thermal collector to partly cover the heating and SHW demand and to operate a thermally driven chiller which covers part of the cooling demand. A natural gas-fuelled condensation boiler is used to cover the rest of the energy demand for heating and SHW and a vapor compression chiller to cover the rest of the cooling demand. Electricity demand is completely covered by the public grid.
- A system consisting of a natural gas-fuelled condensation boiler to cover the energy demand for heating and SHW and a vapor compression chiller to cover the cooling demand. In addition, a photovoltaic (PV) system is used to cover part of the electricity demand. Electricity demand which is not covered by the PV is covered by the public grid. PV electricity which exceeds the actual electricity demand is fed into the public grid.

The general approach of the study is shown in Fig. 28, and schematics of the four different system configurations are shown in Fig. 29.

The assumed hotel has a total floor area of 3,050 m^2, and the building was divided in four different zones for generation of the load file (guest rooms, restaurant, kitchen, lobby, and others) using dynamic multizone building simulation. The annual values for the energy demand add up to 166 MWh for electricity (54.4 kWh/m^2a), 164 MWh for heating (53.6 kWh/m^2a), 78 MWh for cooling (25.4 kWh/m^2a), and 155 MWh for sanitary hot water (51.0 kWh/m^2a).

The key components used in the simulation are the following:

- Advanced flat-plate collector tilted 30° toward south with different sizes (100, 200, 500 m^2)
- Heat buffer storage with a size of 55 l m^{-2} of solar collector aperture area

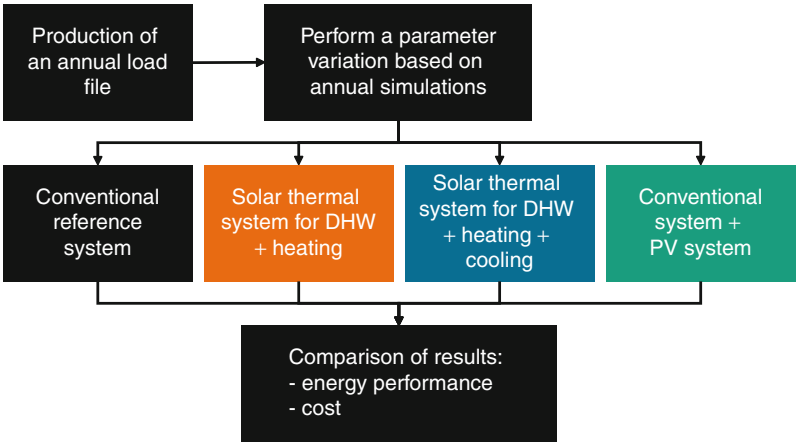

Solar Cooling Systems. Figure 28
Methodology of the simulation study

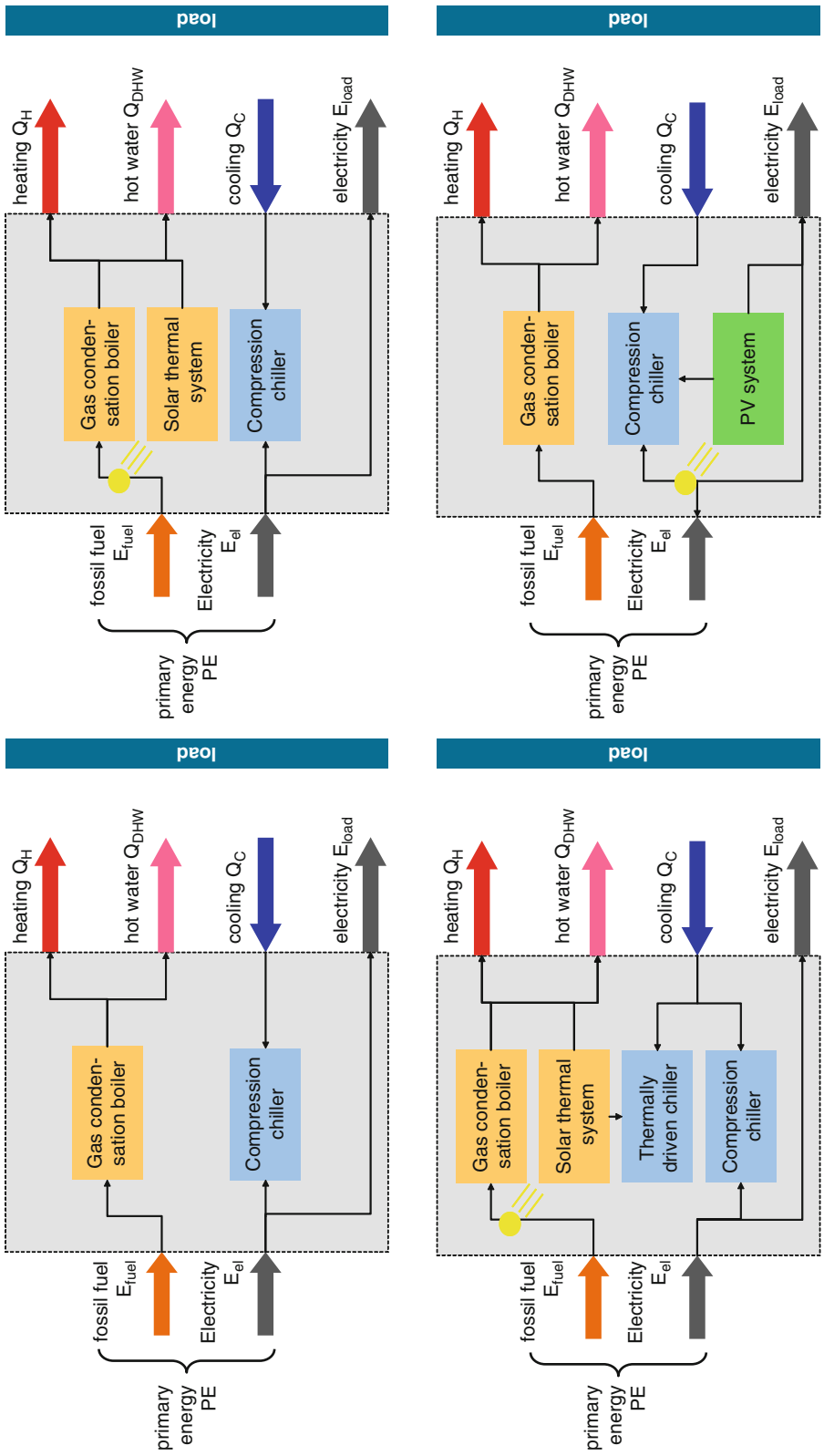

Solar Cooling Systems. Figure 29
Schematics of four compared system configurations: conventional reference (*top left*), solar thermal heating (*top right*), solar thermal heating and cooling (*bottom left*), and PV system (*bottom right*)

- Thermally driven chiller with average thermal COP of 0.68 with different sizes (10-kW, 20-kW, 40-kW cooling capacity)
- Cooling tower with a nominal electric efficiency factor of the heat rejection subsystem of 0.04 (i.e., 1 kWh of consumed electricity per 25 kWh of rejected heat)
- Vapor compression chiller with an average EER of 3.0
- Natural gas condensation boiler with an average efficiency of 0.9
- PV system: PV system using monocrystalline Si wafer PV modules tilted 30° toward south with different sizes (8, 80 kW_{peak})

Regarding costs, the following assumptions were used:

- For all components with a strong dependence of the first cost on the size cost curves have been used (see Fig. 30). These values do not include planning and installation.
- For the PV system, a fix price of 3 € per W_{peak} was assumed. This value includes planning and installation cost.
- No subsidies or incentive schemes for any of the technologies were used in order to generate a fair picture about the real cost of the different technologies.
- The rate of reimbursement for electricity produced by the PV system which exceeds the actual demand and which is fed into grid amounts 50% of the tariff for which electricity is purchased.
- Other important parameters used in the simulation such as energy prices, system lifetime, interest rate, primary energy conversion rates, etc., are summarized in Table 7.

As a first result, Fig. 31 presents the solar fraction achieved with the various solar thermal solutions. Five different variants are shown: two system configurations where solar thermal energy was used for heating and SHW only, and three configurations where a thermally driven chiller was installed additionally. The smallest solar thermal system considered (collector aperture area, A_{coll}, 100 m^2) covers about 40% of the SHW demand and a little less than 20% of the heating demand. Doubling the collector area leads not to a doubling of the useful output of the solar thermal system. Reason is that, in many hours, solar gains exist, but no actual load is available and the heat buffer is fully charged. This happens particularly in summer and in transition periods (fall, spring) when no demand for heating exists. Some use of this surplus heat can be made by adding a thermally driven chiller to the system. About 20% of the cooling demand can be covered by the solar thermal cooling system if, for instance,

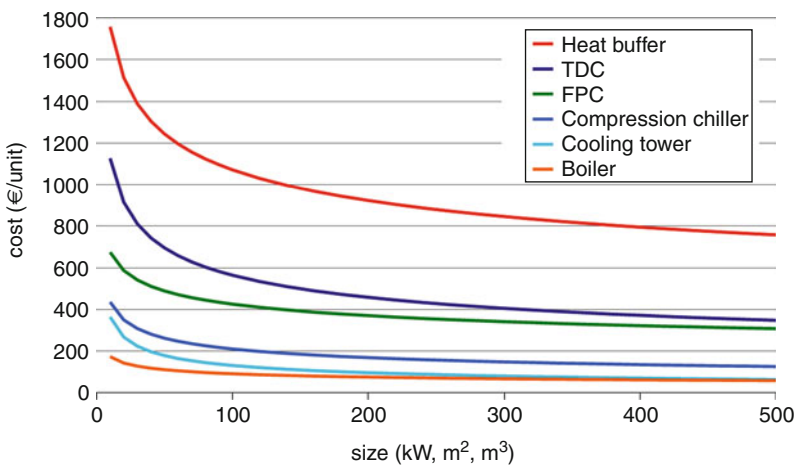

Solar Cooling Systems. Figure 30
Cost curves of key components expressed in cost per unit as function of the size (*TDC* thermally driven chiller, *FPC* flat-plate collector)

Solar Cooling Systems. Table 7 Values of other parameters used in the simulation study (PE = primary energy)

Other cost	Planning	% of invest	20.0%
	Installation	% of invest	30.0%
	Maintenance	% of invest p.a.	1.5%
Energy cost	Electricity	€/kWh	0.15
	Peak electricity cost	€/kW	50.00
	Fuel	€/kWh	0.07
	Increase rate electricity cost	% p.a.	3%
	Increase rate fuel cost	% p.a.	3%
Other parameters	Lifetime	a	20
	Interest rate	%	5.0%
	PE factor electricity $f_{PE,el}$	kWh_{PE}/kWh_{el}	2.7
	PE factor fuel $f_{PE,fuel}$	kWh_{PE}/kWh_{fuel}	1.1

a chiller with a maximum cooling capacity of 20 kW is used. However, this leads only to a small increase when looking at the total thermal energy demand for heating, cooling, and SHW. A significant contribution to the cooling demand (close to 60%) is achieved by the solar thermal system with a much larger solar collector field (500 m^2) and a thermally driven chiller with a cooling capacity of 40 kW. Such configuration allows almost 70% of the total thermal energy demand to be covered by solar energy.

A comparison of solar-assisted systems and the conventional reference can be expressed by both primary energy saving and cost difference. Figure 32 shows the fractional primary energy saving (according to Eq. 22 in section "Energy Balance") and the fractional cost saving (according to Eq. 24 in section "Energy Balance") for different system configurations.

All investigated systems lead to primary energy savings. Figure 32 also indicates that a comparatively small solar thermal system (100, 200 m^2) for heating and sanitary hot water leads to cost saving. The system amortizes within its lifetime under the conditions made. The cost saving is less pronounced when the solar thermal system is also for cooling. Large solar thermal systems (500 m^2) lead to higher total annual cost compared to the conventional solution or – in other words – such system does not amortize within its assumed lifetime. Installation of a small- to medium-sized photovoltaic system (8–40 kW_{peak}) in addition to the conventional system leads to a negligible difference in total annual cost. A large PV system (80 kW_{peak}), however, leads to an increase in total annual cost. Reason is that, at many times, electricity is produced which cannot be consumed onsite and is therefore fed into the grid at a feed-in tariff which amounts 50% of the rate for purchased electricity.

In addition to the systems described previously, Fig. 32 also shows a configuration with a small solar thermal system (100 m^2) and a small PV system (8 kW_{peak}) being installed together. It is interesting to note that this solution leads to the highest decrease in total annual cost and it has the shortest payback period.

For a combined energy-cost-performance assessment, the goal functions defined in section "Energy Balance" may be applied. In Fig. 33, the goal functions F_1 and F_2 are presented for those solutions which lead to a lower total annual cost in comparison to the conventional reference system. Both definitions of goal functions lead to the same result about the three best solutions of the studied configurations: these are a solar thermal system used for heating and sanitary hot water with 200 m^2 of collector area, followed by the combined solar thermal (100 m^2) and small PV system (8 kW_{peak}), and then the solar thermal system with 200 m^2 of collector area with an additional small thermally driven chiller (10-kW cooling capacity). The results shown in Fig. 33 confirm that the second goal function F_2 leads to a more pronounced difference between the different solutions.

The results shown for the example of the hotel in Madrid are specific for the given boundary conditions, particularly meaning climatic conditions which influence both solar gains and load demand. The load conditions are typical for a hotel but will vary significantly in case of other buildings and purposes. Nevertheless, some general conclusions can be drawn which are valid for the system design of building energy supply and, in particular, for the use of solar energy systems in buildings.

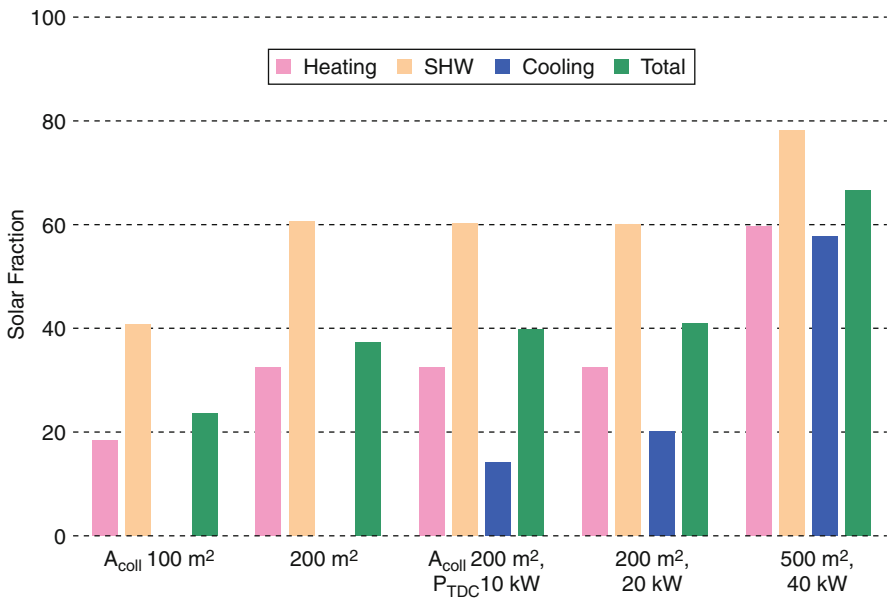

Solar Cooling Systems. Figure 31
Solar fraction for heating, sanitary hot water (SHW), cooling, and total thermal energy demand for different solar thermal system configurations (A_{coll} collector aperture area; PTDC: nominal cooling capacity of the thermally driven chiller)

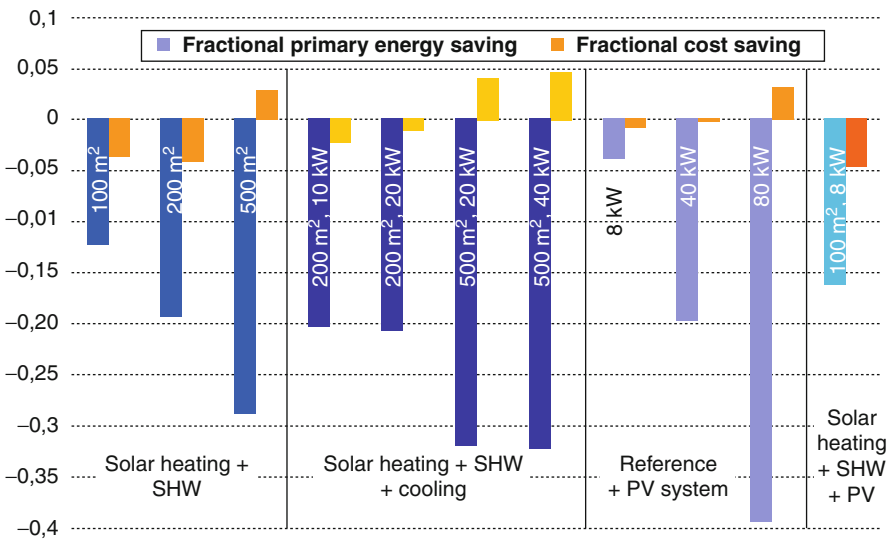

Solar Cooling Systems. Figure 32
Fractional primary energy saving and fractional cost saving for different solar-assisted solutions in comparison to a conventional reference system

- Solar thermal systems will be justified in most cases where a high demand of sanitary hot water exists. These systems are most cost-efficient if they are sized in such way that no significant excess heat is produced by the solar collectors and the solar fraction is not maximized.
- Solar thermally driven cooling is an interesting option in order to make use of high solar gains during the

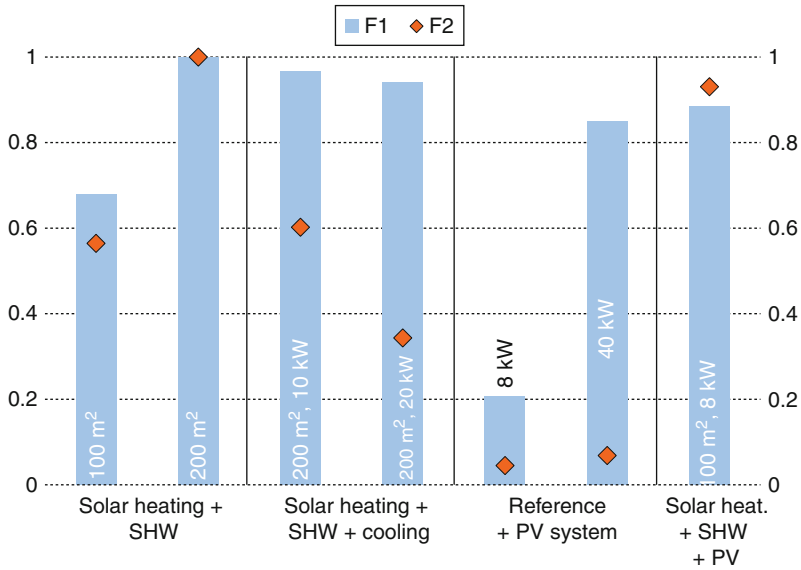

Solar Cooling Systems. Figure 33
Comparison of different system configurations using the combined energy-cost-performance goal functions F_1 (Eq. 25) and F_2 (Eq. 26) (y-axis arbitrary units)

cooling period. The system will be more cost-efficient if it is designed with limited solar fractions. However, this solution is still less cost-efficient in comparison to solar thermal systems without cooling. Future improvements will lead to cost reductions such as higher production rates – and corresponding lower cost – of thermally driven cooling devices and more standardized system designs which will lead to lower planning and installation costs.

- Today, photovoltaic systems rely on high feed-in tariffs in many countries and on an almost infinite grid capacity in comparison to the electricity production by solar energy. Therefore, if the high feed-in tariff is taken into account today, any PV solution will be much more interesting from a cost point of view than most solar thermal systems. However, with increasing production of electricity from renewable sources, this situation will change drastically in the future. Grid issues will become much more important and, among others, the pressure on locally produced electricity (e.g., from PV) will increase to be consumed onsite, too.
- In particular, for solar thermal systems – but in future also for PV systems – a detailed assessment of the correlation between solar gains and onsite loads is important. This analysis can usually only be done appropriately by a simulation of both the load side and the production systems on a sufficiently low time scale. Typically, simulations based on hourly values provide a not only helpful but also reliable basis for a detailed analysis.
- A holistic approach which includes an analysis of different combinations and configurations of technologies is needed in order to identify the optimal solution for a given project with its particular boundary conditions. Combined energy-cost-performance analysis and corresponding goal functions can provide a guide to these optimal solutions.

The large amount and diversity of results and newly gained know-how affirms the fact that performance and operation of (solar or solar-assisted) cooling systems depend on many aspects which are not completely fathomed. Therefore, further research and development actions are needed. One of the most important parts of running research projects are demonstration projects to gain practical insight. Some examples of practical projects are depicted in section "System Experiences."

System Experiences

The first part of section "System Experiences" points out some examples of the existing systems. Examples of

absorption or adsorption cooling as well as examples of solid and liquid desiccative air-conditioning are displayed. Relevant facts like size of the installations, climate zones, and the type of the utilized solar collectors are mentioned. In the second part, experiences which have been made with these installations are discussed.

Examples of Existing Installations: Closed Absorption Systems, Single-Effect

See Table 8.

Examples of Existing Installations: Closed Absorption Systems, Double-Effect

See Table 9.

Examples of Existing Installations: Closed Adsorption Systems

See Table 10.

Examples of Existing Installations: Open Solid Desiccant Systems

See Table 11.

Example of an Existing Installation (Pilot Plant): Open Liquid Desiccant System

See Table 12.

Summary of Experiences

The experiences obtained in demonstration projects and by monitoring of solar cooling plants lead to a valuable collection of know-how in the field of solar and solar-assisted cooling systems.

A major result of the R&D and demonstration work so far is that solar and solar-assisted cooling and air-conditioning systems can lead to significant primary energy savings. That and the fact that the interest of planners, building facility managements, solar companies – and the public in general – in solar thermal air-conditioning increases could give the necessary drive and the still indispensable support to make such systems an unconditional alternative. To sum up some important collected experiences following technical aspects might help to take the right steps into the right directions.

The design phase as well as the commissioning and operation phases has to be carried out accurately and under strict quality criteria.

A software tool is more than useful to design a solar cooling system. There is a need for careful design with particular focus on minimizing parasitic electric demand. Design and simulation studies support the selection and sizing of the appropriate components and determine the potential savings in primary energy. Experiences from monitored systems reveal optimization potential in system control and hydraulic schemes, as the designed systems are often too complex and the system performance was often not able to fulfill the expectations (relevant for Solar Cooling are the projects SACE, ASODECO, MITES, ROCCOCO, SOLAIR, SOLERA, MEDISCO, HIGHCOMBI, SOLARCOMBIPLUS). The planning and installation of large solar collector areas require special attention with respect to well-balanced mass flow and stagnation safety. Size and type of the solar collector and storage volume depends strongly on the site conditions, load structure and applied air-conditioning technology.

The choice of market introduction is quite deliberate, too. Best niches for market introduction are places with high electricity cost and limited quality and security of electricity supply, for example hotels on islands.

Main challenges are that in most cases solar-assisted cooling is not yet economically competitive under present market conditions without funding measures. And even if cost-competitive over the complete life cycle their operation will not lead to a short return-on-invest period. Also, well-trained installation and operation staff is needed in order to assure high quality.

The prepared solar cooling concepts have to be evaluated reasonably with respect to savings in primary energy and greenhouse gas emissions. For thermally-operated cooling processes with low COP and use of fossil fuels (backup heat), a high percentage of solar thermal coverage is required in order to achieve savings in primary energy and CO_2 emissions. Alternatively, an electrically driven compression chiller may be installed as backup solution for the cooling case. In general, further efforts to increase the thermal COP of thermally driven chillers and electric performance of the entire systems are required to exploit the existing saving potential.

Another finding is that improvements in the building shell are prerequisite to reduce the cooling loads for

Solar Cooling Systems. Table 8 Closed Absorption Systems, Single-Effect

Solar-assisted air-conditioning of the European Academy EURAC, Italy	
Boundary conditions	Collectors on the roof of the EURAC building in Bolzano, Italy. © EURAC
• Hot summer, cold winter	
• Academy building	
Installation and operation	Cooling installation at the EURAC building in Bolzano, Italy. © EURAC
• Heat production: 480-m^2 vacuum tube collectors, cogeneration 330-kW_{th}, condensation boilers	
• Cold production: absorption chiller 300 kW, compression chiller 630 kW	
• Heat storage 10 m^3	
• Cold storage 5 m^3	
• In operation since 2005	

Solar Cooling Systems. Table 8 (Continued)

Solar-assisted air-conditioning for offices in Lisbon, Portugal	
Boundary conditions	
• Southern European, Atlantic climate, hot summer	
• Office building with 100,000-m^2 office area	
Installation and operation	
• 545-kW absorption chiller	
• Approximately 1,600-m^2 flat-plate collectors designed for high efficiency at high operation temperatures	
• Backup: thermal, 700 kW	
• In operation since 2008	Collectors on the roof of the CGD bank building in Lisbon, Portugal. © www.solid.at
Solar-assisted air-conditioning at Guadeloupe, Caribbean Sea	
Boundary conditions	
• Tropical climate	
• DIREN office building with 570-m^2 air-conditioned area	
Installation and operation	
• Absorption chiller 35-kW (10 RT) capacity	
• 100-m^2 evacuated tube collectors	
• Wet cooling tower	
• Backup: compression chiller with 55-kW (16 RT) capacity	
• Was in operation since 2004, situation 2010: not working mainly because of administrative reasons	Collectors on the roof of the DIREN building in Guadeloupe, Caribbean Sea. © Tecsol

Solar Cooling Systems. Table 8 (Continued)

Air-conditioning in Dubai, United Arab Emirates (UAE)	
Boundary conditions	Collectors on the roof of the ESAB office building, Dubai, UAE. © Climatewell
• Arid, tropical [48]	
• Air-conditioning of an 2,000-m^2 office building and warehouse	
Installation and operation	Cooling system at the ESAB office building, Dubai, UAE. © Climatewell
• Triple-state absorption chiller (cooling power 10 kW)	
• Storage with 55-kWh capacity for cooling	
• 161-m^2 evacuated tube collector field	
• Wet cooling tower	
• Distribution: Hollow Core Slab system	
• In operation since 2010	

the installation of a solar thermal air-conditioning system. The load (and climatic) conditions mainly effect the ROI, namely the number of operation hours, and cost of conventional energy sources. In general, the implementation of storages – either on the hot side or on the cold side – is essential to handle time shifts between solar thermal heat generation profile and load profile. A high correlation between solar gains and cooling loads occurs mainly in buildings with dominating external loads and usage during day hours.

A promising direction are new developments of small chillers (<15-kW capacity) for residential and commercial use as these systems open new market sectors, especially in southern European areas.

Solar Cooling Systems. Table 9 Closed Absorption Systems, Double-Effect

Solar-assisted air-conditioning in Seville, Spain	
Boundary conditions	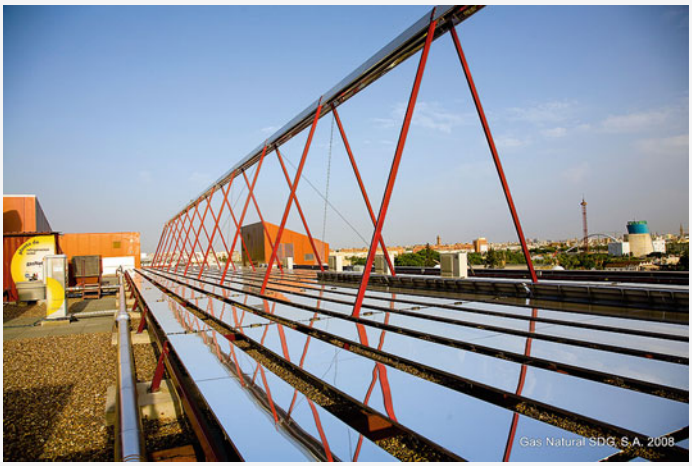 Collectors on the roof of the University Seville in Seville promoted by Gas Natural Fenosa, Spain. © AICIA – Universidad de Sevilla
• Mediterranean hot summer	
• Demonstration system at the University Seville for building air-conditioning	
Installation and operation	Cooling system at the University Seville in Seville promoted by Gas Natural Fenosa, Spain. © AICIA – Universidad de Sevilla
• 2-effect absorption chiller (broad) with 175-kW (50 RT) capacity	
• 1-axis tracked Fresnel-solar collector with 350 m^2 aperture area (PSE/Mirroxx)	
• Solar collector fluid: water/steam (approximately 180°C)	
• In operation since 2008	

Solar Cooling Systems. Table 10 Closed Absorption Systems

Air-conditioning in Freiburg, Germany	
Boundary conditions	Collectors on the roof of the laboratory building, Freiburg, Germany. © Fraunhofer ISE
• Temperate, central European climate	
• Air-conditioning of a laboratory building of a hospital	
Installation and operation	Cooling system at the hospital, Freiburg, Germany. © Fraunhofer ISE
• Adsorption chiller with 70 kW	
• 170-m^2 vacuum tube solar collector	
• Backup: thermally driven by steam network of the hospital	
• Two 3-m^3 solar buffer storage	
• 2 m^3 return flow to buffer storage	
• 2 m^3 cold storage	
• In operation since 1999	
Solar assisted air-conditioning at Viotias, Greece	
Boundary conditions	Collectors at the Inofita site in Viotias, Greece. © GBU mbH Zwingenberg
• Mediterranean hot summer	
• Electricity saving in a cosmetics production factory	
• Supply air cooling, fan coils	

Solar Cooling Systems. Table 10 (Continued)

Installation and operation	Cooling machine at the Inofita site in Viotias, Greece. © GBU mbH Zwingenberg
• 2 adsorption chillers with 350-kW (100 RT) capacity each	
• 2,700-m^2 flat-plate collectors	
• Backup: 3 compression chiller with 350-kW (100 RT) capacity each	
• Wet cooling tower	
• In operation since 1999	
Solar-assisted air-conditioning in Esslingen, Germany	
Boundary conditions	Collectors at the FESTO site in Esslingen, Germany. © FESTO
• Temperate, central European climate	
• Technology Center: 26,000-m^2 office area	
• Concept: electricity saving (prior operation of adsorption chiller)	
Installation and operation	View of the entire collector-covered roof of FESTO site. © FESTO
• 3 × 350-kW adsorption chillers = 1.05 MW total	
• Waste heat, gas boiler	
• 1,218-m^2 evacuated tube collectors	
• Backup: 3 compression chiller with 350 kW (100 RT) capacity each	
• In operation: adsorption chiller since 2001, collectors since 2007	

Solar Cooling Systems. Table 11 Open Solid Desiccant Systems

Solar air-conditioning in Freiburg, Germany	
Boundary conditions	Seminar room of the chamber of trade and commerce in Freiburg, Germany. © Fraunhofer ISE
• Temperate, central European climate	
• Air-conditioning of two seminar rooms (ca. 210 m^2)	
Installation and operation	Collectors on the roof of the chamber of trade and commerce in Freiburg, Germany. © Fraunhofer ISE
• Solid desiccant with rotor; 10,200-m^3/h nominal air volume flow rate	
• 100-m^2 solar air collectors (cooling and preheating)	
• No storage	
• Solar autonomous in summer	
• In operation since 2001	
Solar air-conditioning in Palermo, Italy	
Boundary conditions	Collectors on the roof of DREAM in Palermo, Italy. © DREAM
• Mediterranean, hot, humid	
• University building	

Solar Cooling Systems. Table 11 (Continued)

Installation and operation	
• Solid desiccant system, 1,500 m^3/h	
• 22.5-m^2 flat-plate collectors	
• For winter operation: gas boiler 11 kW	
• Cold-side backup: 24.3 kW	
• In operation since 2008	DEC system at DREAM in Palermo, Italy. © DREAM

Although the reliability of such system operations and environmental savings exist, there is still a large potential for further improvements in terms of efficiency, compactness of the systems and cost. Production capacities of the involved manufacturers are still low and increased volume of production rates would allow highly increased automation. To decrease the investment costs, it is also necessary to create more standardized system solutions for small (and medium size) applications.

For any economical working application, the exploitation of the solar thermal system should be maximized using the system for space heating support and – if needed – production of SHW. The combination of heating support, domestic hot water preparation and solar cooling optimizes the use of the solar thermal system throughout the year and improves the cost effectiveness.

Besides small chillers and SHW different concepts to extend existing HVAC plants to solar assistance at large scale level is a point of interest of commercial applicants.

Future Directions

Several thermally driven air-conditioning technologies are available on the market and enable the use of solar thermal energy for this large field of possible applications. Solar or solar-assisted air-conditioning can lead to remarkable primary energy savings if the corresponding systems are properly designed. Aspects are an appropriate dimensioning of the size of the collector field and the storage devices as well as heat and cold backup source.

In the last years, several efforts have been made in order to develop new thermally driven cooling equipment. Two main directions have been the development of thermally driven water chillers in the range of low cooling capacities (<50 kW down to less than 5 kW) and the further development of advanced open cycles. Different technologies are employed for the purpose of low-capacity water chillers with concepts using liquid sorption materials such as LiBr or NH_3 as well as solid ones such as silica gel and zeolite or solid absorption using salt/water systems. Several R&D activities have focused on the development of open cooling cycles using liquid desiccants. Liquid desiccants have some important advantages compared to systems using sorption wheels as described above. With liquid desiccants, it is possible to separate the processes of absorption and regeneration in time and thereby to use the liquid sorption material as thermochemical storage. The precondition to achieve high storage densities is to establish a highly efficient absorption process which leads to a large difference between concentration of concentrated and diluted solution. Another advantage of using liquid desiccants is that it is easier to cool the sorption process and thereby to realize a higher dehumidification with low regeneration temperatures compared to the usual desiccant cooling system. One of the recent R&D projects also deals with an advanced solid sorption process in which the sorption process is cooled in order to obtain a large dehumidification of

Solar Cooling Systems. Table 12 Open Liquid Desiccant System

Pilot plant with liquid DEC system in Freiburg, Germany	
Boundary conditions	Collectors on the roof of Solar Info Centre, Freiburg, Germany. © Fraunhofer ISE
• Temperate, central European climate	
• Air-conditioning of 310-m^2 office area	
Installation and operation	Liquid desiccant system (Menerga) at Solar Info Centre, Freiburg, Germany. © Fraunhofer ISE
• Liquid desiccant system with LiCl-solution	
• 1,500-m^3 air volume flow rate	
• 17-m^2 flat-plate collectors	
• Solar autonomous in summer	
• In operation since 2004	

the process air. Improvements in the performance of thermally driven chillers and open cooling cycles play a key role in order to approach economic feasibility. New developments of chillers with small capacity will open new market segments. For hot climates, high temperature lifts, that is, temperature differences between temperature of the produced cooling and the heat rejection are necessary. Under these conditions, high-efficiency solar collector systems which are tracking the sun in combination with efficient single-effect systems are a promising future option. Also in this area, a number of promising pilot installations have been realized and opened a broader market deployment, in particular in sunny regions like the Mediterranean countries [14].

Numerous simulation and demonstration projects, many of them supported by the European Commission (relevant for Solar Cooling are the projects SACE, ASODECO, MITES, ROCCOCO, SOLAIR, SOLERA, MEDISCO, HIGHCOMBI, SOLARCOMBIPLUS),

made it possible to provide a lot of useful information and develop strategies concerning further steps and future directions. Recently, many demonstration projects have been realized within the framework of the Solar Heating & Cooling Programme of the International Energy Agency IEA. TASK 25 "Solar Assisted Air-Conditioning of Buildings" (1999–2005) and TASK 38 "Solar Air-Conditioning and Refrigeration" (2006–2010) were large international activities with participation of research institutes, universities, and commercial partners (manufacturers, installation companies, planning offices) which contributed to technology development of solar cooling and provided accompanying measures for a faster and solid market development. For further information, see [50].

Future research has to focus on all levels starting from material research, in particular in the field of advanced sorption materials through process design and system optimization, up to the provision of accompanying measures for a broader and sustainable market introduction. All the concepts and technologies which were described in this chapter will contribute to the use of solar energy for air-conditioning of buildings and refrigeration. Well-adjusted solutions for the various boundary conditions, different climatic situations and different load conditions will be developed. Always an integrated approach is needed in which all the energy flows within a process or building are taken into consideration in a holistic approach in order to identify the best suited solar energy solution.

Bibliography

Primary Literature

1. ÅF-Energikonsult AB, Energi och Miljö, Elisabeth Ekener Petersen et al (2001) cHose Energy savings by CHCP plants in the hotel sector. Within SAVE II Programme (European Commission Directorate General). Dissemination of results seminars. http://www.inescc.pt/urepe/chose/reports/Final_report.pdf
2. Alizadeh S, Saman W (2002) An experimental study of a forced-flow solar collector/regenerator using liquid desiccants. Solar Energy 73(5):345–362
3. American Society of Heating, Refrigerating, and Air-Conditioning Engineers (2005) ASHRAE handbook – fundamentals, chapter 36. American Society of Heating, Refrigerating, and Air-Conditioning Engineers, Atlanta
4. Anyanwu EE (2004) Review of solid adsorption solar refrigeration II: an overview of the principles and theory. Energy Convers Manag 45:1279–1295
5. Bejan A, Tsatsaronis G, Moran M (1996) Thermal design & optimization. Wiley, New York
6. Daniel Keller D, Ochsner E (2008) Absorptionskältemaschinen als Alternative. friscaldo 5:28–30
7. Eicker U, Pietruschka D (2009) Optimization and economics of solar cooling systems advances in building energy research aber. Earthscan 3(1):45–82
8. Fan Y, Luo L, Souyri B (2007) Review of solar sorption refrigeration technologies: development and applications. Renew Sustain Energy Rev 11:1758–1775
9. Florides GA, Tassou SA, Kalogirou SA, Wrobel LC (2002) Review of solar and low energy cooling technologies for buildings. Renew Sustain Energy Rev 6:557–572, Elsevier Science Ltd
10. Gaderer M (2000) Rauchgaskondensationsanlagen Stand der Technik, Schaltungsvarianten, Entwicklungen. ZAE Bayern, München
11. Gassel A (2002) Die Adsorptionskältemaschine-Betriebserfahrungen, thermodynam. Model und TRNSYS-simulation. KI Luft- und Kältetechnik 10:479–483
12. Haider M, Luedeking G (2005) Auslegung und Wirtschaftlichkeit von KWKK-Anlagen Teil 1. KI Luft- und Kältetechnik 7:267–271
13. Heimrat R, Haller M (2007) The reference heating system, the template solar system. IEA-SHC Task 32 project report. www.iea-shc.org/publications/. . ./task32-Reference_Heating_System.pdf
14. Henning H-M (2005) Solar thermal energy for air-conditioning of buildings – advanced technologies adapted to local climatic conditions. IN: Proceedings of the 1st IBME conference, Bahrain, 5–7 Dec 2005
15. Henning H-M (ed) (2007) Solar assisted air conditioning in buildings – a handbook for planners, 2nd revised edn. Springer-Verlag, Wien New York
16. Henning H-M (2007) Solar assisted air conditioning of buildings – an overview. Appl Thermal Eng 27:1734–1749
17. Henning H-M, Pagano T, Mola S, Wiemken E (2005) Micro trigeneration system for indoor air conditioning in the Mediterranean climate. Appl Thermal Eng 27:2188–2194, Elsevier Ltd
18. Henning H-M, Urbaneck T, Morgenstern A, Nunez T, Wiemke E, Thümmler E, Uhlig U (2009) Kühlen und Klimatisieren mit Wärme. Solarpraxis AG, Berlin
19. Henning H-M, Urbaneck T et al (2009) Kühlen und klimatisieren mit Wärme. Bine Informationsdienst. FIZ Karlsruhe, Solarpraxis
20. Höfker G, Eicker U, Lomas K, Eppel H (2001) Desiccant cooling with solar energy. In: Proceedings of the CIBSE conference, London. www.cibse.org/pdfs/desiccant.pdf
21. Jakob U (2010) Solar cooling. Solar thermal markets in Europe: trends and market statistics 2009, p 14. www.estif.org
22. Keßling W, Lävemann E, Kapfhammer C (1998) Energy storage for desiccant cooling systems component development. Solar Energy 64(4–6):209–221
23. Keßling W, Lävemann E, Peltzer M (1998) Energy storage in open cycle liquid desiccant cooling systems. Int J Refrig 21(2):150–156

24. Krause M, Saman W, Heinzen R, Jordan U, Halawa E, Vajen K (2007) Absorber and regenerator models for liquid desiccant air conditioning systems: validation and comparison using experimental data. In: Proceedings of the international solar energy conference ISES2007, Beijing
25. Krause M, Saman W, Heinzen R, Jordan U, Halawa E, Vajen K (2007) Validation and comparison of absorber and regenerator models for liquid desiccant air conditioning systems. In: Proceedings of the 2nd international conference solar air-conditioning, Tarragona (ES), 18–19 Oct 2007
26. Krause M, Saman W, Vajen K (2005) Open cycle liquid desiccant air conditioning systems – theoretical and experimental investigations. In: Proceedings of the 43rd ANZSES conference solar, Dunedin, 28–30 Nov 2005
27. Krause M, Saman W, Vajen K (2006) Optimisation of a regenerator for open cycle liquid desiccant air conditioning systems. In: Proceedings of the EuroSun 2006, Glasgow, 27–29 June 2006
28. Kreider JF, Curtiss PS, Rabl A (2005) Heating and cooling of buildings design for efficiency, 2nd edn. McGraw-Hill, Singapore
29. Kren C (2008) Flue gas fired absorption chillers. Dissertation. Technische Universität München – TUM Physik Department, Lehrstuhl für Physik E19
30. Löf G (1993) Active solar systems. In: Bankston CA (ed) Solar heat technologies, vol 6. MIT Press, Cambridge, MA
31. Lowenstein A (2008) Review of liquid desiccant technology for HVAC applications. HVAC&R Res 14(6):819–840. American Society of Heating, Refrigerating and Air-Conditioning Engineers, Inc. (www.ashrae.org)
32. Lowenstein A, Slayzak S, Kozubal E (2006) A zero carryover liquid-desiccant air conditioner for solar applications. In: Proceedings of the ISEC 2006, Denver, Paper No. ISEC2006-99079
33. Löwenstein A, Slayzak S, Ryan J, Pesaran A (1998) Advanced commercial liquid-desiccant technology development study, NREL/TP-550-24688. National Technical Information Service (NTIS), U.S. Department of Commerce
34. Matsunaga K (2002) Comparison of environmental impacts and physical properties of refrigerants. http://www.engineering.columbia.edu/
35. Medrano M, Bourouis M, Coronas A (2001) Double-lift absorption refrigeration cycles driven by low-temperature heat sources using organic fluid mixtures as working pairs. Appl Energy 68:173–185
36. Mesquita LCS, Harrison SJ, Thomey D (2006) Modeling of heat and mass transfer in parallel plate liquid-desiccant dehumidifiers. Solar Energy 80(11):1475–1482
37. Morgenstern A, Bongs C, Wagner C, Henning H-M (2009) Experimental evaluation of a sorptive coated heat exchanger prototype for dehumidification. In: Proceedings of the 3rd international conference on solar air-conditioning, OTTI, Palermo, 30 Sept–02 Oct 2009
38. Motta M, Henning H-M (2004) An advanced solar assisted sorption cycle for building airconditioning: the ECOS potential and performance assessment. In: Proceedings of the EuroSun 2004, 5th ISES Europe solar congress, Freiburg, 1–4 June 2004
39. Mouchot A (1987) La chaleur Solaire et ses Applications Industrielles (German translation Die Sonnenwärme und ihre industriellen Anwendungen). Olynthus Verlag, Oberbözberg
40. Podesser E (2004) Desiccant-Klimatechnik mit Antriebswärme aus Sonne und Biomasse: Prototypanlage "DEC-ÖKOPARK Hartberg". Joanneum Research, Graz. www.energytech.at/pdf/solares_kuehlen_podesser1.pdf
41. Reichelt J (2000) Wo steht die Kältetechnik in Deutschland und weltweit? Die Kälte & Klimatechnik 53(10):22–32, www.treffpunkt-**kaelte**.de
42. Richter L (2008) Mehrstufige Absorptionskälteanlagen in Energieverbundanlagen. KI Luft- und Kältetechnik 3:131–135
43. Ross S (1948) On physical adsorption. II. A comparison of methods of estimating surface areas of crystalline solids by gas adsorption. J Am Chem Soc 70(11):3830–3837
44. SACE, Solar Assisted Air Conditioning in Europe. http://www.solair-project.eu/218.0.html
45. Simader GR, Rakos C (2005) Klimatisierung, Kühlung und Klimaschutz: Technologien, Wirtschaftlichkeit und CO_2-Reduktionspotentiale Materialband Stand der Technologie, Wirtschaftlichkeit, Potenziale, Emissionen und Fallstudien. Austrian Energy Agency, Vienna, www.energyagency.at
46. Stadler M, Lipman T, Marnay C (2007) Current trends of decentralized CHP integration – The Californian investment subsidy system and its implication for the energy efficiency directive. Office of Electric Transmission and Distribution, Office of Electric Transmission and Distribution, U.S. Department of Energy under Contract No DE-AC02-05CH11231. http://eetd.lbl.gov/
47. TRNSYS, A transient system simulation program – a program developed at the Solar Energy Laboratory, University of Wisconsin, Madison. http://sel.me.wisc.edu/trnsys
48. Troll C, Wissmann VH, Creutzburg N, Paffen KH (1982) Alexander Weltatlas Neue Gesamtausgabe. Ernst Klett Verlage GmbH und Co, Stuttgart
49. von Cube H-L, Steimle F, Lotz H, Kunis J (1997) Lehrbuch der Kältetechnik, Band 2, 4th edn. C. F. Müller Verlag, Heidelberg
50. www.iea-shc.org
51. Yattara A, Zhu Y, Mosa AM (2003) Comparison between solar single-effect and single-effect double-lift absorption machines (Part I). Appl Thermal Eng 23(15):1981–1992, Elsevier Ltd
52. Ziegler F (1997) *Sorptionswärmepumpen*, Forschungsberichte des DKV Nr. 57. Habilitation, Deutscher Kälte- und Klimatechnischer Verein e.V. (DKV), Stuttgart
53. Ziegler F (2002) State of the art in sorption heat pumping and cooling technologies. Int J Refrig 25:450–459

Books and Reviews

Abdulateef JM, Sopian K, Alghoul MA, Sulaiman MY (2009) Review on solar-driven ejector refrigeration technologies. Renew Sustain Energy Rev 13:1338–1349

Adnot J (1999) Energy efficiency of room air-conditioners (EERAC). Study for the Directorate-General for Energy (DGXVII) of the Commission of the EC. Final report

Alefeld G, Rademacher R (1994) Heat conversion systems. CRC Press, London
Alizadeh S, Saman WY (2002) Modeling and performance of a forced flow solar collector/regenerator using liquid desiccant. Solar Energy 72(2):143–154
ASHRAE (2000) Handbook 2000 HVAC systems and equipment, SIth edn. American Society of Heating, Refrigeration and Air-Conditioning, Atlanta
ASHRAE (2002) Absorption cooling, heating and refrigeration equipment, chapter 41. In: Handbook 2002 refrigeration, SI edn. American Society of Heating, Refrigeration, and Air-Conditioning, Atlanta
Bermejo P, Pino FJ, Rosa F (2010) Solar absorption cooling plant in Seville. Solar Energy 84:1503–1512
Chang W-S, Wang C-C, Shieh C-C (2009) Design and performance of a solar-powered heating and cooling system using silica gel/water adsorption chiller. Appl Thermal Eng 29: 2100–2105
Choudhury B, Chatterjee K, Sarkar JP (2010) Review paper on solar-powered air-conditioning through adsorption route. Renew Sustain Energy Rev 14:2189–2195
Collier RKJ (1997) Desiccant dehumidification and cooling systems assessment and analysis. Pacific Northwest National Laboratory, Richland/Washington, DC
Dannies JH (1951) Die Absorptionskältemaschine. Brücke Verlag Kurt Schmersow, Hannover
Duffie JA, Beckman WA (1991) Solar engineering of thermal processes, 2nd edn. Wiley, New York
Eicker U, Pietruschka D (2009) Design and performance of solar powered absorption cooling systems in office buildings. Energy Build 41:81–91
European standard: floor heating – systems and components (/EN-1264-1,2,3 1997 and EN-1264-4 2001/)
Franzke U (2001) Personal communication, Institut für Luft- und Kältetechnik (ILK), Dresden
Lane GA (1986) Phase change materials. In: Solar heat storage: latent heat material, vol II. CRC-Press, Boca Raton
Marc O, Lucas F, Sinama F, Monceyron E (2010) Experimental investigation of a solar cooling absorption system operating without any backup system under tropical climate. Energy Build 42:774–782
Niebergall W (1981) Handbuch der Kältetechnik Band 7: Sorptionskältemaschinen. Springer, Berlin
Pesaran AA, Penney TR, Czanderna AW (1992) Desiccant cooling: state-of-the-art assessment. NREL, Golden
Santamouris M, Asimakopoulos D (1996) Passive cooling of buildings. James & James, London
Sayigh AAM, McVeigh JC (1992) Solar air conditioning and refrigeration. Pergamon Press, Oxford, UK
Schicktanz M, Nunez T (2009) Modelling of an adsorption chiller for dynamic system Simulation. Int J Refrig 32: 588–595
Wang RZ, Ge TS, Chen CJ, Ma Q, Xiong ZQ (2009) Solar sorption cooling systems for residential applications: options and guidelines. Int J Refrig 32:638–660

Solar Detoxification and Disinfection of Water

Sixto Malato, P. Fernández-Ibáñez, M. I. Maldonado, I. Oller, A. Zapata
Plataforma Solar de Almería (CIEMAT), Tabernas, Almería, Spain

Article Outline

Glossary
Definition of the Subject and Its Importance
Introduction
Solar TiO_2 (Heterogeneous) Photocatalysis Applied to Water Decontamination
Fundamental Parameters Affecting Kinetics in Solar TiO_2 (Heterogeneous) Photocatalysis Applied to Water Decontamination
Solar Photo-Fenton
Solar Disinfection and Photocatalytic Disinfection
Solar Hardware for Water Decontamination and Disinfection
Future Directions
Acknowledgments
Bibliography

Glossary

Absorber tube The tube through which the fluid is to be illuminated and/or heated up in a solar collector.

CPC Compound parabolic collector. They are static collectors with a reflective surface following an involute around a cylindrical reactor and have been found to provide the best optics for low-concentration systems.

Electron/hole Negative and positive charge generated in an illuminated semiconductor. The excited electrons are transferred to the reducible specimen at the same time that the catalyst accepts electrons from the oxidizable specimen, which occupies the holes. In both directions, the net flow of electrons is null and the catalyst remains unaltered.

Immobilized catalyst Anchoring the catalyst onto some type of inert support inside the reactor.

Mineralization Conversion of organic compounds to inorganic ones. These inorganic compounds are

usually carbon dioxide, water, and acids (nontoxic substances).

Photocatalysis Combination of photochemistry with catalysis. Both light and catalyst are necessary to achieve or to accelerate a chemical reaction. Photocatalysis may be defined as the "acceleration of a photoreaction by the presence of a catalyst." Heterogeneous processes employ semiconductor slurries for catalysis, whereas homogeneous photocatalysis is used in a single-phase system.

Photo-Fenton Combination of Fe^{2+}, H_2O_2, and irradiation for producing hydroxyl radicals. The main advantage of the photo-Fenton process is the light sensitivity up to a wavelength of 550 nm.

Photoreactor Reactor where a photochemical reaction takes place.

Quantum yield The ratio between the number of reacting molecules of target compound or product formed and the quantity of photons absorbed by the system.

Semiconductor Material with an appropriate energetic separation between its valence and conduction bands which can be surpassed applying external energy (e.g., light). Metal oxides and sulfides represent a large class of semiconductor materials suitable for photocatalytic purposes.

Solar photochemistry This term includes those chemical processes which use the sun to drive specific chemical reactions by direct absorption of solar photons.

Definition of the Subject and Its Importance

One of the most pervasive problems affecting people throughout the world is inadequate access to clean water and sanitation. Problems with water are expected to grow worse in the coming decades, with water scarcity occurring globally, even in regions currently considered water rich. Addressing these problems calls out for a tremendous amount of research to be conducted to identify robust new methods of purifying water at lower cost and with less energy while at the same time minimizing the use of chemicals and impact on the environment. More effective, lower-cost, robust methods to disinfect and decontaminate waters from source to point-of-use are needed, without further stressing the environment or endangering human health by the treatment itself.

Advanced oxidation processes (AOPs) may be used for decontamination of water containing organic pollutants, classified as biorecalcitrant, and/or for disinfection removing current and emerging pathogens. These methods rely on the formation of highly reactive chemical species which degrade even the most recalcitrant molecules into biodegradable compounds. Although there are different reacting systems, all of them are characterized by the same chemical feature: production of hydroxyl radicals (•OH), which are able to oxidize and mineralize almost any organic molecule, yielding CO_2 and inorganic ions. Methods based on UV, H_2O_2/UV, O_3/UV, and other combinations use photolysis of H_2O_2 and ozone to produce the hydroxyl radicals, but generation of UV radiation by lamps or ozone production is expensive. So, future applications of these processes could be improved through the use of catalysis and solar energy. Therefore, research is focusing more and more on those AOPs which can be driven by solar irradiation, permitting solar detoxification and disinfection of water.

Introduction

Conventional methods of water disinfection and decontamination are often chemically, energetically, and operationally intensive, focused on large systems, and thus require considerable infusion of capital, engineering expertise, and infrastructure, all of which preclude their use in much of the world. Furthermore, intensive chemical treatments (such as those involving ammonia, chlorine compounds, hydrochloric acid, sodium hydroxide, ozone, permanganate, alum and ferric salts, coagulation and filtration aids, antiscalants, corrosion control chemicals, and ion-exchange resins and regenerants) and residuals resulting from treatment (sludge, brines, toxic waste) can add to the problems of contamination and salting of freshwater sources.

Rate constants (k_{OH}, $r = k_{OH}$ [•OH] C) for most reactions involving hydroxyl radicals in aqueous solution are usually on the order of 10^6 to 10^9 M^{-1} s^{-1}. They are also characterized by their nonselective attack, which is a useful attribute for wastewater treatment and solution of pollution problems. The versatility of the AOPs is also enhanced by the fact that there are different ways of producing hydroxyl radicals, facilitating compliance with the specific treatment requirements [1].

Heterogeneous photocatalysis and homogeneous photo-Fenton are based on the use of a wide-bandgap semiconductor and addition of H_2O_2 to dissolved iron salts, respectively, and irradiation with UV–VIS light [2]. Both processes are of special interest since sunlight can be used for them.

The overarching goal for the future of reclamation and reuse of water is to capture water directly from nontraditional sources such as industrial or municipal wastewaters and restore it. Municipal wastewaters are commonly treated by activated sludge systems that use suspended microbes to remove organics and nutrients, and large sedimentation tanks to separate the solid and liquid fractions. This level of treatment produces wastewater effluent suitable for discharge to surface waters or for restricted irrigation and some industrial applications. Current wastewater reuse systems use a conventional activated sludge process, followed by a microfiltration pretreatment of the secondary effluent, which has high quantities of suspended and dissolved solids. The effluent water still partially contains dissolved species and colloidal substances that act to foul the membranes of the subsequent RO (reverse osmosis) system used as a final barrier to contaminants in the product water. Futuristic direct reuse systems envisioned [3] involve only two steps: a single-stage membrane bioreactor (MBR) with an immersed nanofiltration membrane (obviating the need for an RO stage), followed by a photocatalytic reactor to provide an absolute barrier to pathogens and to destroy low-molecular-weight organic contaminants that may pass the nanofiltration barrier.

Industrial wastewater is often polluted by toxic or nonbiodegradable organic compounds. Alternatives to the conventional activated sludge treatment need to be employed. Among these, chemical oxidative treatments, and especially advanced oxidation processes (AOPs), are well known for their capacity for oxidizing and mineralizing almost any organic contaminant. Nevertheless, technical applications are still scarce [4]. As the process costs may be considered the main obstacle to their commercial application, several promising cost-cutting approaches have been proposed, such as integration of AOPs as part of a treatment train. It has been demonstrated that AOPs are able to enhance biodegradability of real wastewaters containing biorecalcitrant compounds [5], but it has been also pointed out that the process should be optimized by a proper selection of treatment time [6–8]. Operational conditions should be selected in a suitable range ensuring proper managing of real wastewaters of unpredictable composition. This coupled technology can be applied in industrial plants with difficult access to the municipal sanitation and sewage system, making possible the direct discharge of the effluent or its reutilization in industrial facilities. On the other hand, the correct operation of the system could very often permit the disposal of the pretreated wastewater in conventional sewage systems. In the typical basic process design approach, an AOP pretreats nonbiodegradable or toxic wastewater, and once biodegradability has been achieved, the effluent is transferred to a cheaper biological treatment.

The most important issue in water disinfection is, of course, safe drinking water. According to the WHO and UNICEF, polluted drinking water and lack of sanitation is responsible for the death of approximately 4,500–5,000 children every day, and one billion people still lack access to safe drinking water [9]. In addition to the well-known task of drinking-water disinfection, the second most critical issue is the disinfection of water for agriculture. Bearing in mind that the daily drinking-water requirement per person is only 2–4 L, it is often forgotten that it still takes 2,000–5,000 L of water to produce a person's daily food requirement [10]. Eighty percent of land cultivated worldwide is today still exclusively rainfed. Stored rainwater or surface water used for irrigation accumulates phytopathogens as phytopathogenic bacteria and fungi can be found almost everywhere. The plant and human pathogen *F. solani* has been reported as found almost everywhere, even in hospital water distribution systems [11]. Phytopathogens may be fought with organic disinfectants, also referred to as pesticides, which can be employed for disinfection of irrigation water, but this involves many negative aspects. Chlorine is used extensively, but has the drawback of the disinfection byproducts and resistance. Recent research on solar and solar photocatalytic disinfection attempts to combine sustainability with low cost, leading to an efficient disinfection method, not only for drinking water, but also for irrigation [12, 13].

The publications regarding the photocatalytic process rose continuously over the last years, surpassing

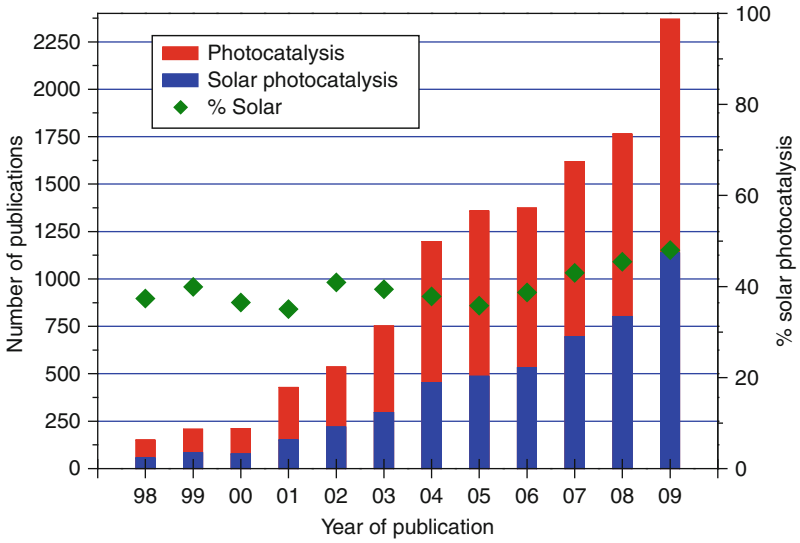

Solar Detoxification and Disinfection of Water. Figure 1
Publication treating photocatalysis and the share treating solar-driven photocatalysis (Source: www.scopus.com, 2010; search terms "photocatalysis" and "solar" within these results)

meanwhile a total number of more than 2,000 peer-reviewed publications per year in 2009. Though such a simple search does not necessarily include every single article correctly, it still serves to prove the general trend of an increasing interest of the scientific community. Figure 1 shows the evolution of these publication activities. Figure 1 also illustrates that much of the literature takes into account the possibility of driving the process with solar radiation. This fact is due to that a priori the photocatalytic process seems to be the most apt of all AOPs to be driven by sunlight. This chapter highlights some of the science and technology being developed to improve the solar photocatalytic disinfection and decontamination of water, as well as efforts to increase water supplies through the safe reuse of wastewater and adequate treatment of industrial wastewater.

Solar TiO_2 (Heterogeneous) Photocatalysis Applied to Water Decontamination

The heterogeneous solar photocatalytic detoxification process consists of making use of the near-ultraviolet band of the solar spectrum ($\lambda < 400$ nm), to photoexcite a semiconductor catalyst in contact with water and in the presence of oxygen. Some semiconductor catalysts can absorb above 400 nm. Oxidizing species (hydroxyl radicals, •OH, produced due to the photogenerated holes), which attack oxidizable contaminants, are generated, producing a progressive breakup of molecules yielding CO_2, H_2O, and diluted inorganic acids. The most important features of this process making it applicable to the treatment of contaminated aqueous effluents are:

- The process takes place at ambient temperature and without overpressure.
- Oxidation of the substances into CO_2 and other inorganic species is complete.
- The oxygen necessary for the reaction can be directly obtained from atmosphere.
- The catalyst is innocuous and can be reused or attached to different types of inert matrices.
- The energy for photoexciting the catalyst can be obtained from the sun.

Semiconductors (e.g., TiO_2, ZnO, Fe_2O_3, CdS, and ZnS) can act as sensitizers for light-induced redox processes due to their electronic structure which is characterized by a filled valence band and an empty conduction band. Absorption of a photon of energy greater than the bandgap energy leads to the formation of an electron/hole pair (Reaction 1). In the absence of suitable scavengers, the stored energy is dissipated within a few nanoseconds by recombination.

If a suitable scavenger or surface defect state is available to trap the electron or hole, recombination is prevented, and subsequent redox reactions (Reactions 2 and 3) may occur. The valence band holes are powerful oxidants (+1.0 to +3.5 V vs NHE depending on the semiconductor and pH), while the conduction band electrons are good reductants (+0.5 to −1.5 V vs NHE):

$$C \xrightarrow{h\nu} C(e^- + h^+) \quad (1)$$

$$h^+ + Red_2 \rightarrow Ox_2 \quad (2)$$

$$e^- + Ox_1 \rightarrow Red_1 \quad (3)$$

In the presence of a fluid (contaminated water), a spontaneous adsorption occurs (water and pollutant), and according to the redox potential of each adsorbate, an electron transfer proceeds toward acceptor molecules, whereas a positive hole is transferred to a donor molecule. Each ion formed subsequently reacts to form the intermediates and final products. Since the photonic excitation of the catalyst appears as the initial step of the activation of the whole catalytic system, being necessary that the photon has enough energy to be absorbed by the catalyst, not by the reactants. Subsequently, the activation of the process goes through the excitation of the solid, but not through that of the reactants. Furthermore, the oxidative species formed (in particular the hydroxyl radicals, $^{\bullet}OH$) react with the majority of organic substances (contaminants). For example, in aromatic compounds, the aromatic part is hydroxylated, and successive steps in oxidation/addition lead to ring opening. The resulting aldehydes and carboxylic acids are decarboxylated and finally produce CO_2. However, the important issue governing the efficiency of photocatalytic oxidative degradation is minimizing electron/hole recombination by maximizing the rate of interfacial electron transfer to capture the photogenerated electron and/or hole. This issue is discussed in more detail later.

Whenever different semiconductor materials have been tested under comparable conditions for the degradation of the same compounds, TiO_2 has generally been demonstrated to be the most active. Furthermore, TiO_2 is of special interest since it can use natural (solar) UV. This is because it has an appropriate energetic separation between its valence and conduction bands which can be surpassed by the energy content of a solar photon (see Table 1). Other semiconductor particles, for example, CdS or GaP, absorb larger fractions of the solar spectrum and can form chemically activated surface-bond intermediates, but unfortunately, these photocatalysts are degraded during the repeated catalytic cycles involved in heterogeneous photocatalysis. To date, evidence supports the idea that the $^{\bullet}OH$ is the main oxidizing specimen responsible for photooxidation of the majority of the organic compounds studied. In TiO_2, after absorption of near-ultraviolet radiation, $\lambda < 390$ nm, electron/hole pairs are generated. In order to avoid recombination of the pairs generated, if the solvent is oxidoreductively active (water), it also acts as a donor and acceptor of electrons. Thus, on a hydrated and hydroxylated TiO_2 surface, the holes trap $^{\bullet}OH$ radicals linked to the surface (Reaction 4). In any case, it should be emphasized that even trapped electrons and holes can rapidly recombine on the surface of a particle (Reaction 5). This can be partially avoided through the capture of the electron by preadsorbed molecular oxygen, forming a superoxide radical (Reaction 6):

$$\begin{aligned}&(TiO^{IV} - O^{2-} - Ti^{IV}) - OH_2 + h^+ \\ &\quad \rightarrow (TiO^{IV} - O^{2-} - Ti^{IV}) - {}^{\bullet}OH + H^+\end{aligned} \quad (4)$$

Solar Detoxification and Disinfection of Water. Table 1 Band position (water at pH = 1) for some common semiconductor photocatalyst. E_G bandgap energy

	TiO_2	SnO_2	ZnO	ZnS	WO_3	CdS	CdSe	GaAs	GaP
Valence band (V vs NHE)	3.1	4.1	3.0	1.4	3.0	2.1	1.6	1.0	2.2
Conduction band (V vs NHE)	−0.1	0.3	−0.2	−2.3	0.2	−0.4	−0.1	−0.4	−1.0
E_G (eV)	3.0	3.9	2.8	3.7	2.8	2.5	1.7	1.4	2.3
Bandgap λ (nm)	390	318	440	336	443	497	730	887	540

$$e^- + h^+ + TiO_2 \rightarrow TiO_2 + \text{heat or } h\nu \quad (5)$$

$$O_2 + e^- \rightarrow O_2^{\bullet -} \quad (6)$$

Degradation by photocatalysis has been most investigated in dimethoxybenzenes, halobenzenes, nitrobenzene, chlorophenols, nitrophenols, benzamide, aniline, etc., most of which are recognized as priority pollutants. In addition to these, several other types of molecules have also been investigated as substrates for photocatalytic degradation: haloaliphatics (trichloroethylene, tetrachloromethane, etc.), pesticides (triazines, organophosphorus, carbamates, phenoxyacids, organochlorines, chloronicotinics, etc.), surfactants, dyes, etc. Until now, the absence of total mineralization has been observed only in s-triazine herbicides, for which the final product obtained was essentially 1,3,5-triazine-2,4,6, trihydroxy (cyanuric acid), which is, fortunately, nontoxic. Special attention has recently been given to the so-called emerging contaminants, mostly unregulated compounds that may be candidates for future regulation depending on research on their potential effects on health and monitoring data regarding their occurrence. Particularly relevant examples of such emerging compounds are those which do not need to persist in the environment to cause a negative effect because their high transformation/removal rates can be compensated by their continuous introduction into the environment [14]. The solar photocatalytic degradation of these new environmental contaminants (pharmaceuticals, antibiotics, analgesics, steroids, hormones, MTBE, cyanotoxins, etc., and their hydrolysis/photolysis reaction intermediates), many of them until recently unknown, is the focus of much research [15].

In photocatalysis, transformation of the parent organic compound is desirable in order to eliminate its toxicity and persistence, but the principal objective is to mineralize all pollutants. The effectiveness of degradation is not demonstrated only because the entire initial compound is decomposed. Reactants and products might be lost (evaporation, adsorption on reactor components, etc.) which introduces uncertainty in results. The mineralization rate is determined by monitoring inorganic compounds, such as CO_2, Cl^-, SO_4^{2-}, NO_3^-, PO_4^{3-}, etc. For chlorinated molecules, Cl^- ions are easily released in the solution and are the first of the ions appearing during the photocatalytic degradation (see Fig. 2). Nitrogen-containing molecules are mineralized mostly into NO_3^- and NH_4^+. Ammonium ions are relatively stable, and the proportion depends mainly on the oxidation stage of organic nitrogen and irradiation time [16]. By comparing the sequence of appearance, NH_4^+ appears as the primary product with respect to NO_3^- in the case of amine compounds. The nitrogen atoms in the amino groups can lead to NH_4^+ ions by successive attacks by hydrogen-containing species. The total amount of nitrogen-containing ions present in the solution at the end of the experiments is usually lower than that

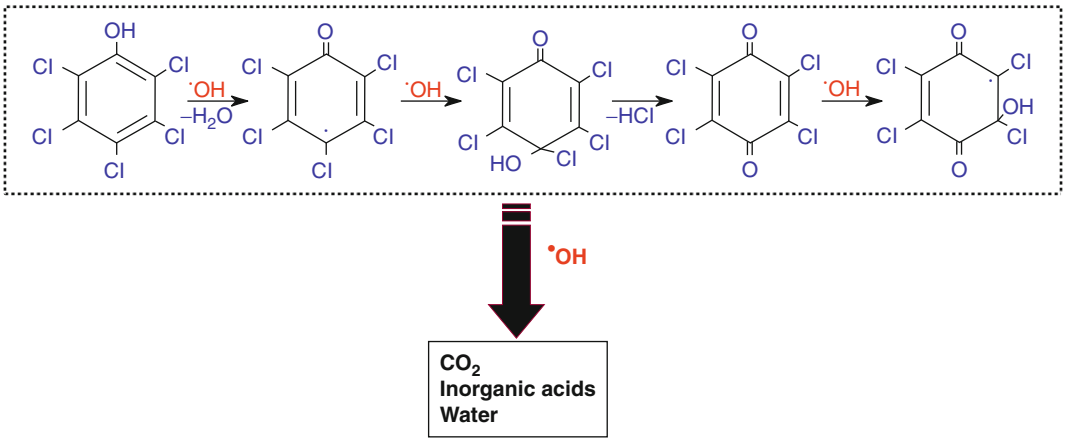

Solar Detoxification and Disinfection of Water. Figure 2
Degradation until complete mineralization of a model contaminant (pentachlorophenol) dissolved in water by •OH radicals

expected from stoichiometry, indicating that N-containing species remain adsorbed in the photocatalyst surface or most probably that significant quantities of N_2 and/or NH_3 have been produced and transferred to the gas phase. The formation of N_2 in azo bounds can be accounted for by the same processes responsible for NH_4^+ formation [17]. N_2 evolution constitutes the ideal case for a decontamination reaction involving totally innocuous nitrogen-containing final product.

Organophosphorus contaminants produce phosphate ions. However, in the pH range used (usually >4), phosphate ions remain adsorbed on TiO_2. This strong adsorption somewhat inhibits the reaction rate, though it is still acceptable. The release of SO_4^{2-} can be accounted by an initial attack by a photoinduced $^{\bullet}OH$ radical. In all the studies, the formation of SO_4^{2-} was always observed, and in most cases, its stoichiometric formation was found in the final steps of the photoreaction when organic intermediates were still present. Initial rate was high, indicating that SO_4^{2-} ions are initial products, directly resulting from the initial attack on the sulfonyl group. Nonstoichiometric formation of sulfate ions is usually explained by a strong adsorption on the photocatalyst surface. This strong adsorption could partially inhibit the reaction rate which, however, remains acceptable. Sulfate, chloride, and phosphate ions, especially at concentrations greater than 1 mM, can reduce the rate due to the competitive adsorption at the photoactivated reaction sites.

Treatment of industrial wastewater seems to be one of the most promising fields of application of solar photocatalysis. There is no general rule at all, each case being completely different [18]. Consequently, preliminary research is always required to assess potential pollutant treatments and optimize the best option for any specific problem, on a nearly case-by-case basis. Reaction 7 generally holds true for an organic compound of general formula $C_nH_mO_p$:

$$C_nH_mO_p + \left(\frac{(m-2p)}{4} + n\right)O_2 \rightarrow nCO_2 + \frac{m}{2}H_2O \tag{7}$$

The oxidation of carbon atoms into CO_2 is relatively easy. In general, at low reactant levels or for compounds which do not form important intermediates, complete mineralization and reactant disappearance proceed with similar half lives, but at higher reactant levels where important intermediates occur, mineralization is slower than the degradation of the parent compound. However, before TiO_2 photocatalytic treatment can be proposed as a general and trouble-free method, it is required that the chemistry of various classes of pollutants under these conditions is known in detail. Since the chemistry of such processes is complex, careful analytical monitoring using different techniques is essential in order to control all transformation steps, to identify harmful intermediates, and to understand and interpret the reaction mechanism. The assessment of pollutant disappearance in the early steps is not sufficient to ensure the absence of residual products because the heterogeneous photocatalytic treatment may give rise to a variety of organic intermediates which can themselves be toxic, and in some cases, more persistent than the original substrate [19].

From an analytical viewpoint, the task that entails the most difficulty is, without doubt, qualitative and quantitative evaluation of the intermediates or degradation products (DPs). As hydroxyl radicals are not selective in their attacks, numerous DPs form on the path toward complete mineralization. There are five main types of DPs:

- Hydroxylated and dehalogenated products, the latter of these derived from the loss of the halogenated substitute in the original contaminant, if it had one
- Products from the oxidation of the alkali chain, if it had one
- Products derived from the opening of the aromatic ring in aromatic contaminants
- Products of decarboxylation
- Products of isomerization and cyclation

The chemical analysis of these complex reaction mixtures is difficult, so that in the majority of the cases, not much attention is paid to their identification and analytical evaluation is limited to tracing the disappearance of the initial pollutant, combined with following decrease in TOC and the appearance of inorganic ions. Thus, the kinetic degradation of contaminants and the mineralization rate during the process are evaluated. However, a greater knowledge of the DPs originated would be necessary. It may be

observed in Fig. 3 the different DPs with high molecular weight appearing during photocatalytic treatment at short treatment time. From here on, they begin to decrease and carboxylic acids appear.

The basic parameters (necessary for relevant information on process kinetics and assure consistent results) to be evaluated are:

- Mineralization, as described below.
- Concentration of the original pollutant. Use of liquid chromatography with UV detection (LC-UV) is recommended for this as the most reliable and versatile technique for analysis of organic pollutants dissolved in water.
- Concentration of inorganic ions. In this case, liquid chromatography with electric conductivity detection (LC-IC) is recommended. This analytical method also makes it possible to determine low-molecular-weight carboxylic acids, which assists in establishing the degradation pathway of the compounds treated since these acids are usually the last step before pollutant mineralization. The most common are formic, acetic, oxalic, glycolic, propanoic, and pyruvic acid, etc.

A complete mass balance of photocatalytic degradation processes is imperative and is generally reported in studies that envisage application of photocatalytic water treatment. The determination of total organic carbon (TOC) and/or the measurement of the chemical oxygen demand (COD) of the irradiated solution are generally used for monitoring the mineralization. It is appropriate to analyze the chemical oxygen demand (COD) when CO_2 or TOC determination is unavailable since it is a cheaper method. However, the information that it provides on mineralization of the

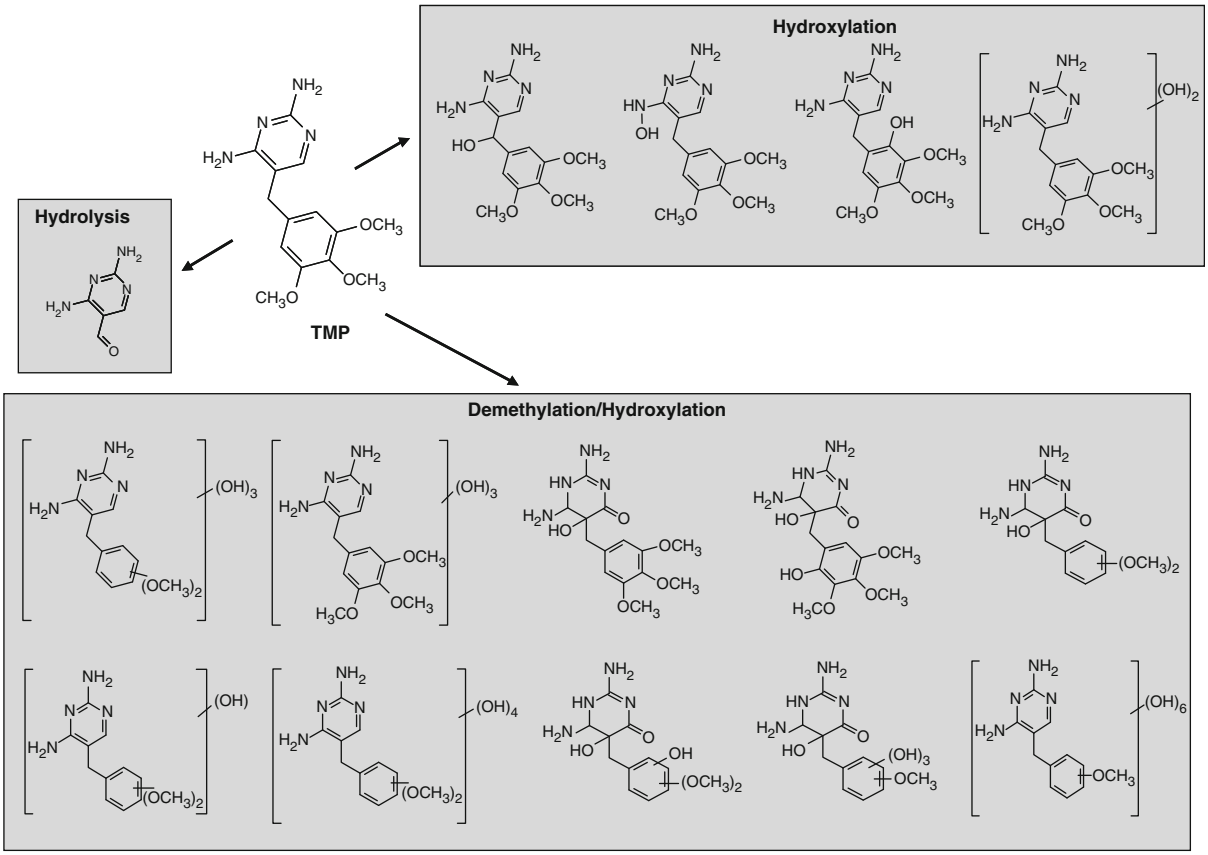

Solar Detoxification and Disinfection of Water. Figure 3
Photodegradation products identified during the TiO_2 photocatalysis of trimethoprim (TMP)

compounds is not as reliable as TOC because COD analyses are usually not accurate for pollutant concentrations in the order of milligrams per liter (very common in photocatalysis) and because oxidizable inorganic species cannot be distinguished from the organic pollutants.

Therefore, the analysis of reaction mixtures containing one or several contaminants and their DPs requires analytical methods that enable the separation and identification of the large number of compounds, with very different chemical properties present in a wide interval of concentrations. In practice, this is possible through the use of sophisticated analytical tools, such as gas chromatography coupled with mass spectrometry (GC-MS) and liquid chromatography coupled also to mass spectrometry (LC-MS). These methods or combinations of them can confirm the identity of the DPs present in a reaction mixture; however, they require specific expertise and the process is usually time consuming. In the last 10 years, analytical instrumentation and techniques have undergone rapid development. Very sophisticated equipment and techniques, especially in the field of GC-MS and LC-MS, have been developed to enable efficient determination of organic compounds [20, 21].

Fundamental Parameters Affecting Kinetics in Solar TiO_2 (Heterogeneous) Photocatalysis Applied to Water Decontamination

Mass of Catalyst

TiO_2 is often used as a suspension, and the rate of photomineralization is generally found to increase with catalyst concentration toward a limiting value at high TiO_2 concentration. This limit depends on the geometry and working conditions of the photoreactor and is for a definite amount of TiO_2 in which all the particles, that is, all the surface exposed, are totally illuminated. When catalyst concentration is very high, after travelling a certain distance on an optical path, turbidity impedes further penetration of light in the reactor. In any given application, this optimum catalyst mass has to be found in order to avoid excess catalyst and ensure total absorption of efficient photons [22, 23]. There are a number of studies in the literature on the influence of catalyst concentration on process efficiency. The results are very different, but from all of them, it may be deduced that radiation incident on the reactor and path length inside the reactor are fundamental in determining the optimum catalyst concentration. In the case of solar photoreactors where the path length is several centimeters long, the appropriate catalyst concentration is several hundreds of milligrams per liter. In this case, it is very clear that the highest rate (i.e., lowest collector area per mass of catalyst) is attained at lower catalyst concentrations when the photoreactor diameter is increased. In the case of the heterogeneous process with TiO_2 in suspension, sedimentation and deposition of the catalyst along the hydraulic circuit must also be avoided, so that turbulent flow in the reactor must be guaranteed [24]. Turbulent flow makes pressure loss an important parameter that can condition design, especially in the case of an industrial plant with long reactor tube lengths. For these reasons, diameters of less than 20–25 mm are not feasible. On the other hand, diameters over 50–60 mm are not considered practical. Furthermore, every photoreactor design must guarantee that all the useful incoming photons are used and do not escape without having intercepted a particle in the reactor.

Although TiO_2 suspensions absorb solar photons with less than 390–400 nm wavelengths, there is also a strong light-scattering effect due to particles. Both effects must be considered in determining the optimum catalyst load as a function of optical path length in the photoreactor. Wavelengths where the catalyst does not absorb light are better for determining the optimum catalyst concentration as a function of light-path length. Under these conditions, measurement of photon losses is only affected by turbidity and it is easy to evaluate the effect of the photoreactor diameter. In Fig. 4, where these results are shown for different photoreactor designs, it may be seen how solar photoreactors present lower optimum catalyst concentration, compared with artificial light devices.

If the lamp is inside the reactor and coaxial with it (Fig. 4a), the optimum catalyst concentration is very high (on the order of several grams per liter). On the other hand, the optimum catalyst concentration is medium (1–2 g/l) if the lamp is outside (Fig. 4b). In the case of solar photoreactors (Fig. 4c), the appropriate catalyst concentration is several hundreds of milligrams per liter. In any case, these are only

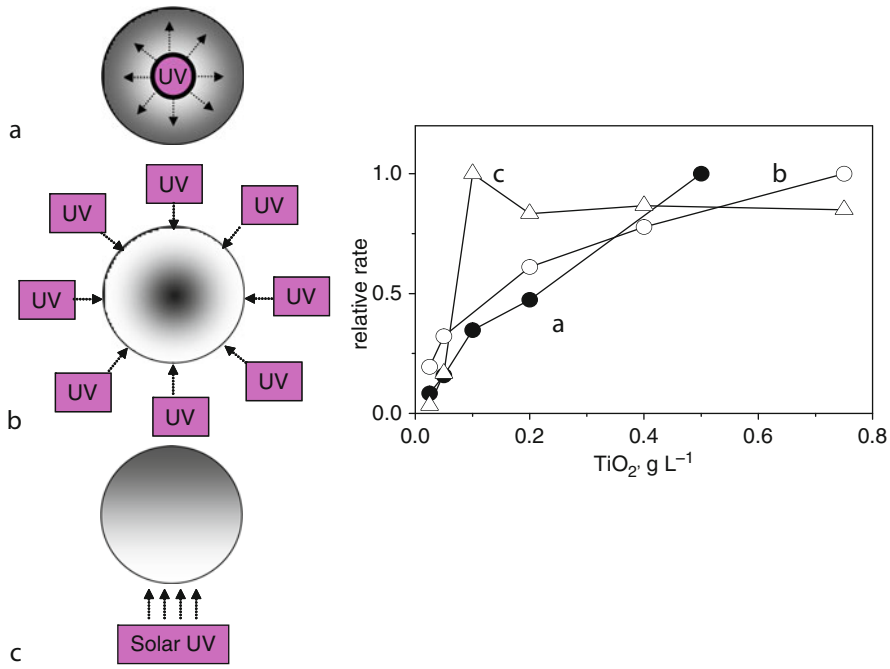

Solar Detoxification and Disinfection of Water. Figure 4
Different photoreactor designs and zones of radiation penetration when illuminated in different ways. The influence of catalyst concentration on the rate of photocatalysis in the different photoreactors is also shown

approximations based on the results obtained by different authors, and because of all of the above, it is always necessary to find out, experimentally, the optimum catalyst concentration for the solar collector studied. That is, the minimum concentration of photocatalyst at which the maximum reaction rate is obtained.

pH

The pH of the aqueous solution significantly affects TiO_2, including the charge on the particles, the size of the aggregates it forms, and the positions of the conductance and valence bands. It is somewhat surprising, therefore, that the rate of photocatalytic mineralization is not usually found to be strongly dependent upon pH between values ranging from 4 to 10. To work outside these values is not logical due to environmental and economical reasons, if the wastewater pH would need to be adjusted. Often, the pH of industrial wastewater can be very acidic or basic. In this case, the effect of pH on TiO_2 photocatalytic efficiency should be taken into account as the process could be enhanced, varying the pH by simple/cheap methods as, for example, mixing different streams.

The pH at which the surface of an oxide is uncharged is defined as the zero point charge (pH_{zpc}), which for TiO_2 depends on the production method ($4.5 < pH_{zpc} < \sim 7$). Above and below this value, the catalyst is negatively or positively charged according to Reactions 8 and 9:

$$-\,TiOH_2^+ \leftrightarrow TiOH + H^+ \tag{8}$$

$$-\,TiOH \leftrightarrow -TiO^- + H^+ \tag{9}$$

The equilibrium constants of these reactions [25] are $pK_{TiOH2+} = 2.4$ and $pK_{TiOH} = 8.0$, the abundance of all the species as a function of pH being $-\,TiOH \geq 80\%$ when $3 < pH < 10$, $-TiO^- \geq 20\%$ when $pH > 10$, and $-\,TiOH_2^+ \geq 20\%$ when $pH < 3$. A very important feature of photocatalysis that must be taken into account when it is to be used for decontamination of water is that during the reaction, a multitude of intermediate products are produced (see Fig. 3) that may behave differently depending on the pH of the solution.

To use only the rate of decomposition of the original substrate could yield an erroneous pH as the best for contaminant degradation. Therefore, a detailed analysis of the pH conditions should include not only the initial substrate but also the rest of the compounds produced during the process. Measurement of an overall parameter as TOC (or COD, or toxicity, or biodegradability, etc.) should be used for choosing the optimum pH or at least to determine the effect of pH on the behavior of the chosen key parameter.

The size of the aggregates formed by TiO_2 particles is also affected by pH. Mean particle-size measurements have been found to be constant at pH far from pH_{zpc}. Several hundred nanometer sizes increase to 2–4 μm when dispersion reaches pH_{zpc} [26]. The zero surface charge yields zero electrostatic surface potential that cannot produce the interactive rejection necessary to separate the particles within the liquid. This induces a phenomenon of aggregation, and TiO_2 clusters become larger. This effect is clearly related to the capability of the suspension for transmitting and/or absorbing light. Furthermore, larger clusters sediment more quickly than small particles; thus, the agitation necessary to maintain good catalyst uniformity must be more vigorous. Therefore, pH close to zero point charge should be avoided in order to not promote TiO_2 particle aggregation.

Temperature

Because of the photonic activation, the photocatalytic systems do not require heating and are operating at room temperature. The true activation energy is nil, whereas the apparent activation energy is often very small (a few kJ/mol) in the medium temperature range (between 20°C and 80°C). However, at very low temperatures (below 0°C), the apparent activation energy increases. The desorption of the final product becomes the rate-limiting step and trends to the heat of adsorption of the product. On the other hand, when temperature increases above 80°C and approaching to the boiling point of water, the exothermic adsorption of reactants becomes disfavored and tends to become the rate-limiting step. Correspondingly, the activity decreases, and the apparent activation energy becomes negative. As a consequence, the optimum temperature is generally comprised between 20°C and 80°C.

This absence of heating is attractive for photocatalytic reactions carried out in aqueous media and, in particular, for photocatalytic water purification. There is no need to waste energy in heating water which possesses a high heat capacity. It is also necessary to take into account that the solubility of oxygen decreases with increasing temperature, affecting therefore to the kinetics described in section "Concentration of Oxygen." Temperature does become a factor in photocatalytic disinfection and as such is commented in section "Solar Disinfection and Photocatalytic Disinfection." This behavior can be easily explained within the frame of the Langmuir–Hinshelwood mechanism described above. The decrease in temperature favors adsorption, which is a spontaneous exothermic phenomenon; θ_x approaches to unity; and KC becomes >> 1. The lowering in T also favors the adsorption (K_P) of the final reaction products, inhibiting the reaction as the term $K_P C_P$ appears in the denominator of Eq. 10. Above 80°C, the adsorption of reactants is disfavored and KC becomes <<1, being $r = k_{ap}C$.

In the photomineralization of organic pollutants sensitized by TiO_2, it has been traditionally reported that the initial rate of disappearance of the pollutant (X) fits a Langmuir–Hinshelwood (L–H) kinetic scheme. According to the L–H model (Eq. 10), the reaction rate (r) is proportional to the fraction of surface of photocatalyst covered by the substrate (θ_x), k_r the reaction rate constant, C the concentration of species X, and K the reactant adsorption constant:

$$r = -\frac{dC}{dt} = k_r\,\theta_x = \frac{k_r\,KC}{1 + KC} \tag{10}$$

As oxidation proceeds, less and less of the surface of the TiO_2 particles is covered as the contaminant is decomposed. Evidently, at total decomposition, the rate of degradation is zero, and a decreased photocatalytic rate is to be expected with increasing illumination time. Most authors agree that, with minor variations, the expression for the rate of photomineralization of organic substrates with irradiated TiO_2 follows the L–H law. Although the L–H isotherm has been rather useful in modeling the process, it is generally agreed that both rate constants and orders are only "apparent" [27–29]. They serve to describe the rate of degradation, and may be used for reactor optimization,

but they have no physical meaning, and may not be used to identify surface processes. Thus, while not an useful tool for describing the active species involved in oxidation, engineers and solar designers seem to have a common understanding of the usefulness of the unmodified L–H model.

Traditionally, K is taken to represent the Langmuir absorption constant of the species X on the surface of TiO_2, and k_r is a proportionality constant which provides a measure of the intrinsic reactivity of the photoactivated surface with X. It is found that k is proportional to Φ_e^n, where Φ_e is the rate of effective (able to form electron/hole pairs) light absorption, and n is a power term which is less than 1 or 1, at high or low light intensities, respectively. In section "Radiant Flux," the effect of Φ on the reaction rate is discussed in more detail.

Radiant Flux

Since 1990, there has been a clarification of the kind of solar technology which should be involved in photocatalysis. The question was if it is necessary to concentrate the radiation for the photocatalysis technology and if a nonconcentrating collector can be as efficient as concentrating ones. Initially, it was thought that concentrating collectors were the ideal alternative, and in fact, the first large pilot plants operated were using them. However, their high cost and the fact that they can only operate with direct solar radiation (this implies their location in highly irradiated areas with few cloud cover) led to consider static nonconcentrating collectors as an alternative [30]. The reason of using one-sun systems for water treatment is firmly based on two factors: first, the high percentage of UV photons in the diffuse component of solar radiation, and second, the low-order dependence of rates on light intensity.

It has been shown, for all types of photocatalytic reactions, that the rate of reaction is proportional to the radiant flux (Φ). This confirms the photoinduced nature of the activation of the catalytic process, with the participation of photoinduced electrical charge (electrons and holes) to the reaction mechanism. However, above a certain value, the reaction rate becomes proportional to Φ^n ($0 > n > 1$). This modification does not seem to happen at well-established radiation intensity, as different researchers obtain different results. It is presumable that the experimental conditions affect significantly, but it has been stated that with a typical solar UV flux of 20–30 Wm^{-2} (0.2–0.3 mol photons m^{-2} h^{-1} in the 300–400 nm), the concentration of sunlight (R_C) on the photoreactor using specific solar concentrating collectors ($R_C = A/2\pi r$, being A the collector aperture width and r the reactor tube radius) is not convenient as reaction rate is usually proportional to $\Phi^{0.5}$. A practical appraisal to this statement is that more than 50 W (<400 nm) per square meter of photoreactor (being tubular or flat-plate) will produce a loss of photonic efficiency. Most authors [31–34] impute the transition of $r = f(\Phi)$ to $r = f(\Phi^{0.5})$, to the excess of photogenerated species (e^-, h^+, and $^{\bullet}OH$). When Φ is very high, a large number of holes and electrons are generated. As the reaction rate depends on the amount of hydroxyl radicals present, and these are generated in the holes (see Eqs. 4, 5), then r is proportional $\Phi^{0.5}$ when Φ is high. Under these conditions, the quantum yield diminishes because the rate of electron/hole formation becomes greater than the photocatalytic rate, which favors the electron/hole recombination.

At much higher radiation intensities, another transition from $r = f(\Phi^{0.5})$ to $r = f(\Phi^0)$ is produced. At this moment, the photocatalytic reaction leaves its dependence on the received radiation, to depend only on the mass transfer within the reaction. So, the rate is constant, although the radiation increases. This effect can be due to different causes, as can be the lack of electrons scavengers (i.e., O_2), or organic molecules in the proximity of TiO_2 surface and/or excess of products occupying active centers of the catalyst, etc. In practical applications, these phenomena are observed more frequently when working with supported catalyst and/or at low agitation level. This implies low catalyst surface in contact with the liquid and smaller turbulence. Thus, the contact of reactants with the catalyst and the diffusion of products from the proximity of the catalyst to the liquid are not favored.

Concentration of Oxygen

In semiconductor photocatalysis for water purification, the pollutants are usually organic, and therefore, the overall process can be summarized by Eq. 11. Given the reaction stoichiometry of this equation, there is no

photomineralization unless O_2 is present. The literature provides a consensus regarding the influence of oxygen. Oxygen is necessary for complete mineralization and does not seem to be competitive with other reactives during the adsorption on TiO_2 since oxidation takes place at a different location from where reduction occurs (see Reactions 4–6). The concentration of oxygen also affects the reaction rate, but it seems that the difference between using air or pure oxygen is not drastic. In an industrial plant, it would be purely a matter of economy of design. It has been reported that the rate of oxidation was independent of oxygen concentrations below air saturation values, suggesting also that the mass transfer of oxygen to the surface could be rate limiting:

$$\text{organic pollutant} + O_2 \xrightarrow[\text{ultra-bandgap energy}]{TiO_2} CO_2 + H_2O + \text{mineral acids} \tag{11}$$

Due to its availability in water, adsorbed oxygen serves as the electron acceptor in semiconductor photocatalysis. Rate equations (see Fig. 5) have been derived assuming a Langmuir adsorption of oxygen onto the titanium dioxide surface. The role of oxygen may not only be that of an electron acceptor. Oxygen, for instance, may be involved in the formation of other oxidative species (superoxide, hydrogen peroxide, hydroxyl radicals), in the prevention of reduction reactions, in the stabilization of radical intermediates, mineralization, and direct photocatalytic reactions.

It is generally assumed that oxygen adsorbs on titania from the liquid phase, where it is dissolved following Henry's law. If the oxygen is regularly supplied, it can be assumed that its coverage at the surface of titania is constant and can be integrated into the apparent rate constant (k_{ap}). In most kinetic studies, the observed variation of the rate of photomineralization as a function of concentration of oxygen is described as shown in Fig. 5, where plots of r versus $\%O_2$ during the photodegradation of a contaminant by TiO_2 photocatalysis are illustrated. Thus, increasing the oxygen concentration in aqueous solution from air saturated (21% O_2) to O_2 saturated (100% O_2) conditions will typically increase the rate by only a small quantity.

Solar Photo-Fenton

For the treatment of industrial wastewater, Fenton and Fenton-like processes are probably among the most

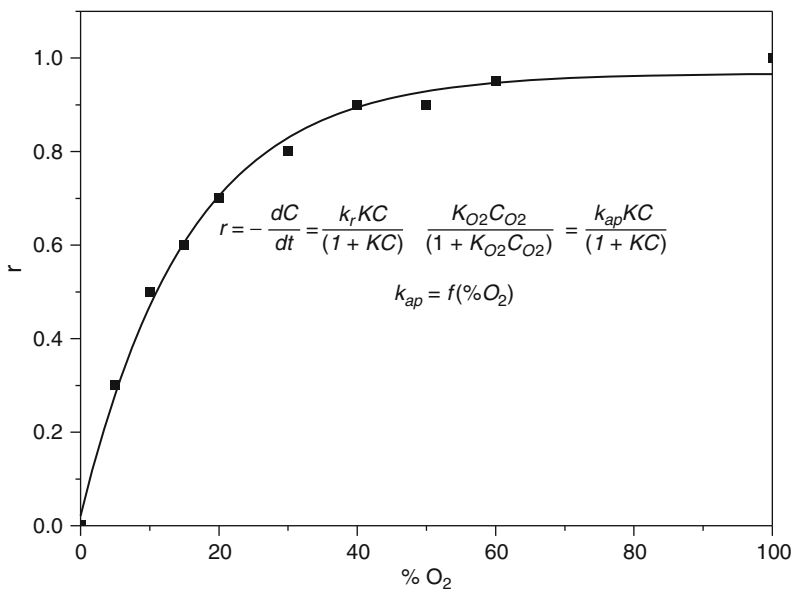

Solar Detoxification and Disinfection of Water. Figure 5
Plots of initial relative rate (r) versus concentration of oxygen ($\%O_2$)

applied advanced oxidation processes. The first proposals for wastewater treatment applications were reported in the 1960s. Quite recent reviews give good overviews of the Fenton chemistry [35, 36]. Yet, it was not until the early 1990s when the first works of the application of the photo-Fenton process (or photoassisted/light-enhanced Fenton process) for the treatment of wastewater were published. Since then, the publication activities regarding the photo-Fenton process rose continuously, surpassing 700 peer-reviewed publications up-to-date (source: www.scopus.com, 07.08.2010; search criteria "photo-Fenton" and "solar photo-Fenton"). Much of the literature treating the photo-Fenton process takes into account the possibility of driving the process with solar radiation. This fact is due to that a priori the photo-Fenton process seems to be the most apt of all AOPs to be driven by sunlight because soluble iron–hydroxy and especially iron–organic acid complexes absorb even part of the visible light spectrum, not only ultraviolet radiation. Consequently, the photo-Fenton system is a very efficient reaction system for the generation of radicals available for oxidative processes.

Hydrogen peroxide is decomposed to water and oxygen in the presence of iron ions in aqueous solution in the Fenton reaction, Eq. 12, which was first reported by H.J.H. Fenton in 1894 [37]. Mixtures of ferrous iron and hydrogen peroxide are called Fenton reagent. If ferrous is replaced by ferric iron, it is called Fenton-like reagent. Equations 12–14 summarize briefly the reactions of ferrous iron, ferric iron, and hydrogen peroxide in the absence of other interfering ions and organic substances. The regeneration of ferrous iron from ferric iron by Eqs. 13, 14 is the rate-limiting step in the catalytic iron cycle, if iron is added in small amounts:

$$Fe^{2+} + H_2O_2 \rightarrow Fe^{3+} + OH^- + {}^{\bullet}OH \tag{12}$$

$$Fe^{3+} + H_2O_2 \rightarrow Fe^{2+} + HO_2^{\bullet} + H^+ \tag{13}$$

$$Fe^{3+} + HO_2^{\bullet} \rightarrow Fe^{2+} + O_2 + H^+ \tag{14}$$

If organic substances (quenchers, scavengers, or in the case of wastewater treatment pollutants) are present in the system $Fe^{2+}/Fe^{3+}/H_2O_2$, they react in many ways with the generated hydroxyl radicals. Yet, in all cases, the oxidative attack is electrophilic and the rate constants are close to the diffusion-controlled limit. There is one great setback of the Fenton method. Especially when the treatment goal is the total mineralization of organic pollutants, carboxylic intermediates cannot be further degraded. Carboxylic and dicarboxylic acids are known to form stable iron complexes, which inhibit the reaction with peroxide [38]. Hence, the catalytic iron cycle reaches a standstill before total mineralization is accomplished, Eq. 15:

$$Fe^{3+} + nL \rightarrow [FeL_n]^{x+} \xrightarrow{H_2O_2,\text{dark}} \text{no further reaction}$$
$$L: \text{mono} - \text{and dicarboxylic acids} \tag{15}$$

The primary step of the photoreduction of dissolved ferric iron is a ligand-to-metal charge-transfer (LMCT) reaction. Subsequently, intermediate complexes dissociate as shown in Reaction 16 [39]. The ligand can be any Lewis base able to form a complex with ferric iron (OH^-, H_2O, HO_2^-, Cl^-, R–COO^-, R–OH, R–NH_2, etc.). Depending on the reacting ligand, the product may be a hydroxyl radical such as in Eqs. 17 and 18 or another radical derived from the ligand:

$$[Fe^{3+}L] + h\nu \rightarrow [Fe^{3+}L]^* \rightarrow Fe^{2+} + L^{\bullet} \tag{16}$$

$$[Fe(H_2O)]^{3+} + h\nu \rightarrow Fe^{2+} + {}^{\bullet}OH + H^+ \tag{17}$$

$$[Fe(OH)]^{2+} + h\nu \rightarrow Fe^{2+} + {}^{\bullet}OH \tag{18}$$

$$[Fe(OOC-R)]^{2+} + h\nu \rightarrow Fe^{2+} + CO_2 + R^{\bullet} \tag{19}$$

$$Fe(C_2O_4)_3{}^{3-} + h\nu \rightarrow Fe^{2+} + 2\,C_2O_4{}^{2-} + C_2O_4{}^{\bullet-} \tag{20}$$

Depending on the ligand, the ferric iron complex has different light absorption properties, and Reaction 16 takes place with different quantum yields and also at different wavelengths. Consequently, the pH plays a crucial role in the efficiency of the photo-Fenton reaction because it strongly influences which complexes are formed. Thus, pH 2.8 was frequently postulated as an optimum pH for photo-Fenton treatment because at this pH, precipitation does not take place yet and the dominant iron species in solution is $[Fe(OH)]^{2+}$, the most photoactive ferric iron–water complex. In fact, as shown in its general form in

Eq. 16, ferric iron can form complexes with many substances and undergo photoreduction. Of special importance are carboxylic acids because they are frequent intermediate products in an oxidative treatment. Such ferric iron–carboxylate complexes can have much higher quantum yields than ferric iron–water complexes. It is therefore a typical observation that a reaction shows an initial lag phase, until intermediates are formed, which can regenerate more efficiently ferrous iron from ferric iron accelerating the process. This can either happen through a photochemical pathway, Eq. 19, a thermal pathway, or a combination of both.

Fe(III) complexes present in mildly acidic solution, such as $Fe(OH)^{2+}$ absorb light appreciably in the UV and into the visible region. The quantum yield for Fe^{2+} formation in Eq. 17 is wavelength-dependent. It is 0.14–0.19 at 313 nm and 0.017 at 360 nm [40]. Fe(III) may complex with certain target compounds or their by-products. These complexes typically have higher molar absorption coefficients in the near-UV and visible regions than the aquo complexes. Polychromatic quantum efficiencies in the UV-visible range from 0.05 to 0.95 are common [36]. Fe(III)–oxalate complexes (Eq. 20) are efficient up to 500 nm (quantum efficiency 1.0–1.2).

Effect of pH

The need for acidification in the photo-Fenton process is often outlined as one of its major drawbacks. Not only does this mean additional cost through the consumption of reagents for acidification and subsequent neutralization but also an increase of the treated water's salt load. A pH of 2.8 avoids iron precipitation (at least under low to moderate iron concentration below approximately 1 mM) but maximizes the concentration of mono- and dihydroxylated iron(III) aquo complexes, which absorb UV light more efficiently than the nonhydroxylated iron(III) complexes. This was accepted by many authors as a matter of fact, and henceforth, many publications appeared applying this pH (see Fig. 6). Usually, the reduction of ferric iron is the rate-limiting step in Fenton and photo-Fenton applications. Photoreduction of ferric iron complexes (Eqs. 16–19) takes place at longer wavelengths, when aquo and hydroxyl ligands are replaced with stronger complexing agents. Hence, if present, upon irradiation with sunlight, these complexes contribute more to the photoreduction than the aquo and hydroxyl complexes. Consequently, one must state that the early explanation for an optimum pH of 2.8 based on the

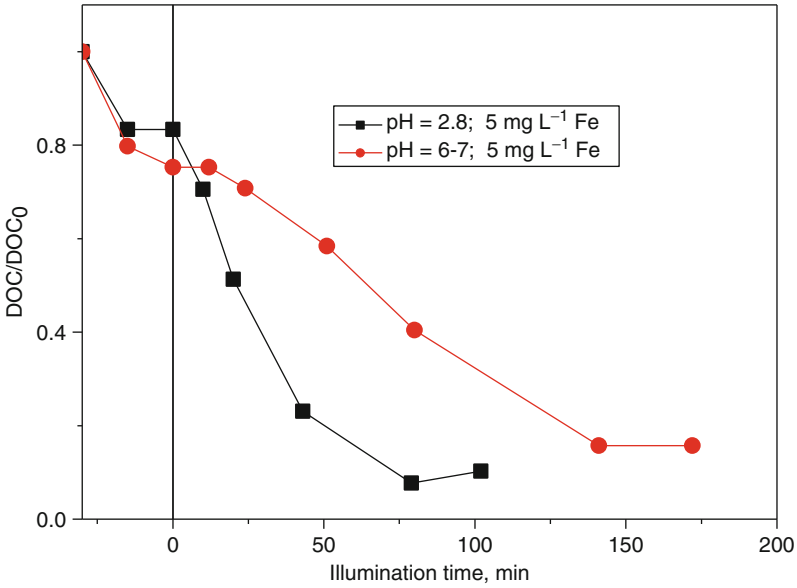

Solar Detoxification and Disinfection of Water. Figure 6
Mineralization (*DOC* dissolved organic carbon) by photo-Fenton of a model contaminant under solar irradiation at pH = 2.8 and at neutral pH

absorbance spectra of different aquo and hydroxyl ferric iron complexes seems only plausible in the absence of complexing agents. This is seldom the case, as carboxylic acids are formed in the oxidation process. Hence, the only real constraint seems to be the need of avoiding iron precipitation.

Effect of Iron Concentration and Iron Source

One of the principal characteristics of a photoreactor is its optical path length, for example, in the case of a tubular photoreactor, the tube diameter. A ray of light is attenuated along the optical path length as a function of the solution's extinction coefficient, which is closely related to the iron concentration. In general, the solar photoreactor constitutes a substantial part of the investment cost of the installation. Hence, one aim in the design of a photoreactor is that nearly the whole volume of the photoreactor is illuminated. A too-high iron concentration generates dark zones in the photoreactor because the incident ray is attenuated too strongly along the optical path length. The inner filter effects present in the solution are another important issue regarding the effect of iron concentration on the reaction rate. Inner filter effects are the competitive absorption of photons by other light-absorbing species, usually the contaminants present in the wastewater.

Consequently, one may state that iron concentration optimization must take into account the solar collector geometry and the inner filter effects. Also, to reduce inner filter effects, sunlight seems an ideal irradiance source. This ability to make use of photons of a wavelength beyond the UV region may also be one of the main reasons why photo-Fenton compares favorably to TiO_2 photocatalysis, when applied to highly colored wastewaters. Only logically following then is that another strategy to overcome inner filter effects is procuring iron complexes that absorb at higher wavelengths than the contaminants present in wastewater, which is part of the reason why applying iron sources containing already iron chelating ligands have been proposed, such as ferric oxalate [41], ferric citrate [42], or also other chelating agents [43]. Whereas there are several obvious advantages, there are also additional costs for adding the chelating agent, as the chelating agent is being oxidized as well more hydrogen peroxide ought to be needed to abate the target contamination.

Figure 7 shows mineralization of a mixture of five pesticides at three Fe^{2+} concentrations and the

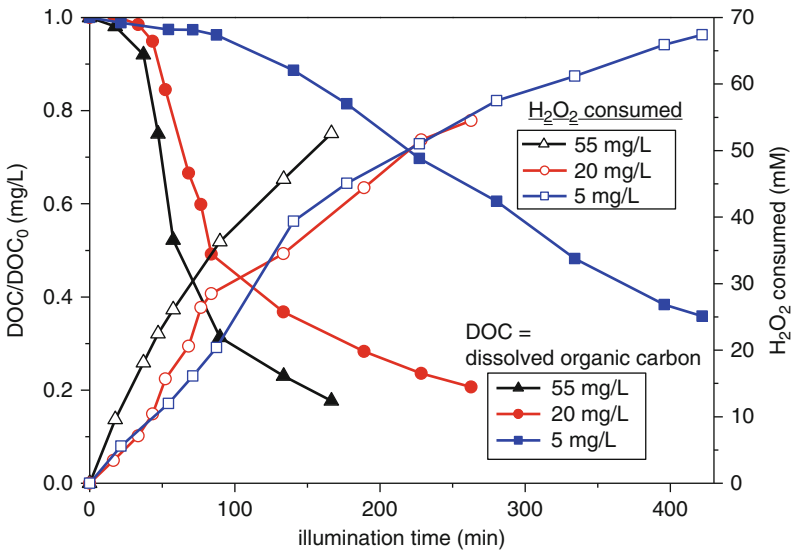

Solar Detoxification and Disinfection of Water. Figure 7
Mineralization of a pesticide mixture at different Fe^{2+} concentrations, with H_2O_2 consumed during photo-Fenton treatment

Solar Detoxification and Disinfection of Water. Table 2 Zero-order kinetic constants (mg/L min) for each pesticide in the mixture treated by photo-Fenton shown in Fig. 7

Compounds	Fe^{2+}(mg/L)			Fe^{3+}(mg/L)		
	5	20	55	5	20	55
Oxamyl	0.47	1.48	3.62	0.29	1.34	2.50
Methomyl	0.11	0.40	0.55	0.10	0.36	0.47
Imidacloprid	0.11	0.44	1.08	0.10	0.41	0.69
Pyrimethanil	0.24	0.89	0.99	0.24	0.75	1.14
Dimethoate	0.32	0.99	1.69	0.39	1.16	1.56

corresponding hydrogen peroxide requirements during the processes [44]. The results were very similar to those with Fe^{3+}, especially at low iron concentrations. No significant difference in DOC was observed between Fe species, although this was not the case for degradation of each individual pesticide, as discussed later (see Table 2). Fe^{2+} salt is rapidly converted to Fe^{3+} if there is excess H_2O_2 (during the first seconds after adding H_2O_2), but the $^{\bullet}OH$ produced by Fenton reaction (Eq. 12) is not enough for significant oxidation of organics. When Fe^{3+} salt is used, it is reduced to Fe^{2+}, mainly by solar irradiation and by H_2O_2 (Eqs. 17 and 18). As the system behaves independently of the initial oxidation state of iron, ferrous iron cannot usually be distinguished from ferric iron by the reaction mechanism. However, in practice, differences in degradation rates may be observed. The presence of Fe^{2+} promotes an initial rapid degradation phase. The extent of this phase depends on the Fe/contaminant molar ratio. On the contrary, when Fe^{3+} is the initial iron source, the oxidation rate is slower than observed with Fe^{2+}, probably due to the fact that as Fe^{3+} is reduced to Fe^{2+}, the free radicals are generated more slowly. It is worth mentioning that with 5 mg/L of iron, treatment is noticeably less efficient (slower pesticide degradation, longer time required for any substantial mineralization, and more hydrogen peroxide consumed). This is because when the iron concentration is very low, H_2O_2 is consumed by less desirable reactions, such as Reactions 13, 21, and 22.

There were no significant differences between the other two iron concentrations (20 mg/L and 55 mg/L), although, as expected, results were slightly better with 55 mg/L. This can be explained because, due to the solar photoreactor design, iron concentration is enough to absorb all the solar irradiation in both cases. Therefore, Reactions 16–19 are maximized permitting quick regeneration of the ferrous ions. Under these conditions, the amount of absorbed photons is quite similar at 20 and 55 mg/L of Fe in a solar photoreactor with a 5-cm light-path length [45]. It should be noticed that the higher the concentration of iron, the fewer photons reach the axis of the photoreactor. However, it may also be said that as iron concentration increases, less hydrogen peroxide is needed for the same degradation. This is because in the presence of higher iron concentrations, the process is accelerated by two added benefits. Firstly, the photocatalytic regeneration of ferrous iron from ferric iron is faster, and there are always ferrous ions available to consume H_2O_2 and produce hydroxyl radicals. H_2O_2 is also more efficient, as it is mainly consumed in "useful" reactions. When the process is too slow, part of the H_2O_2 is decomposed into molecular oxygen and water but does not participate in the oxidation of the polluting molecules. Equations 21–23 show some simultaneous inefficient reactions occurring in the matrix when the hydrogen peroxide concentration in the solution is too high:

$$2H_2O_2 \rightarrow 2H_2O + O_2 \tag{21}$$

$$^{\bullet}OH + H_2O_2 \rightarrow H_2O + HO_2^{\bullet} \tag{22}$$

$$HO_2^{\bullet} + {}^{\bullet}OH \rightarrow H_2O + O_2 \tag{23}$$

Table 2 shows the zero-order kinetic constants for each pesticide with regard to photo-Fenton degradation of the commercial pesticide mixture shown in Fig. 7, employing both iron species at the three tested

concentrations. As expected, the kinetic constants increase with iron concentration and more so with Fe^{2+} than with Fe^{3+} due to the initial fast degradation phase explained above. This effect becomes more noticeable as the iron concentration rises (higher Fe/contaminant molar ratio). It might therefore be concluded that when the main purpose is to substantially reduce the organic content of wastewater, it is irrelevant which species of iron is used as long as its concentration is not too high (mM range). The same is true when the reaction time is expected to be longer than a few minutes.

Effect of Temperature

Increasing temperature always has a beneficial effect on reaction kinetics [46, 47], for example, by about five times by raising temperature from 20°C to 50°C. This can be explained by looking at the thermal reactions involved in the reduction of ferric iron, particularly Eqs. 13, 14, as opposed to the photoreduction of ferric iron. Whereas in the thermal pathway hydrogen peroxide is consumed for the reduction of ferric iron without producing hydroxyl radicals, in the photoreduction pathway, hydrogen peroxide is not consumed. This seems an obvious and easy explanation, but normally, the issue becomes complicated when other reactions are involved. However, a fast, significant loss of dissolved iron could be observed at 50°C, decreasing the degradation rate dramatically due to the reduction in the catalyst concentration, which limits the process [48]. Obviously, the decreased catalyst concentration had a negative effect on the process (longer treatment time required), neutralizing the advantage of higher temperatures. Ferric hydroxides precipitate at a lower pH than ferrous iron. In the absence of further complexing substances, because of the low-solubility product of ferric iron hydroxide ($K_S(Fe(OH)_3) \approx 10^{-37}$), precipitation starts at pH 2.5–3.5 depending on the iron concentration, while the ferrous hydroxides precipitate mainly at a pH up to 6. Precipitation, which also depends on temperature, according to Sapieszko [49], is higher and faster as temperature increases from 25°C to 80°C.

But it is important to remark that the design of the solar plant should take it into consideration to (1) avoid solar light concentration, (2) avoid to operate, if possible, during so hot hours in summer or add more Fe if operation is compulsory, (3) recuperate heat from waste water before applying photo-Fenton when the source is too hot, and (4) keep under shadow pipelines and tanks of the solar plant or apply white paint to them. There are so different design decisions related with this statement.

Solar Disinfection and Photocatalytic Disinfection

Solar Disinfection

Outbreaks of disease as a result of the consumption of untreated or improperly treated drinking water contaminated with viral, bacterial, or parasitic agents that cause diarrheal diseases occur on a daily basis worldwide. In developing countries, global death from diarrhea of children aged less than 5 years were estimated at 1.87 million, approximately 19% of total child deaths [50]. The WHO and the United Nations Children's Fund (UNICEF) have recently claimed that improvement of drinking-water quality and basic sanitation are required to decrease childhood morbidity and mortality and to combat the main transmission route of diarrheal diseases (WHO/UNICEF 2007). Chlorine is used extensively, but has the drawback of the disinfection by-products and resistance. Nonchemical disinfection methods are rare in developing countries (UV-C, H_2O_2, and ozone) as energy costs are very high. Recent research attempts to combine sustainability with low cost, leading to an efficient disinfection method not only for drinking water but also for irrigation. One strategy for solving this problem consists of the use of natural sunlight, an abundant source of energy in many developing regions. The bactericidal effect of sunlight has been known for many years. Acra et al. [51] carried out the first practical study of solar disinfection by filling polyethylene bags with water and exposing them to full sunlight and suggested that natural sunlight could destroy pathogenic microorganisms present in the water. Since 1991, the Department of Water and Sanitation in Developing Countries (SANDEC) at the Swiss Federal Institute of Aquatic Science and Technology (EAWAG) has supported the development and application of solar water disinfection, and at present, about one million people worldwide use this system for treating drinking water [52]. Solar water

disinfection (SODIS) is a simple, environmentally sustainable, and inexpensive point-of-use treatment for drinking water, in which contaminated drinking water is placed in transparent plastic polyethylene terephthalate (PET) bottles and exposed to full sunlight for at least 6 h (or 2 consecutive days if there is more than 50% cloud cover) during daylight hours when the maximum intensity of radiation occurs. Sunlight disinfects contaminated water via the action of radiation in the spectrum of UV light and the high temperatures reached in the water. Numerous studies in the last 15 years have demonstrated the effectiveness of simulated and natural SODIS on the inactivation of viruses, bacteria, fungi, and protozoan parasites [18]. At present, SODIS is one of the recommended methods for disinfection of household drinking water [53].

It is widely accepted that solar UV inactivation of microbial cells occurs through a variety of mechanisms depending, inter alia, on the type of UV used for inactivation. Sunlight used during the SODIS process consists mainly of UV-A, and hence, the main inactivation mechanism is a photooxidative process as well as the generation of reactive oxygen species (ROS). ROS [54] include free radicals such as the superoxide anion as well as nonradicals such as hydrogen peroxide. When ROS interacts with DNA, single strand breaks occur as well as nucleic base modifications which may be lethal and mutagenic. Furthermore, oxidation of proteins and membrane damage is also induced. However, many aspects of solar UV-A inactivation are still unclear. Some studies have shown that UV-A damage depends on irradiance and dose [55], defining the first as the power incident per unit area (Wm^{-2}) and the second as the energy reaching a unit area (Jm^{-2}) of the target system during a given exposure time. Other studies indicate the manner in which the dose is delivered (continuously or intermittently) has an effect on the subsequent inactivation observed [56, 57]. Due to a variety of experimental conditions, (the use or non-use of simulation lamps, natural sunlight, volumes and types of water, as well as different organisms) it is very difficult to compare these inactivation results and draw concrete conclusions as to what drives UV-A inactivation. The usual practice of using plastic bottles in SODIS does not allow for a precise determination of the intensity reaching the surface of the bottle mainly because there are a wide variety of bottle geometries and designs in use throughout the developing world. Nevertheless, disinfection efficacy of the SODIS treatment can easily be affected by water turbidity, low irradiation intensity, and regrowth of bacteria after the solar treatment, probably due to photorepair mechanisms [58].

Solar Photocatalytic Disinfection

Solar photocatalytic disinfection with TiO_2 makes use of the reactive hydroxyl radicals produced by the semiconductor surface in contact with the water under irradiation by sunlight. Hydroxyl radical generation takes place in various reaction steps and is accompanied by coreactions depending on the catalyst surface and the molecules in the water, as fully described in section "Solar TiO_2 (Heterogeneous) Photocatalysis Applied to Water Decontamination." Due to the strong reactivity of the radicals, disinfection with TiO_2 was first reported in the 1980s for the Gram-positive bacteria *Lactobacillus acidophilus*, the Gram-negative bacteria *E. coli*, and the yeast *S. cerevisiae* [59].Very recently, the disinfection of water containing the oocysts of the important, very chlorine-resistant pathogen, *C. parvum* [60], and spores of several species of the fungus genus *Fusarium* have been reported at laboratory scale and in distilled water [61]. Although the interaction of the catalyst and the cell wall was neglected in the beginning, recent literature explains the disinfection process by lipid peroxidation of the cell wall followed by lesions on microbial cell walls and leakage of cell content into the media [62]. Probably, in most of these cases, the TiO_2 sticks to the microbial cell wall where the radicals generated produce these lesions, as observed (Fig. 8) in disinfection of *Fusarium* spores with TiO_2 slurry [63]. This disinfection mechanism is only applicable to slurry systems as in immobilized systems particles cannot be absorbed onto pathogen surface.

The configuration of the catalyst in the reactor can significantly affect the disinfection result. Typically, there are two ways to use the TiO_2 for water treatment purposes: (1) as aqueous suspensions of TiO_2 particles, which are usually called *slurry*, and (2) as immobilized TiO_2 over an inert matrix. If the system is designed for drinking-water purification for human consumption,

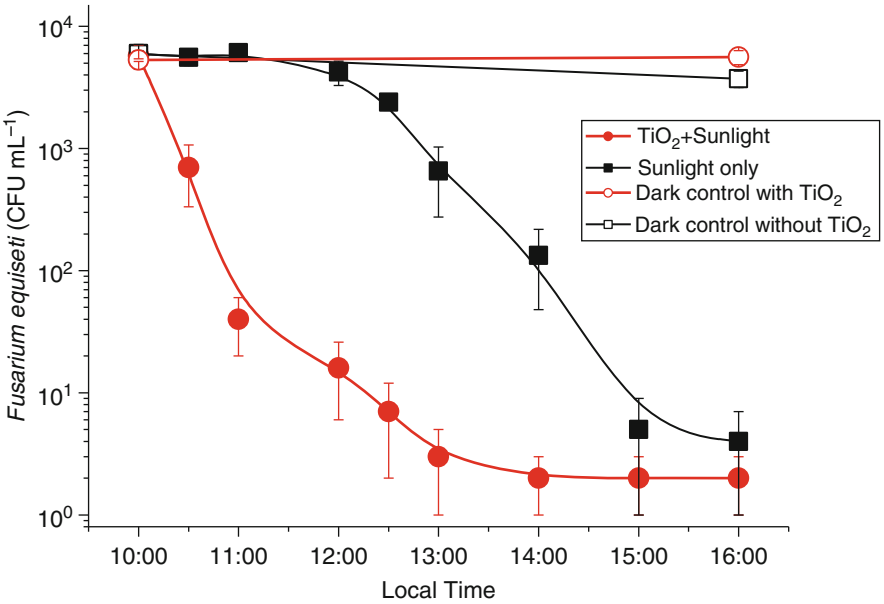

Solar Detoxification and Disinfection of Water. Figure 8
Inactivation of *Fusarium equiseti* spores (in terms of colony-forming units per milliliter, CFU mL^{-1}) in the presence of water and 35 mg L^{-1} of TiO_2 Degussa P25 in a bottle reactor (200 mL) during a 6-h sunlight exposure

the use of TiO_2 in suspension, as a part of a routine intervention for improving the potability of water at household level (point-of-use water treatment), is not feasible. The photocatalyst particles would have to be removed after solar exposure and before consumption. Unfortunately, in photocatalytic disinfection, almost all immobilized TiO_2 either had very limited yields or involved technical effort leading to high cost. It was even reported that immobilization of TiO_2 produces lower disinfection activity compared to slurry systems [64]. In one of the most important publications on the use of TiO_2 nanoparticles in disinfection, Yu et al. even reported positive results for doping with nonmetals. The authors found that sulfur-doped TiO_2 nanoparticles showed strong visible-light-induced activity that effectively kills *Micrococcus lylae*, a common Gram-positive bacterium, within 1 h on S-doped TiO_2 under visible light irradiation [65].

Comparison of experiments in different seasons, early and later in the day, and under cloudy and sunny conditions, leads one to conclude that solar photocatalytic disinfection does not depend proportionally on solar UV irradiance (solar UV intensity) as long as enough photons have been received for disinfection. The minimum UV energy necessary to reach complete inactivation depends on the microorganism and the reactor configuration. The irradiation mode in the photoreactor has also a high influence on the disinfection behavior. When light exposure is continuous (without temporal interruptions), the bactericidal effect of the process is faster and more efficient than when the light is applied intermittently [66]. Some contributions suggest that this effect can be due to bacterial dark-repair mechanisms which allow bacteria to reactivate after treatment [63]. This fact can also be attributed to the partial damage produced by the radiation which cannot totally inactivate all colonies of bacteria present in the water. It is also known that some damaged cells by UV radiation (not completely died or destroyed) can recover viability by means of DNA repair mechanisms. Rincón and Pulgarin designed the first method of assessing the bactericidal inactivation rate in solar photocatalytic processes for drinking water [56]. They demonstrated that the solar UV dose necessary to reach target disinfection levels cannot be the only indicator of system efficiency and proposed a new parameter called "effective disinfection time" (EDT), defined as the treatment

Solar Detoxification and Disinfection of Water. Figure 9 Photo of a solar disinfection CPC reactor to treat 25 L of drinking water at Plataforma Solar de Almeria facilities

time necessary to avoid bacterial regrowth after 24 h (or 48 h) in the dark after phototreatment.

Vidal et al. [67] published the first pilot plant study about TiO_2 solar photocatalysis for water disinfection. These authors constructed a new low-cost CPC prototype to better use the solar radiation for water disinfection objectives. Very recent work has studied improvement of solar disinfection using supported TiO_2 on resistant flexible materials, like cylinders, pills, balls, mesh, etc. One example is TiO_2 deposited on glass fiber inserted in a tubular photoreactor in a CPC solar collector [68]. Recent research work for concrete applications in the field of solar photocatalytic water treatment has also been sponsored by the European Commission in two different projects. As a final research step, both projects developed solar reactors (Fig. 9) to decontaminate and disinfect small volumes of water [69].

Solar Hardware for Water Decontamination and Disinfection

The specific hardware needed for solar photocatalytic applications has much in common with those used for thermal applications. As a result, both reactors and photocatalytic systems have followed conventional solar thermal collector designs, such as parabolic troughs and nonconcentrating collectors. At this point, their designs begin to diverge, since: (1) the fluid must be exposed to ultraviolet solar radiation, and therefore, the absorber must be UV-transparent, and (2) high temperature does not play a significant role in the photocatalytic process, so no insulation is required.

For many of the solar photocatalytic system components [70], the equipment is identical to that used for other types of water treatment and construction materials are commercially available. Most piping may be made of polyethylene or polypropylene, avoiding the use of metallic or composite materials that could be degraded by the oxidant conditions of the process. All materials used must be inert to degradation by UV solar light in order to be compatible with the minimum required lifetime of the system (10 years). Photocatalytic reactors must transmit UV light efficiently because of the process requirements. With regard to the reflecting/concentrating materials, aluminum is the best option due to its low cost and high reflectivity in the solar UV spectrum on earth surface. The photocatalytic reactor must contain the catalyst and be transparent to UV radiation, providing good mass transfer of the contaminant from the fluid stream to an illuminated photocatalyst surface with minimal pressure drop across the system. Aluminum is the only metal surface that is highly reflective throughout the ultraviolet spectrum. Reflectivities range from 92.3% at 280 nm to 92.5% at 385 nm. Comparable values for silver are 25.2% and 92.8%, respectively. The surfaces currently available that best fit these requirements are (1) electropolished anodized aluminum and (2) organic plastic films with an aluminum coating.

The choice of materials that are both transmissive to UV light and resistant to its destructive effects is limited. Common materials that meet these requirements are fluoropolymers, acrylic polymers, and several types of glass. Quartz has excellent UV transmission as well as good temperature and chemical resistance, but high cost makes it completely unfeasible for photocatalytic applications. Fluoropolymers are a good choice of plastic for photoreactors due to their good UV transmittance, excellent ultraviolet stability, and chemical inertness. One of their greatest disadvantages is that, in order to achieve a desired minimum

pressure rating, the wall thickness of a fluoropolymer tube has to be increased, which in turn will lower its UV transmittance. Acrylics could also potentially be used, but they are very brittle. Other low-cost polymeric materials are significantly more susceptible to be attacked by •OH radicals. Standard glass is not satisfactory because it absorbs part of the UV radiation that reaches it, due to its iron content. Borosilicate glass has good transmissive properties in the solar range with a cutoff of about 285 nm [71]. Therefore, such a low-iron-content glass would seem to be the most adequate.

The original solar photoreactor designs [72] for photochemical applications were based on line-focus parabolic-trough concentrators (PTCs). In part, this was a logical extension of the historical emphasis on trough units for solar thermal applications. Furthermore, PTC technology was relatively mature and existing hardware could be easily modified for photochemical processes. The main disadvantages are that the collectors (1) use only direct radiation, (2) are expensive, and (3) have low optical and quantum efficiencies [73].

One-sun (nonconcentrating) collectors have no moving parts or solar tracking devices. They do not concentrate radiation, so efficiency is not reduced by factors associated with concentration and solar tracking. An extensive effort in the design of small nontracking collectors has resulted in the testing of several different nonconcentrating solar reactors [30, 74]. Although one-sun collector designs possess important advantages, the design of a robust one-sun photoreactor is not trivial, due to the need for weather-resistant and chemically inert ultraviolet-transmitting reactors. In addition, nonconcentrating systems require significantly more photoreactor area than concentrating photoreactors, and, as a consequence, full-scale systems (normally composed of hundreds of square meters of collectors) must be designed to withstand the operating pressures anticipated for fluid circulation through a large field. In uncovered, nonconcentrating systems exposed to the ambient, reactants and catalyst could become contaminated. Very often, the chemical inertness of the materials used (to resist corrosion caused by outdoor operation and exposure to solar irradiation) for constructing the nonconcentrating collector would be difficult to guarantee.

Compound parabolic concentrators (CPCs) are static collectors with a reflective surface that can be designed for any given reactor shape. CPCs were invented in the 1960s [75] to achieve solar concentration with static devices, since they were able to concentrate on the receiver all the radiation that arrives within the collector's "angle of acceptance." They do so illuminating the complete perimeter of the receiver, rather than just the "front" of it, as in conventional flat plates. These concentrating devices have ideal optics, thus maintaining both the advantages of the PTC and static systems. The concentration factor (R_C) of a two-dimensional CPC collector is given by Eq. 24:

$$R_{C,CPC} = \frac{1}{\sin\theta_a} = \frac{A}{2\pi\ r} \tag{24}$$

The normal values for the semiangle of acceptance (θ_a), for photocatalytic applications, are between 60° and 90°. A special case is the one in which $\theta_a = 90°$, whereby $R_C = 1$ (nonconcentrating solar system). When this occurs, all the UV radiation that reaches the aperture area of the CPC (direct and diffuse) can be collected and redirected to the reactor. If the CPC is designed for an acceptance angle of +90° to −90°, all incident solar diffuse radiation can be collected (Fig. 10). The light reflected by the CPC is distributed all around the tubular receiver so that almost the entire circumference of the receiver tube is illuminated and the light incident on the photoreactor is the same that would be impinging on a flat plate [76]. They can make highly efficient use of both direct and diffuse solar radiation, without the need for solar tracking. There is no evaporation of possible volatile compounds, and water does not heat up. They have high optical efficiency, since they make use of almost all the available radiation, and high quantum efficiency, as they do not receive a concentrated flow of photons. Flow also can be easily maintained turbulent inside the tube reactor. Reports exist that provide excellent reviews of the needs toward the solar hardware for photocatalytic processes based on TiO_2 and photo-Fenton application including aspects of optics, geometry, and reactor materials [2, 18, 45, 73]. This literature also reviews the different solar collectors developed up-to-date and pilot-plant and industrial applications.

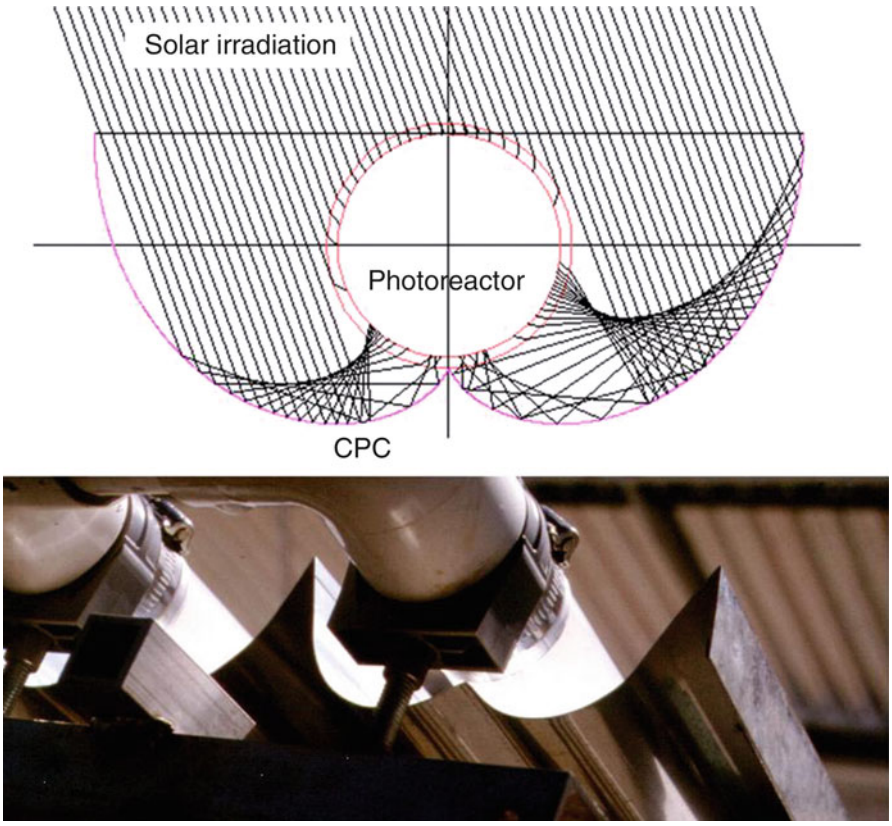

Solar Detoxification and Disinfection of Water. Figure 10
Schematic drawing and photograph of CPC with a semiangle of acceptance of 90º

Future Directions

TiO_2 is a cheap photostable catalyst, and the process may run at ambient temperature and pressure. Additionally, the oxidant, molecular oxygen (O_2), is the mildest. Therefore, in principle, the process involves a mild catalyst working under mild conditions with mild oxidants. However, as concentration and number of contaminants increase, the process becomes more complicated and challenging problems such as slow kinetics, low photoefficiency, and unpredictable mechanisms need to be solved. It is clear that naked TiO_2 needs extra help to undertake practical applications, and this may cause it to lose some of the charm of its mild operation. Therefore, there is a need to find new catalysts able to work with bandgaps which better overlap the solar spectrum, and no "cheap" solution to be used in wastewater treatment has yet been developed.

Photo-Fenton process has the potential of becoming widely applied, especially for wastewaters with medium pollution concentrations (TOC from tens of milligrams per liter up to around 1 g per liter). Several aspects, which in part are currently under development, may also greatly contribute to market introduction upon achieving maturity: (1) catalysts based on immobilized iron; (2) additives which enhance the process performance, regarding either kinetics or pH operation range; (3) optimization of photoreactors, taking into account the processes' specific requirements; and (4) ways to minimize hydrogen peroxide consumption, which is the main cost factor regarding consumables.

Little by little, TiO_2 disinfection research went from basic laboratory studies to the first trials with real disinfection applications. Microorganisms that are very resistant to UV-A irradiation have been successfully inactivated by TiO_2 photocatalysis, and therefore, recent TiO_2 disinfection research focuses more on disinfection applied to more resistant microorganisms.

The irradiation way on the photoreactor has a high influence on the disinfection behavior. When light exposure is made continuously, (without temporal interruptions) the disinfection effect of the process is faster and more efficient than when the light is applied intermittently. The minimum UV energy necessary to reach complete inactivation depends on the microorganism and the reactor configuration. Therefore, there are aspects that are essential to develope a technology, as (1) optimization of photoreactors, taking into account the processes' specific requirements; (2) development of viable process schemes (batch, continuous, semicontinuous); (3) development of process control strategies; (4) study of the influence of process parameters; (5) assessment of the influence of the water chemical parameters; and (6) finding out applications different to potable water disinfection (as a chemical-free system to control pathogens in agriculture).

The current lack of data for comparison of solar photocatalysis with other technologies definitely presents an obstacle toward an industrial application. One issue would be to give sound examples of techno-economic studies. Another aspect should be the assessment of the environmental impact in its broadest sense. One excellent tool is the application of technologies such as life cycle analysis comparing different technologies [77–79]. These studies confirm that solar photocatalysis is a promising technology compared to other investigated technologies, showing the least impact in most of the investigated categories.

Acknowledgments

The authors wish to thank the Spanish Ministry of Science and Innovation for financial support (EDARSOL project http://www.psa.es/webesp/projects/edarsol/index.php, CTQ2009-13459-C05-01).

Bibliography

Primary Literature

1. Gogate PR, Pandit AB (2004) A review of imperative technologies for wastewater treatment I: oxidation technologies at ambient conditions. Adv Environ Res 8:501–551
2. Malato S, Blanco J, Alarcón DC, Maldonado MI, Fernández P, Gernjak W (2007) Photocatalytic decontamination and disinfection of water with solar collectors. Catal Today 122: 137–149
3. Shannon MA, Bohn PW, Elimelech M, Georgiadis JG, Mariñas BJ, Mayes AM (2008) Science and technology for water purification in the coming decades. Nature 452: 301–310
4. Oller I, Malato S, Sánchez-Pérez JA (2011) Combination of advanced oxidation processes and biological treatments for wastewater decontamination-a review. Sci Total Environ 409:4141–4166
5. Mantzavinos D, Psillakis E (2004) Enhancement of biodegradability of industrial wastewaters by chemical oxidation pretreatment. J Chem Technol Biotechnol 79:431–454
6. Augugliaro V, Litter M, Palmisano L, Soria J (2006) The combination of heterogeneous photocatalysis with chemical and physical operations: a tool for improving the photoprocess performance. J Photochem Photobiol 7: 127–144
7. Comninellis C, Kapalka A, Malato S, Parsons SA, Poulios I, Mantzavinos D (2008) Perspective advanced oxidation processes for water treatment: advances and trends for R&D. J Chem Technol Biotechnol 83:769–776
8. Ikehata K, Gamal El-Din M (2006) Aqueous pesticide degradation by hydrogen peroxide/ultraviolet irradiation and Fenton-type advanced oxidation processes: a review. J Environ Eng Sci 5:81–135
9. WHO (2007) Economic and health effects of increasing coverage of low cost household drinking-water supply and sanitation interventions to countries off-track to meet MDG target 10. WHO Press, Geneva, Switzerland
10. FAO, AQUASTAT (2008) FAO's information system on water and agriculture. NRL http://www.fao.org/nr/water/aquastat/main/index.stm. Accessed Nov 2011
11. Anaissie EJ, Kuchar RT, Rex JH, Francesconi A, Kasai M, Müller FC, Lozano-Chiu M, Summerbell RC, Dignani MC, Chanock SJ, Walsh TJ (2001) Fusariosis associated with pathogenic *Fusarium* species colonization of a hospital water system: a new paradigm for the epidemiology of opportunistic mold infections. Clin Infect Dis 33:1871–1878
12. Polo-López MI, Fernández-Ibáñez P, García-Fernández I, Oller I, Salgado-Tránsito I, Sichel C (2010) Resistance of *Fusarium* sp spores to solar TiO_2 photocatalysis: influence of spore type and water (scaling-up results). J Chem Technol Biotechnol 85:1038–1048
13. Fernández-Ibáñez P, Sichel C, Polo-López I, de Cara-García M, Tello JC (2009) Photocatalytic disinfection of natural well water contaminated with *Fusarium solani* using TiO_2 slurry in solar CPC photo-reactors. Catal Today 144:62–68
14. Petrović M, Gonzalez S, Barceló D (2003) Analysis and removal of emerging contaminants in wastewater and drinking water. Trend Anal Chem 22:685–696
15. Klavarioti M, Mantzavinos D, Kassinos D (2009) Removal of residual pharmaceuticals from aqueous systems by advanced oxidation processes. Environ Int 35:402–417
16. Calza P, Pelizzetti E, Minero C (2005) The fate of organic nitrogen in photocatalysis: an overview. J Appl Electrochem 35:665–673

17. Konstantinou IK, Albanis TA (2004) TiO_2-assisted catalytic degradation of azodyes in aqueous solutions: kinetic and mechanistic investigations. A review. Appl Catal B: Environ 49:1–14
18. Malato S, Fernández-Ibáñez P, Maldonado MI, Blanco J, Gernjak W (2009) Decontamination and disinfection of water by solar photocatalysis: recent overview and trends. Catal Today 147:1–59
19. Konstantinou IK, Albanis TA (2003) Photocatalytic transformation of pesticides in aqueous titanium dioxide suspensions using artificial and solar light: intermediates and degradation pathways. Appl Catal B: Environ 42:319–335
20. Petrovic M, Farré M, Lopez de Alda M, Perez S, Postigo C, Köck M, Radjenovic J, Gros M, Barcelo D (2010) Recent trends in the liquid chromatography–mass spectrometry analysis of organic contaminants in environmental samples. J Chromatogr A 1217:4004–4017
21. Gómez MJ, Gómez-Ramos MM, Agüera A, Mezcua M, Herrera S, Fernández-Alba AR (2009) A new gas chromatography/mass spectrometry method for the simultaneous analysis of target and non-target organic contaminants in waters. J Chromatogr A 1216:4071–4082
22. Cassano AE, Alfano OE (2000) Reaction engineering of suspended solids heterogeneous photocatalytic reactors. Catal Today 58:167–197
23. Herrmann JM (2005) Heterogeneous photocatalysis: state of the art and present applications. Top Catal 14:48–65
24. Malato S, Blanco J, Campos A, Cáceres J, Guillard C, Herrmann JM, Fernández-Alba AR (2003) Effect of operating parameters on the testing of new industrial Titania catalysts at solar pilot plant scale. Appl Catal B: Environ 42:349–357
25. Kormann C, Bahnemann DW, Hoffmann MR (2001) Photolysis of chloroform and other organic molecules in aqueous TiO_2 suspensions. Environ Sci Technol 25:494–500
26. Fernández-Ibáñez P, Blanco J, Malato S, de las Nieves FJ (2003) Application of the colloidal stability of TiO_2 particles for recovery and reuse in solar photocatalysis. Water Res 37:3180–3188
27. Cunningham J, Sedlak J (1996) Kinetic studies of depollution process in TiO_2 slurries: interdependences of adsorption and UV-intensity. Catal Today 29:309–315
28. Monllor-Satoca D, Gómez R, González-Hidalgo M, Salvador P (2007) The "Direct–Indirect" model: an alternative kinetic approach in heterogeneous photocatalysis based on the degree of interaction of dissolved pollutant species with the semiconductor surface. Catal Today 129:247–255
29. Minero C (1999) Kinetic analysis of photoinduced reactions at the water semiconductor interface. Catal Today 54:205–216
30. Bahnemann D (2004) Photocatalytic water treatment: solar energy applications. Sol Energy 77:445–459
31. Turchi CS, Ollis DF (1990) Photocatalytic degradation of organic water contaminants: mechanisms involving hydroxyl radical attack. J Catal 122:178–192
32. Gerischer H (1995) The impact of semiconductors on the concepts of electrochemistry. Electrochim Acta 40:1277–1699
33. Martin ST, Lee AT, Hoffmann MR (1995) Chemical mechanism of inorganic oxidants in the TiO_2/UV process: increased rates of degradation of chlorinated hydrocarbons. Environ Sci Technol 29:2567–2573
34. Herrmann JM (1999) Heterogeneous photocatalysis: fundamentals and applications to the removal of various types of aqueous pollutants. Catal Today 53:115–129
35. Neyens E, Baeyens J (2003) A review of classic Fenton's peroxidation as an advanced oxidation technique. J Hazard Mater B98:33–50
36. Pignatello JJ, Oliveros E, MacKay A (2006) Advanced oxidation processes for organic contaminant destruction based on the Fenton reaction and related chemistry. Crit Rev Environ Sci Technol 3:1–84
37. Fenton HJH (1894) Oxidation of tartaric acid in presence of iron. J Chem Soc 65:899–910
38. Kavitha V, Palanivelu K (2004) The role of ferrous ion in Fenton and photo-Fenton processes for the degradation of phenol. Chemosphere 55:1235–1243
39. Zepp RG, Faust BC, Hoigné J (1992) Hydroxyl radical formation in aqueous reactions (pH 3–8) of iron (II) with hydrogen peroxide: the photo-Fenton reaction. Environ Sci Technol 26:313–319
40. Faust BC, Hoigne J (1990) Photolysis of Fe(III)-hydroxy complexes as sources of OH radicals in clouds, fog and rain. Atmos Environ 24:79–89
41. Safarzadeh-Amiri A, Bolton JR, Carter SR (1996) Ferrioxalate-mediated solar degradation of organic contaminants in water. Sol Energy 56:439–443
42. Silva MRA, Trovó AG, Nogueira RFP (2007) Degradation of the herbicide tebuthiuron using solar photo-Fenton process and ferric citrate complex at circumneutral pH. J Photochem Photobiol A: Chem 191:187–192
43. Sun Y, Pignatello JJ (1993) Activation of hydrogen peroxide by iron (III) chelates for abiotic degradation of herbicides and insecticides in water. J Agric Food Chem 41:308–312
44. Zapata A, Velegraki T, Sánchez-Pérez JA, Mantzavinos D, Maldonado MI, Malato S (2009) Solar photo-Fenton treatment of pesticides in water: effect of iron concentration on degradation and assessment of ecotoxicity and biodegradability. Appl Catal B: Environ 88:448–454
45. Malato S, Blanco J, Maldonado MI, Fernández P, Alarcon D, Collares M, Farinha J, Correia J (2004) Engineering of solar photocatalytic collectors. Sol Energy 77:513–524
46. Sagawe G, Lehnard A, Lubber M, Rochendorf G, Bahnemann D (2001) The insulated solar Fenton hybrid process: fundamental investigations. Helv Chim Acta 84:3742–3758
47. Gernjak W, Fuerhacker M, Fernández-Ibañez P, Blanco J, Malato S (2006) Solar photo-Fenton treatment—process parameters and process control. Appl Catal B: Environ 64:121–130
48. Zapata A, Oller I, Rizzo L, Hilgert S, Maldonado MI, Sánchez-Pérez JA, Malato S (2010) Evaluation of operating parameters involved in solar photo-Fenton treatment of wastewater:

interdependence of initial pollutant concentration, temperature and iron concentration. Appl Catal B: Environ 97:292–298
49. Sapieszko RS, Patel RC, Matijevic E (1977) Ferric hydrous oxide sols. 2. Thermodynamics of aqueous hydroxo and sulfato ferric complexes. J Phys Chem 81:1061–1068
50. Boschi-Pinto C, Velebit L, Shibuya K (2008) Estimating child mortality due to diarrhoea in developing countries. Bull World Health Organ 86:710–717
51. Acra A, Karahagopian Y, Raffoul Z, Dajani R (1980) Disinfection of oral rehydration solutions by sunlight. Lancet 2:1257–1258
52. EAWAG (2008) Solar water disinfection: the method. http://www.sodis.ch/methode/index_EN. Accessed 15 Sept 2010
53. WHO/ UNICEF (2005) Water for life: making it happen. http://www.who.int/water_sanitation_health/monitoring/jmp2005/en/index.html. Accessed 15 Sept 2008
54. Miller RV, Jeffrey W, Mitchell D, Elasri M (1999) Bacterial responses to ultraviolet light. ASM News 65:535–541
55. Hoerter JD, Arnold AA, Kuczynska DA (2005) Effects of sublethal UVA irradiation on activity levels of oxidative defense enzymes and protein oxidation in *Escherichia coli*. J Photochem Photobiol B: Biol 81:171–180
56. Rincón AG, Pulgarin C (2004) Field Solar *E coli* inactivation in the absence and presence of TiO_2: is UV solar dose an appropriate parameter for standardization of water solar disinfection? Sol Energy 77:635–648
57. Sichel C, Tello J, de Cara M, Fernandez-Ibanez P (2007) Effect of UV solar intensity and dose on the photocatalytic disinfection of bacteria and fungi. Catal Today 129:152–160
58. Rincón AG, Pulgarín C (2004) Bactericidal action of illuminated TiO_2 on pure *E. coli* and natural bacteria consortia: post-irradiation events in the dark assessment of the effective disinfection time. Appl Catal B: Environ 49:99–112
59. Matsunaga T, Tomoda R, Nakajima T, Nakamura N, Komine T (1988) Continuous-sterilization system that uses photosemiconductor powders. Appl Environ Microbiol 54:1330–1333
60. Méndez-Hermida F, Ares-Mazás E, McGuigan KG, Boyle M, Sichel C, Fernández-Ibáñez P (2007) Disinfection of drinking water contaminated with *Cryptosporidium parvum* oocysts under natural sunlight and using the photocatalyst TiO_2. J Photochem Photobiol B: Biol 88:105–111
61. Lonnen J, Kilvington S, Kehoe SC, Al-Touati F, McGuigan KG (2005) Solar and photocatalytic disinfection of protozoan, fungal and bacterial microbes in drinking water. Water Res 39:877–883
62. Kiwi J, Nadtochenko V (2005) Evidence for the mechanism of photocatalytic degradation of the bacterial wall membrane at the TiO_2 interface by ATR-FTIR and laser kinetic spectroscopy. Langmuir 21:4631–4641
63. Sichel C, de Cara M, Tello J, Blanco J, Fernández-Ibáñez P (2007) Solar photocatalytic disinfection of agricultural pathogenic fungi: *Fusarium* species. Appl Catal B: Environ 74:152–160
64. Gumy D, Rincón AG, Hajdu R, Pulgarin C (2006) Solar photocatalysis for detoxification and disinfection of water: different types of suspended and fixed TiO_2 catalysts study. Sol Energy 80:1376–1381
65. Yu JC, Ho W, Yu J, Yip H, Po KW, Zhao J (2005) Efficient visible-light-induced photocatalytic disinfection on sulfur-doped nanocrystalline titania. Environ Sci Technol 39:1175–1179
66. Rincón AG, Pulgarin C (2003) Photocatalytical inactivaton of *E. coli*: effect of (continuous-intermittent) light intensity and of (suspended-fixed) TiO_2 concentration. App Catal B: Environ 44:263–284
67. Vidal A, Díaz AI, El Hraiki A, Romero M, Muguruza I, Senhaji F, González J (1999) Solar photocatalysis for detoxification and disinfection of contaminated water: pilot plant studies. Catal Today 54:183–190
68. Fernández P, Blanco J, Sichel C, Malato S (2005) Water disinfection by solar photocatalysis using compound parabolic collectors. Catal Today 101:345–352
69. Navntoft C, Araujo P, Litter MI, Apella MC, Fernández D, Puchulu ME, Del Margarita VH, Blesa MA (2007) Field tests of the solar water detoxification SOLWATER reactor in Los Pereyra, Tucumán, Argentina. J Sol Energ-Trans ASME 129:127–134
70. Blanco J, Malato S (2003) Solar detoxification. UNESCO, France
71. Blanco J, Malato S, Fernández P, Vidal A, Morales A, Trincado P, de Oliveira JC, Minero C, Musci M, Casalle C, Brunotte M, Tratzky S, Dischinger N, Funken KH, Sattler C, Vincent M, Collares-Pereira M, Mendes JF, Rangel CM (2000) Compound parabolic concentrator technology development to commercial solar detoxification applications. Sol Energy 67:317–330
72. Goswami DY, Böer KW (1995) Engineering of solar photocatalytic detoxification and disinfection processes. Adv Sol Energy 10:165–209
73. Malato S, Blanco J, Vidal A, Richter C (2002) Photocatalysis with solar energy at a pilot-plant scale: an overview. Appl Catal B: Environ 37:1–15
74. Blanco-Galvez J, Fernández-Ibáñez P, Malato-Rodríguez S (2007) Solar photocatalytic detoxification and disinfection of water: recent overview. J Sol Energy Eng 129:4–15
75. Welford WT, Winston R (1978) The optics of non-imaging concentrators light solar energy. Academic, New York
76. Colina-Márquez J, Machuca-Martínez F, Li Puma JL (2009) Photocatalytic mineralization of commercial herbicides in a pilot-scale solar CPC reactor: photoreactor modeling and reaction kinetics constants independent of radiation field. Environ Sci Technol 43:8953–8960
77. Muñoz I, Peral J, Ayllón AJ, Malato S, Passarinho P, Domènech X (2006) Life cycle assessment of a coupled solar photocatalytic-biological process for wastewater treatment. Water Res 40:3533–3540
78. Muñoz I, Peral J, Ayllón AJ, Malato S, Martin MJ, Perrot JY, Vincent M, Domènech X (2007) Life cycle assessment of

a coupled advanced oxidation-biological process for wastewater treatment. Comparison with granular activated carbon adsorption. Environ Eng Sci 24:638–651
79. Muñoz I, Malato S, Rodríguez A, Doménech X (2008) Integration of environmental and economic performance of processes. Case study on advanced oxidation processes for wastewater treatment. J Adv Oxid Technol 11:270–275

Books and Reviews

Alfano OM, Bahnemann D, Cassano AE, Dillert D, Goslich R (2000) Photocatalysis in water environments using artificial and solar light. Catal Today 58:199–230
Augugliaro V, Litter M, Palmisano L, Soria J (2007) The combination of heterogeneous photocatalysis with chemical and physical operations: a tool for improving the photo process performance. J Photochem Photobiol C: Photochem Rev 7:123–144
Augugliaro V, Palmisano L, Malato S, Gernjak W (2009) Selected papers at the 5th European conference on solar chemistry and photocatalysis: environmental applications (SPEA5). Catal Today 144(3–4):183–366
Augugliaro V, Palmisano L, Malato S (2009) Solar chemistry and photocatalysis – environmental applications. Photochem Photobiol Sci 8(5)
Cassano AE, Alfano OE (2000) Reaction engineering of suspended solids heterogeneous photocatalytic reactors. Catal Today 58:167–197
Fujishima A, Rao TN, Tryk DA (2000) Titanium dioxide photocatalysis. J Photochem Photobiol C: Photochem Rev 1:1–21
Helz GR, Zepp RG, Crosby DG (1994) Aquatic and surface photochemistry. Lewis, Boca Raton
Herrmann JM (2007) Environmental green chemistry as defined by photocatalysis. J Hazard Mater 146:624–629
Legrini O, Oliveros E, Braun AM (1993) Photochemical processes for water treatment. Chem Rev 93:671–698
Malato S, Blanco J, Herrmann JM (1999) Solar catalysis for water decontamination. Catal Today 54(2–3)
Malato S, Blanco J, Estrada CA (2004) Photocatalysis. Sol Energy 77(5)
Malato S, Fernández-Ibáñez P, Giménez J (2005) Environmental applications of photocatalysis, 3rd European meeting on solar chemistry and photocatalysis: environmental applications. Catal Today 101(3–4)
Malato S, Fernández-Ibáñez P, Giménez J (2005) Environmental applications of solar energy. Sol Energy 79(4)
Malato Rodriguez S, Blanco Gálvez J (2007) Solar water detoxification. J Sol Energy Eng 129(1)
Malato Rodriguez S, Gernjak W, Pérez Peña J, Doña JM (2007) Selected contributions of the 4th European meeting on solar chemistry and photocatalysis: environmental applications (SPEA4). Catal Today 129(1–2):1–262
Serpone N, Pelizzetti E (1989) Photocatalysis: fundamental and applications. Wiley, New York

Solar Energy in Thermochemical Processing*

Anton Meier[1], Aldo Steinfeld[2]
[1]Solar Technology Laboratory, Department of General Energy Research, Paul Scherrer Institute, Villigen PSI, Switzerland
[2]Institute of Energy Technology, Department of Mechanical and Process Engineering, ETH Zurich, Zurich, Switzerland

Article Outline

Glossary
Definition of the Subject and Its Importance
Introduction
Thermodynamics of Solar Thermochemical Conversion
Solar Thermochemical Processes
Life Cycle and Economic Analyses
Future Directions
Note
Nomenclature
Bibliography

Glossary

Aperture Opening of a solar cavity receiver.

Carnot efficiency Maximum efficiency for converting heat from a high-temperature thermal reservoir at T_H into work in a cyclic process, and rejecting heat to a low-temperature thermal reservoir at T_L, given by $1-T_L/T_H$.

CB (carbon black) Important industrial raw material used as pigment and reinforcement in rubber and plastic products.

CPC (compound parabolic concentrator) Non-imaging concentrating device that is usually positioned in tandem with the primary parabolic concentrating system to further augment the solar concentration ratio.

CSP (concentrating solar power) CSP plants generate electricity by converting solar energy into high-temperature heat using various mirror configurations.

Endothermic Absorbs heat.

Exothermic Rejects heat.

Exergy efficiency (for a solar thermochemical process) The efficiency for converting solar energy into chemical energy, given by the ratio of the maximum work that may be extracted from a solar fuel to the solar energy input for producing such a fuel.

Direct normal solar irradiance Power flux of direct solar irradiation on a surface perpendicular to the sun's rays.

Fuel cell A fuel cell is an electrochemical cell that converts a fuel into electricity. In the presence of an electrolyte, a fuel (e.g., hydrogen) and an oxidant (e.g., oxygen or air) react and generate an electric current.

PEM (polymer electrolyte membrane) fuel cell PEM fuel cells – also called proton exchange membrane fuel cells – deliver high-power density and offer the advantages of low weight and volume, compared with other fuel cells.

Quench Rapid cooling, e.g., of a high-temperature gas mixture to avoid recombination of products.

Solar cavity receiver A well-insulated enclosure, with a small opening to let in concentrated solar energy, which approaches a blackbody absorber in its ability to capture solar energy.

Solar chemical heat pipe Concept for storing and transporting solar energy using a reversible endothermic reaction.

Solar concentration ratio Non-dimensional ratio of the solar flux intensity (e.g., in "suns") achieved after concentration to the normal insolation of incident beam.

Solar fuels Fuels produced with solar energy.

Solar thermochemical process Any endothermic process that uses concentrated solar energy as the source of high-temperature process heat.

Syngas Synthesis gas (a mixture of primarily hydrogen and carbon monoxide), which serves as the building block for a wide variety of synthetic fuels including Fischer-Tropsch type chemicals, hydrogen, ammonia, and methanol.

Definition of the Subject and Its Importance

This entry develops the underlying science of solar-driven thermochemical processes and describes their applications for efficiently producing clean fuels and material commodities.

Introduction

Sunlight is by far the most abundant carbon-neutral energy resource on earth. More energy from the sun strikes the earth's surface in 1 h than is consumed annually by all of the fossil fuels. In fact, using only 0.1% of the earth's land space with solar collectors that operate with a collection efficiency of merely 20%, one could gather more than enough energy to supply the current yearly energy needs of all the citizens of the planet (about $1.3 \cdot 10^{14}$ kWh) [1]. Furthermore, the solar energy reserve is essentially unlimited and its utilization is ecologically benign. However, solar radiation is dilute (only about 1 $kW \cdot m^{-2}$), intermittent (available only during day-time and under clear-sky conditions), and unequally distributed (mostly by the equator). These drawbacks can be overcome by converting solar energy into chemical energy carriers, that is, *Solar Fuels,* that can be long-term stored and long-range transported, from the sunny and desert regions of the earth to the industrialized and populated centers, where much of the energy is needed. Solar fuels can be burnt to generate heat, further processed into electrical or mechanical work, or used directly to generate electricity in fuel cells and batteries, to meet whenever and wherever the customer's energy demands. Solar process heat can also assist in the processing and recycling of energy-intensive materials, thus avoiding greenhouse gas emissions and other pollutants derived from the combustion of fossil fuels for heat and electricity generation.

There are basically three routes that can be used alone or in combination for producing storable and transportable fuels from solar energy [1]: The *electrochemical* route uses solar electricity made from photovoltaic or concentrating solar thermal systems followed by an electrolytic process; the *photochemical/photobiological* route makes direct use of solar photon energy for photochemical and photobiological processes; the *thermochemical* route uses concentrated solar radiation as the source of high-temperature heat for endothermic thermochemical processes.

The thermochemical route offers some intriguing thermodynamic advantages with direct economic implications. It is this approach that is the subject of this entry; the other two routes are beyond its scope.

Figure 1 illustrates the basic idea of the solar thermochemical route [1]. By concentrating the diluted

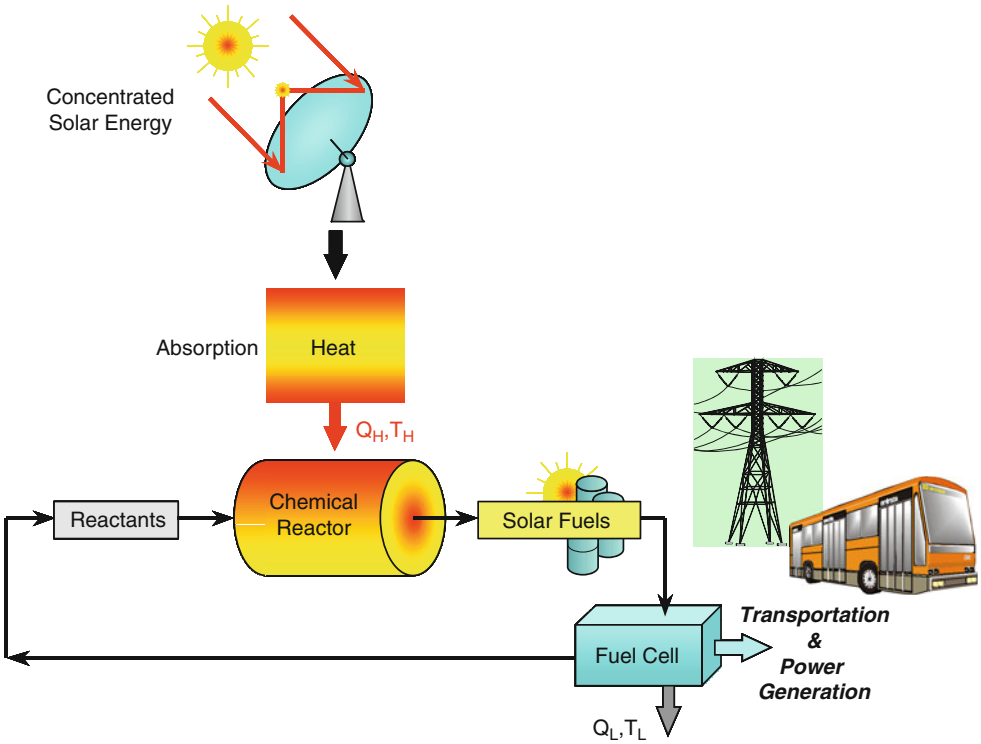

Solar Energy in Thermochemical Processing. Figure 1
Energy conversion into solar fuels for transportation and power generation – Concentrated solar radiation is used as the energy source of high-temperature process heat for driving thermochemical reactions toward the production of storable and transportable fuels (Adapted from [1])

sunlight over a small area with the help of parabolic mirrors, and then capturing the radiant energy with the help of suitable receivers and reactors, heat at high temperatures can be obtained for carrying out an *endothermic* chemical transformation and producing storable and transportable fuels. These solar fuels ultimately store solar energy within their chemical bonds. Regardless of the fuel, the higher the temperature of the reaction process, the higher the efficiency of energy conversion. Higher temperatures, however, also lead to greater losses by re-radiation from the solar receiver. The thermodynamic implications of such phenomena are examined in the following section.

Thermodynamics of Solar Thermochemical Conversion

The state-of-the-art technology for large-scale collection and concentration of solar energy is based on three main optical configurations using parabolic-shaped mirror reflectors. These are the trough, tower, and dish systems, shown schematically in Fig. 2 [2]. Trough systems use linear, two-dimensional, parabolic mirrors to focus sunlight onto a tubular receiver positioned along their focal line. Tower systems use a field of heliostats (two-axis tracking parabolic mirrors) that focus the sunrays onto a receiver mounted on top of a centrally located tower. Dish systems use paraboloidal mirrors to focus sunlight on a receiver positioned at their focus. Solar furnaces are concentrating research facilities, in which high-flux solar intensities are usually obtained at a fixed location inside a housed laboratory. The traditional design consists of a sun-tracking, flat heliostat on-axis with a stationary primary paraboloidal concentrator [3]; off-axis configurations have also been designed.

The capability of these collection systems to concentrate solar energy is often expressed in terms of their mean flux concentration ratio $\widetilde{C}$ over a targeted area A

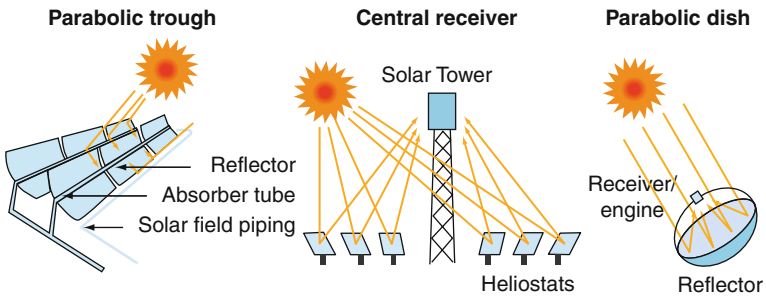

Solar Energy in Thermochemical Processing. Figure 2
Schematic of the three main optical configurations for large-scale collection and concentration of solar energy: Parabolic trough, central receiver (tower system), and parabolic dish (From [2])

at the focal plane, normalized with respect to the incident *direct normal solar irradiance I*:

$$\widetilde{C} = \frac{\dot{Q}_{solar}}{I \cdot A} \tag{1}$$

Here, $\dot{Q}_{solar}$ is the solar radiative power input into the target. $\widetilde{C}$ is often given in units of "suns" when normalized to $I = 1\ \mathrm{kW{\cdot}m^{-2}}$. The *solar concentration ratio* typically obtained at the focal plane varies between 30 and 100 suns for trough systems, 500–2,500 suns for tower systems, and 1,000–10,000 suns for dish systems. Higher concentration ratios imply lower heat losses from smaller receivers and, consequently, higher attainable temperatures at the receiver. To some extent, the flux concentration can be further augmented with the help of a non-imaging secondary concentrator, for example, a *compound parabolic concentrator*, referred to as *CPC*, which is positioned in tandem with the primary concentrating system [4].

The solar concentrating systems have been proven to be technically feasible in large-scale pilot and commercial plants aimed mainly at producing electricity. They make use of a working fluid (typically air, water, synthetic oil, helium, sodium, or molten salt) that is heated by solar energy and then used in traditional steam or gas turbines. As of early 2010, the global stock of commercial CSP plants neared 1 GW capacity, mainly in Spain and the United States [2]. Parabolic troughs account for the largest share of the current CSP market, but competing technologies such as towers are emerging. Some plants incorporate thermal energy storage to guarantee continuous capacity and to expand production time.

Solar thermochemical applications, although not developed as far as solar thermal electricity generation, employ similar solar concentrating technologies, mainly based on the solar tower concept capable of achieving high process temperatures [5]. However, high-temperature thermochemical processes require higher solar concentration than state-of-the-art CSP plants, which has an impact on heliostat field layout and plant operation. An advanced concept is the "beam-down" Cassegrain optical configuration for the tower system that makes use of a hyperboloidal reflector at the top of the tower to redirect sunlight to a receiver located on the ground level [6].

Solar chemical reactors for highly concentrated solar systems usually feature the use of a cavity-receiver type configuration, that is, a well-insulated enclosure with a small opening (the *aperture*) to let in concentrated solar radiation. Because of multiple internal reflections, the fraction of the incoming energy absorbed by the cavity greatly exceeds the simple surface absorptance of the inner walls. The larger the ratio of the characteristic length to the aperture diameter of the cavity, the closer the cavity-receiver approaches a blackbody absorber. Smaller apertures also serve to reduce re-radiation losses. However, they intercept a reduced fraction of the sunlight reflected from the concentrators. Consequently, the optimum aperture size is a compromise between maximizing radiation capture and minimizing radiation losses.

The solar energy absorption efficiency of a solar reactor, $\eta_{absorption}$, is defined as the net rate, at which energy is being absorbed, divided by the solar power coming from the concentrator. At temperatures above

about 1,000 K, the net power absorbed is diminished mostly by radiant losses through the aperture. For a perfectly insulated blackbody cavity-receiver, it is given by

$$\eta_{absorption} = 1 - \frac{\sigma T^4}{I\widetilde{C}} \tag{2}$$

T is the nominal cavity-receiver temperature, and σ the Stefan–Boltzmann constant. The absorbed concentrated solar radiation drives an endothermic chemical reaction. The measure of how well solar energy is converted into chemical energy for a given process is the exergy efficiency, defined as

$$\eta_{exergy} = \frac{-\dot{n}\Delta G|_{T_L}}{\dot{Q}_{solar}} \tag{3}$$

$\dot{Q}_{solar}$ is the solar power input, $\dot{n}$ is the molar flow rate of the products, and ΔG is the maximum possible amount of work (Gibbs free energy change) that may be extracted from the products as they are transformed back to reactants at ambient temperature, $T_L = 298$ K. The second law of thermodynamics is now applied to calculate the theoretical maximum *exergy efficiency* $\eta_{exergy,ideal}$. Since the conversion of solar process heat to chemical energy is limited by both the solar absorption efficiency and the Carnot efficiency, the maximum ideal exergy efficiency is given by [7]

$$\begin{aligned}\eta_{exergy,\,ideal} &= \eta_{absorption} \cdot \eta_{Carnot} \\ &= \left(1 - \frac{\sigma T_H^4}{I\widetilde{C}}\right) \times \left(1 - \frac{T_L}{T_H}\right)\end{aligned} \tag{4}$$

where T_H and T_L are the upper and lower operating temperatures of the equivalent Carnot heat engine. In Fig. 3, $\eta_{exergy,ideal}$ is plotted as a function of T_H for $T_L = 298$ K and for various solar concentration ratios. Because of the Carnot limit, one should try to operate thermochemical processes at the highest upper temperature possible; however, from a heat-transfer perspective, the higher the temperature, the higher the re-radiation losses. The highest temperature an

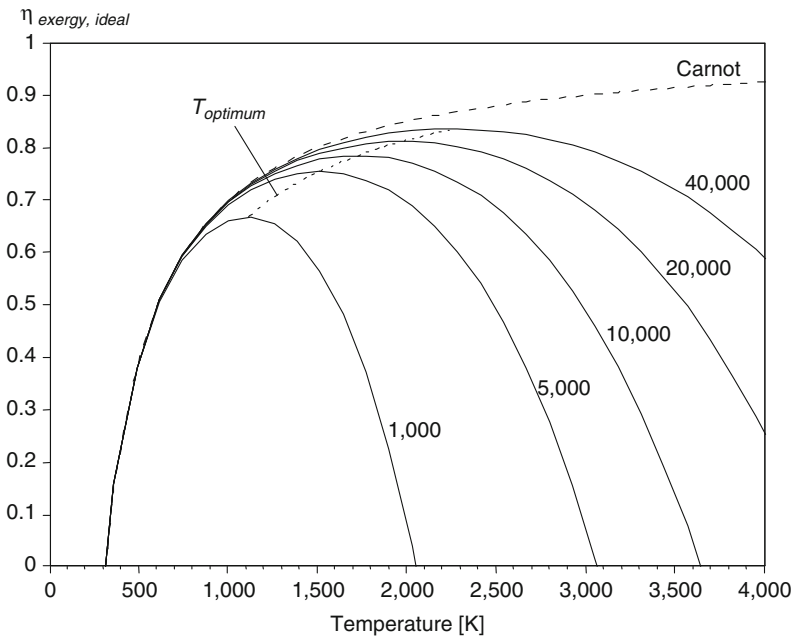

Solar Energy in Thermochemical Processing. Figure 3

Variation of the ideal exergy efficiency $\eta_{exergy,ideal}$ as a function of the operating temperature T_H, for a blackbody cavity-receiver converting concentrated solar energy into chemical energy. The mean solar flux concentration is the parameter: 1,000. . .40,000. Also plotted are the Carnot efficiency and the locus of the optimum cavity temperature $T_{optimum}$ (Adapted from [1])

ideal *solar cavity-receiver* is capable of achieving, defined as the stagnation temperature $T_{stagnation}$, is calculated by setting $\eta_{exergy,ideal}$ equal to zero, yielding

$$T_{stagnation} = \left(\frac{I\widetilde{C}}{\sigma}\right)^{0.25} \tag{5}$$

At this temperature, energy is being re-radiated as fast as it is absorbed. Stagnation temperatures exceeding 3,000 K are attainable with solar concentration ratios above 5,000 suns. However, an energy-efficient process must run at temperatures that are substantially below $T_{stagnation}$. There is an optimum temperature $T_{optimum}$ for maximum efficiency obtained by setting

$$\frac{\partial \eta_{exergy,\,ideal}}{\partial T} = 0 \tag{6}$$

Assuming a uniform power flux distribution, this relation yields the following implicit equation for $T_{optimum}$ [8]:

$$T_{optimum}^5 - \frac{3}{4} T_L T_{optimum}^4 - T_L \frac{I\widetilde{C}}{4\sigma} = 0 \tag{7}$$

The locus of $T_{optimum}$ is shown in Fig. 3. For example, for a solar concentration ratio of 5,000, the optimum temperature of a solar receiver is 1,500 K, giving a maximum theoretical efficiency of 75%, that is, the portion of solar energy that could – in principle – be converted into the chemical energy of fuels. In practice, however, when considering convection and conduction losses in addition to re-radiation losses, the efficiency will peak at a somewhat lower temperature.

The process modeling described in the following paragraphs establishes a base for evaluating and comparing different *solar thermochemical processes* in terms of their ideal exergy efficiency.

Figure 4 depicts a flow diagram of an ideal cyclic process that leads to a fuel, which uses a solar reactor, a quenching device, and a fuel cell. The complete process is carried out at constant pressure. In practice, pressure drops will occur throughout the system. If one assumes, however, frictionless operating conditions, no pumping work is required. The reactants may be pre-heated in an adiabatic heat exchanger where some portion of the sensible and latent heat of the products is transferred to the reactants; for simplicity, a heat exchanger has been omitted. The reactor is

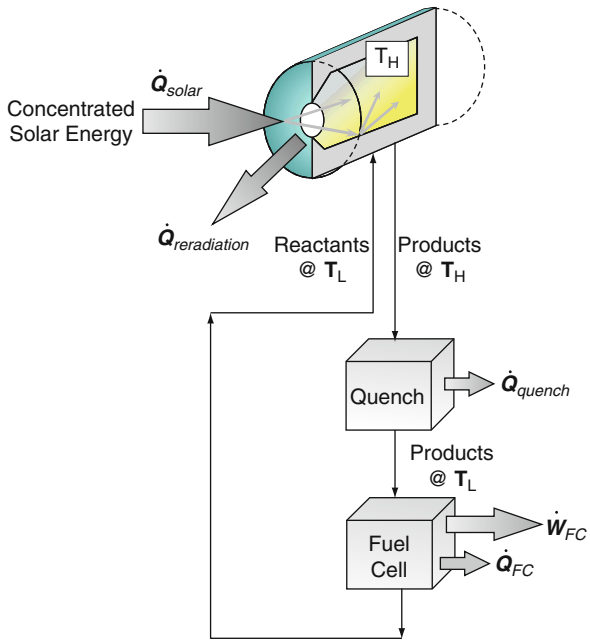

Solar Energy in Thermochemical Processing. Figure 4 Model flow diagram of an ideal cyclic process for calculating the maximum exergy efficiency of a solar thermochemical process (Adapted from [1])

assumed to be a perfect blackbody cavity-receiver. The reactants enter the solar reactor at T_L and are further heated to the reaction temperature T_H. Chemical equilibrium is assumed inside the reactor. The net power absorbed in the solar reactor should match the enthalpy change per unit time of the reaction,

$$\dot{Q}_{reactor,\,net} = \dot{n}\Delta H\,|_{\,Reactants\,@\,T_L \,\rightarrow\, Products\,@\,T_H} \tag{8}$$

Irreversibility in the solar reactor arises from the non-reversible chemical transformation and re-radiation losses $\dot{Q}_{reradiation}$ to the surroundings at T_L. It is found that

$$Irr_{reactor} = \frac{-\dot{Q}_{solar}}{T_H} + \frac{\dot{Q}_{reradiation}}{T_L} + \dot{n}\Delta S|_{\,Reactants\,@\,T_L \,\rightarrow\, Products\,@\,T_H} \tag{9}$$

Products exit the solar reactor at T_H and are cooled rapidly to T_L. The amount of power lost during quenching is

$$\dot{Q}_{quench} = -\dot{n}\Delta H\,|_{\,Products\,@\,T_H \,\rightarrow\, Products\,@\,T_L} \tag{10}$$

The irreversibility associated with quenching is

$$Irr_{quench} = \frac{\dot{Q}_{quench}}{T_L} + \dot{n}\Delta S|_{Products\ @\ T_H \rightarrow Products\ @\ T_L} \tag{11}$$

Introducing a reversible, ideal fuel cell, in which the products recombine to form the original reactants and thereby generate electrical power, closes the cycle. The maximum amount of work that the products leaving the reactor could produce if they combined at T_L and a total pressure of 1 bar is given by

$$\dot{W}_{FC} = -\dot{n}\Delta G|_{Products\ @\ T_L \rightarrow Reactants\ @\ T_L} \tag{12}$$

This work value is also known as the exergy of the products at ambient temperature T_L. The fuel cell operates isothermally; the amount of heat rejected to the surroundings is

$$\dot{Q}_{FC} = -T_L \cdot \dot{n}\Delta S|_{Products\ @\ T_L \rightarrow Reactants\ @\ T_L} \tag{13}$$

The exergy system efficiency of the closed cycle is then calculated using (Eq. 3) as

$$\eta_{exergy} = \frac{\dot{W}_{FC}}{\dot{Q}_{solar}} \tag{14}$$

This thermodynamic analysis can be verified by performing an energy balance and by evaluating the maximum achievable efficiency (Carnot efficiency) from the total available work and from the total power input. The energy balance should satisfy

$$\dot{W}_{FC} = \dot{Q}_{solar} - (\dot{Q}_{reradiation} + \dot{Q}_{quench} + \dot{Q}_{FC}) \tag{15}$$

The available work is calculated as the sum of the fuel-cell work plus the lost work due to the irreversibility associated with the solar reactor and with quenching. Thus,

$$\eta_{\max} = \frac{\dot{W}_{FC} + T_L \cdot (Irr_{reactor} + Irr_{quench})}{\dot{Q}_{solar}} = 1 - \frac{T_L}{T_H} = \eta_{Carnot} \tag{16}$$

Any solar thermochemical process can be thought of in this manner, and their exergy efficiencies can be compared as one criterion for judging their relative industrial potential. The higher the exergy efficiency, the lower is the required solar collection area for producing a given amount of solar fuel and, consequently, the lower are the costs incurred for the solar concentrating system, which usually correspond to half of the total investments for the entire solar chemical plant. Thus, high exergy efficiency implies favorable competitiveness.

Solar Thermochemical Processes

Solar Production of Fuels

Metals are attractive candidates for storage and transport of solar energy [1]. They may be used to generate either high-temperature heat via combustion or electricity via fuel cells and batteries. Metals can also be used to produce solar fuels, such as H_2 from H_2O via hydrolysis, or synthesis gas (*syngas*) from H_2O and CO_2. The chemical products from any of these power- or fuels-generating processes are metal oxides, which, in turn, need to be recycled.

Solar Production of Metals The conventional extraction of metals from their oxides by carbothermic and electrolytic processes is characterized by its high energy consumption and its concomitant environmental pollution. The extractive metallurgical industry discharges vast amounts of greenhouse gases and other pollutants to the environment, derived mainly from the combustion of fossil fuels for heat and electricity generation. These emissions can be substantially reduced, or even completely eliminated, by using concentrated solar energy as the source of high-temperature process heat.

The thermal dissociation and electrothermal reduction of metal oxides proceed without reducing agent, while the carbothermal reduction of metal oxides uses solid carbon C(s) or gaseous hydrocarbons (e.g., CH_4) as reducing agents. The corresponding overall chemical reactions may be represented as follows:

$$M_xO_y \rightarrow xM + \frac{y}{2}O_2 \tag{17}$$

$$M_xO_y + yC(s) \rightarrow xM + yCO \tag{18}$$

$$M_xO_y + yCH_4 \rightarrow xM + y(2H_2 + CO) \tag{19}$$

Here, M denotes the metal and M_xO_y the corresponding metal oxide. The Gibbs free energy of formation, $\Delta_f G^\circ$, of many stable metallic oxides such as

ZnO, MgO, SiO_2, CaO, Al_2O_3, and TiO_2 are large negative numbers that decrease in magnitude with temperature, while their enthalpy of formation, $\Delta_f H^\circ$, remains relatively independent of temperature. Table 1 lists the approximate temperatures at which the standard Gibbs free energy $\Delta_r G^\circ$ for reactions (17), (18), and (19) equals zero for various metal oxides of interest [9, 10].

Thermal Dissociation of Metal Oxides. The solar thermal dissociation of ZnO is among the most promising metal oxide processes. A kinetic study reported an apparent activation energy of $E_a = 361 \pm 53$ kJ·mol^{-1}, which was experimentally determined from isothermal runs in the range 1,800–2,100 K using a solar-driven thermogravimeter – a setup closely approximating the heat and mass transfer characteristics of solar reactors [11]. The E_a is in agreement with previous values ranging from 310 to 350 kJ·mol^{-1} [12] and comparable to non-solar thermogravimetric [13] and solar non-gravimetric [14] analyses. Kinetic parameters determined in an aerosol flow reactor resulted in a pre-exponential factor three orders of magnitude faster than that in stationary reactors [15, 16]. The product gases Zn(g) and O_2 need to be quenched to avoid recombination, which introduces irreversibility and may be a factor of complexity in large-scale utilization [17]. In particular, the quench efficiency is sensitive to the dilution ratio of zinc and oxygen in an inert gas flow and to the temperature of the surface on which the products are quenched [18]. Maximum exergy efficiencies exceeding 50% are possible for a molar ratio of an inert gas to ZnO(s) less than 1 [12]. The condensation of Zn(g) in the presence of O_2 was studied by fractional crystallization in a temperature-gradient tube furnace. The oxidation of Zn is a heterogeneous process and, in the absence of nucleation sites, Zn(g) and O_2 can coexist in a meta-stable state [13].

Except for the thermal dissociation of ZnO, the required temperature for effecting reaction (17) exceeds 3,000 K (Table 1). At temperatures for which $\Delta_r G^\circ$ is positive, solar process heat alone will not make the reaction proceed; some amount of high-quality energy is required in the form of work. It may be supplied in the form of electrical energy in electrolytic processes or in the form of chemical energy by introducing a reducing agent in thermochemical processes.

Electrothermal Reduction of Metal Oxides. An example of a solar electrothermal reduction process that has been demonstrated experimentally in small-scale reactors is the electrolysis of ZnO(s) [19, 20]. At 1,000 K, up to 30% of the total amount of energy required to produce Zn could be supplied by solar process heat using an electrolytic cell housed in a solar cavity-receiver. ZnO(s) is dissolved into an electrolyte composed of a combination of sodium, aluminum, and/or calcium fluoride with a melting point near the process temperature. This choice prevents excess loss of electrolyte due to evaporation. Electric energy is then supplied to two electrodes immersed in a saturated solution. The previous solar thermal electrolytic research [21, 22] identified workable electrolytes as well as crucible and electrode materials; some initial estimates were made of cell resistances and current densities, which were near those found in the industrial

Solar Energy in Thermochemical Processing. Table 1 Approximate temperatures for which $\Delta_r G^\circ$ of reactions (17), (18), and (19) equals zero (From [9, 10])

Metal oxide	Reaction (17): $\Delta_r G^\circ = 0$ at T ~	Reaction (18): $\Delta_r G^\circ = 0$ at T ~	Reaction (19): $\Delta_r G^\circ = 0$ at T ~
Fe_2O_3[a]	3,050 K	920 K	890 K
Al_2O_3	> 4,000 K	2,320 K	1,770 K
MgO	3,700 K	2,120 K	1,760 K
ZnO	2,340 K	1,220 K	1,110 K
TiO_2[a]	> 4,000 K	2,040 K	1,570 K
SiO_2[a]	4,500 K	1,950 K	1,520 K
CaO	> 4,000 K	2,440 K	1,970 K

[a] Fe_2O_3, TiO_2, and SiO_2 decompose to lower-valence metal oxides before complete dissociation to the metal

Hall–Heroult smelting process; materials for the solar reactor were also identified and shown to be reliable under the severe thermal environment of concentrated solar energy. In contrast to the direct solar thermal reduction of ZnO, the solar thermal electrolytic path produces unmixed Zn(g) and O_2 [23]. High-temperature separation of Zn(g) and O_2 further enables recovery of the sensible and latent heat of the products, for example, 116 $kJ \cdot mol^{-1}$ during Zn condensation [24]. Recently, the ionic conductivity was established for electrolytes that have been shown in previous research to support the electrolysis of ZnO (s) at temperatures exceeding 1,200 K [25].

Solar electrochemistry research in this field has been almost exclusively dedicated to ZnO and H_2O, but the investigation could be extended to the high-temperature electrolysis or quasi-electrolysis of MgO, Al_2O_3, and other interesting candidate materials [20].

Carbothermal Reduction of Metal Oxides. For the thermal decomposition of metal oxides into their elements without the application of electrical work, a chemical reducing agent is necessary to lower the dissociation temperature. Coal (as coke) and natural gas (NG, as methane) are preferred reducing agents in blast-furnace processes because of their availability and relatively low price. In the presence of carbon, the uptake of O_2 by the formation of CO brings about reduction of the oxides at much lower temperatures. While reactions (18) and (19) have favorable free energies above the temperatures indicated in Table 1, a more detailed calculation of the chemical equilibrium composition shows that only the carbothermic reduction of Fe_2O_3, MgO, and ZnO will result in significant free metal formation [26]. The carbides Al_3C_4, CaC_2, SiC, and TiC are thermodynamically stable in an inert atmosphere; the nitrides AlN, Si_3N_4, and TiN are stable in N_2 atmosphere. These valuable high-temperature materials were produced in solar furnaces.

Using NG as reducing agent, (Eq. 19) combines in a single process the reduction of metal oxides with the reforming of NG for the co-production of metals and syngas. Thus, CH_4 is reformed in the absence of catalysts and may be tailored to produce high-quality syngas with a molar ratio of H_2 to CO equal to 2, which is especially suitable for synthesizing methanol, a potential substitute for petrol. Thermal reductions of Fe_3O_4 and ZnO with C(s) and CH_4 to produce Fe, Zn, and syngas have been demonstrated in solar furnaces using fluidized bed and vortex-type reactors [27–32]. These reactions are highly endothermic and proceed to completion at temperatures above about 1,300 K.

Example: Carbothermal reduction of ZnO. Zinc production by solar carbothermic reduction of ZnO offers CO_2 emission reduction by a factor of 5, vis-à-vis the conventional fossil-fuel-based electrolytic or Imperial Smelting processes [33]. Furthermore, the use of solar energy for supplying the enthalpy of the reaction upgrades the calorific value of the initial reactants by 39%.

Two examples of solar chemical reactor concepts for producing Zn by reactions (18) and (19) are shown in Figs. 5 and 6, respectively: the "two-cavity" solar reactor based on the indirect irradiation of ZnO + C(gr) [34, 35], and the "vortex" solar reactor based on the direct irradiation of ZnO + CH_4 [30]. A solar chemical "two-cavity" reactor was scaled up in the framework of the European P&D project *SOLZINC*. Testing of the 300 kW solar chemical reactor at a solar tower research facility at temperatures ranging from 1,300 to 1,500 K yielded up to 50 kg/h of 95%-purity Zn with a solar-to-fuel energy conversion efficiency of 30% [36, 37]. The process can be CO_2-neutral if charcoal is used for reducing ZnO.

Solar Production of H_2/CO from H_2O/CO_2 Splitting and/or Fossil Fuels In the long term, the sustainable and carbon-neutral H_2 and synthesis gas (syngas) production from H_2O and/or CO_2 is a promising route involving endothermic thermochemical processes that make use of concentrated solar radiation as the energy source of high-temperature process heat [24]. Syngas is a precursor to liquid hydrocarbons via Fischer–Tropsch or other catalytic reforming processes that are required to power the transportation sectors. Figure 7 illustrates possible solar thermochemical routes to produce H_2 or syngas from H_2O and/or fossil fuels [38]. Feedstocks include *inorganic* compounds such as H_2O and/or CO_2, and *organic* sources such as coal, biomass, and natural gas (NG). The forms of solar fuels are H_2, syngas (with H_2 and CO as main constituents), and their derivatives such as methanol, dimethyl ether (DME), and synthetic oil.

Electrolysis of H_2O – Solar electricity generated by photovoltaics (PV) or concentrating solar thermal

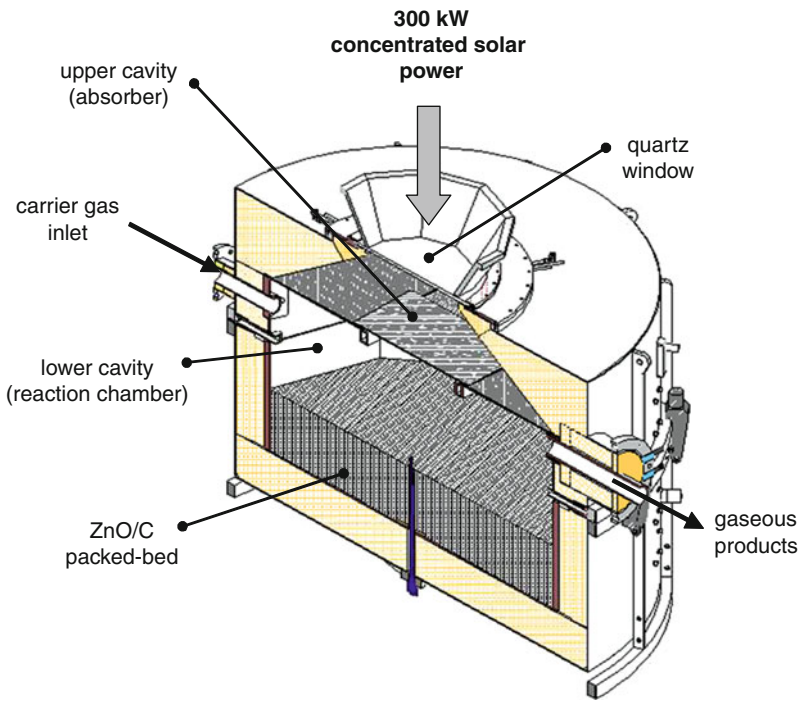

Solar Energy in Thermochemical Processing. Figure 5
Two-cavity solar reactor concept for the carbothermal reduction of ZnO – The upper cavity (absorber) serves as the solar receiver and radiant emitter. The lower cavity is a well-insulated enclosure containing a ZnO/C packed bed. It serves as the reaction chamber and is subjected to thermal radiation from the upper cavity. With this arrangement, the upper cavity protects the quartz window against particles and condensable gases coming from the reaction chamber. The reactor is specifically designed for beam-down incident radiation, as obtained through a Cassegrain optical configuration that makes use of a hyperbolical reflector at the top of the tower to redirect sunlight to a receiver located on the ground level (From [36])

technology (CSP), and followed by electrolysis of water, can be considered as a benchmark [38]. With current technologies, the overall solar-to-H_2 energy conversion efficiency ranges between 10% and 14%, assuming electrolyzers working at 70% efficiency and solar electricity being produced at 15% (PV) and 20% (CSP) annual efficiency. The electricity demand for electrolysis can be significantly reduced if the electrolysis of water proceeds at higher temperatures (1,000–1,200 K) via solid oxide electrolyzer cells (SOEC) [39]. In this case, concentrated solar energy can be applied to provide both the high-temperature process heat and the electricity needed for the high-temperature electrolysis.

Thermolysis of H_2O – The single-step thermal dissociation of H_2O to H_2 and O_2 is known as water thermolysis. Although conceptually simple, its realization is challenging since it needs a heat source above 2,500 K for achieving a reasonable degree of dissociation, reliable materials to operate at these high temperatures, and an effective technique for separating H_2 and O_2 to avoid an explosive mixture. Among the ideas proposed for separating H_2 from the products are effusion separation [7, 40] and electrolytic separation [20, 41]. Rapid quench by injecting a cold gas, expansion in a nozzle, or submerging a solar-irradiated target in liquid water is simple and workable [42, 43], but the quench introduces a significant drop in the efficiency and produces an explosive gas mixture.

H_2O-Splitting Thermochemical Cycles – Water-splitting thermochemical cycles bypass the separation problem and further allow operation at moderately

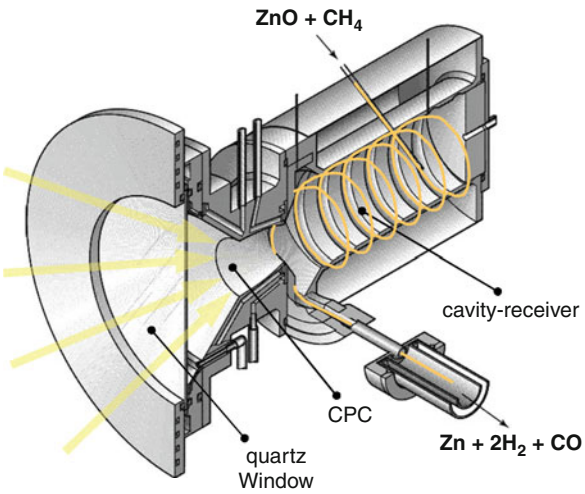

Solar Energy in Thermochemical Processing. Figure 6 Schematic of a "vortex" solar chemical reactor concept for the combined ZnO reduction and CH_4 reforming – It consists of a cylindrical cavity that contains a windowed aperture with a CPC to let in concentrated solar energy. Particles of ZnO, conveyed in a flow of CH_4, are continuously injected into the reactor's cavity via a tangential inlet port. Inside the reactor's cavity, the gas-particle stream forms a vortex flow that progresses toward the front following a helical path. The chemical products, Zn vapor and syngas, continuously exit the cavity via a tangential outlet port located at the front of the cavity, behind the aperture. Energy absorbed by the reactants is used to raise their temperature to above about 1,300 K and to drive reaction (19) (Adapted from [1])

high temperatures [1]. Previous studies performed on thermochemical cycles were mostly characterized by using process heat at temperatures below 950°C, which are expected to be available in the future from very-high-temperature nuclear reactors (VHTR). Leading candidates for multi-step thermochemical cycles are the three-step sulfur iodine cycle and the two-step sulfur hybrid cycle (with one electrolysis step), both based on the thermal decomposition of sulfuric acid at 1,120 K in a catalytic receiver reactor or at 1,470 K without catalyzer [44, 45]. In recent years, significant progress has been made in the development of optical systems for large-scale solar concentrators capable of achieving mean solar concentration ratios that exceed 5,000 suns. Such high-radiation fluxes allow temperatures above 1,500 K, which are needed for the more efficient two-step thermochemical cycles using metal oxide redox reactions [46–53]:

First step (solar):

$$M_xO_y \rightarrow xM + \frac{y}{2}O_2 \tag{17}$$

Second step (non-solar):

$$xM + yH_2O \rightarrow M_xO_y + yH_2 \tag{20}$$

Here, M denotes a metal and M_xO_y the corresponding metal oxide. The generic cycle is represented in Fig. 8. The first, *endothermic* step is the solar thermal dissociation of the metal oxide to the metal or the lower-valence metal oxide. The second, non-solar, *exothermic* step is the hydrolysis of the metal to form H_2 and the corresponding metal oxide. The net reaction is $H_2O = H_2 + ½O_2$, but since H_2 and O_2 are formed in different steps, the need for high-temperature gas separation is thereby eliminated. Among the most favorable candidate metal oxide redox pairs for this cycle are Fe_3O_4/FeO [54, 55] and ZnO/Zn [56–58]. In both cases, the minimum temperature requirement for the solar step is 2,000 K, and the products need to be either quenched or separated at high temperatures to prevent their recombination. Quenching introduces irreversibility and may be a factor of complexity in large-scale utilization.

Example: Zn/ZnO Cycle. The two-step cycle based on the Zn/ZnO redox pair is one of the most researched solar water-splitting processes. The first step is the thermal dissociation of ZnO using solar process heat, represented as:

$$ZnO \rightarrow Zn + \frac{1}{2}O_2 \tag{21}$$

The second non-solar step is the exothermal reaction of Zn with H_2O to generate H_2, represented as:

$$Zn + H_2O \rightarrow ZnO + H_2 \tag{22}$$

The resulting ZnO is recycled to the first step to close the material cycle, with net reaction being $H_2O \rightarrow H_2 + ½\ O_2$. The products are delivered in separate steps, thereby eliminating their high temperature separation. Since the steps are decoupled, the production of H_2 can be carried out on demand at convenient sites and independent of solar energy availability [59].

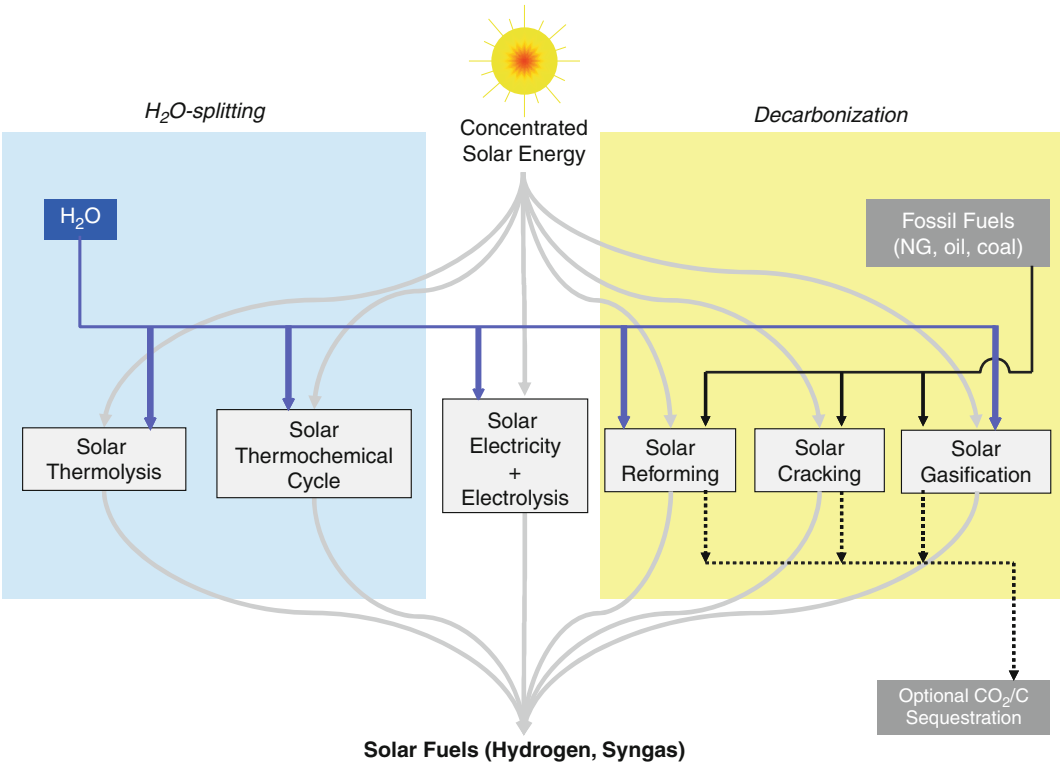

Solar Energy in Thermochemical Processing. Figure 7
Thermochemical routes for solar H_2 and syngas production – Indicated is the chemical source of H_2: H_2O for the solar thermolysis and the solar thermochemical cycles; fossil fuels for the solar cracking, and a combination of fossil fuels and H_2O for the solar reforming and gasification. For the solar decarbonization processes, optional CO_2/C sequestration is considered. All of those routes involve energy consuming (endothermic) reactions that make use of concentrated solar radiation as the energy source of high-temperature process heat (Reproduced from [38])

The second law of thermodynamic analysis – derived in (Eqs. 1–16) – is applied for calculating the theoretical maximum exergy efficiency of the two-step Zn/ZnO cycle [1]. Figure 9 depicts the ideal cyclic process for splitting H_2O. The solar reactor is assumed to be a cavity-receiver operating at 2,000 K. The reactant ZnO(s) enters the solar reactor at 298 K and is further heated to the reaction temperature at 2,000 K. The molar feed rate of ZnO to the solar reactor, $\dot{n}$, is set to 1 mol s^{-1}, and is equal to that of H_2O fed to the hydrolysis reactor. After quenching, the products are assumed to separate naturally (without expending work) into gaseous O_2 and condensed phase Zn. Zinc is sent to the hydrolysis reactor to react exothermally with H_2O and form H_2, according to (Eq. 22).

The heat liberated is assumed lost to the surroundings, as given by:

$$\dot{Q}_{hydrolyzer} = -\dot{n}\Delta H|_{Zn+H_2O\,@\,298\,K \rightarrow ZnO+H_2\,@\,298\,K} \tag{23}$$

Thus, the irreversibility associated with the hydrolyzer is:

$$Irr_{hydrolyzer} = \frac{\dot{Q}_{hydrolyzer}}{298K} + \dot{n}\Delta S|_{Zn+H_2O\,@\,298\,K \rightarrow ZnO+H_2\,@\,298\,K} \tag{24}$$

Introducing an ideal H_2/O_2 fuel cell, in which the products recombine to form H_2O and thereby generate electrical power, closes the cycle. $\dot{W}_{FC}$ and $\dot{Q}_{FC}$ are the work output and the heat rejected, respectively, given by

$$\dot{W}_{FC} = -\eta_{FC}\dot{n}\Delta G|_{H_2+0.5O_2\,@\,298K \rightarrow H_2O\,@\,298K} \tag{25}$$

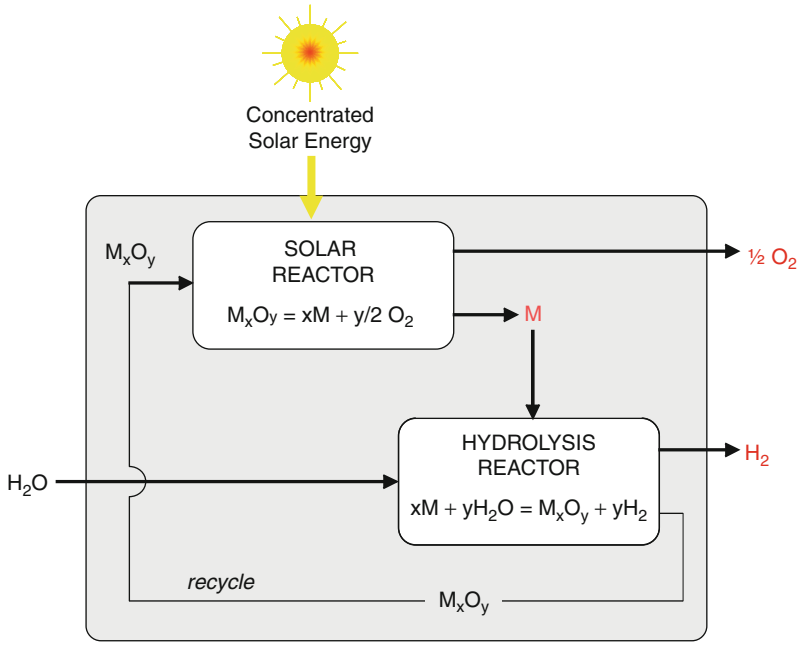

Solar Energy in Thermochemical Processing. Figure 8
Representation of a two-step water-splitting solar thermochemical cycle using metal oxide redox reactions (Adapted from [1])

$$\dot{Q}_{FC} = -T_L \cdot \dot{n}\Delta S|_{H_2+0.5O_2\ @\ 298K\ \rightarrow\ H_2O\ @\ 298K} \qquad (26)$$

The H_2/O_2 fuel cell efficiency η_{FC} is assumed 100% when based on the maximum work output of H_2 (also known as its exergy). Finally, the exergy efficiency is calculated using (Eq. 14). Table 2 gives the results of the calculation for two values of the solar concentration ratio: 5,000 and 10,000. The estimated solar-to-fuel efficiency of the two-step cycle based on the Zn/ZnO redox pair is in the range of 35–39% without heat recovery (h.r.). Recovery of the heat rejected by the quench ($\dot{Q}_{quench}$) and hydrolyzer ($\dot{Q}_{hydrolyzer}$) to preheat the reactants can boost the efficiency to a theoretical maximum of 58–70%.

Figure 10 shows a solar chemical reactor concept for performing the thermal dissociation of ZnO that features a windowed rotating cavity-receiver lined with ZnO particles that are held by centrifugal force [60]. The reactor has a dynamic feeder that extends and retracts within the cavity, allowing for batch-wise formation of a packed bed of ZnO particles evenly distributed over the entire cavity surface. The absorption of concentrated solar energy by directly irradiated reactants provides efficient radiation heat transfer to the reaction site where the energy is needed, by-passing the limitations imposed by indirect heat transport via heat exchangers. 3D computational fluid dynamics (CFD) was employed to determine the optimal flow configuration for an aerodynamic protection of the quartz window against condensable Zn(g).

A 10-kW reactor prototype was fabricated, consisting of a multilayer cylindrical cavity made of sintered ZnO tiles placed on top of a porous 80% Al_2O_3–20%SiO_2 insulation and reinforced by a 95% Al_2O_3–5%Y_2O_3 ceramic matrix composite, providing mechanical, chemical, and thermal stability and a diffusion barrier for product gases. A quenching unit was incorporated at the exit of the cavity to rapidly decrease temperature by injecting Ar into a water-cooled annular outlet [61]. Experimentation was carried out with the 10-kW reactor subjected to mean concentration of 3,000 suns and peak concentration of 5,880 suns [60]. All reactor components performed well at operating temperatures in the range 1,807–1907 K, measured behind the ZnO tiles. The reactor was operated in a transient ablation mode with semi-continuous feed cycles of ZnO particles, characterized by a rate of heat transfer, predominantly by radiation,

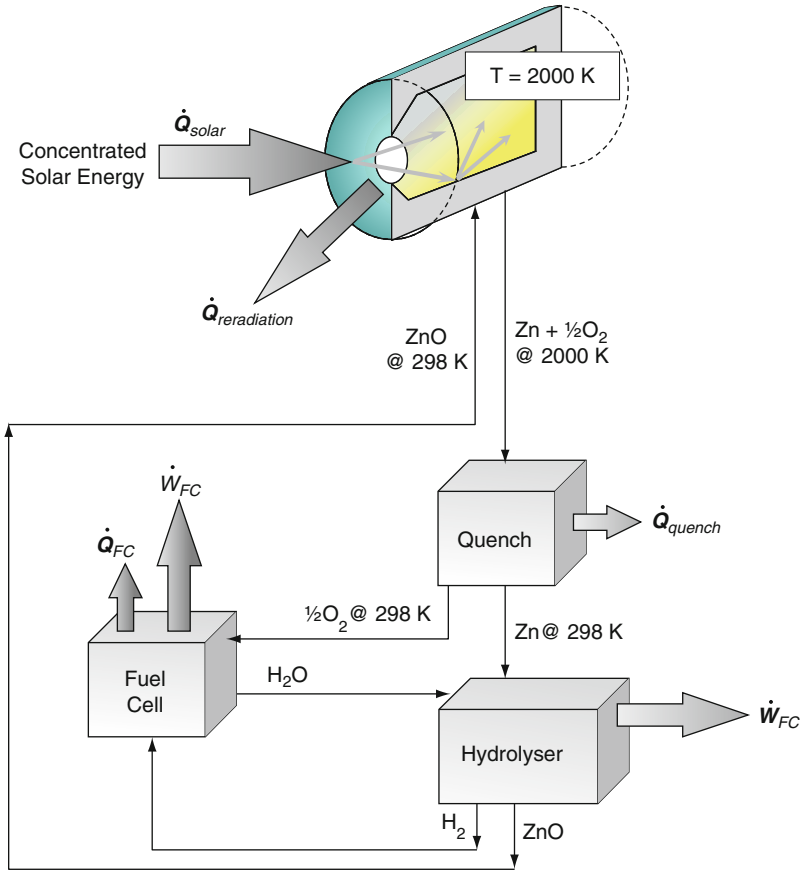

Solar Energy in Thermochemical Processing. Figure 9
Model flow diagram of the two-step water-splitting solar thermochemical Zn/ZnO cycle used for the exergy analysis (Adapted from [1])

to the layer of ZnO particles undergoing endothermic dissociation that proceeded faster than the rate of heat transfer, predominantly by conduction, through the cavity walls. Reactor modeling has enabled a more comprehensive and in-depth understanding of the competing mechanisms and the identification of major sources of energy losses, which lead to optimization and scaling up [62–68].

Tubular aerosol flow reactors were designed for the formation of Zn nanoparticles followed by their in situ reaction with H_2O. They featured three zones for Zn evaporation, steam quenching, and Zn/H_2O reaction, respectively [69–74]. These aerosol flow configurations offered high Zn-to-ZnO conversions over short residence times due to augmented reaction kinetics and heat/mass transfer. However, the reactions primarily occurred heterogeneously outside the aerosol jet flow on surfaces with Zn deposition, making the ZnO recovery, process control, and scale-up problematic [59].

Example: SnO/SnO_2 cycle. Another promising metal oxide cycle is based on SnO/SnO_2. Exergy and energy efficiencies of the cycle are 30% and 36% respectively [75]. Atmospheric and reduced pressure experiments showed that the SnO_2 reduction can be performed efficiently at 1,770 K and the SnO hydrolysis at 820 K. A 1-kW solar reactor prototype was successfully tested for continuous operation [38].

Example: CeO_2/Ce_2O_3 cycle. The feasibility of the two-step cycle based on CeO_2/Ce_2O_3 has been demonstrated using a lab-scale solar reactor at 2,300 K and a fixed bed reactor at 700–900 K, where the water-splitting reaction was completed with fast kinetics [53, 76]. In contrast to the Zn-based system, the ceria remains in solid form throughout [38]. The complete

Solar Energy in Thermochemical Processing. Table 2
Exergy analysis of the two-step water-splitting solar Zn/ZnO cycle using the process modeling scheme depicted in Fig. 9. The ZnO and H_2O molar rates are set to 1 mol s^{-1} (Adapted from [57])

$\widetilde{C}$	5,000	10,000
$\dot{Q}_{solar}$	680 kW	613 kW
$\dot{Q}_{reradiation}$	123 kW	56 kW
$\dot{Q}_{reactor,net}$	557 kW	
$Irr_{reactor}$	0.33 kW·K^{-1}	0.13 kW·K^{-1}
$\dot{Q}_{quench}$	209 kW	
Irr_{quench}	0.55 kW·K^{-1}	
$\dot{Q}_{hydrolyzer}$	64 kW	
$Irr_{hydrolyzer}$	0.26 kW·K^{-1}	
$\dot{Q}_{FC}$	49 kW	
$\dot{W}_{FC}$	237 kW	
$\eta_{absorption}$	82%	91%
η_{exergy}	35%	39%
η_{exergy} *(with h.r.)*	58%	70%

cycle was demonstrated with a 2-kW cavity-receiver containing porous foam made of ceria [77].

Example: Mixed iron oxide cycle. Other metal oxides such as manganese oxide or cobalt oxide, as well as mixed oxides redox pairs – mainly based on iron – have also been considered [78–81]. For example, a mixed iron oxide cycle was demonstrated at the 100-kW power level using a monolithic dual chamber solar reactor (Fig. 11) [82]. A quasi-continuous H_2 flow is produced by cyclic operation of the two reaction chambers through sequential oxidation and reduction steps at 1,050 K and 1,500 K, respectively.

CO_2-Splitting Thermochemical Cycles. A promising alternative to direct CO_2 sequestration is to decompose CO_2 into CO and O_2 using metal oxide redox reactions and concentrated solar radiation:

First step (solar):

$$M_xO_y \rightarrow xM + \frac{y}{2}O_2 \tag{17}$$

Second step (non-solar):

$$xM + yCO_2 \rightarrow M_xO_y + yCO \tag{27}$$

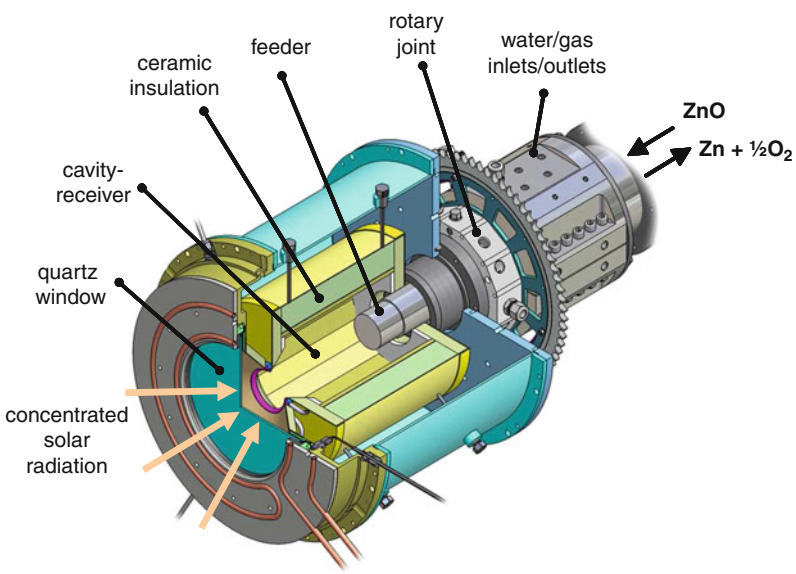

Solar Energy in Thermochemical Processing. Figure 10
Scheme of the solar reactor configuration for the thermal dissociation of ZnO to Zn and O_2 at above 2,000 K – The concept features a windowed rotating cavity-receiver lined with ZnO particles and exposed to high-flux solar irradiation. With this arrangement, ZnO serves simultaneously the functions of radiant absorber, thermal insulator, and chemical reactant (Adapted from [60])

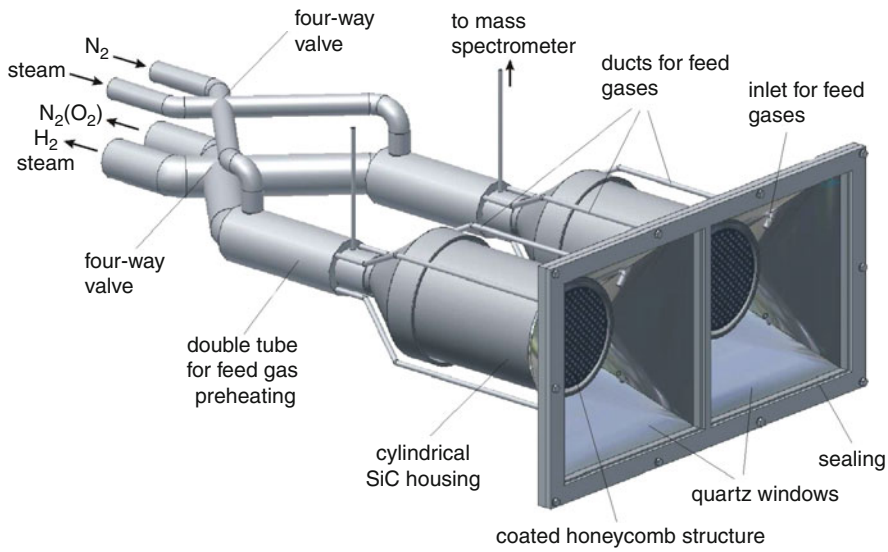

Solar Energy in Thermochemical Processing. Figure 11
Monolithic dual chamber solar receiver-reactor for continuous H_2 production – The concept features a closed receiver-reactor constructed from ceramic multichanneled monoliths. Cyclic operation of the water-splitting and regeneration steps is established in two reaction chambers. Their individual temperature levels are controlled by focusing and defocusing heliostats (Reproduced from [83])

CO can be used as combustion fuel or further processed to synthetic liquid fuels for transportation. O_2 is needed for the oxy-combustion and gasification technologies. Thermodynamic and thermogravimetric-based kinetic analyses were performed for two-step thermochemical cycles based on the Zn/ZnO and FeO/Fe_3O_4 redox reactions [84, 85].

H_2O/CO_2-Splitting Thermochemical Cycles. Producing synthesis gas (syngas) with concentrated solar energy from co-feeding H_2O and CO_2 – the latter eventually captured from air [86–88] – represents a promising path toward sustainable energy utilization [89, 90]:

First step (solar):

$$M_xO_y \rightarrow xM + \frac{y}{2}O_2 \tag{17}$$

Second step (non-solar):

$$xM + y(H_2O + CO_2) \rightarrow M_xO_y + \frac{y}{2}(2H_2 + 2CO + O_2) \tag{28}$$

A solar reactor that incorporates heat recuperation between the reduction and oxidation steps is being developed [52]. The resulting syngas can either be directly combusted for electricity generation in highly efficient combined Brayton–Rankine cycles [91] or further processed via Fischer–Tropsch to liquid hydrocarbon fuels, such as methanol or gasoline [92]. Figure 12 shows the solar reactor technology applied for splitting CO_2 and H_2O using nonstoichiometric ceria redox reactions [77].

Solar Production of H_2 from Fossil Fuels Short-term to mid-term transition processes to solar H_2 encompass the decarbonization of fossil fuels via solar cracking, reforming, and gasification routes that are being investigated in various P&D projects at the power level of several hundred kilowatts [1, 38]. These routes are shown schematically in Fig. 13.

Some of these processes are practiced at an industrial scale, with the process heat supplied by burning a significant portion of the feedstock. Internal combustion results in the contamination of the gaseous products, while external combustion results in a lower thermal efficiency because of the irreversibility associated with indirect heat transfer. Alternatively, using solar energy for process heat offers a threefold advantage: (1) the discharge of pollutants is avoided; (2) the

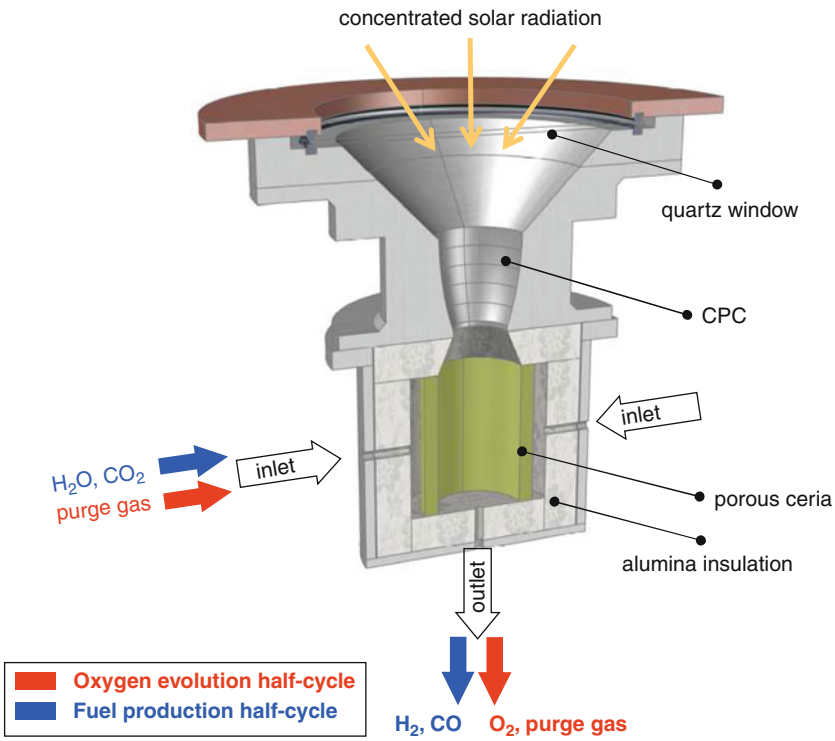

Solar Energy in Thermochemical Processing. Figure 12
Schematic of the solar reactor configuration for the two-step solar thermochemical cycle for splitting H_2O and CO_2 via ceria redox reactions. It consists of a cavity-receiver containing a porous monolithic ceria cylinder. Concentrated solar radiation enters through a windowed aperture and impinges on the ceria inner walls. Reacting gases flow radially across the porous ceria, while product gases exit the cavity through an axial outlet port. *Red arrow* indicates ceria reduction (oxygen evolution); *blue arrow* indicates oxidation (fuel production) (From [77])

gaseous products are not contaminated by combustion by-products; and (3) the calorific value of the fuel is upgraded by adding solar energy in an amount equal to the ΔH of the reaction [1].

Solar Cracking. The solar cracking route refers to the thermal decomposition of natural gas (NG) and other hydrocarbons, and can be represented by the simplified net reaction:

$$C_xH_y = xC(gr) + \frac{y}{2}H_2 \tag{29}$$

The process thermally decomposes NG in a high-temperature solar chemical reactor, yielding two valuable products: a H_2-rich gas and a marketable high-value nano-material called "*Carbon Black*" (CB). Thus, both H_2 and CB are produced by renewable energy, resulting in potential CO_2 emission reduction of 14 kg of CO_2 and energy saving of 277 MJ/kg H_2 compared to conventional NG steam reforming and standard CB processing [93]. Other compounds may also be formed, depending on the reaction kinetics and on the presence of impurities in the raw materials. The carbonaceous solid product can either be sequestered without CO_2 release or used as valuable material commodity (CB) under less-severe CO_2 restraints. It can also be applied as reducing agent in metallurgical processes. The H_2-rich gas mixture can be further processed to high-purity H_2 that is not contaminated with oxides of carbon and, thus, can be used in *PEM fuel cells* without inhibiting platinum-made electrodes. From the point of view of carbon sequestration, it is easier to separate, handle, transport, and store solid carbon than gaseous CO_2. Further, while the steam reforming and gasification methods require additional steps for shifting CO and for separating CO_2, the thermal cracking accomplishes the removal and separation

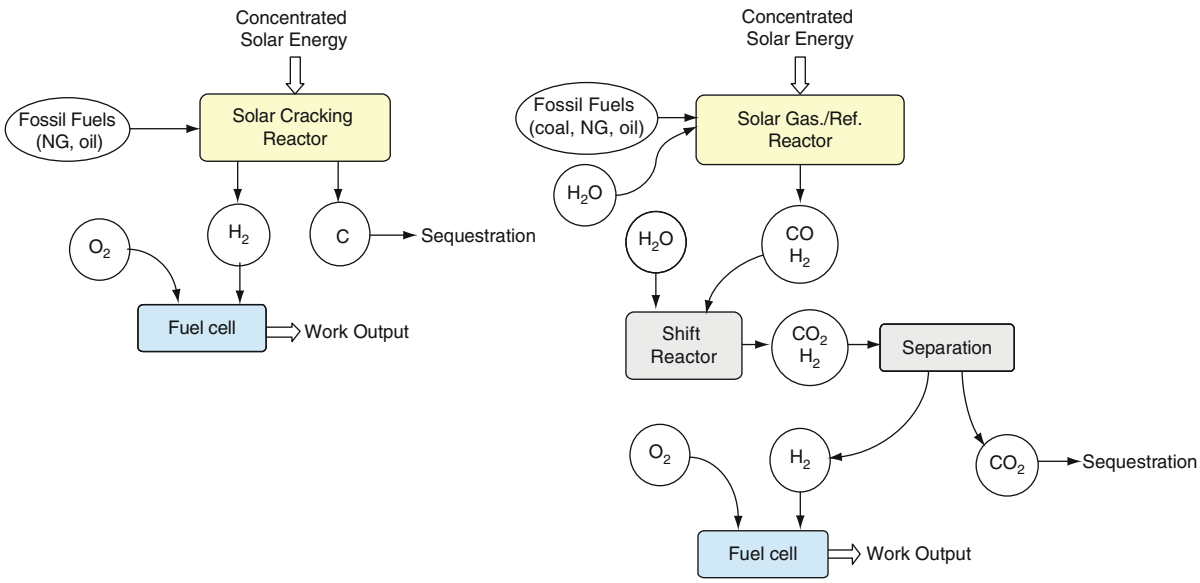

Solar Energy in Thermochemical Processing. Figure 13
Solar thermochemical routes for H_2 production using fossil fuels and H_2O as the chemical source – Solar cracking (*left*), and solar reforming and gasification (*right*) (From [1])

of carbon in a single step. In contrast, the major drawback of the thermal decomposition method is the energy loss associated with the sequestration of carbon. Thus, the solar cracking may be the preferred option for NG and other hydrocarbons with high H_2/C ratio. The exergy efficiency for these routes is defined as the ratio of the work output by the fuel cell to the total thermal energy input by both the solar energy and the heating value of the reactants:

$$\eta_{exergy} = \frac{\dot{W}_{FC}}{\dot{Q}_{solar} + HHV_{\text{reactant}}} \tag{30}$$

Here, $HHV_{reactant}$ is the higher heating value of the fossil fuel being processed, for example, about 890 kJ·mol^{-1} for NG. Assuming a 65%-efficient H_2/O_2 fuel cell, η_{exergy} = 30%. This route offers zero CO_2 emissions as a result of carbon sequestration. However, the energy penalty for completely avoiding CO_2 reaches 30% of the electrical output, vis-à-vis the direct use of NG for fueling a 55%-efficient combined Brayton–Rankine cycle.

An experimental investigation on the thermal decomposition of CH_4 into C and H_2 was carried out using a direct-irradiated 5-kW particle-flow solar chemical reactor tested in a solar furnace in the 1,300–1,600 K range [94]. The reactor features a continuous flow of CH_4 laden with μm-sized carbon particles, confined to a cavity receiver and directly exposed to concentrated solar irradiation. Figure 14 shows a novel indirect-irradiated multi-tubular cavity-type solar reactor. A 10-kW solar reactor prototype was successfully tested in the temperature range of 1,823–2,073 K, reaching 97% CH_4 conversion and 75% H_2 yield [95]. This reactor was scaled up to 50 kW and tested in a large solar furnace.

Solar Reforming. The solar reforming of NG and other hydrocarbons, using either steam or CO_2, has been extensively studied in solar-concentrating research facilities with small-scale solar reactor prototypes. Recently, pilot scale test installations have been commissioned.

Example: Solar steam reforming. The steam-reforming of NG and other hydrocarbons can be represented by the simplified net reaction:

$$C_xH_y + x\text{H}_2\text{O} = \left(\frac{y}{2} + x\right)\text{H}_2 + x\text{CO} \tag{31}$$

This process has been scaled up to power levels of 400 kW and tested at 1,120 K and 8–10 bars in a solar tower facility using a solar volumetric reactor [96], as shown schematically in Fig. 15. A concave quartz

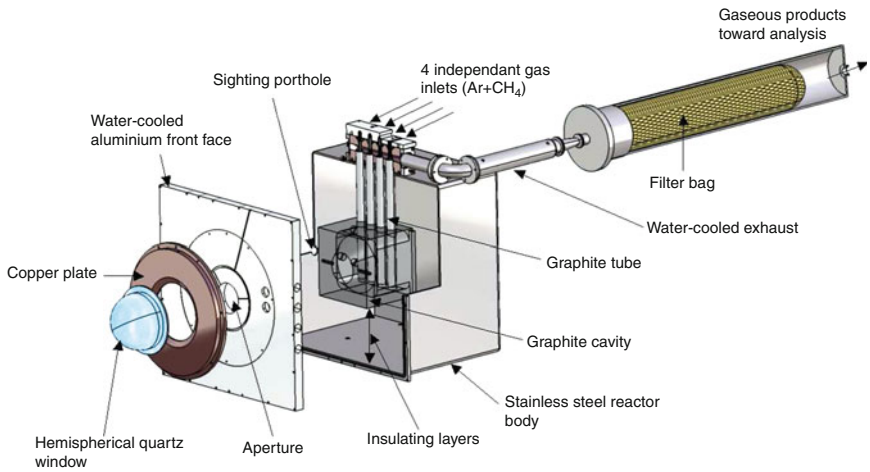

Solar Energy in Thermochemical Processing. Figure 14
Schematic of tubular solar reactor for NG cracking – Reactants (CH_4 in Ar) are indirectly heated inside graphite tubes (From [95])

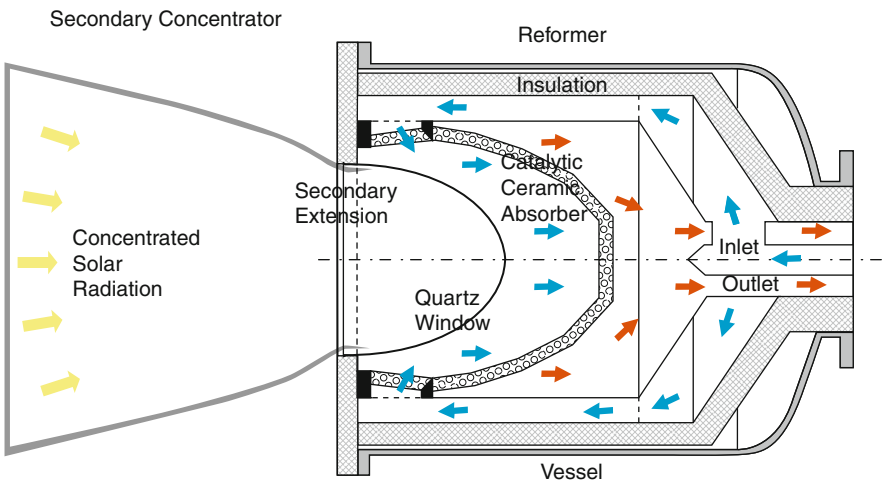

Solar Energy in Thermochemical Processing. Figure 15
Scheme of a direct-irradiated solar reforming chemical reactor (From [96])

window, mounted at the aperture, minimizes reflection losses and permits operation at high pressures. A CPC is implemented at the aperture. The main component is the reticulate porous ceramics (RPC) absorber made of SiC foams and coated with Rh catalyst. A computer tomography–based methodology was applied to determine the transport properties of fluid flow across porous media [97, 98].

Direct-irradiated reactors have the advantage of providing efficient radiation heat transfer directly to the reaction. Furthermore, under proper conditions, direct irradiation may photochemically enhance the kinetics of the reaction. The major drawback, when working with reducing or inert atmospheres, is the requirement of a transparent window, which is a critical and troublesome component under high-pressure and severe gas environment.

Example: Solar chemical heat pipe. The solar dry-reforming of CH_4 with CO_2 offers a sink for CO_2 and – relative to steam methane reforming – produces a more

desirable ratio of H_2 to CO for feed to a Fischer–Tropsch synthesis process [99]. It can be applied in a closed-loop *solar chemical heat pipe* (Fig. 16). The product of this reversible reaction is syngas that can be stored at ambient temperatures and transported to the site where the energy is needed. By the reverse exothermic reaction, stored solar energy is released in the form of high-temperature heat, which can be used, for example, for generating electricity via a Rankine cycle. The products of this reverse reaction are again recycled to the solar reactor, where the process is repeated.

The dissociation/synthesis of ammonia can also be applied in a chemical heat pipe for storage and transportation of solar energy [100]. The endothermic NH_3 dissociation reaction proceeds catalytically at high pressures of 50–200 bar and at temperatures above 700 K. The reverse synthesis of H_2/N_2 delivers heat to a Rankine cycle. The NH_3 fraction in storage is present largely as a liquid, thus automatic phase separation of NH_3 and H_2/N_2 is provided.

Solar Steam Gasification. The solar steam gasification of coal and other carbonaceous materials to produce high-quality syngas is an attractive industrial process represented by the simplified net stoichiometric reaction:

$$C_xH_yO_z + (x-z)H_2O = \left(\frac{y}{2} + x - z\right)H_2 + xCO \tag{32}$$

Other compounds may also be formed, especially with coal, but some impurities contained in the raw materials are cleaned out prior to the decarbonization process. The principal product is high-quality syngas, the building block for a wide variety of synthetic fuels including Fischer–Tropsch type chemicals, hydrogen, ammonia, and methanol. Its quality is determined mainly by the H_2:CO and CO_2:CO molar ratios.

Feedstock: Petcoke. The solar chemical technology for the steam-gasification of heavy crude oil derivatives, such as solid petroleum coke (petcoke) particles, is being developed with participation of the oil industry. For this process, a 5-kW solar reactor was designed that featured a continuous gas-particle vortex flow confined to a cavity receiver and directly exposed to concentrated solar radiation (Fig. 17) [101]. For the 300-kW pilot reactor, complete reaction extent is predicted for an initial feedstock particle size up to 35 μm at residence times of less than 10 s and peak temperatures of 1818 K, yielding high-quality syngas with a calorific content that has been solar-upgraded by 19% over that of the petcoke gasified [102].

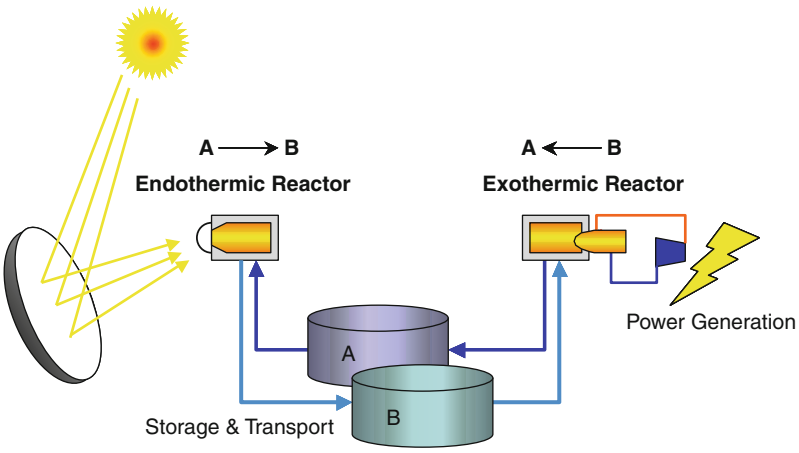

Solar Energy in Thermochemical Processing. Figure 16
Solar chemical heat pipe for storage and transportation of solar energy – High-temperature solar process heat is used to drive the endothermic reversible reaction $A \rightarrow B$. The product B may be long-term stored and long-range transported to the site where the energy is needed. At that site, the exothermic reverse reaction $B \rightarrow A$ is effected and yields high-temperature process heat in an amount equal to the stored solar energy $\Delta H_{A\rightarrow B}$. The chemical product A of the reverse reaction is returned to the solar reactor for reuse (From [1])

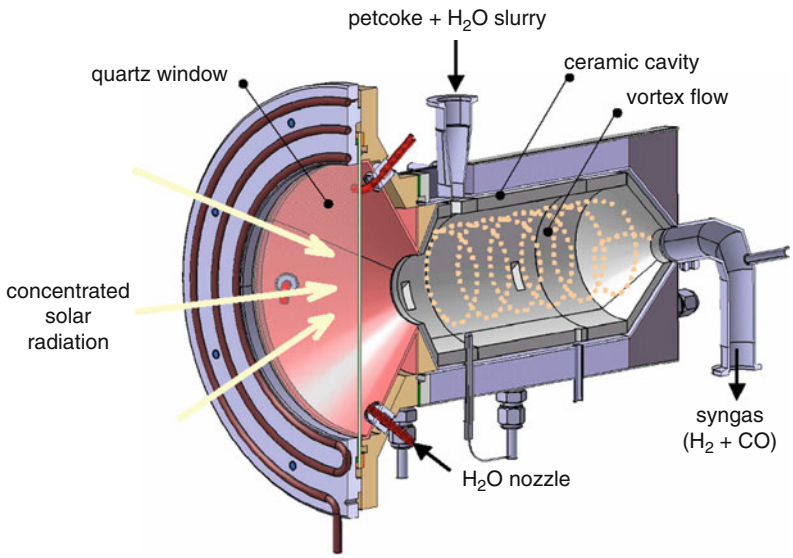

Solar Energy in Thermochemical Processing. Figure 17
Vortex solar reactor for the steam-gasification of petcoke – This configuration features a continuous gas-particle vortex flow confined to a cavity receiver and directly exposed to concentrated solar radiation. The reactants are injected as liquid slurry of petcoke particles and water (Adapted from [101])

Feedstock: Coal and carbonaceous wastes. High-temperature solar process heat is applied for upgrading low-grade carbonaceous feedstock to produce high-quality syngas for substituting fossil fuels in a cement kiln. Figure 18 shows a 5-kW solar reactor prototype that operated at temperatures up to 1,500 K, yielding high-quality syngas of typical molar ratios $H_2/CO = 1.5$ and $CO_2/CO = 0.2$, and with a calorific content up to 30% upgraded over that of the input feedstock [103]. Solar-to-chemical energy conversion efficiencies varied between 17% and 29%. Experimental demonstration of the high-temperature solar reactor technology at pilot scale of 250 kW is in progress.

Feedstock: Biomass. Solar thermal energy is applied to biomass gasification in a solar reactor that creates temperatures of more than 1,500 K, gasifying any feedstock within seconds [46, 104, 105]. Because the process is driven by solar thermal energy, combustion of the valuable biomass resource is not required. As shown by experiments, nearly all of the carbon in the biomass can be converted to syngas, stretching the ability of the biomass resource to meet energy demand and improving the overall economics of the process. Given these advantages and demonstrated experimental work, solar thermal gasification of biomass appears to be the most promising pathway to near-term renewable hydrogen production from solar resources. Following successful completion of laboratory and on-sun demonstration systems, a 1-MW solar plant was commissioned to transform wood waste and other forms of biomass into synthesis gas that can be converted into gasoline [106].

Solar Production of H_2 from H_2S An optional source of H_2 is H_2S, a highly toxic industrial product recovered in large quantities in the sweetening of NG and in the removal of organically bound sulfur from petroleum and coal [1]. Current industrial practice uses the Claus process to recover the sulfur from H_2S, but the process wastes H_2 to produce low-grade process heat. A thermodynamic and economic study indicates that the pure solar process has the potential of lowering the disposal costs of H_2S vis-à-vis the conventional Claus process while coproducing H_2 without concomitant CO_2 emissions [107].

Solar Production of Material Commodities

Solar Metals and Metal Oxides, Metallic Carbides and Nitrides The extractive metallurgical industry is a major consumer of process heat and electricity, and as such responsible for about 10% of global anthropogenic

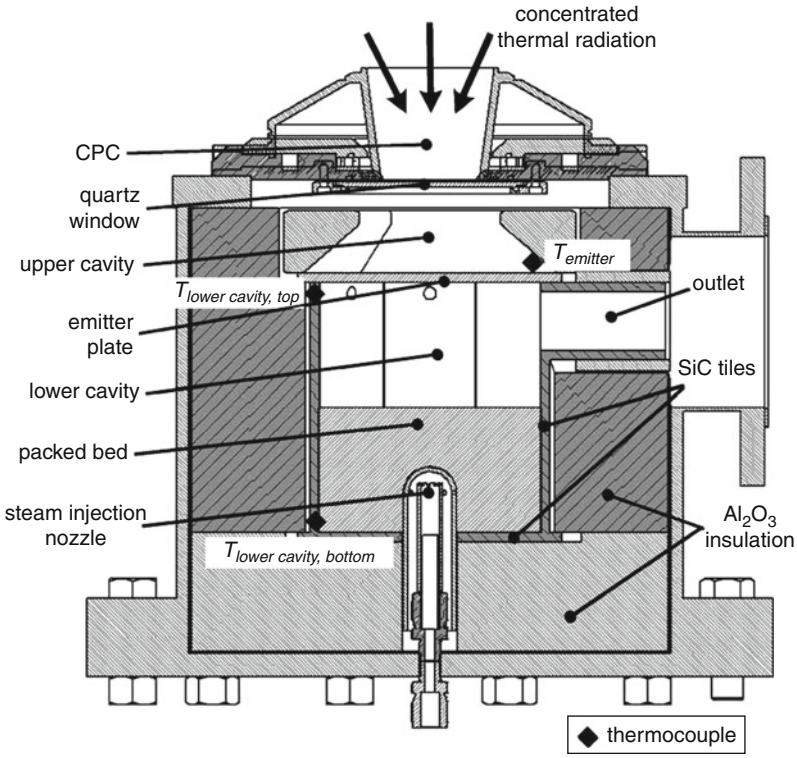

Solar Energy in Thermochemical Processing. Figure 18
Section view of a "two-cavity" packed-bed solar reactor for syngas production from carbonaceous wastes – The two cavities are separated by an emitter plate, with the upper one serving as the radiative absorber and the lower one containing the reacting packed bed that shrinks as the reaction progresses (From [103])

greenhouse gas emissions [1]. A solar thermal process would drastically reduce these emissions.

Example: Solar aluminum processing. Solar processing of aluminum could reduce the CO_2 emissions from 44 to 5 t per ton of aluminum. The temperature required to reduce aluminum ores with carbon is in the range 2,400–2,600 K, that is, at the upper limit for practical process heat addition from a combustion source alone. Preliminary tests performed in a concentrating solar facility suggest two feasible solar thermal routes: (1) at about 2,400 K, a mixture of Al_2O_3, SiO_2, and carbon results in an Al–Si alloy, which can be purified after its production; (2) at above 2,500 K, Al_2O_3 and carbon result in an Al-Al_3C_4 mixture of varying compositions [108]. Thermochemical equilibrium calculations indicate the possibility of significantly lowering the onset temperature of aluminum vapor formation via carbothermal reduction of Al_2O_3 by decreasing the total pressure, enabling its vacuum distillation, while bypassing the formation of undesired byproducts Al_2O, Al_4C_3, and Al-oxycarbides. When the reducing agent is derived from a biomass source, the solar-driven carbothermal reduction is CO_2-neutral. Exploratory experimental runs using a solar reactor were carried out at temperatures in the range 1,300–2,000 K and total pressures in the range 3.5–12 mbar, with reactants Al_2O_3 and bio-charcoal directly exposed to simulated high-flux solar irradiation, yielding up to 19% Al by condensation of product gases, accompanied by the formation of Al_4C_3 and Al_4O_4C within the crucible. Based on the measured CO generation, integrated over the duration of the experimental run, the reaction extent reached 55% at 2,000 K [109].

Example: Solar silicon processing. The solar carbothermal reduction of silica to silicon was examined thermodynamically and demonstrated experimentally at vacuum pressures. Reducing the system pressure favors Si(g) formation, enabling its vacuum distillation.

Experimentation in a solar reactor was performed in the range 1,997–2,263 K at $\sim 3 \cdot 10^{-3}$ bar with mixtures of charcoal and silica directly exposed to radiative flux intensities equivalent to 6500 suns, yielding Si purities ranging from 66.1 wt.% to 79.2 wt.%. The Si purity increased with temperature. Solid characterizations showed SiC and SiO as important reaction intermediaries. When the reducing agent is derived from a biomass source, the solar-driven carbothermal process is CO_2-neutral [110]. An additional energy-intensive refining step is required for obtaining high-purity Si employed in electronic and PV applications. The purification of metallurgical grade silicon (MGS) by extraction of boron and phosphorus was experimentally demonstrated using concentrated solar energy in the temperature range 1,823–1,975 K [111].

Example: Solar zinc processing. As described in section "Solar Production of Metals", Zn can be produced from ZnO by a solar thermal, electrothermal, or carbothermal reduction process. Other examples of solar thermal reduction processes that have been demonstrated in solar furnace exploratory runs are the production of Zn by dissociation of its natural ore willemite (Zn_2SiO_4), the combined ZnO reduction and biomass pyrolysis, and the production of Mg and Fe by carbothermal reduction of their oxides.

Metallic carbides and nitrides can be produced by the solar carbothermic reduction of metal oxides. The reaction is generally given by:

$$M_xO_y + C(gr)\{+N_2\} \rightarrow \{M_{x'}C_{y'}, M_{x''}N_{y''}\} + CO \quad (33)$$

Exploratory experimental studies were conducted in solar furnaces, in which nitrides (AlN, Si_3N_4, TiN, and ZrN) were formed for the systems run in N_2, and carbides (Al_4C_3, CaC_2, SiC, TiC) were formed for the systems run in inert atmosphere [24, 26]. These ceramics are valuable materials for high-temperature applications because of their high hardness, excellent corrosion resistance, high melting points, and low coefficients of thermal expansion. CaC_2 is well known as the feedstock for the production of acetylene. The nitrides and carbides AlN, Fe_3C, and Mn_3C may also be used in cyclic processes as feedstock to produce H_2 and hydrocarbons, or may serve as intermediaries in the production of the metal. The hydrolysis of AlN yields NH_3, the hydrolysis or acidolysis of Fe_3C yields liquid hydrocarbons, and the hydrolysis of the various carbides of manganese yields H_2 and hydrocarbons in different proportions. Thus, reaction (33) may be incorporated in cyclic processes of the type shown in Fig. 19, in which the metal oxides resulting from the hydrolysis are recycled to the solar reactor, and CO from reaction (33) may be shifted to H_2 via the water–gas shift reaction.

Solar Fullerenes and Carbon Nanotubes Fullerenes and carbon nanotubes have become a major field in condensed matter physics and chemistry. However, the large-scale production of these materials with high yield and selectivity is still a crucial problem.

Example: Solar fullerene synthesis. Conventional methods for the synthesis of fullerenes like electric arc discharge and laser ablation fail when the process is being scaled up to higher power levels. The solar vaporization process seems to be more promising using the solar reactor shown in Fig. 20, in which a graphite rod contained under vacuum pressure behind a hemispherical quartz window is directly irradiated with peak solar concentration ratios exceeding 7,000 suns, and the vaporized carbon (at temperatures above 3,300 K) is swept out by Ar, quenched, and collected in a bag filter [112]. The key parameters characterizing this process are the carbon soot mass flow rate and the desired product yield. The former is a function of the target temperature, while the latter is a function of specific reactor variables such as fluid flow pattern, residence time, carbon vapor concentration in the carrier gas, target temperature, and temperature distribution in the cooling zone. Single-walled carbon nanotubes were synthesized in gram quantities with a 50-kW solar reactor [113].

Example: Solar-produced carbon nanotubes and nanofibers. Catalytic filamentous carbon (CFC) can be produced by the solar thermal decomposition of hydrocarbons in the presence of small metal catalyst particles. Solar furnace experiments confirmed that nanotubes can be obtained using Co/MgO catalyst for CO and $CH_4 + H_2$, and nanofibers can be obtained on Ni/Al_2O_3 catalyst for CO, CH_4, $CH_4 + H_2$, and C_4H_{10} [114]. Figure 21 shows a solar chemical reactor used for such experimental runs. It consists of a quartz tube containing a fluidized bed of catalyst and Al_2O_3 grains. A secondary reflector, composed of a 2D-CPC coupled

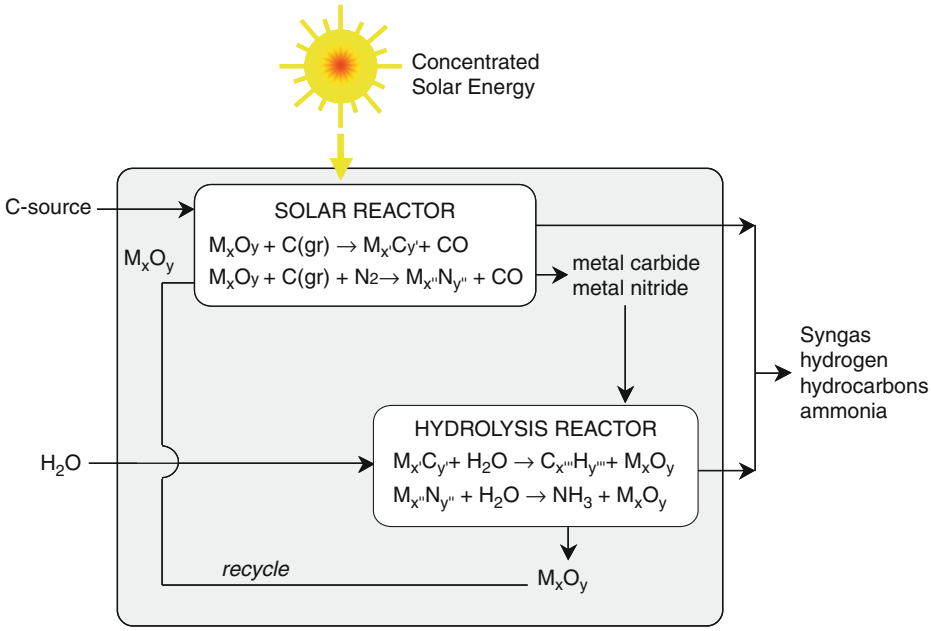

Solar Energy in Thermochemical Processing. Figure 19
Schematic of a two-step thermochemical process for the production of syngas, hydrogen, hydrocarbons, and ammonia, using metal oxides and solar energy – In the first, endothermic step, the metal oxide is carbothermally reduced to a metal carbide or nitride using solar process heat. Subsequently, the carbide or nitride is reacted with water to produce hydrocarbons or ammonia, and CO is water-gas shifted to syngas, while the metal oxide is recycled to the solar step. *M* denotes metal; M_xO_y metal oxide; $M_{x'}C_{y'}$ metal carbide; and $M_{x''}N_{y''}$ metal nitride (From [1])

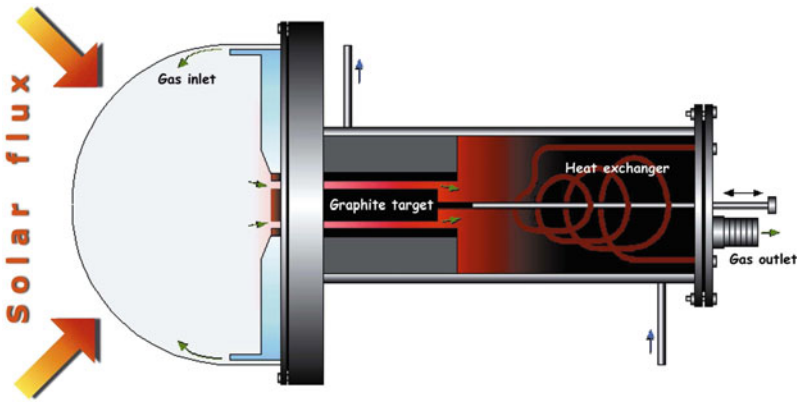

Solar Energy in Thermochemical Processing. Figure 20
Scheme of a solar reactor for fullerene synthesis (Source: Processes, Materials, and Solar Energy Laboratory, PROMES-CNRS, France)

to an involute, provides uniform irradiation on the tubular reactor. CFC formed has typically the following properties: surface area 100–170 m^2/g, pore volume 0.4–0.8 cm^3/g, micropore volume 0.004–0.008 cm^3/g, and average pore diameter 10–40 nm.

Solar Lime and Cement The thermal decomposition of calcium carbonate (limestone) to calcium oxide (lime)

$$CaCO_3 \rightarrow CaO + CO_2 \tag{34}$$

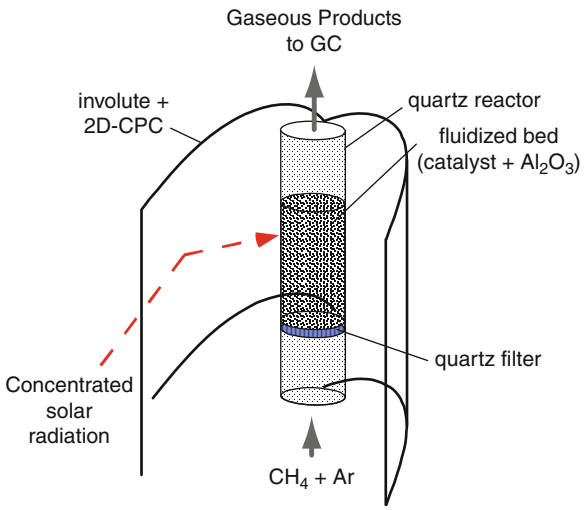

Solar Energy in Thermochemical Processing. Figure 21 Schematic of a solar reactor for CFC production (Adapted from [115])

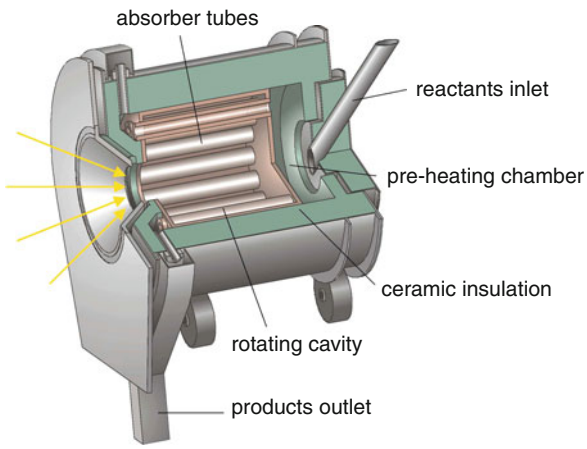

Solar Energy in Thermochemical Processing. Figure 22 Schematic of a direct-irradiated rotary reactor for the solar production of lime (Adapted from [116])

is the main endothermic step in the production of lime and cement at 1,300 K. Substituting concentrated solar energy in place of carbonaceous fuels, as the source of high-temperature process heat, is a means to reduce the dependence on conventional energy resources and to reduce emissions of CO_2 and other pollutants.

Figure 22 shows the solar reactor concept for the solar calcination process [116]. The indirect-heating rotary kiln consists of a tilted cylindrical steel drum lined with ceramic insulation and comprising a multi-tube reaction chamber made from high-temperature-resistant SiC. The kiln works with any conventional external heat source in place of concentrated solar radiation, allowing for continuous operation in case of missing or insufficient solar irradiation. A 10-kW solar reactor prototype has been tested at a solar furnace. It processes 1–5 mm limestone particles, producing high purity lime with a degree of calcination exceeding 98% and any desired reactivity. The reactor efficiency, defined as the enthalpy of the calcination reaction at ambient temperature (3,184 kJ kg^{-1}) divided by the solar energy input, reached 30–35% for solar flux intensities of about 2,000 kW m^{-2} and for quicklime production rates up to 4 kg h^{-1}. The kiln prototype operated reliably for more than 100 h, withstanding thermal shocks that occur in solar high-temperature applications. An economic assessment indicates that the cost of solar lime produced in an industrial solar calcination plant of 20–25 MW solar thermal power input is about 2–3 times the current selling price of conventional lime. The solar production of high-purity lime might be an economically viable path for reducing CO_2 emissions in specific market sectors of the lime industry.

Solar Thermal Recycling of Hazardous Waste Materials Solid waste materials from a wide variety of sources, for example, municipal waste incineration residuals, discharged batteries, dirty scraps, automobile shredded residue, contaminated soil, dusts, sludge, and by-products from the metallurgical industry, contain hazardous compounds that are usually vitrified in a non-leaching slag and finally disposed of at hazardous waste-storage sites. However, limited storage space, increasing storage costs, and environmental regulations have led the need for developing technologies that recycle these toxic materials into useful commodities rather than deposit them in dump sites for an undetermined period of time. Thermal processes are well suited for the treatment of these complex solid waste materials. Waste materials containing carbonaceous compounds can be converted by thermal pyrolysis and gasification into syngas and hydrocarbons that can be further processed into other valuable synthetic

chemicals. Those containing metal oxides may be converted by carbothermal reduction into metals, nitrides, carbides, and other metallic compounds.

The commercial recycling techniques by blast, induction, arc, and plasma furnaces are major consumers of fossil-fuel-based electricity and heat. Concentrated solar energy offers the possibility of converting hazardous solid waste material into valuable commodities for processes in closed and sustainable material cycles. Examples of recycling processes demonstrated in solar furnaces are the processing of electric arc furnace dust (EAFD) using the "two-cavity" reactor depicted in Fig. 23 [117], and the melting of Al scrap using a SiC-lined rotary kiln shown in Fig. 24, which can be tilted for discharging molten metal and slag into moulds [118].

Other applications in the area of solar thermal processing of materials that are being explored include hardening of carbon steel, production of Expanded Natural Graphite (ENG) by exfoliation of graphite

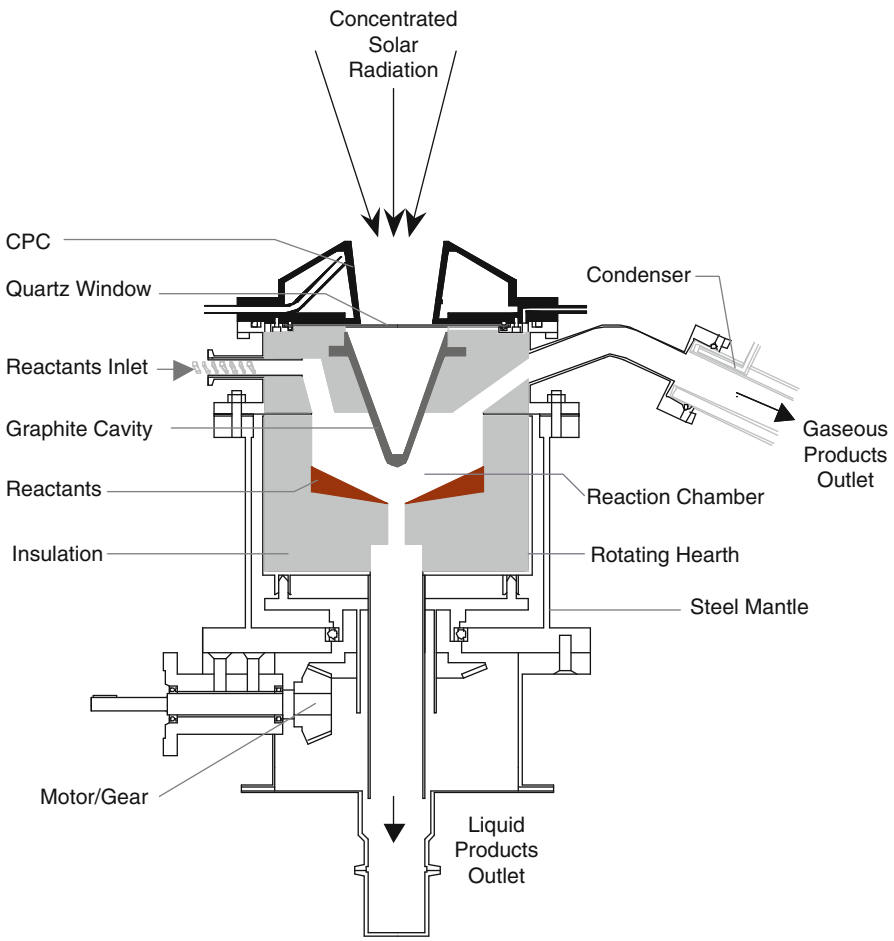

Solar Energy in Thermochemical Processing. Figure 23
Schematic of a "two-cavity" solar chemical reactor concept for the thermal recycling of hazardous waste materials – It features two cavities in series. The inner cavity (absorber) is made of graphite and contains a windowed aperture to let in concentrated solar radiation. A CPC is implemented at the reactor aperture. The outer cavity (reaction chamber) is well insulated and contains the waste material that is subjected to irradiation by the graphite absorber separating the two cavities. With this arrangement, the inner cavity protects the window against particles and condensable gases coming from the reaction chamber. Uniform distribution of continuously fed reactants is achieved by rotating the outer cavity (From [117])

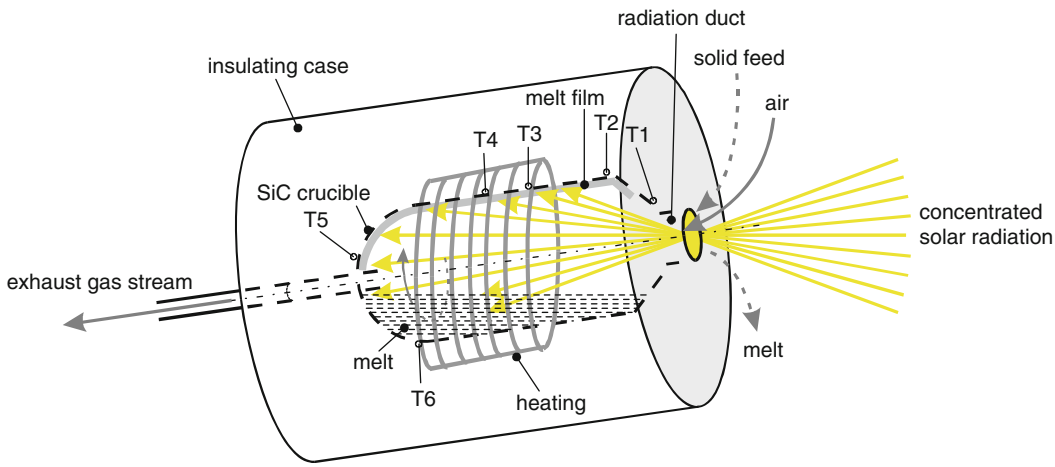

Solar Energy in Thermochemical Processing. Figure 24
Schematic of a solar rotary kiln for aluminum melting (Adapted from [118])

intercalated compounds, synthesis of advanced ceramics, and purification of metallurgical grade silicon for photovoltaic applications.

Life Cycle and Economic Analyses

Environmental Impacts. Solar thermochemical processes use concentrated solar radiation as the main or sole source of high-temperature process heat. A solar thermal plant consists of a central receiver system comprising a heliostat field focusing direct solar radiation on a receiver which is mounted on a tower. The receiver includes a chemical reactor or a heat exchanging device. Land consumption and impacts on local flora and wildlife during the build-up of the heliostat field and other facilities are the main environmental issues of the concentrating solar systems [119]. Other impacts are associated with the construction of the steel-intensive infrastructure for solar energy collection due to mineral and fossil resource consumption as well as discharge of pollutants related to today's steel production technology [120]. Direct CO_2 emissions released by the processes are negligible or significantly lower than those from the current fossil-fuel-based processes [119]. All other possible effects are comparable to the conventional processes or can be prevented by safety measures and equipment which are common practice in the chemical industry.

Economics. Economic assessments indicate that solar thermochemical processes for the production of hydrogen and other solar fuels have the potential of becoming economically competitive vis-à-vis alternative paths for producing solar fuels, such as via electrolysis using solar-generated electricity. These studies further indicate that the heliostat field is responsible for about half of the total investment costs for the entire chemical plant, while the cost of the solar reactor represents 10–15%. However, for a fixed product throughput, the solar reactor's efficiency dictates the size of the heliostat field. Thus, reaching high solar reactor efficiencies and reducing the cost of the heliostats per unit area will have a significant impact on reducing the unit cost of the solar fuel. Application of credits for CO_2 mitigation and pollution avoidance will further enable the solar thermochemical technologies to compete favorably with fossil-fuel-based processes. The weaknesses of these economic evaluations are related primarily to the uncertainties in the viable efficiencies and investment costs of the various components due to their early stage of development and their economy of scale [1].

Future Directions

Solar thermochemical processes have favorable long-term prospects because they avoid or reduce costs for CO_2 mitigation and pollution abatement. The products are renewable fuels and material commodities for delivering clean and sustainable energy services. Further research and development toward optimization and scale-up of the solar thermochemical process and reactor technology is warranted.

The various solar fuels production and materials processing technologies are at diverse stages of maturity. Short-to-mid-term "transition" processes such as solar reforming of NG, solar gasification of carbonaceous materials, or solar carbothermal reduction of ZnO are expected to be ready for large-scale industrial implementation by 2015–2020. The long-term thermochemical cycles for splitting H_2O and CO_2, such as the ZnO/Zn cycle, the mixed iron oxide cycle, the iodine-sulfur cycle, and others, will require further fundamental research and prototype reactor development. Their large-scale industrial implementation is predicted for 2020–2025, provided the price of fuel will account for the external costs of greenhouse gas mitigation and pollution abatement.

Note

This entry provides an update and extension of a previous publication [1]. Reprinted in part from Encyclopedia of Energy, vol. 5, Steinfeld A. and Meier A., Solar Fuels and Materials, 623–637, Copyright (2004), with permission from Elsevier.

Nomenclature

A	Area of reactor aperture (m^2)
$\widetilde{C}$	Mean solar flux concentration ratio (−)
HHV	Higher heating value of a fuel
I	Direct normal solar irradiance ($kW \cdot m^{-2}$)
Irr_{quench}	Irreversibility associated with quenching ($kW \cdot K^{-1}$)
$Irr_{reactor}$	Irreversibility associated with solar reactor ($kW \cdot K^{-1}$)
$Irr_{hydrolyzer}$	Irreversibility associated with hydrolyzer ($kW \cdot K^{-1}$)
$\dot{n}$	Molar flow rate ($mol \cdot s^{-1}$)
$\dot{Q}_{FC}$	Rate of heat rejected to surroundings from fuel cell (kW)
$\dot{Q}_{hydrolyzer}$	Rate of heat rejected to surroundings from hydrolyzer (kW)
$\dot{Q}_{quench}$	Rate of heat rejected to surroundings from the quench (kW)
$\dot{Q}_{reactor,net}$	Net power absorbed by solar reactor (kW)
$\dot{Q}_{reradiation}$	Re-radiated power from solar reactor (kW)
$\dot{Q}_{solar}$	Solar power input to solar reactor (kW)
T	Temperature (K)
T_H	High reservoir temperature (K)
T_L	Low reservoir temperature (K)
$T_{optimum}$	Optimum temperature of solar cavity receiver for maximum η_{exergy} (K)
$T_{stagnation}$	Maximum temperature of a blackbody absorber (K)
$\dot{W}_{FC}$	Rate of maximum theoretical work from fuel cell (kW)
ΔG	Gibbs free energy change ($kJ \cdot mol^{-1}$)
ΔH	Enthalpy change ($kJ \cdot mol^{-1}$)
ΔS	Entropy change ($kJ \cdot mol^{-1} \cdot K^{-1}$)
$\eta_{absorption}$	Solar energy absorption efficiency (−)
η_{Carnot}	Carnot efficiency (−)
η_{exergy}	Exergy efficiency of the thermochemical cycle (−)
η_{FC}	Efficiency of H_2/O_2 fuel cell (−)
σ	Stefan-Boltzmann constant ($5.6705 \cdot 10^{-8}$ $W \cdot m^{-2} \cdot K^{-4}$)

Bibliography

Primary Literature

1. Steinfeld A, Meier A (2004) Solar fuels and materials. In: Cleveland C (ed) Encyclopedia of energy, vol 5. Elsevier, Amsterdam, pp 623–637
2. IEA (2010) IEA technology roadmap – concentrating solar power. International Energy Agency, Paris
3. Haueter P, Seitz T, Steinfeld A (1999) A new high-flux solar furnace for high-temperature thermochemical research. J Sol Energy Eng 121:77–80
4. Welford WT, Winston R (1989) High collection nonimaging optics. Academic, San Diego
5. Romero M, Buck R, Pacheco JE (2002) An update on solar central receiver systems, projects, and technologies. J Sol Energy Eng 124(2):98–108
6. Yogev A, Kribus A, Epstein M, Kogan A (1998) Solar tower reflector systems: a new approach for high-temperature solar plants. Int J Hydrogen Energy 23:239–245
7. Fletcher EA, Moen RL (1977) Hydrogen and oxygen from water. Science 197:1050–1056
8. Steinfeld A, Schubnell M (1993) Optimum aperture size and operating temperature of a solar cavity-receiver. Sol Energy 50:19–25
9. JANAF Thermochemical Tables (1985) National bureau of standards, 3rd edn. National Bureau of Standards, Washington, DC
10. Steinfeld A, Kuhn P, Reller A, Palumbo R, Murray J, Tamaura Y (1998) Solar-processed metals as clean energy carriers and water-splitters. Int J Hydrogen Energy 23:767–774
11. Schunk LO, Steinfeld A (2009) Kinetics of the thermal dissociation of ZnO exposed to concentrated solar irradiation using a solar-driven thermogravimeter in the 1800–2100 K range. AIChE J 55:1497–1504

12. Palumbo R, Lédé J, Boutin O, Elorza-Ricart E, Steinfeld A, Möller S, Weidenkaff A, Fletcher EA, Bielicki J (1998) The production of Zn from ZnO in a single step high temperature solar decomposition process I. The scientific framework for the process. Chem Eng Sci 53:2503–2518
13. Weidenkaff A, Reller AW, Wokaun A, Steinfeld A (2000) Thermogravimetric analysis of the ZnO/Zn water splitting cycle. Thermochim Acta 359:69–75
14. Möller S, Palumbo R (2001) Solar thermal decomposition kinetics of ZnO in the temperature range 1950–2400 K. Chem Eng Sci 56:4505–4515
15. Perkins C, Lichty P, Weimer AW (2007) Determination of aerosol kinetics of thermal ZnO dissociation by thermogravimetry. Chem Eng Sci 62:5952–5962
16. Perkins C, Lichty PR, Weimer A (2008) Thermal ZnO dissociation in a rapid aerosol reactor as part of a solar hydrogen production cycle. Int J Hydrogen Energy 33:499–510
17. Haueter P, Moeller S, Palumbo R, Steinfeld A (1999) The production of zinc by thermal dissociation of zinc oxide – Solar chemical reactor design. Sol Energy 67:161–167
18. Alxneit I (2008) Assessing the feasibility of separating a stoichiometric mixture of zinc vapor and oxygen by a fast quench – Model calculations. Sol Energy 82:959–964
19. Steinfeld A, Palumbo R (2001) Solar thermochemical process technology. In: Meyers RA (ed) Encyclopedia of physical science and technology, vol 15. Academic, San Diego, pp 237–256
20. Fletcher EA (1999) Solarthermal and solar quasi-electrolytic processing and separations: Zinc from Zinc Oxide as an example. Ind Eng Chem Res 38:2275–2282
21. Fletcher EA, Macdonald F, Kunnerth D (1985) High temperature solar electrothermal processing II. Zinc from zinc oxide. Energy 10:1255–1272
22. Palumbo RD, Fletcher EA (1988) High temperature solar electro-thermal processing III. Zinc from zinc oxide at 1200–1675 K using a non-consumable anode. Energy 13:319–332
23. Parks DJ, Scholl KL, Fletcher EA (1988) A study of the use of Y_2O_3 doped ZrO_2 membranes for solar electrothermal and solar thermal separations. Energy 13:121–136
24. Steinfeld A (2005) Solar thermochemical production of hydrogen – a review. Sol Energy 78:603–615
25. Venstrom L, Krueger K, Leonard N, Tomlinson B, Duncan S, Palumbo RD (2009) Solar thermal electrolytic process for the production of Zn from ZnO: an ionic conductivity study. J Sol Energy Eng 131:031005–1
26. Murray JP, Steinfeld A, Fletcher EA (1995) Metals, nitrides, and carbides via solar carbothermal reduction of metal oxides. Energy 20:695–704
27. Steinfeld A, Fletcher EA (1991) Theoretical and experimental investigation of the carbothermic reduction of Fe_2O_3 using solar energy. Energy 16:1011–1019
28. Steinfeld A, Kuhn P, Karni J (1993) High temperature solar thermochemistry: production of iron and synthesis gas by Fe_3O_4-reduction with methane. Energy 18:239–249
29. Steinfeld A, Frei A, Kuhn P, Wuillemin D (1995) Solarthermal production of zinc and syngas via combined ZnO-reduction and CH_4-reforming processes. Int J Hydrogen Energy 20:793–804
30. Steinfeld A, Brack M, Meier A, Weidenkaff A, Wuillemin D (1998) A solar chemical reactor for the co-production of zinc and synthesis gas. Energy 23:803–814
31. Kräupl S, Steinfeld A (2001) Experimental investigation of a vortex-flow solar chemical reactor for the combined ZnO-reduction and CH_4-reforming. J Sol Energy Eng 123:237–243
32. Kräupl S, Steinfeld A (2003) Operational performance of a 5 kW solar chemical reactor for the co-production of zinc and syngas. J Sol Energy Eng 125:124–126
33. Wieckert C, Steinfeld A (2002) Solar thermal reduction of ZnO using CH_4:ZnO and C:ZnO molar ratios less than 1. J Sol Energy Eng 124:55–62
34. Osinga T, Frommherz U, Steinfeld A, Wieckert C (2004) Experimental investigation of the solar carbothermic reduction of ZnO using a two-cavity solar reactor. J Sol Energy Eng 126:633–637
35. Osinga T, Olalde G, Steinfeld A (2004) The solar carbothermal reduction of ZnO – shrinking packed-bed reactor modeling and experimental validation. Ind Eng Chem Res 43:7981–7988
36. Wieckert C, Frommherz U, Kräupl S, Guillot E, Olalde G, Epstein M, Santén S, Osinga T, Steinfeld A (2007) A 300 kW solar chemical pilot plant for the carbothermic production of zinc. J Sol Energy Eng 129(2):190–196
37. Epstein M, Olalde G, Santén S, Steinfeld A, Wieckert C (2008) Towards the industrial solar carbothermal production of zinc. J Sol Energy Eng 130(1):014505
38. Meier A, Steinfeld A (2010) Solar thermochemical production of fuels. Adv Sci Technol 74:303–312
39. Jensen SH, Larsen PJ, Mogensen M (2007) Hydrogen and synthetic fuel production from renewable energy sources. Int J Hydrogen Energy 32(15):3253–3257
40. Kogan A (1998) Direct solar thermal splitting of water and on-site separation of the products. II. Experimental feasibility study. Int J Hydrogen Energy 23:89–98
41. Ihara S (1980) On the study of hydrogen production from water using solar thermal energy. Int J Hydrogen Energy 5:527–534
42. Diver RB, Pederson S, Kappauf T, Fletcher EA (1983) Hydrogen and oxygen from water – VI. Quenching the effluent from a solar furnace. Energy 12:947–955
43. Lédé J, Villermaux J, Ouzane R, Hossain MA, Ouahes R (1987) Production of hydrogen by simple impingement of a turbulent jet of steam upon a high temperature zirconia surface. Int J Hydrogen Energy 12:3–11
44. Le Duigou A, Borgard JM, Larousse B, Doizi D, Allen R, Ewan B et al (2007) HYTHEC: an EC funded search for a long term massive hydrogen production route using solar and nuclear technologies. Int J Hydrogen Energy 32:1516–1529
45. Kolb GJ, Diver RB, Siegel N (2007) Central-station solar hydrogen power plant. J Sol Energy Eng 129:179–183
46. Perkins C, Weimer AW (2009) Solar-thermal production of renewable hydrogen. AIChE J 55:286–293

47. Abanades S, Charvin P, Flamant G, Neveu P (2006) Screening of water-splitting thermochemical cycles potentially attractive for hydrogen production by concentrated solar energy. Energy 31:2805–2822
48. Kodama T (2003) High-temperature solar chemistry for converting solar heat to chemical fuels. Prog Energ Combust 29:567–597
49. Kodama T, Gokon N (2007) Thermochemical cycles for high-temperature solar hydrogen production. Coordin Chem Rev 107:4048–4077
50. Fletcher EA (2001) Solarthermal processing: a review. J Sol Energy Eng 123:63–74
51. Inoue M, Hasegawa N, Uehara R, Gokon N, Kaneko H, Tamaura Y (2004) Solar hydrogen generation with $H_2O/ZnO/MnFe_2O_4$ system. Sol Energy 76:309–315
52. Miller JE, Allendorf MD, Diver RB, Evans LR, Siegel NP, Stuecker JN (2008) Metal oxide composites and structures for ultra-high temperature solar thermochemical cycles. J Mater Sci 43:4714–4728
53. Chueh WC, Haile SM (2009) Ceria as a thermochemical reaction medium for selectively generating syngas or methane from H_2O and CO_2. ChemSusChem 2:735–739
54. Nakamura T (1977) Hydrogen production from water utilizing solar heat at high temperatures. Sol Energy 19:467–475
55. Sibieude F, Ducarroir M, Tofighi A, Ambriz J (1982) High-temperature experiments with a solar furnace: the decomposition of Fe_3O_4, Mn_3O_4, CdO. Int J Hydrogen Energy 7:79–88
56. Bilgen E, Ducarroir M, Foex M, Sibieude F, Trombe F (1977) Use of solar energy for direct and two -step water decomposition cycles. Int J Hydrogen Energy 2:251–257
57. Steinfeld A (2002) Solar hydrogen production via a two-step water-splitting thermochemical cycle based on Zn/ZnO redox reactions. Int J Hydrogen Energy 27:611–619
58. Perkins C, Weimer AW (2004) Likely near-term solar-thermal water splitting technologies. Int J Hydrogen Energy 29: 1587–1599
59. Loutzenhiser PG, Meier A, Steinfeld A (2010) Review of the two-step H_2O/CO_2-splitting solar thermochemical cycle based on Zn/ZnO redox reactions. Materials 3:4922–4938
60. Schunk L, Haeberling P, Wepf S, Wuillemin D, Meier A, Steinfeld A (2008) A solar receiver-reactor for the thermal dissociation of zinc oxide. J Sol Energy Eng 130:021009
61. Müller R, Steinfeld A (2008) H_2O-splitting thermochemical cycle based on ZnO-Zn-redox – Quenching the effluents from the ZnO dissociation. Chem Eng Sci 63:217–227
62. Abanades S, Charvin P, Flamant G (2007) Design and simulation of a solar chemical reactor for the thermal reduction of metal oxides – Case study of zinc oxide dissociation. Chem Eng Sci 62:6323–6333
63. Dombrovsky LA, Lipiński W, Steinfeld A (2007) A diffusion-based approximate model for radiation heat transfer in a solar thermochemical reactor. J Quant Spectrosc Radiat Transf 103:601–610
64. Müller R, Steinfeld A (2007) Band-approximated radiative heat transfer analysis of a solar chemical reactor for the thermal dissociation of zinc oxide. Sol Energy 81:1285–1294
65. Müller R, Lipiński W, Steinfeld A (2008) Transient heat transfer in a directly-irradiated solar chemical reactor for the thermal dissociation of ZnO. Appl Therm Eng 28:524–531
66. Dombrovsky LA, Schunk L, Lipiński W, Steinfeld A (2009) An ablation model for the thermal decomposition of porous zinc oxide layer heated by concentrated solar radiation. Int J Heat Mass Transf 52:2444–2452
67. Schunk LO, Lipiński W, Steinfeld A (2009) Ablative heat transfer in a shrinking packed-bed of ZnO undergoing solar thermal dissociation. AIChE J 55:1659–1666
68. Schunk LO, Lipiński W, Steinfeld A (2009) Heat transfer model of a solar receiver-reactor for the thermal dissociation of ZnO – Experimental validation at 10 kW and scale-up to 1 MW. Chem Eng J 150:502–508
69. Weiss RJ, Ly HC, Wegner K, Pratsinis SE, Steinfeld A (2005) H_2 production by Zn hydrolysis in a hot-wall aerosol reactor. AIChE J 51:1966–1970
70. Wegner K, Ly HC, Weiss RJ, Pratsinis SE, Steinfeld A (2006) In situ formation and hydrolysis of Zn nanoparticles for H_2 production by the two-step ZnO/Zn water-splitting thermochemical cycle. Int J Hydrogen Energy 31:55–61
71. Ernst FO, Tricoli A, Pratsinis SE, Steinfeld A (2006) Co-synthesis of H_2 and ZnO by in-situ Zn aerosol formation and hydrolysis. AIChE J 52:3297–3303
72. Funke HH, Diaz H, Liang X, Carney CS, Weimer AW, Lib P (2008) Hydrogen generation by hydrolysis of zinc powder aerosol. Int J Hydrogen Energy 33:1127–1134
73. Melchior T, Piatkowski N, Steinfeld A (2009) H_2 production by steam-quenching of Zn vapor in a hot-wall aerosol flow reactor. Chem Eng Sci 64:1095–1101
74. Abu Hamed T, Venstrom L, Alshare A, Brülhart M, Davidson JH (2009) Study of a quench device for simultaneous synthesis and hydrolysis of Zn nanoparticles: modeling and experiments. J Sol Energy Eng 131:031018-1-9
75. Abanades S, Charvin P, Lemont F, Flamant G (2008) Novel two-step SnO_2/SnO water-splitting cycle for solar thermochemical production of hydrogen. Int J Hydrogen Energy 33:6021–6030
76. Charvin P, Abanades S, Bêche E, Lemont F, Flamant G (2009) Hydrogen production from mixed cerium oxides via three-step water-splitting cycles. Solid State Ionics 180:1003–1010
77. Chueh WC, Falter C, Abbott M, Scipio D, Furler P, Haile SM, Steinfeld A (2010) High-flux solar-driven thermochemical dissociation of CO_2 and H_2O using nonstoichiometric ceria. Science 330:1797–1801
78. Lemort F, Charvin P, Lafon C, Romnicianu M (2006) Technological and chemical assessment of various thermochemical cycles: from the UT3 cycle up to the two steps iron oxide cycle. Int J Hydrogen Energy 31:2063–2075
79. Kodama T, Nakamuro Y, Mizuno T (2006) A two-step thermochemical water splitting by iron-oxide on stabilized zirconia. J Sol Energy Eng 128:3–7
80. Kaneko H, Miura T, Fuse A, Ishihara H, Taku S, Fukuzumi H, Naganuma Y, Tamaura Y (2007) Rotary-type solar reactor for solar hydrogen production with two-step water splitting process. Energy Fuels 21:2287–2293

81. Diver RB, Miller JE, Allendorf MD, Siegel N, Hogan RE (2008) Solar thermochemical water-splitting ferrite-cycle heat engines. J Sol Energy Eng 130:041001–1
82. Roeb M, Neises M, Säck J-P, Rietbrock P, Monnerie N, Dersch J, Schmitz M, Sattler C (2009) Operational strategy of a two-step thermochemical process for solar hydrogen production. Int J Hydrogen Energy 34:4537–4545
83. Meier A, Sattler C (2010) Solar fuels from concentrated sunlight, IEA SolarPACES Implementing Agreement, Tabernas, Spain. http://www.solarpaces.org/Library/docs/Solar_Fuels.pdf
84. Gálvez E, Loutzenhiser P, Hischier I, Steinfeld A (2008) CO_2 splitting via two-step solar thermochemical cycles with Zn/ZnO and FeO/Fe_3O_4 redox reactions: thermodynamic analysis. Energy Fuels 22:3544–3550
85. Loutzenhiser PG, Gálvez ME, Hischier I, Stamatiou A, Frei A, Steinfeld A (2009) CO_2 splitting via two-step solar thermochemical cycles with Zn/ZnO and FeO/Fe_3O_4 redox reactions II: kinetic analysis. Energy Fuels 23:2832–2839
86. Nikulshina V, Hirsch D, Mazzotti M, Steinfeld A (2006) CO_2 capture from air and co-production of H_2 via the $Ca(OH)_2$-$CaCO_3$ cycle using concentrated solar power – thermodynamic analysis. Energy 31:1379–1389
87. Nikulshina V, Steinfeld A (2009) CO_2 capture from air via CaO-carbonation using a solar-driven fluidized bed reactor – Effect of temperature and water vapor concentration. Chem Eng J 155:867–873
88. Nikulshina V, Gebald C, Steinfeld A (2009) CO_2 capture from atmospheric air via consecutive CaO-carbonation and $CaCO_3$-calcination cycles in a fluidized-bed solar reactor. Chem Eng J 146:244–248
89. Stamatiou A, Loutzenhiser PG, Steinfeld A (2010) Solar syngas production via H_2O/CO_2-splitting thermochemical cycles with Zn/ZnO and FeO/Fe_3O_4 redox reactions. Chem Mater 22:851–859
90. Stamatiou A, Loutzenhiser PG, Steinfeld A (2010) Solar syngas production from H_2O and CO_2 via two-step thermochemical cycles based on Zn/ZnO and FeO/Fe_3O_4 redox reactions: kinetic analysis. Energy Fuels 24:2716–2722
91. Mantzaras J (2008) Catalytic combustion of syngas. J Combust Sci Technol 180:1137–1168
92. Dry ME (2002) The Fischer–Tropsch process: 1950–2000. Catal Today 71:227–241
93. Dahl J, Buechler K, Finley R, Stanislaus T, Weimer A, Lewandowski A, Bingham C, Smeets A, Schneider A (2004) Rapid solar-thermal dissociation of natural gas in an aerosol flow reactor. Energy 29:715–725
94. Maag G, Zanganeh G, Steinfeld A (2009) Solar thermal cracking of methane in a particle-flow reactor for the co-production of hydrogen and carbon. Int J Hydrogen Energy 34:7676–7685
95. Rodat S, Abanades S, Flamant G (2009) High-temperature solar methane dissociation in a multitubular cavity-type reactor in the temperature range 1823–2073 K. Energy Fuels 23:2666–2674
96. Möller S, Kaucic D, Sattler C (2006) Hydrogen production by solar reforming of natural gas: a comparison study of two possible process configurations. J Sol Energy Eng 128:16–23
97. Petrasch J, Meier F, Friess H, Steinfeld A (2008) Tomography based determination of permeability, Dupuit–Forchheimer coefficient, and interfacial heat transfer coefficient in reticulate porous ceramics. Int J Heat Fluid Flow 29:315–326
98. Petrasch J, Wyss P, Stämpfli R, Friess H, Steinfeld A (2008) Tomography-based multi-scale analyses of the 3D geometrical morphology of reticulated porous ceramics. J Am Ceram Soc 91:2659–2665
99. Dahl JK, Weimer AW, Lewandowski A, Bingham C, Brütsch F, Steinfeld A (2004) Dry reforming of methane using a solar-thermal aerosol flow reactor. Ind Eng Chem Res 43:5489–5495
100. Lovegrove K, Luzzi A, Soldiani I, Kreetz H (2004) Developing ammonia based thermochemical energy storage for dish power plants. Sol Energy 76:331–337
101. Z'Graggen A, Haueter P, Maag G, Vidal A, Romero M, Steinfeld A (2007) Hydrogen production by steam-gasification of petroleum coke using concentrated solar power – III. Reactor experimentation with slurry feeding. Int J Hydrogen Energy 32:992–996
102. Z'Graggen A, Steinfeld A (2009) Hydrogen production by steam-gasification of carbonaceous materials using concentrated solar energy – V. reactor modeling, optimization, and scale-up. Int J Hydrogen Energy 33:5484–5492
103. Piatkowski N, Wieckert C, Steinfeld A (2009) Experimental investigation of a packed-bed solar reactor for the steam-gasification of carbonaceous feedstocks. Fuel Process Technol 90:360–366
104. Melchior T, Perkins C, Lichty P, Weimer AW, Steinfeld A (2009) Solar-driven biochar gasification in a particle-flow reactor. Chem Eng Process 48:1279–1287
105. Lichty P, Perkins C, Woodruff B, Bingham C, Weimer AW (2010) Rapid high temperature solar thermal biomass gasification in a prototype cavity reactor. J Sol Energy Eng 132:011012–1
106. Service RF (2009) Sunlight in your tank. Science 326:1471–1475
107. Villasmil W, Steinfeld A (2010) Hydrogen production by hydrogen sulfide splitting using concentrated solar energy – Thermodynamics and economic evaluation. Energy Conv Manag 51:2353–2361
108. Murray JP (1999) Aluminum-silicon carbo-thermal reduction using high-temperature solar process heat. In: Eckert CE (ed) Light metals. The Minerals, Metals, and Materials Society, Warrendale, pp 399–405
109. Kruesi M, Galvez ME, Halmann M, Steinfeld A (2011) Solar aluminum production by vacuum carbothermal reduction of alumina – thermodynamic and experimental analyses. Metall Mater Trans B 42B:254–260
110. Loutzenhiser P, Tuerk O, Steinfeld A (2010) Production of Si by vacuum carbothermal reduction of SiO_2 using concentrated solar energy. J Metals 62:49–54
111. Flamant G, Kurtcuoglu V, Murray J, Steinfeld A (2006) Purification of metallurgical grade silicon by a solar process. Sol Energy Mater Sol Cells 90:2099–2106
112. Guillard T, Alvarez L, Anglaret E, Sauvajol JL, Bernier P, Flamant G, Laplaze D (1999) Production of fullerenes and carbon nanotubes by the solar energy route. J Phys IV France 9:399–404

113. Luxembourg D, Flamant G, Laplaze D (2005) Solar synthesis of single-walled carbon nanotubes at medium scale. Carbon 43:2302–2310
114. Meier A, Kirillov V, Kuvshinov G, Mogilnykh Y, Reller A, Steinfeld A, Weidenkaff A (1999) Solar thermal decomposition of hydrocarbons and carbon monoxide for the production of catalytic filamentous carbon. Chem Eng Sci 54:3341–3348
115. Tamaura Y, Steinfeld A, Kuhn P, Ehrensberger K (1995) Production of solar hydrogen by a novel, 2-step, water-splitting thermochemical cycle. Energy 20:325–330
116. Meier A, Bonaldi E, Cella GM, Lipinski W (2005) Multitube rotary kiln for the industrial solar production of lime. J Sol Energy Eng 127:386–395
117. Schaffner B, Meier A, Wuillemin D, Hoffelner W, Steinfeld A (2003) Recycling of hazardous solid waste material using high-temperature solar process heat. 2. Reactor design and experimentation. Environ Sci Technol 37:165–170
118. Funken K-H, Roeb M, Schwarzboezl P, Warneke H (2001) Aluminum remelting using directly solar-heated rotary kilns. J Sol Energy Eng 123:117–124
119. Pregger T, Graf D, Krewitt W, Sattler C, Roeb M, Möller S (2009) Prospects of solar thermal hydrogen production processes. Int J Hydrogen Energy 34:4256–4267
120. Felder R, Meier A (2008) Well-to-wheel analysis of solar hydrogen production and utilization for passenger car transportation. J Sol Energy Eng 130:011017–1

Books and Reviews

Wieckert C, Epstein M, Olalde G, Santén S, Steinfeld A (2009) Zinc electrodes: solar thermal production. In: Garche J (ed) Encyclopedia of electrochemical power sources, vol 5. Elsevier, Amsterdam, pp 469–486

Solar Irradiance, Global Distribution

Richard W. Mueller
Deutscher Wetterdienst, Offenbach, Germany

Article Outline

Glossary
Definition
Introduction
The Sun and the Earth
Global Distribution of the Top of Atmosphere Irradiance
Global Distribution of Surface Irradiance
Future Directions
Acknowledgments
Bibliography

Glossary

Albedo The albedo is a unitless measure of the reflectivity of an object. Albedo is defined as the ratio of reflected to incident electromagnetic radiation. Here, albedo is related to the reflection of solar irradiance.

Earth's orbit The path of the Earth around the Sun.

Earth's revolution The movement of the Earth around the Sun.

Equinox The days when daylight hours and night hours are equal, halfway between summer and winter.

Hadley circulation Large-scale equatorial circulation of air, driven by gradients in surface and air heating caused by surface irradiance. The Hadley circulation is characterized by rising motion near the equator, poleward horizontal flow of the arisen air at an altitude of 10–15 km, with a subsequent descending motion in the subtropics. The descended air flows then in turn back to the equator near to the surface. The Hadley circulation is closely related to the trade winds, tropical rainbelts, subtropical deserts, and jet streams.

Insolation Solar irradiance is also called insolation.

Inter tropical convergence zone The ITCZ appears as a belt of clouds encircling the globe close to the equator. It is the region where the trade winds originating in the Northern and Southern hemispheres come together.

Luminosity The amount of electromagnetic energy a body radiates per unit of time.

Solar irradiance The quantity of the incoming sun "rays" or, in other words, the amount of electromagnetic power per area. The direct irradiance is the part which comes from the direction of the Sun without scattering. The diffuse direction is the irradiance which comes from all directions.

Stratosphere The atmospheric layer above the troposphere.

Summer solstice The day when the altitude of the Sun is the greatest, close to the first day of summer.

Teleconnection Teleconnection in atmospheric science refers to climate anomalies or anomalies on the flow regime being related to each other at large distances (typically thousands of kilometers).

Top of atmosphere The top of atmosphere (TOA) is approximately 100 km above the Earth's surface. It is the border between the Earth's atmosphere and

space. The number density of the particles decreases logarithmic Al with increasing altitude. At a certain point (TOA) the density is close to zero, the atmosphere ends and space begins.

Troposphere The atmosphere of the Earth is divided into different layers. The layer near to the surface is called the troposphere. The altitude of this layer varies but is typically around 10 km. Above the troposphere the stratospheric layer begins. The transition between troposphere and stratosphere is called stratopause.

Winter solstice When the Northern hemisphere has the fewest daylight hours.

Definition

Solar irradiance is a driving factor of life on Earth and the Earth's energy budget. It is the driving factor also for wind and solar energy and thus guarantees the energy supply in a world running out of fossil energy. The distribution of land surface and vegetation types as well as the different climate regions of the world is predominantly a result of the ratio between the amount of solar surface irradiance and precipitation. For example, a large amount of solar surface irradiance combined with a lack of precipitation leads to decertification. Hence, the distribution of solar irradiance plays a dominant role for the diversity and distribution of plants, animals, and cultures.

Solar irradiance leads to energy uptake by the ocean and land surfaces and a subsequent warming of these surfaces. It is also a key quantity for evaporation. The energy cycle of absorbed solar irradiance, evaporation, emitted heat, and transport drives weather and climate. The distribution of solar irradiance is therefore key to the energy and water cycle of the Earth and hence the weather and climate system.

Solar irradiance affects also the well-being of humans. Large amounts of solar irradiance could easily lead to heat stress, sun burning, and the need for large local noon siestas, while low amounts during a period of several months increases the danger of depression, sometimes called the seasonal affective disorder (SAD).

The above-mentioned interactions of solar surface irradiance distribution with the distribution of animals, plants, climate zones, and weather regimes, demonstrate that the distribution of solar irradiance is important for life on Earth and for the development, establishment, and modifications of cultures. Solar irradiance distribution is the driving factor for wind circulation systems. Further on, knowledge of the solar irradiance distribution is needed for infrastructure planning of solar energy. The distribution of solar irradiance will be the dominant factor for the distribution of solar energy systems.

Introduction

The solar irradiance at the top of atmosphere (TOA) and at the Earth's surface is a key parameter for climate monitoring and analysis. It plays a dominant role in the energy fluxes between the surface and the atmosphere. Solar irradiance is a forcing quantity for heat fluxes, which compensates negative or positive values of the Earth's radiation budget, forcing atmospheric motions.

Solar surface irradiance with a large geographical coverage and a high resolution in space-time are necessary for a better understanding of climate variability and climate dynamics (extremes) and for assessing the radiative forcing of the climate system. Moreover, these data are quite well suitable for the verification of regional climate model output or reanalysis data respectively (e.g., [1]). Finally, irradiance went into climate indices, which are of value for monitoring and seasonal prediction of specific climate impacts (e.g., [2]).

Beside its importance for climate, the solar surface irradiance is also necessary for an efficient planning and monitoring of solar energy systems. Furthermore, it is of importance for the satellite-based estimation of drought and evaporation. Solar surface irradiance assessment from geostationary satellites constitutes a powerful alternative to meteorological ground networks for climatological data [3] and is the primary source of information in regions where ground-based measurements are sparse (e.g., Ocean, Africa). The top of atmosphere irradiance can only be observed from satellites. Knowledge about the global distribution and its temporal variation is quite important for all the above-mentioned applications and research fields.

The Sun and the Earth

The Sun emits a nearly constant flux of energy in the form of electromagnetic waves. The average total energy per unit time is called the solar luminosity and has a value of about $3.839*10^{26}$ W [4]. The solar luminosity is related to the solar irradiance, which is defined

as the electromagnetic energy per unit area and time or power per unit area. In physical terms the solar irradiance is defined as the flux density. The flux density of solar irradiance decreases with increasing distance from the Sun in the power of $1/r^2$. The irradiance (flux density) at the top of atmosphere at a distance of 149.5 million kilometers from the sun is approximately I_0 = 1,366 W/m^2 (see article of Gueymard for further details). I_0 is sometimes called the solar constant, but this term is somehow misleading, since the solar irradiance at the top of atmosphere is by no means constant. There are significant variations in the solar irradiance at the top of atmosphere due to variations in the sun activity (luminosity) and in the distance of the Earth relative to the Sun. The variation of the sun activity affects the solar emission and so the solar irradiance. The changes in solar irradiance due to variations in sun activity are usually within the range of 2–3 W/m^2. The variation in the distance between the Sun and the Earth arises from the orbit of the Earth around the Sun. It is not a circle, which would mean equal distance throughout the year, but an ellipse, see Fig. 1. It takes the Earth one year to make one revolution around the Sun on an elliptical orbit (1). As a consequence, the Earth-Sun distance varies sinusoidally throughout the year in the order of ±1.7%. This leads to a small variation of the solar irradiance. Often a distance factor f, varying between 1.03 and 0.97, is used to account for the seasonal variations in the solar "constant" within models. Along the Earth's elliptical orbit around the Sun, the Earth performs a complete rotation around its tilted spinning axis each day (Fig. 1, red line). One rotation takes 24 h and is responsible for the daily cycles of day and night and the change of the solar altitude throughout the day.

Both the distance between the Earth and the Sun as well as the sun activity affects the whole globe and not only parts of it. It is therefore obvious that both phenomena do not affect the distribution of solar irradiance and are therefore not discussed in more detail in this entry.

Global Distribution of the Top of Atmosphere Irradiance

There are two effects that define the global distribution of the solar irradiance at the top of atmosphere (TOA): the spherical shape of the Earth and the tilt of the Earth's rotation axis relative to the Sun. The Earth's rotation axis is currently tilted at 23.5° with respect to the ecliptic axis, the line drawn from the center of the Earth perpendicular to the ecliptic plane (Fig. 1). This tilt is called the obliquity of the Earth's axis.

The Earth has a spherical shape; hence, close to the equator the incoming solar irradiance covers a smaller region than at higher latitudes. Here, the same amount of incoming solar irradiance is spread over a larger region; hence the solar irradiance is lower per unit area. In mathematical terms, this effect is expressed by the cosine of the solar zenith angle (SZA). The solar zenith angle equals 90° minus the solar altitude of the Sun above the horizon, as illustrated in Fig. 2. The effect of the spherical shape of the Earth leads to a latitude dependency of the solar zenith angles (solar altitudes), as illustrated in Fig. 3. The higher the latitude the lower the highest possible solar altitude, hence, the lower the solar irradiance. (The effect of the solar altitude on the solar irradiance (both at TOA and surface) is by far larger than that of the Sun-Earth distance, as it modifies the solar irradiance in the range between 0 and 1,366. If the solar zenith angle is 60°, the irradiance is only half the value at 0°.) The maximum possible solar irradiance is not at the equator throughout the year, but moves up and down within +/−23.5 degrees latitude as a consequence of the Earth's obliquity (the tilted rotation axis of the Earth). This leads to a seasonal variation of the solar irradiance and hence the global solar irradiance patterns. This effect is illustrated in Fig. 4. The maximum solar altitude at each latitude is therefore dependent on the date of the year. The highest possible solar altitude at local noon at the equinoxes around March 20 and September 23 is 90° minus the local latitude. The highest possible solar altitude (local noon of the day) at the local latitude varies with ±23.5° throughout the year (Fig. 5, left). In the Northern hemisphere it is +23.5° around June 21 and −23.5° around December 21; in the Southern hemisphere this is reversed. This in turn leads to seasonal variations in the maximum and mean solar irradiance. The local noon solar irradiance (maximal possible value during any day) at a given latitude is given by Eq. 1 for every longitude and date.

$$I_{max} = I_0 * cos(latitude + \omega_t) \quad (1)$$

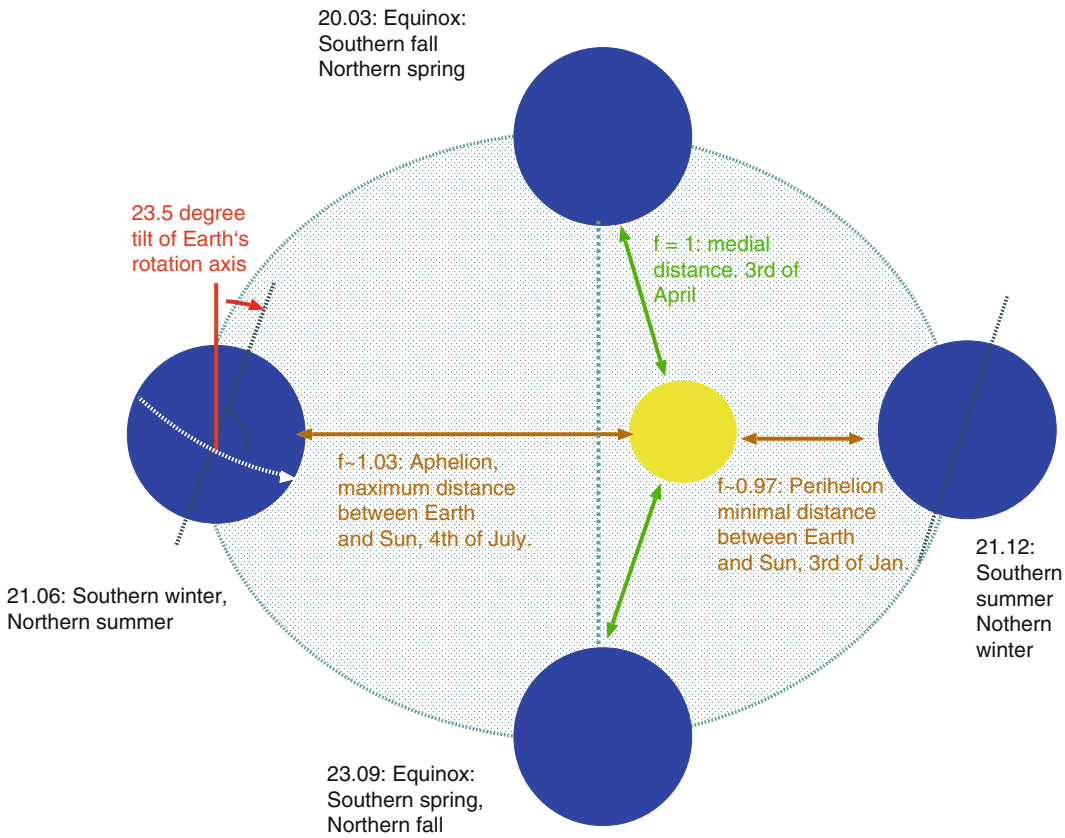

Solar Irradiance, Global Distribution. Figure 1
Illustration of the Earth's orbit around the Sun leading to a seasonal change of distance between the Sun and the Earth. The Sun is not positioned exactly in the center of the ellipse (cross of *gray lines*); rather it lies in one of the two focal points of the ellipse. Once a year (at so-called Perihelion), the Earth is closest to the Sun. At present, the Earth will be closest to the Sun on January 3. At that time the solar irradiance at the top of the atmosphere (TOA) is about 1,415 W/m^2. Six months later, the Sun-Earth distance reaches a maximum (so-called Aphelion). The solar irradiance during Aphelion is only about 1,322 W/m^2 at TOA. Thus, the solar irradiance has a pronounced seasonal cycle, which has a range of about 93 W/m^2 or $\pm$3.3% of the solar constant. The date for Perihelion and Aphelion is slightly changing throughout the decades

whereby ω_t varies between $\pm 23.5°$ throughout the year. Figure 5 (right) provides the distribution of the TOA solar irradiance at local noon, calculated with Eq. 1 for a fixed solar constant. The tilt of the Earth's rotation axis leads also to a seasonal increase or decrease in daylight hours – the farther away from the equator, the greater the effect. Moving from the equator to the north the number of daylight hours decreases with increasing latitude during the northern winter. For each degree change of latitude there is a reduction in daylight hours and a commensurate increase in the hours of darkness. North of the so-called polar circle the Sun does not rise above the horizon during winter time. (Of course from the equator to the South it is the same.) Daylight hours and SZA can be calculated by the use of the so-called equation of time for every date and location [5]; daylight hours can be also calculated online, e.g., at http://www.jgiesen.de/daylight.

The amount of daylight hours does significantly affect the global distribution of solar irradiance at the top of atmosphere. The maximum solar irradiance is reached at a latitude of $\sim 25°$ in each hemisphere, but due to the amount of daylight hours, the solar irradiance does not decrease with increasing latitude but remains constant at this level during the respective summer solstice period. This is illustrated in Fig. 6.

The number of daylight hours together with the maximum available solar altitude defines the distribution of solar irradiance at the top of atmosphere. Both effects are in turn a result of the Earth's rotation around a tilted axis together with the Earth's orbit around the Sun.

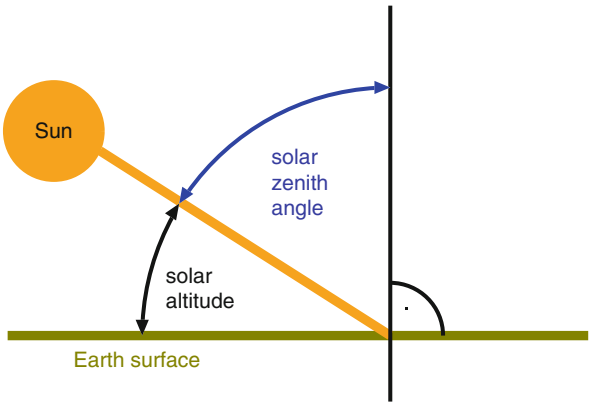

Solar Irradiance, Global Distribution. Figure 2
Illustration of the definition of solar altitude and solar zenith angle

It is important to note that the driving factor for summer and winter is the tilt of the Earth and not the distance between the Earth and the Sun.

Figure 7 shows the mean solar irradiance at the top of atmosphere averaged over 25 years. The seasonal effect of the rotation-axis tilt is compensated and the distribution is symmetric around the equator. Figure 8 illustrates the seasonal effect of the tilt on the solar irradiance at the top of the atmosphere. For individual months or seasons, the distribution is not symmetric around the equator, but leads to low irradiance values in either the southern or northern part of the Earth, especially toward the poles. The data illustrated here is from the NASA/GEWEX surface radiation budget project [6]. The Global Energy and Water-cycle Experiment (GEWEX) is an integrated program of research, observations, and science activities with the goal of providing data sets to support global and regional climate monitoring and analysis. The NASA/GEWEX SRB project is a major component of the GEWEX experiment. The objective of this project is to determine solar and thermal flux densities at the top of atmosphere and at the surface with the precision

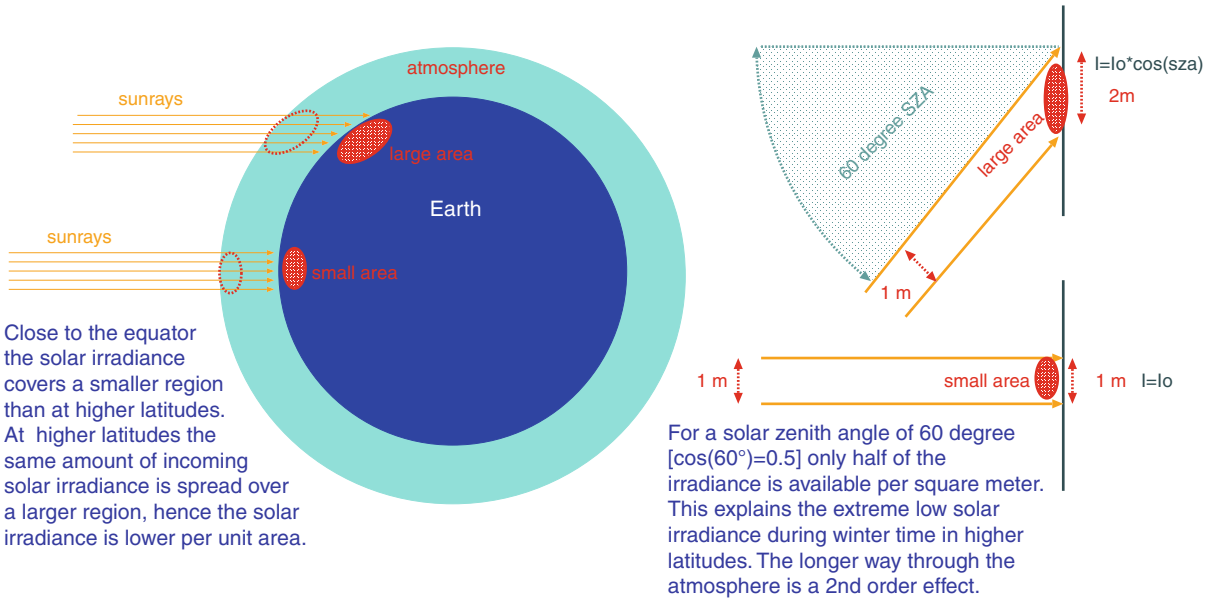

Solar Irradiance, Global Distribution. Figure 3
Illustration of the effect of the spherical shape of the Earth, which leads to different solar zenith angles (solar altitude) in different regions of the world. The higher the latitude the lower the highest possible solar altitude, hence, the lower the solar irradiance

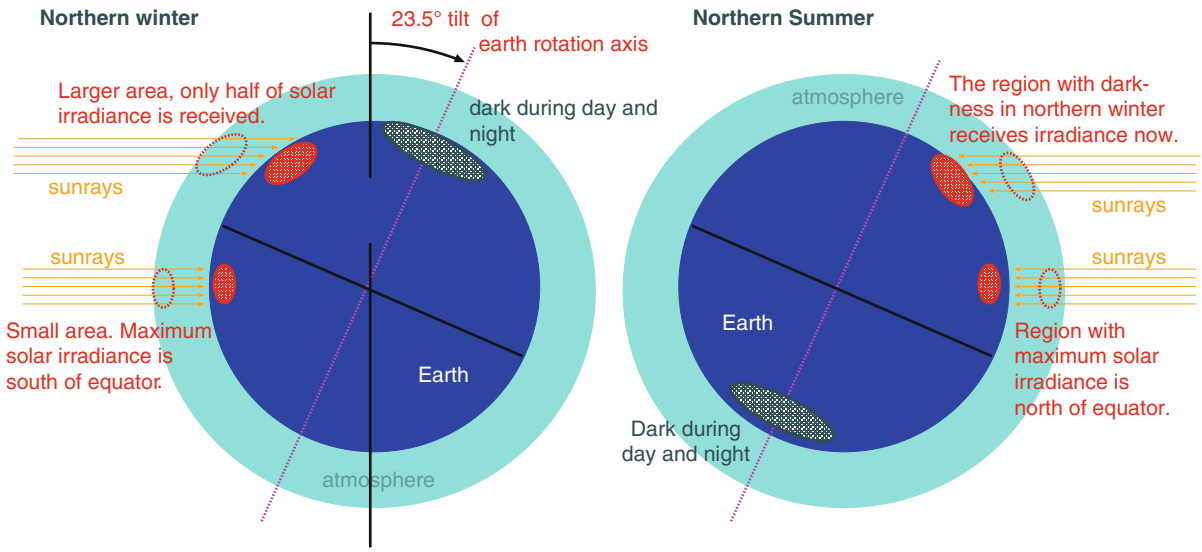

Solar Irradiance, Global Distribution. Figure 4
Illustration of the effect of the Earth's tilt on the global solar irradiance distribution. In spring and autumn the solar irradiance distribution is centered around the equator, but in summer and winter it is not

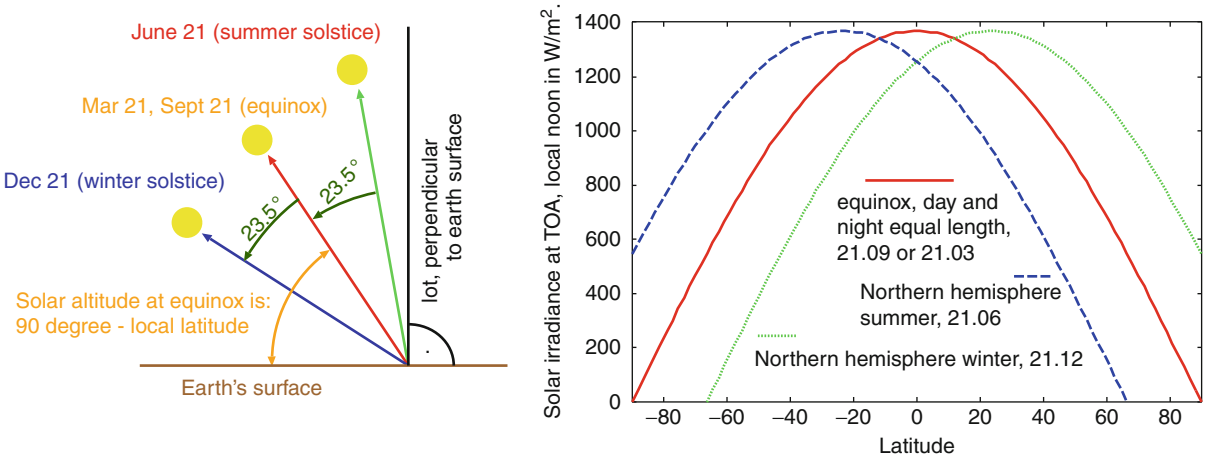

Solar Irradiance, Global Distribution. Figure 5
The *left* figure illustrates the effect of the tilted rotation axis on the seasonal variation of the solar altitude which in turn affects the seasonal variation of the solar irradiance. The seasonal variation of the local noon solar irradiance at the top of atmosphere is illustrated in the *right* figure. It is important to note that the shape and amount of the latitudinal solar irradiance distribution is significantly modified by the increase or decrease of daylight hours resulting from the Earth's rotation around the tilted spinning axis

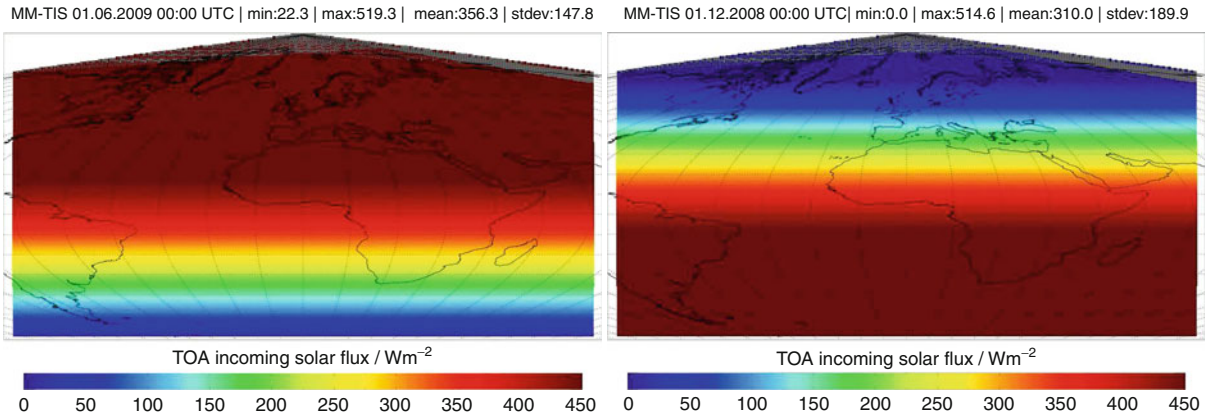

Solar Irradiance, Global Distribution. Figure 6

It is important to note that the shape and amount of the latitudinal solar irradiance distribution is significantly modified by the increase or decrease of daylight hours resulting from the Earth's rotation around the tilted spinning axis. Night hours reduce the amount of available irradiance. The number of night hours varies for a given site throughout the year. The further away from the equator the greater the difference between the maximum and minimum amount of night hours. The *left* figure demonstrates the effect on the latitudinal distribution for December and the *right* for June. The maximum solar irradiance is still reached close to a latitude of 23.5° but remains constant at this level for increasing latitudes in the respective summer season (December in the southern hemisphere and June in the northern hemisphere). The pattern of the latitudinal solar irradiance distribution at the equinoxes is almost not affected, as the tilt of the earth does not affect the relation between daylight and night hours at equinox

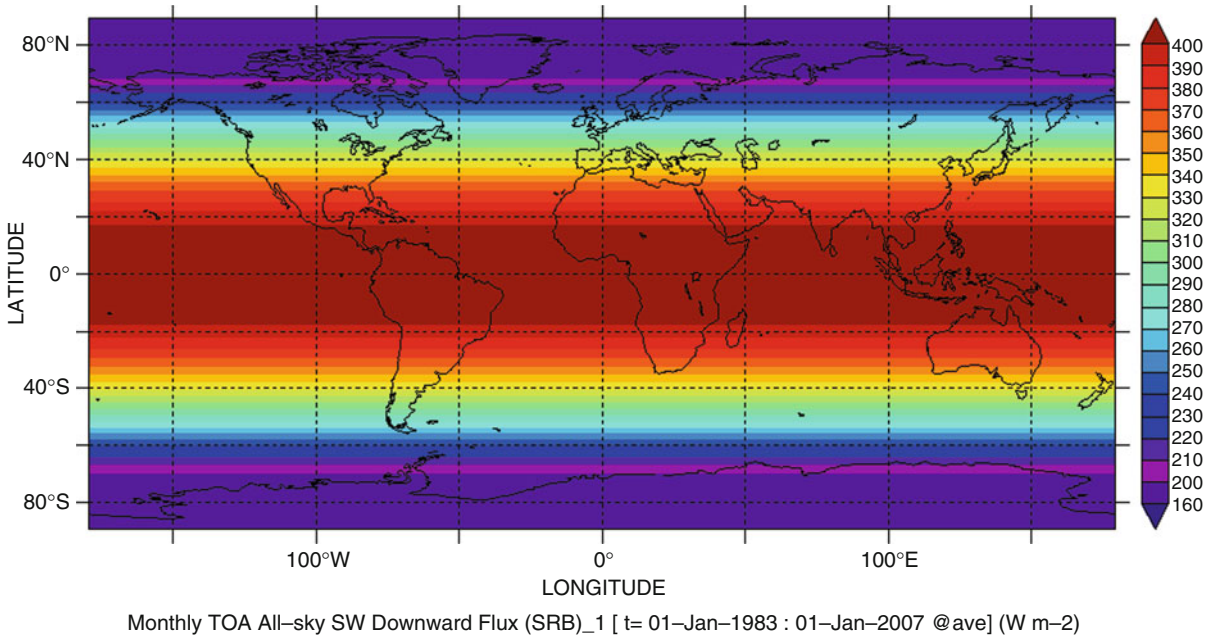

Solar Irradiance, Global Distribution. Figure 7

An 25-year average of monthly mean solar irradiance at the top of atmosphere. The annual mean is symmetric around the equator (Data source: Surface Radiation Budget Project http://gewex-srb.larc.nasa.gov/. Figure generated with NASA NCAR web plotting tool http://mynasadata.larc.nasa.gov/las/servlets/dataset)

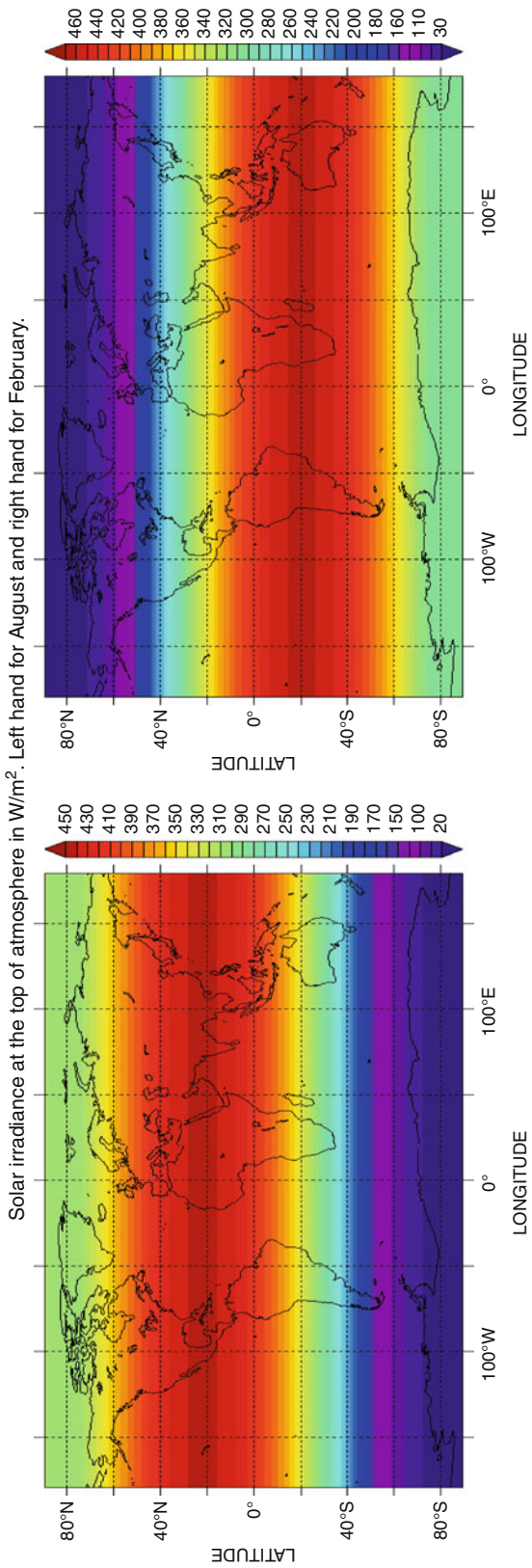

Solar Irradiance, Global Distribution. Figure 8
Distribution of solar irradiance at the top of atmosphere in W/m for August (*left*) and February (*right*). The figures illustrate the seasonal change of the solar irradiance at the top of atmosphere (Data source: Surface Radiation Budget Project http://gewex-srb.larc.nasa.gov/. Figure generated with NASA NCAR web plotting tool http://mynasadata.larc.nasa.gov/las/servlets/dataset)

needed to monitor and analyze climate variations and decadal-to-centennial climate trends. More details are available at http://gewex-srb.larc.nasa.gov/. The data is available and can be visualized with the web service provided by http://mynasadata.larc.nasa.gov/las/servlets/dataset. This tool has been also used for the visualization of all SRB plots within this document.

Role of Satellites

The top of atmosphere albedo (ratio upwelling and downwelling irradiance) is an essential climate variable. The incoming irradiance and outgoing radiation at the top of atmosphere can only be observed continually by satellites. Satellite sensors observe the radiation reflected by the Earth. The observed radiation has to be converted to flux densities in order to derive the top of atmosphere albedo. The radiation observed by satellite sensors can also be used to derive the solar surface irradiance. The law of energy conservation provides the basis for the satellite-based retrieval of solar surface irradiance. Solar irradiance cannot get lost, it is either reflected or absorbed by the atmosphere or it reaches the surface. The absorption effect of the atmosphere is well defined by radiative transfer; the satellite-observed reflections allow, therefore, the estimation of solar surface irradiance.

The radiation reflected by the Earth can be monitored by instruments with a broadband channel or by multispectral instruments, which observe the radiation in several different solar and thermal regions. Satellites have significantly increased the knowledge of the Earth's radiation budget and the distribution of solar irradiance at the top of atmosphere and the surface. In contrast to ground-based observations, space-borne observations have the advantage of a large geographical coverage (geostationary satellites) up to global coverage (polar orbiting satellites such as ERBE and CERES). This is especially important for direct irradiance since the network of ground-based measurements is very sparse.

Different satellites with calibrated broadband radiometers on board have been operated during the last decades. Typical examples for polar orbiting satellites are the Earth Radiation Budget (ERB) sensors aboard Nimbus-7 [7], the Earth Radiation Budget Experiment (ERBE) sensors [8] and the Clouds and the Earth's Radiant Energy System (CERES) [9]. On geostationary satellites, the Geostationary Earth Radiation Budget (GERB) sensor on-board of the Meteosat Second Generation satellites [10]. The multispectral sensors on both polar orbiting and geostationary satellites are also used to produce surface radiation products, as well as top of atmosphere albedo. Examples are the Spinning Enhanced Visible and Infrared Imager (SEVIRI) radiometers onboard the METEOSAT Second Generation (MSG) satellites [11], Geostationary Operational Environmental Satellites (GOES) ([12] and references therein), and Moderate Resolution Imaging Spectroradiometer (MODIS) [13].

Global Distribution of Surface Irradiance

Effect of Atmosphere

Solar surface irradiance is radiation from the Sun received on a given surface area, and its unit is usually Watts per square meter W/m^2. The solar surface irradiance results from the solar irradiance at the top of atmosphere (TOA). Without atmosphere, the solar irradiance at the top of atmosphere (TOA) and at the surface would be identical. The atmosphere affects the amount and distribution of the solar surface irradiance by scattering and absorption, as illustrated in Fig. 9.

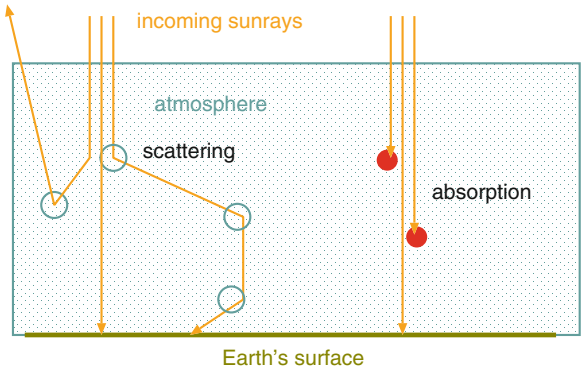

Solar Irradiance, Global Distribution. Figure 9 Illustration of the scattering and absorption effects. Scattering changes the direction of the incoming solar irradiance and leads therefore to an attenuation of the incoming irradiance, as parts of the irradiance are scattered back to space. Parts of the radiation are also scattered forward and reach the Earth surface. In addition, scattering leads to a longer optical path length through the Earth's atmosphere and hence to an increased absorption

This leads to a significant mismatch between the distribution of the solar irradiance at the surface and at the top of atmosphere.

At the top of atmosphere all solar radiation is in the form of direct irradiance. This means that all incoming irradiance is received from the direction of the Sun. Constituents of the atmosphere lead to scattering and absorption of solar radiation. Scattering adds a significant diffuse component to the incoming solar irradiance. Diffuse irradiance is predominantly uniformly distributed over the sky sphere and originates from all directions.

Irradiance consists of electromagnetic waves. These waves have the ability to force oscillations (and electronic transitions) within air molecules. The energy of the wave is reduced as part of the energy is "absorbed" by energy transfer to "vibrational" energy, which in turn leads to attenuation of irradiance. The respective process is called absorption. The higher the "particle" density along the optical path of the irradiance the higher the attenuation by absorption.

The magnitude of irradiance attenuation induced by the atmospheric components due to absorption or scattering is generally expressed in terms of optical depth.

$$I = I_o \cdot exp(\tau) \tag{2}$$

Here I_0 is the incoming irradiance, τ is the optical depth resulting from absorption or scattering and I is the direct irradiance reaching the ground. Optical depth is always defined for a vertical column. The attenuation due to absorption/scattering increases with increasing optical path through the atmosphere given by an increase of the solar zenith angle. For a slant column, Eq. 2 transforms into:

$$I = I_0 * exp\left(\frac{\tau}{cos(sza)}\right) \tag{3}$$

here, *sza* is the solar zenith angle. The term $\frac{\tau}{cos(sza)}$ is called the optical thickness of the respective quantity.

The sum of diffuse and direct irradiance is called global irradiance (which refers to the integration over the sphere) or solar surface irradiance. Global distribution of global irradiance sounds a bit confusing; hence, we prefer here to use the term "solar surface irradiance." The relevant atmospheric scattering and absorption processes comply Rayleigh scattering on air molecules, absorption by air molecules, absorption by water vapor and ozone, the absorption and scattering by aerosols, and cloud water droplets or cloud ice particles, respectively. The effect of cloud absorption is in general quite low relative to the scattering effect [14]. These processes are described in more detail in other articles of this book (e.g., Gueymard); here, their role in the spatial distribution of solar irradiance is discussed. Both absorption and scattering lead to an attenuation of the incoming solar irradiance. The magnitude of attenuation depends on the amount of the respective atmospheric components, hence, the optical depth of the atmospheric components. Consequently, atmospheric components which are not uniformly mixed but show specific spatial patterns affect the distribution of solar irradiance at the surface, leading to a significant mismatch with the distribution at the top of atmosphere. However, well-mixed (uniformly distributed) atmospheric components do not affect the distribution of solar irradiance on the Earth's surface, and would only copy and paste the distribution given at the top of atmosphere to the surface. For example, air molecules in the atmosphere scatters the solar irradiance, the respective process is called Rayleigh scattering. Air molecules are (horizontally) well mixed and uniformly distributed; hence they do not have specific spatial patterns and do not affect the global distribution of solar surface irradiance. However, Rayleigh scattering affects the amount and the spectral distribution of the incoming solar irradiance, leading to blue sky (Rayleigh scattering decreases in the power of 4 with increasing wavelength, hence blue light is much more scattered than the rest of the visible light. As significant parts of the blue light "is scattered" out of the white light, the sky is illuminated by blue light). Also stratospheric aerosols (above $\tilde{1}0$ km) are in general (horizontally) well mixed and do not affect the distribution of solar surface irradiance (with exceptions of fresh large volcanic eruptions). Ozone shows large spatial patterns on a global scale but the effect on the broadband solar irradiance is quite small as the absorption takes place in the UV. Deviations of 100 DU correspond to a change of 5 W/m, which is in the range of the uncertainty of solar irradiance measurements. Thus, the effect of ozone on the spatial distribution of irradiance is rather small.

While air molecules are well mixed and show a homogeneous distribution, this is not the case for clouds, water vapor, and tropospheric aerosols. They are not uniformly distributed, but show specific spatial distribution patterns with large spatial gradients (inhomogeneous spatial distribution). Hence, the magnitude of attenuation resulting from these components differs in different regions of the world as well as on the smaller local scales. Consequently, they affect the global distribution of the irradiance at the Earth surface leading to specific spatial and seasonal patterns. The solar irradiance distribution is dominated by clouds on a global scale. However, especially for direct irradiance, the effect of the spatial aerosol distribution is also quite important. This outlines that the distribution of the surface solar irradiance depends significantly on the distribution of the above-mentioned atmospheric parameters and is not only defined by top of atmosphere distribution.

Figure 10 shows the effect of the atmosphere on the solar surface irradiance in relation to the top of

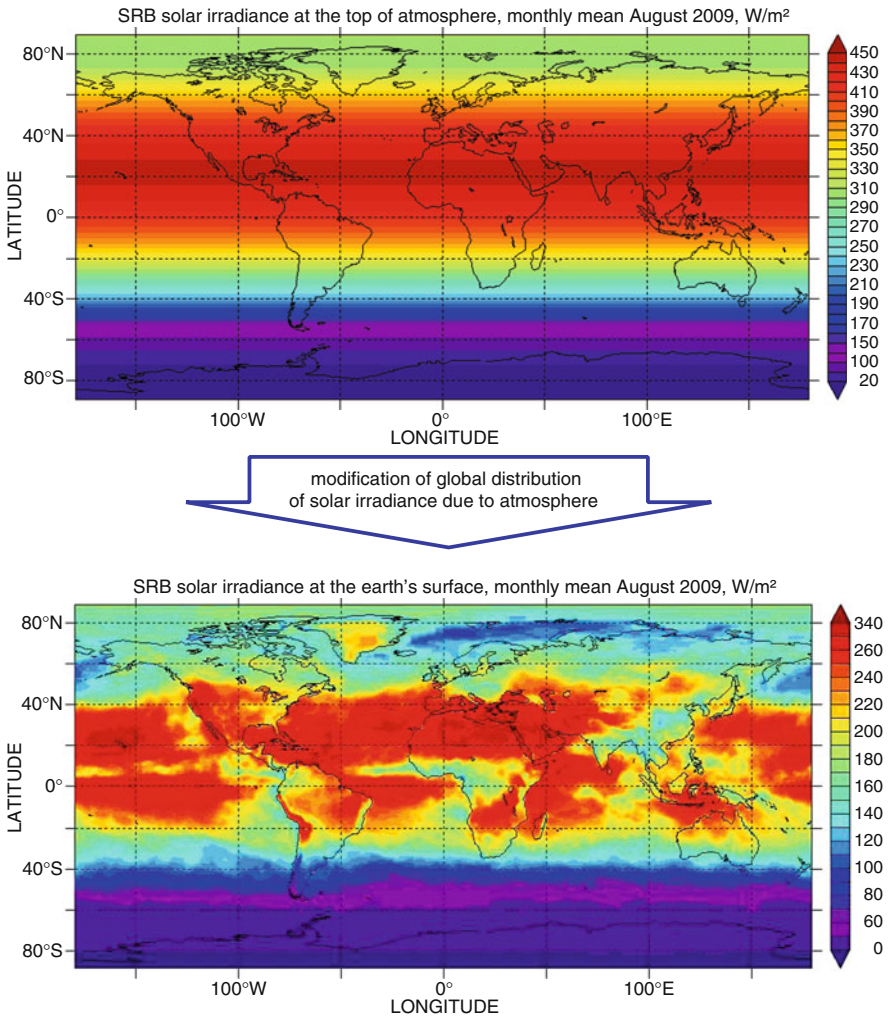

Solar Irradiance, Global Distribution. Figure 10
Effect of the atmosphere on the solar surface irradiance in relation to the top of atmosphere irradiance. The monthly mean solar irradiance at TOA (*top*) and at the earth surface (*bottom*) is quite different due to atmospheric attenuation (Data source: Surface Radiation Budget Project http://gewex-srb.larc.nasa.gov/. Figure generated with NASA NCAR web plotting tool http://mynasadata.larc.nasa.gov/las/servlets/dataset)

atmosphere distribution. The constant amounts of solar irradiance along the latitudes given at TOA are not apparent at the surface due to the effect of atmospheric attenuation dominated by clouds. Significant gradients in the solar irradiance do also occur along latitudes.

Direct irradiance is much more sensitive to aerosols and clouds than solar surface irradiance. This is a result of scattering induced by these variables. Scattering of irradiance leads to an attenuation of the direct irradiance and in turn "generates" diffuse radiation. Parts of the diffuse radiation are scattered back to space, but parts reach the ground and add to the solar surface irradiance. Diffuse irradiance reaching the ground is lost for direct irradiance but counts to the (overall) solar surface irradiance, hence solar surface irradiance is less sensitive to scattering induced by clouds and aerosols.

Therefore direct irradiance is much more affected by the global distribution of clouds and aerosols than solar surface irradiance. In contrast, direct irradiance shows no significant higher sensitivity regarding water vapor and ozone absorption. Water vapor and ozone are pure absorbers, do not scatter, and are therefore not a source for diffuse radiation. The remaining slight differences in the sensitivity between direct and (overall) solar surface irradiance are due to the different optical path length through the atmosphere. Direct irradiance takes per definition always the shortest way through the atmosphere. Diffuse radiation reaching the surface is affected by a longer optical path through the atmosphere due to multi-scattering, leading to increased absorption.

Figures 11 and 12 illustrate the larger effect of clouds and aerosols on direct irradiance comparatively to (overall) solar surface irradiance, respectively.

Figure 12 shows the effect of aerosol optical depth on the direct irradiance in comparison to the (overall) solar surface irradiance.

Direct Irradiance and Direct Normal Irradiance

Solar irradiance is usually discussed with reference to horizontal planes. This is motivated by the close relation of solar surface irradiance with the energy uptake of the Earth's surface. For example, for climate applications the solar irradiance on the Earth's surface is of main concern. Therefore, the solar irradiance is usually given on a horizontal plane in order to provide the energy per square meter surface and not for a surface tilted toward the Sun.

However, for solar energy systems, the irradiance on a plane (surface) tilted toward the Sun is of main concern. The direct irradiance received by a surface tilted toward the direction of the irradiance is called direct normalized irradiance (DNI), because the surface is always normal to the direction of the Sun. Conversely, "direct irradiance" usually refers to a horizontal plane (e.g., the ocean surface). Next, the differences between the direct irradiance and DNI are briefly discussed.

Figure 13 shows the difference between direct irradiance and DNI for a diurnal cycle and a standard atmosphere. It is evident that DNI is much higher than direct irradiance for systems with a surface directed toward the Sun, leading in turn to a much higher energy potential.

The pure geometrical effect of the solar zenith angle on solar irradiance discussed and illustrated in Fig. 3 is compensated by the tilt of the (moving) surface receiving the direct irradiance.

Of course, DNI is in the same relative way affected by clouds and aerosols as the direct irradiance. The global distributions of direct horizontal irradiance and DNI are therefore similar, although DNI values are always larger. A surface which is always normal to the direction of the Sun (e.g., by use of a tracking system) collects the maximum possible direct irradiance throughout the year. This reduces the effect of lower solar altitudes at higher latitudes. The magnitude of the seasonal (winter-summer) variation in DNI is significantly reduced compared to that of direct irradiance due to a reduced dependency of DNI on the solar zenith angle effect. However, the amount of annual daylight hours in combination with the increase of air mass (AM) at higher latitudes still lead to large latitudinal gradients in annual means of DNI and seasonal variations of DNI induced by the Earth-Sun geometry discussed in section "The Sun and the Earth".

The global distribution of DNI and direct irradiance is similar but not identical. This has to be considered for the following discussion of direct irradiance.

Effect and Distribution of Clouds, Water Vapor, and Aerosols

Clouds *Clouds* consist of particles (water and ice droplets) that predominantly scatter the incident radiation (Mie-Scattering). Only a small amount of solar

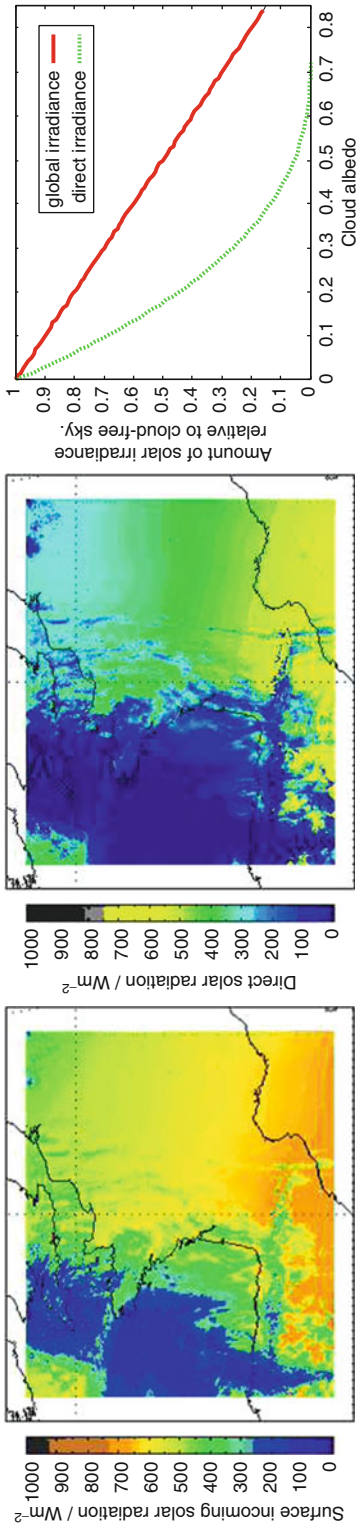

Solar Irradiance, Global Distribution. Figure 11
Solar surface irradiance (*left*) and direct irradiance (*middle*) for an instantaneous satellite overpass in June 2006. The effect of clouds is much higher for direct irradiance, as can be seen by the increase of the *blue* colored area (identical color range). On the *right*, the effect of cloud albedo on the irradiance is illustrated (Data source: CM-SAF, www.cmsaf.eu)

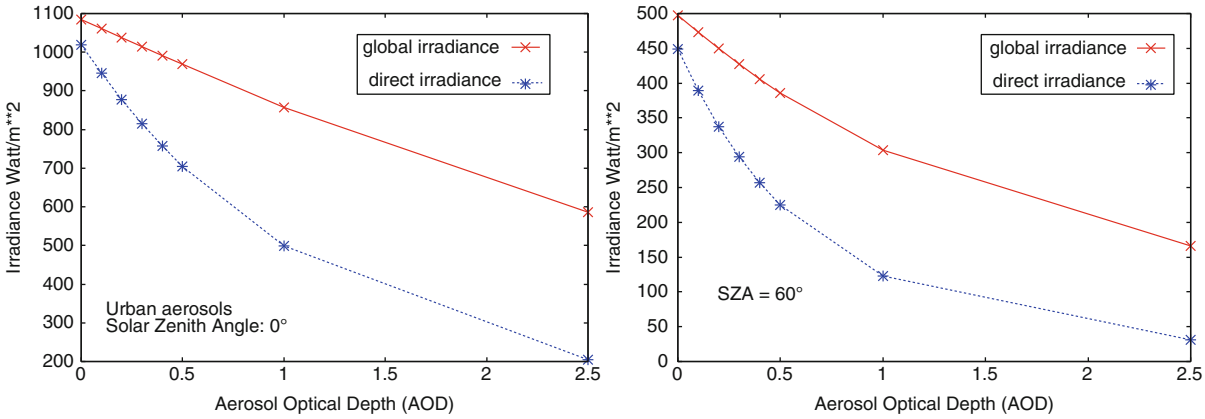

Solar Irradiance, Global Distribution. Figure 12

Effect of aerosol optical depth on the global and direct solar surface irradiance for a fixed water vapor content of 15 mm, a single scattering albedo of 0.8 (urban aerosol) and an air mass of 2 and 1, corresponding to a solar zenith angle of 0° and 60°

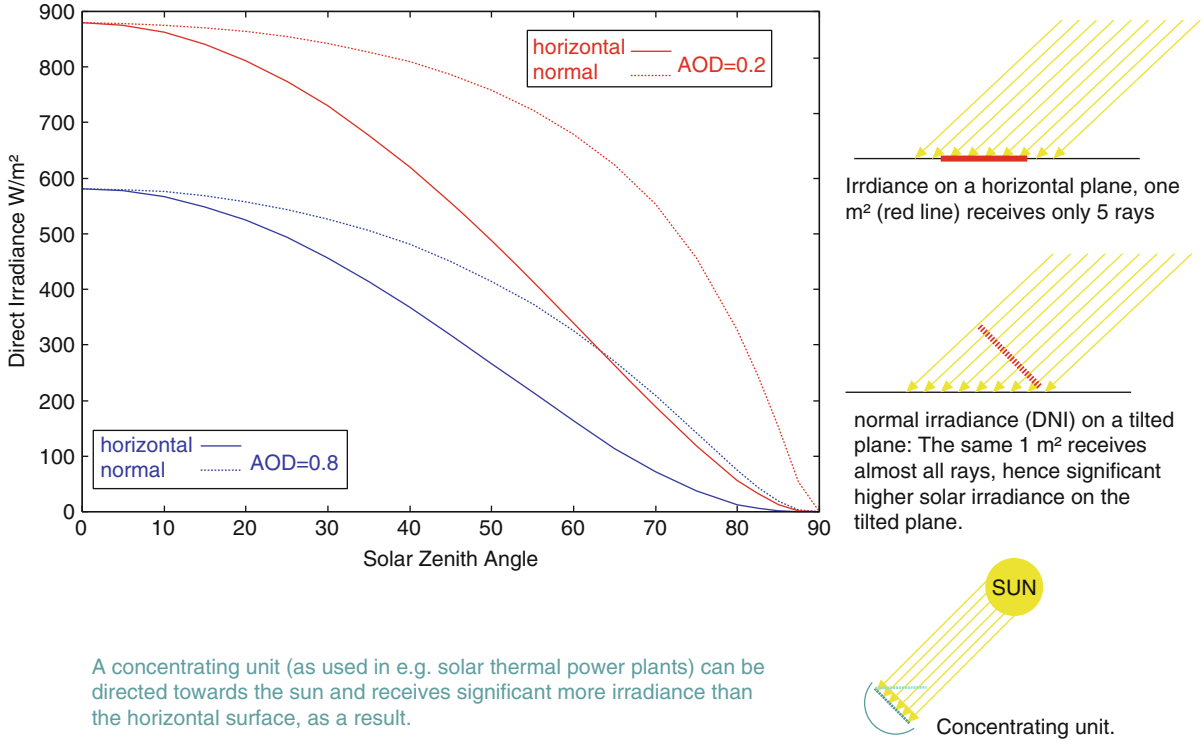

Solar Irradiance, Global Distribution. Figure 13

Left: The difference between the direct irradiance on a horizontal plane and on a tilted plane normal to the direction toward the Sun (Direct Normalized Irradiance). For typical AOD background value of 0.2, the effect is quite large, especially for SZA above 30°. However, for higher aerosol load, here 0.8 a typical value for polluted areas or biomass burning regions, the effect is significantly smaller in absolute terms. *Right*: Illustration of the DNI effect. *Bottom*, short link to the importance of this effect for solar thermal power plants

radiation is absorbed by clouds. The ratio between the incident and reflected radiation is called cloud albedo. The cloud albedo depends on the size and amount of water or ice droplets constituting the cloud. For water clouds, this is usually specified by the liquid water content (or Cloud Optical Depth) and the effective radii of the water droplets.

Clouds show specific spatial and temporal distribution patterns in different scales, affecting significantly the distribution of solar irradiance. It is well known that huge regional differences in cloudiness do exist, even though clouds appear rather chaotic sometimes. For example, the Sahara desert has a permanent low cloud cover throughout the year, while Northern England is almost permanently covered by clouds during winter time.

Figure 14 shows the long-term spatial distribution of clouds and their effect on direct irradiance. It is evident that clouds strongly impact the direct irradiance in regions close to the equator, where tropical (humid) conditions prevail. These regions would otherwise have outstanding conditions for solar energy. It is remarkable that due to high cloudiness, regions at higher latitude such as Southern Europe (Spain, Italy, Turkey) provide a higher solar energy potential than "cloudy" regions close to the equator. The Sahara has a high potential for solar energy since it is predominantly cloud free. However, in Western Sahara, lower values of direct irradiance are apparent, because high aerosol loads strongly affect direct irradiance. The effect of aerosols on direct irradiance is discussed in more detail later on. Next, the cloud distribution and its effect are discussed.

Operational cloud observations are usually made at synoptical weather stations and by meteorological satellites. Cloud information can be well retrieved from satellites due to the large reflection signal. Estimates based on these observations result in a global mean cloud cover of around 60–70% [15–17]. However, there is a huge regional diversity in the overall cloud coverage and cloud optical depth. Both quantities define the magnitude of the cloud albedo and hence of the reflection of irradiance due to the presence of clouds. Dominant drivers for the global cloud cover distribution are large-scale circulation systems and the spatial distribution of moisture. The Hadley

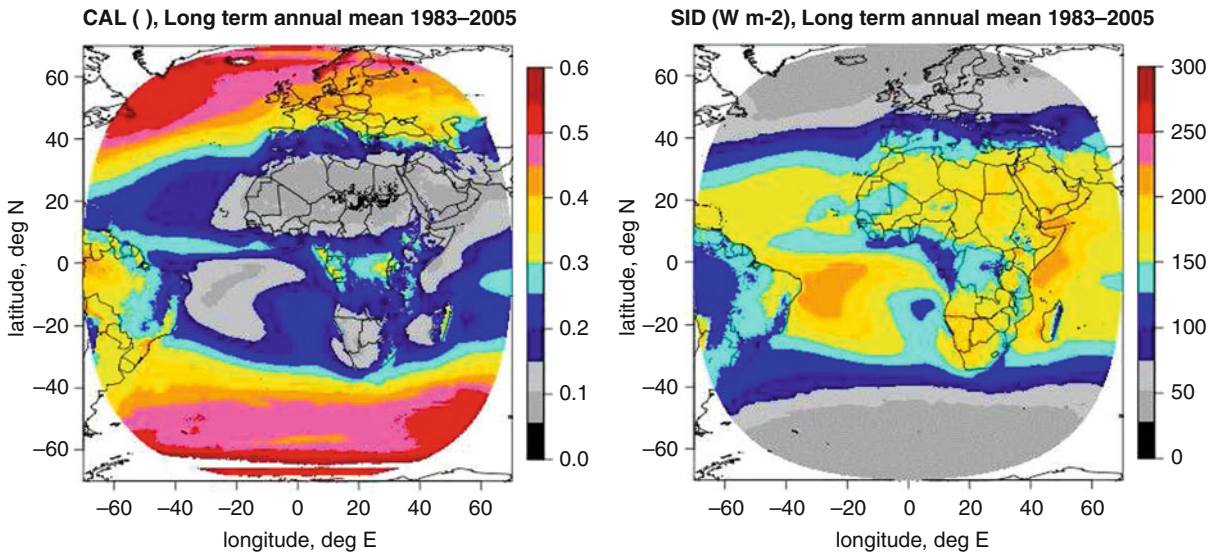

Solar Irradiance, Global Distribution. Figure 14

A 23-year mean of effective cloud albedo (*left*) and direct irradiance at the surface (*right*). Regions of large cloudiness are associated with low direct irradiance and vice versa. The spatial distribution of clouds is reflected in the direct irradiance at the surface. Although the effect of clouds is more pronounced for direct irradiance it constitutes the most important effect for the spatial distribution of solar surface irradiance (global irradiance), too (Data source: CM-SAF, www.cmsaf.eu)

circulation, an essential circulation system, is the generator of the Inter-Tropical Convergence Zone (ITCZ). At the ITCZ humid air is forced upward. As a consequence, optical thick clouds are formed quite regularly, leading to a relatively low solar irradiance. Consequently, the equatorial tropics exhibit a maximum of cloud cover of more than 65%.

The ITCZ is not always located at the same latitudes, but moves up and down. The magnitude of the movement differs for different regions around the equator. Moreover, the ITCZ has different widths around the world. The up and down movement (dynamics) of the ITCZ leads to a large seasonal change in solar irradiance, especially in Africa and surrounding oceans. However, over the eastern Pacific Ocean and over the Atlantic Ocean in the Northern hemisphere, the ITCZ remains nearly permanently over the same latitudes. This is due to the fact that the temperatures of the sea surface in the Atlantic in the Southern hemisphere are nearly always relatively low just south of the equator. This is also the case in the eastern Pacific Ocean [18, 19].

On both sides of the ITCZ, strong meridional gradients in cloud cover are apparent over the oceans, with large cloud cover on the eastern side of the large ocean basins and relative minima further west. This is caused by the existing large gradients in sea surface temperature. In contrast, the subtropical land areas contain the absolute minima in cloud cover over the desert regions of the planet. Here, the humidity needed to generate clouds is not available from the surface and the drying effect of the subsiding motion leads to the most arid regions in the world. The discussion so far demonstrates the extreme effect of the ITCZ on the distribution of clouds and hence on solar irradiance. It is one of the main drivers of solar surface irradiance distribution in the tropics and subtropics.

An additional feature affecting the global distribution of solar irradiance is the presence of very cloudy areas over certain subtropical ocean regions. Examples are the coastal waters close to the coastlines of Peru, California, and also close to Namibia, as illustrated in Fig. 15.

All these regions are characterized by cold ocean water and hence low sea surface temperatures. As a consequence, a relatively stable and very humid boundary layer forms in these areas, which is almost always linked to a relative thick layer of clouds.

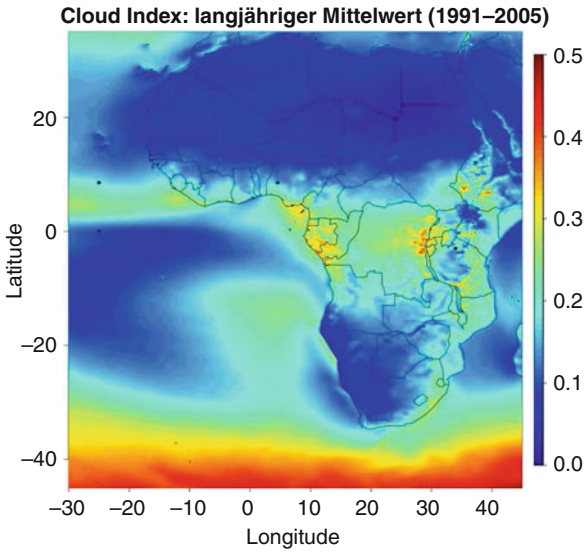

Solar Irradiance, Global Distribution. Figure 15
A 11-year average of monthly mean cloud albedo, derived with the MAGICSOL method [20]. The cloud albedo indicates the amount of solar irradiance that is reflected back to space. The effect of the ITCZ (*yellow*/*green* regions around the equator) and increased cloud albedo close to Namibia is "clearly" apparent (Data source: CM-SAF, www.cmsaf.eu)

The extratropical oceans are the regions of maximum cloud cover across the globe. In these regions a mean cloud cover in excess of 80% is observed. Different types of clouds such as those produced in and around mid-latitude cyclones [21], and low-level stratus clouds which have a high optical thickness, contribute to this large overall coverage with clouds [22]. The maximum cloud cover over land in extratropical regions can be found over North-West Europe where the absence of large north-south-oriented mountain ranges allows clouds and humidity to penetrate well inland, forced by eastward-moving low-pressure systems. Over the rest of the extratropical continental, the cloud cover is typically around 50%.

The distribution of clouds has to be taken carefully into account for the planning of solar power plants due to their quite large effect on direct irradiance. Even relative small regional trends in the mean cloudiness could lead to a large decrease in the solar energy resource.

Hence, for an accurate estimation of the energy yield of solar power plants, accurate information

about the (effective) cloud albedo or cloud fraction and cloud optical depth is needed.

Water vapor (absorption) affects the global distribution of solar irradiance. Water vapor only absorbs and does not scatter solar radiation. The distribution depends on the amount of evaporation and the subsequent transport of water vapor by wind systems. The attenuation effect of water vapor is much smaller than that of clouds. Clouds consist of water droplets or ice droplets, hence of water vapor in liquid or solid phase. Thus, high values of water vapor are often correlated with high cloudiness. In contrast to aerosols, water vapor is available with appropriate accuracy by reanalysis data. It constitutes therefore not a major challenge for an accurate estimation of solar irradiance distribution.

Also tropospheric aerosols are irregularly distributed and affect significantly the global distribution of solar surface irradiance, particularly that of direct irradiance. Aerosols absorb and scatter irradiance. The relation between scattering and absorption depends on the aerosol type and, hence, the composition of the aerosols. This relation can be expressed by the single scattering albedo. A single scattering albedo of 1 means that the aerosols only scatter. A single scattering albedo of 0.8 means that the attenuation of the irradiance resulting from the aerosols is to 80% due to scattering and to 20% due to absorption. Soot is a typical component which leads to "urban" aerosol types with relative high absorption, whereas irradiance is mainly scattered by maritime nonpolluted aerosols. Direct irradiance is only affected by the aerosol optical depth (AOD). However, the spectral distribution of the AOD depends on the aerosol type. This has to be considered if AOD values measured at certain wavelength are used within solar irradiance prediction models.

The distribution of aerosols is predominantly a result of three different sources in combination with their subsequent transport by wind systems. The main sources leading to high aerosol load are:

- Burning of fossils. This leads to hot spots in the aerosol distribution around large cities or industry regions. The aerosols are characterized by a high soot portion.
- Biomass burning. Regions with regular biomass burning events exists, e.g., in Africa and South America. Biomass burning leads to significant increase of aerosol load.
- Desert aerosols and dust outbreaks due to desert storms, which are naturally linked to large desert regions. Desert aerosols are usually larger relative to other aerosol types and have therefore a significantly different spectral effect.

A low aerosol load is usually common over oceans (see article of Gueymard for details). The predominant aerosol type is called maritime aerosol and is characterized by a low aerosol optical depth in combination with a low amount of soot. Naturally, this aerosol type contains a significant amount of sea salt. Over oceanic areas close to significant sources of dust outbreaks (desert storms), biomass burning, or industrial regions, high aerosol loads may regularly occur. Depending on the direction and strength of the wind systems, aerosols are transported away from the original source and high aerosol load can be found far away from the coastlines.

Solar energy systems are predominantly of interest in regions of low cloudiness, hence in regions with high frequency of cloud-free sky. The aerosol distribution is therefore quite important for solar energy systems, particularly those using concentrators, even though clouds dominate the global distribution of solar irradiance. High aerosol loads, e.g., due to biomass burning, desert storms, or industrial pollution, can significantly decrease the solar irradiance in regions with low cloudiness, hence with, otherwise, high potential for solar energy. As power plants are expected to play a significant role in the future energy system, accurate knowledge of aerosol information is needed for appropriate energy predictions. This outlines the importance of accurate aerosol information for the planning of solar energy systems. Within this framework, it is remarkable that there is a huge regional diversity in the overall aerosol load and optical depth data provided by the existing data sources [23] and [24].

Figure 16 shows the global distribution of aerosol optical depth and its extreme effect on the direct normal irradiance (DNI) for clear sky conditions and a solar zenith angle of 60°. The illustrated aerosol optical depth is the median of the values provided by Chemical Transport Models participating in the AeroCom project [23]. Of course, the depleting effect

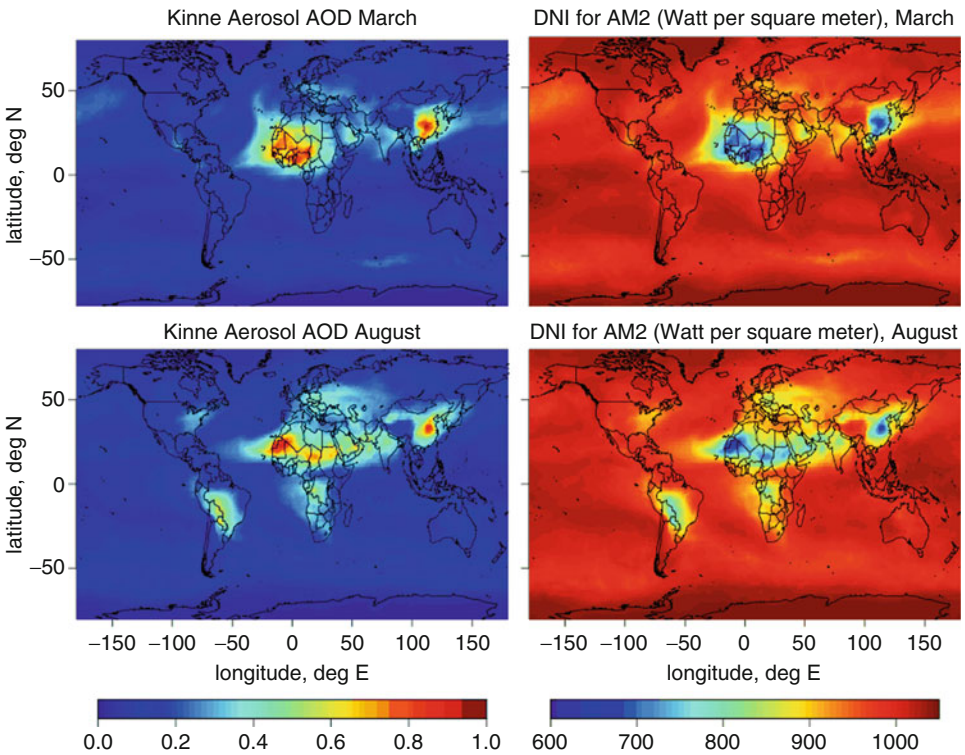

Solar Irradiance, Global Distribution. Figure 16
Aerosol optical depth (*left*) and direct normal irradiance (*right*) for March and August, using the aerosol climatology based on median values of the AeroCom project [23]. The DNI is given for an air mass of 2 (solar zenith angle of 60) throughout the globe. It illustrates the effect of aerosols on DNI for identical SZA, but is not representative for monthly means. Especially in regions with high aerosol load, the attenuation induced by aerosols reduces the direct irradiance extremely. Also evident, the large variation in the distribution illustrated here by the differences between March and August (Data source: Data derived with gnu-MAGIC)

of aerosols is only a fraction of the cloud effect in many regions of the world, but not in regions with low cloudiness, where accurate knowledge of the aerosol optical depth becomes very important. Moreover, the differences between March and August illustrate the large seasonal variation in the aerosol distribution and the subsequent effect on DNI.

In regions with large aerosol loads, specific patterns in the global distribution of DNI become apparent. Hence, accurate estimation of energy yield of solar power plants requires accurate information about the aerosol optical depth. Unfortunately, aerosol information is currently known only with a relative high uncertainty. Figure 17 provides the difference between the predicted DNI using an aerosol climatology based on AeroCom median values [23] and that using the GADS/OPAC climatology [25]. The latter is well established but somehow outdated aerosol climatology. The large differences obtained over some regions illustrate the need for accurate aerosol information for the planning of solar power plants. The effect of uncertainties in aerosol information on DNI will be discussed in more detail in section 5.5

Land Surface Snow can increase the diffuse irradiance and hence the solar surface irradiance, especially under cloudy conditions. For polar regions, this means that the distribution of irradiance is also affected by ocean/snow patterns. This leads to quite high values of solar surface irradiance for the snow-covered Greenland relative to the surrounding ocean, as shown in Fig. 10. Additionally, the low difference in the

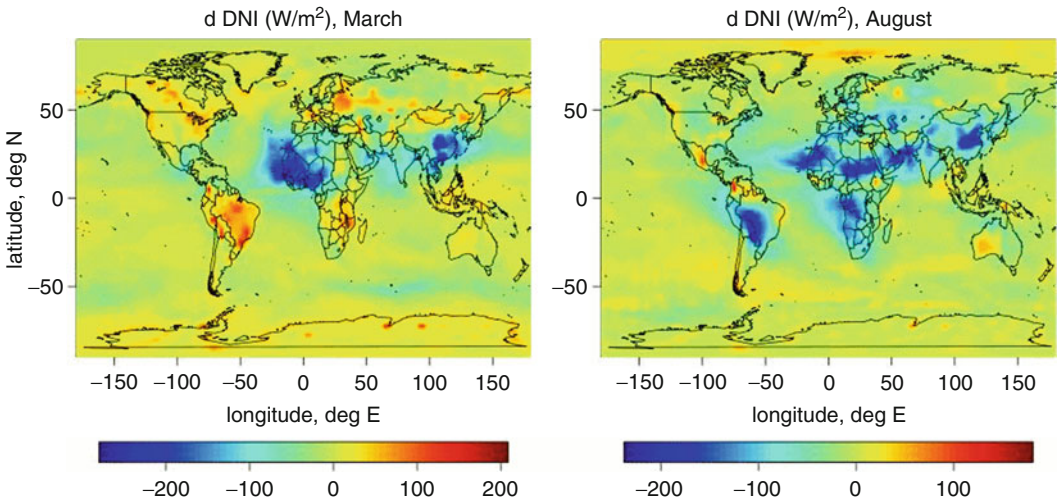

Solar Irradiance, Global Distribution. Figure 17
Difference in DNI for March and August and an AM of 2. The difference in DNI arises from the use of two different aerosol climatologies, AeroCom based on one hand and GADS/OPAC on the other. The differences are quite large, demonstrating the importance of accurate aerosol information (Data source: Image derived with gnu-MAGIC, http://sourceforge.net/projects/gnu-magic)

brightness between clouds and snow (ice) as seen from satellites increases extremely the uncertainty in the estimation of cloud parameters and in turn also that of satellite-based solar irradiance.

Discussion of Surface Irradiance Distribution

The spatial and temporal distribution of the solar irradiance at the surface is a result of the top of atmosphere distribution and its changes due to the atmospheric attenuation induced by clouds, aerosols and water vapor. The distribution of solar irradiance at the top of atmosphere shows the highest values in regions close to the equator. However, the effects of clouds, aerosols, and water vapor significantly alter the distribution at the surface. This in turn has significant consequences for the global distribution of the solar irradiance, e.g., relative low solar irradiance observed in the equatorial belt.

The spatial and temporal variations in the distribution of the atmospheric variables (clouds, aerosols, water vapor) are driven by atmospheric physics and dynamics and the resulting circulation systems of wind and humidity. This leads to specific distributions and typical periodic variations of cloudiness, water vapor content, and aerosol load, resulting in specific solar surface irradiance variations on different spatial and temporal scales.

Some important processes are briefly discussed in the following. The Hadley circulation [19] is a main driver of atmospheric dynamics and affects significantly the solar distribution in the "equatorial belt." The equatorial tropics are dominated by the ascending branch of the Hadley circulation. The ascent of wet air leads to cooling and ultimately to areas with very high cloudiness known as the Intertropical Convergence Zone (ITCZ). The seasonal variation of solar irradiance at the top of the atmosphere is a driver for the up and down "movement" of the Hadley circulation from the north to the south of the equator. This movement (dynamics) leads to a large seasonal change in solar irradiance, especially over Central Africa and the surrounding oceans. However, over the Eastern Pacific Ocean and over the Atlantic Ocean, the ITCZ remains in the northern hemisphere nearly permanently [19] and [18]. The Hadley circulation, generating the ITCZ, is very important for the solar irradiance distribution as it occurs in a region with maximum solar irradiance at the top of atmosphere and, hence, in regions with a theoretically high solar resource. In the ITCZ, high

water vapor content and cloudiness strongly attenuate solar radiation. As a consequence, the solar surface irradiance in the equatorial belt is lower than at higher latitudes, although solar irradiance at the top of atmosphere is maximal. This mismatch illustrates the effect of atmospheric variables on solar irradiance. Moreover, the seasonal variation of the top of atmosphere irradiance is rather small in the equatorial belt, whereas seasonal variations of the ITCZ lead to large seasonal variations in the available solar surface irradiance.

Figure 18 shows the distribution of solar irradiance over Africa, as affected by the ITCZ.

Similarly Fig. 19 shows the spatial distribution of the mean solar surface irradiance (based on a 25-year average).

As a consequence of the ITCZ, the maximum solar surface irradiance over land surfaces is located in a subtropical belt between ca. 15°–35°N/S and not in the equatorial belt. Around 80% of the solar surface irradiance there is available as direct irradiance as a consequence of low cloudiness. Many of the developing nations in northern Africa and southern parts of Asia lie within this "sun" belt and have therefore optimal conditions for the use of solar energy. The solar resource is in particular extremely high in the tropical and subtropical deserts of the Earth, due to high sun angles and a low frequency of cloudiness. However, missing infrastructure together with heavy dust storms is a big handicap for the use of solar energy in these regions.

In the descending branches of the Hadley circulation on both sides of the ITCZ, strong meridional gradients in solar irradiance are apparent over the oceans, with relatively low solar irradiance on the eastern side of the large ocean basins and relative maxima further west.

In the belts close to mid-latitudes (35°–45°), the solar irradiance is significantly decreased because of the lower solar altitudes given at higher latitudes. In addition, cloudiness and atmospheric pollution are important factors that decrease the solar surface irradiance in many regions.

Large cloud amounts in storm tracks in combination with low solar irradiance at TOA account for the much lower values over mid-latitudes, especially outside the respective summer seasons. In addition, numerous cyclones generate a relatively persistent cloud cover.

In general regions beyond 45°–50° North or South have quite low amounts of solar irradiance and therefore less favorable conditions for the use of solar energy.

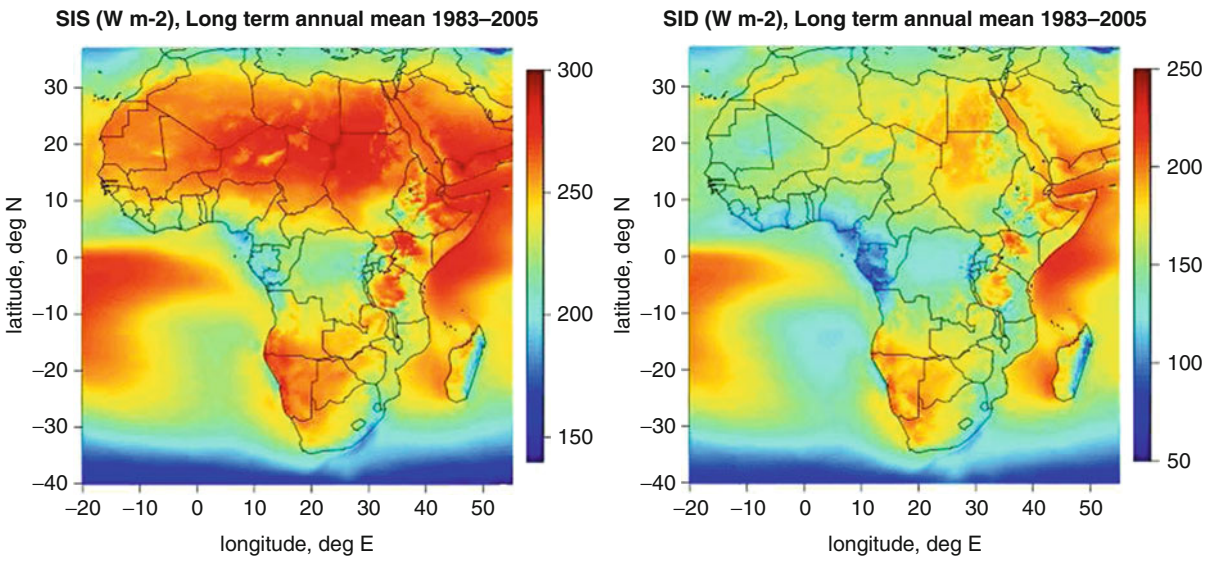

Solar Irradiance, Global Distribution. Figure 18
Long-term annual mean solar irradiance for Africa. Solar surface irradiance (*left*) and direct irradiance (*right*) (Data source: www.cmsaf.eu)

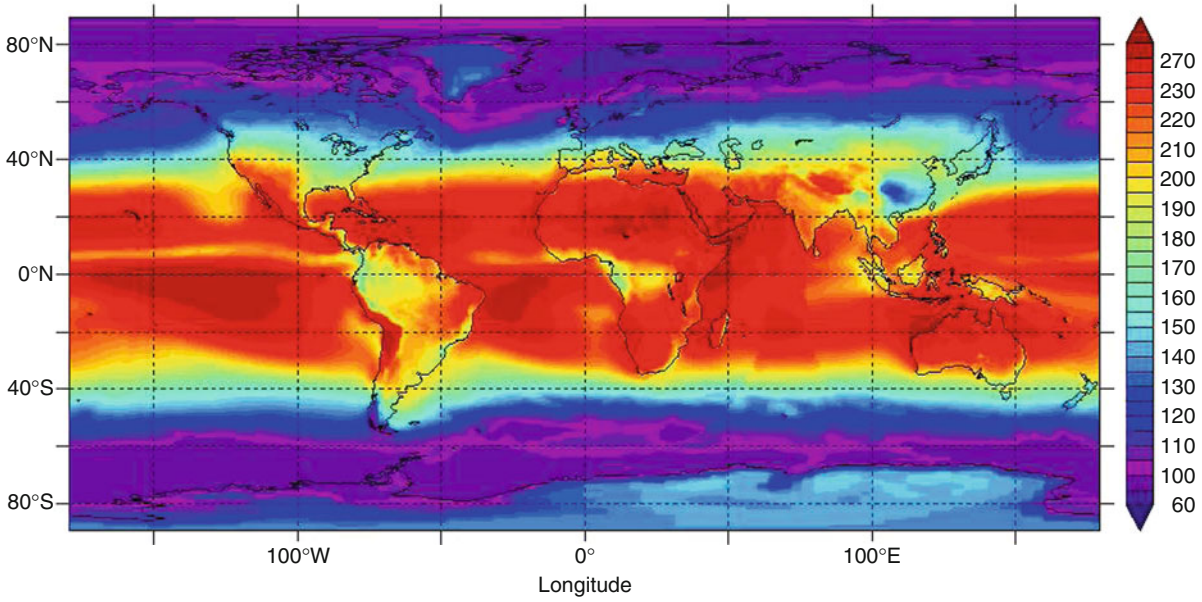

Solar Irradiance, Global Distribution. Figure 19

A 25-year average of monthly mean solar surface irradiance (global irradiance). The effect of atmospheric attenuation is clearly visible in comparison with Fig. 7 (Data source: Surface Radiation Budget Project http://gewex-srb.larc.nasa.gov/. Figure generated with NASA/NCAR web plotting tool http://mynasadata.larc.nasa.gov/las/servlets/dataset)

Solar surface irradiance decreases to a minimum near the poles because of low sun angles and the fact that the Sun does not rise above the horizon during long periods of the year, even though the daily solar irradiance may be high during summertime.

Atmospheric oscillations also contribute to the spatial and temporal distribution of solar irradiance, e.g., ENSO, the El Nino-Southern Oscillation. ENSO episodes are among the most important interannual phenomena occurring in the climate system. The eastward advance of connective activity from the warm pool region to the central and eastern equatorial Pacific and the increase of high thick clouds over those regions are associated with a large decrease in solar irradiance. Hence, ENSO largely affects the solar distribution and also leads to anomalies in the spatial patterns of solar irradiance at the surface [26].

One of the most prominent oscillations (teleconnection pattern) in the northern hemisphere is the North Atlantic Oscillation (NAO) [27]. The NAO combines parts of the East Atlantic and West Atlantic patterns originally identified for the Northern hemisphere winter season by Wallace et al. [28]. The NAO is associated with basin-wide changes in the intensity and location of the North Atlantic jet stream and storm tracks and in large-scale modulations of the normal patterns of zonal and meridional heat and moisture transport [29]. These effects in turn result in changes of cloudiness.

The distribution of atmospheric variables and the resulting attenuation of solar radiation is by no means constant throughout the year as a result of the discussed circulation (oscillation) systems. This results in typical seasonal distribution patterns of solar surface irradiance. Figure 20 shows the seasonal variation of solar surface irradiance and direct irradiance for the Meteosat click. Figure 21 shows the mean solar surface irradiance distribution for two specific months as an example.

Trends in the circulation system, e.g., an increase of the intensity of the Hadley circulation, can significantly affect the solar resource and therefore need to be considered seriously.

On a regional scale, the decrease of water vapor and aerosols with altitude leads to a concomitant increase in clear-sky solar irradiance. In contrast, "mountains" are often associated with an increased cloudiness relative to the surroundings, which leads to a decrease in solar irradiance. These orographic clouds develop in

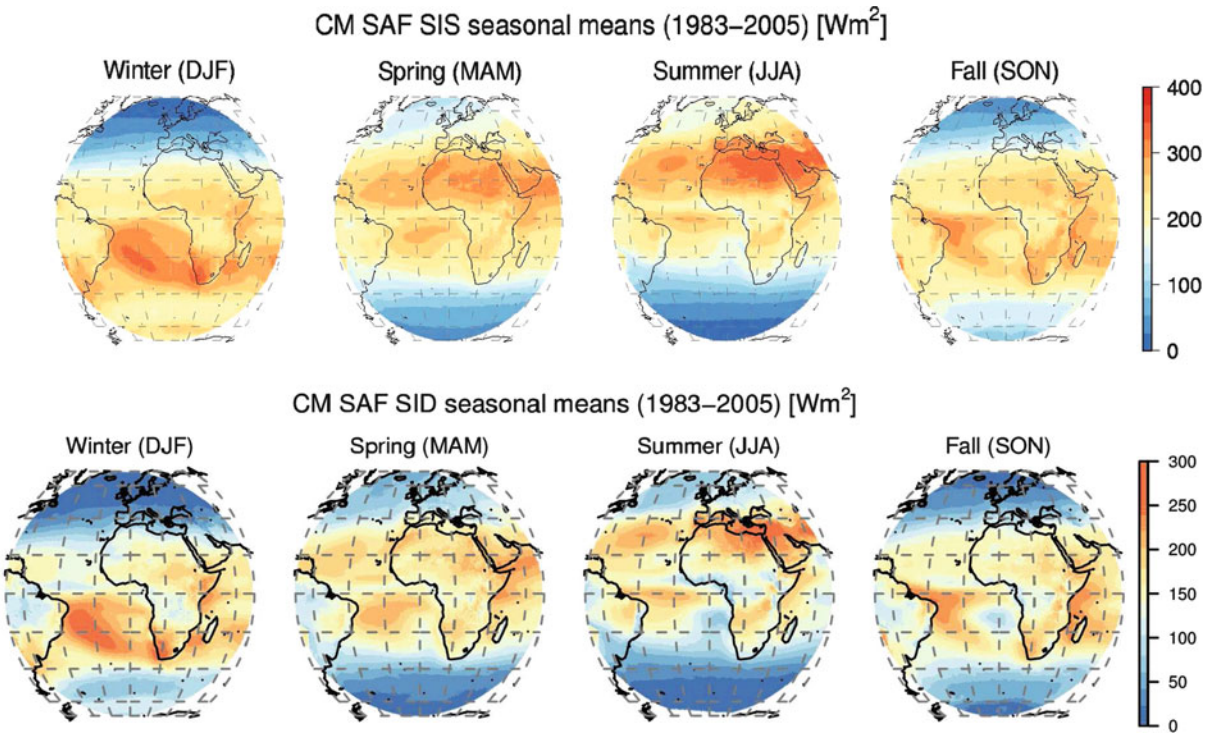

Solar Irradiance, Global Distribution. Figure 20
Seasonal long-term means of solar irradiance for the Meteosat disk. The spatial distribution of direct horizontal irradiance (SID) and solar surface irradiance (SIS, also called global irradiance) is similar on a larger scale. However, in general much lower amounts of direct irradiance are present and on a smaller spatial scale significant differences occur (Data source: CM-SAF, www.cmsaf.eu. Figure generated by R. Posselt, MeteoSwiss)

response to the forced lifting of air caused by the Earth's topography. The subsequent cooling leads to the generation of clouds. The attenuation effect of orographic clouds is usually only partially compensated by the increase in clear sky irradiance. This effect is also present over low mountain ranges and can be additionally forced by temperature differences between sea and land surfaces at coastlines. This in turn leads to specific regional patterns in mean values of solar irradiance, which have to be considered within the planning of solar energy systems, an example is given in Fig. 22.

Even though clouds dominate the distribution of atmospheric attenuation on a global scale, special attention has to be paid to the aerosol effect in regions with low cloud frequency in connection with solar energy applications. Figure 23 illustrates the effect of water vapor and aerosols on the distribution of solar irradiance in the absence of clouds.

Accuracy and Uncertainty of Solar Irradiance

Currently, different solar irradiance data sets are available for solar energy applications. Some of them are available free of charge via a web user interface. Satellite-derived and reanalysis data sets usually cover the whole globe. This indicated the main problem for solar energy prediction is not to locate sources of data, but to get accurate data or at least reliable accuracy information about the data. It is essential that the accuracy of the data is well defined in order to evaluate the applicability of the data and to provide information about the uncertainty of energy predictions to potential users. However, appropriate measures of accuracy are often missing and the performance indicators are often misleading. For example, in many publications and validation reports dealing with gridded solar irradiance data, the mean bias deviation of monthly means (or daily means) and root mean square deviation of

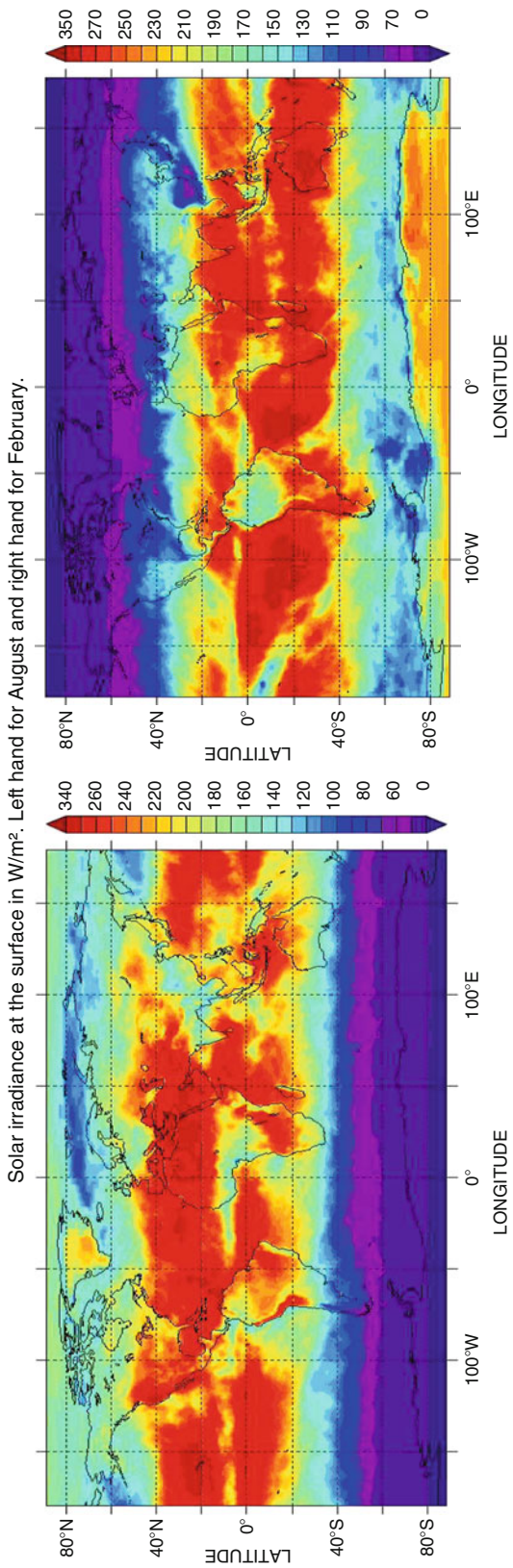

Solar Irradiance, Global Distribution. Figure 21
Solar surface irradiance for August (*left*) and February (*right*) 2005 (Data source: SRB project)

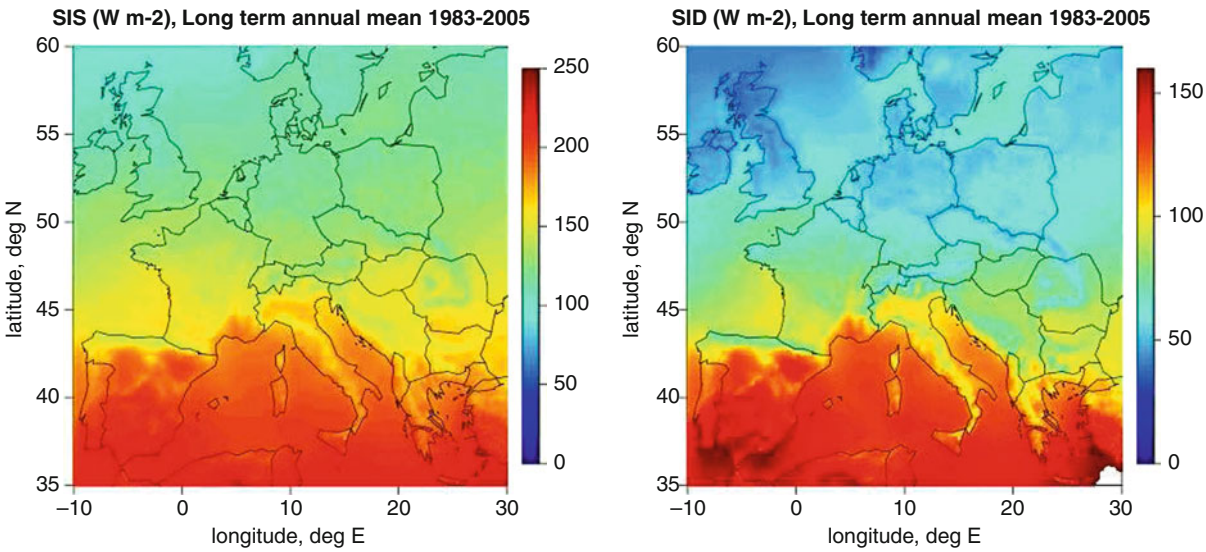

Solar Irradiance, Global Distribution. Figure 22
Annual mean of solar surface irradiance (SIS, *left*) and direct horizontal irradiance (SID, *right*) over Europe. Even on a small scale it is evident that cloudiness modifies the irradiance distribution. Orographic cloud effects can be seen along the North coast of Spain and the Pyrenees, as well as along the Balkan Mountains and the Alpine region. The low solar irradiance in North-West Europe results from large cloudiness (Data source: CM-SAF, www.cmsaf.eu)

hourly means are given, usually derived by comparison with reference ground-based radiometric stations. Unfortunately, these quantities may not be appropriate to define the accuracy of the data. For gridded solar irradiance data (e.g., remote sensing, reanalysis data) the Root Mean Square Deviation (RMSD) for hourly values is of limited value for the estimation of errors in the predicted solar resource. On an hourly basis, large parts of the deviation are due to the mismatch between the grid size of the data and point-specific ground measurements and, therefore, do not provide reliable information about true accuracy. The bias evaluated in publications is often averaged over several months and measurement stations and provides therefore only limited information on the accuracy of solar irradiance for a specific site and period. The bias contains always a cancellation of errors. For example, a bias of −100 in one region and +100 in another region leads to an overall bias of zero. However, data with such regional bias values might be of limited value. Moreover, averaging bias over time may result in misleading information, e.g., a bias of −20 W/m^2 during winter time and +20 W/m^2 during summer time results in a yearly bias of 0. Hence, neglecting seasonal variation may lead to significant errors in the predicted energy yield of solar systems, for instance. Hence, error information given in publications must be interpreted with care. In order to improve the evaluation of accuracy, CM-SAF introduces three additional accuracy measures, the mean absolute difference, the fraction of month with bias above a certain threshold, and the anomaly correlation. These statistical quantities (error measures) have been introduced for climate monitoring but might be of value for accuracy definition within solar energy applications, too. Table 1 illustrates the shortcoming and partly misleading information about accuracy arising from the use of bias as the main error information.

In the discussion that follows, the selected accuracy measure is the mean absolute deviation and not the bias. Nowadays, monthly means of solar surface irradiance can be retrieved from satellites by state-of-the-art retrieval schemes with an overall accuracy of 8–10 W/m^2 or even better. Accuracy here means mean absolute differences in the order of 8–10 W/m^2, or even below, and that at least 90% of the monthly bias values are below 10 W/m^2 plus the uncertainty of ground measurements of 5 W/m.

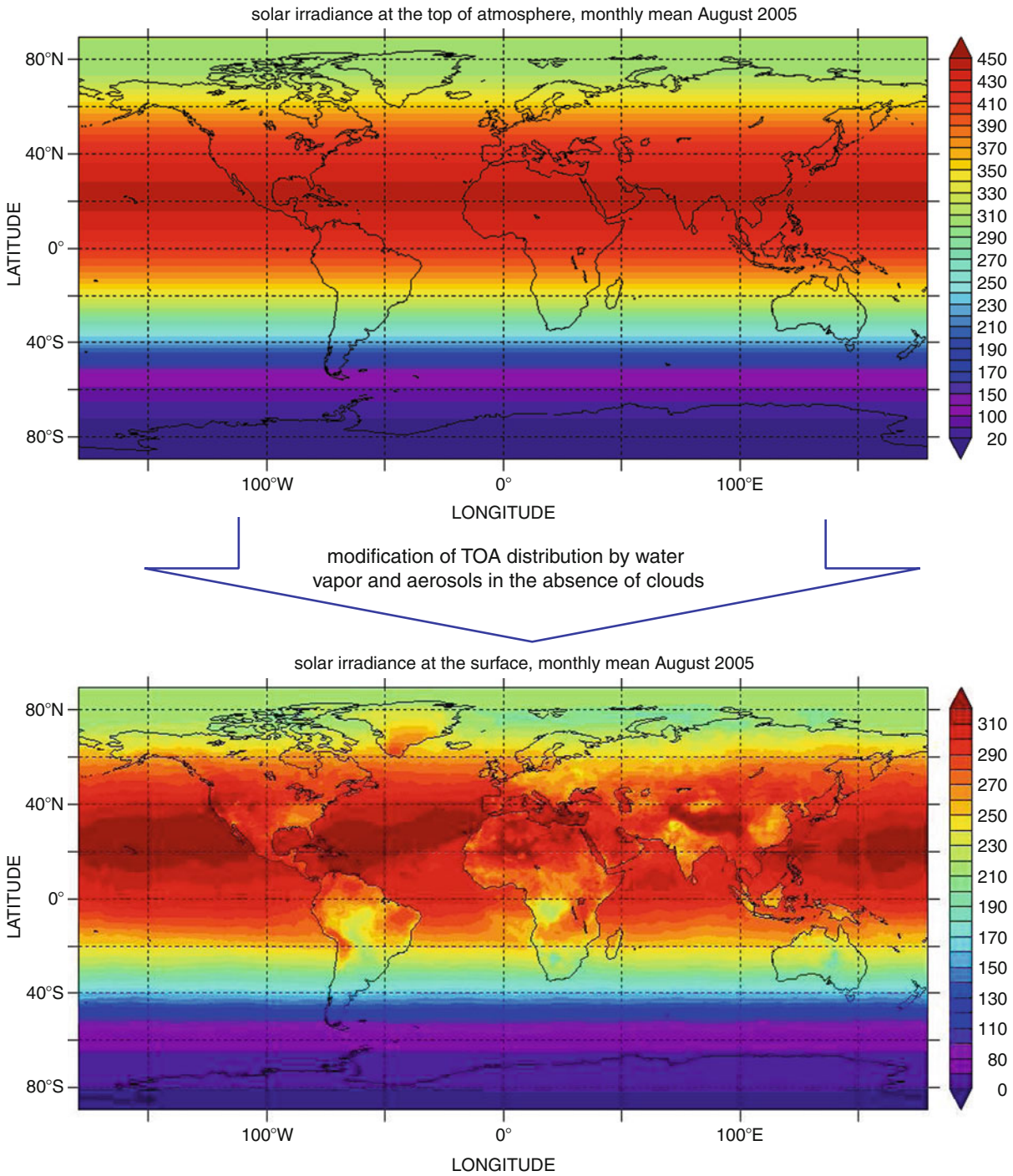

Solar Irradiance, Global Distribution. Figure 23

Modification of the TOA irradiance distribution in the absence of clouds (the sky is assumed to be cloudless throughout the globe) by atmospheric attenuation due to water vapor and aerosols for August 2005 (Data source: Surface Radiation Budget Project http://gewex-srb.larc.nasa.gov/. Figure generated with NASA NCAR web plotting tool http://mynasadata.larc.nasa.gov/las/servlets/dataset)

Solar Irradiance, Global Distribution. Table 1 Comparison of different data sources with BSRN ground measurements. GEWEX and ISCCP show low bias values. However, the additional error measures demonstrate the limited value of ISCCP [30] and GEWEX data [31] for solar energy applications. The relative low accuracy is partly a result of the coarse spatial resolution

SSI (monthly)	n_{mon}	Bias W/m^2	MAD W/m^2	SD W/m^2	AC	$Frac_{mon} > 15$ W/m^2 %
CM SAF-BSRN	855	4.40	7.99	8.14	0.89	11.35
GEWEX-BSRN	855	−2.56	12.26	11.12	0.82	32.75
ISCCP-BSRN	855	−0.03	11.79	11.37	0.78	29.94

MAD mean absolute difference of the monthly bias values, *SD* standard deviation, *AC* anomaly correlation and finally the fraction of months with bias larger than 15 W/m^2

Due to the lack of ground measurements, only rudimentary validations can be performed in some regions of the world, e.g., the ocean and large parts of Africa, including the Sahara desert. BSRN has only four well working radiometric stations in Africa. Similarly, data measured by Fluxnet [32] radiometric stations are partly suspicious and cannot be used for validation without sophisticated quality control [33]. Substantial disparities in different solar radiation maps are apparent, in particular in DNI. These differences may arise from the use of different aerosol data sets. However, in regions with a lack of reference data from ground measurements, the reason for differences can only be analyzed rudimentarily. As discussed, the effect of uncertainties and errors in aerosol and cloud classification is much higher on direct irradiance than on (overall) solar surface irradiance, which explains the difficulties to generate consistent and accurate data sets. Gueymard [34] has analyzed the performance of eight DNI datasets (from both free and commercial sources) using high-quality radiation data from 14 sites in North Africa and bordering regions. He found that these datasets are reasonably accurate over southern Europe. Over North Africa and the Middle East, however, the results presented in his study indicate a significantly lower accuracy, and even reveal some important problematic areas. He found a large monthly scatter in many cases. Even the annual mean DNI predictions may be affected by considerable biases (such as for Cairo and Ilorin). Based on an analysis of coincident radiation and aerosol data from collocated instruments, Gueymard showed that, in most cases, these biases are caused by inaccurate aerosol data being used to model DNI. Unfortunately, away from in situ measurements, the available aerosol information is linked with a high uncertainty. Based on recent publications it can be expected that the uncertainty in AOD may be more than $\pm$ 0.1 over many regions of the world. Figure 16 illustrates the large effect of different aerosol climatologies on DNI. Based on these results, it has to be expected that the accuracy of DNI is much lower than that of solar surface irradiance. Suri [35] compared five databases of DNI for Europe.

The average of these databases shows three regions with high annual DNI above 1,800 kWh/m^2 – South and Central Spain and Portugal, Sicily and Provence. The variability defined by the relative standard deviation stays generally within 7–8% for these regions, but for the large Mediterranean islands and parts of Andalusia, a larger variability is apparent.

The DNI resource seems to be significantly lower over South-Eastern Europe and Italy (with the exception of Sicily). However, outdated aerosol information in some of the data bases might have affected the findings of [35]. Here, the data bases show large deviations, hence a higher disagreement (standard deviation sometimes above 20%). North of the Alps, the DNI potential is below 1,400 kWh/m^2 with decreasing values for increasing latitudes. Here, a higher level of disagreement between the data bases can be observed as well. Suri et al. [35] concluded that aerosols are the main cause for the differences between the data bases, which is indeed highly likely for some sunny regions. However, in cloudier regions (Northern part of Great Britain, Belgium, regions close to the North-Sea, Pyrenees, Denmark, coastline of Croatia) it is likely that clouds or fog are the main cause for the large differences between the data bases.

Lohmann [36] found that at least 15 years of DNI data are needed to overcome uncertainties in energy predictions arising from interannual variations in DNI. Of course, well-maintained, ground-based radiometric measurements covering a period of 15 years are not available in the vicinity of most potential solar energy sites. Satellite data cover such long periods, but their accuracy is mostly not well defined and uncertainties caused by inaccurate aerosol information cannot be evaluated without ground measurements. Setting up and maintaining private aerosol and radiometric ground measurements and subsequent operation for decades is very cost intensive and would anyway lead to an unacceptable delay in the planning and construction of solar energy systems. One reasonable option to overcome this problem is the combination of long-term meteorological data gained from existing data sets with shorter-term in situ measurements of solar irradiance at the site of interest. With a sophisticated method such as Model Output Statistics (MOS) or correlation analysis, the long-term data (satellite-derived or reanalysis) can be corrected with reference to short-term ground measurements to obtain an unbiased long-term solar radiation data base. This method is already applied successfully for wind energy planning.

As a result of the discussed uncertainties in existing gridded data sets, it is obvious that there is a need to improve the accuracy and evaluation of these data sets. Moreover, it is evident that additional well-maintained radiometric stations would be very helpful for the validation of gridded data sets and the improvement of solar energy prediction, especially in regions with a pare density of operated meteorological measurements, like Africa.

Figure 24 shows the temporal variability of DNI over the USA derived by analysis of data from the National Solar Radiation Database [37]. The temporal variability is evaluated by the standard deviation of annual means relative to the 8-year long-term mean. The temporal variability is relatively low in areas of low cloudiness (such as the southwest), and may be high in areas where both high cloudiness and complex topography features are present. Figure 25 shows the Direct Normal Irradiance (DNI) for the USA. In the South-West low temporal variability is associated with high DNI values.

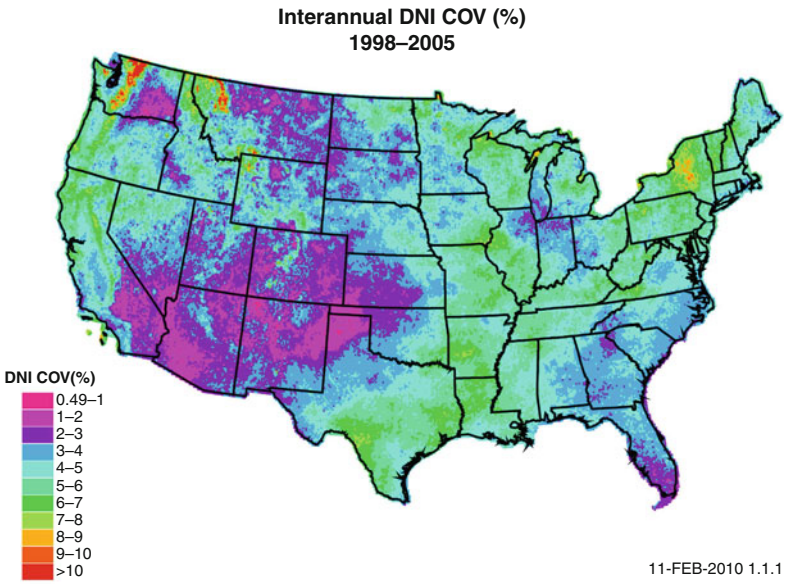

Solar Irradiance, Global Distribution. Figure 24

Temporal variation of DNI in the USA, expressed by the coefficient of variation (COV), i.e., the standard deviation divided by the mean. Large regional differences in the interannual variability are obvious. The higher the temporal variability the longer the needed time period to enable an accurate energy prediction (Source: http://rredc.nrel.gov/solar/newdata/variability)

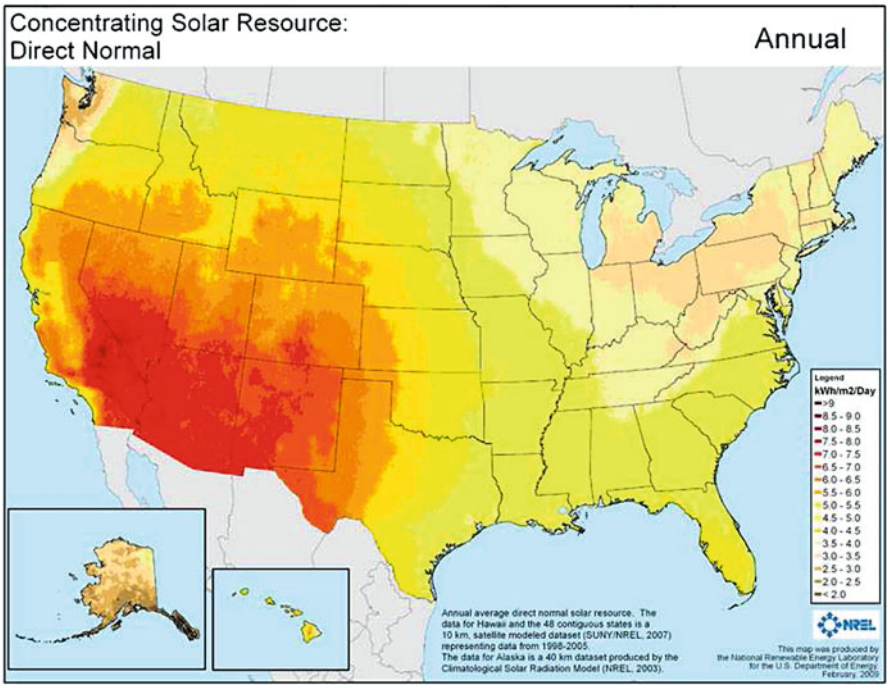

Solar Irradiance, Global Distribution. Figure 25
DNI potential in the USA. The map shows large longitudinal gradients, which are mainly a result of gradients in cloud cover, aerosol load, humidity, and elevation. This Map was produced by the National Renewable Energy Laboratory for the US Department of Energy, 2009, www.nrel.gov. (World maps of solar irradiance, globally or for specific regions, can be obtained (including data download) from http://mynasadata.larc.nasa.gov/las/servlets/dataset)

Summary The distribution of solar irradiance at the top of atmosphere is defined by the Earth-Sun geometry discussed in section "Global Distribution of the Top of Atmosphere Irradiance". The annual mean is only dependent on latitude, with highest values at the equator and lowest values at the poles. The solar irradiance decreases with increasing latitude mostly according to a cosine of latitude. No longitudinal dependency of solar irradiance exists there.

The solar energy potential or solar resource is defined by the solar surface irradiance, which is determined by the solar irradiance at the top of atmosphere and by atmospheric attenuation induced by the atmospheric variables such as water vapor, aerosols, and clouds. The spatial and temporal distribution of these atmospheric variables does significantly affect the distribution of surface irradiance. In contrast to the top of atmosphere distribution, significant latitudinal gradients are apparent in the solar irradiance distribution. As a consequence, the equatorial belt is not the region with the highest solar irradiance, in particular due to the effect of cloudiness.

The distribution of surface irradiance relative to the TOA distribution is essentially defined by the cloud albedo (cloud cover) on a global scale. Main features are the Intertropical Convergence Zone (ITCZ) and mid-latitude with a frequent occurrence of "storms," which are characterized along their tracks by high cloud cover of more than 70%. In Africa and South America the largest amounts of surface irradiance are not located close to the equator, as a consequence of the high cloudiness induced by the ITCZ. The surface irradiance is partly even lower there than in mid-latitudes. The region with maximum surface irradiance over land surfaces is located in a subtropical belt between ca. 15° and 35°N. Around 80% of the solar

surface irradiance is available as direct irradiance in these regions. Many of the developing nations in northern Africa and southern parts of Asia lie within this belt and have therefore optimal conditions for the use of solar energy. Above 35° latitude, the amount of available irradiance decreases with increasing latitude. However, in regions with low cloudiness and air pollution, relative high amounts of solar irradiance are received and thus a good solar energy potential still exists. In general, regions beyond 50° North or South receive much lower amounts of solar irradiance and hence offer less favorable conditions for solar energy systems. This results from a combination of lower solar irradiance at the top of atmosphere and of high cloudiness. For direct irradiance, the effect of clouds and aerosols on its distribution is much more pronounced than in the case of (overall) solar surface irradiance, as a result of the high sensitivity of direct irradiance on these atmospheric variables.

Regions with low cloudiness have a very high solar energy potential. However, in these regions the effect of aerosols becomes relatively more important, especially in the case of direct irradiance. Nowadays it is possible to obtain gridded solar surface irradiance data with an accuracy better than 10 W/m^2. For direct irradiance, less data sets are available and the uncertainty is much larger. This is partly due to the high uncertainty in the available aerosol information, which is, in turn, a result of the quite limited number of stations measuring aerosol properties, which slows scientific progress in this field.

Future Directions

Solar irradiance and its distribution are a driving factor of life on Earth, playing a dominant role in the distribution of climate zones, plants, animals, and to some extent human settlements. In this context, it is important to improve our knowledge of the global distribution of solar irradiance, including issues on accuracy and resolution. In this context, it is also necessary to improve our understanding of the processes affecting the global distribution of solar radiation. While the astronomical physics determining the distribution of solar irradiance at the top of atmosphere is well understood, there are still gaps in our knowledge about the distribution of solar radiation induced by the atmospheric variables. In particular, the accuracy of cloud properties and aerosol properties has to be improved. Also the affect of the greenhouse warming (climate change) on the global distribution of clouds and hence on solar radiation should be investigated in more detail. In turn, it should be investigated in more detail how changes in the global distribution, resulting, e.g., from changes in cloudiness, affect the observation and analysis of greenhouse warming. Increase of cloud albedo can partially compensate greenhouse warming, whereas a decrease in cloud albedo would force further warming [38]. There seems to be also room for improvement in our knowledge of the interaction between solar irradiance distribution and animal, plant, and surface types.

The accuracy of direct irradiance data needs to be improved in order to provide reliable solar radiation data for the energy prediction of solar power plants. Therefore data sets of aerosols with higher accuracy are required. Also, appropriate correction of broken cloud effects is expected to improve the accuracy of satellite-derived direct irradiance data sets. There is still a lack of public-domain solar surface irradiance and direct irradiance data sets. Moreover, the accuracy information in existing data sets needs to be improved by additional accuracy measures and more independent intercomparison studies. In general, the international activities of institutions such as the International Energy Agency concerning quality monitoring and consistency of solar irradiance data sets and algorithms should be intensified. The extension of existing high-quality ground measurement networks such as the BSRN (for solar radiation) and Aeronet (for aerosols) would be very important. This would support scientific developments in various disciplines, such as climate change and solar energy utilization.

Finally, concerning the bridge between natural sciences and social sciences there seems to be a need for an extension of studies concerning the interaction between solar surface irradiance distribution and the history, status, and modifications of cultures. This should also include a discussion of modifications of these interactions due to technical progress and, hence, the interaction between culture and technical adaptations to specific extreme solar irradiance conditions.

Acknowledgments

We acknowledge NCEP/NCAR, SRB/GEWES/NASA for the open, easy and free web access to their high-quality data. Many thanks to Anke Kniffka and Susanne Vlpel for proofreading and to Rebekka Posselt for the seasonal mean figures of solar irradiance.

Bibliography

1. Babst F, Mueller RW, Hollmann R (2008) Verification of NCEP reanalysis shortwave radiation with mesoscale remote sensing data. Geosci Remote Sens Lett 5(1):34–37
2. Wang L, Qu JJ (2007) NMDI: a normalized multi-band drought index for monitoring soil and vegetation moisture with satellite remote sensing. Geophys Res Lett 34: L20405
3. Perez R, Renne D, Seals R, Zelenka A (1998) The strength of satellite-based solar resource assessment. Production of site/time-specific irradiances from satellite and ground data, report 98–3. New York State Energy Research and Development Authority, Corporate Plaza West, 286 Washington Evenue Extension, Albany, NY, pp 12203–6399
4. Carroll BW, Ostlie DA (2007) An introduction to modern astrophysics. Pearson Addison-Wesley, San Francisco. ISBN 0-8053-0402-9
5. Whitman AM (2007) A simple expression for the equation of time. J North American Sundial Soc 14:29–33
6. Lin B, Stackhouse PW, Minnis P Jr, Wielicki BA, Hu Y, Sun W, Fan T-F, Hinkelman LM (2008) Assessment of global annual atmospheric energy balance from satellite observations. J Geophys Res 113:D16114
7. Jacobowitz H, Tighe RJ et al (1984) The earth radiation budget derived from the Nimbus-7 ERB experiment. J Geophys Res 89:4997–5010
8. Barkstrom BR, Smith GL (1986) The earth radiation budget experiment: science and implementation. Rev Geophys 24:379–390
9. Wielicki BA, Barkstrom BR, Baum BA, Charlock TP, Green RN, Kratz DP, Lee RBI, Minnis P, Smith GT, Wong T, Young DF, Cess RD, Coakley JAJ, Crommelynck DA, Donner L, Kandel R, King MD, Miller AJ, Ramanathan V, Randall DA, Stowe LL, Welch RM (1998) Clouds and the earth's radiant energy system (ceres): algorithm overview. IEEE Trans Geosci Remote Sens 36:1127–1141
10. Harries JE, Russel JE, Hanafin JA, Brindley H, Futyan J, Rufus J, Kellock S, Matthews G, Wrigley R, Last A, Mueller J, Mossavati R, Ashmall J, Sawyer E, Parker D, Caldwell P, Allan PM, Smith A, Bates J, Coan B, Stewart BC, Lepine DR, Cornwall DR, Corney DR, Rickets MJ, Drummond D, Smart D, Cutler R, Dewitte S, Clerbaux N, Gonzales A, Ipe A, Bertrand C, Joukoff A, CrommelYnck D, Nelms N, LLewellyn-Jone DT, Butcher G, Smith LG, Szewczyk ZP, Mlynczak PE, Slingo A, Allan RP, Ringer MA (2005) The geostationary earth radiation budget project. BAMS 86:945–960
11. Schmetz J, Pili P, Tjemkes S, Just D, Kerkmann J, Rota S, Ratier A (2002) An introduction to Meteosat Second Generation (MSG). Bull Amer Meteor Soc 83:977–992
12. Pinker RT, Frouin R, Li Z (1995) A review of satellite methods to derive surface shortwave irradiance. Remote Sens Environ 51:108–124
13. Tang B, Li Z-L, Zhang R (2006) A direct method for estimating net surface shortwave radiation from modis data. Remote Sens Environ 103(1):115–126
14. Kokhanovsky AA (2006) Cloud optics. Atmospheric and oceanographic sciences library. Springer, Dordrecht. ISBN 10 1-4020-3955-7
15. Warren SG, Hahn CJ, London J, Chervin RM, Jenne RL (1986) Global distribution of total cloud cover and cloud type amounts over land. Technical Report NCAR Tech. Note NCAR/TN-273 + STR, 29 pp
16. Warren SG, Hahn CJ, London J, Chervin RM, Jenne RL (1986) Global distribution of total cloud cover and cloud type amounts over land. Technical Report NCAR Tech. Note NCAR/TN-317 + STR, National Center for Atmospheric Research, 42 pp
17. Rossow WB, Schiffer RA (1999) Advances in understanding clouds from ISCCP. Bull Amer Meteor Soc 80:2261–2287
18. Aarnout van Delden (2010). Atmospheric dynamics. Lecture notes
19. Holton JR (2004) An introduction to dynamic meteorology. Elsevier, Oxford. ISBN -10:0-12-354015-1
20. Mueller R, Posselt R, Trentmann J, Stckli R (2011) Meteosat (mviri) solar surface irradiance and effective cloud albedo climate data sets: the magicsol method. Technical report, climate monitoring satellite application facility, CM-SAF. www.cmsaf.eu, menu publications and documents
21. Lau N-C, Crane MW (1995) A satellite view of the synoptic-scale organization of cloud properties in midlatitude and tropical circulation systems. Mon Weather Rev 7: 1984–2006
22. Klein SA, Hartmann DL (1993) The seasonal cycle of low stratiform clouds. J Clim 6:1587–1606
23. Kinne S, Schulz M, Textor C, Guibert S, Balkanski Y, Bauer SE, Berntsen T, Berglen TF, Boucher O, Chin M, Collins W, Dentener F, Diehl T, Easter R, Feichter J, Fillmore D, Ghan S, Ginoux P, Gong S, Grini A, Hendricks J, Herzog M, Horowitz L, Isaksen I, Iversen T, Kirkevåg A, Kloster S, Koch D, Kristjansson JE, Krol M, Lauer A, Lamarque JF, Lesins G, Liu X, Lohmann U, Montanaro V, Myhre G, Penner J, Pitari G, Reddy S, Seland O, Stier P, Takemura T, Tie X (2006) An aerocom initial assessment optical properties in aerosol component modules of global models. Atmos Chem Phys 6(7):1815–1834
24. Textor C, Schulz M, Guibert S, Kinne S, Balkanski Y, Bauer S, Berntsen T, Berglen T, Boucher O, Chin M, Dentener F, Diehl T, Easter R, Feichter H, Fillmore D, Ghan S, Ginoux P, Gong S, Grini A, Hendricks J, Horowitz L, Huang P, Isaksen I, Iversen I,

Kloster S, Koch D, Kirkevåg A, Kristjansson JE, Krol M, Lauer A, Lamarque JF, Liu X, Montanaro V, Myhre G, Penner J, Pitari G, Reddy S, Seland O, Stier P, Takemura T, Tie X (2006) Analysis and quantification of the diversities of aerosol life cycles within aerocom. Atmos Chem Phys 6(7): 1777–1813
25. Hess M, Koepke P, Schult I (1998) Optical properties of aerosols and clouds: the software package OPAC. Bull Amer Meteor Soc 79:831–844
26. Gupta SK, Ritchey NA, Wilber AC, Whitlock CH (1999) A climatology of surface radiation budget derived from satellite data. J Clim 12:2691–2709
27. Barnston AG, Livezey RE (1987) Classification, seasonality and persistence of low-frequency atmospheric circulation patterns. Mon Wea Rev 115:1083–1126
28. Wallace JM, Gutzler DS (1981) Teleconnections in the geopotential height field during the northern hemisphere winter. Mon Wea Rev 109:784–812
29. Hurrel JW (1995) Decadal trends in the north Atlantic oscillation: regional temperatures and precipitation. Science 269:676–679
30. Rossow WB, Dueñas EN (2004) The international satellite cloud climatology project (ISCCP) web site: an online resource for research. Bull Am Meteorol Soc 85(2):167–172
31. Gupta S, Stackhouse P Jr, Cox S, Mikovitz J, Zhang T (2006) Surface radiation budget project completes 22-year data set. GEWEX News 16(4):12–13
32. Baldocchi D (2001) Coauthors Fluxnet: a new tool to study the temporal and spatial variability of ecosystemscale carbon dioxide, water vapor, and energy flux densities. Bull Amer Meteor Soc 82(11):2415–2434
33. Pierre Ineichen (2010) Satellite based short wave irradiance validation over Africa. Technical report, climate monitoring satellite application facility, visiting scientist report. www.cmsaf.eu
34. Gueymard CA (2010) Variability in direct irradiance around the Sahara: are the modeled data sets of bankable quality? In: Solar paces conference, Perpingnan, France, 2010
35. Suri M, Remund J, Cebecauer T, Hoyer-Klick C, Dumortier D, Huld T, Stackhouse PW, Ineichen P (2009) Comparison of direct normal irradiation spatial products for Europe. Extended abstract. In: Solar paces conference, Berlin, 2009
36. Lohmann S, Schillings C, Mayer B, Meyer R (2006) Long-term variability of solar direct and global radiation derived from ISCCP data and comparison with reanalysis data. Solar Energy 80:1390–1401
37. Wilcox S et al (2007) Completing production of the updated national solar radiation database for the United States. In: Number ASES, solar conference, Cleveland, 2007
38. Mueller R, Trentmann J, Träger-Chatterjee C, Posselt R, Stökli R (2011) The role of the effective cloud albedo for climate monitoring and analysis. Remote Sens 3: 2305–2320

Solar Radiation and Human Health

Gunther Seckmeyer[1], Armin Zittermann[2], Richard McKenzie[3], Ruediger Greinert[4]
[1]Institute of Meteorology and Climatology, Leibniz University of Hannover, Hannover, Germany
[2]Clinic for Thoracic and Cardiovascular Surgery, Heart Center North Rhine-Westphalia, Ruhr University Bochum, Bad Oeynhausen, Germany
[3]National Institute for Water and Atmospheric Research (NIWA), Lauder, New Zealand
[4]Centre of Dermatology, Elbe Kliniken Buxtehude, Buxtehude, Germany

Article outline

Glossary
Definition of the Subject
Introduction
UV Radiation and Health Effects
UV Index
Visible Radiation and Health Effects
Infrared Effects
Effects for Which the Spectral Responsivity Is Not Yet Known
Future Directions
Bibliography

Glossary

Action spectrum Weighting function describing the wavelength dependence of the biological response. Usually, it is normalized to 1 at a specific wavelength. In the UV, action spectra need to be known accurately over several orders of magnitude.

Direct spectral irradiance $E_{\lambda,D}$ Radiant energy dQ arriving from the disk of the sun per time interval dt, per wavelength interval $d\lambda$, and per area dA on a surface normal to the solar beam.

$$E_{\lambda,D} = \frac{dQ}{dt\, dA\, d\lambda}$$

The angular field of view of an instrument measuring direct normal spectral irradiance must be sufficiently small to reduce uncertainties caused by circumscolar radiation. Recommendations for

view-limiting geometries can be found in WMO [166].

Erythemally weighted irradiance E_{CIE} Global spectral irradiance $E_G(\lambda)$ multiplied with the action spectrum for erythema, $C(\lambda)$, proposed by CIE [1] and integrated over wavelengths λ:

$$E_{CIE} = \int_{250\text{nm}}^{400\text{ nm}} E_G(\lambda) \cdot C(\lambda)\, d\lambda$$

Exposure The spectral exposure Ex_λ is the radiance L_λ integrated over the relevant areas dA of the human body. In this context, the spectral radiance originates from the Sun's direct beam and any scattered components.

$$Ex_\lambda = \int_{t_1}^{t_2} \left(\oint_{(A)} L_\lambda(\varepsilon, \varphi, t, \lambda) \cdot dA \cos\varepsilon \right) dt$$

where $T = t_2 - t_1$ is the exposure time. $Ex_\lambda(\lambda)$ may be weighted with a biological action spectrum and integrated over the wavelength to assess its biological impact. In this case the exposure is no longer a function of the wavelength and has the unit J.

Global spectral irradiance $E_{\lambda,G}$ Radiant energy dQ arriving per time interval dt, per wavelength interval $d\lambda$, and per area dA on a horizontally oriented surface from all parts of the sky above the horizontal, including the disk of the sun itself:

$$E_{\lambda,G} = \frac{dQ}{dt\, dA\, d\lambda} = E_{\lambda,D} \cdot \cos(\vartheta) + E_{\lambda,S}$$

where ϑ is the solar zenith angle.

Spectral radiance L_λ, This can be defined in terms of emitted or received radiation. Here the latter applies. Radiant energy dQ per time interval dt, per wavelength interval $d\lambda$, per area dA, and per solid angle $d\Omega$ on a receiver oriented normal to the source.

$$L_\lambda = \frac{dQ}{dt\, dA\, d\lambda d\Omega}$$

UV index A measure of solar UV radiation at the Earth's surface that is used for public information. According to [2], the UV index is calculated considering the following items:

1. Calculation of the erythemally weighted irradiance E_{CIE} (see above) by utilization of the CIE action spectrum [1] normalized to 1.0 at 298 nm.
2. A minimum requirement is to report the daily maximum UV index.
3. The index is expressed by multiplying the weighted irradiance in W m^{-2} by 40.0 (this leads to an open-ended index which is normally between 0 and 16 at sea level, but with larger values possible at high altitudes).

Remarks:

(a) The definition of the UV index given above may be revised in the future.
(b) According to the alternative definition given in [3], the UV index is calculated as the daily maximum erythemally weighted irradiance in W m^{-2}, averaged over a duration of between 10 and 30 min and multiplied by 40.

UV-A radiation Electromagnetic radiation between 315 and 400 nm [4]. UV-A radiation is a summarizing term only and, unlike UVA irradiance, not a physical quantity.

UV-B radiation Electromagnetic radiation between 280 and 315 nm [4]. UV-B radiation is a summarizing term only and, unlike UVB irradiance, not a physical quantity.

Vitamin D Vitamin D is produced photochemically by UV exposure and conversion of 7-dehydrocholesterol into previtamin D_3, which is rapidly converted to vitamin D_3. The active form of vitamin D_3, 1,25-dihydroxyvitamin D_3, is a hormone.

Definition of the Subject

Solar radiation has both direct and indirect impacts on human health. Only direct effects are described here. (Space is too limited to describe the indirect effects, which are numerous, complex and imbedded into important feedback mechanisms; the most important indirect effects for human health are on the availability and quality of food, effects on aquatic and terrestrial plants and ecosystems, deterioration in air quality, damage to materials, and energy-related issues that drive the world economy.)

While solar energy has been stored in the form of oil and gas for millions of years, it has become evident that these resources are limited and that harnessing renewable energies will be necessary in the future. Closely related are the effects on the environment for food production, which relies on solar energy.

The sun's spectrum extends over a much-broader range of wavelengths than what is detected by the human eye, which responds only from 380 (violet light) to 780 nm (red light), with a peak response near 550 nm (green light). About 50% of the total solar irradiance originates from the near-infrared region. A relatively small but nevertheless important component is contained in the ultraviolet (UV).

Usually, any effect of solar radiation on biological organisms is wavelength dependent. A frequent concept is to describe these effects by means of biological weighting functions, often called action spectra, which quantify the wavelength dependence of effects introduced by electromagnetic radiation on biological matter. Depending on the effect and the organism involved, different biological weighting functions $W(\lambda)$ are used. The biologically effective irradiance, E_{weighted}, is calculated by multiplying the global spectral irradiance, $E_G(\lambda)$, with the action spectrum $W(\lambda)$, and integrating over wavelengths λ:

$$E_{\text{weighted}} = \int E_G(\lambda) \times W(\lambda)\, d\lambda$$

Note that the equation above is applicable for additive effects only (the so-called Bunsen–Roscoe law). Whether the concept is applicable or not must be proven or judged for each individual case. An important weighting function is the action spectrum for erythema (sunburn), as proposed by CIE [1], which describes the wavelength dependence of the reddening of human skin by UV radiation (see also below "erythemally weighted irradiance" E_{CIE}).

Introduction

Humans have long been aware of a close relationship between human health and solar radiation. This is reflected by the fact that in many religions, the sun plays an important role. In many ancient cultures, the sun itself was considered as a god (e.g., in Egypt). The systematic study of the effects of solar radiation progressed in parallel with the evolution of science and medicine. For an assessment of the spectral dependencies of solar radiation, a separation of the different spectra was necessary. A major step was probably the analysis by Joseph von Fraunhofer in the early nineteenth century, who separated the different components of sunlight with high precision using his newly constructed prisms. Later on, the investigations carried out by Carl Dorno, and his publication about "light and air in mountainous regions" that he published in 1911, were other important milestones. For a long time, the UVB radiation was actually called "Dorno radiation."

In this chapter, the present knowledge of the relationship between solar radiation and human health is described. Historical aspects, which are course interesting in their own right, are not considered further. This chapter is separated into the knowledge of spectral effects (UV, visible, and infrared), followed by a short section that deals with effects for which the spectral dependence is not yet known. Solar radiation has both negative and positive effects on human health. The negative effects of UV radiation have been emphasized in recent decades – on the background that skin cancer has been the cancer with the highest rate of increase. In recent years, however, more attention is being given to the positive side of solar radiation. At the end of this chapter, the benefits and dangers of solar radiation are summarized.

UV Radiation and Health Effects

The atmosphere is largely transparent in the visible region. Conversely, gaseous absorption is important in the UV. The latter is subdivided into three spectral bands: UV-A (315–400 nm) radiation, UV-B (280–315 nm) radiation, and UV-C (100–280 nm) radiation. (some authors still use 320 nm as the boundary between UV-A and UV-B radiation.) This separation has been originally introduced due to its relation with human effects. Nowadays, it is better understood that these effects cannot be strictly separated and, thus, only the general term "UV" is often used. UV-A radiation is largely unaffected by gases in the atmosphere. Conversely, only a small amount of UV-B radiation proceeds to the Earth's surface because it is strongly

absorbed by atmospheric ozone, whose absorption cross section increases rapidly toward shorter wavelengths in this spectral region. UV-C comprises less than 0.6% of the incident solar spectrum at the top of the atmosphere, but none of it reaches the surface. Radiation below 240 nm is absorbed by molecular oxygen (O_2, which comprises 20% of the atmosphere). This radiation is capable of photo-dissociating molecules to form two oxygen atoms. The atoms so formed then recombine with another oxygen molecule to form ozone (O_3). Under the terms of the Montreal Protocol on Protection of the Ozone Layer, assessments of the knowledge about the science of Ozone Depletion and UV radiation [5, 6] and assessments of the Environmental Impacts of Ozone Depletion [7] are produced regularly.

If human eyes were sensitive to UV radiation rather than to visible radiation, perceptions of the world would be very different. The sky appears blue because air molecules scatter blue light more strongly than red light. This dependence on the wavelength (λ) of light is very strong. Rayleigh scattering theory shows that it varies as λ^{-4} so, at 300 nm, the strength of this scattering is about 32 times greater than at 600 nm. That is why photographers choose to use blue-blocking filters (i.e., red filters) if they want to obtain dramatic images of cloudy skies in black and white pictures since such filters can greatly enhance the contrast between the bright cloud and dark background.

Because of this wavelength-dependent scattering by air molecules, the UV radiation field is much more diffuse than visible radiation (light). An eye sensitive to UV radiation would therefore perceive a much smaller contrast between clouds and sky, and a smaller contrast between sky and sun. Under clear skies, the diffuse UV component would normally dominate over the direct beam component, whereas in the visible, the diffuse component is typically only 5–15% of the direct. When the sun is low in the sky, Rayleigh extinction becomes so large that the solar disk in the UV region would not even be detectable from the surrounding skylight. The sphere of consciousness would be greatly reduced because objects more distant than even a few kilometers would be completely lost in the gloom of diffuse light. It would be like living in a light fog. Shadows would be less distinct. When the sky is overcast, places normally in the shade would receive more light than under clear skies. One practical implication of this more diffuse field is that any reduction in UV radiation in a shaded area is smaller than the reduction in visible light, as perceived with the eye. Therefore, the protection from the sun offered by shade may be less complete that anticipated from the standpoint of UV effects. The brightness of objects would appear very different too. Most natural surfaces reflect a significant fraction of the incoming visible radiation. But in the UV region, very few surfaces are strongly reflecting. Most natural surfaces would appear quite dark because they reflect less than 5% of the incoming UV-B radiation. Snow and clouds are two of the few exceptions to this rule.

Another aspect of UV radiation is the ratio of diffuse to direct irradiance is much higher in the UV compared to visible wavelengths. Therefore, under clear skies, hazy skies, or very lightly cloudy skies, the diffuse UV irradiance comes from all possible directions, rather than preferentially from around the sun disk (Fig. 1). This further decreases the effectiveness of partial shading structures.

The variability in UV irradiance between common sources is described in Table 1.

Vitamin D

Vitamin D Metabolism Solar UV-B irradiation (280–315 nm) of the skin is the major source of vitamin D3 for humans, whereas dietary intake of vitamin D2 or vitamin D3 is a second, less important source. The dietary contribution to vitamin D supply usually does not exceed 10–20% in free-living persons. Only few fatty salt water fish such as herring, salmon, and sardines are good sources of vitamin D. Skin synthesis of vitamin D3 is very effective. The relevant quantity is the exposure, as defined above (in units of W). Some authors consider summer exposure of arms and legs for 5–30 min (depending on latitude and skin pigmentation) between the hours of 10 a.m. and 3 p.m. twice a week to be adequate. However, it has been found that the vitamin D action spectrum is more uncertain than previously thought. Consequently, in winter, it may not be possible to gain enough vitamin D by casual exposure to sunlight. Exposure of skin to sunlight at regular intervals results in the photochemical conversion of 7-dehydrocholesterol into previtamin D_3, which is rapidly converted to vitamin D_3. In the midsummer

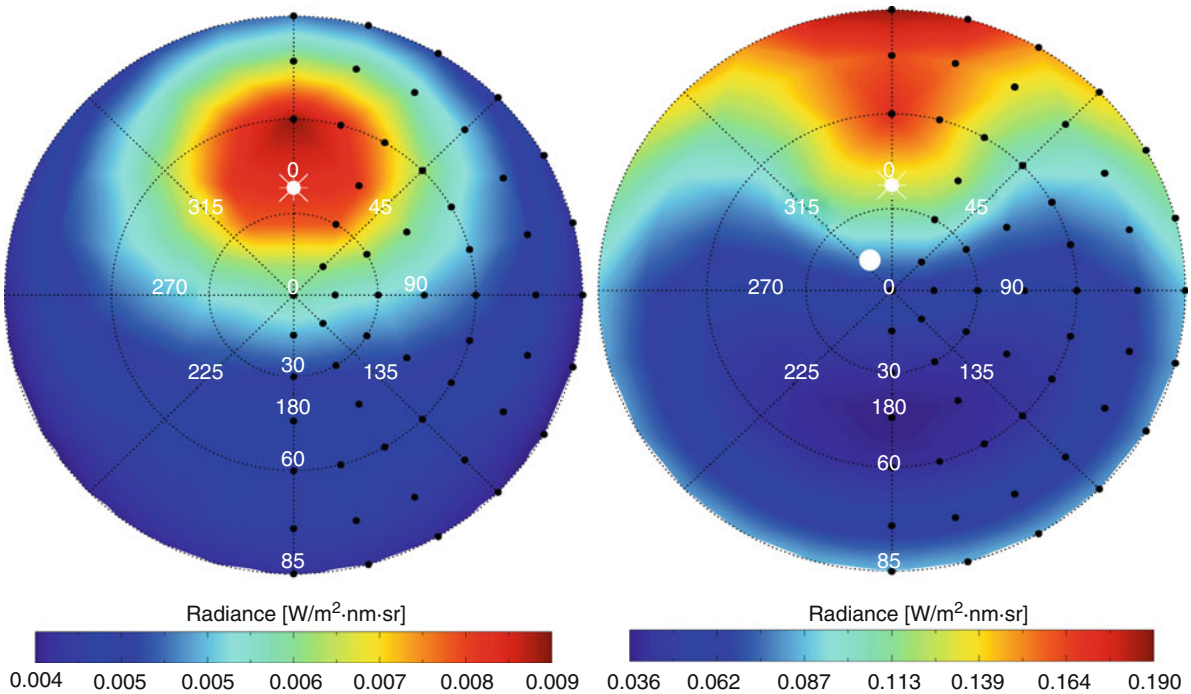

Solar Radiation and Human Health. Figure 1

Radiance distribution measured during clear skies in Hannover during noon. The position of the sun – south at noon – is given by the white symbol. *Left* panel 305 nm, *right* panel 500 nm. It can be recognized that the spatial distribution is quite different at these two wavelengths and that the distribution of sky radiance is more uniform in the UV, which can be understood as a result of double scattering by Rayleigh scattering

months (e.g., June and July in the northern hemisphere), the amount of vitamin D_3 increases to a maximum of approximately 12% of the amount of 7-dehydrocholesterol at latitudes of 34° and below, to 9% in one hour in Boston (42° N) and 11% in 3 h in Edmonton (52° N). Analyses after exposure of the 7-dehydrocholesterol solution at several places in the southern hemisphere showed concordant results [8]. The sunlight-generated vitamin D_3 is a precursor of the active hormonal form of vitamin D_3. Because any excess in previtamin D3 or vitamin D3 is destroyed by sunlight, excessive exposure to sunlight does not cause vitamin D intoxication. It has been reported that exposure to one minimal erythemal dose while wearing only a bathing suit is equivalent to ingestion of approximately 500 μg of vitamin D [9]. Because of its skin synthesis, vitamin D_3 is not really a vitamin for humans. However, if skin exposure to UV-B radiation is negligible (e.g., in winter) or if people live exclusively indoors (institutionalized people), then there is indeed an absolute regular requirement for the fat soluble vitamin D, which must be met through proper dietary intake.

Once in circulation through the body, vitamin D is metabolized by a hepatic hydroxylase into 25-hydroxyvitamin D (25[OH]D) and by a renal 1α-hydroxylase into the vitamin D hormone 1,25-dihydroxyvitamin D (1,25-dihydroxyvitamin D) (Fig. 2). The latter step is under the control of parathyroid hormone (PTH) and serum phosphate. However, in case of vitamin D deficiency/insufficiency, renal synthesis of 1,25-dihydroxyvitamin D becomes substrate dependent, i.e., dependent on the circulating 25(OH)D concentration [10].

The active form of vitamin D, 1,25-dihydroxyvitamin D, is known as a regulator of systemic calcium homeostasis. Together with the parathyroid hormone (PTH) and calcitonin, 1,25-dihydroxyvitamin D carries out the policing job of regulating serum calcium levels in highly evolved

Solar Radiation and Human Health. Table 1 Relationships between various weightings for a typical dermatological UV-A tanning salon compared with natural sunlight (noon sun in summer and winter at 45° S (Lauder New Zealand) and a powerful 1,000 W quartz halogen lamp at a distance of 0.5 m. UV_Ery and UV-VitD are erythemally weighted and vitamin D-weighted UV radiation, respectively

Quantity	Unit	UV-A tanning salon	Winter sun	Summer sun	1,000 W FEL at 0.5 m
UV-A	(μW cm^{-2})	17,598	1797	6161.5	106.2
UV-B	(μW cm^{-2})	208.3	17.9	206.6	6.6
UV_Ery	(μW cm^{-2})	51.5	2.6	28.2	7.0
UV_VitD	(μW cm^{-2})	63.8	3.2	56.7	3.8
UVI		20.6	1	11.3	2.8
T(2SED*)	(min)	6.5	128.2	11.8	47.4
Vit. D/Ery		1.2	1.2	2	0.5
UV-B / UV-A		0.012	0.010	0.034	0.062

mammals. This regulating mechanism is done with astounding efficiency, indicating the importance of serum calcium homeostasis. Serum calcium homeostasis is essential for blood coagulation, activation of various intracellular processes, and bone health. Therefore, serum calcium level of 2.5 mmol/L is maintained in all vertebrate life forms (both aquatic and terrestrial). The regulatory system of calciotropic hormones appears to have developed after transition of life from water (calcium–phosphorus rich environment) to land (environment poor in calcium and phosphorus). This assumption is supported by the fact that, in fish, PTH is missing and calcitonin is inactive [11]. Together with PTH, vitamin D is responsible for maintaining serum calcium levels by increasing intestinal calcium absorption, renal calcium reabsorption, and calcium resorption from bone. Without vitamin D, only 10–15% of dietary calcium and about 60% of phosphorus can be absorbed. vitamin D increases the efficiency of intestinal calcium absorption to 30–40% and phosphorus absorption to approximately 80% [11].

1,25-dihydroxyvitamin D also plays a pivotal role in the intracellular calcium homeostasis and has pleiotropic effects in various tissues. The biological actions of 1,25-dihydroxyvitamin D are mediated through the vitamin D receptor (VDR). In this context, 1,25-dihydroxyvitamin D functions as a steroid hormone that binds to a cytosolic VDR, resulting in a selective demasking of the genome of the nucleolus. The vitamin D receptor is nearly ubiquitously expressed, and almost all cells respond to 1,25-dihydroxyvitamin D exposure. About 3% of the human genome is regulated, directly and/or indirectly, by the vitamin D endocrine system [12]. Apart from the kidney, 1,25-dihydroxyvitamin D can be locally produced in several tissues. These tissues include monocytes, dendritic cells, B lymphocytes, colonocytes, vascular smooth muscle cells, and endothelial cells. Consequently, for 1,25-dihydroxyvitamin D, a paracrine role separate from its calcium-regulating function has been proposed.

Reference Values There is general agreement that the measurement of 25(OH)D is the appropriate tool for the assessment of vitamin D status. Nevertheless, there is currently no consensus on adequate/optimal circulating 25(OH)D concentrations. Cutoff values range between 50 nmol/L [13], 90–100 nmol/L [14], and more than 100 nmol/L [15]. This inconsistency is in part due to different criteria of defining inadequacy. Many researchers do not differentiate between different stages of vitamin D status. However, similar to other vitamins, it is possible to categorize the stages of vitamin D status into deficiency, insufficiency, hypovitaminosis, adequacy, and intoxication. In the deficiency range, severe vitamin D-specific clinical symptoms such as rickets, osteomalacia, calcium malabsorption, severe hyperparathyroidism, low 1,25-dihydroxyvitamin D concentrations, impaired immune system, and ultimately death can occur. In the insufficiency range, reduced bone mineral density, impaired muscle function, low intestinal calcium absorption rates, elevated PTH levels, and slightly reduced 1,25-dihydroxyvitamin D concentration are encountered. In the stage of hypovitaminosis, the body's vitamin reserves are already low, and slightly enhanced PTH levels may be present,

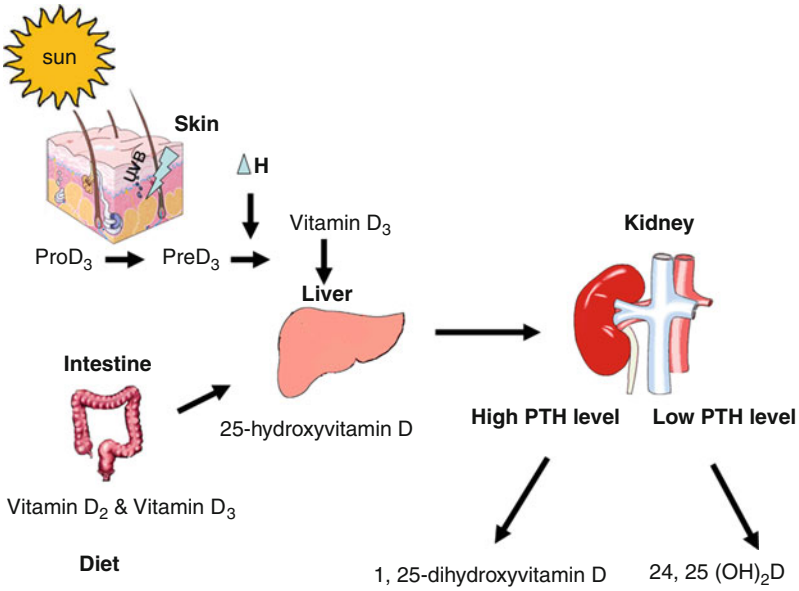

Solar Radiation and Human Health. Figure 2
Vitamin D metabolism

although the corresponding concentrations are usually still in the reference range. In the stage of adequacy, no disturbances in vitamin D-dependent body functions do occur. Only excessive oral intake can lead to vitamin D intoxication, resulting in intestinal calcium hyperabsorption, hypercalcemia, soft tissue calcification, and death. On an individual basis, the consequences of an insufficient vitamin D status may be mild, but the consequences on a population scale may be more important because of the large number of people who are affected. People with long-lasting vitamin D insufficiency may have the highest risk to develop vitamin-D-related chronic diseases.

Unfortunately, insufficient vitamin D status is prevalent around the world. Over the six regions Asia, Europe, Middle East and Africa, Latin America, North America, and Oceania, it has been found that between 50% and more than 90% of people have 25(OH)D concentrations below 50 nmol/L [16]. Low vitamin D status is most common in South Asia and the Middle East. Insufficient vitamin D status and even vitamin D deficiency is widespread, and is actually reemerging as a major health problem globally. Urbanization is an important risk factor for vitamin D insufficiency/deficiency in large parts of the adult population. Other factors include short daylight periods, long cold or hot seasons – or strict cultural traditions – imposing extensive clothing, modern and also traditional lifestyles such as indoor working, predominantly indoor leisure time activities, and the aging factor (institutionalization of elder persons). In a British study in the 1958 birth cohort, for example, 25-hydroxyvitamin D concentrations below 40 nmol/L were more prevalent in Scotland than in the South of England [17]. In highly urbanized or polluted areas, individual daily sun exposure is usually too low to achieve a 25(OH)D level of 75 nmol/L. Without food supplementation, the diet is then not able to close the gap in vitamin D supply. There have been studies linking vitamin D deficiency to latitude [18–21], but there are also studies that could not confirm such correlations [22].

Musculoskeletal Disease Urbanization and industrialization (with their associated air pollution problems) have long been known as a major cause of childhood rickets in western countries. Rickets is now on the increase in many developing countries and is also reemerging as an important health problem in countries with strong sun avoidance policies, or in cultures requiring strictly modest dressing codes. In adults, severe vitamin D deficiency causes osteomalacia, a disease resulting in bone demineralization and muscle weakness.

Due to low calcium absorption rates, vitamin D insufficiency can also contribute to the bone disease osteoporosis. It is estimated that up to 50% of women and more than 20% of men 50 years of age or older will sustain an osteoporotic fracture in their remaining lifetime. A meta-analysis of randomized clinical trials that evaluated the effect of vitamin D supplementation came to the conclusion that the fracture preventing effect of vitamin D is approximately 20% when serum 25(OH)D levels of 75–80 nmol/L are achieved [23]. Another meta-analysis of randomized controlled trials (RCTs) came to the conclusion that daily doses of 17.5–20 μg supplemental vitamin D are able to prevent elderly adults to fall down by improving muscle function [24]. The relative risk of falls was reduced by approximately 20% when serum 25(OH)D concentrations of 60 nmol/L or more could be maintained. In contrast to "high-dose" supplemental vitamin D, low-dose daily supplemental vitamin D (5–15 μg) is not able to prevent falls.

Cancer Since vitamin D is a key regulator of various cellular metabolic pathways, it is important for cellular maturation, differentiation, and apoptosis [25]. In 2008, the WHO published a report from the International Agency for Research on cancer [26] that came to the conclusion that there is (1) consistent epidemiological evidence for an inverse association between 25(OH)D and colorectal cancer and colorectal adenomas, (2) suggested epidemiological evidence for an inverse association between 25(OH)D and breast cancer, (3) insufficient evidence for an inverse association between 25(OH)D and other types of cancer, and (4) the need for new RCTs. One such RCT has recently been published [27]: In a 4-year, population-based study, where the primary outcome was fracture incidence and the principal secondary outcome was cancer incidence, 1,179 community-dwelling women were randomly assigned to receive 1,500 mg supplemental calcium/day alone (Ca-only), supplemental calcium plus 27.5 μg vitamin D/day (Ca + D), or placebo. The cancer incidence was 60–77% lower in the Ca + D women and 43% lower in the Ca-only group than in the placebo control subjects ($P < 0.03$).

Diabetes Mellitus In vitro and in vivo studies suggest that vitamin D can prevent pancreatic beta-cell destruction and reduce the incidence of autoimmune diabetes. This may be due, at least in part, to a suppression of proinflammatory cytokines such as the tumor necrosis factor (TNF)-α. Recently, the relationship between UVB irradiance and age-standardized incidence rates of type-1 diabetes mellitus in children aged 14 years or less was analyzed according to 51 regions of the world [28]. Incidence rates were generally greater at higher latitudes and were inversely associated with UV-B irradiance. As early as 2001, Hyppönen et al. [29] demonstrated, in a birth cohort study, that vitamin D supplementation was associated with a decreased frequency of type-1 diabetes. In contrast, children suspected of having rickets during the first year of life had a three times higher relative risk compared with those without such a suspicion. A meta-analysis of four case-control studies has shown that the risk of type-1 diabetes is reduced by 29% in infants who are supplemented with vitamin D compared to those who are not supplemented [30]. There is also some evidence of a dose-response effect, with those using higher amounts of vitamin D being at lower risk of developing type-1 diabetes.

Observational studies, e.g., Pittas et al. [31], show a relatively consistent association between low vitamin D status and prevalent type-2 diabetes, with an odds ratio of 0.36 for highest vs. lowest 25-hydroxyvitamin D among nonblacks. Evidence from RCTs with vitamin D and/or calcium supplementation suggests that combined vitamin D and calcium supplementation may have a role in the prevention of type-2 diabetes only in populations at high risk (i.e., individuals with glucose intolerance). Whereas vitamin D supplementation did not improve glycemic control in diabetic subjects with initial serum 25(OH)D levels above 50 nmol/L [32], administration of 100 μg vitamin D3 improved insulin sensitivity in vitamin D deficient and insulin-resistant South Asian women [33]. Insulin resistance was most improved when endpoint serum 25(OH)D reached at least 80 nmol/L. Optimal vitamin D concentrations for reducing insulin resistance were shown to be 80–119 nmol/L.

Cardiovascular Disease Globally, cardiovascular disease (CVD) is the number one cause of death. In 2005, it was responsible for approximately 30% of deaths worldwide. CVD includes various illnesses such as

coronary heart disease, peripheral arterial disease, cerebrovascular disease such as stroke, and congestive heart failure. There is accumulating evidence that the vitamin D hormone 1,25-dihydroxyvitamin D exerts important physiological effects in cardiomyocytes, vascular smooth muscle cells, and the vascular endothelium. The mechanisms have been reviewed in detail elsewhere [34]. Hypertension is a key risk factor for CVD. A recently published systematic review and meta-analysis came to the conclusion that vitamin D produces a fall in systolic blood pressure of −6.18 mmHg and a nonsignificant fall in diastolic blood pressure of −2.56 mmHg in hypertensive patients. No reduction in blood pressure is seen in studies examining patients who are normotensive at baseline [35].

Several large prospective observational or cohort studies have demonstrated that a higher vitamin D status is associated with approximately 50% lower cardiovascular morbidity and mortality risk compared with low vitamin D status (Table 2).

Mortality In 2007, a meta-analysis was published, including RCTs on vitamin D and mortality that were not primarily designed to assess mortality [29]. The authors concluded that vitamin D supplementation is linked to lower all-cause mortality rates in middle-aged and elderly patients with low serum concentrations of 25(OH)D than in unsupplemented subjects. Daily doses of vitamin D ranged between 10 and 50 μg. Risk reduction was 7% during a mean follow-up of 5.7 years. Several large prospective cohort studies published in 2008 and 2009 have provided further evidence for association of low circulating 25(OH)D levels with enhanced all-cause mortality (Table 3). However, there is some concern that vitamin D has a biphasic effect on mortality with an enhanced risk at deficient 25(OH)D levels but also at levels above 125 nmol/L [41]. The scientific background of this point of view has recently been questioned [42].

Sunburn (Erythema)

Since UV radiation is not detected by the human eye, or by usual light meters, a different standard is needed to quantify how much of it is present at any time. The erythemally weighted irradiance is defined as above, in units of W m^{-2}. For health purposes, the erythemally weighted UV irradiance is generally reported to the public in terms of a dimensionless number called the UV Index (i.e., UVI, – see below). Rather than referring to the response of the human eye (i.e., the "photopic" response) for light, it refers to the response of human skin to sunburn (i.e., the "erythemal" response), which has no contribution from visible radiation but increases rapidly toward shorter wavelengths within the UV range.

Solar Radiation and Human Health. Table 2 Evidence for association of circulating 25-hydroxyvitamin D level with cardiovascular morbidity and mortality

Study	Design	Population	Comparator	Odds/hazard ratio or Relative risk (95% CI)
Fatal stroke [36]	Prospective cohort study with coronary angiography	3,258	Per z value of 25(OH)D	OR 0.58 (0.43–0.78)
Cardiovascular morbidity [37]	Prospective observational study	1,739	25(OH)D > 37.5 nmol/L vs. < 25 nmol/L	HR 0.55 (0.32–0.97)
Myocardial infarction [38]	Nested case control study	1,354	25(OH)D > 75 nmol/L vs < 37.5 nmol/L	RR 0.48 (0.28–0.81)
Cardiovascular mortality [39]	Prospective cohort study with coronary angiography	3,258	Median 25(OH)D 70 nmol/L vs 19 nmol/L	HR 0.45 (0.32–0.64)
Cardiovascular mortality [36]	Prospective observational study in individuals 50–75 years	614	Three highest vs. lowest 25 (OH)D quartile	HR 0.19 (0.07–0.50)
Cardiovascular mortality [40]	Prospective observational study in individuals > 65 years.	3,408	25(OH)D > 100 nmol/L vs < 25 nmol	HR 0.42 (0.21–0.86)

Solar Radiation and Human Health. Table 3 Evidence for association of circulating 25-hydroxyvitamin D level or vitamin D supplementation with all-cause mortality

Study	Design	Population	Comparator	Hazard ratio or relative risk (95% CI)
[43]	Meta-analysis of 18 vitamin D supplementation studies	57,311	Supplemented vs unsupplemented	RR 0.93 (0.87–0.99)
[39]	Prospective cohort study with coronary angiography	3,258	Median 25(OH)D 70 nmol/L vs 19 nmol/L	HR 0.48 (0.37–0.63)
[44]	Prospective observational study in postmenopausal women	1,232	$\geq$ 50 nmol/L vs. $<$ 50 nmol/L	HR 0.46 (0.27–0.79)
[45]	Prospective cohort study in patients with colorectal cancer	304	Mean 41 nmol/L vs. 100 nmol/L	HR 0.52 (0.29–0.94)
[40]	Prospective observational study in individuals $>$ 65 years.	3,408	25(OH)D $>$ 100 nmol/L vs $<$ 25 nmol/L	HR 0.55 (0.34–0.88)
[36]	Prospective observational study in individuals 50–75 years	614	Three highest quartiles vs. lowest quartile	HR 0.51 (0.28–0.93)

Although UVI was developed to represent damage to human skin, it may be applied to other processes because many biological UV effects have similar action spectra. Since UVI is based on the erythemal action spectrum, its sensitivity to ozone change is the same as for erythema. For a 1% reduction in ozone, UVI increases by approximately 1.1%. The UVI is an open-ended scale. In the British Isles, it peaks at ~6, whereas at northern midlatitudes, it peaks at ~10. Peak values are higher in the southern hemisphere because of the lower ozone amounts, closer summertime Sun–Earth separation, and generally cleaner air. For example, the peak UVI in New Zealand is approximately 40–50% larger than at corresponding northern latitudes, and it often exceeds 12 [46]. In the tropics, it is even much higher. The highest values on Earth occur in the Peruvian Andes at latitudes 10–15° S, where UVI can reach 25 [47]. Outside the Earth's atmosphere, the UVI would be ~300.

The relatively high UV levels in New Zealand and Australia [46, 48] are a contributing factor to the high rates of skin cancer in those countries. There are other factors, however. For those of European extraction, skin types are better adapted to the lower UV levels in Europe, especially in the north [48]. Outdoor lifestyle choices can also be important. In temperate climates, it is quite comfortable to spend long periods of time in direct sunlight. The folly of that behavior manifests itself only later – when the discomfort of sunburn is felt, and much later when skin cancer is experienced.

UV Index

Sunburning UV is often reported to the public in terms of UVI. The upper panel in Fig. 3 shows the spectral UV irradiance for two sun angles and an ozone column of 300 Dobson Units (DU) (Note the log scale for the y-axis). The erythemal (i.e., the "skin-reddening," or "sunburning") weighting function is shown on the right axis. The lower panel shows the corresponding spectra of erythemally weighted UV irradiance (UV_{Ery}).

The internationally agreed UVI is defined in terms of UV_{Ery}. The weighting function involves an arbitrary normalization to unity at wavelengths shorter than 298 nm, so UV_{Ery} is not strictly an SI unit. Furthermore, when UV information was first provided to the public, another normalization was applied to give a maximum UVI of ~10 in Canada, where it was first used. The UVI is therefore a unitless number corresponding to the integral under the curves in the lower panels, multiplied by 40 m^2/W. Mathematically,

$$\mathrm{UVI} = 40 \int \mathrm{I}(\lambda)\mathrm{w}(\lambda)d\lambda,$$

where

λ is the wavelength in nm

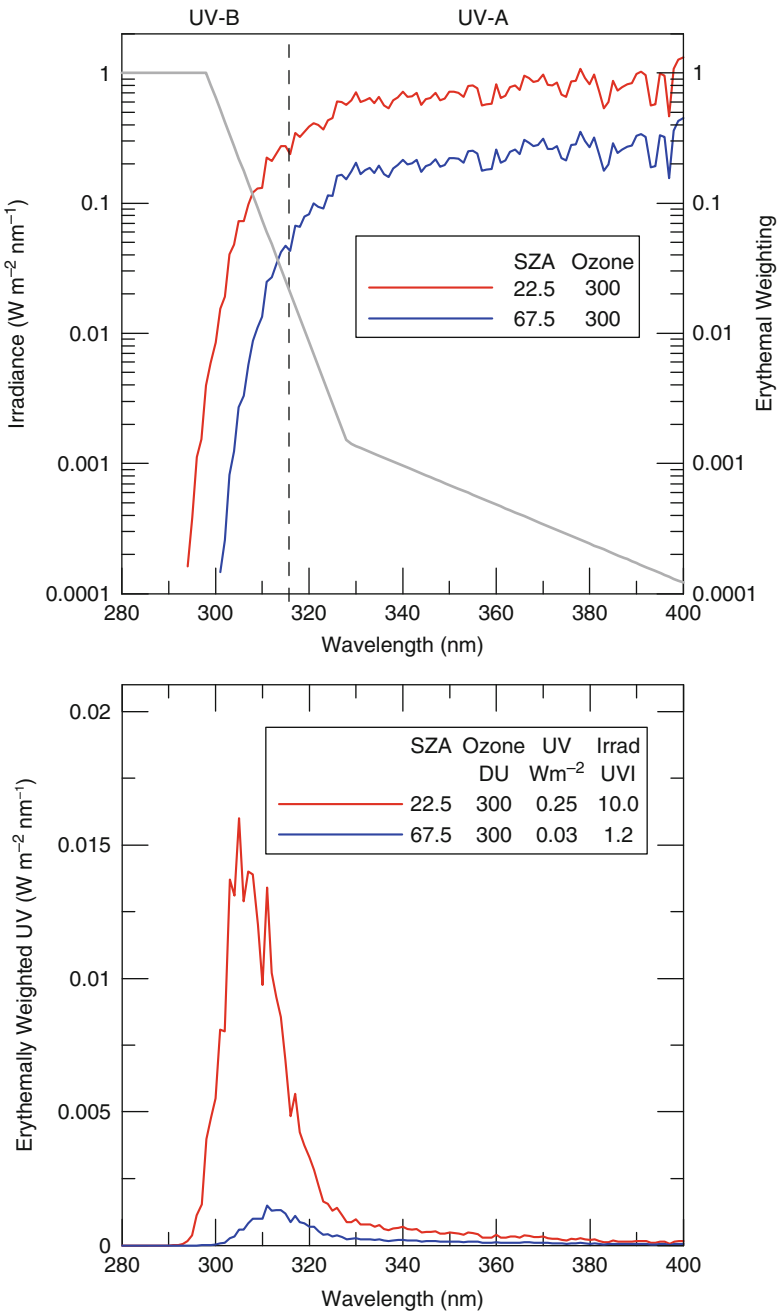

Solar Radiation and Human Health. Figure 3

Upper panel: UV irradiance spectra for noon sunlight at midlatitude (45° S) in summer and winter. The *grey* line shows the erythemal action spectrum. Note the logarithmic scale on the y-axis. *Lower panel*: The same solar irradiance spectra weighted by the erythemal action spectrum

$I(\lambda)$ is the irradiance in W m^{-2} nm^{-1} and
$w(\lambda)$ is the erythemal weighting function, defined as:

$w(\lambda) = 1.0$ for $250 < \lambda \leq 298$ nm

$w(\lambda) = 10^{0.094(298 - \lambda)}$ for $298 < \lambda \leq 328$ nm

$w(\lambda) = 10^{0.015(139 - \lambda)}$ for $328 < \lambda \leq 400$ nm

$w(\lambda) = 0.0$ for $\lambda > 400$ nm

Exposure Times to Optimize Health Effects of UV Radiation

Attempts have been made to estimate the exposure times from sunlight to optimize health [49]. Results are given in terms of UVI (Fig. 4). The exposure times also depend on skin type and possible application of any sunscreens. In the case of vitamin D production, the optimal exposure time also depends on the area of skin exposed. There is a huge variation between the optimal exposure times in summer and winter at mid-latitude sites. There is no simple relationship between UVI and visible radiation. In the case of sunlight, it is true that as light levels increase, so does UV radiation, but the relationship is complex and nonlinear.

The large seasonal variations are also a health risk. In winter, the UV irradiation may not be high enough to maintain adequate vitamin D. The problem is exacerbated because the skin becomes tanned to protect the body from further damage in summer, and this tan persists into the winter, therefore inhibiting the ability to absorb further UV radiation. Those with darker skins (e.g., Africans, many Maoris, Pacific Islanders, and Asians) are at greater risk.

Some published weighting functions for vitamin D production are similar to that for erythema but do

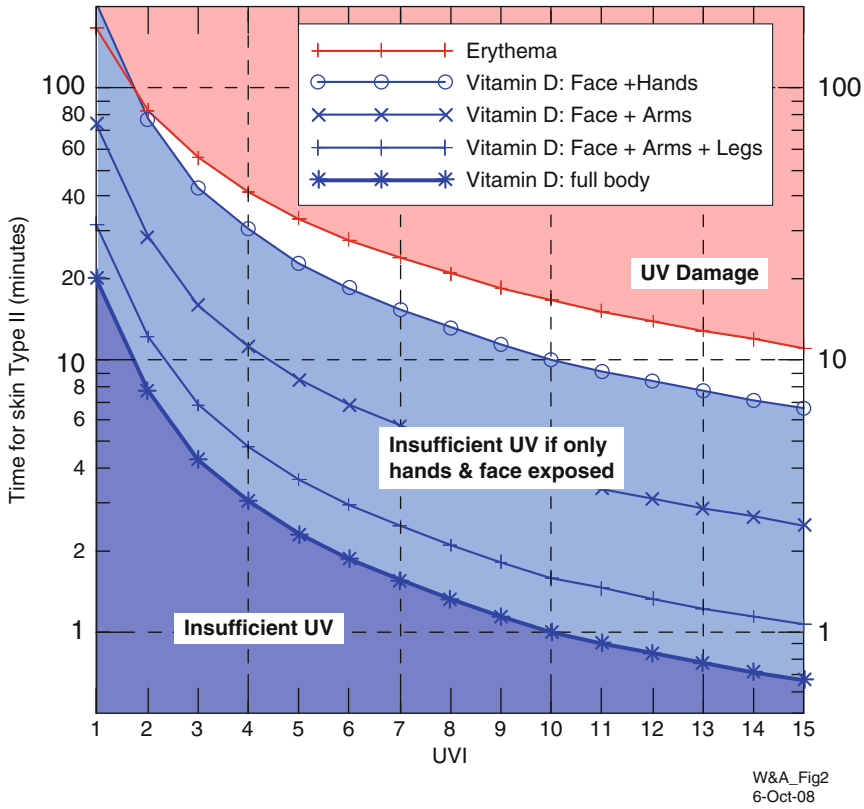

Solar Radiation and Human Health. Figure 4
Approximate exposure times leading to erythema or to sustained adequate vitamin D production, as a function of UVI. Exposure times corresponding to the *red*-shaded area represent too much UV, leading to erythema (skin reddening- and sunburn). Exposures within the dark *blue* region represents too little UV to maintain an intake of 1,000 IU with full-body exposure. The *unshaded* area represents the range of times for optimal exposure, assuming only the hands and face are exposed. The other *blue* curves give the lower exposure limits for adequate vitamin D for different areas of skin exposed. All times shown are for fair skin (skin type II). For brown skin or black skin (skin types IV and VI), all exposure times should be multiplied by 2 and 5, respectively

not extend as far into the UV-A region. Consequently, it is a stronger function of ozone amount and sun angle. Nevertheless, the minimum exposure time for sufficient vitamin D production may still be estimated in terms of UVI. It also depends on the skin type, the SPF of any sunscreen applied, and the area of skin that is exposed to sunlight. The estimated exposure times for sufficient vitamin D production are compared with the exposure times for erythema in Fig. 2 [49].

In summer, when UVI can exceed 10, skin damage occurs in about 15 min for fair-skinned people, whereas for full-body exposure sufficient vitamin D can be produced in less than 1 min. In winter, when the maximum UVI is ~1, skin damage occurs in 150 min, and even with full-body exposure (unlikely in winter), it would take at least 20 min to produce sufficient vitamin D. If only the hands and face are exposed, there is only a small margin between receiving too little or too much UV; and in winter, it would be impossible to receive sufficient vitamin D without skin damage. For darker skins, or if sunscreens are applied, these exposure times must be increased.

Note that there are large uncertainties in these relationships. Firstly, the action spectra may not be correct; secondly, the relevant quantity is really the irradiance on the surface of the body, rather than on the assumed horizontal surface; and thirdly, both the sensitivity of skin to damage and its ability to synthesize vitamin D depend on previous exposure and on the anatomical site [50, 51].

Skin Cancer

Three types of skin cancer, basal cell carcinoma (BCC), squamous cell carcinoma (SCC), and malignant melanoma (MM), sum up to the most frequent type of cancer in the white population worldwide. For MM, the incidence increases more rapidly than for any other type of cancer. Data for the non-melanocytic skin cancers, NMSCs (BCC and SCC), for e.g., USA and Germany show incidences in the range of 1,000,000 new cases per year (USA, 2005) [52] and about 100,000 new cases per year (Germany, 2003) [53]; 80% of these are found on sun-exposed areas of the human body [54].

Corresponding numbers for MM (the most deadly skin cancer, 20–25% of diagnosed patients die) are about 62,000 new cases per year (USA, 2006) [55] and about 15,000 (Germany, 2004, Robert-Koch-Institut: http://www.rki.de). Most of melanoma cases occur on sun-exposed areas of the body. The estimated 10-year survival rates for patients without evident metastases range from 88% for those patients with tumors smaller than 1mm without ulceration, to 32% for those patients with tumors larger than 4 mm with ulceration [56].

The skin cancer incidence is still increasing in most countries [57, 58], although some stabilization has been observed for parts of western Europe and Scandinavia [59, 60]. Nevertheless, being the most frequent cancer, skin cancer represents a huge problem for the public. The personal, medical, clinical and, last but not least, the final burden of skin cancer has therefore to be reduced by means of primary prevention and early detection.

Environmental Risk Factor(s) Although environmental arsenic exposure [60] or certain types of human papillomaviruses (as cofactors in association with UV) [61], as well as ionizing radiation [62] have been considered to play a role during the pathogenesis of NMSC, the overwhelming number of epidemiological and experimental investigations recognize UV-radiation as the main environmental risk factor [63–68]. The role of UV-radiation in melanogenesis has been discussed in past decades because the MM etiology strongly depends on genetic predispositions (e.g., allelic variances in the melanocortin 1 receptor [69]). However, recent epidemiological and experimental investigations, which are mainly dealing with UV-associated induction of benign nevi and the UV-induced mutation patterns, e.g., in the *BRAF* – gene (in nevi), clearly underline once more the important role of UV-radiation as a risk factor for malignant melanoma [63, 70–74]. It is furthermore important to consider that different types of skin cancer have a different dependence on UV-exposure patterns. Whereas MMs are mainly induced by intermittent UV-exposure (e.g., sunburns) [63, 71, 72], SCC-induction is highly dependent on cumulative UV-exposure, and BCC-induction depends on both cumulative and intermittent exposure patterns [63].

Because the main environmental risk factor in the etiology of skin cancer – UV-radiation (regardless of

natural (sun) or artificial (sunbeds) origin) – is known, skin cancer is one of the key cancers that can be prevented by means of primary prevention (i.e., avoiding or reducing risks).

The importance of UV-radiation as *the* environmental (and artificial) risk factor for the induction of skin cancer has recently been underscored by the International Agency for the Research of Cancer (IARC) which characterized UV-radiation from the sun (and from sunbeds) as a group-1 carcinogen ("carcinogenic to humans") [75]. IARC has also been able to show in a meta-analysis that regular use of sunbeds before the age of 35 increases melanoma risk later in life by 75% [76].

Biological Damage Leading to Skin Cancer UV-photon absorption of DNA leads to photochemical conversion of absorbed energy into photodimerization between adjacent pyrimidine bases. According to an action spectrum, UVB is about 1,000 times more effective than UVA in inducing this kind of photodimerization [77]. UVB also induces, at a much lower frequency, inter- and intra-strand crosslinks, protein-DNA crosslinks, DNA strand-breaks, and rare base adducts [78–80]. Photodimerizations between adjacent pyrimidine bases are by far the most prevalent photoreactions resulting from the direct action of UV-radiation. Two major photoproducts are formed via this reaction pathway: the cyclobutyl pyrimidine dimer (CPD) and the pyrimidine(6–4)pyrimidone photoproduct (6-4PP). CPDs are formed between adjacent pyrimidines linked by a cyclobutyl ring between the five and six carbons of adjacent thymine (Thy) and/or cytosine (Cyt) bases. The 6-4PP links the 6 carbons on a 3' Cyt or Thy with the four carbons of a 5' Cyt. However, using the same wavelength of excitation in the UVB, 6-4PPs are induced only at 15–30% the rate of CPDs [81]. Using fluorescently labeled monoclonal antibodies against CPD and a calibration with a radioimmunoassay (RIA) [82], it was shown that a UVB dose of 300 Jm^{-2} is able to induce several hundred thousands of CPDs per genome per cell [83]. Both induction of CPDs and repair of these lesions via nucleotide-excision repair (NER) are UV-dose dependent. Increasing both the UVB dose and the amount of premutagenic CPDs leads to a increase of the time constant for NER to remove CDPs [83]. Furthermore, deficiencies in NER of CPDs have been linked with increased risk of cutaneous malignant melanoma and non-melanoma skin cancers [84–86].

When CPDs are not repaired, these DNA lesions can lead to mutations in the DNA sequence. Mutations are in the form of C→T and CC→TT transitions, known as "UV-signature mutations" [87–90]. These mutations have long been believed to be a specific signature for UVB-radiation. However, recent work suggests that UV-A also induces CPDs that lead to UV-signature mutations [91–93]. This view is supported by results showing that UV-A induces mainly CPDs in human skin [94]. A so called "A-rule" has been proposed to explain how these signature mutations arise [95]. According to the A-rule, DNA polymerase (pol η) inserts, in a default-mechanism, adenine (A) residues,opposite to those lesions it cannot interpret. A mutation is then created upon DNA replication of the strand containing base-pair changes. At a CC cyclobutane dimer, therefore, a CC → TT transition occurs because two A-residues are placed opposite the dimer by default, in place of two guanine (G)-residues. A similar default mechanism for 6–4 PPs might be responsible for C→T transitions [95]. Recent findings show that defects in efficiency of translesion polymerase η (despite other polymerases) seem to play an important role in UV-induced mutagenesis [96, 97].

UV-signature mutations have been detected in a number of tumor suppressor genes and oncogenes (including, e.g., *patched, p16, ras* and *p53*) in human SCC, BCC, and malignant melanoma [95]. Because the important biological function of p53 results from transcriptional activation of a large number of genes involved in fundamental cellular processes like cell cycle control, apoptosis, DNA replication, repair, genome instability, and senescence, it is not surprising that genetic alterations of the p53 gene have most frequently been found in human tumors [98]: especially in skin cancers like SCC, BCC, and precancerous actinic keratoses [99–103]. Convincing models for the initial steps of UV-carcinogenesis, especially for SCC, already exist [104, 105] based on findings that p53 mutations in non-melanoma skin cancers are detected at higher frequency (50–90%) than those in internal malignancy, and that the predominant alterations are

C→T and CC→TT transitions at dipyrimidine sites [103]. Very recent investigations, exploring the melanoma genome, furthermore show that UV-induced signature mutations play the primary role in melanoma induction in humans [106].

Etiology of Skin Cancer In recent years, a huge amount of information has been obtained in the fields of genetics, molecular pathways, and cellular changes, which are important players in skin cancer induction, promotion, progression, and metastasis. Excellent reviews are now available [107–112]. Very briefly, there is convincing evidence that the BCC etiology is highly dependent on dysregulation of the hedgehog signaling pathway, whereas for the SCC etiology, p53-regulated pathways are of outstanding importance. For malignant melanoma, at least three molecular pathways have been found to be nearly invariably disregulated in melanocytic tumors, including the RAS-RAF-MEK-ERK pathway (through mutation of BRAF, NRAS or KIT), the p16 INK4A-CDK4-RB pathway (through mutation of INK4A or CDK4), and the ARF-p53 pathway (through mutation of ARF or TP53). Less frequently targeted pathways include the PI3K-AKT pathway (through mutation of NRAS, PTEN, or PIK3CA) and the canonical Wnt signaling pathway (through mutation of CTNNB1 or APC) [113].

It is to be expected that future research dealing with biological markers will give further insight into the etiology of skin cancer. Furthermore, very recent findings in the field of stem-cell research very clearly show that epidermal stem cells and their regulation on the genetic and epigenetic levels are the main cell targets involved in skin carcinogenesis [113–120]. Investigating the genetic and epigenetic regulation of (cancer-) stem cell fate, therefore, will enduringly increase knowledge about the etiology, as well as about (bio-) markers indicative for progression, staging, and metastasis of skin cancers.

Immunosuppression

It is now generally accepted that chronic and/or intermittent UV-exposure from the sun or from artificial sources (e.g., sunbeds) can initiate and promote skin cancer development through two major mechanisms: (1) induction of UV-dependent mutations; and (2) UV-induced immunosuppression, which might impair recognition of, e.g., UV-induced tumors (as an antigen source) by immunocompetent cells in the skin [121]. The "skin immune system" (SIS) is composed of several different cell types: keratinocytes (KC), melanocytes (MC), fibroblasts, monocytes, epidermal homing T cells, dermal macrophages, and Langerhans cells. These cells interact in a complex network via a number of soluble mediators like cytokines, interleukines, and prostaglandins and build up immune response and immunosurveillance of the skin [122].

UV-induced immunosuppression has been demonstrated initially by in vivo experiments with mice. These studies were able to show that (UV-induced) skin tumors are not rejected when transplanted to previously UV-irradiated mice. Later on, it was shown that UV-radiation mostly impaired the cellular immune response, leaving humoral immunological pathways almost untouched. The cell-mediated immune response was then studied in a large number of investigations with contact or delayed hypersensitivity reactions (CHS or DTH) as a biological endpoint in human skin [122, 123]. These investigations show that antigenes applied to the skin are taken up by antigen presenting cells (APC), where they are processed and finally presented to T lymphocytes to induce the complex immune response to eliminate the antigen.

UV-induced immunosuppression works both locally and systemically. Locally, the site of hapten application corresponds to the UV-irradiated area of skin. Systemic immunosuppression, on the other hand, induces the effect far away from hapten application. Local immunosuppression is mediated by direct UV-induced alterations in APC function, whereas systemic immunosuppresion needs mediators like e.g., Interleukin-1, 10, 12, tumor necrosis factor (TNF-α) or tumor-growth factor β (TGF-β). Furthermore, dose-rate effects of UV-irradiation seem to have an influence on whether immunosuppresion is induced locally or systemically [124].

UV-radiation needs photoreceptors that are able to "translate" UV-interaction into immunomodulatory effects at the cellular level. According to absorption- (and action-) spectra, the most important chromophores involved in immunosuppression are: urocanic acid (UCA) and DNA [123].

UCA is one of the major UV absorbing components in the *stratum corneum* of human skin and undergoes *trans* to *cis* isomerization after UVB irradiation [125]. Cis-UCA then modulates the action of several cytokines, including TNF-α, IL-6, IL-8, IL-12, and others [126, 127], in this way influencing the complex reaction pathways of SIS. It is well accepted now that UV-B-radiation-induced UCA changes, which are involved in immunosuppressive pathways, both work locally and systemically in mice and humans [122, 125, 128], although there exists some evidence that UV-induced production of cis-UCA might be insufficient to suppress CHS [129].

Another, possibly more important molecular target to interact with UV-radiation and to induce immunosuppresion, is DNA [130]. DNA is able to absorb UV-B irradiation directly, which creates cyclobutane pyrimidine dimers (CPD) and (with lower yield) 6–4 photoproducts [90]. These are known to be pre-cancerogenic DNA lesions, giving rise to UV-signature mutations, prominantely involved in the skin cancer etiology. However, these lesions (if not repaired) are also responsible for direct activation of genes involved in immune reactions [131]. CPD play an important role in immunosuppression through alterations of APC function [132], cytokine production, e.g., IL-10, and inhibition of transcription factors [133]. An increase of enzymatic repair activity for CPDs (via support of repair enzymes T4 endonuclease V) restores CHS and DTH response after UV-irradiation [134].

There is convincing evidence that cis-UCA and CPDs mediate their immunosuppressive properties through the impairment of immunocompetent cells populations like APCs, especially Langehans cells [135, 136]. One of the major actions of UV radiation on LC is that it makes them unable to prime Th1 lymphocytes, therefore inducing some tolerance against antigenes [137]. This leads to the hypothesis that UV induced cytokine might affect the critical balance between Th1 and Th2 cells in favor of an (immunosuppressive) Th2 response [138, 139]. There is a convergence of evidence now supporting this hypothesis.

Most of the immunosuppressive effects of UV-radiation have been documented after experimental UV-B irradiation on subjects [122]. However, there is increasing evidence that UVA-radiation (315–400 nm) might also be capable of inducing immunosuppression in human skin [140–143]. From a mechanistic point of view, this seems reasonable because it has recently been shown that UVA (apart from other premutagenic DNA-lesions) predominantly induces CPDs [94] (known to be involved in immunosuppression, see above) in human skin.

Skin Treatments

During the past decade, UV-radiation has been used extensively to cure certain types of skin diseases, especially psoriasis, which is shortly discussed here as an example.

Psoriasis is one of the most frequent inflammatory skin disorders. Its prevalence is estimated to be 2% in the Caucasian population, and it may develop at any age [144]. Immunological mechanisms play an important role, and it is now recognized that psoriasis is the most important T-cell mediated inflammatory disease in humans [145]. The primary immune defect in psoriasis appears to be an increase in cell signaling via chemokines and cytokines that act on upregulation of gene expression and cause hyperproliferation of keratinocytes [146]. There exists, however, strong evidence for an equally important role of polygenetic inheritance in complex genetics of psoriasis [147]. At least eight genetic loci (PSORS1–PSORS8) have been identified so far [147, 148].

Classic psoriarsis treatments use UV radiation. Broadband UV-B, narrowband UV-B (311 nm), as well as psoralen plus UV-A (PUVA) treatments have been used in the past [149]. Among other things, UV radiation reduces the number of antigen presenting cells and affects cell signaling pathways responsible for a decrease of hyperproliferating keratinocytes. UV-B-radiation seems to be less effective than PUVA-therapy. However, the latter carries an elevated risk of skin cancer induction [150–153]. For instance, high-dose PUVA patients (with more than 337 PUVA treatments) carry a 68-fold increase in overall risk of SCC (fourfold increased risk of BCC) [154].

Eye Damage

With the exception of snow- and ice-covered surfaces, most surfaces have a very low UV reflectivity. However, over ice- or snow-covered areas, reflections can directly

increase the eye exposure. In some case, this natural reflectance can be as high as 100% [155]. These enhanced radiation fields can contribute to eye damage. Some impacts on the eye are described below. For more details, see [7].

Photoconjunctivitis

Photoconjunctivitis is an inflammation of the conjunctiva of the eye caused by UV radiation. The action spectrum is similar to DNA damaging radiation. The threshold irradiation for photoconjunctivitis is 50 J m^{-2} [156].

Photokeratitis

Photokeratitis is an inflammation of the cornea's epithelial layer caused by UV radiation. The action spectrum is again similar to DNA damaging radiation. The threshold irradiation is 50 J m^{-2} [156].

Cataract

Cataracts are irreversible turbidities of the eye that can be caused by infrared (IR) or UV radiation. IR cataracts are caused by direct absorption of IR radiation or, indirectly, by heat transfer from the iris to the lens. They are usually caused by long-term (many years) exposure to large infrared sources and are therefore rare as a result of sun exposure only. UV cataracts are quite common. However, there is no known action spectrum for IR or UV cataracts [156].

Visible Radiation and Health Effects

Circadian Effects

It is well known that visible radiation has an impact on human health by affecting the eyes. The major task for the eyes is to gather and further process incoming visible radiation. Basically, the eye acts like a camera. In this "picture," the retina is the film or, more appropriately, the sensitive array that converts incoming photons to electrical signals that are further processed in the brain. For 150 years, it has been known that there are two types of sensors in the retina: the rods and the cones. There is some evidence that visual perception has an indirect impact on human health through psychological effects. However, this is not discussed further here.

In recent years, another photoreceptor, called melanopsin, has been found. It is likely that this photoreceptor has been developed early in the evolution of man. Melanopsin has a lower sensitivity and a coarser spatial resolution compared to the rods and cones. It is "designed" to help synchronizing the inner clock with the solar day.

The inner clock is thought to be essential to human health. The concentrations of many hormones are regulated by the inner clock, and it is known that a long-term disturbance of the inner clock has negative impact on humans [157]. For example, it is known that night-shift workers have a higher incidence of cancer.

The suppression of melatonin is closely linked with melanopsin concentration. The known action spectrum of melatonin suppression has its maximum in the blue part of the spectrum, at about 460 nm and almost no sensitivity in the red part [156]. Since the spectral transmission of the aging human eye progressively shifts toward longer wavelengths, it is assumed that elderly people have a reduced ability to synchronize the inner clock from blue light.

Since the solar spectrum changes appreciably during the day (see chapter ?) – certainly much more than the visual impression, which is regulated by the brain to recognize objects regardless of the incoming solar spectrum – it can be assumed that the red-shift of the solar spectrum during mornings and evenings may also have an impact on the melatonin suppression as well. This is an example of impacts of the solar spectrum on human health that is being understood, and that should be regarded when artificial lighting is used.

Damage of the Retina

Radiation (including infrared) that is absorbed by the retina can cause thermal damage. UV does not play a role in this case because it has a relatively low thermal contribution and is mostly absorbed before it reaches the retina. What is relevant to the damage of the retina is not the irradiance but its thermal impact [156].

Infrared Effects

For a long time, infrared radiation was considered as biologically irrelevant for human health. Consequently,

the study of the impact of infrared radiation only began relatively recently [158]. Infrared radiation produces a high concentration of reactive oxygen species (ROS), i.e., free radicals, that can damage the skin. It was shown that the generation of free radicals depends not only on the incident irradiance but also on the temperature of the skin, which is increased by infrared radiation [159]. A doubling of the irradiance from 400 to 800 W/m^2 can increase the temperature by ~10°C. Such a temperature change enables biochemical reactions in the skin. There are nonlinear dose-effect relationships. The production of free radicals starts at about 37°C and becomes much stronger at about 41°C. However, further increase in temperature to 43°C causes little additional damage. At low latitude sites or in a likely warmer climate of the near future, increased infrared irradiation will lead to an increased formation of ROS, which is potentially dangerous for human health [159]. As a consequence, infrared protection may be beneficial, in as much as the threshold skin temperature of 41°C is not reached. For example, at a latitude of 43.4° N (corresponding to Monaco), these experiments value can be reached after only 20 min of sun exposure. However, these experiments were made with artificial light (Sullux 500 W), which emits a nearly continuous spectrum, whereas the solar irradiance has absorption bands, especially from water vapor. It is not known to what extent such effects can play a role when evaluating the potential danger of infrared radiation for humans. In addition, the spectral transmittance of infrared radiation must be considered. In the near-infrared (IR-A), the spectral transmittance of the skin varies between 2% and 10%. The maximum transmittance is reached at about 1,150 nm.

Several other studies of infrared affects have been undertaken [160, 161] Schieke 2002 [155]; Jantschitsch 2009 [163]. They use a special infrared light source (called "hydrasun") that includes a water filter to minimize heating from long-wave radiation. Experiments with this source show that there is a time- and dose-dependent metalloproteinase-1 (MMP-1) that leads to increased skin aging [162], similar to that from UV exposure. The necessary dose may be reached after 2.5 h of exposure at midlatitudes in summer. However, another study [160] found that even with a high irradiance (380 W/cm^2), there is no systematic induction of MMP-1, which is clearly in contradiction with the findings in [162]. Another study [161] found that, without increased temperature, there is a protection of infrared radiation to UV exposure – a result confirmed by another study [163].

In summary: there are clear indications for effects of infrared radiation for human health, but the complete process is far from being well understood.

Effects for Which the Spectral Responsivity Is Not Yet Known

Depression

Depression can occur as a result of a lack of light in winter. This is often described as seasonal affective disorder (SAD), also known as winter depression. The U.S. national library of medicine notes that some people experience a serious mood change when the seasons change. They may sleep too much, have little energy, and crave sweets and starchy foods. They may also feel depressed. Though symptoms can be severe, they usually clear up naturally. It has been estimated that 1.5–9% of adults in the U.S. experience SAD [164]. There are many different treatments for classic (*winter*-based) SAD, usually using artificial bright lights, or a temporary stay at a southern, sunny location. However, the spectral sensitivity of SAD is not known yet. It may be cured just by exposing the eyes with bright light, but it may be also connected to a deficiency in vitamin D.

Human Behavior in Response to Solar Radiation

Humans change their behavior in response to changes in solar radiation. Possible reactions include: avoiding too intense solar irradiation by seeking shadow, or seeking high level of solar irradiance for cultural or cosmetic reasons. As a consequence, human health is not only influenced by changes in solar irradiation (geographically, daily, seasonally), but to a large extent also by human behavior. Of course, such reactions depend on many factors, both socioeconomic and individual, and it is therefore hard to give general statements on the advantages or disadvantages of changes induced by human behavior in response to solar radiation.

Future Directions

The descriptions above clearly show that solar radiation has both positive and negative effects on human health. Positive effects are the synchronization of the inner clock by natural sunlight and avoidance of winter depression, which affects many people at higher latitudes. Another positive effect is the vitamin D production, for which an overdose by natural sunlight is not known. There is clear evidence that high vitamin D levels are very beneficial to humans. The list of the resulting positive effects has increased considerably in recent years.

On the other hand, there is also clear evidence that UV radiation is mainly responsible for skin cancer, for which the incidence rates are rapidly increasing, probably as a result of changed behavior. Also, negative effects of UV radiation on the eyes are well known. Strong indications of negative impacts of infrared radiation have been found recently.

The positive aspects just mentioned have already led to changes in the "sun-smart" recommendations given by some national cancer agencies. In the past, the most frequent recommendation may have been along the lines "avoid the sun as much as possible." This is now altered to "avoid being sunburnt." Other suggestions are "avoid the sun in summer, seek it in winter." Despite the great number of studies and publications on these topics, there seems to be still insufficient scientific knowledge to convey simple messages to the public about the optimum solar exposure. It is clear that overexposure leads to severe negative effects, whereas underexposure has a negative impact on human health. It is concluded that more research is needed to assess under which conditions either overexposure or underexposure occur and must be considered. This is a rather difficult question for which simple answers are not to be expected soon due to the complexity of human health and of varying physical and meteorological conditions [165]. In addition, the relevant quantity to consider in vitamin D studies is not the irradiance on a horizontal surface but the actual exposure, which requires knowledge of the spectral radiance. This quantity, however, is far from being as well known as the widely used irradiance. More studies are required since the solar radiation regime is expected to be modified as a consequence of climate change.

Bibliography

1. McKinlay AF, Diffey BL (1987) A reference action spectrum for ultra-violet induced erythema in human skin. In: Passchier WF, Bosnajakovic BFM (eds) Human exposure to ultraviolet radiation: risks and regulations. Elsevier, Amsterdam, pp 83–87
2. Kerr JB, Seckmeyer G et al Surface ultraviolet radiation: past, present and future. In: Chapter 7 of Scientific assessment of ozone depletion: 2006, Global ozone research and monitoring project, report no. 50. World Meteorological Organization, Geneva
3. ICNRP/UNEP (1995) Global solar UV Index. Oberschleissheim, Germany
4. CIE (1970) Internationales Wörterbuch der Lichttechnik, Commission International de l'Éclairage, Paris
5. WMO (2007) Scientific Assessment of Ozone Depletion: 2006, vol Global ozone research and monitoring project – report no. 50. (World Meteorological Organization), Geneva
6. Bais AF, Lubin D, Coauthors: Arola A, Bernhard G, Blumthaler M, Chubarova N, Erlick C, Gies HP, Krotkov N, Lantz K, Mayer B, McKenzie RL, Piacentini RD, Seckmeyer G, Slusser JR, Zerefos CS (2007) Surface ultraviolet radiation: past, present and future. In: Albritton DL, Ajavon AN, Watson RT (eds) Chapter 7 of WMO scientific assessment of ozone depletion: 2006, Global ozone research and monitoring project, report no. 55. World Meteorological Organization, Geneva, p 58
7. UNEP (2007) Environmental effects of ozone depletion and its interactions with climate change: 2006 assessment. Photochem Photobiol Sci 6:201–332
8. Holick MF (1994) McCollum award lecture, vitamin D: new horizons for the 21st cen-tury. Am J Clin Nutr 60:619–630
9. Holick MF (2007) Vitamin D deficiency. N Engl J Med 357:266–281
10. Hewison M, Burke F, Evans KN, Lammas DA (2007) Extra-renal 25-hydroxyvitamin D3-1alpha-hydroxylase in human health and disease. J Steroid Biochem Mol Biol 103:316–321
11. Rao D, Raghuramulu N (1999) Is vitamin D redundant in an aquatic habitat? J Nutr Sci Vitaminol 45:1–8
12. Bouillon R, Carmeliet G, Daci E, Segaert S, Verstuyf A (1998) Vitamin D metabolism and action. Osteoporos Int 8:S13–S19
13. Hintzpeter B, Mensink G, Thierfelder W, Müller M, Scheidt-Nave C (2008) Vitamin D status and health correlates among German adults. Eur J Clin Nutr 62:1079–1089
14. Bischoff-Ferrari HA, Giovannucci E, Willett WC, Dietrich T, Dawson-Hughes B (2006) Estimation of optimal serum concentrations of 25-hydroxyvitamin D for multiple health outcomes. Am J Clin Nutr 84:18–28
15. Gorham E, Mohr S, Garland F, Garland C (2009) Vitamin D for cancer prevention and survival. Clin Rev Bone Miner Metab 7:159–175
16. Mithal A, Wahl D, Bonjour J, Burckhardt P, Dawson-Hughes B, Eisman J, El-Hajj Fuleihan G, Josse R, Lips P, Morales-Torres J, IOF Committee of Scientific Advisors (CSA) Nutrition Working Group (2009) Global vitamin D status and determinants of hypovitaminosis D. Osteoporos Int 20:1807–1820

17. Chris Power C, Hyppönen E (2007) Hypovitaminosis D in British adults at age 45 y: nationwide cohort study of dietary and lifestyle predictors. Am J Clin Nutr 85:860–868
18. Engelsen O, Brustad M, Aksnes L, Lund E (2005) Daily duration of vitamin D synthesis in human skin with relation to latitude, total ozone, altitude, ground cover, aerosols and cloud thickness. Photochem Photobiol 81:1287–1290
19. Genuis SJ, Schwalfenberg GK, Hiltz MN, Vaselenak SA (2009) Vitamin d status of clinical practice populations at higher latitudes: analysis and applications. Int J Environ Res Public Health 6:151–173
20. Grant W (2004) Geographic variation of prostate cancer mortality rates in the United States: Implications for prostate cancer risk related to vitamin D. Int J Cancer 111:470–471
21. Kimlin MG (2008) Geographic location and vitamin D synthesis. Mol Aspects Med 29(6):453–461
22. van der Mei IAF, Ponsonby A-L, Engelsen O, Pasco JA, McGrath JJ, Eyles DW, Blizzard L, Dwyer T, Lucas R, Jones G (2007) The high prevalence of vitamin D insufficiency across Australian populations is only partly explained by season and latitude. Environ Health Perspect 115:1132–1139
23. Bischoff-Ferrari H, Willett W, Wong J, Stuck A, Staehelin H, Orav E, Thoma A, Kiel D, Henschkowski J (2009) Prevention of nonvertebral fractures with oral vitamin D and dose dependency: a meta-analysis of randomized controlled trials. Arch Intern Med 169:551–561
24. Bischoff-Ferrari H, Dawson-Hughes B, Staehelin H, Orav J, Stuck A, Theiler R, Wong J, Egli A, Kiel D, Henschkowski J (2009) Fall prevention with supplemental and active forms of vitamin D: a meta-analysis of randomised controlled trials. BMJ 339:b3692, <javascript:AL_get(this,%20'jour',%20'BMJ.');>
25. Zittermann A (2003) Vitamin D in preventive medicine: are we ignoring the evidence? Br J Nutr 89:552–572
26. WHO (2008) International agency for research on cancer. Vitamin D and cancer. IARC working group reports, vol 5. WHO Press, Geneva, p 148
27. Lappe JM, Travers-Gustafson D, Davies KM, Recker RR, Heaney RP (2007) Vitamin D and calcium supplementation reduces cancer risk: results of a randomized trial. Am J Clin Nutr 85:1586–1591
28. Mohr S, Garland C, Gorham E, Garland F (2008) The association between ultraviolet B irradiance, vitamin D status and incidence rates of type 1 diabetes in 51 regions worldwide. Diabetologia 51:1391–1398
29. Hyppönen E (2001) Intake of vitamin D and risk of type 1 diabetes: a birth-cohort study. Lancet 358:1500–1503
30. Zipitis C, Akobeng A (2008) Vitamin D supplementation in early childhood and risk of type 1 diabetes: a systematic review and meta-analysis. Arch Dis Child 93:512–517
31. Pittas A, Lau J, Hu F, Dawson-Hughes B (2007) The role of vitamin D and calcium in type 2 diabetes. A systematic review and meta-analysis. J Clin Endocrinol Metab 92: 2017–2029
32. Jorde R, Figenschau Y (2009) Supplementation with cholecalciferol does not improve glycemic control in diabtetic subjects with normal serum 25-hydroxyvitamin D levels. Eur J Nutr 48:349–354
33. von Hurst P, Stonehouse W, Coad J (2009) Vitamin D supplementation reduces insulin resistance in South Asian women living in New Zealand who are insulin resistant and vitamin D deficient – a randomised, placebo-controlled trial. Br J Nutr 103(4):549–555
34. Zittermann A, Koerfer R (2008) Vitamin D in the prevention and treatment of coronary heart disease. Curr Opin Clin Nutr Metab Care 11:752–757
35. Witham M, Nadir M, Struthers A (2009) Effect of vitamin D on blood pressure: a systematic review and meta-analysis. J Hypertens 27:1948–1954
36. Pilz S, Dobnig H, Nijpels G, Heine R, Stehouwer C, Snijder M, van Dam R, Dekker J (2009) Vitamin D and mortality in older men and women. Clin Endocrinol 71:666–672
37. Wang T, Pencina M, Booth S, Jacques P, Ingelsson E, Lanier K, Benjamin E, D'Agostino R, Wolf M, Vasan R (2008) Vitamin D deficiency and risk of cardiovascular disease. Circulation 117:503–511
38. Giovannucci E, Liu Y, Hollis B, Rimm E (2008) 25-hydroxyvitamin D and risk of myocardial infarction in men: a prospective study. Arch Intern Med 168:1174–1180
39. Dobnig H, Pilz S, Scharnagl H, Renner W, Seelhorst U, Wellnitz B, Kinkeldei J, Boehm B, Weihrauch G, Maerz W (2008) Independent association of low serum 25-hydroxyvitamin D and 1,25-dihydroxyvitamin D levels with all-cause and cardiovascular mortality. Arch Intern Med 168:1340–1349
40. Ginde A, Scragg R, Schwartz R, Camargo C (2009) Prospective study of serum 25-Hydroxyvitamin D level, cardiovascular disease mortality, and all-cause mortality in older U.S. adults. J Am Geriatr Soc 57:1595–1603
41. Melamed M, Michos E, Post W, Astor B (2008) 25-hydroxyvitamin D levels and the risk of mortality in the general population. Arch Intern Med 168:1629–1637
42. Zittermann A, Grant W (2009) 25-hydroxyvitamin D levels and all-cause mortality. Arch Intern Med 169:1075–1076
43. Autier P, Gandini S (2007) Vitamin D supplementation and total mortality: a meta-analysis of randomized controlled trials. Arch Intern Med 167:1730–1737
44. Kuroda T, Shiraki M, Tanaka S, Ohta H (2009) Contributions of 25-hydroxyvitamin D, co-morbidities and bone mass to mortality in Japanese postmenopausal women. Bone 44:168–172
45. Ng K, Meyerhardt J, Wu K, Feskanich D, Hollis B, Giovannucci E, Fuchs C (2008) Circulating 25-hydroxyvitamin d levels and survival in patients with colorectal cancer. J Clin Oncol 26:2984–2991
46. McKenzie RL, Bodeker GE, Scott G, Slusser J (2006) Geographical differences in erythemally-weighted UV measured at mid-latitude USDA sites. Photochem Photobiol Sci 5:343–352
47. Liley JB, McKenzie RL (2006) Where on Earth has the highest UV? In: UV Radiation and its effects: an update, 2006, pp. 26–37. http://www.niwa.co.nz/our-services/online-services/uv-and-ozone/workshops/2006/Liley_2.pdf

48. Seckmeyer G, Glandorf M, Wichers C, McKenzie RL, Henriques D, Carvalho F, Webb AR, Siani AM, Bais A, Kjeldstad B, Brogniez C, Werle P, Koskela T, Lakkala K, Lenoble J, Groebner J, Slaper H, denOuter PN, Feister U (2008) Europe's darker atmosphere in the UV-B. Photochem Photobiol Sci 7:925–930. doi:10.1039/b804109a
49. McKenzie RL, Liley JB, Björn LO (2009) UV radiation: balancing risks and benefits. Photochem Photobiol 85:88–98
50. Knuschke P, Unverricht I, Ott G (2007) "Baseline reference of solar UV exposures" to assess individual UV exposure levels in the population. In: Grobner J (ed) One century of UV radiation research. PMOD, Davos pp 127–128
51. Knuschke P, Unverricht I, Ott G, Jansen M (2007) Personenbezogene messung der UV-Exposition von Arbeitnehmern im freien, Bundesanstalt fur Arbeitsschutz und Arbeitsmedian (BAUA) report no. Dortmund/Berlin/Dresden, p 195. Available from: http://www.baua.de/cae/servlet/contentblob/699494/publicationFile/46848/F1777.pdf
52. Jemal A, Ward E, Hao Y, Thun M (2005) Trends in the leading causes of death in the United States, 1970–2002. JAMA 294:1255–1259
53. Katalinic A, Kunze U, Schafer T (2003) Epidemiology of cutaneous melanoma and non-melanoma skin cancer in Schleswig-Holstein, Germany: incidence, clinical subtypes, tumour stages and localization (epidemiology of skin cancer). Br J Dermatol 149:1200–1206
54. Diepgen TL, Mahler V (2002) The epidemiology of skin cancer. Br J Dermatol 146(Suppl 61):1–6
55. Jemal A, Siegel R, Ward E, Murray T, Xu J, Smigal C, Thun MJ (2006) Cancer statistics, 2006. CA Cancer J Clin 56:106–130
56. Balch CM, Buzaid AC, Soong SJ, Atkins MB, Cascinelli N, Coit DG, Fleming ID, Gershenwald JE, Houghton A Jr, Kirkwood JM, McMasters KM, Mihm MF, Morton DL, Reintgen DS, Ross MI, Sober A, Thompson JA, Thompson JF (2001) Final version of the American joint committee on cancer staging system for cutaneous melanoma. J Clin Oncol 19:3635–3648
57. Boyle P, Dore JF, Autier P, Ringborg U (2004) Cancer of the skin: a forgotten problem in Europe. Ann Oncol 15:5–6
58. de Vries E, Bray FI, Coebergh JW, Parkin DM (2003) Changing epidemiology of malignant cutaneous melanoma in Europe 1953–1997: rising trends in incidence and mortality but recent stabilizations in western Europe and decreases in Scandinavia. Int J Cancer 107:119–126
59. de Vries E, Coebergh JW (2004) Cutaneous malignant melanoma in Europe. Eur J Cancer 40:2355–2366
60. Pesch B, Ranft U, Jakubis P, Nieuwenhuijsen MJ, Hergemoller A, Unfried K, Jakubis M, Miskovic P, Keegan T (2002) Environmental arsenic exposure from a coal-burning power plant as a potential risk factor for nonmelanoma skin carcinoma: results from a case-control study in the district of Prievidza, Slovakia. Am J Epidemiol 155:798–809
61. Nindl I, Gottschling M, Stockfleth E (2007) Human papillomaviruses and non-melanoma skin cancer: basic virology and clinical manifestations. Dis Markers 23:247–259
62. Lichter MD, Karagas MR, Mott LA, Spencer SK, Stukel TA, Greenberg ER, The New Hampshire Skin Cancer Study Group (2000) Therapeutic ionizing radiation and the incidence of basal cell carcinoma and squamous cell carcinoma. Arch Dermatol 136:1007–1011
63. Armstrong BK, Kricker A (2001) The epidemiology of UV induced skin cancer. J Photochem Photobiol B 63:8–18
64. Cleaver JE, Crowley E (2002) UV damage, DNA repair and skin carcinogenesis. Front Biosci 7:d1024–d1043
65. de Gruijl FR, van Kranen HJ, Mullenders LH (2001) UV-induced DNA damage, repair, mutations and oncogenic pathways in skin cancer. J Photochem Photobiol B 63:9–27
66. Madan V, Hoban P, Strange RC, Fryer AA, Lear JT (2006) Genetics and risk factors for basal cell carcinoma. Br J Dermatol 154(Suppl 1):5–7
67. Norval M, Cullen AP, de Gruijl FR, Longstreth J, Takizawa Y, Lucas RM, Noonan FP, van der Leun JC (2007) The effects on human health from stratospheric ozone depletion and its interactions with climate change. Photochem Photobiol Sci 6:232–251
68. Ramos J, Villa J, Ruiz A, Armstrong R, Matta J (2004) UV dose determines key characteristics of nonmelanoma skin cancer. Cancer Epidemiol Biomark Prev 13:2006–2011
69. Abdel-Malek ZA, Knittel J, Kadekaro AL, Swope VB, Starner R (2008) The melanocortin 1 receptor and the UV response of human melanocytes–a shift in paradigm. Photochem Photobiol 84:501–508
70. Besaratinia A, Pfeifer GP (2008) Sunlight ultraviolet irradiation and BRAF V600 mutagenesis in human melanoma. Hum Mutat 29:983–991
71. Dulon M, Weichenthal M, Blettner M, Breitbart M, Hetzer M, Greinert R, Baumgardt-Elms C, Breitbart EW (2002) Sun exposure and number of nevi in 5- to 6-year-old European children. J Clin Epidemiol 55:1075–1081
72. Harrison SL, MacLennan R, Buettner PG (2008) Sun exposure and the incidence of melanocytic nevi in young Australian children. Cancer Epidemiol Biomark Prev 17: 2318–2324
73. Leiter U, Garbe C (2008) Epidemiology of melanoma and nonmelanoma skin cancer–the role of sunlight. Adv Exp Med Biol 624:89–103
74. Thomas NE, Edmiston SN, Alexander A, Millikan RC, Groben PA, Hao H, Tolbert D, Berwick M, Busam K, Begg CB, Mattingly D, Ollila DW, Tse CK, Hummer A, Lee-Taylor J, Conway K (2007) Number of nevi and early-life ambient UV exposure are associated with BRAF-mutant melanoma. Cancer Epidemiol Biomark Prev 16:991–997
75. El Ghissassi F, Baan R, Straif K, Grosse Y, Secretan B, Bouvard V, Benbrahim-Tallaa L, Guha N, Freeman C, Galichet L, Cogliano V (2009) A review of human carcinogens–part D: radiation. Lancet Oncol 10:751–752
76. International Agency for Research on Cancer Working Group (2007) The association of use of sunbeds with cutaneous malignant melanoma and other skin cancers: a systematic review. Int J Cancer 120:116–1122

77. Rosenstein BS, Mitchell DL (1987) Action spectra for the induction of pyrimidine(6–4)pyrimidone photoproducts and cyclobutane pyrimidine dimers in normal human skin fibroblasts. Photochem Photobiol 45:775–780
78. Cadet J, Anselmino C, Douki T, Voituriez L (1992) Photochemistry of nucleic acids in cells. J Photochem Photobiol B 15:277–298
79. Cadet J, Sage E, Douki T (2005) Ultraviolet radiation-mediated damage to cellular DNA. Mutat Res 571:3–17
80. Douki T, Court M, Sauvaigo S, Odin F, Cadet J (2000) Formation of the main UV-induced thymine dimeric lesions within isolated and cellular DNA as measured by high performance liquid chromatography-tandem mass spectrometry. J Biol Chem 275:11678–11685
81. Mitchell DL, Brash DE, Nairn RS (1990) Rapid repair kinetics of pyrimidine(6–4)pyrimidone photoproducts in human cells are due to excision rather than conformational change. Nucleic Acids Res 18:963–971
82. Mitchell DL (2006) Quantification of photoproducts in mammalian cell DNA using radioimmunoassay. Method Mol Biol 314:239–249
83. Greinert R, Boguhn O, Harder D, Breitbart EW, Mitchell DL, Volkmer B (2000) The dose dependence of cyclobutane dimer induction and repair in UVB-irradiated human keratinocytes. Photochem Photobiol 72:701–708
84. Wang LE, Li C, Strom SS, Goldberg LH, Brewster A, Guo Z, Qiao Y, Clayman GL, Lee JJ, El Naggar AK, Prieto VG, Duvic M, Lippman SM, Weber RS, Kripke ML, Wei Q (2007) Repair capacity for UV light induced DNA damage associated with risk of nonmelanoma skin cancer and tumor progression. Clin Cancer Res 13:6532–6539
85. Wang LE, Xiong P, Strom SS, Goldberg LH, Lee JE, Ross MI, Mansfield PF, Gershenwald JE, Prieto VG, Cormier JN, Duvic M, Clayman GL, Weber RS, Lippman SM, Amos CI, Spitz MR, Wei Q (2005) In vitro sensitivity to ultraviolet B light and skin cancer risk: a case-control analysis. J Natl Cancer Inst 97: 1822–1831
86. Wei Q, Lee JE, Gershenwald JE, Ross MI, Mansfield PF, Strom SS, Wang LE, Guo Z, Qiao Y, Amos CI, Spitz MR, Duvic M (2003) Repair of UV light-induced DNA damage and risk of cutaneous malignant melanoma. J Natl Cancer Inst 95:308–315
87. Dumaz N, Drougard C, Sarasin A, Daya-Grosjean L (1993) Specific UV-induced mutation spectrum in the p53 gene of skin tumors from DNA-repair-deficient xeroderma pigmentosum patients. Proc Natl Acad Sci U S A 90:10529–10533
88. Nakazawa H, English D, Randell PL, Nakazawa K, Martel N, Armstrong BK, Yamasaki H (1994) UV and skin cancer: specific p53 gene mutation in normal skin as a biologically relevant exposure measurement. Proc Natl Acad Sci U S A 91:360–364
89. Ravanat JL, Douki T, Cadet J (2001) Direct and indirect effects of UV radiation on DNA and its components. J Photochem Photobiol 63:88–102
90. Sage E, Lamolet B, Brulay E, Moustacchi E, Chteauneuf A, Drobetsky EA (1996) Mutagenic specificity of solar UV light in nucleotide excision repair-deficient rodent cells. Proc Natl Acad Sci U S A 93:176–180
91. Besaratinia A, Kim SI, Pfeifer GP (2008) Rapid repair of UVA-induced oxidized purines and persistence of UVB-induced dipyrimidine lesions determine the mutagenicity of sunlight in mouse cells. FASEB J 22:2379–2392
92. Ikehata H, Kudo H, Masuda T, Ono T (2003) UVA induces C–> T transitions at methyl-CpG-associated dipyrimidine sites in mouse skin epidermis more frequently than UVB. Mutagenesis 18:511–519
93. Runger TM, Kappes UP (2008) Mechanisms of mutation formation with long-wave ultraviolet light (UVA). Photodermatol Photoimmunol Photomed 24:2–10
94. Mouret S, Baudouin C, Charveron M, Favier A, Cadet J, Douki T (2006) Cyclobutane pyrimidine dimers are predominant DNA lesions in whole human skin exposed to UVA radiation. Proc Natl Acad Sci U S A 103: 13765–13770
95. Matsumura Y, Ananthaswamy HN (2002) Molecular mechanisms of photocarcinogenesis. Front Biosci 7:d765–d783
96. Cruet-Hennequart S, Gallagher K, Sokol AM, Villalan S, Prendergast AM, Carty MP (2010) DNA Polymerase eta, a key protein in translesion synthesis in human cells. Subcell Biochem 50:189–209
97. Hendel A, Ziv O, Gueranger Q, Geacintov N, Livneh Z (2008) Reduced efficiency and increased mutagenicity of translesion DNA synthesis across a TT cyclobutane pyrimidine dimer, but not a TT 6–4 photoproduct, in human cells lacking DNA polymerase eta. DNA Repair Amst 7: 1636–1646
98. Hussain SP, Hollstein MH, Harris CC (2000) p53 tumor suppressor gene: at the crossroads of molecular carcinogenesis, molecular epidemiology, and human risk assessment. Ann NY Acad Sci 919:79–85
99. Benjamin CL, Ullrich SE, Kripke ML, Ananthaswamy HN (2008) p53 tumor suppressor gene: a critical molecular target for UV induction and prevention of skin cancer. Photochem Photobiol 84:55–62
100. Brash DE (2006) Roles of the transcription factor p53 in keratinocyte carcinomas. Br J Dermatol 154(Suppl 1): 8–10
101. Brash DE, Ziegler A, Jonason AS, Simon JA, Kunala S, Leffell DJ (1996) Sunlight and sunburn in human skin cancer: p53, apoptosis, and tumor promotion. J Investig Dermatol Symp Proc 1:136–142
102. Nelson MA, Einspahr JG, Alberts DS, Balfour CA, Wymer JA, Welch KL, Salasche SJ, Bangert JL, Grogan TM, Bozzo PO (1994) Analysis of the p53 gene in human precancerous actinic keratosis lesions and squamous cell cancers. Cancer Lett 85:23–29
103. Ziegler A, Leffell DJ, Kunala S, Sharma HW, Gailani M, Simon JA, Halperin AJ, Baden HP, Shapiro PE, Bale AE, Brash DE (1993) Mutation hotspots due to sunlight in the p53 gene of nonmelanoma skin cancers. Proc Natl Acad Sci U S A 90:4216–4220
104. Brash DE (1997) Sunlight and the onset of skin cancer. Trends Genet 13:410–414

105. Fusenig NE, Boukamp P (1998) Multiple stages and genetic alterations in immortalization, malignant transformation, and tumor progression of human skin keratinocytes. Mol Carcinog 23:144–158
106. Pleasance ED, Cheetham RK, Stephens PJ, McBride DJ, Humphray SJ, Greenman CD, Varela I, Lin ML, Ordonez GR, Bignell GR, Ye K, Alipaz J, Bauer MJ, Beare D, Butler A, Carter RJ, Chen L, Cox AJ, Edkins S, Kokko-Gonzales PI, Gormley NA, Grocock RJ, Haudenschild CD, Hims MM, James T, Jia M, Kingsbury Z, Leroy C, Marshall J, Menzies A, Mudie LJ, Ning Z, Royce T, Schulz-Trieglaff OB, Spiridou A, Stebbings LA, Szajkowski L, Teague J, Williamson D, Chin L, Ross MT, Campbell PJ, Bentley DR, Futreal PA, Stratton MR (2010) A comprehensive catalogue of somatic mutations from a human cancer genome. Nature 463: 191–196
107. Benjamin CL, Melnikova VO, Ananthaswamy HN (2008) P53 protein and pathogenesis of melanoma and nonmelanoma skin cancer. Adv Exp Med Biol 624:265–282
108. Bosserhoff AK (2006) Novel biomarkers in malignant melanoma. Clin Chim Acta 367:28–35
109. Daya-Grosjean L, Couve-Privat S (2005) Sonic hedgehog signaling in basal cell carcinomas. Cancer Lett 225:181–192
110. Hussein MR (2005) Ultraviolet radiation and skin cancer: molecular mechanisms. J Cutan Pathol 32:191–205
111. Lupi O (2007) Correlations between the sonic Hedgehog pathway and basal cell carcinoma. Int J Dermatol 46: 1113–1117
112. Sekulic A, Haluska P Jr, Miller AJ, Genebriera DL, Ejadi S, Pulido JS, Salomao DR, Thorland EC, Vile RG, Swanson DL, Pockaj BA, Laman SD, Pittelkow MR, Markovic SN (2008) Malignant melanoma in the 21st century: the emerging molecular landscape. Mayo Clin Proc 83:825–846
113. Dahl C, Guldberg P (2007) The genome and epigenome of malignant melanoma. APMIS 115:1161–1176
114. Faurschou A, Haedersdal M, Poulsen T, Wulf HC (2007) Squamous cell carcinoma induced by ultraviolet radiation originates from cells of the hair follicle in mice. Exp Dermatol 16:485–489
115. Gerdes MJ, Yuspa SH (2005) The contribution of epidermal stem cells to skin cancer. Stem Cell Rev 1:225–231
116. Greinert R (2009) Skin cancer: new markers for better prevention. Pathobiology 76:64–81
117. Grichnik JM (2008) Melanoma, nevogenesis, and stem cell biology. J Invest Dermatol 128:2365–2380
118. Schwabe M, Lubbert M (2007) Epigenetic lesions in malignant melanoma. Curr Pharm Biotechnol 8:382–387
119. Yan X, Owens DM (2008) The skin: a home to multiple classes of epithelial progenitor cells. Stem Cell Rev 4:113–118
120. Zabierowski SE, Herlyn M (2008) Melanoma stem cells: the dark seed of melanoma. J Clin Oncol 26:2890–2894
121. Muller HK, Malley RC, McGee HM, Scott DK, Wozniak T, Woods GM (2008) Effect of UV radiation on the neonatal skin immune system- implications for melanoma. Photochem Photobiol 84:47–54
122. Amerio P, Carbone A, Auriemma M, Varrati S, Tulli A (2009) UV induced skin immunosuppression. Anti-Infamm Anti-Allergy Agents Med Chem 8:3–13
123. Norval M (2000) The impact of ultraviolet radiation on immune response. Radiat Prot Dosim 91:51–56
124. Shimizu T, Streilein JW (1994) Local and systemic consequences of acute, low-dose ultraviolet B radiation are mediated by different immune regulatory mechanisms. Eur J Immunol 24:1765–1770
125. Noonan FP, De Fabo EC (1992) Immunosuppression by ultraviolet B radiation: initiation by urocanic acid. Immunol Today 13:250–254
126. Kaneko K, Smetana-Just U, Matsui M, Young AR, John S, Norval M, Walker SL (2008) cis-Urocanic acid initiates gene transcription in primary human keratinocytes. J Immunol 181:217–224
127. Kurimoto I, Streilein JW (1992) cis-urocanic acid suppression of contact hypersensitivity induction is mediated via tumor necrosis factor-alpha. J Immunol 148:3072–3078
128. Kondo S, Sauder DN, McKenzie RC, Fujisawa H, Shivji GM, El Ghorr A, Norval M (1995) The role of cis-urocanic acid in UVB-induced suppression of contact hypersensitivity. Immunol Lett 48:181–186
129. el Ghorr AA, Norval M (1995) A monoclonal antibody to cis-urocanic acid prevents the ultraviolet-induced changes in Langerhans cells and delayed hypersensitivity responses in mice, although not preventing dendritic cell accumulation in lymph nodes draining the site of irradiation and contact hypersensitivity responses. J Invest Dermatol 105:264–268
130. Kuchel JM, Barnetson RS, Halliday GM (2005) Cyclobutane pyrimidine dimer formation is a molecular trigger for solar-simulated ultraviolet radiation-induced suppression of memory immunity in humans. Photochem Photobiol Sci 4:577–582
131. Yarosh DB (2002) Enhanced DNA repair of cyclobutane pyrimidine dimers changes the biological response to UV-B radiation. Mutat Res 509:221–226
132. Vink AA, Strickland FM, Bucana C, Cox PA, Roza L, Yarosh DB, Kripke ML (1996) Localization of DNA damage and its role in altered antigen-presenting cell function in ultraviolet-irradiated mice. J Exp Med 183:1491–1500
133. Tommasi S, Swiderski PM, Tu Y, Kaplan BE, Pfeifer GP (1996) Inhibition of transcription factor binding by ultraviolet-induced pyrimidine dimers. Biochemistry 35: 15693–15703
134. Kripke ML, Cox PA, Alas LG, Yarosh DB (1992) Pyrimidine dimers in DNA initiate systemic immunosuppression in UV-irradiated mice. Proc Natl Acad Sci U S A 89:7516–7520
135. Donawho CK, Muller HK, Bucana CD, Kripke ML (1996) Enhanced growth of murine melanoma in ultraviolet-irradiated skin is associated with local inhibition of immune effector mechanisms. J Immunol 157:781–786
136. Ullrich SE (1995) Modulation of immunity by ultraviolet radiation: key effects on antigen presentation. J Invest Dermatol 105:30S–36S

137. Simon JC, Tigelaar RE, Bergstresser PR, Edelbaum D, Cruz PD (1991) Ultraviolet B radiation converts Langerhans cells from immunogenic to tolerogenic antigen-presenting cells. Induction of specific clonal anergy in CD4+ T helper 1 cells. J Immunol 146:485–491
138. Shreedhar V, Giese T, Sung VW, Ullrich SE (1998) A cytokine cascade including prostaglandin E2, IL-4, and IL-10 is responsible for UV-induced systemic immune suppression. J Immunol 160:3783–3789
139. Ullrich SE (1996) Does exposure to UV radiation induce a shift to a Th-2-like immune reaction? Photochem Photobiol 64:254–258
140. Clement-Lacroix P, Michel L, Moysan A, Morliere P, Dubertret L (1996) UVA-induced immune suppression in human skin: protective effect of vitamin E in human epidermal cells in vitro. Br J Dermatol 134:77–84
141. Rana S, Rogers LJ, Halliday GM (2010) Immunosuppressive ultraviolet-A radiation inhibits the development of skin memory CD8 T cells. Photochem Photobiol Sci 9:25–30
142. Seite S, Zucchi H, Moyal D, Tison S, Compan D, Christiaens F, Gueniche A, Fourtanier A (2003) Alterations in human epidermal Langerhans cells by ultraviolet radiation: quantitative and morphological study. Br J Dermatol 148:291–299
143. Stoebner PE, Poosti R, Djoukelfit K, Martinez J, Meunier L (2007) Decreased human epidermal antigen-presenting cell activity after ultraviolet A exposure: dose-response effects and protection by sunscreens. Br J Dermatol 156: 1315–1320
144. Christophers E (2001) Psoriasis–epidemiology and clinical spectrum. Clin Exp Dermatol 26:314–320
145. Krueger JG (2002) The immunologic basis for the treatment of psoriasis with new biologic agents. J Am Acad Dermatol 46:1–23
146. Traub M, Marshall K (2007) Psoriasis–pathophysiology, conventional, and alternative approaches to treatment. Altern Med Rev 12:319–330
147. Barker JN (2001) Genetic aspects of psoriasis. Clin Exp Dermatol 26:321–325
148. Valdimarsson H (2007) The genetic basis of psoriasis. Clin Dermatol 25:563–567
149. Gambichler T, Breuckmann F, Boms S, Altmeyer P, Kreuter A (2005) Narrowband UVB phototherapy in skin conditions beyond psoriasis. J Am Acad Dermatol 52:660–670
150. Lim JL, Stern RS (2005) High levels of ultraviolet B exposure increase the risk of non-melanoma skin cancer in psoralen and ultraviolet A-treated patients. J Invest Dermatol 124: 505–513
151. Nijsten TE, Stern RS (2003) The increased risk of skin cancer is persistent after discontinuation of psoralen+ultraviolet A: a cohort study. J Invest Dermatol 121:252–258
152. Stern RS, Bolshakov S, Nataraj AJ, Ananthaswamy HN (2002) p53 mutation in nonmelanoma skin cancers occurring in psoralen ultraviolet a-treated patients: evidence for heterogeneity and field cancerization. J Invest Dermatol 119: 522–526
153. Stern RS, Liebman EJ, Vakeva L (1998) Oral psoralen and ultraviolet-A light (PUVA) treatment of psoriasis and persistent risk of nonmelanoma skin cancer. PUVA follow-up study. J Natl Cancer Inst 90:1278–1284
154. Peritz AE, Gasparro FP (1999) Psoriasis, PUVA, and skin cancer–molecular epidemiology: the curious question of T–>A transversions. J Investig Dermatol Symp Proc 4:11–16
155. Wuttke S, Seckmeyer G, Konig-Langlo G (2006) Measurements of spectral snow albedo at Neumayer, Antarctica. Annles Geophysicae 24:7–21
156. DIN (2008) German Institute for Normalisation Report – Several papers, ISBN 978-3-410-16938. In: *2. DIN Expertenforum, Wirkung des Lichts auf Menschen*, Beuth, Berlin, p 43
157. Schmidt C, Collette F, Leclercq Y, Sterpenich V, Vandewalle G, Berthomier P, Berthomier C, Phillips C, Tinguely G, Darsaud A, Gais S, Schabus M, Desseilles M, Dang-Vu TT, Salmon E, Balteau E, Degueldre C, Luxen A, Maquet P, Cajochen C, Peigneux P (2009) Homeostatic sleep pressure and responses to sustained attention in the suprachiasmatic area Science 465:516–519
158. Kligman LH (1982) Intensification of ultraviolet-induced dermal damage by infrared radiation. Arch Dermatol Res 272:229–267
159. Zastrow L, Groth N (2008) The missing link – light-induced (280–1600 nm) free radical formation in human skin. Skin Pharmacol Physiol 22:31–44
160. Gebbers N, Hirt-Burri N (2007) Water-filtered infrared-a radiation (wira) is not implicated in cellular degeneration of human skin. GMS Ger Med Sci 5:1–14
161. Menendez S, Coulomb B (1998) Non-coherent near infrared radiation protects normal human dermal fibroplasts from solar ultraviolet toxicity. J Investig Dermatol 111: 629–633
162. Schieke SM, Stege H (2002) Infrared-a radiation-induced matrix metalloproteinase 1 expression is mediated through exracellular signal-regulated kinase 1/2 activation in human dermal fibroblasts. J Investig Dermatol 119:1323–1329
163. Jantschitsch C, Majewski S (2009) Infrared radiation confers resistanse to uv-induces apoptosus via reduction of DNA damage and upregulation of antiapoptotic proteins. Soc Investig Dermatol 129:1271–1279
164. Modell J, Rosenthal N, Harriett A, Krishen A, Asgharian A, Foster V, Metz A, Rockett C, Wightman D (2005) Seasonal affective disorder and its prevention by anticipatory treatment with bupropion XL biological psychiatry. Biol Psychiatry 58:658–667
165. Pissulla D, Seckmeyer G, Cordero RR, Blumthaler M, Schallhart B, Webb A, Kifte ASR, Bais AF, Kouremeti N, Cede A, Herman J, Kowalewski M (2009) Comparison of different calibration methods to derive spectral radiance as a function of incident and azimuth angle. Photochem Photobiol Sci 8:516–527
166. WMO (1983) Guide to meteorological instruments and methods of observation (Fifth edn), World Meteorological Organization, Report No. 8, Geneva

Solar Radiation for Solar Energy Utilization

Daryl R. Myers
Resource Information and Forecasting Group, Electricity, Resources, and Building Systems Integration Center, National Renewable Energy Laboratory, Golden, CO, USA

Article Outline

Glossary
Definition of the Subject and Its Importance
Introduction
Brief History of Solar Radiation Instrumentation
The Solar Radiation Measurement Scale: World Radiation Reference
Calibrations and Traceability
Pyrheliometer Calibration
Pyranometer Calibration
Uncertainty Analysis
Solar Radiation Measurements Summary
Modeling Solar Radiation Resources for Solar Energy Conversion
Future Directions
Bibliography

Glossary

Aerosol optical depth A dimensionless parameter for the extinction of solar radiation by scattering and absorption by aerosol particles between the point of observation and the top of the atmosphere.

Air mass The length of the path from an observer's location to the top of the atmosphere, which passes through the center of the sun, relative to the zenith (perpendicular to the local horizontal = air mass 1).

Broadband radiation Photons in a wide electromagnetic spectral wavelength range, typically several hundred nanometers (nm) wide.

Diffuse hemispherical radiation Photons scattered in the atmosphere, excluding those from the solar disk, arriving on a horizontal surface originating from the 2π steradian hemisphere of the sky dome.

Direct normal radiation Nearly parallel rays of photons arriving on a surface perpendicular to the line from the observer to the center of the solar disk originating from within the 0.5° solid angle centered on the solar disk. Experimentally, this also includes additional sky radiation within 2.5°–3° of the center of the solar disk.

Extinction Gradual loss of amplitude in a signal propagating though an absorbing or scattering medium.

Extraterrestrial solar radiation Direct normal radiation at the top of the Earth's atmosphere. Acronym: ETR.

Global hemispherical radiation The combination of photons from the sky dome and solar disk (diffuse hemispherical and projection of the direct normal radiation) received on a horizontal surface.

Incidence angle The angle between the center of the solar disk and the foot of the normal (perpendicular) of a receiving surface.

Pyranometer A radiometer with a 2π steradian (hemispherical) field of view used to measure global hemispherical or diffuse hemispherical radiation.

Pyrheliometer A radiometer with a restricted field of view (typically 5°–6°) used to measure direct normal radiation.

Responsivity The ratio of the output signal of a radiometer to the optical power intercepted by the sensor.

Solar radiation Electromagnetic emissions from the sun between at least 250 and 2,500 nm.

Zenith angle The angle between the local vertical and the center of the solar disk; complement of the solar elevation angle (angle from the center of the solar disk to the horizon).

Definition of the Subject and Its Importance

Present-day concerns of looming energy shortages and drastic climate change resulting from human activities have stimulated deployment of renewable energy systems, including systems to convert solar energy directly into heat or electricity and to substitute sunlight for artificial light.

Solar radiation provides the energy driving the ecosystems and climate of planet Earth. This radiation spans the electromagnetic spectrum from the highly energetic X-ray region through the ultraviolet, visible, and infrared to the far infrared and radio regions. The radiation interacts with the Earth's electromagnetic and atmospheric envelope, resulting in large variations in

the magnitude of solar radiation available for conversion into other forms of useful energy. Most conversion systems utilize only part of the solar spectrum. For daylighting, the energy in the human visual response range (wavelengths of 380–850 nm) is important. Crystal silicon photovoltaic cells convert radiation from 350 to 1,100 nm, and plants use photosynthetically active radiation between 400 and 700 nm. Efficiency and performance of these systems is usually based on the total solar broadband radiation measured between 250 and at least 2,500 nm.

Specialized instruments have been developed to quantify the available broadband solar resource and spectral regions utilized by each technology. The cost and labor-intensive nature of solar radiation measurements has stimulated efforts to develop empirical and theoretical mathematical models of broadband and spectral solar radiation at the Earth's surface. A brief historical introduction is followed by current information on broadband solar radiation components, instrumentation, and modeling.

Introduction

The sun is a star, with radiant emittance of 2.009×10^7 watts per square meter per steradian ($W/m^2/sr$), or 2.845×10^{26} W in total. The Earth's elliptical orbit has an eccentricity of 0.0167 (1.4710×10^6 km at perihelion, 1.5210×10^6 km at aphelion). At the mean Earth–sun distance, the sun subtends a solid angle of 9.24 mrad, or 0.529°. Thus, the sun is not truly a point source, and the rays from the sun are not truly parallel but diverge into a cone with a nominal cone angle of 0.529° [1]. At the mean distance of the Earth from the sun (1.495979×10^6 km), the solar radiation reaching the top of the Earth's atmosphere is 1366.1 $W/m^2 \pm 7.0$ W/m^2 [2]. A very slender cone, or beam, of photons, the direct normal radiation (because it is typically measured with a sensor surface perpendicular to the beam), or direct beam, is intercepted by the Earth and passes through the atmosphere. Photons scattered by molecules and particles in the atmosphere that are not further absorbed contribute to uncollimated diffuse irradiance of the sky dome. The combination of direct normal and diffuse sky radiation constitutes the total solar radiation (usually total hemispherical or "global" total) available from the sky dome.

Figure 1 shows typical spectral power distributions, or magnitude of solar energy as a function of wavelength, over the "optical" part of the spectrum. The Earth's 100-km thick atmosphere filters solar radiation in a manner that protects and promotes life, provides the energy to drive the Earth's weather and climate, and affects the quality and quantity of resources available for solar energy conversion systems. The bars at the top of Fig. 1 show the portions of the spectral distribution utilized by various natural and manmade energy conversion systems. The extraterrestrial curve in Fig. 1 is the radiation reaching the top of the Earth's atmosphere. The other curves represent the effects of the atmosphere on the extraterrestrial energy as it propagates through the atmosphere. Broadband terrestrial solar radiation for solar renewable energy applications is represented by the integrated or total energy bounded by the direct, total, and diffuse curves represented in Fig. 1. Energy between the wavelengths of 280 and 4,000 nm, the so-called shortwave or optical radiation, is the primary subject of this article. (Note that, at the Earth's surface, the energy received between 2,500 and 4,000 nm is only about 3% of the total.) Shortwave radiation is relevant to photoconversion systems, such as photovoltaic (PV) and photo-thermal systems, daylighting, and photosynthesis by plants. Longwave radiation, 4,000–50,000 nm or 4–50 μm, has some application in solar thermal energy systems but is primarily important in climate change and infrared thermal studies. Some radiation is reflected back into space or away from the ground by the atmosphere, clouds, or ground. Figure 2 shows these processes schematically.

Solar Radiation Components

The combination of direct-beam radiation and diffuse radiation on a horizontal surface is the total (hemispherical), often called the global horizontal irradiance. Daily, the sun moves through a range of elevation angles from 0° at sunup, to a maximum at solar noon, to 0° at sunset. Thus, for a horizontal surface, the direct beam is usually not perpendicular to the horizontal surface, but incident at some angle i. The angle i is referred to as the zenith angle, Z (the angle between the local vertical and the center of the solar disk) for a horizontal surface. The direct-beam flux

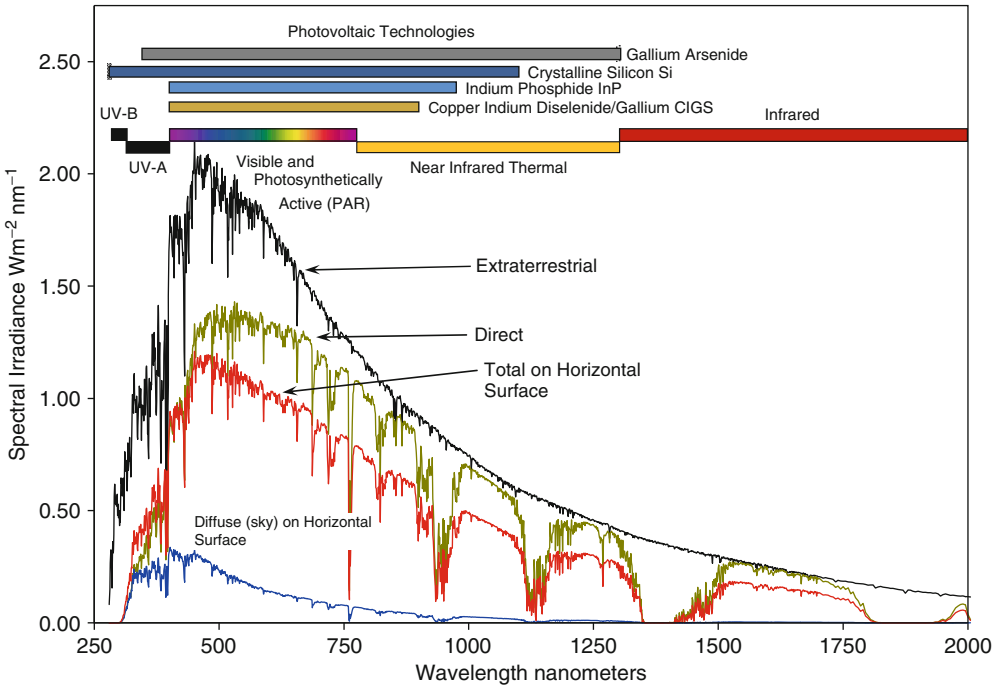

Solar Radiation for Solar Energy Utilization. Figure 1

Representative distributions of power as a function of wavelength for solar energy at the top of the atmosphere (extraterrestrial), solar beam radiation, diffuse sky radiation, and total radiation on a horizontal surface for clear sky conditions. *Bars* show regions of energy utilization by conversion systems

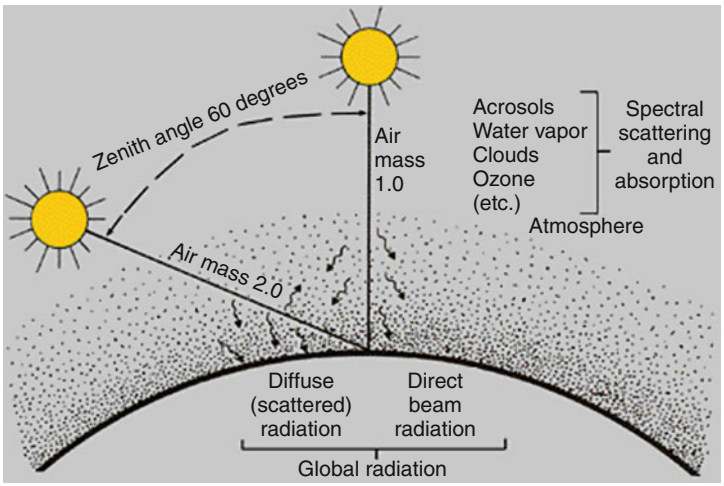

Solar Radiation for Solar Energy Utilization. Figure 2

Scattering of the direct-beam photons from the sun by the atmosphere produces diffuse sky irradiance

density multiplied by the cosine of the incidence or zenith angle produces the flux density on a surface (Lambert's cosine law).

The total irradiance on a horizontal surface, G, is equal to the (direct beam, B) $\times \cos(Z)$ plus the diffuse irradiance (F) from the rest of the sky impinging on the horizontal surface, as in Eq. 1.

$$G = B\cos(Z) + F \tag{1}$$

The rest of this article is devoted to the calibration, measurement, and modeling of the global, direct, and diffuse terrestrial solar radiation components for renewable energy applications.

Brief History of Solar Radiation Instrumentation

Excellent detailed reviews of the history of solar research are given in Whipple [3], Coulson [4], and Hufbauer [5]. Ancient civilizations fully appreciated the life-supporting properties of the sun and the annual solar cycle [6, 7]. The earliest recorded speculations on the physics of the sun in Western natural philosophy are those of the Greeks, beginning about 340 BC with Aristotle, Aristarchus (270 BC), Apollonius (220 BC), Hipparchus (140 BC), and Ptolemy (AD 140). The first to publish a non-Aristotelian view of the solar system was Copernicus (d.1543), who greatly influenced near contemporaries, especially Galileo (d.1642) and Kepler (d.1630). With the advent of the telescope, Galileo discovered sunspots (1610) and the solar rotation. In the late seventeenth century, Flamsteed, Cassini, Halley, Newton, and others devoted efforts to determining the sun's mass, size, and distance as well as developing the now familiar model of the solar system. Sir Isaac Newton (1642–1727) performed scientific study of light from the sun with his well-known experiments involving prisms in a darkened room. Newton described sunlight as composed of "all colors" of light. In 1800, William Herschel (d.1822) used thermometers mounted just beyond the red end of the simple Newtonian optical spectrum to measure infrared (IR) or heat energy in the solar spectrum. Similarly, Johann Wilhelm Ritter detected ultraviolet radiation beyond the blue end of the Newtonian spectrum with silver iodide salts in 1802.

While Hershel attempted to estimate the solar "heat" output, in 1837 Claude Pouillet made the first estimate of the "solar constant" as the amount of heat from the sun impinging on a square centimeter of the top of the Earth's atmosphere. He coined the term "pyrheliometer" and derived a value of 1.76 cal/cm^2/min (1,227 W/m^2), which is within 10% of the presently accepted value.

In the first half of the nineteenth century, Fraunhofer (d.1826) identified more than 500 dark lines in the solar spectrum. By 1823, William Herschel's son, John Herschel, proposed that these lines were associated with absorption by constituents of the solar atmosphere. In 1859, the chemists Gustav Kirchoff (d.1887) and Robert Bunsen (d. 1899) proved John Herschel's absorption hypothesis by associating the laboratory emission spectra and the solar absorption spectra of several key elements, especially sodium.

Samuel Pierpont Langley (d. 1906) spent much of the period from 1870 to 1900 attempting to determine the total spectral energy content of the sun with his bolometers (based on the change in resistance of material with temperature). Langley's solar spectrum, published in 1883, is shown in Fig. 3 (compare with Fig. 1) [8].

Table 1 presents a summarized timeline of the development of solar radiation measurement instrumentation.

Figure 4a–i show the evolution and variety of solar radiometers for measuring global hemispherical, direct normal, and diffuse sky radiation.

The Solar Radiation Measurement Scale: World Radiation Reference

In 1970, Kendall [19], and later Willson [20], at the Jet Propulsion Laboratory developed electrical compensation radiometers (see Fig. 5) utilizing conical blackened-silver cavities with thermojunctions that could be calibrated using electrical heating in place of heating from solar radiation.

These and instruments of similar design by Crommelynck [21], Brusa and Fröhlich [22], and Hickey [23, 24] became the standard for the World Radiometric Reference (WRR) established by the World Meteorological Organization/World Radiation Center (WMO/WRC) and now in use [25]. Figure 6 shows the relationship of a group of absolute cavity radiometers to the definition of WRR, determined by

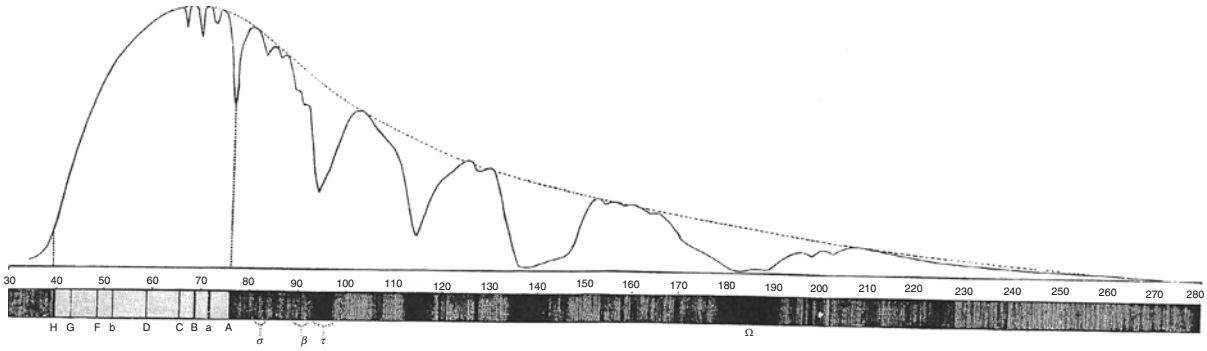

Solar Radiation for Solar Energy Utilization. Figure 3
Langley's 1883 solar spectral distribution

periodic international intercomparisons. Figure 7 is a photograph of the instruments that constitute the World Standard Group (WSG), which is used to define the WRR. As mentioned above, the WRR is the measurement standard for the International System, or *Systeme International* (SI), unit of solar irradiance [26]. The WRR was introduced to ensure homogeneity of solar radiation measurements and has been in use since 1980 [27]. There have been laboratory comparisons between WMO/WRC cavity radiometers and cryogenic absolute cavity radiometer, the SI standard for realizing the radiometric scale for laboratory measurements. The comparison showed that the PMO6 serial numbers −9 and −11 cavity radiometers (corrected to WRR) reproduced the SI laboratory irradiance scale to within 0.05% [28].

Calibrations and Traceability

The traceability of measurements requires an unbroken chain of comparisons with defined uncertainties to stated references. The traceability of the WSG cavity radiometers to SI units is with respect to electrical (volt, ohm, and ampere) and physical-dimensional (length, area) standards maintained by national standardizing laboratories. Detailed characterization of the aperture area, absorption of the cavity, and electrical components of the measurement system substantiates the "absolute" nature of the WSG measurements.

Every 5 years, WMO sponsors the International Pyrheliometer Comparisons (IPC). The WMO representatives of any country are invited to bring their reference solar radiometers to the PMOD/WRC institute in Davos, Switzerland to compare them with the WSG and derive a WRR correction factor [29]. The test radiometers are compared with the WSG using a rigorous data collection and processing protocol documented in Reda [30]. Periodically, regional and local intercomparisons are conducted using at least one, and preferably more, reference cavity pyrheliometer. Radiometers participating in such local intercomparisons are assigned suitable WRR correction factors. Radiometers under calibration include instruments behind quartz or Schott WG295 glass domes (pyranometers) and Corning 7250 quartz Infrasil windows (pyrheliometers) that transmit shortwave radiation over the spectral intervals 295–2,800 nm and 200–4,000 nm, respectively. However, as the reference absolute cavity radiometers providing the reference direct-beam irradiance have no windows, effectively measuring the total beam solar radiation over all possible wavelengths, the spectral cutoff of the domes and windows is effectively "calibrated out" in the comparison process.

Figure 8 shows the traceability path for working field radiometers to WRR through the WSG. Increasing uncertainty at each level is for field radiometer calibrations including transfer process and test radiometer stability.

Pyrheliometer Calibration

Pyrheliometer responsivities (Rs, or output signal per stimulus unit) are derived by direct comparisons with reference cavity pyrheliometers traceable to WRR. The approach is much like the transfer of WRR between cavity radiometers. The ratio of test pyrheliometer signals to the reference irradiance from the reference cavity pyrheliometer is computed over the course of

Solar Radiation for Solar Energy Utilization. Table 1 Outline of history of solar radiation investigation. See references in brackets

Aristotle, Aristarchus, Apollonius, Hipparchus, Ptolemy	~340 BC to AD 140	Various speculations on physics and natural philosophy related to the sun's properties and interactions with the Earth
Nicholas Copernicus	d. 1543	Sun-centric solar system
Galileo	d. 1642	Sunspots, solar rotation
Johannes Kepler	d. 1630	Conic section solar system orbits
Isaac Newton	d. 1727	Solar spectral decomposition
William Herschel	d. 1822	Discovered infrared
Johann Wilhelm Ritter	1802	Discovered ultraviolet
Fraunhofer	d. 1826	Solar absorption lines
Claude Pouillet	1837	Estimated solar constant 1.76 cal/cm^2/min = 1,227 W/m^2
John Herschel	1823	Proposed Fraunhofer lines are due to absorption in sun atmosphere
Gustav Kirchoff/Robert Bunsen	d. 1887/d. 1899	Laboratory detection spectral lines
Samuel P. Langley	1883	Bolometric measurement terrestrial solar spectrum Est. solar constant 3.0 cal/cm^2/min = 2,050 W/m^2
H.S. Callendar [9]	1898	Platinum wire grid pyranometer, U.S. Weather Bureau 1908–1941
Charles Greely Abbot [10, 11]	1872–1973	Silver disk and water flow pyrheliometer, Smithsonian solar scale 1913
Knut Ångström [12, 13]	~1910	Electrical compensation pyrheliometer, International Pyrheliometric Scale 1956 (Å-210)
C.G. Abbot, Aldrich [14, 15]	1916	Thermoelectric pyranometer
Eppley Laboratory, Newport, Rhode Island	1930	10-junction/50-junction "light bulb" thermopile pyranometers, U.S. Weather Bureau until 1965
Robitzsh [16]	1932	Bi-metallic recording pyranograph
Eppley Laboratory, Newport, Rhode Island	~1950	Black-and-white pattern thermopile pyranometers
Dirmhirn-Saber (Philip Schenk) [17]		
Yanishevski (USSR) [18]		
W.J. Moll/L. Gorczynsky	~1960	80-junction Kipp and Zonen thermopile pyranometers
Eppley Laboratory, Newport, Rhode Island	~1970	All-black thermopile sensor pyranometer (Precision Spectral Pyranometer, PSP; Normal Incidence Pyrheliometer, NIP)
Kipp and Zonen, Delft, Netherlands		CM -6; CM-11; CM-21/22; EQ series)
Spectrolab, Sylmar, California		
Australian CSIRO Middleton, Brunswick, Victoria, Australia		
Eko Instruments, Japan		
Li-Cor Inc., Lincoln, Nebraska	1975	Silicon photodiode pyranometer, luminance meter

Solar Radiation for Solar Energy Utilization. Table 1 (Continued)

Kendall and Willson, Jet Propulsion Laboratory, Pasadena CA.	1980	Absolute cavity radiometer and active cavity radiometer absolute pyrheliometers [19, 20].
Yankee Environmental Systems, Turner Falls, New Hampshire		Thin-film platinum resistance thermometer pyranometer; rotating shadow band radiometers for global, direct, diffuse measurements
Ascension Technology Irradiance Inc.		

a clear day or several clear days. Figure 9 shows typical data for such a calibration. National [31] and international [32] standards documents describe the procedures for calibration of field pyrheliometers from primary (absolute cavity) pyrheliometers and reference pyrheliometers.

The shape of the response function for a field pyrheliometer seen in Fig. 9 is of concern, as the distribution of the responsivities is not random but biased differently in the morning and afternoon. The cause for this bias is a current topic of research. Possible explanations are the different fields of view of the reference (5°) and test (5.7°) pyrheliometers, environmental influences (ambient temperature, wind speed, and direction), and test instrument design (thermal gradients between detector and reference thermocouples).

Pyranometer calibration

Pyranometer responsivities may be derived from one of two techniques. The first is a "shade/unshade" technique. Responsivity for a diffuse-measuring reference pyranometer, shown as Rsd, is derived in a shade/unshade calibration using the formula $\mathrm{Rsd} = (U - S)/[B\cos(Z)]$, where U and S are the unshaded and shaded output voltages from the sensor, Z is the zenith angle, and B is measured by a reference pyrheliometer. Procedures for this calibration are described in the American Society for Testing and Materials Standard G167 [33] and international standard ISO 9060 [34].

Significant issues affect the apparently simple shade/unshade calibration. The pyranometer under test has several time constants, caused by differing heating and cooling rates of the domes and detectors as the shade is imposed and removed. In contrast, the diffuse sky radiation, particularly the IR radiation temperature, remains relatively constant. Therefore, the net IR exchange between the instrument and the sky is different in the shade and unshade condition, which leads to changing thermal offsets in the detector, discussed below. Variations in the direct-beam radiation over the shade and unshade periods (at the beginning and end of the shade period) can lead to errors. A modification to the standard shade/unshade pyranometer calibration that determines an average responsivity at 45° zenith angle for three instrument azimuth angles provides an integration over geometric response variations [35, 36].

With this modified shade/unshade technique, clear-sky diffuse irradiance can be measured with an uncertainty of ±(3% of reading + 1.0 W/m^2). For typical clear-sky calibration conditions, the diffuse irradiance is on the order of 10% of the total global hemispherical irradiance. This means that the uncertainty in the total global reference irradiance because of uncertainty in the diffuse reference irradiance is on the order of ±(0.3% of the total reference irradiance, +0.3 W/m^2).

For a "component summation" calibration of a pyranometer, the reference global irradiance (G_r) is derived from an absolute cavity radiometer beam measurement (B) and shaded pyranometer (diffuse) measurement (F) using $G_r = B\cos(Z) + F$, shown symbolically in Fig. 10. The ratio of the test pyranometer signal to the reference global irradiance is then the responsivity, or calibration value, for the pyranometer.

This technique requires a shade/unshade calibrated pyranometer to measure the "reference diffuse" irradiance, F, during the calibration. The instantaneous voltage signals of the test radiometers are divided by the reference global irradiance G_r to generate instantaneous responsivities typically in units of μV/W/m^2. Figure 11 shows a typical plot of responsivity versus zenith angle throughout a day. As with the pyrheliometer example discussed above, the response of the pyranometer is not constant with respect to the solar incidence angle. In the band of incidence angles from 0° (normal incidence) to 60° (solar elevation of 30°), responsivity may vary by 5% or more. Every individual

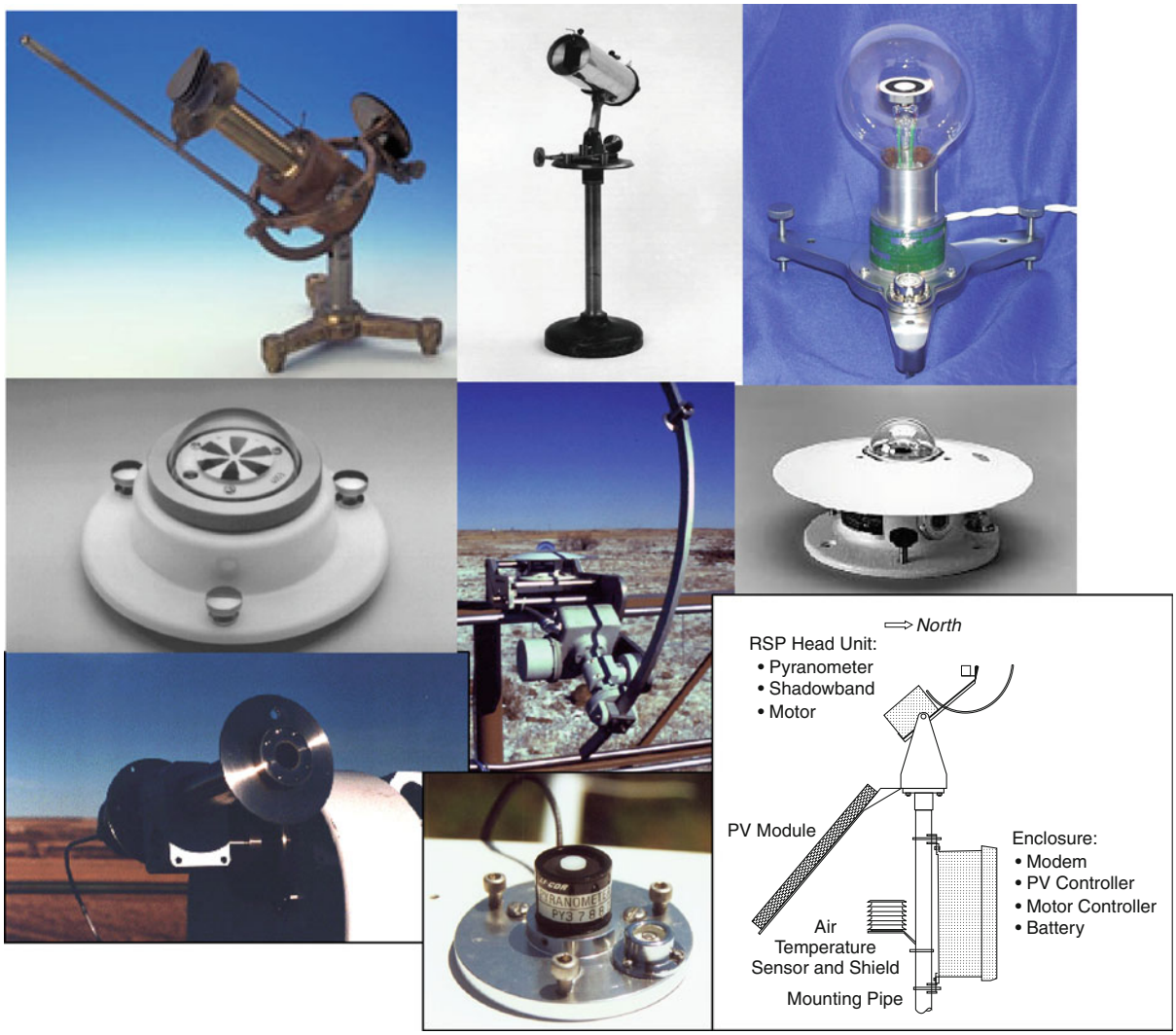

Solar Radiation for Solar Energy Utilization. Figure 4
(**a**) Abbott Silver disk pyrheliometer [10], (**b**) Ångström's pyrheliometer [12], (**c**) Eppley Model 50 pyranometer, (**d**) Schenk Star pyranometer [17], (**e**) tracking shading disk and shaded pyranometer, (**f**) Eppley Model PSP pyranometer, (**g**) Eppley normal incidence pyrheliometer on tracker, (**h**) Li-Cor Inc. silicon photodiode pyranometer, and (**i**) sketch of rotating shadow band radiometer with silicon photodiode detector

pyranometer will have a distinct, unique, individual "signature," even for a given model designation. Similar signatures are obtained from pyranometers calibrated if the shade/unshade techniques are used over a large range of zenith angles. Thus, it is important that calibration methods, selection criteria for a responsivity (or calibration factor, Cf, equal to 1/Rs), and range of Rs (or Cf) be described to adequately characterize the uncertainty in solar radiation measured with the pyranometer.

Uncertainty Analysis

All measurements only approximate the quantity being measured and are incomplete without a quantitative uncertainty. The Guide to Measurement Uncertainty (GUM) of the International Bureau of Weights and Measures (BIPM) [37] is the accepted international guide for conducting measurement uncertainty analysis. The GUM defines Type A uncertainty values as derived from statistical methods and Type B sources

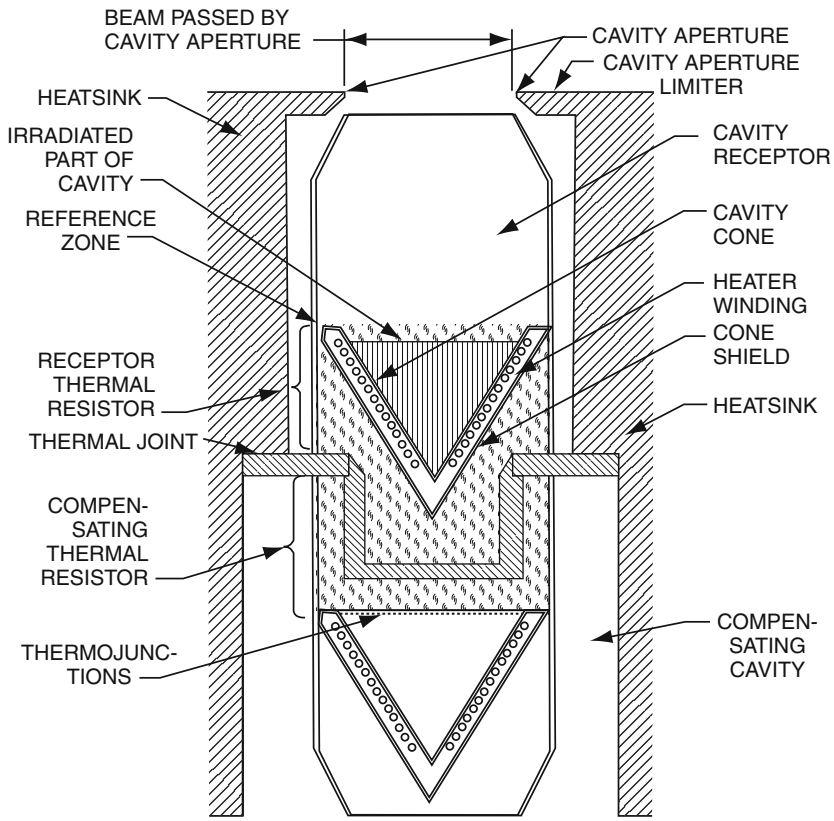

Solar Radiation for Solar Energy Utilization. Figure 5
Kendall's design [21] for an absolute cavity radiometer receiver. Electrical current through the heater winding set to match solar heating of the cavity

as evaluated by "other means," such as scientific judgment, experience, specifications, comparisons, or calibration data.

Every element of a measurement system contributes elements of uncertainty. When a result, R, is functionally dependent on several $i=1,...,n$ variables, x_i, the familiar propagation of error formula $U^2 = \sum_i (\partial_{Xi} R \cdot e_{Xi})^2$ is used, where U is the uncertainty in the resultant, e_{xi} is the estimated uncertainty in variable x_i, and $\partial_{xi} R$ is the partial derivative of the response R with respect to variable x_i, called the sensitivity function for variable x_i.

Previously, uncertainty analysis treated sources of uncertainty in terms of "random" and "bias" types. Total uncertainty, U, was computed from: $U^2 = \sqrt{[(\text{Bias})^2 + (2^*\text{Random})^2}$ [38]. The factor of 2 was applied to the "random" or statistical uncertainty component because this component usually represented a standard deviation. This method was considered to report uncertainty with a 95% "confidence interval." The resulting uncertainty in calibration of pyranometer responsivity and field measurements was 2.4% and 5%, respectively. The GUM replaces the factor of 2 with a "coverage factor," k and $U^2 = \sqrt{[(\text{Type B})^2 + (k^* \text{ Type A})^2]}$. For small ($n<20$) samples, from a Gaussian distribution of measurements, k may be selected from the t-distribution [37, 39]. U is the "expanded uncertainty," and k is usually in the range of 2–3, for confidence intervals of 95% and 99%, respectively. In the following, the GUM approach is followed in an uncertainty analysis.

Radiometer Calibration Sources of Uncertainty

Several types of detectors, including silicon cells and thermal detectors such as resistance thermometers and thermopiles, are used for pyrheliometer and pyranometer instruments.

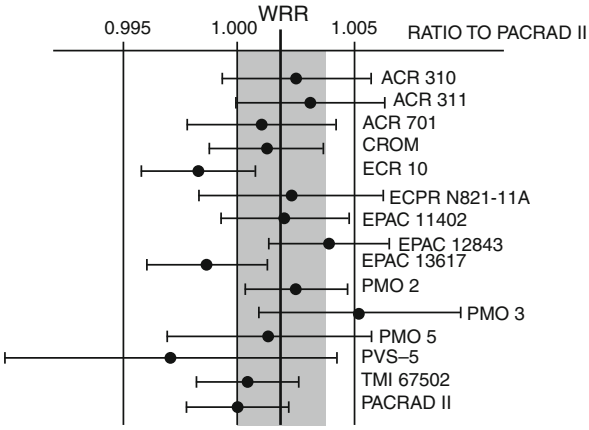

Solar Radiation for Solar Energy Utilization. Figure 6 Relationship of various absolute cavity radiometers to the WRR scale defined by the present WSG

All-Black Detector Thermal Offsets Studies of solar radiation instrumentation in climate research, such as those by the World Climate Change Research Program Baseline Surface Radiation Network (BSRN) participants [40] and others [41–44], have characterized thermal "zero offsets" in thermopile pyranometers with all-black sensors measuring diffuse radiation. The offsets produce negative engineering data at night and clear-sky diffuse irradiances lower than what pure Rayleigh scattering theory predicts. Thermal offsets occur because the cold junctions of the all-black detector thermopile are in a different thermal environment (inside the radiometer) than the exposed absorbing hot junctions. Empirical tests [43] show that thermal infrared exchange among the warm sensors, domes, and cold sky generates these offsets. Some have proposed that shade/unshade calibrations result in "cancellation" of the thermal offsets in the shaded and unshaded state [45]. For black-and-white sensors, the reference and absorbing thermopile junctions are in a similar thermal environment when shaded and unshaded. These radiometers have lower (~1–2 W/m^2) offsets and should produce more accurate diffuse sky measurements. Experiments have been conducted [43–45] that characterized thermal "zero offset" signals in thermopile pyranometers with all-black sensors. Silicon photodiode instruments do not have thermal offsets, though they do have temperature coefficient of responsivity typical of silicon – about 0.15%/°C.

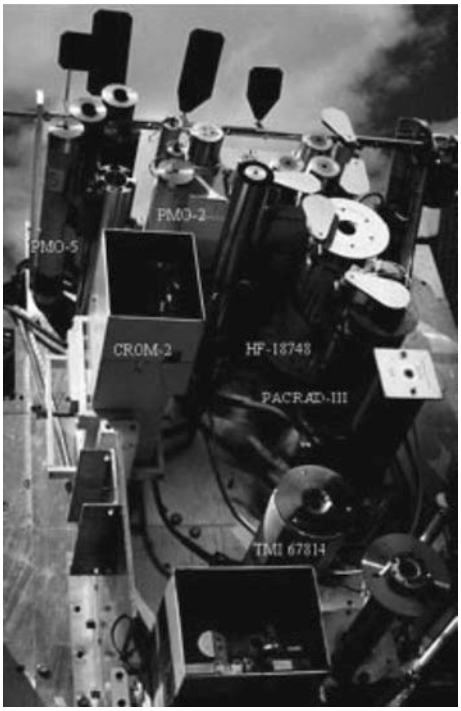

Solar Radiation for Solar Energy Utilization. Figure 7 Six absolute cavity radiometers of various designs constitute the WSG of pyrheliometers that define the solar radiometric scale, the WRR (WRC, Davos, Switzerland)

Spectral Effects There is spectral effect on the shade/unshade calibration. The diffuse sky radiation has very little energy in the shortwave region from 1,000 to 2,500 nm, while direct-beam radiation has significant energy in that region (see Fig. 12). Therefore, anything affecting the direct-beam (hence total global) irradiance, and unshaded pyranometer signal, such as variations in atmospheric water vapor, does *not* affect the *shaded* pyranometer signal. That is, for *different* atmospheric water vapor concentrations and differing direct normal and global total irradiances, the *same* "shaded" signal from the pyranometer is possible. The light areas between the global-irradiance plots show the difference between the low and high water vapor conditions. The concomitant changes in the diffuse spectral distribution are minimal. For essentially the same diffuse radiation, varying water vapor content results in changes of up to 0.5% in shaded/unshade responsivities for both all-black and black-and-white detector pyranometers with respect to the global reference spectrum.

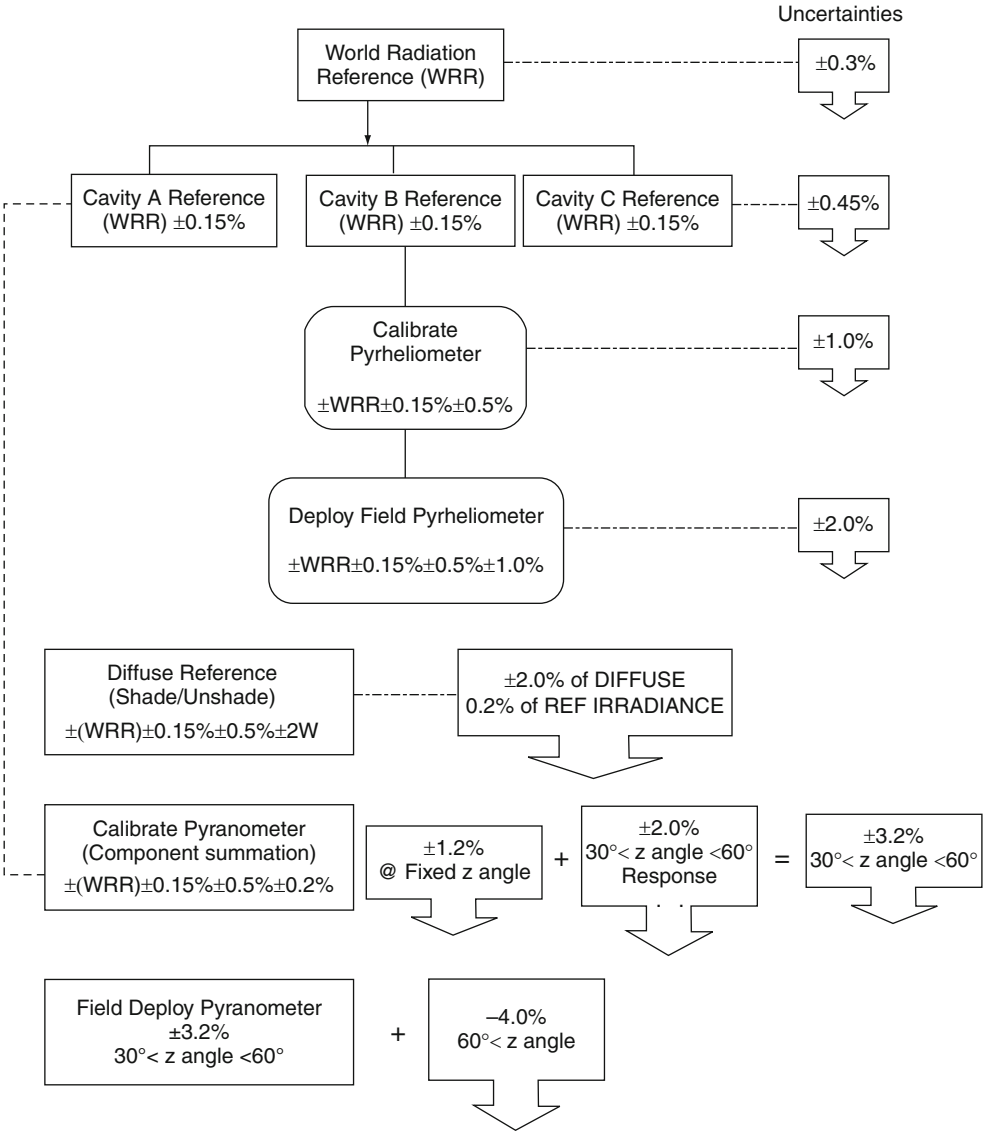

Solar Radiation for Solar Energy Utilization. Figure 8
Traceability diagram and buildup of uncertainty through calibration transfers for radiometers

Geometric, Environmental, and Equipment Uncertainty Additional well-known contributors to radiometer calibration and measurement uncertainty include accuracy of the calculation of the zenith angle, non-Lambertian cosine response of the detector surface (see Fig. 13), temperature coefficients, linearity, thermal electromotive forces (sun shining on connectors), and electromagnetic interference (EMI) [38]. Finally, the specifications and performance of the data-logging equipment (resolution, precision, and accuracy) deployed in the field must be considered. Table 2 lists these uncertainties.

Pyranometer Responsivity Functions A pyranometer responsivity function derived from calibration data should be used to retrieve accurate irradiance from a pyranometer. The uncertainty in each pyranometer calibration responsivity *point* in Fig. 11 is summarized in Table 2. The expanded uncertainty for each point in the curves of Fig. 11 is about 1.8%, with coverage

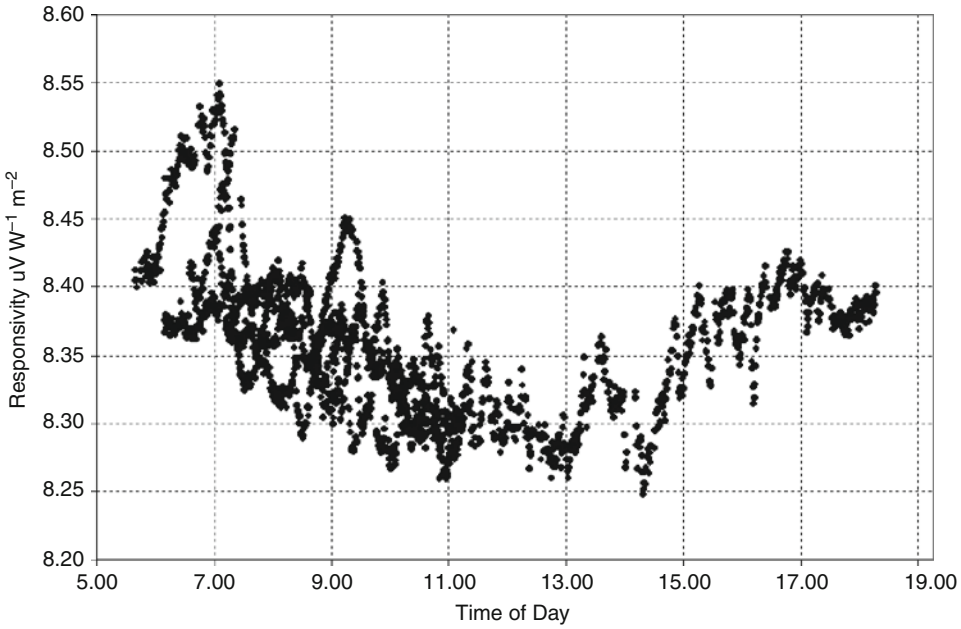

Solar Radiation for Solar Energy Utilization. Figure 9
Pyrheliometer calibration data showing variation in responsivity (ratio of signal to reference irradiance) over several days

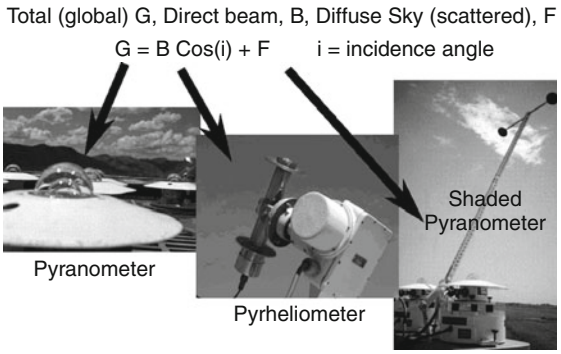

Solar Radiation for Solar Energy Utilization. Figure 10
Solar radiation instruments and the components they measure

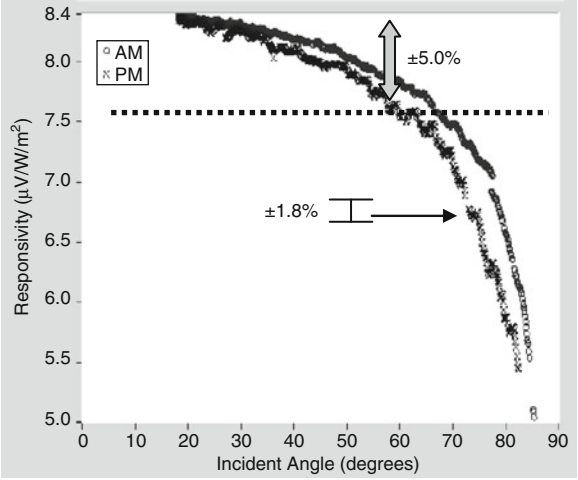

Solar Radiation for Solar Energy Utilization. Figure 11
Example pyranometer responsivity versus solar zenith angle from component summation calibration. *Dotted line* is −5% of Rs (45°)

factor $k=2$. This is the *smallest* uncertainty that can be expected of a pyranometer under conditions identical to the calibration conditions, including the "thermal offset" conditions, at a specific zenith angle. It is possible to *estimate* the thermal offset during calibration, using longwave radiometers (pyrgeometers, with their own inherent uncertainties) and compensate for this effect during calibration [44–47]. Responsivity at a given zenith angle at the time of measurement, Rs(m), can be obtained from a fit to the response curve from calibration data versus zenith angle. Figure 13 shows approximately ±1% repeatability for the responsivity functions for a single all-black detector pyranometer over seven component summation

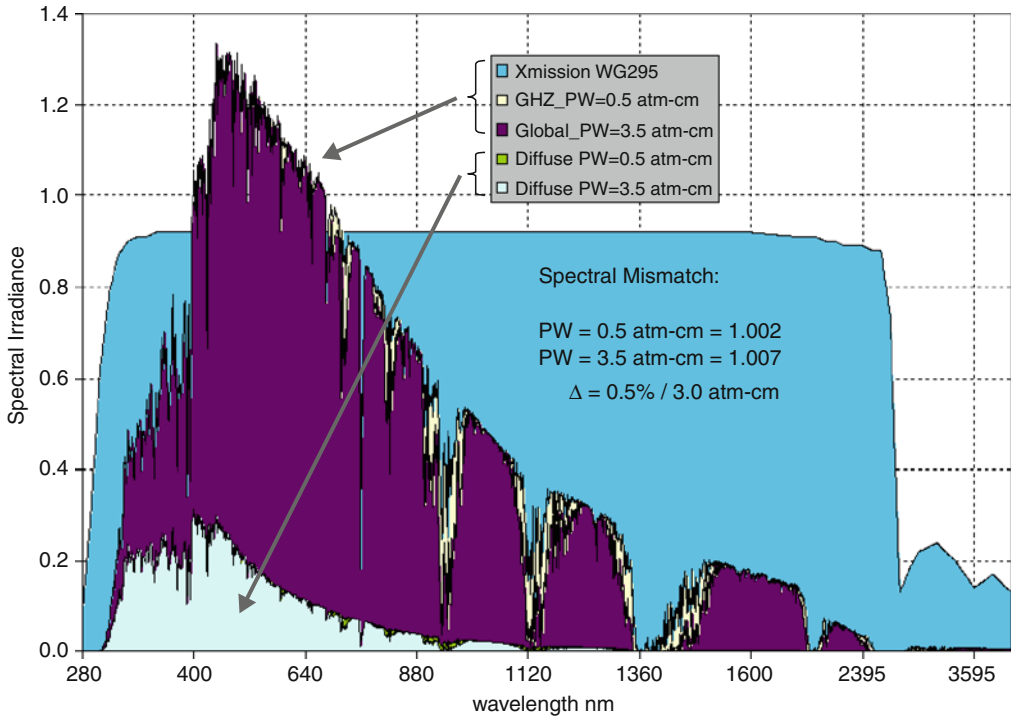

Solar Radiation for Solar Energy Utilization. Figure 12
Global (large-amplitude) and diffuse (low-amplitude) horizontal spectral distributions for water vapor content of 0.5 atm-cm and 3.5 atm-cm. Blue filled area is transmission curve for quartz (WG 295) pyranometer dome material

calibrations in a 2-year period. For radiometers deployed to the field, further sources of uncertainty arise, such as differing accuracy or resolution data recorders, cleanliness, and climatological conditions (i.e., varying net-infrared exchange conditions) – all of which may exist in addition to the calibration uncertainty computed in Table 2. This will lead to field measurements with uncertainty greater than the 1.8% calibration uncertainty [46].

Pyrheliometer Uncertainties As described in the section on "Pyrheliometer Calibrations", pyrheliometer signals are compared directly with the reference (cavity) pyrheliometer signals. There are no concerns with geometric response, computation of the zenith angle, or apparent thermal offsets (nighttime data $\sim \pm 1.0$ W/m^2). Many of the contributions to total uncertainty listed in Table 3 disappear. However, there are new contributions to uncertainty: Pyrheliometers have windows for continuous outdoor operation, and the reference pyrheliometer has no window. This may lead to spectral effects similar to those seen with respect to pyranometer domes. Errors in tracking the sun may arise because the reference pyrheliometer and pyrheliometer must be pointed at the sun. The fields of view of the reference cavity radiometer and pyrheliometer may be different. This would make the calibration dependent on the circumsolar radiation field. The final tally of the pyrheliometer uncertainty components is shown in Table 3. The expanded uncertainty for each Rs is 1.6%. With deployment to the field, pyrheliometer data become subject to additional tracking and window cleanliness issues, differing data logger specifications, etc. These require additional analysis specific to the deployment for estimating a total uncertainty in the field measurement, which must be greater than the 1.6% calibration uncertainty [48].

Solar Radiation Measurements Summary

Today's broadband solar radiation measuring instruments, absolute cavity radiometers, pyranometers, and

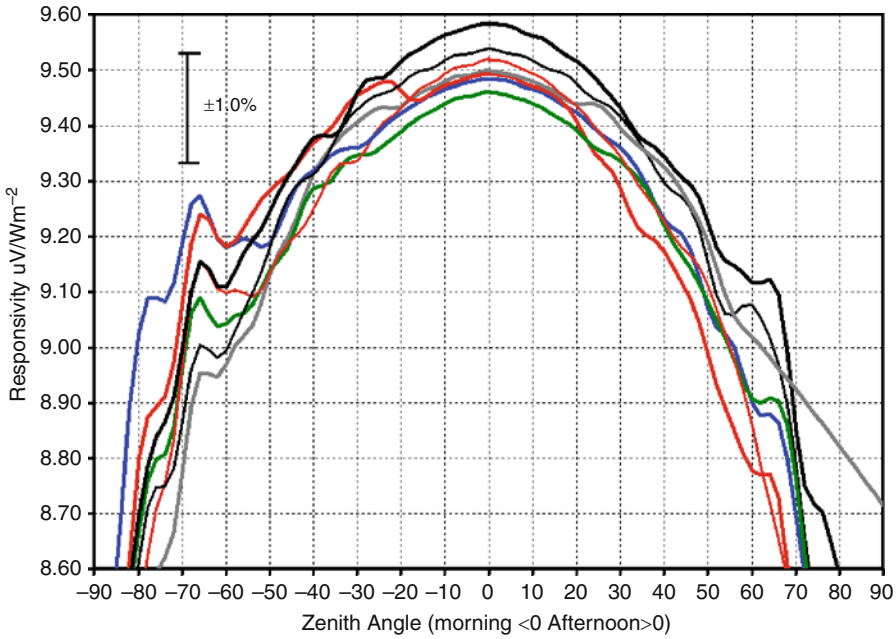

Solar Radiation for Solar Energy Utilization. Figure 13
Repeatability of responsivity functions for a single all-black detector pyranometer over seven calibration events in a 2-year period

pyrheliometers use improved materials and manufacturing processes above and beyond their historical predecessors. Fundamental accuracy for direct-beam and total hemispherical solar radiation as low as 2–5% or better is achievable with simple calibrations. An improvement by a factor of 2 in uncertainty to about 1.5–2.5% is possible *only with extensively characterized instrument responses*, or applications requiring only a very narrowly defined set of conditions (zenith angle or solar geometry). These percentage uncertainties translate to absolute magnitudes of 15, 25, and 50 W/m^2 for clear-sky irradiances of 1,000 W/m^2. Global climate change and general circulation models (GCMs) produce results relating to global warming, temperature trends, and fluctuations that are derived from changes in the Earth's radiation budget of only 1, 2, or 5 W/m^2. Further, the global average daily solar input is only about 325 W/m^2 at the Earth's surface. The GCMs are reporting changes of only 0.3–1.5% in this average value. Only one solar radiation measurement instrument, the absolute cavity radiometer reference pyrheliometer, has accuracy approaching the 0.3% lower value. All other solar broadband measurements have an accuracy exceeding this fundamental lowest limit. Therefore, it is very difficult to verify with any great accuracy the predictions of GCM radiation budget results using current broadband solar radiation instrumentation. A great deal more work in the field of solar radiation measurements needs to be done to significantly shorten the time required to answer questions critical to the energy economy of the planet and human societies.

Modeling Solar Radiation Resources for Solar Energy Conversion

Determining the component(s) – hemispherical, direct, or diffuse – of solar radiation applicable to a conversion system is the first step in evaluating design criteria and performance. Systems with concentrating optics rely on the availability of direct-beam radiation. Low-concentration systems may be able to utilize some diffuse sky radiation through "light trapping" techniques. Flat plate collectors, fixed or variable in their mounting, can utilize all radiation components, including reflected ground radiation from behind the panels in the case of bi-facial modules. Buildings and daylighting applications require solar components

Solar Radiation for Solar Energy Utilization. Table 2
Uncertainties in individual pyranometer Rs for summation calibration

	UNC (%)	STD UNC (%)
Type A (statistical)		
WRR transfer	0.200	0.200
Cos(Z) (2° Z bin)	0.010	0.005
Diffuse reference	0.125	0.063
Temperature (2° Z bin)	0.100	0.050
Data logger precision	0.005	0.0025
Cavity (wind)	0.025	0.013
Temp chg (10°C)	0.250	0.125
Diff offset B&W	0.125	0.063
IR offset	0.250	0.125
EMI/thermal EMF	0.010	0.005
Type B		
Logger bas (9 uV/10 mv)	0.090	0.090
WRR Std U95	0.300	0.300
Cos(Z); Z < 89°; 2° bin	0.010	0.005
Temperature (2° Z bin)	0.100	0.050
Cavity bias (wind)	0.025	0.013
Temp B (event to event) 10°C	0.250	0.125
Diff offset B&W	0.125	0.063
IR offset	0.625	0.625
Spectral error	0.500	0.250
EMI/thermal EMF	0.010	0.005
Total		
Type A	0.455	0.286
Type B	0.910	0.872
Combined	**1.017**	**0.918**
Effective deg. of freedom	>100	
Coverage factor (k)	2	
Expanded uncertainty	**1.84%**	

Solar Radiation for Solar Energy Utilization. Table 3
Uncertainties for 95% confidence interval for individual pyrheliometer Rs

	UNC (%)	STD UNC (%)
Type A (statistical)		
WRR transfer	0.200	0.200
Temp response UUT	0.500	0.050
Data logger precision	0.005	0.003
Linearity (empirical)	0.200	0.100
Cavity (wind, T)	0.025	0.013
Tracking variations	0.250	0.125
Spectral (window)	0.500	0.500
EMI/thermal EMF	0.010	0.005
Type B		
Logger bias (9 uV/10 mv)	0.090	0.090
WRR Std U95	0.300	0.300
Temp response UUT	0.500	0.250
Cavity bias (M, wind, T)	0.025	0.013
Temp B (event to event) 10°	0.250	0.125
Field of view differences	0.050	0.050
Spectral error	0.500	0.500
Tracking bias	0.250	0.013
EMI/thermal EMF	0.010	0.005
Total		
Type A	0.802	0.615
Type B	0.851	0.504
Combined	**1.169**	**0.918**
Effective deg. of freedom	>100	
Coverage factor (k)	2	
Expanded uncertainty	**1.59%**	

contributing to heat loads or available for skylight and window configurations. Most often, the only available measured or modeled solar radiation data are global horizontal total hemispherical radiation. In this case, "conversion" models are used to derive *estimates* of the appropriate quantities. The solar radiation scientific research community, peer-reviewed publications, and published reports are presently relied upon to evaluate, validate, and assess the quality of these conversion algorithms [49]. Table 4 lists the types of solar radiation data needs often requested for specific applications.

Given the variety of solar radiation applications, and the small number of available measurements,

Solar Radiation for Solar Energy Utilization. Table 4 Data formats requested by solar energy system designers and planners

Type of solar data	Time resolution	Application
Hemispherical, vertical surface, cardinal directions	Seasonal/daily	Glazing, building energy balance
Illuminance, vertical surfaces, cardinal directions	Seasonal/daily	Daylighting
Hemispherical tilt	Monthly/annual	Fixed flat plate
Hemispherical tracking	Monthly/annual	Tracking flat plate
Direct normal (beam)	Monthly/annual	Focusing/concentrating system
Sunshape (disk+circumsolar) variation	Varies	Concentrating tracking collector
Monthly mean daily total	Monthly/daily	Economics, design specification
Monthly mean	Monthly	Economics, design specification
Daily profiles	Hourly	System simulation, design, rating
8,760 hourly data for year, hemispherical and/or direct	Hourly	System simulation, design, rating
Hourly time series 10–30 year hourly power	Hourly	Performance and economics, system lifetime
High time resolution time series daily profiles power	Sub-hourly	System transient response

models are frequently needed to provide suitable information for solar energy conversion systems. The following sections describe the principles of modeling solar radiation to meet the requirements for such a wide variety of applications.

Solar Radiation Model Approaches

Long-term measured solar radiation data sets are rare, have variable periods of record (with usually many data gaps), and vary in their ease of access. Measurement networks or stations providing high-accuracy, "up-to-the-minute" measured data are typically oriented toward scientific research and are rare. Agricultural research station solar radiation data for total horizontal solar radiation of highly variable quality is available, usually from state agricultural agencies. However, this data can be episodic (e.g., growing season only) and requires careful evaluation and comparison with other (perhaps estimated or modeled data) sources to establish its appropriateness for use. As a result of the lack of definitive solar radiation measurements for applications listed in Table 4, many models and modeled data solar radiation sets have been developed. Muneer [50, 51], Iqbal [52], and Badescu [53] all describe a myriad of model approaches. The most common models and data sets address total global hemispherical on a horizontal surface, occasionally the direct beam, and sometimes diffuse hemispherical on a horizontal surface.

There are several approaches to modeling solar radiation data. Empirical or parametric models are based on correlations developed between input "independent variables" and solar radiation data. Regression analysis is applied to express the solar radiation parameter in terms of the independent variables. Examples of independent variables often used are sunshine hours, temperature, cloud cover, and so on. Caution is needed in this approach, as the "independent" variables are often cross-correlated (e.g., temperature can be correlated with the solar radiation and relative humidity with temperature and dew point). This multicollinearity results in inflated correlation and sometimes unstable model coefficients derived from the regressions. These models are often site-dependent and not generally applicable worldwide, unless the development data sets are very comprehensive.

Physical models are based on principles of physics, radiative transfer, and the properties of the atmosphere. These models can be complex and require

esoteric, rarely found input parameters. Examples are cloud droplet radii, aerosol size distributions, single scattering albedo, and so on. On the other hand, simple transmission and scattering functions for the atmosphere can be derived from the complex functions in the most complicated physical models. These models often first generate clear-sky direct-beam radiation and use correlations or special algorithms to generate the total hemispherical and or diffuse sky radiation. Examples include Bird and Hulstrom [54], and Gueymard [55]. Survey articles covering such models have been published by Ineichen [56], Wong and Chow [57], Muneer [58], and Gueymard [59]. The model output is usually the product of the extraterrestrial solar radiation and the transmission functions, along with any geometric considerations. An example of a model for all sky conditions is that of Kasten and Czeplak [60].

Satellite-based models transform brightness (radiance) data from images into solar radiation fluxes at the surface. A combination of physical and empirical correlations of solar radiation with variables such as surface albedo, cloud cover, and relations between radiation components are then used to produce radiation total hemispherical, diffuse sky on a horizontal surface, and direct-beam radiation components. Figure 14 illustrates how various gridded layers of information from satellite images (pixel brightness) and ancillary information about atmospheric constituents, ground albedo, etc., are combined to produce surface flux estimates.

Detailed descriptions of these models – including the concepts of cloud index formation for modifying clear sky irradiances and derivation of the total hemispherical, direct-beam, and diffuse sky components – can be found in Cano et al. [61], Diabaté et al. [62], and Perez et al. [63].

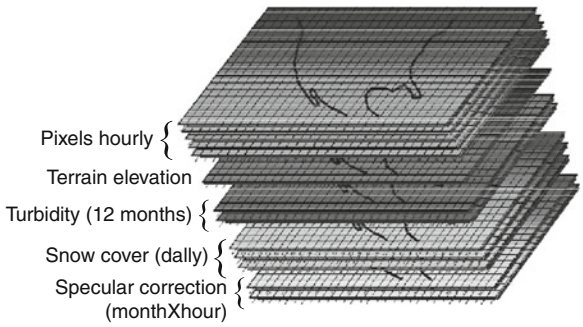

Solar Radiation for Solar Energy Utilization. Figure 14 Gridded layers of information to be combined to estimate solar fluxes from satellite imagery

Temporal Resolution The most prevalent time resolution for solar radiation data (measured or modeled) is hourly average data. Measured data are usually averaged over an hour, based on measurements at higher-resolution (e.g., 1-, 5-, or 10-min) intervals. The underlying higher time-resolution data are usually not available. The WMO World Radiation Data Center (WRC) in St. Petersburg, Russia, is the designated WMO archive for daily solar radiation data in the form of daily total radiation, typically global hemispherical radiation, summed over daylight hours. Often, only monthly averages (e.g., monthly average daily total of hourly data) are popular to evaluate the suitability of a proposed solar energy conversion system. Efforts at making both measured and modeled higher time-resolution data (e.g., intervals of less than 1 h, down to 1 min, or even less) are under way. Such high-resolution data are just beginning to be considered because of the impact of the transient response of large photovoltaic systems might have on the stability of the electric grid over long [64] and short periods [65].

Period of Record Few sets of measured data for long periods of record (i.e., more than a few years) are available to the public. Examples are the University of Oregon Solar monitoring network (since 1975 at some sites), the National Renewable Energy Laboratory Solar Radiation Research Laboratory (since 1981), the US Department of Energy (DOE) Atmospheric Radiation Measurement sites (since 1997), and the BSRN (since approximately the mid-1990s but varies by station). Some modeled data sets, such as the US National Solar Radiation Data Base (NSRDB) and the National Aeronautics and Space Administration (NASA) Surface Solar Energy data set (NASA SSE) contain modeled data over extended periods of time (20–30 years). The NSRDB host hourly data; the highest time-resolution NASA SSE data are daily totals. Stations in the WMO/WRC data archive report daily totals (usually of percent sunshine and/or global horizontal daily totals), and the period of record for individual stations varies widely from a few months to years.

Modeled Data Sets

A sample of modeled data sets available to the public, either free online or for purchase, are the NSRDB, the Swiss Meteotest METEONORM software, the European Solar Radiation Atlas and other European data sets, the NASA SSE Data Set, and the DOE EnergyPlus weather data sets.

An important popular modeled data set is the so-called "Typical Meteorological Year" (TMY) for a specific location. TMY data sets were originally designed for building heating and cooling load calculations. The TMY consists of 8,760 hourly data points for a single, synthetic year. Data for a given TMY month are "near" (but *not* "equal to") the weighted mean of meteorological parameters (e.g., temperature, wind speed, etc.) and solar radiation for all months in the period of record (generally, 30 years is preferred) that the TMY represents. The representative months may come from different years but are spliced together to give the continuous yearly time series. These data sets are used mainly to evaluate *relative performance* of different conversion system designs with respect to a "standard" data set and *may not be appropriate for optimizing performance*. The DOE EnergyPlus data sets contain TMY-derived and TMY-like data sets for many world cities, as well as access to some real-time measurement data.

The primary objective of many of the models described above is to compute total (global) hemispherical irradiance, sometimes decomposed into the direct normal irradiance and the sky diffuse irradiance. Examples include the METSTAT model of Maxwell [66] and models based on meteorological inputs, as described by Muneer [58]. The next step is to try and estimate the solar resources available on various solar energy collector configurations. This means algorithms are needed to convert either available measured or modeled data (e.g., total hemispherical on a horizontal surface) to the radiation on some other configuration – a tilted plane, tracking focusing collector, window area, tilted roof, or building façade. These conversion or transposition models are discussed in the following sections.

Estimating Hemispherical Radiation on a Tilt

Tilted surfaces may be fixed or variable in tilt angle. Examples of the former are south-facing surfaces tilted at the latitude of a location and vertical surfaces facing various azimuth directions. Examples of the latter are surfaces that track the sun or change their tilt from vertical east at sunrise, to horizontal at noon, to vertical west at sunset. The radiation falling on these surfaces is made up of components from the direct beam (if the surface is hit by the beam radiation), a portion of the sky radiation from that portion of the sky seen by the surface, and ground-reflected radiation within the field of view of the surface. Figure 15 illustrates these components.

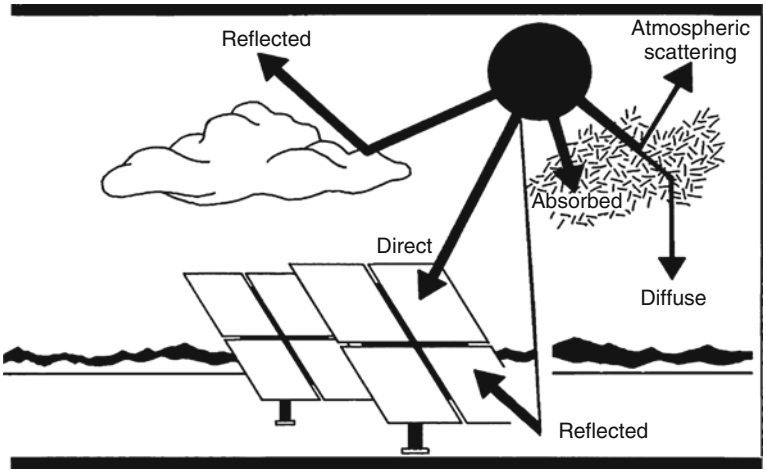

Solar Radiation for Solar Energy Utilization. Figure 15
Schematic of solar radiation components for a tilted surface

Similar to horizontal surfaces, the incidence angle, i, of the direct beam with respect to the normal perpendicular to the surface will determine the contribution of the direct-beam component on a tilted surface (hereafter called plane of array, or POA), Bt, through the relation $\mathrm{Bt} = B\cos(i)$. The contributions of the portions of the sky and ground-reflected radiation hitting the POA are much more variable and difficult to describe without direct measurement of the total hemispherical radiation in the POA. If the total hemispherical radiation on the POA, Hs, can be measured, and the direct beam, B, can be measured independently, the total diffuse on a titled surface, Fs, can be computed using the relation $\mathrm{Fs} = \mathrm{Hs} - \mathrm{Bt} = \mathrm{Hs} - B\cos(i)$.

Note that the total diffuse on a tilted surface, Fs, is the sum of the sky radiation, Ss, and ground-reflected radiation Gs, or Fs = Ss + Gs. It is a difficult measurement problem to separate the sky and ground-reflected radiation from the total hemispherical radiation less the incident beam radiation on a POA. However, models have been developed to accomplish this, depending on the optical properties of the ground in the field of view of the tilted surface.

Many models have been derived for computing hemispherical radiation on a tilt from global horizontal hemispherical radiation. Gueymard [67] evaluated ten models. The most accurate models use at least two measured components to compute the irradiance on the tilted surface; however, a few (less accurate) estimate the irradiance on a tilted surface from a single parameter, usually global horizontal irradiance. Validation of the modeled data against experimentally measured data has shown that these models possess systematic bias errors of 2–5% and random errors of 5–10% with respect to the validation data sets. One of the most popular and accurate of the former is the Perez Anisotropic Model for Diffuse on a tilted surface [68]. This model is embedded in many flat plate photovoltaic performance models. The Perez model was developed using hourly average data and thermopile radiometer data. The Perez model has systematic and random errors on the lower end of the range of errors mentioned above. Applicability of the Perez model, or any of the transposition models, to higher time-resolution (e.g., sub-hourly) periods or data derived from non-thermopile radiometers is also an open research question.

Estimating Direct Beam (DNI) from Global Horizontal Radiation One of the few models to estimate direct beam from global horizontal radiation is the Maxwell DISC (Direct Solar Insolation Code) and the Perez variation on this approach, DIRINT. This model is based on empirical relations between clearness indices [69, 70] Kt, the ratio of ground global hemispherical radiation to extraterrestrial radiation (ETR) on a horizontal surface, ETR $\cos(Z)$, and Kn, the ratio of ground-measured direct beam to ETR direct beam. The model was derived using hourly average data and thermopile radiometer data. Applicability to higher time-resolution data and non-thermopile radiometers, which do not sense the entire solar spectrum, is an open research question. Basic systematic error in the DISC model is around ± 50 W/m^2, with random errors on the order of ± 150 W/m^2 in hourly data. The model was developed and validated using mid-latitude data in the United States, so it may not have included a wide enough range of solar elevation angles to be appropriate for worldwide application. However, Perez et al. [70] evaluated the model for northern European as well as US sites with results similar to those quoted above.

Estimating Diffuse Hemispherical Radiation from Global or DNI Under clear and partly cloudy conditions, diffuse sky radiation is often a relatively small part (<30%) of the total hemispherical radiation. Under dense overcast conditions, the global hemispherical and diffuse sky radiation should be identical. When diffuse sky measurements are not available, estimates of the diffuse may be needed in conjunction with global hemispherical data to estimate direct beam (as in the Maxwell DISC model discussed above). Diffuse sky radiation is also useful for daylighting applications. Many models based on empirical correlations between global hemispherical and diffuse sky radiation data have been developed. Liu and Jordan developed a model for estimating monthly average hourly diffuse. Examples of algorithms for estimating hourly diffuse have been developed by Orgill and Hollands [72], Erbs et al. [73], Spencer [74], Iqbal [52], and many others. These algorithms generally use correlations of global clearness index, Kt [hemispherical radiation divided by ETR $\cos(Z)$] and Kd [diffuse sky radiation/ETR $\cos(Z)$], which have relatively large (~30%) scatter about regression formulas of Kd vs Kt.

Solar Radiation for Solar Energy Utilization. Table 5 Typical model and validation measurement data uncertainty limits

Uncertainty source	Total hemispherical (%)	Direct normal (%)	Diffuse (%)
Measurement (development/validation)	6	5	6
Station meteorological data bias	2	4	2
Station meteorological data random (2 sigma)	8	15	8
Total expanded uncertainty: station meteorological model	10	16	10
Satellite data bias	0	4	1
Satellite data random	5	14	5
Total expanded uncertainty: satellite model	8	15	8

Model Estimate Uncertainties Empirical models derived from measured data correlations with "independent" parameters inherently carry measurement uncertainty embedded in the ultimate model accuracy. Models based on 2% or 5% or 10% accurate data can be no more accurate than the data used to generate the model. Typically, scatter about model regression lines increases the random component of uncertainty further. Models based on first principles of physics and radiation transfer cannot be validated or verified to accuracy any greater than that of the measurements. The typical accumulation of uncertainties, including validation data uncertainties similar to the accumulation of calibration transfer uncertainty in Fig. 8, is shown in Table 5. In this table, "measurement" uncertainty accounts for accuracy of measurement instrumentation as discussed in "Radiometer Calibration Sources of Uncertainty" section, accounting for sources of additional uncertainty in field measurements, such as environmental influences, above and beyond calibration uncertainty. "Station meteorological" and "Satellite data" systematic (bias) and random values are typical values derived from mean bias differences and root-mean-square published in available satellite model validation studies. "Total expanded" uncertainties are root-sum-square combinations of the bias and (two-standard deviation) random components of uncertainty along with the measurement component, which cannot be eliminated. The latter, measurement component, is itself treated as random to account for the wide variety of conditions in which the limits of uncertainty can be achieved. For the satellite data, additional sources of uncertainty – such as poor spatial resolution at high latitudes imaged at low incidence angles and coarse (typically 15- to 30-min) time resolution of images – can come into play.

Sample benchmarking of satellite-based data by the European Management and Exploitation of Solar Resource (MESOR) group has arrived at similar uncertainties for daily average estimates for total hemispherical radiation of about 9% and 20% for direct-beam radiation. Model versus measurement validation of many of the empirical and "station"-based models can be found in Muneer et al. [58].

Future Directions

The imperative to develop clean, quickly deployed, cost-effective, sustainable, and solar energy conversion systems will require more abundant and accurate solar radiation data and models. The measurement technology now in use is more than 40 years old and not adequate to meet many of the needs of the financial as well as technical communities. The mantra of "more, faster, better, cheaper," with the additional need of "higher accuracy" is highly applicable to the solar radiation measurement needs of today and the future. Instruments with improved characteristics and lower cost can be achieved with the advances in materials and detector technologies occurring now and over the past few years. Historical solar radiation data are becoming of less importance relative to data representing the present conditions where new systems might be deployed. It is much more difficult to rehabilitate old, less-accurate data than to produce very good measurement data in the first place.

Better solar instrumentation is needed to monitor more closely the performance and degradation of installed systems to ensure reliable and consistent

energy supplies. Financiers are more likely to fund those projects in which the projected risks have been mitigated by high-quality resource and performance data. For many years, 5% accuracy for solar resource data has been considered adequate. With potential investment in tens, hundreds, and thousands of megawatts of generating potential (and corresponding units of currency), single-percentage differences amount to large amounts of money (and risk).

Both measurements and modeling at much higher resolution in time and space are needed to meet the demands of risk reduction. Operational solar plants will rely on relative dense measurement networks, spread over square kilometers, to monitor system performance and identify potential problems, as well as help plan for the mitigation of transient events such as cloud passage. Forecasting models will be needed to address the next 15 min, 1 hour, 1 day, and 1 week of operations so that reliable, continuous operations of a stable input to the electrical grid can be provided. Operational considerations such as repair/replacement and cleaning of solar conversion system will depend on having adequate resource forecasts and performance data all derived from much-improved solar measurements or models that engender trust in the physical and fiscal operators of solar power plants, whether on a single building roof or a utility-scale implementation.

Applications of solar radiation measurement and model data include predicting heat and cooling loads – from the single building to city and statewide scales. These loads are directly related to energy demand and may result in integration of some aspect of solar radiation monitoring into the new "smart grid" applications of the future.

Lastly, the question of mankind's impact on the global climate and redirection of trends in climate change that can be addressed by human intervention depend on data of adequate accuracy to make a timely decision regarding human activities. More accurate measured data, and models validated to higher accuracy based on such data, provide a larger safety margin for making a timely effort to correct problems of any nature – but none more important than the climate future generations will live under. For these reasons, at least, improved solar radiation measurements are needed. A small investment in this area could be leveraged many times over both energy and climate environments.

Satellite-based observations of Earth are incrementally being improved in terms of time, space, and signal resolution. However, these resources depend on a few countries' ability to finance the design, construction, launch, maintenance, and eventual replacement of these sophisticated tools. The replacement time for these tools can be years, and the risks involved in a stressful launch are not always small.

Direct ground-based observations will always be considered the most definitive type of solar resource data and the basis for the validation of any model, no matter how sophisticated. Such measurement stations will be more accessible than any space-based observation and much more flexible. With denser, more capable, and rational measurement networks, nagging questions about long-term trends, microclimate effects, and statistical variation in multiple space/time coordinates can be addressed and quantified. More capable, accurate, and useful (in terms of worldwide, generally applicable) models will be a result of improved measurement density, accuracy, and temporal resolution. At this point, the need for these improvements is being realized. The action items that need to be undertaken are just beginning to be addressed.

Bibliography

Primary Literature

1. Cox AN (1999) Allen's astrophysical quantities, 4th edn. AIP/Springer, New York
2. Frohlich CJ (1998) Total solar irradiance variations: the construction of a composite and its comparison with models. In: International Astronomical Union Symposium 185: New eyes to see inside the sun and stars. Kluwer Academic, Dortrect
3. Whipple RS (1915) Instruments for the measurement of solar radiation. Trans Opt Soc Lond 15(1):106–182
4. Coulson KL (1975) Solar and terrestrial radiation. Academic, New York
5. Hufbauer K (1991) Exploring the sun: solar science since Galileo (Series in NASA history). Johns Hopkins University Press, Baltimore
6. Krupp EC (1978) In search of ancient astronomers. Doubleday, New York
7. Brecher K, Feirtag M (1979) Astronomy of the ancients. MIT Press, Cambridge
8. Langley SP (1883) The selective absorption of solar energy. Am J Sci Ser 3(25):169–196
9. Callendar HL, Fowler A (1906) The horizontal bolometer. Proc Phys Soc Lond A 77:15–16

10. Abbot CG, Aldrich LB (1932) An improved water-flow pyrheliometer and the standard scale of solar radiation. Smithson Misc Coll 87(15)
11. Abbot CG (1911) The silver disk pyrheliometer. Smithson Misc Coll 56(11)
12. Angstrom K (1899) The absolute determination of the radiation of heat with the electric compensation pyrheliometer with examples of application of this instrument. Astrophysical J 9:332–346
13. Angstrom AK (1919) A new instrument for measuring sky radiation. Q J R Meteorol Soc 50:124–126
14. Aldrich LB, Abbot CG (1948) Smithsonian pyrheliometry and the standard scale of solar radiation. Smithson Misc Coll 110(5)
15. Abbot CG, Aldrich LB (1916) The pyranometer – an instrument for measuring sky radiation. Smithson Misc Coll 66(7):9
16. Robitzsh M (1932) Uber den bimetallaktinographen reuss-robitzsh. Gerlands Beitr Geophys 35:387–394
17. Dirmhirn I (1958) Untersuchengen an sternpyranometern. Arch Meteorol Geophysik Bioklimat B 7:124–128
18. Yanishevski YD (1957) Actinometric instruments and methods of observation. Hydrometeorological Publishing House, Leningrad
19. Kendall JM, Berdahl CM (1970) Two blackbody radiometers of high accuracy. Appl Opt 9(5):1082–1091
20. Willson RC (1973) Active cavity radiometer. Appl Opt 12(4):810–817
21. Crommelynck D, Hall JB (1982) Fundamentals of absolute pyrheliometry and objective characterization. NASA CP-2239. National Aeronautics and Space Administration
22. Brusa RW, Frohlich C (1980) The PMO-6 radiometer and its characterization. World Radiation Center, Davos
23. Hickey JR, Drummond AJ, Thekaekara MP (1973) A satellite experiment to establish the principal extraterrestrial solar energetic fluxes and their variances. The Extraterrestrial Solar Spectrum, Institute of Environmental Sciences, Mount Prospect
24. Smith WL, Hickey J, Howell HB, Jacobowitz H, Hilleary DT, Drummond AJ (1973) Nimbus-6 earth radiation budget experiment. Appl Opt 13(3):306–318
25. Frohlich C (1978) World radiometric reference. WMO/CIMO Final Report WMO No. 490. World Meteorological Organization, Geneva, pp 108–112
26. WMO (1983) OMM No. 8 guide to meteorological instruments and methods of observation, 5th edn, vol 8. Secretariat of the World Meteorological Organization, Geneva
27. Frohlich C (1991) History of solar radiometry and the world radiation reference. Metrologia 28:111–115
28. Romero J, Fox NP, Frohlich C (1996) Improved comparison of the world radiometric reference and the SI radiometric scale. Metrologia 32(6):523–524
29. Ruedi I (2001) International pyrheliometer comparison IPC IX. Meteoswiss Working Report No. 197. Davos, Zurich, http://www.pmodwrc.ch/pdf/ipc9-final.pdf
30. Reda I, Stoffel T, Myers D (1996) Calibration of a solar absolute cavity radiometer with traceability to the World Radiometric Reference. NREL/TP-463-20619. National Renewable Energy Laboratory, Golden. http://www.nrel.gov/docs/legosti/fy96/20619.pdf
31. ASTM E816-05 (2005) Standard test method for calibration of pyrheliometers by comparison to reference pyrheliometers. ASTM International, West Conshocken
32. ISO (1990) Standard 9050: solar energy – calibration of field pyrheliometers by comparison to a reference pyrheliometer. American National Standards Institute, New York
33. ASTM G167-05 (2005) Standard test method for calibration of a pyranometer using a pyrheliometer. ASTM International, West Conshocken
34. ISO (1990) Standard 9060: solar energy – specification and classification of instruments for measuring hemispherical solar and direct solar radiation. American National Standards Institute, New York
35. Reda I, Myers D (1999) Calculating the diffuse responsivity of solar pyranometers. NREL/TP-560-26483, National Renewable Energy Laboratory, Golden
36. Reda I, Stoffel T, Myers D (2003) A method to calibrate a solar pyranometer for measuring reference diffuse irradiance. Sol Energy 74:103–112
37. BIPM (1995) Guide to the expression of uncertainty in measurement. BIPM, http://www.bipm.org/utils/common/documents/jcgm/JCGM_100_2008_E.pdf
38. Myers DR, Emery KA, Stoffel TL (1989) Uncertainty estimates of global solar irradiance measurements used to evaluate PV device performance. Sol Cells 27:455–464
39. Taylor BN, Kuyatt CE (1993) Guidelines for evaluation and expressing the uncertainty of NIST measurement results, NIST Technical Note 1297. National Institute of Standards and Technology, Gaithersburg
40. Ohmura A, Dutton E, Forgan B, Fröhlich C, Gilgen H, Hegner H, Heimo A, König-Langlo G, McArthur B, Muller G, Phillapona R, Pinker R, Whitlock C, Dehne K, Wild M (1998) Baseline Surface Radiation Network (BSRN/WCRP): New precision radiometry for climate change research. Bull Am Meteorol Soc 79(10):2115–2136
41. Gulbrandsen A (1978) On the use of pyranometers in the study of spectral solar radiation and atmospheric aerosols. J Appl Meteorol 17:899–904
42. Haeffelin M, Smith AM, Mahan JR, Rutledge CK, Kato S (1999) Surface shortwave radiation measurements: experimental tests and numerical simulations of pyranometers. Ninth ARM Science Team Meeting, U.S. Department of Energy, San Antonio
43. Haeffelin M, Kato S, Smith AM, Rutledge CK, Charlock TP, Mahan JR (2001) Determination of the thermal offset of the Eppley precision spectral pyranometer. Appl Opt 40(4): 472–484
44. Dutton EG, Michalsky JJ, Stoffel T, Forgan BW, Hickey J, Alberta TL, Reda I (2001) Measurement of broadband diffuse solar irradiance using current commercial instrumentation with a correction for thermal offset errors. J Atmos Oceanic Technol 18(3):297–314

45. Philipona R (2002) Underestimation of solar global and diffuse radiation measured at the Earth's surface. J Geophys Res 107(D22):ACL 15-1-ACL 15-8
46. Reda I (1998) Improving the accuracy of using pyranometers to measure clear sky global irradiance. NREL/TP-560-24833, National Renewable Energy Laboratory, Golden
47. Reda I, Myers D, Stoffel T (2009) Uncertainty estimate for the outdoor calibration of solar pyranometers: a metrologist perspective. J Meas 3(4):58–66 NCSL International, Boulder
48. Vignola F, Reda I (1998) Responsivity of an Eppley NIP as a function of time and temperature. In: Proceedings of the 1998 American Solar Energy Conference, Albuquerque. American Solar Energy Society, Boulder
49. Perez R, Stewart R (1986) Solar irradiance conversion models. Sol Cells 18:213–222
50. Muneer T, Younes S, Munnawar S (2007) Discourses on solar radiation modeling. Renewable Sustainable Energy Rev 11:551–602
51. Muneer T (2004) Solar radiation and daylight models. Elsevier. Butterworth and Heinemann, Oxford
52. Iqbal M (1983) An introduction to solar radiation. Academic, New York
53. Badescu V (2008) Modeling solar radiation at the earth surface. Springer, Berlin
54. Bird RE, Hulstrom RL (1981) Review, evaluation, and improvement of direct irradiance models. J Sol Energy Eng Am Soc Mech Eng 103:182–192
55. Gueymard C (2008) REST2: high performance solar radiation model for cloudless-sky irradiance, illuminance, and photosynthetically active radiation-validation with a benchmark data set. Sol Energy 82:272–285
56. Ineichen P (2006) Comparison of eight clear sky broadband models against 16 independent data banks. Sol Energy 80:468–478
57. Wong LT, Chow WK (2001) Solar radiation model. Appl Energy 69:191–224
58. Muneer T, Gul MS, Kubie J (2000) Models for estimating solar radiation and illuminance from meteorological parameters. J Sol Energy Eng Am Soc Mech Eng 122:146–153
59. Gueymard C (2003) Direct solar transmittance and irradiance predictions with broadband models. Part I: detailed theoretical performance assessment. Sol Energy 74:355–379
60. Kasten F, Czeplak G (1980) Solar and terrestrial radiation dependent on the amount and type of cloud. Sol Energy 24:177–189
61. Cano D, Monget JM, Albuisson M, Guillard H, Regas N, Wald L (1986) A method for the determination of the global solar radiation from meteorological satellites data. Sol Energy 37:31–39
62. Diabaté L, Moussu G, Wald L (1989) Description of an operational tool for determining global solar radiation at ground using geostationary satellite images. Sol Energy 42:201–207
63. Perez R, Ineichen P, Moore K, Kmiecik M, Chain C, George R, Vignola F (2002) A new operational model for satellite derived irradiances: description and validation. Sol Energy 73(5): 307–317
64. Šúri M, Huld T, Dunlop ED, Albuisson M, Lefèvre M, Wald L (2007) Uncertainties in photovoltaic electricity yield prediction from fluctuation of solar radiation. In: Proceedings of the 22nd European Photovoltaic Solar Energy Conference, Milano
65. Gueymard C, Wilcox S (2009) Spatial and temporal variability in the solar resource: assessing the value of short term measurements at potential solar power plant sites. In: Proceedings of Solar 2009, Buffalo, May 11–16, 2009. American Solar Energy Society, Boulder
66. Maxwell EL (1998) METSTAT – The solar radiation model used in the production of the National Solar Radiation Data Base (NSRDB). Sol Energy 62(4):263–279
67. Gueymard C (2009) Direct and indirect uncertainties in the prediction of tilted irradiance for solar engineering applications. Sol Energy 83:432–444
68. Perez R, Seals R, Ineichen P, Stewart R, Menicucci D (1987) A new simplified version of the Perez diffuse irradiance model for tilted surfaces. Sol Energy 39(3):221–231
69. Maxwell E (1987) A quasi-physical model for converting hourly global horizontal to direct normal insolation. SERI/TR-215-3087, Solar Energy Research Institute, Golden
70. Liu BYH, Jordan RC (1960) The interrelationship and characteristic distribution of direct diffuse and total solar radiation. Sol Energy 3:1–19
71. Perez R, Seals R, Zelenka A, Ineichen P (1990) Climatic evaluation of models that predict hourly direct irradiance from hourly global irradiance: prospects for performance improvements. Sol Energy 44(2):99–108
72. Orgill JF, Hollands KG (1977) Correlation equation for hourly diffuse radiation on a horizontal surface. Sol Energy 19(4): 357–359
73. Erbs DG, Klein SA, Duffie JA (1982) Estimation of the diffuse radiation fraction for hourly, daily, and monthly average solar radiation. Sol Energy 28(4):293–304
74. Spencer JW (1982) A comparison of methods for estimating hourly diffuse solar radiation from global solar radiation. Sol Energy 29(1):19–32

Books and Reviews

Bohren CF (1989) Selected papers on scattering in the atmosphere. SPIE Milestone Series vol MS 7, SPIE Optical Engineering Press. Bellingham, WA

Chandrasekhar S (1960) Radiative transfer. Dover, New York

Deick RH (1992) Measurement uncertainty methods and applications. Instrument Society of America, Research Triangle Park

Dogniaux R (1994) Prediction of solar radiation in areas with a specific microclimate. Commission of the European Communities. Kluwer Academic, Dordrecht

Duffie JA, Beckman WA (1975) Solar energy thermal processes. Wiley, New York

Farmer WM (2001) The atmospheric filter, vol 1. Sources. JCD, Winter Park

Farmer WM (2001) The atmospheric filter, vol 2. Effects. JCD, Winter Park

Fleagle RG, Businger JA (1980) An introduction to atmospheric physics, 2nd edn. International Geophysics Series Vol 25, Academic, New York
Hulstrom RL (1989) Solar resources. MIT Press, Cambridge
Kondratyev KY (1965) Radiation in the atmosphere. International Geophysics Series Vol 12, Academic, New York
Kreith F, Kreider JF (1978) Principles of solar engineering. McGraw Hill, Hemisphere
Kyle TG (1991) Atmospheric transmission. Pergamon, Oxford
Liou K (1980) An introduction to atmospheric radiation. International Geophysics Series Vol 26, Academic, New York
Martin CL, Goswami DY (2005) Solar energy pocket reference. James and James, Earthscan
McCluney R (1994) Introduction to radiometry and photometry. Artech House, Boston
Marshak A, Davis AB (2005) 3 D radiative transfer in cloudy atmospheres. Springer, Berlin
Osborn DE (1993) Selected papers on solar radiation and solar thermal systems. SPIE Milestones Series Vol MS 34 SPIE Optical Engineering Press. Bellingham, WA
Paltridge GW, Platt CMR (1976) Radiative processes in meteorology and climatology. Elsevier, Amsterdam
Sayigh AAM (1977) Solar energy engineering. Academic, New York
Sen Z (2008) Solar energy fundamentals and modeling techniques: atmosphere, environment, climate change and renewable energy. Springer, Berlin
Spiro IJ (1990) Selected papers on radiometry. SPIE Milestones Series Vol MS 14, SPIE Optical Engineering Press. Bellingham, WA
Thomas GE, Stamnes K (1999) Radiative transfer in the atmosphere and ocean. Cambridge University Press, Cambridge
White OR (1977) The solar output and its variation. Colorado Associated University Press, Boulder

Solar Radiation Management, Cloud Albedo Enhancement

Stephen H. Salter
Institute for Energy Systems, School of Engineering, The University of Edinburgh, Scotland, UK

Article Outline

Glossary
Definition of the Subject
Introduction
Energy Requirements
Treatment Sites
Environmental Impacts
Future Directions
Conclusions
Bibliography

Glossary

Albedo Whiteness or reflectivity. The ratio of outgoing to incoming radiation power.

Cloud condensation nuclei The small fragment of material needed to start the growth of a cloud drop when the local relative humidity exceeds 100%.

MODIS An acronym for moderate resolution imaging spectroradiometer. This is an instrument carried by two NASA satellites Aqua and Terra. The systems measure 36 spectral bands of radiation of the entire earth surface. Results are available free and are an invaluable aid to research into climate change.

Permafrost Ground which remains frozen throughout the year. It can trap very large amounts of methane which would be released if it were to melt.

Positive feedback A change in the value of a variable which leads to a further change in the same direction. It can often produce explosive effects and oscillations.

Relative humidity The ratio of the amount of water vapor in a parcel of air to the maximum amount that it could hold if nucleating particles were present. Values can exceed 100% and even reach 300% if all nuclei are absent.

Solar constant The rate at which solar energy of all wavelengths crosses unit area at the top of the atmosphere. It is about 1,366 W/m^2 but is strictly not quite constant. There are cyclical variations with an amplitude of about 3.5% due the ellipticity of the earth's orbit around the sun, 11 year cycles and faster random variations of about 0.1%.

Twomey effect The relationship of cloud albedo to cloud depth, liquid water content and concentration of cloud condensation nuclei elucidated by Sean Twomey. His work began following observation of increased albedo of ships tracks in satellite photographs.

Definition of the Subject

Cloud albedo enhancement is one of several possible methods of solar radiation management by which the rate of increase in world temperatures could be reduced

or even reversed. It depends on a well-known phenomenon in atmospheric physics known as the Twomey effect. Twomey argued that the reflectivity of clouds is a function of the size distribution of the drops in the cloud top. In clean mid-ocean air masses, there is a shortage of the condensation nuclei necessary for initial drop formation in addition to high relative humidity. This means that the liquid water in a cloud has to be in relatively large drops. If extra nuclei could be artificially introduced, the same amount of liquid water would be shared among a larger number of smaller drops which would have a larger surface area to reflect a larger fraction of the incoming solar energy back out to space.

Introduction

At noon in the tropics, the top of the Earths' atmosphere receives about 1,350 W/m^2 from the sun. This is known as the solar constant but varies slightly with solar activity and orbital changes. Because of the high source temperature, most of the solar energy is spread over the short wavelengths – those to which our eyes have evolved. Some is reflected back to space, and some is absorbed by gases and particles in the atmosphere, thereby increasing their temperature. The amount reaching cloud level over 24h is about 440 W/m^{2}at the equator and about 340 W/m^2 globally. Some radiation is absorbed by clouds. Some passes through to reach the ground. Radiation from bodies at lower temperatures is at much longer wavelengths where atmospheric gases have different absorption properties.

Changes in the concentrations of atmospheric gases will affect the amount of heat retained, and the temperature then has to rise to restore the energy balance by increasing outward radiation. While much attention is given to carbon dioxide, many other gases are involved, some with stronger absorbing properties, particularly water vapor and methane. The maximum atmospheric water vapor concentration increases with temperature giving a positive feedback, but it can be rapidly returned to the sea as precipitation and condensation. A more abrupt and less reversible positive feedback could be triggered by the release of methane from melting permafrost.

It is widely thought that the change of atmospheric carbon dioxide and other greenhouse gases since pre-industrial times together with the resulting water vapor amplification has increased the amount of heat retained by the earth at a rate of about 1.6 W/m^2. This is only 0.0047 or one part in 212 of the 340 W/m^2 mean 24 h input. It is therefore possible that a very small increase in the reflectivity of the earth could reduce, cancel, or even reverse the anthropogenic increase and so provide time for the development of low-carbon energy sources and carbon sequestration.

Clouds cover a substantial fraction of the earth's surface and are good reflectors of solar energy. However, cloud drops cannot form without an initial small "seed" known as a condensation nucleus. In 1990, John Latham [1] proposed that the reflectivity of marine stratocumulus clouds could be increased by spraying submicron drops of sea water into the marine boundary layer. The drops would evaporate to leave salty residues. Air flows in the marine boundary layer are quite turbulent, and the residues would soon be well mixed through it. Salty particles are hydrophilic and so are ideal condensation nuclei. The most effective size range for nucleation is between 0.5 and 1 μm. Those nuclei which reach cloud level provide the seeds for new drops and so trigger the Twomey effect. Twomey [2] argued that the reflectivity of a cloud depends on its depth Z in meters, the liquid water content L in milliliters of water per cubic meter of air, and the drop concentration expressed in the number per cubic centimeter.

It may be convenient to rewrite the equations in Twomey's original paper with an intermediate term $K(Z, L, n) = 0.15\, Z\, L^{2/3} n^{1/3}$. Cloud albedo A is then

$$A(Z, L, n) = \frac{K(Z, L, n)}{K(Z, L, n) + 0.827}$$

Figure 1, adapted from Schwarz and Slingo [3], shows a plot of the relationship. For the typical range of conditions, a doubling of the number of nuclei will increase reflectivity by 0.056 from an initial value of 0.3–0.7. The vertical bars mark present condensation nuclei concentrations for clean mid-Pacific air and dirtier Atlantic air suggested by Bennartz [4] based on analysis of satellite observations.

It is the fractional increase in the number of nuclei in the effective diameter range that matters, not the amount of water sprayed. This means that the technique is far more effective in clean air and has

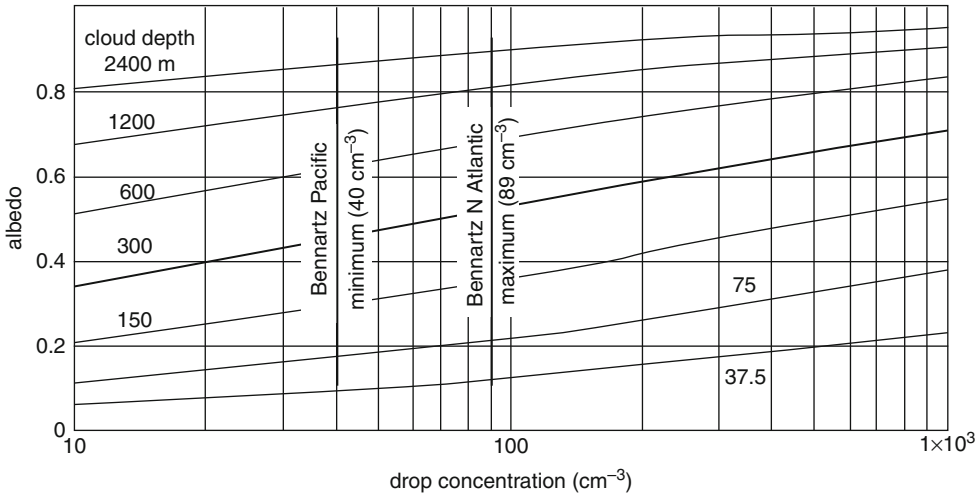

Solar Radiation Management, Cloud Albedo Enhancement. Figure 1
Twomey's results for cloud albedo as a function of cloud depth, a typical liquid water content of 0.3 g/m^3 of air and drop concentration (Adapted from Schwarz and Slingo [3] with Bennartz [4] data for drop concentration)

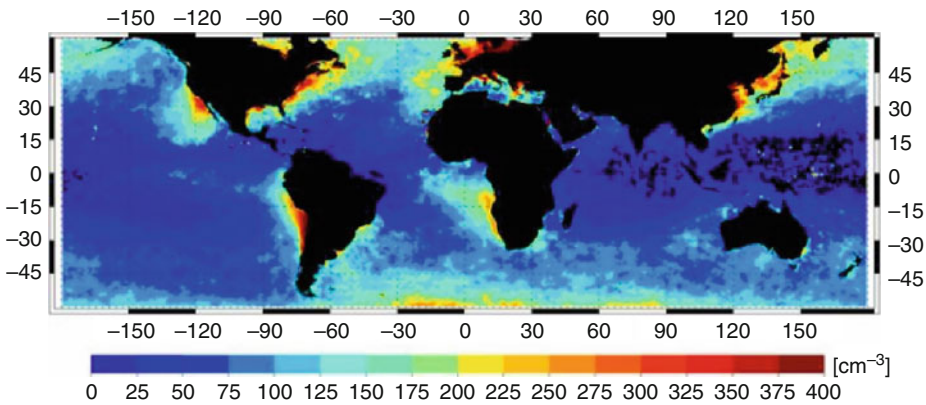

Solar Radiation Management, Cloud Albedo Enhancement. Figure 2
Cloud droplet concentration for warm clouds as estimated by the MODIS instruments (Courtesy of NASA and Robert Wood of the University of Washington)

diminishing returns as treatment progresses. If atmospheric observations are taken from short-range aircraft, there will be a bias towards higher numbers. Figure 2 shows worldwide drop concentration supplied by Wood [5] from the MODIS instrument on Aqua and Terra satellites [6]. Large areas of mid oceans have concentrations below 50 cm^{-3}. In some air masses, which have been over Antarctica for long periods or washed by recent rain, the concentration can be as low as 10 cm^{-3}. In contrast, values over land can be 1,000–5,000 cm^{-3}.

Latham found that, with the correct drop size, the amounts of spray needed to give a useful reduction of incoming power are surprisingly small. Figure 3 shows cooling for 340 W/m^2, a fairly typical selection of cloud depth liquid water content, the nuclei concentrations suggested by Bennartz and their mean. There is some uncertainty about lifetime of the condensation nuclei. This graph uses a half-life of 59 h from Smith et al. [7] and is in good agreement with Hoppel et al. [8] which shows half-life as a function of drop diameter. If the assumptions on the right of the figure are reasonable,

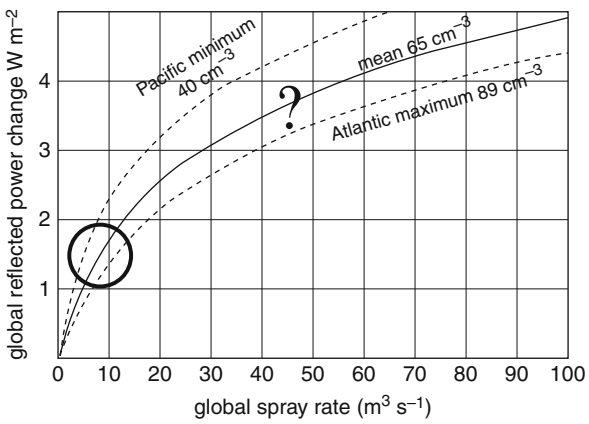

assumptions and sources

boundary layer depth	1000 m
cloud depth	300 m
Schwartz and Slingo (1996)	
liquid water	0.3 ml m^{-3}
Schwartz and Slingo (1996)	
drop life	59 h
Smith et al. (1991)	
low, not high, cloud fraction 0.18	
Charlson et al. (1987)	
initial albedo	0.495
24 h power in	340 Wm^{-2}

Solar Radiation Management, Cloud Albedo Enhancement. Figure 3
Global cooling as a function of spray rate for the assumptions in the table to the right. The circle shows 1.6 W/m^2, often taken as a figure for anthropogenic change since pre-industrial times. The question mark might be the result of a doubling of carbon dioxide

then the thermal damage since pre-industrial times could be offset by spraying about 10 m^3/s worldwide.

Several independent climate models [9, 10] support the effectiveness of Latham's proposal, and in some conditions, in clouds with no internal drizzle, the models predict an albedo change exceeding 0.4. In very rare circumstances with exceptionally clean air, it may be possible to produce clouds from a clear sky. However, the intention is to make existing clouds whiter.

Energy Requirements

The minimum energy requirement to produce a drop is the product of its surface area and its surface tension. For sea water, the surface tension is 0.078 N/m, a little higher than for fresh water, so making a 0.8 μm diameter drop needs at least 1.57×10^{-13} J. When a condensation nucleus reaches the cloud level, it will split an existing drop into two smaller ones with the same volume of liquid but with a reflecting area increased by the cube root of two, about 1.26. Figure 4 shows the range of drop sizes (in radius as used by scientists, not in diameter used by engineers) with much larger ones over mid ocean.

The solar energy that will be reflected by the two new drops will depend on the input power density, the time before the two drops coalesce and the effective reflection coefficient. The reflection coefficient of drops is an extremely complicated function, Mie [11] Laven [12], of wavelength, polarization, and angle of incidence but is of the order of 10%. Few people can believe the magnitude of the ratio of energies of reflected solar radiation to nucleus creation until they have done the calculations for themselves. Figure 5 demonstrates the effect of drop sizes on reflectivity using glass balls.

Treatment Sites

Good sites for spraying need incoming sunshine, low marine stratocumulus clouds, and clean air. The clean air requirement points to regions away from land masses and shipping routes. The sunshine requirement suggests the ability to migrate with the seasons so as to make use of the long hours of summer sunshine at high latitudes. The cloud requirement is less critical than the other variables. Cloud coverage may be inversely related to longer drop life. Spray produced under clear skies evaporates to leave a crystal of dry salt which would be much smaller than the typical 25 μm diameter liquid drop in a cloud but which would have an albedo well above a liquid drop and a lifetime which could be much longer. Furthermore, it is better to have a low dose over wide a area, and spray under clear skies would be more widely dispersed. It might be attractive to spray in air which we expect will later move to a cloudy region.

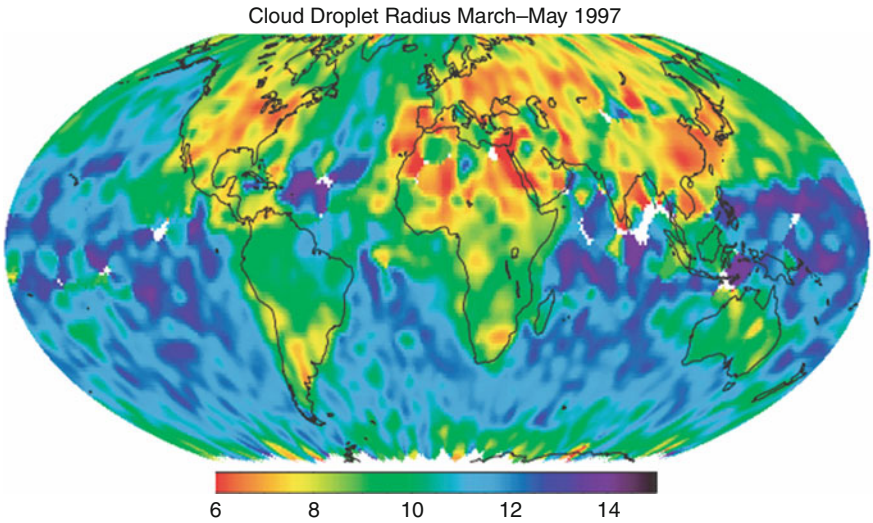

Solar Radiation Management, Cloud Albedo Enhancement. Figure 4
Cloud droplet *radius* derived by Breon Tanre and Generoso (Courtesy of Science. From http://www.sciencemag.org/content/295/5556/834.full.pdf)

Solar Radiation Management, Cloud Albedo Enhancement. Figure 5
The jar on the *left* contains 4 mm glass balls. The *grey scale* behind the jars has 10 bars going from roughly zero to nearly 100% whiteness depending on your printer and paper quality. This shows that the albedo of the 4 mm balls is about 0.6. The jar on the *right* contains 40 μm glass balls, 100 times smaller, and has an albedo of about 0.95

Mobility, energy, and long duty periods can be provided by unmanned sailing vessels. The chief engineering problem is the production of the correct diameter spray from a mechanism with a long service life, low energy requirements, and no need of supplies from land. A narrow range of diameters may reduce the probability of drop collision leading to coalescence which would shorten drop life and it may turn out to be useful to adjust diameter with remote commands. A number of techniques are being studied by Neukermans (2010, 2011, personal communication), Salter [13].

Environmental Impacts

Evaporation of water from the oceans is about 14 million tonnes a second of which about 12.8 million tonnes per second is precipitated back to the sea. There is no need to fear anything from the direct water output from spray vessels.

Breaking waves produce a wide range of drop sizes all over the oceans but especially at beaches. It is not easy to get a number for the salt transfer but Blanchard [13] explains the ways that an attempt could be made. Grini et al. [14] survey more recent estimates. These range from 1000 to 10,000 million tonnes a year or from 30 to 300 tonnes a second. Ten tonnes of sea water, a second needed to cancel 1.6 W/m^2, would transfer 350 kg of salt per second. What makes the salt from spray vessels so much more effective is the controlled size of the salt residues. Most of them would be returned to the sea and so would be very small compared with spray from beaches, much of which goes inland.

However, Victorian doctors knew very well that sea air was good for lung infections. A Polish doctor F Boshkowsky noticed that his patients who worked in the salt mines had no lung illness and enjoyed long lives despite hardworking conditions. In Eastern Europe, salt mine exposure is used for treating asthma, and in the West, there is a brisk trade in salt pipes. There is no need to worry about the effect of salt from spray vessels on human health.

The immediate effect of albedo control is a reduction of the sea surface temperature below the treated cloud. The reduction will be small compared with the normal changes from cloud to clear sky and even less compared with the change from day to night. But sea surface temperatures are a very strong driver for many other meteorological parameters. The laws of thermodynamics predict that although the effect will eventually diffuse worldwide, there can also be local deviations, and operators will have to build up a clear understanding of all the outcomes.

The greatest anxiety about side effects concerns changes to precipitation. Changes in either direction could be bad. During 2010 and 2011, there was severe drought in Russia and the most violent flooding in Pakistan, Queensland, Brazil, and Sri Lanka before anyone had attempted any form of intentional geoengineering. It may be that we have to choose the least bad outcome. But if we understand meteorology properly, we may be able to improve things in different places by drying out wet regions and getting more rain to dry ones. At least eight mechanisms are involved, and some, especially precipitation, are not well represented in present climate models. As so often in meteorology, factors can work in opposite directions, and we may be ignorant even of the polarity, let alone the magnitude, of the final outcome.

The mechanisms so far identified are:

1. The production of rain needs some large drops to fall through deep clouds fast enough to coalesce with other drops in their path so that they grow large enough to fall fast enough to reach the ground without evaporating in the dry air below a cloud. It is known from Albrecht [15] and Konwar et al. [16] that rain is less likely if there are too many small drops due to smoke and fine dust. This happens over land and could happen as a result of cloud albedo control but the depth of marine stratocumulus is mostly too thin to form rain and the effect might be to extend cloud lifetime.
2. However, if more small cloud drops means that there is less rainfall *over the sea*, it follows that there will be more water left in the air mass when it reaches land. The air mass will travel further inland before the original drop numbers are restored by coalescence. Rain inland is more valuable than rain at the coast.
3. Any reduction in sea temperature will tend to reduce evaporation and increase condensation from air back to the sea surface and this will reduce the water content of the atmosphere. The increase in evaporation rate increases sharply at sea surface temperatures around 28°C [17] and may have contributed to recent floods.
4. But cooling the sea means a larger difference between the temperatures of sea and land, more monsoon effect, with stronger winds bringing more water to land.
5. Wind is caused by differences in pressure which are a result of local temperature gradients. Wind causes turbulence in the marine boundary layer. The relative humidity is very high in the stagnant layer of air at distances of millimeters above the sea surface but falls to around 65% a few meters above. Turbulence has a much greater influence on evaporation rate than water temperature except at temperatures above about 27.5°C.
6. Wind makes waves steeper. Spilling breakers mix the thin top layer of water that has been chilled by evaporation and warm it with heat from below. Plunging breakers drive bubbles below the surface and throw spray above it to transfer more water vapor in the air. Evaporation rises steeply if wind speeds exceed 13 m/s.
7. If cloud albedo control at sea reduces temperatures on land, it will also reduce the evaporation rate so more of the precipitation will be retained as ground water.
8. Finally, we know that the regions with the most severe drought problems are dry because air which has been dried by being high in the atmosphere is subsiding and moving out to sea. This means what we do at sea cannot immediately affect the very driest land nearby.

A computer experiment by Jones, Hayward and Boucher [18] illustrates the possibilities. Their world climate model was set to allow the concentration of condensation nuclei to be increased in three small regions together representing 3.3% of the world area. Spray off California nearly doubled rainfall in the drought-stricken region of central Australia and caused a smaller increase in the Southern part of the Amazon basin. Spray off Peru increased rain in Brazil but reduced it in Argentina. But spray off Namibia produced a reduction of about 320 mm a year over most of the Amazon basin which could be partly offset by spray from the Pacific sites.

The spray was applied through the year rather than in any way related to the monsoon phase or wind direction and was confined to the small areas, which would probably not be realistic. But the important result of this work is that we can get changes in precipitation in either direction at distances far from the spray source. It would be no great surprise if the effects were strongly affected by the spray season relative to the monsoon cycle but this has not yet been established.

Other workers [10] have used treatment over much wider areas and have not observed similar effects. In particular, Bala [19] has found the net effect for the Indian subcontinent of widespread long-term cloud albedo control was slightly lower precipitation but a slightly greater run off from the Indian subcontinent because of slower evaporation of ground water in lower temperatures. Another result from [10] is that cloud albedo control carried out well away from the Arctic can reduce the rate of Arctic ice loss and so might prevent an irreversible tipping point. However, the better the climate modeler, the more caveats will accompany the predictions. Present models are not good at predicting precipitation.

It may be possible to use climate models to predict an everywhere-to-everywhere transfer function using pseudo random sequences of increases and reductions of the concentration numbers of condensation nuclei with different sequences in many regions. The sequences would be correlated with the computer model results of all the many meteorological parameters of interest. If small random changes are made to a signal consisting of 20 years of daily observations of temperature records, the scatter of the correlation is about 1% of the standard deviation of the variation of the original record, so very small signals can be detected. More importantly, the processes do not interfere with each other, so all can be done at the same time. By doing the correlations with variable time delays, we can gain information about the frequency response of the climate system.

Engineers know that an accurate control system needs a good way to measure the deviation from the desired state. The resulting error signal should then drive some form of correcting mechanism. Small errors need a high loop gain but require a high-frequency response with a low phase-shift if oscillations are to be avoided. Satellites, perhaps with their temperature-sensing analysis algorithms improved by true data collected from spray vessels, will be able to give fast and accurate measurements of worldwide sea temperatures. Particular attractions of cloud albedo control are that the introduction can be progressive and that the response is both fast and, initially at least, locally precise.

If we understand the flow patterns of winds and currents, we can aim immediate effects at specific regions to preserve Arctic sea ice and coral reefs or protect flood sensitive areas. Even if our understanding is not perfect, we can still apply neural network technology to guide deployment. Few people can explain how to ride a bicycle but many people can ride one. Some atmospheric physicists have said, perhaps not entirely seriously, that while saving humanity's existence on the planet might be regarded as a useful spin-off, the real value of cloud albedo control would be the gain in understanding of atmospheric aerosols.

It is reasonable to suppose that attempts to keep sea surface temperature at previous levels would be less damaging than unbridled increases which seem to be occurring now. Cloud albedo control is like adding steering, brakes and a reverse gear to an unfamiliar vehicle in which the foot of a criminal lunatic is pressing hard on the accelerator. One's first training in the use of a new machine tool should be finding the emergency stop button. It is comforting to know that if we command all vessels to stop spraying, the status quo ante will be restored in a few days. This offsets the frequent criticism of geoengineering by people hostile to it – that once you start using it you have to keep on doing it. This of course could also be an objection raised against electricity generation, sewage treatment, computing, money, and kidney dialysis machines.

If you cut the strings of a parachute, you will quickly revert to your previous, rather high terminal velocity. It is a good idea not to cut the strings until you are on the ground being dragged along by a cross wind. In fact, we only have to keep using cloud albedo control until low carbon sources have been developed and excess atmospheric carbon dioxide or methane have sequestrated down to acceptable levels. The fact that the models say that the system quickly reverts gives comfort that we have done nothing irreversible.

Future Directions

Most people working in geoengineering do so with reluctance in the fear that action may be needed before low-carbon energy technologies can be deployed or atmospheric carbon dioxide removed on a sufficient scale. Even if politically impossible, reductions in emissions could take place today; our past emissions have still to take full effect. It is also possible that carbon dioxide may not be the only source of climate change with methane from permafrost increasing fast and possibly able to take the dominant role.

However, humanity is very ingenious at inventing reasons not to take unpleasant actions and ignoring reality. There are many organizations which have to protect their investments and which have perfected the skills to lobby politicians, some of whom were the same people who played a leading part in delaying the development of renewable energy. Despite achieving no reduction in atmospheric carbon dioxide, as shown by the continued acceleration of the Keeling curve, the carbon trading market has been very profitable, and people taking the profits have no wish to have competition from a parallel thermal trading market.

The near future will see activity on computer modeling of all the possible geoengineering techniques with about half the funding aimed at discrediting the ideas. Politicians try to follow public opinion rather than lead it, and until there has been much more suffering from climate extremes, there will be no political advantage in supporting the development of practical working hardware.

However, if spray hardware can be built, there are problems about producing experimental proof of successful operation because the change of cloud brightness needed is well below the contrast detection threshold of the human eye. A possible solution involves taking a large number of satellite photographs of cloud fields, shifting them to align the spray source, rotating them to align the local wind directions, and taking a pixel by pixel average of the full set. The cloud variations will be suppressed to converge towards a middle grey while the wakes downwind of the spray source emerge from the mist. Figure 6 (left) shows a single cloud image with

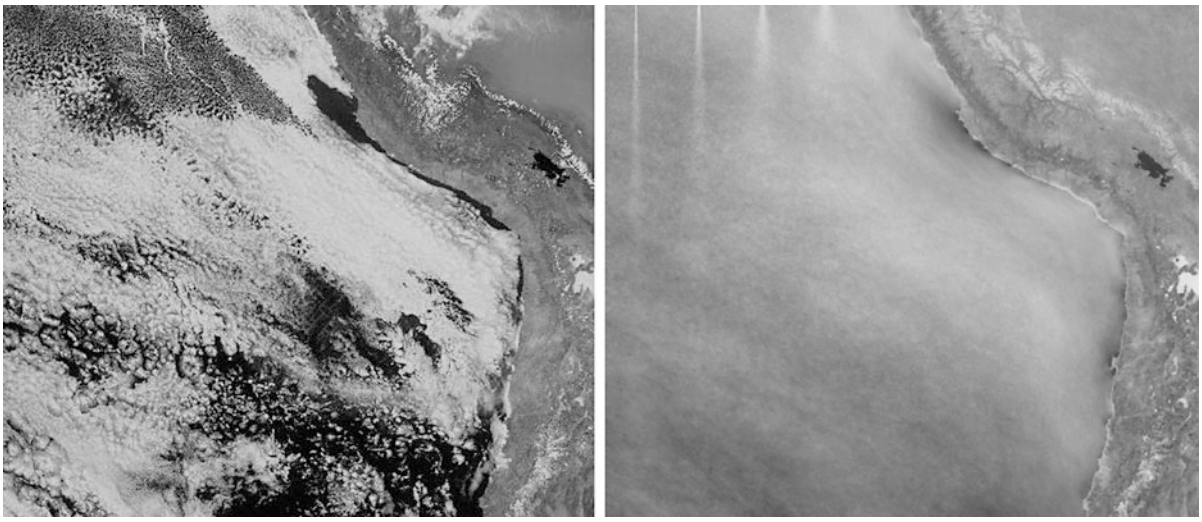

Solar Radiation Management, Cloud Albedo Enhancement. Figure 6
Contrast enhancement by image superposition to demonstrate the effectiveness of small spray sources (Courtesy of NASA and Robert Wood and the VOCALS experiment)

four, mathematically generated 30-kg/s spray sources at four dispersion angles and contrast set by the Twomey equation. It would take a great deal of confidence to use the very faint vertical streak at the top left as proof. Figure 6 (right) shows the same wake patterns in 100 real superimposed images supplied from the VOCALS experiment off South America. The experiment should be done in a long cruise covering many sea areas and several months because the places where the system does not work will be just as interesting as those where it does.

Conclusions

By 2010, four independent climate models confirmed that the Twomey effect could be exploited to control world temperatures by the deliberate increase of cloud condensation nuclei produced from submicron sea spray.

One model shows that spray from small regions can affect precipitation in either direction at other, very distant regions, but this is not confirmed by studies of wider treatment areas.

With proper understanding of the results of pseudorandom increase and decrease of the concentration of cloud condensation nuclei in climate models, we may learn how to control fleets of spray vessels to obtain beneficial reduction of droughts, the prevention of floods, and increases in ice cover by the correct choices of place and season for spray operations.

The chief engineering problem for the cloud albedo system is the development of mobile, energy efficient spray sources of submicron monodisperse spray which can operate for long periods in any chosen set of mid-oceanic sites.

The effectiveness of cloud albedo control can be demonstrated with a small spray source by superimposing and aligning around 100 satellite images.

Bibliography

1. Latham J (1990) Control of global warming? Nature 347: 339–340. doi:10.1038/347339b0E
2. Twomey S (1977) Influence of pollution on the short-wave albedo of clouds. J Atmos Sci 34:1149–1152. doi:10.1175/1520 0469(1977) 034!1149:TIOPOTO2.0.CO;2
3. Schwartz SE, Slingo A (1996) Enhanced shortwave radiative forcing due to anthropogenic aerosols. In: Crutzen P, Ramanathan V (eds) Clouds, chemistry and climate. Springer, Heidelberg, pp 191–236
4. Bennartz R (2007) Global assessment of marine boundary layer cloud droplet number concentration from satellite. J Geophys Res 112:D02201. doi:10.1029/2006JD007547
5. Wood R (in press) http://www.atmos.washington.edu/%7Erobwood/papers/geoengineering/final_jl_philtv17101104.pdf
6. NASA website http://modis.gsfc.nasa.gov/
7. Smith MH, Park PM, Consterdine IE (1991) North Atlantic aerosol remote concentrations measured at a Hebridean coastal site. Atmos Environ A 25:547–555. doi:10.1016/0960-1686(91) 90051-8
8. Hoppel WA, Frick GM, Fitzgerald JW (2002). Surface ocean function for sea-salt aerosol dry deposition to the ocean surface. J Geophys Res 107(D19) doi:10.1029/2001JD002014 See Figure 5
9. Latham J, Rasch P, Chen C, Kettles L, Gadian A, Gettelman A, Morrison H, Bower K, Choularton T (2008) Global temperature stabilization via controlled albedo enhancement of low-level maritime clouds. Phil Trans Roy Soc A 366. doi:10.1098/rsta.2008.0137
10. Wang HP, Rasch PJ, Feingold G (2011) Manipulating marine stratocumulus cloud amount and albedo: a process-modelling study of aerosol-cloud-precipitation interactions in response to injection of cloud condensation nuclei. Atmos Chem Phys Discuss 11:885–916. doi:10.5194/acpd-11-885-2011, www.atmos-chem-phys-discuss.net/11/885/2011
11. Mie G (1908) Beitrage zur Optik tru¨ber Medien, speziell kolloidaler metallosungen. Ann Phys Leipzig 25:377–445
12. Laven P (2004) Simulation of rainbows, coronas and glories using Mie theory and the Debye series. J Quant Spectrosc Radiat Trans 89:257–269. See also software from http://www.philiplaven.com/mieplot.htm
13. Blanchard D (1985) The oceanic production of atmospheric sea salt. J Geophys Res 90:961–963
14. Grini A, Myhre G, Sundet JK, Isaksen ISA (2002) Modelling the annual cycle of sea salt in the global 3D Oslo CTM2: concentrations fluxes and radiative impact. J Clim 15:1717–1730
15. Albrecht B (1989) Aerosols, cloud microphysics, and fractional cloudiness. Science 245:1227–1230
16. Konwar M, Maheskumar R, Kulkarni JK, Freud E, Goswami BN, Rosenfeld D (2010) Suppression of warm rain by aerosols in rain-shadow areas of India. Atmos Chem Phys Discuss 10:17009–17027. doi:10.5194/acpd-10-17009-2010
17. Webster PJ, Clayson CA, Curry JA (1996) Clouds radiation and the diurnal cycle of sea surface temperature in the tropical western Pacific. J Clim 9:1712–1730
18. Jones A, Hayward J, Boucher O (2009) Climate impacts of geoengineering marine stratocumulus clouds. J Geophys Res 114 (doi:10.1029/2008JD011450)
19. Bala G, Caldeira K, Nemani R, Cao L, Ban-Weiss G, Shin HJ (2010) Albedo enhancement of marine clouds to counteract global warming: impacts on the hydrological cycle. Clim Dyn. doi: 10.1007/s00382-010-0868-1
20. Salter SH, Latham J, Sortino G (2008) Sea-going hardware for the cloud albedo method of reversing global warming. Phil Trans Roy Soc A 366:2989–4006. doi:10.1098/rsta.2008.0136

Solar Radiation Spectrum

Christian A. Gueymard
Solar Consulting Services, Colebrook, NH, USA

Article Outline

Glossary
Definition of the Subject
Introduction
Solar Radiation Outside of the Earth's Atmosphere
Solar Radiation and the Earth's Atmosphere
Solar Geometry
Instrumentation and Units
Radiative Transfer Modeling
Direct, Diffuse, and Global Spectral Irradiance
Input Data to Radiative Models
Standard Spectra
Future Directions
Bibliography

Glossary

Air mass In meteorology, the air mass characterizes the transport of a large system away from where it originates (e.g., continental air mass, tropical air mass). In radiative transfer, the air mass (or, more accurately, "optical air mass") is the idealized dimensionless optical pathlength of the solar photons from the limit of the atmosphere to a specific point at the surface, relative to the pathlength corresponding to the vertical of that same point. An air mass of 1 corresponds to an overhead sun, and an air mass of about 38 to a rising or setting sun. By extension, "air mass zero" refers to conditions just outside the limit of the atmosphere. See also "Optical mass."

Albedo Overall dimensionless reflectance property of a surface, varying from 0 (perfectly black, nonreflecting surface) to 1 (perfectly white, totally reflecting surface).

Geographic information system (GIS) A computerized system that is used to analyze various layers of data that are linked to geographical locations, by merging cartography and database technology.

Global positioning system (GPS) A global navigation satellite system providing accurate location and time information at any location with an unobstructed line of sight to at least four dedicated satellites. Special GPS antennae can be used to derive information on the water vapor content of the atmosphere by measuring the propagation delay of the GPS signal.

Irradiance Radiant power of electromagnetic radiation per unit area of a surface on which it is incident. It is equivalent to the radiance of the electromagnetic source integrated over all angles. Spectral irradiance is usually measured in W m^{-2} nm^{-1}.

Langley plot Method of extrapolation of ground-based spectral measurements (with sunphotometers, in particular) to obtain the corresponding extraterrestrial value at the same wavelength. This was developed by Samuel P. Langley, based on the Bouguer–Lambert–Beer law, and is now commonly used to derive the absolute calibration of an instrument. To be valid, the atmospheric transmission must remain constant during the experiment, which is carried out throughout a very clear day or half-day.

Longwave Relates to wavelengths longer than about 4 μm, corresponding to the infrared (or thermal) part of the spectrum, which can be of solar or terrestrial origin.

Luminous efficacy Characteristic illuminance (total luminous flux incident on a surface, per unit area) created by the sun (or an artificial lamp), relative to the power radiated by the sun (or the electric power used by the lamp). Its unit is the lumen per watt.

Mie scattering Refers to the theory developed by Gustav Mie to evaluate the electromagnetic extinction caused by particles whose size is larger than molecules, or even wavelength.

Monte Carlo code Radiative transfer computer program using the Monte Carlo method, which is a statistical-numerical method of solution of complex physical problems that relies on repeated random sampling. A large number of photons are virtually sent through the atmosphere and their disposition is recorded. This method can solve many complex problems, but is computationally intensive.

Optical depth A measure of transparency of an atmospheric layer, characterizing the fraction of radiation that is altered (scattered or absorbed) along its path through that layer.

Optical mass Idealized dimensionless optical pathlength of the solar photons from the limit of the atmosphere to a specific point at the surface, relative to the pathlength corresponding to the vertical of that same point. An optical mass of 1 corresponds to an overhead sun. An optical mass can be defined for each possible radiatively active constituent, and depends on the vertical profiles of its concentration and refractive index, combined with that of pressure and temperature. The optical mass corresponding to the scattering by air molecules (Rayleigh scattering) is the optical air mass, or simply air mass.

Photovoltaics Related to the property of photosensitive semiconductor materials (like silicon) to generate a photonic current (and thus electricity) when irradiated by a light source, such as solar radiation.

Precipitable water Depth of water inside a fictitious vertical atmospheric column, after all the water vapor originally contained in that column has condensed.

Radiance Radiometric quantity describing the amount of radiation that is emitted from a particular area (e.g., of the sky), within a given solid angle. Spectral radiance is usually measured in $W\,m^{-2}\,nm^{-1}\,sr^{-1}$.

Radiative transfer Describes the energy transfer of electromagnetic radiation through absorbing, scattering, and emitting media.

Radiometry Scientific field that studies the measurement of electromagnetic radiation with instruments called radiometers.

Rayleigh scattering Extinction process for the elastic scattering of electromagnetic radiation by small particles, such as air molecules. The cloudless sky is normally blue as a result of Rayleigh scattering.

Shadowband Small arm used to block the sun in front of a radiometer. It can be a fixed band to measure diffuse radiation only, or a motorized rotating band to measure diffuse and global radiation alternatively.

Shortwave Relates to wavelengths shorter than about 4 μm, corresponding to the ultraviolet, visible, and near-infrared parts of the solar spectrum.

Solar spectral irradiance (SSI) Radiative power received from the sun at 1 AU at normal incidence on a surface of unit area (1 m^2) at a specific wavelength.

Spectroradiometry A part of radiometry dedicated to the measurement of radiation quantities in narrow spectral bands, using instruments called spectroradiometers or spectrometers.

Stratosphere Upper region of the terrestrial atmosphere extending from about 18 to 50 km.

Sunphotometry A part of radiometry dedicated to the measurement of narrow spectral bands of the solar spectrum with an instrument pointing at the sun called sunphotometer.

Total solar irradiance (TSI) Radiative power received from the sun at 1 AU at normal incidence on a surface of unit area (1 m^2).

Troposphere Lowest portion of the Earth's atmosphere, below about 18 km altitude, in which most of atmospheric extinction occurs.

Definition of the Subject

Solar radiation is significantly altered along its path throughout the atmosphere. This has important implications in many natural and technological processes, including meteorology, biology, ecology, and energy production. This entry examines the characteristics of the solar electromagnetic spectrum as it can be observed from just outside the Earth's atmosphere, how atmospheric extinction processes affect the shortwave portion of this spectrum, how all these processes can be modeled, and how the resulting spectrum can be determined experimentally. Furthermore, discussions are provided about the availability of various modeling tools to evaluate the spectral irradiance at the Earth's surface, and about sources of measured or modeled data regarding the solar spectrum.

Introduction

Life on Earth is totally dependent on the quantity and quality of the electromagnetic radiation it receives from the sun. All physicochemical processes in the atmosphere, at the Earth's surface or in the oceans, are also affected by the quantity of energy received from the sun. However, the quality of this source of energy (i.e., its spectral distribution) is also important, since most natural reactions are sensitive to certain spectral bands. The increasing use of solar radiation as a sustainable source of energy also results in the accelerated development of efficient spectrally selective materials

(e.g., for photovoltaic applications), whose optical properties must be designed or determined as a function of the incident solar spectrum.

As in many other science fields, knowledge of the properties of the solar spectrum has progressed through both measurement and theory. The difficulties here are that the spectral distribution of the solar spectrum changes over time for many different reasons, and that the spectral intensity varies by orders of magnitude over the whole possible spectral range. Contrarily to most existing radiometers used to measure spectral radiation, the human eye is well adapted to rapid changes in both intensity and visual quality of light when, for instance, a thick cloud suddenly masks the sun. Even above the atmosphere, the solar spectrum changes over time due to solar activity. Still, the major source of variability at the Earth's surface is caused by changes in atmospheric extinction processes, since many of its constituents (such as gases, particles, and clouds) vary over both space and time. Modeling the solar spectrum is needed to predict its spatial and temporal variations, and this implies the appropriate development of two different things: radiative transfer models, which must correctly simulate the main extinction processes of radiation in the atmosphere when its constitution is known, and precise supporting input data about the spatial and temporal distributions of these constituents. The current developments in these fields are discussed here.

Solar Radiation Outside of the Earth's Atmosphere

The sun is now known as a variable star. As early as 1881, Samuel P. Langley of the Smithsonian Institution conducted initial attempts to measure the solar constant from a high-altitude site (Mt. Whitney). He then initiated what became the longest program of ground observations of the sun's output, the Smithsonian "solar constant program." His assistant, Charles G. Abbot, started this new series of measurements in 1902 and continued for 6 decades. He later summarized the premises and goals of this program in a 1966 review paper [1]: "Langley suspected that this (the radiation of the sun) might be variable, and that its variation might be a cause of weather changes. If the suspected solar variations proved periodic, they might lead to long-range weather forecasts of great value for agriculture and water supply."

The large amount of data collected by Abbot and collaborators indeed revealed short-term and long-term variations in what was still called the solar constant. Because of this variability, the more proper term used now is Total Solar Irradiance (TSI). Still, the concept of solar constant is still used to refer to the long-term average value of TSI. Although the goal of the Smithsonian scientists was to detect any variations in the solar constant (which is the integrated sun's irradiance over its whole spectrum), their basic measurements were done spectrally. Substantial experimental and logistical difficulties made such measurements not accurate enough to detect TSI variations to the correct magnitude [2]. Furthermore, evaluating the transmission of the atmosphere in strong absorption bands (such as those of ozone and water vapor) introduced large uncertainties. Nowadays, instruments are much more sophisticated, precise and stable, but the difficulty just mentioned still remains when trying to evaluate the solar spectrum from terrestrial measurements. In the modern era, this "extrapolation" method has provided important milestones in the knowledge of the Solar Spectral Irradiance (SSI), also called Extraterrestrial Spectrum (ETS) [3–7], but this method's limits have probably been reached.

The current research on SSI is dominated by two approaches: direct measurement from spaceborne instruments, and physical or semiempirical models of the sun's radiative output. The existing models (e.g., [8–12]) may be necessary for long-term space-system specifications and operations [13], but are much too sophisticated for everyday use in most earth sciences or engineering/technology applications. For such instances, the use of reference spectra mostly based on spaceborne data (e.g., [14–18]) is well adapted. Since detectors used in spectrometers have only a limited spectral range, data from various instruments must usually be combined to obtain a reference solar spectrum with a sufficiently large spectral range. Various methodologies have been proposed to derive reference spectra, and a standard [19] now exists to specify the representations of solar irradiance. This standard is actually applicable not only to reference spectra, but also to measurements and physical or empirical solar models.

Space missions dedicated to spectral irradiance measurements have revolved around different spectral domains of observation, depending on scientific need. The extreme ultraviolet (EUV) was first to be scrutinized, with the goal of studying the properties of the Earth's upper ionosphere. Later, the discovery of the ozone hole led to the need of monitoring the UV spectrum as accurately as possible. In recent years, the importance of the climate change issue and the specific needs of atmospheric or climate models led to measuring a much larger part of the solar spectrum, up to the infrared (IR).

In the 1990s, the SUSIM [20] and SOLSTICE [21] spectrometers placed onboard the Upper Atmosphere Research Satellite (UARS), started to measure the UV spectrum from the Lyman-α emission line (121.6 nm) to 400 nm, and covered a large part of solar cycle 22 (1986–1996). Based on these measurements, the short-term UV variability of SSI could be evaluated [22]. Independent measurements were also obtained from three instruments that flew during the ATLAS 1, 2, and 3 space shuttle missions [23–25]. These missions lasted about 10 days each, and allowed retrieval of the instruments for postflight laboratory optical characterization. Furthermore, a comparison of the simultaneous solar irradiance measurements obtained by the ATLAS and UARS instruments showed that their absolute irradiance uncertainty was of the order of 5% [23, 25].

SOLSPEC was the first spectrometer designed to measure the visible and infrared domains (200–2400 nm) from space [24]. From the acquired dataset, two composite spectra were generated for two different levels of solar activity corresponding to the ATLAS 1 and 3 missions [17].

The most recent spectral measurement missions include: (1) the Solar EUV Experiment (0.1–195 nm) on board TIMED; (2) the XPS (0.1–40 nm), SOLSTICE (115–310 nm), and SIM (200–2400 nm) instruments onboard SORCE; (3) the NOAA-SBUV (170–400 nm); and (4) two instruments onboard ESA's Columbus laboratory on the International Space Station (ISS): SolACES (16–220 nm) and a redesigned version of SOLSTICE with an expanded spectral range (165–3080 nm). The latter two instruments are accompanied by SOVIM, which monitors the spectral irradiance at three discrete wavelengths (402, 500, and 862 nm), and also measures TSI with a broadband radiometer. The combined ISS experimental setup (SolACES, SOLSTICE, and SOVIM) is shown in Fig. 1.

A comparison between the Gueymard's moderate-resolution composite spectrum [15] (available from http://www.solarconsultingservices.com/Gueymard_ET_spectrum_2004.txt or http://rredc.nrel.gov/solar/spectra/am0/special.html#newgueymard) and the Planck distribution for blackbody temperatures of 5,500, 5,776, and 6,000 K is shown in Fig.2. For 5,776 K, the integrated blackbody irradiance equals the current solar constant value of 1,366 W m^{-2} [26]. It is clear that the sun does not behave like a blackbody below about 650 nm. It is noticeably "hotter" than its average blackbody temperature around its peak, and colder in the UV, with a sharp transition around 400 nm. Below that wavelength, a lot of structure also appears, which is caused by various emission and absorption lines.

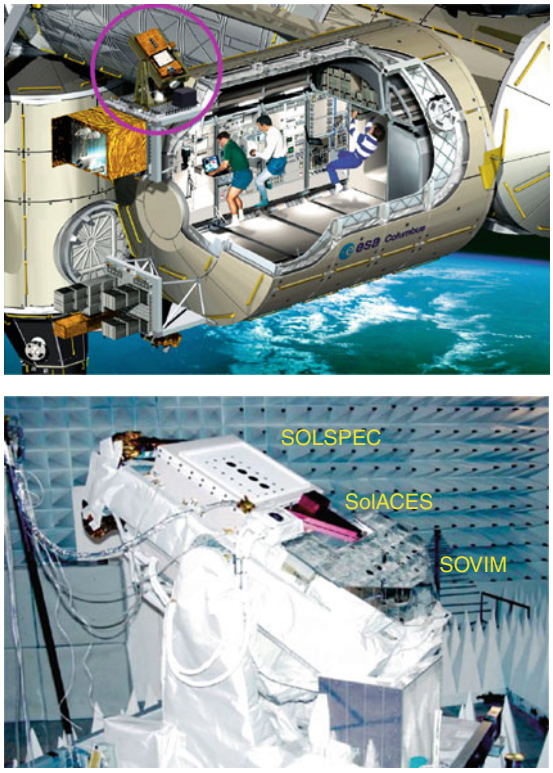

Solar Radiation Spectrum. Figure 1
Artist impression of the SolACES, SOLSPEC, and SOVIM instruments mounted on a single sun-pointing device outside of ESA's Columbus laboratory of the ISS (*top*); the same apparatus during preflight electromagnetic compatibility laboratory tests. (Photos ESA)

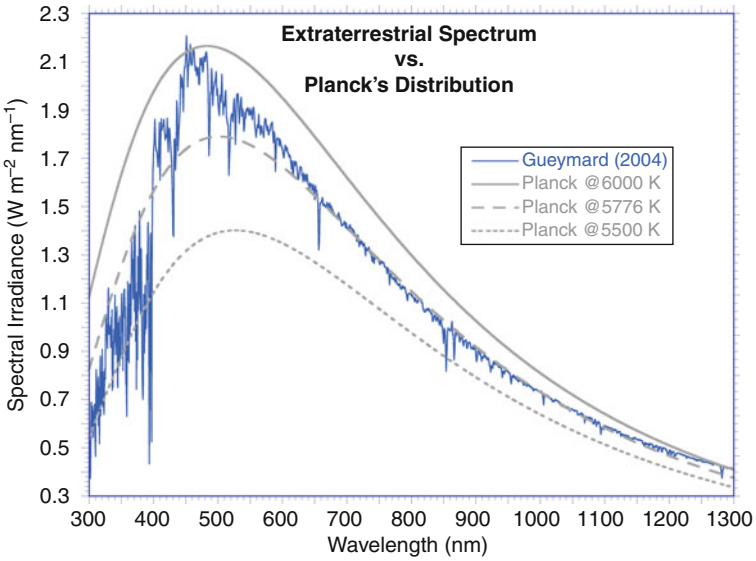

Solar Radiation Spectrum. Figure 2
Solar spectral irradiance from 300 to 1,300 nm compared to blackbody distributions (from Planck's theory) at various temperatures

During periods of high solar activity, the UV part of the spectrum is enhanced, whereas the visible and IR parts remain relatively stable. Since the UV is significantly absorbed by the Earth's atmosphere, solar activity only results in minute changes in the absolute irradiance at the Earth's surface. For most terrestrial applications, a unique SSI distribution can thus be used, without considering the day-to-day changes in solar activity. In contrast, seasonal changes in the magnitude of the spectrum do occur because of the obliquity of the Earth's orbit around the sun. Like with TSI, all reference spectra are evaluated at the average sun-earth distance ($\approx$1 AU). Therefore, they must be corrected by up to $\pm$3.4%, depending on the day of the year. This correction is systematic, affects all wavelengths evenly, and can be calculated with a simple, yet accurate formula [26].

Solar Radiation and the Earth's Atmosphere

The composition of this planet's atmosphere is dominated (at 98% in volume) by nitrogen and oxygen. Some gases, such as ozone, carbon dioxide, methane, or water vapor, can absorb the energy from sun rays in various parts of the spectrum, and therefore have a strong radiative impact on solar radiation and climate in general, even though their concentration is very low in comparison with the two main gases just cited. In a broader way, all gases contribute to the atmospheric extinction of solar radiation through molecular scattering – the process that creates the blue color of the atmosphere. This was demonstrated by Lord Rayleigh at the end of the nineteenth century. His theory applies to the interaction of electromagnetic radiation with microscopic particles (in this case, molecules) whose size is smaller than the wavelength of incident radiation. The atmosphere also contains particulates of various origins, both natural and anthropogenic. They too have a strong impact on solar radiation and climate through scattering and absorption. The size of these small particles, or aerosols as they are called now, varies widely according to their origin, but it is larger than the wavelength of incident radiation. For such a case, the theory proposed by Gustav Mie in 1908 needs to be applied to evaluate the aerosol extinction. Finally, the sky is frequently covered with clouds, which are made of liquid water droplets or ice crystals, depending on their altitude and other factors. Among all atmospheric constituents, clouds are normally those that have the largest impact on solar radiation, weather, and climate.

The unperturbed SSI that exists at about 100 km above the Earth's surface is progressively affected by all constituents just mentioned through absorption and

scattering along its path to the surface. Solar radiation that is reflected upward by the Earth's surface or atmosphere (clouds in particular) needs to be considered too. It participates to what is called the planetary albedo. Surface-reflected radiation is also a component of the total radiation incident on natural formations (e.g., mountain sides), human constructions (e.g., buildings or solar collectors), or living organisms (e.g., trees or standing humans).

Not all atmospheric gases are distributed vertically the same way. Some, such as oxygen (O_2), nitrogen (N_2), or carbon dioxide (CO_2) have a concentration (by volume) that is essentially constant with altitude. As a result, their total columnar amount above any given altitude is proportional to the atmospheric pressure at that level. Others, such as methane (CH_4), ozone (O_3), nitrogen dioxide (NO_2), carbon monoxide (CO), nitrous oxide (N_2O), or water vapor (H_2O) have intricate vertical profiles. Figure 3 shows such vertical profiles for different gases, as well as the main layers (troposphere, stratosphere, mesosphere, and thermosphere) as defined in the 1976 US Standard Atmosphere [27]. The temperature and gaseous profiles of this reference atmosphere, which is meant to be representative of typical "pristine" conditions at mid-latitude (45°N) locations, are widely used in idealized studies of radiative transfer. Whereas water vapor is most abundant in the lower troposphere, O_3 and NO_2 are concentrated in the mid-stratosphere, also known as the ozone layer, where NO_2 participates in the chain of chemical reactions that produce or destroy ozone,

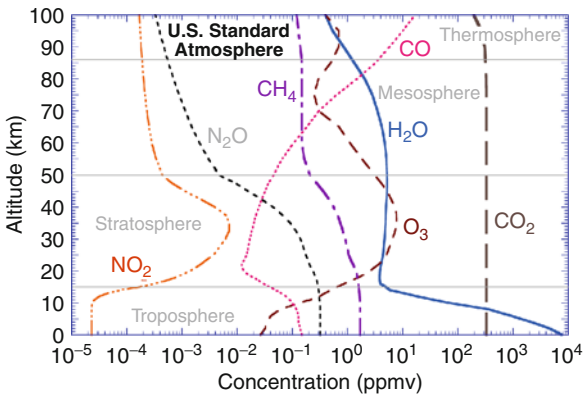

Solar Radiation Spectrum. Figure 3
Vertical concentration profiles of some radiatively active gases in the US Standard Atmosphere of 1976

depending on temperature and abundance of other gases (such as chlorofluorocarbons). In the lower atmosphere around urban or industrial areas in particular, the concentration of O_3 and NO_2 may be considerably larger than indicated by the US Standard Atmosphere due to anthropogenic emissions and/or photochemical reactions. The other atmospheric constituents, for which reference atmospheres such as the US Standard Atmosphere do not provide a vertical profile, are those that are highly variable and not in gaseous state: aerosols and clouds.

Most clouds exist at an altitude below about 18 km above mean sea level. There are different types of clouds, and they are classified according to their form and height. Three layers are usually considered: low, middle and high. These correspond to cloud bases typically below 2 km, between 2 and 6 km, and above 6 km, respectively. To each layer (or "étage") correspond different cloud types (or "genera"). Normally, water clouds are concentrated in the two lower layers and ice clouds in the highest layer. Ice clouds are thin and therefore generally do not completely mask the sun. Water clouds are optically thicker so that their effect on solar radiation is considerable. The optical properties of clouds can be described in various ways. At the microphysical level, the concentration and size distribution of water droplets or ice crystals are necessary to calculate their bulk properties. When this information is not available, which is frequently the case, a convenient way to evaluate the overall optical properties of clouds is to use their fractional amount (the fraction of sky covered by the clouds) and their optical depth (or optical thickness), which both directly condition their radiative impact. A simplified cloud typology is provided in Table 1. For more details, see e.g., http://www.weatheronline.co.uk/reports/wxfacts/Cloud-classification.htm; http://en.wikipedia.org/wiki/International_Cloud_Atlas; and http://isccp.giss.nasa.gov/cloudtypes.html. Fog is a particular type of cloud whose base height is at surface level. It is normally reported as an obstruction to vision rather than as a cloud, hence it does not appear in Table 1.

Aerosols are particulates of various natural or anthropogenic origins: dust, salt, sand, smoke, pollutants, etc. Their size depends on their origin, and is highly variable, from about 0.01 to 100 μm. The size of hygroscopic aerosols (e.g., salt) also increases with

Solar Radiation Spectrum. Table 1 Classification of clouds and their optical depth

Level	Genera	Symbol	Base height (km)	Top pressure (hPa)	Optical depth
Low	Stratus	St	0.0–1.2	680	23–379
	Stratocumulus	Sc	0.3–2.0	680	3.6–23
	Cumulus	Cu	0.3–2.0	680	0.0–3.6
	Cumulonimbus	Cb	0.3–2.0	680	0.0–60
Middle	Nimbostratus	Ns	0–3	440	23–379
	Altostratus	As	2–6	440	3.6–23
	Altocumulus	Ac	2–6	440	0.0–3.6
High	Cirrus	Ci	6–12	50	0.0–3.6
	Cirrostratus	Cs	6–12	50	3.6–23
	Cirrocumulus	Cc	6–12	50	3.6–23

relative humidity, particularly above 70%, or even more so, near saturation. Like for clouds, the microphysical properties (concentration and size distribution) of aerosols are necessary to evaluate their optical characteristics using first principles (Mie scattering theory). In practice however, bulk properties (such as spectral optical depth) are easier to obtain experimentally, and are therefore more readily available. Like water vapor, aerosols are concentrated in the lower troposphere, or mixing layer, within the first 2 km above the surface. Nevertheless, aerosol clouds originating from intense biomass fires or dust storms can be lifted to heights of 6 km or more, and can then travel over huge distances, up to thousands of kilometers, before dissipating (Fig. 4). Additionally, the concentration of aerosols in the lower stratosphere can be noticeable, due to meteoric dust and, more importantly, volcanic activity. In recent history for instance, the eruptions of El Chichón (1982) and Pinatubo (1991) sent aerosol clouds that circled the globe and had a profound impact on solar radiation transmission and climate in general. These effects leave their trace as sharp dips in solar transmission records, and can be felt during a few years after the eruption (Fig. 5).

Aerosols and clouds have strong direct effects on solar radiation transmission. Furthermore, they also interact through various physicochemical processes (e.g., cloud nucleation around aerosol particles), thus creating intricate indirect radiative effects, which are now known to affect climate. For instance, although aerosols tend to increase cloudiness, dark aerosols in smoke plumes from forest fires can actually prevent cloud formation.

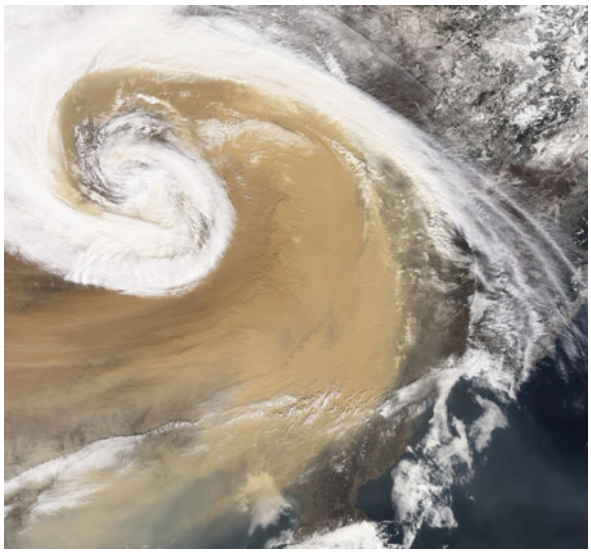

Solar Radiation Spectrum. Figure 4
A "perfect dust storm" over China, as seen from space by the MODIS instrument, April 7, 2001 (Image courtesy NASA's Earth Observatory)

Solar Geometry

Solar radiation transmission through the atmosphere – and by way of consequence, the planet's climate – is directly affected by the earth–sun geometry. Outside of

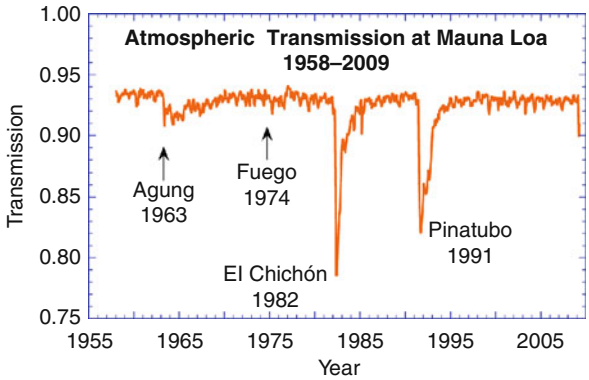

Solar Radiation Spectrum. Figure 5
Atmospheric transmission above Mauna Loa's observatory, Hawaii. (Data courtesy Ellsworth Dutton, NOAA)

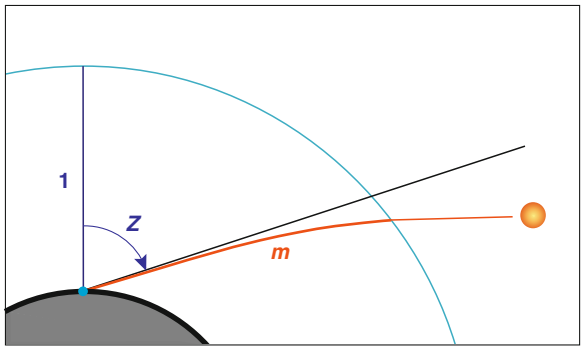

Solar Radiation Spectrum. Figure 6
Solar geometry relative to a surface location, showing the solar zenith angle Z and the air mass m

the intertropical zone, the sun's position above the horizon is markedly lower in winter than in summer, which in turn is the cause of alternating seasonal differences in climate. The apparent position of the sun in the sky can be characterized by two angles, whose selection depends on the system of reference. The vertical position of the sun can be determined from the zenith through the zenith angle, Z, or with reference to the horizon with the solar elevation angle, H. These angles being obviously the complement of each other, the two reference systems are equivalent. However, the literature reveals that the use of Z is more frequent than that of H. The lateral position of the sun is characterized by its azimuth, ψ. It is usually measured clockwise from north. The vertical position of the sun is more critical than its lateral position since the former angle conditions the sun rays' pathlength through the atmosphere. The longer this pathlength, the higher the probability that solar photons will undergo some form of atmospheric extinction before hitting the surface. The optical mass of an atmospheric constituent, m, is defined as the ratio between a slant pathlength and a vertical pathlength for a zenith sun (Fig. 6). For a hypothetical plane-parallel atmosphere, one would have simply $m = 1/\cos Z$. Due to the atmosphere's sphericity, m does not reach an infinite value at sunrise or sunset. A precise evaluation of m as a function of Z is intricate since each atmospheric constituent has a specific vertical profile, while the refractive index is progressively varying along the path due to changes in pressure and temperature [28].

The optical air mass (or in short, "air mass"), m_R, is the optical mass corresponding to molecular (or Rayleigh) scattering. It is also the appropriate optical mass in calculations of absorption by uniformly mixed gases, such as CO_2 (Fig. 3). By extension, the air mass is frequently used to evaluate all possible extinctions, even though this is not strictly correct. In actuality, the optical mass of constituents that are concentrated at high altitude (such as ozone) is lower than the air mass, for any given $Z > 0°$. Reciprocally, the optical mass of constituents concentrated in the lower atmosphere (such as water vapor or aerosols) is larger than the air mass. However, such differences become only noticeable for Z larger than about 80° (Fig. 7). For applications where low-sun situations are frequent and accuracy is important, distinct optical masses for each extinction process should be considered. A set of fitting functions of Z has been proposed to obtain the optical mass of each significant extinction process as a function of Z [29, 30] thus advantageously replacing the repetitive and tedious calculations behind Fig. 7. Such optical mass calculations are accurate only to the extent that Z is itself obtained accurately. The ultimate accuracy requires Ephemeris-type calculations. Since these are impractical in most applications, various levels of simplification have been proposed in the literature, from sophisticated algorithms [31], methods of high accuracy but with efficient computational techniques [32, 33], and highly simplified equations that do not take long-term drifts in astronomical quantities or atmospheric refraction into consideration [34]. Typically, the former methods may be accurate to

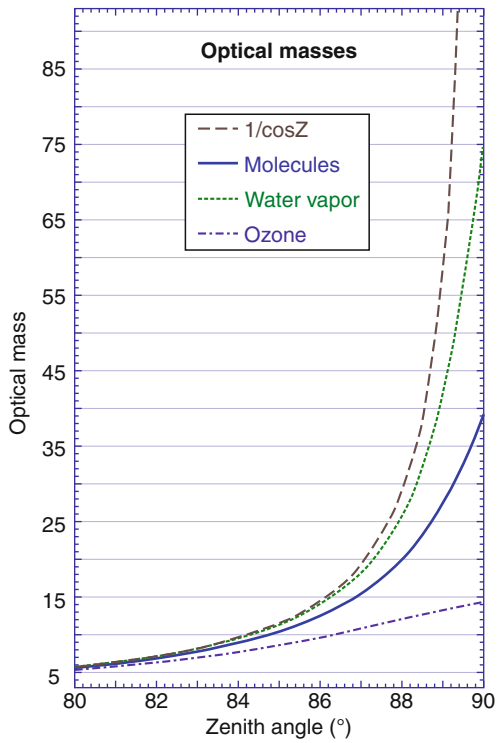

Solar Radiation Spectrum. Figure 7
Optical masses for some atmospheric extinction processes

within about $\pm 0.001°$, whereas the latter equations are more in the $\pm 1°$ range, which may still be sufficient for engineering-type calculations. Online tools are also available. See, e.g., http://www.nrel.gov/midc/solpos/solpos.html http://www.esrl.noaa.gov/gmd/grad/solcalc/ http://solardat.uoregon.edu/SolarPositionCalculator.html http://www.volker-quaschning.de/datserv/sunpos/index_e.php.

In applications where solar radiation interacts with optical surface properties (reflection, absorption, or transmission), the angle of incidence, θ, of the sun rays on the surface must also be known. For a horizontal surface, θ is simply equal to Z. For incidence on a surface tilted at an angle s from the horizontal with an azimuth γ from north

$$\cos\theta = \cos s \cos Z + \sin s \sin Z \cos(\psi - \gamma). \quad (1)$$

Instrumentation and Units

Radiometry is the scientific field related to the measurement of electromagnetic radiation with radiometers. Spectroradiometry is the subfield that studies methods to measure spectral radiation with spectrometers or spectroradiometers – instruments that can discriminate narrow wavelength intervals. Photometry is the related field that involves the measurement of visible light by photometers that imitate the human eye's spectral response over the limited spectral band 360–830 nm. The fundamentals of radiometry and photometry are described in textbooks (e.g., [35]) or in online resources, such as http://www.optics.arizona.edu/Palmer/. Note that some confusion in terminology exists because astronomers tend to use the term "photometry" to refer to radiometry. An unfortunate consequence is that the astronomy-related science of studying radiometric quantities by pointing an instrument at the sun is still termed "sunphotometry," even though it does not involve the subjective perception of light by the human eye [36, 37]. The practical use of sunphotometers is discussed in section "Input Data to Radiative Model".

The measurement of spectral radiation involves a much more elaborate and costly experimental setup than what is needed to measure broadband irradiances with more conventional radiometers. Moreover, the absolute calibration of spectral radiometers is more challenging than that of broadband radiometers. Therefore, it must be borne in mind that the uncertainty in spectral measurements is usually larger than that in broadband measurements.

Although the measurement of spectral *radiance* is possible (to evaluate the variations in intensity and color over the sky vault, for instance), it is not common. Most experimental setups rather deal with the measurement of the spectrum directly emanating from the sun (direct irradiance), from the sky (diffuse irradiance), or from all possible directions (global irradiance). The SI unit for spectral irradiance, E_λ, is W m^{-3}, but it is most often reported in the more convenient units of W m^{-2} nm^{-1} (for wavelengths in nm) or W m^{-2} μm^{-1} (for wavelengths in μm). For some energy-related applications, such as photovoltaics, the quantum effect of photons needs to be characterized by the photon flux, F_λ, such that

$$F_\lambda = kE_\lambda \lambda/(hc) \quad (2)$$

where λ is wavelength, c is the speed of light in vacuum (2.99792458×10^8 m s^{-1}), h is the Planck constant ($6.62606896 \times 10^{-34}$ J s), and k is a numerical constant

used to reconcile units. It equals 1×10^{-13} for λ in nm, E_λ in W m^{-2} nm^{-1}, and F_λ in cm^{-2} s^{-1} nm^{-1}.

A similar conversion from energy to photonic units is used to study photosynthesis in many fields related to plant science. The *photosynthetically active radiation* (PAR) spectrum extends between about 400 and 700 nm. The correspondence between the spectral PAR irradiance in photonic units, P_λ, and its equivalent in energy units is obtained here as a slightly modified version of Eq. 2 [38]:

$$P_\lambda = E_\lambda \lambda / (N_A hc) \tag{3}$$

where N_A is Avogadro's constant ($6.02214179 \times 10^{23}$ mol^{-1}). (All physical constants used in this section are from CODATA 2006 [13], available from http://physics.nist.gov/cuu/Constants/papers.html.) Although PAR can be measured or modeled spectrally, only its integrated value over the PAR band is reported widely. This band-integrated quantity is measured either in energy units by a filtered radiometer, or in photon units by a quantum sensor, which is the preferred method. This defines the *photosynthetic photon flux density* (PPFD), usually expressed in μmol m^{-2} s^{-1}.

Throughout this section, the focus is on the part of the shortwave solar spectrum (from ≈300 to ≈4,000 nm) that can be measured from the Earth's surface. This includes the most energetic part of the spectrum (300–1,100 nm), which can be monitored with spectroradiometers equipped with a silicon (Si) detector. Such devices are fast, stable, well characterized and very common. For the near-infrared part of the spectrum between about 1 and 4 μm, other types of detectors become necessary, such as germanium (Ge), indium-gallium-arsenide (InGaAs), lead sulfide (PbS), or lead selenide (PbSe). Silicon photodiode arrays are increasingly used in spectroradiometers for their critical ability to sense the whole spectrum instantaneously over their spectral range. Instruments based on older types of designs have to progressively scan the spectrum, wavelength by wavelength, with an electromechanical system. This process can typically take a few seconds to a few minutes, which presents a difficulty since the sun and sky conditions may vary during that time. Spectroradiometers or sunphotometers that cover a very large wavelength range (e.g., 300–2,500 nm) must use at least two different types of detectors, making them more complex and expensive than instruments with silicon-only detectors. Other types of detectors and instruments are necessary to study the far-infrared spectrum (above ≈4 μm) that emanates from the sun, or is radiated upward and downward by the planetary surface–atmosphere system.

A spectroradiometer can be equipped with a flat diffuser to measure the global spectrum, or with a limiting tube (or collimator) to measure the direct spectrum. For continuous operation in the latter case, the instrument must be installed on a sun tracker. A temperature-controlled and weatherproof container is also needed for automated operation outdoors. Whereas laboratory instruments are sturdy, heavy, and need electricity, there are portable instruments specifically designed to operate autonomously in the field.

Like with any instrument, absolute accuracy, precision, resolution, and repeatability are important characteristics that contribute to the price of the instrument. Moreover, it needs to be frequently calibrated. This is usually accomplished in the laboratory with the help of a standard lamp (or with a calibrated lamp traceable to a standard lamp), whose spectral output is precisely known. Another technique, in the case of a spectroradiometer mounted on a tracker to measure the direct spectrum, is to use the sun as the source, through the "Langley plot" technique. This can be more accurate than the standard lamp technique, but has many limitations: it has to be done at a very clear site during very stable atmospheric conditions, wavelength by wavelength, and would not be advisable in the case of scanning instruments.

To compare a measured spectrum to a modeled spectrum, three characteristics of the instrument must be known: its spectral step, the shape of its filtering function (usually Gaussian or triangular), and its bandwidth. The latter is expressed as the full width at half maximum (FWHM). It is usually in the 0.5–5 nm range for good instruments, sometimes even less for instruments specifically designed for UV measurement (a lower value means a higher resolving power between one wavelength and the next). The FWHM may not be constant with wavelength, particularly with solid-state detector arrays. For instance, the FWHM of the Rotating Shadowband Spectroradiometer (RSS) varies from 0.3 nm in the UV to 3.9 nm in the near IR. The RSS is a particular type of instrument that records the global and diffuse spectra in alternation [39] and derives the

direct spectrum through Eq. 12 without the need for a collimator tube or tracking. Its sensor is a horizontal silicon array that is rapidly and alternatively unshaded and shaded from the sun with a little motorized shadowband.

Owing to the complexity and cost of monitoring the solar spectrum with instruments of dependable accuracy and reliability (especially in continuous operation under all-weather conditions), most spectral records are obtained at a few sites in the world for short experimental campaigns, or specific conditions (e.g., clear sky only). Long series of publicly available datasets providing quality-assessed data from various spectral instruments and ancillary meteorological data are extremely rare. It is worth mentioning the resources offered by the Atmospheric Radiation Measurement Program (http://www.arm.gov/instruments/location), the National Renewable Energy Laboratory (http://www.nrel.gov/midc/srrl_bms/; http://rredc.nrel.gov/solar/old_data/spectral/), and the NOAA-EPA Brewer Spectrophotometer UV and Ozone Network (NEUBrew, http://www.esrl.noaa.gov/gmd/grad/neubrew/). The latter is limited to the spectral range 286.5–363.0 nm for ultraviolet (UV) research, however.

Radiative Transfer Modeling

Considering the just-mentioned difficulties and cost of obtaining high-quality experimental data of spectral radiation, it is not surprising that modeling has become an essential tool to obtain spectral irradiance data. Based on the work of pioneers, such as Lord Rayleigh (1870s), Langley (1880s), Schuster (1905), Schwarzschild (1906, 1914), Mie (1908), or Eddington (1916), the field of radiative transfer modeling began to emerge in the 1940s under the impulse of astrophysicists, such as Chandrasekhar, who published *Radiative Transfer* – the first treatise on the topic – in 1950. (Incidentally, Subramanyan Chandrasekhar was awarded the Nobel Prize in Physics, 1983.) From then on, radiative transfer modeling became an essential tool in the hands of physicists, meteorologists, climatologists, energy engineers, etc. Recent textbooks on the topic should be consulted for current methodological and computational details [40–47].

In its basic form, the equation of radiative transfer simply expresses that a beam of radiation, initially of intensity (or radiance) I, that travels through any attenuating layer of thickness ds loses some energy through absorption, redistributes some energy through scattering, and gains another fraction of energy by emission, according to

$$dI_\lambda/ds = -\alpha_\lambda I_\lambda - \sigma_\lambda I_\lambda + B_\lambda \tag{4}$$

where α_λ and σ_λ are the absorption and scattering coefficients at wavelength λ, respectively, and B_λ is the emitted energy. By defining $k_\lambda = \alpha_\lambda + \sigma_\lambda$ as the total extinction coefficient and $k_\lambda\, ds = d\tau_s$ as the layer's total optical depth (due to both absorption and scattering), Eq. 3 becomes

$$dI_\lambda/d\tau_s = -I_\lambda + B_\lambda/k_\lambda. \tag{5}$$

Note that "optical depth" is also called "optical thickness." Emission only occurs in the far infrared, so that the last term can be ignored when dealing only with the solar (shortwave) domain. Still, the apparent simplicity of Eq. 5 hides the fact that all possible directions of propagation are involved, which precludes a simple algebraic resolution unless various simplifications are used. A highly effective simplification is to consider a plane-parallel atmosphere. Other simplifications are frequently used to specify the hemispherical directionality of σ_λ relative to the direction of propagation, which is defined by Z. For instance, for an ideally isotropic medium, σ_λ would be constant over all possible directions. Such a simple case never occurs in reality, however.

Using the popular *two-stream approximation*, it is possible to resolve Eq. 5 algebraically in the simplest way possible. This solution is fast and convenient, but its accuracy usually degrades noticeably when Z increases. More sophisticated solutions, such as the delta-Eddington approximation, the discrete-ordinate method, or purely numerical methods, are currently used in practice. Their features are compared in some textbooks [42, 47]. For optimal handling with modern computers, the models that allow the calculation of radiance and irradiance under various possible atmospheric conditions are packaged into Radiative Transfer (RT) codes. Most of them are not user friendly, and therefore require sufficient expertise to manipulate them correctly. A succinct description of some of these codes is available in textbooks (e.g., [30]) and online (http://www.statemaster.com/encyclopedia/

List-of-atmospheric-radiative-transfer-codes). RT codes are used routinely to solve various problems in atmospheric physics, including how the vertical irradiance profile varies with altitude over complex surface reflectance patterns [48].

In recent years, 3D radiative transfer modeling, using computationally intensive Monte Carlo codes (some of which are listed at http://i3rc.gsfc.nasa.gov/Public_codes_3DRT.htm), has gathered much interest to improve predictions of radiation transmission under complex conditions, such as cloud fields or surface reflectance properties with strong inhomogeneities [49–51]. An overview of the general principles of Monte Carlo modeling appears in [52]. Because of their importance in atmospheric sciences in general, and climate issues in particular, all types of RT codes are frequently intercompared by international teams for consistency and quality assurance [49, 53–56].

For engineering and other terrestrial applications, many more simplifications are desirable. They are motivated by various considerations: accuracy requirements are typically less stringent, results are needed fast, they often need to provide the irradiance incident on surfaces of various orientations (i.e., not just on the horizontal, as most atmospheric models are limited to), and, finally, intermediate results through the atmosphere (such as the vertical irradiance profiles) are superfluous, since only radiative results near the system being studied matter in this case. Many such simplified models have been proposed in the literature, to predict the spectral irradiance, and often also its integrated value over the whole shortwave spectrum, called broadband (or sometimes "total") irradiance. Spectral irradiance predictions can also be used to derive irradiances or photonic fluxes in narrower bands (e.g., photosynthetically active radiation, illuminance, or ultraviolet irradiance combined with any kind of action spectrum). Examples of spectral irradiance models for cloudless conditions include SPCTRAL2 [57] and SMARTS [29], whose codes are available online (http://rredc.nrel.gov/solar/models/spectral/; http://www.solarconsultingservices.com/smarts.php). In particular, SMARTS (Simple Model of the Atmospheric Radiative Transfer of Sunshine) has been thoroughly validated (e.g., [58, 59]), and is versatile enough to be used in a large variety of applications [60], such as the derivation of standard spectra (see Section Standard Spectra), the design optimization or power output simulation of photovoltaic (PV) or other solar energy systems [61–64], as well as the evaluation of the luminous efficacies of solar radiation under sunlight and daylight [65, 66]. To manage cloudy conditions, the simple empirical spectral cloud correction factors proposed for models such as BRGC [67] or SEDES2 [68] may be considered for very approximate results.

Direct, Diffuse, and Global Spectral Irradiance

Due to the more or less intense scattering effects that solar photons undergo while penetrating deeper through the atmosphere, solar radiation can exist in two different forms: direct, or "beam," radiation (directly emanating from the sun) and diffuse radiation (emanating from the rest of the sky hemisphere). Under clear skies, direct radiation is very intense and peaks at yellow to orange wavelengths (at noon and sunrise/sunset, respectively), while diffuse radiation is low and peaks at blue to violet wavelengths. Clouds tend to act as a neutral density filter, and therefore appear white or grey. Under overcast cloudiness, direct radiation disappears if the cloud is dense enough, and is then transformed into diffuse radiation, which is therefore normally more intense than under clear conditions. All kinds of intermediate situations may occur due to, e.g., haze (caused by aerosols) or partial cloudiness. Figure 8 provides a schematic representation of the main processes occurring in the atmosphere from the standpoint of a surface structure, such as a tree, a building, a solar system (as depicted here), etc. From this standpoint, three radiation components must be determined in most applications: the direct component from the sun, the diffuse component from the sky, and the diffuse component from surface reflections. The latter component is normally small, except in the case of a highly reflective ground (e.g., snow or white sand). Moreover, natural nondiffuse reflectors (such as water and ice at grazing angles) or man-made reflectors (glass, mirrors, and metals) may also add an intense direct (or "specular") component to the reflected radiation.

Since direct radiation propagates along only one direction, it is much easier to evaluate than diffuse radiation. Consider that direct radiation is attenuated along n different layers (or "slabs") of the atmosphere,

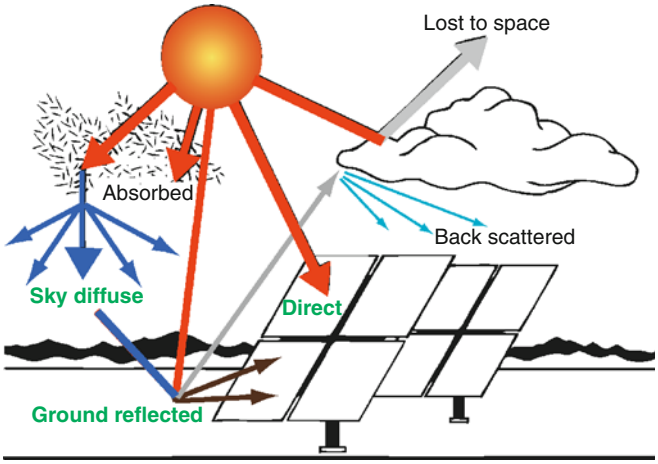

Solar Radiation Spectrum. Figure 8
Irradiance components relative to a tilted receiver

which may or may not be contiguous. From the Bouguer–Lambert–Beer law, the spectral transmittance, $T_{i\lambda}$, of the ith layer may be expressed by

$$T_{i\lambda} = \exp(-k_\lambda s_i) \tag{6}$$

where k_λ is an attenuation factor (due to scattering or absorption) for a single attenuation process per unit length, and s_i is the sun ray's pathlength through the layer. Assuming k_λ does not vary from one layer to the other, the total transmittance through the whole atmosphere is

$$T_\lambda = T_{1\lambda} T_{2\lambda} T_{3\lambda} \ldots T_{n\lambda} = \exp(-k_\lambda s) \tag{7}$$

where s is the total pathlength, i.e., the sum of all individual pathlengths s_i. This means that the order in which the layers are piled up has no effect on the result. Since s is difficult to measure in practice and the product $k_\lambda s$ is nondimensional, the latter can be advantageously replaced by the product of the air mass m (see Section Solar Geometry) and optical depth (or "optical thickness") at wavelength λ, τ_λ, which is to be evaluated along a vertical column above the point of interest (Fig. 4). The spectral transmittance at the bottom of the nth layer (e.g., at the Earth's surface) is then

$$T_\lambda = \exp(-m\tau_\lambda). \tag{8}$$

All atmospheric extinction processes $a, b, c \ldots p$ can be considered independently, each with a specific optical depth $\tau_{a\lambda}, \tau_{b\lambda}, \tau_{c\lambda}, \ldots \tau_{p\lambda}$, and transmittance $T_{a\lambda}, T_{b\lambda}, T_{c\lambda}, \ldots T_{p\lambda}$. Transmittances are multiplicative, so that the spectral irradiance at the bottom of the atmosphere, E_λ, can be expressed as

$$E_\lambda = T_{a\lambda} T_{b\lambda} T_{c\lambda} \ldots T_{p\lambda} E_{0\lambda} = T_{t\lambda} E_{0\lambda} \tag{9a}$$

or, equivalently,

$$E_\lambda = E_{0\lambda} \exp(-m\tau_{t\lambda}) = E_{0\lambda} \exp[-m(\tau_{a\lambda} + \tau_{b\lambda} + \tau_{c\lambda} + \ldots + \tau_{p\lambda})] \tag{9b}$$

where $E_{0\lambda}$ is the SSI, and $\tau_{t\lambda}$ is the total atmospheric optical depth. Since m is a pure geometric factor and $E_{0\lambda}$ is known from other sources, the only difficulty left in the prediction of E_λ is the evaluation of each individual optical depth at each wavelength.

For absorbing gases, τ_λ can be conveniently considered as the product of the total abundance of the gas along the vertical column, u, and its spectral absorption coefficient, α_λ. The latter is usually derived from spectroscopic measurements under well-controlled laboratory conditions. This simplified approach has been used in various engineering-type radiative models [57, 69], which have relatively coarse spectral resolution (typically 1–10 nm). The case of water vapor is the main exception to this rule and is much more difficult to handle accurately. High accuracies command the best possible spectral resolutions (with line-by-line data and codes) or "band-model" approximations derived from the latter.

For scattering processes by molecules and aerosols, the optical depth is still a convenient concept.

The optical depth for molecular scattering, $\tau_{R\lambda}$, decreases smoothly but strongly with wavelength (such as λ^{-4}) and can be derived from Rayleigh's theory. Different mathematical expressions, in the form of continuous functions of λ, have been proposed to simplify calculations while maintaining high accuracy. One such expression is used in SMARTS [30]:

$$\tau_{R\lambda} = (p/p_0)[117.3405\lambda^4 - 1.5107\lambda^2 + 0.017535 - 0.00087743\lambda^{-2}]^{-1} \quad (10)$$

where p is the actual site pressure, p_0 is standard pressure at sea level (1013.25 hPa), and λ is expressed in μm.

The aerosol optical depth (AOD; alternatively called "aerosol optical thickness," AOT), $\tau_{A\lambda}$, varies largely over space and time because it depends directly on both the quantity and type of aerosols, which are rapidly changing characteristics (see section "Input Data to Radiative Models" for sources of data). At wavelengths between about 350 and 1,000 nm – where the solar spectrum is most intense – the variation of AOD resembles that of $\tau_{R\lambda}$ albeit with a much flatter way, according to the empirical Ångström's law [70]:

$$\tau_{A\lambda} = \beta\lambda^{-\alpha} \quad (11)$$

where λ is expressed in μm, β is AOD at 1 μm, and α is the wavelength exponent, also called "Ångström coefficient," which varies usually between about 0.5 (for aerosols constituted of mostly large particles, such as from oceanic origin) to about 2.5 (for aerosols constituted of mostly fine particles, such as from urban origin). A typical average for rural-type aerosols, which are prevalently found in "clean" rural areas only subjected to local, natural aerosol sources, is 1–1.5. The value of β is site and time specific, and can vary from close to 0 at remote pristine sites (such as over mountain peaks) to 1 or more under extreme conditions, such as intense smoke from forest fires or dust storms around deserts. The measurement of α and β is discussed further in section "Input Data to Radiative Models". The extinction effect of aerosols is mostly in the form of scattering (with a strong forward scattering component), but some types of aerosols (particularly soot) can also absorb the incident radiation.

Finally, the cloud optical depth (COD) can be derived experimentally from spectral or broadband radiometric measurements, or can be derived from spaceborne sensor data using elaborate radiative-transfer calculations. COD can vary from less than 0.5 for very thin cirrus-type clouds to 100 or more for very thick and dark precipitation clouds (Table 1). As far as scattering is concerned, COD depends little on wavelength, and can therefore be approximated with Eq. 11 using $\alpha \approx 0$, so that COD values are usually quoted without a reference wavelength. However, clouds additionally exhibit strong absorption bands in the near infrared, due to their water content (liquid droplets or ice crystals).

Figure 9 compares the optical depths of the main extinction processes in the cloudless atmosphere, based on ideal conditions (such as USSA for the abundance of gases). The resulting individual transmittances for a zenith sun ($m = 1$) are illustrated in Fig. 10. It is obvious that wavelengths below 0.7 μm are dominated by scattering (with the exception of the UV below 0.35 μm, where ozone absorption is extremely strong), whereas the extinction at wavelengths above 0.7 μm is dominated by absorption.

When m increases, some extinction effects are exacerbated more than others. As a general rule, the extinction then increases relatively more at the shorter wavelengths than at the longer wavelengths, resulting in a red shift of the direct spectrum when the sun is low (explaining its reddish color at sunrise and sunset). This is illustrated in Fig. 11, which shows actual spectra measured under clear-sky summer conditions at the Solar Radiation Research Laboratory of Golden, Colorado (latitude 39.74°N, longitude 105.18°W, elevation 1829 m; data available online from http://www.nrel.gov/midc/srrl_bms). These direct irradiance spectra are measured automatically at 5-min intervals with a silicon-based spectroradiometer equipped with a tracker to follow the sun, and a collimator tube to block the radiation from the sky. With this arrangement, the sensor is continually facing the sun. Since the sun rays impinge on the sensor at normal incidence, what it measures is usually called direct normal irradiance (DNI), $E_{bn\lambda}$. Only a limited number of spectra are shown here (at uneven intervals) for legibility. Spectra measured under similar cloudless conditions, but for a winter day, are shown in Fig. 12.

The fraction of radiation that is scattered out of the direct beam is either lost to space (upward) or regained

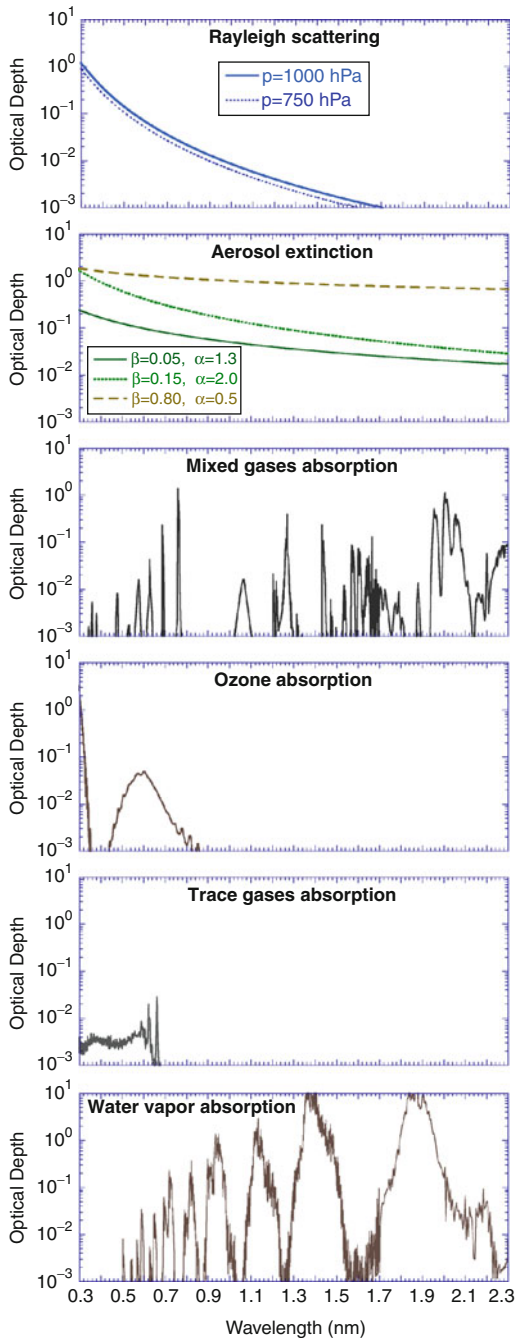

Solar Radiation Spectrum. Figure 9
Optical depth of various atmospheric extinction processes for the conditions of the US Standard Atmosphere and various aerosol models, using SMARTS version 2.9.5

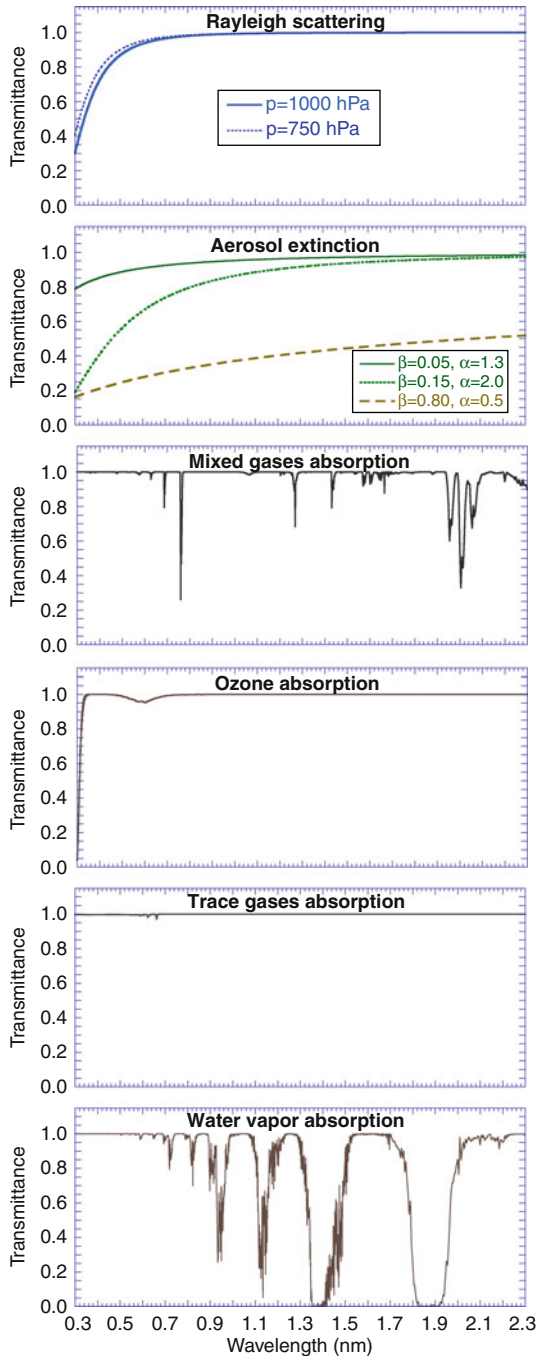

Solar Radiation Spectrum. Figure 10
Transmittance for the various extinction processes of Fig. 9 and an overhead sun ($Z = 0$ and $m = 1$), using SMARTS version 2.9.5

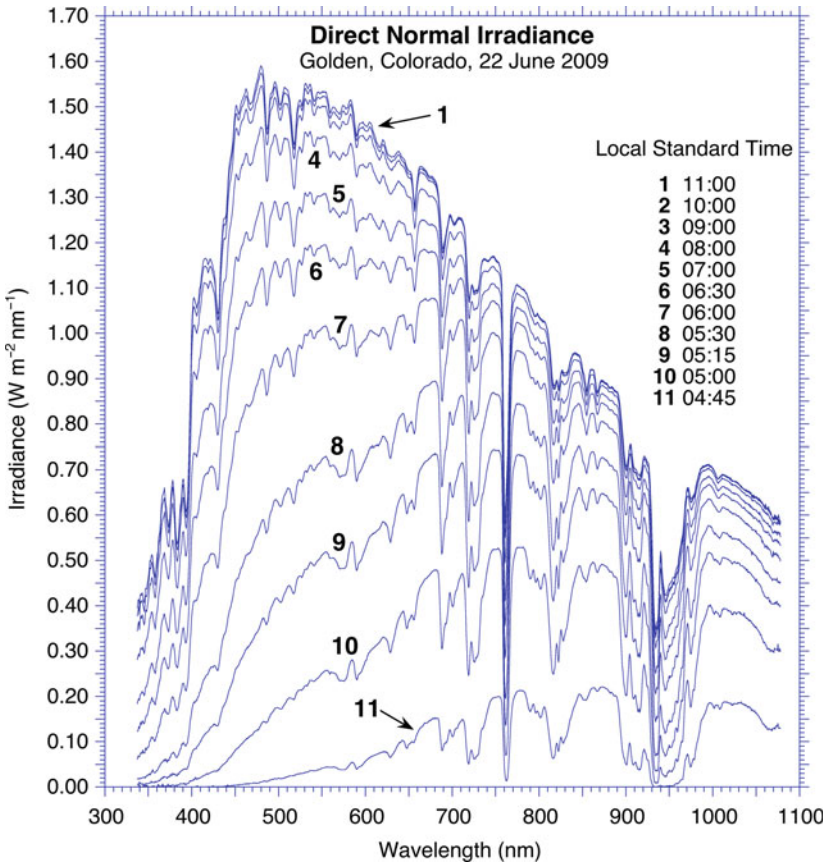

Solar Radiation Spectrum. Figure 11

Direct irradiance spectrum as measured automatically by a scanning spectroradiometer at Golden, Colorado, during a clear summer day. Not all recorded spectra are shown for clarity

(downward) as diffuse sky radiation. Since molecular scattering is most effective at short wavelengths, this downward diffuse radiation is characteristically blue rich, and even more so, ultraviolet rich. Below about 320 nm, where scattering is extremely intense, it is normal to find that the diffuse component is of comparable magnitude to – if not larger than – the direct beam component. Above that threshold wavelength, however, diffuse radiation is only a small part of the global spectrum, at least under clear skies with low to moderate AODs. Similarly to Figs. 11 and 12, Fig. 13 compares diffuse spectra measured at the Southern Great Plains experimental site (near Lamont, Oklahoma; latitude 36.61°N, longitude 97.49°W, elevation 310 m) of the Atmospheric Radiation Measurement program, at different times during May 2003. The instrument used here is an RSS, described previously in section "Instrumentation and Unit". The diffuse spectrum, $E_{d\lambda}$, is obtained when the shadowband blocks the sun. In the unshaded position, the global spectrum is rather obtained. This global irradiance, $E_{g\lambda}$, is the sum of the diffuse irradiance and the projected component of DNI on the horizontal, such as:

$$E_{g_\lambda} = E_{d\lambda} + E_{bn\lambda}\cos Z. \quad (12)$$

Under very clear conditions, $E_{g\lambda}$ is very close to ($E_{bn\lambda}$ cos$Z$) since the diffuse irradiance is small. Conversely, under a thick cloud cover, $E_{bn\lambda}$ becomes zero, so that $E_{g\lambda} = E_{d\lambda}$. More generally, the global irradiance below a uniform cloud cover, $E_{gc\lambda}$, can be estimated from that under similar cloudless conditions, $E_{g0\lambda}$, if the global transmittance of the cloud cover, $T_{gc\lambda}$, and the fractional cloud amount, C, are known, using the so-called independent column approximation [52]:

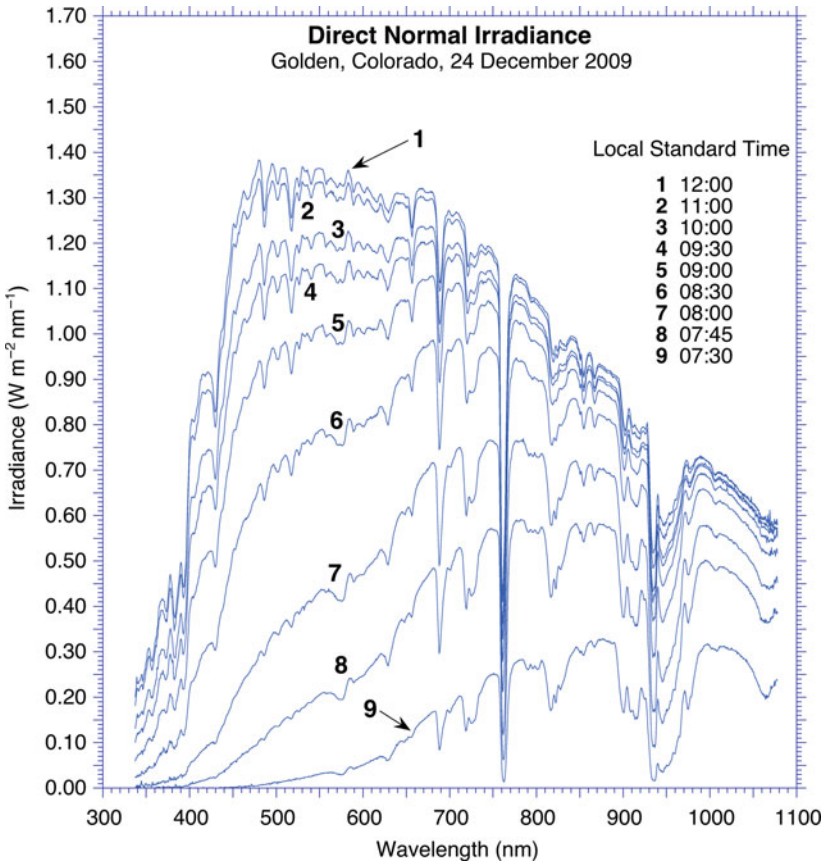

Solar Radiation Spectrum. Figure 12
Same as Fig. 11, but for a clear winter day

$$E_{gc_\lambda} = [CT_{gc_\lambda} + (1 - C)]E_{g0_\lambda}. \quad (13)$$

This approximation progressively deteriorates when Z increases under broken cloud conditions, because of shading and inter-reflections. An accurate solution would require 3D modeling in such a case. In the visible, $T_{gc\lambda}$ is mostly a function of COD and type of cloud (ice vs. water) for any specific Z. In the near-infrared, $T_{gc\lambda}$ is further reduced due to strong water (or ice) absorption bands, as shown in Fig. 14 for a few typical cases. Note that, for a specified COD, $T_{gc\lambda}$ is different for an ice cloud and a water cloud, even though their *direct* transmittance is essentially the same. The latter is not affected by absorption or wavelength, and can be approximated by $\exp(-m_c \bullet \mathrm{COD})$, from the Bouguer–Lambert–Beer law, where m_c is the cloud optical mass. Since the latter is difficult to calculate in practice, the optical air mass can be used instead, as a first approximation. No measurable direct radiation is transmitted when the product $m_c \bullet \mathrm{COD}$ is larger than about 5. The function $T_{gc\lambda}$ is calculated here with version 1.5b of the libRadtran RT code [71], which is publicly available online (http://www.libradtran.org). Another highly complex situation occurs whenever a realistic scene with more than one cloud layer must be modeled. Various approximation methods have been devised to provide a reasonable solution in such a case [72].

Figure 15 shows an example of comparison between the global, diffuse, and direct spectra predicted by SMARTS (using information on AOD and PW from a collocated sunphotometer) and the corresponding spectra measured by an RSS under clear-sky conditions. Since the model has a much higher spectral resolution than the instrument, the modeled spectra must be convolved with the spectral transfer function

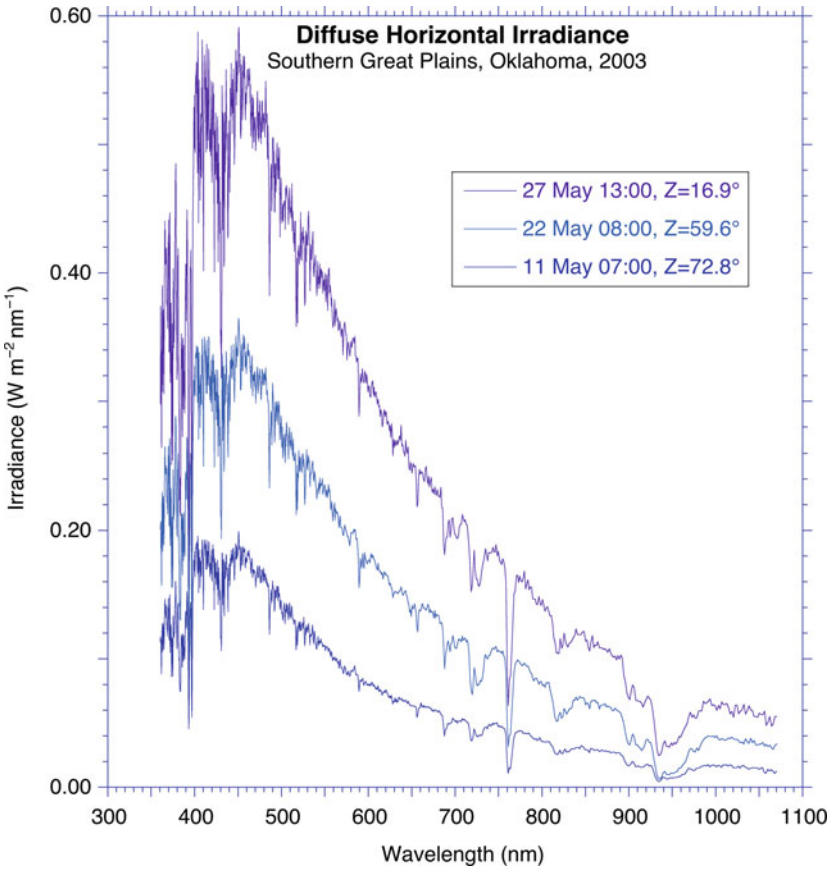

Solar Radiation Spectrum. Figure 13
Diffuse spectral irradiance measured with a spectroradiometer under clear conditions in Oklahoma. Note the change of vertical scale compared to Figs. 11 and 12

of the instrument to simulate the smoothing effect of its bandwidth and provide a meaningful comparison.

For some applications, such as the performance simulation of flat-plate PV systems, it may be necessary to determine the global irradiance on a tilted surface. This "plane-of-array" irradiance, $E_{gs\lambda}$, must take into account the changes in geometry for both the direct and sky diffuse components, and the addition of reflected irradiance from the surroundings (natural environment, nearby constructions, boosting mirrors, etc.). This can be accomplished with Monte Carlo models, which can essentially handle any type of spatial environment and atmospheric conditions. However, their usage is complex, computationally intensive, and is generally too difficult or costly for nonexperts. Among the more conventional models, there are currently two radiative transfer models with such capabilities. SMARTS [58] can handle all possible tilt geometries, but it is limited to clear-sky conditions. Conversely, SEDES2 [68] can handle cloudy sky conditions, but only for surfaces tilted toward the equator, and with less spectral resolution and overall capabilities than SMARTS. Such calculations require some data on the spectral reflectance properties of all these intervening surfaces, which adds to the difficulty. In the absence of local reflectance measurements, SMARTS includes a library of spectral reflectance data for typical surfaces.

Input Data to Radiative Models

Although RT models are available to predict the components of solar irradiance under a variety of situations, they all need a variety of input data to describe the state of the atmosphere aloft. To obtain accurate

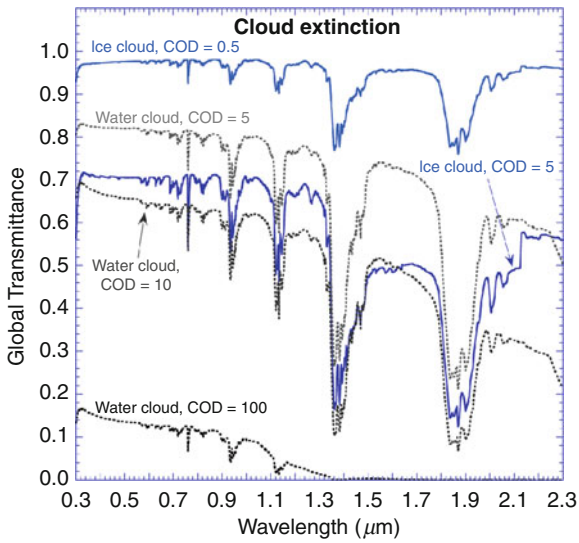

Solar Radiation Spectrum. Figure 14
Spectral transmittance for global irradiance under overcast conditions for various types of clouds, characterized by their optical depth (COD): thin ice cloud (COD = 0.5), thick ice cloud (COD = 5), thin water cloud (COD = 5), medium water cloud (COD = 10), and very thick water cloud (COD = 100). Calculations performed with libRadtran version 1.5b for an overhead sun (m = 1)

spectral irradiances, the difficulty is therefore twofold: the intricacies of the radiative model used must be understood, and the best input data for the cases under scrutiny must be obtained in detail (including appropriate time resolution, accuracy, and format), which is usually not a trivial task. Input data requirements differ from one model to the other, but there are general similarities. For instance, two completely different types of situations can be encountered depending on the problem at hand. The simplest possible case occurs when predetermined typical atmospheric conditions can be considered to obtain general "theoretical" results. A "model atmosphere" is then chosen by the user to represent the assumed average vertical profiles of all radiatively active atmospheric gases. Similarly, an "aerosol model" must be added since there are always some aerosols in the atmosphere, particularly in its lower layers. The only remaining variable is the apparent position of the sun. Such ideal situations are useful to develop parametric functions and explore "what if" scenarios.

A more difficult case arises when realistic atmospheric conditions must be simulated, such as for a specific location and time. The vertical profiles of gases and aerosols must then be obtained for this location and time, which usually requires precise specialized measurements. As a general statement, the accuracy in the predicted spectral irradiance (i.e., the model's output) depends on both the intrinsic performance of the model and on the quality of its input data. The spectral range and the spectral resolution are also elements to take into consideration. For instance, the total ozone amount conditions the ultraviolet spectrum, but has only a small impact in the visible or near-infrared (NIR) spectrum. Conversely, water vapor is a significant absorber in the NIR, but has no impact in the UV, and virtually none in the visible. Therefore, if only the visible spectrum is to be predicted, for instance, approximate determinations of ozone and water vapor can be tolerated.

From section "Direct, Diffuse, and Global Spectral Irradiance" and Fig. 10, it is obvious that, in general and over large spectral bands, there are three *variable* atmospheric constituents that influence the clear-sky shortwave spectrum most: ozone, water vapor, and aerosols. The most common sources of data for these constituents are reviewed next.

Ozone has been measured for decades from a world network of ground-based spectroradiometers called the World Ozone and Ultraviolet Radiation Data Centre (WOUDC; http://www.woudc.org/). The common unit for the vertical column amount of ozone is the Dobson Unit (DU), which commemorates the influential pioneering work of Gordon Dobson (1889–1976), who built the first instrument to measure ozone, known as the "Dobson spectrophotometer." One DU is equivalent to a depth of one hundredth of a millimeter along a vertical column maintained at standard pressure/temperature, i.e., 100 DU equals 1 atm-mm. The ozone amount typically varies day by day with a seasonal pattern, and is normally in the range 200–500 DU. Very low ozone amounts (<100 DU) are referred to as "ozone hole" conditions. Another source of ozone data, with better geographic coverage, but slightly lower accuracy, is from spaceborne sensors, such as TOMS, OMI, and SCIAMACHY (see, e.g., http://toms.gsfc.nasa.gov/teacher/ozone_overhead_v8.html and http://www.temis.nl/protocols/O3total.html). The vertical profile of ozone is measured by ozonesondes.

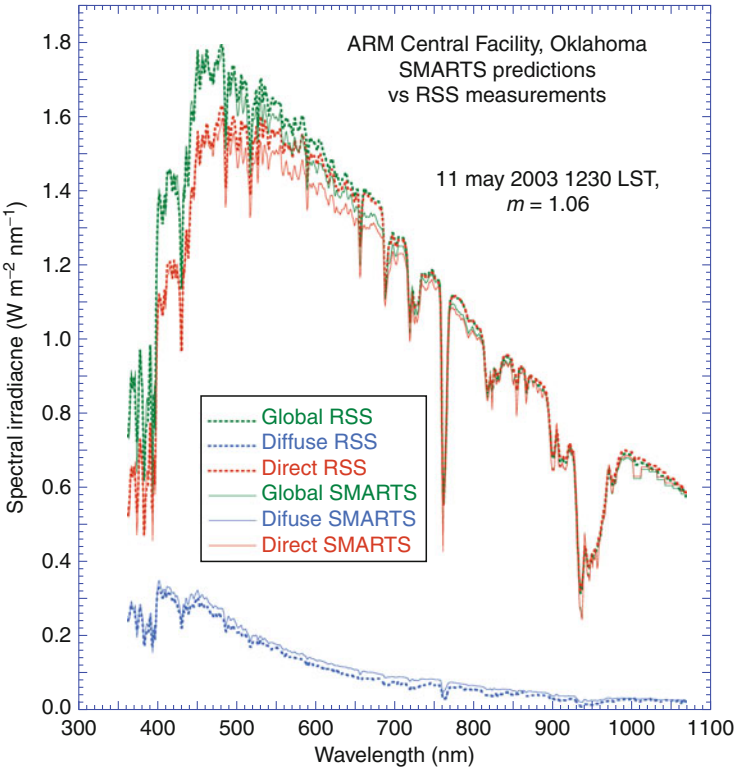

Solar Radiation Spectrum. Figure 15
Modeled global, direct, and diffuse spectra compared to their measured counterpart obtained with rotating shadowband spectroradiometer under clear skies in Oklahoma

Water vapor is also highly variable in both space and time. Contrarily to ozone, which is concentrated at high altitude, water vapor is concentrated in the boundary layer, up to 2–3 km above surface. Consequently, it is normal to observe very low water vapor amounts at elevated sites, such as mountain peaks and elevated plateaus. Moreover, there are seasonal variations (more water vapor in summer than winter), climatological variations (low water vapor in dry zones vs. high water vapor in humid tropical zones), and daily meteorological variations linked to the general circulation of air masses, cold fronts, etc. The vertical profile of water vapor concentration has been measured with radiosondes (or rawinsondes) for many decades. There are usually two ascents per day, at 0000 and 1200 Universal Time. Such data may be requested from each country's meteorological service, or obtained online from sites such as http://www.esrl.noaa.gov/raobs/. The total amount of water vapor is usually measured in terms of precipitable water (PW), also called "integrated water vapor (IWV)," which can be defined as the height that would occupy all the water vapor aloft if it were condensed inside a virtual vertical tube of 1 cm^2 section. This height is usually indicated in cm. Since 1 cm^3 of water weighs 1 gram, equivalent PW units are g/cm^3 or g/cm^2. (A better SI unit is kg/m^2, with 1 cm of precipitable water being equivalent to 10 kg/m^2.) Other ground-based determinations of PW can now be made by a variety of instruments, including special GPS sensors (see, e.g., http://www.suominet.ucar.edu/ and http://gpsmet.noaa.gov/jsp/index.jsp), sunphotometers (e.g., http://aeronet.gsfc.nasa.gov/), Fourier transform infrared spectrometers (FTIR), microwave radiometers (MWR), lidars, or millimeter-wave imaging radiometers (MIR). All these methods have upsides and downsides, and they are frequently compared and reviewed in the literature [73–76]. Some of these techniques also provide information on

the vertical distribution of water vapor. Other sources of data with a broader geographical coverage include spaceborne sensors (e.g., AMSU, AVHRR, GOME, MODIS, SEVIRI, SSM/I, or TOVS), datasets using assimilation of ground and satellite measurements such as NVAP [77], and reanalysis data [78–81].

Aerosol information is usually the most critical input, and yet the most difficult to obtain with good accuracy for a specific location and time. The recognized importance of local and global effects of aerosols in the current climate change research has led to considerable efforts being deployed to monitor their optical characteristics, particularly AOD. Four main methods are currently being used:

- Sunphotometry from ground sites, which can provide the spectral AOD after filtering of cloud occurrences, and by further derivation, the Ångström coefficient, the aerosols' single-scattering albedo (which characterizes their relative fraction of scattering and absorption), the phase function (which characterizes the directional scattering properties), and the size distribution of the particles in the vertical mix. The main world network is that of AERONET [82], http://aeronet.gsfc.nasa.gov/), but other, more limited, networks also exist (e.g., GAW, http://wdca.jrc.it/data/parameters/data_AOD.html, SKYNET, http://atmos.cr.chiba-u.ac.jp/index.html, and SURFRAD, http://www.srrb.noaa.gov/surfrad/aod/).
- Lidar measurements from ground sites, mostly used to evaluate the vertical profile of the aerosol concentration.
- Spectraradiometry from space platforms, with instruments such as MODIS and MISR. Since most of these satellites are polar orbiters, they cannot provide time-continuous AOD retrievals for any specific site, but they can accumulate long-term data series with good spatial resolution and provide useful aerosol climatologies over time. Because of the uncertainties in the measurements and retrieval algorithms, their AOD predictions must be validated against ground-truth data from ground-based sunphotometers.
- Chemical transport models, which predict the distribution of AOD over time and space by using source information about when and where natural or anthropogenic particles were released in the atmosphere, chemical information about their evolution and transformation, and meteorological information about the continuous movement of air masses. These models also need to be validated against ground truth [83]. The international Aerocom project (http://nansen.ipsl.jussieu.fr/AEROCOM/aerocomhome.html) has the mission to improve these models and facilitate their intercomparisons, or their comparisons with ground or satellite data.

Once AOD is obtained at various wavelengths, it is possible to extrapolate to other wavelengths through Eq. 11. For instance, most current AOD datasets derived from spaceborne sensors or chemical transport models report the AOD at 550 nm. Moreover, the Ångström turbidity coefficients α and β can be derived from such simultaneous measurements of $\tau_{A\lambda}$ at a few (usually 4–10) wavelengths $\lambda_0 \ldots \lambda_n$ by fitting these points to a linearized version of Eq. 11:

$$\ln(\tau_{A\lambda}) = \ln(\beta) - \alpha \ln(\lambda). \tag{14}$$

The intercept and slope of this fitted straight line provide $\ln(\beta)$ and α, respectively. The Ångström law expressed by Eqs. 11 or 14 is convenient and is observed to be of general validity in practice, although exceptions are possible and can be explained by theory [84, 85]. A few typical cases (for low to high turbidity) recorded with a sunphotometer equipped with eight AOD-dedicated filters appear in Fig. 16, which also shows variable curvature in the log-log plot of $\tau_{A\lambda} = f(\lambda)$.

Standard Spectra

The solar spectrum at the Earth's surface is variable in both space and time. Due to compensation effects, the direct and diffuse spectra are more variable than the global spectrum. Various physical, chemical, or biological processes are also dependent on the spectral distribution of incident radiation. In particular, scientists and engineers are confronted with determining the performance of PV devices that use solar cells, of spectrally selective fenestration used in energy-efficient buildings, or of natural daylighting systems. They also need to address how various materials degrade over time, due in part to the action of the UV spectrum.

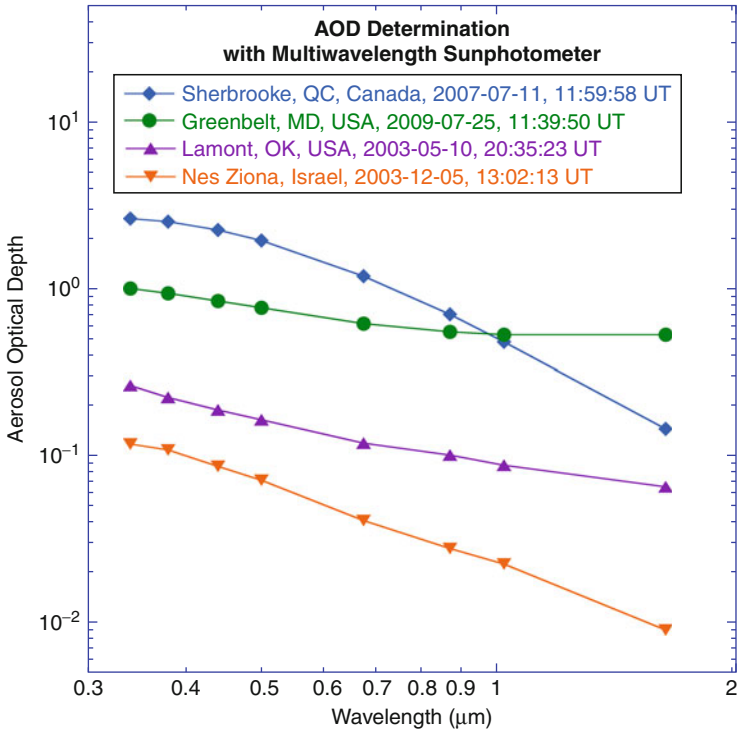

Solar Radiation Spectrum. Figure 16
Variation of spectral aerosol optical depth with wavelength for selected measurements using a sunphotometer equipped with eight dedicated aerosol filters from 340 to 1,640 nm

All these applications rely on spectral information, and may require measured and/or modeled data. Such information may not be available at the design stage of an engineering project, however. In this case, the designer is interested in using reference spectral data. Moreover, when different products (such as PV panels or coated windows) must be compared or rated, some reference conditions must be agreed upon so that the performance of all competitive products can be evaluated fairly, using identical test conditions. These concerns have fueled the impetus to develop reference spectra for standardization purposes.

The American Society for Testing and Materials (now known as ASTM International) has proposed various standard reference spectra over the years. For space applications, their current standard is E490 [14]. For terrestrial applications, two older standard spectra [86, 87] are still referred to in the current literature or in other standards, even though they have been deprecated by ASTM and replaced in 2003 by their revised version, contained in a single standard, G173 [88]. One spectrum is for the shortwave direct irradiance. The other spectrum is for the shortwave global irradiance incident on a surface tilted at 37° toward the sun. Both are evaluated for clear-sky conditions at sea level for an air mass of 1.5 (i.e., a zenith angle of 48.24°), and for the whole spectral range (280–4,000 nm) covered by SMARTS. They integrate to 900 and 1,000 W/m^2, respectively. A slightly different version of G173's global spectrum has been adopted in 2008 by the International Electrotechnical Commission (IEC) for the testing of PV devices [89]. The justification and technical details behind the transition from the older spectra to the newer ones are detailed elsewhere [90, 91].

Recognizing the importance for users of these reference spectra to evaluate the possible effects of incremental changes in the spectrum on the performance of their systems, ASTM elevated SMARTS to the status of "adjunct standard" (ASTM reference: ADJG173CD). Although the spectra specially created by any user with this adjunct standard have no official validity, they are convenient since they are consistent with the

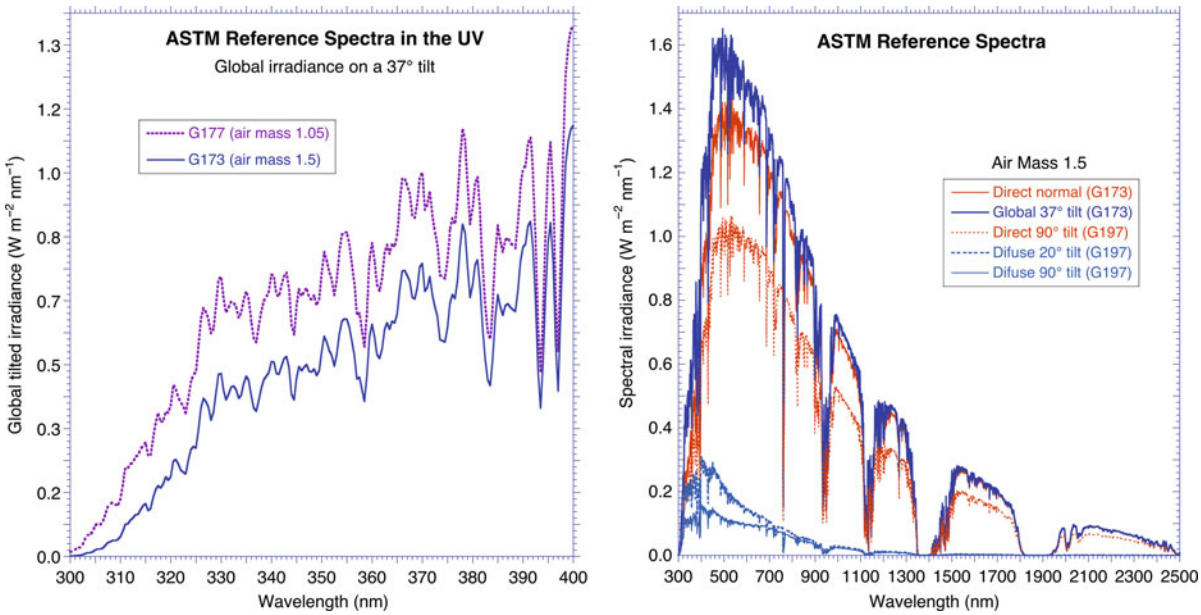

Solar Radiation Spectrum. Figure 17
(*Left*) Reference global spectra in the UV from ASTM G173 and G177. (*Right*) Direct, global, and diffuse reference spectra from ASTM G173 and G197. The G197 direct spectrum for a 20° tilt is not shown for clarity

reference spectra, and, most importantly, have the exact same spectral resolution. Using the same model for consistency, another global irradiance spectrum, limited to the UV spectral range (280–400 nm) and targeting material degradation applications, was also standardized to represent "high UV" and low air-mass conditions [92]. Finally, two direct irradiance spectra and two diffuse spectra for building and PV applications were standardized later, still using the G173 adjunct standard. These spectra correspond to the irradiance incident on either a vertical surface (representing a wall) or a 20°-tilted surface (representing a roof), and are directly compatible with those in G173 since they are for the same atmospheric conditions and same air mass of 1.5 [93]. A comparison of the current reference spectra is shown in Fig. 17.

Future Directions

Information on spectral solar radiation is available in different forms for many applications. The extraterrestrial spectrum and its short-term or long-term variations will continue to be improved from analysis of continuous spaceborne measurements. For terrestrial applications, spectral measurements are relatively scarce due to their initial cost, need for regular maintenance and specialized laboratory work for calibration. However, with appropriate weatherproofing, spectroradiometers can monitor the solar spectrum even under variable cloudiness, including precipitating conditions.

Solar spectra can alternatively be generated by radiative transfer models for a much lower cost, but they require specialized input data to represent the specific atmospheric conditions being modeled. Such data may be difficult to obtain without additional instrumentation, depending on the type of problem at hand. Research continues to improve the availability, accuracy, and resolution (both spatial and temporal) of the main atmospheric data that control the transfer of radiation: clouds, aerosols, water vapor, and ozone, most importantly. Improvements need to be done in different ways: additional networks of high-quality instrumented sites for continuous monitoring and ground truthing, deployment of more specialized spaceborne sensors, and development of high-resolution 3D models to predict and forecast the evolution of cloud and aerosol fields. Their integration with GIS tools would be extremely useful too.

If provided with accurate input data, the best models can predict accurate spectra, with an uncertainty similar to that of measurements under clear skies. Models also tend to have better spectral resolution and a larger spectral range than most instruments. Conversely, it might be extremely difficult to model the solar spectrum under rapidly changing cloudiness. Measurements have a definite advantage in this case. The current trend toward the development of compact, portable, low-cost, and easy-to-use solid-state spectrometers should continue, opening new windows of opportunities for the field of spectral measurement and radiometry, which is still mostly the realm of experts.

Finally, reference spectra have been standardized and are being used routinely in many engineering applications. New standards may have to be developed to accommodate the needs of emerging applications, such as concentrated PV or high-end daylighting devices.

Bibliography

1. Abbot CG (1966) Solar variation, a weather element. Proc Natl Acad Sci 56:1627–1634
2. Hoyt DV (1979) The Smithsonian Astrophysical Observatory solar constant program. Rev Geophys Space Phys 17:427–458
3. Burlov-Vasiljev KA, Gurtovenko EA, Matvejev YB (1995) New absolute measurements of the solar spectrum 310-685 nm. Sol Phys 157:51
4. Burlov-Vasiljev KA, Matvejev YB, Lasiljeva IE (1998) New measurements of the solar disk-center spectral intensity in the near IR from 645 nm to 1070 nm. Sol Phys 177:25–40
5. Harrison L, Kiedron P, Berndt J, Schlemmer J (2003) The solar spectrum 360 to 1050 nm from rotating shadowband spectroradiometer (RSS) measurements at the Southern Great Plains site. J Geophys Res 108(D14)4424. doi:10.1029/2001JD001311
6. Kurucz RL, Furenlid I, Brault J, Testerman L (1984) Solar flux atlas from 296 to 1300 nm. National Solar Observatory Atlas No.1, NOAO, Sunspot, NM
7. Neckel H, Labs D (1981) Improved data of solar spectral irradiance from 0.33 to 1.25μ. Sol Phys 74:231–249
8. Fontenla J, Harder G (2005) Physical modeling of spectral irradiance variations. Mem Soc Astron Ital 76:826–833
9. Fontenla J, White OR, Fox PA, Avrett EH, Kurucz RL (1999) Calculation of solar irradiances I: synthesis of the solar spectrum. Astrophys J 518:480–499
10. Kurucz RL (1995) The solar irradiance by computation. In: 17th annual conference transmission models. Report PL-TR-95-2060. Phillips Lab, Hanscom AFB, MA, pp 333–334
11. Shapiro AI, Schmutz W, Schoell M, Hanberreiter M, Rozanov E (2010) NLTE solar irradiance modeling with the COSI code. Astronomy Astrophys 517. doi:10.1051/0004-6361/200913987
12. Tobiska WK, Woods T, Eparvier F, Viereck R, Floyd L, Bouwer D, Rottman G, White OR (2000) The SOLAR2000 empirical solar irradiance model and forecast tool. J Atm Solar Terr Phys 62:1233–1250
13. Tobiska WK, Bouwer SD (2006) New developments in SOLAR2000 for space research and operations. Adv Space Res 37:347–358
14. ASTM (2000) Standard solar constant and air mass zero solar spectral irradiance tables, Standard E490-00. American Society for Testing and Materials, West Conshohocken
15. Gueymard CA (2004) The sun's total and spectral irradiance for solar energy applications and solar radiation models. Sol Energy 76:423–453
16. Gueymard CA (2006) Reference solar spectra: their evolution, standardization and comparison to recent measurements. Adv Space Res 37:323–340
17. Thuillier G, Floyd L, Woods TN, Cebula R, Hilsenrath E, Hersé M, Labs D (2004) Solar irradiance reference spectra. In: Pap JM, Fox J (eds) Solar variability and its effects on climate. American Geophysical Union, Washington, DC
18. Woods TN, Chamberlin PC, Harder JW, Hock RA, Snow M, Eparvier F, Fontenla J, McClintock WE, Richard E (2009) Solar irradiance reference spectra (SIRS) for the 2008 whole heliosphere interval (WHI). Geophys Res Lett 36:5. doi:10.1029/2008GL036373
19. ISO (2007) Space environment (natural and artificial) – process for determining solar irradiances, Standard 21348:2007. Geneva, Switzerland
20. Brueckner GE et al (1993) The solar ultraviolet spectral irradiance monitor (SUSIM) experiment on board the Upper Atmosphere Research Satellite (UARS). J Geophys Res 98D:10695–10711
21. Rottman GJ, Woods TN, Sparn TP (1993) Solar stellar irradiance comparison experiment I: instrument design and operation. J Geophys Res 98:10667–10677
22. Floyd LE, Reiser PA, Crane PC, Herring LC, Prinz DK, Brueckner GE (1998) Solar cycle 22 UV spectral irradiance variability: current measurements by SUSIM UARS. Sol Phys 177:79–87
23. Cebula RP, Thuillier GO, VanHoosier ME, Hilsenrath E, Herse M, Brueckner GE, Simon PC (1996) Observations of the solar irradiance in the 200-350 nm interval during the ATLAS-1 mission: a comparison among three sets of measurements – SSBUV, SOLSPEC, and SUSIM. Geophys Res Lett 23:2289–2292
24. Thuillier G, Hersé M, Labs D, Foujols T, Petermans W, Gillotay D, Simon PC, Mandel H (2003) The solar spectral irradiance from 200 to 2400 nm as measured by the SOLSPEC spectrometer from the ATLAS and EURECA missions. Sol Phys 214:1–22
25. Woods TN, Prinz DK, Rottman GJ, London J, Crane PC, Cebula RP, Hilsenrath E, Brueckner GE, Andrews MD, White OR, VanHoosier ME, Floyd LE, Herring LC, Knapp BG, Pankratz CK, Reiser PA (1996) Validation of the UARS solar ultraviolet irradiances: comparison with the ATLAS 1 and 2 measurements. J Geophys Res 101D:9541–9569
26. Gueymard CA, Myers DR (2010) Solar resource for space and terrestrial applications. In: Fraas LM, Partain LD (eds) Solar cells and their applications, 2nd edn. Wiley, Hoboken

27. Anon (1976) U.S. Standard Atmosphere 1976, NOAA/NASA/USAF, Washington, DC
28. Kasten F, Young AT (1989) Revised optical air mass tables and approximation formula. Appl Opt 28:4735–4738
29. Gueymard CA (2001) Parameterized transmittance model for direct beam and circumsolar spectral irradiance. Sol Energy 71:325–346
30. Gueymard CA, Kambezidis HD (2004) Solar spectral radiation. In: Muneer T (ed) Solar radiation and daylight models. Elsevier, Amsterdam, pp 221–301
31. Reda I, Andreas A (2004) Solar position algorithm for solar radiation applications. Sol Energy 76:577–589
32. Blanco-Muriel M, Alarcon-Padilla DC, Lopez-Moratalla T, Lara-Coira M (2001) Computing the solar vector. Sol Energy 70:431–441
33. Grena R (2008) An algorithm for the computation of the solar position. Sol Energy 82:462–470
34. Iqbal M (1983) An introduction to solar radiation. Academic, Toronto
35. McCluney WR (1994) Introduction to radiometry and photometry. Artech House, Boston
36. Shaw GE (2007) Genesis of sun photometry. J Appl Remote Sens 1:012503–012513
37. Shaw GE (1983) Sun photometry. B Am Meteorol Soc 64:4–10
38. Ross J, Sulev M (2000) Sources of errors in measurements of PAR. Agric For Meteorol 100:103–125
39. Harrison L, Beauharnois M, Berndt J, Kiedron P, Michalsky J, Min Q (1999) The rotating shadowband spectroradiometer (RSS) at SGP. Geophys Res Lett 26:1715–1718
40. Bohren CF, Clothiaux EE (2006) Fundamentals of atmospheric radiation: an introduction with 400 problems. Wiley, Weinheim
41. Goody RM, Yung YL (1995) Atmospheric radiation: theoretical basis, 2nd edn. Oxford University Press, New York
42. Lenoble J (1985) Radiative transfer in scattering and absorbing atmospheres: standard computational procedures. A. Deepak Publ, Hampton
43. Lenoble J (1993) Atmospheric radiative transfer. A. Deepak Publ, Hampton
44. Liou KN (1992) Radiation and cloud processes in the atmosphere: theory, observation, and modeling. Oxford University Press, New York
45. Liou KN (2002) An introduction to atmospheric radiation, 2nd edn, vol 84. Academic, New York
46. Petty GW (2006) A first course in atmospheric radiation, 2nd edn. Sundog Publ, Madison
47. Thomas GE, Stamnes K (1999) Radiative transfer in the atmosphere and ocean. Cambridge University Press, Cambridge
48. Wendisch M, Mayer B (2003) Vertical distribution of spectral solar irradiance in the cloudless sky: a case study. Geophys Res Lett 30:1183. doi:10.1029/2002GL016529
49. Cahalan RF, Oreopoulos L, Marshak A, Evans KF, Davis AB, Pincus R, Yetzer KH, Mayer B, Davies R, Ackerman TP, Barker HW, Clothiaux EE, Ellingsom RG, Garay MJ, Kassianov E, Kinne S, Macke A, O'Hirock W, Partain PT, Prigarin SM, Rublev AN, Stephens GL, Szczap F, Takara EE, Varnai T, Wen G, Zhuravleva TB (2005) The I3RC – bringing together the most advanced radiative transfer tools for cloudy atmospheres. B Am Meteorol Soc 86:1275–1293
50. Kylling A, Mayer B (2001) Ultraviolet radiation in partly snow covered terrain: observations and three-dimensional simulations. Geophys Res Lett 28:3365–3368
51. Marshak A, Davis A (eds) (2005) 3D radiative transfer in cloudy atmospheres. Springer, Berlin
52. Mayer B (2009) Radiative transfer in the cloudy atmosphere. Eur Phys J Conf 1:75–99
53. Barker HW, Stephens GL, Partain PT, Bergman JW, Bonnel B, Campana K, Clothiaux EE, Clough SA, Cusack S, Delamere J, Edwards J, Evans KF, Fouquart Y, Freidenreich S, Galin V, Hou Y, Kato S, Li J, Mlawer E, Morcrette JJ, O'Hirok W, Raisanen P, Ramaswamy V, Ritter B, Rozanov E, Schlesinger M, Shibata K, Sporyshev P, Sun Z, Wendisch M, Wood N, Yang F (2003) Assessing 1D atmospheric solar radiative transfer models: interpretation and handling of unresolved clouds. J Clim 16:2676–2699
54. Halthore RN, Crisp D, Schwartz SE, Anderson GP, Berk A, Bonnel B, Boucher O, Chang F-L, Chou M-D, Clothiaux EE, Dubuisson P, Fomin B, Fouquart Y, Freidenreich S, Gautier C, Kato S, Laszlo I, Li Z, Mather JH, Plana-Fattori A, Ramaswamy V, Ricchiazzi P, Shiren Y, Trishchenko A, Wiscombe W (2005) Intercomparison of shortwave radiative transfer codes and measurements. J Geophys Res 110D. doi:10.1029/2004JD005293
55. Kotchenova SY, Vermote E, Levy R, Lyapustin A (2008) Radiative transfer codes for atmospheric correction and aerosol retrieval: intercomparison study. Appl Opt 47:2215–2226
56. Oreopoulos L, Mlawer E (2010) The Continual Intercomparison of Radiation Codes (CIRC): assessing anew the quality of GCM radiation algorithms. B Am Meteorol Soc 91:305–310
57. Bird RE (1984) A simple, solar spectral model for direct-normal and diffuse horizontal irradiance. Sol Energy 32:461–471
58. Gueymard CA (2008) Prediction and validation of cloudless shortwave solar spectra incident on horizontal, tilted, or tracking surfaces. Sol Energy 82:260–271
59. Tadros MTY, El-Metwally M, Hamed AB (2005) A comparative study on SPCTRAL2, SPCTR-1881 and SMARTS2 models using direct normal irradiance in different bands for Cairo and Aswan Egypt. J Atmos Sol Terr Phy 67:1343–1356
60. Gueymard CA (2005) Interdisciplinary applications of a versatile spectral solar irradiance model: a review. Energy 30:1551–1576
61. Chu SX, Liu LH (2009) Analysis of terrestrial solar radiation exergy. Sol Energy 83:1390–1404
62. Guechi A, Chegaar M (2007) Effects of diffuse spectral illumination on microcrystalline solar cells. J Electron Devices 5:116–121
63. Kinsey GS, Pien P, Hebert P, Sherif RA (2009) Operating characteristics of multijunction solar cells. Sol Energ Mat Sol C 93:950–951
64. Myers DR, Gueymard CA (2004) Description and availability of the SMARTS spectral model for photovoltaic applications.

In: Organic photovoltaics V, conference proceedings, vol 5520. SPIE, Bellingham, WA, pp 56–67
65. Cucumo M, De Rosa A, Ferraro V, Kaliakatsos D, Marinelli V (2008) Correlations of global and diffuse solar luminous efficacy for all sky conditions and comparisons with experimental data of five localities. Renew Energy 33:2036–2047
66. Lopez G, Gueymard CA (2007) Clear-sky solar luminous efficacy determination using artificial neural networks. Sol Energy 81:929–939
67. Bartlett JS, Ciotti AM, Davis RF, Cullen JJ (1998) The spectral effects of clouds on solar irradiance. J Geophys Res 103C:31017–31031
68. Nann S, Riordan C (1991) Solar spectral irradiance under clear and cloudy skies: measurements and a semiempirical model. J Appl Meteorol 30:447–462
69. Leckner B (1978) The spectral distribution of solar radiation at the Earth's surface – elements of a model. Sol Energy 20:143–150
70. Ångström A (1929) On the atmospheric transmission of sun radiation and on dust in the air. Geografis Annal 2:156–166
71. Mayer B, Kylling A (2005) The libRadtran software package for radiative transfer calculations: description and examples of use. Atmos Chem Phys 5:1855–1877
72. Zdunkowski W, Trautmann T, Bott A (2007) Radiation in the atmosphere – a course in theoretical meteorology. Cambridge Universuty Press, Cambridge, UK
73. Liou Y-A, Teng Y-T, Van Hove T, Liljegren JC (2001) Comparison of precipitable water observations in the near Tropics by GPS, microwave radiometer, and radiosondes. J Appl Meteorol 40:5–15
74. Pacione R, Fionda E, Ferrara R, Lanotte R, Sciarretta C, Vespe F (2002) Comparison of atmospheric parameters derived from GPS VLBI ground based microwave radiometer Italy. Phys Chem Earth 27:309–316
75. Schneider M, Romero PM, Hase F, Blumenstock T, Cuevas E, Ramos R (2010) Continuous quality assessment of atmospheric water vapour measurement techniques: FTIR, Cimel, MFRSR, GPS, and Vaisala RS92. Atmos Meas Tech 3:323–338
76. Wang JR, Melfi SH, Racette P, Whitemen DN, Chang LA, Ferrare RA, Evans KD, Schmidlin FJ (1995) Simultaneous measurements of atmospheric water vapor with MIR, Raman lidar, and rawinsondes. J Appl Meteorol 34:1595–1607
77. Randel DL, Vonder Haar TH, Rngerud MA, Stephens GL, Greenwald TJ, Combs CL (1996) A new global water vapor dataset. B Am Meteorol Soc 77:1233–1246
78. Amenu GG, Kumar P (2005) NVAP and Reanalysis-2 global precipitable water products: intercomparison and variability studies. B Am Meteorol Soc 86:245–256
79. Kistler R, Kalnay E, Collins W, Saha S, White G, Woollen J, Chelliah M, Ebisuzaki W, Kanamitsu M, Kousky V, van den Dool H, Jenne R, Fiorino M (2001) The NCEP–NCAR 50-year reanalysis: monthly means CD-ROM and documentation. B Am Meteorol Soc 82:247–268
80. Morland J, Liniger MA, Kunz H, Balin I, Nyeki S, Mätzler C, Kämpfer N (2006) Comparison of GPS and ERA40 IWV in the Alpine region, including correction of GPS observations at Jungfraujoch (3584 m). J Geophys Res 111D. doi:10.1029/2005JD006043
81. Sudradjat A, Ferraro RR, Fiorino M (2005) A comparison of total precipitable water between reanalyses and NVAP. J Clim 18:1790–1807
82. Holben BN, Eck TF, Slutsker I, Tanré D, Buis JP, Setzer A, Vermote E, Reagan JA, Kaufman YJ, Nakajima T, Lavenu F, Jankowiak I, Smirnov A (1998) AERONET – a federated instrument network and data archive for aerosol characterization. Remote Sens Environ 66:1–16
83. Kinne S, Schulz M, Textor C, Guibert S, Balkanski Y, Bauer SE, Berntsen T, Berglen TF, Boucher O, Chin M, Collins W, Dentener F, Diehl T, Easter R, Feichter J, Fillmore D, Ghan S, Ginoux P, Gong S, Grini A, Hendricks J, Herzog M, Horowitz L, Isaksen I, Iversen T, Kirkevag A, Kloseter S, Koch D, Krsitjansson JE, Krol M, Lauer A, Lamarque JF, Lesins G, Liu X, Lohmann U, Montanaro V, Myhre G, Penner JE, Pitari G, Reddy S, Seland O, Stier P, Takemura T, Tie X (2006) An AeroCom initial assessment – optical properties in aerosol component modules of global models. Atmos Chem Phys 6:1815–1834
84. Eck TF, Holben BN, Reid JS, Dubovik O, Smirnov A, O'Neill NT, Slutsker I, Kinne S (1999) Wavelength dependence of the optical depth of biomass burning, urban, and desert dust aerosols. J Geophys Res 104D:31333–31349
85. Weller M, Leiterer U (1988) Experimental data on spectral aerosol optical thickness and its global distribution. Contr Atmos Phys 61:1–9
86. ASTM (1987) Standard tables for terrestrial direct normal solar spectral irradiance for air mass 1.5, Standard E891-87. American Society for Testing and Materials, Philadelphia
87. ASTM (1987) Standard tables for terrestrial solar spectral irradiance at air mass 1.5 for a 37° tilted surface, Standard E892-87. American Society for Testing and Materials, Philadelphia
88. ASTM (2003) Standard tables for reference solar spectral irradiances: direct normal and hemispherical on 37° tilted surface. American Society for Testing and Materials, West Conshohocken
89. IEC (2008) Photovoltaic devices, Part 3: measurement principles for terrestrial photovoltaic (PV) solar devices with reference spectral irradiance data. International Electrotechnical Commission, Geneva, Switzerland
90. Gueymard CA, Myers D, Emery K (2002) Proposed reference irradiance spectra for solar energy systems testing. Sol Energy 73:443–467
91. Myers DR, Emery K, Gueymard CA (2004) Revising and validating spectral irradiance reference standards for photovoltaic performance evaluation. J Sol Energ-T ASME 126:567–574
92. ASTM (2003) Standard tables for reference solar ultraviolet spectral distributions: hemispherical on 37° tilted surface. American Society for Testing and Materials, West Conshohocken
93. ASTM (2008) Table for reference solar spectral distributions: direct and diffuse on 20° tilted and vertical surfaces. American Society for Testing and Materials, West Conshohocken

Solar Radiation Versus Climate Change

Martin Wild
Institute for Atmospheric and Climate Science, ETH Zurich, Zurich, Switzerland

Article Outline

Glossary
Definition of the Subject
Introduction
Available Observational Data
Variations in Surface Solar Radiation
Impacts on the Climate System
Future Directions
Acknowledgments
Bibliography

Glossary

Brightening Describes the evidence for a partial recovery from prior dimming at many locations between the 1980s and 2000.

Dimming Also known as "global dimming," a popular expression coined to describe the evidence for a widespread decline in surface solar radiation between the 1950s and 1980s.

Early brightening Describes the evidence for an increase in surface solar radiation during the 1930s and 1940s seen in the longest surface radiation records in Europe.

Pyranometer Measurement device to record the total flux (diffuse and direct) of solar radiation incident on a horizontal plane at the Earth surface.

Surface solar radiation Also known as "global radiation" or "surface insolation," refers to the solar radiation (sunlight) incident at the Earth's surface.

Definition of the Subject

Solar radiation incident at the Earth's surface is the ultimate energy source for life on the planet, and largely determines the climatic conditions of our habitats. The amount of solar energy reaching the surface is a major component of the surface energy balance and governs a large number of diverse surface processes, such as evaporation and associated hydrological components, snow and glacier melt, plant photosynthesis and related terrestrial carbon uptake, as well as the diurnal and seasonal course of surface temperatures.

It has also major practical implications, for example, for solar energy technologies and agricultural productivity. Changes in the amount of solar energy reaching the Earth's surface can therefore have profound environmental, societal, and economic implications. There is increasing evidence that the amount of solar radiation incident at the Earth's surface is not stable over the years but undergoes significant decadal variations. This entry discusses the evidence for these changes, their magnitude, their possible causes, their representation in climate models, and their potential implications for climate change.

Introduction

The major anthropogenic impact on climate occurs through a modification of the Earth radiation balance by changing the amount of greenhouse gases and aerosol in the atmosphere. The amount of solar radiation reaching the Earth surface is thereby particularly important as a driver of a variety of climate-relevant physical and chemical processes. Observational and modeling studies emerging in the past two decades suggest that surface solar radiation is not necessary constant on decadal timescales as often assumed for simplicity, but shows substantial decadal variations. Largely unnoticed over a decade or more, this phenomenon recently gained a rapid growth of attention under the popular expressions "global dimming" and "brightening," which refer to decadal decreases and increases in surface solar radiation, respectively. This is, for example, documented in a recent special issue in the *Journal of Geophysical Research* dedicated to the topic of global dimming and brightening [1].

Available Observational Data

Monitoring of surface radiative fluxes started in the early twentieth century at selected sites, predominantly measuring the downwelling solar component (also known as "global radiation," and referred to as surface solar radiation (SSR) in this chapter). For example, continuous measurements of SSR began in 1923 at the Stockholm observatory, and in 1937 at Potsdam (Fig. 1).

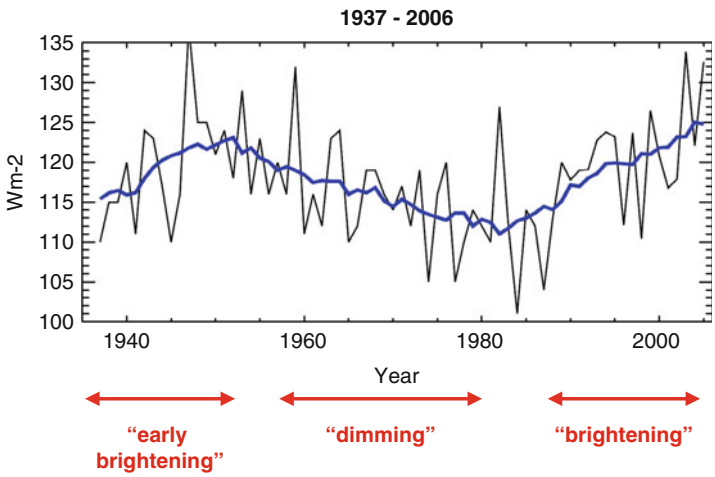

Solar Radiation Versus Climate Change. Figure 1
Annual mean surface solar radiation (in W m^{-2}) as observed at Potsdam, Germany, from 1937 to 2006. Five-year moving average in blue. Distinct phases of inclines (1930s–1940s, "early brightening"), declines (1950s–1980s, "dimming"), and renewed inclines (since 1980s, "brightening") can be seen

More widespread measurements of this quantity with thermopile pyranometers were initiated during the International Geophysical Year (IGY, 1957/1958). Many of these historic measurements have been compiled in the Global Energy Balance Archive (GEBA) at ETH Zürich [2, 3], and in the World Radiation Data Centre (WRDC) of the Main Geophysical Observatory in St. Petersburg, Russia. The data in GEBA underwent different quality checks to assure homogeneity in the records [3]. Homogeneous climatological records assert that any changes and variations in the data are induced by natural phenomena and are not an artifact. The accuracy of these historic measurements has been estimated in [3] at 2% on an annual basis. However, the quality of the measurements, performed predominantly under the auspices of the national weather services, is highly variable and not always well established. Rigorous quality control is necessary to avoid spurious trends in these data [3–5], and not all records are properly homogenized yet. In addition, possible "urbanization effects" in the surface solar radiation data [6] may have to be taken into account and need better quantification.

In the late 1980s the necessity for a reference network of surface radiation measurements with improved and defined accuracy was recognized. As a result, the Baseline Surface Radiation Network (BSRN) was established [7]. The first BSRN sites, equipped with instruments of the highest possible accuracy, became operational in the early 1990s. To date, more than 40 anchor sites in different climate regimes provide data at high temporal resolution (1-min data) for both solar (total, diffuse/direct, and reflected) and thermal (downward and upward) components. The BSRN accuracy targets are for surface solar radiation 2% or 5 W m^{-2} (ventilated pyranometer), for direct solar radiation 1% or 2 W m^{-2} (normal incidence pyrheliometer), for diffuse radiation 4% or 5 W m^{-2} (ventilated shaded pyranometer), for reflected SW radiation 5% (ventilated pyranometer), and for downward and upward thermal radiation ± 2 W m^{-2} (pyrgeometer). Other radiation networks with comparable quality standards were established around the world in recent years: the Atmospheric Radiation Measurement (ARM) Program with several worldwide distributed sites [8, 9], the SURFRAD (SURFace RADiation) network maintained by the National Oceanic and Atmospheric Administration (NOAA) with seven sites within the USA [10], the NOAA Earth System Research Laboratory (ESRL) Network with five worldwide distributed remote sites [4], the Australian Network maintained by the Bureau of Meteorology, and the Alpine Surface Radiation Budget network (ASRB) with seven sites in the Swiss Alps [11].

Despite the increasing number of high-accuracy surface radiation stations, large regions are insufficiently covered by direct surface radiation stations, such as vast areas of Africa, South America, and the Maritime Continent, and particularly ocean areas, which prevent a true global assessment.

Satellite-derived fluxes can provide a near-global picture, but their records are of limited lengths and go back to the early 1980s at most [12–14]. Furthermore, they do not directly measure the surface fluxes, but have to infer them from measurable top-of-atmosphere signals using, in addition, empirical or physical models to remove atmospheric perturbations. Satellite-inferred SSR records may also suffer from potential inhomogeneities due to changes in satellites, viewing geometries, inaccurate positioning, or sensor degradation, particularly in the earlier records [15].

In addition, reconstructions of SSR from more widely performed meteorological measurement quantities may be used to extend the information spatially and temporally, such as surface solar radiation changes inferred from observed changes in sunshine duration, diurnal temperature range, or pan evaporation [16–19].

Variations in Surface Solar Radiation

The earliest studies analyzing extended observational records of surface solar radiation appeared in the early 1990s [20–26] (see [27, 28] for a more complete overview). These pioneering studies presented the first evidence that solar radiation at the Earth's surface had not been constant over time as previously assumed, but showed significant decadal variations. Specifically, they pointed to declines in surface solar radiation since the 1950s in different regions of the globe. The first analyses with comprehensive datasets of sites distributed worldwide, as available from GEBA/WRDC, were performed by [3, 27, 29]. These studies reported an overall decrease of solar radiation at widespread locations over land surfaces on the order of 6–9 W m^{-2} between 1960 and 1990, corresponding to 4–6% over 30 years. The popular term "global dimming" was coined by Stanhill and Cohen (2001) [27] to describe this decrease. Increasing air pollution and associated increases in aerosol concentration have been suggested as major cause of this phenomenon, although changes in cloud amount and cloud optical properties may also contribute (see [28] for an overview). A direct assessment of the origins of surface solar dimming is complicated by the lack of adequate long-term observational datasets on variations of cloud and aerosol properties.

The studies on "global dimming" were all limited to data prior to 1990, since GEBA contained no data after 1990 at the time these studies were completed. More recently, ETH Zürich undertook a major effort to update the worldwide measured surface radiation data in GEBA for the period from 1990 to present. Wild et al. (2005) [30] evaluated the newly available surface observational records from GEBA and BSRN to investigate the trends in solar radiation in the more recent years. This analysis showed that the decline in solar radiation at land surfaces seen in earlier data is no longer visible in the 1990s at many locations. Instead, a brightening is observed since the late 1980s at the majority of the available observation sites (see also [28] for a recent review). A major exception is India, where the records show a persistent dimming throughout [30–32]. The brightening during the 1990s is not just found under all sky conditions, but also seen under clear skies at various sites, pointing to aerosol as a major cause of this trend reversal [28, 30, 33, 34]. The trend reversal is reconcilable with trends in aerosol emission, aerosol optical depth, and atmospheric transmission, which also show a distinct trend reversal during the 1980s [30, 35–39] (Fig. 2, taken from [30]). The trend reversal toward a reduction in aerosol emission and the associated increasing atmospheric transmission since the mid-1980s may be related to the adoption of more stringent air pollution regulations in developed countries, and the breakdown of the economy in the former communist countries. Changes in cloud properties also play a role in some regions and seem to be responsible, for example, for the dimming and brightening in New Zealand [40] and the recent brightening in the USA [41]. Overall, at many sites the brightening could not fully compensate for prior dimming, so that insolation levels around the year 2000 were still below those of the 1950s [28, 42].

The latest updates on solar radiation changes observed at the surface beyond the year 2000 suggest a continuation of the brightening at sites in Europe, in the USA, and in parts of Asia, particularly Korea [43]. Brightening seems to level off at sites in Japan and

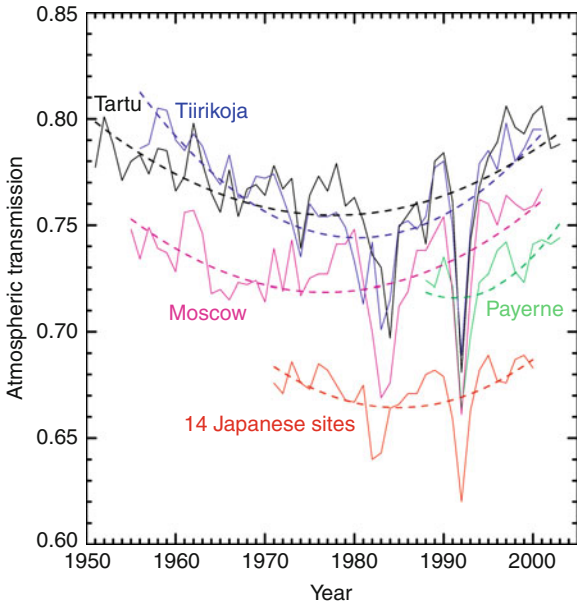

Solar Radiation Versus Climate Change. Figure 2 Time series of annual mean atmospheric transmission under cloud-free conditions determined from pyrheliometer measurements at various sites in Russia (Moscow), Estonia (Tartu-Toravere and Tiirikoja), Switzerland (Payerne), and Japan (average of 14 sites) (From [30], online supporting material)

Antarctica after 2000, while indications for a renewed dimming are seen in China, likely associated with large emission increases in China after 2000. The compensating tendencies in various regions of the globe may tentatively indicate that the overall surface solar radiation signal inferred from ground-based observations did not undergo dramatic changes since 2000 [43]. This fits with the general picture provided by satellite observations, which suggest that the global mean planetary albedo as well as the background aerosol burden of the atmosphere may not have undergone substantial changes in the early 2000s, at least globally [37, 43, 44].

The longest direct observational records, which go back to the 1920s and 1930s at a few sites in Europe, further indicate some brightening tendencies during the first half of the twentieth century, known as "early brightening" [28, 45]. This suggests that dimming, at least in Europe, was restricted to a period between the 1950s and 1980s (see Fig. 1). A potential origin of this early brightening could have been the transition from the use of coal to oil as the main fossil energy source, which temporally reduced the emission of sulfur and black carbon [28, 46].

The early brightening up to the 1950s, the subsequent dimming until the 1980s, and the more recent brightening from the 1980s to 2000 are illustrated in the long-term solar radiation record measured at Potsdam (Fig. 1).

Climate-relevant surface radiative forcing is not only determined by surface solar radiation variations, but also strongly governed by the reduced thermal surface cooling with enhanced greenhouse capacity of the atmosphere, manifest in increased downward thermal radiation from the atmosphere to the surface. Compared to the solar component, much less information from direct observations is available on the temporal evolution of the downward thermal component. Operational monitoring of this quantity started in the 1990s in the abovementioned networks of BSRN, ARM, SURFRAD, and ASRB. The first analyses of the still very short time series of downward thermal radiation indicate an overall average increase in this quantity of 2–3 W m^{-2} per decade since the early 1990s at the globally distributed measurement sites of BSRN [47, 48]. Measurements taken in the Swiss Alps show an even larger increase in downward thermal radiation since 1995 in this particular region [11]. An increase in the downward thermal radiation is in line with the expectations from greenhouse theory and climate model scenarios [49], and gives direct evidence for the real existence of an increasing greenhouse effect [11].

Impacts on the Climate System

A growing number of studies provide evidence that the variations in SSR have a considerable impact on climate change. Wild et al. (2007) [42] investigated the impact of dimming and brightening on global warming. They presented evidence that surface solar dimming was effective in masking and suppressing greenhouse warming, but only up to 1980s, when dimming gradually transformed into brightening. Since then, the uncovered greenhouse effect reveals its full dimension, as manifested in a rapid temperature rise (+0.38°C per decade over land since mid-1980s). The early brightening may have contributed to the rapid warming during the 1930s and 1940s (Fig. 3, taken

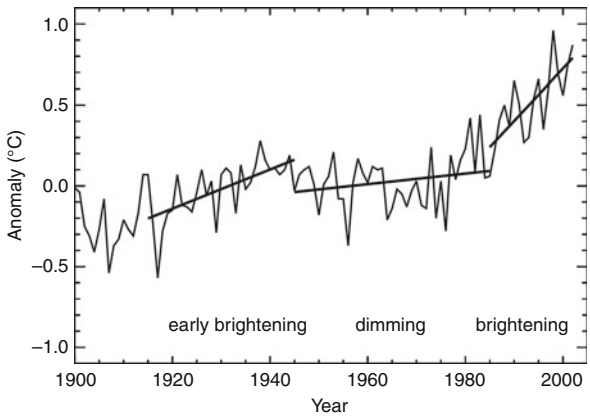

Solar Radiation Versus Climate Change. Figure 3 Two-meter temperature anomalies over global land surfaces during the twentieth century. There is indication for a suppression of greenhouse-induced warming through "global dimming" between the 1950s and 1980s, and an enhancement through "brightening" between the 1920s and 1940s as well as from the 1980s onward. Anomalies are with respect to the twentieth-century average. Unit °C (From [28])

from [28]). Ruckstuhl et al. (2008) [50] and Philipona et al. (2009) [51] came to similar conclusions for the area of Europe, where brightening due to the substantial reduction in aerosol optical depth (up to 60% since 1986 at six remote locations in Europe) may have significantly contributed to the recent rapid warming in this region. Brightening, however, cannot supersede the greenhouse effect as main cause of global warming, since land temperatures increased by 0.8°C since 1960, even though solar brightening did not fully outweigh prior dimming over this period [42].

The climate models used in IPCC-AR4 do not seem to fully account for these observed decadal modulations of global warming through solar dimming and brightening, even if all known forcings are included in the models (Fig. 4) [52, 53]. They underestimate the suppression of warming through dimming between the 1950s and 1980s over global land surfaces, and simulate a higher rate of temperature rise than observed during this period (Fig. 4). On the other hand, for the more recent decades the models underestimate the rate of global warming, indicative of a lack of brightening (Fig. 4) [52]. The potential explanations that have been put forward for these modeling problems include the large uncertainties in historic emission inventories and associated aerosol burdens in the atmosphere, which may not consider the full extent of decadal variations, the inadequate representation of the direct and indirect aerosol forcings, as well as a general underestimation of the unforced natural variability in the models [52–54].

Wild et al. (2007) [42] provided further evidence for a strong impact of dimming and brightening on global warming, based on analyses of decadal changes in observed daily maximum and minimum temperatures and related diurnal temperature range (DTR). They found a slight decrease in the daily maximum temperatures over the "dimming" period from the 1960s to the 1980s, which is in line with the reduction of SSR over this period. Daily minimum temperatures, on the other hand, have been increasing over the same period, causing a decline in DTR. In contrast, since the mid-1980s, observed minimum and maximum temperatures increase at a very similar pace. This is indicative of a major change in the surface radiative forcing regime, where the maximum temperature rise is no longer suppressed as in the decades before, due to the transition from dimming to brightening [42]. The close correlation between DTR and SSR changes may also allow a reconstruction of SSR trends back to the first part of the twentieth century, when radiation measurements were lacking, but DTR observations were already abundant. This is at least feasible for the Northern Hemisphere with much more long-term observational temperature records than for the Southern Hemisphere (P. Jones, personal communication 2008). Figure 5 (taken from [28]) depicts the annual mean DTR evolution over Northern Hemisphere land surfaces during the twentieth century, as determined here from the CRU dataset. The figure not only suggests a downward tendency in DTR predominantly between the 1950s and 1980s and a leveling off thereafter as discussed above, but also a slight upward tendency in the 1930 and 1940s. This gives, on the one hand, support for two episodes of "brightening," one at the end of the twentieth century, and a second one in the 1930s and 1940s ("early brightening"). On the other hand, it implies that "global dimming" was essentially a phenomenon confined to about a 30–40 years period in the second half of the twentieth century [28]. This behavior is again not found in the IPCC-AR4 models [28].

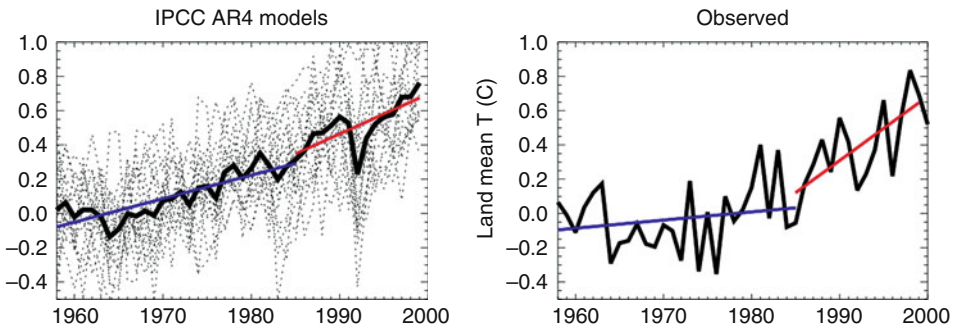

Solar Radiation Versus Climate Change. Figure 4

Annual mean temperature anomalies (°C) over land surfaces from 1958 to 1999, as simulated by 18 Global Climate Models in "all forcings" twentieth-century experiments performed for the Fourth IPCC assessment report (*left panel*), and as observed (*right panel*). Multimodel mean given as thick black lines. Individual model realizations shown as dashed lines. Linear regressions for the periods 1958–1985 in blue and 1985–1999 in red. Observations from the CRU dataset [60]. Reference period for anomalies is the entire twentieth century (From [52])

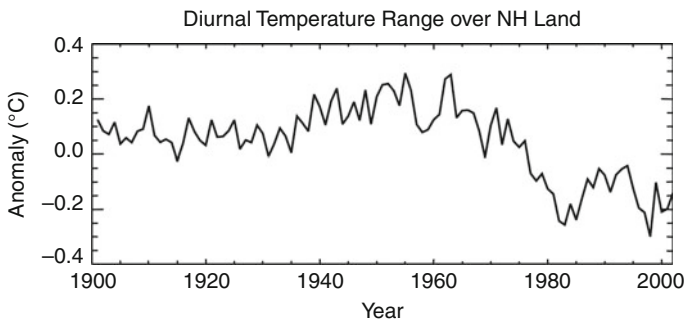

Solar Radiation Versus Climate Change. Figure 5

Annual mean diurnal temperature range (°C) anomalies averaged over Northern Hemispheric land surfaces, from 1900 to 2002. Variations of diurnal temperature range may provide a useful proxy for variations in surface solar radiation. Data from CRU [60]. Anomalies are shown with respect to the 1961–1990 mean (From [28])

Solar energy available at the earth's surface is also a major determinant of surface evaporation and thereby the main driver of the global water cycle. Wild et al. (2004) [55] suggested that surface solar energy reductions outweighed the increasing thermal energy from the greenhouse effect from the 1960s to 1980s, resulting in a reduction of surface net radiation and associated evaporation over land surfaces, causing an attenuation of the intensity of the associated hydrological cycle (Fig. 6). In contrast, for the more recent period 1980s to 2000, Wild et al. (2008) [48] pointed out that the surface solar brightening adds to the increasing energy from the enhanced greenhouse effect, leading to higher evaporation and an intensification of the global terrestrial water cycle since the 1980s (Fig. 6). Again, current climate models are not capable of adequately reproducing these decadal variations in the hydrological cycle [28, 56]. Robock and Li (2006) [57] used the dimming phenomenon to explain the increasing soil moisture and decreasing evaporation between the 1960s and 1980s, as seen in long-term soil moisture records in the Ukraine. Impacts of the transition from dimming to brightening can further be seen in the more rapid retreats of glaciers and snow cover, which became evident since the 1980s as soon as the dimming disappeared [28, 58].

There are also indications that dimming and brightening may impact the terrestrial carbon cycle

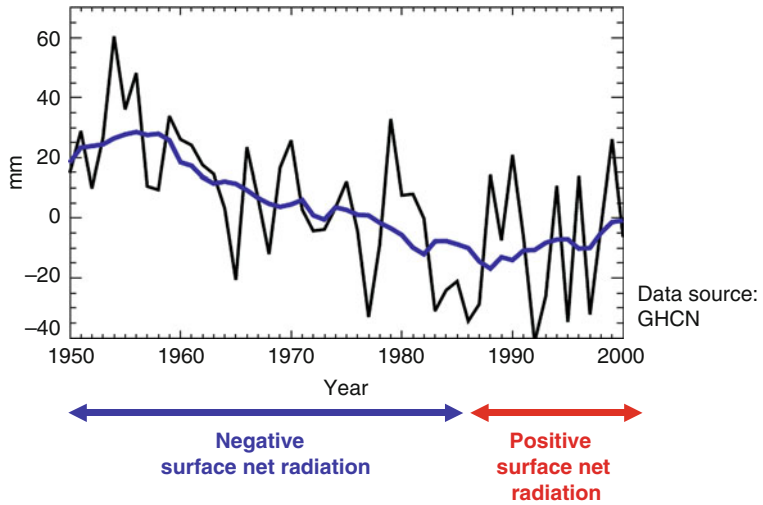

Solar Radiation Versus Climate Change. Figure 6
Northern Hemispheric terrestrial precipitation anomalies (in mm) during the second half of the twentieth century. During the "dimming" phase (1950s–1980s), the decline in downwelling solar radiation may have outweighed increasing downwelling thermal radiation from enhanced greenhouse gases, and thereby reduced the surface net radiation, causing reductions in evaporation and associated intensity of the hydrological cycle. During the "brightening" phase (1980s–2000), the disappearance of the dimming no longer compensated for the enhanced greenhouse effect, leading to an increase in surface net radiation and an intensification of the hydrological cycle. Data from the Global Historic Climate Network (GHCN)

and plant growth [59]. During dimming, plant photosynthesis and associated terrestrial carbon uptake might have been enhanced despite a reduction in surface solar radiation, since the stronger aerosol and cloud scattering increased the diffuse radiative fraction during this period. Diffuse light penetrates deeper into the vegetation canopies than the direct sunbeam and can therefore be more effectively used by plants for photosynthesis. The modeling results of this study suggests that the effect of the increasing diffuse fraction dominates over the reduced surface solar radiation during dimming, leading to an enhanced terrestrial carbon uptake in this period, which fades thereafter during the brightening period with declining diffuse fraction [59].

Further research will be required to establish the full dimension of impacts of surface solar dimming and brightening on the climate system and climate change.

Future Directions

To the extent that decadal variations in surface solar radiation are caused by anthropogenic air pollution, dimming and brightening will depend on future anthropogenic emissions of aerosols and aerosol precursors [28]. These emissions may change substantially in the future in response to economic growth, energy consumption, and air pollution regulations. The tendency toward a renewed dimming seen in the radiation data in China since 2000, for example, is not unexpected, because coal consumption in China has doubled between 2002 and 2007 (data available from the US Energy Information Administration) [28]. On the other hand, not much further brightening might be expected in Western industrialized countries, since aerosol levels stabilized since about 2000 at low values [36, 51]. A renewed overall dimming can therefore not be excluded for a few years to come, with the air pollution mitigation potential approaching saturation in many of the industrialized nations on the one hand, thus preventing further policy-related brightening, and continued increase of air pollution and associated dimming in developing and emerging nations on the other hand. This could also have implications for the near-term global warming. However, such a potential renewed dimming clearly should not be persistent, as in developing countries as well as in East Asia and India, new air pollution regulations will become

inevitable to prevent drastic health or environmental problems. Therefore, in the longer run, a turn into brightening can be expected also in these countries. Under these perspectives, effective greenhouse gas mitigation measures call for urgent implementation to prevent drastic temperature rise under foreseeable future brightening.

The continuation of accurate monitoring from both surface and space, along with the development of advanced global modeling systems, will be of utmost importance to diagnose, understand, and control these anticipated fundamental changes in the radiation balance of the globe.

Acknowledgments

I acknowledge support from the National Centre for Competence in Climate Research (NCCR Climate) of the Swiss National Science Foundation. This entry contributes to the efforts of the working group "Global Energy Balance" of the International Radiation Commission (IRC).

Bibliography

1. Wild M (2010) Introduction to special section on global dimming and brightening. J Geophys Res Atmos 115:D00d00. doi:10.1029/2009jd012841
2. Ohmura A, Gilgen H, Wild M (1989) Global energy balance archive GEBA, world climate program – water project A7. Rep, Zuerich
3. Gilgen H, Wild M, Ohmura A (1998) Means and trends of shortwave irradiance at the surface estimated from global energy balance archive data. J Climate 11:2042–2061
4. Dutton EG, Nelson DW, Stone RS, Longenecker D, Carbaugh G, Harris JM, Wendell J (2006) Decadal variations in surface solar irradiance as observed in a globally remote network. J Geophys Res Atmos 111:D19101. doi:10.1029/2005jd006901
5. Shi GY, Hayasaka T, Ohmura A, Chen ZH, Wang B, Zhao JQ, Che HZ, Xu L (2008) Data quality assessment and the long-term trend of ground solar radiation in China. J Appl Meteorol Climatol 47:1006–1016. doi:10.1175/2007jamc1493.1
6. Alpert P, Kishcha P, Kaufman YJ, Schwarzbard R (2005) Global dimming or local dimming?: effect of urbanization on sunlight availability. Geophys Res Lett 32:L17802. doi:10.1029/2005gl023320
7. Ohmura A, Dutton EG, Forgan B, Frohlich C, Gilgen H, Hegner H, Heimo A, Konig-Langlo G, McArthur B, Muller G, Philipona R, Pinker R, Whitlock CH, Dehne K, Wild M (1998) Baseline Surface Radiation Network (BSRN/WCRP): new precision radiometry for climate research. Bull Am Meteorol Soc 79:2115–2136
8. Ackerman TP, Stokes GM (2003) The atmospheric radiation measurement program. Phys Today 56:38–44
9. Stokes GM, Schwartz SE (1994) The atmospheric radiation – measurement (Arm) program – programmatic background and design of the cloud and radiation test-bed. Bull Am Meteorol Soc 75:1201–1221
10. Augustine JA, DeLuisi JJ, Long CN (2000) SURFRAD – a national surface radiation budget network for atmospheric research. Bull Am Meteorol Soc 81:2341–2357
11. Philipona R, Durr B, Marty C, Ohmura A, Wild M (2004) Radiative forcing – measured at Earth's surface – corroborate the increasing greenhouse effect. Geophys Res Lett 31:L03202. doi:10.1029/2003gl018765
12. Pinker RT, Zhang B, Dutton EG (2005) Do satellites detect trends in surface solar radiation? Science 308:850–854. doi:10.1126/science.1103159
13. Hatzianastassiou N, Matsoukas C, Fotiadi A, Pavlakis KG, Drakakis E, Hatzidimitriou D, Vardavas I (2005) Global distribution of Earth's surface shortwave radiation budget. Atmos Chem Phys 5:2847–2867
14. Hinkelman LM, Stackhouse PW, Wielicki BA, Zhang TP, Wilson SR (2009) Surface insolation trends from satellite and ground measurements: comparisons and challenges. J Geophys Res Atmos 114:D00d20. doi:10.1029/2008jd011004
15. Evan AT, Heidinger AK, Vimont DJ (2007) Arguments against a physical long-term trend in global ISCCP cloud amounts. Geophys Res Lett 34:L04701. doi:10.1029/2006gl028083
16. Makowski K, Jaeger EB, Chiacchio M, Wild M, Ewen T, Ohmura A (2009) On the relationship between diurnal temperature range and surface solar radiation in Europe. J Geophys Res Atmos 114:D00d07. doi:10.1029/2008jd011104
17. Sanchez-Lorenzo A, Brunetti M, Calbo J, Martin-Vide J (2007) Recent spatial and temporal variability and trends of sunshine duration over the Iberian Peninsula from a homogenized data set. J Geophys Res Atmos 112:D20115. doi:10.1029/2007jd008677
18. Sanchez-Lorenzo A, Calbo J, Martin-Vide J (2008) Spatial and temporal trends in sunshine duration over Western Europe (1938–2004). J Climate 21:6089–6098. doi:10.1175/2008jcli2442.1
19. Roderick ML, Farquhar GD (2002) The cause of decreased pan evaporation over the past 50 years. Science 298:1410–1411
20. Ohmura A, Lang H (1989) Secular variations of global radiation in Europe. A. Deepak, Lille, pp 98–301
21. Russak V (1990) Trends of solar radiation, cloudiness and atmospheric transparency during recent decades in Estonia. Tellus 42B:206–210
22. Dutton EG, Stone RS, Nelson DW, Mendonca BG (1991) Recent interannual variations in solar-radiation, cloudiness, and surface-temperature at the south-pole. J Climate 4:848–858
23. Stanhill G, Moreshet S (1992) Global radiation climate changes – the world network. Clim Change 21:57–75
24. Stanhill G, Moreshet S (1994) Global radiation climate-change at 7 sites remote from surface sources of pollution. Clim Change 26:89–103

25. Liepert BG, Fabian P, Grassl H (1994) Solar radiation in Germany – observed trends and assessment of their causes; Part I: regional approach. Beitr Phys Atmos 67:15–29
26. Abakumova GM, Feigelson EM, Russak V, Stadnik VV (1996) Evaluation of long-term changes in radiation, cloudiness, and surface temperature on the territory of the former soviet union. J Climate 9:1319–1327
27. Stanhill G, Cohen S (2001) Global dimming: a review of the evidence for a widespread and significant reduction in global radiation with discussion of its probable causes and possible agricultural consequences. Agric Forest Meteorol 107:255–278
28. Wild M (2009) Global dimming and brightening: a review. J Geophys Res Atmos 114:D00d16. doi:10.1029/2008jd011470
29. Liepert BG (2002) Observed reductions of surface solar radiation at sites in the United States and worldwide from 1961 to 1990. Geophys Res Lett 29:1421. doi:10.1029/2002gl014910
30. Wild M, Gilgen H, Roesch A, Ohmura A, Long CN, Dutton EG, Forgan B, Kallis A, Russak V, Tsvetkov A (2005) From dimming to brightening: decadal changes in solar radiation at Earth's surface. Science 308:847–850. doi:10.1126/science.1103215
31. Ramanathan V, Chung C, Kim D, Bettge T, Buja L, Kiehl JT, Washington WM, Fu Q, Sikka DR, Wild M (2005) Atmospheric brown clouds: impacts on South Asian climate and hydrological cycle. Proc Natl Acad Sci USA 102:5326–5333. doi:10.1073/pnas.0500656102
32. Kumari BP, Londhe AL, Daniel S, Jadhav DB (2007) Observational evidence of solar dimming: offsetting surface warming over India. Geophys Res Lett 34:L21810. doi:10.1029/2007gl031133
33. Norris JR, Wild M (2007) Trends in aerosol radiative effects over Europe inferred from observed cloud cover, solar "dimming" and solar "brightening". J Geophys Res Atmos 112:D08214. doi:10.1029/2006jd007794
34. Norris JR, Wild M (2009) Trends in aerosol radiative effects over China and Japan inferred from observed cloud cover, solar "dimming," and solar "brightening". J Geophys Res Atmos 114:D00d15. doi:10.1029/2008jd011378
35. Streets DG, Wu Y, Chin M (2006) Two-decadal aerosol trends as a likely explanation of the global dimming/brightening transition. Geophys Res Lett 33:L15806. doi:10.1029/2006gl026471
36. Streets DG, Yan F, Chin M, Diehl T, Mahowald N, Schultz M, Wild M, Wu Y, Yu C (2009) Anthropogenic and natural contributions to regional trends in aerosol optical depth, 1980–2006. J Geophys Res Atmos 114:D00d18. doi:10.1029/2008jd011624
37. Mishchenko MI, Geogdzhayev IV, Rossow WB, Cairns B, Carlson BE, Lacis AA, Liu L, Travis LD (2007) Long-term satellite record reveals likely recent aerosol trend. Science 315:1543–1543. doi:10.1126/science.1136709
38. Russak V (2009) Changes in solar radiation and their influence on temperature trend in Estonia (1955–2007). J Geophys Res Atmos 114:D00d01. doi:10.1029/2008jd010613
39. Ohvril H, Teral H, Neiman L, Kannel M, Uustare M, Tee M, Russak V, Okulov O, Joeveer A, Kallis A, Ohvril T, Terez EI, Terez GA, Gushchin GK, Abakumova GM, Gorbarenko EV, Tsvetkov AV, Laulainen N (2009) Global dimming and brightening versus atmospheric column transparency, Europe, 1906–2007. J Geophys Res Atmos 114:D00d12. doi:10.1029/2008jd010644
40. Liley JB (2009) New Zealand dimming and brightening. J Geophys Res Atmos 114:D00d10. doi:10.1029/2008jd011401
41. Long CN, Dutton EG, Augustine JA, Wiscombe W, Wild M, McFarlane SA, Flynn CJ (2009) Significant decadal brightening of downwelling shortwave in the continental United States. J Geophys Res Atmos 114:D00d06. doi:10.1029/2008jd011263
42. Wild M, Ohmura A, Makowski K (2007) Impact of global dimming and brightening on global warming. Geophys Res Lett 34:L04702. doi:10.1029/2006gl028031
43. Wild M, Truessel B, Ohmura A, Long CN, Konig-Langlo G, Dutton EG, Tsvetkov A (2009) Global dimming and brightening: an update beyond 2000. J Geophys Res Atmos 114:D00d13. doi:10.1029/2008jd011382
44. Loeb NG, Wielicki BA, Rose FG, Doelling DR (2007) Variability in global top-of-atmosphere shortwave radiation between 2000 and 2005. Geophys Res Lett 34:L03704. doi:10.1029/2006gl028196
45. Ohmura A (2009) Observed decadal variations in surface solar radiation and their causes. J Geophys Res Atmos 114:D00d05. doi:10.1029/2008jd011290
46. McConnell JR, Edwards R, Kok GL, Flanner MG, Zender CS, Saltzman ES, Banta JR, Pasteris DR, Carter MM, Kahl JDW (2007) 20th-century industrial black carbon emissions altered arctic climate forcing. Science 317:1381–1384. doi:10.1126/science.1144856
47. Wild M, Ohmura A (2004) BSRN longwave downward radiation measurements combined with GCMs show promise for greenhouse detection studies. GEWEX News 14:9–10
48. Wild M, Grieser J, Schaer C (2008) Combined surface solar brightening and increasing greenhouse effect support recent intensification of the global land-based hydrological cycle. Geophys Res Lett 35:L17706. doi:10.1029/2008gl034842
49. Wild M, Ohmura A, Cubasch U (1997) GCM-simulated surface energy fluxes in climate change experiments. J Climate 10:3093–3110
50. Ruckstuhl C, Philipona R, Behrens K, Coen MC, Durr B, Heimo A, Matzler C, Nyeki S, Ohmura A, Vuilleumier L, Weller M, Wehrli C, Zelenka A (2008) Aerosol and cloud effects on solar brightening and the recent rapid warming. Geophys Res Lett 35:L12708. doi:10.1029/2008gl034228
51. Philipona R, Behrens K, Ruckstuhl C (2009) How declining aerosols and rising greenhouse gases forced rapid warming in Europe since the 1980s. Geophys Res Lett 36:L02806. doi:10.1029/2008gl036350
52. Wild M (2009) How well do IPCC-AR4/CMIP3 climate models simulate global dimming/brightening and twentieth-century daytime and nighttime warming? J Geophys Res Atmos 114:D00d11. doi:10.1029/2008jd011372
53. Wild M, Schmucki E (2010) Assessment of global dimming and brightening in IPCC-AR4/CMIP3 models and ERA40. Clim Dynam. doi:10.1007/s00382-010-0939-3

54. Ruckstuhl C, Norris JR (2009) How do aerosol histories affect solar "dimming" and "brightening" over Europe?: IPCC-AR4 models versus observations. J Geophys Res Atmos 114: D00d04. doi:10.1029/2008jd011066
55. Wild M, Ohmura A, Gilgen H, Rosenfeld D (2004) On the consistency of trends in radiation and temperature records and implications for the global hydrological cycle. Geophys Res Lett 31:L11201. doi:10.1029/2003gl019188
56. Wild M, Liepert B (2010) The Earth radiation balance as driver of the global hydrological cycle. Environ Res Lett 5:Artn 025003. doi:10.1088/1748-9326/5/2/025003
57. Robock A, Li HB (2006) Solar dimming and CO2 effects on soil moisture trends. Geophys Res Lett 33:L20708. doi:10.1029/2006gl027585
58. Ohmura A, Bauder A, Muller H, Kappenberger G (2007) Long-term change of mass balance and the role of radiation. Ann Glaciol 46:367–374
59. Mercado LM, Bellouin N, Sitch S, Boucher O, Huntingford C, Wild M, Cox PM (2009) Impact of changes in diffuse radiation on the global land carbon sink. Nature 458:1014–U87. doi:10.1038/Nature07949
60. Mitchell TD, Jones PD (2005) An improved method of constructing a database of monthly climate observations and associated high-resolution grids. Int J Climatol 25:693–712. doi:10.1002/Joc.1181

Solar Radiation, Introduction

Christian A. Gueymard
Solar Consulting Services, Colebrook, NH, USA

Article Outline

Solar Radiation and Sustainability
Historical Perspective
Multidisciplinary Perspective
Bibliography

Solar Radiation and Sustainability

Solar radiation is ultimately what directly brings two essential conditions that are needed to maintain life on Earth: light and heat. Light is obviously what is most directly needed by photosynthesis to absorb carbon dioxide and produce oxygen. Indirectly, various chemical reactions in the atmosphere induced by solar radiation – particularly in the ultraviolet (UV) – produce some critical elements (such as ozone and oxygen) in the right quantities and at the right altitude. The result of these direct and indirect effects is to maintain atmospheric gases to levels compatible with life as it is known. By extension, the quantity and quality of solar radiation is what totally determines the delicate balance of the Earth's ecosystems, the agricultural and forestry resources needed for human or animal food, and even the development of our civilizations.

In the present era, various factors are contributing to a stronger-than-ever need for a detailed understanding of how constant the sun's energy output is, how it propagates through the Earth's atmosphere, how its local or global variations affect our climate and life forms (including human health and behavior), how human activities induce changes in solar radiation as well as climate, and how or where it can be efficiently harnessed to develop advanced solar technologies. Such "clean" technologies are particularly necessary today to solve three critical and interrelated problems of our industrial civilization: climate change, pollution, and near complete dependence on nonrenewable energy sources. The latter factor is a major cause of the two others, and all three are fundamental reasons why our current civilization is *not* sustainable. The societies of the future will need to be based on a zero-emission renewable energy economy. This is a necessary (but not sufficient) condition to achieve sustainability.

Historical Perspective

Interest for solar radiation, and solar energy applications in general, is not new. Many textbooks or other sources provide historical accounts of discoveries or technological breakthroughs from some solar pioneers since the Antiquity. One barely known pioneer was Frank Schuman (1862–1918), an American engineer who developed various solar thermal engines that could produce steam. These were similar to those that are currently being developed throughout the world with a technology known as Concentrating Solar Power (CSP), which uses parabolic troughs (or other concentrating devices) to heat a fluid, produce steam, and ultimately electricity. Unfortunately, Schuman's inventions, and even a full-scale 88-kW demonstration plant in Egypt, progressively fell into oblivion while the reign of cheap oil was starting. Schuman was not just an engineer, but also a visionary, as exemplified by this surprising statement of his: "*One thing I feel sure of. . . is*

that the human race must finally utilize direct sun power or revert to barbarism" [1]. Although this doom's day scenario might sound extreme or utterly simplistic, there is some truth in this 100-year old warning. A more balanced and science-based statement could be "Since it is a finite system, the technological human civilization must only utilize renewable sources of energy, maintain its expansion below the limit of the Earth's 'carrying capacity' or 'planetary boundary,' and maintain sustainability for all aspects of life in that system, or eventually disappear."

In more recent history, the last 4 decades have seen considerable developments in the field of solar radiation. In the early 1970s, the oil embargo crisis sprung interest for alternative energy sources, such as solar, as well as sustainable architecture (then known as "passive solar" or "bioclimatic" architecture). Solar radiation models were developed to provide engineers and architects with modeled solar radiation data, which were necessary because very few meteorological stations were measuring it over the world. The political support for the development of solar energy applications was short-lived, unfortunately, but the field of solar radiation modeling and measurement for energy applications remained relatively active. In recent years, the interest for renewable energy applications surged again, as an anticipated way of curbing climate change, and also as a way to decrease dependence on fossil energy sources, which are not as cheap now as they were before.

Still in the 1970s, the discovery that anthropogenic emissions of halocarbons were a threat to the ozone layer [2] generated considerable interest for the study of ultraviolet radiation (UV). The main orientations of these studies were: the relationship between ozone and UV, the geographic, historic, and projected variations in the quantity and spectral quality of UV, its effect on the ecosystem and various food chains, and its effect on human health. By the mid-2000s, the halocarbon concentrations had considerably decreased, as a direct effect of the Montreal protocol. There were indications that the ozone layer had stopped its decline, and might even show the first signs of recovery [3]. This slowed down the research on UV, although new topics of interest surfaced. For instance, there is now less emphasis on the erythema and other negative health effects of UV (e.g., skin cancer), but there is more interest for the positive side of it, particularly the synthesis of vitamin D.

The 1970s also saw the developing awareness of what was originally called "global warming" [5], but is now more generally referred to as "climate change." Since solar radiation is the most important source of *natural* heating of the atmosphere, it is obvious that the whole field of climate change is directly dependent on a better understanding of the transfer of solar radiation through the atmosphere. Rapid progress followed in various areas of research: radiative transfer modeling, remote sensing of atmospheric constituents using ground-based or satellite-based instruments, improved measurements of solar radiation both outside of the atmosphere (with satellite-based sensors) and at surface level (with ground instruments using advanced radiometric methods), and evaluation of solar radiation on a global scale based on satellite-based observations. In 2005, the national science academies of the G8 nations and Brazil, China, and India signed a statement on the global response to climate change. One of the recommendations of this statement was "Show leadership in developing and deploying clean energy technologies and approaches to energy efficiency, and share this knowledge with all other nations." In 2007, the Intergovernmental Panel on Climate Change (IPCC), Nobel Peace Prize co-awardee that year, published its fourth assessment report [6], which introduced the notion that renewable sources of energy would have an important role to mitigate climate change. The report also contained an entire chapter dedicated to the importance of sustainable development. Then, in 2011, the IPCC published a special report on the role of renewable energy sources, again for the mitigation of climate change [7], providing more coverage of the role of renewable energy than was included in the 2007 report [6], as well as a stronger push for appropriate renewable energy policies.

All these important developments are obvious indicators that the study of solar radiation (in a broad sense) is now central to the very sustainability of our civilization, and is thus more important than ever. Throughout this entry (13 articles), the term "solar radiation" generally refers to electromagnetic radiation at wavelengths shorter than about 4 μm, which contains most of the solar spectrum's total energy. This is also referred to as "shortwave radiation" in the literature. In contrast, the "longwave radiation" from the sun (beyond 4 μm, i.e., in the infrared region of the

spectrum) is relatively weak, so that the thermal emission from the Earth's surface is of similar magnitude. A large part of the global warming process is caused by the blanketing action of the so-called greenhouse gases, which tend to decrease the thermal (or longwave) radiation emitted to space, and thus the natural cooling of the Earth's surface and its lower atmosphere. Since the longwave part of the solar spectrum is of too small magnitude to be of direct use in the context of sustainable technologies, only the shortwave part of the spectrum is investigated here.

Multidisciplinary Perspective

As can be understood from the above discussion, there are many disciplines directly or indirectly related to solar radiation. Essentially, all of them can now benefit from recent advances in remote sensing, particularly from satellites. Satellite-based information brings large geographical coverage at continuously improving spatial and temporal resolutions. Among other things, the retrieved variables include the solar radiative output, various atmospheric constituents (e.g., ozone, water vapor, aerosols, clouds), surface reflectance and land use, temperature and precipitation, and various components of solar radiation incident on the Earth surface.

It is logical to start the study of solar radiation by characterizing the solar radiative output, in terms of both its total radiative power and its spectral distribution (see ► Solar Constant and Total Solar Irradiance Variations and ► Solar Radiation Spectrum). Since these articles were written, new and important progress has been made in the measurement of the total radiative output of the sun, now referred to as *Total Solar Irradiance* (TSI). Validation of the recent results from the SORCE satellite mission indicated that the previous satellite-based determinations of TSI were too high. This important development may have implications in many disciplines, such as climate change [8]. The PREMOS instrument on the PICARD satellite (launched June 15, 2010) is the first space radiometer with a calibration that is fully traceable to SI, and with an extremely low uncertainty (0.05%) compared to ground-based field instruments (1–5%). The PREMOS observations have the potential to resolve the disagreement on the absolute value of TSI that followed the introduction of the SORCE data in mid-2003. Based on the preliminary PREMOS data available as of this writing (November 2011), and their comparison with other sources of longer duration (including SORCE), the long-term average value of TSI (referred to as the "solar constant" in the past) would be about 1361.2 W m^{-2}, which is $\approx$5 W m^{-2} lower than previous determinations (e.g., [9]).

Variations in the solar output and its spectral distribution have a direct effect on climate (see ► Solar-induced Climate Effects and ► Solar Radiation Versus Climate Change). In recent years, the quiet period between the sun's Cycles 23 and 24 appeared much longer than usual. Since low solar activity normally corresponds to a lower TSI and much lower UV or extreme UV (which affect the upper terrestrial atmosphere), there were concerns about a possible "Little Ice Age" syndrome, which obviously would have directly affected our lives. New research [10] shows that the radiative forcing of climate from solar origin is not necessarily in phase with solar activity in the ultraviolet (UV), as was generally considered before. The sun-climate relationship is complex, but ultimately, the sustainability of our civilization depends on the sun not being too variable. Studies of the propagation of UV radiation through the atmosphere, and of its fraction reaching the surface, in relation with variations in the ozone layer and with climate change, are important to many aspects of life on Earth, including human health (see ► Ultraviolet Radiation: Distribution and Variability, ► UV Effects on Living Organisms, and ► Solar Radiation and Human Health). Daylight is another aspect of solar radiation that affects human health and behavior. Thus, natural illumination is also an essential component of the good design of energy-efficient buildings, which is a key aspect of sustainable architecture (see ► Daylight, Indoor Illumination, and Human Behavior).

The fraction of solar radiation that is directly used by plants for photosynthesis also needs to be studied to better understand the potential of plant production (in agriculture and forestry) and their indirect effect on climate (through absorption of carbon dioxide in particular). It is obvious that appropriate food production is essential to guarantee the sustainability of our civilization (see ► Photosynthetically Active Radiation: Measurement and Modeling).

The most direct link between solar radiation and sustainability science and technology remains the utilization of solar radiation as a source of "clean" energy. Considerable developments in this direction have been made in the last few years, for reasons explained above. The early developments in solar energy (from the early 1970s to the late 1990s) were focused around small systems for the heating of residences (passive solar architecture) or the heating of water with solar collectors. Then the photovoltaic (PV) revolution started, fueled by the rapidly decreasing price and increasing availability of such systems. Mass production and still decreasing costs now make this technology appealing to the power industry and electric utilities as well. The size of solar projects thus rapidly increased from a few kilowatts to multi-megawatts in a matter of a few years. Other large solar systems use concentrators, either to heat a fluid and produce electric power with a turbine (the CSP path) or to use high-efficiency PV cells for the direct production of electricity (the CPV path).

The considerable costs of large projects force them to obey the bankability rules of financial institutions. The revenue from a solar power plant is essentially proportional to the local solar resource. The field of *solar resource assessment* thus rapidly became an important component of the whole financing process. It consists of an analysis of the local solar resource, in terms of magnitude, variability and risk assessment of "bad years," and the production of a dataset of solar radiation and important meteorological variables (temperature, precipitation and wind speed, in particular) covering a period of at least 10 years with a time step of 1 h or shorter. The development of such data series is based on radiative models using satellite-derived observations and/or on local radiometric/weather measurements (see ► Solar Irradiance, Global Distribution, ► Solar Radiation for Solar Energy Utilization, and ► Topographic Solar Radiation Modeling for Environmental Applications).

Spatial and temporal variability is another important factor here. Spatial variability conditions the confidence that analysts can have in spatial extrapolations of solar radiation data, which is often necessary. Short-term temporal variability (at a time scale of seconds to minutes) is of interest to CSP operators (to optimize the use of heat storage, if available), and to electric utilities (to study the impact of intermittent electric production on the stability of the electric grid). Long-term temporal variability (at a time scale of days to years) is a key aspect of solar resource assessment (see ► Solar Radiation, Spatial and Temporal Variability).

Various solar technologies (such as PV) or building technologies (such as energy-efficient glazings) employ materials that are spectrally selective, that is, whose response depends on wavelength. Similarly, most materials degrade over time when exposed to sunlight, and this process is spectrally selective too. For such applications, detailed knowledge of the spectral distribution of solar radiation and its variations over time is necessary. This can be obtained by radiative modeling, measurement, or their appropriate combination (see ► Solar Radiation Spectrum).

Finally, the field of *solar radiation forecasting* is still in its infancy, and thus is not covered here. It combines solar radiation modeling with advanced numerical weather prediction techniques used in meteorology and/or statistical techniques [11–16]. Rapid developments are expected in the near future, for instance, to help electric utilities improve the management of their solar power plants, or prepare optimal schedules for the use of storage or reserves in anticipation of cloudy periods.

Bibliography

1. Cleveland C et al (2008) Shuman, Frank. In: The encyclopedia of Earth. http://www.eoearth.org/article/Shuman,_Frank. Accessed 26 Aug 2011
2. National Academy of Sciences (1976) Halocarbons, effects on stratospheric ozone. National Academy of Sciences, Washington, DC
3. WMO (2007) Scientific assessment of ozone depletion: 2006. http://www.wmo.int/pages/prog/arep/gaw/ozone_2006/ozone_asst_report.html
4. Oreskes N (2004) Beyond the ivory tower: the scientific consensus on climate change. Science 306(5702):1686. doi:10.1126/science.1103618 DOI:dx.doi.org
5. Broecker WS (1975) Climatic change: are we on the brink of a pronounced global warming? Science 189(4201):460–463
6. IPCC Working Group III (2007) Fourth assessment report—mitigation of climate change. http://www.ipcc-wg3.de/publications/assessment-reports/ar4/working-group-iii-fourth-assessment-report
7. IPCC Working Group III (2011) Special report on renewable energy sources and climate change mitigation. http://www.ipcc-wg3.de/publications/special-reports/srren/special-report-renewable-energy-sources

8. Kopp G, Lean JL (2011) A new, lower value of total solar irradiance: evidence and climate significance. Geophys Res Lett 38. doi:10.1029/2010GL045777
9. Gueymard CA (2004) The sun's total and spectral irradiance for solar energy applications and solar radiation models. Sol Energy 76:423–453
10. Haigh JD et al (2010) An influence of solar spectral variations on radiative forcing of climate. Nature 467:696–699. doi:10.1038/nature09426
11. Lorenz E et al (2010) Regional PV power prediction for improved grid integration. Prog Photovoltaics. doi:10.1002/pip. 1033
12. Martin L et al (2010) Prediction of global solar irradiance based on time series analysis: application to solar thermal power plants energy production planning. Sol Energy 84:1772–1781
13. Perez R et al (2010) Validation of short and medium term operational solar radiation forecasts in the US. Sol Energy 84:2161–2172
14. Marquez R, Coimbra CFM (2011) Forecasting of global and direct solar irradiance using stochastic learning methods, ground experiments and the NWS database. Sol Energy 85:746–756
15. Mathiesen P, Kleissl J (2011) Evaluation of numerical weather prediction for intra-day solar forecasting in the continental United States. Sol Energy 85:967–977
16. Lara-Fanego V et al (2012) Evaluation of the WRF model solar irradiance forecasts in Andalusia (southern Spain). Sol Energy. doi:10.1016/j.solener.2011.02.014, http://www.sciencedirect.com/science/article/pii/S0038092X11000582

Solar Radiation, Spatial and Temporal Variability

Annette Hammer[1], H. G. Beyer[2]
[1]Energy Meteorology Group, Energy and Semiconductor Research Laboratory, Institute of Physics, University of Oldenburg, Oldenburg, Germany
[2]Department of Engineering, University of Agder, Grimstad, Norway

Article Outline

Glossary
Definition of the Subject
Introduction
Examples for Spatial and Temporal Variability on Different Scales
Databases for the Statistical Analysis of Solar Radiation
Temporal Variability
Spatial Variability
Large-Scale and Long-Term Variability from Satellite Observations
Future Directions
Bibliography

Glossary

Autocorrelation The autocorrelation of a random process describes the statistical analogy between values of the process at different points in time, as a function of the two times or of the time difference.

Clearness index Ratio of the global irradiance on a horizontal plane (on the earth surface) to the respective irradiance just outside of the atmosphere.

Clear-sky index Ratio of the global irradiance on a horizontal plane to the irradiance expected under clear-sky conditions.

DNI Direct normal irradiance.

GHI Global horizontal irradiance.

Ground albedo Measure of how strongly the ground reflects sunlight.

Residual time series A time series in which the trends have been removed.

Definition of the Subject

Solar irradiance is a highly variable and fluctuating resource. This characteristic directly and strongly affects the performance of solar energy systems, such as the electricity production from photovoltaic (PV) systems or solar thermal power plants. This entry describes databases and appropriate methods to characterize spatial and temporal variability in solar radiation. The regional distribution of solar energy depends on the meteorological situation characterized by clouds, aerosols, and water vapor content, but also on topography and ground albedo. Within this entry the focus is laid on cloud-induced fluctuations. The spatial variability caused by the topography of the terrain is not accounted for here, since it is the topic of another entry in this encyclopedia.

Introduction

As fluctuations in solar radiation are directly coupled to the output power and yield of a grid-connected PV system, for instance, efforts have been taken to measure and characterize the solar resource's spatial and temporal variability. At first, studies focused on the impact of temporal variations. With the growing PV market and

ever increasing amounts of PV power fed into the utility grid since the early 1990s, studies of the spatial characterization of solar radiation became necessary.

Spatial variability of the solar radiation field may influence the performance of a distributed solar energy system in two ways. The collection of solar energy at different points in space leads to a smoothing of temporal fluctuations in the overall solar energy input and thus in the total power output. On one hand, this smoothing is beneficial to the system's performance, while on the other hand it must be assured that local differences in energy flow can be handled by the power distribution network.

For systems distributed over a small area only, in general the spatial variability of high temporal resolution data (with samples taken every minute, or even every second) needs to be accounted for so as to fully characterize the power fluctuations. If large-scale systems, such as grid-connected PV systems that are scattered over the whole area of a large-scale utility network, are analyzed the investigation of the temporal structure of the irradiance field with a coarser temporal resolution is adequate. Hourly data can be used in this case.

This entry gives a summary on appropriate methods to characterize the spatial and temporal variability in solar radiation. An overview about databases and methods proposed by different authors is given.

The variations of solar radiation are studied with respect to time and location. As long as the temporal and regional evolutions are controlled by temporal and spatial correlation structures, common tools in statistical analysis of time series can be applied. Other methods model the cloud field structures that induce fluctuations in solar radiation on small scales. For larger scales, satellite data have been used.

Examples for Spatial and Temporal Variability on Different Scales

This section is meant to provide a sense of the temporal and spatial variability of solar radiation, using 1 year of modelled radiation data in Germany as an example. The temporal variability induced by cloudiness is analyzed on different timescales.

Figure 1 shows the variability of daily irradiance sums and their monthly averages at three sites in Germany for the year 2009. The data has been derived from satellite images of Meteosat Second Generation with the Heliosat method [1]. Seasonal variations of the monthly averages are mainly caused by the varying position of the earth's polar axis with respect to the sun. For sites in Northern Germany with a distance of 55 km this annual course and the daily values are closely related but not identical. The Southern site lies at a distance of more than 600 km; the annual course shows similar seasons but with notable differences compared to the Northern sites. All sites show considerable fluctuations of the daily sums of irradiance around the monthly average values.

The variability within a day and from site to site is exemplified in Fig. 2. Hourly values of global horizontal irradiance (GHI) are shown for 15 days in May 2009 and for seven German sites. The obvious day/night pattern is deterministic; its annual and daily variations can be described by analytic models of the sun–earth geometry. Other differences in the time series are caused by clouds; their occurrence is of a stochastic, rather than deterministic, nature.

The temporal variability within a day is given in more detail in Fig. 3. This example of minute-by-minute values shows that the passing of a field of opaque clouds may lead to changes of the incoming irradiance of up to ~80% of the clear-sky value within a minute. For a proper analysis of these fluctuations, it is reasonable to separate the deterministic annual and daily trends from the stochastic variability of the atmospheric conditions.

Information about the interannual variability of GHI can only be obtained with long-term data. An example for the interannual variability is shown in Fig. 4 for monthly sums of GHI. Here, for two Italian sites, the satellite-derived averages, maxima and minima within a 15-year period are compared to ground-measured averages (climate normals) of a disjoint 30-year period. For these sites the long-term averages are similar for both sources with relative deviations within ±10% for Torino and ±4% for Brindisi. The monthly sum of an individual year can strongly deviate from the long-term average by ±30% for Torino and ±20% for Brindisi.

Databases for the Statistical Analysis of Solar Radiation

The meteorological services of most countries operate a network for solar radiation. For instance, the German

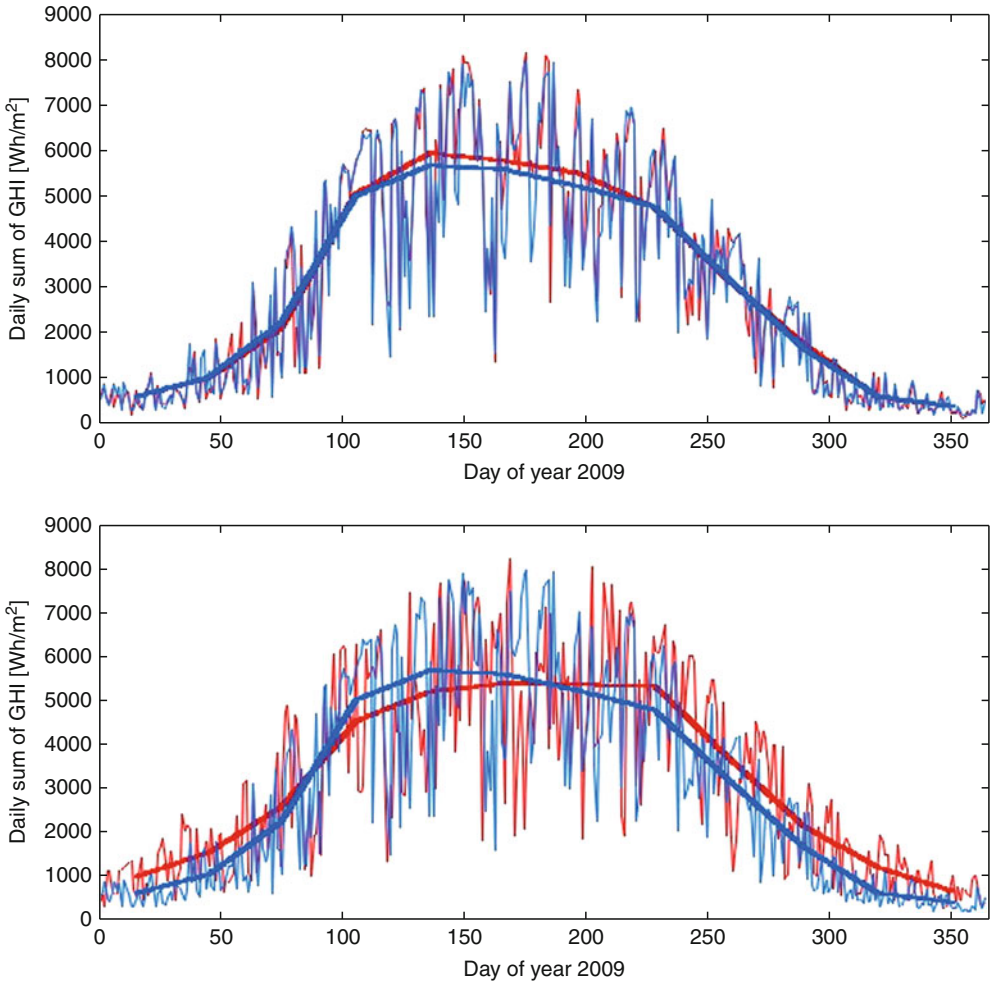

Solar Radiation, Spatial and Temporal Variability. Figure 1
One year of daily sums of satellite-derived global horizontal irradiance, GHI for three German sites in comparison to the monthly average of daily sum. *Upper image*: two sites in North Germany with a distance of 55 km (blue Neuhaus/Oste, 53.8034°N, 9.0027°E, red Nesserdeich, 54.3139°N, 9.0027°E). *Lower image*: one site in North Germany (blue Neuhaus/Oste), one in South Germany (red Lengenfeld, 48.0745°N, 9.0045°E), distance 633 km

service (Deutscher Wetterdienst, or DWD) monitors GHI at about 50 stations with interstation distances of 25–800 km. Usually the data are made available as hourly averages.

The analysis of the structure of the irradiance field over smaller spatial distances has to rely on networks that are specially designed for this purpose. The first measurement campaigns of this kind have been reported in [2, 3]. A network of 11 pyranometers distributed across an area of 75×75 km^2 in Pennsylvania was operated during 2 weeks collecting 1-min averages of GHI [4]. In Scotland, data have been recorded in the Pentland Hills (1987–1989, 10-min averages) and Edinburgh (1993–1995, 30-s averages) within an area of 10×30 km^2 [5]. A similar network of ten stations has been operated at Saarbrücken, Germany. Here, 10-min averages of GHI have been recorded for 1.5 years [6].

Mesoscale and small-scale networks had been installed by University of Oldenburg. The irradiance on horizontal and inclined planes was recorded with a temporal resolution of 10 s at five stations [7]. During

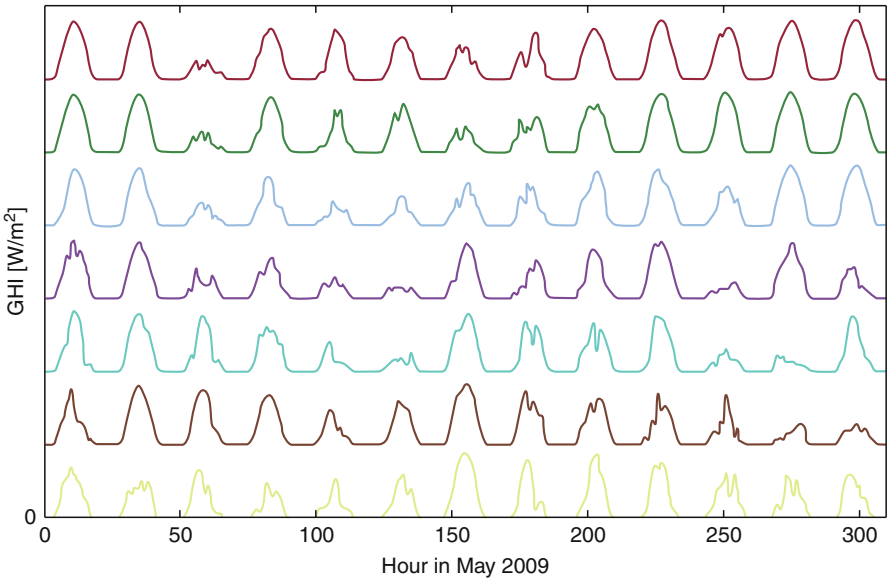

Solar Radiation, Spatial and Temporal Variability. Figure 2
Satellite-derived hourly global horizontal irradiance for 15 days of May 2009 for seven German sites at approximately 9°E, with latitudes ranging from 54.3°N (*top*) to 48°N (*bottom*). The irradiance values are ranging from 0 to 900 W/m^2

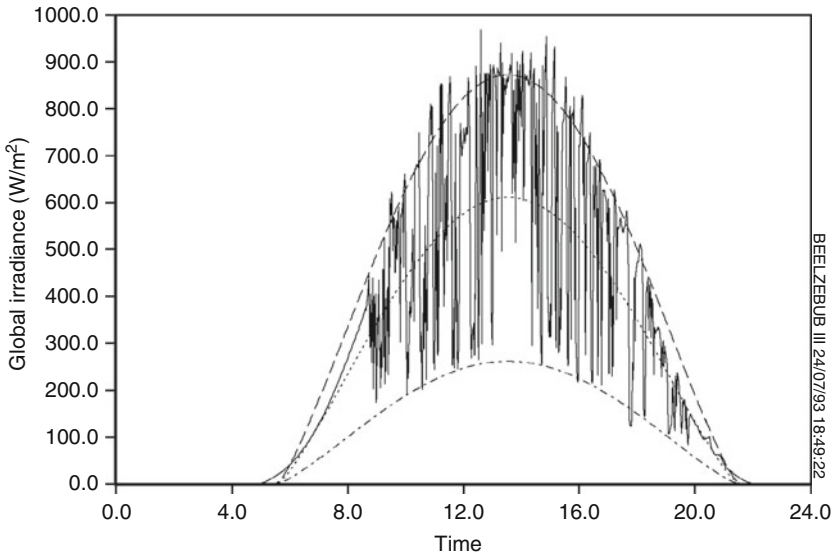

Solar Radiation, Spatial and Temporal Variability. Figure 3
One day of instantaneous values (minutes) of global horizontal irradiance measured at Oldenburg, Germany, 1993 (*solid line*). The *dashed lines* are empirical values for clear and cloudy states and a threshold value to distinguish between them

different measurement phases, the station distances ranged from a few hundred meters to a few hundred kilometers. For very small separations, a network of 15 sensors at distances of 50–300 m has been installed on roofs of the Oldenburg University Campus. Data have been recorded with a time resolution of 1 s during 1 year [8].

In Japan, a lattice of nine pyranometers within an area of 4 × 4 km^2 has been installed to record 1-min GHI data [9].

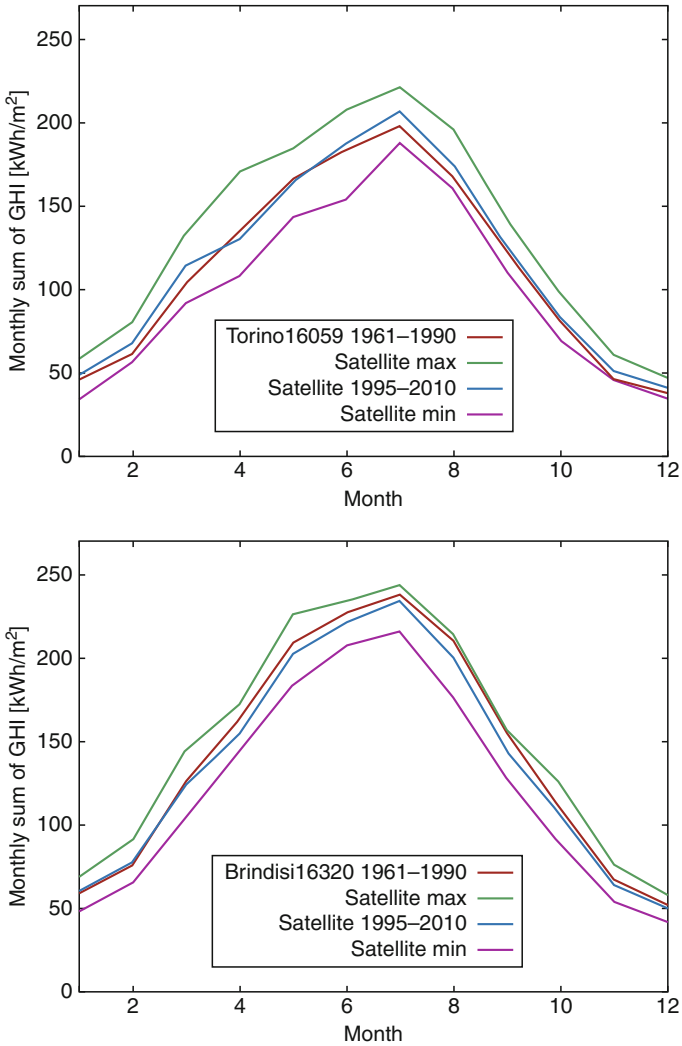

Solar Radiation, Spatial and Temporal Variability. Figure 4
Presentation of the interannual variability of monthly sums of GHI for the two Italian sites Torino (45.220°N, 7.650°E) and Brindisi (40.660°N, 17.950°E) given by the annual course of multiyear averages (from a 30-year period of ground measurements [Servizio Meteorologia dell'Aeronautica Militaire, http://clima.meteoam.it/Clino61–90.php] and a 15-year period of satellite-derived data) and the annual course of maxima and minima of the monthly sums

The Israel Meteorological Service and Ben Gurion University established the Negev Radiation Survey in the 1980s collecting data of 10-min GHI and direct normal irradiance (DNI) at nine stations in Israel's Negev desert [DOI: 10.1115/1.1756138].

In the USA, several databases of this type have been established. The Southern Great Plains (SGP) site was the first field measurement site established by the Atmospheric Radiation Measurement (ARM) Program in 1992. A site map is shown on http://www.arm.gov/sites/sgp. The Oklahoma Mesonet network consists of over 100 automated observing stations located throughout the state. It provides 5- and 15-min averaged surface meteorological data in near-real time. In addition, the Kansas Mesonet provides surface meteorology and radiation data. The 60-min data are available for 16 stations in Kansas. Data of these networks can be obtained from http://www.arm.gov.

The networks described above consist of sensors giving data for discrete points in space. In principle, the time resolution of the data sampling and the total length of the recording period may be varied within a large range. This enables an almost continuous monitoring of the irradiance field in time. In contrast, the spatial characterization of the irradiance field is limited and restricted by the number of stations used. The field can only be monitored at discrete distances. This also restricts the types of methods that can be applied to analyze the data.

For solar radiation, a supplementary source of data is given by imaging techniques. The irradiance at the earth's surface is determined by the atmospheric transmission, itself a strong function of cloudiness. Thus, automatic optical observations of clouds provide a representation of the radiation conditions. Using satellites, an almost continuous spatial coverage is obtained by cloud images sampled at discrete time intervals [10]. Another source for images is available, using ground-based cameras. The latter have been used to monitor total cloud cover [11, 12] or for studies on diffuse radiation [13, 14]. In this context, the images are analyzed with respect to the distribution of the sky dome radiance or luminance [15, 16]. For the determination of cloud structures under very inhomogeneous radiation conditions, sky images have been used for cloud field analyses [8, 17].

Images of the earth, containing information on the atmospheric state, are routinely obtained by polar orbiting or geostationary satellites, the latter provide pixel sizes of $1 \times 1\ km^2$ to $2.5 \times 2.5\ km^2$, and a temporal sampling of 15–30 min. This enables to derive hourly GHI values with a high spatial resolution and geographical coverage. The following irradiance databases all use satellite cloud data as an input to radiative models.

The server Satel-Light [18] is a European database of daylight and half-hourly solar radiation. It is based on the analysis of cloud radiance derived from Meteosat images and contains 5 years of data, with 30-min irradiance values at about 250,000 sites, http://www.satellight.com.

The SoDa Intelligent System (SoDa IS) [19] performs the integration and exploitation of diverse networked information sources that are geographically dispersed. The SoDa Service accumulates solar irradiance information from all over the world. The spatial and temporal resolution of the data is determined by the remote information sources, http://www.soda-is.com.

The 1991–2005 National Solar Radiation Database (NSRDB) [20] contains hourly global, direct, and diffuse solar radiation and meteorological data for 1,454 US stations. These time series are evaluated using cloud observations from as many ground stations. The NSRDB also offers a gridded dataset that contains satellite-derived hourly solar records for 8 years (1998–2005) for the USA (except Alaska above 60° latitude), representing about 100,000 pixel locations (at a nominal $10 \times 10\ km^2$ pixel size) (http://rredc.nrel.gov/solar/old_data/nsrdb/).

The Surface meteorology and Solar Energy (SSE) dataset (http://eosweb.larc.nasa.gov/sse/) contains parameters formulated for assessing and designing renewable energy systems [21]. It is capable to obtain data for locations, global/regional areas, and daily and monthly ground measurements. The SSE dataset is based on NASA satellite- and reanalysis-derived insolation and meteorological data for the 22-year period July 1983 through June 2005. Results are provided for 1° latitude by 1° longitude grid cells over the globe. Average daily and monthly measurements for 1,195 World Radiation Data Centre ground sites are also available. The Prediction of Worldwide Energy Resource (POWER) project (http://power.larc.nasa.gov/) was initiated to extend the SSE data till near-real time [21]. For this purpose, for example, FLASHFlux data are continuously included, which provide daily average solar irradiance derived from the polar orbiting satellites Terra and Aqua within 1 week of observation [22]. A comparative analysis of both, coarse SSE and finer-resolved NSRDB data, with SGP ground measurements has been performed to evaluate resolution-induced uncertainties in the assessment of the solar energy potential [23].

The DLR-ISIS [24] dataset is based on cloud data from the International Satellite Cloud Climatology Project (ISCCP) and radiative transfer calculations. It gives an overview of the available total solar irradiance worldwide for GHI and DNI. Its long temporal coverage over more than 21 years makes it possible to derive stable long-term averages, to evaluate the variability of irradiance from year to year and to study the effect of

extreme atmospheric conditions on the irradiance at the surface, for example, after a volcanic eruption. The temporal resolution of ISIS is 3 h, and its spatial resolution is $280 \times 280\,km^2$ (http://www.pa.op.dlr.de/ISIS/).

Apart from these satellite-based methods, the database Meteonorm [25] is a software-based collection of ground-measured monthly averages of GHI and temperature. It contains 2,400 stations with at least 10 years of data. The user is proposed interpolated monthly data for intermediate sites as well as synthesized hourly values. For the generation of these values the inclusion of the spatial and temporal variability of the irradiance field is required. The user gets site-specific data containing the temporal variability. Nevertheless, this dataset is not usable for statistical correlation analysis, since all short-term data are synthetic.

Finally, the European Solar Radiation Atlas (ESRA) [26] contains digital maps of monthly averages of direct, global, and diffuse radiation at a resolution of approximately $10 \times 10\,km^2$. These maps result from the merging of ground-measured radiation data and coarse resolution satellite-based irradiance maps [27]. Measurements of daily sums of irradiance at 90 sites and of hourly averages at six sites are additionally included.

Temporal Variability

Different authors investigated the variability of solar radiation time series with traditional statistical characterization tools. As a measure of temporal variability, it is common practice to calculate the mean and standard deviation of the time series. Moreover, efforts have been made to characterize the distribution functions of the irradiance data and to study the sequential characteristics of the time series.

In some cases, knowledge of the statistical characteristics allows a direct evaluation of the performance of solar energy systems without a detailed hourly simulation. In other cases, for example, for systems including storage, an explicit time-step simulation is needed. For these systems, the statistical characteristics can be used to generate synthetic solar radiation time series as input for time-step simulations. Starting with a monthly average of GHI – as taken from an atlas, for instance – it is possible to generate consecutive synthetic time series of daily sums, hourly averages, and minute-by-minute values. Hopefully, such time series should carry the natural statistical characteristics by reproducing the distribution functions and sequential patterns found in measured datasets. Procedures of this kind are executed by the Meteonorm tools and within specialized photovoltaic (PV) simulation software.

If solar radiation at the Earth's surface showed strong annual variations, this could seriously harm the return of investment for solar energy projects. While long-term radiation trends are handled in detail in a different entry of this encyclopedia, brief information about their annual variations is given here in a later section about large-scale and long-term variability from satellite images.

Distribution Function of Solar Radiation

The analysis of the distribution function focuses on the identification of analytical models with a reasonable representation but only a limited number of free parameters to characterize a given situation. Authors detected different types of probability functions when observing daily values, hourly values, or instantaneous data. A summary of their findings is given in the following sections.

Probability Function of Daily Mean Irradiance

For daily mean values of irradiance, a commonly used procedure is to calculate the overall atmospheric transmission represented by the clearness index, K_t. It is defined as the ratio of the irradiance on a horizontal plane on the earth surface divided by the respective irradiance just outside of the atmosphere [28]. Ideally, K_t time series should be free from deterministic trends. However, due to systematic seasonal variations of the climatic conditions see (Fig. 5) and the dependence of K_t on the sun's zenith angle, the clearness index does not qualify as a stationary process for long time series. Shorter sections, such as monthly datasets, can approximate stationary processes.

The first distribution function of daily K_t was presented in the seminal contribution of Liu and Jordan [28]. They stated that the distribution function is mainly determined by the monthly mean value of K_t. Starting from this assumption, several models for the monthly distribution functions of daily K_t have been developed [29–32] to represent various climatic conditions, including the Tropics, and medium to high

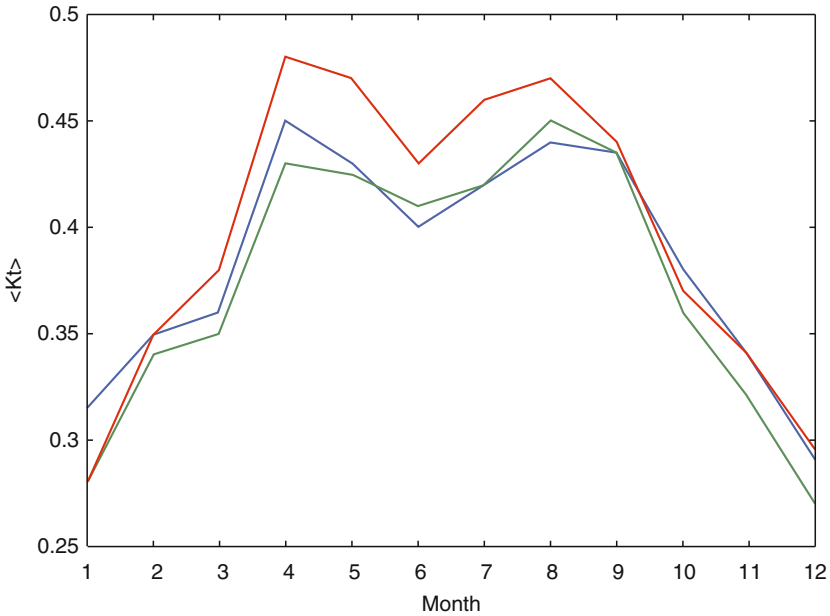

Solar Radiation, Spatial and Temporal Variability. Figure 5
Annual course of the mean monthly clearness index (average value of 10 years) for three North German stations

latitudes. Noticing that for fixed mean values of daily K_t the standard deviation varies with location, a model for the probability density function was introduced to provide both the required mean value and variance [33].

Probability Distribution of Hourly Clearness Index Values

To properly model the distribution of hourly irradiance data as a function of the daily clearness index, it has to be considered that a daily trend of the hourly clearness index remains, which is caused by different optical paths through the atmosphere. Such models are given in [34, 35]. As an alternative, a model for the irradiance under clear-sky conditions may be used to analyze the clear-sky index K^*, defined by the ratio of the actual irradiance to the irradiance expected under clear-sky conditions. In particular, this approach has been used for the analysis of instantaneous irradiance data, as discussed below.

Instantaneous Clearness Index, Clear-Sky Index Values, and Irradiance Distributions

Data with higher time resolution have been dealt with in various studies [36–38]. They found that the probability densities of 1-min clearness index values tend to show a distinct bimodal shape. This is explained by the fact that short-term data are dominated by either one of two opposite sky conditions – *clear sky* and *cloud shadow* – whereas in hourly time series these two states are mixed by the averaging. As a model for the distribution function of 1-min clear-sky index (K^*) data, the use of two beta functions was proposed [39]. This type of model has been implemented in procedures to generate synthetic time series, which are usually applied in solar system simulation studies [40].

The variability of irradiance within an hour is important for the correct inverter sizing in PV systems, for instance. In most cases, this design is done assuming a clear-sky situation and using hourly averages of irradiance data. These hourly averages smooth out extreme values, which may, due to scattering at complex cloud structures, even be higher than the irradiance expected for a clear-sky situation. If these higher instantaneous irradiance values are neglected, an undersizing of system components as the inverter will occur. This in turn causes a loss in the system's energy output [41, 42].

The variability of irradiance within an hour can be advantageously accounted for when modeling the

diffuse fraction of hourly GHI [43]. A high variability is an indicator for sunny intervals in alteration with the occurrence of thick clouds. The diffuse fraction for a given value of GHI is in this case expected to be higher than in a clear situation with low variability. Nevertheless, for time series of hourly GHI the variability within the hour is not known, but can be estimated from the variability from hour to hour [43].

Solar Radiation Time Series Characteristics

The irradiance incident on a solar system shows variations with respect to time and location. The temporal and regional patterns are controlled by temporal and spatial correlation structures.

For the analysis of time series characteristics in solar radiation datasets, the quasi-deterministic trend function must be separated from the stochastic fluctuations. When this is done, it becomes possible to represent the stochastic part of the time evolution by a simple model process.

To model the temporal evolution of solar radiation data, autoregressive processes or Markov chain approaches have been proposed. Stochastic processes for daily and hourly data are, in general, analyzed separately. The key of the process identification is the analysis of the autocorrelation function of the residual trend-free data, for example, K_t. It is stated by several authors [33, 44–48] that the autocorrelation function of the daily radiation within 1 month can be well approximated by an exponential function see (Fig. 6). This leads to the conclusion that a model process that is discrete in time may be represented by a first-order autoregressive process or Markov chain. Examples for the application of Markov chain models for daily clearness index are given in [48, 49]. For the time evolution of hourly data within 1 day, see [34, 35].

Short-term DNI data are governed by an on/off pattern due to their distinct sensitivity to obstruction of the sun by clouds. This leads to a characterization of the temporal evolution by the respective durations of clear and cloudy periods. Probability distributions of these duration times have been presented [36, 50].

An analysis of irradiance fluctuations that focuses on their amplitude, persistence, and frequency of occurrence can be performed by a localized spectral analysis. As an outcome of such an analysis, a fluctuation power index and a fluctuation energy index have been introduced [51].

Spatial Variability

Sufficient knowledge of the spatial variability of solar radiation can help to evaluate the ideal spacing of

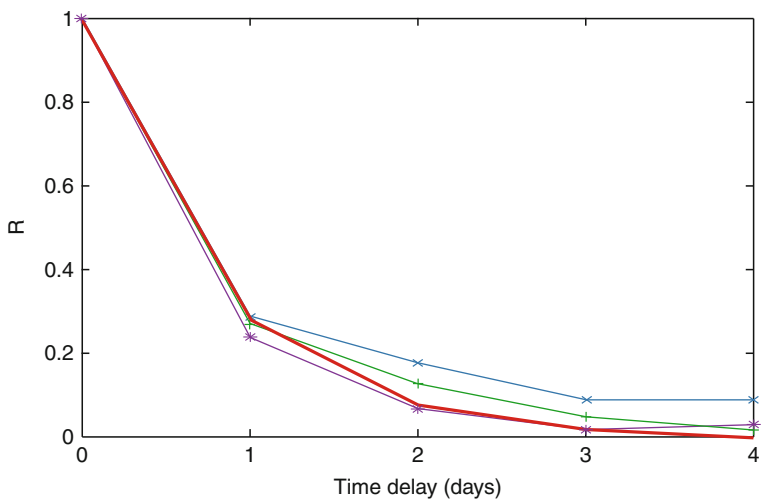

Solar Radiation, Spatial and Temporal Variability. Figure 6
Autocorrelation functions for time series of daily clearness index values. The curves are gained from monthly datasets from three North German stations with average clearness index value lower than 0.37. The *red line* refers to an exponential autocorrelation characteristic

measurement stations in a network. Measurements from each station shall be representative of a large area. In this kind of application, it is possible to benefit from the fact that observations at different sites are not independent, but rather that nearby sites share more similarities than sites that are far apart.

A common method to evaluate spatial variability from a set of measurement sites is the cross-correlation analysis. More details are given in the following section.

For the spatial interpolation of solar radiation data between measurement sites, advanced methods have been developed which include a representation of the spatial correlation. Other methods combine measurements with satellite data, see below.

Satellite-derived irradiance values are widely used in solar energy applications. Nevertheless, these data show a typical relative bias for GHI in the range of ±5 to ±10% and a relative rmse between 15% and 30% [52], which will affect site audit and yield prognosis. Here the question arises, whether it is better to rely on experimental measurements from a station located at y km from the site under scrutiny or on data derived from a satellite pixel containing that site [53].

Moreover, the spatial variability of irradiance causes fluctuations in the power output of large PV arrays, and may possibly affect electricity production negatively due to load imbalances. This typically occurs when a part of a large array is in the sun while another is in the shade, and is discussed in the section about small-scale variability.

Cross-correlation Analysis

The correlation of time series measured at two different sites is often calculated to analyze spatial variability. This cross correlation is expected to decrease when the distance between the sites increases. In addition, the correlation between station pairs increases with increasing averaging times.

With the knowledge of the cross-correlation structure of a set of single-point radiation time series, some global characteristics of these time series defined by their ensemble average can be described. Regarding the analysis of large renewable energy systems, this is helpful to describe the smoothing of relative fluctuations in the lumped power output of a number of spatially dispersed collectors, compared to those for a single collector [54].

It has been found [7] that the correlation of hourly residuals of German irradiance data would obey a simple exponential decay of the form $r = e^{-ad}$, where d is the distance between stations (km). A decay constant of $a = 3.38\ \mathrm{km}^{-1}$ was reported in that study. Therefore, for those conditions, the correlation coefficient drops from $r \approx 0.845$ at a distance of 50 km to $r \approx 0.5$ at approximately 200 km, and $r \approx 0.09$ at a distance of 700 km. It is generally accepted that at a distance of more than 50 km from a measurement station, it is better to use local satellite-based modelled irradiance estimates than to extrapolate those measurements. This critical distance may vary significantly as a function of terrain homogeneity, however.

Using radiation data from a network in Pennsylvania, the expected decrease in correlation with increasing distance and the increase in correlation with increasing averaging times was confirmed [4]. For daily values the correlation was found to decrease only slightly to $r = 0.97$, at a distance of 90 km. The authors found a spacing of 150 km between measurement sites reasonable to measure daily irradiance in that hilly area.

In Scotland, the time delay for maximum correlation between sites was directly coupled to their Easterly distance, between 0 and 20 km [5]. It was postulated that the correlation is a function of a combined space-time distance.

Spatial Interpolation

Spatial interpolation methods are needed to estimate solar irradiance at uninstrumented sites in a given geographic area, based on known irradiance values at some distant measurement sites. All methods estimate the unknown irradiance by a weighted sum of the irradiance measured at surrounding sites. In a commonly used approach, the weights are proportional to the inverse of the distance.

Kriging is a more sophisticated method in geostatistics. It extracts information about spatial variability from the available measurements. The spatial variability information is then used to determine the values of the weights in such a way that the error in the interpolated irradiance is minimized. For this method, the spatial correlation structure of solar irradiance is expressed by the so-called semivariogram [55, 56].

A combination of semicontinuous (gridded) satellite data with accurate local radiometric measurements can be performed by the data fusion method called Kriging of Differences. When applied to monthly irradiance values, this method was proven superior to pure satellite-derived data or to data interpolated with ordinary Kriging. The data fusion method has been selected to perform spatial interpolation for the European Solar Radiation Atlas [27], and to derive highly accurate daily irradiances for the remote monitoring of PV systems [57].

Small-Scale Variability

The passage of a field of opaque clouds may lead to large changes in the incoming irradiance when compared to the corresponding clear-sky value, for example, up to ~80% for GHI or 100% for DNI. The dynamics of the irradiance field can be assumed to be caused by wind-induced movements of such a cloud field.

Simple cloud field models have been introduced using ideal rectangular clouds [58] or ensembles of circular clouds [59].

An analysis of more realistic irregular cloud patterns resulted in a general model for the synthesis of radiation fields and their temporal evolution [8]. For this analysis, cloud field structures were extracted from sky photographs and described as fractal objects. Based on this representation, synthetic cloud patterns and their induced radiation fields could be generated, as shown in Figs. 7 and 8. Such modeled radiation fields were shown to correctly reproduce the actual measurements from an array of ground sensors, with respect to the frequency of transitions between the clear and cloudy states and the duration of either state. This method would also be applicable to obtain the probability that two measurement sites are in the same state or in opposite states. Artificial time series, as well as measured time series, show a dampening effect of fluctuations when ensemble averages are considered.

Solar Radiation, Spatial and Temporal Variability. Figure 7
A synthetic cloud shadow pattern generated by a fractal model. It is used for the generation of irradiance datasets with high spatial and temporal resolution. The cloud band covers an area of 14 × 3.5 km^2. With the assumption of a cloud drift speed of 15 m/s the clouds need 16 min to pass over this area

A similar synthesis approach was proposed [7] to expand observations of the binary cloud/no-cloud state from at least a pair of points to a synthetic cloud field. Based on the hypothesis of a rigid cloud pattern and knowledge of the drift speed, the temporal correlation structure of the cloud field is transformed into a spatial correlation structure, representing the probability of co-occurrence of clouds at points with a given spatial separation. Based on this information, a shifting cloud field showing a realistic correlation structure over space and time can be expanded from the measured radiation time series.

The dampening effect of fluctuations created by ensemble averages has been confirmed in this case by a frequency analysis of irradiance fluctuations as measured at nine sites within an area of 4 × 4 km^2 [60].

Large-Scale and Long-Term Variability from Satellite Observations

For the integration of a high share of renewable energy on a nationwide or European scale, the interaction of the renewable production with the conventional power park has to be considered. As it is necessary to balance local deficits and surpluses of supply and demand, the scheduling of the conventional power plants must be adapted and the transport capacity of the network must be sufficient. Analyses of this type that take the structure of the irradiance field explicitly into account have been performed with satellite-derived hourly maps of the irradiance field [61], giving an insight into the balancing energy flows. In this case, the structure of the irradiance field was analyzed with the help of a multi-resolution analysis of clearness index images [62].

PV electricity yield prediction should reflect the energy gain accumulated over longer periods, for example, 20 years. Thus the variability of the irradiance sum over longer averaging periods is of interest. For Potsdam and Germany, a time series of GHI has been measured for more than 60 years. Here, the yearly sum

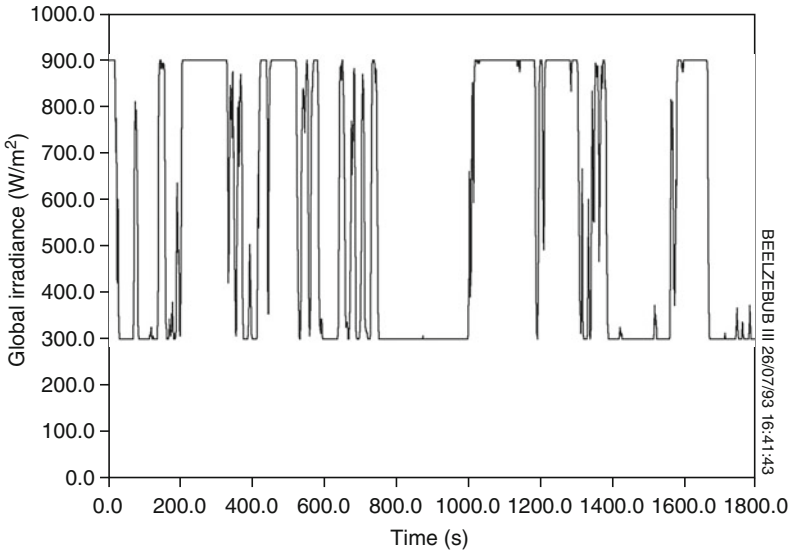

Solar Radiation, Spatial and Temporal Variability. Figure 8
Synthetic time series of global horizontal irradiance (30 min of 1 s data) generated with a fractal cloud model as shown in Fig. 7

of a single year can deviate by ±15% from the long-term average [63]. Moreover, a minimum of 8 years is necessary to approximate the long-term average with less than 5% deviation. As this number of recommended years may vary from region to region and may be different for DNI the interannual variability was analyzed with satellite data [64]. Here, the annual sum of DNI was derived from Meteosat data for Spain for 5 years. In Spain, the individual deviation of each year (1999–2003) from the 5-year average was 30% for sites in the Pyrenees, and 10% for other large regions. This means that for DNI it is necessary to average over far more than 5 years to derive reliable long-term averages for planning.

The topic of another study was the estimation of uncertainties in yield prediction caused by fluctuations in solar radiation [65]. For this, the interannual variability of GHI was analyzed by comparing the yearly and monthly averages to the long-term values. The results are presented as standard deviation maps for the regions around the Mediterranean and Black Seas.

A study of the spatial and temporal variability of GHI, global tilted irradiance (GTI), and DNI in the USA has been performed recently [66]. Eight years of data from the National Solar Radiation Database have been analyzed. The results are presented as maps of both the interannual and spatial variations in yearly and monthly values of DNI and GTI. Besides this, the authors observed that DNI is always more variable than global irradiance. The long-term annual average of global irradiance could be estimated within ±5% after only 1 or 2 years of local measurements, whereas a similar approximation of the long-term annual average of DNI could take 10–15 years.

The long-term variability of irradiance has also been analyzed on a global scale [24]. The study is based on 18 years of DLR-ISIS data (1984–2001). It was found that, during that period, DNI significantly increased (up to +4 W/m^2 per year) over several regions in the subtropics with the exception of Australia, where a small decrease of −1 W/m^2 per year was observed. The interannual DNI variability was found very strong, and sometimes exceeded 20% relative to the long-term average. Changes in GHI were found much smaller and less significant, with a maximum increase of 0.8 W/m^2 per year and an annual variability of less than 4%. Large volcanic eruptions were found to reduce annual averages of DNI by up to 16% and annual averages of global horizontal irradiance by less than 2.2%.

The strong variability of DNI from year to year must be accounted for in estimating the energy yield of concentrating solar power plants. To that effect,

a promising method has been proposed [67]. It consists in combining precision DNI data from a measurement campaign with long-term satellite-derived data from two different sources, each spanning over a period of at least 10 years. From these separate datasets, a quality-weighted average is calculated depending on the individual uncertainties of each of them. With the help of long-term data, the most representative climatological values are determined for the final best estimate, which is required for bankable simulations of energy yields.

Future Directions

In view of future energy supply systems that will presumably include large shares of both solar and wind energy converters, the analysis of cross-statistics of solar and wind fields is important. For the treatment of the structure of the solar irradiance field, large-scale information derived from satellite images, and large-scale meteorological modeling results have to be taken into account.

The spatial variability in solar radiation has been discussed in the context of energy generation planning and of optimal structure of the supply system. In addition to these topics, forecasts of the energy flows are necessary for the operation of any electricity network. In networks with a high share of generation from wind farms and PV systems, the stochastic nature of these energy flows dominates the uncertainties in power generation and load balance, which in turn affects the load scheduling of conventional power generating capacity. Due to the high share of wind generation in national supply grids, such as in Germany and Denmark, wind power forecasts have become an integral part of everyday operations, which involve power station dispatch and power trading. Considering the expected rapid growth of installed PV capacity, short-term forecasts of PV electrical generation will have to be added. Various schemes are considered for this task, and are already under active development.

Bibliography

1. Kemper A, Lorenz E, Hammer A, Heinemann D (2008) Evaluation of a new model to calculate direct normal irradiance based on satellite images of Meteosat Second Generation. In: EUROSUN 2008 – first international conference on solar heating, cooling and buildings, Lisbon, Portugal, 7–10 Oct 2008
2. Kern SA, Gulachenski EM, Kern GA (1988) Cloud effects on the distributed photovoltaic generation, slow transients at the Gardner Massachusetts photovoltaic experiment. IEEE Trans Energy Convers 4:184–190
3. Longhetto A, Elisei G, Giraud C (1989) Effect of correlation in time and spatial extent on performance of very large solar conversion systems. Sol Energy 43:77–84
4. Long CN, Ackerman TP (1995) Surface measurements of solar irradiance: a study of the spatial correlation between simultaneous measurements at separated sites. J Appl Meteorol 34:1039–1046
5. Glasbey CA, Graham R, Hunter AGM (2001) Spatio-temporal variability of solar energy across a region: a statistical modelling approach. Sol Energy 70:373–381
6. Luther G (1992) The regional function of solar energy. In: Proceedings of the 11th EC PV solar energy conference, Montreux, Switzerland
7. Steinberger-Willms R (1993) Analyse der Fluktuationen der Leistungsabgabe großer Wind- und Solarenergiesysteme in Hinblick auf deren Einbindung in elektrische Versorgungsnetze. PhD thesis, University of Oldenburg, Germany
8. Beyer HG, Hammer A, Luther J, Poplawska J, Stolzenburg K, Wieting P (1994) Analysis and synthesis of cloud pattern for radiation field studies. Sol Energy 52:379–390
9. Otani K, Minowa J, Kurokawa K (1997) Study on areal solar irradiance for analyzing areally-totalized PV systems. Sol Energy Mater Sol Cells 47:281
10. Li Z, Cribb C, Chang FL, Trishchenko AP (2004) Validation of MODIS-retrieved cloud fractions using whole sky imager measurements at three ARM sites. In: Fourteenth ARM science team meeting proceedings, Albuquerque, NM, 22–26 March 2004
11. Willard JH, Steeves J (1991) Sky-cover correlation within a sky dome. J Appl Meteorol 30:1037–1039
12. Slater DW, Long CN, Tooman TP (2001) Total sky imager/whole sky imager cloud fraction comparison. In: Eleventh ARM science team meeting proceedings, Atlanta, GA, 19–23 March 2001
13. Robbins CL, Hunter KC, Cannon T (1984) Mapping sky and surface luminance distribution using a flux mapper. Energy Build 6:247–252
14. Rosen MA, Hooper FC (1987) A calibration of the three discrete radiance component model. In: Proceedings of the ISES solar world congress, Hamburg, Germany
15. Brunger AP, Hooper FC (1993) Anisotropic radiance model based on narrow field of view measurements of shortwave radiance. Sol Energy 50:53–64
16. Perez R, Seals R, Michalsky J (1993) All weather model for sky luminance distribution – preliminary results and validation. Sol Energy 50:235–245
17. Reinhardt ER, Schwarzmann P, Straub B, Dörrer R (1983) Sky image analysis. Final Report ESF-032-D, Institut für physikalische Elektronik, University of Stuttgart, Germany
18. Fontoynont M, Dumortier D, Heinemann D, Hammer A, Olseth J, Skartveit A, Ineichen P, Reise C, Page J, Roche L, Beyer HG, Wald L (1998) Satellight: a WWW server which provides high

quality daylight and solar radiation data for Western and Central Europe. In: Proceedings of the ninth conference on satellite meteorology and oceanography, Paris
19. Wald L, Albuisson M, Best C, Delamare C, Dumortier D, Gaboardi E, Hammer A, Heinemann D, Kift R, Kunz S, Lefèvre M, Leroy S, Martinoli M, Ménard L, Page J, Prager T, Ratto C, Reise C, Remund J, Rimoczi-Paal A, Van der Goot E, Vanroy F, Webb A (2004) SoDa: a Web service on solar radiation. In: Proceedings of EUROSUN 2004, vol 3. PSE, Freiburg, pp 921–927. ISBN 3-9809656-4-3
20. Wilcox S et al (2007) Completing production of the updated National Solar Radiation Database for the United States. In: Solar 2007 conference, Cleveland, OH. ASES
21. Chandler WS, Stackhouse PW, Whitlock CH, Hoell JM, Westberg D, Zhang T (2010) Near real-time global radiation and meteorology Web services available from NASA. In: Proceedings of ASES annual conference, Phoenix, USA
22. Stackhouse PW, Kratz DP, McGarragh GR, Gupta SK, Geier EB (2006) Fast Longwave and Shortwave Radiative Flux (FLASHFlux) products from CERES and MODIS measurements. In: Proceedings of the 12th conference on atmospheric radiation, Madison, USA
23. Anderberg M, Renne D, Stoffel T, Sengupta M, Perez R, Stackhouse P (2010) Evaluating solar resource variability from satellite and ground-based observations. In: Proceedings of ASES annual conference, Phoenix, USA
24. Lohmann S, Schillings C, Mayer B, Meyer R (2006) Long-term variability of solar direct and global radiation derived from ISCCP data and comparison with reanalysis data. Sol Energy 80:1390–1401
25. Remund J, Kunz S, Lang R (2003) MeteoNorm. includ. CD-ROM, 5th edn. Meteotest, Bern
26. Scharmer K, Greif J (2000) ESRA, European Solar Radiation Atlas, 4th edn (includ. CD-ROM). Scientific advisors: Dogniaux R, Page JK. Authors: Wald L, Albuisson M, Czeplak G, Bourges B, Aguiar R, Lund H, Joukoff A, Terzenbach U, Beyer HG, Borisenko EP. Published for the Commission of the European Communities by Presses de l'Ecole, Ecole des Mines de Paris, Paris
27. Beyer HG, Czeplak G, Terzenbach U, Wald L (1997) Assessment of the method used to construct clearness index maps for the new European Solar Radiation Atlas (ESRA). Sol Energy 61:389–397
28. Liu BYH, Jordan RC (1960) The interrelationship and characteristic distribution of direct, diffuse and total solar radiation. Sol Energy 4:1–19
29. Hollands KGT, Huget RG (1983) A probability density function for the clearness index, with applications. Sol Energy 30:195–209
30. Bendt P, Collares-Pereira M, Rabl A (1981) The frequency distribution of daily insolation values. Sol Energy 27:1–5
31. Saunier GY, Reddy TA, Kumar S (1987) A monthly probability distribution function of daily global irradiation values appropriate for both tropical and temperate locations. Sol Energy 38:169–177
32. Olseth JA, Skartveit A (1984) A probability density function for daily insolation within the temperate storm belt. Sol Energy 33:533–542
33. Gordon JM, Reddy TA (1988) Time series analysis of daily horizontal solar radiation. Sol Energy 41:215
34. Graham VA, Hollands KGT, Unny TE (1987) Stochastic variation of hourly solar radiation over the day. In: Proceedings of ISES solar world congress, Hamburg, Germany
35. Aguiar R, Collares-Pereira M (1992) TAG: a time dependent autoregressive model for generating synthetic hourly radiation. Sol Energy 49:167
36. Mejon MJ, Bois P, Lestienne R (1980) Simulation de l'energie solaire directe au pas de temps de la minute. L'exemple de Saint-Chamas (Marseille). Rev Phys Appl 15:113–122
37. Louche A, Notton G, Poggi P, Simonnot C (1991) Classification of direct irradiation days in view of energetic applications. Sol Energy 46:255–259
38. Suehrcke H, McCormick PG (1988) The frequency distribution of instantaneous insolation values. Sol Energy 40:413–422
39. Skartveit A, Olseth JA (1992) The probability density and autocorrelation of short-term global and beam irradiance. Sol Energy 49:477–487
40. Walkenhorst O, Luther J, Reinhart C, Timmer J (2002) Dynamic annual daylight simulations based on one-hour and one-minute means of irradiance data. Sol Energy 72(5):385–395
41. Burger B, Rüther R (2006) Inverter sizing of grid-connected photovoltaic systems in the light of local solar resource distribution characteristics and temperature. Sol Energy 80:32–45
42. Zehner M, Hartmann M, Weizenbeck J, Gratzl T, Weigl T, Mayer B, Wirth G, Krawczynski M, Betts T, Gottschalg R, Hammer A, Giesler B, Becker G, Mayer O (2010) Systematic analysis of meteorological irradiation effects. In: Twenty-fifth European photovoltaic solar energy conference, Valencia, Spain, 6–9 Sept 2010
43. Skartveit A, Olseth JA, Tuft ME (1998) An hourly diffuse fraction model with correction for variability and surface albedo. Sol Energy 63:173–183
44. Brinkworth BJ (1977) Autocorrelation and stochastic modelling of insolation sequences. Sol Energy 19:343–347
45. Amato U, Andretta A, Bartoli B, Coluzzi B, Cuomo V, Fontanta F, Serio C (1986) Markov processes and Fourier analysis as a tool to describe and simulate daily solar irradiance. Sol Energy 37:179–194
46. Klein SA, Beckman WA (1987) Loss-of-load probabilities for stand-alone photovoltaic systems. Sol Energy 39:499–512
47. Graham VA, Hollands KGT, Unny TE (1988) A time series model for K_t with application to global synthetic weather generation. Sol Energy 40:83–92
48. Aguiar R, Collares-Pereira M, Conde JP (1988) Simple procedure for generating sequences of daily radiation values using a library of Markov transition matrices. Sol Energy 40:269–279
49. Beyer HG (1988) Zur Bestimmung des energetischen Verhaltens regenerativer Elekrtizitätsversorgungssysteme unter besonderer Berücksichtigung statistischer Eigenschaften des Windes und der Solarstrahlung. PhD thesis, University of Oldenburg, Germany
50. Manier G, Traup S (1991) Kurzzeitvariation der solaren Bestrahlung. Meteorol Rundsch 43:178–186

51. Woyte A, Belmans R, Nijs J (2007) Localized spectral analysis of fluctuating power generation from solar energy systems. EURASIP J Adv Signal Process, Article ID 80919, 8 pages. doi:10.1155/2007/80919
52. Beyer HG, Martinez JP, Suri M, Torres JL, Lorenz E, Müller SC, Hoyer-Klick C, Ineichen P (2009) D 1.1.3 report on benchmarking of radiation products. Technical Report MESOR (Management and Exploitation of Solar Resource Knowledge). http://www.mesor.org/. Accessed May 15, 2010
53. Zelenka A, Perez P, Seals R, Renné D (1999) Effective accuracy of satellite-derived hourly irradiances. Theor Appl Climatol 62:199–207. doi:10.1007/s007040050084
54. Beyer HG, Luther J, Steinberger-Willms R (1991) Reduction in fluctuations in lumped power output from distantly spaced PV-arrays. In: Proceedings of ISES solar world conference, Denver, USA
55. Zelenka A, Czeplak G, D'Agostino V, Weine J, Maxwell E, Perez R (1992) Techniques for supplementing solar radiation network data. Report IEA task 9, vol 2. Report no. IEA-SHCP-9D-1
56. Sen Z, Sahin AD (2001) Spatial interpolation and estimation of solar irradiance by cumulative semivariograms. Sol Energy 71:11–21
57. Betcke J, Beyer HG (2004) Accuracy improvement of irradiation data by combining ground and satellite measurements. In: Proceedings of EuroSun2004, Freiburg, Germany, vol 3, pp 764–770
58. Jewell WT, Ramakumar R (1988) The effect of moving clouds on electric utilities with dispersed photovoltaic generation. IEEE Trans Energy Convers 3:570–576
59. Garret DL, Jeter SM (1989) A photovoltaic voltage regulation impact investigation technique. Part I – model development. IEEE Trans Energy Convers 4:47–53
60. Kawasaki N, Takashi O, Otani K, Kurokawa K (2006) An evaluation method of the fluctuation characteristics of photovoltaic systems by using frequency analysis. Sol Energy Mater Sol Cells 90:3356–3363
61. Reise C (2003) Entwicklung von Verfahren zur Prognose des Ertrags großflächiger Energieversorgungssysteme auf der Basis von Satelliteninformationen. PhD thesis, University of Oldenburg, Germany
62. Beyer HG, Costanzo C, Reise C (1995) Multiresolution analysis of satellite-derived irradiance maps – an evaluation of a new tool for the spatial characterization of hourly irradiance fields. Sol Energy 55:9–20
63. Quaschning V, Geuder N, Ortmanns W (2002) Vergleich und Bewertung verschiedener Verfahren zur Solarstrahlungsbestimmung, 13. In: Internationales Sonnenforum, Berlin, Germany
64. Meyer R, Lohmann S, Schillings C, Hoyer C (2007) Climate statistics for planning and siting of solar energy systems. In: Solar resource from the local level to global scale in support of the resource management of renewable electricity generation. Nova Science/Earthlink, Nova Science Publisher, New York, 11 pp
65. Suri M, Huld T, Dunlop ED, Albuisson M, Lefevre M, Wald L (2007) Uncertainties in photovoltaic electricity yield prediction from fluctuations of solar radiation. In: Proceedings of the 22nd EuPVSEC conference, Milano, Italy
66. Wilcox S, Gueymard CA (2010) Spatial and temporal variability of the solar resource in the United States. In: Proceedings of the ASES annual conference, Phoenix, USA
67. Meyer R, Butron JT, Marquardt G, Schwandt M, Geuder N, Hoyer-Klick C, Lorenz E, Hammer A, Beyer HG (2008) Combining solar irradiance measurements and various satellite derived products to a site-specific best estimate. In: Fourteenth SolarPACES symposium, Las Vegas, USA

Solar Thermal Desalination

Claus R. Mertes
Geschäftsbereich Energie/Business Group Energy
Borsteler Chausse, Poyry Deutschland GmbH,
Hamburg, Germany

Article Outline

Glossary
Definition of the Subject
Introduction
Solar Driers
Acknowledgments
Bibliography

Glossary

CSP Concentrating solar power generation, solar fuel, thermal process
Desalination To desalinate water production power generation, solar fuel, thermal process
MED Multi-effect distillation
MSF Multi-stage flash, evaporation
RO Reverse osmosis
ZLD Zero liquid discharge brine, effluent, environmental impact, EIA

Definition of the Subject

Based on 20 years of experience, the author will inform readers on solar-driven desalination using different types of solar systems and also different desalination systems. These simple and robust devices and the use of clean solar fuel not only conserve conventional fuels but also help to produce additional water and to reduce pollutants, thus reducing global warming.

Introduction

Renewable energy–powered desalination plants operate with either a mechanical process or a thermal distillation process. In the mechanical process (reverse osmosis and vapor compression), a distinction is made between network-bound and non-network systems (isolated systems). The electrical energy needs may be provided by wind power or solar power using a photovoltaic (PV) system. Hybrid systems are often used in order to continue operation in low wind periods or at low irradiance. Some facilities, for example, use diesel engines.

In several countries (Spain, Kuwait, Abu Dhabi, Mexico, USA) test facilities have been built with larger collector arrays for multi-stage flash (MSF) and multi-effect distillation (MED) desalination plants. The collectors act through vacuum tubes and flat plate collectors. Some plants are operated with solar ponds. MSF technology does not play a significant role in low-thermal-driven desalination plants using renewable energy because of their low daily production (e.g., a few liters per day to a few cubic meters per day).

For future large-scale solar power plants, however, these processes will useful applications. Studies show the advantages of thermal desalination processes, e.g., the MED process using mechanical energy or the coupling of reverse osmosis (RO) and mechanical vapor compression (MVC). These systems offer flexibility in operation. If electrical energy from the grid is not available, energy from a MVC or RO system can be used. By combining electricity generation and the use of power plant waste heat for desalination, an overall improvement in system efficiency can be achieved.

Such a system exists in the Plataforma Solar de Almería solar field trial in Spain. The MED test facility has a parabolic field of 2672 m^2, 14 distillation stages, a gained output ratio (GOR) value of about 9, and a maximum water production of about 72 m^3/day. Another demonstration plant based on the MED process was built in 1984 in Abu Dhabi with vacuum tubes and 18 distillation stages. The maximum daily production of drinking water was about 80 m^3/day.

A new generation of solar power plants is already under construction in Spain and the US. Solar power plants are in the design stage in Algeria, Morocco, Egypt, Libya, United Arab Emirates, South Africa, Israel, Italy, Iran, and India. Development in this area is dependent on politics, industry, and science. Germany, which is actively involved in this development, has a solar tower power plant with 1.5 MW of electrical power in Jülich, which was built for research purposes.

The coupled solar desalination plants require more or less continuous operation. New thermal desalination plants are able to utilize the available energy more effectively. The specified water production ranges from 110% to 20% of nominal water output. A priority for further research is the development of appropriate energy or heat storage, which allows for both overnight electricity and ensures continuous operation of the desalination plants.

RO desalination plants must operate continuously. Their coupling with a solar power plant provides electricity for the operation of desalination; the electricity must be available both day and night. This is a process-integrated project. Because the power plants are connected to the grid, it is possible to ensure continuous operation even without advanced storage technology.

Solar Driers

Water desalination is both costly and energy consuming. Today's desalination plants operate largely with fossil fuels. Of all the world's desalinated water today, only about 0.02% is generated from renewable sources. Rising oil and gas prices, however, will exert pressure in the future on energy-intensive processes such as desalination. Solar energy provides an interesting alternative, especially because desalination is most needed where there is enough solar energy available. Many areas in the world have water shortages and also annual solar irradiance of more than 1,500 kWh per square meter.

For these areas, which are often areas with poor infrastructure, renewable-powered desalination plants could provide an alternative market with great development opportunity. Following are several different variants of desalination with renewable energies.

Simple Greenhouse Distillery

Since the end of the last century, the simplest and most-used solar thermal desalination system is the simple solar distiller: a simple container with a black base and

glass cover that evaporates seawater by the greenhouse principle and the water condenses on the glass cover. Disadvantages of simple solar stills are their low production rates of about 2 to 5 l/m^2 per day, depending on global radiation.

A variety of studies have focused on improvements in the area of single distilleries. Here the objective is first to increase the production rate and, second, to reduce costs. For small and very small plants, it is difficult to estimate the typical cost because there are many different systems around the world.

Solar Water Stills in a Large-Format Pyramid Aqua-Aero WaterSystems (Delft, Netherlands) has developed the WaterPyramid. It is basically a simple solar still at a larger scale. It consists of a transparent film stretched in a pyramid shape. The salt water is heated in the pelvic area by the incoming solar radiation and is evaporated. The condensate is discharged at the sides and can be used with appropriate treatment for drinking. In addition, the roof of the pyramid serves as a collection area for rain water, which can also be used as drinking water. The water pyramid has a total floor area of 650 m^2 and a production of about 1 to 1.2 m^3 of drinking water per day in good light. The system is used in Africa and India.

Humid Air Distillation

Another type of thermal desalination system with a heat recovery system operates with moist air. This procedure, called multi-effect humidification, is also known as humid air distillation (HAD) and was developed by ZAE Bayern and the University of Bochum. Incoming salt water is heated in the condenser by capturing the heat of condensation of the distillate. Then the raw water is heated by solar collectors or waste heat from a heat process and further heated and fed into a vaporizer. The evaporated water is absorbed by the circulating air stream and condenses back to the salt water inlet. The distillate is collected separately and taken away. This type of system is now distributed by the Terrawater (Kiel, Germany). The company offers water systems in sizes from 1, 5, and 10 up to 50 m^3 per day in modular construction. The systems can be operated from a power station with solar process heat or waste heat.

Membrane Distillation Membrane distillation (MD) is a thermal process that has been studied by Fraunhofer Institute for Solar Energy Systems ISE (Freiburg, Germany) and TNO (Delft, Netherlands). The separation of water and salt is achieved by the evaporation of water through a microporous hydrophobic membrane (e.g., PTFE), which on one side is not wetted by the surface properties of liquid water, and on the other by side, because of its high porosity, water vapor does pass through very well. The driving force here is the temperature difference between the partial vapor pressures of the evaporator and the condenser surface on the other side. Between the two surfaces is the distillate channel, which is separated by the vapor-permeable membrane from the hot brine and a waterproof membrane from the inflowing water in the condenser. Since only vapor can penetrate the membrane, the result is pure distillate.

Solar Desalination Using Multi-stage Desalination with Heat Recovery Another type of solar still uses multi-stage desalination (MSD) with heat recovery. They work with a number of stacked shelves and use the heat of condensation of each deeper level. This is an open system, the pressure in each stage corresponding to the ambient pressure. Unlike with MSF or MED plants, this system cannot be adjusted by changing the boiling temperature of the pressure levels. The heat supply is the salt water at the lowest level at about 95–100°C and caused to evaporate. The vapor in the rising, moist air condenses on the lower side of the overlying evaporative stage. The condensation freed by the evaporation is released into the overlying stage and heats the salt water therein. The condensate runs off at the bottom of the capacitor steps and is collected and directed into a sump at the deepest point of the system. The heat inputs into the next higher level for re-evaporation and condensation. The resultant heat recovery reduces the specific heat consumption per liter of distillate.

The maximum size of the plant is estimated at about 5–10 m^3/day. The systems can also operate with vacuum tubes or flat plate collectors. No external electrical power is required to operate the plants. The systems regulate themselves and require very little maintenance. The plants can be operated, for example, with waste heat from diesel engines. This is increased by

the continuous operation of desalination plants on the daily output by about a factor of 3. The Solar Institute Jülich and the engineering firm IBEU (Jülich, Germany) have developed and tested this system.

Reverse Osmosis with Photovoltaic Reverse osmosis (RO) and multi-effect desalination with mechanical vapor compression (MED TVC) are mechanically driven processes. Solar-powered reverse osmosis is, in remote areas, an attractive alternative because it can be used on proven components and consumes little power. This system represents about 60% of the total drinking water that is produced worldwide with renewable energy sources. Solar-thermal-powered MSF or MED account for 25%. The cost for water systems with a daily capacity of 12–120 m^3 per day is at 3.5–20 €/m^3. However, this system requires the chemicals for water treatment, replacement of membranes, and trained users. Furthermore, larger RO plants must be uniformly supplied with energy, because they can suffer substantial damage to the operation of the fluctuating energy. When operating with unpredictable energy sources such as solar and wind power, it is necessary to have uninterrupted energy, e.g., with storage, which increases the cost of the system.

Thermodynamic and Electrical Characteristics Thermal desalination is energy intensive. The evaporation of 1 kg of water requires 0.645 kWh of energy. Therefore, all major systems work with heat recovery. Efficiency increases with a heat recovery system compared with a simple solar still without heat recovery.

To compare solar-thermal with mechanical desalination plants, there are several specific characteristics to be assessed. A measure of the degree of heat recovery is the GOR value, the utilization of energy provided for the process. It is advantageous to consider the GOR value for the desalination system and for the overall system (with collector field). Other important benchmarks are the specific daily amount of drinking water produced in kilograms per m^2 collector area and the specific electrical energy consumption (ECsp) counted in kWh per m^3 drinking water. It should be noted that, in thermal systems, the drive is electrical energy (pumps etc.), e.g., energy related to PV generation must be taken into account.

$$GOR = \frac{m_{DES}{}^{*}\Delta h}{Q_{Solar}{}^{*}A_{Koll}}$$

$$GOR = \frac{m_{DES}{}^{*}\Delta h}{Q_{Solar}{}^{*}A_{Koll} + E_{PV}/\eta_{Pv}}$$

$$m_{sp} = \frac{m_{Des}}{A_{Koll} + A_{PV}}$$

$$EB_{sp} = \frac{E_{Strom}}{\dot{V}_{Des}}$$

= temporal distillate quantity in kg/h
m_{DES} = distillate=weight in kg/day
= temporal distillate quantity in kg/h
(t) = global radiation in W/m
EB_{sp} = specific energy consumption in kWh/m^3
E_{PV} = electrical energy consumption of the system in kWh/day
E_{Strom} = current consumed amount of investment in kWh/day
Δh evaporation = 0.645 kWh/kg
Q_{Solar} = total solar radiation on the collector surface in kWh/m^2 d
A_{Koll} = total collector area in m^2
A_{PV} = PV area in m^2
η_{Pv} = chain efficiency of the PV system as a whole
$\dot{m}_{Des}(t)$ = Temporal distillate quantity in kg/h
m_{Des} = temporal distillate quantity in kg/h
$\dot{V}_{Des}$ = temporal distillate volume in m^3/day
$\dot{E}(t)$ = global radiation in W/m^2
EB_{sp} = specific energy consumption in kWh/m^3
E_{PV} = electrical energy consumption of the system in kWh/day
E_{Str} = consumed electrical energy in the System in kWh/day
Δh = evaporation enthalpy 0.645 kWh/kg
Q_{Solar} = total solar radiation on the collector surface in kWh/m^2d
A_{Koll} = total collector area in m^2
A_{PV} = PV area in m^2
η_{PV} = Overall efficiency of the PV system

Comparison with Renewable Energy Powered Desalination Table 1 provides information such as specific energy consumption in kWh/m^3 of drinking

Solar Thermal Desalination. Table 1

	Typ. capacaty m^3/day	Spec. energy needed kWh/m^3	Cost for water €/m^3	Technical status
Solar still	<0.1	Therm: 645	1–5	Developed
Solar-MEH&ZLD	1–100	Therm: 100–150	4–10	Developed
		Electr. 1.5		R&D
Solar-MSD	0.05–5	Therm:150–200	5–10	Prototype
				R&D
Solar-MD	0.15–10	Therm: 150–200	8–15	Developed
		Electr:1.5		
Solar-CSP	10–5,000	Therm: 60–70	1.8–2.2	Developed
MED, MED-TVC		Electr: 0.8–2		Prototype, R&D
PV-RO	<100	Electr.		Developed
		BW: 0.5–1.5	BW: 5–7	R&D
		SW: 4–5	SW: 9–12	
PV-ED	<100	Electr: 3–4	BW: 8–9	R&D
		nur BW		
Wind-RO	50–2,000	Electr.	BW: 3–5	Developed
		BW: 0.5–1.5	SW: 5–7	R&D
		SW: 4–5	>1,000 m^3/day (1.5–4)	
Wind-MVC	<250	Electr.	SW: 4–6	Developed
		SW: 10–14		

water, the approximate production costs in €/m^3, and the state of technological development of different plant types. In the water development costs, the cost of building infrastructure is not included. These costs vary depending on location; for small water systems, the development costs more than double. Note also that many plants are not yet in the mature stage of development and, therefore, the specific values are approximate and objective.

Small Rural Infrastructure Facilities for Poor Regions For small systems there is a high demand, especially in arid zones of structurally weakness in developing and emerging countries, but most users do not have the money to finance such plants. For the distribution of these small plants there is a big need for national or international financial support. This requirement is not limited to the desalination of brackish water and seawater, but also in regions with naturally contaminated groundwater. Particularly noteworthy are boron, arsenic, fluoride, and lead, which occur often in such high concentrations that drinking this water is very harmful.

Solar Thermal Desalination Markets

There is currently no functioning market for small solar-thermal desalination. Previous installations of various small plant types were usually subsidized research and development projects. However, interest has increased in large solar-thermal power plants combined with big desalination units that co-generate of water and electricity. In markets with a high demand for drinking water, desalination systems that use waste heat from the power plant process are cost-effective. Studies of the DLR (German Aerospace Agency) show that it is advantageous to combine, for example, thermal desalination processes such as MED with

mechanical processes such as RO or MVC. This variability optimizes the operation of all units in use. Electrical energy from the grid can ensure the continuous operation of MVC or RO systems.

Acknowledgments

The author is grateful to the DME (German Desalination Society) Duisburg, Germany, and the Solar Insitute Jülich, Jülich, Germany

Bibliography

1. 978-3-86861-000-0, 978-3-86861-001-7 Einführung in die Meerwasserentsalzung (German) (S-003-2004+S-004-2004)
2. 978-3-86861-002-4 Seawater desalination in Saudi Arabia (English) (C-001-2004)
3. 978-3-86861-003-1 Meerwasserentsalzung und Erneuerbare Energien (German) (S-001-2005)
4. 978-3-86861-004-8 Wasservorbehandlung in der Meerwasserentsalzung (German) (S-002-2005)
5. 978-3-86861-006-2, 978-3-86861-010-9, 978-3-86861-012-3 Introduction to seawater desalination (English) (S-004-2005 +S-004-2006+S-002-2007)
6. 978-3-86861-007-9 Seawater desalination in Iran (English) (C-002-2005)
7. 978-3-86861-005-5 Fouling and scaling in seawater desalination (English) (S-2003-2005)
8. 978-3-86861-008-6 Seawater desalination in U.A.E. (English) (C-003-2006)
9. 978-3-86861-009-3 Financing of projects in desalination (English) (S-001-2006)
10. 978-3-86861-011-6 Instrumentation and control systems (English) (S-001-2007)
11. 978-3-86861-013-0 Materials and corrosion in desalination plants (English) (S-003-2007)
12. 978-3-86861-014-7 Membrane technology for saline waters (Engl.) (W-002-2007)
13. 978-3-86861-015-4 Thermal desalination of saline waters (Engl.) (W-001-2008)
14. 978-3-86861-016-1 Pumps and valves in desalination plants (S-005-2008)
15. 978-3-86861-017-8 Desalination and renewable energies (S-007-2008)
16. 978-3-86861-018-5 Introduction to seawater desalination (S-008-2008)
17. 978-3-86861-019-2 Membrane technology for saline waters (W-002-2008)
18. 978-3-86861-020-8 Thermal desalination of saline waters (W-001-2009)
19. 978-3-86861-081-9 Environmental issues in seawater desalination (S-002-2009)
20. 978-3-86861-082-6 Introduction to seawater desalination (Engl.) (S-004-2009)
21. 978-3-86861-083-3 Materials and corrosion in seawater desalination (S-007-2009)
22. 978-3-86861-084-0 Design of MED, MED-TVC and MVC desalination plants (S-008-2009)
23. 978-3-86861-085-7 Desalination and renewable energies (S-009-2009)
24. 978-3-86861-086-4 Chemicals and pretreatment in seawater desalination (S-004-2010)
25. 978-3-86861-087-1 Introduction to seawater desalination (Engl.) (S-005-2010)
26. 978-3-86861-088-8 Seawater desalination and the environment (S-006-2010)
27. 978-3-86861-089-5 Einführung in die Meerwasserentsalzung (Ger.) (S-007-2010)
28. 978-3-86861-090-1 Thermal desalination of saline waters (W-001-2011)
29. 978-3-86861-091-8 Membrane technology for saline waters (W-002-2011)
30. 978-3-86861-092-5 Introduction to seawater desalination (Engl.) (S-001-2011)
31. 978-3-86861-093-2 Desalination and renewable energies (S-002-2011)
32. 978-3-86861-094-9 Introduction to seawater desalination (Engl.) (S-003-2011)
33. 978-3-86861-095-6 Enhanced membrane technology (S-004-2011)

Solar Thermal Energy, Introduction

Christoph Richter
Project Manager Solar Research,
Plataforma Solar de Almeria , Institute of Solar Research, DLR – German Aerospace Centre, Germany

Contrary to a common saying, rather than money it's the sun that moves our world, makes it "go round." The tiny portion of the energy, this huge fusion reactor emits continuously that reaches the earth in 1 year is about 10,000 times more than the energy consumption of mankind during the same time. Absorbed in the atmosphere and on the earth surface itself, it provides the temperature range enabling our ecosystems to exist and is also responsible for a large part of our available renewable (wind, waves, biomass) and fossil energy sources.

This section deals with technologies that actively convert solar radiation into useful heat, in a temperature range from little above ambient up to more than 1,000°C, covering a broad range of energy services such as space heating, cooking, domestic hot water supply,

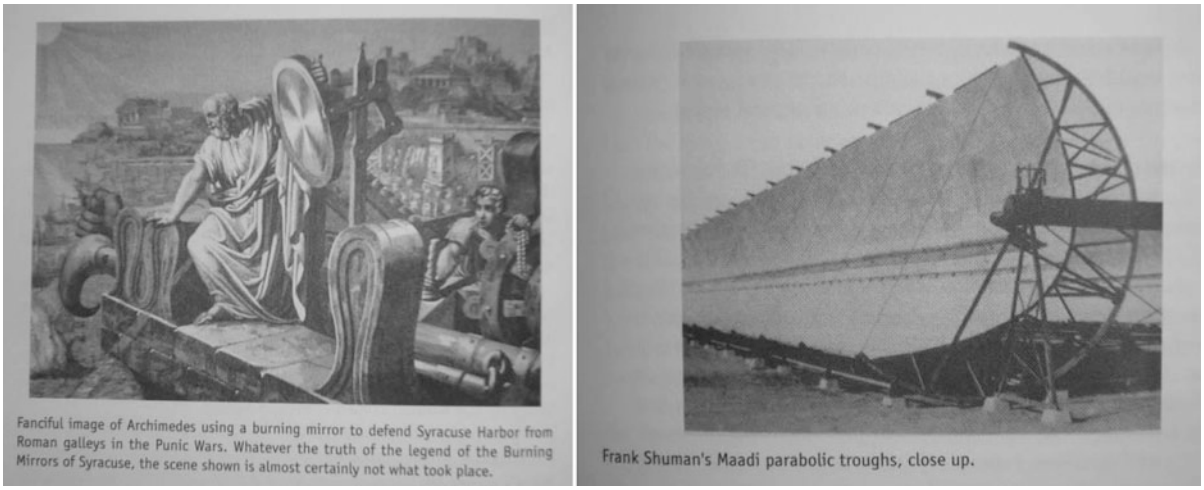

Solar Thermal Energy, Introduction. Figure 1
Early attempts of solar thermal energy applications. (Ref. [1])

electrical power generation, and high temperature thermochemical processes.

The history of ideas and devices to use solar thermal energy is very long. Archimedes is said to have defeated the Roman fleet attacking Syracus 300 B.C. by concentrating solar radiation with mirrors on the wooden ships to set them on fire. Though this is certainly not true as depicted, it illustrates an early understanding of the important principle of applying solar thermal energy, the concentration of light to achieve higher temperatures and therefore more application possibilities. In the late nineteenth century, A. Mouchot, a French engineer, developed several prototypes of solar engines, using concentrated solar light to operate a steam engine. Similarly, in 1912, the American engineer, F. Shuman constructed in Egypt a first parabolic trough collector (see Fig. 1, left) to drive a steam engine for water-pumping purposes. The major developments however that lead to the currently available technologies for solar thermal energy applications have been initiated mainly after the first oil crisis in 1973.

Section Content Overview

Solar thermal energy use can be classified in one way by the temperature range achieved and the corresponding applications. It is widely used already for heating purposes (water, space) in the "low" temperature range up to about 100°C, using mainly nonconcentrating collectors, higher temperatures can be achieved with more sophisticated solar collector technologies and over 200°C require concentrating solar radiation through typically mirror systems. The different technologies are described in detail in the following entries of this entry. The entry "► Solar Collectors, Non-concentrating" gives an overview of solar collector systems in the lower temperature range. Another traditional application the direct use of solar radiation for food processing, namely cooking and drying is resumed in the entry "► Solar Cookers and Dryers to Conserve Human and Planet Health." Solar energy can also be applied for cooling purposes, which can offer the advantage of a good overlap of resource (solar radiation) and demand (cooling). This is described in detail in the entry "► Solar Cooling Systems."

Another group of sections deals with technologies that have as a primary application focus the production of electricity through conversion of solar radiation first to heat, driving a mechanical conversion system coupled to an electric generator. This approach offers the intrinsic option for intermediate and cost-effective storage of the heat generated in the first step and therefore decoupling electricity production from solar radiation availability. The entry dealing with different systems for concentrating solar energy for conversion to electricity are "► Parabolic Trough Solar Technology," "► Linear Fresnel Collectors," and "► Concentrating Receiver Systems (Solar Power Tower)." Nevertheless, the high temperature heat generated in

these systems can also be applied to industrial process heat applications of all kind. The entry on "► Solar Updraft Towers" describes another approach to generate electricity using the primarily production of warm air to drive a wind turbine in a very high tower for electricity production.

The intermittent character of solar radiation makes storage systems highly desirable to match demand and thereby increase the range of application of solar energy. Technologies for this purpose are described in the respective entry "► Thermal Energy Storage." One important potential application of solar thermal energy is desalination, last not least because of the typical overlap of regions with high insolation and low water availability. This is the topic of the entry "► Solar Thermal Desalination."

The Solar Radiation can also be applied to drive chemical processes. One branch of applications in the future can be high temperature thermochemical processes to produce, for example, hydrogen or other chemical commodities for either energy or material applications. Solar Furnaces are one tool to develop such applications. The entry "► Solar Energy in Thermochemical Processing" deals with these applications. Detoxification of contaminated waters is an interesting application that has received much attention by researchers during the last decades to tackle the growing water problems. Technically, it does not rely primarily on thermal processes but direct photochemical processes induced by sunlight. It is described in detail in the entry "► Solar Detoxification and Disinfection of Water." In this area, different demonstration plants have been recently developed. An industrial plant with 100 m^2 of CPC collector surface (for photo-Fenton oxidation), combined with a biological treatment plant based on an immobilized biomass activated sludge reactor (1 m^3 of total volume) was designed and constructed for the treatment of 4 m^3/day of saline industrial wastewater containing around 600 mg/L of a nonbiodegradable compounds and from 400 to 600 mg/L of dissolved organic carbon [2]. The technical feasibility of a large-scale combined solar photocatalysis/aerobic biological process for the treatment of wastewater polluted with pesticides has recently been evaluated. Partial photo- oxidation was carried out under sunlight in a 150 m^2 CPC-based plant. Afterward, complete wastewater treatment was performed in a biological system based on immobilized biomass reactors filled with Pall®Ring supports colonized by activated sludge from the municipal WWTP [4].

Overall, the perspectives for the future contribution of solar energy to the global energy mix are very high, as one example the possible development of solar electricity from solar thermal power plants according to the roadmap of the International Energy Agency is shown in Fig. 2, with about 11% of contribution to electricity supply.

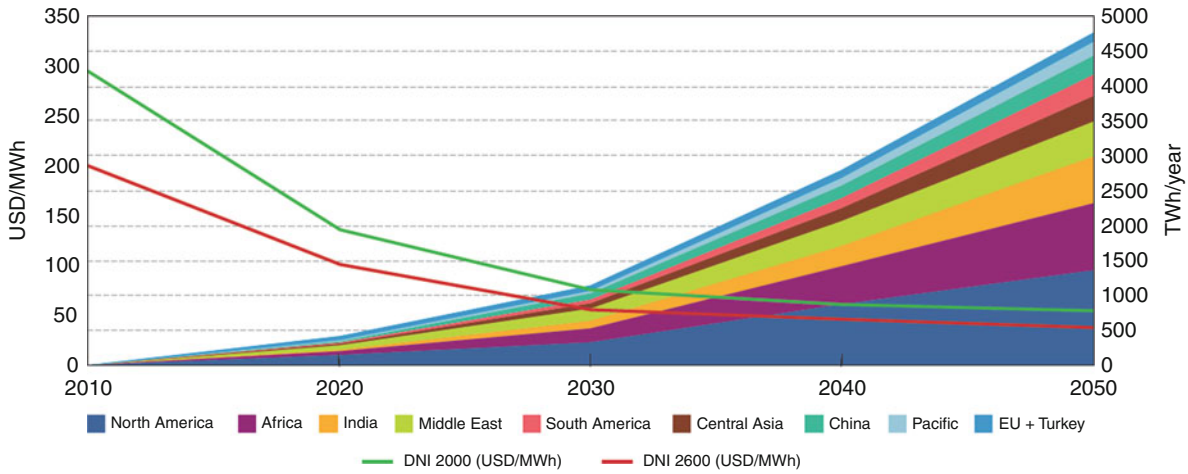

Solar Thermal Energy, Introduction. Figure 2
Possible development of electricity supply from solar thermal energy (CSP) and cost development (Ref. [3])

Bibliography

1. Butti K, Perlin J (1981) A golden thread
2. Oller I, Malato S, Sánchez-Pérez JA, Maldonado MI, Gernjak W, Pérez-Estrada LA, Muñoz JA, Ramos C, Pulgarín C (2007) Pre-industrial-scale combined solar photo-Fenton and immobilized biomass activated-sludge biotreatment. Ind Eng Chem Res 46:7467–7475
3. IEA CSP Roadmap (2010) www.iea.org/roadmaps/
4. Zapata A, Oller I, Sirtori C, Rodríguez A, Sánchez-Pérez JA, López A, Mezcua M, Malato S (2010) Decontamination of industrial wastewater containing pesticides by combining large-scale homogeneous solar photocatalysis and biological treatment. Chem Eng J 160:447–456

Solar Updraft Towers

Gerhard Weinrebe, Rudolf Bergermann, Jörg Schlaich
Schlaich Bergermann Solar GmbH, Stuttgart, Germany

Article Outline

Glossary
Definition of the Subject and Its Importance
Introduction
Solar Updraft Tower Technical Concept
Prototype
Transferring the Results to Large-Scale Plants
Large-Scale Solar Updraft Towers
Future Directions
Bibliography

Glossary

Greenhouse Large translucent solar collector roof under which air is heated by solar radiation.

Solar updraft tower (SUT) Solar Power Plant where ambient air is heated in a greenhouse and rises in a centrally installed tower tube. This convective flow drives one or more turbines to generate electricity.

Solar energy utilization Conversion of the electromagnetic radiation from the sun into usable energy, mostly heat, electricity, or chemically stored energy.

Levelized electricity cost (LEC) LEC is an economic assessment of the cost of an energy-generating system including all the costs over its lifetime: initial investment, operations and maintenance, cost of fuel, and cost of capital. The LEC is the minimum price at which energy must be sold for an energy project to break even.

Definition of the Subject and Its Importance

Electricity generation based on renewable energy is of utmost importance to replace power generation using fossil fuels, as the latter is damaging the environment and exhaustible [1, 2]. Solar energy as a resource is abundant. Several technological options exist to utilize solar radiation. Solar Updraft Towers (SUTs) are one of them. They work on a simple well-known principle: Hot air rises. To make use of this simple physical fact for power generation, air is heated by the sun under a large translucent roof (greenhouse effect). The heated air is then sucked in by a central vertical cylindrical tube (chimney effect). The updraft wind, thus created, drives turbines with generators and so generates electricity. The principle has been proven by building and successfully operating a prototype in Spain for 7 years.

Introduction

Current electricity production from coal, oil, and natural gas is damaging the environment; it is nonsustainable, and many developing countries cannot afford these energy sources. Nuclear power stations are an unacceptable risk in most locations. But inadequate energy supply leads to or maintains poverty, which commonly is accompanied by population explosion: a vicious circle.

Sensible technology for the wide use of renewable energy must be simple and reliable, accessible to the technologically less developed countries that are sunny and often have limited raw material resources; it should not need cooling water or produce waste and should be based on environmentally sound production from renewable or recyclable materials.

The solar updraft tower meets these conditions and makes it possible to take the crucial step toward a global solar energy economy. Economic appraisals based on experience and knowledge already gathered have shown that large-scale solar updraft towers ($\geq$100 MW) are capable of generating energy at costs close to those of conventional power plants [3, 4]. This is reason enough to further develop this form of solar energy utilization, up to large, economically viable

units. In a future energy economy, solar updraft towers could thus help assure the economic and environmentally benign provision of energy in sunny regions.

Although invented by others already 100 years ago [5], it was the German engineering office Schlaich Bergermann und Partner that has taken up the solar updraft tower concept about 30 years back and developed it to the present stage of technical and economical feasibility [3, 6–12]. Thermodynamic behavior has been investigated and tested in a pilot plant in Manzanares in Spain, forming the basis for the layout of large plants. (In 1903, Spanish Army Colonel Isidoro Cabanyes first proposed a solar chimney power plant in the magazine *La energía eléctrica*. One of the earliest descriptions of a solar chimney power plant was written in 1931 by a German author, Hanns Günther. He already described the Desertec concept [see http://www.desertec.org] too.)

Extensive research work and detailed analyses have proven the constructibility of huge towers in general and have resulted in an economically optimized structural concept for tower and collector [9].

Solar Updraft Tower Technical Concept

Principle

Man learned to make active use of solar energy at a very early stage: Greenhouses helped to grow food, chimney suction ventilated and cooled buildings, and windmills ground corn and pumped water.

The solar updraft tower's three essential elements – solar air collector, chimney/tower, and wind turbines – have thus been familiar for centuries, but are combined now in a novel way.

The principle is shown in Fig. 1: Air is heated by solar radiation under a low circular transparent roof open at the periphery; the roof and the natural ground below form an air collector. In the middle of the roof, there is a vertical tower with large air inlets at its base. The joint between the roof and the tower base is airtight. As hot air is lighter than cold air, it rises up the tower. Suction from the tower then draws in more hot air from the collector, and cold air comes in from the outer perimeter.

Thus, solar radiation causes a constant updraft in the tower. The energy contained in the updraft is converted into mechanical energy by pressure-staged turbines at the base of the tower and into electrical energy by conventional generators.

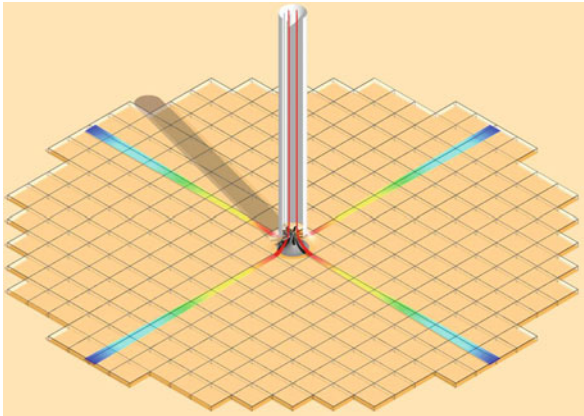

Solar Updraft Towers. Figure 1
Solar updraft tower principle

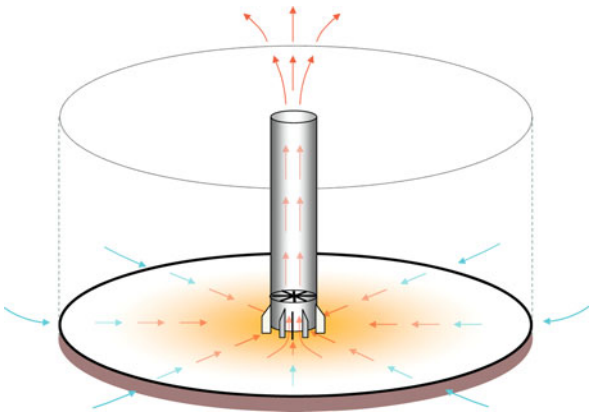

Solar Updraft Towers. Figure 2
Electricity generation of a solar updraft tower is in proportion to the volume defined by tower height and collector diameter

Continuous 24-h operation can be achieved by placing tight water-filled tubes or bags under the roof (Figs. 9 and 10). The water heats up during daytime and releases its heat at night. These tubes are filled only once; no further water is needed.

Electrical output of a solar updraft tower is proportional to the volume included within the tower height and collector area (Fig. 2). The same output may result from a larger tower with a smaller collector area and vice versa.

Components

The main SUT components are collector with (natural and optionally additional) storage, tower tube, and turbine(s). They are described in this section.

Collector The air in a solar chimney is heated by making use of the greenhouse effect in a simple air collector consisting of a glass or plastic roof (either sheet plastic or plastic membrane) a few meters above the ground and the ground beneath it. Only near the chimney's base does the roof rise to 20 or 25 m in order to keep the air velocity within reasonable bounds and thereby reduce friction losses, afterward at the center redirecting the air upward. This roof allows the short-wave solar radiation to penetrate and retains long-wave reradiation from the heated ground. Thus, the ground under the roof is heated and releases its heat to the air flowing radially across it from the edge to the center of the collector.

The natural heat storage capacity of the ground can be enhanced by laying out tubes or casks filled with water [4, 13]. This evens out daily variations in power output up to continuous 24-h operation and complete independence of energy yield from actual insolation.

As will be later described in the section on SUT physics, air mass flow is controlled by the turbines. If the pressure differential at the turbine increases, the flow rate is reduced, and the temperature inside the collector increases. This results in an increase in collector roof surface temperature and thus an increase in thermal losses (infrared emission and convection). Thus, the pressure intake and temperature determine plant output in varying degrees. The insolation incident on the collector roof is partly transformed into usable energy by heating the air and, if additional thermal storage is installed, the water under it. The balance is lost due to reflection, convection, and emission losses as well as heat lost in the ground.

Several alternative designs have been developed for different situations. The decisive selection criteria are the delivery, manufacturing, and assembly costs at the location in relation to the expected service life and amortization period for the roof. Service life for especially durable plastic sheet and membrane roofs is roughly 15–25 years and practically endless for a glass roof. Another solution is to combine several options. Because of the temperature increase under the roof toward the chimney, a sheet-plastic roof with its higher heat transfer rate on the edge of the roof in combination with a glass roof toward the tower, perhaps with partial double glazing, might be ideal.

Glass Roof *Glass Sheet Dimensions*: Normal plate or float glass can be produced to a thickness of between 2 and 12 mm. In the test installation at Manzanares, 4 m × 1 m sections have proven themselves for years (Fig. 3). Comparative tests have shown that a 4-mm thickness can be regarded as ideal for 1–1.2-m sections.

Three millimeters would be sufficient for 1–1.2-m widths with heat-strengthened glass, and 4 mm could be used for 1.5–1.65-m panes. The final selection depends on cost.

Coated Glass: Low-E glass, i.e., glass with a low coefficient of emission in the infrared range, can be used to improve collector efficiency, reducing heat loss to between 1/4 and 1/5. The cost of coating the glass may be compensated for by improved efficiency. From a structural design point of view, it is no different from uncoated regular glass.

Double Glazing: Double glazing or insulating glass with sealed facet joints can be used to reduce heat loss; however, the higher cost is very likely not compensated for by heat savings achieved. Furthermore, support structure loads are greater, and work-intensive sealing of the glass joints is also costly.

Solar Updraft Towers. Figure 3
Manzanares prototype glass roof

Therefore, coating and double glazing are, at most, options for the area around the chimney where air temperatures increase significantly.

Acrylic Glass: If a net savings is involved, transparent plastic panels, e.g., PMMA or polycarbonates, may be used instead of glass.

Glass Roof on Hanging Steel Bands: Slightly sagging steel bands at 1–1.2-m intervals between thin tube supports in concrete bore-pile foundations (depending on construction site) with lightweight 9/9-m^2-grid trussed support girders in one direction at right angles to them, support the glass panes attached to them (Figs. 3 and 4). Total roof area should therefore be divided into 90/90–135/135-m^2 segments. The upper rail of the support girders could be used for "vacuum cleaner" tracks.

This design was proven in Manzanares for many years with no damage even during heavy storms.

The wind wake behind the tower can negate the weight of the light support construction so that it curves upward (as it did in Manzanares without being damaged in the process). Especially where wages are high and steel cost is relatively low, the right solution might be to use bending supports in both directions. The amount of steel required is minimal, with a 6.0/4.8-m^2 support grid. Rolled beams (again with rails) cross the 6 m, and folded sheet-metal support purlins are placed at right angles to them every 1.8 m. This roof is completely level (Fig. 5). As an alternative, it can be finished with plastic panels instead of glass.

Sheet-Plastic Roof: Sheet plastics have a shorter service life than glass, but today, they are very resilient and transparent while they are not only cheaper to produce but also surprisingly advanced with regard to energy consumption.

For producing 1 m^2 of 0.2-mm-thick HP-PE plastic sheet, ~4.4 kWh per square meter of sheet plastic are required, whereas for 1 m^2 of 4-mm-thick glass, ~38 kWh per square meter of glass are required, almost nine times as much energy. However, in the future, the energy source for making the glass could be the inexhaustible sun, whereas oil is always required for plastic (with 1 l oil ≅ 10 kWh).

Plastic Sheet Funnel Roof: This option with several plastic sheets, which were not yet very resilient at the time, was tested in Manzanares (Fig. 6). Clip profiles were arranged in a 6/4-m^2 support grid onto which plastic sheets, heat-sealed – not cut – from parallel strips, were clipped. A hole with a perforated plastic disk was placed in the center of each square for draining rain water, and the sheet was anchored to a foundation in the ground, stretching it into a funnel. Because of the central anchoring foundations which have to absorb the entire wind wake, this design can only be efficient under very favorable site conditions. On the other hand, this roof can be set up by untrained labor without problem.

Plastic Sheet Roof on Arches: For long service life without wrinkles and local tears, the sheets should, if possible, curve evenly and be continuously clipped onto the edges. With a low-cost commercial thin polyethylene sheet (coated on both sides), sufficient weft, warp, and seam strengths can be achieved. In this option, arches typically form a 4/10-m^2 grid with

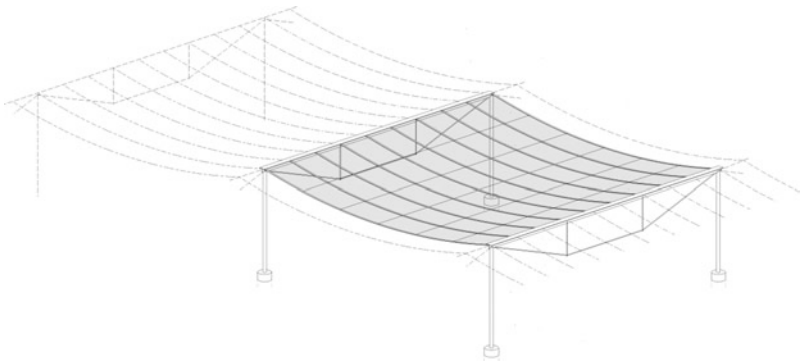

Solar Updraft Towers. Figure 4
Schematic of glass roof on purlins (bending supports)

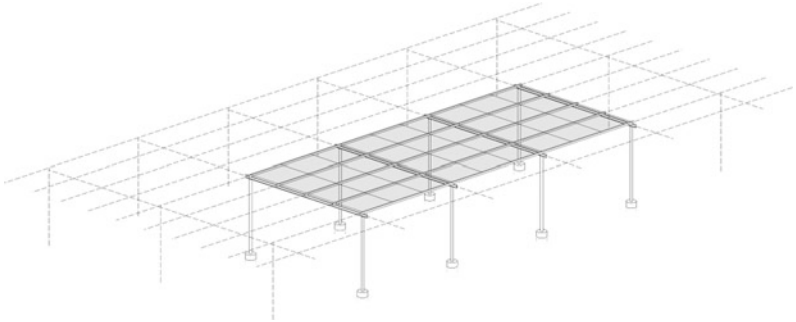

Solar Updraft Towers. Figure 5
Schematic of collector roof with purlins

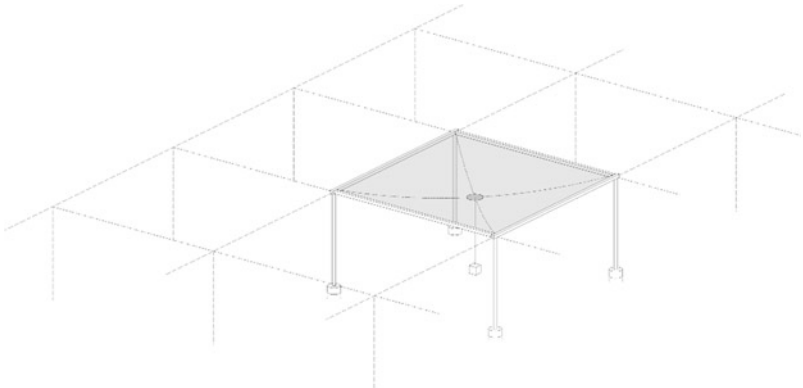

Solar Updraft Towers. Figure 6
Manzanares prototype plastic sheet roof

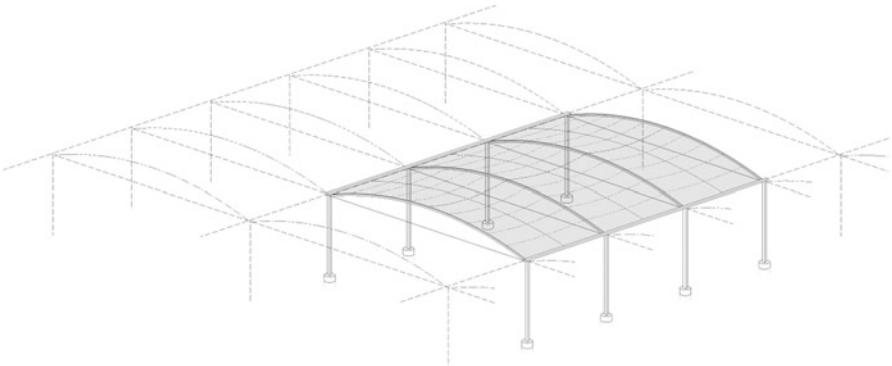

Solar Updraft Towers. Figure 7
Drawing of saddle-shaped plastic sheet roof

10-m tie rods every 4 m and simple supports placed at right angles to them (which also support the vacuum cleaner). Plastic sheets of 10 × 40-m^2 are then spread over them like a saddle (Fig. 7).

Designing the Canopy near the Tower There are high wind wake loads near the tower, and the air temperature under the roof increases so steeply that in the region closer to the tower stronger (toughened)

and/or thicker glass or double glazing must be used. Very close to the tower, in the area where also the turbines are, a solid trapeze sheet-metal roof should be considered.

Vacuum-Cleaning the Roof In the Manzanares experiment, the collector roof could safely be relied upon to be cleaned by occasional rain showers; however, this depends on the site. Of course, pure sand deserts are unsuitable (not only) because of the infrequency of rain on one hand and sandstorms resulting in grit and sand deposits on the other. In some cases, operators will have to provide some active cleaning. Especially designed vacuum cleaners are a useful, simple, and affordable solution for this purpose. They can ride on tracks that are an integral part of the roof supports (Fig. 8).

The amount of sand to be cleaned away and the power requirements for the fan and the drive are now estimated. Three alternatives are compared below for the vacuum cleaner power supply: photovoltaics, motor-driven winch, and engine.

The simplest solution would be the engine. Guiding a winch cable is complicated. Photovoltaics is simple and reliable in keeping with the plant's technology, but as the batteries are too heavy and expensive, such cleaners can currently only be used for about 10 h at a time.

Sand containers at the end of every lane must be emptied, and the cleaner has to move up or down the track. The transfer position is recognized by sensors, a second set of wheels at right angles to the first set emerges, and the cleaner goes over onto the next track up or down on transfer tracks.

Storage If additional thermal storage capacity is desired, water-filled black tubes or other casks or containers are laid down side by side on the

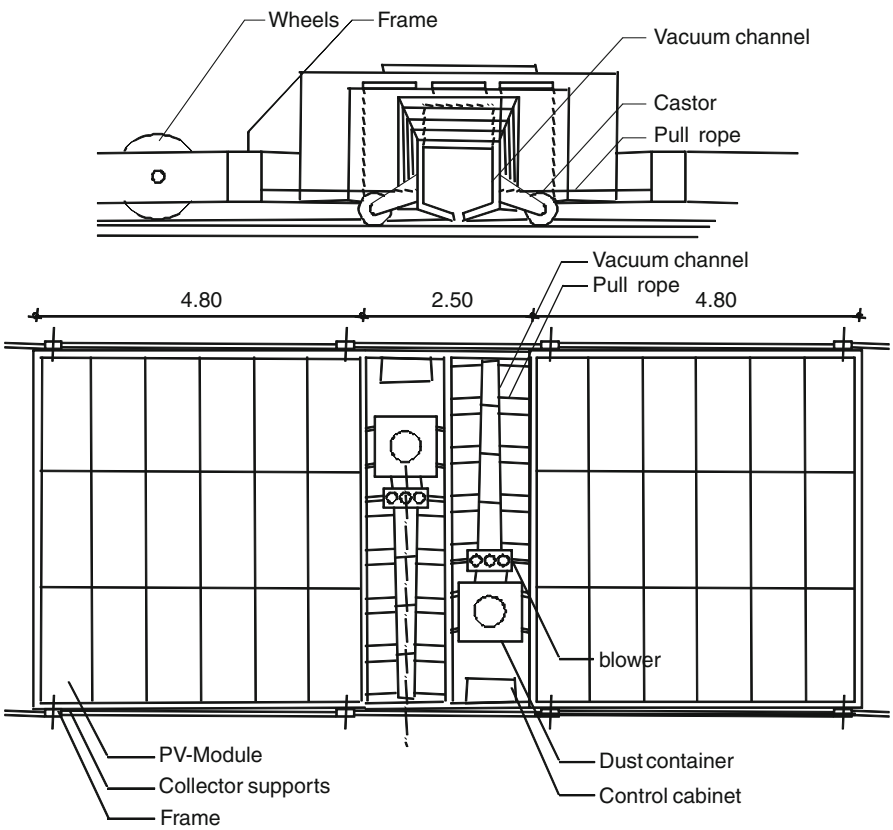

Solar Updraft Towers. Figure 8
Vacuum cleaner (conceptual design)

radiation-absorbing soil under the collector [13]. The tubes are filled with water once and remain closed thereafter so that no evaporation can take place.

The water inside the tubes stores a part of the solar heat and releases it during the night when the air in the collector cools down. This enables the plant to run for 24 h/day on pure solar energy (Fig. 9).

The volume of water in the tubes is selected to correspond to a water layer with a depth of 5–20 cm depending on the desired power output characteristics (Fig. 10).

Heat storage with water works more efficiently than with soil alone, since even at low water velocities – from natural convection in the tubes – the heat transfer between water tubes and water is much higher than that between ground surface and the soil layers underneath, and since the heat capacity of water is about five times higher than that of soil.

Because of their strong impact on the service life of the storage system and the cost of power generation, the materials suitable for these hoses and related manufacturing and assembly techniques were

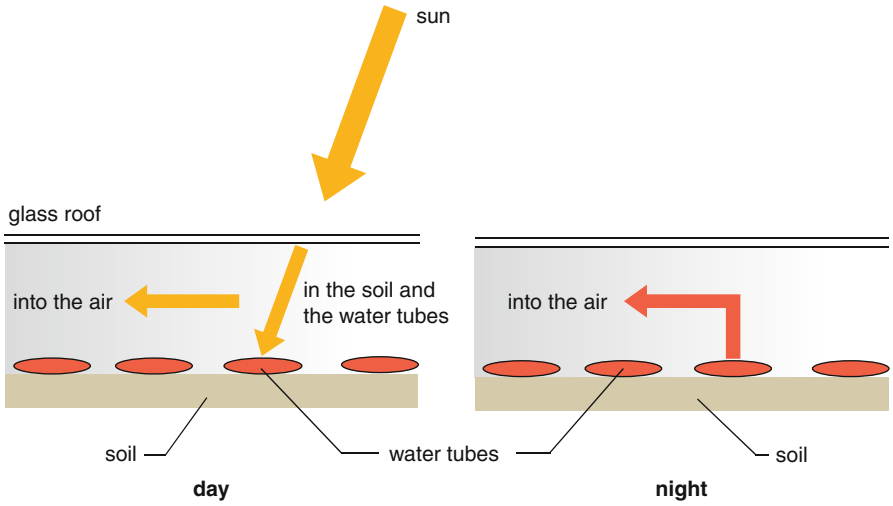

Solar Updraft Towers. Figure 9
Principle of thermal energy storage with water-filled tubes

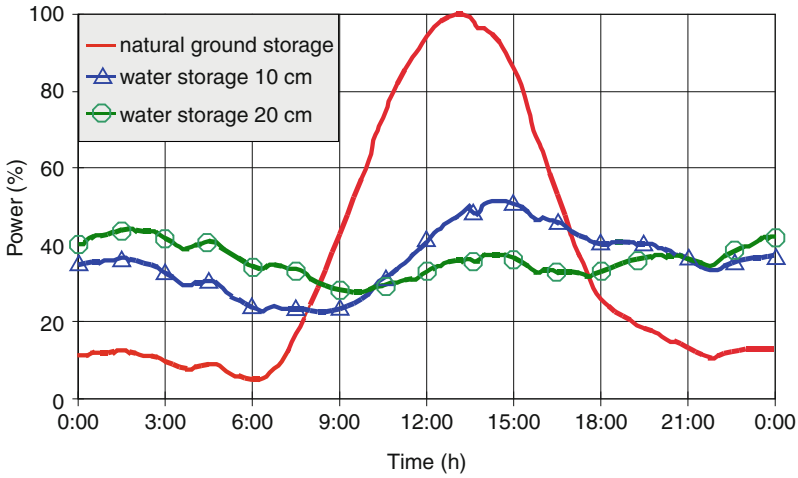

Solar Updraft Towers. Figure 10
Effect of heat storage underneath the collector roof using water-filled black tubes

examined in detail according to a list of required properties: short- and long-term mechanical resilience, heat resistance, UV resistance, aging and long-term properties, width, joining techniques, and cost. The materials compared were glass, textile materials, plastics (PE, PP, PVC, PTFC, ETFE, polyester), and aluminum.

Glass had to be excluded for design and cost reasons. Water tightness is a problem for using aluminum, especially at the welding seams, and is not to be recommended for ecological reasons because of the high energy expense during its production.

High-performance plastic materials, such as PTFE, ETFE, and others, are not an option because of their high cost and because they are still hard to weld. Polyester, which is otherwise highly suitable, is excluded because at temperatures exceeding approximately 80°C hydrolysis tends to make the material brittle, provided this tendency cannot be eliminated. PVC is also only heat resistant up to 75°C.

Polyethylene (PE), a low-cost, worldwide available standard plastic material, available in widths of up to 11 m because it is manufactured by extrusion, seems to be suitable for the application in question, despite its sensitivity to heat and UV radiation. One factor in favor of PE is the fact that a glass collector roof absorbs much of the UV radiation. Quenchers and UV absorbers as well as heat stabilizers added to the plastic material increase durability and thus the service life of the material if it is thick enough (though unfortunately, also raising the material price). PE sheets are used in construction and for reservoirs and have a proven service life of more than 20 years.

PE is easy to weld and the seams are watertight. Cushions are spread radially on the leveled collector floor. Another factor in favor of "airbed storage" is the fact that ground leveling is hardly necessary as the water circulates in a closed circuit. The pressure created by irregularities in the ground and expansion of the water because of temperature changes has to be absorbed by the hose/cushion material.

The cushion consists of a thin plastic sheet above water level and a second one below it, the latter being thicker to provide mechanical protection against irregularities on the ground (Fig. 11).

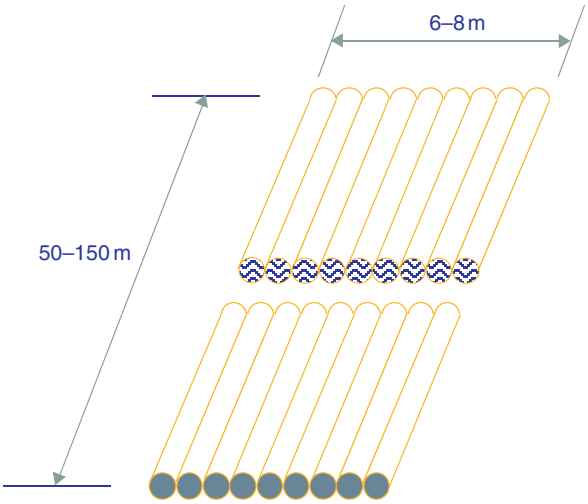

Solar Updraft Towers. Figure 11
Water cushions as heat storage

Tower The tower is the plant's actual thermal engine [14]. It is a pressure tube with low friction loss (like a hydropower station penstock) because of its favorably low surface–volume ratio. The updraft of the air heated in the collector is approximately proportional to the air temperature rise (ΔT) in the collector and to the height of the tower. In a large solar updraft tower, the collector raises the air temperature by about 30–35 K. This produces an updraft velocity in the tower of about 15 m/s at full load. It is thus possible to enter into an operating solar tower power plant for maintenance without danger from high air velocities.

Loads on the Tower The main wind, seismic, and settling loads on the tower depend on the site. Added to this are site-independent differences in temperature and construction imperfections other than defects.

Wind Wind being the main load, detailed expert reports on wind conditions up to a height of 1,000 m were obtained from leading specialists in their field [15–18].

The mean wind speed curve at different heights and gust frequencies greatly depends on topography.

Potential solar tower sites are usually characterized by level surroundings having no natural obstacles. This means that during the first 100 m above ground, wind speed increases sharply, slowly becoming nearly constant after that. Above 300 m, no significant increase in wind speed need be expected.

Gusts are mainly caused by irregularities in the ground. At greater heights, the influence of the

topography, and thus frequency of gusts, drops off. This can be expressed as turbulence intensity (Fig. 12).

The development of wind speed and turbulence can be explained very well with theoretical models which have been confirmed by actual measurements. The Deaves and Harris wind development model [19] is recognized around the world. Theoretical models for the particular site can be calibrated by measuring wind speeds at a fixed reference height for several years.

How much a gust influences a building strongly depends on how large the gust is, and how fast it is moving, compared to the size of the building. The smaller a gust is, the faster it moves. A gust over 1,000 m wide will hit the whole tower, but it is only 10% faster than the mean wind speed. Smaller gusts of only 50 × 50 m can double the wind speed in the area they hit. However, their effect on the tower and its foundations will again be slight because of their limited size. Therefore, several combinations of gust patterns have to be applied to the tower during the planning stage.

The impact pushing or pulling on the surface of the cylinder can easily be determined based on gust speed. Figure 13 shows the distribution of pressure and suction on the cylinder surface and how it was determined by experiments on circular tanks.

The pulsating effect of gusts can, furthermore, cause structural oscillation. Factors increasing this dynamic load are calculated by analyzing oscillation inherent in the structure.

Apart from induced oscillation in the direction of the wind, shear vibration can be induced in towers with circular profiles because vortices are regularly shed when their inherent oscillation (eigenfrequency) f_e equals the shedding frequency in the von-Kármán vortex street (Fig. 14) $f_w = v * S/D$ (with S = 0.2 for the circular profile).

Because of its large diameter, the critical wind speed,

$$v_{krit} = f_E * D/S,$$

for the tower of a solar tower power plant is larger than the maximum wind speed attained. Therefore, shear vibration cannot be induced.

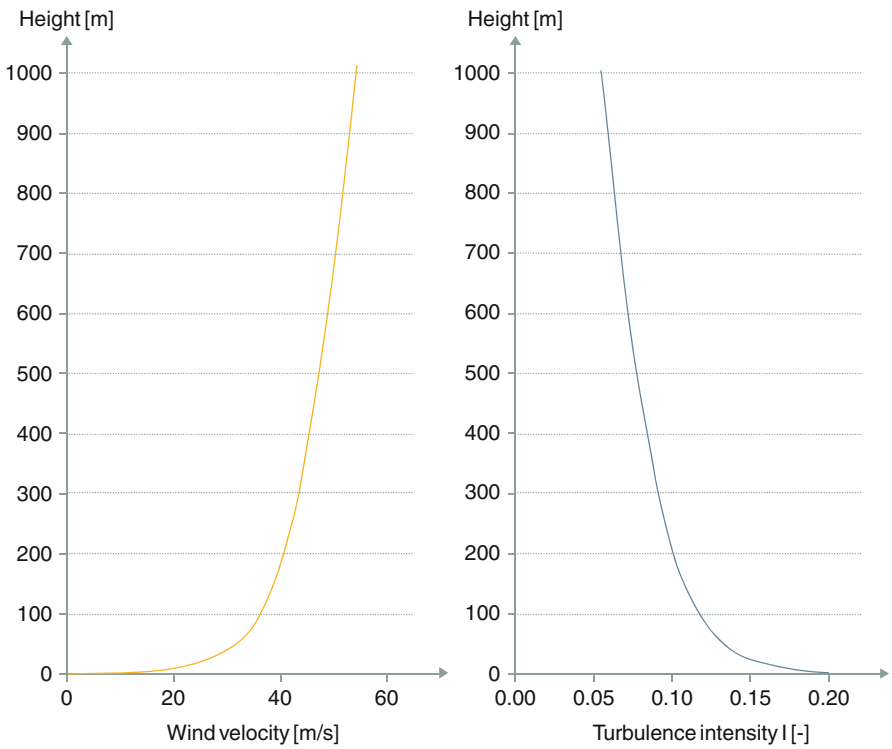

Solar Updraft Towers. Figure 12
Wind speed distribution and turbulence intensity up to a height of 1,000 m above ground (Deaves-Harris model, [19])

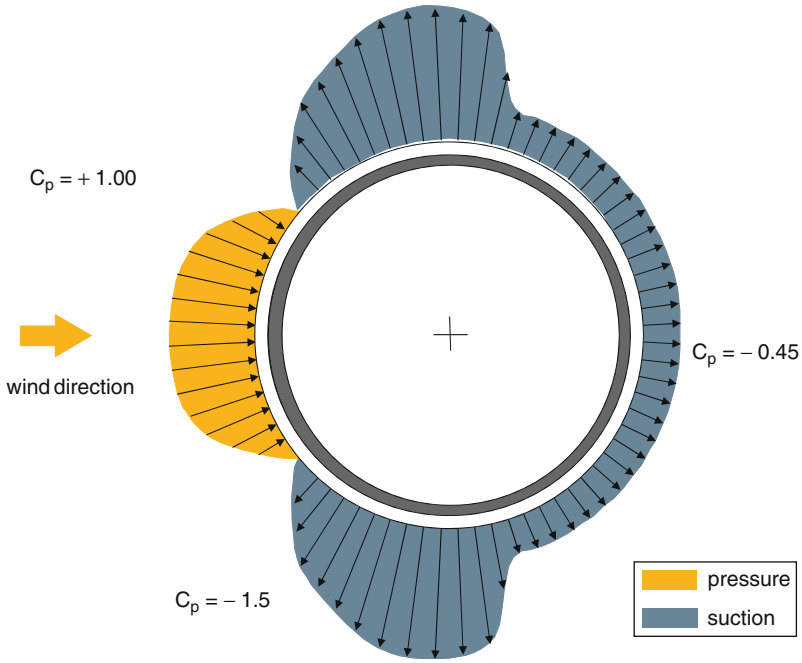

Solar Updraft Towers. Figure 13
Distribution of impact on the circumference of a cylinder

Earthquakes In choosing large-scale power plant sites, extreme danger of earthquake must usually be eliminated. Earthquakes accelerate a building's mass, which results in certain horizontal forces. If the maximum acceleration to be expected at a site as a result of an earthquake results in weaker horizontal forces than from wind, there is no danger to the tower because the probability of maximum wind strength and a very strong earthquake occurring at the same time is negligible.

Settlement The soil under the tower's foundation settles to a certain degree depending on the composition of the ground. Regular settlement is not critical for the layout of the tower and does not affect its operation. However, if the ground under the foundation settles irregularly, it can cause the tower to lean, resulting in additional loads. To avoid this, on less suitable construction sites, the tower foundation is built on a rigid concrete slab, or the tower can be built on piles which, if possible, reach down to a solid rock layer in the ground. Usually, however, suitable construction sites with regular settlement patterns may be expected in arid regions and deserts considered possible sites for solar updraft towers.

The foundation design depends on the site and ground conditions there. For example, soil compacting under the foundation varies greatly depending on the soil's rigidity although the weight is distributed.

Temperature The differences in temperature between inside and outside can greatly affect curved shell structures. For example, there are wide temperature differences when the sun shines on only one side of the tower in the morning when the plant is offline, resulting in relatively low air temperatures inside the tower. Other typical cases are night operation from heat storage or morning operation. The air rising in the tower can easily reach temperatures in excess of 50°C. With a morning ambient temperature of 10°C, temperature differences could exceed 40 K, often leading to cracks in the concrete surface. However, calculations have proven that this does not endanger tower stability.

Imperfections There are always small, unavoidable imperfections in construction. On a building site exposed to the elements at an altitude of over 800 m, it must be assumed that the tower is not always built perfectly vertical and that the walls will have larger or smaller dents in them. From measurements of many cooling towers, however, the usual tolerances for such

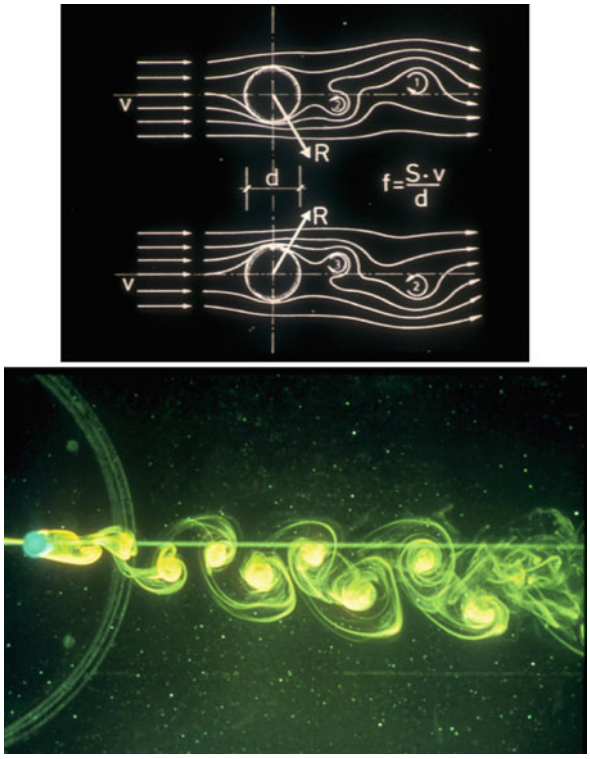

Solar Updraft Towers. Figure 14
Regular shedding of vortices on a circular cylinder (Kármán vortex street). *Top*: schematic and formula, bottom: photo from laboratory tests in water channel

imperfections are known. Special measuring programs using laser and GPS ensure that these tolerances are not exceeded even at heights of 1,000 m. In tunnel construction, perforations several kilometers long are made right on target.

The influence of unavoidable imperfections must be taken into account in the plant layout as they often have considerable impact on shell stability.

Spoked wheels (Fig. 15) are used to stiffen the thin shell wall in such a way as to prevent classic buckling.

Calculations and *Layout for 1,000-m Tubes*: The finite elements method can be used to efficiently calculate linear elasticity for the entire tower. Of course, it is not sufficient to rely on a single computer program, but results of various independently developed finite element software packages have to be compared.

Even the linear calculation clearly demonstrates the favorable effect of spoked wheels. The strong membrane forces of an unstiffened cylindrical shell are almost reduced to those of a cylindrical shaft (Fig. 16).

The suction bulge of the tube without spoked wheels – a reference for the amount of reinforcement steel required – and the pressure dent – a reference for the wall thickness required – are completely leveled out when spoked wheels are used so that construction cost can be reduced and stability increased (Fig. 17). Furthermore, the spoked wheels prevent oscillation of the entire cylinder wall over almost 1,000 m (Fig. 18). This type of oscillation could otherwise be caused by vortex shedding and quickly lead to the building's collapse because of the significant distortion. The spoked wheels completely prevent this type of oscillation. Figure 18 shows oscillation with spoked wheels on the right. No load caused by natural wind would result in such a curve. Therefore, with regular vortex shedding, there is no danger to the spoked-wheel shell.

Modern finite element software, furthermore, makes it possible to use nonlinear geometric and material calculation methods which take into account crack in the concrete surface as well as plastic deformation in the steel reinforcements. All of this makes for a very realistic representation of the tower's actual characteristics and thus provides a good understanding of its load-bearing properties, giving the impression that it is sufficiently safe (Fig. 19).

The German standard for steel-reinforced concrete construction (DIN 1045–1) stipulates a load-bearing factor of at least 1.3. The calculations carried out so far, in part at the University of Stuttgart, have shown a load-bearing factor of approximately 1.7. By taking into account the nonlinear properties of steel-reinforced concrete, the reinforcement distribution shown above can be further improved as the loads are displaced (Fig. 20).

Calculations and Layout for Base and Foundation: The lower support structure is also calculated with the finite elements method, taking the ground's rigidity into account (Fig. 21). This makes it possible to comprehensively determine the impact of settlement and the maximum soil compression. The stability of the wall sections is ensured by a geometrically nonlinear calculation method.

Tie-and-strut models are used for the highly stressed area at the transition from the circular cylinder to the wall sections on which the cylinder rests (Fig. 22). The load on the steel-reinforced concrete can be accurately calculated so that it is well within safety tolerances.

Solar Updraft Towers. Figure 15
Tower tube of a solar updraft tower power plant with spoked wheel to stiffen it

Turbines Using turbines, mechanical output in the form of rotational energy can be derived from the airflow in the tower. Turbines in a solar updraft tower do not work with staged velocity like free-running wind energy converters, but as a shrouded pressure-staged wind turbo generator, in which, similarly to a hydroelectric power station's Kaplan turbine, static pressure is converted to rotational energy [20]. The specific power output (power per area swept by the rotor) of a shrouded pressure-staged turbine in the solar updraft tower is roughly one order of magnitude higher than that of a velocity-staged wind turbine, i.e., SUT turbines are more compact as compared to wind energy converters of the same capacity. Air speed, before and after the turbine, is about the same. The output achieved is proportional to the product of volume flow per time unit and the pressure differential over the turbine. With a view to maximum energy yield, the aim of the turbine control system is to maximize this product, i.e., power output, under all operating conditions.

To this end, blade pitch is adjusted during operation to regulate power output according to the altering airspeed and airflow. If the flat sides of the blades are perpendicular to the airflow, the turbine does not turn. If the blades are parallel to the air flow and allow the air to flow through undisturbed, there is no drop in pressure at the turbine and no electricity is generated. Between these two extremes there is an optimum blade setting: The output is maximized if the pressure drop at the turbine is about 80–90% of the total pressure differential available, depending on weather and operating conditions as well as on plant design.

SUT rotors will have a larger number of comparatively thick blades (e.g., from 5 to 13 blades, compared to 2 or 3 in current wind power plants). There is a clear relationship between the solar tower turbine and the Kaplan hydroturbine, as shown in Fig. 23.

Turbine Layout Today, the state of the art places *many* small horizontal-axis turbines around the perimeter of the tower base, but for smaller plants up to a few megawatts one may install a single turbine with horizontal axis in the tower shaft.

Airflow The turbines in the solar tower are driven by the pressure difference caused by the updraft inside the tower. In order to maximize usable plant power output, it is designed in such a way as to minimize the unavoidable friction losses as air flows through the

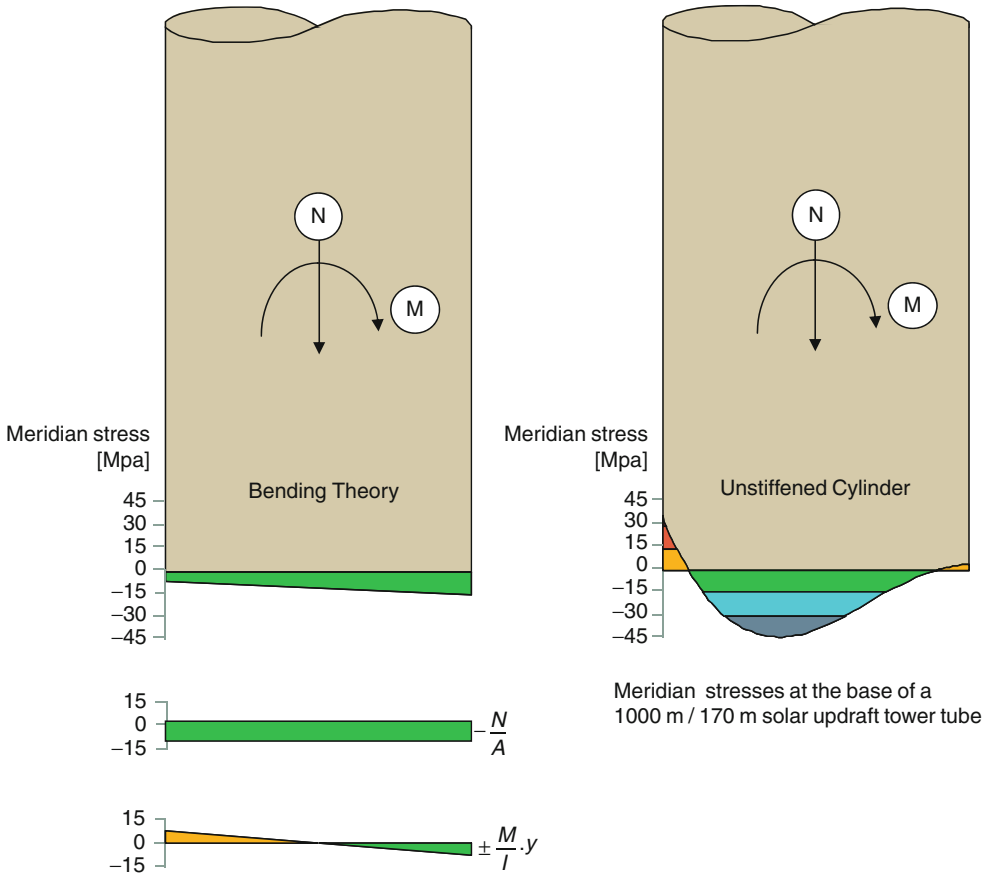

Solar Updraft Towers. Figure 16
Sectional distribution of meridian stresses in a shaft and a shell

plant. This is achieved through the geometric design of the flow duct. The following sections aim to give an idea of the calculations and measurements required.

Calculations Flows on which the turbine layout is based are increasingly computer-calculated, and in some cases, wind tunnel experiments are conducted as well. The technical term for computerized flow calculations is Computational Fluid Dynamics (CFD). Figure 24 shows how the flow area to be investigated is divided into a mesh of numerous small control volumes for which the flow conservation equations (e.g., conservation of mass and impulse) are performed numerically by the computer. The resulting "mesh" showing the edges of the control volumes is shown.

Figure 25 shows such calculations for the flow pattern around the turbine housing graphically. Here, too, the aim is to minimize friction losses while achieving a practical shape which can be manufactured economically.

Suitable turbine blade profiles, thickness, and twist as a function of radius have to be found. The result of this process is shown in Fig. 26.

Flow Redirection into the Tower After the air has blown horizontally through the collector and possibly through the turbines (provided the turbine is not inside the tower shaft), its flow has to be redirected 90° upward into the tower shaft with minimum friction. Internal tower parts can contribute to keeping friction losses low (Fig. 27).

This also has to be ensured for asymmetrical flow patterns, e.g., if individual turbines are off-line or a part of the collector should be in shadow.

Figure 28 shows an example of the speed profiles for one option of redirectional geometry.

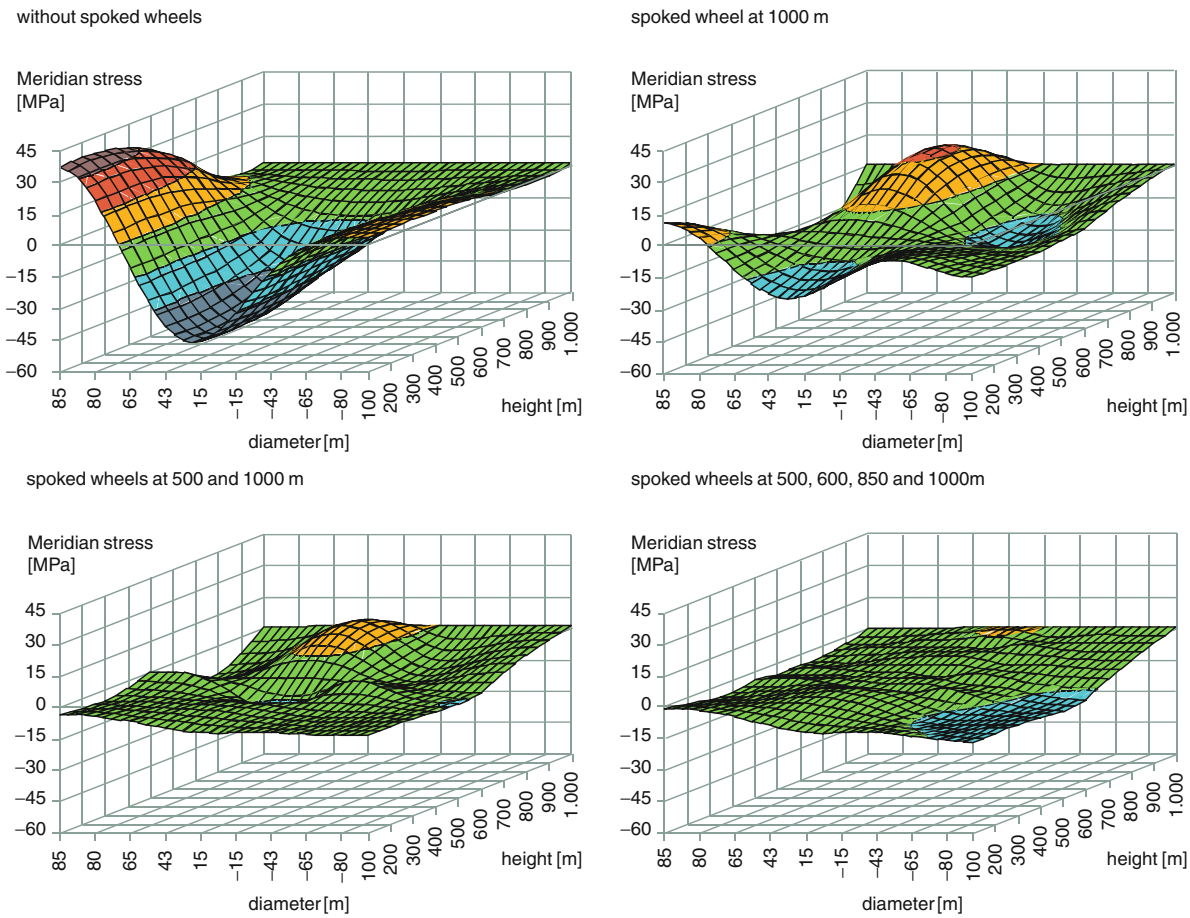

Solar Updraft Towers. Figure 17
Distribution of meridian forces along the wall of the tower under wind load with increasing numbers of spoked wheels

Generator The generator, which converts mechanical energy into electricity, is driven by the turbine runner. The alternating current delivered to the public distribution grid must have exactly the same frequency as the grid. Because the synchronized speed is the quotient of grid frequency and the number of pole pairs, there are certain suitable generator speed and pole pair number combinations. This is illustrated in the following example:

Grid frequency = 50 Hz (50 s^{-1})
Number of pole pairs = 2, therefore
Synchronized speed n_d = 50 $s^{-1}/2$ = 25 s^{-1} = 1500 min^{-1}

The generator in our example has to be run at exactly 1,500 rpm to generate alternating current with the required grid frequency. Alternatively, a frequency transformer can be used to match different frequencies of the SUT generator and the grid (see below).

Because of the required size (runner diameter) of the turbine and the aerodynamic requirement that the blade tips may not reach supersonic speeds during regular operation, the turbine speeds permissible in a solar tower are significantly lower than the 1,500 min^{-1} in our example. Take as an illustration a permissible 75 min^{-1} speed in a 25-m-diameter turbine. This would correspond to a blade tip speed of roughly 100 m/s. Even considering the increase in speed on the turbine blade – also at runaway speeds – the blade tip speed thus remains below the speed of sound (roughly 320 m/s at normal temperature). The following options are then still available to match the required grid frequency:

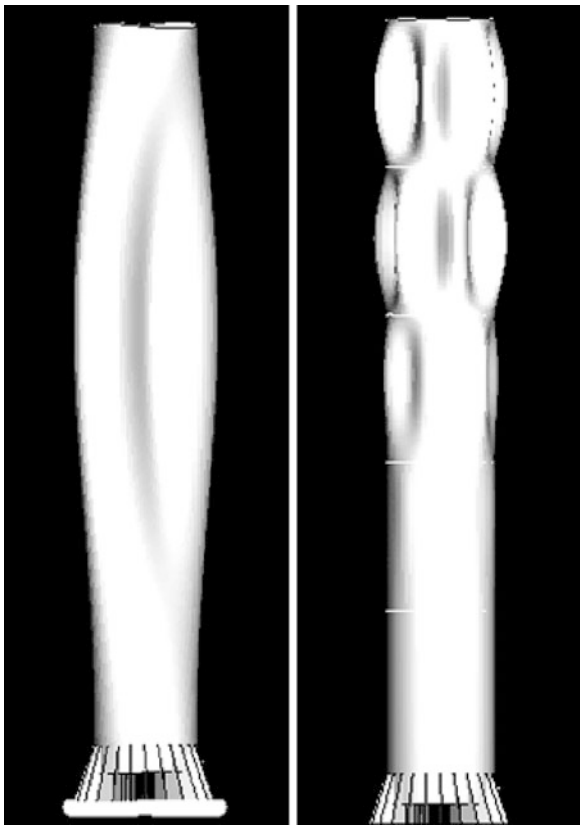

Solar Updraft Towers. Figure 18
Oscillation figures with one spoked wheel at the top (left) and with five spoked wheels

Gearing. The generator can be driven by the runner through a gear unit making it possible to adapt the speed of rotation. This solution has the advantage that cost-effective standard generators can be used. Its disadvantages are mechanical losses in the gear unit and the longer time and greater expense required for maintenance.

Larger number of pole pairs. The frequency of the alternating current generated can be increased by increasing the number of pole pairs. As pole size cannot be reduced indefinitely, this solution unfortunately requires a larger circumference and thus a greater runner diameter. Consequently, cost increases with the number of pairs of poles.

Frequency transformer. A frequency transformer inserted between the generator and the grid disconnects the two frequencies so that the turbine can also be operated at variable speed. This technology is already being used in some wind power plants where variable-frequency operation is especially advantageous.

Safety The situation becomes critical when the turbine is not slowed down by the generator, i.e., when the latter is no longer "absorbing" energy. This can happen if the generator and the grid are disconnected ("load shedding"). Without the braking effect of the generator, the speed of the turbine increases. Its acceleration is

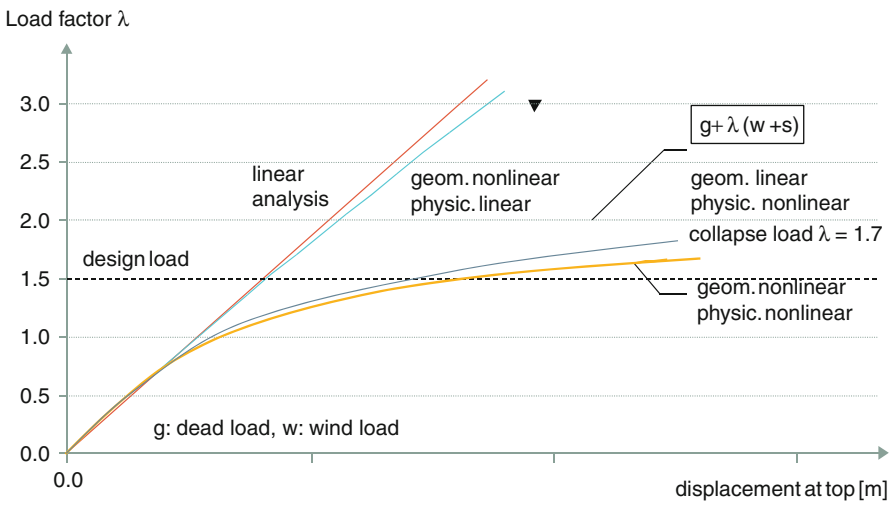

Solar Updraft Towers. Figure 19
Shell structure load displacement properties

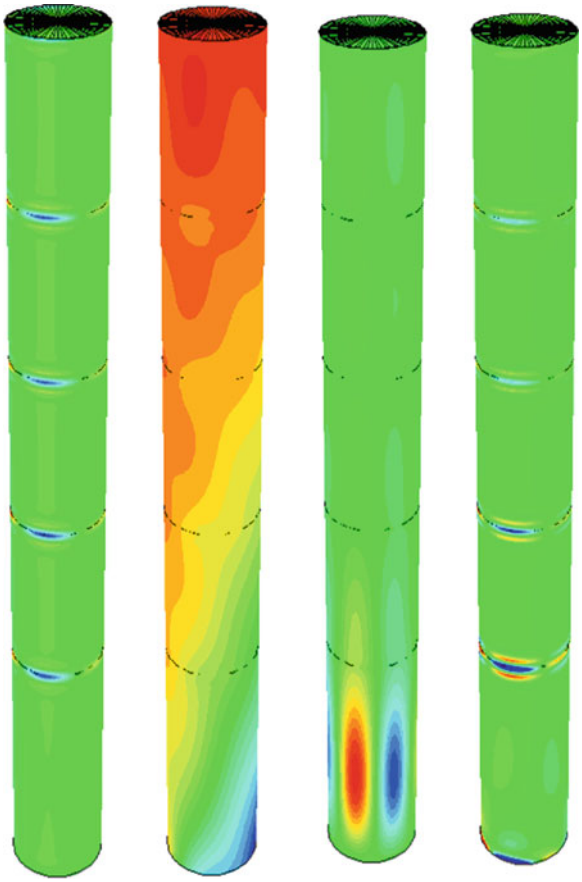

Solar Updraft Towers. Figure 20
Nonlinear calculation of distribution of stress from wind load

limited by the inertia of the rotating mass (meaning that the larger the rotating mass and the greater its distance from the axis of rotation, the more "leisurely" turbine speed increases). If no further precaution is taken, turbine speed increases until equilibrium is reached between the accelerating and braking forces, which also increase at higher speeds. This rotation speed is called runaway speed. Usually a turbine is designed to withstand the forces acting on it even at runaway speed, though this speed should never be reached.

The turbine blade tips should never reach supersonic speeds out of consideration of the strength required, although, if necessary, slight excess of the speed of sound might be permissible for a short time. This establishes the turbine runaway speed and thereby, the turbine's operating speed (rule of thumb: runaway speed = 2 × operating speed).

To keep turbine speed within the operating tolerance range, measures have to be taken to reduce it as soon as it exceeds the permissible operating speed, or – as a last resort – the plant must be shut down.

Pitch control. The blades are automatically oriented by control mechanisms so as to minimize torque in case of load shedding. If necessary, the blade pitch can be adjusted so far as to actively slowdown the turbine. Even if individual blades should not adjust their pitch, the braking torque of the remaining blades would be enough to slow the turbine down. Dr. Viktor Kaplan (1876–1934) had already patented a hydraulic turbine with adjustable blades in 1914 (Fig. 29). Such turbines, known as the Kaplan turbine, are used around the world today.

Only if – failing all precautions and redundancies – the turbine cannot be stopped by adjusting the blade pitch, another step has to be taken.

Blocking the flow. Like the hydroelectric power plant bulkheads that stop the flow of water and drain the turbine (e.g., for inspection), SUTs also have a blocking mechanism. But as air is approximately 1,000 times less dense than water, much less material is required for the solar tower. A "parachute" membrane is one option. Sliding doors similar to those used for airport hangars can also be used.

Physical Model

The exact description of the output behavior of a solar updraft tower under specific meteorological conditions and with specified tower height, tower diameter, and collector radius is only possible with a comprehensive thermodynamic and fluid dynamic finite elements computer program. It includes finding and describing the influence of heat transfer between the soil and the air in the collector, friction losses in the collector and the tower, and heat storage in the soil and output control, all of which can be very complex.

With certain simplifications, however, the basic concept and the influence of significant parameters on expected total plant efficiency and output can be seen in the following equations.

Generally speaking, power output P of the solar tower can be calculated as the solar input $\dot{Q}_{solar}$

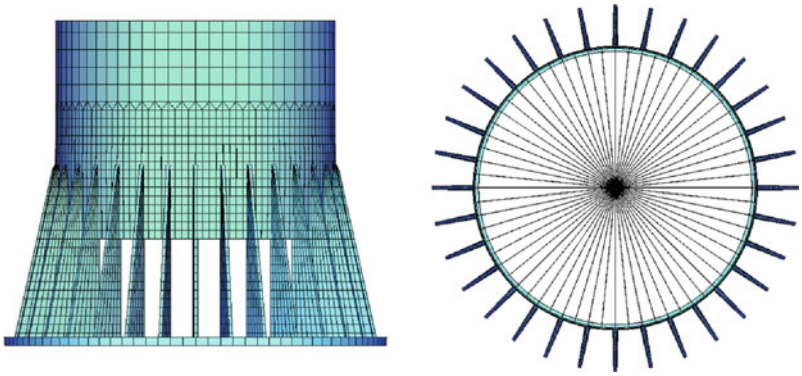

Solar Updraft Towers. Figure 21
Elevation and layout from the finite elements model

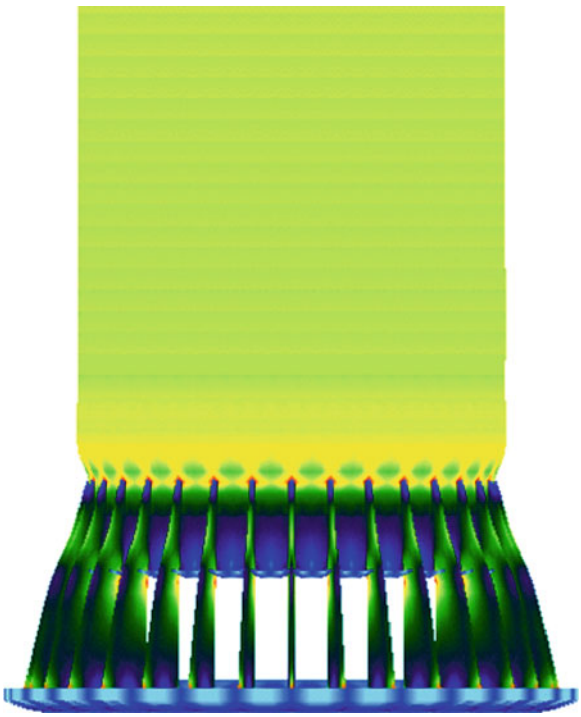

Solar Updraft Towers. Figure 22
Deformation and stress distribution in the support structure (red = points of maximum stress)

multiplied by the respective efficiencies of collector, tower, and turbine(s):

$$P = \dot{Q}_{solar} \cdot \eta_{coll} \cdot \eta_{tower} \cdot \eta_{turbine} = \dot{Q}_{solar} \cdot \eta_{plant} \quad (1)$$

The solar energy input $\dot{Q}_{solar}$ into the system can be written as the product of global horizontal radiation G_h and collector area A_{coll}.

$$\dot{Q}_{solar} = G_h \cdot A_{coll} \quad (2)$$

The tower (chimney) converts the heat flow produced by the collector into kinetic energy (convection current) and potential energy (pressure drop at the turbine). Thus, the density difference of the air caused by the temperature rise in the collector works as a driving force. The lighter column of air in the tower is connected with the surrounding atmosphere at the base (inside the collector) and at the top of the tower, and thus acquires lift. A pressure difference Δp_{tot} is produced between tower base (collector outlet) and the ambient:

$$\Delta p_{tot} = g \cdot \int_0^{Htower} (\rho_a - \rho_{tower}) \cdot dH \quad (3)$$

Thus Δp_{tot} increases with tower height.

The pressure difference Δp_{tot} can be subdivided into a static and a dynamic component, neglecting friction losses:

$$\Delta p_{tot} = \Delta p_s + \Delta p_d \quad (4)$$

The static pressure difference drops at the turbines; the dynamic component describes the kinetic energy of the airflow.

With the total pressure difference and the volume flow of the air at $\Delta p_s = 0$, the power P_{tot} contained in the flow is now:

$$P_{tot} = \Delta p_{tot} \cdot v_{tower,max} \cdot A_{tower} \quad (5)$$

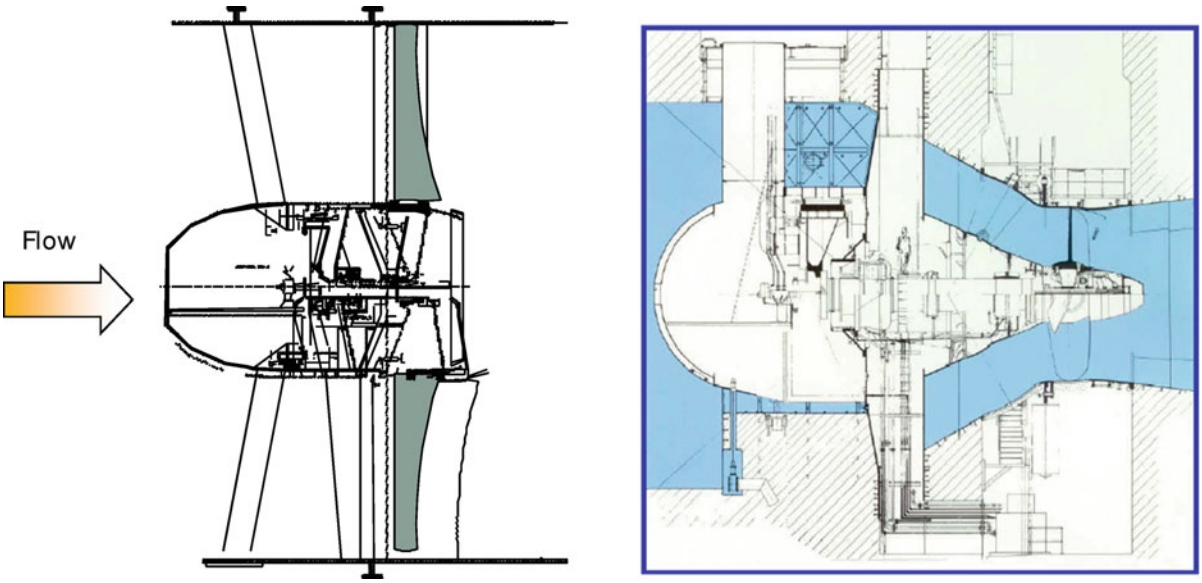

Solar Updraft Towers. Figure 23
Close relatives: horizontal solar tower turbine (left) and Kaplan turbine (right) (Source Kaplan turbine: VATECH Hydro)

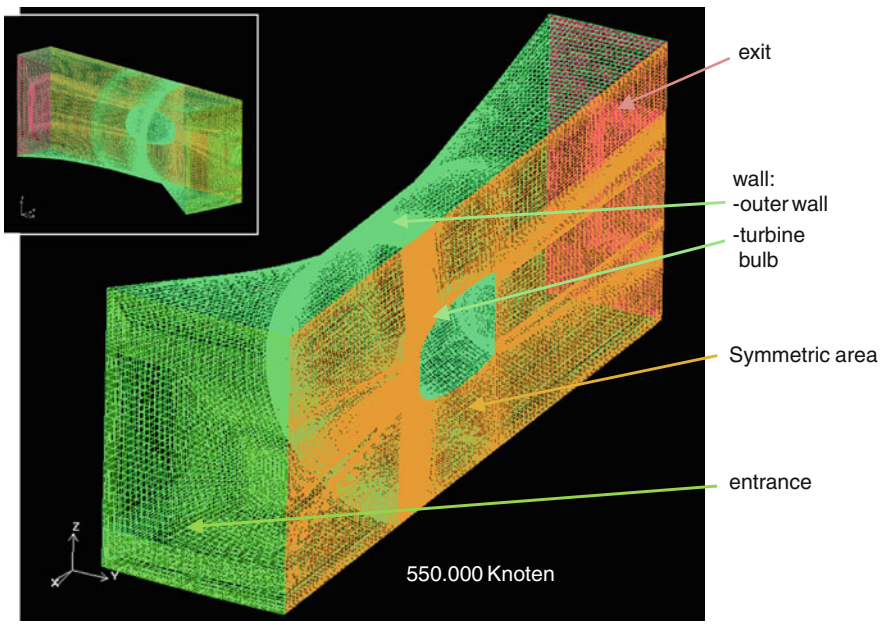

Solar Updraft Towers. Figure 24
Turbine flow calculation mesh (IHS, University of Stuttgart)

from which the efficiency of the tower can be established:

$$\Delta_{\text{tower}} = \frac{P_{tot}}{\dot{Q}} \tag{6}$$

Actual subdivision of the pressure difference into a static and a dynamic component depends on the energy taken up by the turbine. Without turbine, a maximum flow speed of $v_{\text{tower, max}}$ is achieved, and the whole pressure difference is used to

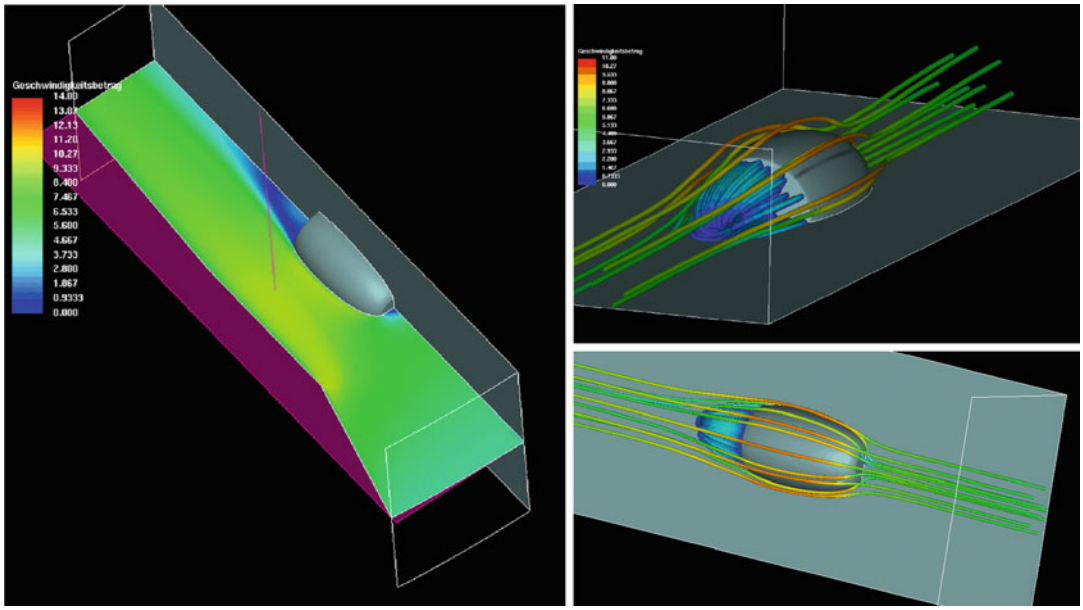

Solar Updraft Towers. Figure 25
How the turbine housing influences the flow pattern

accelerate the air and is thus converted into kinetic energy:

$$P_{tot} = \frac{1}{2} \Delta \dot{m}\, v^2_{\text{tower, max}} \tag{7}$$

Using the Boussinesq approximation [14], the speed reached by free convection currents can be expressed as

$$v_{\text{tower, max}} = \sqrt{2 \cdot g \cdot H_{\text{tower}} \cdot \frac{\Delta T}{T_0}} \tag{8}$$

where ΔT is the temperature rise between ambient and collector outlet (=tower inflow).

Tower efficiency is given in equation 9 [8]:

$$\Delta_{\text{tower}} = \frac{g \cdot H}{c_p \cdot T_0} \tag{9}$$

This simplified representation explains one of the basic characteristics of the solar tower, which is that the tower efficiency is fundamentally dependent only on its height. For heights of 1,000 m, the deviation from the exact solution, caused by the Boussinesq approximation, is negligible.

Using equations (1), (2), and (9), it can be found that solar updraft tower power output is proportional to collector area and tower height, i.e., proportional to the cylinder depicted in Fig. 2.

As electrical output of the solar tower is proportional to the volume included within the tower height and collector area, the same output may result from a large tower with a small collector area and vice versa. As soon as friction losses in the collector are included in a detailed simulation, the linear correlation between power output and the product "collector area times tower height" is not strictly valid any more. Still, it is a good rule of thumb as long as the collector diameter is not too large.

Prototype

Detailed theoretical preliminary research and a wide range of wind tunnel experiments led to the establishment of an experimental plant with a peak output of 50 kW on a site made available by the Spanish utility Union Electrica Fenosa in Manzanares (about 150 km south of Madrid) in 1981/82 (Fig. 30), with funds provided by the German Ministry of Research and Technology (BMFT) [3, 6, 7].

The aim of this research project was to verify, through field measurements, the performance projected from calculations based on theory, and to examine the influence of individual components on

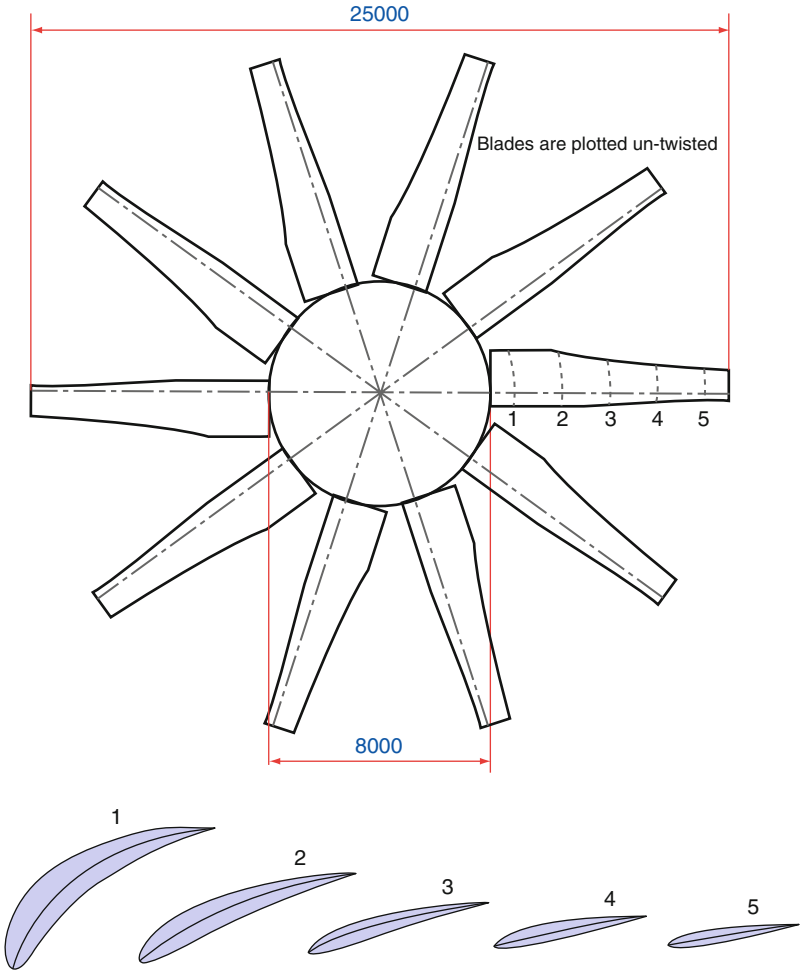

Solar Updraft Towers. Figure 26
Sketch of a 25-m-diameter solar tower turbine runner and the corresponding blade profile sections

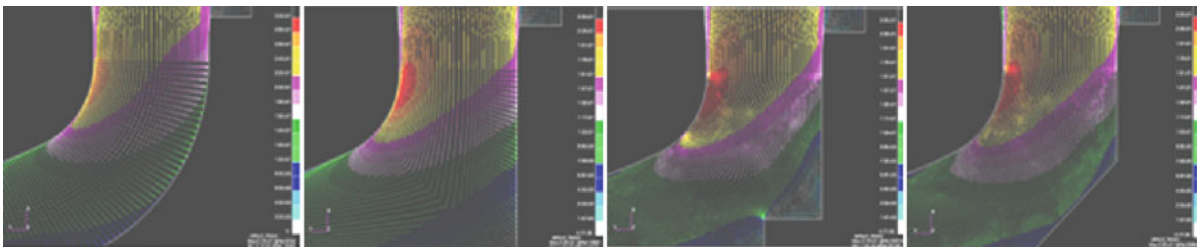

Solar Updraft Towers. Figure 27
Several solutions for redirection (schematics, *top*) and calculated flow patterns (*bottom*). Because of rotational symmetry, only the left half of the cross section is shown

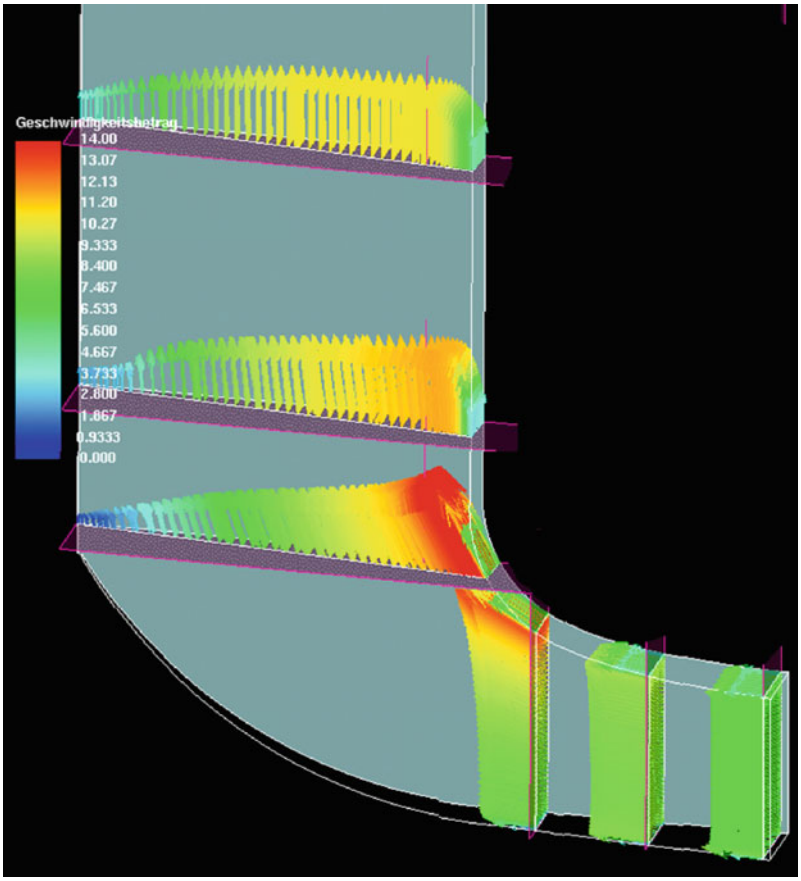

Solar Updraft Towers. Figure 28
Flow pattern in the area of redirection. The figure shows speed profiles (*blue*: low speed, *red*: high speed)

the plant's output and efficiency under realistic engineering and meteorological conditions.

The main dimensions and technical data for the facility are listed in Table 1.

The tower comprises a guyed tube of trapezoidal sheets, gauge 1.25 mm and corrugation depth 150 mm. The tube stands on a supporting ring 10 m above ground level; this ring is carried by eight thin tubular columns, so that the warm air can flow in practically unhindered at the base of the tower. A prestressed membrane of plastic-coated fabric, shaped to provide good flow characteristics, forms the transition between the roof and the tower. The tower is guyed at four levels, and in three directions, to foundations secured with rock anchors. The tower was erected at ground level, utilizing a specially developed incremental lifting method: First, the top section of the tower was installed on a lifting ring on the ground, and then it was raised onto the supporting ring by means of hydraulic presses. Subsequently, the other sections were assembled on the ground, connected to the already installed top tower section(s), and then the whole assembly was lifted. So the complete tower was built in 20 shots of 10 m each.

The turbine (Fig. 31) is supported independently of the tower on a steel framework 9 m above ground level. It has four blades, which are adjustable according to the face velocity of the air in order to achieve an optimal pressure drop across the turbine blades.

Vertical wind velocity is 2.5 m/s on start-up and can attain a maximum of 12 m/s during turbine operation.

The collector roof of the solar tower not only has to have a transparent or translucent covering, it must also be durable and reasonably priced.

A variety of types of plastic sheet, as well as glass, were selected in order to determine which was the best – and in the long term, most cost effective – material (Fig. 32).

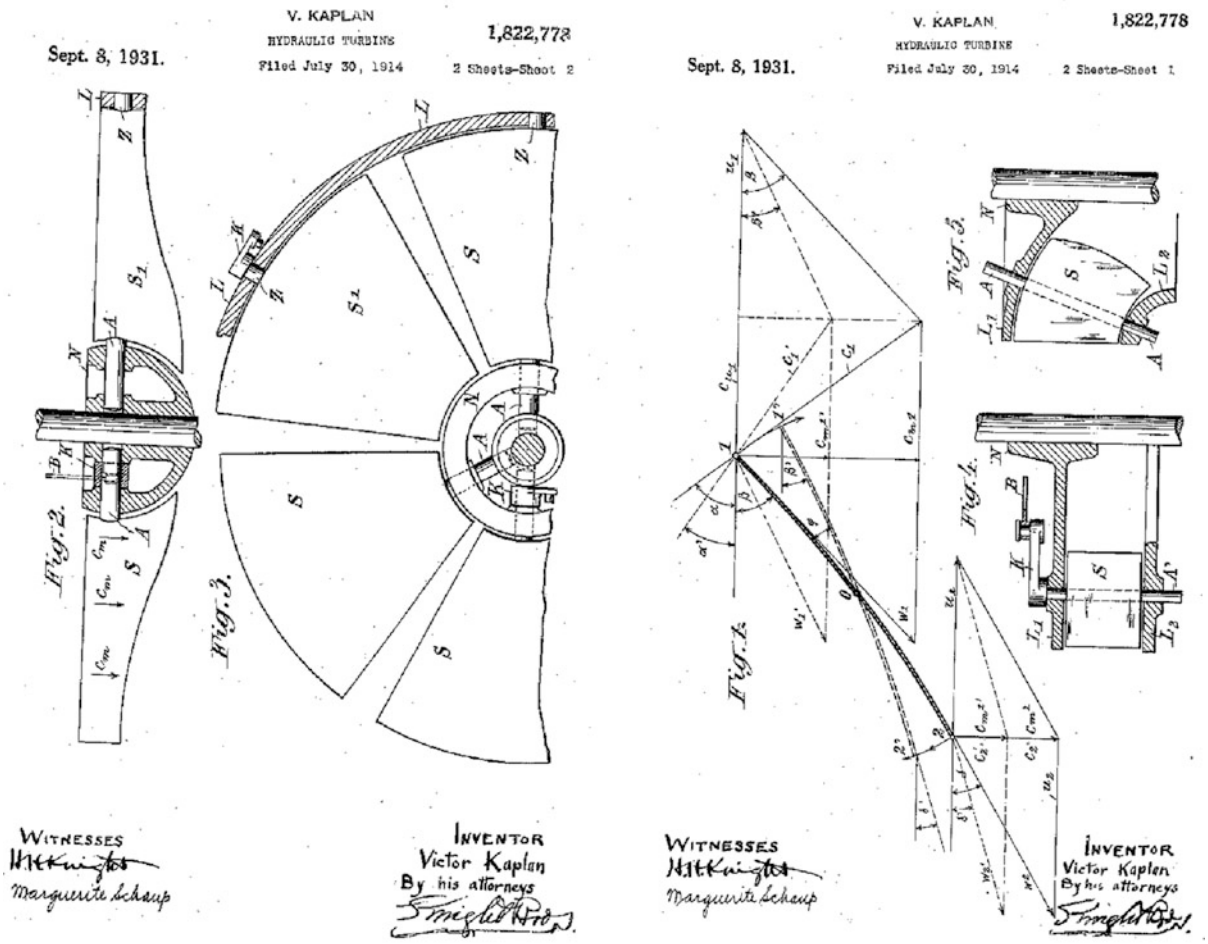

Solar Updraft Towers. Figure 29

Dr. Viktor Kaplan's US patent for a hydraulic turbine with adjustable blades (Source: European Patent Office)

Glass resisted heavy storms for many years without harm and proved to be self-cleaning thanks to the occasional rain showers.

The plastic membranes are clamped to a frame and stressed down to the ground at the center by use of a plate with drain holes. The initial investment cost of plastic membranes is lower than that of glass; however, in Manzanares the membranes got brittle with time and thus tended to tear. Material (temperature and UV stability) and design improvements (e.g., membrane domes) achieved in the last years may help to overcome this particular disadvantage.

Completion of the construction phase in 1982 was followed by an experimental phase, the purpose of which was to demonstrate the operating principle of a solar tower. The goals of this phase of the project were (1) to obtain data on the efficiency of the technology developed, (2) to demonstrate fully automatic, power-plant-like operation with a high degree of reliability, and (3) to record and analyze operational behavior and physical relationships on the basis of long-term measurements.

In Fig. 33, the main operational data, i.e., solar insolation, updraft velocity, and electric power output, are shown for a typical day. Two things shall be pointed out: Firstly, that power output during the day correlates closely with solar insolation for this small plant without additional storage. But, second, there is still an updraft during the night, which can be used to generate power during some hours of the night.

Solar Updraft Towers. Figure 30
Aerial photo of SUT prototype in Spain

Solar Updraft Towers. Table 1 Main dimensions and technical data of the Manzanares prototype

Tower height	194.6 m
Tower radius	5.08 m
Mean collector radius	122.0 m
Mean roof height	1.85 m
Number of turbine blades	4
Turbine blade profile	FX W-151-A
Blade tip speed to air transport velocity ratio	1:10
Operation modes	Stand-alone or grid connected mode
Typical collector air temperature increase	$\Delta T = 20$ K
Nominal output	50 kW
Collector covered with plastic membrane	40,000 m^2
Collector covered with glass	6,000 m^2

With increasing collector size, i.e., generally speaking with increasing thermal inertia of the system, this effect increases, as will be seen later from the results of simulation runs for large-scale plants (Fig. 34).

In order to arrive at a thorough understanding of the physical relationships and to evolve and identify points of approach for possible improvements, a computer simulation code was developed that describes the individual components, their performance, and their dynamic interaction. This program was verified on the basis of experimental measurement results from Manzanares. Today, it is a development tool that takes all known effects into account and with the aid of which the thermodynamic behavior of large-scale plants under given meteorological conditions can be calculated in advance [7, 21].

From mid-1986 to early 1989, the plant was run on a regular daily basis. As soon as the air velocity in the tower exceeded a set value, typically 2.5 m/s, the plant started up automatically and was automatically connected to the public grid. During this 32-month period, the plant ran, fully automatically, an average of 8.9 h per day. In 1987, there were 3,067 h with a solar global horizontal irradiation of over 150 W/m^2 at the Manzanares site. Total operation time of the plant with net positive power to the grid was 3,157 h, including 244 h of net positive power to the grid at night.

These results show that the system and its components are dependable and that the plant as a whole is capable of highly reliable operation. Thermodynamic

Solar Updraft Towers. Figure 31
Turbine of prototype SUT, three of the four fast-moving blades can be seen (view from below the turbine up to the tower top)

Solar Updraft Towers. Figure 32
Collector types tested (*left*: glass, *right*: plastic sheet)

inertia is a characteristic feature of the system, continuous operation throughout the day is possible, and for large systems, even abrupt fluctuations in energy supply are effectively cushioned.

Using the custom-made thermodynamic simulation code based on finite elements that solves the equations for conservation of energy, momentum, and mass, the theoretical performance of the plant was calculated and the results compared with the measurements obtained. The code includes simulation of collector performance based on standard collector theory [22], extended by an integration of thermal storage effects of the natural collector ground and – if required – additional thermal storage by water-filled bags into the model [13, 23]. Fluid dynamics of collector, turbine, and tower are calculated, taking into consideration friction in the respective system components. Calculation of pressure losses relies on standard calculation procedures [24] and, where this is considered not to be applicable or sufficient, on experimental

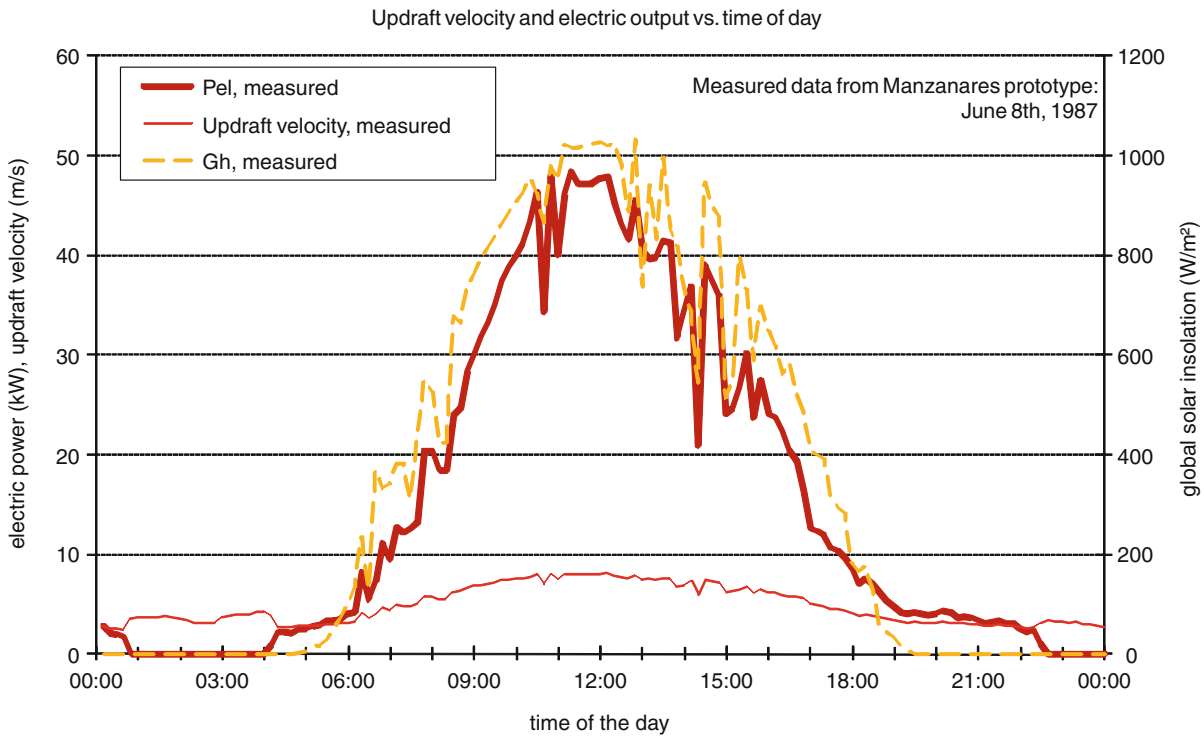

Solar Updraft Towers. Figure 33
Main operational data for a typical day

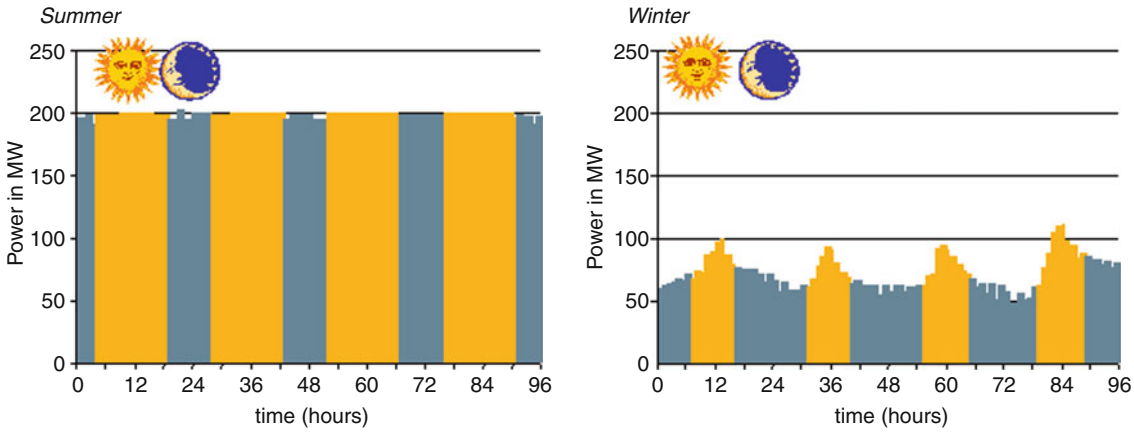

Solar Updraft Towers. Figure 34
Results of simulation runs for a large plant with additional thermal storage, for a site with pronounced seasonal variations

data including wind tunnel tests. Turbine behavior is modeled based on the CFD design calculations done by the "Institute of Fluid Dynamics and Hydraulics Machinery" of the University of Stuttgart [25].

Figure 35 shows a comparison between the measured and calculated average monthly energy outputs, showing that there is good agreement between the theoretical and measured values.

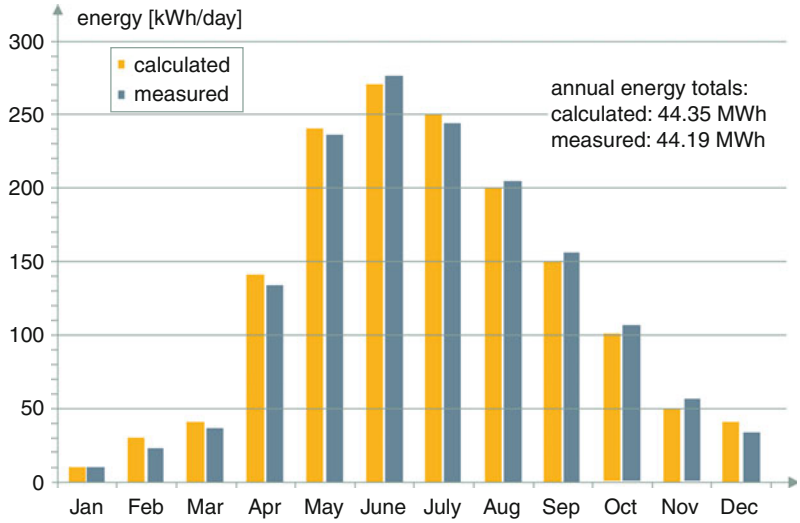

Solar Updraft Towers. Figure 35
Comparison between measured and calculated average monthly energy output

Overall, it may be said that the optical and thermodynamic processes in a solar tower are well understood and that models have attained a degree of maturity that accurately reproduces plant behavior under given meteorological conditions.

Transferring the Results to Large-Scale Plants

Detailed investigations, supported by extensive wind tunnel experiments, show that thermodynamic calculations for collector, tower, and turbine are very reliable for large plants as well.

Despite considerable area and volume differences between the Manzanares pilot plant and a projected 100-MW facility, the key thermodynamic factors are of similar size in both cases. Using the temperature rise and air velocity in the collector as examples, the measured temperature rise at Manzanares was a daily average of 8 K, wind speed was average 4 m/s, while the corresponding calculated average figures for a 100-MW facility are 11 K and 9 m/s.

Therefore measurements taken from the experimental plant in Manzanares and solar updraft tower thermodynamic behavior simulation codes are used to design large plants with an output of up to 200 MW.

In this way, the overall performance of the plant, by day and by season, given the prescribed plant geometry and climate, considering all physical phenomena including single and double glazing of the collector, heat storage system, and pressure losses in collector, tower, and turbine, can be calculated rather accurately.

Large-Scale Solar Updraft Towers

General System Advantages

Apart from working on a very simple principle, solar updraft towers have a number of special features:

1. The collector can use all solar radiation, both direct and diffuse. This is crucial for tropical countries where the sky is frequently overcast.
2. Due to the soil under the collector working as a natural heat storage system, solar updraft towers will operate 24/7 on pure solar energy, at reduced output at night time. If desired, additional water tubes or bags placed under the collector roof absorb part of the radiated energy during the day and release it into the collector at night. Thus solar updraft towers can operate as base load power plants. As the plant's prime mover is the air temperature *difference* (=air density difference) between the air in the tower and ambient air, lower ambient temperatures at night help to keep the output at an almost constant level even when the temperature of natural and additional thermal storage also decreases without sunshine, as the temperature *difference* remains practically the same.

Solar Updraft Towers. Table 2 Typical dimensions and electricity output

Capacity		50 MW	100 MW	200 MW
Tower height	m	750	1,000	1,000
Tower diameter	m	90	110	120
Collector diameter	m	3,750	4,300	7,000
Electricity output at 2,300 kWh/(m^2yr)[a]	GWh/a	153	320	680
Electricity output at 1,800 kWh/(m^2yr)[b]	GWh/a	120	250	532

[a]Annual global horizontal solar radiation of 2,300 kWh/(m^2a), a value found at the best sites worldwide
[b]Annual global horizontal solar radiation of 1,800 kWh/(m^2a), a typical value for Spain

3. Solar updraft towers are particularly reliable. Turbines and generators – subject to a steady flow of air – are the plant's only moving parts. This simple and robust structure guarantees operation that needs little maintenance and of course no combustible fuel.
4. Unlike conventional power stations (and also some other solar thermal power station types), solar updraft towers do not need cooling water. This is a key advantage in the many sunny countries that already have major problems with water supply.
5. The building materials needed for solar updraft towers, mainly concrete and glass, are available everywhere in sufficient quantities. In fact, with the energy taken from the solar tower itself and the stone and sand available in the desert, they can be reproduced partly on site.
6. Solar updraft towers can be built now, even in less industrially developed countries. The industry already available in most countries is entirely adequate for solar updraft tower requirements. No investment in high-tech manufacturing plants is needed.
7. Even in less developed countries, it is possible to build a large plant without high foreign currency expenditure by using local resources and work force; this creates large numbers of jobs while significantly reducing the required capital investment and thus the cost of generating electricity.

Solar Updraft Towers. Table 3 Investment cost and electricity cost

Capacity		50 MW	100 MW	200 MW	
Tower cost	Mio. €	72	156	188	188
Average labor cost for collector construction		18 €/h	18 €/h	18 €/h	5 €/h
Collector cost	Mio. €	140	166	388	320
Turbine cost including housing	Mio. €	56	80	146	146
Engineering, tests, miscellaneous	Mio. €	32	45	49	48
Total investment cost	Mio. €	300	447	771	702
Annuity on investment	Mio. €/a	28.1	41.9	72.2	65.7
Annual operation and maintenance cost	Mio. €/a	1.6	2.3	3.7	3.7
Electricity cost at 2,300 kWh/(m^2yr)[a]	€/kWh	0.19	0.14	0.11	0.10
Electricity cost at 1,800 kWh/(m^2yr)[a]	€/kWh	0.25	0.18	0.14	0.13

[a]Using an average interest rate of 8% and a depreciation time of 25 years

Nevertheless, solar updraft towers also have a feature that makes them less suitable for some sites: They require large areas of flat land. This land should be available at low cost, which means that there should be no competing usage, e.g., intensive agriculture for the land. The siting of the solar updraft tower has to be carefully considered in extremely earthquake prone areas.

Electricity Generation Costs

Electricity yielded by a solar updraft tower is in proportion to the intensity of global solar radiation, collector area, and tower height. There is in fact no

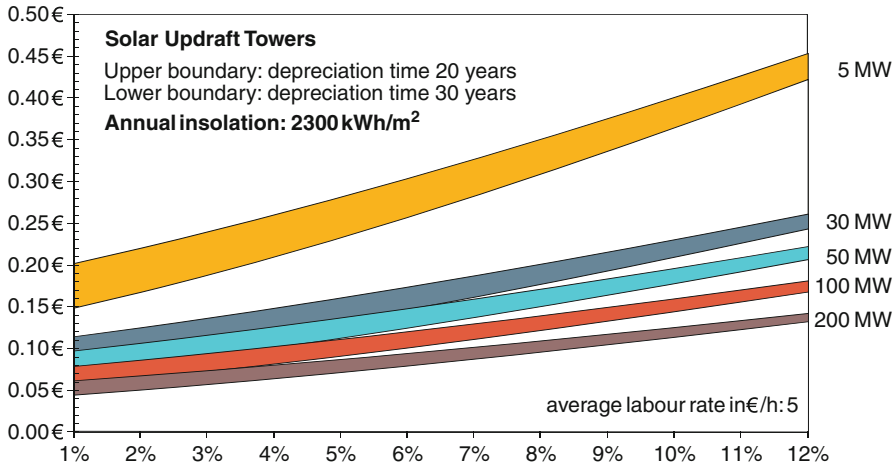

Solar Updraft Towers. Figure 36
Levelized electricity costs vs. average cost of capital for solar updraft towers (high-insolation, low labor cost country)

optimum physical size for such plants. Optimum dimensions can be calculated only by including specific component costs (collector, tower, turbines) for individual sites. And so plants of different optimum key dimensions will be built for different sites – but always at optimum cost: If collector area is cheap and concrete expensive, then the collector will be large and the tower relatively small; if the collector is expensive, there will be a smaller collector and a tall tower.

To give an overview, typical dimensions for selected solar updraft tower capacities are given in Table 2. The numbers are based on typical material and construction costs.

Based on specific costs and the dimensions from Table 2, investment costs were calculated. For the 50-MW solar updraft tower, for example, investment costs of 300 M€ are estimated (see Table 3).

With the respective annual energy outputs from simulation runs, electricity costs (EC) are calculated using an average cost of capital (interest rate) of 8% and a depreciation time of 25 years. Results are shown in Table 3 for a 50-MW, a 100-MW, and a 200-MW power plant. For all plants, two generic reference sites are considered with an annual global horizontal insolation of 1,800 and 2,300 kWh/(m^{2}yr), respectively, to show the effect of this important site characteristic (bottom rows of Table 2 and Table 3). For the 200-MW solar updraft tower, there is an additional column to the very right with data assuming average labor cost of 5 €/h, as compared to the value of 18 €/h being used before. An average labor cost for collector construction of 5 €/h, or even significantly below, can be expected in low-wage countries, e.g., North Africa, Mexico, or China.

From Table 3 and Fig. 36, it becomes obvious that with increasing plant size, a significant reduction of electricity generation cost is associated, leading to EC of 0.11 €/kWh for a 200-MW plant at a high-insolation site, with a further reduction in low-wage countries of about half a €-Cent (see examples given in Table 3).

The financial parameters interest rate and depreciation time are varied to illustrate their influence (Fig. 36). The upper boundary was calculated for a depreciation time of 20 years, the lower boundary for 30 years. As expected, electricity generating costs of the capital intensive solar updraft towers are dominated by interest rate. Depreciation time has a significant influence, too. Assuming an average interest rate of, e.g., 12% and a depreciation time of 20 years leads to EC of 0.14 €/kWh for the 200-MW system at a location with 2,300 kWh/(m^{2}yr) of global solar radiation and average collector labor costs of 5€/h. When, e.g., by clever financial engineering, an interest rate of 5% and a depreciation time of 30 years is achieved, EC drop to 0.07 €/kWh, i.e., half the formerly calculated value.

Future Directions

Designing and building such large structures as solar updraft towers cost efficiently is a challenge, but

finding investors for the construction of solar updraft towers is the main hurdle today. The risk margins an investor puts on top of the "normal" interest rate when investing into this nonproven technology are high and therefore prevented all commercial projects until today. What is missing is a medium-scale power plant in the, say, 1–10 MW range to make SUTs a proven technology. Small-scale solar updraft towers are not economically viable today. Only large plants with a capacity of 100 MW or more are characterized by power generation costs that are competitive (cf. Fig. 36).

The only way to overcome this vicious circle is a considerable subsidy for the first large plant by a government, a foundation, or similar. So today, it is not clear if a large scale solar updraft tower will ever be built.

If they will ever be built, there are various fields to further improve the technology and adapt it to the needs of electricity consumers:

- Higher towers may further reduce electricity generation costs.
- Better control mechanisms, strategies, and algorithms will help to closely match the power generation curve to the demand curve.
- Water production by either using the collector roof as a giant rain catcher or condensation of water vapor inside the SUT as part of the process may help to provide water in arid areas.

Bibliography

Primary Literature

1. Kaltschmitt M, Wiese A, Streicher W (eds) (2008) Renewable energy. Springer, Berlin
2. Weinrebe G (1999) Greenhouse gas mitigation with solar thermal power plants. In: Proceedings of the powergen Europe 1999 conference. Frankfurt, 1–3 June 1999
3. Schlaich J, Schiel W, Friedrich K, Schwarz G, Wehowsky P, Meinecke W, Kiera M (1990) Abschlußbericht Aufwindkraftwerk, Übertragbarkeit der Ergebnisse von Manzanares auf größere Anlagen. BMFT-Förderkennzeichen 0324249D, Stuttgart
4. Schlaich J, Bergermann R, Schiel W, Weinrebe G (2005) Design of commercial solar updraft tower systems,–utilization of solar induced convective flows. Stuttgart
5. Günther H (1931) In hundert Jahren – Die künftige Energieversorgung der Welt. Kosmos, Gesellschaft der Naturfreunde, Franckh'sche Verlagshandlung, Stuttgart
6. Haaf W, Friedrich K, Mayr G, Schlaich J (1983) Solar chimneys, part I: principle and construction of the pilot plant in Manzanares. Sol Energy 2:3–20
7. Haaf W (1984) Solar towers, part II: preliminary test results from the Manzanares pilot plant. Sol Energy 2: 141–161
8. Schlaich J (1995) The solar chimney. Axel Menges, Stuttgart
9. Schlaich J et al (2004) Aufwindkraftwerke zur solaren Stromerzeugung, erschwinglich – unerschöpflich – global. Bauwerk, Berlin
10. Gannon AJ, Backström TW (2000) Solar chimney cycle analysis with system loss and solar collector performance. J Sol Energy Eng 122(3):133–137
11. Gannon AJ, von Backström TW (2000) Thermal and technical analyses of solar chimneys. In: Pacheco JE, Thornbloom MD (eds) Proceedings of solar 2000. ASME, New York
12. Dos Santos Bernardes MA, Voß A, Weinrebe G (2003) Thermal and technical analyses of solar chimneys. Sol Energy 75:511–524
13. Kreetz H (1997) Theoretische Untersuchungen und Auslegung eines temporären Wasserspeichers für das Aufwindkraftwerk. Diploma thesis, Technical University Berlin, Berlin
14. Unger J (1988) Konvektionsströmungen. Teubner, Stuttgart
15. Davenport AG (1961) The application of statistical concepts to the wind loading of structures. In: Proceedings of the institution of civil engineers, London, vol 19, May–August 1961, paper no. 6480, pp 449–472
16. Davenport AG (1967) Gust loading factors. J Struct Div, ASCE 93(ST3):11–35
17. Niemann H-J (1993) Windwirkung auf hohe Schalenkühltürme. In Bautechnik bei Wärmekraftwerken, 1st edn, vol 9 of the series "Kraftwerkstechnik." Verlag VGB-Kraftwerkstechnik GmbH, Essen, pp 248–305
18. Niemann H-J, Zerna W (1986) Impact of research on development of large cooling towers. Eng Struct 8:74–86
19. Harris RI, Deaves DM (1980) The structure of strong winds. In: Proceedings of the CIRIA conference held on 12–13 Nov 1980. Construction Industry Research and Information Association, London, pp 4/1–4/93
20. von Backström TW, Gannon AJ (2003) Solar chimney turbine characteristics. Sol Energy 76(1–3):235–241
21. Weinrebe G (2000) Solar chimney simulation. In: Proceedings of the IEA Solarpaces task III simulation of solar thermal power systems workshop, 28–29 Sept 2000, Cologne
22. Duffie JA, Beckman WA (1991) Solar engineering of thermal processes, 2nd edn. Wiley Interscience, New York
23. Baehr HD (1998) Wärme- und Stoffübertragung, 3rd edn. Springer, Berlin
24. Verein Deutscher Ingenieure (1998) VDI-Gesellschaft Verfahrenstechnik und Chemieingenieurwesen (GVC): "VDI-Wärmeatlas". Springer, Berlin
25. Ruprecht A et al (2003) Strömungstechnische Gestaltung eines Aufwindkraftwerks (Fluid dynamic design of a solar updraft power plant). In: Proceedings of the Internationales symposium über Anwendungen der Informatik und Mathematik in Architektur und Bauwesen. Bauhaus-University Weimar, Germany, 10–12 June 2003

Books and Reviews

Von Backström TW, Gannon AJ (2000) Compressible flow through tall chimneys. In: Proceedings of solar 2000: solar powers life, share the energy. Madison, Wisconsin, USA June 2000

Berdahl P, Martin M (1984) Emissivity of clear skies. Sol Energy 32(5):663–664

Bernardes MAdS, Valle RM, Cortez MF-B (1999) Numerical analysis of natural laminar convection in a radial solar heater. Int J Therm Sci 38:42–50

Castillo MA (1984) A new solar chimney design to harness energy from the atmosphere. In: Nagai M, Heiniger AJ (eds) Spirit of enterprise: the 1984 Rolex Awards. Aurum Press, London, pp 58–59

Churchill SW (1977) Comprehensive correlating equations for heat, mass and momentum transfer in fully developed flow in smooth tubes. Ind Eng Chem/Fundam 16(1):109–116

Churchill SW, Chu HHS (1975) Correlating equations for laminar and turbulent free convection from a vertical plate. Int J Heat Mass Transf 18:1323–1329

Colebrook CF (1939) Turbulent flow in pipes with particular reference to the transition region between the smooth and rough pipes law. J Inst Civil Eng 11:133–156

Mullet LB (1987) The solar chimney overall efficiency, design and performance. Int J Ambient Energy 8(1):35–40

Padki MM, Sherif SA (1989a) Solar chimney for medium-to-large scale power generation. In: Proceedings of the manila international symposium on the development and management of energy resources, vol 1. Manila, pp 432–437

Padki MM, Sherif SA (1989b) A mathematical model for solar chimneys. Seminar on energy conservation and generation through renewable resources. Ranchi, pp. 91–96

Pasumarthi N, Sherif SA (1997) Performance of a demonstration solar chimney model for power generation. In: Reardon FH, Ngo TD (eds) Proceedings of the 35th Heat Transfer and Fluid Mechanics Institute. California State University at Sacramento, School of Engineering and Computer Science, Sacramento, California, pp 203–240

Petukhov BS, Popov NV (1963) Theoretical calculation of heat transfer and frictional resistance in turbulent flow in tubes of an incompressible fluid with variable physical properties. High Temp 1:69–83

Schlaich J, Bergermann R, Schiel W, Weinrebe G (2003) Multi-megawatt updraft solar tower systems. In: ISES solar world congress, Göteborg, 16–19 June 2003

Schlichting H, Gersten K, Krause E, Mayes K, Oertel H (1999) Boundary-layer theory. Springer, Berlin

Yan M-Q, Sherif SA, Kridli GT, Lee SS, Padki MM (1991) Thermo-fluid analysis of solar chimneys. In: Morrow TB, Marshall LR, Sherif SA (eds) Industrial Applications of Fluid Mechanics-1991. Proceedings of the 112th ASME winter annual meeting, Atlanta, GA, Dec 1–6 1991, FED-vol. 132, Book #H00720. The American Society of Mechanical Engineers, New York, pp 125–130

Solar-Induced Climate Effects

Mike Lockwood
Department of Meteorology, University of Reading, Reading, UK
RAL Space, Rutherford Appleton Laboratory, Oxfordshire, UK

Article Outline

Glossary
Definition
Introduction
Solar Variability
Paleoclimate Studies
Observations of Solar Effects in Earth's Atmosphere
Regional Climate Effects
Modeling Studies and Detection–Attribution
Stratosphere–Troposphere Coupling and Top-Down Solar Forcing of Climate
Cosmic Ray Modulation of Clouds
Solar Energetic Particles and Ozone
Are the GMAST Data Correct?
Future Directions
Bibliography

Glossary

Anomaly The deviation of a parameter from its mean value over a defined reference period.

Blackbody radiator A body that emits the maximum radiation possible for its temperature, at all wavelengths.

Chromosphere The lower solar atmosphere, within about 2,000 km of the photosphere.

Cloud condensation nuclei An aerosol particle or air ion on which water can condense such that it grows into a cloud water droplet.

Diffuse fraction The ratio of the intensity in shade divided by the intensity in direct sunlight; for clear skies the diffuse fraction approaches zero, whereas for cloudy skies (and/or with heavy aerosol loading) the diffuse fraction approaches unity.

El Niño Southern Oscillation (ENSO) The extremes of this quasi-periodic (period of 3–7 years) coupled ocean–atmosphere circulation oscillation are El

Niño and La Niña events in which the sea surface temperature in the equatorial Pacific is, respectively, warmer and colder than average. ENSO is one of the predominant causes of interannual variability of regional climates around the globe.

Forbush decrease A transient decrease in GCR fluxes reaching Earth lasting typically 1–4 days, caused by the shielding properties of transient events released from the solar atmosphere.

Galactic cosmic rays (GCRs) Charged particles ranging in mass from electrons and protons up to iron and silicon ions with energies typically of order 0.1–100 GeV. They are generated by explosive galactic events such as supernovae. The flux of GCRs at Earth is modulated by the extension of the solar magnetic field into interplanetary space.

Global albedo (A) The fraction of the total electromagnetic energy from the Sun incident on the Earth that is reflected back into space.

Global circulation model (GCM) Also called a General Climate Model. A numerical model of Earth's global climate system incorporating best available knowledge of the fluid dynamical, chemical, and, increasingly, biological aspects of Earth's climate system.

Global Mean Air Surface Temperature (GMAST) The average of the temperature measured 2 m above the ground by a global network of meteorological stations. The number of stations available declines further back into the past and is consistently lower in the southern hemisphere. Note that it is usually expressed as an anomaly by taking global averages of the station temperature anomalies.

Heliosphere The area of space surrounding the Sun and solar system dominated by the solar wind and the magnetic field of solar origin embedded in it.

Jet stream Narrow bands of fast westerly (eastward) wind in the upper troposphere caused by the combination of equatorial solar heating and Earth's rotation. There are two in each hemisphere: the polar jets are typically found at latitudes of 30–60° whereas the weaker subtropical jets are at 25–30°.

Laschamp event An example of a geomagnetic excursion that occurred around 40 kyr ago. These events are "short-lived" (typically 1–10 kyr in duration) decreases in the geomagnetic field intensity (often to below 20% of normal) with a variation in pole orientation of up to 45°, but no polarity reversal. Any confirmed and consistent paleoclimate signatures of climate change associated with this event would be very significant because the GCR flux reaching Earth's atmosphere would increase but with no simultaneous solar irradiance change.

North Atlantic Oscillation (NAO) An oscillation in the pattern and strengths of westerly winds and storm tracks in the north Atlantic. It is quantified by the fluctuations in sea level pressure between the Icelandic low and the Azores high. The NAO is very closely related to the Arctic Oscillation (AO – which is also called the Northern Annular Mode, NAM).

Northern annular mode (NAM) Also called the Arctic Oscillation: see "North Atlantic Oscillation."

Open solar flux The magnetic field of solar origin that leaves the top of the solar atmosphere and fills the heliosphere.

Paleoclimatology The reconstruction of past climate from a variety of sources such as tree growth from tree rings (dendrochronology); analysis of air bubbles trapped in snow and ice; chemical and isotopic analysis of speliothems, lake deposits, ocean sediments, ice-rafted debris and corals; and documentary evidence.

Photosphere The visible surface of the Sun (mean radius $R_\odot$).

Radiative forcing The change in the difference between the incoming radiation energy and the outgoing radiation energy per unit area at the atmospheric boundary between the troposphere and the stratosphere (the tropopause). It is measured in Wm^{-2}. Consider the case of a TSI change of ΔS: the change in the total power incident on Earth is $\Delta S \pi R_E^2$, where R_E is a mean Earth radius. The change per unit surface area of the Earth is $\Delta S \pi R_E^2/(4\pi R_E^2) = \Delta S/4$. The part not reflected back into space is $\Delta S(1 - A)/4$, where A is Earth's global albedo. Therefore, a TSI change of ΔS corresponds to a radiative forcing of $\Delta S(1 - A)/4$. For other influences on climate the equivalent value can be computed in each case.

Solar energetic particles (SEPs) Charged particles ranging in mass from electrons and protons up to iron and silicon ions of energies of order 0.1–100 MeV. They are generated by transient events in the solar atmosphere and heliosphere.

Solar wind The continuous, supersonic and super Alfvénic outflow of thermal plasma (ionized gas) from the solar atmosphere driven by its high temperatures.

Spectral solar irradiance (SSI) The solar electromagnetic power at a given wavelength, per unit wavelength, falling on unit area normal to the Sun–Earth line (often considered in the UV band of the spectrum).

Stratosphere Atmospheric layer at about 20–55 km altitude, between the tropopause and the stratopause.

Super-Alfvénic In a plasma (ionized gas) a family of waves which modulate both the plasma and the magnetic field can propagate. These are called Alfvén waves, and particles that move faster than them are called Super-Alfvénic.

Total solar irradiance (TSI) The total solar electromagnetic power falling on unit area normal to the Sun–Earth line.

Troposphere The Atmospheric layer between Earth's surface and the tropopause, which lies at an altitude of about 11 km at the poles and 17 km at the equator. All climate and weather processes reside in the troposphere.

Definition

Solar electromagnetic radiation powers Earth's climate system and, consequently, it is often naively assumed that changes in this solar output must be responsible for changes in Earth's climate. However, the Sun emits according to its surface temperature and the huge thermal time constant of the outer part of the Sun limits the variability in surface temperature and hence output. As a result, on all timescales of interest, changes in total power output are limited to small changes in effective surface temperature (associated with magnetic fields) and potential, although as yet undetected, solar radius variations. Larger variations are seen in the UV part of the spectrum which is emitted from the lower solar atmosphere (the chromosphere) and which influences Earth's stratosphere. There is interest in "top-down" mechanisms whereby solar UV irradiance modulates stratospheric temperatures and winds which, in turn, may influence the underlying troposphere where Earth's climate and weather reside. This contrasts with "bottom-up" effects in which the small total solar irradiance (dominated by the visible and near-IR) variations cause surface temperature changes which drive atmospheric circulations. In addition to these electromagnetic outputs, the Sun modulates energetic particle fluxes incident on the Earth. Solar Energetic Particles (SEP) are emitted by solar flares and from the shock fronts ahead of supersonic (and super-Alfvénic) ejections of material from the solar atmosphere. These SEPs enhance the destruction of polar stratospheric ozone which could be an additional form of top-down climate forcing. Even more energetic are Galactic Cosmic Rays (GCRs). These particles are not generated by the Sun, rather they originate at the shock fronts emanating from violent galactic events such as supernovae explosions; however, the expansion of the solar magnetic field into interplanetary space means that the Sun modulates the number of GCRs reaching Earth. These play a key role in enabling Earth's global electric (thunderstorm) circuit and it has been proposed that they also modulate the formation of clouds. Both electromagnetic and corpuscular solar effects are known to vary over the solar magnetic cycle which is typically between 10 and 14 years in length (with an average close to 11 years). The solar magnetic field polarity at any one phase of one of these activity cycles is opposite to that at the same phase of the next cycle and this influences some phenomena, for example GCRs, which therefore show a 22-years ("Hale") cycle. Other phenomena, such as irradiance modulation, do not depend on the polarity of the magnetic field and so show only the basic 11-year activity cycle. However, any effects on climate are much more significant for solar drifts over centennial timescales. This chapter discusses and evaluates potential effects on Earth's climate system of variations in these solar inputs. Because of the great variety of proposed mechanisms, the wide range of timescales studied (from days to millennia), and the many debates (often triggered by the application of inadequate statistical methods), the literature on this subject is vast, complex, divergent, and rapidly changing: consequently the number of references cited in this review is very large (yet still only a small fraction of the total).

Introduction

It is interesting to ponder what the author h-index of the astronomer Sir Frederick William Herschel

(1738–1822) would be (an author with an h-index of *n* means he/she has authored *n* publications each of which has been cited in other publications at least *n* times). Certainly his 1801 paper [1], in which he speculated on a connection between sunspots and the regional climate of the UK, has been cited a great many times and continues to be cited regularly today. Herschel appears to have been more aware of the limitations of his apparent correlation (writing "this prediction ought not to be relied on by anyone") than many who have subsequently cited his paper. He notes limitations to his speculation that many subsequent studies of solar influence on climate have failed to adequately consider. Specifically:

1. Sunspots are, at best, only indirectly related to the solar outputs that are relevant to climate. (Hershel attempts to build an argument about enhanced emission from sunspots which is now known to be incorrect.)
2. The lack of suitable measurements of Earth's global climate leads to the use of indirect proxies (Herschel used the price of wheat) and there are many other factors which can influence such proxies. (Note that some modern studies continue to try to use the price of wheat as a climate proxy [e.g., 2].)
3. The datasets are not homogeneous and measurements show instrumental drifts and discrete jumps. (Herschel notes this in respect of the sunspot data available to him.)
4. The climate data are usually regional and not global. (Herschel used the price of wheat in the UK and not on the global market.)
5. The climate data are often for a limited season (in Herschel's case, this is effectively the growing season of wheat).
6. Correlations readily occur by chance and the probability of that happening must be evaluated. In geophysics (including climate science) this test must allow for the "persistence" in the data time series. Also called "conservation," this is a measure of the tendency of one data point to be similar to its predecessors, and it lowers the effective number of independent samples and hence the significance of any correlation. In addition, tests are needed to prevent "data snooping," i.e., exploiting a feature in the data that turns out to be a statistical or instrumental artifact. To ensure wrong conclusions are not drawn from statistical coincidences, clear null hypotheses must be formulated and proper statistical tests performed [3, 4].
7. Even when the proxies are reliable indicators of a climate variable, there are a great many other influences on it besides solar variability. For example, Herschel neglected the effects of volcanic eruptions that occurred during the interval that he studied. Multiple regression analysis is often used [5–7] but it can be misleading if intercorrelations exist between the data series that are input into the study or if genuine factors are omitted. Naive regression analyses may also be misleading due to convoluted nonlinear response associated with feedback processes, the use of non-optimal regression techniques, and the presence of internal system variability [8], particularly arising from ocean circulation changes [9]. Hence such results need to be interpreted with caution and judgment.
8. The potential for selection effects mean one must ask "would the correlation coefficient be as high if an equivalent dataset were substituted?" (For example, in Herschel's case, was the behavior of the price or barley similar to that of wheat?) Selection effects can often arise (unintentionally or otherwise) from restricted data intervals. For example, Lockwood and Fröhlich [10] showed that whereas solar irradiance and cosmic ray trends before 1985 had been in the direction needed to explain the observed global temperature rise, after that date (which marks the peak of a grand solar maximum [11]) they have been in the opposite direction. Hence, studies based only on data from before 1985 are more likely to be misleading.
9. Even a statistically significant correlation or detected periodic signal does not establish causality. Neither do lags and phases for coupled systems involving stationary oscillations. There are a huge number of publications looking at oscillations at periods close to that of the solar cycle and/or correlations with the solar cycle at a fixed lag. Tests of some of these reveal that they are unlikely to be driven by solar forcing, and that they are more likely to reflect other natural cycles of the

climate system, such as the 14-year cycle, or a harmonic combination of multi-year cycles [12, 13].

10. Is there a realistic mechanism or series of mechanisms that could have given rise to the correlation? (Herschel's proposal invoked solar physics, climate science, agricultural science, and the effect of supply-and-demand in economics.)

The reason why the citation rate for Herschel's speculation is so high is that a great many subsequent studies have explored the same ideas. The growth in modern-day interest can be traced to John A. "Jack" Eddy (1931–2009). (Incidentally, Eddy's h-index is known and is just 13, but his most influential paper, published in 1976 [14], has been cited 797 times at the time of writing – citation analysis using Web of Science, May 2010.) The academic reputation of the field of Sun–climate relations is poor because many, perhaps most, studies do not address all, or even some, of the limitations listed above. It is also a field that in recent years has been corrupted by unwelcome political and financial influence as climate change skeptics have seized upon solar effects as an excuse for inaction on anthropogenic effects. In particular, figures and statistics with known errors, limitations, and inaccuracies are repeatedly reproduced on the internet and in the media [15]. None of this makes any difference to the scientific reality, or otherwise, of mechanisms connecting solar variability and Earth's climate; however, it does make evaluation of the evidence much more difficult. Recent reviews have been presented by Reid (2000), Rind (2002), Haigh (2003, 2007), Beer (2006), Foukal et al. (2006), de Jaeger (2008), and Gray et al. (2010) [16–23].

Solar Variability

Solar outputs reaching Earth undergo periodic variations over a range of time scales. These include the 27-day variation due to solar rotation, the decadal-scale solar magnetic (sunspot), and Hale cycles and oscillations between grand solar maxima and minima on timescales of several centuries. How a key climate parameter, such as the Global Mean Air Surface Temperature (GMAST), varies in response to these solar variations will depend on its response timescales. Estimates of the GMAST response time have varied from less than 1 year to several decades [24–34]. Knutti et al. [28] discuss the time constants of different parts of the climate system: short time scales (1 year or less) apply to atmospheric adjustments and land surface processes, medium time scales (of order decades) to the melting of sea ice, and long time scales (many decades) to warming of the whole ocean surface layer. Ocean warming effects are complex because of mixing behavior [29, 30]. In the absence of heat uptake by ocean circulations, diffusion through the upper ocean layers leads to a spectrum of GMAST response times (rather than a single value) up to about 20 years [28, 299]. However, an estimated 40–50% of heat uptake is by deeper meridional circulation and this has a much longer (>500 years) response time [298]. Climate response modeling [31] and analysis of preindustrial data [32, 33] has yielded effective response times of up to 10 years. Hence, it is clear that responses to 27-day solar variations will be damped to undetectable levels in GMAST whereas the centennial solar variations should be reflected in ocean surface layer temperatures. The extent to which the solar cycle variations will be damped is still a matter of debate. Lockwood and Fröhlich [11] showed that solar trends since 1985 have been in the opposite direction to that needed to explain the observed GMAST rise. This could be explained by solar forcing only (with large amplification) using a very long (of order several decades) response time, but without shorter response times and this would also mean that all associations of decadal-scale oscillations in GMAST with the solar cycle were coincidental as the true solar cycle signal would be highly damped [34]. Hence there is a paradox: attributing large fractions of the centennial global warming to solar changes means that decadal-scale correlations on global scales must be regarded as coincidences, whereas accepting the validity of evidence for a solar cycle global climate response would mean that recent climate trends were not related to solar changes. This does not mean that components of the global system, which may have a shorter response time than GMAST, would not show solar cycle variations.

Elsewhere in this section on Solar Radiation, the article by Fröhlich discusses the observations of total solar irradiance (TSI) covering three solar cycles. This variability is well explained by the effects of magnetic

structures threading the photosphere [35, 37], i.e., the darkening effect of sunspots and the brightening effect of smaller magnetic flux tubes called faculae. To evaluate the solar contribution of TSI variability to centennial climate change requires its reconstruction over the past few centuries. Figure 1 shows a collection of TSI reconstructions covering the interval from just before the Maunder minimum (the period in the second half of the seventeenth century when almost no sunspots were seen) up to the present day. The figure shows that estimates of the magnitude of the centennial drift in TSI have declined: initial estimates [38–40] were based on a limited survey of putative Sun-like stars [36, 49]. However, larger surveys with stricter criteria for Sun-like stellar analogues did not reproduce the key result employed in these early TSI reconstructions [50, 51]. As a result, information on long-term drift of the solar magnetic field from geomagnetic activity [11, 45, 52] was employed in the later reconstructions. Reliable geomagnetic activity data are available back to 1868 and can be used to derive the open solar flux (OSF), the magnetic flux leaving the top of the solar atmosphere. OSF correlates well with TSI over the solar cycle [42, 53] and recent studies indicate that observed TSI may also reflect some of the longer-term drift in OSF [43]. Modeling of the OSF variation [54–58] showed that the total flux threading the photosphere could be constrained by the OSF variation and this could be combined with sunspot observations to reconstruct TSI back to 1600. Figure 1 shows that these second methods are yielding considerably smaller changes in TSI since the Maunder minimum than the early reconstructions based on stellar analogues.

In evaluating some reported associations between TSI and climate, it is important to note the implications of the debate about the intercalibration of TSI data across the "ACRIM gap" in modern TSI data composites (see Fig. 1 in the article by Fröhlich), after the end of the available data from the ACRIM1 space-based radiometer but before its successor, ACRIM2,

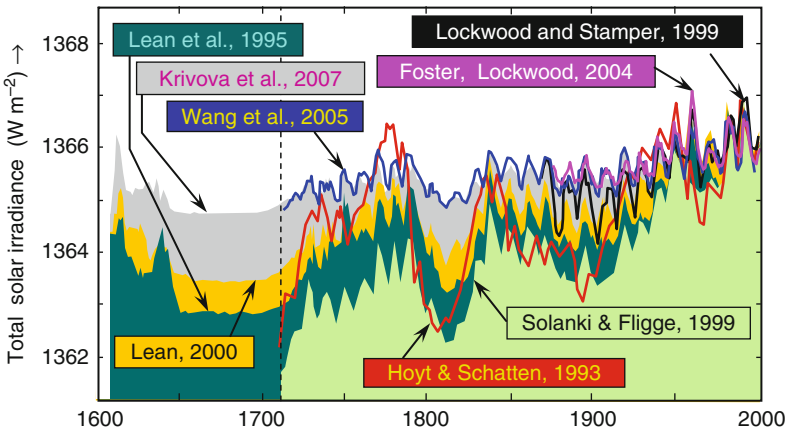

Solar-Induced Climate Effects. Figure 1

Reconstructions of past variations in TSI using different solar proxies. The Hoyt and Schatten (1993) [38] estimates are based on solar cycle length, L. Solanki and Fligge (1999) [39] used the annual sunspot number, R (available back to 1713, the *dotted line*). Lean et al. (1995) [40] and Lean (2000) [69] used a combination of the group sunspot number R_G (available back to 1611), and its 11-year running mean. In these early reconstructions, the amplitude of the slowly-varying component was derived by comparison of the modern-day Sun and Maunder minimum Sun to distributions of the luminosity of cyclic and noncyclic Sun-like stars. Lockwood and Stamper (1999) [53] used the observed correlation between the variations of TSI and the open solar flux on decadal timescales [42]. Wang et al. (2005) [58] used a solar magnetic flux transport model constrained to fit the observed open solar flux variation [11, 45]. Foster (2004) [46] and Lockwood (2004) [47] used Greenwich sunspot observations (available back to 1874). Krivova et al. (2007) [48] used R_G and the open solar flux variation

started to take data. These composites use many of the same raw data series but differ in the degree to which they allow for instrument degradation and in the instrument intercalibrations. Lockwood and Fröhlich [34] note that the anticorrelation between TSI and GCR fluxes (see below) is found for the reconstructed TSI data time series known as the "PMOD data composite" but does not hold for the alternative "ACRIM" composite [44, 59]. Scafetta and Willson (2009) [60] argue that the long-term reconstruction of TSI by Krivova et al. (2007) [48] supports the ACRIM composite but Krivova et al. (2009) [61], and Wenzler et al. (2009) [62] point out that the more precise TSI reconstruction from modern magnetograph data is inconsistent with the ACRIM composite but consistent with the PMOD composite. The implications of this debate are discussed later in relation to Fig. 2.

The UV part of the solar spectrum is much more variable than TSI and is an essential factor that modulates ozone abundance, temperatures, and winds in Earth's stratosphere (see review by Gray et al. [23]). Composites of UV spectral solar irradiance (SSI) had shown little variation in the spectral shape, such that different wavelengths exhibit a similar waveform to TSI [68, 69] and this has been reflected in centennial reconstructions of SSI [63]. However, recent observations of the descent into the current unusual solar minimum [41] cast doubt on this as they show more variability in the UV and considerable change in spectral shape [67], although the validity of these data has been questioned [70]. If valid, they imply that at the wavelengths responsible for stratospheric modulation, centennial variation may be greater than previously thought [72]. There is debate about the degree of centennial drift in historic observations of the UV Ca "K" absorption line [71, 73, 74] but this may, anyway, be of limited relevance because the absorption arises higher in the solar atmosphere than does the UV continuum emission.

The degree of uncertainty in long-term variability of TSI and SSI should be noted. Reconstructions allow for the effect of large active regions (groups of dark sunspots surrounded by bright faculae) which vary with the decadal- and centennial-scale changes in the large-scale solar dynamo. However, the long-term variability and effect of small-scale fields in the quiet Sun (away from active regions) driven by the turbulent, small-scale dynamo [75] is not well known. Furthermore, it has been suggested that magnetic fields below the solar surface may have an influence [76] and although the success of modeling TSI variations using surface fields means there is no evidence for these "shadow effects" over recent solar cycles, this does not necessarily mean that they could not have an effect on longer timescales. Another potential source of additional long-term drift arises from changes in the solar radius, $R_\odot$. A great many studies over many years have searched for such variations, both over recent solar cycles and, using eclipse data, on centennial timescales. These studies are inconclusive and often contradictory: it is unclear that any changes detected are bigger than the experimental uncertainties. For example, there are a number of reports that $R_\odot$ increases with solar activity [77] whereas other measurements show the reverse or no consistent change [78, 79]. Bruls and Solanki (2004) [80] demonstrated that surface luminosity features can perturb many techniques and the results from helioseismology show small and inconsistent changes [81]. The best observations place an upper limit of about 0.01% on variations in $R_\odot$ over decades [82–84] and reports of larger changes (e.g., [85]) remain controversial.

As well as being used in reconstructions of TSI, the OSF is highly anticorrelated with the flux of GCRs incident on Earth [87]. As discussed later, GCRs have been proposed as a direct modulator of Earth's climate; however, the anticorrelation of GCRs with OSF and irradiance means that GCRs may just be a proxy indicator of TSI and SSI variations. Indeed, the cosmogenic isotopes that GCRs produce are routinely used in paleoclimate studies as a proxy indicator of irradiance [87]. Lockwood [89] showed that the relationship between cosmogenic isotope production and TSI is monotonic but may not be linear, depending on the effect of unknowns in the long-term irradiance behavior discussed above. Steinhilber et al. [90] have recently reconstructed TSI variability on centennial scales using cosmogenic isotope data and for recent centuries their results are similar to the modern TSI reconstructions shown in Fig. 1. A number of cosmogenic isotope data sequences have been generated [91–93]. A key point to note is that the Maunder minimum is just one of a number of "grand solar minima" (and far from the deepest one in the record over the last 10^4 years),

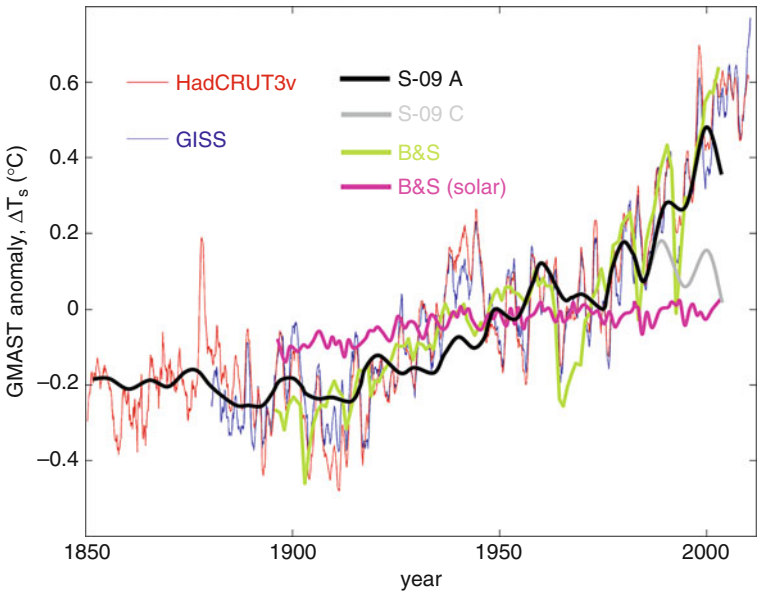

Solar-Induced Climate Effects. Figure 2

Estimates in the literature of the contributions of solar change to observed global temperature rise vary widely. The *blue line* shows the global mean surface temperature (GMAST) anomaly compiled from observations by NASA/GISS [64], the *red line* the equivalent HadCRUT3v compilation by UEA and the UK Meteorological Office [65]. (Both GISS and HadCRUT3v have here been re-normalized to a reference period of 1900–2000.) The *black* and *grey lines* are estimates of the solar contribution from multivariate fits by Scafetta [66]: these employ only solar forcing and use as input the TSI reconstruction of Krivova et al. (2007) [48] (see Fig. 1), splined to different data composites of modern-day TSI measurements. The black curve (S-09A) is consistent with the ACRIM data composite whereas S-09C (in *grey*) is consistent with the PMOD data composite. The *green line* is the fit by Benestad and Schmidt [8] from full GCM modeling of all known climate forcings, the solar contribution to which is shown in mauve. The main issue is not so much the closeness of fit, it is the robustness and appropriateness of the procedures used, as discussed in the text. Only robust procedures have predictive power which is the key test of all science. Note the effect of extreme sensitivity of the solar-only multivariate fit to small features and hence the potential for "data snooping": the fit to the data after 1990 of the S-09A curve relies on the ACRIM composite which differs from the PMOD by what many believe to be a single (and rather small) erroneous calibration skip during the so-called ACRIM gap (see Lockwood and Fröhlich 2007 [35]). Using the PMOD composite (S-09C), the limitations of the multivariate fit begin to become apparent after around 1985 (with the oppositely-directed solar and GMAST trends noted by Lockwood and Fröhlich [10]). The fits of Scafetta [66] continue up to 2002: the subsequent exceptionally low solar minimum reveals that even curve S-09A will have a downward trend after 1997 and it too fails to reproduce the most recent GMAST data [67]

whereas modern space-based measurements are all within a "grand solar maximum." There has been debate as to the degree to which the current grand maximum is an exceptional one in terms of its amplitude [94, 95]. However, it is clear that its duration is relatively long and hence a return to more average solar conditions is somewhat overdue [96]. The OSF variation suggests that this decline commenced around 1985 [10, 11] and that the recent solar minimum (between cycles 23 and 24), which was exceptionally low compared to previous examples during the space age [41], is a symptom of that decline. From the composite of cosmogenic isotope records by Steinhilber et al. [93], Lockwood [41] estimates that there is about an 8% chance of a rapid return to Maunder minimum conditions within the next 50 years.

One last solar output is the continuous, but highly variable, stream of low-energy thermal particles in the solar wind which has been invoked in some climate studies (e.g., [97, 98]). The power incident on Earth's atmosphere delivered by the solar wind is smaller than that from solar electromagnetic radiation by a factor of between 10^4 and 10^5 [47]. Nevertheless, energy extracted from the solar wind undoubtedly dominates the uppermost atmosphere (the thermosphere), but this contains a tiny fraction of the total mass of the atmosphere. Other studies find relationships with geomagnetic activity (caused by electrical currents in the upper atmosphere): for example, Bochníček and Hejda [99] report variations in the North Atlantic Oscillation (NAO) to be more related to geomagnetic activity than sunspots. Thejll et al. [100] also investigated correlations between geomagnetic activity indices and the NAO and found significant correlations in winter for some but not all years. However, solar wind and geomagnetic activity are both highly correlated with OSF which, in turn, is highly correlated with spectral and total solar irradiance (and also correlated with SEP occurrence and anticorrelated with GCR flux). Given that the total masses in the troposphere, stratosphere, and thermosphere are approximately 80%, 19.9%, and 0.1%, respectively, of the total atmospheric mass, any mechanism connecting the solar wind and climate would require a mechanism of truly extraordinary amplification; hence any relationships are most likely to be due to other, correlated, solar outputs.

Paleoclimate Studies

A great many studies have indicated that solar variations had an effect on preindustrial climate throughout the Holocene (the warm interval since the last ice age). These studies have been made in many parts of the world and employ a huge variety of paleoclimate proxies [101–128]. Studies on timescales of up to 1–2 kyr are, in some ways, optimum since such periods are short enough to avoid complications from changes in the geomagnetic field and Earth's orbit [129]. In all cases, the solar change is evaluated from cosmogenic isotopes. The most interesting of these studies employed terrestrial data that are indicators of more than just local climate. For example, Bond et al. [110] studied the average abundance of ice-rafted debris (IRD), as measured in the cores of ocean bed sediment throughout the middle and North Atlantic. IRD are glasses, grains, and crystals that are gouged out by known glaciers, which are then carved off in icebergs and deposited in the sediment when and where the icebergs melt. The sediment is dated using microfossils found at the same level in the core. The abundances of this IRD are sensitive indicators of currents, winds, and temperatures throughout the North Atlantic and reveal high, and highly significant, correlations with both the ^{10}Be and ^{14}C cosmogenic isotopes. A second example has been obtained from the deviation of the oxygen isotope ratio from a reference standard variation, δ^{18}O, as measured in stalagmites in Oman and China in two separate studies [111, 124]. These studies reveal an exceptional correspondence with the cosmogenic isotopes on all time scales between decades and several thousand years. The δ^{18}O is, in each case, a proxy for local rainfall [130] and reveals enhanced precipitation caused by small north–south migrations of the intertropical convergence zone. Large effects are seen because the latitudinal gradients around the sites are large. The fact that the effect is seen at widely spaced locations is evidence for coherent shifts in the latitude of the monsoon belt.

These correlations of paleoclimate indicators are found for both the ^{14}C and ^{10}Be cosmogenic isotopes. The ^{10}Be is a spallation product of galactic cosmic rays hitting atmospheric O, N, and Ar atoms; the ^{14}C is produced by thermal neutrons, generated by cosmic rays, interacting with N. About two thirds of the ^{10}Be is formed in the stratosphere and about one third in the troposphere from where precipitation times into the reservoirs are typically 1 year and 1 week, respectively, and the deposition into any one reservoir is influenced by climate conditions [131–134]. On the other hand, the ^{14}C generated by GCRs takes part in the carbon cycle and is exchanged with the two major reservoirs, the oceans and the biomass. Hence, the transport and deposition into the reservoirs where they are detected (e.g., ancient tree trunks for ^{14}C and ice sheets in the case of ^{10}Be) are vastly different for these two major cosmogenic isotopes. As a result, the possibility that the isotope abundances in their respective reservoirs are similarly influenced by climate during their terrestrial life history can be discounted because the transport and

deposition of each is so different. Thus, it is concluded that the correlations are found for both isotopes because of the one common denominator in their production, namely the incident cosmic ray flux.

One method used to try to understand global climate change from local and regional paleoclimate indicators is "forward prediction of proxies" in which global circulation models (GCMs) are used to simulate the time series of one or more proxies at a number of locations. These modeled time series are then compared to the observed proxy data. In many of these studies, the climate proxies used relate to tropical hydrology and the connections have not yet been fully explained. Shindell et al. [135] used a coupled ocean–atmosphere-composition model, forced by sustained multi-decadal irradiance increases, to show that greater tropical temperatures alter the hydrologic cycle, enhancing the climatological precipitation maxima in the tropics while drying the subtropical regions. The model captures the pattern inferred from paleoclimate records. This may explain drought conditions experienced by the Mayans, Moche, and Ancestral Puebloans civilizations during the late "medieval maximum" (900–1250), and other cultures, which experienced a weakened monsoon during the "Little Ice Age" (c. 1400–1750).

The flux of the GCRs that generate the cosmogenic isotopes is modulated by three influences [129]: (1) the interstellar flux of GCRs incident on the Sun's heliosphere, (2) the GCR shielding by the heliosphere, and (3) the GCR shielding by the Earth's geomagnetic field. The spatial scale of interstellar GCR flux variation in the galaxy is sufficiently large that, compared to distances moved by the solar system through the galaxy, the incident GCR variations on timescales of million years (Myr) and smaller can be neglected. The geomagnetic field shield has varied on timescales of 10 kyr. This variation has, in the main, been gradual during the Holocene [136, 137], although there have been shorter-lived weakenings of the field (which may be geomagnetic reversal onsets that did not develop) such as the Laschamp event around 40 kyr ago [138]. These events complicate the cosmogenic isotope record [139, 140] but are not consistent with the variations seen on timescales of order 1 kyr and less seen, for example by Bond et al. [110], Neff et al. [111], and Wang et al. [124]. This being the case, most of the variations on these timescales arise from heliospheric shielding, i.e., the Sun. To study solar variability effects during the Holocene, several studies have corrected the cosmogenic isotope record to allow for the secular geomagnetic variations [e.g., 90, 93].

With paleoclimate studies, it is important to bear in mind all ten of the potential pitfalls listed in the introduction. An additional problem with the data sequences, which is not a factor for direct observations, is dating [141]. Because record dates are uncertain, "wiggle matching" is often used [142, 143]. Even if this is done with great care, such that the date of any one data point is not moved by more than the accurately computed dating uncertainty, there is inevitably a selection effect at work. This is because the adjustments are made to improve correlations and not to degrade them. For this reason, there is a marked tendency for reported correlations to degrade as the accuracy of the dating is improved.

Observations of Solar Effects in Earth's Atmosphere

This review does not cover the great volume of literature describing and detailing the correlations and connections between solar activity and the ozone concentration, UV heating, and consequent temperatures and dynamics in the stratosphere. Instead, the reader is referred to the recent comprehensive review by Gray et al. (2010) [23]. A later section will discuss mechanisms whereby these stratospheric changes could influence the much larger air mass of the underlying troposphere. This section evaluates the connections between solar variability and the troposphere (on local, regional, and global scales) that have been reported.

A hugely-cited cited paper (cited 405 times in citation analysis using Web of Science, May 2010) by Friis-Christensen and Lassen (1991) [144], reporting a correlation between GMAST and solar cycle length L, highlights several of the problems discussed in the introduction. Firstly, one has to worry about selection effects and the mechanism. Why would L be relevant to climate-effective solar outputs (or was it used only because a correlation was found for L only)? But a more serious problem relates to the data handling and its effects on the significance of the correlation.

Some of the L values in this paper were smoothed using a very long time constant filter. Such smoothing introduces great persistence into the data to the extent that the correlation has no significance [145]. Such correlations can arise, and may even continue for a while, by chance. Lack of significance does not prove the correlation is not present. If it is real it will continue to hold while more data are taken until statistical significance tells us that it has some validity. However, if it is not real it will eventually fail, as was found in this case [146, 147].

As well as persistence of the data series, using a large number of fit variables also reduces the significance of a correlation. This is one issue for multiple regression fits of terrestrial parameters using a combination of one or more solar and other parameters. Scafetta and West (2007) and Scafetta (2009) [66, 148 and a series of previous papers cited therein] (hereafter referred to as SW) propose in their so-called phenomenological methods that multiple time constants are required from which they derived multivariate fits that give up to 65% of the GMAST attributable to TSI change (see Fig. 2). However, SW do not evaluate the significance of the resulting correlations given that they employ a larger number of solar fit variables (the amplitude and time constant of each of the responses). Full understanding needs to also consider the effect of other known external inputs into the climate system (volcanoes, man-made aerosols, greenhouse gasses, land use, etc.) and ensure that fits are not influenced by internal variability and oscillations such as the El Niño Southern Oscillation (ENSO) and the North Atlantic Oscillation (NAO). Many other multivariate fits in this area also fail to test the significance of the best-fit correlation against a well-posed null hypothesis and a properly defined noise model; however, the papers of SW have attracted particular attention because they derive much larger solar contributions to the temperature change. The largest estimates of the solar contribution by SW required use of the ACRIM TSI composite, rather than the PMOD composite, and tests show that both other data and proxies are more consistent with the PMOD composite [35, 41, 62] . This is just one of a number of arbitrary choices made by SW: Benestad and Schmidt (2009) [8] have found that the methodology used in the SW papers is not robust, and sensitivity tests performed on some of SW's choices showed that errors are significantly larger than SW report. They applied the SW procedure to GMAST modeled from known inputs and found that it returned very much larger solar variations than were initially input into the model. As for all multivariate fits, the addition of internal variability and additional forcings greatly confounded the accuracy of the SW procedure. Benestad and Schmidt find that the most likely contribution from solar forcing to GMAST is $7 \pm 1\%$ for the twentieth century and is negligible for warming since 1980 (see Fig. 2). This degree of solar influence is consistent with many modeling and detection–attribution studies (see below) and broadly in line with the computed ratio of solar to anthropogenic radiative forcings: the IPCC report of 2007 assessed that the change in solar radiative forcing over the interval 1750–2005 was in the range 0.06–0.30 W m^{-2} (at the 90% confidence level) with a most likely value of 0.12 W m^{-2} (consistent with the later TSI reconstructions in Fig. 2), whereas the net anthropogenic forcing is in the range 0.6–2.4 W m^{-2} [149, 150]. The TSI change of 1.3 W m^{-2} derived by Krivova et al. [48] for this interval gives a slightly larger radiative forcing of 0.21 W m^{-2}. These forcings should be compared with a total required value to explain the observed GMAST rise, including all feedbacks, of 5.1 Wm^{-2} [41]. The conclusion that global climate early in the twentieth century may show some solar influence, but that in recent decades it has been swamped by anthropogenic effects, is consistent with a great many studies, ranging from correlation studies [7, 8, 151, 152] to detection–attribution studies using GCMs [e.g., 149, 153–157].

The majority of reports of solar signals in global and regional climate are of solar cycle variations and so are subject to the major caveat that these can be easily confused with internal decadal-scale oscillations of the climate system [12, 13, 191]. A statistically significant solar cycle signal throughout the troposphere was reported by Coughlin [293]. Camp and Tung [158] showed significant (and large) differences between mean GMAST for composite surface temperature maps at low and high sunspot activity levels. Such a signal can also be seen in both the ECMWF ERA40 and NCEP/NCAR re-analysis datasets, in which observations have been assimilated with model data [159]. This signal is weaker in the ERA40 set and varies

regionally [160, 161]. Both temperature and mean zonal winds at all heights in the troposphere and stratosphere show significant decadal signal estimated from a multiple regression analysis [162, 163].

A great many studies have reported solar cycle signals in oscillatory modes and features in Earth's troposphere, including: the Northern Annular Mode, NAM [164–166] and the related north Atlantic Oscillation, NAO [167, 168]; the Indian Ocean monsoon [169]; the Southern Annular Mode, SAM [170]; tropical circulation [171–173]; Pacific variability patterns [174–179], in particular, the El Niño Southern Oscillation, ENSO [180, 181]. In addition, observations of temperature variations in the ocean mixing layer are thought to be evidence for resonant responses and "bottom-up" mechanisms [182–185], suggesting a strengthening of the Hadley circulation induced by an increased equator-to-pole temperature gradient.

Regional Climate Effects

Using both a climate model and empirical reconstructions, Shindell et al. [185–187] found that even though solar-induced GMAST changes are small (about 0.3–0.4°C), regional temperature changes associated with solar variability can be quite large. In the model, these occur primarily through a forced shift toward the low index state of the Arctic Oscillation/North Atlantic Oscillation as solar irradiance decreases. This leads to colder temperatures over the Northern Hemisphere continents, especially in winter (1–2°C), in agreement with historical records and proxy data for surface temperatures. Using a stratosphere-resolving GCM, these authors also found that long-term regional changes during the preindustrial period appear to have been dominated by solar forcing [187]. Studies by Mann et al. [188] and Trout et al. [189] have recently supported this idea for the little ice age and medieval maximum, respectively, although other modeling of the medieval maximum suggests that the role of solar changes is not as great as might be expected compared to other factors such as land use [190].

For post-industrial measurements, North and Stevens [191] applied optimal signal detection theory to data from 36 regions around the globe and found the solar signal was small and not highly significant. On the other hand, multivariate fits by Lean and Rind [88] do find strong solar responses in certain regions. Of these regions, this review concentrates on Europe for which the instrumental record is strongest. In this area, as for global responses, the issues of robust procedures and appropriate statistical methods are key considerations. For example, statistically significant signatures of multi-decadal solar activity changes in atmospheric temperatures in Europe have recently been reported by Kossobokov et al. [192] and Le Mouël et al. [193–195], but Yiou et al. [3] and Legras et al. [4] argue that they do not survive proper null-hypothesis testing.

Figure 3 stresses how different the behavior of a regional/seasonal climate in Europe can be from the global or hemispheric mean. The fluctuations for different regions tend to cancel, giving global means that are less variable, more clearly revealing the trends. The plot uses winter means, T_{DJF}, of the Central England Temperatures (CET), which is the world's longest instrumental record and extends back to 1659, at the start of the Maunder minimum. The CET covers a spatial scale of ≈300 km, which makes it a "small regional" climate indicator. In winter, the North Atlantic Oscillation (NAO), and associated changes in thermal advection, contributes to a large fraction of the observed variability of CET [196, 197]. Comparison of parts (a) and (b) shows that T_{DJF} correlates with both open solar flux and the hemispheric mean surface temperature ΔT_{N}. However, the correlation is weak in both cases. Lockwood et al. [198] show that there is a subtle solar influence on winter CET in that it is statistically significant that more cold winters, relative to the hemispheric trend, occur when the open solar flux is low (i.e., when TSI and UV SSI are low and GCR fluxes are high; see Fig. 3c). A number of mechanisms are possible (discussed in the following sections). Early instrumental records from the Maunder minimum indicate an increased frequency of easterly winds influencing the UK temperatures. This has also been deduced from indirect proxies [197], including the spatial patterns of changes in recorded harvest dates [199]. This suggests a link with the incidence of long-lived winter "blocking events" in the eastern Atlantic at low solar activity. Blocking episodes comprise extensive and quasi-stationary anticyclones that can persist for several weeks, leading to extended cold periods in

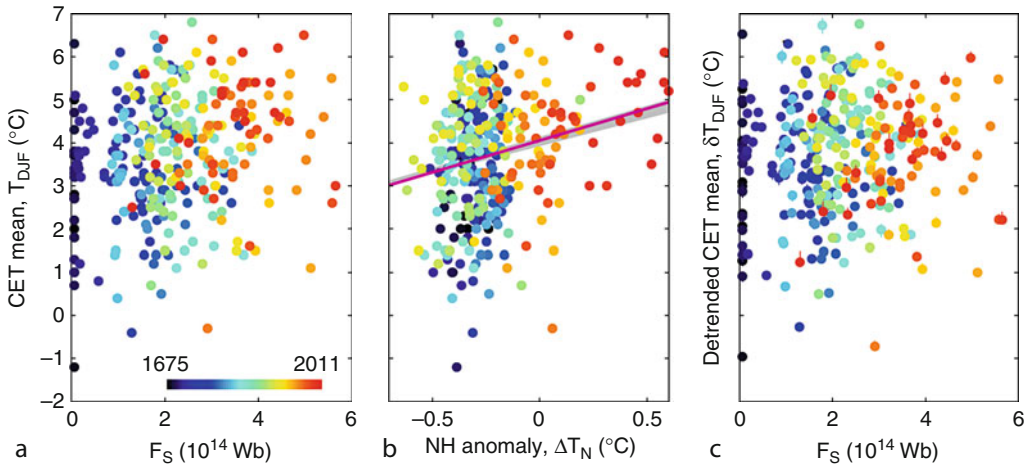

Solar-Induced Climate Effects. Figure 3

Scatter plots of mean winter Central England Temperature (CET), T_{DJF}, as a function of (**a**) open solar flux, F_S, and (**b**) the hemispheric mean surface temperature anomaly ΔT_N (extended to before 1850 using the median of a basket of proxy reconstructions). Points are colored according to the date using the scale shown in (**a**). The line in (**b**) is the ordinary least squares linear regression fit and the *grey* area bounds the uncertainty range set by the use of proxy reconstructions for ΔT_N prior to 1850. The correlation coefficients for (**a**) and (**b**) are low at 0.23 and 0.25 (significant at the 99.1% and 99.6% levels). In the case of (**b**) this demonstrates the great variability of a regional/seasonal temperature around a global-scale mean. (**c**) is the same as (**a**), for the detrended winter CET data δT_{DJF}, where the detrending allows for the hemispheric change ΔT_N and uses the regression line shown in (**b**). Part (**c**) shows that, even after allowing for the hemispheric trend, most of the coldest winters in central England occur at low solar activity, as quantified by F_S. Lockwood et al. [198] test this against the null hypothesis that F_S has no effect on winter CET values and show that this tendency is statistically significant at around the 95% level

winter as the mild maritime westerly winds are replaced by continental north-easterlies and the land surface cools under cloudless skies. Long-lived Atlantic blocking events at more eastward locations have been found to be more prevalent at sunspot minimum than at higher solar activity, and this leads to colder winters in Europe [200]. This evidence suggests that changes in the occurrence of blocking could be acting to amplify the solar-induced perturbations to the tropospheric jet stream. Other evidence supports this idea. For example, the effects of the changed position and frequency of blocking events may be seen as a manifestation of modes of low-frequency circulation variability that have been found to respond to solar activity, giving increased/decreased frequencies of easterly/westerly circulation patterns over Europe under low solar activity conditions [201, 202]. Winter CET values are known to be strongly modulated by the NAO [196] and modeling has shown that stratospheric trends over recent decades, along with downward links to surface, are indeed strong enough to explain much of the prominent trend in the NAO and hence regional winter climate in Europe between the 1960s and the 1990s [203]. The GCM runs experiments by Rind et al. [204] produce a relative negative phase of the North Atlantic Oscillation/Arctic Oscillation (NAO/AO) during the Maunder Minimum which contributes to the lower European winter temperatures.

Modeling Studies and Detection–Attribution

GCMs have developed rapidly over the last 2 decades, and this has changed the details of the predictions of solar effects. Predicted solar-induced changes in

GMAST have generally been small, even for the larger drifts in solar radiative forcing predicted by the early TSI reconstructions (see Fig. 1). Full comparisons are complex because the TSI reconstructions have evolved at the same time as have the complexity and resolution of the models. As expected, weaker solar effects are found for the smaller TSI drift predicted by the more recent reconstructions: for example, compare the results and inputs of Wigley and Raper [24], Zorita et al. [205], and Stendel et al. [206]. Examples of recent GCM experiments giving a relatively large bottom-up solar effect have been presented by Rind et al. [207]. The input solar forcing change between the Maunder minimum and the present day used was 0.68 W m^{-2} (with an input of 1.9 W m^{-2} from anthropogenic forcing change). This solar forcing is relatively large, compared with the range 0.06–0.30 W m^{-2} quoted by Hergel et al. [149] and Solomon et al. [150], and the experiments generally gave a large solar contribution (near 30%) to the total GMAST rise (the total rise being larger than observed). The tropical response, in particular, was much greater than observed, consistent with the excessive TSI change input to the experiments.

Rind et al. [207] used a model with a coupled stratosphere at four different resolutions to investigate various aspects of top-down solar cycle influence on the troposphere/stratosphere system. The results show that the stratospheric response is highly repeatable and significant. Stratospheric westerly wind increases were found to extend down into the troposphere and in some experiments the jet stream weakened and moved poleward. The predominant tropospheric response consisted of a warming of the troposphere, with coherent changes in regional precipitation. The tropospheric response was often not great, but was similar in all the different simulations. All runs revealed both top-down and bottom-up solar effects but they account for only a small percentage of the total GMAST variance. A model described by Meehl et al. [174–176] includes ocean–atmosphere coupling and a stratosphere, and so can include both top-down and bottom-up solar forcing. This model suggests potential resonant connections between solar forcing and the ENSO oscillation.

Model predictions are a key part of "detection–attribution" studies, in which the effect of varying an input to the GCM must be detected above the internal variability of the climate system modeled by the GCM. Results do depend on which GCM is used, although there is also a considerable degree of agreement between the different models. In many studies, the input forcings are multiplied by variable amplification "β" factors to get the best fit to the variation of the global spatial pattern of surface temperature. For example, studies by Stott et al. [153] found that for solar forcing $\beta = 3$ was required, but this unexplained amplification of the solar radiative forcing may have been overestimated because of the characteristics of the GCM used (see review by Ingram [157]) and/or because of instrumental problems with the data sequence [209]. A comprehensive review of detection–attribution methods and results has been given by Hegerl et al. [210].

Stratosphere –Troposphere Coupling and Top-Down Solar Forcing of Climate

Dynamical coupling across the tropopause [211] means that stratospheric forcing can influence the underlying troposphere [e.g., 212–214], and under some circumstances, robust tropospheric responses are indeed predicted by the models. Observational studies show that stratospheric perturbations (e.g., stratospheric warmings) typically last for at least a month and on average affect the troposphere within approximately 2 weeks [208, 215]. Tropospheric jet streams have been shown to be sensitive to the solar forcing of stratospheric temperatures [18, 19, 216, 217]. This could occur through disturbances to the stratospheric polar vortex [218], which can propagate downward to affect the tropospheric jets [219–221], or through the effects of tropical stratospheric temperature changes on the refraction of tropospheric eddies [222, 223]. Models [e.g., 187] predict that perturbations can descend from the stratosphere to the surface by altering the propagation of planetary waves coming up from the surface – an effect that has been observed in data [224]. However, models that do not yield realistic stratospheric dynamics fail to capture these wave flux changes. The tropospheric response is reduced when planetary waves are suppressed in the stratosphere by additional damping or when the strength of

the stratospheric jet is increased. The models show that the stratosphere could play a crucial role in recent trends. For example, Scaife et al. [203] have demonstrated that stratospheric trends over recent decades, along with downward links to surface, are indeed strong enough to explain much of the prominent trend in the NAO and hence regional winter climate in Europe between the 1960s and the 1990s. Such effects are not just found in the northern hemisphere [225].

A wide variety of tropospheric responses have been suggested [e.g., 226–229]. A predicted effect on tropospheric jet stream latitude is that increased heating of the equatorial stratosphere causes a slight poleward motion, an effect that has been reproduced in simple GCM simulations [230], deduced from other data [231], and has been suggested as a cause of equatorial precipitation changes in the little ice age [232].

The solar influence on winter European temperatures, discussed in the section above, suggests that the occurrence of the blocking phenomenon could be acting to amplify the solar-induced perturbations to the tropospheric jet stream [233]. Solar cycle control of the location, strength, and occurrence of blocking events has been detected by Barriopedro et al. [200] and Woollings et al. [295].

Cosmic Ray Modulation of Clouds

A long-standing suggestion is that cosmic rays can aid the formation of clouds (see reviews by Carslaw et al. [234] and Kirkby, [235]). This would be a highly significant effect because clouds modulate Earth's energy balance by (1) changing Earth's albedo, A, and (2) by enhancing the IR greenhouse trapping effect. The balance between these two competing effects is dependent on the cloud altitude: for low clouds the albedo effect dominates whereas the lower temperature of higher altitude clouds means that the greenhouse trapping dominates. Variations in Earth's albedo are particularly poorly known [236, 237]. A great many papers have been written about low-altitude global cloud cover arguing that it shows a statistically significant solar cycle variation, consistent with GCR modulation of the growth of cloud condensation nuclei [238–242]. Other studies find no significant effect [243–248]. A third set of studies finds significant correlations but only in restricted regions [249, 250], whereas a fourth set reports a solar cycle variation but finds it to be more consistent with solar UV irradiance variability [249, 251, 252]. Voiculescu et al. [253] argue that both UV and GCRs have an effect. Harrison [254] detected a 1.68-year oscillation in the long diffuse fraction data series from the Lerwick (maritime) station – an oscillation found in the open solar flux and GCR fluxes but not in the SSI or TSI variations [86], hence supporting a direct effect of GCRs. It is expected that the effect would be more significant in clean maritime air where there is a shortage of CCNs for water vapor to condense on, and thus air ions generated by GCRs may be a more significant factor in maritime regions [255, 256].

The arguments against such direct cosmic ray-cloud connection have been: (1) given the atmospheric supersaturations, there is no established mechanism that can cause the effect; (2) the intercalibrations involved in the composite cloud cover dataset used render it unsuitable for this type of long-term variability analysis [e.g., 257]; (3) the data sequences are too short and so the significance of the correlations is low or marginal (For example, Sun and Bradley [246] show that the uniquely high cosmic ray-cloud cover correlation in the period 1983–1999 over the Atlantic Ocean, is greatly weakened when an extended data set is used); (4) Periods of low geomagnetic field, particularly the Laschamp event, gave enhanced GCR fluxes in the Earth's atmosphere but did not influence climate in the Greenland area [20]. Of these objections, only argument (4) suggests that such a mechanism is not effective, whereas arguments (1–3) all indicate that the evidence in its favor is inadequate (but cannot be used to argue that it is not active). In relation to (4), there is some evidence that the failure to see an effect of the Laschamp event [258] may have been a local characteristic of the climate in the Greenland area [116]. Other studies give indications of an influence of the geomagnetic field on preindustrial climate. Recent reports of associations between the main geomagnetic field and climatic changes [259–263] would be very significant, if confirmed. These changes have also been linked to latitudinal motions of the intertropical convergence zone [259, 264] and effects on civilizations

that had a critical dependence on rainfall [260, 264–267]. Nevertheless, objection (4) remains a key debate.

Harrison and Stephenson [268] found evidence for a GCR effect on diffuse fraction measurements at a variety of UK meteorological stations. As these are homogeneous sequences of simple measurements, this does counter objection (2) to some extent; however, the effect was small and no allowance is made for the effect of the variable aerosol optical depth. The best chance of answering objection (1) is the CLOUD experiment at CERN [269], which has just begun to studying the "ion-aerosol clear-air" mechanism. However, Pierce and Adams [270] have estimated that this mechanism is two orders of magnitude too small to explain the reported effects. Other mechanisms involving the atmospheric electric field [271] have been proposed [272–275].

In addition to the solar cycle variation in GCRs, there are sudden decreases in GCR fluxes (Forbush decreases) and these have been reported as giving responses in ground-based cloud data [276] and in satellite cloud cover data [277] using "compositing" analysis (also called "superposed epoch" and "Chree" analysis). The problem with these studies (particularly if the satellite dataset are employed) is that there are very few large Forbush decreases and the results appear to be dominated by one or two very large events and other studies have failed to find this response [296]. The delay of the putative effect is also a puzzle. Nevertheless, it has been independently reported that 3% of cloud variability on short timescales may be associated with GCRs [278]. The potential importance of this effect is that there are long-term changes in the open solar flux [11] that yield the long-term changes in GCRs [91–93], which could in turn introduce long-term changes in climate if the mechanism is sufficiently effective [94].

Solar Energetic Particles and Ozone

SEPs are directed toward Earth poles by the geomagnetic field where they generate nitrates on hitting Earth's atmosphere as demonstrated, for example, in observations by Mlynczak et al. [279]. These nitrates are seen to migrate downward over time [280, 281], resulting in catalytic destruction of stratospheric ozone [282]. Large SEP events generate considerable transient polar ozone depletions, which persist in winter until UV irradiance of the polar stratosphere resumes [283–286]. Recently, Seppälä et al. [287] reported changes in polar winter surface temperatures, which they associate with large SEP events, based on the modeling predictions of such effects by Rozanov et al. [288].

Are the GMAST Data Correct?

There are difficulties in combining the available data into a single homogeneous GMAST anomaly time series. Different approaches are taken and different data used. An example is the way that regions of missing data are handled varies – GISS [64] interpolates into areas of missing data, whereas HadCRUT3v [65] does not. Nevertheless, as shown in Fig. 2, the GISS and HadCRUT3v reconstructions agree rather well and both show a recent plateau in GMAST anomaly, such that the HadCRUT3v value is still below the 1998 level although this is not true of GISS.

There are, however, potential issues that could influence both reconstructions. For example, Thompson et al. [209] report that sea surface temperature measurement biases may have contributed a downward step in the GMAST of about 0.3°C in the middle of the twentieth century. Correcting this would probably improve the agreement in Fig. 2 with the GCM model fit shown, but initial indications are that this correction would also lead to a lower solar contribution being derived by detection–attribution studies. In other words, if Thompson et al. are correct, the amplification of the solar forcing (with a beta factor >1) in some detection–attribution studies would be an example of data "snooping" because it relied on an artifact in the data.

Lockwood [7] carried out a simple multivariate fit analysis that fits the plateau in the HadCRUT3v GMAST well. In this fit, the plateau arises mainly because of the lack of El-Niño events since the major 1998 event, with a small contribution from the solar decline. This fit demonstrates that this feature could be readily explained as the combined effect of known influences. (Note that this statement can be no more definitive than this because of the limitations inherent in the multivariate fits, as discussed earlier.) The plateau is also nothing unusual, compared to past variations around the upward trend [41, 289, 290]. The same is true for the corresponding plateau

(or even slight fall) in global mean ocean surface layer temperature [297].

Future Directions

From solar-induced variations of cosmogenic isotopes over the past 10^4 years, Lockwood [67] has deduced there is an 8% chance that the Sun will return to Maunder minimum conditions within 50 years. Feulner and Rahmstorf [291] used a coupled model to predict that this will offset anthropogenically rising global mean temperatures by no more than 0.3°C in the year 2100, relative to what would happen if the solar output remained constant. Similarly Lean and Rind [292] found that the solar decline would delay reaching a given temperature level by no more than a decade. Thus these predictions show that continued solar decline will do little to alleviate global warming. However, the decline will do much to end the debate about the fraction of global warming that can be attributed to solar change. For the first time since anthropogenic climate change became rapid, solar and anthropogenic trends are now in opposite directions. Non-robust fits (of low statistical significance, suffering from data snooping and selection effects, and which have not isolated internal variability) will fail sooner rather than later because of the change in solar behavior. Thus the next few years will provide much better estimates of the solar contribution. Concerning the global temperature rise, there is every indication that these new estimates will, if anything, be smaller than previous estimates. On the other hand, there are indications that some regional climates are much more susceptible to solar changes than others. Understanding and differentiating "top-down" and "bottom-up" solar forcings will be key because these will have very different effects on the spatial patterns of the responses. Key advances in this area will be made in modeling, with higher resolution in time and space, better understanding of numerical noise and of the relationship of natural climate variability to that in the model behavior, fewer parameterizations, better definition of the inputs forcings, and inclusion of more biological responses alongside the physical and chemical. However, these developments will take time and in many cases mitigation and adaptation decisions may have to be taken based on the most successful of the current model simulations.

Bibliography

1. Herschel W (1801) Observations tending to investigate the nature of the Sun, in order to find the causes or symptoms of its variable of light and heat; with remarks on the use that may possibly be drawn from solar observations. Philos Trans R Soc Lond 91:265–318
2. Pustilnik LA, Yom Din G (2004) Influence of solar activity on the state of the wheat market in medieval England. Sol Phys 223:335
3. Yiou P, Bard E, Dandin P, Legras B, Naveau P, Rust HW, Terray L, Vrac M (2010) Statistical issues about solar-climate relations. Clim Past Discuss 6:461–487 (http://www.clim-past-discuss.net/6/461/2010/)
4. Legras B, Mestre O, Bard E, Yiou P (2010) On misleading solar-climate relationship. Clim Past Discuss 6:767–800
5. Santer BD, Wigley TML, Doutriaux C, Boyle JS, Hansen JE, Jones PD, Meehl GA, Roeckner E, Sengupta S, Taylor KE (2001) Accounting for the effects of volcanoes and ENSO in comparisons of modelled and observed temperature trends. J Geophys Res 106:28033–28059
6. Lean J (2006) Comment on "Estimated solar contribution to the global surface warming using the ACRIM TSI satellite composite" by N. Scafetta and B. J. West. Geophys Res Lett 33:L15701. doi:10.1029/2005GL025342
7. Lockwood M (2008) Recent changes in solar outputs and the global mean surface temperature. III. Analysis of contributions to global mean air surface temperature rise. Proc R Soc A 464(2094):1387–1404
8. Benestad RE, Schmidt GA (2009) Solar trends and global warming. J Geophys Res 114:D14101. doi:10.1029/2008JD011639
9. Palmer MD, Good SA, Haines K, Rayner NA, Stott PA (2009) A new perspective on warming of the global oceans. Geophys Res Lett 36:L20709. doi:10.1029/2009GL039491
10. Lockwood M, Fröhlich C (2007) Recent oppositely-directed trends in solar climate forcings and the global mean surface air temperature. Proc R Soc Lond A 463(2086):2447–2460. doi:10.1098/rspa2007.1880
11. Lockwood M, Rouillard AP, Finch ID (2009) The rise and fall of open solar flux during the current grand solar maximum. Astrophys J 700:937–944. doi:10.1088/0004-637X/700/2/937
12. Drijfhout SS, Haarsma RJ, Opsteegh JD, Selten FM (1999) Solar-induced versus internal variability in a coupled climate model. Geophys Res Lett 26:205–208
13. Moore J, Grinsted A, Jevrejeva S (2006) Is there evidence for sunspot forcing of climate at multi-year and decadal periods? Geophys Res Lett 33:L17705. doi:10.1029/2006GL026501
14. Eddy JA (1976) The maunder minimum. Science 192(4245):1189–1202
15. Damon PE, Laut P (2004) Pattern of strange errors plagues solar activity and terrestrial climate data. EOS Trans Am Geophys Union 85(39):370. doi:10.1029/2004EO390005, 2004

16. Reid G (2000) Solar variability and the Earth's climate: introduction and overview. Space Sci Rev 94:1–11
17. Rind D (2002) The Sun's role in climate variations. Science 296:673–678
18. Haigh JD (2003) The effects of solar variability on the Earth's climate. Philos Trans R Soc Lond A 361(95):111. doi:10.1098/rsta.2002.1111
19. Haigh JD (2007) The Sun and the Earth's climate. Living Rev Solar Phys 4:2, URL (cited on 26 September 2009): http://www.livingreviews.org/lrsp-2007-2
20. Beer J (2006) Solar variability and climate change. Sol Variability Earth's Climate 76:751–754
21. Foukal P, Fröhlich C, Spruit H, Wigley TML (2006) Variations in solar luminosity and their effect on the Earth's climate. Nature 443:161–166. doi:10.1038/nature05072
22. de Jager C (2008) Solar activity and its influence on climate. Neth J Geosci Geol En Mijnbouw 87(3):207–213
23. Gray LJ, Beer J, Geller M, Haigh J, Lockwood M, Matthes K, Cubasch U, Fleitmann D, Harrison G, Hood L, Luterbacher J, Marsh N, Shindell D, van Geel B, White W (2010) Solar influences on climate. Rev Geophys 48:RG4001. doi:10.1029/2009RG000282
24. Wigley TML, Raper SCB (1990) Climatic change due to solar irradiance changes. Geophys Res Lett 17:2169–2172
25. Douglass DH, Clader BD (2002) Climate sensitivity of the Earth to solar irradiance. Geophys Res Lett 29:1786. doi:10.1029/2002GL015345
26. Schwartz SE (2007) Heat capacity, time constant, and sensitivity of Earth's climate system. J Geophys Res 112:D24S05. doi:10.1029/2007JD008746
27. Stouffer RJ (2004) Time scales of climate response. J Climate 17(1):209–217
28. Knutti R, Krähenmann S, Frame DJ, Allen MR (2008) Comment on "Heat capacity, time constant, and sensitivity of Earth's climate system" by S. E. Schwartz. J Geophys Res 113: D15103. doi:10.1029/2007JD009473
29. Hansen J, Russell G, Lacis AA, Fung I, Rind D, Stone P (1985) Climate response times: dependence on climate sensitivity and ocean mixing. Science 229:857–859
30. Dickinson RE, Schaudt KJ (1998) Analysis of timescales of response of a simple climate model. J Climate 11:97–106
31. Rind D, Lean J, Healy R (1999) Simulated time-dependent climate response to solar radiative forcing since 1600. J Geophys Res 104:1973–1990
32. Waple AM, Mann ME, Bradley RS (2002) Long-term patterns of solar irradiance forcing in model experiments and proxy-based surface temperature reconstructions. Climate Dyn 18:563–578
33. Weber SL (2005) A timescale analysis of the Northern Hemisphere temperature response to volcanic and solar forcing. Clim Past Discuss 1:9–17
34. Lockwood M, Fröhlich C (2008) Recent oppositely-directed trends in solar climate forcings and the global mean surface air temperature: II. Different reconstructions of the Total Solar Irradiance variation and dependence on response timescale. Proc R Soc Lond 464(2094):1367–1385
35. Solanki SK, Krivova NA, Wenzler T (2005) Irradiance models. Adv Space Res 35:376–383
36. Baliunas S, Jastrow R (1990) Evidence for long-term brightness changes of solar-type stars. Nature 348:520–523
37. Wenzler T, Solanki SK, Kirova NA, Fröhlich C (2006) Reconstruction of solar irradiance variations in cycles 21–23 based on surface magnetic fields. Astron Astrophys 460: 583–595
38. Hoyt D, Schatten K (1993) A discussion of plausible solar irradiance variations 1700–1992. J Geophys Res 98:18895–18906
39. Solanki SK, Fligge M (1999) A reconstruction of total solar irradiance since 1700. Geophys Res Lett 26:2465–2468
40. Lean J, Beer J, Bradley R (1995) Reconstruction of solar irradiance since 1610: implications for climate change. Geophys Res Lett 22:3195–3319. doi:10.1029/95GL03093
41. Lockwood M (2010) Solar change and climate: an update in the light of the current exceptional solar minimum. Proc R Soc A 466(2114):303–329. doi:10.1098/rspa.2009.0519
42. Lockwood M (2002) An evaluation of the correlation between open solar flux and total solar irradiance. Astron Astrophys 382:678–687
43. Fröhlich C (2009) Evidence of a long-term trend in total solar irradiance. Astron Astrophys 501(3):L27–L30. doi:10.1051/0004-6361/200912318
44. Willson RC (1997) Total solar irradiance trend during solar cycles 21 and 22. Science 277:1963–1965
45. Rouillard AP, Lockwood M, Finch ID (2007) Centennial changes in the solar wind speed and in the open solar flux. J Geophys Res 112:A05103. doi:10.1029/2006JA012130
46. Foster SS (2004) Reconstruction of solar irradiance variations, for use in studies of global climate change: application of recent SoHO observations with historic data from the Greenwich observations. PhD thesis, School of Physics and Astronomy, University of Southampton, Southampton
47. Lockwood M (2004) Solar outputs, their variations and their effects of Earth. In: Rüedi I, Güdel M, Schmutz W (eds) The Sun, solar analogs and the climate, Proceedings of Saas-Fee advanced course 34. Springer, Berlin, pp 107–304 (ISBN 3-540-23856-5)
48. Krivova NA, Balmaceda L, Solanki SK (2007) Reconstruction of solar total irradiance since 1700 from the surface magnetic flux. Astron Astrophys 467:335–346. doi:10.1051/0004-6361:20066725
49. Zhang Q, Soon WH, Baliunas SL, Lockwood GW, Skiff BA, Raddick RR (1994) A method of determining possible brightness variations of the Sun in past centuries from observations of solar-type stars. Astrophys J 427:L111–L114
50. Hall JC, Lockwood GW (2004) The chromospheric activity and variability of cycling and flat activity solar-analog stars. Astrophys J 614(1):942–946

51. Giampapa M (2004) Stellar analogs of solar activity: the Sun in a stellar context. In: Redi I, Güdel M, Schmutz W (eds) The Sun, solar analogs and the climate. Springer, Berlin/Heidelberg/New York, pp 305–423
52. Lockwood M, Stamper R, Wild MN (1999) A doubling of the sun's coronal magnetic field during the last 100 years. Nature 399:437–439
53. Lockwood M, Stamper R (1999) Long-term drift of the coronal source magnetic flux and the total solar irradiance. Geophys Res Lett 26:2461–2464. doi:10.1029/1999GL900485
54. Solanki SK, Schüssler M, Fligge M (2000) Secular evolution of the Sun's magnetic field since the Maunder minimum. Nature 480:445–446. doi:10.1038/35044027
55. Solanki SK, Schüssler M, Fligge M (2001) Secular evolution of the Sun's magnetic flux. Astron Astrophys 383:706–712. doi:10.1051/0004-6361:20011790
56. Vieira LEA, Solanki SK (2010) Evolution of the solar magnetic flux on time scales of years to millennia. Astron Astrophys 509(1):A100. doi:10.1051/0004-6361/200913276
57. Lean J, Wang Y-M, Sheeley NR Jr (2002) The effect of increasing solar activity on the Suns total and open magnetic flux during multiple cycles: implications for solar forcing of climate. Geophys Res Lett 29(24):2224
58. Wang Y-M, Lean JL, Sheeley NR Jr (2005) Modeling the Sun's magnetic field and irradiance since 1713. Astrophys J 625:522–538. doi:10.1086/429689
59. Willson RC, Mordvinov AV (2003) Secular total solar irradiance trend during solar cycles 21–23. Geophys Res Lett 30:1199–1202. doi:10.1029/2002GL016038
60. Scafetta N, Willson RC (2009) ACRIM-gap and TSI trend issue resolved using a surface magnetic flux TSI proxy model. Geophys Res Lett 36:L05701. doi:10.1029/2008GL036307
61. Krivova NA, Solanki SK, Wenzler T (2009) ACRIM-gap and total solar irradiance revisited: is there a secular trend between 1986 and 1996? Geophys Res Lett 36:L20101. doi:10.1029/2009GL040707
62. Wenzler T, Solanki SK, Krivova NA (2009) Reconstructed and measured total solar irradiance: is there a secular trend between 1978 and 2003? Geophys Res Lett 36:L11102. doi:10.1029/2009GL037519
63. Lean JL, Rottman GJ, Kyle HL, Woods TN, Hickey JR, Puga LC (1997) Detection and parameterization of variations in solar midand near-ultraviolet radiation (200–400 nm). J Geophys Res 102(29):939
64. Hansen J, Ruedy R, Glascoe J, Sato Mki (1999) GISS analysis of surface temperature change. J Geophys Res 104:30997–31022. doi:10.1029/1999JD900835
65. Brohan P, Kennedy JJ, Haris I, Tett SFB, Jones PD (2006) Uncertainty estimates in regional and global observed temperature changes: a new dataset from 1850. J Geophys Res 111:D12106. doi:10.1029/2005JD006548
66. Scafetta N (2009) Empirical analysis of the solar contribution to global mean air surface temperature change. J Atmos Solar Terr Phys 71:1916–1923. doi:10.1016/j.jastp.2009.07.007
67. Harder JW, Fontenla JM, Pilewskie P, Richard EC, Woods TN (2009) Trends in solar spectral irradiance variability in the visible and infrared. Geophys Res Lett 36:L07801. doi:10.1029/2008GL036797
68. Krivova NA, Solanki SK, Wenzler T, Podlipnik B (2009) Reconstruction of solar UV irradiance since 1974. J Geophys Res 114: D00I04. doi:10.1029/2009JD012375
69. Lean J (2000) Evolution of the Sun's spectral irradiance since the Maunder Minimum. Geophys Res Lett 27:2425–2428
70. Lean JL (2010) How bright is the sun? How does it vary? Why do we care? Bull Am Meteor Soc (in press)
71. Foukal P, Bertello L, Livingston WC, Pevtsov AA, Singh J, Tlatov AG, Ulrich RK (2009) A century of Solar Ca II measurements and their implication for solar UV driving of climate. Sol Phys 255(2):229–238
72. Lockwood M, Bell C, Woollings T, Harrison RG, Gray LJ, Haigh JD (2010) Top-down solar modulation of climate: evidence for centennial-scale change. Environ Res Lett 5:034008. doi:10.1088/1748-9326/5/3/034008
73. Ermolli I, Solanki SK, Tlatov AG, Krivova NA, Ulrich RK, Singh J (2009) Comparison among Ca ii K spectroheliogram time series with an application to solar activity studies. Astrophys J 698(2):1000–1009
74. Tlatov AG, Pevtsov AA, Singh JA (2009) New method of calibration of photographic plates from three historic data sets. Sol Phys 255(2):239–251
75. Cattaneo F, Hughes DW (2001) Solar dynamo theory: a new look at the origin of small-scale magnetic fields. Astron Geophys 42:3.18–3.22
76. Kuhn JR, Libbrecht KG, Dicke RH (1988) The surface temperature of the Sun and changes in the solar constant. Science 242:908–911
77. Chapman GA, Dobias JJ, Walton SR (2008) On the variability of the apparent solar radius. Astrophys J 681:1698–1702. doi:10.1086/588512
78. Sofia S, Basu S, Demarque P, Li L, Thuillier G (2005) The nonhomologous nature of solar diameter variations. Astrophys J 632:L147–L150
79. Egidi A, Caccin B, Sofia S, Heaps W, Hoegy W, Twigg L (2006) High-precision measurements of the solar diameter and oblateness by the Solar Disk Sextant (SDS) experiment. Sol Phys 235(1/2):407–418
80. Bruls JHMJ, Solanki SK (2004) Apparent solar radius variations: the influence of magnetic network and plage. Astron Astrophys 427:735–743. doi:10.1051/0004-6361:20041311
81. Lefebvre S, Bertello L, Ulrich RK, Boyden JE, Rozelot JP (2006) Solar radius measurements at Mount Wilson observatory. Astrophys J 649(1):444–451
82. Djafer D, Thuillier G, Sofia S (2008) A comparison among solar diameter measurements carried out from the ground and outside Earth's atmosphere. Astrophys J 676(1): 651–657

83. Lefebvre S, Kosovichev AG, Rozelot JP (2007) Helioseismic test of nonhomologous solar radius changes with the 11 year activity cycle. Astrophys J 658:L135–L138
84. Kuhn JR, Bush RI, Emilio M, Scherrer PH (2004) On the constancy of the solar diameter. II. Astrophys J 613(2): 1241–1252
85. Noël F (2004) Solar cycle dependence of the apparent radius of the Sun. Astron Astrophys 413:725–732
86. Rouillard AP, Lockwood M (2004) Oscillations in the open solar magnetic flux with period 1.68 years: imprint on galactic cosmic rays and implications for heliospheric shielding. Ann Geophys 22:4381–4396
87. Bard E, Raisbeck G, Yiou F, Jouzel J (2000) Solar irradiance during the last 1200 years based on cosmogenic nuclides. Tellus 52B:985–992
88. Lean JL, Rind DH (2008) How natural and anthropogenic influences alter global and regional surface temperatures: 1889 to 2006. Geophys Res Lett 35:L18701. doi:10.1029/2008GL034864
89. Lockwood M (2006) What do cosmogenic isotopes tell us about past solar forcing of climate? Space Sci Rev 125:95–109. doi:10.1007/s11214-006-9049-2
90. Steinhilber F, Beer J, Fröhlich C (2009) Total solar irradiance during the Holocene. Geophys Res Lett 36:L19704. doi:10.1029/2009GL040142
91. McCracken KG, Beer J (2007) Long-term changes in the cosmic ray intensity at Earth, 1428–2005. J Geophys Res 112:A10101. doi:10.1029/2006JA012117
92. Muscheler R, Joos F, Beer J, Muller SA, Vonmoos M, Snowball I (2007) Solar activity during the last 1000 yr inferred from radionucleide records. Quat Sci Rev 26:82–97
93. Steinhilber F, Abreu JA, Beer J (2008) Solar modulation during the Holocene. Astrophys Space Sci Trans 4:1–6
94. Usoskin IG, Schuessler M, Solanki SK, Mursula K (2005) Solar activity, cosmic rays, and Earth's temperature: a millennium-scale comparison. J Geophys Res 110:A10102. doi:10.1029/2004JA010946
95. Solanki SK, Usoskin IG, Kromer B, Schüssler M, Beer J (2004) Unusual activity of the Sun during recent decades compared to the previous 11000 years. Nature 431:1084–1087. doi:10.1038/nature02995
96. Abreu JA, Beer J, Steinhilber F, Tobias SM, Weiss NO (2008) For how long will the current grand maximum of solar activity persist? Geophys Res Lett 35(20):L20109
97. Boberg F, Lundstedt H (2002) Solar wind variations related to fluctuations of the North Atlantic Oscillation. Geophys Res Lett 29:1718
98. Lu H, Jarvis MJ, Hibbins RE (2008) Possible solar wind effect on the northern annular mode and northern hemispheric circulation during winter and spring. J Geophys Res 113:D23104. doi:10.1029/2008JD010848
99. Bochníček J, Hejda P (2005) The winter NAO pattern changes in association with solar and geomagnetic activity. J Atmos Sol Terr Phys 67:17–32
100. Thejll P, Christiansen B, Gleisner H (2003) On correlations between the North Atlantic Oscillation, geopotential heights and geomagnetic activity. Geophys Res Lett 30(6):1347. doi:10.1029/2002GL016598
101. Davis OK, Shafer DS (1992) An Early-Holocene maximum for the Arizona monsoon recorded at Montezuma Well, central Arizona. Palaeogeogr Palaeoclimatol Palaeoecol 92:107–119. doi:10.1016/0031-0182(92)90137-T
102. Jirikowic JL, Kalin RM, Davis OK (1993) Tree-ring ^{14}C as an indicator of climate change. In: Climatic change in continental isotopic records, vol 78, AGU geophysical monograph. American Geophysical Union, Washington, pp 353–366
103. Davis OK (1994) The correlation of summer precipitation in the southwestern USA with isotopic records of solar activity during the Medieval Warm Period. Clim Change 26:271–287. doi:10.1007/BF01092418
104. Crowley TJ, Kim K-Y (1996) Comparison of proxy records of climate change and solar forcing. Geophys Res Lett 23:359–362
105. van Geel B, Van der Plicht J, Kilian MR, Klaver ER, Kouwenberg JHM, Renssen H, Reynaud-Farrera I, Waterbolk HT (1998) The sharp rise of $\Delta^{14}C$ ca. 800 cal BC: possible causes, related climatic teleconnections and the impact on human environments. Radiocarbon 40:535–550
106. de Putter T, Loutre MF, Wansard G (1998) Decadal periodicities of Nile river historical discharge (A.D. 622–1470) and climatic implications. Geophys Res Lett 25:3193–3196
107. Beer J, van Geel B (1998) Holocene climate change and the evidence for solar and other forcings. In: Batterbee RW, Binney HA (eds) Natural climate variability and global warming: a holocene perspective. Wiley-Blackwell, Oxford, pp 138–162
108. Yu Z, Ito E (1999) Possible solar forcing of century-scale drought frequency in the northern Great Plains. Geology 27:263–266. doi:10.1130/0091-7613(1999) 027<0263: PSFOCSO2.3>CO;2
109. Verschuren D, Laird KR, Cumming BF (2000) Rainfall and drought in equatorial east Africa during the past 1100 years. Nature 403:410–414
110. Bond G, Kromer B, Beer J, Muscheler R, Evans MN, Showers W, Hoffman S, Lotti-Bond R, Hajdas I, Bonani G (2001) Persistent solar influence on North Atlantic climate during the Holocene. Science 294:2130–2136. doi:10.1126/science.1065680
111. Neff U, Burns SJ, Mangini A, Mudelsee M, Fleitmann D, Matter A (2001) Strong coherence between solar variability and the monsoon in Oman between 9 and 6 kyr ago. Nature 411:290–293. doi:10.1038/35077048
112. Speranza A, van Geel B, van der Plicht J (2002) Evidence for solar forcing of climate change at ca. 850 cal BC from a Czech peat sequence. Glob Planet Change 35:51–65
113. Mauquoy D, van Geel B, Blaauw M, van der Plicht J (2002) Evidence from northwest European bogs shows "Little Ice Age" climatic changes driven by variations in solar activity. Holocene 12:1–6

114. Hu FS, Kaufman D, Yoneji S, Nelson D, Shemesh A, Huang Y, Tian J, Bond G, Clegg B, Brown T (2003) Cyclic variation and solar forcing of Holocene climate in the Alaskan subarctic. Science 301:1890–1893. doi:10.1126/science.1088568
115. Sarnthein M, van Kreveld S, Erlenkeuser H, Grootes PM, Kucera M, Pflaumann U, Schulz M (2003) Centennial-to-millennial-scale periodicities of Holocene climate and sediment injections off the western Barents shelf, 75° N. Boreas 32:447–461. doi:10.1080/03009480301813
116. Christla M, Manginia A, Holzkäampera S, Spötlb C (2004) Evidence for a link between the flux of galactic cosmic rays and Earth's climate during the past 200 000 years. J Atmos Sol Terr Phys 66:313–322. doi:10.1016/j.jastp.2003.12.004
117. van der Plicht J, van Geel B, Bohncke SJP, Bos JAA, Blaauw M, Speranza AOM, Muscheler R, Björck S (2004) The Preboreal climate reversal and a subsequent solar-forced climate shift. J Quat Sci 19:263–269
118. Prasad S, Vos H, Negendank JFW, Waldmann N, Goldstein SL, Stein M (2004) Evidence from Lake Lisan of solar influence on decadal to centennial climate variability during marine oxygen isotope stage 2. Geology 32:581–584. doi:10.1130/G20553.1
119. Wei J, Wang H (2004) A possible role of solar radiation and ocean in the Mid-Holocene east Asian monsoon climate. Adv Atmos Sci 21:1–12
120. Wiles GC, D'Arrigo RD, Villalba R, Calkin PE, Barclay DJ (2004) Century-scale solar variability and Alaskan temperature change over the past millennium. Geophys Res Lett 31: L15203
121. Maasch K, Mayewski PA, Rohling E, Stager C, Karlen K, Meeker LD, Meyerson E (2005) Climate of the past 2000 years. Geogr Ann A 87:7–15. doi:10.1111/j.0435-3676.2005.00241.x
122. Ammann CM et al (2007) Solar influence on climate during the past millenium: results from transient simulations with the NCAR climate system model. Proc Natl Acad Sci 104:3713–3718
123. Mayewski PA et al (2005) Solar forcing of the polar atmosphere. Ann Glaciol 41:147–154
124. Wang Y et al (2005) The Holocene Asian monsoon: links to solar changes and North Atlantic climate. Science 308:854–857. doi:10.1126/science.1106296
125. Bard E, Frank M (2006) Climate change and solar variability: what's new under the Sun? Earth Planet Sci Lett 248:1–14. doi:10.1016/j.epsl.2006.06.016
126. Ruzmaikin JF, Yung YL (2006) Is solar variability reflected in the Nile River? J Geophys Res 111:D21114
127. Polissar PJ, Abbott MB, Wolfe AP, Bezada M, Rull V, Bradley RS (2006) Solar modulation of Little Ice Age climate in the tropical Andes. Proc Natl Acad Sci 103:8937–8942. doi:10.1073/pnas.0603118103
128. Zhang P, Cheng H, Edwards RL, Chen F, Wang Y, Yang X, Liu J, Tan M, Wang X, Liu J, An C, Dai Z, Zhou J, Zhang D, Jia J, Jin L, Johnson KR (2008) A test of climate, Sun, and culture relationships from an 1810-year Chinese cave record. Science 322(5903):940–942. doi:10.1126/science.1163965
129. Beer J, Vonmoos M, Müscheler R (2006) Solar variability over the past several millennia. Space Sci Rev 125:67–79. doi:10.1007/s11214-006-9047-4
130. Fleitmann D, Burns SJ, Mudelsee M, Neff U, Kramers J, Mangini A, Matter A (2003) Holocene forcing of the Indian monsoon recorded in a stalagmite from Southern Oman. Science 300:1737–1739
131. Vonmoos M, Beer J, Muscheler R (2006) Large variations in Holocene solar activity: constraints from Be-10 in the Greenland Ice Core Project ice core. J Geophys Res 111:A10105. doi:10.1029/2005JA011500
132. Field CV, Schmidt GA, Koch D, Salyk C (2006) Modeling production and climate-related impacts on Be-10 concentrations in ice cores. J Geophys Res 111:D15107. doi:10.1029/2005JD006410
133. Aldahan A, Hedfors J, Possnert G, Kulan A, Berggren A-M, Söderström C (2008) Atmospheric impact on beryllium isotopes as solar activity proxy. Geophys Res Lett 35:L21812. doi:10.1029/2008GL035189
134. Heikkila U, Beer J, Feichter J (2008) Modeling cosmogenic radionucleides Be-10 and Be-7 during the Maunder Minimum using the ECHAM5-HAM General Circulation Model. Atmos Chem Phys 8:2797–2809
135. Shindell DT, Faluvegi G, Miller RL, Schmidt GA, Hansen JE, Sun S (2006) Solar and anthropogenic forcing of tropical hydrology. Geophys Res Lett 33:L24706. doi:10.1029/2006GL027468
136. Tric E (1992) Paleointensity of the geomagnetic field during the last 80,000 years. J Geophys Res 97:9337–9351
137. Baumgartner S, Beer J, Masarik J, Wagner G, Meynadier L, Synal H-A (1998) Geomagnetic Modulation of the 36Cl Flux in the GRIP Ice Core Greenland. Science 279:1330–1331
138. Laj C et al (2001) North Atlantic paleointensity stack since 75 ka (NAPIS-75) and the duration of the Laschamp event. Philos Trans R Soc Lond 358:1009–1025
139. Bhattacharyya A, Mitra B (1997) Changes in cosmic ray cut-off rigidities due to secular variations of the geomagnetic field. Ann Geophys 15:734–739
140. Damon PE, Lerman JC, Long A (1978) Temporal fluctuations of atmospheric 14C: causal factors and implications. Ann Rev Earth Planet Sci 6:457
141. van Geel B, Mook WG (1989) High resolution 14C dating of organic deposits using natural atmospheric 14C variations. Radiocarbon 31:151–155
142. Kilian MR, van der Plicht J, van Geel B (1995) Dating raised bogs: new aspects of AMS ^{14}C wiggle matching, a reservoir effect and climatic change. Quat Sci Rev 14: 959–966
143. Blaauw M, Heuvelink GBM, Mauquoy D, van der Plicht J, van Geel B (2003) A numerical approach to ^{14}C wiggle-match dating of organic deposits: best fits and confidence intervals. Quat Sci Rev 22:1485–1500

144. Friis-Christensen E, Lassen K (1991) Length of the solar cycle: an indicator of solar activity closely associated with climate. Science 245:698–700. doi:10.1126/science.254.5032.698
145. Laut P (2003) Solar activity and terrestrial climate: an analysis of some purported correlations. J Atmos Sol Terr Phys 65:801–812
146. Thejll P, Lassen K (2000) Solar forcing of the Northern hemisphere land air temperature: new data. J Atmos Terr Phys 62(13):1207–1213
147. Benestad RE (2005) A review of the solar cycle length estimates. Geophys Res Lett 32:L15714. doi:10.1029/2005GL023621
148. Scafetta N, West BJ (2007) Phenomenological reconstructions of the solar signature in the Northern Hemisphere surface temperature records since 1600. J Geophys Res 112(D24):D24S03
149. Hegerl GC, Zwiers FW, Braconnot P, Gillett NP, Luo Y, Marengo Orsini JA, Nicholls N, Penner JE, Stott PA (2007) Understanding and attributing climate change. In: Solomon S, Qin D, Manning M, Chen Z, Marquis M, Averyt KB, Tignor M, Miller HL (eds) Climate change 2007: the physical science basis, Contribution of working group I to the fourth assessment report of the intergovernmental panel on climate change. Cambridge University Press, Cambridge/New York
150. Solomon S, Quin D, Manning M, Chen Z, Marquis M, Averyt KB, Tignotr M, Miller HL (eds) (2007) Climate change: the physical science basis, Contribution of working group I to the fourth assessment report of the intergovernmental panel on climate change. Cambridge University Press, Cambridge
151. Solanki SK, Krivova NA (2003) Can solar variability explain global warming since 1970? J Geophys Res 108(A5):1200
152. Erlykin AD, Sloan T, Wolfendale AW (2009) Solar activity and the mean global temperature. Environ Res Lett 4(1):014006
153. Stott PA, Jones GS, Mitchell JF (2003) Do models underestimate the solar contribution to recent climate change? J Climate 16:4079–4093
154. Crowley TJ (2000) Causes of climate change over the past 1000 years. Science 289:270–277
155. Cubasch U, Voss R (2000) The influence of total solar irradiance on climate. Space Sci Rev 94:185–198
156. Cubasch U, Voss R, Hegerl GC, Waszkewitz J, Crowley TJ (1997) Simulation of the influence of solar radiation variations on the global climate with an ocean–atmosphere general circulation model. Climate Dyn 13:757–767. doi:10.1007/s003820050196
157. Ingram WJ (2006) Detection and attribution of climate change, and understanding solar influence on climate. Space Sci Rev 125:199–211. doi:10.1007/s11214-006-9057-2
158. Camp CD, Tung KK (2007) Surface warming by the solar cycle as revealed by the composite mean difference projection. Geophys Res Lett 34:L14703
159. Gleisner H, Thejll P, Stendel M, Kaas E, Machenhauer B (2005) Solar signals in tropospheric re-analysis data: comparing NCEP/NCAR and ERA40. J Atmos Sol Terr Phys 67(8–9): 785–791
160. Gleisner H, Thejll P (2003) Patterns of tropospheric response to solar variability. Geophys Res Lett 30:17129
161. Frame T, Gray LJ (2010) The 11-year solar cycle in ERA-40 data: an update to 2008. J Climate 23:2213–2222
162. Crooks SA, Gray LJ (2005) Characterisation of the 11-year solar signal using a multiple regression analysis of the ERA-40 dataset. J Climate 18:996–1015
163. Ruzmaikin A, Feynman J (2002) Solar influence on a major mode of atmospheric variability. J Geophys Res 107:4209
164. Lee JN, Hameed S (2007) The Northern Hemisphere annular mode in summer: its physical significance and its relation to solar activity variations. J Geophys Res 112:D15111
165. Lee JN, Hameed S, Shindell DT (2008) Northern annular mode in summer and its relation to solar activity variations in the GISS Model E. J Atmos Sol Terr Phys 70:730–741
166. Kodera K (2002) Solar cycle modulation of the North Atlantic Oscillation: implications in the spatial structure of the NAO. Geophys Res Lett 29(8):1218. doi:10.1029/2001GL014557
167. Kodera K, Kuroda Y (2005) A possible mechanism of solar modulation of the spatial structure of the North Atlantic Oscillation. J Geophys Res 110:D02111. doi:10.1029/2004JD005258
168. Kodera K (2004) Solar influence on the Indian Ocean monsoon through dynamical processes. Geophys Res Lett 31: L24209. doi:10.1029/2004GL020928
169. Kuroda Y, Kodera K (2005) Solar cycle modulation of the Southern Annular Mode. Geophys Res Lett 32:L13802. doi:10.1029/2005GL022516
170. Salby ML, Callaghan PF (2006) Evidence of the solar cycle in the tropical troposphere. J Geophys Res 111:D21113. doi:10.1029/2006JD007133
171. Kodera K, Shibata K (2006) Solar influence on the tropical stratosphere and troposphere in the northern summer. Geophys Res Lett 33:L19704. doi:10.1029/2006GL026659
172. Brönnimann S, Ewen T, Griesser T, Jenne R (2007) Multidecadal signal of solar variability in the upper troposphere during the 20th century. Space Sci Rev 125:305–315
173. Kodera K, Coughlin K, Arakawa O (2007) Possible modulation of the connection between the Pacific and Indian Ocean variability by the solar cycle. Geophys Res Lett 34:L03710. doi:10.1029/2006GL027827
174. Meehl GA, Washington WM, Wigley TML, Arblaster JM, Dai A (2003) Solar and greenhouse gas forcing and climate response in the twentieth century. J Climate 16:426–444. doi:10.1175/15200442
175. Meehl GA, Arblaster JM, Branstator G, van Loon H (2008) A coupled air-sea response mechanism to solar forcing in the Pacific region. J Climate 21:2883–2897
176. Meehl GA, Arblaster JM, Matthes K, Sassi F, van Loon H (2009) Amplifying the Pacific climate system response to a small 11-year solar cycle forcing. Science 325:1114–1118. doi:10.1126/science.1172872

177. van Loon H, Meehl GA, Shea DJ (2007) Coupled air-sea response to solar forcing in the Pacific region during northern winter. J Geophys Res 112:D02108. doi:10.1029/2006JD007378
178. van Loon H, Meehl GA (2008) The response in the Pacific to the Sun's decadal peaks and contrasts to cold events in the Southern Oscillation. J Atmos Sol Terr Phys 70: 1046–1055
179. White WB, Liu Z (2008) Non-linear alignment of El Nino to the 11-yr solar cycle. Geophys Res Lett 35:L19607. doi:10.1029/2008GL034831
180. Emile-Geay J, Cane M, Seager R, Kaplan A, Allmasi P (2007) El Niño as a mediator of the solar influence on climate. Paleoceanography 22:PA3210. doi:10.1029/2006PA001304
181. White WB, Cayan DR, Lean J (1998) Global upper ocean heat storage response to radiative forcing from changing solar irradiance and increasing greenhouse gas/aerosol concentrations. J Geophys Res 103:21355–21366
182. White WB, Lean J, Cayan DR, Dettinger MD (1997) Response of global upper ocean temperature to changing solar irradiance. J Geophys Res 102:3255–3266
183. White WB, Dettinger MD, Cayan DR (2003) Sources of global warming in the upper-ocean on decadal period scales. J Geophys Res 108(C8):3248. doi:10.1029/2002JC001396
184. White WB, Liu Z (2008) Resonant response of the quasi-decadal oscillation to the 11-yr period signal in the Sun's irradiance. J Geophys Res 113:C01002. doi:10.1029/2006JC004057
185. Shindell DT, Schmidt GA, Miller RL, Rind D (2001) Northern hemisphere winter climate response to greenhouse gas, ozone, solar, and volcanic forcing. J Geophys Res 106: 7193–7210
186. Shindell DT, Schmidt GA, Mann ME, Rind D, Waple A (2001) Solar Forcing of Regional Climate Change during the Maunder Minimum. Science 294(5549):2149–2152
187. Shindell DT, Schmidt GA, Miller RL, Mann ME (2003) Volcanic and solar forcing of climate change during the preindustrial era. J Climate 16:4094–4107
188. Mann ME, Zhang Z, Rutherford S, Bradley R, Hughes MK, Shindell D, Ammann C, Faluvegi G, Ni F (2009) Global signatures of the Little Ice Age and Medieval climate anomaly and plausible dynamical origins. Science 326: 1256–1260
189. Trouet V, Esper J, Graham NE, Baker A, Scourse JD, Frank DC (2009) Persistent positive North Atlantic Oscillation mode dominated the Medieval climate anomaly. Science 324:78–80
190. Goosse H, Arzel O, Luterbacher J, Mann ME, Renssen H, Riedwyl N, Timmermann A, Xoplaki E, Wanner H (2006) The origin of the European Medieval Warm Period. Clim Past Discuss 2:99–113
191. North GR, Stevens MJ (1998) Detecting climate signals in the surface temperature record. J Climate 11:563–577
192. Kossobokov V, Le Mouël J-L, Courtillot V (2010) A statistically significant signature of multidecadal solar activity changes in atmospheric temperatures at three European stations. J Atmos Sol Terr Phys 72:595–606. doi:10.1016/j.jastp.2010.02.016
193. Le Mouël J-L, Courtillot V, Blanter E, Shnirman M (2008) Evidence for a solar signature in 20th-century temperature data from the USA and Europe. C R Geosci 340:421–430
194. Le Mouël J-L, Blanter E, Shnirman M, Courtillot V (2009) Evidence for solar forcing in variability of temperature and pressure in Europe. J Atmos Sol Terr Phys 71:1309–1321. doi:10.1016/j.jastp. 2009.05.006
195. Le Mouël J-L, Kossobokov V, Courtillot V (2010) A solar pattern in the longest temperature series from three stations in Europe. J Atmos Sol Terr Phys 72:62–76. doi:10.1016/j.jastp.2009.10.009
196. Karoly DJ, Stott PA (2006) Anthropogenic warming of central England temperature. Atmos Sci Lett 7:81–85. doi:10.1002/asl.136, 2006
197. Luterbacher J et al (2001) The late Maunder Minimum (1675–1715) – a key period for studying decadal scale climatic change in Europe. Clim Change 49:441–462
198. Lockwood M, Harrison RG, Woollings T, Solanki SK (2010) Are cold winters in Europe associated with low solar activity? Environ Res Lett 5:024001. doi:10.1088/1748-9326/5/2/024001
199. Wanner H, Pfister C, Brázdil R, Frich P, Frydendahl K, Jónsson T, Kington J, Lamb HH, Rosenørn S, Wishman E (1995) Wintertime European circulation patterns during the late Maunder Minimum cooling period (1675–1704). Theor Appl Climatol 51:167–175. doi:10.1007/BF00867443
200. Barriopedro D, Garcia-Herrera R, Huth R (2008) Solar modulation of Northern Hemisphere winter blocking. J Geophys Res 113:D14118. doi:10.1029/2008JD009789
201. Huth R, Pokorná L, Bochníček J, Hejda P (2006) Solar cycle effects on modes of low-frequency circulation variability. J Geophys Res 111:D22107
202. Huth R, Kyselý J, Bochníček J, Hejda P (2008) Solar activity affects the occurrence of synoptic types over Europe. Ann Geophys 26:1999–2004
203. Scaife AA, Knight JR, Vallis GK, Folland CK (2005) A stratospheric influence on the winter NAO and North Atlantic surface climate. Geophys Res Lett 32:L18715
204. Rind D, Shindell D, Perlwitz J, Lerner J, Lonergan P, Lean J, McLinden C (2004) The relative importance of solar and anthropogenic forcing of climate change between the Maunder Minimum and the present. J Climate 17:906–929
205. Zorita E, von Storch H, Gonzalez-Rouco F, Cubasch U, Luterbacher J, Legutke S, Fischer-Bruns I, Schlese U (2004) Climate evolution in the last five centuries simulated by an atmosphere-ocean model: global temperatures, the North Atlantic Oscillation and the Late Maunder Minimum. Meteor Zeit 13:271–289
206. Stendel M, Mogensen IA, Christensen JH (2006) Influence of various forcings on global climate in historical times using

a coupled atmosphere-ocean general circulation model. Climate Dyn 26(1):1–15
207. Rind D, Lean J, Lerner J, Lonergan P, Leboissitier A (2008) Exploring the stratospheric/tropospheric response to solar forcing. J Geophys Res Atmos 113:D24103
208. Baldwin MP (2003) Comment on "Tropospheric response to stratospheric perturbations in a relatively simple general circulation model" by Lorenzo M. Polvani and Paul J. Kushner. Geophys Res Lett 30(15):1812. doi:10.1029/2003GL017793
209. Thompson DWJ, Kennedy J, Wallace JM, Jones PD (2008) A large discontinuity in the mid-twentieth century in observed global-mean surface temperature. Nature 453(7195):646–649
210. Hegerl GC, Crowley TJ, Baum SK, Kim KY, Hyde WT (2003) Detection of volcanic, solar and greenhouse gas signals in paleo-reconstructions of Northern Hemisphere temperature. Geophys Res Lett 30:1242
211. Shepherd TG (2002) Issues in stratosphere-troposphere coupling. J Meterol Soc Jpn 80:769–792
212. Hartley DE, Villarin JT, Black RX, Davis CA (1998) A new perspective on the dynamical link between the stratosphere and troposphere. Nature 391:471–474
213. Song YC, Robinson WA (2004) Dynamical mechanisms for stratospheric influences on the troposphere. J Atmos Sci 61:1711–1725
214. Matthes K, Kuroda Y, Kodera K, Langematz U (2006) Transfer of the solar signal from the stratosphere to the troposphere: Northern winter. J Geophys Res 111:D06108. doi:10.1029/2005JD006283
215. Baldwin MP, Dunkerton TJ (2001) The solar cycle and stratosphere-troposphere dynamical coupling. Science 294:581–584
216. Haigh JD (1996) The impact of solar variability on climate. Science 272:981–984
217. Haigh JD (2001) Climate variability and the influence of the Sun. Science 294:2109–2111. doi:10.1126/science.1067013
218. Gray LJ, Crooks S, Pascoe C, Sparrow S, Palmer M (2004) Solar and QBO Influences on the Timing of Stratospheric Sudden Warmings. J Atmos Sci 61:2777–2796
219. Plumb RA, Semeniuk K (2003) Downward propagation of extra-tropical zonal wind anomalies. J Geophys Res 108:4223. doi:10.1029/2002JD002773
220. Polvani LM, Kushner PJ (2002) Tropospheric response to stratospheric perturbations in a relatively simple general circulation model. Geophys Res Lett 29:1114. doi:10.1029/2001GL014284
221. Barriopedro D, García-Herrera R, Lupo AR, Hernández E (2006) A climatology of Northern Hemisphere blocking. J Climate 19:1042–1063
222. Kushner PJ, Polvani LM (2004) Stratosphere-troposphere coupling in a relatively simple AGCM: the role of eddies. J Climate 17:629–639
223. Simpson IR, Blackburn M, Haigh JD (2009) The role of eddies in driving the tropospheric response to stratospheric heating perturbations. J Atmos Sci 66(5):1347–1365
224. Perlwitz J, Harnik N (2003) Observational evidence of a stratospheric influence on the troposphere by planetary wave reflection. J Climate 16:3011–3026
225. Thompson DWJ, Baldwin MP, Solomon S (2005) Stratosphere-troposphere coupling in the Southern Hemisphere. J Atmos Sci 62:708–715
226. Castanheira JM, Graf H-F (2003) North Pacific – North Atlantic relationships under stratospheric control? J Geophys Res 108(D1):4036
227. Kuroda Y, Deushi M, Shibata K (2007) Role of solar activity in the troposphere-stratosphere coupling in the southern Hemisphere winter. Geophys Res Lett 34:L21704. doi:10.1029/2007GL030983
228. Labitzke K, van Loon H (1988) Associations between the 11-year solar cycle, the QBO and the atmosphere, Part I: the troposphere and stratosphere in the northern hemisphere in winter. J Atmos Terr Phys 50:197–206
229. Haigh JD, Blackburn M (2006) Solar influences on dynamical coupling between the stratosphere and troposphere. Space Sci Rev 125:331–344
230. Haigh JD (1994) The role of stratospheric ozone in modulating the solar radiative forcing of climate. Nature 370:544–546
231. Poore RZ, Quinn TM, Verardo S (2004) Century-scale movement of the Atlantic Intertropical Convergence Zone linked to solar variability. Geophys Res Lett 31:L12214. doi:10.1029/2004GL019940
232. Russell JM, Johnson TC (2007) Little Ice Age drought in equatorial Africa: intertropical convergence zone migrations and El-Nino Southern Oscillation variability. Geology 35:21–24
233. Woollings T, Charlton-Perez A, Ineson S, Marshall AG, Masato G (2010) Associations between stratospheric variability and tropospheric blocking. J Geophys Res 115:D06108. doi:10.1029/2009JD012742
234. Carslaw KS, Harrison RG, Kirkby J (2002) Cosmic rays, clouds and climate. Science 298:1732–1737. doi:10.1126/science.1076964
235. Kirkby J (2007) Cosmic rays and climate. Surv Geophys 28 (5/6):333–375
236. Charlson RJ, Valero FPJ, Seinfeld JH (2005) In search of balance. Science 308(5723):806–807. doi:10.1126/science.1108162
237. Pallé E, Goode PR, Montañés-Rodríguez P (2009) Interannual variations in Earth's reflectance 1999–2007. J Geophys Res 114:D00D03. doi:10.1029/2008JD010734
238. Svensmark H, Friis-Christensen E (1997) Variations of cosmic ray flux and global cloud coverage – a missing link in solar-climate relationships. J Atmos Terr Phys 59:1225–1232
239. Svensmark H (2007) Cosmoclimatology: a new theory emerges. Astron Geophys 48:118–124. doi:10.1111/j.1468-4004.2007.48118.x
240. Marsh N, Svensmark H (2000) Cosmic rays, clouds, and climate. Space Sci Rev 94:215–230
241. Marsh N, Svensmark H (2003) Galactic cosmic ray and El Nino Southern Oscillation trends in International Satellite Cloud Climatology Project D2 low-cloud properties. J Geophys Res 108(D6):4195

242. Marsh N, Svensmark H (2004) Comment on "Solar influences on cosmic rays and cloud formation: A reassessment" by Bomin Sun and Raymond S. Bradley. J Geophys Res 109: D14205. doi:10.1029/2003JD004063
243. Sloan T, Wolfendale AW (2008) Testing the proposed causal link between cosmic rays and cloud cover. Environ Res Lett 3(2):024001. doi:10.1088/1748-9326/3/2/024001
244. Kernthaler SC, Toumi R, Haigh JD (1999) Some doubts concerning a link between cosmic ray fluxes and global cloudiness. Geophys Res Lett 26(7):863–865
245. Kristjánsson JE, Kristiansen J (2000) Is there a cosmic ray signal in recent variations in global cloudiness and cloud radiative forcing? J Geophys Res 105(D9):11851–11863
246. Sun B, Bradley RS (2002) Solar influences on cosmic rays and cloud formation: a reassessment. J Geophys Res 107(D14):4211. doi:10.1029/2001JD000560
247. Kulmala M, Riipinen I, Nieminen T, Hulkkonen M, Sogacheva L, Manninen HE, Paasonen P, Petäjä T, Dal Maso M, Aalto PP, Viljanen A, Usoskin I, Vainio R, Mirme S, Mirme A, Minikin A, Petzold A, Hõrrak U, Plaß-Dülmer C, Birmili W, Kerminen V-M (2010) Atmospheric data over a solar cycle: no connection between galactic cosmic rays and new particle formation. Atmos Chem Phys 10:1885–1898. doi:10.5194/acp-10-1885-2010
248. Sun B, Bradley RS (2004) Reply to comment by N. D. Marsh and H. Svensmark on "Solar influences on cosmic rays and cloud formation: a reassessment". J Geophys Res 109: D14206. doi:10.1029/2003JD004479
249. Erlykin AD, Sloan T, Wolfendale AW (2010) Correlations of clouds, cosmic rays and solar irradiation over the Earth. J Atmos Sol Terr Phys 72(2/3):151–156. doi:10.1016/j.jastp.2009.11.002) |
250. Kristjánsson JE, Stjern CW, Stordal F et al (2008) Cosmic rays, cloud condensation nuclei and clouds – a reassessment using MODIS data. Atmos Chem Phys 8(24):7373–7387
251. de Jager C, Usoskin I (2006) On possible drivers of Sun-induced climate changes. J Atmos Sol Terr Phys 68:2053–2060
252. Udelhofen PM, Cess RD (2001) Cloud cover variations over the United States: an influence of cosmic rays or Solar variability? Geophys Res Lett 28(13):2617–2620
253. Voiculescu M, Usoskin IG, Mursula K (2006) Different response of clouds to solar input. Geophys Res Lett 33:L21802. doi:10.1029/2006GL027820
254. Harrison R (2008) Discrimination between cosmic ray and solar irradiance effects on clouds, and evidence for geophysical modulation of cloud thickness. Proc R Soc A 464(2098): 2575–2590
255. Kazil J, Lovejoy ER, Barth MC, O'Brien K (2006) Aerosol nucleation over oceans and the role of galactic cosmic rays. Atmos Chem Phys 6:4905–4924
256. Laken B, Wolfendale A, Kniveton D (2009) Cosmic ray decreases and changes in the liquid water cloud fraction over the oceans. Geophys Res Lett 36:L23803
257. Klein SA, Hartmann DL (1993) Spurious changes in the ISCCP dataset. Geophys Res Lett 20:455–458
258. Palmer MA, Gray LJ, Allen MR, Norton WA (2004) Solar forcing of climate: model results. Adv Space Res 34:343–348
259. Haug G, Hughen K, Sigman D, Peterson L, Röhl U (2001) Southward migration of the Intertropical Convergence Zone through the Holocene. Science 293:1304–1308. doi:10.1126/science.1059725
260. Gallet Y, Genevey A (2007) The Mayans: climate determinism or geomagnetic determinism? EOS Trans Am Geophys Union 88:129–130. doi:10.1029/2007EO110001
261. Gallet Y, Genevey A, Fluteau F (2005) Does Earth's magnetic field secular variation control centennial climate change? Earth Planet Sci Lett 236:339–347. doi:10.1016/j.epsl.2005.04.045
262. Gallet Y, Genevey A, Le Goff M, Fluteau F, Eshraghi SA (2006) Possible impact of the Earth's magnetic field on the history of ancient civilizations. Earth Planet Sci Lett 246:17–26. doi:10.1016/j.epsl.2006.04.001
263. Courtillot V, Gallet Y, Le Mouël J-L, Fluteau F, Genevey A (2007) Are there connections between the Earth's magnetic field and climate? Earth Planet Sci Lett 253:328–339. doi:10.1016/j.epsl.2006.10.032
264. Haug G, Günther D, Peterson L, Sigman D, Hughen K, Aeschlimann B (2003) Climate and the collapse of Maya civilization. Science 299:1731–1735. doi:10.1126/science.1080444
265. Hodell D, Curtis J, Brenner M (1995) Possible role of climate in the collapse of Classic Maya civilization. Nature 375:391–394. doi:10.1038/375391a0
266. Curtis J, Hodell D, Brenner M (1996) Climate variability on the Yucatan Peninsula (Mexico) during the past 3500 years, and implications for Mayan cultural evolution. Quat Res 46:37–47. doi:10.1006/qres.1996.0042
267. de Menocal P (2001) Cultural response to climate change during the late Holocene. Science 292:667–673. doi:10.1126/science.1059827
268. Harrison RG, Stephenson DB (2006) Empirical evidence for a nonlinear effect of galactic cosmic rays on clouds. Proc R Soc A 462:1221–1233. doi:10.1098/rspa.2005.1628
269. Duplissy J, Enghoff MB, Aplin KL, Arnold F, Aufmhoff H, Avngaard M, Baltensperger U, Bondo T, Bingham R, Carslaw K, Curtius J, David A, Fastrup B, Gagne S, Hahn F, Harrison RG, Kellett B, Kirkby J, Kulmala M, Laakso L, Laaksonen A, Lillestol E, Lockwood M, Makela J, Makhmutov V, Marsh ND, Nieminen T, Onnela A, Pedersen E, Pedersen JOP, Polny J, Reichl U, Seinfeld JH, Sipila M, Stozhkov Y, Stratmann F, Svensmark H, Svensmark J, Veenhof R, Verheggen B, Viisanen Y, Wagner PE, Wehrle G, Weingartner E, Wex H, Wilhelmsson M, Winkler PM (2010) Results from the CERN pilot CLOUD experiment. Atmos Chem Phys 10(4):1635–1647
270. Pierce JR, Adams PJ (2009) Can cosmic rays affect cloud condensation nuclei by altering new particle formation rates? Geophys Res Lett 36:L09820. doi:10.1029/2009GL037946
271. Rycroft MJ, Israelsson S, Price C (2000) The global atmospheric electric circuit, solar activity and climate change. J Atmos Sol Terr Phys 62:1563–1576

272. Harrison RG (2000) Cloud formation and the possible significance of charge for atmospheric condensation and ice nuclei. Space Sci Rev 94:381–396
273. Harrison RG, Ambaum MHP (2008) Enhancement of cloud formation by droplet charging. Proc R Soc A 464: 2561–2573
274. Tinsley BA, Brown GM, Scherrer PH (1989) Solar variability influences on weather and climate: possible connections through cosmic ray-fluxes and storm intensification. J Geophys Res 94:14783–14792
275. Kniveton DR, Tinsley BA, Burns GB, Bering EA, Troshichev OA (2008) Variations in global cloud cover and the fair-weather vertical electric field. J Atmos Sol Terr Phys 70: 1633–1642
276. Pudovkin MI, Veretenenko VS (1997) Effects of the galactic cosmic ray variations on the solar radiation input in the lower atmosphere. J Atmos Terr Phys 59(14):1739–1746
277. Svensmark H, Bondo T, Svensmark J (2009) Cosmic rays decreases affect atmospheric aerosols and cloud. Geophys Res Lett 36:L15101. doi:10.1029/2009GL038429, 2009
278. Brown BH (2008) Short-term changes in global cloud cover and in cosmic radiation. J Atmos Sol Terr Phys 70(7): 1122–1131
279. Mlynczak M et al (2003) The natural thermostat of nitric oxide emission at 5.3 μm in the thermosphere observed during the solar storms of April 2002. Geophys Res Lett 30:2100. doi:10.1029/2003GL017693
280. Siskind DE, Nedoluha GE, Randall CE, Fromm M, Russell JM III (2000) An assessment of Southern Hemisphere stratospheric NOx enhancements due to transport from the upper atmosphere. Geophys Res Lett 27:329–332
281. Funke B, Lopez-Puertas M, Gil-Lopez S, von Clarmann T, Stiller G, Fischer H, Kellman S (2005) Downward transport of upper atmospheric NO_x into the polar stratosphere and lower mesosphere during the Antarctic 2003 and Arctic 2002/2003 winters. J Geophys Res 110:D24308. doi:10.1029/2005JD006463
282. Callis LB, Natarajan M, Lambeth J (2000) Calculated upper stratospheric effects of solar UV flux and NO_y variations during the 11-year solar cycle. Geophys Res Lett 27:3869–3872
283. Jackman CH, DeLand MT, Labow GJ, Fleming EI, Lopez-Puertas M (2006) Satellite measurements of middle atmospheric impacts by solar proton events in solar cycle 23. Space Sci Rev 125:381–391
284. Jackman CH, Marsh DR, Vitt FM, Garcia RR, Fleming EL, Labow GJ, Randall CE, Lopez-Puertas M, Funke B, von Clarmann T, Stiller GP (2008) Short- and medium-term atmospheric constituent effects of very large solar proton events. Atmos Chem Phys 8:765–785
285. Randall CE, Harvey V, Singleton CS, Bailey S, Bernath P, Codrescu M, Nakajima H, Russell JM III (2007) Energetic particle precipitation effects on the Southern Hemisphere stratosphere in 1992–2005. J Geophys Res 112:D08308. doi:10.1029/2006JD007696
286. Randall CE, Harvey VL, Manney GL, Orsolini Y, Codrescu M, Sioris C, Brohede S, Haley C, Gordley L, Zawodny J, Russell J III (2005) Stratospheric effects of energetic particle precipitation in 2003–2004. Geophys Res Lett 32:L05802. doi:10.1029/2004GL022003
287. Seppälä A, Randall CE, Clilverd MA, Rozanov E, Rodger CJ (2009) Geomagnetic activity and polar surface air temperature variability. J Geophys Res 114:A10312. doi:10.1029/2008JA014029
288. Rozanov EV, Callis L, Schlesinger E, Yang F, Andronova N, Zubov VA (2005) Atmospheric response to NOy source due to Energetic electron precipitation. J Geophys Res 32:L14811. doi:10.1029/2005GL023041
289. Easterling DR, Wehner MF (2009) Is the climate warming or cooling? Geophys Res Lett 36:L08706. doi:10.1029/2009GL037810
290. Knight J, Kenney JJ, Folland C, Harris G, Jones GS, Palmer M, Parker D, Scaife A, Stott P (2009) Do global temperature trends over the last decade falsify climate predictions. BAMS 90(8):S75–S79
291. Feulner G, Rahmstorf S (2010) On the effect of a new grand minimum of solar activity on the future climate on Earth. Geophys Res Lett 37:L05707. doi:10.1029/2010GL042710
292. Lean JL, Rind DH (2009) How will Earth's surface temperature change in future decades? Geophys Res Lett 36:L15708. doi:10.1029/2009GL038932
293. Coughlin K (2004) Eleven-year solar cycle signal throughout the lower atmosphere. J Geophys Res 109:D21105
294. Wagner G, Lvingstone DM, Masarik J, Muscheler R, Beer J (2001) Some results relevant to the discussion of a possible link between cosmic rays and the Earth's climate. J Geophys Res 106(D4):3381–3387
295. Woollings T, Lockwood M, Masato G, Bell C, Gray L (2010) Enhanced signature of solar variability in Eurasian winter climate. Geophys Res Lett 37:L20805. doi:10.1029/2010GL044601
296. Calogovic J, Albert C, Arnold F, Beer J, Desorgher L, Flueckiger EO (2010) Sudden cosmic ray decreases: No change of global cloud cover. Geophys Res Lett 37:L03802. doi:10.1029/2009GL041327
297. Katsman CA, van Oldenborgh GJ (2011) Tracing the upper ocean's "missing heat". Geophys Res Lett 38:L14610. doi:10.1029/2011GL048417
298. Jarvis A, Li S (2011) The contribution of timescales to the temperature response of climate models. Clim Dyn 36: pp 523–531
299. Foster G, Annan JD, Schmidt GA, Mann ME (2008) Comment on "Heat capacity, time constant, and sensitivity of Earth's climate system" by S. E. Schwartz. J Geophys Res 113:D15102. doi:10.1029/2007JD009373

Solid Biofuels, Fuels and Their Characteristics

Hans Hartmann
Technologie- und Förderzentrum im Kompetenzzentrum für Nachwachsende Rohstoffe (TFZ), Straubing, Bavaria, Germany

Article Outline

Glossary
Definition of the Subject
Introduction
Fuel Characterization Schemes and Overview
Fuel Composition
Technical Combustion Properties
Physical-Mechanical Properties
Future Directions
Bibliography

Glossary

Woody fuels Biomass from trees, bushes, and shrubs.

Herbaceous fuels Biomass from plants that have a non-woody stem and which die back at the end of the growing season.

Pellets Densified biofuel made from pulverized biomass with or without additives usually with a cylindrical form, random length typically 5–40 mm, and broken ends. Max diameter: 25 mm.

Physical-mechanical properties Fuel characteristics such as surface properties, geometry, size and size distribution, fine matter content, flowing and bridging properties, resistance to abrasion, bulk, and particle density.

Biomass ash Solid mineral residue obtained from complete fuel combustion.

Energy density Ratio of net energy content and bulk volume.

Definition of the Subject

In the context of the future energy supply and renewable energies biomass is an energy source with a high potential and it has raised many expectations in society and politics. This high interest is also caused by the huge variety of possible resources and the many technical options of application for heating, electricity production, or mobility. The physical appearance of biofuels is also quite variable: biomass can be provided as solid, liquid, or gaseous fuel determining different technological conversion paths.

However, the overview presented here is limited to solid biomass resources. The paper aims at understanding the specialties of natural solid biomass fuels, which are directly used for thermochemical conversion mainly by an end user who has the goal to produce heat and/or electricity. Therefore, raw materials for biological conversion (e.g., fermentation for biogas production) are not characterized. This is also true for those resources that are relevant for non-thermochemical upgrading processes as applied for the production of liquid biofuels (e.g., physical extraction or ethanol fermentation).

Any biomass-containing waste streams are also not considered here, even if they are used for energetic purposes. The goal is rather to define, present and discuss the properties of the main natural untreated solid biomass fuels, which are either residues or field crops, and to indicate the consequences for the conversion process.

Introduction

The provision of solid biofuels that meet high quality standards is becoming increasingly important in order to fulfill the rising technical and environmental requirements for their utilization. The process of a thermochemical conversion is largely influenced by the fuel properties, and this applies to the pollutant formation. Therefore, the specific characteristics of the respective fuels have to be adequately regarded. It is also essential to understand their impact in the conversion process in order to assess their importance and to evaluate chances for improvements. This is a major goal of the here presented study.

The avoidance of unfavorable fuel properties can only be considered if the reasons for any excessive fuel related phenomenons are known and can be explained. It is therefore important to analyze the production chain and to identify the key impacts for fuel quality.

In general, quality-determining factors of biomass fuels can be attributed to two major phases of the life cycle: the growing phase, in which mainly the compositional characteristics are developed, and the supply

phase, in which mostly the physical-mechanical parameters determined (Fig. 1). Only some of the quality influencing factors identified during these phases have been studied and can be quantified at least to some extend with regard to their effectiveness [27].

In view of the influences and the history of the fuel provision as outlined in Fig. 1, the selection and specification of the suitable fuel for a given process is thus an essential part of the optimization strategy of an energy use concept for biomass. Both, the direct determination of the critical quality parameters as well as the fuel assessment by knowing the species and the influences along the provision chain can lead to a sound assessment of the fuels applicability.

Fuel Characterization Schemes and Overview

Fuel specification can either be done directly, by determining the relevant fuel parameters, or indirectly, by retracing the fuel to the origin and/or to the actual species which allows fuel assessment through experience. Both approaches are discussed in the following.

Characterization by Determining Specific Fuel Properties

For the energetic use, three groups of characteristics are decisive: the elementary composition, the technical combustion properties, and the physical-mechanical properties (Table 1). Sometimes the last two groups are also compiled as "physical parameters." Most of the parameters allocated to the three groups are quality-relevant parameters, because they can influence the thermochemical and the pollutant formation processes or they are determining the usability of the produced ash or slag residues.

Below therefore the significance of each of the presented fuel parameter is discussed individually. This applies to the characteristics as listed in Table 1, which can serve as an overview of important fuel properties. For better understanding of the thermochemical conversion processes (i.e., pyrolytic decomposition, gasification and oxidation) the main macromolecular constituents of lignocellulose biomass fuels are also presented in the following.

Characterization by Origin

Many of the measurable fuel parameters and their usual variation are already determined by the fuel origin, which is described either by the species or raw material type or by the processes for harvesting and treatment. The description and the retracing of fuels to their origin is therefore an essential element of an effective quality assurance management for solid biofuels. Therefore,

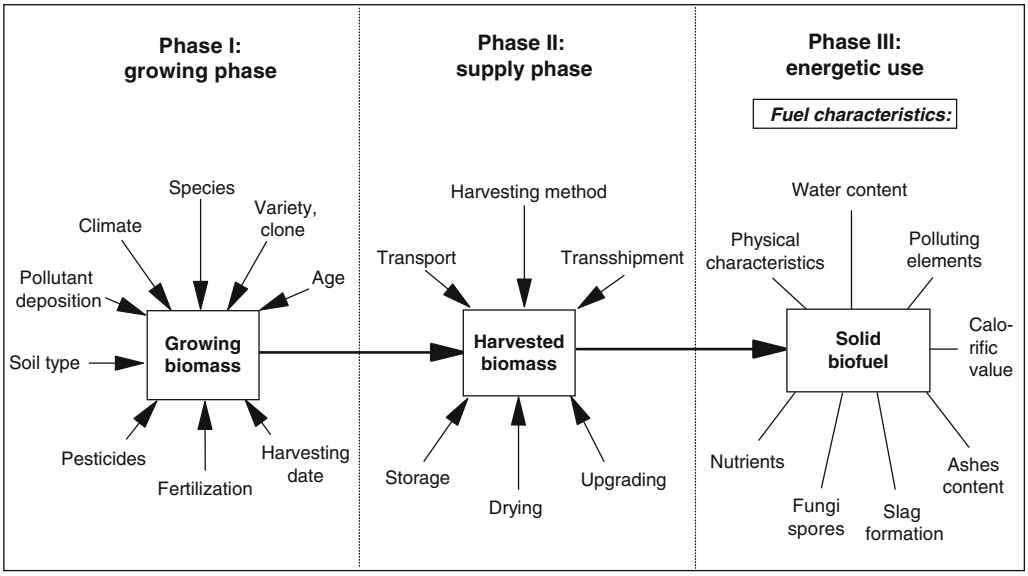

Solid Biofuels, Fuels and Their Characteristics. Figure 1
Factors influencing the quality of solid biofuels ([27], modified)

Solid Biofuels, Fuels and Their Characteristics. Table 1 Quality relevant characteristics of biomass fuels and their impact in the utilization chain

Quality parameter	Main impact
Element concentration	
Carbon (C)	Calorific value, oxygen demand, particle emissions
Hydrogen (H)	Calorific value, oxygen demand
Oxygen (O)	Calorific value, oxygen demand
Nitrogen (N)	NO_x- and N_2O-emission
Potassium (K)	Ash softening behavior, high temperature corrosion, particle emission
Magnesium (Mg)	Ash softening behavior, ash embedding of pollutants, ash utilization, particle emission
Calcium (Ca)	Ash softening behavior, ash embedding of pollutants, ash utilization, particle emission
Sulfur (S)	SO_x-emissions, high temperature corrosion, particle emission
Chlorine (Cl)	Emissions of HCl and halogen-organic compounds (e.g., PCDD/F), high temperature chlorine corrosion, particle emission
Heavy metals	Ash utilization, heavy metal emissions, catalytic impacts (e.g., in PCDD/F-formation), particle emission
Technical combustion properties	
Moisture content	Calorific value, storability (losses by biodegradation, self ignition), fuel weight, combustion temperature
Calorific value	Energy content of fuel, dimensioning of combustion plant
Ash content	Particle emission, residue management and utilization
Ash melting behavior	Slag formation and deposits, operational safety and -continuity, maintenance requirements
Physical-mechanical properties	
Shape and dimensions	Allocation to mechanical systems and furnace types, bridging properties, ignitability, drying speed
Size classification/Fine matter content	Clogging in conveyors, flowability and bridging properties, aeration and drying properties, dust formation, risk of explosion
Bridging properties	Flowability, failures during transhipment and storage extraction
Bulk density	Storage and transport efforts, power requirement of conveyor motors, volume of storage
Particle density	Bulk density, pneumatic conveying properties, combustion properties (specific heat conductivity, etc.)
Resistance to abrasion	Amount of fines (dust formation, demixing)

a uniform identification system was elaborated in the course of the European standardization process for solid biofuels [18]. In this system, the possible features of origin and/or the biomass fractions are comprehensively defined following a hierarchical classification and enumeration scheme. It allows characterizing the given fuel with variable levels of detail, depending on the knowledge about the fuel. This is done by distinguishing four major groups [18]:

- Woody biomass (digit 1)
- Herbaceous biomass (digit 2)
- Fruit biomass (digit 3)
- Blends and mixtures (digit 4)

Theses major groups are divided into several other groups and subgroups. As an example, Figs. 2 and 3 show the classification for the two largest groups, the woody and herbaceous fuels. The given labeling numbers allow a simple reference to specific fuels or fuel groups (e.g., to be used in directives, contracts, or fuel quality standards).

Also the third major group (fruit biomass) is divided into several subclasses. Here a differentiation between orchard and horticulture fruits, by-products and residues from fruit processing industry, as well as blends and mixtures is made. Both subgroups have further subdivisions [18].

The term "blends and mixtures" not only used for the fourth major group but also for several sub-groups is addressing raw materials of variable origin within the given group in the classification scheme and it appears on all four levels. Blends are defined as intentionally mixed biomass, whereas mixtures are unintentionally mixed biomass. A mixture between chemically treated and untreated material is to be classified as a chemically treated fuel [18].

Fuel Composition

Molecular Composition

Biomass fuels are consisting of the three biopolymers cellulose, hemicellulose, and lignin. They usually provide more than 95% of the plants dry matter. As further groups of components, the extractives (e.g., fat and resin) and the ash need to be mentioned. Annually harvested crops can also contain a significant amount of protein. The share of masses for these main constituents in wood and herbaceous fuels is given in Table 2.

Among all organic substances, the cellulose is most widespread in nature. Cellulose forms the structural

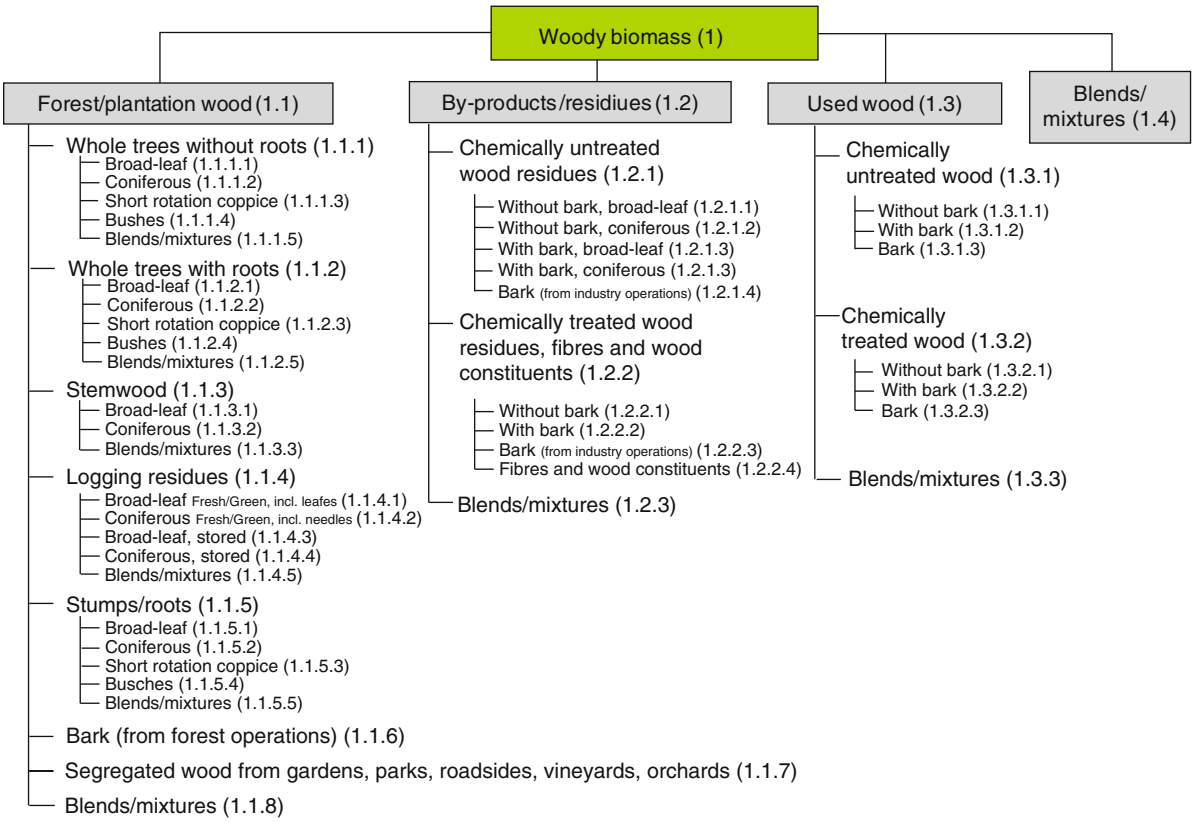

Solid Biofuels, Fuels and Their Characteristics. Figure 2

Classification and enumeration scheme for woody biomass by origin and biomass fractions (according to EN 14 961-1 [18])

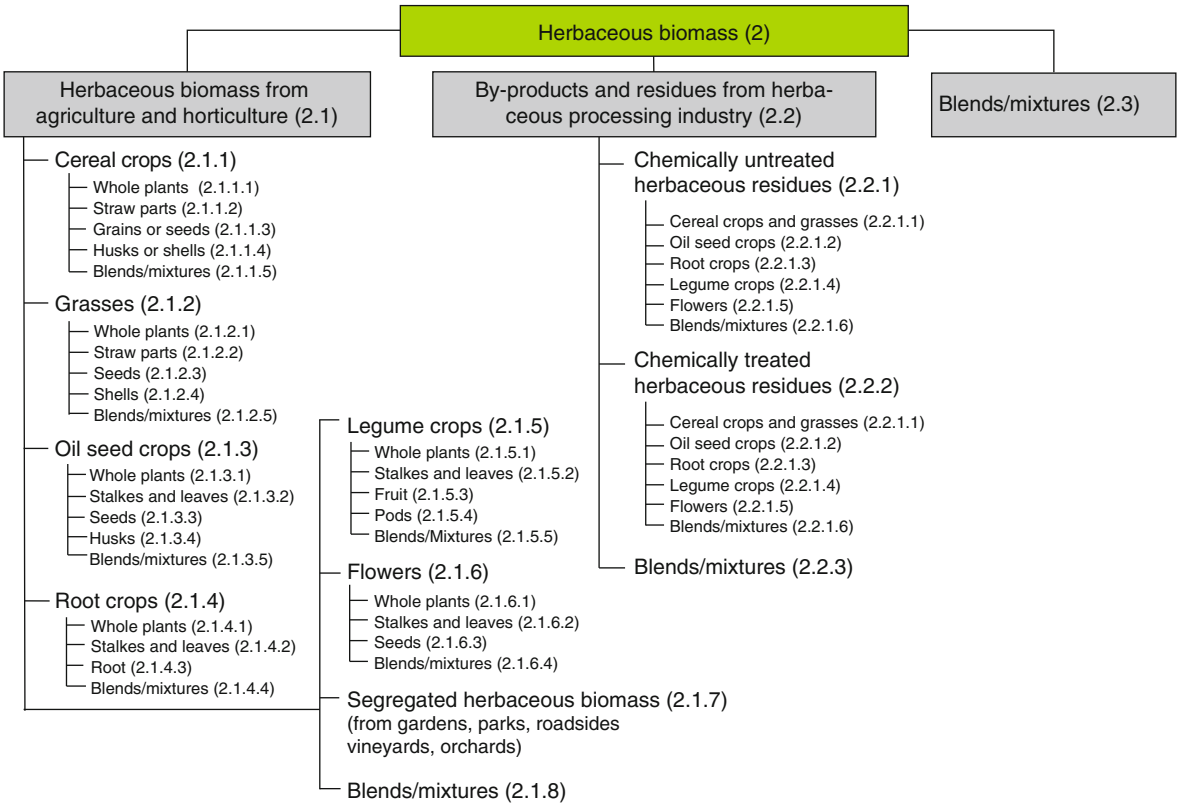

Solid Biofuels, Fuels and Their Characteristics. Figure 3
Classification and enumeration scheme for herbaceous biomass by origin and biomass fractions (according to EN 14 961-1 [18])

substance of the cell wall and it is responsible for the tensile strength of biomass. Cellulose consists almost fully of congenerous D-glycoside molecules which are linked via a ß-(1–4)-binding to form an unbranched polysaccharide (Fig. 4). The degree of polymerization or the length of the chain can vary widely. Depending on the wood species it can reach up to 14,000 molecules [47].

The term hemicellulose (also polyose) specifies a second important group of biopolymers. Hemicellulose is a branched polysaccharide formed by various monomeric units. Their function in the plant is manifold. They serve as structural element in the cell membrane, as reserve material, or they act cell wall cementating through their adhesive properties. Hemicellulose in detail is either hexose (glucose, mannose and galactose), pentose (arabinose, xylose), desoxyhexose, or one of various hexuronic acids.

The actual filling material of lignocellulose materials is lignin. It does not appear as independent material but it is always a companion of the cellulose. Due to its cementation properties it is responsible for the pressure resistance of wood. Lignin is a three dimensionally linked aromatic polymer compound with alcyl-benzol-structure. It consists of variously bound phenylpropane units substituted by hydroxyl and methoxyl groups (Fig. 5). A strong lignification ensures that the sprout of the plant can remain in the upright position when the water pressure (turgor) usually responsible for stability of less lignified plants becomes weak. Therefore, strongly lignified materials (e.g., wood) have relatively low moisture content. Wood fuels have a lignin content of 20–30%, while for annually harvested plants it is usually below 20% (Table 2).

In lignin the carbon content is significantly higher (64%) than for cellulose (42%). Differences in the

Solid Biofuels, Fuels and Their Characteristics. Table 2 Share of cellulose, hemicellulose, lignin, and other components in various biomass fuels ([24, 41, 40]; no specification is made concerning the deviation to 100% mass; *na* not available)

Fuel	Cellulose	Hemicellulose	Lignin	Resin/fat	Protein	Ash
Wood fuel species (data given in % of dry matter)						
Fir	42.3	22.5	28.6	2.3	–	1.2
Pine	41.9	21.5	29.5	3.2	–	1.3
Spruce	41.0	24.3	30.0	n.a.		na
Ash	40.2	25.0	26.0	2.2	–	1.3
Beech	45.4	22.2	22.7	0.7	–	1.6
Birch	40.9	27.1	27.3	2.2	–	1.8
Poplar	48.4	18.2	21.6	2.4	–	1.3
Willow	42.9	21.9	24.7	2.0	–	1.2
Herbaceous fuels (data given in % of dry matter)						
Wheat straw	38	29	15	–	4	6
Prairie grass	37	29	19	–	3	6
Miscanthus	43	24	19	–	3	2
Sweet sorghum	23	14	11	–	n.a.	5
Tall fescue	25	25	14	–	13	11
Maize straw	38	26	19	–	5	6

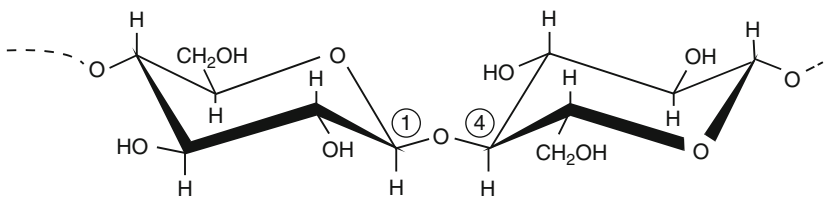

Solid Biofuels, Fuels and Their Characteristics. Figure 4 Chemical structure of cellulose

macromolecular composition are therefore directly influencing the total carbon content as the main determinant for the calorific value of the dry matter. High contents of lignin and extractives are therefore raising the calorific value (section "Calorific Value").

Elemental Composition

Plant biomass is composed of many elements, of which 26 are known to be essential for growth. They can be distinguished between main elements and trace elements.

The main elements are carbon (C), oxygen (O), and hydrogen (H), which arise from the CO_2-assimilation and the H_2O-uptake, and the six major nutrients nitrogen (N), potassium (K), phosphorus (P), calcium (Ca), magnesium (Mg), and sulfur (S), as well as the also relatively prevalent chlorine (Cl), which does not count as a nutrient. These elements are either decisively contributing to biomass formation or they play an important role as associated material in plant nutrition.

Apart from these elements the plant mass also contains trace elements such as silicon (Si), sodium (Na),

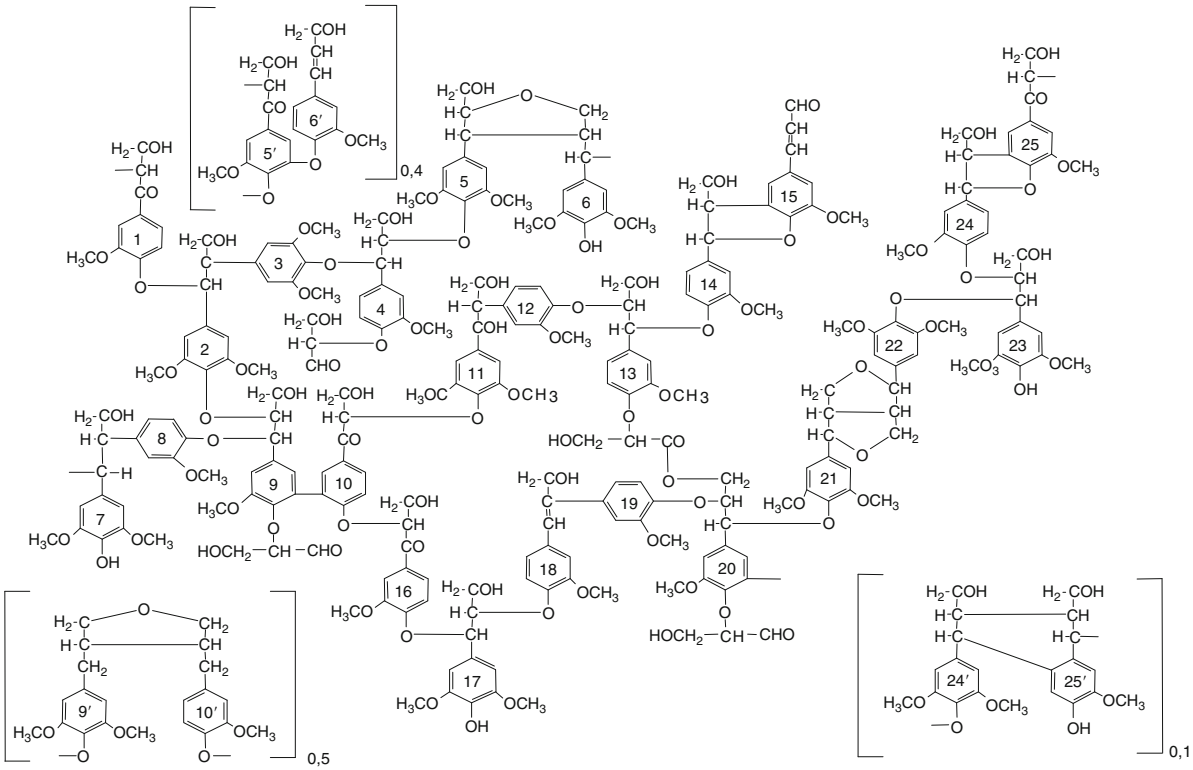

Solid Biofuels, Fuels and Their Characteristics. Figure 5
Chemical structure of beech wood lignin [45]

iron (Fe), manganese (Mn), zinc (Zn), copper (Cu), molybdenum (Mo), cobalt (Co), lead (Pb), aluminum (Al), chrome (Cr), cadmium (Cd), nickel (Ni), mercury (Hg) or arsenic (As). Several of them are listed as essential micro nutrients while others can be harmful to plant life. The usual concentrations of these elements and their impact on in thermochemical conversion are discussed below.

Main Elements *Carbon, oxygen, hydrogen.* Solid biomass consists mainly of carbon (C), oxygen (O), and hydrogen (H). The component that most determines the release of heat via oxidation is the carbon. Hydrogen also provides energy by oxidations while oxygen supports these reactions. Woody fuels contain the highest carbon content among the biomass materials (about 47–50 mass-% in dry matter). Non-woody biomass fuels have a carbon content of 43–48%. Their oxygen content is between 40% and 45% (dry basis) and for hydrogen the content is between 5% and 7% (see Table 3).

From these data the molecular formula for wood is around $CH_{1.44}O_{0.66}$. Significantly, higher carbon contents are given for biomass with high oil content (e.g., rapeseeds). A higher share of non-burning constituents (ash) can cause lower carbon content. This, for example, applies to roadside woodcuttings with usually have a higher ash content.

Opposite to coal (e.g., hard coal, brown coal), which are an outcome of a natural carbonization process, the carbon in solid biofuels is prevailing in a partly oxidized mode with a respectively higher oxygen content, thus having a lower carbon concentration. This explains the lower caloric value compared to fossil coal (Table 6).

Nitrogen. The nitrogen(N)-content varies significantly between different biomass types. This variation reflects the differences in composition of solid biomass. High protein containing plants or plant fractions are always higher in nitrogen content than typical lignocellulose materials as wood or straw. This applies mainly to the generative parts of crops like grain, oil

Solid Biofuels, Fuels and Their Characteristics. Table 3 Contents of main elements in untreated natural biomass fuels compared to hard and brown coal (mean values according to [31], for coal: [56])

Biomass fuel	C	H	O	N	K	Ca	Mg	P	S	Cl
	in % of dry matter									
Hard coal	72.5	5.6	11.1	1.3					0.94	<0.13
Brown coal	65.9	4.9	23.0	0.7					0.39	<0.1
Spruce wood (with bark)	49.8	6.3	43.2	0.13	0.13	0.70	0.08	0.03	0.015	0.005
Beech wood (with bark)	47.9	6.2	45.2	0.22	0.15	0.29	0.04	0.04	0.015	0.006
Poplar (short rotation)	47.5	6.2	44.1	0.42	0.35	0.51	0.05	0.10	0.031	0.004
Willow (short rotation)	47.1	6.1	44.3	0.54	0.26	0.68	0.05	0.09	0.045	0.004
Bark (coniferous)	51.4	5.7	38.7	0.48	0.24	1.27	0.14	0.05	0.085	0.019
Rye straw	46.6	6.0	42.1	0.55	1.68	0.36	0.06	0.15	0.085	0.40
Wheat straw	45.6	5.8	42.4	0.48	1.01	0.31	0.10	0.10	0.082	0.19
Triticale straw	43.9	5.9	43.8	0.42	1.05	0.31	0.05	0.08	0.056	0.27
Barley straw	47.5	5.8	41.4	0.46	1.38	0.49	0.07	0.21	0.089	0.40
Rapeseed straw	47.1	5.9	40.0	0.84	0.79	1.70	0.22	0.13	0.27	0.47
Maize straw	45.7	5.3	41.7	0.65					0.12	0.35
Sunflower straw	42.5	5.1	39.1	1.11	5.00	1.90	0.21	0.20	0.15	0.81
Hemp straw	46.1	5.9	42.5	0.74	1.54	1.34	0.20	0.25	0.10	0.20
Rye whole plants	48.0	5.8	40.9	1.14	1.11		0.07	0.28	0.11	0.34
Wheat whole plants	45.2	6.4	42.9	1.41	0.71	0.21	0.12	0.24	0.12	0.09
Triticale whole plants	44.0	6.0	44.6	1.08	0.90	0.19	0.09	0.22	0.18	0.14
Rye kernels	45.7	6.4	44.0	1.91	0.66		0.17	0.49	0.11	0.16
Wheat kernels	43.6	6.5	44.9	2.28	0.46	0.05	0.13	0.39	0.12	0.04
Triticale kernels	43.5	6.4	46.4	1.68	0.62	0.06	0.10	0.35	0.11	0.07
Rapeseed kernels	60.5	7.2	23.8	3.94					0.10	
Miscanthus	47.5	6.2	41.7	0.73	0.72	0.16	0.06	0.07	0.15	0.22
Hay (nature conservation)	45.5	6.1	41.5	1.14	1.49	0.50	0.16	0.19	0.16	0.31
Tall fescue	41.4	6.3	43.0	0.87	1.94	0.38	0.17	0.17	0.14	0.50
Ryegras	46.1	5.6	38.1	1.34					0.14	1.39
Gras from roadsides	37.1	5.1	33.2	1.49	1.30	2.38	0.63	0.19	0.19	0.88

seeds, and protein plants, but it is also true for herbaceous crops, which have a high value as animal feed. Correspondingly, the nitrogen content is relatively high for grain kernels, whole grain plants and animal feed grass. Spruce wood contains only little nitrogen of around 0.1–0.2% (1,000–2,000 mg/kg) in the dry matter, while grain straw ranges in the order of 0.5% (Table 3). Also slightly increased nitrogen contents are observed for short rotation coppice; this is explained by the higher content of bark in the total wood mass.

The variations within a specific biomass assortment are usually relatively low for wood. This is demonstrated by the frequency distribution of certain

concentration classes (Fig. 7). Concentrations of above 0.6% or below 0.3% are, for example, quite rare in wood fuels. Higher values and variation are given for straw from rapeseed, maize, sunflower, or hemp crops. The higher variation of nitrogen concentrations in herbaceous fuels is mainly due to differences in fertilization (e.g., different fertilization level or fertilization timing).

The nitrogen content of the fuel is directly affecting the formation of nitrogen oxides (NO_x) because this element is usually completely released into the volatile phase during combustion or gasification. The oxidation of the chemically bound nitrogen in the fuel is by far the most relevant formation path for NO_x. Therefore, the NO_x formation is usually declining with lower N-content in the fuel. Nitrogen embedding into the ash hardly happens. Nitrogen can also be responsible for the formation of N_2O (laughing gas) which is harmful to the climate.

Potassium. Similar to nitrogen there are also major differences in the potassium (K)-content between periodically fertilized field crops and perennial wood cultures usually not fertilized (e.g., forest or short rotation coppice). However, the potassium is – other than for nitrogen – not mostly prevalent in the generative parts of the plants, but it occurs mainly in the sprout and leaves. Therefore the potassium content of grain kernels is low (ca. 0.5–0.7% or 5,000–7,000 mg/kg, dry basis) while grain straw usually has K-concentrations around or above 1% (Table 3). Wood fuels however show potassium contents of hardly higher than 0.35% and their variation is low. This is not the case for grain straw, where the concentration varies between 0.2% and 2.5%. This larger bandwidth is not only a result of variable fertilization levels. It can be caused by differences in leaching by precipitation during the phase between ripening and harvest [31, 53].

Potassium is involved in the corrosion process on heat exchangers or on flue gas conducting parts of a furnace. The participation of potassium (and sodium) in corrosion is based on the fact that these elements can form gaseous alkali chlorides which condense and deposit on heat exchanger surfaces or on fine particles during cooling. These deposits can react with sulfur dioxide (SO_2) from the flue gas on heat exchanger surfaces and form alkali sulfates and elementary chlorine (Cl_2). The latter can diffuse though the porous cinder layers toward the tube surface of the heat exchanger where it is reduced to iron chloride ($FeCl_2$) due to the prevailing reductive conditions. Under the large temperature differences within the layer of deposits on the heat exchanger the partial pressure of $FeCl_2$ is differing largely. This allows the $FeCl_2$ gaseous under the prevailing conditions to diffuse away from the tube surface where they again undergo oxidizing conditions. The iron is thus oxidized again and a part of the released chlorine is repeatedly available for the corrosion process (so-called high temperature chlorine corrosion, Fig. 6) [48].

In the oxide state, potassium becomes volatile during combustion and only after cooling in the course of the flue gas tract it is condensed as fine particle. Therefore, potassium is listed among the aerosol forming elements of biofuel components [3]; this property can cause significant increases of particle emissions [35].

Potassium also influences the ash softening properties of a biofuel as it lowers the melting temperature of the ash (section "Ash Melting Properties"). The largest share of the potassium is thus embedded into the solid ash residues.

Calcium, magnesium, phosphorus. Biomass contains calcium (Ca), magnesium (Mg), and phosphorus (P). The calcium content ranges between 0.3% and 1% (for bark even higher), but in herbaceous fuels it can be significantly higher. The calcium content is low in grain straw and kernels. But it can be high in straw from other crops (e.g., rapeseed straw, sunflower straw) (Table 3).

In the combustion process, calcium improves the ash softening behavior by increasing the melting temperature of the ash (section "Ash Melting Properties"). For several fuels with an unfavorable ash-melting behavior, it can therefore be useful to mix calcium-containing additives (e.g., lime) to the fuel in order to raise the ash melting point [57]. High contents of alkaline earth elements (mainly Ca) can also lead to a higher embedding of sulfur into the ash, thus preventing the sulfur to be released as harmful SO_2 via the flue gas.

The manganese(Mg)-content in wood fuels is relatively low (ca. 0.04–0.1%). This is also true for phosphorus which is usually found in concentrations of <0.1% (for wood) or about 0.2% (herbaceous fuels) (Table 3). The three elements calcium, magnesium, and phosphorus increase the fertilization value of the ash.

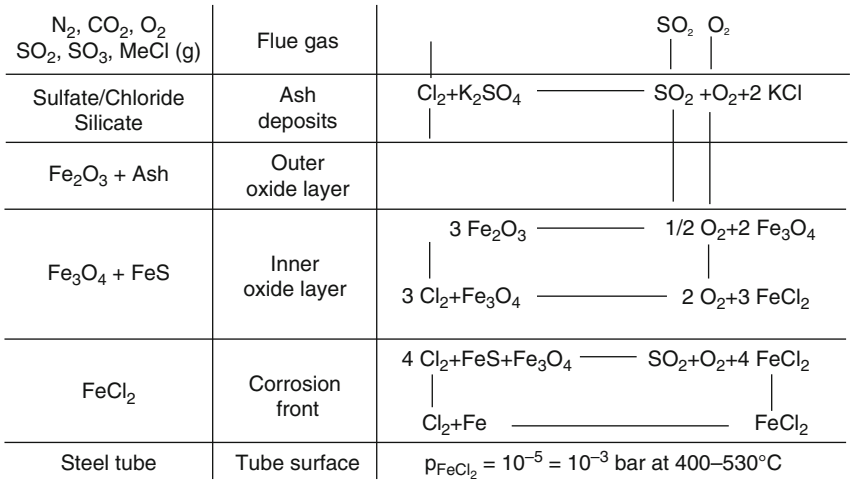

Solid Biofuels, Fuels and Their Characteristics. Figure 6
Mechanism of high temperature chlorine corrosion at a heat exchanger surface [48]

Sulfur. The sulfur(S)-content in biomass fuels is strongly depending on the given macromolecular composition. For some amino acids and enzymes sulfur is required as an essential crop nutrient, but mostly only low quantities have to be provided by fertilization. However, the sulfur supply is usually significantly higher for field crops than for unfertilised woodland or for hardly fertilized short rotation coppice. Rapeseed straw has an average sulfur content of 0.3% in the dry matter. This is the highest among the biomass fuels. For wood fuels a sulfur content in the range of 0.02–0.05% can be expected and for grain straw the S-content is usually below 0.1% (Table 3). In general biomass fuels are low sulfur containing fuels.

In a complete thermochemical conversion, the sulfur oxide emissions are mainly determined by the sulfur content in the applied fuel. Sulfur is mostly changing into the gaseous phase by forming SO_2, SO_3, and alkali sulfates [48]. Similar to chloride, sulfur compounds can also condense during the cooling phase of the flue gas while forming alkaline or alkaline earth sulfates which are deposited either on heat exchanger surfaces or on other flue gas particles. A large portion of the sulfur content in the fuel (ca. 40–90%) is embedded into the ash, depending on the degree of particle separation by the applied flue gas purification system.

Sulfur can also indirectly contribute to increased corrosion (e.g., on heat exchanger surfaces). This can occur at higher SO_2-concentrations in the flue gas. Due to an increased sulfate binding in the prevailing alkaline and alkaline earth chloride compounds a release of corrosive chlorine (Cl_2) is supported [48].

Under certain circumstances, sulfur can also play a role in preventing the formation of dioxin and furan (PCDD/F). This can happen by changing and inactivating the catalytically acting copper oxides. In coal combustion, for example, a PCDD/F inhibiting effect is observed when the Cl/S-ratio in the fuel falls below 1.0. The chlorination or aromatics during PCDD/F-formation is usually even fully prevented at a Cl/S-ratio below 0.1 [25, 56].

Chlorine. Chlorine (Cl) is a major associated material in potassium fertilizers [31]. Therefore its content in herbaceous biomass fuels is significantly higher than in wood fuels. This is because in forest operations and in short rotation forestry practice fertilization does usually not happen.

Consequently wood fuels show very low chlorine contents of about 0.005–0.02% in the dry matter. Often these contents are even below the detection limits of the applied methods. But for grain straw the chlorine content is several times higher (ca. 0.2–0.5%) and in coastal areas even concentrations of more than 1% are possible. Very high Cl-content is often observed in straw from rapeseed and sunflower (ca. 0.5–0.8%). This is also true for conventional hay (e.g., from ryegrass) (Table 3).

For the chlorine content, the bandwidth of variation is relatively high. In non-wood crops [31] this variation is on the one hand caused by the variable chlorine freight transported onto the land by fertilization and on the other hand it is influenced by leaching from the soil or from the died-off crop through precipitation. Such leaching from the crop can account for 60–80% chlorine reduction in the fuel [31, 53]. Therefore the leached "gray" straw is – from the viewpoint of combustion – always preferable compared to any fresh "yellow" straw. Both straw qualities are usually available in a region or during a harvesting season, thus the frequency distribution curve for the chlorine concentrations follows a pattern with a peak on the left side (Fig. 7).

The significance of chlorine in a thermochemical conversion process is manifold. For example, Chlorine is participating in the formation of hydrogen chloride (HCl) and dioxin/furan (PCDD/F) [38, 39, 48]. In spite of a high chlorine embedding into the ash between 40% and 95% [48], the HCl emissions via flue gas can be critical for certain Cl-rich fuels (e.g., grain straw) which then require secondary flue gas treatment. Furthermore, chlorine is acting corrosive at the surface of heat exchangers. This happens in interaction with alkaline and alkaline earth metals and with sulfur dioxide (SO_2). Additionally, chlorine is known to be an aerosol forming element [3], which can contribute to increasing particulate matter emissions during combustion [35].

Trace Elements All remaining elements are defined as trace elements. They are mostly heavy metals. These elements mainly determine the quality and usability of

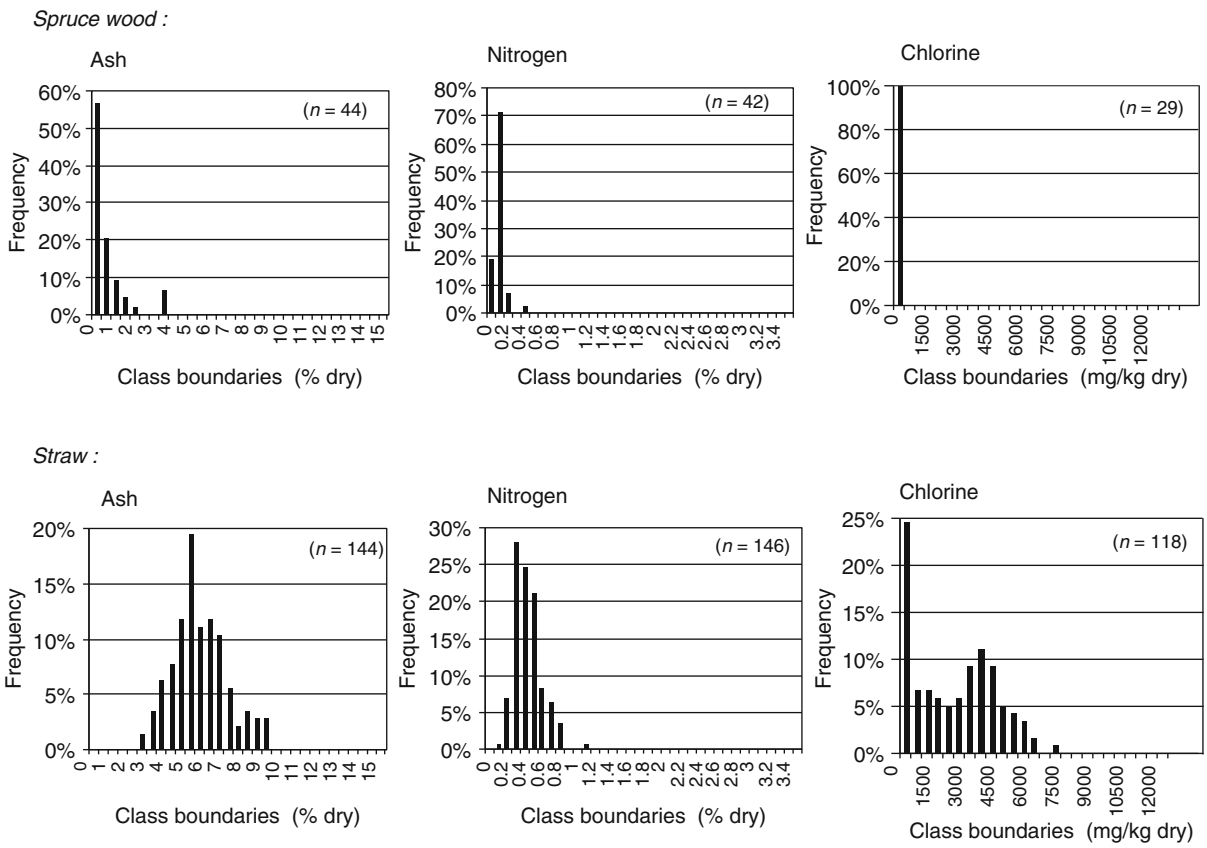

Solid Biofuels, Fuels and Their Characteristics. Figure 7
Frequency distribution of values for selected fuel parameters measured in spruce wood and grain straw (*n* number of data) [31]

the ash accumulated during combustion or gasification. The easy volatile heavy metals cadmium (Cd), lead (Pb), and zinc (Zn) are listed as major aerosol forming elements increasing the emissions of particulate matter during combustion [3].

Opposite to the main elements, the variation of the trace element content is largely higher and less predictable. But some general trends and differences between the untreated natural fuels can be identified. Wood fuels from the forests, for example, are usually higher in heavy metal content than annually harvested crops. Particularly the bark from spruce wood takes here a top position for most heavy metals (for As, Cd, Co, Fe, Hg, Mn, Mo, Ni, and Zn). For the other wood fuels a differentiation has to be made between the long-term growing forest trees and the short rotation coppice (e.g., poplar, willow), where forest wood has almost consistently higher heavy metal contents. This is primarily due to the long rotation time where the forest trees are exposed to heavy metal depositions from the atmosphere. A second explanation is given by the fact that the pH-value of forest soils are usually low, which leads to a higher heavy metal solubility and thus to an increased element uptake via the roots.

An exception is here given for cadmium, which is relatively high in young willow trees due to a specific capturing ability which is given for this crop. Therefore, willow can be used for melioration of cadmium polluted fields [31, 54]. Apart from cadmium, the content of nickel, chrome, and mainly mercury, lead, and molybdenum is usually quite low for short rotation coppice.

The heavy metal content represents an important characteristic for the differentiation between naturally untreated and treated or used fuels. Increased heavy metal contents are often observed for grass cuttings or wood from roadsides [31]. Therefore some heavy metals are used as lead indicators for any nonnatural or untreated background. For example, a rapid test was developed for zinc (combined with the element chlorine) which is determined in the accumulated ash of a furnace in order to find evidence for illegal fuel use [46].

Also for compressed biomass such as briquettes the proof for using only natural untreated raw material can be provided by meeting the limitations of a fuel standard. For example, in Germany the requirements for wood briquettes concerning heavy metals were fixed according to the standard DIN 51 731 [8]. It requires staying below the following threshold values:

- Arsenic (As) < 0.8 mg/kg
- Cadmium (Cd) < 0.5 mg/kg
- Chrome (Cr) < 8 mg/kg
- Copper (Cu) < 5 mg/kg
- Mercury (Hg) < 0.05 mg/kg
- Lead (Pb) < 10 mg/kg
- Zinc (Zn) < 100 mg/kg

Heavy metals can primarily influence the ash quality, as they largely remain in the combustion residues and can limit their reuse for fertilization purposes. But, the heavy metal concentrations of different ash fractions from a thermochemical process can largely differ. Cadmium, zinc and lead are easier volatilized than other heavy metals. In the flue gas they are thus condensed on fly ash particles during the cooling phase and therefore they are accumulated in these particles (e.g., fabric filters, electrostatic precipitators). By separating the bed ashes from the cyclone or filter ashes for reuse or disposal the pollution risks by fertilization can be controlled and minimized [48].

Some heavy metals can act catalytically in the formation of dioxin and furan (PCDD/F). Copper and iron chloride play a leading role in this process; they serve as source for chlorine. Particularly the Cu^{2+} ions can catalyze the formation of C-Cl bindings and the oxidation of carbon [1].

Technical Combustion Properties

The technical combustion properties of biofuels described below are determining the possibilities and boundaries for thermochemical conversion or they play an important role in this process. Apart from the calorific value, the moisture and ash content as well as the ash-softening behavior of the fuels are here presented and discussed.

Calorific Value

Definition. For the calorific value (heating value) a differentiation between the gross calorific value and the net calorific value is made. Both definitions are given and the differences are discussed.

Definition of net calorific value. The net calorific value (q_{net}) is the specific heat released during complete

oxidation of a fuel without regarding the latent heat by condensation of any water vapor in the flue gas (EN 14918 [10]). It is defined as absolute value of the specific heat (enthalpy) of combustion, in joules, for unit mass of the biofuel burned in oxygen at constant pressure or at constant volume under such conditions that all the water of the reaction products remains as water vapor (hypothetically at a pressure of 0.1 MPa). If the latent heat of the water vapor would be recovered the released heat would be slightly higher. Therefore the net calorific value was formerly been named as "lower calorific value."

Definition of gross calorific value. Opposite to the net calorific value the gross calorific value (q_{gr}) is the specific heat released at complete oxidation of a fuel when the latent heat by condensation of any water vapor in the flue gas is regarded and utilized. In order to do this the flue gas has to be cooled to condense the water vapor. According to the method for determination (EN 14918 [10]) the reference temperature is here set to 25°C. Compared to the net calorific value the heat yield is higher. Therefore, the gross calorific value was formerly named as "higher calorific value."

Difference between gross and net calorific value. The water vapor which is formed during the thermochemical reaction and which is the main reason for the two different definitions of the calorific value is either produced in the chemical reaction of the fuel-bound hydrogen or from the free water in the solid biofuel. For each percentage point of hydrogen content in the dry matter, a latent heat of 218.3 J (related to 1 g of fuel) can be calculated (at 25°C flue gas temperature). For the free and bound water in the biomass, the specific latent heat yield per percentage point of moisture content is 24.43 J, related to 1 g fuel mass.

With these specific values, the deviation between gross and net calorific value can be calculated. The terms can therefore not be used alternatively. For the calculation of the chemically bound fuel energy in a given fuel mass, the net calorific value represents the commonly used parameter. This is because in a heating plant the latent heat via flue gas condensation can only be used if the heat use system is designed for low temperature levels. Furthermore, the combustion unit itself and the chimney system must be able to manage the produced condensates without damage (e.g., condensing boilers). These circumstances are however rarely given. The common use of the net calorific value is therefore a technical convention, which regards the currently given practice of solid fuel conversion systems. This agreement however leads to the paradox, that conversion plants, where the respective technical infrastructure for flue gas condensation and low temperature heat use is given, can thus achieve efficiencies of more than 100% [33]. If the fuel input would be calculated by using then gross calorific value the efficiency would always be below 100%.

The gross calorific value (q_{gr}) of biomass fuels is usually about 6% (bark), 7% (wood), or 7.5% (herbaceous fuels) higher than the net calorific value (q_{net}) (Table 6). This, however, only applies to absolutely dry biomass fuels. For wet fuels this relative difference between the two parameters increases, because the possible heat yield through re-condensation of the produced water vapor is respectively higher (Fig. 8).

Determination. The determination of the gross calorific value – from which afterwards the net calorific value is calculated – is done by the calorimetric method according to EN/TS 14918 [10]. It consists of two separate tests: (1) the combustion of the calibration substance (benzoic acid) and (2) the combustion of the fuel sample itself. For both combustion tests, the same conditions have to be guaranteed.

The determination of the gross calorific value is done by performing a combustion reaction (in pure oxygen under high pressure) after which the combustion products are in defined conditions. This happens in a so-called calorimetric bomb enclosed by a water

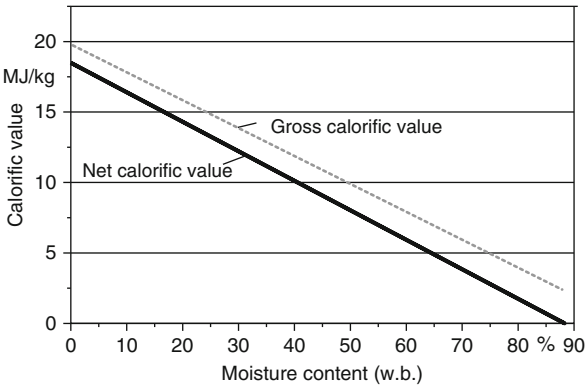

Solid Biofuels, Fuels and Their Characteristics. Figure 8 Difference between gross and net calorific value at variable fuel moisture contents

jacket at temperatures of about 25°C (bomb calorimeter). In the water jacket the temperature change can be determined. It represents the released heat during the performed combustion.

After having determined the gross calorific value, the net calorific value is calculated. This is done by reducing the energy content according to the above given correction factors for each percentage point of hydrogen content. In addition, for moisture content a correction is needed by using the above given correction factors. Both corrections account for the heat by condensation usually not recovered (see above). Therefore, an analysis of the hydrogen and the moisture content of the test sample are always needed for the determination of calorific value. Furthermore, the content of oxygen, sulfur, and nitrogen in the fuel is required.

Calorific value of *dry fuels*. For solid biofuels the net calorific value (q_{net}) of the absolutely dry matter is between 16.5 and 19 MJ/kg (Table 6). In practice the rule of thumb applies, it say that about 2.5 kg of air-dried wood represents about 1 l of heating oil (≈10 kWh or ≈36 MJ). For coniferous wood approximately 2% higher net calorific value is observed compared to wood from broad leaf trees [31]. This increase is due to the higher lignin content. For bark from coniferous, another 2% increase is given due to the content of extractives (e.g., resin, oils, and fats). Both component groups are characterized by a relatively high partial calorific value (27.0 and 35.9 MJ/kg), compared to cellulose (about 17.3 MJ/kg) or hemicellulose (about ca. 16.2 MJ/kg) [42].

Wood fuels show a mean increase of net calorific value of about 9% compared to herbaceous fuels. It varies between 16.5 and 17.5 MJ/kg (Fig. 7). Marked differences between grain straw and grain kernels are not given, this also applies to the different grass species. Oil containing fuels (e.g., rapeseed kernels, rapeseed press cake) have a higher calorific value, depending on the individual oil content. This is due to the high calorific value of the oil, which is around 36 MJ/kg (see Table 6).

The calorific value of dry biomass fuels is mainly depending on the content of oxidizable elements (primarily carbon and hydrogen). Additional heat is also released by the oxidation of several main nutrient elements such as sulfur and nitrogen. Due to the usually low contents of these elements, the calorific value of solid biofuels is not influenced significantly. The oxygen content, however, reduces the calorific value because the oxidizable components of oxygen-containing compounds are already available at a higher oxidation state and thus any further oxidation can only provide limited heat yields.

Because of the above interrelation, the net calorific value can be estimated from the knowledge of the elemental composition. This is frequently done by using Eq. 1 (approximation according to BOIE [44]). For biomass, this equation was found best fitting in empirical studies [31]. The net calorific value of dry biomass fuels ($q_{net,\,d}$) in MJ/kg is thus calculated from the element content of carbon (C), hydrogen (H), and the main nutrients sulfur (S) and nitrogen (N). Additionally, the oxygen (O) content in percent of the dry matter is required. When using Eq. 1 a mean error of 4% is given [31]:

$$\left(q_{net,\,d}\right) = 34.8\mathrm{C} + 93.9\mathrm{H} + 10.5\mathrm{S} + 6.3\mathrm{N} - 10.8\mathrm{O} \tag{1}$$

Recently also a new biomass specific estimation for the gross calorific value (dry basis) was derived from 122 data sets [23]. This estimation is given in Eq. 2.

$$\left(q_{gross,\,d}\right) = 1.87\mathrm{C}^2 - 144\mathrm{C} - 2.802\mathrm{H} + 63.8\mathrm{CH} + 129\mathrm{N} + 20.147 \tag{2}$$

$q_{gross,\,d}$ in kJ/kg is given when for carbon (C), hydrogen (H), and nitrogen (N) the values are entered in mass-% from the elementary analyses of the dry biomass fuel.

Impact of moisture content. The highest influence on the net calorific value of a biomass is given by the moisture content. Because moisture content is highly variable, comparisons between fuel types are always made on dry matter basis. Between moisture content and actual calorific value, a linear correlation is given (Fig. 8).

For an estimation of the actual amount of energy, the net calorific value as given at moisture content upon delivery or energetic use is relevant. The respective calculation is done using Eq. 3. $q_{net,\,ar}$ is the net calorific value of the biomass as received (in MJ/kg), M is the given moisture content (in %), $q_{net,\,d}$ is the calorific value of the dry biomass, and the constant

2.443 results from the evaporation heat of water (in MJ/kg), at a temperature of 25°C.

$$q_{\text{net, ar}} = \frac{q_{\text{net, d}}(100 - M) - 2.443M}{100} \quad (3)$$

Impact of ash content. The ash content is an influencing factor, too. This, for example, becomes visible when regarding the reduced net calorific value of sunflower straw and grass cuttings from roadsides compared to wood (Table 6). Figure 9 demonstrates this dependency. The usually limited bandwidth of ash content in the fuels leads to a relatively low impact in calorific value. Only if heavy secondary pollution with minerals occur (e.g., for roadside grass cuttings) this can be different.

Estimating an amount of energy. On the basis of the calorific value and the moisture content of the fuel the amount of energy of a given batch can be calculated. To do this the mass has to be determined. For wood logs, which are mainly traded by the volume (stacked cubic meter) a rough estimation of the mass can be made via conversion into solid cubic meters (massive wood), for example by using the conversion factors given in Table 10. From the solid cubic meters the total wood mass can be calculated, this is done by using mean values for the wood density (Table 11). Because in nature wood is not available at absolutely dry stage the wood densities at given moisture content should be applied. For three different wood types, this conversion is made in Table 4 for several assortments [29].

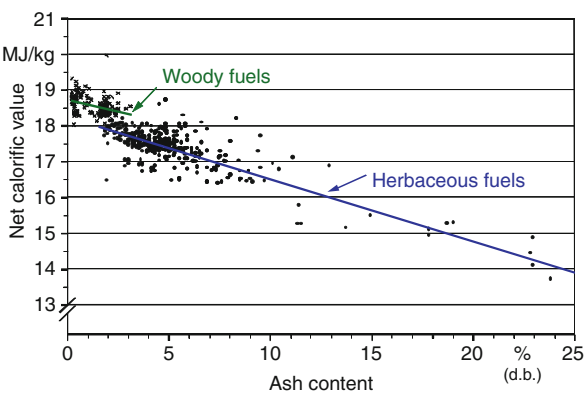

Solid Biofuels, Fuels and Their Characteristics. Figure 9 Net calorific value as a function of the ash content of wood and herbaceous fuels (related to dry basis) [31]

The conversions for wood logs was performed using uniform factors (1 solid m^3 = 0.65 stacked m^3 wood logs or 1 solid m^3 = 2.43 m^3 wood chips).

The estimation of an amount of energy of a given batch is finally calculated from the determined (or estimated) mass (Table 4), multiplied by the net calorific value of a respective biomass type at the given moisture content (Eq. 3). In Table 5 some planning figures are given for typical biomass fuels and assortments. In order to convert from mega-joule (MJ) into kilowatt hours (kWh) a division by 3.6 is made. One liter of heating oil equivalent (light heating oil) is calculated by dividing the energy content given in kWh by 10 (10 kWh ≈ 1 l heating oil).

The increase of the available fuel energy by drying is usually overestimated. It is fact that the reduction of moisture content leads to a linear increase of the net calorific value (Fig. 8). However, this parameter is related to the fuel mass with water. Thus the drying also reduces the total fuel mass of a given batch. Therefore, the energy increase by drying is not proportional to the increasing net calorific value (as received).

Figure 10 shows the actual impact of drying on the fuel energy of a given cubic meter of stacked or poured bulk material. For example, the drying of spruce wood logs (1 m^3) from 50% to 15% moisture content leads to an fuel energy increase of 135 kWh, this is equivalent to 13% (see variant B in Fig. 10, left figure). For wood chips, e.g., 1 m^3 spruce wood chips, the energy content of freshly harvested material at 50% moisture content increases by 85 kWh if the fuel is dried down to 15% moisture content (i.e., 13% increase, see variant B in Fig. 10, right figure). If, however, air-dried material is assessed the shrinkage has mostly already happened. Then the valuation of the fuel energy in a given cubic meter of stacked or bulk fuel follows variant A in Fig. 10.

Consequently, the drying of biomass fuels can only lead to significant energy increases if the starting point of drying is at high moisture content. At lower moisture content, the drying mainly improves fuel quality and minimizes fuel losses by biological processes during storage. However, drying is often also a requirement to achieve higher combustion temperatures, which can lead to improved burnout (mainly for residential furnaces). For some thermochemical processes drying is even essential (e.g., log wood stoves or updraft gasification).

Solid Biofuels, Fuels and Their Characteristics. Table 4 Mass of various volume assortments and wood types as a function of moisture content. Solid: solid cubic meter; log: wood logs 33 cm stacked; chips: wood chips; sm^3: solid cubic meter

Moisture content in %	Beech			Spruce			Pine		
	solid 1 m^3	log 1 sm^3	chips 1 m^3	solid 1 m^3	log 1 sm^3	chips 1 m^3	solid 1 m^3	log 1 sm^3	chips 1 m^3
	Mass per unit[a] in kg								
0	680	422	280	430	277	177	490	316	202
10	704	437	290	457	295	188	514	332	212
15	716	445	295	472	304	194	527	340	217
20	730	453	300	*488*	315	201	541	349	223
30	798	495	328	541	349	223	615	397	253
40	930	578	383	631	407	260	718	463	295
50	1,117	694	459	758	489	312	861	556	354

[a]Regarding the fact that wood looses volume while drying; the dry matter densities used here (at 0% moisture) are representing the particle density of dried wood according to Table 11. The respective wood density (incl. moisture) was corrected by the maximum shrinkage (beech 17.9%, spruce 11.9%, pine 12.1%). Between the dry matter density and the density at fiber saturation point (moisture content of 25%, 25% and 21% for beech, spruce, and pine, respectively, see [41]) a linear volume change is assumed

Volatile Matter

All products released from the dry organic substance during pyrolytic decomposition under defined heating conditions are volatile matter. Depending on the fuel type, this fraction is variable. Thus, it is a useful parameter to characterize the fuel's ability to disintegrate into combustible gaseous compounds under heat impact.

The volatile matter content is not an absolute figure. It was defined through convention. It is determined under standardized conditions following EN 15148 [16]. A test portion is heated without contact to ambient air at 900°C ± 10°C for 7 min. The percentage of volatile matter is calculated from the loss in mass of the test portion after deducting the loss in mass due to moisture. In order to achieve a reproducible measurement, the end temperature and the total time of the test have to be monitored carefully. Furthermore, the access to air is to be prevented in order to avoid oxidation.

The volatile matter content allows conclusions on the flame length during combustion or on the gas build-up in gasification. It is thus a relevant characteristic for furnace construction. For example, it can be necessary to increase the amount of secondary air flow if the fuel has high volatile matter content. Also, the combustion space in the furnace has to be larger for high volatile matter contents in order to ensure a sufficiently high residence time of the larger gas volume released.

For lignocellulose fuels, the volatile matter content in the total dry mass is between 74% and 83%. The upper end of this bandwidth is marked by wood fuels (around 82% volatile matter) while for grain straw and grassland cuttings lower values of 74% and 76% are reported (Table 6). In coal the volatile matter is significantly lower. For hard coal a range of 6–45% and for lignite values between 45% and 63% are reported.

Moisture Content

The moisture content is the share of water which can be removed from the fuel under defined conditions. It is usually related to the total mass including water. Sometimes it is also related to the dry matter (e.g., in Germany it is then denominated as "wood moisture" instead of "moisture content"; this term is common in forestry and wood processing industry). However, for energy purposes the moisture content (based on the total mass) is internationally more commonly used [9].

Solid Biofuels, Fuels and Their Characteristics. Table 5 Planning figures for the evaluation of the energy content in a given fuel batch (for wood logs and wood chips the volume change which happens below 25% moisture content was considered) (*OE* oil equivalent, based on light heating oil)

Fuel	Unit	Moisture content *M* in %	Mass (at *M*) in kg	Net calorific value (at *M*) in MJ/kg	Fuel value		
					in MJ	in kWh	in l OE
Wood logs, stacked							
Beech 33 cm, dry	1 sm^3	15	445	15.3	6,797	1,888	189
Beech 33 cm, skin-dry	1 sm^3	30	495	12.1	6,018	1,672	167
Spruce 33 cm, dry	1 sm^3	15	304	15.6	4,753	1,320	132
Spruce 33 cm, skin-dry	1 sm^3	30	349	12.4	4,339	1,205	121
Wood chips							
Beech, dry	1 m^3	15	295	15.3	4,503	1,251	125
Beech, skin-dry	1 m^3	30	328	12.1	3,987	1,107	111
Spruce, dry	1 m^3	15	194	15.6	3,032	842	84
Spruce, skin-dry	1 m^3	30	223	12.4	2,768	769	77
Pellets							
Wood pellets, by volume	1 m^3	8	650	17.1	11,115	3,088	309
Wood pellets, by weight	1 t	8	1,000	17.1	17,101	4,750	475
Fuels by weight							
Beech, dry	1 t	15	1,000	15.3	15,274	4,243	424
Beech, skin dry	1 t	30	1,000	12.1	12,148	3,374	337
Spruce, dry	1 t	15	1,000	15.6	15,614	4,337	434
Spruce, skin dry	1 t	30	1,000	12.4	12,428	3,452	345
Herbaceous (e.g., straw)	1 t	15	1,000	14.3	14,254	3,959	396

It is determined by placing a sample in a drying cabinet at 105°C until constant mass (i.e., drying until no further mass differences can be recorded). This procedure follows the European Standard EN 14774-1 [22].

Natural untreated biomass fuels can also contain some small amount of highly volatile extractives with high-energy content (section "Molecular Composition"). These substances can become volatile during the moisture content determination in a drying cabinet. They are mostly α-pinenes. However, the difference in the measured moisture content is usually below 1%. Only for oil containing materials (e.g., rapeseed press cake) slightly higher deviations are observed when drying is performed at 80°C instead of the usual 105°C [52]. For vast majority of solid biomass fuels the possible error by accepting any volatilization of non-water substances can be neglected in the assessment of a given fuel (e.g., for the determination of the calorific value).

Higher measuring errors are however possible if – as it is realized in practice – rapid methods are applied for moisture content determination. This applies particularly to measuring devices operating according to the electrical conductivity principle as used for wood logs. They usually underestimate the actual moisture content [51]. Rapid test methods for wood chips using capacitance or infrared-reflection methods (NIR) are significantly more accurate. Their measuring inaccuracy is around 3–10% and it remains constant over a large range of moisture contents up to 50% [2, 62].

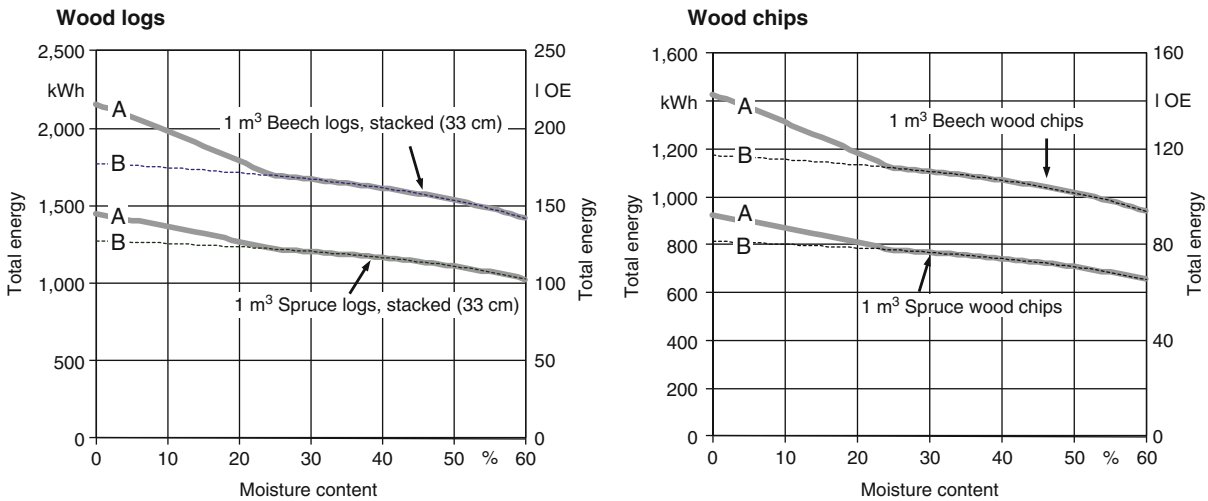

Solid Biofuels, Fuels and Their Characteristics. Figure 10
Energy content in a stacked cubic meter of wood logs (*left figure*) or in a cubic meter of wood chips (*right figure*) as a function of fuel moisture content. Variant A and B: with and without regarding volume changes by swelling and shrinkage (i.e., for variant A the shrinkage volume is replaced while for variant B the dry matter content remains the same) (*OE* oil equivalent, for light heating oil)

Any false estimation of the moisture content affects the valuation of the fuel energy; this is because the moisture content is the major determinant for the net calorific value at the given drying stage. In nature, totally dry biomass material is not available. Thus the remaining moisture content has to be evaporated during thermochemical conversion. The required energy for this process is obtained from the released process heat and thus it reduces the net energy yield if – as it is common – no condensation of the water vapor in the flue gas is performed.

This impact of moisture content on the net calorific value of the biomass (as received) is shown in Eq. 3. Figure 8 illustrates the described function (section "Calorific Value"). It shows that the net calorific value of wood (here: 18.5 MJ/kg) deceases linearly with rising moisture content. At around 88% moisture content the net calorific value is zero.

In the lower moisture range, an effect on volume of wood is given (section "Physical-Mechanical Properties"). Nevertheless, moisture mainly affects the fuel mass and the combustion temperatures to be achieved under adiabatic conditions. Furthermore, the storability of the fuel is influenced. Moisture content above 16% usually speeds up biological degradation and conversion processes associated with energy losses. Additionally there is an increasing risk of fire due to self-heating and possible self-ignition.

Moisture content of biomass fuels is highly variable, depending on the biomass type, the season and the time between provision and energetic use. The usual bandwidth is between 8% and 65%. Fresh from the forest the moisture content of wood is between 45% and 60%. Hard wood has lower moisture content than soft wood. For coniferous wood, the moisture content is higher in winter when assimilation is low compared to summer [4]. This is not true for broad leaf trees. In short rotation forestry (e.g., poplar, willow) there is an increase of moisture content at the beginning of the vegetation period of 5%-points [31]; this results in higher moisture contents if harvesting is delayed to spring.

Equilibrium moisture content of air-dried wood in Central Europe is given between 10% and 20%, depending on the season. This results in a net calorific value between 14.5 and 16.5 MJ/kg. Herbaceous fuels which are died-off or have been field dried and grain kernels can usually be stored at 15% moisture content. Pellets which follow the European pellet standard EN 14961–2 shall have a maximum moisture content of 10% [18].

Solid Biofuels, Fuels and Their Characteristics. Table 6 Technical combustion properties of untreated natural biomass fuels compared to hard and brown coal (mean values according to [31], for coal: [56])

Biomass fuel	Net calorific value in MJ/kg	Gross calorific value in MJ/kg	Ash content in %	Volatile matter content in %	Ash melting properties		
					DT[a] in °C	HT[a] in °C	FT[b] in °C
Hard coal	29.7[c]		8.3	34.7	1,250		
Brown coal	20.6[c]		5.1	52.1	1,050		
Spruce wood (with bark)	18.8	20.2	0.6	82.9	1,426		1,583
Beech wood (with bark)	18.4	19.7	0.5	84.0			
Poplar (short rotation)	18.5	19.8	1.8	81.2	1,335		1,475
Willow (short rotation)	18.4	19.7	2.0	80.3	1,283		1,490
Bark (coniferous)	19.2	20.4	3.8	77.2	1,440	1,460	1,490
Rye straw	17.4	18.5	4.8	76.4	1,002	1,147	1,188
Wheat straw	17.2	18.5	5.7	77.0	998	1,246	1,302
Triticale straw	17.1	18.3	5.9	75.2	911	1,125	1,167
Barley straw	17.5	18.5	4.8	77.3	980	1,113	1,173
Rapeseed straw	17.1	18.1	6.2	75.8	1,273		1,403
Maize straw	17.7	18.9	6.7	76.8	1,050	1,120	1,140
Sunflower straw	15.8	16.9	12.2	72.7	839	1,178	1,270
Hemp straw	17.0	18.2	4.8	81.4	1,336	1,420	1,456
Rye whole plants	17.7	19.0	4.2	79.1			
Wheat whole plants	17.1	18.7	4.1	77.6	977	1,155	1,207
Triticale whole plants	17.0	18.4	4.4	78.2	833	982	1,019
Rye kernels	17.1	18.4	2.0	80.9	710		810
Wheat kernels	17.0	18.4	2.7	80.0	687	887	933
Triticale kernels	16.9	18.2	2.1	81.0	730	795	840
Rapeseed kernels	26.5		4.6	85.2			
Miscanthus	17.6	19.1	3.9	77.6	973	1,097	1,170
Hay (nature conservation)	17.4	18.9	5.7	75.4	1,061		1,228
Tall fescue	16.4	17.8	8.5	72.0	869	1,197	1,233
Ryegras	16.5	18.0	8.8	74.8			
Gras from roadsides	14.1	15.2	23.1	61.7	1,200	1,270	1,286

[a]*DT* deformation temperature, *HT* hemisphere temperature, *FT* flow temperature (according to CEN/TS 15370-1 [15])
[b]Here: determination acc. to DIN 51 730 [7], deviation to results achieved with newer method are possible
[c]Typical moisture content hard coal: 5%; crude brown coal 50% [56]

Ash Content

The inorganic residue after combustion of a solid biofuels is the ash. It can originate directly from the (unpolluted) fuel or it can be caused by mineral pollutants which have been entrained during the supply chain (e.g., during harvesting, comminution, transport, storage).

The ash content is calculated by the mass of the residue remaining when a sample is heated under defined conditions EN 14775 [20]. This is done by rising the oven temperature over 30–50 min to 250°C and then keeping the temperature constant over 60 min to allow any volatiles to leave the sample before combustion. Then the oven temperature rises at a constant increase of 10 K/min to 550°C, where it remains constant over minimum of 120 min.

In previous test methods (e.g., ISO 1171) the ash determination was performed at a much higher temperature of 815°C, which is still common for coal fuels. The results between the two methods can deviate because at high temperatures inorganic matter can partly become volatile by further oxidation or a release of CO_2 from the disintegration of carbonates can lead to material losses. This systematic deviation can be between zero and several percentage points, depending on the fuel type and ash content level [31].

Of all biomass fuels wood has the lowest ash content in the dry matter (about 0.5%). Higher values are thus usually due to secondary pollution (e.g., by adhering soil). This can be read from the frequency distribution curve for the ash content following a pattern with a peak on the left side (Fig. 7). Accordingly, ash content above 1% is rare for wood alone (without needles or leaves). Only wood from short rotation forestry (e.g., poplar, willow) contains usually higher amounts of ash (about 2%). This is due to the higher bark content of young wood and because bark contains more ash than the heartwood. Bark from spruce, for example, has ash content between 2.5% and 5% (Table 6). The ash content is even higher for most herbaceous fuels.

The ash content of a fuel has an environmental impact and it influences the technical design of a furnace. Higher ash content in the fuel can lead to increased particle emissions or to further requirements for particle separation. Additionally, special technical solutions may be required for the deashing and cleaning of heat exchanger surfaces. Furthermore, the higher efforts for ash handling and disposal are increasing the process costs.

In the ash, several elements described in section "Elemental Composition" are accumulated. These elements are mainly calcium (Ca), magnesium (Mg), potassium (K), phosphorous (P), and sodium (Na). The mean composition of coarse ash from combustion of wood is about 42% CaO, about 6% K_2O, about 6% MgO, about 3% P_2O_5, and about 1% Na_2O. Additionally there is a minor content of iron (Fe) and manganese (Mn). Ashes from straw fuels also have higher shares of K_2O and P_2O_5.

Ash Melting Properties

Due to the induced processes during thermochemical conversion, the physical properties of the ash are modified. Depending on the temperature level, phenomenon like sinterification or even a complete meltdown of ash particles can occur in the fire bed. This can be associated with severe technical disadvantages in the conversion plant and it has to be considered for the design of the combustion process.

The ash melting behavior is depending on the ash constituents and it is thus directly correlated with the fuel composition. Therefore, the ash melting behavior is listed among the fuel-specific properties. As measuring parameters, four characteristic temperatures are used. At these temperatures certain observations concerning ash modifications are made. They are the Shrinkage Starting Temperature (SST), the Deformation Temperature (DT), the Hemisphere Temperature (HT), and the Flow Temperature (FT).

Their determination is done following CEN/TS 15370–1 [15]. A fuel sample is first incinerated according to the principles for the ash content determination (i.e., at 550°C [20]), then the ash is milled and mixed with an additive (water, dextrin, or ethanol) before it is pressed to a sharp edged cylindrical sample piece of 3–5 mm height and the same diameter. The produced test piece is then heated in a defined temperature rise while the observed changes are recorded via a digital camera. The temperatures at which the sample piece is noticeably changing by softening and deformation describe the ash melting behavior. They are defined as follows:

- *Shrinkage starting temperature, SST.* At this temperature the shrinking of the test piece occurs. This temperature is defined as when the area of the test piece falls below 95% of the test piece area at 550°C (Fig. 11). Shrinking may be due to liberation of carbon dioxide, volatile alkali compounds, or sintering. The shrinkage is not always easily detectable but it provides additional information on the

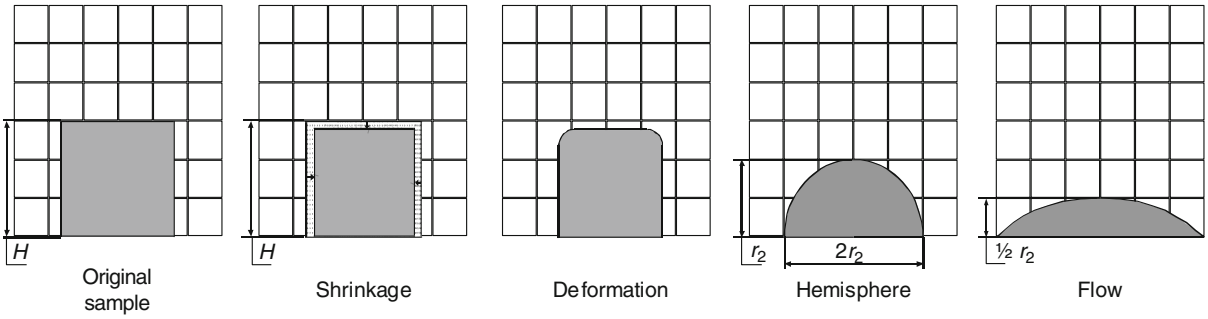

Solid Biofuels, Fuels and Their Characteristics. Figure 11
Characteristic phases during the melting process of a cylindrical ash sample piece according to the standard test method [15] (Original sample = form and size at 550°C; *H* height of sample piece, r_2 radius of hemisphere)

fuel ash behavior. Currently few data are available for shrinkage; Table 6 is therefore incomplete concerning this new parameter.

- *Deformation temperature, DT.* At this temperature the first signs of rounding of the edges due to melting of the test piece occur (Fig. 11).
- *Hemisphere temperature, HT.* It is the temperature at which the test piece forms approximately a hemisphere; this is given when the height becomes equal to half the base diameter (Fig. 11).
- *Flow temperature, FT.* At the flow temperature the ash is spread out over the supporting tile in a layer; the height of this layer is half of the height of the test piece at the hemisphere temperature (Fig. 11).

For fuels with a low ash melting point a high risk of slag deposition and adhesion in the conversion plant is given (e.g., in the combustion chamber, at the grate, on heat exchanger surfaces). Such coatings can lead to blockages, breakdowns, and to an inhibited combustion air supply. They also promote high temperature corrosion. By complex technical attachments, such as water-cooled grates or furnace beds, moving elements in the fire bed, flue gas recirculation, slag breaking elements, fuel turbulence, or fuel additives, the problems can be avoided.

Because wood and bark show high deformation temperatures of about 1,300°C to more than 1,400°C they are usually uncritical in most energetic processes (Table 6). For herbaceous fuels, however, the deformation temperature is almost consistently below 1,200°C. Thus, the described disadvantages bear a technical risk for combustion. For grain straw, for example, a mean deformation temperature of 900–950°C is observed (Fig. 7). However, most critical are grain kernels, where even the flow temperature is usually below 900°C (Table 6).

Similar to the calorific value, the ash deformation temperature is depending on the content of relevant elements. In this context, calcium has a positive impact because it raises the critical temperatures. For potassium, the opposite effect is observed. From these correlations it can be concluded that the ash melting behavior can be improved by mixing the fuel with calcium-containing additives (lime) or by using additives which capture alkaline compounds (e.g., kaolin) [57]. On the other side, the depletion of critical elements from the fuel is a different path for improvements. Therefore the leaching of potassium by precipitation during field-drying or the ripening phase of the crop (e.g., for straw or hay) can have a positive effect under practical conditions. Thus, the ash deformation temperature can be raised in a magnitude of 100–150°C [31].

Physical-Mechanical Properties

Physical-mechanical fuel parameters mainly describe those properties determined during the harvesting and upgrading process. They comprise characteristics such as the surface properties, geometry, size and size distribution, fine matter content, flowing and bridging properties, resistance to abrasion, bulk, and particle density. As for the parameters described in section "Technical Combustion Properties," international standards for their determination are also available for most parameters described here.

In opposite to the fuel composition parameters (section "Fuel Composition"), the technical and physical-mechanical characteristics are largely interacting among each other. The moisture content is also playing a major role in this context of interactions (Fig. 12) and it influences the physical mechanical properties. These parameters are presented and discussed in below.

Shape and Dimensions

Solid biofuels can be characterized by their shape, which is described by length, height, and width, or by the volume and the geometrical form (i.e., geometric solid).

For hand charged furnaces, specific requirements concerning the maximum fuel expansion are usually given for each furnace type. Firewood can, for example, have a maximum end-user size of 1 m (for meter-wood boilers). But mostly such wood logs are cut one, two, or three times to pieces of 50, 33, or 25 cm in length, depending on the depth of the combustion chamber. Log lengths of 33 cm are here clearly predominant.

For briquettes, produced by mechanical compaction of biomass, variable sizes and shapes are available on the market today. A differentiation between pellets and briquettes is here mainly made by the diameter. From a diameter above 25 mm they are briquettes, below this diameter they are pellets [17].

For pellets European standard size classes are defined:

- Class D06: diameter $\leq$ 6 mm $\pm$ 1.0 mm und length (L) 3.15 $\leq$ L $\leq$ 40 mm

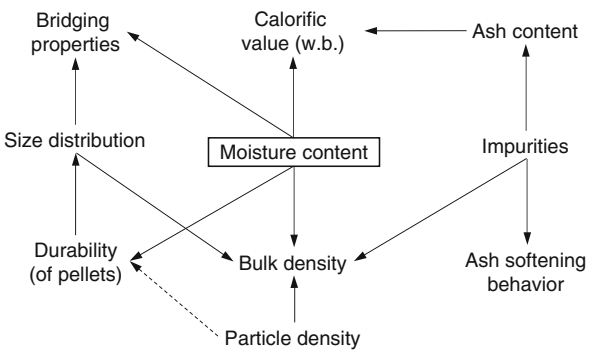

Solid Biofuels, Fuels and Their Characteristics. Figure 12 Interactions between physical-mechanical and technical combustion properties of solid biomass fuels [28]

- Class D08: diameter $\leq$ 8 mm $\pm$ 1.0 mm und length (L) 3.15 $\leq$ L $\leq$ 40 mm
- Class D10: diameter $\leq$ 10 mm $\pm$ 1.0 mm und length (L) 3.15 $\leq$ L $\leq$ 40 mm
- Class D12: diameter $\leq$ 12 mm $\pm$ 1.0 mm und length (L) 3.15 $\leq$ L $\leq$ 40 mm
- Class D25: diameter $\leq$ 25 mm $\pm$ 1.0 mm und length (L) 10 $\leq$ L $\leq$ 50 mm

In addition, herbaceous fuels can be compressed to either round or square bales of variable dimensions (Table 7). Recently also pellets und briquettes are produced. Loose unchopped material is not directly applied as a fuel, but the comminution to chopped material (pieces of 2–40 mm length) can lead to similar mechanization benefits as for wood chips.

Size Classes and Fine Matter

The flow and transport properties of pourable materials are also described by the particle size distribution and the share of fine materials (e.g., by abrasion of pellets). To describe the physical properties of a given wood chip batch, for example, the determination of a mean particle diameter or the mean length alone is not sufficient. Rather the information about the share of certain size classes is needed for proper description. Therefore, a classification using several size classes is useful. Such a system is described in Table 8.

The particle size distribution is relevant for several technical reasons. A larger impact of an unsuitable size distribution is given for mechanical systems in silo emptying, conveying, or charging systems of thermochemical conversion plants. Too long particles can, for

Solid Biofuels, Fuels and Their Characteristics. Table 7 Geometry and dimensions of various compressed herbaceous fuels

Fuel form	Geometry	Dimension in cm
Small square bales	Cuboid	40 × 50 × 50–120
Round bales	Cylindrical	Ø 80–200 × 120–170
Big square bales	Cuboid	80–130 × 80–130 × 120–250
Highly compressed fuels: pellets briquettes	Cylindrical, cuboid, etc.	Ø 0.3–2 × variable length variable forms

Solid Biofuels, Fuels and Their Characteristics. Table 8 Requirements for size classes of wood chips according to the European wood chip standard EN 14961-4 [19]

Size class	Minimum 75 wt% in main fraction, mm[a]	Fines fraction, wt % (<3.15 mm)	Coarse fraction, (wt%), max. length of particle (mm), max. cross-sectional area (cm^2)
P16A	$3.15 \leq P \leq 16$ mm	≤12%	≤ 3% > 16 mm, and all < 31.5 mm The cross-sectional area of the oversized particles <1 cm^2
P16B	$3.15 \leq P \leq 16$ mm	≤12%	≤ 3% > 45 mm and all <120 mm The cross-sectional area of the oversized particles <1 cm^2
P31.5	$8 \leq P \leq 31.5$ mm	≤8%	≤ 6% > 45 mm, and all <120 mm The cross-sectional area of the oversized particles <2 cm^2
P45A	$8 \leq P \leq 45$ mm	≤8%	≤ 6% > 63 mm and maximum 3.5% > 100 mm, all <120 mm The cross sectional area of the oversized particles <5 cm^2

[a]The numerical values (P-class) for dimension refer to the particle sizes (at least 75 wt%) passing through the mentioned round hole sieve size

example, lead to blockages and damages of the conveyor and they can lower the material throughput. In addition, the flowability and the resistance to air flow during ventilation or drying are affected. Furthermore, the tendency to form a bridge during transhipment (e.g., at the bottom of a silo) is determined by an unsuitable size distribution. Finally, also the possibility for fine material to disintegrate from the bulk (e.g., during transportation) and thus to increase non-uniformity within the fuel bulk is facilitated by an unfavorable size distribution.

The determination of particle size distribution is performed by sieving. This is done using a set of horizontally shaking sieves placed above each other. The particles of a sample are then passed through the screen set starting with the largest hole apertures. Then they are separated according to their size in the respective screen, which is finally weighed. The share of mass in each fraction, assuming that particle density of smaller and larger particles is consistent, then determines the size distribution. For the determination of a particle size distribution according to the European wood chip standard a set of screens with round holes was selected (hole diameters of 3.15, 8, 16, 31.5, 45, and 63 mm). Additionally it can be useful to add a 1 mm (mesh wire sieve) [21].

During sieving the particles are rather separated by their width than by their length. Therefore, a considerable amount of particles which are significantly longer than the screen hole aperture width are found in one of the following size class. The median value of a size distribution determined by horizontal screening is therefore mostly only half of the value to be found if the median value was determined from the distribution of the actual lengths (maximum particle expansion) [34]. In particular, higher shares of overlong particles are always determined when the particles largely differ from an ideal sphere shape. This is, for example, the case when the sample is a hog fuel type produced by using blunt tools rather than sharp cutting knifes as applied in wood chip production [34]. Hog fuel usually has a largely higher length-diameter ratio.

Consequently, the classification during sieving is mainly done by sorting according to the maximum particle diameter. However, for the assessment of mechanical fuel properties the results from a size distribution determination by length (i.e., largest expansion) would be the more relevant parameter. This approach would also be more decisive for the mechanical properties of the fuel. But at sufficient accuracy such a measurement can only be performed using continuous image analysis [34]. However, this method is still not widely available. Therefore, the results from a particle size distribution analysis by screening according to EN 15149–1 [21] shall not be interpreted as absolute figures.

During the particle size analysis, the amount of fine material is also determined. It is characterized as the fraction of particles falling through screen hole apertures of about 3.15 or 1.0 mm diameter (internationally

inconsistent). The share of fines is often regarded as an independent fuel parameter. This particle fraction is particularly relevant for wood pellets, because dry wood dust can lead to drastic dust formation during pneumatic conveying. It can also increase the risk of explosion by deflagration.

Flowing and Bridging Properties

The fuel extraction from silos and day storages can be inhibited by technical problems created by unfavorable flow properties. The formation of hollow spaces (bridges or arches) or shafts in a silo is possible (Fig. 13). The latter is associated with a core flow of the material instead of the desired mass flow. Both phenomenons finally lead to the problem that the fuel will sooner or later not any more fall downward to the conveyors or the flow becomes unsteady. Frequently there is also an alternating build-up and breakdown of bridges or shafts. Furthermore, the volume of the container is incompletely used and the retention time of the fuel compartments is inhomogeneous. This means that the fuel remains much longer in the dead layers of a shaft silo and this can lead to severe quality losses. The described phenomenons can also be the reason for fuel segregation by particle size, density, and form; a high quality variation is then a consequence.

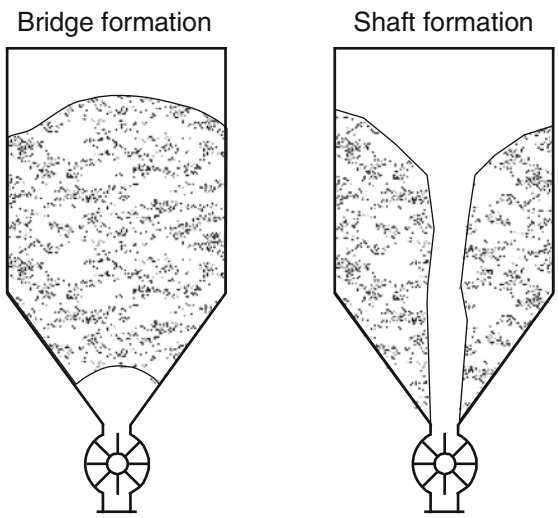

Solid Biofuels, Fuels and Their Characteristics. Figure 13 Phenomenons of unfavorable flowability of fuels [55]

The problems created by unsuitable flow properties are increasing with the moisture content, the filling depth, and the share of overlong and branched particles while uniform particle sizes and smooth surfaces (e.g., pellets, wood chips without bark) are beneficial [36, 43]. A supplementary sorting to achieve uniform material conditions can thus lead to considerable improvements of the flow properties.

Usual shear cells are not suitable for the determination of flow properties due to the sometimes large particle sizes. Therefore a method for a direct determination of the bridging properties was developed. It uses a special apparatus where a fuel sample of 1.65 m^3 is forced to form a bridge over an opening slot under controlled conditions. The opening width of the slot at the moment when the fuel bridge collapses is taken as a measure for the bridge building properties of the sample. This requires a frictionless opening of the bottom slot. It is achieved by the fact that a flat steel bottom is sliding away underneath a PVC mat on which the fuel sample is resting [36].

Bulk Density

The required storage and transport volume is determined by the bulk density of a pourable fuel or by the stacked density of logs and briquettes. The respective definitions and conversion factors are described below.

Definition. The bulk density is defined as the quotient of the mass of a material filled into a container and the filling volume of the container. The hollow space between the fuel particles is thus not reducing the volume; this also applies to the staked density of wood logs. Typical density values are given in Table 9.

Determination. For determination of the bulk density a sample is being filled in a defined mode into a cylindrical container of 50 l volume (EN 15103 [11]). The container is filled over the edge and is then exposed to controlled shock by dropping it three times from 150 mm height onto a wooden floor. Then the filling volume created by the shock operation is refilled and leveled to the rim of the container. Then the net weight is determined and related to the container volume.

Settling factor. The defined shock exposure operation leads to a certain volume reduction due to compaction effects occurring during the supply chain. These

Solid Biofuels, Fuels and Their Characteristics. Table 9 Typical bulk and staked densities of biomass fuels at a moisture content of 15%

Wood fuels		Density in kg/m^3	Herbaceous fuels		Density in kg/m^3
Wood logs (stacked)	Beech	445	Round bale	Straw	85
	Spruce	305		Hay	100
Wood chips	Soft wood	200	Square bale	Straw, miscanthus	140
				Hay	160
	Hard wood	280		Whole grain crop	190
Wood bark	(coniferous)	175	Chopped	Miscanthus	110
Saw dust		160		Whole grain crop	150
Shavings		90	Grain kernels		750
Wood pellets		650	Pellets		550

compaction effects are mainly due the fact that the fuel is usually transported and/or stored in containers or silos much larger than the measuring container chosen for the method described here. Thus in practice the higher mass load in a storage leads to an increased load pressure and to fuel settling, which can additionally be enhanced by the vibrations during transportation. Furthermore, filling or unloading operations in practice usually apply a higher falling depth than the one chosen for the here performed test. This will also result in a respectively higher compaction due to the increased kinetic energy of the particles falling. The procedure with applying a controlled shock to the sample is thus believed to reflect the practically prevailing bulk density in a better way than a method without shock. This is particularly true when the mass of a delivered fuel has to be estimated from the volume load of a transporting vehicle, which is a common procedure in many countries.

The difference between a measurement with and without shock can be interpreted as the settling factor. The measured results for this factor are given in Fig. 14 for several biomass fuels. It shows that the compaction effect during handling and transhipment is low for wood pellets or grain kernels (only 6–7% settling). However, this effect is largely higher when chopped herbaceous fuel such as Miscanthus is regarded (max. 18% settling). For wood chips the bulk density increase due to controlled shock is around 11%; differences between high or low density wood chips are negligible here (fuels above 180 kg dry matter per m^3 were in Fig. 14 defined as high density fuels).

Transformation to other moisture content bases. For comparability the determined densities should be converted to uniform moisture content or to dry basis. If for practical reasons the swelling and shrinkage is here disregarded, the dry matter based bulk density (D_d) is calculated from the actual bulk density as received (D_{ar}) by regarding the given moisture content (M) according to Eq. 4.

$$D_d = D_{ar} \times \frac{100 - M_{ar}}{100} \tag{4}$$

Equation 4 disregards shrinkage or expansion, which usually cause significant deviations when the sample is measured at different drying stages. For uncompressed wood fuels, these volume changes usually occur at moisture contents below the fiber saturation point, which is at around 25%, depending on the wood species. A true comparison between fuel samples would therefore require a determination at similar moisture contents. Alternatively, a correction factor can be used if sample materials of different moisture content shall be compared and at least one sample is below the fiber saturation point. Here the usual effect of swelling or shrinkage is in the order of around 0.7% volume change per percentage point of moisture difference [32].

Conversion of volumes. In practice, a fuel volume often needs to be converted to another volume basis.

Solid Biofuels, Fuels and Their Characteristics. Table 10 Conversion factors between different wood log assortments (with bark) [37] (sm^3: stacked cubic meter)

Wood type	Solid wood volume in solid m^3	Round wood, stacked in sm^3	1-m logs, split, stacked in sm^3	33-cm logs, split stacked in sm^3	33-cm logs, loose in m^3
For 1 solid cubic meter (with bark)					
Beech	1.00	1.70	1.98	1.61	2.38
Spruce	1.00	1.55	1.80	1.55	2.52
For 1 cubic meter of round wood					
Beech	0.59	1.00	1.17	0.95	1.40
Spruce	0.65	1.00	1.16	1.00	1.63
For 1 cubic meter of 1-m logs (split)					
Beech	0.50	0.86	1.00	0.81	1.20
Spruce	0.56	0.86	1.00	0.86	1.40
For 1 cubic meter of 33-cm logs (split)					
Beech	0.62	1.05	1.23	1.00	1.48
Spruce	0.64	1.00	1.16	1.00	1.62
For 1 cubic meter of 33-cm logs (split)					
Beech	0.42	0.71	0.83	0.68	1.00
Spruce	0.40	0.62	0.72	0.62	1.00

In the untreated state wood is often rated by the solid cubic meter (i.e., without regarding any hollow space). However, when supplied to the final customer as wood logs, the fuel is usually rated as staked or bulk cubic meter. For conversion from solid cubic meters (solid m^3) to staked cubic meters (sm^3) a general factor of 1.43 had in the past widely been used (i.e., 1 solid m^3 is 1.43 sm^3). However, a more differentiated calculation is useful, particularly because the general conversion factor of 1.43 is too low even for very densely piled oven-ready and dry wood logs [37]. Table 10 shows that a staked cubic meter of firewood at 33 cm length is in average produced from 0.62 m^3 of solid beech wood or from 0.64 m^3 of spruce wood. For a single cubic meter of stacked 33 cm-logs a volume of 1.23 sm^3 of 1 m-logs is required. Significantly different conversion factors between spruce and beech wood also observed within the loose logwood assortment (Table 10).

In reality, however, the conversion factors can largely differ from the figures given in Table 10, depending on the processing technology and the physical growth shape of the tree. This applies particularly to the conversion factors from solid to any form of stacked cubic meter.

For wood chips, the conversion from massive (solid) cubic meter to the volume of bulk material is usually done using a general factor [5]. It is:

- 1 solid cubic meter (m^3) (massive wood) $\approx$ 2.43 m^3 wood chips
- 1 stacked cubic meter (sm^3) of stacked wood $\approx$ 1.7 m^3 wood chips

Larger deviations from this general factor are also likely. But to date no differentiations between wood species or between the applied comminution technologies can yet be made. The shrinkage by drying or the volume losses by shock or vibration (settling factor) can be estimated using the data given in the previous chapters.

Energy density. When assessing biofuels and their specific storage room demand the term "energy density" is sometimes used. It is defined as the respective

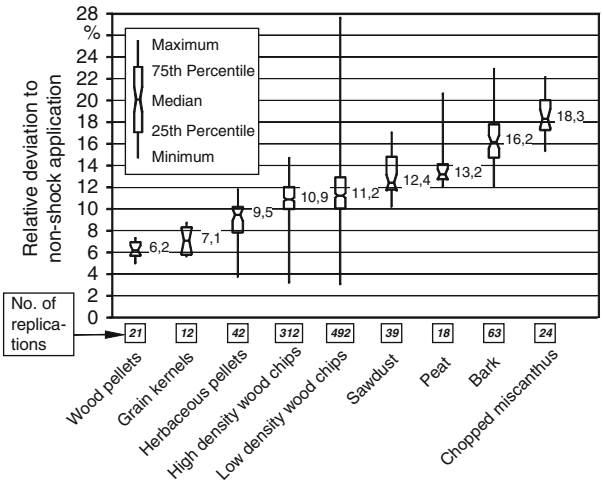

Solid Biofuels, Fuels and Their Characteristics. Figure 14 Relative effect of shock impact compared to a non-shock application in bulk density determination ("settling factor") derived from measurements in a 50-l-container, which is dropped three times before refilling, surface leveling and weighing [32]

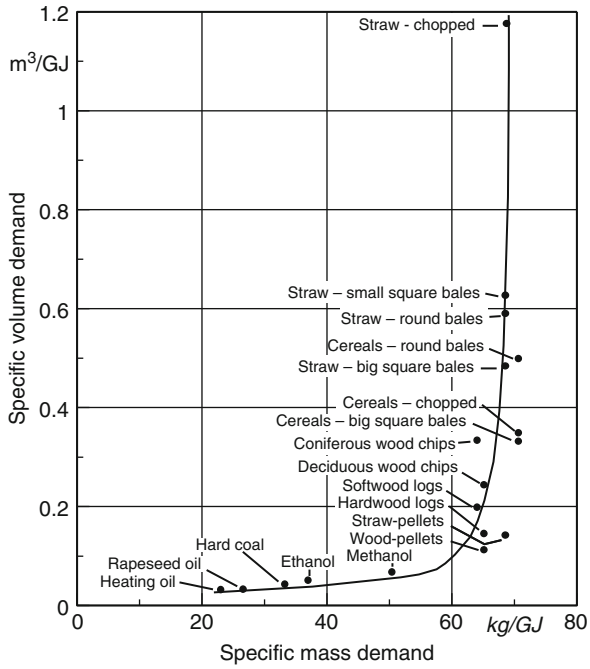

Solid Biofuels, Fuels and Their Characteristics. Figure 15 Specific mass and storage room demand of different energy sources (for solid fuels a moisture content of 15% is assumed) [26]

mass or volume needed to provide a given unit of fuel energy at a given moisture content. A comparison of selected fuels regarding their energy density is given in Fig. 15.

Particle Density

The particle density of a fuel describes the actual material density (i.e., without regarding the hollow space between the particles). It influences the bulk or stacked density and some combustion properties (e.g., the specific heat transfer rate): Also, the pneumatic transportability is depending on it. Physically the particle density can only be influenced by compaction to pellets or briquettes.

When determining the particle density of compressed biomass fuels (pellets or briquettes), the volume of a single particle is first determined by measuring its buoyancy in a liquid (water with wetting agent) according to EN 15150 [12]. Then the mass as determined in ambient air is set into relation to this volume.

Table 11 shows the particle densities of various wood species given at an absolutely dry stage. When the moisture content of fiber saturation is given (ca. 19–25%) the volume is higher. The difference is the so-called shrinkage factor. This has a respective effect on the particle density of the wetter fuel. The volume change by shrinkage is 17.9% and 12.2% for beech and oak or 11.9% and 12.1% for spruce and pine [41].

The parameter particle density is sometimes used to characterize the intensity and quality of a compaction process. A high particle density indicates a high hardness and thus only little risk of abrasion or fine material losses. However, a significant correlation between particle density and resistance to abrasion has never been clearly observed [58]. For pellets therefore the direct determination of abrasion using a mechanical test method is today preferred (section "Resistance to Abrasion").

Compared to compressed materials the particle density of grain kernels is usually not lower. For oat kernels (with husk), for example, the density is around 1.0 g/cm^3 while wheat kernels without husks have an average density of 1.35 g/cm^3. The density of a grain

Solid Biofuels, Fuels and Their Characteristics. Table 11 Particle density (including shrinkage) of absolutely dry wood [41, 49]

Soft wood (max. 0.55 g/cm^3)		Hard wood (above 0.55 g/cm^3)	
Spruce	0.43 g/cm^3	Oak	0.67 g/cm^3
Fir	0.41 g/cm^3	Sycamore	0.50 g/cm^3
Pine	0.49 g/cm^3	Ash	0.67 g/cm^3
Douglas fir	0.47 g/cm^3	Beech	0.68 g/cm^3
Larch	0.55 g/cm^3	Birch	0.64 g/cm^3
Alder	0.49 g/cm^3	White beech	0.75 g/cm^3
Lime tree	0.49 g/cm^3	Black pine	0.56 g/cm^3
Aspen	0.45 g/cm^3	Hazelnut	0.56 g/cm^3
Poplar	0.41 g/cm^3	Black locust acacia	0.73 g/cm^3
Willow	0.52 g/cm^3	Elm	0.64 g/cm^3

haulm is however significantly lower, for wheat straw it is in average around 0.20 g/cm^3 (considering only wall material) [30].

Resistance to Abrasion

Resistance to abrasion describes the coherence of fuel particles in a compressed material (pellets or briquettes). This property is mainly important for all processes of loading and transhipment, where the material is exposed to mechanical wear, and where small particles are removed and can thus contribute to the release of fine dust. Such dust is usually formed when a silo or storage is pneumatically filled with pellets, because fine wood dust can easily penetrate through small cracks in silos or rooms. With briquettes, an unsuitable mechanical strength can lead to a breaking of the material during hand charging or transport. Moreover, it leads to dirt accumulation near the furnace (e.g., in the living space). A high dust formation can lead to explosion reactions when either a high heat impact or freely flying sparks are given. This can happen in the storage, the feeding system, or within the furnace itself.

For the determination of resistance to abrasion a standard method is applied (EN 15210–1 [13]). A sieved pellet sample is filled into a dust-tight rotating test box of a rectangular geometry (300 × 300 × 125 mm). In the inside, the box is equipped with a baffle. The sample is then exposed to defined mechanical wear by rotating it in the box over 10 min at a speed of 50 rpm. Then the sample is again screened using the previously applied round hole sieve (3.15 mm hole diameter) and the weight difference to the original sample is determined. For high quality pellets, the pellet mass remaining on the screen after the mechanical treatment should be above 97.5%. Such a durability is then classified by "DU97.5" according to the EN 14961–1 [17]. Further quality steps are, for example, DU96.5 and DU95.0 with less remaining mass fraction after the described mechanical treatment and sieving.

For briquettes the mechanical treatment is similar (EN 15210–2 [14]). Instead of the rectangular tumbling chamber, a lying cylinder is used for rotating the sample (diameter and height both being 598 mm). An inbuilt baffle ensures that the sample is exposed to significant mechanical stress over 5 min of rotation at 21 rpm [14]. The applied sample mass of 2 kg is higher because of the larger briquettes.

The stability of pellets or briquettes during mechanical stress depends on several factors. They are, for example, the form (for briquette), the chosen compaction method, or the use of any binding agents. An unsuitable cooling after compaction reduces the mechanical strength. High air humidity during storage can lead to an increased fuel moisture content which also lowers the mechanical stability [28]. The type of material itself also gives a decisive role, because composition and macromolecular structure can influence the effectiveness of the binding forces. Therefore the stability of straw pellets is usually lower than of wood pellets [58].

Future Directions

In some regions, biomass fuels are already becoming scarce. Countries with high ambitions or obligations concerning their future share of renewable energy or CO_2-reduction goals are therefore increasingly depending on imported biomass. In such a scenario, the energetic density is a decisive criterion. Therefore, pelletization of biomass is an increasingly important technical option to realize long-distant trade relations. International standardization in this field is now providing the necessary directions and enables

the introduction of sound and comprehensive quality assurance systems.

The growing importance of pelletization does not only apply to wood fuels but also to agricultural residues and non-woody energy crops. However, the scope of using herbaceous fuels is today still limited due to their unfavorable properties. The upcoming search for new resources therefore needs to be associated with developing and applying new methods for fuel improvements. This can, for example, be the application of additives or applying other pretreatment measures before pelletizing. Desirable changes in fuel composition can also be achieved by depleting pollutants through active leaching with water or by thermochemical pretreatment measures such as heat application (torrefaction) or the use of steam and pressure (hydrothermal carbonization). In such cases, largely homogenized high-value fuels are produced and not only their chemical composition but also their physical-mechanical properties are thus adapted to new requirements. This development can enable to establish new technical applications for the fuel (e.g., higher rates of co-combustion with fossil coal).

In general, the now introduced European and ISO-standards for biomass are about to boost possibilities for quality increases and they allow the introduction of high grade market fuels which finally can stimulate technologically and environmentally more sophisticated conversion routes. Nevertheless, in view of the increasing depletion of existing potentials – particularly for low value biomass residues and by-products – the future challenge is to select, improve, and process suitable energy crops, and to monitor all quality relevant influences in order to achieve consistently high biomass fuel quality. However, the knowledge base for such comprehensive quality manipulations is still thin and sound, and predictable technical measures are yet few.

Bibliography

1. Ballschmiter KH, Bacher R (1996) Dioxine – Chemie, Analytik, Vorkommen Umweltverhalten und Toxikologie der halogenierten Dibenzo-p-Dioxine und Dibenzofurane. VHC, Weinheim
2. Böhm T, Hartmann H (2000) Wassergehalt von Holzhackschnitzeln – Ein Vergleich der Bestimmungsmethoden. Landtechnik 55(4):280–281
3. Brunner T (2006) Aerosol and coarse fly ashes in fixed-bed biomass combustion. Dissertation an der Eindhoven University of Technology (Faculty of Mechanical Engineering), The Netherlands, Eigenverlag
4. Burmester A (1980) Holzfeuchtigkeit in Nadelhölzern – Jahreszeitliche Einflüsse auf die Eigenschaften des Splint- und Kernholzes von Nadelbäumen. Holz Zentralbl 106(91): 1303–1304
5. Centrale Marketinggesellschaft der deutschen Agrarwirtschaft (Hrsg.) (1988) Holz als Energierohstoff; Centrale Marketinggesellschaft der deutschen Agrarwirtschaft, Selbstverlag, Bonn, 2 Auflage
6. Daugbjerg Jensen P, Hartmann H, Böhm T, Temmerman M, Rabier F, Morsing M (2006) Moisture content determination in solid biofuels by dielectric and NIR reflection methods. Biomass Bioenergy 30:935–943
7. Deutsches Institut für Normung (Hrsg.) (1984) DIN 51 730 (Prüfung fester Brennstoffe – Bestimmung des Ascheschmelzverhaltens). Beuth, Berlin
8. Deutsches Institut für Normung (Hrsg.) (1996) DIN 51 731 Prüfung fester Brennstoffe – Presslinge aus naturbelassenem Holz – Anforderungen und Prüfung. Beuth, Berlin
9. Deutsches Institut für Normung (Hrsg.) (2003) CEN/TS 14588:2003: Feste Biobrennstoffe – Terminologie, Definitionen und Beschreibungen. Beuth, Berlin
10. Deutsches Institut für Normung (Hrsg.) (2005) CEN/TS 14918:2005: Feste Biobrennstoffe – Verfahren zur Bestimmung des Heizwertes. Beuth, Berlin
11. Deutsches Institut für Normung (Hrsg.) (2005) FprEN 15103:2009: Solid biofuels – determination of bulk density. Beuth, Berlin
12. Deutsches Institut für Normung (Hrsg.) (2005) prCEN/TS 15150:2005: Solid biofuels – methods for the determination of particle density. Beuth, Berlin
13. Deutsches Institut für Normung (Hrsg.) (2005) prCEN/TS 15210-1:2005: Feste Biobrennstoffe – Verfahren zur Bestimmung mechanischen Festigkeit – Teil 1 – Pellets. Beuth, Berlin
14. Deutsches Institut für Normung (Hrsg.) (2005) CEN/TS 15210-2:2005 Feste Biobrennstoffe – Verfahren zur Bestimmung mechanischen Festigkeit – Teil 2 – Briketts. Beuth, Berlin
15. Deutsches Institut für Normung (Hrsg.) (2006) CEN/TS 15370-1:2006 Solid biofuels – method for the determination of ash melting behaviour – Part 1: characteristic temperatures method. Beuth, Berlin
16. Deutsches Institut für Normung (Hrsg.) (2009) CEN/TS 15148:2005: Solid biofuels – solid biofuels – determination of the content of volatile matter, Final draft, April 2009. Beuth, Berlin
17. Deutsches Institut für Normung (Hrsg.) (2010) EN 14961-1:2010: Solid biofuels –fuel specifications and classes – Part 1: general requirements. Beuth Verlag, Berlin
18. Deutsches Institut für Normung (Hrsg.) (2010) EN 14961-2:2010: Solid biofuels – fuel specifications and classes – Part 2: wood pellets for non-industrial use. Beuth Verlag, Berlin

19. Deutsches Institut für Normung (Hrsg.) (2010) FprEN 14961-4:2010: Solid biofuels – fuel specifications and classes – Part 4: wood chips for non-industrial use. Beuth Verlag, Berlin
20. Deutsches Institut für Normung (Hrsg.) (2010) EN 14775: 2009: Solid biofuels – determination of ash content. Beuth, Berlin
21. Deutsches Institut für Normung (Hrsg.) (2010) FprEN/TS 15149-1:2010: Solid biofuels – determination of particle size distribution – Part 1: oscillating screen method using sieve apertures of 1 mm and above. Beuth, Berlin
22. Deutsches Institut für Normung (Hrsg.) EN 14774:2010 (2010): Solid biofuels – determination of moisture content – oven dry method – Parts 1 to 3. Beuth, Berlin
23. Friedl A et al (2005) Prediction of heating value of biomass fuel from elemental composition. Anal Chem 554:191–198
24. Gammel R (1989) Forstbenutzung – Technologie, Verwertung und Verwendung des Holzes. Verlag Paul Parey, Hamburg, Pareys Studientexte 67, 193S
25. Griffin RD (1986) A new theory of dioxin formation in municipal solid waste combustion. Chemosphere 9–12: 1987–1990
26. Hartmann H (1996) Analyse und Bewertung der Systeme zur Hochdruckverdichtung von Halmgut; Bayerisches Staatsministerium für Ernährung, Landwirtschaft und Forsten (Hrsg.), Selbstverlag, München, Reihe "Gelbes Heft" 60
27. Hartmann H (1998) Influences on the quality of solid biofuels – causes for variations and measures for improvement. In: Biomass for energy and industry, proceedings of the 10th European conference and technology exhibition, Würzburg, 8–11 June 1998. C.A.R.M.E.N in Würzburg-Rimpar, Germany, pp 184–187
28. Hartmann H (2004) Physical-mechanical fuel properties – significance and impacts. In: Hein M, Kaltschmitt M (eds) Standardisation of solid biofuels – international conference, 6–7 Oct 2004. Institute for Energy and Environment (IE), Leipzig, pp 106–S115
29. Hartmann H (Hrsg.) (2007) Handbuch Bioenergie-Kleinanlagen (2. vollst. überarbeitete -Auflage). Sonderpublikation des Bundesministeriums für Verbraucherschutz, Ernährung und Landwirtschaft (BMVEL) und der Fachagentur Nachwachsende Rohstoffe (FNR), Gülzow, 224 S
30. Hartmann H, Böhm T (2000) Messverfahren zur Bestimmung der Rohdichte von biogenen Festbrennstoffen. Bayerische Landesanstalt für Landtechnik, Freising, (noch unveröffentlicht)
31. Hartmann H, Böhm T, Maier L (2000) Naturbelassene biogene Festbrennstoffe – Umweltrelevante Eigenschaften und Einflussmöglichkeiten. Bayerisches Staatsministerium für Landesentwicklung und Umweltfragen (Hrsg.), München, Reihe "Materialien", 154 Download
32. Hartmann H, Böhm T, Daugbjerg Jensen P, Temmerman M, Rabier F, Jirjis R, Hersener J-L, Rathbauer J (2004) Methods for bulk density determination of solid biofuels. In: Van Swaaij WPM, Fjällström T, Helm P, Grassi A (Hrsg.) 2nd world conference and technology exhibition on biomass for energy, industry and climate protection, Rome, 10–14 May 2004. Energy research Centre of the Netherlands ECN, Petten, pp 662–665
33. Hartmann H, Roßmann P, Link H, Marks A, Müller R, Amann E (2004) Secondary flue gas condensation for domestic wood chip boilers. In: Van Swaaij WPM, Fjällström T, Helm P, Grassi A (Hrsg.) 2nd world conference and technology exhibition on biomass for energy, industry and climate protection, Rome, 10–14 May 2004. Energy research Centre of the Netherlands ECN, Petten, pp 1334–1337
34. Hartmann H, Böhm T, Daugbjerg Jensen P, Temmerman M, Rabier F, Golser M (2006) Methods for size classification of wood chips. Biomass Bioenergy 30:944–953
35. Hartmann H, Turowski P, Roßmann P, Ellner-Schuberth F, Hopf N (2007) Grain and straw combustion in domestic furnaces – influences of fuel types and fuel pretreatment. In: Maniatis K, Grimm H-P, Helm P, Grassi A (eds) Proceedings 15th European biomass conference and exhibition, Berlin, Germany, 7–11 May 2007. ETA Renewable Energies, Florence, Italy, pp 1564–1569
36. Hinterreiter S, Hartmann H, Turowski P, Kallio M, Lazdiņš A, Zimelis A, Rathbauer J, Sulzbacher L, Sønderstgaard Sørensen K, Temmerman M (2010) Determination of bridging properties – experimental and model approach. In: ETA Renewable Energies (eds) Proceedings 18th European biomass conference and exhibition – from research to industry and markets. Lyon, France, 03–07 May 2010. ETA Renewable Energies, Florence, Italy, pp 1688–1698
37. Höldrich A, Hartmann H, Decker T, Reisinger K, Schardt M, Sommer W, Wittkopf S, Ohrner G (2006) Rationelle Scheitholzbereitstellungsverfahren. Berichte aus dem TFZ, 11, Technologie- und Förderzentrum (TFZ), Selbstverlag, Straubing, 274 S. www.tfz.bayern.de
38. Huber S, Friess H (1998) Emissions of biomass combustion plants. In: Kopetz Hua (Hrsg.) Biomass for energy and industry. C.A.R.M.E.N., Würzburg-Rimpar, pp 1405–1408
39. Launhardt T, Hartmann H, Link H, Schmid V (2000) Verbrennungsversuche mit naturbelassenen biogenen Festbrennstoffen in einer Kleinfeuerungsanlage – Emissionen und Aschequalität. Bayerisches Staatsministerium für Landesentwicklung und Umweltfragen (Hrsg.), München, Reihe "Materialien", 156
40. Lee D, Owens VN, Boe A, Jeranyama P (2007) Composition of herbaceous biomass feedstocks. North Central Sun Grant Center (Hrsg.), South Dakota State University, Selbstverlag, Brookings, 16 S
41. Lohmann U (1993) Handbuch Holz, DRW-Verlag, Stuttgart, 4. Auflage, 312 S
42. Marutzky R (1993) Moderne Holzfeuerungsanlagen. Centrale Marketinggesellschaft der deutschen Agrarwirtschaft (Hrsg.), Selbstverlag, Bonn
43. Mattsson JE (1990) Basic handling characteristics of wood fuel: angle of repose, friction against surfaces and tendency to

bridge building for different assortments. Scand J Forest Res 5:583–597
44. Netz H (1982) Verbrennung und Gasgewinnung bei Festbrennstoffen; Technischer Verlag Resch, München
45. Nimz H (1974) Beech lignin-proposal of a constitutional lignin. Angew Chem Int Edit 13:313–321
46. Noger D, Pletscher E (1998) Brennstoffkriminalität – Schnelltest. In: Siebtes symposium Biobrennstoffe und umweltfreundliche Energietechnik, November 1998; OTTI-Technologie Kolleg, Selbstverlag, Regensburg, pp 173–180
47. Nultsch W (1982) Angewandte Botanik. Thieme, Stuttgart, 7. Auflage
48. Obernberger I (1997) Nutzung fester Biomasse in Verbrennungsanlagen unter besonderer Berücksichtigung des Verhaltens aschebildender Elemente; Schriftenreihe Thermische Biomassenutzung (1), dbv, Graz, p 349
49. Österreichisches Normungsinstitut (Hrsg.) (1998) ÖNORM M7132 Energiewirtschaftliche Nutzung von Holz und Rinde als Brennstoff – Begriffsbestimmungen und brennstofftechnologische Merkmale; Selbstverlag, Wien
50. Rau JA (1989) Composition and size distribution of residential wood smoke particles. J Aerosol Sci Tech 10:181–192
51. Reisinger K, Hartmann H, Turowski P, Nürnberger K (2009) Schnellbestimmung des Wassergehaltes im Holzscheit – Vergleich marktgängiger Messgeräte. Berichte aus dem TFZ 16. Eigenverlag Technologie- und Förderzentrum, Straubing 2009, p 110. www.tfz.bayern.de
52. Samuelsson R, Burvall J, Jirjis R (2006) Comparison of different methods for the determination of moisture content in biomass. Biomass Bioenergy 30:929–934
53. Sander B (1996) Fuel data for Danish biofuels and improvement of the quality of straw and whole crops. In: Chartier P (ed) Biomass for energy and the environment. Elsevier Science, Oxford, pp 490–495
54. Sander M-L, Ericsson T (1998) Vertical distributions of plant nutrients and heavy metals in salix viminalis stems and their implications for sampling. Biomass Bioenergy 14(1):57–66
55. Schultze D (2007) Fließeigenschaften von Schüttgütern und verfahrenstechnische Siloauslegung. Schwedes und Schultze Schüttguttechnik GmbH, Eigenverlag, Braunschweig, www.schwedes-und-schulze.de
56. Spliethoff H, Siegle V, Hein KRG (1996) Erforderliche Eigenschaften holz- und halmgutartiger Biomasse bei einer Zufeuerung in existierenden Kraftwerksanlagen; Tagung "Biomasse als Festbrennstoff – Anforderungen, Einflussmöglichkeiten, Normung", Schriftenreihe "Nachwachsende Rohstoffe" Band 6, Landwirtschaftsverlag, Münster, pp 155–175
57. Steenari B-M, Lindqvist O (1998) High-temperature reactions of straw ash and the anti-sintering additives kaolin and dolomite. Biomass Bioenergy 14(1):67–76
58. Temmerman M, Rabier F, Daugbjerg Jensen P, Hartmann H, Böhm T (2006) Comparative study on durability test methods for pellets and briquettes. Biomass Bioenergy 30:964–972

Solid Oxide Fuel Cell Materials: Durability, Reliability and Cost

Harumi Yokokawa[1,2], Teruhisa Horita[2]
[1]Advanced Research Laboratories, Tokyo City University, Tokyo, Japan
[2]National Institute of Advanced Industrial Science and Technology (AIST), Tsukuba, Ibaraki, Japan

Article Outline

Glossary
Definition of the Subject
Introduction
Historical Aspects of Reliability, Durability, and Cost Issues
Durability/Reliability of SOFC Systems
Cost Issues
Future Directions
Bibliography

Glossary

Acceleration method Generally speaking, there is no appropriate acceleration method for stack performance degradation as a whole. Therefore, individual factors should be carefully accelerated to know the degradation phenomena. One degradation phenomena should consist of several processes having different activation processes. It is highly required to have an acceleration method which should not create additional sources of different origin and mask the original sources of degradation to be investigated.

Cr poisoning Catastrophic degradation of lanthanum manganite–based cathode due to the chromium–oxygen vapors emitted from Cr_2O_3 oxide scale as a result of reaction with (humidified) air. Cr poisoning for other cathodes such as cobaltite or ferrites are completely different in mechanism. The $SrCrO_4$ formation is a key phenomena causing the lowering in cathode performance.

EVD cells Sealless tubular cells fabricated by the electrochemical vapor deposition (EVD) technique. The durability is excellent, whereas the fabrication

cost is expected to be quite high. This cell can be regarded as the standard cell when the relation among durability, efficiency, and cost is considered.

First-generation cells Cells to be operated in the temperature region of 900–1,000°C. Usually oxide interconnects are used together with electrolyte made of YSZ. Since materials compatibility is severe at higher temperatures, stable lanthanum manganite-base cathode is adopted, whereas nickel anodes are used in a similar manner to other types. Electrolyte-self-support or cathode-support types are adopted.

Metal-support cells Cells are fabricated on metal substrates. Compared with ceramic substrates, adoptable fabrication conditions are limited to prevent metals from being oxidized severely. Instead, metals as a main structural component provide many benefits such as better stability against thermal shocks and milder temperature distribution inside the stacks, etc.

Redox stability When anode-support cells are adopted, the mechanical behavior of anode substrate becomes important. During redox cycles, an anode layer is expanded to destroy the nickel connection or to make cracks on YSZ framework/YSZ electrolyte plate.

Reliability versus cost reduction In many cases, achievement of reliability is in trade-off relation to cost reduction. To overcome this, it is required to make breakthroughs in the fabrication technologies.

Second-generation cells Cells to be operated in the temperature region of around 800°C. Metal interconnects are used together with anode-support cells and sealing materials. The active cathode such as LSCF (lanthanum strontium cobaltite ferrites) is used so that the durability is one of the main issues.

Stress caused by volume changes Mechanical stability is dominated by volume changes in components; these are caused by thermal expansion with temperature, chemical volume change due to the valence change within the same lattice at the constant temperature.

Sulfur poisoning Degradation of nickel-cermet anodes due to the adsorption of sulfur originated from H_2S in fuels. An initial drop in performance after introducing H_2S is maintained without further degradation. After switching back to the normal fuels without sulfur, anode performance is recovered slowly. In cathodes, some degradation is observed due to the contamination as SO_2/SO_3; in such a case, $SrSO_4$ is formed.

Third-generation cells Cells to be operated below 800°C. Instead of oxide ceramics, metal is used to support cells. Fabrication technique is most challenging.

Definition of the Subject

Solid Oxide Fuel Cells (SOFCs) are devices of converting chemical energy (fuels) into electrical energy using an oxide ion conducting materials as electrolyte together with cathode for oxygen incorporation process and anode for oxidation of fuels. For fuel cells to be continuously operated, there arise four flows inside fuel cells: air flow and fuel flow, electrical current, and heat flow. Historically, only a small number of SOFC stack types have been successfully established because it is rather difficult to construct electrochemical cells/stacks with solid materials alone in keeping good electrical contacts among components, good gaseous permeability along the gas channels, or complete gaseous tightness across dense parts such as electrolyte and interconnects [1–3]. This leads to additional requirements concerning the chemical compatibility [4] among the cell components and the mechanical stability [5] of stack as a whole during fabrication and long-term operation including a certain number of thermal cycles. This makes materials selection difficult. Not only the functional properties but also the compatibility with adjacent materials is quite important. Durability and reliability of SOFC stacks are therefore strongly dependent on such materials compatibility [6]. Stress comes from any volume changes in the cell components; for example, thermal expansion mismatch, chemical volume expansion due to changes in valence state [7], volume change on precipitation of products of reactive diffusion or reaction with gaseous impurities, pore formation, etc. These changes may cause the mechanical instability among the stack components and also affecting the functional parts of cells; that is, the electrical path can be damaged or the gaseous permeability through gas channel to and from the electrochemical reaction sites are influenced. When cracks are formed inside

electrolytes or interconnects, fuels and oxidants will meet and burn without generating electricity, causing local heating. The electrochemical performance may also be degraded directly by gaseous impurities attacking the electrochemical reaction sites which are located at the electrode/electrolyte interface region. Changes in microstructure of electrodes also lead to degradation of performance; nickel sintering is a typical example. In these processes, solid-state diffusion makes important contribution [8].

Historically speaking, reliability issues are always associated with an important feature that developments of stack design, fabrication methods, and cell materials are mutually related with each other. Even when the same materials are used in different stack designs, a fabrication method must be different so that materials compatibility appears in different manners. Main issues in the early stage of research and development were interface stability between cathode and electrolyte [9], interconnect chemistry associated with sinterability of lanthanum chromites [10], and chemical volume expansion [7]. Sealless tubular cells fabricated with electrochemical vapor deposition (EVD) [11, 12] were the first ones which have been successfully developed by solving those issues [13, 14]. Durability of the sealless tubular cells was found to be excellent as shown in quite low degradation rates: 0.1%/1,000 h for cell performance and less than 0.1%/1,000 h for system performance at the operation temperature of 1,000°C [10]. Demerits of tubular cells, however, were analyzed as their low-volume power density and high fabrication cost [15]. These sealless tubular cells are recognized as the first-generation cells. After this success, many attempts have been made to overcome those demerits by testing new materials, new cell designs, and new stack designs. The most typical ones can be called as the second-generation cells which are operated around 750–800°C. Here, metal interconnects were adopted instead of oxide interconnect, active cathodes such as lanthanum strontium cobaltites (LSC) or lanthanum strontium cobaltite ferrites (LSCF) [16] were used instead of stable but less active lanthanum strontium manganites (LSM), and an anode-support-type cell design was adopted. As a result, performance of such second-generation cells has been rapidly improved and in many cases has become much better than that of the first generation. On the other hand, durability was not better because metal interconnects and active cathodes were adopted in spite of their low chemical stability [17]. More recently, the third generation based on the metal support cells [18–20] has attracted much attention, because of its expecting low costs and lower operating temperatures. Based on the idea adopted for this generation, nickel can be regarded as a rather expensive material. Instead, cheaper stainless steel should be utilized as a main cell component. This inevitably leads to a requirement that appropriate fabrication methods should be developed so as to fabricate metal-support cells with a reasonable cost. In other words, chemical stability becomes a big issue even in the fabrication processes.

Introduction

The most important features associated with fuel cell technologies are energy conversion efficiency, durability (or life time), and cost. These are common characteristic features among various fuel cells such as phosphoric acid fuel cells (PAFC), molten carbonate fuel cells (MCFC), polymer electrolyte fuel cells (PEFC), and solid oxide fuel cells (SOFC). For comparison among fuel cells, applications in which fuel cells are utilized are important aspects of fuel cells: stationary application in several 100 kW or larger, small stationary applications for residential houses, and automotive or mobile applications.

For the first stationary application, comparison was made in 1980s–mid-1990s among PAFC, MCFC, and SOFC. Efficiency, based on the methane fuel, was regarded as about 40% for PAFC operated at 180°C, 45% for MCFC operated at 650°C and 40% for SOFC operated at 1,000°C when the first attempt by Westinghouse for tubular cells was succeeded [21]. Later, it is clarified that the higher efficiency of MCFC compared with SOFC is due mainly to the operation temperature. Actually, with decreasing operation temperature of SOFCs, the efficiency increases even for SOFCs. The most surprisingly impressive achievement of Westinghouse's SOFCs is their stable performance for a long period of operation time, although their fabrication cost was evaluated to be too high. Alternative efforts of constructing SOFCs in planar design with metal interconnects were, on the other hand, suffered from poor durability in its early

stage of development. One of plausible reasons for such technological dead-rock seems to be at a point that the target application was stationary so that they aimed at constructing larger flat cells with sealant materials. In such a larger planar stack, temperature distribution developed within planar cells may cause strong mechanical stresses, leading to failure in sealing or to crack formation.

From the mid-1990s, there arose a new wave in fuel cell applications, that is, the automotive application and closely related applications of small stationary. It began with PEFC. Even so, SOFC has also received the impacts of new applications. This leads to two important efforts on SOFC developments: (1) severer requirements for mechanical stability in automotive applications [22] and (2) smaller stationary application. The former has come from the new application proposed by BMW, Delphi, and Renault to utilize SOFC systems as auxiliary power unit in combustion engine cars. Since BMW and Delphi have cooperated with National Laboratories in their own countries, materials development has been made to improve mechanical instability. Development of simulation technique also helps to improve the stack technologies. The latter case of the small stationary systems gave rise to a big impact in Japan, Australia, Switzerland, and UK where the SOFC cogeneration systems have attracted strong attention.

Current issues of SOFC technologies, namely, reliability/durability and cost appear in different manners in respective applications which have different historical background.

This entry is organized as follows: In section "Historical Aspects of Reliability, Durability and Cost Issues," historical aspects are first described to provide essential points of SOFC stack/system development. The technological features of the first-generation cells, namely, sealless tubular cells, will be described in comparison with the second- and the third-generation cells in critical technological issues; these are materials selection of interconnect (oxide or metal), sealing scheme, redox issues of nickel cermets, metal support cells, trade-off relation between reliability and performance, and materials chemistry associated with lowering operation temperature. Section "Durability/Reliability of SOFC Systems" describes durability/reliability of SOFC systems. Failures of system operation are first described. Then, failures of stacks and degradation of cell performances are described in detail with focuses on chromium poisoning, nickel sintering, carbon deposition, sulfur poisoning, etc. Results of field tests are also described in relation to reliability. Section "Cost Issues" describes the cost issue and "Future Directions of SOFC development" are given finally in section "Future Directions."

Historical Aspects of Reliability, Durability, and Cost Issues

Materials compatibility is important in construction of SOFCs. Particularly, chemical and mechanical stabilities are crucial in simultaneously optimizing materials, materials processing and stack design. First success has been achieved by Westinghouse Power Corp. (later Siemens Westinghouse Power Corp. and now Siemens Power Generation Corp.) in the 1980s by adopting the first-generation cell materials, the electrochemical deposition technique to fabricate a dense yttria-stabilized zirconia (YSZ) electrolyte film on porous LSM cathode tubes and subsequent Ni anode on the dense YSZ film as described in Fig. 1. This is called sealless tubular cells, because no use of sealing materials is the important key point. The cells exhibit high performance and also long stability; only a small degradation rate of performance (less than 0.1%/1000 h) has been confirmed for more than 70,000 h for the cell level (see Fig. 2) and more than 30,000 h for the system level. Two demerits, however, were pointed out for those cells by Ackermann et al. [15] in Argonne National Laboratory; one is high cost because of the adoption of electrochemical vapor deposition (EVD) technique which utilizes metal chlorides in vacuum vessels, the other one being low-volume power density. Since then, many attempts have been made to overcome these demerits, namely, alternative materials have been investigated, new materials processing methods have been developed, and alternative stack designs have been attempted (Table 1).

In recent years, rapid progress has been made in the development of SOFC cogeneration systems with several kW scale for residential houses [23–26]; its demonstration has been successfully made in real residential circumstances [23]. In such a situation, degradation, durability, and reliability have appeared again

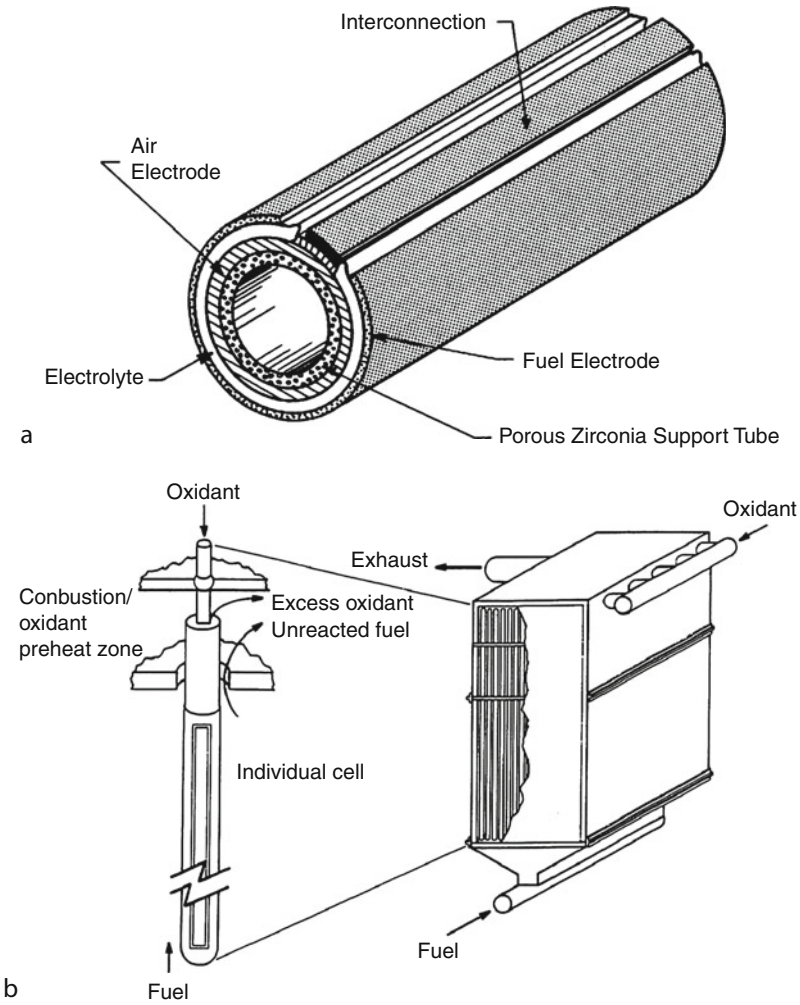

Solid Oxide Fuel Cell Materials: Durability, Reliability and Cost. Figure 1
Sealless tubular cell: (**a**) cell configuration and (**b**) stack configuration (From [13, 14])

as important issues. Now these should be related with cost issues, because it is already well established that the excellent long stability can be achieved with the electrochemical vapor deposition (EVD) technique despite high cost. The most important point is that the low cost has to be obtained at the same time together with high efficiency and long stability.

First Generation Stack: Sealless Tubular Performance as Standard

Westinghouse Power Corp. made a breakthrough by adopting sealless tubular cells after examining several other types of SOFC stack design such as planar cells or segment-in-series cells. This implies that the sealless tubular cells have many advantages against other designs. Actually, after the breakthrough, they succeeded in demonstrating the long-term stability. From the current knowledge of durability of other cells, their success in long-term stability can be ascribed to the following:

1. The electrochemical vapor deposition (EVD) process has been successfully developed as fabricating a dense electrolyte film on porous cathodes and fixing anode nickel particles on the electrolyte plate with YSZ. This provides a nearly ideal microstructure for electrolyte/electrode interfaces.

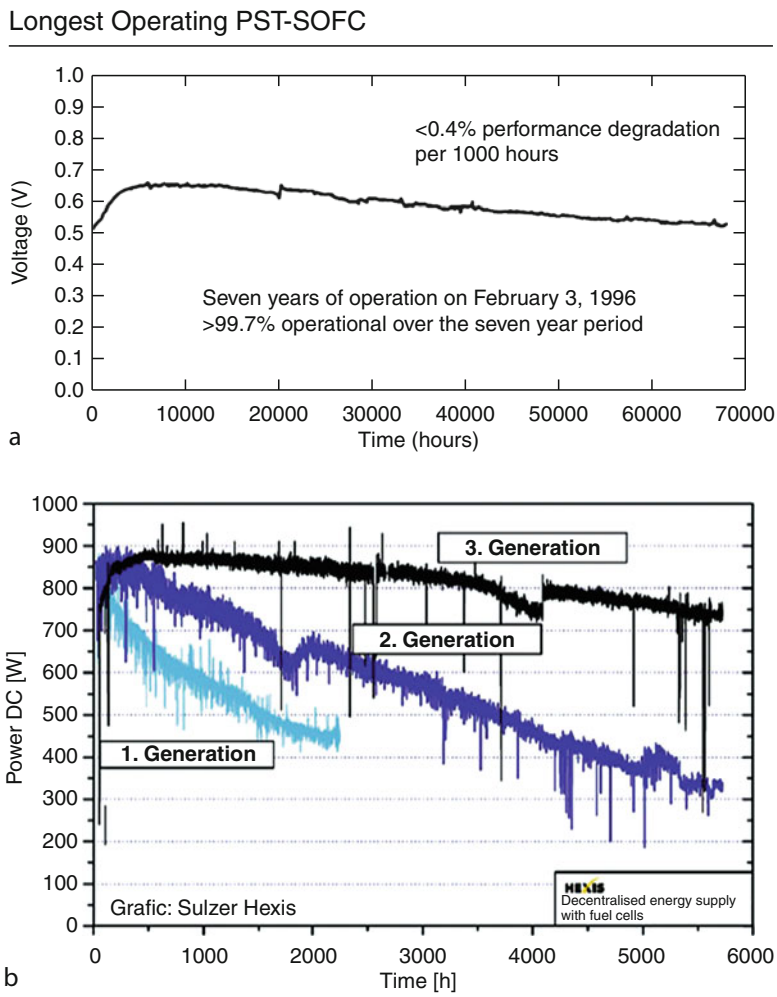

Solid Oxide Fuel Cell Materials: Durability, Reliability and Cost. Figure 2
Cell performance degradation of (**a**) the first generation sealless tubular cells by Westinghouse (Currently Siemens, From [13, 14]) and (**b**) the second generation planar cells by Sulzer Hexis (Currently Hexis, From [17])

2. Sealing materials are not used. Particularly, this cell is free from silica; silica is one of materials to be carefully treated.
3. Other metals than nickel are not used in anode atmosphere or in air. Alloys (Fe–Cr, Ni–Cr) sometimes caused troubles such as anomalous corrosion. In sealless tubular cells, nickel is used as anode materials and also as cell-to-cell connecting materials. Note that nickel is stable in the fuel atmosphere without forming oxide scale. Furthermore, a small amount of oxygen can be dissolved so that even when oxygen permeates from the air side on nickel in the fuel side, a steady state flow of oxygen can be established across the nickel/$LaCrO_3$-based interconnects. Nickel connection can be made because this is the cathode-support cell. Note that when the anode-support tubular cell is adopted in a similar design, cell-to-cell connection has to be made in the air side, leading to a severer materials problem.
4. Alumina tubes are used for providing air at the bottom of the cathode compartment. This is acted as heat exchanger to remove heats out of cells. This provides an excellent situation for thermal management on larger stacks.

Immediately after the success of sealless tubular cells, one important analysis was made to clarify the technological features by Argonne National Laboratory [15]. Their main conclusions are given as follows:

1. Fabrication cost is too high
2. Power density per unit volume is less

Status of the sealless tubular cells concerning cost, efficiency, and durability can be summarized as shown in Fig. 3a.

After knowing the success of Westinghouse and technological assessments by ANL, many people started to develop various kinds of SOFC stacks to overcome demerits of the sealless tubular cells. Depending on their technological strategies, several different attempts have been made. These can be summarized as follows:

1. Improvement of sealless tubular cells. To improve the volume power density, flatten tube type or delta type designs have been investigated by Siemens (Westinghouse) themselves [27]. To lower the fabrication cost, sintering-wet process has been successfully adopted by TOTO [28], whereas atmospheric plasma spray was adopted by Siemens themselves [27]. These attempts are based on the idea that tubular cells or their modified cells must be superior to other designs.

Solid Oxide Fuel Cell Materials: Durability, Reliability and Cost. Table 1 Comparison in typical materials and fabrication methods among the first-, second-, and third-generation SOFCs

	First	Second	Third
Cathode	LSM	LSCF	LSCF
Electrolyte	YSZ (50 μm)	YSZ (10 μm) Ni ScSZ, LSGM GDC	ScSZ, GDC
Anode	Ni/YSZ	Ni/YSZ, Ni/SSZ, Ni/DGC	Ni
Interconnect	$LaCrO_3$-based $SrTiO_3$-based	Ferritic, Cr-based	Ferritic
Cell to cell connection	Ni	Ferritic	ferritic
Operation temperature	900–1,000°C	750–800°C	500–650°C
Typical fabrication method	EVD, plasma spray	Wet-sintering	Sintering in reducing atmosphere

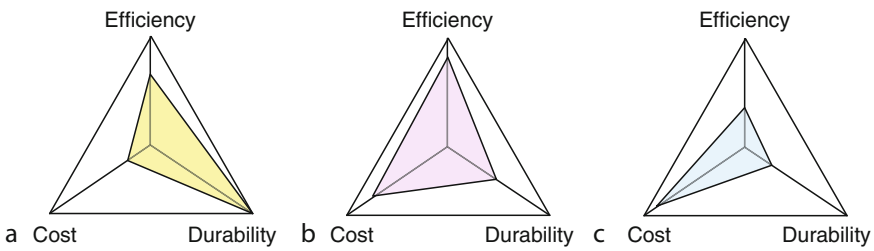

Solid Oxide Fuel Cell Materials: Durability, Reliability and Cost. Figure 3
Schematic representation of the current status of technology for achieving three targets of fuel cells, namely, efficiency, cost, and durability; (**a**) the first generation SOFC based on Electrochemical vapor deposition technique; (**b**) the second generation SOFC based on anode-support cells with wet-sintering processes; and (**c**) the third generation based on metal support cells

2. Planar design has been recognized as better in achieving the higher power density in an analogous manner to other fuel cells such as PAFC or MCFC. One approach is to adopt the oxide interconnect, the other being the metal interconnects. Only few developers have adopted the oxide interconnect in planar stacks [29, 30]. One technological reason is that sintering of lanthanum chromite–based ceramics is difficult, particularly in air. Another reason is originated from the cost consideration; when rather thick plates of $LaCrO_3$-based interconnects are used in planar cells, the contribution of La to the total material cost becomes quite large [31]. Adoption of metal interconnects becomes important in stack developments probably because of their technological merits [32, 33]; the use of metal inside SOFC stacks is quite useful for better thermal management, and for controlling the mechanical stress, etc. Even so, demerits can be seen in poisoning of cathodes by Cr originated from oxide scale [34], chemical interactions with sealing materials, and also increasing interface resistivity across the oxide scale. In many cases, utilization of metal interconnect is combined with the adoption of anode support cells.
3. There have been also many efforts in improving stack design such as flatten tubes, micro tubes, or honeycomb type cells. This is mainly from the thermo-mechanical considerations. In order to avoid the thermal shock effectively, utilization of materials having low thermal expansion and high thermal diffusivity are highly required; Al_2O_3 and Si_3N_4 can be regarded as one of such materials for high-temperature use. Unfortunately, YSZ exhibits high thermal expansion and low thermal conductivity and there is no good way of improving those inappropriate properties. Thus, the most effective way of overcoming thermal shock is to shorten the thermal diffusion length so as to relax changes in temperature on thermal shocks. For this purpose, micro-tube or honeycomb structures become attractive.
4. Metal support cells are proposed to realize cost reduction from the materials cost and fabrication cost simultaneously. Compared with nickel which is the major component in the anode support cells, the metal support cells aim at using cheaper Fe–Cr alloy as supporting materials [19]. Instead, the fabrication process becomes rather difficult compared with other cell design.

These activities can be summarized as the second or the third generations of SOFCs. These characteristic features are compared with the first generation in fundamental aspects in Fig. 3. Cost and efficiency are expected to be satisfied, whereas durability has not been confirmed yet. Thus, the main issue associated with the second generation becomes the establishment of durability/reliability (Fig. 4).

Oxide Interconnect Versus Metal Interconnect

Interconnect materials are quite important in fabricating SOFC stacks. To meet the chemical and mechanical stability requirements under an oxygen potential gradient, only a few materials have remained; some spinel compounds such as $NiCr_2O_4$ or $CoCr_2O_4$ were tested as interconnects in the early stage of development without success because of their poor materials stability. Remaining materials are $LaCrO_3$-based or $SrTiO_3$-based perovskite oxides. The interconnect materials need to meet two requirements: good electrical conductivity (at the same time, essentially no oxide ion conductivity) and the good gaseous tightness. This can be met by fabricating into dense plates/films. Furthermore, an additional requirement is derived from the mechanical point of view, that is, the thermal expansion coefficient should match with that of YSZ, and the chemical volume expansion due to valence change should be small enough [35].

The technical issues associated with oxide interconnect can be summarized as follows:

1. Establishment of inexpensive fabrication process for making dense films of $LaCrO_3$-based ceramics. This is because the sintering of $LaCrO_3$ in air is quite difficult since the chromium component tends to volatilize during sintering and to subsequently deposit at interparticle necks as Cr_2O_3; This deposited chromia hinders further sintering [10].
2. Thermal expansion coefficient is another issue. The thermal expansion coefficient of non-doped $LaCrO_3$ is small compared with YSZ. To match the thermal expansion coefficient, there are two ways: one is the heavy alkaline earth doping up to 30 mol%,

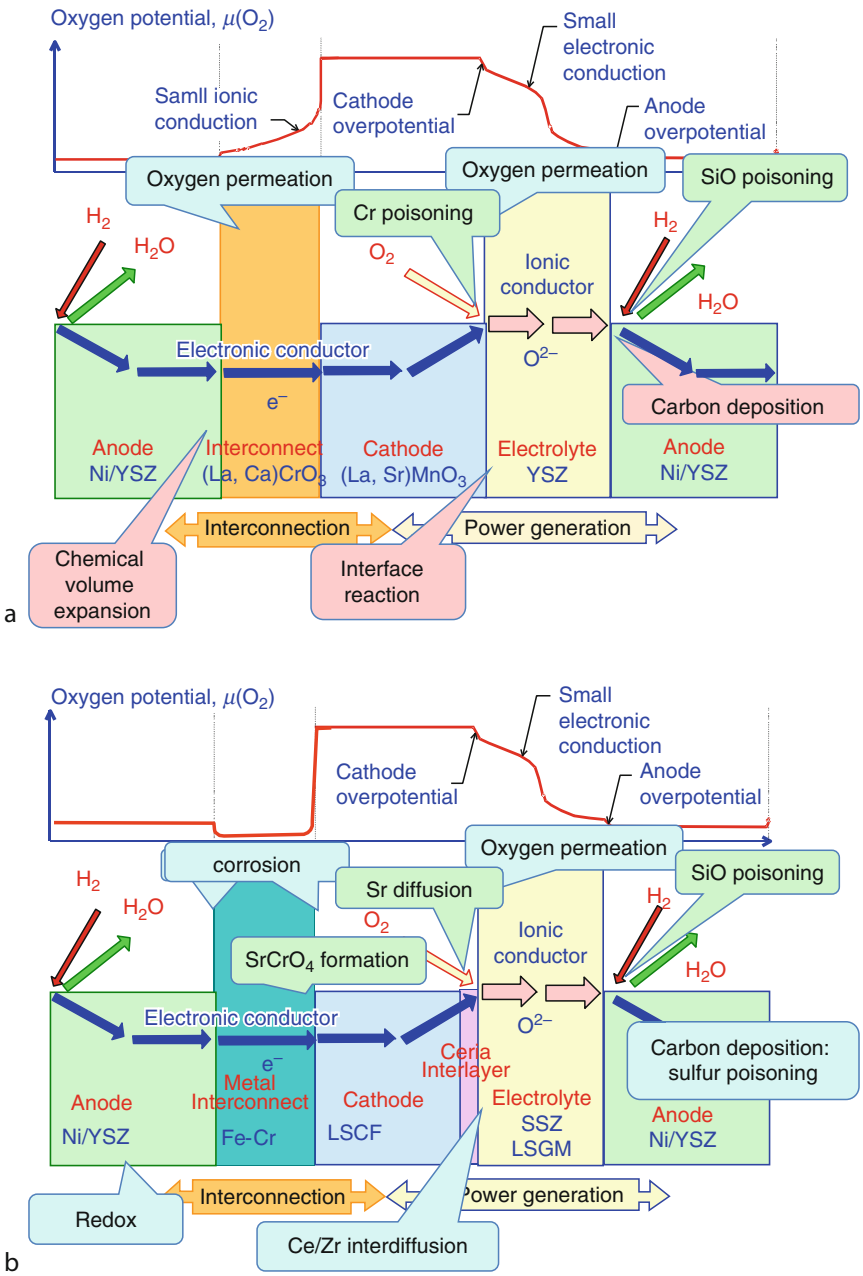

Solid Oxide Fuel Cell Materials: Durability, Reliability and Cost. Figure 4
Schematic representation of the materials and associated degradation issues (**a**) the first-generation cells and (**b**) the second-generation cells

the other being addition of alumina to YSZ to reduce the effective thermal expansion coefficient of a mixture of YSZ and Al_2O_3 [35]. This makes it possible to adopt the low concentration (about 10%) doping of alkaline earth.

3. The high electrical conductivity is achieved by holes created as a result of doping of alkali earth oxide; however, in reducing atmosphere, hole and Cr^{4+} is reduced to Cr^{3+} and oxide ion vacancies. This valence change gives rise to the volume expansion,

which is called the chemical volume expansion [7]. For the heavily doped system, this chemical volume expansion is too big so that additional B-site doping is necessarily made to reduce the chemical volume expansion.

4. The material cost of lanthanum is high so that the thickness of the oxide interconnects should be thin enough to reduce the amount used in cells [31]. On the other hand, the $LaCrO_3$-based interconnects should be thick enough to prevent the electrochemical oxygen permeation which takes place as the bipolar diffusion of oxide ions and holes inside the interconnect. For such a purpose, Ca-doped $LaCrO_3$ is not appropriate because those ceramics are highest in gas permeation among the alkali earth-doped $LaCrO_3$ [36, 37].
5. For the $SrTiO_3$-based interconnects, sintering is much easier than $LaCrO_3$-based ceramics, whereas the electrical properties are not good, particularly in the air side [38].

When the metal interconnects are adopted in the second generation stack, there arise other technical issues:

1. Metal interconnects typically made of ferritic alloys have slightly higher thermal expansion coefficients than YSZ. A new alloy was produced so as to fit the thermal expansion of YSZ; this is a Cr-based alloy, $Cr5Fe1Y_2O_3$ [39]. Since this alloy is oxide dispersed and therefore quite hard, it is not easy to fabricate it into a desired shape. For this purpose, powder metallurgy process has been developed [40].
2. Most important difference of metal interconnects from oxide interconnects is that such alloys will be oxidized during the cell operation. This inevitably involves kinetic aspects in durability of materials. The most important aspect related with durability is materials behavior under a steep oxygen potential gradient. Electrolyte and interconnect materials should be stable under such a gradient. In addition, alloys have to be stable on both sides of materials, namely, the air side as well as the fuel side, because the oxygen potential inside normal Fe–Cr alloys is maintained to be quite low compared with the fuel atmosphere. One difference from oxide interconnect is that oxygen atoms to be transferred inside oxide interconnects will permeate through the interconnect plate, whereas oxygen atoms reacted with or dissolved into alloys do not permeate but will be accumulated in the surface area to form oxide scale. This increasing amount of oxide scales with operational time becomes an important factor of limiting life time. Note here that in the first-generation sealless tubular cells, only nickel is used in the fuel compartment and such nickel is oxygen permeable when oxygen flux is low enough to maintain the reducing condition.
3. Immediately after starting the utilization of metal interconnects, the chromium poisoning for lanthanum manganite–based cathode was recognized as a severe degradation [34, 41–43]. The Cr_2O_3 component of the oxide scales reacts with oxygen molecule in air with/without water vapor to emit the vapors of $CrO_3(g)$ or $CrO_2(OH)_2(g)$. Such vapors come to the electrochemically active sites of LSM cathode (namely, three phase boundaries) and deposited as Cr_2O_3 or $MnCr_2O_4$. Although detailed mechanism is different, similar poisoning effects due to Cr vapors were found for other cathodes such as LSCF through the $SrCrO_4$ formation.
4. A most effective way of overcoming Cr poisoning is to reduce Cr vapors from oxide scales [44]. As a result, coating technique becomes crucial in the utilization of metal interconnect. Materials to be coated should meet several requirements concerning the stability under a steep oxygen potential gradient. Such requirements are quite similar to those for the oxide interconnects. Thus, perovskite oxides have been tested as coating materials [45]. As far as the cation diffusivity and the oxygen permeability are concerned, the lanthanum chromite–based materials will be most appropriate. Even so, the fabrication technique to form a dense film on alloys is quite limited. Attempts have been made to try to utilize other perovskite materials such as cobaltites and manganites. Since those perovskites are oxygen permeable, oxide scales should grow under the coating materials. In addition to Cr_2O_3, some spinel phases are formed between the alloys and the coating. Investigations on such complicated oxide layers lead to selection of $MnCo_2O_4$ spinels as coating materials [46].
5. From the viewpoint of cost, utilization of metal interconnects should be considered as the combined

technology with coating. Although raw alloy materials are cheaper than lanthanum, the fabrication cost will increase due to the sophisticated coating technique. If coating cannot be avoided, it is essential to reduce the fabrication cost for coating as well as to reduce further the raw materials cost because the development of mother alloys alone cannot lead to low cost enough as interconnects.

From the materials design point of view for those electrical conductive oxides which are stable under an oxygen potential gradient, oxide interconnects and coating materials for alloys are quite similar. From the fabrication method, however, there are several differences. Inexpensive sintering process can be applied for oxide interconnects, whereas high-temperature heat treatment is limited for coating. The low-pressure plasma splay technique was successfully adopted to form dense films; however, from the cost point of view, this is not appropriate. The atmospheric pressure plasma splay is more cost effective, but the quality of fabricated films is not excellent.

Seals

Seal technology is quite sophisticated among the stacking technologies. As described above, the first success of stacking SOFCs by Westinghouse has been made by adopting the sealless design combined with the electrochemical vapor deposition technique. This clearly indicates that when seals are adopted, there arise many materials problems and without solving those problems, any stacks cannot survive.

The most severe requirements for sealing materials are

1. Appropriate bonding to prevent gaseous leakage. Compared with PEFC which can be easily sealed gas-tightly by just compressing the main cell components, it is impossible for SOFC to achieve the gas-tightness among the ceramic cell components without activation in the atomic level.
2. Sometimes, not quite often, sealing can be achieved by co-sintering two materials to be joined at a relatively high temperature. This can be regarded as a thermally activated process at interfaces.
3. In many cases, glasses or crystallized glasses will be used as sealing materials. This is because glasses are convenient for achieving the gas-tightness due to their deformable nature. Even so, glasses are non-stable materials and tend to undergo the transformation into crystalline phases on reactions with other cell components. This changes the mechanical property or the gas permeability at the bonding places. Such processes are dependent on various factors; temperature, reaction rate, crystallization rate, etc. This implies that their mechanical strength depends on their thermal history. Since there is a large temperature distribution among the places where sealing is needed, deterioration of sealed parts takes place in a different manner from place to place. Note that the durability/reliability of stacks is determined by the weakest place.
4. When no glasses will be used and compression sealing [47] will be adopted, complete gas tightness cannot be necessarily achieved. Thus effects due to gas leakage will appear in various aspects of stack behavior. Since the SOFC stacks consist of the oxide ion conductive and/or electronic conductive materials, local gas leakage gives rise to those effects which will be spread throughout the stack [48]. In this sense, to make an analysis on gas leakage and to overcome this issue, it will be needed to understand a whole behavior of stacks.

In view of these features, sealing is not the localized materials issue but it is a matter of whole stacks. In this sense, the characteristic features of the adopted stack design and the sequential of fabrication depends on the way of making seals.

Redox Issues

In a typical case, the stack fabrication will be completed by reducing NiO to Ni metal to form the electrical path in the anode side. On this reduction, the sintered NiO will be reduced by hydrogen to become nickel powders first and then to make an electrical path after some coagulation; during this process, the mechanical constrains introduced at the high temperature heat treatment will be released at the anode side and a new constrained state will start under the oxygen potential gradient [49].

When the sealless structure is adopted and the remaining fuels are combusted inside the stack, there is always some possibility that combusted gases

will diffuse backward to the nickel anode area and will reoxidize nickel.

For anode support cells, one needs to have an appropriate method of sealing edges of cells where the porous supporting anode should be appropriately closed. The flatten tubes provide one good way of sealing sides by high-temperature sintering without using seals.

For small power-unit systems such as the SOFC cogeneration systems for the residential applications, usually no purge gas will be used. Thus, there arises a big possibility that the anodes can be reoxidized during the start-up and shutdown cycles.

Metal Support Cells

The metal support cells can be regarded as the third generation. The major driving forces for making the metal support cells can be summarized as follows;

1. For the mobile/transportation application, it is highly required to start up rapidly, to make stacks mechanically strong enough against mechanical or thermal shocks. For this purpose, ANL adopted the metal-supported cells and they made attempts of fabricating metal parts in essentially the same manner as those for ceramics, that is, they tested to fabricate by sintering metal powders in the reducing atmosphere [18].
2 Another major driving force for metal support cells is cost reduction [19]. For the anode-supported cells, a relatively large amount of nickel will be used because the nickel cermet becomes the major structural supporting component. To achieve a drastic change in row materials cost, therefore, cheaper alloys should be used as the major component. Note also that from the raw materials point of view, ceramics are more expensive than metals in general.
3. The use of metal as supporting component implies that the operational temperature will be below 800°C which is the typical operational temperature for the second-generation cells. At such a low temperature, brazing will be used instead of glass-based sealing methods. This will make materials chemistry much simpler.

Despite expected low cost, it is expected that the fabrication technology is much more difficult for metal support cells. This is illustrated in Fig. 3c.

Reliability Versus Performance and Its Relation to Operation Temperature

Utilization of metal interconnects requires lower temperature operation, and this low operation temperature is generally expected to lead to less severe conditions for degradations because of the Arrhenius-type behavior of processes involved in degradations. Accumulated knowledge on durability, however, exhibits an interesting feature that on contrary to this expectation, some degradations become more severe at lower temperatures. That is because with lowering operation temperature, there arise an increasing number of factors affecting durability as indicated as follows:

1. In order to achieve the same performance as the first generation, the more active electrodes are needed. In particular, cathode performance exhibit rather large temperature dependence [50]. Thus, instead of the stable LSM cathode, it is needed to utilize more active cathodes such as LSCF. The electrode activity of LSCF is high because this material exhibits ionic and electronic mixed conductivity and also shows high surface reaction rate for the oxygen incorporation reaction. These features are originated from the high concentration of oxide ion vacancies in LSCF. This is chemically represented as follows: the $SrFeO_3$ or $SrCoO_3$ components in perovskite are reduced to form Fe^{3+}/Co^{+3} ions together with the oxide ion vacancies. Chemically speaking, the oxide ion vacancy formation is due to the fact that unstable $SrFeO_3$ is reduced to be $SrFeO_{3-x}$ and $O_2(g)$. In other words, the valence stability of Fe^{4+}/Co^{+4} is weak compared with that of Mn^{4+} in the perovskite lattice.
2. This in turn indicates that LSCF is also reactive to other materials/gases; typical reactions are those with YSZ to form zirconates ($SrZrO_4$ or $La_2Zr_2O_7$) and with chromium containing vapors($CrO_3(g)$ or $CrO_2(OH)_2$) to form $SrCrO_4$. In this reaction, the $SrFeO_{3-x}$ component is reductively decomposed into SrO in $SrZrO_4/SrCrO_4$ and $FeO+O_2(g)$. Thus, this chemical reactivity is originated from the same physicochemical properties described above. In this sense, the performance and the durability are in trade-off relation. This is summarized in Table 2 [4, 51].

Solid Oxide Fuel Cell Materials: Durability, Reliability and Cost. Table 2 Comparison of cathodes among lanthanum strontium manganites, ferrites, and cobaltites in their chemical reactivity, functionality as cathode, and tolerance against Cr poisoning

Items	LSM	LSF	LSC
Valence stability	Mn^{4+}Stable	Fe^{4+}unstable	$Co^{4+}Co^{3+}$ unstable
O^{2-}conductive	Nearly zero	High	High
Cathode mechanism	Three phase boundaries	Two phase boundaries (surface)	
Reactivity with YSZ	Stable (A-site deficient)	$SrZrO_3$ formation	$La_2Zr_2O_7$ $SrZrO_3$ formation
Reactivity with Cr	Cr^{3+} substitute	$SrCrO_4/Cr^{3+}$ substitution	$SrCrO_4/Cr^{3+}$ Cr^{4+} substitution
Cr poisoning	Significant	Not seen in early stage but causes various deteriorations	

3. Instead of stable YSZ, use is frequently made of other electrolytes showing higher oxide-ion conductivity; these are ScSZ (Scandia-stabilized zirconia), GDC (gadolinia-doped ceria), and LSGM (lanthanum strontium gallium magnesium oxide). The chemical reactivity of these electrolytes is, however, higher than YSZ. In many cases, ceria is thought to be more stable than zirconia. This is true when comparison is made just between ceria and zirconia. However, when comparison is made among the dopants, this is not the case; dopants in ceria are not well stabilized so that they are more reactive than yttria in YSZ [52].
4. Use of metal interconnect gives rise to a new situation that materials are not necessarily used in their most stable states. This means that the durability is determined not only by equilibrium properties but also by kinetic properties. Thus, corrosion becomes one of the main issues at lower temperatures.
5. The equilibrium properties tend to shift to a more reactive side with decreasing temperature [52]. In particular, those reactions which involve the condensation of the gaseous component become more favored at lower operation temperatures. A typical example is the adsorption of sulfur from H_2S gases on nickel. Another important example is the redox reactions which emit or adsorb oxygen gas. At low temperatures, the oxidation becomes thermodynamically favored. Those reactions with gaseous impurities (including water vapor, CO_2) exhibit the same tendency. With decreasing temperature, the driving force for such reaction increases due to the negative entropy effect. Those features are shown as the oxygen potential vs. temperature plot in Fig. 5.
6. From the Arrhenius behavior of kinetic processes, the reaction rate decreases exponentially at low temperatures. This in turn gives rise to larger driving force for degradation. For example, the overpotential of LSM cathode increases with decreasing temperature as expected. This is understandable from the Arrhenius behavior. This larger overpotential at lower temperatures promotes Cr poisoning because the oxygen potential difference corresponding to the overpotential assists the Cr vapor to reach the electrochemically active sites at the three-phase boundaries (TPBs) and to be electrochemically reduced to form Cr_2O_3 (see Fig. 6). In another example using the samarium strontium cobaltite (SSC) cathode, reactions with SO_2 proceed fast at a high temperature so that only a small amount of SO_2 can reach the electrochemically active zone. With decreasing temperature, however, this trapping ability is weakened; as a result, a larger amount of SO_2 can attack the sites, leading to faster degradation compared with high temperature [53, 54]. These examples indicate that one degradation phenomenon consists of several processes which have their own temperature dependence. Thus, the apparent degradation rate becomes fast at lower temperatures.
7. So-called inert metals such as Pt and Ag are not necessarily chemically inert at lower temperatures [55].

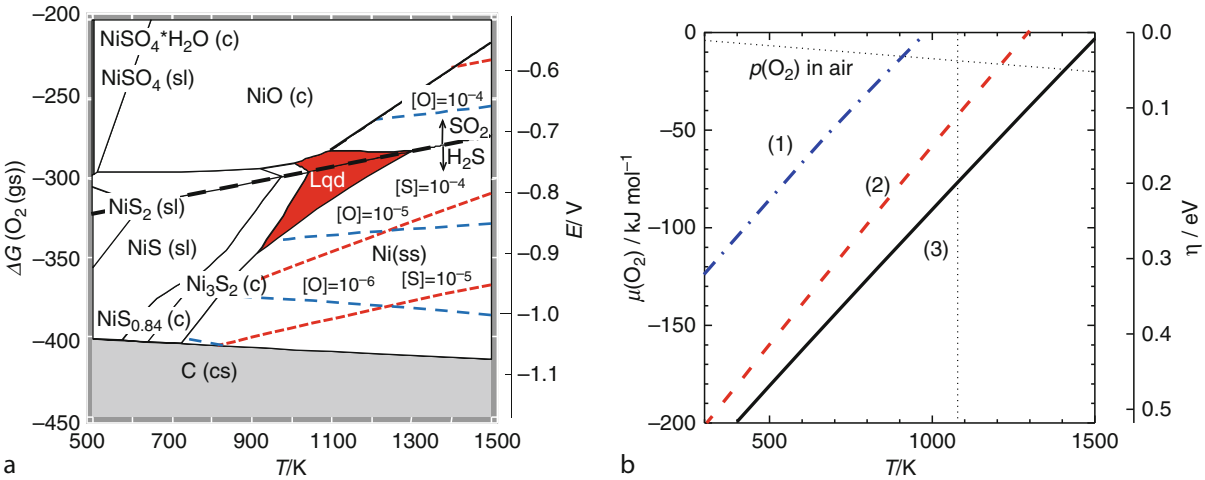

Solid Oxide Fuel Cell Materials: Durability, Reliability and Cost. Figure 5
Ellingham diagrams plotted as $\mu(O_2)$ vs. T (**a**) Ni-S-O-H system for interaction of nickel and impurities (From [85]); (**b**) Borderlines for separating $SrCrO_4$ formation region and $LaCrO_3$ solid solution formation region for interaction of perovskite cathodes and chromium containing vapors; (1) $2SrCrO_4 + 2LaMnO_3 = 2LaCrO_3 + 2SrMnO_3 + O_2(g)$; (2) $1.33SrCrO_4 + 1.33LaFeO_3 = 1.33LaCrO_3 + 1.33SrFeO_{2.5} + O_2(g)$; (3) $2SrCrO_4 = 2SrCrO_3 + O_2(g)$ (From [42])

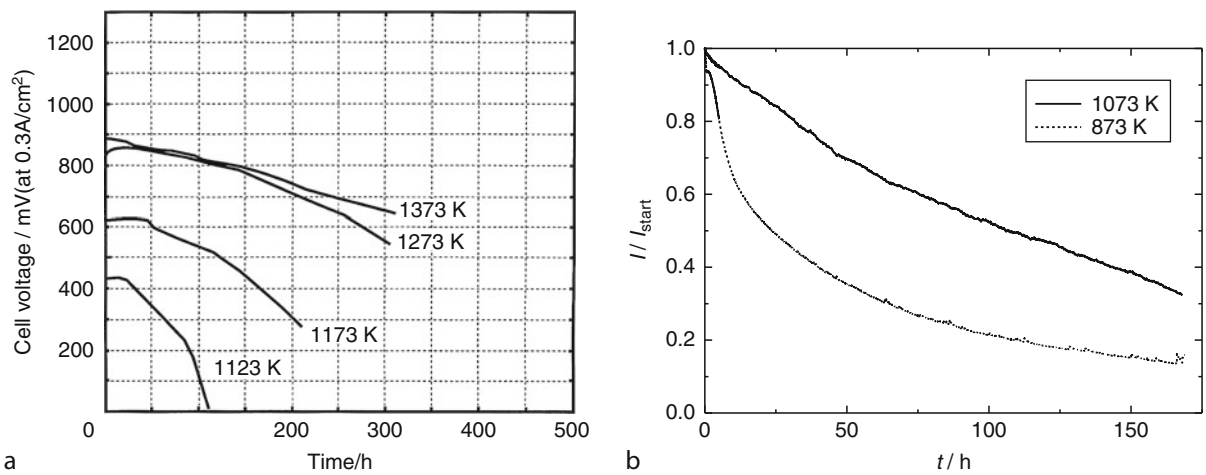

Solid Oxide Fuel Cell Materials: Durability, Reliability and Cost. Figure 6
Temperature dependence of cathode degradation (**a**) Cr poisoning on LSM cathodes (From [34]) (**b**) SO_2 poisoning on SSC cathode (From [53])

8. For active cathodes, an interlayer is inserted between such cathodes and the YSZ electrolyte to prevent chemical reactions, leading to a complicated interconnect/electrode/electrolyte structure. This introduces another technical requirement for fabricating those layers durable enough.

9. Effects of impurities may appear in a more significant manner at low temperatures. One example is sintering of nickel at low temperatures. Compared with the first-generation cells, there are many reports suggesting more significant sintering in the second-generation cells [56]. This is probably

due to gaseous impurities which tend to condensate at low temperatures.

10. With decreasing temperature, nature of electrochemical reactions may change. Particularly, degradation may depend not only on the major electrochemical reactions but also on the secondary reactions. For example, protons in YSZ or GDC do not contribute to the major electrochemical reaction because of its extremely low transport number. However, it is not adequate to neglect completely possible effects of protons in electrolytes or in cathodes. In particular, GDC exhibits two-orders-of-magnitude higher proton solubility than YSZ [57, 58]. This makes it reasonable to assume that protons can contribute to side electrochemical reactions.

When consideration is made on chemical compatibility of cathodes with other components/impurities, it becomes clear that the selection of elements in the major components is critically important. Differences between LSM, LSC, LSF, and LSCF are originated mainly from the thermodynamic activity of SrO component in coexistence with transition metal oxides. Thus, no use of the SrO component in cathodes can be good attempts of avoiding gap between the stability and the performance. Actually, LNF ($La(Ni,Fe)O_3$) proposed by NTT [59] seems to indicate some progress in this issue.

Durability/Reliability of SOFC Systems

Failures in Flow Systems

The SOFC system is an energy converter from fuels as chemical energy to electricity and heats. There are four flows inside stacks, namely, fuel flow, air flow, electrical flow, and heat flow. In order to maintain the proper function as energy converter, these four flows have to be well maintained and controlled so as to harmonize to generate electricity and remove heats [60].

SOFC systems frequently have to be stopped in their operation due to unexpected failures in controlling systematic flows of fuels, water to be used in reforming, air, or electricity. Typical examples are given as follows:

1. Air flow: When air blower malfunctions, systems will be in trouble. Oxygen starvation takes place in cathodes. Perovskite oxide cathodes will be reduced to provide oxygen if oxygen gas is not sufficiently available. As a result, such cathodes are heavily damaged.
2. Fuel and fuel treatment: Except for hydrogen gas, normal fuels need to be reformed before utilization. The water reforming needs to add water to hydrocarbons; when water is not supplied in a proper amount, carbon deposition will take place. Deposited carbon can act as catalyst for further carbon deposition, leading to collapse of fuel flow. Similarly, when an amount of air for partial oxidation or autothermal oxidation is not well controlled, essentially the same situation can be reproduced. When fuel supply is stopped accidentally, fuel starvation takes place and nickel anodes will be oxidized by water vapors.
3. Concerning the electrical path, there can be two failure modes: one is shorting, the other being cut-off of path. When shorting will start, the current should pass until generated electrical potential is cancelled out with the ohmic loss in the shorting circuit path; typically, this happens when one of the chemicals (fuel or oxygen) becomes empty. A large current will be concentrated in a limited area, leading to damage in local area. The latter case of cut-off corresponds to the so-called death of the electrochemical cells. This will happen on the electrochemical sites or along the path.
4. Heats are by-products of the electrochemical conversion and therefore have to be removed effectively. Usually this removal of heats is made with the air flow which is supplied in an excess amount to the stoichiometrically required one. When this removal becomes insufficient, the temperature will increase and enhance various kinds of activation processes. The contribution of radiation loss from the stack surface will increase; in other words, temperature distribution inside stacks becomes large.

These failures should be avoided by well-designed and well-trained control systems.

Field Tests

Field tests of the SOFC systems have been made in several places. In Germany, field test was initiated by the utility companies. Among them, the test on the

Sulzer Hexis system has been made in recent years and well documented in the literature [17]. After the field test, Sulzer Hexis made improvements on the system configurations; these seem to be interesting in knowing what kinds of materials issues were involved. First to be considered is the effect of sulfur. Those SOFC systems in Europe are designed to be utilized with natural gases available from natural gas pipelines. This implies that the sulfur content is rather high and changeable. They chose to operate at a higher temperature instead of applying the desulfurization process. As a result, their cells with Cr-base alloys are operated at around 900°C. Another issue was $CaSO_4$. To avoid the contamination by $CaSO_4$, they decided not to use the external water.

In Japan, a demonstration program for the SOFC cogeneration systems for residential houses has been initiated for the period 2007–2010. Kyocera reported the statistics of troubles during the demonstration program [61, 62]; this is summarized in Fig. 7. Troubles in systems were well treated to be improved so that a number of troubles decrease year by year.

Failures/Degradation in SOFC Stacks

Since there are many kinds of SOFC stacks which are fabricated by different fabrication methods in different sequences, it looks rather hard to describe the failure/degradation modes of stacks in a proper manner. Even so, it seems possible to extract some common features out of various failure/degradation modes.

Long-Term Operation During a long period of operation time, some changes may happen on the following aspects:

1. Deformation due to creep when cells are stacked into a tower consisting of a large number of cells.
2. Change in microstructure and related electrode structure due to diffusion in the vicinity of active sites.
3. Change in mechanical strength due to surface segregation, other aging effects or impurities effects.
4. Those changes in small parts may cause accumulated effects on the durability against thermal shocks or mechanical shocks.

Driving forces for such phenomena are diffusion in solid materials and reactions of solid components with gaseous components. These effects are expected to determine the life time beyond 10,000 h.

These features have been found to be highly correlated with the fabrication method/sequence as well as materials selected. For example, anode support cells have stable anodes but there remain several points to be optimized for a cathode-complex-layer structure.

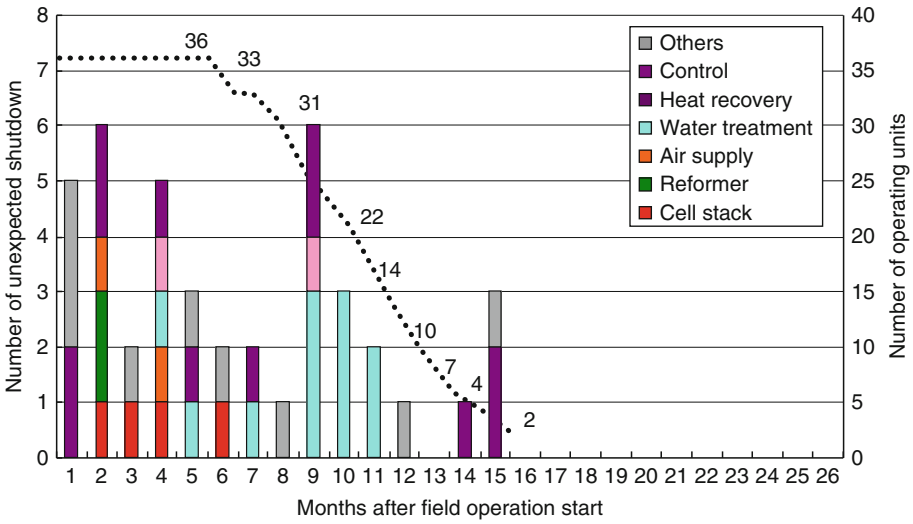

Solid Oxide Fuel Cell Materials: Durability, Reliability and Cost. Figure 7
Summary of troubles during the field test for the 2007 fiscal year's SOFC units. These are categorized into troubles in Control system, heat recovery system, water treatment system air supply system, reformer, and cell stack itself (From [61])

On contrary, cathode-support cells have the stable performance for cathodes, but anodes may have some changed in microstructure because of nickel sintering [63].

Failures Originating from Thermal Cycles or Redox Cycles The SOFC stacks consist all of solid materials. Except for nickel anode and metal interconnects, all other materials are ceramics so that the mechanical instability during thermal cycles and redox cycles can be one of possible failures.

In many cases, failures are associated with stress concentration during thermal cycles or redox cycles. Mechanical stresses are closely related with volume changes of one component leading to mismatch along interfaces.

Volume changes are ascribed to

1. Thermal expansion
2. Chemical volume change due to valence change within the same crystal lattice
3. Redox of the main component such as Ni
4. Precipitation of new phases at interfaces or bonded regions

During operation, temperature distribution can be determined by the current density distribution and related heat release from the surface. This implies that the thermal stress can be properly treated only by the combined analyses on electrochemical performance, gaseous concentration, and thermal conduction. When stacks will be cooled down, temperature distribution can be determined by cooling mechanism so that the thermal stress distribution may change from those under operation.

Effects Appearing in Stacks

1. Edge effect: Small changes in the shape of repeating elements may be accumulated and appear as an edge effect. In many cases, ceramic cells have their own structure to keep the electrical path and gaseous tightness inside stacks. During a long-term operation or frequent thermal cycles, deformation can appear as a sum of the accumulated small changes in shape. In this sense, edges tend to have troubles in loss of the electrical loss, gaseous tightness, etc. In addition, temperature gradient tends to be steep in the vicinity of edges. As a result, degradation is apparently worsened in edge parts.
2. Effect of stack weight: When the horizontal cells are vertically stacked to form tower stacks/modules, an effect of gravitational weight may appear at the bottom of the stacks. This is a similar situation to the stacks of MCFC where a large number of horizontal cells are stacked and the effect of creep will appear when the selection of anode materials is not appropriate, for example, copper is recognized as such materials. For the SOFC stacks, no report has been made on creep behavior of the nickel cermet anodes so far. Ferritic steels are recognized as weaker against creep than austenite steels.
3. Gas distribution: Gas manifold system is critically important in the stack technology. When this malfunctions, supplying rate of gases become different from cell to cell, whereas the same electrical current passes through such cells connected in series. As a result, there can be a shortage of fuels in a particular cell, leading to damage of the cell [64].
4. Distribution of current: The SOFC stacks consist of highly electronic conductive electrodes and of highly ionic conductive electrolyte so that the current distribution can be easily reestablished when some parts in flows of fuel or air becomes ineffective or some parts of electrode area are damaged [65]. This electrochemical response to degradation makes it difficult to find out symptom of deteriorated parts while such deterioration continues to take place. In many cases, the degradation of stack performance appears to be linear with operation time.
5. Contamination: The only one appropriate method for investigating on the significance of contamination from other components and on plausible effects on electrode reactivity, electrical resistivity, or gaseous permeability is utilization of secondary ion mass spectrometry (SIMS) [66, 67]. Attempts by AIST clarified the interesting behavior of elements inside the SOFC stacks [68] as shown in Fig. 8.
   (a) Impurities are common in many cases. For example, sodium is quite frequently observed contaminant, whereas potassium is much less than sodium. In addition, aluminum and silicon are also always detected; frequently, but not always, phosphor is detected. Sulfur is also found to be a frequently observed contaminant.

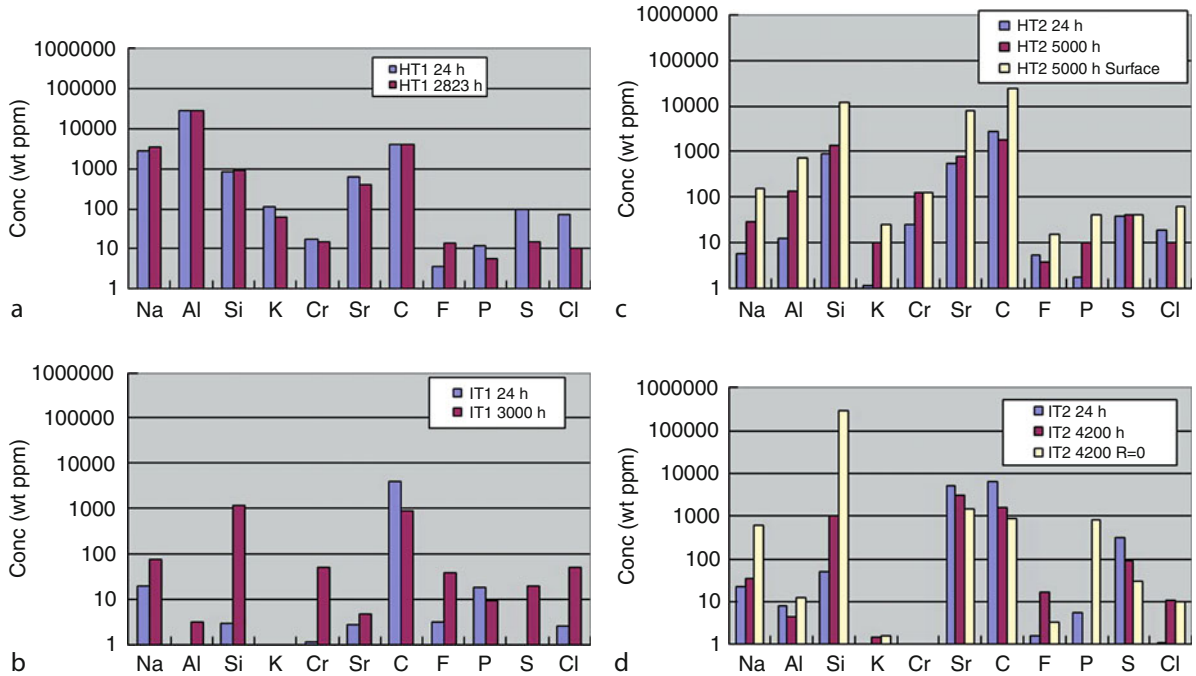

Solid Oxide Fuel Cell Materials: Durability, Reliability and Cost. Figure 8
Impurities in anodes for four SOFC stacks with different materials and designs. Impurities were determined with SIMS on the 24 h operation and on the longer (about 5,000 h) operations. (**a**) High-temperature segment-in-series cell by MHI, (**b**) intermediate flatten tubular cell by Kyocera, (**c**) high temperature sealless tubular cells by TOTO, and (**d**) intermediate temperature disk-type planar cells by Mitsubishi Materials corp

This is not necessarily derived from fuels. Even in air side, sulfur can be detected. Halogen such as Cl and F can also be detected. Note that Se, As, and Sb are not detected although those elements are major impurities in coal-derived gases.

(b) Impurity levels however depend on stacks/systems. For example, the Na contamination depends largely on raw materials or on the fabrication process.

(c) There are several elements which increase in concentration during a long-term operation. Apparently, such elements are transported as the gaseous species in fuel or air atmospheres. Generally speaking, contamination is much severer in the fuel side compared with the air side. This is due to the presence of water vapors in fuel sides, enhancing the volatilization by forming metal hydroxide vapors or metal suboxide vapors. Actually, the contamination level is higher in many cases in the downstream where water vapors are increased.

(d) Some particular elements are deposited on electrodes. Those elements which are known as poisons for the electrode activity, for example, chromium in cathode and phosphor in anode, are detected in a more concentrated manner at the three-phase boundaries where the main electrochemical reactions take place.

(e) Sources of contaminants can be suggested as follows: thermal insulating materials, alloys, sealing materials, if any.

6. Behavior during emergency stop: Many durability tests have suffered from emergency stops which are caused, for example, by failures of controlling system for the test facilities. Such accidental stop tends to cause changes in performance or mechanical failure. Severest situation is rapid cooling with the purge gases which will be introduced mandatorily, leading to mechanical failure or heavy damage of cells [69].

Anomalous Situation

1. Gaseous leakage: Anomalous gaseous leakage can take place as a result of crack formation of electrolyte, interconnect, or seals. In addition, oxygen can be permeable through the oxide electrolyte/interconnect in a form of bipolar diffusion of oxide ion and electrons. In any case, gaseous leakage gives rise to combustion without generating electricity. This releases heats locally at the place where combustion occurs. This may provide a local hot spot of electrolyte/interconnect. Since gaseous leakage tends to increase with temperature, local heating enhances further gaseous leakage regardless of leakage through pores/cracks or electrochemical oxygen permeation.
2. Shorting: When electrical shorting takes place, current will pass within the shorting circuit until fuel/air becomes in shortage and as a result, high resistive materials are formed on the electrical path. Current density is determined so as to cancel out electromotive force by the overpotential and ohmic loss inside shortened circuit. Unlike the electrochemical oxygen permeation, electrons move quite fast. Therefore, combustion rate and heat generation rate are fast. Since the ionic conductivity and the electrode activity are higher at higher temperatures, consumption rate increases until there is shortage of fuel or air.
3. Back diffusion of combusted gases: Some stacks are designed not to have sealing parts. In such a case, combustion of remaining fuels takes place just outside the electricity-generating cell area. In other words, there is a great possibility that the combusted gas will diffuse backward to the electrode area. To protect particularly nickels against such an oxidative atmosphere, an appropriate distance should be maintained between combusting area and the electrochemical active area.

Redistribution of Current Flow Among Cells Connected in Parallel or Series

When a cell or a part of a cell is degraded, this should appear as change in cell performances. When the electrical potential decrease takes place in one cell among cells connected in series, it can be detected easily by watching the respective cell performance. On the other hand, when there are many other cells which are connected in parallel with a degraded cell, the current redistribution takes place so as to minimize effects of degraded cells. In such a case, it becomes difficult to detect those degradations from changes in cell performance alone.

Degradation in Cell Performance

Cell performance is degraded from various reasons. Some degradations are caused from the main components of fuel, others being from contaminants. In many cases, operation temperature plays an important role, whereas the overpotential can become the major factor of controlling degradation. First of all, the places causing potential drops are listed and their relation to other operation conditions is described in section "Operation Conditions and Their Relations to Degradation of Repeat Elements" and then respective poisoning effects will be described.

Operation Conditions and Their Relations to Degradation of Repeat Elements

1. Exothermic and Endothermic Effects

   Figure 9 summarizes schematically those places where exothermic or endothermic processes take place in repeated elements.

   (a) Most important heat effects are the exothermic process due to the electrochemical reaction at the active reaction sites. This contribution increases with increasing temperature. This is due to the reversible reaction so that this effect cannot be detected in AC impedance spectroscopic measurements under OCV conditions; the exothermal and endothermic effects are cancelled out in AC. This effect can appear in the DC polarization measurements; with increasing current density, exothermic heats increase, leading to local heating in the vicinity of the active sites.

   (b) Potential drop due to the electrode overpotential appear also in the electrochemical active sites. This is however irreversible.

   (c) Ohmic loss is also irreversible but appearing along the electrical path with low conductivity.

   (d) Interface resistivity: between cells and interconnects or at cell-to-cell connection potential drop can arise.

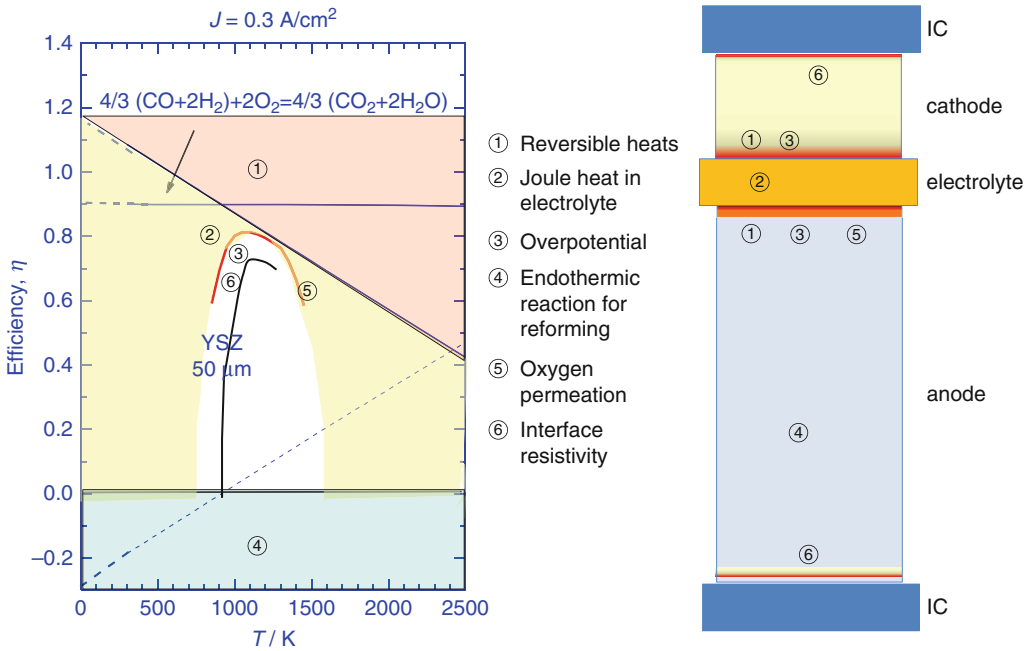

Solid Oxide Fuel Cell Materials: Durability, Reliability and Cost. Figure 9
Analyses on endothermic or exothermic effects in the theoretical efficiency for SOFC and corresponding places inside cells

(e) Oxygen permeation, if any, results in local heating due to combustion without generating electricity.
(f) For internal reforming inside anode layers, local cooling takes place at those places where reforming reactions proceed.

2. Effects of current density

In addition to temperature, there are several operational variables which should be examined carefully in their relations to degradation. One of such variables is the current density. In what follows, plausible effects of increasing current density will be examined in two levels: cell level and stack level.

In cell level:

(a) With increasing current density, heats are emitted at the electrochemical active sites, therefore, temperature at the active sites increases.
(b) With increasing current density, the overpotential around the active sites increases. When the overpotential is the driving force, degradation should be given as a function of overpotential as will be shown in Cr poisoning for LSM cathodes.
(c) When the oxygen potential at the active sites plays an important role in determining the equilibrium for a particular degradation, it can be related to the current density in an indirect way.
(d) With increasing current density, gaseous flow rates for air and fuel increase if the utilization of air or fuel is kept constant. When poisons for electrode activities are carried with air or fuels, increasing flow rates implies that an amount of transported poisons increases at active sites.

In stacks level:

(a) Since the conversion efficiency decreases with increasing current density, heats to be removed increase in two aspects: (1) Reversible heats increase linearly with current density and (2) Irreversible heats increase nonlinearly under the same fuel utilization.
(b) Thermal balance will be achieved (1) when air flow rate increases resulting in lower air utilization or (2) when a larger temperature distribution is allowed to have the larger heat exchange with the same amount of gas flow.

For the latter case, the maximum cell temperature should be increased.

3. Oxygen Potential

Another important variable related with the operation condition is oxygen potential.

When the degradation of electrode performance is considered, the oxygen potential distribution inside electrode layer or at the electrode/electrolyte interfaces becomes important. In particular, the oxygen potential at the electrochemical reaction sites is critical.

Furthermore, oxygen potential distribution may change during operations. Typical examples are schematically shown in Fig. 10. for the oxygen potential ($\mu(O_2)$) distribution in relation to electron electrochemical potential ($\eta(e^-)$) and oxide-ion electrical potential ($\mu(O^{2-})$)and are summarized as follows:

(a) Normal cases: the electrode overpotential corresponds to a drop of the oxygen potential at the active sites. In cathodes, the overpotential can be interpreted in terms of the oxygen atom diffusion potential on the LSM surface, whereas the oxygen potential drop should appear across the surface of active LSCF cathodes. For nickel anodes, the oxygen potential drop corresponds to the diffusion of hydrogen atoms on nickel. Even when there is a distribution of electrode activity or gaseous concentration inside one cell, the oxygen potential at the active sites is controlled to provide the same electrical potential throughout the cell.

(b) Fuel/air starvation. Oxygen potential in the starvation side changes drastically from the normal oxygen potential. As a result, some damage may occur on the electrode. In such a case, nickel can be oxidized while LSCF cathodes can be partially decomposed, when the oxygen potential changes beyond the thermodynamic limit.

(c) Degradation of one electrode of a cell among in-series connected cells. In a series connection, the same current passes through all cells in the

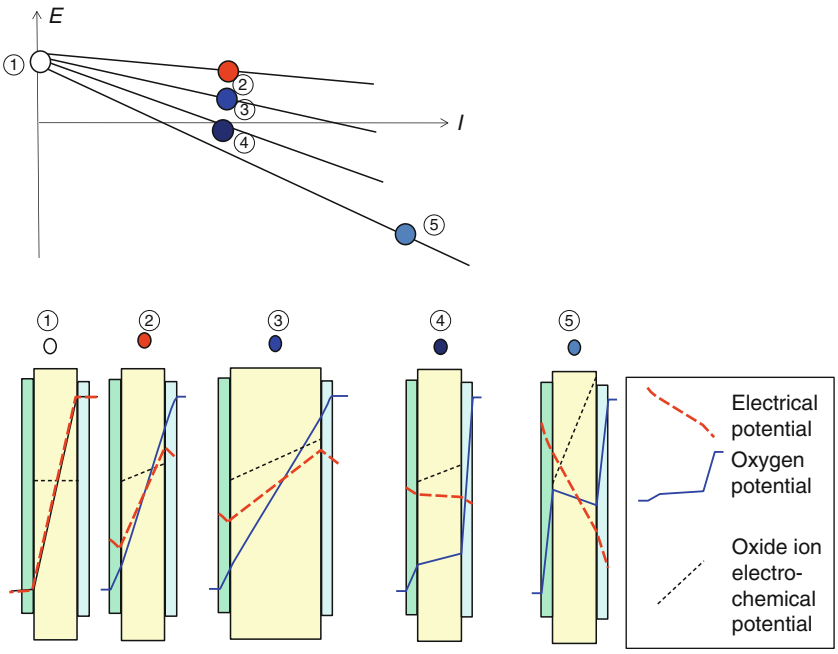

Solid Oxide Fuel Cell Materials: Durability, Reliability and Cost. Figure 10

Typical changes in electrical potential, oxygen potential and oxide ion electrochemical potential for (1) OCV, (2) normal operation, (3) normal operation with thicker electrolyte, and (4) cathode damaged cell and weakest cell on shorting cells in series

series. When one electrode is degraded, the overpotential increases under the same current density. The generating voltage decreases. Even when a damaged cell cannot generate the electricity, the current is mandatorily passed through the cell. In such a case, the oxygen potential at the electrode/electrolyte interface is shifted to an extremely oxidative/reductive side.

(d) Short circuit with/without outer resistance. When shorting takes place among in-series connected cells, a large amount of current may pass through to cancel out the generated voltage with the resistivity/overpotential of damaged cells. At the beginning, the current is limited by the gas diffusion of air or fuels. Once there appears difference in cell performance including gas diffusion, the generated voltage tends to be cancelled out with the electrode resistivity or gas diffusion resistivity of a particular damaged cell. This suggests that heats are generated locally at the damaged cells. Since the Ohmic loss inside the electrolyte and other places are essentially the same between the damaged and the normal cells, a drastic difference should appear as electrode resistivity. When there are differences in electrode activities among the damaged cells, the current tends to be concentrated in an area with better electrode activity. This will continue to a situation where air or fuel will be in starvation in a major part of cells, leading to lowering in generated voltage.

Chromium Poisoning Chromium poisoning was first observed during the investigation of utilization of metal interconnect at a rather high temperature like 900°C together with LSM cathodes. Therefore many investigations [34, 70–76] have been made on the chromium poisoning effects of lanthanum strontium manganite cathodes. Among them, the work by Taniguchi et al. [34] is excellent in a sense that from a large number of experimental results obtained by changing cathode materials and testing conditions such as temperature, etc., they eventually found an interesting fact that the half-life time of any manganite cathodes is governed by a simple quantity, namely, log a(O), derived directly from the overpotential of the cathodes with a conversion factor of $4F/2.303\ RT$. This is well interpreted in terms of the cathode reaction model for the lanthanum strontium manganites [77]; essentially no oxide ion conduction is available in LSM. TPBs become only electrochemically active sites and, as a result, there arises a large oxygen potential gradient in the TPB vicinity which in turn provides a driving force for chromium-containing vapors to attack the electrochemical sites. In an actual segment-in-series cell, the chromium concentration at TPBs was observed by using SIMS technique [68] (see Fig. 11). The observed change in an accumulated amount of chromium was found to have excellent correlation with the cell performance degradation. That is, degradation in a level of several percent in operating potential is caused by the chromium accumulated at TPBs in the order of several hundred parts per million. This strongly suggests that without measuring with SIMS, no proper examination can be made on a long life time of LSM cathodes in an order of several ten thousand hours.

Another interesting finding is obtained by Matsuzaki and Yasuda [69] – they found that the chromium poisoning depends not only on cathode materials but also on electrolyte to be used with cathodes. From four possible combinations made with LSM and LSCF as cathode and YSZ and SDC as electrolyte, they found that the LSCF/SDC combination does not show any degradation under the same conditions. Since then, many efforts have been made on the non-LSM cathode/ceria interlayer/YSZ systems [78, 79]. In some cases, cell performance is linearly degraded from beginning, whereas the performance is not directly related with the $SrCrO_4$ formation which is always observed. From analyses on the chemical stability of cathodes and their electrode reaction mechanism based on the mixed conductivity, the generalized degradation mechanism [42, 51] can be derived to cover phenomena occurring at the chemical reactions sites as well as the electrochemically active sites. The important physicochemical feature is the probability of poisoning substances arriving at the sites by penetrating though a trapping zone.

Lanthanum nickel-iron oxide cathodes, $La(Ni,Fe)O_3$, have attracted much attention because they show essentially no effects of chromium poisoning [59]. This is mainly because there is no chance of $SrCrO_4$ formation. From the thermodynamic point of view, there is

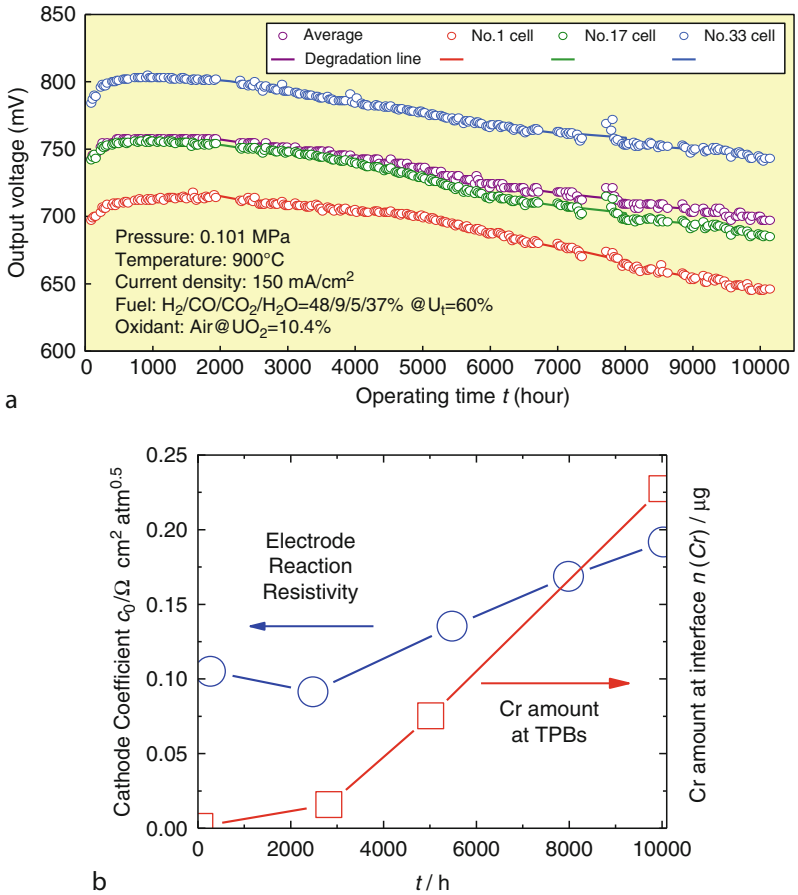

Solid Oxide Fuel Cell Materials: Durability, Reliability and Cost. Figure 11
(**a**) The time-dependent degradation of segment-in-series cells by Mitsubishi heavy industry. (**b**) Correlation of electrode reaction resistivity and the amount of accumulated chromium at the three phase boundaries

a possibility that the $La(Ni,Fe)O_3$ perovskites react with chromium-containing vapors to form the $La(Ni,Fe,Cr)O_3$ solid solution [42]. Even so, such perovskites must still be electro-conductive, although some surface kinetic activity will be lowered due to the fact that lanthanum chromite has lower catalytic activity among the transition metal perovskite oxides.

In recent years, an interesting but troublesome fact has been revealed, that is, Pt wire reacts with oxygen in air to form $PtO_2(g)$ and will be deposited on the three phase boundaries of LSM cathodes [80]. Usually, Pt cathodes are not better than perovskite cathodes so that the electrode activity may be lowered when such Pt will be deposited on cathodes. However, the situation for the chromium poisoning for the LSM cathode is quite different. When Pt is deposited on TPB of LSM cathodes, the cathode performance can be improved or lowered depending on the state of deposited Pt. This disturbs the effects of chromium on the LSM cathodes. This makes it difficult to examine the chromium poisoning in a laboratory scale.

Other effects such as potassium are reported [81]. The most recent trend to prevent Cr poisoning is to reduce the chromium volatilization from alloys [82]. This is related to the interconnect issues.

Nickel Sintering Since the EVD nickel anode is fabricated so as to be firmly fixed to the YSZ electrolyte, the degradation rate of such electrode is small. Compared with the EVD nickel anode, normal Nickel

cermet anodes are fabricated by sintering after slurry coating. This implies that the mechanical strength between YSZ and nickel is not necessarily good enough so that pre-annealing process is needed to have a good contact.

For the first-generation cells to be operated at 900–1,000°C, sintering of nickel appears as a result of bulk diffusion based on the normal thermal activation process; note that the melting temperature of nickel is 1,728 K and therefore above two thirds of melting temperature, i.e., 1,152 K = 880°C, sintering can be significant. Actually, experimental observation indicates the change in microstructure in the range of several thousand hours due to sintering.

For the second-generation cells to be operated at 800°C or below, sintering exhibits more complicated features. Sintering depends largely on stacks or cells. This implies that the fabrication as well as operation conditions may affect sintering.

About the operation condition, details of nickel electrode degradation have been investigated by Karlsruhe Institute of technology group [83, 84]; they changed the fuel composition and current density separately with a parameter of operating potential and found that the degradation is severe with increasing water content in fuel and with increasing current density (see Fig. 12). Although there is no examination on relation between such degradation and sintering, this seems to be due to sintering. In a cell test, Topsøe Fuel Cells reported that the degradation of nickel anode is severe in the region where the fuel utilization is high, and correspondingly they observed actual sintering of nickel [56].

An interesting feature associated with sintering is that it can take place on thermal cycles alone between operation temperature and room temperature [63]. It seems plausible due to sulfur contamination on nickel since the nickel–sulfur system exhibits significant lowering of liquidus temperature due to the eutectic formation; thus eutectics appear even below 800°C.

In any case, change in microstructure is a complicated matter, and detailed analyses should be made not only on nickel but also on oxide component or pore [85]. In recent years, the investigation on microstructure with FIB-SEM or XCT has been rapidly progressed [86–88]. It is therefore expected that sintering behavior and related phenomena will be well clarified in its relation to degradation.

Carbon Deposition Since hydrocarbons are important fuels for SOFC, carbon deposition should be avoided [89]. When carbon deposition once starts, this destroys the microstructure of Ni-cermet anode and deposited carbon acts as catalyst for further deposition so that a large amount of carbon can block the flow of fuels. Since the decomposition temperature of hydrocarbons decreases with increasing carbon number in hydrocarbons, the possibility of carbon

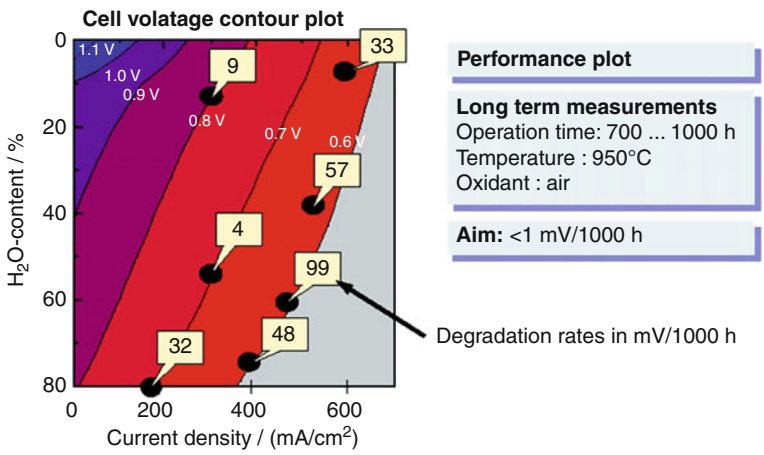

Solid Oxide Fuel Cell Materials: Durability, Reliability and Cost. Figure 12
Systematic investigation on the anode degradation as functions of current density and water content in fuels with a parameter of electrical potential (From [83, 84])

deposition increases with carbon number. On the other hand, water vapors are emitted from the electrochemically active sites and this promotes the steam reforming. Thus, under cell operation, the possibility of carbon deposition decreases in the vicinity of active sites.

Sulfur Poisoning Sulfur contaminations inside SOFC stacks depend on the system configuration. For the small stationary applications, desulfurization process is first placed before the reforming process; this is because the reforming catalysis is week against sulfur contamination. In such a case, essentially no sulfur poisoning can be expected during the normal procedure of SOFC operation.

For diesel fuels, on the other hand, the presence of sulfur, and possible sulfur poisoning, is strongly related with the degree of reforming [90].

In recent years, it has been found that sulfur contamination appears even when sulfur-free fuel such as hydrogen is utilized [66]. This strongly suggests that sulfur sources are not only from fuels but also from other components. Most probable source is metal components in stacks and thermal insulating substances containing metal sulfates.

Performance degradation of nickel anode due to sulfur consists typically of two stages [90–100]. The first stage is the prompt response against the introduction of hydrogen sulfur, namely, stepwise decrease of electrical potential. The potential drop is well correlated with the sulfur coverage on Ni [96]. This is usually recovered when sulfur-containing fuels switch back to noncontaminated fuels; this is quite a slow process. The second stage is a process following the first stepwise change; when concentration is low, there is no further change, whereas some irreversible lowering in electrical potential is observed when concentration is high.

Furthermore, effects of sulfur can appear in a more significant and fatal manner. In an experiment by Julich research center, the cell performance was tested in hydrogen fuel containing 50 ppm H_2S. After the initial decrease in potential, the performance was maintained at this low level. However, after about 150 h, the cell suddenly died. Posttest examination clarified that NiS spread out in the interface region between YSZ electrolyte and nickel cermets. In addition, $NiSO_4$ was formed inside the anode layer. These features contradicted with the expected Ni-S interaction predicted from the thermodynamic equilibrium [85]. There must be some mechanism to enhance the effect of sulfur and to accumulate sulfur at the TPB vicinity. One possible explanation is the irreversible nature of the electrochemical side reactions under the anodically polarized current, that is, the sulfur deposition is described as the following anodic reaction:

$$H_2S(g) + 0.5\ O^{2-} = S(\text{on Ni}) + H_2O(g) + e^- \quad (1)$$

On the other hand, the volatilization reaction can be written as follows:

$$S(\text{on Ni}) + 2O^{2-} = SO_2(g) + 4e^- \quad (2)$$

When two reactions take place continuously, adsorption sulfur can be maintained at a certain coverage on Ni. For a long period of operation time, sulfur can be accumulated inside nickel particle as a result of dissolution and diffusion of sulfur.

Other Impurities Figure 8 shows the actually observed impurities. Among them, effects of silicon have been extensively investigated [101–106].

Recently, investigation on the impurities derived from coal-base gases has been made extensively in the SECA project of US Department of Energy (DOE), which promotes the utilization of coals in SOFC [107]. They first made thermodynamic analyses on chemical behavior of impurities in gasification process and hot gas cleaning process, and then categorized impurity elements into several classes [108, 109]; furthermore, they made a series of experiments to examine those elements which are regarded as possible poisoning elements to nickel anodes [110–114]; the following is a brief summary of their results in comparison with other related investigations [115–123].

1. Phosphor and Arsine show the strong affinity with nickel to form intermetallic compounds. In button cell experiments, intermetallic compounds are formed outside of the anode layer, which indicates that the reaction rate is fast and the diffusion of Ni to reaction sites is fast too. For AsH_3 gas, cell performance does not show any changes for a while despite the formation of intermetallic compound and suddenly dies. This is probably because the electrical path was broken due to the nickel deformation. For PH_3, on the contrary, the cell performance

degrades from the starting time. This is probably due to the formation of $HPO_2(g)$ [116–123] which attacks the electrochemical sites.

2. Sulfur and Selenium exhibit similar behavior when the concentration of H_2S or H_2Se is low. Namely, the abrupt initial change occurs first and then constant performance is maintained. Difference can be seen in the recovery behavior from the contaminated fuel to noncontaminated fuel. For H_2S, a slow recovery process appears, whereas no recovery process appears for H_2Se. Furthermore, severe damage may be caused for H_2Se. The common feature is that damage parts are always in the interface region between electrolyte and anodes.

Generalized Model for Degradation due to Gaseous Impurities

Yokokawa et al. [8] made thermodynamic analyses on the interaction between cathodes/anodes and gaseous impurities. By comparison between the thermodynamic reactivity and the electrode degradation behaviors, they have extracted generalized models for degradation. It can be summarized as in Fig. 13, where the characteristic features concerning degradations are plotted by using variables for the transported amount of impurities and for the thermodynamic affinity between electrode and gaseous impurities, for example, for perovskite cathodes, the thermodynamic activity of SrO can be adopted, whereas for anodes, the interaction parameters of systems for forming nickel intermetallic alloys can be used. Essential points in the generalized models are:

1. When the electrochemical activity is lowered due to the impurities, the electrochemical reaction sites should be covered by such impurities. In this case, it is no need that the covered atoms have the strong chemical interactions with electrode materials. The deposition or adsorption is enough to disturb the fundamental steps in the electrode reaction mechanisms. On the other hand, when cell performance is changed due to changes in electrical path or gaseous channel, the accumulated amount of deposited or reacted impurities should be large. This difference should be quite significant. For example, in the Cr poisoning, only a thin layer of deposited chromium in the order of several nanometers on reaction sites is enough to lower the cell performance in the order of 10%. On the other hand, since the electrical path or gas channel are made of the particles or pores in the order of several micrometers in size. This implies that a large amount of $SrCrO_4$ is needed to block the electrical current or the gaseous flow.
2. There can be two different reactions for impurity behaviors, namely, electrochemical side reaction and normal chemical reaction. The most important feature of the degradation is that the degradation reaction takes place under the flow of the electrochemically active species. This suggests that in the cathodic polarization, the electrochemical reduction (cathodic reaction) is accelerated. For example, chromium-containing vapors, $CrO_3(g)$ or $CrO_2(OH)_2(g)$, can be easily reduced to form Cr_2O_3 at the electrochemically active sites and as a result, the electrochemical activity of active sites decreases due to the coverage of no electrical conductive and no catalytically active substances.
3. On the other hand, recovery processes also have two contributions from the chemical and the electrochemical reactions; the latter is given in equation [2], which was derived from considerations on the difference in the recovery process between S and Se.
4. When the chemical interaction between the electrode components and the gaseous impurities is strong, there arise many processes inside the electrode area and respective processes have their own activated process. As a result, their appearance as degradation behavior is quite different from experiment to experiment. Typical example is the effect of Cr vapors on the electrode activity of LSF- or LSC-based active cathodes.

After establishing the general model for degradation due to impurities, it becomes possible to consider all possible effects on a particular case of specified electrode and impurity.

Cost Issues

Cost Issues in Relation to Durability/Reliability and Performance

Cost, performance, and durability are important figures of fuel cell systems and for SOFCs, these three

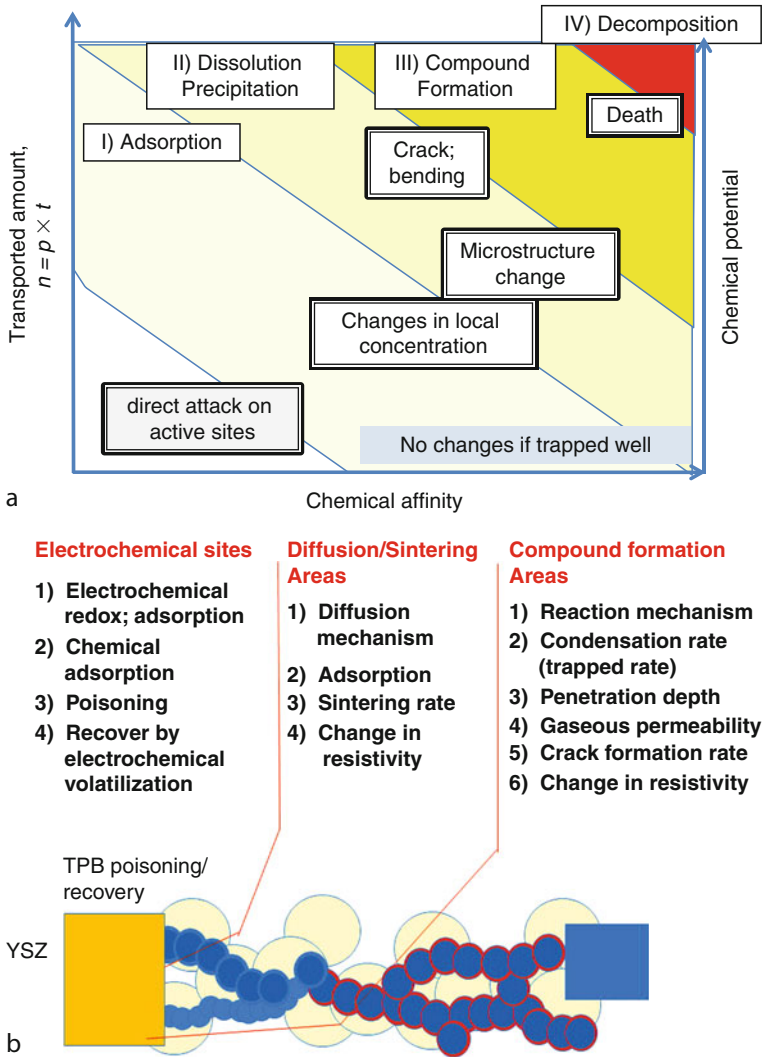

Solid Oxide Fuel Cell Materials: Durability, Reliability and Cost. Figure 13
Generalized model for electrode-impurity interactions and their relation to degradation: (**a**) chemical phenomena as functions of transported amount of impurities and chemical affinity between electrode materials and (**b**) three fundamental regions for electrode-impurity interaction

aspects are closely related with each other. This can be summarized as follows:

1. Costs consist of materials cost, cell/stack fabrication cost, and system cost. Whenever durability has been improved by changing materials or materials processing, usually it costs more due to additional treatments, etc. Thus, there is a trade-off relation between durability and cost. To overcome this relation, innovative breakthrough is needed to stage up this relation.
2. When cell performance will be improved, this benefit can be used in increasing the conversion efficiency or in increasing operating current density to reduce the mass to realize rated power, leading to cost reduction per rated power.

As described in the introduction, SOFC stack development started with the breakthrough by Westinghouse; the sealless tubular cells can be categorized as stable but expensive stacks. Since then, many efforts

have been focused on reducing the fabrication cost in the first-generation cells.

On the other hand, there has been a big wave to construct the second-generation cells to be operated at lower temperatures around 800°C. When the first-generation cells are operated at low temperatures, the Ohmic loss in electrolyte and the overpotential in cathode become quite big. Therefore, in the second-generation cells, use is made of thinner electrolytes and more active cathode materials. Interestingly enough, the performance (conversion efficiency) of second-generation cells becomes much better than that of the first generation. This is mainly because the active cathodes such as LSCF exhibit excellent performance even at low temperatures and also handling of the thinner electrolyte provides some improvement even for fabricating the cathode layer; as a result, performance becomes better. Even so, the active cathodes such as LSCF are chemically reactive, for example, LSCF reacts with CO_2(g), CrO_3(g) and SO_2(g) to form $SrCO_3$, $SrCrO_4$ or $SrSO_4$. This is directly related with the long-term durability.

Cost in Relation to Applications

Since the first-generation cells were aimed at larger stationary applications, several cost evaluations were made on such applications [31, 124–130]. These considerations are focused on the followings points:

1. Identification of high cost element. The most expensive elements are Y in YSZ, La in cathodes or oxide interconnects; Co in LSCF, Ni in anode can be also categorized as rather expensive materials. To avoid the utilization of such elements, it is required to adopt redesigned stack structure with appropriate fabrication methods.
2. Cheaper materials if acceptable; particularly, impurities will be an issue.
3. Reduction of the number of the components in repetitive units of stacks.
4. Reduction of losses during fabrication.
5. Automation of production.

There are generalized arguments on the relation between cost and performance:

1. Roles of raw materials: as the structural component, the low price materials are thought to be used, whereas for the highly functional materials, there are some arguments: A typical example is the utilization of scandium [131]. Although the raw materials cost for scandium oxides is much higher than that for yttrium oxide, there are many groups who are interested in utilizing ScSZ instead of YSZ. This is based on an idea that despite higher raw materials cost, the higher performance leads to reduction of total cost of stacks to be required to achieve a given rated power.
2. Even when low-cost materials are used, additional procedures are needed to achieve the required reliability and durability. Therefore, cost should be considered in combination of raw materials cost and fabrication cost. This is particularly true for metal interconnects; metal interconnects are cheap in materials cost compared with La-based oxide but additional procedure of coating increases the fabrication cost.

In 1998, BMW, Delphi, and Renault announced the application of SOFC as APU (Auxiliary Power Units) of automotive. This gave rise to drastic changes in applications of SOFC systems. The US Department of Energy started a new project called SECA (Solid State Energy Converter Alliance). Their cost target is about \$150/kW for stacks and \$700/kW for system in the mass production level. Recently, an interesting analysis [132] has been made on the operation modes of the degraded stacks in its relation to total system cost. There can be two operation modes; one is to keep the same current density, the other being to keep the same electrical potential. This difference gives rise to a large difference in strategies in the replacement of the stack itself and overdesign.

1. Under constant current operation, some degradation leads to lowering the electrical potential and as a result, power output is correspondingly lowered. Since the conversion efficiency is also lowered, heats produced inside stacks increases. To remove excess heats, a larger amount of air has to be flowed. For this purpose, additional energy is required and total efficiency is further decreased. In this sense, operation is continued under a rather severer condition. Further degradation can take place under such a condition. In addition, one needs to keep a large capacity of BOP to ensure the capacity for air flow

in an excess amount. In view of these features, this operation mode must only be appropriate for stacks with extremely low degradation rate.

2. Under constant voltage operation, current density decreases largely in contrast and as a result, power output is also correspondingly lowered significantly. However, efficiency is maintained rather constant and therefore there is no need to keep a large capacity of BOP. Since power output per one unit decreases significantly, additional stack capacity is required to offset for such a loss of capacity. In this operation mode, damage on stacks is not severe so that stacks can be operated for a longer period of time, and this is an important advantage against the constant current operation mode.

Future Directions

There are a number of degradation issues which are still unclear and need to be addressed in the future:

Stack Behavior

Stack behaviors are characterized in terms of temperature distribution, current density distribution, flow distribution, etc. Among them, current distribution is very important in determining stack performance, stack temperature distribution, etc., but is hard to be measured in real stacks. In many cases, the information on current distribution is obtained from the simulation technique. In this sense, simulation technique becomes quite important. It is still highly hoped that progress in experimental technique will be made in obtaining the current density distribution in stacks.

From the materials point of view, many stacks consist of ceramics and metals. Ceramics may exhibit oxygen nonstoichiometry and change their volume in a complicated manner as functions of temperature and pressure. On the other hand, metals and alloys can be deformed under stresses/loads. When those two materials are utilized under a long-term operation at constant temperature or under frequent thermal cycles, mechanical interactions between two materials become important.

Effects of High Conductive Electrolyte

There can be seen one interesting feature in the low-temperature SOFC, that is, the cell performance of the anode support cells has been much improved compared with electrolyte self support cells. This is apparently due to the lowering of the ohmic resistance inside electrolyte. Furthermore, the electrode performance is also improved very much. This can be ascribed to better fabrication procedure. When thin electrolyte is fabricated, very fine structure is designed and fabricated. In a similar manner, cathodes are fabricated carefully so that it is expected that microstructure of cathodes is well established. These features can be summarized as follows: When the conductance is improved and the homogeneous current flow is established inside electrolyte, electrode performance can be maximized by fabricating the electrode layer without faults. This is a matter of the current density distribution inside one cell. This is determined in terms of the homogeneous ionic current, homogeneously distributed electrochemical sites, and homogeneous electronic current. If there is some fault among them, this leads to inhomogeneous current flow and therefore some degradation may take place.

Here, an interesting finding by Watanabe and Uchida [133] should be referred to: that the electrode performance becomes higher with those electrolytes having the higher ionic conductivity. The proper mechanism of this finding has not been given fully but the current density distribution in the vicinity of electrochemically active sites may be different between those electrolytes having different ionic conductivities.

Advances in Characterization

The electrode performance is determined by many factors. Among them, the microstructure is one of the very important factors. Even so, it has not been easy to make characterization on the microstructure in an appropriate way. For example, in nickel cermet electrode, the connection of nickel is important in addition to the skeleton structure of oxide network. Since nickel is dissolved into acid, it is easy to extract the skeleton structure of zirconia. On the other hand, nickel network is not well determined experimentally. Recent advances in the experimental determination of three-dimensional electrode structures by FIB-SEM or by XCT techniques make it possible to evaluate details of microstructure changes in nickel cermets. For example, the most important physicochemical measure of the

electrode is the length of three phase (electrolyte oxide, electronic conductive metal, and gases) boundaries. Recent experimental and related theoretical progress makes it possible to reconstruct the cermet electrode in computer space and to identify the ionic path, electron path, and electrochemically active sites in combination with appropriate electrode reaction mechanisms. This provides a powerful tool for investigating the mechanism of degradation in terms of fuel cell operation variables such as time, current density, etc. Thus, it is highly recommended to investigate in more details the microstructure and its relation to electrode activity.

Intermediate Temperature Gaseous Species

Most typical degradation is chromium poisoning. This is caused by the gaseous species such as $CrO_3(g)$ or $Cr_2O_2(OH)(g)$. In order to understand the chromium poisoning, thermodynamic analyses on those gaseous species are essential. Fortunately, those data are available so that detailed analyses were made successfully. For the Ni-P system, the vapors, $HPO_x(X = 1,2,3)$ play an important role according to Bao et al. [116–118]. Without considerations on such gaseous species, no proper transportation mechanism can be obtained. An important point of these analyses is that the partial pressure of such species is extremely small in the range of 10^{-12} to 10^{-6} atm.

Although the accurate determination of the partial pressure of electrochemically important species is highly required, there can be some difficulties:

(a) Lack of the thermodynamic properties of those gaseous species which can be dominant in the intermediate temperature region. This is particularly true for species which are emitted in the presence of water vapors.
(b) Some uncertainty in the already available thermodynamic data.

Thus, the intermediate temperature gas chemistry should progress for the electrochemical purpose.

Effects of Minor Species

Minor carriers in electrolyte can also make contributions to degradation, although apparent effects have not been fully clarified. Most important minor carrier in the fluorite-type oxides is proton. It is well know that the proton concentration in YSZ is in the order of 10^{-5} in mole base. Correspondingly, the transportation number can be evaluated to be in the same order. Normally, it is quite difficult to detect this effect in the electrical performance so that in many electrode reaction models, any role of protons is neglected particularly in cathodes. In the fuel cell operation mode, protons are formed in anode and migrated to cathodes, leading to the emission of water vapors on the cathode side. In view of this nature, it is expected that the formation of hydroxide compounds can be expected as an electrochemical side reaction. $Sr(OH)_2(g)$ must be interesting in view of the proposed mechanism of Sr migration in the form of gaseous species. In addition, the $Cr_2O_2(OH)_2(g)$ emission can also be expected from the reaction of deposited Cr_2O_3 with transported protons and oxygen atom. This reaction should be considered as the recovering (heeling) process of Cr poisoning. Note also that because proton concentrations in doped ceria is two orders of magnitude higher than that in YSZ, the utilization of doped ceria as reaction/diffusion barrier can also provide enhancing effects of such recovering (heeling) process. It is hoped to clarify such effects in relation to a long-term stability of cathode materials.

Bibliography

Primary Literature

1. Yokokawa H, Sakai N (2003) Part 4. Fuel cell principle, systems and applications, Chapter 13 History of high temperature fuel cell development. In: Vielstich W, Lamm A, Gasteiger HA (eds) Handbook of fuel cells fundamentals technology and application, vol 1. Fundamentals and survey of systems. Wiley, Chichester, pp 219–266
2. Möbius HH (1997) On the history of solid electrolyte fuel cells. J Solid State Electrochem 1:2–16
3. Brown JT (1985) High temperature solid-oxide fuel cells (SOFCs). Energy, Int J 209–229
4. Yokokawa H (2003) Understanding materials compatibility. Annu Rev Mater Res 33:581–610
5. Atkinson A, Marquis AJ (2009) Mechanical stability. In: Vielstich W, Yokokawa H, Gasteiger HA (eds) Handbook of fuel cells fundamental technology and applications vol 5. Advanced in electrocatalysis, materials, diagnostics and durability: Part 1. Wiley, Chichester, pp 463–474
6. Yokokawa H, Tu H, Iwanschitz B, Mai A (2008) Fundamental mechanism limiting solid oxide fuel cell durability. J Power Sources 182:400–412

7. Yasuda I, Hishinuma M (1995) Mathematical analysis of stress distribution in acceptor doped lanthanum chromites under an oxygen potential gradient. In: Dokiya M, Yamamoto O, Tagawa H, Singhal SC (eds) Solid oxide fuel cells IV, PV 95-1. The Electrochem. Soc. Inc., Pennington, NJ, pp 924–933
8. Yokokawa H, Yamaji K, Brito ME, Kishimoto H, Horita T (2010) General considerations on degradation of SOFC anodes and cathodes to impurities in gases. J Power Sources (to be published). doi:10.1016/j.powersour.2010.07.093
9. Yokokawa H, Sakai N, Kawada T, Dokiya M (1991) Thermodynamic analysis of reaction profiles between $LaMO_3$ (M = Ni, Co, Mn) and ZrO_2. J Electrochem Soc 138:2719
10. Yokokawa H, Sakai N, Kawada T, Dokiya M (1991) Chemical thermodynamic considerations in sinterability of $LaCrO_3$-based perovskites. J Electrochem Soc 138:1018
11. Pal UB, Singhal SC (1981) Electrochemical vapor deposition of Yttria-stabilized zirconia films. J Electrochem Soc 137(9): 2937–2941
12. Isenberg AO (1981) Energy conversion via solid oxide electrolyte electrochemical-cells at high-temperatures. Solid State Ionics 3(4):431–437
13. Singhal SC (1995) Advance in tubular solid oxide fuel cell technology. In: Dokiya M, Yamamoto O, Tagawa H, Singhal SC (eds) Solid oxide fuel cells IV PV 95-1. The Electrochem. Soc. Inc, Pennington, NJ, pp 195–207
14. Singhal SC (1997) Recent progress in tubular solid oxide fuel cell technology. In: Stimming U, Singhal SC, Tagawa H, Lehnett W (eds) Solid oxide fuel cells V, PV 97-40. The Electrochem Soc. Inc., Pennington, pp 37–50
15. Fee DC, Zwick SA, Ackerman JP (1983) Solid oxide fuel cell performance. In: Salzano FJ (ed) Proceedings of the conference on high temperature solid oxide electrolytes anion conductors, vol 1. Brookhaven National Laboratory, Upton, New York pp 29–38
16. Steele BCH, Hori KM, Uchino S (2000) Kinetic parameters influencing the performance of IT-SOFC composite electrodes. Solid State Ionics 135:445–450
17. Frey H, Kessler A, Münch W, Edel M, Nerlich V (2009) Chapter 68 Field experience with molten carbonate fuel cells (MCFCs) and solid oxide fuel cells (SOFCs) with an emphasis on degradation. In: Vielstich W, Yokokawa H, Gasteiger HA (eds) Handbook of fuel cells fundamental technology and applications, vol 6. Advanced in electrocatalysis, materials, diagnostics and durability: part 2. Wiley, Chichester, pp 992–1001
18. Carter JD, Myers D, Kumar R (2006) Recent progress on the development of TuffCell, a metal-supported SOFC/SOEC. In: Presented in the 30th International Conference & Exposition on Advanced Ceramics and Composites, Cocoa Beach, Florida, pp 22–27
19. Tucker MC (2010) Progress in metal supported solid oxide fuel cells: a review. J Power Sources 195(15):4570–4582
20. Brandon NP, Blake A, Corcoran D, Cumming D, Duckett A, El-Koury K, Haigh D, Kidd C, Leah R, Lewis G, Matthews C, Maynard N, Oishi N, McColm T, Trezona R, Selcuk A, Schmidt M, Verdugo L (2004) Development of metal supported solid oxide fuel cells for operation at 500–600°C. J Fuel Cell Sci Technol 1(1):61–65
21. Hooie DT, Camara EH (1985) Onsite industrial applications for natural gas-fueled fuel cells. Fuel Cell Semin 182–185
22. Stolten D, de Haart LGJ, Blum L (2003) Design criteria for SOFC generators. In: Proceedings of the 27th Annul Cocoa Beach conference and exposition on advanced ceramics and composites, Cocoa Beach, Florida, USA. American Ceramic Society, Westerville, OH, pp 263–272
23. Suzuki M, Iwata S, Higaki K, Inoue S, Shigehisa T, Miyoshi I, Nakabayashi H, Shimazu K (2009) Development and field test results of residential SOFC CHP system. In: Singhal SC, Yokokawa H (eds) Solid oxide fuel cells XI –Part 1. ECS Trans 25(2):143–148
24. Mai A, Iwanschitz B, Weissen U, Denzler R, Haberstock D, Nerlich V, Sfeir J, Schler A (2009) Status of Hexis SOFC stack development and the Galileo 1000 N Micro-CHP System. In: Singhal SC, Yokokawa H (eds) Solid oxide fuel cells XI – Part 1. ECS Trans 25(2):149–158
25. Love J, Amarasinghe S, Selvey D, Zheng X, Christiansen L (2009) Development of SOFC stacks at ceramic fuel cells limited. In: Singhal SC, Yokokawa H (eds) Solid oxide fuel cells XI – Part 1. ECS Trans 25(2):115–124
26. Hinnells M (2008) Combined heat and power in industry and buildings. Energy Policy 36(12):4522–4526
27. Singhal SC (1999) Progress in tubular solid oxide fuel cell technology. In: Singhal SC, Dokiya M (eds) Solid oxide fuel cell VI PV 99-19. The Electrochem Soc. Inc., Pennington, pp 39–51
28. Takeuchi H, Nishiyama H, Ueno A, Aikawa S, Aizawa M (1999) Current status of SOFC development by wet process. In: Singhal SC, Dokiya M (eds) Solid oxide fuel cell VI, PV 99-19. The Electrochem Soc. Inc., Pennington, pp 879–884
29. Dönitz W, Erdle E, Schäfer W, Schamm R, Späh R (1991) Status of SOFC development at dornier. In: Grosz F, Zegers P, Singhal SC, Yamamoto O (eds) Proceedings of the 2nd International Symposium solid oxide fuel cells. Commission of the European Communities, Brussels and Luxembourg, pp 75–84
30. Nakanishi A, Hattori M, Sakaki Y, Kimura K, Ando Y, Miyamoto H, Oozawa H (2005) Development of MOLB type SOFC. In: Singhal SC, MIzusaki J (eds) Solid oxide fuel cells IX, PV-2005-07. The Electrochem Soc. Inc., Pennington, pp 82–88
31. Bagger C, Christiansen N, Hendriksen PV, Jensen EJ, Larsen SS, Mogensen M (1996) Technical problems to be solved before the solid oxide fuel cell commercialized. Fuel Cell Semin 44–47
32. Hilpert K, Quadakkers J, Singheiser L (2003) Chapter 74 Interconnects. In: Vielstich W, Lamm A, Gasteiger HA (eds) Handbook of fuel cells fundamental technologies and applications, vol 4. Fuel cell technology and applications, Part 2. Wiley, Chichester, pp 1037–1054
33. Yang ZG, Stevenson J (2009) Chapter 35 Durability of metallic interconnects and protective coatings. In: Vielstich W, Yokokawa H, Gasteiger HA (eds) Handbook of fuel cells fundamental technology and applications vol 5. Advanced in

electrocatalysis, materials, diagnostics and durability: part 1. Wiley, Chichester, pp 531–542
34. Taniguchi S, Kadwaki M, Kawamura H, Yasuo T, Akiyama Y, Miyake Y, Saitoh T (1995) Degradation phenomena in the cathode of a solid oxide fuel cell with an alloy separator. Power Sources 55:73–79
35. Yokokawa H (2001) Recent developments in solid oxide fuel cell materials. Fuel Cells Fundam Syst 1(2):1–15
36. Sakai N, Horita T, Yokokawa H, Dokiya M (1996) Oxygen permeation measurement of $La_{1-x}Ca_xCrO_{3-d}$ by using an electrochemical method. Solid State Ionics 86–88:1273–1278
37. Sakai N, Yamaji K, Horita T, Yokokawa H, Kawada T, Dokiya M, Hiwatashi K, Ueno A, Aizawa M (1999) Determination of oxygen permeation flux through $La_{0.75}Ca_{0.25}CrO_{3-d}$ by electrochemical method. J Electrochem Soc 146(4): 1341–1345
38. Nishi T et al (2003) Solid electrolyte fuel cell. Japan Patent 3453283
39. Kȍck W, Martinz H-P, Greiner H, Janousek M (1995) Development and processing of metallic Cr based materials for SOFC parts. In: Dokiya M, Yamamoto O, Tagawa H, Singhal SC (eds) Soli oxide fuel cells IV, PV 95-1. The Electrochem. Soc. Inc., Pennington, pp 841–849
40. Glatz W, Kunschert G, Janousek M, Venskutonis A (2005) P/M processing and properties of high performance interconnect materials and components for SOFC applications. In: Singhal SC, Dokiya M (eds) Solid oxide fuel cell IX, PV 2005-07. The Electrochem. Soc. Inc., Pennington, pp 1773–1780
41. Yokokawa H, Horita T (2003) Chapter 5. Cathode. In: Singhal SC, Kendall K (eds) High temperature solid oxide fuel cells fundamentals design and application. Elsevier, Oxford, pp 119–147
42. Yokokawa H, Horita T, Sakai N, Yamaji K, Brito ME, Xiong XP, Kishimoto H (2006) Thermodynamic considerations on Cr poisoning in SOFC cathodes. Solid State Ionics 177:3193–3198
43. Mentzer NH, Mai A, Stöver D (2009) Durability of cathodes including Cr poisoning. In: Vielstich W, Yokokawa H, Gasteiger HA (eds) Handbook of fuel cells fundamental technology and applications vol 5. Advanced in electrocatalysis, materials, diagnostics and durability: Part 1. Wiley, Chichester, pp 566–578
44. Hilpert K, Das D, Miller M, Peck DH, Weiss R (1996) Chromium vapor species over solid oxide fuel cell interconnect materials and their potential for degradation processes. J Electrochem Soc 143:3642
45. Batawi E, Plas A, Straub W, Honneger K, Diethelm R (1999) New cost-effective ceramic oxide phases used as protective coatings for chromium-based interconnects. In: Singhal SC, Dokiya M (eds) Solid oxide fuel cells VI, PV 99-19. The Electrochem. Soc. Inc., Pennington, pp 767–773
46. Larring Y, Norby T (2000) Spinel and Perovskite functional layers between plansee metallic interconnect (Cr-5 wt% Fe-1wr% Y_2O_3) and ceramic $(La_{0.85}Sr_{0.15})_{0.91}MnO_3$ cathode materials for solid oxide fuel cells. J Electrochem Soc 147(9):3251–3256
47. Ghosh D, Tang E, Perry M, Prediger D, Pastula M, Boersuma R (2001) Status of SOFC developments at global thermoelectric. In: Yokokawa H, Singhal SC (eds) Solid oxide fuel cells VII, PV-2001-16. The Electrochem. Soc. Inc., Pennington, pp 100–110
48. Wuilleman Z, Autissier N, Nakajo A, Luong M, Van herle J, Favrat D (2008) Modeling and study of the influence of sealing on solid oxide fuel cell. J Fuel Cell Sci Technol 5:011016
49. Ivers-Tiffẽe E, Timmermann H, Leonide A, Mentzer NH, Malzbender J (2009) Methane reforming kinetics, carbon deposition, and redox durability of Ni/8 yttria stabilized zirconia (YSZ) anodes. In: Vielstich W, Yokokawa H, Gasteiger HA (eds) Handbook of fuel cells fundamental technology and applications vol 6. Advanced in electrocatalysis, materials, diagnostics and durability: Part 2. Wiley, Chichester, pp 933–956
50. Steinberger-Wilckens R, Blum L, Buchkrember H-P, de Haart LGJ, Pap M, Steinbrech RW, Uhlenbruck S, Tietz F (2009) Overview of solid oxide fuel cell development at Forschungzentrum Juelich. ECS Trans 25(2):213–220
51. Yokokawa H, Sakai H, Horita T, Yamaji K, Brito ME, Kishimoto H (2008) Thermodynamic and kinetic considerations on degradations in solid oxide fuel cell cathodes. J Alloy Comp 452:41–47
52. Sakai N, Kishimoto H, Yamaji K, Horita T, Brito ME, Yokokawa H (2007) Interface stability of Perovskite cathodes and rare-earth doped ceria interlayer in SOFCs. J Electrochem Soc 154(12):B1331–B1337
53. Xiong YP, Yamaji K, Horita T, Yokokawa H, Akikusa J, Eto H, Inagaki T (2009) Sulfur poisoning of SOFC cathodes. J Electrochem Soc 156(5):B588–B592
54. Yamaji K, Kishimoto H, Horita T, Yokokawa H, Akikusa J, Kawano M (2010) Effect of temperature on SO_2 poisoning for SSC Cathode. In: Proceedings 77th meeting of electrochemical society of Japan, March 29–31, Toyama, Japan, 1G20, p 209
55. Simner SP, Anderson MD, Pederson LR, Stevenson JW (2005) Performance variability of $La(Sr)FeO_3$ SOFC cathode with Pt, Ag, and Au current collectors. J Electrochem Soc 152:A1851
56. Christiansen N, Hansen JB, Holm-Larsen H, Jørgensen MJ, Larsen P, Hendriksen P, Hagen A, Linderoth S (2008) Solid oxide fuel cell research and development at tops – fuel cell A/S and Risø. In: Proceedings of the 8th European solid oxide fuel cell forum. The European Fuel Cell Forum, Switzerland, B0201
57. Yokokawa H, Horita T, Sakai N, Yamaji K, Brito ME, Xiong YP, Kishimoto H (2004) Protons in ceria and their roles in SOFC electrode reactions from thermodynamic and SIMS analyses. Solid State Ionics 174:205–221
58. Yokokawa H, Horita T, Sakai N, Yamaji K, Brito ME, Xiong YP, Kishimoto H (2006) Ceria: relation among thermodynamic, electronic hole and proton properties. Solid State Ionics 177:1705–1714
59. Komatsu T, Arai H, Chiba R, Nozawa K, Arakawa M, Sato K (2006) Cr poisoning suppression in solid oxide fuel cells

using LaNi(Fe)O3 electrodes. Electrochem Solid State Lett 9(1): A9–A12
60. Hartvingsen JJ, Elangovan S, Khandkar AC (2003) Chapter 76 System design. In: Vielstich W, Lamm A, Gasteiger HA (eds) Handbook of fuel cells fundamentals technology and applications, vol 4. Fuel cell technology and applications: Part 2. Wiley, Chichester, pp 1070–1085
61. Okuda M (2010) Solid oxide fuel cell demonstration program. In: Proceedings of the report symposium of NEDO projects on fuel cells and hydrogen, Tokyo, July 7–9, NEDO, Kawasaki, pp 141–148
62. Okuda M (2010) SOFC demonstrative research project. In: Proceedings of the progress report symposium of solid oxide fuel cell demonstrative research project, March 8, 2010, New Energy Foundation, Tokyo, Japan
63. Yokokawa H (2010) NEDO SOFC project on durability/reliability. In: Proceedings of the report symposium of NEDO projects on Fuel Cells and Hydrogen, Tokyo, July 7–9, NEDO, Kawasaki, pp 95–107
64. Yoshida H, Fujita K, Yakabe H, Yamashita S, Sobue T, Seyama T (2006) Subjects to be solved in SOFC system development. In: 15th symposium on solid oxide fuel cells in Japan, Extended abstracts, The solid oxide fuel cell society of Japan, Tokyo, pp 18–21
65. Wuillemin Z, Nakajo A, Müller A, Schuler JA, Diethelm S, Van herle J, Favrat D (2009) Locally-resolved study of degradation in a SOFC repeat element. ECS Trans 25(2):457–466
66. Yokokawa H, Sakai N, Horita T, Yamaji K (2009) Impact of impurities on reliability of materials in solid oxide fuel cell (SOFC) stack/modules. In: Vielstich W, Yokokawa H, Gasteiger HA (eds) Handbook of fuel cells fundamentals technology and application, vol 6. Advances in electrocatalysis, materials, diagnostics and durability: Part 2. Wiley, Chichester, pp 979–991
67. Yamaji K, Sakai N, Kishimoto H, Horita T, Brito ME, Yokokawa H (2009) Application of secondary ion mass spectrometry (SIMS) technique on the durability of solid oxide fuel cell (SOFC). In: Vielstich W, Yokokawa H, Gasteiger HA (eds) Handbook of Fuel Cells Fundamentals technology and application, vol 5. Advances in electrocatalysis, materials, diagnostics and durability: Part 1. Wiley, Chichester, pp 555–565
68. Yokokawa H, Horita T, Yamaji K, Kishimoto H, Brito ME (2010) Materials chemical point of view for durability issues in solid oxide fuel cells. J Korean Ceram Soc 47(1):26–38
69. Wunderlich C (2007) Staxera SOFC stacks in series production. Abstracts for oral presentations for 2007 fuel cell seminar and exposition. October 15–19, 2007, San Antonio, p 322
70. Matsuzaki Y, Yasuda I (2001) Dependence of SOFC cathode degradation by chromium-containing alloy on compositions of electrodes and electrolytes. J Electrochem Soc 148:A126
71. Badwal SPS, Deller R, Foger K, Ramprakash Y, Zhang JP (1997) Interaction between chromia forming alloy interconnects and air electrode of solid oxide fuel cells. Solid State Ionics 99:297–310
72. Simner SP, Anderson MD, Xia G-G, Yang Z, Pederson LR, Stevenson JW (2005) SOFC performance with Fe-Cr-Mn alloy interconnect. J Electrochem Soc 152(4):A740–A745
73. Jiang SP, Zhang JP, Fõger K (2000) Deposition of chromium species at Sr-doped $LaMnO_3$ electrodes in solid oxide fuel cells. J Electrochem Soc 147(1):4013–4022; (2000) 147(9): 3195–3205; (2001) 148(7):C447–C455
74. Paulson SC, Birss VI (2004) Chromium poisoning of LSM-YSZ SOFC cathodes I. Detailed study of the distribution of chromium species at a porous, Single-phase cathode. J Electrochem Soc 151(1):A1961–A1968
75. Konysheva E, Penkalla H, Wessel E, Mertens J, Seeling U, Singheiser L, Hilpert K (2006) Chromium poisoning of Perovskite cathodes by the ODS alloy $Cr5Fe1Y_2O_3$ and the high chromium ferritic steel Croffer 22APU. J Electrochem Soc 153(4):A765–A773
76. Konysheva E, Mertens J, Penkalla H, Singheiser L, Hilpert K (2007) Chromium poisoning of the porous composite cathode effect of cathode thickness and current density. J Electrochem Soc 154(12):B1252–B1264
77. Tsuneyoshi K, Mori K, Sawata A, Mizusaki J, Tagawa H (1989) Kinetic studies on the reaction at the $La_{0.6}Ca_{0.4}MnO_3$/YSZ interface, as an SOFC air electrode. Solid State Ionics 35: 263–268
78. Jiang SP, Zhang S, Zhen YD (2006) Deposition of Cr species at (La, Sr) (Co, Fe)O3 cathodes of solid oxide fuel cells. J Electrochem Soc 153(1):A127–A134
79. Kim JY, Sprenkle VL, Canfield NL, Meinhardt KD, Chick LA (2006) Effects of chrome contamination on the performance of $La_{0.6}Sr_{0.4}Co_{0.2}Fe_{0.8}O_3$ cathode used in solid oxide fuel cells. J Electrochem Soc 153(5):A880–A886
80. Xiong YP, Yamaji K, Kishimoto H, Brito ME, Horita T, Yokokawa H (2009) Deposition of platinum particles at LSM/ScSZ/Air three-phase boundaries using a platinum current collector. Electrochem Solid State Lett 12(3):B31–B33
81. Ingram BJ, Cruse TA, Krumpelt M (2007) Potassium-assisted chromium transport in solid oxide fuel cells. J Electrohcem Soc 154(11):B1200–B1205
82. Stanislowsli M, Froitzheim J, Niewolak L, Quadakkers WJ, Hilpert K, Markus T, Singheiser L (2007) Reduction of chromium vaporization from SOFC interconnectors by highly effective coatings. J Power Sources 164:578–589
83. Müller AC, Weber A, Beie HJ, Krügel A, Gerthsen D, Ivers-Tiffée E (1998) Influence of current density and fuel utilization on the degradation of the anode. In: Stevens P (ed) Proceedings of the 3rd European solid oxide fuel cell forum, The European Fuel Cell Forum, pp 353–362
84. Weber A, Sauer B, Müller AC, Herbstritt D, Ivers-Tiffée E (2002) Oxidation of H2, CO and methane in SOFCs with Ni/YSZ-cermet anodes. Solid State Ionics 152–153:543–550
85. Kishimoto H, Horita T, Yamaji K, Brito ME, Xiong YP, Yokokawa H (2010) Sulfur poisoning on SOFC Ni anodes: thermodynamic analyses within local equilibrium anode reaction model. J Electrochem Soc 157(6):B802–B813
86. Wilson JR, Kobsciriphat W, Mendoza R, Chen H-Y, Hiller JM, Miller DJ, Thornton K, Voorhees PW, Adler SB, Barnett SA (July 2006) Three-dimensional reconstruction of a solid-oxide fuel-cell anode. Nat Mater 5:541–544

87. Abbaspour A, Nandakumar K, Luo J, Chuang KT (2006) A novel approach to study the structure versus performance relationship of SOFC electrodes. J Power Sources 161:965–970
88. Smith JR, Chen A, Gostovic D, Hickey D, Kundinger D, Duncan KL, DeHoff RT, Jones KS, Wachsman ED (2009) Evaluation of the relation between cathode microstructure and electrochemical behavior for SOFCs. Solid State Ionics 180:90–98
89. Timmermann H, Sawady W, Campbell D, Weber A, Reimert R, Ivers-Tiffée E (2008) Coke formation and degradation in SOFC operation with a model reformate from liquid hydrocarbons. J Electrochem Soc 155(4):B356–B359
90. Mukerjee S, Kerr R, Shaffer S (2009) Solid oxide fuel cell development for transportation and stationary applications: latest update on stack and system performance. In: Abstracts for the oral and poster presentations for 2009 Fuel cell seminar and exposition, November 16–19, 2009, Palm Springs, CA, HRD 24-1
91. Matsuzaki Y, Yasuda I (2000) The poisoning effect of sulfur-containing impurity gas on a SOFC anode: part I. Dependence on temperature, time, and impurity concentration. Solid State Ionics 132:261–269
92. Sasaki K, Susuki K, Iyoshi A, Uchimura M, Imamura N, Kusaba H, Teraoka Y, Fuchino H, Tsujimoto K, Uchida Y, Jingo N (2006) H_2S poisoning of solid oxide fuel cells. J Electrochem Soc 153(11):A2023–A2029
93. Lohsoontorn P, Brett DJL, Brandon NP (2008) The effect of fuel composition and temperature on the interaction of H_2S with nickel-ceria anodes for Solid Oxide Fuel Cells. J Power Sources 183:232–239
94. Lohsoontorn P, Brett DJL, Brandon NP (2008) Thermodynamic predictions of the impact of fuel composition on the propensity of sulphur to interact with Ni and ceria-based anodes for solid oxide fuel cells. J Power Sources 175:60–67
95. Dong J, Cheng Z, Zha S, Liu M (2006) Identification of nickel sulfides on Ni-YSZ cermet exposed to H_2 fuel containing H_2S using Raman spectroscopy. J Power Sources 156:461–465
96. Hansen JB (2008) Correlating sulfur poisoning of SOFC nickel anodes by Temkin isotherm. Electrochem Solid State Lett 11(10):B178–B180
97. Marques AI, Abreu YD, Botte GG (2006) Theoretical investigations of Ni/YSZ in the presence of H_2S. Electrochem Solid State Lett 9(3):A163–A166
98. Wang J-H, Liu M (2007) Computational study of sulfur-nickel interactions: a new S-Ni phase diagram. Electrochem Commun 9:2213–2218
99. Zha S, Cheng Z, Liu M (2007) Sulfur poisoning and regeneration of Ni-based anodes in solid oxide fuel cells. J Electrochem Soc 154(2):B201–B206
100. Ferrizz RM, Gorte RJ, Vohs JM (2003) Determining the Ce_2O_2S-CeO_x phase boundary for conditions relevant to adsorption and catalysis. Appl Catal B43:273–280
101. Chou Y-S, Stevenson JW, Hardy JS, Singh P (2006) Material degradation during isothermal aging and thermal cycling of hybrid mica seal with Ag interlayer under SOFC exposure conditions. J Electrochem Soc 153(8):A1591–A1598
102. Hansen KV, Norrman K, Mogensen M (2004) H_2-H_2O-Ni-YSZ electrode performance effect of segregation to the interface. J Electrochem Soc 151(9):A1436–A1444
103. Hauch A, Jensen SH, Bilde-Sørensen JB, Mogensen M (2007) Silica segregation in the Ni/YSZ electrode. J Electrochem Soc 154(7):A619–A626
104. Aravind PV, Ouweltjes JP, Woudstra N, Rietveld G (2008) Impact of biomass-derived contaminants on SOFCs with Ni/Gadolinia-doped ceria anodes. Electrochem Solid State Lett 11(2):B24–B28
105. Yang Z, Meihardt KD, Stevenson JW (2003) Chemical compatibility of barium-calcuium-aluminosilicate-based sealing glasses with tge ferritic stainless steel interconnect in SOFCs. J Electrochem Soc 150(8):A1095–A1101
106. Hofmann P, Panopoulos KD, Fryda LE, Schweiger A, Ouweltjes JP, Karl J (2008) Integrating biomass gasification with solid oxide fuel cells: effect of real product gas tars, fluctuations and particulates on Ni-GDC anode. Int J Hydrogen Energy 33:2834–2844
107. Marina OA, Pederson LR, Gemmen R, Finklea K, Celik IB (2009) Overview of SOFC anode interactions with coal gas impurities. In: 2009 Fuel cell seminar, Palm Spring, CA, HRD43b-1
108. Gemmen RS, Trembly J (2006) On the mechanisms and behavior of coal syngas transport and reaction within the anode of a solid oxide fuel cell. J Power Sources 161: 1084–1095
109. Trembly JP, Gemmen RS, Bayless DJ (2007) The effect of IGFC warm gas cleanup system conditions on the gas-solid partitioning and form of trace species in coal syngas and their interactions with SOFC anodes. J Power Sources 163:986–996
110. Trembly JP, Gemmen RS, Bayless DJ (2007) The effect of coal syngas containing HCl on the performance of solid oxide fuel cells: investigations into the effect of operational temperature and HCl concentration. J Power Sources 169:347–354
111. Trembly JP, Gemmen RS, Bayless DJ (2007) The effect of coal syngas containing AsH_3 on the performance of SOFCs: Investigations into the effect of operational temperature, current density and AsH_3 concentration. J Power Sources 171:818–825
112. Xu B, Zondlo JW, Finklea HO, Demircan O, Gong M, Liu XB (2009) The effect of phosphine in syngas on Ni-YSZ anode-supported solid oxide fuel cells. J Power Sources 193:739–746
113. Trembly JP, Marques AI, Ohrn TR, Bayless DJ (2006) Effects of coal syngas and H_2S on the performance of solid oxide fuel cells: single-cell tests. J Power Sources 158:263–273
114. Zhi M, Chen X, Finklea H, Celik I, Wu NQ (2008) Electrochemical and microstructural analysis of nickel-yttria-stabilized zirconia electrode operated in phosphorus-containing syngas. J Power Sources 183:485–490
115. Haga K, Adachi S, Shiratori Y, Itoh K, Sasaki K (2008) Poisoning of SOFC anodes by various fuel impurities. Solid State Ionics 179:1427–1431

116. Bao J, Krishnan GN, Jayaweera P, Perez-Mariano J, Sanjurjo A (2009) Effect of various coal contaminants on the performance of solid oxide fuel cells: part I accelerated testing. J Power Sources 193:607–616
117. Bao J, Krishnan GN, Jayaweera P, Kau KH, Sanjurjo A (2009) Effect of various coal contaminants on the performance of solid oxide fuel cells: part II. ppm and sub-ppm level testing. J Power Sources 193:617–624
118. Bao J, Krishnan GN, Jayaweera P, Sanjurojo A (2010) Effect of various coal gas contaminants on the performance of solid oxide fuel cells: part III Synergistic effects. J Power Sources 195(5):1316–1324
119. Burnette DD, Kremer GG, Bayless DJ (2008) The use of hydrogen-depleted coal syngas in solid oxide fuel cells. J Power Sources 182:329–333
120. Huang T-J, Chou C-L, Chen W-J, Huang M-C (2009) Coal syngas reactivity over Ni-added LSCF-GDC anode of solid oxide fuel cells. Electrochem Commun 11:294–297
121. Marques AI, Ohrn TR, Trembly JP, Ingram DC, Bayless DJ (2007) Effect of coal syngas and H_2S on the performance of solid oxide fuel cells part 2 Stack tests. J Power Sources 164:659–667
122. Cayan FN, Zhi M, Pakalapati SR, Celik I, Wu NQ, Gemmen R (2008) Effects of coal syngas impurities on anodes of solid oxide fuel cells. J Power Sources 185:595–602
123. Casleton KH, Breault RW, Richards GA (2008) System issues and tradeoffs associated with syngas production and combustion. Combust Sci Tech 180:1013–1052
124. Itoh H, Mori M, Mori N, Abe T (1993) Development of solid oxide fuel cells – producing cost estimation. Yokosuka Research Laboratory Rep. No. W92028, CRIEPI, Tokyo, Japan
125. Itoh H, Mori M, Mori N, Abe T (1994) Production cost estimation of solid oxide fuel cells. J Power Sources 49: 315–332
126. Romero C, Wright J (1996) The value and manufacturing costs of planar solid oxide fuel cell stacks. Topical Report no. TDA-GRI-96/0210 for Gas Research Institute
127. Krist K, Wright JD, Romero C, Chen TP (1996) Cost projections for planar solid oxide fuel cell systems. In: Fuel Cell Seminar, Orlando, FL, pp 497–500
128. Krist K, Wright JD, Romero C (1995) Manufacturing costs for planar solid oxide fuel cells. In: Dokiya M, Yamamoto O, Tagawa T, Singhal SC (eds) Solid oxide fuel cells IV, PV 95-1. The Electrochem. Soc. Inc., Pennington, pp 24–32
129. Ipponmatsu M, Sasaki H, Otoshi S (1996) Evaluation of the cost performance of the SOFC cell in the market. Int J Hydrogen Energy 21(2):129–135
130. George RA, Bessette N (1998) Reducing the manufacturing cost of tubular SOFC technology. J Power Sources 71:131–137
131. Mizutani Y, Tamura M, Kawai M, Nomura K, Nakamura Y, Yamamoto O (1995) Characterization of the Sc2O3-ZrO2 system and its application as the electrolyte in Planar SOFC. In: Dokiya M, Yamamoto O, Tagawa T, Singhal SC (eds) Solid oxide fuel cells IV, PV 95-1. The Electrochem. Soc. Inc., Pennington, pp 301–317
132. Thijssen JH, Surdval WA (2009) Stack operating strategies for central station SOFC. In: 2009 Fuel cell seminar and exposition. November 16–19, Palm Springs, CA, HRD32-3
133. Watanabe M, Uchida H, Yoshida M (1997) Effect of ionic conductivity of zirconia electrolytes on the polarization behavior of ceria-based anodes in solid oxide fuel cells. J Electrochem Soc 144(5):1739–11743

Books and Reviews

Ishihara T (ed) (2009) Perovskite oxide for solid oxide fuel cells. Springer, Dordrecht
Minh Q, Takahashi T (1995) Science and technology of ceramic fuel cells. Elsevier, Amsterdam
Singhal SC, Kendall K (eds) (2003) Solid oxide fuel cells. Elsevier, Oxford
Vielstrich W, Yokokawa H, Gasteiger HA (eds) (2009) Hand book of fuel cells fundamentals technology and application, vols 5 and 6. Advances in electrocatalysis, materials, diagnostics and durability. Wiley, Chichester

Solid Oxide Fuel Cells

A. Atkinson, S. J. Skinner, J. A. Kilner
Department of Materials, Imperial College London, London, UK

Article Outline

Glossary
Definition of the Subject and Its Importance
Introduction
Novel Devices and Configurations
Novel Materials
Development of In situ Diagnostics
Future Directions
Acknowledgments
Bibliography

Glossary

Anode The negative terminal of the SOFC where oxygen ions from the electrolyte react with fuel releasing electrons to the external circuit.

Cathode The positive terminal of the SOFC where oxygen molecules from the air are reduced to oxygen ions by absorbing electrons from the external circuit.

Electrolyte The central component of the SOFC which conducts electricity by the movement of oxygen ions. This is the solid analogue of the liquid electrolyte used in a battery.

Fuel cell stack A fuel cell composed of several individual fuel cell (anode/electrolyte/cathode) units electrically interconnected in order to provide a useful device in terms of power output.

Heterostructure A structure consisting of two closely matched materials with properties superior to those of the individual components due primarily to interface effects. Can be further enhanced through creation of multilayer heterostructures where many repeats are generated.

Planar device A fuel cell constructed from sequential functional layers of anode, electrolyte, and cathode in a planar geometry.

Solid oxide fuel cell (SOFC) An electrochemical device for the conversion of a gaseous fuel into electrical energy using oxide ion-conducting ceramic membranes.

Definition of the Subject and Its Importance

The Solid Oxide Fuel Cell is an electrochemical device for the conversion of hydrogen or a hydrocarbon fuel directly into electrical power. They are clean, modular, and efficient and retain this efficiency across a wide range of sizes. This fuel flexibility and efficiency makes them very attractive for a number of power-generation roles, including distributed generation and combined heat and power applications, where they could make a significant impact on carbon-emission reductions and provide a pathway towards an eventual low carbon economy. There are some significant hurdles to be overcome before there is a global uptake of SOFC technology, and it is very likely that the technology will evolve markedly over the next few decades. It is thus important to take a forward look at how the technology may evolve and what kinds of devices, materials, and diagnostics will be needed to assure this continued development.

Introduction

Although Solid Oxide Fuel Cells (SOFCs) have been investigated since their discovery by Sir William Grove in the nineteenth century, little progress was made until almost a century later when the twin drivers of security of supply and the reduction of carbon emissions provided the necessary financial and political imperatives to accelerate SOFC development. Since that time, there have been a number of generations of devices, from the early tubular cells developed by Westinghouse and Mitsubishi Heavy Industries, through planar electrolyte supported cells, to the current generation of supported thin-film planar devices, which are nearing commercial exploitation, operating at intermediate temperatures (ITSOFCs). Much has been written on the materials and device characteristics in journal articles, conference proceedings, and there are many reference books [1, 2]. The aim of this article is not to replicate these many excellent texts, but to present quite a different view, one which looks towards the future of SOFC technology and what new designs, new materials, and new diagnostic techniques will be required to meet the demands of future SOFC developments.

From the current perspective, the future of SOFC technology looks promising. SOFCs will have many roles to play in the global energy scenario, from large-scale central power generation, distributed generation roles in domestic and district Combined Heat and Power (CHP), to mobile, remote, and standby power. If this outlook is correct, then the SOFC will undergo continued development to achieve improved performance and durability and will become more commercially viable in the very near future, delivering substantial increases in the efficient use of hydrocarbon fuels and a consequent drop in carbon emissions. In considering the future, it is thus important to look at how the technology will develop into new SOFC concepts. These have lagged behind mainstream SOFC development, but could quickly benefit from any significant technological advances made in their development. One thing is clear; these developments are underpinned by the requirements for new materials and new diagnostic techniques. The materials must meet stringent requirements for electrical and mechanical properties coupled with long-term stability in the appropriate environment. The purpose of this contribution is to describe these possible novel SOFC and SOFC-related concepts, describe their strengths and their drawbacks, and in parallel to explore the advances

in materials and materials characterization that will be necessary to ensure application and commercialization in the future.

Novel Devices and Configurations

SOFCs have largely converged on standard configurations, such as tubular or planar, with the structural support provided by the electrolyte, the anode, the metallic interconnector, or an inert porous support material. Each of these concepts has its own combination of advantages and disadvantages. In this section, some "unconventional" SOFC configurations and devices are discussed, and their performance and potential applications are considered in comparison with the more conventional approaches. This will include microtubular fuel cells, mixed reactant fuel cells, micro-planar fuel cells, and dual proton-oxygen ion fuel cells.

Microtubular SOFCs

Tubular SOFCs are not new and have been developed for large-scale stationary CHP applications with both circular and flat-cross sections. A major advantage of tubular SOFCs is better tolerance of thermal cycling, especially if one end is closed and therefore unconstrained to allow thermal expansion-length changes. A major disadvantage is that the volumetric power density is smaller than for a planar configuration, although this is partially offset with a flat cross-section tube. However, another way of improving the volumetric power density is to make the tubes smaller in diameter. When the diameter is less than approximately 3 mm, these are referred to as microtubular cells and their development has recently been reviewed by Lawlor et al. [3] and Kendall [4]. The reduction in diameter brings additional advantages in that the small tubes tend to have higher mean strength because the stressed volumes are smaller and lower variability in strength as the processing tends to give a more uniform microstructure. Consequently, microtubular SOFCs tend to have excellent thermal cycling durability.

The most usual configuration is a thin film of electrolyte on an anode support tube and an outer thick-film cathode. However, a major problem with the microtubular concept is with current collection from the electrodes and interconnection into stacks. Since the tubes are so small, large numbers are required for applications requiring appreciable power. For example, a typical tube with diameter 2 mm and length 100 mm operating at 0.2 W cm^{-2} only produces 1.25 W. Sammes et al. [5] have described a serpentine interconnection system for anode-supported tubes of conventional SOFC materials that are somewhat larger than the usual microtubular size, being 13 mm diameter and 110 mm long. However, at 850°C, the maximum power density was only 0.1 W cm^{-2} and was limited by the current collection along the cathode.

Suzuki et al. [6, 7] have attempted to overcome this problem with a cubic stack design (Fig. 1) in which microtubular SOFCs are assembled in layers joined by a porous matrix of cathode material. The layers are assembled in stacks in which individual layers are electrically insulated from each other by a glass and the cathodes of one layer are connected to the anodes of the next using silver. Each microtube was 0.8 mm in diameter and 8 mm in length and made from a Ni/$Ce_{1-x}Gd_xO_{2-\delta}$ (CGO) composite anode material. The electrolyte was CGO and the cathode an $La_{1-x}Sr_xCo_{1-y}Fe_yO_{3-\delta}$ (LSCF)/CGO composite. The stack consisted of 20 cells; 4 layers of 5 cells; and its performance is also shown in Fig. 1. At 500°C, the power output of a single tube was 0.32 W cm^{-2} at 0.7 V, and the total-bundle power at 490°C and 0.7 V per cell was approximately 1.3 W; corresponding to 0.25 W cm^{-2}. These are impressive performance figures at such low operating temperatures. However, the fabrication of these stacks could be difficult to automate and the final structure is monolithic, so that much of the tolerance of the tubular configuration to thermal gradient stresses is compromised.

Mixed Reactant Fuel Cells

A major problem with almost all SOFC designs is the requirement to seal the structure in order to prevent the fuel and oxidant gases from coming into direct contact and causing direct combustion of the fuel. One possible way around this is to operate the cell at a temperature below which no direct combustion will take place and to allow the fuel and oxidant to mix. The cell then requires very selective electro-catalytic electrodes in order to generate electrochemical power. Ideally, the anode should only catalyze the

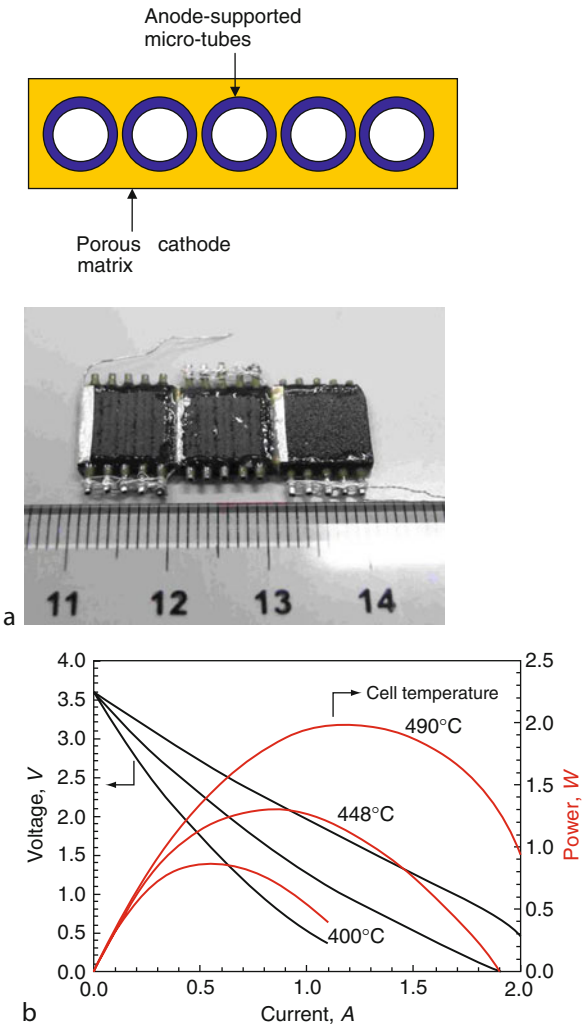

Solid Oxide Fuel Cells. Figure 1
(**a**) Micro-tubular SOFC stack layer concept and (**b**) performance of a 20 cell (4 layers) bundle [6, 7]. Reproduced with permission

fuel-electrochemical oxidation and the cathode the electrochemical reduction of the oxidant. Neither electrode should catalyze direct chemical reaction of fuel and oxidant.

The first attempts at such a configuration were reported by Hibino and Iwahara, [8] and there have been many subsequently. The area has recently been reviewed by Yano et al. [9], and some typical configurations are illustrated in Fig. 2. There are many reports of good power densities when operating on hydrocarbon fuels, which are more resistant to direct oxidation

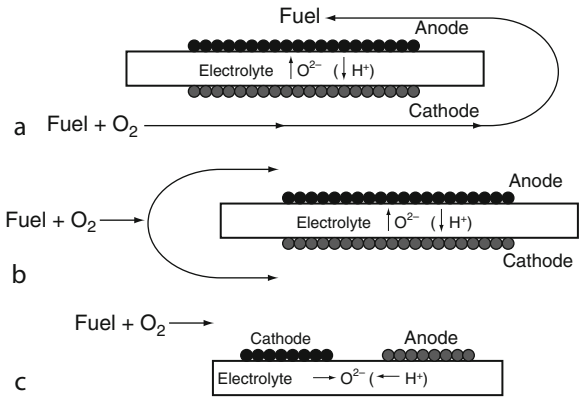

Solid Oxide Fuel Cells. Figure 2
Geometries for planar mixed reactant SOFCs [7]

than hydrogen. However, there is always some direct combustion and the cell temperature can be considerably higher than the nominal ambient temperature as a result, which makes the performance difficult to judge. Some direct combustion might even be regarded as an advantage since it can help small SOFCs to be thermally self-sustaining. Riess [10] has discussed the issues involved in mixed-reactant mode and pointed out that to date they can only operate with low fuel utilization and short gas residence times (high-flow rates). He proposes a configuration similar to that being investigated in mixed reactant PEMFCs that is illustrated in Fig. 3. All the components are porous, so that the mixed-reactant gas stream flows through the whole unit. This concept enables high fuel utilization to be achieved in principle, but has not yet been realized in practice since the selectivity of the electrode catalysis is not good enough for the materials investigated thus far.

Micro-planar SOFCs

These devices feature the use of micro-fabrication techniques adapted from the micro-electronics industry. These encompass substrate etching, thin-film deposition, lithography, and film-etching steps. This field has recently been reviewed by Evans et al. [11], and all devices exhibit the beautiful structural quality resulting from the micro-fabrication techniques. An example of a micro-planar SOFC fabricated on a silicon substrate is illustrated in Fig. 4 [12]. Figure 4a shows the sequence of fabrication steps used to make the edge-supported SOFC membrane which spans an aperture

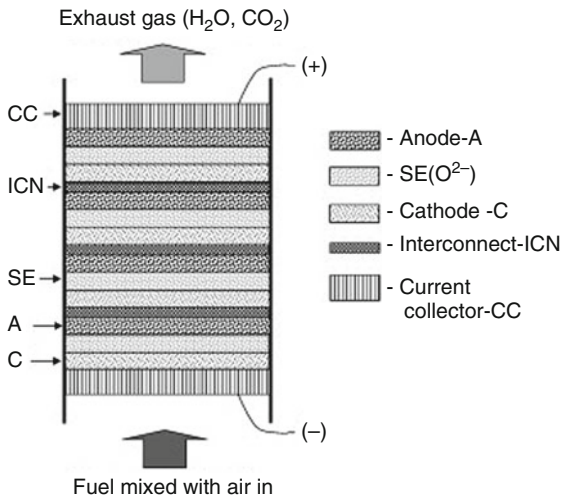

Solid Oxide Fuel Cells. Figure 3
Proposed configuration for a flow-through mixed reactant SOFC [10]. Reproduced with permission

with dimensions 600 × 600 μm. The yttria stabilized zirconia (YSZ) electrolyte, which is only 70-nm thick, was deposited by atomic-layer deposition and is corrugated in order to increase the active area and accommodate thermal and fabrication strains. An image of the corrugated electrolyte is shown in Fig. 4b. The electrodes are 120-nm thick porous-Pt deposited by sputtering. The performance, of both flat and corrugated cells, on hydrogen is remarkable (Fig. 4c), with a maximum power density of 0.86 W cm^{-2} at 450°C. The shape of the *V–I* characteristic indicates large overpotentials at the electrodes and therefore the possibility of large power density at more useful terminal voltage with improved electrodes.

At this stage of development, the reported results indicate that good performance is likely to be achievable with micro-fabricated SOFCs. However, more problematic are the engineering issues related to thermal management and fuel utilization that are more difficult to deal with as the device becomes smaller. Even if these problems are solved, the power levels and total energies are so small that the impact on sustainable electrical energy generation will be small and the development of these devices will be driven by convenience of operation (e.g., in consumer electronics) rather than energy efficiency.

Dual Proton-Oxygen Ion-Conducting Cells

Recently, a new concept (Fig. 5) has been proposed, called the IDEAL-Cell which attempts to combine the advantages of both proton-conducting and oxygen ion-conducting SOFCs [13]. The anode electrode reaction is as in a proton-conducting SOFC, and the cathode reaction as in an oxygen ion-conducting SOFC. In the central chamber, which contains a porous mixture of the two electrolytes, the protons and oxygen ions combine to give the product water. In this way, the water reaction product does not interfere with either of the electrode reactions. A "proof-of-concept" small cell was fabricated with yttrium-doped barium cerate as the proton-conducting electrolyte and yttrium-doped ceria as the oxygen ion-conducting electrolyte. The test cell achieved an encouraging maximum power output approaching 0.5 W cm^{-2} at 600°C on oxygen and humidified hydrogen. It will be interesting to see whether this concept can actually deliver the anticipated benefits on a larger scale.

Novel Materials

In the preceding section, new design concepts for the SOFC for application in the near future were discussed. One common feature of most of these new concepts is the lowering of the operating temperature into a new regime (400–600°C), where high performance materials should make a significant impact. The active components of such solid oxide fuel cells must conform to some very stringent materials requirements. The prime need is to have very high diffusion coefficients for the oxide ion at these low temperatures which will require considerable materials development for both electrolytes and the mixed conductors used as electrodes. In this lower temperature regime, the three active components: anode, cathode, and electrolyte, each contribute towards the overall area specific resistance (ASR) of the cell. Of these three components, the two that have received the most attention are the electrolyte and the cathode, which is known to give rise to the largest ASR below temperatures of 650°C [2].

Before moving to the details of these materials, it is instructive to examine the atomistic quantities that govern the transport of oxygen in these oxides. A simple Arrhenius-type expression describes the diffusion coefficient of oxygen, D, in oxide materials.

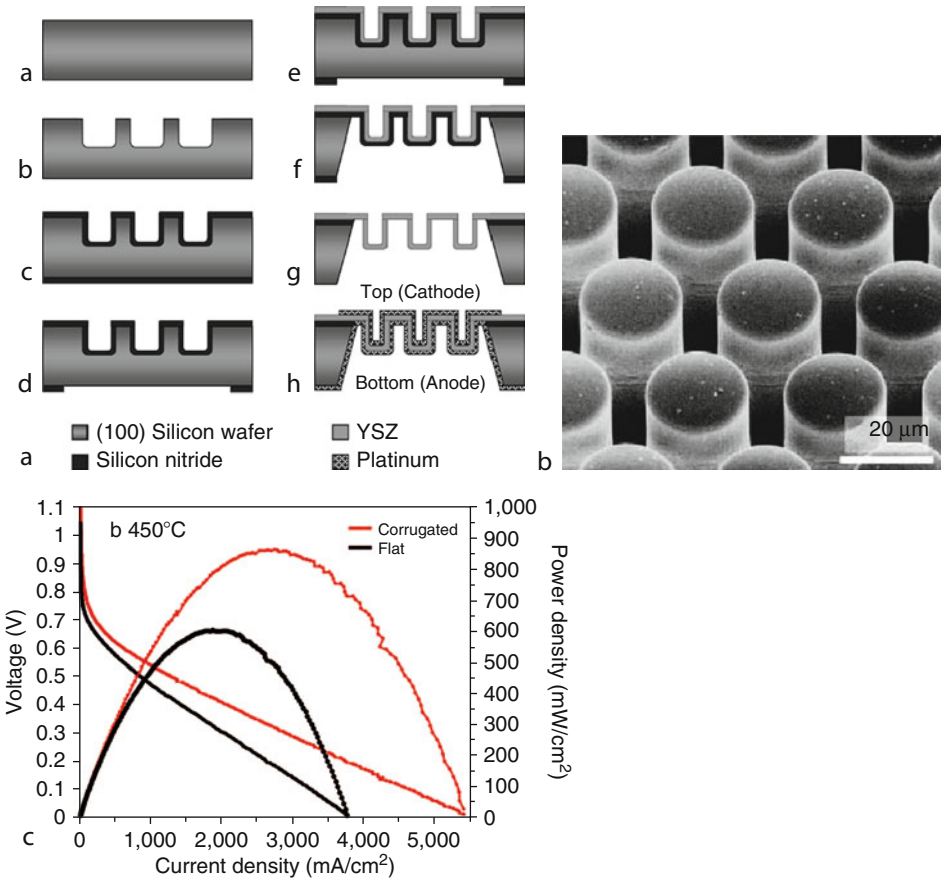

Solid Oxide Fuel Cells. Figure 4

An example of a micro-planar SOFC produced by micro-fabrication methods. (**a**) The sequence of fabrication steps, (**b**) the corrugated electrolyte membrane before deposition of the electrodes, and (**c**) the electrochemical performance [12]. Reproduced with permission

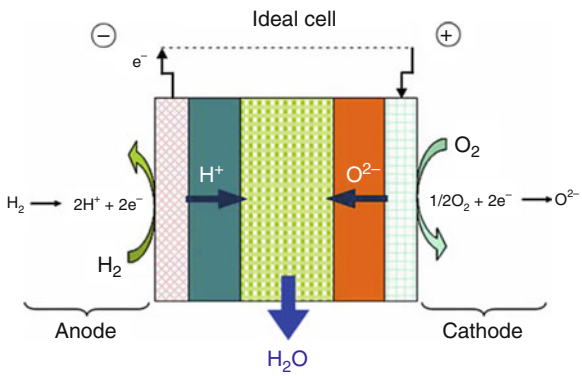

Solid Oxide Fuel Cells. Figure 5

The concept of a dual proton and oxygen ion SOFC [13]. Reproduced with permission

$$D = D_0 \exp\left\{\frac{-E_a}{RT}\right\}$$

where D_0 is the pre-exponential factor which contains terms relating to the concentration of oxygen defects and E_a is the activation energy for diffusion which can contain terms relating to the formation, association, and migration of the defects on the oxygen sublattice [14]. Both terms are important in achieving high diffusivities. Materials with highly defective oxygen sublattices or high concentrations of interstitials are commonly investigated to give high diffusion coefficients; however, a low activation energy is essential to retaining the high-diffusion coefficient to low temperatures. This means minimizing (or removing) any

terms due to the formation or association of defects and ensuring that the mobile oxygen ions can migrate with the minimum of hindrance. These criteria apply to materials that have very high ionic transport numbers for use as electrolyte materials as well as to mixed conducting materials used as electrodes.

An additional criterion for mixed conducting materials used as cathodes is that they should have a high surface exchange rate (k) for oxygen. This quantity also follows Arrhenius-type behavior, although the atomistic parameters that govern the exchange process are still somewhat obscure. However, it is well known that materials that have high oxygen-diffusion coefficients usually have high oxygen-exchange coefficients because both are related to the oxygen mobility in the material [15]. It should be remembered that the selection criteria described above are only part of the process of the selection and optimization of new materials for the application in solid oxide fuel cells, and that a significant part of the application of new materials relies upon the development of appropriate ceramic processing to yield a suitable microstructure for the SOFC cathode [16].

In the following paragraphs some of the current materials research that could give rise to suitable materials for applications in SOFCs is described.

Electrolyte Materials

The materials requirements described above for obtaining high oxygen transport can be further developed [17] and have been used for many years in the optimization of new oxygen ion conductors. A good example of this are the materials formed from ceria gadolinia solid solutions that have some of the highest conductivities at low temperatures. Fig. 6 shows an Arrhenius plot of the conductivity of most of the conventional oxide ion conductors used as electrolytes. New ionic conductors are emerging as further compositions are explored, such as the $La_2Mo_2O_9$ (LAMOX) family and the apatite-structure materials, however they usually offer incremental advantages and do not have either the low-temperature conductivity offered by the cerias or the very high stability offered by the stabilized zirconia materials. At 600°C, some very high ionic conductivities can be achieved by bismuth-based

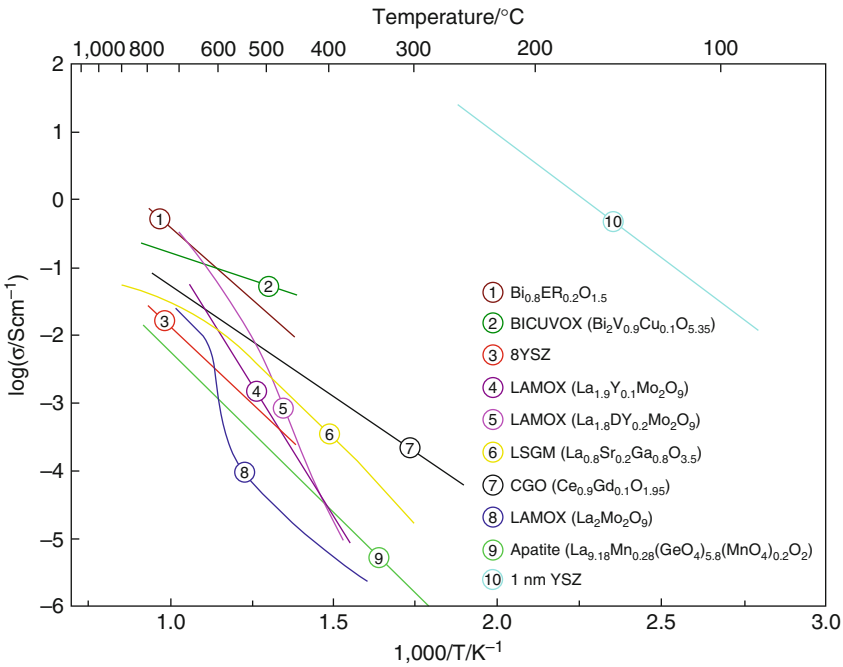

Solid Oxide Fuel Cells. Figure 6
Comparison of the lattice conductivity of some well known oxide ion conductors. Data taken from [18–26]

materials, on the order of 10^{-1} S cm^{-1} which is equivalent to that of yttria-stabilized zirconia at 1,000°C; however, these materials suffer from poor stability in reducing atmospheres and are thus not suitable to act as SOFC electrolytes without some form of protective layer. Other than the bismuth materials, there is a paucity of materials that can display conductivities of this order below temperatures of around 650–700°C.

Thin-Film Heterostructures

The continued search for materials that show better ionic transport, especially at low temperatures, has been a quest that has been pursued for many years. In the main, there have been two ways in which this search has been pursued: by the discovery of new materials, i.e., the optimization of the lattice mobility for the oxygen ion, as mentioned above, and more recently, by the investigation of nanomaterials and nanostructures, i.e., by the optimization of the interfacial transport of oxygen. Early work with thin (down to ~15nm) epitaxial yttria-stabilized zirconia (YSZ) films by Kosacki et al. [27] and Karthikeyan et al. [28] instigated a number of investigations into the effect of interfaces on conductivity. Kosacki et al.'s findings implied that the oxygen conductivity of the interfacial layer between the MgO substrate and the YSZ was strongly enhanced, by up to 3 or 4 orders of magnitude, and more significantly, that the activation energy was more than halved from 1.04 to 0.45 eV, important for achieving high values of conductivity at low temperatures. These findings prompted a number of subsequent investigations into the ionic conductivity of heterostructures, produced by pulsed laser deposition, involving thin layers of an oxide ion conductor (mostly YSZ) sandwiched between layers of insulating materials. The temperature dependence of the ionic conductivity for these materials is shown in Fig. 7, which shows that the conductivity can be either enhanced or suppressed over that for single crystal zirconia. By far the most significant result is that obtained by Garcia-Barriocanal et al. [18] (trace 10 in Figs. 6 and 7a in Fig. 7) who investigated very thin layers of YSZ and strontium titanate (STO) in samples made by sputtering. They observe that for epitaxial trilayers of 10 nm STO/1 nm YSZ/10 nm STO the conductivity was highly enhanced (trace 7a in Fig. 7), showing over 8 orders of magnitude of enhancement at 100°C. This is clearly much larger than any of the enhancements seen by other workers, most of which are grouped around 1–2 orders of enhancement of the conductivity of zirconia, depending upon the temperature. There is still much debate over these findings as, at the date of writing, they have not been repeated and there is controversy over the nature of the carrier, an electronic carrier would be much easier to reconcile with these high conductivities [31–33]. The interfacial strain at the STO/YSZ interface should be on the order of 7% which should not lead to a coherent interface as was observed by electron microscopy. Despite the lack of experimental evidence, there have been some theoretical studies including simulations by Density Functional Theory (DFT) which would tend to support the idea that the observed effects could indeed be ionic [34], although there is some doubt about the magnitude of the conductivity enhancement [35].

The most systematic of the subsequent investigations of heterostructures has been by Korte and coworkers [30, 36, 37], who have investigated a number of different interfaces by fabricating stabilized zirconia-insulator heterostructures using pulsed laser deposition. Recently, Korte et al. [38] have reviewed the current status of their (and other) work on multilayer structures and have classified them according to the degree of coherency of the crystal structure across the interfaces. They show that the lattice strain in the zirconia layers is important in determining the magnitude of the change in both conductivity and in activation energy. Tensile strain leads to an enhancement of the conductivity by up to an order of magnitude; however, the largest enhancement seen is in structures formed with calcia-stabilized zirconia (CSZ) and Al_2O_3 as the insulating layer, which have an incoherent interface and a disordered region and a high density of mismatch dislocations. The enhancement of conductivity seen is around a factor of 60 at 575°C with a lowering of the activation energy of almost 0.5 eV, a significant decrease, leading to increased low-temperature conductivity.

Korte et al. [38] speculate on the role of any misfit dislocations in the conductivity enhancement. This seems to be a likely explanation, as conductivity enhancement has been seen in YSZ single crystals that have been plastically deformed at high temperatures.

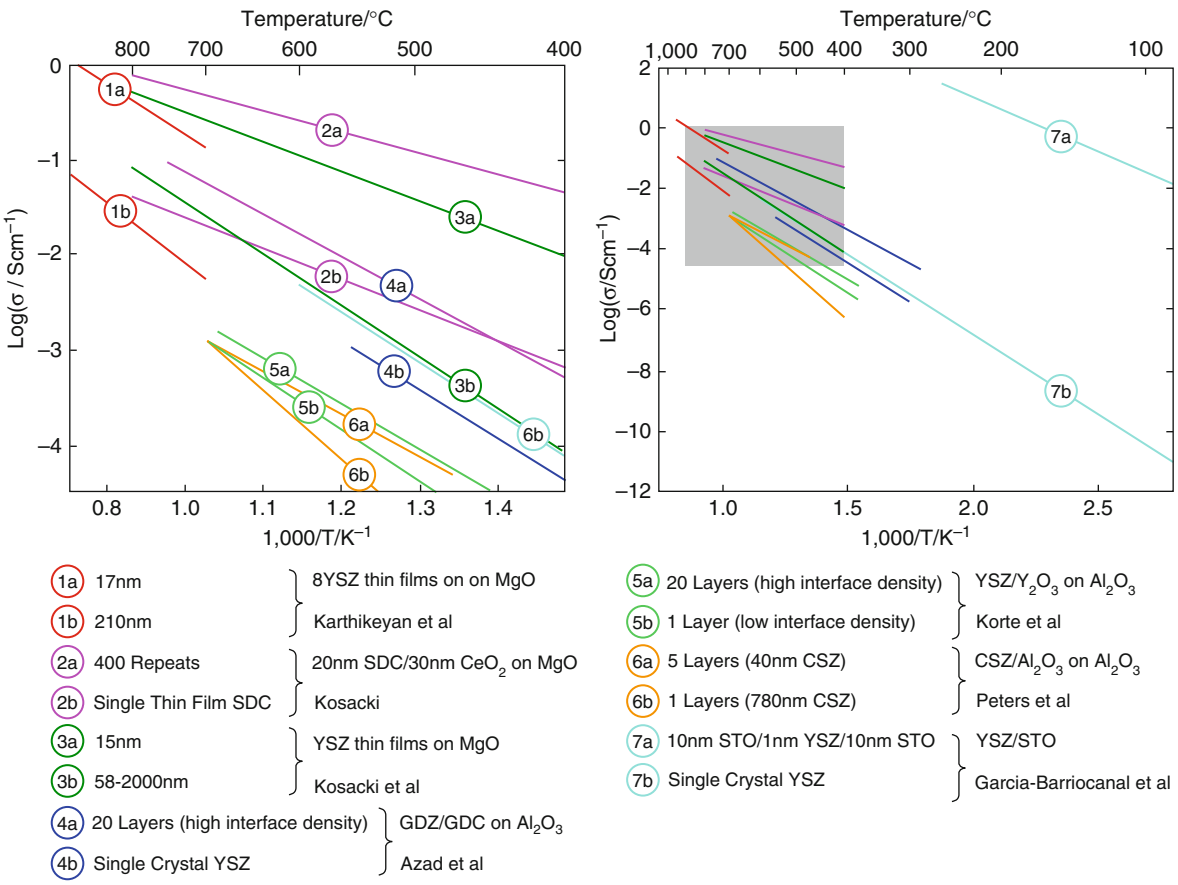

Solid Oxide Fuel Cells. Figure 7

Temperature dependence of the conductivity of oxide heterostructures. Data taken from Karthekeyan et al. [28], Kosacki et al. [27], Azad et al. [29], Korte et al. [30], Garcia-Barriocanal et al. [18]

Otsuka and coworkers [39, 40] have shown that the conductivity of material with high dislocation densities does show an enhancement of the conductivity and they estimate that the conductivity could be enhanced by a factor of 10^2–10^4. These findings clearly indicate a possible method for the enhancement of low-temperature conductivity in oxygen-ion conductors by the introduction of structures, such as heterointerfaces that give rise to either tensile strain or to large numbers of dislocations.

Electrode Materials

The search for new materials for electrodes has also been a long-term quest similar to the one mentioned above for electrolyte materials. Because of the importance of developing new cathode materials for low-temperature operation, much recent work has focussed on mixed electronic-ionic conducting materials for this particular application. Like the electrolyte materials, there have been indications that heterogeneous interfaces in mixed conductors can show some enhanced behavior [41], although there has been little published on this subject to date. Much of the conventional bulk materials have been based on highly substituted perovskite materials, such as $La_{1-x}Sr_xCoO_{3-\delta}$ for which substitution (x) can be as high as 0.6. There materials have very high strontium contents and high degrees of non-stoichiometry which give the materials high performance as cathodes, but bring a set of problems. The materials that have the highest levels of oxygen diffusivity, such as the cobalt-based materials mentioned above, also have high values of expansion coefficient (>20 ppm K^{-1}) [42], making them

thermo-mechanically incompatible with the electrolyte materials. In addition, the high strontium contents lead to vulnerability to long-term degradation problems [16] and possibly to chromium poisoning. In order to combat some of these problems, there has been a move towards materials that do not need high degrees of substitution and that could show greater stability while retaining the high electrochemical activity.

Of current interest is the work on layered crystal structures (which are almost a natural analogue of the heterostructures described above) in either polycrystalline or single crystal form. An example of a family of oxides with this layered structure is the Ln_2NiO_4 materials such as $La_2NiO_{4+\delta}$ or $Nd_2NiO_{4+\delta}$. These materials are the first member of the Ruddlesden Popper homologous series with the K_2NiF_4 structure, and they are unusual in that they show highly anisotropic conductivity (see for example Fig. 9 next section). The general structure of such $A_2BO_{4+\delta}$ oxides is shown in Fig. 8 and consist of alternating layers of perovskite ABO_3 and rocksalt AO layers. These materials are not substituted, but due to the variable valency of the B, cation tend to oxygen excess in air, i.e., $\delta > 0$, which can reach values of around 0.14. The oxygen interstitials are mobile in the AO layers and can give rise to substantial values of oxygen diffusivity. The expansion coefficients of these materials do not suffer from the very high values seen for the substituted perovskites, and so these materials are good candidates for next generation cathodes; however, their durability in cathode environments needs to be verified. Their performance, as ITSOFC cathode, has recently been reviewed and their suitability as candidates has been confirmed [43].

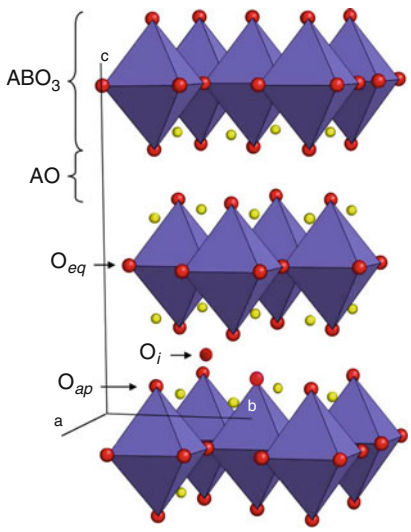

Solid Oxide Fuel Cells. Figure 8
Schematic of the crystal structure of $A_2BO_{4+\delta}$

Accelerated Materials Discovery

Accelerated materials discovery is of great interest for the development of the SOFC and a key goal for further development is the lowering of the operational temperature to below 600°C, the so-called intermediate-temperature regime. In this regime, cheap and readily available materials can be used for the balance of plant. When considering the need for novel materials, it is pertinent to consider the timescales needed for the introduction of new materials into devices to meet emissions reductions targets for 2030 and 2050 and beyond. Historically, the timescales for adoption of new materials/new technologies has been rather long, especially where the drivers (at least initially) are not financial. In order to have significant impact on the reduction of carbon emissions, wide-scale adoption of fuel cells has to take place over the timescale of the 20–30 years from 2010. Moving back down the development chain, this implies that any new materials must be adopted within the next decade or so, and the real scope of the task becomes apparent. How this can be achieved has been described in a short editorial by Kilner [44].

- Clearly, conventional trial and error methods of materials discovery are not going to meet this aggressive agenda and an accelerated form of materials discovery is needed. The important question is what type of accelerated materials development tools will become available? A new topic of "Materials Informatics" has emerged, which employs the use of large databases of materials properties obtained from conventional, combinatorial, or computational sources. The databases are then interrogated using techniques, such as data mining, neural networks, etc. This new and developing technique is still in its infancy, and very few databases exist which cover the functional properties of oxide ceramics.

  Much has been made of combinatorial approaches to materials discovery; however, there are many

barriers to the introduction of these methods to SOFC materials, not least their suitability to synthesize libraries of complex multicomponent oxides, such as the cathode materials $La_{1-x}Sr_xCo_{1-y}Fe_yO_{3-\delta}$ [45]. In addition to these limitations, there is the requirement for rapid screening methods to allow combinatorial libraries to be measured in an accelerated manner. This is not an easy problem to solve for applications that rely upon measuring complex electro-catalytic activity in very aggressive environments, such as SOFC electrodes.

Computer simulation offers an alternative way of providing guidelines for materials searching. For example, atomistic simulation of defects and transport in materials is well established; however, it is hardly a rapid process and much of the effort is expended in the rationalization of existing experimental data. A change in scope is needed to exploit the potential of such techniques to predictive materials screening.

It is important that these rather more pragmatic techniques, mentioned above, are developed in parallel with the more conventional intuitive methods to give development engineers rapid access to new materials.

Development of In Situ Diagnostics

Identifying and developing new materials for all components of a solid oxide fuel-cell system is only the first stage in producing a device. There are several key requirements, such as durability and compatibility, which have to be fully investigated before a material can be incorporated into a working fuel cell. As detailed earlier, this type of cell operates in a relatively harsh environment with a high temperature of operation and a wide pO_2 range. It is therefore essential to gain a full understanding of the behavior of each of the cell components and the stack itself as a function of all of these parameters in situ. Consequently, there has been an increasing demand for in situ characterization techniques to give real-time insights into device performance. Of course, in situ characterization covers a wide variety of techniques and properties. When discussing in situ characterization, it has to be considered that measurements are obtained as a function of either high temperature, variable pO_2, or electrical load, or indeed a combination of each of these. Many in situ studies focus on the structural characterization of individual materials, while further studies map the temperature distribution over a single fuel cell. In this section, the current status of in situ characterization of fuel cells and fuel cell materials are considered using a variety of techniques including diffraction and spectroscopy and some of the challenges are detailed that remain in fully understanding all of the processes; mechanical, structural, and electrochemical, that govern fuel-cell performance and durability.

In Situ Materials Characterization

In considering the development of new materials for fuel cells, many authors have used diffraction techniques to probe the high-temperature stability of individual components and to investigate any potential phase-transformation problems on thermal cycling. Information that can be obtained readily can be classified as either crystallographic (phase evolution/reactivity) or mechanical (stress evolution in ceramics). Initially, users are likely to consider the use of powder x-ray diffraction to investigate all of the individual functional components, given the relative ease of access to the equipment. However, the information obtained from x-ray techniques is limited by a number of factors, including the limited resolution of instruments and the dependence of the x-ray-scattering factors on atomic number, meaning access to information from elements, such as oxygen, is limited. There are many examples of information being derived successfully from x-ray diffraction studies with perhaps the simplest examples being the study of the reactivity of functional components at operating temperatures. Zhu et al. [46], for instance, have investigated the novel cathode material $PrBaCo_2O_{5+\delta}$ in contact with $Ce_{0.8}Sm_{0.2}O_{1.9}$ as a composite, finding no discernible reaction at temperatures up to 1,100°C, over only a short period of 3 h; while Sayers et al. [47] investigated nickelate cathodes on both Ce_{1-x} Gd_xO_{2-d} (CGO) and La_{1-x} Sr_x Ga_{1-y} Mg_yO_{3-d} (LSGM) electrolytes, finding differing degrees of reaction depending upon both time and temperature. Significant reactivity was identified by these authors with CGO at temperatures greater than 800°C. It was however noted that the in situ characterization of these reactions was limited by the data collection time and instrument resolution.

In determining the residual stress of an anode-supported SOFC, Fischer et al. [48] have used x-ray

diffraction to map the stress distribution as a function of processing and also have monitored the change in the stress state at room temperature and at 800°C. However, this study is limited by the operating temperature data having to be recorded after annealing, once the sample has returned to room temperature. Evidently, in situ characterization is of considerable value, but can be limited by the capabilities of the instrumentation/technique, and for SOFCs laboratory, x-ray techniques are certainly restricted.

For either higher resolution or greater phase discrimination, there are two main alternatives to laboratory x-ray techniques: synchrotron powder diffraction or neutron diffraction. Each of these techniques has its own advantages, with neutron-powder diffraction enabling access to light elements while synchrotron-diffraction experiments offer exceptionally high-peak resolution. The use of neutron diffraction at elevated temperature has proven to be invaluable in providing information on cathode materials in particular [49–54], while synchrotron sources have been at the forefront of the development of new techniques, such as 3 dimensional imaging of components.

Neutron Scattering Studies of Fuel Cell Oxides

Neutron diffraction has long been viewed as an essential tool for the structural characterization of novel materials [55, 56]. It is only relatively recently, however, that neutron diffraction has been used to characterize fuel cell oxides. Recent developments that have attracted researchers to the technique include the production of instruments that can offer small sample sizes and high-temperature stages with variable atmosphere capabilities, extending the in situ capabilities of this technique. Some of the earliest studies of fuel cell oxides were by necessity under ambient conditions and focussed on proton-conducting barium cerates [57–59] in which a structural distortion of $BaCe_{1-x}Nd_xO_{3-\delta}$ was determined and related to the release of spontaneous strain with increasing Nd content. Since these initial works, several authors have turned to neutron diffraction to gain additional structural information. Slater et al. [60] were among the first to use this technique to characterize an electrolyte material, $La_{0.9}Sr_{0.1}Ga_{0.8}Mg_{0.2}O_{3-\delta}$. Here the authors identified a significant structural difference between the substituted material and the parent $LaGaO_3$, with the Sr- and Mg-substituted material adopting a more complex monoclinic structure at room temperature and undergoing several phase transitions on heating to 1,000°C. A tilting of GaO_6 octahedra was observed and related to the change in activation energy of conduction on heating identified from previous studies.

Use of neutron diffraction to study electrode materials in situ is a relatively recent development, with much of the current interest directed toward the phase evolution in novel cathodes with complex crystallography. Alonso [49] has provided an excellent review of the potential of neutron diffraction for characterizing fuel cell materials and detailed work on the La_2MO_{4+d} (M = Ni, Cu, Co) series of cathodes stating that the relationship between M–O distances and electrical properties can be readily determined as a function of temperature. With the $La_2MO_{4+\delta}$ materials, electrical changes occur on introduction of an A-site substituent, such as Sr, and the relationship between Sr content, apical M–O bond length, and total conductivity is resolved from this high resolution structural data. Further work by Skinner [54] focussed on the location of the oxygen interstitial, a particular strength of neutron scattering, identifying the relationship between oxygen content and phase, varying both temperature and atmosphere. Additionally, the two phase nature of the $La_2Ni_{1-x}Co_xO_{4+\delta}$ was clearly determined [61] from in situ studies where previous x-ray techniques had indicated a single phase. Information on the nature of the conduction properties of cathode materials can be inferred from the structural data obtained from these measurements, with Hou et al. [62] arguing that the nature of the Ni redox couple in $LaNi_{1-x}Mo_xO_3$ cathodes can be determined from the crystallographic data obtained. They also suggest that oxygen deficiency was observed leading to the potentially high oxide ion mobility required for a mixed conductor.

While this information on the crystal chemistry is of importance in determining the potential for new materials, it is the latest advances in data processing and interpretation that enable both structural and chemical information to be extracted from one data set. The advent of the Maximum Entropy Method (MEM) [63] for analysis of neutron-diffraction data has enabled authors to extract chemical-pathway data from the neutron density. Yashima et al. [64, 65] used

the MEM technique to visualize the diffusion pathway of the oxide ions in an anisotropic $Pr_2NiO_{4+\delta}$-based interstitial oxide ion conductor. The data obtained, Fig. 9, at temperatures of up to 812°C clearly illustrate 2-D diffusional pathways in the *ab* plane of the anisotropic crystal structure. This method has also been used to verify molecular dynamics studies of the isostructural $La_2NiO_{4+\delta}$ material [66], highlighting the benefits of combining both the experimental studies with simulation techniques.

Identification of novel conduction mechanisms is a particular strength of neutron techniques, and these studies have been extended to include the novel electrolyte apatite materials, with local defects identified [67–70]. Further electrolyte studies have included determining the total conductivity of the potential electrolyte, $La_2Mo_2O_9$, in situ through impedance spectroscopy and correlating these time-resolved data with structural transformations revealed through neutron-diffraction measurements [71, 72]. This relies upon the availability of well-designed experimental stages optimized for diffraction beamlines [71]. Engaging with central facilities to design, build, and commission this equipment is therefore essential.

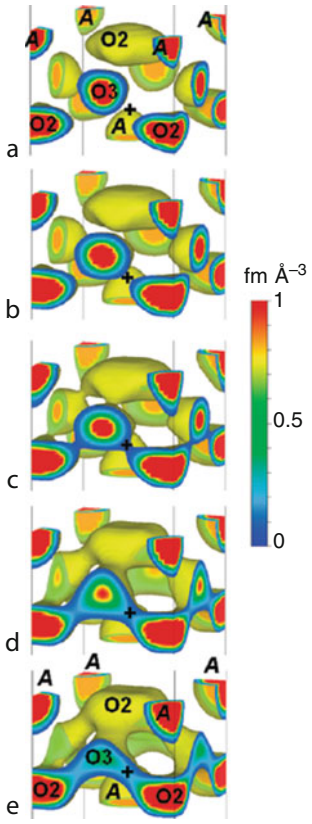

Solid Oxide Fuel Cells. Figure 9
Distribution of nuclear density as a function of temperature in $(Pr_{0.9}La_{0.1})(Ni_{0.74}Cu_{0.21}Ga_{0.05})O_{4+d}$ as determined by MEM fitting of neutron diffraction data at (**a**) 27°C, (**b**) 395°C, (**c**) 607°C, (**d**) 813°C, and (**e**) 1,016°C (Reproduced with permission from Yashima et al. JACS)

Synchrotron X-ray Studies

Synchrotron radiation is incredibly versatile allowing a wide variety of experimental techniques to be developed. Of direct interest to solid oxide fuel-cell science and technology are both diffraction and spectroscopy. Diffraction beamlines offer the potential to access complex structural information that is not revealed by competing diffraction techniques, while the spectroscopic techniques (X-ray Absorption Near Edge Spectroscopy [XANES]) and Extended X-ray Absorption Fine Structure [EXAFS]) allow users to access chemical information, such as redox kinetics. The latest developments include 3D tomography of complete cells which give unparalled information about the microstructure of composite electrodes [73, 74].

Synchrotron Diffraction In situ synchrotron x-ray-powder diffraction of fuel cell components has developed significantly over recent years as sample stages, and instrument development has enabled rapid data collection as a function of atmosphere with unprecedented resolution [75]. As the MEM technique can be applied to neutron diffraction data, so it can also be applied to synchrotron diffraction data, with Itoh et al. [76, 77] showing the complementary data obtained from combining both techniques. Through their investigation of $La_{1-x}Sr_xMnO_{3-\delta}$ (LSM)/$Ba_{1-x}Sr_xCo_{1-y}Fe_yO_3$ (BSCF) composites, they have determined both the ionic and electronic conduction pathways, with the synchrotron data highlighting isotropic Mn–O covalent bonds through which the electrons will pass, leading to good electronic conductivity.

As well as obtaining data as a function of temperature and atmosphere, Hagen et al. [78] have demonstrated that depth-resolved data acquisition from

NiO/YSZ cermets is possible. Using an advanced data collection mode employing a spiral slit and beamstop, the authors were able to follow the redox process between Ni and NiO. As the distance from the free anode surface increased, a reduction of the reaction rate was observed which is attributed to the difficulty of gas penetration to the electrode/electrolyte interface. As these data were obtained as a function of depth under redox conditions, a logical extension is to include larger operating cells in this environment to fully characterize structural/chemical changes under realistic conditions. These measurements could therefore have a dramatic impact upon cell development.

Residual stress within cells and components is evidently a key concern for developers of SOFCs [79], and analysis of this can readily be achieved using synchrotron x-ray studies. Villanova et al. [80] demonstrated the complementarity of both laboratory and synchrotron x-ray sources through their investigation of all components of the fuel cell. From lab x-ray studies they were able to determine residual stress in an anode-supported SOFC. Macroscopic stresses were determined in each layer through the analysis of lattice deformation. A significant finding of inhomogeneous stress distribution in the electrolyte led these authors to use the synchrotron technique to investigate the local stress from analysis of the stress tensor in the individual electrolyte grains.

A further study [81] examined the development of internal stress as a function of temperature for an anode-supported cell based on a Sc stabilized zirconia (ScSZ) electrolyte with a NiO-3 mol%-YSZ anode, finding that there were significant changes in the internal stress in both NiO and ScSZ that were not fully reversible, Fig. 10. Residual stress in the electrolyte was measured as a function of the reduction cycle and found to be 400 MPa in air, but decreased to 200 MPa on reduction of the NiO, and concluded that this redox cycle would be detrimental to SOFC performance.

While these studies are of importance, there are no studies of stress evolution in a complete functioning cell under electrical load, or indeed in a fuel cell stack, and this is evidently the next development step. The data obtained so far from synchrotron and laboratory x-ray studies highlight the potential of these techniques to advance the current understanding of failure mechanisms in operating SOFCs.

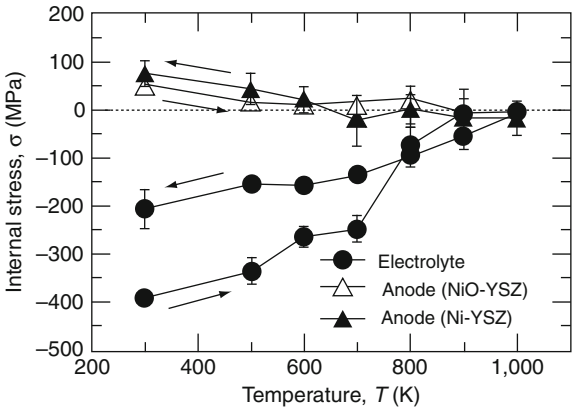

Solid Oxide Fuel Cells. Figure 10
Changes in internal stress of a Scandia stabilized zirconia electrolyte and NiO-YSZ anode as determined by in situ synchrotron measurements. (Reproduced with permissions Sumi et al. J Fuel cell Sci Tech)

Spectroscopy – XANES and EXAFS Spectroscopic techniques complement the diffraction measurements previously discussed as these target the local structure, giving details of the coordination environment surrounding particular chemical species. Thus, through control of the experimental conditions, it is feasible to extract chemical information from in situ measurements of fuel cell materials. There have been a number of initial studies of the room temperature and local structure of SOFC electrolytes, with Yamazaki et al. [82–84] considering the effect of dopants on the defect structure of $CeO_{2-\delta}$-based electrolytes. Further investigation of the Ce L_{III} edge spectra of ceria electrolytes was reported by Hormes et al. [85], who have also applied the same techniques to the cathode material $La_{1-x}Sr_xMnO_{3-\delta}$ (LSM). Each of these studies considered the bulk polycrystalline material, whereas Zhang et al. [86, 87] have used XANES to investigate the growth mechanism and crystallization of CeO_2 nanoparticles.

In considering LSM samples, significant differences in the local structure of thin film samples when compared with bulk LSM were observed [88], leading to the conclusion that the coordination environment of the Mn species is less distorted in the thin film. With the recent surge in interest in thin-film technologies for fuel cells, this may prove to be a significant finding and highlights the power of x-ray spectroscopy to

detect subtle differences that may have a dramatic impact on material performance.

The real strength of x-ray-absorption spectroscopy, however, is in extending these measurements to both time-resolved and temperature-dependent measurements. Species that are commonly found in solid oxide fuel-cell components are easily accessed as the techniques are element specific. As well as accessing element-specific information, the XANES technique is also sensitive to valence state, and hence redox processes and kinetic information can be extracted from in situ data. It is also straightforward to control the atmosphere under which the measurements are undertaken, so kinetics of both anode and cathode materials as functions of temperature, time, and pO_2 can be obtained. Indeed, this has recently been demonstrated with redox kinetics for fast oxide ion-conducting $CeNbO_{4+\delta}$ having been determined from Ce L_{III} edge XANES data [89].

3D Microtomography Perhaps one of the most exciting developments involving synchrotron radiation has been the advent of three-dimensional tomography [73, 74]. With this technique, it has been shown that detailed information about the internal structure of complex composites can be obtained, enabling researchers to gain vital information on the length of triple phase boundaries (TPB). This also allows the differentiation between active and inactive TPBs and has so far been demonstrated with anode cermets (Ni-YSZ). While not currently available as an in situ measurement, this is an obvious extension and is no doubt a future development for this technique. Currently these measurements are only available at a small number of sites worldwide, and hence this is a clear limitation. But as interest grows in this technique, it is highly likely that future developments at synchrotron sources will include this capability.

Wilson et al. [74] pioneered this technique using a Focussed Ion Beam slice and view method to allow the electrochemical performance and microstructure of materials to be quantitatively connected. In their pioneering work, a direct measurement of the TPB length was achieved through analysis of the reconstructed 3D anode, Fig. 11. From the analysis, they differentiate between interconnected and unconnected pathways, finding 63% of TPBs are interconnected. A high level

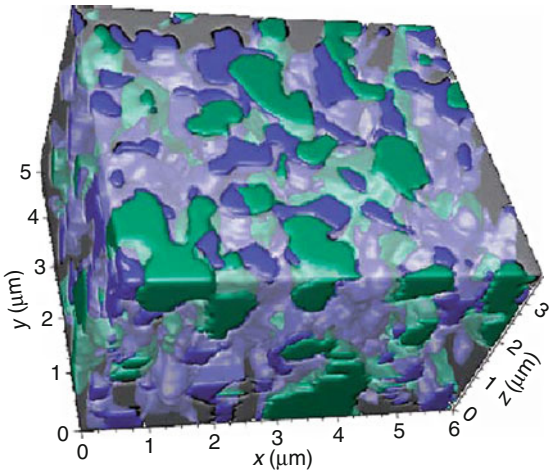

Solid Oxide Fuel Cells. Figure 11
3D reconstruction of the anode microstructure of a Ni-YSZ anode determined through the use of Focussed Ion Beam Imaging. (Reproduced with permission Wilson et al. Nat Mats)

of interconnection is required for electrochemical reactions to occur, and quantifying the microstructure in this way enables further optimization to proceed.

Shearing has adapted this process to incorporate a focussed ion beam lift-out technique, and in combination with software development, has shown that detailed phase contrast can be obtained from the Ni-YSZ couple, Fig. 12, leading to greater data quality and reduced uncertainty regarding redeposition of sputtered material. The use of this FIB tomography technique is unfortunately destructive [90], and hence the use of x-ray tomography presents an ideal opportunity to extract similar TPB information non-destructively [91]. While these data can be collected from standard x-ray systems, the use of a nano-CT system at a synchrotron source will enable higher resolutions to be achieved.

Raman Spectroscopy

Another promising in situ characterization method to have been proposed recently relies on the use of Raman spectroscopy [90, 92–94] to optically detect changes in the fuel cell under examination. Using Raman spectroscopy is entirely complementary to the previously discussed techniques and delivers data, for instance, on the heat distribution across a cell. Maher et al. [93] have

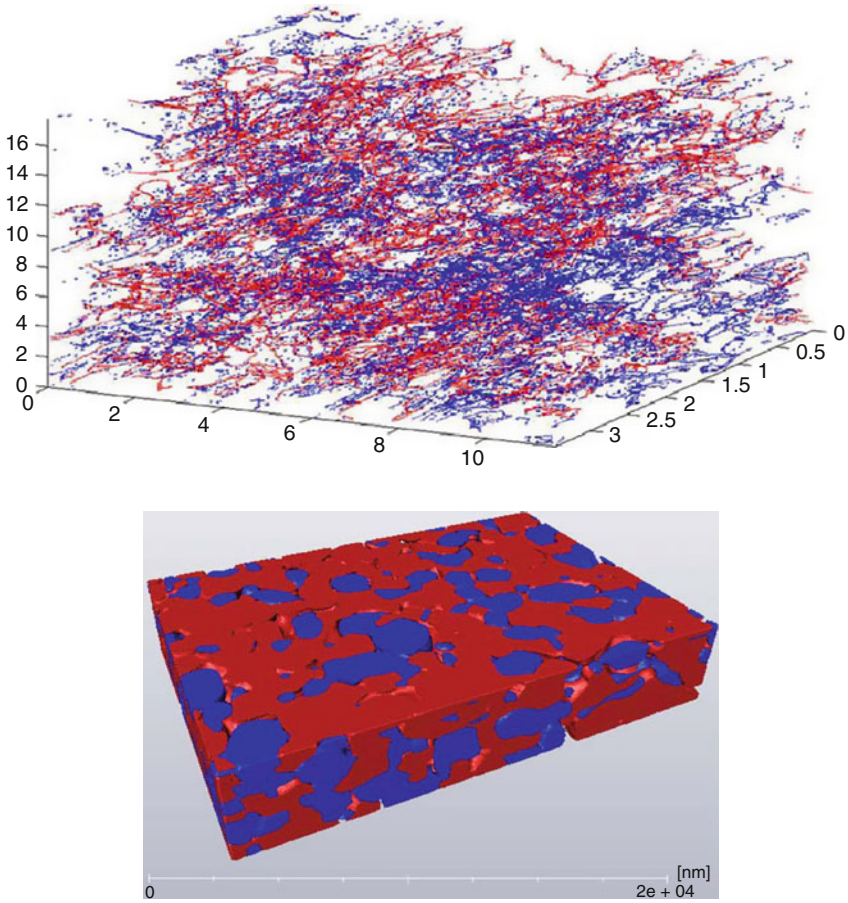

Solid Oxide Fuel Cells. Figure 12
Determination of anode microstructure and the extraction of active TPB length determined through FIB tomography. (Reproduced with permission Shearing et al. Figs. 4 and 5)

demonstrated the effective use of Raman spectroscopy with a Gd-substituted ceria in which the shift of a characteristic peak at 460 cm^{-1} can be correlated accurately with temperature and thus provides a method by which temperature distribution with high spatial resolution can be measured. Previously, the use of the Raman technique to determine the chemistry occurring at electrodes in SOFCs was highlighted [90], with particular emphasis on the monitoring of electrochemical processes at the anode. In this work, the disappearance of graphitic carbon was monitored as well as the kinetics of the Ni-NiO redox, and finally it was suggested that phonon modes of YSZ electrolytes could be correlated with lattice parameter changes, leading to a diagnostic for thermal gradients within cells. Subsequent work [95] has highlighted that oxidation processes can be monitored in situ and the effect of using carbon based fuels determined. Deposition of graphitic species (either ordered or disordered) was found to vary depending on carbon source and potential.

Summary

In situ characterization of solid oxide fuel cells can be achieved through the use of a variety of techniques to produce direct information on the chemistry, structure, and mechanical properties of the material/cell of interest. Rapid developments in test equipment offer ever greater levels of detail, with many techniques providing submicron resolution, and below, of the critical processes affecting solid oxide fuel-cell operation.

Particularly the non-destructive nature of many of these techniques allows full cycles of operation to potentially be analyzed and the causes of performance degradation to be determined.

Future Directions

Although the main aim of this article is to look at the future of the SOFC, this has been in the main a look at the near-term future and the possible designs and materials that the SOFC might move toward. The long-term future of the SOFC is much more difficult to predict because it will depend very heavily upon the diversity of renewable energy sources, what energy vectors are employed, and what fuels evolve to form the future energy mix. Most forecasters agree that the supply of usable hydrocarbons is limited and may already have peaked in the early part of the twenty-first century. The relative roles of newer fuels, such as bio-derived hydrocarbons and hydrogen in this future mix remains unclear; however, because of their high efficiency and fuel flexibility, it is likely that SOFCs will see widespread adoption and continued development in both the short- and long-term future.

Acknowledgments

The authors would like to acknowledge the support of the EPSRC through grant no. EP/F009720/1. We would also like to thank Mr Stuart Cook for the preparation of Figs. 6 and 7.

Bibliography

Primary Literature

1. Huang K, Goodenough JB (2009) Solid oxide fuel cell technology principles, performance and operations, Woodhead Energy Series. Woodhead Publishing Ltd, Cambridge, p 344
2. Singhal SC, Kendall K (2003) High-temperature solid oxide fuel cells: fundamentals, design and applications. Elsevier Advanced Technology, Oxford, p xvi, 405 p
3. Lawlor V, Griesser S, Buchinger G, Olabi AG, Cordiner S, Meissner D (2010) Review of the micro-tubular solid oxide fuel cell: Part I. Stack design issues and research activities (vol 193, pg 387, 2009). J Power Sources 195(3):936–936
4. Kendall K (2010) Progress in microtubular solid oxide fuel cells. Int J Appl Ceram Technol 7(1):1–9
5. Sammes NM, Du Y, Bove R (2005) Design and fabrication of a 100 W anode supported micro-tubular SOFC stack. J Power Sources 145(2):428–434
6. Suzuki T, Funahashi Y, Yamaguchi T, Fujishiro Y, Awano M (2008) Cube-type micro SOFC stacks using sub-millimeter tubular SOFCs. J Power Sources 183(2):544–550
7. Suzuki T, Funahashi Y, Yamaguchi T, Fujishiro Y, Awano M (2009) Performance of the micro-SOFC module using submillimeter tubular cells. J Electrochem Soc 156(3):B318–B321
8. Hibino T, Iwahara H (1993) Simplification of solid oxide fuel-cell system using partial oxidation of methane. Chem Lett 1993(7):1131–1134
9. Yano M, Tomita A, Sano M, Hibino T (2007) Recent advances in single-chamber solid oxide fuel cells: a review. Solid State Ionics 177(39–40):3351–3359
10. Riess I (2008) On the single chamber solid oxide fuel cells. J Power Sources 175(1):325–337
11. Evans A, Bieberle-Hutter A, Rupp JLM, Gauckler LJ (2009) Review on microfabricated micro-solid oxide fuel cell membranes. J Power Sources 194(1):119–129
12. Su PC, Chao CC, Shim JH, Fasching R, Prinz FB (2008) Solid oxide fuel cell with corrugated thin film electrolyte. Nano Lett 8(8):2289–2292
13. Thorel AS, Chesnaud A, Viviani M, Barbucci A, Presto S, Piccardo P, Ilhan Z, Vladikova D, Stoynov Z (2009) IDEAL-cell, a high temperature innovative dual membrane fuel cell. ECS Trans 25(2):753–762
14. Kilner JA (2000) Fast oxygen transport in acceptor doped oxides. Solid State Ionics 129(1):13–23
15. Merkle R, Maier J, Bouwmeester HJM (2004) A linear free energy relationship for gas-solid interactions: correlation between surface rate constant and diffusion coefficient of oxygen tracer exchange for electron-rich perovskites. Angew Chem Int Ed 43(38):5069–5073
16. Tietz F, Mai A, Stover D (2008) From powder properties to fuel cell performance – a holistic approach for SOFC cathode development. Solid State Ionics 179(27–32):1509–1515
17. Kilner JA (2007) Optimisation of oxygen ion transport in materials for ceramic membrane devices. Faraday Discuss 134:9–15
18. Garcia-Barriocanal J, Rivera-Calzada A, Varela M, Sefrioui Z, Iborra E, Leon C, Pennycook SJ, Santamaria J (2008) Colossal ionic conductivity at interfaces of epitaxial ZrO_2:Y_2O_3/$SrTiO_3$ heterostructures. Science 321(5889):676–680
19. Georges S, Goutenoire F, Altorfer F, Sheptyakov D, Fauth F, Suard E, Lacorre P (2003) Thermal, structural and transport properties of the fast oxide-ion conductors $La_{2-x}R_xMo_2O_9$ (R=Nd, Gd, Y). Solid State Ionics 161(3–4):231–241
20. Kendrick E, Knight KS, Slater PR (2009) Ambi-site substitution of Mn in lanthanum germanate apatites. Mater Res Bull 44(8):1806–1809
21. Lacorre P, Goutenoire F, Bohnke O, Retoux R, Laligant Y (2000) Designing fast oxide-ion conductors based on $La_2Mo_2O_9$. Nature 404(6780):856–858
22. Li Q, Xia T, Liu XD, Ma XF, Meng J, Cao XQ (2007) Fast densification and electrical conductivity of yttria-stabilized zirconia nanoceramics. Mater Sci Eng B 138(1):78–83
23. Thangadurai V, Weppner W (2005) Studies on electrical properties of $La_{0.8}Sr_{0.2}Ga_{0.8}Mg_{0.2}O_{2.80}$ (LSGM) and LSGM-$SrSn_{1-x}Fe_xO_3$

(x=0.8; 0.9) composites and their chemical reactivity. Electrochim Acta 50(9):1871–1877
24. Tsai D-S, Hsieh M-J, Tseng J-C, Lee H-Y (2005) Ionic conductivities and phase transitions of lanthanide rare-earth substituted $La_2Mo_2O_9$. J Eur Ceram Soc 25(4):481–487
25. Vannier RN, Skinner SJ, Chater RJ, Kilner JA, Mairesse G (2003) Oxygen transfer in BIMEVOX materials. Solid State Ionics 160(1–2):85–92
26. Verkerk MJ, Keizer K, Burggraaf AJ (1980) High oxygen ion conduction in sintered oxides of the Bi_2O_3-Er_2O_3 system. J Appl Electrochem 10(1):81–90
27. Kosacki I, Rouleau CM, Becher PF, Bentley J, Lowndes DH (2005) Nanoscale effects on the ionic conductivity in highly textured YSZ thin films. Solid State Ionics 176(13–14):1319–1326
28. Karthikeyan A, Chang CL, Ramanathan S (2006) High temperature conductivity studies on nanoscale yttria-doped zirconia thin films and size effects. Appl Phys Lett 89(18):183116
29. Azad S, Marina OA, Wang CM, Saraf L, Shutthanandan V, McCready DE, El-Azab A, Jaffe JE, Engelhard MH, Peden CHF, Thevuthasan S (2005) Nanoscale effects on ion conductance of layer-by-layer structures of gadolinia-doped ceria and zirconia. Appl Phys Lett 86(13):131906
30. Korte C, Peters A, Janek J, Hesse D, Zakharov N (2008) Ionic conductivity and activation energy for oxygen ion transport in superlattices – the semicoherent multilayer system YSZ (ZrO_2+9.5 mol% Y_2O_3)/Y_2O_3. Phys Chem Chem Phys 10(31): 4623–4635
31. Guo X (2009) Comment on "Colossal ionic conductivity at interfaces of epitaxial ZrO_2:Y_2O_3/$SrTiO_3$ heterostructures". Science 324(5926):465
32. Cavallaro A, Burriel M, Roqueta J, Apostolidis A, Bernardi A, Tarancón A, Srinivasan R, Cook SN, Fraser HL, Kilner JA, McComb DW, Santiso J (2010) Electronic nature of the enhanced conductivity in YSZ-STO multilayers deposited by PLD. Solid State Ionics 181(13–14):592–601
33. Kilner JA (2008) Ionic conductors feel the strain. Nat Mater 7(11):838–839
34. Pennycook TJ, Beck MJ, Varga K, Varela M, Pennycook SJ, Pantelides ST (2010) Origin of colossal ionic conductivity in oxide multilayers: interface induced sublattice disorder. Phys Rev Lett 104(11):115901
35. Kushima A, Yildiz B (2010) Oxygen ion diffusivity in strained yttria stabilized zirconia: where is the fastest strain? J Mater Chem 20(23):4809–4819
36. Schichtel N, Korte C, Hesse D, Janek J (2009) Elastic strain at interfaces and its influence on ionic conductivity in nanoscaled solid electrolyte thin films-theoretical considerations and experimental studies. Phys Chem Chem Phys 11(17):3043–3048
37. Peters A, Korte C, Hesse D, Zakharov N, Janek J (2007) Ionic conductivity and activation energy for oxygen ion transport in superlattices – the multilayer system CSZ (ZrO_2+CaO)/Al_2O_3. Solid State Ionics 178(1–2):67–76
38. Korte C, Schichtel N, Hesse D, Janek J (2009) Influence of interface structure on mass transport in phase boundaries between different ionic materials experimental studies and formal considerations. Monatshefte Fur Chemie 140(9): 1069–1080
39. Otsuka K, Matsunaga K, Nakamura A, Ji S, Kuwabara A, Yamamoto T, Ikuhara Y (2004) Effects of dislocations on the oxygen ionic conduction in yttria stabilized zirconia. Mater Trans 45(7):2042–2047
40. Otsuka K, Kuwabara A, Nakamura A, Yamamoto T, Matsunaga K, Ikuhara Y (2003) Dislocation-enhanced ionic conductivity of yttria-stabilized zirconia. Appl Phys Lett 82(6):877–879
41. Sase M, Yashiro K, Sato K, Mizusaki J, Kawada T, Sakai N, Yamaji K, Horita T, Yokokawa H (2008) Enhancement of oxygen exchange at the hetero interface of (La, Sr)CoO_3/(La, Sr)$_2CoO_4$ in composite ceramics. Solid State Ionics 178(35–36):1843–1852
42. Ullmann H, Trofimenko N, Tietz F, Stover D, Ahmad-Khanlou A (2000) Correlation between thermal expansion and oxide ion transport in mixed conducting perovskite-type oxides for SOFC cathodes. Solid State Ionics 138(1–2):79–90
43. Tarancon M, Burriel M, Santiso J, Skinner SJ, Kilner JA (2010) Advances in layered oxide cathodes for intermediate temperature solid oxide fuel cells. J Mater Chem 20:3799–3813
44. Kilner JA (2009) Accelerated R&D of solid oxide fuel cells with lowering operation temperature vision. Electrochemistry 77(2):113–113
45. Rossiny JCH, Julis J, Fearn S, Kilner JA, Zhang Y, Chen LF, Yang SF, Evans JRG (2008) Combinatorial characterisation of mixed conducting perovskites. Solid State Ionics 179(21–26): 1085–1089
46. Zhu CJ, Liu XM, Yi CS, Pei L, Wang DJ, Yan DT, Yao KG, Lu TQ, Su WH (2010) High-performance $PrBaCo_2O_5$+delta-$Ce_{0.8}Sm_{0.2}O_{1.9}$ composite cathodes for intermediate temperature solid oxide fuel cell. J Power Sources 195(11):3504–3507
47. Sayers R, Liu J, Rustumji B, Skinner SJ (2008) Novel K_2NiF_4-type materials for solid oxide fuel cells: compatibility with electrolytes in the intermediate temperature range. Fuel Cells 8(5):338–343
48. Fischer W, Malzbender J, Blass G, Steinbrech RW (2005) Residual stresses in planar solid oxide fuel cells. J Power Sources 150:73–77
49. Alonso JA, Martinez-Lope MJ, Aguadero A, Daza L (2008) Neutron powder diffraction as a characterization tool of solid oxide fuel cell materials. Prog Solid State Chem 36(1–2): 134–150
50. Aguadero A, Alonso JA, Daza L (2008) Oxygen excess in La2CoO_4+delta: A neutron diffraction study. Z Naturfsch Sect B J Chem Sci 63(6):615–622
51. Aguadero A, Alonso JA, Fernandez-Diaz MT, Escudero MJ, Daza L (2007) In situ high temperature neutron powder diffraction study of $La_2Ni_{0.6}Cu_{0.4}O_4$+delta in air: correlation with the electrical behaviour. J Power Sources 169(1):17–24
52. Aguadero A, Perez M, Alonso JA, Daza L (2005) Neutron powder diffraction study of the influence of high oxygen pressure treatments on La_2NiO_4+delta and structural analysis of $La_2Ni_{1-x}Cu_xO_4$+delta (0 <= x <= 1). J Power Sources 151:52–56

53. Bartolome JF, Bruno G, Deaza AH (2008) Neutron diffraction residual stress analysis of zirconia toughened alumina (ZTA) composites. J Eur Ceram Soc 28(9):1809–1814
54. Skinner SJ (2003) Characterisation of La_2NiO_4+delta using in situ high temperature neutron powder diffraction. Solid State Sci 5(3):419–426
55. Goodenough JB (2004) Electronic and ionic transport properties and other physical aspects of perovskites. Rep Prog Phys 67(11):1915–1993
56. Goodenough JB (2003) Oxide-ion electrolytes. Annu Rev Mater Res 33:91–128
57. Knight KS, Soar M, Bonanos N (1992) Crystal-structures of gadolinium-doped and yttrium-doped barium cerate. J Mater Chem 2(7):709–712
58. Knight KS, Bonanos N (1995) A high-resolution neutron powder diffraction study of neodymium doping in barium cerate. Solid State Ionics 77:189–194
59. Jacobson AJ, Tofield BC, Fender BEF (1972) Structures of $BaCeO_3$, $BaPrO_3$ and $BaTbO_3$ by neutron-diffraction – lattice-parameter relations and ionic radii in O-perovskites. Acta Crystallogr Sect B Struct Crystallogr Crystal Chem B 28(Mar 15):956–961
60. Slater PR, Irvine JTS, Ishihara T, Takita Y (1998) High-temperature powder neutron diffraction study of the oxide ion conductor $La_{0.9}Sr_{0.1}Ga_{0.8}Mg_{0.2}O_{2.85}$. J Solid State Chem 139(1):135–143
61. Skinner SJ, Amow G (2007) Structural observations on La-2(Ni, CO)O-4 +/-delta phases determined from in situ neutron powder diffraction. J Solid State Chem 180(7): 1977–1983
62. Hou SE, Alonso JA, Rajasekhara S, Martinez-Lope MJ, Fernandez-Diaz MT, Goodenough JB (2010) Defective Ni perovskites as cathode materials in intermediate-temperature solid-oxide fuel cells: a structure-properties correlation. Chem Mater 22(3):1071–1079
63. Sakata M, Mori R, Kumazawa S, Takata M, Toraya H (1990) Electron-density distribution from x-ray-powder data by use of profile fits and the maximum-entropy method. J Appl Crystallogr 23:526–534
64. Yashima M, Sirikanda N, Ishihara T (2010) Crystal structure, diffusion path, and oxygen permeability of a Pr_2NiO_4-based mixed conductor $(Pr_{0.9}La_{0.1})(2)(Ni_{0.74}Cu_{0.21}Ga_{0.05})O_4$+delta. J Am Chem Soc 132(7):2385–2392
65. Yashima M, Enoki M, Wakita T, Ali R, Matsushita Y, Izumi F, Ishihara T (2008) Structural disorder and diffusional pathway of oxide ions in a doped Pr_2NiO_4-based mixed conductor. J Am Chem Soc 130(9):2762
66. Chroneos A, Parfitt D, Kilner JA, Grimes RW (2010) Anisotropic oxygen diffusion in tetragonal La_2NiO_4+delta: molecular dynamics calculations. J Mater Chem 20(2):266–270
67. Guillot S, Beaudet-Savignat S, Lambert S, Vannier RN, Rousse P, Porcher F (2009) Evidence of local defects in the oxygen excess apatite La-9.67(SiO4)(6)O-2.5 from high resolution neutron powder diffraction. J Solid State Chem 182(12): 3358–3364
68. Leon-Reina L, Porras-Vazquez JM, Losilla ER, Aranda MAG (2006) Interstitial oxide positions in oxygen-excess oxyapatites. Solid State Ionics 177(15–16):1307–1315
69. Leon-Reina L, Losilla ER, Martinez-Lara M, Bruque S, Llobet A, Sheptyakov DV, Aranda MAG (2005) Interstitial oxygen in oxygen-stoichiometric apatites. J Mater Chem 15(25): 2489–2498
70. Leon-Reina L, Losilla ER, Martinez-Lara M, Bruque S, Aranda MAG (2004) Interstitial oxygen conduction in lanthanum oxyapatite electrolytes. J Mater Chem 14(7):1142–1149
71. Engin TE, Powell AV, Haynes R, Chowdhury MAH, Goodway CM, Done R, Kirichek O, Hull S (2008) A high temperature cell for simultaneous electrical resistance and neutron diffraction measurements. Rev Sci Instrum 79(9):095104
72. Liu J (2010) Department of Materials. Imperial College London, London
73. Shearing PR, Golbert J, Chater RJ, Brandon NP (2009) 3D reconstruction of SOFC anodes using a focused ion beam lift-out technique. Chem Eng Sci 64(17):3928–3933
74. Wilson JR, Kobsiriphat W, Mendoza R, Chen HY, Hiller JM, Miller DJ, Thornton K, Voorhees PW, Adler SB, Barnett SA (2006) Three-dimensional reconstruction of a solid-oxide fuel-cell anode. Nat Mater 5(7):541–544
75. Thompson SP, Parker JE, Potter J, Hill TP, Birt A, Cobb TM, Yuan F, Tang CC (2009) Beamline I11 at diamond: a new instrument for high resolution powder diffraction. Rev Sci Instrum 80(7):075107
76. Itoh T, Shirasaki S, Fujie Y, Kitamura N, Idemoto Y, Osaka K, Ofuchi H, Hirayama S, Honma T, Hirosawa I (2010) Study of charge density and crystal structure of $(La_{0.75}Sr_{0.25})MnO_{3.00}$ and $(Ba_{0.5}Sr_{0.5})(Co_{0.8}Fe_{0.2})O_{2.33}$-delta at 500–900 K by in situ synchrotron x-ray diffraction. J Alloy Comp 491(1–2): 527–535
77. Itoh T, Shirasaki S, Fujie Y, Kitamura N, Idemoto Y, Osaka K, Hirosawa I, Igawa N (2009) Study of Mechanism of Mixed Conduction Due to Electrons and Oxygen Ions in $(La_{0.75}Sr_{0.25})MnO_{3.00}$ and $(Ba_{0.5}Sr_{0.5})(Co_{0.8}Fe_{0.2})O$-2.33 through Rietveld Refinement and MEM Analysis. Electrochemistry 77(2):161–168
78. Hagen A, Poulsen HF, Klemenso T, Martins RV, Honkimaki V, Buslaps T, Feidenshans'l R (2006) A depth-resolved in situ study of the reduction and oxidation of Ni-based anodes in solid oxide fuel cells. Fuel Cells 6(5):361–366
79. Atkinson A, Sun B (2007) Residual stress and thermal cycling of planar solid oxide fuel cells. Mater Sci Technol 23(10): 1135–1143
80. Villanova J, Sicardy O, Fortunier R, Micha JS, Bleuet P (2010) Determination of global and local residual stresses in SOFC by X-ray diffraction. Nucl Instrum Methods Phys Res Sect B 268(3–4):282–286
81. Sumi H, Ukai K, Yokoyama M, Mizutani Y, Doi Y, Machiya S, Akiniwa Y, Tanaka K (2006) Changes of internal stress in solid-oxide fuel cell during red-ox cycle evaluated by in situ measurement with synchrotron radiation. J Fuel Cell Sci Technol 3(1):68–74

82. Yamazaki S, Matsui T, Sato T, Arita Y, Nagasaki T (2002) EXAFS study of reduced ceria doped with lanthanide oxides. Solid State Ionics 154:113–118
83. Yamazaki S, Matsui T, Ohashi T, Arita Y (2000) Defect structures in doped CeO_2 studied by using XAFS spectrometry. Solid State Ionics 136:913–920
84. Ohashi T, Yamazaki S, Tokunaga T, Arita Y, Matsui T, Harami T, Kobayashi K (1998) EXAFS study of $Ce_{1-x}Gd_xO_{2-x/2}$. Solid State Ionics 113:559–564
85. Hormes J, Pantelouris M, Balazs GB, Rambabu B (2000) X-ray absorption near edge structure (XANES) measurements of ceria-based solid electrolytes. Solid State Ionics 136:945–954
86. Zhang J, Wu ZY, Liu T, Hu TD, Wu ZH, Ju X (2001) XANES study on the valence transitions in cerium oxide nanoparticles. J Synchrotron Radiat 8:531–532
87. Zhang J, Wu ZY, Rong LX, Dong BZ (2005) Temperature dependence of the growth of cerium oxide nanoparticles investigated by SAXS and XANES. Phys Scr T115:661–663
88. Gnanasekar KI, Jiang X, Jiang JC, Aghasyan M, Tiltsworth R, Hormes J, Rambabu B (2002) Nanocrystalline bulk and thin films of $La_{1-x}SrMnO_3$ (0 <= x <= 0.3). Solid State Ionics 148(3–4):575–581
89. Skinner SJ, Packer RJ, Bayliss RD, Illy B, Prestipino C, Ryan MP (in press) Redox chemistry of the novel fast oxide ion conductor $CeNbO_4$+d determined through an in situ spectroscopic technique. Solid State Ionics. doi:10.1016/j.ssi.2009.12.008
90. Pomfret MB, Owrutsky JC, Walker RA (2006) High-temperature Raman spectroscopy of solid oxide fuel cell materials and processes. J Phys Chem B 110(35):17305–17308
91. Izzo JR, Joshi AS, Grew KN, Chiu WKS, Tkachuk A, Wang SH, Yun WB (2008) Nondestructive reconstruction and analysis of SOFC anodes using x-ray computed tomography at sub-50 nm resolution. J Electrochem Soc 155(5):B504–B508
92. Malzbender J, Steinbrech RW, Singheiser L (2009) A review of advanced techniques for characterising SOFC behaviour. Fuel Cells 9(6):785–793
93. Maher RC, Cohen LF (2008) Raman spectroscopy as a probe of temperature and oxidation state for gadolinium-doped ceria used in solid oxide fuel cells. J Phys Chem A 112(7):1497–1501
94. Charrier-Cougoulic I, Pagnier T, Lucazeau G (1999) Raman spectroscopy of perovskite-type $BaCe_xZr_{1-x}O_3$(0 <= x <= 1). J Solid State Chem 142(1):220–227
95. Pomfret MB, Owrutsky JC, Walker RA (2007) In situ studies of fuel oxidation in solid oxide fuel cells. Anal Chem 79(6): 2367–2372

Books and Reviews

Gellings PJ, Bouwmeester HJM (1997) The CRC handbook of solid state electrochemistry. CRC Press, Boca Raton, p 630

Kisi EH, Howard CJ (2008) Applications of neutron powder diffraction, vol 15, Oxford series on neutron scattering in condensed matter. Oxford University Press, Oxford/New York, p xvii, p 486

Larminie J, Dicks A (2003) Fuel cell systems explained, 2nd edn. Wiley, Chichester, West Sussex, p xxii, p 406

Maier J (2004) Physical chemistry of ionic materials: ions and electrons in solids. Wiley, Chichester/Hoboken, p 537

Rand DAJ, Dell R (2008) Hydrogen energy: challenges and prospects, RSC energy series. RSC Pub, Cambridge, p xxxviii, p 300

Will G (2006) Powder diffraction: the Rietveld method and the two-stage method to determine and refine crystal structures from powder diffraction data. Springer, Berlin/New York, p ix, p 224

Solid Oxide Fuel Cells, Marketing Issues

John Bøgild Hansen[1], Niels Christiansen[2]
[1]Haldor Topsøe A/S, Lyngby, Denmark
[2]Topsoe Fuel Cell A/S, Lyngby, Denmark

Article Outline

Glossary
Definition of the Subject
Introduction
The Global Energy Challenge
Briefly on the SOFC Technology
Markets
Major SOFC Players
Steps in Commercialization
Competitiveness
Summing Up
Future Directions
Conclusions
Bibliography

Glossary

APU Auxiliary power unit – device providing power in addition to main power train.

DG Distributed generation. Combined heat and power plant with typical capacities from 50 kW to several MW.

micro-CHP Micro-combined heat and power. Capacities up to say 10-kW.

SOEC Solid oxide electrolyzer cell.

SOFC Solid oxide fuel cell.

Definition of the Subject

Clean and sufficient energy is an important precondition for the continued growth in global wealth. Solutions must be found to utilize the remaining fossil fuels more efficiently and also to ensure that new environmentally friendly fuels can secure power production in the post-fossil fuel era. This is the essence of the global energy challenge.

Fuel cells hold the promise of an efficient, low-pollution technology for production of electricity. Because fuel cells rely on electrochemical rather than thermo-mechanical processes in the conversion of fuel into electricity, the fuel cell is not limited by the Carnot efficiency as is the case for conventional generators. High-temperature fuel cells hold the promise of an efficient, low-pollution technology for production of electricity and efficient use of waste heat including low transmission losses. Scalability, decentralization, and load following capabilities are major advantages that can play an effective role in future power grids and power supply.

Solid oxide fuel cells offer the potential of high volumetric power density, cost-efficiency, and fuel flexibility, and significant progress has been made during the last 5 years in bringing SOFC technology closer to commercialization.

This entry will endeavor to answer the question whether SOFC technology is now ready for the market or perhaps put in another way: Is the market ready for SOFC technology and which challenges still need to be addressed?

Introduction

The entry will describe how SOFC technology can contribute to solving the energy challenges in the future. The current status of the SOFC technology and industry will be briefly discussed and the possible markets described. Three main challenges on the road to competiveness – lifetime, reliability, and cost – are addressed. Techno-economic studies of the different market segments are used to define the threshold for market entry. The entry ends by looking ahead and concluding that the SOFC technology is ready for the market with respect to the projected cost and lifetimes, but that reliability under real-life conditions still remains to be demonstrated. The learning investments needed, however, do not appear to be prohibitive considering the benefits which this game-changing technology has to offer.

The Global Energy Challenge

Increasing Power Demand

The increasing global demand for energy and power mainly comes from the growth in industrialization, population, and living standards.

Forecasts from International Energy Agency (IEA – all forecasts in the following comes from the publication World Energy Outlook 2010 [1]) show that the population will grow from 6.7 billion in 2008 to 8.5 billion in 2035. Almost all of the increase will take place in the non-OECD area.

On a global scale, the demand for primary energy is expected to increase by 1.2% per year until 2035. More than one third of the total primary energy consumed is used for power generation (Table 1).

The rapid population growth in the non-OECD area is further followed by a sharp increase in urbanization, which will have a significant impact on the demand for power coming from industrialization and improvements in housing and level of welfare. The demand for electricity generation will therefore increase accordingly and at an even higher rate than the energy demand. Total electricity consumption is expected to increase by 2.5% per year until 2035 (Table 2).

The growth in primary energy demand together with the decreasing accessibility of fossil fuels is expected to result in increasing energy prices. This makes efficiency in power production an important issue. Technologies with higher efficiency will be in demand.

In 2035, a very large number of people will not have access to power in the quantities known to us in the

Solid Oxide Fuel Cells, Marketing Issues. Table 1 World primary energy demand

	1980	2008	2020 F	2035 F	Annual growth rate 2008–2035
Energy demand (Mtoe)	7,229	12,271	14,556	16,748	1.2%

Solid Oxide Fuel Cells, Marketing Issues. Table 2 World electricity consumption

TWh	1980	2008	2020F	2035F	Annual growth rate 2008–2035
OECD	4,739	8,244	10,339	11,566	1.0%
Non-OECD	971	7,575	12,841	18,763	3.8%
Total, world	**5,711**	**16,819**	**23,180**	**30,329**	2.5%

Solid Oxide Fuel Cells, Marketing Issues. Table 3 Projected capacity additions and investment in power infrastructure 2008–2035

	Capacity addition (GW)	Investments, new plants (billion US dollars)
OECD	1,985	3,992
Non-OECD	3,688	5,642
Total, world	**5,673**	**9,634**

OECD area today, despite the rapid growth and urbanization within the non-OECD area. Although the total power consumption is expected to double from 2008 to 2035, 38% of the world's power consumption will still be in the OECD area, having only 15% of the world population. While the per capita electricity consumption in the non-OECD countries will be doubled by 2035 to 2,600 kWh/year, it will at that time only be around one fourth of the level of the OECD area.

Significant Structural Investments Needed

In order to meet this high level of consumption, significant investments in energy production and power generation will be needed. The figure below shows the expected growth and the expected investments in power generation capacity (Table 3).

The majority of investments will take place in the non-OECD area. The total growth in capacity, including replacement and expansion, will be about 5,700 GW or almost 10 trillion US dollars over the forecasted period. This corresponds to 220-GW new capacity or investments in new plants of 370 billion US dollars per year.

The total investment in new power generation capacity constitutes more than half of the total world energy investments. This means that in future, a high dependency on the power grids remains, and the cost of improving poor grids and in establishing new grids where these do not yet exist will be significant.

Despite the expected high level of investments, the power grid and other power infrastructure will impose a limitation on the capacity and efficiency of the present infrastructure. This will be a driver toward a more decentralized power production with production taking place closer to the end user and with combined production of heat and power.

The transmission losses throughout the grid existing today will also exist in future. On a global average, the energy content of the primary fuel that is actually converted into consumed power will not exceed 35%.

Renewable-Based Power Production Increase

The increasing scarcity of oil and other fossil fuels makes the exploration efforts more expensive and the transport routes to the consumers longer. This will concentrate the remaining reserves to a limited number of countries. This is a growing concern to the net-importing Western world.

Power generation based on renewables is expected to increase over the forecasted period due to higher fossil fuel prices, growing concerns over pollution and greenhouse gas emissions, and declining technology costs and government support. Renewable electricity generation is expected to grow globally and will in the OECD area constitute 26% of the total power generation in 2035, and in the non-OECD area 22% (Table 4).

The rising share of wind and solar power (PV) poses a challenge of integration into the power grid and a challenge of how to match power production with power demand in due time. Power production from wind and PV fluctuates according to the prevailing conditions with regard to weather, season, and time of the day. Problems due to variability affecting the reliability of a power production system are manageable when the shares of wind and other variable renewable capacity are small, but with a larger share of power from renewables, such problems will increase.

This makes it necessary to balance the growth in renewables in the overall production system with

Solid Oxide Fuel Cells, Marketing Issues. Table 4 Fuel sources of power generation

TWh	1990	2008	2020F	2035F	Annual growth rate 2008–2035
Coal	4,427	8,273	10,630	11,241	1.1%
Oil	1,338	1,104	689	480	−3.0%
Gas	1,726	4,303	5,881	7,557	2.1%
Nuclear	2,013	2,731	3,712	4,883	2.2%
Hydro	2,145	3,208	4,367	5,533	2.0%
Biomass	131	267	547	1,476	6.5%
Wind	4	219	1,229	2,851	10.0%
Others	38	79	319	1,314	11.0%
Total generation	**11,821**	**20,183**	**27,373**	**35,336**	2.1%

smaller, scalable units capable of equalizing the fluctuations created by solar cells and wind turbines.

Restrictions on Pollution and Emissions Still Tighter

The extensive use of fossil fuel globally will continue to drive up power-generation-related CO_2 emissions, from 11.9 Gt in 2008 to 14 Gt in 2035 in the base scenario. Nearly all the increase in power-related CO_2 emissions is expected to come from non-OECD countries, where urbanization and higher living standards – together with rising reliance on fossil fuels – are particularly pronounced. The non-OECD area is projected to increase its power-related CO_2 emission by more than 50% by 2035, corresponding to 76% of the total amount.

Continuously, stricter legislation on emissions and pollution is introduced in most countries. This will be supported by incentive schemes given to energy technologies that have inherently lower emissions.

This is already the case in Europe and the USA. The high-growth countries in the Far East and South America have less focus on climate end environment at present. But along with their development, an increasing awareness of the environmental issues is expected to emerge. This will be followed by willingness and ability to pay for advanced, cleaner energy technologies.

Global Challenges

All in all, the situation can be summarized in the headlines below. The world urgently needs new technologies that can help solve the challenges of access to clean and sufficient energy (Table 5).

Fuel cells are one of the most promising technologies capable of delivering solutions to the world's energy challenges.

Briefly on the SOFC Technology

A fuel cell system produces electricity from a cleaner and more efficient fuel than conventional technologies. The fuel can be natural gas, diesel, biogas, hydrogen, or similar. Like batteries, a fuel cell generates power by an electrochemical process.

In physical terms, an SOFC fuel cell is a very thin, planar "sheet" of flexible, ceramic material consisting of three functional layers – the anode, the cathode, and the electrolyte (Figs. 1 and 2).

Fuel is supplied and passes over the anode side, and air passes over the cathode. The electrolyte – a thin, gas-tight, ion-conducting layer – is placed between the anode and the cathode.

An external circuit connects the anode to the cathode and provides the mechanism to power electrical devices (Fig. 3).

A single fuel cell can create a voltage of approximately 0.7–0.9 V.

The current state-of-the-art SOFC anode-supported cells based on doped zircona ceramic electrolytes, ceramic LSM cathodes, and Ni/YSZ cermet anodes are operated in the temperature range 700–800°C with a cell area specific resistance (ASR) of about 0.5 Ω/cm^2 at 750°C. Using the more active ceramic lanthanum

Solid Oxide Fuel Cells, Marketing Issues. Table 5 Global challenges in the energy complex

GLOBAL CHALLENGES *urge decision makers to set*	TARGETS *which will need radical*	SOLUTIONS
– Global growth in future power demand – Global warming increasing – Risk linked to accessibility and location of fossil fuels – Energy security and dependency – Balance problems in supply due to increasing renewable share – Increasing energy prices – Limited capacity and potential expansion in existing grid	– Significantly increase power output per volume of fuel input through higher efficiency – Reduce CO_2 – and other emissions – by higher efficiency and by use of emission neutral renewable fuels – Provide sufficient power for everybody everywhere	– Raising electrical efficiency – Reduction in CO_2 by change in fuels and power generation technologies – Decentralisation and scalability of power supply – Fuel flexibility and increased use of renewable fuels – Heat and power coproduction – Energy storage technology

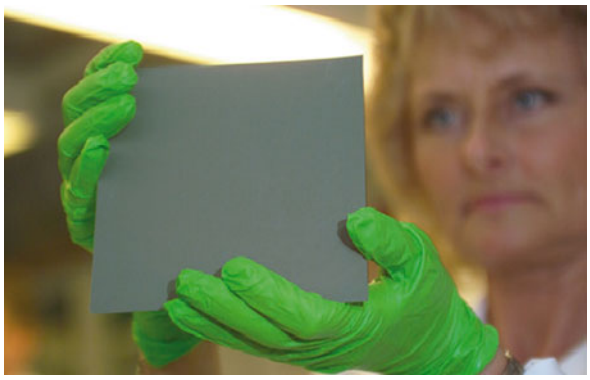

Solid Oxide Fuel Cells, Marketing Issues. Figure 1 Electrolyte/electrode assembly

strontium cobalt ferrite (LSFC)-based cathodes, the ASR is decreased to about 0.25 Ω/cm^2 at this temperature, which is a more favorable value regarding overall stack power density and cost-effectiveness.

Fuel Cell Stack, Stack Modules, and PowerCore

Single cells are combined in a stack to generate power in useful quantities.

Solid Oxide Fuel Cells, Marketing Issues. Figure 2 Highly flexible material

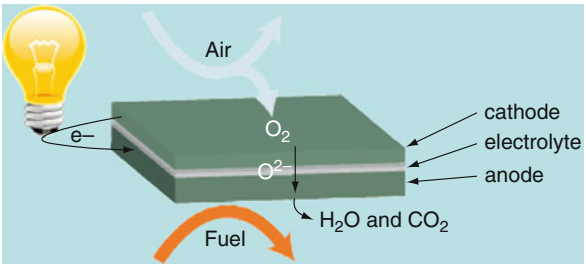

Solid Oxide Fuel Cells, Marketing Issues. Figure 3
The electrochemical process of a fuel cell

A stack is a multilayer construction of fuel cells separated by metal sheets (the "interconnect plate") guiding the flow of air and fuel to the individual cells. The number of repeated cell/interconnect plates determines the stack capacity. The stack is the heart of a fuel cell system (Figs. 4 and 5).

With the current technology, a stack can generate up to about 3 kW of power. For larger power levels, stacks are combined into stack modules, which in turn also can be combined, thus providing for power output, in principle, approaching indefinite sizes.

In addition to a stack or stack module, a fuel cell system comprises components for handling of fuel, heat, electric power conditioning, and other components required for the operation.

The fuel cell process on which Topsoe Fuel Cell's technology is based (SOFC) takes place at temperatures of 700–900°C. The parts of the system operating above 300°C are integrated into a module called a PowerCore™. The PowerCore is a highly integrated "black box" with defined operating responsibility suitable for installation into complete systems (Fig. 6).

Comparing Fuel Cells to Conventional Technologies

A conventional combustion engine converts the energy stored in the fuel to electricity through a combustion, which in turn drives a generator that produces electricity. In contrast, a fuel cell converts the same initial energy into electricity via a direct electrochemical path.

This direct conversion of energy to electrical power means that fuel cells have higher energy efficiency, and at the same time, lower emissions of CO_2, VOC, and NO_X than the dominating power generation technologies based on combustion. This makes fuel

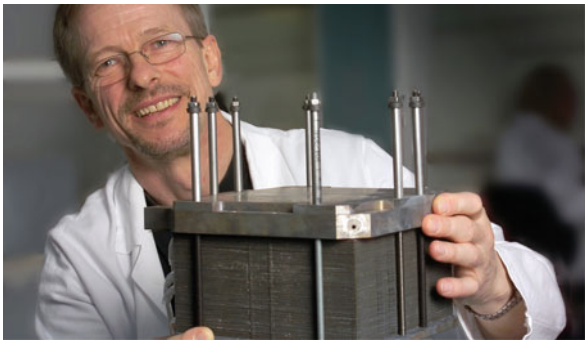

Solid Oxide Fuel Cells, Marketing Issues. Figure 4
Fuel cell stack

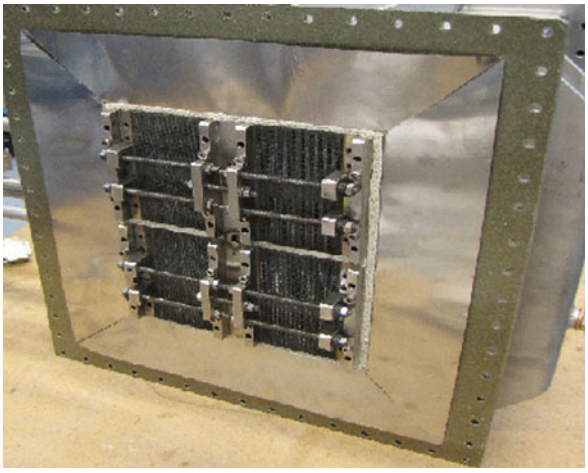

Solid Oxide Fuel Cells, Marketing Issues. Figure 5
Stack module

Solid Oxide Fuel Cells, Marketing Issues. Figure 6
PowerCore™

cell technology economic and very environmentally friendly and accordingly addresses the major challenges of the energy sector: economy, securing energy supplies, and protection of the environment.

Different Types of Fuel Cells

Different types of fuel cell technologies exist. They are all based on the same electrochemical principle but differentiated by the materials used for the electrolytes. The six major types are:

- Proton exchange membrane (PEMFC)
- Alkaline (AFC)
- Phosphoric acid (PAFC)
- Molten carbonate (MCFC)
- Direct methanol (DMFC)
- Solid oxide (SOFC)

The difference in materials between the fuel cell types results in large differences in performance parameters and operational requirements. This makes the different types specifically suited for different applications.

With some exceptions, higher-temperature systems (MCFC, SOFC, PAFC) tend to be best suited for larger applications, while low-temperature systems (DMFC, PEMFC, AFC) can, in addition to units up to some hundred of kilowatts, be configured to provide as little as a few watts of power or less and hence be applied for portable equipment etc. (Fig. 7).

Advantages of SOFC Fuel Cells

Analyses made by Haldor Topsøe and Topsoe Fuel Cell have shown that SOFC technology possesses the highest potential to become a main contributor to the global power market because of:

Higher electrical efficiency. The SOFC technology will be able to provide an electrical efficiency of up to 60%. This efficiency is very high compared to worldwide power plants operating at average electric efficiencies of 30–35% and to existing decentralized, smaller power generation equipment (engines and generators) operating at as low as 5–10% for engines and 15–25% for generators. Application of SOFC units with higher electrical efficiency will result in substantial savings in fuel and money, and for operation on fossil fuels also in a proportional reduction in CO_2 emissions.

High efficiency for all capacities. The SOFC technology is scalable and can cover the complete range from 1 kW to 1 MW, or even higher, with almost no loss of efficiency. The technology offers a very competitive output per weight or volume compared to power plants. Because of this, the SOFC technology addresses a wide range of applications and finds use both in urban and remote areas and both for stationary and mobile purposes.

Fuel flexibility. The SOFC technology is (together with MCFC) the only technology among the different fuel cell technologies which is able to effectively

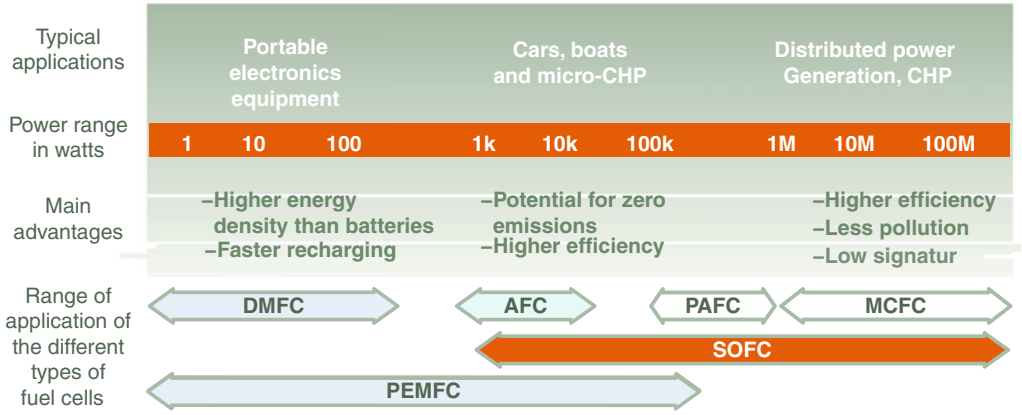

Solid Oxide Fuel Cells, Marketing Issues. Figure 7
Primary applications for different fuel cell technologies

generate power directly based on the fossil fuels in use today, and at the same time, the technology has a clear path to renewables and CO_2-neutral energy systems. This is due to the higher operating temperatures and the superior ability of the SOFC to convert hydrocarbon in the fuel cell stack.

Lower maintenance cost. The SOFC system provides a highly effective and direct electrochemical conversion of fuel to power. The only rotating parts in the system are a fuel pump and a small air blower. Accordingly, maintenance costs are expected to be substantially lower, and operating periods between overhauls are substantially longer than conventional technologies.

Lower emission and noise levels. Since no combustion is involved, the acoustic and heat signatures and particle (NO_X or other particles) emissions will be small. This is crucial for some applications.

Synergies with coupled technologies. SOFC systems are very well suited for integration in coupled technologies. Examples include SOFC systems with heat pumps or air-conditioning systems in which SOFC systems can produce power and interchangeable heat or cooling. SOFC can also be coupled with gas turbine to provide extremely high electrical efficiencies up to 70%.

Solid oxide electrolysis (*SOEC*). The SOFC technology deals with conversion of fuel to power. However, the system can be designed to handle the reverse process converting excess production of power to fuel (electrolysis). This is especially interesting in relation to balancing fluctuating power generating sources, like wind turbines or PV systems, but it is also of interest in relation to nuclear power plants, where change from stable base load operation to match supply and demand is not accepted. Commercialization of SOEC is still some years ahead but is an extremely important future feature of the SOFC technology, especially because SOEC is the only electrolysis technology with the capability to electrolyze CO_2 so that synthesis gas (CO plus H_2) can be produced. This opens up the possibility of production of renewable transportation fuels from power, water, and CO_2 without having to rely on limited biomass resources and renewable fuels.

Competing Conventional Power Generation Technologies

SOFC systems will, in the coming commercial phase, face competition primarily from the conventional power generation technologies such as boilers, Stirling engines, diesel generators, gas engines, batteries, etc., much more than competition from other fuel cell producers. Most of the conventional technologies are advanced, mature technologies (Fig. 8).

The fuel cell industry in general has to prove that fuel cell systems can provide superior performance (taking all technical, financial, and environmental parameters into account) compared to existing technologies.

The strength of competition from other power generation technologies differs between the different applications and markets.

Markets

Solid oxide fuel cells have a higher efficiency than existing power generation technologies, meaning that attractive and competitive applications of SOFC systems are almost endless – provided the cost and performance targets are met. This includes applications of small and large capacity, stationary and mobile applications, and centralized and decentralized applications, running on fossil fuels as well as on renewables.

Figure 9 groups the potential applications according to power range and mobility. The applications are described in more detail below.

Each market has specific requirements to the technology with regard to, e.g., capacity, cost, and lifetime. Accordingly, there will be a difference as to when the SOFC technology is ready for a given market. Some of the early opportunities, such as smaller units for military applications and secondary power, are characterized by having relatively low capacity requirements and accepting a slightly higher price compared to consumer markets.

Topsoe Fuel Cell uses a classification of the potential target applications in three generic market segments: micro-combined heat and power (micro-CHP), auxiliary power units (APU), and distributed generation (DG). In Fig. 10, the market segments are grouped following this classification.

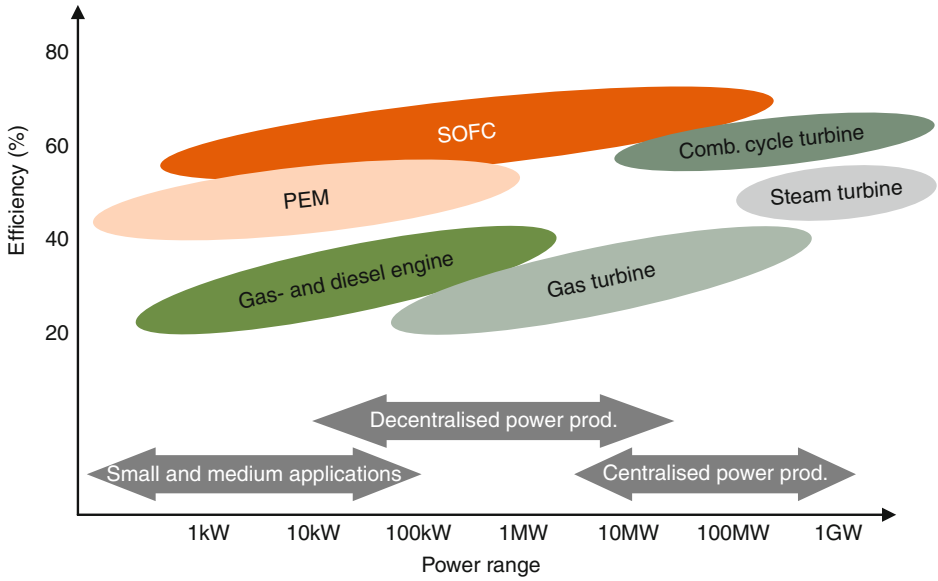

Solid Oxide Fuel Cells, Marketing Issues. Figure 8
SOFC compared with other power production technologies (illustrative figures)

		Small 1–5 kW	Medium 5–50 kW	Large 50–250 kW	Mega large >250 kW
Stationary	Grid	– ***micro-CHP (residential)***	– ***Apartment buildings*** – ***Hotels*** – ***Small industry***	– ***Medium industry*** – ***Super markets*** – ***Hospitals***	– Power plants – Airports – Large industry – Electrolysis
	Off-grid	– ***Telecom base stations*** – Remote holiday houses	– ***Military camps*** – Emergency aid camps – Large screens, light and sound at concerts, circus etc. – Oil and gas industry (power for pipeline pumps and surveillance) – Hotels, ski lifts etc.		– Remote villages and towns – Offshore platforms
Mobile		– ***Unmanned aerial vehicles*** – ***Truck cab power*** – Recreational vehicles – Yachts – Golf cars	– ***Military vehicles*** – Buses – Range extenders (battery charger for electric battery vehicles) – Cooling containers	– Coastal vessels – Airplanes	– Trains – Ocean going vessels
SOEC (electrolysis)					– Storage for renewable energy – Smart grids – Nuclear plants

Solid Oxide Fuel Cells, Marketing Issues. Figure 9
Applications for SOFC fuel cells – Topsoe Fuel Cell target applications are highlighted

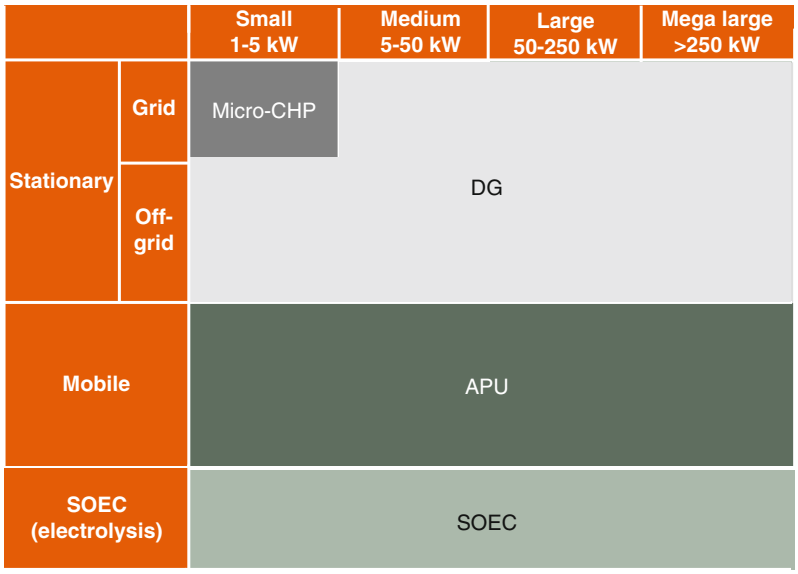

Solid Oxide Fuel Cells, Marketing Issues. Figure 10
Market segments grouped by Topsoe Fuel Cell segmentation

Topsoe Fuel Cell has chosen initially to target the markets for residential micro-CHP, smaller CHP units (up to 250 kW) within DG, and APU for trucks and military applications first because these applications pose early opportunities for demonstration and at the same time lead to high volume markets later on.

Micro-combined Heat and Power (micro-CHP)

micro-CHP units are small stationary systems with an electricity capacity of 1-5 kW intended mainly for private households. The systems are typically based on natural gas using the existing gas pipeline system.

The existing market for domestic power and hearting is dominated by gas-based systems, based on an internal combustion engine technology (ICE) or a Stirling engine. In addition, some 8,000 PEM fuel cell systems are installed in Japan, and some hundred PEM units have been sold in the USA.

All the existing technologies in the market today provide significantly more heat than power (cf. Fig. 11 below). The electrical power is the more valuable output and should be maximized, but at the same time, legislation dictates that heat must not be wasted. Since heat cannot easily be transported over long distances, it should preferentially be consumed on site. This means that when the need for heating is low, such as during summer, the system must be run at a lower capacity or be turned off, jeopardizing the return on investment. Therefore, a low heat to power ratio will enable the system to run at full capacity during a larger part of the year.

Compared to other technologies, SOFC systems have a superior heat to power ratio as it appears from the figure below.

The attractive markets for micro-CHP products for domestic application are:

- Large markets with access to piped natural gas or other SOFC suited fuel
- A significant price differential between primary fuel (e.g., natural gas) and power
- Legislation which favors clean technology and distributed generation

Based on this, the attractive markets are the Northern part of Europe, South Korea, Japan, and the Northeastern USA.

micro-CHP in Europe In Europe, there are three main market drivers:

The consumer wants to save money on the combined electricity/gas bill. A more efficient SOFC system with a power generation efficiency which is higher than that of a central power plant will meet this need.

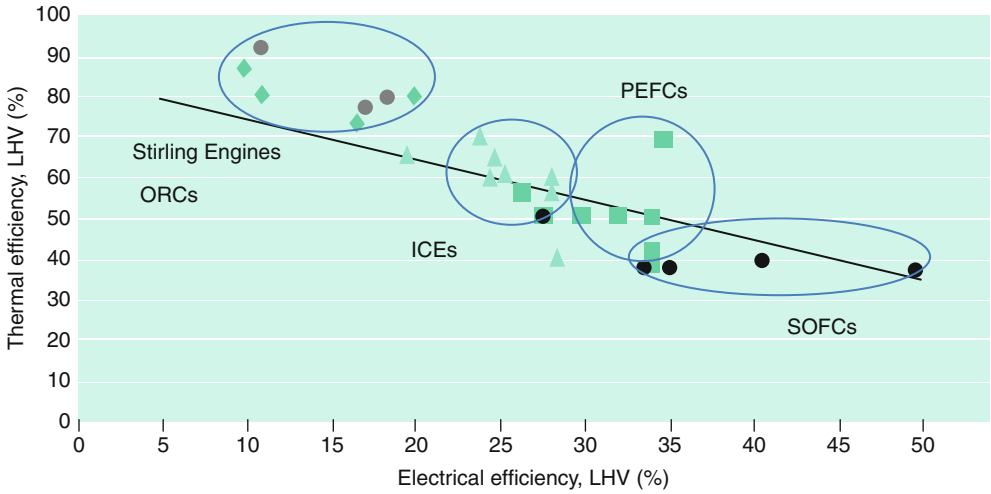

Solid Oxide Fuel Cells, Marketing Issues. Figure 11
SOFC compared with other micro-CHP technologies

Government subsidies to the households who install fuel cell systems as introduced in a number of countries may further boost the commercialization of the technology.

The energy companies are interested in more decentralized and flexible power generation. SOFC systems installed with consumers will satisfy this demand.

New building regulations demand measures to be taken to reduce the energy consumption when a building is refurbished. In many cases, it is easier to replace the domestic heating and power system (with, e.g., an SOFC unit) than to modify an existing system or install additional thermal insulation.

The market potential in Europe is given by the replacement of oil and gas boilers in private homes and by sales to new houses. One of Europe's largest boiler manufacturers, who is also involved in development of micro-CHP systems, estimates this market eventually to be about 2 million units per year (Western Europe).

micro-CHP in North America In North America, there is an increasing focus on energy efficiency and energy conservation. Currently, legislation and programs demanding higher energy efficiency in buildings and production are being implemented. It is estimated that this focus will trickle down to the consumer market. In addition, the demand will be driven by an interest in grid-independent technology because of the relatively unstable electricity grids in many parts of the USA.

In North America, 1.6 million houses are considered eligible for micro-CHP (access to natural gas, attractive ratio between natural gas and electricity price).

micro-CHP in Japan and South Korea The demand in Japan and South Korea is driven by both the environmental impact of the technology and its business potential. Japan has made a massive public investment in fuel cell development, and in South Korea, investment in a fuel cell unit is subsidized. Consultants (Delta EE and Fuel Cell Today) estimate the annual markets to be 1–2 million units in Japan and about half a million units in South Korea.

Auxiliary Power Unit (APU)

Auxiliary power units (APU) range from a few kilowatts to megawatts. They are intended for mobile applications in connection with heavy duty trucks and reefer containers (3–10 kW), leisure applications such as yachts and recreational vehicles (RV), military vehicles, and tanks (10–20 kW). APU systems are used as power generators, either in support of the main engine during peak periods or instead of the main engine when this has been switched off. These systems can also be used in connection with electric cars

running on batteries as an integrated, continued charger of the main battery. These systems can be run on diesel, LPG, or methanol.

APUs find their use in many different applications. In the 3–20 kW range, this includes heavy duty trucks, military vehicles, ground generators, and unmanned aerial vehicles (UAV). Each application is described in more detail below.

APU: Heavy Duty Truck The primary market for APUs for heavy duty trucks is the USA. Heavy duty trucks commute long distances and often have a sleeper cabin equipped with fridge, consumer electronics, coffee maker, etc., all equipment which requires more power than the battery can supply.

Currently, the power is supplied by an idling main engine or by electrified truck stops. An idling main engine is running at very low efficiency and is polluting, and electrified truck stops do not meet the drivers' demand for flexibility.

An SOFC APU unit will provide a clean and efficient power supply, meeting these demands.

Demand is driven by potential savings in fuel and maintenance costs and by anti-idling legislation, which entails that idling is allowed only for very short time. Based on the current diesel price of 3.1 $/gal and US Department of Energy standard assumptions on truck driving, Topsoe Fuel Cell calculations show that $4,200 can be saved annually in operational cost by installing an SOFC APU on a truck compared to an idling engine. In addition, all the environmental benefits should be considered.

It is estimated that the potential market in the USA alone is around 200,000 units annually.

APU: Military Applications In the military commands, there is an increasing focus on fuel savings, as transport of fuel to the battle field is vulnerable and expensive (between 15 and 40 $/gal depending on the mode of transport and type of engagement). Any savings in fuel will reduce costs, and low signature energy supply can reduce casualties. Three applications are of specific interest for SOFC units: as a substitute for diesel generators in military camps, as a silent APU for military vehicles, and as power for unmanned aerial vehicles (UAV):

Power generator in camps. Today, diesel generators supply electricity generation in military camps. A lower number of large generators (200–750 kW) and some smaller towable generators (5–20 kW) are used. The military has an interest in optimizing the energy infrastructure by distributing a larger number of smaller generators in the camp.

In the field. Military vehicles have an increasing need for electricity for powering air condition, reconnaissance equipment, and weapon systems. Currently, this electricity need is satisfied by the main engine, by batteries, or by a diesel generator. However, none of the existing solutions are satisfactory.

If a single 10-kW generator is replaced by an SOFC APU, savings in fuel cost will be about $100 per day or $40,000 on an annual basis.

Considering the thousands of generators in the field, the potential saving is enormous.

Reconnaissance from the air. UAVs come in many different sizes and are today powered by various engines running on jet fuel. Depending of the size of the UAV, it can carry a certain payload including fuel.

There is thus an interest in reducing fuel consumption in order to increase mission length and also in decreasing the signature. Both can be accomplished by a fuel-cell-based generator.

The primary markets for military applications are North America and Europe.

Distributed Generation (DG)

Distributed generation (DG) covers a large range of capacities, from 10-kW for building installations up to the low megawatt range for decentralized power

plants. Applications in this size are mostly stationary, but can also be ships and trains and thereby become mobile. These large systems can be used as either primary power generators, as APUs, or as backup support. A wide range of fuels is used for DG. Natural gas from the grid is the most common fossil fuel. Biogas from fermentation, landfill gas, and sewage gas are important renewable fuels. Coal gas is considered for future large-scale power generation. Liquid fuels such as diesel, LPG, or methanol are normally fuels of choice for off-grid applications and for mobile applications. The DG segment can be subdivided into four major subsegments: prime power, combined heat and power (CHP), off-grid and secondary power, and mobile power (Fig. 12).

Prime Power Prime power is defined as megawatt-class power plants, delivering electrical power to the grid. Today, mid-size gas turbines or very large stationary engines are used as prime movers. The demand for SOFC units for prime power is driven by the energy companies' need for load balancing the electricity production because a large and increasing share of the production comes from renewable energy such as wind, solar, and hydro power and from a need to reduce the CO_2 emissions. SOFC units can solve these problems because they are efficient (and consequently has a lower CO_2 footprint), have excellent load following capabilities, and enable carbon sequestration and storage.

Combined Heat and Power (CHP) CHP is an optimal way of utilizing fuel. In a traditional central power station, only about 35-45% of the primary energy is transformed to electrical power, while the remaining is waste heat which is not used. In a CHP plant, the heat is not wasted but used as steam or hot water to provide heat to homes, buildings, or industry. This requires

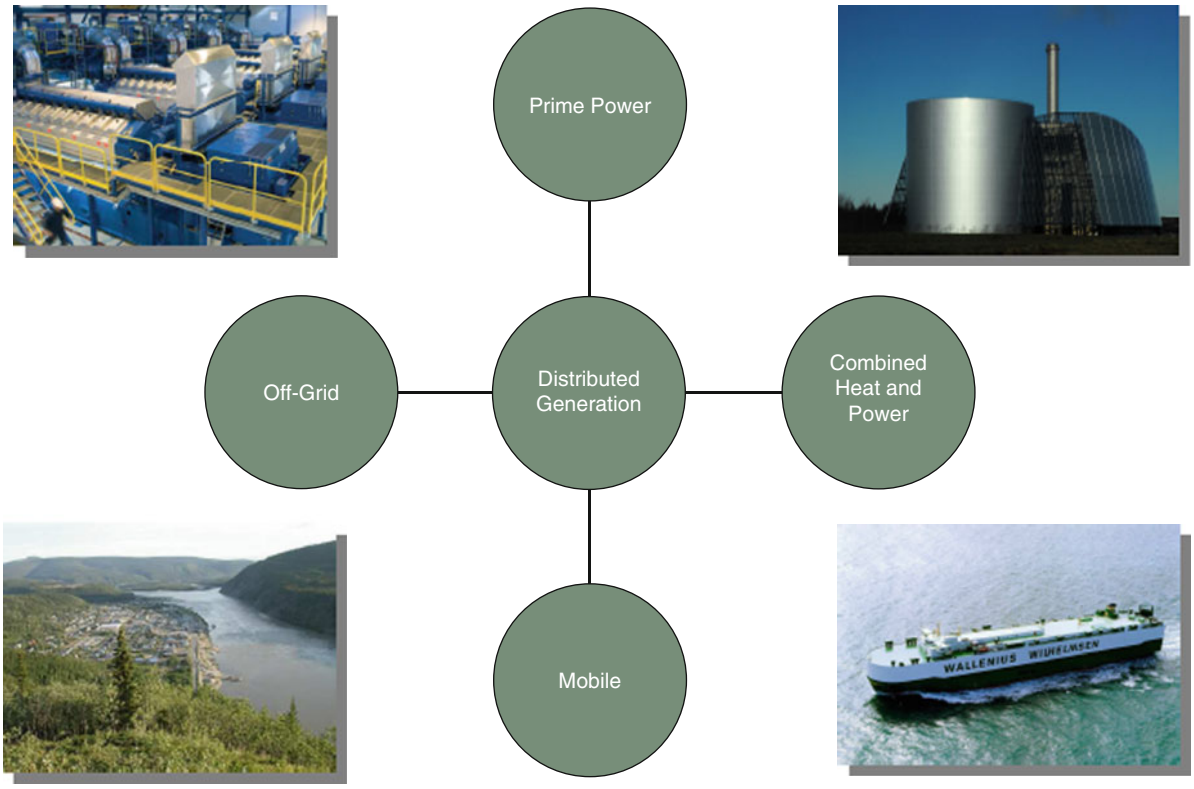

Solid Oxide Fuel Cells, Marketing Issues. Figure 12
Sub-segments in the market of distributed generation

a heat network, and consequently, CHP solutions are primarily implemented as small decentral units situated together with hospitals, hotels, airports, etc., where the heat can be consumed on site.

The CHP market today is dominated by the internal combustion engine technology (ICE), and for high-power systems (above 2 MW) also by gas turbines. These technologies produce more heat than what is typically required by the customer. Since heat is not allowed to be wasted, this limits the time during which a system can operate or limits the overall efficiency. Since the SOFC technology offers a much better power to heat ratio than competing technologies, the SOFC system can either be operated for a longer time or a higher capacity CHP system can be installed.

Off-Grid and Secondary Power Many power consumers are located in areas without electricity grid or in weak grid areas. Examples are telecom base stations and pipeline and border surveillance. In India, many of the telecom base stations are connected to the grid, but the power is very unreliable, and often the power is out for 8–10 h daily. In such areas, an SOFC unit fueled by, e.g., natural gas would provide an attractive alternative since it would offer a reliable power source.

In areas where there is no grid, diesel generators are often used as power sources. The value added by an SOFC unit is higher efficiency (longer time between fueling), less maintenance, and the ability to use nonconventional fuels (in some areas, diesel is often stolen from such sites). Less maintenance and longer time between fueling is of very high value in remote areas because they can often only be reached with off-road vehicles or even helicopters.

Mobile Applications The marine industry has an increased focus on the environment because many ports around the world and many coastal regions have started to implement strict emission requirements. One way of fulfilling these requirements is an APU which generates electric power more efficiently and cleaner than the main engine. This unit can be run in ports in order to provide the total load of the ship, but can also be run at sea, reducing the fuel consumption of the main engine.

Once the SOFC technology has been established for marine APUs, the technology can be extended to the main drive of the ship in order to make it even more efficient, more quiet, and less polluting.

Just as in marine transport, the fuel economy and environmental impact of trains can be optimized. Many countries around the world have a desire to switch from diesel engines to electric trains but cannot justify the infrastructure cost of electrifying main train lines, let alone secondary lines. A potential solution to this problem is a battery-powered train that is equipped with a so-called range extender, which is an onboard power plant that constantly recharges the battery, thereby extending the operating range of the train way beyond the limited capacity of a battery.

In 2009, the world market for power generation equipment (<2 MW) for distributed generation was 28 GW. Geographically, the largest share of this market is in Asia with 12.3 GW annually. Naturally, not all of this potential market is accessible for the fuel cell technology in the short term. Especially interesting in Asia are countries such as South Korea which creates programs for clean energy generation including fuel cells.

In South Korea, the Renewable Portfolio Standard that will come into effect in 2012 demands an increasing share of power generated from renewable sources and fuel cells. It is estimated that the impact of the RPS will be an annual installation of renewable generation capacity including fuel cells of more than 300 MW in 2012 and reaching more than 900 MW toward the end of the decade.

Focusing on Europe, the market for CHP generation equipment has been substantial for more than a decade; from the mid-1990s to 2007, the installed CHP generation capacity has increased from 4.7 GW to 10.6 GW, resulting in average annual sales of about 550 MW. Assuming that the implementation of CHP continues toward the goal set by the European policy (EU directive 2004/8/EC), the annual sales volume over the next decade is expected to be between 600 MW and up to 1 GW toward the end of this decade.

In addition to this figure, there is also a European market for replacement (repowering) of existing CHP installations of about 400 MW annually (Fig. 13).

Solid Oxide Electrolysis (SOEC)

This reverse SOFC process (SOEC) produces fuel from excess power production. SOEC units will be attractive

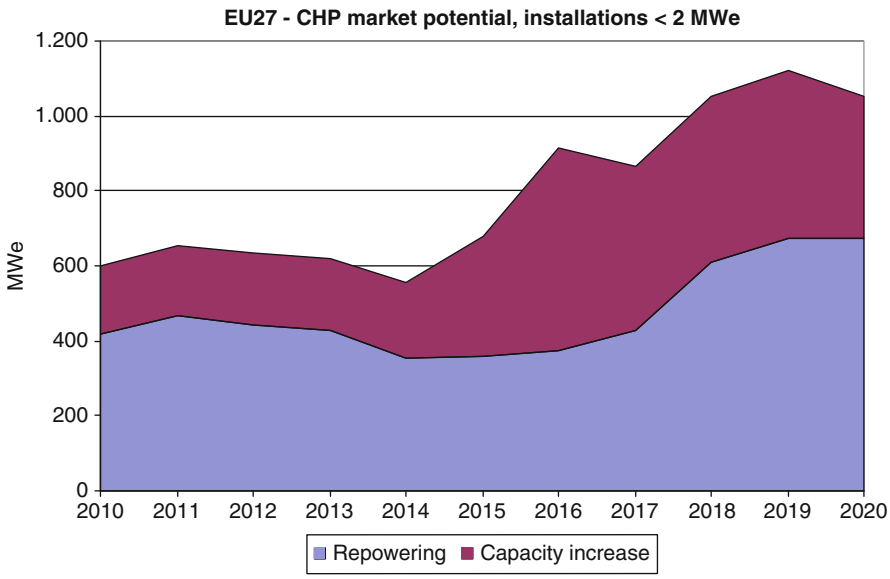

Solid Oxide Fuel Cells, Marketing Issues. Figure 13
Potential European market for CHP power generation equipment

as energy storage in relation with excess power produced on wind turbines or solar panels. SOEC can be used to help balance supply and demand. This market, as well as the technology serving it, is still some years ahead.

Market Summary

In all the market segments where commercial SOFC products can be a competitive alternative, the potential market size is overwhelming. All of them are global multibillion-dollar markets.

The size and the market drivers for the market segments are summarized in Table 6.

Major SOFC Players

A number of important companies are active today within the development of SOFC technology. Although some of these will ultimately become competitors, they are currently mainly seen as important contributors in a common effort to promote the technology. The main players are listed in the table below (Table 7).

None of the SOFC companies have yet reached a commercial phase. Like Topsoe Fuel Cell, some have started marketing their products and signing up with commercial partners, e.g., CFCL with E.ON and Ceres with Centrica. However, everybody in the industry is still on a prototype level without industrial production and sales, thus creating large yearly deficits.

A number of large European and US companies like GE and Siemens Westinghouse with commercial interest in power generation have, during recent years, either withdrawn or dramatically scaled down their participation in SOFC R&D. This means that today, no major player in the industry is directly funded by any of the larger energy technology companies. These companies will most probably re-enter the market when a commercial breakthrough has occurred. Their strategy has merely changed from home-grown development to acquisition.

Instead, new players originating from Asia (Korea, India, and China) with access to large R&D budgets are entering the industry.

One of the first companies to develop solid oxide fuel cells was Westinghouse in the USA. They developed a tubular cell design that proved to have advantages such as robustness and easy sealing and manifolding [2]. The tubular cells had a diameter of 2″ (25 mm) and a length of 180 cm (150 cm active length) and were building upon a porous ceramic cathode support tube. Each tube was interconnected by nickel felt and bundled to a stack of 1,152 tubes for 100-kW_{el} overall rating [3]. Tubular cells possess some

Solid Oxide Fuel Cells, Marketing Issues. Table 6 Primary market drivers and estimated market sizes

	Market drivers	Estimated market size p.a.
micro-CHP	*Europe:* Economic savings, green image, incentives, lower natural gas price, higher electricity price. *North America*: Economic savings, reliable electricity supply	Europe: 2 million units N. America: 1.6 million units Asia: 2 million units
APU	*Europe*: Expected anti-idling legislation, savings in diesel consumption (high diesel price). *North America*: Anti-idling legislation, savings in diesel consumption (high diesel price).	Truck, USA: 200,000 units
	Military: Size and weight, low noise, higher efficiency	
DG	*Europe*: Economic savings, increasing decentralization of electricity generation, partly driven by the local availability of renewable fuels, increasing requirement for load balancing *Asia*: Growing demand for electrical power, grid instability, incentives	World: 28 GW Europe: 5.3 GW Asia: 12.3 GW
DG-CHP	*Europe*: Economic savings, increase in energy efficiency, European and country policies on CHP, feed-in tariffs and incentives	World: 2 GW Europe: 1 GW

characteristic advantages compared to other cell designs. The tubular symmetry tolerates larger thermal gradients and offers the possibility to design stacks with very low pressure drop. However, tubular cells have a quite long in-cell current path leading to significant, resistive losses. The internal losses are reduced by operating the cells at high temperatures. Although the tubes are operated at temperatures around 1,000°C, long lifetimes of up to 70,000 h could be proven in a ceramic test housing with very low degradation. It is quite likely that avoidance of any impurities and contaminants is a prerequisite for the very low degradation.

In 1998, Siemens acquired Westinghouse SOFC and the tubular SOFC concept. Siemens dropped their leading position with their proprietary planar electrolyte-supported concept and metallic interconnects developed in the early 1990s in Germany. Upscaling of the tubular SOFC concept resulted in two 100-kW_{el} prototypes of which one was installed in Arnhem, The Netherlands, in 1999. After successful demonstration of the system, it was refurbished and removed to Torino, Italy, to the Siemens Turbocare plant [4]. Here, it completed a total of 30,000 h of systems operation. Until now, this SOFC concept based on cathode-supported tubular cells is the only one that has surpassed 20,000 h operation on system level. Due to the termination of Siemens' development of the original tubes, the system finally had to be shut down in 2007 [5]. Two Siemens Westinghouse units were built for pressurized operation. Pressurized operation of fuel cells results in an increased cell voltage. A pressure around 4 bar results in approximately 15% higher performance. The Siemens pressurized systems underwent up to 3,500 h of testing before being abandoned [6]. Siemens adopted several concepts of improved power density tubes in which the current path and compactness of the tube bundles was improved. These "high power density" ("HPD") tubes used a "flattened" design with current transporting ribs across the air transport channel. The "Delta 9" was a further improved design based on a flat tubular geometry. Both HPD and Delta were tested in the 5-kW_{el} class. Siemens entered the SECA Phase 2 after having completed the SECA Phase 1 with a 5-kW system built in cooperation with Fuel Cell Technologies. Apparently, the manufacturing and volume power density of the different Siemens tubular designs prevented Siemens from suitably reducing the manufacturing costs. The Siemens SOFC operations in Pittsburgh were up for sale in 2008. A number of other SOFC organizations continue to develop SOFC technology based on tubular cells primarily due to their robustness, reliability, and suitability for large pressurized systems.

Global Thermoelectric from Calgary, Canada, acquired the base technology of anode-supported SOFC from Forschungszentrum Jülich in 1997 [7].

Solid Oxide Fuel Cells, Marketing Issues. Table 7 Major SOFC players

Company	Country	Market focus	No. of employees (est)	Ownership	Remarks
Ceramic fuel cell	Australia	micro-CHP	120	Listed	Currently marketing systems. More than fifty systems sold. Partnerships with European utility comp. Close relation to E.ON. Stack manufacturing facility in Germany started 2009. Full in-house system assembly from 2011
Ceres power	UK	micro-CHP	100	Listed	Close partnership with Centrica. Expected launch in 2012
Versa power	USA	DG	40	Owned 42% by Fuel Cell Energy, a leading MCFC company (listed)	Pre-commercial development of 2–10 kW prototype systems. They will be used as building blocks for larger systems which are the focus area. Focus on projects under the public-supported US SECA program
Accumentrics	USA	Sec. power. APU	–	Holding comp. focusing on UPS for military	Small systems for off-grid use. Focus on military applications. Developing a 10-kW system together with US military
Hexis	CH	micro-CHP	20	Private	Close relation with EnBW. Focusing on heat-driven products for residential applications
Delphi	USA	APU	–	Part of automotive group	Focus on automotive applications. Group being reconstructed following Chap. 11 after GM collapse
Bloom Energy	USA	DG, CHP	4–500	Venture funds headed by Kleiner Perkins	More than fifty 100-kW systems sold and operating at trophy clients. More than 400 million US dollars invested so far
Kyocera	Japan	micro-CHP	–	Part of larger industrial group	Expected to be close to marketing commercial stacks for micro-CHP
Rolls Royce	USA	DG	80	Part of larger industrial group	Partly relocated to US. Limited commercial activity
Topsoe Fuel Cell	Denmark	micro-CHP, APU, DG	125	Haldor Topsøe A/S	Partnership with Wärtsilä. 5-MW production facilities

In 2003, the SOFC operations were bought by the US company FuelCell Energy and transferred into a joint venture with FCE and became Versa Power. Versa successfully accomplished the SECA Phase 1. Today, Versa is the main supplier of large stack units in the SECA Phase 2, working on a 10-kW_{el}-plus stack unit [8] which is one of the largest known worldwide with a stack footprint of about 500 cm^2. Versa is the only SOFC organization that builds and demonstrates stacks with flat planar anode-supported cells with footprint as large as 25 × 25 cm^2 and even 30 × 30 cm^2. Already, in 2009, they obtained more than 5,000 h of continuous testing. The aim is to demonstrate a 250-kW module in 2012 and a 5-MW proof of concept system in 2015. The objective of the DoE/SECA Phase 2 is to develop the SOFC technology for combination with coal gasification and CO_2 capture.

Bloom Energy, formerly known as Ion America, are active in the development of 100-kW_{el}-class SOFC systems [9]. After a long period where little was known of

their activities, Bloom disclosed details of their SOFC technology in April 2010. The 100-kW_{el} systems called ES-5000 Energy Server are built of a multitude of stacks of 1–2-kW_{el} rating based on planar electrolyte-supported cells with a footprint of about 10×10 cm^2 and metallic interconnects. It delivers 480 V AC at an electrical efficiency of about 50% LHV on natural gas. The unit weighs 10 t with the dimensions $224'' \times 84'' \times 81''$. It is well known that for planar cells, a small footprint offers higher stack reliability due to a smaller failure probability for a smaller cell volume. However, small cell footprint leads to increased manifolding cost and use of nonactive stack materials.

In Japan, the main emphasis of SOFC development has been on residential units and distributed generation. Mitsubishi Heavy Industries (MHI) have been working on 150-kW_{el} and 200-kW_{el} pressurized SOFC system for industrial CHP and larger coal-gas-fueled power plants. These units are based on high-temperature (900°C) segmented anode-supported tubular cells which have been under development since 1991. By 2009, a 200-kW class system was operated, pressurized for about 3,000 h at 52.1% electrical efficiency LHV [10]. The MHI planar MOLB design (Mono Block Layer Build') was developed from about 1995 to 2005. It consists of a "corrugated" electrolyte-supported cell design which integrates functions of interconnect and electrode and operates at a high temperature of around 950°C. The corrugated cell design has an extended active cell area which promises an increased volume power density compared to more traditional planar stack designs. After the presentation of two units at around 30 kW_{el} at the World Exposition in 2005 with few operation hours until failure, activities have reverted back to basic development work.

Ceramic Fuel Cell Ltd. (CFCL) from Australia pursued a 10-kW class design in the 1990s [11]. This was abandoned, and all activities were directed toward small CHP units for residential application. CFCL is now heavily and successfully active in building 1–2 kW_{el} units for residential CHP based on planar stack technology in which each repeatable unit consists of four relatively small (7×7 cm^2) anode-supported cells sealed in a stainless steel window frame. For these small units, they have claimed to have system electrical efficiencies of about 60% due to a strongly integrated system design. Although CFCL possesses a comprehensive experience on development and manufacturing of electrolyte-supported as well as anode-supported cells through many years of engagement in SOFC development, they have decided to outsource their cell manufacturing to leading German ceramic manufacturing companies [12, 13].

Rolls Royce Fuel Cell Systems (UK) is working on medium-sized industrial power generation units up to and above 250 kW, eventually up to several megawatts of electrical power. The basic component is a flattened ceramic tube with a sequence of cells (segmented) printed on it. In contrast to the Siemens concept, fuel flows within the tube and air outside. The design is named as "integrated planar" since it uses characteristics of both tubular (gas supply) and planar (printing on flat surface) designs. The tube units are combined to sub-stacks that are again arranged around a "hub." This module is pressurized and combined with a turbocharger [14, 15]. In this way, the RRFCS has the possibility to make use of the higher voltage achievable with pressurized operation. RRFCS are targeting the US power generation market with the help of SOFCo, which they acquired in 2007. Recently, considerable funding was awarded by the DoE within the SECA Phase 2 program. At the SECA 2009 workshop, RRFC announced that their experience with a 125-kW scale up on the way to 250 kW and further MW class units revealed that scale up was much more challenging than anticipated.

A number of smaller European developers adopted the planar SOFC concept. This has now evolved into a high-performance technology, especially with the anode-supported variant. Development groups including cell and stack manufactures have successfully developed the planar anode-supported technology at a scale above 10 kW_{el}. These industrial developers include: Topsoe Fuel Cell (TOFC, Denmark), ProtoTech (Norway), SOFCPower (Italy), Hexis (Switzerland), Staxera (Germany), and Ceres Power (UK).

Ceres Power in UK was founded based on development of low-temperature SOFC carried out at Imperial College in the 1990s. Their cells with ceria electrolyte operate at 500–600°C and are metal-supported. Both cell and short stack durability have been demonstrated during 2,500–3,000 h of operation on reformed fuels. The inevitable electronic leakage current in the ceria electrolyte limits the stack efficiency and constricts the

operating temperature to 500–600°C. However, they have, with more than 140 mW/cm^2 at 570°C, achieved commercially meaningful performance of metal-supported SOFCs. Ceres Power has not provided a public update of recent progress due to commercialization activities. Their primary focus is on the manufacturing of small wall-hanging 1-kW CHP units which are now ready for extended field test [16, 17].

Topsoe Fuel Cell is a subsidiary of the Haldor Topsøe Group. Topsoe Fuel Cell was established as a separate company in 2004, based on more than a decade of fuel cell research activities in Haldor Topsøe. Haldor Topsøe is an internationally recognized company within the catalysis industry with worldwide presence and a turnover exceeding 500 million €. Haldor Topsøe holds a top three position in all of its business areas and has a strong track record for bringing new technology from R&D to global commercial success.

Topsoe Fuel Cell is engaged in development, manufacturing, and marketing of solid oxide fuel cells (SOFC). Until now, 170 million € has been invested in bringing Topsoe Fuel Cell to the leading edge of SOFC technology globally.

Topsoe Fuel Cell is commercializing its technology through a platform strategy where a few basic technology platforms, all coming from the core captive proprietary technology of Topsoe Fuel Cell, can be commercialized and customized to fit into different market segments.

Topsoe Fuel Cell has identified a number of market applications with early commercial opportunities in order to secure a broad market penetration as early as 2013.

Topsoe Fuel Cell has entered into partnerships with a number of important customers, especially for those market applications chosen as early commercial focus areas. Final product development is a mutual effort of the partnership. Field tests and real-life demonstration projects are scaled up.

TOFC has in 2009 started a pilot-scale facility for production of planar anode-supported cells and stacks. The TOFC stack concept aims at cost-efficiency by using thin-sheet metallic interconnects and minimizing stack component materials. Their stacks have been operated with a stable performance for more than 12,000 h. Currently, TOFC is supplying stacks up to 3 kW and stack modules in the 10-kW size range. Multi-stack arrays are developed for larger systems. For smaller capacities, it is of paramount importance to have a very tight integration, both mechanically and thermally, of all the hot components of the SOFC system. TOFC therefore has a program to develop a so-called PowerCore unit comprising fuel processing, the stack, feed effluent heat exchangers, and catalytic burner(s). A complete 5-kW PowerCore unit based on methanol has been constructed and tested successfully under dynamic load following operating conditions. In similar systems based on diesel fuel, strategies to counteract the impact of sulfur are under investigation. For the micro-CHP applications, 1-kW PowerCore unit has been designed and will be deployed in field tests [18].

Wärtsilä is a Finnish company with a steel and shipbuilding background. Their main interest is the application of SOFC systems as auxiliary power unit (onboard electricity generation) on ships and as multi-sized (100 kW$_{el}$ to 100 MW$_{el}$) DG units. With TOFC as a stack supplier, a complete 20-kW demonstration unit based on pre-reforming of natural gas with anode recycle was operated for more than 1,000 h with 24 stacks of the 75 cell (12 × 12 cm^2) type in 2007. Another 24-stack prototype, now based on methanol, was built by Wärtsilä in the project METHAPU, another one for biogas use. The methanol is converted into methane upstream the anode, using a proprietary catalyst. More recently, within the EU project LargeSOFC, Wärtsilä has built a 50-kW$_{el}$ system due for operation in 2009/2010. This will be the first SOFC system worldwide in this power class operating at ambient pressure and using planar cells. Follow-up test units of up to 150 kW$_{el}$ are expected within the next few years [19–22].

Steps in Commercialization

Recently, different SOFC companies have been able to show performance records of their fuel cells that prove the commercial viability of the technology.

The proof of competitiveness is taking place in the three phases:

Validation and proof of concept. This phase demonstrates that the technology works and that operation can be controlled. This phase has been completed by most of today's SOFC manufacturers.

Large-scale test and demonstration. This phase demonstrates that the technology can also work under

harsh real-life conditions, and special attention is on robustness and reliability. Most of today's SOFC manufacturers are currently in this phase.

High-volume field testing and production. This phase shall go through a very large number of field tests to demonstrate that reproducibility is possible without failures and that competitive manufacturing costs can be achieved. Some SOFC manufacturers are currently preparing for this phase through establishment of manufacturing facilities.

In general, the technology is on its way to prove that it, under real-life conditions, can achieve low production cost, sufficient reliability, and required lifetime to produce an overall performance in line with existing technologies.

Major Challenges

The major challenges to be focused on are shown below (Fig. 14):

Lifetime

One of the major hurdles on the way to competitiveness for SOFC technology development has been to develop cells and interconnects, which degrades at an acceptable rate to obtain commercially viable lifetimes for the stacks.

In an integrated EU effort to improve the durability of SOFC components, REAL-SOFC, under the Sixth Framework Programme, quite significant progress was made to that effect. The degradation rates were decreased from 2% to 3% voltage drop per 1,000 h of operation at 300 mA/cm^2 at the beginning of the project in 2004 to 0.5–0.75%/1,000 h at the end of the project in 2009. This reduction in degradation rate was even achieved at a higher current density of 500 mA/cm^2. More than a 100 thermal cycles from room temperature to 800°C and 250 full red-ox cycles were also demonstrated [23].

Similar progress has also been demonstrated in the US SECA program: As an example, the degradation rate has been brought down from 3.6% per 1,000 h for the Versa stacks in the 2005-2007 time frame to 1.7% per 1,000 h in the 2008–2009 time frame in tests for more than 5,000 h [24]. The latest results indicate an aging rate of 0.64%/1,000 h for a 32-cell stack operating at 700°C furnace temperature at 390 mA/cm^2 [25].

At Topsoe Fuel Cell, the measured degradation rate has also been dramatically improved as exemplified in Fig. 15 below:

It can thus be concluded that SOFC stacks – under continuous operation – can be expected to have a useful lifetime, defined as a maximum 10–20% loss of performance, in excess of 30,000 h. Strategies to counteract aging – like gradually increasing operating temperature during the lifetime of the stacks and

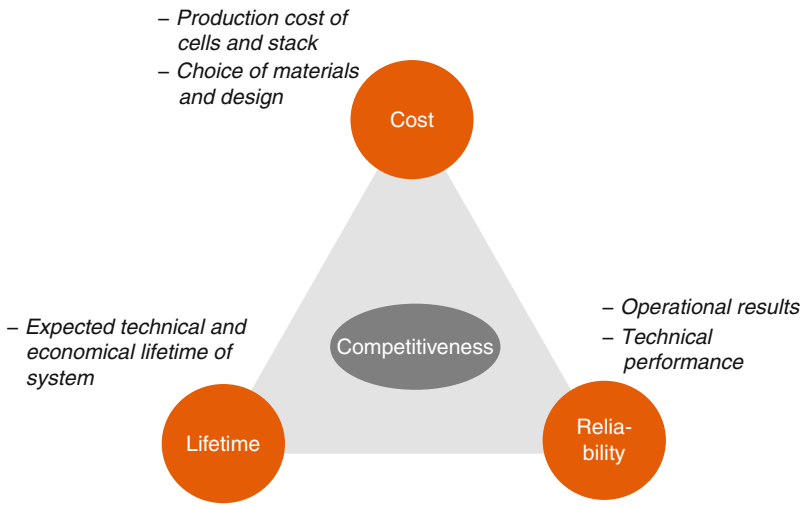

Solid Oxide Fuel Cells, Marketing Issues. Figure 14
Interrelated challenges in SOFC development

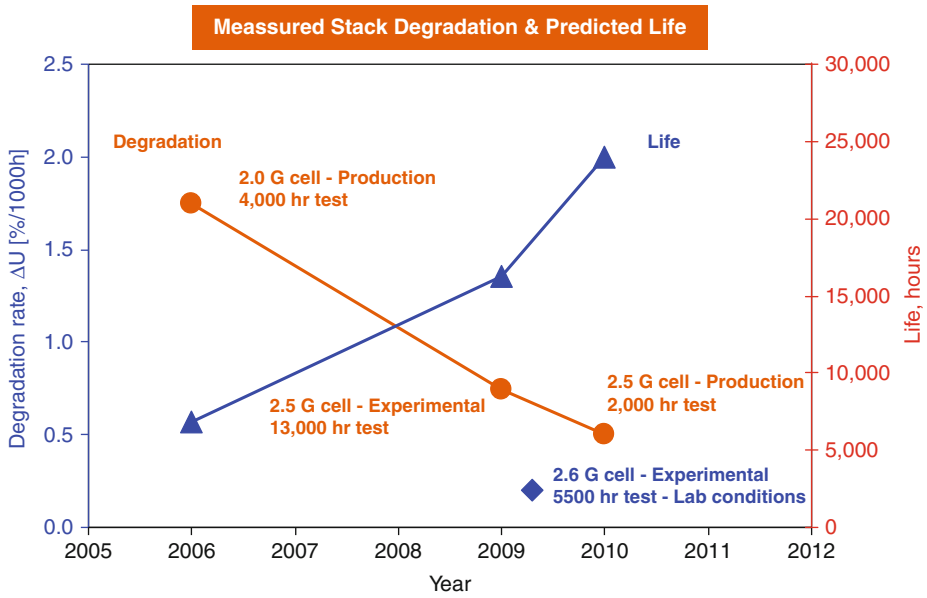

Solid Oxide Fuel Cells, Marketing Issues. Figure 15
Degradation rate for TOFC stacks

thus keep the internal resistance constant despite degradation – can also be used to maintain system performance [26]. This is a unique opportunity offered by SOFC systems because the stacks can operate in a wide temperature window unlike other fuel cell types.

Reliability

Many of the demonstrations with ceramic cells in real system operation have until now revealed problems regarding reliability and degradation in combination with low robustness of system components. Attention to these issues has to be paid in connection with SOFC technology for mobile as well as stationary application. Recent demonstration studies as well as practical experience in the past have proved how upscaling of cells and stacks to larger, more industrially relevant sizes generally leads to lower reliability and some unforeseen challenges. In real system operation failure, abuse or malfunction of auxiliary components can cause harmful conditions for the SOFC stack. Successful verification of long-term operation for more than 10,000 h of current system technologies is still needed and has only been demonstrated so far for the costly tubular designs.

It is important to apply meticulous care in designing *all* the system components in order to avoid operational incidents leading to hard failures [27].

In order to improve durability and cost-efficiency of the cells, the stacks, and the system, much of the development has in the past focused on lower operating temperature, increased power density, and material savings based on reduced cell and stack component thickness. Current SOFC technology is relying upon cells made of ceramics with their inherent, somewhat unreliable properties in addition to their intolerance toward thermo-mechanical stresses [28–32]. Therefore, industrialization of SOFC concepts based on the current materials requires implication of large safety factors, which leaves further cost reduction as well as reliability improvements challenging.

The low value of fracture toughness makes ceramic cells sensitive to material defects and unsuspected flaws. The consequence is that the ultimate strength of ceramic cells deviates from their nominal mean value, and significant safety factors (maximum tolerated intrinsic load/applied extrinsic load) have to be used in order to obtain a reasonably safe design. Furthermore, defect sensitivity means that quality control in all manufacturing steps becomes very critical and costly.

One interesting development concept aiming at increased robustness and reduced cost is to replace the critical structural components in cells and stacks with metallic materials [33]. The numbers of R&D activities related to the so-called metal-supported SOFC (also called third-generation SOFC) have increased significantly in recent years. It is expected that many SOFC applications would benefit from increased mechanical ruggedness, red-ox tolerance, and thermal cycling promised by metal-supported cells. Future commercial success depends on a continued development where more emphasis is devoted to an integrated engineering approach and innovative solutions. Introduction of materials such as metals with easily predictive properties makes it possible to design cells, stacks, and system peripheries without over-engineering and without requirements of large safety factors in design. SOFC organizations that have published their development results on metal-supported SOFC are German Aerospace Centre (DLR), Plansee SE, Lawrence Berkeley National Laboratory/Worldwide Energy Inc., JPower, Ikerlan, National Research Council of Canada (NRCIFCI), Ceres Power, and Risø-DTU/Topsoe Fuel Cell A/S. Furthermore, a significant number of R&D institutes worldwide have, during the last 5 years, initiated development activities on next-generation SOFC technology including metal-supported cells.

Cost

Although great progress has been made toward solving most of the technical problems associated with the use of SOFC technology, it is generally acknowledged that the cost of the stacks and systems is today about one order of magnitude too high for commercial breakthrough.

Manufacturing Cost Calculations There are only a few bottom-up calculations available in the open literature of the manufacturing costs for SOFC stack. The best estimates done by the manufacturers are for obvious reasons not published, but as part of the SECA program, DOE has commissioned three very detailed studies carried out in close contact with major SOFC cell and stack developers. These studies have been used by the DOE to set target and monitor progress of the program [34].

The cost of manufacturing cells and stacks was calculated from the cost of raw materials, manufacturing facility investments, and the operation thereof. The costs were calculated both as function of cell size and manufacturing capacity. It was concluded that the benefits of upscaling the size of the cells from 100 cm^2 to 1,000 cm^2 was relatively modest, in the order of 10–20%, mainly due to lower production yields.

The results as function of manufacturing scale for the most competitive option, anode-supported planar cells, are shown in Fig. 16.

It is interesting to note that the cost first of all can reach the DOE goals of 175 $/kW for the stack but also that the cost can be reduced by a factor 8 by moving from a production capacity of 5–500 MW/year. Even more noteworthy is the reduction by a factor 4 by going to 25 MW/year from 5 MW/year. This indicates that there is a viable stepping stone toward competitive pricing without incurring enormous investment before the major market breakthrough has occurred.

State-of-the-art SOFC cells contain critical rare earth elements. The impact of the dramatic price increases last year, by a factor 4–5 imposed by the mainly Chinese suppliers, has also been calculated for the DOE [35]. The result for the planar, anode-supported cells was an increase in the price of the stack, so that the rare earth component constitutes a cost of 12 $/kW. In pre-2008 prices, the cost would have been around 1 $/kW. For the tubular SOFCs, the implications are much more serious, resulting in a dramatic price increase because they contain up to 1.7 kg rare earth elements per kilowatt whereas anode-supported, planar cells only contain 35 g/kW in the stack architecture studied.

The sustainability of using this amount of rare earth elements was also studied, assuming 90% recycling of spent stack material in a scenario where 4-GW new SOFC plants were added per year together with replacement of another 4-GW capacity. The results are shown in Table 8 below:

This demonstrates that the amount of rare earth elements (REE) could be used in a sustainable manner without upsetting the market. It was also concluded that the price would not rise much further without attracting new mining capacity outside China, thus stabilizing the price level.

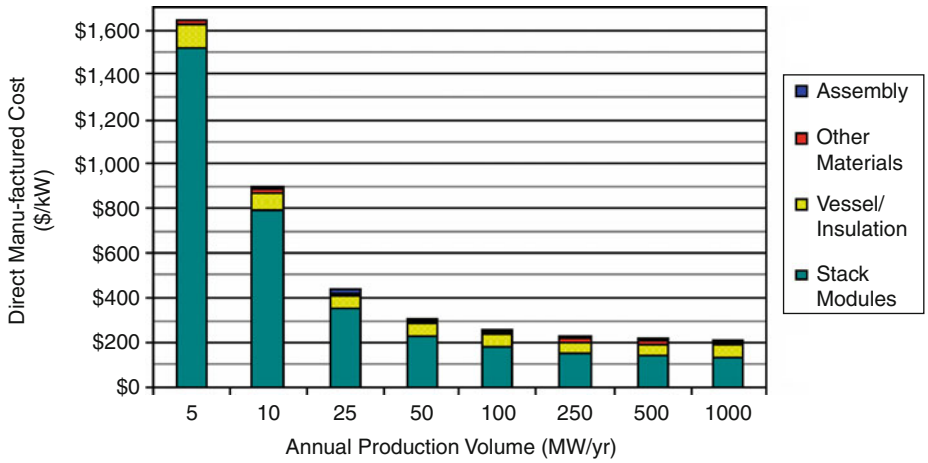

Solid Oxide Fuel Cells, Marketing Issues. Figure 16
Manufacturing cost of planar SOFC stacks

Solid Oxide Fuel Cells, Marketing Issues. Table 8 Cost and availability of rare earth used in SOFC

	REE content of SOFC g/kW	SOFC-driven Net REE demand t/year (2030)	REE production (2009) t/year	Estimated reserves T
Yttria	21	40	9,000	540,000
Lanthanum oxide	9.2	95	>12,000	>10 million
Other REE (Ce, Gd, Sm)	<3	<12	20,000	~50 million

Experience or Learning Curves Another approach to forecast the future cost is to make use of empirically observed experience curves. Such curves reflect the observation, first made in the aircraft industry and later expanded by the Boston Consulting Group, that the cost of a product drops with the same fraction (the learning rate LR) every time the installed or sold volume has been doubled [36–40].

Mathematically, this can be expressed by the formula:

$$\frac{C_v}{C_0} = \left(\frac{V}{V_0}\right)^{\alpha} \tag{1}$$

where c = the unit cost, and V is the cumulative volume sold or installed; α is defined by

$$\alpha = \frac{\ln(1 - LR)}{\ln 2} \tag{2}$$

and the subscript 0 refers to the initial state.

If the cost target for the product to reach a competitive level is C_{br}, then the accumulated volume before market breakthrough occurs, V_{br}, can be calculated from Eq. 1. The extra cost incurred to reach breakthrough can be calculated by integrating Eq. 1 from V_0 to V_{br} and subtract the reference energy cost over the same interval.

The concept is illustrated on Fig. 17.

The learning curve concept clearly breaks down if extrapolated too far because there will always be a floor price set by the raw materials and manufacturing cost and also allowing for a fair profit, so that the producers will enter the market and can recuperate their investment and carry out the necessary R&D to keep abreast of the competition.

The learning investment will obviously have to be paid by somebody, most likely a combination of funding agencies identifying long-term societal benefits, the investors in the industry, and the early adopter customers.

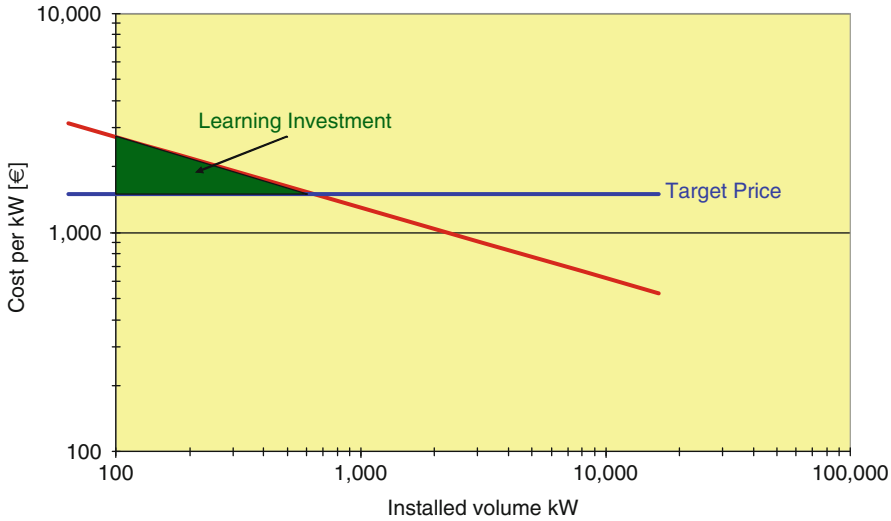

Solid Oxide Fuel Cells, Marketing Issues. Figure 17
Learning or experience curve concept

The concept has been used by agencies guiding policy-makers like the IEA or the DOE, and numerous studies have proven their worth.

The learning rate observed varies between 2% and 3% for very mature technologies like gas and steam turbines, whereas emerging technologies with a significant R&D and scale-up potential portion normally have learning rates around 15–25%.

As the accumulated, installed, or produced volumes of SOFC stacks of all varieties are probably below 5-MW and for the most promising, anode-supported planar variety more likely below 1 MW, there is not enough data available to perform analyses yet, but studies have been made on other types of fuel cells like AFC, PAFC, and notably PEMFC where richer data material is available. The studies show learning rates centered around 20–21% with an error around 4% [41–43].

The predictions made by using the experience curve due to its logarithmic nature are obviously very sensitive to the initial assumptions as illustrated in Table 9 where the target cost is assumed to be 1,500 €/kW.

The base case in the first row assumes that a cost price of 12,000 €/kW has been attained after production/installation of 1-MW capacity and that the learning rate is 20%. It can then be calculated that 639 MW needs to be installed before the breakthrough cost of 1,500 €/kW is reached and the learning investment cost is 439 million €. If the installed capacity then increases exponentially by 75% each year, then it would take 10 years to reach the breakthrough target.

Solid Oxide Fuel Cells, Marketing Issues. Table 9 Initial cost and volume installed versus learning rate, break even volume and learning investment

Initial cost (€/kw)	V_0 (MW)	Learning (LR, %)	V_{br} (MW)	Cost (Mio €)	Beta (%)	Years (to target)
12,000	1	20	639	439	75	10
24,000	1	20	5,500	3,883	75	14
12,000	**5**	20	3,193	7,064	75	13
12,000	1	**15**	7,107	3,250	75	15
12,000	1	*25*	150	141	75	7
12,000	1	20	639	439	**100**	8
12,000	1	20	639	439	75	13

In the subsequent rows, the consequences of changing the parameter (in bold) compared to the base case are illustrated. As pointed out by Lund [44] and also Jamasb [45], RTD could bring about a low entry cost and a high learning rate, and it can be seen that such investments in R&D could pay out handsomely.

The learning investment cost may appear very high but is actually quite modest considering the required total investments in new electricity generation capacity discussed in section "The Global Energy Change." This learning investment is furthermore paid back within a few years provided that the price can be brought below the reference breakthrough price.

Competitiveness

The break-even point for introduction of SOFC systems is normally defined as the selling price for the system which makes it competitive with respect to incumbent technology. A more precise definition would be that the equivalent annual cost for the owner should provide an acceptable payback time for the investment, which will typically be higher than the incumbent technology, but the SOFC will benefit from higher efficiency. Unfortunately, it will normally not be possible to take credit for the lowered environmental impact in the form of lower emissions of CO_2 and the virtual complete avoidance of sulfur, particulates, and NO_x emissions.

The economic comparison is based on the equivalent annual cost (EAC). The EAC is the cost per year of owning and operating an asset over its entire lifespan. EAC is often used as a decision-making tool in capital budgeting when comparing investment projects. The EAC can be calculated by multiplying the net present value (NPV) of a project by the loan repayment factor LRF. The loan repayment factor (LRF) is calculated by the total time n (years) of the project and the discount rate (i). The net present value (NPV) of a project or investment is defined as the sum of the present values of the annual cash flows C_i minus the initial investment C_0.

$$\mathrm{EAC}_W = \frac{1}{P_{\text{Net, Average}} \cdot t_{Annual}} \cdot \left(C_0 \cdot \mathrm{LRF} \cdot \frac{P_{\text{Net, Peak}}}{P_{\text{Net, Average}}} + \frac{P_{\text{Net, Average}} \cdot t_{\text{Annual}}}{\eta_{\text{Net}}} \cdot c_{\text{Fuel}} + C_{\text{Maintenance}} \right) \quad (3)$$

Distributed Generation

Wärtsilä Corporation and Haldor Topsøe together performed a conceptual study of a 250-kW planar SOFC system for CHP application [46]. They cost estimated the price based on obtained offers or estimated costs for the bottom-up designed components. They found that the major cost components were stacks (31%), power electronics (15%), control system (17%), and labor and overheads (15%) (see Fig. 18 for details).

They also evaluated the competitiveness compared with gas engines, of which Wärtsilä is a major supplier. The lifetime of the stacks was assumed to be 40,000 and 50,000 h in 2015 and 2020, respectively. The cost of the system was predicted to be between 680 and 1,080 €/kW in 2020 when the cost of a gas engine would be 660 €/kW. The efficiency of the SOFC was, however, calculated to be 55% and the net electric and total cogeneration efficiency 90%. For the gas engine, the corresponding numbers were 37% and 81%, respectively, so that the SOFC plant would indeed be the most economical.

It was concluded that the SOFC power unit would become competitive at an investment cost below 1,500 €/kW, e.g., at a stack cost of around 500 €/kW. There should be cost-saving potential by especially simplifying the control system, whereas it was presumed that the cost reduction potential for the power electronics would depend on the general cost development within the technology.

The above analyses emphasize the importance of cost reductions related to the balance of plant components.

Auxiliary Power Units Based on Diesel

Nehter et al. [47] have analyzed the technology and economics of different fuel processing options for mobile auxiliary power units using ultra-low sulfur diesel as fuel.

At present, trucks generate power when idling by letting the main engine run the generator. The cost of this operation is given in Table 10.

By analyzing the different layouts discussed above and using a payback time of 3 years, the allowable cost of the SOFC APU systems was calculated as function of electrical efficiency. It was found that a system employing an autothermal reformer (ATR) with an average efficiency would have an allowable price of 2,660 €/kW with the fuel price in Table 10. Operation without desulfurization is feasible even with conventional Ni/YSZ anodes because the penalty incurred in the form of extra stack area needed is relatively modest with ULSD. Other studies have arrived at similar results [48–52].

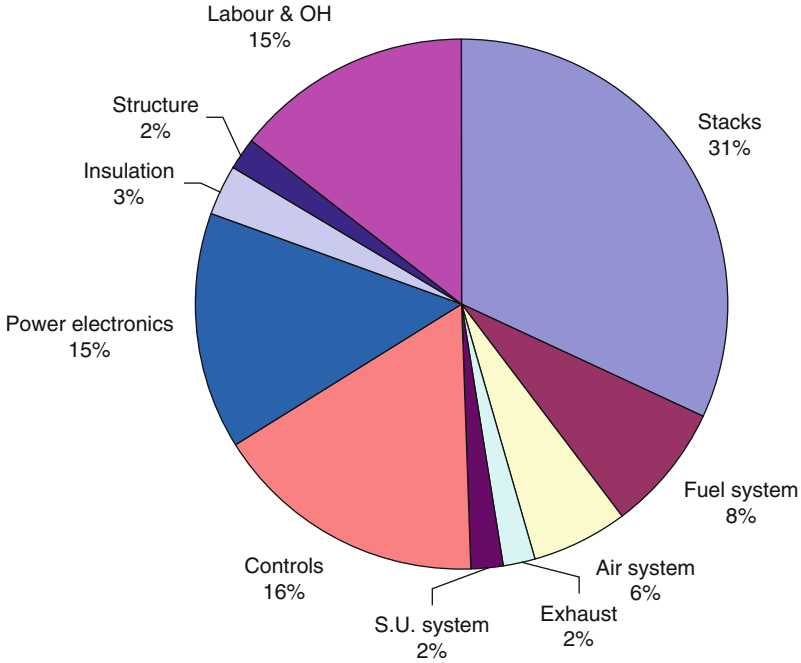

Solid Oxide Fuel Cells, Marketing Issues. Figure 18
Breakdown of capital cost for 250-kW system

Solid Oxide Fuel Cells, Marketing Issues. Table 10 Cost of truck idling

	Truck idling
Electrical net efficiency	4%
Power average (kWel)	1.3
Power peak (kWel)	3.9
Electrical work (kWh/year) (1,830 h/year)	2,379
Fuel consumption (gal/year) (37 kWh/gal)	1,607
Fuel cost ($/year) (2.9 $/gal)	4,661
Maintenance cost ($/h)	0.16
Maintenance cost ($/year)	292
Variable cost (fuel + maintenance) ($/year)	4,953

Micro-CHP Units

There are quite a number of techno-economic studies on micro-CHP units based on SOFC for residential use. They exhibit quite different results, mainly due to geographical differences, which give rise to quite different boundary conditions due to climatic conditions, e.g., the need for heat versus electricity and annual variations thereof, operating strategy (electric load versus heat load following), sparks spread and installed capacity determined by dwelling size, electrical consumption patterns, state of insulation, need for cooling, etc. [53–63].

In general, it can be said that micro-CHP requirements are quite severe: Low maintenance need is a must, as well as high durability (in some analyses, more than 80,000 h lifetime is required).

Large Central Power Plants

The main focus of DOE's SECA program has been on using SOFC in large coal-fired power plants with CO_2 sequestration. The 2015 goals are:

1. 90% CO_2 capture
2. Less than 10% increase in cost of electricity
3. Efficiency of 60% (without CO_2 capture)

Solid Oxide Fuel Cells, Marketing Issues. Table 11 Advanced power systems with CO_2 capture, compression and storage

	PC baseline	IGCC baseline	IGFC Atm.	IG pressure
Efficiency HHV(%)	28.4	32.6	51.1	57.0
Capital cost $/kW	3,570	3,330	2,150	2,100
Water withdrawal gpm/MW_{net}	10.7	18.3	2.5	1.8
Levelized cost-of-electricity ¢/kW-h	15.0	15.1	10.8	10.3

The analyses carried out for DOE have shown that SOFC is the only technology which can lead to these goals [64].

The main results of the analyses are shown in Table 11.

It is interesting to note that the advanced integrated gasification fuel cell plant (IGFC) is in fact producing electricity at a lower cost than the baseline pressurized combustion (PC) plant, sequesters all the CO_2 instead of only 90%, and uses less than one fifth of the fresh water.

These encouraging results, however, presume that a number of innovative, non-proven technologies can be scaled up – catalytic gasification, dry coal pumps, warm gas clean up, ion transport membranes for oxygen generation, and hydrogen membranes – and finally that the cost of the SOFC power block is lower than 700 $/kW (stack less than 175 $/kW). Compared to a plant using pressurized combustion with supercritical steam data without CO_2 capture, it can be calculated that the cost incurred to avoid CO_2 emission is as low as $18 per ton of CO_2.

Summing Up

It is evident from the discussion above that the criteria for commercialization are or can under the right circumstances be met with respect to lifetime and cost. The required reliability still needs to be proven in long-term demonstration tests under real-life conditions. In fact, it is quite remarkable what has been achieved in the last decade, considering the fact that the total staff engaged in SOFC development worldwide is probably only a few thousand [65], e.g., less than the R&D Division of many large, industrial companies. One could argue that one of the reasons why a market breakthrough has not occurred before is the somewhat fragmented efforts without the necessary critical mass. International collaboration has on the other hand been quite extensive also among companies, who will eventually become competitors.

There are, however, other challenges than the technical alone. Discussing the challenges of the commercialization process of mainly automotive fuel cells, Hellman et al. [66] have listed the following:

- Immaturity characterized by rapid technological progress still with no dominant design emerging yet, which increases the risk of choosing the wrong technical path.
- Application diversity: This obvious, long-term very beneficial aspect of fuel cell technology does in the short term present the developers with difficulties in business development decisions, and mistakes can be very detrimental especially with respect to timing.
- Replacement technology: Fuel cells basically provide power and heat, two commodities which are already supplied reliably with incumbent technologies. Fuel cell companies thus have to compete/collaborate with entrenched large OEM's with well-established products, where a lot of investments has been made in R&D, manufacturing equipment, and infrastructure.
- Sub-system of a product: The fuel cell is obviously the heart of the new power/heat plant, but it needs to be carefully integrated into a complete system with many interrelated critical components. It has proven difficult to spur significant interest among balance of plant component suppliers to adapt their equipment in order to obtain the necessary reliability and cost.
- Complexity: Although the SOFC technology requires relatively simple system designs compared to other fuel cell systems, an SOFC system is still rather complex, requiring a broad variety of skills to design and construct.

To this can be added the difficulties in attracting the large amount of capital needed to establish mass

manufacturing facilities, which in turn are needed to bring the cost down to a competitive level. The efforts needed to have stakeholders pay for the necessary learning investments should neither be underestimated, and a certain amount of hype and overselling fuel cells in general have not been helpful.

Future Directions

Despite the remarkable progress made in the last decade, especially with respect to technical performance parameters, it is of course difficult to predict accurately when the commercial breakthrough for SOFC technology will happen because this hinges on several factors beyond the control of the SOFC industry. Among the more important factors can be mentioned:

1. The global economic situation in general
2. The evolution of fuel prices
3. Legislative initiatives with respect to pollution and greenhouse gases
4. The funding levels for upscaling and demonstrating the technology
5. Progress in development and mass production of balance of plant components
6. The ability of the industry to attract the necessary investment for upscaling manufacturing facilities

There is, however, a momentum in the industry toward commercialization, and as an example, Topsoe Fuel Cell plans to reduce manufacturing costs by a factor 3 by 2012 and a factor 20 by 2020. The required investments and changes in production methods required to become a high-volume manufacturer have already been defined.

The path toward commercialization of SOFC technology could be envisaged as shown in the figure below:

Once the technology has reached commercially competitive levels in performance and cost, the potential market for fuel cells will be a double-digit percentage share of the global power generation market, totaling more than 350 billion US dollars per year.

Conclusions

The reader should, hopefully, after reading the above, be better equipped to answer the question: Is SOFC ready for the market, or is the market ready for SOFC?

We believe the answer is: Yes, but not quite yet. It will still require some years of development, buildup of manufacturing facilities, and demonstrations before the reservation can be omitted. A significant and concerted effort is still required by the funding authorities, the industry itself, investors, sub-suppliers, and other stakeholders before this promising technology will contribute in a major way to solving the energy challenges ahead. The uncertainties and risks involved are significant but so are the benefits to society at large if the endeavors are successful.

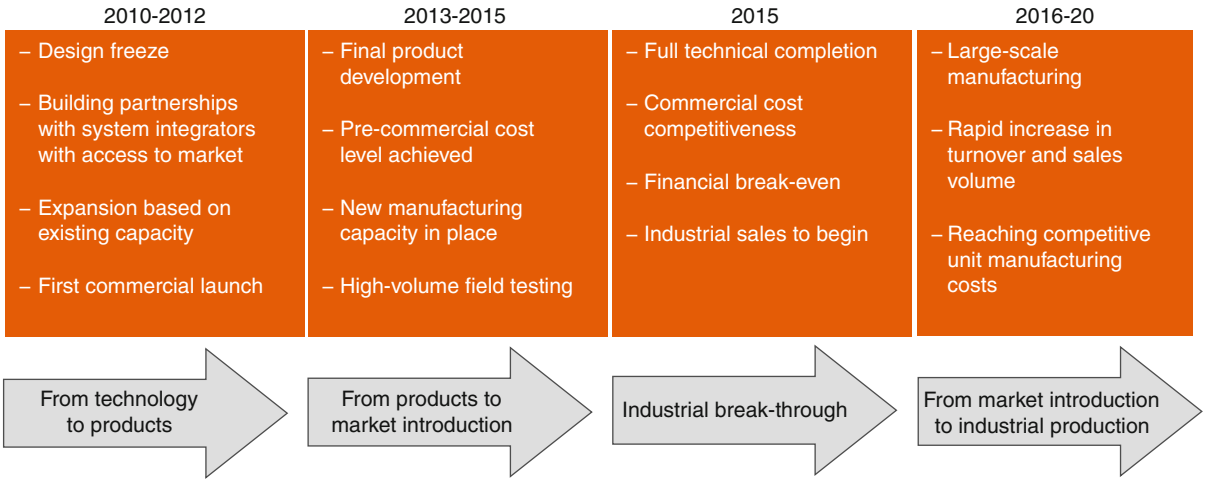

Bibliography

1. World energy outlook 2010. IEA, Paris, 2010
2. Singhal SC (1993) Advances in tubular solid oxide fuel cell technology. In: Dokiya M, Yamamoto Y, Takagawa H, Singhal SC (eds) ECS transactions, PV95-1. Electrochemical Society, Pennington, pp 195–207
3. Kendall K, Minh NQ, Singhal SC (2003) Cell and stack designs. In: Singhal SC, Kendall K (eds) High temperature solid oxide fuel cells - fundamentals, design and applications. Elsevier, Oxford, UK
4. Orsello G, Casanova A, Hoffman J (2008) Latest info about operation of the Siemens SOFC Generators CHP100 and SFC5 in a factory. In: Proceedings of the 8th European fuel cell forum, Lucerne, pp B0204
5. Gariglio M, De Benedictis F, Santarelli M, Calm M, Orsello G (2009) Experimental activity on two tubular solid oxide fuel cell cogeneration plants in a real industrial environment. Int J Hydrogen Energy 34:4661–4668
6. Hassmann K (2001) SOFC power plants, the Siemens-Westinghouse approach. Fuel Cells 1:78–84
7. Borglum B, Fan JJ, Neary E (2003) Following the critical path to commercialization: an update on global thermoelectrics technology and product development. In: Proceedings of the 8th ECS SOFC Symposium, SOFC VIII, Paris. The Electrochemical Society, Pennington, pp 60–69
8. Borglum B, Tang E, Pastula M (2009) The status of SOFC development at versa power systems. In: ECS Transactions, vol 25, pp 65–70
9. Seeking Alpha: eBay installing bloom energy fuel cells, 9-10-2009. http://seekingalpha.com/article/167936-ebay-installing-bloom-energy-fuel-cells. Accessed 12 Feb 2011
10. JCN Newswires MHI achieves 3,000 hour operation, unprecedented in Japan for SOFC/MGT combined-cycle power generation systems, 2 Oct 2009
11. Föger K, Love JG (2004) Fifteen years of SOFC development in Australia. Solid State Ionics 174:119–126
12. Love J, Amarasinghe S, Selvey D, Zheng X, Christiansen L (2009) Development of SOFC stacks at ceramic fuel cells limited. In: ECS Transactions, vol 25, pp 115–124
13. Payne R, Love J, Kah M (2009) Generating electricity at 60% electrical efficiency from 1–2 kWe SOFC products. In: ECS Transactions, vol 25, pp 231–239
14. Agnew GD, Collins RD, Jorger M, Pyke SH, Travis RP (2007) The components of a Rolls-Royce 1 MW SOFC system. In: ECS Transactions, vol 7, pp 105–111
15. Magistri L, Bozzolo M, Tarnowski O, Agnew G, Massardo AF (2007) Design and off-design analysis of a MW hybrid system based on Rolls-Royce integrated planar solid oxide fuel cells. J Eng Gas Turbines Power 129:792–797
16. Bance P, Brandon NP, Girvan B, Holbeche P, O'Dea S, Steele BCH (2004) Spinning-out a fuel cell company from a UK University – 2 years of progress at Ceres power. J Power Sources 131:86–90, 5-14-2004
17. Brandon NP, Blake A, Corcoran D, Cumming D, Duckett A, El-Koury K, Haigh D, Kidd C, Leah R, Lewis G, Matthews C, Maynard N, Oishi N, McColm T, Trezona R, Selcuk A, Schmidt M, Verdugo L (2004) Development of metal supported solid oxide fuel cells for operation at 500–600°C. J Fuel Cell Sci Technol 1:61–65
18. Christiansen N, Hansen JB, Holm-Larsen H, Jørgensen MJ, Wandel M, Hendriksen PV, Hagen A, Ramousse S (2009) Status of development and manufacture of solid oxide fuel cells at Topsoe Fuel Cell A/S and Risø DTU. In: ECS Transactions, vol 25, pp 133–142
19. Fontell E (2008) Fuel cell fed with landfill biogas provides power. Industrial Bioprocess 30:10
20. Fontell E, Phan T, Kivisaari T, Kerañnen K (2006) Solid oxide fuel cell system and the economical feasibility. J Fuel Cell Sci Technol 3:242–253
21. Fontell E, Jussila M, Hansen JB, Pålsson J, Kivisaari T, Nielsen JU (2005) Wärtsilä-Haldor Topsøe SOFC test system. In: Proceedings of the Electrochemical Society, PV 2005-07, pp 123–132
22. METHAPU. 12-1-2012. http://www.methapu.eu/Oskari2.aspx?cmd=15. Accessed 10 Jan 2011
23. Steinberger-Wilckens R, Bucheli O, De Haart LGJ, Hagen A, Kiviaho J, Larsen J, Pyke S, Rietveld B, Sfeir J, Tietz F, Zahid M (2009) Real-SOFC – a joint European effort to improve SOFC durability. In: ECS Transactions, vol 25, pp 43–56
24. Vora S (2010) SECA program accomplishment and future challenges. In: 11th annual SECA workshop, Pittsburg, PA
25. Ghezedl-Ayagh H, Borglum B (2010) Coal based SECA program – fuel cell energy. In: 11th annual SECA workshop, Pittsburg, PA
26. Hansen JB, Pålsson J, Nielsen JU, Fontell E, Kivisaari T, Jumppanen P, Hendriksen PV (2003) Design aspects of a 250 kW NG fuelled SOFC system – strategies to counteract stack performance degradation. In: Abstract fuel cell seminar, Miami Beach, FL, 3 Nov 2003, pp 790–793
27. Åström K, Fontell E, Virtanen S (2007) Reliability analysis and initial requirements for FC systems and stacks. J Power Sources 171:46–54
28. Nakajo A, Wuillemin Z, Vanherle J, Favrat D (2009) Simulation of thermal stresses in anode-supported solid oxide fuel cell stacks. Part I: probability of failure of the cells. J Power Sources 193:203–215
29. Nakajo A, Wuillemin Z, Vanherle J, Favrat D (2009) Simulation of thermal stresses in anode-supported solid oxide fuel cell stacks. Part II: loss of gas-tightness, electrical contact and thermal buckling. J Power Sources 193:216–226
30. Anandakumar G, Li N, Verma A, Singh P, Kim JH (2010) Thermal stress and probability of failure analyses of functionally graded solid oxide fuel cells. J Power Sources 195:6659–6670
31. Anandakumar G, Kim JH (2010) A thermomechanical fracture modeling and simulation for functionally graded solids using a residual-strain formulation. Int J Fracture 164:31–55
32. Zhang Y, Xia C (2010) A durability model for solid oxide fuel cell electrodes in thermal cycle processes. J Power Sources 195:6611–6618

33. Tucker MC (2010) Progress in metal-supported solid oxide fuel cells: a review. J Power Sources 195:4570–4582
34. Thijssen J (2007) The impact of scale-up and production volume on SOFC manufacturing cost, 4 Feb 2007. http://www.netl.doe.gov/technologies/coalpower/fuelcells/publications/JT%20Manufacturing%20Study%20Report%20070522.pdf. Accessed 10 Jan 2011
35. Thijssen J (2010) Market impact of rare element use in solid oxide fuel cells, 18 Oct 2010. http://www.netl.doe.gov/technologies/coalpower/fuelcells/publications/Rare%20Earth%20Markets%20and%20Solid%20Oxide%20Fuel%20Cells%20101018.pdf. Accessed 10 Jan 2011
36. Mattsson N, Wene GO (1997) Assessing new energy technologies using an energy system model with endogenized experience curves. Int J Energy Res 21:385–393
37. Neij L (1997) Use of experience curves to analyse the prospects for diffusion and adoption of renewable energy technology. Energy Policy 25:1099–1107
38. Norberg-Bohm V (2000) Creating incentives for environmentally enhancing technological change: lessons from 30 years of U.S. Energy Technology Policy. Technol Forecast Soc Change 65:125–148
39. Rivers N, Jaccard M (2006) Choice of environmental policy in the presence of learning by doing. Energ Econ 28:223–242
40. Woerlen C (2004) Experience curves for energy technologies. In: Cleveland CJ (ed) Encyclopedia of energy. Elsevier, New York, pp 641–649
41. Schoots K, Kramer GJ, van der Zwaan BCC (2010) Technology learning for fuel cells: an assessment of past and potential cost reductions. Energ Policy 38:2887–2897
42. Schwoon M (2008) Learning by doing, learning spillovers and the diffusion of fuel cell vehicles. Simulat Model Pract Theor 16:1463–1476
43. Staffell I, Green RJ (2009) Estimating future prices for stationary fuel cells with empirically derived experience curves. Int J Hydrogen Energy 34:5617–5628
44. Lund PD (2010) Importance of integrated strategies and innovations for commercial breakthrough of fuel cells. Int J Hydrogen Energy 35:2602–2605
45. Jamasb T (2007) Technical change theory and learning curves: patterns of progress in electricity generation technologies. Energy J 28:51–71
46. Fontell E, Kivisaari T, Christiansen N, Hansen JB, Pålsson J (2004) Conceptual study of a 250 kW planar SOFC system for CHP application. J Power Sources 131:49–56
47. Nehter P, Hansen JB, Larsen PK (2011) J Power Sources 196(17): 7347–7354
48. Baratto F, Diwekar UM (2005) Life cycle assessment of fuel cell-based APUs. J Power Sources 139:188–196
49. Baratto F, Diwekar UM, Manca D (2005) Impacts assessment and trade-offs of fuel cell-based auxiliary power units Part I: system performance and cost modeling. J Power Sources 139:205–213
50. Baratto F, Diwekar UM, Manca D (2005) Impacts assessment and tradeoffs of fuel cell based auxiliary power units Part II. Environmental and health impacts, LCA, and multi-objective optimization. J Power Sources 139:214–222
51. Hansen JB (2005) Oxygenates as SOFC fuels for APU applications. In: 15th international symposia on alcohol fuels (ISAF XV), San Diego, CA, Sep 2005, 2006
52. Rechberger J, Schauperl R, Hansen JB, Larsen PK (2009) Development of a methanol SOFC APU demonstration system. In: ECS Transactions, vol 25, pp 1085–1092
53. Alanne K, Saari A, Ugursal VI, Good J (2006) The financial viability of an SOFC cogeneration system in single-family dwellings. J Power Sources 158:403–416
54. Alanne K, Salo A, Saari A, Gustafsson SI (2007) Multi-criteria evaluation of residential energy supply systems. Energ Buildings 39:1218–1226
55. Alanne K, Saari A (2008) Estimating the environmental burdens of residential energy supply systems through material input and emission factors. Build Environ 43:1734–1748
56. Bompard E, Napoli R, Wan B, Orsello G (2008) Economics evaluation of a 5 kW SOFC power system for residential use. Int J Hydrogen Energy 33:3243–3247
57. Braun RJ, Klein SA, Reindl DT (2006) Evaluation of system configurations for solid oxide fuel cell-based micro-combined heat and power generators in residential applications. J Power Sources 158:1290–1305
58. Braun RJ (2010) Techno-economic optimal design of solid oxide fuel cell systems for micro-combined heat and power applications in the U.S. J Fuel Cell Sci Technol 7:0310181–03101815
59. Hawkes AD, Aguiar P, Hernandez-Aramburo CA, Leach MA, Brandon NP, Green TC, Adjiman CS (2006) Techno-economic modelling of a solid oxide fuel cell stack for micro combined heat and power. J Power Sources 156:321–333
60. Hawkes AD, Leach MA (2007) Cost-effective operating strategy for residential micro-combined heat and power. Energy 32:711–723
61. Hawkes AD, Aguiar P, Croxford B, Leach MA, Adjiman CS, Brandon NP (2007) Solid oxide fuel cell micro combined heat and power system operating strategy: Options for provision of residential space and water heating. J Power Sources 164:260–271
62. Palazzi F, Autissier N, François MAM, Favrat D (2007) A methodology for thermo-economic modeling and optimization of solid oxide fuel cell systems. Appl Thermal Eng 27:2703–2712
63. Staffell I, Green R, Kendall K (2008) Cost targets for domestic fuel cell CHP. J Power Sources 181:339–349
64. Gray D (2010) Current and future technologies for gasification-based power generation. Vol 2 – revision 1", 11 Nov 2010. http://www.netl.doe.gov/energy-analyses/pubs/Advanced-PowerSystemsPathwayVol2.pdf. Accessed 10 Jan 2011
65. Steinberger-Wilckens R (2009) European SOFC R&D – Status and trends. In: ECS Transactions, vol 25, 2009, pp 3–10
66. Hellman HL, van den Hoed R (2007) Characterising fuel cell technology: challenges of the commercialisation process. Int J Hydrogen Energy 32:305–315

Solid Oxide Fuel Cells, Sustainability Aspects

K. U. Birnbaum, R. Steinberger-Wilkens, P. Zapp
Institute of Energy Research, Forschungszentrum Jülich, Juelich, Germany

Article Outline

Glossary
Definition of the Subject
Introduction
SOFC as High-Efficiency Energy Converters
CO_2 Emission Reductions from SOFC Implementation
Materials Inventory of SOFC Concepts
Environmental Impacts
Future Directions
Acknowledgments
Bibliography

Glossary

BoP Balance of plant – summary term for all components of a fuel cell system, apart from the stack.
CHP Combined heat and power.
DG Distributed generation.
LCA Life cycle assessment.
LCI Life cycle inventory.
Life cycle Period of time and/or use of an object (product) spanning the time from the production over use to final disposal (cradle to grave).
SOFC Solid oxide fuel cell.
Stack Fuel cell assembly, including the single cells and the interconnecting plates.

Definition of the Subject

The introduction of environmentally relevant issues in the planning, development, and design phase of a product is today an important subject besides the usual technical, economical, social, and legal framework conditions [1]. Fuel cells as future energy conversion systems are expected to have a high potential for environmental benefits. They offer a potentially high electrical efficiency, which implies reductions in fossil fuel use and greenhouse gas emissions relative to today's generating equipment, and they display extremely low local pollutant emission levels.

Especially for new and supposedly environmentally beneficial technology, it is important to prove these benefits and identify any possible pitfalls. Under the headline of "sustainability," this article therefore discusses several aspects of environmental impact of solid oxide fuel cell (SOFC) technology: the improvements delivered by increased (primary) energy efficiency and carbon dioxide emissions on the one hand and the prospective impacts of the materials used in manufacturing the SOFC on the other hand, using an inventory analysis approach.

Introduction

Solid oxide fuel cells (SOFC) are one type of high-temperature fuel cells operating in the range of 500–850°C. The active components consist of ceramics, and electrolyte is a ceramic layer in most cases made of zirconia or ceria material. Due to the high temperature, the SOFC can use methane directly as a fuel which is then internally converted to hydrogen and carbon dioxide. The electrical efficiency of SOFC systems can reach very high values up to and above 60%, depending on operational parameters, which makes SOFC very interesting for stationary power generation at all scales from one to several hundred kilowatts but also for onboard electricity generation on vehicles.

The first part of this article looks at the impact of SOFC operation on primary energy efficiency and carbon dioxide emission from electricity generation. These two factors will have a major influence on benefits fuel cell operation will bring to the environmental footprint of the electricity supply system.

The active parts of SOFC (air electrode, electrolyte, and fuel electrode) are made of materials which are not commonly used in conventional power generating equipment. The second part of this article presents outlines of an inventory analysis, evaluating the environmental impact of the materials implemented and that of the processing chains involved using the rules of a life cycle assessment (LCA) [2]. This analysis is an important tool in testing the overall advantages of SOFC technology since environmental benefits of operating a technology may be offset by hazards and impacts that emanate from the materials and processes

used in manufacturing. Another point of interest is the end-of-use phase of dismantling and recycling.

Fuel cells are an evolving technology and require a very different set of materials for the core system parts (especially the fuel cell stack) than today's power generating equipment. Consequently, many manufacturing processes are involved which are not yet fully commercialized or well characterized. Moreover, the options for end-of-life material reclamation, recycling, and disposal are less well defined today than for other power equipment.

Much of the analysis presented in this article is thus of a preliminary nature and is based on laboratory prototypes rather than commercially available products. The data on SOFC referred to here rather reflect differences of concepts and tendencies in development than absolute values. Nevertheless, the information compiled on the materials inventory can be seen as quite representative of SOFC technology. Developments are currently taking place that might introduce novel materials and processes for certain components. Updates of the analysis will therefore be necessary as SOFC technology progresses.

SOFC as High-Efficiency Energy Converters

Worldwide, central electricity generation based on coal, nuclear, and other fossil sources has an average net efficiency of 32% [3]. The remaining 68% of the fuel energy is rejected to the atmosphere as waste heat. Average European or German efficiencies only marginally differ from this figure [4]. Another 5–10% of the electricity generated is lost during transport in the supply grids [5, 6]. Central electricity supply based on fossil fuels thus has an overall efficiency of around and below 35% and is one major cause of CO_2 emissions and depletion of fossil fuels. This relation can be written as

$$\eta_{el} = E_{el,output}/E_{fuel,input} = \eta_{conversion} * \eta_{transmission} \quad (1)$$

Therefore, high-efficiency electricity producing equipment is of great value in decreasing the environmental impact of electric power production and securing a sustainable use of primary energy resources. In the energy industry, pollution of the atmosphere with CO_2 is measured relative to end energy units, i.e., to the useful energy or energy service, generally in units of kg CO_2 per kWh of delivered energy (thermal or electrical). For carbon-containing fossil fuels, a reduction in primary energy consumption per unit of electricity delivered will obviously immediately translate into a reduction of the carbon footprint of this energy service. This effect will be discussed in the following section.

All fossil primary energy sources (from natural gas all the way to uranium) are limited in availability [7]. Their more efficient use will not automatically lead to a sustainable energy supply system since depletion will simply occur later but not be totally avoided. Nevertheless, increased energy efficiency buys time to further develop sustainable energy supply technologies, based on renewable energies. As will be shown later, SOFC technology is specifically helpful in such a transition phase since it can use both fossil- and renewables-based fuels.

As indicated in Eq. 1, increases in efficiency can be achieved both by reducing the losses in energy conversion as well as in the distribution system. While the former calls for improved efficiency in energy conversion, the latter can only partly be met by technology improvements in energy distribution. The concept of "distributed generation" addresses distribution losses of central electricity generation (at least partly) by replacing this by local electricity generating units that will be considerably closer to the electricity consumers or even are located on-site their premises (with larger building complexes, industrial and commercial facilities, etc.).

Distributed generation has been employed for decades already as a means for companies to produce their own power during periods of peak load in order to valorise waste gases emanating from a variety of production processes (in chemical industry, steel making, etc.), to supply backup or uninterruptible power, or simply to reduce electricity expenses. The main equipment applied is gas or diesel internal combustion engines and gas turbines. In the region between 1 and 500 kW_{el}, these have a limited electrical efficiency ranging from 25% to 35% [8]. The electrical efficiency will in most cases thus be below the average efficiency of central electric power delivery. Therefore, the cost of electricity produced is very sensitive to the spark spread [9], i.e., the price relation between fuel and electricity price. Especially industrial customers can reduce their

electricity bills by exploiting this price difference and produce electricity themselves at competitive cost. Following the sharp increases in the natural gas prices in Europe in the 1990s, though, many DG units were shut down due to a lack of economic competitiveness in regular electricity generation (apart from units operating in peak shaving and backup power generation).

On the other hand, the employment of relatively small generator units (tens of kW_{el} to tens of MW_{el}) near to the point of use allows for new ways of utilizing the reject heat of the units. Instead of rejecting this to the atmosphere, it can be integrated in heating buildings, hot-water and process heat supply, etc. In this way, the grid losses are minimized as well as the total efficiency of energy conversion increased. The input of primary energy will now not only result in electricity but also heat supplied. This coupling of energy streams is termed "combined heat and power generation" (CHP). The overall efficiency of primary energy use will increase by the fraction of thermal energy put to use:

$$\eta_{total} = \eta_{el} + \eta_{th} \quad (2)$$

The European Directive on CHP [10] demands that η_{tot} be higher than 70% in order for a CHP installation to qualify for the preferred conditions granted for CHP units in Europe. It has to be noted, of course, that Eq. 2 cannot be based on the maximum theoretical amount of heat that can be extracted but has to take into account what part of the heat generated could actually be put to effective use. Hot weather or hot climate conditions will prevent the utilization of off-heat for heating purposes and limit the operation of the CHP plant to hot-water production, unless other applications, for instance, coupling with chillers, are developed. A lack of demand for heat will require the CHP unit to be reduced in power output or even shut down. Ultimately, a heat rejection unit (cooler) can transfer excess heat to the ambient, if electricity demand so requires and the 70% minimum efficiency rule is not violated.

Only large gas turbines of multi-MW_{el} size and low rpm diesel engine generators of 1 MW and more can display efficiencies above 40% [11], thus competing with modern coal-fired power plants. Nevertheless, considering the avoidance of grid losses and the dramatically increased total conversion efficiency, a clear case can be made for CHP units with respect to reductions in CO_2 emissions and fossil fuel savings.

Figure 1 shows an energy flow analysis of a gas engine CHP unit. Assuming generalized figures of 30% electrical and 65% thermal conversion efficiency (relative to the lower heating value, LHV), we obtain an overall primary energy efficiency of 95%. The right side of the graph shows a comparison with a state-of-the-art heating boiler (condensing boiler) and the average electricity supply as a reference. To the right, the primary energy input into the reference system is stated that would lead to the same useful energy delivered to the customer.

The primary energy input is calculated from the useful energy using the efficiencies of 33% and 98% for the electricity delivery and heating boiler, respectively. The summation of primary energy input clearly reveals the superiority of the CHP application and displays a substantial primary energy savings of 34%. As mentioned before, the results of this energy balance of course depends on the amount of heat actually put

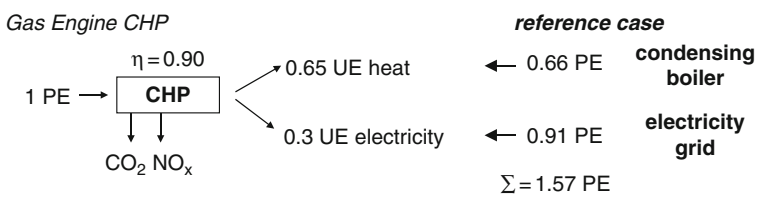

Solid Oxide Fuel Cells, Sustainability Aspects. Figure 1
Block diagram of a gas engine CHP unit producing heat and electricity. It is compared with a condensing boiler and the German electricity grid as systems of reference with respect to their delivery of useful energy (energy services). Calibrating to the energy delivery, the total primary energy effort for both scenarios can be compared as 1:1.57, i.e., resulting in a 34% decrease in primary energy effort for the gas engine CHP case

to use in the system. If excess heat is produced that has to be rejected to the environment, the total efficiency will obviously be lower.

As a result of the typical spark spread observed in Europe in the last decades, CHP units have to be operated as long as possible in order to produce as much electricity as possible. Typically, a minimum of 6,000–7,000 h in operation are required for units to be economically competitive with grid electricity [12]. Switching off units due to lack of heating demand therefore has to be reduced to a minimum.

This means that CHP units are often sized to cover little more than hot-water demand in heating systems. The situation only changes when process heat or heat for absorption or adsorption chillers is required as well. Also, the minimum size of units is more or less limited to around 5 kW_{el} since the efficiency of smaller engines and turbines dramatically drops [8]. Single family (four persons) buildings in Central Europe will typically require 1–1.5 kW_{el} of peak electric power (with an average power demand around 450 W_{el}) and summer hot-water heat demand of 500–750 W_{th} [13]. This will limit CHP units to below 1 kW_{el}. Therefore, only very few CHP units suitable for single family housing (micro-CHP) exist. These mostly use Stirling engines which have an even lower electrical efficiency, although their total energy utilization is high. Nevertheless, they suffer from an aggravated problem of heat removal in summer.

SOFC technology, on the other hand, offers interesting options to improve the effectiveness of CHP units. The reasons are many: the prospects for high efficiency, low emissions, low noise, scalability, reliability, and, finally, potentially low cost. However, the main attractiveness in CHP is the high system efficiency even for small units and at part load operation [14]. Among the most interesting applications are stationary distributed power generation (incl. CHP), small residential combined heat and power units (micro CHP), various transport applications (auxiliary power units, APU), and medium-sized portable systems up to 5 kW_{el}.

With a properly designed fuel processing system, SOFC can use many available fuel types. Operating at temperatures above 600°C, SOFC can reform methane (the main component of natural gas) directly on the cell anode or operate on CO-containing gas or even on ammonia.

The fact that thermodynamically, some of the heat generated in the electrochemical reaction can be "reinvested" into the chemical fuel conversion explains that SOFC have the potential to reach a net electrical system efficiency above 60% with natural gas fuel [14]. In a combined cycle system, where the exhaust gas from the high-temperature fuel cell is used to drive a gas turbine, the overall system electrical efficiency may even reach over 70% [15]. The efficiencies of gas turbines and diesel engines decrease at part load, whereas the efficiency of the fuel-cell-based systems will be almost independent of part load up to very high turndown ratios [14].

These high efficiencies are possible due to a marked increase in cell performance during recent years (for instance, [16]), resulting in significantly reduced overpotentials, i.e., increased cell efficiencies. An SOFC CHP unit can reach fossil fuel savings of over 45% (Fig. 2) whilst delivering the same energy services as the reference system from Fig. 1.

Figure 2 shows a comparison of two systems generating electric power at 50% (upper graph) and 60% (lower graph) efficiency. Obviously, the increase in primary energy efficiency strongly depends on the efficiency of electricity generation, which is clear since the difference in efficiency between CHP unit and reference system is highest for electricity generation. A high-electrical-efficiency CHP device will thus bring the highest gains in total efficiency. It should be noted that with SOFC CHP units, it is difficult to obtain very high total efficiency values. This is a result of the system flow sheet most of today's developments use [17], where the cathode airflow is used for cooling as well as for oxygen supply. When cathode and anode off-gas are combined in an afterburner to combust any unconverted fuel, the dilution of the resulting exhaust gas with air is so high that it is virtually impossible to reclaim the sensible heat in the water vapor within the exhaust gas stream. Due to the typically high lambda values of 4–8, the dew temperature of the exhaust gas is far below the 50°C condensing boilers display. Therefore, Fig. 2 shows the total energy efficiency to remain constant at 80%, independent of electrical efficiency. Total energy efficiency can be increased using larger heat exchangers (which will also imply higher pressure drops and air blower energy requirements). The dew temperature on the other hand can only be increased by

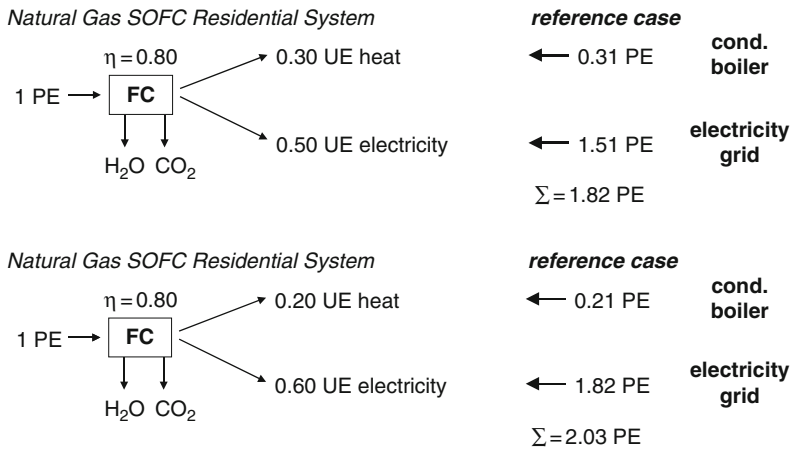

Solid Oxide Fuel Cells, Sustainability Aspects. Figure 2
Modification of Fig. 1 with parameters for a high-efficiency SOFC system. Electrical efficiency is taken as 50% and 60%, while the overall efficiency remains constant (80%). Primary energy use is decreased by 45% and 51%, respectively, for the two energy services

reducing the diluting effect, for instance, by condensing the water out of the anode gas stream before mixing.

Nevertheless, the graphs also show an imminent problem: the more electricity is generated, the less heat is available for further use. This is of course also a result from high conversion efficiencies because due to the second law of thermodynamics, the higher the proportion of electrical energy (useful energy), the lower the losses (entropy), which in the case of CHP are partly turned into useful heat (theoretically, if the fuel cell extracted heat from the environment, the entropy could even be negative and the efficiency higher than 100%; this effect is used in high-temperature electrolysis, SOEC). As a result, the units have to be scaled up again in order to produce sufficient heat for a specific application, for instance, summertime hot-water demand. High electricity production in a single family housing, on the other hand, generally means a high fraction of electricity fed to the grid. This is not a problem in itself since low-efficiency generated, centrally produced electricity is displaced by high-efficiency generated electrical energy. Since CHP electricity fed to the grid is supported by guaranteed pricing or regulated tariffs in most parts of Europe [18], though, a high fraction of grid feed-in will make the economics of the unit strongly dependent on the political framework. This will often be fragile and may change during the lifetime of the unit, thus causing an additional operational risk for the owner.

With high-temperature fuel cells, the off-heat offers further possibilities. Polygeneration is the parallel production of electricity, heat, and other products like steam, hydrogen, etc., or heat supplied to air conditioning and cooling equipment. The temperature level of the SOFC exhaust gas is sufficiently high to serve as efficient heat source for both ad- and absorption chiller regeneration. The exhaust gas from the fuel cell can also be adjusted to a syngas composition with carbon monoxide concentrations that can be used by downstream chemical processes as, for instance, reported in [19].

One final thought should be spent on the heat use in distributed generation. There are applications, for instance, in grid stabilization and peak load production, where the exhaust heat of small electricity generating units is not used. This can be the case when there are no heat sinks in the vicinity of the DG unit and the electricity generating costs are competitive even without marketing the off-heat. The aspect of high electrical efficiency will in these cases be the main specification of interest, again making an SOFC system or even a hybrid system of SOFC and gas turbine with electricity generating efficiencies of 60–75%, respectively, specially attractive [20].

CO_2 Emission Reductions from SOFC Implementation

Working on hydrogen as a fuel, SOFC will obviously achieve a 100% reduction in local CO_2 emissions for a given energy service providing electricity and heat (as, for instance, depicted in Fig. 2). Of course, the environmentally relevant emissions from the hydrogen production process have to be acknowledged for also, so that an analysis here cannot be definite since the source of hydrogen would be arbitrary. Since, on the other hand, the main applications of SOFC are the area of stationary or diesel-based vehicle systems, the question of hydrogen fuel is – at least for the time being – a marginal one.

Once large quantities of renewable, fluctuating energy streams have to be stored in order to balance power production and demand in the supply grids, especially under the framework conditions of a high fraction of renewable energies in the supply system, this situation will change [20, 21]. SOFC and their twin technology, the solid oxide electrolyzers (high-temperature electrolysis) [22], will receive an important role for producing hydrogen and reconverting it to electricity at high efficiencies.

Nevertheless, stationary electricity generation, whether in micro-CHP, CHP, or distributed generation, will heavily rely on carbon-containing fuels for many years to come. This is due to the fact that distributed generation units are generally run on natural gas (more rarely on diesel or fuel oil) [23] and rely on the natural gas distribution infrastructure for fuel supply. Figure 3 shows a selection of fuels suitable for high-temperature fuel cells (in effect, both for MCFC and SOFC). The conversion of the majority of these fuels will lead to a release of CO_2. The improvement in electrical efficiency of the conversion as compared to conventional technology will inherently bring considerable reductions in CO_2 emissions, in parallel with the primary energy savings mentioned in the previous section.

Therefore, high-efficiency electricity-producing equipment is important in decreasing the environmental impact of electric power production. In energy services, pollution of the atmosphere with CO_2 is measured relative to end energy units, i.e., to the form of energy delivered to the customer (electricity, fuels, etc.), generally in units of kg CO_2 per kWh. The figure not only includes the emissions from the energy conversion

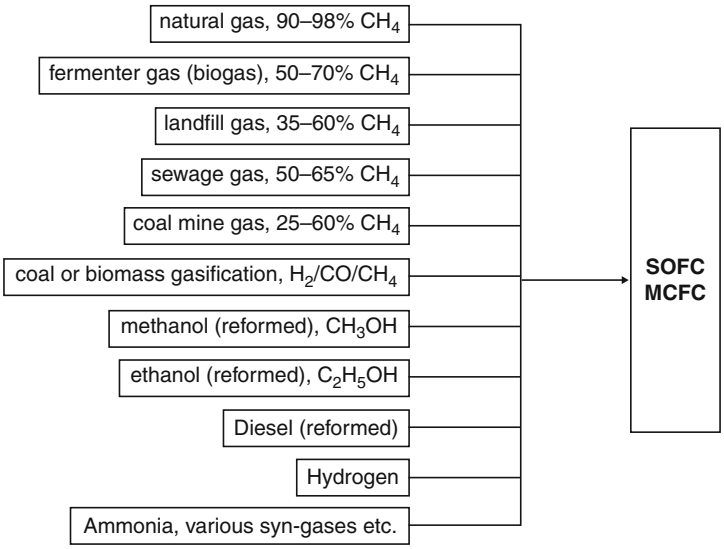

Solid Oxide Fuel Cells, Sustainability Aspects. Figure 3
Fuels suitable for high-temperature fuel cells. Most of these are gases and can be converted internally within the fuel cells without preprocessing (apart from eliminating corrosive elements and pollutants). The higher-order hydrocarbons, though, including diesel, generally require reforming (Values from [23, 24])

itself but also all emissions emanating from the processing steps leading up from the primary energy source (oil well, coal mine, gas well, etc.) up to the energy form delivered to the customer.

In order to compare energy conversion processes on site of the customer, the respective consumption of fuel has to be calculated and the CO_2 emissions evaluated from this. Table 1 compares some processes in building energy supply (heating and electricity). In the CHP processes, the figures for heat and electricity production alone are also stated. They are not practically relevant but show that only the combined use of all energy forms produced leads to the desired increase in system performance. For carbon-containing fossil fuels, a reduction in primary energy demand per unit of electricity produced (and delivered) will obviously immediately translate into a reduction of the carbon footprint of the energy service. Comparison of the emission values for gas engine and SOFC CHP shows that values can be misleading, if not properly compared to a reference system. Assuming a high total efficiency of the gas engine (by using latent heat from the exhaust gas water content), the total emission from the energy generated (electric plus thermal) is lower than with the fuel cell. With today's system architecture, the latter will not reach heat removal efficiencies as high as with the gas engine. Nevertheless, looking at the electrical efficiency alone, the SOFC has a clear advantage. A full analysis, though, will have to consider the alternative (or reference) cases as, for instance, shown in Figs. 1 and 2 and compare the emissions with this (see below).

Reduction effects can also be achieved by using primary energy sources with reduced carbon content in the chemical energy stored (for instance, natural gas in place of coal, where the methane in the natural gas contributes three atoms of hydrogen per atom of carbon).

Within Fig. 3, three fossil fuels are mentioned (natural gas, coal, and mineral oil/diesel), all three of which require some pretreatment, i.e., pre-reforming, gasification, and reforming, respectively. The pretreatment requires heat which again can, at least partly, be recovered from the SOFC exhaust heat. Nevertheless, gas treatment will generally reduce the total efficiency of conversion since these processing steps will incur additional losses.

The gases from renewable sources, on the other hand, have a twofold advantage:

- They only contain ingredients that can be directly fed to an SOFC (apart from pollutants that have to be removed in any case).
- They only contain carbon in the form of methane, carbon monoxide, and carbon dioxide, all of which are either an SOFC fuel or an inert gas (from the perspective of the fuel cell).

Therefore, the use of these gases merely requires gas cleanup but no further processing. The carbon dioxide emissions from electricity generated using biogas (fermenter gas), sewage, coal mine, or landfill gas are extremely low since the carbon chemically bound in the gas molecules was originally extracted from the

Solid Oxide Fuel Cells, Sustainability Aspects. Table 1 CO_2 emissions per unit of useful energy (kWh electricity or heat) and for combined heat and power generation (From [25] and own calculations)

Process	Fuel	CO_2 emission/kWh useful energy (LHV)
Condensing boiler	Natural gas	235 g/kWh (heat)
German electricity supply grid	Various	560 g/kWh (electricity)
Gas engine CHP (30% el.effic., 95% total effic.)	Natural gas	362 g/kWh (heat)
		783 g/kWh (electricity)
		247 g/kWh (combined)
SOFC CHP (60% el.effic., 80% total effic.)	Natural gas	1,175 g/kWh (heat)
		392 g/kWh (electricity)
		294 g/kWh (combined)

atmosphere, thus leading to a net zero release. The only remaining carbon dioxide contribution originates from fossil energy that was consumed in the growing, harvesting, and transporting the feedstock and in building the plants and devices necessary for producing the gases. In the cases of landfill and coal mine gas, even these contributions may be extremely low since the only effort is to capture and channel the gases which are produced anyhow. Landfills and coal mines as such have been known to be attributed high values of CO_2 equivalent values due to the highly adverse effect methane emissions have to the atmosphere [26]. Once these gases are used for energy production, though, this effect is avoided and the CO_2 footprint is dramatically reduced. Table 2 shows the CO_2 emission factors for various renewable gases from Fig. 3.

In comparing and assessing the carbon reduction potential of SOFC in CHP applications, a balance of emissions has to be drawn in analogy to Fig. 1. Such a balance is shown to the left in Fig. 4. The black bar above the axis indicates the CO_2 release from 1 kWh of feedstock gas (for instance, natural gas) for an ignition engine CHP unit with a heat and electricity production in the ratio 0.65:0.3 (as indicated in Fig. 1). The patterned bars below the axis show the carbon dioxide release for the reference case producing the same amount of useful heat and electricity (condensing boiler and grid electricity, emission values as in Table 1 for the German grid). The resulting balance between the two cases is indicated as the gray bar above the x-axis. In the case shown, the CO_2 reduction amounts to 27%. The middle set of bars shows the relationship for an SOFC micro-CHP unit with 60% electrical efficiency (as in Fig. 2).

Solid Oxide Fuel Cells, Sustainability Aspects. Table 2 CO_2 emission factors for various renewable fuels from Fig. 3 [87, 91]

Fuel	CO_2 emission/kWh (LHV)
Fermenter biogas (energy crops)	~0 g/kWh
Fermenter biogas (manure)	~0 g/kWh
Fermenter biogas (wastes)	~0 g/kWh
Landfill gas	4 g/kWh
Sewage gas	0 g/kWh
Coal mine gas	195 g/kWh

It is clear that the CO_2 emissions reduction is considerably higher (−39%) than in the first case due to the increased electrical efficiency, even though the total efficiency is lower. Finally, on the right side, the same (SOFC) case is shown using fermenter biogas. Since the net CO_2 emission of this process is near to zero, the CO_2 emission reduction dramatically increases to minus 74% with the parameters assumed for this example.

Total CO_2 emission reduction is lower than the primary energy savings since part of the primary energy used in electricity generation is free of CO_2 already today. Therefore, the ratio between the emission factors from Table 1 does not reflect the ratio in efficiencies as displayed in Figs. 1 and 2.

The total energy efficiency of a CHP unit will have a distinct effect on the CO_2 emission reduction. The less energy is lost to the environment, the less CO_2 is effectively emitted per unit of final energy (electricity and heat), especially as the electrical efficiency is increased. On the other hand, the savings in comparison with a reference case will depend on the balance between heat and electricity production (as represented by the respective system efficiencies). This is analyzed in Fig. 5. The y-axis shows the absolute CO_2 reduction in comparison with a German reference system as in Figs. 1 and 2. The three lines correspond to 70%, 80%, and 95% total energy conversion efficiency, as may be attributed to low-, medium-, and high-efficiency CHP units, 70% being the minimum set by European Regulations [9]. The x-axis shows the electrical efficiency of the CHP unit.

The SOFC CHP installation with the total energy efficiency (η_{tot}) comparable to up-to-date gas engine units (95%) displays emission savings all across the electrical efficiency (η_{el}) range. With other words, due to the high η_{tot}, the unit can even save emissions at low η_{el}. On the other hand, the low η_{tot} units will not improve but even deteriorate the CO_2 emission balance at low η_{el}. It is therefore essential to analyze the overall primary energy and emission situation when choosing and installing CHP units. As with many other examples, the simple replacement of conventional technology with technological alternatives will not automatically create a more intelligent solution. It is

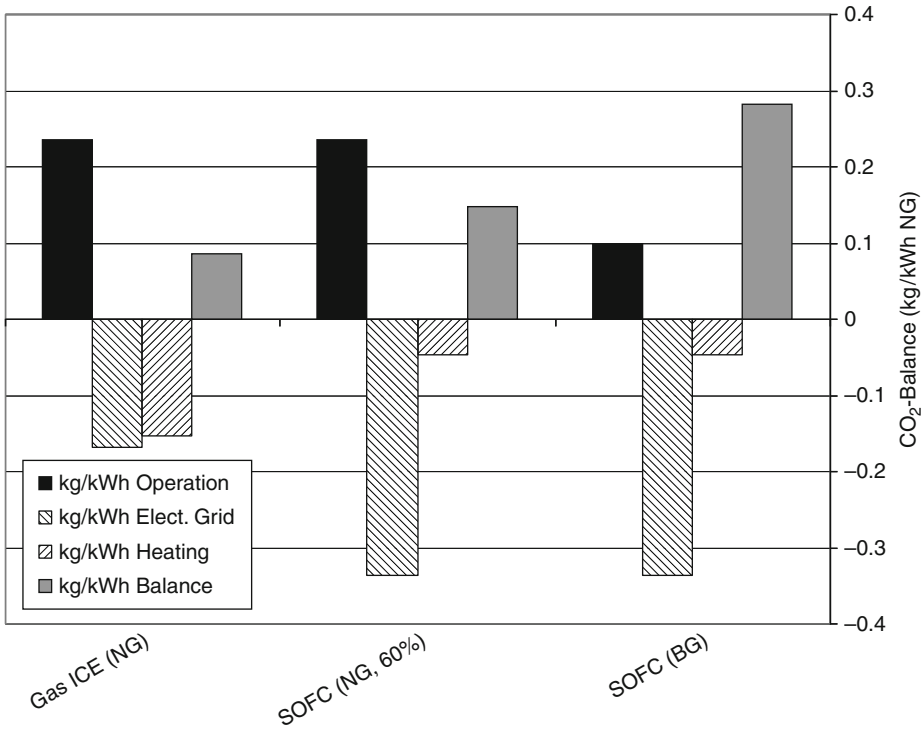

Solid Oxide Fuel Cells, Sustainability Aspects. Figure 4

Emission balances for a gas engine CHP system as depicted in Fig. 1 (*left*) for the SOFC system depicted in Fig. 2 (η_{el} = 60% case, *middle*) and the same SOFC system operated on biogas (*right*). The *black bars* show the CO_2 emissions from the CHP system. The patterned bars below the axis represent the CO_2 emission from the reference system (cf. Fig. 1), and the *gray bar* shows the difference between CHP unit and reference case. If the balance is positive (*above the axis*), the CHP unit saves the amount of CO_2 shown

equally apparent that high η_{el} is a necessary requirement, if major CO_2 emission reductions are targeted and that a high η_{tot} can only partly offset a low η_{el}. Since a condensing boiler displays a conversion efficiency of around 98%, this sets the benchmark for the limiting case of zero electrical efficiency.

The case of pure electricity generation with an SOFC unit is represented by the data points with equal η_{el} and η_{tot}, for instance, 0.7, 0.7. At this specific point, the CO_2 reduction is about 35% and not more, due to the considerable loss of 30% of the energy input. A higher electrical efficiency hardly appears feasible, though a combination of an SOFC with a (micro) gas turbine could lead to η_{el} of up to 75% [15]. Total energy efficiency, nevertheless, is doubled.

The examples above were calculated for the situation of the German electricity grid and the CO_2 footprint shown in Table 1. It can easily be argued that the CO_2 savings will strongly depend on this footprint, i.e., in a grid with no CO_2 emissions from electricity generation, a CHP installation will not be able to reduce emissions. Figure 6 shows the parameter analysis with 200, 400, and 600 g of CO_2 per kWh of grid electricity. The total energy efficiency η_{tot} is set to 80% as a point of reference. As may have been expected, the CHP units cannot deliver emission savings in grid environments with low CO_2 footprint.

If the carbon footprint is even lower than that of a condensing boiler, higher electrical efficiencies will even lead to a further deterioration of the emission balance. It is therefore rather obvious that not only the situation at the point of installation but also the total system configuration into which the CHP unit is integrated need careful analysis.

The analysis up to here has been based on the energy output of a single gas engine or SOFC CHP

unit. This is of course a rather limited view, since the requirements of a building or household being supplied with electricity and heat will most probably not be covered by the CHP system alone. Generally, CHP systems are built with the CHP unit as a base load unit supplying the major part of the electricity and some heat, with a (condensing) boiler as the main and backup heat source. Any electricity demand that cannot be covered by the CHP unit – for lack of heat demand, for instance – would be covered by the grid, into which also the excess electricity is fed when heat demand is high and electricity demand not sufficient to use all electrical output.

Due to the higher value of the electricity as compared to heat delivery, CHP units are designed to operate as continuously as possible and mostly at a minimum of 5,500–6,500 h per year, thus delivering the base load. The layout of such a system is shown in Fig. 7. The total CO_2 balance of such a system will not only depend on the balances for the CHP unit alone, as shown in Figs. 5 and 6, but on the annual displacement of grid electricity and conventional heating. Figure 8 depicts the situation for a household with 20.000 kWh_{th} of annual heat demand and a CHP installation of 1 kW_{el}. The gas engine CHP unit will deliver 2.17 kW_{th}, the two SOFC units (with 80% and 95% total efficiency) 0.33 and 0.58, respectively. A heating boiler is added that will supply the remaining heating and hot-water requirements. The gas engine is limited to around 6,600 h of annual operation. Above this, the heat demand is lower than the heat produced and the unit is shut down.

Both fuel cell units have a maximum heat production of below and around 500 W. This will just cover the hot-water demand of a typical household (12 kWh/day). Therefore, these units will not be shut down at all, maybe with the exception of holidays.

As a results, the η_{tot} = 80% SOFC and the gas engine unit are roughly equivalent in CO_2 reduction. The percentage of reduction, though, is slightly lower because the overall level of CO_2 emission is higher due to the lower η_{tot}. The η_{tot} = 95% SOFC system achieves higher savings in CO_2 emissions. Nevertheless, a comparison with Fig. 4 shows that the differences between the scenarios have been reduced. This is due to the emissions from the heating boiler that amount to roughly half of total emissions in all scenarios and thus form a kind of base emission to which the CHP unit then adds.

The percentage of CO_2 saved is between 22% and 23% (left and middle set of columns), and 28% (right set of columns). These figures are smaller than those displayed in Fig. 4 due to the base level set by the heating system.

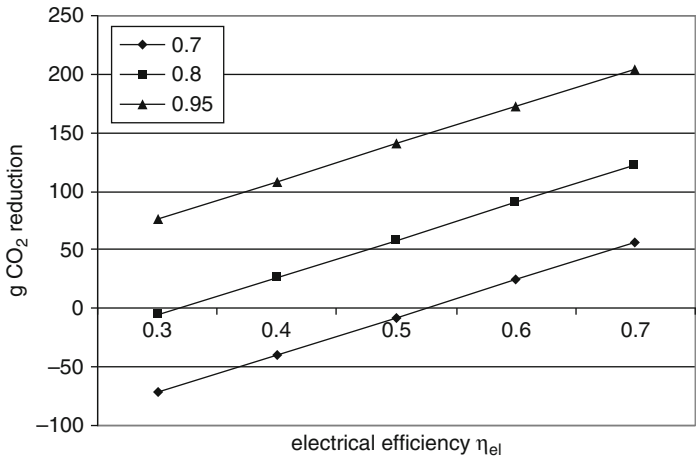

Solid Oxide Fuel Cells, Sustainability Aspects. Figure 5
Dependence of total CO_2 savings from a CHP unit running on natural gas on the total energy conversion efficiency η_{tot} (parameter) and the electrical efficiency η_{el} (x axis). A condensing boiler and the German electricity grid are taken as a reference

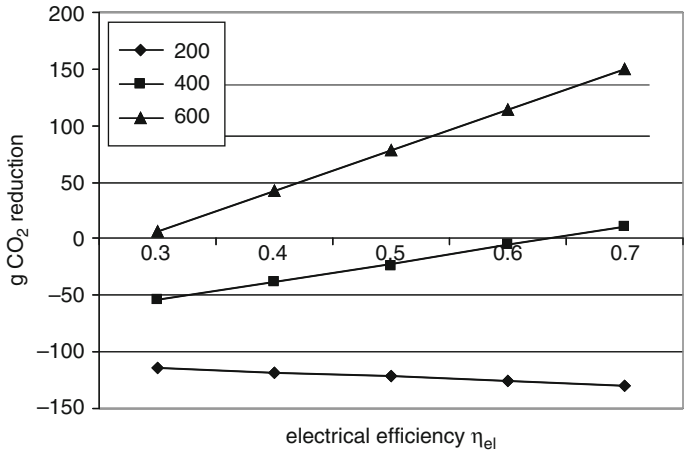

Solid Oxide Fuel Cells, Sustainability Aspects. Figure 6
Dependence of total CO_2 savings from a CHP unit running on natural gas on the electrical efficiency of the unit, η_{el} (x axis), and the CO_2 footprint of the electricity grid in g CO_2/kWh_{el} (parameter). Again, a condensing boiler and an electricity grid with the respective footprint are taken as a reference. Total energy efficiency (η_{tot}) of the SOFC CHP unit is set to 80% in this example

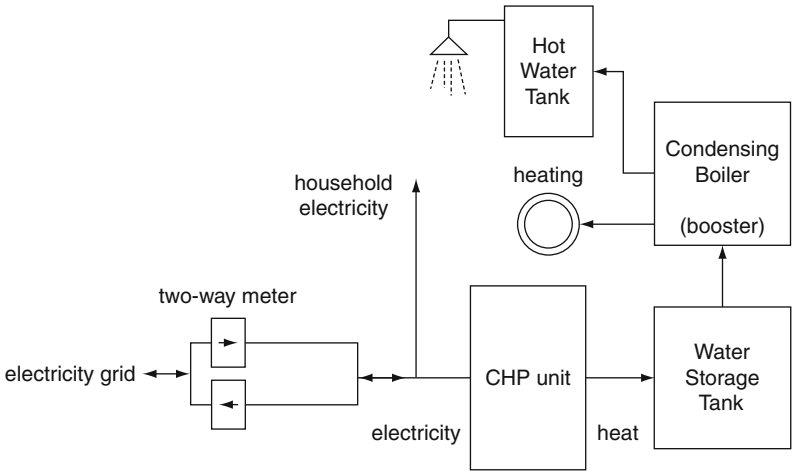

Solid Oxide Fuel Cells, Sustainability Aspects. Figure 7
Typical layout of a residential CHP system. For typical German households, the heat demand is around 20,000 kWh/year (heating and hot water) and electricity consumption amounts to 4,000 kWh/year [13]. A 1 kW_{el} CHP system will therefore require a heating boiler and the electricity grid as backup and as a sink for excess electricity

Materials Inventory of SOFC Concepts

An Introduction to Life Cycle Assessment

An environmental evaluation of the entire life cycle of an SOFC system is necessary to ensure that no environmental effects are neglected, right from the start of the development. A well-developed tool to investigate all stages of a product's life cycle is the life cycle assessment (LCA). It addresses the environmental aspects and potential impacts (e.g., global warming potential, acidification potential, ozone depletion potential, and toxicological potential) throughout the life cycle of

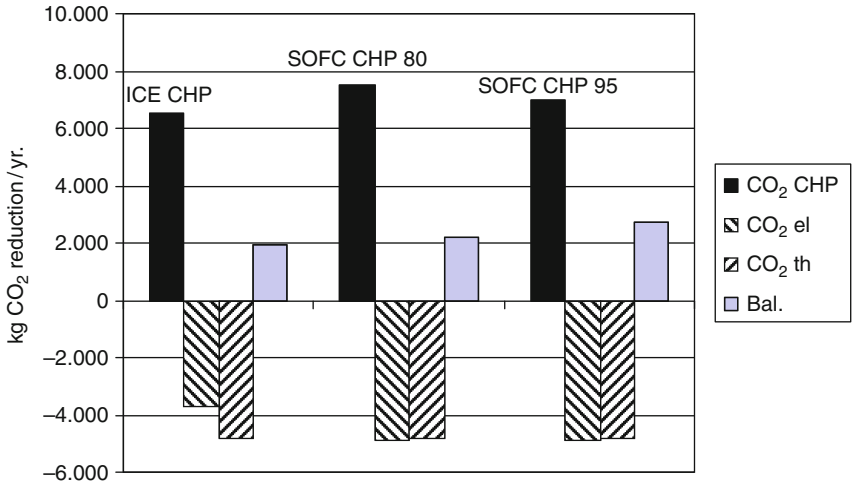

Solid Oxide Fuel Cells, Sustainability Aspects. Figure 8
CO_2 emission balances in analogy to Fig. 4 for a system according to Fig. 7 for three selected CHP units. Total heating consumption is 20,000 kWh/year and total electricity consumption 4,000 kWh/year

a product or a technique from "cradle to grave" [2]. This not only covers the emissions and energy consumption during operation, as discussed in the previous sections, but also the materials inventory and all environmental effects emanating from the raw materials extraction (for instance, mining, etc.), over the materials processing to the final manufacturing steps. A complete analysis includes the end-of-life provisions, as, for instance, recycling, waste treatment, or waste disposal.

An LCA is divided into four distinct, though interdependent, phases: (1) goal and scope definition, (2) inventory, (3) impact assessment, and (4) interpretation (see Fig. 9).

1. In the first step, the extent of the analysis as well as the specific methods used is described. A precise definition of the product, comparison basis (functional unit), system boundaries, time frame, and geographical coverage, as well as methodological choices such as allocation methods and impact categories of the assessment are made during this initial phase.
2. Secondly, all environmental inputs and outputs of the investigated system are collected, calculated, and analyzed. For every life cycle stage, inputs (energy and materials) and outputs (emissions to air and water, solid wastes) are gathered and aggregated over the entire life cycle. As one has to deal with a huge amount of data in this step, databases are usually used. For process technology that is not yet commercially available, the only possibility to collect data is often contact with industrial manufacturers and researchers. When the data situation is unclear, an assumption has to be made and its influence has to be investigated via a sensitivity analysis in the discussion of the results.
3. Thirdly, the inputs and outputs of the system are categorized and allocated to impact categories, such as global warming, acidification, ozone depletion, eutrophication, human- or ecotoxicity, etc. After calculating the environmental effects in the different categories, optional steps are normalization, grouping, and weighting.
4. In the last step, results have to be summarized and discussed as a basis for conclusions and recommendations. Limitations are to be detected. Sensitivity analysis can be used as an appropriate tool for this purpose. Iteration between life cycle interpretation and the other LCA phases often occurs to refine results, further explore sensitivities, or clarify critical problems unveiled in the analysis.

Demarcation of the Analysis Area

Figure 10 provides an overview of the complexity of an operational fuel cell system which is an ensemble of

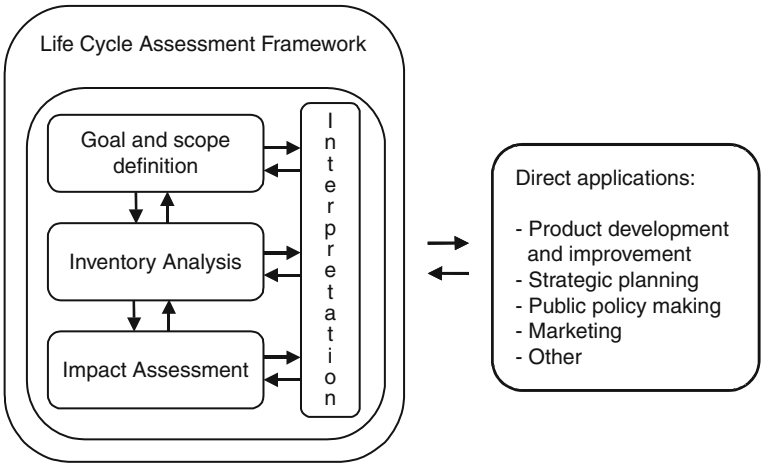

Solid Oxide Fuel Cells, Sustainability Aspects. Figure 9
Phases of an LCA according to [2]

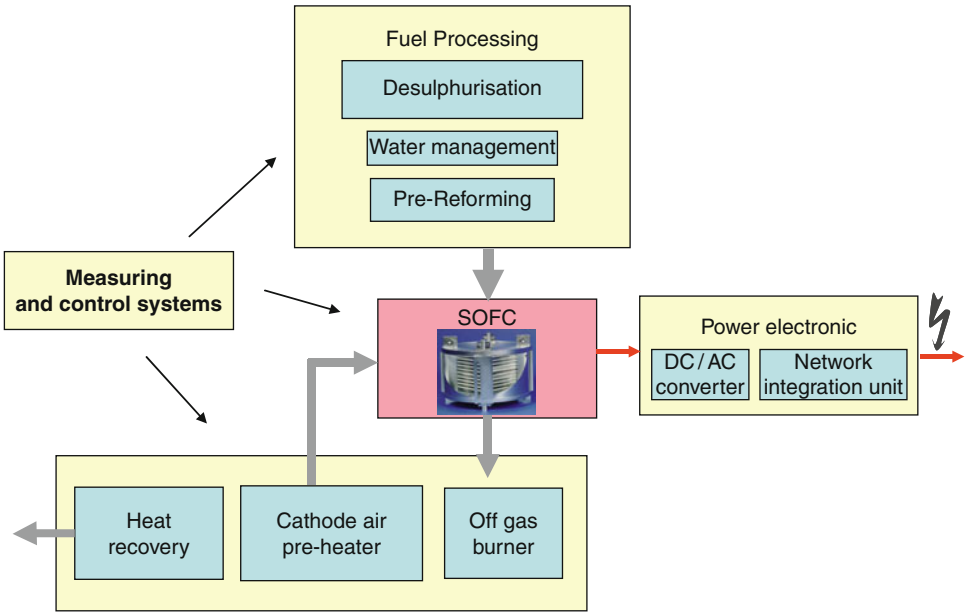

Solid Oxide Fuel Cells, Sustainability Aspects. Figure 10
Layout of a fuel cell system with its main components

technical components. Five main sections can be distinguished:

- The fuel cell stack at the center
- The upstream fuel processing unit with desulfurization, pre-reforming, and water management
- The Balance of Plant (BoP) of which only the off-gas burner, the preheater, and the heat recovery unit are shown
- The measuring and control system
- The power electronic components like DC/AC converter and the grid integration unit

Although all equipment components of an operable system should be considered working out an LCA, the analysis presented here only covers the fuel cell stack and is based on findings of the EU-project REAL-SOFC [29] in which three different SOFC concepts were analyzed.

These stack concepts include:

- A planar stack with anode-supported ceramic cells designed for stationary applications, as, for instance, developed by Forschungszentrum Jülich [30], referred to in the following as "stationary design"
- A planar, lightweight stack with metal-supported cells made by plasma spraying, as, for instance, developed by DLR [31], referred to in the following as "lightweight plasma-sprayed design"
- An "integrated planar" stack as a hybrid between tubular and planar technology, as, for instance, developed by Rolls-Royce Fuel Cell Systems [32], referred to in the following as "IP design"

All of these designs are still in a development stage and do not represent commercially available components. Insofar the data presented in the following is preliminary and should be considered "indicative." What the data does show, nevertheless, is the principal differences between the concepts and their weak points that require further consideration in the development process.

Raw Materials for the Cell Components

The materials for the SOFC, mostly mixtures and not pure elements, must be extracted/manufactured from raw materials. Besides iron ore and chromite, which supply the main components for the steel parts, especially rare earths, nickel ore, and alkaline earth minerals are important sources of raw materials. For the LCA of a fuel cell, the upstream mining and processing chains are of equal interest to the processing of the pure materials.

Due to the expected demand in future applications, i.e., batteries for electric mobility, long-term bottlenecks in raw materials availability cannot be ruled out. This possibly applies for strategically important metals such as rare earth elements or others, as the regional distribution of the reserves and resources is very diverse [33].

The following section presents examples of main raw materials as a first indication of the environmental impact and of possible contributions from the upstream processes of materials extraction and purification.

Zirconium (Zr) Zirconium is one of the main constituents of SOFC electrolytes today (in YSZ, yttrium stabilized zirconia). As indicated in the previous chapter, it is not only the main element in the electrolyte but also an important ingredient in anode substrates and composite cathodes.

Occurrence The share of zirconium in the structure of the earth's crust amounts to roughly 0.02 weight percentage. It does not occur in pure form in nature. The most important zirconium minerals are alvit (zircon, $ZrSiO_4$) and brasilit, and/or baddeleyit (zirconia, ZrO_2). Deposits are found on the coasts of Australia, as well as in South Africa, in the USA (Florida), Brazil, China, India, Sri Lanka, Madagascar, Scandinavia, Greenland, and in the GUS states.

Production Zirconia is usually produced from zircon, $ZrSiO_4$. Zircon sands are first melted with sodium hydroxide and transferred to zirconium (IV) oxide. With addition of coal, the zirconium oxide is transferred to zirconium carbonitride in a plasma arc, which is converted again to zirconium (IV) chloride with chlorine. The chloride is reduced to zirconium with magnesium in a helium atmosphere at 800°C in the so-called Kroll-process: $ZrCl_4 + 2Mg \rightarrow Zr + 2\ MgCl_2$.

After the distillation of the magnesium chloride and the separation of excess magnesium, the retrieved raw zirconium is cleaned in a vapor deposition process.

Australia is the largest producer with a share of nearly 50% at the world production and also has the largest reserves. The second position is held by South Africa, with regard to the yearly production as well as to the reserve situation (cf. Table 3).

Yttrium (Y) Yttrium is used in SOFC cells to stabilize the zirconia lattice in electrolyte materials and used within a range of 3–10 mol% (3YSZ, 8YSZ, 10YSZ, etc.).

Occurrence Yttrium is a rare earth element and occurs in nearly all of the rare earth minerals. Rare earths are defined as a group of 17 elements, comprised of

Solid Oxide Fuel Cells, Sustainability Aspects. Table 3 World production and reserves of zirconium [34]

	Mine production Zircon and baddeleyite		Reserves[6] (thousand metric tons)		Reserve base[6] (thousand metric tons)	
	2005	2006[e]	ZrO_2 content	HfO_2 content	ZrO_2 content	HfO_2 content
United States	W	W	3,400	68	5,700	97
Austalia	445	480	9,100	180	30,000	600
Brazil	35	35	2,200	44	4,600	91
China	17	20	500	NA	3,700	NA
India	20	20	3,400	42	3,800	46
South Africa	305	310	14,000	280	14,000	290
Ukraine	35	37	4,000	NA	6,000	NA
Other countries	20	20	900	NA	4,100	NA
World total (rounded)	880	920	38,000	610	72,000	1,100

scandium, yttrium, and the lanthanides. The similar radii and oxidation states of the rare earths allows liberal substitution of the rare earths for one another into the crystal lattice sites of minerals. This substitution accounts for their wide dispersion in the earth's crust and the characteristic occurrence as a group of elements within more than 100 minerals. The principal ores of the rare earths are bastnäsite, monazite, and xenotime. Several of the ores occur in unique geologic settings, whereas others are found in similar occurrences worldwide.

Bastnäsite ($CeFCO_3$) – a fluorocarbonate of cerium containing 60–70% rare earth oxides (REO), including lanthanum and neodymium – is the world's major source of rare earths. Host rocks include carbonatite, dolomite breccia with syenite intrusives, pegmatite, and amphibole skarn. Since 1985, the bastnäsite production in China has increased very fast and has dominated the market from the 1990s to the present.

The mineral xenotime (YPO_4) was the principal ore of yttrium and the other heavy rare earth elements. The ion-adsorption lateritic clays from Southern China replaced xenotime as the principal source of yttrium and the other heavy rare earth elements in the 1990s. These intensely weathered clays have rare earth ions adsorbed into the clay mineral structure.

Monazite ($(Ce,La,Y,Th)PO_4$) is a rare earth phosphate containing 50–78% REO. It is recovered as a component of heavy mineral sands and is a major source of thorium which imparts radioactive properties to the mineral [35, 36].

Production World production of rare earths was estimated at 98,200 metric tons of equivalent rare earth oxides in 2002. The graph in Fig. 11 only shows the development of production up to 2006. China was by far the largest producer, with ~90% of the world's total. Smaller amounts of ore came from the U.S.A. and other countries like India, Kazakhstan, Kyrgyzstan, Malaysia, Russia, and the Ukraine [37].

In 2008, the approximate distribution of rare earths by use was as follows: magnets 21%, metal alloy 18%, catalysts 19%, polishing 12%, glass 10%, phosphors 7%, ceramics 6%, and miscellaneous 7% [38].

Reserves Large resources of yttrium in monazite and xenotime are available worldwide in ancient and recent placer deposits, carbonatites, uranium ores, and weathered clay deposits (ion-adsorption ore). Additional large subeconomic resources of yttrium occur in apatite-magnetite rocks, deposits of niobium-tantalum minerals, nonplacer monazite-bearing deposits, sedimentary phosphate deposits, and uranium ores. The world's resources of yttrium are probably very large [39].

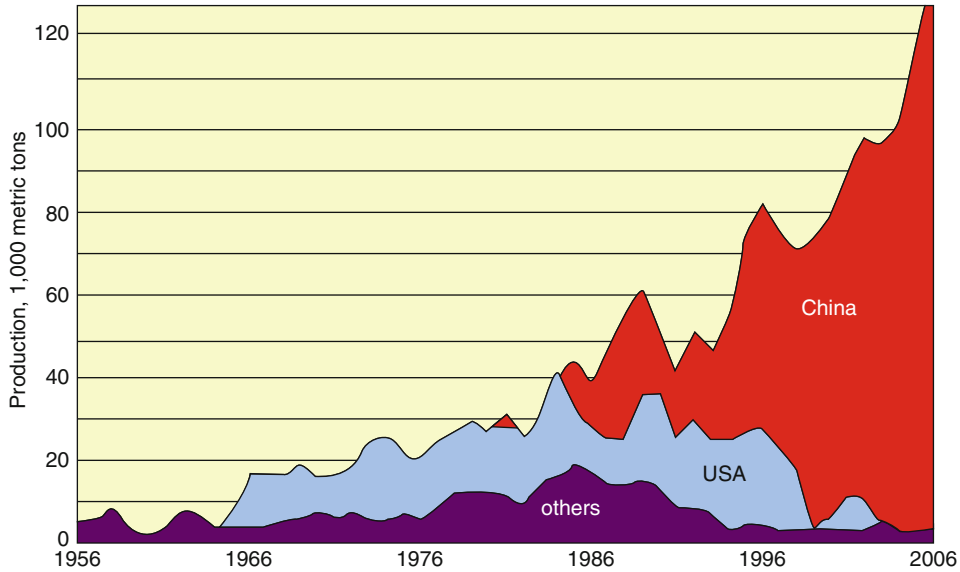

Solid Oxide Fuel Cells, Sustainability Aspects. Figure 11
Worldwide rare earth oxide production [36]

Biological rating: No known benefits to life processes [40].
Biological benefits: Yttrium has no known biological use [40].

Lanthanum, La Lanthanum is a main constituent of cathode materials but is also used in ceramic interconnects and in electrolytes or contact pastes.

Occurrence Lanthanum has a share in the earth's crust of 0.0017%. In nature, it always occurs in compounds with other rare earth metals and in minerals like bastnäsit, monazit, cerit, or orthit, with percentages up to 25% and 38%, respectively. Misch metal, used in making lighter flints, contains about 25% of lanthanum.

Lanthanum is one of the most reactive of the rare earth metals. It oxidizes rapidly when exposed to air. Cold water attacks lanthanum slowly, and hot water attacks it much more rapidly. The metal reacts directly with elemental carbon, nitrogen, boron, selenium, silicon, phosphorus, sulfur, and with halogens [41].

Production The most important base minerals are xenotime, monazite, and bastnäsite. The first two are orthophosphate minerals $LaPO_4$ and the third is a fluoride carbonate $LaCO_3F$. Lanthanoids with even atomic numbers are more common. Monazite also contains thorium and yttrium which makes handling difficult since thorium and its decomposition products are radioactive.

For many purposes it is not particularly necessary to separate the metals, but if separation is required, the process is complex. Initially, the metals are extracted as salts from the ores by extraction with sulfuric acid (H_2SO_4), hydrochloric acid (HCl), and sodium hydroxide (NaOH). Modern purification techniques for these lanthanoid salt mixtures are ingenious and involve selective complexation techniques, solvent extractions, and ion exchange chromatography.

Pure lanthanum is available through the reduction of LaF_3 with calcium metal.

$$2LaF_3 + 3Ca \rightarrow 2La + 3CaF_2$$

This would work for the other calcium halides as well, but the product CaF_2 is easier to handle under the reaction conditions (heated to 50°C above the melting point of the element in an argon atmosphere). Excess calcium is removed from the reaction mixture under vacuum [42].

Biological rating: No known benefits for life processes in plants and animals.
Biological benefits: Lanthanum has no known biological use [43].

Obtained from: Lanthanum mainly is obtained from lanthanum-rich monazite and bastnäsite. Other lanthanum-bearing minerals include allanite and cerite. It is mined in the USA, China, Russia, Australia, and India [43].

Strontium, Sr Strontium belongs to group 2 of the periodic table and is one of the alkaline earth metals. Strontium, with atomic number 38, lies between calcium and barium in this group. The discovery of strontium carbonate, which was originally thought to be barium carbonate, is associated with a lead mine located in Strontian, Scotland, hence the name strontium.

Occurrence Strontium is present in the Earth's crust at an average concentration of 0.04% and is therefore 15th in abundance. Of the naturally occurring strontium compounds, only the minerals strontianite (strontium carbonate, $SrCO_3$) and celestite (strontium sulfate, $SrSO_4$) are of economic importance.

Celestite occurs principally as nodules, lenses, beds, and materials filling crevices in sedimentary rocks such as carbonates, gypsums, clays, and evaporites. The economic importance of celestite is considerably greater than that of strontianite.

Production Celestite ores are obtained by both open-pit and underground mining. In most cases, only coarsely intergrown rich ores are worked, which can be further enriched by hand picking to give a material containing >90% $SrSO_4$. Demands for increasing purity in chemically produced strontium salts together with the growth of mechanized mining techniques necessitate a continually increasing amount of processing. Finely divided impurities are removed by desliming. By means of density separation, celestite is separated from limestone, quartz, gypsum, and dolomite, which have densities of <3 g/cm^3, giving end products containing >95% $SrSO_4$. In Spain, a flotation plant for separating finely intergrown celestite ores has been in operation since 1990. The introduction of this technology has markedly increased the number of deposits worldwide that can be profitably worked.

Many important deposits cannot be mined because of unacceptably high levels of barium and deposit-specific trace elements that cannot be removed by available processing technologies.

Production of Strontium Carbonate Black Ash Method, Reduction with Carbon. To enable the chemical reduction of $SrSo_4$, celestite is mixed with powdered coal and then heated up to about 1,100°C. The chemical reaction follows the equation $SrSO_4 + 2C \rightarrow SrS + 2CO_2$ and produces carbon dioxide and strontium sulfide. In the next process step, the strontium sulfide is dissolved in water, before carbon dioxide passes through $SrS + H_2O + CO_2 \rightarrow SrCO_3 + H_2S$ the solution, forming and precipitating strontium carbonate from the solution. The by-product sulfur is recovered as elemental sulfur.

Soda Ash Process. Ground celestite ($SrSO_4$) is converted to strontium carbonate by adding it to hot sodium carbonate solution. Numerous variations of this process have been proposed. Typically, an excess of Na_2CO_3 solution is used. The crude product so obtained is not usually acceptable without further treatment. A product sufficiently pure for most applications is obtained by dissolving the crude material in hydrochloric acid, neutralizing with sodium carbonate solution to precipitate iron and aluminum, filtering, and reprecipitating with caustic soda. This process also produces impure sodium sulfate solution as a by-product which must be further treated or disposed. The high consumption of sodium carbonate is a further drawback [44].

Production of Strontium Metal Metallic strontium can be produced by aluminothermic reduction of the oxide or by electrolysis in the dry way of a $SrCl_2$–KCI blend. The refining takes place via vacuum distillation.

Transportation, Storage, and Safety Due to its reactive nature, strontium must be handled with care. The pure metal and the commercial eutectic alloy (90% Sr, 10% Al) are classified as alkaline earth metals NOS (not otherwise specified), UN no. 1393, for the purposes of transportation. This classification is indicative of materials requiring special approved packaging for transport. These two forms of commercial strontium are packed under an inert atmosphere to prevent formation of an oxide coating. Strontium is a strong reducing agent and forms explosive hydrogen gas when in contact with water. Strontium is therefore classified as a flammable solid. Hence, strontium is a Class 4.3 material, i.e., one that emits a flammable gas on contact with water. Strontium should therefore be stored in

a well-ventilated dry place, avoiding all contact with water. However, commercial alloys of strontium, such as the Sr–Mg–Al master alloy or the family of aluminum–strontium master alloys which contain up to 10% strontium, do not require these special precautions.

Use Metallic strontium and master alloys containing strontium have experienced significant expansion in application in modern foundry practice. In aluminum foundries, strontium is used as an additive to Al–Si alloys to enhance their mechanical properties and improve the machining performance. Strontium improves the mechanical properties of Al–Si castings by changing the morphology of the eutectic silicon phase. In an unmodified Al–Si alloy, this eutectic silicon phase precipitates as coarse acicular plates, which causes the casting to exhibit poor mechanical properties. Modification causes the silicon to assume a fine, interconnected fibrous morphology, resulting in higher tensile strength and greatly improved ductility. Impact resistance and machining characteristics are also enhanced through modification.

Strontium improves the properties and processing of wrought aluminum alloys.

In an aluminum alloy sheet which requires high formability, the presence of strontium is reported to reduce the number of intermetallic precipitates. This improves the alloy's formability and reduces the incidence of edge cracking.

In ferrous metallurgy, strontium finds application as a component in certain foundry grades of ferrosilicon, used as inoculants in gray iron casting. The addition of 0.65–1.05% strontium controls the carbon structure in an iron casting and inhibits the chill. The chill, which is in some cases a desired phenomenon, is a rapidly solidified zone in a casting where the formation of mottled iron (cementite and graphite) is favored over a pearlite structure with graphite. By controlling the chill, the foundry may be able to decrease the minimum section size in a casting keeping it free from the brittle carbides which would most likely form without inoculation. In addition, strontium-bearing inoculants are particularly effective in helping to control internal shrinkage in these castings and thereby enhancing the pressure tightness of the casting [44].

Economic Aspects and Reserves Whereas strontianite was the principal starting material used in the production of strontium compounds between 1870 and 1920, it has now been almost completely replaced by celestite for this purpose.

Practically the only use for celestite is the production of other strontium compounds. It is used only to a small extent as a white filler in competition with ground barite (barium sulfate).

World production of celestite in the early 1990s was estimated at ca. 250,000–300,000 t/annum. The most important producing countries are Spain, Turkey, United Kingdom, China, Mexico, Iran, and Morocco.

The world production in 2003 was around 370,000 metric tons of strontium minerals, and the reserves are expected to exceed 1 billion tons.

Large exploited deposits exist in Spain, Mexico, Turkey, China, and Iran. There are much less important deposits in Algeria, Cyprus, Argentina, and Morocco. Mining in the United Kingdom, the traditional producer, ended in 1992.

Manganese, Mn

Occurrence Manganese is a silver-gray metal, resembling iron. It is hard and very brittle, and its primary uses in a metallic form are as an alloying, desulfurizing, and deoxidizing agent for steel, cast iron, and nonferrous metals. It has a high tendency to oxidize.

Manganese is the twelfth most abundant element in the Earth's crust, at 950 ppm.

Manganese is contained in many minerals, of which approximately 250 can be regarded as true manganese minerals. The major ores, generally with manganese contents above 35%, are hydrated or anhydrous oxides. The silicates and carbonates occur to a lesser extent.

Economically significant manganese deposits are all of sedimentary origin, having been dissolved from crystalline rocks and deposited as the oxide, hydroxide, or carbonate.

Typically, only ores containing a minimum of 35% Mn are regarded as manganese ores. Ores containing 10–35% Mn are categorized as ferruginous manganese ores, and iron ores with 5–10% Mn are referred to as manganiferous ores.

The three most important areas of application of manganese ores and the specific requirements are as follows:

1. Metallurgical grade ore for the iron and steel industry, which generally contains 38–55% Mn. The phosphorus content should preferably be below 0.1%, and the concentrations of Al_2O_3, SiO_2, CaO, MgO, and S are important. The manganese/iron ratio is critical; a 7.5:1 ratio, e.g., is required for a standard ferromanganese alloy with 78% Mn.
2. Battery grade ore, containing 70–85% MnO_2 (44–54% Mn). The ore should generally contain less than 0.05% of metals more electronegative than zinc, such as copper, nickel, cobalt, and arsenic. The suitability of manganese dioxide for use in batteries depends on a number of factors, including the crystal structure, surface area, pore size distribution, particle shape and size, electrical conductivity, surface conditions, chemical composition, and structure defects.
3. Chemical grade ore whose specifications vary considerably depending on the end use. Included in this category are feedstocks for electrolytic manganese and manganese dioxide, manganese chemicals, colorants, and, in the Republic of South Africa, an oxidant in uranium extraction.

Production The major producers of manganese ore apply both underground and open-pit mining techniques. In the Republic of South Africa, Samancor extracts ore from the open-cast Mamatwan mine and the underground Wessels mine. At Mamatwan, e.g., the ore body attains a maximum thickness of 45.2 m and is overlain by, on average, 45 m of overburden. The open pit is approximately 1,900 m by 300 m, and the ore is extracted from three benches by drilling, blasting, loading, and hauling to an in-pit crusher. At Wessels, the ore body is located at a depth of ca. 300 m and a room and pillar mining system is employed. The average stope height is ca. 5 m, and the ore is drilled, blasted, loaded, and hauled to underground primary crushing facilities.

The most important methods for the production of relatively pure manganese metal are the electrolysis of aqueous manganese salts and the electrothermal decomposition of manganese ores [45].

Reserves The most important manganese ore deposits are located in the Republic of South Africa, Russia, Australia, Gabon in West Africa, and Brazil. The deposits in India and Mexico are of declining importance, and the majority of the production is consumed domestically.

The largest known land-based manganese deposit is the Kalahari Field, located in the Northern Cape Province of the Republic of South Africa, which contains ca. 78% (13,600 × 106 t) of the world's potential resources. The surface area underlain by this deposit is approximately 320 km^2. The deposit is sedimentary and interlayered with banded ironstone.

Nickel, Ni

Occurrence Nickel is a frequent element and with a share of 0.015% of the earth's crust inhabits the 21st place of the list of frequency of elements. It is more abundant than copper, zinc, or lead. In elemental form, it occurs only in meteorites. On the earth, it is component of so-called nickel ores. An important example is pentlandit which has a close association with other sulfides such as pyrite, chalcopyrite, and pyrrhotite in basic igneous rock intrusions. Garnierite and nickeliferous limonite are other nickel ores of economic significance. The term garnierite is commonly used as a generic name for a series of mixed nickeliferous silicates with a wide range of nickel contents and can include colloidal mixtures of silica and nickel hydroxide. Nickeliferous limonite is the term used to describe poorly crystalline nickel-bearing ferric oxides of which the main constituent is goethite (α-FeO • OH).

Production The methods for the extraction and refining of nickel minerals depend on the mineralogical and geological characteristics of the ore. Nickel has mainly been extracted from sulfide and laterite ores.

Nickel sulfide ores are mostly mined underground using drilling, blasting, and other techniques. Milling procedures include liberation, flotation, and magnetic separation. Liberation of the sulfides from the gangue includes grinding of the rock material. Then the sulfides are concentrated by flotation processes. Flotation involves streaming air bubbles through an aqueous slurry of the ore particles in a flotation cell. The particles that are not wetted by the liquid adhere to the air

bubbles, rise to the surface of the slurry, and can be removed. The addition of different chemicals to the flotation medium allows the selective flotation of nickel- and copper-rich fractions.

Most of the pyrrhotite (both lump ore and ground ore) can be separated magnetically because of its magnetic properties.

Laterite nickel deposits are mined from open pits using earthmoving equipment.

Both sulfide ore concentrates and laterite ores are subjected to pyro- and hydrometallurgical processes. The pyrometallurgical processing basically involves three operations, i.e., roasting, smelting, and converting.

During roasting, the concentrate is oxidized by hot air. Most of the iron is oxidized, while nickel, copper, and cobalt remain combined with sulfur. Part of the sulfur is removed as gaseous sulfur dioxide.

The roasted product is smelted in a furnace together with a siliceous flux to obtain two immiscible phases, an iron-rich silicate slag and a nickel-rich sulfide matte, which also contains iron, copper, and cobalt.

The matte is treated in a "converter" where more sulfur is driven off and the remaining iron is oxidized and removed as slag.

The matte is allowed to cool and treated in different ways. It may be, e.g., cast into anodes for electrolytic refining or cooled slowly to facilitate crystallization to nickel sulfide, copper sulfide, and a nickel–copper alloy containing the desired metals. These three phases can then be separated by flotation and magnetic separation. The species of nickel likely to be present during roasting, smelting, and converting include the ore, nickel subsulfides, nickel-copper sulfides, nickel oxides, nickel-copper oxides, arsenides, and anhydrous nickel sulfate. The extraction of nickel from laterite ores is similar to the extraction of nickel from sulfide ores with the exception that sulfur (commonly gypsum) has to be added. The molten matte is charged into a converter where the iron is oxidized, and the sulfur combines with nickel to form Ni_3S_2.

Smelting to ferronickel is essentially the same as matte smelting, except that no sulfur is added. It is often applied to laterite ores. The resulting iron–nickel alloy contains 20–50% nickel [46].

Most of the nickel matte obtained from sulfide or laterite ore smelting undergoes further refining techniques, such as electro-, vapo-, or hydrometallurgical refining, but a part of the matte is roasted to marketable nickel oxide sinter.

Hydrometallurgical refining can be applied both to laterite ore and sulfide ore or sulfide ore concentrates. Soluble nickel amines are formed during pressure leaching of the sulfide ore concentrate with strong ammoniacal solution at a moderately elevated temperature. The saturated solution is boiled to drive off ammonia and precipitate copper as sulfide. Sulfur is oxidized. Nickel and cobalt are recovered as pure metal powders by reduction with hydrogen under pressure.

Laterite ores must first be reduced. The reduced ore is leached with an ammonia–ammonium carbonate solution. Nickel dissolves as nickel amine. The saturated solution is heated by steam, ammonia is driven off, and nickel is precipitated as a basic carbonate.

Pure nickel (99.9%) can be produced by electrolytic refining. Generally, an impure metal anode (produced by reducing nickel oxide) and a cathode starting sheet are placed in an acidic electrolytic solution. When a current flows, nickel and other metals are dissolved from the anode. The electrolyte is then removed, purified, and returned to the cathode compartment, where nickel is deposited on the cathode.

During vapometallurgical refining, impure metal obtained by the reduction of nickel oxide is subjected to the action of carbon monoxide forming volatile nickel carbonyl [$Ni(CO)_4$] (carbonyl or Mond process). This reaction is reversed by heat, and the nickel carbonyl decomposes to pure nickel metal and carbon monoxide. The carbonyl process produces the purest nickel (99.97% or more) [47–51].

Chromium

Occurrence Chromium is practically only found as chromite or chrome iron stone, ($FeCr_2O_4$), in open-pit mining or in near-surface underground mining. Metallic chromium is obtained by reduction of the ore with aluminum or silicon. Untapped chromite deposits are plentiful and geographically concentrated in Kazakhstan and southern Africa.

Production South Africa extracts approximately half of the world's demand of chromite. Other substantial producing countries are Kazakhstan, India, and Turkey.

Approximately 15 million tons of marketable chromite ore were produced in 2000 and converted into approximately 4 million tons of ferrochrome.

Stationary SOFC Stack Design

The "stationary" SOFC design used for analysis in the following is based on the F-Design stacks as developed by Forschungszentrum Jülich since 2002. It was established as a laboratory platform for evaluation of SOFC cell developments, protective layers, thermal cycling capabilities, and long-term degradation [30, 52, 53]. Nevertheless, it is also a concept that can be used in stationary fuel cell applications, i.e., for power generation and CHP. For practical, commercial employment, though, some critical parameters, like the amount of steel used for interconnects (see below), will need to be improved, for instance, in order to reduce the manufacturing costs.

The central element of the solid oxide fuel cell stack is the SOFC cell which consists of the fuel electrode (anode), the oxygen electrode (cathode), and the ion-conducting electrolyte. To reach the desired electrical voltage, single cells are stacked (cf. Fig. 11). They are separated by interconnects (plates) and sealed by glass ceramics.

In the case discussed here, the anode substrate is the mechanically supporting component of the fuel cell. The thickness of the anode is set at ~1,500 μm due to laboratory manufacturing constraints in warm pressing. More recent anode substrates produced by tape casting are reduced to 300–1,000 μm thickness, still supplying the required mechanical stability. In choosing the anode material, attention must be paid to the fact that the electrochemical reactions are not impaired by the thickness. As the electrolyte has no mechanical function in this concept, its thickness can be reduced from the typical ~150 μm seen with electrolyte-supported cells to ~5 μm. In this way, the resistance of the electrolyte decreases dramatically. This opens the possibility to reduce the operating temperature to below 800°C, without any efficiency losses. The reduced operating temperature promises several advantages such as simpler and cheaper materials and manufacturing processes, or longer lifetime.

A variety of new materials have been and still are being developed and applied in this SOFC concept. Due to the operating temperature range of 600–800°C, heat-resistant steels, ceramics, and glasses are preferentially used. Depending on the function and requirement specifications, the components differ with respect to the choice of materials.

Figure 12 gives an impression of the cell design, the different layers (components), and of the materials used in a stack repeating unit (interconnect to interconnect). The respective functions are described on the following pages.

The tasks of the *interconnect* (equivalent to the bipolar plate in low-temperature fuel cells) are the separation of the gas supply streams for the electrodes and the electrical contacting of the cells. An important requirement with contacting is the reduction of the

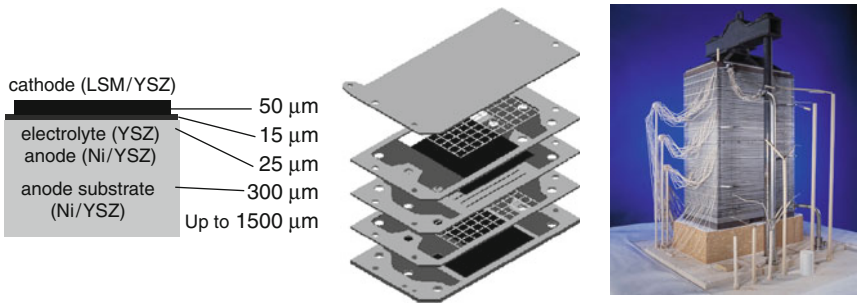

Solid Oxide Fuel Cells, Sustainability Aspects. Figure 12
Stationary SOFC concept, stacking principle, and example of a 15 kW stack [30, 52, 53]. The F10 stack shown in the middle has cells of size 10 × 10 cm^2 and a footprint of approx. 12 x 20 cm^2. The 15 kW class stack has a footprint of approx. 22 × 30 cm^2 and a height of about 40 cm

transition resistance to the electrodes of the SOFC. For the guidance of the gaseous fuels, gas distribution structures can be machined into the interconnects. Highly alloyed ferritic steel can be used as material for the interconnect, if the operating temperature of the SOFC is appropriate and not above 850°C. This condition can be fulfilled with the anode-supported concept. The new developed chromium–nickel alloy steel (CroFer22APU) is very suitable to fulfill the requirements. It ensures a permanently good electrical conductivity, and the expansion coefficient differs only slightly from that of the ceramic membrane. It fulfills further requirements like high thermal conductivity, favorable corrosion properties, commercial availability, low product costs, and simple machining [54, 55].

The *cathode* (the air electrode of the fuel cell) has to reduce the oxygen molecules (O_2) of the air to oxygen ions (O^{2-}) which then migrate to (and through) the electrolyte. Its porous structure enables the gas transport to the electrolyte surface. It must also supply electrons for the reduction of the oxygen so that good electron conductivity is necessary. Lanthanum strontium manganite (LSM), a complex oxide with a perovskite structure, is used as a standard cathode material today. This fulfills the requirements with respect to processing and to the chemical stability during operation. The coefficient of thermal expansion also matches well to that of the electrolyte. LSM exhibits high electronic conductivity; nevertheless, the ionic conductivity is nearly zero. Electron conducting materials like LSM have a disadvantage since the electrochemically active area ("three phase boundary" of cathode, electrolyte, and gas space) is limited to the direct vicinity of the electrolyte. To overcome this drawback, the cathode material is mixed with electrolyte material – forming the actual cathode (composite cathode) – and covered with a current collecting layer of pure cathode material (bilayer cathode) [56]. More advanced SOFC cells use perovskites where the manganese is replaced by cobalt or iron or replaced by a combination of these (LSCF cathodes) [57]. Further modifications include doping with copper or the use of nickelate materials.

To achieve the desired power output, repeating units are piled up to form a "stack." A gas-tight separation of the anode- and cathode-side gas supply with, at the same time, good electrical contact between the cells is a prerequisite of this design. Two problems occur with this assembly. On one hand, the cell might be uneven and slightly curved, which can lead to contact problems with the interconnect. On the other hand, the process temperature of the fuel cell (700–900°C) may lead to chromium evaporation from the steel interconnect which can cause an inhibition of the electrochemical process at the cathode side and contributes thereby substantially to the degradation of the cell and to the impairment of the life span of the SOFC [58]. To solve these problems, *contact layers* and chromium evaporation *protective layers* are applied. The requirements for these layers are a good chemical and thermodynamical stability at the operating temperatures of the fuel cell with, at the same time, good electrical conductivity. Furthermore, the layers should not interact chemically with each other nor the interconnect or the electrodes. For this purpose, special ceramic oxides with perovskite or spinel structure were developed which fulfill these requirements. For the cathode side contact layer, perovskites are often used. Sputtered, plasma-sprayed, galvanically applied or vapor-deposited perovskite, metal, and metal oxide coatings on the interconnect show good results as evaporation protection [59].

Within the *electrolyte*, the oxygen ions (O^{2-}) are transported from the air electrode to the fuel electrode side (anode). Well suitable material is zirconia (ZrO_2), which is a poor ionic conductor at ambient conditions, but if heated up to temperatures above 2,000°C, it becomes ionic conducting due to a phase transformation from tetragonal to cubic structure. By adding stabilizing agents like yttria (YSZ), calcium (CSZ), or scandia (ScSZ), the cubic structure is stabilized even at ambient conditions. Because of this stabilization, zirconia becomes a reasonable ionic conductor at SOFC operating temperatures (600–850°C) [60].

The *anode* must be an effective oxidation catalyst so that the oxygen ions, diffused through the electrolyte, react with the fuel hydrogen. Further requirements are, amongst others, high electronic conductivity, chemical, and mechanical stability. For nickel-YSZ anodes (the YSZ provides structural support for separated Ni particles, preventing them from sintering together while matching the thermal expansions) nickel oxide and YSZ are mixed and thermally treated through several steps to form the anode substrate, which has the necessary mechanical stability to be used as the base

component for the cell. When the SOFC cell is heated up in reducing conditions (for instance, hydrogen atmosphere), the nickel oxide is reduced to metallic nickel and the resulting ceramic and metal structure, the so-called cermet, is characterized by an excellent electrical conductivity due to its nickel content. A pore structure is achieved by mixing organic particles into the substrate before sintering and permits the fuel gas to flow to the anode interface with the electrolyte. The electrocatalytic effect is based on the metallic nickel, which not only binds hydrogen on its surface but also carries the electrons resulting from the oxidation of the hydrogen. The necessary oxygen ions are supplied by the electrolyte and the ramified YSZ network, whereas the transport of the fuel gas and its corresponding products takes place through the pores. The selective tuning of the pore structure, nickel, and YSZ content leads to an optimized electrochemical conversion [61].

Thermal cyclability and redox stability are crucial requirements for SOFC stacks. Reliable *sealing* of the gas-filled compartments is necessary to ensure a high effectiveness and safe operation of the stacks. The difference in coefficients of thermal expansion (CTE) of the stack components requires long-term separation of the oxidant and fuel-gas compartments of planar stacks under dynamic operation conditions. Glass-ceramic sealants are, for instance, developed basing on the ternary system $BaO–CaO–SiO_2$ with additions of transition metal oxides. Chemical interaction of the sealing glass with the interconnect steel may deteriorate the corrosion resistance of both chromia-forming as well as alumina-forming alloys [62]. The inherent brittleness of glass ceramics and the rigid bonding of the stack components limit the compensation of mechanical and thermal stresses and promote growth of defects or cracks at the interconnect/glass-ceramic interface. Due to the stiff stack assembly, the reduction of mechanical or thermal stresses by elastic or plastic deformation or by free expansion and contraction of stack components is hampered. Furthermore, a nondestructive dismantling of stacks to replace malfunctioning components is impossible [63].

Manufacturing of Components and Cell A description of the manufacturing process chain is given for the example of an anode-supported SOFC with warm pressed substrate.

The anode substrate is the mechanical supporting component of the cell (cf. Fig. 13). The substrate consists of nickel oxide (NiO) and yttria-stabilized

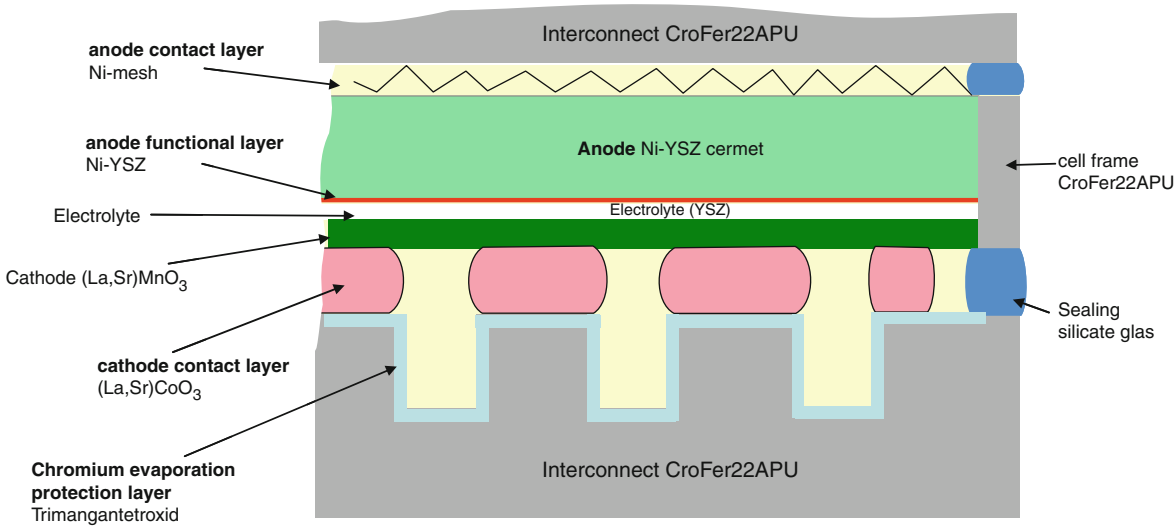

Solid Oxide Fuel Cells, Sustainability Aspects. Figure 13
Cross section of a planar SOFC stack single repeating unit [30]

zirconia (8YSZ) and is fabricated by conditioning of the ceramic powders using the Coat-Mix® Process with polymeric resin and subsequent warm pressing; Figure 14 shows the various processing steps. After burning out the resin, which makes the powder flowable and strengthens the components during pressing, the substrate is fired at temperatures >1,000°C. Thereafter, the substrate has sufficient mechanical stability and the necessary porosity for the subsequent coating processes. The substrate does not act as anode since a triple phase boundary with the electrolyte is necessary for this function. Making the substrate of essentially the same material as the anode, though, reduces problems of CTE matching and chemical compatibility while it adds considerable reforming capabilities for methane reforming. During the next processing step, the actual anode layer and the electrolyte are deposited by vacuum slip casting. For the coatings, alcoholic suspensions of NiO/8YSZ and pure 8YSZ are deposited in sequence on the substrate, dried, and sintered at a temperature of ca. 1,400°C during a cofiring process. After sintering, the electrolyte is gastight and the "half-cell" can be cut to the required dimensions with a diamond saw or by laser cutting. The cathode layer (for instance, LSM) is then deposited by wet powder spraying or screen printing on the anode-electrolyte unit as a bilayer of differently processed powders. The completed cell is dried and subsequently sintered at about 1,100°C.

Anode The Coat-Mix Process® is a procedure patented by FZ Jülich, in which different nonsoluble powders (called fillers) are coated with phenol formaldehyde resin (binder). The manufacturing takes place by mixing NiO, YSZ, and ethanol in a roll container using zirconia balls for milling. The NiO agglomerates, existing in the NiO powder, are destroyed, and both powders are finely grinded. Thus, one receives a homogeneous mud-like alcoholic suspension of the raw materials. After transfer into

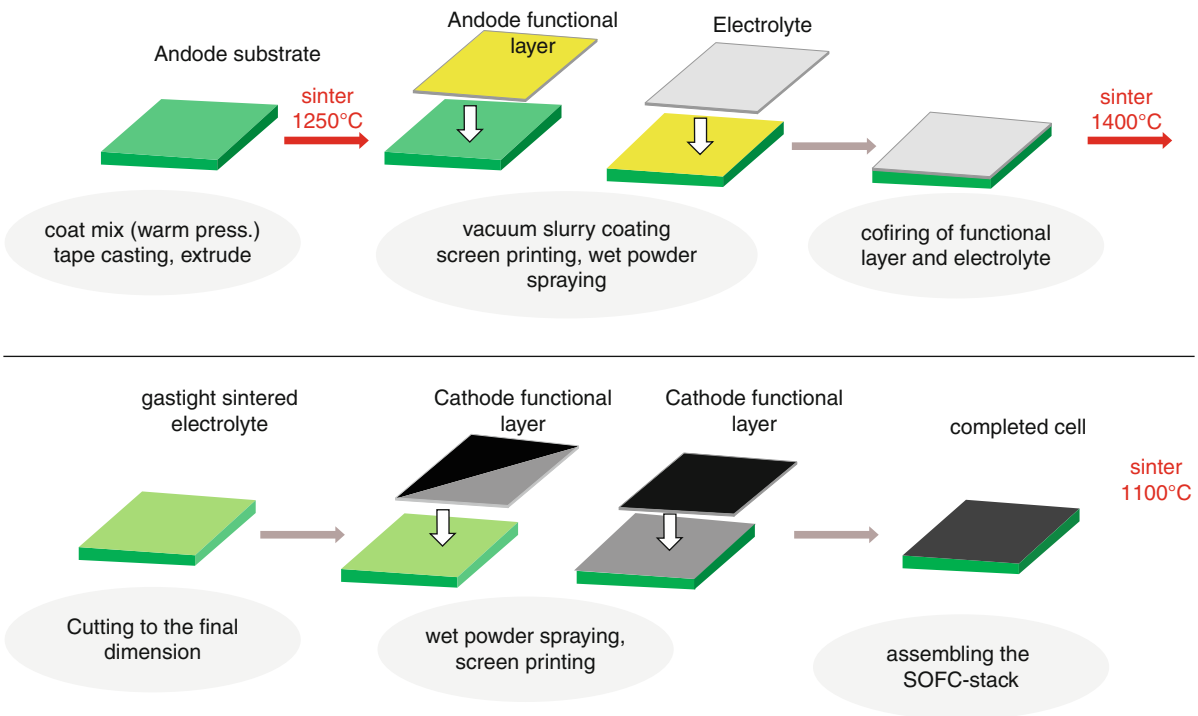

Solid Oxide Fuel Cells, Sustainability Aspects. Figure 14
Processing scheme of Jülich's SOFC (the fabrication technologies stated for each process step are alternatives in production technologies) [64]

the coating container, Fig. 15, phenol formaldehyde resin is added to the alcoholic suspension, which dissolves in the existing alcohol after short warming, so that a slurry in binder-lotion is produced. In the following step, acidified water with defined supply rate is added slowly and continuously to this mixture. The phenol formaldehyde resin is hardly soluble in water and precipitates again with the addition of the insoluble phase. The powder grains, which are held in suspense by milling, are coated in this phase with the phenol formaldehyde resin and stick together easily with one another to larger agglomerates (coat mixing). After a subsequent thermal treatment and a washing process, the precipitation settles and the liquid is removed on a suction filter.

The filter cake is transferred to dishes and dried in a vacuum condensation drying furnace at low temperature. The advantage of this manufacturing method is that no further additives are needed in the mixing process. The powder, which is obtained in this way, is well processible after sieving <80 μm and is filled in pressing forms. Under low pressure, at temperatures above the melting range of the binder, it is processed to the desired anode substrates [65].

Alternatively to this discontinuous anode production process, tape casting can be used, a standard industrial production technology in electronics, by which the anode substrate can be produced continuously (Fig. 16).

The first step of the process is the preparation/mixing of a slurry consisting of nickel oxide with yttria-stabilized zirconia and graphite powder, as well as several organic additives like solvent, disperging agents, binder, and softener. The slurry is subsequently cast by means of the tape casting facility. During the process, the slurry flows from a storage container onto a plastic or metallic foil, which is continuously moved at a controlled velocity beneath the container. The height of the slurry layer is controlled by a doctor blade, which determines the final layer thickness and which creates a smooth and even slurry coating on the carrier foil. After casting the slurry, the formed ceramic foil passes a drying chamber, in which the foil is dried at given temperatures. Thus, a flexible ceramic foil is manufactured ("green tape"), which can be cut, sawn, or punched. Once it is sintered at temperatures >1,000°C, it is rigid and can be coated. The advantage of the procedure in relation to other methods,

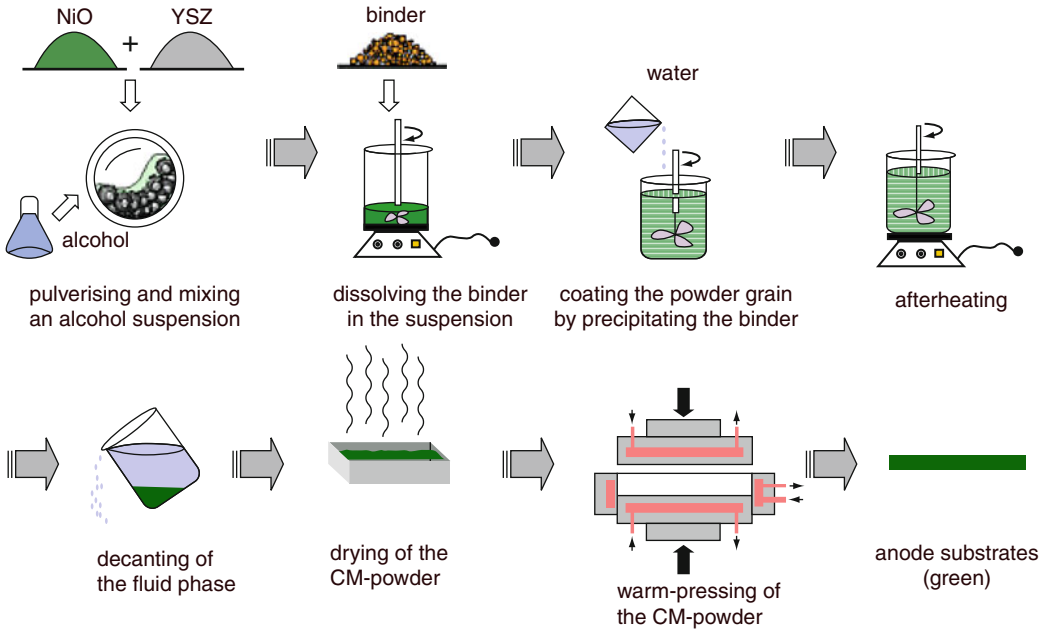

Solid Oxide Fuel Cells, Sustainability Aspects. Figure 15
Manufacturing the anode substrate by means of the Coat-Mix® Process (CM) with subsequent thermal pressing

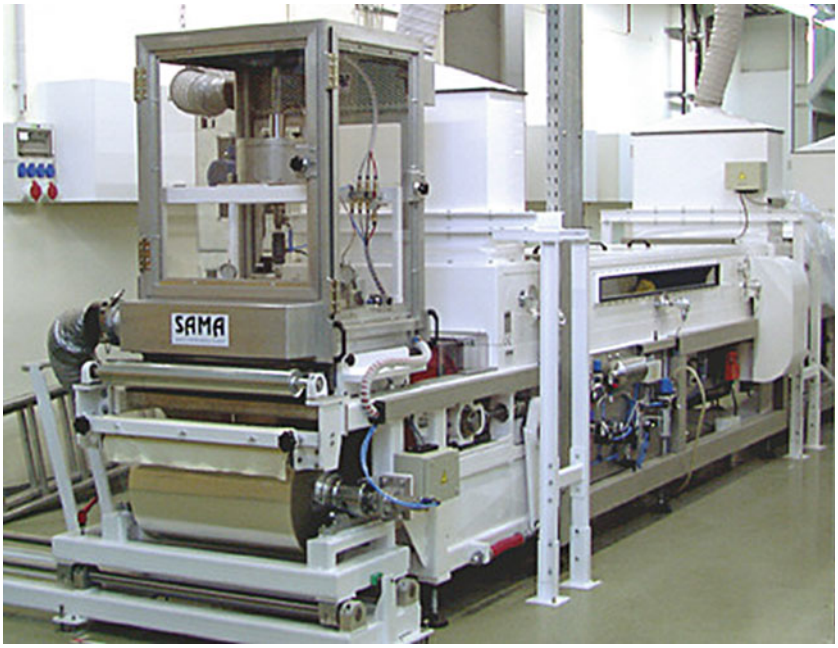

Solid Oxide Fuel Cells, Sustainability Aspects. Figure 16
Tape casting equipment at Forschungszentrum Jülich

e.g., pressing, are a higher manufacturing throughput, an economical production, the high reproducibility, the possibility to recycle green tape leftovers, and the compatibility with standard industrial manufacturing processes [64].

Electrolyte The electrolyte is deposited by slip casting on the anode substrate.

In general, the slip casting process is used to manufacture three-dimensional ceramic components. With the vacuum slip casting process, the process flow is accelerated using vacuum suction. In principle, slip casting processes base upon filling a porous casting mold with a solid-containing suspension (slip). The solvents of the slip will be drawn into the pores of the casting mold, taking along the solid. The solid is deposited at the outline of the casting mold and adds up in a layer that can be separated from the casting mold after drying.

For the production of thin anode functional layers and electrolyte layers when producing planar solid oxide fuel cells, a modified slip casting process is used. Here, the suspension is applied on a planar, porous anode substrate in a special apparatus as shown in Fig. 17. The solvent is drawn through the pores by a vacuum. When the substrate is aligned horizontally, the solids of the suspension deposit evenly on the surface. This process to manufacture thin layers has the following advantages:

- Easy and straightforward handling.
- Series production, if automated.
- Excellent quality of the produced layers.
- Reproducibility of the layer thickness, uniform thickness, and structure throughout the layer.
- Two to 50 μm layers can be realized.
- Little waste (the solvent can be reused).
- Long-term stable suspensions can be produced with little effort.

The disadvantage of this process is the handling of large quantities of solvents and the limitation in the thickness of the layer. There is also a big influence of the structure of the substrate (surface topography, pore size, pore distribution, density distribution, and absorbency) on the quality of the layer in terms of voids and impermeability [66].

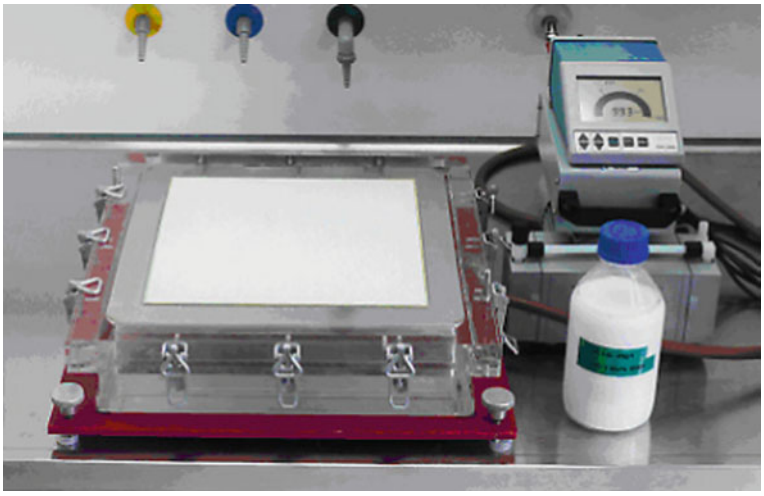

Solid Oxide Fuel Cells, Sustainability Aspects. Figure 17
Vacuum slip casting equipment for production of planar SOFCs

Cathode

Wet Powder Spraying Bilayer cathodes consisting of cathode and cathode current collector layer can be manufactured by wet powder spraying (WPS). The cathode contact layer is also applied on the metallic interconnects by spraying. Limitations of the technology are the overspray (the amount of suspension which is sprayed past the object to be coated) and the formation of a suspension mist which needs to be extracted by suction. The overspray can be recycled, though.

By WPS, a suspension composed of solvent, powder, and additives is sprayed by a nozzle (cf. Fig. 18). The thickness of the coating is adjusted by the amount of spray runs with intermediate drying steps. Various geometries, e.g., planar-type or tubular-type SOFC, can be coated by a PC-controlled x-y-axis system and a rotational system in case of the tubes. The thickness obtained so far varies between 5 and 100 μm. The major parameters affecting the spray result are the spray pressure, the spray distance, the nozzle type (with varying aperture), the viscosity and the solid fraction of the suspension, and the grain size distribution and grain morphology of the powder. The intermediate drying steps to obtain thicker layers are necessary to suppress cracking during drying.

The major advantages of WPS compared to screen printing or plasma spraying are the low-cost fabrication, the flexibility concerning size and shape of the samples to be coated, and the easy integration into an industrial process chain.

Screen Printing With the screen printing process, a standard industrial manufacturing process can also be applied to manufacture the cathode.

It is characteristic of this process that the cathode material paste is squeezed through the mesh openings of a screen and onto the underlying object. The high-viscosity paste contains particles, binder, and solvent. After drying, i.e., evaporation of the solvent, the layer adheres to the object (cf. Fig. 19). Reproducibility, continuity, state-of-the-art, and the low material consumption are the main advantages of the process. Increasing the cycle time reduces the costs. A variety of patterns can be printed (used, for instance, in electronics industry for integrated circuits) on various surfaces, depending on the size of the printer. Evenness of the substrate, size and resolution of the screen, given by the mesh openings, are the main limitation factors. Another limitation is the layer thickness. Only certain thicknesses are producible as the thickness of the resulting layer is given by the screen [67].

Screen printing is expected to replace wet powder spraying in cathode production in the long run. The same procedure can also be applied for electrolyte production. The development target is multilayer printing, i.e., all layers will be printed on top of an

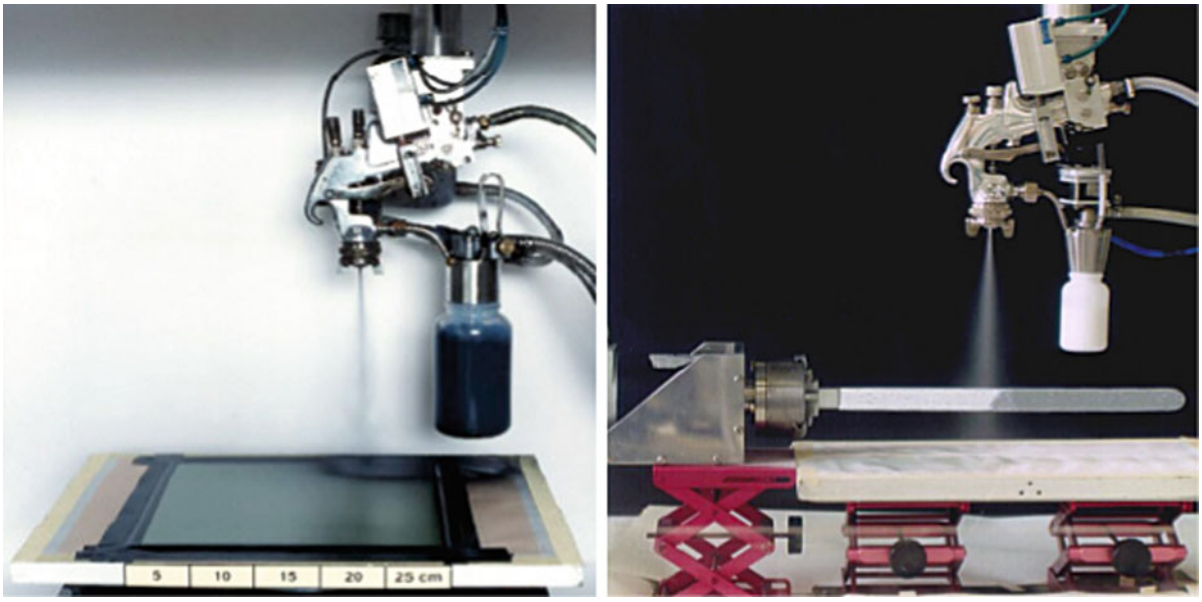

Solid Oxide Fuel Cells, Sustainability Aspects. Figure 18
Wet powder spraying process for planar (*left*) and tubular (*right*) geometries

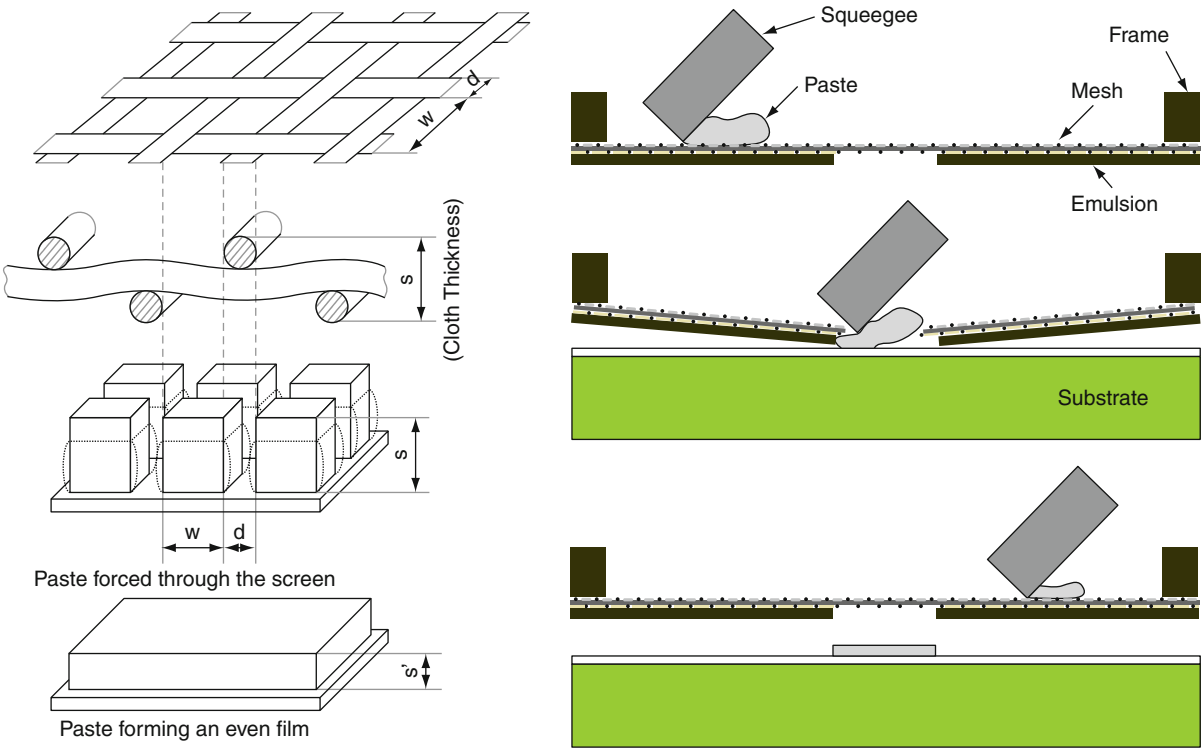

Solid Oxide Fuel Cells, Sustainability Aspects. Figure 19
Concept of screen printing (*left*); schematic screen printer (*right*)

anode substrate to form the SOFC cell. This would result in a reduction of sintering steps and therefore in considerable effort and cost reduction.

Material and Energy Demand for Processing/Manufacturing Table 4 gives an overview of the materials used for SOFC fabrication. The third and fourth columns refer to the raw material and the upstream processes, preparing the final product/material from the raw material.

Figure 20 illustrates that stainless steel is the main material of a stack. The interconnects, which separate the cells, are metallic, and their weight dominates the complete unit.

The second most used material is nickel oxide which is processed from nickel ore and used for the anode substrate and anode together with yttrium-stabilized zirkonia in form of a cermet and as a nickel mesh for the anode contact layer. Yttrium-stabilized zirconia is produced from rare earths and mineral sands.

The manufacturing process is relatively energy intensive as several electricity-operated high-temperature processes are necessary, for instance, the sintering of the anode substrate, the sheet metal working, the melting of the sealing material, or the heating while assembling, as shown in Table 5. Major processes contributing to environmental impacts are the anode-substrate sintering, the production of the metallic interconnectors, and of course the assembling of the components to a stack.

Lightweight SOFC Cassette-Type Stack Design

Since automotive applications require a rather robust SOFC design with rapid starting capability, good thermal cycling properties and high tolerance of the anode to oxidizing atmospheres, the replacement of the nickel cermet anode substrate by a material less sensitive to oxygen and with improved thermomechanical stability appears advisable.

In an alternative approach to standard SOFC manufacturing techniques using sintering of ceramics, various groups are developing cells with a porous metal sheet as the supporting layer for the thin active layers

Solid Oxide Fuel Cells, Sustainability Aspects. Table 4 Materials for the stationary design SOFC. The processing includes mining and metallurgical and chemical processes for all these materials

Material	Abbreviation	Occurrence
Nickeloxid	NiO	Nickelore
Yttrium-stabilzed Zirkonia	8YSZ	Y: rare earth metal
		Zr: in minerals
Lanthanum Manganite doped with strontium Oxide (LSM)	$(La_{0.8}SR_{0.2})_{0.98}MnO_{3-\delta}$	La: rare earth metal
		Sr: as mineral
		Mn: ore component
Lanthanum Nitrate hexahydrate	$La(NO_3)_3*6H_2O$	La: rare earth metal
Strontium Nitate	$Sr(NO_3)_2$	Sr: alkaline earth metal
Lanthanum Cobalt oxide	$LaCoO_3$	La: rare earth metal
		Co: Cobalt ore
Manganese Nitrate	$Mn(NO_3)_2*4H_2O$	Mn: ore component
Barium Oxide	BaO	Ba: alkaline-earth metal
Calcium Oxide	CaO	Ca: component of minerals
Aluminium Oxide	Al_2O_3	Al: component of minerals (i.e., bauxite)
Silicium Oxide	SiO_2	Si: quartz, silicate minerals
Nickel	Nickel mesh	Nickelore

Solid Oxide Fuel Cells, Sustainability Aspects. Figure 20
Single repeating units and 15 kW class stack of the stationary SOFC design

of the cell. The Deutsches Zentrum für Luft- und Raumfahrt (DLR), for instance, has developed a planar thin-film concept which is based on vacuum plasma spray technology for the manufacture of the cell layers. This concept, whose principle is schematically shown in Fig. 21, enables an electrolyte thickness of 20–30 μm which allows for operating temperatures of 800°C or below with still sufficiently high performance. Similar to the "stationary" concept described previously, the lower operating temperature allows for inexpensive materials in the stack as well as for the peripheral high-temperature components [31]. The metal-supported cell (MSC) concept is coupled with thin metal frames and interconnects in a so-called cassette design [68] especially interesting for automobile applications. Therefore, the stack concept referred to in this section is termed "lightweight plasma-sprayed design."

The mechanical strength of the thin-film cell as well as the electrical and thermal conductivity are provided by an open porous metallic substrate which also serves as a fuel gas distributor. The functional layers of the cell – anode, electrolyte, and cathode – are consecutively deposited onto this substrate by a multistep vacuum plasma spray process. The contact from the cathode to the ferritic steel interconnect (bipolar plate) is provided by a flexible and ductile perovskite coating. An important precondition for this design concept is the availability of a long-term stable and corrosion-resistant substrate material with an adequate thermal expansion behavior related to the ceramic cell components [31, 69].

SOFC Components and Stack Manufacturing Processes *Interconnect, cell frame, and metallic substrate* are made from the ferritic steels CroFer22APU [55] and IT-11 [70].

For the soldering of substrate and interconnect, a nickel-based solder foil is required.

The *anode* of the lightweight SOFC is made from Nickel oxide (NiO) and yttria-stabilized zirconia. For the *electrolyte*, yttria-stabilized zirconia is also used, while the cathode is made from lanthanum strontium manganite (LSM) (cf. previous section). The same material is used for the *contact layer*. Lanthanum strontium chromite is applied as a ceramic *protective coating* for chromium retention. The noble gas argon is used as an auxiliary medium in the vacuum plasma spraying process [71].

A summary of the material categories used in this lightweight concept is given in Table 6.

Three technical processes are characteristic for the plasma spray SOFC manufacturing.

The central technology is the multistep vacuum plasma spray process (Fig. 22) by which the SOFC cell is deposited onto the substrate-interconnect unit. For an optimum cermet anode layer, doped zirconia (with yttria) and NiO powders are internally injected into

Solid Oxide Fuel Cells, Sustainability Aspects. Table 5 Electricity intensive steps in stationary SOFC design production

Anode-substrat	
Preparation powder & suspension	
Anode substract	Coat Mix
Sintering	1250°C
Anode substrate/ande functional layer	
Mixing powder & suspension	
Applying anode functional layer	Slip casting process
Electrolyte	
Prepar. powder & suspension	
Applying the elektolyte	Slip casting process
Firing	1400°C
Cathode functional layer	
Catho de functional layer – paste	
Applying catho de functional layer	Screen printing
Cathode	
Catho de-paste, preparation	
Applying the cathode	Screen printing
Co-firing	1100°C
Inteconnector, cell frames	
Metal plate processing	sheet metal working
Facing the interconnector	
Ceramic-powder suspension preparation	
Interconnect coating	Wet powder spraying
Glass sealing	
Glass preparation	melting
Glass sealant paste preparation	milling – mixing
Stak assembling	
Joining and sealing the stack	~ 800°C

a nozzle. At a pressure of 200 mbar and a power level of 30 kW resulting in a relatively low velocity of the particles at impact in the range of 250–350 m/s, a porous cermet anode layer is formed as a result of the weak flattening and densification. At the cell's operating conditions, the NiO in the anode is completely reduced by hydrogen to pure Ni. This leads to a further increase in porosity to about 20–25 vol% which ensures sufficiently high gas diffusion. The thickness of the anode layer depends on the surface properties of the substrate used; generally, it is in the range of 30–40 μm. For the production of high performance SOFCs, it is necessary to spray thin gastight electrolyte layers with high deposition efficiency. This is only achievable with completely molten particles which are accelerated to high velocity in the plasma jet and therefore flattened to dense lamellae on impact. Lamellar microstructured and dense electrolyte layers with high interparticle bonding can be achieved with a thickness of only 20–40 μm [31].

The plasma-sprayed cathodes are obtained in a similar way as the anodes. The variation of the spray parameters has shown that the perovskite phase tends to decompose, especially when H_2 is added to the plasma gas. With an Ar/He or a pure Ar plasma, best results were achieved with a standard F4V nozzle at a power level of 20 kW, 100 mbar and internal injection of the powder with 15° in opposite direction to the plasma gas flow. With identical parameters, LSF and LSCF powders in addition to LSM have also been processed to cathode coatings. The lack of a "pore forming process" as it is used with the reduction process of the anodes leads to a significantly lower overall porosity of plasma-sprayed cathodes in the range of only 10 vol%. This results in a relatively high cathodic polarization resistance and, hence, strong efforts are made to improve the cathode's pore structure. A promising approach is given by the possibility of the in situ synthesis and deposition of cathode coatings by applying RF plasma technology.

A vacuum soldering process is the second technical process of relevance. It is used to solder the porous metallic substrate on the interconnect whereby a nickel-based solder foil is applied [73].

The third characteristic process is wet powder spraying, by which the contact layer (between cathode and interconnector) is applied on the cathode.

Feedstock Material for the Cell Components The "lightweight plasma-sprayed" SOFC concept in principle uses the same materials set as the "stationary"

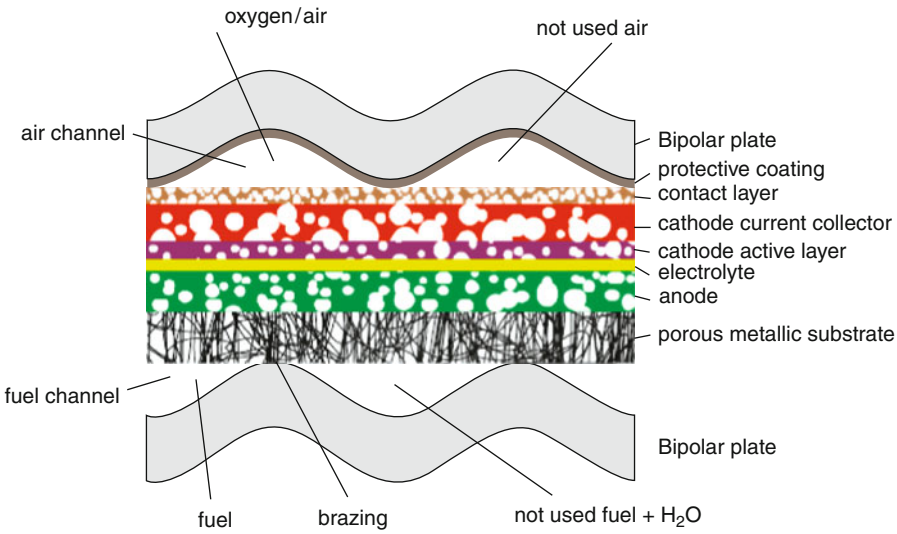

Solid Oxide Fuel Cells, Sustainability Aspects. Figure 21
Principle of the planar metal substrate-supported lightweight SOFC concept [69]

Solid Oxide Fuel Cells, Sustainability Aspects. Table 6 Materials for metallic substrate, plasma-sprayed lightweight SOFC [31, 69, 71]. The processing includes mining and metallurgical and chemical processes for all these materials

Material	Abbreviation	Occurrence
Nickeloxid	NiO	Nickelore
Yttrium-stabilzed Zirkonia	8YSZ	Y: rare earth metal
		Zr: in minerals
LSM	$(La_{0.8}SR_{0.2})_{0.98}MnO_{3-\delta}$	La: rare earth metal
		Sr: as mineral
	$La_{0.8}Sr_{0.2}MnO_3$	Mn: ore component
LSCr	$La_{0.7}Sr_{0.15}Ca_{0.15}CrO_3$	La: rare earth metal
		Sr: as mineral
		Ca: in minerals
		CrO_3: in minerals
Barium Oxide	BaO	Ba: alkaline-earth metal
Calcium Oxide	CaO	Ca: component of minerals
Alumina (Aluminium Oxide)	Al_2O_3	Al: component of minerals (i.e., bauxit)
Silicium Oxide	SiO_2	Si: quartz, silicate minerals
Nickel	Nickel mesh	Nickelore

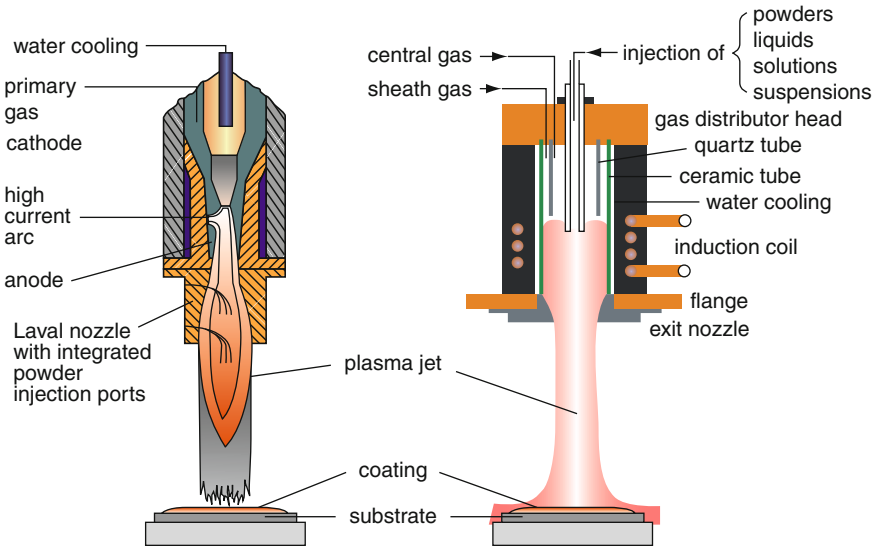

Solid Oxide Fuel Cells, Sustainability Aspects. Figure 22
Principles of direct-current plasma (*left*) and radio frequency plasma (*right*) torches [72]

concept. The plasma spray process consumes a certain amount of the noble gas argon, which has its own process chain and the specific feature that it is produced by air separation technologies [74, 75].

Integrated Planar SOFC Concept

The "integrated planar" (IP) SOFC stack concept, for instance, applied by Rolls-Royce Fuel Cell Systems, uses an array of series-connected cells deposited by screen printing onto a flat support tube, a schematic cross section of which is shown Fig. 23. The support tube, an inert, porous ceramic, is fabricated from a magnesia magnesium aluminate spinel (MMA), whereby the desired coefficient of thermal expansion is adjusted by the ratio of the base materials [76].

On the left, Fig. 24 shows an IP-SOFC assembly and on the right the ceramic substrate with the channels shown in front. These channels enable the fuel supply through the support structure and the removal of the reaction products (H_2O, CO_2). The support tube is made by extrusion. The properties of the MMA ceramic are a function of the precursor powder and the extrusion process used to produce the support tubes. The extrusion process involves combining the MMA with a binder system to produce a dough-like mix.

This is then extruded through an appropriately shaped form to produce a 1.5 m length of support module. Following a drying process, the module supports are cut to approximate length before firing at high temperature to burn out the binders and partially sinter the extrudate. The module supports are then finished by accurately machining to length [78].

Each of the three functional layers of the cell, *anode*, *electrolyte*, and *cathode*, are deposited onto the substrate using screen printing. In practice, each of the functional components requires multiple layers to provide the necessary functionality and manufacturability. Unlike other SOFC designs and similar to the metal-supported cell, the IP-SOFC uses neither the electrolyte nor electrodes to provide structural support. This allows very thin cells with consequently very small material quantities (cf. previous section). The cell functional layers again are made of conventional SOFC materials: yttria-stabilized zirconia electrolyte, nickel cermet anode, and rare earth manganese oxide cathode. The choice of conventional materials allows the use of standard materials suppliers. This ensures that high-quality material can be obtained which is essential in producing the quantity of product for scale up and future production. It also allows the efforts in research activities to focus on fine tuning the material

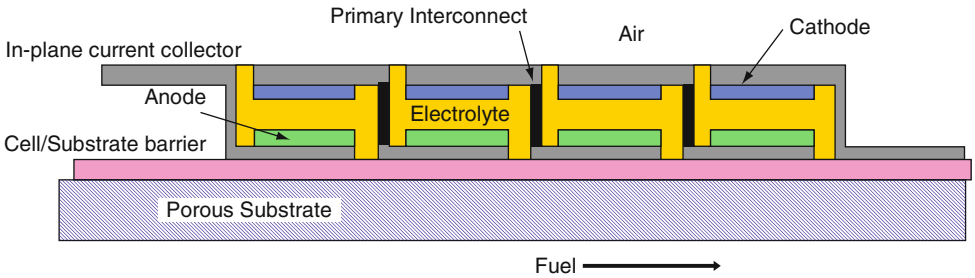

Solid Oxide Fuel Cells, Sustainability Aspects. Figure 23
Integrated planar solid oxide fuel cell concept [77]

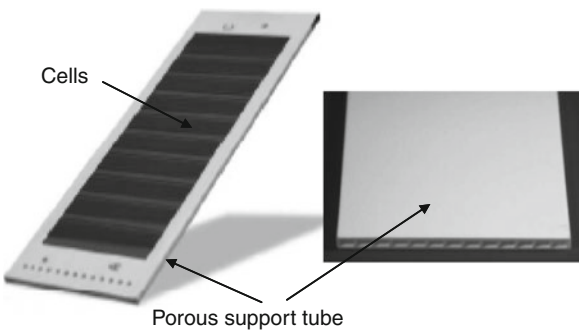

Solid Oxide Fuel Cells, Sustainability Aspects. Figure 24
Active tube and extruded porous support tube [76, 77]

performance and not developing fundamentally new materials. New materials can be introduced as future enhancements after a first product is produced [76].

For the *anode*, a nickel-oxide-YSZ cermet is applied, though the limitations of the current state of that type with respect to redox stability, coking, and sulfur tolerance are known. More recently, the integration of oxide anodes into the concept has been analyzed and tested [78].

Like other concepts, the IP-SOFC design uses yttria-stabilized zirconia as *electrolyte* material. By screen printing, the electrolyte is fabricated with a layer thickness of about 10 μm, which leads to a minimal ionic resistance so that the electrolyte resistance has only a small contribution to the total losses in the cell [76].

For the *cathode*, a mixture of strontium-doped lanthanum manganite (LSM) proved most suitable, and as the slurry spray process was not scalable to larger modules and production volumes, the screen printing process was chosen for the cathode fabrication [76].

The stack assembly includes ceramic manifold components not further specified, metallic interconnect compounds, and glass ceramics for sealing and joining. The main components are silicon dioxide, calcium oxide, aluminum oxide, and barium oxide.

Environmental Impacts

LCA Studies of SOFC

Life cycle assessment of SOFC technology is still uncommon due to the relatively early stage in technical development. However, several studies have been performed since the end of the 1990s. Since there is a lack of "standard" commercial equipment that could serve as a basis and reference point for analysis, LCA studies mostly refer to hypothetical concepts and/or extrapolate from laboratory and early market prototypes to commercial units. While the first studies had only little access to operation data at all (for the fuel cell system itself but also for production processes), the main effort was set in the assessment of inventory data using assumptions, simplifications, and correlations [79, 80]. The main outcomes of these studies were the identification of weak points and the setting of benchmarks for further development. With more information about fuel cells available today and a simultaneous advancement in LCA methodology, the studies became more reliable and detailed, regarding system description [81] as well as the assessment of environmental impacts connected with inputs and outputs [82]. Especially the extensive data of these two studies found their way to commercial databases for LCA [83] and thereby became available to LCA practitioners. In 2005, the Federal Ministry for the Environment, Nature Conservation and Nuclear Safety (BMU)

commissioned a study investigating ecological aspects of fuel cells beside economical factors [84]. The most recent LCA analyses were performed in the European integrated projects Real-SOFC [85, 86] and Large SOFC [87]. In the NEEDS project, fuel cells are one technology among others to build up future sustainable energy systems [88].

LCA Results

With increasing environmental operating standards for modern energy conversion systems, the up and downstream processes, e.g., fuel supply or system production as well as waste treatment or recycling, are becoming increasingly relevant. More important than the relative contribution of the production is the absolute impact of production. Very often, technologies showing good characteristics in the use phase lead to high absolute environmental impacts in the production phase due to the use of more "sophisticated" materials and components as well as newly developed or adjusted production processes. Therefore, the entire life cycle has to be included in the investigation.

Goal and Scope In the different LCA studies, the investigated fuel cell systems vary in their system boundaries. While some studies focus exclusively on the stack itself, others also include the Balance-of-Plant into the investigations. Major impacts on the results can also be identified due to the variation of fuels used and the end-of-life concept considered in the analysis.

The main goals of the studies are twofold:

- Determination of weak points along the life cycle of fuel cells through identification of materials or processes with potentially high environmental impacts. The results can be used to give some recommendations to avoid or reduce them.
- Comparison of ecological characteristics of fuel cell systems and future competing systems to help decision makers in terms of optimal applications for fuel cells.

Depending on the focus of the study, the functional unit varies for the different studies. In all studies, the manufacturing of the fuel cell itself is included. Input and output data are related to a 1 kW_{el} fuel cell stack, distinguished in tubular or planar cell concepts. The Real-SOFC study focuses exclusively on the stacks, accompanying the research activities performed in this project. The other studies include the Balance of Plant (BoP) and auxiliary components as well. All other studies expand the investigated life cycle by integrating the use phases as well, thus defining 1 kWh of electricity produced as the basis for comparison.

The impact assessment varies also between the projects. While older studies consider mostly material and energy inputs as well as selected emissions to the atmosphere, the newer studies describe the environmental effects using aggregated impact categories.

Parameters with high impact on the results are technical data like cell performance, electrical efficiency and technical lifetime of the stack, the end-of-life concept considered, and the fuel used. Methodologically speaking, the evaluation and allocation of the coproduct "heat" plays an important role. These parameters are not handled equally in the different studies and thus make comparison between the studies difficult.

Inventory

Stack Manufacturing The environmental impacts of the fuel cell stack can be classified on one hand into the life cycle stage material provision and manufacturing of the stack and on the other hand into the operation phase of the fuel cell. The sensitive parameters for the stack system manufacturing are the material input, the manufacturing processes, and the cell performance. The materials used in the planar, sintered fuel cell concept are described in detail in section "Stationary SOFC Stack Design". It is typical for this type of stacks for stationary applications that the stacks include a high amount of chrome alloy for the interconnect. More recent designs already tackle this issue for reasons of materials, weight, and cost reduction. The relatively high amount of NiO is specific for cells with a thick anode substrate (up to 1.5 mm in Fig. 12, for instance). Again, more recent developments reduce this thickness to 300–1,000 μm. The amount of $ZrO_2(Y_2O)$ is caused by the comparatively low yield of the first sintering phase (~80%), where a number of plates crack or bend and have to be rejected [81]. In contrast, the materials used in tubular cell design are dominated by ceramics. However, the manufacturing process is far more complex. Major material is $LaMnO_3$. $ZrCl_4$ and

YCl_3 amounts are increased due to a low material utilization of electrochemical vapor deposition (EVD) (~20%). This process consumes about 15% of the energy necessary for the production of the cell. Together with atmospheric plasma spraying, it sums up to almost 90% of the total energy required for manufacturing. This equals the energy necessary to supply the materials used. The sum of this energy requirement for the tubular concept is lower than that for the sintered ceramic planar design (stationary design), almost by a factor 7. For the sintered ceramic planar concept, energy inputs for materials production are almost 100 times higher than the energy used during manufacturing, mostly related to the supply of the chromium alloy. However, detailed information about the production of some key materials is not available. To compensate the data gaps, assumptions had to be made. The materials affected are $LaMnO_3$, doped $LaCrO_3$, $ZrCl_4$, YCl_3, and YSZ. In a sensitivity study [81], it was shown that a doubling of the energy values of these materials only results in a 1.6% increase in total energy requirement. For tubular concepts, this source finds the opposite trend. With the dominant material being $LaMnO_3$, a doubling would cause an increase to the total figure of about 96%. For the sintered ceramic planar concept, a possible recycling of the interconnect Cr alloy material would reduce the energy requirement significantly [82]. The energy demand for the manufacturing stage is dominated by thermal processes such as sintering and drying. According to furnace manufacturers, the energy demand for a sintering furnace can be decreased by 65% for series production in an industrial furnace and optimized packing of samples in the furnace [82]. The Real-SOFC project also showed that the manufacturing processes of slip casting (Fig. 17) and screen printing (Fig. 19) require more than five times more energy than the vacuum plasma-sprayed layers (Fig. 22) of the plasma spray metal support concept. The energy intensive manufacturing processes for the tubular concept are also expected to decrease for mass production [81].

Balance of Plant Manufacturing The Balance of Plant (BoP) of a fuel cell system consists of all system components except the fuel cell stack itself. The BoP therefore includes the complete set of heat exchangers, reformer, afterburner, pumps, blowers, control, etc., that is necessary to build the operational fuel cell system. In contrast to the stack, the BoP for both planar and tubular designs consists mostly of conventional materials. This is predominately steel (~99% for the stationary planar concept). Additionally, alumina (~7%) is used in the tubular concept to a greater extent. As the components are well established, the energy requirements for the manufacturing processes are lower compared to the stack manufacturing. In the NEEDS project, which is more oriented toward future developments and in which technology descriptions for 2025 and 2050 are evaluated, no improvements for heat exchanger, inverter, or gas turbine are expected due to the high maturity of these components. The other BoP components are expected to reduce material intensity by 20% until 2025 and further 30% until 2050, which results in a 42% material reduction (mainly steel). For the fuel cell stack itself, an improvement of 10% for each time step is estimated.

Sensitivity Analysis of Power Density Another sensitive parameter for the results is the cell performance, regulating the amount of cells necessary. In a sensitivity analysis, Karakoussis [81] shows the effects of a change in power density of the cell from 0.2 to 0.5 W/cm^2. As more cells with lower power density are necessary for a 1 kW stack, the material and energy demand for manufacturing increases in a linear relationship. A shift from 0.2 to 0.5 W/cm^2 decreases the values for materials consumption by 40%.

Key Emissions The key emissions to air for BoP-related emissions are higher than those for manufacturing the stack. This reflects the higher specific mass of the materials used for the BoP and the associated energy requirements. Figure 25 shows the share of some key emissions differentiated for material production and process energy [81].

All emissions are much higher from activities related to material production than from the processes involved in manufacturing fuel cell and BoP. The share of some process-related emissions is more significant for the tubular type, reflecting primarily the much higher process energy requirements for manufacturing. The Real-SOFC project additionally showed high argon emissions for the plasma deposition process [85].

Comparison of the Manufacturing and the Operation Phase Finally, the manufacturing phase must be compared with the operation phase of the fuel cell. Because fuel cell systems do not involve a combustion process like that of reciprocating engines, most of the atmospheric emissions during operation are much lower. Due to the low operating temperatures, the NO_x emissions are very low. The higher reaction temperatures lead to low CO and hydrocarbon emissions. The SO_2 emissions are derived from the sulfur content of the fuel. Because sulfur is toxic to the catalysts, it is removed before entering the fuel cell. The SO_2 emissions therefore do not occur during operation but when the catalyst is regenerated.

Table 7 shows emission values during operation with natural gas from some studies.

Including also the fuel supply into the investigation, CO_2 and other GHG are mainly emitted during operation, with about 80% of the total. The rest is mainly related to the fuel supply, whereas the manufacturing is negligible. For all other emissions, the fuel supply is responsible for the biggest share (between 50% and

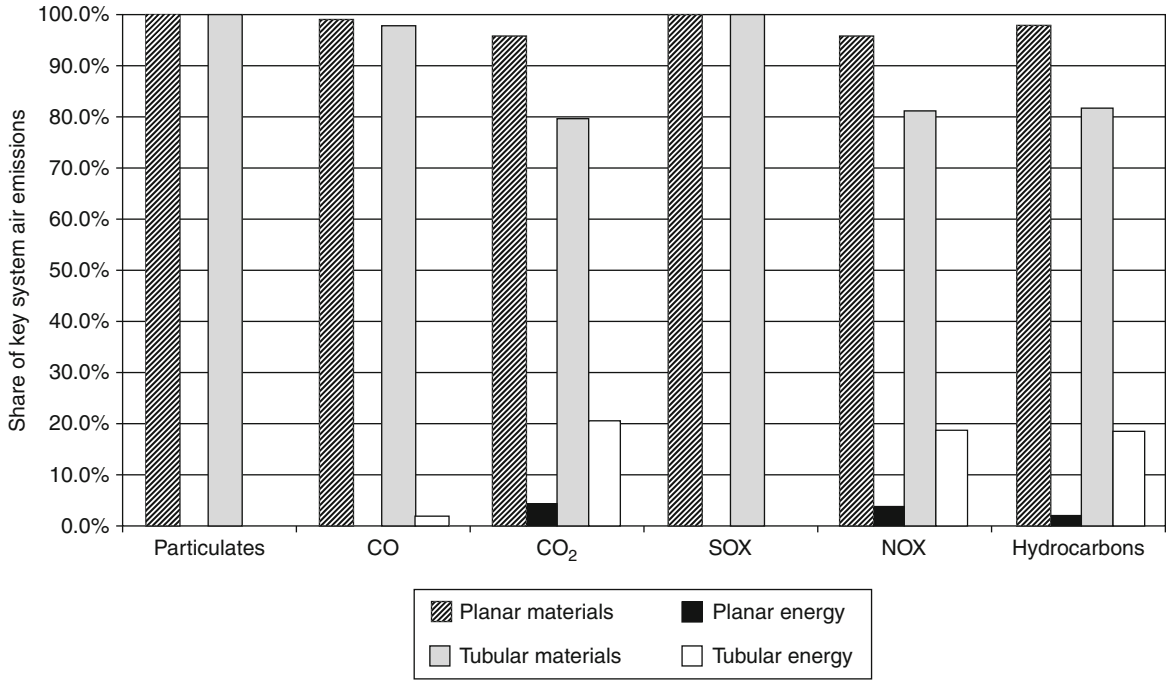

Solid Oxide Fuel Cells, Sustainability Aspects. Figure 25
Share of key atmospheric emissions from material production and process energy [81]

Solid Oxide Fuel Cells, Sustainability Aspects. Table 7 Atmospheric emissions for SOFC systems operated on natural gas

CO [g/kWh]	CO_2 [g/kWh]	So_x	No_x [g/kWh]	Hydrocarb ones [g/kWh]	Sources
0.001	218	0.005	0.021	0.202	Karakoussis [81]
0.004	218	0.005	0.021	0.15	Bauen & Hart [92]
0.006	213	0	0.003	0.03	Pehnt [82]
0.006	202	0.002	0.007	0.016	Ecoinvent [83]

90%), with the construction phase mainly causing the rest. In the case of SO_2 emissions, the construction phase is significant because no SO_2 is emitted during operation and natural gas has a small sulfur content. Additionally, some materials employed in the fuel cells (e.g., Nickel and other metals) are produced from sulfidic ores [88].

Impact Assessment In the third phase of an LCA, the life cycle impact assessment (LCIA), the inventory data are allocated to possible environmental impacts. Thereby, different impact categories can be considered. Table 8 summarizes the different impact categories considered in the various studies, the allocated inventory data, and the chosen characterization factor.

Stack Manufacturing The differences in the stationary planar and integrated tubular concepts are also visible in the impact assessment, as shown in Fig. 26. The high amount of chromium in the stationary planar concept is decisive for the impacts in all emission-related

Solid Oxide Fuel Cells, Sustainability Aspects. Table 8 Impact categories of LCIA (Adopted from [89])

Impact category	Allocated inventory data	Characterisation factor	Studies
Resource depletion	Material and energy resources	Cumulated energy demand (CEA) kg antimony-eq.	[DLR], [Large SOFC], [Pehnt], [Real-SOFC]
Global warming potential (GWP)	CO_2, CH_4, N_2O, C_2F_6, CF_4	kg CO_2-eq.	[DLR], [LargeSOFC], [Pehnt], [Real-SOFC]
Acidification potential (AP)	SO_2, No_x, NH_3, HCI, HF, H_2S	kg SO_2-eq.	[DLR], [LargeSOFC], [Pehnt], [Real-SOFC]
Eutrophication potential (EP)	No_x, NH_3	kg PO_4^{3-}-eq.	[DLR], [LargeSOFC] [Pehnt], [Real-SOFC]
Human toxicity potential (HTP)	Particles, SO_2, No_x, NMHC, CO	Years of Lost Life (YOLL)	[DLR], [Pehnt], [Real-SOFC]
		Unit risk Factor kg 1.4 DCB-eq.	
Photochemical ozone formation potential (POCP)	NO_x, NMHC, CH_4, ethanol, butane, hexane,	kg ehtylene-eq.	[DLR], [LargeSOFC], [Pehnt],
Ecotoxicity potential (FAETP, FSETP)	NH_3, chromium, HCI, Ni, NO_2, SO_2	kg 1.4 DCB-eq.	[Real-SOFC]
Ozone depletion potential (ODP)	CFC, trichloroethane	kg CFC-11-eq.	[LargeSOFC]

[DLR] = [84], [LargeSOFC] = [87], [Pehnt] = [82], [RealSOFC] = [85]

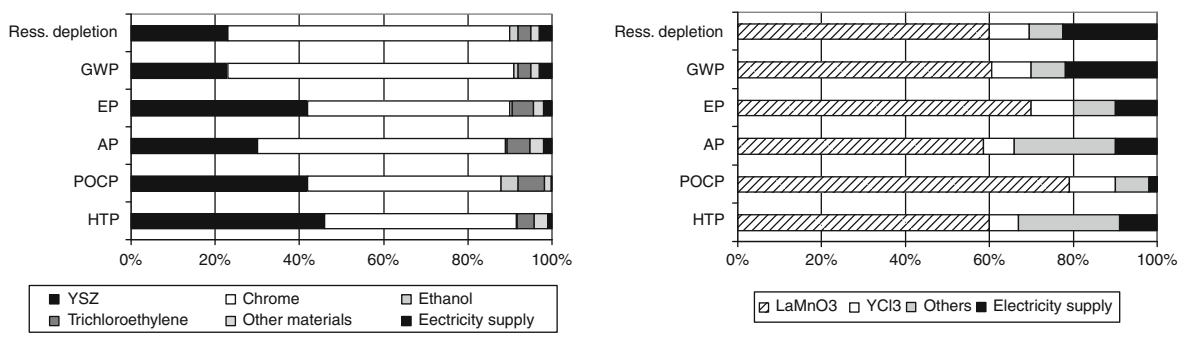

Solid Oxide Fuel Cells, Sustainability Aspects. Figure 26
Material- and energy-related impacts for the planar (*left*) and the tubular system (*right*) [84]

categories. Also for energy-related emissions, the chromium production shows the highest figures. It has to be kept in mind that no recycling of the interconnect is considered in any of the studies reviewed, but it is technically possible and would result in a considerable reduction in emissions. The impacts of the yttrium-stabilized zirconium is also significant in all categories. Although the mass fraction of yttrium is only 8%, it has a high environmental impact and in some categories shows higher impacts than the production of ZrO_2. For the integrated tubular concept, this environmental sensitivity becomes visible in the impact of YCl. Although its specific amount is quite small, it is noticeable in the environmental impacts. However, $LaMnO_3$ dominates the environmental impacts, being the material with the highest weight fraction in the support tube. Additionally, the use of electricity in the production phase has a considerable impact on the environment.

During manufacturing of the cells, solvents are used. Although some of them are specified in the inventory of some studies, the environmental relevance is not analyzed in any of the studies due to the lack of detailed information. It is often not clear whether these solvents have a toxic potential or contribute to the creation of photochemical ozone. Therefore, further analysis on the solvent management (for instance, venting of solvent vapor to the atmosphere or condensation and recycling) is necessary.

Environmental Impacts of the Life Cycle Stages The particular life cycle stages have different effects on the various environmental impacts. Figure 27 compares the qualitative distribution of impacts for the two fuel cell systems investigated in the Real-SOFC project [85], differentiating in the three life cycle stage manufacturing (only fuel cell without BoP), operation phase, and supply of natural gas.

Both fuel cell designs have almost the same impact distribution for all chosen impact categories. Especially the global warming potential is dominated by the operation phase. It is directly connected to the assumed efficiency of the system and the use of natural gas fuel. With comparable efficiencies assumed in all

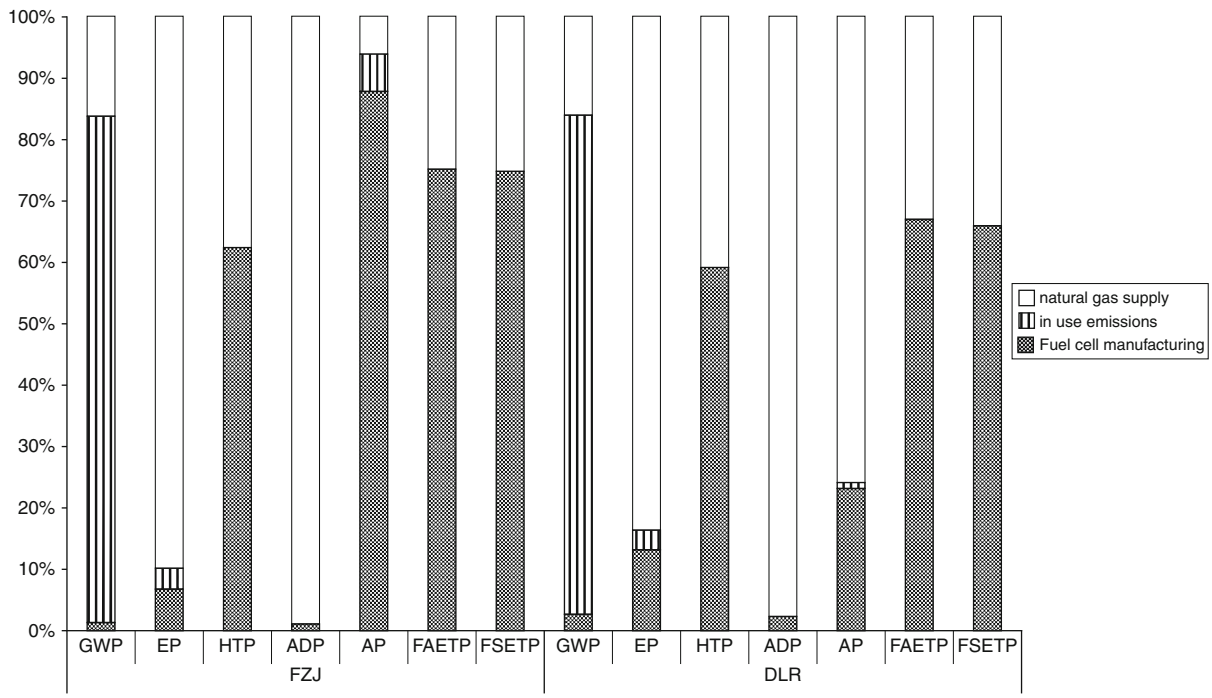

Solid Oxide Fuel Cells, Sustainability Aspects. Figure 27
Qualitative distribution or the impacts for the stationary sintered cell and lightweight plasma-sprayed planar concepts [85]

studies, the results are similar. Further contributions are related to methane emissions in fuel distribution.

As expected, the use of resources is nearly exclusively related to the fuel supply chain (about 98%). The eutrophication potential, the potential to form photochemical ozone (only considered in [82, 84, 87]), and the acidification potential are strongly affected by the supply of fuel. However, the results of the stationary sintered cell concept show a high impact of the fuel cell manufacturing also for AP. This is caused by the amount of steel used in this concept. Again, no recycling is considered here.

The effect of fuel cell manufacturing of the cells on the human toxicity is also not consistent in the different studies. While [85] shows a high share for both concepts analyzed, [82] and [84] estimate a higher share of the fuel supply chain.

Variation of Fuel Supply As many impact categories are dominated by emissions from the fuel supply chain, the analysis in [87] focuses on the variation of fuels. The study compares methanol (conventional and produced from biomass), natural gas, syngas, and biogas from landfill sites. Figure 28 summarizes the impacts of the overall system for the different fuels used during operation.

For the different categories, no clear winner can be defined. The SOFC fuelled with landfill biogas shows the lowest values for all impact categories except global warming potential. Methanol from biomass has the lowest global warming potential but in nearly all other categories the worst performance. In the Real-SOFC project [88], another fuel option considered was hydrogen produced by water electrolysis using electricity from wind turbines. All figures, except the results related to human toxicity, show a significant reduction in impacts. The ten times higher HTP value is exclusively linked to the high amount of steel consumed in the manufacturing of wind turbines.

Allocation Between Electricity and Heat As the SOFC systems produce electricity and heat simultaneously, it is necessary to allocate the emissions to the two products. The different studies proceed differently. While some studies allocate all emissions exclusively to the production of electricity, some studies value the heat as well. Two ways are possible to allocate the emissions. One is to give the system a credit for producing heat also, and the other is to allocate in a way that reflects the physical relationship. References [82] and [84] credit the heat production with reference to a modern natural gas burner. This means the impacts of producing the same amount of heat with a natural gas burner are subtracted from the impact of the fuel cell CHP system because it substitutes this energy conversion process (cf. Sections "SOFC as High-Efficiency Energy Converters" and "CO_2 Emission Reductions from SOFC Implementation"). This leads to a reduction in the overall impacts of the system proportionally to the amount of heat produced (and utilized). In the NEEDS project, it was chosen to share the emissions between the two products. An often used allocation basis for combined heat and power systems is the exergy. Exergy describes the amount of useful energy that is contained within a product. As exergy of heat is very low, this implies that fuel cell systems with high amounts of heat generated turn out worse in the comparison of electricity compared to fuel cell systems with higher electrical efficiency [88]. In the Real-SOFC project [85], both methods are used. The impacts obtained using the credit method differ much more than those using exergy as allocation base. However, both methods do not lead to a change in ranking of the different systems investigated.

End-of-Life Treatment No study considers end-of-life treatment in its analysis due to the lack of information available at this time of development. However, nearly all studies point out that a reuse or recycling of components would decrease the impacts considerably. In the Real-SOFC project, possible end-of-life options are described qualitatively considering high thermal and chemical processes to show possible solutions to decrease the amount of primary material [85].

Future Directions

Efficiency and emission balances, as well as materials inventories and end-of-life considerations, are necessary tools in evaluating the environmental performance of fuel cell technology. Due to the complex system of materials and the integration into energy supply systems, for instance, as combined heat and power (CHP) units, the results are not intuitively predictable.

All in all, SOFC show a considerable potential for increasing energy conversion efficiencies, especially

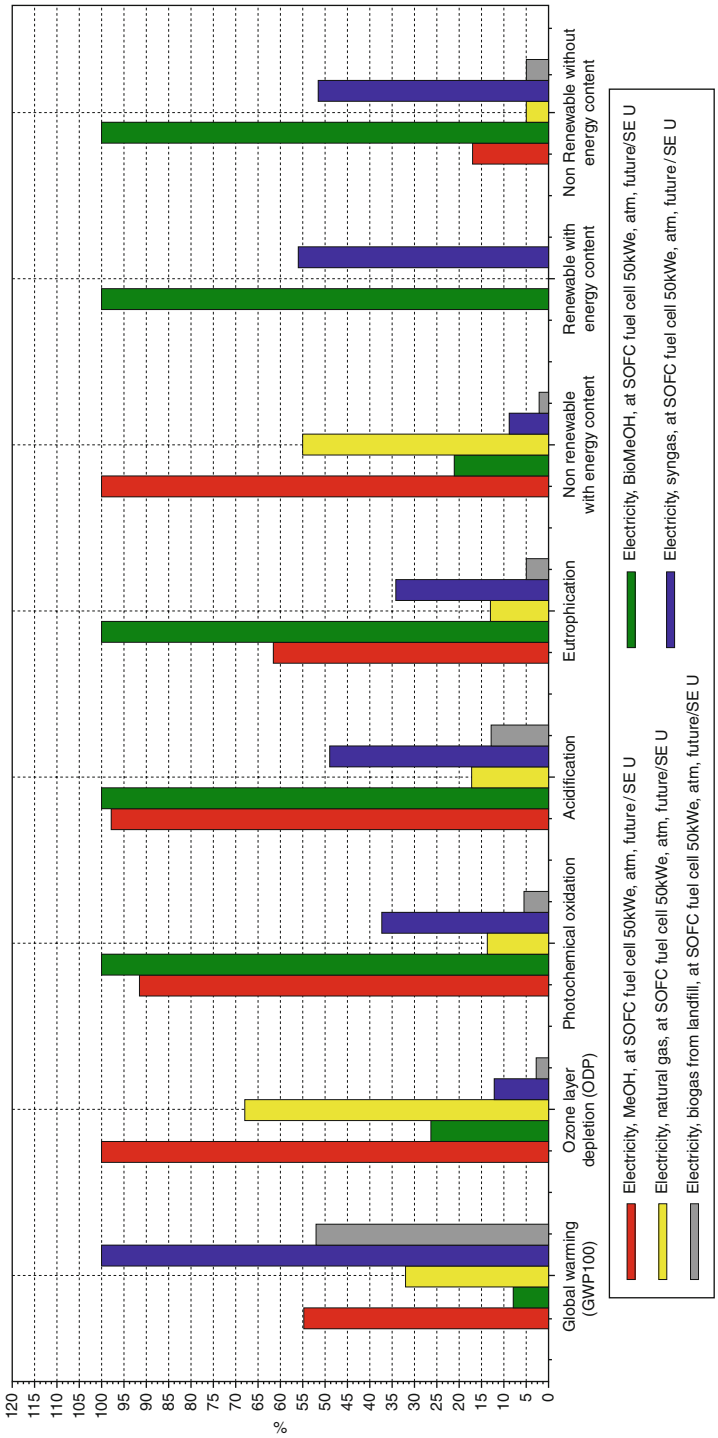

Solid Oxide Fuel Cells, Sustainability Aspects. Figure 28
Environmental impacts of a 50 kW fuel cell system using different fuels (per kWh) [87]

in electricity generation and in CO_2 emission reduction. They do not cause major concerns due to environmental impacts emanating from manufacturing or recycling. SOFC have the advantage that they do not rely on noble metal catalysts, and the ceramic materials used cause little environmental harm. One of the more serious problems is the working environment hazard of nickel powders that has to be addressed when designing SOFC cell manufacturing plants.

As SOFC technology progresses toward a reduction in the amounts of material, especially for interconnects (cf. Section "Materials Inventory of SOFC Concepts"), the analyses presented in the previous sections have to be updated and modified. The same is true for the analysis of the types of materials implemented and their environmental impact from ore mining over materials processing to recycling. New materials and new recipes for pastes and raw materials are gradually introduced, and processes for application of layers modified or totally changed. Physical vapor deposition and solgel techniques may be used in the manufacturing of high-performance layers [90], as well as roll coating as a cheap and fast method of applying pastes. These processes have not been evaluated to date.

Further analysis is also necessary for the manufacturing processes as they are implemented in industry. The principal methods used in laboratories may deviate considerably from large-scale industrial procedures for a variety of reasons. On one hand, there is of course the necessity to reduce costs, often at the expense of quality, which may also be coupled to inferior qualities of raw materials with a different environmental footprint (both positive or negative, depending on the circumstances). On the other hand, some processes cannot be implemented under conditions of large-scale manufacturing, whether for reasons of a low speed of the process, unfulfillable requirements to process parameter control, or simply size restrictions. Therefore, the exact setting of an industrial production will have to be analyzed and assessed for every manufacturer separately, unless specific standardized processes establish themselves in SOFC industry.

As the analysis in Section "CO_2 Emission Reductions from SOFC Implementation" indicates, the potential of SOFC for contributing toward CO_2 emission reduction obviously depends on the fuels but also on the footprint of the electricity grid an SOFC unit is connected to. This is a rather complex problem that has been recognized by the European Commission and the Fuel Cell and Hydrogen Joint Undertaking (FCH JU) in the formulation of the FCH JU Multi-Annual Implementation Plan [27]. A European project – EuroFC-Grid – will be performing a comprehensive analysis of this problem in the years 2010–2012 [28]. This will lead up to a better understanding of the dependencies of SOFC CO_2 reduction potential on electricity grid carbon footprints and integration of CHP units into heating and electricity supply systems. Eventually, the formulation of minimum efficiency requirements for electrical efficiency, as well as for total energy efficiency and CO_2 release – for a particular fuel – will result from this project. These figures can form the basis for funding decisions in the European programs or, for instance, become elements in certifying fuel cell CHP units under the specific European regulations [10].

Acknowledgments

The authors wish to thank the teams at Forschungszentrum Jülich (FZJ), Deutsches Zentrum für Luft- und Raumfahrt (DLR), Rolls-Royce Fuel Cell Systems (RRFCS), ECN, and EdF/EIfER for their support in the project Real-SOFC, as well as the other consortium members for the fruitful discussions on life cycle analysis issues.

Further thanks go to the members of staff at FZJ who supplied details on cell and stack manufacturing.

Bibliography

Primary Literature

1. European Parliament: Directive 2005/32/EC of the European Parliament and of the Council, Official Journal of the European Union, 22.7.2005, http://eurlex.europa.eu/LexUriServ/LexUriServ.do?uri=OJ:L:2005:191:0029:0058:EN:PDF. Accessed March 2010
2. ISO 14040/14044 (2006) Environmental management - life cycle assessment - principles and framework, - requirements and guidelines. Deutsches Institut für Normung e. V
3. Grausa W, Worrella E (2009) Trends in efficiency and capacity of fossil power generation in the EU. Energ Policy 376: 2147–2160

4. Arbeitsgemeinschaft Energiebilanzen e.V (2010) Ausgewählte Effizienzindikatoren zur Energiebilanz Deutschland. Daten für die Jahre von 1990 bis 2008 (Selected efficiency indicators for the German energy balances. Data for the years 1990 to 2008). Berlin
5. Brown MH, Sedano RP (2004) Electricity transmission – a primer. National Council on Electric Policy, Washington, DC. ISBN 1-58024-352-5
6. Viebahn P, Patyk A, Fritsche UR, Beer M, Corradini R, Ciroth A, Blesl M, Mayer-Spohn O, Macharey U, Schnettler A, Smolka Th, Fischer M, Schuller O, Große Böckmann Th, Wagner H-J, Mayer H (2008) Erstellung der Grundlagen für einen harmonisierten und fortschreibbaren Datensatz des deutschen Strommixes (Development of base data for a harmonised and updateable data set of the German electricity mix). Stuttgart/Heidelberg/Darmstadt, May 2008
7. Bundesanstalt für Geowissenschaften und Rohstoffe/ Bundesministerium für Wirtschaft und Arbeit (German Ministry of the Economy) (2002) Reserven, Ressourcen und Verfügbarkeit von Energierohstoffen 2002 (Reserves, resources and availability of energy raw materials 2002). E. Schweizerbart'sche Verlagsbuchhandlung, Stuttgart. ISSN 0342 – 9288
8. ASUE (2002) Mikro-KWK - Motoren, Turbinen und Brennstoffzellen (Micro CHP – engines, turbines and fuel cells). Kaiserslautern
9. Slowe J (2008) Market prospects for the CHP equipment industry. Journal of Cogeneration and On-Site Power Production. http://www.delta-ee.com/downloads/ARTICLES_COSPP_%2008_3_p29_33_Slowe.pdf. Accessed May 2011
10. Cogeneration Directive 2004/8/EC. European Commission, Brussels, 2004
11. Herdin GR (2000) Increasing gas engine efficiency. In: Proceedings of the world energy engineering congress, Atlanta
12. Obernberger I, Thek G (2004) Techno-economic evaluation of selected decentralised CHP applications based on biomass combustion in IEA partner countries. IEA Task 32 report, Graz 2004
13. VDI 2067 and VDEW-Lastprofile Materialien M-28/99
14. Föger K (2010) Commercialisation of CFCL's residential power station – BlueGen. In: Proceedings of the 9th European SOFC forum, Lucerne. Paper 0203
15. Birnbaum KU (2010) Brennstoffzellen / Brennstoffzellen Hybridkraftwerke. In Energietechnologien 2050 – Schwerpunkte für Forschung und Entwicklung, Technologiebericht, Fraunhofer Verlag, ISBN: 978-3-8396-0102-0
16. Steinberger-Wilckens R, Buchkremer H-P, Malzbender J, Blum L, de Haart LGJ, Pap M (2010) Recent developments in SOFC research at Forschungszentrum Jülich. In: Proceedings of the 9th European SOFC forum, Lucerne, 30 June – 2 July 2010. Paper A0105
17. Blum L, Peters Ro, David P, Au SF, Deja R, Tiedemann W (2004) Integrated stack module development for a 20 kW system. In: Proceedings of the 6th European SOFC forum, Lucerne, 30 June – 2 July 2004
18. Esdaile-Bouquet T (2011) CHP support mechanisms in the EU, CODE final dissemination workshop, Brussels, 25 Mar 2011. http://www.code-project.eu/wp-content/uploads/2011/03/Thomas-Bouquet.pdf. Accessed May 2010
19. Pillai MR, Bierschenk DM, Barnett SA (2008) Electrochemical partial oxidation of methane in solid oxide fuel cells: effect of anode reforming activity. Catal Lett 121:19–23
20. European Commission (2011) A roadmap for moving to a competitive low carbon economy in 2050. COM (2011) 112 final, Brussels, 8 Mar 2011
21. Steinberger-Wilckens R (2005) Hydrogen as a means of transporting and controlling wind power. In: Ackermann Th (ed) Wind energy in power systems. Wiley, Chichester, pp 505–519. ISBN 0-470-85508-8
22. Brisse A, Schefold J, Stoots C, O'Brien J (2010) Electrolysis using fuel cell technology. In: Steinberger-Wilckens R, Lehnert W (eds) Innovations in fuel cell technologies, vol 2, RSC energy and environment series. Royal Society of Chemistry, London, pp 267–286. ISBN 978-1-84973-033-4
23. Jönsson O, Polman E, Jensen JK, Eklund R, Schyl H, Ivarsson S (2003) Sustainable gas enters the European gas distribution system. In: Proceedings world gas conference, Tokyo
24. Oasmaa A Report on biofuels for SOFC applications, part 1: fuel options (D6.1). Report to the large SOFC project. VTT Technical Research Centre of Finland. http://www.vtt.fi/files/projects/largesofc/large_sofc_biofuels_wp6_public.pdf. Accessed May 2011
25. Global Emission Model for Integrated Systems (GEMIS). http://www.oeko.de/service/gemis/en/index.htm. Accessed May 2011
26. Machat M, Werner K (2007) Entwicklung der spezifischen Kohlendioxid-Emissionen des deutschen Strommix (Development of the specific CO2 emissions of the German electricity mix). Umweltbundesamt, Dessau, ISSN 1862-4359
27. Fuel Cell and Hydrogen Joint Undertaking (FCH JU) (2008) Multi-annual implementation plan (MAIP). Brussels
28. Project documentation and deliverables of EuroFC-Grid, project funded by the FCH JU, 2010-2012
29. Steinberger-Wilckens R, Bucheli O, de Haart LGJ, Hagen A, Kiviaho J, Larsen J, Pyke S, Rietveld B, Sfeir J, Tietz F, Zahid M (2009) Real-SOFC – a joint European effort to improve SOFC durability. ECS transactions: solid oxide fuel cells 11 (SOFC XI). In: Proceedings of the SOFC XI meeting, Vienna; ECS Transactions, vol 25, issue 2, "SOFC XI", The Electrochemical Society, Pennington, p 43–56
30. Blum L, H–P Buchkremer, Gross SM, de Haart LGJ, Quadakkers J, Reisgen U, Steinberger-Wilckens R, Steinbrech RW, Tietz F (2006) Overview of the development of solid oxide fuel cells at Forschungszentrum Juelich. Int J Appl Ceram Technol 3(6):470–476
31. Schiller G, Henne R, Lang M, Müller M (2004) Development of solid oxide fuel cells by applying DC and RF plasma deposition technologies. J Fuel Cell Sci Technol 4(1–2):56–61

32. Cunningham R (2011) Fuel cell gas turbine hybrids – a key part of a clean future, The Rolls-Royce development programme for pressurised hybrid fuel cell systems. http://www.fuelcellmarkets.com/content/images/articles/H2net%20RAL%20Sep01.pdf. Accessed May 2011
33. German Federal Government's National Electromobility Development Plan, Berlin, Aug 2009. http://www.bmwi.de/English/Redaktion/Pdf/national-electromobility-development-plan,property=pdf,bereich=bmwi,sprache=en,rwb=true.pdf. Accessed May 2011
34. U.S. Geological Survey web-site. http://minerals.usgs.gov/minerals/pubs/commodity/zirconium/zircomcs07.pdf. Accessed Sept 2011
35. Hedrick JB (2003) U.S. geological survey, mineral commodity, summaries, January 2003. http://minerals.usgs.gov/minerals/pubs/commodity/rare_earths/740303.pdf. Accessed Sept 2011
36. U.S. Geological Survey: Fact Sheet 087-02 - Rare earth elements—critical resources for high technology. http://pubs.usgs.gov/fs/2002/fs087-02/. Accessed Sept 2011
37. U.S. Geological Survey: rare earths. http://minerals.usgs.gov/minerals/pubs/commodity/rare_earths/mcs-2010-raree.pdf. Accessed Sept 2011
38. Kingsnorth DJ (2009) The rare earth market: can supply meet demand in 2014? Industrial minerals company of Australia, PDAC 2009, Toronto
39. U.S. Geological Survey. http://minerals.usgs.gov/minerals/pubs/commodity/rare_earths/mcs-2009-yttri.pdf/. Accessed Sept 2011
40. Mineral Information Institute. http://www.mii.org/periodic/Y.htm. Accessed Sept 2011
41. Seilnacht T, Binder H (1999) Lexikon der chemischen Elemente. Stuttgart/Leipzig
42. http://www.webelements.com/lanthanum/. Accessed Sept 2011
43. Mineral Information Institute: Lanthanum. http://www.mii.org/periodic/La.htm. Accessed Sept 2011
44. MacMillan JP (2004) Strontium. In: Ullmann's encyclopedia of industrial chemistry. Wiley, New York
45. International Manganese Institute. http://www.manganese.org/. Accessed Sept 2011
46. Duke JM (1980) Nickel in rocks and ores. In: Nriagu JO (ed) Nickel in the environment. Wiley, New York/Chichester/Brisbane/Toronto, pp 27–50
47. Mining, smelting and refining of nickel. http://www.nickelinstitute.org/en/NickelUseInSociety/AboutNickel/HowNickelIsProduced.aspx. Accessed Sept 2011
48. Sanborn D, et al. (1995–1996) Amethyst Galleries, Inc. (updated several times by Covey S.). http://www.galleries.com/minerals/sulfides/pentland/pentland.htm. Accessed Sept 2011
49. Hertel RF, Maass T, Muller VR (1991) Nickel. World Health Organization, Geneva. http://www.inchem.org/pages/ehc.html. Accessed Sept 2011
50. Nickel. http://www.seilnacht.com/Lexikon/28Nickel.htm. Accessed Sept 2011
51. Kerfoot DGE (2004) Nickel. In: Ullmann's encyclopedia of industrial chemistry. Wiley-VCH Verlag GmbH & Co. KGaA. doi:10.1002/14356007.a17_157
52. Buchkremer HP, Diekmann U, de Haart LGJ, Kabs H, Stimming U, Stöver D (1997) In: Stimming U, Singhal SC, Tagawa H, Lehnert W (eds), Proceedings of the 5th international symposium. Solid oxide fuel cells (SOFC-V), The Electrochemical Society, Pennington, p 160
53. de Haart LGJ, Vinke IC, Janke A, Ringel H, Tietz F (2001) New developments in stack technology for anode substrate based SOFC. In: Yokokawa H, Singhal SC (eds) Solid oxide fuel cells VII. The Electrochemical Society, PV 2001-16. Proceedings series, Pennington, p 111
54. Piron-Abellan J, Shement V, Tietz F, Singheiser L, Quadakkers WJ, Gil A (2001) Ferritic steel interconnect for reduced temperature SOFC. In: Yokokawa H (ed) Proceedings of the 7th international symposium on solid oxide fuel cells (SOFC-VII), Tsukuba, 3–8 Juni 2001 (Proceedings of the electrochemical society; 2001-16, Pennington, 2001) p 811–819. ISBN 1-56677-322-9
55. Thyssen Krupp VDM, CroFer22APU Material data sheet No. 8005
56. Haanappel VAC, Mertens J, Rutenbeck D, Tropartz C, Herzhof W, Sebold D, Tietz F (2005) Optimization of processing and microstructural parameters of LSM cathodes to improve the electrochemical performance of anode-supported SOFCs. J Power Sources 141:216
57. Mai A, Haanappel VAC, Uhlenbruck S, Tietz F, Stöver D (2005) Ferrite-based perovskites as cathode materials for anode-supported solid oxide fuel cells: part I. Variation of composition. Solid State Ionics 176:1341–1350
58. Konysheva E, Penkalla H, Wessel E, Mertens J, Seeling U, Singheiser L, Hilpert K (2006) Chromium poisoning of perovskite cathodes by the ODS alloy Cr5Fe1Y2O3 and the high chromium ferritic steel CroFer22APU. J Electrochem Soc 153:A765
59. Shaigana N, Qua W, Iveyb DG, Chen W (2010) A review of recent progress in coatings, surface modifications and alloy developments for solid oxide fuel cell ferritic stainless steel interconnects. J Power Sources 195(6):1529–1542
60. Ishihara T, Sammes NM, Yamamoto O (2003) Electrolytes. In: Singhal SC, Kendall K (eds) High temperature solid oxide fuel cells. Elsevier, Oxford/New York/Tokyo. ISBN 1 856 173 879
61. Stöver D, Buchkremer HP, Huijsmans JPP (2003) MEA/cell preparation methods: Europe/USA. In: Vielstich W, Lamm A, Gasteiger HA (eds) Handbook of fuel cells, vol 4, Fuel cell technology and applications, part 2. Wiley, Chichester, pp 1013–1031
62. Haanappel VAC, Shemet V, Vinke IC, Gross SM, Koppitz Th, Menzler N, Zahid M, Quadakkers WJ (2005) Evaluation of the suitability of various glass sealant-alloy combinations under SOFC stack conditions. J Mater Sci 40:1583–1592
63. Gross SM, Koppitz T, Remmel J, Reisgen U (2005) Glass-ceramic materials of the system BaO-CaO-SiO_2 as sealants for SOFC applications. Ceramic engineering and science proceedings CODEN CESPDK, 26(4): 239–245. ISSN 0196-6219

64. Stöver D, Mai HPA, Menzler NH, Zahid M (2006) Processing and properties of advanced solid oxide fuel cells. In: Chandra T, Tsuzaki K, Militzer M, Ravindran C (eds) Proceedings of the THERMEC 2006, Materials Science Forum (vol 539–543), pp1367–1372
65. Hellerbrand H (1995) Processing of ceramics, Part I. In: Cahn RW, Haasen I, Kramer EJ (eds) Materials science and technology, vol 17A. Wiley, Weinheim, p 190
66. Gaudon M, Menzler NH, Djurado E, Buchkremer HP (2005) YSZ electrolyte of anode-supported SOFCs prepared from sub micron YSZ powders. J Mater Science 40:3735–3743
67. Holmes PJ, Loasby RG (1976) Handbook of thick film technology. Electrochemical Publications, Scotland, p 14
68. Gubner A, Nguyen-Xuan T, Bram M, Remmel J, de Haart (2006) Lightweight cassette type SOFC stacks for automotive applications. In: Proceedings of the 7th European SOFC forum, Lucerne, Paper B0402
69. Franco T, Ruckdäschel R (2006) Diffusion and protecting barrier layers in a substrate supported SOFC concept. In: Proceedings of the 7th European solid oxide fuel cell forum, European Fuel Cell Forum, Oberrohrdorf. Paper No. P0802-051
70. Montero X, Tietz F, Stöver D, Cassir M, Villarreal I (2009) Evaluation of commercial alloys as cathode current collector for metal-supported tubular solid oxide fuel cells. Corros Sci 51(1):110–118
71. Henne R, Arnold J, Kavka T, Maslani A (2004) Influence of injection mode on properties of DC plasma jets for thermal plasma spraying. Czech J Phys 54(3):C766–C771, Springer, Netherlands
72. Henne R (2003) Was können Brennstoffzellen zur Lösung unserer Energieversorgungsprobleme beitragen? Presentation, VDI Arbeitskreis Technische Gebäudeausrüstung Stuttgart, 20 Oct 2003. wiv.vdi-bezirksverein.de/HenneVDI.pdf. Accessed May 2011
73. Schiller G (2006) Metallgestützte SOFC-Zellen. Fortbildungsseminar Werkstofffragen der Hochtemperatur-Brennstoffzelle, Deutsche Gesellschaft für Materialkunde (Hrsg.), Jülich, 26–28 Apr 2006. http://elib.dlr.de/45395/1/J%C3%BClich_DGM_2006_G._Schiller.pdf. Accessed May 2011
74. Lenntech BV (2011). http://www.lenntech.com/periodic/elements/ar.htm. Accessed Feb 2011
75. Praxair, gases, production of argon. www.praxair.com. Accessed Feb 2011
76. Hart NT (2004) Scale up of the IP-SOFC to multi kilowatt levels. Report F/01/00197/REP, URN 04/556, DTI. www.berr.gov.uk/files/file15317.pdf. Accessed May 2011
77. Goettler R (2009) Overview of the Rolls-Royce SOFC technology and SECA program. http://www.netl.doe.gov/publications/proceedings/09/seca/presentations/Goettler_Presentation.pdf. Accessed May 2011
78. Cassidy M, Boulfrad S, Irvine J, Chung C, Jorger M, Munnings C, Pyke S (2008) Integration of oxide anodes into the Rolls-Royce IP-SOFC concept. J Fuel Cell Sci Technol 9(6):891–898
79. Hart D, Hörmandinger G (1997) Initial assessment of the environmental characteristics of fuel cells and competing technologies. ETSU F/02/00111/REP/1, ETSU, Harwell
80. Zapp P (1998) Ganzheitliche Material- und Energieflussanalyse von SOFC-Brennstoffzellen. Dissertation Universität–GH Essen, Jülich, Jül-3497
81. Karakoussis V, Brandon NP, Leach M, van der Vorst P (2001) The environmental impact of manufacturing planar and tubular solid oxide fuel cells. J Power Sources 101:10–26
82. Pehnt M (2003) Assessing future energy and transport systems: the case of fuel cells, Part 2: environmental performance. Int J Life Cycle Ass 8(6):365–378
83. http://ecoinvent.ch. Accessed Aug 2011
84. Krewitt W, Pehnt M, Fischedick M, Temming H (2005) Brennstoffzellen in der Kraft-Wärme-Kopplung - Ökobilanzen, Szenarien, Marktpotentiale. Beiträge zur Umweltgestaltung Band A 156, Erich Schmidt Verlag, Berlin
85. European Institute for Energy Research (EIFER) (2008) Final report on evaluation on the sustainability of the stacks produced in the project. Real-SOFC Project, Realising reliable, durable energy efficient and cost effective SOFC systems, Integrated EU project under the 6th framework programme
86. Rolls-Royce Fuel Cell Systems Limited (2008) Life cycle inventory analysis of the IP-SOFC stack concept. Real-SOFC Project, Realising reliable, durable energy efficient and cost effective SOFC systems, Integrated EU project under the 6th framework programme
87. Del Borghi A, et al. (2009) Final report on environmental impact of the operation of high temperature FC. LargeSOFC-Project, Towards a large SOFC power plant, Integrated EU project under the 6th framework programme
88. Gerboni R, Pehnt M, Viebahn P, Lavagno E (2008) Final report on technical data, costs and life cycle inventories of fuel cells. NEEDS-Project, New energy externalities developments for sustainability, Integrated EU project under the 6th framework programme
89. Guinée J, Gorrée M, Heijungs R, Huppes G, Kleijn R, de Koning A, van Oers L, Wegener Sleeswijk A, Suh S, de Haes HAU, de Bruijn H, van Duin R, Huijbregts MAJ (2002) Handbook on life cycle assessment: operational guide to the ISO standards. Kluwer, Dordrecht
90. Han F, Leonide A, van Gestel T, Buchkremer HP (2010) Excellent electrochemical performance with thin YSZ electrolyte for IT-SOFCs. In: Proceedings of the 9th European SOFC forum, European Fuel Cell Forum, Oberrohrdorf/Lucerne
91. BMU (2003) Bundeseinheitliche Liste der CO_2-Emissionsfaktoren. Bundesministerium für Umwelt, Berlin, 1 Nov 2003
92. Bauen A, Hart D (2000) Assessment of the environmental benefits of transport and stationary fuel cells. J Power Sources 86:482–494

Books and Reviews

Seilnacht T, Binder H (1999) Lexikon der chemischen Elemente, Stuttgart/Leipzig, publishing house Hirzel Stuttgart

Solid Waste Disposal and Recycling, Environmental Impacts

Jess W. Everett
Civil and Environmental Engineering, Rowan University, Glassboro, NJ, USA

Article Outline

Glossary
Definition of the Subject and Its Importance
Introduction
Hierarchy of Solid Waste Management
Environmental Impacts
Future Directions
Bibliography

Glossary

Composting Controlled aerobic or anaerobic biodegradation in which microbes consume the more biodegradable portions of a waste.

Incinerator A facility for the volume and mass reduction of solid waste via combustion.

Landfill A facility where waste is disposed of on or in land.

Reuse When a new use is found for a waste, either directly or after refurbishment.

Recycling Processing a waste for use in manufacturing a new product.

Sanitary landfill A landfill with many modern components, including daily cover, liners, and leachate collection.

Solid waste An unwanted item that is not liquid or gas.

Source reduction Not making a waste in the first place.

Waste disposal Removing a waste from the human sphere.

Waste-to-energy An incinerator with energy recovery.

Definition of the Subject and Its Importance

A waste is anything humans do not want. Solid wastes are unwanted items that are not liquid or gas. Waste disposal involves removing a waste from the human sphere. This is often done by placing the waste in a landfill or burning it and placing the ashes in a landfill. Recycling involves processing a waste for use in manufacturing a new product. Reusing waste means using it again, either directly or after repair or improvement. Finally, source reduction involves not making waste in the first place.

Humans have disposed of waste since the creation of the species. Initially, this involved discarding an object at the point it became waste, in time and space. Where population centers developed, disposal became more involved. Waste had to be disposed of by combustion and/or deposition in an out-of-the-way place. In modern times, high population density, high waste generation, and toxic waste characteristics resulted in the need for sophisticated waste disposal and recycling methods to avoid unacceptable environmental impacts.

Introduction

In the nonhuman environment, there is no waste. Rocks weather into soil. New plants grow; animals are born and eat the plants. Plants and animals die or are killed and return to the earth by natural processes. Urine and feces are diluted and biodegraded and also returned to the earth. Nature is a cycle of birth, growth, death, and decay.

In the human world, wastes are things humans no longer want. Solid wastes are unwanted items that are not liquid or gas. Nonindustrial human populations typically generate small amounts of solid waste per person. They depend directly on animal husbandry and agriculture. The bare minimum of products, e.g., tools, pottery, food, and shelter, are made by hand using available natural materials. The resulting solid wastes are little different from materials found in nature: feces, plant debris, animal by-products, ceramic, stone and wood objects, and perhaps smaller amounts of metallic items. Sparse nonindustrial human populations can essentially follow the way of nature without undo harm to themselves or the environment. Solid wastes can be left where they are produced or a short distance from camps and villages. Biodegradable wastes – feces, spoiled food, broken wood products, worn-out furs and textiles, and the dead – naturally break down and return to the environment quickly. Non-biodegradable wastes, such

as stone, ceramic, and metallic products, remain intact longer but do not cause environmental harm.

For larger and denser nonindustrial populations, the quantity of solid wastes can overwhelm the natural assimilative capacity of the local environment. Greater effort is required to manage the biodegradable wastes generated by humans and their domesticated animals. Of special concern are feces and edible wastes.

Feces can contain pathogenic organisms. Improper management can spread disease. Pit latrines are often used in such societies, and are still in common use in rural areas, especially in less developed countries. Pit latrines located too close to water sources can lead to contamination of drinking water. Where possible, rivers may be used to dispose of feces, with negative consequences for downstream populations. Feces have also been used as fertilizer, i.e., night soil. Care must be taken to avoid the spread of diseases from the pathogenic organisms in the feces, especially when night soil is used to fertilize human food crops. Composting feces before application can be used to destroy pathogenic organisms. Composting is controlled aerobic or anaerobic biodegradation; microbes consume the more biodegradable portions of a waste. During the composting process, temperature and time work to kill pathogens, which have evolved to live in host organisms, not a compost pile.

The improper management of edible solid wastes can result in the proliferation of disease vectors, i.e., animals and insects that feed on the waste and carry disease, such as flies, rats, and birds. Edible wastes may be fed to domestic animals. Of course, the subsequent increase in animal numbers will increase the amount of feces requiring proper management. Composting can be used to turn any biodegradable waste into a useful soil amendment that is not attractive to vectors. Burning or burying solid waste can also be used to avoid the proliferation of vectors. Burning also reduces the volume of waste; however, negative air impacts result if too much waste is burned or inadequate pollution controls are used.

The sheer quantity of non-biodegradable or slowly-biodegrading wastes produced by more dense human populations, e.g., building debris, pottery, tools, and fabrics, can cause inconvenience if not isolated from the human environment. Inconvenience can include aesthetic impacts, rising street levels, and impediments to travel. Isolation can be accomplished by depositing the wastes in dry wells, pits, ravines, water bodies, or swamps. In many cases, dump sites can eventually be built upon if the fraction of biodegradables wastes is low or sufficient time passes for the biodegradable wastes to fully decay. Otherwise, the dump site will have poor structural properties and it will be difficult to build good foundations. Cities in unindustrialized societies have historically used all of the options presented above to manage solid wastes.

Industrial societies typically have higher population densities, generate more solid waste per person, and generate waste with different characteristics, as compared to nonindustrial societies. Better food, water, sanitation, and medicine allows for higher population density. The higher per capita generation results largely from a higher quality of life and the consumerism inherent in the modern industrialist system. Population density and per capita generation together result in significantly more waste generation in modern industrial societies. Whereas the waste of the nonindustrial society is primarily associated with food production and shelter, the industrial society produces a huge number of different products which ultimately must be disposed of, including large quantities of manufacturing by-products, broken or obsolete products, and packaging. The waste of industrial nations is high in paper, plastic, glass, and metal. Special waste types include electronic wastes, florescent light bulbs, batteries, and hazardous wastes. Though ideally handled through separate management systems, special wastes can impact solid waste management in general. For example, the modern US landfill is designed to contain household hazardous waste contained within municipal solid waste.

The remainder of this entry is focused on the environmental impacts of solid waste disposal and recycling. Because feces are typically mixed with urine and water and handled as a liquid waste, they are not included here. Furthermore, collection and transport are covered in a separate entry. Here, the hierarchy of solid waste management is used to introduce the various disposal and recycling options. Then, the environmental impacts of the disposal and recycling elements of the hierarchy are explored.

Hierarchy of Solid Waste Management

A commonly used hierarchy of solid waste management is

- Source reduction and reuse
- Recycling and composting
- Landfilling and incineration

The hierarchy can be interpreted as follows. One should reduce the amount of waste generated, or reuse wastes directly, as much as is warranted. Waste that is not avoided or reused should be recycled or composted, again, as warranted. Finally, waste that cannot be reasonably avoided, reused, recycled, or composted must be incinerated (with energy recovery) and/or landfilled. Note the use of the word "warranted." The hierarchy is not meant to suggest that all possible source reduction and reuse should be done before any consideration of recycling and composting. It is a case of "if all else is equal" source reduction and reuse are more valued than recycling and composting which in turn are more valued than landfilling and incineration. In the European Union, the order of importance, by directive, is minimization at source, reuse, recycling, incineration with energy recovery, and landfilling [1].

Source Reduction

Source reduction avoids the production of waste altogether, either because products are manufactured in ways that result in less waste or fewer products come to the end of their useful life. It is accomplished primarily through changes in product design or personal lifestyle.

Products can be designed using fewer materials, e.g., the walls of beverage containers have been "thinned" significantly since first introduced. Those who used early plastic bottles and aluminum cans may remember how much thicker and sturdier the walls were compared to later examples. In this case, a given amount of product, e.g., soda, can be delivered with less waste upon disposal. Some products can be made smaller, e.g., a sound system that used to consist of a receiver, CD player, and large speakers can be replaced by an mp3 player the size of a deck of cards and ear bud speakers.

Reducing the toxicity of waste is also a worthwhile goal. This is typically accomplished by making the product using less toxic materials, e.g., many newspapers moved from petroleum-based inks to soy-based inks in the later part of the twentieth century. In 2009, more than 90% of the nation's daily newspapers were printed with color soy ink [2]. Significant reduction in the metal content of batteries was also accomplished [3, 4].

Products can be designed to be more durable, e.g., a product that lasts twice as long but uses only 50% more material causes 25% less waste when it reaches the end of its useful life. Examples of items where increased durability is desirable include clothing, toys, and furniture. Durable items can be resold if one grows tired of them.

A consumer lifestyle arose in the twentieth century. Centralized efficient manufacturing made more products available at reduced cost, while simultaneously giving rise to a prosperous middle class that could afford more goods. More and more people purchased more and more products. While the consumerist lifestyle supports economic growth, it also greatly increases waste per capita. Examples of the consumerist lifestyle that affect waste generation include a greater reliance on disposable items or items with planned obsolescence, increased packaging, and simply having more "stuff" to eventually throw away.

Disposable items are typically used once or a very limited number of times. Examples include razors, rain ponchos, foam coolers, and plastic plates, glasses, and utensils. Consumers wishing to generate less waste should avoid disposable items in favor of more durable ones, assuming they will obtain the full benefit of the durable item, i.e., repeated use. The environmental superiority of durable items over disposable depends on how the items are used. A study conducted by the Dutch Environment Ministry found that the superiority of a ceramic coffee mug over a polystyrene one depended on how many times the ceramic mug was reused before it broke and how much water, soap, and energy were used to clean it [5]. Ceramic mugs used twice between washings had to be used 114 times before they had less environmental impact than one-use polystyrene cups.

Many items are built and marketed with planned obsolescence in mind. In some cases, the obsolescence is at least partly a function of technological advance, e.g., electronics such as computers, audio equipment, and video equipment are quickly superseded by

products that are faster, smaller, or have more features. In other cases, the obsolescence is solely a function of fashion, e.g., clothing. Consumers can resist planned obsolescence by purchasing durable items, when appropriate.

Centralized manufacturing and the resulting long transport distances to market make packaging a requirement to safely deliver the vast array of items for sale. In 2008, 30.8% of the US Municipal waste stream consisted of containers and packaging [6]. Efficient packaging design can minimize this waste stream. Purchasing locally manufactured items and food can also avoid packaging waste. Finally, purchasing in bulk will often reduce packaging waste.

Affluence, and the availability of affordable products, encourages people to purchase more items, nearly all of which become waste in a relatively short time. A return to a more frugal and simple lifestyle can greatly reduce waste. Avoiding disposable items, buying in bulk, and avoiding unnecessary purchases can lead to significant reduction in waste generation. A popular example is using reusable cloth bags at the grocery store, rather than disposable paper or plastic. Another example is using cloth diapers instead of disposable. In many communities, a service can be hired that provides fresh diapers and takes used ones for cleaning.

The City of Greensboro, NC, USA, demonstrated the effectiveness of using education to encourage source reduction [7]. An education program was carried out in one neighborhood, consisting of monthly newsletters, public meetings, and small group meetings in homes, while a control neighborhood was provided with no educational activities. Waste decreased by only 1.3% in the control neighborhood. Waste in the educated neighborhood decreased by 23.4%.

The potential for waste reduction through lifestyle change is high. In numerous communities, residents pay different rates depending on the volume or mass of waste collected. This is commonly called unit pricing or pay as you throw (PAYT). One typical scenario is for residents to select from a range of waste container volumes; the smaller the container, the lower the monthly charge. In other systems, residents pay a fee for each bag of waste set out or a fee assessed relative to the mass of material collected.

In the late 1990s in Olympia, Washington, USA, the standard collection scenario was biweekly collection with a 65 gal (246 L) container, but 10% of residents opted for a 35 gal (133 L) container [8]. A small number were able to use a 20 gal (76 L) container. Considering that a typical waste collection scenario in the US is weekly collection with a 96 gal (363 L) container, biweekly collection of a 20 gal container shows the potential for reduction associated with lifestyle changes, whether motivated by environmental or financial concerns. Of course, reduction was not the only strategy used to reduce waste; reuse, recycling, and composting were also employed.

Reuse

At the United Nations Conference on Environment and Development in 1992,178 governments agreed on the need for more sustainable municipal solid waste management in developed and developing nations [9]. Chapter 21 of Agenda 21, the Rio Declaration on Environment and Development, describes environmentally sound solid waste management, including the maximization of environmentally sound waste reuse and recycling.

Reuse involves taking an item that has come to the end of its useful life and finding a new use that requires no change to the item (direct reuse) or some repair or improvement (refurbishing). Direct reuse examples include using the back side of waste paper for notes, using glass jars as drinking glasses, using plastic bread bags as sandwich bags, and using plastic or paper shopping bags as garbage bags. The waste savings is related to the number of reuses. Many opportunities only afford one reuse; for example, using a grocery bag as a garbage bag reduces waste by the amount of garbage bags one avoids purchasing.

Refurbishing opportunities involve repairing or upgrading items that would otherwise be discarded. A number of car parts, including alternators and engines are commonly refurbished and resold. Wood from old barns, warehouses, and homes is replaned and used to make furniture or new floors. This is sometimes called deconstruction.

In some cases, products can be designed for easy repair and upgrading, i.e., reuse, rather than early obsolescence. This increases product lifetime with only the minor waste associated with the replaced components. However, this may not be financially

rewarding to companies unless the externalities associated with waste management are built into the economic system through taxes and fees.

Recycling

Recycling involves using a waste product as a raw material to make a new product. The recycling cycle is shown in Fig. 1. The most commonly recycled waste products are paper, cardboard, plastic, glass, aluminum, and steel. Post consumer recycling, i.e., recycling that occurs after an item is sold to a consumer, typically involves collection, transfer to a processing facility, and transport to a manufacturing facility. At processing facilities, materials are sorted to remove impurities and compacted for efficient transport. At the manufacturing facility, waste materials are often mixed with virgin materials when making new products.

Paper and cardboard wastes are repulped to make new paper, cardboard, or tarpaper products. Each time wood is pulped, the fibers become shorter. For this reason, paper fibers can only be recycled a finite number of times. Care must be taken to ensure the quality of items made from recycled fiber.

There are a number of different plastic resins. The two that are most commonly recycled are Polyethylene Terephthalate (PET) and High-Density Polyethylene (HDPE). In the USA, these are identified with the numbers 1 and 2, respectively, found surrounded by three recycling "arrows" on the bottom of any container made from PET and HDPE. PET is the most common soda, water, and juice bottle material, while HDPE is used in milk containers and a host of other plastic containers, including shampoo and cleaners. Plastic wastes are cleaned, ground, and remelted to form pellets which are used in the manufacture of new products. Except for certain applications, such as plastic lumber, the different resins must be kept separate. Colors must be kept from nonpigmented, if nonpigmented products are to be made from the recycled plastic.

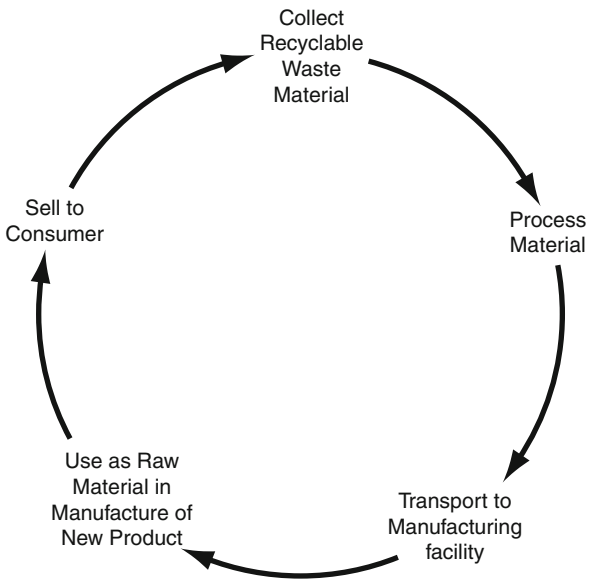

Solid Waste Disposal and Recycling, Environmental Impacts. Figure 1
The recycling cycle

Different colors of glass are often recycled separately. Different types of metals are recycled separately, except to make a particular alloy. Glass and metals are melted at a recycling plant. Glass is immediately formed into new products. Metals are often formed into ingots which are later formed into new products.

Product design can make products easier to recycle, especially products with multiple components. For example, automobile recycling often entails dismantling [10], which can be aided by reducing the number of different materials used and by labeling parts, especially plastics, for easy identification. One way to encourage appropriate product design is called "extended producer responsibility." This concept, incorporated into European law, makes producers responsible for the management of the waste resulting from their products. In this system, for example, producers must ensure that appropriate percentages of their waste products are collected for recycling. This includes the packaging associated with their products. When extended producer responsibility laws are employed properly, producers have a financial incentive to redesign their products to produce less waste, be easier to reuse, recycle, or compost, and be safer to landfill or incinerate.

Recycling can be an important part of solid waste management in developed and developing countries. After assessing recycling in 23 developing countries, Troschinetz and Mihelcic [9] estimated an average MSW generation rate of 0.77 kg/person/day with recovery rates varying from 5% to 40%.The waste streams of 19 of these case studies consisted of 0–70% recyclable material and 17–80% organic material.

This can be compared to the USA with an average MSW generation rate of 2 kg/person/day and a recovery rate of 33% [6]. The US municipal waste stream is 25.9% food scraps and yard trimmings. The percent of the US waste stream that is recyclable has been estimated to be as low as 38.4% [11] and at least as high as 72%, given that San Francisco announced a 72% recycling rate in 2009 [12].

Twelve factors have been identified that influence the sustainable recycling of municipal solid waste management (MSWM) in developing countries: government policy, government finances, waste characterization, waste collection and segregation, household education, household economics, MSWM administration, MSWM personnel education, MSWM plan, local recycled-material market, technological and human resources, and land availability [9]. These same factors are important in developed countries.

It is best to consider source reduction, reuse, and recycling simultaneously. According to the IWIEMEF [13], the solution to solid waste management requires us to:

- Recycle materials from discarded products so they can be reprocessed and used to manufacture "new" products
- Remanufacture discarded goods, involving disassembly, cleaning, and reassembly into "rebuilt" products
- Redesign products and processes to dramatically improve efficiency of material and energy use and make recycling easier
- Rethink how goods and services can meet human wants more efficiently

Composting

Composting is a process in which biodegradable wastes are turned into a soil amendment by microbes. If done under anaerobic conditions, methane and carbon dioxide are the main gaseous end products. If accomplished under aerobic conditions, the major gaseous end product is carbon dioxide. Aerobic composting is most common. Composting can be considered a recycling process, as waste material is turned into a new product, a soil amendment.

Grass, leaves, and yard waste are the most commonly composted materials; however, any biodegradable material can be incorporated, including food waste, agricultural waste, sawdust, wood chips, waste paper, manure, and wastewater sludge. Bulking agents may be added to create a mix that is easy to aerate. Woodchips and saw dust are examples of bulking agents.

The most important factors in aerobic composting are moisture content, oxygen level, and carbon to nitrogen ratio. Typical recommendations are 50–65% moisture content, a reduction in oxygen content of no more than 50%, and 15:1–35:1 by weight carbon to nitrogen ratio [14, 15]. Under these conditions, bacteria and other microbes will consume the easily degradable materials via respiration, leaving an organic material that can be safely stored and applied to land. While not a fertilizer, compost applied to land will slowly release low levels of nitrogen. It also adds valuable organic matter to soil.

The simplest composting process involves forming waste into windrows, long piles, which are turned periodically to introduce oxygen. Special windrow turning machines can be used, but manual labor or front end loaders can also be used. Static windrows can be used if perforated pipes are placed within the pile and used to introduce air. In-vessel composting systems often use an inclined rotating cylinder to mix and introduce oxygen. Typically, the windrow process takes the longest time to produce stable compost, while in-vessel takes the least time. Times can vary from as long as 6 months, when composting materials with high carbon to nitrogen ratios using the windrow process, to less than a week for in-vessel composting of readily biodegradable wastes [16].

Landfilling

Landfilling is the land disposal of waste. Typically, some excavation occurs when building a landfill, but waste is often built up to a level well above the original ground surface. Landfilling is a direct descendant of the largely uncontrolled dumps that were used previously in the developed world and are still used in many parts of the developing world. In uncontrolled dumps, waste is deposited directly on the Earth's surface, often in low points such as ravines or gullies, or in water bodies or swamps. It is often burned to reduce volume. Scavengers may pick through the waste to recover items of value.

A modern landfill is shown in Fig. 2. It has a liner and leachate collection system. Leachate is any liquid that comes in contact with the waste. The liner system consists of clay and/or thick plastic membranes. To minimize leaks, the leachate collection system collects any leachate that reaches the liner. The collection system consists of a drainage layer, often sand, with perforated pipes that quickly convey leachate to a sump. A pump typically sends the collected leachate to an on-site treatment facility and/or a sanitary sewer. Located up and down gradient of the landfill, monitoring wells are used to identify any contamination of groundwater.

The working face of the landfill is a relatively small section where waste is unloaded from collection or transport vehicles. The working face is kept as small as possible, to minimize litter and vectors. At the end of each day, any exposed waste is covered with soil, tarps

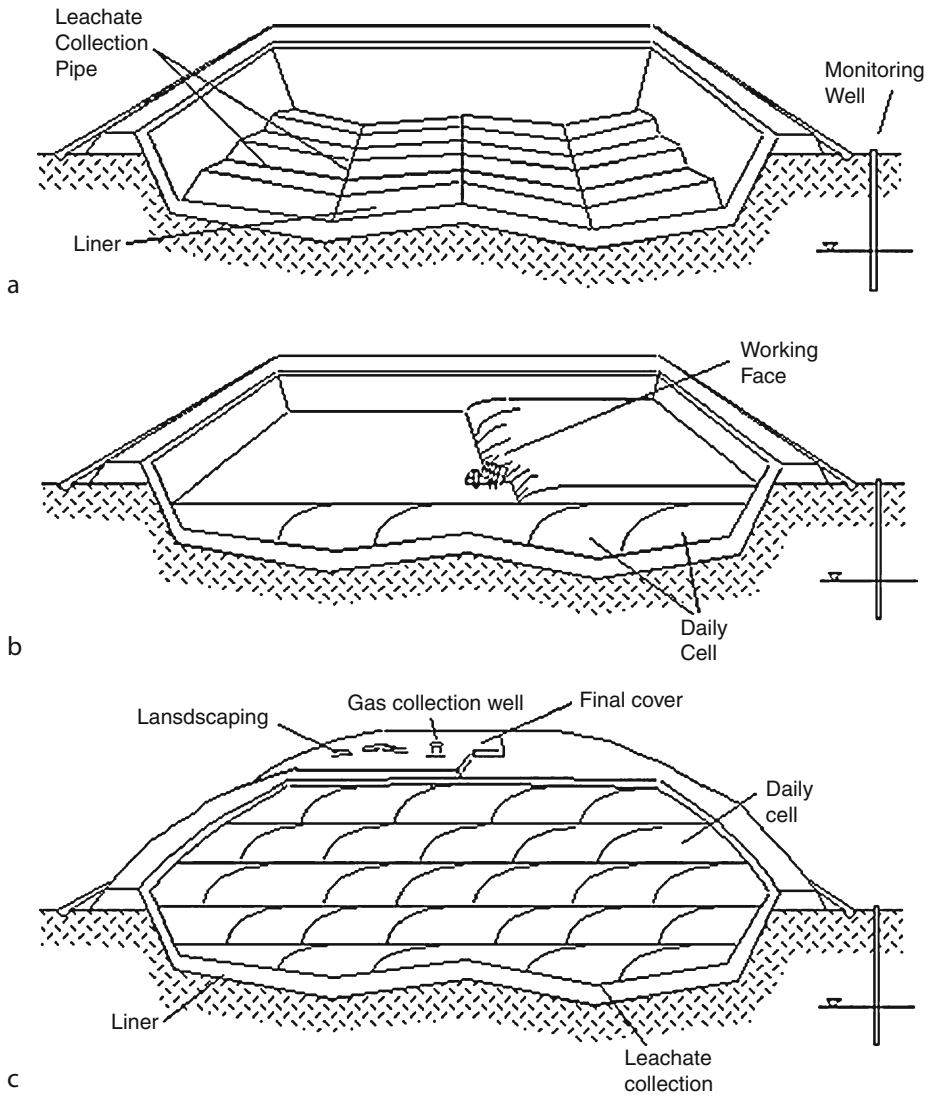

Solid Waste Disposal and Recycling, Environmental Impacts. Figure 2
Development of a Landfill: (**a**) excavation and installation of landfill liner, (**b**) placement of solid waste in landfill, (**c**) cutaway through completed landfill (Adapted from [17])

or foam, both for fire and vector control. This is called daily cover. Fires still occur at landfills, more frequently if landfill operations are lax [18]. Daily cover and litter fences keep litter contained at the landfill site.

Final slopes are covered with a top liner, to minimize rain infiltration and to keep landfill gas from escaping. A gas recovery system is installed consisting of vertical or horizontal perforated pipes. The typical landfill becomes anaerobic; in this case, the landfill gas is comprised of roughly half CO_2 and half methane, with some trace gases [19]. Landfill gases may be flared or used to run a turbine to generate electricity.

Because of the poor structural properties of the waste, plus the rapid settlement cause by biodegradation, it is difficult to build on landfills, especially while significant settling is occurring. However, special foundations can be used if buildings are to be located on a closed landfill.

In bioreactor landfills, water and/or air are circulated to increase the rate of biodegradation. If air is circulated, the landfill will degrade under aerobic processes and the landfill gas will largely be comprised of CO_2. Once the waste is sufficiently degraded, it may be possible to recover it for use as a daily cover.

Incineration

The uncontrolled combustion of unwanted wastes probably started shortly after humankind learned to control fire. The first waste-to-energy incineration plant was constructed in Hamburg, Germany in 1896. It used steam to create electricity. By 1979, there were 522 worldwide [20]. Incineration is a relatively expensive method for pretreating MSW before landfilling. The main objective is to convert biodegradable waste to an inert material while minimizing its volume before disposal in landfills [21].

Waste-to-energy plants combust waste in the presence of excess oxygen to promote complete combustion. Heat is transferred to water circulating in tubes around the furnace, turning the water into steam. The steam is used to turn a turbine, generating electricity. In some cases, the waste heat is used for district heating; hot water or steam is distributed through pipes to provide heat and hot water to buildings in surroundings of the incinerator. All modern incinerators employ energy recovery. In addition to energy recovery, incinerators reduce the volume and weight of material that must be landfilled. The typical incinerator produces ash that is 10% by volume and 30% by weight of the materials incinerated. Unfortunately, only about 50% of municipal waste is combustible [22].

Control of temperature and oxygen, as well as treatment of emissions are the main methods by which incinerators control pollution. Air Pollution control systems include acid gas and dioxin control, scrubbers, and particulate control devices [23]. The primary emission is CO_2, though oxides of nitrogen, acids, metals, and dioxins can be released.

Environmental Impacts

The environmental impacts associated with disposal and recycling include aesthetic degradation, vectors, pollution, and resource depletion. They occur throughout the entire life cycle of a product, shown in Fig. 3. The focus here is on the waste management portion of the cycle, but optimal minimization of a product's environmental impact requires examination of the entire cycle.

Aesthetic Degradation

Aesthetic impacts include litter, odors, and noise. Various factors may be used to both predict littering behavior and design interventions, such as education, gender, income, marital status, and religious convictions. In a study conducted in the town of Nablus, Israel, Al-Khatib et al. [24] determined that males littered more than females, widowers and married individuals littered less than single and divorced individuals and people who identified themselves as "strongly religious" littered less than those who self-described weak or no religious convictions. There were even correlations with the type of material littered, e.g., females and strongly religious individuals rarely littered cigarette butts. In a related study, children reported that the most effective means of discouraging littering were moral and religious conventions and street cleanliness [25]. Santosa et al. [26] found that litter on Cassino beach in Southern Brazil was directly related to beachgoer density and socioeconomic characteristics. Litter generation was approximately twice as high in an area occupied by people with lower average annual income and degree of literacy.

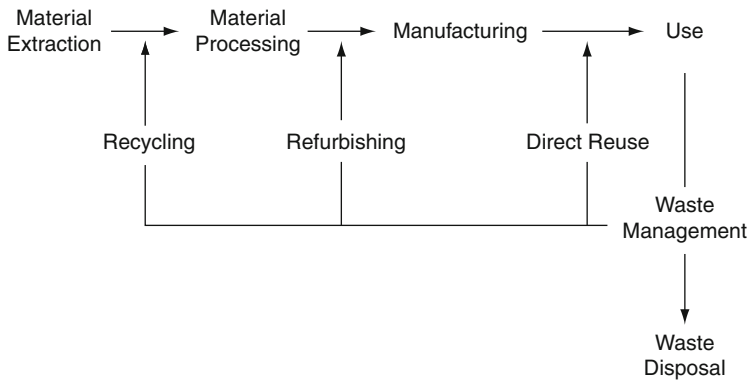

Solid Waste Disposal and Recycling, Environmental Impacts. Figure 3
Product life cycle

Packaging can influence littering behavior, e.g., anti-litter labels on single-use coffee cups reduced litter significantly in a cafeteria [27]. The reclosability of soft-drink packaging can also be important. In one study, a reclosable PET bottle resulted in significantly less litter than carton packaging with a tear-off closure [27].

Litter can also occur as a result of improper waste management. Storage containers should be kept closed to prevent wind from spreading litter. Landfill working faces are kept small and waste is covered at the end of each day in part to minimize litter. Proper placement of litter fences and regular litter collection can keep litter from migrating off-site.

Unpleasant odors can emanate from waste storage, composting, and landfills. Frequent collection will reduce odors associated with storage. Operational procedures can be used to reduce odors at composting facilities and landfills. At composting facilities managing feedstocks, pH monitoring, controlling emissions from conveyors, using aerated static piles, and biofilters have been used successfully [28]. Proper facility siting can also minimize the impact of odors. According to Sironi et al., [29] landfill odor emission factors are directly proportional to the amount of waste deposited annually, the area of the working face, and the area where waste has already been deposited, and inversely proportional to waste density, working days per year, and the height of the daily waste deposit.

Noise impacts associated with recycling and landfills can be minimized by establishing buffers around facilities. Most noise issues associated with solid wastes arise in collection, covered elsewhere.

Vectors

Vectors are creatures that eat waste, such as flies, rats, and birds. Where waste is easily accessed, vectors proliferate and can spread disease. Vectors are minimized by covering the working face at the end of each work day. Birds can also interfere with air traffic. In the USA, landfills are required to be further than 3,500 m (10,000 ft) from airports with turbojet aircraft in order to avoid plane-bird impacts.

Pollution

Pollution impacts from solid waste disposal and recycling include greenhouse gases (GHG), nutrient enrichment, ozone depletion, photochemical ozone formation, acidification, human toxicity, and ecotoxicity. The GHG emissions associated with the material life cycle are given in Fig. 4 and Table 1.

Calabrò [21] evaluated the influence of recycling on greenhouse gas emissions (GHG) emissions from the entire management process, using a waste composition appropriate for Italy. Three different recycling scenarios were investigated. In the first, food and garden waste, paper and cardboard, plastic, glass, wood, metals, textiles were recycled. In the second, plastic was omitted from the list of recycled materials. In the third, food and garden waste was omitted. For each scenario, different recycling rates were investigated. The final disposition of non-recycled materials could be composting, anaerobic digestion, incineration, incineration with energy recovery, or landfilling.

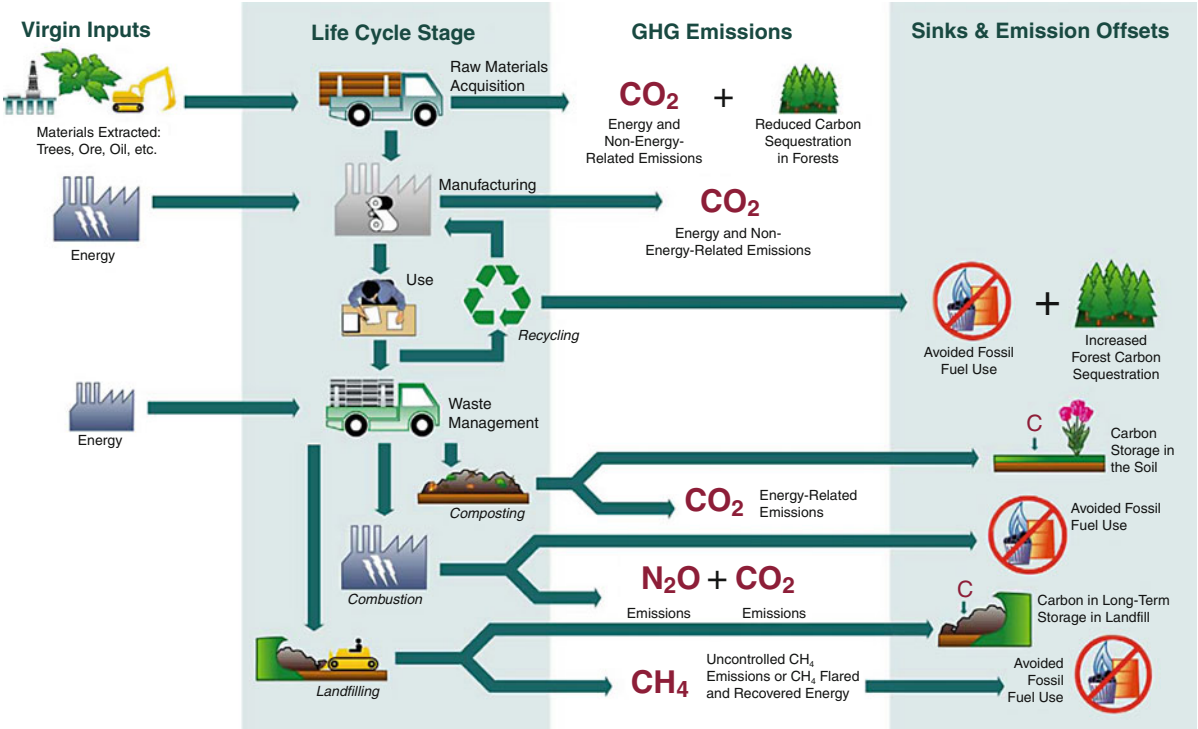

Solid Waste Disposal and Recycling, Environmental Impacts. Figure 4
Greenhouse gas sources and sinks associated with the material life cycle [30]

GHG avoided emissions from recycling are given in Table 2 [21]. The amounts exclude any emissions associated with collection. Emissions reductions are associated with energy savings from reducing the need for virgin materials.

GHG emissions from landfills depend on the efficiency of the biogas collection system [21]. If 90% of the biogas is recovered, the net emissions due to CH_4 are negative, i.e., landfills can be carbon sinks because the combined effect of biogas recovery and energy production canceled the GHG emissions from landfill disposal. For incinerators, the net CO_2 emissions are the CO_2 emissions from the combustion of non-biodegradable materials, such as plastic, minus the avoided emissions due to energy production. Net emissions were positive for all combinations; however, there were a few scenarios where the net emissions were lower than conventional energy processes, such as clean coal.

Disposal in a landfill equipped with 90% biogas collection systems and energy recovery was the best option for residual MSW management in all the scenarios tested [21]. These scenarios actually operated as carbon sinks. Higher recycling rates coupled with landfilling with energy recovery always resulted in higher emissions reductions. Incinerators with energy recovery could also act as carbon sinks, with high recycling rates and high efficiency energy recovery.

In 2008, the USA recycled and composted 83 million US tons of municipal solid waste, providing an annual reduction of 182 million metric tons of carbon dioxide equivalent emissions, comparable to the annual GHG emissions from more than 33 million passenger vehicles [6]. According to the US EPA, source reduction and recycling [31, 32]:

- *Reduce emissions from energy consumption.* Manufacturing goods from recycled materials typically requires less energy than producing goods from virgin materials. Waste prevention is even more effective. When people reuse things or when products are made with less material, less energy is needed to extract, transport, and process raw materials and to manufacture products. With

Solid Waste Disposal and Recycling, Environmental Impacts. Table 1 Net GHG emissions from source reduction and MSW management options, MTCE/Ton[a] [30]

Material	Source reduction[b]	Recycling	Composting	Combustion[c]	Landfilling[d]
Aluminum cans	−2.24	−3.70	NA	0.02	0.02
Steel cans	−0.87	−0.49	NA	−0.42	−0.42
Copper wire	−2.00	−1.34	NA	0.01	0.01
Glass	−0.16	−0.08	NA	0.01	0.01
HDPE	−0.49	−0.38	NA	0.25	0.25
LDPE	−0.62	−0.46	NA	0.25	0.25
PET	−0.57	−0.42	NA	0.30	0.30
Corr. cardboard	−1.52	−0.85	NA	−0.18	−0.18
Magazines/3rd-class mail	−2.36	−0.84	NA	−0.13	−0.13
Newspaper	−1.33	−0.76	NA	−0.20	−0.20
Office paper	−2.18	−0.78	NA	−0.17	−0.17
Phonebooks	−1.72	−0.72	NA	−0.20	−0.20
Textbooks	−2.50	−0.85	NA	−0.17	−0.17
Dimensional lumber	−0.55	−0.67	NA	−0.21	−0.21
Medium-density fiberboard	−0.60	−0.67	NA	−0.21	−0.21
Food discards	NA	NA	−0.05	−0.05	−0.05
Yard trimmings	NA	NA	−0.05	−0.06	−0.06
Mixed paper					
-Broad definition	NA	−0.96	NA	−0.18	−0.18
-Residential definition	NA	−0.96	NA	−0.18	−0.18
-Office paper definition	NA	−0.93	NA	−0.16	−0.16
Mixed metals	NA	−1.43	NA	−0.29	−0.29
Mixed plastics	NA	−0.41	NA	0.27	0.27
Mixed recyclables	NA	−0.79	NA	−0.17	−0.17
Mixed organics	NA	NA	−0.05	−0.05	−0.05
Mixed MSW as disposed	NA	NA	NA	−0.03	−0.03
Carpet	−1.09	−1.96	NA	0.11	0.11
Personal computers	−15.13	−0.62	NA	−0.05	−0.05
Clay bricks	−0.08	NA	NA	NA	NA
Concrete	NA	0.00	NA	NA	NA
Fly ash	NA	−0.24	NA	NA	NA
Tires	−1.09	−0.50e	NA	0.05	0.05

Note that totals may not add due to rounding, and more digits may be displayed than are significant

NA Not applicable, or in the case of composting of paper, not analyzed

[a]MTCE/t: Metric tons of carbon equivalent per short ton of material. Material tonnages are on an as-managed (wet weight) basis

[b]Source reduction assumes initial production using the current mix of virgin and recycled inputs

[c]Values are for mass burn facilities with national average rate of ferrous recovery

[d]Values reflect estimated national average CH4 recovery in year 2003

[e]Recycling of tires, as modeled in this analysis, consists only of retreading the tires

recycling or source reduction, fewer fossil fuels are burned and less carbon dioxide is emitted to the atmosphere.

- *Reduce emissions from incinerators.* Recycling and source reduction allow materials to be diverted from incinerators and thus reduce greenhouse gas emissions from waste combustion.
- *Reduce methane emissions from landfills.* Source reduction and recycling (including composting) divert organic wastes from landfills, reducing the methane released when these materials decompose.
- *Increase storage of carbon in trees.* Trees absorb and store carbon dioxide from the atmosphere, a natural example of "carbon sequestration." Source reduction and recycling of paper products allow more trees to remain in the forest.

Reducing the waste generated in the USA from 2003 to 1990 levels would reduce greenhouse gas emissions by 18 million metric tons of carbon equivalent (MTCE). An MTCE is an amount of GHGs (e.g., CO_2, Methane, water vapor, or ozone) with the greenhouse potential of an amount of CO_2 containing one metric ton of carbon. Increasing the US recycling rate 5% would reduce greenhouse gas emissions by another 10 million MTCE, compared to landfilling the same material. Together, this is comparable to the annual emissions from the electricity consumption of nearly 4.9 million households [31]. Pay-as-you-throw (PAYT) programs are an effective method for encouraging source reduction and recycling. The US EPA [33] estimated that each person participating in a PAYT program reduced their annual greenhouse gas emissions by an average of 0.085 MTCE.

Some wastes can cause environmental or ecological problems when littered. Billions of household batteries are discarded in municipal waste in the USA annually, 35–90 batteries per person per year [4]. The mercury content of new batteries has decreased over time, but the accumulation of mercury, cadmium, and other metals still constitutes a health risk. Nickel-cadmium batteries are a significant source of cadmium in municipal solid waste. Potential health effects of metals in batteries are described in Table 3.

Car batteries rapidly deteriorate when abandoned as litter, releasing Ag, Ba, Cd, Cr, Cu, Hg, Li, Mn, Ni, Pb, Ti, and Zn to storm-water runoff. Results from a study in Cleveland, Ohio, USA, documented annual battery litter as high as 215 batteries/ha of parking lot pavement and 0.4 batteries/m of street curb [34].

Litter can also have a negative impact on animals. An extensive review conducted by Darraik [35] identified a number of impacts on animals caused by plastic litter found in oceans, including physical problems from ingestion, absorption of chemicals leaching

Solid Waste Disposal and Recycling, Environmental Impacts. Table 2 Avoided emissions due to recycling for different materials [21]

Material	Avoided emissions [kg CO_2/metric ton]
Paper and cardboard	565
Plastic (mixed)	396
Glass	159
Metals (mix of aluminum and steel)	3,205
Food and garden waste – composting	−42[a]
Food and garden waste – anaerobic digestion	92

[a]Composting is energy consuming and for this reason CO_2 is emitted

Solid Waste Disposal and Recycling, Environmental Impacts. Table 3 Potential health effects of metals in batteries [4]

Metal	Health effect
Cadmium	Pulmonary edema, emphysema, anemia, lung cancer, anosmia
Lithium	Parkinson's disease, hyperpyrexia, gastroenteritis, diabetes
Manganese	Liver cirrhosis, pneumonia, bronchitis, influenza
Mercury	Bronchitis, gingivitis, pulmonary edema, nervous system disorders
Nickel	Dermatitis, pneumonia, lung and nasal cancer
Silver	Blindness, skin lesions, pneumoconiosis
Zinc	Cornea ulceration, esophagus damage, pulmonary edema

from ingested plastics, and entanglement. Some plastic litter consists of the pellets used to make plastic products, other types degrade into the pellet size range or smaller. These types of plastic litter are easily ingested by many animals. Bags, beverage rings, and fishing nets are particularly likely to cause entanglement.

Improper waste management leads to significant amounts of plastic finding its way into the Earth's oceans. A study conducted in the Pacific Ocean gyre compared the occurrence of plastic and plankton. The mass of plastic was approximately six times higher than plankton. Thin films and polypropylene/monofilament line were the most common types of identifiable plastic [36]. While fishing wastes are a large source of plastic litter in the oceans, land-origin plastic is also significant. Packaging design can be used to minimize it as a source of dangerous litter, e.g., entanglement problems can be reduced by making plastics that break apart in the environment, though one should ensure that this does not increase problems associated with ingestion. Litter is best reduced through proper management of solid waste through source reduction, reuse, recycling, composting, incineration, and landfilling.

Source reduction and reuse reduce pollution. Recycling municipal solid waste also typically reduces pollution. According to the New Jersey Department of Environmental Protection [37], producing new paper from old creates 74% less air pollution and 35% less water pollution than virgin paper production, while glass recycling results in 20% less air pollution and steel recycling creates 85% less air pollution and 40% less water pollution. Recycling also reduces mining wastes, e.g., a metric ton of glass made with 50% recycled materials reduces mining wastes by 125 kg of mining waste [37].

Low and Nair [38] conducted a review of landfills and composting sites. The results of their literature review suggest that GHG emissions from waste decomposition are typically higher for landfills than for composting facilities, primarily because anaerobic decomposition (landfills) produces methane which has a global warming potential (GWP) 25 times that of CO_2. Energy recovery at landfills is an effective mitigation strategy, but requires a good landfill cap and gas recovery system. Even flaring the captured landfill gas will reduce GHG emissions, by converting methane to CO_2. Landfill caps can also reduce water infiltration, slowing the rate of decay and spreading the release of GHGs over a longer time period. Aerobic bioreactor landfills will release less methane, lowering GHG emissions; however, they also consume more energy in forcing oxygen into the landfill. The GHGs associated with the fuel used to blow oxygen into the bioreactor must be considered. Similarly, composting operations that are more energy intensive, such as in-vessel composting, may emit more GHG emissions than relatively passive anaerobic landfills.

All landfills release pollution to the environment through air or groundwater. Potential impacts include nutrient enrichment, ozone depletion, photochemical ozone formation, acidification, human toxicity, and ecotoxicity [39]. Landfills without liners, caps, and leachate and gas collection are particularly prone. Many sites that have required remediation are old landfill sites. A modeling study of the closed Ano Liosia landfill in the greater Athens area estimated air concentrations in the Aspropirgos and the Ano Liosia areas that exceed the reference continuous lifetime exposure levels of priority gas pollutants vinyl chloride and benzene [40]. The landfill was used for co-disposal of hazardous (industrial) and municipal waste. Approximately 50% of the waste entering the landfill was decomposable. There was no gas collection system in use or leachate collection system installed at the site. An assessment of 30 landfills in Chile and Spain indicated that environmental impacts on soil and groundwater are greater than the impacts on surface water, air, and health [41].

The solid waste management model EASEWASTE can be used to assess the environmental impact of a landfill over its life cycle [42]. The results of a case study used to describe the model, based on data from the US EPA, indicate that the normalized environmental effects of landfill gas on global warming and photochemical smog are much greater than the environmental effects of landfill leachate or landfill construction. Niskanen et al. [43] used EASEWASTE to study the Ämmässuo Landfill in Finland. The life cycle assessment results showed substantial impact potentials for spoiled groundwater, global warming, ozone depletion, human toxicity via soil, and chronic ecotoxicity in water.

Simone and Christensen [39] used EASEWASTE to compare the environmental performance of six

landfilling technologies, including open dump, conventional landfill with flares, conventional landfill with energy recovery, standard bioreactor landfill, flushing bioreactor landfill, and semi-aerobic landfill. The assessment criteria included global warming, nutrient enrichment, ozone depletion, photochemical ozone formation, acidification, human toxicity, ecotoxicity, and groundwater resources. Model results demonstrated the importance of collecting landfill gas and leachate. Energy recovery leads to reduced emissions and avoided impacts in several environmental categories. While bioreactors did not reduce total emissions, they did shorten the time frame during which emissions lead to significant environmental impacts.

Mendesa et al. [44] used a life cycle assessment to compare the environmental impact of incineration and the landfilling of municipal solid waste in São Paulo City, Brazil. Three incineration scenarios with different ash treatment systems were evaluated. Two landfilling scenarios were evaluated, with and without energy recovery. Three impact factors were evaluated: Global warming, acidification, and nutrient enrichment. Electricity generation did not result in a significant reduction in overall environmental impact, because of the prevalence of hydropower in Brazil. Significant reductions in environmental impact could be obtained by shifting from landfilling to incineration with ash disposal in a landfill.

The environmental impact of landfilling, incineration, composting, and anaerobic digestion was compared by Seo et al. [45]. Environmental impact categories included global warming, eutrophication, acidification, photochemical oxidant creation, abiotic resource depletion, and ozone depletion. Only the first three contributed significantly to the impact of the considered solid waste management methods. Incineration and anaerobic digestion were found to be the most environmentally friendly, while the landfill method had the highest environmental impact.

Proper landfill controls can significantly reduce emissions to groundwater. A study in which landfills in semiarid regions were modeled using the Hydrologic Evaluation of Landfill Performance and Multimedia Exposure Assessment Models found that requiring landfill cover, leachate collection systems, and compacted soil liners could reduce leachate emission by 56%. Simply requiring a cover reduced leachate emission by 28%.

Study conclusions have varied regarding the relative merits of landfills and incinerators. In some studies, landfills have been found to have less impact than incinerators, while other studies have found the reverse. Study outcomes are dependent on the many assumptions required. The efficiency of landfill gas collection and utilization can have a significant effect on landfill evaluations.

Assessment of the environmental impact potential of solid waste management must include consideration of natural disasters, such as earthquakes and floods. Landfill flooding can contaminate surface water, groundwater, and soil. Of 1,064 landfills investigated in Austria, 312 were located in or next to areas flooded on average once in 200 years [46]. Only 5% of these landfills were equipped with flood protection facilities. Material inventories of 147 landfill sites endangered by flooding indicated that the emission potential of flooded landfills is high, but not relative to expected emissions from the totality of facilities expected to be flooded.

Resource Depletion

While estimates vary depending on the types of technologies considered, many forms of recycling save energy. According the New Jersey Department of Environmental Protection [37], aluminum produced from used beverage cans requires 90–95% less energy than aluminum produced from bauxite ore, recycled glass production requires 20% less energy than glass production from virgin materials, and recycled paper production also requires between 23% and 74% less energy than virgin paper production. Savings for steel and copper recycling are 74% and 87%, respectively [13].

The recovery of energy when wastes are incinerated avoids resource depletion. According to Korzun [47], there is a saving of approximately 1.3 barrels of No. 2 fuel oil for each US ton of municipal solid waste used to generate electrical power. Incinerating a US ton of newsprint, polyethylene, or lawn grass with 65% moisture saves 2.4, 5.63, and 0.81 barrels, respectively. In 2006, the State of New Jersey, USA, population 8.6M [48], recycled over 11 million metric tons of solid waste [37]. Over 1.8 million metric tons of iron ore, coal, limestone, sand, soda ash, and feldspar were saved by recycling scrap metal and glass.

Each kilogram of waste recycled reduces mining needs, e.g., recycling 1 kg of aluminum reduces mining needs by 4 kg of bauxite ore [37].

Future Directions

Futures directions for waste recycling and disposal include increasing adoption of modern techniques in the developing world. Bernache [49] reported on the municipal management system in the Guadalajara metropolitan area, the second largest in Mexico. The average generation of household waste per person was estimated to be 0.51 kg/day. The general breakdown was 53.8% organic (kitchen and garden), 17.5% packaging, and 28.6% other wastes. The daily average per capita production of municipal solid wastes in the metropolitan area was estimated to be 0.91 kg. Collection ranged from daily in urban areas to one per week or less in marginal areas. Approximately 77% of the collection trucks travelled long distances to dump at municipal dumps, because only two transfer stations were in operation. Only 2% of the total municipal solid waste was separated for recycling. Scavengers (pepenadores) were responsible for most of the recycling, with over 600 registered scavengers operating at one site. The quality of life for pepenadores is poor.

Open and controlled dumps were used to dispose of 98% of the MSW in the Guadalajara metropolitan area [49]. None of the dump locations were selected for geological or hydrological reasons. Rather, properties were selected because they were inexpensive and close to population centers. Pollution control structures were absent at many dumps; in some cases, they were added after initial construction but typically do not operate to a high standard. At a number of dumps, leachate was contaminating surrounding water supplies. Some closed dump sites had been divided into building lots; lots were sold to people unaware of the site history. A number of houses built on landfill material have been abandoned due to differential settling. The problems in the Guadalajara area have been ascribed to poor municipal solid waste management, the result of low political value attributed to MSW management, limited experience with environmental issues, little incentive for workers, and lack of knowledge concerning technological innovations. In the future, it is hoped that more communities across the world will adopt modern methods of solid waste management.

Additional future directions include advances in product design, recycling, landfilling, and incineration technology. Advanced product design includes design for reuse and recycling and reducing toxicity. Recycling advancement will increase the types of materials that can be recycled and improve the quality of products made with recycled materials. Future landfills will degrade wastes faster and more completely, and more completely recover and use landfill gases to produce energy. Future incinerators will generate more energy and release less pollutants.

Bibliography

1. Iriarte A, Gabarrell X, Rieradevall J (2009) LCA of selective waste collection systems in dense urban areas. Waste Manag 29:903–914
2. Soya (2009) History of soy ink. www.soya.be. Accessed 1 Nov 2009
3. Montgomery County MD DEP (2009) Batteries: hazardous waste or not? www.montgomerycountymd.gov. Accessed 1 Nov 2009
4. Shapek R (1995) Local government household battery collection programs: costs and benefits. Resour Conserv Recycl 15:1–19
5. Hackett S (2006) Environmental and natural resource economics: theory, policy, and the sustainable society, 3rd edn. M.E. Sharpe, Inc., Armonk
6. USEPA (2009) Municipal solid waste generation, recycling, and disposal in the United States: facts and figures for 2008. United States Environmental Protection Agency, EPA-530-F-009-021, Washington, DC
7. GEPD (1992) Solid waste: source reduction education program. Greensboro Environmental Programs Division, Greensboro
8. Canterburry J (1998) How to succeed with pay-as-you-throw. Biocycle 39(12):30–35
9. Troschinetz A, Mihelcic JR (2009) Sustainable recycling of municipal solid waste in developing countries. Waste Manag 29:915–923
10. Ferrão P, Amaral J (2006) Design for recycling in the automobile industry: new approaches and new tools. J Eng Des 17(5):447–462
11. NCDPPEA (2004) Recyclable materials in North Carolina's disposed waste stream. North Carolina Division of Pollution Prevention and Environmental Assistance, DPPEA-FY03-30, Raleigh, NC
12. SFOM (2009) Mayor Newsom announces San Francisco's highest in the nation recycling rate now at 72% SF Office of the Mayer. www.sfgov.org. Accessed 12 May 2009

13. IWIEMEF (1998) Materials, interagency workgroup on industrial ecology, materials, and energy flows. President's Council on Sustainable Development, Washington, DC
14. Switzenbaum M (1997) Composting. In: David L, Béla L (eds) Environmental engineer's handbook, 2nd edn. Lewis, Boca Raton
15. Glysson E (1990) Solid waste. In: Robert C (ed) Standard handbook of environmental engineering. McGraw-Hill, New York
16. Vesilind A, Worrell W, Reinhart D (2002) Solid waste engineering. Brooks/Cole, Pacific Grove
17. Tchobanoglous G, Theisen H, Vigil S (1993) Integrated solid waste management: engineering principles and management issues. Irwin/Mc-Graw-Hill, New York
18. Wichmann H, Kolb M, Jopke P, Schmidt C, Alawi M, Bahadir M (2006) Assessment of the environmental impact of landfill sites with open combustion located in arid regions by combined chemical and ecotoxicological studies. Chemosphere 65:1778–1783
19. Ham R (1979) Recovery, processing, and utilization of gas from sanitary landfills, United States Environmental Protection Agency, EPA 600/2-79-001, Washington, DC
20. Korzun E (1990) Economic value of municipal solid waste. J Energy Eng 116(1):39–50
21. Calabrò P (2009) Greenhouse gases emission from municipal waste management: the role of separate collection. Waste Manag 29:2178–2187
22. Rhyner C, Schwartz L, Wenger R, Kohrell M (1995) Waste management and resource recovery. Lewis, Boca Raton
23. Shah K (2000) Basics of solid and hazardous waste management technology. Prentice Hall, Upper Saddle River
24. Al-Khatib I, Arafat H, Daoud R, Shwahneh H (2009) Enhanced solid waste management by understanding the effects of gender, income, marital status, and religious convictions on attitudes and practices related to street littering in Nablus – Palestinian territory. Waste Manag 29:449–455
25. Al-Khatib I (2009) Children's perceptions and behavior with respect to glass littering in developing countries: a case study in Palestine's Nablus district. Waste Manag 29: 1434–1437
26. Santosa I, Friedricha A, Wallner-Kersanachb M, Fillmann G (2005) Influence of socio-economic characteristics of beach users on litter generation. Ocean Coast Manag 48: 742–752
27. Wever R (2006) Influence of packaging design on littering behavior. IAPRI World Conf Packaging 15:274–278
28. Goldstein J, Goldstein N (2005) Controlling odors at composting facilities. BioCycle 46(5):22–25
29. Selena S, Capelli L, Céntola P, DelRosso R, Grande M Il (2005) Odour emission factors for assessment and prediction of Italian MSW landfills odour impact. Atmos Environ 39:5387–5394
30. USEPA (2006) Solid waste management and greenhouse gases – a life-cycle assessment of emissions and sinks, 3rd edn. United States Environmental Protection Agency, Washington, DC
31. USEPA (2003a) Climate change and waste – reducing waste can make a difference. United States Environmental Protection Agency, EPA 530-E-03-002, Washington, DC
32. USEPA (2003c) WasteWise: climate benefits from reducing waste. United States Environmental Protection Agency, EPA 530-F-03-009, Washington, DC
33. USEPA (2003b) Pay-as-you-throw: a cooling effect on climate change. United States Environmental Protection Agency, EPA 530-F-03-008, Washington, DC
34. Jennings A, Hise S, Kiedrowski B, Krouse C (2009) Urban battery litter. J Environ Eng 135(1):46–57
35. Derraik J (2002) The pollution of the marine environment by plastic debris: a review. Mar Pollut Bull 44:842–852
36. Moore C, Moore S, Leecaster M, Weisberg S (2001) A comparison of plastic and plankton in the North Pacific Central Gyre. Mar Pollut Bull 42(12):1297–1300
37. NJDEP (2009) Recycling in New Jersey New Jersey Department of Environmental Protection. www.state.nj.us/dep/dshw. Accessed 2 Dec 2009
38. Lou X, Nair J (2009) The impact of landfilling and composting on greenhouse gas emissions – a review. Bioresour Technol 100:3792–3798
39. Simone M, Christensen TH (2009) Environmental assessment of solid waste landfilling technologies by means of LCA-modeling. Waste Manag 29:32–43
40. Paraskaki I, Lazaridis M (2005) Quantification of landfill emissions to air: a case study of the Ano Liosia landfill site in the greater Athens area. Waste Manag Res 23:199–208
41. Calvo F, Moreno B, Zamorano M, Szanto M (2005) Environmental diagnosis methodology for municipal waste landfills. Waste Manag 25:768–779
42. Kirkeby J, Birgisdottir H, Bhander GS (2007) Modelling of environmental impacts of solid waste landfilling within the life-cycle analysis program EASEWASTE. Waste Manag 27:961–970
43. Niskanen A, Manfredi S, Christensen TH, Anderson R (2009) Environmental assessment of Ämmässuo Landfill (Finland) by means of LCA-modelling (EASEWASTE). Waste Manag Res 27:542–550
44. Mendesa M, Aramaki T, Hanaki K (2004) Comparison of the environmental impact of incineration and landfilling in São Paulo City as determined by LCA. Resour Conserv Recycl 41:47–63
45. Seo S, Aramaki T, Hwang Y, Hanaki K (2004) Environmental impact of solid waste treatment methods in Korea. J Environ Eng 130(1):81–89
46. Laner D, Fellner J, Brunner PH (2009) Flooding of municipal solid waste landfills – an environmental hazard? Sci Total Environ 407:3674–3680
47. Korzun E (1991) Recycling energy value of municipal solid waste. J Energy Eng 117(3):133–150
48. USCB (2009) Population estimates, U.S. Census Bureau. www.census.gov. Accessed 2 Dec 2009
49. Bernache G (2003) The environmental impact of municipal waste management: the case of Guadalajara metro area. Resour Conserv Recycl 39:223–237

Solid Waste Disposal and Recycling, Introduction

Ronald L. Mersky
Department of Civil Engineering, Widener University, Chester, PA, USA

Article Outline

Glossary
Definition of the Subject
Introduction
Historical Perspective
Development of Solid Waste Management Systems
Contemporary Solid Waste Disposal and Recycling
Future Directions
Bibliography

Glossary

Hazardous waste Waste that has the potential to harm human health or the environment (including the biological environment). Typically, this is waste that exhibits one or more of the following characteristics: toxicity, flammability, reactivity, corrosivity, radioactivity, or pathogenicity. In some countries the definition of what constitutes hazardous waste is set by law rather than the actual physical, chemical, or biological characteristics of the waste. So, wastes that exhibit one or more of the preceding characteristics may be legally declared nonhazardous if produced in small quantities or by typical residential, commercial, institutional, recreational, or construction activities.

Municipal solid waste (MSW) Nonhazardous solid waste that results from typical residential, commercial, institutional, recreational, and construction activities. It is important to note that this definition varies among governments, organizations, and professionals working in the solid waste management field. This term may sometimes also include nonhazardous solid waste that results from some industrial activities and water and wastewater treatment sludges. It will usually exclude wastes produced from agricultural, forestry, and mining activities, and fly ash from air pollution control systems.

Solid waste Waste that is solid in form. It may include gas and liquid contained in pores or cavities of the waste. It includes solid materials removed from gaseous waste (fly ash from air pollution control systems) or from liquid waste (sludge from water or wastewater treatment plants).

Solid waste composition* The percentages (usually by weight) of individual constituents (e.g., paper, aluminum, plastics) of the waste generated in a community.

Solid waste discarding* The sending of generated solid wastes to the solid waste management system. This is often used synonymously with "solid waste generation," but there is a difference: some solid waste is disposed of at the generation site and never enters the solid waste management system.

Solid waste disposal* Placement, intended to be permanent, of waste in a containment location. Current regulations limit disposal to placement in or on land. During containment, waste may undergo changes due to physical, chemical, and biological actions.

Solid waste generation* The production of solid wastes.

Solid waste generation rate* The weight per time (e.g., kg/day) or weight per time per person (e.g., kg/day/person) of solid waste generation in a community. In most communities the discarding rate is used as the generation rate. This is because the actual generation rate is difficult to measure and also because it is the discarding rate that is useful in designing features of the solid waste management system.

Solid waste management* The application of technologies and managerial techniques to handle solid wastes in the best manner. What is "best" is subjective and will vary among communities due to economic, social, political, and practical considerations.

Solid waste management system* The discarding of solid wastes plus the set of solid waste management activities within a community.

Solid waste recycling* The use of solid waste as input material for the production of a product. It is synonymous with "solid waste materials recovery." The waste is usually used in place of a virgin material.

Solid waste reuse* The use of a solid waste product for that product's original purpose or a different purpose without significant modification of the product.

Waste* Material that has been determined by its owner to be of negative value (the cost of keeping is greater than the benefit of keeping) and therefore designated for removal from, or disposal at, its current location.

*Each of the definitions when preceded by "Municipal" will refer specifically to municipal solid waste.

Definition of the Subject

Waste is one of society's frustrations. If efficiency is defined as the ratio of output value to input, the generation of waste materials – outputs of negative value – is an obvious reminder of the inefficiencies of a system.

Agricultural, forestry, and mining solid wastes are commonly managed at or near the site of generation and do not enter a community's solid waste management system. Municipal solid wastes are mostly discarded into a management system. Therefore, management of MSW and management of other solid wastes can largely be discussed separately. The following sections' discussion of solid waste management systems will primarily refer to MSW.

Waste that is discarded into a municipal solid waste management system can be managed in several different ways: it can be directly disposed of, it can be recycled, it can be reused, or it can be processed prior to disposal, recycling, or reuse. These activities are done at sites other than the generation site, sometimes a considerable distance from the point of generation. This requires a system of solid waste storage and transportation.

The MSW management system of a community is a combination of technological and managerial methods. In the solid waste field, it is often difficult to clearly separate technologies from management approaches as the two are significantly intertwined. Landfill, as an example, can be correctly categorized as a disposal technology and a disposal management technique.

Introduction

A solid waste management system for a community can be described as a set of modules. A module is the technological and managerial features of one broad component, or a set of logically related components, of the system.

All solid waste management systems must contain three basic modules: generation; generation-site storage, collection, and short-haul; and disposal. Some systems will contain one or more optional modules, commonly: transfer and long-haul, burning (with or without energy recovery), recycling, and composting.

The generation module consists of the details of the community's waste generation rate and waste composition. These are the basic data that are needed to design the waste management system. Depending on the size and structure of the community and the scope of the system, these data may be aggregated or may be broken down by neighborhood and by sector (residential, commercial, etc.). These data are typically gathered at more than one time per year to account for seasonal variations.

The generation-site storage, collection, and short-haul module consists of the plan for storing waste at the generation sites (homes, businesses, etc.) until the next collection time; the equipment, personnel, and vehicles for collecting the waste; and the method for transporting the waste, in the collection vehicles, short distances to the location of tipping. The details contained in this module include storage containers to be used at the generation sites (sizes, locations, styles), collection vehicle routes, methods of transferring waste from the storage containers to the vehicles (manual, mechanical), the assigned tasks of the crew members (driving, loading, container moving/preparation), and the short-haul plan (routing, which crew members accompany the vehicle). These items are combined into one module as they must be planned together to be compatible.

The disposal module is the plan for permanent waste containment. In the past, dumping in water was sometimes used, but that method has been prohibited by law. Today the only option for disposal is land disposal. There are two variations of land disposal: landfilling and open dumping.

Landfilling is the preferred option. A landfill is a planned facility designed to contain the waste in a manner that minimizes environmental damage and health and safety risks and permits the site to be used productively after the landfill has closed. The primary protections designed into landfills are the control of leachate and gas and the covering of the waste.

Open dumping is the placing of waste on land without a means of collecting leachate and gas. The waste

material is exposed, posing a risk to health and safety as well as environmental damage. Open dumping is prohibited in many countries.

The transfer and long-haul module is included in solid waste management systems when the tipping location (disposal site, burning facility, recycling facility) is located at a long distance from the waste generation sites. Solid waste collection vehicles are generally small to allow for ease of use on crowded or narrow streets and to reduce loading times. These small vehicles are not an economical means of transporting waste long distances, especially if multiple crew members accompany the vehicle to the tipping location. In such cases, a transfer station is built near the generation sites for the transfer of waste from the short-haul collection vehicles to larger (more economical) long-haul vehicles. Long-haul vehicles may be trucks, railcars, or ships.

The burning module reduces the volume of waste. That means less cost of transport to the land treatment site and also extension of the time before the capacity of the land treatment facility is reached (and a new site is needed). Burning is also often used to generate electricity and steam (referred to as waste-to-energy), resulting in income from the sale of that energy and reduced need for fuels. In some burning facilities the waste is highly processed prior to burning, the product being called refuse derived fuel (RDF). The term mass burn facility is used to describe burning operations without significant processing of the waste before burning.

Recycling modules have become very common in solid waste management systems in the past 25 years. By removing some materials from the waste generated, there are lower quantities for which disposal must be provided. There may also be environmental and resource benefits to avoiding the production and transport of virgin materials that would have been needed if recycling were not done. A recycling module is a complex plan that includes selection of materials to recycle (which will be dependent on availability of materials buyers, cost of collection, and expected revenue from sale of materials), style of collection vehicles, materials separation methodology (will individual recyclable materials be separated from each other by the waste generators, the collection crew, the materials buyers, or a combination of these), and an education program for waste generators.

Composting is a planned accelerated biological decomposition of organic wastes. If waste generators can be persuaded to compost on site, the collection and disposal costs of the composted materials are avoided. If organic materials are collected from the generation sites and composted at a community facility, disposal is still avoided as the resulting compost can be used as a soil conditioner. Cut decorative grasses are often left in place to degrade. Leaves and small branches are generally easily collected for composting. Some food wastes can also be composted with somewhat more effort required.

Historical Perspective

The primary goal of solid waste management in most societies has been sanitation, the elimination or reduction of negative health, and aesthetic impacts. It is therefore not surprising that the development of formal solid waste systems is often associated with urbanization. Prior to the establishment of densely populated cities, individuals could manage wastes by carrying to outlying areas or simply allowing on-site accumulation of cleaner materials. When population densities and city areas increased, those methods became impractical or inadequate.

In the literature there are reports of some form of solid waste management system in operation in several ancient cities. The oldest recorded landfill sites served the city of Knossos, Crete, which had designated disposal sites for organic wastes by 1500 BCE [1–3]. Mohenjo-Daro, founded about 1,000 years earlier (near modern Karachi), had homes with waste chutes and on-site waste storage bins and may have had a solid waste collection system [1, 3]. The Mayans (who inhabited the North America/Central America border areas) had designated disposal areas for organic wastes and used broken pottery as fill material [1].

The first documented solid waste regulation was issued in Athens approximately 400–500 BCE, requiring that waste be disposed of at least 1.5 km outside of the city walls. Interestingly this was not done primarily for sanitation but rather as a defense measure: waste piled just outside the walls could be used as elevation from which attackers could scale the walls. (About 1,900 years later, Paris experienced a similar waste-related defense problem.) Transport of the waste to

the distant dumps was carried out by households or scavengers. The first formal waste collection service was established in Rome in 14 CE. Waste was thrown into streets from where collection crews loaded it onto wagons [1–5].

After Europe entered the middle ages and beyond, the continent had little significant advancement in solid waste management for hundreds of years [1–3]. As cities grew, some did have collection and regulations, but not with great effect. Disposal in waterways was common. In 1388 the English Parliament prohibited water disposal, but that did not stop the practice. As an example of the damage caused by water disposal, by 1597, Naples considered the replacement of a ship mooring area that had become clogged with waste. The new cities of North America had some waste management deficiencies similar to those of Europe, although America benefited from having much more land availability. In 1657, New York (then known as New Amsterdam) prohibited garbage from being thrown into streets [1–3].

The beginning of the industrial age in the late 1700s brought about greatly increased urbanization and a concomitant increase in the need to better manage solid wastes. While smaller communities could rely on dilution to reduce the negative effects of open burning and street and water dumping, the newly enlarged cities needed new technological and managerial approaches. By the mid-1800s, as disease and discomfort emerged from the combination of crowded environments and industrial by-products, a new approach to waste management began to be developed – an approach built on scientifically based methodologies and formal procedures backed by regulations and enforcement.

Development of Solid Waste Management Systems

While some early collection and disposal schemes could be classified as solid waste management systems, their limited goals and simplicity make them weak analogies for what is contemporarily viewed as an acceptable system.

Perhaps the most significant advance in 1800s solid waste management was the realization that individual waste generators could not be responsible for completely managing their own discards. Large crowded cities needed waste service providers to collect, haul, dispose off, and regulate refuse. Communities established or expanded formal governmental sanitation offices (sometimes part of a more general health department) to manage these responsibilities. These departments, because of their size and official standing, could establish effective systems and develop or encourage advancements in the field [1].

Along with formalization of administrative functions came organized scientific designs of solid waste systems. In 1906, H. de B. Parsons wrote what might be the first book dealing exclusively with solid waste engineering [6].

Contemporary Solid Waste Disposal and Recycling

Solid waste management today can be described as both established and developing. It is established in that there are well-proven technical and managerial methods readily available for dealing with discarded solid wastes in a manner that is affordable (in more affluent countries) and reasonably environmentally sound. It is developing in that the modules of the system are often improved or modified to meet changing environmental standards, political and social goals, or new concerns (climate change, land availability, etc.). The Solid Waste and Recycling sections of this encyclopedia describe both established practice and current areas of advancement.

The first step in designing or improving a solid waste management system for a community is the determination of its waste generation rate and composition (► Solid Waste Generation and Characterization). These values vary greatly among communities, so it is best to gather actual data for the area to be served by the management system rather than to rely on national or regional averages. The generation-site storage, collection, and short-haul module (► Waste Collection and Transport) should be designed with consideration of multiple factors, including sanitation, cost, and residents' preferences.

► Land disposal is necessary in all solid waste management systems. Landfills are complex systems that require ► landfill leachate control for protection of water and a plan to eventually return the site to a nondisposal use (► landfill closure and reuse of land).

Traditional landfilling has focused primarily on permanent storage of waste, allowing passive decomposition of the stored material. A newer approach, ► Landfill Bioreactors, actively accelerates biodegradation with several potential benefits.

Recycling modules require a methodology for collecting materials to be recycled separately from other wastes and, additionally, separating the recyclable components from each other (► recycling collection and materials separation). The latter separation may be done by the collection entity or an intermediate business that prepares the materials for use as a replacement for virgin materials (► recycling technologies). One area of particular recycling interest is ► Waste Materials in Construction, Utilization of.

Some solid wastes are commonly managed in a manner different from that of other solid wastes because of special circumstances. ► Mining solid wastes, because of their very large generation rates and often remote locations of generation, are an example. ► Fly ash, generated from the pollution control systems of coal burning facilities, is another. ► Construction and demolition wastes, because they are often bulkier, less biodegradable, or more easily reusable or recyclable, would also fit this category. ► Electronic Waste and Its Regulation are of special concern because their generation rate has been rapidly increasing in recent years and they contain components that may be hazardous.

All solid waste management activities have a potential for impacting the environment (► Solid Waste Disposal and Recycling, Environmental Impacts). With increased regulation and complexity of solid waste management has come increased need for ► solid waste public involvement and education.

One point that is obvious, but has not always been addressed in solid waste management systems, is that the waste that requires management is the waste that is generated. Therefore many communities have begun to encourage ► Waste Diversion – lowering the generation rate to reduce the costs (economic, environmental, and otherwise) associated with waste management.

Future Directions

Changes in the direction of solid waste management result from influences outside of the field (introduction of new materials and products, political and social concerns, land use patterns, etc.) as well as internal technological and managerial advances. Significant changes usually occur over periods of several years because of the substantial system infrastructure that exists at any time. While current trends in solid waste management will likely change to some degree in the near future, an extrapolation of those trends and areas of research can yield the following expectations for the next several years:

1. Landfilling will remain the preferred (in many countries the only) disposal method, with a greater percentage of landfilled waste going to accelerated decomposition (bioreactor) landfills and waste-segregated landfills (e.g., landfills for construction/demolition wastes only or ash only).
2. Landfills in economically wealthy countries will become fewer in number and larger in capacity, requiring more transportation of solid waste. This will result in greater percentages of waste long-haul being conducted by rail, rather than truck.
3. There will be an increase in recovery of energy from solid waste, including waste-to-energy burning and landfill gas utilization.
4. Recycling will continue to increase as a result of anticipated environmental benefits and increased costs of disposal.
5. Highly planned waste management methods (landfill, energy recovery) will replace open dumping as urbanization increases and sanitation and environmental protection become higher priority issues internationally.

Bibliography

1. Melosi MV (2005) Garbage in the cities: refuse, reform, and the environment. University of Pittsburgh Press, Pittsburgh
2. Tammemagi H (1999) The waste crisis: landfills, incinerators, and the search for a sustainable future. Oxford University Press, New York
3. Vesilind PA, Worrell W, Reinhart D (2002) Solid waste engineering. Brooks/Cole, Pacific Grove
4. Franchetti MJ (2009) Solid waste analysis & minimization: a systems approach. McGraw-Hill, New York
5. Nickolsen JW (2008) Timeline of waste management 1. http://www.timeline-help.com/timeline-of-waste-management.html. Accessed 22 Dec 2010
6. Tchobanoglous G, Theisen H, Vigil S (1993) Integrated solid waste management: engineering principles and management issues. Irwin McGraw-Hill, New York

7. Mersky RL (2006) Municipal solid waste engineering. Widener University Course Notes
8. Gupta JP, Suresh Babu B (2009) A new hazardous waste index. J Hazard Mater 67:1–7
9. US EPA, Waste disposal. http://www.epa.gov/ebtpages/wastwastedisposal.html. Accessed 22 Dec 2010
10. US EPA, Wastes – non-hazardous waste – municipal solid waste. http://www.epa.gov/epawaste/nonhaz/municipal/. Accessed 22 Dec 2010
11. US Code of Federal Regulation, Title 40: Protection of Environment. http://ecfr.gpoaccess.gov/cgi/t/text/text-idx?c=ecfr&sid=305f91b17ec541820b9e4948af6f35af&rgn=div8&view=text&node=40:25.0.1.1.2.1.1.2&idno=40. Accessed 22 Dec 2010
12. FedCenter.gov, Open dumping. http://www.fedcenter.gov/resources/facilitytour/solid/dumping/. Accessed 22 Dec 2010
13. Working Group on Environmental Information and Outlooks, OECD, OECD Environmental Data COMPENDIUM 2006–2008. http://www.oecd.org/dataoecd/22/58/41878186.pdf. Accessed 22 Dec 2010
14. US EPA, Wastes. http://www.epa.gov/osw/. Accessed 22 Dec 2010

Solid Waste Generation and Characterization

Anders Lagerkvist, Lisa Dahlén
Civil, Mining and Environmental Engineering, Waste Science and Technology, Luleå University of Technology, Luleå, Sweden

Article Outline

Glossary
Definition of the Subject and Its Importance
Introduction
Waste Flows
Future Directions
Bibliography

Glossary

Agricultural waste Plant and animal residues from agricultural production. Straw, fruit-stones, peels, manure are examples of agricultural waste.

Construction and demolition waste Waste generated from the construction, reconstruction or deconstruction of buildings, roads and other infrastructure.

Disaster waste Waste generated from and arising due to a disaster like a natural disaster as earthquakes, floods, tsunamis, hurricanes/typhoons/cyclones, wildfires, winter storms, and volcanoes or larger accidents caused by humans.

Industrial waste Solid wastes that are generated during the manufacture of products. Material spills, dusts, sludges, defect products, etc., belong to this group of wastes.

Municipal solid waste Household waste and other waste under municipal responsibility, e.g., street sweepings and waste from public institutions.

Waste characterization To learn about the intrinsic properties of waste materials and how the materials will influence and be influenced by different environments.

Waste That which cannot be sold, but the owner wants to or is required to get rid of.

Definition of the Subject and Its Importance

The generation of solid waste is the inevitable consequence of all processes where materials are used. Extraction of raw materials, manufacture of products, consumption, and waste management all generate wastes. The rate of material use today is so large, both with regard to the total amounts and seen as a *per capita* average, that the waste generated will impact on the environmental quality and human health worldwide if it is not managed properly.

A few centuries, or even decades ago, the solid waste generated was a small fraction of what it is today, the drivers of the generation are primarily the increased availability of energy and secondly the population growth.

Waste generation is also related to urbanization and global trade. Archeologists derive information of old times through the wastes that most old cities are built on. From the subsurface strata, it is possible to learn that waste generation has varied much over time, increased when the economy was flourishing, and decreased during poor times. This reflects that the value of material resources has fluctuated, and underpins the definition of waste presented in the glossary above.

Any definition of waste is bound to be interpreted differently, to begin with because it includes a decision

by someone regarding the usefulness of some material matter, and that which is worthless for one may have a value for another. Thus one cannot define any material properties which define waste, but rather a situation where waste appears.

Within the European Union, a considerable effort has gone into creating a definition of the term waste, and it was formulated as: "Waste" shall mean any substance or object which the holder discards or intends or is required to discard [12]. The Basel convention on international movement of hazardous waste has a similar definition, but related to national legislations; "Wastes" are substances or objects which are disposed of or are intended to be disposed of or are required to be disposed of by the provisions of national law [4]. The words "discard" and "dispose" is another difference between these definitions, the meaning of which has been disputed. Later [13] the European Union added definitions of "by-products" and criteria for when waste ceased to be waste, "end of waste." The theme will probably be discussed for a long time yet.

The interest of the legislators in waste is not so much related to its value as it is to the potential it has to create problems, i.e., its negative value. The link between human health and wastes was first proved in the last part of the nineteenth century, when it was discovered that bacteria could transmit diseases. This led to a worldwide development of city cleansing and sanitary infrastructure, which has considerably increased the life expectancy of those that enjoy its services. Next, the impact of emissions from industry and society was found to impact on the environment on a local and regional scale, a perspective which was established in the mid-twentieth century. At present global impacts, such as global warming, are on the agenda. Solid waste and its management is a significant part of human impact on health and environmental quality.

Introduction

Waste is generated in all processes. According to the laws of thermodynamics, materials and energy can be transformed but never destroyed. Even if material is substantially transformed, all matter which is introduced in any kind of process will come out of the process in exactly the same number of kilograms, either as products, by-products, or waste. Waste may be solid, liquid, or gaseous. In many cases, gaseous waste is a dominating outflow when processing solid matter. However, the focus in this article is on solid waste.

Waste is often perceived as the remains from consumption. However, the major part of all solid waste is generated already by consumers' demand for products, i.e., before the products were consumed and thrown away. In general, the extraction of natural resources and industrial production processes produce massively more solid waste than the consumer products amount to, e.g., about 20 times according to European waste data [14]. As material flows through society, waste is formed in each step, as illustrated in Fig. 1. The material wastes can either end up in landfills or they can be dispersed in water, air, or soil. The dispersion in liquid phases typically exits the material from the waste management domain and turns it into pollution, albeit solid wastes can also form pollution, such as the floating plastic of the oceans.

Solid wastes are often categorized by their origin, e.g.:

- Waste from mining and quarrying
- Commercial and industrial waste (including agricultural waste)
- Construction and demolition waste
- Municipal solid waste

Alternatively, the properties or the possible management may serve to classify materials, e.g.:

- Recyclables
- Combustible waste

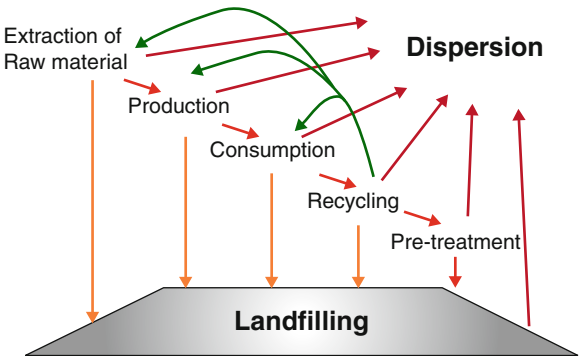

Solid Waste Generation and Characterization. Figure 1 Major waste generation steps in society

- Biodegradable waste
- Wet waste (sludges)
- Residual waste

The waste categories based on treatment alternatives are overlapping, since most wastes have several treatment options. For example, paper can be recycled in a paper mill, incinerated in a power plant, or decomposed by biological treatment. Another example is waste water treatment sludges, which are biodegradable as well as burnable and the content of nutrients may be recycled in agriculture.

Often waste management is governed by environmental concerns which provide a base for another classification used in legal terms such as:

- Hazardous waste
- Nonhazardous waste
- Inert waste

Although the origin of waste carries some information on the nature of the material, additional information on the waste material is often needed for its classification and management. *Waste characterization* is a term that is broadly used to denominate the actions undertaken to learn about the intrinsic properties of a waste and how these properties affect the environment where the material is, and how the environment affects the material. The aspects covered by a characterization depend on the purpose of the characterization and various limitations of time and resources.

A common purpose of waste characterization is for legal classification, e.g., as hazardous or nonhazardous, which then forms the basis for decisions on the further management of the material in question. The legislation may require certain testing to be undertaken and advice criteria to be used in such classification. Such testing typically relies on simple standardized routines that yield results which can easily be evaluated, e.g., by comparison with some list of limit values for some variables. Often the waste's intrinsic properties are considered, such as its content of some compounds or elements. A major path of pollution from solid wastes is leaching, and in consequence different leaching tests are frequently used in a similar fashion as a composition analysis, i.e., the leached amounts or concentrations are compared with some limit values and the waste is classified accordingly. There is a multitude of different leaching tests applied around the world, the most commonly used ones being batch tests where one places a sample together with a solute in a container and agitates it for a defined time before separating the remaining solid material and the solution (see the leftmost test of Fig. 2). One often used

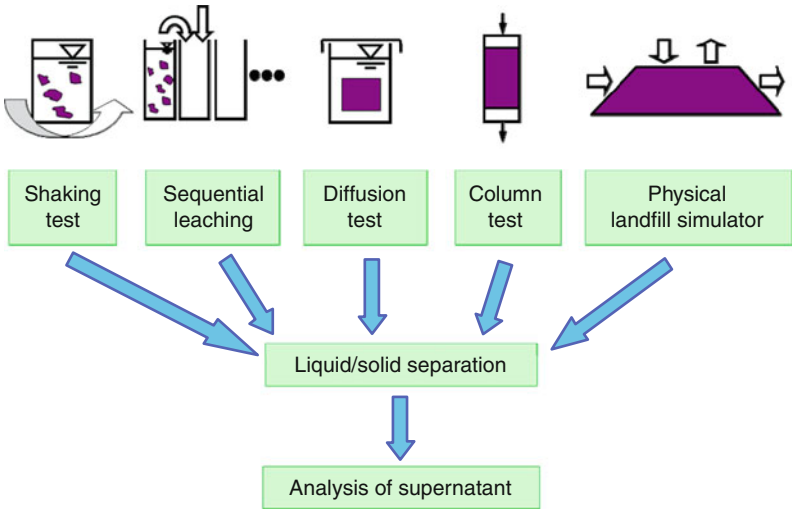

Solid Waste Generation and Characterization. Figure 2
Principal approaches of leaching tests. There are many varieties of each test type, e.g., different proportions between solids and liquids, different leaching media, etc.

batch test is the DIN S4 standard leaching test [9] another is the Toxicity characteristics leaching procedure [28]. All the types of tests described in Fig. 2 except the physical landfill simulators are routinely used to classify wastes in different countries, the effort involved to perform the tests roughly increases from left to right in the figure, so the ones to the left are most commonly used and prescribed for in different regulations. Landfill simulators have the advantage of a better representation of the actual leaching environment for landfilled waste, but are time consuming and expensive.

Other purposes of waste characterization may be to choose a treatment method for a material, judge its potential use for some purpose or to learn about the process that generated the waste. Depending on the information need, the characterization can include a wide range of analyses and tests, e.g., to elucidate the degradability, toxicity, compressibility, etc., of the material. Often the knowledge on relevant factors may be incomplete, so experimental simulations may be needed. An introduction to the art of waste characterization is found in the textbook edited by Christensen [7]. Different standardized tests are published by national and international organizations and authorities such as:

- The Swedish Institute for Standards, SIS [25]
- The International Organization for Standardization, ISO [17]
- The American Society of Testing and Materials [3]
- Deutsches Institut für Normung (Standardization) e.V. [10]
- United States Environmental Agency, USEPA [29]
- Nordtest [22]

All in all, there are still fairly few testing methods that have been developed purely for waste characterization. Often tests developed for other types of materials are used, modified or not.

Thus, there is a great need of further development within the area of waste characterization, especially concerning the long-term behavior and interaction of wastes with different environments.

Using the traditional grouping by origin, some waste streams will be discussed in the following sections.

Waste Flows

Industrial Waste

The generic rule that waste is that which cannot be sold is especially fitting to industrial waste. In this context, the term "industry" is understood as the manufacture of material products excluding primary production from natural resources such as mining and agriculture. With regard to the quality and quantity of industrial waste, almost anything is possible since the choice of materials, processes, and the organization of global production chains, as well as, e.g., the market for recycling of materials in different locations will impact on the waste flux leaving one specific industry. For example, the production of one car may generate wastes in half a dozen different countries, and, depending on the market situation, almost all or nothing of the wastes may be recycled. As an example, the uneven distribution of industrial waste generation in Japan due to the geographical separation of different steps of production chains was discussed by Kagawa et al. [19].

Waste Generation Commonly industrial wastes are grouped after the nature of the industrial activity and not necessarily by material properties. One attempt to structure is the European waste list [11]. The list is structured according to a mixture of criteria regarding the origin, material quality, and commercial sectors generating the wastes (Table 1).

Most of the categories above could include industrial wastes according to the definition used here and give little advice with regard to the management of waste. However, the waste list forms the basis of a code system by which waste is registered and statistics are generated from.

Due to the many affecting factors mentioned above, it is difficult to estimate the amount of wastes from a given industry or even from a sector or a country. In Table 2, some aggregated data on waste generation within the European Union are shown.

According to the Eurostat data, the 27 member states of the European Union generated about three billion tons of wastes in total in 2004 and 2006, i.e., about ten tons per person and year, the proportion of industrial wastes is mostly found under the heading "Manufacturing industry," and it accounts for about

Solid Waste Generation and Characterization. Table 1 Main chapters of European List of Waste (Commission Decision 2000/532/EC)

01	Wastes resulting from exploration, mining, dressing, and further treatment of minerals and quarry
02	Wastes from agricultural, horticultural, hunting, fishing, and aquacultural primary production, food preparation, and processing
03	Wastes from wood processing and the production of paper, cardboard, pulp, panels, and furniture
04	Wastes from the leather, fur, and textile industries
05	Wastes from petroleum refining, natural gas purification, and pyrolytic treatment of coal
06	Wastes from inorganic chemical processes
07	Wastes from organic chemical processes
08	Wastes from the manufacture, formulation, supply and use (MFSU) of coatings (paints, varnishes, and vitreous enamels), adhesives, sealants, and printing inks
09	Wastes from the photographic industry
10	Inorganic wastes from thermal processes
11	Inorganic metal-containing wastes from metal treatment and the coating of metals, and non-ferrous hydrometallurgy
12	Wastes from shaping and surface treatment of metals and plastics
13	Oil wastes (except edible oils, 05 and 12)
14	Wastes from organic substances used as solvents (except 07 and 08)
15	Waste packaging; absorbents, wiping cloths, filter materials, and protective clothing not otherwise specified
16	Wastes not otherwise specified in the list
17	Construction and demolition wastes (including road construction)
18	Wastes from human or animal health care and/or related research (except kitchen and restaurant wastes not arising from immediate health care)
19	Wastes from waste treatment facilities, off-site waste water treatment plants, and the water industry
20	Municipal wastes and similar commercial, industrial, and institutional wastes including separately collected fractions

12% of the total waste generation. The data quality is at best questionable, but representative of the data quality available. If one scales the industrial waste to municipal solid waste, MSW (consumption wastes), the data suggest that the amounts of wastes generated from industrial production would range between half to about 15 times the mass of MSW among the different countries, i.e., a variation of 30 times. The average is about three times, which is not that unreasonable, when considering global production chains and the regions and the sectors import of products and materials from other areas and economic sectors.

Waste Characterization The properties of industrial wastes depend on the materials used and the processes applied. Thus it has to be assessed on an individual case basis. The proportion of that which is defined as hazardous wastes will vary accordingly. In the Eurostat data, the average proportion of hazardous industrial waste is about 1% of the total, but variations are huge. Similarly as the amounts, the composition and properties of wastes from a given industry may also change much over time as the production changes.

Outlook The amounts of industrial wastes vary with the economic activity, as the economy grows, the waste generation will increase and when it shrinks it will diminish. For the industry, a constant optimization of cost will tend toward more and more efficient use of materials, which is a likely undercurrent to the variations caused by economic ups and downs. The variation caused by shifts in demand will be balanced to some degree by changes in the recycling markets. However, the amount of industrial wastes will be significant in a foreseeable future. Further, the development of more complex products will make recycling more challenging and costly.

Agricultural Waste

Agricultural waste is a mix of natural and manufactured products. By far the dominating fluxes are vegetable and animal residues such as straw, peels, stones, and manure. Slaughter waste is a smaller part of the waste stream, but it requires special attention due to its composition and hazard as a disease vector. With a more industrialized agriculture, the amounts of

Solid Waste Generation and Characterization. Table 2 Eurostat data on waste generation (ktons) in different economic sectors

	Total waste from economic activities and households		Manufacturing industry		Mining and quarrying activities		Construction and demolition activities		Other economic activities (services)	
	2004	2006	2004	2006	2004	2006	2004	2006	2004	2006
EU -11	*2,918,220*	*2,946,667*	*384,676*	*363,743*	*862,155*	*740,743*	:	:	*146,754*	*155,807*
Belgium	52,809	59,352	*18,177*	*15,308*	*384*	*159*	*11,037*	*13,090*	*8,689*	*7,039*
Bulgaria	252,058	242,489	5,611	4,316	222,231	225,338	2,999	1,023	9,181	1,473
Czech Republic	29,276	24,746	8,618	5,932	708	472	8,131	8,380	933	1,025
Denmark	12,814	12,821	1,555	1,179	0	0	4,274	5,802	1,515	1,486
Germany	364,022	363,786	30,163	31,705	55,880	47,222	191,563	196,536	16,343	15,107
Estonia	20,861	18,933	6,288	3,981	5,306	5,961	489	717	1,720	1,601
Ireland	24,513	*30,005*	*5,356*	*4,067*	4,046	4,793	11,287	16,599	1,184	1,327
Greece	34,953	51,325	4,554	5,285	1,902	14,888	3,324	6,829	1,518	1,518
Spain	*160,668*	160,947	28,377	22,427	21,780	26,015	46,320	47,323	14,194	15,376
France	429,153	445,865	21,434	22,973	166	1,040	:	:	*24,158*	*24,158*
Italy	139,806	155,025	39,472	39,997	761	1,005	49,151	52,316	3,360	5,534
Cyprus	2,332	1,870	557	413	119	60	488	307	403	403
Latvia	1,257	1,859	349	570	0	0	8	19	99	239
Lithuania	7,010	7,665	2,632	*2,948*	4	6	357	*349*	158	586
Luxembourg	8,322	9,586	725	604	46	56	6,985	6,775	179	243

Solid Waste Generation and Characterization. Table 2 (Continued)

	Total waste from economic activities and households		Manufacturing industry		Mining and quarrying activities		Construction and demolition activities		Other economic activities (services)	
	2004	2006	2004	2006	2004	2006	2004	2006	2004	2006
Hungary	*24,661*	*22,287*	*5,071*	*5,528*	*1,640*	*27*	*1,736*	*3,045*	*1,965*	*2,445*
Malta	2,482	2,861	10	50	0	0	2,206	2,493	160	173
Netherlands	*88,099*	*93,808*	*16,086*	*15,562*	*296*	*213*	*49,612*	*56,610*	*5,276*	*5,349*
Austria	53,021	54,287	15,073	11,470	622	1,043	27,935	31,322	2,856	3,458
Poland	251,243	266,741	61,514	61,131	38,311	38,671	1,993	14,141	1,965	3,512
Portugal	*29,272*	*34,077*	*10,123*	*14,699*	*4,761*	*3,563*	*2,626*	*3,607*	*4,202*	*10,352*
Romania	371,503	331,863	11,156	9,184	326,553	199,138	54	34	3,096	3,841
Slovenia	5,771	6,036	1,960	2,385	129	377	908	995	426	429
Slovakia	10,668	14,502	3,878	5,527	211	332	1,404	916	761	4,859
Finland	74,361	72,205	23,266	17,976	23,819	21,501	20,843	23,146	1,276	1,668
Sweden	109,741	115,583	27,614	30,363	58,600	62,084	10,272	8,943	*1,517*	1,517
United Kingdom	357,544	346,144	35,056	28,161	93,883	86,779	99,234	109,546	39,120	41,088
Croatia	7,209	:	3,695	:	347	:	646	:	116	:
Turkey	58,820	46,092	16,325	:	:	:	:	:	62	:
Iceland	501	:	*61*	:	1	:	19	:	6	:
Norway	7,454	9,051	2,956	3,519	116	136	1,101	1,248	865	1,472

Source: Eurostat [15].

manufactured products are growing, e.g., different containers and wrappings and other consumables. The latter type of wastes may be included in other waste streams such as commercial or industrial wastes. Often the natural wastes are taken care of on site, through burning, biogas production, depositing, or reuse, e.g., as fertilizer, on the own farm. In the more industrialized food production, also the natural wastes may need to be taken care of externally.

Waste Generation There are no reliable data on the production of agricultural wastes. The generation depends on the type of production, the efficiency of the production and the recycling of materials. The total world production of grain in 2008/2009 was about 2.2 billion metric tons according to the USDA [27]. The grain is only a few percent of the mass of the plant, and a substantial, but highly variable, portion of the harvested grain will be wasted in the following processes leading up to the consumption. FAO, the food and agriculture organization of the United Nations [16], is another source of information on agricultural production, but little data are available on waste.

Waste Characterization In contrast to production and consumption wastes, the character of agricultural wastes remains fairly constant. The large volume of plant materials consists mainly of carbohydrates and lignins, with minor contributions of fats, inorganics, and proteins. The main elements are carbon and oxygen, which each typically range from about 30–50%. Hydrogen may vary around 5% and the nitrogen content ranges from a fraction of a percent to about 5%. Other elements usually total up to 5% combined. Manure has a similar composition, but typically a higher nitrogen content. Slaughter waste contains considerably higher amounts of nitrogen. Some wastes such as peach stones [2] may contain fairly high phosphorus content, and depending on plant and soil conditions, various elements may appear in higher concentrations, e.g., some plants are known to accumulate particular metals. Most of the agricultural wastes are prone to biodegradation and may cause oxygen depletion in streams and lakes as well as foul smells. The energy can also be beneficially used, e.g., through biogas production or in thermal conversion processes. A high lignin content will hamper biogas production, as may also a high nitrogen content. The heating value of the plant residues is commonly in the range of 10–20 MJ/kg of DS, and animal wastes have a somewhat higher energy content.

Outlook According to the FAO [16], a billion people live in chronic hunger today. The reason is not just the lacking production, but the distribution of food. At the same time, the competition for agricultural land is getting fiercer due to the increased demand for energy crops. This is already an established conflict. In the coming years, it is likely that waste from agriculture and forestry will become much more in demand as energy carriers and the integration of the agriculture with the energy supply chain will develop on a global scale. A great portion of the agricultural waste may become a commodity in the process.

Construction and Demolition Waste

Waste Generation Construction and demolition (C D) wastes are generated from the construction, reconstruction, or deconstruction of buildings, roads, and other infrastructure. Thus the waste generation rate is a direct consequence of the rate of construction activities. Waste generation per produced unit may change substantially only if construction methods are radically changed, e.g., by off-site construction of buildings.

A waste index and equation for prediction of waste mass from construction of houses has been presented by Lipsmeier [21]; see examples of potential waste masses per m^2 gross floor space in Table 3.

Demolition waste is predetermined to contain the mass and characteristics of the materials which were used when the construction was built. According to

Solid Waste Generation and Characterization. Table 3 Potential construction waste mass per m^2 gross floor space (GFS) in constructed building

Type of building	Construction waste
Office building (low–high equipment standard)	57–67 kg/m^2 GFS
Apartment building (low–high equipment standard)	47–61 kg/m^2 GFS

Source: Lipsmeier [21].

Solid Waste Generation and Characterization. Table 4
Chapter 17 of European waste list

17 Construction and demolition wastes (including road construction)
17 01 Concrete, bricks, tiles, ceramics, and gypsum-based materials
17 01 01 Concrete
17 01 02 Bricks
17 01 03 Tiles and ceramics
17 01 04 Gypsum-based construction materials
17 01 05 Asbestos-based construction materials
17 02 Wood, glass, and plastic
17 02 01 Wood
17 02 02 Glass
17 02 03 Plastic
17 03 Asphalt, tar, and tarred products
17 03 01 Asphalt containing tar
17 03 02 Asphalt not containing tar
17 03 03 Tar and tar products
17 04 Metals (including their alloys)
17 04 01 Copper, bronze, brass
17 04 02 Aluminium
17 04 03 Lead
17 04 04 Zinc
17 04 05 Iron and steel
17 04 06 Tin
17 04 07 Mixed metals
17 04 08 Cables
17 05 Soil and dredging spoil
17 05 03[a] Soil and stones containing dangerous substances
17 05 04 Soil and stones other than those mentioned in 17 05 03
17 05 05[a] Dredging spoil containing dangerous substances
17 05 06 Dredging spoil other than those mentioned in 17 05 05
17 06 Insulation materials
17 06 01[a] Insulation materials containing asbestos
17 06 02 Other insulation materials

Solid Waste Generation and Characterization. Table 4 (Continued)

17 07 Mixed construction and demolition waste
17 07 02[a] Mixed construction and demolition waste or separated fractions containing dangerous substances
17 07 03 Mixed construction and demolition waste other than those mentioned in 17 07

[a]Hazardous waste
Source: European Commission [11]

a Danish study, demolition of modern houses contributes to about 1,600–1,800 kg waste per m^2 floor space demolished [7].

Roads and pavements represent large amounts of material. During construction typically 8–15 tons of materials are used per meter of a road lane. The main part of the waste generated during road construction is what appears from clearing the site, i.e., excavated soil, green (garden) waste, and demolition waste if the site was a built-up area. Demolition of paved areas is rare, but maintenance of roads usually involves regular intervals of renewing the wearing course. Asphalt may be landfilled, but asphalt is more and more often recycled and reused as asphalt, sometimes directly on-site [7].

Waste Characterization The construction waste materials typically include soils, gravel, concrete, bricks, glass, wood, plasterboard, asbestos, metals and plastics. One attempt to classify construction and demolition waste is the European waste list, Chap. 17, which can be seen in Table 4.

Construction waste will contain both nonhazardous and hazardous materials, which is a distinction important from management, cost and environmental perspectives. The majority of the nonhazardous materials in construction and demolition waste can be easily recycled, whereas hazardous materials will require further treatment. Excavated contaminated soils and asphalt containing polycyclic aromatic hydrocarbons (PAH) represent a large part of the hazardous materials in construction wastes.

Outlook There are considerable opportunities for improvements in the resource efficiency of construction and demolition waste management. The waste

stream contains a high proportion of inert materials that are relatively simple to process and that can be used for various secondary applications instead of being disposed. It also contains many valuable components with high embodied environmental impacts in terms of the investment that has gone into producing them. Reusing or recycling these can avoid the need for further investment in primary production.

Municipal Solid Waste

Waste Generation The waste category municipal solid waste consists predominantly of household waste. Other wastes under municipal responsibility are, e.g., street sweepings, waste from public institutions, litter collected in public litterbins, and green waste from tending public parks. In addition, the municipal waste management system commonly cares for waste from small businesses and commercial establishments.

Household waste is a generic term including a number of different types of consumption wastes originating from activities in private homes. Similar waste from, e.g., institutions is sometimes included as "household waste," and sometimes not. There is no standardized or common definition of household waste, which has led to numerous locally defined terms and definitions. Common main categories of household waste are listed in Table 5.

Solid Waste Generation and Characterization. Table 5
Household waste categories

Residual household waste (mingled waste mainly from the kitchen area in households, containing materials that have not been sorted out and sent for reprocessing, with waste components small enough to fit in ordinary waste bins and bags)
Separated food waste
Separated recyclables (paper, plastic, metal, glass)
Waste electric and electronic equipment (WEEE)
Garden waste
Bulky waste (e.g., furniture, private home repair and construction waste, private workshop/garage waste)
Hazardous waste
Infrequent special waste, e.g., vehicles, dead pets

The generation rate and composition of household solid waste depend on many factors related to lifestyle and behavior. A general influential factor is economic development, i.e., the rate of production and consumption of goods, which consequently is reflected in waste generation [5]. The waste composition is decided by product and packaging design, and householders' choice of products.

The collected amount and composition of household waste in bins and bags may also be affected by householders' waste handling, e.g., the use of garbage grinders, home composting, and separate collection of recyclables, where the material flow is redistributed but the total waste generation is unchanged.

Waste Characterization All products and materials introduced into society will end up somewhere. Hence, life cycle thinking is an important basis for the analysis of waste management systems. Household waste generation may be predicted based on production data for materials and products put on the market. In such predictions, adjustments need to be made for the lifetime of products, imports and exports, and for diversions from the waste stream. However, statistical information on imported and exported goods is only available at a national level and because of the varying product turnover times such waste generation prediction will be very general [24]. Instead a common method for household waste component studies is manual sorting of waste samples, where the results are presented as weight percent of different materials found in the waste samples. In waste component studies, a limited number of primary sorting categories is recommended, based as far as possible on physical material (Table 6, [8]). In most cases, food waste is the decidedly dominating material in household waste (by wet-weight).

Outlook Sanitary concerns will remain the primary reason why household waste management is regulated by law and cared for by the authorities in most countries.

Concerns about natural resource depletion and sustainability arguments are other reasons why household waste management is regulated. Household waste sorting and recycling schemes are developing in most parts of the world, at different levels. As mentioned above the major part of all solid waste is generated

during the production of consumer products, which might have occurred in another country before the products were shipped to consumption and later thrown away as household waste. Therefore, a global perspective and systems thinking are needed to understand the waste generation due to consumption.

In the foreseeable future, the lack of international waste characterization standards and reliable waste flow data will continue to obstruct evaluation and benchmarking of waste policy measures.

Disaster Waste

Waste Generation An irregular but relevant form of waste generation is that occurring during major disasters such as strong earthquakes, storms, fires, floods or major oil spills, nuclear accidents, etc. The regular waste management is also affected by such events, e.g., through the blockage of roads, and indirect hazards associated with the management of ordinary municipal waste can occur, e.g., water pollution and other sanitary problems.

The amounts of waste that can be generated through disasters of different kinds are staggering, as is exemplified in Table 7 which shows statistics on the amounts of collapsed buildings during an earthquake in China and the composition of such waste. Another example is the Tsunami of 2004 which has been estimated to generate a quarter of a million tons of waste in Sri Lanka alone [20], the disposal of which undoubtedly caused numerous problems. The hurricane Katrina that struck New Orleans in 2006 has been estimated to generate more than five million tons of waste brought to emergency landfills in the period 2006–2008 as well as an increase of a similar amount that was brought to existing landfills. Most of the waste was building remains which, while containing potentially useful material, for the most part was landfilled due to a lacking infrastructure [1]. Further data on disaster waste management can be found in Brown et al. [6].

Waste statistics often contain large errors and reflect a number of site specific characteristics, such as the efficiency of waste collection and the monitoring of waste fluxes, which is highly variable. For disaster waste, it is likely that the margin of error is considerably larger than in regular waste statistics, but it is safe to assume that the quantities are substantial and out of the

Solid Waste Generation and Characterization. Table 6 Main components of household waste in bins and bags

Primary category	Examples
1. Biowaste	Food waste
	Garden waste
2. Paper	Newsprint, magazines, paper packaging, writing paper
3. Plastic	Plastic bags and plastic film
	Foam plastic
	Dense plastic packaging
	Other plastic
4. Glass	Glass packaging
	Other glass
5. Metal	Metal packaging
	Other metal
6. Other inorganics	Ash, cat sand, ceramics
Hazardous waste	E.g., paint residues, solvents, chemicals, pharmaceuticals, mineral oil
WEEE	Waste electronic and electrical equipment
Miscellaneous	Wood
	Textiles
	Diapers, sanitary napkins
	Everything else that does not belong to any other category (e.g., leather, shoes, soap, complex products)

Solid Waste Generation and Characterization. Table 7 Breakdown of construction wastes generated by an earthquake in Wenchuan, China, in May 2008

Materials	Amount (tons)	Proportion (%)
Concrete	2.08665×10^8	54.5
Bricks	1.52156×10^8	39.8
Steel	0.08431×10^8	2.2
Timber	0.12564×10^8	3.3
Other	0.00616×10^8	0.2
Total	3.82432×10^8	100

Source: Jian-Zhuang et al. [18].

range of normal waste management capacity even in highly developed countries.

Waste Characterization Disaster waste will vary in character as well as in amounts. Basically all material resources which have accumulated in society will form disaster waste, and since a good part of the mass of urban environments is buildings, the materials used in construction will often be dominating. These wastes are typically not poisonous or prone to spread diseases, but materials mixed into the building remains may cause such problems. In some instances, the wastes generated will have a direct impact on the environment and human health, e.g., oil spills or radioactive masses, but typically the problem is more the overload on the waste management system, as well as the quick fixes applied that may cause problems. For example, when organic wastes must be destroyed quickly and there is a lack of suitable facilities, a common method is putting it to fire, with the associated smoke problems.

The stored amounts of toxic wastes have been identified as a major factor worsening the impact of natural disasters [23]. In order to assess the existence of hazardous materials in the disaster waste, it is a necessary precaution to routinely perform a mapping of materials used in different processes, buildings, and storage facilities to enable a rough risk assessment when disaster strikes. The on-site assessment may be too time consuming, so backup storage facilities for the rubble is an essential resource in order to buy time for testing and treating the wastes

Outlook With an increasing world population, and an increasing concentration of people in urban areas, and an increased dependency on transports and infrastructure, it would seem likely that disasters will strike harder and generate more waste in the future. The UNISDR [26] global assessment report points out that a small portion of the world's surface carries a large concentration of disaster risks, e.g., areas such as tropical cyclone prone coastal cities. In spite of efforts to reduce the impacts of disasters in such areas, the increase of exposure due to population growth in these areas is said to outweigh the countermeasures, thus increasing the impact of future disasters.

Today waste issues are found to be off focus for most agencies involved in disaster management planning [20], in spite of its large importance for the post disaster health and environmental situation. Countermeasures in the form of planning and provision of back-up storage and treatment schemes will undoubtedly be necessary as a matter of routine, and may limit the impact on catastrophic events where applied. Where such measures are not applied, the impact on health and environment from disaster waste will add considerably to the direct impact of catastrophic events. There is and will be a need for the environmental engineering equivalency to Medicins Sans Frontiers.

Monitoring Waste Generation

Waste generation data are preferably measured and presented in comparable units, e.g., *tons per year* or *tons per produced unit* in industry and *kg/capita per year* or *kg/household per week* in household waste management.

Important questions to answer when monitoring waste flows are (a) what do we measure and why and (b) what is the magnitude of errors in the measurements. The lack of standardized collection data, and the general lack of metadata (i.e., data about data), affects all evaluations and comparisons of waste generation data. No method of evaluation or statistical processing of data can produce results of better quality than the quality of input data.

Sources of errors and uncertainties in waste generation data are numerous.

Examples:

- The waste categories are not clearly defined and/or understood.
- Data are not comparable over time because of radical changes in the outline of collections systems and definition of waste categories.
- Variations in local waste management organization and administration lead to different routines for data compilation.
- Waste flow data have undefined data gaps due to waste not dealt with in the normal waste management system, e.g., illegally dumped waste, secondary markets, waste flushed into the sewage system.
- Data concerning waste collection at drop-off points (intended for a specific waste category) include an unknown amount of wrongly disposed materials.

- Recycling is defined in various ways, which makes the key indicator "recycling ratio" ambiguous.

An example of unclear definitions of "recycling" is the production of wood chips from secondary wood. When used as a solid fuel in thermal power stations it might be classified as waste incineration *or* as recycling of biofuel. Note the term recycling is sometimes used in the sense "make use of," however complete recycling of wood should include not only energy recovery but also bringing the nutrients (ashes) back to the forest.

The uncertainties and unclear definitions in waste generation data call for caution when drawing conclusions about factors influencing waste generation and recycling rates, e.g., declared regional differences may be differences in monitoring methods only, not in actual waste generation.

Future Directions

Waste is the unwanted result of all material conversion processes, or life, or development of material wealth in the world. During the last decades, the economic development of the world has accelerated and its driver has been the availability of cheap energy, mainly in the form of fossil fuels. Oil consumption is fairly proportional to economic wealth, and also to some degree to waste generation.

The use of fossil fuels is certainly still climbing and there are no signs that it should stabilize or be reduced in the next decades. The increased energy demand of large populations such as India and China seem to outweigh the reductions of some industrialized countries massively.

So it may be expected that the amounts of waste will grow at about present rates, i.e., a few percent per year. The increased population, urbanization, and energy consumption all speaks for this trend. Thus, the demand for waste collection, treatment, disposal, and recovery and recycling will also increase. Considering the state of these activities today, the expansion of the waste management sector will need to increase more than the economy in general in order to catch up. Waste management may be more crucial for the development of human society than is commonly recognized, both directly as it deals with environmental and health hazards, but also indirectly as it reduces the deterioration of environmental quality on a local and global scale. The dispersion of material from society does change the quality of all recipients globally and will in the end be limiting for our use of soil, water, and air, as well as it will impact on all other living creatures. Ultimately, the harmless reintroduction of waste materials into natural cycles is the goal of waste management. Recycling and reuse of materials is of course beneficial as it reduces the stress on all recipients, and leaner and more efficient production processes will act in the same direction, but as long as there is an uncontrolled, long-term increase of the background concentrations of various compounds due to emissions from human activities, we have not achieved the goal of waste management.

The growing amount of wastes is one challenge for waste management and a second is the distribution of the wastes. Regions with heavy industry and raw material extraction will have the bulk of the waste to deal with and service based economies will have little more than consumption and construction and demolition wastes. The long distance transfer of wastes may be one result of this unbalance, and it may cause severe problems as has already been seen, e.g., with electronic waste in some regions of western Africa.

A third problem is an increasing waste complexity, which results in a need of more elaborate waste management practices. Products with flame retardants will not burn, mixtures of polymers will not recycle as easily and so on. The present development within nanotechnology is already adding to the complexity of products and will increase to do so, and new challenges are likely to emerge in the waste management sector.

A developed waste management is a sign of an advanced culture. It has been developed as a part of government and is expressed by laws. At present, waste management is lacking in many aspects. To begin with, the data on waste generation are ranging from unprecise to absurdly poor and the understanding of waste characterization needs to be much improved among those that work with waste management or make decisions about it. The consequences of these shortcomings are suboptimal practices and a waste of resources, human as well as natural. Coming to terms with these fundamental issues, the long-term challenge remains: to fit the output of society into the material cycles of nature without damaging the recipients. It does not suffice to talk about the weather, now it is time to do something about it.

Bibliography

1. Ardani KB, Reith CC, Donlan CJ (2009) Harnessing catastrophe to promote resource recovery and eco-industrial development. J Ind Ecol 13(4):579–591
2. Arvelakisa S, Gehrmannb H, Beckmannc M, Koukiosa EG (2005) Preliminary results on the ash behavior of peach stones during fluidized bed gasification: evaluation of fractionation and leaching as pre-treatments. Biomass Bioenerg 8:331–338
3. ASTM (2010) American Society of Testing and Materials. http://www.astm.org/. The American Society of Testing and Materials
4. Basel Convention (1992) Basel convention on the control of transboundary movements of hazardous wastes and their disposalASEL. http://www.basel.int/text/con-e.pdf
5. Beigl P, Lebersorger S, Salhofer S (2008) Modelling municipal solid waste generation: a review. Waste Manag 28(1):200–214
6. Brown C, Milke M, Seville E (2011) Disaster waste management: a review article. Waste Manag 31:1085–1098
7. Christensen TH (ed) (2010) Solid waste technology management, 1st edn. Wiley, Hoboken, p 1072
8. Dahlén L, Lagerkvist A (2008) Methods for household waste composition studies. Review. Waste Manag 28(7):1100–1112
9. DIN (1984) Deutsches Einheitsverfahren zur Wasser-, Abwasser- und Schlammuntersuchung; Schlamm und Sedimente (Gruppe S); Bestimmung der Eluierbarkeit mit Wasser (S4). DIN 38 414 Teil 4
10. DIN (2010) DIN Deutsches Institut für Normung e.V. http://www.din.de/. DIN Deutsches Institut für Normung e.V
11. European Commission (2000) European list of waste. Commission Decision 2000/532/EC. Off J Eur Comm L226:3–24
12. European Commission (2006) Directive 2006/12/EC. Off J Eur Comm L 114:9, 27.4.2006
13. European Commission (2008) Directive 2008/98/EC of the European parliament and of the council of 19 November 2008 on waste and repealing certain directives. Off J Eur Comm L312:3–30
14. European Commission (2010) The Eurostat database waste statistics/generation of waste. http://epp.eurostat.ec.europa.eu/portal/page/portal/waste/data/database
15. Eurostat (2010) Waste statistics. http://epp.eurostat.ec.europa.eu/statistics_explained/index.php?title=File:Generation_of_waste,_total_arising_and_by_selected_economic_activities.PNGoldid=12882
16. FAO (2010) The Food and Agriculture Organization of the United Nations. http://www.fao.org/
17. ISO (2010) The International Organization for Standardization. http://www.iso.ch/. The International Organization for Standardization
18. Jian-Zhuang X, He X, Chang-Qing W, Li G (2009) Statistical analysis on building waste in Wenchuan Earthquake-hit area. J Sichuan Univ 41(3):188–194, Engineering Science Edition
19. Kagawa S, Inamura H, Moriguchi Y (2004) A simple multi-regional input–output account for waste analysis. Econ Systems Res 16(1):1–20, Retrieved from Business Source Elite database
20. Karunasena G, Amaratunga D, Haigh R, Lill I (2009) Post disaster waste management strategies in developing countries: case of Sri Lanka. Int J Strat Property Manag 13:171–190
21. Lipsmeier K (2004) Abfallkennzahlen fuer Neubauleistungen im Hochbau, Hochbaukonstruktionen und Neubauvorhaben in Hochbau nach abfallwirtschaftlichen Gesichtspunkten. Dissertation, Technische Universität Dresden
22. Nordtest (2010) http://www.nordicinnovation.net/nordtest.cfm
23. Petrova E (2006) Vulnerability of Russian regions to natural risk: experience of quantitative assessment. Nat Hazard Earth Sys Sci 6:49–54
24. Rugg FM (1997) Solid waste/characterization methods. In: Liu DHF, Lipták BG (eds) Environmental engineers' handbook. Lewis, Boca Raton, pp 1158–1174. ISBN 0-8493-9971-8
25. SIS (2010) Swedish Institute for Standards. http://www.sis.se/. Swedish Institute for Standards
26. UNISDR (2009) Global assessment report on disaster risk reduction, United Nations international strategy for disaster reduction secretariat. ISBN/ISSN: 9789211320282, p 207. http://www.preventionweb.net
27. USDA (2010) Table 01 world crop production summary. United States Department of Agriculture. http://www.fas.usda.gov
28. USEPA (1992) EPA test method 1311 – TCLP, toxicity characteristic leaching procedure, p 38. www.ehso.com
29. USEPA (2010) http://www.epa.gov/wastes/index.htm

Solid Waste Public Involvement and Education

Matthew J. Franchetti
Department of Mechanical, Industrial, and Manufacturing Engineering, The University of Toledo, Toledo, OH, USA

S

Article Outline

Glossary
Definition of the Subject and Its Importance
Introduction
Overview of Environmental Concerns
Key Environmental Regulations
Components of Environmental Education
Public Involvement and Planning Framework
Examples of Successful Programs
Future Directions
Bibliography

Glossary

Environmental education Process in which individuals gain awareness of their environment and acquire knowledge, skills, values, and experiences to solve present and future environmental problems, including solid waste minimization.

Municipal solid waste A waste type that includes predominantly household and commercial wastes collected by a municipality within a given area. They are in either solid or semisolid form and generally exclude industrial hazardous wastes.

Public involvement The full range of activities utilized by an organization to engage the public in the decision-making process.

Recycling The act of processing used or abandoned materials for use in creating new products.

Source reduction Refers to any change in the design, manufacture, purchase, or use of materials or products (including packaging) to reduce their amount or toxicity before they become municipal solid waste.

Definition of the Subject and Its Importance

Solid waste public involvement and education are critical components of successful solid waste minimization. Public involvement is defined as the full range of activities utilized by an organization to engage the public in the decision-making process. Through environmental education, people gain an understanding of how individual actions affect the environment, acquire skills to weigh various sides of issues, and become better equipped to make informed decisions. The components of environmental education are:

- Awareness and sensitivity
- Knowledge and understanding
- Attitudes
- Skills
- Participation

Public involvement and education are important components for effective solid waste minimization efforts at local and national levels. These efforts, combined with strong solid waste minimization programs, are the cornerstones that allow organizations to reach waste minimization goals by informing and motivating stakeholders to participate in these programs.

Introduction

Municipal Solid Waste (MSW), more commonly known as trash or garbage, consists of everyday items such as product packaging, grass clippings, furniture, clothing, bottles, food scraps, newspapers, appliances, paint, and batteries. In the year 2006, US residents, businesses, and institutions generated more than 228 t (251 million US tons) of MSW, which is approximately 2.1 kg (4.6 lb) of waste per person per day, up from 1.2 kg (2.7 lb) per person per day in 1960 [1]. Governments must work through their constituents to address these issues. Public involvement and education are critical components to increase the awareness and to help drive down these trends. This chapter provides an overview of public involvement and education for solid waste reduction. First, background information is provided, including an overview of environmental concerns related to solid waste reduction and an overview of key environmental regulations. Next, the main components of environmental education are discussed including education and public involvement tools, the public involvement plan framework, and an overview of several successful solid waste education and involvement plans. Finally, a discussion of future directions in this field is provided.

Overview of Environmental Concerns

The world has changed significantly over the past century. Societies are shifting to a convenience oriented mind set, world population is increasing, and subsequently waste generation is shifting, which is creating new environmental impacts. For example, from a convenience standpoint, solid waste generation rates are increasing due to the proliferation of individually packaged food servings, fast food containers, and disposable diapers.

The average American discards 2.1 kg (4.6 lb) of garbage every day [1]. Most of this waste is compacted and buried in landfills, and as it continues to grow, so will pressure on the landfills, the resources, and the environment. The impacts are intensified by an ever increasing population. The US Census Bureau estimates the current world population at 6.6 billion people, with a projected annual growth rate of approximately 1.2% [2]. By 2050, the world population is projected to be over nine billion [2]. Globalization

and the development of Third World countries are compounding these issues as well. More people, generating more waste is not a good combination for the environment.

One of the central purposes of solid waste education is to inform the public of the need to reduce or eliminate the environmental impacts of individuals, companies, and industries. An understanding of these impacts is critical when addressing solid waste issues to provide direction for reduction efforts. Some of these impacts are more important than others, thus a comprehensive understanding will allow citizens, managers, and engineers to focus on more serious problems. This section provides an overview of these impacts with a focus on the effects and not the sources. These impacts are:

- *Space availability*: as the world population increases and cities grow, the available space to dispose of solid waste decreases. By minimizing solid waste levels, disposal space will also decrease making land available for other uses.
- *Landfill leachate*: leachate is liquid that is generated from a landfill that is created from decomposing waste, created after rainwater mixes with the chemical waste in a landfill, or liquids present in the landfill. Once it enters the environment, the leachate is at risk for mixing with groundwater near the site which can have very negative effects. Groundwater is the source of drinking water for over 40% of the US population, and up to 90% of the population in rural areas. It was formerly assumed that this source of water was not subject to contamination, but recent studies have shown that this source of water can in fact become contaminated. Landfill leachate may be virtually harmless or dangerously toxic, depending upon the characteristics of the material in the landfill. Typically, landfill leachate has high concentrations of nitrogen, iron, organic carbon, manganese, chloride, and phenols. Other chemicals including pesticides, solvents, and heavy metals may also be present. Modern landfill sites require that the landfill leachate be collected and treated. Since there is no method to ensure that rainwater cannot enter the landfill site, landfill sites must now have an impermeable layer at the bottom. The landfill leachate that collects at the bottom must be monitored and treated if required. This liquid can be treated in a similar manner to sewage, and the treated water can then be safely released into the environment.
- *Global warming*: One study reports that US landfills are responsible for 3.8% of the global warming damage from humans. Sources in the US Municipal solid waste landfills are the largest source of human-related methane emissions in the USA, accounting for about 25% of these emissions in 2004 [1]. This gas consists of about 50% methane (CH_4), the primary component of natural gas, about 50% carbon dioxide (CO_2), and a small amount of non-methane organic compounds. In 2003, US landfills generated 131.2 Tg (teragrams) methane in terms of carbon dioxide CO_2 equivalents (where a teragram is one million tons). Reducing the amounts of solid waste disposed in landfills would reduce methane generation and subsequently reduce global warming.
- *Consumption of natural resources*: a large component of solid waste minimization is recycling. Recycling reduces the consumption of virgin natural resources by utilizing perceived waste materials. For example, production of recycled paper uses 80% less water and 65% less energy, and produces 95% less air pollution than virgin paper production. If every American recycled their newspaper just 1 day a week, the USA would save approximately 36 million trees a year. For every four-foot stack of paper recycled, one tree is saved and deforestation is minimized. Recycling also reduces environmental impacts due to mining. For example, by recycling aluminum, the need for the raw mineral bauxite is eliminated, which in turn eliminates the need for mining and smelting.
- *Loss of habitat*: although it is difficult to accurately quantify habitat loss, many animal species are displaced by the creation of landfills and the effects of deforestation. By minimizing solid waste levels and increasing recycling, available habitats for animals will not be disrupted by the development or expansion of landfills and the effects of deforestation to acquire virgin raw materials.

Key Environmental Regulations

Governments play a critical role in managing the environment including the atmosphere, land, water bodies,

and all natural resources. Governments are valuable institutions for resolving problems involving natural resources at both the local and global scales. Although in recent decades the economic market has been identified as a suitable mechanism for managing environmental quality, markets have serious failures and governmental intervention, and regulation and the rule of law are still required for the proper, just, and sustainable management of the environment. This section discusses several of the key US environmental laws and regulations that pertain to solid waste management.

Solid Waste Disposal Act (SWDA) of 1965

The Solid Waste Disposal Act (SWDA) (P.L. 89–272, 79 Stat. 992) became law on October 20, 1965. In its original form, it was a broad attempt to address the solid waste problems confronting the nation through a series of research projects, investigations, experiments, training, demonstrations, surveys, and studies. The key points of the SWDA were as follows:

- Promoted better management of solid wastes
- Supported resource recovery
- Directed that the US Public Health Service (PHS) promulgate and enforce regulations for solid waste collection, transportation, recycling, and disposal (The US EPA was not formed until 1970)
- Provided financial assistance for states to study and develop solid waste management plans
- Provided support for research and development of improved methods of solid waste management

The decade following its passage revealed that the SWDA was not sufficiently structured to resolve the growing mountain of waste disposal issues facing the country. As a result, significant amendments were made to the act with the passage of the Resource Conservation and Recovery Act of 1976 (RCRA).

The National Environmental Policy Act (NEPA) of 1969

The National Environmental Policy Act (NEPA), established in 1969 by the US Government (42 U.S.C. 4321), was one of the first laws written related to environmental protection. NEPA, which is pronounced NEE-pa, established a basic policy to assure that all branches of government give proper consideration to the environment prior to undertaking any major federal action that significantly affects the environment. One of the key phrases from this document that relates to recycling is "to enhance the quality of renewable resources and approach the maximum attainable recycling of depletable resources."

NEPA requires federal agencies to integrate environmental values into their decision-making processes by considering the environmental impacts of their proposed actions and reasonable alternatives to those actions. To meet this requirement, federal agencies prepare a detailed statement known as an Environmental Impact Statement (EIS). EPA reviews and comments on EISs prepared by other federal agencies, maintain a national filing system for all EISs, and assure that its own actions comply with NEPA.

Resource Recovery Act (RRA) of 1970

Increasing concerns over protection for human health and the environment led to amendments of the 1965 SWDA, and the 1970 Resource Recovery Act (RRA) was passed. The RAA increased federal involvement with management of solid waste; it encouraged waste reduction and resource recovery and created national disposal criteria for hazardous wastes. This Act was the forerunner of the Resource Conservation and Recovery Act (RCRA) of 1976. Below are the key points of RAA:

- Directed that the nation would change its emphasis from solid waste disposal to recycling and energy recovery
- Required the US Public Health Systems to investigate and report on the disposal of hazardous waste in the nation

This was an important guidance document for the early stages of solid and hazardous waste management. The RRA also marked the birth of the Environmental Protection Agency (EPA), as it was formed in the interim.

Resource Conservation and Recovery Act (RCRA) of 1976

The RCRA is the US's primary law governing the disposal of solid and hazardous waste. Congress passed

RCRA on October 21, 1976 to address the increasing problems the nation faced from our growing volume of municipal and industrial waste. RCRA, which amended the Solid Waste Disposal Act of 1965, set national goals for:

1. Protecting human health and the environment from the potential hazards of waste disposal
2. Conserving energy and natural resources
3. Reducing the amount of waste generated
4. Ensuring that wastes are managed in an environmentally sound manner
5. RCRA also included directives that the US EPA establishes regulations to control solid waste disposal. To achieve these goals, RCRA established three distinct, yet interrelated, programs:
   (a) The solid waste program: under RCRA Subtitle D, encourages states to develop comprehensive plans to manage nonhazardous industrial solid waste and municipal solid waste, sets criteria for municipal solid waste landfills and other solid waste disposal facilities, and prohibits the open dumping of solid waste.
   (b) The hazardous waste program: under RCRA Subtitle C, establishes a system for controlling hazardous waste from the time it is generated units its ultimate disposal – in effect, from "cradle to grave."
   (c) The underground storage tank (UST) program: under RCRA Subtitle I, regulates underground storage tanks containing hazardous substances and petroleum products.

RCRA banned all open dumping of waste, encouraged source reduction and recycling, and promoted the safe disposal of municipal waste. RCRA also mandated strict controls over the treatment, storage, and disposal of hazardous waste. The first RCRA regulations, "Hazardous Waste and Consolidated Permit Regulations," published in the Federal Register on May 19, 1980 (45 FR 33066; May 19, 1980), established the basic "cradle to grave" approach to hazardous waste management that exists today. RCRA focuses only on active and future facilities and does not address abandoned or historical sites which are managed under the Comprehensive Environmental Response, Compensation, and Liability Act (CERCLA) – commonly known as Superfund.

The Hazardous and Solid Waste Amendment (HSWA) of 1984

RCRA was amended and strengthened by Congress in November 1984 with the passing of the Federal Hazardous and Solid Waste Amendments (HSWA). These amendments to RCRA required phasing out land disposal of hazardous waste. Some of the other mandates of this strict law include increased enforcement authority for EPA, more stringent hazardous waste management standards, and a comprehensive underground storage tank program. Key points from the HSWA are the following:

- Directed the US EPA to revise criteria for landfills which receive hazardous household waste or small quantities of industrial hazardous waste.
- Treatment of all contaminated surface water running off of landfills.
- Methods for disposing of wastewater sewage sludge at landfills are included in the Clean Water Act as amended.
- Increased enforcement authority for EPA.
- Provided more stringent hazardous waste management standards.
- Created a comprehensive underground storage tank program.

The HSWA marked the most significant set of amendments to RCRA with a complex law with many detailed technical requirements. Additional restrictions on land disposal and the inclusion of small-quantity hazardous waste generators (those producing between 100 and 1,000 kg of waste per month) in the hazardous waste regulatory scheme were added. The EPA was directed to issue regulations governing those who produce, distribute, and use fuels produced from hazardous waste, including used oil. Under HSWA, hazardous waste facilities owned or operated by federal, state, or local government agencies must be inspected annually, and privately owned facilities must be inspected at least every 2 years. Each federal agency was required to submit to EPA an inventory of hazardous waste facilities it has possessed in its history. The HSWA also imposed on EPA a timetable for issuing or denying permits for treatment, storage, and disposal facilities; required permits to be for fixed terms not exceeding 10 years; terminated in 1985 the "interim status" of

land disposal facilities that existed prior to RCRA's enactment, unless they met certain requirements; required permit applications to be accompanied by information regarding the potential for public exposure to hazardous substances in connection with the facility; and authorized EPA to issue experimental permits for facilities demonstrating new technologies. EPA's enforcement powers were increased, the list of prohibited actions constituting crimes was expanded, penalties were increased, and the citizen suit provisions were expanded. Other provisions prohibited the export of hazardous waste unless the government of the receiving country formally consented to accept it; created an ombudsman's office in EPA to deal with RCRA-associated complaints, grievances, and requests for information; and reauthorized RCRA through FY88 at a level of about $250 million per year. Finally, HSWA called for a National Ground Water Commission to assess and report to Congress in 2 years on groundwater issues and contamination from hazardous wastes. The commission was never funded and never established, however.

Pollution Prevention Act of 1990

The Pollution Prevention Act of 1990 (PPA) was passed as part of the Omnibus Budget Reconciliation Act of 1991. The measure declared pollution prevention to be the national policy, and directed EPA to undertake a series of activities aimed at preventing the generation of pollutants, rather than controlling pollutants after they are created. Matching grants were authorized for states to establish technical assistance programs for businesses, and EPA was directed to establish a Source Reduction Clearinghouse to disseminate information. The Act also imposed new reporting requirements on industry. Firms that were required to file an annual toxic chemical release form under the Emergency Planning and Community Right-to-Know Act of 1986 must also file a report detailing their source reduction and recycling efforts over the previous year. A more complete description of the Act, which addresses air and water pollution as well as waste, is provided in the first section of this report.

Federal Facility Compliance Act of 1992

The Federal Facility Compliance Act, 1992 (FFCA) amended RCRA with the primary purpose of ensuring a complete and unambiguous waiver of sovereign immunity with regard to imposition of administrative and civil fines and penalties on federal facilities. It requires compliance with all federal, state, interstate, and local requirements in the same manner and extent as any person. The objectives of the FFCA bring all federal facilities into compliance with applicable federal and state hazardous waste laws, of waiving federal sovereign immunity under those laws, and of allowing the imposition of fines and penalties. The law also requires the US Department of Energy (DOE) to submit an inventory of all its mixed waste and to develop a treatment plan for mixed waste. The FFCA has ten sections, concerning extent of waiver of sovereign immunity, application of RCRA to radioactive mixed wastes, application to public vessels, waste munitions, and to federally owned treatment works. The language of RCRA waiver of sovereign immunity prior to FFCA was unclear on whether federal facilities had to pay civil and administrative penalties for violations of hazardous waste provisions. Cases have involved the determination of whether federal facilities have to pay penalties, even though there was no waiver of sovereign immunity. Legislatively, there were many failed attempts at passing the act. But due to increasing support for environmental movements and frustration at state regulatory agencies that could not strike federal facilities with fines and penalties, the act was passed in 1992. Key points of the FFC are:

- All Federal agencies are subject to all substantive and procedural requirements of Federal, State, and local solid and hazardous waste laws in the same manner as any private party.
- The sovereign immunity of the USA is expressly waived in all such cases.
- "Substantive and procedural requirements" of such law include all administrative orders, civil, and administrative fines and penalties, and reasonable service charges imposed for issuing and reviewing permits, plans and studies, and inspecting facilities.
- Employees, officers, and agents of the USA may not be liable for civil penalties under any such law for actions committed within the scope of that person's official duties, but such persons may be liable for criminal penalties.
- The Administrator of EPA is authorized to commence an administrative enforcement action against

any Federal agency or department in the same manner as against a private party.

- Agencies must reimburse EPA for the required annual inspections of agency hazardous waste facilities, and for EPA to conduct a comprehensive ground water monitoring evaluation at the first inspection of each such site conducted after October 6, 1992 (unless such an evaluation has been conducted within the preceding year).
- In consultation with the Secretary of Defense, EPA is required to propose regulations identifying when military munitions become hazardous waste, and providing for the safe transportation and storage of such waste.
- Federally owned wastewater treatment works are not to be considered hazardous waste facilities if most of the water treated consists of domestic sewage, and certain other specified requirements are met. Introduction of a hazardous waste into a federally owned wastewater treatment works is prohibited.

Landfill Disposal Program Flexibility Act of 1996

Land Disposal Program Flexibility Act of 1996 provided regulatory flexibility for land disposal of certain wastes as amendments to RCRA. This act exempts hazardous waste from RCRA regulation if it is treated to a point where it no longer exhibits the characteristics that made it hazardous, and is subsequently disposed in a facility regulated under the Clean Water Act or in a Class I deep injection well regulated under the Safe Drinking Water Act. A second provision of the bill exempted small landfills located in arid or remote areas from ground water monitoring requirements, provided there is no evidence of ground water contamination.

Components of Environmental Education

Environmental Education (EE) is a process in which individuals gain awareness of their environment and acquire knowledge, skills, values, and experiences to solve present and future environmental problems, including solid waste minimization. The goal of EE should also motivate individuals and organizations and enable them to act to address solid waste issues.

EE is a complex process, covering not just events, but also a strong underlying approach to society building as a whole. EE provides people with the awareness needed to build partnerships, understand government activities/programs, develop participatory approaches to urban planning, and ensure future markets for eco-business.

Environmental education is a learning process that increases people's knowledge and awareness about the environment and associated challenges, develops the necessary skills and expertise to address the challenges, and fosters attitudes, motivations, and commitments to make informed decisions and take responsible action. The US EPA provides the following definitions that are helpful in understanding this subject matter:

- "Environmental Education (EE)" increases public awareness and knowledge about environmental issues and provides the skills necessary to make informed environmental decisions and to take responsible actions. EE is based on objective and scientifically sound information, and does not advocate a particular viewpoint or a course of action. EE teaches individuals how to weigh various sides of an issue through critical thinking and enhances their own problem-solving and decision-making skills on environmental topics.
- "Environmental Information" provides facts or opinions about environmental issues or problems. Information is essential to any educational effort. However, environmental information is not, by itself, environmental education. Information provides facts or opinions whereas education teaches people how to think, analyze, and solve problems.
- "Environmental Outreach" disseminates information and sometimes asks audiences to take specific action, but does not necessarily teach people how to analyze an issue. Outreach often presents a particular point of view, and often in pursuit of a particular goal. Examples may include a community meeting to inform residents about a toxic site in their area and where they can go for help, or a campaign to get volunteer participants for a beach or stream clean-up event.
- "Environmental Stewardship" is voluntary commitment, behavior, and action that results in environmental protection or improvement. Stewardship refers to an acceptance of personal responsibility for actions to improve environmental

quality and to achieve sustainable outcomes. Stewardship involves lifestyles and business practices, initiatives, and actions that enhance the state of the environment. Some examples are: living or conducting business in such a way as to minimize or eliminate pollution at its source; use energy and natural resources efficiently; decrease the use of hazardous chemicals; recycle wastes effectively; and conserve or restore forests, prairies, wetlands, rivers, and urban parks. Stewardship can be practiced by individuals, groups, schools, organizations, companies, communities, and state and local governments.

Environmental education enhances critical thinking, problem-solving, and effective decision-making skills, and teaches individuals to weigh various sides of an environmental issue to make informed and responsible decisions. The components of environmental education are:

- Awareness and sensitivity to the environment and environmental challenges
- Knowledge and understanding of the environment and environmental challenges
- Attitudes of concern for the environment and motivation to improve or maintain environmental quality
- Skills to identify and help resolve environmental challenges
- Participation in activities that lead to the resolution of environmental challenges

Awareness and sensitivity to environmental issues and challenges involve disseminating information to the public. This is accomplished through a variety of means including television advertisement, printed media, outreach programs, or the internet. The purpose is to create a knowledgeable society that understands the negative impacts of solid waste generation and to motivate them to take action. These activities can take place in a school classroom or through ad campaigns. Several notable examples are listed below:

- Recycling one aluminum can saves enough energy to run a TV for 3 h – or the equivalent of a half a gallon of gasoline.
- We use over 80 billion aluminum soda cans every year.
- To produce each week's Sunday newspapers, 500,000 trees must be cut down.
- Recycling a single run of the Sunday *New York Times* would save 75,000 trees.
- The average American uses seven trees a year in paper, wood, and other products made from trees. This amounts to about two billion trees per year!
- The 17 trees saved (above) can absorb a total of 250 lb of carbon dioxide from the air each year. Burning that same ton of paper would create 1,500 lb of carbon dioxide.
- Americans use 2.5 million plastic bottles every hour! Most of them are thrown away!
- The energy saved from recycling one glass bottle can run a 100-W light bulb for 4 h. It also causes 20% less air pollution and 50% less water pollution than when a new bottle is made from raw materials.
- A modern glass bottle would take 4,000 years or more to decompose – and even longer if it is in the landfill.
- Mining and transporting raw materials for glass produces about 385 lb of waste for every ton of glass that is made. If recycled glass is substituted for half of the raw materials, the waste is cut by more than 80%.

These facts help illustrate the awareness and motivation components of EE. They highlight brief solid waste examples that compel individuals and companies to recognize solid waste challenges and take action.

The final components of EE focus on providing the public the necessary skills to take action. For example, instructions and information regarding setting up a recycling station at home or the workplace, plus a list of local vendor and nonprofits that may be able help. In addition, local and state governments can provide no cost activities and workshops to assist individuals in the process. Many local government agencies sponsor no-cost hazardous waste collection days to aid in the minimization process.

Environmental education is aimed at producing a public that is knowledgeable concerning the biophysical environment and its associated problems, aware of how to help solve these problems, and motivated to work toward their solution.

Public Involvement and Planning Framework

Public involvement is defined as the procedures for obtaining and considering the views of the general public in planning and decision-making processes. As related to solid waste, this includes gathering input with regard to solid waste removal processes and collection schedules, locations of landfills, and recycling processes (drop off sites or curbside recycling). The public involvement plan is a key component of this process. The goal of the plan is to provide the public with accurate information about solid waste removal and minimization in a convenient and timely manner. The plan should be made available to the public and periodically reviewed. The main parts of this plan are:

- The goal, policies, and objectives of the public involvement plan
- The public involvement techniques to be utilized
- The public involvement evaluation plan
- A list of revisions and amendments

Generally, objectives of the plan include maintaining an accurate database of solid waste contacts (vendors and elected officials), providing regular meeting announcements, making all work and documents readily assessable to the public (usually through the Internet), maintaining a staffed office to answer questions, and continually improving/reviewing the plan.

Common public involvement techniques include maintaining a web site, maintaining a master database, providing legal advertisements, providing a periodic newsletter (and a newsletter discussing specific projects), displaying adds, mailing information directly to the public, press releases, television/radio messaging, billboard messaging, hosting project workshops/open houses, providing posters/flyers, and conducting surveys to gauge opinions.

The evaluation plan describes public involvement techniques, outlines the steps to be taken to evaluate those techniques, identifies measures to quantify success rates, and outlines strategies to improve the public involvement process. The appendices of the plan may contain samples of public involvement tools, general and project-specific evaluations, and general and project-specific improvement strategies.

Examples of Successful Programs

Throughout the USA there have been several programs and research studies linking colleges, government agencies, and businesses involved with environmental education. Universities play an important role in environmental education and often "set the bar" for outreach and innovation. This section provides a brief overview and comparison concerning some of these research studies and programs. These programs include:

- US Department of Energy's Industrial Assessment Centers
- The University of Toledo Business Waste Reduction Assistance Program
- Youngtown State University's Industrial Waste Minimization Project
- Cornell University's Waste Management Institute
- Indiana University's Institute on Recycling
- Iowa State University's Total Assessment Audits

US Department of Energy Industrial Assessment Centers

The Federal Government has been funding industrial assessments for small- and medium-sized manufacturing firms under the Industrial Assessment Center (IAC) program (formerly called the Energy Analysis and Diagnostic Center [EADC] program) since 1976. The program is funded through the US Department of Energy's Office of Industrial Technologies [3].

The industrial assessments provide an in-depth assessment of a plant site: its facilities, services, and manufacturing operations. This term is used to refer to a process which involves a thorough examination of potential savings from energy efficiency improvements, waste minimization and pollution prevention, and productivity improvements. Assessments are performed by local teams of engineering faculty and students from 26 participating universities across the country. The 26 participating universities are listed below:

- Arizona State University, Tempe, AZ
- Bradley University, Peoria, IL
- Colorado State University, Fort Collins, CO
- Loyola Marymount University, Los Angeles, CA

- Iowa State University, Ames, IA
- Lehigh University, Bethlehem, PA
- Mississippi State University, Mississippi State, MS
- North Carolina State University, Raleigh, NC
- Oklahoma State University, Stillwater, OK
- Oregon State University, Corvallis, OR
- Rutgers University
- San Diego State University, San Diego, CA
- San Francisco State University, San Francisco, CA
- Syracuse University, Syracuse, NY
- Texas A&M University, College Station, TX
- University of Dayton, Dayton, OH
- University of Florida, Gainesville, FL
- University of Illinois at Chicago, Chicago, IL
- University of Louisiana at Lafayette, Lafayette, LA
- University of Massachusetts, Amherst, MA
- University of Miami, Coral Gables, FL
- University of Michigan, Ann Arbor, MI
- University of Texas at Arlington, Arlington, TX
- University of Utah, Salt Lake City, UT
- University of Wisconsin-Milwaukee, Milwaukee, WI
- West Virginia University, Morgantown, WV

The assessment begins with a university-based IAC team conducting a survey of the eligible plant, followed by a 1 or 2 day site visit, taking engineering measurements as a basis for assessment recommendations. The team then performs a detailed analysis for specific recommendations with related estimates of costs, performance, and payback times. Within 60 days, a confidential report, detailing the analysis, findings, and recommendations of the team is sent to the plant. In 2–6 months, follow-up phone calls are placed to the plant manager to verify recommendations that will be implemented.

Manufacturers are not the only beneficiaries of the IAC program. Students involved in the program have a unique opportunity to see a range of manufacturing operations first hand. This results in more motivated students who more often than not enter energy management as a career field.

Business Waste Reduction Assistance Program (The University of Toledo, Ohio)

In 1996, an innovative partnership between the Lucas County Solid Waste Management District and The University of Toledo, College of Engineering was formed to help improve environmental and economic conditions in Lucas County, OH, USA by providing no cost solid waste assessments to Lucas County manufacturers and businesses [4]. Since the inception of the project, over 70 waste assessments have been completed, over 109,000 t of solid waste has been identified for reuse, reduction, or recycling and over $3.1 million have been identified as potential cost savings for Lucas County business. The project demonstrates that through a cooperative effort and a creative alliance, businesses, governments, universities, and industries can work together to improve environmental quality, reduce waste, and improve profitability. The project also educates college students through practical, real-world environmental work experience and trains them to become future environmental leaders.

Industrial Waste Minimization Research Project (Youngtown State University, Ohio)

In 1995, the Mahoning County Industrial Waste Minimization Project, in a cooperative effort between the Mahoning County Solid Waste District and Youngstown State University began using interns to provide free waste minimization audits [5]. The project team attended a training seminar titled "Integrated Manufacturing Assessments" to develop their waste audit process. Between 1995 and 1999, the project conducted 22 waste audits. In 1997, the project received the Governor's Award for Outstanding Achievement in Pollution Prevention and received additional grants in 1998 [6]. In 1999, the project was discontinued due to lack of resources. This project was very similar to the WAMRP at The University of Toledo. Both projects involved a joint effort between government and academia and conducted no cost waste audits. The major difference between the programs was the college departments involved. The WAMRP used industrial engineering students and faculty, while this project used environmental science majors. For this type of waste audits, industrial engineering majors have an advantage over environmental science majors due to the industrial engineering curriculum based process analysis, engineering economics, and systems improvement.

Waste Management Institute (Cornell University)

The Cornell Waste Management Institute (CWMI) was established in 1987 to address environmental and

social issues associated with waste management [7]. Researchers and educators work to develop technical solutions to waste management problems and to address broader issues of waste generation and composition, waste reduction, risk management, environmental equity, and public decision making. Current areas of research for the CWMI are composting as a component of integrated waste management; assessing the benefits and impacts of agricultural application of sewage sludges, manures and fertilizers; and source reduction.

Major goals of the CWMI outreach program are to improve the ability of local officials, businesses, and the public to make informed waste management decisions and to enhance the competency of solid waste professionals through increased training opportunities. The Cornell Cooperative Extension network, with offices in every New York State county, provides useful means of reaching these audiences. Outreach activities are based on research, with a goal of extending up to date, objective, research-based knowledge to a wide range of audiences from state agencies to America's youth.

The Institute develops and sponsors technical and management workshops and conferences. The CWMI staff also produces reports, audio-visual, and computer-based training materials. The CWMI houses a publication library with over 5,700 reference materials and is open to the public. A database of the library materials can be accessed and searched through the CWMI web site.

Institute on Recycling (Indiana University)

The Indiana Institute on Recycling, a state-run agency created in 1989 by the General Assembly of Indiana, is located at Indiana State University, in Terre Haute, Indiana. The Institute developed concepts, methods, and procedures for assisting Indiana residents in reducing and recycling solid waste. The Institute has conducted over 90 solid waste reduction studies with emphasis on cost benefits. The studies have developed economical and environmental solutions for companies to address specific solid waste issues at their facilities, e.g., cost analyses on the use of reusable shipping containers.

The Institute is similar to the WAMRP in that both are supported by State funding, utilize college students to conduct the studies, and apply economic benefit analyses as an incentive for companies to reduce waste. The primary difference is that the Institute addresses very focused, specific waste reduction needs of companies covering a broad range of areas and the WAMRP specifically conducts solid waste audits to characterize the companies' waste streams and target areas for reduction.

Total Assessment Audits (Iowa State University)

In 1993, Iowa State University and the Iowa Energy Center developed a Total Assessment Audit (TAA) project that conducted energy, waste reduction, and productivity audits simultaneously for manufacturing facilities [8]. The TAA concept originated from the belief that a manufacturing facility is better served using a holistic approach to problem solving rather than the more conventional isolated approach. The TAA approach assumes energy, waste reduction, and productivity objectives are interrelated and that simultaneous evaluation will produce synergistic results.

The TAA methodology utilized in Iowa has evolved over a 6-year time frame and was utilized on 25 audits. The TAA procedure emphasizes top management support and the use of cross-functional teams. Benchmarking exercises and energy usage analyses have been conducted to help the audit process identify improvement opportunities.

An initial 2–3 day on-site audit is conducted with the aid of key facility operating and management personnel. The TAA team members are paired with the appropriate facility personnel to collect specific data, gather a working knowledge of operations, and identify opportunities for improvement. Workshops are conducted at the end of the day to exchange information and are structured to encourage open discussion and debate regarding the merit of each identified opportunity.

The TAA method is a very powerful tool for small- and medium-sized manufacturers and identifies and evaluates improvement opportunities, while accounting for the interconnected levels of energy, waste, and process analyses. This method allows for an efficient, cost-effective analysis, in essence combining three audits into one.

EPA Environmental Education Initiatives

The US EPA also plays a critical role in environmental education and public involvement. Since 1992, the US EPA has awarded over 3,300 environmental education grants to various organizations at an amount of $2–3 million annually [9]. Any local education agency, college or university, state education or environmental agency, non-profit organization as described in Section 501(C) [3] of the Internal Revenue Code, or a noncommercial educational broadcasting entity as defined and licensed by Federal Communications Commission may submit a proposal for these grants. The Grants Program sponsored by EPA's Environmental Education Division (EED), Office of Children's Health Protection and Environmental Education, supports environmental education projects that enhance the public's awareness, knowledge, and skills to help people make informed decisions that affect environmental quality. The US EPA has indentified the following education priorities in the USA:

- EE Capacity Building: Building the capacity of agencies and organizations to develop, deliver, and sustain comprehensive environmental education programs statewide. Capacity building proposals may focus on one state, multiple states across the country, or multiple states in one geographic region.
- Educational Advancement: Utilizing environmental education as a catalyst to advance state or local education improvement goals.
- Community Projects: "Community Projects" address environmental stewardship in a local context and use community-based stewardship activities as the primary teaching tool.
- Human Health and the Environment: Educating teachers, students, parents, community leaders, or the public about human health threats from environmental pollution and how to minimize human exposure to preserve good health.
- EE Teaching Skills: Providing pre-service and in-service professional development for teachers, faculty, or non-formal educators to improve their environmental education teaching skills and/or knowledge about environmental issues and content, such as sustainability, water and air quality, chemical risks, hazardous wastes, climate change, and greenhouse gas emissions.

Below is a snapshot of several public involvement and environmental education projects that were funded from this grant. These projects demonstrate several real-world examples of public involvement and environmental education that may be applied in other regions to reduce solid waste generation. For each project, the name or the organization, organization contact, address, project title, and brief description are provided [9].

Eastern Michigan University Rebecca Martusewicz, Starkweather Hall, 2nd Floor, Ypsilanti, MI 48197
Building Leadership Capacity for Sustainability Education
This project targets kindergarten through grade 12 teachers, administrators, and community partners to strengthen the capacity of four public school districts in New Hampshire, New York, Michigan, and Minnesota to reorient themselves around sustainability and become models for other schools. The goals of this project are to develop a network of effective school leaders who can demonstrate and advance education in sustainability as a critical reform approach and to disseminate a model process for building this leadership capacity. To achieve these goals, four leadership teams are completing status reports to outline the strengths, weaknesses, and needs in student achievement, opportunities for involving students in environmental stewardship, existing reform efforts in sustainability education, and internal capacity. Based on these data, a 2-day retreat is designed where the teams are provided with training in strategic planning, planning assistance, and existing resources in sustainability education. After the retreat, the teams develop a strategic plan that outlines 1-, 3-, and 5-year goals and budgets for: (1) implementing programming to meet the needs identified, (2) involving students in stewardship, (3) evaluating the impacts of their efforts on student achievement and environmental stewardship, (4) sustaining their work through funding, and (5) promoting the reform work to other educators. Teams are provided with a rigorous framework in strategic planning, technical assistance, evaluation methods, and networking to achieve the objectives. Creative Change Educational Solutions and four public school districts

in New Hampshire, New York, Michigan, and Minnesota are the partners on this project.

Creative Change Educational Solutions Susan Santone, 229 Miles Street, Ypsilanti, MI 48198
Land Use Education for Youth
Under this grant, high school teachers from across southeast Michigan attend a 2-day workshop to learn about local land issues. The teachers then integrate lessons learned into the classrooms. The culmination of the project is a youth leadership forum where students share what they have learned, identify priorities, and create action plans that address land-use issues, specifically urban sprawl. One important feature of "Lessons in Leadership" is the content flexibility of its model (teacher education plus classroom instruction plus youth leadership). The flexibility offers the potential for other regions to adapt the model to pertinent environmental issues.

The Greening of Detroit Rebecca Salminen Witt, 1418 Michigan Avenue, Detroit, MI 48216
Green Heroes Program
The Green Heroes program increases environmental awareness among Detroit's youth by providing elementary school students and adult partners with out-of-school training, guidance, and materials to create cleaner and greener spaces in their own neighborhoods. The program partners with two groups to promote a better understanding of the environment to children and adults. It provides resources to participants for areas selected for revitalization. Additionally, community groups and youth investigate their neighborhoods by creating maps of areas that need to be cleaned up and planted with vegetation to create a healthier ecosystem. All participants are recognized for their efforts in protecting their environment and creating a cleaner and healthier Detroit.

Copper County Intermediate School District Shawn Oppliger, 809 Hecla Street, Hancock, MI 49930
Developing Environmentally Informed Scientists, Educators, and Stewards for the Future
In this project, Michigan Tech University students are recruited and trained to support two programs for elementary and middle school students: an after-school environmental science class and a forest and pond ecology field trip. Approximately 600 students in kindergarten through grade 8 participate in the environmental science class, and about 2,500 students complete the field trip. Pre-serve education and environmental engineering students conduct and facilitate the after-school program and field trips. University students gain valuable training and presentation skills while introducing young students to environmental careers. While on the field trips, educators are involved in modeling environmental education methods.

Michigan Technological University Joan Chadde, 1400 Townsend Drive, Houghton, MI 49931
Kids Make a Difference
The Kids Make a Difference program provides incentives for kindergarten through 12th-grade students, teachers, and youth groups to develop projects that promote environmental education, community service, and environmental enhancement. School classes and youth groups select environmental topics to study and to teach others about, or they design and implement projects that address environmental issues in their communities. Students share their projects through presentations to other students or by publishing articles in the newspaper. All program participants receive Earth Day award certificates and tokens of recognition. In addition, their names are entered in a drawing in which they could win an educational tool kit or an environmental education field trip.

Ypsilanti Public Schools Tulani Smith, Office of Academic Services, Ypsilanti, MI 48197
Sustainability Education for Sustainable Communities
The project addresses a critical need in Washtenaw County to bring together teachers and students to use education reform as a means of addressing the links among student achievement, urban sprawl, and sustainability of communities. The target audiences of the project, middle- and high-school teachers and students, are developing a model for education reform that is based on sustainability education. The goals of the project are to: (1) train science and social studies teachers to lead students through investigations of contemporary environmental, social, and economic issues; (2) support and mentor teachers as they implement classroom investigations; (3) use presentations, newsletters, and reports developed by the students to

educate the community about positive responses to contemporary challenges; (4) evaluate the effect of the project on the practices of the teachers and the students' achievements; and (5) disseminate the components of the project – workshop designs, lesson plans, assessment tools, and case studies – to promote its replication. The outcomes of the project are evaluated against state educational standards, and the principal components of the project are distributed at the local, state, and national levels. Partners in the project include Washtenaw Intermediate School District, Washtenaw County Government, Sustainable Washtenaw, the Michigan Alliance for Environmental and Outdoor Education, the Northeast Initiative, the New Jersey Sustainable Schools Network, the BESS Project, and consultants from the University of Michigan and Eastern Michigan University.

The Creation Station Lori Thomas, P.O. Box 26113, Lansing, MI 48909-6113
Environmental Literacy Through Creative Educational Projects
The Creation Station provides teachers and child-care providers in the greater Lansing area with creative and educational resources related to waste management and pollution prevention. Material guidelines provided by the North American Association for Environmental Education are used to develop classroom kits for preschoolers and third graders that meet the Michigan curriculum frameworks. Along with its collaborators, The Creation Station also develops workshops to show teachers how the materials integrate environmental education and science with art and creativity. More than 15,000 preschool, day-care and third-grade students are reached.

Michigan Recycling Coalition Kerrin O'Brien, P.O. Box 10240, Lansing, MI 48901-0240
Master Recycler Program
After revising and adapting a recycling curriculum developed by the Oregon State University Extension Service, the Michigan Recycling Coalition conducts two training programs in the community. The first pilot program seeks to educate community members about recycling, and the second pilot program seeks to educate business leaders about that subject. After completing the pilot programs, participants are identified as Master Recyclers. The Michigan Recycling Coalition then conducts a train-the-trainer workshop during which potential facilitators are trained to conduct the community-based program.

Ecology Center of Ann Arbor Rebecca Kanner, 117 N. Division, Ann Arbor, MI 48104
The Re-Bicycle Project
The Ecology Center of Ann Arbor provides a summer program for young people through which participants learn how to repair used bicycles. In addition to learning the technical skills of repairing a bicycle, students learn the important environmental concepts of reuse and recycling. Participants reduce the amount of solid waste going into the landfill by repairing discarded bicycles. They also obtain an affordable and environmentally friendly form of transportation. The program targets middle school children living in public and subsidized housing developments. Approximately 45–60 young people participate in the program.

The University of Michigan Peggy Britt, Michigan Sea Grant, 3003 S. State Street, Room 1066, Ann Arbor, MI 48109
Environmental Journalism
The Michigan Sea Grant Program provides a handbook and fact sheet for high school writing teachers. The handbook and fact sheet provide teachers with the information they need to incorporate environmental journalism into their curricula. The materials provide teachers with an understanding of key environmental concepts and address the elements of science-based environmental writing. Students are introduced to environmental journalism and related careers in environmental communication. The handbook and accompanying fact sheet address critical-thinking skills, such as investigating and analyzing environmental issues and assessing the threats that pollution poses to human health. Although a needs assessment indicated that educators were not interested in workshops, staff at Michigan Sea Grant are committed to assisting teachers in fully integrating the lessons from the handbook into their classroom criteria.

City of Ann Arbor Cheryl Saam, 1831 Traver Road, Ann Arbor, MI 48105
Taking Action in Recycling

Taking Action in Recycling provides 19 full-day field trips for students in area schools. Through the field trips, approximately 1,140 students become familiar with the recycling process and learn how to implement recycling programs at their schools. Each field trip begins at the Leslie Science Center, where staff members introduce the concepts of natural cycles, ecosystems, and interdependency. Students participate in hands-on activities, nature hikes, simulation games, and group discussions. They then have the opportunity to see recycling in action at the Solid Waste Department's material recovery facility. After the field trip, students and teachers receive recycling boxes and are encouraged to establish recycling programs in their schools. The Leslie Science Center and the City of Ann Arbor Solid Waste Department work in partnership to sponsor the project.

U-SNAP-BAC, Inc. Linda Smith, Executive Director, 11101 Morang, Detroit, MI 48224
Environmental Negotiations Skills Seminars
Environmental Negotiations Skills Seminars are 2-day seminars offered by U-SNAP-BAC and several partners to residents in the east side of Detroit. The seminars teach participants how to negotiate with financial institutions, developers, and state and local governmental agencies on residential, commercial, and industrial redevelopment of Brownfields and other urban sites. Brownfields are abandoned or under-used industrial sites. These model seminars employ an innovative role-play technique and include a feedback tool that enables groups to monitor their negotiation behaviors and evaluate progress. U-SNAP-BAC will develop a final product that describes the process of planning and offering these seminars to enable other communities to offer similar programs.

Communities in Schools Beth Urban, 510 East Broadway, Columbus, OH 43214
Recycling Awareness
Communities in Schools provides environmental education opportunities to students in after-school programs. The opportunities focus on community issues of (1) litter, (2) lack of environmental stewardship, (3) waste reduction, (4) limited willingness to recycle, and (5) limited access to free recycling centers in low-income areas of Columbus. Students learn the effects of littering along with the value of recycling and environmental stewardship. Goals are achieved through use of EPA's Planet Protector and Make a Difference curriculum and field trips and by starting recycling programs in each participating school. The project is implemented in three phases: (1) educational programming during the after-school program, (2) active participation in school and community recycling, and (3) promoting greater access to recycling bins for the school community. Students involved in the project educate the Solid Waste Authority of Central Ohio and the local government about the importance of recycling.

Youngstown State University Marcia Barr, One University Plaza, Youngstown, OH 44555-3355
Waste Minimization Workshop for Youngstown Students and Teachers
In this project, fifth- and sixth-grade teachers from the Youngstown public and Catholic schools participate in "train the trainer" workshops that meet the Ohio Department of Education's technology standards. The workshops, with the participation of 11 public and 5 Catholic schools, provide an interactive chemistry demonstration and instruction on waste reduction and pollution prevention as well as ecosystem protection. The teachers learn how to access databases in order to determine what waste minimization regulations affect their schools. Tests are given before and after workshops so that project staff members can determine the training's effectiveness.

Mahoning Valley/Northeast Ohio Camp Fire Council Barbara Smith, P.O. Box 516, 3712 Leffingwell Road, Canfield, OH 44406
Environmental Olympics
Mahoning Valley/Northeast Ohio Camp Fire Council teams with Organizacfon Civica y Cultural Hispana Americana, Inc. (OCCHA) to bring environmental education activities to OCCHA's after-school site on the south side of Youngstown. The program teaches 40 inner-city, high-risk youth from 8 to 13 years of age about their local environment through field trips and hands-on service learning projects. Among other evaluation measures, Mahoning Valley/Northeast Ohio Camp Fire Council tracks student self-esteem throughout different phases of the project.

Texas Discovery Gardens Fran Anderson, 3601 Martin Luther King Boulevard, Dallas, TX 75210
After-School EE Program
Texas Discovery Gardens is an organic, botanic gardens located in historic Fair Park in Dallas, Texas. The garden has created a program called the "After-School Environmental Education Program" for children to attend after school lets out for the day. Students from local school groups participate in the "Life in the Compost Bin Earthkeepers." In this program, students focus on sustainable urban development and waste management through composting and recycling education. This program reaches many local households by working with and empowering the children of these communities. The students who participate in this program learn about community stewardship and environmental issues. The student participants develop a community project and conduct outreach programs in their neighborhoods. While they are involved in these outreach programs, the students coordinate with media outlets to produce newsletters and brochures to use in these outreach efforts. The students also produce a short-film documentary of the outreach efforts for use as a public service announcement.

The Artist Boat, Inc. Karla Klay, 4919 Austin, Galveston, TX 77551
Eco-Art Adventure via Kayak Program
The Artist Boat increases awareness among and instills an environmental ethic in middle school students. The program employs an innovative and effective inquiry-based teaching methodology, which integrates art and science to engage all types of learners – visual, auditory, and tactile. The program consists of Eco-Art Workshops (2-h in-class workshops); Eco-Art adventures (4-h waterborne field classes) on kayaks at Galveston Island State Park; and interdisciplinary environmental curricula in art, math, science, social studies, and English (8 pre- and post-classroom lessons teachers deliver). The nonprofit organization also provides faculty members with Eco-Art Professional Development training. This program meets the goals of the Texas Education Agency – Texas Essential Knowledge and Skills and Galveston Bay Estuary Program's goals for public participation and education in the Galveston Bay watershed.

Keep Texas Beautiful, Inc. Stacy Cantu, 1524 South IH-35, Suite 150, Austin, TX 78704
Stop Trashing Texas — It's the Law
The goal of Keep Texas Beautiful, Inc. (KTB) is to implement Stop Trashing Texas – It's the Law, an illegal dumping educational program. KTB engages its statewide network of community affiliates to promote workshops held in geographically and economically diverse areas of Texas in order to support elimination of illegal dumping. KTB's efforts concentrate on law enforcement personnel, such as code enforcement officials, police officers, and sheriff's office representatives. This program gives law enforcement personnel the opportunity to attend workshops and gather training tools and resource materials that can be used to support community enforcement efforts with the ultimate goal of eliminating illegal dumping in Texas.

National Wildlife Federation Marya Fowler, 44 East Avenue, Suite 200, Austin, TX 78701
Earth Tomorrow
The project initiates Earth Tomorrow, an interdisciplinary, after-school and summer program in environmental education and leadership for under-served high school students. The goal of the project is to address the environmental education and leadership needs of today's young people by increasing their environmental literacy. This is being accomplished by means of teacher training to align after-school enrichment with classroom instruction, field trips, career mentoring in the environmental sciences, and a 5-day residential summer institute at a local university. At this institute, students, teachers, and community leaders have the opportunity to explore the environmental sciences through field trips, hands-on data collection and analysis, discussions with environmental professionals, and planning for a community action project.

Texas Southern University Laura Solitare, 3100 Cleburne Street, Houston, TX 77004
Environmental Education for Environmental Justice
The goal of this project is to educate local residents and community leaders about environmental justice, environmental planning, and urban revitalization issues through six interactive, hands-on workshops. The workshops give the participants a basic understanding of environmental systems and the regulations

that frame the field of environmental planning. In particular, the workshops focus on water issues, municipal solid waste, and contaminated land. The workshops also examine how local residents and community leaders can help achieve environmental justice in their communities.

Keep Texas Beautiful Stacey George Cantu, 823 Congress Avenue, Suite 230, Austin, TX 78701
Waste In Place
This project hosts eight Waste in Place curriculum workshops and distributes Keep Texas Beautiful youth environmental education kits. Waste in Place is a hands-on youth environmental education curriculum. The interdisciplinary curriculum for grades kindergarten through 8 provides resource materials and hands-on activities for educators and students to examine their environment, including land, water, and air issues. The goals are to provide materials to increase the environmental awareness of educators and youth, to offer formal and informal educators a proven resource tool, and to provide regional workshops. The objectives include training educators through workshops offered in eight locations in the state to reach formal and informal educators, and to reach thousands of youths. Partners include Texas Department of Transportation, Texas Natural Resource Conservation Commission, and Texas Forest Service.

Art from Scrap Cay Sanchez, 302 East Cota Street, Santa Barbara, CA 93101
AFS Green Schools Teacher Training Workshops
Getting "back to the garden" is the method Art from Scrap uses to teach elementary school children in Santa Barbara County to foster appreciation of the natural world. This teacher education program is the first step to promoting positive messages about environmental stewardship in Santa Barbara County schools. It offers the beginnings of a social foundation for encouraging environmental practices that enhance land use for tourism and mitigate the potential for groundwater contamination from commercial use of pesticides and fertilizers in regional agriculture. Art from Scrap sponsors workshops in organic gardening and in composting to classroom teachers, student teachers, classroom aides, parent volunteers, and administrators. Program partner Healing Grounds Nursery provides free plant seedlings and composting worms, the living beginnings for a laboratory where age-appropriate experiments are conducted every day in the most natural way, as children cognitively and physically engage with nature. The fruit of the garden for the community is the opportunity it provides children to internalize positive associations with stewardship of the environment.

California Integrated Waste Management Board Christy Humpert, 1001 I Street, P.O. Box 4025, Sacramento, CA 95812
Strategies for Incorporating the EEI Curriculum into California Classrooms
The California Integrated Waste Management Board (CIWMB) is responsible for implementing the Education and the Environment Initiative (EEI), a program developed under a California law that was enacted in 2003. It requires development and dissemination of a kindergarten through grade 12 environment-based education program for all students in the state's public schools. The EEI curriculum focuses on the relationship between humans and the environment and addresses various environmental issues, including sustainability, water, air, and pollution prevention. Under this project, CIWMB is developing and implementing a strategy for incorporating the EEI curriculum into California school districts to produce more environmentally literate students. In addition, CIWMB is developing a professional development plan for training educators in use of the EEI curriculum. Teachers attend workshops to learn about EEI and participate in focus group meetings. This project serves as a model for bringing environment-based education into public schools nationwide, institutionalizes environment-based education, and helps to develop more environmentally literate students. Partners in this project include the California Environmental Protection Agency (EPA), the California Department of Education, the State Education and Environmental Roundtable, and the National Geographic Society.

Catholic Charities CYO Deidre Rettenmaier, 180 Howard Street, Suite 100, San Francisco, CA 94105
Developing Youth as Environmental Leaders and Stewards
This project, "Developing Youth as Environmental Leaders and Stewards," addresses challenges to the

riparian corridor of two discrete stretches of Salmon Creek and one of its tributaries that run through 220 acres of coastal redwood forest in Sonoma County. The program will serve students and teachers during 5-day retreats offered 24 times throughout the year. A new creek and watershed curriculum has been introduced, emphasizing on-the-ground restoration activities that are the direct result of student field study, observation, evaluation, decision making, and problem solving. The goal is to develop the environmental leadership and stewardship skills of the students through direct exposure to local environmental challenges.

Generation Green R.C. Ferris, 2066 Donald Drive, Moraga, CA 94556
Traveling Trash Transformations
Generation Green will provide at least 20 hands-on workshops on recycled art at libraries and farmer's markets throughout Contra Costa County. The objective is to inspire people, through creative endeavors, to see the potential value of the raw materials that are recycled. The organization hopes to attract participants at the farmer's markets and students at county and school libraries, who will take part in "eco art" activities that generate enthusiasm and fun, while teaching folks to use unused, recycled materials, and to think before it is thrown away. Generation Green wants to enable people to create, make, and make do; to inspire people to experiment with junk. The organization wants to help create a generation of recyclers so that it will be second nature to look at something discarded and wonder, "What else can this be?" or "What can I make with this?"

California Integrated Waste Management Board Joanne Vorhies, 1001 I Street, P.O. Box 4025, Sacramento, CA 95812-4025
Education and the Environment Initiative Implementation Project
In an effort to improve implementation of the Education and the Environment Initiative (EEI), the California Integrated Waste Management Board (CIWMB) provides environmental nongovernment organizations (NGO) in the state with professional development opportunities and technical assistance. Established by a state law in 2003, the EEI requires CIWMB, the California Environmental Protection Agency (Cal/EPA), and the California State Department of Education to develop principles and approaches for incorporating environmental education into elementary and secondary school curriculums. The EEI also requires the agencies to create a model environmental education curriculum based on California's academic content standards. As part of the EEI implementation project, representatives of environmental NGOs attend professional development workshops conducted in six regions across the state followed by a series of technical assistance workshops. These workshops are intended to help the NGO community revise existing environmental education materials in order to better align them with California's model curriculum. The workshops also provide increased opportunities for the NGOs to collaborate with schools on environmental education reform. As a result, environmental concepts are being further integrated into the education of California's elementary and secondary school students. Each environmental NGO works with California teachers to help them integrate the revised materials into their curriculums, a process that also builds the capacity of the NGOs. As another element of the project, CIWMB is creating a web-based environmental education provider database that gives teachers and organizations the ability to communicate and exchange expertise. Key CIWMB partners in the project include Cal/EPA, the California Resources Agency, the California State Department of Education, the Office of the Secretary for Education, and the State Board of Education. The project is also supported by a large number of associated partners.

Los Angeles County Education Foundation Roberta Gerarde, 9300 Imperial Highway, Room 106, Downey, CA 90242
EarthWorks — Careers That Serve the Earth
Earth Works – Careers that Serve the Earth is a new program that educates students in grades 10 and 11 about environmental careers such as forestry and the atmospheric, space, and earth sciences. Earth Works addresses crosscutting topics using presentations by career professionals and small group work through use of the property known as Blue Sky Meadow in the San Bernardino Mountains. These presentations emphasize local environmental issues, field study, and service learning projects, such as habitat

improvement and modification or native plant restoration. Through interactive discussions, written materials, and guided activities, students learn how to identify and achieve their academic and vocational goals. The students learn about the steps that lead to careers in geology, meteorology, astronomy, teaching, environmental engineering, and forest management.

Imperial Valley Regional Occupational Program Madaleine O. Macholtz, 687 State Street, El Centro, CA 92243
Imperial Valley Student Entrepreneurs for Recycling
The Imperial Valley Student Entrepreneurs for Recycling program raises students' awareness about recycling and resource management to improve their overall academic performance. Another goal of the program is to help students explore environmental careers and find ways to make positive contributions to the local environment. As part of the program, middle and high school teachers are being trained using the California Integrated Waste Management Board's "Closing the Loop" curriculum guide. The teachers work with six middle and high school groups to develop school-based recycling businesses. Information about the students' efforts is disseminated throughout the community. The target audience for this grant includes students from a low-income, culturally diverse, rural community.

Placer Land Trust and Nature Center Linda Desai, 3700 Christian Valley Road, Auburn, CA 95602
Waste Busters
In this project, the Waste Busters program will be added to the Environmental Science Travels (EST) program, which is a set of five interactive programs for elementary school students that brings environmental science into the classroom. Subjects of the EST program include water resources; recycling; food chains; and birds, bats, and bugs. For example, the Water Basins program enhances middle school science curriculums by making connections between the physical science concepts that students learn about in the classroom and the energy and natural resources that they use in everyday life. Although a traditional science curriculum addresses the concepts of energy and its application, it does not make energy issues personal for students. The EST program connects the concepts taught in the classroom with students, their homes, and their community. Thus, the program offers students a fuller understanding of energy and natural resources and their application in every aspect of the students' lives.

Venice High School Julie Mann, 13000 Venice Boulevard, Los Angeles, CA 90066
The Learning Garden Composting Demonstration Site
The Venice High School Learning Garden includes a functional and educational composting demonstration site that serves as a learning center for students and community members. The Learning Garden is a green waste reduction post for the high school and surrounding neighborhoods, and it produces rich soil amendment for its own use. The goal of the project is to incorporate the theory and practice of composting into the school system and the curriculum by utilizing existing environmental education materials. Local businesses are encouraged to compost their wastes at the site. Weekend workshops are held every 2 months targeting different areas of the community. The workshops educate residents about composting options and landfill issues. Through community use of the composting site, participants learn how to reduce the amount of waste being landfilled while producing a beneficial soil amendment that can be used to green their homes and neighborhoods.

California Academy of Sciences J. Patrick Kociolek, Golden Gate Park, San Francisco, CA 94118
Wild City! Urban Environmental Education
Wild City! Urban Environmental Education activities are for fourth and fifth grade public school students in San Francisco communities where residents are traditionally underrepresented in the sciences. The project connects scientific and environmental concepts to everyday life and experiences in order to make learning science fun and interesting for children, many of whom have had little or no previous experience in the natural world. Wild City! helps participants understand biodiversity at the species and ecosystem levels, emphasizes the importance of local biodiversity as well as the problems facing biodiversity and possible solutions, gives each child the opportunity to contribute personally to the preservation of biodiversity through a restoration or cleanup project, and establishes a connection and a potential ongoing relationship

between each child and the resources of the California Academy of Sciences.

CEC Stuyvesant Cove, Inc Christopher Collins, 24–20 FDR Drive Service Road East, New York, NY 10010
The Green Design Lab
The Green Design Lab teaches high school students to assess energy, water, waste, and food flows in the Manhattan Comprehensive high school building. They create a detailed proposal for how to "green" the school, including a plan for capital renovations. This project uses existing curricula and resources to pioneer a new environmental educational strategy that incorporates science, art, design, community stewardship, and career development, with an emphasis on creativity, applied problem solving, and career training.

Friends of Van Cortlandt Park $15,000 Christina Taylor, 124 Gale Place, Apt. GRA, Bronx, NY 10463
Summer Environmental Internship Program
The Friends of Van Cortlandt Park runs the Summer Environmental Internship Program for New York City high school students. The program provides hands-on summer employment within Van Cortlandt and other parks in the city. The summer environmental interns obtain first-hand experience maintaining and learning about the ecosystems in urban parks, in the process developing an understanding of the need to protect the natural environment and the ways visitors to a natural area affect its ecosystems. Students work with staff and volunteers from environmental and natural resource providers, agencies, and organizations to acquire increased knowledge of career opportunities in the environment as well as basic job skills. By working in this urban ecosystem, participants acquire environmental knowledge and skills and undertake tasks reflecting their commitment to environmental stewardship.

Long Island Regional Envirothon, Ltd. Sharon Frost, 423 Griffing Avenue, Riverhead, NY 11901
Long Island Regional Envirothon
Participation of high school students in New York's Nassau and Suffolk Counties in an annual environmental education competition is supported through this grant. Students prepare by studying various topics and issues, such as aquatics, forestry, soils, wildlife, and current environmental issues. They then compete by responding to questions and challenges on these environmental topics, demonstrating what they have learned. Their involvement in the program fosters interest in environmental careers and develops environmental stewardship.

Capitol District YMCA Camp Chingachgook Outdoor Center Brian Leibacher, 1872 Pilot Knob Road, Kattskill Bay, NY 12844
Food Source Reduction and Composting
The goal of this project is to reduce Chingachgook's food waste, create a useful compost product, and educate participants in the annual program on the ease and benefits of Food Source Reduction and Composting. The target audiences for this project are school children, summer campers, and adults and family members from diverse backgrounds. These participants are taught about the value of waste reduction and the amount of energy that is required to produce a meal from "grow to throw." Students and campers weigh food waste and learn to separate out composting materials. Source reduction and composting is also incorporated into Chingachgook's free semiannual teacher training day and camp food and maintenance conferences.

City Parks Foundation David Rivel, 830 Fifth Avenue, New York, NY 10021
Green Girls
Green Girls introduces seventh- and eighth-grade girls in East Harlem and the Bronx to career opportunities in the sciences and supports the girls' academic achievement. The City Parks Foundation in New York City provides these middle school girls with after-school, weekend, and summer activities to promote environmental stewardship. The Green Girls program encourages the girls to consider careers in the sciences, enriches their understanding of science by introducing the girls to successful female scientists who share their knowledge and love for the field. The program also exposes them to environmental and social issues that affect their communities. The girls also become familiar with New York City's educational resources and develop their critical-thinking, leadership, and teamwork skills.

Cornell University Jeff Corbin, 120 Day Hall, Ithaca, NY 14853
Environmental Careers Skills Program
The Environmental Careers Skills Program focuses on ecosystem protection. This program provides college students with the skills and knowledge they need to become better environmental stewards and to explore potential environmental careers. Program participants learn about field sampling techniques, study environmental issues, are introduced to environmental career paths, and learn leadership and team-building skills that improve their ability to work with others to protect the environment. In addition, students attend a 3–4-day training workshop that teaches them strategies for networking with professionals and their peers.

Friends of the High School for Environmental Studies M'Lis Bartlett, 444 West 56th Street, New York, NY 10019
Environmental Science Literacy Training Project
The Friends of the High School for Environmental Studies (HSES) offers professional development programs for HSES teachers to increase their environmental literacy and understanding of environmental stewardship. These interdisciplinary programs are designed to help teachers feel comfortable in incorporating environmental issues into any subject area. HSES is implementing a project to support science literacy efforts as a means of promoting understanding of environmental issues. This project offers training to both English and science teachers through inquiry-based discussions of environmental readings that reinforce concepts taught in high school science classes.

Prospect Park Alliance Carol Giangreco, 95 Prospect Park West, Brooklyn, NY 11215
Midwood Green Team Project
The Prospect Park Audubon Center's Midwood Green Team Project engages 20 pre-teens in hands-on study, restoration, protection, and interpretation of Prospect Park's Midwood, a natural habitat. The project is intended to improve the development and implementation of ecological programs for underserved youth. Project participants design, produce, and install educational signage to encourage environmental stewardship among park visitors.

Old First Ward Community Association, Inc. Laura Kelly, 62 Republic Street, Buffalo, NY 14204
Community Environmental Education Demonstration
The Community Environmental Education Demonstration project educates the children and teenagers in the traditionally underserved areas of the Old First Ward community about ecological problems such as pollution, contaminated soils, and numerous Brownfields associated with industrial development in their neighborhood. The Old First Ward Community Center is conducting workshops that include field trips to the nearby Tifft Nature Reserve, local greenhouses, grain elevators, and polluted industrial sites along the Buffalo River. The workshop participants focus on community garden projects as a means to explore various environmental practices that can improve their quality of life and lower their contribution to Buffalo River contamination.

Dream in Green Jane Gilbert, 2000 Ponce de Leon Boulevard, Suite 647, Coral Gables, FL 33134
Green Schools Challenge
The aim of this grant is to make concrete steps toward a more "green" society. This goal is accomplished by integrating hands-on, inquiry-based learning about the local and global environmental impacts of greenhouse gas (GHG) emissions, sources of and conversion factors for GHG emissions, energy assessments, and conservation methods to teach science, math, and language arts. This project supports the training, resources, coaching, and tracking support necessary for its participating schools to educate students about energy and resource conservation, reduce the carbon footprint of the schools and students' homes, and provide highly engaging, real-world learning opportunities for students through the use of professional energy analysis tools.

University of Central Florida Terri Vallery, 12201 Research Parkway, Suite 501, Orlando, FL 32826-3246
Education Recycling
Education Recycling aims to increase recycling rates on the university campus by conducting workshops on environmental stewardship and recycling that targets students living in University of Central Florida (UCF) housing on campus and the building managers for all 123 campus buildings and the entire staff of the UCF

library. This project focuses on the community and national issue of recycling and the need to increase recycling rates on a national basis to approach a zero waste stream goal. This project empowers the UCF community to think about its role in stewardship of the environment and the need to increase recycling toward the goal of a zero waste stream campus. Education leads to further knowledge in the community that is carried back home, and to a new generation, about the role recycling plays in environmental stewardship.

911 Media Arts Center Malory Graham, 117 Yale Avenue North, Seattle, WA 98109
STUFF: The Secret Life of Everyday Things
In this environmental educational program, 25 high school students explore the relationship between consumerism and waste production and their own consumption habits. They mentor with professional media producers to create a 10-min video that takes a behind-the-scenes look at the production, distribution, and consumption of an everyday household object. The project increases the capacity of three organizations: the 911 Media Arts center (non-profit educational organization), King County Solid Waste (government natural resources agency), and Foster High School (public high school) to develop a strategic model for producing and delivering environmental education video projects on a county level.

Future Directions

One of the current trends within environmental education seeks to move from an approach of ideology and activism to one that allows students to make informed decisions and take action based on experience as well as data. Within this process, environmental curricula have progressively been integrated into governmental education standards. Some environmental educators find this movement distressing and a move away from the original political and activist approach to environmental education while others find this approach more valid and accessible.

There is a movement that has progressed since the relatively recent founding (1960s) of the idea of environmental education in industrial societies, which has transported the participant from nature appreciation and awareness to education for an ecologically sustainable future. This trend may be viewed as a microcosm of how many environmental education programs seek to first engage with participants through developing a sense of nature appreciation which is then translated into actions that affect conservation and sustainability.

Bibliography

Primary Literature

1. US EPA (2008) Municipal solid waste in the United States 2007 Facts and Figures, EPA-350-R-08-101, Washington, DC
2. http://www.census2010.gov/ipc/www/idb/worldpopinfo.html. Accessed 22 Dec 2009
3. US Department of Energy, Office of Energy Efficiency and Renewable Energy (2001) Industrial Assessment Center Brochure 2001. Washington, DC
4. Franchetti M (2009) The solid waste analysis and minimization research project: a collaborative economic stimulus and environmental protection initiative in Northwest Ohio. J Solid Waste Technol Manage 25(2):88–94
5. Covey SK (2000) Building partnerships – the Ohio materials exchange. Resour Conserv Recycl 28:265–277
6. Ohio EPA (1997) Governor's Pollution Prevention Award Recipient: Mahoning County's Industrial Waste Minimization Project. Fact Sheet #41
7. Harris E (2000) Cornell Waste Management Institute Update June 2000. Ithaca
8. Haman W (2000) Total assessment audits (TAA) in Iowa. Resour Conserv Recycl 28:189–198
9. www.epa.gov. Accessed 22 Dec 2009

Books and Reviews

Berenyi EB (2002) K2001–2002 materials recycling and processing in the United States, 4th edn. Governmental Advisory Associates, Westport

Diaz LF, Savage GM, Eggerth LL, Golueke CG (1993) Composting and recycling municipal solid waste. Lewis, Boca Raton

Dowie W, McCartney D, Tamm J (1998) A case study of an institutional solid waste environmental management system. J Environ Manage 53:137–146

Environment at a glance: OCED Environmental Indicators, OCED, Paris 2006

Environmental management and monitoring for sport events and facilities: a practical toolkit for managers. Prepared for Department of Canadian Heritage Sport Canada by Green & Gold Inc., March 1999

EPA (1988) Waste minimization opportunity assessment manual. US Environmental Protection Agency, Cincinnati

Fishbein B (1994) Germany, garbage, and the green dot: challenging the throwaway society. Inform Publishing, New York

Franchetti M (2008) One company's trash is another company's treasure. Resour Recycling N Am Recycling Composting J 31: 40–42
Modern Marvels: History of Garbage. Video produced by The History Channel
National Wildlife Federation (2001) State of the campus environment. Washington, DC
NC Division of Pollution Prevention and Environmental Assistance (1997) Mixed waste processing. http://www.p2pays.org/ref/01/00028.htm. Accessed Feb 2006
OECD Environmental Data Compendium 2004, OCED, Paris 2005
Petrell R, Duff S, Felder M (2001) A solid waste audit and directions at the University of British Columbia, Canada. Waste Manage Res 19:354–365
Rathje W, Murphy C (2001) Rubbish!: the archeology of garbage. University of Arizona Press, Tucson
Rhyner CR, Schwartz LJ, Wenger RB, Kohrell MG (1995) Waste management and resource recovery. Lewis, Boca Raton
Ryding S (1994) International experiences of environmentally sound product development based on life cycle assessment. Swedish Waste Research Council, ARF Report 36, Stockholm, May 1994
Shimberg SJ (1985) The hazardous and solid waste amendments of 1984: What congress did ... and why. The Environmental Forum. March 1985, pp 8–19
Siegler T, Starr N (1999) Sorting out recycling rates. Resour Recycling 22:29–34
Strong DL (1997) Recycling in America, 2nd edn. ABC-CLIO, Santa Barbara
United States Congress of Technology Assessment (US Congress OTA) (1992) Green products by design: choices for a cleaner environment. OTA-E-541, U.S. Government Printing Office, Washington, DC
US Environmental Protection Agency (1990) The Nation's hazardous waste management program at a crossroads. Report No. EPA/530-SW-90-069. EPA, Washington, DC, 114 p
US Environmental Protection Agency (1992) The guardian: origins of the EPA. EPA Historical Publication-1, Spring 1992
US Environmental Protection Agency (1993) Household hazardous waste management: a manual for one-day community collection programs. U.S. Environmental Protection Agency, Washington, DC
United States Environmental Protection Agency (2006a) Recycling. http://www.epa.gov/epaoswer/non-hw/muncpl/recycle.htm. Accessed Feb 2006
United States Environmental Protection Agency (2006b) Municipal solid waste – basic facts. http://www.epa.gov/epaoswer/non-hw/muncpl/facts.htm
US Department of Energy, Office of Energy Efficiency and Renewable Energy (2001) Industrial Assessment Center Brochure. Washington, DC
US Environmental Protection Agency. Office of Solid Waste (1998) RCRA orientation manual. US Government Printing Office, Washington, DC, 160 p
US EPA (1988) Waste minimization assessment manual. Hazardous Waste Engineering Research Laboratory, Cincinnati
Wang Q, Dong L, Xi B, Zhou B, Huang Q (2006) The current situation of solid waste management in China. J Mater Cycles Waste Manage 8:63–69
www.indstate.edu/recycle
www.oit.doe.gov/iac

Spatial Crop Structure in Agricultural Systems

Emilio H. Satorre
Cátedra de Cerealicultura, University of Buenos Aires, Buenos Aires, Argentina
CONICET (National Research Council), University of Buenos Aires, Buenos Aires, Argentina
AACREA, Buenos Aires, Argentina

Article Outline

Glossary
Definition of the Subject
Introduction
Ecophysiological Basis of Response to Crop Structure
Crop Structure Responses in Monocultures
Crop Structure Responses in Polycultures
Future Directions
Bibliography

Glossary

Competition Refers to the process whereby plants share resources (e.g., mineral nutrients, water, and light) which are in insufficient supply for their joint requirements [71].

Crop structure Refers to the spatial, temporal, and genetic arrangement of a particular crop species or genotype within a sown area.

Density Is the number of individuals of a plant species in a unit of area within a crop.

Facilitation Is the process whereby one crop species provides some sort of benefit for another species when in a polyculture. Usually, when facilitation occurs, at least one crop may positively alter the environment for the other crop [77].

Policulture (also intercrop) Refers to crop arrangements that include more than one crop species or genotypes grown together partially or totally during the growth period of a particular area.

Potential yield Is the crop yield obtained when available resource use is maximized in a particular environmental condition and limiting factors, such as soil nutrients, or reduction factors, such as insect and plant pests and diseases, are absent [41, 78].

Rectangularity Is a measure used to describe the spatial distribution of individual plants in crops sown in rows. It is the ratio of the mean distance between rows and the distance between individual plants within a row.

Resource complementarity Is a measure of the extent to which the crop species components in a polyculture share common limiting resources, i.e., plant components in a crop that show complete resource complementarity do not compete [71].

Spatial arrangement Refers to the way that crop plants are distributed in a field. For example, they may be randomly distributed, when seeds or propagules are randomly broadcast or they may be sown in rows, in a regular pattern when drillers are used.

Definition of the Subject

Crop yields mostly depend on the growth rate experienced by the plant during particular critical periods. The amount of the resources captured and the resource use efficiency determine the growth rate of the crop plants at those crucial stages for yield determination. Since plants stand still in the land, the way they are distributed greatly influence the ability of a crop to capture and use environmental resources (radiation, water, and nutrients), which are necessary for growth and yield. The spatial arrangement of plants and the temporal development of their structures (mainly leaves and roots) define the crop structure. Crop structure may be then analyzed and described in many ways. However, most effort has been concentrated on describing the size and distribution of leaves, which capture the radiant energy, since they are aboveground and easy to measure. The study of yield response to crop structure has conformed to the scientific basis for important technical management decisions and technologies involving crop density, and distance between rows and rectangularity in both mono- and polycultures in various agricultural systems of the world. Crop structure, as a research topic, is one of the few examples in which science dynamically contributes to develop crop management strategies and to guide genetic improvement among crop species. At present, the manipulation of crop structure is not only explored in controlled, semi-controlled, and field research experiments, but also in mathematical modeling, which evidences the complexity of the interactions that need to be explored and, at the same time, the maturity of the knowledge reached in this area.

Introduction

Crop structure is one of the major determinants of the ability of a crop to capture resources and to produce high yields. It has received much attention from producers, agronomists, and researchers because it is under fairly close control by the farmer in most crop systems of the world. Crop structure is a complex crop attribute, determined by the crop genotype, its sowing date, density (i.e., the number of plants per unit area), and the spatial plant arrangement. Therefore, crop structure in general has a genetic, temporal, and spatial component. However, the spatial component determined by the plant density and spatial arrangement of the plants are largely considered the main modifier of crop resource capture and use and, therefore, a strong determinant of crop yield. For this reason, just for simplicity, in this entry, attention will be centered on the spatial structure of crops, since it would be very difficult to cover all the effects and interactions from other factors, such as temporal ones, in a single entry.

The structural component of a crop may be seen as determining its potential yield in any particular region. Decisions affecting the structure of the crop and so its ability to capture light and other resources may modify the potential yield of the crop. The potential yield is the yield attainable by the crop when its growth is only limited by the radiation and carbon dioxide available, and so is only affected by the temperature of the site and the crop structure. Crop structure factors may directly (for example, in the case of density) or

indirectly (for example, in the case of the genotype sown, due to its length or appropriate sowing date) modify the potential yield of a crop. Although actual (real) yields harvested may usually be lower than potential yields due to the effect of limiting (i.e., water or nutrients) and reducing (i.e., diseases, pests, and weeds) factors [78], the interaction of crop structure with environment and other crop management decisions are crucial to produce high yields efficiently.

Most crops in mechanized agriculture are sown in monocultures, i.e., single-species stands are grown every growing period in the same region. However, in most subsistence and few mechanized modern agricultural systems, crops are sown in polycultures, i.e., more than one species are grown in the same area during each growing period. Crop structure characteristics are crucial in determining crop yield responses both in single species and polycultures. Usually, the interest was concentrated in defining the relationships between density and crop yield quantitatively in order to establish optimum crop populations and maximum attainable yields under various situations. As a result, the effect of density on crop productivity in mono- and polycultures has been deeply studied since mid last century [22, 34, 82]. However, due to the high contribution of single-species crops to grain crop production, the study of spatial crop structure determinants has called the attention of researchers all over the world, particularly under this modern and technologically advanced crop production system.

Crops in monocultures are usually heavily selected for uniformity so that most individuals are genetically and phenotypically similar or even identical because of the uniformity of seed size and the fact that sown seeds tend to germinate synchronously. In such crops stands, intraspecific competition (competition between plants of the same species) may be intense and is largely the process commanding crop responses and yield. When in polycultures, intra- and interspecific competition together with resource complementarities or facilitation processes determines yield of each crop species in the stand. For most of the modern agricultural systems, plant competition is therefore the ecological process largely determining the yield response to spatial crop structure arrangements.

Crop density largely determines interplant competition causing a reduction in survival, dry-matter growth, and grain yield of individual plants. Despite the fact that interplant competition causes a negative effect in the individual plants, the management of crop competition through density selection may allow maximum yields per unit area to be achieved. Identifying and understanding crops yield-density response allow researchers to predict the effect of crop management practices on yield and help farmers, agronomists, and consultants to properly design crop production structure under various ecological conditions. Spatial arrangement also determines not only interplant competition at any density (since it may modify the competition between plants within a row with respect to plants in different rows) but also resource use efficiency. Therefore, crop-plants arrangement or crop structure affects intraspecific competition and resource use efficiency, allowing a full or partial use of available resources and how they are transformed during the various stages of crop growth. In this entry, I will discuss how density and spatial arrangement affects crop functioning and how some environmental conditions or crop management decisions may affect those relationships. Most of the information comes from crops in monocultures, but the performance of these spatial components of crop structure in polycultures will be also briefly addressed.

Ecophysiological Basis of Response to Crop Structure

Resource Use and Dry-Matter Production

Crop dry-matter production under potential conditions is determined by the intercepted solar radiation and the radiation use efficiency of the crop canopy. From both aspects, crop density mainly affects the ability of the crop to intercept radiation (or to capture the light resource, from an ecological perspective) since there is little evidence on the effects of density on resource use efficiency. However, spatial arrangement may modify both the capture and use efficiency of resources [42, 83].

It is known that much of the incident solar radiation is not available for annual crop species growth during the early stages, due to the fact that low leaf area expansion determines low light interception. At early crop stages, increasing density may contribute to increase Leaf Area Index (LAI) of the crop (i.e., the

green leaf surface per unit of area) and the amount of light intercepted. For this reason, there is a strong positive, although nonlinear, relationship between density, LAI, and the proportion of the incident light that is intercepted in early stages of crop development. When the crop grows, light resource capture increases as leaves expand and LAI increases, and a nonlinear relationship establishes among both variables. Although density may modify the number of leaves, particularly at early crop stages, the relationship between density and leaf area becomes weak when the crop advances in its development. Improving plants spatial distribution (for example, by changing the distance between rows) may also help to intercept more light at early stages of crop growth, when Leaf Area Index (LAI) values are low. To illustrate these points, early results from Puckridge and Donald in wheat [56] clearly showed that density manipulation in the range 1.4–1078 pl/m^2 could successfully increase light interception of wheat crops under the Western Australia conditions. The greater proportion of intercepted light in high-density crops explained most of the differences in early crop growth rates calculated from the results of that research; i.e., early crop growth rates were greater in crops sown at the higher densities. Similar results were also obtained with other crops, such as those reported in recent experiments for maize (e.g., [79], soybean, and sunflower [76]. There are experimental evidences that increasing density not only improve light capture early in the season but also the uptake of soil resources such as water [75]). For example, in a Mediterranean environment, high crop-sowing densities contributed to reduce soil evaporation and to increase biomass production and water use in the early phases of wheat growth [16].

During the early stages of development, competition among small crop plants may be evident only at very high densities; therefore, young individual plants tend to have similar dry-matter production, while crop productivity per unit area tends to increase linearly with density. Plotting the logarithm of plant dry matter against the logarithm of density as suggested by Kira et al. [39] helps to show the way individual plants and crops would tend to respond as they grow (Fig. 1). It is clear from the figure that, as time goes by and crop development progresses, plants increase in size and leaf area, and the onset of competition is evident even at low densities; i.e., individual plant size is continuously reduced as density increases above a density threshold (Fig. 1, see arrows). As plant size increases, crop growth rate may depend more on resource availability than on plant density; therefore, crop growth rates may be only influenced by density if plant number is below the competition threshold. This density threshold varies according to the crop or genotype characteristics and the environmental conditions.

For any crop, when crop stands are above the threshold density, LAI tends to allow full light interception and use of the available resources; therefore, crop growth rate will be maximum for the set of environmental conditions explored by the crop. At this stage, any crop density above the competition threshold (Fig. 1) would maximize crop growth rate per unit area. Sustaining maximum crop growth rates is important for high yields to be obtained, especially when that occurs during the critical period for yield determination of the crop.

The phenological period that is critical for yield determination varies among species; i.e., the period when reductions in crop growth rate significantly reduce grain number or yield depends on the species considered. For example, for wheat, it extends from the

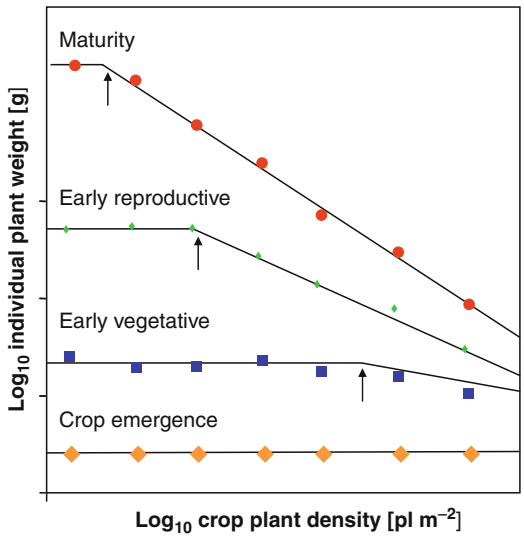

Spatial Crop Structure in Agricultural Systems. Figure 1 Influence of density on individual plant weight at various stages of crop development, following Kira et al. [39] proposal. *Arrows* indicate competition thresholds at the various crop stages (see text for details)

beginning of ear growth to the beginning of grain growth [29, 68], but for maize, it is considered to be centered 15 days before and after crop silking [3]. High crop yield per unit area would then be expected when crop structure, density, and plant arrangement have been suitable for the crop to reach 95% light interception, which allows maximum crop growth rate when non-limiting or reduction factors are present, before the beginning of the critical period and during it. Environmental and management practices such as fertilizer application or disease control could alter the crop yield-density response, altering the density above which crop growth rate is maximum.

In general, crop structures are aimed to use above- and belowground resources completely, allowing the crop to maximize its growth rate during critical stages. However, it has to be mentioned that increasing early resource capture through great plant densities may not necessarily maximize growth rate at critical crop stages. For example, large quantities of water use by a crop in the early phases of growth may reduce soil-water availability late in the season, leading to biomass yields similar to those obtained with lower plant densities [20, 51]. In temperate subhumid areas, this pattern of crop water use may led to reduce crop sowing rates, as in wheat in the southern pampas of Argentina [32] or the semiarid Brown soil zone of Canada during dry years [45].

Due to the relationship described in Fig. 1, the total shoot weight of a crop per unit area of land usually increases asymptotically as density increases (Fig. 2). Therefore, the performance of crops sown at low densities may depend on their ability to compensate for low plant populations by producing more tillers, branches of bigger leaves. Tillers offer vegetative plasticity in the case of barley or wheat, while branches do so in the case of soybean. Crops that do not produce tillers or branches may express some vegetative plasticity by altering leaf size or height as in the case of maize or sunflower. Moreover, in some crops, the dry-matter asymptote in Fig. 2 extends over a wide range of densities, due mainly to the large plasticity of individual plant size which determines that mean plant weight declines to exactly compensate for increases in density; i.e., proportionate reductions in plant weight occur as densities increase above the normal sown density [22, 35, 69]. Examples of such phenotypic plasticity

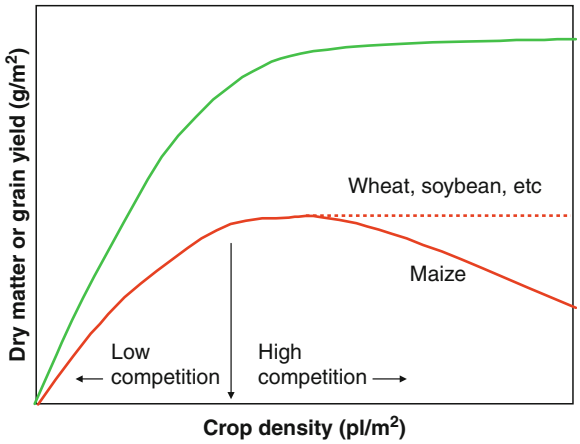

Spatial Crop Structure in Agricultural Systems. Figure 2 Influence of density on crop dry matter (*green line*) and grain yield (*red line*). Low and high competition range is indicated, together with the expected response of yield to density in maize (*solid red*) and wheat or soybean (*dotted red*)

may be found in crop species, such as wheat, soybean, or barley. Forty-fold differences in plant weight have been reported to occur between widely spaced wheat plants and plants growing in stands at normal seed rates [9, 56].

The supply of limiting resources and the genetic ability to capture and use them largely determine the maximum total biomass yield per unit area of any particular crop in a particular environment [82]. Environmental factors such as temperature or daylength, which may affect the length of the growing season, can also affect maximum shoot weight (Potential yield) by modifying the ability of the crop to capture resources. For example, in the case of wheat, a crop with large vegetative plasticity (see Fig. 2), long days at high latitudes reduce wheat tillering, which determines that sowing rates of 500–700 pl/m^2 are commonly used for spring wheat crops in places such as Finland [55] in contrast with the 200–300 pl/m^2 used in temperate areas. In some cases, the relationship between density and total shoot weight per unit area is better described by a parabolic model; i.e., there is a distinct maximum yield at a particular density, and shoot yield declines as density increases above this point. In these cases, it is expected that crowding reduces the efficiency of the crop to capture or use environmental resources [22].

Grain Yield Production

Grain yield increases as density increase up to a value which determines maximum use of available resources (i.e., at suboptimal densities). However, performance of yield at supraoptimal densities may vary among species. It has generally been accepted that the response to density of harvest or storage organs (e.g., grains) is better described by a parabolic model [35]; i.e., grain yield decreases at higher or supraoptimal plant densities due to the fact that the allocation of resources to storage organs or grains is greatly altered by competition [34]. In general, the proportion of the total biomass allocated in the grains, i.e., harvest index (HI), declines progressively with increasing density [23]. Despite the fact that parabolic responses are generally accepted for grain yield–density relationships, some studies indicate that yield–density relationships for grain may sometimes be better described by asymptotic models (e.g., [38, 43]). In this case, the range of densities that maximize grain yield could be wide and strongly dependent upon crop genotype and environmental characteristics.

When crop plants are under severe competition due to relatively high crop densities, they show a reduction in individual growth rate. This will markedly affect grain number determination of any grain crop, particularly if the per plant low growth rates occur during its critical period. Therefore, shoot growth may become less affected than grain yield, causing a reduction in harvest index. Crops such as maize, with low reproductive plasticity, may experience severe grain yield reductions at high crop densities, mainly under limiting environments, such as with low water availability. Grain yield reductions at supraoptimal densities depend on how crops determine yield. In most grain crops, the number of grains per plant, firstly, and per unit area, lately, is strongly related to yield. However, the relationship differs between crop species (Fig. 3).

In the case of maize and sunflower, a minimum plant growth rate is necessary to fix grains, and the relationship is not linear, while in the case of soybean or wheat, it is linear, and the minimum plant growth rate necessary to fix grains is very close to zero (Fig. 3; [5, 79]). It is clear from much data that the number of grains fixed per unit area is the main factor controlling the grain yield-density response of grain crops and, since number of grains determination varies between species, density rules and decisions have to be carefully explored in any particular case. In high-yielding environments or cropping systems (i.e., with irrigation and high fertilizer rates), it appears that large plant populations will determine large number of grains per unit area and high yields.

Low seeding rates or low crop stands may be compensated by the contribution of tillers or branches. Therefore, in low-density crops, either tillering, branching, or the reproductive plasticity of the species is an essential component in determining the number of grains per unit area at harvest. However, tillering and branching have been recognized as complex phenomenon, controlled by endogenous (genetically) and environmental factors [60]. It has been accepted that a large

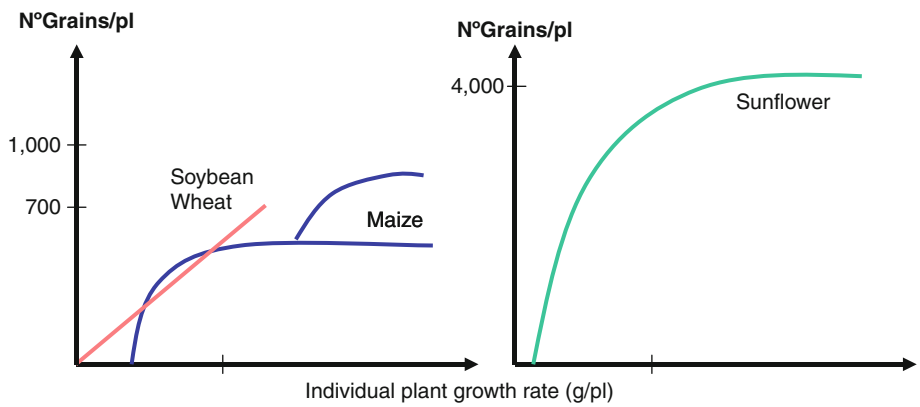

Spatial Crop Structure in Agricultural Systems. Figure 3
Expected relationship between the individual grain number and growth rate of four grain crops

number of tillers or branches are produced by plants when the availability of resources is high. However, recent studies have found that light quality may affect tiller or branch responses. Light composition with low Red/Far Red ratio in a crop canopy reduces tillering or branching of individual plants [13]. These results indicate that, within a wide range of resource availability, photomorphogenic reactions mediated by light quality may also affect responses to various crop structures. Therefore, density and plant arrangement responses will ultimately be the result of the interaction between resource-based and non-resource-based environmental signals.

High density in crops may produce adverse agronomic effects, such as lodging or higher susceptibility to pest or disease damage. Although different plant densities may have little effect on carbon photoassimilation in top plant structures, including reproductive structures, high densities may tend to reduce partitioning to the stem internodes and to increase leaf senescence among other effects [61, 80, 81]. For example, when stems export photoassimilates due to high competition pressure by crop plants, the rate of leaf senescence is increased and basal nodes weaken, which contributes to increase lodge susceptibility and to reduce grain yields under high sowing rates.

Crop Structure Responses in Monocultures

The Effect of Soil Resources

As mentioned above, the supply of limiting resources, i.e., water, light, and nutrients may affect the form and parameters of the biomass and yield–density relationships, largely through their effect on the maximum yield per unit area that can be achieved at very high densities. Resources have little effect on the yield of widely spaced plants, i.e., yield per plant at very low densities, since in that case, biomass and yield productivity is limited by the possibility to capture resources due to the low-density crop structure. For example, nitrogen fertilizer applications tended to increase maximum wheat yields per unit area under field conditions, but only slightly affect the maximum yield per plant when plants were sown widely spaced [9]. However, in most agricultural conditions, the response to density is dependent upon the supply of limiting resources since it is competition for limiting resources the driving process in crop stands. Generally, increasing the availability of soil resources through fertilizer applications (nutrients) of irrigation (water) will relax or reduce the interplant competition so that the environment may support a higher number of plants. This will be so if the addition of a limiting factor does not affect the competition or availability of other competition factor; i.e., increasing the availability of soil resources, such as water or nitrogen, may reduce competition for soil factors, but it may increase competition for aboveground resources, such as light [22].

Nitrogen, a major soil limiting factor, strongly interacts with density in most grain crop species [70]. The optimum density and, therefore, the maximum grain yield tend to be greater by increasing nitrogen applications if nitrogen is a yield limiting factor. For example, optimum maize crop density tends to be higher as nitrogen [47, 49] or water [3] availability increases. When supplies of the major limiting resource (either water or nitrogen) are made, the crop system might be enabled to sustain a higher crop density and hence a greater grain yield. Since individual plant growth is reduced as density increases within the range of crop densities that allow maximum grain yields, the overall demand of growth resources per unit of area will tend to be similar; therefore, the nitrogen application rate or water provision required will tend to be similar between the lowest and highest density that allow maximum yields [59].

Nitrogen or water availability have a great impact on early vegetative growth by promoting plant tillering or branching, or by increasing leaf area and its activity; However, while this increases the shoot weight of the crop plants in most species, it may reduce the harvest index, particularly at high crop density (see above) if resources during the critical period of yield determination are scarce.

Crop species and genotypes within species may present different responses to density at various soil resource conditions. Differences are usually associated to the way resources are partitioned between vegetative and reproductive structures within the plant, to the ability to produce tillers or branches, and to the morphological and geometrical characteristics of their canopies. Sowing date and plant arrangements may modify the performance of the plants under various crop structures by altering the phenotypic plasticity of the crops.

The Effect of Plant Arrangement

Among the management factors that determine crop structure and that may affect crop yield–density relationships, the planting arrangement of the crop is the most important. Plant spatial arrangement, usually the distance between rows, is under close control by farmers. At any given crop density, sowing patterns can be considered random, clumped, or regular; extensive and mechanized grain crops are normally sown in rows, i.e., in a clumped arrangement, although in some cases regular patterns may be found. Historically, planting arrangement in a crop was determined to allow mechanical weed control or other labor, i.e., to let the tractor, the animal, and the tool to do its labor on the weeds between rows of the crop. However, in various parts of the world, herbicide technology and the tolerance of modern genotypes to herbicides have allowed modifying planting arrangements since no secondary, mechanical weed control labors are necessary. The planting arrangement of crops is often described by its "rectangularity," i.e., the ratio of the distance between rows to the distance between plants within a row. In general, crop yield tends to be the greatest, at any density, if the plants are arranged regularly, i.e., the rectangularity is 1 [10, 30, 33, 36, 53]. However, the effect of planting arrangement is often not significant if densities are at or above those required to achieve maximum use of resources and yield [3, 10, 50]. The extent to which rectangularity affects the yield of a crop is dependent on the plasticity of the individual plants of any particular genotype, variety, or hybrid and the environmental conditions. Grain crops yield patterns are not consistent through literature when rectangularity is analyzed. In maize crop, [17] found that contrasting crop genotypes regularly sown in narrow rows (38 cm between rows) produced significant higher yields than crops in a more rectangular pattern (70 cm between rows) in 2 years. They observed that crop growth rate was higher early, and light interception was greater at the critical period of maize (flowering) when crops were sown regularly spaced. However, Cirilo [20] found no significant differences between maize crops sown at 52 vs 70 cm between rows, since at the critical period of yield determination (see above), crop growth rate was similar among cropping patterns. Similarly, in the case of wheat crops, Holliday [36] reported yield increases between 8% and 33% due to reducing row spacing from 20 to 10 cm. In the case of wheat crop, most research worldwide has shown that closer row spacing (15–18 cm) gave higher grain yields than wider row spacing (usually greater than 23 cm; [32, 54, 73, 52]), though a few experiments showed that wider row spacing did not result in wheat yield losses [40]. Differences in cycle length among varieties or sowing dates may help to explain such results, as in the case of soybean in the Southern Pampas. When long-cycle soybean varieties are sown, no yield differences between various row widths may be found (i.e., 52 vs 35 cm between rows). However, when short-cycle soybean varieties are sown, yields tend to increase consistently as distance between rows is reduced. Similarly, consistent yield increases are found when soybean varieties are sown late in the season at narrow rows, while no differences may be found, particularly in long cycle varieties, at optimum sowing dates among various row distances.

Planting arrangement may be used in crops to overcome water plant stress. For example, in the case of wheat, in some subhumid areas with late water stress periods, wide cropping patterns (for example, 52 cm between rows) proved to be more stable and productive than narrow ones, mainly due to a better water use efficiency in those environments. This sowing pattern is presently used in the low-producing areas of the Northwest of Argentina under a monsoonal climate. However, also in wheat crops, several experiments reported that there was a consistent yield depression at low sowing rates as rectangularity was increased [10, 26]. In some other cases, wheat crop yields per unit area gradually declined as rectangularity increases either by increasing plant density or increasing row width, though yield declines at high density were greater than at low-density crops [82]. When crops have enough phenotypic and reproductive plasticity, results are consistent in showing that there are better possibilities to equal high-density crop yields if low-density crops are sown in a square pattern; i.e., a better plant spatial distribution may promote grain yield advantages when crops are sown at low density rather than at high density.

The reported evidence suggests that any advantage derived from spatial arrangement is brought about by improving crops ability to exploit available

resources (e.g., [84]). Low rectangularity crops increase yield due to the its effect on (1) improving the capture of incident radiation, particularly in early crop stages; (2) allowing the crop to reach 95% light interception during the critical period of yield determination (see above and [4]); (3) improving resource use efficiency, for example, water use efficiency by reducing water-soil losses through direct evaporation; and (4) improving weed control or reducing weed competition. Therefore, it may be also inferred that positive effects of improving plant arrangement by reducing rectangularity is particularly important when productive conditions may reduce plant growth due to limiting factors (i.e., low-resource availability, late sown crops under short growth periods, short cycle varieties, etc.) and when environmental or management conditions may affect crop resource capture during the critical periods.

Rectangular, more clumped, arrangements possibly cause an early reduction of crop growth rate, which in some cases may delayed or even avoid use of distant resources. On the other hand, as mentioned above, reducing the distance between rows and rectangularity and increasing plant density contributes to rapidly exploit resources by intercepting more light or capturing more water or soil resources which in most crops enhance the competitiveness of the crops against weeds [8, 31, 58, 65, 66, 72]. For example, Solie et al. [72] concluded that wheat yield increases of 18% could be obtained when row spacing was reduced from 23 to 7.5 cm when cheat (Bromus secalinus)-free and cheat-infested fields were evaluated. Similarly, [14]found that weed yield reduction was lower when soybean crops were sown at narrow rows than when they were sown widely spaced. Conversely, weed production increases with increasing weed density, or by increasing crop rectangularity or by reducing crop density. For example, Felton [28] found that increasing the row spacing in soybeans from 50 to 100 cm increased weed yield 3.5 times.

Mathematical Relationships Between Plant Yield and Density

Since density is a main determinant of crop structure responses, mathematical models have been proposed for interpreting and predicting the effect of density on yield. Interest in quantitative relationships between crop yield and density was largely stimulated by the need to clearly define optimum sowing densities for crop production. Such relationships should, ideally, take account of environmental factors, such as limiting resources, or spatial arrangement (rectangularity) which may affect the response to density. Willey & Heath [82], Mead [46], and Ratkowsky [57] among others made a comprehensive review of the various models used to describe yield–density relationships pointing out the advantages and disadvantages of the various mathematical functions proposed. Several types of equations have been described, but only the so-called reciprocal equations for yield per plant have proved to be satisfactory for a wide range of crops and conditions. Some forms of the reciprocal equation that have been proposed are:

$$\text{Yield} = \text{density}/(a + b^{*}\text{density}) \quad (1)$$

In Eq. 1, yield is the shoot or grain yield per unit area and density is number of crop plants per unit area, and “a” and “b” are parameters of the equation. This is the simplest equation and describes only the asymptotic model; i.e., yield increases asymptotically toward a maximum yield as density increases. A basic form of Eq. 1 was first proposed by Shinozaki and Kira [69], and its beauty relies on the fact that parameters (“a” & “b”) have biological meaning [82]. In this equation, parameter “a” is the reciprocal of the yield per plant (w^{-1}) when a crop genotype is sown at an infinitely low density, i.e., it is an estimation of the yield of wide-spaced plants, in competition-free conditions. This may be regarded as a measure of the “genetic potential” of individual plants of the crop. The fitted value of “a” indeed largely depends on the genetic characteristics of a particular genotype. If the yield–density relationship is truly asymptotic, parameter “b” is inversely related to the value of the asymptote, i.e., the maximum yield per unit area at very high densities; Willey & Heath [82] regarded this parameter as a measure of the “environmental potential,” i.e., as an estimator of the maximum crop yield that can be attained in a particular environment and crop production system.

Other reciprocal equations incorporate a third parameter so that they can also describe parabolic yield–density relationships, i.e., the possibility of a

reduction of shoot or grain yield at high densities. For example, Holliday [35] proposed the expression:

$$\text{Yield} = \text{density}/\left(a + b^{*}\text{density} + c^{*}\text{density}^{2}\right) \quad (2)$$

In Eq. 2, the quadratic term accounts for parabolic relationships; if the parameter "c" is equal to 0.0, then the equation reduces to that of Shinozaki & Kira [69]. Similarly, Farazdaghi and Harris [25] proposed the expression:

$$\text{Yield} = \text{density}/(a + b^{*}\text{density}^{z}) \quad (3)$$

Like in Eq. 2, this becomes identical to Eq. 1 when $z = 1$.

In spite of the good fit provided in several cases by these mathematical approaches [57], the reciprocal equations have some statistical limitations. However, novel statistical techniques, using data transformation and nonlinear procedures, have improved the statistical treatment of these models [57].

For modeling purposes, the response of crops to plant density should be also defined in terms of the spatial arrangement of the plants. Few researchers have intended to distinguish between density and plant arrangement (rectangularity) when modelling crop response, since usually responses to different densities have been studied at a constant row width. Although the extent to which spatial arrangement may affect the yield of crops is strongly dependent on the plasticity of the genotype [82] and the availability of environmental resources (see above), it appears to be important to consider the effect of rectangularity on the yield-density equations, particularly when crops may be sown at various densities and distances between rows. In these cases, equations should be able to describe the effects of density as well as those of rectangularity. For this purpose, it has been proposed to include intrarow and interrow spacing (rectangularity) as variables in Eqs. 1–3 [82]. However, there has been insufficient research on the effect of rectangularity on yield-density responses, and the yield-density-arrangement equations have been only tested on wheat and maize crops in few cases. Recently, Satorre [64] suggested that optimum density decreases as rectangularity increases in maize crops sown at 53, 104, and 157 cm between rows (Fig. 4). Moreover, and more important, the authors found that the magnitude of the yield increase obtained due to improving plant arrangement, by

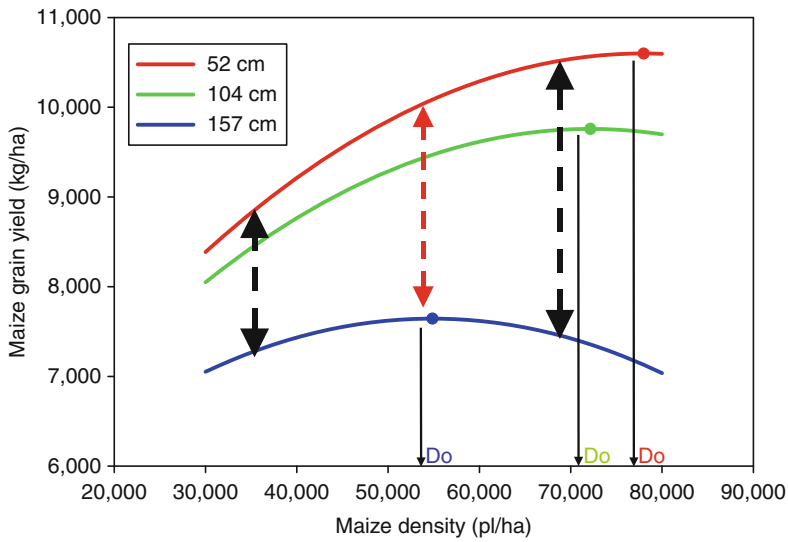

Spatial Crop Structure in Agricultural Systems. Figure 4
Yield density response in maize crops sown at 52, 104, 157 cm between rows. Optimum density (Do) at each planting arrangement is indicated by solid vertical rows. Optimum density (Do) decreases 214 plants/ha for every centimeter of increase in the distance between rows above 52 cm. Nonsolid vertical *arrows* indicate the magnitude of resource reduction found between extreme plant arrangements due to plant rectangularity increment

reducing rectangularity or the distance between rows, was greater in high-yielding environments than in low yielding, since vegetative growth at early crop stages was unaffected.

The reciprocal equations have proved to be robust and provide a tool to describe asymptotic or parabolic yield–density relationships. However, despite these efforts to describe the effect of crop structure on crop yield, there is still a huge work to be done since, also for modeling purposes, the response of crops to plant density should be also defined in terms of the planting arrangement and management, and environmental conditions that may modify them. In this case, the effect of environmental conditions on the performance of the yield-density model parameters also needs to be described.

Crop Structure Responses in Polycultures

Crops, in developed countries, are normally grown in single-species stands or monocultures. As was discussed above, in such crop structures, there is little or no interspecific competition, but usually intense intraspecific competition. However, in the tropics and at present in some temperate areas, mixed crops are very common [7]. The concept of mixed crop or polycultures refers to the practice of growing more than one specie or genotype in the same land at the same time [6]. In such polycultures, competition occurs between plants of different species or genotypes, as well as between plants of a single genotype. In this general concept, the space and time component of the mixture allows the recognition of a whole gradient of intensity of interactions among component crops. For example, crops may be sown in sequence, i.e., a second crop is sown in the growing period immediately after a first crop is harvested, or partially or totally overlapped (i.e., two or more crops are sown and grown simultaneously in the same field). Similarly, crops may be sown in strips or in alternate rows. As the overlap of time or space between individuals of the various crop species increases, the opportunity to capture positive interactions among crop components also increases if they complement or facilitate the use of environmental resources. By this means, mixed crops or polycultures have showed some evidence of greater yield, greater stability of yield, and lower pest and disease damage than monocultures [1, 2]. Particularly, mixes of legumes and non-legumes species have shown greater yield when sown together than when they are sown alone [74].

Mixed crops are far less common in temperate areas under mechanized agricultural systems than in tropical subsistence farming [37]. However, recent biotechnological advances which helped to improve weed control with the use of previously nonselective herbicides in crops such as soybean, maize, and sunflower has opened new alternatives for the development of polycultures in extensive grain crops. For example, this increasing interest in exploring the performance of mixtures of cultivars and species in modern, mechanized grain-cropping systems has been slowly expanding in some regions of the Pampas. In the Argentinean Pampas, one of the most productive areas of the world, mixed grain crops may be found in various patterns depending on the component crops species, the degree of temporal overlap among species, and on the spatial arrangement and relative density of the plants [62, 85].

Within the concept of polycultures, successive crops is defined when two or more species are grown in the same land in the same cropping or calendar year but without any overlapping; i.e., a second crop is sown immediately after harvesting the previous crop. In this plant arrangement, the use of resources is intensified per unit of time when compared to a single crop per year, but the interaction between crop species is reduced to the interference produced by the use of resources by one species on the resources available to the following crop [6]. As mentioned before, in the Pampas, nearly three million hectares are sown every year in a successive crops planting pattern. Wheat/double-cropped soybean, maize, or sorghum, and Barley/double-cropped soybean are examples of such extensive crops planting arrangements. In such systems, wheat crop structure (variety, density, distance between rows, and sowing dates) remains unaffected, while the soybean structure is usually modified by reducing the distance between rows and by increasing the plant density [11, 19, 67]. Wheat/double-cropped soybean, the more extensively used successive multiple-crop pattern, has proved to be more productive in terms of total yield and income per hectare and less variable than either sole wheat or sole soybean crops in the same unit of land.

As previously mentioned, the term intercrop is applied when two or more species or genotypes are grown simultaneously during part or the whole crop growing period in the same land. Intercrops are also used in the Pampas in a wheat/soybean mixture when the soybean growing period left by the wheat is short enough to affect its productivity, i.e., the yield of the second crop. In the case of such intercrops, the wheat (winter crop) and the soybean (summer crop) crop structures are both modified. The soybean is sown in spaces previously unsown with wheat, usually after wheat flowering and well before it is harvested. In wheat/soybean intercrop, wheat crop is sown in rows widely apart (for example, at 52 cm between rows) or in a variable spatial pattern, some rows are left unsown, and others follow the usual planting pattern for the region (i.e., 17.5 or 19 cm between rows; see Pictures 1 and 2). In intercrops, the soybean varieties are frequently sown at 52, 38, 35, or 19 cm between rows. Therefore, one row of wheat remains unsown in every three rows when at 17 cm between rows (i.e., 66% wheat, 100% soybean), or 1 every other row is sown when the wheat is at 19 cm between rows (i.e., 50% wheat, 100% soybean). Since the wheat plants tend to compensate with a higher vegetative and reproductive growth in the absence of crop plants, wheat yield is reduced by only 20–25% when compared to 100% monocultures (e.g., [24]). Successive and partially overlapped winter–summer intercrops increase the radiation use efficiency [86] and the weed and soil erosion control. However, it increases management complexities and requires well-trained people to conduct mechanized operations.

More recently, summer–summer crop species intercrops have been also evaluated in mechanized temperate agriculture. Intercrops of soybean in maize crops or soybean in sunflower crops have been evaluated at commercial fields in various regions of the Pampas in Argentina [18, 19]. The release of transgenic glyphosate-resistant soybean and maize has been crucial to explore this planting arrangement at commercial fields. Similarly, biotechnology and the release of imidazolinone resistant sunflower have been crucial to explore sunflower–soybean intercrops. A less complex

Spatial Crop Structure in Agricultural Systems. Picture 1
Interplanting soybean in a wheat crop

Spatial Crop Structure in Agricultural Systems. Picture 2
Harvesting wheat in a wheat/soybean intercrop. See soybean plants growing in the harvested crop

intercrop may be obtained when each crop species is sown in wide strips in the field. Some yield and pest control advantages have been reported in maize–soybean strip patterns, although they are dependent on the width of the strip and its orientation, among other factors [48]. It is well documented that yield advantages (greater grain yield and yield stability) were often found when, particularly, grass and legume crops were mixed [74] mainly due to the complementary use of belowground resources. In such cases, it has been proposed that legume plants may use both soil and atmospheric nitrogen, while grass species may only use soil nitrogen; in such circumstances, both species complementary use nitrogen. However, it has also been proposed that in some cases, atmospheric nitrogen previously fixed by the legume species may be transferred to the belowground environment of the grass species. In such cases, growth of grasses in the presence of legumes tends to be greater than when they are alone. In this case, facilitation tends to be the dominant process. It has been also found that the incidence of pest and diseases have sometimes been reduced when species or genotypes are grown in mixtures [12, 27, 77]. Such advantages may support the interest and promote the increase of area sown with more complex crop structures.

Future Directions

Attaining high yields per unit area requires that individual crop plants may usually experiences a competitive stress. Therefore, highly productive crops depend on crop structure by controlling the amount of resources used and their use efficiency which will determine the extent of competition experienced by the crop plants. In this respect, the discussion in this entry has deliberately concentrated on the effect of density and plant arrangement on crop growth and yield determination, and it has avoided any discussion on the effect of crop structure on the mortality of plants since this hardly occurs, at least as a density dependant process, in most crop production conditions. Interpreting the response of crops to crop structure from an ecophysiological and ecological approach was aimed to help construct a framework in which the temporal and spatial aspects of crop structure may be understood. Plant

functional responses, determining individual species' requirements and critical periods for yield determination, and competitive interactions are responsible of the effects of density and plant arrangement on yield under various environments and crop management situations. The conceptual framework built may provide a rationale for predicting and manipulating crop structure under various conditions since modifying crop structure (density, plant arrangement, genotype) may be seen as a way to change crop spatial and temporal structure and, by this means, the use of crop resources. Although high densities for any particular environment should provide a greater use of early available environmental resources, yield-density responses still rely strongly on the way resources are used during the critical periods of yield components determination of the various crops. Taking this into account, density or plant arrangement manipulation should be effective only when it assures that the crop must be able to achieve high plant growth rates during those periods. Moreover, since genetic improvement has successfully widened the adaptation of crop species and genotypes to various production conditions, genotype specific interactions and characteristics need to be individually considered within the framework presented here to develop effective crop structures.

Although interspecific plant interactions, such as crop–weed interactions, are frequent in extensive grain crops. Polycultures increase the complexity of crop structures by adding the influence of crop plant–crop plant interactions and new crop management complexities to the result of the cropping system. Analysis of the "ecological combining ability" of crop species and genotypes in modern agriculture opens a whole new world to explore more productive and sustainable cropping practices, partially resembling the complexity and functioning of natural systems. The evaluation of the yield advantages of mixtures or polycultures compare to pure-stand yields or monocultures is also crucial. It has for long been based upon the absolute or relative yield differences between mixtures and polycultures [34, 44], but other criteria including resource use efficiency and environment health will surely need to be considered. In any case, the design and management of crop structure remains one, perhaps the most, important decision that farmers and agronomists face every time they plan to grow a grain crop.

Bibliography

Primary Literature

1. Alexander HL, Roelfs AP, Cobbs G (1986) Effects of disease and plant competition on yield in monocultures and mixtures of two wheat cultivars. Plant Pathol 35:457–465
2. Allard RW, Adams J (1969) Population studies in predominantly self-pollinating species. XIII Intergenotypic competition and population structure in barley and wheat. The American Naturalist 103:621–645
3. Andrade F, Cirilo A, Uhart S, Otegui M (1996) Ecofisiología del cultivo de maíz. Editorial La Barrosa & Dekalb Press, Argentina
4. Andrade FH, Calviño P, Cirilo A, Barbieri P (2002) Yield responses to narrow rows depends on increased radiation interception. Agron J 94:975–980
5. Andrade HF, Otegui ME, Vega C (2000) Intercepted radiation at flowering and kernel number in maize. Agron J 92:92–97
6. Andrews DJ, Kassam AH (1976) Importance of multiple cropping in increasing world food supplies. In: Sánchez A, Triplett GB (eds) Multiple cropping. American Society of Agronomy (ASA) Spec. Pub. 27, Madison, pp 1–10
7. Francis CA (1986) Multiple cropping: practices and potentials. Macmillan, New York
8. Arias S, Satorre EH (1991) Competencia entre trigo (*Triticum aestivum*) y Brassica sp. El efecto de la densidad del cultivo y la maleza sobre el rendimiento de grano. Actas de la XII Reunión Argentina sobre la maleza y su control (Mar del Plata, Argentina) 2:5–10
9. Arias S, Satorre EH, Guglielmini A (1994) Competencia entre trigo (*Triticum aestivum* L.) y Brassica sp. El efecto de la densidad del cultivo y la maleza en dos niveles de fertilización nitrogenada. Actas III Congreso Nacional de Trigo (Bahía Blanca, Argentina) 1:193–194
10. Auld BA, Kemp DR, Medd RW (1983) The influence of spatial arrangement on grain yield of wheat. Aust J Agric Res 34:99–108
11. Baigorrí HE (2008) Elección de variedades. In: Satorre EH (ed) Producción de Soja. AACREA Unidad de Comunicación y Marketing, Buenos Aires, Argentina, pp 33–42
12. Baker RJ, Briggs KG (1982) Effects of plant density on the performance of 10 barley cultivars. Crop Sci 22:1164–1167
13. Barnes C, Bugbee B (1991) Morphological responses of wheat to changes in phytocrome photoequilibrium. Plant Physiol 97:359–365
14. Bedmar F, Eyherabide JJ, Satorre EH (2000) Bases para el manejo de malezas. In: Andrade y FH, Sadras VO (eds) Bases para el manejo del maíz, el girasol y la soja. Editorial Médica Panamericana SA, Argentina. ISBN 987-521-016-1, pp 269–307; 443 pp
15. Bleasdale JKA (1966) Plant growth and crop yield. Ann Appl Biol 57:173–182
16. van den Boogaard R, Veneklass EJ, Peacock JM, Lambers H (1996) Yield and water use of wheat (*Triticum aestivum*) in a mediterranean environment: cultivar differences and sowing density effects. Plant Soil 181(2):251–262

17. Bullock D, Nielsen R, Nyquist W (1988) A growth analysis of corn grown in conventional and equidistant plant spacing. Crop Sci 28:254–258
18. Calviño P (2007) Intensificación de Sistemas de producción de granos y el manejo del riesgo en agricultura. In: Actas del Congreso Mundo Soja 2007. SEMA, Buenos Aires, Argentina, pp 75–76
19. Calviño P (2008) El cultivo de Soja de Segunda. In: Satorre EH (ed) Producción de Soja. AACREA, Unidad de Comunicación y Marketing, Buenos Aires, Argentina, pp 33–42, pp 93–98
20. Cirilo A (2002) Respuesta a la densidad y distribución de plantas del cultivo de Maíz. In: Satorre EH (ed) Maíz. Cuaderno de Actualización técnica Nº 65, AACREA, Buenos Aires, Argentina, pp 62–71
21. Darwinkel A (1978) Patterns of tillering and grain production of winter wheat at a wide range of plant densities. Netherland J Agric Sci 26:383–398
22. Donald CM (1963) Competition among crop and pasture plants. Adv Agron 15:1–118
23. Donald CM, Hamblin J (1976) The biological yield and harvest index of cereals as agronomic and plant breeding criteria. Adv Agron 28:361–405
24. Dodds P, Slafer GA, Satorre EH (1990) Sistemas de producción de trigo y soja en el norte de Buenos Aires. Evaluación del cultivo de Trigo. Actas II Congreso Nacional de Trigo, vol 1. Pergamino, Argentina, pp 198–208
25. Farazdaghi H, Harris PM (1968) Plant competition and crop yield. Nature 217:289–290
26. Fawcett RG (1964) Effect of certain conditions on yield of crop plants. Nature 204:858–860
27. Federer WT, Conningale JC, Rutger JN, Wijesinha A (1982) Statistical analysis of yields from uniblends and biblends of eight dry bean cultivars. Crop Sci 22:111–115
28. Felton WL (1976) The influence of row spacing and plant population on the effect of weed competition in soybeans (*Glycine max*). Aust J Exp Agric Anim Husb 16:926–931
29. Fischer RA (1984) Wheat. In: Smith WH, Barta SJ (eds) Symposium on potential productivity of field crops under different environments. Philippines, IRRI, Los Baños, pp 129–153
30. Fischer RA, Miles RE (1973) The role of spatial pattern in the competition between crop plants and weeds. A theoretical analysis. Math Biosci 18:335–350
31. Flemming GF, Young FL, Ogg AC (1988) Competitive relationships among winter wheat (*Triticum aestivum*), jointed goatgrass (*Aegilop scylindrica*), and downy brome (*Bromus tectorum*). Weed Sci 36:479–486
32. Gallez LM, Mockel FE, Cantamutto MA, Gullace GD, Vallati AR (1986) Densidad de siembra y separación entre hileras: Su influencia sobre el rendimiento de trigo en la región pampeana semiárida. Actas I Congreso Nacional de Trigo (Pergamino, Argentina) 3:167–177
33. Goodall DW (1960) Quantitative effects of intraspecific competition: an experiment with marigolds. Bull Res Council Israel 8:181–194
34. Harper JL (1977) Population biology of plants. Academic, London
35. Holliday R (1960) Plant population and crop yield. Field Crop Abstr 13(3):159–167
36. Holliday R (1963) The effect of row width on the yield of cereals. Field Crop Abstr 16:71–81
37. Horwith B (1985) A role for intercropping in modern agriculture. Bioscience 35(5):286
38. Kantolic A (2008) Fecha y densidad de siembra en soja. In: Satorre E (ed) Producción de Soja. AACREA, Unidad de Comunicación y Marketing, Buenos Aires, pp 23–32
39. Kira T, Ogawa H, Shinozaki K (1953) Intraespecific competition among higher plants. 1- Competition-density-yield interrelationships in regularly dispersed populations. J Inst Polytech Osaka City Univ 4:1–16
40. Lafond GP, Domitruk D, Bailey KL, Derksen D (1996) Effects of row spacing, seeding rate and seed-placed phosphorus on wheat and barley in the canadian prairies. Better Crop Plant Food 80(4):20–22
41. Loomis RS, Connor DJ (1992) Crop ecology: productivity and management in agricultural systems. Cambridge University Press, Cambridge
42. Maddonni GA, Cirilo AG, Otegui ME (2006) Row width and maize grain yield. Agron J 98:1532–1543
43. Martin MPLD, Field RJ (1987) Competition between vegetative plants of wild oat (*A. fatua*) and wheat (*Triticum aestivum* L.). Weed Res 27:119–124
44. McGilchrist CA, Trenbath BR (1971) A revised analysis of plant competition experiments. Biometrics 27:659–671
45. McLeod JG, Campbell CA, Gan Y, Dyck FB, Vera CL (1996) Seeding depth, rate and row spacing for winter wheat grown on stubble and chemical fallow in the semiarid prairies. Can J Plant Sci 76(2):207–214
46. Mead R (1979) Competition experiments. Biometrics 35:41–54
47. Mitchell R (1970) Crop growth and culture. Iowa State University Press, Ames, p 349
48. Monzon JP, Carrozza TJ, Calviño P, Andrade FH (2005) Efectos del Intercultivo en franjas de maíz y soja sobre el rendimiento- In: Actas del VIII Congreso Nacional de Maíz. AIANBA, Rosario, Argentina, pp 64–66
49. Nafziger E (1998) Corn. Chapter 2. In: Agronomy handbook, Illinois. 1997–1998. University of Illinois at Urbana-Champaign. College of Agricultural, Consumer and Environmental Sciences Department of crop Sciences. Cooperative Extension Service. Circular 1344, pp 16–26
50. Nerson H (1980) Effects of population density and number of ears on wheat yield and its components. Field Crop Res 3:225–234
51. Otegui ME, Ruiz R (1993) Performance of six maize hybrids sown at three population densities in Argentina. Test of agrochemicals and cultivars. Ann Appl Biol 122(Suppl): 172–173
52. Panda SC, Pattanaik A, Rath BS, Tripathy RK, Behera B (1996) Response of wheat (*Triticum aestivum*) to crop geometry and weed management. Indian J Agron 41(4):553–557

53. Panda SC, Pattanaik A, Rath BS, Tripathy RK, Behera BP, Pant MM (1979) Dependence of plant yield on density and planting pattern. Ann Bot 44:513–516
54. Panwar RS, Malik RK, Balyan RS, Singh DP (1995) Effect of isoproturon, sowing method and seed rate on weeds and yield of wheat (*Triticum aestivum*). Indian J Agric Sci 65(2):109–111
55. Peltonen J, Peltonen-Sainio P (1997) Breaking uniculm growth habit of spring cereals at high latitudes by crop management. II Tillering, grain yield and yield components. J Agron Crop Sci 178(2):87–95
56. Puckridge DW, Donald CM (1967) Competition among wheat plants sown at a wide range of densities. Aust J Agric Res 18:193–211
57. Ratkowsky DA (1983) Nonlinear regression modelling. A unified practical approach. Marcel Dekker, New York and Basel
58. Ross MA, Harper JL (1972) Occupation of biological space during seedling establishment. J Ecol 60:77–88
59. Salazar GM, Moreno RO, Salazar GR, Carrillo ML (1996) Wheat production as affected by seeding rate x fertilization interaction. Cereal Res Commun 24(2):231–237
60. Sánchez RA, Casal JJ, Ballaré CL, Scopel AL (1993) Plant responses to canopy density mediated by photomorphogenic processes. In: Buxton DR, Shibles R, Forsberg RA, Blad BL, Asay KH, Paulsen GM, Wilson RF (eds) International crop science I. Crop Science Society of America, Madison, pp 779–786
61. Sarandon SJ, Chidichimo HO (1985) Efecto de la densidad de siembra sobre la acumulación y redistribución del nitrógeno en tres cultivares de T. aestivum L. Revista de la Facultad de Agronomía (La Plata) 61–62:105–122
62. Sarandon SJ, Chamorro AM (2003) Policultivos en los sistemas de producción de granos. In: Satorre EH, Arnold B, Slafer GA, de La Fuente EB, Miralles DJ, Otegui ME, Savin R (eds) Producción de Granos. Bases funcionales para su manejo. Ed. Facultad de Agronomía, University of Buenos Aires, Argentina, pp 353–376
63. Satorre EH (1988) The competitive ability of spring cereals. Ph.D. thesis, University of Reading, Reading
64. Satorre EH (2008) Estructura especial: respuesta del cultivo a la densidad, distancia entre hileras y uniformidad. In: Satorre EH (ed) Producción de Maíz. AACREA, Unidad de Comunicación y Marketing, Buenos Aires, pp 25–32
65. Satorre EH, Arias SP (1990) Competencia entre trigo (*Triticum aestivum*) y malezas. III El efecto de la densidad del cultivo y la maleza. Actas II Congreso Nacional de Trigo. Pergamino, Argentina, vol 4, pp 1–10
66. Satorre EH, Ghersa CM (1987) Relationship between canopy structure and weed biomass. Field Crop Res 17:37–43
67. Satorre EH, Slafer GA (1999) Wheat production systems of the Pampas. In: Satorre EH, Slafer GA (eds) Wheat. Ecology and physiology of yield determination. Food products Press, New York, pp 333–350
68. Savin R, Slafer GA (1991) Shading effects on yield of an Argentinian wheat cultivar. J Agric Sci Camb 116:1–7
69. Shinozaki K, Kira T (1956) Intraspecific competition among higher plants VII logistic theory of the C-D effect. J Inst Polytech Osaka City Univ 7:35–72
70. Snaydon RW (1984) Plant demography in an agricultural context. In: Dirzo R, Sarukhan J (eds) Perspectives on plant population biology. Sinauer Associates, Sunderland, pp 389–408
71. Snaydon RW, Satorre EH (1989) Modifications and interpretations of bivariate diagrams for plant competition data. J Appl Ecol 26:1043–1057
72. Solie JB, Solomon SG Jr, Self KP, Peeper TF, Koscelny JA (1991) Reduced row spacing for improved wheat yields in weed-free and weed-infested fields. Trans ASAE 34(4): 1654–1660
73. Thakur SS, Pandey IB, Singh SJ, Mishra SS (1996) Effect of seed rate and row spacing on late sown wheat in alluvial calcareous soil. J Res Birsa Agric Univ 8(2):123–125
74. Trenbath BR (1974) Biomass productivity of mixtures. Adv Agron 26:177–210
75. Trenbath BR (1976) Plant interactions in mixed crop communities. In: Papendick RI, Sánchez PA, Triplett GB (eds) Multiple cropping. ASA special pub. N° 27 (ASA), pp 129–170
76. Valentinuz O (1996) Crecimiento y rendimiento comparados de girasol, maíz y soja ante cambios en la densidad de plantas. M.Sc. thesis, Fac. de Ciencias Agrarias, Universidad de Mar del Plata, Argentina, p 45
77. Vandermeer J (1992) The ecology of intercropping. Cambridge University Press, Cambridge
78. Van Ittersum MK, Rabbinge R (1997) Concepts in production ecology for analysis and quantification of agricultural input-output combinations. Field Crop Res 52:197–208
79. Vega CRC, Andrade FH, Sadras VO, Uhart SA, Valentinuz OR (2001) Seed number as a function of growth. A comparative study in soybean, sunflower, and maize. Crop Sci 41:748–754
80. Verona CA, Loffer CM, Fernández ON (1980) Efecto de la densidad de plantas sobre el rendimiento y la distribución de N en T. durum Def. Revista de Investigaciones Agropecuarias. INTA 15(1):75–95
81. Lin WZ, Min FJ, Rong HM, Ping YY, Min CH (1997) Planting density effects on assimilation and partitioning of photosynthates during grain filling in the late sown wheat. Photosynthetica 33(2):199–204
82. Willey RW, Heath SB (1969) The quantitative relationships between plant population and crop yield. Adv Agron 21:281–321
83. Yunusa IAM (1989) Effects of planting density and plant arrangement pattern on growth and yields of maize (*Zea mays* L.) and soya bean (Glycine max L. Merr.) grown in mixtures. J Agric Sci Cambridge 112:1–8
84. Kemp DR, Auld BA, Medd RW (1983) Does optimizing plant arrangement reduce interference or improve the utilization of space? Agric Syst 12:31–36

85. Satorre EH (1998) Aumentar los rendimientos en forma sustentable en la Pampa Argentina: Aspectos Generales. In: Solbrig, Vainesman (eds) Hacia una agricultura productiva y sostenible en la Pampa. Orientación Gráfica Editora, Buenos Aires, Argentina, pp 72–98
86. Ghersa CM, Martinez-Ghersa MA (1989) Cambios ecológicos en los agroecosistemas de la pampa ondulada. Efectos de la introducción de la soja. Ecología 2:182–188

Speciation of Metals, Effects on Aquatic Biota

James C. McGeer[1], D. Scott Smith[2], Kevin V. Brix[3], William J. Adams[4]
[1]Department of Biology, Wilfrid Laurier University, Waterloo, ON, Canada
[2]Department of Chemistry, Wilfrid Laurier University, Waterloo, ON, Canada
[3]University of Miami, RSMAS, Marine Biology and Fisheries, Miami, FL, USA
[4]Rio Tinto, Murray, UT, USA

Article Outline

Glossary
Definition of the Subject
Introduction
Speciation, Uptake, and Bioaccumulation
Modeling
Predicting Toxicity in Algae
Conclusions
Future Directions
Bibliography

Glossary

Biotic ligand model (BLM) Is a conceptual model where toxicity is assumed to be proportional to metal binding at a site of toxic action (the Biotic Ligand often assumed to be the gill). Bound metal is influenced by metal complexation reactions in solution and competition with other cations for the biotic ligand. The amount of metal bound to the biotic ligand can be calculated using geochemical modeling techniques and tabulated equilibrium constants. In practice, BLM often refers to the computer code and/or set of constants predicting toxicity for a given dataset (organism and metal).

Free ion activity model (FIAM) Is conceptually similar to the BLM. Here toxicity is assumed to be proportional to the free metal concentration. The free metal ion is assumed to be the most bioavailable. FIAM can take into account solution complexation protective effects but not cation competition protective effects on metal toxicity.

Geochemical modeling Refers to calculated equilibrium distribution of elements based on defined reaction stoichiometries and equilibrium constants. Numerically, simultaneous equilibria must be satisfied within the constraint of system mass balance and electroneutrality.

Natural organic matter (NOM) Is a ubiquitous and important ligand for metal complexation in solution. NOM comes from breakdown of terrestrial organic matter (terrigenous carbon) or is generated in situ in the water column (autochthonous carbon) by the activity of microorganisms (i.e., bacteria, algae). For BLM predictions, NOM is approximated by the measurable quantity dissolved organic carbon (DOC). In many aquatic systems the most important components of NOM are humic and fulvic acids, which are macromolecular polyelectrolytes with metal binding functional groups such as phenolic and carboxylic.

Speciation Distribution of an element among its possible chemical and physical forms. For metallic elements, the terminology would be metal speciation. Speciation can refer to an analytical measurement or a chemical equilibrium calculation. Speciation can be coarsely resolved such as filtered (dissolved) versus unfilterable (particulate) metal, for example, or very specific such as measured or calculated molecular species (i.e., M, MOH, MCl, M-NOM, etc.). The sum of all chemical species corresponds to the total element (metal).

Definition of the Subject

The interaction of dissolved metal with biological surfaces of organisms is dependent on a full understanding of speciation in aquatic media. The understanding has

been recently developed as a method for predicting the toxicity of metals in aquatic systems on a site-specific (i.e., water chemistry) basis. The approach has also been extended, with appropriate modifications, to predict metal toxicity soils and sediments. The biotic ligand modeling approach is mechanistically based and relies on the fact that waterborne metals bind to and/or are taken up at specific sites, that this uptake/binding can be reliably characterized, and that there is a direct correlation between bioaccumulation and toxicity. The conceptual foundation of the biotic ligand model (BLM) was originally described for fish as the Gill Site Interaction Model (GSIM) by Pagenkopf [1]. The GSIM modeling approach was further elucidated by Campbell [2] to the free ion activity model (FIAM) and then subsequently developed into the BLM [3]. This development of models was directed at predicting the toxicity of metals to aquatic biota and was anchored in toxicological, geochemical, and physiological research. The robust nature of this approach is evidenced by its promotion as a regulatory tool [4] and subsequent acceptance [5, 6] for developing site-specific water quality criteria, for risk assessment, and for setting site-specific discharge objectives. The following discussion focuses on metal speciation, its importance in understanding metal bioavailability and impact, how speciation and bioavailability are incorporated into the BLM approach, and the application of the BLM as a tissue residue-based toxicity prediction model. This work does not discuss radioisotopic uptake and effects as such but is designed to contribute understanding of the factors influencing their uptake and accumulation. Previous work by Fortin et al. [7] has shown that this speciation and tissue burden approach to predicting inorganic metal toxicity can also be applied toward the chemical toxicity of uranium to algae.

Introduction

Metal speciation is the distribution of total metal among different physical and chemical forms. Speciation can refer to analytical techniques used to determine different fractions or individual molecular species or it can refer to calculated speciation. Metal speciation can be calculated by solving the simultaneous set of equilibrium reactions for a metal in an aquatic system. Species for a metal with oxidation state *n* could include inorganic species such as free aquo metal ion (M^{n+}), chlorocomplexes ($MCl^{(n-1)+}$, $MCl_2^{(n-2)+}$), hydrolysis species ($MOH^{(n-1)+}$, $MOH_2^{(n-2)+}$), and others. Organic metal species include complexes with organic acids such as citrate or oxalate but also with macromolecular acids such as humic and fulvic acids found in naturally occurring organic matter. The influence of this latter complexation is a key factor in determining the potential impact of metals in natural waters but is not well understood and is an area of active research. For many metals, including some radionuclides, inorganic complexes are fairly well defined through established equilibrium constant databases such as NIST. The biotic ligand approach develops reactions at biota surfaces are included as additional ligands in the simultaneous set of metal complexation equilibria.

The BLM approach integrates metal interactions along the exposure – uptake – accumulation – and toxicity pathway. Integration is achieved using equilibrium-based geochemical modeling approaches that characterize the reaction of a metal with aquatic ligands. The exposure component applies standard aquatic speciation modeling software to predict the binding of metal to inorganic ligands as well as dissolved organic matter (DOM) to produce a profile of dissolved species that occur in particular defined water chemistry. This speciation is via commercially available (but relatively inexpensive) software packages such as the Windemere Humic Aqueous Model (WHAM, [8] Tipping 1994; http://www.windermere.ceh.ac.uk/aquatic_processes/wham/) and MINEQL+ ([9]; http://www.mineql.com) as well as freeware such as MINTEQA2 ([10]; http://www.epa.gov/ceampubl/mmedia/minteq/index.htm). In general, the database of conditional equilibrium constants (Log K values) is similar between models; however, there are important differences between programs and also within different versions of programs and the science continues to evolve [11, 12].

The prediction of metal uptake within the BLM is based on estimates of the relative bioavailability of different dissolved species of metal. These interactions between metal species and the biotic ligand (BL) are incorporated into the equilibrium modeling framework via description of additional ligands that account for biological interactions. The additional ligands describe the binding constants of a metal species, for example, free metal ions, hyroxides, or carbonates, at

the site of toxic action as well as other cations that competitively bind to that site and reduce toxicity. The exposure, uptake, and accumulation interactions illustrated through schematic diagram shown in Fig. 1, also see Figure 1 of Di Toro et al. [3].

As shown in Fig. 1, there are three main components to BLMs: chemistry, physiology, and toxicology. The chemical equilibrium component represents complexation of the metal of interest in solution as well as competition with other cations for the biotic ligand. The biotic ligand is represented in Fig. 1 as a fish gill. Biological processes on the fish gill and associated biological transformations of the metal are indicated as physiology in Fig. 1. Finally, the relationship between external chemistry and internal physiology results in measures of toxicology, which can be used for regulatory purposes.

Speciation, Uptake, and Bioaccumulation

The strength of biotic ligand models is that they simultaneously account for the geochemical speciation as well as the relative binding of metal species (or not) to the site of toxicity. The total concentration of metal bound to the BL is the parameter used to predict toxicity endpoints within BLMs and therefore, the accumulation–toxicity relationship is a central feature that must be characterized. From a modeling perspective, the BL-bound metal is assumed to accumulate at the site of toxic action where impacts will follow a dose–response threshold paradigm. With increased exposure to bioavailable metal, there is increased uptake/accumulation until the threshold concentration is reached. The threshold concentration is derived to be predictive of the toxicity endpoint (e.g., for acute toxicity the concentration of metal lethal to half the fish (LC50) or effecting half the fish as some other toxic endpoint (EC50)). This threshold accumulation for toxicity is termed the LA (lethal accumulation, e.g., for acute toxicity the LA50). As such, application of the BLM in water quality criteria or guidelines is unique because it is a site-specific bioaccumulation-based methodology.

While accumulation at the site of toxicity is at the heart of the BLM, understanding the relative bioavailability of various metal species is fundamental. The free ion form is universally, and often the only bioavailable form of metal [3]. However, in some cases other dissolved metal species have been implicated in accumulation and toxicity. For example, in the case of the

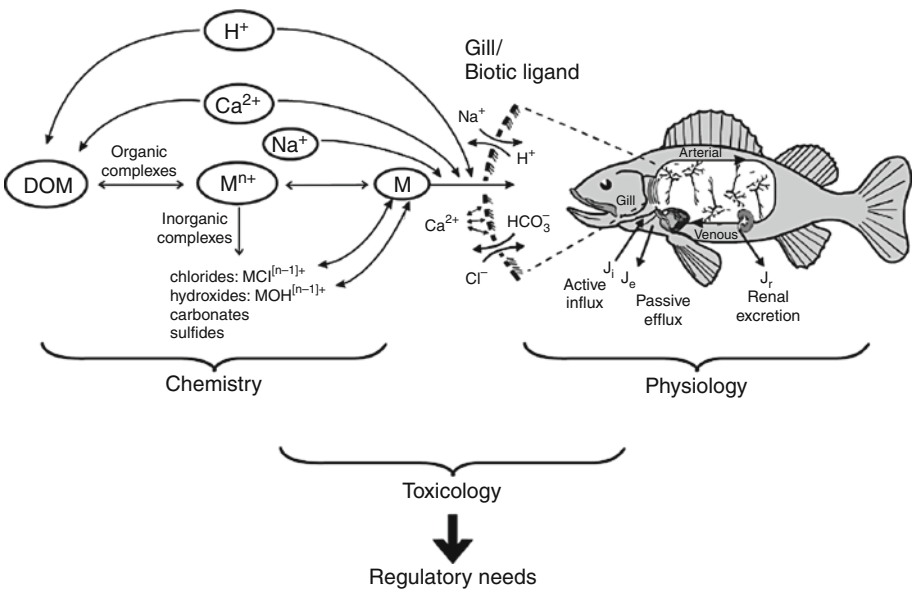

Speciation of Metals, Effects on Aquatic Biota. Figure 1
Schematic diagram, from Fig. 1 of [13] describing the integration of chemistry, physiology, bioaccumulation, and toxicology within BLMs

effects of Ag on fathead minnows it is both Ag^+ and AgCl, which have been shown to contribute to toxicity [14]. Similarly, the model derived by De Schamphelaere and coworkers [15] for the acute effects of Cu on *Daphnia magna* included not only the toxicity of the Cu^{2+} ion, but also the contributions that CuOH and also $CuCO_3$ make to toxicity.

The uptake of bioavailable metal onto the BL is characterized through conditional equilibrium constants that describe short-term binding (typically 3–24 h). The first descriptions were made by Playle et al. [16–18] for Cd and Cu using 3-h accumulations in the presence of various organic ligands to quantify the relative binding of metal to the rainbow trout gill. The study of MacRae et al. [19] measured Cu binding to fish (rainbow and brook trout) gills at 24 h, and linked this accumulation to subsequent acute toxicity. The use of short-term accumulation is appropriate, at least for acute toxicity, because the initial rapid uptake of metal occurs via essential ion uptake processes that, when overloaded, result in toxic impacts. As reviewed by Niyogi and Wood [20], Cu^{2+} and Ag^+ act via Na^+ and secondarily Cl^-, while Cd^{2+}, Zn^{2+}, Pb^{2+}, and Co^{2+} disrupt Ca^{2+} transport (Fig. 2). The site of Ni^{2+} binding

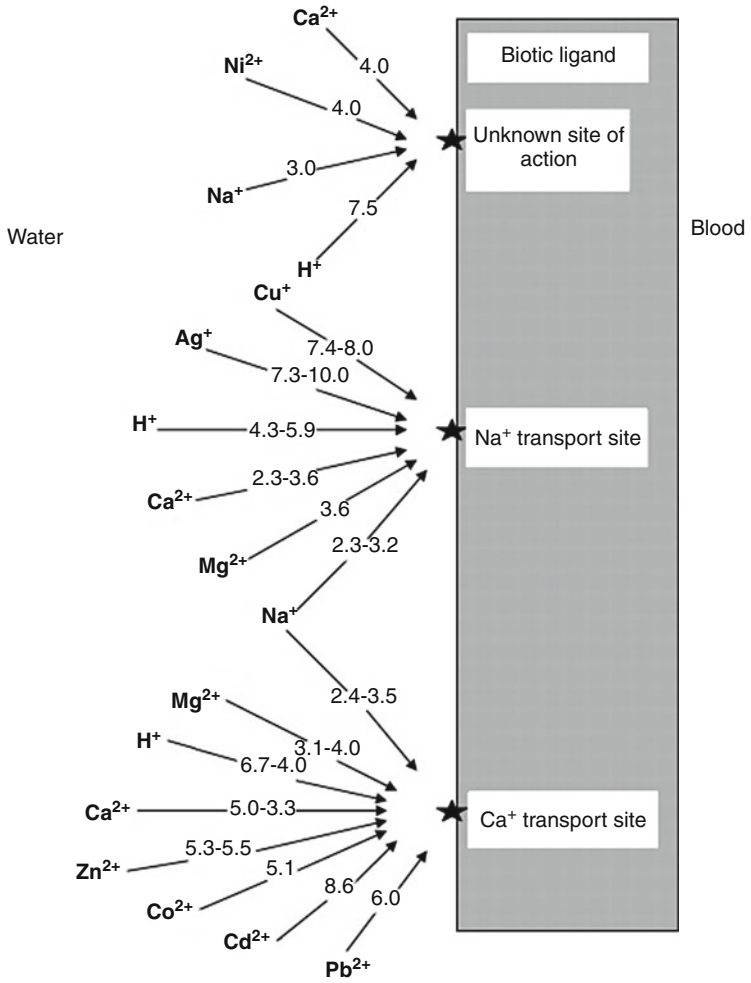

Speciation of Metals, Effects on Aquatic Biota. Figure 2
Binding affinities of free ions of different metals and environmental cations, interacting at different sites of toxic action on the biotic ligand. From Fig. 1 of the BLM review of Niyogi and Wood [20]

has not been conclusively identified, but may be involved in Mg^{2+} regulation. Much of the work illustrating the effects of metals on ionic balance and the relationship between ionic imbalance and toxicity has been done with fish; however, some studies have shown that these mechanisms are likely consistent with effects in invertebrates as well. For example, Pane et al. [21] showed that Ni^{2+} impairs Mg^{2+} regulation in *Daphnia magna*, while Bianchini et al. [22] illustrated that Ag^{+} disruption of Na^{+} balance was similar across many species. Whether it is disruption of Na^{+}, Ca^{2+}, or Mg^{2+}, the consequences leading to toxic impacts are general and related to the effects of ion loss on the cardiovascular system [23, 24], and similar in nature to the effects of acidification [25].

While both metal bioaccumulation and toxicity are, by definition, not equilibrium events, it is possible to describe the events using equilibrium-based models and this approach is supported mechanistically (physiologically). In terms of acute toxicity, short-term accumulation has been linked to the subsequent lethal consequences, at least in a few studies, for example, [26] and [19]. As a process that is typically described via Michaelis Menton kinetics, short-term metal binding is characterized by a rapid increase to a maximum that can be described as a Langmuir isotherm [18]. The descriptive variables (maximum capacity (Bmax) and binding strength (Km)), derived through Scatchard (for example) analysis can be applied within an equilibrium context to characterize the metal accumulation that results from a given exposure. In terms of metal bioaccumulation, as Niyogi and Wood [20] point out, gill metal burdens will increase as exposure continues beyond the short term, particularly if conditions are lethal. However, it is the initial rapid uptake, before pathological deterioration of the exchange surface occurs, that is correlated to the later acute toxicity endpoint. One of the key mechanistic links of the BLM approach is that initial rapid bioaccumulation is via ion uptake processes and that mortality result from the consequences of inhibition of ion uptake.

The protective effect that cations can have on metal toxicity supports the mechanistic linkage between metal accumulation, ion uptake, and toxic impacts. As discussed above, the reduction of toxicity is specific to a particular metal–ion combination and reflects the ionic mechanism through which the metal is taken up. This protective effect is modeled via competitive interactions as defined by affinity constants for ions on the biotic ligand (reviewed by [20], Fig. 2). Although the BLM considers the protective effects of cations only from the point of view of competitive binding to the BL, the actual protective effects arise through two potential mechanisms. In addition to competition, ions such as Mg^{2+} and Ca^{2+} can have a stabilizing effect on membrane permeability thus alleviating some of the severity of impacts (i.e., ion loss) that a given metal concentration may induce.

Modeling

The BLM considers bioaccumulation of metal by establishing thresholds (LA values) for binding to the BL, accounting for the relative bioavailability of different species of metal in the exposure medium and including the role of cationic competition for occupancy of BL sites. Therefore, within a given water chemistry, the prediction of toxicity depends on the interplay between equilibrium constants for BL–metal interactions, BL–ion interactions (including complexation reactions that reduce the availability of the free ion, such as binding by natural organic matter), and the LA value itself. Table 1 provides a summary of some of the biotic ligand models and the metal bioaccumulation-based parameters (Log $K_{BL\text{-}Me}$ and LA values). In general, particularly for aquatic media, two types of approaches have been developed. The more detailed approach is to establish a full BLM by applying experimental results to develop and refine a full suite of conditional equilibrium constants, for both metal–BL interaction(s) and cationic competition, as well as the relevant LA50 value (e.g., [3, 15, 27, 30]). The other approach to developing a BLM model is to use some or all of the Log K values from an existing model and to adjust the threshold at the BL (i.e., LA50) value to match the sensitivity of the organism under study (e.g., [28, 29, 32]). This latter approach has been developed for the water chemistry normalization procedures within the derivation of the draft water quality criteria for Cu [6]. An associated and less-common approach is to use a fixed LA50 value and to adjust the log $K_{BL\text{-}Me}$ constants to account for different species sensitivities (e.g., [35]).

Speciation of Metals, Effects on Aquatic Biota. Table 1 Summary of bioaccumulation variables for metal within some of the currently available BLM models including affinity constants (Log K values) for metal uptake as well as the tissue residue concentrations associated with specific toxicological endpoints (the LA50 value) associated with the toxicity endpoint

hMetal	Media	Type	Affinity constant		Species	Toxicity endpoint	LA50 (nmol/g)	References
			Interaction	Value				
Cu	Aquat	Acute	Log $K_{BL\text{-}Cu}^{2+}$	7.4	Fathead minnow	96 h LC50	7.32	[3] [27], current version is 2.2.3
			Log $K_{BL\text{-}CuOH}^{-}$		*Ceriodaphnia dubia*	48 h EC50	0.077	
				−1.3	*Daphnia magna*	48 h EC50	0.069	
					Daphnia pulex	48 h EC50	0.062	
Cu	Aquat	Acute	Log $K_{BL\text{-}Cu}^{2+}$	7.4	*Gasterosteus aculeatus*	96 h LC50	8.5	[28]
			Log $K_{BL\text{-}CuOH}^{-}$	−1.3				
Cu	Aquat	Chronic	Log $K_{BL\text{-}Cu}$	7.4	*Mytilus* sp.	48 h EC50	0.0006	[29] using the BLM framework of [27]
			Log $K_{BL\text{-}CuOH}^{-}$	−1.3				
Cu	Aquat	Acute	Log $K_{BL\text{-}Cu}^{2+}$	8.02	*Daphnia magna*	48 h EC50	6.10	[30]
			Log $K_{BL\text{-}CuOH}^{-}$	7.45				
Cu	Aquat	Acute	Log $K_{BL\text{-}Cu}^{2+}$	8.02	*Daphnia magna*	48 h EC50	0.47	[15]
			Log $K_{BL\text{-}CuOH}^{-}$	7.32				
			Log $K_{BL\text{-}CuCO3}$	7.01				
Cu	Aquat	Chronic	Log $K_{BL\text{-}Cu}^{2+}$	8.02	*Daphnia magna*	21 days $EC50_{reprod}$	0.39	[31]
			Log $K_{BL\text{-}CuOH}^{-}$	8.02				
			Log $K_{BL\text{-}CuCO3}$	7.44		21 days $NOEC_{reprod}$	0.26	
Cu	Aquat	Chronic	Log $K_{BL\text{-}Cu}^{2+}$	8.02	*Brachionus calyciflorus*	48 h NOEC	2.1	[32]
			Log $K_{BL\text{-}CuOH}^{-}$	8.02		48 h LOEC	3.6	
			Log $K_{BL\text{-}CuCO3}$	7.44				
Cu	Terrest	Acute	Log $K_{BL\text{-}Cu}$	5.9	*Aporrectodea caliginosa*	7 days LC50	0.2	[33]
Cu	Terrest	Acute	Log $K_{BL\text{-}Cu}$	7.41	*Hordeum vulgare*	4 days LC50	0.05	[34]
Cu	Terrest	Mixed	Log $K_{BL\text{-}Cu}$	5.65	*Lycopersicon esculentum*	4 days EC50	0.05	[35]
				4.62	*Folsomia candida*	4 weeks EC50		
				6.50	*Eisenia fetida*	4 weeks EC50		
				6.69	*Microbial – respiration*	24 h EC50		
				4.93	*Microbial – nitrification*	24 h EC50		
Zn	Aquat	Acute	Log $K_{BL\text{-}Zn}^{2+}$	8.6	Fathead minnow	96 h LC50	4.94	Based on [27] and [3] with data from [36], current model is 2.2.3
			Log $K_{BL\text{-}ZnOH}^{-}$	−3.8	Rainbow trout	96 h LC50	1.59	
					Ceriodaphnia dubia	48 h EC50	9.98	

Speciation of Metals, Effects on Aquatic Biota. Table 1 (Continued)

hMetal	Media	Type	Affinity constant		Species	Toxicity endpoint	LA50 (nmol/g)	References
			Interaction	Value				
Zn	Aquat	Acute	Log $K_{BL\text{-}Zn}^{2+}$	5.31	*Daphnia magna*	48 h EC50	0.417	[37]
Zn	Aquat	Chronic	Log $K_{BL\text{-}Zn}^{2+}$	5.31	*Daphnia magna*	21 days $EC50_{reprod}$	0.127	[38]
						21 days $NOEC_{reprod}$	0.084	
Zn	Aquat	Acute	Log $K_{BL\text{-}Zn}^{2+}$	5.5	*Rainbow trout*	96 h LC50	1.73	[39]
Zn	Aquat	Chronic	Log $K_{BL\text{-}Zn}^{2+}$	5.5	*Rainbow trout*	30 days $EC50_{survive}$	0.25	[39]
						30 days $EC10_{survive}$	0.09	
Ag	Aquat	Acute	Log $K_{BL\text{-}Ag}^{+}$	6.8	Fathead minnow	96 h LC50	9.98	based on [27] and [3] with specifics from [40] current model is 2.2.3.
					Rainbow trout	96 h LC50	9.98	
			Log $K_{BL\text{-}AgCl}$	9.7	*Ceriodaphnia dubia*	48 h EC50	0.344	
					Daphnia magna	48 h EC50	1.13	
Ag	Aquat	Acute	Log $K_{BL\text{-}Ag}^{+}$	7.6	Rainbow trout	96 h LC50	0.65	[41]
Ag	Aquat	Acute	Log $K_{BL\text{-}Ag}^{+}$	8.88	*Daphnia magna*	48 h EC50	0.733	[14]
					Daphnia pulex			
					Gammarus pulex			
Ni	Terrest	Acute	Log $K_{BL\text{-}Ni}^{2+}$	5.27	*Hordeum vulgare*	4 days EC50	0.57	[42]
Ni	Terrest	Acute	Log $K_{BL\text{-}Ni}$	3.6	*Hordeum vulgare*	4 days LC50	0.05	[34]
Ni	Terrest	Mixed	Log $K_{BL\text{-}Ni}$	6.05	*Lycopersicon esculentum*	4 days EC50	0.05	[35]
				5.12	*Folsomia candida*	4 weeks EC50		
				5.33	*Eisenia.fetida*	4 weeks EC50		
				4.53	*Microbial – respiration*	24 h EC50		
				5.72	*Microbial – nitrification*	24 h EC50		
Cd	Aquat	Acute	Log $K_{BL\text{-}Cd}^{2+}$	8.6	Fathead minnow	96 h LC50	4.75	[27] and [3], current model is 2.2.3.
					Rainbow trout	96 h LC50	3.16	
					Ceriodaphnia dubia	48 h EC50	7.53	
Co	Terrest	Acute	Log $K_{BL\text{-}Co}^{2+}$	5.13	*Enchytraeus albidus*	14 days LC50	0.32	y

Examples of some of the aquatic as well as terrestrial models that have been published are given. Note that for some models, a common Log $K_{BL\text{-}MeX+}$ interaction is applied across multiple species and adjustments for sensitivity are provided via alteration of the LA50

When establishing a full BLM de novo, there are three different methodologies that have been successfully employed: the bioaccumulation, the physiological, and the toxicity based approaches. The BLM model described by [3] and [27] for the acute effects of Cu is an example of the bioaccumulation-based method. In establishing this model, experimental data from the gill accumulation studies of Playle et al. [16–18] as well as the binding and toxicity study of MacRae et al. [19] were used as the source of the conditional equilibrium constants and LA50 value. These bioaccumulation-based values were subsequently adjusted to achieve a fit with existing toxicity data to give a tissue residue-based prediction model for acute toxicity. The Playle studies used fathead minnows and extrapolation to other species, including invertebrates, was done through adjustments of the LA50 values (see Table 1). The Cu version of this model has been widely tested and it has proved too robust and consistent. For example, the study of Villavicencio et al. [43] tested the Cu BLM for *Daphnia magna* on a number of field populations of *Daphnia* throughout Chile and convincingly illustrated the ability of that BLM to predicted Cu toxicity in natural populations (Fig. 3).

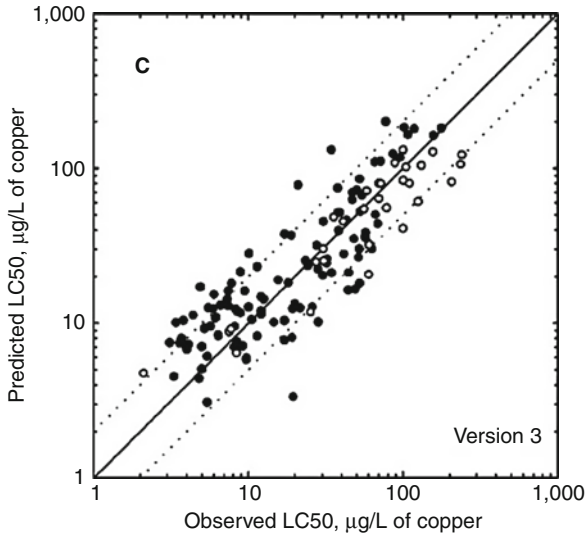

Speciation of Metals, Effects on Aquatic Biota. Figure 3 Illustration of the ability of an acute BLM for Cu to predict toxicity on populations of *Daphnia* sp. (*D. magna*, *D. pulex*, and *D. obtuse*) in different natural waters from throughout Chile. Data from the study is shown as a log–log plot and predictions are shown for the final version (version 3) of the adjusted model. The solid line shows the 1:1 line of perfect prediction and the dotted lines show a factor of ±2-fold. Figure is from [43]

The physiologically based approach used by McGeer et al. [41] derived binding constants for the effects of Ag^+ on rainbow trout using the direct mechanism of toxicity in rainbow trout, inhibition of gill Na^+/K^+ ATPase as the basis for Log $K_{BL\text{-}Ag}$. This physiologically based value (representing the 85% inhibition associated with the 96 h LC50) was combined with the competitive cation affinity constants and the LA50 value from the short-term gill binding study of Janes and Playle [44]. As with the bioaccumulation model development approach, Log K values were adjusted to achieve the best fit to the toxicity dataset. In this study, McGeer et al. [41] used MINEQL+ as the geochemical speciation model, in contrast to the models developed by Di Toro et al. [3] and Santore et al. [27], which is tied to WHAM (version 5).

The toxicity-based approach for deriving BLMs has been used by De Schamphelaere and colleagues (e.g., [15] and [45]). In this approach, speciation modeling and regression analysis are used to establish the conditional equilibrium constants for the effects of the bioavailable metal species as well as cationic competition. These values are developed into a lab-water model, which is then validated using natural waters where the effects of DOM are characterized and then integrated into the model. As with other models, the constants are subject to minor adjustments to optimize the fit to the toxicity data. An example of this is shown in Fig. 4, where a preliminary model was developed from lab-based data and subsequently adjusted to improve predictions in natural waters. In this particular case [31], the initial model considered all natural organic matter (NOM) sources in the same way and the final model adjusted for source by incorporating the relative absorbance of NOM at 350 nm into the model. The advantage of the toxicity-based approach is that it is endpoint-driven and therefore can be used to develop chronic BLMs as well as acute BLM's, something that has not been possible using other methods. Additionally, the choice of geochemical speciation modeling software can be varied as appropriate. However, this toxicity-based approach is not tissue residue based, even though it is a BLM (i.e., it accounts for speciation and cationic competition as well as predicting

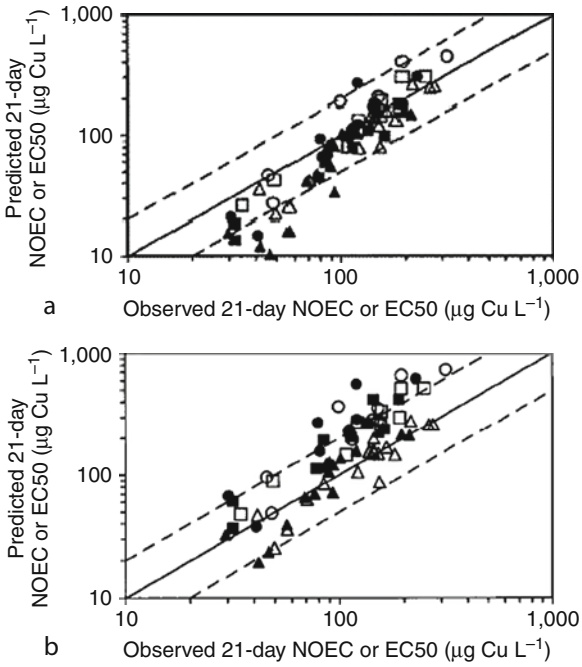

Speciation of Metals, Effects on Aquatic Biota. Figure 4 Illustration of the adjustments made to incorporate natural waters into a BLM framework, taken from Fig. 3 of [31]. Panel A show the initial BLM derivation with all NOM modeled in the same way, panel B shows the fit when metal–NOM interactions are adjusted for each source water. The solid line shows the line of perfect prediction and the dashed lines show ± a factor of 2

bioaccumulation and using a threshold LA50 value). In other words, short-term metal binding data and data linking short-term accumulation to subsequent toxicity are not required. In this approach, the LA50 is entirely an inferred value fitted so as to best predict the actual toxicity data.

Predicting Toxicity in Algae

The development and application of the BLM framework to predict effects on algae has proven to be challenging. Certainly the biotic ligand principles generally apply to metal uptake into or onto algae [46] though there are exceptions (e.g., [7]). Other than H^+, cationic competition appears less important, at least for Cu and Zn [45] and [47]. As a result, geochemical modeling has been used to apply a FIAM approach in conjunction with regression analysis to derive bioavailability models that account for the effect of Zn^{2+} and Cu^{2+} to *Pseudokirchneriella subcapitata* over a range of pH values [45, 47]. The models are therefore, not bioaccumulation based.

Conclusions

The biotic ligand model (BLM) approach to predicting metal toxicity in aquatic media has proven to be successful in explaining the variability that arises due to the influence of water chemistry on bioavailability. Mechanistically, the BLM is based on the relationship between bioaccumulation, tissue residue concentrations (i.e., BL–Me interactions), and toxicity. This methodology has proven to be robust, allowing for its application to Cu, Ni, Ag, Zn, Co, and Cd. Its strength lies in the fact that in principle, it is a tissue residue-based model (LA50) with a mechanistic basis, which accounts for the central role that bioaccumulation plays in expression of toxicity. The biotic ligand model is a useful conceptual tool as well as potential regulatory tool. The methods were developed for metals such as Cu, Ni, Zn, and Pb but can easily be generalized to capture effects of radionuclide toxicity. An additional consideration in radionuclide applications of BLM framework is not only radionuclides blocking essential transport pathways but also the inherent toxicity of radioactive decay particles if bound to the surface of a biotic ligand, such as a fish gill. This added mode of toxicity should still be accounted for in a BLM approach because the assumption that toxicity is proportional to the amount of bound radionuclide should still be satisfied.

Future Directions

Metal toxicity predictions and biotic ligand models in particular are an active area of research. These predictive tools have the potential for effective use in environmental protection, including risk assessment as well as regulatory practices. The site-specific nature of BLMs allow for optimal environmental protection taking the chemistry of the receiving water into account and reduces the needs for animal testing. The application of these BLM techniques for many transition metals (Cu, Ni, Pb, Zn, Cd) is fairly mature and there is a large body of literature on these metals. For radioactive metals, there has been much less experimental

work, but the concepts of BLM should apply for radionuclides as well as transition metals. Future research must continue to test BLM concepts for radionuclides and start to develop radionuclide-specific BLMs for potential use in reactive transport modeling and risk assessment.

Bibliography

1. Pagenkopf GK (1983) Gill surface interaction model for trace-metal toxicity to fishes: role of complexation, pH, and water chemistry. Environ Sci Technol 17:342–346
2. Campbell PGC (1995) Interactions between trace metals and aquatic organisms: a critique of the free-ion activity model in metal speciation and bioavailability in aquatic systems. In: Tessier A, Turner DR (eds) Trace metal speciation and bioavailability in aquatic systems. Wiley, Chichester, pp 45–102
3. Di Toro DM, Allen HE, Bergman H, Meyer JS, Paquin PR, Santore CS (2001) Biotic ligand model of the acute toxicity of metals. 1. Technical basis. Environ Toxicol Chem 20:2383–2396
4. Bergman HL, Dorward-King EJ (1997) Reassessment of metals criteria for aquatic life protection. Society for Environmental Toxicology and Chemistry Press, Pensacola
5. CCME (2007) A protocol for the derivation of water quality guidelines for the protection of aquatic life. Canadian Council of Ministers of the Environment. Winnipeg, Manitoba, Canada
6. EPA (2007) Aquatic life ambient freshwater quality criteria, copper, EPA-822-R-07-001. EPA, Washington
7. Fortin C, Dutel L, Garnier-Laplace J (2004) Uranium complexation and uptake by a green alga in relation to chemical speciation: the importance of the free uranyl ion. Environ Toxicol Chem 23:974–981
8. Tipping E (1994) WHAM A computer equilibrium model and computer code for waters, sediments, and soils incorporating a discrete site/electrostatic model of ion-binding by humic substances. Comput Geosci 20:973–1023
9. Schecher WD, McAvoy DC (2001) MINEQL+, version 4.5. Environmental Research Software, Hallowell
10. Allison JD, Brown DS, Novo-Gradac KJ (1991) MINTEQA2/PRODEFA2, a geochemical assessment model for environmental systems, version 3.0, user's manual. U.S. Environmental Protection Agency, Washington
11. Unsworth ER, Warnken KW, Zhang H, Davison W, Black F, Buffle J, Cao J, Cleven R, Galceran J, Gunkel P, Kalis E, Kistler D, Van Leeuwen HP, Martin M, Noel S, Nur Y, Odzak N, Puy J, Van Riemsdijk W, Sigg L, Temminghoff E, Tercier-Waeber ML, Toepperwien S, Town RM, Weng LP, Xue HB (2006) Model predictions of metal speciation in freshwaters compared to measurements by in situ techniques. Environ Sci Technol 40:1942–1949
12. van Leeuwen HP, Town RM, Buffle J, Cleven RFMJ, Davison W, Puy J, van Riemsdijk WH, Sigg L (2005) Dynamic speciation analysis and bioavailability of metals in aquatic systems. Environ Sci Technol 39:8545–8556
13. Paquin PR, Gorsuch JW, Apte S, Batley GE, Bowles KC, Campbell PGC, Delos CG, Di Toro DM, Dwyer RL, Galvez F, Gensemer RW, Goss GG, Hogstrand C, Janssen CR, McGeer JC, Naddy RB, Playle RC, Santore RC, Schneider U, Stubblefield WA, Wood CM, Wu BK (2002) The biotic ligand model: a historic overview. Comp Biochem Physiol 133C:3–35
14. Bury NR, Shaw J, Glover C, Hogstrand C (2002) Derivation of a toxicity-based model to predict how water chemistry influences silver toxicity to invertebrates. Comp Biochem Physiol 133C:259–270
15. De Schamphelaere KAC, Heijerick DG, Janssen CR (2002) Refinement and field validation of a biotic ligand model predicting acute copper toxicity to *Daphnia magna*. Comp Biochem Physiol 133C:243–258
16. Playle RC, Gensemer RW, Dixon DG (1992) Copper accumulation on gills of fathead minnows – influence of water hardness, complexation and pH of the gill microenvironment. Environ Toxicol Chem 11:381–391
17. Playle RC, Dixon DG, Burnison K (1993) Copper and cadmium-binding to fish gills – modification by dissolved organic-carbon and synthetic ligands. Can J Fish Aquat Sci 50:2667–2677
18. Playle RC, Dixon DG, Burnison K (1993) Copper and cadmium-binding to fish gills – estimates of metal gill stability-constants and modeling of metal accumulation. Can J Fish Aquat Sci 50:2678–2687
19. MacRae RK, Smith DE, Swoboda-Colberg N, Meyer JS, Bergman HL (1999) Copper binding affinity of rainbow trout (*Oncorhynchus mykiss*) and brook trout (*Salvelinus fontinalis*) gills: implications for assessing bioavailable metal. Environ Toxicol Chem 18:1180–1189
20. Niyogi S, Wood CM (2004) Biotic ligand model, a flexible tool for developing site – specific water quality guidelines for metals. Environ Sci Technol 38:6177–6192
21. Pane EF, Smith C, McGeer JC, Wood CM (2004) Mechanisms of acute and chronic waterborne nickel toxicity in the freshwater cladoceran, *Daphnia magna*. Environ Sci Technol 37:4382–4389
22. Bianchini A, Grosell M, Gregory SM, Wood CM (2002) Acute silver toxicity in aquatic animals is a function of sodium uptake rate. Environ Sci Technol 36:1763–1766
23. Hogstrand C, Wood CM (1998) Toward a better understanding of the bioavailability, physiology, and acute toxicity of silver in fish: implications for water quality criteria. Environ Toxicol Chem 17:547–561
24. Wilson RW, Taylor EW (1993) The physiological response of freshwater rainbow trout *Oncorhynchus mykiss*, during acutely lethal copper exposure. J Comp Physiol 163B:38–47
25. Wood CM (1998) The physiological problems of fish in waters. In: Morris R, Taylor EW, Brown DJA, Brown JA (eds) Acid toxicity and aquatic animals, Society for Experimental Biology Seminar Series. Cambridge University Press, Cambridge, pp 125–152
26. Morgan TP, Wood CM (2004) A relationship between gill silver accumulation and acute silver toxicity in the freshwater rainbow trout: support for the acute silver biotic ligand model. Environ Toxicol Chem 23:1261–1267

27. Santore RC, Di Toro DM, Paquin PR, Allen HE, Meyer JS (2001) Biotic ligand model of the acute toxicity of metals. 2. Application to acute copper toxicity in freshwater fish and *Daphnia*. Environ Toxicol Chem 20:2397–2402
28. Gravenmier JJ, Johnston DW, Santore RC, Arnold WS (2005) Acute toxicity of copper to the threespine stickleback, *Gasterosteus aculeatus*. Environ Toxicol 20:150–159
29. Arnold WR, Santore RC, Cotsifas S (2005) Predicting copper toxicity in estuarine and marine waters using the biotic ligand model. Mar Pollut Bull 12:1634–1640
30. De Schamphelaere KAC, Janssen CR (2002) A biotic ligand model predicting acute copper toxicity for *Daphnia magna*: the effects of calcium, magnesium, sodium, potassium, and pH. Environ Sci Technol 36:48–54
31. De Schamphelaere KAC, Janssen CR (2004) Development and field validation of a biotic ligand model predicting chronic copper toxicity to Daphnia magna. Environ Toxicol Chem 23:1365–1375
32. De Schamphelaere KAC, Heijerick DG, Janssen CR (2006) Cross-phylum comparison of a chronic biotic ligand model to predict chronic toxicity of copper to a freshwater rotifer, *Brachionus calyciflorus* (Pallas). Ecotoxicol Environ Saf 63:189–195
33. Steenbergen NTTM, Iaccino F, De Winkel M, Reijnders L, Peijnenburg WJGM (2005) Development of a biotic ligand model and a regression model predicting acute copper toxicity to the earthworm *Aporrectodea caliginosa*. Environ Sci Technol 39:5694–5702
34. Thakali S, Allen HE, Di Toro D, Ponizovsky AA, Rooney CP, Zhao FJ, McGrath SP (2006) A terrestrial biotic ligand model. 1. Development and application to Cu and Ni toxicities to barley root elongation in soils. Environ Sci Technol 40:7085–7093
35. Thakali S, Allen HE, Di Toro D, Ponizovsky AA, Rooney CP, Zhao FJ, McGrath SP (2006) Terrestrial biotic ligand model. 2. Application to Ni and Cu toxicities to plants, invertebrates, and microbes in soil. Environ Sci Technol 40:7094–7100
36. Santore RC, Mathew R, Paquin PR, Di Toro D (2002) Application of the biotic ligand model to predicting zinc toxicity to rainbow trout, fathead minnow and Daphnia magna. Comp Biochem Physiol 133C:271–285
37. Heijerick DG, De Schamphelaere KAC, Janssen CR (2002) Predicting acute zinc toxicity for Daphnia magna as a function of key water chemistry characteristics: development and validation of a biotic ligand model. Environ Toxicol Chem 21:1309–1315
38. Heijerick DG, De Schamphelaere KAC, Van Sprang PA, Janssen CR (2005) Development of a chronic zinc biotic ligand model for *Daphnia magna*. Ecotoxicol Environ Saf 62:1–10
39. De Schamphelaere KAC, Janssen CR (2004) Bioavailability and chronic toxicity of zinc to juvenile rainbow trout (*Oncorhynchus mykiss*): comparison with other fish species and development of a biotic ligand model. Environ Sci Technol 38:6201–6209
40. Paquin PR, Di Toro DM, Santore RC, Trivedi D, Wu K-B (1999) A biotic ligand model of the acute toxicity of metals. III. Application to fish and daphnia exposure to fish, EPA-822-E-99-001. EPA, Washington
41. McGeer JC, Playle RC, Wood CM, Galvez F (2000) A physiologically based biotic ligand model for predicting the acute toxicity of waterborne silver to rainbow trout in fresh waters. Environ Sci Technol 34:4199–4207
42. Lock K, De Schamphelaere KAC, Because S, Criel P, Van Eeckhout H, Janssen C (2006) Development and validation of an acute biotic ligand model (BLM) predicting cobalt toxicity in soil to the potworm *Enchytraeus albidus*. Soil Biol Biochem 38:1924–1932
43. Villavicencio G, Urrestarazu P, Carvajal C, De Schamphelaere KAC, Janssen CR, Torres JC, Rodriguez PH (2005) Biotic ligand model prediction of copper toxicity to daphnids in a range of natural waters in Chile. Environ Toxicol Chem 24:1287–1299
44. Janes N, Playle RC (1995) Modeling silver-binding to gills of rainbow trout (*Oncorhynchus mykiss*). Environ Toxicol Chem 14:1847–1858
45. Heijerick DG, De Schamphelaere KAC, Janssen CR (2002) Biotic ligand model development predicting Zn toxicity to the algae *Raphidocelis subcapitata*: possibilities and limitations. Comp Biochem Physiol 133C:207–218
46. De Schamphelaere KAC, Lofts S, Janssen CR (2005) Bioavailability models for predicting acute and chronic toxicity of zinc to algae, daphnids, and fish in natural surface waters. Environ Toxicol Chem 4:1190–1197
47. De Schamphelaere KAC, Vasconcelos FM, Heijerick DG, Tack FMG, Delbeke K, Allen HE, Janssen CR (2003) Development and field validation of a predictive copper toxicity model for the green alga *Pseudokirchneriella subcapitata*. Environ Toxicol Chem 22:2454–2465

Species Competition and Predation

Peter Chesson
Department of Ecology and Evolutionary Biology, The University of Arizona, Tucson, AZ, USA

S

Article Outline

Glossary
Definition of the Subject
Introduction
Feedback Loops
Exclusion Principles
Stabilizing and Equalizing Mechanisms
Competition-Based and Predation-Based Coexistence Mechanisms
Complexities of Foraging Behavior and Resource Acquisition

Environmental Variation and Population Fluctuations
Spatial Structure
Applications
Future Directions
Acknowledgments
Bibliography

Glossary

Apparent competition The tendency for an increase in the density of a species to increase the impact of a natural enemy on that same species or other species.

Competition The tendency for an increase in the density of a species to have a negative effect on the survival or reproduction of individuals of the same species or of other species by reducing resource abundance, reducing access to resources, or by direct harm of one individual organism on another associated with resource acquisition.

Density dependence The tendency for an increase in the density of a species to have a negative effect on the survival or reproduction of individuals of the same or different species. As used in this essay, the species in question are in the same guild. Competition and apparent competition are special cases of density dependence.

Feedback loop A chain of species interactions from one member of a guild, through other species, back to a species in that same guild. Feedback loops transmit density dependence.

Guild A group of species potentially co-occurring in the same locality and having similar ecology in the sense of depending on the same or similar resources, often seeking those resources in similar ways, and susceptible to the same or similar natural enemies. The standard of similarity in this definition is not precise, and varies depending on the purpose of the investigator.

Natural enemy An organism that benefits its own reproduction or survival by harming the individuals of a given species, commonly by feeding on them.

Niche overlap For any pair of species, the degree to which density dependence through feedback loops is concentrated between species compared to within species. It is measured by the quantity ρ which varies between zero for no overlap (no interspecific density dependence) and 1 for complete overlap (interspecific density dependence is on average equal to intraspecific density dependence).

Predator A species that gains food by killing and consuming individuals of the species in the ecological guild in question.

Species average fitness For a given species in a guild, it is a numerical measure of how well that species is adapted to the environment with the property that it predicts which species would dominate if the niche overlaps, ρ, were all equal to 1. It is normally related to the long-term average per capita growth rates of the species measured at fixed levels of competition and apparent competition. In this essay, the fitnesses κ are obtained from per capita growth rates at zero levels of competition and apparent competition, which are achieved by setting all members of a guild at zero density. These growth rates are then divided by scaling factors that correct for differences between species in their levels of sensitivity to competition and apparent competition.

Stable coexistence The tendency of the members of a guild to recover when individually perturbed to low density, allowing their long-term persistence in the presence of interactions with other guild members.

Definition of the Subject

Competition and predation are key interactions between species, and are major foci of thought and study in community ecology. They are believed to be major forces structuring natural communities, having critical roles in the determination of species diversity and species composition, and are regarded as important drivers of evolutionary processes. The relationships between the niches of different species determine how they interact through competition and predation, which then have key roles in assembly of local communities, and their reassembly following perturbations. Niches define patterns of linkages between species, their resources, and their natural enemies. These patterns include how linkages change over time, and between different spatial locations, and define mechanisms by which similar species are able to coexist by their effects on competition and predation relationships. The human element in the environment has profound effects

on these phenomena. Changing the environment shifts interactions between species, and profoundly modifies the structure of food webs. In the modern day, there is much community reassembly, potentially involving major shifts in competition and predation. Humans transport invasive species that act as predators, prey, and competitors with potentially major effects on the community reassembly process.

Introduction

Competition and predation are key species interactions that are believed to structure natural ecosystems and to have major roles in systems dominated by humans. Both of these interactions involve consumer–resource relationships in one form or another [1]. The relationship between a predator and one of its prey species is of necessity a consumer–resource relationship with the predator being the consumer and the prey its resource. Competition is mostly commonly resource competition, where several consumer species share one or more resources and compete for these resources [2–4]. A resource may or may not be a biological species. When the resources are biological species that are killed by the consumer, competition necessary involves predator–prey relationships. However, resource species may instead be grazed or browsed, parasitized or infected. In these cases, the consumer species are natural enemies of their resources, harming them without necessarily killing them, which generalizes the idea of a predator–prey relationship to a species–enemy relationship.

The resources of plants are generally not biological species, and indeed this is the case with the resources of most plants, which are instead broadly light energy, water, and chemical elements [5]. Plants are often thought of as requiring space to grow as a resource [4]. Space then provides their other needs. In general, not all space is equal, and plant species tend to be somewhat specialized, leading to the concept of safe sites [6] (places that satisfy the requirements for establishment, growth, and reproduction for a particular species), and the regeneration niche [5] (an elaboration of the idea of a safe site with a particular view to how species compete with one another). Sedentary animal species that either settle in a particular place and do not move, or establish territories, can also be regarded as having space as a resource [7]. Animal species require particular places for particular uses, such as nest holes and wallows, and use various dead organic and inorganic materials in their lives. These all count as resources if they are used or occupied by an individual to its benefit.

Both competition and predation are assumed to involve harm. In the case of predation, of course the predators benefit from the relationship, and prey are harmed because individual prey are killed. This does not, however, preclude some positive benefits of predation, or more generally of natural enemies, on species that are attacked, as these species may well be adapted to their natural enemies, and suffer some negative effects when natural enemies are removed. For example, grasses may be adapted to grazers that remove old, less productive biomass as well as enhancing nutrient recycling [8]. In the case of competition, harm is mutually negative for the participant species, though it is often lopsided with some species being harmed much more than others.

Resource consumption may reduce resource availability to individuals in species that depend on the resource. In this case, harm occurs when lowered resource availability leads to reduced fitness of individuals because they suffer directly by consuming less resource, have to expend more energy or materials to obtain the resource, take greater risks to obtain it, or have to divert time from other beneficial activities to do so. Competition is also assumed to occur by direct negative interactions between individuals seeking the resource. It is not necessary in such instances for resource consumption to lower resource availability, but the presence of other individuals decreases the ability of a given individual to consume resources, or in the process of seeking resources, individuals harm each other in other ways, for instance through fighting [9, 10].

Predation and species–enemy relationships necessarily have strong effects in ecosystems, as they form the paths of energy and material flows [1]. The role of competition between species is less obvious, often indirect, and frequently controversial [11]. Although it is easy to verify that a predator consumes a prey species, it is much more difficult to demonstrate that one consumer species harms another consumer species through their resource consumption activities. While numerous

rigorous experimental studies have firmly established that competition between species is frequently a strong force in nature, the effects of interspecific competition on various community properties have been difficult to establish. An abundance of theoretical work provides hypotheses, but rigorously testing of them in nature has proved to be difficult and often controversial [12–14]. Thus, although competition as a strong force is well established, the effects of that force are not.

Several difficulties arise in the study of competition. First, the consequences of competition between species (interspecific competition) do not rest with its absolute strength but with its strength relative to competition within species (intraspecific competition) [15]. Competition within species constrains the tendency of one species to harm another. Second, competition can be constrained by other interactions, such as predation, in some cases limiting its effects, but potentially interacting with competition in complex ways [16, 17]. Third, the natural world is extremely variable in time and space. This variability not only makes clear trends difficult to discern, it potentially interacts with competition modifying the outcome [15]. Thus, although competition can be shown to be present and strong, and is believed to have important implications for numerous community phenomena, clear tests of predictions have often been elusive.

The predictions from predation are most often of a different character from those of competition, yet they need not be. Competition comes from the interactions between consumers as a result of consumption of shared resources. Turning that on its head, when the resources are prey, they affect each other indirectly by providing food for common predators, potential increasing danger from those predator species. This indirect interaction between prey species is known to have analogous effects to competition, and has thus been termed apparent competition [18]. Although first suggested in a single-species context many years ago [19], it has only recently been generally understood, and so has received far less direct study than competition, but it is also likely that studies of competition have inadvertently included the effects of apparent competition: protocols to cleanly separate the two effects have yet to be developed.

Conceptual difficulties have plagued understanding of how competition and predation structure communities owing to the intrinsic complexity of the subject. The theory, however, has been making steady progress, and a much more comprehensive theoretical framework is available now than even a few years ago. The body of this essay explains the fundamentals of how competition and predation are hypothesized to structure communities in the light of these recent advances. Included are the intricacies introduced by the complex behavior organisms, and the often conceptually difficult area of how predictions about competition and predation can be made in the face of temporal and spatial variation in the physical environment, and in the presence of fluctuations in the populations of the organisms themselves. Applications to a theory of invasive species are then presented. Invasions of alien species represent perturbations to natural systems that can lead to a process of reassembly of communities of organisms. Competition and predation are believed to have large roles in this reassembly process, and explaining it is a critical challenge in community ecology. Because of the impacts of alien species on native communities, there are major implications for conservation biology also. Finally, challenges in the study of competition and predation, and promising future directions, are presented.

Feedback Loops

The fundamentals of competition and predation can be best understood in terms of feedback loops within a food web. Figure 1 shows a simplified food web, which should be considered as part of a food web rather than being any reasonably complete web that one might find in nature. It shows three trophic levels allowing understanding of how the middle trophic level is affected by the trophic levels above and below, which represent, respectively, predators and resources of that middle trophic level. Species in the same trophic level, by sharing trophic position, have strong similarities in their ecology. There may be other ecological similarities, and also differences within a trophic level, in the way the species relate to other trophic levels and to other elements in their environment. Species with similar ecology are commonly referred to as a *guild* and here the middle trophic level is the focus of discussion and is referred to as the focal guild, or just "the guild." How species in a guild interact with each other, and

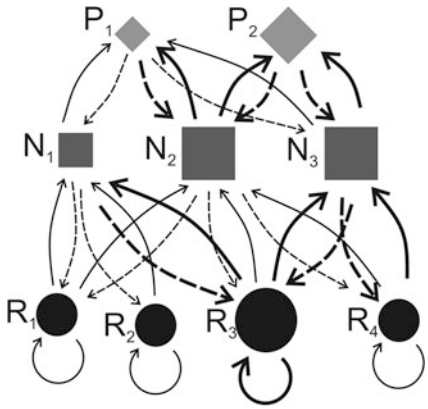

Species Competition and Predation. Figure 1
Representation of a subset of a food web with arrows showing directions of effects from one species to another. Differences in the thicknesses of arrows are meant to indicate differences in the strengths of effects. The different symbols distinguish trophic levels, and their size differences are meant to imply differences between species in population size within a trophic level. The letters *R* and *P* indicate that they are respectively resources and predators of the species, *N*, in the middle trophic level, with subscripts labeling species within a trophic level. These subscripted letters serve simultaneously as species labels and as the population densities of the species. The recursive arrows for resources mean they experience direct intraspecific competition of some form giving density feedback to themselves, but not direct interspecific feedback within the resource trophic level. An assumption like this is common in the Lotka–Volterra models discussed in this essay, and may also be applied to the predators too

ultimately coexist or instead exclude each other, leads to an understanding of how communities are structured, that is, an understanding of the relationships between the traits of different species that allow them to come together to form a long-lasting community, or in other words are assembled [20, 21]. Competition can be understood by considering the linkages between focal-guild species and their resources in the trophic level below. Linkages with the tropic level above lead to an understanding of apparent competition [22].

The arrows in the diagram show directions of effects. A species benefits from arrows pointing to it from a lower trophic level and suffers from arrows pointing to it from a higher trophic level. Chains of arrows define pathways of effects. Competition and apparent competition can be understood by pathways leading from the middle trophic level back to that level. For example, the species N_2 has pathways going from itself to each resource species, *R*, back to itself. These pathways contribute to intraspecific competition for N_2. The idea is that an increase in the density of N_2 leads to greater consumption of each resource species, *R*, reducing their densities and thereby reducing the availability of these resources for N_2. Pathways from these resources back to other species contribute interspecific competition. Thus, the pathways from N_2 through R_3 and R_4 back to N_3 lead to interspecific competition for N_2 on N_3. Through these various pathways, increasing the density of N_2 feeds back negatively to itself and to other species in the same trophic level. Critical to understanding of the ultimate effects of competition is the extent to which negative feedback of a species on itself limits its ability to increase and harm other species.

Apparent competition is understood by entirely analogous effects. In this case, we note that N_2 is preyed upon by P_1 and P_2. An increase in N_2 benefits both P_1 and P_2. These predators may therefore increase in abundance, and as a consequence, predation on the second trophic level will increase. Again, increasing the density of a species in the middle trophic level feeds back negatively to itself and to other species. Thus, in a food web, multispecies density dependence occurs when changes in the density of a species within a given trophic level feed back to that trophic level through linkages to other trophic levels, modifying the growth rates of the species. The term "density dependence" is traditionally used in ecology just for feedback from a species to itself, but understanding of the joint effects of predation and competition requires broadening of this concept to *interspecific density dependence* where increasing the density of one species affects the per capita growth rate of another species. Consistent with this usage, the traditional density dependence concept of ecology becomes *intraspecific density dependence*. Competition and predation both contribute to intraspecific and interspecific density dependence [17].

Basic understanding of the role of competition in ecological communities is usually represented by the Lotka–Volterra competition equations. Using the

species labels to mean also their densities, these equations can be written in the form

$$\frac{1}{N_i}\frac{dN_i}{dt} = r_i\left(1 - \sum_{j=1}^{n}\alpha_{ij}N_j\right), i = 1, \ldots, n. \quad (1)$$

These equations define the per capita growth rate of each species in the focal guild, which reflect the average conditions that individuals of each species experience. The quantity r_i is the maximum per capita growth rate of species i, which is reduced by the terms representing density dependence inside the parenthesis. The coefficient α_{ij} measures density dependence of species j on species i. It measures how much the per capita growth rate of species i, as a proportion of its maximum value r_i, is decreased by increasing the density of species j by one unit. This coefficient measures interspecific density dependence if j is different from i, and intraspecific density dependence if $i = j$. The coefficient of intraspecific density dependence defines the so-called carrying capacity for a species: $K_i = 1/\alpha_{ii}$. Traditionally, the Lotka–Volterra competition equations have been parameterized with the competition coefficients defined as multiples of the carrying capacity, with the carrying capacity itself appearing explicitly in the equations, but this approach is now known to obscure the workings of the equations [15], and so is not done here.

Recent understanding shows that the Eq. 1 can also represent apparent competition, not just competition, and indeed they can represent the combined effects of competition and apparent competition. To do this, the equations are derived from a larger set of equations that take account of the direct interactions of the focal species with other species in the food web [17]. Thus, these equations have explicit formulae defining the effects of the arrows for a food web like Fig. 1. Equation 1 is then able to define the long-term growth of the species in the focal guild in terms of feedback loops from other species. The α_{ij} are given by formulae derived from this larger set of equations and depend specifically on how species forage for their resources, how they are preyed upon by their predators, and how these resources and predators change in density in response to density changes in the focal guild [17]. It is important to note, however, that Eq. 1 does not apply to short-term prediction, but to long-term outcomes such as long-term recovery of a population from low density, or eventual extinction [17]. Although the Lotka–Volterra competition equations are used generically in ecology, it should be appreciated that they are very specific, and can only be used to illustrate general principles, not to give precise outcomes in any given system. Fortunately, there are means of matching Lotka–Volterra models with models for particular systems that validate their use for general principles when treated appropriately [4, 15, 23].

The key issue to be addressed with the Eq. 1 is when species coexistence will occur, and when some species will be excluded from the community. This is easy and straightforward in the case of a guild of two species, and this case gives some key general principles [17]. The fundamental result in the two-species case is that species j can exclude i from a community if

$$\alpha_{ij} > \alpha_{jj}. \quad (2)$$

The reverse inequality means that species i is always able to invade the system when dominated by species j. The mutual invasibility criterion [24] then says that two species, labeled 1 and 2, will coexist stably whenever they are both able to recover from low density in the presence of the other species. In the two-species Lotka–Volterra equations, this criterion leads to the condition

$$\alpha_{11} > \alpha_{21} \text{ and } \alpha_{22} > \alpha_{12}. \quad (3)$$

Fundamentally, this means that for stable coexistence, each species must depress its own growth more strongly than it depresses the growth of the other species as it increases in population density. It is a very simple and general criterion that ensures stable coexistence [15]. If one of the inequalities in (Eq. 3) is reversed, then one species can exclude the other, and not vice versa. This means that one species always drives the other extinct. On the other hand, if both inequalities are reversed, then each species can exclude the other. This means that neither species can invade a system consisting of the other species. Whichever species establishes first remains the sole occupant in the guild in question in that locality.

The Lotka–Volterra competition Eq. 1 can be interpreted directly as meaning direct interference of individuals of all species with individuals of other species, harming them by reducing foraging time or in

some cases by cannibalism or *intraguild predation*, which refers to predation by one species in a guild by another species in that guild [25]. In this case of direct interference, resource shortages or predators need not have a role [9–11]. Indeed, it is in this form that the Lotka–Volterra equations are in principle most accurate, given that they do not explicitly represent the dynamics of resources or natural enemies outside the guild in question. In these cases, they are valid for short-term as well as long-term predictions. In these cases of direct interference, conditions (Eq. 2) and (Eq. 3) then apply, respectively, to exclusion and coexistence, showing in particular that coexistence requires each species to interfere more strongly intraspecifically than interspecifically.

When the Lotka–Volterra equations are used to represent trophic interactions such as those of the food web Fig. 1, the coefficients of density dependence α can be defined in terms of quantities that summarize the interactions in the food web: niche overlap, ρ, and species-level average fitness, κ [17]. The niche overlap, ρ, between any pair of species is a measure of the relative strength of the density-dependent feedback between versus within species through resources and through predators. This quantity takes the value 1 when there is complete overlap, and zero when then there is no overlap. No overlap occurs when the members of the pair of species under consideration do not share resources and do not share predators. Thus, they do not have arrows to or from any of the same resources or predators in Fig. 1. With complete overlap, they have arrows to and from all of the same resources and predators, and these predators and resources are of the same relative importance for each species in the guild. If the resources and predators vary in importance for different species, but nevertheless both species under consideration are affected by them, then ρ will be between 0 and 1. Figure 2 gives various scenarios for different strengths of niche overlap.

The average fitness measure, κ, for any given species measures its ability to meet its energy needs and avoid predation when all species in the guild are at low density and thus not providing any feedback through density changes. This measurement is also expressed in special units, namely, in units of average sensitivity of the per capita growth rate of the species to changes in resources and predators. These quantities ρ and κ now relate to the coefficients of density dependence according to the relationship

$$\frac{\alpha_{ij}}{\alpha_{jj}} = \frac{\kappa_j}{\kappa_i}\rho. \tag{4}$$

Thus, the ratio of interspecific to intraspecific density dependence for species j's impact on species i is equal to the ratio of the fitness of species j to species i, multiplied by the overlap measure. This relationship is correct regardless of how many species are present in the guild in question. However, when there are just two species, the condition that the ratio (Eq. 4) be greater than 1 is the condition (Eq. 2) for species j to exclude species i. The ratio being less than 1 means that exclusion does not occur. These conditions in terms of the fitness ratio, multiplied by the overlap measure, are also strongly intuitive and instructive in terms of how stable coexistence occurs.

Consider the case of complete niche overlap, $\rho = 1$. Then the formula (Eq. 4) implies that whichever species has the larger fitness will exclude the other species. In other words, a simple fitness ratio greater than 1 is sufficient for one species to exclude the other. When $\rho < 1$, the fitness ratio is discounted by the overlap measure to determine if exclusion will occur. For example, if the overlap is ½, a species has to have fitness more than twice as high as the other to exclude it. The mathematics implies this outcome, but intuitively the idea is that the less species overlap in their niches, the more difficult it is for one species to exclude the other, but this can still occur if a species has a strong enough fitness advantage.

It is also worth noting that ρ is a symmetric measure of the ratio of interspecific to interspecific density dependence for any pair of species i and j, as formula (Eq. 4) implies that

$$\rho = \sqrt{\frac{\alpha_{ij}}{\alpha_{jj}} \cdot \frac{\alpha_{ji}}{\alpha_{ii}}}. \tag{5}$$

Thus, ρ can be thought of as niche overlap, and at the same time as the geometric mean of the ratios of interspecific versus intraspecific density feedback for any pair of species. Thus, it measures the potential for stabilization of coexistence without taking into account the fact the ratio might be different for one species compared with other and lead to dominance instead

of coexistence. The formula (Eq. 4) shows how that bias changes as the fitness ratio changes, suggesting, as we shall see below, how changes in circumstances can change the opportunities for coexistence.

Niches and Species Coexistence Mechanisms

The results of the Lotka–Volterra equations can now be applied to see how a guild of coexisting species is constrained by trophic relationships. For two species to coexist, the conditions (Eq. 3) together with the formula (Eq. 4) imply that

$$\rho < \frac{\kappa_1}{\kappa_2} < \frac{1}{\rho}. \tag{6}$$

Fundamentally, this says that species 1 and 2 will coexist stably if their fitness ratio lies between ρ and $1/\rho$. Thus, the less the niche overlap, the greater the difference in fitness that is tolerated compatible with species coexistence. These conditions involve two kinds of differences between species that affect species coexistence in opposite ways. First are fitness differences, which are measured in terms of the deviation of the fitness ratios from 1. This ratio fundamentally measures the overall relative degrees of adaptedness of the species to their common environment. A species with a larger value of κ can be thought of as a better performer, and therefore inequality in this respect understandably favors exclusion.

A complication arises due to the fact that when different focal species are present, the resource species or predator species maintained in the food web may be different [17]. When we ask if species 1 can exclude species 2, those resources and predators present when species 1 is present alone are used to calculate the fitnesses and niche overlap for both species 1 and 2. When we ask if species 2 can exclude species 1, a different set of resources and predators might be present. This means that in some cases, the ρ and κ ratio for each end of the inequality in (Eq. 6) will be different, and will have to be calculated based on which focal species is present. While, this complication does not alter the fundamentals as to whether a given species can exclude another species from a community, it is important to keep in mind that ρ and the κ's may change with the circumstances [26, 27].

What do these critical quantities measure? Although the κ's and ρ both involve aspects of resource consumption and predation, they measure independent aspects. In particular, the quantity ρ is independent of how well the species are adapted to the environment. Instead it compares species in terms of which trophic links (links to resources and predators) are most important to them, and how important they are, as illustrated in Fig. 2. Importance is measured in terms of the ability of that link to generate density-dependent feedback [17]. This comparison shows how much the species interact with each other through their resources and natural enemies and so how much conflict there is between them: the larger ρ is, the larger the conflict. Naturally, two individual organisms have greater similarity and therefore greater conflict through trophic relationships within species than between species (not counting the effects of overall fitness differences), and ρ is a relative measure comparing between-species interactions through trophic links to within-species interactions. In other words, it compares the strength of interspecific feedback loops with intraspecific feedback loops, in essence adjusted to equal overall fitness. Thus, the ratio κ_1/κ_2 and niche overlap ρ represent two different kinds of comparison between species.

Exclusion Principles

Recognition of these two separate kinds of ecological comparison between species resolves a conundrum about the competitive exclusion principle [28], which is often stated as "no two species can occupy the same ecological niche." It has been a problematic principle because often the niche is not defined precisely enough to give the principle content. Indeed, there are many and various definitions of the niche [29], but perhaps the one most usefully behind the principle is the Eltonian niche which is about how an organism uses the environment [29]. However, when natural enemies are considered, the niche must include not just how a species uses the environment, but also how other organisms in the environment use that species. Thus, the niche needs to be defined as how an organism relates to the environment [15, 29]. Regardless of whether this idea can be measured in an absolute sense, the quantity ρ provides a relative sense in which two species relate to the environment. This definition specifically removes the overall level of adaptedness to the environment from

the comparison between species, focusing on how they relate to it. This way of comparing niches differs markedly from what would be concluded from comparing niches according to the recent niche definition of Chase and Leibold [29]. Under their definition, the conditions in the environment defining zero per capita growth rates are the niche. That means species would only overlap completely if their growth rates were zero under exactly the same conditions. Species with $\rho = 1$ would overlap completely according to the approach here, but would not have zero growth under the same conditions unless their κ values were the same too.

The sense in which the competitive exclusion principle is correct is that no two species can coexist stably if their niches overlap completely, i.e., $\rho = 1$. The Lotka–Volterra approach defines this idea here, and makes it precise, but it is important to realize that it in fact emerges from a broad array of models, as will be discussed further below, without evidently any contrary models. More important, these ideas allow a quantitative approach to the competitive exclusion principle. A niche overlap value of $\rho = 1$ is an unlikely occurrence in nature, but a value near 1 is not unreasonable. Here condition (Eq. 6) shows that when species have high niche overlap, their fitnesses are very closely constrained to be more nearly equal. Thus, there is a more quantitative exclusion principle that relates not just to competition, but to apparent competition too, and states that species with high niche overlap must have correspondingly high similarity in average fitness if they are to coexist. This principle then replaces a statement with limited application to a more significant one about the difficulty of coexistence for species with strongly overlapping niches. That degree of difficulty is measured by how similar in average fitness the species must be to allow coexistence with that degree of overlap.

Stabilizing and Equalizing Mechanisms

The expanded exclusion principle defined here is broadened with the realization that there are two general but not equivalent ways in which species coexistence can be favored. First is low overlap in niches, and second is similarity in average fitness. Mechanisms that lead to low niche overlap are called stabilizing mechanisms, and those that lead to similar average fitnesses are termed equalizing mechanisms. The issue that distinguishes these two ways of achieving coexistence is the role of feedback loops. Niche overlap, ρ, is fundamentally about feedback loops. Low niche overlap means feedback loops between species are weak relative to those within species. As emphasized above, this is essential for coexistence to be stabilized. Thus, mechanisms that bring about low niche overlap are called stabilizing mechanisms. Stabilizing mechanisms vary from the obvious to the subtle. Specialization of the members of a guild on different resources is the stabilizing mechanism termed resource partitioning [30], which quite directly leads to low contributions to ρ (Fig. 2a, d, and e). Likewise, if the natural enemies of the guild members are specialists, feedback loops through predation are separated (Fig. 2a and c). This is natural enemy partitioning [17]. As we shall see below, these direct and obvious stabilizing mechanisms are far from the only ones. Likely involved in these scenarios are trade-offs that provide advantages to specialization. For instance, consumers well equipped to exploit a particular resource, or predators well equipped to attack a particular species, may not be so well equipped to exploit a different resource or attack a different species because the very equipment that works well in a specific situation does not work so well in another [11, 31].

Equalizing mechanisms do not have to involve the feedback loops at all. In the Lotka–Volterra model considered here, the fitnesses are measured at low density, and so density feedback has no direct role [17]. One can ask what mechanisms might lead species to be similar in average fitness in a given environment. It is clear that the laws of physics come in at the ultimate level and constrain performance differences between species. But there are still numerous ways in which species might differ in efficiency at a given task. Many trade-offs might be seen as equalizing mechanisms in that doing well in one respect might mean doing less well in another respect [29]. For instance, defense against predation or harsh physical environmental conditions might lead to lower growth rates of individual organisms and perhaps slower rates of reproduction. Thus, one species might have higher survival rates but suffer in reproduction relative to another species, thus limiting the fitness differences between species that are possible.

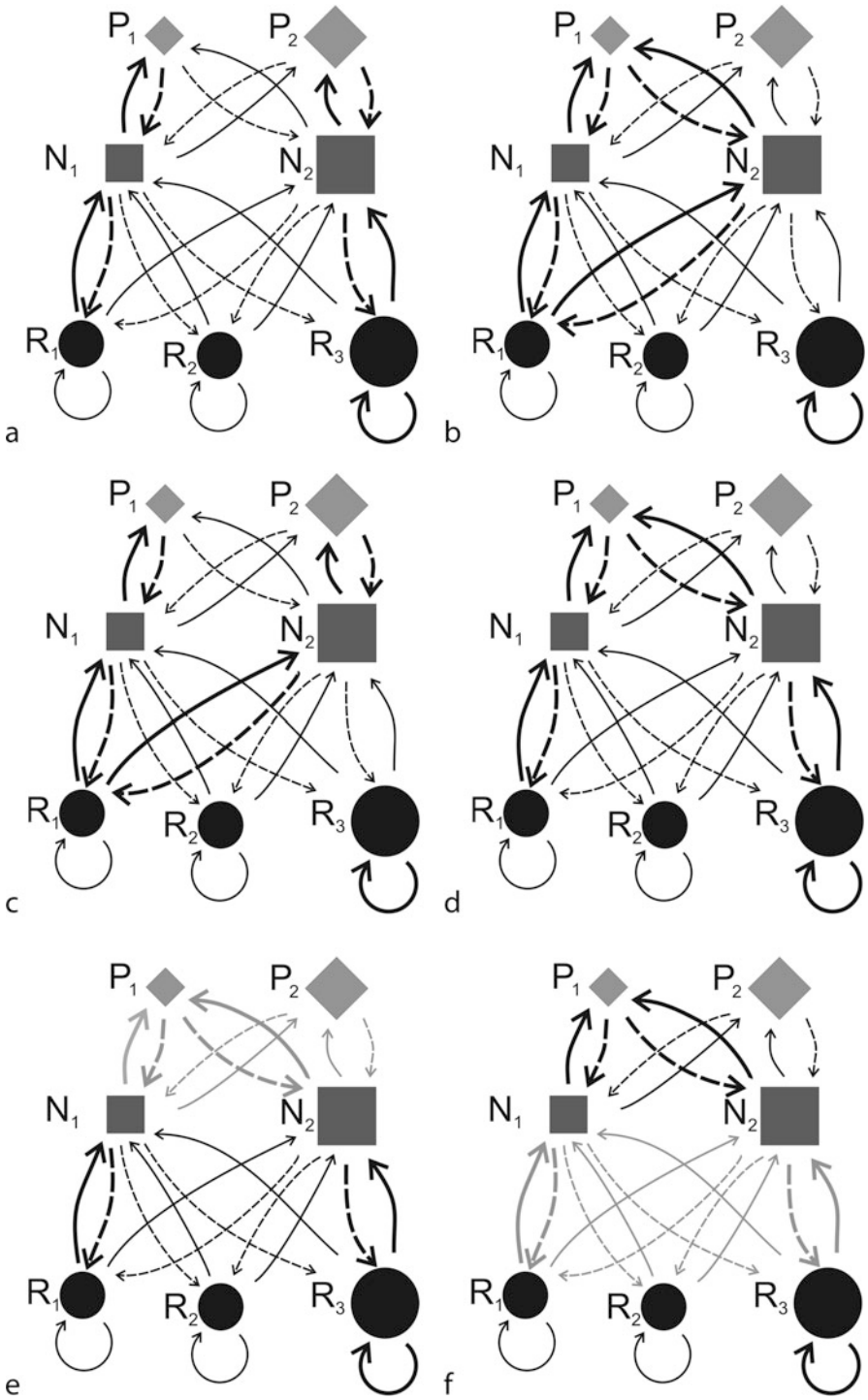

Species Competition and Predation. Figure 2
(Continued)

There is as yet no general theory of equalizing mechanisms, but one is likely to emerge from general principles of community assembly and natural selection. Natural selection drives species to the limits of what is possible: for instance, not being defended against harsh conditions, while not growing fast, are certainly possible in an organism, but if it is also possible through a genetic change to grow faster if expenditures on defense are low, or to be defended if growth is slow, then that character is likely to evolve. The constraint on what is possible is approached, which enforces the trade-off [4]. This process happens within species, as it involves natural selection at the individual level. The process of relevance between species is community assembly. More efficient species arriving in a particular locality are likely to displace others there, and that process will continue until constraints on efficiency are approached, trade-offs apply, and fitness differences are minimized.

It should be recognized that many constraints in nature may have both stabilizing and equalizing aspects to them. Trade-offs associated with resource partitioning may lead to stabilization as well as equalization, provided similar profit is derived from use of the various different resources involved. There is also a body of thought leading to the neutral theory of community ecology which says that highly diverse natural communities, such as tropical forests, behave as if all average fitnesses are equal, and stabilizing mechanisms are absent [32]. In terms of the theory here, this would mean that the average fitnesses, κ, are the same for all species and $\rho = 1$ for every species. Coexistence cannot be stabilized in these circumstances: invader growth rates are zero, and in the Lotka–Volterra model, the total abundance of all species is stabilized, but relative abundances are not. They are instead predicted to drift as a consequence of the chance processes of individual birth and death. However, there is no general reason to expect this extreme situation to arise in nature. The patterns that agree with those in nature can also be predicted by models with stabilizing mechanisms present [33], and fitness differences in systems without stabilizing mechanisms quickly lead to the collapse of diversity [34].

Competition-Based and Predation-Based Coexistence Mechanisms

Competition is often thought of as a major factor that limits species diversity, without a clear distinction being made between interspecific and intraspecific competition. That thought quickly leads to the idea that lower population densities will lessen the magnitude of competition and therefore promote the maintenance of species diversity [16]. In particular, that line of reasoning leads to the idea that high mortality rates, or harsh and stressful conditions, might generally promote species diversity [35]. However, as emphasized above, it is the ratio of interspecific competition to intraspecific competition that is critical to species coexistence and not the absolute value. Thus, lowering densities, and indeed lowering the intensity of

Species Competition and Predation. Figure 2
Different scenarios for indirect linkages between the focal species, N_1 and N_2, through their resources and predators, leading to different degrees of niche overlap, ρ. Thick arrows indicate relatively strong linkages compared with thin arrows. A gray arrow indicates that although the linkage might be important, it is not a strong source of density-dependent feedback for focal species. (**a**) Low niche overlap because the strong links to both resources and predators differ between N_1 and N_2. (**b**) High niche overlap because the strength of the links between N_1 and the various resources and predators has the same pattern as the strength of the links between N_2 and these resources and predators. Although these two species do discriminate between these resources and predators, they do so in an identical way. (**c**) High niche overlap through resources, but low niche overlap through predators, leading overall to an intermediate level of niche overlap. (**d**) Low niche overlap through resources, but high niche overlap through predators, leading overall to an intermediate level of niche overlap. (**e**) As in **d**, but predation is not strongly density dependent, and so overall niche overlap is low due to the low overlap through resources. (**f**) As in **d**, but resource consumption is not strongly density dependent, and so overall niche overlap is high due to the high overlap through predators

competition, need not have any effect on the ratio of interspecific to intraspecific competition, and therefore need have not have any effect on species coexistence. In fact, competition can be important for stable coexistence. If competition is the only form of density dependence, then it is essential for stable coexistence. The challenge for species coexistence is not competition per se but interspecific competition that is strong relative to intraspecific competition. A pattern of species interactions that intensifies intraspecific competition relative to interspecific competition is a competition-based species coexistence mechanism [17].

Recent appreciation that density dependence from predation can play a similar role to competition leads to the idea of predation-based coexistence mechanisms. These are mechanisms that concentrate intraspecific apparent competition relative to interspecific apparent competition [17]. What then are the joint effects of competition and predation on species coexistence? Both natural enemy attack and resource competition are likely to be important in most guilds of coexisting species simply because it is difficult to avoid these phenomena. In discussions of species coexistence, predation has sometimes been viewed as important primarily as a cause of high mortality, and therefore not distinguished from harsh or stressful conditions in its effects [16]. However, as remarked above, such conditions need have no effect on species coexistence because they need not be associated with density-dependent effects, although they would alter species average fitness ratios if they were species-specific in effect.

The feedback loops expected with trophic interactions mean that predation would likely act in a density-dependent way. However, it is also possible that its density dependence might be weak relative to other sources and function on different spatial and temporal scales. For instance, predators that range over a much larger area than the focal guild might not be very responsive to the changes in the density of the focal guild. Predators might also live much longer and so change in density much more slowly than their prey in the focal guild, and they might also depend more heavily on species outside the focal guild and so not be so responsive to the focal guild even though they inflict mortality on them. Thus, it is not unreasonable to entertain the hypothesis that in some situations predation acts in an approximately density-independent way.

Density-independent predation would reduce the fitnesses κ of the species in the focal guild. From the two-species coexistence condition, it is clear that it would only affect coexistence if the ratio κ_1/κ_2 were affected, or in the multispecies case, if the ratio of any species' fitness to the guild average fitness were affected [15]. If fitnesses are unequal in the absence of predation, the same reduction for each fitness has the effect of making the fitness ratio deviate further from the value 1, which is more likely to lead to exclusion than coexistence. However, a trade-off that led to a disproportionately large reduction in fitness for the species with larger fitness ("selective predation on the competitive dominant") [16, 36] would make the fitness ratios more equal provided predation was not too strong. The requirement that the predation be not too strong leads to an intermediate predation prediction: predation promotes diversity for intermediate intensities of predation [16, 36].

Empirical studies have noted strong effects of predators in some guilds [37]. Of particular note are those consisting of sessile intertidal organisms, where the predator or herbivore is necessary for the maintenance of diversity [36, 38]. These predators are often termed keystone predators due to their essential role [38, 39]. Discussions of keystone predators often emphasize selective predation without regard for a density-dependent role of predation [37]. However, density-independent selective predation is purely equalizing and would be incapable of stabilizing coexistence in the absence of a separate stabilizing mechanism, such as resource partitioning [16].

It is reasonable to expect that a keystone predator would respond at least to some extent in a density-dependent way to its prey. A density-dependent but nonselective predator, i.e., one that does not affect the fitness ratio, would in fact have the effect of undermining competition-based coexistence, and thereby undermine coexistence overall. This would occur because such a predator adds equally to intraspecific and interspecific density dependence, diluting the effect of resource partitioning and increasing the value of ρ, weakening coexistence. A density-dependent but selective predator need not have negative effects on coexistence provided it is selective on the competitive dominant [40],

but it would still be limited in its effects on coexistence without the presence of other stabilizing mechanisms, because alone it would not add the sort of structure to feedback loops able to separate many species [16, 35]. Indeed, the patterning of feedback loops would be quite limited. Lotka–Volterra theory in this case predicts that at most two species can coexist stably when species in the focal guild do not partition resources, and there is only one predator present, regardless of how the predator distributes its attacks [41].

Fundamentally, development of the keystone species concept has viewed predation and competition as very different kinds of interactions, and has not focused adequately on the true requirement that density dependence needs to be concentrated more strongly within species than between species to promote stable coexistence [16]. Simply reducing the magnitude of competition uniformly does not achieve this, and equalizing fitnesses alone does not achieve this in the absence of a separate and strong stabilizing mechanism [16]. Certainly it is conceivable that a keystone predator might focus its attacks in such a way that fitness is approximately equalized across species, which would achieve approximate neutrality, but there is no mechanism that makes this likely. Trade-offs between susceptibility to predation and competitive ability would work in the right direction [40], but there is no reason for these trade-offs to be sufficiently precise to yield approximate neutrality, which nevertheless would not stabilize diversity, just slow its loss. Though keystone predation can indeed be shown to have strong effects in some communities [16], the stabilizing mechanisms needed to make it effective have neither been identified nor sought.

The theory discussed above identifies predator partitioning as an important way in which predation can promote diversity. Indeed, predators and other natural enemies can have very strong effects on their prey populations, and it is not uncommon for predators to be relatively specialized [11]. In fact, if the predators of a guild partition their resources (the prey populations in the guild in question), it follows reciprocally that the prey are partitioning predators. Thus, predator partitioning should have about the same prevalence in nature as resource partitioning. If both predator partitioning and resource partitioning are present for any given guild (Fig. 2a), the reasonable expectation is that the strength of coexistence would be stronger than if only one of these were partitioned (Fig. 2c and d). Indeed, the evidence from models points in this direction [17]. However, this outcome applies when predators that partition their prey are substituted for predators that do not partition their prey. A situation of great importance in nature is removal, addition, or restoration of predators, as occurs with human activities, although human activities might sometimes substitute one kind of predator for another [42–44]. In this case, adding predators that partition the focal guild to a comparable extent to the partitioning of resources in the focal guild would not greatly change the strength of coexistence. The reason is that there would be little change in the ratio of interspecific to intraspecific density dependence. However, adding predators that do not partition would increase the ratio of interspecific to intraspecific density dependence, undermining resource partitioning and therefore undermining coexistence, as noted above.

These effects of adding or removing predators, or changing their properties, can be summarized in terms of changing values of ρ as the scenario changes. Note that ρ is the niche overlap measure, but is also a symmetric measure of the ratio of interspecific to intraspecific density dependence by Eq. 5. Defining the case under consideration in parentheses gives the following chain of inequalities:

$$\begin{aligned} &\rho(R_p, P_p) \approx \rho(R_p) \approx \rho(P_p) \\ &< \rho(R_p, P_{np}) \approx \rho(R_{np}, P_p) \\ &< \rho(R_{np}, P_{np}) = \rho(R_{np}) = \rho(P_{np}) = 1. \end{aligned} \tag{7}$$

Here R or P indicates the presence of resource competition or apparent competition, and the subscripts "p" and "np" indicate partitioned and not partitioned interactions. As smaller values of ρ mean stronger coexistence, the situations are ranked from strongest coexistence to no coexistence, from left to right. The approximate equality of $\rho(R_p)$ and $\rho(P_p)$ in (Eq. 7) is not a conclusion, but the assumption that resources and predators are partitioned about equally, specifying the scenario considered here. The rest of the inequalities and approximations are conclusions. When P or R is not listed in parentheses, predators or resources may still be present, but are not important sources of density dependence. For instance, strongly density-dependent predation can prevent resource competition

from occurring even though resources are still consumed and contribute essentially to fitness.

When competition and apparent competition are both present, the value of ρ is intermediate between the values that occur when only one of these is present. Thus, when they are both partitioned in inequalities (Eq. 7), the value of ρ does not change much, regardless of whether competition and predation are both present, or only one is present (e.g., Fig 2a vs. 2e). When they are both present, but only one is partitioned, the value of ρ is necessarily higher than when they are both partitioned because then a smaller fraction of all density-dependent interactions are partitioned, reducing the distinction between interspecific and intraspecific density dependence (Fig. 2c and d vs. 2a). The reason is that there is less partitioning overall among the array of density-dependent interactions experienced. No partitioning leads to a value of ρ equal to 1 (Fig. 2b), regardless of which interactions are present, and therefore no possibility for stable coexistence.

The situation not considered in the inequalities (Eq. 7) is when there is partitioning between predation and competition (Fig. 3). In this case, although there is no partitioning of resources or predators, there is joint

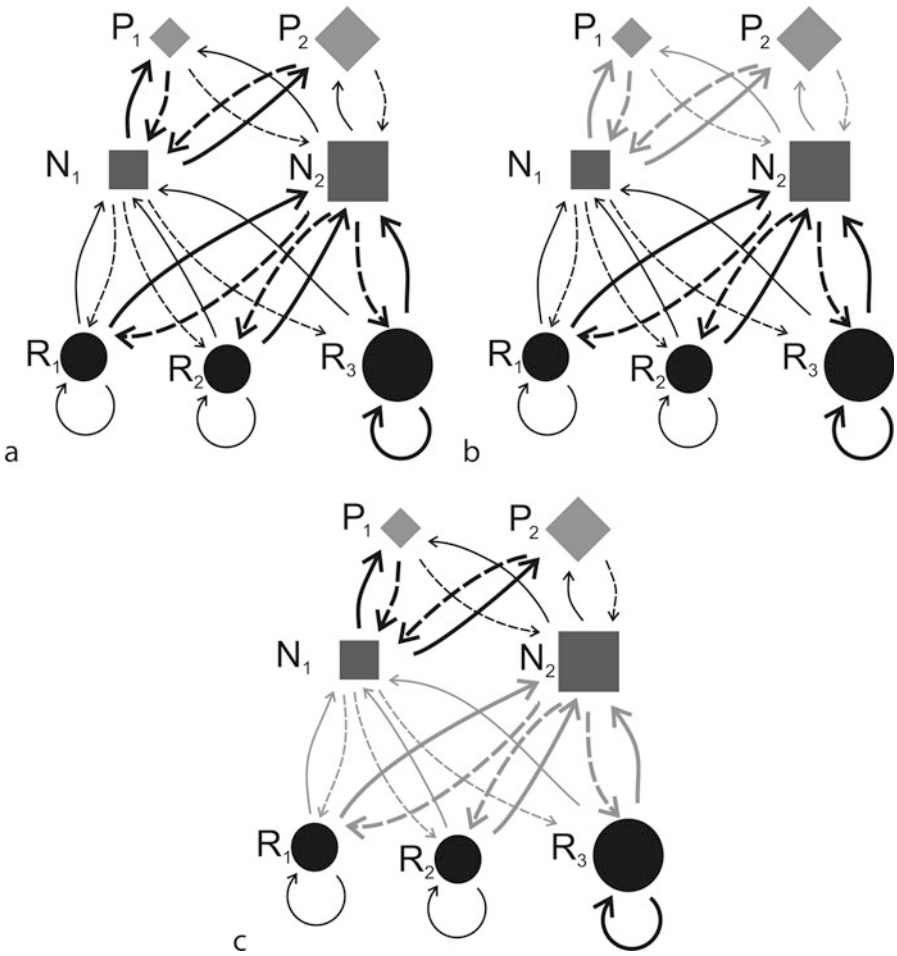

Species Competition and Predation. Figure 3

General features as for Fig. 2. (**a**) Trade-off between competition and predation (apparent competition). Species 1 is more sensitive to predation, and species 2 is more sensitive to resources. Both resource consumption and predation are density dependent. Niche overlap is low. (**b**) As for (a), but only resource consumption is strongly density dependent. Niche overlap is high. (**c**) As for (a), but only predation is strongly density dependent. Niche overlap is high

partitioning of them in that some species have strong predator feedback loops, being particularly susceptible to predation, and some species have strong resource feedback loops and therefore are particularly susceptible to resource competition [40]. This is a predation-competition trade-off. But without partitioning within these interactions, at most two species can coexist. The predator is selective in this case, and it is simply the keystone species case once again. It implies

$$\rho(R_{\mathrm{np}}, P_{\mathrm{np}}) < \rho(R_{\mathrm{np}}) = \rho(P_{\mathrm{np}}) = 1 \tag{8}$$

as illustrated in Fig. 3. Although theoretically interesting in that it leads to coexistence in the absence of resource partitioning, it is not a serious solution to the maintenance of high diversity by means of predation because, by itself, it allows stable coexistence of at most two species as discussed in detail above.

Complexities of Foraging Behavior and Resource Acquisition

Predation and resource competition intimately involve the behavior of the organisms in seeking food and resources, or avoiding predation [45]. Interference competition is one behavior that is accounted for reasonably well in the Lotka–Volterra competition equations, as discussed above, as direct contributions to the coefficients of density-dependence α. However, other aspects of the behavior of organisms are not accounted for well because all resource acquisition rates and foraging rates are assumed to be linear, i.e., the amount of any resource or prey consumed or captured by an individual organism per unit time is simply proportional to the abundance of that resource or prey [17]. One very simple and almost unavoidable deviation from the linearity of Lotka–Volterra equations occurs through the simple fact that an individual organism is generally limited in how much resource can be consumed per unit time, or how many prey can be captured and consumed. As a resource or prey becomes very abundant, the rate of consumption normally plateaus. Such plateaus weaken density-dependent feedback as densities increase, creating instabilities in population dynamics and promoting population fluctuations [1].

There is a vast literature on how these fluctuations might be stabilized and the extent to which they are indeed responsible for population fluctuations in nature [1]. Some scenarios involving population fluctuations provide further mechanisms of coexistence, because they enable population fluctuations to be partitioned by the various species, as discussed below (*environmental and population fluctuations*). However, when such nonlinearities are not strong enough to destabilize dynamics, and even in many cases when they do, the general principles for the Lotka–Volterra case continue to apply to the extent that they have been studied theoretically. For instance, a very general development of Levin [41], though lacking specific detail, is entirely consistent with the messages from the Lotka–Volterra development on partitioning resources and predators.

Resource-competition models where the resources do not regenerate in a Lotka–Volterra manner have also been studied [46], reproducing much of the detail, even quantitatively, for the Lotka–Volterra case. For plants, the key resources are light energy and simple inorganic compounds. Obtaining them in the right proportions is key to optimum plant growth, which makes the equations not just nonlinear, but nonadditive in the different resources. Despite these differences, the qualitative picture given here reappears in a different quantitative form [29, 31]. Nonlinear predation for equilibrium scenarios has been studied in limited situations [40, 47–49]. Quantitative variations on the results from the Lotka–Volterra case are found, but again in general the qualitative messages here remain intact. The reason is the fundamental nature of the requirement for coexistence that a species should inhibit its own growth more than it inhibits the growth of other species if it is to coexist with them. Thus, the requirement that intraspecific density dependence be stronger than interspecific density dependence is a robust requirement [15]. More complex nonlinear situations differ only in providing alternative ways of achieving this outcome. Partitioning of the environment, in one form or another, remains common among these alternative models. The major exception is for complex behaviors that lead to frequency dependence, as discussed next.

Some of the strongest effects occur when the per capita rates of foraging depend on the relative abundances of the species. The linear rates assumed in the Lotka–Volterra development mean that the fraction that any particular prey species represents in the diet

of a predator is proportional to the abundance of that prey species. This makes intuitive sense as a prey species might be expected to be encountered at a rate proportional to its abundance. However, if a predator's efficiency at finding a prey species, or capturing it, increases with the rate at which it is encountered, then the actual rate of capture is super-proportional to the abundance of the prey species. The effect of this on the prey mortality rates is to make them increasing functions of intraspecific prey density, and possibly decreasing functions of the densities of other species. This phenomenon is known as frequency-dependent predation [50]. An important outcome is the intensification of intraspecific apparent competition relative to interspecific apparent competition. In models, frequency-dependent predation has been shown to be a powerful species coexistence mechanism. At a qualitative level, the outcome is similar to predator partitioning (or natural enemy partitioning) where each prey species has its own specialist natural enemy [50, 51]. Thus, frequency-dependent predation achieves with one natural enemy the same effect as several specialist natural enemies that do not have frequency-dependent behavior.

Frequency-dependent predation, which is also called "switching" in the ecological literature [52, 53] and "apostatic selection" in the evolutionary literature [54], has considerable empirical support to the extent that it has been studied [50]. Most studies reporting this phenomenon have been laboratory studies, with few prey species, and much less is known empirically from field studies. Moreover, the theoretical studies have only demonstrated multispecies coexistence from symmetrically acting forms of frequency-dependent predation: those that might be expected from increasing prey encounter and capture efficiency with increasing prey abundance [51]. The theory of optimal diet selection, however, leads to an asymmetrical form of frequency-dependent predation where the per capita predation rate on prey of low value to a predator depends on the absolute abundance of higher ranked prey, and not directly on the abundance of that prey itself [55]. Although coexistence can be promoted also by this form of behavior [56, 57], it is much less well investigated than symmetrically acting frequency dependence, and its performance in multispecies situations is not understood.

Environmental Variation and Population Fluctuations

Environmental fluctuations are often intuitively expected to undermine equilibrium perspectives such as those developed on the basis of Lotka–Volterra models [58]. In fact, however, rather than undermine them, they provide new contexts in which the critical phenomena considered here are realized. Fundamentally, they allow resource partitioning and predator partitioning to occur on large scales of time even though they do not occur on small scales [51, 59]. This is possible because different species in the same guild may have different responses to the physical environment, such as weather. Annual plant species, for instance, often have species-specific weather-dependent germination requirements. As weather patterns vary from year to year, and sometimes very markedly, this means that guilds of annual plants often show very marked variation from year to year in the relative abundances of the plants that successfully germinate, grow, and flower [59, 60]. Those that are not successful in given year can bide their time as dormant seeds in the soil, with good chances of success in some future year. In this way, intraspecific competition becomes concentrated relative to interspecific competition when a sequence of years of different environments are considered, as this behavior means that a given individual is likely to experience more intraspecific competition than interspecific competition from any given other species. The outcome is partitioning of resources over time [59]. Indeed, it is possible to derive Lotka–Volterra equations or very similar ones that represent the outcome of integration of short-term fluctuations over time, even based on random fluctuations on that short timescale [15, 23].

The details of these effects of temporal partitioning are important. It is critical for instance, that competition between individuals growing at different times does not occur [61]. For this to be the case, the resources cannot carry over in time. For instance, day and night foragers for a particular resource might still be competing strongly even though they capture the resource at different times. This would be the case if units of resource available at night are used by organisms in the day time if they are missed by night time foragers. The result is that temporal differences in

foraging do not, in this case, concentrate intraspecific competition relative to interspecific competition.

What is possible in this context for competition is also possible with apparent competition, extending the essential symmetries for consideration of these processes before. However, differences do occur because of the potential that apparent competition works on a longer timescale [61]. For example, in annual plants with seed predators, when a good seed crop causes buildup of seed predators through high predator reproduction and survival, it is the seed crop the next year that experiences the higher predator density. The seed crop the next year will likely have different species composition due to species differences in response to the temporally varying physical environment. Thus, the species that cause the predator buildup are not necessarily the species experiencing higher predation. Intraspecific apparent competition is not necessarily concentrated relative to intraspecific competition in his case. When the environment varies randomly from 1 year to the next, predator buildup on good seed crops does not lead to effective temporal partitioning. However, behavioral changes in predation rates can be on short timescales with the potential that effective temporal partitioning can occur. Indeed, the theory implies that frequency-dependent behavior and other density-dependent behaviors can in some circumstances lead to temporal partitioning due to predation [50, 51]. In these cases, frequency-dependent behavior has two effects: an immediate and direct effect of frequency dependence on the ratio of intraspecific to interspecific density dependence, and a longer-term effect that involves an interaction between year to year temporal variation in the physical environment and temporal variation in foraging behavior as the prey species fluctuate in density in response to the environment.

These instances of temporal partitioning due to the responses of species to environmental variation are generally referred to as the storage effect, but another general mechanism termed relative nonlinearity of competition [15] works based on temporal fluctuations in the magnitude of competition and different nonlinear responses to competition by different species. Fundamentally, different species are more sensitive to competition over different ranges of competition. Under certain conditions, they can also generate the kinds of fluctuations that are disadvantageous to them when they are abundant. This mechanism continues the theme that coexistence stems from mechanisms that generate stronger intraspecific density dependence than interspecific density dependence when integrated over time. This mechanism works just as well for apparent competition [62], but it seems to be a relatively weak mechanism to the extent that at best two species can coexist this way in the absence of other mechanisms [15]. However, in the two-species case, models have suggested that it can have comparable strength to resource partitioning [63]. Moreover, there is some suggestion that when interacting with other mechanisms, it can be very powerful in multispecies settings, but there is as yet insufficient information on this possibility [64, 65].

Spatial Structure

Spatially varying environments have long been known to allow spatial partitioning of competition in a very similar way to temporal partitioning [66]. Thus, there are various spatial analogues to temporal partitioning by the storage effect for both competition [67–69] and apparent competition [22, 70]. Indeed, there is every indication that spatial variation powerfully fosters species coexistence due to the different responses that species have to environmental factors that vary in space. From time to time, the idea that species tend to be spatially aggregated intraspecifically is raised as a potential mechanism of species coexistence [71]. Such local aggregation naturally arises due to localized dispersal [72], can also be influenced by habitat selection. Although coexistence by aggregation has sometimes been claimed to be an entirely new mechanism [73], there are good reasons to believe that it functions primarily as a form of spatial resource partitioning [74], or as a form of competition–colonization trade-off [75], as discussed next.

Some spatial mechanisms do not have clear analogues with temporal mechanisms. Of particular note is the mechanism known as competition–colonization trade-offs [76]. In this case, species are assumed to be ranked very strictly in competitive ability such that any given locality will become dominated by just one species, the strongest competitor that has found that locality. In some cases, a locality is assumed to be a site only large enough to be occupied by a single plant

individual. In other cases, it might be a local population of a plant or animal species [77]. Death of the individual, or extinction of the local population, vacates that space. The assumption is that there is a trade-off between competitive ability and colonizing ability, and this means that vacant space is likely to be taken by an inferior competitor. Ecological succession takes place as inferior competitors are replaced by later arriving superior competitors. Because local sites are vacated at different times, and recolonization and succession have stochastic timing, landscapes governed by these process will consist of a mosaic of sites in different successional stages. For this reason, this hypothesis is also known as the successional mosaic hypothesis [35]. It is one version of the intermediate disturbance hypothesis [78–80], and perhaps the version closest to the original intention of the idea [79].

In these discussions, disturbance is a natural process such as fire or extreme weather that destroys local populations patchily in space. In one version, predators are the agents that destroy local populations [37, 81], and thus maintain a patchy landscape in a mosaic of successional states. The competition–colonization trade-off hypothesis, however, can work without an agent of disturbance, but relying on chance mortality of individuals, dispersal and colonization [82]. This successional mosiac process can be modeled well by Lotka–Volterra competition equations with density measured at the landscape scale as the fraction of sites occupied by a species [76, 77, 83]. Its form is the same as an asymmetric interference competition model, but nevertheless governed by the coexistence conditions (Eq. 3) above, which mean that all species inhibit themselves more than they do other species. For superior competitors, this outcome occurs because inferior competitors are better at finding free species and so escape interspecific competition from superior competitors. This idea is also related to nonspatial models of exploitation of leftover resources, for example light not intercepted by a plant canopy, and so available to understorey species [84, 85]. Fundamentally, in the competition–colonization trade-off hypothesis and leftover resource models, superior competitors do not efficiently exploit all resources, leaving some to be exploited by those species that have lesser competitive ability but through a trade-off have achieved the ability to exploit the leftovers.

A final spatial mechanism involves natural enemies. Known as the Janzen-Connell hypothesis [86–88], it was originally proposed for tropical trees, but is closely related to the soil-feedback hypothesis for coexistence of species in grasslands [89]. The idea as applied to trees was that natural enemies specialized on a particular species would build up in abundance on or near a given tree. These natural enemies would then provide strong inhibition to the establishment of individuals of the same species there. Other species, however, would be able to establish. It is clear, however, that this is a form of natural enemy partitioning that does not require a spatial element, although it might well be enhanced by the spatial element. In the soil-feedback hypothesis, soil microorganism communities develop in the root zone of a particular individual plant. A preponderance of relatively species-specific harmful microorganisms leads to a net negative effect of establishment of the same species at that site, favoring others species to replace that individual or to thrive nearby [89, 90].

Applications

These ideas have applications in a number of other areas beyond the basic concept of how communities are structured, including invasion biology [91, 92], conservation biology [93, 94], and ecosystem functioning [95]. The focus here is on invasion biology. The biosphere is undergoing vast changes as a result of human activities. One activity is the introduction of new species to places where they were not previously found either deliberately or as an accidental by-product of commerce. Many transplanted species fail to perform well in a new environment, or if they do perform well enough to establish self-sustaining populations (to "naturalize"), they never become very abundant. However, a few species perform spectacularly well and become major pests or weeds, often displacing native species [96]. Although invasive species are not often responsible for regional extinction of native species, they can displace them locally and dramatically change the character of local communities. The local communities thus undergo a process of reassembly in response to the arrival of these invasive species. The ability of alien species to have these effects is often analyzed in terms of competition and predation, although other mechanisms, such as facilitation of one species by

another can be expected to be important too [97]. The study of coexistence and exclusion mechanisms, as discussed here, fundamentally involves the question of whether a species can increase from very low density in the presence of other members of the guild, or to "invade." This invasibility analysis also applies to the question of how an alien invader successfully enters a local guild, and whether it displaces existing guild members.

The ability of an alien species to invade can be discussed in terms of the concept of niche opportunities [91]. Fundamentally, a niche opportunity means sufficient resources are available for the species in question to invade, given the risk from natural enemies that it will encounter. To some extent, lower risk from natural enemies can enable a species to invade at lower resource levels, as it would be able to do so at lower reproduction or survival based on those resources. A surfeit of resources is called a resource opportunity, while a low risk from natural enemies is an escape opportunity. The overriding question in invasion biology is why native species, in the eons of time, have not used up all opportunities to exploit a particular environment. There are a number of potential answers to this question.

First the local environment may have changed as a result of human activities or climate change, and the local community is therefore no longer well adapted to it, allowing the potential for a species from elsewhere to be better adapted than local species [91, 98]. This idea of change, however, should not be confused with a natural regime of disturbance or environmental variation that might be temporally partitioned by the native species. Like other persistent features of the environment, such environmental variation ought already be exploited by the native species, and so should not provide new opportunities. Unless, the natural regime of environmental variation has changed, there is no change that should be expected to facilitate invasion [98]. Pollution is an example of one common change that humans cause. When this results in deposition of nitrogen in a nutrient-poor environment, it can have a large effect on local plant communities, facilitating the invasion of species adapted to exploit this resource [99]. The invasive species then potentially depress other resources that the native species depend on, harming them.

Second, the native community might have not existed for very long, or in the past was poorly connected to areas that might provide colonists or genetic diversity allowing adaptation to exploit all opportunities well. In a sense, such a local community is immature [91]. In these cases, niche opportunities exist, and species from elsewhere might have the adaptations allowing them to exploit the local environment more successfully than the native species. Islands that have been devastated by invasions might be in this category [96, 100], but so also might aquatic systems which suffer from the problem that dispersal from one place to another was historically much rarer than it is today. This idea has been applied on continental scale, suggesting that the Eurasian continent being larger contains species with stronger competitive ability than species in North America [101]. There is some evidence for this in plant species from Eurasian that use chemical interference successfully in competition with North American species [102]. The idea of biotic resistance says that localities with high species diversity ought to be more difficult to invade [103, 104], which makes sense to the extent that it means that more niche opportunities are foreclosed by the adaptations present in the more diverse community.

Third, invaders potentially arrive in the absence of their specialist natural enemies. Even if diseases, parasites, or predators are introduced with an invader at the same time, unless these natural enemies can exploit other species, they may well be lost early in the introduction because the invader in question was initially at too small a population size to sustain them. Such a species would have a strong natural enemy escape opportunity that would give it an advantage in a novel environment, especially if native species were attacked by natural enemies that do not affect the invader [97, 105]. Of course, native natural enemies do attack and inhibit invaders to varying extents, reducing their success [91, 97].

These various ideas can be analyzed within the Lotka–Volterra framework presented here [92, 106]. Fundamentally, if an invader has overall advantage such as novel competitive weapons for interfering with other species, is less susceptible to enemy attack, or is better overall in its adaptation to the environment, it will have an average fitness advantage over native species (κ ratios greater than 1), allowing it to invade,

with the potential, if this advantage is large enough, to exclude native species, at least locally. Instead, it might not have an overall advantage, but simply an advantage under specific conditions, leading to low niche overlaps, ρ, with native species. This advantage might be that it can specialize better on a particular resource or particular environmental conditions, arising spatially or temporally, that native species are not fully exploiting. In many situations, it seems that elements of both are likely. It might for instance weakly partition resources or predators, but also have some fitness benefits, without average superiority over natives, but together this might be sufficient for invasion. On the other hand, the fact that even strongly successful invaders do not eliminate species in the same guild on a regional scale suggests that spatial partitioning, perhaps coupled with temporal partitioning, is sufficiently strong for natives to persist in a region even if they are eliminated or driven to low abundances locally [92, 107].

Invaders naturally interact with species outside their own guild also. As predators and diseases they have been more frequently the cause of extinctions of native species [44, 96]. However, they can also be the agents that enhance predators or diseases, damaging native species through apparent competition [43, 108]. Ways of controlling such invasives is therefore of substantial interest in conservation biology [43, 108].

Future Directions

The picture of community organization driven by competition and predation presented here has been developing for decades but it is relatively recently gelling on a new synthesis. It is now able to integrate competition, predation, temporal variation, and spatial structure in one common framework to gain understanding of not just individual mechanisms but their interactions as well [17, 51], as exemplified by the simple comparison presented above of how the strength of stabilization of coexistence changes with the circumstances. This picture now leads to comprehensive theoretical understanding that greatly clarifies a confusing picture of numerous potential mechanisms of a few years ago [109]. The most glaring lack now is in rigorous empirical study of mechanisms by which communities are structured, especially stable coexistence mechanisms [14].

Many empirical studies focus on features of mechanisms without truly testing whether they have a role in stabilizing diversity [13, 14]. Patterns of morphology of animals [11] and plants [110] that are related to how they gather resources or avoid predation can provide strong circumstantial evidence, but still leave open numerous possibilities as to the actual mechanisms [110]. One problem has been that the sort of data necessary to test mechanisms has not been clear because the mechanisms have not been truly understood, but that issue is now much less significant. One recent development is a theory of testing mechanisms [13] aimed to guide empirical studies. The key problem is to determine ways of testing whether density feedback loops do indeed concentrate intraspecific density dependence relative to interspecific density dependence in the manner proposed by a specific mechanism. In general, this is not an easy proposition, but it is also not infeasible for well-resourced project, given the right approach. Developing these approaches is the aim of the theory of testing mechanisms [13]. For example, to test for stabilization by temporal or spatial resource partitioning, the concept of covariance between environment and competition has been developed, which specifically measures how competition is linked to environmental factors [111]. Testing whether coexistence is stabilized by partitioning environmental conditions involves showing that covariance between environment and competition weakens as a species is reduced to low density in presence of unmanipulated competitors. More developments along these lines are needed to test other specific mechanisms.

New theoretical understanding has also revealed relatively basic deficiencies in empirical studies. For instance, frequency-dependent predation shows much promise as a strong coexistence mechanism, yet there are few rigorous field studies of this phenomenon [50]. It seems that the dominance of predation–competition trade-offs, including keystone predation ideas, has led to the neglect of frequency-dependent predation as a coexistence mechanism in empirical studies. However, it is also true that studies of keystone predation assumed that the mechanism was powerful when acting alone, and this impression seems likely to have inhibited the search for the stabilizing mechanisms

that must be present also for keystone predation to be effective in promoting multispecies coexistence.

Naturally, the theory, though rich and not rigorously tested, still has some glaring deficiencies. One issue that complicates the Lotka–Volterra theory presented above is that as parameters are changed gradually, species in the resource and predator guilds that interact with the focal guild may not be supportable [27]. This possibility leads to abrupt changes in the coefficients of density dependence and related parameters [26]. It is also true that depressing a given member of the focal guild to low density may mean that only a subset of the resource species or predator species is present [17]. These facts, however, do not alter the invasion criteria presented here provided they are based on the resources and predators actually present in a given invasion scenario. They do, however, complicate interpretation of the criteria as parameters are changed. It is not known how important these issues are, and a comprehensive theory of their effects is needed.

The integrated understanding of the roles of predation and competition in species coexistence and exclusion presented here also raises the critical question of what factors control density dependence through these two processes. Of potentially major significance are other species in food webs beyond those directly linked to the focal guild. For instance, if the major natural enemies of the focal guild are themselves subject to strong density dependence from their natural enemies, they will be limited in their ability to change in abundance in response changes in the density of the focal guild. This means that density-dependent feedback to the focal guild through their natural enemies would be limited to behavioral responses of the natural enemies to focal guild densities. The idea of trophic cascades has long postulated how various density-dependent effects permeate from one part of a food web to another [112–114]. Integration of trophic cascade research with species coexistence research has the potential to make important advances with major implications for understanding the broader impacts that humans are having on the planet through widespread disruption of food webs, especially the destruction of many large carnivorous species [115–117].

Most of the discussion here has been purely ecological focused on interactions between a few species. However, natural populations and communities are shaped by evolution and community assembly processes, of which the considerations discussed above form just a small part. It is now known that evolutionary change can be fast to the extent that ecological dynamics and evolutionary dynamics cannot be completely separated [118]. The field of adaptive dynamics tries to integrate ecological and evolutionary process, but nevertheless still tends to treat these two processes as functioning on different timescales [119]. At the same time, much study of species coexistence focuses on the conditions that allow species coexistence, without considering the processes by which species assemble in communities. A proper treatment of community assembly would include challenging a local community with invaders from the pool species present regionally. There have been only limited theoretical studies of this sort [83, 120, 121]. Without an adequate treatment of these processes of adaptation and assembly, there is no true prediction of the structure of natural communities, and a seriously incomplete understanding of the role of competition and predation in community structure.

Finally, future theoretical research will likely take on the challenge of long-term climate change. The planet faces relative rapid climate change at the hand of human activities, but long-term climate change has always been a feature of the environment. However, theoretical models normally assume that climate fluctuations have stable long-term frequencies. There is a critical need to strip away this assumption, and develop theory that allows predictions even though the climate is not statistically stable. A useful theory would couple long-term climate change with the ability of populations to move on a spatially structured landscape as climate shifts change the viability of parts of their habitat. With such migration, there is the potential that climate fluctuations realized by species will have stable long-term frequencies as species track the shifting climate, but there are bound to be numerous new issues arising due to the fact that different species are likely to track the environment at different rates and in different ways [122].

A few years ago, imagining developments in the directions discussed here would have been daunting given the challenges that simpler theory gave. However, recent progress augers major extensions beyond the current limited contexts.

Acknowledgments

I am grateful for comments on the manuscript by Jonathan Levine and for support from the National Science Foundation grant numbers DEB-0717222 and DEB-0816231.

Bibliography

Primary Literature

1. Murdoch WW, Briggs CJ, Nisbet RM (2003) Consumer-resource dynamics. Princeton University Press, Princeton, NJ
2. MacArthur R (1970) Species packing and competitive equilibrium for many species. Theor Popul Biol 1:1–11
3. MacArthur RH (1972) Geographical ecology: patterns in the distribution of species. Harper & Row, New York
4. Tilman D (1982) Resource competition and community structure. Princeton University Press, Princeton, NJ
5. Grubb PJ (1977) The maintenance of species-richness in plant communities: the importance of the regeneration niche. Biol Rev 52:107–145
6. Harper JL (1977) Population biology of plants. Academic, London
7. Connolly SR, Roughgarden J (1999) Theory of marine communities: competition, predation, and recruitment-dependent interaction strength. Ecol Monogr 69:277–296
8. Frank DA, McNaughton SJ, Tracy BF (1998) The ecology of the Earth's grazing ecosystems. Bioscience 48:513–521
9. Birch LC (1957) The meanings of competition. Am Nat 91:5–18
10. Schoener TW (1983) Field experiments on interspecific competition. Am Nat 122:240–285
11. Dayan T, Simberloff D (2005) Ecological and community-wide character displacement: the next generation. Ecol Lett 8:875–894
12. Adler PB, HilleRisLambers J, Levine JM (2007) A niche for neutrality. Ecol Lett 10:95–104
13. Chesson P (2008) Quantifying and testing species coexistence mechanisms. In: Valladares F, Camacho A, Elosegui A, Gracia C, Estrada M, Senar JC, Gili JM (eds) Unity in diversity: reflections on ecology after the legacy of Ramon Margalef. Fundacion BBVA, Bilbao, pp 119–164
14. Siepielski AM, McPeek MA (2010) On the evidence for species coexistence: a critique of the coexistence program. Ecology 91:3153–3164
15. Chesson P (2000) Mechanisms of maintenance of species diversity. Annu Rev Ecol Syst 31:343–366
16. Chase JM, Abrams PA, Grover JP, Diehl S, Chesson P, Holt RD, Richards SA, Nisbet RM, Case TJ (2002) The interaction between predation and competition: a review and synthesis. Ecol Lett 5:302–315
17. Chesson P, Kuang JJ (2008) The interaction between predation and competition. Nature 456:235–238
18. Holt RD (1977) Predation, apparent competition, and the structure of prey communities. Theor Popul Biol 12:197–229
19. Nicholson AJ (1937) The role of competition in determining animal populations. JSIR (Australia) 10:101–106
20. Hutchinson GE (1959) Homage to Santa Rosalia or why are there so many kinds of animals. Am Nat 93:145–159
21. Roughgarden J (1989) Community structure and assembly. In: Roughgarden J, May RM, Levin SA (eds) Perspectives in ecological theory. Princeton University Press, Princeton, NJ, pp 203–226
22. Holt RD (1984) Spatial heterogeneity, indirect interactions, and the coexistence of prey species. Am Nat 124:377–406
23. Chesson P, Huntly N (1993) Temporal hierarchies of variation and the maintenance of diversity. Plant Species Biol 8:195–206
24. Kang Y, Chesson P (2010) Relative nonlinearity and permanence. Theor Popul Biol 78:26–35
25. Holt RD, Polis GA (1997) A theoretical framework for intraguild predation. Am Nat 149:745–764
26. Abrams PA (1998) High competition with low similarity and low competition with high similarity: exploitative and apparent competition in consumer-resource systems. Am Nat 152:114–128
27. Abrams PA, Rueffler C (2009) Coexistence and limiting similarity of consumer species competing for a linear array of resources. Ecology 90:812–822
28. Hardin G (1960) The competitive exclusion principle. Science 131:1292–1297
29. Chase JM, Leibold MA (2003) Ecological Niches: linking classical and contemporary approaches. The University of Chicago Press, Chicago
30. Schoener TW (1974) Resource partitioning in ecological communities. Science 185:27–39
31. Tilman D (1988) Plant strategies and the dynamics and structure of plant communities. Princeton University Press, Princeton, NJ
32. Hubbell SP (2001) The unified neutral theory of biodiversity and biogeography. Princeton University Press, Princeton, NJ
33. Purves DW, Pacala SW (2005) Ecological drift in niche-structured communities: neutral pattern does not imply neutral process. In: Burslem D, Pinard M, Hartley S (eds) Biotic interactions in the tropics. Cambridge University Press, Cambridge, UK, pp 103–138
34. Zhang DY, Lin K (1997) The effects of competitive asymmetry on the rate of competitive displacement: how robust is Hubbell's community drift model? J Theor Biol 188:361–367
35. Chesson P, Huntly N (1997) The roles of harsh and fluctuating conditions in the dynamics of ecological communities. Am Nat 150:519–553
36. Lubchenco J (1978) Plant species diversity in a marine intertidal community: importance of herbivore food preference and algal competitive abilities. Am Nat 112:23–39
37. Gurevitch J, Morrison JA, Hedges LV (2000) The interaction between competition and predation: a meta-analysis of field experiments. Am Nat 155:435–453
38. Paine RT (1969) A note on trophic complexity and community stability. Am Nat 103:91–93

39. Power ME, Tilman D, Estes JA, Menge BA, Bond WJ, Mills LS, Daily G, Castilla JC, Lubchenco J, Paine RT (1996) Challenges in the quest for keystones. Bioscience 46:609–620
40. Grover JP, Holt RD (1998) Disentangling resource and apparent competition: realistic models for plant-herbivore communities. J Theor Biol 191:353–376
41. Levin SA (1970) Community equilibria and stability, and an extension of the competitive exclusion principle. Am Nat 104:413–423
42. Crooks KR, Soule ME (1999) Mesopredator release and avifaunal extinctions in a fragmented system. Nature 400:563–566
43. Johnson CN, Isaac JL, Fisher DO (2007) Rarity of a top predator triggers continent-wide collapse of mammal prey: dingoes and marsupials in Australia. Proc R Soc B-Biol Sci 274:341–346
44. Knowlton JL, Donlan CJ, Roemer GW, Samaniego-Herrera A, Kertt BS, Wood B, Aguirre-Munoz A, Faulknier KR, Tershy BR (2007) Eradication of non-native mammals and the status of insular mammals on the California Channel Islands, USA, and Pacific Baja California Peninsula Islands, Mexico. Southwest Nat 52:528–540
45. Stephens DW, Brown JS, Ydenberg RC (eds) (2007) Foraging: behavior and ecology. University of Chicago Press, Chicago
46. Haygood R (2002) Coexistence in MacArthur-style consumer–resource models. Theor Popul Biol 61:215–223
47. Holt RD (1985) Density-independent morality, nonlinear competitive interactions and species coexistence. J Theor Biol 116:479–493
48. Kotler BP, Holt RD (1989) Predation and competition: the interaction of two types of species interactions. Oikos 54: 256–260
49. Holt RD, Grover J, Tilman D (1994) Simple rules for interspecific dominance in systems with exploitative and apparent competition. Am Nat 144:741–771
50. Kuang JJ, Chesson P (2010) Interacting coexistence mechanisms in annual plant communities: frequency-dependent predation and the storage effect. Theor Popul Biol 77:56–70
51. Chesson P, Kuang JJ (2010) The storage effect due to frequency-dependent predation in multispecies plant communities. Theor Popul Biol 78:148–164
52. Murdoch WW, Bence J (1987) General predators and unstable prey populations. In: Kerfoot WC, Sih A (eds) Predation: direct and indirect impacts on aquatic communities. University Press of New England, Hanover and London, pp 17–30
53. Abrams PA, Matsuda H (2004) Consequences of behavioral dynamics for the population dynamics of predator-prey systems with switching. Popul Ecol 46:13–25
54. Bond AB (2007) The evolution of color polymorphism: crypticity, searching images, and apostatic selection. Annu Rev Ecol Evol Syst 38:489–514
55. Stephens DW, Krebs JR (1986) Foraging theory. The Princeton University Press, Princeton, NJ
56. Hamback P (1998) Seasonality, optimal foraging and prey coexistence. Am Nat 152:881–895
57. Krivan V (2003) Competitive co-existence by adaptive predators. Evol Ecol Res 5:1163–1182
58. May RM (1974) Stability and complexity in model ecosystems, 2nd edn. Princeton University Press, Princeton, NJ
59. Chesson P, Gebauer RLE, Schwinning S, Huntly N, Wiegand K, Ernest MSK, Sher A, Novoplansky A, Weltzin JF (2004) Resource pulses, species interactions and diversity maintenance in arid and semi-arid environments. Oecologia 141:236–257
60. Angert AL, Huxman TE, Chesson P, Venable DL (2009) Functional tradeoffs determine species coexistence via the storage effect. Proc Natl Acad Sci USA 106:11641–11645
61. Kuang JJ, Chesson P (2009) Coexistence of annual plants: generalist seed predation weakens the storage effect. Ecology 90:170–182
62. Kuang JJ, Chesson P (2008) Predation-competition interactions for seasonally recruiting species. Am Nat 171:E119–E133
63. Abrams P, Holt R (2002) The impact of consumer–resource cycles on the coexistence of competing consumers. Theor Popul Biol 62:281–295
64. Huisman J, Weissing FJ (1999) Biodiversity of plankton by species oscillations and chaos. Nature 402:407–410
65. Huisman J, Weissing FJ (2001) Fundamental unpredictability in multispecies competition. Am Nat 157:488–494
66. Amarasekare P, Nisbet RM (2001) Spatial heterogeneity, source-sink dynamics, and the local coexistence of competing species. Am Nat 158:572–584
67. Muko S, Iwasa Y (2003) Incomplete mixing promotes species coexistence in a lottery model with permanent spatial heterogeneity. Theor Popul Biol 64:359–368
68. Snyder RE, Chesson P (2004) How the spatial scales of dispersal, competition, and environmental heterogeneity interact to affect coexistence. Am Nat 164:633–650
69. Miller AD, Chesson P (2009) Coexistence in disturbance prone communities: how a resistance-resilience trade off generates coexistence via the storage effect. Am Nat 173:E30–E43
70. Amarasekare P (2008) Spatial dynamics of foodwebs. Annu Rev Ecol Evol Syst 39:479–500
71. Ives AR (1988) Covariance, coexistence and the population dynamics of two competitors using a patchy resource. J Theor Biol 133:345–361
72. Murrell DJ, Purves DW, Law R (2001) Uniting pattern and process in plant ecology. Trends Ecol Evol 16:529–530
73. Hartley S, Shorrocks B (2002) A general framework for the aggregation model of coexistence. J Anim Ecol 71:651–662
74. Chesson P, Neuhauser C (2002) Intraspecific aggregation and species coexistence. Trends Ecol Evol 17:210–211
75. Bolker B, Pacala S (1999) Spatial moment equations for plant competition: understanding spatial strategies and the advantages of short dispersal. Am Nat 153:575–602
76. Tilman D (1994) Competition and biodiversity in spatially structured habitats. Ecology 75:2–16
77. Hastings A (1980) Disturbance, coexistence, history, and competition for space. Theor Popul Biol 18:363–373
78. Connell JH (1978) Diversity in tropical rain forests and coral reefs. Science 199:1302–1310
79. Connell JH (1979) Tropical rainforests and coral reefs as open non-equilibrium systems. In: Anderson RM, Turner BD,

Taylor LR (eds) Population dynamics. Blackwell Scientific Publications, Oxford, pp 141–163
80. Roxburgh SH, Shea K, Wilson JB (2004) The intermediate disturbance hypothesis: patch dynamics and mechanisms of species coexistence. Ecology 85:359–371
81. Caswell H (1978) Predator-mediated coexistence: a nonequilibrium model. Am Nat 112:127–154
82. Bolker BM, Pacala SW, Neuhauser C (2003) Spatial dynamics in model plant communities: what do we really know? Am Nat 162:135–148
83. Dushoff J, Worden L, Keymer J, Levin S (2002) Metapopulations, community assenbly, and scale invariance in aspect space. Theor Popul Biol 62:329–338
84. Kohyama T (1993) Size-structured tree populations in gap-dynamic forest–the forest architecture hypothesis for the stable coexistence of species. J Ecol 81:131–143
85. Vance RR, Nevai AL (2007) Plant population growth and competition in a light gradient: a mathematical model of canopy partitioning. J Theor Biol 245:210–219
86. Connell JH (1970) On the role of natural enemies in preventing competitive exclusion in some marine animals and rainforest trees. In: den Boer PJ, Gradwell G (eds) Dynamics of populations. Centre for Agricultural Publishing and Documentation, Wageningen, pp 298–312
87. Janzen DH (1970) Herbivores and the number of tree species in tropical forests. Am Nat 104:501–528
88. Adler FR, Muller-Landau HC (2005) When do localized natural enemies increase species richness? Ecol Lett 8:438–447
89. Bever JD, Dickie IA, Facelli E, Facelli JM, Klironomos J, Moora M, Rillig MC, Stock WD, Tibbett M, Zobel M (2010) Rooting theories of plant community ecology in microbial interactions. Trends Ecol Evol 25:468–478
90. Klironomos JN (2002) Feedback with soil biota contributes to plant rarity and invasiveness in communities. Nature 417:67–70
91. Shea K, Chesson P (2002) Community ecology theory as a framework for biological invasions. Trends Ecol Evol 17: 170–176
92. Melbourne BA, Cornell HV, Davies KF, Dugaw CJ, Elmendorf S, Freestone AL, Hall RJ, Harrison S, Hastings A, Holland M, Holyoak M, Lambrinos J, Moore K, Yokomizo H (2007) Invasion in a heterogeneous world: resistance, coexistence or hostile takeover? Ecol Lett 10:77–94
93. Drury WH (1998) Chance and change: ecology for conservationists. University of California Press, Berkeley, Calif
94. Sergio F, Caro T, Brown D, Clucas B, Hunter J, Ketchum J, McHugh K, Hiraldo F (2008) Top predators as conservation tools: ecological rationale, assumptions, and efficacy. Annu Rev Ecol Evol Syst 39:1–19
95. Kinzig A, Pacala S, Tilman D (eds) (2001) The functional consequences of biodiversity. Princeton University Press, Princeton, NJ
96. Sax DF, Gaines SD (2008) Species invasions and extinction: the future of native biodiversity on islands. Proc Natl Acad Sci USA 105:11490–11497
97. Reinhart KO, Callaway RM (2006) Soil biota and invasive plants. New Phytol 170:445–457
98. Sher AA, Hyatt LA (1999) The disturbed resource-flux invasion matrix: a new framework for patterns of plant invasion. Biological Invasions 1:107–114
99. Brooks ML (2003) Effects of increased soil nitrogen on the dominance of alien annual plants in the Mojave Desert. J Appl Ecol 40:344–353
100. Simberloff D (1995) Why do introduced species appear to devastate islands more than mainland areas? Pac Sci 49: 87–97
101. Huston MA (1994) Biological diversity, 1st edn. Cambridge University Press, Cambridge
102. Callaway RM, Ridenour WM (2004) Novel weapons: invasive success and the evolution of increased competitive ability. Front Ecol Environ 2:436–443
103. Elton C (1958) The ecology of invasions by animals and plants. Methuen and Co, London
104. Levine JM (2000) Species diversity and biological invasions: relating local process to community pattern. Science 288:852–854
105. Keane RM, Crawley MJ (2002) Exotic plant invasions and the enemy release hypothesis. Trends Ecol Evol 17:164–169
106. MacDougall AS, Gilbert B, Levine JM (2009) Plant invasions and the niche. J Ecol 97:609–615
107. Davies KF, Chesson P, Harrison S, Inouye B, Melbourne BA, Rice KJ (2005) Spatial heterogeneity explains the scale dependence of the native-exotic diversity relationship. Ecology 86:1602–1610
108. Courchamp F, Woodroffe R, Roemer G (2003) Removing protected populations to save endangered species. Science 302:1532
109. Wilson JB (2011) The twelve theories of co-existence in plant communities: the doubtful, the important and the unexplored. J Veg Sci 22:184–195
110. Ackerly DD (2003) Community assembly, niche conservatism, and adaptive evolution in changing environments. Int J Plant Sci 164:S165–S184
111. Sears ALW, Chesson P (2007) New methods for quantifying the spatial storage effect: an illustration with desert annuals. Ecology 88:2240–2247
112. Holt RD (2000) Trophic cascades in terrestrial ecosystems. Tree 15:444–445
113. Chase JM (2003) Strong and weak trophic cascades along a productivity gradient. Oikos 101:187–195
114. Terborgh J, Estes JA (2010) Trophic cascades: predators, prey, and the changing dynamics of nature. Island Press, Washington DC
115. Terborgh J, Lopez L, Nunez P, Rao M, Shahabuddin G, Orihuela G, Riveros M, Ascanio R, Adler GH, Lambert TD, Balbas L (2001) Ecological meltdown in predator-free forest fragments. Science 294:1923–1926
116. Myers RA, Baum JK, Shepherd TD, Powers SP, Peterson CH (2007) Cascading effects of the loss of apex predatory sharks from a coastal ocean. Science 315:1846–1850

117. Letnic M, Koch F (2010) Are dingoes a trophic regulator in arid Australia? A comparison of mammal communities on either side of the dingo fence. Austral Ecol 35:167–175
118. Meyer JR, Ellner SP, Hairston NG, Jones LE, Yoshida T (2006) Prey evolution on the time scale of predator-prey dynamics revealed by allele-specific quantitative PCR. Proc Natl Acad Sci USA 103:10690–10695
119. Geritz SAH, Kisdi E, Meszena G, Metz JAJ (1998) Evolutionarily singular strategies and the adaptive growth and branching of the evolutionary tree. Evol Ecol 12:35–57
120. Morton RD, Law R (1997) Regional species pools and the assembly of local ecological communities. J Theor Biol 187:321–331
121. O'Dwyer JP, Lake JK, Ostling A, Savage VM, Green JL (2009) An integrative framework for stochastic, size-structured community assembly. Proc Natl Acad Sci USA 106:6170–6175
122. Davis MB (1986) Climatic instability, time-lags and community disequilibrium. In: Diamond J, Case T (eds) Community ecology. Harper and Row, Cambridge, pp 269–284

Books and Reviews

Eisenberg C (2010) The wolf's tooth: keystone predators, trophic cascades, and biodiversity. Island Press, Washington, DC

Grant PR, Grant BR (2008) How and why species multiply: the radiation of Darwin's finches. Princeton University Press, Princeton

Species Diversity Within and Among Ecosystems

Jonathan E. M. Baillie, Karolyn Upham
Zoological Society of London, London, UK

Article Outline

Glossary
Definition of Species Diversity
Introduction
Patterns of Species Diversity
Vertebrate Species Status, Trends, and Threats
Link Between Species and Ecosystem Function
Species Loss and Extinction
Conservation of Species and Ecosystems
Conclusions
Future Directions
Bibliography

Glossary

Biodiversity The variability among living organisms from all sources and the ecological complexes of which they are part biodiversity includes diversity within species between species and of ecosystems.

Ecosystem A dynamic complex of plant, animal, and microorganism communities and their nonliving environment interacting as a functional unit.

Ecosystem service The benefits people obtain from ecosystems these include provisioning services such as food and water regulating services such as flood and disease control cultural services such as recreation or spiritual benefits and supporting services such as nutrient cycling.

Population A geographic entity within a species that is distinguished either ecologically or genetically.

Species (biological species concept) Interbreeding natural groups whose members are unable to successfully reproduce with members of other such groups.

Definition of Species Diversity

Species diversity is a function of species richness, the number of species in a given locality and species evenness, the degree to which the relative abundances of species are similar [1, 2]. While this notion may be easy to conceptualize, it has proven difficult, and at time contentious, to quantify [1, 2]. Commonly used methods include constructing mathematical indices known as diversity indexes (the Shannon, Simpson, and Margalef indexes being the most widely used) or comparing observed patterns of species abundance to theoretical models [3]. There is no single best metric and often commonly used ones are chosen because they are familiar and not necessarily because they are the most appropriate [1]. The scale of assessment may range from within a single site or habitat (known as α diversity) to the difference between two or more sites (β diversity) [4], which can then be combined to give γ diversity – the diversity of the landscape. Early research tended to be concentrated on largely α diversity, but there has been a marked increase in studies investigating β and γ diversity during the last decade [1].

The species richness aspect of diversity is often considered the iconic measure of biodiversity since it

is well defined and aligns with our intuitive sense of the concept [1, 5]. As the species level is the level at which living organisms are most widely known, species have become the major taxonomic rank for describing biodiversity. Along with populations, it is also the level that most scientists, managers, and policy makers use when referring to biological diversity, and it provides a useful means for both monitoring and priority setting [6]. As the species level is one of three fundamental levels of biodiversity (the others are the genetic level and the ecosystem/community level), species diversity is thus an important component of conservation. This entry will refer to species diversity in the less restrictive sense, that is, the variety of species that inhabit our planet.

Introduction

Ever since naturalists began classifying living organisms, there has been no consensus on how best to define a species [7]; Mayden [8] listed 24 different named species concepts and in a partial listing, Mallet [9] indentified 15. This longstanding failure of scientists to agree on how to identify species is commonly referred to as the species problem, with taxonomists being described as either "lumpers" or "splitters" with the former approach resulting in lower numbers of species and the latter higher. However, despite this proliferation of definitions, most taxonomists agree that species represent a distinct genetic lineage, interact with the environment in similar ways, and are reproductively compatible [1, 5, 7]. More importantly, whether based on gene flow, ecological separation, or morphological distinctiveness, most concepts tend to give similar results due to the independent evolutionary history that has resulted in unique morphological, ecological, and reproductive characteristics. In addition, most populations within a species share common ancestors with other populations in the very recent past, which in turn causes them to not be significantly differentiated [10].

Since the middle of the twentieth century, the most commonly accepted definition has been the biological species concept [10], which defines a species as a group of interbreeding natural populations whose members are unable to successfully reproduce with members of other such groups [11]. As species based on this definition have natural and objective boundaries due to gene flow [12], they provide natural units for biodiversity assessment [5]. While the approach of classifying species will influence both conservation priorities and the scale of intervention [5], the important thing for conservationists is that the commonly understood units can be defined and interventions implemented and assessed. There will always be issues with using species as a basis for biodiversity assessment, but many of these can be overcome [5, 10, 13].

The next question that often arises is how many species exist on Earth. While there are no reliable estimates for prokaryotes [10, 14, 15], many estimates exist for eukaryotic species. Recent studies [16] predict ~8.7 million species globally, of which ~2.2 million are marine species. Earlier estimates have varied greatly, with most falling between five and ten million (see Table 1). However, these estimates could be much higher if poorly known groups such as deep-sea organisms, algae, or fungi have more species than currently believed [10]. Incomplete sampling, lack of robust extrapolation approaches, controversy over the underlying assumptions, and subjectivity are all cited reasons for the uncertainty [16]. However, with only around

Species Diversity Within and Among Ecosystems.
Table 1 Estimates of number of eukaryote species globally, following [10]

Estimate	References	Method
30 million	Erwin [17]	Extrapolation from samples
3–5 million	Raven [18]	Ratios known: unknown species
10–80 million	Stork [19]	Extrapolation from samples
4.9–6.6 million	Stork and Gaston [20]	Ratios known: unknown species
1.84–2.57 million	Hodkinson and Casson [21]	Ratios known: unknown species
5 million	Hodkinson [22]	Ratios known: unknown species
4–6 million	Novotny et al. [23]	Extrapolation from samples
7.4–10 million	Mora et al. [16]	Extrapolation from samples

1.7 million species currently described [16] and only 15,000 newly described species each year [25], the key point is that a major knowledge gap still exists in this area; there is a likelihood of losing species to extinction before ever describing them.

Patterns of Species Diversity

Despite the uncertainty around how to define a species and the total number of species on the planet, the diversity of species is evident in the world around us. Species are unevenly distributed across the globe [10, 26] in terms of both geography and taxonomic groupings, with a disproportionately large number of species in the Class Insecta. It is very difficult to estimate this variability, as data are limited for marine and fresh water ecosystems and for non-vertebrate species, but there are around 10 plant species and at least 100 invertebrate species for each vertebrate species. Despite their low numbers compared to invertebrates, considerable datasets have been compiled for vertebrates, allowing numerous patterns of variations to be explored [10], although the extent to which these patterns can be generalized remains unknown [27].

One of the most obvious patterns is that for virtually all taxonomic groups, species richness tends to decrease from the tropics to the poles [28]; the tropics hold much higher species richness than do temperate, boreal, or polar regions. This is more so than would be expected on the basis of area alone [10], although it is complicated by physiographic and climatic factors such as mountain ranges or rainfall patterns. There is also a broadly similar spatial distribution of diversity between taxa, where differences seem to be driven by particular biological traits [10, 29]. In general, these differences will increase with increasing evolutionary distance between taxa [30]. Patterns of marine and freshwater species richness are less understood, but studies [31, 32] have demonstrated a latitudinal gradient in the shallow water benthos, with decreasing richness toward the poles.

There are also patterns of endemism and evolutionary distinctiveness that are important aspects of species diversity, as species with long and independent evolutionary histories and few surviving relatives contain irreplaceable genetic diversity. Most species have small range sizes [33], which tend to co-occur in centers of endemism [10, 31]. Centers of endemism are also concentrated in the tropics, with overlap, at certain scales, across birds, mammals, and amphibians [34] and a similar pattern is expected for plants [35]. However, this pattern does not appear to represent the situation for invertebrates or microorganisms [10]. There is enormous variation between species in terms of the evolutionary age [36]. Evolutionary distinctiveness among species can be explored using taxonomic relationships and as with species richness, the available data indicates that tropical rainforests are regions with the greatest number of taxa with the longest independent evolutionary history [37].

Vertebrate Species Status, Trends, and Threats

Conservation assessments have been primarily carried out for vertebrates as the conservation community tends to use these species as flagships or indicators of ecosystem health and global biodiversity. Therefore, this section will focus on vertebrate species, as sufficient data exists on the status and trends of the world's mammals, birds, amphibians, and cartilaginous fishes, and weighted approaches can be used to gain an understanding for reptiles and bony fishes [38]. Other taxonomic groups will not be discussed as there is not currently sufficient data for a global assessment. However, vertebrates represent only 5% of animal species and a fraction of the world's overall species [39]. Recent efforts to assess whether vertebrates trends and patterns can be used to extrapolate for other taxonomic groups are ongoing and show promise, with initial assessments indicating that the threat levels seen in invertebrate groups are not dissimilar from that of vertebrates [40].

The IUCN Red List of Threatened Species is the most widely accepted standard for assessing species' risk of extinction [41]. The IUCN Red List assesses species according to five quantitative criteria and classifies them into one of eight categories (see Fig. 1). Regular assessments of taxonomic groups provide information on trends in extinction risk, known as the IUCN Red List Index (RLI). The RLI considers species classified as Critically Endangered, Endangered, or Vulnerable to be threatened with extinction and explicitly accounts for Data Deficient species. Comprehensive datasets exist for mammals [42], birds [43, 44],

and amphibians [45], while sampled assessments can be used for other taxa [38] (Fig. 2).

Trends in vertebrate populations have been measured using the Living Planet Index, a global biodiversity indicator that tracks changes in vertebrate populations in the wild. It contains data on species trends from 1970 to 2005 and is calculated by aggregating population time series for each taxonomic group where data is available [46]. However, results for individual classes are at this point considered preliminary and conservative due to limited data or data biased toward temperate regions [38].

Mammals

Mammals are found across the world's terrestrial and aquatic ecosystems, with South American, sub-Saharan Africa, and Southeast Asia containing the highest concentrations of species of terrestrial mammals. The highest species richness of terrestrial mammals is

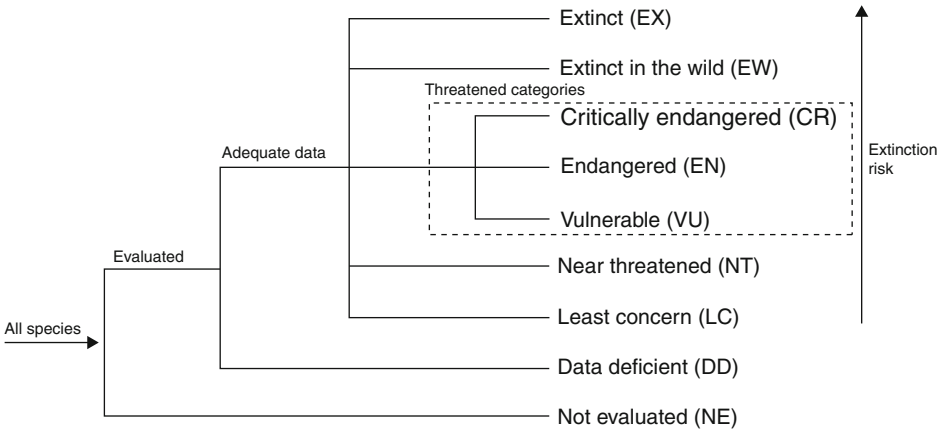

Species Diversity Within and Among Ecosystems. Figure 1
The IUCN red list of threatened species™ provides taxonomic, conservation status, and distribution information on species that have been globally evaluated using the IUCN red list categories and criteria

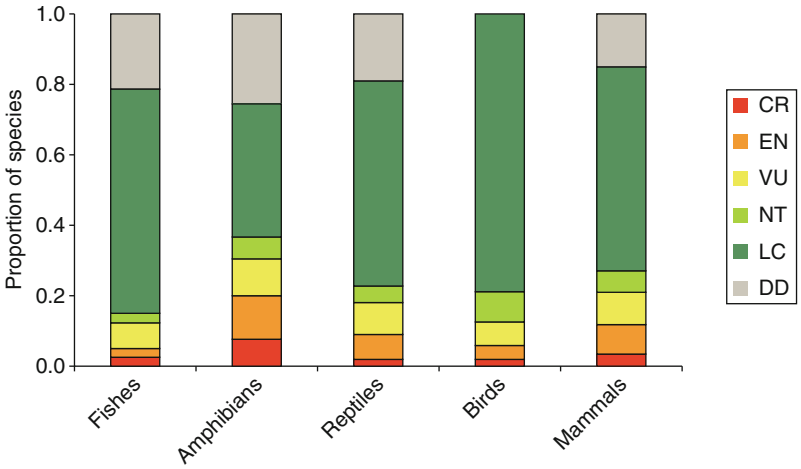

Species Diversity Within and Among Ecosystems. Figure 2
Vertebrate species by IUCN red list categories [38]

found in the tropical rainforests of Brazil and Indonesia and for aquatic mammals, the continental coastlines are the areas of the highest species richness; 21–36% of mammal species are currently threatened with extinction and the highest proportion of threatened species are found in the Monotremes (egg-laying mammals) and Perissodactyla (odd-toed ungulates). Countries with high numbers of threatened terrestrial mammal species include Mexico, Indonesia, Brazil, Papua New Guinea, and Vietnam. For marine mammals, the highest species richness of threatened species is found around the coastal regions of Asia, Japan, North Atlantic, and North Pacific [38, 42].

The LPI shows an overall reduction of 25% for terrestrial mammals. Marine mammals are omitted in the analysis due to sparse data; however, cetaceans have experienced a well-documented decline [47]. Mammal species are threatened from deforestation and coastal development, especially logging, wood harvesting, and smallholder farming. Overexploitation, particularly in the form of hunting for sport, subsistence, or use in traditional medicines, is also a threat to numerous species [38, 42].

Birds

Birds are found on all seven continents, with many migrating thousands of kilometers every year between breeding and wintering grounds. Habitats with high number of bird species include forests, shrubland, grassland, savanna, and inland wetlands [44, 48]. The Neotropics – specifically Colombia, Peru, Brazil and Ecuador – hold the highest numbers of bird species, followed by the Afrotropical, Indomalayan, and Australasian realms. Between 12% and 13% of bird species are currently threatened with extinction; areas with particularly high densities of threatened bird species are the tropical Andes, the Atlantic forests of Brazil, the Eastern Himalayas, Eastern Madagascar, and the archipelagos of Southeast Asia [38, 44].

The LPI shows an overall decline of 8% for birds and 28% for tropical birds alone. The main threats to birds are the spread of logging, wood harvesting, and agriculture in addition to the impacts of invasive alien species. Residential and commercial development, hunting, and pollution are also having serious impacts on bird populations globally [38, 44].

Amphibians

As amphibians are dependent on water for reproduction and other stages of their life cycles, the majority are found in tropical moist forests or freshwater ecosystems. Amphibian species richness is highest in the Neotropical regions of South and Central America and the countries with the highest species richness are Brazil, Colombia, Ecuador, and Peru. The Southeastern USA also has high species richness due to the large number of native salamander species. Roughly 30–56% of all amphibian species are currently threatened with extinction [45]. Among vertebrates, they have the highest proportion of Critically Endangered species and highest number of recent extinctions. The highest species richness of threatened amphibians is found in the dense tropical and subtropical forests of the Northern Andes, Caribbean, Western Ghats, Malaysian Borneo, and West Africa [38, 45].

There is only limited data on amphibian population trends, so the LPI result of an 80% decline should be treated with caution [38]. There is, however, a great deal of supporting evidence that amphibian species have suffered a major decline since the 1970s [40, 45, 49, 50]. Their aquatic habitats are under great human pressures, which included rapid deforestation, habitat degradation, pollution, and overuse of water. In addition, the emergence of the chytrid fungus, *Batrachochytrium dendrobatidis*, is another major threat. First described in the 1990s, the fungus is now found on every continent inhabited by amphibians and evidence suggests that it is responsible for causing mass mortalities among many populations [51, 52].

Fishes

The West and Central Indo-Pacific, South China, and Coral Sea are the areas of the highest marine fish species richness, while Southeast Asia, Eastern Africa's Great Lakes, South American Amazonia, and the forest of Central Africa have the highest species richness of freshwater fish [38]. Of the world's fish species, 41% are obligate freshwater, 58% are obligate marine, and the remaining 1% can tolerate both systems. An assessment of a representative sample of fish species suggests that between 12% and 34% are currently threatened with extinction. The highest species richness of threatened marine fishes is found in the Indo-West Pacific,

Central Indo-Pacific, South China, Coral, Caribbean, and Mediterranean Seas, and the highest species richness of threatened freshwater fish species is found in Southeast Asia [38].

The available data for the LPI for freshwater fish indicates a rapid and steady decline in population abundance approaching a 65% reduction. Marine data are limited, but indicate a gradual decrease of 20% in the number of marine fish populations [38]. The main threat to fish species is overexploitation and pollution; aquatic habitats are routinely treated as limitless sources for human consumption [53, 54]. Over 85% of the world's fisheries are either recovering or fully or partially overexploited [55]. In addition, freshwater fish have been particularly negatively affected by pollution and habitat alteration caused by damming and water management activities such as abstraction for agriculture [56].

Reptiles

While reptiles are the dominant vertebrate of arid systems, like other vertebrates, the highest species richness is found in tropical forests. Indonesia and the Congo Basin have the highest species richness of reptiles. Marine reptiles, such as sea snakes, turtles, and crocodiles, are found in the highest concentrations in the West and Central Indo-Pacific and the South China and Coral Seas. An assessment of a representative sample of species suggests that between 18% and 32% of reptile species are threatened with extinction, although this varies greatly between groups [38]. For example, a high proportion of crocodilians are threatened compared with a relatively lower number of snakes [57]. The highest species richness of threatened reptiles is found in Southeast Asia and the Ganges basin [38].

The available trend data for the LPI for reptile species indicates that the number of reptiles has declined by 7% [38]. However, this figure for the whole class may mask the decline in certain orders such as turtles and tortoises, which have seen large declines in regional-scale analysis [57]. Habitat loss is the greatest threat to reptiles and is principally in the form of agricultural expansion, logging, and urban development. Hunting, trapping, and overharvesting for consumption and the pet trade are particular threats, especially to turtles and tortoises [58] (Fig. 3).

Link Between Species and Ecosystem Function

A key topic in ecology is investigating how the diversity and composition of species in an ecosystem is related to its function. Considerable research has gone into answering this question [59] and ecological theory supports the notion that ecosystem function, and the resultant goods and services, depends on biodiversity. It is generally predicted that a decrease in biodiversity will result in a reduction of ecosystem function, which will in turn lead to the loss of ecosystem goods and services [60–62]. While there is still work to be done

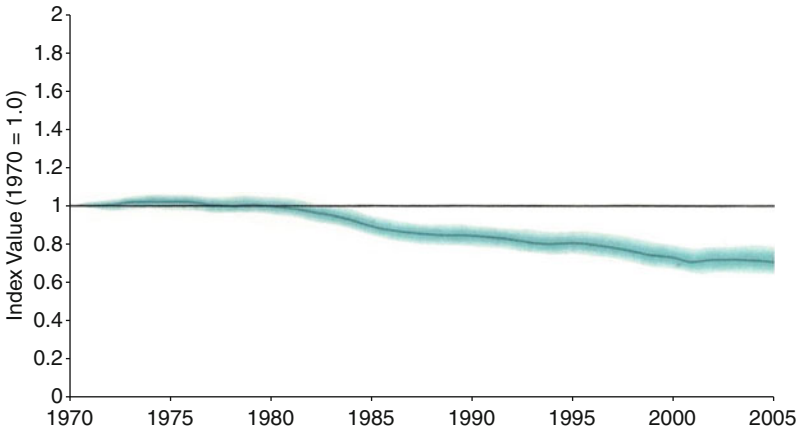

Species Diversity Within and Among Ecosystems. Figure 3
Living planet index for vertebrates. Index value shown in bold; shaded area shows 95% confidence limits [38]

to describe the exact nature of the relationship [63], evidence suggests that species richness, functional characteristics, composition, and interactions influence ecosystem function [64].

The greatest amount of research in this area has focused on the relationship between species richness and ecosystem function [65], with the relationship usually reported as being positive [64]. Evidence suggests that species-rich communities have greater interspecific variation in response to changes and provide more temporally stable ecosystem services [66]. In experimental systems, it has been proven that productivity, nutrient retention, and resistance to invasion and diseases, all tend to increase with increasing species richness [67].

Interactions among species, such as competition, mutualism, and predation, are also crucial to ecosystem functioning [67] and may be more important than species richness [68]. Direct interactions between plants and fungi, plants, and animals, and indirect interactions involving more than two species are essential for ecosystem processes such as transfer of pollen and seeds, transfer of plant biomass production to decomposers or herbivores, construction of habitat complexity, or the spread or suppression of plant, animal, and human pathogens [67]. Interactions between different species trophic levels are also key to regulating the provision of ecosystem services [69]. Certain combinations of species are complementary in their patterns of resource use and can increase average rates of productivity and nutrient retention [64].

Species' functional characteristics also strongly influence ecosystem properties. The loss of species such as ecological engineers or keystone species with unique functional characteristics may have profound effects on ecosystem function [71]. Species composition also plays an important role in ecosystem processes and extinctions of local populations, or their reduction to functionally extinct, can dramatically affect regulating and supporting ecosystem services [71].

Species Loss and Extinction

It is clear that as more species and/or the variability within species disappears, significant loss of ecosystem function, and hence ecosystem goods and services, may occur. While the evolution of species and the extinction of others is a natural process, current extinction rates are estimated to be between 100 and 1,000 times greater than they were in the distant past and future rates may be 10–100 times what they are today [10, 34]. Even among lesser threatened taxa, for example, birds, current extinction rates are several orders of magnitude higher than the natural or background rate. Roughly one-fifth of the world's vertebrates and plants are threatened with extinction [38, 72], and in addition to individual species, entire lineages or ecosystems are threatened [45, 73]. Current rates of population extirpation are probably at least three orders of magnitude higher than species extinction rates [74]. In addition, changes in the relative abundance among species are also capable of causing important changes in ecosystem function [75].

The main cause of extinction across all vertebrate groups is habitat loss or degradation – primarily driven by agricultural development and logging – followed by invasive species and human overexploitation [38, 72]. However as the impacts of climate change increase, it will likely be the greatest driver of extinctions this century. Climate change has already been proven as a cause of species extinction [76] and may likely be the greatest driver of extinction this century. As more distributions shift, it is predicted based on midrange climate warming scenarios for 2050 that 15–37% of species will be committed to extinction, with the most severe impacts resulting from synergistic interactions among a range of threats [77, 78].

Conservation of Species and Ecosystems

Invasive species and human-caused extinctions are already altering ecosystems; there are few places left on the planet that have not been affected by human impacts [79, 80]. Even minor losses may reduce the capacity of ecosystems to adjust to changing environments. As it is often difficult, expensive, or impossible to fix or reverse these changes with technological solutions [64, 81], it is crucial that the diversity of our planet's species and ecosystems is conserved. There are several levels of approach and the appropriate one will depend on the specific goals and resources available. The species level has been the traditional focus of conservation planning and action. Common frameworks include IUCN Species Action Plans and Species

Conservation Strategies, which focus on assessing species and making conservation recommendations, and Range-wide Priority Setting, which is designed for widely distributed species. Other approaches include the EDGE approach, which combines IUCN Red List data on threats with species evolutionary distinctiveness to focus on conserving threatened species with few remaining relatives [82].

Conservation approaches at other levels, such as landscape/ecosystems, are also widely used. Examples include Conservation Action Planning [83], which often focuses on a target landscape, and the Ecosystem Approach, which puts natural resource use at the center of decision making [84]. However, even at the ecosystem/landscape level, conservationists still use species, often iconic and charismatic species ones referred to as flagship species, to act as ambassadors for conservation of the wider area. These species are also a good way to begin engaging with the public, an important part of modern conservation. If people feel a connection to the natural world, they will be more willing to conserve it [85].

Whatever the chosen approach, it must be based on sound science and have a strong conceptual framework to guide action on the ground. Included in this framework should be significant capacity-building component to enable long-term continuation of responses capable of keeping pace with increasing threats, especially climate change. While there have been past conservation successes [73], the conservation community needs to focus more on coordinating large-scale strategic conservation plans around specific objectives. National Biodiversity Strategies and Action Plans, required by Convention on Biological Diversity member countries, have the potential to be very effective, if technical capacity and financial resources are developed to support their creation and implementation [90].

Conclusions

While there is disagreement about the definition and number of species, it is known for sure that species are the building blocks of ecosystems, and their diversity within and among ecosystems is essential to maintaining its function. Species are under threat from numerous anthropogenic factors including habitat loss, overexploitation, introduced and invasive species, and climate change. Current extinction rates are magnitudes higher than those of the past and no one knows for certain how many species the planet can afford to lose before there will be major implications for humanity. As technological solutions to lost or degraded ecosystem services are often expensive, difficult, or even impossible, there is clearly a need to conserve and sustainably manage our ecosystems and the species within them in order to maintain biodiversity and its practical benefits to humanity. However, the current level of conservation action is far outweighed by degree of threat. To halt species loss, there is an urgent need to scale up conservation action. While there have been conservation successes in the past, a coordinated and increased national- and global-level response is urgently need to halt the loss of global biodiversity.

Future Directions

The ecology of species and ecosystems is incredibly complicated and there are still many knowledge gaps regarding species diversity and its exact role within ecosystem function. Further research is needed to more fully explain this relationship and inform conservation action and policy. However, urgent action is also needed to conserve species as it can be confidently predicted that there is already a movement toward the next mass extinction [50, 86]. This is especially critical as the year 2050 is approached when the Earth will need to provide enough natural resources for an estimated 9.2 billion people [87]. Addressing the biodiversity crisis and all its consequences for humanity requires rapid movement toward governance structures and economic systems that encourage the sustainable use of Earth's natural resources. If this effort is to be successful, it cannot be limited to traditional conservationists; it must have the strong support of society as a whole and include leaders from a range of sectors such as engineering, medicine, finance, communications, business, and the arts.

Bibliography

1. Magurran AE, Gill BJ (2011) Biological diversity: frontiers in measurement and assessment. Oxford University Press, Oxford, UK
2. Hurlbert S (1971) The nonconcept of species diversity: a critique and alternative parameters. Ecology 52:577–586

3. Hamilton AJ (2004) Species diversity or biodiversity? J Environ Manage 75:89–92
4. Whittaker RH (1960) Vegetation of the Siskiyou mountains, Oregon and California. Ecol Monogr 30:279–338
5. Mace GM (2004) The role of taxonomy in species conservation. Philos Trans R Soc Lond B Biol Sci 359:711–719
6. Mace GM, Gittleman JL, Purvis A (2003) Preserving the tree of life. Science 300:1707–1709
7. Hey J (2001) The mind of the species problem. Trends Ecol Evol 16:326–329
8. Mayden RL (1997) A hierarchy of species concepts: the denouement in the saga of the species problem. In: Claridge MF et al (eds) Species: the units of biodiversity. Chapman and Hall, London, pp 381–424
9. Mallet J (2006) Species concepts. In: Fox CW, Wolf JB (eds) Evolutionary genetics: concepts and case studies. Oxford University Press, Oxford, UK, pp 367–373
10. Mace GM, Masundire H, Baillie JEM (2005) Biodiversity. In: Hassan R, Sholes R, Ash N (eds) Millennium ecosystem assessment, 2005 Current state and trends: findings of the condition and trends working group Ecosystems and human well-being, vol 1, chapter 4. Island Press, Washington, DC
11. Mayr E (1963) Animal species and evolution. Belknap Press of Harvard University Press, Cambridge, UK
12. Hay J (2000) Genes, categories and species: the evolutionary and cognitive causes of the species problem. Oxford University Press, Oxford, UK
13. Isaac NJB, Mallett J, Mace GM (2004) Taxonomic inflation: its influence on macroecology and conservation. Trends Ecol Evol 19(9):464–469
14. Ward BB (2002) How many species of prokaryotes are there? Proc Natl Acad Sci USA 99:10234–10236
15. Nee S (2003) Unveiling prokaryotic diversity. Trends Ecol Evol 18(2):62–63
16. Mora C, Tittensor DP, Ald S, Simpson AGG, Worm B (2011) How many species are there on Earth and in the ocean? PLoS Biol 9(8):e1001127
17. Erwin TL (1982) Tropical forests: their richness in Coleoptera and other Arthropod species. Coleopt Bull 36:74–75
18. Raven PH (1983) The challenge of tropical biology. Bull Entomol Soc Am 29(1):4–12
19. Stork NE (1988) Insect diversity: facts, fiction and speculation. Biol J Linn Soc 35:321–337
20. Stork NE, Gaston KJ (1990) Counting new species one by one. New Sci 1729:43–47
21. Hodkinson ID, Casson D (1991) A lesser predilection for bugs: Hemiptera (Insecta) diversity in tropical rain forests. Biol J Linn Soc 73:101–109
22. Hodkinson ID (1992) Global insect diversity revisited. J Trop Ecol 8:505–508
23. Novotny V, Basset Y, Miller SE et al (2002) Low host specificity of herbivorous insects in a tropical forest. Nature 419:841–844
24. IUCN (2011) IUCN red list of threatened species, version 2011.2: Table 1. www.iucnredlist.org. Downloaded on 14 Nov 2011
25. May RM (2007) Unanswered questions and why they matter. In: May RN, McLean AR (eds) Theoretical ecology: principles and applications, 3rd edn. Oxford University Press, Oxford, UK
26. Rosenzwieg ML (1995) Species diversity in space and time. Cambridge University Press, Cambridge, UK
27. Prendergast JR, Quinn RM, Lawton JH et al (1993) Rare species, the coincidence of diversity hotspots and conservation strategies. Nature 356:335–337
28. Fischer AG (1960) Latitudinal variations in organic diversity. Evolution 14:64–81
29. Hillebrand H (2004) On the generality of the latitudinal diversity gradient. Am Nat 163:192–211
30. Reid WV (1998) Biodiversity hotspots. Trends Ecol Evol 13:275–280
31. Snelgrove PVR (1999) Getting to the bottom of marine biodiversity: sedimentary habitats – ocean bottoms are the most widespread habitat on Earth and support high biodiversity and ecosystem services. BioScience 49:129–138
32. Crame JA (2002) Evolution of taxonomic diversity gradients in the marine realm: a comparison of Late Jurassic and recent bivalve faunas. Paleobiology 28:184–207
33. Gaston KJ, Spicer JI (1998) Biodiversity: an introduction. Blackwell Science, Oxford, UK
34. Baillie JEM, Hilton-Taylor C, Stuart SN (2004) 2004 IUCN red list of threatened species. A global species assessment. IUCN, Gland
35. Myers N, Mittermeier RA, Mittermeier GC et al (2000) Biodiversity hotspots for conservation priorities. Nature 403:853–858
36. Faith DP (1992) Conservation evaluation and phylogenetic diversity. Biol Conserv 61:1–10
37. Williams PH, Humphries CJ, Gaston KJ (1994) Centres of seed-plant diversity: the family way. Proc Roy Soc Lond B 256:67–70
38. Baillie JEM, Griffiths J, Turvey ST et al (2010) Evolution lost: status and trends of the world's vertebrates. Zoological Society of London, London, UK
39. Ponder W, Lunney D (1999) The other 99%: the conservation and biodiversity of invertebrates. Transactions of the Royal Zoological Society of New South Wales, Chipping Norton
40. Collen B, Ram M, Dewhurst N et al (2009) Broadening the coverage of biodiversity assessments. In: Vié J-C, Hilton-Taylor C, Stuart SN (eds) Wildlife in a changing world: an analysis of the 2008 review of The IUCN red list of threatened species. IUCN, Gland, pp 67–77
41. Rodrigues ASL, Pilgrim JD, Lamoreux JF et al (2005) The value of the IUCN red list for conservation. Trends Ecol Evol 21:71–76
42. Schipper J, Chanson JS, Chiozza F et al (2008) The status of the world's land and marine mammals: diversity, threat and knowledge. Science 10(322):225–230
43. Butchart SHM et al (2004) Measuring global trends in the status of biodiversity: red list indices for birds. PLoS Biol 2:2294–2304. doi:10.1371/journal.pbio.0020383
44. BirdLife International (2004) Threatened birds of the World 2004. (http://www.birdlife.org/datazone/species/index.html)
45. Stuart SN et al (2004) Status and trends of amphibian declines and extinctions worldwide. Science 306:1783–1786

46. Collen B, Loh J, McRae L et al (2009) Monitoring change in vertebrate abundance: the living planet index. Conserv Biol 23:317–327
47. Christensen LB (2006) Marine mammal populations: reconstruction historical abundances at the global scale. University of British Columbia, Vancouver, Canada
48. BirdLife International (2008) State of the world's birds: indicators for our changing world. BirdLife International, Cambridge, UK
49. Bielby J, Cooper N, Cunningham AA et al (2008) Predicting declines in the world's frogs. Conserv Lett 1:82
50. Wake DB, Vredenburg VT (2008) Are we in the midst of the sixth mass extinction? A view from the world of amphibians. Proc Natl Acad Sci 105:11466–11473
51. Blaustein AR, Wake DB (1990) Declining amphibian populations: a global phenomenon? Trends Ecol Evol 5:203–204
52. Daszak P, Cunningham AA, Hyatt AD (2003) Infectious disease and amphibian population declines. Divers Distrib 9(2):141–150
53. Jackson J, Kirby MX, Berger WH et al (2001) Historical overfishing and the recent collapse of coastal ecosystems. Science 293:629–637
54. Thurstan RH, Brockington S, Roberts CM (2010) The effects of 118 years of industrial fishing on UK bottom trawl fisheries. Nat Commun 1. doi:10.1038/ncomms1013
55. Food and Agriculture Organization of the United Nations (FAO) (2010) The state of the world fisheries and aquaculture. FAO, Rome
56. Le Quesne T, Matthews JH, Von der Heyden C et al (2010) Flowing forward: freshwater ecosystem adaption to climate change in water resources management and biodiversity conservation. World Bank and WWF
57. Reading CJ, Luiselli LM, Akani GC et al (2010) Are snake populations in widespread decline? Biol Lett. doi:10.1098/rsbl.2010.0373
58. Whitfield Gibbon J, Scott DE, Ryan TJ et al (2000) The global decline of reptiles, Déjà vu amphibians. Bioscience 50(8):653–666
59. Naeem S, Wright JP (2003) Disentangling biodiversity effects on ecosystem functioning: deriving solutions to a seemingly insurmountable problem. Ecol Lett 6:567–579
60. Naeem S, Thompson LJ, Lawler SP et al (1994) Declining biodiversity can alter the performance of ecosystems. Nature 368:734–737
61. Daily GC, Alexander S, Ehrlich PR (1997) Ecosystem services: benefits supplied to human societies by natural ecosystems. Issues Ecol 2:1–16
62. Chapin FS, Zavaletta ES, Eviner VT et al (2000) Consequences of changing biodiversity. Nature 405:234–242
63. Luck GW, Daily GC, Ehrlich PR (2003) Population diversity and ecosystem services. Trends Ecol Evol 18:331–336
64. Hooper DU et al (2005) Effects of biodiversity on ecosystem functioning: a consensus of current knowledge. Ecol Monogr 75:3–35
65. Kremen C (2005) Managing ecosystem services: what do we need to know about their ecology? Ecol Lett 8:468–479
66. Tilman D (1996) Biodiversity: population versus ecosystem stability. Ecology 77:350–363
67. Diaz S, Tilman D, Fargione (2005) Biodiversity regulation of ecosystem services. In: Hassan R, Sholes R, Ash N (eds) Millennium ecosystem assessment, 2005 current state and trends: findings of the condition and trends working group ecosystems and human well-being, vol 1, chapter 11. Island Press, Washington, DC
68. Grime JP (1997) Biodiversity and ecosystem function: the debate deepens. Science 277:1260–1261
69. Dobson A, Lodge D, Alder J et al (2006) Habitat loss, trophic collapse and the decline of ecosystem services. Ecology 87(8):1915–1924
70. Jones CG, Lawton JH, Shachak M (1994) Organisms as ecosystem engineers. OIKOS 69:3
71. Schindler DE, Hilborn R, Chasco B et al (2010) Population diversity and the portfolio effect in an exploited species. Nature 465:609–612
72. Hoffman M, Hilton-Taylor C, Angulo A et al (2010) The impact of conservation on the status of the world's vertebrates. Science 330:1503
73. Harding S, Clark E, Gardiner-Smith B et al (2010) GLOBE action plan for coral reefs. GLOBE International, London
74. Hughes JB, Daily GW, Ehrlich PR (1997) Population diversity; its extent and extinction. Science 278:689–692
75. Valéry L, Fritz H, Lefueve J-C, Simberloff D (2009) Ecosystem-level consequences of invasion by native species as a way to investigate relationships between evenness and ecosystem function. Biol Invasions 11(3):609–617
76. Parmesan C, Yohe G (2003) A globally coherent fingerprint of climate change impacts across natural systems. Nature 421:37–42
77. Thomas CD, Cameron A, Green RE et al (2004) Extinction risk from climate change. Nature 427:145–148
78. Stork NE (2009) Re-assessing current extinction rates. Biodivers Conserv 19(2):357–371
79. McMichael AJ, Butler CD, Folke C (2003) New visions for addressing sustainability. Science 302:1919–1920
80. Halpern BS, Walbridge S, Selkoe KA et al (2008) A global map of human impact on marine ecosystems. Science 319:948
81. Palmer M, Bernhardt E, Chornesky E et al (2004) Ecology for a crowded planet. Science 304:1251–1252
82. Issac NJB, Turvey ST, Collen B et al (2007) Mammals on the EDGE: conservation priorities based on threat and phylogeny. PLoS One 2(3):e296
83. Hamberg SE, Martin AS (2007) Conservation action planning. Innovations in conservation series. Parks in Peril Programme. The Nature Conservancy, Arlington
84. Convention on Biological Diversity (2000) Decision V/6. Ecosystem approach. In: Proceedings of the fifth conference of the parties, Nairobi
85. Saunders CD (2003) The emerging field of conservation psychology. Human Ecol Forum 10(2):137–149

86. Barnosky AD, Matzke N, Tomiya S et al (2011) Has the Earth's sixth mass extinction already arrived? Nature 471:51–57
87. United Nations, Department of Economic and Social Affairs, Population Division (2007) World population prospects: 2006 revision, highlights. Working Paper No. ESA/P/WP.202
88. Anderson S (1994) Area and endemism. Q Rev Biol 69:451–471
89. Brown JH, Whitman TG, Ernest SKM, Gehring CA (2001) Complex species interactions and the dynamics of ecological systems: long term experiments. Science 293:643–649
90. Baillie JEM, Raffaelli D, Sillero-Zubiri C (in prep) Levels of approach. In: Macdonald D (ed) Key topics in conservation biology 2nd ed. Wiley-Blackwell, Oxford, UK

Stormwater Harvesting and Reuse

G. Singh[1], M. A. H. Johir[1], J. Kandasamy[1], S. Vigneswaran[1], B. Kus[1], R. Naidu[2]
[1]University of Technology, Sydney, NSW, Australia
[2]CRC Care, University of South Australia, Adelaide, Australia

Article Outline

Glossary
Definition of the Subject and Its Importance
Introduction
Stormwater Characteristics
Stormwater Treatment Measures – WSUD
Stormwater Harvesting and Recycling
Assessment Methods for Measuring Treatment Effectiveness of Stormwater Treatment Systems
Future Directions
Bibliography

Glossary

Average recurrence interval (ARI) or return period The size of flood that on average occurs once every return period in years (or ARI).

Best management practice (BMP) The best practicable method of achieving water quality management objectives, similar to treatment measure.

Design flow Similar to treatable flow rate.

Event mean concentration (EMC) The event mean concentration (EMC) is derived from a number of rainfall events. For each rainfall event, the average pollutant concentration is determined based on measurement of pollutant concentration over the rainfall event. The mean of all these event-based average pollutant concentration values is the event mean concentration or EMC.

High rate treatment Treating stormwater at a high discharge rate.

Inline system A treatment system that is part of the main drainage system and treats all flows passing through it.

Major drainage flow paths Also known as overland flow paths that drain water from the catchment to formalized drainage systems. These usually include drainage easements and roadways.

Minor drainage flow paths This is usually the formal drainage system and consists of pipes and stormwater channels.

Modeling Simulating the performance of treatment systems or a series of treatment systems using numerical models.

Off-line system A treatment system not the main drainage system, and treats flows from only a local catchment that drains toward the formalized or main drainage system.

Stormwater havesting Collecting and treating stormwater for beneficial reuse purposes.

Treatable flow Defined as the minimum flow that a stormwater treatment measure must be capable of treating, without bypass, to achieve the desired pollutant retention criteria.

Treatment measures A stormwater treatment device that removes pollutants in the stormwater passing through it.

Treatment train Is a series of BMPs to achieve WQOs.

Water quality objectives (WQOs) WQOs are specific water quality targets agreed between stakeholders, or set by local jurisdictions.

WSUD Water sensitive urban design.

Definition of the Subject and Its Importance

Rapid urbanization has contributed to considerable increases in urban stromwater runoff and pollution, a deterioration of the water quality of urban waterways, and significant threats to its ecosystem. Stormwater runoff is the most neglected resource and, given that it contributes significantly to diffuse pollution of our waterways, it needs to be managed in more sustainable

way to capture its benefits and at the same time to reduce the adverse impacts on waterways and receiving waters. A cultural change is occurring in urban stormwater management practice. Environmental aspects are becoming a major focus, with potentially profound effects on the traditional approach to stormwater management. An integrated approach to stormwater treatment and management and stormwater harvesting regards stormwater as a resource rather than a waste and considers all aspects of runoff within a development, including implementation of water quality/quantity controls, maximizing water reuse/conservation whilst preserving the amenity and environmental values within the catchment. Stormwater harvesting and reuse offers a potential alternative water supply for at least non-potable uses. The benefits of a successful stormwater harvesting systems include reductions in stormwater pollution loads to downstream waterways and estuaries, and in stormwater volumes and discharges. Methods of assessment to check the extent to which stormwater treatment systems are meeting their design objectives and compliance to water quality standards is important.

Introduction

Stormwater is runoff from roof, road and paved surfaces, etc., from residential, commercial, and other urban areas. Pollution from urban catchments is a major problem in waterways. Impervious surfaces accumulate pollutants deposited from the atmosphere, leaked from vehicles, or windblown from adjacent areas. During storm events, these pollutants washoff, and are rapidly transported to waters downstream. Pollutants discharged in stormwater are largely uncontrolled. Stormwater runoff constitutes the primary transport mechanism for nonpoint pollution. Pollution problems associated with land use and development encompass typical pollutants such as pesticides, fertilizers, and petroleum products. A further problem stemming from residential, commercial, and industrial land uses is the higher volume of runoff because of the higher percentage of impervious area and faster catchment runoff times.

Recent developments in stormwater management have focused on detention and retention of water, pollutant removal, and reuse. As the basis of more strategic-based management, the Australian and New Zealand Environment and Conservation Council (ANZECC) Guidelines for Fresh & Marine Water Quality [1] make explicit the water environmental and use values to be protected or in the case of modified waterways, restored, and the major threats to these values, as the focus of a risk management-based approach. Importantly, the guidelines recognize that in the case of some modified waterways, such as urban systems, it may not be practical to "restore" the waterways to predevelopment conditions, but that the waterways may nonetheless sustain, or be capable of sustaining, a range of important environmental and use values worthy of management into the future. The best management practice (BMP) approach or Water Sensitive Urban Design (WSUD) recognizes that runoff cannot be directly treated to ambient receiving water quality, but that the employment of WSUD will provide a practical level of protection for the ecosystem. By its very nature, WSUD can be expected to improve and change over time.

Stormwater harvesting and reuse offers a potential alternative water supply for at least non-potable uses. The benefits of a successful stormwater harvesting systems include reductions in stormwater pollution loads to downstream waterways and estuaries and in stormwater volumes and discharges.

Methods of assessment to check the extent to which stormwater treatment systems are meeting their design objectives and compliance to water quality standards are important. Assessment methods usually require numerical modeling, which is presented in the last part of this chapter.

Stormwater Characteristics

Intense human activities results in many pollutants, such as suspended solids (SS); nutrients and metals; oxygen demanding and inert material; particulate and dissolved substances; chemical, biological, and physical matter; toxic and nontoxic matter; organic and inorganic matter; and polycyclic aromatic hydrocarbons (PAHs). These pollutants have considerable impacts on aquatic community in streams and estuaries. The effect of these pollutants and the likely urban sources of pollutants found in stormwater are outlined in Table 1 [2].

Stormwater Harvesting and Reuse. Table 1 Types and causes of urban stormwater pollution (Adapted from [2])

Pollutant	Effect	Urban source
Sediment	Reduces the amount of light in the water available for plant growth and thereby reducing the supply of food for other organisms. Damages sensitive tissues such as the gills of fish. Smothers organisms, which live on or in the bed of lakes and streams when suspended material settles out.	• Land surface erosion
		• Building and construction sites
		• Organic matter (e.g., leaf litter, grass)
		• Atmospheric deposition.
Nutrients	Stimulates the growth of aquatic plants, aquatic weeds, and algae that may choke lakes and streams and lead to exhaustion of dissolved oxygen levels.	• Fertilizer
		• Sewer overflows, septic tank leaks
		• Detergents (car washing)
Oxygen demanding substances	The drop in oxygen levels may kill fish and other aquatic organisms. Anaerobic conditions may occur, unpleasant odors can result.	• Organic matter decay
		• Sewer overflows, septic tank leaks
		• Animal feces
pH acidity	Increased acidity damages plants and animals	• Organic matter decay
		• Erosion of roofing material.
Microorganisms	Bacteria and viruses can cause illnesses, including hepatitis and gastroenteritis.	• Animal feces
		• Sewer overflows, septic tank leaks
Toxic organics	Can poison living organisms or damage their life processes.	• Pesticides
		• Herbicides
		• Sewer overflows, septic tank.
Heavy metals	Poison living organisms or damage their life processes in some other way. Persists in the environment for a long time.	• Atmospheric deposition
		• Vehicle wear
		• Sewer overflows, septic tank leaks
Gross pollutants (litter, debris)	Unsightly. Animals can eat and choke on this material.	• Pedestrians and vehicles
		• Leaf-fall from trees
		• Shopping precincts
Oils, detergents (surfactants)	Highly toxic poison to fish and other aquatic life.	• Asphalt pavements
		• Spillage, illegal discharges
		• Leaks from vehicles
Increased water temperature	High temperatures are lethal to fish and other aquatic organisms. Elevated water temperatures stimulate the growth of nuisance plants and algae.	• Runoff from impervious surfaces
		• Removal of riparian vegetation.

Pollutants originate from either point or nonpoint sources. Point sources are specific identifiable locations where stormwater pollution origniate. These include illegal discharges of trade wastes and sewer overflows. Nonpoint sources or diffuse sources, are more general, and are comparatively difficult to identify and control. These include litter, sediments, nutrients, oils and grease from road surfaces, toxic material, bacteria, and organic material. Without appropriate stormwater treatment devices, the resulting impacts on receiving waters can be devastating, not only for aquatic ecosystems but also to community values such as aesthetics, recreation, economics, and health of receiving water bodies.

Stormwater quality is further complicated by the variation in pollutant concentration through the period of storm flows. The concentration of pollutant is typically most severe at an early stage of runoff giving rise to a "first flush." In small urban sites, the first flush does not always occur where pollutants (e.g., oils and greases) are not transported as easily or quickly as soluble materials and fine dusts, or where vegetated surfaces are generally not "cleansed" as easily as sealed surfaces or where continuous sources of pollutants may exist. The rainfall intensity and the pollutants largely define the wash-off behavior of pollutants and their control management. It is important to consider the dynamic behavior of pollutants and their concentration through the storm event.

Typical range of stormwater quality data for Australian catchments is presented in Table 2. This is compared with corresponding water quality standards.

Stormwater Treatment Measures – WSUD

A cultural change is occurring in urban stormwater management. Environmental aspects are becoming a major focus, with potentially profound effects on the traditional approach to drainage. WSUD is a catch-all term for environmentally sustainable water resource management in urban areas. In Australia, WSUD is gaining prominence as a contemporary approach for managing urban stormwater to minimize the impact of urban development on waterways and estuaries.

WSUD seeks to minimize the extent of impervious surfaces, treating stormwater runoff and mitigating changes to the natural water balance, through on-site reuse of the water as well as through temporary storage. An integrated approach to stormwater management is the key to WSUD. This integrated approach regards stormwater as a resource rather than a burden and considers all aspects of runoff within a development, including implementation of water quality/quantity controls, maximizing water reuse, conservation and preservation of amenities and environmental values within the catchment (see Fig. 1).

The target pollutants in stormwater treatment are litter, coarse/fine sediments, and nutrients. Treatment measures can be classified into nonstructural measures, which aim to reduce pollution through public education, etc., and structural measures. When assessing structural treatment measures for removal or reducing pollutants, there are three subsets, which describe the type of treatment measure and type of pollutants, which are removed or reduced. These are:

- Primary treatment
- Secondary treatment
- Tertiary treatment

Primary treatment targets the removal of gross pollutants and coarse sediments and any associated nutrients, hydrocarbons attached onto particulates larger than 1.25 μm. Secondary treatment measures attempt to remove finer particles and attached pollutants by using filtration techniques and/or by inducing sedimentation. Tertiary treatment includes a range of physicochemical measures such as enhanced sedimentation, filtration and adsorption, and biological uptake.

Stormwater pollution is effectively managed through a treatment train, which is a sequence of treatment measures formulated to manage specific size ranges of pollutants at appropriate timescales, based on the areas available to suitably site the treatment measures. For example, coarse sediment can settle out in a matter of minutes once stilling of the flow occurs, whereas removal of nutrients can take several hours to days. As such, a treatment measure that is effective at removing coarse sediment is not necessarily suitable for removing nutrients. Further, a treatment measure designed to remove nutrients may require more frequent maintenance if it has to also remove coarse sediment. It is obvious that one treatment measure will not be able to treat a suite of pollutants. While a vegetated swale may be able to remove some nutrients, it will not be effective for removing colloidal and dissolved material. By contrast, the latter are more effectively removed by a wetland or biofilteration. The swale may then become the pretreatment measure for the wetland, creating a treatment train.

Nonstructural Measures

Clearly "prevention is better than cure" – not only is it more effective, it is also cheaper. The cost for removal of trapped pollutants is substantial as is the ongoing associated maintenance costs and the one-off

Stormwater Harvesting and Reuse. Table 2 General characteristics of urban stormwater quality data in Australia

Parameter	Unit	Sydney	Australia	Australian standards [3–6]
		Range of pollutant concentration[a]	Range of pollutant concentration [3]	
Nutirents				
Total nitrogen	mg/L N	0.39–9.5	0.6–8.6	<0.1–0.75
Nitrate	mg/L N	0.38–7.9	–	–
Nitrite	mg/L N	0.069–0.97	–	–
Ammonia	mg/L N	0.4–1.15	0.01–9.8	<0.02–0.03
Total phosphorus	mg/L P	0.021–0.36	0.12–1.6	<0.01–0.1
Orthophosphate	mg/L P	0.02–0.026	–	–
Physical and chemical				
TSS	mg/L	–	20–1,000	<10% change
pH	–	6.68–7.28	–	–
TOC	mg/L	4.25–8.96	–	–
Turbidity	NTU	1.5–90	–	–
True color	PtCo	18–270	–	–
Bicarbonate	mg/L $CaCO_3$ equivalent	30–95	–	–
Water hardness	mg/L $CaCO_3$ equivalent	22–145	–	–
Metals				
Aluminum	mg/L	0.028–0.188	–	–
Arsenic	mg/L	0.001–0.005	–	–
Cadmium	mg/L	0.0009–0.001	0.01–0.09	0.0002–0.002
Chromium	mg/L	0.002–0.002	0.006–0.025	0.01
Copper	mg/L	0.008–0.049	0.027–0.094	0.002–0.005
Iron	mg/L	0.05–2.55	–	–
Manganese	mg/L	0.001–0.024	–	–
Nickel	mg/L	0.003–0.10	0.014–0.025	0.015–0.15
Lead	mg/L	0.001–0.022	0.19–0.53	0.001–0.005
Selenium	mg/L	0.001–0.004	–	–
Zinc	mg/L	0.016–0.123	0.27–1.10	0.27–1.10
Biological				
Fecal coliform	cfu/100 mL	–	4,000–200,000	150 (PR)
				1,000 (SR)

PR primary recreation, *SR* secondary recreation

[a]Data measured in Carlton, Kogarah

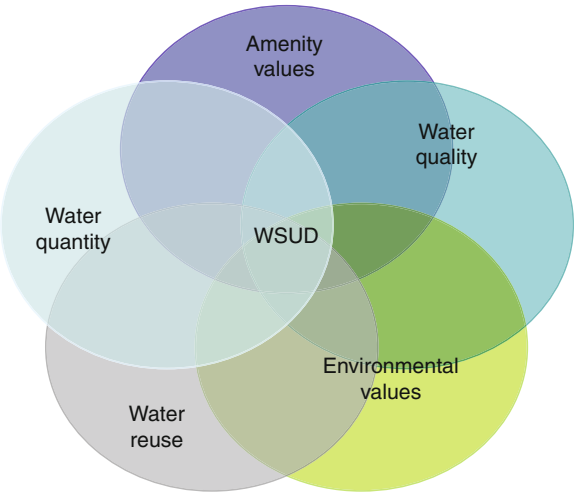

Stormwater Harvesting and Reuse. Figure 1
WSUD conceptual model

capital cost. The following nonstructural options are commonly used for reducing stormwater pollution:

- Educational measures, e.g., advertising in local papers, radio & TV media, school curriculum, shopping centers, etc.
- Planning controls, e.g., council policies and strategies for better planning of existing and new developments in the catchment.
- Site inspections and auditing.
- Review of management practices and program efficiency improvements (e.g., council maintenance activities, etc.).
- Studies and assessments to develop strategies for reducing stormwater pollutants in waterways.

The most commonly used nonstructural method is stormwater education. This involves working on programs that involves education at schools, community workshops, industrial and shopping centers. The program includes distribution of education materials, community and students' involvement, voluntary programs for water quality monitoring, and advertising in newspapers. Nonstructural methods are the most cost-effective approach to water quality management.

Structural Measures

Primary Treatment Primary treatment involves removal of gross pollutants and coarse sediments and any nutrients, or hydrocarbons attached on particulates larger than 1.25 m. The removal method is through entrapment of litter/debris and sedimentation of coarser particles. Trapped pollutants are held until removal in two main ways; by containing pollutants within a wet sump (either in baskets or chambers) or by storing pollutants in baskets, nets, or behind screens that are free draining. A description and comparison between different treatments used in stormwater are given in Table 3 [7].

Secondary Treatment Secondary treatment consists of sedimentation of finer particle or filtration techniques to remove fine particles and attached pollutants. This can be achieved in a natural treatment system. The treatment falls into the following categories:

- Pre-entrance treatments

  This type of secondary treatment uses either filtration techniques to separate out entrained sediment prior to its entry into the drainage network or uses enhanced sedimentation to control contaminants. Some common examples of pre-entrance treatments are filter or buffer strips and grass swales. Infiltration is also promoted in one of two ways; either by stormwater flowing over vegetated land enhancing infiltration, or through the use of purpose-built structures such as porous pavements and infiltration trenches.

  Buffer strips are vegetated grassed areas that treat overland (sheet) flow, and commonly used as a source control measure, particularly adjacent to water courses, and to treat road runoff. They are effective in the removal of coarse to medium-sized sediments and can be an effective pretreatment measure.

  Grass swales are vegetated open channel systems, which utilize the grass as a filter to aid the removal of sediment and suspended solids. These systems are subjected to fairly high hydraulic loading and the removal efficiency is highly dependent on the density and height of the grass.

  The pollutant removal efficiency of swales and buffer strips are summarized in Table 4.
- In-transit treatments

  In-transit secondary treatment systems entrain pollutants flowing through the stormwater system. A typical example is a *biofiltration system*. By reducing the flow, these systems encourage sedimentation,

Stormwater Harvesting and Reuse. Table 3 Stormwater treatment methods and techniques and their advantages, disadvantages (Adapted from [7])

Treatment measures	Description	Advantages	Disadvantages
Trash/Litter racks	Litter racks (or trash racks) are a series of metal bars located across a channel or pipe to trap litter and debris.	(a) Appropriate for retrofitting into existing areas (b) Low downstream maintenance (c) Applicable for areas between 8 and 20 ha	(a) Not suitable in tidal areas as collected litter can move upstream (b) Potential odors and health risk to workers when handling litter (c) Possible safety risk when instaxlled in channels and difficult to clean/maintain
Sediment trap	Sediment traps are designed to trap coarse sediment and can take the form of a "tank" or a less formal pond.	(a) Trap coarse sediments upstream such as a wet basin or constructed wetland (b) Reduce coarse sediment loads to stormwater systems or receiving waters (c) Applicable for areas greater than 5 ha	(a) Limited removal of fine sediment, and pollutants can be remobilized (b) Visually unattractive (c) Trapping of excessive sediment can result in downstream channel erosion (d) Potential for mosquito breeding
Gross pollutant trap	A gross pollutant trap (GPT) is a sediment trap with a litter (or trash) rack, usually located at the downstream end.	(a) GPTs trap coarse sediments before they enter into the waterway (b) Appropriate for retrofitting into existing urban areas (c) Suitable for catchments greater than 6–8 ha	(a) Potential to aggravate upstream flooding (b) Visually unattractive (c) Impose odors and health and safety risk to workers when handling litter (d) Difficult and expensive to clean
Litter booms	Litter booms are floating booms with mesh skirts placed in channels or creeks to collect floating litter and debris.	(a) Enhance aesthetic appeal and recreational potential of downstream waterways (b) Collects litter at a single location (c) No hydraulic head loss (d) Boom can rise and fall with the tide	(a) Traps floating litter/debris (b) Large objects such as branches or boats can reduce boom effectiveness (c) Litter can be blown over the boom's collar in wind (d) Low visual amenity
Oil/Grit separators	Oil/grit separators, also known as water quality inlets, generally consist of three underground retention chambers designed to remove coarse sediment and hydrocarbons.	(a) Appropriate for treating stormwater from areas expected to have significant vehicular pollution (e.g., parking) (b) Can also be used for treating stormwater from areas storing or handling petroleum products (c) Can be appropriate for retrofitting into existing areas	(a) Limited removal of fine or soluble pollutants (b) When turbulent stormwater enters the chambers, this action may resuspend particulates or entrain floating oil (c) Trapped debris is likely to have high concentrations of pollutants, possibly toxicants (d) Needs to be regularly cleaned with safety hazard

and through the use of a porous media, they filter the storm water. In addition, vegetation can consume (biological uptake) the nutrients trapped in the filter media.

Figure 2 shows the biofiltration systems. These systems promote the removal of particulate and soluble contaminants by passing stormwater through the vegetation and filter medium. The type of vegetation and

Stormwater Harvesting and Reuse. Table 4 Pollutant trapping efficiency for natural treatment system

Pollutant	Swale	Buffer strip	Wetland	Biofiltration
Litter	M	L-M	L	N-L
Oxygen demanding material	L	L	M-H	H
Sediment	H	H	H	H
Oil & grease	H	H	H	H
Nutrients	M	M	M	M
Bacteria	H	H	H	H

H high efficiency (75–100% removal), *M* moderate efficiency (50–75% removal), *L* low efficiency (10–50% removal), *N* negligible efficiency (0–10% removal)

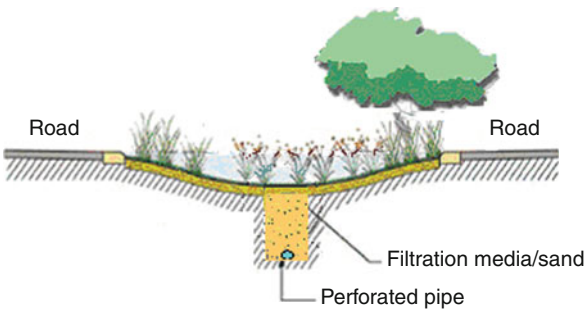

Stormwater Harvesting and Reuse. Figure 2 Biofiltration system as part of road median

filter medium determines the effectiveness of pollutant removal, with the vegetation and material of lower hydraulic conductivity providing the most efficient pollutant removal (owing to longer detention time). Typical filter material ranges from gravel (~10 mm) to fine sand (~0.1 mm). Table 4 gives the pollutant removal efficiency of biofiltration.

Tertiary Treatment *Constructed wetland* systems are shallow, extensively vegetated water bodies that use processes of extended detention, fine filtration, and biological pollutant uptake to remove pollutants from stormwater. Wetlands generally consist of an inlet zone (sedimentation basin), a macrophyte zone, an outlet zone, and a high flow bypass channel. The macrophyte zone generally has an extended detention depth of 0.25–0.5 m, specialist plant species (depending on the desired operation and target pollutant), and a notional detention time of between 48 and 72 h.

The pollutant removal process is through solubilization of nutrients and uptake by plants within the wetlands. Pretreatment is required for removal of gross pollutants and coarser sediments prior to wetland. Heavy metals adsorbed on the sediments are removed from enhanced sedimentation and through solubilization from anaerobic activity followed by uptake by plants and microorganisms. The dissolved metals are removed to some extent from direct uptake by microorganisms, predominantly phytoplanktons in treatment measures such as wetlands and ponds. The pollutant removal efficiency is summarized in Table 4.

Evaluation of WSUD

The potential benefits and limitations of WSUD are summarized in the list below for a range of issues including water balance, water quantity and quality, environmental values, and cost. Among the most significant limitations are the land footprint required for adequate levels of treatment, ongoing maintenance requirement and costs, and the lack of reliability of water quality of the effluent over a range of influents condition.

The potential benefits of WSUD are as follows:

Water balance
- Maintains the hydrological balance by using natural processes of storage, infiltration, and evaporation.
- Aids in groundwater recharge.

Water quantity
- Promotes reuse and recycling of stormwater.

Water quality
- Maintains and, where possible, enhances water quality
- Minimizes waterborne sediment loading
- Minimizes the export of pollutants to surface or groundwater
- Minimizes the export and impact of pollutants from sewage

Environmental values
- Protects environmentally sensitive areas from urban development.

- Restores and enhances urban waterways.
- Minimizes the impact on the environment of urban development.
- Can increase the diversity of natural habitats and suburban landscape.

Visual/Amenity values

- High visual amenity.
- Opportunities to link community nodes through public open space.
- Protects existing riparian or fringing vegetation.

Costs

- May reduce capital costs (pipework and drains) and reduces construction costs (e.g., grading, tree clearing)
- Potentially reduces the costs of water quality improvements, by retaining existing waterways.
- Incorporating water-sensitive features, water frontages, networked public open space, and preserving and enhancing ecological systems tends to make developments more desirable and marketable

The constraints/limitations of WSUD are as follows:

- Potentially increases maintenance and operation costs. Maintenance can potentially reverse the benefits of stormwater treatment by increasing the nutrient loads to the receiving bodies.
- WSUD is not effective for removal of heavy metals, dissolved nutrients (mainly nitrogen) and pathogens. Stormwater filtration may be a more suitable alternative for gross removal of all pollutants and pathogens.
- There may be possible need to supplement WSUD treatments (such as swales) with pipes, to accommodate minor storm events and steep terrain.
- Opportunities are limited in areas with high water tables, deeply dissected terrain and steep slope, or poor soil and shallow depth to bedrock.

Case Studies of WSUD

Shipwrights Bay WSUD The Shipwrights Bay catchment is approximately 59 ha of special use (52%), residential land (37%), and parks/open space (11%) that drains into Shipwrights Bay. In 2005–2006, Kogarah Council, a local government authority in Sydney, investigated strategies to reduce the sediment and nutrient loads to the bay. The most viable measure was the construction of a stormwater treatment train that included rehabilitation of the creek, stormwater pretreatment devices (ski jump and net litter traps), and constructed wetland, see Fig. 3. Pretreatment is required for removal of gross pollutants and coarser sediments before it enters the wetland. The constructed wetland systems are shallow, extensively vegetated

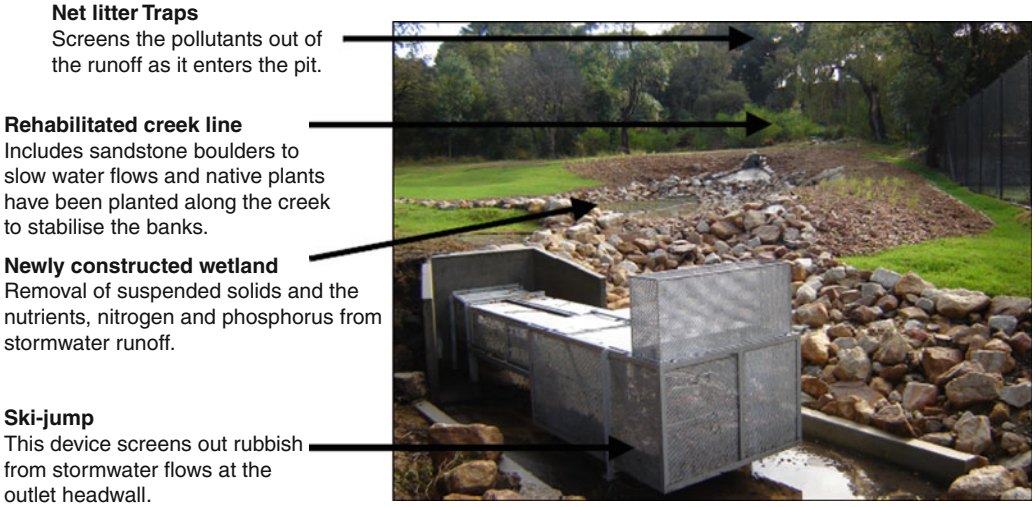

Stormwater Harvesting and Reuse. Figure 3
Shipwrights Bay WSUD

water bodies that use extended detention, fine filtration, and biological pollutant uptake processes to remove pollutants from stormwater.

Following community consultation, an urban wetland was constructed in a natural reserve area in conjunction with GPTs (ski jump and net litter traps) to form a stormwater treatment train to reduce sediment and nutrient loads to the bay.

Post-construction water quality monitoring downstream of the treatment train (August 2006–December 2008), Table 5, indicated significant improvement in water quality of effluent discharging to the bay. The water quality within the bay in proximity to the discharge point to Shipwrights Bay was within limits specified in the ANZECC guidelines [1]. The wetlands have also provided a habitat for flora and fauna and enhanced the recreational amenity of the reserve.

Drummoyne Sand Filter The sand filtration device (SFD) at Drummoyne Park, Sydney is an offline device and was designed to treat pollution contained in the first flush. By intercepting this volume, a large portion of the pollution load may be captured before it discharges into the receiving waters.

The SFD consists of several components including a diversion pit on the main stormwater pipeline, a gross pollutant trap located within the inlet pit, an aboveground storage basin, two sand filter compartments, and a monitoring pit at the filter outlet (Fig. 4). The diversion pit diverts stormwater discharges up to the 6 month average recurrence interval (ARI) event to the sand filtration compartments. A gross pollutant trap within the diversion pit provides prescreening of stormwater to remove gross pollutants and gravel. This helps prevent clogging of the SFD.

The surcharge pit provides access to the stormwater inflow for monitoring and directs the stormwater into the aboveground storage basin. The aboveground storage basin provides storage for runoff. By providing up to 1 m depth of storage above the SFD, the basin can store up to 155 m^3 of stormwater or approximately half of the 6 month (ARI) runoff volume. An overflow weir diverts away inflow volumes greater than this capacity.

The sand filter bed overlays a geotextile fabric layer, which in turn covers a gravel media and an underdrain system that drains filtered runoff away from the SFD. The entire sand filtration unit is covered with removable aluminum grates. The downstream pit provides access for sampling of the treated effluent water and drains back into the main stormwater trunk line.

The performance of the SFD is good and is generally better than reported in literature, Table 6. The SFD removed 61% of total nitrogen (TN), 70% of total kjeldahl nitrogen (TKN) and 53% of oxides of nitrogen (NOx) from the stormwater runoff. It also removed 75% in suspended solids (SS) and 80% of heavy metal (zinc) from the stormwater runoff.

Stormwater Harvesting and Recycling

Stormwater harvesting and reuse offers a potential alternative water supply for at least non-potable uses.

Stormwater Harvesting and Reuse. Table 5 Quality of effluent at Shipwrights Bay WSUD

Pollutant	Maximum	Minimum	Median	Modeled catchment EMC[a]	Potential removal rate (%)
pH	7.16	7.02	7.1	–	–
Turbidity (NTU)	15.00	3.50	7.2	120	87–97
Total nitrogen dry weather (mg/L)	0.2	0.05	0.1	2	90–98
Total nitrogen wet weather (mg/L)	0.25	0.1	0.15	2	88–95
Total phosphorus dry weather (mg/L)	0.07	0.02	0.05	0.20	72–92
Total phosphorus wet weather (mg/L)	0.09	0.04	0.06	0.20	64–84

[a]*EMC* event mean concentration

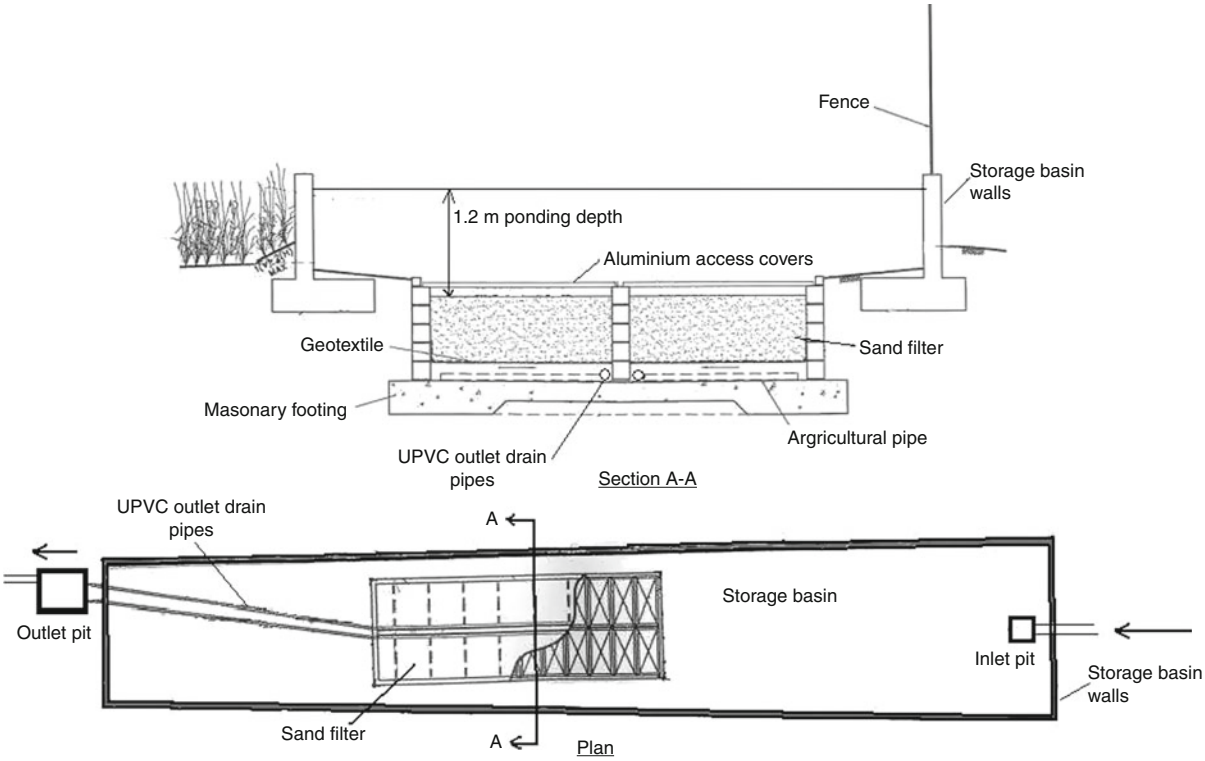

Stormwater Harvesting and Reuse. Figure 4
Schematic of sand filtration device (SFD)

Stormwater Harvesting and Reuse. Table 6 Average EMC of stormwater at the Drummoyne Park SFD (Modified from [8])

Water quality parameter	Inlet	Coarse filter outlet (% removal)	Stormwater filtration systems [9]
Fecal coliforms	57,814 cfu per 100 mL	11,966 cfu per 100 mL (79%)	NA
Suspended solids	14.4 mg/L	3.4 mg/L (76%)	81%
Total phosphorus	0.21 mg/L	0.13 mg/L (39%)	45
Total nitrogen	2.2 mg/L	0.86 mg/L (61%)	32%
Oxidized nitrogen	1.1 mg/L	0.52 mg/L (53%)	−13
Total kjeldahl nitrogen	1.1 mg/L	0.33 mg/L (70%)	NA
Zinc	0.28 mg/L	0.05 mg/L (83%)	69%

NA no information available

It complements other approaches to sustainable urban water management such as rainwater tanks, the reuse of wastewater and greywater, and demand management. Collectively, these areas form the basis of developing sustainable water technologies.

The average annual volume of urban storm water runoff in Australian cities is almost equal to the average annual urban water usages, of which at least 50% is for non-potable use [10]. Urban stormwater is perceived to be of better quality than greywater and wastewater and its reuse has a better public acceptance. The benefits of a successful stormwater harvesting scheme are reductions in (1) demand for town (potable) water, (2) stormwater pollution loads to downstream

waterways and estuaries, (3) stormwater volumes and discharges. Stormwater pollution is a major source of pollution in Sydney Harbour and Melbourne's Port Phillips Bay. Stormwater contributed 94% of sediments and 50–60% of nutrients to Sydney Harbor [11].

Stormwater Treatment Targets and Objectives

The three aspects of stormwater quality of particular relevance to stormwater harvesting and reuse schemes are [12]:

- Pathogens, including fecal coliforms and *E. coli* – for public health implications.
- Chemical constituents – for public health and environmental considerations, and some end-use requirements (e.g., irrigation).
- Suspended solids and turbidity – for their potential impact on both the effectiveness of disinfection and the function of irrigation schemes.

Table 2 gives the quality of stormwater for a range of constituents. To date, the analysis and evaluation of stormwater quality has been on the basis of surrogate components. Further, the assessments have been predominantly targeted for the impacts on receiving water and not for reuse purposes. Table 7 provides indicative values for a range of non-potable uses including residential non-potable uses such as toilet flushing, irrigation, construction applications, and fire fighting. Additional criteria may be applicable for more specific application, e.g., industrial reuse purposes.

WSUD treatment devices such as wetlands, bioretention, permeable pavement are widely used in stormwater management. According to Hatt et al. [13], the current WSUD devices used in Australia for stormwater pollution control do not provide the reliability in water quality necessary for recycling due to their inadequate removal efficiency for a range of inflow conditions. Further, for adequate levels of treatment, WSUD devices take up a considerable land area, which is often not available in urban inner-city areas.

Stormwater discharge is relatively high and therefore needs to be treated at a high rate. The alternative is to store the stormwater before treatment. Raw stormwater in storage has low value and will degrade under anerobic and anoxic condition while pretreatment of stormwater adds value to the stored water and can be beneficially reused.

Stormwater Harvesting and Reuse. Table 7 Stormwater indicative targets criteria for reuse application [12]

Application	Typical indicative targets
Level 1: Reticulated non-potable residential uses (e.g., garden watering, toilet flushing, car washing)	*E. coli* <1 cfu/100 mL, turbidity ≤ 2 NTU
	pH 6.5–8.5, pathogen reduction[b]
Level 2 (with human exposure). Spray or drip irrigation of open spaces, parks and sportsgrounds, dust suppression, construction site, ornamental water bodies, firefighting.	*E. coli* <10 cfu/100 mL, turbidity ≤2 NTU, pH 6.5–8.5, pathogen reduction[b], TP < 0.05 mg/L[a], TN < 5 mg/L[a]
Level 3 (no human exposure) Spray or drip irrigation or subsurface irrigation of open spaces, parks and sportsgrounds, Industrial uses – dust suppression, construction site.	*E. coli* <1,000 cfu/100 mL, pH 6.5–8.5, TP < 0.05 mg/L[a], TN < 5 mg/L[a]

[a]Indicative values for long-term irrigation
[b]1 mg/L Cl_2 residual after 30 min or equivalent

Following high rate treatment, the effluent stormwater is of similar quality to roof rainwater and both can be stored in the same tank. This increases the contributing catchment from just the building roof to the whole site, increasing the amount of water that can be captured and stored for reuse. In medium-scale developments, rainwater tanks typically empty quite quickly due to demand and often are augmented by town water.

High rate treatment systems can be used to create a sustainable urban development with a low demand on town water, low stormwater pollution export, and reduced stormwater discharges. These treatment systems have been used successfully in water and wastewater treatment and include fiber filters, deep bed filters, and biofilters. By-products of the treatment

process (concentrated pollutants and sludge) can be discharged to the sewer, alleviating sludge disposal problems and is attractive in creating a low maintenance system. The use of these treatment systems for water reuse can significantly reduce the stormwater pollution export from a site that is transported downstream into the receiving water.

High Rate Treatment Technology

Physiochemical treatment systems can achieve a relatively high pollutant removal at a high rate. These high rate systems are targeted to enhance water quality to at least level 2 (Table 7).

Fiber Filter High rate fiber filters were developed by Lee et al. [14] and its high efficacy for the tertiary treatment of wastewater was proved in terms of high filtration velocity and good removal of particulate matter. In place of the sand, fiber media consisting of bundles of U-shaped fine polyamide fibers are used, Fig. 5 and Table 8. Compared with the conventional rapid sand filter, the filtration velocity of a fiber filter is more than 5–20 times and the specific surface is more than twice [14, 15]. The fiber packing combines the two advantages of a large specific surface area and very large porosity (more than 90%), which results in high removal efficiency and low pressure drop despite the high filtration velocity [14]. In-line additions of flocculants enhance the pollutant removal capacity for both dissolved organics and trace metals.

The performance of a high rate fiber filter in treating stormwater in conjunction with in-line flocculation ferric chloride ($FeCl_3 \cdot 6H_2O$) was assessed [16]. The performance of the fiber filter was good as measured by turbidity removal (95%), total suspended solids reduction (98%), color removal efficiency (99%), TOC removal (reduced by 30–40%), and total coliform removal (93%). Similar results were obtained for nutrients such as nitrogen and phosphorus where the removal efficiency was significant. The removal efficiency of heavy metal was variable as the concentration in the raw stormwater was small. Eventhough the concentration of some of these metals such as iron, aluminum, copper, and zinc was significantly reduced, others like nickel, chromium, and cadmium showed lower removal rates.

Deep Bed Filter Deep bed filtration is often referred to as media filtration or rapid filtration and has been

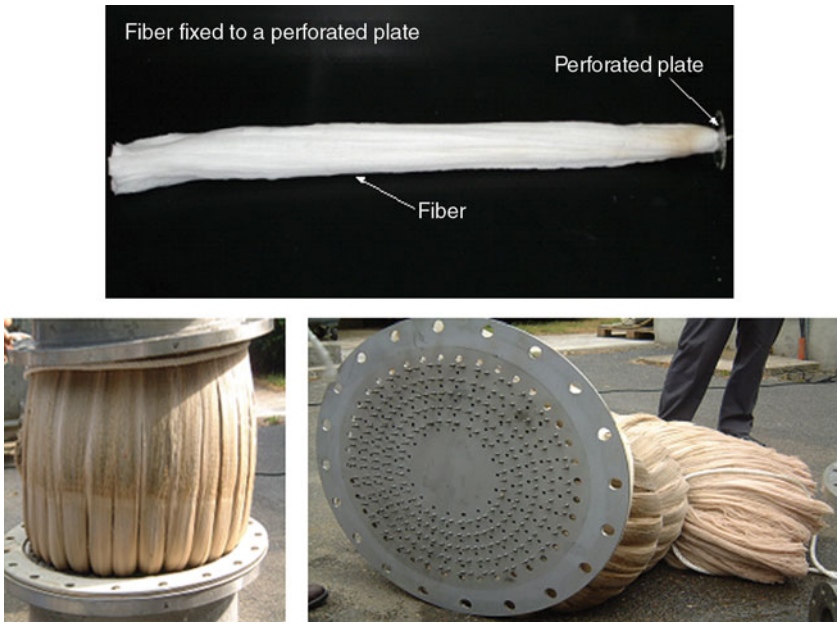

Stormwater Harvesting and Reuse. Figure 5
Fiber filter

Stormwater Harvesting and Reuse. Table 8 Physical properties of Fiber Filter Media [14]

Material	Packing density	Filtration rate
Bundles of U-shaped fine polyamide micro fibers	105–125 kg/m^3	20–60 m/h

widely used for water treatment as a final clarification unit to remove particles. Deep bed filtration is an effective process in removing particles of various nature and sizes that are present in water and wastewater. Deep bed filtration finds its greatest application in the clarification of dilute suspensions (less than 500 mg/L) of particles ranging in size from about 0.1 μm to about 50 μm [17]. Deep bed filter is usually single medium, dual media, or mixed media operating under pressure or gravity [18]. The filtration velocity of deep bed filter is usually 5–20 m/h. The other characteristics are summarized in Table 9. The use of in-line flocculation in conjunction with deep bed filtration has some advantages. This process produces smaller flocs that can be intercepted by the filter media. Further, it is simple, easy to operate, and cheap.

The performance of dual media and single medium deep bed filters in treating stormwater in conjunction with in-line flocculation of ferric chloride ($FeCl_3{\cdot}6H_2O$) was assessed [19]. The single medium filter (80 cm) consisted of either anthracite or sand, and the dual media filter consisted of sand (40 cm at the bottom) and anthracite (40 cm on top). Filtration velocities of 5, 10 and 15 m/h were examined. The removal efficiency for turbidity, suspended solids, and TOC was found to be 95%, 99%, and 30–45%, respectively at a flocculant dose of $FeCl_3$ of 15 mg/L. The removal efficiency for nitrogen was lower than phosphorus, which was relatively good (up to 50%). After filtration, the amount of total coliform reduced significantly (up to 80%). The removal efficiency for heavy metals such as Cd, Pb, Cr, and Ni was found to be already low for all filter systems, partly because the concentrations of these metals in the influent were low.

Membrane Filtration and Membrane Hybrid Systems Advances in low pressure-driven membrane technologies such as microfiltration (MF) and ultrafiltration (UF) have permitted their use in stormwater

Stormwater Harvesting and Reuse. Table 9 Characteristics of rapid filters

Characteristics	Sand filter	Anthracite filter
Filtration rate, m/h	10–20	10–20
Depth of bed, cm	80	80
Particle size, mm	0.35–0.5	0.7–0.8
Max headloss (gravity filter), m	5	5
Max headloss (pressure filter), kPa	200–400	200–400
Backwash rate, m/h	40–50	40–50

due to their high efficiency, ease of operation, and small footprint [20]. MF that is generally used has a pore size of 0.1–0.2 μm, although there are exceptions, as MF membranes with pores sizes of up to 10 μm are available. For UF, pore sizes generally range from 0.01 to 0.05 μm or less [21]. In addition, in terms of a pore size, the lower cutoff for a UF membrane is approximately 0.005 μm [21]. A basic comparison between MF and UF membrane is given in Table 10. The pathogen removal ability from water of each type of membrane (MF/UF) is presented in Fig. 6.

Membrane filtration can reduce the turbidity of stormwater from 25 to 35 NTU to less than 0.29 (i.e., 98% removal) [19]. The average TOC removal by submerged membrane itself was only about 7%. Microfiltration alone cannot remove the TOC due to its large pore size (0.3 μm). The TOC removal is due to adsorption of organics on membrane.

Membrane filtration is usually coupled with a pretreatment of fiber filter or deep bed filter and such systems are called membrane hydrid systems. This significantly improved the removal efficiency of the system yielding high-quality reuse water. An in-line flocculation–filtration followed by hollow fiber membrane system improved the TOC removal efficiency from 7% to 40% while achieving almost complete removal of turbidity.

Other Stormwater Treatments – Biofilter

Biofilter typically comprises a column of support media (typically granular activated carbon, (GAC)) onto which microbes grow. In the initial stage

Stormwater Harvesting and Reuse. Table 10 Comparing MF and UF membrane processes [22]

	MF	UF
Membrane	Symmetrical, asymmetrical	Asymmetrical
Thickness (μm)	10–150	150–250
Thin film (μm)	–	1
Pore size (μm)	4–0.2	0.2–0.02
Excludes	Particles, clay, bacteria	Macro molecules, proteins, polysaccharides, virus
Membrane materials	Polysulfone (PSO), Polyvinylidenedifluoride (PVDF), Polypropylene (PP)	Polysulfone (PSO), cellulose acetate (CA), Polyvinylidenedifluoride (PVDF), polypropylene (PP)
Membrane module	Tubular, hollow fiber	Tubular, hollow fiber, spiral wound, plate-and-frame
Operating pressure (kPa)	100–1,000	<200

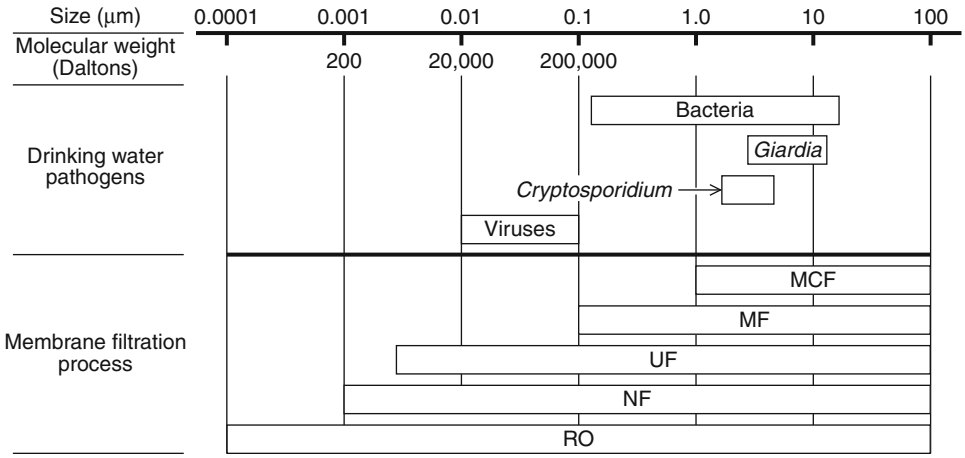

Stormwater Harvesting and Reuse. Figure 6
Pathogen removal ability of membrane filtration (Adapted from [21])

of operating the biofilter, adsorption of substances including microorganisms is the dominant process, while in the later stages organic degradation by microbial activities becomes more important. The activities of microbes determine the performance of biological filtration in removing pollutants.

Thamer [23] presented the results of the long-term biofilter experiments conducted with raw stormwater collected from a stormwater canal in Sydney. GAC were used as a single medium filter in biofilter columns. Media heights of 75 and 40 cm were used. The filter columns were operated at filtration velocities of 0.12 and 0.25 m/h. The removal efficiency for turbidity and DOC for the GAC filter media were found to be 75% and almost 100%, respectively. Based on a limited sample of stormwater, the removal efficiency for phosphorus was upto 74% and that of nitrogen was up to 30%. The removal of zinc, iron, lead, and nickel was good (upto 90%), although the concentration of heavy metals in the raw surface water sample was already low, Table 2.

Biofilter is an environmentally friendly pretreatment, which can remove the majority of organic matter in stormwater. This biofilter (1) removes the majority

of dissolved organic matter and reduces/eliminates the biofouling on the subsequent membrane process; (2) requires only a small amount of energy; (3) does not require regeneration of GAC; (4) does not involve any chemical requirement; (5) achieves significant removal of dissolved organics for a long period of time with little operation and maintenance; and (6) is simple to construct and operate.

Case Study – Carlton Stormwater Reuse Plant

Kogarah Council, a local government authority in Sydney, introduced the Carlton Industrial Sustainable Water Program (CISWP), in part to minimize potable water consumption through the Carlton Industrial area. One major part of the CISWP was the design and installation of a stormwater harvesting plant at Carlton, Kogarah, Fig. 7. The stormwater drains by gravity through a sump pit in the floor of the stormwater canal to an adjacent wet well. It is then pumped through a control valve pit, which monitors the turbidity levels for filtration suitability. If the turbidity is greater than 50 NTU, the water is diverted back through a return pit to the canal. If the water is less than 50 NTU, it proceeds to the stormwater filtration plant at 0.7 L/s or 2.5 kL/h.

The stormwater filtration plant filters the stormwater through an efficient two-stage process. The first stage involves dosing the raw stormwater with coagulant as it enters a fiber filter treatment units. Following fiber filtration, the stormwater passes through two granular activated carbon (GAC) vessels. Based on laboratory trials, it is anticipated that the water quality effluent following GAC treatment will be, at least, classed as level 2 reuse water, Table 7. During this stage, the water quality is being monitored to prove its quality.

During stage two, a membrane filtration unit, an ultraviolet (UV) or chlorination treatment unit, and 50 kL underground storage tanks will be added to the existing stage. The objective of stage two is to produce water similar in quality to the Australian Drinking Water Guidelines (Level 1, Table 7). In stage two, 50 kL of grade A water will be pumped to an adjacent concrete batching plant to supplement or even replace

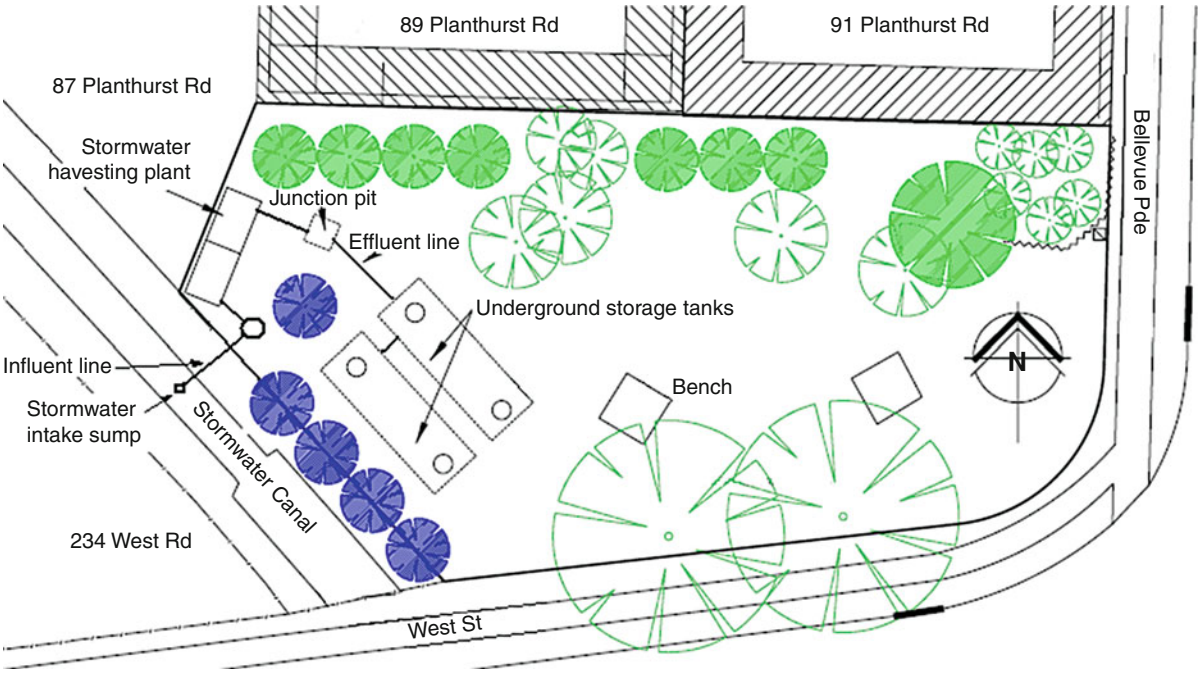

Stormwater Harvesting and Reuse. Figure 7
Carlton Stormwater Harvesting Plant, Kogarah, Sydney

their 20 kL/day potable water requirement, which is currently being supplied by town mains from Sydney Water.

The stormwater harvesting plant has the potential to reduce the potable water usage at the Carlton industrial area by 3–4 mL/year or by 10%. The calculated running cost of the plant including all annual power, maintenance, and licensing costs is approximately $2–$2.50/kL. This is quite acceptable considering Sydney Water's (potable water supplier) current rates are $1.87/kL and are earmarked to rise.

Assessment Methods for Measuring Treatment Effectiveness of Stormwater Treatment Systems

WSUD has been adopted widely in Australia and is being implemented in various local government areas. The major challenge to the success of WSUD is to adequately measure its effectiveness over the life cycle given the high maintenance that is required. Evaluation of treatment effectiveness of any stormwater treatment system requires a large quantity of continuous measured data. The monitoring of water quality is intensive and is expensive to implement given the large variation of inflow and effluent water quality over a range of storm events. It is therefore imperative to reduce cost by the use statistical or mathematical modeling tools to predict the performance of these systems. These models can simulate the processes of generation, export, and transport of pollutants in a catchment for observed storm events. Water quality models are in common use in Australia to design and assess the performance of stormwater treatment trains.

Model for Urban Stormwater Improvement Conceptualization (MUSIC)

The Model for Urban Stormwater Improvement Conceptualization (MUSIC) was developed by the Cooperative Research Center for Catchment Hydrology, Australia [24]. MUSIC provides the ability to model stormwater quality and quantity for catchments of varying sizes, from single house block through to large catchments. The model has a variety of inbuilt treatment measures and has the capacity to model one treatment device through to treatment trains and distributed treatment measures.

The MUSIC model is typically used as an aid to decision making by predicting stormwater quality and quantity for a variety of user input scenarios. The model calculates stormwater quality and runoff using algorithms based on known performance characteristics of stormwater quality treatment measures. These performance characteristics in MUSIC are supported by significant background research conducted by the Cooperative Research Center for Catchment Hydrology (CRCCH).

The model runs on an event or continuous basis enabling short- or long-term analysis. The capacity of MUSIC to model on an event basis allows the designer to revisit the model after an adopted solution has been constructed and to compare water quality samples collected on-site to those predicted by the model. This "calibration" allows users to adequately model different treatment measures in their specific catchments.

EPA SWMM Model

The United Sates Environmental Protection Agencies (EPA) Storm Water Management Model (SWMM) is a comprehensive computer model for the analysis of storm water quantity and quality [25]. SWMM can model both continuous and single rainfall events. The stormwater model can simulate many aspects of the hydrological cycle including snowmelt, surface and subsurface runoff, storage, and treatment.

SWMM is a comprehensive modeling package, which can be used for both planning and design. The model inputs can be tailored to suit a purpose, e.g., the use of rather large catchments for planning purposes, through to very detailed, small sub-catchments analysis for design. The modeling approach unlike MUSIC involves detailed simulation of process for generation, export, and transport of pollutants through urban waterway. It is a more comprehensive modeling tool and requires expert knowledge for setting up and calibrating the models to observed data.

Artificial Neural Networks (ANN)

Artificial Neural Network (ANN) is an adaptable system that can learn relationships through repeated presentation of data and is capable of generalizing new, previously unseen data. Some networks are supervised, in that a human determines how the network should

learn from the data. In this case, the user specifies for the network a set of inputs and the corresponding desired outputs. The network then tries to learn the relationships between input and output data by adapting its free parameters. Other networks are unsupervised, in that the manner they organize information is inherent in their architecture. Neural network is a powerful data modeling tool that is able to capture and represent complex input–output relationship. The use of ANN is growing rapidly with successful applications in many areas including process control, engineering design, financial trading, credit evaluation, medical diagnosis, and cognitive simulation. This method has been also widely applied in prediction of runoff and water quality in water engineering [26, 27].

Case Study – Treatment Effectiveness

The WSUD system that was used in this case study was the Connells Point WSUD. Connells Point is located in the South Eastern part of Sydney, Australia and is part of Kogarah Council local government area. Kogarah Council constructed a stormwater treatment system based on the principles of WSUD in 2005 to improve water quality in the bay. A water quality monitoring program was also put into place to monitor the water quality in the bay and stormwater outlets post construction of the stormwater treatment system.

The treatment train comprises an underground gross pollutant trap (CDS units) (primary treatment), diversion of low flow (up to 6 month ARI) to a bioretention trench, and surcharge of high flows through the nature reserve from surcharge pits (see Fig. 8).

The difficulty in calibration of water quality models is related to the empirical nature of algorithms that simulate water quality processes in models, and the use of these models as tool for measuring effectiveness is therefore limited. This is further exacerbated by the limited water quality sampling data available to

Stormwater Harvesting and Reuse. Figure 8
Connells point water sensitive urban design for stormwater treatment

calibrate the model for representative storm events for a range of typical inflow conditions. A novel approach has been developed that allows a combination of calibrated water quality model and neural-based models to predict the water quality from WSUD. This approach takes the strength of both the modeling techniques to provide a decision support tool that can be used with confidence in testing the efficacy of a stormwater treatment train for range of catchment and rainfall conditions. The methodology has been presented in Fig. 9.

Stage 1: This stage involved calibrating the water quality variables in MUSIC to the observed field data. The hydrological parameters and pollutant generation rates in the MUSIC model are fine-tuned so that it best simulates the observed sampling data (48 samples). It is pertinent to note that no flow calibration was undertaken due to the absence of flow monitoring data. Influent runoff was calculated from rainfall records. This approach was acceptable since the objective was to gauge the effectiveness of treatment devices and not to calculate annual pollutant loads.

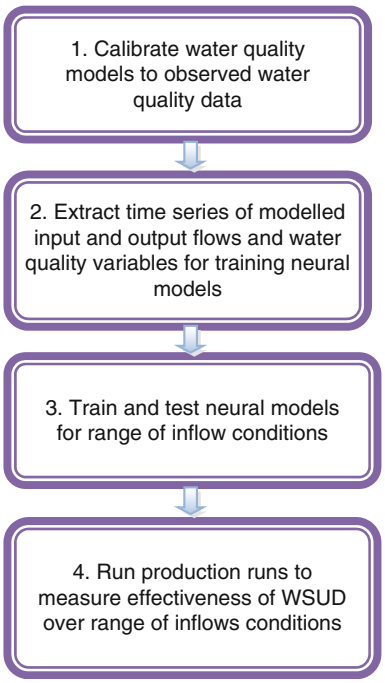

Stormwater Harvesting and Reuse. Figure 9 Methodology for measuring treatment effectiveness

Stage 2: This involved using the calibrated model to generate the time series of the discharge and concentration of water quality parameters of the influent and effluent of the bioretention trench. The time series were extracted for range of catchment and rainfall conditions for testing with the ANN model.

Stage 3: This involves training of the ANN model using time series data from the calibrated MUSIC model. The input parameters were influent discharge, TSS, TP, and TN and the output parameters were TSS, TP, and TN. The trained model was then tested and validated using the modeled input and output parameters. The best model was then adopted.

Stage 4: This involves running the trained and tested ANN model over the whole range of catchment and rainfall conditions. This is the production dataset and the results were then used to assess the treatment effectiveness of the stormwater treatment train.

The ANN model was developed using neural network toolbox in MATLAB [28]. The input parameters were influent discharge, TSS, TP, and TN and the output parameters were TSS, TP, and TN. One fourth of the total data was selected for training, one fourth for validation (observed data), and the remaining one half for testing. Network performance was estimated by linear regression between the observed and predicted water quality parameters after post-processing the output to the original scalar variables. The results of the training, testing, and validation are presented in the Fig. 10. The figure shows that for trained network, a mean square error (MSE) of 0.05 was achieved in just 40 epochs with convergence around 200 epochs. The results show a good convergence in 1,000 epochs for all the datasets and this trained model was then used for the production runs (i.e., predicted ANN model output for an input time series of modeled variables from MUSIC).

The linear regression of the observed TSS and predicted TSS is shown in Fig. 11. It can be seen that the MUSIC model output is poorly correlated with the observed data. ANN is able to generate a pattern of output variables and is better in predicting the observed dataset.

The linear regression of the observed TP and predicted TP is shown in Fig. 12. It can be seen that the MUSIC model output is poorly correlated with the observed data. This is due to the manner in which the

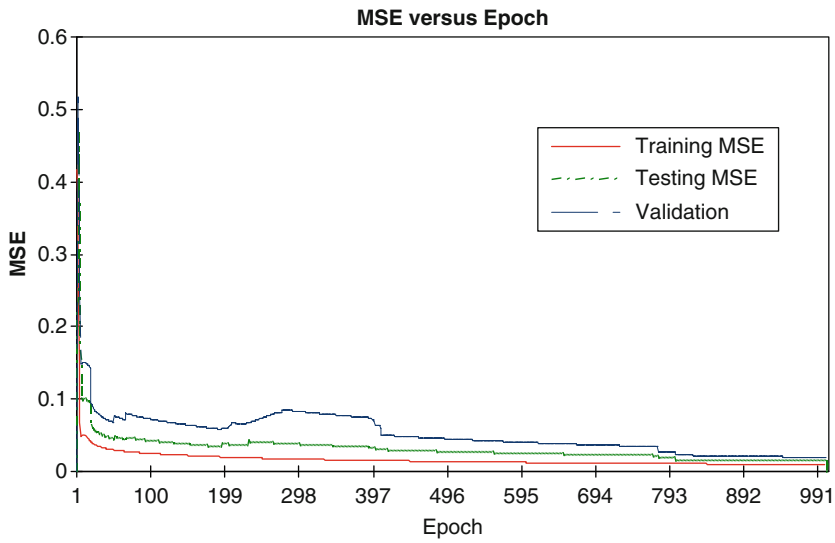

Best network	Training	Testing	Validation
Epoch	1000	1000	1000
Minimum MSE#	0.0098	0.0148	0.0195
Final MSE#	0.0098	0.0148	0.0195

Stormwater Harvesting and Reuse. Figure 10
Results for trained Neural Network

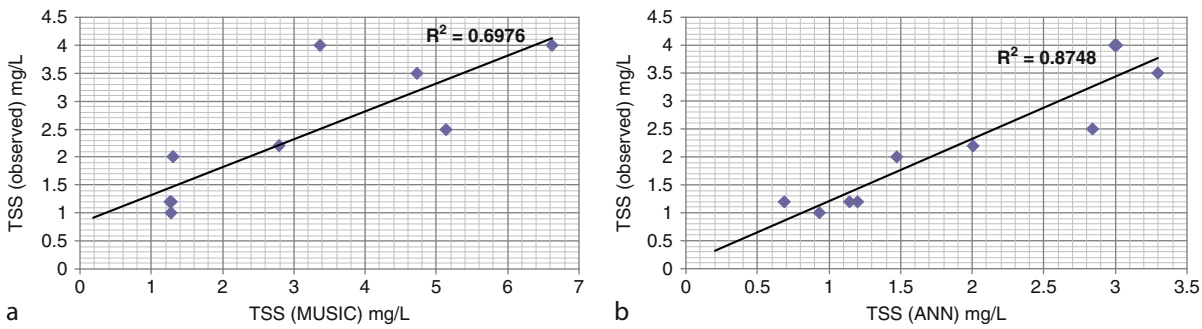

Stormwater Harvesting and Reuse. Figure 11
(**a**, **b**) Linear regression of the observed TSS and predicted TSS from the neural network

MUSIC model specifies removal of TP in the biofilter. The ANN predicted output shows a better correlation with the observed.

The linear regression of the observed TN and predicted TN is shown in Fig. 13. It can be seen that both MUSIC model and ANN output is poorly correlated with the observed data, although ANN is better correlated compared to MUSIC. The results show that the removal process for TN is not well defined in the MUSIC model.

The results show the strengths of using a hybrid modeling approach where strengths of both deterministic and neural-based models can be used for prediction of water quality in a treatment system.

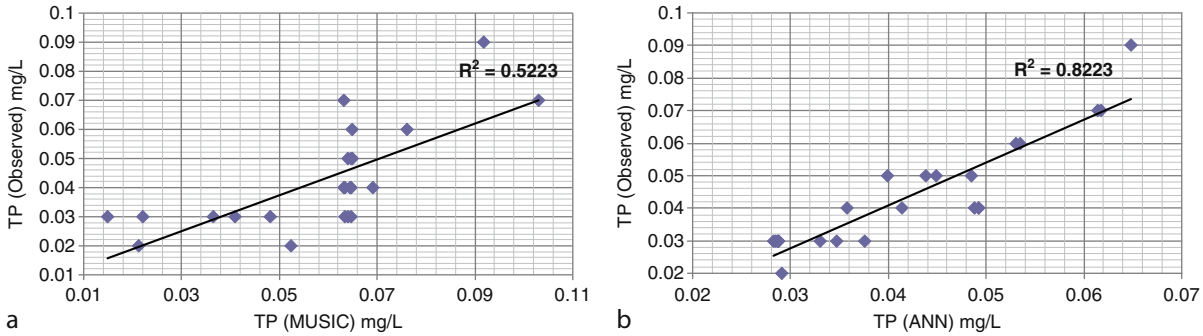

Stormwater Harvesting and Reuse. Figure 12
(**a**, **b**) Linear regression of the observed TP and predicted TP from the neural network

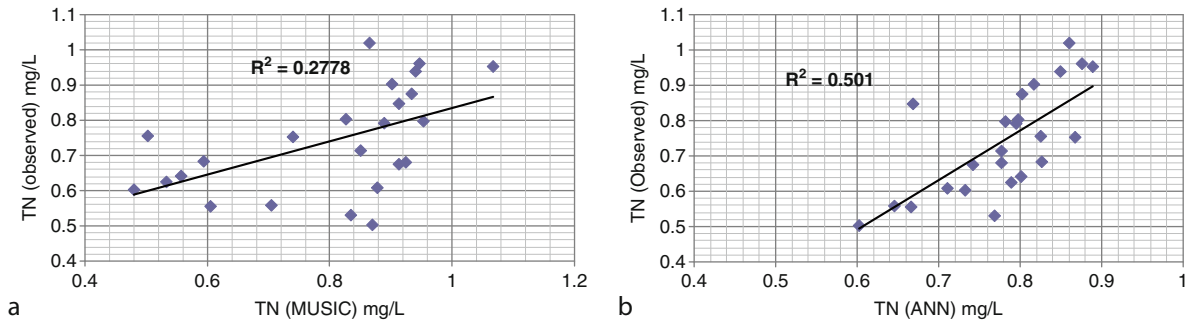

Stormwater Harvesting and Reuse. Figure 13
(**a**, **b**) Linear regression of the observed TN and predicted TN from the neural network

The results from both modeling approaches are presented in Table 11 below. The table shows that the ANN model more closely matches the recorded data of storm event compared with the MUSIC. All the variables are within the expected range from field data observed in biofiltration systems.

The effectiveness of stormwater treatment train is shown in Table 12 below. It is to be noted that upto 99% removal of TSS, 89% removal of TP, and 65% removal of TN is achieved in the treatment train. This is based on the generated pollutants into the treatment train; however, a reasonable match of ANN model output with recorded data gives confidence in the determination of these pollutants in the inflow stream. This analysis also shows the limitations of MUSIC in modeling the treatment processes in the biofilter system. A more sophisticated deterministic model (e.g., : EPA SWMM) may improve the results.

Future Directions

This chapter presents treatment technologies and best management practices for removal of pollutants in stormwater from urban waterways. It presents treatment systems for the emerging stormwater havesting field. Methods of assessment to check the extent to which stormwater treatment systems are meeting their design objectives and compliance to water quality standards are presented. It makes reference to Australian practice applicable to management, harvesting, and modeling of urban runoff. Some specific case studies are also presented to demonstrate what is achievable. Some of the technologies such as fiber filter and

Stormwater Harvesting and Reuse. Table 11 Results from ANN and MUSIC models compared with recorded data

	Minimum	Median	Maximum
Total suspended solids (Observed)	1.10	2.05	4.0
Total suspended solids (MUSIC)	0.18	1.16	6.62
Total suspended solids (ANN)	0.20	1.73	3.30
Total phosphorus (Observed)	0.02	0.04	0.09
Total phosphorus (MUSIC)	0.01	0.06	0.10
Total phosphorus (ANN)	0.03	0.04	0.06
Total nitrogen (Observed)	0.50	0.73	1.02
Total nitrogen (MUSIC)	0.48	0.87	1.07
Total nitrogen (ANN)	0.52	0.79	0.89

Stormwater Harvesting and Reuse. Table 12 Effectiveness of stormwater treatment train

	Event mean concentration (mg/L)	Potential removal	Potential removal
		MUSIC model (%)	ANN model (%)
Total suspended solids	160	96–99	98–99
Total phosphorus	0.25	59–94	74–89
Total nitrogen	2.0	47–76	56–70

deep bed filter with flocculation presented in this chapter are potential candidates for high rate applications in high density urban areas. Further, the biofilter and membrane filter introduced can remove dissolved organic matter and microorganisms, respectively and as such they can be used to produce water of recyclable quality. Methods of assessment presented in this chapter to check the extent to which stormwater treatment systems are meeting their design objectives and compliance to water quality standards are becoming increasingly important and will have major impacts on stormwater management.

Bibliography

Primary Literature

1. Australian and New Zealand Environment and Conservation Council (ANZECC) (2000) Australian guidelines for water quality monitoring and reporting, National water quality management strategy. Australian and New Zealand Environment and Conservation Council, Canberra
2. CSIRO (1999) Urban stormwater: best practice environmental management guidelines. CSIRO, Collingwood
3. Wong T, Breen P, Lloyd S (2000) Water sensitive road design – design options for improving stormwater quality of road runoff. Technical report, Report 00/1, Co-operative research centre for Catchment hydrology, Australia
4. Australian and New Zealand Environment and Conservation Council (ANZECC) (1992) Australian water quality guidelines for fresh and marine waters. Australian and New Zealand Environment and Conservation Council, Canberra
5. NSW-EPA (1996) Managing urban stormwater: treatment techniques, Draft report prepared for the State Stormwater Coordinating Committee. Environment Protection Authority, Chatswood, 68 p
6. Graham R (1989) Urban stormwater quality improvement in a detention pond and wetland system. MEngSc thesis, University of Melbourne,103 p
7. Begum S, Rasul MG, Brown RJ (2008) A comparative review of stormwater treatment and reuse techniques with a new approach: Green Gully. WSEAS Trans Environ Dev 4(11): 1002–1013
8. Kandasamy J, Beecham S, Dunphy A (2008) Effectiveness of stormwater sand filters in water sensitive urban design. In: Proceedings of the institution of civil engineers-water management, WM2, Melbourne, Apr 2008, pp 55–64
9. Brown W, Schueler T (1997) National pollutant removal performance database of current urban stormwater best management practices. Center for Watershed Protection, Ellicott City
10. Mitchell VG, Mein RG, McMahon TA (1999) The reuse potential of urban stormwater and wastewater resources in urban areas. Aust J Water Resour 6(1):31–43
11. NSW Premiers (1997) Report to the NSW Government on the proposal by Sydney Water Corporation for sewage overflow abatement in Sydney Harbour. Waterways Advisory Panel Report, NSW Premiers Department. www.muim.nsw.gov.au/wap/5.htm
12. DEC (2006) Managing urban stormwater: harvesting and reuse, vol 1 and 2. NSW Department of Environment and Conservation, Sydney. ISBN 1741378753

13. Hatt BE, Deletic A, Fletcher TD (2006) Integrated treatment and recycling of stormwater: a review of Australian practice. J Environ Manage 79:102–113
14. Lee JJ, Jeong MK, Im JH, BenAim R, Lee SH, Oh JE, Woo HJ, Kim CW (2006) Enhancing flexible fibre filter (3FM) performance using in-line coagulation. Water Sci Technol 53(7):59–66
15. Lee JJ, Im JH, BenAim R, Kim JR, Kim YJ, Poo KM, Kim CW (2007) Better understanding of the filtration characteristics in the flexible fibre filter module (3FM). Water Sci Technol 55(1–2):77–83
16. Johir MAH, Lee JJ, Vigneswaran S, Kandasamy J, Shaw K (2009) Treatment of stormwater using fibre filter media. Water Air Soil Pollut Focus 9(5):439
17. Vigneswaran S, Chang JS, Janssens JG (1990) Experimental investigation of size distribution of suspended particles in granular bed filtration. Water Res 24:927–930
18. Wilf M (2007) The guidebook to membrane desalination technology: reverse osmosis, nanofiltration and hybrid systems: process, design, applications, and economics. Balaban Desalination, L'Aquila
19. Johir MAH, Vigneswaran S, Kandasamy J (2009) Deep bed filter as pre-treatment to stormwater. Desalin Water Treat 12:313–323
20. Qin JJ, Oo MH, Kekre KA, Knops F, Miller P (2006) Reservoir water treatment using hybrid coagulation–ultrafiltration. Desalination 193:344–349
21. Allgeier S, Alspach B, Vickers J (2005) Membrane filtration guidance manual. United States Environmental Protection Agency, Washington, DC
22. Wagner J (2001) Membrane filtration handbook practical tips and hints, 2nd edn, Revision 2. Osmonics, Minnetonka
23. Mohammed T, Vigneswaran S, Kandasamy J (2010) Biofiltration as pre-treatment to water harvesting and recycling. Water Sci Technol (in press)
24. MUSIC (2005) MUSIC Version 3 User Manual. Cooperative Research Centre for Catchment Hydrology, Melbourne
25. EPA SWMM (2009) EPA SWMM version 5, Stormwater Management Model. US EPA, Cincinnati
26. Lek S, Guiresse M, Giraudel J-L (1999) Predicting stream nitrogen concentration from watershed features using neural networks. Water Res 33(16):3469–3478
27. Poff NL, Tokar S, Johnson P (1996) Stream hydrological and ecological responses to climate change assessed with an artificial neural network. Limnol Oceanogr 41(5):857–863
28. Hines JW (1997) MATLAB supplement to Fuzzy and neural approaches in engineering. Wiley, New York

Book and Reviews

Kandasamy J, Vigneswaran S (2008) Constructed wetland. Nova, New York. ISBN 978-1-60456-613-0

Singh G, Kandasamy J, Vigneswaran S, Aryal R, Naidu R (2010) Stormwater treatment technologies. In: Encyclopedia of Life Support Systems (EOLSS). Developed under the auspices of the UNESCO. EOLSS, Oxford, UK. http://www.eolss.net

Stratospheric Aerosols for Solar Radiation Management

Ben Kravitz
Department of Global Ecology, Carnegie Institution for Science, Stanford, CA, USA

Article Outline

Glossary
Definition of the Subject
Introduction
History and Brief Literature Summary
Types of Aerosols
Future Directions
Acknowledgments
Bibliography

Glossary

Arctic oscillation A pattern of sea-level pressures in the Arctic indicating large-scale circulation patterns. This serves as a proxy for the degree to which Arctic air penetrates to lower latitudes. During a positive mode of the Arctic Oscillation, which occurs both naturally and can be forced by large injections of stratospheric aerosols that enhance the polar jets, cold air gets trapped in the Arctic, resulting in warmer winter temperatures over the northern hemisphere continents.

Carbon dioxide removal (CDR) Removing carbon dioxide from the atmosphere and sequestering it, either in geological formations or in the deep ocean, thereby decreasing the atmospheric concentration of anthropogenic greenhouse gases.

Pyrocumulus A convective cloud that forms from a large amount of heating, and subsequent rising air, created by large fires.

Solar radiation management (SRM) Reducing the amount of sunlight incident at the surface, thereby decreasing the globally averaged surface air temperature of the planet.

Stratospheric aerosols A layer of aerosols into the stratosphere which either scatter or absorb (or a combination of the two) a certain portion of

sunlight that would, under normal circumstances, reach the surface.

Tipping point The point at which global climate transitions from one stable state to another. Some extreme examples include ice ages, in which the climate rapidly cools, forming large ice sheets. The climate in this state is relatively stable, mainly due to an increase in planetary albedo, and is not easily returned to a different state (the present day climate, for example) without a large forcing of some kind.

Definition of the Subject

SRM in the context of this entry involves placing a large amount of aerosols in the stratosphere to reduce the amount of solar radiation reaching the surface, thereby cooling the surface and counteracting some of the warming from anthropogenic greenhouse gases. The way this is accomplished depends on the specific aerosol used, but the basic mechanism involves backscattering and absorbing certain amounts of solar radiation aloft. Since warming from greenhouse gases is due to longwave (thermal) emission, compensating for this warming by reduction of shortwave (solar) energy is inherently imperfect, meaning SRM will have climate effects that are different from the effects of climate change. This will likely manifest in the form of regional inequalities, in that, similarly to climate change, some regions will benefit from SRM, while some will be adversely affected, viewed both in the context of present climate and a climate with high CO_2 concentrations. These effects are highly dependent upon the means of SRM, including the type of aerosol to be used, the particle size and other microphysical concerns, and the methods by which the aerosol is placed in the stratosphere. SRM has never been performed, nor has deployment been tested, so the research up to this point has serious gaps. The amount of aerosols required is large enough that SRM would require a major engineering endeavor, although SRM is potentially cheap enough that it could be conducted unilaterally. Methods of governance must be in place before deployment is attempted, should deployment even be desired. Research in public policy, ethics, and economics, as well as many other disciplines, will be essential to the decision-making process. SRM is only a palliative treatment for climate change, and it is best viewed as part of a portfolio of responses, including mitigation, adaptation, and possibly CDR. At most, SRM is insurance against dangerous consequences that are directly due to increased surface air temperatures.

Introduction

Anthropogenic climate change has come to the forefront of scientific research as one of the most important problems facing society. The primary cause of climate change is the emission of greenhouse gases from fossil fuel combustion for production of energy, and the consequences have the potential to be severe [1]. Mitigation of emissions is the only viable permanent solution to the problem of climate change, but mitigation is likely to be difficult and expensive, and large-scale political will to abate emissions is currently lacking at a sufficient scale to prevent escalation of the problem.

As an alternative, there have been repeated proposals to deliberately alter the climate to counteract these changes, thereby avoiding some of the negative impacts. The proposed methods generally fall into two categories: SRM and CDR. Most of the solar radiation energy is contained within short wavelengths, to which the Earth's atmosphere is mostly transparent. This energy reaches the planet's surface and is absorbed, and the surface then radiates energy in longer wavelengths, which can be broadly interpreted as heat. Anthropogenic greenhouse gases, the predominant one being CO_2, absorb energy in certain bands of these longer wavelengths, thereby reducing the transmissivity of the atmosphere. Since the atmosphere retains this heat for a longer period of time, the atmosphere warms, radiating heat to the surface, and warming the surface. The purpose of SRM is to reduce this problem at the source by decreasing the amount of solar radiation that reaches the surface. Many methods for this have been proposed, but the one that has received the most attention and is likely to be the most feasible is placing a large amount of aerosols in the stratosphere, which will scatter or absorb the incoming solar radiation, preventing it from being converted to longwave energy. Conversely, the purpose of CDR is to remove CO_2 from the atmosphere and sequester it in long-term storage sites, generally in

geologic formations or in the deep ocean. This has the potential to remove the cause of anthropogenic climate change and return the climate to a previous state.

This highlights that SRM and CDR are fundamentally different solutions to the climate change problem. Since climate change is caused by an increase in longwave energy, balancing this with a reduction in shortwave will necessarily result in imperfect compensation [2]. Conversely, CDR directly removes the source of the problem, so it will address all aspects of climate change, not just surface air temperature changes. SRM has the advantage that it will work quickly, reaching full effectiveness on the order of months to years [3]. CDR is likely to be slow and expensive, being effective at reducing climate change after several decades of sustained implementation [4].

Since SRM is only a palliative treatment and does little to reduce ambient concentrations of CO_2, if SRM were to cease, the climate would rebound to its pre-SRM state in a very short time [3, 5]. The ease of adaptation strongly depends on the length of time over which society can adapt, so the suffering felt during this rebound would be prominent. Therefore, if SRM were the only technology used to counteract climate change, due to the long atmospheric lifetime of CO_2 [6, 7], it would need to be done essentially forever.

One of the most commonly discussed methods of SRM is to mimic a large volcanic eruption by placing or creating large amounts of aerosols in the stratosphere. Large volcanic eruptions place SO_2 in the stratosphere which oxidizes to sulfate aerosols. These backscatter solar radiation, preventing it from reaching the surface, and the general effect is cooling for a short time after the eruption. This is primarily a radiative effect, independent of the way the aerosols were created, meaning to achieve surface cooling, aerosols could be placed in the atmosphere deliberately.

For SRM with aerosols to be feasible, the aerosols must be placed in the stratosphere. In the troposphere, the average aerosol lifetime is 1–2 weeks, meaning annual injection rates would need to be approximately two orders of magnitude larger than the desired equilibrium atmospheric loading of aerosol mass. However, the stratosphere is stable, resulting in atmospheric lifetimes of 1–3 years, depending upon the altitude and latitude of injection, as well as the aerosol size. Tropical injections would maximize this lifetime, as well as result in a more equal distribution of the aerosols throughout the global stratosphere, using the general atmospheric circulation to distribute the aerosols and transport them poleward.

Some past simulations have looked at optimizing cooling of the northern hemisphere continents, where the bulk of the world's population lives, instead of creating a worldwide aerosol layer, thus allowing for smaller injection amounts [8, 9]. However, doing so dramatically decreases the atmospheric lifetime of the aerosols, reducing their efficiency for SRM, as well as creating an interhemispheric imbalance of radiative forcing, which has profound implications for the hydrologic cycle, much more so than for tropical injections of aerosols.

The risks of SRM are potentially great, and at best, it is only a temporary measure, so some have questioned why research on SRM should even go forward [10]. The debate on SRM is exploring this question in great detail, but two answers have emerged prominently in the discussions. The first is to treat SRM as an insurance policy. If climate change were to reach dangerous levels, possibly even triggering climate tipping points, SRM gives society a means by which some negative impacts of climate change can be delayed, allowing time for a different, more permanent solution to be developed. Without having these emergency countermeasures available, the only choice for dealing with the impacts is adaptation, which is likely to be painful and costly [1, 11]. The second is pure scientific interest. SRM allows climate scientists to investigate scenarios that may not have previously occurred to them, allowing for new ways of thinking about the climate system and new understanding of physical processes. Regardless of whether SRM is actually implemented, this new knowledge is valuable to the scientific community.

History and Brief Literature Summary

The history of SRM is surprisingly lengthy, considering most of the attention to this topic has been concentrated in the last 5 years [12]. Arguably, the first mention of SRM, although not specifically in those terms, was by von Neumann in 1955 as an editorial opinion piece [13]. Although he understood mechanisms of climate change, including the ability of

large volcanic eruptions to cool the climate and that warming would cause large-scale changes in ice sheet coverage, he made no mention of the connection between anthropogenic greenhouse gases and a warming planet. The first to make this connection in the context of SRM was Budyko [14, 15]. He understood that society's quality of life, obtained from combustion of fossil fuels, had the potential to cause massive changes in the climate system and that society may wish to deliberately cause compensatory cooling of the planet. Knowing that large volcanic eruptions cool the climate due to a layer of stratospheric sulfate aerosols, he did preliminary calculations of the amount of sulfate necessary to cause cooling to a certain level, also suggesting the amount of cooling could be controlled.

The study of SRM proceeded sporadically over the next three decades, with few papers and a small handful of reports. The National Academy of Sciences issued a report dealing with the practicality of inserting large amounts of aerosols into the stratosphere [16]. Some of the ideas they proposed include putting the material into a cargo airplane and flying it up to the stratosphere, firing it into the stratosphere using artillery, lofting it with weather balloons, or pumping it up a large tube, either through a tall tower or tethered to a stationary floating anchor (Fig. 1). Their rough estimates of costs suggested that SRM could be performed cheaply and, in some cases, with already existing technology.

This was followed by one of the first reviews of aerosol approaches to SRM by Dickinson, who provided preliminary estimates based on the eruption of Mount Pinatubo in 1991 of how much SRM would be required to cool the planet [17]. The next decade saw the first climate model simulations of SRM, performed by Govindasamy and Caldeira, in which they simulated a reduction in solar radiation to compensate for an increase in carbon dioxide concentrations [18].

Many of the reports early in the studies of SRM were completed at Lawrence Livermore National Laboratory under the guidance of Edward Teller [19–21]. These reports were often the source for many new ideas of how to perform SRM, including the use of black carbon aerosols, as well as some of the first estimates of costs. Most of the subsequent research over the next few years is summarized in a series of reports and articles [22–24]

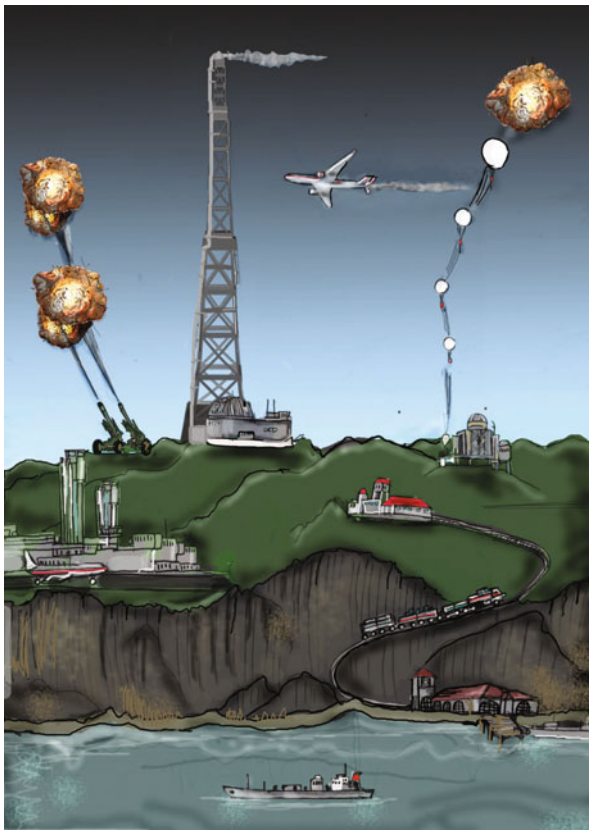

Stratospheric Aerosols for Solar Radiation Management. Figure 1
Various means of accomplishing SRM (Reproduced from Fig. 1 in [56]. Drawing by Brian West)

which tended to concentrate on the evaluation of the climate impacts of SRM.

SRM research received a large rejuvenation from a special issue of *Climatic Change* in 2006, most prominently due to the Nobel Prize winner Paul Crutzen [25]. His salient and timely calculations, showing SRM would likely require a small amount of effort when compared to mitigation, combined with worries about the implications of this conclusion, remain relevant and are often revisited by SRM researchers in all disciplines. He helped legitimize the study of SRM, resulting in an explosion of research and publications over the following years that continues to this day. This article was concurrent with simulations by Wigley, which confirmed that sustained injections of large amounts of stratospheric aerosols will cause surface cooling [5]. However, one of the most important findings of this

study was that if SRM is stopped but CO_2 concentrations are not reduced, the climate will rapidly return to its pre-SRM state, making adaptation to the resulting change nearly impossible.

Another significant effect of SRM, as discussed by Trenberth and Dai the following year, is suppression of the global hydrologic cycle [26]. Although their findings were based on the evaluation of the effects of the eruption of Mount Pinatubo as an analogue, these findings were reinforced by Robock et al., who performed the first simulations of stratospheric aerosol SRM using a fully coupled atmosphere-ocean general circulation model [9]. This study was concurrent with a review paper by Rasch et al., comparing different modeling groups' simulations of SRM [27].

The first study of SRM with stratospheric sulfate aerosols to use a microphysical model found that aerosol microphysics plays a very important role in determining the particle size distribution and that nearly all past simulations of stratospheric sulfate SRM used an aerosol size that was much too small [9, 28, 29]. This suggests that SRM using injections of SO_2 would either require much more care and study or injections of much larger amounts [30].

The next stage of climate model research will largely be conducted under the framework of The Geoengineering Model Intercomparison Project (GeoMIP), which at the time of writing this entry is underway [31]. The need for this project, as well as a description, can be found in the last section.

Some attempts have been made to classify different SRM and CDR schemes and rate their effectiveness [32–35]. The findings generally show that SRM with stratospheric aerosols is likely to be cheap and highly effective, especially when compared to many other means. However, the uncertainties of this idea are quite large, and the adverse consequences are potentially severe, often more so than the other more expensive, less effective means.

Perhaps the most helpful view of SRM has arrived in recent years, in that it should be treated as part of a portfolio approach to climate change. Mitigation and possibly CDR are the only permanent solutions to anthropogenic climate change, but these are expensive and will take a long time to implement, during which time some dangerous levels of warming and their negative impacts could be felt. In this sense, SRM could be used to temporarily alleviate a small amount of warming to stay below the 2°C policy target [5] (Fig. 2).

Types of Aerosols

SRM with stratospheric aerosols implies that different kinds of aerosols could be used, each with their own array of impacts and consequences, some advantageous and some disadvantageous. It is well beyond the scope of this paper to discuss every possible aerosol, but two choices can be treated as bookends of a spectrum study. Sulfate aerosols backscatter sunlight almost perfectly, whereas black carbon aerosols are excellent absorbers, so the scattering properties of nearly any choice of natural aerosol actually used for deployment can, to first order, be seen as a linear combination of these two. Should an engineered, manufactured particle be deployed, perhaps the scattering properties could be tuned to be optimal, so for this case, properties other than extinction become of higher concern. In this sense, a great deal of information regarding the atmospheric physics impacts of SRM with stratospheric aerosols can be gained by study of only three kinds of aerosols: sulfate, black carbon, and engineered particles. Such a study must not only include the physical effects and climate impacts, but also practicality, i.e., how the aerosols can be created, placed in the stratosphere, and whether they will actually work at cooling the surface of the planet.

Sulfate

The most researched aerosol in the context of SRM is sulfate aerosols, mainly due to the well-studied analogue of large volcanic eruptions. The climate effects of large volcanic eruptions are well known [36]. The primary driver of these effects is the layer of stratospheric sulfate aerosols created by injection of SO_2 gas from the volcano. If the eruption is sufficiently large and at the proper time of the year [37], the aerosol layer will backscatter a sufficient amount of solar radiation to cause surface cooling, which primarily occurs over the northern hemisphere continents, since land has a lower heat capacity than the oceans. The summer of the year following the 1991 eruption of Mount Pinatubo, which was the largest volcanic eruption of the last 50 years,

showed reduced globally averaged surface air temperatures by approximately 0.5°C [38].

Although volcanic eruptions are an inspiration for SRM, and many of the effects and impacts of large volcanic eruptions are due to a stratospheric aerosol layer, implying the effects would be similar, they are an imperfect analogue. Volcanic eruptions involve a pulsed injection of sulfate aerosol precursors. After the aerosols form, they begin to coagulate and fall out of the stratosphere, meaning the total stratospheric mass of aerosols decays from an early peak, until it reaches the levels before the eruption. To ensure a constant level of radiative forcing that would be required for SRM, a steady state is required, which necessitates smaller, regular injections, if not continuous injections.

Sustaining an aerosol layer would certainly have some differences from a pulse injection. As the aerosols stay in the stratosphere longer, they will grow from condensation of water onto the aerosols and coagulation of particles [39]. Therefore, the average particle size under SRM would likely be much larger than for volcanic eruptions, which reduces both the scattering efficiency of the aerosols and the atmospheric lifetime by increasing fall speed. Most simulations of stratospheric SRM using general circulation models are highly idealized in terms of the achieved sulfate aerosol forcing per unit mass, as they often neglect coagulation processes [28]. To achieve the radiative forcings that are often reported in the literature for a given stratospheric injection of SO_2 would likely require an order of magnitude more mass due to the microphysical effects [30]. Simulations have suggested that this significant hurdle could be overcome if pulsed injections were used instead of continuous injections [28]. Also, using aerosol precursors such as SO_2 could be bypassed entirely by directly condensing gaseous sulfuric acid into the atmosphere to achieve a monodisperse droplet size,

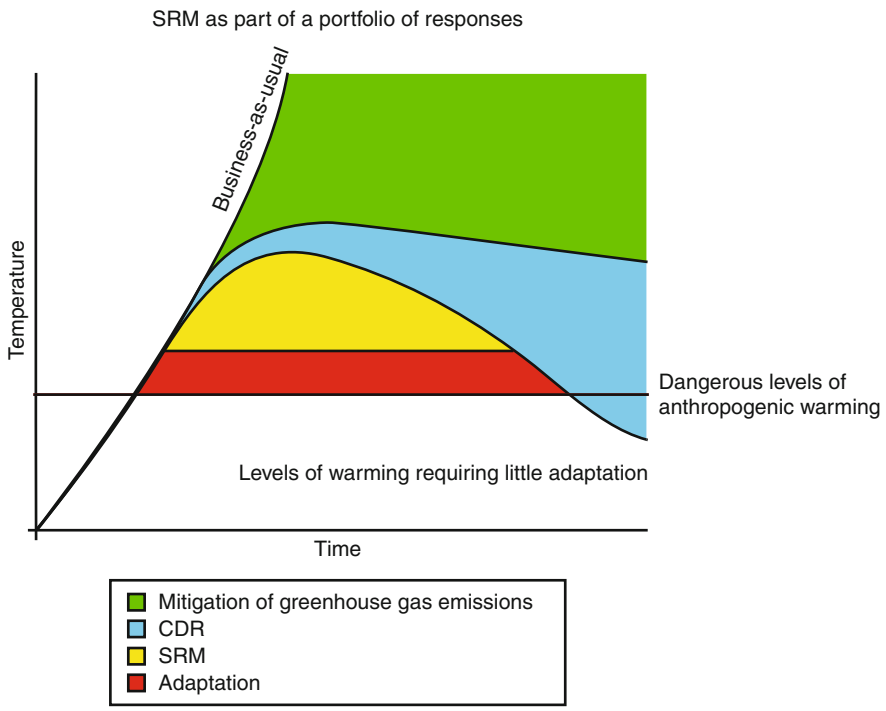

Stratospheric Aerosols for Solar Radiation Management. Figure 2
SRM when viewed as part of a portfolio of responses to climate change, adapted from a personal communication with John Shepherd. Axes are left unlabeled deliberately to avoid assumptions about policy decisions or estimates of climate sensitivity

although this idea requires further study and testing [30]. Moreover, any reduction of solar radiation will result in ocean memory of the cooling due to the ocean's thermal inertia, meaning surface cooling under SRM will necessarily be greater than cooling from a large volcanic eruption [40].

The negative impacts of SRM with sulfate aerosols have the potential to be quite severe. One of the most discussed aspects of the climate effects of SRM is changes to the hydrologic cycle. The eruption of Pinatubo dramatically suppressed the hydrologic cycle, leading to drought in many parts of the world, so SRM could reasonably be expected to have similar effects [26]. Some simulations of sulfate aerosol SRM have confirmed this expectation, showing a large reduction in the Indian/African/Asian monsoon system [9], although efforts to determine whether this effect is robust have not yet been conclusive [31, 41]. The impacts of SRM manifest on both a global and a regional scale, resulting in regional inequalities for any level of globally implemented SRM [2].

Another problem is that introduction of large amounts of aerosols into the stratosphere would damage the ozone layer through enhanced thermal decomposition from increased stratospheric temperatures and enhanced halogen-catalyzed depletion [42–44]. The eruptions of El Chichòn and Pinatubo both resulted in modest but noticeable depletion of the ozone layer [45, 46]. Simulations of SRM using models with sophisticated chemical components have confirmed this, showing a delay in the recovery of the Antarctic ozone hole by decades [47, 48].

Not all ancillary impacts of SRM would be negative. After the eruption of Pinatubo, due to the increased light scattering from the sulfate aerosols, the fraction of diffuse light increased significantly, promoting plant photosynthesis across most of the globe [49]. This showed that stratospheric aerosols could address climate change directly by increasing the biosphere carbon sink. The 2 years after Pinatubo showed an increase in carbon uptake by over 1 Pg a^{-1}, which resulted in a measurable drawdown of atmospheric CO_2 concentrations [50, 51]. The land carbon sink has also steadily increased from global dimming, giving further credence to this mechanism. However, the increase in the diffuse fraction of incident sunlight would negatively impact solar power generated from large thermal generation plants, with the amount of power scaling approximately linearly with the amount of available direct sunlight [52]. These two effects are simply due to the presence of scattering aerosols, meaning SRM would likely have similar effects.

An often cited concern of sulfate SRM is that when the aerosols eventually pass into the troposphere, they will fall as acid rain. However, current worldwide sulfur emissions are over 100 Tg [53], so any reasonable amount of SRM would be at least an order of magnitude less, meaning all but the most poorly buffered ecosystems would be negatively affected by the additional acid rain [54, 55].

Assuming SRM with sulfate aerosols was to be undertaken, the next natural question is how the aerosols can be placed in the stratosphere. The most commonly discussed means is through large injections of SO_2, mimicking volcanic eruptions and allowing the atmosphere to convert the SO_2 gas into sulfate aerosols. However, as discussed previously, microphysical issues would likely make this infeasible, prompting brainstorming of other methods [30].

The next stage of thought is transporting the aerosols or aerosol precursors to the stratosphere. Many means of this have been suggested in the past, including using airplanes, balloons, artillery, and space elevators [16, 56] (Fig. 1). Likely the most efficient means of achieving this, as well as the cheapest, is using planes to transport the material. Engineering considerations aside, this method is probably very cheap when compared to the cost of mitigation or climate change impacts, and cheap enough that it could be done unilaterally [56, 57]. The implications of this invite myriad legal, governance, ethical, and economic issues, but much more work on these topics is needed.

Black Carbon

Despite being repeatedly suggested throughout the history of SRM research [19, 21, 25, 40], formal study of deliberate large stratospheric injections of black carbon aerosols is distinctly lacking. At the time of the preparation of this entry, only one such study has been performed [58].

Black carbon SRM analogues are not nearly as closely related to SRM as is the case for sulfate aerosols.

The only large injections into the stratosphere of black carbon aerosols are from pyrocumulus events, which occur from large fires, but the amount of stratospheric black carbon that results from these events is quite small and localized compared to the amount that would be needed for SRM [58, 59]. Measurements below the plumes of these large fires show surface cooling, lending credence to their consideration for SRM [60, 61].

Another analogue, albeit only in simulation form, is the climate effects of nuclear winter. The fires from nuclear war would cause pyroconvection, similar to pyrocumulus events but on a massive scale, lofting several megatons of soot into the stratosphere, which would reduce sunlight reaching the surface, causing cooling [62–67]. The amount of cooling that would result from such an injection would more than offset anthropogenic warming, causing enough temperature reduction to be catastrophic to agriculture [68]. Also similarly to sulfate aerosol SRM, these analogues involve one-time injections of aerosols, whereas SRM would involve continuous injections and a sustained radiative forcing.

Most of the negative impacts from stratospheric SRM with black carbon aerosols would be from the massive stratospheric heating due to absorption of sunlight by the aerosols. The heating would be much more than for sulfate aerosols, and the soot particles would also self-loft, potentially reaching the mesopause until the ambient air pressure can no longer suspend the particles [58, 69–71].

One of the most prominent side effects would be ozone depletion from accelerated thermal decomposition, much more than would be found for an equivalent mass of sulfate aerosols [42–44, 58, 71]. Additionally, the heating would allow more water vapor to enter the stratosphere, which would cause ozone destruction through chemical interactions [71]. Heterogeneous chemistry on the surface of the particles would also likely cause ozone depletion to some extent, but these effects are largely unknown.

The stratospheric heating would likely cause circulation changes by strengthening the polar vortices, forcing a positive mode of the Arctic Oscillation and potentially introducing an Arctic ozone hole [58]. Additionally, not only is black carbon hazardous to human health [72], but if black carbon falls on fresh snow, it would reduce the surface albedo, causing more absorption of sunlight by the surface, which is counterproductive to the purpose of SRM [73].

The effectiveness of black carbon SRM on reducing surface temperatures strongly depends on the particle size and altitude of injection, which has a direct impact on the feasibility of this choice of aerosol. The more efficiently a certain combination of SRM parameters cools the surface, the more efficiently the aerosols will heat the stratosphere, causing negative impacts. Smaller aerosols are more radiatively efficient and have a slow fall speed, resulting in more surface cooling per unit mass. If the aerosols are too large, they will actually have an effect in the longwave, resulting in warming [74].

The concerns with and mechanisms of deployment of SRM with black carbon aerosols are similar to those of sulfate aerosols. Soot is a by-product of incomplete combustion and not a gaseous aerosol precursor, so the means of creating the aerosols is different, but costs are of a similar order of magnitude. Transporting the aerosols to the stratosphere dominate the costs and feasibility of this method, but these costs are highly variable, dependent upon the way the aerosols are transported up to the stratosphere.

Engineered Particles

The drawbacks of aerosols with natural analogues, like sulfate and black carbon, have prompted the study of manufactured particles that are specifically engineered to optimize scattering of sunlight while avoiding some of the less desirable attributes. These engineered particles have been discussed briefly in the literature, mostly as thought experiments, as the feasibility of producing large amounts of these aerosols is uncertain.

One of the first mentions of this idea was by Edward Teller who wanted to optimize both the scattering properties and atmospheric lifetime by creating an efficient "self-lofting blue/UV chaff" or "resonant scatterers" [20, 21, 40]. Creating particles that photophoretically levitate is also possible, the advantage being that the atmospheric lifetime would be lengthened, so considerably fewer particles would be needed for a given amount of cooling [75, 76]. However, this has the serious problem of irreversibility of SRM unless a mechanism for removing the particles from the mesosphere could be designed.

One could certainly conceive of other desirable properties an aerosol might have as well as potential designs for it. The potential for research on engineered particles is large, as this idea is largely unexplored.

Future Directions

Although SRM with stratospheric aerosols has received a great deal of attention and study, this idea is still far from deployment-ready, notwithstanding the issue of whether deployment is necessary. However, assuming stratospheric aerosols is the method of choice for modifying the climate, the next stage of research must still resolve some serious fundamental questions.

Perhaps the most basic question that can be asked, which still has no satisfactorily all-encompassing answer, is: "What is SRM?" Implicit in this question is not just the method, but also the means. The scientific community, and more importantly, the policy community, has still not defined what SRM is supposed to do. Depending on what kind of aerosol is used, the aerosol size, the method of stratospheric delivery, and the location and timing of injection, as well as myriad other decidable parameters, the cooling effects and climate impacts of SRM can span a very large range and, to some extent, are tunable [9, 30, 37]. This invites a question often asked by Alan Robock, "Whose hand is on the thermostat?" [77, 78]. Moreover, this question suggests the most important variable to be adjusted by SRM is surface air temperature, but perhaps other climate variables could be tuned by adding more "thermostats."

Assuming this decision could be made, SRM will not necessarily behave as predicted or intended. The radiative effects for given aerosol parameters can be determined quite well with various climate models at the disposal of the scientific community, but determining which radiative parameters are applicable to SRM is more uncertain. The recently highlighted issue of aerosol microphysics [28, 30] suggests other physical science issues with SRM could easily arise, dramatically changing the knowledge field. Equally as important are Donald Rumsfeld's famous "unknown unknowns," a phrase particularly applicable to a field with so much uncertainty. The only way to truly be sure of the effects of SRM is to conduct a test, but regarding tests involving actually placing aerosols in the stratosphere, the line between testing and deployment is quite blurred and the ability to observe the results of these tests is severely hampered by low signal-to-noise ratios [79]. Testing also has serious implications for issues of governance, which are well beyond the scope of this paper, although efforts are underway to investigate the issues involved (SRMGI, http://www.srmgi.org).

Despite the issues and inherent uncertainty with climate models, they are one of the most useful tools available to SRM research. Until recently, SRM studies with climate models were sporadic and uncoordinated, leading to modeling groups performing experiments that were insufficiently similar for comparison [27]. Even among modeling groups that did conduct similar experiments, some results were dissimilar enough to prevent robust conclusions on the expected climate effects from SRM from being reached [41]. The Geoengineering Model Intercomparison Project (GeoMIP, http://climate.envsci.rutgers.edu/GeoMIP/) provides a framework of coordinated experiments for all modeling groups wishing to participate, eventually allowing for robustness of results to be achieved [31]. In the project's current stages, the four proposed experiments are underway (Fig. 3) and, as of the time this entry was written, are being conducted by 16 different climate modeling groups.

Climate models used on a global scale have difficulty with accurate resolution of regional and local impacts, which will likely be some of the most important issues in the debate on SRM. Although assessment of these effects has begun [2], this direction will likely be one of the dominant avenues in the future of SRM research. Another important aspect in future research will likely be the increasing problem of ocean acidification, which SRM does little to prevent [80]. These reasons, and many others, have been suggested repeatedly as important investigations in the course of SRM research [77, 78].

If SRM were to be deployed, society's current ability to monitor the effectiveness of deployment has some prominent gaps. For such an endeavor, a global observation network is essential, and one of the most important parts of such a network would be satellites specifically geared to observe stratospheric aerosols and their climatic impacts. Although such instruments for directly observing aerosols have existed in the past, providing excellent observations of past volcanic

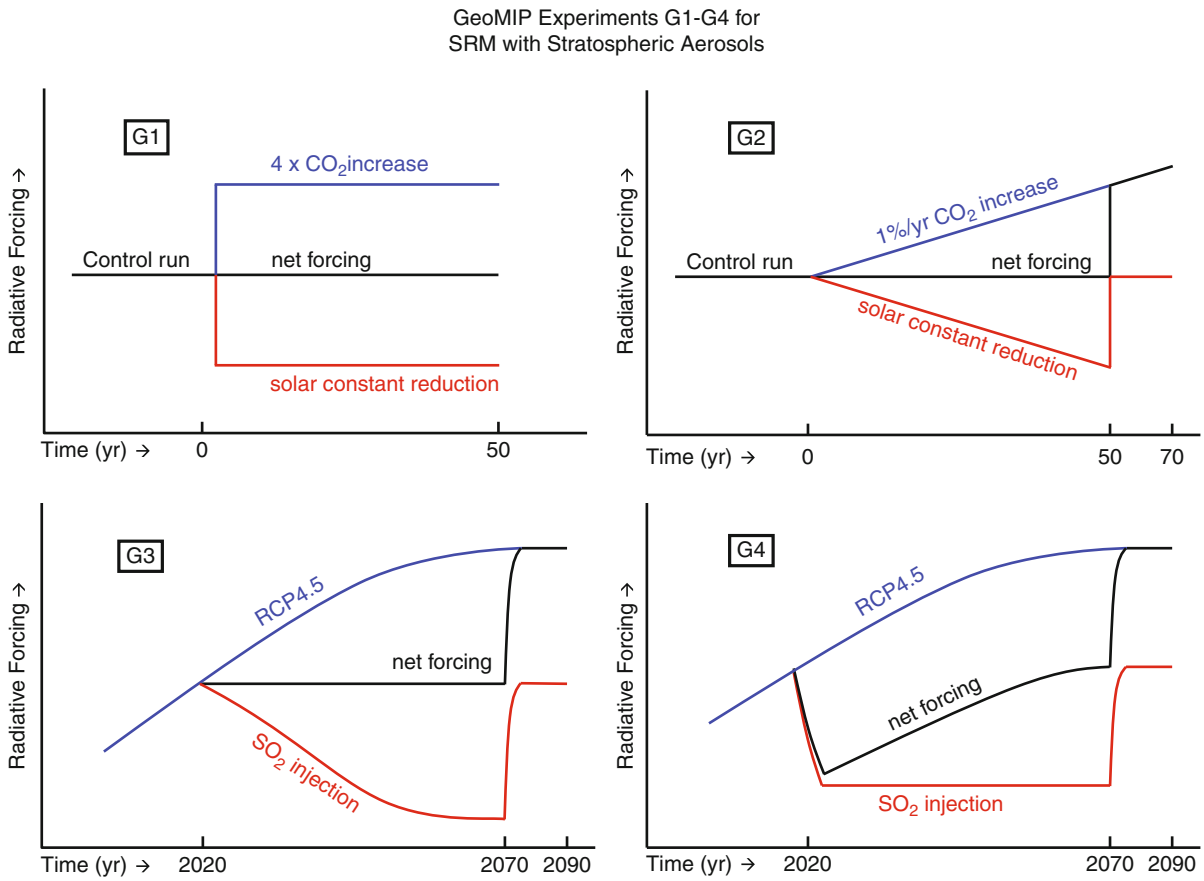

Stratospheric Aerosols for Solar Radiation Management. Figure 3
Outlines of the four coordinated experiments (G1–G4) to be performed by the participants of GeoMIP. Panels are combined from Figs. 1–4 from [31]

eruptions [81], currently only one similar instrument exists [82]. Many of the current instruments in orbit are aging, and replacement plans are desperately needed to ensure uninterrupted observations. Before SRM deployment can even be considered, the observation network will require serious assessment and improvement on a large scale.

This entry has mostly focused on physical science aspects of SRM. Although such concerns are fundamental to understanding SRM, during the decision-making process of whether to undertake SRM, or even some forms of SRM research, physical science results should not and likely will not be the sole determining factor. Discussions will include myriad different values, necessitating research in many different fields, including (but certainly not limited to) law, governance, economics, ethics, and social policy. Research in these fields is essential and ongoing, but like physical science research of SRM, much more work is needed.

SRM has the potential to relieve some of the expected consequences of climate change, but not without numerous possible consequences, all of which must be evaluated. The decision to deploy SRM, as well as how long to deploy until mitigation has taken effect, must include all information possible to achieve the best outcome for society in the face of the daunting problem of climate change.

Acknowledgments

I thank Long Cao, Ken Caldeira, Robin Becht, and the editors for helpful comments.

Bibliography

1. Intergovernmental Panel on Climate Change (IPCC) (2007) Climate change 2007: the fourth assessment report of the intergovernmental panel on climate change. Cambridge University Press, 996 pp
2. Ricke KL, Morgan MG, Allen MR (2010) Regional climate response to solar-radiation management. Nat Geosci 3:537–541. doi:10.1038/ngeo915
3. Matthews HD, Caldeira K (2007) Transient climate-carbon simulations of planetary geoengineering. Proc Natl Acad Sci 104(24):9949–9954. doi:10.1073/pnas.0700419104
4. Cao L, Caldeira K (2010) Atmospheric carbon dioxide removal: long-term consequences and commitment. Environ Res Lett 5:024011. doi:10.1088/1748-9326/5/2/024011
5. Wigley TML (2006) A combined mitigation/geoengineering approach to climate stabilization. Science 314(5798):452–454. doi:10.1126/science.1131728
6. Archer D, Eby M, Brovkin V, Ridgwell A, Cao L, Mikola-jewicz U, Caldeira K, Matsumoto K, Munhoven G, Montenegro A, Tokos K (2009) Atmospheric lifetime of fossil fuel carbon dioxide. Annu Rev Earth Planet Sci 37:117–134. doi:10.1146/annurev.earth.031208.100206
7. Solomon S, Plattner G-K, Knutti R, Friedlingstein P (2009) Irreversible climate change due to carbon dioxide emissions. Proc Natl Acad Sci 106(6):1704–1709. doi:10.1073/pnas.0812721106
8. Caldeira K, Wood L (2008) Global and arctic climate engineering: numerical model studies. Philos Trans R Soc A 366(1882):4039–4056. doi:10.1098/rsta.2008.0132
9. Robock A, Oman L, Stenchikov GL (2008) Regional climate responses to geoengineering with tropical and Arctic SO_2 injections. J Geophys Res 113:D16101. doi:10.1029/2008JD010050
10. ETC (2010) Stop geoengineering – our home is not a laboratory! http://www.etcgroup.org/upload/publication/pdf_file/HOMEBriefingENGsm.pdf. Accessed 30 Oct 2011
11. Stern N (2006) The economics of climate change: the stern review. Executive summary, Her Majesty's treasury, London, 27 pp. http://siteresources.worldbank.org/INTINDONESIA/Resources/226271-1170911056314/3428109-1174614780539/SternReviewEng.pdf. Accessed 30 Oct 2011
12. Fleming JR (2010) Fixing the sky: the checkered history of weather and climate control. Columbia University Press, New York, 344 pp
13. von Neumann J (1955) Can we survive technology? Fortune 106–108:151–152
14. Budyko MI (1974) Climate and life. Academic, New York, 508 pp
15. Budyko MI (1977) Climatic changes. American Geophysical Union, Washington, DC, 261 pp
16. National Academy of Sciences (NAS) (1992) Policy implications of greenhouse warming: mitigation, adaptation, and the science base. National Academy Press, Washington, DC, pp 433–464
17. Dickinson RE (1996) Climate engineering: a review of aerosol approaches to changing the global energy balance. Clim Chang 33(3):279–290. doi:10.1007/BF00142576
18. Govindasamy B, Caldeira K (2000) Geoengineering Earth's radiation balance to mitigate CO_2-induced climate change. Geophys Res Lett 27(14):2141–2144. doi:10.1029/1999GL006086
19. Teller E, Wood L, Hyde R (1997) Global warming and ice ages: I. Prospects for physics-based modulation of global change. U.S. Department of Energy, Lawrence Livermore National Laboratory, UCRL-JC- 128715, 18 pp
20. Teller E, Caldeira K, Canavan G, Govindasamy B, Grossman A, Hyde R, Ishikawa M, Ledebuhr A, Leith C, Molenkamp C, Nuckolls J, Wood L (1999) Long-range weather prediction and prevention of climate catastrophes: a status report. U.S. Department of Energy, Lawrence Livermore National Laboratory, UCRL-JC-135414, 42 pp
21. Teller E, Hyde R, Wood L (2002) Active climate stabilization: Practical physics-based approaches to prevention of climate change. U.S. Department of Energy, Lawrence Livermore National Laboratory, 8 pp
22. Flannery BP, Marland G, Broecker W, Ishatani H, Keshgi H, Komiyama H, MacCracken M, Rosenberg N, Steinberg M, Wigley T (1997) Geoengineering climate, Chapter 8. In: Watts RG (ed) The engineering response to climate change. Lewis, Boca Raton, pp 379–427
23. Khan E, Ferrell W, MacCracken MC, Schwartz SE, Duffy PB, Thompson S, Marland GH (2001) Response options to limit rapid or severe climate change. U.S Department of Energy, Washington, DC, 37 pp
24. Schneider S, Keith D (2001) Earth systems engineering and management. Nature 409:417–421. doi:10.1038/35053203
25. Crutzen PJ (2006) Albedo enhancement by stratospheric sulfur injections: a contribution to resolve a policy dilemma? Clim Chang 77:211–219. doi:10.1007/s10584-006-9101-y
26. Trenberth KE, Dai A (2007) Effects of Mount Pinatubo volcanic eruption on the hydrological cycle as an analog of geoengineering. Geophys Res Lett 34:L15702. doi:10.1029/2007GL030524
27. Rasch PJ, Tilmes S, Turco RP, Robock A, Oman L, Chen C-C, Stenchikov GL, Garcia RR (2008) An overview of geoengineering of climate using stratospheric sulfate aerosols. Philos Trans R Soc A 366:4007–4037. doi:10.1098/rsta.2008.0131
28. Heckendorn P, Weisenstein D, Fueglistaler S, Luo BP, Rozanov E, Schraner M, Thomason LW, Peter T (2009) The impact of geoengineering aerosols on stratospheric temperature and ozone. Environ Res Lett 4:045108. doi:10.1088/1748-9326/4/4/045108
29. Rasch PJ, Crutzen PJ, Coleman DB (2008) Exploring the geoengineering of climate using stratospheric sulfate aerosols: the role of particle size. Geophys Res Lett 35:L02809. doi:10.1029/2007GL032179
30. Pierce JR, Weisenstein DK, Heckendorn P, Peter T, Keith DW (2010) Efficient formulation of stratospheric aerosol for

climate engineering by emission of condensible vapor from aircraft. Geophys Res Lett 37:L18805. doi:10.1029/2010GL043975
31. Kravitz B, Robock A, Boucher O, Schmidt H, Taylor KE, Stenchikov G, Schulz M (2011) The geoengineering model inter-comparison project (GeoMIP). Atm Sci Lett 12:162167. doi:10.1002/asl.316
32. Keith DW (2000) Geoengineering the climate: history and prospect. Annu Rev Energy Environ 25:245–284. doi:10.1146/annurev.energy.25.1.245
33. Boyd PW (2008) Ranking geo-engineering schemes. Nat Geosci 1:722–724. doi:10.1038/ngeo348
34. Lenton TM, Vaughan NE (2009) The radiative forcing potential of different climate geoengineering options. Atm Chem Phys 9:5539–5561. doi:10.5194/acp-9-5539-2009
35. Shepherd J, Caldeira K, Cox P, Haigh J, Keith D, Launder B, Mace G, MacKerron G, Pyle J, Rayner S, Redgwell C, Watson A (2009) Geoengineering the climate: science, governance and uncertainty. Royal Society Policy document 10/09, 82 pp
36. Robock A (2000) Volcanic eruptions and climate. Rev Geophys 38:191–219. doi:10.1029/1998RG000054
37. Kravitz B, Robock A (2011) The climate effects of high latitude eruptions: the role of the time of year. J Geophys Res 116: D01105. doi:10.1029/2010JD014448
38. Lacis AA, Mishchenko MI (1995) Climate forcing, climate sensitivity, and climate response: a radiative modeling persepctive on atmospheric aerosols. In: Charlson RJ, Heintzenberg J (eds) Aerosol forcing of climate: report of the Dahlem workshop on aerosol forcing of climate, Berlin, 24–29 April 1994. Wiley, Chichester/New York
39. Pinto JP, Turco RP, Toon OB (1989) Self-limiting physical and chemical effects in volcanic eruption clouds. J Geophys Res 94(D8):11165–11174, doi:10.1029/JD094iD08p11165
40. Lane L, Caldeira K, Chatfield R, Langhoff S (2007) Workshop report on managing solar radiation. National Aeronautics and Space Administration, NASA/CP-2007-214558, 31 pp
41. Jones A, Haywood J, Boucher O, Kravitz B, Robock A (2010) Geoengineering by stratospheric SO_2 injection: results from the Met Office HadGEM2 climate model and comparison with the Goddard Institute for Space Studies ModelE. Atm Chem Phys 10:5999–6006. doi:10.5194/acp-10-5999-2010
42. Chapman S (1930) On ozone and atomic oxygen in the upper atmosphere. Philos Mag 10:369–383
43. Chapman S (1942) The photochemistry of atmospheric oxygen. Rep Prog Phys 9:92–100. doi:10.1088/0034- 4885/9/1/310
44. Solomon S (1999) Stratospheric ozone depletion: a review of concepts and history. Rev Geophys 37(3):275–316. doi:10.1029/1999RG900008
45. Hofmann DJ, Solomon S (1989) Ozone destruction through heterogeneous chemistry following the eruption of El Chichòn. J Geophys Res 94(D4):5029–5041. doi:10.1029/JD094iD04p05029
46. Kinnison DE, Grant KE, Connell PS, Rotman DA, Wuebbles DJ (1994) The chemical and radiative effects of the Mount Pinatubo eruption. J Geophys Res 99:2570525731. doi:10.1029/94JD02318
47. Tilmes S, Mller R, Salawitch R (2008) The sensitivity of polar ozone depletion to proposed geoengineering schemes. Science 320:1201–1204. doi:10.1126/science.1153966
48. Tilmes S, Garcia RR, Kinnison DE, Gettelman A, Rasch PJ (2009) Impact of geoengineered aerosols on the troposphere and stratosphere. J Geophys Res 114:D12305. doi:10.1029/2008JD011420
49. Gu L, Baldocchi DD, Wofsy SC, Munger JW, Michalsky JJ, Urbanski SP, Boden TA (2003) Response of a deciduous forest to the Mount Pinatubo eruption: enhanced photosynthesis. Science 299(5615):2035–2038. doi:10.1126/science.1078366
50. Mercado LM, Bellouin N, Sitch S, Boucher O, Hunting-ford C, Wild M, Cox PM (2009) Impact of changes in diffuse radiation on the global land carbon sink. Nature 458:1014–1018. doi:10.1038/nature07949
51. Keeling CD, Piper SC, Bacastow RB, Wahlen M, Whorf TP, Heimann M, Meijer HA (2001) Exchanges of atmospheric CO_2 and $^{13}CO_2$ with the terrestrial biosphere and oceans from 1978 to 2000, vol I. Scripps Institution of Oceanography, San Diego Global aspects, SIO Reference Series, No. 01–06, 88pp
52. Murphy DM (2009) Effect of stratospheric aerosols on direct sunlight and implications for concentrating solar power. Environ Sci Technol 43(8):2784–2786. doi:10.1021/es802206b
53. Koch D, Schmidt GA, Field CV (2006) Sulfur, sea salt, and radionuclide aerosols in GISS ModelE. J Geophys Res 111: D06206. doi:10.1029/2004JD005550
54. Kravitz B, Robock A, Oman L, Stenchikov G, Marquardt AB (2009) Sulfuric acid deposition from stratospheric geoengineering with sulfate aerosols. J Geophys Res 114: D14109. doi:10.1029/2009JD011918
55. Kravitz B, Robock A, Oman L, Stenchikov G, Marquardt AB (2010) Correction to Sulfuric acid deposition from stratospheric geo-engineering with sulfate aerosols. J Geophys Res 115:D16119. doi:10.1029/2010JD014579
56. Robock A, Marquardt A, Kravitz B, Stenchikov G (2009) Benefits, risks, and costs of stratospheric geoengineering. Geophys Res Lett 36:L19703. doi:10.1029/2009GL039209
57. McClellan J, Sisco J, Suarez B, Keogh G (2010) Geoengineering cost analysis. Aurora Flight Sciences, AR10-182, 86 pp
58. Kravitz B (2011), Stratospheric geoengineering with black carbon aerosols, Dissertation thesis, available online at http://www.stanford.edu/~bkravitz/research/papers/other/kravitzthesisfinal.pdf
59. Fromm M, Lindsey DT, Servranckx R, Yue G, Trickl T, Sica R, Doucet P, Godin-Beekmann S (2010) The untold story of pyrocumulonimbus. Bull American Meteorol Soc 91:1193–1209. doi:10.1175/2010BAMS3004.1
60. Robock A (1988) Enhancement of surface cooling due to forest fire smoke. Science 242(4880):911–913. doi:10.1126/science.242.4880.911
61. Robock A (1991) Surface cooling due to forest fire smoke. J Geophys Res 96(D11):20869–20878. doi:10.1029/91JD02043
62. Crutzen PJ, Birks JW (1982) Atmosphere after a nuclear war: Twilight at noon. Ambio 11(2/3):114–125

63. Turco RP, Toon OB, Ackerman TP, Pollack JB, Sagan C (1983) Nuclear winter: global consequences of multiple nuclear explosions. Science 222(4630):1283–1292. doi:10.1126/science.222.4630.1283
64. Aleksandrov VV, Stenchikov GL (1983) On the modeling of the climatic consequences of the nuclear war. In: The proceedings of applied mathematics, The Computing Centre of the USSR Academy of Sciences, Moscow, 21 pp
65. Covey C, Schneider SH, Thompson SL (1984) Global atmospheric effects of massive smoke injections from a nuclear war: results from general circulation model simulations. Nature 308:21–25. doi:10.1038/308021a0
66. Pittock AB, Ackerman TP, Crutzen PJ, MacCracken MC, Shapiro CS, Turco RP (eds) (1986) Environmental consequences of nuclear war, SCOPE 28, vol I. Wiley, New York, Physical and Atmospheric Effects
67. Robock A, Oman L, Stenchikov GL, Toon OB, Bardeen C, Turco RP (2007) Climatic consequences of regional nuclear conflicts. Atm Chem Phys 7:2003–2012. doi:10.5194/acp-7-2003-2007
68. Toon OB, Robock A, Turco RP, Bardeen C, Oman L, Stenchikov GL (2007) Consequences of regional-scale nuclear conflicts. Science 315:1224–1225. doi:10.1126/science.1137747
69. Pueschel RF, Verma S, Rohatschek H, Ferry GV, Boiadjieva N, Howard SD, Strawa AW (2000) Vertical transport of anthropogenic soot aerosol into the middle atmosphere. J Geophys Res 105(D3):3727–3736. doi:10.1029/1999JD900505
70. Rohatschek H (1996) Levitation of stratospheric and mesospheric aerosols by gravitophoresis. J Aerosol Sci 27(3):467–475. doi:10.1016/0021-8502(95)00556-0
71. Mills MJ, Toon OB, Turco RP, Kinnison DE, Garcia RR (2008) Massive global ozone loss predicted following regional nuclear conflict. Proc Natl Acad Sci 105(14):5307–5312. doi:10.1073/pnas.0710058105
72. CDC (1999) Elemental carbon (diesel particulate): Method 5040, Issue 3 (Interim), National Institute for Safety and Health, Centers for Disease Control and Prevention. In: NIOSH manual of analytical methods, 4th rev. edn., 5 pp. http://www.cdc.gov/niosh/docs/2003-154/pdfs/5040f3.pdf. Accessed 30 Oct 2011
73. Vogelmann AM, Robock A, Ellingson RG (1988) Effects of dirty snow in nuclear winter simulations. J Geophys Res 93(D5):5319–5332, doi:10.1029/JD093iD05p05319
74. Stenchikov GL, Kirchner I, Robock A, Graf H-F, Antufia JC, Grainger RG, Lambert A, Thomason L (1998) Radiative forcing from the 1991 Mount Pinatubo volcanic eruption. J Geophys Res 103:13837–13857. doi:10.1029/98JD00693
75. Keith DW (2010) Photophoretic levitation of engineered aerosols for geoengineering. Proc Natl Acad Sci 107(38):16428–16431. doi:10.1073/pnas.1009519107
76. Benford G, Benford J (2005) An aero-spacecraft for the far upper atmosphere supported by microwaves. Acta Astronaut 56:529–535. doi:10.1016/j.actaastro.2004.09.050
77. Robock A (2008) 20 reasons why geoengineering may be a bad idea. Bull At Sci 64(2):14–18. doi:10.2968/064002006, 59
78. Robock A (2011) Bubble, bubble, toil and trouble: an editorial comment. Clim Chang 105:383–385. doi:10.1007/s10584-010-0017-1
79. Robock A, Bunzl M, Kravitz B, Stenchikov G (2010) A test for geoengineering? Science (Perspectives) 327(5965):530–531. doi:10.1126/science.1186237
80. Matthews HD, Cao L, Caldeira K (2009) Sensitivity of ocean acidification to geoengineered climate stabilization. Geophys Res Lett 36:L10706. doi:10.1029GL037488
81. Russell PB, McCormick MP (1989) SAGE II aerosol data validation and initial data use: an introduction and overview. J Geophys Res 94:8335–8338. doi:10.1029/JD094iD06p08335.
82. Llewellyn EJ, Lloyd ND, Degenstein DA, Gattinger RL, Petelina SV, Bourassa AE, Wiensz JT, Ivanov EV, McDade IC, Solheim BH, McConnell JC, Haley CS, von Savigny C, Sioris CE, McLinden CA, Griffioen E, Kaminski J, Evans WFJ, Puckrin E, Strong K, Wehrle V, Hum RH, Kendall DJW, Matsushita J, Murtagh DP, Brohede S, Stegman J, Witt G, Barnes G, Payne WF, Piché L, Smith K, Warshaw G, Deslauniers D-L, Marchand P, Richardson EH, King RA, Wevers I, McCreath W, Kyrölä E, Oikarinen L, Leppelmeier GW, Auvinen H, Mégie G, Hauchecorne A, Lefévre F, de La Nöe J, Ricaud P, Frisk U, Sjoberg F, von Schéele F, Nordh L (2004) The OSIRIS instrument on the Odin spacecraft. Can J Phys 82(6):411–422. doi:10.1139/p04?005

Stratospheric Pollution

Martyn P. Chipperfield
Institute for Climate and Atmospheric Science, School of Earth and Environment, University of Leeds, Leeds, UK

Article Outline

Glossary
Definition of the Subject
Introduction
Stratospheric Ozone
Ozone Depletion
Ozone Recovery and Chemistry–Climate Interactions
Future Directions
Bibliography

Glossary

Chemical transport model Three-dimensional model of atmospheric chemistry used to simulate past and present changes.

Chlorofluorocarbon (CFC) Class of chemical compound containing chlorine, fluorine, and carbon.

Coupled chemistry-climate model (CCM) Version of three-dimensional atmospheric climate model with detailed interactive chemistry. Used to simulate past ozone changes and to predict the future ozone layer.

Montreal protocol International agreement to limit and phase out production and emission of chlorine- and bromine-containing ozone-depleting substances.

Ozone Molecule containing three oxygen atoms (O_3).

Ozone-depleting substance (ODS) General term for compounds which, when broken down in the atmosphere, can release chemical species that destroy ozone.

Ozone hole Popular name given to the large seasonal reduction in column ozone over Antarctica, which currently occurs from August to October each year.

Stratosphere Region of atmosphere from about 10–18 km to 50 km altitude. Contains 90% of atmospheric ozone in the ozone layer.

Very short-lived species (VSLS) Source gas with an atmospheric lifetime less than about 6 months.

Definition of the Subject

The stratosphere is the region of the atmosphere between 8–18 km and 50 km altitude. This region contains 90% of the ozone (O_3) in the atmosphere in the so-called ozone layer. Ozone is continually produced naturally in the stratosphere by sunlight and molecular oxygen. It is destroyed by a variety of chemical species that are present in the atmosphere both naturally and through human activities. The ozone layer prevents harmful short wavelength ultraviolet radiation from reaching the Earth's surface and also plays an important role in the atmospheric climate balance. Over the past few decades, increases in atmospheric chlorine and bromine have occurred through human activities (e.g., use of chlorofluorocarbons or CFCs), and this has led to ozone depletion. The most dramatic reduction in the ozone layer has occurred over the Antarctic in springtime where about 70% of the column ozone is removed, corresponding to complete loss in the lower stratosphere. Smaller depletion has been observed in the Arctic winter and spring, and in the middle latitudes. An international agreement (The Montreal Protocol and Amendments) has now acted to ban the production and emission of CFCs and other major ozone-depleting substances (ODSs). Over the timescale of next 50 years or so the ozone layer should recover, though the speed and extent of this recovery will depend on stratospheric climate change.

Introduction

The presence of the Earth's ozone layer is essential for life on Earth. The realization that through human activities we had started to destroy it has been a major science and environmental issue since the late twentieth century. This article briefly discusses the key science and policy issues behind the issue of global stratospheric ozone depletion.

Section "Stratospheric Ozone" describes the chemistry of ozone layer and summarizes the natural and man-made substances, which can lead to its depletion. Section "Ozone Depletion" describes observations of past ozone depletion and the policy measures which have been introduced to reverse this trend. Section "Ozone Recovery and Chemistry–Climate Interactions" discusses the likely future evolution of the ozone layer and how this will depend on interactions with climate change. Some future directions for ozone layer research are outlined in section "Future Directions".

Stratospheric Ozone

The Stratosphere and the Natural Ozone Layer

Ozone is produced in the stratosphere naturally by the action of short wavelength ultraviolet radiation ($\lambda \leq 242$ nm) dissociating oxygen molecules:

$$O_2 + h\nu \rightarrow O + O \tag{1}$$

where $h\nu$ is a photon of light with sufficient energy to break the O–O bond. The O atoms produced can rapidly combine with another O_2 molecule to form ozone:

$$O + O_2 + M \rightarrow O_3 + M \tag{2}$$

where M is any third body. In fact, O and O_3 form a tightly coupled chemical family and are normally considered together as "odd oxygen." The production

and removal of O or O_3 is equivalent; destruction of O leads to O_3 loss. O_3 can be converted back to O via:

$$O_3 + h\nu \rightarrow O + O_2 \quad (3)$$

Ozone (or odd oxygen) is destroyed by conversion to O_2 via:

$$O + O_3 \rightarrow 2O_2 \quad (4)$$

The first theory for the chemistry of the ozone layer was put forward by Chapman in 1930 [1]. His scheme comprised of reactions (1)–(4) and was therefore based on oxygen-only chemistry. The chemical loss of odd oxygen in the Chapman mechanism occurs via reaction (4), i.e., the direct reaction of O and O_3. The Chapman mechanism successfully and qualitatively predicts the occurrence of an ozone layer in the stratosphere. However, by the 1960s, when good observations of the ozone layer became available and improved laboratory measurements gave accurate values of the relevant chemical rate constants, it became clear that the Chapman scheme could not explain the observations quantitatively. While the Chapman scheme does include the source of stratospheric ozone (reaction 1), the direct reaction (4) accounts for only about 20% of the actual loss. The Chapman mechanism ignores the very important destruction of ozone by other chemical families.

Catalytic Ozone Loss

There are a number of cycles which can catalyze the destruction of stratospheric ozone. Many cycles are based on:

$$XO + O \rightarrow X + O_2$$
$$X + O_3 \rightarrow XO + O_2$$
$$\text{Net}: O + O_3 \rightarrow 2O_2$$

In this scheme, the species X (in practice X = OH, NO, Cl, Br) reacts with O_3 to form XO. XO then reacts with O to reform X. Therefore, X is acting catalytically and the net effect of these two reactions is the same as reaction (4) of the Chapman mechanism. In this way a species with an abundance much smaller than O_3 can cause its destruction, i.e., species present at the part per billion (1 in 10^9) or part per trillion (1 in 10^{12}) level can affect ozone that is present in the part per million (1 in 10^6) level in the stratosphere. Concern over stratospheric ozone depletion really started in the early 1970s with the realization that O_3 could be destroyed catalytically by NOx (NO + NO_2) [2], and that large fleets of proposed supersonic aircraft, flying near 18 km, could directly inject NOx into the stratosphere [3]. As it turned out, very few supersonic passenger aircraft (i.e., Concorde) were built so the impact on the ozone layer was small. In 1974, attention turned to chlorine when it was proposed that this family could catalytically destroy ozone [4].

Catalytic cycles can also be based on:

$$X + O_3 \rightarrow XO + O_2$$
$$Y + O_3 \rightarrow YO + O_2$$
$$XO + YO \rightarrow XY + O_2 \quad (5)$$
$$XY + h\nu \rightarrow X + Y \quad (6)$$
$$\text{Net}: 2O_3 \rightarrow 3O_2$$

The details of steps (5) and (6) vary between different cycles (i.e., different species X and Y), though all such cycles catalyze $2O_3 \rightarrow 3O_2$. As these cycles do not depend on the concentration of atomic oxygen they are more efficient in the lower stratosphere.

Stratospheric Chemistry

There are a number of important chemical families whose species can lead to stratospheric ozone destruction. For each of these families there are one or more source gases, reservoirs, and radicals. Source gases are the long-lived species (lifetime many years) which can be transported from the surface to the stratosphere. Once in the stratosphere these source gases decompose to release radicals. These are the species which can catalytically destroy ozone in cycles described in section "Catalytic Ozone Loss". However, the radicals can also become temporarily tied up in reservoir species; these species do not destroy ozone and, therefore, reduce the impact of the radical-catalyzed loss. Table 1 summarizes the main stratospheric chemical families.

The only natural source of chlorine which gets to the stratosphere is methyl chloride (CH_3Cl). This is emitted from oceans and contributes about 600 parts per trillion (pptv) to the atmospheric loading, i.e., about 20% of the current total. The majority of chlorine in the present day atmosphere comes from man-made sources such as chlorofluorocabons (CFCs),

hydrochlorofluorocabons (HCFCs), and solvents (e.g., CCl_4, CH_3CCl_3). The use of these species since the 1930s (e.g., CFCs were used as aerosol propellants and refrigerants) has resulted in a significant increase in chlorine over the natural background levels. Similarly, industrial use of methyl bromide and halons (used in fire extinguishers) has increased the atmospheric bromine loading to about 20 pptv compared to background levels of about half that. Although bromine has a much lower abundance in the atmosphere, it is about 50 times more efficient at destroying ozone because a smaller proportion is tied up in its reservoir species. Concern about the increasing levels of chlorine in the atmosphere started in 1974 when Molina and Rowland [5] suggested that the only atmospheric sink for the stable, inert CFC molecules was transport to the stratosphere where they would be broken down by short wavelength UV radiation to release chlorine, which could catalytically destroy ozone.

Ozone Depletion

Polar Ozone Loss

The most dramatic manifestation of human-induced ozone depletion has occurred over the Antarctic in springtime, the so-called Antarctic Ozone Hole. Reductions in the stratospheric ozone column over Antarctica were first detected by Farman et al. [6] in the early to mid-1980s. Observations of ozone loss in this region were a complete surprise to the scientific community as it was believed that in the cold Antarctic lower stratosphere, ozone should be very stable and long-lived. The publication of the observed decrease initiated an intense period of scientific study with field campaigns to Antarctica, analysis of satellite data and numerical modeling. It was rapidly established that the cause of the ozone loss was high levels of "active chlorine" [7], i.e., chlorine present as ozone-destroying radicals (ClO) rather than in the reservoir form. A new catalytic cycle involving the dimer of ClO (catalyzing $2O_3 \rightarrow 3O_2$) was proposed to explain how ClO could destroy ozone in the cold polar lower stratosphere when sunlight returns in spring [8]. Temperatures in the Antarctic lower stratosphere in winter, when there is 24-h darkness, can reach as low as 185–190 K. Strong westerly winds form a polar vortex which isolates the stratosphere over Antarctica from middle latitudes. A key step to explaining polar ozone depletion was the discovery that polar stratospheric clouds (PSCs), which form at around 20 km in the polar regions despite the low pressures and dry stratosphere, could initiate heterogeneous reactions [9], which convert the normally stable reservoir HCl and $ClONO_2$ to the active radical form. Thus, it is the cold isolated conditions of the Antarctic lower stratosphere in winter and spring which favor ozone loss. Figure 1 shows satellite observations of the Antarctic Ozone

Stratospheric Pollution. Table 1 The four main chemical families in the stratosphere along with example source gases, reservoirs, and radicals

Family	Source gases	Reservoirs	Radicals
Hydrogen	H_2O CH_4	H_2O_2	OH, HO_2
Nitrogen	N_2O	HNO_3, N_2O_5 $ClONO_2$	NO, NO_2
Chlorine	CH_3Cl CFCs HCFCs Solvents	HCl $ClONO_2$	Cl, ClO
Bromine	CH_3Br Halons Shorter-lived organics	HBr $BrONO_2$	Br, BrO

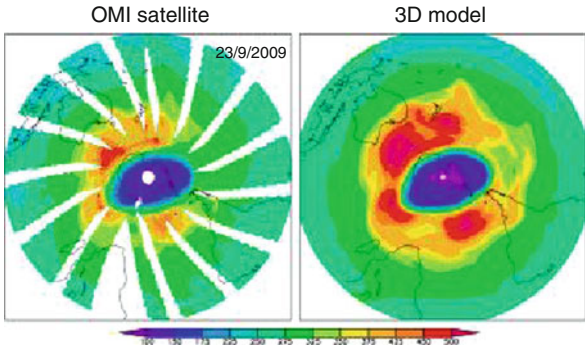

Stratospheric Pollution. Figure 1
Ozone Monitoring Instrument (OMI) satellite observations of total column ozone (Dobson Units) showing the Antarctic Ozone Hole on September 23, 2009 (*left*), along with calculations from the SLIMCAT 3D chemical transport model [10] (*right*) (Image courtesy of W. Feng, University of Leeds)

Hole in 2009, along with calculations from a state-of-the-art 3D model. Such models now include the relevant chemical processes and can reproduce the observed depletion well.

The same chemical and meteorological processes which occur over the Antarctic also occur over the north pole. However, due to differences in surface orography, i.e., the northern hemisphere is more mountainous while the southern hemisphere is largely ocean, the Arctic polar vortex is weaker, more disturbed, more variable, and warmer. Therefore, there is less occurrence of PSCs in the north, less activation of chlorine, and less ozone depletion [11]. In cold Arctic winters ozone loss of about 50% at 20 km, corresponding to about 30% of the column is observed.

Middle Latitudes and Tropics

Ozone depletion has been observed at middle latitudes. This reduction is not as large as observed in the polar regions and amounts to a decreasing trend of about 0.6%/year during the 1980s and 1990s [12] (Fig. 2). The main chemical cause of this midlatitude decrease is also the increases in atmospheric chlorine and bromine. The loss at middle latitudes can be caused by export of ozone-poor or chlorine-activated air from the polar vortex or by chemical processes occurring at midlatitudes [13]. Sulfate aerosols in the lower stratosphere can perform a similar role as PSCs in promoting heterogeneous reactions. Large volcanic eruptions can significantly enhance the stratospheric sulfate aerosol layer, and increased ozone loss was observed after the eruption of Mt Pinatubo in 1991 [14].

No significant decrease in column ozone has been observed in the tropics (Fig. 2). However, it is important to note that the ozone layer is naturally thin in this region of the world – by up to a factor two compared to high latitudes. As the sun elevation is also larger in the tropics, humans can experience a much larger dose of excess ultraviolet radiation naturally at low latitudes than through the effects of ozone depletion at middle or high latitudes.

Effects of Ozone Depletion

The ozone layer prevents wavelengths shorter than about 300 nm from reaching the Earth's surface, i.e., all UV-C radiation and most UV-B radiation.

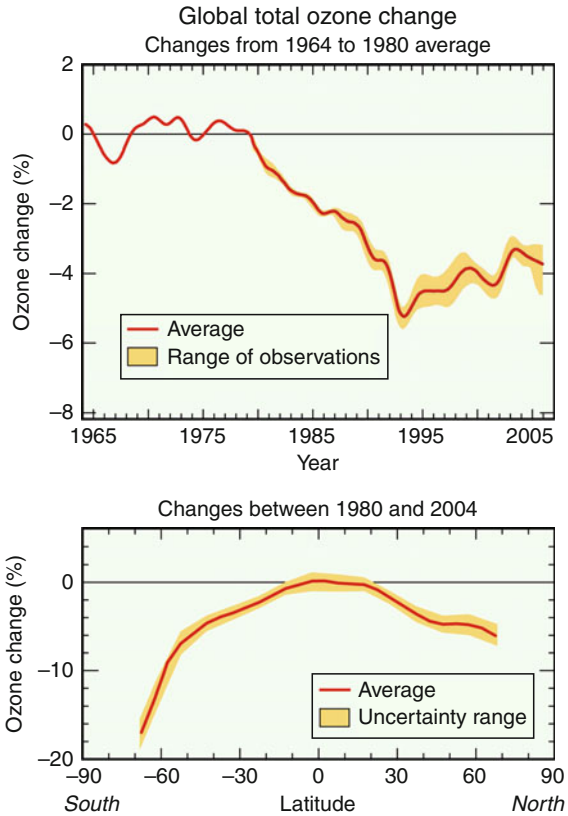

Stratospheric Pollution. Figure 2
Observations of global ozone changes. The *top panel* shows changes in global ozone (based on ground-based and satellite observations) from 1964 to 2005 relative to the 1964–1980 mean. Annual and solar cycle variations have been removed. The *bottom panel* shows ozone changes between 1980 and 2004 as a function of latitude (From [15])

Decreases in stratospheric ozone will increase the amount of UV-B radiation reaching the surface. This will affect human health (skin, eyes, and immune system), animal health, terrestrial ecosystems, aquatic ecosystems, biogeochemical cycles, air quality and materials [16]. As ozone absorbs both in the ultraviolet and infrared parts of the spectrum, it is intimately coupled to atmospheric climate balance. Past ozone depletion has acted to cool the surface of the Earth, thereby offsetting some of the warming caused by GHG increases [17]. Any changes to stratospheric ozone also have the potential to alter the temperature and dynamical structure of the atmosphere.

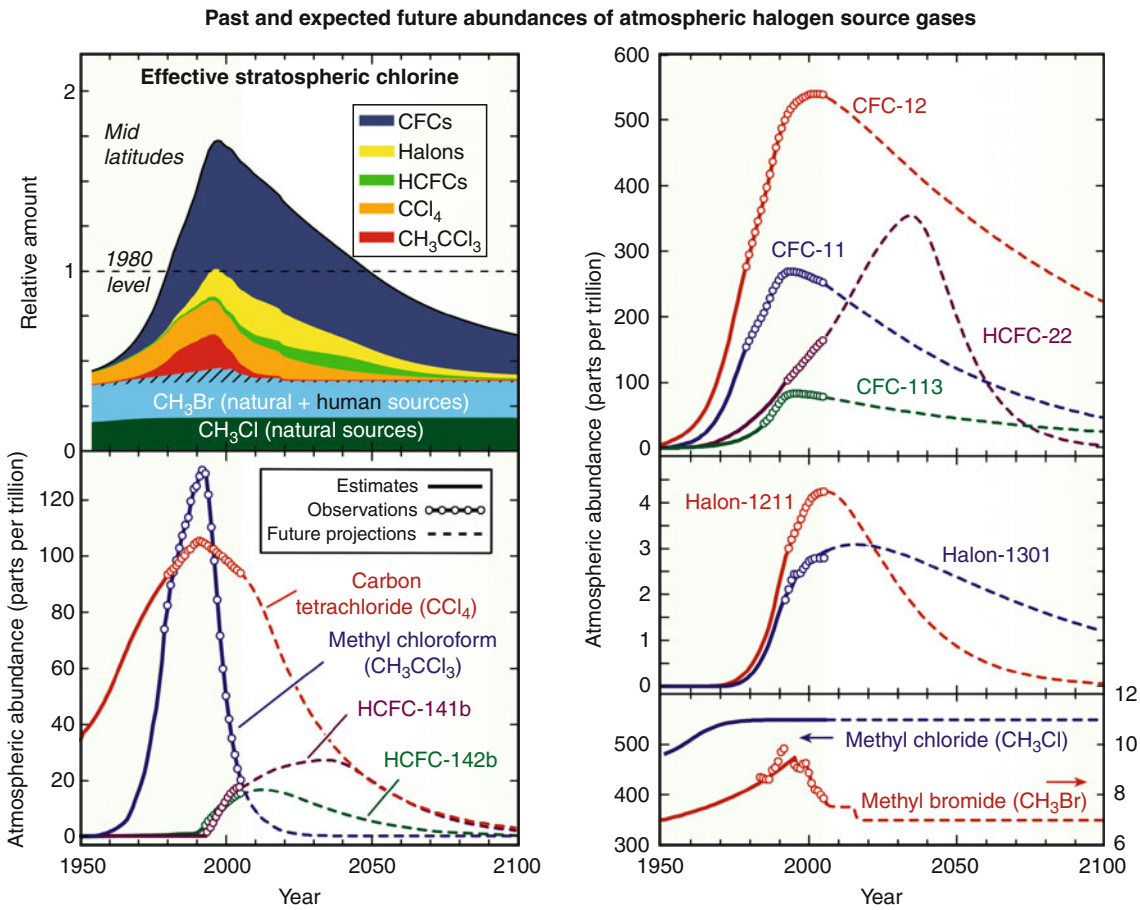

Stratospheric Pollution. Figure 3

The observed abundances of the important bromine and chlorine source gases and their expected future evolution based on current trends and the scope of the Montreal Protocol. The *top left panel* shows the accumulated effective chlorine due to all source gases (From [15])

Montreal Protocol

The seminal paper by Rowland and Molina [5] first suggested that CFCs and other halocarbons could lead to reductions in the global ozone layer. This discovery prompted some efforts at regulation of CFCs within the USA. By 1978, some unilateral action was taken – the US banned the sale of CFCs for use in spray cans. However, because of other uses of CFCs the atmospheric abundance of these species continued to increase. The atmospheric models available at the time predicted only modest decreases in ozone due to CFCs; the models were wrong because they did not contain a description of the role of PSCs and heterogeneous chemistry.

The first significant attempt at international regulation was the Vienna Convention for the Protection of the Ozone Layer in March 1985. This resulted in 22 countries agreeing to reduce CFC emissions and to study the impact of CFCs on ozone further. In September 1987, the Montreal Protocol was signed, initially by 27 countries, leading to some limits in the production of CFCs and halons. There were two key elements to the Montreal Protocol which contributed to its ultimate success. First, a Multilateral Fund was set up to help developing countries phase out the use of ozone-depleting substances. Second, the protocol allowed for strengthening of the regulations should stronger scientific evidence linking CFCs to ozone loss emerge.

Following intense scientific research in the late 1980s and 1990s to determine the cause of polar and global ozone depletion, such unequivocal evidence was found. The Montreal Protocol was strengthened in a series of amendments: London (1990), Copenhagen (1992), Montreal (1997), and Beijing (1999). The past trends and predicted changes in stratospheric chlorine based on these strengthened amendments are shown in Figs. 3 and 4.

Note that CFCs and other gases controlled under the Montreal Protocol are potent greenhouses gases (GHGs). For example, CFC-12 (CF_2Cl_2) has a Global Warming Potential of about 10,000 (on a 100-year time horizon). By removing these species from the atmosphere, the Montreal Protocol has had a significant effect in preventing further climate change [18].

Ozone Recovery and Chemistry–Climate Interactions

Surface observations of halocarbon source gases from global networks have confirmed the success of the Montreal Protocol and Amendments in delaying, and reversing, the increase in atmospheric chlorine concentrations. The abundance of the shorter-lived source gases (e.g., CH_3CCl_3, lifetime 6 years) has peaked and these species are now showing a decline. Longer-lived species (e.g., CFC-12, lifetime 100 years) have shown a slowing down in growth and leveling off in abundance. This is consistent with the behavior expected under regulations imposed by the Montreal Protocol and Amendments. The protocol allows for some continued production of HCFCs until 2030.

Overall, we expect the levels of atmospheric halogens (chlorine and bromine) to return to values when the Antarctic Ozone hole first appeared (1980) by about 2050. This date therefore sets the reference point for the disappearance of the Antarctic Ozone hole if the other atmospheric conditions remain constant. However, because of increases in greenhouse gases (GHGs), and associated climate change, the atmosphere in 2050 will be markedly different to 1980. The main radiative impact of GHG increases is a cooling of the stratosphere (accompanied by the well-known warming of the surface). This cooling of the stratosphere will impact the temperature-dependent ozone chemistry. Colder temperatures in the lower stratosphere will cause more PSCs and so while the

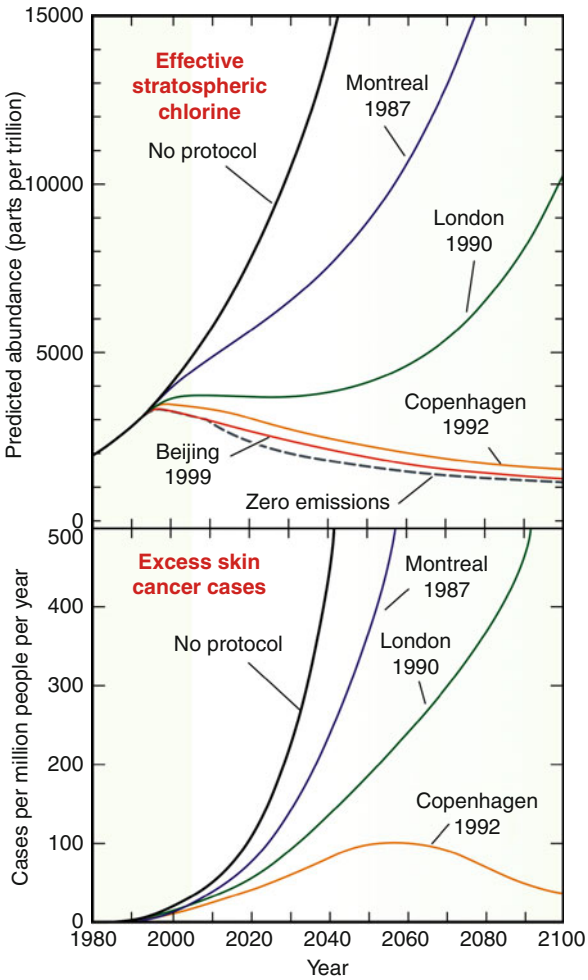

Stratospheric Pollution. Figure 4
The *top panel* shows predicted abundance of effective stratospheric chlorine (which combines chlorine and bromine) based on the Montreal Protocol and its series of amendments. The *bottom panel* shows the estimated excess skin cancers which would have resulted from these different scenarios (From [15])

halogen loading remains high this could lead to increased ozone loss. On the other hand, colder temperatures will tend to slow down the rate of the gas-phase reactions which destroy ozone (from all cycles). This will lead to more stratospheric ozone. Other climate change feedbacks might occur, e.g., a strengthening of the stratospheric meridional circulation [19], which will transport more ozone to higher latitudes. State-of-the-art predictions [20] for the future of the ozone layer are shown in Fig. 5. These CCM

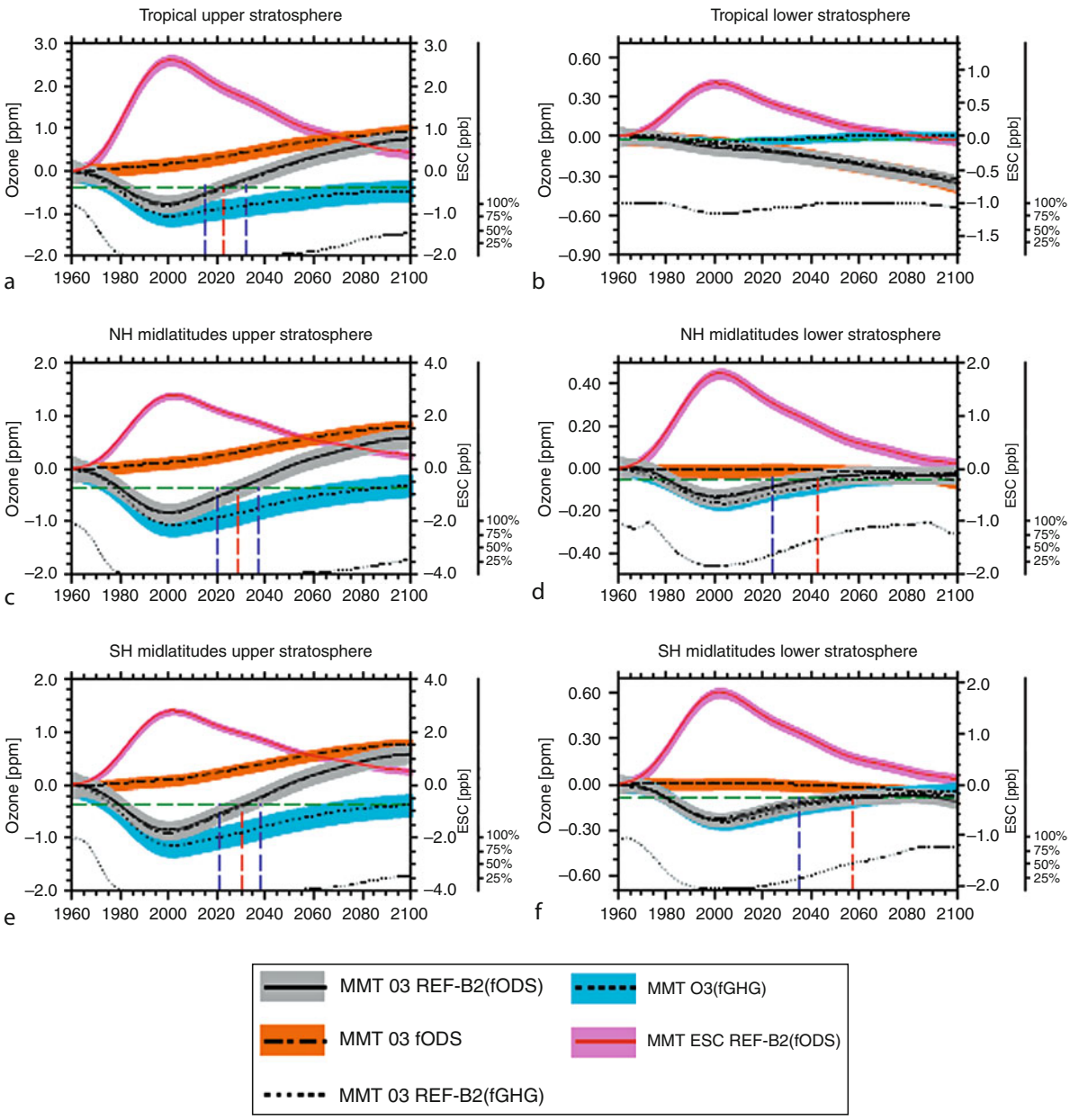

Stratospheric Pollution. Figure 5

Results from chemistry-climate model (CCM) simulations for the past and future evolution of the ozone layer. The *panels* show different geographical and altitude regions. The *model lines* are averages of around 15 CCMs used worldwide. The models ran three experiments to separate the effect of changing ODS and changing greenhouse gases (GHGs). The *gray shaded line* included both changes. The *blue shaded line* shows the effect of ODS changes only. The *orange shaded line* shows the effect of GHG increases only. The *pink line* shows the change in ODS concentrations in the models (*right hand axis*) (From [20])

results show that rate of ozone layer recovery will vary with region. The model experiments also clearly show that climate change (stratospheric cooling) acts to speed up the future increase in ozone.

Future Directions

An important current stratospheric science topic concerns the rate of ozone recovery and the interactions between this and climate change (see section "Ozone Recovery and Chemistry–Climate Interactions"). While the expected decrease in halocarbon ODS is believed to be fairly well constrained, there are many other uncertainties. The future atmospheric concentrations of the major GHGs CO_2, CH_4, and N_2O are uncertain, especially beyond the middle of this century. N_2O itself is the source of stratospheric odd nitrogen, which can cause ozone loss (Table 1). Ravishankara et al. [21] argued that in the future, as halocarbons are now declining, N_2O will be the major anthropogenic ODS. To research these issues of chemistry–climate interactions, and to quantify these impacts, will require the development of detailed Chemistry-Climate Models (CCMs). CCMs are essentially versions of climate models with detailed interactive chemistry. In the future, these models will become part of larger Earth System Models (ESMs), with coupled oceans, cryosphere, vegetation, and so on.

The Montreal Protocol has controlled the major anthropogenic sources of chlorine and bromine which reach the stratosphere. However, a current research area concerns natural sources of similar halogen species. There is clear evidence that around 6 parts per trillion (pptv) of the current stratospheric bromine loading of 21 pptv comes from sources other than CH_3Br and the halons [22]. The species responsible are the so-called very short-lived species (VSLS) such as bromoform ($CHBr_3$) and dibromomethane (CH_2Br_2). Although these species have atmospheric lifetimes of around 6 months or less, they can still be transported to the stratosphere [23]. These species are emitted naturally from the oceans and it is possible that future climate change will increase these emissions. This natural source of halogens offsets some of the reduction in anthropogenic halogens and leads to lower levels of stratospheric ozone.

There is currently a large debate on the possibilities of avoiding climate change by human manipulation of the climate system, so-called geoengineering. Among the various potential geoengineering solutions that have been proposed, one relates directly to the stratosphere. Scientists have suggested that humans could replicate the effect of a large volcanic eruption which injects sulfate aerosol directly into the stratosphere [24]. The most recent such large natural eruption was Mt Pinatubo in the Philippines in June 1991. The impact of enhanced stratospheric aerosol is to cool the surface – the desired effect from a geoengineering point of view. However, while atmospheric chlorine loadings remain high, enhanced stratospheric aerosol will lead to ozone destruction. The eruption of Mt Pinatubo led to a 1–2% reduction in column ozone globally see (2). As halogens decline in the future the impact of aerosol on ozone will be less, as shown by simulations for the period of the large El Chichon eruption in 1982, well before the peak in atmospheric chlorine and bromine [14]. The potential side effects of such geoengineering options need to be fully investigated and quantified with detailed chemistry-climate models.

Bibliography

Primary Literature

1. Chapman S (1930) A theory of upper-atmosphere ozone. Mem R Meteorol Soc 3:103
2. Crutzen PJ (1970) The influence of nitrogen oxide on the atmospheric ozone content. Q J R Meteorol Soc 96:320
3. Johnston HS (1971) Reduction of stratospheric ozone by nitrogen oxide catalysts from supersonic transport exhaust. Science 173:517
4. Stolarski RS, Cicerone RJ (1974) Stratospheric chlorine: a possible sink for ozone. Can J Chem 52:1610
5. Molina MJ, Rowland FS (1974) Stratospheric sink for chlorofluoromethanes: chlorine atom catalysed destruction of ozone. Nature 249:810–812
6. Farman JC, Gardiner BG, Shanklin JD (1985) Large losses of total ozone in Antarctica reveal seasonal ClOx/NOx interaction. Nature 315:207–210
7. Anderson JG, Brune WH, Proffitt MH (1989) Ozone destruction by chlorine radicals within the Antarctic vortex: the spatial and temporal evolution of ClO-O_3 anitcorrelation based on in situ ER-2 data. J Geophys Res 94:11480–11520
8. Molina LT, Molina MJ (1987) Production of Cl_2O_2 by the self reaction of the ClO radical. J Phys Chem 91:433–436
9. Solomon S, Garcia RR, Rowland FS, Wuebbles D (1986) On the depletion of Antarctic ozone. Nature 321:755–758

10. Chipperfield MP (2006) New version of the TOMCAT/SLIMCAT off-line chemical transport model: intercomparison of stratospheric tracer experiments. Q J R Meteorol Soc 132:1179–1203. doi:10.1256/qj.05.51
11. Rex M, Salawitch RJ, von der Gathen P, Harris NRP, Chipperfield MP, Naujokat B (2004) Arctic ozone loss and climate change. Geophys Res Lett 31:L04116. doi:10.1029/2003GL018844
12. Chipperfield MP, Fioletov V (Lead Authors) (2007) Global Ozone. In: Ennis CA (ed) Scientific assessment of ozone depletion, 2006: pursuant to Article 6 of Montreal Protocol on Substances that Deplete the Ozone Layer, Chap 3. Global Ozone Research and Monitoring Project – Report No. 50. World Meteorological Organization, Geneva, p 572
13. Chipperfield MP (1999) Multiannual simulations with a three-dimensional chemical transport model. J Geophys Res 104:1781–1805
14. Tie XX, Brasseur GP (1995) The response of stratospheric ozone to volcanic eruptions: sensitivity to atmospheric chlorine loading. Geophys Res Lett 22:3035–3038
15. Fahey DW (Lead Author) (2007) Twenty questions and answers about the ozone layer: 2006 Update. Scientific assessment of Ozone Depletion: 2006. World Meteorological Organization, Geneva, p 50
16. United Nations Environment Program (UNEP) (1998) Environmental effects of ozone depletion: 1998 assessment. J Photochem Photobiol B Biol 46:1–4
17. IPCC, Solomon S, Qin D, Manning M, Chen Z, Marquis M, Averyt KB, Tignor M, Miller HL (eds) (2007) Climate change 2007: the physical science basis: contribution of Working Group I to the Fourth Assessment Report of the Intergovernmental Panel on Climate Change. Cambridge University Press, Cambridge/New York, p 996
18. Velders GJM, Andersen SO, Daniel JS, Fahey DW, McFarland M (2007) The importance of the Montreal protocol in protecting climate. PNAS. doi:10.1073/pnas.0610328104
19. Butchart N, Scaife AA, Bourqui M, de Grandpré J, Hare SHE, Kettleborough J, Langematz U, Manzini E, Sassi F, Shibata K, Shindell D, Sigmond M (2006) Simulations of anthropogenic change in the strength of the Brewer-Dobson circulation. Climate Dyn 27:727–741
20. Eyring V, Cionni I, Bodeker GE, Charlton-Perez AJ, Kinnison DE, Scinocca JF, Waugh DW, Akiyoshi H, Bekki S, Chipperfield MP, Dameris M, Dhomse S, Frith SM, Garny H, Gettelman A, Kubin A, Langematz U, Mancini E, Marchand M, Nakamura T, Oman LD, Pawson S, Pitari G, Plummer DA, Rozanov E, Shepherd TG, Shibata K, Tian W, Braesicke P, Hardiman SC, Lamarque JF, Morgenstern O, Smale D, Pyle JA, Yamashita Y (2010) Multi-model assessment of stratospheric ozone return dates and ozone recovery in CCMVal-2 models. Atmos Chem Phys 10:9451–9472. doi:10.5194/acp-10-9451-2010
21. Ravishankara AR, Daniel JS, Portmann RW (2009) Nitrous oxide (N_2O): the dominant ozone-depleting substance emitted in the 21st century. Science 326:123–125. doi:10.1126/science.1176985
22. Dorf M, Butz A, Camy-Peyret C, Chipperfield MP, Kritten L, Pfeilsticker K (2008) Bromine in the tropical troposphere and stratosphere as derived from balloon-borne BrO observations. Atmos Chem Phys 8:7265–7271
23. Hossaini R, Chipperfield MP, Monge-Sanz BM, Richards NAD, Atlas E, Blake DR (2010) Bromoform and dibromomethane in the tropics: a 3D model study of chemistry and transport. Atmos Chem Phys 10:719–735
24. Tilmes S, Müller R, Salawitch R (2008) The sensitivity of polar ozone depletion to proposed geoengineering schemes. Science 320:1201–1204

Books and Reviews

Anderson SO, Sarma KM (2002) Protecting the ozone layer. Earthscan, London

Brasseur GP, Orlando JJ, Tyndall GS (1999) Atmospheric chemistry and global change. Oxford University Press, New York

Brasseur GP, Solomon S (1986) Aeronomy of the middle atmosphere: chemistry and physics of the stratosphere and mesosphere, 2nd edn. D. Reidel, Dordrecht

Jacobson MZ (2002) Atmospheric pollution: history, science, and regulation. Cambridge University Press, Cambridge

Wayne RP (2000) Chemistry of atmospheres, 3rd edn. Oxford University Press, Oxford

WMO (World Meteorological Organization) (2007) Scientific assessment of ozone depletion: 2006, Global Ozone Research and Monitoring Project – Report No. 50. World Meteorological Organization, Geneva, p 572

Subsurface Fate and Transport of Chemicals

Frank T. Barranco, Jr., Samantha L. Saalfield, Frederick J. Tenbus, Brian P. Shedd
EA Engineering, Science, and Technology, Inc., Sparks, MD, USA

Article Outline

Glossary
Definition of the Subject and Its Importance
Introduction
Sustainable Remediation Practices for Classes of Typical Subsurface Contaminants
Future Directions
Bibliography

Glossary

Abiotic Not relating to life, as in abiotic chemical reactions that occur independent of living organisms.

Absorption Retention of a chemical within a solid material.

Adsorption Adhesion of a chemical to the surface of a solid.

Advection Transport of a solute within a fluid in the direction of the bulk fluid's flow.

Aerobic Requiring oxygen.

Air sparging Injecting air or oxygen into an aquifer.

Aliphatic Organic compounds not containing an aromatic ring.

Anaerobic Without oxygen.

Best management practice (BMP) Techniques generally accepted as effective for achieving a particular goal, for example minimizing the environmental impact of remediation.

Biodegradation Use of living organisms to clean up contaminated environmental media.

Biotic Relating to life, as in a biotic reaction mediated by living organisms.

Bioventing The addition of air (or oxygen) under, at times, an induced lowering of water table to promote aerobic biodegradation of subsurface contaminants in the unsaturated zone.

Catalytic oxidizer Remediation technology equipment that uses a catalyst to accelerate the chemical oxidation of hydrocarbons with oxygen in a vapor effluent stream.

Chemisorption Adhesion of a chemical to the surface of a solid, specifically through a chemical reaction occurring at the surface.

Confined aquifer A water-bearing geologic strata that is situated between impermeable layers (clays and silt layers), leading to higher pressure of the groundwater in this unit.

Extraction well A well used to remove liquid or gas from the subsurface.

Fate and transport Encompasses how contaminants move through environmental media and how long the contaminants persist or how fast they are degraded.

Feasibility study A document that describes and analyzes potential cleanup alternatives for a site and recommends selection of an effective and efficient alternative.

Green and sustainable remediation Environmental cleanup that is designed and performed with consideration of the environmental impacts of the technologies used.

Half-life Time required for half of the molecules of a chemical to decay or be degraded.

Henry's law Law that is used to describe the volatility of a chemical, by describing the equilibrium between the vapor phase and dissolved forms of the chemical.

Hydrocarbons Chemical compounds that consist of carbon and hydrogen.

Hydrodynamic dispersion Transport within a fluid in directions other than the primary direction of fluid flow. This process decreases contaminant concentrations while increasing the total volume of fluid contaminated.

Hydrodynamics The process of the motion of groundwater.

Hydrogeology Discipline dealing with the properties and characteristics of groundwater.

Hydrolysis Reaction that splits a chemical into two parts by adding a water molecule, through addition of a hydrogen ion to one fragment of the chemical and addition of a hydroxyl group to the other fragment.

Hydrophobic Having an aversion to water. Typically describes a contaminant that associates with nonpolar substances (such as oils and organic matter) rather than polar substances like water.

Injection well A well used for injection of fluids, gases, and/or chemicals for remediation.

Inorganic Describes chemicals that are not organic, including metals and common anions (sulfate, nitrate, etc.).

Interfacial tension Tension at the interface between a liquid of one chemical and a solid, liquid, or gas of another chemical. One of the primary determinants of NAPL mobility in the subsurface.

Interim remedial action A remedial action taken to address immediate risks to human health or the environment before long-term remedial goals are achieved.

Leaching Dissolution of relatively soluble chemicals and removal by water transport.

Life cycle analysis (LCA) Evaluation of the environmental impacts of all stages of a product or process.

Light nonaqueous phase liquid (LNAPL) A nonaqueous phase liquid that is less dense than water and therefore floats on the water table, including petroleum hydrocarbon fuels and lubricating oils.

Liquid density Mass per unit volume of a liquid.

Liquid viscosity Resistance of a liquid to being deformed. Higher viscosity is associated with more resistance to flow, or less fluidity.

Lower explosive limit The concentration of a compound in air below which it will not ignite.

Microaerophilic Requiring only small amounts of oxygen.

Monoaromatic hydrocarbons (MAHs) Organic chemicals containing one aromatic ring, which are common petroleum derivatives.

Nonaqueous phase liquid (NAPL) A liquid, such as oil, that remains in a separate phase in the groundwater and can act as a source of organic contaminants to groundwater and soil.

Organic Describes a category of chemicals that typically contain carbon with hydrogen, oxygen, and/or nitrogen. Most organic compounds can be degraded to carbon dioxide, water, and other simple components.

Oxidation Chemical reaction in which a chemical of interest loses electrons. The chemical that takes the electrons is known as the *oxidant*. Includes "rusting" of metals and processes that degrade organic matter to carbon dioxide.

Partitioning Distribution of a chemical between the solid, fluid, and/or gas phases, in proportions reflecting its affinity for each phase, as described by the *partition coefficient*.

Permeability Tendency of a material to allow fluids to flow through it.

Persistent organic pollutants (POPs) Chemicals that do not readily degrade under environmental conditions and, therefore, persist in environmental media.

Polychlorinated biphenyls (PCBs) Organic chemicals with chlorine atoms attached to two benzene (aromatic) rings, which were widely used as dielectric and coolant fluids, for example in transformers.

Polycyclic aromatic hydrocarbons (PAHs) Organic chemicals containing more than one aromatic ring, which are common by-products of coal combustion.

Porosity Fraction of a material that is void space. Can be primary (original, from when the geological material was formed) or secondary (formed later, by selective dissolution or fracturing).

Precipitation Formation of a solid from dissolved chemicals in a solution.

Preferential flow Faster movement of groundwater through certain, more porous or permeable, portions of the subsurface, which can result in localized, rapid contaminant transport.

Redox Term used to describe the related processes of reduction and oxidation.

Reduction Chemical reaction in which electrons are gained by a chemical of interest. The chemical donating the electrons is known as the *reductant*. Includes the reduction of oxygen gas during aerobic respiration and the reduction of other chemicals (nitrate, iron, carbon dioxide) during anaerobic respiration.

Remedial action Action taken to remove or contain a hazardous substance in the environment.

Remediation Cleanup or other methods used to remove or contain hazardous materials.

Risk assessment Qualitative and quantitative evaluation of the risk posed to human health and/or the environment by contaminants.

Saturated zone The portion of the subsurface below the water table, where the pressure of water within the pores is at a pressure equal to or greater than atmospheric pressure.

Solubility Ability of a chemical to dissolve into (i.e., mix with and become incorporated into) another substance. Unless otherwise specified, in an environmental context, solubility is typically used to refer to solubility of a chemical in water.

Sorption (verb: to sorb) Attachment of a chemical to a solid, which removes the chemical from the dissolved phase. See also adsorption, absorption, and chemisorptions.

Speciation The chemical form (phase, redox state, molecular structure) in which an element exists. Important determinant of metal mobility in the environment.

Subsurface The zone beneath the surface of the earth, including geologic strata and groundwater.

Transport mechanisms Processes by which contaminants move through the environment.

Unsaturated/vadose zone The subsurface zone between land surface and the water table where the moisture content is less than atmospheric pressure (i.e., soil pores are not completely filled with water).

Vapor pressure Pressure of the vapor of a chemical that exists in equilibrium with the chemical's solid or liquid phase.

Volatility Tendency of a chemical to vaporize, or go into the gaseous phase.

Definition of the Subject and Its Importance

Since the onset of subsurface remediation in the 1970s, there has been a need for a more appropriate balance between the protectiveness of environmental cleanup technologies and the concept of environmental sustainability. This entry explores the implementation of innovative green and sustainable practices deemed appropriate for the remedial technologies that address the most common classes of persistent and toxic subsurface contaminants.

Introduction

Preceding and during the early timeframe of environmental remediation, there was a lack of concern and knowledge about the fate and persistence of chemicals released to the subsurface. There was a prevailing but unfounded assumption that the subsurface environment would sorb or attenuate almost unlimited amounts of contaminants. Much to our dismay, this has been shown to be false through major advancements in analytical chemistry techniques over the last 2 decades. Once subsurface transport mechanisms were understood, it became obvious that contaminants released at or near the surface may make their way deep into subsurface environments, including confined aquifers and bedrock settings. The fate and transport of environmental contaminants in subsurface environments are significantly affected by two categories of properties (Table 1): (1) the geologic characteristics of the subsurface environment, which defines the intrinsic properties of the soil (or rock) and imparts the characteristics of groundwater flow through that media, and (2) the properties of the contaminants, which define the physicochemical and biological processes that affect their fate and persistence.

Subsurface Fate and Transport of Chemicals. Table 1 Summary of properties that affect fate and transport of organic and inorganic contaminants in the subsurface

Contaminant properties	
Organic contaminants	*Inorganic contaminants*
Solubility	Solubility
Fluid density	Redox (reduction-oxidation)
Viscosity	Speciation
Interfacial tension	Adsorption
Carbon partition coefficient	Reactivity
Henry's law constant	Vapor pressure
Biological degradation	
Vapor pressure	
Subsurface/hydrogeologic properties	
Rock type and characteristics	
Hydraulic conductivity	
Aquifer redox chemistry	
Specific surface area of minerals	

The prevailing group of processes affecting subsurface fate and contaminant transport are hydrodynamic processes, partitioning, biotic reactions, and abiotic reactions. Hydrodynamic processes impact contaminant transport through groundwater advection, hydrodynamic dispersion, and potential preferential flow. Partitioning affects contaminant distribution and dispersal by allowing interchange of contaminant from one subsurface medium to another (e.g., soil, groundwater, soil gas) through means of adsorption, absorption, or chemisorption. Biotic reactions can affect contaminant transport by degradation (or immobilization) of the contaminant in oxidation or reduction reactions. More specifically, biotic processes, which occur under aerobic, microaerophilic, or anaerobic conditions, can lead to degradation or immobilization (by reaction or precipitation), depending on the type of contaminant. Abiotic reactions affect

contaminant transport in the subsurface by promoting interactions between the contaminant and groundwater or stationary media (e.g., soil, bedrock), causing the contaminant to degrade or change in form (e.g., hydrolysis, redox reactions). These processes take place within the saturated zone and the unsaturated zone of the subsurface. Of these two subsurface zones, heightened concern is often paid to the saturated zone because contaminants are in direct contact with groundwater, which may be used as a potable or irrigational resource or for other purposes. The unsaturated zone, or vadose zone, overlies the saturated zone (i.e., above the water table) and is an important contributor to contaminant fate and transport through processes such as leaching and migration to the saturated groundwater zone.

Sources of chemicals released to the subsurface are varied, but generally include (1) underground and above ground storage tanks, (2) septic tanks, (3) agricultural activities, (4) municipal and industrial landfills and dumps, (5) regulated and abandoned hazardous waste sites, (6) injection wells, and (7) other industrial sites [1]. The types of chemicals that have been historically released to the subsurface and have the potential to cause adverse effects to human health or the environment are generally divided into organic compounds and inorganic compounds (or inorganic elements). Several of the more common classes of organic and inorganic contaminants found in soil and groundwater are as follows:

- Petroleum hydrocarbons and derivatives used as fuels such as gasoline, diesel fuel, jet fuel, and heating oil. These fuels consist of many organic chemical components, including monoaromatic hydrocarbons (MAHs) like benzene, toluene, ethylbenzene, and xylene (BTEX), and low-molecular-weight polycyclic aromatic hydrocarbons (PAHs), such as naphthalene, and are generally less dense in hydrocarbon fluid form than water, contain components that are highly volatile, and are sparingly to moderately soluble in water. When present as an immiscible phase (in water), they tend to persist over reasonably long time frames as light non-aqueous phase liquids (LNAPLs). However, LNAPL constituents will dissolve in water, sorb onto soils, and/or partition into the vapor phase.
- Chlorinated aliphatic hydrocarbons used as solvents, degreasers, and dry cleaning fluids, such as tetrachloroethylene (PCE), trichloroethylene (TCE), and carbon tetrachloride (CT). These compounds generally are distilled for use in industrial settings in a pure form or as relatively simple mixtures. When present as an immiscible phase, they generally are denser than water, highly volatile, and also sparingly soluble in water. Hence, they can exist as dense non-aqueous phase liquids (DNAPLs), dissolved in water, sorbed onto soils, and/or present in the vapor phase.
- Polychlorinated biphenyls (PCBs), pesticides, wood-preserving chemicals (such as creosote), and fossil fuel combustion/gas manufacturing gas by-products, such as coal tars and high-molecular-weight PAHs. These contaminants tend to be dense, highly viscous fluids (when present an immiscible phase) with constituents that sorb strongly onto soils, are nearly insoluble in water, exhibit low volatility, and are persistent in the subsurface environment because they chemically and biologically degrade very slowly. When present as an immiscible phase, they generally are found as DNAPL or are sorbed onto soils.
- Explosives and energetic compounds such as solid-rocket fuels and propellants, including trinitrotoluene (TNT), plastic explosives, perchlorate, and munitions components. These constituents are often found as solids on or near the land surface, although some (such as perchlorate) can be found dissolved in groundwater.
- Metals such as arsenic, lead, chromium (VI), mercury, cadmium, and others. These generally are found either dissolved in groundwater, present as elements in the solid phase, or present within the rock matrices as mineral components.

Each type of contaminant has a distinct set of physicochemical characteristics that define its behavior and migration within subsurface environments. Hydrogeology and rock/mineral geochemistry also have a significant influence on defining the fate and migration of contaminants. As a function of the contaminant's physicochemical properties and geologic characteristics, the above listed classes of organic chemicals exist in the subsurface as one or more of

four phases: (1) mobile or residually entrapped nonaqueous phase liquid (NAPL), (2) dissolved phase in groundwater, (3) sorbed phase to solid aquifer media, and (4) vapor phase in soil gas. Both the properties of the chemical and that of the subsurface control the dynamic evolution of phase transfer, including the duration of time that these organic chemical remains within these phases following a spill or release. From the point of release, organic chemicals generally exist in the NAPL phase, with eventual partitioning to one or more of the other phases with time. Subsurface NAPLs can exist as a pure chemical or as a bulk mixture of chemicals.

Physical and chemical properties that have a major effect on the fate, transport, and persistence of the classes of typical organic contaminants are shown in Table 2. Properties such as solubility (in water) determine the degree to which a contaminant persists in the subsurface as an immiscible fluid or solid. If an immiscible fluid phase persists in the subsurface, fluid density governs whether the fluid acts as an LNAPL or DNAPL (e.g., petroleum hydrocarbons, with a fluid density less than 1 g/mL, form LNAPLs, whereas chlorinated hydrocarbons form DNAPLs). Properties like organic carbon partition coefficient (K_{oc}) and Henry's law constant effect the tendency of a chemical to partition under equilibrium conditions from a source release (e.g., contaminant liquid or solid) to subsurface media (e.g., soil, groundwater, and/or soil gas). The relatively high Henry's law constants and solubilities of hydrocarbons, for example, indicate that hydrocarbons are more likely to partition into air and groundwater than are PAHs, PCBs, and pesticides.

The half-lives for biological degradation of the contaminants, also shown in Table 2, provide an indication (using first order kinetics) of how quickly a chemical will biologically degrade in the subsurface. Petroleum hydrocarbons and chlorinated hydrocarbons have been observed to degrade under aerobic and anaerobic conditions, respectively, at reaction rates determined to be moderate to fast for both natural and engineered remedial systems. Conversely, PCBs and certain PAHs have been shown to undergo very slow to negligible rates of aerobic and/or anaerobic biodegradation in natural subsurface settings. Explosives and energetic compounds have been shown on a constituent by constituent basis to biologically or chemically degrade (in presence of reductants and oxidants, respectively) under subsurface conditions attainable with the aid of remedial technologies.

The most common inorganic compounds identified in the subsurface include metal contaminants. Although metals are natural constituents of soils, anthropogenic metals enter the soil through a variety

Subsurface Fate and Transport of Chemicals. Table 2 Physicochemical properties of organic contaminants that affect contaminant fate, transport, and persistence (Refs. [2–5])

Class of contaminant	Henry's law constant (atm. m^3/mol)	Solubility (g/L)	Fluid density (g/cm^3)	log K_{oc}	Biodegradation half-life	
					Aerobic	Anaerobic
Chlorinated hydrocarbons	0.00674–0.015	0.15–6.3	1.2–1.6	0.4–2.4	4 weeks–1 year	11 weeks–4.5 years
Petroleum hydrocarbons	0.00046–0.015	0.03–200	0.86–0.88	1.5–3.6	2 days–6 months	8 days–2 years
Heavy PAHs	Minimal–0.0003	0.0000003–0.004	NA (solid)	1.3–7.5	12 days–5.2 years	50 days–21 years
PCBs	0.000003–750	0.00001–0.002	1.182–1.566	2.4–6.4	1.5–9 years	–
Pesticides	0.0000002–0.002	0.0000004–0.5	NA (solid)	2.1–6.3	2 days–16 years	1–294 days
Explosives/energetics	Minimal–0.00000002	0.13–250	NA (solid)	NA	4 weeks–6 months (TNT)	4 weeks–6 months (TNT)

NA not applicable

of means including (1) leaching of municipal or industrial solid wastes, (2) storm water runoff and infiltration, (3) industrial by-products, (4) dredged materials, (5) mining and smelting operations, (6) atmospheric emissions from coal or oil combustion, (7) ash and slag from coal or oil combustion, (8) and sludge residues from wastewater treatment. Typical metals identified as contaminants in subsurface environments include arsenic, chromium, cadmium, copper, lead, mercury, nickel, silver, and zinc. Radionuclides are a separate class of contaminants that are inorganic and due to their specificity are not discussed in this entry.

The physicochemical properties of inorganic chemicals that govern their fate, partitioning, and migration within subsurface environments include solubility, reduction–oxidation (redox) speciation, reactivity, and vapor pressure. Properties of subsurface media that play a defining role in the fate of inorganic contaminants within subsurface environments include rock type and characteristics (primary and secondary porosity, mineral composition, fracture density), hydraulic conductivity, redox chemistry, and specific surface area of minerals present. Metals are not degraded by biological or chemical reactions, though they can conveniently be rendered unavailable through precipitation reactions or transformed via oxidation/reduction reactions to less toxic species.

Properties of subsurface media that play a defining role in the fate, partitioning, and transport of organic contaminants within subsurface environments include rock type (i.e., porous or fracture flow), primary and secondary porosity, hydraulic conductivity, and total organic carbon.

Background

Beginning in the 1970s with the advent of subsurface remediation, the environmental industry invested heavily in remediation systems without an adequate understanding of the degree of contaminant cleanup (or the duration of the cleanup). Although these early efforts were well intended, the actions taken with the technologies utilized were not justified based on the costs of the cleanups, the overutilization of resources, the intensive amount of energy consumed, and the insufficient contaminant removal. Past presumptive remedies such as soil "excavation and off-site disposal" and groundwater "pump and treat" are prime examples of these generally wasteful remedies considered unsustainable onto the future.

Beyond this early misunderstanding about remedial technology selection to achieve efficient and sustained removal of subsurface contaminants, there has been a long-standing misperception that cleanup shall continue to pristine conditions, a goal that as turns out is largely unattainable in most circumstances. At the expense of nearly 2 decades of numerous examples of unsuccessful and costly cleanups, we have learned considerably from these early mistakes. Today, in many cases, there is a robust process and a wealth of regulatory guidance to determine more pragmatic yet adequate remedial action objectives and cleanup performance criteria. These cleanup goals and objectives are most often defined by human health risk assessment [6], ecological risk assessment [7], risk-based corrective action [8, 9], or by what is reasonably achievable based on the best practicable remedial technology options (generally referred to as best available technology [BAT]).

In addition to these well-considered approaches that have provided a practicable risk-related basis for cleanup end goals, there is growing interest in the last 5 years to incorporate green and sustainable remediation (GSR) concepts throughout the remedial action process, while continuing to provide acceptable long-term protection of human health and the environment. As suggested by the Sustainable Remediation Forum (SURF), sustainable remediation is defined as a "remedy or combination of remedies whose net benefit on human health and the environment is maximized through the judicious use of limited resources" [10]. To this end, sustainable remediation employs solutions that minimize the environmental footprint while providing maximum net environmental benefit over the remedial lifecycle. To realize the benefits of sustainable remediation requires the use of green and/or renewable energy sources, conservation of water and energy, decreasing waste, and formulating integrated sustainability policies. With sustainable remediation, the goal should be to (1) develop and implement safe remedial solutions that are minimally disruptive to the environment, (2) realize energy savings through creative design and value engineering, (3) embrace waste minimization and recycling concepts, and (4) emit the

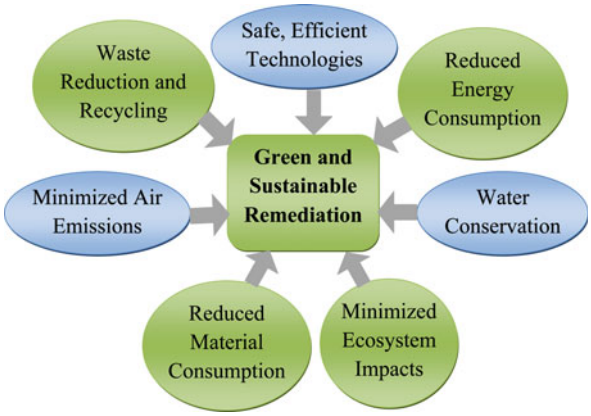

Subsurface Fate and Transport of Chemicals. Figure 1 Key elements of green and sustainable remediation

least amount of pollutants and greenhouse gases to the atmosphere. To the extent practical, the following sustainability elements should be applied to remedial solutions incorporating GSR practices (Fig. 1): (1) short-and long-term energy and water consumption, (2) greenhouse gas emissions and air pollutants, (3) ecosystem impacts, (4) material consumption, and (5) waste minimization and/or recycling.

The recent recognition of the balance between adequacy of cleanup and sustainability concepts has not, in some cases, dispelled the notion of initiating cleanups with little thought to the protective character (human health and environmental), resource utilization, or safety of the action. As evidenced by the continued use of pump and treat systems, there are still regulatory mandates for cleanup with little decrease in contaminant mass (and therefore little decrease in overall risk). There are, in fact, examples of sites where natural attenuation is actively decreasing contaminant concentrations in the subsurface, yet the overseeing regulatory agencies require a more traditional, less sustainably oriented, significantly more costly approach because of outdated or arbitrary remediation goals set for the site. Clearly a new paradigm is warranted, whereby cleanup protectiveness of a remedy is balanced with sustainability elements. The analysis to establish this balance should be evaluated early in remedial planning, such as during a feasibility study of remedial alternatives. Incorporation of sustainability into the balancing criteria evaluated during a feasibility study would help to assure that this process happens. In the interim, many professionals in the environmental industry have been documenting sustainability metrics by qualitatively and/or quantitatively scoring the degree of sustainability core elements to be utilized on cleanup actions. Such evaluations have ranged from simple qualitative review of the available list of best management practices (BMPs), utilizing those that are applicable, to the performance of quantitative and complex life cycle analysis (LCAs) for optimization of the cleanup over the remedial lifetime. The following section provides valuable information on industry lessons learned from implemented LCAs and BMPs for sustainable remediation practices, as applied to the typical classes of subsurface contaminants described in this document.

Sustainable Remediation Practices for Classes of Typical Subsurface Contaminants

Remediation sites comprise a range of sizes, proximity to human and/or ecological receptors, proximity to man-made infrastructure, site accessibility, environmental complexity, type of contaminants and their chemical, physical, and toxicity characteristics, complexity of the circumstances surrounding the release (s), and so on. All of these factors affect the feasibility of corrective actions, and even the ability to implement any corrective action. Because of this, no generalized discussion of sustainable remediation practices can be complete, because the topic is simply too broad. However, the information described below, is comprised of remedial measures applied recently that can be characterized as sustainable practices.

With this in mind, this chapter will focus on sustainable practices honed over time for the general classes of subsurface contaminants discussed above. The discussions are premised on the following assumptions:

- Releases to the subsurface have stopped; i.e., that the pipelines have been repaired, the underground storage tanks have been removed, the uncontrolled landfill is no longer receiving toxic materials and has been capped, etc.
- Any discussion of "sources," with regard to groundwater, refers to concentrated areas of contaminants such as NAPL or highly contaminated soils that are present but relatively stable.

- A risk assessment has been completed (if necessary), and remedial action objectives have been defined before remedial implementation.
- Emergency or interim measures (e.g., protection or replacement of domestic water supplies affected by the release) are in place as needed.
- Site characterization has progressed to a point where remediation methods can be considered within a feasibility study (FS) or a focused feasibility study (FFS).
- Remedial systems are designed to destroy (or remove) contaminants with the knowledge and benefit of exploiting the physical and/or chemical characteristics of the contaminants.
- Sustainable measures for the contaminants discussed have been optimized over time as a result of trial and error evaluation with full-scale remedial systems and technology innovation or breakthroughs.

These discussions readily address the lessons learned and resulting sustainable optimizations (or BMPs) of various technologies for typical contaminants.

Petroleum Hydrocarbons

Petroleum hydrocarbons, including MAHs and low-molecular-weight PAHs, often occur in persistent LNAPLs in the subsurface. Therefore, the primary method of remediation historically has relied on product recovery within a cone of depression produced by water table drawdown from groundwater pumping.

As a result of energy inefficiencies and high cost of groundwater extraction (and treatment), a more sustainable approach evolved involving product recovery with skimmer pumps. Skimmer pumps are designed to remove LNAPL from the water table surface. The skimmer floats on the water table and has an interval with a hydrophobic (water-rejecting) screen that is open to the LNAPL layer within a monitoring well. LNAPL is drawn into the skimmer and flows through a flexible tube to a reservoir where it is pumped to the surface. The following practices are often employed with product recovery systems to reduce energy consumption, minimize site impacts, and improve the overall sustainability of the treatment [11]:

- Power product recovery components or auxiliary equipment with low energy demand, such as renewable energy off-grid wind turbines or photovoltaic (PV) systems.
- Such systems relying on off-grid energy should be equipped with deep-cycle batteries to provide steady power.
- Eliminate the long-distance transport of incoming materials and equipment or outgoing remedial-derived wastes (i.e., recovered product). To that end, consolidate deliveries/pickups to avoid deploying partially filled vehicles.
- Recycle separated product (LNAPL) through local fuel or waste recyclers.
- Optimize product recovery through proper equipment sizing and frequent reassessment based on treatment performance.
- Establish operating or cleanup performance criteria that could trigger use of less intensive polishing technologies as cleanup progresses and LNAPL recovery rates decline.

Skimmer pumps are capable of removing LNAPL down to a sheen, but do not reduce dissolved contaminant concentrations or the mass of contaminants sorbed onto soil. In addition, skimmer pumps, unless supplemented with vacuum enhancements, generally are not capable of providing complete capture of a mobile accumulation of free-phase LNAPL that is migrating under natural subsurface conditions. In such cases, groundwater extraction is sparingly used to capture and contain the mobile, free-phase LNAPL for recovery. The following sustainable practices are often employed to minimize groundwater extraction while optimizing LNAPL capture:

- Perform groundwater capture zone analyses using empirical calculations or numerical groundwater modeling as basis of design for groundwater capture and, therefore, LNAPL containment.
- Calibrate and refine groundwater extraction network and flow rates with calculations or modeling after system startup with observed drawdown conditions from corrected groundwater elevations.
- Monitor and periodically optimize the groundwater extraction network and flow rates to maximize LNAPL recovery rates as a result of higher producing wells.
- Monitor extraction well change in head at a given rate over time, or specific capacity, to ensure

continued efficient well operation. Rehabilitate wells periodically, if decreased specific capacity is observed, to maximize extraction well longevity.

- Design system to minimize the total amount of piping including length, surface area, bends, and elbows to maximize transport efficiency.
- Engineer extraction wells to maximize efficiency through decreased head loss and optimized flow rates by designing the well gravel pack to match the formation and using the largest feasible slot size to maximize open cross-sectional area. This decreases velocity and prevents migration of fines by allowing a less-turbulent flow into the well.

Sustainable features of skimmer pumps are that they require little energy to operate, and the energy can be obtained from sustainable sources such as solar panels (Fig. 2). Recovered LNAPL can be recycled to minimize waste. The method is relatively slow and inefficient for LNAPL removal, but it can be effective at small sites. Skimmer systems can be enhanced by applying a vacuum, which can speed up LNAPL recovery for a relatively minor additional energy input that could also be obtained from sustainable power sources. The use of skimmer pumps generally does not exacerbate existing subsurface conditions or make additional remediation efforts more difficult or less effective.

Soil vapor extraction (SVE) can be effective at removal of volatile organic compounds (VOCs) of petroleum hydrocarbons within the unsaturated zone of the subsurface present as LNAPL, sorbed to contaminated soil, or in the vapor phase. One or more SVE wells (screened in the unsaturated zone above the water table) are constructed, and a vacuum system is installed and manifolded to the wells. The vacuum draws the soil air (which is contaminated with VOCs) out of the subsurface through a treatment system (described below). The contaminated vapors are replaced by fresh air from vent wells or from other parts of the subsurface. This allows the volatile fraction of the VOC to evaporate at a rate that is proportional to the Henry's law coefficient. These volatiles are then carried by the air into the SVE system, allowing for further evaporation into the fresher soil air, and so on.

SVE systems are efficient for VOC removal in the unsaturated zone primarily because volatiles preferentially partition into the vapor phase, and air is relatively easy to move in the subsurface compared to liquids. SVE systems tend to lose efficiency with age as the

Subsurface Fate and Transport of Chemicals. Figure 2
Example of solar powered system with photovoltaic panels for powering product skimming

volatile fractions of the contaminants are removed and the less volatile fractions remain. Because not all of the components of refined petroleum hydrocarbons are volatile, SVE by itself cannot achieve complete subsurface remediation. In addition, SVE does not affect contaminants below the water table, because they are not in contact with the soil air. However, certain adaptations can be made to an SVE system to facilitate contaminant removal from the subsurface. Examples of these adaptations include artificially lowering the water table to expose more soil contaminants to the air or forcing air into the aquifer below the water table to strip out the dissolved or sorbed volatile compounds in the saturated zone through a process known as air sparging.

Nearly all SVE systems require treatment of the vapors removed from the subsurface soil. The most efficient treatment depends on the contaminant concentrations within the vapor stream. Essentially, low concentrations are most cost effectively removed using a sorption medium such as granular activated carbon (GAC), which is a specific type of charcoal. GAC requires no energy input to remove organic compounds from soil vapors while deployed on an SVE system. Because GAC is an absorbent material, however, it does not destroy contaminants, but transfers them to another medium. Once most of the sorption sites are filled and "breakthrough" (i.e., contaminants are no longer captured by the absorbent material) occurs, GAC must be regenerated off-site (requiring energy) or replaced with virgin material (also requiring energy). The virgin material commonly used to manufacture GAC is coconut shells, which are a sustainable resource.

If vapor concentrations are too high, breakthrough will occur quickly and GAC change-out costs can become prohibitive. Above certain concentration threshold, however, a treatment method that uses a catalytic oxidizer may become the most appropriate choice. Catalytic oxidizers are energy intensive because their optimal performance occurs at a relatively high temperature (300–600°C). However, the oxidation of fuel components at sufficient concentrations releases heat that is used to maintain the optimal temperature, greatly increasing efficiency and decreasing or eliminating the need for external energy inputs. As a result, the sustainability of the remediation system is enhanced.

For very high concentrations of VOCs that approach or exceed the lower explosive limit of the vapors, high temperature oxidation of the fuel components can be used to actually run the SVE system in whole or in part. The technology uses an internal combustion engine powered by the extracted vapors and an auxiliary fuel source such as propane if needed. Under the right conditions, such a system requires no external power supply, and if a generator module is added, the system can supply power that can be used to operate lights or other electrical equipment onsite. Off-gas emissions from these units are equivalent to those from operating an automobile engine.

If properly used, SVE does not generally exacerbate existing subsurface conditions or make additional remediation efforts more difficult or less effective. If improperly vented, however, the negative pressure generated by the SVE can cause mounding of the water table that creates a hydraulic gradient capable of spreading LNAPL away from the vapor extraction well(s), possibly increasing the lateral extent of the contaminated area.

Most SVE systems have esthetic impacts that reduce their green characteristics. One undesirable aspect is that they tend to be noisy. This can be mitigated by methods such as surrounding the SVE unit with fences lined with commercially available sound-insulating blankets. Another undesirable aspect is that the systems have a visual impact. They typically are not large, with a footprint on the order of 10 m^2 or less and a height less than 3 m, but they have an "industrial" look about them. This could be mitigated with appropriate landscaping that could include components like fencing with small trees, shrubs, or even large potted plants. Typically, SVE systems are operated almost constantly for a period of approximately 2–3 years, so the esthetic impacts can be a substantial nuisance to nearby workers, passers-by, or residents. The following BMPs are examples of ways to promote a more sustainable SVE approach:

- Optimize extraction configuration and rates by manifolding several vapor points and periodically manipulating valves to minimize "dead zones" and reduce remediation timeframe, energy consumption, and noise.
- Utilize appropriate vapor treatment with GAC by vapor concentration (low concentrations – energy

efficient; low concentrations result in infrequent change out; cat-ox for intermediate to high concentrations – appropriate concentrations improve oxidation efficiency; thermal oxidation for very high concentrations – can utilize contaminant vapors as a fuel source).

Multiphase extraction combines a pump system to remove LNAPL and contaminated groundwater along with SVE to remove soil vapors. The pump system has the effect of lowering the water table, creating a gradient for the LNAPL to migrate toward the extraction well while it removes contaminated water and LNAPL. This effect also exposes more of the subsurface to the soil air, enabling SVE to act on a larger volume of subsurface material.

If the water table is relatively shallow (less than about 8 m below land surface), removal of all three contaminant phases can be accomplished from the surface by applying SVE within the unsaturated zone along with suction to a downhole drop tube with its end located at or slightly below the oil–water interface. At the surface, the oil and water are separated. The oil can then be recycled (or used to power the internal combustion engine if appropriate), and the water gets treated and released back into the environment (Fig. 3).

Multiphase extraction can be energy intensive, but as with SVE, green and sustainable options exist. For example, the power to operate the system can sometimes be obtained from the petroleum hydrocarbon vapors and/or the LNAPL, considerably reducing or possibly eliminating the need for external power

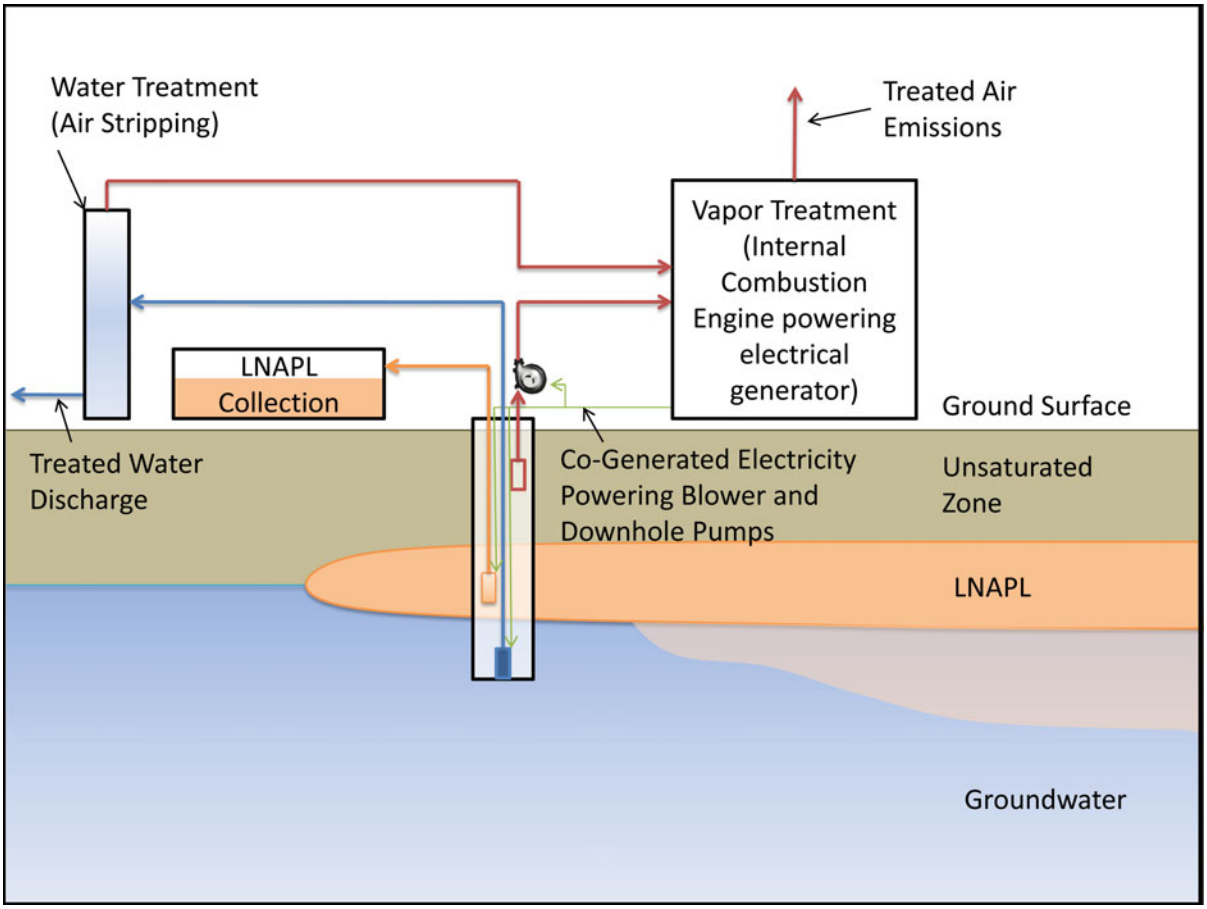

Subsurface Fate and Transport of Chemicals. Figure 3
Concept-level remedial strategy for green and sustainable multiphase NAPL recovery

sources. Multiphase extraction generally is fast and effective, reducing overall energy use along with reducing long-term esthetic impacts from noise and infrastructure. It can be deployed quickly as all or part of an interim remedial action to mitigate urgent cleanup requirements and reduce the need for additional remedial actions that may be less sustainable. Even if it is not effective at a site, multiphase extraction generally does not exacerbate existing conditions or make additional remediation efforts more difficult or less effective. As with SVE, visual and noise impacts from the extraction system can represent an esthetic nuisance, but can be mitigated in a similar fashion with appropriate landscaping and noise dampening components. Although groundwater pumping (and treatment) is included in multiphase extraction for the purpose of exposing subsurface soil to unsaturated conditions, many of the pitfalls (e.g., energy-intensive systems, low dissolved phase contaminant removal, and high treatment cost) described earlier in this entry for pump and treat systems would also apply here. Therefore, caution is warranted when employing groundwater extraction and treatment for multiphase recovery or for product recovery. The following BMPs are offered to provide a sustainable approach to groundwater extraction and treatment with multiphase extraction systems:

- System design should consider modular treatment components that can be removed or added as needed.
- Variable frequency drive pumps can be used to optimize performance and reduce energy usage.
- Use of gravity flow where feasible to reduce the need for transfer pumps.
- System operation should have optimized extraction network to minimize pumping of clean water.
- Use of energy efficient equipment and green energy from alternative energy providers.
- Regenerate GAC onsite; recycle process residuals.

Monitored natural attenuation (MNA) is a highly sustainable remediation method that can be used for releases of petroleum hydrocarbon fuels, distillates, or contamination from other organic compounds. The method utilizes naturally occurring processes such as biodegradation to reduce contaminant mass and concentrations that are dissolved in groundwater, present as LNAPL, or sorbed to the soil. Biodegradation generally destroys most of the components of refined petroleum hydrocarbons, producing innocuous byproducts such as carbon dioxide and water. As a result, MNA requires little to no external energy input and generates minimal waste.

Biodegradation of petroleum hydrocarbons readily occurs in many environments. Microbes have undergone natural selection for millennia, resulting in microbial communities that have evolved remarkable capabilities to utilize every bit of energy that can be extracted from oil constituents [12]. Biodegradation occurs even in extreme conditions. Fouling of fuel system components in aircraft due to microbial growth in kerosene-based jet fuel was recognized as early as 1956 [13]. For practical purposes, this means that in many (if not most) cases, degradation of refined petroleum hydrocarbons will proceed under natural conditions without external energy inputs.

MNA as the sole remediation method has certain limitations that must be addressed prior to and during implementation. First, it must be demonstrated that adverse impacts to human and ecological receptors are not occurring and are unlikely to occur in the future. Second, sufficient evidence for effective natural attenuation must be shown to exist at a given site. Such evidence can include among other things a demonstrably shrinking or stable dissolved plume, a reduction of dissolved concentrations in groundwater over time, and the use of stable isotopes to determine degradation rates. Third, long-term monitoring is required to ensure that conditions do not develop to change the efficacy of natural attenuation as a remedial action. MNA, in a practical sense, does not diverge from the activities associated with site investigation and monitoring. For this reason, the following BMPs utilized for site investigation are introduced with MNA activities [14]:

- Perform fewer field mobilizations through the use of flexible work plans and real-time field measurements as well as onsite mobile laboratory analyses to determine the next course of action during a single sampling event.
- Utilize small-scale direct push technology drilling equipment for invasive work or monitoring well installation to reduce fuel consumption, reduce drilling time, lower air emissions, lower water

consumption, produce less noise, and minimize site clearing and physical impact.

- Use groundwater low-flow sampling equipment to minimize sampling purge volumes, reduce energy consumption, and reduced derived waste.
- Onsite treatment and recycling of MNA-derived wastes, including site clearing by onsite composting or landscaping and treatment/reuse of extracted groundwater for equipment decontamination.
- Collect the meteorological information (e.g., sun duration, wind direction and velocity) necessary to support the design and installation of off-grid alternative energy for auxiliary power for MNA monitoring.
- Use of solar or wind-powered telemetry systems to remotely transmit logging data directly to project offices.

In a variety of circumstances, MNA is used in conjunction with other methods that may not be sufficient to provide complete remediation of a site by themselves. There is a saying within the remediation industry that "90% of the remedial effort goes into cleaning up the last 10% of contamination." While this is not always true, monitored natural attenuation can provide a means in which the "last 10%" of the contamination does not have to be actively remediated because the final cleanup can be accomplished naturally and sustainably.

Enhanced bioremediation is designed to stimulate contaminant biodegradation by indigenous microbial populations [15]. Petroleum hydrocarbons degrade most rapidly under aerobic (i.e., oxygenated) conditions, although other electron acceptors may be utilized as reactants in biodegradation. Enhanced bioremediation of these compounds involves the injection of amendments to the contaminated subsurface to increase oxygen/electron acceptor concentration in the unsaturated and/or saturated zones. Enhanced bioremediation can supplement monitored natural attenuation in many cases to improve performance and reduce the time needed for complete remediation.

Several sustainable methods for promoting bioremediation by adding oxygen to the subsurface exist. One method used for soil remediation is known as bioventing. Bioventing works by injecting atmospheric air at low rates into the unsaturated subsurface zone to displace oxygen-depleted air, thereby stimulating the growth of aerobic microorganisms and improving biodegradation rates. Generally, the air is injected into the ground through well points screened in the contaminated unsaturated zone using a blower similar to that found on many SVE systems operated at low injection rates. Low air injection rates are important, particularly in populated areas, due to the potential for soil vapor migration into basements or other inhabited spaces. The low injection rates are advantageous for sustainable remediation, as external energy inputs are relatively low and could be supplied by renewable sources. A novel approach for air injection using mechanical windmill power (US Patent No. 6,109,358) represents a potential application of green bioventing technology.

Oxygen addition below the water table for bioremediation purposes can be accomplished through chemical or mechanical means. Proprietary slow-release oxygenating compounds for enhancing aerobic bioremediation are available in several forms, including powder (designed to be mixed with water), solids, and filter bags. Compounds in powder form generally are mixed with water and injected into the subsurface using direct push technology. Compounds in solid form or filter bags are typically suspended within the screened or open interval of monitoring-type wells.

Mechanical means of adding oxygen (for bioremediation or physical air stripping) below the water table usually takes the form of air sparging. Air sparging works by injecting air under pressure through one or more wells completely screened in the saturated zone for the purpose of providing oxygen to the groundwater. The air travels upward through the porous medium, along preferred flow paths that form a dendritic pattern (similar to the branches on a tree), until it reaches the unsaturated zone and becomes exposed to the soil.

Introduction of air in this manner will have two desirable outcomes if it is working well. First, the air will strip out volatile organic compounds from the water and saturated soil, transferring these compounds into the vapor phase where they can be removed through SVE (as needed). Second, the groundwater will pick up oxygen and become more aerobic, stimulating biodegradation. Air flow rate and injection pressure generally define whether physical air stripping (of VOCs) or in-place bioremediation will be the

dominant process. If aerobic bioremediation is promoted through air introduction, the process is referred to as biosparging. The following sustainable BMPs can be applied to various types of bioremediation systems for treatment of petroleum hydrocarbons [15]:

- Maximize use of existing or new wells (to avoid resource overutilization) for addition of reagents that will act as electron acceptors in the biodegradation of petroleum hydrocarbons.
- Design and use of bioremediation recirculation cells allowing multiple passes of oxygenated groundwater through fewer wells.
- If oxygen additive is in liquid form, add to the subsurface via trickling gravity-feed system if high-pressure injections are unnecessary to assure proper distribution.
- If pressurized injection of air is required, evaluate the feasibility of pulsing rather than continuous injection to increase the efficiency of delivery.
- Employ modular, portable units that can be modified or incrementally reduced as needed.
- Employ photovoltaic panels or wind turbines to generate auxiliary power for trailer or for equipment, such as air blowers.

Physical air sparging (for the purposes of stripping and removing VOCs from the saturated zone) does not work at every site. It will not succeed if the dendritic patterns of the upwardly traveling sparge zone form with only a few branches, as contact between the air and the contaminants is essential. The efficacy of air sparging can be determined through relatively simple pilot tests, however.

Air sparging will require energy inputs to run the air pumps for a considerable period of time, depending on the size of the impacted area. The systems generally are run in conjunction with SVE, which is needed for vapor control, so 2–3 years of operation is not uncommon. If run with an SVE system, visual and noise esthetic impacts of air sparging are not substantially increased from an SVE system alone.

Phytoremediation is a remedial technology that uses plants to extract, destroy, and/or contain contaminants in environmental media. Petroleum hydrocarbons can be degraded within the plants or by plant by-products that are excreted into the soil, or volatilized into the atmosphere through transpiration.

To date, one of the most commonly implemented types of phytoremediation of petroleum hydrocarbons in shallow soils is rhizodegradation, or the destruction of contaminants by microbes whose activity is promoted by plant roots. Plants used for rhizodegradation include mulberry, hybrid poplars, grasses, cattails, and rice [16]. Phytodegradation, or destruction of the contaminants within the plant, and phytovolatilization of the contaminants can also be performed by a variety of trees, scrubs, and herbaceous plants.

Trees including poplars, cottonwoods, and willows can also be used to achieve hydraulic control to contain groundwater plumes. Often the same plants are used for both contaminant remediation and containment through hydraulic control. BMPs for phytoremediation include techniques for minimizing the impact of generic site operations, including energy conservation, waste minimization, and use of onsite resources.

The sustainability benefits of phytoremediation technologies include minimal site disturbance, leading to operational and esthetic benefits, and minimal energy inputs. Current technologies are limited in their applications by such factors as plants' limited contaminant tolerance, limited depth of influence of plant roots, and often lengthy remediation timeframes. Ongoing research and pilot studies are focused on developing new and improved methodologies for phytoremediation.

In situ chemical oxidation (also known as ISCO or Chem-Ox) is a method designed to oxidize contaminants using reactions that break apart chemical bonds, completely destroying the petroleum hydrocarbon compounds. The primary delivery method for the chemical oxidants is injecting them in liquid form into the aquifer using direct push methods or permanent injection wells. The method can work quite well at many sites, but like any remediation method, it is not universally applicable. Typical problems include daylighting (chemical oxidants flowing out onto the land surface or other inappropriate places), preferential oxidation of ambient organic carbon not related to contamination, desorbing of petroleum hydrocarbons from the soil into LNAPL form, and poor contact between the oxidant and the contaminants.

The sustainability advantages of ISCO is that it is fast acting, that it destroys contaminants rather than transferring them to another medium, and that it is

injected using small equipment with a resultant small carbon footprint and minimal site disturbance. Direct push methods usually leave a boring with a diameter of 5 cm or less, which is filled in accordance with regulations and finished at the surface with a sod plug, asphalt patch, or other material such that little to no visual evidence of the hole exists. Remedial actions using ISCO are most applicable to small sites and generally are completed after two to six injection events, leaving no long-term esthetic impacts. Some or all of the following BMPs are examples of ways to promote a more sustainable ISCO approach:

- Minimize operational impact by constructing little to no long-term or permanent infrastructure.
- Use of extracted groundwater for onsite mixing of ISCO reagents.
- Use of direct push injections over injection wells if minimal injections are required.
- Reuse existing injection wells if multiple ISCO injection events are necessary.

Excavation and treatment or disposal is a remediation method not commonly associated with a green and sustainable approach. However, in many cases, it can be a direct and verifiable way of removing grossly contaminated material, which can then allow for more sustainable remedial methods to be implemented. Excavation can have many undesirable aspects during and after implementation, including things such as noise, dust, heavy equipment, large trucks, scarred landscapes, and so on. While these things may be necessary, they can be mitigated with proper planning and implementation of the remedial action. Some or all of the following BMPs are examples of ways that can help improve the green characteristics of excavation actions [17]:

- Devote time and resources to conducting low-impact site characterization (using direct push methods, field screening, etc.) both before and during the remedial action. Excavation footprints can sometimes be reduced if efforts are made to minimize the removal of clean material.
- Use appropriately sized equipment for excavation and hauling to minimize noise, dust, erosion, and fuel efficiency. Utilize energy efficient operating procedures such as minimizing idling and performing routine maintenance to improve fuel efficiency.
- Consider onsite treatment or using the closest treatment and disposal facility to minimize hauling. Purchase supplies that are produced locally and use local contractors when possible. Scout for local or onsite backfill material in the planning stages and during implementation.
- Salvage uncontaminated vegetation and organic debris for use as mulch or compost.
- Salvage uncontaminated objects and materials (such as steel, storage containers, etc.) for recycling, reuse, resale, or donation if possible.
- Revegetate and restore excavated areas as quickly as possible. Use native rather than imported plants. Judicious use of diverse plants and prior planning of final landforms can be utilized to create valuable habitat.

Chlorinated Hydrocarbons

Chlorinated aliphatic hydrocarbons, which include chlorinated VOCs, are important industrial chemicals frequently used as solvents for dry cleaning, degreasing, metal cleaning, paint stripping, and electronics. They tend to be highly volatile, toxic to humans, and denser than water. Common chlorinated solvents include chlorinated ethenes such as tetrachloroethylene (also known as perchloroethylene or PCE), trichloroethene (TCE), 1,2-dichloroethene (1,2-DCE), and vinyl chloride (VC); chlorinated ethanes such as 1,1,1-trichloroethane and 1,2-dichloroethane; and chlorinated methanes such as carbon tetrachloride, chloroform, and methylene chloride.

Like refined petroleum hydrocarbons, chlorinated VOCs can be found in the vapor phase, dissolved in groundwater, sorbed to soil, or as a NAPL. However, because chlorinated solvents are denser than water, NAPL will be present as DNAPL. Because of its higher density and other properties such as high viscosity, a DNAPL tends to be considerably harder to remove, destroy, or otherwise remediate than LNAPL.

Remediation methods for chlorinated VOCs include some that are the same as or similar to those discussed in the section on petroleum hydrocarbon remediation. These and other remediation methods are discussed below in the context of chlorinated

hydrocarbons cleanup. However, the BMPs offered as sustainable practices discussed previously by technology for petroleum hydrocarbons have not been repeated in this section.

Soil vapor extraction (SVE) can be effective at removal of chlorinated VOCs present in the unsaturated zone of the subsurface that is sorbed to contaminated soil or present in the vapor phase. As described earlier, one or more SVE wells (screened in the unsaturated zone above the water table) are constructed and a vacuum system is installed with a manifold to the wells. The vacuum draws the air from the soil (which is contaminated with VOCs) out of the subsurface through a treatment system. The contaminated vapors are replaced by fresh air from vent wells or from other parts of the subsurface, allowing the VOCs to evaporate and drawn to the SVE for removal. Representative BMPs for SVE systems discussed in the previous section on petroleum hydrocarbons would be applicable for chlorinated VOCs with the exception of those related to vapor control technology.

Treatment of extracted soil vapor for chlorinated VOCs is more complicated than it is for fuel hydrocarbons. Chlorinated VOCs are not combustible, and when oxidized, one of the by-products is hydrochloric acid, which is highly corrosive, and can severely damage or ruin catalytic or thermal oxidizers. The vapors can be treated with GAC, but this is not green or sustainable and could result in considerable change-out expense if concentrations are high.

For higher concentrations, it is sometimes possible to recover the chlorinated solvents from the vapor stream for recycling. One method uses refrigerated condensation to recover VOCs from the vapor phase as liquid [18]. This type of technology is energy intensive, but can be considered a green remediation method based on the high efficiency of product recovery from the vapor stream.

Multiphase extraction is sometimes used to recover DNAPL, contaminated water, and soil vapor from the subsurface. DNAPL, however, is usually more viscous than LNAPL and is more prone to adhering to the soil matrix, making it difficult to draw the liquid into a well for product recovery. In most cases, the recoverable volume is small and the recovered solvent has been degraded to less than commercial quality, so recycling or reuse of the DNAPL generally would not be cost effective. As a result, most of the material would be disposed of off-site. As with the use of multiphase extraction for the recovery of petroleum hydrocarbons, caution is warranted when employing groundwater recovery and treatment. The BMPs offered for groundwater recovery with multiphase extraction of petroleum hydrocarbons would also apply to the recovery of chlorinated VOCs.

Monitored natural attenuation is a highly sustainable remediation method that can be very effective for the destruction of certain chlorinated hydrocarbons, particularly the chlorinated ethenes. The method exploits naturally occurring processes such as abiotic and biotic degradation to reduce contaminant mass and concentrations that are dissolved in groundwater, present as DNAPL, or sorbed to the soil. The process known as reductive dechlorination sequentially strips chlorine atoms off of each compound, starting with highly chlorinated compounds such as PCE and TCE through 1,2-DCE and VC, ultimately producing innocuous by-products such as carbon dioxide, chloride ions, and water. As with petroleum hydrocarbons, monitored natural attenuation of chlorinated ethenes requires little to no external energy input and generates minimal waste.

Biodegradation of chlorinated hydrocarbons through reductive dechlorination does not occur in all subsurface environments. Reductive dechlorination proceeds best under anaerobic (i.e., oxygen-depleted) conditions as opposed to the aerobic conditions that are most favorable for degradation of petroleum hydrocarbons. Additionally, reductive dechlorination requires both electron acceptors (i.e., the chlorinated ethenes) and electron donors (generally organic carbon that can come from anthropogenic sources such as landfill leachate or natural sources such as decaying vegetation) [19]. Third, microbial populations capable of facilitating reductive dechlorination are not always present, even if anaerobic conditions exist and adequate organic carbon is available. Therefore, even though MNA can be a green and sustainable remediation method, it is not always applicable or effective. In such cases, other methods need to be implemented.

Enhanced bioremediation, which is a method designed to stimulate contaminant biodegradation by indigenous microbial populations [15], can be a green and sustainable alternative similar to MNA. Enhanced

bioremediation of chlorinated compounds involves the injection of amendments to the contaminated subsurface to promote bacterial processes that consume oxygen in the unsaturated and/or saturated zones, thereby initiating or enhancing reductive dechlorination. In cases where natural attenuation is actively occurring, enhanced bioremediation can supplement monitored natural attenuation to improve performance and reduce the time needed for complete remediation. If biodegradation is not occurring under natural conditions, enhanced bioremediation can initiate the process by creating conditions that are amenable to reductive dechlorination.

Enhanced biostimulation of chlorinated compounds typically uses fast-acting and/or slow-acting, food-grade carbon sources such as lactate, emulsified oils, molasses, or proprietary compounds developed specifically for this purpose. In many cases, injection of these carbon sources can be done with low energy input (such as controlled gravity feed), and they can be left in the subsurface because they are nontoxic and will eventually be completely consumed by the microbial populations. Enhanced bioremediation also destroys contaminants rather than transferring them to another medium, decreasing undesirable environmental impacts that can occur with some other remedial actions.

Like MNA, enhanced bioremediation can be used as a green and sustainable component of a larger scale remedial action involving media other than groundwater. Specific mixtures of carbon substrate can be used as needed to quickly induce anaerobic conditions or to react slowly and last longer. Other parameters, such as viscosity, density, emulsification, and so on, can be modified based on site conditions and remediation goals or requirements.

In some cases, the natural microbial populations are insufficient to degrade chlorinated hydrocarbons such as PCE and TCE to nontoxic endpoints, which can cause an undesirable buildup of 1,2-DCE and/or VC. Because VC is more toxic than TCE, this result is not acceptable from a regulatory or human health perspective. In such cases, bioaugmentation can be used, in which microbial consortia capable of complete degradation of chlorinated ethenes are grown in a laboratory, acclimated to site conditions, and injected into the subsurface with an appropriate carbon substrate. At present (2011), the only commercially available microbial consortia for this purpose are of the *Dehalococcoides* genus.

In situ chemical oxidation (also known as ISCO or Chem-Ox) is used to directly oxidize chlorinated hydrocarbons, typically by injection of oxidants in liquid form into the aquifer using direct push methods or permanent injection wells. The limitations to using ISCO for chlorinated hydrocarbons are similar to those discussed above for petroleum hydrocarbons and include daylighting, preferential oxidation of ambient organic carbon not related to contamination, and poor contact between the oxidant and the contaminants.

In situ chemical reduction can be used in place of or in conjunction with enhanced bioremediation. Its purpose is to chemically induce strongly reducing conditions capable of abiotically destroying chlorinated hydrocarbons. A typical reducing agent is zero valent iron (ZVI), which is a highly reactive metal that can be deployed as a powder in a permeable reactive barrier or injected into the subsurface in the form of a liquid suspension. The method is considered to be green and sustainable because it is long lasting, not harmful to the environment, and chemically destroys contaminants. The method also can have a residual effect of creating sustained reducing conditions in the subsurface that serve to enhance bioremediation, increasing its utility as a remedial tool.

Phytoremediation can be an effective technology for remediating chlorinated hydrocarbons in soil or groundwater. Plants used for phytodegradation of PCE, TCE, and DCE include poplars and cottonwoods. As discussed above, these trees can also be used to achieve hydraulic control to contain groundwater plumes. Rhizodegradation and phytovolatilization of chlorinated hydrocarbons have also been observed [16].

PCBs, Pesticides, and High-Molecular-Weight PAHs

PCBs, pesticides, and high-molecular weight PAHs are three of the most common classes of persistent organic pollutants (POPs), toxic chemicals that resist chemical and/or biological degradation and therefore persist in the environment. Although many of these compounds are now banned or highly regulated in the United States, their environmental persistence necessitates ongoing remediation efforts of historically contaminated sites.

Many POPs are polychlorinated or polycyclic aromatic compounds. The incorporation of multiple halogen atoms (chlorine, bromine, etc.) or multiple aromatic rings into organic compounds tends to make the compounds more difficult to degrade both chemically and biologically. Because POPs are difficult to degrade under environmental conditions, containment or ex situ treatments are typically required.

POPs are typically characterized by low solubility and, therefore, are most often found contaminating solid materials including soils and sediments. Incineration is often the presumed remedy for solid wastes contaminated with POPs, which are destroyed at high temperatures. Benefits of incineration include near-complete destruction of a wide variety of POPs and the ability to treat large volumes of contaminated material on relatively short timeframes. However, incineration can create toxic by-products (e.g., dioxins and furans) or volatilize heavy metals and, therefore, must be carefully engineered to prevent adverse health effects. Incineration also requires large quantities of energy to excavate the contaminated soil and to reach temperatures that often exceed 1,200°C.

Specialized technologies developed as alternatives to incineration include a variety of techniques for ex situ chemical degradation of POPs [20]. However, these technologies typically require high temperatures and caustic solutions or solvents, due to the innate stability of the chemicals. Onsite reuse of treated soil for backfilling can make these technologies somewhat greener. Vitrification can also be used to destroy POPs at high temperature, while containing any residual contaminants in the resulting glass, though this technology is not considered sustainable, due to excessive energy consumption. The large environmental impacts of most technologies for POP treatment highlight both the difficulty of treating these classes of contaminants and the need for additional innovation in this area of remediation.

In response to the need for innovation, various specialized technologies have been developed for bioremediation of PCBs and specific pesticides, typically via dechlorination. These technologies use specialized organic amendments, nutrients, or proteins to stimulate microbial activity that drives dechlorination of the POPs. Bioremediation is useful only for wastes with low POP concentrations, due to the much slower rate of degradation relative to more energy-intensive processes. Because of the specific nature of microbial processes and the difficulty of either dechlorinating or breaking the polyaromatic structure of POPs, technologies are often specific to the compounds for which they were developed and require testing for applicability to other POPs. These technologies are significantly more sustainable than incineration and chemical degradation processes, due to significantly lower energy requirements and waste production, and because some of the technologies can be utilized in situ at sites where conditions allow.

Another emerging technology uses mechanical agitation of POP-contaminated waste with a chemical reactant in a ball mill or similar machine to drive dechlorination, such as for PCBs. Although this technology requires excavation of the contaminated material, it has relatively low energy requirements, because mechanical energy is substituted for thermal energy in promoting degradation of the POPs. The sustainability of variations on this method is further affected by the nature of the chemical reactant used and waste products created.

Ongoing research into application of phytoremediation to POPs has revealed plants capable of phytoextraction and rhizodegradation of PCBs, pesticides, and PAHs. Phytoremediation is only possible where POP concentrations are low enough so that they are not toxic to the plants, and it is particularly promising for treatment of low-level pesticide contamination of surface soils. Where feasible, this technology offers a highly green and sustainable alternative to the high energy intensity and site disturbance required by most POP remediation technologies.

Explosives and Energetics

Explosive and energetic compounds that are in widespread use in military and industrial applications are common contaminants of concern, on account of their relative solubility and persistence in the environment. Common examples of these contaminants include perchlorate, 2,4,6-trinitrotoluene (TNT), hexahydro-1,3,5-trinitro-1,3,5-triazine (RDX), and octahydro-1,3,5,7-tetranitro-1,3,5,7-tetrazocine (HMX).

As with POPs, costly and energy-intensive remedial technologies such as incineration are often used to treat

energetic compounds in soil. However, these compounds are less recalcitrant than POPs and can be degraded biologically under appropriate conditions.

Although microbial degradation of these compounds is typically slow, enhanced bioremediation of perchlorate, TNT, RMX, and HMX can be achieved by addition of a variety of carbon and/or nutrient amendments to groundwater, either in situ or ex situ. Investigations have shown that bacteria capable of degrading these energetic compounds, under both oxic and anoxic conditions, are widespread in the environment, but specific bacteria can also be added to promote degradation [21, 22]. Ex situ technologies that have been proven effective include a variety of bioreactors and composting operations. Organic energetic compounds (TNT, RMX, HMX) can be degraded to other organic by-products, or mineralized all the way to carbon dioxide. Perchlorate is reduced to chloride and oxygen gas.

Phytoremediation technologies for energetic compounds include rhizodegradation and phytodegradation of TNT by a variety of plants including hybrid poplars. Studies have also provided evidence for phytoremediation of perchlorate, RDX, and HMX. Constructed wetlands have also been found to be effective for remediating a variety of energetic compounds, through a combination of bioremediation and phytoremediation.

The BMPs and sustainability benefits of microbial degradation and phytoremediation of explosive and energetic compounds are similar to those discussed above for other classes of organic contaminants.

Metals

The diversity of metals and sources of metal contamination in the environment necessitates diverse contaminant- and site-specific remedial approaches. Common metal contaminants identified for remediation include arsenic, chromium, lead, and mercury. Modern and historical sources of metal contamination include mining and smelting operations (including acid mine drainage), steel production, landfills, firing ranges, battery recycling and disposal operations, metal plating facilities, wood treatment facilities, coal combustion by-products (e.g., coal ash), dyes and paints, lead arsenical pesticides, and leaded fuels.

Unlike organic contaminants, metals cannot be biologically or chemically degraded to innocuous by-products. Therefore, remediation of metals typically relies either on removal or on sequestration in solids, which limits mobility and potential exposure. Various methods exist for increasing the sustainability of technologies for both removal and sequestration.

In situ stabilization and geochemical fixation of metals uses chemical or biological processes to transform metals in soils or aquifers from soluble and/or toxic to insoluble and/or nontoxic forms. The chemistry of stabilization is dependent on the specific metal(s) of concern. Different metals have distinct properties that affect their mobility and bioavailability under different environmental conditions, and remedial technologies must be designed to address the specific site conditions relative to the properties of the metals of concern.

Redox state can be an important determinant of solubility and toxicity for redox-active metals, such as chromium, arsenic, iron, and manganese. For example, hexavalent (oxidized) chromium is much more soluble and toxic than trivalent (reduced) chromium, whereas iron and manganese are typically less soluble and toxic under oxidized conditions. Reducing conditions can also lead to sulfide production, and sequester metals through the formation of metal sulfide minerals. Therefore, addition of chemicals that stimulate reduction or oxygenation of the contaminated soils or aquifers can be designed to cause the metal(s) of concern to precipitate and become less bioavailable.

Various properties of soil and water geochemistry also affect metal behavior. Many metals are more soluble and bioavailable under acidic (low pH) conditions, and carbonate, in the form of lime or limestone, can be added to increase pH. The presence of other geochemical species (e.g., phosphates or organic matter) can cause metals such as lead, zinc, copper, cadmium, nickel, and uranium to be retained in the solid phase. Phosphate causes metals to precipitate, whereas addition of organic matter tends to increase metal sorption to soils. Addition of solids that tend to adsorb metals, such as iron oxyhydroxides, can also effectively sequester metals.

Implementation of in situ stabilization typically requires that an aqueous or solid chemical reactant be injected into the contaminated aquifer or mixed with impacted soils. Application of this technology in

aquifers therefore requires the installation of injection wells, while remediation of soil requires equipment sufficient to mix to the depth of desired treatment. The BMPs for in situ stabilization include some discussed above for enhanced biodegradation and ISCO, technologies which require similar injection of reactants, and for excavation, which requires site disturbance similar to soil mixing.

As an in situ technology, stabilization offers relatively low energy requirements, as compared to extractive technologies. The environmental impacts of the stabilization as applied to groundwater are dependent on the frequency of injection events and level of automation of the system, which can minimize the number trips to the site for operations and maintenance of the injection system. Metals stabilization in soils has minimal energy requirements after the initial mixing. Use of recycled materials, such as composts, wood or coal fly ash, or red mud from the alumina industry, as treatment additives can further increase the overall sustainability of the remedial effort.

Limitations of this technology include the difficulty of achieving thorough mixing with the contaminated medium, possible limitations to future site use, and the necessity of treatability studies to demonstrate that metal solubilities will meet criteria after treatment. However, in sites where the contaminant and physical characteristics are well suited for in situ stabilization, it can be a highly effective and environmentally sustainable remedial option.

Phytoremediation of metals uses plants to extract and/or contain contaminants in environmental media. Whereas remediation of organic compounds by plants often focuses on contaminant degradation, phytoremediation of metals focuses on accumulating the metals within plant tissues, volatilizing them through the plants, stabilizing them in soils, or otherwise limiting metal mobility and bioavailability.

A wide variety of metals can be removed from solid materials or water through phytoextraction, which results in accumulation of metals in plant tissues. Plants used for phytoextraction are often chosen for their ability to tolerate and/or "hyperaccumulate" a specific metal of concern. For example, Chinese brake ferns are used to remove arsenic from shallow soils (Fig. 4). Because the metals are not degraded, plants typically must be harvested and disposed of as waste following metal uptake. Plants are also used for

Subsurface Fate and Transport of Chemicals. Figure 4
Use of Chinese brake ferns for remediation of arsenic in shallow soils

phytovolatilization of certain metals (e.g., selenium, mercury, and arsenic) through transpiration.

Plant-based containment technologies for metals include phytostabilization within the soil, achieved through chemical or biological processes that decrease metal solubility, and hydraulic control, which uses water uptake by trees to limit the mobility of dissolved metals.

Monitored natural attenuation, discussed in detail above in reference to organic contaminants, is also applicable to dissolved metals in aquifers, in cases where the natural groundwater chemistry results in immobilization of the contaminants. For example, hexavalent chromium may be naturally oxidized in aquifers with sufficient dissolved oxygen. Precipitation of metals at naturally high pH or adsorption of metals to solid materials present in the aquifer (e.g., minerals and organic matter) can also result in the attainment of remedial goals for dissolved metals.

As with remediation of organic contaminants, monitored natural attenuation of metals requires collection of evidence to indicate that natural attenuation is occurring and that no adverse impacts to humans or the environment are present. Where these conditions are met, this remedial strategy is a highly sustainable method for achieving remedial goals with minimal energy inputs.

Excavation is not typically considered a green or sustainable technology, due to its high energy demands and the need to contain excavated waste within a disposal facility. However, as discussed for petroleum hydrocarbons above, certain methods can be incorporated into excavation projects to improve their sustainability. For metals, one additional option is excavation followed by metal recycling, which can be an environmentally responsible remedial option for waste with high metals concentrations, such as slag from metal smelting operations and munitions from firing ranges. The economic feasibility of recycling is often dependent on the concentration of metals, the quantity of contaminated material, and proximity of recycling facilities.

Future Directions

This entry has provided practical concepts, value engineering principles, and BMPs for the current state of remedial technologies for the typical classes of environmental contaminants observed in the subsurface. These concepts and practices represent the qualitative principles currently utilized to improve or increase the sustainability of subsurface remediation.

Although these BMPs are helpful, is it not possible based on BMP application to evaluate their ultimate benefit to improving sustainability. In the near future, the environmental industry will move away from the general practice of subjectively reviewing and applying BMPs from a master list to the practice of applying project-specific, robust, quantitative analyses of sustainability benefit for a project. Green and sustainable remediation organizations like SURF have already created a compilation of comprehensive metrics (Metrics Toolbox) that can be used to evaluate, track, and forecast a remedy's ability to achieve certain outcomes in relation to sustainability goals [23]. In the future, metrics like those in SURF's Metrics Toolbox will be supplemented with a wider suite of metrics to perform analyses of sustainability key elements in remedial program decision making.

Although it is envisioned that greener remedies have a distinct place within regulatory programs, such as the US Environmental Protection Agency (EPA) Comprehensive Environmental Response, Compensation, and Liability Act (CERCLA) or Resource Conservation and Recovery Act (RCRA), program-specific regulatory criteria do not currently address the social and economic considerations of sustainability. The US EPA is presently attempting to clarify the role of green remediation within the CERCLA and RCRA programs; however, its ability to include the social and economic benefits in the remedy selection process may exceed the authority of these programs. The task of defining what is meant by the term "sustainable" in terms of remedial measures remains an ongoing effort [24] and will continue to evolve in coming decades through collaboration between researchers, regulators, and environmental remediation professionals.

Bibliography

Primary Literature

1. Office of Technology Assessment (OTA) (1984) Protecting the nation's groundwater from contamination, report
2. Howard PH, Boethling RS, Jarvis WM, Meylan WM, Michalenko EM (1991) Handbook of environmental degradation rates. Lewis, Chelsea, p 725

3. Suthersan SS (1997) Remediation engineering: design concepts. Lewis, Boca Raton, p 362
4. Kalderis D, Juhasz AL, Boopathy R, Comfort S (2011) Soils contaminated with explosives: environmental fate and evaluation of state-of-the-art remediation processes (IUPAC technical report). Pure Appl Chem 83:1407–1484
5. Liu L, Tindall JA, Friedel MJ (2007) Biodegradation of PAHs and PCBs in soils and sludges. Water Air Soil Pollut 181(1–4): 281–296
6. U.S. Environmental Protection Agency (EPA) (1989) Risk assessment guidance for superfund. Volume I: Human health evaluation manual, Part A, EPA/540/1-89/002. U.S. Environmental Protection Agency, Office of Emergency and Remedial Response, Washington, DC
7. U.S. Environmental Protection Agency (EPA) (1989) Risk assessment guidance for superfund. Volume II: Environmental evaluation manual, EPA/540/1-89/001. U.S. Environmental Protection Agency, Office of Emergency and Remedial Response, Washington, DC
8. Office of Solid Waste and Emergency Response (1995) Use of Risk-based decision making in UST corrective action programs. OSWER Directive 9610.17, Mar 1995. Office of Solid Waste and Emergency Response, Washington, DC
9. Foster Wheeler Environmental Corporation (Foster Wheeler) (1998) RBCA fate and transport models: compendium and selection guidance, prepared for ASTM, Nov 1998, pp 1–26
10. Ellis DE, Hadley PW (2009) Sustainable remediation white paper – integrating sustainable principles, practices, and metrics into remediation projects, remediation. Wiley Interscience. doi:10.1002/rem.20210
11. U.S. Environmental Protection Agency (USEPA) (2011) Green remediation best management practices – sites with leaking underground storage tank systems, EPA 542-F-11-008, June 2011. Office of Solid Waste and Emergency Response, Office of Emergency and Remedial Response, Washington, DC
12. American Academy of Microbiology (2011) Microbes and oil spills (FAQ), p14
13. Crane CR, Sanders DC (1967) Evaluation of a biocidal turbine fuel additive, Aug 1967. Federal Aviation Administration AM 67-21, Washington, DC, p12
14. U.S. Environmental Protection Agency (USEPA) (2009) Green remediation best management practices – site investigation, EPA 542-F-09-004, Dec 2009. Office of Solid Waste and Emergency Response, Office of Emergency and Remedial Response, Washington, DC
15. U.S. Environmental Protection Agency (USEPA) (2010) Green remediation best management practices – bioremediation, EPA 542-F-10-006, Mar 2010. Office of Solid Waste and Emergency Response, Office of Emergency and Remedial Response, Washington, DC
16. U.S. Environmental Protection Agency (USEPA) (2000) Introduction to phytoremediation, EPA/600/R-99/107, Feb 2000. Office of Research and Development, Cincinnati
17. U.S. Environmental Protection Agency (USEPA) (2008) Green remediation – best management practices for excavation and surface restoration, EPA 542-F-08-012, Dec 2008. Office of Solid Waste and Emergency Response, Office of Emergency and Remedial Response, Washington, DC
18. Kessel L, Squire J, Holland K (2008) Sustainable soil remediation by refrigerated condensation at sites with "high-concentration" recalcitrant compounds and NAPL – two case studies. Remediation 19:53–72
19. U.S. Environmental Protection Agency (USEPA) (1998) Technical protocol for evaluating natural attenuation of chlorinated solvents in ground water, EPA/600/R-98/128, Sept 1998. Office of Research and Development, Cincinnati
20. U.S. Environmental Protection Agency (USEPA) (2010) Reference guide to non-combustion technologies for remediation of persistent organic pollutants in soil, 2nd edn. EPA 542-R-09-007, Sept 2010. Office of Solid Waste and Emergency Response, Office of Emergency and Remedial Response, Washington, DC
21. Interstate Technology and Regulatory Council (ITRC) (2005) Perchlorate: overview of issues, status, and remedial options, Sept 2005. ITRC, Washington, DC
22. Esteve-Nunez A, Caballero A, Ramos JL (2001) Biological degradation of 2, 4, 6-trinitrotoluene. Microbiol Mol Biol Rev 63:335–352
23. Butler PB, Larsen-Hallock L, Lewis R, Glenn C, Armstead R (2011) Metrics for integrating sustainability evaluations into remediation projects. Remediation 21(3):81–87
24. Interstate Technology and Regulatory Council (ITRC) (2011) Green and sustainable remediation: state of the science and practice. ITRC, Washington, DC, 43 pp

Books and Reviews

Fetter CW (1999) Contaminant hydrogeology, 2nd edn. Waveland, Long Grove, p500

Holland KS et al (2011) Framework for integrating sustainability into remediation projects. Remediation 21(3):7–38

Illaszewicz J, Gibson K (2009) Green and sustainable remediation: creating a framework for environmentally friendly site cleanup. Environ Qual Manag 18(4):1–8

Pankow JF, Cherry JA (1996) Dense chlorinated solvents and other DNAPLs in groundwater. Waterloo, Portland, 522 pp

Schwarzenback RP, Gschwend PM, Imboden DM (1993) Environmental organic chemistry. Wiley, New York, 681 pp

Stumm WS, Morgan JJ (1981) Aquatic chemistry: an introduction emphasizing chemical equilibria in natural waters, 2nd edn. Wiley, New York, 780 pp

U.S. Environmental Protection Agency (USEPA) (2008a) Green remediation: incorporating sustainable environmental practices into remediation of contaminated sites, EPA 542-R-08-002, Apr 2008. Office of Solid Waste and Emergency Response, Washington, DC

Sunshades for Solar Radiation Management

Daniel J. Lunt
School of Geographical Sciences, University of Bristol, Bristol, UK

Article Outline

Glossary
Definition of the Subject and Its Importance
Introduction
Modeling the Efficacy of Sunshades
Engineering Considerations
Future Directions
Bibliography

Glossary

Geoengineering The intentional large-scale manipulation of the environment.

Solar radiation management Deliberate modification of the solar radiation budget, by either changing the amount of sunlight entering the Earth's atmosphere, or by changing the Earth's reflectivity, normally in an effort to counteract human-induced climate change.

Sunshade A colloquial term for a giant reflector, or array of smaller reflectors, in orbit between the Earth and the Sun. Also known as a "space mirror."

Definition of the Subject and Its Importance

There is strong scientific consensus that the Earth's climate has been warming over the last century and that this warming is primarily due to human influences on the climate system (IPCC 2007). Attempts to curb human emissions of greenhouse gases have so far largely failed; as such, and in an attempt to avoid or delay potential dangerous climate change, several geoengineering schemes have been suggested for modifying Earth's climate directly. One such scheme is the construction of a sunshade in space, in orbit between the Earth and the Sun, with the aim of reducing the effective strength of the Sun's rays, and cooling the Earth's climate. However, it is now thought that such a sunshade, although highly effective in terms of cooling the planet, would have other, perhaps undesirable, impacts on Earth's climate, in particular on precipitation patterns. This highlights the importance of using a whole-Earth system approach when considering the potential impacts of any geoengineering scheme.

Introduction

One of the first references to a space-based sunshade was proposed in the context of modifying the climates of extraterrestrial planets, with the aim of making them habitable [1]. More recently, it has been widely discussed in the context of cooling our own planet, in an attempt to mitigate effects of human-induced global warming (e.g., [2–5]). The basic underlying concept is extremely simple – a reflective or deflecting substance or substances are placed between the Earth and the Sun in order to reduce the intensity of incoming solar radiation at the top of the Earth's atmosphere. The amount of reduction in solar radiation would be chosen to offset, or partially offset, surface warming induced by increases in greenhouse gases in the Earth's atmosphere.

The apparently alluring idea that a sunshade could perfectly offset greenhouse-gas-induced global warming is, perhaps unfortunately, an oversimplification. A sunshade positioned in space between the Earth and the Sun would reduce the effective strength of the Sun, resulting in an absolute change in the local solar forcing at the top of the Earth's atmosphere proportional to the local solar input, meaning that high latitudes and winter seasons receive less solar energy decrease than low latitudes and summer seasons (see Fig. 1). However, the radiative forcing due to increased greenhouse gases is more homogenous seasonally and latitudinally. As such, although the *global annual mean* greenhouse gas forcing could be exactly canceled by a solar shield, in such a "globally corrected" case the tropical and summer regions would be overcompensated, and high latitude and winter regions would be undercompensated. This would result in a surface temperature pattern of a globally corrected geoengineered world which, compared to modern, would be colder in the tropics than in the high latitudes. Along with this imperfect cancelation of temperature, other aspects of the Earth system would also remain unmitigated, such as changes to the hydrological cycle, as well as impacts resulting directly from the high CO_2, such as ocean acidification.

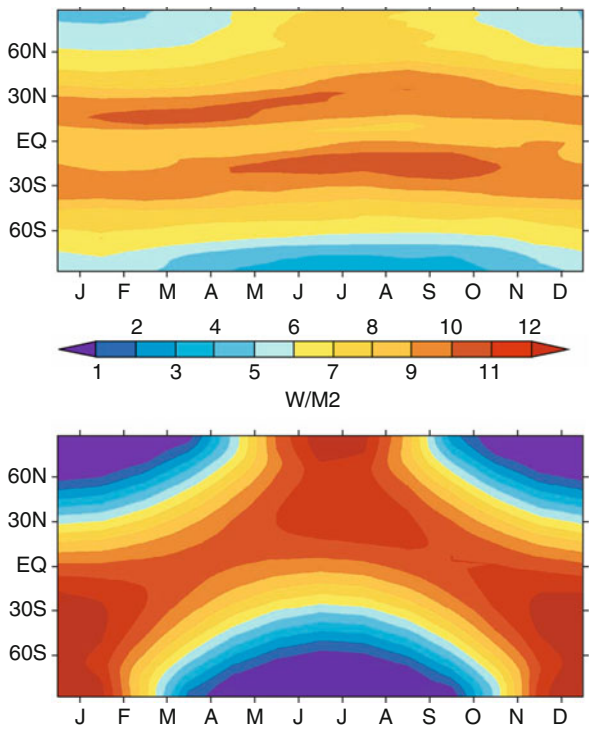

Sunshades for Solar Radiation Management. Figure 1 Change in net long-wave radiative flux at the tropopause when CO_2 is quadrupled (*top panel*) with respect to the Control case and the reduction in incoming solar radiation (*bottom panel*) needed to compensate this forcing. Both values (W m^{-2}) are zonally averaged as a function of time of year. Change in solar radiation has a latitudinal and seasonal pattern markedly different from the radiative forcing of CO_2 (Adapted from [6], Fig. 1)

This entry focuses on the climatic effects (both desired and undesired) of placing sunshades in space. It also touches very briefly on some of the engineering considerations associated with the manufacture and launch of such a system. The substantial governance, political, and ethical considerations are not discussed here. Instead, the reader is referred to Virgoe [21], Blackstock and Long [7], and Corner and Pidgeon [8] for discussion of these more qualitative, but nonetheless important, issues.

Modeling the Efficacy of Sunshades

Background

Because of the incredible complexity of the Earth system, and the expense and potential risks of carrying out large-scale field studies, probably the only way that the success and possible side effects of sunshade geoengineering can be assessed, at least initially, is through numerical climate modeling. Climate models, also known as "General Circulation Models," or GCMs, consist of a numerical representation of our best understanding of the Earth system. In the atmosphere, they typically consist of a "dynamical core" which solves an approximation to the fundamental equations of motion of a perfect gas on a rotating sphere, a representation of radiative processes across a range of wavelengths from the solar to the infrared, and a set of "parameterizations," which represent the large-scale effect of processes which occur at too small a scale to be resolved by the dynamical core, such as small-scale atmospheric waves, turbulence, processes associated with clouds, surface processes such as evaporation, and other aspects of the hydrological cycle. These atmospheric models can either have the temperatures of the ocean surface prescribed as boundary conditions, or can use a simple "slab" representation of the ocean in which the ocean interacts thermodynamically with the atmosphere (e.g., warming up if the atmosphere warms).

The last decade has also seen the development of coupled atmosphere-ocean models, which, as well as the atmosphere, also solve equations related to the fluid flow of the oceans. Given an initial condition (e.g., a static atmosphere and ocean, or the ocean–atmosphere state on a particular historical day since the advent of dense networks of observations) and a set of appropriate boundary conditions (such as the Earth's topography and bathymetry and land-surface characteristics, and atmospheric gas composition), a model will typically solve the equations in the dynamical core and associated parameterizations, and increment the state of the atmosphere forward in time (typically 15 min to 1 h, depending on the spatial resolution of the model – high-resolution models require short timesteps to maintain numerical stability). If the boundary conditions remain fixed over time, then the model will eventually (typically years to decades for an atmosphere-only model, centuries to millennia for an atmosphere-ocean model) reach a quasi-equilibrium, where dynamic weather systems are superimposed on an equilibrium circulation of the atmosphere-ocean system. In this case, the initial

condition of the model becomes unimportant (unless there are multiple equilibrium states of the system for the given boundary conditions).

How can these models be applied to sunshades in space? In a typical numerical experimental design, three model simulations are carried out with three different sets of boundary conditions. Firstly, a "modern" (or "control" or "preindustrial") simulation is carried out, in which the boundary conditions are set as those of the modern era (or alternatively pre-industrialization values for atmospheric gas composition). Secondly a "perturbed" or "future" simulation is carried out, in which greenhouse gas concentrations are set at elevated concentrations (e.g., twice or four times preindustrial or modern values). Thirdly, a "geoengineered" simulation is carried out, in which the greenhouse gas concentrations are elevated and in addition the strength of the Sun's solar output (the "solar constant") is reduced. The reduction of solar constant acts as an approximation to the effect of a sunshade in space. The magnitude of the solar constant reduction is usually chosen so as to balance as closely as possible the global annual mean increase in surface air temperature caused by the elevated greenhouse gas concentrations. An alternative experimental design consists of a transient time-varying simulation, in which greenhouse gas concentrations are slowly increased in the "future" simulation, and a corresponding slow increase in the strength of the solar shield is applied in the "geoengineered" simulation.

Results

The first numerical model study of the impacts of geoengineering was carried out by Govindasamy and Caldeira [2]. Using an atmospheric GCM and a "slab" ocean model, they carried out three equilibrium simulations, as outlined above. They found a cooling in the tropics (20°S–20°N) in their geoengineered simulation compared to their control simulation, and a warming outside these regions. However, because of the relatively short length of the simulation (the climatologies were calculated over only 15 years of model time), only a small fraction of the temperature changes in their geoengineering simulation compared to their modern simulation were deemed statistically significant at a 95% confidence limit. Coupled with their use of a "slab" ocean model compared to a full atmosphere-ocean GCM, some of their other results (e.g., they observed an increase in sea ice in their geoengineered simulation compared to their control, and little change in the hydrological cycle) remained somewhat ambiguous. However, this paper was certainly pioneering, and inspired a series of subsequent studies which used a very similar methodology.

Govindasamy et al. [6] carried out a follow-on study, which increased the forcing to a fourfold increase in greenhouse gas concentration. This resulted in a larger signal to analyze, and, as well as confirming their earlier results regarding temperature changes, also resulted in a more physically realistic decrease in sea ice in their geoengineering simulation compared to their control. They also noted that this form of geoengineering, although doing a relatively good job of returning tropospheric temperatures back to modern levels, does little to counteract the cooling in the stratosphere associated with the warming in the troposphere. There was also a decrease in evaporative water flux from the ocean to the atmosphere in the tropics, associated with the cooler sea surface temperatures. However, they noted that all their results, and especially those associated with sea ice, should be regarded with some caution due to their use of a "slab" ocean model and lack of dynamics in the sea-ice scheme.

This issue was partially addressed by the study of Matthews and Caldeira [5]. They used a model with a representation of ocean dynamics, but due to computational constraints used a simplified representation of the atmosphere compared with Govindasamy and Caldeira [2]. They carried out a set of "transient" geoengineering simulations. Because their model was relatively computationally efficient, they were able to carry out long simulations and obtain statistically meaningful results. Their results largely agreed with those of previous studies regarding temperature change, but were very different in terms of precipitation. Matthews and Caldeira [5] found a widespread decrease in continental precipitation in a geoengineered world compared to modern, in particular over the rainforest regions of Amazonia, Central Africa, and South East Asia. They attributed this to decreased evapotranspiration in a high-CO_2 world, as plants used water more efficiently. Matthews and Caldeira [5] also addressed the question of the "safety"

of sunshade geoengineering. In particular, several of their scenarios included a simulated catastrophic failure of the sunshade, such that the solar constant was instantaneously increased back to its normal value, with CO_2 levels still high. In this case, they found an extremely rapid warming, up to 20 times greater than the current anthropogenic warming. However, as with previous work, there remained some uncertainty in the validity of some of the results (in particular, the large reduction in precipitation in the geoengineered case) due to the lack of complexity in the atmospheric component of their model.

The first study to use a fully coupled atmosphere-ocean climate model to investigate sunshade geoengineering was that of Lunt et al. [4]. They also carried out long simulations with averages calculated over 60 years. In general terms, their temperature estimates for the "sunshade world" were similar to previous, but with some new features, such as a maximum in cooling off the west coast of tropical Africa, associated with increased ocean upwelling in the geoengineered case, and maximum warming in the Arctic north of the Bering Strait, associated with a loss of sea ice (see Fig. 2). They also found new results in terms of precipitation, with a global mean decrease in precipitation predicted (in agreement with Matthews and Caldeira [5]), but instead of maximum reductions over continents, they found maximum reductions over the tropical oceans, in a regional pattern which correlated with that of temperature. The use of a fully coupled model also allowed them to investigate changes in El Nino Southern Oscillation (ENSO). They found a significant decrease in the amplitude of ENSO variability in sunshade world relative to modern, associated with a decrease in the tight coupling of atmosphere and ocean feedbacks due to the cooler tropics, but no significant change in ENSO frequency. They also found that the geoengineered world had a slightly more vigorous ocean circulation than the control, associated with a decrease in the intensity of the hydrological cycle, and decreased poleward moisture transport.

This study was followed up by Irvine et al. [3], who used the same model, but investigated a range of "strengths" of sunshade geoenginering, from 100% (which exactly balances the global annual mean temperature change associated with a greenhouse gas concentration increase), to 0% (no geoengineering). They also looked in more detail at the regional patterns of change following sunshade geoengineering. For example, they found that, relative to modern, the

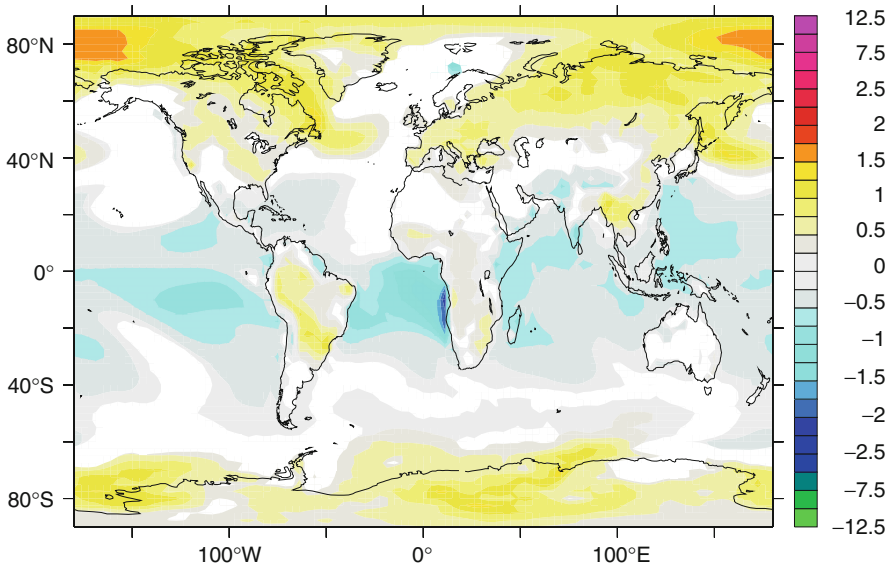

Sunshades for Solar Radiation Management. Figure 2

Change in near-surface air temperature (°C) in a sunshade geoengineered world compared to modern, as predicted by a coupled atmosphere-ocean General Circulation Model. Regions where the difference is not statistically significant at a 95% confidence limit, as given by a Student *T* test, are masked out in white (Adapted from [4], Fig. 2)

USA mainland region experiences a +8% increase in precipitation given 0% geoengineering, and an 11% decrease in precipitation given 100% geoengineering. According to their results, to achieve a precipitation rate close to that of modern, the USA would "choose" a sunshade of strength 40–50%. However, the east China region experiences precipitation back at modern levels with 100% geoengineering. The possible political implications are considerable. They also investigated the effects of sunshade geoengineering on croplands and densely populated regions, and found that in order to obtain modern average values of precipitation in cropland regions would require 75% geoengineering, whereas in urban areas it would require 85% geoengineering. Although this study highlighted the very regional impacts of geoengineering schemes, it should also be noted that no climate model is perfect, and in particular precipitation remains one of the variables which shows the largest inter-model spread. As such, the exact predictions of "ideal" geoengineering levels presented in Irvine et al. [3] should be regarded with some caution.

Several other studies have looked at the implications of sunshade geoeingineering on other aspects of the Earth system. Govindasamy et al. [9] looked at the impact of geoengineering on the biosphere. They used a coupled atmosphere-biosphere model with a slab ocean to carry out the classic three equilibrium geoengineering simulations. They found that the decrease in solar energy in the geoengineered world had very little effect on net primary productivity (NPP) by the biosphere, and instead that the CO_2 increase relative to modern resulted in almost a doubling of NPP. Their model did neglect some possibly important factors such as changes to nutrient cycles in the sunshade world. However, these are likely to be minor compared to the zeroth order result of increased biomass in the geoengineered world compared with modern.

Irvine et al. [10] addressed the possible mitigative potential of sunshade geoengineering for sea-level rise. This question was motivated by the "residual" Arctic warming seen in all of the sunshade geoengineering simulations. Would this residual warming be enough to significantly affect the Greenland ice sheet, and lead to sea-level rise? To address this question they used an offline ice sheet model, which, given fields of temperature and precipitation, calculates the surface mass balance (accumulation vs. melt) and flow of an ice sheet, to obtain an ice sheet geometry that is in equilibrium with the temperature and precipitation. They compared the ice sheets predicted to be in equilibrium with the "control," "future," and "geoengineered" climates from GCM simulations, and found that the "future" climate produced a Greenland ice sheet which was almost completely melted, with only small ice caps remaining on the high-altitude or high-accumulation regions in the east and south of Greenland, equivalent to a sea-level rise of 6.4 m. However, the "geoengineered" climate, despite the residual Arctic warming, was almost identical to the "control" case, with essentially no sea-level rise (see Fig. 3). Irvine et al. [10] went further, simulating a range of strengths of sunshades, and found that a sunshade which reflected only 60% of the sunlight necessary to return global average temperatures back to modern, was sufficient to prevent any melting of the Greenland ice sheet; less than 60% and significant sea-level rise was predicted. Although this study highlighted the potential for sunshade geoengineering to mitigate sea-level rise, its conclusions should be viewed with some caution, as the ice sheet model used lacked some physical processes which could be important, for example, climate-albedo feedbacks, and lubrication of the bedrock by surface melting ice flowing down crevasses (e.g., [11]). It also contained simplified representations of other processes, such as surface mass balance (e.g., [12]) and flow regimes important for ice streams (e.g., [13]).

Many studies have qualitatively highlighted the fact that sunshade geoengineering, despite being predicted to bring temperatures close to those of modern, does nothing to mitigate the effects of increasing anthropogenic CO_2 leading to ocean acidification. Ocean acidification is the process in which a fraction of any increase in atmospheric CO_2 dissolves in the ocean, decreasing the ocean pH. This decrease in pH could have significant effects on ocean ecosystems; corals have been highlighted as being particularly susceptible to relatively small decreases in pH. Matthews et al. [20] noted that actually sunshade geoengineering would have some change on ocean pH compared to a modern world, due to the changes in ocean temperature which result from the sunshade's imperfect

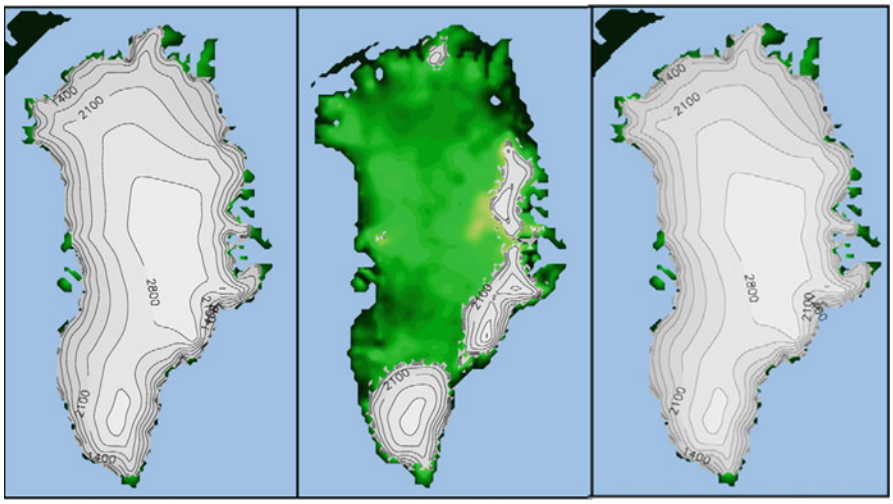

Sunshades for Solar Radiation Management. Figure 3
Equilibrium ice sheets, as predicted by an ice sheet model. *Left*: ice sheet driven by modern climates (temperature and precipitation). *Middle*: ice sheet model driven by climate of a world with quadrupled atmospheric CO_2. *Right*: ice sheet model driven by climate of a world with quadrupled atmospheric CO_2 and a sunshade (Adapted from [10], Figs. 3 and 4)

cancelation of the CO_2-induced warming, and due to changes in the terrestrial uptake of carbon. The cooler tropical temperatures in the tropics in the sunshade world result in increased solubility of CO_2, and therefore decreased pH. However, this is more than offset by the terrestrial carbon cycle change, where the cooler temperatures in the sunshade world result in increased terrestrial biomass compared with the unmitigated world, resulting in slightly lowered atmospheric CO_2, and therefore less dissolved ocean CO_2. So, a sunshade world might have a slightly less acidified ocean than an unmitigated future climate. However, the effect is relatively small, mitigating about 10% of the pH change by the year 2100 in their future scenario.

How does solar radiation management by sunshades compare to other geoengineering schemes? The Royal Society, in their report on geoengineering (2009), rate a number of geoengineering schemes according to their effectiveness, affordability, timeliness (how quickly the technology could be implemented and how quickly it would act once implemented), and safety (possible side effects). They rated sunshades as one of the most effective, but one of the least affordable and least timely, forms of geoengineering. In terms of safety it was ranked medium. A more quantitative assessment was carried out by [14]. They compared sunshade geoengineering with a range of surface albedo Solar radiation management schemes. Unsurprisingly, they found sunshades to be more effective than the other schemes (urban, crop, and desert albedo geoengineering) in terms of returning surface temperatures back to those of modern. And in spite of the previously noted changes to the hydrological cycle, they also found it to be more effective than the other schemes at returning precipitation back to modern levels.

Engineering Considerations

So, could a sunshade be feasibly built? Various engineering solutions have been suggested (e.g., [15, 16]), either fabricating a sunshade on Earth and transporting it to space, or building a sunshade out in space from materials available on asteroids. Sunshades have been suggested which consist of a single superstructure, or an array of millions of tiny reflectors or refractors. For those sunshades built on Earth, electromagnetic rails could launch the individual reflectors into space [15]. Estimates of cost vary, but a value in the region of several trillion dollars has been suggested [15]. Several authors have suggested that an obvious candidate for positioning a sunshade would be at or near the "first Lagrange point" (also known as the "L1 point"), which

is an equilibrium point directly between the Earth and sun, about five times further from the Earth than the moon, at which the gravitational attraction of the Sun and Earth exactly cancel. An object placed at the L1 point is unstable, in that if it is displaced slightly, it will be accelerated further in the same direction, toward either the Earth or Sun. Such a displacement would occur due to the pressure on a sunshade exerted by the Sun's radiation itself. Therefore in practice, a more suitable location for a sunshade would be slightly closer to the Sun than the L1 point, allowing the radiation pressure to balance the offset in gravitational attraction. The ideal location (that which minimizes the mass of sunshade required for a given decrease in solar strength) depends on the density and reflective properties of the sunshades [16]. Others have suggested positioning a sunshade in a near-Earth orbit, or a ring of tiny dust particles, held in place by accompanying satellites [17]. However, these near-Earth solutions would potentially interfere with communications and other satellites.

Future Directions

So, where now for sunshade geoengineering? In terms of modeling, many of the predictions made so far have been carried out with models that can no longer be considered "state of the art." More recent models, such as those that will be used in the forthcoming IPCC fifth assessment report, run at higher resolution than older models, so they are able to resolve more regional features, and are expected to better represent the physics and dynamics of the atmosphere and ocean. Furthermore, they in general include more aspects of the system – they are true "Earth System" models, taking into account previously neglected processes such as atmospheric chemistry, aerosols, the terrestrial biosphere change, and ocean biogeochemistry. However, even these models are far from perfect, evident from the fact that even under identical scenarios, they make differing predictions. As such, it is important to consider predictions from a range of state-of-the art models. Such a task is currently being undertaken in the context of a recent project, "GeoMIP" (Geoengineering Modeling Intercomparison Project; [18]). This project defines two well-defined sunshade geoengineering experiments, which will all be carried out by a range of models (see Fig. 4). However, this multimodel approach still does not sample the full range of possible predictions. Each individual model has a large number of internal parameters which are not well constrained by observations, such as the relative humidity at which clouds start to form on the scale of a single model gridbox. As such, the very latest work is beginning to

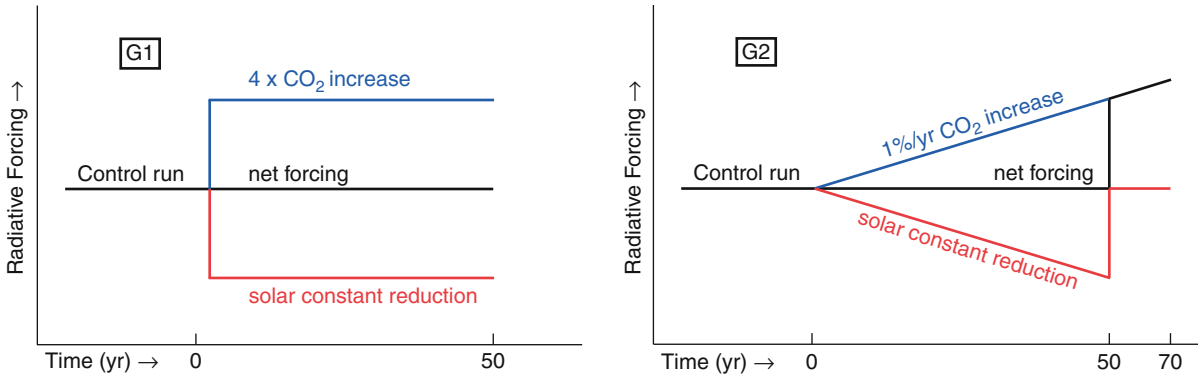

Sunshades for Solar Radiation Management. Figure 4
Schematic of experiments"G1" and "G2" as defined in the GeoMIP project. G1: the experiment is started from a control run. The instantaneous quadrupling of CO_2 concentration from preindustrial levels is balanced by a reduction in the solar constant until year 2050. G2: the experiment is started from a control run. The positive radiative forcing of an increase in CO_2 concentration of 1% per year is balanced by a decrease in the solar constant until year 2050 (Adapted from [18], Figs. 1 and 2)

make predictions with an ensemble of models, which sample some of the model parameter space. This approach has been used for a number for years in future climate prediction (e.g., [19]), but work is just starting on applying this technique to geoengineering.

In terms of engineering solutions, it seems unlikely that a giant sunshade will be launched into space any time soon, due to the high costs associated with fabrication and/or launch, not to mention the possible legal, moral, and ethical questions. Other, cheaper, global geoengineering schemes are likely to be developed first, if at all, such as the injection of aerosols into the stratosphere. However, the concept of a sunshade in space does provide a neat idealized framework in which to study, with numerical models, possible geoengineering options. As such, the concept is likely to be investigated and discussed for some years to come.

Bibliography

Primary Literature

1. Oberg JE (1981) New Earths. New American Library, New York
2. Govindasamy B, Caldeira K (2000) Geoengineering Earth's radiation balance to mitigate CO_2-induced climate change. Geophys Res Lett 27:2141–2144
3. Irvine PJ, Ridgwell A, Lunt DJ (2010) Assessing the regional disparities in geoengineering impacts. Geophys Res Lett 37: L18702. doi:10.1029/2010GL044447
4. Lunt DJ, Ridgwell A, Valdes PJ, Seale A (2008) "Sunshade world": a fully coupled GCM evaluation of the climatic impacts of geoengineering. Geophys Res Lett 35:L12710. doi:10.1029/2008GL033674
5. Matthews HD, Caldeira K (2007) Transient climate-carbon simulations of planetary geoengineering. Proc Natl Acad Sci USA 104:9949–9954
6. Govindasamy B, Caldeira K, Duffy PB (2003) Geoengineering Earth's radiation balance to mitigate climate change from a quadrupling of CO_2. Glob Planet Change 37(1–2):157–168. doi:10.1016/S0921-8181(02)00195-9
7. Blackstock JJ, Long JCS (2010) The politics of geoengineering. Science 327:527. doi:10.1126/science.1183029
8. Corner A, Pidgeon N (2010) Geoengineering the climate: the social and ethical implications. Environ Sci Policy Sustain Dev 52(1):24–37
9. Govindasamy B, Thompson S, Duffy PB, Caldeira K, Delire C (2002) Impact of geoengineering schemes on the terrestrial biosphere. Geophys Res Lett 29(22):2061. doi:10.1029/2002GL015911
10. Irvine PJ, Lunt DJ, Stone EJ, Ridgwell A (2009) The fate of the Greenland ice sheet in a geoengineered, high CO_2 world. Environ Res Lett 4:045109. doi:10.1088/1748-9326/4/4/045109
11. Parizek BR, Alley RB (2004) Implications of increased Greenland surface melt under global warming scenarios: ice sheet simulations. Quat Sci Rev 23:1013–1027. doi:10.1016/j.quascirev.2003.12.024
12. Bougamont M, Bamber JL, Ridley JK, Gladstone RM, Greuell W, Hanna E, Payne AJ, Rutt I (2007) Impact of model physics on estimating the surface mass balance of the Greenland ice sheet. Geophys Res Lett 34:L17501. doi:10.1029/2007GL030700
13. Pattyn F (2003) A new three-dimensional higher-order thermomechanical ice sheet model: basic sensitivity, ice stream development, and ice flow across subglacial lakes. J Geophys Res 108:2382. doi:10.1029/2002JB002329
14. Irvine PJ, Ridgwell A, Lunt DJ (2011) Climatic effects of surface albedo geoengineering. J Geophys Res. doi:10.1029/2011JD016281, in press
15. Angel R (2006) Feasibility of cooling the Earth with a cloud of small spacecraft near the inner Lagrange point (L1). Proc Natl Acad Sci 103:17184–17189
16. McInnes CR (2010) Space-based geoengineering: challenges and requirements. Proc Inst Mech Eng C J Mech Eng Sci 224(3):571–580. doi:10.1243/09544062JMES1439, 1 Mar 2010
17. Mautner M (1991) A space-based solar screen against climate warming. J Br Interplanet Soc 44:135–138
18. Kravitz B, Robock A, Boucher O, Schmidt H, Taylor KE, Stenchikov G, Schulz M (2011) The geoengineering model intercomparison project (GeoMIP). Atmos Sci Lett 12:162–167. doi:10.1002/asl.316
19. Stainforth DA, Aina T, Christensen C, Collins M, Faull N, Frame DJ, Kettleborough JA, Knight S, Martin A, Murphy JM, Piani C, Sexton D, Smith LA, Spicer RA, Thorpe AJ, Allen MR (2005) Uncertainty in predictions of the climate response to rising levels of greenhouse gases. Nature 433(7024):403–406
20. Matthews HD, Cao L, Caldeira K (2009) Sensitivity of ocean acidification to geoengineered climate stabilization. Geophys Res Lett 36:L10706. doi:10.1029/2009GL037488
21. Virgoe J (2009) International governance of a possible geoengineering intervention to combat climate change. Clim Change 95:103–119. doi:10.1007/s10584-008-9523-9

Books and Reviews

Intergovernmental Panel on Climate Change (IPCC), Solomon S et al (eds) (2007) Climate change 2007: the physical science basis: contribution of Working Group 1 to the Fourth Assesment Report of the Intergovernmental Panel on Climate Change. Cambridge University Press, New York, 996 pp

McGuffie K, Henderson-Sellers A (1997) A climate modelling primer. Wiley, Chichester

Shepherd J et al (2009) Geoengineering the climate: science, governance and uncertainty. The Royal Society, London. http://royalsociety.org/ 587geoengineeringclimate. Accessed 1 Aug 2011

Supercritical Carbon Dioxide (CO_2) as Green Solvent

Tianbin Wu, Buxing Han
Institute of Chemistry, Chinese Academy of Sciences, Beijing, China

Article Outline

Glossary
Definition of the Subject
Introduction
The Properties of $scCO_2$
Applications of $scCO_2$
Future Directions
Bibliography

Glossary

Chemical structure of carbon dioxide Carbon dioxide (CO_2) has a structure O=C=O.

Green solvent A green solvent should have some basic properties, such as low toxic, chemically stable, readily available, and easily recyclable.

Ionic liquids Ionic liquids are salts that are liquid at ambient conditions.

Microemulsion A microemulsion is a thermodynamically stable dispersion formed from immiscible substances with the aid of surfactants.

Supercritical fluid A substance is called as a supercritical fluid (SCF) when the temperature and pressure are higher than its critical values.

Definition of the Subject

A substance is called as a supercritical fluid (SCF) when the temperature and pressure are higher than its critical values. Therefore, CO_2 becomes supercritical when its temperature and pressure are higher than 31.1°C (critical temperature, *Tc*) and pressure 7.38 MPa (critical pressure, P_c). SCFs have many unique properties, such as strong solvation power for different solutes, large diffusion coefficient comparing with liquids, zero surface tension, and their physical properties can be tuned continuously by varying the pressure and temperature because the isothermal compressibility of SCFs is very large, especially in the critical region. These unique properties of SCFs lead to great potential for the development of innovative technologies. Besides these common advantages of SCFs, supercritical CO_2 ($scCO_2$) has some other advantages, such as nontoxic, nonflammable, chemically stable, readily available, cheap, and easily recyclable, and it has easily accessible critical parameters. Therefore, $scCO_2$ can be used as green solvent in different fields.

Introduction

It is well known that chemical industry has made great contribution to mankind. However, many volatile, toxic organic solvents are used in chemical processes, which results in environment and safety problems. In recent years, sustainable development has become one of the most important topics in the world, and great effort has been devoted to green chemistry. Green chemistry can be simply defined as "design of chemical products and processes that reduce or eliminate the use and generation of hazardous substances." Effective utilization of green solvents is one of the main topics of green chemistry.

SCFs are typical green solvents. In general, physicochemical properties of SCFs are intermediate to those of the liquid and gaseous states. The ability of a SCF to dissolve low-volatile substances was found more than century ago [1]. However, SCFs did not receive enough attention before 1960s. Systemic study of the properties of SCFs and their applications began in 1970s. It is now well known that SCFs possess many unusual properties, such as strong solvation power for many substances, excellent diffusivity, and near zero surface tension. Moreover, many properties of SCFs can be tuned continuously by varying pressure and/or temperature. Especially, a small change in pressure and temperature remarkably alters the properties of a SCF in the vicinity of its critical point, such as density, viscosity, diffusivity, dielectric constant, and solvent power. The tunable nature of SCFs is favorable to developing new technologies. $ScCO_2$ has the common advantages of SCFs. In addition, it has more advantages because CO_2 is cheap, nontoxic, nonflammable, readily available, and has easily accessible critical point.

Effective utilization of $scCO_2$ and other SCFs as greener media has attracted much attention in recent years. On one hand, they can be used to replace hazardous organic solvents in many chemical processes. On the other hand, the efficiency of some processes can be optimized by using the special properties of SCFs, even some new technologies with obvious advantages can be developed. Both fundamental researches and developing high technologies have achieved significantly over the past decades [2, 3]. In this entry, the basic properties of $scCO_2$ and its applications in extraction and fractionation, chemical reactions, polymeric synthesis, material science, supercritical chromatography, painting, dyeing and cleaning, emulsions related with CO_2, and so on are discussed. It should be emphasized that in each field only some examples are discussed because too many excellent publications are available in the open literature.

The Properties of $scCO_2$

In the immediate vicinity of the critical point, the density of $scCO_2$ is about 0.4 g/mL and increases with increasing pressure and decreases as temperature rises. The diffusion coefficient of $scCO_2$ is much larger than that of liquid solvents. The increase of temperature and decrease of pressure lead to the enlargement of self-diffusion coefficient of $scCO_2$. In general, the viscosity of $scCO_2$ is at least an order of magnitude lower than that of liquid solvents and rapidly increases with pressure near the critical point. $ScCO_2$ shows essentially the properties of nonpolar solvent. It is therefore more suitable for dissolution of weak polar substances. In general, $scCO_2$ is a good solvent for many nonpolar molecules with low molecular weights. It is however a very poor solvent for most high molecular weight polymers under readily achievable conditions. Nevertheless, the addition of some cosolvents (e.g. methanol, ethanol, acetone) to $scCO_2$ can improve the solubility of the polar substances in $scCO_2$ significantly. Its surface tension reduces to zero when temperature exceeds its critical temperature (31.1°C), which makes $scCO_2$ easily penetrate a microporous solid structure. Moreover, $scCO_2$ can swell many polymers. These properties are beneficial for the preparation of porous polymer materials and metal nanoparticles stabilized in porous polymer materials.

Applications of $scCO_2$

Extraction and Fractionation Using $scCO_2$ as Solvent

Supercritical fluid extraction (SFE) is the process of separating one or some components from others using SCFs as the extracting solvent. SFE is an alternative to traditional extraction methods using organic solvents. Extraction is suitable for both solid matrixes and liquids. SFE has some obvious advantages. For example, the process is simple; mild operation temperature; the extraction rate and phase separation can be much faster than those of conventional extraction methods; the extraction efficiency can be controlled through changes of the system pressure and/or temperature because the solubility of a solute in SCFs depends on both vapor pressure of the solute and the solute–solvent interaction; toxic organic solvents can be avoided and the quantity of residual solvent in the products is negligible. Moreover, the addition of small amount of cosolvents to $scCO_2$ can improve the extraction efficiency greatly in many cases. SFE has been studied extensively in food, flavoring, pharmaceutical, petroleum, and coal industries, and some techniques have been commercialized. Some other applications such as catalyst regeneration and soil protection have also been studied.

SFE using $scCO_2$ as the solvent has unusual advantages for the applications in food, flavor, and pharmaceutical industries due to low operation temperature and no solvent residue in the products. Application of SFE in food industry started from 1970s, and this technique has been industrialized [4]. The earliest industrial application of SFE is extracting caffeine from coffee beans using $scCO_2$, and it is shown that the technique has some prominent advantages compared with organic solvent extraction [4]. Another successful application of SFE is the extraction of hops in beer industry [5]. Nonpolar CO_2 is an ineffective solvent for substances of high polarity. Therefore, polar cosolvents are sometimes added to enhance the overall polarity of the fluid phase during extraction. For example, the solubility of phospholipids in neat CO_2 is extremely low in SFE. However, addition of ethanol as cosolvent makes it possible to selectively extract phospholipids from soybeans [6]. Extraction of soybean isoflavones using $scCO_2$ modified with aqueous methanol is studied [7], and the results show that the

isoflavones recovery can be very high at suitable condition.

In the past 3 decades, rapid progress has been obtained for the extraction of essential oils and flavor compounds using $scCO_2$ [8, 9]. On the basis of experimental data of $scCO_2$ extraction of essential oils from plant materials, a mathematical model for the partition of a solute between the solid matrix and the solvent has been proposed [10]. Peach almond oil can also be obtained by means of SFE with a satisfactory yield [11]. The extraction pressure, CO_2 flow rate, and particle size of the matrix on the extraction are evaluated, and the scale-up methodologies are studied.

SFE technique has also been used to upgrade petroleum feedstocks. The separation of petroleum residuum using SFE technique can obtain high-quality deasphalted oil that has been widely used as the raw materials of catalytic cracking and lubricants [12]. The effect of temperature and pressure on the extraction of crude oil and bitumen using $scCO_2$ is investigated [13], and it is demonstrated that higher oil yields can be obtained. In the crude oil and native bitumen extractions, heavier compounds are extracted in supercritical phase as the extraction time and/or the extraction pressure increased. Quantitative recovery of petroleum hydrocarbons from a contaminated soil [14] by SFE technique has also achieved satisfactory results.

Coals can be separated into oils, asphaltenes, and pre-asphaltenes by SFE method. The oil is divided into aliphatics, aromatics, and polar compounds. The prediction method of the solubilities of naphthalene, phenanthrene, phenol, and 2-naphthol in $scCO_2$ has been developed [15]. Study of applications of $scCO_2$ extraction in pharmaceutical industry [16], treatment of nuclear waste [17], and tobacco industry [18] has also obtained satisfactory progress. Some studies have shown that $scCO_2$ can be used to extract triglycerides from a number of natural products effectively. It is concluded that high concentration of triglycerides in the extract and high conversion of methylation lead to a high-quality biodiesel [19].

Chemical Reactions in $scCO_2$

Many chemical reactions have been conducted in $scCO_2$. Besides the solvent is greener, chemical reactions in $scCO_2$ or under supercritical condition have many other advantages. For example, reaction rates, yields, and selectivity can be adjusted by varying temperature and/or pressure; mass transfer can be improved for heterogeneous reactions; and simultaneous reaction and separation can be accomplished more easily for some reactions. In some cases, $scCO_2$ acts as both reactant and solvent.

Hydrogenation Reactions in $scCO_2$ Hydrogenation is a class of important reaction in petroleum, food, and fine chemical industries. The solubility of H_2 in liquids is very small. The excellent miscibility of $scCO_2$ with H_2 and liquid reactants can help to avoid mass-transfer limitation, which are frequently encountered in gas-liquid phase reactions. Application of $scCO_2$ to hydrogenation reactions is particularly attractive [20, 21].

It is known that allyl alcohol easily isomerizes into by-product propanal or acetone during its hydrogenation to produce 1-propanol catalyzed by Pd nanoparticles [22]. To prevent isomerization, Pd nanoparticles can be embedded in polymer to enhance the selectivity of 1-propanol and the stability of the catalysts, but polymer restricted allyl alcohol to access active sites of Pd nanoparticles, which reduce the reaction rate. It is possible improve the reaction rate effectively by using $scCO_2$ due to its higher diffusivity, near zero interfacial tension and swelling effect on polymer. The hydrogenation of allyl alcohol in $scCO_2$ over Pd nanocatalysts on silica support with cross-linked polystyrene coating has been conducted [23]. The selectivity of the reaction can be enhanced significantly by the polymer coating. The catalysts are very stable due to the insoluble nature of the cross-linked polymers, and $scCO_2$ can accelerate the reaction rate of the reaction significantly.

Selective hydrogenation of α, β-unsaturated aldehydes into the corresponding unsaturated alcohols is of importance in flavor, fragrance, and pharmaceutical industries. The selective hydrogenation of citral in $scCO_2$ has been carried out. The selectivity to the partially saturated aldehyde (citronellal) or unsaturated alcohols (geraniol and nerol) can be tuned by varying metal catalysts and CO_2 pressure. The monometallic Pt catalyst is highly selective to the unsaturated alcohol (geraniol and nerol), whereas the bimetallic Pt-Ru catalyst becomes selective to the partially saturated aldehyde (citronellal) under the same $scCO_2$

conditions. The selectivity for the unsaturated alcohols is larger at higher CO_2 pressures. It has also been shown that the selective hydrogenation of citral to produce only geraniol (*trans*) with remarkable selectivity at a very high conversion, and the selectivity for geraniol (*trans*) strongly depends on CO_2 and hydrogen pressure, reaction time, citral concentration, and the reaction temperature [24]. The effect of CO_2 pressure on product distribution for the hydrogenation of citral over Pd and Ru nanoparticles hosted in reverse micelles with $scCO_2$ as the continuous phase has been investigated [25]. The selective formation of a particular hydrogenated product can be achieved by carefully tuning the pressure of the fluid, which can alter the balance between solvation of the molecule into the fluid and its binding affinity to the metal surface.

The selective hydrogenation of nitro compounds is commonly used to manufacture amines, which are important intermediates for dyes, urethanes, agrochemicals, and pharmaceuticals. The hydrogenation of nitrobenzene in $scCO_2$ and in ethanol catalyzed by Pd, Pt, Ru, and Rh supported on C, SiO_2, and Al_2O_3 has been carried out [26]. For all the catalysts, higher selectivity to aniline has been obtained in $scCO_2$ compared with ethanol. The yield to aniline can approach 100% at optimized condition. The hydrogenation of a series of substituted nitro compounds such as 2-,3-,4-nitroanisole, 2-,3-,4-nitrotoluene, 2,4-dinitrobenzene, and 2,4-dinitrotoluene in $scCO_2$ and ethanol has been conducted with carbon supported platinum catalyst [27]. The solubility of these compounds in $scCO_2$ has also been examined at different conditions. The solubility of the nitro compounds increases with increasing CO_2 pressure, but decreases in the presence of hydrogen. Although the total conversion obtained in $scCO_2$ is similar to that in ethanol, the selectivity to amino products is higher in the former reaction medium.

The hydrogenation of phenol is an important approach for preparation of cyclohexanone. Pd is a commonly used catalyst. However, the activity of the reaction is low under mild condition, and the product cyclohexanone can be further hydrogenated to by-product cyclohexanol easily. Therefore, the attainment of high selectivity at elevated conversion with a satisfactory rate is very difficult. Recent work has illustrated that commercial supported Pd catalysts and solid Lewis acids have excellent synergy in the hydrogenation of phenol to cyclohexanone, and the conversion and selectivity of the reaction approach 100% simultaneously under mild condition [28]. Moreover, it is further found that in $scCO_2$ reaction is faster and the reaction efficiency depends on the phase behavior of the reaction system, and the separation process is very easy.

Asymmetric hydrogenation plays a critical role in both the pharmaceutical and agrochemical industries. Hydrogenation of α, β-unsaturated carboxylic acids, such as tiglic acid, has been performed in $scCO_2$ with Ru-based catalyst. The enantiomeric excess (ee) of the product in $scCO_2$ is comparable to that in methanol and greater than that in hexane. $ScCO_2$ has also been used as the medium for the asymmetric hydrogenation of α-enamides using a cationic Rh complex as the catalyst [29]. The reactions can proceed homogeneously at controlled temperature and pressure. The ee is fair to excellent and generally comparable to that obtained in conventional solvents. The asymmetric hydrogenation of C=O [30] and C=N [31] double bonds have also been performed in $scCO_2$. It is demonstrated that $scCO_2$ is an attractive alternative reaction medium for the enantioselective hydrogenation. $ScCO_2$ provides advantages over the organic solvents and enhances the enantioselectivity and catalytic efficiency.

Continuous flow $scCO_2$ has been shown to be a viable medium for conducting continuous asymmetric hydrogenation in the presence of catalysts [32]. The hydrogenation of complex pharmaceutical intermediate, rac-sertraline imine has been optimized in a continuous flow process utilizing a palladium/calcium carbonate catalyst in $scCO_2$ [33]. Superior levels of selectivity can be obtained in the flow system. It is suggested that the excellent heat transfer properties of the $scCO_2$ help to maintain exceptional levels of chemoselectivity even at elevated temperature. The application of $scCO_2$ in continuous, fixed bed reactors has allowed the successful development of a variety of industrially viable synthetic transformations. The multireaction, supercritical flow reactor was commissioned in 2002. The development of this project from laboratory to plant scale is highlighted, particularly in the context of the hydrogenation of isophorone [34].

Oxidation Reactions in $scCO_2$ Oxidation reactions are among the most important processes for introducing functional groups into hydrocarbons. $ScCO_2$ is advantageous because of its inertness towards oxidation, thus providing additional safety and avoiding side products from solvent oxidation. The selective oxidation of hydrocarbons with molecular oxygen is of special interest for synthetic chemistry from an economic as well as an ecological point of view. $ScCO_2$ allows the combination of high concentration of substrates and oxygen with the additional safety. It has been reported that the presence of CO_2 can improve yields, reaction rates, and/or selectivities in some selective alkane and alkene oxidation processes.

The selective oxidation of cyclohexane into cyclohexanol and cyclohexanone is of considerable importance in chemical industry for producing Nylon-6 polymers. The selective oxidation reaction of cyclohexane to produce cyclohexanol and cyclohexanone is carried out in CO_2 at 398.2 K using oxygen as an oxidant, and the reaction mixture is controlled to be in the two-phase region, very close to the critical point, and in the supercritical region of the reaction system. The effect of a small amount of butyric acid cosolvent on the reaction in $scCO_2$ is also studied [35]. The conversion and selectivity of the reaction in $scCO_2$ change considerably with the phase behavior or the apparent density of the reaction system. Addition of a small amount of butyric acid cosolvent to $scCO_2$ enhances the conversion significantly, and the selectivity also changes considerably. The by-products of the reaction in $scCO_2$ with and without the cosolvent are much less than that of the reaction in liquid solvents or in the absence of solvents. The use of supported metal oxides leads to higher yields for target products cyclohexanone and cyclohexanol compared to the immobilized complexes. A series of CoAPO-5 with different Co contents have been synthesized and used to catalyze selective oxidation of cyclohexane in $scCO_2$ [36]. The CoAPO-5 catalysts are effective catalysts for the reaction and the total selectivity of objective products are high in $scCO_2$.

The oxidation of cyclooctane to cyclooctanone with molecular oxygen and acetaldehyde as a coreductant proceeds efficiently in the presence of compressed CO_2 [37]. CO_2 is more effective than other inert diluting gases at the same conditions. The selective oxidation of other alkanes has also been studied, and the results are promising [38]. For example, the oxidation of cycloalkanes or alkylarenes with molecular oxygen and acetaldehyde as sacrificial coreductant occurs efficiently in $scCO_2$ under mild multiphase conditions without catalyst. In comparison with other inert gases, the yields of alkane oxygenates in CO_2 is higher at identical reaction conditions.

Wacker reaction is an efficient way to produce methyl ketones via the Pd(II)-catalyzed oxidation of terminal olefins. It has been shown that the Wacker reaction of oct-1-ene can be proceeded smoothly in $scCO_2$ or methanol/$scCO_2$ mixed SCF [39]. The selectivity of product octa-2-one of the reaction proceeded in $scCO_2$ is obviously higher than that in methanol at the same reaction time. However, the reaction rate in $scCO_2$ is lower than that in methanol due to the insoluble nature of $PdCl_2$ and $CuCl_2$ in $scCO_2$. Nevertheless, addition of cosolvent methanol in $scCO_2$ can accelerate the reaction rate and reduce the isomerization of oct-1-ene. $PdCl_2$/polystyrene-supported benzoquinone can also be employed as the catalyst for the acetalization of terminal olefins with electron-withdrawing groups [40]. In $scCO_2$, the reaction can proceed with high yield and selectivity, and the catalyst can be easily recycled.

The selective oxidation of styrene to acetophenone over Pd-Au bimetallic catalyst using H_2O_2 as the oxidant in $scCO_2$ medium has been studied [41]. The bimetallic catalyst supported on Al_2O_3 is very effective for the reaction. The presence of CO_2 improves the oxidation of styrene to acetophenone and inhibits the formation of the by-products. An electron-donating group at the *para*-position of styrene increases the conversion of styrene, but an electron-withdrawing group at the *meta*-position of styrene reduces both the conversion and the selectivity to acetophenone.

Poly(ethylene glycol) (PEG) is an inexpensive, nonvolatile, and environmentally benign solvent, which is another kind of green reaction medium. Combination of PEG and $scCO_2$ has some obvious advantages for chemical reactions. The $PdCl_2$-catalyzed aerobic oxidation of styrene in a biphasic PEG/$scCO_2$ system results in two possible products, benzaldehyde and the Wacker oxidation product acetophenone [42]. The selectivity of the reaction can be switched by the cocatalyst CuCl, from 92% in favor of acetophenone in the presence of

CuCl to 85% favoring benzaldehyde without any cocatalyst. The PEG in the reaction system can effectively stabilize the catalysts.

Alkyl 3,3-dialkoxypropanoates are important intermediates in organic synthesis and have been used to synthesize a variety of compounds. The oxidation of methyl acrylate catalyzed by Pd(II)/$CuCl_2$ can be carried out in $scCO_2$ to give the dimethyl acetal as major product when an excess amount of methanol is used [43]. A conversion of 99.4% and selectivity of 96.6% can be obtained under the suitable condition. The reaction medium and the electron property of alkene substituent group obviously influence the regioselectivity of oxidation for methyl acrylate.

The aerobic oxidation of alcohols to aldehydes and ketones is a fundamental chemical transformation for the production of a variety of important intermediates and fine chemical products. Aerobic oxidation of benzyl alcohol in $scCO_2$ catalyzed with perruthenate immobilized on polymer supports has been conducted [44]. The catalyst is very active and highly selective in $scCO_2$. The reaction rate in $scCO_2$ depends strongly on pressure and reaches maximum at about 14 MPa, which can be explained by the effects of pressure on the phase behavior of reaction system, diffusivity of the components, and solvent power of $scCO_2$. The catalyst can be reused directly after extraction of the products using $scCO_2$. PEG/CO_2 biphasic system has also been used for aerobic oxidation of alcohols. For example, a highly efficient PEG/CO_2 biphasic catalytic system for the aerobic oxidation for allylic alcohols, primary and secondary benzylic alcohols, cyclic alcohol, and 1-butanol has been reported [45], which is highly active, selective, and stable for a broad range of substrates. In the system, the PEG matrix effectively stabilizes and immobilizes the catalytically active Pd nanoparticles, whereas the unique solubility and mass-transfer properties of $scCO_2$ allow continuous processing at mild conditions, even for the low-volatility substrates. This system well exemplifies the benefits resulting from the combination of $scCO_2$ and PEG for the reactions. Study of aerobic oxidation of benzhydrol, 1-phenylethanol, and cyclohexanol to corresponding ketones in PEG/$scCO_2$ biphasic system using unsupported and supported $CoCl_2{\cdot}6H_2O$ as the catalysts [46] has indicated that the $CoCl_2{\cdot}6H_2O$, Co(II)/Al_2O_3, and Co(II)/ZnO are all active and selective for the reactions, and the yields of the desired products can be optimized by the pressure of $scCO_2$. Co(II)/ZnO is most stable and can be reused. Recently, a miniature catalytic reactor has been developed, which can be used for the continuous oxidation of primary and secondary alcohols with molecular oxygen in $scCO_2$. Satisfactory yields can be achieved at the optimized conditions [47].

Photo-oxidation in $scCO_2$ has become an interesting topic. A continuous photocatalytic reactor for performing reactions of $^1O_2$ in $scCO_2$ has been developed. The reactor has demonstrated the potential of using light-emitting diodes (LED) for performing synthetic photochemistry in a continuous milliliter-scale reactor. This has been accomplished by the combination of high-power LED technology with a high-pressure $scCO_2$ reactor system capable of supporting high concentrations of O_2 with negligible mass-transfer limitations [48].

A $scCO_2$-soluble photosensitiser has been used to perform $^1O_2$ reactions of α-terpinene, 2,3-dimethyl-2-butene, and 1-methyl-cyclohexene in $scCO_2$ [49]. The three reactions show zero-order kinetics and quantitative conversions with reasonable reaction rate. Some insoluble photosensitisers have also been evaluated with highly fluorinated surfactants and dimethyl carbonate cosolvent. It is clear that the applicability of $^1O_2$ reactions in $scCO_2$ has been significantly enhanced by the use of these surfactants and cosolvent.

Carbon–Carbon Bond Forming Reactions The efficient generation of a carbon–carbon bond is the essence of synthetic chemistry. The efficient formation of carbon–carbon bonds is still a synthetic challenge in organic chemistry although this topic has been the focus for many years.

The Diels–Alder reactions are among the most important synthetic reactions for the construction of polycyclic ring compounds. The Diels–Alder reaction in $scCO_2$ is also an interesting topic [50, 51]. Investigation of the Diels–Alder reaction between *p*-benzoquinone and cyclopentandiene in CO_2 illustrates that the reaction effectively occurs throughout the liquid and supercritical range with no discontinuity and that the rate of the reaction is about 20% larger than those obtained in diethyl ether [52]. It has been shown that for the Diels–Alder reaction in $scCO_2$ using scandium tris(heptadecafluorooctanesulfonate)

as a Lewis acid catalyst [53], the catalyst activity is improved by increasing the length of the perfluoroalkyl chain and its solubility. This catalyst has also been used in the aza-Diels–Alder reaction of Danishefsky's diene with the imine in $scCO_2$, and 99% yield of the corresponding aza-Diels–Alder adduct can be obtained.

$PdCl_2$ is a commonly used catalyst for the cyclotrimerization of alkynes to substituted benzene derivatives. Cyclotrimerization of alkynes to substituted benzene derivatives in $scCO_2$ can smoothly proceed [54]. The yields and regioselectivities are high as $CuCl_2$ and methanol are added. $CuCl_2$ can not only accelerate the rate of cyclotrimerization of alkynes, but also is an absolutely indispensable factor for the cyclotrimerization of unsymmetrical alkynes.

The Glaser coupling is a synthesis of symmetric or cyclic bisacetylenes via a coupling reaction of terminal alkynes. There is a competition between coupling and carbonylation reactions when carbonylation reaction is operated in $scCO_2$. The Glaser coupling can be carried out effectively in $scCO_2$ using a solid base instead of amines [55]. The coupling reaction gives low conversion and yield in pure $scCO_2$, in which $CuCl_2$ and NaOAc cannot dissolve. However, the presence of methanol remarkably enhanced the rate of the reaction. The higher CO_2 pressure is favorable to the enhancing the reaction. In $scCO_2$, the coupling can also take place without base with higher conversion and yield than those in the presence of pyridine.

Suzuki and Heck reactions are among the most versatile families of reactions. The catalysts soluble in $scCO_2$ are crucial for high reaction efficiency. Polyfluoroalkylphosphine ligand has been prepared to enhance the solubility of Pd(II) catalysts for coupling reactions of phenyl iodide [56]. While $PdCl_2[P(C_6H_5)_3]_2$ and $Pd(O_2\text{-}CCH_3)_2[P(C_6H_5)_3]_2$ are insoluble in $scCO_2$, their analogues containing $P(C_6H_5)_{3\text{-}n}(CH_2CH_2C_6F_{13})n$ (n = 1 or 2) ligands are partially soluble. In the Suzuki reaction of phenyl boronicacid catalyzed by Pd $[(C_6F_{13}CH_2CH_2)_2PC_6H_5]_2Cl_2$, the yield of biphenyl in $scCO_2$ is higher than that in benzene medium. Study has also indicated that the homocoupling of iodoarenes catalyzed by $Pd(OCOCF_3)_2/P(2\text{-furyl})_3$ occurs effectively in $scCO_2$ [57], which provides an attractive alternative to conventional procedures. In addition, there is preferential solvation effect for the reaction in $scCO_2$.

Study of Heck coupling reaction of phenyl iodide [58] demonstrates that the coupling reaction can proceed in $scCO_2$ with rates and selectivites comparable to those in toluene. The fluorinated phosphines, particularly tris[3,5-bis(trifluoromethyl)phenyl]phosphine, result in high conversions due to the ability of these ligands to enhance the solubility of the metal complexes in $scCO_2$. CO_2-philic ligands can expand the utility of $scCO_2$ for homogeneous catalysis efficiently.

Hydroformylation of olefins is an important industrial reaction used to transform alkenes into aldehydes using carbon monoxide and hydrogen. The reaction of propene with a Co catalyst $Co_2(CO)_8$ occurs at a slightly lower rate in $scCO_2$ than in hydrocarbon solvents such as methylcyclohexane and heptane [59], and the selectivity to the desired linear aldehyde, butanal is higher than that in the organic solvent. The linear-to-branch ratio is slightly influenced by the reaction pressure and temperature [60]. The linear product selectivity increases as pressure increases. One possible explanation for the change in the selectivity is a steric effect of a CO_2 molecule coordinated to the central metal as observed in the CoH $(CO)_3[P(C_4H_9)_3]$ catalyst system. Kinetic study of the reaction has demonstrated that the activation energy obtained in $scCO_2$ is comparable to or somewhat lower than those in organic solvents. More detailed study for the effect of different solvents on hydroformylation of olefins suggests that $scCO_2$ has some obvious advantages. Continuous process for the selective hydroformylation of higher olefins in $scCO_2$ is investigated [61, 62]. The catalyst shows high selectivity and activity over several hours and decrease in performance does not occur over several days.

Olefin metathesis refers to the mutual alkylidene exchange reaction of alkenes. $[Ru(H_2O)_6](OTs)_2$ (Ts=*p*-toluenesulfonyl) can catalyze the ring-opening metathesis polymerization (ROMP) of norbornene in $scCO_2$ [63]. The product can be isolated by just venting the CO_2. The chemical yield and molecular weight of the polymers are comparable to those in conventional solvents. Norbornene is quite soluble in $scCO_2$ under the reaction conditions, although the Ru catalyst is not completely soluble. However, the catalyst is sufficiently soluble for the completion of the reaction.

In the presence of methanol cosolvent, the catalyst dissolved. The polymers obtained in $scCO_2$ have high *cis* olefin content, but adding methanol in $scCO_2$ results in a significant decrease in the *cis* content, indicating that the structure of the polymer is controllable by adjusting the polarity of the CO_2 medium with methanol. The isolable metal-carbene complexes are also highly effective for the ROMP of norbornene in $scCO_2$ [64]. Although the Ru-carbene complex retains catalytic activity even under aqueous emulsion conditions, $scCO_2$ is another environmentally benign solvent besides H_2O and offers the possibility of developing new polymer syntheses without solvent waste. It has also been reported that $scCO_2$ is a versatile reaction medium for ROMP and ring-closing olefin metathesis reactions using ruthenium and molybdenum catalysts. The unique properties of $scCO_2$ provide significant advantages beyond simple solvent replacement. This pertains to highly convenient workup procedures both for polymeric and low molecular weight products, to catalyst immobilization, to reaction tuning by density control, and to applications of $scCO_2$ as a protective medium [65].

Catalysis of Enzyme in $scCO_2$ Enzymes have been used widely as biocatalysts. However, the possibility of using enzymes as heterogeneous catalysts in supercritical media opens up more possibilities for chemical synthesis. Enzyme catalyzed reactions have been studied widely since the mile 1980s [66, 67]. Among enzymes active in $scCO_2$, lipase has been most frequently used because it catalyzes various types of reactions with wide substrate specificity. Thus, lipase-catalyzed reactions in $scCO_2$ have been carried out for different reactions, such as hydrolysis of triacylglycerol [68], alcoholysis of palm kernel oil [69], glycerolysis of soybean oil [70], acylation of glucose with lauric acid [71], transesterifications of milk fat with canola oil [72], and synthesis of poly-L-lactide [73].

The effect of compressed CO_2 on the specific activity of chloroperoxidase to catalyze the chlorination of 1,3-dihydroxybenzene in cetyltrimethylammonium chloride/H_2O/octane/pentanol reverse micellar solution has been studied [74]. The results show that the specific activity of the enzyme can be enhanced significantly by compressed CO_2, and the specific activity can be tuned continuously by changing pressure.

The main advantages of using $scCO_2$ as solvent for biocatalyzed reactions are the tunability of solvent properties and simple downstream processing features that can be readily combined with other unit operations. Although many enzymes are stable in $scCO_2$, attention should be paid to identify the correct reaction conditions for each substrate/enzyme/SCF system. One of the persistent problems is the instability and deactivation of enzymes under pressure and temperature [75].

Some Other Reactions in $scCO_2$ Many other reactions in $scCO_2$ have also been studied, and promising results have been obtained. For example, the reaction between 1,n-terminal diols (n=3 or 6) with simple alcohols (MeOH, EtOH, and n-PrOH) in $scCO_2$ over an acid catalyst leads to two possible products, a mono and a bis-ether [76]. The selectivity of the reaction with 1,6-hexanediol and MeOH can be switched from 1:20 in favor of the bis-ether to 9:1 in favor of the desymmetrized mono-ether with the increase of CO_2 pressure. It is demonstrated that the switch in selectivity is associated with the phase state of the reaction mixture.

High-yielding and greener routes for the continuous synthesis of methyl ethers in $scCO_2$ have been developed [77]. Ethers have been efficiently produced using a methodology which eliminates the use of toxic alkylating agents and reduces the waste generation that is characteristic of traditional etherification processes. The use of acidic heterogeneous catalysts can achieve etherification when using $scCO_2$ as a reaction medium.

The esterification of acetic acid and ethanol in $scCO_2$ has been studied [78]. The phase behavior and the isothermal compressibility of reaction system are also determined under the reaction conditions. The conversion increases with increasing pressure in the two-phase region and reaches a maximum in the critical region of the reaction system where the system just becomes one phase. Then the conversion decreases with pressure after the pressure is higher than the critical value. The study on transesterification between ethyl acetate and *n*-butanol in $scCO_2$ demonstrates that the equilibrium conversion is very sensitive to pressure as the reaction mixture approaches the critical point, bubble point, and dew

point of the reaction mixtures in the critical region, whereas the effect of pressure on equilibrium conversion is not significant outside the critical region [79]. All these results indicate that the equilibrium conversions of the reversible reactions can be tuned effectively by pressure in the critical regions of the reaction mixtures. Continuous dehydration of alcohols in $scCO_2$ shows that CO_2 can provide significant advantages in these heterogeneous, acid-catalyzed reactions over a wide range of temperatures and pressures [80]. Furthermore, using $scCO_2$ as the solvent for ether formation will encourage the phase separation of H_2O, which appears to reduce back reaction via rehydration of the product.

Dimethyl carbonate(DMC) is a very useful chemical. Synthesis of DMC using $scCO_2$ and methanol is studied, and the phase behavior and critical density of the reaction system are also determined [81]. The reaction is carried out at various pressures that correspond to conditions in the two-phase region, the critical region as well as the single-phase supercritical region. The original ratios of the reactants CO_2:CH_3OH are 8:2 and 7:3, and the corresponding reaction temperatures were 353.2 K and 393.2 K, respectively, which are slightly higher than the critical temperatures of the reaction systems. The results indicate that the phase behavior affects the equilibrium conversion of methanol significantly and the conversion reaches a maximum in the critical regions of the reaction system. At 353.2 K, the equilibrium conversion in the critical region is about 7%, and can be about three times as large as those in other phase regions. At 393.15 K, the equilibrium conversion in the critical region is also much higher and can be twice as large as those in other phase regions.

Chemical Reactions in $scCO_2$/Ionic Liquid Systems

Ionic liquids (ILs) are salts that are liquid at ambient conditions. They are a relatively new type of solvents, which have attracted much interest as an alternative for volatile organic compounds. ILs have some unique properties, such as extremely low vapor pressure, excellent solvent power for both organic and inorganic compounds, high thermal and chemical stability. In addition, functions ILs can be designed by varying the cations and anions to afford certain specific properties. Combination of CO_2 and ILs is an interesting topic. The very distinct properties of $scCO_2$ and ILs make them good combination to form biphasic solvent systems with special properties. High-pressure CO_2 is soluble in ILs, while ILs are almost insoluble in $scCO_2$ [82]. Therefore, at suitable conditions the organic compounds can be extracted from the ILs without cross-contamination. With these unique properties, CO_2/IL biphasic systems can be used not only in separation, but also in biphasic reactions. It has been shown that $scCO_2$/IL biphasic system can shift chemical equilibrium of revisable reactions and improve conversion and selectivity of chemical reactions [83].

The oxidation of aromatic alcohol into corresponding aldehyde is an important transformation because aromatic aldehdyes are versatile intermediates for the production of pharmaceuticals, plastic aitives, and perfumes. However, a major drawback of such oxidation reactions is their lack of selectivity owing to the easy over-oxidation of aldehydes into carboxylic acids. Electro-oxidation reaction of benzyl alcohol in $scCO_2$/ILs is investigated using 1-butyl-3-methylimidazolium tetrafluoroborate ([Bmim][BF_4]) and 1-butyl-3-methylimidazolium hexafluorophosphate ([Bmim][PF_6]) as the ILs and electrolytes [84]. It is demonstrated that benzyl alcohol can be efficiently electro-oxidized to benzaldehyde. [Bmim][BF_4] is more effective medium for the electro-oxidation of benzyl alcohol. The product can be easily recovered from the IL by using $scCO_2$ extraction after the electrolysis, and the IL can be reused. The Faradic efficiency (FE) and selectivity of benzaldehyde increase with the pressure of CO_2 when the pressure is lower than about 9.3 MPa, while the FE decreases as the pressure is increased further. This phenomenon can be explained reasonably on the basis of solubility difference of the reactant and product.

Enhancing equilibrium conversion of reversible reactions has been a topic of great importance for a long time. The effect of CO_2 on the phase behavior of the reaction system and equilibrium conversion for esterification of acetic acid and ethanol in IL 1-butyl-3-methylimidazolium hydrogen sulfate ([bmim][HSO_4]) is studied up to 15 MPa [85]. There is only one phase in the reaction system in the absence of CO_2. The reaction system undergoes two-phase→three-phases→two-phase transitions with increasing pressure.

The pressure of CO_2 or the phase behavior of the system affected the equilibrium conversion of the reaction markedly. As the pressure is less than 3.5 MPa, there are two phases in the system, and the equilibrium conversion increases as pressure is increased. In the pressure range of 3.5–9.5 MPa, there exist three phases, and the equilibrium conversion increases more rapidly with increasing pressure. As the pressure is higher than 9.5 MPa, the reaction system enters another two-phase region and the equilibrium conversion is nearly independent of pressure. The total equilibrium conversion was 64% without CO_2 and can be as high as 80% as pressure is higher than 9.0 MPa. The apparent equilibrium constants (Kx) in different phases are also determined, showing that the Kx in the mile phase or top phase is much greater than that in the bottom phase.

Oxidation of 1-hexene by molecular oxygen is conducted in [bmim] [PF_6], $scCO_2$, $scCO_2$/[bmim] [PF_6] biphasic system, and in the absence of solvent [86]. The difference in conversion at various reaction times in $scCO_2$ and in the CO_2/IL mixture is not considerable. However, in the $scCO_2$/IL biphasic system, the selectivity to the desired product is much higher than that in $scCO_2$. Moreover, the selectivity in the biphasic system increases slightly with reaction time, while the selectivity decreases slowly with reaction time in $scCO_2$. The conversion is very high and is nearly independent of pressure. However, the selectivity increases with pressure significantly, especially in the low-pressure range. A reasonable explanation is that the solvent power of CO_2 increases with increasing pressure. Therefore, less reactant exists in the IL-rich phase at higher pressure, which favors reduction of the isomerization of the reactant. Meanwhile, the solubility of CO_2 in the IL increases with pressure, and so the diffusivity of the solvent is improved more significantly at the higher pressures, which may also enhance the selectivity. In addition, the catalyst used is more stable in the $scCO_2$/IL biphasic system than in $scCO_2$.

A continuous flow system for the hydroformylation of relatively low-volatility alkenes in $scCO_2$/IL biphasic systems has been reported [87]. The catalyst is dissolved in an IL, while the substrate and gaseous reagents dissolved in $scCO_2$ are transported into the reactor, which simultaneously acts as a transport vector for aldehyde products. Decompression of the fluid mixture yields products which are free of both reaction solvent and catalyst. The nature of the ILs is very important in achieving high rates, with 1-alkyl-3-methylimidazolium bis(trifluoromethanesulfonyl)amides giving the best activity if the alkyl chain is at least C-8. High catalyst turnover frequencies have been obtained, with the better rates at higher substrate flow rates. The leaching of the catalyst into the product stream can be very low. Under certain process conditions, $scCO_2$/IL biphasic system can be operated continuously for several weeks without any visible sign of catalyst degradation.

Polymerization in $scCO_2$

$ScCO_2$ has received considerable attention as an environmentally benign reaction medium for polymerization. The early research on polymerization in CO_2 can be dated back to the 1960s [88]. However, less attention was received on this because viscous solid or liquid polymer with low molecular weight were produced, which are practically useless. In early 1990s, homogeneous solution polymerization of 1,1-dihydroperfluorooctyl methyl acrylate monomers in $scCO_2$ was reported using azo-bisisobutyronitrile as the initiator [89]. The polymerization in $scCO_2$ has become an interesting topic since then [90–92]. There are some unique aspects of polymerization in $scCO_2$, such as the solvent is green; the molecular weight and the morphologies of the products can be tailored by pressure; the resulting polymer can be isolated from the reaction medium by simple depressurization, resulting in a dry, solvent-free product. These make it possible for $scCO_2$ to replace hazardous volatile organic solvents in some industrial applications.

The solubility of polymer in $scCO_2$ has a decisive effect on the polymerization. While CO_2 is a good solvent for many low molecular weight monomers, it is a very poor solvent for most polymers. The only polymers to have good solubility in pure $scCO_2$ under mild conditions are amorphous fluoropolymers and silicones. This has allowed the synthesis of high molecular weight fluoropolymers by homogeneous solution polymerization in $scCO_2$. Except for the synthesis of fluoropolymers, most polymerizations in $scCO_2$ have

been carried out by heterogeneous polymerization, mainly including suspension, emulsion, dispersion, and precipitation polymerizations. The fore three polymerizations need the addition of special fluoro-surfactants that can dissolve in $scCO_2$. Although some nonfluoro-nonionic-surfactants and nonfluoro-ionic-surfactants have been reported, they cannot meet the requirement satisfactorily.

Although the solubility of most polymers in $scCO_2$ is extremely low, the solubility of $scCO_2$ in many polymers is fairly large. This can lead to a dramatic decrease in the glass transition temperature (*Tg*) of these materials (i.e., plasticisation), even at modest pressures [93]. It has been shown by various methods that CO_2 is a good plasticizing agent for a number of polymeric materials [94]. In heterogeneous polymerization, plasticization can facilitate diffusion of monomer and initiator into the polymer phase to increase the rate of polymerization.

Preparation of Materials

SCF technology has penetrated into various fields of materials science, including generation of superfine particles, microporous materials, composite materials, and semiconductor devices [95]. The material preparation using $scCO_2$ technology has some unique advantages, and some special materials that are difficult to be prepared by other techniques can be fabricated due to the special properties of SCFs. Application of $scCO_2$ in material science has bright future.

Preparation of Fine Particles and Porous Materials

There are two kinds of methods to prepare superfine particles using $scCO_2$, i.e., physical and chemical methods. Physical method mainly includes rapid expansion of SCF solutions (RESS) and supercritical anti-solvent (SAS) process, and some new methods have been derived on the basis of RESS and SAS.

The technique of RESS was developed in the late 1980s [96]. The most attractive advantage of RESS is that it can produce particles with relatively narrow size distribution, which can be particularly important for drug delivery systems. The main disadvantage of RESS is that it can only be applied to produce materials which are soluble in $scCO_2$. Since the solubility of most materials in $scCO_2$ is relatively low, a large amount of CO_2 is used to prepare small amount of particles. Therefore, this technique is relatively costly and is usually used in laboratory or producing high-value-added products. Up to now, many particles have been fabricated by RESS, such as fine particles of composite polymer microparticles [97], semiconductor particles [98], and pharmaceutical particles [99].

Study of SAS technique began in early 1990s [100], which has been developed rapidly. This technique can be used to process the substances that are not soluble in the supercritical medium. In the process, the materials of interesting are dissolved into an organic liquid that is miscible with $scCO_2$ under appropriate process conditions. When in contact with liquid solution, the SCF dissolves into the liquid, a large and fast expansion of the liquid phase occurs, and small particles of solute can be precipitated [101]. The SAS technique has been further developed using compressed CO_2 as antisolvent to recover the nanoparticles and nanocomposites synthesized in reverse micelles, such as protein [102] and ZnS [103], nanoparticles, and Ag/PS nanocomposites [104].

Another method to prepare superfine particles using $scCO_2$ as medium involves chemical reaction. Inorganic materials including metals, semiconductors, nitrides, and oxides are prepared by thermal decomposition reaction or redox reaction in $scCO_2$. $ScCO_2$ can be a good solvent for many organometallic compounds and the ligands, but a poor solvent for the inorganic compounds. Therefore, precursor reduction occurs at the solution/solid interface at significantly lower temperature and higher reagent concentration than those of vapor-phase techniques like chemical vapor deposition. In addition, the presence of $scCO_2$ facilitates desorption of the ligands on the metal surfaces, which are produced from the decomposition of organometallic compounds [105].

Inorganic nanomaterials in $scCO_2$ can be prepared by the reduction of organometallic compounds with H_2 due to the high miscibility of $scCO_2$ with H_2 [106]. Preparation of core-shell magnetic materials from the precursor bis(hexafluoroacetylacetonate)-copper(II) solubilized in the $scCO_2$/ethanol mixture has been studied [107]. The results show that Ni/Cu core-shell

structure particles increase the coercive field due to the existence of Cu shell layer.

The polymerization of tetraalkoxysilanes tetramethoxysilane and 1,4-bis(triethoxysilyl)benzene in $scCO_2$ is carried out by using formic acid as the condensation reagent, and silica aerogels and 1,4-phenylene-bridged polysilsesquioxane aerogels are fabricated, respectively [108]. $ScCO_2$ appears to be an excellent solvent for preparing highly porous architectures with both meso- and macroporous structure, and seems to be a better solvent than ethanol for preparing phenylene-bridged polysilsesquioxane aerogels. In addition, the process can be used to generate monolithic aerogels in a single step from their monomeric precursors. It has also been reported that silica aerogel particles can be obtained in $scCO_2$ using acetic acid as the condensation agent for silicon alkoxides [109]. It is shown that acetic acid is a mild and controllable agent for sol-gel route preparation of silica aerogel particles. By changing the ratio of silicon alkoxide, acetic acid, and water, the polymerization rate is tunable and precipitation can be prevented. Submicron particle sizes can be obtained when the sol-gel solution is destabilized by pressure reduction and particles as small as 100 nm can be formed using the improved RESS process.

The synthesis of hollow silica spheres with mesoporous wall structures via CO_2-in-water emulsion templating in the presence of nonionic PEO-PPO-PEO block copolymer surfactants as mesostructure-directing templates has been investigated under various conditions [110]. The successful synthesis of hollow spheres strongly depends on the pressure and density of CO_2. The pore size and morphology of the silica hollow spheres can be controlled by varying the pressure of CO_2.

Well-ordered mesoporous silicate films have been prepared by infusion and selective condensation of silicon alkoxides within microphase-separated block copolymer templates dilated with $scCO_2$ [111]. Confinement of metal oxide deposition to specific subdomains of the preorganized template yields high-fidelity, three-dimensional replication of the copolymer morphology, enabling the preparation of structures with multiscale order in a process that closely resembles biomineralization. Ordered mesoporous silicate films synthesized have very low dielectric constants and excellent mechanical properties. The films survive the chemical–mechanical polishing step required for device manufacturing.

Polymer foams created using $scCO_2$ as a processing solvent have attracted much interest in recent years, and some progress has been achieved. For example, the foaming of fluorinated ethylene propylene copolymer films using $scCO_2$ is investigated [112]. The films prepared show a homogeneous cellular structure with thin compact polymer layers on both sides. The foaming behavior of the polymer films is dependence on the exposure time of the polymer to the $scCO_2$, the processing temperature and pressure as well as on the pressure drop rate during the foaming process. The resulting density and the foam morphology depend on the pressure during the saturation process. The size of the cells generated depends mainly on the foaming temperature, whereas their number per volume is determined mainly by the applied pressure. Furthermore, the pressure drop rate influences the size of the cells in a way that significantly fewer but larger bubbles are formed for longer times of depressurizing. The properties of $scCO_2$ make it suited to replace organic solvents that are being phased out for environmental reasons. A number of processes and products are already being used in industry [113].

Preparation of Composite Materials and Devices

As mentioned above, SCFs can easily carry dissolved matters into any accessible place, which provides a new approach for the preparation of composite materials. Various composite materials using $scCO_2$ as a medium have been prepared and studied extensively, including polymer composites, organic/inorganic hybrid materials and inorganic/inorganic composites.

The ability of $scCO_2$ to swell polymers is beneficial for the preparation of polymer composites. $ScCO_2$ can carry dissolved small molecules into swollen polymer matrix to prepare polymer-based composites. A number of polymeric composites have been fabricated using this route. For example, styrene monomer and initiator can be infused into polymer substrates such as poly (chlorotrifluoroethy1ene), poly(4-methyl-1-pentne), poly(ethy1ene), nylon 66, poly(oxymethy1ene), and

bisphenol A polycarbonate, and the corresponding polymer blends are formed after free-radical polymerization [114].

Because many organometallic precursors are soluble in $scCO_2$, metal/polymer materials can also be prepared by impregnate metal precursors into polymer matrix using $scCO_2$ as the solvent, followed by chemical or thermal reduction of the precursors to the base metals [115, 116]. Similarly, the swelling property of $scCO_2$ has also been used to fabricate Eu_2O_3/polystyrene composites via decomposition of europium nitrate hexahydrate in $scCO_2$/ethanol solution in the presence of dispersed polymeric hollow spheres [117]. In addition to adhering to the outer surface, the Eu_2O_3 nanoparticles impregnate the shell and the cavity of the polystyrene substrate.

Carbon nanotubes (CNTs) have received much attention owing to their special electrical, mechanical, and optical properties. SCF techniques show intriguing advantages for the synthesis of various CNT-based composites. The composites can be fabricated by deposition of metal and metal oxide on CNTs using $scCO_2$ as the solvent [118, 119]. Because the deposition process involves only H_2 and precursors, it is possible to apply the same method to fabricate other metal/CNT composites, or to coat CNTs with metal films or nanoparticles. From the various results presented, it is clear that chemical fluid deposition in $scCO_2$ provides an effective and clean way to decorate CNTs. For instance, coating of Eu_2O_3 on CNTs in $scCO_2$-ethanol mixture can be accomplished [120]. Similarly, Poly (2,4-hexadiyne-1,6-diol) (poly(HDiD)) can be coated on the outer walls of CNTs with the aid of $scCO_2$, resulting in poly(HDiD)/CNT nanocomposites, which possess optical properties originated from poly (HDiD) [121]. Coating CNTs with solvent resistant polymer in $scCO_2$ has also been achieved [122], which permits the selective deposition of high molecular weight fluorinated graft poly(methyl vinyl ether-alt-maleic anhydride) polymer onto CNTs and forms quasi one-dimensional nanostructures with conducting cores and insulating surfaces.

Some special microporous, mesoporous, and layer composites have also been prepared in $scCO_2$, such as size-controlled Pt nanoparticles in micro- and mesoporous silica. $ScCO_2$ is an excellent solvent for the introduction of nanoparticles into small spaces on a nanometer scale due to its special properties [123].

Zr-TiO_2 nanotubes have been synthesized via a surfactant-free sol-gel route in $scCO_2$. The morphology of the Zr-TiO_2 nanotubes can be tailored by changing the concentration of the starting materials or the acid-to-metal-alkoxide ratio. The formed Zr-TiO_2 nanotubes have high surface area, small crystallite size, and high thermal stability, and are highly desirable as catalysts, support materials, semiconductors, and electrodes in dye-sensitized solar cells. This synthesis procedure is simple and reaction condition is mild, and provides a high yield and high-quality nanotubes [124].

High-purity conformal metal oxide films can be deposited onto planar and etched silicon wafers by surface-selective precursor hydrolysis in $scCO_2$ using a cold wall reactor [125]. Continuous films of cerium, hafnium, titanium, mobium, tantalum, zirconium, and bismuth oxides with different thick are grown using CO_2 soluble precursors. The as-deposited films are pure single-phase oxide in the cases of HfO_2, ZrO_2, and TiO_2 and composed of oxides of mixed oxidation states in the cases of cerium, tantalum, niobium, and bismuth oxides.

Carbon black supported single Pd, Pt and bimetallic Pd-Pt nanoparticles have been prepared utilizing $scCO_2$ deposition method with hydrogen as the reducing agent [126]. Increasing reduction temperature and metal loading caused an increase in Pd particle size. The Pt nanoparticles are homogeneously distributed with a size range of 2–6 nm. Binary metal nanoparticles can also be produced by simultaneous adsorption and subsequent reduction of the precursors. Addition of Pt increases the homogeneity and reduces the particle size on the support compared to single Pd nanoparticles. Pt-rich nanoparticles have diameters of around 4 nm, whereas Pd-rich nanoparticles are larger with diameters of around 10 nm.

Supercritical Chromatography

SCFs have been used as chromatographic mobile phases for several decades [127, 128]. Supercritical fluid chromatography (SFC) using $scCO_2$ as a mobile phase has been applied to analyze a wide variety of materials [129], including chiral separation [130, 131]. It has

also been proven that SFC has high performance to control the enantiomeric purity of the final drug substance [132]. SFC has recently been utilized for the separation of furocoumarins of essential oils [133] and evaluation of a condensation nucleation light scattering detector for the analysis of synthetic polymer [134]. SFC combines some advantages of both liquid chromatography and gas chromatography, including high efficiency, fast separation, low-temperature analysis, and applicability to wide variety of detectors. It permits separation and determination of some compounds that are not conveniently handled by either liquid chromatography or gas chromatography.

Painting and Dyeing

$ScCO_2$ is well suited to spray painting applications because of its excellent solvent power, low toxicity, and nonflammability. Spray painting with $scCO_2$ can reduce volatile organic compounds (VOCs) emissions and increases transfer efficiency [135].

Due to the environmental benefit of avoiding wastewater, an alternative dyeing process in SCFs has been proposed [136]. $ScCO_2$ is widely adopted as a suitable solvent, which has good plasticizing and swelling action on many textiles [137]. Some promising results have been obtained in the dyeing of some synthetic polymers with disperse dyes in $scCO_2$ [138]. Similar to SFE, the presence of small amount of polar or nonpolar cosolvents can remarkably increase the solubility of different dyes in $scCO_2$ and allows good dyeing results at less severe working conditions [139].

Cleaning Using $scCO_2$

Due to special physical properties $scCO_2$, some significant achievements have been made using $scCO_2$ as cleaning solvent in the fields of microelectronics [140], metallic surfaces [141], and printing and packaging industries [142]. Additionally, water-in-CO_2 microemulsion formed from surfactants in nonpolar CO_2 can effectively remove residues. The study for removing post-etch residues from patterned porous low-*k* dielectrics using water-in-CO_2 microemulsions has demonstrated that $scCO_2$ has no effect on the thickness and refractive index, indicating that collapse or voiding of the pores does not occur and post-etch residue can be removed with a solvent containing water, CO_2, and a hydrocarbon surfactant [143]. Combination of $scCO_2$ and hydrocarbon surfactants has also been utilized to remove water from photoresists without pattern collapse due to capillary forces. Moreover, the addition of highly branched hydrocarbon surfactants to CO_2 reduces the amount of solvent required for drying and lowers the interfacial tension [144].

Emulsions Related with CO_2

Surfactants have the ability to self-assemble into morphologically different structures, such as micelles, reverse micelles, vesicles, and liquid crystals. The functions and properties of surfactant systems depend strongly on their microstructures. Therefore, surfactant assemblies have wide applications in different fields of chemical engineering, material science, biology, environmental science, food industry, detergency, and enhanced oil recovery because desired functions can be achieved by controlling the microstructures. To tune the properties of surfactant assemblies is of great importance from both scientific and practical application viewpoints. Formation of water-in-CO_2 microemulsions and tuning the properties of surfactant aggregates using compressed CO_2 have been interesting areas in recent years.

Microemulsions with $scCO_2$ as the continuous phase have been studied extensively, which show some special properties comparing with the conventional water-in-oil microemulsions. For most of the CO_2-continuous microemulsions, water is used as the dispersed phase, forming the water-in-CO_2 microemulsions. The applications of this kind of microemulsions in nanoparticle synthesis and chemical reactions have been studied extensively. The design of surfactants compatible with CO_2 is crucial for the formation of stable water-in-CO_2 microemulsions. The most effective compounds that have been reported to stabilize water-in-CO_2 microemulsions are the partially or fully fluorinated surfactants. On consideration of the environmental and economical factors, some efforts have been made for the hydrocarbon surfactants and hybrid fluorocarbon–hydrocarbon surfactants [145, 146]. Recently, the formation of IL-in-CO_2

microemulsions was reported, of which the nanosized IL droplets are dispersed in $scCO_2$ with the aid of a perfluorinated surfactant [147]. Due to the unique features of $scCO_2$ and ILs, this kind of IL-in-CO_2 microemulsions may find various potential applications.

Controlling the properties of surfactant solutions using compressed CO_2 is another interesting topic, which exhibits unique properties in the synthesis of nanomaterials and chemical reactions because the properties of the microemulsions can be tuned continuously by pressure and the operation pressure is relatively low. Some copolymers can form reverse micelles in organic solvents, and different methods to induce micellization, such as changing temperature and adding salts, have been studied. The formation of copolymer reverse micelles induced by CO_2 has been investigated. It shows that compressed CO_2 can induce the formation of reverse micelles of the PEO-PPO-PEO copolymers [148]. The pressure at which reverse micelles begin to form is defined as critical micelle pressure. The unique advantage of this kind of reverse micelles is that the formation and breaking of reverse micelles can be repeated easily by controlling the pressure, and CO_2 can be removed completely after depressurization.

Recent study demonstrates that compressed CO_2 can switch the phase transition between lamellar liquid crystal and micellar solution of sodium bis (2-ethylhexyl) sulphosuccinate (AOT)/water system [149]. In the low pressure range, the viscosity of the system is very high and gradually decreases with increasing pressure of CO_2. As the pressure reaches an optimum value, the viscosity of the surfactant system reduces dramatically and changes into a transparent solution. Different techniques proved that this phenomenon corresponds to the phase transition from lamellar liquid crystal to micellar solution. The phase transition is reversible and can be repeated by controlling the pressure. This method to induce phase transition has some unique futures. For instance, CO_2 can induce the phase transition at ambient temperature, whereas the phase transition occurs at or above 140°C in the absence of CO_2 for the surfactant system studied. Second, the CO_2-induced phase transition is reversible and can be easily accomplished by the controlling pressure of CO_2. As the CO_2 can be easily removed by release of pressure, the post-processing steps are much easier. Gold and silica nanostructures in the AOT/water lamellar liquid crystal and AOT/water/CO_2 micelles are synthesized using the hydrophilic precursor of $HAuCl_4$ and hydrophobic precursor of tetraethyl orthosilicate, respectively. It is shown that the morphologies of the materials depend on pressure of CO_2. Similarly, compressed CO_2 can also induce micelle-to-vesicle transition (MVT) of dodecyltrimethylammonium bromide/sodium dodecyl sulfate mixed surfactants in aqueous solution reversibly [150]. It is deduced that the MVT induced by CO_2 is not originated from the change of the property of water. The main reason may be that CO_2 can insert into hydrocarbon chain region of the interfacial films, which increases the structural packing parameter. Silica particles with micelle template and vesicle template have prepared by controlling the pressure of CO_2. Switching the MVT by CO_2 may find different applications in material science and chemical reactions.

Future Directions

$ScCO_2$ as a green solvent has been used in different fields, and will be used more widely in extraction and fractionation, chemical reactions, material science, microelectronics, and so on. It also provides many opportunities for developing new technologies using its unusual properties. However, it must be realized that there are some disadvantages of $scCO_2$ in applications. For example, high pressure is always required when using $scCO_2$, and therefore the energy problem, safety aspects, capital investment for equipments must be carefully considered. Nevertheless, it is no doubt that $scCO_2$ will play an important role in the development of new and green technologies, especially those in which the usual properties of $scCO_2$ can be used effectively. Attention should also be paid to combine supercritical technology and other technologies, and therefore makes the processes more efficient. Further studies are surely needed to require true interdisciplinary cooperation involving academic and industrial researchers. With growing environmental concerns, deep realization of the properties of $scCO_2$, and the requirement of sustainable development, $scCO_2$-based technology will be widely applied in many fields.

Bibliography

Primary Literature

1. Hannay JB, Hogarth J (1879) On the solubility of solids in gases. Proc R Soc Lond 29:324–326
2. Poliakoff M, Licence P (2007) Sustainable technology: green chemistry. Nature 450:810–812
3. Eckert CA, Knutson BL, Debenedetti PG (1996) Supercritical fluids as solvents for chemical and materials processing. Nature 383:313–318
4. Zosel K (1978) Separation with supercritical gases: practical applications. Angew Chem Int Ed 17:702–709
5. Daoud IS, Kusinski S (1993) Liquid CO_2 and ethanol extraction of hops. 3. Effect of hop deterioration on utilization and beer quality. J Inst Brew 99:147–152
6. Montanari L, Fantozzi P, Snyder JM, King JW (1999) Selective extraction of phospholipids from soybeans with supercritical carbon dioxide and ethanol. J Supercrit Fluids 14:87–93
7. Zuo YB, Zeng AW, Yuan XG, Yu KT (2008) Extraction of soybean isoflavones from soybean meal with aqueous methanol modified supercritical carbon dioxide. J Food Eng 89:384–389
8. Hawthorne SB, Krieger MS, Miller DJ (1988) Analysis of flavor and fragrance compounds using supercritical fluid extraction coupled with gas chromatography. Anal Chem 60:472–477
9. Abbasi H, Rezaei K, Rashidi L (2008) Extraction of essential oils from the seeds of pomegranate using organic solvents and supercritical CO_2. J Am Oil Chem Soc 85:83–89
10. Araus K, Uquiche E, del Valle JM (2009) Matrix effects in supercritical CO_2 extraction of essential oils from plant material. J Food Eng 92:438–447
11. Mezzomo N, Martinez J, Ferreira SRS (2009) Supercritical fluid extraction of peach (*Prunus persica*) almond oil: kinetics, mathematical modeling and scale-up. J Supercrit Fluids 51:10–16
12. Nelson SR, Roodman RG (1985) Rose-the energy-efficient bottom of the barrel alternative. Chem Eng Prog 81:63–68
13. Deo MD, Hwang J, Hanson FV (1992) Supercritical fluid extraction of a crude oil, bitumen-derived liquid and bitumen by carbon dioxide and propane. Fuel 71:1519–1526
14. Low GKC, Duffy GJ (1995) Supercritical fluid extraction of petroleum hydrocarbons from contaminated soils. Trends Anal Chem 14:218–225
15. Bartle KD, Clifford AA, Shilstone GF (1989) Prediction of solubilities for tar extraction by supercritical carbon dioxide. J Supercrit Fluids 2:30–34
16. Bristow S, Shekunov BY, York P (2001) Solubility analysis of drug compounds in supercritical carbon dioxide using static and dynamic extraction systems. Ind Eng Chem Res 40:1732–1739
17. Lin YH, Smart NG, Wai CM (1995) Supercritical fluid extraction of uranium and thorium from nitric acid solutions with organophosphorus reagents. Environ Sci Technol 29:2706–2708
18. Rincon J, De Lucas A, Garcia MA, Garcia A, Alvarez A, Carnicer A (1998) Preliminary study on the supercritical carbon dioxide extraction of nicotine from tobacco wastes. Sep Sci Technol 33:411–423
19. Chen WH, Chen CH, Chang CMJ, Chiu YH, Hsiang D (2009) Supercritical carbon dioxide extraction of triglycerides from *Jatropha curcas* L. seeds. J Supercrit Fluids 51:174–180
20. Hitzler MG, Poliakoff M (1997) Continuous hydrogenation of organic compounds in supercritical fluids. Chem Commun 1667–1668
21. Baiker A (1999) Supercritical fluids in heterogeneous catalysis. Chem Rev 99:453–474
22. Jiang YJ, Gao QM (2006) Heterogeneous hydrogenation catalyses over recyclable Pd(0) nanoparticle catalysts stabilized by PAMAM-SBA-15 organic−inorganic hybrid composites. J Am Chem Soc 128:716–717
23. Wu TB, Jiang T, Hu BJ, Han BX, He JL, Zhou XS (2009) Cross-linked polymer coated Pd nanocatalysts on SiO_2 support: very selective and stable catalysts for hydrogenation in supercritical CO_2. Green Chem 11:798–803
24. Chatterjee M, Zhao FY, Ikushima Y (2004) Hydrogenation of citral using monometallic Pt and bimetallic Pt-Ru catalysts on a mesoporous support in supercritical carbon dioxide medium. Adv Synth Catal 346:459–466
25. Meric P, Yu KMK, Kong ATS, Tsang SC (2006) Pressure-dependent product distribution of citral hydrogenation over micelle-hosted Pd and Ru nanoparticles in supercritical carbon dioxide. J Catal 237:330–336
26. Zhao FY, Zhang R, Chatterjee M, Ikushima Y, Arai M (2004) Hydrogenation of nitrobenzene with supported transition metal catalysts in supercritical carbon dioxide. Adv Synth Catal 346:661–668
27. Zhao FY, Fujitaa S, Sun JM, Ikushima Y, Arai M (2004) Hydrogenation of nitro compounds with supported platinum catalyst in supercritical carbon dioxide. Catal Today 98:523–528
28. Liu HZ, Jiang T, Han BX, Liang SG, Zhou YX (2009) Selective phenol hydrogenation to cyclohexanone over a dualsupported Pd-Lewis acid catalyst. Science 326:1250–1252
29. Burk MJ, Feng S, Gross MF, Tumas W (1995) Asymmetric catalytic hydrogenation reactions in supercritical carbon dioxide. J Am Chem Soc 117:8277–8278
30. Wang SN, Kienzle F (2000) The syntheses of pharmaceutical intermediates in supercritical fluids. Ind Eng Chem Res 39:4487–4490
31. Kainz S, Brinkmann A, Leitner W, Pfaltz A (1999) Iridium-catalyzed enantioselective hydrogenation of imines in supercritical carbon dioxide. J Am Chem Soc 121:6421–6429
32. Stephenson P, Licence P, Ross SK, Poliakoff M (2004) Continuous catalytic asymmetric hydrogenation in supercritical CO_2. Green Chem 6:521–523
33. Pr C, Poliakoff M, Wells A (2007) Continuous flow hydrogenation of a pharmaceutical intermediate, [4-(3, 4-Dichlorophenyl)-3, 4-dihydro-2H-naphthalenyidene]methylamine, in supercritical carbon dioxide. Adv Synth Catal 349:2655–2659
34. Licence P, Ke J, Sokolova M, Ross SK, Poliakoff M (2003) Chemical reactions in supercritical carbon dioxide: from laboratory to commercial plant. Green Chem 5:99–104

35. Hou ZS, Han BX, Gao L, Liu ZM, Yang GY (2002) Selective oxidation of cyclohexane in compressed CO_2 and in liquid solvents over MnAPO-5 molecular sieve. Green Chem 4:426–430
36. Zhang RZ, Qin ZF, Dong M, Wang GF, Wang JG (2005) Selective oxidation of cyclohexane in supercritical carbon dioxide over CoAPO-5 molecular sieves. Catal Today 110:351–356
37. Theyssen N, Leitner W (2002) Selective oxidation of cyclooctane to cyclootanone with molecular oxygen in the presence of compressed carbon dioxide. Chem Commun 410–411. doi: 10.1039/B111212K
38. Theyssen N, Hou ZS, Leitner W (2006) Selective oxidation of alkanes with molecular oxygen and acetaldehyde in compressed (supercritical) carbon dioxide as reaction Medium. Chem Eur J 12:3401–3409
39. Jiang HF, Jia LQ, Li JH (2000) Wacker reaction in supercritical carbon dioxide. Green Chem 2:161–164
40. Wang ZY, Jiang HF, Qi CR, Wang YG, Dong YS, Liu HL (2005) PS-BQ: an efficient polymer-supported cocatalyst for the Wacker reaction in supercritical carbon dioxide. Green Chem 7:582–585
41. Wang XG, Venkataramanan NS, Kawanami H, Ikushima Y (2007) Selective oxidation of styrene to acetophenone over supported Au-Pd catalyst with hydrogen peroxide in supercritical carbon dioxide. Green Chem 9:1352–1355
42. Wang JQ, Cai F, Wang E, He LN (2007) Supercritical carbon dioxide and poly(ethylene glycol): an environmentally benign biphasic solvent system for aerobic oxidation of styrene. Green Chem 9:882–887
43. Jia LQ, Jiang HF, Li JH (1999) Palladium(II)-catalyzed oxidation of acrylate esters to acetals in supercritical carbon dioxide. Chem Commun 985–986. doi: 10.1039/A901935I
44. Xie Y, Zhang ZF, Hu SQ, Song JL, Li WJ, Han BX (2008) Aerobic oxidation of benzyl alcohol in supercritical CO_2 catalyzed by perruthenate immobilized on polymer supported ionic liquid. Green Chem 10:278–282
45. Hou ZS, Theyssen N, Brinkmann A, Leitner W (2005) Biphasic aerobic oxidation of alcohols catalyzed by poly(ethylene glycol)-stabilized palladium nanoparticles in supercritical carbon dioxide. Angew Chem Int Ed 44:1346–1349
46. He JL, Wu TB, Jiang T, Zhou XS, Hu BJ, Han BX (2008) Aerobic oxidation of secondary alcohols to ketones catalyzed by cobalt(II)/ZnO in poly(ethylene glycol)/CO_2 system. Catal Commun 9:2239–2243
47. Chapman AO, Akien GR, Arrowsmith NJ, Licence P, Poliakoff M (2010) Continuous heterogeneous catalytic oxidation of primary and secondary alcohols in $scCO_2$. Green Chem 12: 310–315
48. Bourne RA, Han X, Poliakoff M, George MW (2009) Cleaner continuous photo-oxidation using singlet oxygen in supercritical carbon dioxide. Angew Chem Int Ed 48:5322–5325
49. Han X, Bourne RA, Poliakoff M, George MW (2009) Strategies for cleaner oxidations using photochemically generated singlet oxygen in supercritical carbon dioxide. Green Chem 11:1787–1792
50. Clifford AA, Pople K, Gaskill WJ, Bartle KD, Rayner CM (1997) Reaction control and potential tuning in a supercritical fluid. Chem Commun 595–596. doi: 10.1039/A608066I
51. Qian J, Timko MT, Allen AJ, Rusell CJ, Winnik B, Buckley B, Steinfeld JI, Tester JW (2004) Solvophobic acceleration of Diels-Alder reactions in supercritical carbon dioxide. J Am Chem Soc 126:5465–5474
52. Isaacs NS, Keating N (1992) The rates of a Diels-Alder reaction in liquid and supercritical carbon dioxide. J Chem Soc Chem Commun 876–877. doi: 10.1039/C39920000876
53. Matsuo J, Tsuchiya T, Odashina K, Kobayashi S (2000) Lewis acid catalysis in supercritical carbon dioxide. use of scandium tris(heptadecafluorooctanesulfonate) as a lewis acid catalyst in Diels-Alder and Aza Diels-Alder reactions. Chem Lett 29:178–179
54. Cheng JS, Jiang HF (2004) Palladium-catalyzed regioselective cyclotrimerization of acetylenes in supercritical carbon dioxide. Eur J Org Chem 643–646. doi: 10.1002/ejoc.200300299
55. Li JH, Jiang HF (1999) Glaser coupling reaction in supercritical carbon dioxide. Chem Commun 2369–2370. doi: 10.1039/A908014G
56. Carroll MA, Holmes AB (1998) Palladium-catalysed carbon-carbon bond formation in supercritical carbon dioxide. Chem Commun 1395–1396. doi: 10.1039/A802235F
57. Shezad N, Clifford AA, Rayner CM (2002) Pd-catalysed coupling reactions in supercritical carbon dioxide and under solventless conditions. Green Chem 4:64–67
58. Morita DK, David SA, Tumas W, Pesiri DR, Glaze WH (1998) Palladium-catalyzed cross-coupling reactions in supercritical carbon dioxide. Chem Commun 1397–1398. doi: 10.1039/A802621A
59. Rathke JW, Klingler RJ, Krause TR (1991) Propylene hydroformylation in supercritical carbon dioxide. Organometallics 10:1350–1355
60. Guo Y, Akgerman A (1997) Hydroformylation of propylene in supercritical carbon dioxide. Ind Eng Chem Res 36: 4581–4585
61. Webb PB, Kunene TE, Cole-Hamilton DJ (2005) Continuous flow homogeneous hydroformylation of alkenes using supercritical fluids. Green Chem 7:373–379
62. Meehan NJ, Poliakoff M, Sandee AJ, Reek JNH, Kamer PCJ, van Leeuwen PWNM (2000) Continuous, selective hydroformylation in supercritical carbon dioxide using an immobilised homogeneous catalyst. Chem Commun 1497–1498. doi: 10.1039/B002526G
63. Mistele CD, Thorp HH, DeSimone JM (1996) Ring-opening metathesis polymerizations in carbon dioxide. J Macromol Sci Pure Appl Chem 33:953–960
64. Fürstner A, Koch D, Langemann K, Leitner W, Six C (1997) Olefin metathesis in compressed carbon dioxide. Angew Chem Int Ed Engl 36:2466–2469
65. Fürstner A, Ackermann L, Beck K, Hori H, Koch D, Langemann K, Liebl M, Six C, Leitner W (2001) Olefin metathesis in supercritical carbon dioxide. J Am Chem Soc 123:9000–9006

66. Randolph TW, Blanch HW, Prausnitz JM, Wilke CR (1985) Enzymatic catalysis in a supercritical fluid. Biotechnol Lett 7:325–328
67. Hobbs HR, Thomas NR (2007) Biocatalysis in supercritical fluids, in fluorous solvents, and under solvent-free conditions. Chem Rev 107:2786–2820
68. Hampson JW, Foglia TA (1999) Effect of moisture content on immobilized lipase-catalyzed triacylglycerol hydrolysis under supercritical carbon dioxide flow in a tubular fixed-bed reactor. J Am Oil Chem Soc 76:777–781
69. Oiveira JV, Oiveira D (2000) Kinetics of the enzymatic alcoholysis of palm kernel oil in supercritical CO_2. Ind Eng Chem Res 39:4450–4454
70. Jackson MA, King JW (1997) Lipase-catalyzed glycerolysis of soybean oil in supercritical carbon dioxide. J Am Oil Chem Soc 74:103–106
71. Tsitsimkou C, Stamatis H, Sereti V, Daflos H, Kolisis FN (1998) Acylation of glucose catalysed by lipases in supercritical carbon dioxide. J Chem Technol Biotechnol 71: 309–314
72. Yu ZR, Rizvi SSH, Zolloweg JA (1992) Enzymic esterification of fatty acid mixtures from milk fat and anhydrous milk fat with canola oil in supercritical carbon dioxide. Biotechnol Prog 8:508–513
73. Garcia-Arrazola R, López-Guerrero DA, Gimeno M, Bárzana E (2009) Lipase-catalyzed synthesis of poly-L-lactide using supercritical carbon dioxide. J Supercrit Fluids 51:197–201
74. Chen J, Zhang JL, Han BX, Li JC, Li ZH, Feng XY (2006) Effect of compressed CO_2 on the chloroperoxidase catalyzed halogenation of 1, 3-dihydroxybenzene in reverse micelles. Phys Chem Chem Phys 8:877–881
75. Knez E (2009) Enzymatic reactions in dense gases. J Supercrit Fluids 47:357–372
76. Licence P, Gray WK, Sokolova M, Poliakoff M (2005) Selective monoprotection of 1, n-terminal diols in supercritical carbon dioxide: a striking example of solvent tunable desymmetrization. J Am Chem Soc 127:293–298
77. Gooden PN, Bourne RA, Parrott AJ, Bevinakatti HS, Irvine DJ, Poliakoff M (2010) Continuous acid-catalyzed methylations in supercritical carbon dioxide: comparison of methanol, dimethyl ether and dimethyl carbonate as methylating agents. Org Process Res Dev 14:411–416
78. Hou ZS, Han BX, Zhang XG, Zhang HF, Liu ZM (2001) Pressure tuning of reaction equilibrium of esterification of acetic acid with ethanol in compressed CO_2. J Phys Chem B 105:4510–4513
79. Gao L, Wu WZ, Hou ZS, Jiang T, Han BX, Liu J, Liu ZM (2003) Transesterification between ethyl acetate and *n*-butanol in compressed CO_2 in the critical region of the reaction system. J Phys Chem B 107:13093–13099
80. Gray WK, Smail FR, Hitzler MG, Ross SK, Poliakoff M (1999) The continuous acid-catalyzed dehydration of alcohols in supercritical fluids: a new approach to the cleaner synthesis of acetals, ketals, and ethers with high selectivity. J Am Chem Soc 121:10711–10718
81. Hou ZS, Han BX, Liu ZM, Jiang T, Yang GY (2002) Synthesis of dimethyl carbonate using CO_2 and methanol: enhancing the conversion by controlling the phase behavior. Green Chem 4:467–471
82. Blanchard LA, Hancu D, Beckman EJ, Brennecke JF (1999) Green processing using ionic liquids and CO_2. Nature 399:28–29
83. Jiang T, Han BX (2009) Ionic liquid catalytic systems and chemical reactions. Curr Org Chem 13:1278–1299
84. Zhao GY, Jiang T, Wu WZ, Han BX, Liu ZM, Gao HX (2004) Electro-oxidation of benzyl alcohol in a biphasic system consisting of supercritical CO_2 and ionic liquids. J Phys Chem B 108:13052–13057
85. Zhang ZF, Wu WZ, Han BX, Jiang T, Wang B, Liu ZM (2005) Phase separation of the reaction system induced by CO_2 and conversion enhancement for the esterification of acetic acid with ethanol in ionic liquid. J Phys Chem B 109:16176–16179
86. Hou ZS, Han BX, Gao L, Jiang T, Liu ZM, Chang YH, Zhang XG, He J (2002) Wacker oxidation of 1-hexene in 1-n-butyl-3-methylimidazolium hexafluorophosphate ([bmim][PF_6]), supercritical (SC) CO_2, and SC CO_2/[bmim][PF_6]mixed solvent. New J Chem 26:1246–1248
87. Webb PB, Sellin MF, Kunene TE, Williamson S, Slawin AMZ, Cole-Hamilton DJ (2003) Continuous flow hydroformylation of alkenes in supercritical fluid-ionic liquid biphasic systems. J Am Chem Soc 125:15577–15588
88. Biddulph RH, Plesch PH (1960) The low-temperature polymerisation of isobutene. Part IV. exploratory experiments. J Chem Soc 3913–3920. doi: 10.1039/JR9600003913
89. Desimone JM, Guan Z, Elsbernd CS (1992) Synthesis of fluoropolymers in supercritical carbon doxide. Science 257:945–947
90. O'Connor P, Zetterlund PB, Aldabbagh F (2010) Effect of monomer loading and pressure on particle formation in nitroxide-mediated precipitation polymerization in supercritical carbon dioxide. Macromolecules 43:914–919
91. Kim J, Dong LB, Kiserow DJ, Roberts GW (2009) Complex effects of the sweep fluid on solid-state polymerization: poly (bisphenol a carbonate) in supercritical carbon dioxide. Macromolecules 42:2472–2479
92. Grignard B, Jerome C, Calberg C, Jerome R, Wang WX, Howdle SM, Detrembleur C (2008) Dispersion atom transfer radical polymerization of vinyl monomers in supercritical carbon dioxide. Macromolecules 41:8575–8583
93. Chiou JS, Barlow JW, Paul DR (1985) Plasticization of glassy polymers by CO_2. J Appl Polym Sci 30:2633–2642
94. Wissinger RG, Paulaitis ME (1991) Molecular thermodynamic model for sorption and swelling in glassy polymer-carbon dioxide systems at elevated pressures. Ind Eng Chem Res 30:842–851
95. Romang AH, Watkins JJ (2010) Supercritical fluids for the fabrication of semiconductor devices: emerging or missed opportunities? Chem Rev 110:459–478

96. Matson DW, Fulton JL, Petersen RC, Smith RD (1987) Rapid expansion of supercritical fluid solutions: solute formation of powders, thin films, and fibers. Ind Eng Chem Res 26:2298–2306
97. Reverchon E, Adami R, Cardea S, Della Porta G (2009) Supercritical fluids processing of polymers for pharmaceutical and medical applications. J Supercrit Fluids 47:484–492
98. Sun YP, Guduru R, Lin F, Whiteside T (2000) Preparation of nanoscale semiconductors through the rapid expansion of supercritical solution (RESS) into liquid solution. Ind Eng Chem Res 39:4663–4669
99. Türk M (2009) Manufacture of submicron drug particles with enhanced dissolution behaviour by rapid expansion processes. J Supercrit Fluids 47:537–545
100. Gallagher PM, Coffey MP, Krukonis VJ, Hillstrom WW (1992) Gas anti-solvent recrystallization of RDX: Formation of ultra-fine particles of a difficult-to-comminute explosive. J Supercrit Fluids 5:130–142
101. Reverchon E, Porta GD, Trolio AD, Pace S (1998) Supercritical antisolvent precipitation of nanoparticles of superconductor precursors. Ind Eng Chem Res 37:952–958
102. Chen J, Zhang JL, Han BX, Li ZH, Li JC, Feng XY (2006) Synthesis of cross-linked enzyme aggregates (CLEAs) in CO_2-expanded micellar solutions. Colloids Surf B Biointerfaces 48:72–76
103. Zhang JL, Han BX, Liu JC, Zhang XG, Liu ZM, He J (2001) A new method to recover the nanoparticles from reverse micelles: recovery of ZnS nanoparticles synthesized in reverse micelles by compressed CO_2. Chem Commun 2724–2725. doi: 10.1039/B109802K
104. Zhang JL, Liu ZM, Han BX, Liu DX, Chen J, He J, Jiang T (2004) A novel method to synthesize polystyrene nanospheres immobilized with silver nanoparticles by using compressed CO_2. Chem Eur J 10:3531–3536
105. Watkins JJ, Blackburn JM, McCarthy TJ (1999) Chemical fluid deposition: reactive deposition of platinum metal from carbon dioxide solution. Chem Mater 11:213–215
106. Blackburn JM, Long DP, Cabañas A, Watkins JJ (2001) Deposition of conformal copper and nickel films from supercritical carbon dioxide. Science 294:141–145
107. Pessey V, Garriga R, Weill F, Chevalier B, Etourneau J, Cansell F (2000) Core-shell materials elaboration in supercritical mixture CO_2/ethanol. Ind Eng Chem Res 39: 4714–4719
108. Loy DA, Russick EM, Yamanaka SA, Baugher BM, Shea KJ (1997) Direct formation of aerogels by sol-gel polymerizations of alkoxysilanes in supercritical carbon dioxide. Chem Mater 9:2264–2268
109. Sui RH, Rizkalla AS, Charpentier PA (2004) Synthesis and formation of silica aerogel particles by a novel sol-gel route in supercritical carbon dioxide. J Phys Chem B 108: 11886–11892
110. Wang JW, Xia YD, Wang WX, Poliakoff M, Mokaya R (2006) Synthesis of mesoporous silica hollow spheres in supercritical CO_2/water systems. J Mater Chem 16:1751–1756
111. Pai RA, Humayun R, Schulberg MT, Sengupta A, Sun JN, Watkins JJ (2004) Mesoporous silicates prepared using preorganized templates in supercritical fluids. Science 303:507–510
112. Zirkel L, Jakob M, Münstedt H (2009) Foaming of thin films of a fluorinated ethylene propylene copolymer using supercritical carbon dioxide. J Supercrit Fluids 49:103–110
113. Tomasko DL, Burley A, Feng L, Yeh SK, Miyazono K, Nirmal-Kumar S, Kusaka I, Koelling K (2009) Development of CO_2 for polymer foam applications. J Supercrit Fluids 47:493–499
114. Watkins JJ, McCarthy TJ (1994) Polymerization in supercritical fluid-swollen polymers: a new route to polymer blends. Macromolecules 27:4845–4847
115. Watkins JJ, McCarthy TJ (1995) Polymer/metal nanocomposite synthesis in supercritical CO_2. Chem Mater 7:1991–1994
116. Liao WS, Pan HB, Liu HW, Chen HJ, Wai CM (2009) Kinetic study of hydrodechlorination of chlorobiphenyl with polymer-stabilized palladium nanoparticles in supercritical carbon dioxide. J Phys Chem A 113:9772–9778
117. Wang JQ, Zhang CL, Liu ZM, Ding KL, Yang ZZ (2006) A simple and efficient route to prepare inorganic compound/polymer composites in supercritical fluids. Macromol Rapid Commun 27:787–792
118. Liu ZM, Han BX (2009) Synthesis of carbon-nanotube composites using supercritical fluids and their potential applications. Adv Mater 21:825–829
119. Ye XR, Lin YH, Wang CM, Wai CM (2003) Supercritical fluid fabrication of metal nanowires and nanorods templated by multiwalled carbon nanotubes. Adv Mater 15:316–319
120. Fu L, Liu ZM, Liu YQ, Han BX, Wang JQ, Hu PA, Cao LC, Zhu DB (2004) Coating carbon nanotubes with rare earth oxide multiwalled nanotubes. Adv Mater 16:350–352
121. Dai XH, Liu ZM, Han BX, Sun ZY, Wang Y, Xu J, Guo XL, Zhao N, Chen J (2004) Carbon nanotube/poly(2,4-hexadiyne-1,6-diol) nanocomposites prepared with the aid of supercritical CO_2. Chem Commun 2190–2191. doi: 10.1039/B407605B
122. Wang JW, Khlobystov AN, Wang WX, Howdle SM, Poliakoff M (2006) Coating carbon nanotubes with polymer in supercritical carbon dioxide. Chem Commun 1670–1672
123. Wakayama H, Setoyama N, Fukushima Y (2003) Size-controlled synthesis and catalytic performance of Pt nanoparticles in micro- and mesoporous silica prepared using supercritical solvents. Adv Mater 15:742–745
124. Lucky RA, Charpentier PA (2008) A one-Step approach to the synthesis of ZrO_2-modified TiO_2 nanotubes in supercritical carbon dioxide. Adv Mater 20:1755–1759
125. O'Neil A, Watkins JJ (2007) Reactive deposition of conformal metal oxide films from supercritical carbon dioxide. Chem Mater 19:5460–5466
126. Cangül B, Zhang LC, Aindow M, Erkey C (2009) Preparation of carbon black supported Pd, Pt and Pd-Pt nanoparticles

using supercritical CO_2 deposition. J Supercrit Fluids 50: 82–90
127. Klesper E, Corwin AH, Turner DA (1962) High pressure gas chromatography above critical temperatures. J Org Chem 27:700–701
128. Lee ML, Markides KE (1987) Chromatography with supercritical fluids. Science 235:1342–1347
129. Taylor LT (2009) Supercritical fluid chromatography for the 21st century. J Supercrit Fluids 47:566–573
130. Zhao YQ, Pritts WA, Zhang SH (2008) Chiral separation of selected proline derivatives using a polysaccharide-type stationary phase by supercritical fluid chromatography and comparison with high-performance liquid chromatography. J Chromatogr A 1189:245–253
131. West C, Bouet A, Gillaizeau I, Coudert G, Lafosse M, Eric L (2010) Chiral separation of phospine-containing α-amino acid derivatives using two complementary cellulosic stationary phases in supercritical fluid chromatography. Chirality 22:242–251
132. Miller L, Potter M (2008) Preparative chromatographic resolution of racemates using HPLC and SFC in a pharmaceutical discovery environment. J Chromatogr B 875:230–236
133. Desmortreux C, Rothaupt M, West C, Lesellier E (2009) Improved separation of furocoumarins of essential oils by supercritical fluid chromatography. J Chromatogr A 1216:7088–7095
134. Takahashi K, Kinugasa S, Yoshihara R, Nakanishi A, Mosing RK, Takahashi R (2009) Evaluation of a condensation nucleation light scattering detector for the analysis of synthetic polymer by supercritical fluid chromatography. J Chromatogr A 1216:9008–9013
135. Munshi P, Bhaduri S (2009) Supercritical CO_2: a twenty-first century solvent for the chemical industry. Curr Sci 97:63–72
136. Liu ZT, Sun ZF, Liu ZW, Lu J, Xiong HP (2008) Benzylated modification and dyeing of ramie fiber in supercritical carbon dioxide. J Appl Polym Sci 107:1872–1878
137. Montero GA, Smith CB, Hendrix WA, Butcher DL (2000) Supercritical fluid technology in textile processing: an overview. Ind Eng Chem Res 39:4806–4812
138. van der Kraan M, Cid MVF, Woerlee GF, Veugelers WJT, Witkamp GJ (2007) Dyeing of natural and synthetic textiles in supercritical carbon dioxide with disperse reactive dyes. J Supercrit Fluids 40:470–476
139. Banchero M, Ferri A, Manna L (2009) The phase partition of disperse dyes in the dyeing of polyethylene terephthalate with a supercritical CO_2/methanol mixture. J Supercrit Fluids 48:72–78
140. Weibel GL, Ober CK (2003) An overview of supercritical CO_2 applications in microelectronics processing. Microelectron Eng 65:145–152
141. Ventosa C, Rébiscoul D, Perrut V, Ivanova V, Renault O, Passemard G (2008) Copper cleaning in supercritical CO_2 for the microprocessor interconnects. Microelectron Eng 85:1629–1638
142. Porta GD, Volpe MC, Reverchon E (2006) Supercritical cleaning of rollers for printing and packaging industry. J Supercrit Fluids 37:409–416
143. Zhang XG, Pham JQ, Martinez HJ, Wolf PJ, Green PF, Johnston KP (2003) Water-in-carbon dioxide microemulsions for removing post-etch residues from patterned porous low-*k* dielectrics. J Vac Sci Technol B 21:2590–2598
144. Zhang XG, Pham JQ, Ryza N, Green PF, Johnston KP (2004) Chemical-mechanical photoresist drying in supercritical carbon dioxide with hydrocarbon surfactants. J Vac Sci Technol B 22:818–825
145. Johnston KP, da Rocha SRP (2009) Colloids in supercritical fluids over the last 20 years and future directions. J Supercrit Fluids 47:523–530
146. Zhang JL, Han BX (2009) Supercritical CO_2-continuous microemulsions and compressed CO_2-expanded reverse microemulsions. J Supercrit Fluids 47:531–536
147. Liu JH, Cheng SQ, Zhang JL, Feng XY, Fu XG, Han BX (2007) Reverse micelles in carbon dioxide with ionic-liquid domains. Angew Chem Int Ed 46:3313–3315
148. Zhang R, Liu J, He J, Han BX, Zhang XG, Liu ZM, Jiang T, Hu GH (2002) Compressed CO_2-assisted formation of reverse micelles of PEO-PPO-PEO copolymer. Macromolecules 35:7869–7871
149. Zhang JL, Han BX, Li W, Zhao YJ, Hou MQ (2008) Reversible switching of lamellar liquid crystals into micellar solutions using CO_2. Angew Chem Int Ed 47:10119–10123
150. Li W, Zhang JL, Zhao YJ, Hou MQ, Han BX, Yu CL, Ye JP (2010) Reversible switching a micelle-to-vesicle transition reversibly by compressed CO_2. Chem Eur J 16:1296–1305

Books and Reviews

Anastas PT, Farris CA (1994) Benign by design: alternative synthetic design for pollution prevention, vol 577. American Chemical Society, Washington, DC

Brunner G (2004) Supercritical fluid as solvents and reaction media. Elsevier, Amsterdam

Centi G, Perathoner S (2002) Selective oxidation-industrial, Encyclopedia of catalysis. Wiley, New York. doi:10.1002/0471227617.eoc188

Clifford AA (1998) Fundamentals of supercritical fluid. Oxford University Press, Oxford, UK

Gupta RB, Shim JJ (2007) Solubility in supercritical carbon dioxide. CRC Press, Boca Raton

Jessop PG, Leitner W (1999) Chemical synthesis using supercritical fluids. Wiley-VCH, Weinheim

McHugh MA, Krukonis VJ (1994) Supercritical fluid extraction, 2nd edn. Butterworth-Heinemann, Stoneham, MA

Noyori R (1994) Asymmetric catalysis in organic Synthesis. John Wiley & Sons, New York

Quinn EL, Jones CL (1936) Carbon dioxide. Reinhold, New York

Sustainability in Water, Introduction

Jaeweon Cho
Gwangju Institute Science and Technology (GIST), Department of Environmental Science and Engineering, Natural Organic Matter Lab, Gwangju, Korea

There have been concepts of water based on the dynamic experiences with nature. Once these concepts are formed, generally people are reluctant to change them. Water itself is a sustainable substance, but problems with water arise from its uneven distribution, relative scarcity, and contamination beyond a self purification capacity. When this project was started with the theme of water sustainability, three classes of water concepts – quantity, quality, and harmony – were considered. Prior to applying engineering or scientific practices, concepts of water have to be understood scientifically, with fundamental principles underlying the concepts. Water concepts formed through our past experiences, with problems and corresponding solutions, research, new visions and even ideas, may face challenges from new problems for which other different water concepts have to be thought of and further development of science and engineering in areas related to water is required. Thus, water itself does not change, but existing types of water change continuously. Sustainability is a unified concept for water. The concept of sustainability can be subdivided into threefold concepts: Quantity, Quality, and Harmony, using regressive way (i.e., from sustainability as consequence to prerequisite conditions). Thus, the three concepts of water are subsumed under the unified sustainability concept, for which two conditions are being used in this section: firstly, succession in time with water acquisition and use, and secondly, the dynamic relationship between humans and nature, with regard to water.

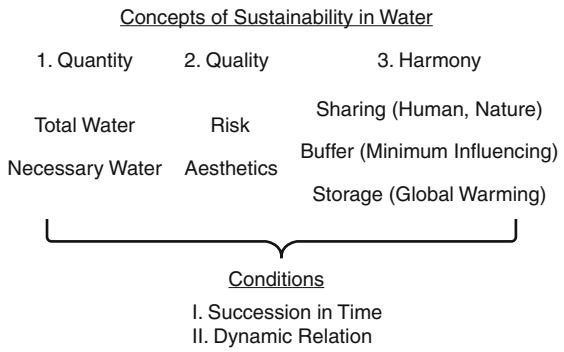

Succession in time of water does not satisfy a big gap in the water continuum between spaces (i.e., small village, community, city, country). Even if there is a big gap, it should be minimized under the condition of the Sustainability Concept. Limited sources of water shared, among humans and even with nature, require not simple aggregation but dynamic interactions with both humans and nature. With the aforementioned conditions (i.e., succession in time of water and dynamic interactions), which are necessary for the Sustainability Concept of water, many subcategorized concepts can now be deduced from the three classes of water concepts. The Quantity of Water is further classified into the total available amount of water (total water) and the necessary amount of water (necessary water). Necessary water includes not only drinking and normal living waters but waters for all other purposes, such as transport, electronics, and many others. If total water is less than necessary water, the status is defined as a water shortage. The Quality of Water is classified by risk and aesthetics; the former is related to risky contaminants, such as particles, colloids, pathogens, pesticides, and micropollutants, such as endocrine disrupting chemicals and pharmaceuticals, and the latter is related to materials concerned by the public. Lastly, the Harmony of Water is classified into sharing, buffering (influencing), and storage. The concept of buffering is related to both, contaminants in, and necessary amount of, water, for nature. The water storage concept arises in conjunction with groundwater especially, which is not exposed to air. This, with the potential of the evaporation and water cycle, ultimately influences global warming by means of water vapor.

Sustainability Concepts can be completed only through practice with the development of technology, to be applied and their actual applications. This encyclopedia practices several application technologies, conceptual designs, and ideas with hypotheses and judgments. From the water quantity concept point of view, chapters include themes of rainwater harvesting, storm water, desalination, wastewater reclamation and water reuse, and weather modification. Some of the chapters also contribute to one or more concepts. For the Water Quality Concepts, chapters mainly include themes such as; the control of the emerging contaminants, sustainable remediation of

groundwater with metals and radionuclides, and membrane technology. However, some contents of the theme "wastewater reclamation," address these themes as well. For the Water Harmony Concepts, chapters include themes of water monitoring (instrumentation, monitoring, and control and automation), nexus between water and energy, water resource managements, roles of constructed wetlands. Readers are requested to first keep the previously introduced concepts in mind and then to look into the contents of the technology and application cases delivered in the each chapter. The chapters are not simply combined but interconnected with dynamic connections to the "water sustainability" concepts; even though authors did not discuss on themes and contents they were supposed to include for their chapters, before they started to write or while they were writing, strong connections among the chapters exist under the concept of "sustainability," as have been found.

Four chapters were used to discuss on alternative water supply, under the water quantity concept: Stormwater harvesting and reuse potential, as an alternative water supply especially for non-potable uses, were introduced, with merit of reduction in stormwater pollution which loads to downstream waterways and estuaries and reduction in stormwater discharging volume, using a few specific case studies with effective biofilter treating contaminants in stormwater (Entry on ► "Stormwater Harvesting and Reuse"). Rainwater harvesting systems were described, with emphases on satisfying ongoing water demand, reduction in reliance on other water sources, control of nonpoint source pollution in urban areas, as well as detailed technologies of catchment, treatment of contaminants in rainwater, and operating and maintenance (Entry on ► "Rainwater Harvesting"). Desalination technology was in depth discussed, with world markets summary and forecast, main processes, including thermal and membrane (reverse osmosis) separation technologies, and future technologies, such as forward osmosis and membrane distillation (Entry on ► "Desalination Technology for Sustainable Water Resource"). Wastewater reclamation and water reuse were discussed to emphasize two important contributions: production of sustainable water resources and reduction of adverse environmental effects. Available processes technologies were introduced, with water quality requirements of wastewater reclamation for various different purposes, information of energy consumption, operating, and maintenance costs. It was also discussed that zero discharges of contaminants resulted from anthropogenic activities, to the environment, can be achieved through the introduced wastewater reclamation technologies (Entry on ► "Wastewater Reclamation").

There are chapters about water quality issues, including treatment processes, remediation, and emerging contaminants. Constructed wetlands can be essential wastewater treatment systems, thus, have been designed and operated as such, though many systems do support other functional values. Constructed wetlands can be built with a much greater degree of control than natural systems, thus allowing the establishment of experimental treatment facilities with well-defined composition of substrate, type of vegetation, and flow pattern. Classification of constructed wetlands, characteristics, in terms of treatment capacity and limitation, and guidelines of applications upon different wastewater types, were described (Entry on ► "Wastewater Treatment and Control through Wetlands"). Water production technologies of membranes having relatively low pore sizes, were introduced, with respects to both advantages, in terms of contaminants removal effectiveness, and limitations, such as fouling, with corresponding overcoming guidelines (Entry on ► "Sustainable Water Treatment using Nanofiltration and Tight Ultrafiltration Membranes").

Case histories and applications of environmental and economic sustainability assessment, with remediation strategic planning and technologies, were presented and illustrated for different groundwater sites with contaminations, such as nonaqueous phase liquids (Entry on ► "Groundwater Remediation, Environmental and Economic Assessment"). Great attention was given to developing detailed definitions and quantitative metrics for the social, environmental, and economic aspects of remediation. Some of these efforts and influences, as well as the benefits of applying sound scientific principles and practices to remediation, were discussed, with much information

on a remediation forum and a few remediation projects (Entry on ► "Sustainable Remediation: Integrating Risk, Science, and Sustainability Principles"). Classical techniques (such as pump and treat) and relatively novel methods (such as permeable reactive barrier) for soil remediation were discussed; detailed description of remediation processes were introduced with metals and radionuclides, with treatment efficiencies and background chemistries (Entry on ► "Sustainable Remediation Methods for Metals and Radionuclides").

Due to rapid development of economic industries, concentrated urbanization, and population growth, issues of micropollutants, including endocrine disrupting chemicals, pharmaceuticals, and personal care products, are getting attention from even publics. Micropollutants were intensively investigated with occurrence survey and reviews for various waters, ranging wastewater, drinking water source, even to tap water of specific sites (Entry on ► "Climate Change Impacts on Emerging Contaminants"). The same issues were rigorously discussed, focusing on wastewater reclamation processes, such as membrane bioreactor (MBR) (Entry on ► "Water Reclamation System and Micropollutants"). Lastly, micropollutants indicator for effective water quality management was suggested based on results obtained from projects conducted for two rivers with pharmaceuticals discharged from wastewater treatment plants (Entry on ► "Wastewater Treatment Plant: Anthropogenic Micropollutant Indicators for Sustainable River Management").

Last part of the book was devoted to the Water Harmony concept. With a global view, link between climate change and water sustainability was reviewed, from both public/government and private/business perspectives (Entry on ► "Climate Change and Global Water Sustainability"). Important issues relating to water quality with connection to wastewater reclamation and rainwater were discussed, and attempts were taken to increase public understanding of multivariate nature of water qualities for effective management of community-owned water resources, with the project of the city of Tokyo (Entry on ► "Community-owned Water Resource and Climate Change, Quality Management"). Importance and incentives of instrumentation, control, and automation (ICA) in all water and wastewater operations were described, with basic control concept, specific examples of control systems for actual treatment processes, and monitoring and feedback system, in connection to upstream and downstream sewer network (Entry on ► "Water and Wastewater Operation: Instrumentation, Monitoring, Control and Automation"). Interrelationship between water production and required energy becomes more important than ever, under several conditions, including climate change, population growth, and environmental standards increase. Efficiencies (i.e., with respect to energy) of water production and wastewater treatment were discussed, from perspectives of types of the relationships, plants design, energy recovery, and monitoring and control system (Entry on ► "Water and Energy Nexus").

As briefly introduced, all the authors shared their precious experiences with water for us to synthesize the concepts. Most of the authors also suggested ideas, derived from the basis of their related experiences, which are anticipated to be problem-solving concepts and corresponding technologies in near future, by the authors again or hopefully by potential readers. Problems as a result from water shortage and with risky contaminants may be harsh and arise in certain forms that are not expected. Then, in order to overcome the problems, existing scientific concepts and application technologies have to be used, and new scientific concepts and technologies may also have to be used. In this case, it is important to bring up the two conditions previously used for the sustainable concepts, succession in time and dynamic relationship. There is no result without cause, and there is no big gap in the arising problems with water. It is imperative to remember this when solving future problems with water. There is a need to educate the next generations with our scientific concepts and technologies to prepare for future problems. It is our responsibility to give both knowledge with the concepts and technologies, and the knowledge of judgment. The latter is supposed to give them (1) the unconditioned goal of ours with water and (2) certain reasonable constraints to be applied to the technologies, for sustainability of water.

Sustainability Performance Simulation Tools for Building Design

Khee Poh Lam
Center for Building Performance and Diagnostics, School of Architecture, Carnegie Mellon University, Pittsburgh, PA, USA

Article Outline

Glossary
Introduction
Brief History of Building Performance Simulation
Principles of Sustainable Building Design
Modeling and Simulation
Building Energy Simulation Tools
Integrated Building Design and Operation Process Modeling
Conclusion and Future Trends
Bibliography

Glossary

Algorithm It is a step-by-step procedure expressed as a finite set of well-defined instructions for calculating a mathematical function related to data processing and system analytics.

Behavioral model It is a virtual model that aims to abstractly represent a real-world system through one-to-one mapping of parameters that can reproduce the behavior of the original analyzed system. A validated model can uniquely predict the future system states based on past system states.

Building information model It is a digital representation of physical and functional characteristics of a facility based on a standardized representation schema to facilitate collaboration by different stakeholders at different phases of the lifecycle of a facility.

Building life cycle A comprehensive overview of a building delivery process that takes into account the design, construction, commissioning, operation, and decommissioning phases.

Building performance A set of qualitative and quantitative metrics that characterizes the behavior of a building, which includes spatial, thermal, air quality, acoustical, visual, building integrity, and energy efficiency considerations.

Interoperability It is a property of a product or system, that conforms to a certain established standard framework, with clear interface connections to other products or systems, present or future, without any restricted access or implementation.

Ontology It is a formal explicit representation of knowledge as a set of related concepts within a certain domain.

Semantics It is the study of meaning and interpretation of human forms of expressions in terms of words, phrases, signs, and symbols in communication.

Stochastic model It is a representation of a system whose behavior is intrinsically nondeterministic, such that the probability of the outcome of a future state is affected by both the process's predictable actions and by a random element.

Taxonomy It is the practice and science of classification of things or concepts as well as principles underlying such classification.

Introduction

Sustainable building, also commonly known as high-performance or green building, is the practice of creating structures and using processes that are environmentally responsible and resource-efficient throughout a building's life cycle from siting to design, construction, operation, maintenance, renovation, and deconstruction [1]. This practice expands and complements the classical building design concerns of economy, utility, durability, and comfort. Historically, there have been many well-established theoretical frameworks that relate building design with its environmental as well as human occupant performance within those buildings [2–5]. Design decision support tools, both physical and computational, have invariably been developed in accordance with the needs of these respective design processes and, in some instances, directly linked to meeting various building code and standard requirements. Therefore, such tools must be understood and appreciated in the context of the building delivery processes adopted in contemporary practices

or are being advocated in response to certain prevailing industry-wide mission (such as sustainable design) in a particular historical milieu.

The building delivery process has commonly been regarded as a discrete and sequential set of activities. This state of affairs is the result of a historical evolution driven by many factors. As building design becomes ever increasingly complex due to changing perceptions and demands of developers in a competitive globalized real estate market, specialist professional communities have emerged, bringing specific knowledge input to the building delivery process beyond the capabilities of the conventional architectural and building engineering professions. While this might seem a rational step toward addressing the complexity involved, it also inevitably and fundamentally transforms the originally integrated process to one of fragmentation and compartmentalization. This in turn necessitated the development of communication frameworks based on the organization of activities for the purpose of establishing a professional fee structure that is commensurate with the scope of work and level of accountability or responsibility at various project phases. The quest for more efficient communication methods has gradually evolved into a *circulus vitiosus* whereby advances in communication and dissemination technologies continuously struggle to cope with unprecedented rate of information growth globally, while continuing (if not intensifying) the trend toward process disintegration. Superficial attempts to patch the current decision-making approaches often lead to miscommunication of intentions, resulting in unsatisfactory solutions which are costly to remedy in terms of time and resources.

The capabilities of design decision support tools are nonetheless expanding but they still fall short of anticipating or challenging the very logic of the industry processes they are supposed to support. Among the major industries in any national economy, it is often observed that the building industry is one that is traditionally most resilient to structural change. In particular, its uptake and exploitation of advanced technology of any form is conservative and slow – the common reason given being cost constraint. The availability and affordability of powerful computer systems and software have transformed the way business is conducted in many other fields. Yet the building industry still tends to deploy this technology in a comparatively rudimentary way. However, over the past decade, the sustainable development movement has been gaining unprecedented momentum globally and is beginning to exert a profound influence on coevolutionary development of the building delivery process and building performance simulation tools.

More elaborate discourse in this matter can be found in [6] and [7]. These authors further address the necessary conditions under which significant structural changes in the building delivery process can evolve and the related implications for future development of decision support tools. They also explore hidden potentials of existing tools and propose enhancements to facilitate effective knowledge transfer and process management.

Brief History of Building Performance Simulation

Building simulation as a discipline can be traced back to the 1960s with the US government's projects to evaluate the thermal environment in fallout shelters by an hour-by-hour simulation of heat and moisture transfer process between human occupants and shelter walls under limited ventilation conditions [8]. Kusuda offered an interesting historical account of the building system simulation focusing on the thermal performance domain. Since then, building simulation has been constantly evolving as a vibrant discipline that produced a variety of tools that are scientifically validated across different climatic domains.

According to Clarke [9], there are four relatively distinct generations of energy simulation tools over the past 4 decades. The first generation of tools tend to be handbook oriented that adopt disparate simulation techniques to address piecemeal design exercises. These tools are easy to apply but the results are difficult to interpret. The second generation tools of the mid-1970s began to focus on the temporal aspects of energy simulation by implementing response functions to derive analytical solutions. HVAC system modeling was confined to steady state assumptions. The third generation of the mid-1980s recognized the importance of systems integration in the simulation approach

whereby all other system parameters are linked and solved numerically while only space, time, and climate remain independent variables. The first graphical-user interfaces (GUI) began to emerge at this time. The fourth generation tools of the mid-1990s continued to pursue and expand the integration framework. The increasing scale and complexity of such integrated design functionalities necessitate the development of a modeling platform (now commonly referred to as building information model or BIM), to organize, manage, and provide seamless exchange of data between various discrete and yet related building system domains. The GUIs became more user-centered, providing support through embedded knowledge bases in the form of data libraries and design task-oriented guidance.

Meanwhile, other building performance related simulation tools, e.g., in lighting, airflow in and around buildings, moisture flow, and acoustics, have also emerged in the 1980s and are continually being refined. One of the most comprehensive sources of literature that document the evolution of the building performance simulation world can be found in the publication archives of the International Building Performance Simulation Association (IBPSA) [10]. The collection of papers dates back to 1985 when the IBPSA held its inaugural conference in Seattle, Washington, USA. The conference proceedings are organized thematically that covered in the early years a limited range of topics on research and development, validations, applications in industry, and user interface design. As the field continues to evolve, the range of topics have expanded significantly to include detailed simulation of advanced building materials, components and systems, control technologies, occupant behavior, health and comfort, code compliance, as well as macrolevel studies of climates and microclimates, landscape and urban heat island effects, and zero- or low-carbon sustainable developments.

In 2008, IBPSA launched its Journal of Building Performance Simulation [11]. At about the same period, another journal titled Building Simulation: An International Journal [12] was also established. These are important milestones that signify the maturation of building performance simulation into a recognized and indispensable discipline for all professions involved in the design, engineering, operation, and management of buildings. In the twenty-first century, the simulation evolution is dominated by two key processes, namely, (1) attaining an increased level of quality assurance and (2) offering efficient integration of simulation expertise and tools in the overall building process, according to Augenbroe [7]. His paper on *Trends in Building Simulation* offers a detailed overview of the achievements and imminent challenges faced by the profession. It also provides a glimpse into the changing "appearance" of simulation tools that is brought about by the internet revolution, as exemplified by new forms of ubiquitous, remote, collaborative, and pervasive applications. There are also experimental attempts to blur the distinction between real and virtual simulation with the deployment of augmented reality, as described in [13]. This technology can potentially allow an observer to interact with a running simulation of himself and his environment while being immersed in the real environment. The results of the simulation can be overlaid in real time on the sensory input of the immersed observer, e.g., via computer generation of an image on a transparent visor.[1]

Principles of Sustainable Building Design

Four fundamental human-related elements should be contemplated in discussing the process of human involvement in the creation of our built environment: theory and practice – knowledge and experience. These elements are always present, but the degree of engagement varies within individuals as well as collectively within a building design team.

Theory and Practice

Theories can be regarded as analytical tools for understanding, explaining, and making predictions about a given subject matter, be it in the arts or sciences. Theoretical constructs are particularly helpful when dealing with complex systems involving multidimensional and multi-domain interactions. It should be noted that a theory is syntactic in nature and is only meaningful when given a semantic component by applying it to some content (i.e., facts and relationships of the actual historical and physical world as it is unfolding) [14]. Green building design is a good case in point.

Green building, also commonly known as sustainable or high-performance building, is the practice of creating structures and using processes that are environmentally responsible and resource-efficient throughout a building's life cycle from siting to design, construction, operation, maintenance, renovation, and deconstruction [15]. This practice expands and complements the classical building design concerns of economy, utility, durability, and comfort. There are many "traditional" theories that relate building design with its environmental as well as human occupant performance within those buildings [16, 17].

A specific example of the performance-based approach to design is a well-established model based on the concept of total building performance and diagnostics (TBPD) [18] (Fig. 1). This concept was originally advocated by a research team at Carnegie Mellon University, USA, in the early 1980s. TBPD is an integrated and holistic knowledge-based framework for conceptualizing, specifying, designing, analyzing, and commissioning a building project. It can provide a comprehensive brief for a client and the project team who are committed to quality and high-performance goals throughout the project duration, from inception to completion, and can even extend to post-occupancy management and maintenance. It can facilitate optimization of the design performance, avoidance of conflicts, elimination of omissions and abortive work, and wastage of resources.

It embraces six principal performance mandates, namely, spatial, acoustical, thermal, visual, indoor air quality, and building integrity. Each mandate comprises a set of performance targets and pertinent diagnostic tools. The targets are occupant-oriented deliverables that pertain to the environmental or physical attributes of the building which impact the physiological, psychological, social, and economic well-being of the occupants. The diagnostic tools are methodologies developed for the appraisal of the building design in terms of the various performance indices.

TBPD is not just about the application of "hi-tech" building systems and/or materials. It seeks to rationally and systematically exploit the synergy of the various relevant technologies and management know-how to

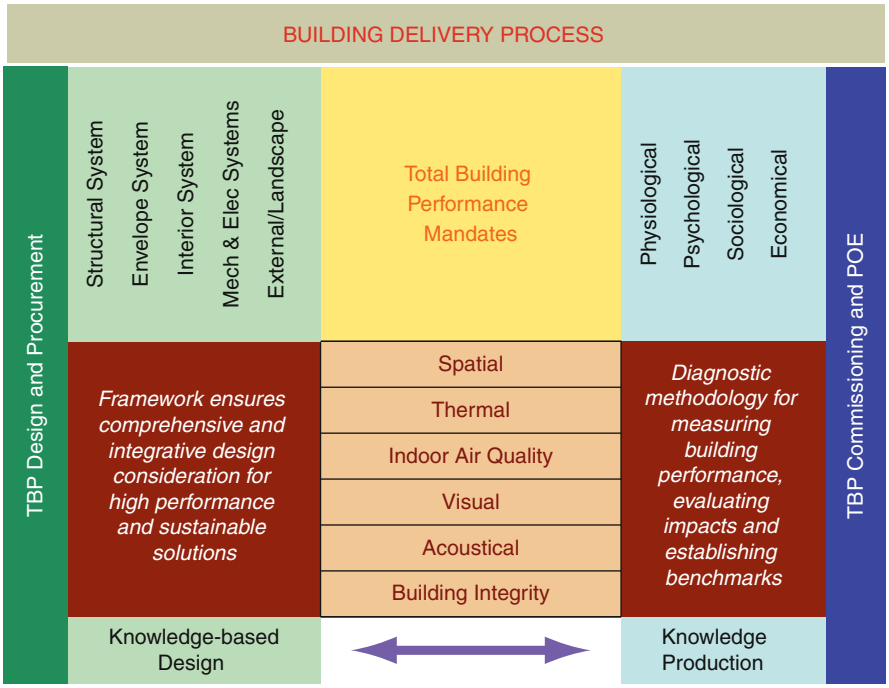

Sustainability Performance Simulation Tools for Building Design. Figure 1
Total building performance and diagnostics concept

bring about desirable building performance at a reasonable cost. Knowledge and experience of an integrated team are clearly essential ingredients within the strategic framework. The ultimate success of a sustainable and high-performance building may be assessed by considering how well it meets the following four principal criteria: (1) occupant satisfaction, (2) organizational flexibility, (3) technological adaptability, and (4) environmental and energy effectiveness.

Knowledge and Experience

Louis Sullivan defines architecture as the crystallization of the thoughts and feelings of a civilization. There is a long tradition in the architectural world of tracing and documenting the changes in building design over the ages and in different geographical, climatic, and sociocultural and even political contexts. Such efforts in the realm of history and theory of architecture tend to focus predominantly on the arts and humanistic aspects. Literature that rigorously records the building-related sciences and technologies of the times is comparatively rare. Occasionally, it is possible to get a glimpse of the work of the ancient master-builders and the incredible technical ingenuity that created architectural masterpieces that is "sustainable" in every sense by today's [re] definition of the term. Knowledge and experience are produced, preserved, and transmitted through the generations often by long-suffering apprenticeships. Arguably, life was simpler and the palette of options was limited in comparison to our modern globalized world but that was not necessarily a disadvantage and certainly did not hamper the creative and innovative spirit that existed during those past milieus.

Witnessing phenomenal advances in science and technology in the world, the building industry at large remains very slow in responding to or capitalizing on the tremendous potentials and opportunities offered compared to other industries or businesses. Building performance–related research is not particularly valued by the industry and society, and consequently, support for such endeavors is dismal. Despite the circumstance, there have been research activities that generated a significant body of knowledge over the past 3–4 decades, way before green design became a contemporary buzzword. However, this knowledge is invariably lodged within highly technical publication archives that continue to serve the academic and research communities but rarely touch the practice world in any meaningful or impactful way. As the knowledge base continues to expand, it is inevitable that the chasm between "what is known" and "what is done" becomes increasingly wide.

Recognizing this state of affair, the building industry then attempts to ameliorate the consequences by simplifying the inherently complex relationships and interactions between humans and the environment in the form of prescriptive solutions that get codified into standards and regulations. Simplification and prescriptive approaches are not inherently bad in themselves and they do provide a cost-effective means of setting certain critical performance benchmarks in building. However, there are always limits of applicability and embodied assumptions that are not often immediately apparent to designers who are increasingly more likely to operate in a globalized practice.

This then leads to the final human element of experience in this discussion. Even in this realm, the building industry is unbelievably weak in "professionalizing" this valuable human resource. The medical and the law industry, two rather diametrically different professions one may add, share a common unifying practice of systematically and meticulously documenting their "experiences" – both the good and the bad as well as the success and the failures. These become the tangible and valuable industry assets that society has come to accept and somehow has to pay for. Whether it is attributable to the educational system and/or a deeply entrenched business structure, the building industry is highly fragmented and often adversarial rather than collaborative in nature. For the fear of professional and financial liability, cases of failure are often buried through private settlement. Experiences gained from such events therefore reside only with the parties involved and not generally accessible for the industry to share and learn from. Even if there is no catastrophic encounter, there is currently no widely adopted practice of monitoring and measuring the performance of buildings in use and comparing the empirical results with the predicted design performance targets. Much can be learned from such provisions and they can also open up new innovation pathways into the field of real-time intelligent sensing

and predictive optimal building control. Unless there is some fundamental paradigm shift in professional practice, especially to address the specific challenge of green building design and operation, the industry may well be condemned to the "Sisyphean task"[2] for a long time to come.

Prerequisites for Building Performance Modeling

An effective process of sustainable building design requires engaging the elements of theory, practice, knowledge, and experience through integrative inputs from multidisciplinary professional teams. Effective communication through information exchange is an important success factor. A study from US National Institute of Standards and Technology shows that 30% of the construction cost is lost due to the information interoperability problem among the building delivery team [19] (Figs. 2 and 3). There is national interest in the USA to strategically address this issue that affects the quality of buildings being designed and constructed as well as productivity loss in the industry.

A multi-prong strategic approach has to be adopted to revolutionize the building industry and to change the "business-as-usual" mindset. It must concurrently address the processes and products involved in green building delivery, and the nature of the hardware, software, and human resources associated with the respective functions. Education is perhaps the most critical starting point to address the fragmented infrastructure as illustrated by Mattar [20] (Fig. 4) and effect lasting change. While architecture is traditionally regarded as "the art and science of building," architectural education around the world is still seeking the balanced curriculum that provides a firm foundation in both the qualitative and quantitative elements of design creativity. The sustainability movement has yielded new and widely recognized building performance standards (e.g., LEED) that are leading building developers to demand design teams to achieve such standards in order to remain competitive in the real estate market. Industry drivers are in motion to hasten the curricula and pedagogical change in schools of architecture and engineering.

Modeling and Simulation

Simulation is the process of designing a model of a real or imagined system and conducting experiments with that model. The purpose of simulation experiments is to understand the behavior of the system or evaluate

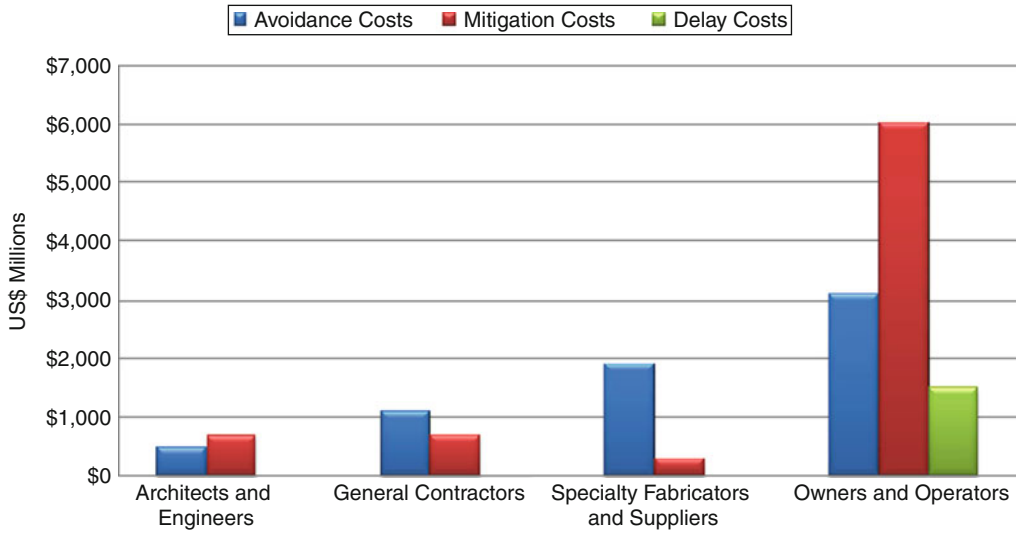

http://www.bfrl.nist.gov/oae/publications/gcrs/04867.pdf

Sustainability Performance Simulation Tools for Building Design. Figure 2
Cost of inadequate interoperability by stakeholder group and cost category

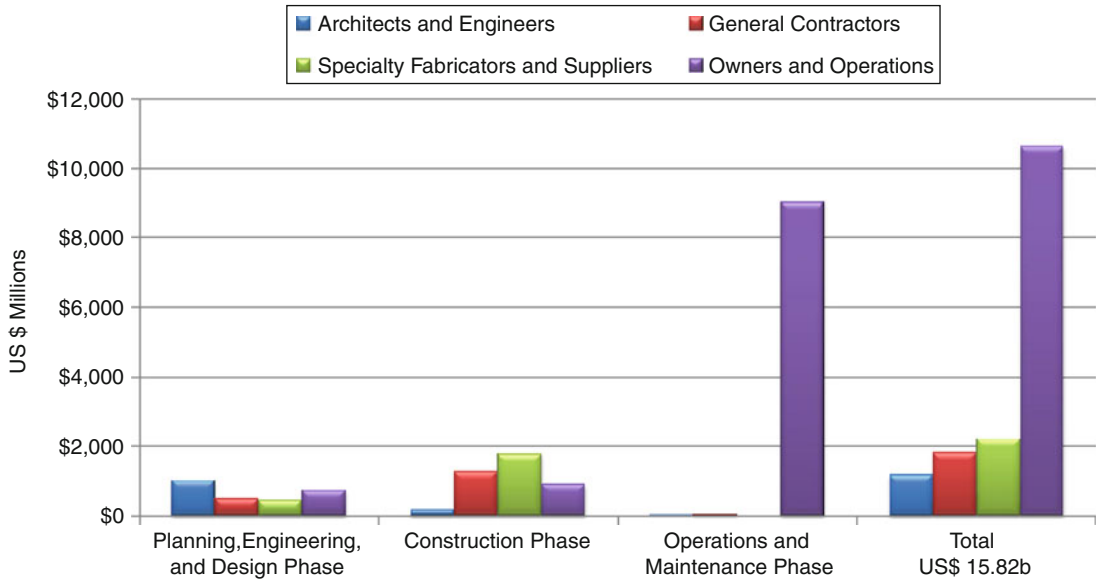

http://www.bfrl.nist.gov/oae/publications/gcrs/04867.pdf

Sustainability Performance Simulation Tools for Building Design. Figure 3
Cost of inadequate interoperability by stakeholder group and building life cycle phase

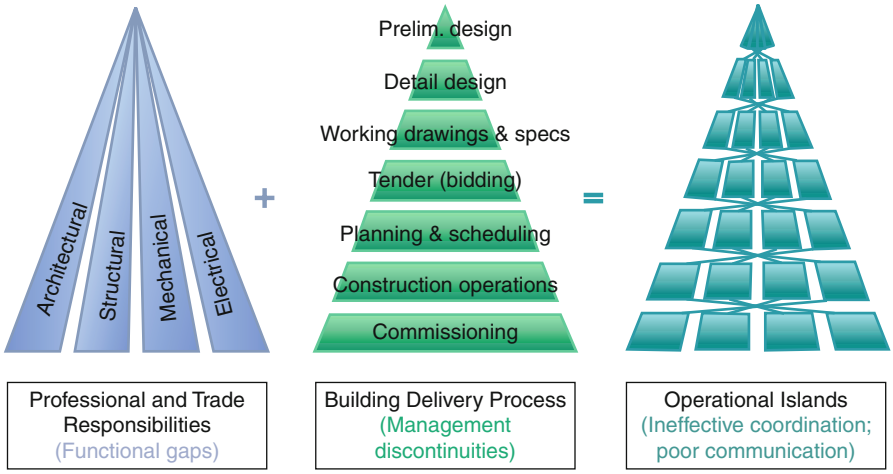

Sustainability Performance Simulation Tools for Building Design. Figure 4
Building industry infrastructure (cp. Mattar [20])

strategies for the operation of the system. Assumptions are made about this system and mathematical algorithms and relationships are derived to describe these assumptions – this constitutes a "model" that can reveal how the system works [21]. Simulation is deployed when the real system cannot be engaged, because it may not be accessible, or it may be dangerous or unacceptable to engage, or it is being designed but not yet built, or it may simply not exist [22]. It can be used to demonstrate the eventual "real" effects of a system when subjected to alternative conditions and courses of action.

Building performance models are developed by reducing real-world physical entities and phenomena to an idealized form on some desired level of abstraction. A classic overview of modeling tasks in the building physics domain can be found in Clarke [9]. Design analysis supported by simulation involves the creation of a behavioral model of a building in a given stage of its development, e.g., reflecting its "as-designed" or "as-built" or "as-operated" specification. The actual simulation involves executing this model on a computer, analyzing its observable states, and mapping these observations to suitable quantifications of performance indicators, e.g., by suitable postprocessing of the outputs of the simulation runs [7].

Critical Elements of Integrated Process and Product Modeling

Data Sharing and Interoperability It is encouraging to note that in the past decade, the building industries in many countries have begun to seriously adopt IT within an integrated and systematic framework that covers the building life cycle, from inception to design, construction, post-occupancy operations, and eventually demolition and recycling of building materials.

A significant catalyst of this movement is the establishment of the International Alliance for Interoperability (IAI), which originated from the USA in 1993. It has since been renamed as buildingSMART International and currently has 15 chapters in North America, Europe, Asia, Australia and Middle East with more than 600 member organizations and companies [23]. One of its mission is to define, publish and promote standard specifications for industry foundation classes (IFC) as a basis for information sharing throughout the project life cycle (including facilitating e-procurement of project-related goods and services), and across all disciplines and technical applications in building industries worldwide. IFC, essentially an object-oriented data model schema, enables interoperability – an environment in which IFC-compliant computer programs of any kind (e.g., CAD, specification documentation, building performance simulation and facilities management software) can share and exchange data, regardless of where the data may be residing. They are information-rich, comprising physical and other attributes that can be shared throughout the supply chain. Data pertaining to a project can be seamlessly organized and linked for ease of communication during the design and construction process, and subsequently archived for future reference by building owners and operations management. Such a data schema forms the core of what is now commonly known as building information modeling or BIM.

Building Information Modeling In the USA, a National Building Information Modeling Standard (NBIMS) has recently been published [24]. This standard is intended to provide the framework and foundation to encourage the flow of information and interoperability between all phases of facility's lifecycle. It defines BIM as "a digital representation of physical and functional characteristics of a facility" and its overall scope is to facilitate "collaboration by different stakeholders at different phases of the lifecycle of a facility to insert, extract, update, or modify information in the BIM to support and reflect the roles of that stakeholder" [23].

The key attribute of a BIM is its ability to organize and relate information for both users and machine-readable approaches. However, to enable interoperability between applications and databases, the inherent semantics of the underlying taxonomy and ontology have to be unambiguous and nonredundant. One of the primary roles of the NBIMS is to provide the ontologies and their associated common languages that will allow information to be machine-readable across different but related domains. NBIMS presents an excellent conceptual model of information exchange in AEC industry. The question then is what approach can be adopted to develop an operative IT platform to realize and implement this conceptual model in practice. Current BIM development work tends to be focused on the design and construction phases (and with minimal interoperability for integrative performance simulation support) but not yet extended to consider ongoing performance monitoring and diagnostics throughout the life cycle of the building. Particularly for complex buildings, effective operations have significant impacts on ensuring that the predicted design performance is actually achieved and sustained throughout the building life cycle. Therefore, a comprehensive dynamic life cycle building information model for the "total building performance and

diagnostics" approach is advocated to address the entire building delivery process and ongoing commissioning of high-performance buildings. The model structure is based on the industry foundation class (IFC) schema (as endorsed by NBIMS) that will capture (a) "static" building information generated during the design and construction process and shared among the design architects and engineers particularly to support building performance predictions using various building simulation tools, benchmark evaluations (e.g., LEED), and advanced design optimizations; (b) "dynamic" (operational) building information generated from large-scale occupancy detection and environmental sensing network for ongoing commissioning, whole building performance monitoring, and advanced adaptive controls based on occupant behavioral studies. This integrated model will also serve as a rich repository of comprehensive evidence-based case studies for ongoing research and development as well as education of professionals for the building industry in the long term (Fig. 5).

Building Performance Modeling While the BIM development work continues, many well-established advanced "stand-alone" performance modeling tools are readily available for use by design teams. The following discussion highlights some of the critical areas of input especially from the architect working within the team. Whether or not the architect personally conducts the modeling work, these points of considerations are vital and must be clearly established for the team. Otherwise, the age-old ugly truth of computing will prevail – garbage in, garbage out (GIGO).

Determining Occupancy Schedule Building performance simulation aims to support sustainable design and the creation of healthy, comfortable, and productive habitats for human activities while minimizing resource utilization and waste generation. Ironically, defining such human activities "accurately" as input factors in performance modeling remains probably the single most complex and challenging task. For example, research has shown that for a variety of reasons, actual occupancy rate in modern office buildings is frequently only 40–60% of the design assumption. This has consequences not only on energy consumption but also on the maintenance of comfort conditions in buildings. Mismatch between designed and actual operating conditions results in excessive

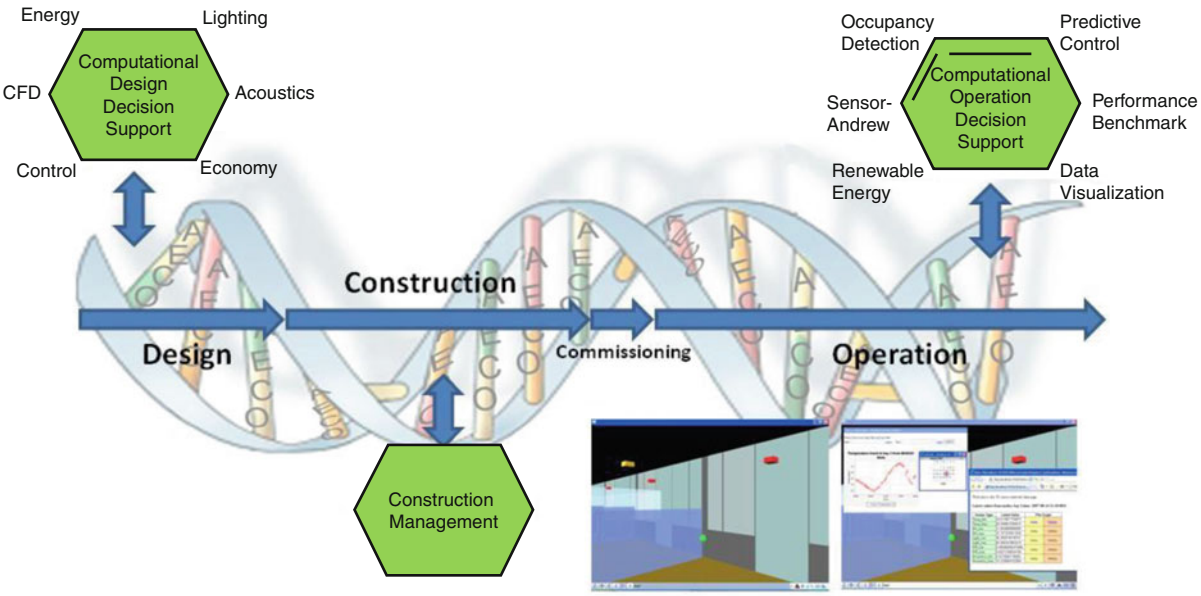

Sustainability Performance Simulation Tools for Building Design. Figure 5
Dynamic Life Cycle Building Information Model (DLC-BIM) in support of an integrated and sustainable building delivery and operation process. (Architecture, Engineering, Construction, Operation – AECO – the "genetic DNA" of DLC-BIM)

provision of heating/cooling and difficulty in optimizing control of building systems. This challenge lies squarely with the architect, whose responsibility is to thoroughly understand the client's operational requirements and translate that "qualitative" descriptive brief into an architectural design solution, accompanied by appropriate quantitative parameters that can be communicated to the engineering design team members for producing concurrent technical solutions. Recognizing this crucial communicative role should prompt architects to play a more proactive leadership role in building performance modeling.

Configuring Thermal Control Zoning Architects and HVAC engineers typically have quite different notions about "zoning" in a building. One views these zones as formal, spatial, and functional demarcations which may be subject to certain design codes such as fire compartmentalizations while the other regards them as volumes that require conditioning according to a desired set-point temperature. The usual HVAC design objective is to size the systems and configure the layout so as to meet peak load conditions while minimizing the number of discrete control zones as far as possible to save on cost. It is not uncommon to witness inadequacies and conflicts in operational control of the systems when there is a lack of cross-disciplinary understanding and communication during the design stage. Coupled with the uncertainties of occupancy schedule mentioned above, the systems may not be able to respond optimally, resulting in energy inefficiency and uncomfortable indoor environment.

The theoretically ideal approach is to map the "architectural" zones which are subjected to difference in location-based exposures according to orientations (e.g., perimeter versus internal core zones) with the thermal control zoning configuration in the building. Possible design solutions can then be generated through parametric energy simulations and an "optimal" decision can be derived through systematic analysis and evaluation of the quantitative results.

In reality, any simulation result is only as good and reliable as the assumed input values for the various parameters. However, if the model is constructed based on "first principle" integrated approach mentioned above, there would be built-in capabilities in the systems for further fine-tuning of the controls when the completed building is in operation. Looking beyond current practice, there are already R&D efforts to "automate" such fine-tuning based on continuous concurrent sensing of the indoor environment and monitoring the system performance as well as micro-climatic conditions throughout the life cycle of the building. The empirical data acquired is the "real deal" and when used as input into a predictive control model, further realistic optimization of the system can be achieved with even greater energy saving. This subject will be further elaborated in section "Integrated Building Design and Operation Process Modeling."

Concurrent Modeling of the Building and the Surrounding Physical and Environmental Context Traditional environmental performance modeling tends to focus mainly on active systems within a "closed" building that rely completely on energy to provide some form of conditioning all year round. Green building design calls for a radical departure from that rigid approach and encourages the exploration of multi-modal environmental control systems in buildings. These would include passive systems that require no energy for operation (e.g., sunshades for solar control, operable windows for natural ventilation, light shelves for daylighting enhancement, etc.), the common active systems as well as mixed-mode conditioning that selectively combine the passive and partially active systems for optimal effects. Furthermore, the concern also extends beyond the performance of the building itself to its potential impact on the surrounding ecological and environmental conditions. The critical consideration for such a holistic design approach necessitates the design team to be fully cognizant of the physical and micro-level environmental conditions surrounding the proposed building, whether present or anticipated (to the extent possible) in the future.

The model should then include every object within the physical domain that will conceivably impact the overall performance outcome. Given that external climatic conditions are naturally dynamic, the parametric study should be carefully structured in order to provide design decision support performance data that sufficiently represent the probabilistic occurrence under the varying conditions over the year or seasons or even at a higher periodic resolution as each case may demand.

Modeling examples of two performance domains (daylighting and natural ventilation) are presented here. Figure 6 shows the sunshine availability and temporal distribution analysis on a multi-block residential development in the Tianjin Eco-city in China. Figure 7 shows the concurrent analysis of daylight factor and daylight illuminance for the same development in meeting China's GB/T 50378: 2006 Evaluation Standard for Green Buildings.

Figure 8a illustrates the concurrent computational fluid dynamics modeling of site and building interiors for the same residential development in Tianjin Eco-city. Figure 8b shows the resulting velocity fields, temperature profiles, and air change rates under different wind directions at an assumed wind speed of 2 m/s. Figure 8c shows the comparative analysis of airflow patterns, assuming same window opening configurations but different interior door opening conditions, under the same external wind conditions. As would be intuitively expected, the results clearly illustrate the importance of considering not only the "static" physical building layout but the inclusion of the "dynamic" configurations under different in-use conditions.

Allocating Resources for Modeling in Early Design Stage The predominant factor in the decision-making process in practice is still based on cost, more specifically first cost. Traditional processes often ignore the operational and occupancy implications while emphasizing first cost despite the fact that tools are available for evaluating cost benefits of a performance-oriented approach to the building delivery process over the life cycle of a project. Yudelson notes that increased economic benefits are the prime driver for change for green buildings. The business case for green development should be based on a comprehensive view of benefits that include economic, financial, productivity, risk managements, public relations and marketing, and funding [5]. It is well acknowledged that decisions at the early project

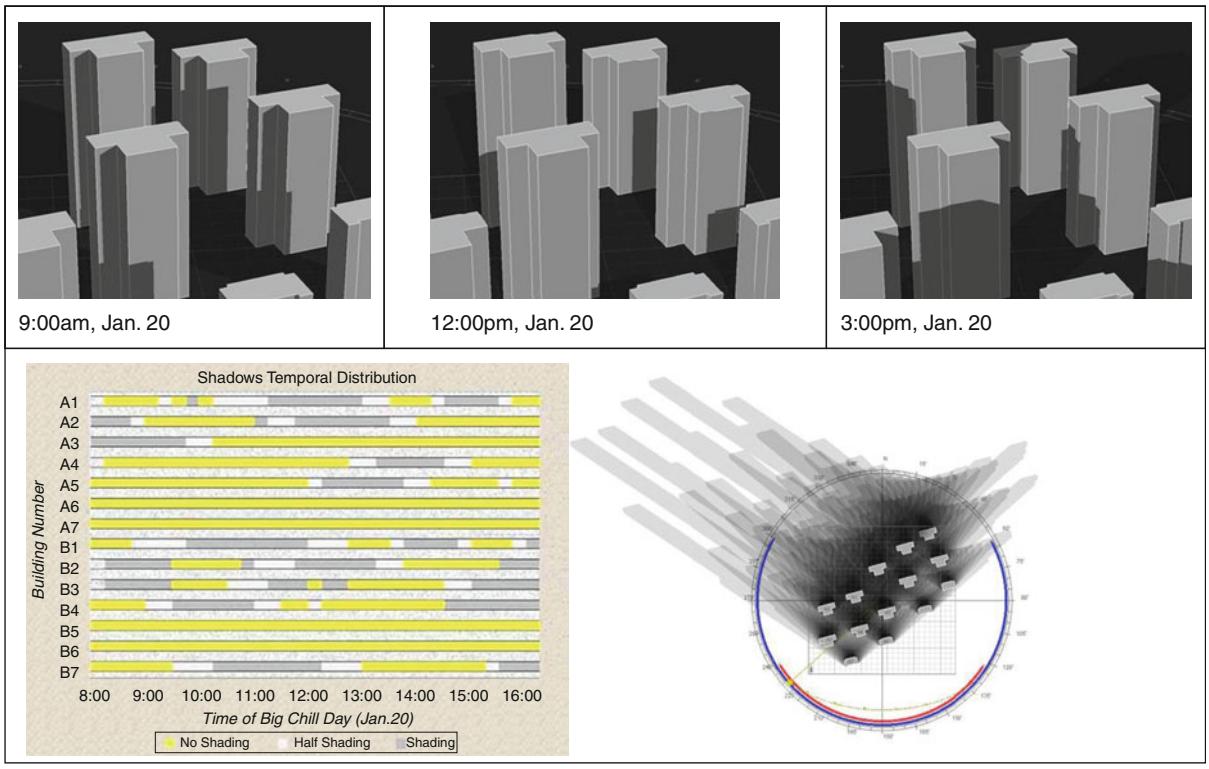

Sustainability Performance Simulation Tools for Building Design. Figure 6
Sunshine availability and temporal distribution analysis of a multi-block residential development in Tianjin Eco-City, China [25]

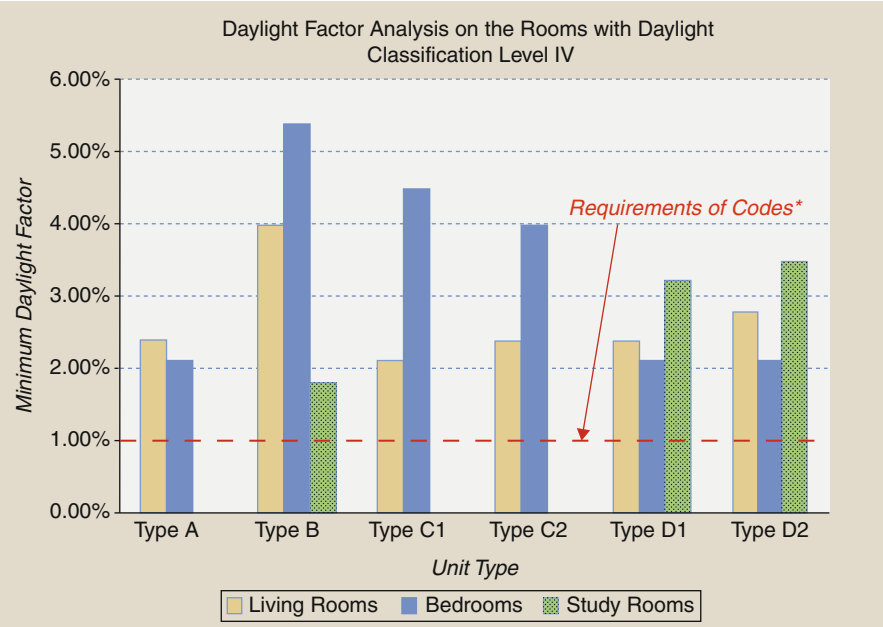

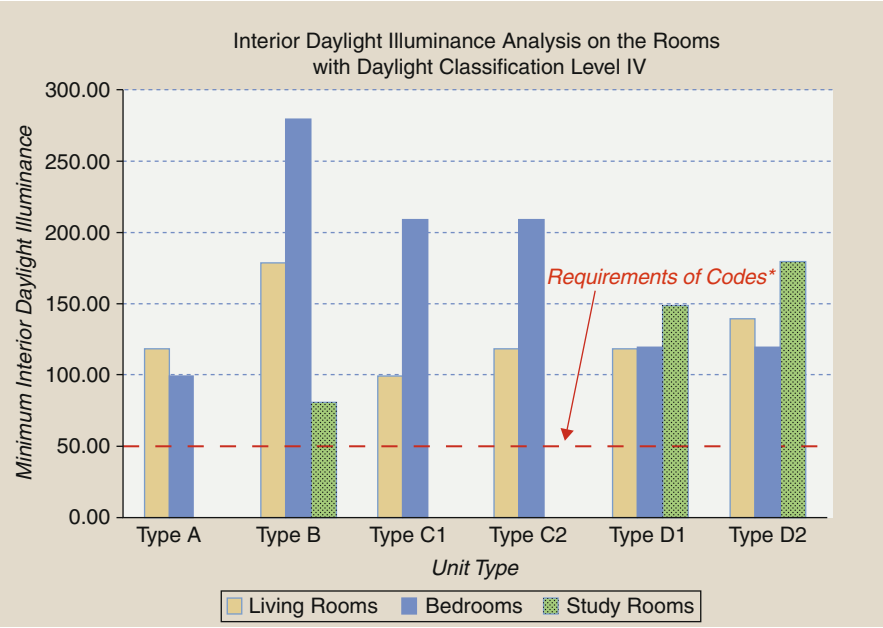

Sustainability Performance Simulation Tools for Building Design. Figure 7
Concurrent analysis of daylight factor and daylight illuminance for the multi-block residential development in Tianjin Eco-City in China in satisfying China's GB/T 50378: 2006 evaluation standard for green buildings [25]

phase can have significant impact on subsequent alternatives and design solutions. But the unwillingness to invest in preliminary investigative design studies in order to keep costs low would invariably result in remedial or even abortive work, thereby increasing the overall costs toward the end of the project phase. The range and nature of existing design support tools that are being applied in practice clearly reflect this scenario, whereby they are almost exclusively developed for the back-end of the design and construction process,

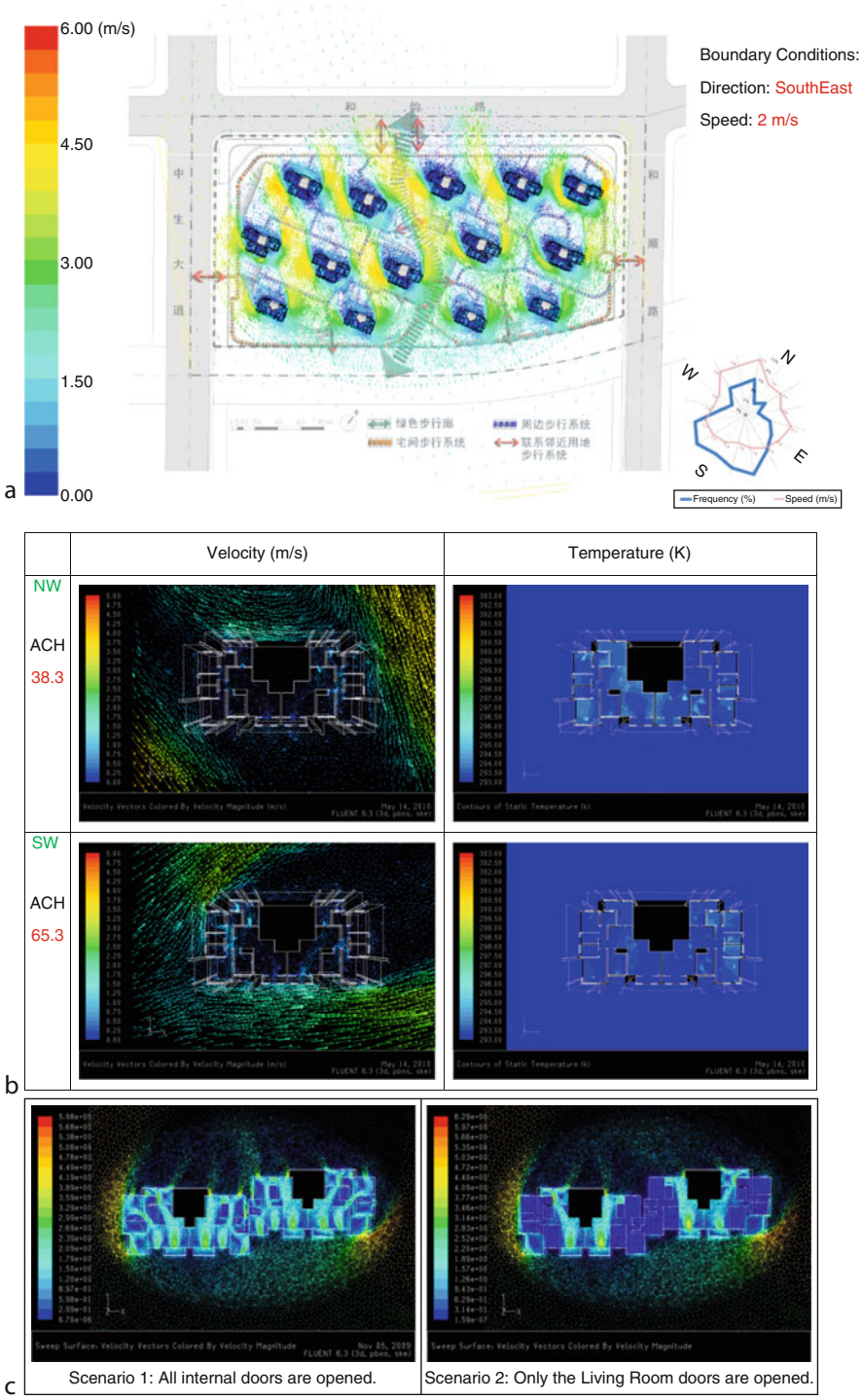

Sustainability Performance Simulation Tools for Building Design. Figure 8

(**a**) Concurrent computational fluid dynamics modeling of site and building interiors [26]. (**b**) Velocity fields, temperature profiles, and air change rates under different wind directions at an assumed wind speed of 2 m/s. (**c**) Air flow patterns assuming same window opening configurations but different interior door opening conditions under same wind conditions

primarily for design verification rather than design generation. It is therefore of strategic advantage to reassess the relative importance of early conceptual design within the whole and to allocate adequate resource toward this stage of work, and to utilize the potential of computer-aided information-processing tools to support a more comprehensive design/construction strategy.

Performance-Based Versus Prescriptive-based Design

There is a trend in building design toward a performance-based rather than the conventional prescriptive-based approach [27]. Advances in computer technology and, perhaps more importantly, the affordability of such powerful technology have made it feasible and cost effective to use computational design support tools to conduct parametric performance studies of various design options, even at the preliminary design phase.

To further encourage the use of performance-based simulation tools, it is essential to shift the current regulatory systems from prescriptive- to performance-based approach. This shift is not a recent phenomenon as the evolution of building legislation from the practice of prescriptive requirements to performance-based solutions has taken place over the last 10 years or so in countries such as Australia [28]. Though the traditional prescriptive approach is relatively simple to understand, and the requirements are treated as "rules" to be complied with, its provisions are often regarded as "cumulative, conservative in nature and in reality only suitable in relation to 'standard' building configurations" [29].

On the other hand, the basic concept of a performance-based approach is not to prescribe solutions but rather to demonstrate that the proposed design meets defined objectives. This approach may result in alternative designs which are more flexible, rational, innovative, and cost effective. This approach can also be multidisciplinary, consciously taking into consideration the implications and synergistic effects of the various performance mandates. A comprehensive performance-based approach necessitates the ability to translate the objectives into quantifiable parameters, to set limits for these parameters, and to have means of estimating performance of proposed design to validate compliance with the required performance parameters [30]. In this respect, simulation tools should be able to play vital roles in achieving such objectives.

Building Energy Simulation Tools

One of the best overviews of the currently available tools can be found on the US Department of Energy Web site: http://apps1.eere.energy.gov/buildings/tools_directory/subjects_sub.cfm [31]. The list reveals that the emphasis has expanded from an early focus on energy consumption to many other related building performance characteristics.

Majority of the tools are developed to address the increasingly complex requirements of the design and evaluation of commercial buildings. Such complexity arises from the changing perception and demands of building owners, facility managers, and tenants with regard to green/sustainable developments and life cycle operating costs (concerning energy use, in particular) as well as a growing awareness of the potential impact of buildings on human productivity, health, and security.

It is well recognized that the key to influencing the building costs and its performance standards (including energy performance) lies at the early stages of a building project's life cycle [32, 33]. Given the complexity involved, there is a need for effective and efficient tools to assess energy impacts early in the conceptual design phase of a new commercial building design process. Some tools currently exist in various stages of development and targeted for different types of applications and users. There is a need to assess what are currently available and, where necessary, make recommendations for improvements to the tools to facilitate their use in the industry.

Application of Energy Modeling Tools in Industry

An industry survey by Wong et al. [34] of the use of performance-based simulation tools for building design and evaluation concluded that usage of tools remains very limited due to several factors: (1) inherent technical limitation of the software, (2) emphasis on initial or capital cost by clients, (3) a fragmented building delivery process that does not routinely include quantifiable assessments of design options by the design team, and (4) the prescriptive nature of current building codes and design guidelines do not promote analytical use of these tools. The paper also provides a comprehensive list of the

well-known simulation tools for energy and HVAC system analyses available in the building industry, providing brief descriptions of the program features and results output. However, commonly deployed energy-related software tools in industry have been dominated by those used for the analysis of energy consumption, selection, and sizing of HVAC equipment by the HVAC designers. Most of these tools are, as mentioned previously, developed for the purpose of design verification and to meet building code requirements at the end of the design phase. They do not necessarily provide "active support" particularly for the early design process.

These points are also echoed in an internal study by the Public Works and Government Services Canada [35]. The study included eight building energy simulation tools (namely, Energy-10, RETScreen, EE4 CBIP, Visual-DOE, BLAST, DOE-2, EnergyPlus, and ESP-r) which focused mainly on their functionalities. The purpose was "to contribute to an increased understanding of energy techniques and consequently, to more rational decision making in building design" among the designers and engineers at PWGSC.

With the increasing consciousness and demand for sustainable building design solutions, the U.S. Green Building Council has provided a national standard for what constitutes a "green building" – the Leadership in Energy and Environmental Design (LEED™) Green Building Rating System. It contains a prerequisite requirement of minimum energy performance for new construction and major renovations. Recommended potential technologies and strategies include the use of a computer simulation model to assess the energy performance and identify the most cost-effective energy measure and quantify energy performance compared to the baseline building. The latest release of LEED V3 incorporated technical advancements to the rating system, offering enhanced online access and help features as well as an expanded certification infrastructure based on ISO standards, administered by the Green Building Certification Institute (GBCI) for improved capacity, speed, and performance [36]. This is a major impetus in promoting the use of energy modeling tools in design.

Besides LEED, there are also other commercial sector endeavors that work to streamline the process of energy ratings for both commercial and residential buildings. One such well-established program is the Residential Energy Services Network (RESNET) [37]. RESNET has just launched the Commercial Energy Services Network (COMNET), which is a new system assessing the energy efficiency of commercial and multifamily buildings. COMNET has published a manual titled "Commercial Buildings Energy Modeling Guidelines and Procedures" [38]. It offers guidance to building energy modelers, ensuring technically rigorous and credible assessment of energy performance of commercial and multifamily residential buildings. It provides a streamlined process that can be used with various existing modeling software and systems, across a range of programs. Notably, the COMNET guidelines will offer applicable procedures for owners to demonstrate that their buildings qualify for federal energy efficient building tax deductions per Section 179 day of the Internal Revenue Code. The guidelines can also be used in calculating percent energy savings for point eligibility for green building rating systems, and in modeling annual energy consumption for use with building energy labels.

Definition of Early Design Phase and Application of Tools

While the term "early design phase" is very commonly used in discussing the building design process, it invariably refers to the stage of work where initial design ideas are being conceptualized in tandem[3] with the formulation of the building project requirements. It is generally recognized that this is an adaptive-iterative process [6]. However, it is often not clear in practice when this phase ends and the next begins.

One essential reference to establish a professional practice definition of early design is the American Institute of Architects Contract Documents. The AIA standard form of contract (see Fig. 9) includes the provision for Energy Studies and Report under the category of planning and evaluation services. The description of supplementary services further describe Energy Studies consisting of special analyses of mechanical systems, fuel costs, on-site energy generation, and energy conservation options for the Owner's consideration. The description of Schematic Design Document also includes electronic modeling. There are also considerations of copyright of electronic documents associated with computational modeling work. These are covered in the Owner-Architect Agreement shown in Fig. 9.

Architect's Services

B141 - 1997 (Owner-Architect Agreement)

Identifying the services needed for the project: Under the Categories of Planning and Evaluation Services *Energy Studies and Report.*
Design Service Articles 2.4.2.1 (p.896): Schematic Design Document may include study models, perspective sketches, *electronic modeling* or combination of these media. Preliminary selections of major building systems and construction materials shall be noted on the drawings or described in writing.

B163 - Part2 (Description of Designated Services for Owner-Architect Agreement)

Article 2.3 – Description of Designated Services:

Project Administration and Management Services - .01 Project Administration – *02 – Research* Design Services - .23 Architectural Design/Documentation - *.07 Study model(s)*
Design Services - .25 Mechanical Design/Documentation - .01 (Schematic Design Phase) - *.01 Energy sources, .02 Energy conservation* and .02 (Design Development Phase)-*.07 Energy conservation measures*
Design Services - .31 Materials Research/Documentation -.01 (Schematic Design Phase) - .02 Investigation of availability and suitability of alternative *architectural materials, systems and equipment.*

Article 2.4 – Description of Supplemental Services:

Supplemental Services - .54 Special Studies consisting of investigation, research and analysis of the Owner's special requirements for the Project and documentation of findings, conclusions and recommendations for: - .01 Master planning *to provide design services relative to future facilities, systems and equipment* which are not intended to be constructed as part of the Project during the Construction Phase. .02 Providing special studies for the project such as *analyzing acoustical or lighting requirements,* record retention, communications and security systems.

Supplemental Services - *.68 Energy Studies* consisting of special analyses of mechanical systems, fuel costs, *on-site energy generation and energy conservation* options for the Owner's consideration.
Supplemental Services - *.78 Computer Applications* consisting of computer program development and/or computer program search and acquisition, plus on-line computer time charges, for: *.08 Architectural analysis and design ; .10 Mechanical analysis and design; .11 Electrical analysis and design.*

Copyright of Electronic Document

B141-1997 (Owner-Architect Agreement)

(P.2) Terms and Conditions
Articles 1.3 contain the "ground rules" of B141, and embodies a number of notable changes from earlier editions. *One such change involves the architect's drawings, specifications and other documents, now defined as "Instruments of Service", which specifically includes documents in electronic form. The owner's right to the use of such documents (and architect's consultant's rights in documents they have prepared) have been clarified by means of nonexclusive licenses.* In place of "basic" and "additional" services, circumstances are identified that may give rise to change in the architect's services, thereby entitling the architects to additional compensation or additional time for performance. Provisions for dispute resolution now include mediation. Provisions for dispute avoidance include a wavier of consequential damages. The waiver is intended to prevent the escalation of dispute by limiting parties to direct damages resulting from a breach. Finally, grounds for termination are clarified, and the owner is given the right to terminate for convenience.

Sustainability Performance Simulation Tools for Building Design. Figure 9
(Continued)

(P.18) Technological advances, such as computer-aided design, have and will continue to have an impact on the architect's services and the manner in which they are provides. *The architect's services are reflected in instruments of service*, such as drawings, specifications, *electronic data* and interpretive sketches which help the owner to reach the final result, a building project. *Because the use or misuse of the architect's instruments of service affects specific rights and obligations of the owner, the construction team and the public, the architect as a licensed professional retains ownership of, control over and responsibility for these documents.*

(P.19) 1.3.2 Instrument of Service: 1.3.2.1 Drawings, specifications and other documents, including those in electronic form, prepared by the Architect and the Architect's consultants are Instruments of Service for use solely with respect to this Project. The Architect and the Architect's consultants shall be deemed the authors and owners of their respective *Instruments of Service and shall retain all common law, statutory and other reserved rights, including copyrights.*

(P.20) *Given the rapid pace of technological changes, it is not practical to address all the varieties of electronic documentation in a standard form document. The parties may wish to develop a separate, written agreement on how to deal with the electronic formats they may use.*

(P.21) 1.3.2.4 Prior the Architect providing to the Owner any Instruments of Service in electronic form or the Owner providing to the Architect any electronic data for incorporation into the Instruments of Service, the Owner and Architect shall by *separate written agreement* set forth the specific conditions governing the format of such *Instrument of Service or electronic data, including any special limitations or licenses not otherwise provided in this Agreement.*

Sustainability Performance Simulation Tools for Building Design. Figure 9
Summary of contractual provisions in the AIA contract document for conducting energy studies in architectural practice

Given these contractual provisions and the drive toward greener designs, it is envisaged that the use of energy modeling tools will become more pervasive in due course. The critical challenge then is to ensure the available tools are indeed effective in supporting the design process.

Many energy modeling tools have been developed over the years by research and development teams in academia, public agencies as well as the private sectors around the world. The conceptual approaches adopted and technical implementation of these tools vary significantly. Some tools employ "simplified" methods that address specific perceived needs of the early design phase while others adopt complex first-principle-based engineering algorithms that can meet detailed design requirements. The potential for continuous development of any of these tools depends largely on the software engineering paradigm adopted, which should consider both data modeling and activity modeling for the entire design process.

In building performance modeling, the fundamental data required may be categorized as contextual (e.g., geographical and climatic), formal (e.g., geometric configuration and orientation), semantic or attributive (e.g., dynamic material properties), and performance indices (e.g., energy consumption targets and code requirements). Activity modeling should recognize the growing necessity to support multidisciplinary collaborative design as building projects become more complex [39]. With increasingly affordable computing power, it is argued that energy modeling tools should adopt rigorous physics- and engineering-based algorithmic principles in the computational prediction of energy performance to ensure acceptable results.

The different functions within a particular design phase can be met through the user interface design which could progressively reveal different levels of pertinent information input demands with associated library support, and generate appropriate output information to assist in decision making at that particular stage. For example, at the early design phase, the architect may explore various building geometries, orientations, and fenestration configurations, and be provided with recommended input parameters derived from an extensive contextual case-based library support in terms of materials, construction, performance targets, etc. The output required at this phase may just be building loads without detailed considerations of mechanical systems and actual energy consumption. As the design progresses, the design team can then be

exposed to greater degrees of freedom, with commensurate application support, in modifying the input parameters, not only in terms of the data model but also in computational algorithmic options that aim toward increasing levels of accuracy and resolution as well as performance details in the results output.

Literature Survey of Some Existing Energy Modeling Tools

As part of a research project titled "Energy Modeling Tools for Early Design Phase" [40], a literature review was conducted on the more well-known energy modeling tools that exist. These tools vary tremendously in many respects. A comparison of the 22 tools was made based on the following criteria:

User interface
CAD interface
Ease of use
Manuals
Computer platform
Expertise required
Input flexibility
Output capability
Functionality
Technical approach
Validation
Audience
Customer support
Price
Usage

Details, including contact information for the respective tools, are given in Table 1. The definitions of the items in the evaluation matrix are given in Table 4.

Five tools are subsequently selected for conducting detailed evaluation of their use in the context of early design support. These are (1) Green Building Studio, (2) eQUEST, (3) Energy Scheming, (4) Ecotect, and (5) TAS. These tools are selected because they are relatively known and considered to hold particular promise for use in schematic design. This selection may be regarded as representative of the broad categories of tools that exist in industry. The same information contained in Table 1 has been extracted and tabulated for these five tools for convenient comparison in Table 2.

Evaluation of Selected Tools for the Early Design Phase

The evaluation of the five selected tools is structured to address the following themes in computational design modeling and analysis:

- Usability
  - System requirements
  - Interoperability with other tools, import/export capabilities
  - User interface
  - Learning and training time required
  - Effort required in updating model/conducting parametric studies
  - Processing time
- Functionality
  - Comprehensiveness of geometric and system modeling
  - Types of energy calculations (e.g., load estimation, HVAC systems performance, etc.)
  - Types of data analysis and presentation
  - Availability of other environmental domain simulations (e.g., lighting)
- Reliability
  - Consistency of results
  - Accuracy of results
- Prevalence
  - Compliance with industry standards
  - Documentation
  - User support
  - Pricing and licensing

The exercise involves two major tasks: (1) development of a comprehensive classification schema for comparing the five selected tools, and (2) application and experimental testing of the tools in "simulated" architectural practice scenarios conducted by graduate students and selected practicing architects under controlled conditions.

A detailed matrix of features is developed to enable a comprehensive comparison of the five selected tools according to the major themes stated above, and represented by the following specific criteria:

1. System
2. Extension
3. Functionality
4. User

Sustainability Performance Simulation Tools for Building Design. Table 1 Summary of a survey of existing energy modeling tools

	ApacheSim (part of VE of IES)	BDA 3.1 (Building design advisor)	BSim	COMFIE v3.0
User interface	Graphical user interface	Graphical schematic editor, building browser and decision desktop	SimView graphical user interface and model editor	Graphical user interface (PLEIADES)
CAD interface	Yes	No	Yes	No
Ease of use	2 days of training is recommended for the basic modules	Easy (according to the developer)	Courses available	Easy (according to the developer)
Manuals		User's guide, online help	User's guide	User's manual
Computer Platform	Windows 2000/XP	Windows 95/98/NT/2000	Windows NT/2000/XP/Vista	PC or Macintosh
Expertise required	2 days of training is recommended for the basic modules, with additional courses available for specific applications	Knowledge of Windows applications	General knowledge of building design and how buildings behave thermally	High level of computer literacy not required
Input Flexibility	Certain energy systems such as PCM and roof ponds not covered	Complex 3-D geometry and sloping roofs not covered	Unlimited rooms and zones	Readable and structured input file generated by Pleiades user interface
Output capability	Presents a wide range of data outputs in tabular and graphical form. All reportage can be copied into word processing and spreadsheet packages	User-selected output parameters displayed in graphic form, including 2-D and 3-D distributions	Tabular or graphic output of any of the calculated parameters on hourly, weekly, monthly, or periodical basis, numeric output is also available	Heating and cooling load, system sizing information, hourly indoor temperature profile and temperature histogram
Functionality	Hourly simulation of solar shading and penetration (SunCast) HVAC systems and control (Apache HVAC) natural ventilation and mixed mode systems (MacroFlo)	Daylighting analysis and electric lighting computation, thermal and energy analysis, comparison of multiple design alternatives	Simultaneous thermal and moisture simulation, dynamic solar and shadow simulation, daylighting calculation, building integrated PV system calculation	Heating and cooling load calculation, system sizing, hourly temperature profile, comfort evaluation

Technical approach	Based on first-principles models of heat transfer and is driven by real weather data	Simplified daylighting analysis and electric lighting computation, DOE-2.1E energy simulation engine	Finite time step, finite difference on building envelope	Finite volume method for building simulation, simplified mechanical system modeling
Validation	Independent testing by other companies and institutions shows good results Development is supported by current research	DOE-2.1E is subject to BESTEST validation procedure	Thermal simulation core has been validated in the IEA Task 12/ Annex 21	Empirical validation and inter-model comparison with ESP-r
Audience	Mechanical building services engineers	Architects and engineers, in early design phases	Engineers, researchers, and students	Architectural engineers, energy consultants, architects
Customer support	Available from the developer	Available from LBNL	Available from the developer	Available from the developer, users' club
Price	Depends on retailers	Free	2,680 EUR annual for up to 5 users/ PCs	Approximately $1,000 for new installations
Usage	Many throughout Europe	800+ as of 09/2010	650 licenses (most of which in Denmark and Germany)	100+
Contact	Don McLean IES Ltd. Helix Building, West of Scotland Science Park Kelvin Campus Glasgow G20 0SP UK Tel: +44 (141) 945 8500 Fax: +44 (141) 945 8501 E-mail: don.mclean@iesve.com Web: http://www.iesve.com	Konstantinos Papamichael Lawrence Berkeley National Laboratory Mail Stop 90-3111 1 Cyclotron Road Berkeley, California 94720 Tel: (510) 486-6854 Fax: (510) 486-4089 E-mail: MAJohnson@lbl.gov Web: http://gaia.lbl.gov/BDA	Kim B. Wittchen Aalborg university Dr. Neergaards Vej 15 Hoersholm DK-2970 Denmark Tel: +45 (45) 86 5533 Fax: +45 (42) 86 7535 E-mail: bsim-support@sbi.dk Web: http://www.bsim.dk	Bruno Peuportier 60, Bd St Michel 75272 Paris Cedex 0 France Tel: +33 1 40 51 9151 Fax: +33 1 46 34 24 91 E-mail: peuportier@cenerg.ensmp.fr Web: http://www-cenerg.ensmp.fr/english/themes
	DEROB-LTH v2.0	*DOE-2.1E*	*Autodesk ECOTECT Analysis*	*EnerCAD 2010*
User interface	User friendly graphical interface	Text input file	Intuitive 3D modeling interface	Graphical interface
Cad interface	No	No	Yes	No

Sustainability Performance Simulation Tools for Building Design. Table 1 (Continued)

	ApacheSim (part of VE of IES)	BDA 3.1 (Building design advisor)	BSim	COMFIE v3.0
Ease of use	Easy (according to the developer)	Recommend 3 days of formal training in basic and advanced DOE-2 use	Easy (according to the developer)	Input assistants make the program easy to use. User interface structured to facilitate error-free inputs
Manuals	NA	User's manual, reference manual, engineer's manual	Tutorials, online help	User's guide
Computer Platform	Windows 95/MS Windows NT	Windows 95/98/ME/2000/NT, UNIX, DOS, VMS	Windows 2000/XP/Vista/7 or Macintosh	Compatible with multi-platform of WIN, MAC-OS, Linux
Expertise required	An overall knowledge of the influence of different design parameters on the thermal behavior of buildings	3-day training recommended	CAD and environmental design experience useful but not essential	None required
Input flexibility	Up to 8 rooms	Up to 200 zones, 512 interior walls, fixed system configurations	Can deal with highly complex 3D models. BIM integration provided	EnerCAD offers default values for all input and extensive building material, window, and wall libraries
Output capability	Simple diagrams for space temperatures, space heating and cooling demand and solar parameters, diagrams for the distribution of the comfort indices PMV and PPD for one space	Numerical output of input verification report, performance summaries, design day summaries and hourly report for building thermal performance, energy consumption, and cost	Graphic output of thermal, lighting, acoustic and cost results, export to RADIANCE, EnergyPlus, ESP-r etc.	Table of monthly values, annual heat demand, monthly histogram, flux diagram
Functionality	Hourly calculation of temperature and comfort level, detailed window and shading modeling, flexible modeling of building	Numerical output of detailed, hourly, whole building energy analysis of multiple zones in buildings of complex design, operational energy cost calculation, daylighting analysis included	Hourly simulation of lighting, thermal and acoustic performance, discomfort level, resource management, daylighting analysis included	Monthly calculation of cooling and heating load, U-value calculator, shading calculator, window calculator
Technical approach	RC-network building thermal model, simplified mechanical system modeling	Hour-by-hour, response factors for walls, weighting factors for zones, rectilinear surface model for daylighting	CIBSE Admittance Method for load calculation, hour-by-hour building, and system thermal performance simulation	Monthly heat balance method

Validation	NA	Subject to BESTEST validation procedure	NA	Based on Swiss "recommendation SIA 380/1" edition 2009 and the European "Thermal performance of buildings EN 832"
Audience	Students, researchers, and energy consultants	Architects, engineers, energy consultants, researchers	Architects, engineers, environmental consultants	Architects and building engineers
Customer support	Support maintained from Lund Institute of Technology, Lund University	LBNL help line, commercial sources	Support forum maintained by Autodesk Support	Support provided by EnerCAD 2010 Web site
Price	500 EUR – Research License 2000 EUR – Commercial License	$300–$2,000	Provided from local re-sellers	CHF 760 Pro version CHF 50 Educational version
Usage	150	800 user organizations in USA. 200 user organizations internationally	NA	500+
Contact	Lund Institute of Technology, Lund University, Box 118, Lund, 221 00, Sweden. Tel: +46 (46) 222 9662 Fax: +46 (46) 222 4719 E-mail: Maria. Wall@Ebd.Lth.Se Web: http://www.derob.se	Fred Winkelmann Lawrence Berkeley National Laboratory, Mail Stop 90-3147, 1 Cyclotron Road, Berkeley, California 94720. Tel: (510) 486–5711, Fax: (510) 486-4089.E-mail: FCWinkelmann@lbl.gov Web: http://simulationresearch.lbl.gov	Autodesk Ecotect Analysis and Green Building Studio Services & Support Web: http://usa.autodesk.com/adsk/servlet/ps/index?siteID=12311 2&id=13740368&linkID=13734 494	CUEPE University of Geneva Battelle bat. A 7, rte de Drize Carouge/Gevera, 1227 Switzerland Fax: +41 (22) 705 96 39 E-mail: info@enercad.ch Web: http://www.enercad.ch
	Energy-10 v1.8	*Energy Scheming v3*	*ENER-WIN Version e9*	*eQUEST*
User interface	Menu-driven input system	Graphical interface	Graphical interface (zone sketch interface)	Graphical interface, schematic design wizard, design development wizard
CAD interface	No	Yes	No	Yes
Ease of use	Autobuild feature makes the tool easy to use	Predefined building elements make the tool easy to use	Easy to use	Knowledge-based default values make the tool easy to use
Manuals	User's manual and help system	User's manual	Users manual/Web-documentation	Tutorials, online help

Sustainability Performance Simulation Tools for Building Design. Table 1 (Continued)

	ApacheSim (part of VE of IES)	BDA 3.1 (Building design advisor)	BSim	COMFIE v3.0
Computer platform	Windows 3.1/95/98/2000/NT	Macintosh or Windows	Windows 95/98/NT/ME/2000/XP/ Vista and 7	Windows 95/98/ME/NT/2000/XP/ Vista
Expertise required	Moderate level of computer literacy required, 2 days of training advised	Understanding of basic concepts of energy design Familiarity with the Mac interface is helpful	Experience with Windows applications. Knowledge of building thermal properties and energy concepts	Understanding of basic concepts of building and HVAC system design
Input flexibility	Building size less than 10,000 sf, up to 2 zones, 10 surfaces per zone, limited HVAC system types	Single zone, do not have HVAC systems, do not intend to be a building simulation program	25 zones per floor, up to 98 zones in total, 200 walls and 400 surfaces, 42 building types from ASHRAE	Inputs can be provided at three levels: schematic design, design development, and detailed interface
Output capability	Comparison of various EEMs between reference and base case building, annual energy cost, cost-effectiveness ranking of EEMs	Graphic and numeric reports showing heat gain and loss by hour for each of the calculation days	Annual utility and energy costs with peaks, thermal comfort analysis, life-cycle cost summary	Output of monthly and annual energy consumption by end use, graphic comparison of alternative designs, detailed numeric load, system, plant and economics reports
Functionality	Automatic generation of base cases and energy-efficient alternative case, rank-ordering of EEMs, annual operation cost calculation, daylighting analysis included Photovoltaic Module, Solar Domestic Hot Water Module, and ASHRAE Material Library are added to v1.8	Loads analysis for 24 h for each of 4 seasonal evaluation days, daylighting analysis included	Peak cooling and heating load calculation and zone sizing, hourly calculation of energy performance, Simplified HVAC system simulation	Hourly simulation of thermal and energy performance as well as energy cost, parametric runs, comparison of alternative designs
Technical approach	CNE thermal network thermal simulation engine, 15-min time step, rectilinear surface model for daylighting (split flux method)	Hourly calculation of 4 evaluation days	Transient modeling based on sol-air temperature, time lag, decrement factor, ETD; zone loads and temperatures based on a heat balance methodology; and daylighting algorithms based on a modified Daylight Factor methodology	DOE-2.2 simulation engine

Validation	Subject to BESTEST validation procedure	NA	Empirical validation	DOE-2 is subject to BESTEST validation procedure
Audience	Building designers, HVAC engineers, utility companies	Architectural professionals, students, and building designers	Architects, engineers, energy analyst, building inspectors, student	Building designers, operators, owners, energy/LEED consultants
Customer support	Commercially available from SBIC	Support maintained from Oikos (Oikos.com)	Available from the developer	Available from Doe2.com
Price	$375 ($315 SBIC Members)	$250	$249 for professional license	Free
Usage	3,200+ as of 09/2010	600+	Estimated to be in low 100s	# of full program downloads is approximately 10,000 per annum
Contact	Sustainable Buildings Industry Council Suite 240 1112 16th Street NW Washington D.C. 20036 U.S. Tel: (202) 628-7400 ext 210 Fax: (202) 393-5043 Email: SBIC@SBICouncil.org Web: http://sbicouncil.org/displayc ommon.cfm?an=1&subarticlenbr=110	G. Z. Brown Energy Studies in Buildings Laboratory Department of Architecture University of Oregon Eugene, Oregon 97403 Tel: (541) 346-5647 Fax: (541) 346-3626 Email: GZBrown@aaa.uoregon.edu	Larry O. Degelman Degelman Engineering Group, Inc. 2206 Quail Run College Station, Texas 77845 U. S. Email: ldegelman@suddenlink.net Web: http://pages.suddenlink.net/en erwin	James J. Hirsch & Associates 12185 Presilla Road Camarillo CA 93012-9243 Email: Jeff.Hirsch@doe2.com Web: www.doe2.com
	Green Building Studio	*HAP*	*PowerDOE*	*RIUSKA*
User interface	Web-based	Explorer style graphical user interface	Graphical interface	Windows-based graphical interface
CAD interface	Yes, integration to BIM tools	No	Yes	Yes, integration with BIM tools
Ease of use	Easy to use focused on early design phases	Requires training or extensive use to be proficient	Training is highly recommended by developer	Default data libraries
Manuals	Online help, tutorials	User's manual and reference guide, online help	Quick start guide, tutorial, online help	
Computer Platform	Windows and MAC-OS	Windows 98/NT/2000/XP/Vista Windows 7	DOS, UNIX, Windows May not operate properly with more recent versions such as XP and Vista	Windows 2000/XP/Vista/7

Sustainability Performance Simulation Tools for Building Design. Table 1 (Continued)

	ApacheSim (part of VE of IES)	BDA 3.1 (Building design advisor)	BSim	COMFIE v3.0
Expertise required	Knowledge of BIM tools and basic understanding of environmental performance outputs	General knowledge of HVAC engineering principles	Training is highly recommended	Engineering background required to analyze calculation results.
Input flexibility	Unlimited number of thermal zones at the expense of increased computation time	100 plants, 250 systems, 2,500 spaces, unlimited building elements fixed system configurations		The flexibility associated with DOE-2.1E
Output capability	Wide range of environmental performance outputs: building energy and carbon emission reporting, daylighting, water usage and costs, ENERGY STAR scoring, natural ventilation potential	Graphical and numerical output of design reports and hourly, daily, monthly, or annual simulation reports	Graphical and numeric outputs of schedules, peak loads, monthly and annual energy consumption	Numerical output of hourly and annual heating and cooling loads, energy consumption and temperature profile
Functionality	Hourly energy performance simulation using DOE-2 engine. Determines appropriate defaults based on building type and location (majority of defaults are ASHRAE 90.1-2004 compliant)	Load calculation, system sizing, hourly thermal and energy performance simulation, operating energy cost calculation	Hourly simulation of thermal and energy performance	Hourly calculation of building and system energy performance, can be used for life-cycle data management
Technical approach	DOE-2 thermal simulation engine	ASHRAE-endorsed transfer function methodology for load calculation, hour-by-hour thermal and energy simulation	DOE-2.2 simulation engine	DOE-2.1E thermal simulation engine
Validation	DOE-2 is subject to BESTEST validation procedure	Comparison studies with DOE-2.1 yielded good correlation	DOE-2 is subject to BESTEST validation procedure	DOE-2 is subject to BESTEST validation procedure
Audience	Architects and designers	Consulting engineers, design/build contractors, HVAC contractors, facility engineers	engineers, energy consultants, and utility staff	architectural engineers
Customer support	Provided by Autodesk	Carrier factory support and training available	Available from the developer	–

Price	$745 Single user annual subscription $4,995 ten user annual subscription	$1,195 for first year and $240 thereafter	$278 for non-expiration license	–
Usage	unknown	Approximately 5,000 worldwide as of 07/2002	Unknown	About 20 in Finland
Contact	Autodesk Green Building Studio Web: http://usa.autodesk.com/adsk/servlet/pc/index?id=11179508&siteID=123112	Carrier Corporation Bldg TR-4 P.O. Box 4808 Syracuse, New York 13221 Tel: (315) 432-6838 Fax: (315) 432-6844 Email: software.systems@carrier.utc.com Web: http://www.carrier-commercial.com/software	James J. Hirsch & Associates Email: Jeff.Hirsch@doe2.com Web: www.doe2.com	Tuomas Laine Olof Granlund Oy Malminkaari 21 P.O. Box 59 Helsinki, FIN-00701 Tel: +358 (9) 351031 Fax: +358 (9) 35103421 Email: Tuomas.Laine@granlund.fi
	TAS 9.1.4.2	*TRACE 700*	*VisualDOE 4.0*	*Energy Plus v6.0*
User interface	Windows-based graphical interface	Windows-based graphical interface, multiple views, drag and drop load assignments	Graphical interface	No “user friendly” graphical interface
CAD interface	Yes	Yes, integration with BIM tools	Yes	No
Ease of use	Qualified engineer or architect, No training courses are required	Formal training recommended for new users	Not as easy as eQUEST or Energy-10 (According to 21CR)	Text input may make it difficult to use compared to graphical interfaces
Manuals	Users manual	Engineer’s manual, online help, modeling guide	User’s manual, online help system	Well-documented input/output and engineering reference
Computer Platform	Windows NT	Windows 95/98/ME/NT/2000/ME/XP/7	Windows 95/98/NT/ME/2000/XP/7	Windows XP/Vista/7, Mac OS and Linux
Expertise required	General knowledge of architectural engineering and building design	General knowledge of HVAC engineering principles	Basic experience with Windows software. Familiarity with building systems is recommended. One to two days of training also recommended	High level of computer literacy not required, engineering background is helpful for analysis portions

Sustainability Performance Simulation Tools for Building Design. Table 1 (Continued)

	ApacheSim (part of VE of IES)	BDA 3.1 (Building design advisor)	BSim	COMFIE v3.0
Input Flexibility	Unlimited number of zones, rooms, and surfaces	Unlimited rooms, systems, and building elements, fixed system configurations	Up to 1,024 zones and 256 systems, analysis of up to 99 alternatives	Unlimited number of zones and surfaces, uses a simple ASCII input file
Output capability	Numerical and graphical output of any simulation parameter over any period of time	Graphical and numerical output of design parameters, hourly building temperature profiles and energy consumption, comparison of various alternatives, predefined reports	Graphical comparison of design alternatives or selected parameters, standard DOE-2.1E numeric output, LEED style end-use report Life cycle cost analysis of design alternatives	Has a number of ASCII output files which can be readily adapted into spreadsheet form for further analysis, reporting of EER, SEER, and IEER for DX cooling coils, enhanced SQLite output.
Functionality	System sizing, Hourly simulation of heating and cooling demand, CFD, daylighting	Load calculation, system sizing, comparison of up to 4 system design alternatives through hour-by-hour simulation, life-cycle cost calculation, daylighting analysis included, ASHRAE 90.1-2004 analysis	Hour-by-hour simulation of thermal and energy performance as well as energy cost, daylighting analysis included, comparison of alternative designs, 95% of DOE-2.1E's functions	Innovative simulation capabilities including steps of less than an hour, modular systems simulation modules integrated with a heat balance–based zone simulation. Multizone airflow, electric power simulation including fuel cells and other distribution systems, water management systems, Model library for DOE reference buildings (including a 130-zone hospital baseline). Life-cycle costing dataset with US regional fuel escalation factors, functionality of running multiple simulations simultaneously, movable and transparent insulation (TIM) modeling, Ecoroof model, separate sizing factors for heating and cooling

Technical approach	Hourly simulation of dynamic building and system performance	Choose from 7 different ASHRAE load methodologies, Hourly calculation available, rectilinear surface model for daylighting	DOE-2.1E simulation engine	Energy Plus simulation engine (BLAST + DOE-2.1E), significant increase with v6.0 (up to 25–40% execution time reduction), surface heat transfer convection coefficient options for adaptive models
Validation	Empirical validation using IEA test data, EPC and Part L, BEEM, ASHRAE 140-1	Tested according to ASHRAE Standard 140	DOE-2 is subject to BESTEST validation procedure	Tested and validated against the IEA BESTEST building load and HVAC tests
Audience	Building services engineers and architects	Engineers, architects, energy consultants, and utility companies	Mechanical/electrical/energy engineers and architects	Mechanical energy and architectural engineers
Customer support	Available from the developer	Free technical support from Trane factory, training available	Available from Architectural Energy Corporation	Provided by US DOE http://apps1.eere.energy.gov/buildings/energyplus/
Price	1,600+	$1,995 for single license, $3,990 for site/LAN license	$1,250 single commercial $650 single educational	free
Usage	250 user sites	Approximately 1,200 worldwide as of 05/2001	1,000+ as of 08/2002	85,000+ downloads since April 2001
Contact	Alan M. Jones EDSL Ltd 13/14 Cofferidge Close Stony Stratford Milton Keynes, Mk11 1BY United Kingdom +44 (1908) 261 461 +44 (1908) 566 553 Email: info@edsl.net Web: http://www.edsl.net/	The Trane Company 3600 Pammel Creek Road La Crosse, Wisconsin 54601 Tel: (608) 787-3926 Fax: (608) 787-3005 Email: CDSHelp@trane.com Web: http://www.trane.com/commercial/software	Architectural Energy Corporation 142 Minna Street, 2nd Floor San Francisco, CA 94105 U.S. Tel: (415) 957-1977 Fax: (415) 957-1381 Email: vdoesupport@archenergy.com Web: http://www.archenergy.com/products/visualdoe/	U.S. Department of Energy EE-2J Building Technologies 1000 Independence Avenue, SW Washington D.C. 20585-0121 U.S. Tel: +1 (202) 586-2344 E-mail: Drury.Crawley@ee.doe.gov Web: http://www.energyplus.gov

Sustainability Performance Simulation Tools for Building Design. Table 2 List of selected energy modeling tools for experimental evaluation

	ECOTECT	TAS	Green building studio	eQUEST	Energy scheming
User interface	Intuitive 3D modeling interface	Windows-based graphical interface	Web-based	Graphical interface, schematic design wizard, design development wizard	Graphical interface
Cad interface	Yes	Yes	Yes	Yes	No
Ease of use	Easy (according to the developer)	Easy to use, No training courses are required		Easy (according to the developer)	Predefined building elements make the tool easy to use
Manuals	Tutorials, online help	Users manual	Online help, tutorials	Tutorials, online help	User's manual
Computer platform	Windows 95/98/ NT/2000/XP or Macintosh	Windows NT		Windows 95/98/ME/NT/2000/ XP	Macintosh or Windows
Expertise required	CAD and environmental design experience useful but not essential	General knowledge of architectural engineering and building design		Understanding of basic concepts of building and HVAC system design	Understanding of basic concepts of energy design
Input Flexibility	Can deal with highly complex 3D models	Unlimited number of zones, rooms, and surfaces		Only 3 floors could be defined (according to Charli_and_Mahabir_Overview_ simulation_model.ppt)	Single zone, do not have HVAC systems, do not intend to be a building simulation program
Output capability	Graphic output of thermal, lighting, acoustic and cost results, export to RADIANCE, EnergyPlus, ESP-r etc.	Numerical and graphical output of any simulation parameter over any period of time		Graphic output of monthly and annual energy consumption by end use, graphic comparison of alternative designs, detailed numeric load, system, plant and economics reports	Graphic and numeric reports showing heat gain and loss by hour for each of the calculation days
Functionality	Hourly simulation of lighting, thermal and acoustic performance, discomfort level, resource management, daylighting analysis included	System sizing, hour-by-hour simulation of heating and cooling demand, CFD, daylighting		Hour-by-hour simulation of thermal and energy performance as well as energy cost, parametric runs, comparison of alternative designs	Loads analysis for 24 h for each of 4 seasonal evaluation days, daylighting analysis included

Sustainability Performance Simulation Tools for Building Design. Table 2 (Continued)

	ECOTECT	TAS	Green building studio	eQUEST	Energy scheming
Technical approach	CIBSE Admittance Method for load calculation, hour-by-hour building and system thermal performance simulation	Hour-by-hour simulation of dynamic building and system performance	DOE-2 thermal simulation engine	DOE-2.2 simulation engine	Hourly calculation of four evaluation days
Validation	Undergoing	Empirical validation using IEA test data	DOE-2 is subject to BESTEST validation procedure	DOE-2 is subject to BESTEST validation procedure	
Audience	Architects, engineers, environmental consultants	Building services engineers and architects		Architects, architectural engineers	Architects
Customer support	Support forum maintained by the developer	Available from the developer	Available from GeoPraxis, Inc.		
Price	$650 for first professional license, $350 for education and $90 for student	UK$1,600+	Free	Free	$250
Usage	2,000+ as of 09/2002	200+	Unknown	Unknown	600+ as of 03/1999
Contact	Square One Research Pty Ltd c/o Center for Research in the Built Environment Cardiff University, Bute Building, Cardiff, Wales CF10 2NB, UK Tel: +44 (29) 2087 5977 Fax: +44 (29) 2087 4623 Email: sales@squ1.com Web: http://www.squ1.com	Alan M. Jones EDSL Ltd 13/14 Cofferidge Close Stony Stratford Milton Keynes, Mk11 1BY United Kingdom +44 (1908) 261 461 +44 (1908) 566 553 Email: info_edsl@csi.com Web: http://ourworld.compuserve.com/homepages/edsl	John F. Kennedy GeoPraxis, Inc. Tel: 707.766.7010 Fax: 707.766.7014 Email: jfk@geopraxis.com Web: www.geopraxis.com	James J. Hirsch & Associates Email: Jeff.Hirsch@doe2.com Web: www.doe2.com	G. Z. Brown Energy Studies in Buildings Laboratory Department of Architecture University of Oregon Eugene, Oregon 97403 Tel: (541) 346-5647 Fax: (541) 346-3626 Email: GZBrown@aaa.uoregon.edu

5. Modeling
   (a) Project information
   (b) Building modeling
   (c) HVAC modeling
6. Result output

Detailed description of these features and the definitions of the items in the evaluation matrix are given in Tables 3 and 4.

Sustainability Performance Simulation Tools for Building Design. Table 3 Selected energy modeling tools: Matrix of features

I. System					
Operating platform					
Windows	Yes	Yes	Yes	Yes	Yes (emulated Mac)
Mac OS	No	No	Yes	No	Yes
Unit system	SI and English	SI	SI and English	English	SI and English
Energy design guidance	No	No	No	Yes (general guidance available in tutorial)	Yes (specific advice in context of the building design, in text or audio format)
Built-in library[a]					
Weather data	Ye	Yes	Yes	Yes	Yes
Material	Yes	Yes	Yes	Yes	Yes
Construction	Yes	Yes	Yes	Yes	Yes
Schedule	No	Yes	Yes	Yes	Yes
Internal heat gain	No	Yes	Yes	Yes	Yes
Infiltration	No	Yes	Yes	Yes	Yes
HVAC system type	No	No (available in separate plug-in)	Yes	Yes	No
HVAC equipment	No	Yes	Yes	Yes	No
Simulation application					
Stand-alone	Yes	Yes	No	Yes	Yes
Web-powered	No	No	Yes (via Internet)	No	No
Program stability	Moderate (Exception errors when working with multiple projects during single session. Program should be restarted when closing one project and opening another project)	Moderate (120MB file size limitation. Program unstable when a larger number of reports are requested)	Stable	Crash occasionally	Crash occasionally (beta version evaluated)

Sustainability Performance Simulation Tools for Building Design. Table 3 (Continued)

I. System					
Weather file	Library and user definable	Library and user definable	According to zip code	According to geographical location (can be downloaded from doe-2.com ftp site by eQUEST)	No separate weather file, weather data is specified in input interface
Types of weather files	.wea (weather tool data)	.twd (TAS weather database)	Unsure	.bin file	N/A
History tracking					
Undo/redo	Yes (single state undo/redo only)	Yes	No (available in CAD tool)	No	No
Error logging	Yes	Yes	Yes (runtime error message)	Yes (separate error log file)	Yes (runtime error message)
II. Extension					
Interoperability					
IFC compliance	No	No	No	No	No
File exchange with other energy simulation tools	Yes (export of EnergyPlus, ESP-r file)	No	Yes (export of.inp and gbxml file, import of gbxml file is not visible to the user)	Yes (import of.inp file)	Yes (export of. doe2 file)
File exchange with CAD tools	Yes (Autodesk Architectural Desktop and 3D studio file)	No	Yes (.dwg from Autodesk Architectural Desktop,.pne from ArchiCAD,.rvt from Revit, unsure from Autodesk Building System All CAD information is imported into GBS through SOAP and a gbXML file)	No	No
Drawing data input					
Import as underlay	Yes (AutoCad DXF, ASCII model, 3D studio, Stereo Lithography, Radiant Scene, HPGL plot, Ray, Analysis Grid files)	Yes (AutoCAD. dwg and dxf files)	No	Yes (AutoCAD.dwg files)	No (copy and paste drawings from other programs as underlay)

Sustainability Performance Simulation Tools for Building Design. Table 3 (Continued)

II. Extension					
Building element import	Yes (AutoCad DXF, ASCII model, 3D studio, Stereo Lithography, Radiant Scene, HPGL plot, Ray, Analysis Grid files) – Element information not included	No	Yes	No	No
III. Functionality					
Technical approach	CIBSE admittance method	TBD (Dynamic Simulation)	DOE-2.2 simulation engine	DOE 2.2 simulation engine	Hourly calculation of building load for 4 evaluation days
Types of energy calculation					
Building load calculation	Yes	Yes	Not visible in GBS result output. Available in gbxml file exported from GBS	Not visible in eQUEST graphic result output. Available in detailed simulation output file	Yes
Building energy simulation	No	No	Yes	Yes	No
Parametric operation					
Single run/single input and output	Yes	Yes	Yes	Yes	Yes
Batch processing	No	Yes	No	Yes	No
Code compliance	Yes (UK Part-L)	Yes (UK Part-L)	No	Yes	No
Cost estimation	Yes (material cost and resource consumptions, energy cost not included)	No	Yes (annual energy cost and lifecycle operating cost)	Yes (monthly and annual energy cost, lifecycle cost)	No
IV. User					
Documentation					
Tutorial/manuals/ wizard	Tutorial, some background of thermal analysis in help file and in html file and example/ tutorial files	Separate help file and video tutorial	Tutorial for installation and basic usage in pdf and video format	Tutorial in pdf format, schematic design and design development wizards	User's manual in hard copy and pdf format
Engineering documentation	No	No	No	Yes (combined in tutorial)	Yes (combined in user's manual)

Sustainability Performance Simulation Tools for Building Design. Table 3 (Continued)

IV. User					
Help function	Yes (help menu, help topic, FAQ, balloon help)	No (in manager, menu list only in modeler in simulator)	Yes (help menu)	Yes (help menu and on-screen help)	No
User support	Yes (homepages, helpdesk, forum, online courses)	Yes (helpdesk, training)	Yes (inquiry and issues submission through Web site)	Unsure	Yes (by phone or email)
File save interval	Anytime	Anytime	Anytime	Anytime with the exception when the building creation wizard window is open	Anytime with the exception of when a specification window is opened, in which case the user is prompted to close it
Navigation between windows	Flexible random	Flexible random	Flexible random	Flexible random	Flexible random
Clarity of menu and tool bars	Yes	Yes	Yes	Yes	Yes
Model view	Yes (2D and 3D)	Yes (2D and 3D)	No (view in VRML in external application)	Yes (2D and 3D)	Yes (2D)
Model display	Wireframe, Shaded, OpenGL and VRML	Wireframe and Shaded	VRML	Shaded	As pasted or drawn
Expertise required	General knowledge about building energy simulation and thermal analysis.	General knowledge about building energy simulation and thermal analysis.	Experience of 3D CAD tool (Autodesk Architectural Desktop, ArchiCAD, Revit, Autodesk Building System)	General knowledge about building energy simulation and thermal analysis. DOE-2 experience required in detailed data edit mode	General knowledge about building thermal analysis
V. Modeling					
Zone management	By zone management dialog	By zones and zone groups	By space list table	By activity area allocation, no information about the specific location in the building in schematic design wizard	By occupancy, lighting, and equipment zones

Sustainability Performance Simulation Tools for Building Design. Table 3 (Continued)

a. Project information					
Building type definition	Yes (Domestic dwelling, commercial residential, office/ shop/assembly, industrial or storage, others) only used in the UK Part-L analysis	No (for project labeling only)	Yes (see appendix, links to default values)	Yes (see appendix, links to default values)	Yes (links to default values)
Space type definition	No (conventionally specified in zone management dialog as zone name)	No	Yes (see appendix, links to default values)	Yes (see appendix, links to default values)	No
b. Building modeling					
Geometry					
Space composition					
Buildup by spaces	Yes	Yes	No (done in CAD tool)	Yes	Yes
Subdivision of floor plate	Yes	Yes	No (done in CAD tool)	Yes	Yes
Direct drawing input					
Primitive shapes	No	No	No (done in CAD tool)	No	No
Extrusion based on closed curve	Yes	Yes	No (done in CAD tool)	Yes	No
Surfaces	Yes	No	No (done in CAD tool)	No	Yes
Building element definition	Yes (void, roof, floor, ceiling, wall, partition, window, panel, door, point, speaker, light, appliance, solar collector, camera, line)	Yes (floor, building element and window)	No (Defined in the CAD input file)	No	Yes
Different heights within floor	Yes	Yes	Yes	Not available in wizard data edit mode, flexible in detailed data edit mode	Yes
Sloped roof	Yes	Yes	No (done in CAD tool)	Yes	Yes
Sloped floor	Yes	No	No (done in CAD tool)	No (except in detailed data edit mode)	No

Sustainability Performance Simulation Tools for Building Design. Table 3 (Continued)

b. Building modeling					
Building orientation	Yes	Yes	Yes	Yes	Orientation of elevations and roof surfaces available
Accessible coordinate data	Yes (Cartesian coordinate and polar coordinate)	No	Not shown in the user interface, available in CAD tool and gbxml file exported from GBS	Yes	No
Snap function	Yes (snap to grid or object)	Yes (snap to overlay only)	No (available in CAD tool)	Yes (to overlay and grid)	No
Modification	Yes (transform(move, rotate, scale, mirror, extrude, revolve, spin), morph, link/unlink, group/ungroup)	Yes (delete, change alignment)	No (done in CAD tool)	Yes	Yes
Geometry checking	Yes	No	Yes	Unsure	No
Building construction					
Material	Selectable from the library and user definable	Selectable from the library and user definable	Not visible, editable, and definable by user. Not visible to user in GBS result output. Accessible and editable in gbxml and DOE-2 files exported from GBS. Gbxml and DOE-2 files cannot be imported into GBS by user.	Selectable from the library, not editable and definable except in detailed data edit mode	Selectable from the library and user definable
Layer	User definable	User definable	Not visible, editable and definable by user. Not visible to user in GBS result output. Accessible and editable in gbxml and DOE-2 files exported from GBS. Gbxml and DOE-2 files cannot be imported into GBS by user	Selectable from the library, not editable and definable except in detailed data edit mode	Selectable from the library and user definable

Sustainability Performance Simulation Tools for Building Design. Table 3 (Continued)

b. Building modeling					
Construction	Selectable from the library and user definable	Selectable from the library and user definable	Not visible, editable, and definable by user. Visible to user in GBS result output. Accessible and editable in gbxml and DOE-2 files exported from GBS. Gbxml and DOE-2 files cannot be imported into GBS by user	Selectable from the library, not editable and definable except in detailed data edit mode	Selectable from the library and user definable
Shades	User definable	User definable	Not visible, editable. and definable by user. Not visible to user in GBS result output. Accessible and editable in gbxml and DOE-2 files exported from GBS. Gbxml and DOE-2 files cannot be imported into GBS by user	Selectable from the library, editable but not definable except in detailed data edit mode	Selectable from the library and user definable
Default values	No	No	Yes	Yes	Yes
Recommendation	No	No	Yes (according to building type and geographical location)	Yes (according to building type)	Yes (according to building type)
Internal loads					
Occupant					
Load					
Density	Yes (user definable)	Yes (user definable)	No	Yes (editable)	Yes (selectable from the library and user definable)
Total number of occupants	Yes	Yes	Yes (Not visible, editable, and definable by user except in ABS. Visible to user in GBS result output. Accessible and editable in gbxml and DOE-2 files exported from GBS. Gbxml and DOE-2 files cannot be imported into GBS by user)	Yes	No

Sustainability Performance Simulation Tools for Building Design. Table 3 (Continued)

b. Building modeling					
Schedule	Yes (User definable)	Yes (Selectable from the library and user definable)	Yes (Not visible, editable and definable by user. Not visible to user in GBS result output. Accessible and editable in gbxml and DOE-2 files exported from GBS. Gbxml and DOE-2 files cannot be imported into GBS by user)	Yes (selectable from the library, not editable, and definable except in detailed data edit mode)	Yes (user editable, occupied/ unoccupied only, one schedule per day for all occupancy zones)
Lighting					
Load					
Density	Yes (User definable combined with Equipment Load)	Yes (User definable)	Yes (Not visible, editable, and definable by user. Visible to user in GBS result output. Accessible and editable in gbxml and DOE-2 files exported from GBS. Gbxml and DOE-2 files cannot be imported into GBS by user)	Yes (editable)	Yes(selectable from the library and user definable)
Individual appliance	Yes (User definable)	Yes	Yes (Not visible, editable and definable by user except in ABS)	No	No
Schedule	Yes (user definable)	Yes (Selectable from the library and user definable)	Yes (Not visible, editable, and definable by user. Not visible to user in GBS result output. Accessible and editable in gbxml and DOE-2 files exported from GBS. Gbxml and DOE-2 files cannot be imported into GBS by user)	Yes (selectable from the library, not editable, and definable except in detailed data edit mode)	Yes (user editable, on/ off only, one schedule per day for all lighting zones

Sustainability Performance Simulation Tools for Building Design. Table 3 (Continued)

b. Building modeling					
Equipment					
Load					
Density	Yes (User definable combined with Lighting Load)	Yes (User definable)	Yes (Not visible, editable, and definable by user. Visible to user in GBS result output. Accessible and editable in gbxml and DOE-2 files exported from GBS. Gbxml and DOE-2 files cannot be imported into GBS by user)	Yes (editable)	Yes (selectable from the library and user definable)
Individual appliance	Yes	Yes	Yes (Not visible, editable, and definable by user except in ABS)	No	Yes (selectable from the library and user definable)
Schedule	Yes (User definable)	Yes (Selectable from the library and user definable)	Yes (Not visible, editable, and definable by user. Not visible to user in GBS result output. Accessible and editable in gbxml and DOE-2 files exported from GBS. Gbxml and DOE-2 files cannot be imported into GBS by user)	Yes (Selectable from the library, not editable, and definable except in detailed data edit mode)	Yes (user editable, on/off only, one schedule per day for all equipment zones)
Default values	No	No	Yes	Yes	Yes
Recommendation	No	No	Yes (according to building type, location, floor area, and ratio of surface to floor area)	Yes (according to building type and activity area type)	Yes (according to building type)

Sustainability Performance Simulation Tools for Building Design. Table 3 (Continued)

b. Building modeling					
Infiltration					
Rate	Yes (User definable)	Yes (User definable)	Yes (Not visible, editable, and definable by user. Not visible to user in GBS result output. Accessible and editable in gbxml and DOE-2 files exported from GBS. Gbxml and DOE-2 files cannot be imported into GBS by user)	Yes (editable)	Yes (selectable from the library and user definable)
Schedule	Yes (User definable)	Yes (Selectable from the library and user definable)	Yes (Not visible, editable, and definable by user. Not visible to user in GBS result output. Accessible and editable in gbxml and DOE-2 files exported from GBS. Gbxml and DOE-2 files cannot be imported into GBS by user)	Yes	Yes (follows occupant schedule)
Default values	No	No	Yes	Yes	Yes
Recommendation	No	No	Yes (according to building type)	Yes	Unavailable in input process, available in design guidance advice
Utility					
Rate	Yes (for equipment only)	No	Yes (Not visible, editable, and definable by user. Not visible to user in GBS result output. Accessible and editable in gbxml and DOE-2 files exported from GBS. Gbxml and DOE-2 files cannot be imported into GBS by user)	Yes (selectable from the library, and user definable)	No

Sustainability Performance Simulation Tools for Building Design. Table 3 (Continued)

b. Building modeling					
Schedule	Yes (User definable)	No	Yes (Not visible, editable and definable by user. Not visible to user in GBS result output. Accessible and editable in gbxml and DOE-2 files exported from GBS. Gbxml and DOE-2 files cannot be imported into GBS by user)	Yes (selectable from the library, and user definable)	No
Default values	No	No	Yes	Yes (for California only)	No
Recommendation	No	No	Yes (according to building location)	Yes (according to climate zone and estimated peak electrical demand)	No
c. HVAC modeling					
Thermostat setpoint	Yes	Yes	Yes (Not visible, editable, and definable by user. Not visible to user in GBS result output. Accessible and editable in gbxml and DOE-2 files exported from GBS. Gbxml and DOE-2 files cannot be imported into GBS by user)	Yes (editable)	Yes
HVAC zoning	Yes (multizones)	Yes (multizones)	Yes (multizones)	Yes (multizones)	No
Relationship between HVAC zone and building space	HVAC zone same as the building space	One HVAC zone can have multiple spaces	HVAC zone same as the building space	HVAC zone different from building space	N/A
Zone grouping	No	Yes	No	Yes	No

Sustainability Performance Simulation Tools for Building Design. Table 3 (Continued)

c. HVAC modeling					
HVAC schedule	Yes (Fixed on/off timing for entire year)	Yes	Yes (Not visible, editable, and definable by user. Not visible to user in GBS result output. Accessible and editable in gbxml and DOE-2 files exported from GBS. Gbxml and DOE-2 files cannot be imported into GBS by user.)	Yes (editable)	No
Default values	No	No	Yes	Yes	No
Recommendation	No	No	Yes (according to building type)	Yes (according to building type)	No
Outside air requirement	No	No	Yes (Not visible, editable, and definable by user except in ABS. Not visible to user in GBS result output. Accessible and editable in gbxml and DOE-2 files exported from GBS. Gbxml and DOE-2 files cannot be imported into GBS by user)	Yes (editable)	Yes (selectable from the library and user definable)
Default values	N/A	N/A	Yes	Yes	Yes
Recommendation			Yes (according to space type)	Yes (according to activity area type)	Unavailable in input process, available in design guidance advice

Sustainability Performance Simulation Tools for Building Design. Table 3 (Continued)

c. HVAC modeling					
HVAC system	No	No	Yes (Not visible, editable, and definable by user. Not visible to user in GBS result output. Accessible and editable in gbxml and DOE-2 files exported from GBS. Gbxml and DOE-2 files cannot be imported into GBS by user)	Yes (editable and user definable)	No
Default system	No	No	Yes	Yes	No
Recommendation	No	No	Yes (according to building type and floor area)	Yes (according to building type and heating/cooling source)	No
System sizing	No	No	Yes (Not visible in GBS result output)	Yes (Autosize available. Sizing info not visible in eQUEST report output)	No
VI. Result output					
Output export	Yes (text, bitmap output)	Yes	No	No	No
Format of report					
Numeric	Yes	Yes	Yes	Yes	Yes (total net heat flow and breakdown by building element)
Graphic	Yes	Yes	Yes	Yes	Yes (total net heat flow, breakdown of heat gains and losses by building element)
Tabulated data	Yes	Yes	Yes	Yes	Yes
Spreadsheet	No	No	No	No	No
Data visualization	Yes	Yes	No	No	Yes (with animation and sound effect)
Types of report					
Single runs report	Yes	Yes	Yes	Yes	Yes

Sustainability Performance Simulation Tools for Building Design. Table 3 (Continued)

VI. Result output					
Comparative runs report	No	No	No	Yes	No
Content of report					
Parameter					
Temperature profile	Yes	Yes	No	No	No
Heat gain/loss	Yes (fabric, indirect solar, direct solar, ventilation, internal, interzonal gains)	Yes	Not visible in GBS result output. Available in gbxml file exported from GBS	Not visible in eQUEST graphic result output. Available in detailed simulation output file	Yes
Zone load	Yes	Yes	Not visible in GBS result output. Available in gbxml file exported from GBS	Not visible in eQUEST graphic result output. Available in detailed simulation output file	No
Building load	Yes	Yes	Not visible in GBS result output. Available in gbxml file exported from GBS	Not visible in eQUEST graphic result output. Available in detailed simulation output file.	No
Building energy use	No	No	Yes	Yes	No
Breakdown of building energy use	No	No	Yes	Yes	No
Utility bills	Yes (equipment only)	No	Yes	Yes	No
Frequency					
Building lifecycle value	Yes	No	Yes (30 years)	Yes	No
Annual value	Yes	Yes	Yes	Yes	No
Monthly values	Yes	Yes	No	Yes	No
Daily values	Yes	Yes	No	No	Yes
Hourly values	Yes	Yes	No	No	Yes
Summary					
Total	Yes	Yes	Yes	Yes	Yes
Average	No	No	No	Yes	No
Peak	Yes	Yes	Yes	Yes	Yes

Sustainability Performance Simulation Tools for Building Design. Table 3 (Continued)

Building types in GBS	Space types in GBS		
Automotive facility	Active storage	Electrical or mechanical	Other televised playing area sports
Convention center	Active storage hospital or healthcare	Elevator lobbies	arena
Courthouse	Air or train or bus baggage area	Emergency hospital or healthcare	Parking area attendant only parking
Dining bar lounge or leisure	Airport concourse	Equipment room manufacturing facility	garage
Dining cafeteria fast food	Atrium each additional floor	Exam or treatment hospital or healthcare	Parking area pedestrian parking garage
Dining family	Atrium first three floors	Exercise area exercise center	Patient room hospital or healthcare
Dormitory	Audience or seating area penitentiary	Exercise area gymnasium	Personal services sales area retail
Exercise center	Audience or seating area exercise center	Exhibit space convention center	Pharmacy hospital or healthcare
Fire station	Audience or seating area gymnasium	Fellowship hall religious buildings	Physical therapy hospital or healthcare
Gymnasium	Audience or seating area sports arena	Fine material warehouse	Playing area gymnasium
Hospital or healthcare	Audience or seating area convention center	Fine merchandise sales area retail	Police station laboratory police or fire
Hotel	Audience or seating area motion picture theatre	Fire station engine room police or fire station	station
Library	Audience or seating area performing arts theatre	Food preparation	Public and staff lounge hospital or healthcare
Manufacturing	Audience or seating area religious	Garage service or repair automotive facility	
Motel	Audience or seating area police or fire stations	General high bay manufacturing facility	Reading area library
Motion picture theatre	Audience or seating area courthouse	General low bay manufacturing facility	Reception or waiting transportation
Multi family	Audience or seating area auditorium	General exhibition museum	Reception or waiting motel
Museum	Bank customer area	Hospital nursery hospital or healthcare	Reception or waiting hotel
Office	Banking activity area office	Hospital or medical supplies hospital or healthcare	Recovery hospital or healthcare
Parking garage	Barber and beauty parlor		Restoration museum
Penitentiary	Card file and cataloguing library	Hospital or radiology hospital or healthcare	Restrooms

Sustainability Performance Simulation Tools for Building Design. Table 3 (Continued)

Building types in GBS	Space types in GBS		
Performing arts theatre	Classroom or lecture or training penitentiary	Hotel or conference center conference or meeting	Ring sports area sport arena
Police station	Classroom or lecture or training		Sleeping quarters police or fire station
Post office	Confinement cells penitentiary	Inactive storage	Sorting area post office
Religious building	Confinement cells court house	Judges chambers court house	Specialty store sales area retail
Retail	Conference meeting or multipurpose	Laboratory office	Stacks library
School or university	Corridor or transition	Laundry ironing and sorting	Stairs inactive
Sports arena	Corridor or transition manufacturing	Laundry washing hospital or healthcare	Stairway
Town hall	Corridors with patient waiting exam hospital or healthcare	Library audio visual library audio visual	Supermarket sales area retail
Transportation		Living quarters dormitory	Terminal ticket counter transportation
Warehouse	Court sports area sports arena	Living quarters motel	Workshop workshop
Workshop	Courtroom court house	Living quarters hotel	Worship pulpit choir religious
	Department store sales area retail	Lobby	
	Detailed manufacturing facility	Lobby religious buildings	
	Dining area	Lobby motion picture theatre	
	Dining area hotel	Lobby auditorium	
	Dining area family dining	Lobby performing arts theatre	
	Dining area lounge or leisure dining	Lobby post office	
	Dining area motel	Lobby hotel	
	Dining area transportation	Lounge or recreation	
	Dining area penitentiary	Mall concourse sales area retail	
	Dining area civil services	Mass merchandising sales area retail	
	Dormitory bedroom	Medium or bulky material warehouse	
	Dormitory study hall	Merchandising sales area retail	
	Dressing or locker or fitting room gymnasium	Museum and gallery storage	
	Dressing or locker or fitting room court house	Nurse station hospital or healthcare	

Sustainability Performance Simulation Tools for Building Design. Table 3 (Continued)

Building types in GBS	Space types in GBS		
	Dressing or locker or fitting room performing arts	Office enclosed	
	theatre	Office open plan	
	Dressing or locker or fitting room auditorium	Office common activity areas inactive storage	
	Dressing or locker or fitting room exercise center	Operating room hospital or healthcare	

Building Types in eQUEST	Activity Area Types in eQUEST
Community center	Auditorium
Conference/convention center	Auto repair workshop
Health/fitness center	Bank/financial institution
Heath, hospital (inpatient)	Bar, cocktail lounge
Health, long-term care (nursing home)	Barber and beauty shop
Health, medical clinic/prof. building (outpatient)	Casino/gaming
Lodging, motel	Classroom/lecture
Lodging, high-rise hotel	Courtroom
Multifamily, low-rise (exterior entries)	Comm/ind work (general, high bay)
Multifamily, mid-rise (interior entries)	Comm/ind work (general, low bay)
Multifamily, high-rise (interior entries)	Comm/ind work (precision)
Museum	Conference room
Office bldg, high-rise	Convention and meeting center
Office bldg, mid-rise	Copy room (photocopying equipment)
Office bldg, two story	Corridor
Office bldg, bank/financial	Dining area
Religious worship	Dry cleaning (coin operated)
Restaurant, full service (full menu)	Dry cleaning (full service commercial)
Restaurant, quick service (fast food)	Exercising centers and gymnasium
Restaurant, bar/lounge	Exhibit display area/museum
Retail, department store	Hotel/motel guest room (incl. toilets)
Retail, large single story	Kitchen and food preparation
Retail, stand-alone structure	Laboratory, medical
Retail, single storefront	Laundry
Retail, strip mall	Library (reading areas)
Retail, service station	Library (stacks)
Retail, service station/convenience store	Lobby (hotel)
Retail, warehouse sales	Lobby (main entry and assembly)

Sustainability Performance Simulation Tools for Building Design. Table 3 (Continued)

Building Types in eQUEST	Activity Area Types in eQUEST
School, preschool/daycare	Lobby (office reception/waiting)
School, k-6 elementary	Locker and dressing room
School, middle school	Mall, arcade and atrium
School, college/university	Mechanical/electrical room
Storage, conditioned high bay	Medical and clinical care
Storage, unconditioned high bay	Office (general)
Storage, conditioned low bay	Office (executive/private)
Storage, unconditioned low bay	Office (open plan)
Theater/performing arts	Police station and fire station
Unknown, custom or mixed use	Religious worship
	Residential (high-rise)
	Residential (multifamily dwelling unit)
	Residential (single family)
	Restrooms
	Retail sales and wholesale showroom
	Smoking lounge
	Storage (conditioned)
	Storage (unconditioned)
	Theater (motion picture)
	Theater (performance)
	Vocational areas
	Unknown

[a]Definition of *Built-in Library* as a selection of specific cases with complete and realistic description of relevant input parameter

Conclusions and Recommendations

Research by Lam et al. [41] has demonstrated the web-based service approach to energy modeling tool design has distinct advantages of being platform independent, allowing distributed collaborations, ease of maintenance and updates, better resource support and availability, and arguably lower costs. The development of GBS as a web-based service has shown the same benefits.

The user interface should be designed such that it is familiar, cognitive, and complements the concepts and processes of architectural design and energy modeling. With respect to operation within the Windows environment, Ecotect has been exemplary in providing a well-designed user interface that is easy to use.

Technical help, guidance, and documentation are important to the usability of software. Ecotect has comprehensive help files, tutorials, and the user forum was very useful. TAS and GBS have taken a new approach to providing guidance by providing videos. Only eQUEST provides detailed technical documentation, which is considered to be important given the nature of energy modeling, but may not be a dominant issue during the early design phase.

Geometric acquisition for energy modeling has traditionally been a tedious and error-prone process.

Sustainability Performance Simulation Tools for Building Design. Table 4 Definition of items in the evaluation matrix

Item	Description
1. SYSTEM	
Operating platform	
Windows	Tool operates within Windows environment without additional software or emulators
Mac OS	Tool operates within Macintosh environment without additional software or emulators
Unit system	Measurement units used by the tool
Energy design guidance	Assistance in conducting energy simulations, such as guidance on simulation workflow and appropriate modeling methods
Built-in library	
Weather data	Availability of selection of specific cases with complete and realistic description of relevant input parameter
Material	
Construction	
Schedule	
Internal heat gain	
Infiltration	
HVAC system type	
HVAC equipment	
Simulation application	
Stand-alone	Simulation conducted on local workstation
Web-powered	Simulation conducted on off-site server via network
Program stability	The ability of the tool to continue operations and maintain correctness under an amplitude of input changes
Weather file	Method used to select climatic data
Types of weather files	Format of climatic data used
History Tracking	
Undo/redo	The tool keeps track of states allowing the feature of redo and undo
Error logging	The tool maintains an error log upon failures
II. Extension	
Interoperability	
IFC compliance	The tool allows import/export of data in IFC format without additional software
File exchange with other energy simulation tools	The tool allows import/export of complete energy model data with other simulation tools without additional software or intervention
File exchange with CAD tools	The tool allows import/export of complete geometric data with CAD systems without additional software or intervention
Drawing data input	
Import as underlay	The tool allows import of 2D drawings from CAD systems to facilitate geometric modeling

Sustainability Performance Simulation Tools for Building Design. Table 4 (Continued)

Item	Description
Building element import	The tool allows import of 3D elements from CAD systems to facilitate geometric modeling
III. Functionality	
Technical approach	Simulation engine used by the tool
Types of energy calculation	
Building load calculation	Calculation of building heating, cooling, and electricity load
Building energy simulation	Calculation of energy consumption by the various equipments in the mechanical system, in order to meet the building heating, cooling, and electricity load
Parametric operation	
Single run/single input and output	Tool allows simulation of a model and presents the results
Batch Processing	Tool allows queuing of multiple models for simulation
Code compliance	Tool includes features to consider if the results of the energy models comply with regulations
Cost estimation	Tool includes features to estimate the costs related to the building that is being modeled
IV. User	
Documentation	
Tutorial/manuals/wizard	Types of documentation available to assist in learning how to use the tool and understanding the workflow
Engineering documentation	Technical documentation explaining the computational processes, methods, and assumptions used by the tool
Help function	Integrated help feature by button, keystroke, or menu to assist in using the tool interface and explaining the workflow
User support	Types of resources available to users in learning the tool
File save interval	Restrictions on when the user can invoke the save command
Navigation between windows	Restrictions on the user to toggle between different windows: Flexible – Tool allows user to toggle between windows in no particular sequence, Random – Tool allows user to toggle between any two windows
Clarity of menu and tool bars	The organization and naming of the menu and tool bars are with clarity
Model view	Allows user to view the energy model geometrically
Model display	Shading methods available when viewing the energy model
Expertise required	General expertise required of user to use the tool effectively
V. Modeling	
Zone management	Method used to manage the thermal zones in the energy model
a. Project information	
Building type definition	Tool allows user specification of building type to check, modify, or recommend various parameter settings
Space type definition	Tool allows user specification of space type to check, modify, or recommend various parameter settings

Sustainability Performance Simulation Tools for Building Design. Table 4 (Continued)

Item	Description
b. Building modeling	
Geometry	
Space composition	
Buildup by spaces	Tool allows geometric model to be constructed additively
Subdivision of floor plate	Tool allows modeled elements to be subdivided
Direct drawing input	
Primitive shapes	Tool allows modeling by selecting basic forms Boolean operations
Extrusion based on closed curve	Tool allows modeling by drawing profiles and extruding
Surfaces	Tool allows modeling by constructing surfaces
Building element definition	Tool allows specification and modification of individual elements as various building element types
Different heights within floor	Tool allows different spaces on the same level of the model to have different floor to ceiling heights
Sloped roof	Tool allows the modeling of sloped roofs
Sloped floor	Tool allows the modeling of sloped floors
Building orientation	Tool allows the north direction to be modified via a single orientation parameter
Accessible coordinate data	Tool shows the dimensions of each element and allows them to be changed by direct numerical input
Snap function	Tool provides modeling snap-to-point features
Modification	Tool allows modeled elements to be transformed geometrically
Geometry checking	Tool provides features to check that the geometric model has been constructed properly
Building construction	
Material	Notes on how the tool allows the user to define materials
Layer	Notes on how the tool allows the user to define layers
Construction	Notes on how the tool allows the user to define constructions
Shades	Notes on how the tool allows the user to model sun shading devices
Default values	Tool specifies some realistic default construction properties for building elements based on some project information such as type of building or space being modeled
Recommendations	Tool makes recommendations for construction types and material values based on some project information such as type of building or space being modeled
Internal loads	
Occupant	
Load	
Density	Tool allows variation of occupancy density across different spaces
Total Number of occupants	Tool allows specification and modification of number of occupants
Schedule	Tool allows specification of a schedule for occupancy

Sustainability Performance Simulation Tools for Building Design. Table 4 (Continued)

Item	Description
Lighting	
Load	
Density	Tool allows variation of lighting loads across different spaces
Individual appliance	Tool allows specification of individual light appliances within each space
Schedule	Tool allows specification of a schedule for lighting loads
Equipment	
Load	
Density	Tool allows variation of equipment loads across different spaces
Individual appliance	Tool allows specification of individual electrical appliances within each space
Schedule	Tool allows specification of a schedule for electrical loads
Default values	Tool specifies some realistic default internal loads conditions based on the type of building or space being modeled
Recommendations	Tool makes recommendations for internal load conditions based on some project information such as type of building or space being modeled
Infiltration	
Rate	Tool allows specification of infiltration rates
Schedule	Tool allows specification of a schedule for infiltration
Default values	Tool specifies some realistic default infiltration conditions based on the type of building or space being modeled
Recommendations	Tool makes recommendations for infiltration conditions based on some project information such as type of building or space being modeled
Utility	
Rate	Tool allows specification of utility rates
Schedule	Tool allows specification of a schedule utility rates
Default values	Tool specifies some realistic default utility rates based on some project information such as type of building being modeled or location of building
Recommendations	Tool makes recommendations for infiltration conditions based on some project information such as type of building being modeled or location of building
c. HVAC modeling	
Thermostat set point	Tool allows specification of heating and cooling set points for each zone in the HVAC system
HVAC zoning	Tool allows specification of HVAC zones from the spaces defined by the geometric building model
Relationship between HVAC zone and building space	Relationship between HVAC zones and spaces defined by the geometric building model
Zone Grouping	Tool allows several zones to be grouped in a hierarchical manner
HVAC schedule	Tool allows specification of a schedule for HVAC operations
Default values	Tool specifies some realistic default HVAC schedules based on some project information such as type of building or space being modeled

Sustainability Performance Simulation Tools for Building Design. Table 4 (Continued)

Item	Description
Recommendations	Tool makes recommendations for HVAC scheduling based on some project information such as type of building or space being modeled
Outside air requirement	Tool allows specification of outside air requirements as part of HVAC system
Default values	Tool specifies some realistic default outside air requirements based on some project information such as type of building or occupancy being modeled
Recommendations	Tool makes recommendations for outside air requirements based on some project information such as type of building or occupancy being modeled
HVAC system	Tool allows specification of the type of HVAC system
Default system	Tool specifies some realistic default HVAC system based on some project information such as type of building being modeled
Recommendations	Tool makes recommendations for HVAC system based on some project information such as type of building being modeled
System sizing	Tool includes feature to size the HVAC system accordingly
VI. Result output	
Output export	Tool allows simulation results to be exported for processing in other spreadsheet or analysis applications
Format of Report	
Numeric	Tool produces numerical reports of simulation results
Graphic	Tool produces graphical reports of simulation results
Tabulated data	Tool produces tabular reports of simulation results
Spreadsheet	Tool produces spreadsheets from simulation results
Data visualization	Tool includes some features of presenting the data in visuals that assist in understanding the thermal performance predicted by simulation
Types of report	
Single runs report	Tool produces reports for a single simulation
Comparative runs report	Tool presents results from multiple simulations on a single report for comparison
Content of report	
Parameter	
Temperature profile	Report on outdoor mean air temperature and mean space temperature for all spaces
Heat gain/loss	Report on heat gain/loss for all spaces
Zone load	Report on all zone loads
Building load	Report on building load
Building energy use	Report on active building energy use
Breakdown of building energy use	Report on active building energy use breakdown
Utility bills	Report on building utility bills
Frequency	
Building lifecycle value	Reports presented over lifecycle of building with appropriate time values

Sustainability Performance Simulation Tools for Building Design. Table 4 (Continued)

Item	Description
Annual value	Reports presented as cumulative annual values
Monthly values	Reports presented as 12 monthly values
Daily values	Reports presented as 365 daily values
Hourly values	Reports presented as 8,760 hourly values
Summary	
Total	Reports include a total value
Average	Reports include an averaged values
Peak	Reports indicate maximum and minimum value occurrences

The advances of Ecotect in allowing 3D CAD model import and fully automatic geometric acquisition from imported CAD files by GBS is heartening.

Different technical approaches have different semantic and spatial limitations. It is important that the user receives timely and detailed feedback on the correctness of the geometry that he/she has defined. This should be the case even if the geometry acquisition is totally automated.

In general, extensive library support and appropriate recommendations for constructions and materials are important for the designers, especially in the early design phase. Comprehensive weather data should also be made available.

The postprocessing functionalities in the selected tools are limited to conventional numerical and graphical reports of values such as loads and temperatures. It would be desirable to develop visualizations that would better facilitate a qualitative understanding of the design performance to the user and provide appropriate guidance in the context of early design decision making.

With respect to the early design phase as an adaptive-iterative process, energy modeling tools should ideally be able to support parametric studies. This is generally lacking in contemporary energy modeling tools.

The information content provided by the various tools varies tremendously. There is a need to clarify the information needs of the early design phase and to match the provisions accordingly.

For a tool to be beneficial and remain relevant throughout the building delivery process, it would be advantageous if it is developed based on comprehensive and fundamental principles in modeling the building-environment interactions. The tendency to adopt abstraction and rule-of-thumb approaches in an attempt to meet the time and resource constraints encountered in early design should be avoided. By offering different sets of user interfaces that automate and reveal parameters on different levels of granularity, it is possible for a tool to support various design phases effectively.

Integrated Building Design and Operation Process Modeling

Notwithstanding the advancement in modeling tool developments, it can be argued that any model that is created during the design phase will never be able to truly and accurately represent the as-built and operational realities of a building. There are simply too many variables involved in the building delivery process and the building operation phase that are difficult to assure that the specified properties are achieved and assumed occupational schedules are indeed maintained. However, if the model is created with high fidelity and solidly based on first-principle physical constructs, it can in fact be continuously used in the operational phase of the building as part of the integrated building management and control system. The assumed values of parameters used in the original design for predicting the building performance can now be replaced by real

operational data acquired through an environmental sensor network (both indoor and outdoor) and from the building management system. The model can thus be empirically recalibrated[5] and then used to conduct advanced predictive control of building operations.

Role of Building Control in Energy Consumption Reduction

Buildings are responsible for at least 40% of energy use in many countries, mostly derived from fossil fuels. Worldwide building energy consumption is expected to grow 45% over the next 20 years [42]. In the United States, commercial buildings consume almost 17% of national energy use. Seventy-six percent of the services used by buildings (e.g., heating, cooling, lighting, etc.) are powered by electricity, and these account for 35% of the total electricity consumed nationally [43]. Heating, ventilation, and air-conditioning (HVAC) systems in commercial buildings account for nearly 37% of the total building energy.

According to the market surveys conducted by Brambley et al. [44], building controls can potentially reduce energy consumption significantly in commercial buildings. Table 5 demonstrates how a traditional Energy Management and Control System (EMCS) can save between 5% and 15% of a building's energy with an 8–10-year return on investment for the system, while occupancy sensors for lighting control can save 20–28% energy with 1–5 years payback on the initial investment. In addition, one of the objectives of control system is to improve the indoor environmental performance (e.g., thermal, lighting, and air quality). Figure 10 further illustrates that HVAC controls have potentially the biggest impact on the building energy consumption, yet there are relatively few installations in multifamily residential developments [45]. Furthermore, the Building Investment Decision Support Tool developed by the Center for Building Performance and Diagnostics at Carnegie Mellon University has identified 20 studies that link improved temperature control to productivity gains, with an average 5.5% productivity increase within a range of between 1.2% and 24% [46].

Typical control functions in buildings can be divided into two categories: local control and

Sustainability Performance Simulation Tools for Building Design. Table 5 Summary of energy-saving potentials for different control approaches (Brambley et al. [44])

Control technology	Technical market size (billions ft^2)	Relevant primary energy (quads)	Energy savings (%)	Technical energy savings potential (quads)	Simple payback period (years)	Remaining market penetration	Market-achievable energy savings (quads)
Energy management and control system (EMCS)	33	6.2	5–15%	0.3–0.9	8–10	5–10%	0.02–0.09
Commissioning	55	9.8[a]	5–15%	0.5–1.5	2–10	3–30%	0.015–0.5
Automatic fault detection and diagnostics (AFDD)/ Continuous commissioning	55	9.8[a]	5–15%	0.5–1.5	1–3	15–55%/ 6–24%	0.07–0.8/ 0.03–0.35
Occupancy sensors for lighting control	50	3.5	20–28%	0.7–1.0	1–5	0–45%	0–0.45
Photosensor-based lighting control	55	3.9	20–60%	0.8–2.3	1–7	8–55%	0.08–1.3
Demand controlled ventilation (DCV)	55	5.4	10–15%	0.5–0.8	2–3	15–30%	0.08–0.25

[a]This figure includes 0.5 quads for supermarket refrigeration systems and walk-in refrigeration

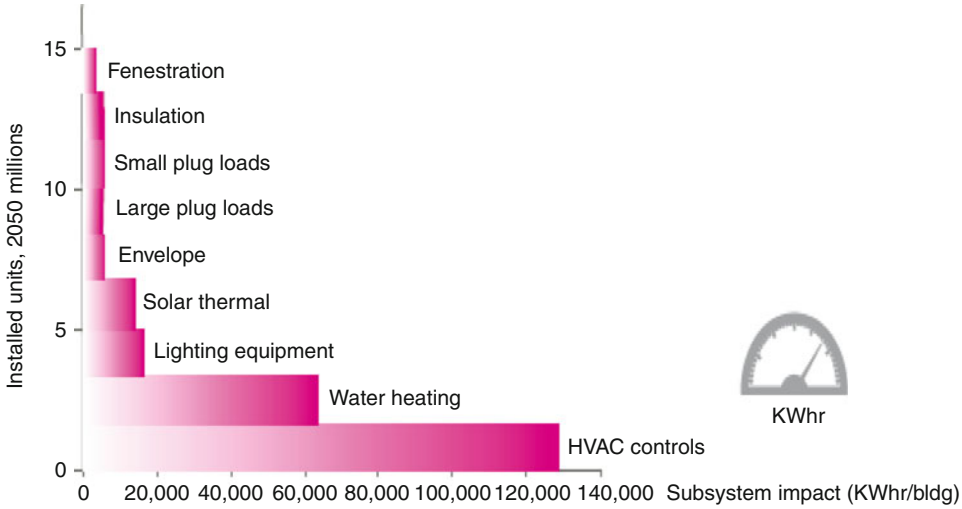

Sustainability Performance Simulation Tools for Building Design. Figure 10
Energy-saving potentials for HVAC control (cp. World Business Council for sustainable development [45])

supervisory control. Local control provides basic control and automation functions, such as ON/OFF control and proportional-integral-derivative (PID) control that allow building services to operate properly. Many studies show that local controls can provide thermal comfort and satisfy goals for indoor air quality (Moore and Fisher [47]; Nassif et al. [48]; Zhang and Hanby [49]). Supervisory control functions are higher level controls that include local control functions while considering whole system characteristics (both active HVAC and passive systems), interaction, and energy optimization for total building energy saving. Supervisory control functions are developed using the physical model–based method, hybrid method, performance mapping method, and data learning approach [50]. In the last decade, research has increasingly focused on supervisory control to expand the opportunities for greater energy savings.

Modeling Building Control Design and Operation

Building control design and operation need consistent and reliable static and dynamic information from various resources to feed into the set of fundamental governing thermal dynamic equations. Table 6 summarizes the informational requirements for the design and operation of a model-based building control system.

Model-based predicted control can help optimize energy use while maintaining the appropriate indoor set-point temperature when the spaces are occupied. However, several barriers in many of the current approaches of building control design and operation impede the full achievement of this goal. For instance, (a) dynamic data are not readily available such as real-time site weather (e.g., temperature, wind speed, and solar radiation) and occupancy status (number as well as duration in the space); (b) a comprehensive whole building energy model is not fully integrated into advanced controls for accuracy and robustness; (c) real-time implementation cases of such control on indoor thermal environment are rare.

Dong [51] recently published his PhD dissertation to address some of these limitations in implementing integrated building control. A comprehensive literature review was conducted on the topics of (1) model-based supervisory control and optimization techniques for building HVAC systems and (2) occupancy detection and behavior prediction in buildings.

Model-Based Supervisory Control and Optimization Techniques A summary of main optimization techniques used in building HVAC supervisory controls is given in Table 7.

Sustainability Performance Simulation Tools for Building Design. Table 6 Information requirements for the design and operation of a model-based building control system

Information type	Information elements	
Input parameters during control design stage		
Geometry information	Static information	Wall, doors, and windows surface areas
		Number of thermal zones and volumes
		External surface orientation, tilt and azimuth
Construction information	Static information	External/internal wall, window, and door construction type
		Material properties: thickness, thermal conductivity, specific heat, solar transmission, etc.
Internal zone information	Dynamic information	Internal gains: occupancy number and schedule, equipment, and use schedule
		Indoor temperature set-point, air flow rate, etc.
System information	Static information	HVAC system type (chiller, heat pump, fan coil, etc.) and their physical parameters
		Duct or pipe physical parameters such as length
	Dynamic information	Designed operation information
Weather information	Dynamic information	Outdoor temperature, solar radiation, wind velocity, etc.
Data resources during operation		
Static information	CAD MEP drawings, construction, and material specification	
	Predefined schedules for HVAC systems, occupancy, lighting, etc.	
Dynamic information	Real-time HVAC system performance from sensors in systems such as supply air temperature, supply air flow rate, return air temperature, relative humidity	
	Real-time indoor environmental measures from sensors such as temperature, RH, CO_2, air flow, etc. and dynamic occupancy information from sensors	
	Dynamic usage of internal equipment from power metering	
	Historical/simulated weather information, on-site weather measurements	

Occupancy Detection and Behavior Prediction Occupant presence and behavior in buildings has been shown to have large impacts on space heating, cooling and ventilation demand, energy consumption of lighting and space appliances, and building controls [66]. Several stochastic models have been developed to model occupant presence and interactions with space appliances and equipment. Fritsch et al. [67] proposed a model based on Markov chains to model the random opening of windows by occupants. Degelman [68] developed a Monte Carlo modeling approach for space occupancy predictions based on survey statistics. Reinhart [69] determined occupant presence for lighting simulation by using a simplified stochastic model of arrival and departure. Wang et al. [70] applied Poisson distributions to generate daily occupancy profiles in a single-occupied office. Bourgeois et al. [71] integrated an occupancy model based on Reinhart's algorithm into ESP-r to investigate lighting application. Most of these occupancy presence models were either tested on a single-person office or presented as a specific application such as lighting control. More

Sustainability Performance Simulation Tools for Building Design. Table 7 Summary of main optimization techniques used in building HVAC supervisory controls

	Techniques	Research studies	Strength	Weakness
Nonlinear local techniques	Direct search	Zaheer-uddin and Zheng [52]; Xu and Haves [53]	Simple and easy to be understood and implemented. No derivatives are required	Often fails to obtain an optimal solution and less computationally efficient
	Sequential quadratic programming	House and Smith [54]; Kota et al. [55]; Sun and Reddy [56]	Handles a large number of inequality	Has to start from initial guess values and the speed is affected by its initial values
			Constraints efficiently	
	Lagrange method	Chang [57]; Sane and Guay [58]	Easy to be implemented since Lagrange formula does not depend on the order in which the nodes are arranged	The convergence is not always guaranteed
Nonlinear global techniques	Simulated annealing	Flake [59]; Chang et al. [60]	Relatively easy to be implemented	High computational costs and memory demands
	Evolutionary algorithms and genetic algorithm	Henze et al. [61]; Wang and Jin [62]; Xing [63]; Kummert [64]; Zhang and Hanby [49]; Coffey [65]	With high generalities and flexibilities, and they are also robust in finding the global minimum	Extensive computational costs and memory demands due to a high number of fitness evaluations

recently, Page et al. [72] targeted individual occupancy behaviors by developing a generalized stochastic model for the simulation of occupant presence with derived probability distributions based on Markov chains. However, such a stochastic model was based on the assumption that occupants will interact with different appliances in the space, and the validation was conducted in single-person-occupied offices. Other current approaches to occupancy detection take place mostly in commercial buildings through the use of passive infrared (PIR) motion detectors. Motion detectors have inherent limitations when occupants remain relatively still. Moreover, motion detectors alone only provide information regarding the presence or absence of people in a space rather than the number of occupants, information which is highly useful for building control tasks such as demand controlled ventilation [73].

Video cameras have also been used to detect human movements in buildings. Trivedi et al. [74] conducted rigorous experimental investigations on the processing and control modules for the active camera networks and the microphone array which are embedded in an intelligent room. The integrated system has the functionality of human tracking, active camera control, face recognition, and speaker recognition. Lymberopoulos et al. [75] developed a system called BehaviorScope for interpreting human activity patterns using a camera network and its application to elder monitoring in assisted living. Notwithstanding the tremendous value of this technique, video capture raises privacy concerns and requires large amounts of data storage.

Other work has focused on the use of carbon dioxide (CO_2) sensors in conjunction with building models for estimating the number of people generating the measured CO_2 level [76, 77]. Recent research on so-called smart environments involves the use of a diverse set of sensors to monitor and infer human activity in a building. Examples include the MIT Intelligent Room [78], the University of Colorado Boulder Neural Network Adaptive Home [79], Georgia Tech Aware Home [80] and the University of Texas at Arlington MavHome [81, 82]. Most of these efforts focus on behavioral modeling or mobility tracking and do not exploit additional sensing capability for the detection of occupancy numbers. In addition to these test beds, Duong et al. [83] used Hidden Semi-Markov models

for modeling and detecting activities of daily living such as cooking and eating, and Youngblood and Cook [82] introduced a new method of automatically constructing Hierarchical Hidden Markov models using the output of a sequential data mining algorithm to control a smart environment. Other research endeavors investigate HVAC preconditioning and device automation via mined location and device interaction patterns and the energy-saving potential is estimated through a relatively simple consumption model [84].

A Demonstrative Case Study: The CMU Solar Decathlon House 2005

Based on the above literature review and identification of the apparent "gaps" in the current techniques (see Table 8), Dong [51] introduces and illustrates a novel methodology for integrated building heating, cooling, and ventilation control with the objective to reduce energy consumption and maintain indoor temperature set-point, based on the prediction of occupant behavior patterns and weather conditions. Several advanced machine learning methods such as Adaptive Gaussian Process, Hidden Markov Model, Episode Discovery, and Semi-Markov Model were modified and implemented. A nonlinear model predictive control (NMPC) was designed and implemented in real time based on dynamic programming. The experiment test bed was set up in the Solar Decathlon House (2005) (Fig. 11), with over 100 sensor points measuring indoor environmental parameters such as temperature, relative humidity, CO_2, lighting, motion and acoustics, and the power consumption for electrical plugs, HVAC, and lighting. The outdoor environmental parameters such as temperature, relative humidity, CO_2, global horizontal solar radiation, and wind speed are obtained from an on-site weather station. The designed controller was implemented through LabView.

A first-principle physically based detailed and integrated model of the test bed was constructed which comprises the constituent models of the building geometry, construction materials and thermal zoning (Fig. 12), the energy supply and demand (HVAC) systems (Fig. 13), as well as the optimal building control schema (Fig. 14).

Sustainability Performance Simulation Tools for Building Design. Table 8 Comparisons of integrated HVAC control approaches

Author	Input information for control modeling		Actual implementation		
	Local weather forecasting	Dynamic occupancy patterns	Real time	Fully model-based	High computational speed
Wang and Jin [62]			√		√
Henze et al. [61, 85, 86]			√		
Xu and Haves[53]				√	√
Xing [63]				√	
Sun and Reddy [56]			√		
Kummert and Andre [64]			√	√	
Zhang and Hanby [49]					
Sane and Guay [58]			√		√
Coffey [65]			√	√	
Dong [51]	√	√	√	√	√

Sustainability Performance Simulation Tools for Building Design. Figure 11
The Carnegie Mellon University Solar Decathlon House 2005

The models were validated through empirical experiments, and studies were conducted for two continuous months in the heating season and for a week in cooling season. Some selected results are presented below.

Figure 15 shows the measured results of energy consumption profile of the NMPC model, which integrates the weather forecasting and occupant behavior pattern prediction. Due to the thermal mass effect of the concrete floor slab, there is no need for additional heating during the daytime on most days during the experimental period, while maintaining the temperature within the set-point bands (see Fig. 16).

It also shows the comparison of the energy profile between the NMPC model and a "conventional" scheduled set-point model. The scheduled temperature set-point normally has a night setback, which is 17°C in this study. The heating system remains off until the indoor temperature drops below the setback temperature. Hence, the heating system often starts after midnight and at its full capacity in order to reach the desired set-point in the morning. In addition, the actual occupancy period often does not quite match with the scheduled daily temperature set-point period. These conditions result in more energy consumption for scheduled temperature set-points control compared with the proposed integrated control. The energy saving from the integrated control is illustrated in dashed boxes. The integrated control can save 30.1% of energy compared with the scheduled control. Furthermore, the temperature set-point was not met only for 2 h for the integrated control while it was 8 h for the schedule temperature set-point control (see Table 9). This is because during some cold nights when the indoor air temperature is around the night setback (17°C), the daily set-point in the morning cannot be met. Instead, the integrated controls keep the indoor air temperature warm enough at night to meet the set-point in the morning.

Figure 17 compares the energy consumption between NMPC and scheduled set-points during a week in the cooling season. The energy saving mainly comes from the dynamic occupancy scheduling, while the scheduled control set-point method tries to maintain the set-point regardless of whether there is any occupant in the space.

Figure 18 provides a more detailed look at the daily behavior and performance of the system on July 1, 2010. The scheduled set-point maintains the indoor temperature at the set-point, 25°C. The NMPC

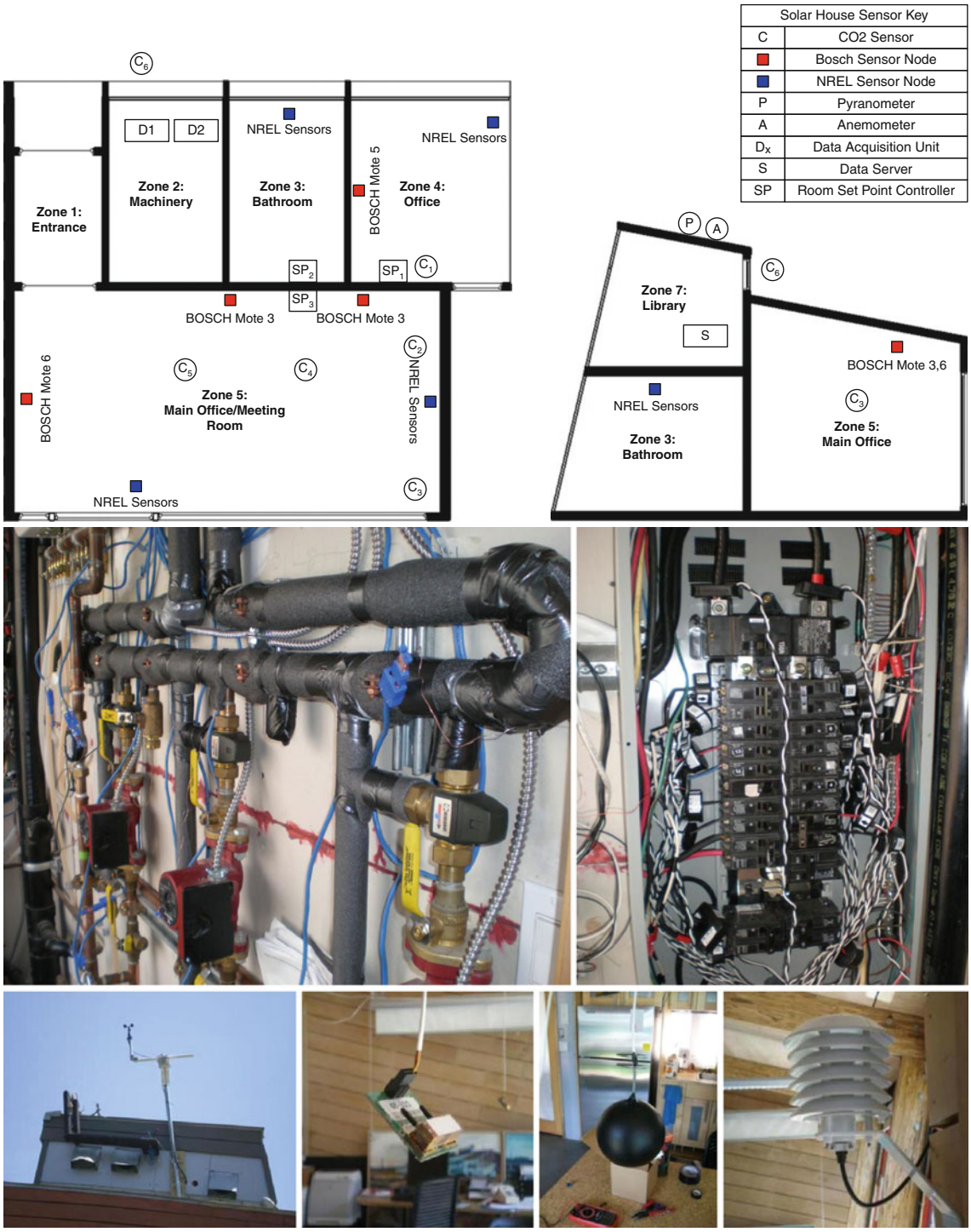

Sustainability Performance Simulation Tools for Building Design. Figure 12
Building geometry, thermal zoning, and sensor system layout

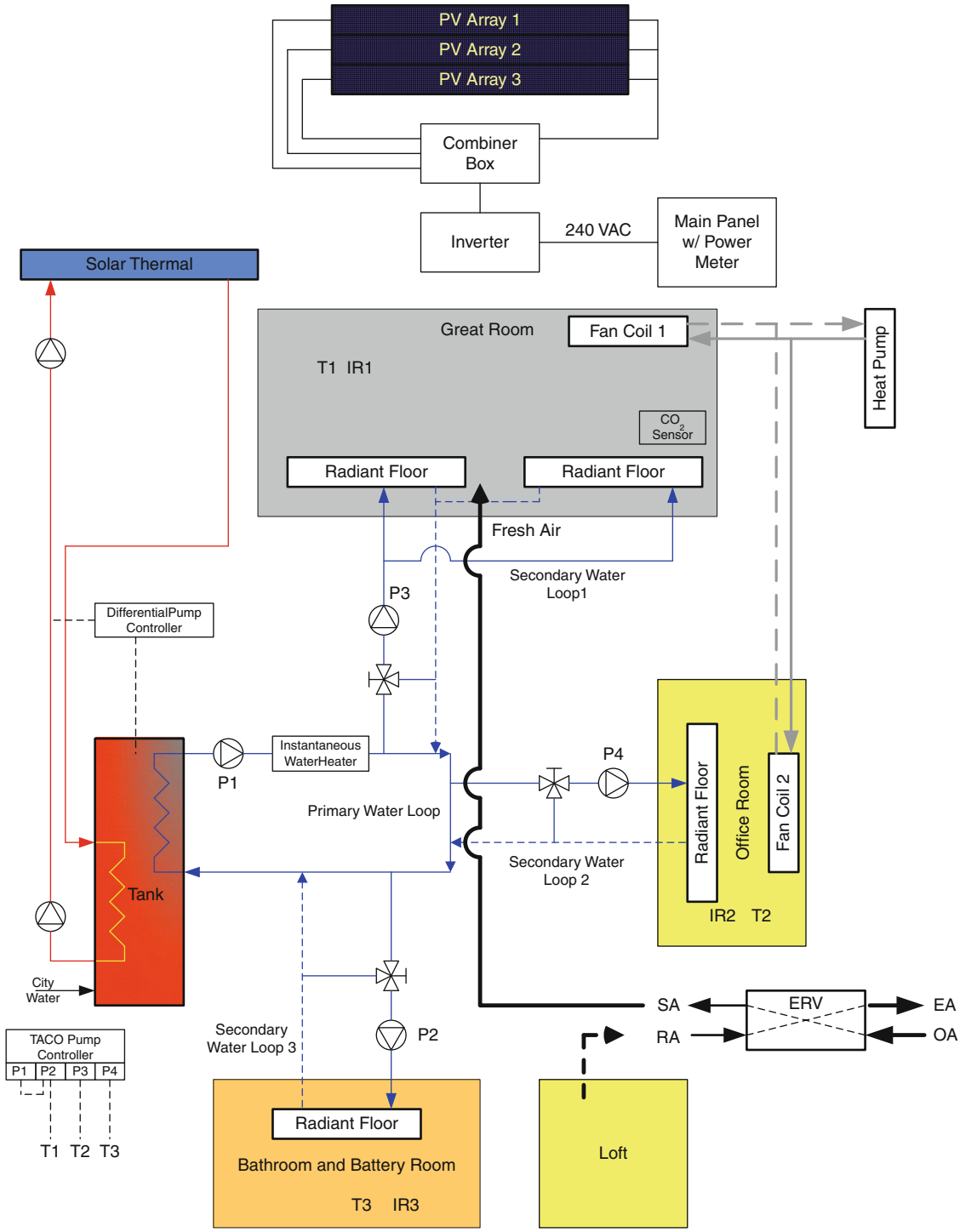

Sustainability Performance Simulation Tools for Building Design. Figure 13
Overview of the energy supply and demand systems

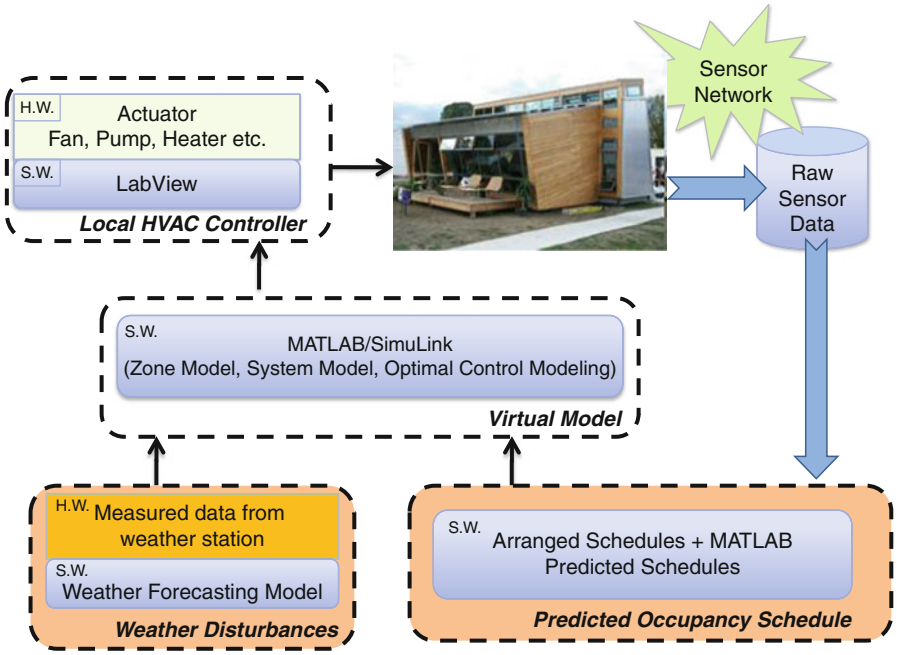

Sustainability Performance Simulation Tools for Building Design. Figure 14
Overview of integrated control (NMPC) implementation schema

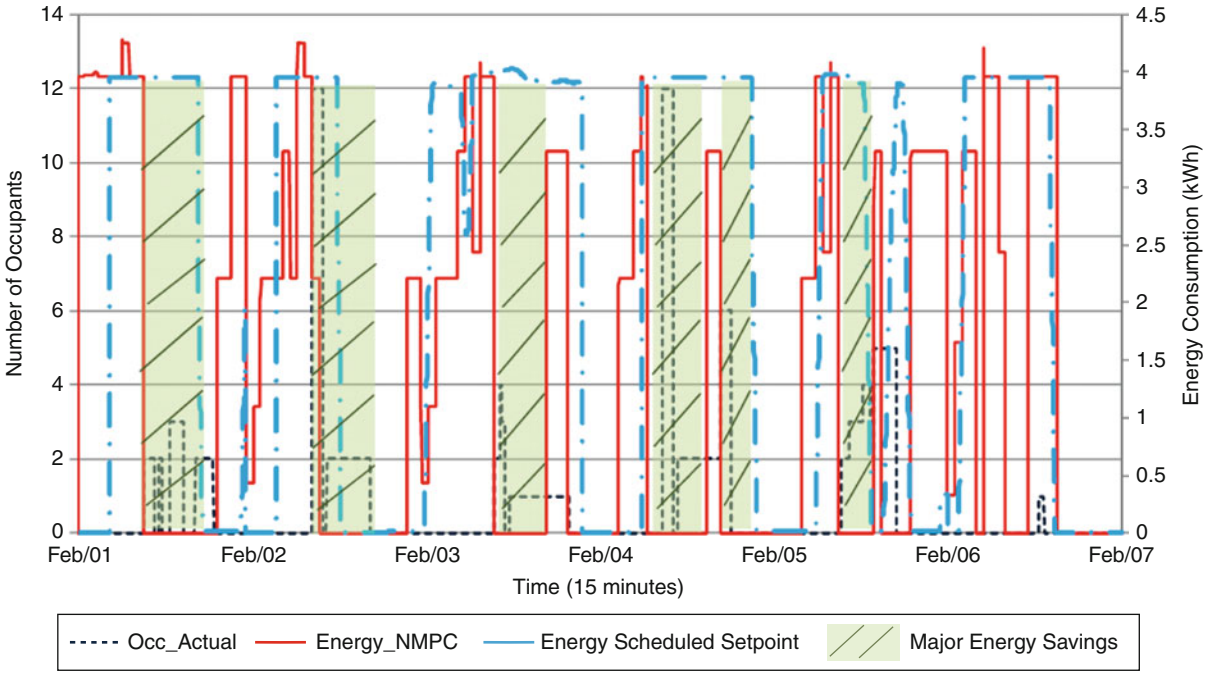

Sustainability Performance Simulation Tools for Building Design. Figure 15
Comparison of energy profiles between NMPC and scheduled temperature set-points for the heating season in February 2010

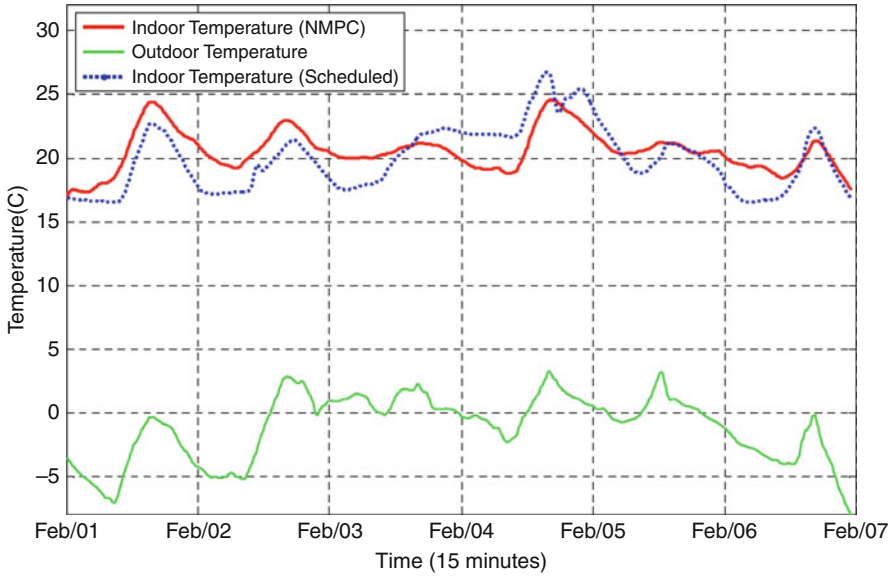

Sustainability Performance Simulation Tools for Building Design. Figure 16
Indoor and outdoor temperature profile from February 1 to February 7, 2010

Sustainability Performance Simulation Tools for Building Design. Table 9 Comparison of heating energy consumption and number of hours when temperature set-points are not met

Energy consumption (kWh)		Energy saving (%)
Scheduled temperature set-points	343	30.1
NMPC optimization	240	
Temperature set-point not met while occupied (h)		*Better set-point met time (%)*
Scheduled temperature set-points	8	75
NMPC optimization	2	

dynamically controls the temperature based on the actual occupancy level. In addition, the scheduled set-point assumes the occupants vacated the premise at 7:00 p.m., while in reality it happened at 5:30 p.m. The NMPC cools down the space in two time steps (30 min) before the occupants arrive, and allows the room temperature to float during lunchtime.

Table 10 compares the simulated energy consumption of schedule set-points and measured NMPC optimization. The total cooling energy saving for the week is 17.8%. Although the dynamic occupancy schedule varies with cooling set-points in the space, the temperature of the space changes quickly so that the energy saving is only realized over a short duration of about an hour (four 15-min time steps).

To investigate further energy saving possibilities, a model with better building envelop performance is conducted. The air infiltration rate for the meeting room in the test bed is found to be 0.6 air change per hour (ACH). However, a good benchmark of a tight envelop should be 0.3 ACH. With this improved value, there is a further increase in energy saving and the number of hours whereby the set-point temperature is not met is also reduced. While the pre-cooling time becomes slighting longer with 3–4 time step ahead of occupant's morning arrival instead of 1 time step, the

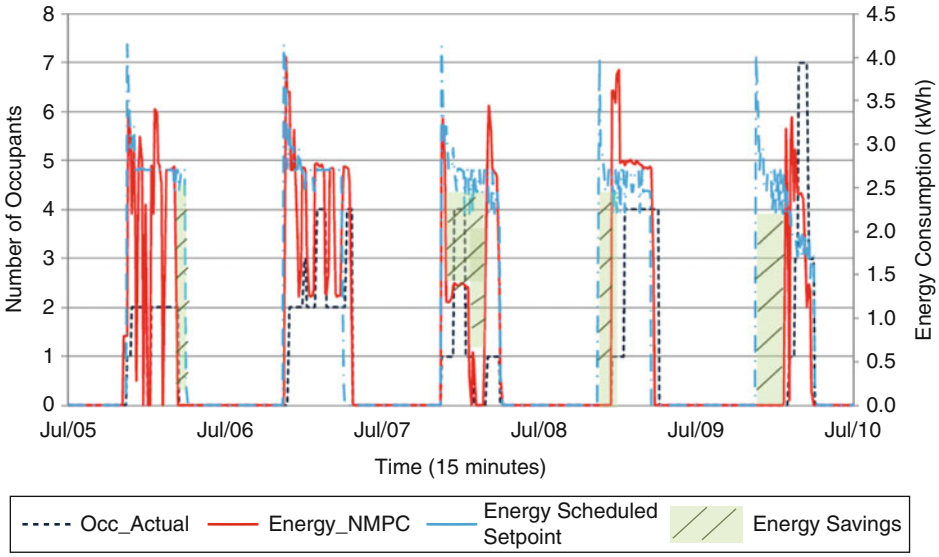

Sustainability Performance Simulation Tools for Building Design. Figure 17
Comparison of energy profiles between NMPC and scheduled temperature set-points for the cooling season in July 2010

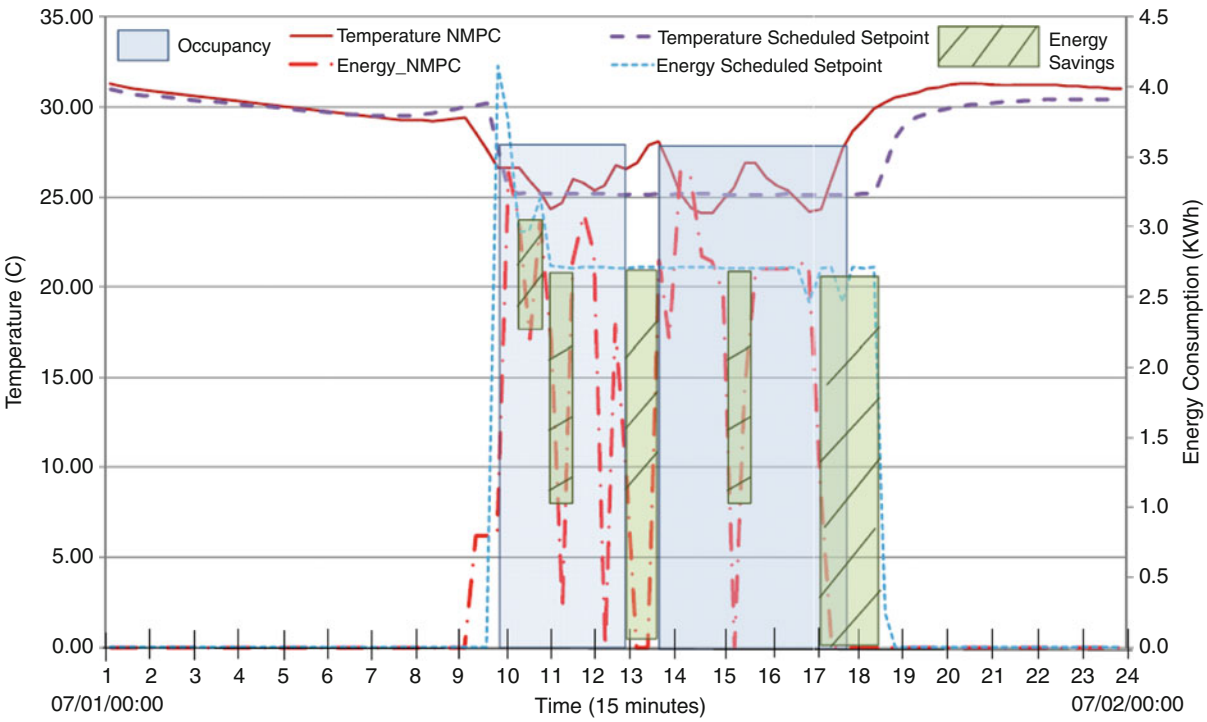

Sustainability Performance Simulation Tools for Building Design. Figure 18
Comparison of energy profiles between NMPC and scheduled temperature set-points on July 1, 2010

Sustainability Performance Simulation Tools for Building Design. Table 10 Comparison of cooling energy consumption and number of hours when temperature set-points are not met

Energy consumption (kWh)		Energy saving (%)
Scheduled temperature set-points	96.83	
NMPC optimization	76.92	17.8
Simulated NMPC optimization with reduced infiltration	77.3	20.2
Temperature set-point not met while occupied (h)		*Improved set-point met time (%)*
Scheduled temperature set-points	3	
NMPC optimization	2	33%
Simulated NMPC optimization with reduced infiltration	1	66%

cooling system shuts down several time steps earlier before the occupants leave the room.

In summary, it can be seen that NMPC-based control of HVAC systems is an active "self-learning" process compared to the passive conventional HVAC system which only responds to a rigid predetermined indoor set-point temperature schedule. The integrated HVAC control can dynamically predict the control profile and state variables (e.g., indoor air temperature) based on information derived from the validated building HVAC and weather forecasting models. With the predicted information, the energy consumption of HVAC system can be optimized. Furthermore, the real-time occupant behavior patterns are integrated with the HVAC controls. Hence, when the space is unoccupied, there is no need to maintain the conventional temperature set-point. In addition, the operation of HVAC at night is also integrated with the prediction of occupants' arrival time on the next day. The ventilation rate can be adjusted according to the number of occupants in the space. Such control can operate the HVAC system dynamically and result in energy saving while maintaining desirable set-point temperature as well as indoor air quality. The new features of this integrated HVAC control contribute to the next generation of building energy management systems in both residential and commercial buildings.

Conclusion and Future Trends

Future trends in the development and application of simulation tools will continue to be driven by the needs for knowledge-based design decisions, as demanded by knowledgeable clients, and better quality assurance of the performance assessments. Multidisciplinary teamwork that draws upon relevant expertise across geographical boundaries and the adoption of integrative design approaches to achieve high-performance buildings will be critical factors of success in the design and construction business, particularly in an increasingly global and competitive world market.

The potential use of contemporary information technology (e.g., for architectural and engineering design) in the building industry is extensive, and so are the potential performance benefits and cost savings through more efficient and productive processes. However, all the sophisticated IT in the world will not guarantee a decisive transformation of the industry if it is not accompanied by a new level of commitment from players in the industry. The ultimate key to the successful exploitation of IT is "professionalism" and "discipline" in the way our business is conducted in the building industry to create a high-quality and sustainable living environment.

Meanwhile, the capabilities of simulation tools will continue to evolve to address, among others, two major objectives: Firstly to make simulation tools more accessible to the architectural profession to support the open-ended nature of design inquiry, and secondly, to enable effective "real-time" sharing of design information between the entire team through a web-based infrastructure. The pervasive use of these tools will ultimately depend on how they can effectively support the design decision-making process (providing a level

of confidence on the predicted performance of the solution) while reducing project overheads such as time, manpower, training, and computational resources typically associated with advanced performance simulations. If a model is carefully created with high fidelity and solidly based on first-principle physical constructs, which are available in some advanced simulation tools, there can be a significant return on upfront time investment by deploying the same model continuously during the operational phase of the building as part of the integrated building management of control system.

As a collaborative activity, the building delivery process relies heavily on the effectiveness of communication structures and means. While it was initially expected that the application of innovative information technologies would qualitatively enhance the information transfer mechanisms within this process, this has not occurred, at least not to the desired extent. To facilitate better understanding of this evolving circumstance, continuous critical review of the status quo and thoughtful theoretical reflections on the complex relations between process evolution and tool development is necessary.

Bibliography

1. http://www.epa.gov/greenbuilding/pubs/about.htm#1. Accessed 15 Nov 2010
2. Ruck NC (1989) Building design and human performance. Van Nostrand Reinhold, New York
3. Hartkopf V, Loftness VE, Mill PAD (1986) The concept of total building performance and building diagnostics. In: Building performance: function, preservation, and rehabilitation. ASTM special technical publication. STP901 American Society for Testing and. Materials, Philadelphia, pp 5–22
4. Thomas R (ed) (2002) Environmental design: an introduction for architects and engineers, 2nd edn. Spon Press, London
5. Yudelson J (2009) Green building through integrated design. McGraw-Hill, New York
6. Mahdavi A, Lam KP (1993) A dialectic of process and tool: knowledge transfer and decision-making strategies in the building delivery process. In: Krishan M, Martin B, Kwok WT (eds) Management of information technology for construction. World Scientific, Singapore, pp 345–356
7. Augenbroe G (2002) Trends in building simulation. Build Environ 37:891–902
8. Kusuda T(1999) Early history and future prospects of buildings system simulation. In: IBPSA, Japan
9. Clarke JA (2001) Energy simulation in building design. Butterworth-Heinemann, Oxford
10. International building performance simulation association. http://www.ibpsa.org/m_papers.asp.
11. Journal of Building Performance Simulation (2008) Taylor and Francis, UK
12. Building simulation: an international journal (2008) Springer and Tsinghua University Press
13. Malkawi A, Choudhary R (1999) Visualizing the sensed environment in the real world. J Hum Environ Syst 1:61–69
14. http://en.wikipedia.org/wiki/Theory. Accessed 15 Nov 2010
15. http://www.epa.gov/greenbuilding/pubs/about.htm#1. Accessed 15 Nov 2010
16. Ruck NC (ed) (1989) Building design and human performance. Van Nostrand Reinhold, New York
17. Thomas R (ed) (2002) Environmental design: an introduction for architects and engineers, 2nd edn. Spon Press, London
18. Loftness V, Hartkopf V, Mill P (1989) Chapter 9. A critical framework for building evaluation: total building performance, systems integration, and levels of measurement and assessment. In: Preiser WFE (ed) Building evaluation. Plenum, New York
19. Gallaher MP, O'Connor AC, Dettbarn JL Jr, Gilday LT (2004) Cost analysis of inadequate interoperability in the U.S. Capital Facilities Industry. Research report sponsored by National Institute of Standards and Technology, Advanced technology program, Aug 2004
20. Mattar SG (1983) Buildability and building envelope design. In: Proceedings of the second Canadian conference on building science and technology, Waterloo, Nov 1983
21. Smith RD (1998) Simulation http://www.modelbenders.com/encyclopedia/encyclopedia.html. Accessed 15 Nov 2010
22. Sokolowski JA, Banks CM (2009) Principles of modeling and simulation. Wiley, Hoboken
23. www.buildingsmart.com. Accessed 8 Feb 2012
24. US National Institute of Building Sciences (2007) National building information model, version 1, part 1, overview, principles and methodologies. http://www.buildingsmartalliance.org/nbims/. Accessed 15 Nov 2010
25. Lam KP and Zhang R (2010) Plot 12a Tianjin Eco-City Project - Sunlight and Daylight Simulation Report, July
26. Lam KP and Zhang R (2010) Plot 12a Tianjin Eco-City Project - Sunlight and Daylight Simulation Report, May
27. Lam KP (2002) Performance-based design. In: Batimat Asia specifiers' forum, Singapore, 6–8 Nov 2002
28. Chang W, Lim B, Williamson J (1998) Fire legislation reform and the architect. Royal Australian Institute of Architects (Queensland Chapter) Seminar, Oct 1998
29. Hatton T (1996) Problems of the prescriptive. In: Fire code reform national seminar series: performance-based approach to building fire safety design, Adelaide, Aug 1996
30. Beck V (1997) Performance-based fire engineering design and its application in Australia. In: Fire safety science-proceedings of the fifth international symposium of the international association of fire safety science, Fire Protection Research Foundation, Quincy MA, pp 23–40

31. Department of energy building energy software tools directory. http://apps1.eere.energy.gov/buildings/tools_directory/subjects_sub.cfm. Accessed 15 Nov 2010
32. Augenbroe G (1992) Integrated building performance evaluation in the early design stages. Build Environ 27(2): 149–161
33. Mahdavi A, Lam KP (1991) Performance simulation as a front-end tool for integrative conceptual design evaluation. In: Proceedings of the 2nd international conference of the international building performance simulation association (IBPSA), France, pp 185–192
34. Wong NH, Lam KP, Feriadi H (2000) The use of performance-based simulation tools for building design and evaluation – a Singapore perspective. Build Environ 35:709–736
35. Ma C (2001) Analysis of building energy simulation tools. Public Works and Government Services Canada, Summer 2001
36. http://www.usgbc.org/DisplayPage.aspx?CMSPageID=220#v3. Accessed 15 Nov 2010
37. http://www.resnet.us/. Accessed on 15 Nov 2010
38. COMNET: Commercial buildings energy modeling guidelines and procedures. August 2010. http://www.comnet.org/sites/default/files/images/COMNET-MGP-2.pdf. Accessed 15 Nov 2010
39. Lam KP, Mahdavi A (1995) Representation and performance: Interface design for building performance modeling. In: Tan M, Teh R (eds) CAAD Futures 1995: International conference on computer aided architectural design, 24–26 September 1995, Centre for advanced studies in architecture, Singapore, December 1995, pp 141–152
40. Energy modeling tools assessment for early design phase. Final research report prepared for the Northwest energy efficiency alliance, Portland, OR 97204. December 31, 2004
41. Lam KP, Mahdavi A, Gupta S, Wong NH, Brahme R, Kang Z (2002) Integrated and distributed computational support for building performance evaluation. Adv Eng Software 33:199–206
42. World Business Council for Sustainable Development (2007) Energy efficiency in buildings: facts and trends. http://www.wbcsd.org/DocRoot/H94WhkJoIYq5uDtsLfxR/WBCSD_EEB_final.pdf
43. EIA (2009) Commercial buildings energy consumption survey data. http://www.eia.doe.gov/emeu/cbecs/. Accessed 15 Nov 2010
44. Brambley M, Hasen D, Haves P, Holmberg D, McDonald S, Roth K, Torcellini P (2005) Advanced sensors and controls for building applications: market assessment and potential R&D pathways. Pacific Northwest National Lab. Report No. 15149
45. World Business Council for Sustainable Development (2009) Transforming the market: energy efficiency in buildings. WBCSD, Washington DC
46. eBIDS. http://cbpd.arc.cmu.edu/ebids/pages/home.aspx. Accessed 15 Nov 2010
47. Moore BJ, Fisher DS (2003) Pump differential pressure setpoint reset based on chilled water valve position. ASHRAE Transactions 109(1):373–379
48. Nassif N, Kajl S, Sabourin R (2005) Optimization of HVAC control system strategy using two-objective genetic algorithm. HVAC & R Research 11(3):459–486
49. Zhang Y, Hanby VI (2006) HVAC & R research. Model-based control of renewable energy systems in buildings. HVAC & R Research 12(3a):577–598
50. Wang SW, Ma ZJ (2008) Supervisory and optimal control of building HVAC systems: a review. HVAC & R Research 14(1):3–32
51. Dong B (2010) Integrated building heating, cooling and ventilation control. Doctor of Philosophy Dissertation, Carnegie Mellon University, Pittsburgh, PA, USA
52. Zaheer-uddin M, Zheng GR (2001) Multistage optimal operating strategies for HVAC systems. ASHRAE Trans 107(2):346–352
53. Xu P, Haves P (2004) A simulation-based testing and training environment for building controls. In: Proceedings of SimBuild, Boulder, CO, 2004
54. House JM, Smith TF (1995) A system approach to optimal control for HVAC and building system. ASHRAE Trans 101(2):647–640
55. Kota NN, House JM, Arora JS, Smith TF (1996) Optimal control of HVAC systems using DDP and NLP techniques. Opt Control Appl Meth 17(1):71–78
56. Sun J, Reddy A (2005) Optimal control of building HVAC&R systems using complete simulation-based sequential quadratic programming (CSB-SQP). Building Environ 40(5):657–669
57. Chang YC (2004) A novel energy conservation method- optimal chiller loading. Electric Power Syst Res 69(2):221–226
58. Sane H, Guay M (2008) Minmax dynamic optimization over a finite-time horizon for building demand control. In: Proceedings of American control conference. June 11–13, Seattle, Washington, USA
59. Flake BA (1998) Parameter estimation and optimal supervisory control of chilled water plants. PhD Thesis, University of Wisconsin-Madison, USA
60. Chang YC, Chen WH, Lee CY, Huang CN (2006) Simulated annealing based optimal chiller loading for saving energy. Energ Convers Manage 47(15–16):2044–2058
61. Henze GP, Dodier RH, Krarti M (1997) Development of a predictive optimal controller for thermal energy-storage systems. HVAC & R Research 3(3):233–264
62. Wang SW, Jin XQ (2000) Model-based optimal control of VAV air-conditioning system using genertic algorithm. Building Environ 35(6):471–487
63. Xing HY (2004) Building load control and optimization. Doctor of Philosophy Dissertation, MIT, Cambridge, MA
64. Kummert K, Andre P (2005) Simulation of a model-based optimal controller for heating systems under realistic hypotheses. In: Proceedings of 9th IBPSA 2005. Montreal, Canada.
65. Coffey B (2008) A development and testing framework for simulation-based supervisory control with application to optimal zone temperature ramping demand response using

a modified genetic algorithm. Master Thesis, Concordia University, Quebec, Canada
66. Page J, Robinson D, Page, Morel N, Scartezzini JL (2007) A generalised stochastic model for the simulation of occupant presence. Energ Buildings 40(2):83–98
67. Fritsch R, Kohler A, Nygard-Ferguson M, Scartezzini J-L (1990) A stochastic model of user behaviour regarding ventilation. Build Environ 25(2):173–181
68. Degelman LO (1999) A model for simulation of daylighting and occupancy sensors as an energy control strategy for office buildings. In: Proceedings of building simulation'99, an IBPSA conference, Kyoto, pp 571–578
69. Reinhart C (2004) Lightswitch-2002: a model for manual and automated control of electric lighting and blinds. Solar Energy 77:15–28
70. Wang D, Federspiel C, Rubinstein F (2005) Modelling occupancy in single person offices. Energ Buildings 37:121–126
71. Bourgeois D, Reinhart C, Macdonald I (2006) Adding advanced behavioural models in whole building energy simulation: a study on the total energy impact of manual and automated lighting control. Energ Buildings 38:814–823
72. Page J, Robinson D, Morel N, Scartezzini JL (2007) A generalised stochastic model for the simulation of occupant presence. Energ Buildings 40(2):83–98
73. Emmerich SJ, Persily AK (2001) State-of-the-art review of CO_2 demand controlled ventilation technology and application, NISTIR 6729. NIST, US Department of Commerce
74. Trivedi M, Huang K, Mikic I (2000) Intelligent environment and active networks. In: Proceedings of IEEE international conference on systems, man, and cybernetics, Nashville, Tennessee
75. Lymberopoulos DA, Bamis T, Teixeira and A. Savvides. 2008. BehaviorScope: Real-time remote human monitoring using sensor networks. In: Proceedings of international conference on information processing in sensor networks, IPSN 2008, St. Louis, Missouri
76. Federspiel CC (1997) Estimating the inputs of gas transport processes in buildings. IEEE Trans Control Syst Technol 5:480–489
77. Wang SW, Jin XQ (1998) CO_2-based occupancy detection for on-lin outdoor air flow control. Indoor Built Environ 7:165–181
78. Torrance MC (1995) Advances in human-computer interaction: the intelligent room. In: Working notes of the CHI 95 research symposium, Denver, CO
79. Mozer MC (1998) The neural network house: an environment that adapts to its inhabitants. In: Coen M (ed) Proceedings of the American association for artificial intelligence spring symposium on intelligent environments. AAAI Press, Menlo Park, CA, pp 110–114
80. Lesser V, Atighetchi M, Benyo B, Horling B, Raja A, Vincent R, Wagner T, Ping X, Zhang SX (1999) The intelligent home testbed. In: Proceedings of the autonomy control software workshop, Seattle, WA
81. Cook D, Das S (2004) Smart environments: technology, protocols and applications. Wiley, Hoboken, NJ
82. Youngblood GM, Cook D (2007) Data mining for hierarchical model creation. IEEE Trans Syst Man Cybernet 37(4):561–572
83. Duong TV, Phung DQ, Bui HH, Venkatesh S (2006) Human behavior recognition with generic exponential family duration modeling in the hidden Semi-Markov model. In: Proceedings of the 18th international Conference on Pattern Recognition, IEEE, vol 3, pp 202–207
84. Roy A, Das SK, Basu K (2007) A predictive framework for location-aware resource management in smart homes. IEEE Trans Mobile Comput 6(11):1270–1283
85. Henze GP, Clemens F, Gottfried K (2004) Evaluation of optimal control for active and passive building thermal storage. Int J Thermal Sciences 43:173–183
86. Henze GP, Kalz DE, Liu S, Felsmann C (2005) Experimental analysis of model-based predictive optimal control for active and passive building thermal storage inventory. HVAC & R Research 11(2):189–214

Sustainable and Healthy Built Environment

Vivian Loftness[1], Megan Snyder[2]
[1]Center for Building Performance and Diagnostics, Carnegie Mellon University, Pittsburgh, PA, USA
[2]School of Architecture and Center for Building Performance & Diagnostics, Carnegie Mellon University, Pittsburgh, PA, USA

Article Outline

Glossary
Definition of the Subject
Introduction: Linking Definitions of Sustainability and Health
CMU: Seven Principles for the Design of Sustainable Built Environments
A Definition of Health to Be Integral with Sustainable Design
Linking Health and the Built Environment
Sustainable Land Use and Health
Sustainable Building Massing/Enclosure and Health
Sustainable HVAC and Health
Sustainable Lighting and Health
Sustainable Interior Systems and Health: Materials and Ergonomics
Sustainable Maintenance and Operations and Health
Calculating the Life Cycle Benefits of Sustainable Design and Health

Health and the Built Environment: A Research Mandate
Note
Bibliography

Glossary

BIDS™ The Building Investment Decision Support tool developed by the Center for Building Performance at Carnegie Mellon University to both assemble research from around the world linking design decisions to performance outcomes and to create a "triple bottom line" calculator to support changes in design decision making.

Biophilia Introduced by E.O. Wilson, the biophilia hypothesis suggests that there is an instinctive bond between human beings and other living systems that must be met by buildings that ensure critical connections.

Cornell medical index An index and questionnaire created by Cornell in 1949 to consistently collect the breadth of pertinent medical and psychiatric data on patients given limited physician time.

Epidemiological case studies Quantitative studies of a group of individuals in controlled environmental conditions with controlled changes in those conditions – interventions that may be evident, blind or double blind – with statistical analysis to demonstrate linkages between the physical environment and outcomes.

Evidenced-based design Use of laboratory and field gathered evidence in design decision making. Evidenced-based design was adopted by the Center for Health Design to improve patient health and safety outcomes through improvements in design.

LEED™, BREEAM™, Greenstar™, CASBEE™ Rigorous, voluntary sustainability standards developed in the USA, UK, Australia, and Japan, respectively, that span land use and site, energy and atmosphere, water, materials and resources, and indoor environmental quality goals.

Mixed mode or hybrid HVAC An approach to space conditioning that combines natural ventilation from operable windows or vents with mechanical heating, cooling, and ventilation systems (HVAC).

Precautionary principle Adopted by the European Community and several nations around the world, the precautionary principle argues that if an action or policy has a suspected risk of causing harm to the public or to the environment, even in the absence of scientific consensus that the action or policy is harmful, the burden of proof that it is not harmful falls on those taking the action.

Triple bottom line Expanding the criteria for evaluating a project's success from economic benefits alone to include ecological and social cost benefits, adopted by the United Nations and others to ensure public sector decision making reflects full cost accounting, and colloquialized as "people, planet, and profit."

Definition of the Subject

While sustainable design is focused on reducing the environmental footprint, the resources consumed, and the waste produced, it is also critically linked to our health. Design decision making for sustainability – land use, building massing and enclosure, lighting systems, mechanical systems, interior systems, building operation and management – can not only reduce our environmental footprint, it can and must enhance our visual, aural, dermal, musculoskeletal, circulatory, respiratory, reproductive, and mental health. The challenge is to explore the linkages between critical design decisions, from land use to material and system design to building maintenance and operations, to critical health outcomes. Based on years of gathering emerging laboratory, field, and epidemiological case studies, the Center for Building Performance and Diagnostics at Carnegie Mellon University has been assembling the research on environmental, health, and productivity benefits of the range of high-performance building systems that are the basis for sustainable design. Captured in a Building Investment Decision Support tool (BIDS™), the cost-benefits of investing in a sustainable built environment revealed in these case studies should drive measurable changes in building design, construction, and management. Given critical data sets linking sustainable design solutions and health, triple bottom line accounting can support strategic, long-term decision making in the built environment, commensurate with its intended life of 30–50 to hundreds of years. At the same time, the funding for ongoing research and the aggregation of knowledge linking health and the

built environment within an international data base will be critical to ensuring the necessary investment in the quality of our buildings and communities – the foundation of sustainability.

Introduction: Linking Definitions of Sustainability and Health

Many decision makers assume that sustainable design is about resource conservation – energy, water, and material resources. The last 10 years, however, has seen a dramatic broadening of the definition of sustainability to include commitments to mobility through improvements in land use and transportation, commitments to health and productivity through improvements in indoor environmental quality, and commitments to the protection of regional strengths a more globally shared quality of life is pursued. In the USA, this broader definition of sustainability is most often ensured through the LEED™ standard (Leadership in Energy and Environmental Design) of the US Green Building Council. Paralleled by developments in the UK (BREEAM), Australia (Greenstar), and Japan (CASBEE), the 100 or more credits in the LEED sustainability rating systems for new and existing buildings extend beyond conservation goals for energy, water, and materials, to include sustainable sites and transportation, indoor environmental quality, and regional sustainability (usgbc.org/LEED).

The Center for Building Performance and Diagnostics at Carnegie Mellon University would argue for expanding this definition even further, to give even greater emphasis to contextual and regional design goals, to accessible and flexible infrastructures that support change, to natural/passive conditioning, and to human engagement, motivation, and health. Indeed, the CBPD research team proposes the following definition:

- Sustainable design is the result of a trans-disciplinary, collective design process driven to ensure that the built environment achieves greater levels of ecological balance in new and retrofit construction, toward the long term viability and humanization of architecture. Focusing on environmental context, sustainable design merges the natural, minimum resource conditioning solutions of the past (daylight, solar heat and natural ventilation) with the innovative technologies of the present, into an integrated "intelligent" system that supports individual control with expert negotiation for environmental quality and resource consciousness. Sustainable design rediscovers the social, environmental and technical values of pedestrian, mixed-use communities, fully using existing infrastructures, including "main streets" and small town planning principles, and recapturing indoor-outdoor relationships. Sustainable design avoids the further thinning out of land use, and the dislocated placement of buildings and functions caused by single-use zoning. Sustainable design introduces benign, non-polluting materials and assemblies with lower embodied and operating energy requirements, and higher durability and recyclability. Finally, sustainable design offers architecture of long term value through "forgiving" and modifiable building systems, through life-cycle instead of least-cost investments, and through timeless delight and craftsmanship [44].

The depth of the definition of sustainability matters, especially when assessing the relevance of sustainable design, construction, and operations of buildings for long-term human and environmental health. This chapter explores the range of health outcomes that can be linked to these important principles for the design of a sustainable built environment:

CMU: Seven Principles for the Design of Sustainable Built Environments

1. Sustainable design depends on an integrative, human-ecological design approach.
2. Sustainable design depends on changing approaches to land use and community fabric.
3. Sustainable design depends on the promotion of infrastructures to neighborhood amenities.
4. Sustainable design depends on the effective use of natural, local, and global resources to reduce resource demands and maximize resource use.
5. Sustainable design depends on the design of flexible, forgiving systems.

6. Sustainable design depends on the use of healthy, renewable materials and assemblies.
7. Sustainable design depends on design for life cycle instead of first cost.

A Definition of Health to Be Integral with Sustainable Design

Equally critical to a shared definition of sustainable design is the exploration of a shared definition of human health. Building on the Cornell Medical Index of 1949 [13], the Center for Building Performance at Carnegie Mellon is using the following 10 indices for evaluating the importance of design, construction, and operation decisions on human health:

Ten qualities of human health integral with sustainable design

1. Respiratory health
2. Digestive health
3. Visual health
4. Aural health
5. Skin/dermal health (integumentum system)
6. Musculoskeletal health
7. Circulatory health
8. Nervous system health
9. Genitourinary (including reproductive) health
10. Mental health

To date, evidence from research suggests six primary clusters of health issues related to the built environment: respiratory (chest, wheeze, allergies, asthma, colds, flu), mucosal (eye, nose, throat), dermal (face, hand skin); neurological (e.g., headache, migraine, dizziness, heavy-headedness), musculoskeletal (to include body mass today), and mental health.

The challenge is to definitively link these health issues to the quality of the built environment. Given the unbounded variations in physical settings and their management over time, arguments for causality between a single design decision, such as type of ventilation system, and health outcome will be very difficult. Moreover, funding for these multivariate research questions is scarce. The challenge is to identify the controlled experiments, field intervention studies, and portfolio wide studies that might support effective design decision making for sustainability. The Center for Health Design (http://www.healthdesign.org/) has made the case for evidenced-based design that "is the process of basing decisions about the built environment on credible research to achieve the best possible outcomes." They have launched the "Pebble Project" to capture profiles of healthcare organizations whose facility design has made a difference in the quality of care – as well as their financial performance. These case studies explore the potential benefits of daylight and view, acoustics, variations in ventilation, hospital room layout and configuration, and more, on hospital outcomes. These projects are changing design practice, but some might argue they are not based on definitive research finding that can explain the mechanisms whereby health outcomes are improved. For this to occur, multiyear epidemiological studies as well as controlled laboratory and field experiments must be undertaken by collaborative teams of health and building professionals. In the meantime, the design community is making decisions every day that can positively or negatively impact human health. To this community, it is argued that every study available must contribute to informed decision making, and every act must be based on the European Union's precautionary principle:

- Where there is uncertainty as to the existence or extent of risks of serious or irreversible damage to the environment, or injury to human health, adequate protective measures must be taken without having to wait until the reality and seriousness of those risks become fully apparent.
  http://www.sustainable-design.ie/arch/precautionaryprinciple.htm.

The precautionary principle argues for the building community to take responsibility to protect the public from exposure to harm, whenever scientific investigation has found a plausible risk. These protections can be relaxed only if further scientific findings emerge that provide sound evidence that no harm will result. For example, scientific investigation suggests that outdoor air ventilation rates should be doubled in buildings to reduce the risks of colds, flus, and respiratory illnesses.

Research further argues that these increased ventilation rates should be accompanied by economizer cycles and/or heat recovery to ensure that primary energy loads will not increase, since power plant pollution also poses measurable health risks. The following sections will elaborate on the sustainable building design decisions for which scientific evidence is emerging, but not yet definitive given our weak commitment to funding research on health and the built environment.

Linking Health and the Built Environment

By setting a definition of the attributes of sustainable design against the characteristics of human health, even intuitive judgment would illuminate the importance of building design, construction, and operation for human health (Fig. 1).

With over 10 years of intense study by faculty, researchers, and graduate students, the Center for Building Performance and Diagnostics at Carnegie Mellon have been collecting building case studies as well as laboratory and simulation studies in an effort to statistically link the quality of buildings – system by system – to productivity, health, and life cycle sustainability.

Amassed in the BIDS™ (Building Investment Decision Support) tool, these case studies enable building decision makers to calculate return on investments for high-performance building components and systems, and will lead to greater understandings of the importance of buildings and communities to human health (see http://cbpd.arc.cmu.edu/bidstrial). The following six sections explore design innovations and the potential health impacts of changes in land use, building massing and enclosure, HVAC engineering, daylight and lighting system design, interior systems, and long-term building maintenance and operations.

Sustainable Land Use and Health

One of the most significant design shifts needed for the long-term health of humans is to move away from the automobile-centric land-use planning that makes pedestrian lifestyles impossible. The dramatic reductions in walking and biking that have resulted from sprawl and single-use zoning have contributed to increasing rates of obesity in industrialized nations [10, 20, 26, 55]. At the same time, the increased reliance upon automobiles has resulted in ever-increasing levels of particulate and ozone levels that are respiratory and cardiovascular hazards [24]. David L. Skole of the Center for Global Change and Earth Observations at Michigan State University identifies a range of health effects from sprawl: air pollution, CO_2 emissions, heat island effect, reduced physical exercise, increased car accidents, and pedestrian injuries, as well as declining water quality [58].

Numerous studies have revealed the seriousness of particulate-related health concerns. Wordley et al. [75] identified a 2.4% increase in respiratory hospital admissions and a 2.1% increase in cerebrovascular admissions associated with a 10 $\mu g/m^3$ increase in PM10 in the air, which, according to Dockery & Pope [15], increases respiratory admissions by 0.8 $\sim$ 3.4%. Tenias et al. [64] found that a 10 $\mu g/m^3$ increase of NO_2 and O_3 in the air causes increases in the number of emergency visits for asthma by 7.6% and 6.3%, respectively.

Moreover, automobile-centric land use and single-use zoning has led to increasing inactivity in children, teens, and senior citizens that contributes to obesity and all the associated health impacts of obesity, as well as potentially contributing to attention deficit and depression. In a 2004 cross-sectional survey of 10,878 adults from the Atlanta, Georgia region, Frank et al. identify a 12.2% decline in the likelihood of obesity for each quartile increase in land use mix, which was defined on a scale from 0 (indicating a single-use environment) to 1 (indicating a perfectly equal mix of residential, commercial, office, and institutional uses). They also found a significant relationship between reductions in vehicle miles travel and reductions in particulate matter, NOX and VOC pollution, which have other health ramifications (see Fig. 2), [23].

The US studies on land use and obesity are summarized and advanced in the 2006 National Institute of Health study of the "Relationship Between Urban Sprawl and Weight of United States Youth" [21]. "The first studies reporting a direct relationship between the built environment and obesity were published in 2003 [10, 19, 26, 55]. After controlling for age, education, fruit and vegetable consumption, and other socio-demographic and behavioral covariates, Ewing et al. [20] found that adults living in sprawling counties had higher body mass indices (BMIs) and were more

	Respiratory system	Digestive system	Eyes, vision, circadian system	Ears, hearing, concentration	Skin	Musculo-skeletal	Circulatory system	Nervous system	Genitourinary system	Mental health, stress, biophilia
Land use										
Design live - work - walk communities		●				●	●			
Design mixed mode mobility	●	●				●	●			
Increase landscape/reduce paving	●					●		●		●
Distributed/ renewable power sources	●									
Building Massing and Enclosure										
Design for Daylighting/View /Passive Solar			●					●		●
Design for Natural Ventilation	●									●
Engineer Thermal Load Balancing							●			
Design Enclosure Integrity	●			●			●			
Lighting and HVAC Systems										
Separate ambient and task lighting			●							
Specify high performance lighting & controls			●							
Separate ventilation & thermal conditioning	●						●			●
Increase outside air & ventilation effectiveness	●									
Engineer moisture humidity management	●				●					
Engineer individual control of temperature							●			
Interior Systems										
Specify ergonomic furniture						●	●			
Design spatial layout/density for health/safety						●				
Specify acoustic quality				●						
Specify materials vs. out gassing/ degradation	●							●		
Specify materials vs. irritation/ re-infection	●	●			●					
Specify materials vs. mold	●									
Operations										
Continuously Commission Systems	●									
Eliminate standing water, dampness & mold	●									
Design for non toxic pest/plant management	●	●						●		
Design for environmentally benign cleaning	●				●			●		
Improve food/vending quality for health		●								
Improve water quality for health		●								
Reduce waste/ manage waste vs. pests	●									●

Sustainable and Healthy Built Environment. Figure 1
Correlating decision making in the built environment to improving human health should be a major international initiative

Increased density + mixed land use = Health

Frank et al 2004

In a 2004 cross-sectional survey of 10,878 adults from the atlanta, Georgia region, Frank et al identify a 12.2% decline in the likelihood of obesity for each quartile increase in land use mix, which was defined on a scale from 0 (indicating a single-use environment) to 1 (indicating a perfectly equal mix of residential, commercial, office, and institutional uses).

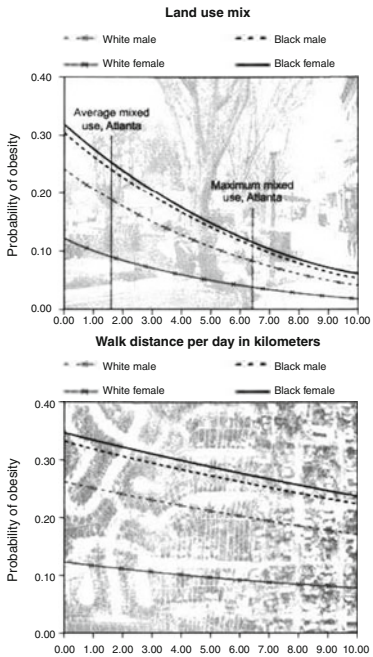

First cost savings:	$4,408 / person
Annual health savings:	$51 / person
RoI:	Immediate

Reference: D. Frank, M. Andresen, T. Schmid. Obesity relationships with community design, physical activity, and time spent in cars. American Journal of Preventive Medicine, Volume 27, Issue 2, August 2004.

Center for Building Performance and Diagnostics, a NSF/IUCRC, and ABSIC at Carnegie Mellon

Sustainable and Healthy Built Environment. Figure 2
Land use can significantly reduce vehicle miles traveled which in turn reduces the pollution that causes growing respiratory health concerns

likely to be obese (BMI $\geq$ 30) than were their counterparts living in compact counties. Independent studies have since generally confirmed these original findings. Specifically, all macro-level (county or larger) studies, and all but one micro-level (neighborhood) studies, have found significant relationships, in the expected direction, between sprawl-like development patterns and BMI, after controlling for socio-demographic and other influences" [21].

Moreover, automobile-based design is "paving" the countryside, with the elimination of landscapes that act as natural lungs for filtering our air, and with the increasing salts, oils, and storm-sewer overflows that result in toxic runoff into our drinking water. The quantification of these serious health hazards should fully justify the shift in sustainable design to: live-work-walk lifestyles with mixed-use communities; multigenerational mobility with mixed mode transportation; and the preservation and celebration of natural landscapes and sustainable infrastructures.

Guidelines Linking Sustainable Land Use and Health
Design live-work-walk communities to reduce car pollution – particulates and ozone – that trigger asthma
Design for pedestrian, bicycle, transit mobility to reduce obesity
Minimize paving for roads and parking to reduce salting and oil runoff, as well as standing water concerns
Design landscape dominant environments to reduce thermal heat islands, heat stress, and rebuild nature's lungs for air quality

Sustainable Building Massing/Enclosure and Health

After land use design, the second most critical design decision for human health might be building massing

and enclosure specifications. On the one hand, access to nature's assets – daylight, natural ventilation, natural comfort and thermal variation, views and physical access to outdoor activity - are becoming increasingly linked to human health. On the other hand, humans need protection from nature's liabilities – overheating, excessive cold, wind, rain, and snow. The design of the building enclosure is critical for managing both these climatic assets and liabilities.

The CBPD has identified a range of international case studies linking access to the natural environment – daylight, views, and natural ventilation – to improved health outcomes, including reductions in headaches, colds, sick building symptoms (SBS), and patient length of stay (see Fig. 3). Beyond the health benefits, a number of international case studies demonstrate that access to the natural environment increases individual productivity between 3% and 18%, reduces absenteeism between 9% and 71%, and offers over 50% lighting and HVAC energy savings (CBPD).

While the debate continues as to the mechanisms by which *daylight* improves health, research continues to reveal that sunlight, especially morning sunlight, reduces length of stay for patients recovering from surgery, bipolar, and SAD treatment [3, 4, 12, 71]. In a 2005 building case study of Inha University Hospital in Korea, Choi identifies a 41% reduction in average length of stay among gynecology patients in bright (sunlit) rooms, as compared to those in dull rooms, in spring, and an average 26% reduction in average length of stay among surgery ward patients in bright rooms, as compared to those in dull rooms, during spring and fall [12]. In a separate study of pain medication use among 89 patients undergoing elective cervical and lumbar spinal surgery at Montefiore Hospital in Pittsburgh, PA, Walch et al. identify a 22% reduction in analgesic medication use among patients in bright rooms who were exposed to more natural sunlight after surgery, as compared to patients located in dim rooms after surgery [71] (Fig. 4).

The work of the Lighting Research Institute at RPI has begun to reveal the possible mechanisms of these health outcomes, identifying the relationship of ultraviolet light exposure to the production of melatonin,

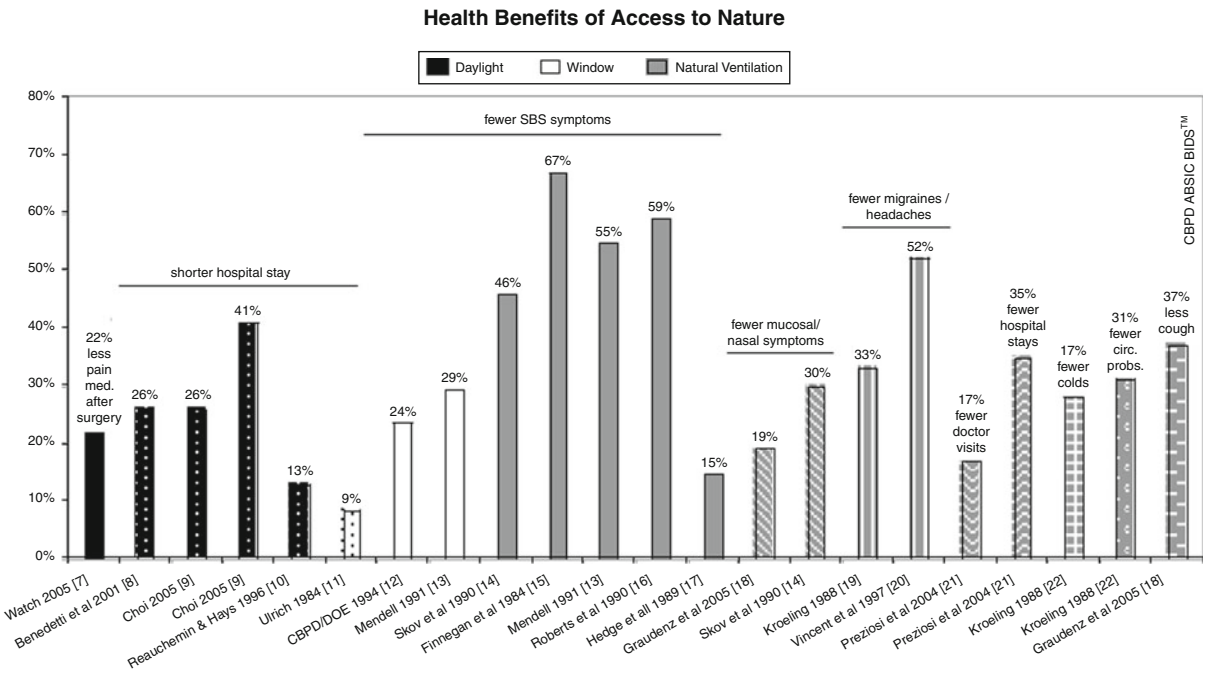

Sustainable and Healthy Built Environment. Figure 3
A range of international case studies link access to the natural environment – daylight, views, and natural ventilation to improved health outcomes – reductions in headaches, colds, sick building symptoms (SBS), and patient length of stay

Daylight = Health

Inha University Hospital / Choi 2005 (Hospital)

In a 2005 building case study of Inha University Hospital in Korea, Choi identifies a 41% reduction in average length of stay among gynecology patients in bright (sunlit) rooms, as compared to those in dull rooms, in spring, and an average 26% reduction in average length of stay among surgery ward patients in bright rooms, as compared to those in dull rooms, during spring and fall.

First cost increase:	$ 1,000 / bed
Annual health savings:	$ 10,115 / bed
ROI:	**1,011%**

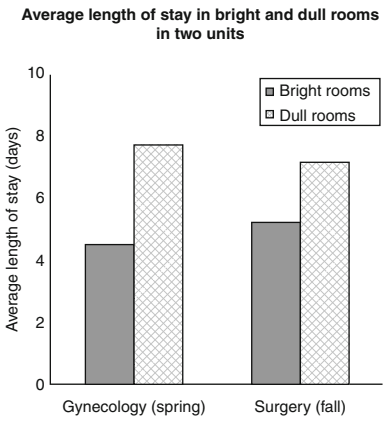

Reference: Choi, Joonho. (2005). Study of the Relationship between Indoor daylight Environments and Patient Average Length of Stay (ALOS) in Healthcare Facilities, Unpublished master's thesis, Department of Architecture, Texas A&M University. College Station, TX.

Center for Building Performance and Diagnostics, a NSF/IUCRC, and ABSIC at Carnegie Mellon

Daylight = Health

Montefiore Hospital / Walch et al 2005 (Hospital)

In a 2005 study of pain medication use among 89 patients undergoing elective cervical and lumbar spinal surgery at Montefiore Hospital in Pittsburgh, PA, Walch et al identify a 22% reduction in analgesic medication use among patients in bright rooms who were exposed to more natural sunlight after surgery, as compared to patients located in dim rooms after surgery.

First cost increase:	$ 1,000 / bed
Annual health savings:	$ 28 / bed
ROI:	**3%**

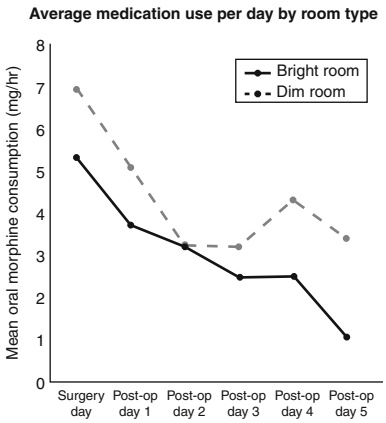

Reference: Walch JM, Rabin BS, Day R, Williams JN, Choi K, Kang JD (2005) The effect of sunlight on postoperative analgesic medication use: a prospective study of patients undergoing spinal surgery. Psychosom Med 67:156–163

Center for Building Performance and Diagnostics, a NSF/IUCRC, and ABSIC at Carnegie Mellon

Sustainable and Healthy Built Environment. Figure 4
In extensive hospital record studies, Choi and Walch identified the value of southern and south eastern rooms to reduced patient length of stay.

a natural hormone that controls circadian rhythms that are related to sleep cycles and potentially to reduced cancer cell development [7]. At the same time daylight, and most especially sunlight, can introduce glare and overheating that might negatively affect human health outcomes.

The importance of *views* of nature and proximity to windows for human health is equally important for study, with the work of Ulrich [68], Mendell [45], Heschong Mahone Group [31] now Kellert [41] identifying possible links between views and reduced length of hospital stay after surgery, reduced sick building syndrome, improved overall emotional health, and improved performance at task. In a 1991 11-building study of office buildings in San Francisco, Mendell [45] identifies 25–52% reductions in reported SBS

symptoms among occupants located within 15 ft of a window, as compared to those seated further from a window.

In addition to confirming the importance of seated views for all building occupants, research is critically needed to understand the importance of the content of those views from windows for human health (e.g., the benefit of landscape views over parking lots, building walls, and sky). In a seminal 1984 field study at a Pennsylvania hospital, Ulrich [68] identifies an 8.5% reduction in postoperative hospital stay (8.7 vs. 7.96 days) for gall bladder surgery patients who had a view of a natural scene from their hospital room, as compared to those with a view of the brick wall of the adjacent building wing. Patients with a view of nature also received fewer negative evaluations from nurses and took fewer strong analgesics (see Fig. 5).

In addition to sunlight and views, it is critical to understand the benefits of direct access to outdoor air and outdoor spaces through operable windows and doors. The value of increasing outside air delivery rates is becoming increasingly evident, as will be described in the section on HVAC design. It is not clear, however, whether increased levels of outside air are more effectively delivered through *natural ventilation* (operable windows) or through mechanical systems that incorporate filtration, dehumidification, and thermal conditioning of that outside air. There are over a dozen studies that reveal the benefits of natural ventilation in existing buildings as compared to mechanically ventilated buildings – benefits that range from reduced headaches, mucosal symptoms, colds, coughs and circulatory problems, to reduced SBS symptoms. In a 1992 study of two London hospitals, Kelland [40] identifies a 40% reduction in sick building syndrome (SBS) symptoms among staff of a naturally ventilated hospital, as compared to those of a mechanically ventilated hospital (see Fig. 6). In a 2004 multiple building study of professional middle-aged women in France, Preziosi et al. [52] identify a 57.1% reduction in sickness absence, a 16.7% reduction in medical services use (doctor visits), and a 34.8% reduction in hospital stays among subjects with natural ventilation in their workplace, as compared to those with air conditioning (see Fig. 6). In a 2007 study of 104 child care centers in Singapore, Zuraimi et al. identifies a 10.7% decrease in cough with cold/flu symptoms, a 31% decrease in phlegm with cold/flu, a 27.3% decrease in coughing attacks lasting more than 1 week, and a 33.3% decrease in lower respiratory illness in children attending naturally ventilated child care centers as opposed to centers with hybrid ventilation [77].

While operable windows can bring in higher quantities of outside air, they can also bring in unwanted outdoor pollution, humidity, rain, and noise. The pros and cons of increasing outside air rates through natural versus mechanical means are outlined in Fig. 3, with a bias to the value of natural ventilation, especially given the variable long-term performance of HVAC systems and controls in operation (Fig. 7).

The design decisions central to ensuring daylight, view, and natural ventilation include increasing surface area with thinner floor plates and resolving glare, overheating, heat loss, and rain penetration through appropriate enclosure design. In some respects, sustainable, healthy buildings have many of the characteristics of sustainable, healthy humans – they are physically fit rather than obese (thin floor plans, finger plans, and courtyard buildings); they have circulatory systems that take the heat from the core out to the surface (through water mullions or air flow windows described in Chap. 2); and they absorb sunlight and breathe fresh air. At the same time, sustainable buildings are designed to reduce or make use of climatic liabilities – rain, cold and hot temperatures, diurnal temperature swings, excessive sun, freeze-thaw – with completely regional design solutions.

Guidelines Linking Sustainable Building Massing/Enclosure and Health
Design for daylighting without glare to support visual acuity and reduce headaches
Design for natural ventilation without drafts and rain penetration to reduce respiratory symptoms
Engineer thermal load balancing to eliminate radiant asymmetry associated with arthritis and circulatory disorders
Design for passive solar heating where climate appropriate for thermal comfort and UV benefits
Design enclosure integrity to eliminate mold affecting SBS, respiratory/allergy and asthma

Seated Access to Views = Health

PA Hospital / Ulrich 1984

In a 1984 observational field study at a Pennsylvania hospital, Uirich identifies an 8.5% reduction in post-operative hospital stay (8.7 vs 7.96 days) for gall bladder surgery patients who had a view of a natural scene from their hospital room, as compared to those with a view of a brick wall. Patients with a view of nature also received fewer negative evaluations from nurses and took fewer strong analgesics.

First cost increase:	$ 5,000 / bed
Annual health savings:	$ 2,237 / bed
ROI:	**45%**

Floor plan at a hospital

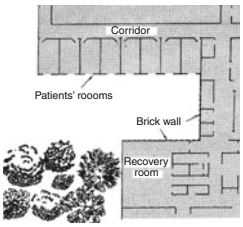

Average length of stay with a view of nature vs without a view of nature

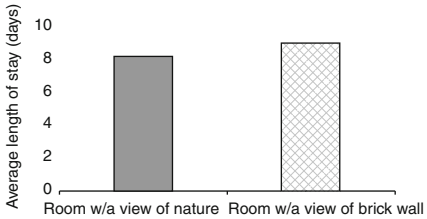

Reference: Ulrich, R. (1984) View Through a Window May Influence Recovery From Surgery. Science, 224(4647), pp. 420-421.

Center for Building Performance and Diagnostics, a NSF/IUCRC, and ABSIC at Carnegie Mellon

Seated Access to Windows = Health + Individual Productivity

CA Healthy Building Study / Mendell 1991 (Wargocki et al 2000)

In a 1991 multiple building study of 11 office buildings in San Francisco, Mendell identifies 25% - 52% reductions in reported SBS symptoms among occupants located within 15 feet of a window, as compared to those seated further from a window.

In a 2000 study, Wargocki et al identify a 1.1% productivity increase for every 10% reduction in SBS complaints, suggesting an average 4.3% productivity gain for workers seated near a window.

First cost increase:	$1,000 / employee
Annual productivity savings:	$1,935 / employee
Annual health savings:	$40
ROI:	**198%**

Reported symptoms by distance to window

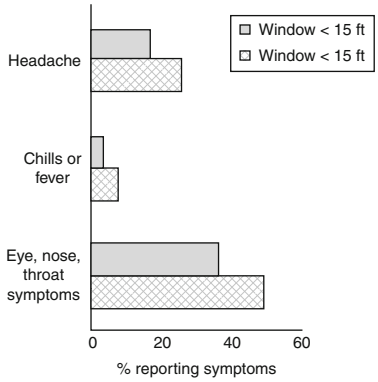

Reference: Mendell, Mark J. (1991) Risk Factors for work-Related Symptoms in Northern California Office Workers. Wargocki, P, Wyon, D, and Fanger, P.O. (2000) Pollution Source Control and Ventilation Improve Heath, Comfort and Productivity. In Proceedings of Cold Climate HVAC 2000, Sapporo, Japan, November 1-3, 2000, pp. 445-450.

Center for Building Performance and Diagnostics, a NSF/IUCRC, and ABSIC at Carnegie Mellon

Sustainable and Healthy Built Environment. Figure 5

Ulrich and Mendell identified the importance of views and view content to sick building syndrome and reduced patient length of stay

Natural Ventilation = Health + Individual Productivity

Preziosi et al 2004

In a 2004 multiple building study of professional middle-aged women in France, Preziosi et al identify a 57.1% reduction in sickness absence, a 16.7% reduction in medical services use (doctor visits), and a 34.8% reduction in hospital stays among subjects with natural ventilation in their workplace, as compared to those with air conditioning.

First cost increase:	$1,000 / employee
Annual health savings:	$181 / employee
Annual productivity savings:	$85 / employee
ROI:	**27%**

Per capita health services use and absenteeism in naturally ventilated vs. mechanically ventilated buildings

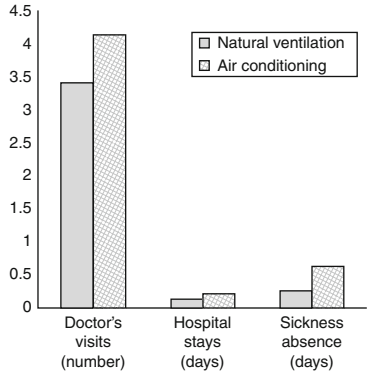

Reference: Preziosi P., S. Czerniichow, P. Gehanne, and S. Hercberg (2004) Workplace air-conditioning and health services attendance among French middle-aged women: a prospective cohort study. International Journal of Epidemiology, 33(5), pp. 1120-1123.

Center for Building Performance and Diagnostics, a NSF/IUCRC, and ABSIC at Carnegie Mellon

Natural Ventilation = Health

London Hospitals / Kelland 1992 (Wargocki et al 2000)

In a 1992 multiple building study of two London hospitals, Kelland identifies a 40% reduction in sick building syndrome (SBS) symptoms among staff of a naturally ventilated hospital, as compared to those of a mechanically ventilated hospital.

In a 2000 study, Wargocki et al identify a 1.1% increase in productivity for every 10% reduction in SBS complaints, suggesting a 4.4% productivity gain due to natural ventilation.

First cost increase:	$543 / employee
Annual productivity savings:	$1,980 / employee
ROI:	**365%**

SBS symptom prevalence at a naturally ventilated and a mechanically ventilated hospital

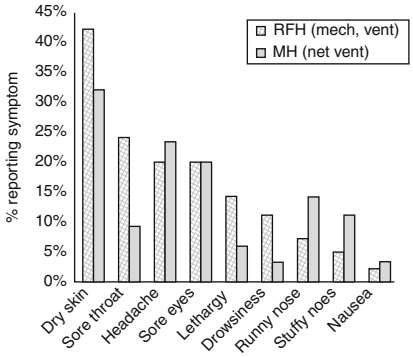

Reference: Kelland, P (1992) Sick Building Syndrome, Working Environments and Hospital Staff. Indoor Environment, v1, PP. 335-340; Wargocki, P, Wyon, D, and Fanger, P. O. (2000) Pollution Source Control and Ventilation Improve Health, Comfort and Productivity. In Proceedings of Cold Climate HVAC 2000, Sapporo, Japan, November 1-3 2000, pp. 445-450.

Center for Building Performance and Diagnostics, a NSF/IUCRC, and ABSIC at Carnegie Mellon

Sustainable and Healthy Built Environment. Figure 6
Kelland identified a reduction in hospital staff SBS and Preziosi identified reductions in absenteeism and doctor visits in buildings with natural ventilation as compared to those with mechanical ventilation

Sustainable HVAC and Health

The design of heating, ventilation, and air conditioning systems (HVAC) for human health are based on at least three improvements in individual occupant conditions: increased outside air rates and filtration; improved moisture/humidity control; and improved thermal comfort control.

In addition to managing sources of pollution, healthy indoor air is dependent on a commitment to improving the quality and quantity of outside air. Increasing outside ventilation rates for health has substantial research justification – a doubling or tripling of code requirements for outside air measurably reduces headaches, colds, flus, nasal symptoms, coughs, and

Should Windows Open?

No	Yes
Avoid outdoor pollution	Dilute indoor pollution from HVAC sources
	Dilute indoor pollution from materials/ activities
Avoid outdoor humidity	Diffuse indoor humidity build up
Avoid outdoor noise (traffic, HVAC, mowers)	Connect to nature – air, sounds
Well designed/maintained HVAC ensures temperature control and ventilation rates	Increase local ventilation rates as needed
	Increase local thermal control in cool periods
Avoid rain penetration	Design windows to shed rain

Sustainable and Healthy Built Environment. Figure 7
Operable windows are critical to long term sustainability and human health, so challenges should be addressed through design

SBS symptoms [5, 6, 16, 22, 34, 47, 49, 59, 62, 65]. Increasing outside air rates without energy penalty may be achieved by maximizing natural ventilation with mixed-mode HVAC systems that support natural ventilation; by designing HVAC systems with *separate* ventilation air and thermal conditioning systems, which permits thermal conditioning to be water or air based; or at a minimum by increasing outside air quantities with effective filtration and heat recovery for energy efficiency. In a meta-analysis of 20 ventilation rate studies, Seppanen, Fisk, and Mendell found that the relative risks of respiratory illnesses were 1.5–2 higher in low ventilation rate buildings (below 10 L/s/person) as compared to high ventilation rate buildings (up to 20 L/s/person), alongside a 1.1–6 higher risk of sick building syndrome symptoms in low ventilation rate buildings [56].

A recent international study of papers published in peer-reviewed scientific journals identified a "biological plausibility for an association of health outcomes with ventilation rates, although the literature does not provide clear evidence on particular agent(s) for the effects. Higher ventilation rates in offices, up to about 25 L/s per person, are associated with reduced prevalence of sick building syndrome (SBS) symptoms. The limited available data suggest that inflammation, respiratory infections, asthma symptoms, and short-term sick leave increase with lower ventilation rates. Home ventilation rates above 0.5 air changes per hour (h^{-1}) have been associated with a reduced risk of allergic manifestations among children in a Nordic climate. The need remains for more studies of the relationship between ventilation rates and health, especially in diverse climates, in locations with polluted outdoor air and in buildings other than offices [61]."

To ensure ventilation effectiveness, the ventilation system must be designed to provide air *to the individual* with "task" air systems, ideally with some level of individual control to address local pollutant buildup. In a 2000 building intervention study in 39 Swedish schools, Smedje and Norback identify a 69% reduction in the 2-year incidence of asthma among students in schools that received a new displacement ventilation system with increased fresh air supply rates, as compared to students in schools that did not receive a new ventilation system (see Fig. 8, [59]. In a 2002 controlled experiment, Kaczmarczyk et al. identify a 23.5% reduction in headache symptoms when workers are provided with individually controlled task air systems supplying outdoor air, as compared to a conventional mixing ventilation system, in a room with a typical office pollutant source [39] (see Fig. 8). Both of these studies reveal the health benefits of ensuring that fresh air reaches the nose of every occupant. At the same time, a healthy HVAC system must guarantee outdoor and indoor pollution source control through building design, HVAC configuration, maintenance, and effective filtration. In a 2003 multiple building study of three Montreal office buildings, Menzies et al. identify a 25% reduction in reported mucosal symptoms and a 25% reduction in reported respiratory symptoms due to ultraviolet germicidal irradiation (UVGI) of drip pans and cooling coils within ventilation systems [48]. Additional studies are critically needed to address the importance of

Floor-based ventilation + Increased outside air = Health

Smedje & Norback 2000 (School)

In a 2000 multiple building study of 39 schools in Sweden, Smedje and Norback identify a 69% reduction in the 2-year incidence of asthma among students in schools that received a new displacement ventilation system with increased fresh air supply rates, as compared to students in schools that did not receive a new ventilation system .

First cost increase:	$38 / student
Annual energy cost increase:	$2 / student
Annual health savings:	$36 / student
ROI:	**89%**

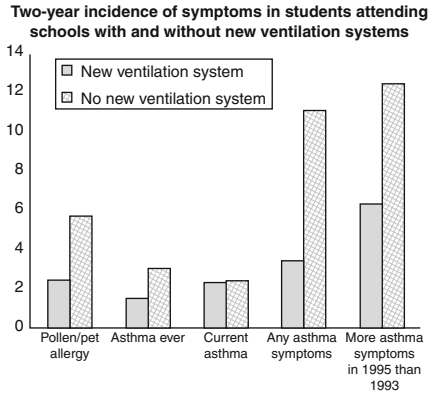

Reference: Smedje, G and Norback, D. (2000) New ventilation systems at select schools in Sweden–Ettects on Asthma and Exposure. Archives of Environmental Health, 35(1), pp. 18-25.

Center for Building Performance and Diagnostics, a NSF/IUCRC, and ABSIC at Carnegie Mellon

Individual air control + Increased outside air = Health

Kaczmarczyk et al 2002

In a 2002 controlled experiment, Kaczmarczyk et al identify a 23.5% reduction in headache symptoms when workers are provided with individually-controlled task air systems supplying outdoor air, as compared to a conventional mixing ventilation system, in a room with a typical office pollutant source.

First cost increase:	$800 / employee
Annual energy cost increase:	$8 / employee
Annual health savings:	$17 / employee
Annual productivity savings:	$106 / employee
ROI:	**14%**

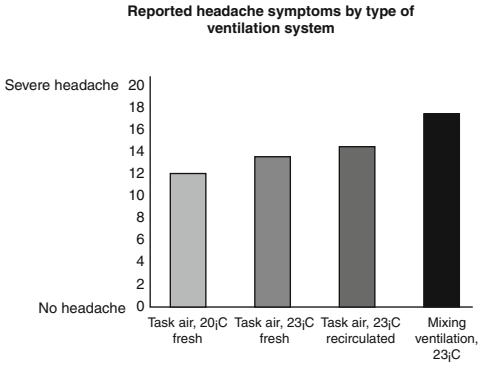

Reference: Kaczmarczk, J., Zeng, Q., Melikov, A., and Fanger, P.O. (2002) The effect of a personalized ventilation system on perceived air quality and SBS symptoms. In Proceedings of Indoor Air 2002, Monterey, CA, June 30-July 5, 2002; Office of Pollution Prevention and Toxics, U.S. Environmental Protection Agency. Cost of Illness Handbook. http://www.epa. gov/oppt/coi; Schwartz et al (1997) Lost Workdays and Reduced Work Effectiveness Associated with Headache in the Workplace. Journal of Occupational and Environmental Medicine. 39(4), pp. 320-327.

Center for Building Performance and Diagnostics, a NSF/IUCRC, and ABSIC at Carnegie Mellon

Sustainable and Healthy Built Environment. Figure 8
Smedje and Norback [59] identify a 69% reduction in 2-year incidences of asthma in schoolchildren, and Kaczmarczyk [39] identifies a 23.5% reduction in headache symptoms in offices when ventilation is delivered more effectively to individuals

both filtration and ongoing HVAC maintenance for human health.

The CBPD has summarized a range of international case studies that link high-performance ventilation strategies to 10–90% reductions in respiratory illnesses, including asthma and allergies, as well as studies that demonstrate reductions in SBS, headaches, flus, and colds (see Fig. 9). In these studies, the critical HVAC improvements are increasing outside air rates, ensuring mold/moisture control and air stream management and maintenance, as well as quality filtration. In addition to health benefits, the

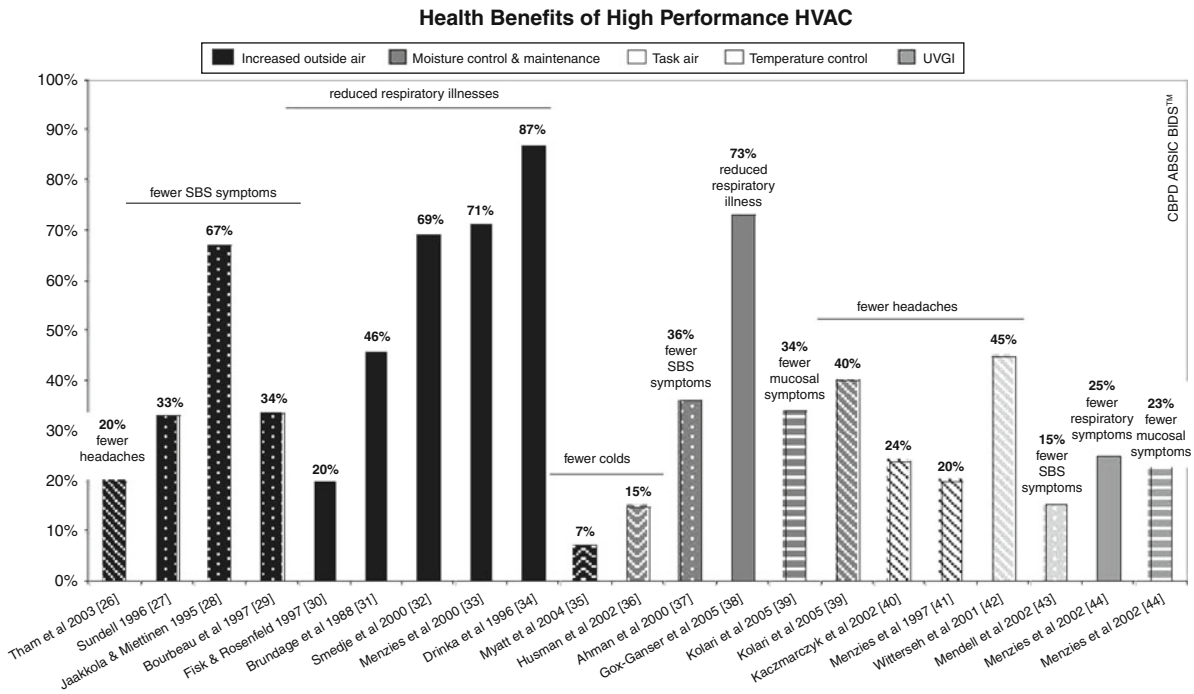

Sustainable and Healthy Built Environment. Figure 9

A range of international case studies link improvements in HVAC to reduce colds, headaches, respiratory, mucosal, and SBS symptoms

CBPD has identified studies that link individual productivity gains of 1.7–11% to high-performance ventilation strategies. Studies also reveal that the energy penalty for increasing outside air rates can be easily eliminated with heat recovery or the use of mixed mode ventilation and conditioning, to generate up to 50–80% energy savings in sustainable HVAC systems (CBPD).

Sustainable HVAC systems must also be designed to provide individual thermal controls. Several laboratory and field experiments link temperature control to individual productivity gains between 0.2% and 7% to 15% energy savings through task thermal conditioning (CBPD), and to reduced headache and SBS symptoms [39, 46]. The challenges for HVAC design for thermal comfort are to design for dynamic thermal zone sizes (anticipating changing density and uses); provide individual thermal controls (through under floor air and task air distribution systems); design for building load balancing and radiant comfort; and finally, to engineer prototyped, robust systems that provide air quality and thermal comfort consistently in the field, over time.

Sustainable HVAC for Health
Increase outside air rates, through natural ventilation or HVAC with heat recovery – to reduce respiratory, allergy, asthma, colds, headaches, SBS
Engineer ventilation effectiveness, including air path and filtration management – to reduce respiratory, throat, and mucosal symptoms
Engineer moisture/humidity management – to reduce mold affecting respiratory illnesses, colds, SBS
Separate ventilation and thermal conditioning systems for individual thermal control – to reduce headaches and SBS symptoms

Sustainable Lighting and Health

Sustainable design must maximize the use of daylight for both sustainability and health, as long as it can be provided without glare and excessive heat loss or heat gain.

Daylight can provide the higher light levels needed for fine work, improve color rendition and sculptural definition, give the full spectrum and ultraviolet content that might be critical to circadian rhythms, and provide access to views of nature. Subsequently, electric lighting systems have the responsibility to effectively interface with daylight to meet the needs of specific tasks, and provide the appropriate quantity and quality of light when daylight is not available. To this end, sustainable lighting is dependent on selecting the highest quality lighting fixtures, lamps, ballasts, reflectors, lenses, and controls to light each specific task or task surface in an energy-effective manner.

The benefits of well-designed daylight for human health have been previously discussed. If daylight is well designed to control glare and brightness contrast, it is a low energy source that can significantly improve task performance and reduce headaches. In addition, the spectral distribution of daylight, critical to plant health, as well as time-of-day variations in light, may have a measurable impact on our circadian rhythms that impact sleep cycles and energy levels. Finally, as previously discussed, views that may be associated with daylight sources may have a measurable impact on reducing depression and SBS symptoms, while improving hospital recovery rates.

The high-quality lighting fixtures, lamps, ballasts, reflectors, lenses, and controls to light each specific task or task surface also have measurable benefits for human health. For example, in a 1989 controlled field experiment at a government legal office in the UK, Wilkins et al. identify a 74% reduction in the incidence of headaches among office workers when magnetic ballasts are replaced by high-frequency electronic ballasts (see Fig. 10, [74].

Given the shift from paper-based to computer-based tasks, lighting design must be improved for task performance, for energy effectiveness, and for human health. Sustainable lighting design supports the separation of task and ambient lighting – to enable lower overall ambient light levels at 200–300 lux for computer-based work and face-to-face discussions, to be augmented by higher task light levels at 500–800 lux for fine print work. In a 1998 multiple building study in Germany, Çakir and Çakir identify a 19% reduction in headaches for workers with separate task and ambient lighting, as compared to workers with ceiling-only combined task and ambient lighting (see Fig. 10) [9].

Three international case studies demonstrate that improved lighting design reduces headache symptoms, as shown in Fig. 11. The CBPD has also identified 12 international case studies that indicate that improved lighting design increases individual productivity between 0.7% and 23% while reducing annual energy loads by 27–88% (CBPD).

Guidelines for Sustainable Lighting for Health
Design for daylighting without glare to support visual acuity, color rendition, circadian rhythms, view content to reduce headaches, hospital length of stay
Specify high-performance fixtures for maximum lumens/watt, reduced glare, shadowing and noise and to reduce headaches
Separate ambient and task lighting delivery to match light levels to task and provide individual control

Sustainable Interior Systems and Health: Materials and Ergonomics

Among a range of interior design decisions that affect both sustainability and productivity, at least three design decisions also have measurable health impacts – healthy material selection, acoustic/noise management, and the ergonomics of furniture and space layout.

Interior material selection is critical to thermal performance, air quality (due to outgassing), toxicity in fires, cancer-causing fibers, and mold growth, which in turn impact our respiratory and digestive systems, our eyes and skin. The CBPD has identified six studies linking materials selection to health outcomes including SBS, mucosal irritation, allergies, and asthma (see Fig. 12, [25, 35, 36, 43, 72, 73]. In a 1996 study of 80 homes in Victoria, Australia, Garrett et al. identify a 60% reduction in the prevalence of asthma and a 63% reduction in the prevalence of allergies among children whose homes contain formaldehyde-free composite wood products, as compared to those exposed to formaldehyde from furnishings and products in their home [25]. While sustainable design depends on the use of materials and assemblies that support healthy indoor environments, it also mandates the selection of

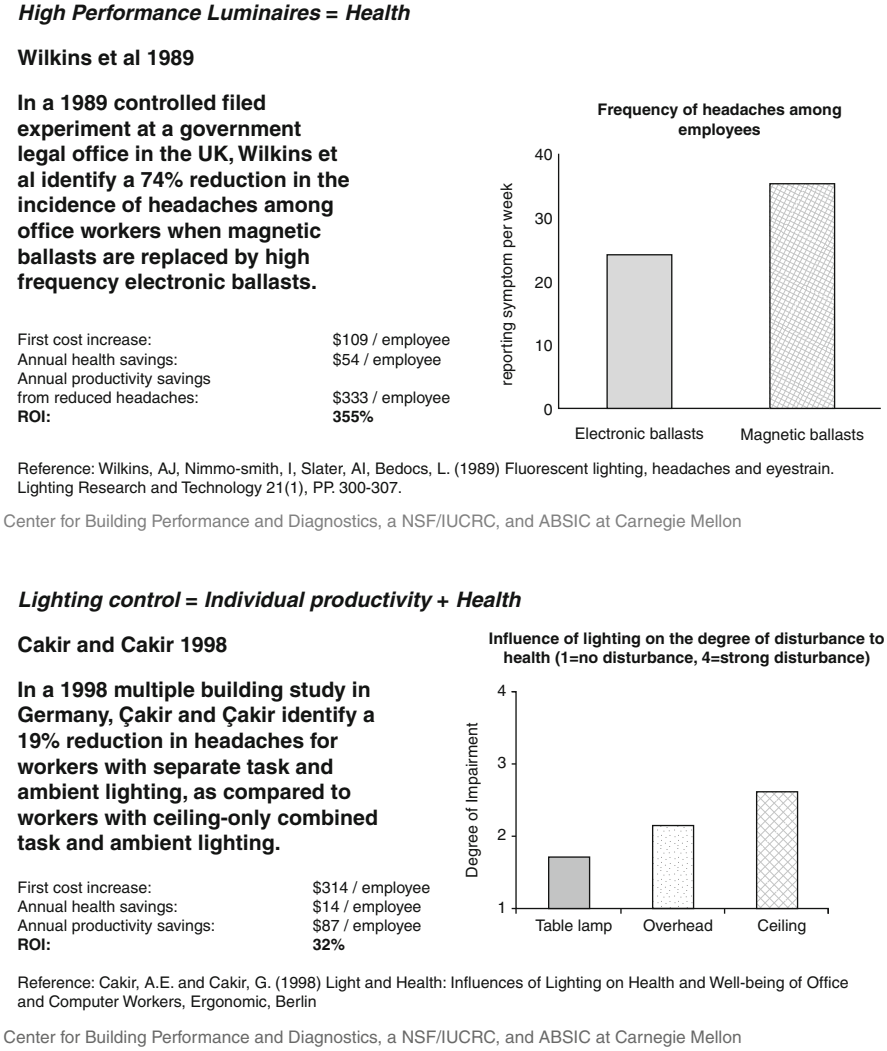

Sustainable and Healthy Built Environment. Figure 10
Wilkins identified a 74% reduction in headaches with updated lighting ballasts, and Cakir and Cakir identified 19% reduction in headaches with the separation of ambient and task lighting

materials with low embodied and transportation energy, since these environmental costs carry secondary health concerns.

The most rapidly emerging body of research linking interior materials and health may be related to the infections transferred by contact with surfaces, door handles, faucets, keyboards, telephones, even elevator buttons, and the importance of hands-free design and frequent hand washing. One study by Rheinbaben et al. in a household or dormitory setting, viruses can be transferred to six people successively from contaminated door handles [54]. Contact infection can be addressed through hand washing and green cleaning techniques that are an element in sustainability standards, as well as through hands-free design innovations for shared facilities and equipment.

Managing acoustic quality in indoor environments is critical to both productivity and human health. The importance of reducing unnecessary noise sources while ensuring appropriate sound transmission must continue to be a major requirement for high-performance and sustainable indoor environments.

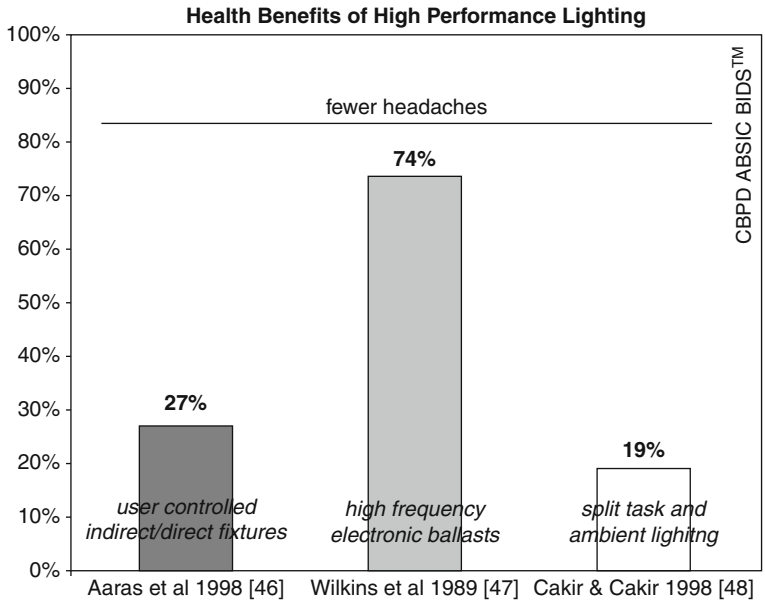

Sustainable and Healthy Built Environment. Figure 11
Case studies link improvements in lighting – ballast quality and individual control – to reduced headache symptoms

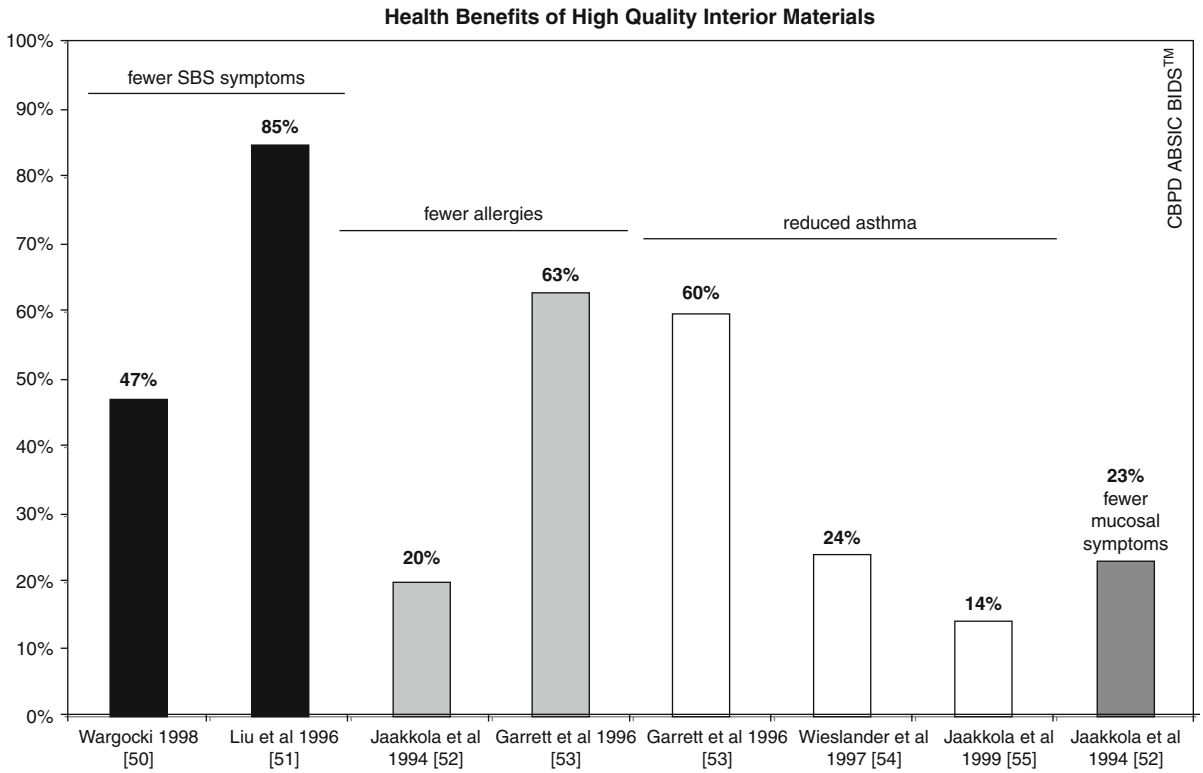

Sustainable and Healthy Built Environment. Figure 12
A number of international studies link the quality of building materials and assemblies to allergies, asthma, SBS, and mucosal symptoms

In a 2002 study of ten volunteer teachers from ten randomly selected preschools in Stockholm, Sweden, Sodersten et al. identify an 11% reduction in vocal strain among teachers in classrooms with background noise levels of 55 dB, as compared to those in classrooms with background noise levels of 75.2 dB [60]. Managing unnecessary background noise and ensuring appropriate and necessary sound distribution are as critical to defining indoor environmental quality (IEQ) as visual, thermal, and air quality.

While less tied to today's definition of sustainability, the importance of ergonomic furniture and space configuration for human health must continue to be emphasized in the design of high-performance indoor environments. Given the growing preponderance of computer-based work today, work surfaces, chairs, keyboards, and mouse design must be ergonomically designed to reduce musculoskeletal disorders (MSD). According to a Washington State study, 1.7–3.2% of MSD complaints result in medical costs averaging $22,000 per affected occupant and in many cases permanent consequences for the employee [57]. The CBPD has identified seven international case studies that demonstrate that ergonomic workstations reduce MSD symptoms between 48% and 84% (Fig. 13) [1, 27–29, 32, 69, 76].

Ergonomic design goes beyond anthropometric concerns, however, to also address building layout and densities that support human health and productivity. Jaakkola and Heinonen [33] identified a 35% lower rate of colds among occupants of individual offices, compared to those in shared offices. John Templer [63], the author of a two-volume reference on *Stairs*, carefully illustrates critical design decisions for stairs, ramps, curbs, and surfaces to reduce the

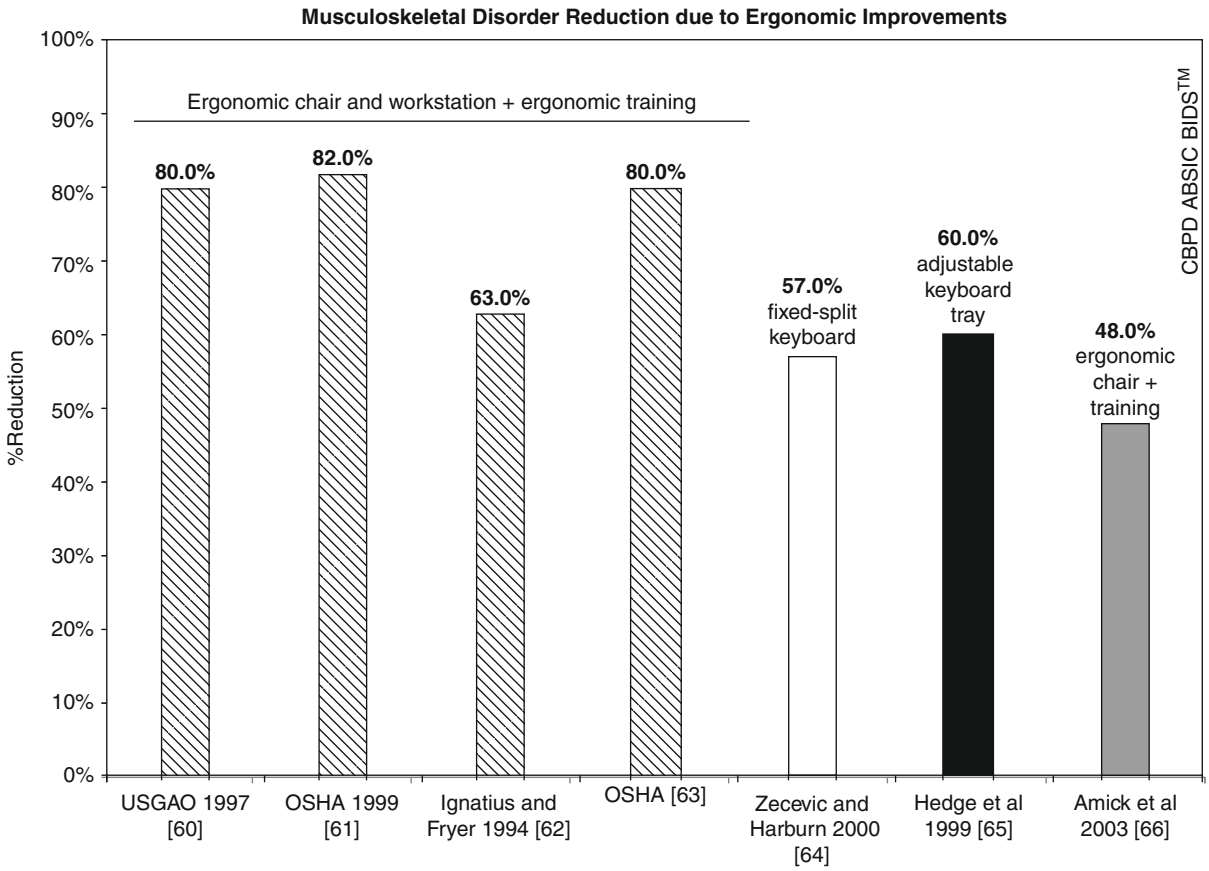

Sustainable and Healthy Built Environment. Figure 13
A number of international studies link Musculoskeletal disorder reduction due to ergonomic improvements

frequency of falls, the most frequent cause of injury and death in buildings.

Moving beyond the importance of land use and community design to increase physical activity and health, interior design also plays a major role. An emerging effort in the New York City public health department is the development of design guidelines for new and existing buildings to promote physical activity in an effort to address obesity and its related diseases (http://ddcftp.nyc.gov/adg/downloads/adguidelines.pdf). The *Active Design Guidelines* provides architects and urban designers with a manual of strategies for creating healthier buildings, streets, and urban spaces, based on the latest academic research and best practices in the field. With this addition, the role of interior architecture, engineering, and design on human health is extensive, and suggests a rich mix of critical design guidelines for improved human health over time.

Guidelines for Sustainable Material Selection for Health
Specify materials that do not irritate the skin with contact to avoid dermatological conditions
Specify materials that do not outgas toxins to avoid respiratory/allergy and asthma
Specify materials that do not degenerate into respirable fibers or emit radon to avoid cancers
Specify materials that are not fire hazards causing respiratory illness or death
Specify materials that do not foster mold or mildew leading to respiratory symptoms
Specify materials with low embodied energy and low transportation costs to reduce outdoor air pollution
Guidelines for Sustainable Interior Design and Furnishings for Health
Specify furniture ergonomics to reduce musculoskeletal disorders (MSD)
Design spatial layout/density to reduce transmission of contagious illnesses (flus, colds)
Design spatial layout to reduce falls and tripping
Design layout and specify surfaces to reduce infections transferred by contact with hands-free design
Design spatial layout for enhanced physical activity to reduce obesity and related health concerns

Sustainable Maintenance and Operations and Health

Needless to say, each of these design decisions will become obsolete if there is no commitment to long-term maintenance and operational standards. The building enclosure, HVAC, and lighting systems must be continuously commissioned to maintain the healthy conditions intended. Standing water, dampness, and mold must be prevented. Occupant densities must be managed, and furniture and finishes must continue to meet the health standards set.

In addition, human activities in buildings and the products they bring in must also be selected for health. Cleaning supplies, plants, fertilizers and herbicides, office and teaching supplies must all be environmentally benign. In addition, food and water quality should be monitored for health, including guidelines for vending machines. Waste must be effectively managed since it is a natural breeding ground for roaches, rodents, and other pests, *and* an opportunity for recycling or composting. While this research team has not evaluated the studies that may link poor maintenance and operation practices to health concerns, it is clear that any degradation in as-built performance will result in health consequences equally serious as those of poor design, engineering, and construction.

Calculating the Life Cycle Benefits of Sustainable Design and Health

The work of the faculty, researchers, and graduate students of the Center for Building Performance and Diagnostics at Carnegie Mellon and the Advanced Building Systems Integration Consortium extends beyond the pursuit of building case studies that link the quality of buildings to productivity, health, and life cycle sustainability. The development of the BIDS™ tool is based on the identification of economic, environmental, and human life cycle cost benefits related to buildings and communities in order to calculate the return on investment of high-performance building systems (see http://cbpd.arc.cmu.edu/ebids). Figure 14 helps to reveal the diverse building-related costs of doing business in US offices, including salaries and health benefits, technological and spatial churn, rent, energy and maintenance costs. This cost is

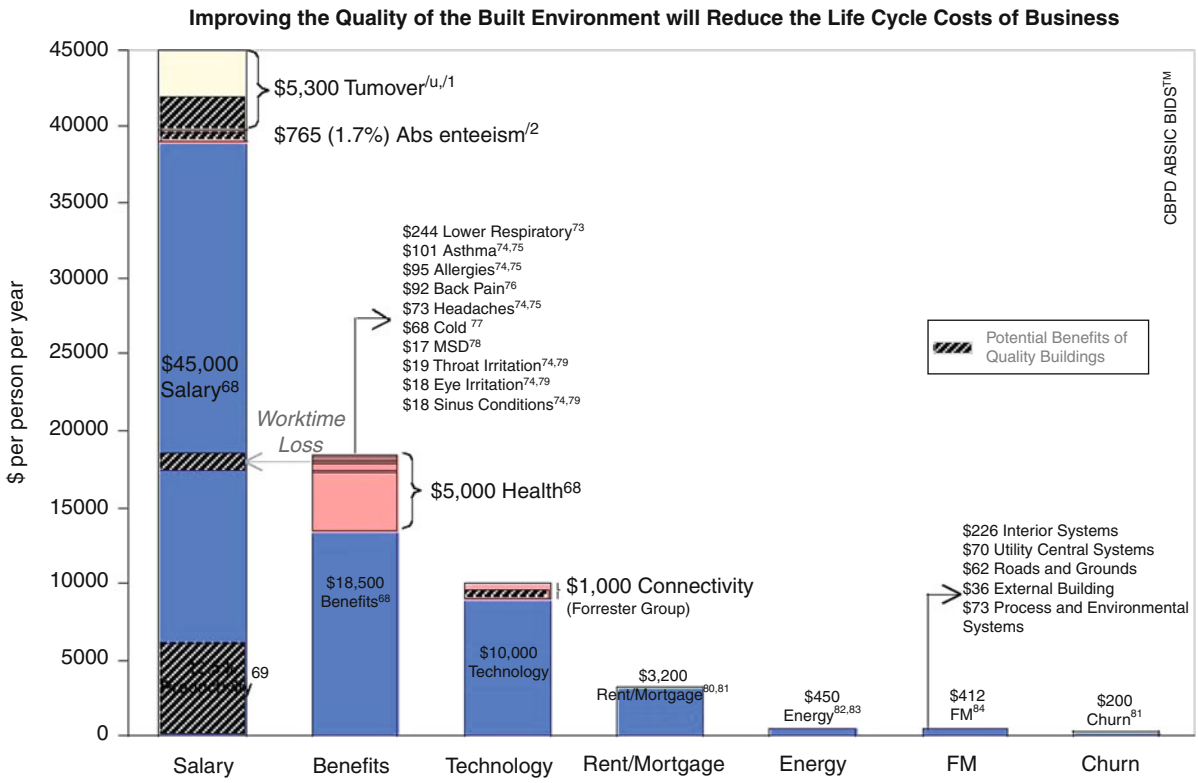

Sustainable and Healthy Built Environment. Figure 14

The true cost of business extends well beyond mortgage and energy costs, to include salaries, benefits, technological and spatial churn. Improving the quality of the built environment can be offset by sustained health benefits

normalized in dollars per person per year, rather than cost per square foot, since the employee represents both the greatest cost and the greatest asset to an organization.

The CBPD research identified that across independent nonprofit organizations, human resource research firms, and the US government, the average employer cost for health insurance was approximately $5,000 per employee per year in 2003 [8, 14, 17, 66, 70]. Within this $5,000 expense, the CBPD has been able to identify the cost of several specific health conditions and illnesses that can be linked to the quality of the indoor environment, including: colds, headaches, respiratory illnesses, musculoskeletal disorders, back pain (shown in Fig. 14), which account for roughly $750 of the $5,000 annually spent per employee, or 14% of all annual health insurance expenditures.

The direct costs for medical attention and pharmaceuticals would be multiplied further with the indirect costs of reduced speed and accuracy on task, and lost work time due to absenteeism. Beyond the organizational and human costs of worker absenteeism, however, Paul Kemp in Harvard Business Review introduced the term "presenteeism" to reflect the more typical and serious condition of individuals coming to work sick because they cannot afford to miss more work hours or important meetings [30]. While the measured costs of presenteeism are not well documented, there is a modest literature to help quantify the effective work time that is lost on the job due to headaches, colds, flus, and back pain (see Fig. 15), [42].

The importance of quantifying the financial, environmental, as well as human health and productivity

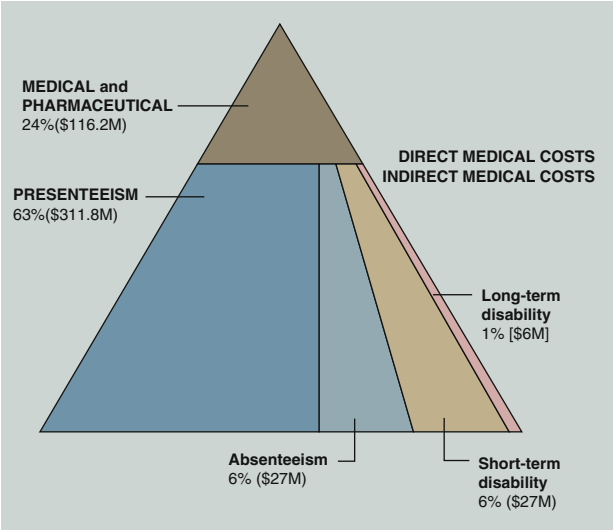

Source: Back One
Figures are based on annual data for 2000 workers' compensation accounted for less than 7% of indirect medical costs

Condition	Prevalence	Average productivity loss	Aggregate ammual loss
Migraine	12.0%	4.9%	$434,385
Arthritis	19.7	5.9	865,530
Chronic lower-back pain (without leg rain)	21.3	5.5	858,825
Allergies or sinus trouble	59.8	4.1	1,809,945
Asthma	6.8	5.2	259,740
GERD (acid reflux disease)	15.2	5.2	582,660
Dermatitis or other skin condition	16.1	5.2	610,740
Flu in the past two weeks	17.5	4.7	607,005
Depression	13.9	7.6	786,600

Source: Debra Lerner, William M. Rogers, and Mong Chang, & Tofts-New England Medical Center

Sustainable and Healthy Built Environment. Figure 15
While absenteeism is a cost of business, presenteeism – coming to work with colds, flus, and back pain for example – may have an even greater impact on the *bottom line*

impacts of design decisions is critical to the advancement of sustainable buildings and communities. In his 1998 book *Cannibals with Forks: The Triple Bottom Line of 21st Century Business*, John Elkington [18] introduces the importance of adding social and environmental impacts to economic performance in a triple net present value calculation. To accomplish this, it is critical to quantify the environmental costs of using energy and raw materials without caution, as well as the human health and performance costs of poor land use planning and building design and operation. For the past 10 years, the CMU Center for Building Performance and Diagnostics has been building the economic baselines for triple bottom line calculations for offices, schools, and hospitals (see Fig. 16).

The calculation of life cycle benefits of better design, engineering, and management of hospitals, for example, would include variables such as the average length of stay per illness, at 4.6 days per patient in US hospitals [53]; average cost of hospital stay, set at $1,217 per day in US hospitals [67]; patient reinfection rates, estimated at 2.16/10,000 patient days in US hospitals [51]; average cost of these nosocomial infections, estimated at $27,000 plus 12 day increase in hospital stay [50]; and the average cost of nurse turnover, at $13,800 per nurse per year [2, 37, 38]. The magnitude of these costs would clearly justify significant investment and reinvestment in the quality of hospitals to ensure long-term health and productivity.

Cars and laptops are purchased with far more comprehensive life cycle considerations than buildings, and yet the life span of cars and laptops are often 5 years or less. Since buildings are built for 30, 50, or even hundreds of years, it is imperative that the client and design community begin to address life cycle costs of materials, components, and integrated systems with triple bottom line decision making to ensure the sustainability of economic, environmental, and human health and productivity.

Health and the Built Environment: A Research Mandate

Sustainability is in truth all about health. Energy/material extraction and use and atmospheric, water, and land pollution are as significantly health-related issues as they

Example Measures of Cost-Benefit Performance for Different Building Types

Offices	Schools	Hospitals
O&M, Energy & Water Worker Health Attraction-Retention Individual productivity Absenteeism/ Presenteeism Organizational productivity Market share Customer speed to market waste cost/ benefits Litigation/ Insurance/ Tax SBS	O & M, Energy & Water Teacher health Student health Teacher turnover Student test scores college placement Absenteeism/ Plasenteeism Drop-out rates No child left behind waste cost/ benefits	O & M, Energy & Water Length of stay/ Recovery rates Nosocomial infections Patient falls Staff health Staff turnover Absenteeism/ Presenteeism Bed vacancies cost/ Bed profit Bed waste cost/ benefits Medication errors

Sustainable and Healthy Built Environment. Figure 16
Measuring "productivity and health" in different building types will require careful identification of critical outcomes and consistent data collection

are environmental conservation issues. Certainly the design and maintenance of building enclosures, HVAC, lighting, and interior systems are directly linked to our short- and long-term health, as the evidence collected in this chapter has begun to prove. Human health in relation to the built environment is one of the most critically needed research efforts, requiring both extensive experimental and field research efforts. Controlled laboratory experiments need to be carried out simultaneously with experiments in the field – to map chains of consequence, and identify possible building-related causes for respiratory, digestive, circadian, musculoskeletal, circulatory, and nervous system illnesses, as well as other health-related concerns. Yet in the USA, at least, there is remarkably little federal investment in defining and valuing healthy buildings and communities.

One cannot overstress the importance of defining key national and international research directions for addressing the impact of the built environment on health. Bringing together emerging knowledge about the importance of land use, building enclosure, HVAC, lighting, and interior design decisions, with the life cycle justifications to ensure their implementation, is critically needed. Sustainable buildings and communities have the potential to deliver the highest quality air, thermal control, light, ergonomics and acoustic quality, as well as regionally appropriate access to the natural environment, which are integral to human health.

In the face of rapid changes in the built environment, the importance of proving that sustainable design and engineering improves health, productivity, and quality of life has never been more important. Indeed, the advances most critically needed for environmental sustainability will constantly be slowed by least first-cost decision making, unless the health-related benefits of sustainable buildings and communities are definitively revealed.

Note

This chapter builds upon the paper "Sustainability and Health are Integral Goals for the Built Environment" by Loftness, Hartkopf, Lam, Snyder et al., published in Healthy Buildings 2006 Lisbon, Portugal June 4–8, 2006.

Bibliography

1. Amick B, Robertson M, DeRango K, Bazzani L, Moore A, Rooney T et al (2003) Effect of office ergonomics intervention on reducing musculoskeletal symptoms. Spine 28(24):2706–2711
2. AONE AO (2002) Acute care hospital survey of RN vacancies and turnover rates in 2000.American organization of nurse executives
3. Beauchemin KM, Hays P (1996) Sunny hospital rooms expedite recovery from severe and refractory depression. J Affect Disord 40:49–51
4. Benedetti F, Colombo C, Barbini B, Campori E, Smeraldi E (2001) Morning sunlight reduces length of hospitalization in bipolar depression. J Affect Disord 62:221–223
5. Bourbeau J, Brisson C, Allaire S (1997) Prevalence of the sick building syndrome symptoms in office workers before and six months and three years after being exposed to a building with an improved ventilation system. Occup Environ Med 54:49–53

6. Brundage J, McNeil R, Lednar W, Smith D, Miller R (1988) Building-associated risk of febrile acute respiratory diseases in army trainees. JAMA 259(14):2108–2112
7. Bullough JD, Rea M (2006) Of mice and women: light as a circadian stimulus in breast cancer research. Cancer Causes Control 17(4):375–383
8. Bureau of Labor Statistics, U. D (2002) National compensation survey: occupational wages in the United States 2001. Bureau of Labor Statistics, US Department of Labor
9. Çakir AE, Çakir G (1998) Light and health: influences of lighting on health and well-being of office and computer workers. Ergonomic, Berlin
10. Catlin T, Simoes E, Brownson R (2003) Environmental and policy factors associated with overweight among adults in Missouri. Am J Health Promot 17(4):249–258
11. CBPD (n.d.) eBIDS – energy building investment building support. Retrieved from center for building performance and diagnostics; School of Architecture; Carnegie Mellon University. http://cbpd.arc.cmu.edu/ebids/pages/home.aspx. Accessed 27 Dec 2011
12. Choi J (2005) Study of the relationship between indoor daylight environments and patient average length of stay (ALOS) in healthcare facilities. Unpublished master's thesis, Department of Architecture, Texas A&M University. College Station
13. Cornell University Medical College, C. U (1949) A brief history of the cornell medical index. Retrieved from Weill Cornell Medical Library. http://library.med.cornell.edu/About/cornellmedindex.html. Accessed 27 Dec 2011
14. Deloitte and Touche D (2003) Employer health care strategy survey 2003
15. Dockery D, Pope C (1994) Acute respiratory effects of particulate air pollution. Annu Rev Public Health 15:107–132
16. Drinka P, Krause P, Schilling M, Miller B, Shult P, Gravenstein S (1996) Report of an outbreak: nursing home architecture and influenza-A attack rates. J Am Geriatr Soc 44:910–913
17. Kaiser Family Foundation and Health Research and Educational Trust K. F (2003) Employer health benefits: 2003 annual survey.Retrieved from Kaiser Family Foundation and Health Research and Educational Trust. http://ehbs.kff.org/. Accessed 27 Dec 2011
18. Elkington J (1998) Cannibals with forks: the triple bottom line of 21st century business. New Society, Gabriola Island
19. Ewing R, Schmid T (2003) Relationship between urban sprawl and physical activity, obesity, and morbidity. Am J Health Promot 18(1):47–57
20. Ewing R, Schmid T, Killingsworth R, Zlot A, Raudenbush S (2003) Relationship between urban sprawl and physical activity, obesity, and morbidity. Am J Health Promot 18(1):47–57
21. Ewing R, Brownson RC, Berrigan AD (2006) Relationship between urban sprawl and weight of United States youth. Am J Prev Med 31(6):464–474
22. Fisk W, Rosenfeld A (1997) Estimates of improved productivity and health from better indoor environments. Indoor Air 7:158–172
23. Frank D, Andresen M, Schmid T (2004) Obesity relationships with community design, physical activity, and time spent in cars. Am J Prev Med 27(2):87–96
24. Frumkin H (2002) Urban sprawl and public health. Public Health Rep 117(3):201–217
25. Garrett M, Hooper M, Hooper B (1996) Low levels of formaldehyde in residential homes and a correlation with asthma and allergy in children. In: Proceedings of the 7th International conference of indoor air quality and climate (Indoor Air996), vol 1, pp 617–622, Nagoya, Japan
26. Giles-Corti B, Macintyre S (2003) Environmental and lifestyle factors associated with overweight and obesity in Perth, Australia. Am J Health Promot 18(1):93–102
27. Occupational Safety and Health Administration, U. D (1999) Preliminary economic analysis and initial regulatory flexibility analysis for the occupational safety and health administration's proposed ergonomics programs standard (Chapter III–V and Appendix III-A, Scenario No. OGI14). US Department of Labor
28. Occupational Safety and Health Administration, U. D (2006) Success with Ergonomics
29. Hedge A, Morimoto S, McCrobie D (1999) Effects of keyboard tray geometry on upper body posture and comfort. Ergonomics 42(10):1333–1349
30. Hemp P (2004) Presenteeism: at work – but out of it. Harv Bus Rev 82(10):49–58
31. Heschong Mahone Group (2003) Windows and offices: a study of office worker performance and the indoor environment. Program, funded by the California Energy Commission's Public Interest Energy Research (PIER) program
32. Ignatius EA (1994) The high cost of keyboard injuries. 12(3): 45–46
33. Jaakkola JJ (1995) Shared office space and the risk of the common cold. Eur J Epidemiol 11:213–216
34. Jaakkola J, Miettinen P (1995) Ventilation rates in office buildings and sick building syndrome. Occup Environ Health 94(2):709–714
35. Jaakkola J, Tuomaala P, Seppanen O (1994) Textile wall materials and sick building syndrome. Arch Environ Health 49(3):175–182
36. Jaakkola JJ, Oie L, Nafstad P, Botten G, Samuelson SO, Magnus P (1999) Interior surface materials in the home and the development of bronchial obstruction in young children in Oslo, Norway. Am J Public Health 89:188–192
37. Jones C (2004) The costs of nurse turnover. Part 1: an economic perspective. J Nurs Adm 34(12):362–370
38. Jones C (2005) The costs of nurse turnover. Part 2: application of the nursing turnover cost calculation methodology. J Nurs Adm 35(1):41–49
39. Kaczmarczyk J, Zeng Q, Melikov A, Fanger P (2002) The effect of a personalized ventilation system on perceived air quality and SBS symptoms. In: Proceedings of indoor air 2002, Monterey
40. Kelland P (1992) Sick building syndrome, working environments and hospital staff. Indoor Environ 1:335–340

41. Kellert SR (2005) Building for life: designing and understanding the human-nature connection. Island Press, Washington, DC
42. Lerner D, Chang H, Rogers WH, Benson C, Schein J, Allaire S (2009) A method for imputing the impact of health problems on at-work performance and productivity from available health data. J Occup Environ Med 51(5):515–524
43. Liu JZ, Tao YX, Hao L (1996) The relationship between sick building syndrome and indoor decoration. In: Proceedings of the 7th international conference on indoor air quality and climate (Indoor Air'96), vol 2, pp 321–324, Nagoya, Japan
44. Loftness VE (2005) Building Investment Decision Support (BIDS™) – cost-benefit tool to promote high performance components, flexible infrastructures & systems integration for sustainable commercial buildings and productive organizations. AIA pilot report on university research, pp 12–31, AIA, Washington, DC
45. Mendell MJ (1991) Risk factors for work-related symptoms in Northern California office workers.Unpublished doctoral dissertation, University of California, CA Dept. of Health Services, and NIOSH, indoor environment program Lawrence Berkeley Lab., CA. Sponsoring Org. USDOE, Washington, DC
46. Menzies D, Pasztor J, Nunes F, Leduc J, Chan C (1997) Effect of a new ventilation system on health and well-being of office workers. Arch Environ Health 52(5):360–367
47. Menzies DF, Yuan L, Fitzgerald J (2000) Hospital ventilation and risk for tuberculosis infection in Canadian Health Care Workers. Ann Intern Med 133(10):779–789
48. Menzies D, Popa J, Hanley J, Rand T, Milton D (2003) Effect of ultraviolet germicidal lights installed in office ventilation systems on workers' health and wellbeing: double-blind multiple crossover trial. Lancet 362:1785–1791
49. Myatt T, Johnston S, Zuo Z, Wand M, Kebadze T, Rudnick S et al (2004) Detection of airborne rhinovirus and its relation to outdoor air supply in office environments. Am J Respir Crit Care Med 169:1187
50. North Carolina Statewide Program for Infection Control and Epidemiology S (n.d.) SPICE (North Carolina statewide program for infection control and epidemiology). Retrieved from http://www.unc.edu/depts/spice/MRSA-VRE-Surveillance.ppt. Accessed 27 Dec 2011
51. Pittet D, Hugonnet S, Harbarth S, Mourouga P, Sauvan V, Touveneau S et al (2000) Effectiveness of a hospital-wide program to improve compliance with hand hygiene. Lancet 356:1307–1312
52. Preziosi P, Czernichow S (2004) Workplace air-conditioning and health services attendance among French middle-aged women: a prospective cohort study. Int J Epidemiol 33(5):1120–1123
53. Project H (n.d.) Agency for healthcare research and quality. Retrieved from http://hcupnet.ahrq.gov/HCUPnet.app/. Accessed 27 Dec 2011
54. Rheinbaben F, Schünemann S (2000) Transmission of viruses via contact in a household setting: experiments using bacteriophage φX174 as a model virus. J Hosp Infect 46:61–66
55. Saelens BE, Sallis JF, Black J, Chen D (2003) Neighborhood-based differences in physical activity: an environment scale evaluation. Am J Public Health 93(9):1552–1558
56. Seppänen OA, Fisk WJ, Mendell MJ (1999) Association of ventilation rates and CO_2 concentrations with health and other responses in commercial and institutional buildings. Indoor Air 9(4):226–252
57. Silverstein B, Vilkari-Juntura E, Kalat J (2000) Work-related musculoskeletal disorders of the neck, back, and upper extremity in Washington state, 1990–1988, technical report number 40-4a-2000. Safety and Health Assessment & Research for Prevention, Washington State Department of Labor and Industries, Washington, DC
58. Skole DL (n.d.) Land use, human health and climate change: convergence of planning problems for Michigan. Retrieved from http://www.landuse.msu.edu/. Accessed 27 Dec 2011
59. Smedje G, Norback D (2000) New ventilation systems at select schools in Sweden – effects on asthma and exposure. Arch Environ Health 35(1):18–25
60. Sordersten MG (2002) Vocal loading factors for preschool teachers at work studied with binaural DAT recordings. Department of Speech Music and Hearing, Royal Institute of Technology, Stockholm
61. Sundel J, Levin H, Nazaroff WW, Cain WS, Fisk WJ, Grimsrud DT et al (2011) Ventilation rates and health: multidisciplinary review of the scientific literature. Indoor Air 21(3):191–204
62. Sundell J (1996) What we know, and don't know, about sick building syndrome. ASHRAE J 38:51–57
63. Templer J (1995) The staircase: studies of hazards, falls, and safer design. MIT Press, Cambridge
64. Tenias JM, Ballester F, Rivera ML (1998) Association between hospital emergency visits for asthma and air pollution in Valencia, Spain. Occup Environ Med 55:541–547
65. Tham KH (2003) Temperature and ventilation effects on the work performance of office workers (study of a call center in the tropics). In: Proceedings of healthy buildings 2003, Singapore
66. Towers Perrin HR Services TP (2003) Towers Perrin 2004 health care cost survey
67. U.S. Census Bureau, U. C (2003) Statistical abstract of the United States: 2003, 123rd edn. U.S. Census Bureau, Washington, DC
68. Ulrich RS (1984) View through a window may influence recovery from surgery. Science 224(4647):420–421
69. United State General Accounting Office, U. S (1997) Worker protection: private sector ergonomics programs yield positive results.GAO/HEHS-97-163
70. US Chamber of Commerce Statistics and Research Center, U. C (2003) 2003 Employee benefits study
71. Walch JM, Rabin BS, Day R, Williams JN, Choi K, Kang JD (2005) The effect of sunlight on postoperative analgesic medication use: a prospective study of patients undergoing spinal surgery. Psychosom Med 67:156–163
72. Wargocki P (1998) Human perception, productivity, and symptoms related to indoor air quality. Doctoral thesis. Center for

Indoor Environment and Energy, Technical University of Denmark
73. Wieslander G, Norback D, Bjornsson E, Janson C, Boman G (1997) Asthma and the indoor environment: the significance of emission of formaldehyde and volatile organic compounds from newly painted surfaces. Int Arch Occup Environ Health 79(2):115–124
74. Wilkins AN-S (1989) Fluorescent lighting, headaches and eyestrain. Light Res Technol 21(1):300–307
75. Wordley J, Walters S, Ayres J (1997) Short term variations in hospital admissions and mortality and particulate air pollution. Occup Environ Med 54:108–116
76. Zecevic A, Miller DI, Harburn K (2000) An evaluation of the ergonomics of three computer keyboards. Ergonomics 43(1):55–72
77. Zuraimi MK (2007) The effect of ventilation strategies of child care centers on indoor air quality and respiratory health of children in Singapore. Indoor Air 17:317–327

Sustainable Built Environment, Introduction

Vivian Loftness
Center for Building Performance and Diagnostics, Carnegie Mellon University, Pittsburgh, PA, USA

Article Outline

Defining Sustainability in the Built Environment
How Does this Broad Definition Translate into an Encyclopedia for Sustainable Built Environments?
The Scale of the Sustainability Problem and the Opportunity
Building Enclosures for Sustainability
Building Mechanical Systems for Sustainability
Daylighting and Lighting for Sustainability
Interior Systems and Materials for Sustainability
Energy Generation and Sustainable Buildings
Water and the Built Environment
Landscape Sustainability
Land Use and Sustainability
Integrated Delivery Processes for Sustainability
Conclusion for Sustainable Built Environments: Policy Matters: the Market Will not Take Care of It
Bibliography

Defining Sustainability in the Built Environment

Sustainable design is a collective process whereby the built environment achieves unprecedented levels of ecological balance through new and retrofit construction, toward the long-term viability and humanization of architecture. Focusing on environmental context, sustainable design merges the natural, minimum resource conditioning solutions of the past (daylight, solar heat, and natural ventilation) with the innovative technologies of the present, into an integrated "intelligent" system that supports individual control with expert negotiation for resource consciousness. Sustainable design rediscovers the social, environmental, and technical values of pedestrian, mixed-use communities, fully using the existing infrastructures, including "main streets" and small town planning principles, and recapturing indoor-outdoor relationships. Sustainable design avoids the further thinning out of land use, and the dislocated placement of buildings and functions caused by single use zoning. Sustainable design introduces benign, nonpolluting materials and assemblies with lower embodied and operating energy requirements, and higher durability and recyclability. Finally, sustainable design offers architecture of long-term value through "forgiving" and modifiable building systems, through life cycle instead of least-cost investments, and through timeless delight and craftsmanship.

Seven Principles for the Design of a Sustainable Built Environment

A sustainable built environment depends on the following seven principles:

1. An integrative, human-ecological design approach
2. Changing approaches to land use and community fabric
3. The effective use of natural, local, and global resources to reduce infrastructure loading and maximize infrastructure use
4. The design of flexible systems, integrated for comprehensive performance delivery
5. The use of sustainable materials and assemblies
6. The design for life cycle instead of first cost

7. The promotion of infrastructures for water, energy, transportation, and connectivity to sustainable neighborhood amenities

How Does this Broad Definition Translate into an Encyclopedia for Sustainable Built Environments?

While it may not be immediately evident, a sustainable built environment spans dozens of professions, from urban planning to architecture to engineering to interior design to material science to social science and beyond. Sustainability is a revolution for educational pedagogy and content. Moreover, it requires a level of transdisciplinarity that challenges professional roles and creates new collaborative processes. To profile the breadth of science and engineering knowledge that is critical to advancing sustainable built environments, multiple encyclopedia sections would be needed, one each for: public policy and economics of a sustainable built environment, architecture, mechanical engineering, lighting engineering, material engineering, water engineering, energy engineering, as well as urban design, landscape and urban infrastructure engineering. By necessity a single section on sustainable built environments must offer a sampling of the science and technology expertise required. This section has gathered 15 leading authors from around the world to provide insight into the breadth of knowledge needed, leaving substantial content for expansion around each of the following critical knowledge bases:

1. The scale of the building sustainability problem and the opportunity
2. Building enclosures for sustainability
3. Building mechanical systems for sustainability
4. Daylighting and lighting for sustainability
5. Interior systems and materials for sustainability
6. Water and the built environment
7. Energy generation and sustainable buildings
8. Landscape sustainability
9. Land use and sustainability
10. Integrated delivery processes for sustainability

The following sections introduce these chapters within the broader knowledge base for substantially advancing our built environment from one that consumes and destroys to one that generates and revitalizes.

The Scale of the Sustainability Problem and the Opportunity

The building sector is the biggest "player" in the energy use equation and can have the greatest impact on maximizing energy supply and minimizing energy demand while providing measurable gains for productivity, health, and the environment. In the USA, commercial and residential buildings use 70% of total US electricity and are responsible for over 35% of total U.S. greenhouse gas emissions [17] (Fig. 1, CBPD).

Equally significantly, however, are other environmental statistics related to the built environment: material use, water use, waste production, health, productivity, manufacturing and transportation costs, and climate change. Buildings use 40% of the raw materials globally and 14% of the potable water in the USA. Building activity in the USA also contributes over 136 million tons of construction and demolition waste (2.8 lbs/person/day), and 35% of US greenhouse gas emissions [1].

These statistics underscore the impact of buildings and the built environment on global energy use and climate change, on water and material use. Through land use policies and actions, the built environment generated most of the increases in transportation energy use in the last decade. The impact is even more substantial when human and environmental health, land use and community, as well as indoor environmental quality are factored into sustainability. In short, the scale of the sustainability challenge in the built environment must include:

The role of the built environment on global energy use and climate change
The role of the built environment on health and indoor environmental quality
The role of the built environment on water use
The role of the built environment on material depletion
The role of the built environment on mobility and sustainable infrastructures

Two chapters have been included in this section to begin the dialogue. In the entry entitled "► Sustainable and Healthy Built Environment," Vivian Loftness has introduced a framework for ensuring that building and communities are designed to achieve the highest level of human health outcomes while generating the lowest

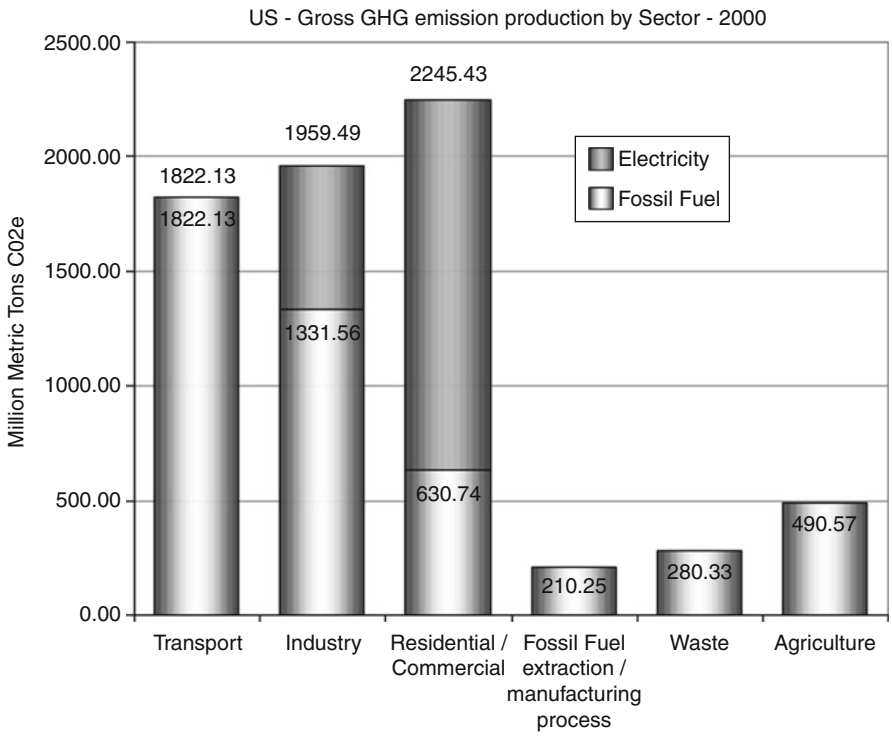

Created 2009 Carnegie Mellon Center for Building Performance and Diagnostics, based on US data:
www.epa.gov/climatechange/emissions
http://apps1.eere.energy.gov/states/electricity.cfm
December 27, 2011

Sustainable Built Environment, Introduction. Figure 1
The building sector is the greatest contributor to climate change, exceeding both industry and transportation

environmental footprint [25]. Across 30 years of teaching, researching, and even administration as Head of the School of Architecture at Carnegie Mellon, the author has been developing a data base of research linking building components and systems, land use approaches and infrastructures, to health, productivity, and other outcomes of critical importance to decision-makers, captured in this chapter on buildings and health.

In the entry "► Resource Repletion, Role of Buildings," Braungart, Hansen, and Mulhall introduce the massive responsibility of the design community to not only select materials and assemblies for human health and sustainability, but to use environmental life cycle analysis to design for the regeneration of material resources rather than the ongoing depletion. Michael Braungart is the founder of EPEA International Umweltforschung GmbH, and co-founder of McDonough Braungart Design Chemistry (MBDC). A professor of Process Engineering at the University of Applied Sciences in Suderburg (Fachhochschule Nordostniedersachsen), Dr. Braungart is the co-author of the seminal book *Cradle to Cradle* with William McDonough [2].

These discourses are critical to public policy and to public and private investment. They are also critical to setting the stage for standards, research, and innovation to ensure that the built environment is no longer the cause of depleting resources and reduced health, but a source of sustainable actions for regenerating those resources and for expanding access to a shared quality of life.

Building Enclosures for Sustainability

Entire civilizations have successfully prospered in highly diverse and challenging climates without depleting natural resources beyond the ability of those

resources to naturally regenerate. In large part, this success has been achieved through highly responsive, even intelligent building enclosures. Each climate commands a different strategy for natural conditioning, as so eloquently introduced in Don Watson's entry on "► Bioclimatic Design." Emeritus Chair and Professor of Yale University and former Dean of RPI's School of Architecture, Don Watson is a leading sustainability practitioner and author who received the 2008 US Green Building Council Leadership Award, and the American Institute of Architect's Presidential Citation, for his contributions to sustainability in the built environment. Most critically, Don Watson is a preeminent scholar on the subject of Climate and Architecture, and author of standards and textbooks used worldwide, beginning with his McGraw-Hill textbook *Climatic Building Design: Energy Efficient Building Principles and Practices* [3]. *Buildings and Climate Change* [4], the United Nations Environment Program (UNEP) captures the breadth of these regional design responses and reminds the design community of their continuing importance for sustainability (Fig. 2, www.unep.org/sbci/pdfs/SBCI-BCCSummary.pdf).

Dr. Volker Hartkopf and Senior Researcher, Azizan Aziz build on these climatic imperatives and introduce the richness of design responses in their entry on "► Facades and Enclosures, Building for Sustainability." Professor of Architecture and Director of the Center for Building Performance and Diagnostics at Carnegie Mellon University, Volker Hartkopf has led an industrial and government consortium dedicated to advanced building systems integration for performance through collaborative research, demonstration, and policy for over 30 years. In collaboration with a faculty team that includes Azizan Aziz, Dr. Hartkopf's leadership led to the construction of the Intelligent Workplace, a living laboratory for innovation in building materials, components, and integrated systems for improving human comfort and health, individual and organizational productivity, and environmental sustainability [5].

To fully explain the enclosure science and the engineering innovation that is critically needed to ensure the highest performance outcomes for each climate and building type, a wide range of chapters would be needed:

Energy conserving enclosures – insulation and airtightness
Energy conserving enclosures – shading
Radiant barriers and roof ventilation
Passive solar heating
Natural and stack ventilation
Time lag cooling
Night sky cooling
Earth tubes and radiant cooling
Evaporative and desiccant cooling
Earth sheltered design

While the ecological functions of green roofs are discussed in the Sustainable Landscape Design section, three critical topics are in this section. Professor Robert Hastings of the EcolePolytechniqueFederale de Lausanne has written the entry "► Passive Solar Heating in Built Environment." As managing director of Architecture, Energy & Environment GmbH in Switzerland, Robert Hastings is a leader in the IEA Task 28 – Solar Heating and Cooling. A prolific author with a long list of technical publications on energy efficiency, he co-edited *Solar Energy Houses: Strategies, Technologies and Examples* published by Earthscan [6]. This chapter gives a highly illustrated overview of the breadth of passive solar systems in use throughout Europe and North America, and sets the stage for the next chapter by Kathrin Klingenberg on the *PassivHaus*.

Kathrin Klingenberg is the Co-Founder and Director of the Ecological Construction Laboratory and the Passive House Institute in the USA (PHIUS). A long-term collaborator with the PassivHaus Institute in Europe, she co-authored the book *Homes for a Changing Climate: Passive Houses in the US* [7], to emphasize both the potential of passive house design to dramatically reduce or eliminate thermal conditioning in homes, and the importance of climate-specific approaches to balancing conservation and passive conditioning.

The final entry in this critical area of science and technology for building sustainability is "► Natural Ventilation in Built Environment" by Derek Clements-Croome and Tong Yang. Editor of Intelligent Buildings International Journal and Emeritus Professor of the University of Reading, Derek Clements-Croome is the CIB Coordinator for WO98 Intelligent and

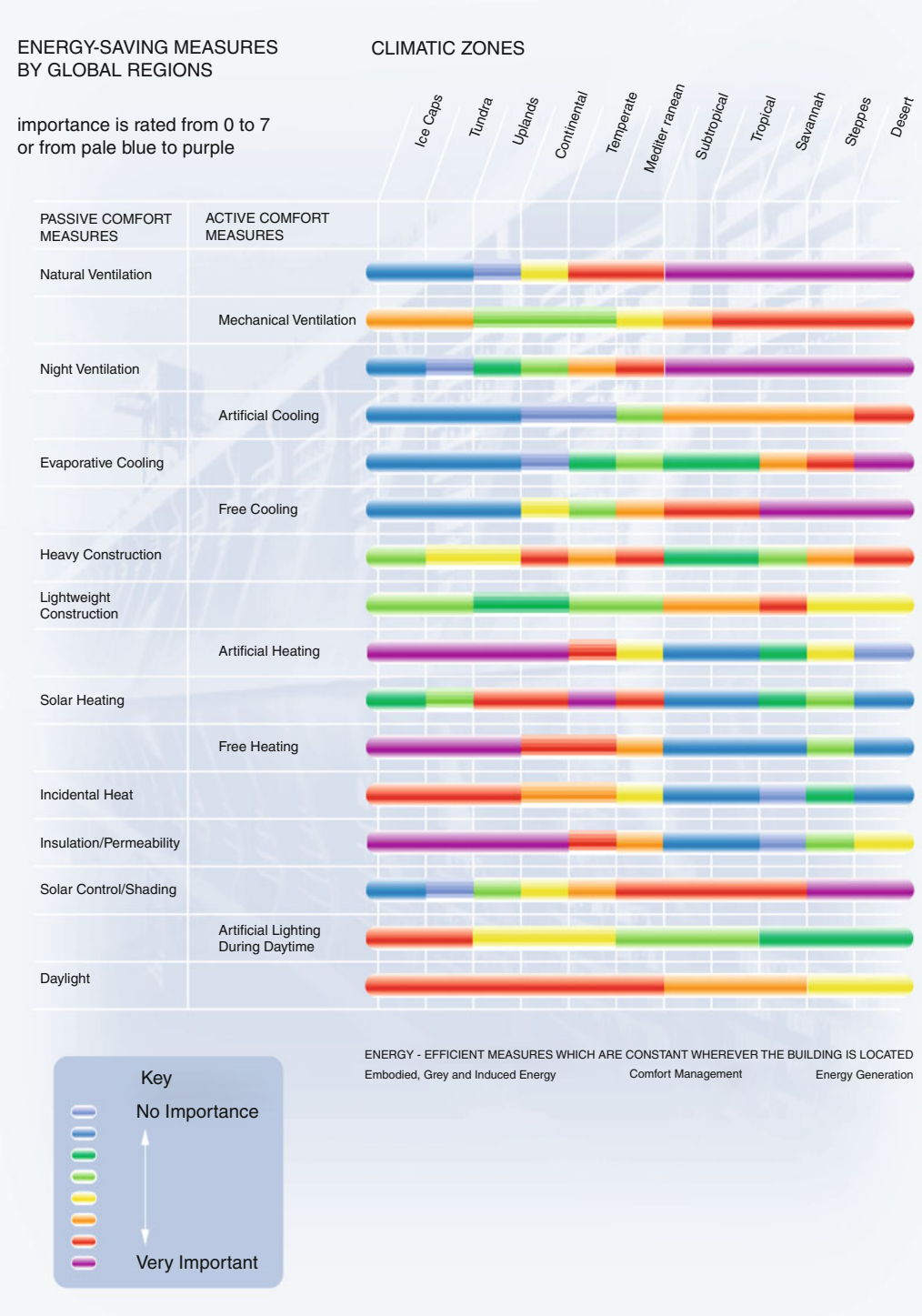

Table. 2.20
Energy saving measures by global regions.
Source: Jones 1998.

Sustainable Built Environment, Introduction. Figure 2
Climate-specific natural conditioning can displace significant energy loads ([4], *Buildings and Climate Change*)

Responsive Buildings and co-author of the book *Naturally Ventilated Buildings* published by E & F N Spon [8]. Co-authored with Dr. Tong Yang, research associate at Loughborough University, this chapter illustrates the potential for natural ventilation and natural cooling to ensure the highest level of thermal comfort and air quality at the lowest energy cost – through design and engineering innovation.

Building Mechanical Systems for Sustainability

"The best mechanical system is one that you never need to turn on." In a prophetic and visionary statement by one of the leading engineers worldwide, Kevin Hydes PE calls for dramatic changes in the role of the mechanical engineers in practice. Former President of Keen Engineering, later Stantec, Kevin Hydes is today President and CEO of the Integral Group – an interactive global network of design professionals collaborating to achieve deep green engineering. A founder of the Canadian GBC, Past Chair of the Board of Directors of the USGBC and the World Green Building Council, he co-authored the *Ecological Engineer* from Ecotone Publishing [9]. Kevin Hydes introduces the breadth and importance of sustainable mechanical engineering, and the changes in practice that will be critical to a sustainable future, in the entry "► Sustainable Heating Ventilation and Air Conditioning." A dedicated section on the science and engineering of building mechanical systems for sustainability could include:

Heating and cooling integrated systems for delivered energy efficiency
Water based thermal conditioning systems
Displacement ventilation and underfloor air systems
Heat recovery, energy recovery and desiccant ventilation
Commissioning for sustainability
Building automation systems and occupant controls for sustainability
Integrated solar power, hot water, heating and cooling systems

Daylighting and Lighting for Sustainability

Over 10% of all US energy is used for lighting buildings, much of this during the daytime when daylight is abundant. Effective daylighting can yield 30–60% reductions in annual lighting energy consumption. If complemented by cutting-edge electric lighting, the residual energy demands for lighting would be less than 10% of today's demand. For this reason, design and engineering for daylighting with integrated electric lighting sustainability would have the most significant impact on energy savings of any investments in the built environment. Helmut Koester's entry on "► Daylighting Controls, Performance and Global Impacts" addresses the most critical design and engineering innovations needed for ensuring daylight's massive contribution to energy and carbon savings. Architect and inventor of one of the most innovative daylight management technologies, Helmut Koester is the author of *Dynamic Daylighting Architecture: Basics, Systems, Projects* published by Birkhauser Press [10]. This chapter introduces glazing innovations with external and internal layers for effective daylighting and view, as well as shading, glare, and brightness contrast control, with a companion chapter on Daylight, Indoor Illumination and Human Behavior in the Solar Radiation section of the Encyclopedia. Alongside daylight innovations, low-energy high-performance electric lighting advances are also critical for sustainability, suggesting a number of other important topics for future articles:

Electric lighting innovations for sustainability
Electric lighting control innovations for sustainability
Regional design/engineering innovations for balancing view, light, heat, and air

Interior Systems and Materials for Sustainability

While enclosure, mechanical, and lighting systems dominate the energy conservation and carbon footprint discussions, interior systems play a significant role in energy use over time and become a dominant driver for indoor environment quality, material conservation, and human health and productivity outcomes. Innovation is occurring in number of important arenas, with one included in this section:

Interior systems for indoor environmental quality
Interior systems and systems integration for energy conservation
Interior systems for material/resource conservation

Interiors for organizational and individual productivity
Evidence based design for improving IEQ and health
Biophilia

In the entry "► Indoor Environmental Quality and Health Improvement, Evidence-Based Design for," Dr. Charlene Bayer provides a critical introduction to the breadth of challenges and opportunities for the design of interior systems for sustainability. As Leader of the Environmental Exposures and Analysis Group at the Georgia Tech Research Institute (GTRI) and Director of Georgia Institute of Technology's Indoor Environment Research Program, Dr. Bayer brings over 30 years of experience to the discussion of indoor environmental quality. She introduces the power of a field research–based approach to facilities design "that treats the building and its occupants as a system and gives importance to design features that impact health, well-being, mood and stress, safety, operational efficiency, and economics." Evidence Based Design (EBD) is one of the most important recent contributions to ensuring sustainable built environments – shifting the focus from designed performance to the installed performance of integrated building systems, and re-centering goals to focus on the productivity and health of individuals and organizations.

Energy Generation and Sustainable Buildings

In 2002 [11], architect Edward Mazria issued the 2030 challenge, asking the global architecture and building community to adopt 60% energy savings goals by 2010, 70% by 2015, advancing each 5 years by 10% to achieve carbon neutrality by 2030 for all new buildings and major renovations (http://www.architecture2030.org/). The 2030 challenge demonstrated that these targets can be accomplished by "implementing innovative sustainable design strategies, generating on-site renewable power, and purchasing renewable energy (up to a 20% maximum)." While green house gases do not define the entire story of sustainable built environments, they present the largest challenge for designers today because of the multiplied impacts of declining resource availability, increasing outdoor air and water pollution, as well as global warming with all of its serious ramifications for survivability. Demand reduction is the critical first step, with huge potential for dramatic reduction. Sustainable alternatives to energy supply, fully integrated with community and building design, is the critical next step. Alternative energy supply choices and their ramification for building design, engineering and land use planning are introduced in this and other sections of the Encyclopedia:

Managing electricity – plug and process loads, parasitic loads
Combined heat and power (CHP) & building integrated CHP
Site and building integrated PV
Site and building integrated solar thermal
Geothermal, aquathermal, ground coupled HVAC
Bio-fuels and sustainable buildings

This section includes two chapters on thermal and power energy systems with major implications for the building industry. The authors have the most cutting-edge knowledge of the breadth and depth of the engineering challenges and opportunities because they have recent dissertations on the topics. Nina Baird, an expert on open and closed loop aqua-thermal district energy systems, gives a rigorous overview of the breadth of ground coupled heating and cooling systems that can serve individual buildings, campuses, or entire communities, in the entry "► Geothermal Conditioning: Critical Sources for Sustainability." Fred Betz, senior sustainable engineer at Affiliated Engineers, gives a rigorous overview of innovations in renewable fuels for power and heat generation in the chapter *Bio-fuels and Sustainable Buildings*.

Combined heat and power, photovoltaics, and solar thermal have been included in the other sections of this encyclopedia. In pursuing these innovative energy sources, it is critical for the design community to aggressively pursue both "exergy" and energy cascades. In their PLEA 2004 [12] paper, "Critical analysis of exergy efficiency definitions applicable to buildings and building services," Boelman and Sakulpipatsin discuss the importance of matching each type of energy (electricity, low and high temperature thermal), and their energy potential, to their thermodynamically optimal uses in buildings and building services. Exergy begs the question 'if the Earth provides moderate temperature cooling and the Sun provides moderate temperature heating, can we design thermal conditioning

systems that use these sources directly with maximum effect, leaving electricity for more challenging tasks?'

At the same time, a sustainable built environment would use the building as a critical element in energy cascades, using the "waste" heat from one process for the next, and using the building mass as a "battery" for thermal energy. In conceiving the "Building as Power Plant," Volker Hartkopf suggests that each new building should be a net energy exporter: first combining energy efficiency with passive conditioning in an "ascending" strategy of daylighting, natural ventilation, passive cooling, and passive solar heating; then integrating "cascading" energy uses, with the waste heat from power generation cascading to cooling energy, waste heat from cooling cascading to heating energy, and waste heat from heating cascading to hot water through the integrated design of the building, including the management of peak loads and time shifts for each energy source [13] (Fig. 3).

Water and the Built Environment

While energy is the central focus of most sustainability chapters, due to the rapid depletion of nonrenewable sources and the serious global warming and green house gases produced, water is an equally serious challenge. Global demands for freshwater are depleting freshwater availability at a rate that is alarming. While 70% of global freshwater demand is for agriculture, the 20% freshwater used in the building sector is growing at a rapid rate – with the highest level of inefficiency. As with energy, the greatest opportunities for conservation at the lowest first cost and the highest payback reside in the building sector. UNEP illustrates this with charts that differentiate extraction and consumption per end use sector (see Fig. 4), highlighting the major opportunities for the building sector to dramatically reduce its extraction demands through efficiency, gray water, and black water innovations [14].

Sustainable Built Environments include a range of innovations for water conservation and cascading water use, including:

Water conservation in buildings
Rainwater capture and use
Grey water systems
Black water systems
Closing the loop – regenerative fresh water systems

The concept of "cascading" water use parallels the concept of exergy – ensuring the use of potable or

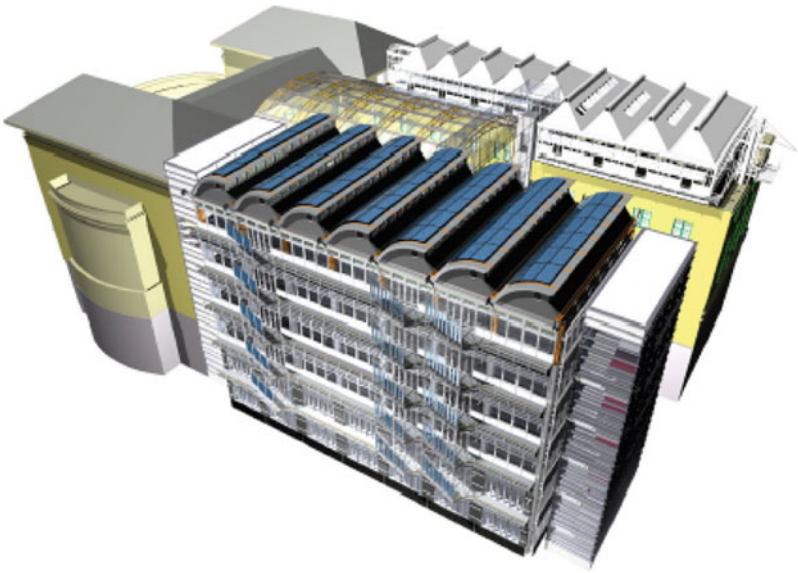

Sustainable Built Environment, Introduction. Figure 3
Carnegie Mellon's vision for a "Building as Power Plant" uses energy cascades to meet power, cooling, heating, and hot water demands, matching loads to optimize the 'exergy' of each source, with excess energy for export to the campus grid

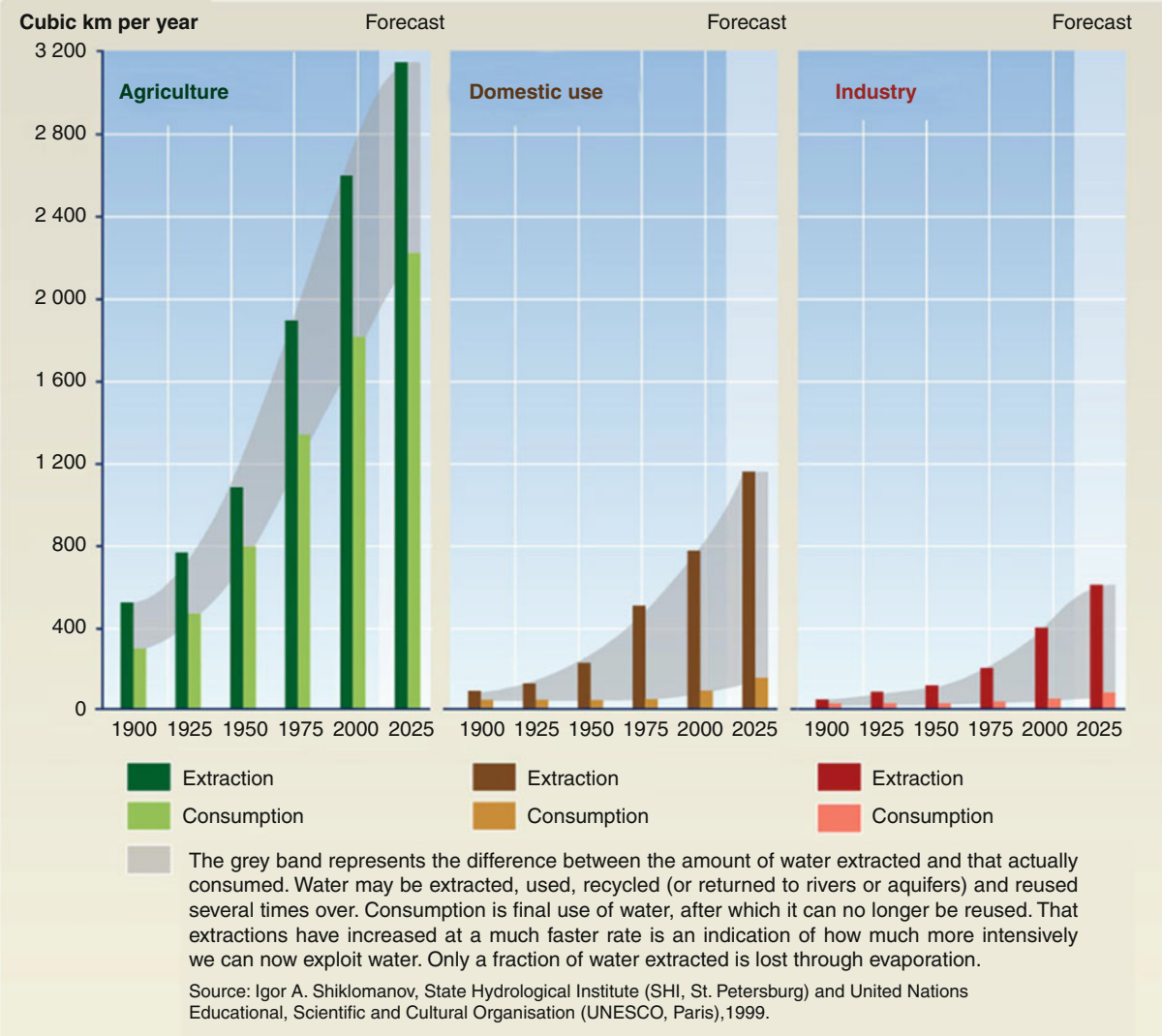

Sustainable Built Environment, Introduction. Figure 4
While agriculture represents the largest consumer of freshwater worldwide, the greatest waste in freshwater use is the built environment, shown in the difference between extraction and consumption

freshwater for its highest and best use, then using the gray "waste" water for its highest and best use, and finally the reuse of black water through innovations in sustainable filtration, with the intention of designing closed loop systems for returning freshwater to the aquifer. In addition, a sustainable built environment must ensure that deluge and drought, hurricanes and floods do not devastate buildings and communities, or the infrastructures that ensure habitability.

Landscape Sustainability

Explored in the section on Sustainable Landscape Design, the design of landscapes for sustainable sites, neighborhoods, and entire regions has the potential to address a broad range of environmental challenges: water shortages, flooding, brownfields, carbon sequestration, habitats, edible landscapes, and even human health. Through collaborative design, the building

community should fully engage the science and technology of:

Watershed planning
Landscape design for brownfields
Landscape design to reduce climate change
Landscape design for net zero water and aquifer recharge
Landscape design for shrinking land
Building and landscape design for biotopes and habitats
Landscape design and quality of life
Cool roofs and cool communities

Many of the tools described in the final chapters of this section embrace the importance of water and landscape sustainability. Ray Cole's entry on "► Rating Systems for Sustainability" highlights how sustainable sites and water are as important as energy, materials, and indoor environmental quality to the sustainable design community. Bill Reed's entry on "► Regenerative Development and Design" erases the lines completely between energy, materials, water, land, and the assurance of a sustainable quality of life.

Land Use and Sustainability

At this point, an encyclopedia on Sustainable Built Environments would move outside the boundaries of the building or even the campus to embrace the growing challenges of land use. There are two divergent challenges that this section would address: rapid urbanization in the developing world and ongoing sprawl in industrialized nations. Both of these rapid changes in land use generate massive and long-term consequences for: energy, water, material resources, infrastructures, abandonment, transportation, agriculture, industry, and a sustainable, shared quality of life. Further explored in the encyclopedia section on Environmental Geology and on Mass Transit, land use practices for sustainability include:

Sustainable urbanism
Urban growth boundaries and transit-oriented development
Town planning for sustainability
Regional planning for sustainability
Coastal planning for sustainability
Civil infrastructures for sustainability
Future sustainable cities
Ecological footprints

All sustainable building designers today reach a point where they realize that even net zero energy and net zero water buildings can be overwhelmed by environmental demands of poor siting, community design, and infrastructures. In the USA, there is an emerging effort to ensure that sustainability includes a number of the most egregious environmental demands. The Center for Neighborhood Technology, for example, is developing a Transit Energy Index (TEI) for buildings, in an effort to ensure that the distance traveled, the type of vehicles and the environmental consequences of that travel are included in the sustainability assessment (http://www.cnt.org). The 2007 book *Sustainable Urbanism: Urban Design with Nature* by Douglas Farr provides a comprehensive introduction to the integration of density and mix, land use and transportation, design for universal accessibility, for human health and for a long-term partnership with nature [15].

Integrated Delivery Processes for Sustainability

The final four chapters in this section define the cutting-edge processes that ensure integrated design and engineering innovation for sustainability. Raymond Cole, Professor at the University of British Columbia and Head of the Environmental Research Group (ERG), provides a worldwide overview of "► Rating Systems for Sustainability." One of the leading experts on sustainable building practices, Dr. Cole has helped to forge the evolution in standards to ensure broad environmental responsibilities for designers – from energy to water to materials to indoor environmental quality to land use – a breadth that has been critical to defining sustainability science and technology for the built environment.

Dr. Khee Poh Lam, Professor of Architecture at Carnegie Mellon University and former Dean at the National University of Singapore, has written the critical entry on "► Sustainability Performance Simulation Tools for Building Design." His leadership in the development and application of energy, lighting, and computational fluid dynamics tools, as well as his development of design compliance tools for sustainable practices, contributes to this expert overview of computational tools and their contributions to ensuring measured environmental outcomes. Laura Lesniewski,

a principal in the leading sustainability firm of BNIM, has written the entry on "► Sustainable Design and Construction, Integrated Delivery Processes and Building Information Modeling." An architect with a significant portfolio of LEED, net-zero and Living Building projects, Laura brings critical insight to the changes needed in professional practice for sustainability, and the changes that range from early multidisciplinary collaboration to the most advanced Building Information Modeling, to embrace the science and technology of sustainability.

A comprehensive description of integrated building delivery processes for Sustainable Built Environments should also include:

Post occupancy evaluation (POE) for quantitative and qualitative feedback
Sustainable specifications and life cycle assessment (LCA)
Cradle to cradle™ design

While textbooks are sorely lacking in POE or LCA for the sustainable design community, the manifesto *Cradle to Cradle*™ by William McDonough and Michael Braungart is unquestionably one of the most critical references for our time [2].

Equally important is the emerging understanding of living buildings, restorative buildings, and regenerative buildings. The deep green efforts of the Living Future Institute to create a visionary path to a restorative future through the Living Building Challenge are critical aspirations for transformational changes in sustainability (https://ilbi.org/lbc). Bill Reed takes these goals and the integrated design processes critical to their success, even further in the final entry of this section – "► Regenerative Development and Design." A principal in three firms, the Integrative Design Collaborative, Regenesis, Inc., and Delving Deeper, Bill Reed was a founding board member of the USGBC and co-author with the Seven Group of *The Integrative Design Guide to Green Building* published in 2009 [16] by John Wiley. In collaboration with Pamela Mang, Bill Reed has written the culminating chapter for this section, creating a framework for an integrative, whole-systems design process to ensure that "projects and processes achieve the highest level of performance across every sustainability metric – and beyond, into regenerating the health of our ecological systems."

Conclusion for Sustainable Built Environments: Policy Matters: the Market Will not Take Care of It

Energy is cheap, especially if the externalities of climate change, pollution, or health are not considered. In the USA, governments, building owners, and consumers do not see energy as a large enough component of their disposable income to even evaluate the return on investing in energy efficiency, much less water efficiency or other sustainability goals. Deregulation has reduced the efforts of major utilities to pursue demand side management and weatherization. At the same time, power unreliability has led residential and commercial building owners to purchase inefficient and polluting standby power rather than consider the significant opportunity to invest in energy efficiency and renewable energy sources. Policy is critical because the market will not act quickly or forcefully. The contributions of buildings to the discharge of four primary pollutants – NO_X, SO_X, CO_2, and particulates – should be fully recognized in the cost of energy, to catalyze owners and occupants to pursue more environmentally responsible buildings and building use patterns.

Federal and state energy efficiency standards, as well as tax incentives, are critical to finally balancing investment between energy supply and demand. Given the major energy excesses in the built environment, reducing demand must be seen as a major energy *source*. The McKinsey report "Unlocking Energy Efficiency in the US Economy" was a revelation for the energy world, finding that carbon reductions through building energy efficiency are the lowest cost per ton with the highest return on investment of any GHG action (Fig. 5, [18]). Investments in "mining" this new energy supply will yield greater economic benefit for a broader array of industries; provide significant gains in reducing environmental pollution; and ensure a longevity to energy "supply" that few other sources can ensure.

Even though the return on investment for energy efficiency dramatically exceeds that of creating new sources, the US dollars in energy supply research and development (R&D) are six times the R&D dollars for reducing energy demand [19]. Yet the modest national investments by the US DOE (of around $3 million per program) in R&D for energy-efficient ballasts, low-E windows, and refrigerator standards reaped national benefits of $9,000, $7,000, and $23,000 per dollar

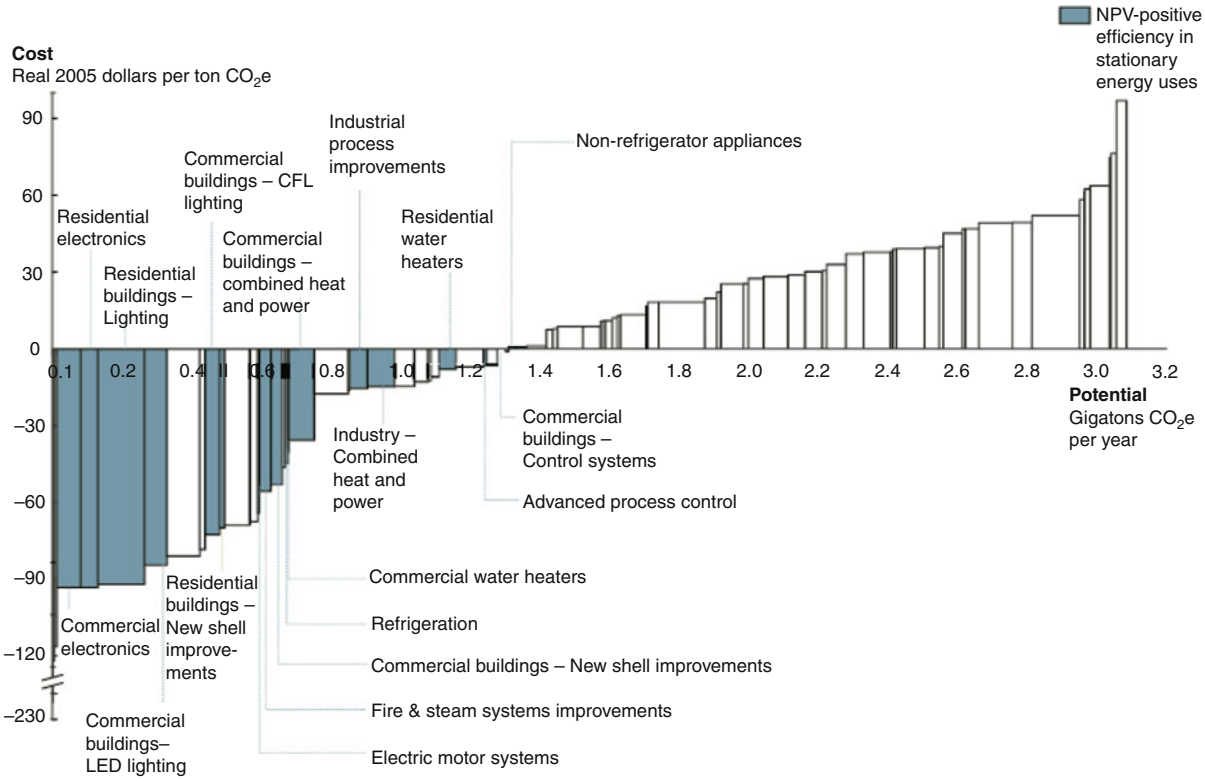

Source: McKinsey analysis

Sustainable Built Environment, Introduction. Figure 5
Carbon reductions through building energy efficiency are the lowest cost per ton with the highest return on investment (http://www.mckinsey.com)

invested [20]. In addition to the obvious benefits of reduced energy demand, dramatically accelerated national investments and policies focused on building energy efficiency will contribute to the following:

Reduced unnecessary annual energy consumption
Reduced emissions and climate change impacts
Increased peak power capacitance and reliability (energy security)
Improved health, human safety, and security
Improved productivity
Improved quality of life
Increased exports of products and services
Setting a proven example for emerging nations with growing demands

This last point is especially important – setting a proven example in mitigating climate change for emerging economies that will depend on expanding energy resources. Greg Kats argues in a study of the costs and financial benefits of green buildings, "The vast majority of the world's climate change scientists have concluded that anthropogenic emissions – principally from burning fossil fuels – are the root cause of global warming. The USA is responsible for about 22% of global greenhouse gas emissions. Of this 22%, the US building sector is responsible for about 35% of US CO_2 emissions, the dominant global warming gas" [21]. The critical actions needed include massively improving building energy efficiency, building land use, and infrastructure efficiency – in the very near term. This can only be achieved by immediate changes in policy, investment, and research at the national, regional, and industrial level.

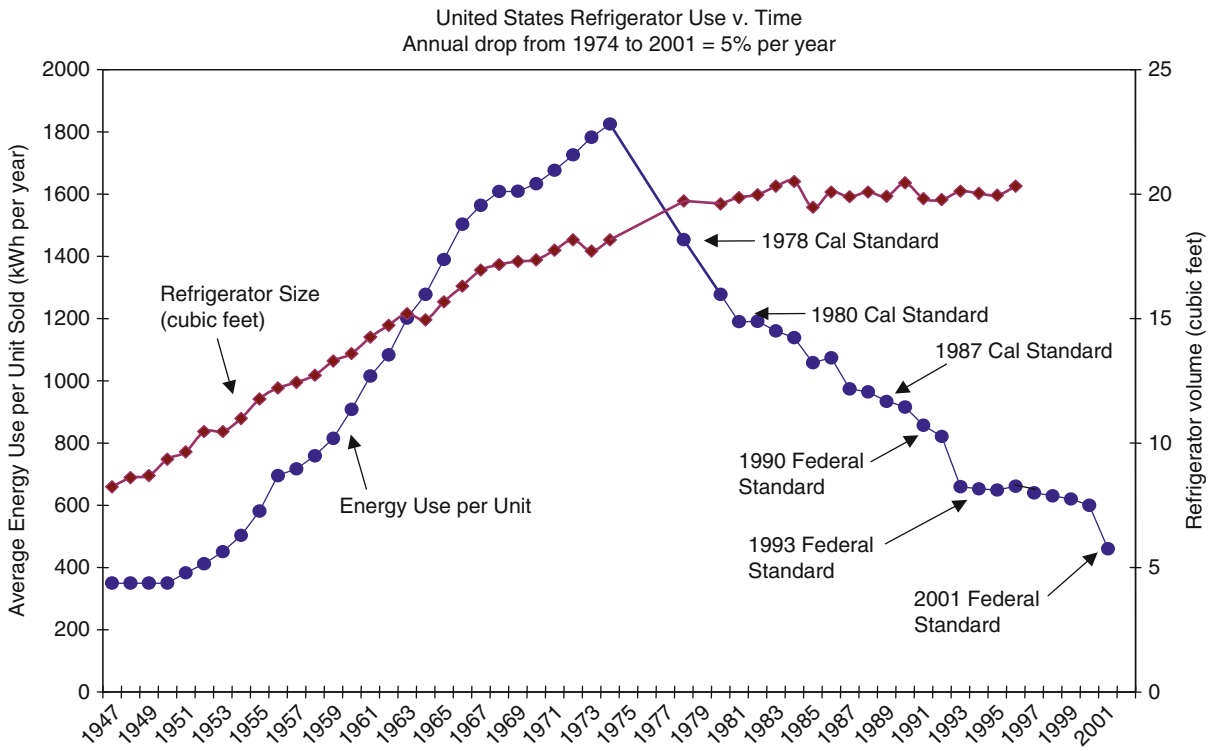

Sustainable Built Environment, Introduction. Figure 6
Driven by California, national standards led to significant reductions in energy use from key buildings technologies – a major "source" of new energy for the USA

Energy efficiency in buildings represents a major untapped resource for energy supply. The development of national standards and the removal of market barriers can lead to significant reductions in energy use from key buildings technologies through their natural replacement cycle ([22], Fig. 6). A 1997 study undertaken by all five national laboratories determined that building energy efficiency could achieve 230MTC of the 400MTC savings needed by 2010 to meet US targets under the Kyoto Protocol [23]. With the addition of innovative combined cooling, heat and power technologies, a further 170MTC could be achieved, fully meeting 2010 goals through the building sector alone. Over the longer term, expanded building R&D budgets, industry- and university-based research, and continuing national policies that focus on building energy efficiency could trigger dramatic improvements in energy and environmental quality in the built environment. Moreover, these investments would ensure ancillary benefits including the revitalization of existing buildings and infrastructures, measurable gains in health and productivity, and a positive influence on energy-efficient growth in the built environment of developing nations.

Investing in building energy efficiency as a new energy "supply" would dramatically surpass production from new oil supplies and power plant investments, as well as offer sustained "sources" of energy that do not generate greenhouse gases. Yet the combined budgets for building research across US government agencies is less than 2% of federally funded R&D, in no way commensurate with the importance of the built environment to our economy and quality of life [24]. Given this paucity of research support, there are only a handful of university Ph.D. programs in the USA focused on energy efficiency and environmental quality in the built environment, an inadequacy that leaves the US industry lagging in its ability to innovate for building energy efficiency.

Given that buildings in the USA account for 70% of electricity consumption, 40% of energy use, 38% of all carbon dioxide (CO2) emissions, 40% of raw materials

use, 30% of waste output (136 million tons annually), and 14% of potable water consumption, and are significantly linked to health and competitiveness, it is critical for the USA to invest in policy, research, and innovation toward more sustainable built environments.

At the same time, all nations need to enact collaborative efforts to ensure that decision-making in the built environment contributes to a shared future of sustainable energy, air, water, land, and material resources, while ensuring a sustainable quality of life for all nations.

Bibliography

1. USGBC (2007) A national green building research agenda, November 2007. http://www.usgbc.org/ShowFile.aspx?DocumentID=3402. Accessed 27 Dec 2011
2. McDonough W, Braungart M (2002) Cradle to cradle: remaking the way we make things. North Point, New York. ISBN 10: 0865475873
3. Watson D, Labs K (1993) Climatic building design: energy-efficient building principles and practices. McGraw Hill, New York. ISBN 10: 007068488X
4. UNEP (2007) Buildings and climate change. United Nations environment program. www.unep.org/sbci/pdfs/SBCI-BCCSummary.pdf
5. Resnick D, Scott D (2004) Innovative university. CMU Press, Pittsburgh. ISBN 10: 0887483763
6. Hestnes AG, Hastings R, Saxhof B (2003) Solar energy houses: strategies technologies examples. Earthscan, London. ISBN 10: 1902916433
7. Klingenberg K, Kernagis M, James M (2009) Homes for a changing climate passive houses in the U.S. Aspen, Colorado
8. Derek C-C (1998) Naturally ventilated buildings: building for the senses, the economy and society. Spon Press, New York. ISBN 10: 0419215204
9. Macauly D, McLennan JF (2005) The ecological engineer. Ecotone, Kansas. ISBN 10: 0974903345
10. Koster H (2004) Dynamic daylighting architecture. Springer verlag, Vienna, Austria. ISBN: 9783764367305
11. Mazria E (2002-present) The 2030 challenge. http://www.architecture2030.org/
12. Boelman EC, Sakulpipatsin P (2004) Critical analysis of exergy efficiency definitions applicable to buildings and building services. In: Plea 2004 – the 21st conference on passive and low energy architecture, Eindhoven, 19–22 Sept 2004
13. Hartkopf V et al (2002) Building as power plant. The Austin papers, Building Green. ISBN 1-929884-10-9, Austin TX
14. UNEP (2009) water demands. Drawn from Igor A. Shiklomanow, state hydrological institute (SHI, St. Petersburg) and United Nations Educational, Scientific and Cultural Organisation, UNESCO, Paris. http://www.grida.no/publications/vg/water2/page/3229.aspx
15. Farr D (2007) Sustainable urbanism: urban design with nature. Wiley, Hoboken. ISBN 10: 047177751X
16. 7 group and Reed B (2009) The integrative design guide to green building: redefining the practice of sustainability (sustainable design). Wiley, Hoboken. ISBN-10: 0470181109
17. U.S. DOE, Energy Information Administration (2010) EIA, annual energy review. http://38.96.246.204/totalenergy/data/annual/index.cfm
18. McKinsey Report (2009) Unlocking energy efficiency in the US economy. http://www.mckinsey.com/en/Client_Service/Electric_Power_and_Natural_Gas/Latest_thinking/Unlocking_energy_efficiency_in_the_US_economy.aspx
19. Rosenfeld AH (1999) The art of energy efficiency: protecting the environment with better technology. Ann Rev Energy Environ 24:33–82
20. Rosenfeld AH, McAuliffe P, Wilson J (2004) Energy efficiency and climate change. In: Braungart M (ed) Encyclopedia on energy. Cutler Cleveland, Academic Press, Elsevier Science
21. Kats G (2009) Greening our built world: costs, benefits, and strategies. Island Press, Washington, DC. ISBN 10: 159726668X
22. Rosenfeld AH (2003) Improving energy efficiency 2–3% year to save money and avoid global warming. In: Sessler symposium, LBNL, 15 March 2003, Berkeley, CA
23. Interlaboratory Working Group (1997). Scenarios of US carbon reductions: potential impacts of energy technologies by 2010 and beyond. ORNL CON 444. www.ornl.gov/ORNL/Energy_Eff/labweb.htm
24. Loftness V (2000) E-vision: energy, productivity and the critical role of the built environment. In: RAND/DOE E-vision workshop proceedings, Arlington, 11–13 Oct 2000
25. Loftness V, Harktopf V (2002) Building investment decision support (BIDS): cost-benefit tool to promote high performance components, flexible infrastructures and systems integration for sustainable commercial buildings and productive organizations. The Austin Papers, Building Green. ISBN 1-929884-10-9

Sustainable Design and Construction, Integrated Delivery Processes and Building Information Modeling

Laura Lesniewski[1], Bob Berkebile[2]
[1]AIA, BNIM – Berkebile Nelson Immenschuh McDowell Architects, Kansas City, MO, USA
[2]FAIA, BNIM – Berkebile Nelson Immenschuh McDowell Architects, Kansas City, MO, USA

Article Outline

Glossary
Definition of the Subject
Introduction: Sustainability Through Reintegration

Sustainable Design and Construction
Integrated Delivery Processes
Building Information Modeling to Support Integrated Project Delivery
Future Directions
Bibliography

Glossary

BIM model A three-dimensional digital simulation, typically of a building or other built form, which is both parametric and database driven.

Building information modeling (BIM) The methodology or process of creating a parametric database-driven digital model of a building or built environment. Understood within the practice of building information modeling, especially on large complex projects, is the collaboration required of various team members during all design and construction phases to add, delete, modify, enhance, or otherwise update the BIM model for the benefit of the overall project and team.

Integrated project delivery (IPD) A project delivery approach that integrates people, systems, business structures, and practices into a process that collaboratively harnesses the talents and insights of all participants to optimize project results, increase value to the owner, reduce waste, and maximize efficiency through all phases of design, fabrication, and construction [1].

Lean thinking A way to do more and more with less and less – less human effort, less equipment, less time, and less space – while coming closer and closer to providing customers with exactly what they want (value) [2].

Sustainable design An approach to design whereby the needs of the present are met without compromising the ability of future generations to meet their own needs [3].

Definition of the Subject

While a nascent understanding of the need for a more sustainable approach to design and construction has been around for decades, only recently have there been appropriate methods and tools available that are substantial and mature enough to help move a design and construction team toward a more integrated approach and, therefore, a more sustainable project. For these last few decades, progress toward sustainable thinking in both academia and practice has occurred in fits and starts, relying on old tools and methods while attempting to accomplish fundamentally different (i.e., truly sustainable) results. The mainstream availability of integrated delivery processes as well as building information modeling tools that have been tested in the field with positive results suggest that the industry has turned a corner on an integration that matters.

Introduction: Sustainability Through Reintegration

Since Descartes and Bacon, western civilization has clung to two critical notions: humanity's dominance over nature as a God-given right and specialization as the means to dissect nature in order to understand it. Since then the slow evolution of deconstructing the natural world leaves the current generation in a severe state of naiveté, particularly as it struggles to understand the global impact of humanity's collective and cumulative decisions and actions. This gradual loss of wisdom of the interconnected whole leaves today's societies puzzled and overwhelmed in trying to understand what sustainability really means, as specialized behaviors, methodologies, and policies have been developed over the centuries. This disintegrated approach, which has been codified and held dear within the design and construction industry, directly reflects a Baconesque tendency toward separation.

As the effects of design and building decisions have become more measurable through quantitative metrics for sustainability, and the impact of these decisions is made more evident, architects and engineers are radically rethinking their approach to design. In addition to engaging numerous disciplines early in the design process, new methods for collaboration have been developed to reduce the traditional redundancy and suboptimization of project goals. Transformational methodologies and tools, particularly integrated delivery processes and building information modeling, are finally dovetailing with comprehensive sustainability goals in buildings and communities.

Sustainable Design and Construction

Indigenous Architecture

In an abbreviated history of sustainable design, McLennan [4] refers to four "beginnings": the Biological Beginning, the Indigenous Vernacular Beginning, the Industrial Beginning, and the Modern Beginning. A brief overview of the last three is noted here, while the biological beginning is addressed under section Future Directions.

A quick survey of the architecture of indigenous cultures reveals a profound understanding of sustainability borne from the realities of their environments. Without the ability to transport materials over great distances, and without the benefit of technological advances such as electricity, combustion engines, and elevators, for example – indigenous populations founded their architecture firmly within the limits of their culture, climate, and place. The use of the term "limits" here is not to be considered pejorative, but rather as a foundational principle of sustainability. Benyus [5] refers to "tapping the power of limits" as a mature understanding of one's place within a whole, as contrasted to the more domineering mentality of a culture that seeks to find boundaries in order to overcome them, as described by Descartes.

The beauty of the Anasazi rock dwellings in Colorado and Utah lies not just in their formal qualities, but in their direct and readily apparent response to their climate and place. An experiential understanding of their climate informs a number of design decisions: orientation, mass, overhangs, the use of local materials, and seasonal variations for protection from hot and cold temperatures, sun, wind, and rain.

Similarly, the nomadic tribes of the North American plains developed portable tipis to support their nomadic culture, made from wood and animal skins readily available in their place, designed to take advantage of prevailing winds for natural ventilation and to protect from sun and wind as needed (Fig. 1).

Sustainable Design and Construction, Integrated Delivery Processes and Building Information Modeling. Figure 1
Indigenous architecture. The tipis of the Crow Nation are built for their portability, with materials readily available. The form and construction of the tipi also encourage natural ventilation

The igloos of the Inuit in northern climates suggest a multifaceted and deep understanding of snow and ice as a building material. In its stacked form, it provides protection from winds and introduces a thermal insulation critical in their climate. The rounded form is appropriate to deflect strong winds and for structural stability with a building block that is not otherwise mechanically secured or tied in place.

Though these, indigenous structures are familiar to many in the western world, each one reveals a profound understanding of sustainability in design and construction that is overlooked today, and all come from a deep understanding of climate, culture, and place. When seen only as rudimentary or sentimental structures irrelevant to current lifestyles, an opportunity for deep learning from multigenerational cultures is missed. The ability to respond intelligently to climate, culture, and place emerges from the time spent in that place, measured in generations rather than years. A generational understanding of place allows

sustainable design or building activity to become intuitive. Shy of that, a project team that is not from the place is relegated to an extensive research effort, which at best becomes knowledge, but may not ensure intuitive wisdom.

On the one hand, generational knowledge of place is critical to informing sustainable design. On the other hand, designing for durability can be equally important to sustainability. As societies expanded, larger structures were designed and built to reflect religious, cultural, or political institutions. These structures similarly reflected the climate, culture, and place and were built to last far beyond the generation that built them. In many instances, the generation of builders that began the construction of such buildings, for example the Duomo in Florence, knew that they would not even see the completion of the structure in their lifetime [6]. As defined by the Brundtland Commission, sustainable development is development "that meets the needs of the present without compromising the ability of future generations to meet their own needs" [7]. The concept of time in terms of generations rather than years is fundamental to understanding true sustainably. As will be explored later in this chapter, the use of integrated project delivery and BIM cannot makeup entirely for the loss of intuitive wisdom born from multigenerational familiarity with place, nor for the cultural shift away from long-term (durable) structures and toward short-term paybacks. These tools do, however, have potential to reconnect that which is lost by way of access to pertinent data (in lieu of experiential learning) and collective wisdom of a diverse and integrated team.

Unsustainable Design and Construction

In the late eighteenth century, the transition from custom-made to machine-made goods as part of the Industrial Revolution impacted the design and construction industry profoundly. Mass production gradually became the norm, suggesting a shift toward interchangeable building parts and materials that were no longer customized for each project. With primary goals of conserving human labor and increasing production, the slow evolution away from culture-, climate-, and place-based structures began. Concurrent with this transformation in the delivery of buildings was a prevailing attitude that natural resources were abundant, even unlimited, and relatively inexpensive to extract. The shift away from generational thinking also began, both in terms of wisdom of the place, as well as building for generations.

While the technological shift in building production was underway, the architecture of the early 1900s preserved a number of place-based principles for daylighting, natural ventilation, thermal mass for cooling, and mixed-use pedestrian lifestyles. As building technology developed, however – introducing automobiles, air conditioners, high-rise elevators, and others – the remaining sustainable principles were lost. With the increased use of manufactured materials, as well as a willingness to transport materials over great distances, projects relied less and less on materials harvested in close proximity to the site (Fig. 2).

With the rise in access to and use of electric lighting, it was possible to design buildings without access to daylight in each space. With air-conditioning, deep floor areas, and windowless spaces, unshaded and sealed building envelopes could provide thermal comfort regardless of climate and place. Each of these innovations gradually and significantly contributed to more energy-intensive buildings and an ever-increasing separation of humans and nature.

Over time, heating, cooling, and lighting were predominantly handled with mechanical systems, rather

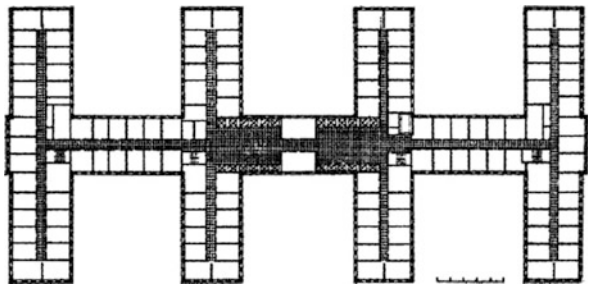

Sustainable Design and Construction, Integrated Delivery Processes and Building Information Modeling. Figure 2
Narrow footprints. The plan for Detroit's General Motors headquarters, built in 1921, places each worker within 20 ft of an operable window and provides access to views and daylight for almost every room in the building (Architect: Albert Kahn, Inc.)

than taking advantage of climate for natural conditioning. Building codes gradually required uniform comfort standards to be maintained, leading the design industry to rely even more on mechanical (and not natural) solutions. Eventually, manufacturers of building products limited their warranties to these tightly controlled conditions, providing even less incentive for the building owner to allow the building to be "open" to the opportunities of natural conditioning and direct contact with place, season, and even time of day. By the mid-twentieth century, the independence of building design and construction from culture, climate, and place had been achieved. A mid-rise building design for Anchorage, Alaska, was indistinguishable from a similar structure in Phoenix, Arizona. No specific reference to place was integrated other than by way of name or superficial decoration.

Eventually, through case studies demonstrating the human health implications of the design of such spaces, a renewed understanding of both the interconnectedness of natural systems to themselves as well as the inherent affiliation between humans and natural systems has emerged. As Kellert suggests in *Biophilic Design* [8]:

- Most of our emotional, problem-solving, critical-thinking, and constructive abilities continue to reflect skills and aptitudes learned in close association with natural systems and processes that remain critical in human health, maturation, and productivity. The assumption that human progress and civilization is measured by our separation from if not transcendence of nature is an erroneous and dangerous illusion. People's physical and mental well-being remains highly contingent on contact with the natural environment, which is a necessity rather than a luxury for achieving lives of fitness and satisfaction even in our modern urban society.

It is a similar renewed understanding of the power of integration that has influenced the explosion in the late twentieth and early twenty-first centuries of new integrated tools and processes, such as BIM and integrated project delivery. As we will see, this relatively recent and renewed understanding of the need for deep integration, including the way in which designers design and builders build, is critical to achieving regenerative design, which will create the foundation for true sustainability in our built environments.

The Modern Sustainable Design Movement

Many consider Rachel Carson's *Silent Spring* [9] of 1962 to be the catalyst of the modern environmental movement and a precursor to the modern sustainable design movement. In her position as a marine biologist with the US Fish and Wildlife Service, she was overwhelmed by the detrimental impacts of the cumulative actions of humans on the environment. In "A Fable for Tomorrow," Carson illustrates the interconnectivity of ecological diversity and the health of humans.

Carson was a catalyst for a new era of environmental thinkers within the EPA, yet the building professions lagged until the energy crisis of the 1970s, when a group of architects, including Sim Van der Ryn and others, focused their efforts on building designs that minimized reliance on oil and maximized reliance on solar energy. In the 1980s, the seeds were being sown to significantly expand the environmental movement beyond the issues of energy conservation. Leaders including BNIM Architects and William McDonough Architects broadened the dialog to include design for material and water resources, indoor air quality, and livable communities. In 1993, the US Green Building Council (USGBC) launched the Leadership in Energy and Environmental Design (LEED) Green Building Rating System, transforming US attitudes and behaviors toward sustainable design and construction.

The LEED tools, and those emerging in other countries such as BREEAM and CASBEE, were developed for a variety of reasons: to define standards for measuring sustainability; to compare buildings evenly; to transform the construction industry; to raise consumer and client awareness; to stimulate competition; to establish a recognized name for sustainable design; and to educate and integrate the building industry, building owners, and design practitioners. Most significantly for the discussion of integrated design practice, the LEED credit system seeks to promote integrated design; encourage innovative design solutions; improve the life-cycle economics of the project; provide a healthy, productive, and safe workplace for employees; reduce resource consumption; and reduce

the negative impact on the environment. These methodologies place real attention on the performance of buildings and communities and their impact on the environment. However, they tend to focus on reducing environmental impact rather than the more challenging goals of rebalancing the relationship between humans and nature, closing the ecological cycles, and restoring or regenerating the earth. A number of far-reaching approaches are challenging the professions even further: Architecture 2030, Living Building Challenge, Cradle to Cradle, REGEN, and One Planet Communities. A key tenet of these approaches to sustainable design is the need for an integrated delivery process that recaptures the integration of human–climate–place embodied by indigenous populations, the integration of nature–human ecosystems illustrated by Rachel Carson, and the integration of disciplines central to introducing buildings and communities that are truly regenerative.

Integrated Delivery Processes

Legacy of a Fragmented Infrastructure

S.G. Mattar identifies the operational islands that exist in the building industry that contribute to ongoing performance failures in economic, environmental, and human terms [10]. By overlaying the functional gaps of increasingly multidisciplinary teams with the management discontinuities of sequential stages of the work, potential points of missed interconnectedness or disintegration are revealed. Integrated delivery processes, including the use of BIM as a tool, begin to coordinate the separate disciplines in the design stages and the trades in the building delivery process. Section "Integrated Delivery Processes" will illustrate first how the building delivery process is evolving to integrate the expertise of design-construction-management, and section "Building Information Modeling to Support Integrated Project Delivery" will illustrate how the design process is evolving to integrate the diverse expertise of the comprehensive design team (Fig. 3).

Lean Thinking as a Path to Integrated Project Delivery

In the Japanese language, the term for waste is *muda*, which is fundamentally based on an understanding value. In the world of lean manufacturing, at least seven types of *muda* have been identified: overproduction, waiting, transporting, inappropriate processing, unnecessary inventory, unnecessary/excess motion, and defects [2]. Further, lean thinking places value on the delivered product and its performance

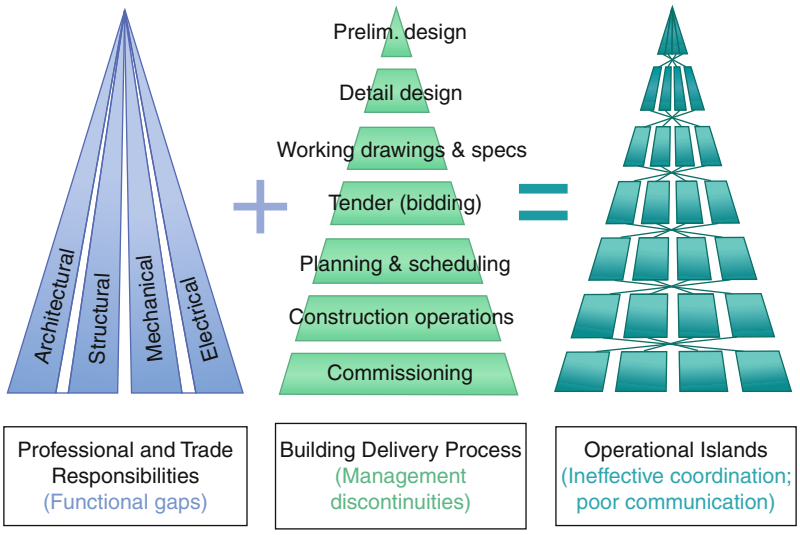

Sustainable Design and Construction, Integrated Delivery Processes and Building Information Modeling. Figure 3 Fragmented infrastructure. These diagrams by S.G. Mattar in "Buildability and Building Envelope Design" illustrate the operational islands (opportunities for disintegration) in the traditional delivery model

rather than just the cost of production, not unlike the concept of life cycle analysis as compared to simple first cost comparisons in the building industry.

Lean Production/Manufacturing Advances in the manufacturing world, specifically the automotive industry, provide context and insight into potential breakthroughs in the design and construction industry. In their book, *The Machine That Changed the World: The Story of Lean Production* [11], Womack, Jones, and Roos trace the history of production methodologies in the automotive industry, from craft production to mass production and most recently to lean production. In the mid- to late-1800s, craft production was the norm, characterized by a highly skilled workforce, decentralized organizations, use of general-purpose machine tools, and a very low production volume. In the early 1900s, Henry Ford introduced revolutionary changes to car manufacturing, thus beginning the era of mass production, coincidental with the aforementioned transformation of the design and construction industry's emerging reliance on technological innovation. As Womack suggests, it was not the assembly line that marked Ford's innovation, but rather "the complete and consistent interchangeability of parts and the simplicity of attaching them to each other."

Though considered to be a breakthrough in efficient product delivery, mass production held the same primary characteristics of building design and construction coming out of the Industrial Revolution, namely, "principles of specialization, division of labor, and standardization of parts to the manufacturing of goods on a large scale" [12]. Though considered to be a breakthrough in efficient production, costs of specialization within the workforce remained hidden. In yet another example of the dangers of specialization, Holstein explains:

- . . . the division of labor, the specialization of narrow skills, the detailed engineering specification of how each task is to be carried out, and the assemblage of large numbers of employees in great manufacturing plants have greatly diluted the identification of employees with their productive functions and with their employers. Many surveys in the United States and in the industrialized countries of Europe have shown that workers do not fully understand and appreciate their roles and positions in society. In addition, the division and specialization of labor may lead to such narrowly defined skills and highly repetitive operations, paced by the steady progression of a machine or conveyor line, that tedium and fatigue arise to reduce the sense of satisfaction inherent in productive work. [12]

As discussed under Future Directions, engaging mind, body, and spirit is also essential to understanding a truly comprehensive integrated delivery process, which is addressed in the lean production model.

By the 1950s, Eiji Toyoda and Taiichi Ohno at the Toyota Motor Company determined that mass production was an inappropriate approach for their organization, and so they set about on a different path, which would eventually become synonymous with lean production. Considered by many as the next significant organizational/production model, lean production finds its roots in an integrated approach to improvement. The mainstays of the Toyota Production System are "continuous improvement" and "respect for people," both of which suggest a strong reliance on integration within the process, the product, and the people creating them.

- "The key to the Toyota Way and what makes Toyota stand out is not any of the individual elements. . .. But what is important is having all the elements together as a system. It must be practiced every day in a very consistent manner—not in spurts." [13]

Though perhaps *revolutionary* in its conception, lean production is in reality a philosophy of *evolution*. It is an attitude toward innovation that is focused on continuous and incremental improvements, not in breakthrough transformations, or in essence multigenerational learning.

After in-depth observation of their processes in action, Liker derived 14 management principles that characterize the "Toyota way," all stemming from the fundamental commitment to "respect for people" and "continuous improvement" [13]:

I. Long-term philosophy.
   1. Base your management decisions on long-term philosophy, even at the expense of short-term financial goals.

II. The right process will produce the Right results.
   2. Create continuous process flow to bring problems to the surface.

3. Use "pull" systems to avoid overproduction.
4. Level out the workload (*heijunka*) (Work like a tortoise, not a hare).
5. Build a culture of stopping to fix problems, to get quality right the first time.
6. Standardized tasks are the foundation for continuous improvement and employee empowerment.
7. Use visual control so no problems are hidden.
8. Use only reliable, thoroughly tested technology that serves your people and processes.

III. Add value to the organization by developing your people and partners.
   9. Grow leaders who thoroughly understand the work, live the philosophy, and teach it to others.
   10. Develop exceptional people and teams who follow your company's philosophy.
   11. Respect your extended network of partners and suppliers by challenging them and helping them improve.

IV. Continuously solving root problems drives organizational learning.
   12. Go and see for yourself to thoroughly understand the situation (*genchi genbutsu*).
   13. Make decisions slowly by consensus, thoroughly considering all options; implement decisions rapidly.
   14. Become a learning organization through relentless reflection (*hansei*) and continuous improvement (*kaizen*).

Liker cautions others away from rigidly applying these principles to their own organizations and encourages others to develop their own principles appropriate to their own situation, not unlike indigenous designs being culture based.

Lean Design and Construction Koskela, Howell, Ballard, and Tommelein [14] suggest that lean construction is both inspired and challenged by the theory of lean production. The Lean Construction Institute is an evolutionary framework of individuals and organizations (both theorists and practitioners) involved in a conversation on the application of this theoretical framework in the construction field.

Like lean production, lean construction seeks to eliminate waste while maintaining or adding value, a measure of productivity in product per man-hour. Data from the US Department of Commerce illustrate the decrease in productivity within the design and construction industry as compared to other industries in recent decades.

Those involved in the lean construction movement continue to explore the benefits of lean thinking on traditional design and construction processes. From its roots in production management, lean principles have been applied to and studied on large, complex, and short-schedule projects. Lean construction is a project delivery system that emphasizes the reliable and timely delivery of value. It does not hold the notion that there is a trade-off between quality, time, and cost on a project, but believes that all can and should be achieved. Significant to note is the fundamental difference between manufacturing and construction whereby construction is project/function based and site based, with each project unique by definition. Methodologies and/or tools that have been developed to work within a lean design and construction environment can be categorized into lean production management, lean design, lean supply, and lean assembly [15]:

Lean production management	Lean work structuring
	Scheduling
	Last planner system
	Look-Ahead Planning
Lean design	Cross-functional teams
	Set-based strategies
	Structured design work
	Optimization of design iteration
	Design production control
	Building information modeling (BIM)
	Communication flow protocols
	Big room
	Target value costing
	Reliable promising
	A3 reports

Lean supply	Communication flow protocols
	Information transparency
	Lean product supply
	Supply chain design and control
	Reliable promising
Lean assembly	Lean installation
	Continuous flow

In direct response to the fragmented infrastructure of the traditional delivery models in design and construction, the Lean Production Delivery System, as illustrated in Fig. 4, reconsiders traditional linear phasing of production with a more integrated approach of overlapping processes. Not unlike other fields, such as quantum physics, social modeling, and software networks, those studying lean design and construction have been recognizing the significance of interconnectedness rather than separation between individual components (Fig. 5).

Integrated Delivery Processes

Integrated Form of Agreement In 2005, Sutter Health, a not-for-profit community-based health care and hospital system in California developed a contracting model that supports Lean Project Delivery [16]. This model was based on the research of the Lean Construction Institute, including an attempt to address management of workflow, team relationships, and contractual relationships. "Five Big Ideas" emerged as a framework that focused on the concept of maximizing value to the customer (in this case, Sutter Health):

1. Collaborate, really collaborate (throughout design, planning, and execution).
2. Increase relatedness among all project participants.
3. Consider projects as networks of commitments.
4. Optimize the project, not the pieces of the project.
5. Tightly couple action with learning.

Not unlike Toyota's lean production model, the foundation of an integrated delivery approach resides in a team's mutual trust and respect for the knowledge and expertise brought by each team member. For this

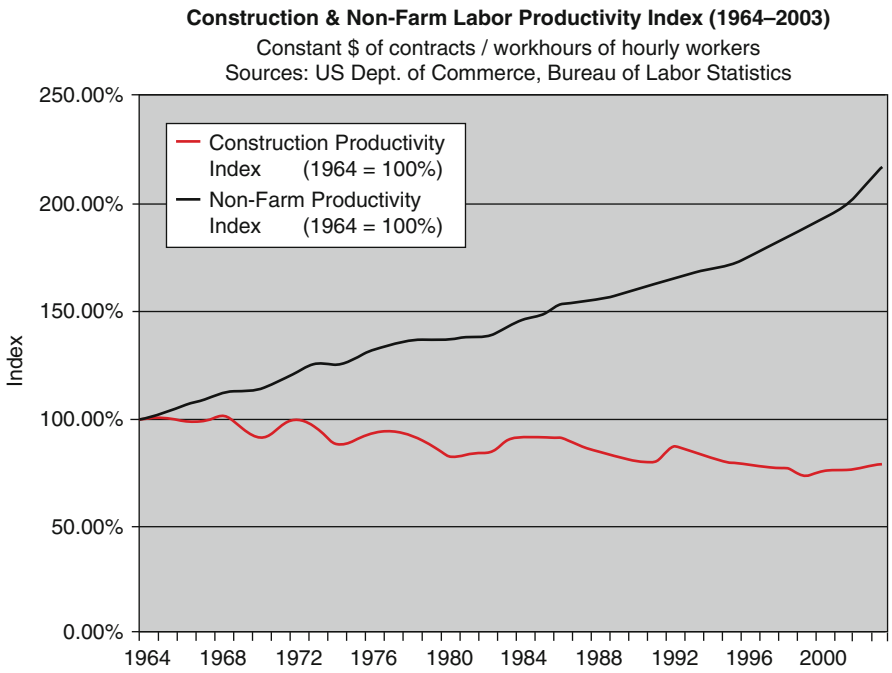

Sustainable Design and Construction, Integrated Delivery Processes and Building Information Modeling. Figure 4 Declining productivity. Data from US Department of Commerce, Bureau of Labor Statistics illustrating the decline in productivity in the design and construction industry as contrasted with other fields

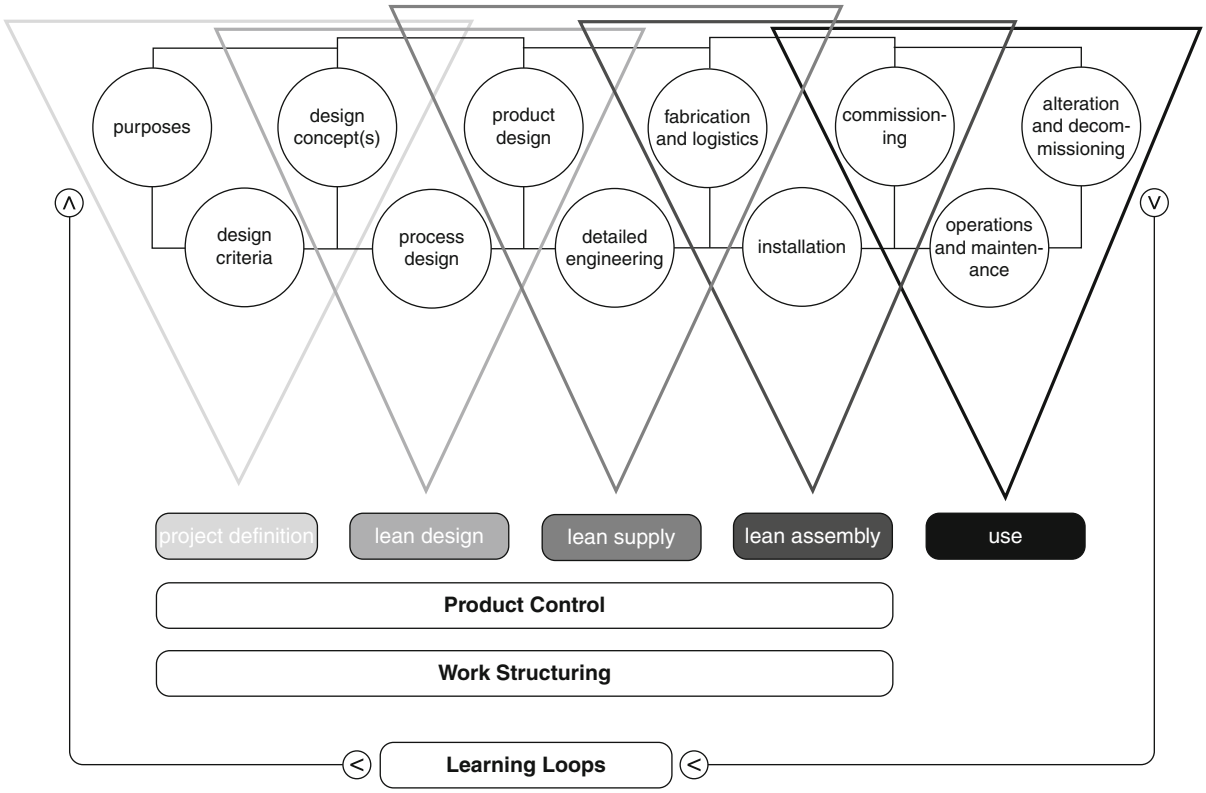

Sustainable Design and Construction, Integrated Delivery Processes and Building Information Modeling. Figure 5 Lean project delivery system. From project definition through to product use, project phases overlap and a learning loop is introduced to reflect the goal of continuous improvement [21]

reason, prior experience working together is a significant benefit, another access point to multigenerational wisdom. While collaborative skills of the team can be developed between newly congregated team members, intentional work is required upfront to build the mutual trust and respect and, therefore, take advantage of meaningful integration. Integrated project delivery is not simply getting everyone in a room together, but rather practicing a deep and significant collaboration of individuals, their knowledge and wisdom, and shared values – as suggested above by the first big idea: "Collaborate, really collaborate." Though not required to achieve integrated delivery, an integrated form of agreement as a relational contractual model can beneficially support this desired type of team behavior.

Integrated Project Delivery (IPD) In 2007, the American Institute of Architects (AIA) and AIA California Council introduced Integrated Project Delivery (IPD) as a "project delivery approach that integrates people, systems, business structures, and practices into a process that collaboratively harnesses the talents and insights of all participants to optimize project results, increase value to the owner, reduce waste, and maximize efficiency through all phases of design, fabrication, and construction." In this model, the multiparty agreement shifts dramatically from the traditional design-bid-build or design-build contracts to a focus on shared responsibilities for project delivery by the three primary players: owner, designer, and constructor.

Connection to Sustainable Design and Construction A critical tenet of sustainable design is collaborative decision-making in the early design stages to ensure that preliminary decisions strategically support sustainability goals and do not compromise the ability of later decisions or actions in meeting those goals. Figure 6 illustrates the time and cost benefits of early design collaboration, with the promise of an even greater benefit of increased quality in the final building product.

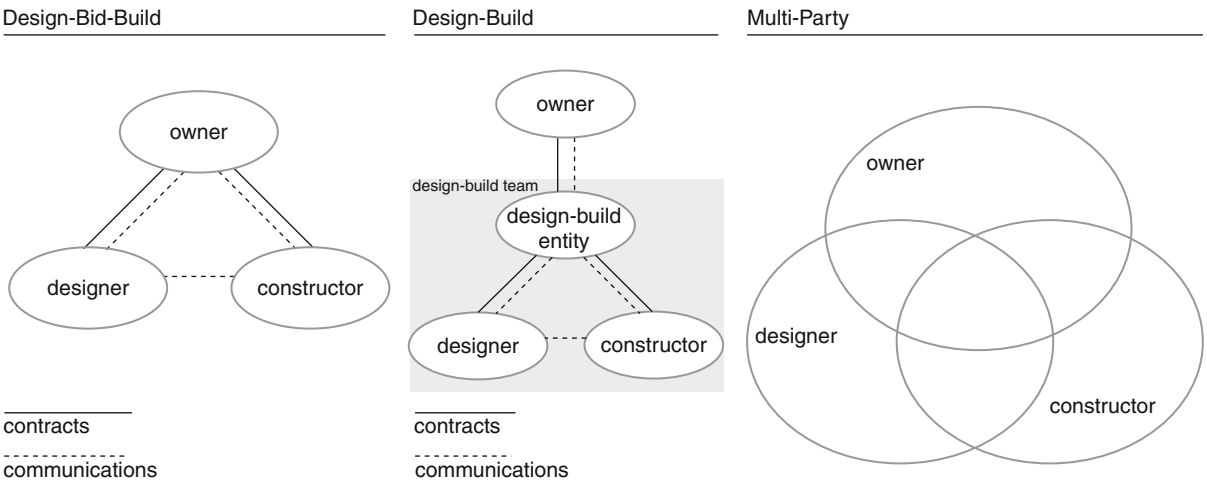

Sustainable Design and Construction, Integrated Delivery Processes and Building Information Modeling. Figure 6 Project delivery models. As compared with traditional delivery system models of design-bid-build and design-build, a multiparty relational agreement is one contract signed by owner, architect, and contractor (plus any additional key project partners), indicating the shared risk and reward nature of the relationship

Numerous recent publications document the shift toward a more integrated approach in the building delivery process and the value of integrated design for high-performance buildings [17, 18, 19]. The changes in the building delivery process, especially with respect to when various project participants are brought on board, are illustrated in Figs. 7 and 8.

Since the introduction of integrated design processes, codified in LEED for example, the benefits to building performance and sustainability are just beginning to be quantified. Through integrated decision-making early in the design process, measurable gains in energy and water efficiency and material and land conservation have been recorded in new buildings, major retrofits, interior retrofits, and existing building operations [17, 19, 20]. The key is to *integrate, really integrate*. The advent of building information modeling as a mainstream design and construction tool is helping to facilitate an integrated team and therefore an integrated design process.

Building Information Modeling to Support Integrated Project Delivery

CAD to BIM

Building information modeling (BIM) moves well beyond traditional computer-aided drafting (CAD) by tying component properties and characteristics to a geometric model that supports parametric changes by each expert in the building delivery process. Parametric modeling takes its name from the project parameters or variables that are modified as work progresses. It also refers to the model's content as interconnected components and views, all of which are updated when modifications are made to one component in any view. Common in the shipbuilding, automotive, and airplane industries for decades, the integration of parametric modeling within the architectural design process is relatively recent. With significant investment by software developers such as Autodesk and Bentley, BIM now supports integrated design development by architects, engineers, and contractors, generating as-built documents that can be updated and modified by building managers.

BIM in the Design Phase The most obvious benefit of BIM use in the design and construction industry comes in the form of three-dimensional design visualization. Three-dimensional models (be they physical or electronic) convey a better sense of the final project than two-dimensional representations of abstract views of the building. Site, floor, ceiling, and roof plans, and interior and exterior elevations are complex abstractions of the actual building, often unintelligible to those that need to understand them the most, from

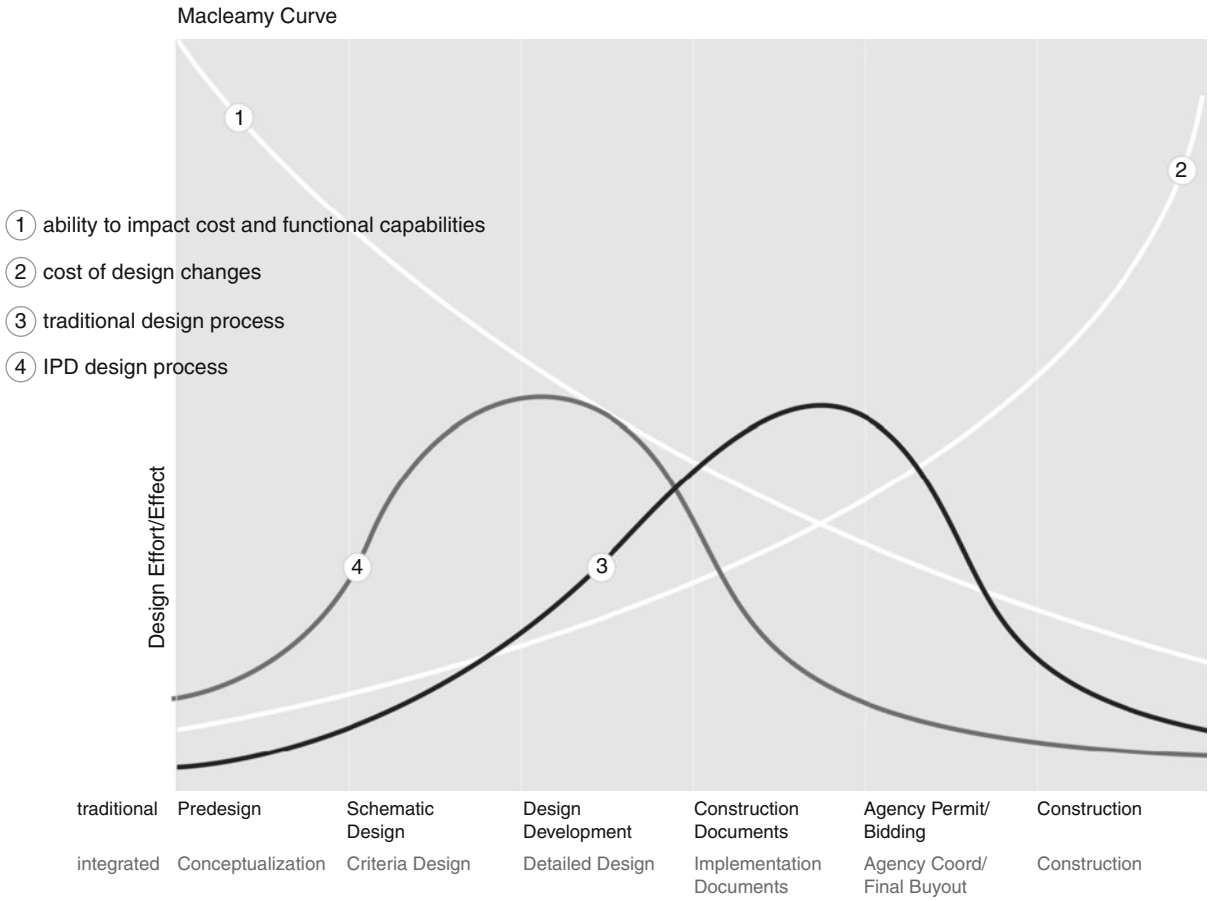

Sustainable Design and Construction, Integrated Delivery Processes and Building Information Modeling. Figure 7 The case for informed decisions in early design. Mcleamy Curve comparing design effort, project phase, and impact on costs. The implication of this diagram is that it is highly beneficial to the overall project success for key stakeholders to be at the table early in the design process making informed decisions

the client to future occupants. Three-dimensional models afford a much greater opportunity to understand the building during design before construction begins, when key decisions are being made. Not only is this beneficial with the client and user groups in making informed decisions, but it is also valuable in communicating the design intent to officials of regulatory agencies (code, zoning, public utilities, etc.), neighborhood groups, and any other stakeholders that would benefit from fully understanding the project. So, in its most basic form, BIM affords real integration with the client and ultimate occupants/users of the building. As mentioned earlier, the full integration of these constituents in the overall process makes for a more integrated and ultimately successful solution.

To support an integrated design and construction team, another critical difference between BIM models and CAD models is the parametric nature of the model information. Because the model is being updated concurrently by various members of the design team, there is no lag time of sharing information between the various disciplines responsible for the design of the project. Also, discrepancies within the separated two-dimensional drawings of the building are also minimized. Design options can be rapidly generated for study and review to afford quick and informed decision-making, and to ensure that the latest decisions are communicated to the entire team. Cost estimating and construction review can occur iteratively and quickly (reminiscent of rapid prototyping or small batching in

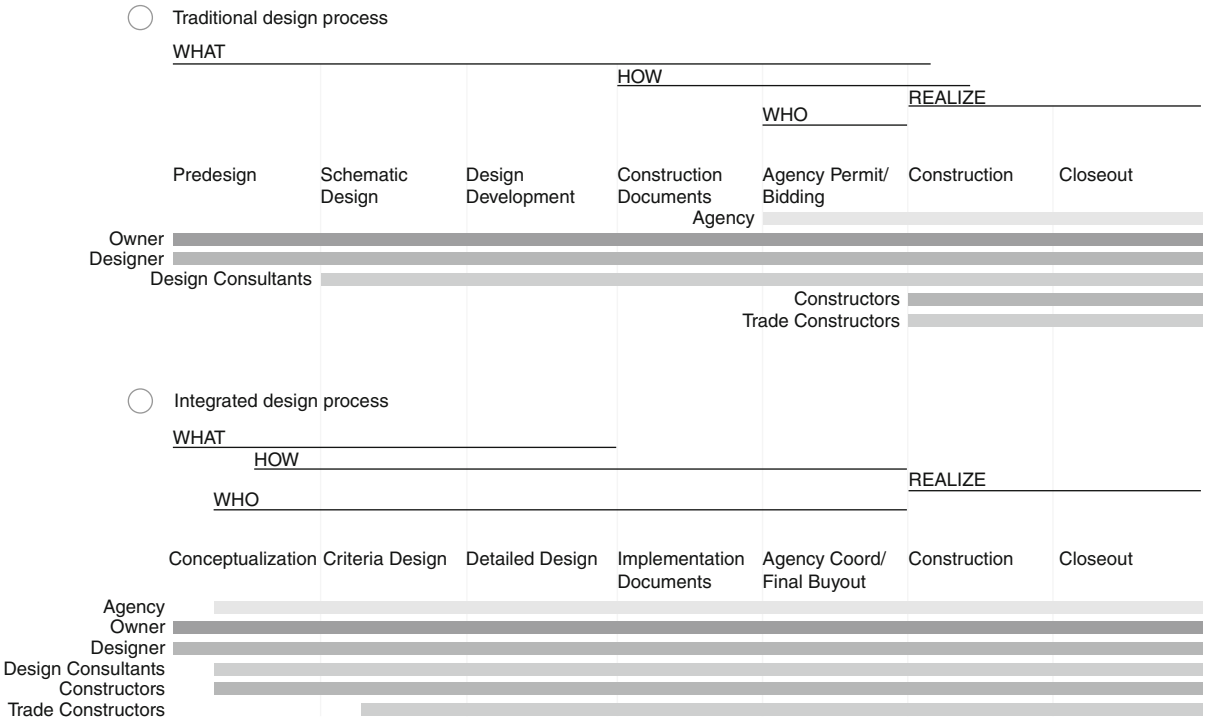

Sustainable Design and Construction, Integrated Delivery Processes and Building Information Modeling. Figure 8 Project team integration. Comparison of team member involvement for a traditional design process and an integrated design process as illustrated within AIA's integrated project delivery guide

the lean world), rather than waiting until a benchmark set of documents is produced.

Manufacturers and trade partners, including curtain wall, mechanical, electrical, plumbing, furniture, and other manufactured products, have the potential to contribute key information regarding constructability and cost implications during design. The use of BIM in the design stage supports a level of iterative and early collaborative decision-making that is critical in the integration of the more rigorous design goals for sustainability.

BIM in the Construction Phase Contractor input is becoming a valuable component of the design process at times contributing to early design decision-making, cost estimating, and constructability assessments, pulling construction planning up into the design phases. In some instances, the BIM model is further used by the general contractor as well as trade partners for staging and sequencing, and as an effective communication tool to "see" the construction workflow in advance. Clarity of this kind of information eliminates waste at multiple levels, from early interference checking to the timing of on-site construction equipment (tower cranes, etc.) – allowing team members to coordinate their work effectively.

A highly beneficial feature of a BIM model is its capacity for interference checking. When all of the building's systems – structure, enclosure, mechanical, plumbing, and others – coexist in the same three-dimensional space, the team can collectively and virtually see space constraints and interferences, sometimes called clash detection. This is impossible without integration of multiple disciplines and without cultural integration of project team members from the owner, design and builder teams. Resolving such conditions virtually rather than out in the field eliminates waste at multiple levels – in time, materials, and cost. The economic, human, and environmental costs of change orders are significant, and integrated design practices combined with the use of BIM have the potential to measurably reduce these costs. This process blurs the

line between design and construction phases as design modifications are made ahead of construction as informed by physical/construction realities.

BIM in the Manufacturing Phase Reducing short-term or long-term costs, however, is not ambitious enough for the sustainable design community. There is a long-standing and built-up need for improving installed performance of integrated systems, with the least amount of resources, which might also be enhanced through BIM. When the design team's BIM model is developed with the manufacturers and fabricators (direct to fabrication), an iterative "design assist" model is initiated, similar to lean design. Instead of fabricators redrawing the design documents and submitting for approval (in the traditional delivery model), the fabricator takes over the BIM design model or one portion of it and makes adjustments for improved performance for the design team to review and approve for fabrication.

Kieran and Timberlake's explorations in "refabricating architecture" are a vivid illustration of this approach [22]. In this model, BIM geometry and data are sent direct to fabricators for off-site fabrication or manufacturing in controlled environments where tolerances and performance can be optimized. In lieu of on-site *construction*, on-site *assembly* is maximized, shortening overall construction time and improving quality of workmanship. The migration of BIM models into the CAD/CAM arena offers significant gains in integrated design decision-making across the professional disciplines and through the building delivery process.

BIM and Building Performance Simulation As discussed in Chap. X, BIM models are beginning to support building performance simulation directly. Thermal, lighting, acoustic, structural, energy, and other performance simulation models have been advancing rapidly over the past decades. However, in almost every case, these models have needed independent geometric and performance specification profiles to be built in customized computer models before the simulation could be completed. Today, we see the first instances of the direct use of BIM models for performance simulation. Since geographical coordinates are resident in most BIM models, solar access and sunshading studies can be performed directly. More extensive modeling for daylighting and energy studies still requires separate interfaces, but progress in the interoperability of software packages is gradually allowing the original BIM model to be exported directly to the analysis software. This is especially true for energy analysis software in early design when a broad spectrum of options are generated and when comparative analysis and quick turnaround times are needed. As the design develops and more detailed material and component specifications are required for real projections of energy use or natural ventilation effectiveness for example, the interoperability of software still needs development.

Beyond energy simulation, BIM models can be instantly mined for area and material calculations to support the planning of other sustainable strategies, such as rainwater harvesting, material savings, and recycled content [23]. Interoperability advances beyond spreadsheet calculations are still needed, however, as will be discussed in Future Directions.

BIM and Materials Life-Cycle Cost Analysis (LCA) While BIM is often perceived to be simply a three-dimensional model, it has the capacity to accommodate additional dimensions by addressing systems integration in 3-D, design-construction-use phasing in the fourth dimension, performance outcomes in the fifth, costing, and more. One of the more important yet complex opportunities for building information modeling is the incorporation of material life-cycle properties. Wall, door, hardware, finish, and window schedules are all generated and updated automatically as the model is built with carefully chosen component libraries. Additional information about project materials embedded in the model – from raw materials to assembly and transport, from physical properties of components to those of assembled systems – would be even more helpful in iteratively assessing LCA impact of design decisions. The most immediate benefit of this database is the ability to report out material quantity takeoffs normally handled by a contractor or cost consultant. In addition to pure quantities, material qualities can also be embedded in the model. To ensure that manufacturers offer reliable and clear specifications for these BIM libraries, national standards are being created by the National Building Information Model Standard (NBIMS) Project

Committee, under the National Institute of Building Sciences (NIBS) *buildingSMART alliance*™ with a broad constituency of industry partners [24]. As the material and product specification libraries become populated with reliable data, the design and construction teams will be able to make more environmentally sound decisions, driven first by simpler goals of recycled content and recyclability, cost, and physical performance (or durability/life expectancy). In the near future, as the inventory is populated with data about the full life cycle assessment of components, decisions for the most sustainable built environment will be better informed. Insert LCA criteria figure

The David and Lucile Packard Foundation Sustainability Report and Matrix is an early tool developed by the BNIM project team for a new headquarters building in Los Altos, California. It reflects an extensive study in understanding not only the first costs of sustainable design and construction but also long-term (generational) cost benefits, examined over 30-, 60-, and 100-year cost models [25] (Fig. 9).

BIM and Computer-Aided Facilities Management (CAFM) CAFM is a communication and tracking tool for ongoing operations and maintenance of a building and assets inside it, such as fixtures, furnishings, equipment, and people. To consider that the building information model has expended, its usefulness at the time of construction completion is to miss a significant opportunity for further integration of the BIM model into the project delivery process as it relates to its stored data. As noted in a 2004 NIST study on the

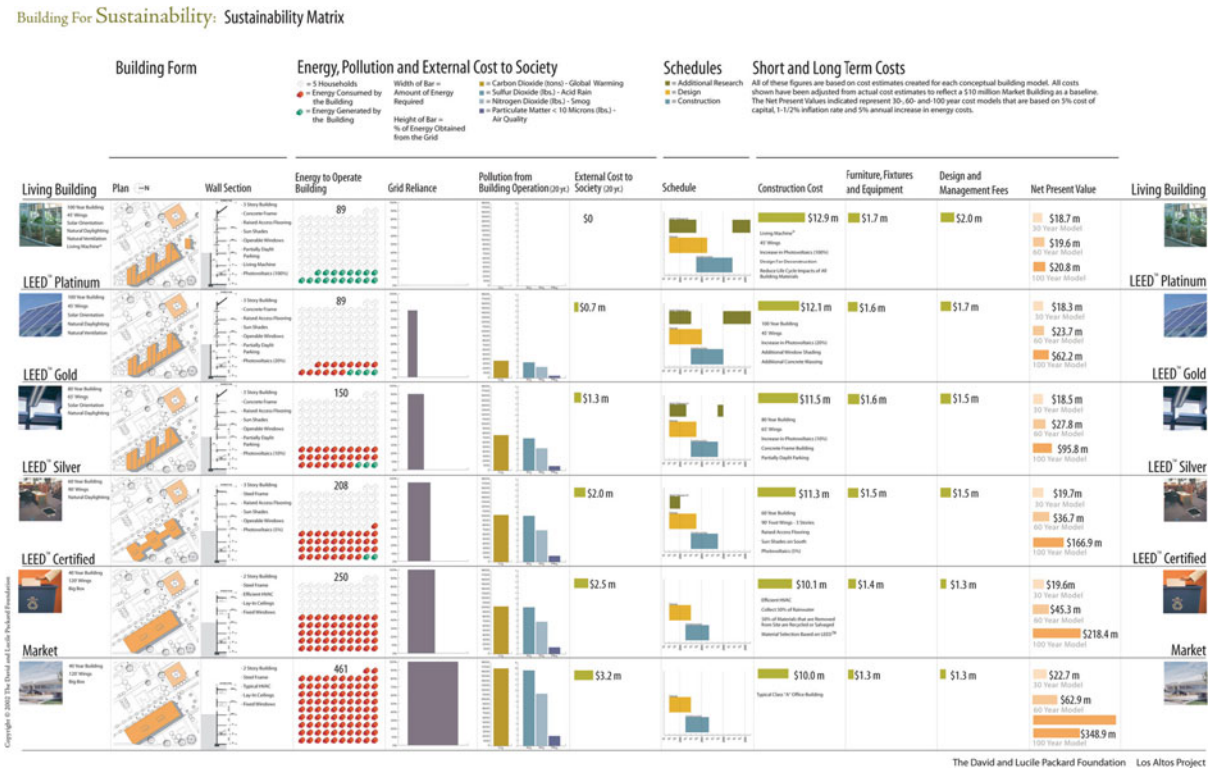

Sustainable Design and Construction, Integrated Delivery Processes and Building Information Modeling. Figure 9 Packard sustainability report illustrating long-term financial impacts. The project team evaluated six conceptual designs for the same building program, each representing various levels of sustainable design and construction, including Market, four levels of LEED, and a Living Building. The 30-, 60-, and 100-year cost models were developed to demonstrate the long-term benefits of sustainable thinking

costs of inadequate interoperability in the facilities industry:

- Owners and operators have the largest interoperability costs of all the stakeholders: over $10.6 billion, or about 68 percent of the total $15.8 billion of inadequate interoperability costs calculated for the capital facilities supply chain . . . This is because owners and operators carry the burden of ongoing interoperability costs during the operations and maintenance phase. . . Eighty-five percent of owners and operators' interoperability costs are incurred during the operations and maintenance phase. Quantified costs were estimated at approximately $9 billion in 2002. Although inefficient business process management costs are significant during this phase ($1.6 billion), the costs related to facilities management and maintenance are even larger. [26]

In an attempt to address these losses, use of the project's BIM model for facilities management, once the owner or tenant has begun occupancy of the building, is emerging. Activities such as employee tracking (moves/adds/changes) and asset management (spaces, equipment, furniture) are being handled within CAFM systems, yet it is rare for the BIM model that was built during design and modified during construction to be carried through to the facility management phase. BIM holds the component information for building materials, systems, and components, while CAFM holds the ongoing operations and maintenance information. The current goal in bridging this interoperability divide is the successful communication between in asset knowledge (BIM) and asset maintenance (CAFM). Similar to the development of compatible software for daylight and energy modeling that seamlessly accept appropriate data from a BIM model, bridging the BIM–CAFM means allowing the BIM and CAFM models to directly influence each other via data transfer, data such as manufacturers data on building materials and systems, including fixtures, furnishings and equipment (especially mechanical), and the subsequent history of ongoing maintenance.

Workflow Transformation

Advancing sustainable design with integrated project delivery and building information modeling requires a traditional project team to fundamentally change the way the work is performed. Traditional sequential relationships between architects, engineers, manufacturers, contractors, and facility managers are eliminated, as teams rely on each others' expertise throughout the entire process to ensure higher quality outcomes. When project goals are met, all team members benefit, including the owner. When projects encounter unforeseen conditions or when oversight errors occur, the team solves the problem together rather than wasting energy determining fault. A full client and building delivery team is at the same table early in the process and collectively accepts risks and responsibilities for the entire project (see Fig. 7). Performance goals are set, and building design processes are established collectively to ensure integrated decision-making and collaborative problem-solving required to meet those goals. (See HPBDP outline.)

Architects, engineers, manufacturers, and builders are working within the same BIM environment to ensure the virtual building is coordinated prior to work on-site. To ensure high-performance buildings, critical building science consultants are engaged from project kickoff, participating in the generation and evaluation of design alternatives. The collaboration is fundamental because the integration of diverse ideas and feedback is critical to a more sustainable process and product. If the call for a truly sustainable built environment is real, this kind of fundamental transformation in how the design and construction industry works together must also be real.

Future Directions

Toward Interdependence

In the spirit of learning from indigenous cultures to help western civilization regains its connection to nature, reference to the term "ubuntu" from the Bantu language group is appropriate. This term has been translated in variant ways, all with the common thread of interdependence – one among others rather than one separate from others. Its simplest translation – "I am because we are" – suggests a fundamental understanding of self as inseparable from community. This embodies the spirit of what has been lost in our culture and what is required to achieve true sustainability of humanity and planet. This first principle of interdependence underpins all conversations on sustainable design and integrated delivery.

Connecting Data and Decisions

There are some basic and solvable ways that integrated practice, and building information modeling can be enhanced from its current forms to catalyze project teams toward better decision-making. On the one hand, strong benefits are gained by a project team that engages individuals who are local to a place – who bring some measure of historical wisdom and/or knowledge – particularly if that knowledge is multigenerational. Similarly, in-depth research on the environmental and ecological characteristics of a place is invaluable to design efforts geared toward true sustainability and restoration (Fig. 10).

Other solutions are technological in nature and solvable over time. BIM software is available today that alerts teams when a design is in conflict with local codes and ordinances. BIM parametric data can provide the design team with live LEED documentation as the design evolves – not all credits yet, but those that are dependent on quantities and dimensions, such as the percent of occupied spaces that have seated views and access to daylight. BIM models tie material data to product specifications, which support pricing models and alert the team when LEED material credits are met. These are all highly beneficial uses of a BIM model to automatically and parametrically calculate design-related performance outcomes as the design evolves.

Critical to the next generation of parametric modeling is the ability of the model to be located in time and space in order to support extensive data acquisition from external sources. As a project model is initiated,

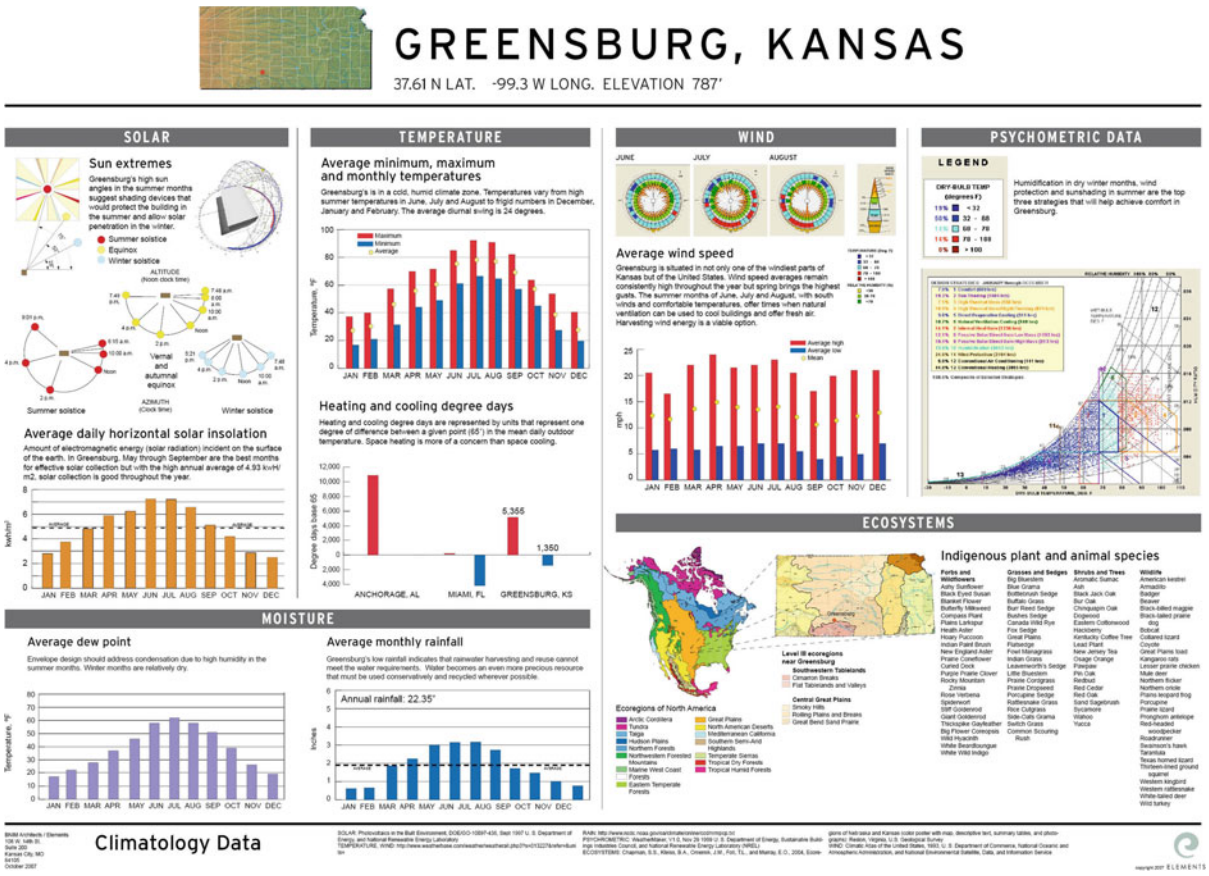

Sustainable Design and Construction, Integrated Delivery Processes and Building Information Modeling. Figure 10 Climate data chart. A sample collection of basic environmental data collected for work in a specific locale. Primary categories of data minimally include solar, temperature, wind, psychometric data, moisture, and ecosystems (Courtesy of BNIM/Elements)

project site parameters would immediately connect live external data to the project. Imagine a model that pulls detailed data regarding rainfall expected at a project site – not just annual rainfall, but data from the last 100 years of rainfall, providing the team with trends in high and low years and potential expectations based on a more global understanding of climate change. Imagine a model that is linked to a product database that monitors product data and availability within close proximity to the site, or that identifies appropriate building systems or materials based on the project location. Imagine a model that, once "placed" within its geographical coordinates, identifies not only expected solar access and informs the team on appropriate orientation, massing, and sunshading, but also pulls available data on solar products and calculates anticipated solar income available at the building based on the efficacy of those products. The potential of BIM models to support data and analysis input from a diverse set of sources begins to bridge the sustainability gaps previously described, but only the technological gaps.

Reconnecting Nature and Human Nature

Integrated design practice methodologies and BIM tools have emerged to challenge and transform the "old" way of thinking. It is not clear, however, if they will be adequate for understanding nature's principles of interconnectivity and interdependence or for actively contributing to this regenerative loop. Native cultures throughout time have spoken out on the wisdom of nature and have given warnings against ignoring her interconnectedness, or "consilience" as E.O. Wilson would suggest [27]. John Muir left us with his observation, after spending extended time in the wilderness, that "When we try to pick out anything by itself, we find it hitched to everything else in the universe." Similarly, the David Suzuki Foundation, in preparation for the 1992 United Nations Earth Summit in Rio de Janeiro, issued their own Declaration of Interdependence [28], one they hoped would be adopted by all (italics mine):

- **DECLARATION OF INTERDEPENDENCE**

  This we know

  We are the earth, through the plants and animals that nourish us.

  We are the rains and the oceans that flow through our veins.

  We are the breath of the forests of the land, and the plants of the sea.

  We are human animals, related to all other life as descendants of the firstborn cell.

  We share with these kin a common history, written in our genes.

  We share a common present, filled with uncertainty.

  And we share a common future, as yet untold.

  We humans are but one of thirty million species weaving the thin layer of life enveloping the world.

  The stability of communities of living things depends upon this diversity.

  Linked in that web, we are interconnected — using, cleansing, sharing and replenishing the fundamental elements of life.

  Our home, planet Earth, is finite; all life shares its resources and the energy from the sun, and therefore has limits to growth.

  For the first time, we have touched those limits.

  When we compromise the air, the water, the soil and the variety of life, we steal from the endless future to serve the fleeting present.

  This we believe

  Humans have become so numerous and our tools so powerful that we have driven fellow creatures to extinction, dammed the great rivers, torn down ancient forests, poisoned the earth, rain and wind, and ripped holes in the sky.

  Our science has brought pain as well as joy; our comfort is paid for by the suffering of millions.

  We are learning from our mistakes, we are mourning our vanished kin, and we now build a new politics of hope.

  We respect and uphold the absolute need for clean air, water and soil. We see that economic activities that benefit the few while shrinking the inheritance of many are wrong.

  And since environmental degradation erodes biological capital forever, full ecological and social cost must enter all equations of development.

  We are one brief generation in the long March of time; the future is not ours to erase.

  So where knowledge is limited, we will remember all those who will walk after us, and err on the side of caution.

  This we resolve

  All this that we know and believe must now become the foundation of the way we live.

> At this turning point in our relationship with Earth, we work for an evolution:
> *from dominance to partnership;*
> *from fragmentation to connection;*
> *from insecurity to interdependence.*

Important to note is Suzuki's final imperative that we work from "insecurity" – not to "security" but rather – to "interdependence," suggesting the stronger alternative to just security.

In a similar fashion, Benyus [5] provokes the designers of today to reconsider their source of inspiration and to look deeply into nature to find the "genius of place," the "biological beginning." *Biomimicry* – a call to study and absorb nature's principles for the purposes of design – is the other side of Carson's *Silent Spring* coin, a call in response to the warning. In it Benyus identifies a new science that views nature as model, measure, and mentor, searching for wisdom instead of knowledge to inform innovation in agriculture, energy, textiles, medicine, computation, business, and architecture.

Reconnecting Mind, Body, and Spirit

While it may be unorthodox to incorporate the notion of spirit within a scientific text, it is precisely the separation of spirit from mind and body that has distorted our thinking and has taken humanity out of alignment with nature. To underscore the need for integration, or reintegration in the case of the twenty-first century condition, one must reengage the spirit.

Chrisna du Plessis, at the first national convention of the US Green Building Council in 2002 in Austin, Texas [29], shared what the developing world can offer the rest of humanity in terms of sustainable thinking:

- In lieu of mastery of nature, consider mastery of self.
- In lieu of progress above all, consider humanity above all.
- In lieu of pursuit of knowledge, consider pursuit of wisdom.

As technology such as BIM bridges the knowledge gap, humanity's recognition of our own interdependence with nature can bridge the wisdom gap, leading us back to an integrated whole: the integration of man–climate–place honored by indigenous populations, the integration of nature–human ecosystems honored by Rachel Carson, and the integration of diverse disciplines central to introducing buildings and communities that are truly regenerative.

Bibliography

1. AIA National (2007) AIA California Council integrated project delivery a guide. The American Institute of Architects, Washington, DC
2. Womack JP, Jones DT (2003) Lean thinking: banish waste and create wealth in your corporation. Free Press, New York. ISBN 0-7432-4927-5
3. World Commission on Environment and Development (1987) Report of the World commission on environment and development: our common future. Annex to document A/42/427. United Nations, Geneva
4. McLennan JF (2004) The philosophy of sustainable design: the future of architecture. Ecotone, Kansas Ctiy. ISBN 0-9749033-0-2
5. Benyus JM (1998) Biomimicry: innovation inspired by nature. Harper Collins, New York. ISBN 0-06-053322-6
6. King R (2000) Brunelleschi's dome: how a renaissance genius reinvented architecture. Penguin Group, New York. ISBN 0-8027-1366-1
7. World Commission on Environment and Development (1987) Report of the World commission on environment and development: our common future. Annex to general assembly document A/42/427. Development and International Cooperation: Environment, New York
8. Kellert SR, Heerwagen JH, Mador ML (2008) Biophilic design: the theory, science, and practice of bringing buildings to life. Wiley, Hoboken. ISBN 978-0-470-16334-4
9. Carson R (1962) Silent spring. Houghton Mifflin, New York. ISBN 0-618-25305-x
10. Mattar SG (1983) Buildability and building envelope design. In: Second Canadian conference on building science and technology, Waterloo
11. Womack JP, Jones DT, Roos D (1991) The machine that changed the world: the story of lean production. Harper Perennial Modern Classics, New York. ISBN 0-06-097417-6
12. Holstein WK, Tanenbaum M (2011) Mass production: Encyclopaedia Brittanica. *eb.com*. [Online] Encyclopedia Brittanica Online. http://www.britannica.com/EBchecked/topic/368270/mass-production. Accessed 9 May 2011
13. Liker JK (2004) The Toyota way: 14 management principles from the world's greatest manufacturer. McGraw-Hill, New York. ISBN 0-07-139231-9
14. Koskela L et al (2002) The foundations of lean construction. In: Best R, de Valence G (eds) Design and construction: building in value. Butterworth-Heinemann, Oxford
15. Ballard G et al (2002) Lean construction tools and techniques. In: Best R, de Valence G (eds) Design and construction: building in value. Butterworth-Heinemann, Oxford
16. Lichtig WA (2005) Sutter health: developing a contracting model to support lean project delivery. Lean Constr J 2:105–112

17. 7group, Reed BG (2009) The integrative design guide to green building: redefining the practice of sustainability. Wiley, Hoboken. ISBN 978-0-470-18110-2
18. Yudelson J (2009) Green building through integrated design. McGraw-Hill, New York. ISBN 978-0-07-154601-0
19. Williams K et al (2000) The NIST report for the MSU EPICenter. NIST, Washington, DC
20. Kats G (2009) Greening our built world: costs, benefits, and strategies. Island Press, Washington, DC. ISBN 9781597266680
21. Ballard G (2000) Lean project delivery system, revision 1. White paper #8, Lean Construction Institute, Sep 23, 6 pp
22. Kieran S, Timberlake J (2004) Refabricating architecture: how manufacturing methodologies are poised to transform building construction. McGraw-Hill, New York. ISBN 0-07-143321-X
23. Krygiel E, Nies B (2008) Green BIM: successful sustainable design with building information modeling. Wiley, Indianapolis. ISBN 978-0-470-23960-5
24. Building smart alliance (2010) About National BIM Standards. National Institute of Building Sciences, 19 Aug 2010 [Online]. http://www.buildingsmartalliance.org/index.php/nbims/about/
25. The David and Lucile Packard Foundation (2002) Sustainability report: six scenarios for the David and Lucile Packard Foundation, Los Altos Project. BNIM Architects, Kansas City
26. Gallaher MP et al (2004) Cost analysis of inadequate interoperability in the U.S. Capital Facilties Industry. GCR 04–867. National Institute of Standards and Technology, Gaithersburg
27. Wilson EO (1998) Consilience: the unity of knowledge. Alfred A. Knopf, New York. ISBN 0-679-45077-7
28. David Suzuki Foundation (1992) Declaration of interdependence. David Suzuki Foundation [Online]. http://www.davidsuzuki.org/about/declaration/
29. du Plessis C (2002) Keynote speech at the U.S. Green Building Council Greenbuild National Conference, Austin

Sustainable Ecological Aquaculture

Stephen F. Cross
Coastal Aquaculture Research & Training (CART) Network, Department of Geography, University of Victoria, Victoria, BC, Canada
SEA-Vision Group of Companies, Courtenay, BC, Canada

Article Outline

Glossary
Definition of the Subject and Its Importance
Introduction
Future Directions
Bibliography

Glossary

Alternative energy Is a generic term that refers to any source of usable energy intended to replace fuel sources without the undesired consequences of the replaced fuels. It is typically used to describe renewable forms of energy that can be used in place of fossil fuels and thereby reducing, mitigating, or eliminating the negative environmental consequences associated with the traditionally used fuels.

Aquaculture Is the farming of aquatic organisms and represents a controlled approach to the production of marine or freshwater species – differentiating it from fishing, which is the harvest of wild organisms.

Integrated multi-trophic aquaculture (IMTA) An ecologically designed recycling process in which the organic wastes generated from one species become inputs (food or nutrients) for another. A fed aquaculture species, such as fish or shrimp, are combined with inorganic extractive (e.g., seaweed) and organic extractive (e.g., shellfish) aquaculture to create an ecologically "balanced" food production system.

Ocean ranching A seafood production approach that combines aquaculture techniques with traditional fishery methods. Juveniles are produced in hatchery and controlled rearing facilities, and then released to the ocean environment where they grow under natural (no containment) conditions to harvest size and then captured (fished) using standard industry methods (e.g., trolling, seining, divers, etc.).

Polyculture An agriculture or aquaculture approach that uses multiple crops (or species) in the same space, typically in an effort to avoid the production issues (e.g., disease susceptibility) associated with single-species, or monoculture production. Differentiated from IMTA, which selects species based upon ecosystem function (trophic relationships), polyculture simply supports species diversification within the production model.

Sustainability Meeting the environmental, social, and economic needs of the present generation without compromising the ability of future generations to meet their needs.

Definition of the Subject and Its Importance

An increasing global demand for seafood has resulted in considerable and increasing pressure on world

fisheries, with a number having already collapsed and others in serious decline [1]. Satisfying the growing seafood demand has seen aquaculture production increase significantly over the past few decades, with the current contribution of aquaculture to the global seafood supply equal to or exceeding that of the wild fisheries. However, commensurate with this controlled, although often intensive, approach to seafood production are a number of environmental consequences that have called into question, as with the pressured growth in the wild fisheries, the ultimate sustainability of these approaches.

Sustainable ecological aquaculture (SEA) systems endeavor to address the socioeconomic and environmental facets of sustainability by integrating ecological and engineering system design with comprehensive best management practices. Operational efficiency is considered a keystone element in such designs, and one which will ultimately demonstrate that an industry focus on sustainability can also be profitable – a critical argument in encouraging innovation and facilitating long-term change within the corporate environment of global food production.

Introduction

The United Nations Food and Agriculture Organization (FAO) defines sustainability as "*Meeting the needs of the present without compromising the ability of future generations to meet their needs*" [2]. This definition requires that mankind keeps population densities below the carrying capacity of a region, facilitates the *renewal* of renewable resources, conserves and establishes priorities for the use of nonrenewable resources, and keeps environmental impact below the level required to allow affected systems to recover and continue to evolve.

In a simple, yet technical-based definition, sustainability – in reference to natural resource management – has also been described as the "*long-term maintenance of ecosystem components and functions for future generations*" [3]. Linking economic, social, and environmental aspects of human society this concept is intended to configure civilization and human activities so that society, its members and its economies are able to meet their needs and express their greatest potential in the present, while preserving biodiversity and ecosystem integrity, and planning and acting for the ability to maintain these ideals indefinitely [4].

Although sustainability values may vary greatly among cultures, there is a fundamental commonality among these details that is best described as a "*parallel care and respect for the ecosystem and for the people within*." From these common values emerges the goal of sustainability – to concurrently achieve human and ecosystem well-being. It thus follows that the measure of sustainability for any activity (including aquaculture) be the achievement of, or the contribution to, human and ecosystem well-being together. In this way, the concept of sustainability can be considered a positive concept that has as much to do with achieving well-being for people and ecosystems as it has to do strictly (as is often the focus) with environmental protection.

In general, society has been moving steadily toward sustainable industrial activities for a number of decades, recovering "waste" in an effort to recycle and reuse such materials [5]. Industry and government have both recognized that these waste streams are in fact a valuable resource, and society now expects the use of recoverable materials and the integration of natural design into most product development. These ideals are further promulgated through initiatives such as eco-labeling, eco-certification, eco-design, etc. – all of which are becoming more prevalent in the seafood production industry [6].

Consumers now use their purchasing power to ensure that the products they acquire meet these ever-changing social criteria. A growing awareness of sustainability issues has placed pressure on business (industry) to shift or to modify their production processes to accommodate the eco-ethical consumer needs [7]. This has become increasingly critical to both the wild fisheries and the aquaculture industry sectors as demand for a high quality, and sustainable supply of seafood continues to rise.

While it is indisputable that the achievement of sustainability for coastal aquaculture – embracing social, economic and environmental objectives – is necessary, the motivation for fundamental change in current industry production approaches, where required, has not yet been clearly established. The development of sustainable ecological aquaculture (SEA)

systems represents a movement toward this goal, and commercialization efforts are now in place to provide working models and the basis for future innovations [8]. The following sections provide an example of SEA-System development in coastal British Columbia, a region renowned for the social conflicts associated with open netcage (finfish) aquaculture. The environmental issues associated with this approach to finfish aquaculture are summarized and then used to exemplify how a sustainable ecological aquaculture (SEA) system approach can be developed to resolve these issues, and further to illustrate how a comprehensive approach to SEA system design and operation can satisfy the environmental, economic, and social aspects of aquatic food production sustainability.

Sustainability Issues in Coastal Aquaculture Production

The development of coastal aquaculture, and the subsequent increase in its global role for seafood production, has not been without its environmental and socioeconomic risks and negative impacts [9]. The rapid development in Asian shrimp production through pond culture, for example, stimulated significant socioeconomic activity in traditionally poor, rural coastal communities – resulting, as envisioned, in increased livelihood opportunities in the wake of declining subsistence fisheries. Although successful in addressing a number of social issues associated with the coastal fisheries situation, the inherent value in shrimp production and the local and regional wealth it generated facilitated the tendency to further increase production, despite exceeding environmental sustainability criteria, to support further wealth creation, with a predictable result – catastrophic production collapses with serious socioeconomic and environmental consequences [10]. The three pillars of sustainability – environmental, social, and economic – are truly in balance, and ignoring one can have serious consequences to this integral relationship.

In the global salmon aquaculture industry, with farm production originating in Norway, Chile, United Kingdom, Canada, United States, Australia, and New Zealand, a standardized production approach, including infrastructure configuration and general management practices, has resulted in a common suite of sustainability issues associated with the industry. The net-cage aquaculture operational procedures that will ultimately influence whether this approach is considered environmentally sustainable will also form the basis upon which social and economic criteria for sustainability are determined. As with many new coastal activities, social "acceptance" of open net-cage aquaculture has, in many jurisdictions, waned as inherent environmental issues have been identified during the early stages of its development. Issues that currently jeopardize the sustainability of this form of coastal aquaculture include the following.

Species selection is typically seen as a serious risk when exotic (non-indigenous) species are used [11]. Should escapes occur, the potential for disruption of ecosystem structure through displacement of indigenous species, or the potential for interbreeding that could weaken the natural, resident populations are associated with use of such species – despite their selection and obvious benefits as farm stock (disease resistance, faster growth rates, etc.). Farming of high densities of animals in proximity to wild populations of similar phylogeny may also pose threats of disease and/or parasite transfer both to and from the farm facility.

Stock escapes have occurred both incidentally, as a result of human error during the husbandry process, or catastrophically due to containment system failure during extreme weather episodes, and marine mammal interactions causing severe subsurface net damage. The risks associated with stock escapes include interactions with wild populations – genetic dilution – as well as those associated with the escapes of farm stock comprised of non-indigenous species (referenced above) [12, 13].

Chemotherapeutic compounds represent a wide range of complex chemical and antimicrobial compounds that have been developed to manage farm stock disease and parasite issues. Their use is considered a site management activity, and is recognized as a stressor due to the periodic release of the respective compounds (and residues) into the environment [14]. The environmental effects of this stressor could manifest itself in a number of ways – changes to contaminant concentrations

(partitioned in various ways within the ecosystem), and through a suite of potential effects determined by the bioavailability of these residues to nontarget organisms within the ecosystem.

Chemicals used in net-cage aquaculture comprise a variety of compounds and include the micronutrients of fish feed (trace metals), disinfectants, anaesthetics, and antifoulants. All are released to the marine environment, albeit typically in very low concentrations and at differing release rates. The fate and effects of these residues within the environment, like that of the chemotherapeutic compounds, pose a risk to a variety of ecosystem components through environmental partitioning, accumulation and persistence, and the bioavailability and effects to nontarget species [15].

Organic fish wastes are a natural product comprised of fecal material and incidental wasted feed. These materials are released from the fish and enter the environment where they can have localized impacts to benthic habitat, changing biophysical conditions and displacing or disrupting species composition of these communities [16, 17]. While localized in nature, these impacts are of considerable concern when considered with respect to aquaculture expansion and the potential for broader, cumulative effects.

Inorganic fish wastes, comprise of dissolved nutrients (e.g., nitrogen, nitrate/nitrites, ammonium, phosphorus) are excreted as a result of fish metabolism and primarily released to the environment through the urine [18–20]. While localized effects of nutrient release are often associated with enrichment effects, nutrient loading from large or multi-farm operations have been implicated in potential eutrophication processes, with speculation that harmful algal blooms can be generated and sustained as a result of the cumulative nutrient enrichment (far-field) effects from such aquaculture facilities.

Energy consumption, and particularly that component generated from hydrocarbon-based (fossil) fuels, is currently a globally recognized sustainability issue – regardless of the associated activity [21]. Salmon, and other temperate finish aquaculture, currently operate in remote coastal areas and as a result, rely upon off-grid source of power for much of the required operational needs. Expansion of these industry sectors to satisfy increasing seafood supply will likely result in further use of such coastal areas and thereby increase the use and hence the broader scale effects associated with this use.

The significance of these open net-cage aquaculture issues, in terms of impact upon environmental and socioeconomic sustainability, varies among the farm operational regions and reflects local concerns, values, and hence how, where, and what priority research effort is focused. Many of these sustainability issues are addressed independently, through a variety of ongoing private sector and/or academic-based research initiatives, and usually in an effort to continually improve environmental and economic performance of the present production model [22].

While a continual improvement paradigm is a recognized and essential component to maintain sustainability, typically characterized with ongoing and relatively minor changes to operational procedures or infrastructure design (e.g., materials use), a more dramatic step in the development of sustainable aquaculture will be required in order to supply increasing demands for seafood. The evolution toward sustainable ecological aquaculture (SEA) systems considers the array of stressor-impact concerns associated within current production models with the objective of designing an approach that incorporates innovative infrastructure and proactive operational controls [23].

Design and Operational Framework for SEA Systems: Considerations for Socioeconomic Sustainability

A sustainable ecological aquaculture (SEA) system can be defined as *a holistic aquaculture approach that uses the principles of ecology to achieve the goal of sustainability*. It is essentially a blend of two developmental pathways for aquaculture systems, whether referring to a freshwater or to a marine environment scenario, i.e., sustainable aquaculture and ecological aquaculture. In terms of the *sustainable* aquaculture component, a sustainable ecological aquaculture system endeavors to satisfy the perpetual needs of society (e.g., ensuring food security, maintaining livelihoods) while protecting the environment – and do so in a manner that is efficient and hence economically viable [22].

Figure 1 illustrates the relationship among the three facets of sustainability. While the range of

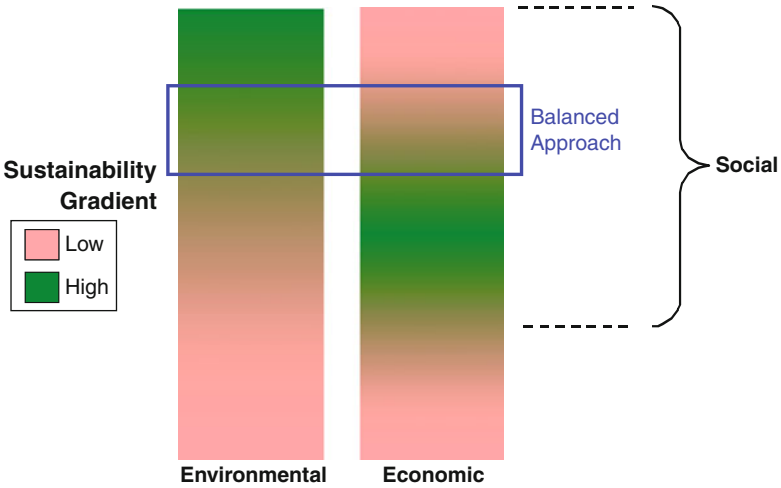

Sustainable Ecological Aquaculture. Figure 1
The inherent balance between environmental and economic sustainability gradients, based upon a comprehensive suite of sustainability factors/indicators, the associated need for compromise, and the relationship to social acceptance

Social acceptance may vary considerably among communities, and/or given a specific form of aquaculture, the balance between environmental and economic sustainability is much more objective in nature with their concurrent evaluation typically resulting in a compromise that may in fact represent a narrow range of opportunity. If, for example, all of the criteria considered necessary to achieve environmental sustainability (top portion of the left gradient) is the goal, then the associated economic costs may increase and actually exceed the ability to accomplish the environmental objectives (illustrated with a pink portion at the top of the right gradient). Hence, to achieve economic sustainability, a sacrifice along the environmental gradient of sustainability may be required in the short-term. As system innovation addresses operational efficiencies and costs, then the balanced approach shown with the blue box (Fig. 1) will move toward the top of both gradients – improving environmental performance while remaining, and potentially increasing, social acceptance.

Environmental Sustainability: The Ecological Design of SEA Systems

The configuration and operational design of many current aquaculture systems are, or could with minor modifications, be considered environmentally sustainable. Minor ongoing operational improvements, typically introduced as efficiencies in husbandry practices, have and will continue to result in the reduction of environmental effects. For example, the development and introduction of effective vaccines has dramatically reduced the use of antibiotics, the residues from which are released to the environment and presumably neutralized through natural assimilative processes. The engineering and introduction of new structural materials (e.g., netting), with greater breaking strengths and increased antifouling properties, prevent negative interactions with predators and reduce maintenance (net washing) costs while optimizing water quality and flows through the cages.

However, as the demand pressures on current seafood supply continues to rise, the scale of coastal production (individual farm configuration and/or regional allocation of farming units) will need to increase at a rate faster than minor adaptive changes to existing system design will be able to occur to remain environmentally sustainable. Figure 2 illustrates the hypothetical impacts of increased production on sustainability using seven environmental stressors – stock escapes (and use of exotic species), release of therapeutic and chemical residues, discharge of organic and inorganic wastes, and energy use.

Scenario I in Fig. 2 (upper portion) represents the projected effects of present farm operational models

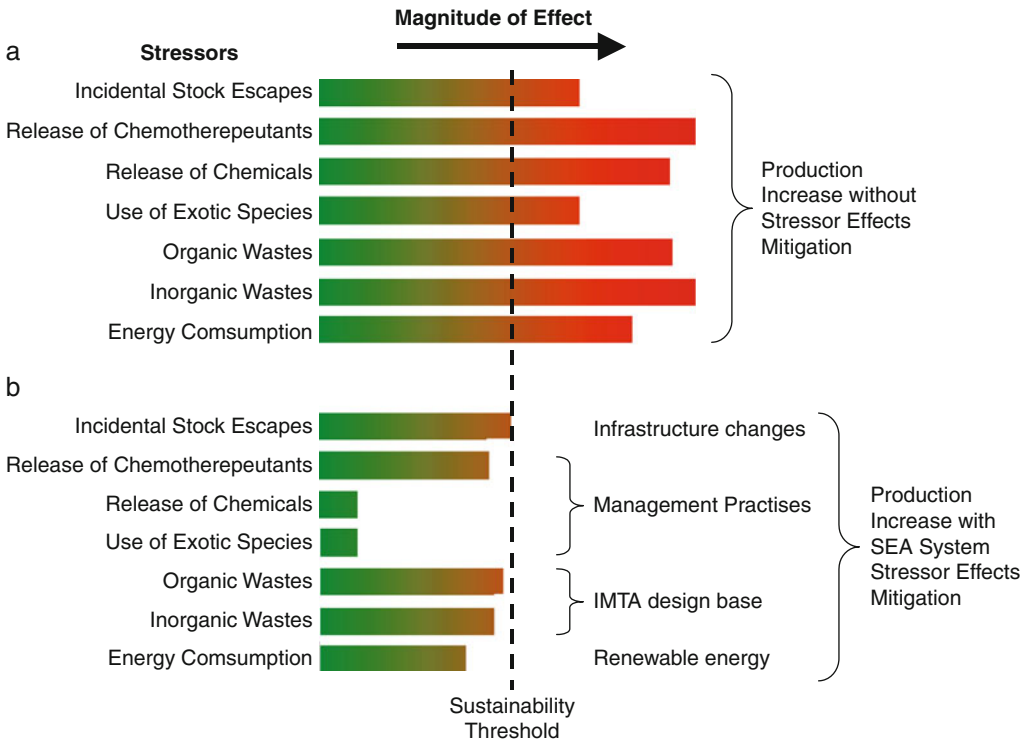

Sustainable Ecological Aquaculture. Figure 2
Anticipated sustainability impacts of increased farm/regional production based on two developmental scenarios: (**a**) magnitude of individual environmental stressor effects without the introduction of appropriate mitigation measures; and (**b**) potential mitigation of these stressor effects using a sustainable ecological aquaculture approach to production

given a dramatic increase in production with a limited adaptive response to mitigate the associated environmental impacts. At present, the magnitude of independent environmental effects resulting from each of these seven stressor effects is likely to the left of the vertical dashed line, which represents the sustainability threshold for each stressor effect. As production is increased, through increased farm size and/or the number of farms within an operational area (density), the magnitude of stressor effects of any number of these (and other) operational factors will exceed the environmental, and eventually the social and economic sustainability thresholds.

Scenario II in Fig. 2 (lower portion) suggests how a sustainable ecological aquaculture approach, representing a significant shift in fundamental system design and operational considerations, would proactively mitigate (or eliminate) the impacts of the example stressor effects and thereby accommodate increased production needs. First – use of an *integrated multi-trophic aquaculture (IMTA)* production model provides an inherent increase in system productivity (and product diversification), yet represents a design and change in *infrastructure configuration* that facilitates interception and use of the organic and inorganic wastes, generated and released from the fed (fish) component, by extractive species such as shellfish, echinoderms and seaweeds/kelps [24–27]. Second – revised *management practices* that comprise protocols committing to best (e.g., *organic)* practices/standards result in strict control over all operational inputs, including elimination of therapeutics and other process chemicals, restricted introduction/use of non-indigenous species, and sourcing of feeds.

Third – integration of renewable energy into system operations provides a significant and ongoing reduction in the use of fossil fuels and hence the carbon footprint of the operation.

Example: Commercialization of the SEA-System Approach

The principles of sustainable ecological aquaculture are currently being applied by the SEA-Vision Group of companies of western Canada (www.SEAvisiongroup.ca) in the development and commercialization of its own SEAfood System. This unique coastal aquaculture production system is based on the predominant open netcage approach used in finfish aquaculture but incorporates engineering and ecological design components that facilitate a scalable transition from single to multiple species production. In the development of this new system, the SEA-Vision Group has considered the social, environmental, and economic pillars of sustainability – resulting in an environmentally efficient, cost-effective production system that meets the scrutiny of both the local community and the consumer. A description of the key socioeconomic and environment design aspects of the SEAfood System are provided in the following sections.

Social Sustainability Considerations Social sustainability is based on *acceptance* and on *involvement*. Introduction and commercialization of the SEAfood System in coastal British Columbia considered three levels of social engagement – community design input, operational involvement, and satisfaction of consumer demand.

Community design input was considered essential in establishing the conceptual framework upon which the local coastal community would be willing to accept and support the introduction of a new commercial-scale production system/operation – one intended to address the ongoing controversies associated with coastal aquaculture in the region. In British Columbia, the aquaculture industry comprises two independent sectors – shellfish and finfish. Shellfish, which primarily encompasses self-feeding extractive species such as oysters, scallops, mussels, and intertidal clams, also includes (and refers to) other extractive invertebrates that have had their historical use as a harvest fishery and have recently garnered attention as potential culture candidates, for example, urchins, sea cucumbers, geoduck clams, and abalone. The finfish sector was developed with salmon (indigenous and introduced species) but has begun to diversify with the introduction of marine species such as sablefish and rock cod.

Sites best suited to aquaculture in British Columbia are generally located in remote coastal areas, substantially removed from urban centers and populations. These areas remain resource-based and under joint management control of Provincial/Federal governments and the local aboriginal (First Nation) peoples that maintain claim over their traditional coastal territories. In soliciting *community design input* for the new SEA-Vision Group production model, the integration of traditional ecological knowledge (TEK) of the residing coastal first nation community (the Ka:'yu:'k't'h'/Che:k:tles7et'h' First Nation = KCFN) was a critical social engagement step [28] in the commercialization process. Discussion of the SEAfood System conceptual design with the KCFN allowed input as to species selection that satisfied the ecological design criteria of the system yet met the needs and concerns of the local community. The KCFN conveyed their specific concerns regarding coastal aquaculture, identified a suite of indigenous species candidates for the system design, and provided valuable input into which of these species would be of most value to their people's tradition. A formal agreement as to species use, restrictions, and other operational criteria was prepared and has formed the basis for local social acceptance of the SEA-system approach in this case – one that also supports the social sustainability issues of the community.

Operational involvement has also been an important social sustainability factor for the SEAfood System development, providing and supporting direct and indirect coastal community livelihoods – for example, farm staff, contract services (divers, harvest vessels), investment. Integration of local workers into the business, including those from the KCFN, further supports the social acceptance of the approach, allowing ongoing input into system operational improvements. A continuing working partnership with the local community is critical to the success of current operations and the potential for future operational expansion and corporate growth.

Consumer demand for seafood sustainability was also an important consideration of the social engagement process. Many of the environmental issues associated with open netcage aquaculture have had a direct influence on consumer acceptance of the product (farmed salmon), and with an associated and growing demand for wholesome, sustainably produced seafood, the design and operational attributes of the SEAfood System deliberately focused on these consumer criteria to provide a supply of seafood that would satisfy these demands. By systematically addressing this range of environmental concerns, and by continually and immediately addressing new issues/concerns as they are realized, the sustainable ecological approach allows the consumer to be integrated into the continual improvement paradigm of the approach – and thereby further supporting the sustainability of the SEAfood System.

Environmental Sustainability Attributes In order to address, and facilitate improvement among all of the socio-environmental issues of open netcage aquaculture in the region, the SEA-Vision Group system focuses on three design components – its production model, energy needs, and operational practices (Fig. 3). This combination effectively encompasses ecological design (multispecies, IMTA approach) to reduce the waste/nutrient foot-print, integrated energy alternatives to reduce the carbon foot-print; and implementation of best, organic practices to mitigate the potential effects of antibiotics and chemical use.

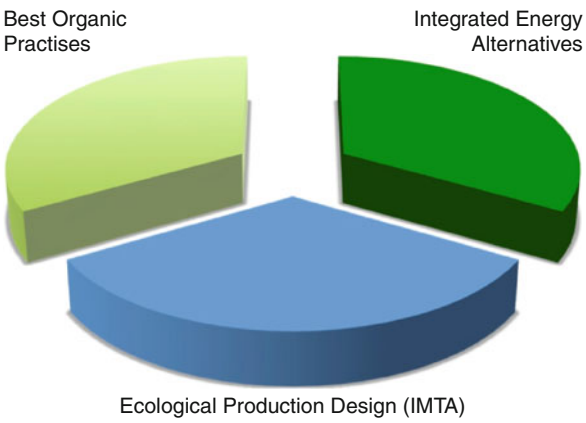

Sustainable Ecological Aquaculture. Figure 3
The SEAfood System™ addresses the majority of socio-environmental issues of open netcage aquaculture using an effective combination of ecological (multispecies, IMTA) system design, integrated energy alternatives, and a suite of best organic practices

Production Model The ecological production design of the SEAfood System is based on that of an Integrated Multi-Trophic Aquaculture (IMTA) model [29]. This multispecies approach expands upon the monoculture model for fed (fish) production by integrating a number of extractive species to intercept and remove the organic and inorganic wastes generated by the fish. Two simple criteria are used in the selection of species for the SEAfood System: (a) each species must fill an ecological role in the removal of organic and/or inorganic wastes; and (b) each must have economic value – a marketable and profitable product [30, 31].

The SEAfood System model developed in British Columbia combines a single fed species – sablefish (*Anoplopoma fimbria*) or Chinook salmon (*Oncorhynchus tshawytscha*), with a variety of extractive species positioned deliberately to facilitate interception and removal of the organic and inorganic fish wastes that are released into the environment as particulates and dissolved nutrients. Downstream of the fish component is a shellfish (bivalve mollusk) system that is situated and configured to maximize the extraction of the fine particulate fraction of the organic waste streams [32]. Further downstream is a series of kelp/seaweed grids (*Saccharina lattisima* or *Porphyra sp.*) that are positioned to intercept and capitalize on the enriched dissolved nitrogenous wastes. Beneath the entire floating infrastructure of the farm, sea cucumbers (*Parastichopus californicus*) are grown in an ocean-ranching style – released as juveniles, these animals consume the rich settleable organic material that would otherwise accumulate over the seafloor.

Figure 4 illustrates the infrastructure configuration and spatial relationship of the SEAfood System species. The various extractive components of the SEAfood System are situated in such a manner so as to maximize receipt of the organic and inorganic wastes originating from the fish. SEAfood System sites – SEAfarms – are configured with the extractive species downstream and to one side of the fish component to allow for

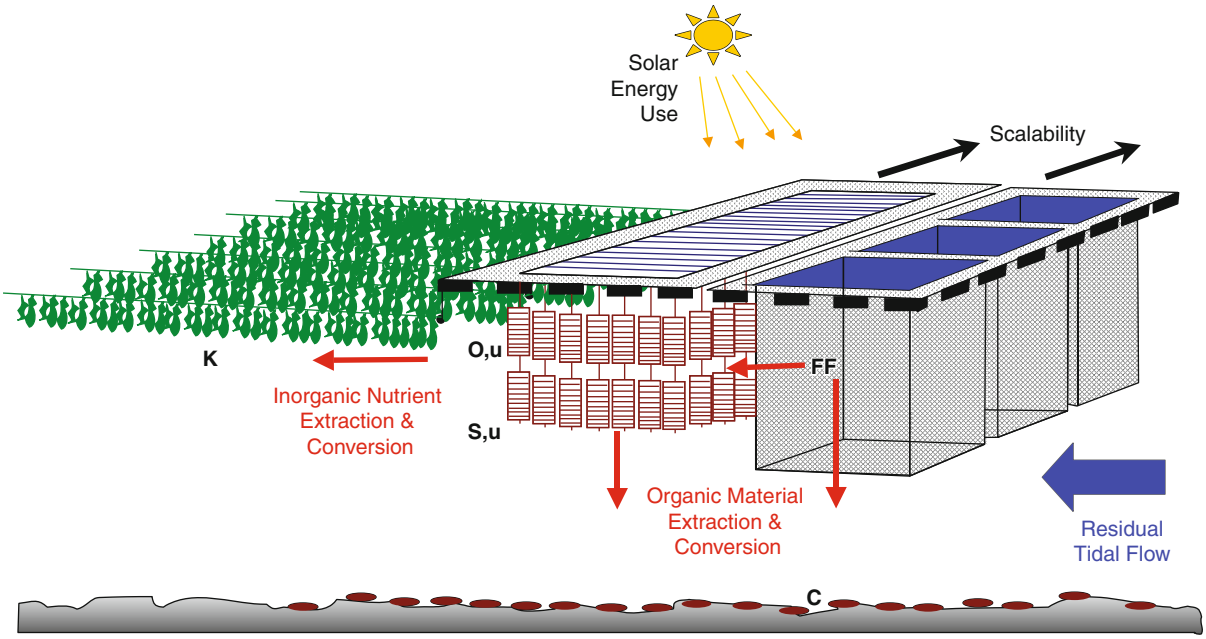

Sustainable Ecological Aquaculture. Figure 4
Infrastructure configuration, orientation with respect to tidal flow, and the spatial relationship of the SEAfood System™ species. The integrated multi-trophic aquaculture (IMTA) design aspects of the system support a single-fed component (**FF** – sablefish or salmon), a 2-tiered shellfish component (**O** – oysters; **S** – scallops) to extract fine organic particulates, a deposit feeding component comprised of sea cucumbers (**C**) to remove settleable organics, and a large kelp/seaweed component to assimilate dissolved nutrients. Urchins (**u**) are integrated with the shellfish to reduce biofouling and solar energy is used to power operational components of the system

operational logistics around the cages (e.g., vessels used for net changes, harvesting, etc.). Site selection and subsequent system orientation thus requires a thorough physical oceanographic assessment to ensure that system component placement is in the direction of the residual tidal flow (downstream).

The total length and production capacity of a SEAfarm is scalable and is determined by the finfish production component. In the initial model each SEAfarm is 200 m in length and includes twelve 15-m square cages or six 30-m cages. This small operational foot-print for the fish production component (by current industry standards) is considered an additional environmental benefit to the SEAfood System design, allowing for better water flow, waste transfer, and overall assimilative efficiencies among the species components.

Infrastructure compatibility between the extractive components and that of the base finfish production system is considered key to SEAfood System production capacity and operational efficiencies. A new suspended shellfish aquaculture system was therefore designed and engineered to meet the unique needs of multispecies production. The system, shown in Fig. 5, uses similar construction materials to that of the finfish cage (e.g., galvanized steel, high-density polyethylene flotation billets), provides a production platform with a number of benefits: (a) strong connection points for securing to the finfish cage system, (b) a very high floatation capacity that supports considerable shellfish production – both in surface area and in depth, (c) a moving *SEA-Tram* system that supports multiple, wind/solar-powered winch systems for on-system handling of shellfish product, (d) adjustable cross-beams to allow changes to spacing of the shellfish droplines, and (e) standardized outboard attachment points for kelp/seaweed lines.

The shellfish component of the first SEAfood System production model, shown in Fig. 5, comprises Pacific oysters (*Crassostrea gigas*) in the surface layer (1–4 m) and Pacific scallops (*Patinopecten yessoensis*) in

Sustainable Ecological Aquaculture. Figure 5
Left photograph: a segment of the SEAfood System's shellfish component showing the powered SEA-Tram and gantry for hoisting shellfish droplines. *Right photograph*: SEA-Tram gantry showing author lifting dropline of scallop nets using one of the winch components; these six winches have subsequently been changed to electric units with a solar panel system mounted at the top of the gantry. Battery storage is at the base of the gantry

the lower (5–10 m) portion of the water column. With 1.0 m spacing between vertical lines of shellfish trays/nets, the overall 2-tiered shellfish system comprises a biofiltration component that is 15 m wide (immediately downstream of the fish), 10 m deep, and extends parallel to the finfish cages and the entire length of the farm (200 m). A SEAfarm of this size thus has the capacity to physically support approximately 2,600 vertical shellfish lines with each line comprised of 8 oyster trays and 12 scallop nets – a total of 52,000 shellfish production units.

Kelp lines are attached to the downstream side of the shellfish component, with a 1.0-m spacing, which in the current British Columbia SEAfarm model results in a total of 200 kelp/seaweed production lines. These lines run perpendicular to the shellfish system with the production grid extending 80 m downstream of the shellfish structure (although length is only limited by available space).

The sea cucumber component of the SEAfood System is managed using an ocean-ranching approach that makes it independent of the floating aquaculture production units that support the finfish, shellfish, and kelp/seaweed. Cucumber seed (small juveniles: 2–3 cm) are sowed over the ocean floor (5–10 m^2) and allowed to move freely in the vicinity of the farm structures, taking advantage of the continual input of organics originating from the overlying species assemblage – fed and extractive components. Once achieving market size these animals are harvested using divers, and although a somewhat labor-intensive method, this extensive approach allows for waste management across the entire farm rather than just below the source of the settleable organics (the finfish).

Energy Needs Widespread recognition and growing concern over fossil fuel consumption trends, associated carbon emissions, and the global/regional climatalogical effects of these atmospheric loads are also reflected at the aquaculture farm scale, representing a significant environmental as well as economic (business) impact. For example, in remote coastal aquaculture operations, the reliance on diesel fuel to power boats and associated equipment (hydraulic pumps, winches) represents a significant impact on operations. In an analysis of the current shellfish aquaculture industry, it has been estimated that to produce a dozen [12] oysters using a suspended (raft) culture approach requires 0.24 l of diesel fuel over the entire production cycle – this

includes on-farm activities only and does not account for seed and harvest transport to/from the farm.

Integration of sustainable energy alternatives (SEA-Power) within the SEAfood System design was envisioned as another approach to improve upon environmental performance (reducing the carbon footprint) while addressing this inherent and increasing operational cost of aquaculture production. As alternative energy systems continue to increase in efficiency, their unit size, weight, materials use, and life cycle characteristics now lends itself to uses other than satisfying the energy needs of large facilities (e.g., homes, commercial buildings).

Following a detailed site-specific meteorological assessment, selection, and integration of a solar energy system has been used within the first SEAfood System operation to operate the winch systems within the shellfish production component. Panels at the top of the SEA-Tram collect solar-derived electrical energy to maintain a battery storage unit at the base. The 2.0-kW system for the first SEAfarm site has been designed for independent operation of six electric winches, each capable of lifting a maximum of 240 kg (shellfish droplines). The energy use pattern for the SEA-Tram is unique, in terms of typical alternative energy system uses, in that operation of the winch units occur over a 10–12-h working day, and comprise a series of long-lift (entire dropline) retrieval as well as short lifts (vertical moves from one layer of shellfish to the next for product handling).

Each proposed SEAfarm site will have different alternative energy sources and will require different energy extraction and storage configurations. The shift between small solar and wind power units, or using a combination of the two, may be needed to maintain operational energy needs for this intended use within a SEAfarm. The size of the farm may also dictate the need for additional SEA-Tram (and associated energy units) in order to efficiently manage shellfish production levels within this SEAfood System component. The current model considers a SEA-Tram for each 100-m length of farm – a total of two for the one discussed in this example (one operating on each end of the SEAfarm).

Operational Practices Application of organic operational standards is considered an effective approach by which many of the other environmental issues associated with coastal aquaculture, including food formulations, use of antibiotics and other chemicals, animal welfare (stocking density), etc., can be addressed [33]. While certified organic standards are currently under development in North America, it is anticipated that these operational protocols will be similar to Standards that are currently in practice in other jurisdictions (e.g., *Naturland organic standards* in the EU).

Organic standards include strict operational requirements for all aspects of the food production. In aquaculture, the standards dictate specifications for environmental management, prohibitions on use of antibiotics and chemicals, animal welfare (stocking densities, humane forms of dispatch), feed composition and sources, product handling (husbandry, harvesting, transport), biosecurity, emergency protocols, auditing requirements, staff training, branding, sales, etc.

Integrating these rigorous practices within the ecologically designed SEAfood System further supports the goal of achieving environmental as well as socio-economic sustainability. As a third-party-verified (audited) operational program, a certified organic aspect provides an important linkage between environmental sustainability practices and the inherent and ongoing need for social acceptability – a level of assurance to the consumer and to other coastal stakeholders. The implementation of a certified organic approach is also beneficial from a business/economic perspective, in that the approach will allow for further product differentiation and market access.

Economic Sustainability: The Business Model As discussed above, the ecological design and operational practices associated with the SEAfood System address many of the environmental issues/stressors associated with current methods of coastal aquaculture production, and in doing provides an additional measure of social acceptability (and sustainability) for this growing seafood producing sector. However, the sustainable ecological aquaculture (SEA) system approach is also inherently more complex than that of traditional production approaches – and with increased complexity comes increased operational (and business) risk. A cost-benefit analysis of the SEAfood System

production model, implemented during the early design stage of system development, is thus an essential exercise in terms of achieving economic (and business) sustainability [30, 31]. Basic criteria that have been incorporated into this assessment include the following: (a) species selection, value and production capacity, (b) operational efficiencies; (c) economy of scale; and (d) vertical integration.

Species Selection, Value, and Production Capacity The choice of species used in the SEAfood System developed for British Columbia considered social sustainability, ecological function within the production model, and market value (profitability). First, all species used in the system are native (or long established through introductions), and thereby satisfy the social issues and potential ecological risks of using exotic species – particularly in regard to the fed (finfish) component of the system. Sablefish and Pacific salmon, although slightly more difficult to culture than the Atlantic salmon, receive a significantly higher farm-gate value given the comparatively lower regional supply but increasing demand for these particular species. This inherent price premium, coupled with the *green* nature of the SEAfood System approach, offsets the cost of implementing and maintaining the operational standards required for *organic* certification – adding additional value to the fish and offering a variety of new market segment opportunities.

The selection of the organic extractive species is a much more difficult task given the number of species available to satisfy this role within the SEAfood System [34–37]. Choice of appropriate species ultimately requires a compromise between extractive efficiency and product value. For example, although blue mussels (*Mytilus edulis*) are known to be the most efficient shellfish species in terms of filtration capacity, their commercial value is much lower than that of other shellfish species candidates. Therefore, to maximize the profitability of the shellfish extractive component, a 2-tiered approach was introduced into the design – oysters in the surface layer (replacing a mussel) and scallops in the lower portion of the water column. The combination of the two extractive species not only increases the operational efficiency for this component but also provides a significantly higher farm-gate value to the overall seafood production model.

The business decision to adapt a much more complex, multispecies production system, and ultimately the economic sustainability of this approach, will be determined not only by the values of the individual species but also by the level of combined production that can be achieved for the additional, extractive species, the cost of production (CoP) for these integrated components, and continued consumer demand for the products.

Assuming that consumer demand remains constant (although it will likely continue to grow), Fig. 6 illustrates the relative proportions of annual production (harvest volumes) among the system components, as well as the farm-gate value for the various SEAfood System species in the first SEAfood System operation established on the Canadian west coast. For each kilogram of sablefish produced from the system, approximately 5 dozen half-shell oysters, 5–6 scallops, 1–2 sea cucumbers, and a kilogram of kelp are harvested. It should be noted that this proportion of species represents a starting commercial balance for the SEAfood System and one that will be refined over time to ensure extractive efficiency of the system. These values also represent the proportion of annually harvested stock, and the SEAfood System maintains multiple year classes of each species.

The pie chart in Fig. 6 illustrates the proportion (percent) of farm-gate revenue generated annually from each of the component species. These values were generated from total annual revenue projected for four regional SEAfarms, and averaged to provide standardized estimate of farm-gate sales for a single facility. The fed component of the system (e.g., sablefish) remains the highest value (66.4%), with oysters contributing 13.9%, scallops 12.5%, sea cucumbers 5.5%, and kelp 1.8% of the total annual sales revenue. With operating expenses of 63.5% of the total sales, the Net Revenue (Total Expenses – Total Gross Revenue) is 36.5%. This analysis indicates that from a business/economic perspective the SEAfood System is potentially quite profitable, and given these margins would not only be considered sustainable but would also support future growth.

Operational Efficiencies The SEAfood System maintains multiple-year classes for each component species, ensuring an annual balance between seed

Annual Harvest Proportions

Sablefish	1.0 kg (harvest weight)
Oysters	63.4 individuals
Scallops	5.3 individuals
Sea cucumbers	1.4 individuals
Kelp	1.0 kg

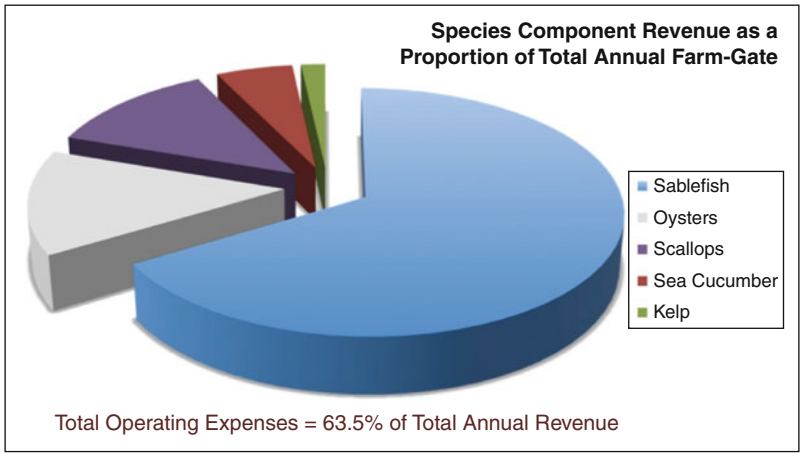

Sustainable Ecological Aquaculture. Figure 6
Annual harvest proportions and the individual species component revenues represented as a proportion of her total annual farm-gate sales

entry and product removal (harvest) for each of these species. Although intuitively a much more complex management challenge than a process involving a single species/product, there are inherent operational efficiencies – and economic (profitability) gains – that can be realized within this type of operational system.

The infrastructure design and configuration of this multispecies SEAfood System represents an adaptation of the galvanized steel netcage array used in the finfish aquaculture industry. The majority of species components (fish, shellfish, urchins, and attachment points for the kelp/seaweed) are directly accessible from the consolidated SEAfood System infrastructure components and thus do not require transportation of staff, materials, and vessels among what might otherwise comprise independently moored structures. The operational efficiencies gained through this design are significant, and are associated primarily with savings in labor and the requirement for dedicated working vessels (with fuel and equipment costs). Development of unique infrastructure (e.g., the shellfish SEA-Tram component) has further reduced the Cost of Production (CoP) within the consolidated multispecies SEAfood System model. By introducing alternative energy components to power shellfish winches, the saving in fuel (estimated from traditional shellfish production methods) is projected at over 43,000 l annually for each SEAfarm (based on 0.23 l/dozen shellfish produced). Fuel costs have continued to burden CoP over the past decade, and the present and future projections for the cost of fuel is a continual increase. The shift from fossil fuels to wind/solar energy is therefore readily justified, and in fact, represents a significant reduction in CoP and in business (economic) risk.

A shared labor pool will also result in a significant reduction in overall CoP. While each farm will require staff for finfish husbandry (feeding, net maintenance, grading, harvesting, etc.) as well as for the additional, extractive species component (shellfish grading, net maintenance, harvesting, etc.), in a consolidated multispecies system, there is opportunity for staff to assist in all tasks and thereby eliminate traditional slow periods in workloads. It is estimated that the SEAfood System will require 75–80% of the staff that would be cumulatively needed to independently operate the various production components.

While these inherent operational efficiencies are evident within the single SEAfarm operation, further CoP reductions can be realized through economy of scale – the addition of multiple SEAfarm sites.

Economy of Scale Compatibility and scalability were the key design criteria in developing the SEAfood System. Engineering of unique extractive species infrastructure, using comparable materials and assembly lengths, makes the system compatible with most of the current finfish cage system designs. Further, and as illustrated in Fig. 4, this manufacturing flexibility allows scalability in each SEAfarm. The configuration described in this chapter, for example, is based on a single array of 12 steel fish cages – approximately 200 m in length – with the extractive system components paralleling these structures. Other farms may choose to use large fish cages, perhaps with a fewer number, while others may establish very long farms with greater numbers of fish cages.

Economy of scale for the present *SEA*food System production operation is further realized through the development of a vertically integrated *SEA*farm Cluster – an operational aggregate of 4–5 production SEAfarm sites and an affiliated seed (hatchery) facility (see following section). Each of the production sites is configured identically as per the first *SEA*farm – the operational template – including infrastructure configuration and species composition and stocking densities. The joint management/operation of the *SEA*farm Cluster facilities allow increased production with a commensurate reduction in the cost of operations resulting regional efficiencies. Spatial distribution of a number of smaller SEAfarm units, rather than establishing large farm facilities, is considered an additional design feature in reducing the environmental footprint of the commercial production system.

Vertical Integration One of the greatest operational risks associated with a multispecies production model is the assurance of annual seed supply. While this is always a challenge for aquaculture (fish, shellfish) companies, this becomes even more difficult when the function of the ecological production system relies on an established biomass for each species component – fish, shellfish, echinoderms, and kelp/seaweed.

To optimize and fully control the *SEA*food System production model, vertical integration within the operational framework includes a small, floating "*marine species*" hatchery. The *SEA*food-Hatchery capacity is small by comparison to the current hatchery model, and is designed to accommodate seed/juvenile production for no more than 4–5 *SEA*farm sites – allowing control of seed production of all marine component species (if salmon is used, these are acquired through other commercial facilities). The floating (barge-based) design of the *SEA*food-Hatchery supports placement of this aspect of the overall aquaculture production system directly *within* a *SEA*farm cluster (4–5 farms in an operational area), facilitating use of farm infrastructure for broodstock management, juvenile rearing, and other activities that would otherwise be conducted within a land-based hatchery – saving capital infrastructure costs, operational expenses, and lowering the overall cost of production for these integrated aquaculture systems. This becomes particularly relevant in remote coastal areas where transportation expenditures for all aspects of production can be limiting.

Summary of Cost–Benefits Risk associated with any form of aquaculture, including that of the SEAfood System approach, the business risks, and hence the determinants of economic sustainability, are mitigated largely by the inherent ecological design and business framework established for this new aquaculture approach. In addition to the intuitive environmental benefits associated with the SEAfood System approach, which directly address societal concerns associated with traditional aquaculture, this new production model provides significant economic benefits/incentives for future industry commercialization efforts. Specifically, the mitigation of these risks increase profitability of this ecological approach that stem jointly from the:

- Selection and integration of high-valued commercial species to the SEAfood System, thereby ensuring a higher combined farm-gate value
- Coproduction of multiple species, providing an inherent product diversification and reducing the potential operational or financial risks associated with single species production
- Reduced Cost of Production, resulting from a shared labor pool, integrated infrastructure, and lower per-unit production expenditures for the SEA-system components

- Inherent, potentially higher margins associated with a sustainable ecological aquaculture (SEA) system production approach that is viewed by consumers as *natural*, and that follows the operational standards established for organic certification

Future Directions

The sustainability of aquatic food production systems is currently recognized as a critical issue in global seafood supply and demand. Environmental effects resulting from many aquaculture approaches may represent ecosystem stressors that will not support long-term sustainability goals given the inherent and increasing need for marine protein. With the dramatic shift from a reliance on global fisheries to the production of seafood through controlled aquaculture systems, innovation in design and operational practices will facilitate the sustainable growth of global aquatic food production.

The vision for sustainable ecological aquaculture (SEA) systems is one that will continue to evolve under a *continual improvement* paradigm. All three pillars of sustainability – social, economic, environmental – and how these will effectively be integrated into the global seafood production process will necessarily require a multi-disciplinary and collaborative approach of science. Ongoing social pressures including demand for seafood, concerns over environmental degradation, and growing competition for space by other coastal foreshore stakeholder will further dictate the need for increased production efficiency. Modifications to SEA system design, improvements to infrastructure, and integration of new species, will all support a long-term sustainable ecological aquaculture (SEA) vision.

Bibliography

1. FAO (Food and Agriculture Organization) (2009) The state of world fisheries and aquaculture 2008. Fisheries Department, Food and Agriculture Organization of the United Nations (FAO), Rome
2. United Nations (1987) Report of the world commission on Environment and Development – our growing future. Annex to Document A/42/427
3. Munro DA (1991) Caring for the earth – a strategy for sustainable living. Published (1991-12-31) in partnership by IUCN, UNEP, WWF, 228 p
4. Holling CS (2000) Theories for sustainable futures. Conserv Ecol 4(2):7
5. Anderberg S (1998) Industrial metabolism and linkages between economics, ethics, and the environment. Ecol Econ 24:311–320
6. D'Souza CM, Taghian POLamb, Peretiatko R (2007) Green decisions: demographics and consumer understanding of environmental labels. Int J Consum Stud 31:311–376
7. Lavallee S, Plouffe S (2009) The eco-label and sustainable development. Int J Life Cycle Ass 9(6):349–354
8. Costa Pierce B (2010) Sustainable ecological aquaculture systems: the need for a new social contract for aquaculture development. Mar Technol Soc J 44:1–25
9. GESAMP (2008) (imo/fao/unesco-ioc/unido/wmo/iaea/un/unep joint group of experts on scientific aspects of marine environmental protection) assessment and communication of environmental risks in coastal aquaculture. Reports and studies GESAMP no. 76. FAO, Rome, 198 pp
10. Flaherty M, Vandergeest P, Miller P (1999) Rice paddy or shrimp pond: tough decision in rural Thailand. World Dev 27(18):2045–2060
11. Leung KMY, Dudgeon D (2008) Ecological risk assessment and management of exotic organisms associated with aquaculture activities. In: Bondad-Reantaso GG, Arthur JR, Subasinghe RP (eds) Understanding and applying risk analysis in aquaculture. FAO fisheries and aquaculture technical paper 519. FAO, Rome, pp 67–100
12. Kolar CS, Lodge DM (2002) Ecological predictions and risk assessment for alien fishes in North America. Science 298:1233–1236
13. Youngson AF, Dousat A, Saroglia M, Jordan WC (2001) Genetic interactions between escaped finfish species n European aquaculture and wild conspecifics. J Appl Ichthyol 17:153–162
14. Haya K, Sephton D, Martin J, Chopin T (2004) Monitoring of therapeutants and phycotoxins in kelps and mussels co-cultured with Atlantic salmon in an integrated multi-trophic aquaculture system. Bull Aquac Assoc Can 104(3):29–34
15. Cross SF (2004) Marine finfish and suspended shellfish aquaculture: water quality interactions and the potential for integrated aquaculture. PhD thesis, University of Stirling (UK), 368 p
16. Weise AM, Cromey CJ, Callier MD, Archambault P, Chamberlain J, McKindsey CW (2009) Shellfish – DEPMOD: modeling the biodeposition from suspended shellfish aquaculture and assessing benthic effects. Aquaculture 288(3–4):239–253
17. Cromey CJ, Nickell TD, Black KD (2002) DEPOMOD modeling the deposition and biological effects of waste solids from marine cage farms. Aquaculture 214:211–239
18. Chopin T, Robinson S, Sawhney M, Bastarache S, Belyea E, Shea R, Armstrong W, Stewart I, Fitzgerald P (2004) The AquaNet integrated multi-trophic aquaculture project: rationale of the project and development of kelp cultivation as the inorganic extractive component of the system. Bull Aquac Assoc Can 104(3):11–18

19. Neori A, Chopin T, Troell M, Buschmann AH, Kraemer GP, Halling C, Shpigel M, Yarish C (2004) Integrated aquaculture: rationale, evolution and state of the art emphasizing seaweed biofiltration in modern mariculture. Aquaculture 231:361–391
20. Troell M, Halling C, Neori A, Chopin T, Buschmann AH, Kautsky N, Yarish C (2003) Integrated mariculture: asking the right questions. Aquaculture 226:69–90
21. Caldeira K, Wickett ME (2003) Anthropogenic carbon and ocean pH. Nature 424:365
22. CostaPierce BA (2002) Farming systems research and extension methods for the development of sustainable aquaculture ecosystems. In: Costa-Pierce BA (ed) Ecological aquaculture: the evolution of the blue revolution. Blackwell, Oxford, UK, pp 103–124
23. Soto D, AguilarManjarrez J, Brugère C, Angel D, Bailey C, Black K, Edwards P, Costa-Pierce B, Chopin T, Deudero S, Freeman S, Hambrey J, Hishamunda N, Knowler D, Silvert W, Marba N, Mathe S, Norambuena R, Simard F, Tett P, Troell M, Wainberg A (2008) Applying an ecosystembased approach to aquaculture: principles, scales and some management measures. In: Soto D, Aguilar-Manjarrez J, Hishamunda N (eds) Building an ecosystem approach to aquaculture. FAO/Universitat de les Illes Balears expert workshop, 7–11 May 2007, Palma de Mallorca. FAO fisheries and aquaculture proceedings, No. 14. FAO, Rome, pp 15–35
24. Chopin T, Buschmann AH, Halling C, Troell M, Kautsky N, Neori A, Kraemer GP, Zertuche-Gonzalez JA, Yarish C, Neefus C (2001) Integrating seaweeds into marine aquaculture systems: a key toward sustainability. J Phycol 37:975–986
25. Cross SF (2004) Finfish-shellfish integrated aquaculture: water quality interactions and the implication for multi-trophic aquaculture policy development. Bull Aquac Assoc Can 104–3:44–55
26. Duarte P, Meneses R, Hawkins AJS, Zhu M, Fang J, Grant J (2003) Mathematical modeling to assess the carrying capacity for multi-species culture within coastal waters. Ecol Model 168:109–143
27. Lander T, Barrington K, Robinson S, MacDonald B, Martin J (2004) Dynamics of the blue mussel as an extractive organism in an integrated multi-trophic aquaculture system. Bull Aquac Assoc Can 104(3):19–28
28. Huntington HP (2000) Using traditional ecological knowledge (TEK) in science – methods and applications. Ecol Appl 10:1270–1274
29. Neori A, Troell M, Chopin T, Yarish C, Critchley A, Buschmann AH (2007) The need for a balanced ecosystem approach to blue revolution aquaculture. Environment 49(3):36–43
30. Ridler N, Robinson B, Chopin T, Robinson S, Page F (2006) Development of integrated multi-trophic aquaculture in the Bay of Fundy, Canada: a socio-economic case study. World Aquac 37(3):43–48
31. Ridler N, Wowchuk M, Robinson B, Barrington K, Chopin T, Robinson S, Page F, Reid G, Haya K (2007) Integrated multi-trophic aquaculture (IMTA): a potential strategic choice for farmers. Aquac Econ Manage 11:99–110
32. Mazzola A, Sarà G (2001) The effect of fish farming organic waste on food availability for bivalve molluscs (Gaeta Gulf, Central Tyrrhenian, MED): stable carbon isotopic analysis. Aquaculture 192:361–379
33. Mansfield B (2006) Orgaic views of nature: the debate over organic certification of aquatic animals. Sociologia Ruralis 44(2):216–232
34. Shpigel M, Lee J, Soohoo B, Fridman R, Gordin H (1993) The use of effluent water from fish ponds as a food source for the pacific oyster Crassostrea gigas Tunberg. Aquac Fish Manage 24:529–543
35. Shpigel M, Blaylock RA (1991) The Pacific oyster, Crassostrea gigas, as a biological filter for a marine fish aquaculture pond. Aquaculture 92:187–197
36. Smaal A, van Stralen M, Schuiling E (2001) The interaction between shellfish culture and ecosystem processes. Can J Fish Aquat Sci 58:991–1002
37. Shpigel M, Fridman R (1990) Propagation of the Manila clam Tapes semidecussatus in the effluent of marine aquaculture ponds in Eilat, Israel. Aquaculture 90:113–122

Sustainable Heating Ventilation and Air Conditioning

Kevin Hydes[1], Jennifer Foskett[2]
[1]Integral Group, Oakland, CA, USA
[2]Social Green, Berkeley, CA, USA

Article Outline

Glossary
Definition of the Subject
Introduction
Fundamentals
Philosophy
Future Directions
Bibliography

Glossary

Biomimicry Imitate or use models found in nature as inspiration for designs and processes to solve human problems. Nature becomes the measure by which a designer assesses the rightness of a design.

Green building High-performance building designed to be less resource intensive, have a lower environmental footprint, and reduce the life cycle environmental impacts of the material used.

HVAC The tools and technologies that heat, ventilate, and air-condition buildings to provide healthy and comfortable indoor environments.

Hybrid ventilation Mixed mode building systems that use natural ventilation when feasible and supplement with mechanical systems when not, either sequentially or simultaneously. Hybrid ventilation combines the best features of natural ventilation with mechanical systems.

Indoor environmental quality (IEQ) The quality of air inside the built environment.

Living building A net-zero building conceptualized as a living organism, integrated within a living system and having a positive impact on that system, including energy, air, water, and waste.

Natural ventilation Cooling and ventilating through design choices that permit outdoor airflow. Natural ventilation plays an important role in low-tech building design and seasonal strategies to reduce energy.

Net-zero buildings Buildings that not only achieve extreme levels of energy efficiency but that supply their own sources of energy on a net annual basis through renewable energy resources. The first goal is to reduce loads and maximize efficiency and then to provide for all of the rest of its energy requirements through on-site, nonpolluting, renewable resources.

Order-of-operations thinking The idea that by doing things in the right order, the engineer of sustainable HVAC can ensure the best fit between performance and cost. The first step is to reduce loads – to conceptualize a system that requires less heating and cooling to begin with. The second step is to utilize free energy resources like natural ventilation and passive solar. Step three is to select efficient and appropriately sized systems.

Regenerative design Regenerative design goes several steps beyond sustainability, encouraging the designer to participate *as part of* nature instead of acting *upon* nature. While net-zero buildings neutralize the impact of the built environment on the planet, regenerative design systems have a positive impact, often on a community scale.

Right-sizing systems Designing HVAC systems that are tailored to a specific building, at a specific time and place. The move toward downsized systems that fit the job.

Sustainable building Often used interchangeably with green building but with an emphasis on longer term and broader goals.

Thermal mass The ability of a material to absorb heat and re-release it later, using external energy to change the temperature of a high-density material such as concrete, or a material that absorbs and releases heat through phase change. Thermal mass plays an important role in low-tech building design.

Whole systems thinking Understanding the built environment as an organism, a coming together of interrelated elements instead of a series of discrete and separate parts.

Definition of the Subject

Sustainable HVAC is the collection of tools, technologies, techniques, practices, and methodologies that heat, ventilate, and air-condition buildings with minimal consumption and environmental impact. Sustainable HVAC seeks to find ways, through integrated thinking, to minimize and reduce the capacity of primary heating/cooling and energy-moving equipment in order to achieve the low energy, zero energy, and increasingly "energy plus" buildings of tomorrow.

Introduction

Commercial and residential buildings are an enormous drain of energy, consuming almost 40% of the annual US primary energy and 70% of the annual electric power [1, 2]. Green buildings, by contrast, are designed to be less resource intensive, have a lower environmental footprint, and reduce the life cycle environmental impacts of the materials used [2]. The enormity of the environmental footprint associated with the built environment means that engineers, whose work critically shapes that footprint, have a unique responsibility to practice sustainability [3]. Sustainable heating, ventilating, and air-conditioning (HVAC) prioritizes energy efficiency and low environmental impacts in creating the tools, technologies, techniques, practices, and methodologies that heat, ventilate, and air-condition buildings. Sustainable HVAC is part of broader systems, decisions, and practices that together constitute a successfully designed, constructed, and operated building. In essence, sustainable HVAC is a

complimentary and supportive strategy to sustainable communities and buildings.

The HVAC field emerged at a time when society began expecting a controlled, predictable, and comfortable interior environment within which to live, work, and play [4]. From this expectation, the perceived need for human-made solutions to control or condition buildings arose. From the origins of Victorian-era heating and plumbing systems to warm buildings to the advent of air-conditioning and elevators which allowed buildings to be compact and comfortable in ever-denser urbanized environments, various systems, equipment, and methodologies have emerged and become defined as "standard practice" in the twentieth century.

The roots of sustainable HVAC are not new. In 1923, "Ventilation: A Report of the New York State Commission on Ventilation" [5] analyzed a variety of systems in New York schools with a view to determining the healthiest and most productive system at that time. The members of the commission included doctors and academics as well as Dwight. D. Kimball, a practicing mechanical engineer. The study concluded "...that window ventilation (i.e., natural), with ample direct radiation, window deflectors and adequate gravity exhaust, seems the most generally promising method of ventilation of a classroom, where conditions permit" [5, pp. 529]. Almost a century later, this is still a definitive volume on the subject and its early and enduring importance, and demonstrates that "hybrid ventilation" has been a system of interest for almost a century.

During the pre- and post-war eras, the move toward urban density, especially in the world of commercial and government office space, led increasingly to a typology of buildings with deeper floor plates and increased distances between occupants and sources of daylight and natural ventilation through windows [4]. The preeminent architectural boom of the 1950s and 1960s effectively led to a new norm of sealed buildings, relying entirely on artificial systems regardless of geographical locations. This defined a new "standard" for the time which influenced other building types and ultimately global building practices. Regional and cultural variation diminished [6]. In effect, an international standard had emerged during a period of prosperity and cheap, abundant fuel.

The oil crisis of the 1970s began to reframe and change ideas and attitudes within this industry as both the cost and certainty of energy came into question for the first time in the modern HVAC era [7]. From this point forward, various pressures were exerted on the notion of standard practice. Energy efficiency became a topic of interest as both the cost and security of fuel was no longer certain. The challenges of the 1970s continued in the 1980s when concerns emerged regarding the depletion of the ozone layer, attributed in large part to the commercial refrigerants of the day. In the 1990s, amplified concerns emerged around climate change and the direct link to CO_2 emissions from the use of fossil fuels to provide the higher quality of life demanded in developed and developing economies. Throughout these decades, the costs and environmental consequences of standard HVAC approaches were being scrutinized as were the levels of service required or even appropriate.

Today, a new paradigm is emerging where engineers are increasingly asked to optimize, minimize, downsize, or "right-size" systems and equipment, catering them to a specific purpose, in a specific location, at a specific time or day or year [8–10]. The profession has undergone a meta transformation, entering a new millennium where HVAC has shifted from a language of capacity (peak heating, peak cooling, etc.) to a language of consumption (kwh/ft^2 t CO_2/person). Sustainable HVAC has become a critical requirement of the industry today.

Sustainable HVAC seeks to find ways, through integrated thinking, to minimize and reduce the capacity of primary heating/cooling and energy-moving equipment in order to achieve the low energy and increasingly net-zero energy buildings of tomorrow. Ultimately, in a world of finite resources and fixed constraints, the engineer/designer must open their minds constantly to new ways of making building systems more efficient while having less of an impact on the infrastructures and environments that supports us.

Fundamentals

Understanding Context

When considering system choices, sustainable HVAC begins by understanding context. No two buildings

or system solutions are the same. Instead, the designer should begin by asking the following key questions:

- Why is the building needed; for what purpose now and in the future?
- Where is the building to be placed geographically, given the nested contexts of surrounding buildings, communities, and natural or urban environments? Is it a single structure or one of many?
- What functions and sub-functions will the building perform? In asking this question, it is most effective to break the building down into its subcomponents: transient spaces, fully occupied spaces, and partially occupied spaces, and set standards and energy targets for each.
- When is the building used (by space, by time of day, by season)?
- Who will occupy and manage the building? Are the users permanent (as in the case of a government office) or transient (as in the case of a hotel)?
- How will the building be operated and by whom? Do you need to allow different operating strategies and system choices?
- What are the desired goals for the building now and over time? How do these goals vary from the owner/users perspective as well as from the city or state perspective on the building stock in 10, 20, and 50 years? Is there in fact a specific goal for the building (the tallest, greenest, quietest, etc.)?

By fully imagining the place the building will occupy, the designer can carefully consider all of the unique issues that may affect system requirements and performance. Both internal and external environmental factors are important. Contextualizing the building externally is critical: Temperature, humidity, wind, rainfall, solar energy, air quality, vegetation, and surrounding topography are all key. Each of these issues needs to be understood hourly, daily, seasonally, and annually to maximize natural benefits and deals with natural constraints. Hard data on climate variations is readily available from public data sets published by national weather data sources. The more subtle factors of site and building responses to variations in the natural environment also need to be understood (i.e., deciduous trees shed leaves in winter allowing increased solar radiation and wind which could benefit or hinder a design).

Internal environmental demands are also important: What the space is being used for (i.e., is it a building for machines, such as a data center or microelectronics factory or is it a building for human comfort)? What are the space needs and purposes? Who will occupy the space (now and in the future)? When and why is it being built (or increasingly renovated)? This will determine the desired indoor environmental quality (IEQ) and the acceptable ranges for air temperature, radiant temperature, humidity, air movement, air cleanliness, light, acoustics, and more [11–13]. Being able to imagine future use and users means imagining seasonal clothing patterns, desired access to nature and views of nature, permanent vs. transient occupancy, and the importance of the ability of an occupant to control their environment.

This may seem obvious, but its importance cannot be overstated. The system needs of a building hinge upon the specific contexts of that building. For example, a world class art collection might require highly controlled and largely artificial systems to ensure the preservation and protection of the collection. Conversely, a seasonally occupied retreat camp for outdoor adventurers in mountain regions far from urban infrastructure may trigger a much more natural set of choices in harmony with nature. A hotel in a hot, humid climate should be quite different than one in a temperate location, independent of the standard of service expected by the owner/user.

Considering these external and internal environmental factors will maximize the potential for sustainable HVAC. For example, two approaches could be taken to a three-story office building in a suburban Midwest location: First, a fully air-conditioned, code-compliant building with roof-mounted HVAC and sealed windows; second, a two-story courtyard design with operable windows and a hybrid system using decentralized geo-exchange heat pumps. Among the many differences these two choices would reveal, beyond more or less energy at the source, is the consideration of more or less noise from external HVAC equipment to the surroundings. Internally, the ability to operate/control local ventilation via operable windows supplementing or replacing active systems offers indoor environmental quality (IEQ) advantages.

At the earliest stages of design, these impacts and differences need to be identified, discussed, and understood to enable the best decisions.

Developing Engineering Alternatives

The formal sustainable HVAC design process typically considers multiple solutions to a given design project: three or four architectural designs and the corresponding engineering choices and/or alternatives. This formality allows the designer and extended team to understand the implications both of architecture as well as engineering design decision-making.

When developing the alternative designs, there is a methodology that is common to each. All buildings can be separated into three types of spaces: passive; active/passive (or hybrid); and active. In some cases, a larger percentage of the building may be able to operate passively with the associated reductions in capital and operating costs. Conversely, some spaces may need to be fully treated with active systems. Most often, however, the solutions can come down to a combination of active/passive systems capable of operating differently depending upon season and occupancy.

Regardless of the split between these three approaches, a rigorous assessment and analysis of system requirements both physical and nonphysical (i.e., costs, energy, etc.) must be undertaken. In the case of passive or hybrid system design, it is especially important to consider the implications on comfort/operator interface. For example, a designer may choose to explore natural ventilation in an entrance area with low occupancies, but must anticipate occupant densities that are occasionally high. The design calculations must predict the increases in temperatures that are likely to occur and for how long. This allows the designer to engage in a dialogue with others and come to agreement moving forward with the notion of "informed consent."

A good place to begin in sustainable HVAC design is to identify an ideal design diagram to articulate the principles of what the engineer wants the building and systems to do.

For example, consider a building in a challenging inner-city site intended for a holistic health treatment center. The owner wants to use operable windows and natural systems, which they believe will be an asset to patient health. However, the adjacent streets have significant traffic and associated noise and air pollution, making an intuitive, simple, cross-ventilated section solution problematic. The problem is further compounded by the fact that the site is surrounded by large buildings which block sun and wind. Taking the ideal solution into consideration along with all of the elements of place and their attendant opportunities and constraints, the solution emerges: the creation of an inner courtyard which will become a green oasis and the "lungs" of the building. The courtyard will be used to draw clean air into the building both naturally and mechanically while the perimeter windows will be sealed to prevent dirty air and noise from entering. This system exemplifies a hybrid choice driven by an understanding of place together with a clear vision of the principles and philosophies guiding sustainable design. In this case, the methodology of interchanging the external and internal conditions iteratively led to the most logical solution.

Order-of-Operations Thinking Order-of-operations thinking is the idea that by doing things in the right order, the engineer of sustainable HVAC can ensure the best fit between performance and cost [3, 14, 15]. The first step is to reduce loads – to conceptualize a system that requires less heating and cooling to begin with. "Load reduction is the most powerful way to reduce the environmental footprint of a project (Macaulay and McLennan 2006, pp. 98)." Sometimes this means challenging preconceived expectations of clients and architects, and requires working with the design team in early phases to encourage architectural and siting choices that will ultimate reduce the heating and cooling loads of the HVAC system.

The second step in order-of-operations thinking is to find free energy resources [3]. Using natural ventilation and passive solar, for example, the engineer can harness the energy that is naturally available to heat and cool a building. As with step one, this requires the engineer to participate in design discussions at the outset.

Finally, step three in order-of-operations thinking is to select efficient and right-sized mechanical and electrical systems [3, 8–10]. Once the loads have been

reduced and free energy utilized, the engineer can think about what systems should be designed to do the rest of the HVAC work of the building. The benefit of order-of-operations thinking is that by doing step one and step two, step three is often far less expensive and far more resource intensive than in mainstream engineering practice [3].

Integrated Design Process Sustainable HVAC benefits from participation in integrative design processes [3, 16–18]. As illustrated in the above discussion of order-of-operations thinking, sustainable HVAC looks for solutions in the earliest stages of building design. Finding ways to reduce loads and utilize free energy resources means being involved in discussions of building site and architectural design; it means having a stake in landscaping, structural engineering, urban planning, water management, and more. Sustainable design requires understanding the interconnections between all of the design choices for a building and its environmental and social contexts. Some of these relationships may be invisible at first and a single designer cannot possibly grasp them all. "Since no one has all of this knowledge individually, the role of the team takes on great importance in systems understanding [17, pp. 132]. Integrated design processes allow the engineer (and all other members of the design team) to find synergies early on that can maximize the sustainability of the building.

A key activity of the integrated design process is the design charette – a design meeting that brings together clients, engineers, architects, landscape architects, and other relevant disciplines or stakeholders to explore areas of overlapping and mutually beneficial solutions. The charette is inclusive, collaborative, and goal-driven [16]. It is often facilitated by someone whose investment is primarily in the design process itself rather than the ultimate product, and it brings in nontraditional expertise [16]. Each member brings their wealth of knowledge and research to the dialogue, applying it to the project at hand, with the intention of generating design opportunities for research and exploration [18]. "The ecological engineer embraces the charrette as the main engine for eco-innovation and integration that makes sustainability affordable and effective [3, pp. 97]."

LEED and Other Tools Green building rating tools are important assets for ensuring sustainable HVAC design. The increasingly standardized and third party verified tools provide a framework that can guide sustainable HVAC choices, reinforcing order-of-operations thinking in HVAC design. The most widely used rating system for green buildings is LEED (Leadership in Energy and Environmental Design), a point-based rating system that brings together diverse elements of a green building from materials and construction to water use to siting to energy systems and rates the degree to which that building has adhered to widely accepted standards of green building [19]. Developed by the US Green Building council and adapted for an ever-increasing number of situations and building types [20], LEED has been widely adopted in policy, building practices, and design.

Pursue Architectural/Engineering Integration

Unlike traditional engineering, sustainable HVAC encourages an actively symbiotic relationship between the architect and engineer [3, 21]. "The ecological engineer. . .realizes that unless the architectural process is understood and appreciated, then an optimized solution is not possible." [3, pp. 84]. Thus, once the context of the building has been determined and its implications understood, the sustainable HVAC engineer must consider architectural issues.

In early stages of the design process, the architect will be making decisions about site, orientation, density, and massing. These decisions are critical to order-of-operations thinking and will have a fundamental impact on the possibilities, constraints, and needs of the building systems. Architectural design is integral to sustainable HVAC engineering as well as a constraining feature.

The HVAC system requirements that result from architectural design decisions may, themselves, affect the architecture of the building. For example, a community college with low massing and shallow floor plates providing good access to daylight and operable windows may increase the cost of the perimeter envelope of the building skin, but reduce the sizes of mechanical rooms and distribution together with lowering the building's energy and emissions.

As a result, practicing sustainable HVAC design requires constant dialogue to balance architectural and engineering considerations throughout the design process. Engineers can explain the implications of primary architectural design decisions as they relate to system size, style, and first costs, as well as operating and environmental costs. Truly elegant architectural/engineering system integration is where you do not see the system itself and it performs at its optimal level discreetly.

Consider the choices of HVAC systems for a large international airport. The characteristics of the space are well known: Large transient populations in high ceiling open spaces; areas of peak gathering (i.e., ticketing and gates), and large areas of transient movement (halls, concourses). A conventional approach might be to utilize overhead ducts hidden behind acoustic ceilings high overhead. This approach uses large quantities of energy and system capacity to condition the occupied zone that is often more than 20 ft below the ceiling. Such an option is not, however, an elegant choice or one that integrates architecture and engineering. An alternative choice might involve decentralized localized conditioning equipment at floor level, integrated with TV screens, for example, and a largely passive conditioning strategy for the high volume above the occupants' heads, with roof relief vents and minor ductwork. Working with the architecture and furnishings often allows an efficient, cost-effective solution that results in lower energy consumption.

Philosophy

Sustainability demands a commitment to understanding the broad philosophical issues pertaining to buildings as part of communities and the broader built environment including infrastructure, transportation, the natural environment, and society itself. These philosophical issues demand a broader commitment from the design profession to defining and realizing bioregionalism, systems thinking, appropriate technologies, and innovations for sustainability.

Bioregional and Bioclimatic Thinking

Bioregional and bioclimatic thinking all but disappeared from HVAC design considerations in the last century along with the rise of the international/global standardization of building systems. The sustainable HVAC engineer must bring an understanding of bioregionalism and bioclimate back into design. This begins with the exploration of place: Where is the building? What are the natural characteristics of that place (temperature, humidity, highs, lows, averages, snow/rain/drought, wind intensity, and direction)? How does it vary by season? By time of day? Are there on-shore/off-shore winds to consider? Fog? Cloud cover? Sun? What kind of flora and fauna exist at the site? What is the natural vegetation and preexisting topographies? How have the traditional, vernacular buildings in that location been designed?

The importance of considering all permutations of place and its effect on systems cannot be overstated. For instance, sites in steep ravines will open up discussions of topographic sun shading and axial river winds unlike high desert sites with unobstructed skies and intense sun and wind. Large diurnal and contextual variations in environmental conditions may trigger diverse system choices to meet identical comfort or energy-performance goals for the two sites, even when they are in the same geographic region.

It is possible to find accurate weather data for most sites, but in cases where there are unusual microclimate conditions, local site testing is encouraged to fully understand challenges and explore opportunities. It is worth noting that the historic climate data that is relied on is no longer as predictable due to climate change, heat island effects, etc., so an ability to forecast future change is also needed.

Whole Systems Thinking

A fundamental philosophy underpinning sustainable HVAC design is "whole systems thinking." Whole systems thinking anticipates the interconnectedness of all things – natural systems, mechanical systems, social systems [22]. In green building design, whole systems thinking means understanding the built environment as a coming together of interrelated elements instead of a series of discrete and separate parts. Whole systems thinking allows the designer to deeply understand all of the attributes of the system and their implications and interrelationships. It also means using the health of the ecological system as a basis for design [17, 22].

Sustainable HVAC explores and discovers multiple layers of interconnections between energy flows, air flows, and water flows and looks for synergies to ensure use and reuse of resources flowing through a building and its systems. Whole systems thinking in sustainable HVAC utilizes an iterative approach to exploring these opportunities and tunnels deeper as the design proceeds.

For example, one approach to an office building in a cold climate might be to design a building with a code-compliant skin that incorporates a perimeter skin heating system for comfort. This is a classic example of linear, nonintegrated system thinking. By focusing only on one element at a time, this approach misses opportunities to make design choices that will have synergistic benefits across the system. Alternatively, whole system thinking might lead to spending more money to create a better envelope, switching, for example, from double to triple glazing, which would increase the insulation value *and* increase the surface temperature, allowing the designer to eliminate the hydronic system altogether saving both capital and energy. This whole systems thinking reflects what Hawkins, Lovins and Lovins refer to as "tunneling though the cost barrier" [15], the idea that active and passive strategies can be considered that may eliminate the need for entire systems resulting in large gains in efficiency and lower cost.

Prioritizing Low Tech, Optimizing High Tech

Traditionally, heating, cooling, and ventilation design was a matter of siting and constructing buildings in ways that took advantage of natural heating, cooling, and ventilation [4, 23]. It was not until the early decades of the twentieth century that totally artificial indoor environments became possible. Since then, the possibilities have grown exponentially and much of the history of modern HVAC is a history of technological innovation to achieve new and exciting possibilities in building systems. As illustrated in the discussion of order-of-operations thinking, sustainable HVAC turns these traditions on their head seeking simple, low-tech solutions before high-tech solutions.

At the heart of sustainable HVAC is the idea that wherever, and to the greatest extent, possible, design problems should be solved by using the natural benefits of air, water, sun, and shade. Designs that take advantage of natural ventilation [23], night ventilation, and thermal mass [24, 25] are important low-tech strategies for sustainable HVAC. Another important set of strategies stem from enhancing the building facades: appropriately specified and configured windows, sunshades, overhangs, trellises, awnings, and roofing can all be manipulated to support natural heating, cooling, and ventilation in a building [26].

In all likelihood, HVAC technologies will be added once the natural systems have exhausted their potential or to enhance the potential of the low-tech solutions. Sustainable HVAC has a plethora of cutting-edge solutions within its tool kit: underfloor air distribution, displacement ventilation, radiant heating and cooling systems, geo-exchange heat pump systems, thermal storage systems, labyrinth natural cooling methods [26–30], and more.

Yet even at this point, a commitment to prioritizing lower-tech solutions can lead to optimizing higher-tech solutions that remain sustainably focused. Increasingly, engineers are opting for mixed-mode buildings or hybrid ventilation using natural ventilation during times of the day, year, or use cycle that are feasible, and supplementing nature with building mechanical systems when natural ventilation is not feasible [31, 32]. Such strategies combine the best elements of natural ventilation with high-tech options. Technologies integrated into walls [33], roofs [34–36], and windows [37, 38] as well as attention to how these components are installed and interconnected [39] can facilitate and increase the efficiency of natural, low-tech conditioning.

Keeping simplicity at the forefront and engaging in critical, self-reflexive questions is essential to sustainable HVAC: Has this system been done before? If not, why? What measures are needed to mitigate or share risk? Who will operate and maintain the systems? How much user interface is needed or encouraged?

Asking these questions will maintain some of the benefits of low-tech solutions, even as higher-tech solutions inevitably come into play and result in a high-tech/low-tech hybrid that optimizes sustainability. As an illustration, a design team was exploring the introduction of a double facade to an existing downtown office building. The goals were to reduce energy while allowing the reuse of 70-year-old operable

windows that had been fixed shut for two decades due to concern about noise and external pollution. The design team developed a scheme which allowed the original windows to be opened manually by the occupant again (low tech). They created a buffer zone via the double facade (low tech) and allowed air to come into the buffer zone at different levels seasonally through temperature sensors (high tech). The buffer zone was vented during hot summer days via fans with DC motors that were powered by DC PV panels directly (high tech). The balance of high-tech and low-tech solutions through whole systems thinking and integrated decision-making ensured that the project achieved the highest level of sustainability.

Innovation

Committing to low tech, passive conditioning and simplicity in high tech does not mean the abandonment of innovation. Indeed, it is essential to continue to search for innovation in sustainable HVAC and there are at least four categories of innovation that are critical to explore: tools, techniques, technologies, and timing.

Tools There are many recent innovations in engineering design and simulation tools for the sustainable engineer. Building information modeling supports integrated design. Energy Plus under ongoing refinement by the US DOE and the Lawrence Berkeley National Lab illustrates the advancement of building simulation tools that support accurate predictions of performance for hybrid HVAC systems. The advancement in measuring and predicting microclimate weather data provides increasingly accurate information for designing buildings that rely on natural energies. Modeling the ability of a building's potential to cycle energy in and out of thermal mass can reduce or even eliminate the need for mechanical refrigeration.

Techniques As previously discussed, the most dramatic shift in engineering techniques is integrated design. Integrated design ensures that all disciplines are engaged at the earliest design stage in decision-making, and establishes processes to ensure they remain engaged for critical decision-making as design develops. Other innovations in engineering processes include blurring the line between designing, building, and operating buildings to ensure the delivery of the highest sustained performance at the lowest cost. Building commissioning is becoming a critical service of the engineering profession, and in the future peer review of design drawings – a form of pre-commissioning by an independent expert – may also become the norm. Collaboration with industry to ensure the delivery of integrated systems that deliver sustained performance may replace the delivery of a series of independent technologies that may be difficult to integrate and operate effectively. The list of opportunities is substantial and global connectivity allows us to learn from each successful project.

Technologies Clearly, new technologies are allowing us to lower energy and resource consumption. Breakthrough technologies, however, are often expensive unless coupled with incentive programs or with whole systems thinking to change systematically how the buildings are designed and built.

Confidence in the market may be critical to allow the rapid uptake of these new products and a similar reduction in capital cost. Photovoltaics are a case in point. Initially invented for the exploration in space, PV panels became a choice for building renewable energy in the 1970s but were cost prohibitive for most buildings other than prototype demonstrations or pilots. A number of countries, states, and other jurisdictions began aggressive incentive programs, the most publicized and successful of which were in Germany and California. In Germany the approach was to give three times as much money for electricity sold back into the grid than the utility would charge to sell electricity (known as a feed in tariff). The factor of three to one makes the economics of purchasing the PV panels more lucrative on a life cycle cost basis, and has resulted in a shared public-private investment into substantial renewable energy for the country. Similarly, the state of California embarked on a utility incentive program that provided incentives and rebates to reduce the capital cost of PV panels installed in the state.

In both cases, the increase in volume of PVs required in the marketplace led indirectly to reduced costs for purchase, greater industry growth, and measurable creation of new energy sources. This trend continues on a global scale as the interest in renewables and particularly PV is driving up the volume of manufacture and

down the price. Simultaneously, ongoing research and development is increasing the efficiency of the PV equipment as competitive forces drive the innovation cycle through mass market adoption.

Designers, however, must be aware of the consequences of introducing new technologies into a new market and build in resiliencies that ensure adequate training and ongoing technical support as needed. The global interest in "green technology" is exciting and will no doubt bring to market much needed new technologies (wireless control, advanced glazing, renewables, to name but a few).

Timing The introduction of innovation requires consideration of the timescale.

Sometimes a new product or system is available but the market – locally, regionally, or nationally – is not ready for any number of reasons: price, attitude, knowledge, public/private constraints, etc. However, since a building takes multiple years to be designed and built, "future pricing" will need to be factored in to make educated decisions regarding technologies which will be purchased years down the line. At the same time, long-term goals for sustainability must be determined: a minimum life cycle for materials and systems; energy resource goals with an eye to long-term costs; material resource goals with an eye to employment and regional strength; human health goals; and even survivability goals in the face of brown-outs and blackouts. Discussions about the lifetime of the building and its systems ensure that sustainability will be paramount.

Replication

It is often the case that sustainable HVAC designers looking to innovative solutions are thought of as inventors. This is an incorrect perception. Instead, it is the HVAC engineer's job to seek out new ways of solving problems through the use of innovative tools, technologies, and techniques and then to reuse them on a broader scale, through knowledge transfer within the industry. Efficiency is gained from the replication of successful design processes that in turn allow us to spend more time exploring new ideas of design.

However, the identification of "successful" designs does place a demand on the engineering profession to undertake post-occupancy evaluation, to ascertain the success of their engineered solutions for delivering thermal comfort, air quality, acoustic quality, and more.

The Human Factor

Designing HVAC systems to be sustainable is a very pragmatic goal. Buildings are tangible assets. They are designed, built, and operated by real people of various social, economic, and educational backgrounds. Addressing the requirements of all of the users is critical to bringing to life a well-functioning building. In the end our buildings must be practical, affordable, and enduring. A level of pragmatism should be used at every step of the process: Can this be done here and now? Are the right skills, tools, techniques, and training available? Can future operators and users manage these systems?

Not only are real people designing the systems, but importantly, real people will be operating them [40]. Research demonstrates that predicted building performance does not match actual performance in part because of the behavior of occupants and facility managers [41, 42]. Cultural, social, and economic factors can all shape how people will use building systems and how that may change over time [40, 43]. It is critical to anticipate how buildings will be used in real life and use that information in HVAC design decisions so that otherwise sustainable systems are not undermined by incorrect use, or that opportunities for user-based savings are not missed [44–48]. While there is an element of unpredictability to the behavioral effects on HVAC systems, models exist to guage human influence [49].

If people are seen as active participants in their built environments, providing and maintaining the conditions that they desire, instead of as passive recipients of predetermined comfort conditions, the demands for comfort itself can shift from energy-intensive HVAC to integrated systems that are more sustainable [41]. Ray Cole of UBC argues that conventional approaches to comfort which do not take into consideration behavioral aspects result in HVAC systems designed for predictability and uniformity rather than resilience and adaptability [41]. Research is demonstrating that human comfort in buildings is

shaped by more than thermal, luminous, and acoustic conditions [41, 50] and that people tolerate and even enjoy a wider range of conditions than previously assumed [13].

Engaging building occupants in environmental conditioning requires clear and concise communication and feedback among building inhabitants, building managers, engineers, and the systems themselves. Several communications technologies have been developed to facilitate such ongoing interaction: dashboards, smart meters, mobile technology, and many others [41].

Future Directions

The applied science of HVAC has shifted from a system-intensive emphasis in the middle of the last century to a much more integrated combination of natural and artificial systems. The HVAC designer of the future should have a broad understanding of both high- and low-tech solutions as well as an understanding of the place-based, contextual, environmental, and human factors that allow particular system choices to be used.

Rating systems such as LEED and BREEAM have allowed decision makers to request, incent, and explore higher levels of environmental performance at similar costs and service qualities. Increasingly, sights have been set on producing net-zero buildings – buildings that not only achieve extreme levels of energy efficiency but that supply their own sources of energy through renewable energy resources [51–54]. Ideally, a zero energy building meets all its energy requirements through on-site, nonpolluting, renewable resources. As with sustainable HVAC overall, the first goal is to reduce loads and maximize efficiency and then to provide for the remaining needs with renewables.

In the future, there will be greater exploration of the potential of the net-zero approach at the level of communities [54, 55]. Understanding buildings not as isolated units, but as interconnected elements of larger built environments can ultimately reap even greater environmental rewards. The potential for net-zero design at the community and campus level, determining optimal ways to extend the conceptual boundaries of net-zero buildings, will most effectively utilize renewable resources globally [54].

As net-zero buildings move into the future, it is also important to consider not only operating energy but the *embodied energy* of a building – the energy necessary to deliver the products and services that are used across the life cycle of a building [56–59]. Originally, most definitions of zero energy buildings focused on operational energy rather than embodied energy. Hernandez and Kenny propose the net-zero building of the future is one in which the "primary energy use in operation plus the energy embedded in materials and systems over the life of the building is equal or less than the energy produced by renewable energy systems within the building" [56, pp. 819].

Some argue that net-zero buildings do not go far enough and that one should be striving for living buildings. A living building conceptualizes the building as a living organism, integrated within a living system [6]. The Living Building Challenge lays out advanced measures of sustainability for the built environment, working to diminish the gap between current limits and ideal solutions [60]. Through its seven performance areas: site, water, energy, health, materials, equity, and beauty, the Living Building Challenge provides a framework for design, construction, and the symbiotic relationship between people, the built environment, and nature.

Moving beyond carbon neutrality, the buildings of the future should actively participate in restoring and renewing natural systems [17, 22]. Regenerative design goes several steps beyond sustainability, encouraging the designer to participate *as part of* nature instead of acting *upon* nature [22]. If net-zero buildings neutralize the impact of the built environment on the planet, restorative and regenerative design actively engages and interacts with local earth systems to have a positive impact. Following principles of bio-mimicry, regenerative design seeks to use nature as its model and inspiration [6, 61, 62]. Nature becomes the measure by which a designer assesses the rightness of a design, asking, is there a precedent for this in nature? [61]. Constant feedback and ongoing learning allow the design to shape and evolve in concert with the natural systems of which it is a part.

Realizing the future of sustainable HVAC will require a constant thirst for curiosity and innovation to explore, define, and redefine approaches, methods, techniques, and technologies that will support the quest for a cleaner and healthier built environment: in pursuit of zero.

Bibliography

Primary Literature

1. Torcellini PA, Judkoff R, Crawley DB (2004) High-performance buildings. ASHRAE J 46(9):S4–S12
2. Yudelson J (2008) The green building revolution. Island Press, Washington
3. Macaulay DR, McLennan JF (2006) The ecological engineer. Ecotone, Kansas City
4. Cooper G (1998) Air-conditioning America: engineers and the controlled environment, 1900–1960. Johns Hopkins University Press, Baltimore
5. Winslow C-EA, Kimball DD, Lee FS, Miller JA, Phelps EB, Thorndike EL (1923) Ventilation: report of the New York state commission of ventilation. E.P. Dutton and Company, New York
6. Berkebile R, McLennan JF (1999) The living building. The World I 14(10):160
7. Gore A (2006) An inconvenient truth: the planetary emergency of global warming and what we can do about it. Simon and Schuster, Inc
8. Mathew P, Greenberg S, Frenze D, Morehead M, Sartor D, Starr W (2005a) Right-sizing laboratory HVAC systems–part I. HPAC Engineering, Sep
9. Mathew P, Greenberg S, Frenze D, Morehead M, Sartor D, Starr W (2005b) Right-sizing laboratory HVAC systems–part II. HPAC Engineering, Oct
10. Thomas PC, Moller S (2006) HVAC system size–getting it right. In: Clients driving innovation: moving ideas into practice, 12–14 Mar. Cooperative Research Centre for Construction Innovation, Brisbane
11. Olesen BW, Brager GS (2004) A better way to predict comfort. ASHRAE J 46:20–28
12. deDear R, Brager GS (1998) Developing an adaptive model of thermal comfort and preference. ASHRAE Trans 104(1a):145–167
13. deDear R, Brager GS (2001) The adaptive model of thermal comfort and energy conservation in the built environment. Int J Biometeorol 45:100–108
14. McLennan J (2004) The philosophy of sustainable design. Ecotone, Bainbridge Island
15. Hawkins P, Amory L, Hunter L (1999) Natural capitalism: creating the next industrial revolution. Little Brown and Company, Boston
16. Zimmerman A (2006) Integrated design process guide. Canadian Mortgage Housing Corporation, Ottawa
17. Reed B (2008) The integrative design process, changing our mental model. In: Guenther R, Vittor G (eds) Sustainable Healthcare Architecture. Wiley, Hoboken, pp 132–135
18. Yudelson J (2009) Green building through integrative design. McGraw-Hill, New York
19. Yudelson J (2007) Green building a to z: understanding the language of green building. NewSociety Publisher, Gabriola Island
20. McLennan JF, Rumsey P (2003) Is LEED the holy grail of sustainable design? Environ Des Constr 6(5):34–35
21. McConahey E, Haves D, Christ T (2002) The integration of engineering and architecture: a perspective on natural ventilation for the new San Francisco federal building. In: Proceedings of ACEEE summer study on energy efficiency in buildings, Asilomar, CA
22. Reed B (2007) Shifting from "sustainability" to regeneration. Build Res Inf 35(6):674–680
23. Brager GS, de Dear R (2000) A standard for natural ventilation. ASHRAE J 42:21–29
24. Givoni B (1994) Passive and low energy cooling of buildings. Van Nostrand Reinhold, New York
25. Brown GZ, Cartwright V (1985) Sun, wind, and light: architectural design strategies. Wiley, New York
26. Saelens D (2003) Energy performance assessment of multiple-skin facades. Int J HVAC & R 9:167–186
27. Lehrer D, Bauman F (2003) Hype vs. reality: newresearch on underfloor air distribution systems. In: Proceedings, Greenbuild 2003, Pittsburgh, PA. http://escholarship.org/uc/item/2bb1c9t0
28. Bauman F (2002) Underfloor air distribution (UFAD) design guide. ASHRAE J
29. Schiavon S, Bauman F, Lee KH, Webster T (2010) Development of a simplified cooling load design tool for underfloor air distribution systems. Final report to CEC PIER program. CEC contract no. 500-06-049, July
30. Schiavon S, Lee KH, Bauman F, Webster T (2010) Simplified calculation method for design cooling loads in underfloor air distribution (UFAD) systems. Energ Build 43:517–528
31. Li Y, Heisleberg P (2002) Analysis methods for natural and hybrid ventilation: a critical literature review and recent developments. Int J Vent 1(4):3–20, special edition on hybrid ventilation
32. Brager G (2006) Mixed mode cooling. ASHRAE 48:30–37
33. Kilkis BI (2006) Cost optimization of a hybrid HVAC system with composite radiant wall panels. Appl Therm Eng 26(1):10–17
34. Rangsit S, Chaicharn C, Charoenporn L, Rungsiyopasc M (2011) Thermal performance analysis and economic evaluation of roof-integrated solar concrete collector. Energ Build 43(6):1403–1408
35. Suehrcke H, Peterson EL, Selby N (2008) Effect of roof solar reflectance on the building heat gain in a hot climatic. Energ Build 40:2224–2235
36. Juanico L (2008) A new design of roof-integrated water solar collector for domestic heating and cooling. Solar Energy 82:481–492
37. Karlsson J, Roos A (2001) Annual energy window performance vs. glazing thermal emittance—the relevance of very low emittance values. Thin Solid Films 391:345–348
38. Roos A, Wall M (2006) Influence of windows size in the energy balance of low energy houses. Energ Build 38:181–188
39. Cappellettia F, Gasparellab A, Romagnonia P, Baggioc P (2011) Analysis of the influence of installation thermal bridges on

windows performance: The case of clay block walls. Energ Build 43(6):1435–1442
40. Fosket J, Mamo L (2009) Living green: communities that sustain. New Society Publishers, Gabriola Island
41. Cole R, Robinson J, Brown Z, O'Shea M (2008) Recontextualizing the notion of comfort. Build Res Inf 36(4):323–336
42. Owen B, Frankel M, Turner C (2007) The energy performance of LEED buildings. Paper presented at the Greenbuild conference and expo, Nov 2007
43. Nakagami H (1996) Lifestyle change and energy use in Japan: household equipment and energy consumption. Energy 21(12):1157–1167
44. Heerwagen J, Zagreus L (2005) The human factors of sustainable design: post occupancy evaluation of the Philip Merrill Environmental Center, Annapolis, MD. Report prepared for the US Department of Energy Building Technology Program Centre for the Built Environment, University of California, Berkeley, Apr 2005
45. Rijal HB, Tuohy P, Humphreys MA, Nicol JF, Samuel A, Clarke J (2007) Using results from field surveys to predict the effect of open windows on thermal comfort and energy use in buildings. Energ Build 39(7):823–836
46. Hensen JLM, Loomans MGLC, de Vries B, Bourgeois D (2009) User behavior in whole building simulation. Energ Build 41(3):295–302
47. Emery AF, Kippenhan CJ (2006) A long-term study of residential home heating consumption and the effect of occupant behavior on homes in the Pacific Northwest constructed according to improved thermal standards. Energy 31(5):677–693
48. Ouyang J, Hokao K (2009) Energy-saving potential by improving occupants' behavior in urban residential sector in Hangzhou City, China. Energ Build 41(7):711–720
49. Yu Z, Fung BCM, Haghighat F, Yoshino H, Morofsky E (2011) A systematic procedure to study the influence of occupant behavior on building energy consumption. Energ Build 43(6):1409–1411
50. Brager G, deDear RJ (2003) Historical and cultural influences on comfort expectation. In: Cole RJ, Lorch R (eds) Buildings, culture and environment. Blackwell, Oxford, pp 177–200
51. Marszala AJ, Heiselberga P, Bourrelleb JS, Musallc E, Vossc K, Sartorid I, Napolitanoe A (2011) Zero energy building – A review of definitions and calculation. Energ Build 43(4):971–979
52. Torcellini P, Pless S, Deru M, Crawley D (2006) Zero energy buildings: a critical look at the definition. ACEEE summer study on energy efficiency in buildings. National Renewable Energy Laboratory, Golden, CO
53. Torcellini P, Pless S, Deru M, Griffith B, Long N, Judkoff R (2006b) Lessons learned from case studies of six high-performance buildings. NREL report no. TP-550-37542. National Renewable Energy Laboratory, Golden
54. Crawley D, Pless S, Torcellini P (2009) Getting to net zero. ASHRAE Sep
55. Busby P, Wardle K (2008) Ecodensity initiative. Municipal World, 31–34 Sep
56. Hernandez P, Kenny P (2010) From net energy to zero energy buildings: defining life cycle zero energy buildings (LC-ZEB). Energ Build 42(6):815–821
57. Adalberth K (1997) Energy use during the life cycle of buildings: a method. Build Environ 32(4):317–320
58. Thormark C (2002) A low energy building in a life cycle—its embodied energy, energy need for operation and recycling potential. Build Environ 37(4):429–435
59. McDonough W, Braungart M (2002) Cradle to cradle: remaking the way we make things. North Point Press, New York
60. Cascadia Region Green Building Council (2006) The living building challenge v1.0: in pursuit of true sustainability in the built environment. Cascadia Region Green Building Council, Portaland, OR
61. Benyus JM (1997) Biomimicry: invention inspired by nature. William Morrow and Company, New York
62. Zari MP (2010) Biomimetic design for climate change adaptation and mitigation. Archit Sci Rev 53(2)

Books and Reviews

Allard F (ed) (1998) Natural ventilation in buildings. James and James, London

Anderson R (1998) Mid-course correction: toward a sustainable enterprise: the interface model. The Peregrinzilla press, Atlanta

Brand S (1995) How buildings learn. Penguin books, New York

Daniels K, Schwaiger E (1998) Low-tech light-tech high-tech: building in the information age. Princeton Architectural Press, New York

Mendler S, Odell W (2000) The HOK guidebook to sustainable design. Wiley, Hoboken

Orr DW (2004) The nature of design: ecology, culture and human intention. Oxford University Press, Oxford

Sustainable Herbicide-Resistant Crops

Jonathan Gressel
Plant Sciences Department, Weizmann Institute of Science, Rehovot, Israel

Article Outline

Glossary
Definition of the Subject
Introduction
Problems with the Present Transgenic Herbicide-Resistant Crops

Non-transgenic Strategies to Sustain Transgenic Herbicide Resistances
Genetic Engineering Strategies to Extend the Sustainability of Transgenic Herbicide Resistances
Future Directions
Bibliography

Glossary

Gene stacking Developing transgenic crops containing two or more transgenes, either by simultaneous transformation or by hybridizing plants with different transgenes.

Graminicide A herbicide that specifically controls weeds in the grass family (Graminae – Poaceae).

Harvest index The ratio of grain to total biomass in a crop.

Herbicide hypersensitivity The property of certain genetically engineered crops to be susceptible to herbicides to which the wild type is naturally resistant.

Herbicide resistance The ability to withstand a critical level of herbicide with little or no effect on yield. Resistance can be natural, evolved, or generated by mutagenesis as well as by using recombinant DNA technology (genetic engineering).

Selectivity The ability to differentially control weeds with little or no effect on a specific crop.

Shattering Premature dropping of seeds before they can be harvested.

Systemic herbicide A herbicide that is applied to the leaves but spreads to underground plant organs, and affects these parts of the plant as well as leaves, or is applied to the soil and also affects leaves.

Target site The specific site to which a herbicide binds, beginning the cascade leading to plant death.

Transposon A DNA element that can move from one location in the genome to another.

Volunteer weed Weeds of a plant species that had been a crop in a previous season.

Definition of the Subject

While transgenic herbicide-resistant crops have been a boon to agriculture, reducing both production costs and ecological impacts of farming, weeds have rapidly evolved resistance to the major herbicide used in transgenic crops (glyphosate) [1], rapidly rendering the technology less sustainable than had been thought [2]. While no practice in agriculture has been sustainable forever, the period of sustainability can be extended. Methods are outlined to extend both the usefulness to crops where needed as well as the sustainability of transgenic herbicide technologies such as rotations of crops and herbicides, increasing the targets of herbicide action, suppressing herbicide targets in rotation. Transgenically inducing hypersensitivity to herbicides can be considered as an option for some weeds.

Introduction

Chemical weed control with herbicides has been a major quantum step that has allowed agriculture to supply food to a rapidly growing population, decreasing the drudgery of mechanical and manual (too often fe-manual) control of weeds. It allowed the switch in the direction of crop domestication from selection of ever taller grain crops (with lower harvest index) that were more competitive with weeds, to dwarf "green revolution" high harvest index crops. This broke the cycle of weeds continuing to evolve taller forms as a consequence of farmer and breeder selecting for height in crops so that the crop would compete with weeds.

The amount of additional arable land that would have been needed to feed the present populations of India and China just does not exist in these countries, and there would have been massive famine had it not been for the green revolution dwarfing wheat and rice, and the availability and use of herbicides to control the highly competitive, taller weeds. There would have been this famine even if all available natural wild ecosystems were brought under the plow. Still, the chemical industry has not been able to generate new herbicides needed for each cropping situation where they are needed. Some of the older generation herbicides were found to have environmental or toxicological issues and have been de-registered as regulatory standards change. Additionally, weeds continue to evolve, just as they had to previous efforts to deal with them. Agriculture is not statically sustainable. New strategies must continuously be developed as previous ones are lost. So far, agricultural scientists have been successful at this continuing exercise, coming up with new technologies to replace lost ones, and delaying Malthus's nineteenth century predictions

that due to population increasing at a higher rate than yields, there would be starvation. Indeed, typical annual yield increases would not keep up with population increases, but in every generation or so a new technology appears, providing quantum leaps. These included the use of hybrid vigor, tractors, selective herbicides, the green revolution, etc., all leading to major jumps in yield.

Genetically engineered herbicide resistance was another quantum leap; it allows taking a desired herbicide with limited use because it is not selective with a particular crop and then expand its use by transgenically rendering the crop resistant [3]. The major herbicide being used transgenically, glyphosate, indeed has excellent properties; no mammalian toxicity in realistic amounts; little environmental toxicity, it kills most weeds, including many that are hard to control [4]. The latter include weeds that have hidden buds and/or underground organs that require that a herbicide be systemic and penetrate to all parts of a plant to prevent resprouting.

Successes of Transgenic Herbicide-Resistant Crops

It has been argued that no technology has been taken up as rapidly and as massively as transgenic herbicide resistance to the herbicide glyphosate [5, 6]. This resistance has only been released in four crops: soy, maize, cotton, and oilseed rape (canola). Over 80% of the world's soybean and most of the maize and oilseed rape are glyphosate resistant, as is most of the North American cotton [5]. In the latter case, farmers had a choice of herbicide-resistant cotton with or without a transgene encoding the Bt insecticidal gene, and more farmers cultivated transgenic cotton with herbicide resistance than with the insecticidal gene. This rapid adoption by growers occurred despite high "technology fees" for the seeds, the availability of non-transgenic varieties, and a predominantly bad public perception generated by antitechnology, anti-multinational, and antiglobalization groups. The reasons are simple; the herbicide is inexpensive and the control package costs less, a larger spectrum of weeds is controlled, and the farmers had more flexibility in application timing than with previous herbicides [3, 6]. This had a major (positive) environmental impact. Many of the previous herbicides used were applied to cultivated bare ground before planting and much herbicide washed (with soil) into rivers or percolated into underground aquifers. The rapid dissipation of glyphosate allowed farmers to apply herbicide to standing weeds before planting, without cultivation, and then plant into soil-holding stubble. Spraying requires far less energy than plowing followed by disk cultivating, with considerable saving in fossil fuels. It has been estimated that the amount of fossil fuel saved per year is equivalent to that which would be saved from removing over five million automobiles from the roads [6]. This lack of preplant cultivation (no-, minimum, or eco-tilling) reduces soil erosion by 95% [6, 7]. It was not just in industrial USA and Canada where the technology was rapidly adopted. Argentina had a problem with a mistake made generations ago; they repeated an earlier mistake of a Mr. Johnson in the USA who introduced a Middle-Eastern weed, *Sorghum halepense* to the USA as a pasture grass. This "johnsongrass" turned out to be a poor pasture grass in both countries, but especially in Argentina, an excellent weed that propagates by seed as well as by underground buds on rhizomes. Other herbicides would burn off the tops only to have it resprout; cultivation cut the rhizomes into multiple propagules, spreading the weed. Transgenic glyphosate-resistant soybeans, planted into "johnsongrass" and other weed stubble that kept the soil from overheating, became a hit [7]. This transgenic soybean spread rapidly to neighboring Brazil where it was cultivated illegally until the government changed its policies due to massive farmer civil disobedience.

Countries in Europe, though reluctant to allow farmers the choice to cultivate transgenic herbicide-resistant maize and soy, have had no choice but to import them to feed their livestock. The claim that European agriculture is sustainable without cultivation of transgenic crops is only correct when the importation of transgenic feed grains to sustain European livestock is politely ignored.

There are those who argue that transgenic crops are not needed; modern breeding using DNA marker-assisted techniques can meet all needs. This author knows only of cases where marker-assisted breeding has allowed more rapid stabilization of inherent traits, such as a naturally occurring mutation for herbicide resistance that also occurs in weeds at a high frequency. Breeding cannot bring in herbicide resistance traits that

do not exist in that crop species. This can only be done with recombinant technologies. Mutation breeding is counter-indicated with crops having related weeds, as this is not even sustainable in the short term, as discussed below.

Problems with the Present Transgenic Herbicide-Resistant Crops

There has never been a rapidly adopted technology that is not without drawbacks, despite widespread use. A case in point is the Model T Ford that revolutionized personal transport, cityscapes, suburbia, and lifestyles. It was inexpensive and met unforeseen needs. Still, it could never meet present day fuel, pollution, or safety standards with its arm breaking hand crank, poor suspension, steering and brakes, and tires that rapidly blew out. Early cars had detractors who passed regulations such as to have flagmen run in front of cars so as not scare horses, not too unlike some of the irrelevant regulatory requirements for transgenics (e.g., knowing flanking sequences of insertion sites). Such detractors rarely call for the rational and much needed regulation concomitant with all technologies.

The next generations of herbicide-resistant crops need to evolve to meet new needs and higher standards. They will be more sophisticated, more efficient, and their use far more complex than the present ones. The author hopes that he will not be misconstrued from the following sections: he is clearly not against the use of transgenic herbicide-resistant crops, but there are far too many cases where they are being used injudiciously, compromising the long-term effectiveness of the technology. The agronomic, economic, environmental, and toxicological benefits discussed above should make it clear that they are needed. Just for those reasons it is discussed at length how to sustain such useful products.

There Are Not Enough Herbicide-Resistant Crops

Industry has decided for its own (arguably misdirected) reasons to both limit the crops rendered herbicide resistant, as well as the markets where they are sold. Weeds are a major problem in "truck" crops (intensively cultivated fruit and vegetable crops). There are very few herbicides registered for use in these crops and most such crops are hardly competitive with weeds (imagine un-weeded lettuce or radishes). They must be intensively mechanically and manually cultivated. Many such crops have already been transformed using resistance to the herbicide glufosinate as the selectable marker. Despite the need for these crops in the field, the company that owns patent rights to both the gene and the herbicide steadfastly refuses to register the use of their gene and herbicide in such crops.

Hand weeding is de rigueur in much of the developing world, especially Africa due to the small farm sizes, lack of capital for machinery as well as chemicals. When transgenic glyphosate-resistant maize was finally released in South Africa (and marketed to rich, large-scale farmers) adoption was rapid among resource-poor farmers. A lady farmer could spray down weeds on 2 ha with a backpack sprayer in a day, where she could only hoe weeds on 1 ha in a month, with much weeded too late. There has been no major effort to market this maize in other African countries, despite its potential use in controlling parasitic weeds [8]. Parasitic weeds that attach to roots of major crops and suck the crops dry before emerging from the soil and flower are a scourge of major crops in Africa, the Mediterranean basin, and eastern Europe. They cannot be controlled by cultivation or conventional herbicides, facilitating their spread and gain in importance. Fifteen years ago, it was demonstrated that transgenic crops with resistance to systemic herbicides with three different targets sites of action could be successfully used to control parasitic weeds [9]. No transgenic crop has yet to be marketed with this use in mind. Non-transgenic maize [10, 11] and sunflowers [12, 13] with mutant acetolactate synthase genes have been marketed, and can be used for this purpose. A similar herbicide-resistant sorghum is also being developed for use in *Striga* control in Africa [14]. Parasitic weeds have not rapidly evolved resistance in maize because at the high local herbicide levels used with maize seed dressings, resistance is recessive [15]. At the levels used in field spraying sunflowers, both parasitic weeds and regular weeds are rapidly expected to evolve resistance.

Wheat and rice are humanity's two major food crops. Before the advent of selective herbicides, wheat fields were biodiversely multicolored red (from poppies) or white or yellow (various mustards or other weeds). These weeds severely reduced yields and grain quality. The advent of the herbicide 2,4-D after

World War II rid wheat and rice fields of broad leaf weeds that made fields so pretty to city folk, but devastated farmers. No real sustainable fit resistance has evolved to 2,4-D among the weeds it so successfully controlled. Grass weeds, which could not compete with broad leaf weeds, quickly filled the ecological vacuum for weeds in wheat and rice. Industry countered by developing selective graminicides that could control the grass weeds in wheat and rice, grasses themselves. One by one grass weeds evolved resistance to the various graminicides, most often by using the same enzymes the crops uses to degrade and detoxify the herbicide. Initially, the weeds had too low a level of these enzymes and they slowly evolved upregulated levels, probably by gene duplication or modifications in controlling elements such as promoters and enhancers of gene expression [3]. Thus, wheat and rice are ideal targets for transformation with genes endowing resistance to general broad spectrum herbicides such as glyphosate. Such new transgenic wheat or rice varieties could then be treated with a single broad spectrum herbicide instead of 2,4-D (or a related herbicide) together with a graminicide, a more expensive technology. Both transgenic glyphosate- and glufosinate-resistant rice and wheat have been generated and tested, but neither has been marketed.

There is good evidence that transgenic herbicide resistance, as presently generated, may well not be sustainable, even in the short term in wheat and rice. This is rather certain for rice on a broad scale and for wheat on a more limited scale. This is due to two particular weeds, one more limited in distribution (*Aegilops cylindrica*) in wheat, and weedy rice in rice. Neither weed can be controlled by the selective herbicides in these crops, as each is too closely related to the crop, and are naturally resistant to the same herbicides. Wheat and rice are thus problematic targets for transgenic herbicide resistances that can then provide selectivity between weed and crop. Both weeds are able to introgress genes (hybridize and then internalize genes) from the respective crop. *Aegilops cylindrica* is a weed composed of two related but distinct genomes and wheat is made up of three. One genome is common to both wheat and its hard-to-control weed. When one mutant non-transgenic herbicide-resistant (Clearfield™) wheat was developed, the resistant gene quickly appeared in *Aegilops cylindrica* in the USA [16], and other herbicide resistances were shown to move from wheat to two other *Aegilops* species in Europe [17, 18]. Thus, instead of being controlled by the herbicide, these weeds could again become uncontrollable problems.

Weedy rice (also called feral rice or red rice) is a large group of varied de-domesticated rice strains, but almost all are the same species as cultivated rice [19]. The consistent trait of weedy rice is that it shatters seed; a dominant back mutation from the recessive non-shattering of the crop. Weedy rice can have other dominant mutations rendering it ever more feral and weedy, a regain of secondary dormancy such that some seeds remain dormant for a few seasons; a dominant mutation to reddish or purple seed color; long awns, a dominant mutation to height and to tillering [19]. Weedy rice had been controlled by transplanting nursery-grown non-weedy domestic rice into cultivated paddies, giving the crop a month head start. This labor intensive, backbreaking process is rapidly being replaced by direct seeding, and weedy rice is celebrating. The only chemical answer has been a non-transgenic Clearfield™ rice, and the mutant gene quickly moves into weedy rice [20]. The Clearfield™ technology quickly became "passé" in tropical Latin America where it had been used season after season even during the same years [21, 22].

Thus, it can be seen that where a crop has a related introgressing weed in the same agroecosystem, transgene flow from crop to weed can be a real issue, especially with a trait such as herbicide resistance. Transgene flow from crop to related wild species would be an ecological nonissue as herbicides are not used in the wild, so there would be no selective advantage to resistance. One must carefully read and interpret the literature claims of gene flow from transgenic crops to "wild" relatives, (for example, [23]). A close perusal of the data quickly reveals that there was no gene flow to wild relatives, but that all the gene flow was to weeds of agroecosystems or of ruderal (human disturbed) ecosystems such as roadsides. There are many basic differences between weedy species and wild species [24].

There are many crops with weedy or feral relatives in the same agroecosystems, and these weeds are major problems in those crops. They include weedy beets, weedy radish, weedy sunflowers, and especially weedy

sorghum (shattercane) [23, 25–28]. All the weeds are the same botanical species as the crop, even if botanists have tagged them with different Latin binomials. There are no known weedy forms of cotton, maize, or soybeans in the vast majority of the areas where these crops are cultivated. There are no weedy relatives of oilseed rape in the western provinces of Canada where transgenic herbicide-resistant oilseed rape was initially introduced, but there are in the eastern provinces and gene flow is a problem there. Thus, there is a Catch 22 situation with many crops: transgenic herbicide resistance is needed to control weeds related to the crop, but the transgene will quickly hybridize into the weed, abrogating the utility of the technology. As will be discussed in a later Section, the problem can be overcome by more sophisticated transgenic technologies.

The Evolution of Weed Resistance

More than 90% of the area covered by transgenic herbicide-resistant crops is devoted to one gene (CP4 type EPSP synthase) and the herbicide glyphosate (Roundup Ready™) [5, 6]. When this was just released and being rapidly adopted, the manufacturer saw no reason to institute any strategies that might delay resistance from evolving, and the company scientists claimed that the nature of the herbicide and its mode of action precluded the evolution of resistance, a view they maintained well after the first cases of evolved resistance were confirmed [2]. This was despite ample evidence that there was diversity in the level of resistance among weeds due to a multiplicity of factors, and these factors could either combine to provide resilient resistance or any given factor could intensify with the same result [29]. Nature has a way of making fools of those who claim that something cannot evolve, and has done so with a vengeance. There has been a propensity of some of the most pernicious weeds to have the variability and mutability to rapidly evolve resistance to many different herbicides.

It may be a question of numbers, these are weeds that shed thousands of seeds where one or two would be enough for replacement of parents or it could be that they are more mutable than others. Thus, weeds in the genus *Amaranthus* and *Lolium* have rapidly evolved resistance to most herbicides controlling them [3, 30], and they proceeded to evolve resistance to glyphosate in various locations around the globe [1], often with different populations evolving differing modes of resistance. Some of the weeds that evolved resistance were those where glyphosate was most needed; those requiring a systemic herbicide. Some of these weeds evolved a "phoenix" resistance. The leaves burnt off and new shoots emerged from the ashes in a manner similar to the mythical bird. In *Conyza*, they emerged from dormant buds at the base of the rosette of leaves [31]; in *Sorghum halepense* (johnsongrass) in Argentina and the USA from the underground rhizomes [30, 32, 33]. In many of these cases, glyphosate was the herbicide of last resort, the weeds had evolved resistance (or were naturally resistant) to other herbicides.

Very Few Herbicide-Resistant Genes Have Been Commercialized

The ease of use, the low price of herbicide, the broad spectrum of weed control quickly rendered glyphosate resistance the choice of farmers. The farmers either believed or wished that weeds would not evolve resistance to glyphosate. Worse yet, competitors of the producers of glyphosate believed this hype and severely cut back on research on discovery of new herbicides and on developing transgenic resistances to their own preexisting herbicides, which they thought could never compete with glyphosate, and by not bringing new products to market self-fulfilled their predictions. The options available to farmers were further reduced when it came time for industry to reregister older herbicides. Many companies decided that they could not justify the outlay for renewed registration because they thought that other herbicides will never again compete with glyphosate. Many transgenic herbicide resistances under development that had value were never released and at least one that had been commercialized was withdrawn. When glyphosate resistance was initially released, seed companies continued to breed conventional varieties to provide farmers with choice. The less farmers chose conventional varieties, the less incentive remained to breed them.

The lack of alternatives clearly exacerbated the rate at which glyphosate resistance evolved and spread. This in turn was made worse by policies of the manufacturer who convinced many that resistance could not be an

issue and no management strategies were needed that might involve competitors' products that could assist in sustaining their own technology.

Non-transgenic Strategies to Sustain Transgenic Herbicide Resistances

There are a series of strategies used to sustain the useful lifetime of conventional herbicide technologies. These can extend the useful lifetime of the transgenic herbicide only where there is a no similarity between the transgenic crop and the weed; that is, such technologies are poor at dealing with problems such as transgene flow from crop to related weed. One strategic mistake with glyphosate-resistant crops was the promotion of glyphosate for all applications, including preplant where crop herbicide resistance is not required. There are other herbicides such as paraquat and inhibitors of protoporphyrinogen oxidase that provide rapid burn down of most weeds; with the notable exception being those that require a systemic herbicide. Thus, any weeds that might have evolved glyphosate resistance in previous seasons and germinate before planting would be controlled by these preplant herbicides. At least by changing the preplant herbicide, glyphosate-resistant weeds will not have a head start on the crop.

Crop and herbicide rotations have always been excellent tools to delay herbicide resistance using conventional herbicides, and they could have delayed glyphosate resistance, had they been applied. The best herbicides for use in rotation are those that exert negative cross-resistance; that is, they are more effective at controlling resistant individuals that in controlling the wild type [34]. Still, there have been no reports about herbicides that preferentially control glyphosate-resistant weeds. Most cases of glyphosate resistance evolved following the sole use of glyphosate, season after season, with no other herbicide that controls the target weeds used in the interim.

Some herbicide mixtures have been highly effective in delaying resistance in the past. Resistance evolved to atrazine in maize where atrazine was used alone, but not where it was mixed with herbicides in the chloroacetamide group inhibiting long-chain fatty acid biosynthesis [35]. These chloroacetamide herbicides even prevented the evolution of resistance in weed species that they did not control; but they must have weakened them to the point that they were unable to compete. Not all mixtures work equally well, and there are some rule-of-thumb criteria for choosing good mixtures, such as having the same persistence, different targets of action, overlapping weed control spectra, etc. [36].

Genetic Engineering Strategies to Extend the Sustainability of Transgenic Herbicide Resistances

From the foregoing, it is clear that many of the problems with what had been and still is a most useful agricultural tool, transgenic herbicide resistance, are derived from the overreliance on a single technology. If there were more transgenic herbicides to rotate, the risk would have been spread and each would last for much longer, and each in turn would have controlled resistance to the previous one. There are herbicide chemistries that have less propensity to having herbicide resistance evolve, and should be used more often in rotations and mixtures. The chloroacetomide herbicides inhibiting long-chain fatty acid biosynthesis have been heavily used for over 4 decades. The only major case of resistance reported for this group was when a rice weed evolved resistance to one herbicide in the group [37]. The cross-resistance of the weed to herbicides of a different group suggests that resistance probably was not at the target site of herbicide action. These chloroacetamide herbicides inhibit more than one fatty acid elongase, and resistance at all the target sites would require the exceedingly rare confluence of a few mutations appearing simultaneously. Resistance due to catabolism could continue to evolve to members of this group of herbicides, but the diversity of chemistries preclude the probability of a single metabolic system degrading them all.

Industry has dedicated most of its efforts to finding herbicides that affect single targets of action. Nature has been wiser; it evolved natural herbicides (allelochemicals) as part of one of its strategies of using chemical warfare for one plant species to compete with others. Many of these allelochemicals inhibit more than one target site [3]. For example, sorghum secretes the phytotoxin sorgoleone that inhibits two separate targets in plants, the psbA protein in photosystem II and the enzyme HPPD

(4-hydroxyphenylpyruvate dioxygenase) [38], which are key targets of two separate groups of commercial herbicides. Two targets would have to simultaneously mutate for target site resistance to evolve. If the chemical industry could find such multisite inhibitors, the biotech industry could find or generate genes encoding enzymes that will degrade them to provide crops with selective transgenic herbicide resistance. Technologies such as gene shuffling allow researchers to take genes that encode enzymes that inefficiently degrade a herbicide and turn them into usable genes. This has been elegantly used to generate herbicide-resistant maize, but so far only published for generating metabolic resistance to the herbicide glyphosate [39], where additional resistant genes are redundant.

There are ways to extend useful life of the present and future transgenic herbicide resistances by stacking genes. There are also ways to deal with crops where gene flow is an issue, as well as to develop sophisticated systems using herbicide hypersensitivity to both prevent volunteer weeds and crop × weed hybrids from going feral. One can even envisage ways of overcoming weed resistance after it has evolved, all as outlined below.

Stacking Herbicide Resistances

Two companies have announced that they are stacking herbicide resistances to preclude some of the problems that at least one [2] had denied would occur. This will require the farmer to use both herbicides, effectively raising production costs. Convincing them to do so may not be easy. One company is stacking glyphosate resistance with resistance to dicamba, a herbicide similar to 2,4-D in structure and mode of action [40]. Another is stacking glyphosate resistance with resistance to acetolactate synthase inhibiting herbicides [41]. These may solve many problems, but not all. Dicamba controls only broad leaf weeds so it may be effective against the *Amaranthus* species that evolved resistance to glyphosate [30], but will have no effect on the populations of grass weeds such as johnsongrass and *Lolium* spp. that have already or will evolve resistance to glyphosate. At high rates, dicamba will kill some perennial broad leaf weeds, but a high level of transgenic resistance will be required.

The choice of acetolactate synthase inhibiting herbicides as a mixing partner for stacked-gene crops raises questions, even though these are systemic herbicide. Too many weeds that have evolved glyphosate resistance such as *Lolium* spp., the *Amaranthus* spp., *Conyza* spp., as well as the *Sorghum halepense* have already evolved resistance to these acetolactate synthase herbicides [30, 32], the most resistance-prone group of herbicides known. Even if this has not occurred in all populations, it easily can.

The best stacking partners will be with genes encoding resistance to systemic general herbicides with multiple target sites of action (mostly yet undiscovered), and/or with genes encoding resistance to graminicides, as these are cases where the needs are the greatest.

Mitigating Gene Flow with Tandemly Coupled Genes for Herbicide Resistance and Non-weediness

As discussed above, there is a major reservation to conferring transgenic herbicide resistance on major crops such as rice, wheat, sorghum, sunflowers as well as others having related weeds. This is because such herbicide resistances would be non-sustainable. The ability to control the closely related feral, weedy forms of these crops or other closely related weeds residing in the same agroecosystem as the crop, will soon be lost due to gene flow. This problem can be precluded by assuring that any hybrid and future offspring from a cross of a transgenic herbicide-resistant crop with an interbreeding weed will lose at least one weediness trait, rendering it less fit to compete with its wild-type brethren, as well as less fit to compete with other species. In highly competitive ecosystems such as agricultural fields, where hundreds of weed seeds germinate in a small area, and competitive "self thinning" leaves a single survivor, "less fit" usually means "unfit." Thus offspring having lost a weediness trait are offspring that cannot establish as a majority of a population; at worst, these offspring will remain in an insignificant frequency in the population, at best, they will die off completely. This use of a tandem construct of a herbicide resistance gene coupled with an anti-weediness gene or genes is the basis of the concept of transgenic mitigation [42]. The mitigating genes used can be those genes causing dwarfing, genes preventing seed shattering, genes preventing secondary dormancy, and with "root" or "head" crops, genes

preventing "bolting" (premature flowering) [26]. The result is offspring that are more like the crop and cannot compete with weeds. Because a tandem construct is used, the herbicide resistance and the mitigating genes are genetically linked and will not segregate from each other. Where goes resistance, so goes mitigation. That this strategy might work has been demonstrated with transgenically mitigated tobacco competing with wild-type tobacco as a model system [43, 44], and with oilseed rape in the screenhouse [45, 46] as well as in the field [47].

A Special Endogenous Mitigator for Wheat Wheat has a propensity to naturally introgress genes into wild and weedy *Aegilops* species [16–18], including those with which it has no homologous chromosomes, such as *Aegilops peregrina* [48]. It transfers such genes by the process of homoeologous recombination by which similar but not identical (homoeologous) chromosomes recombine. This recombination does not occur in the F_1 generation, only in backcrosses after some wheat chromosomes are lost, most notably chromosome 4B. Homoeologous recombination would be deadly to wheat itself; the chromosomes of its three different genomes would pair with each other during meiosis causing a spaghetti-like mess. There is a gene *ph*1 on this long arm of chromosome 4 in the B genome (4BL) that prevents homoeologous recombination, and thus this type of gene flow from wheat to related *Aegilops* species can occur only after 4BL is lost. Thus, it was suggested to insert the gene of choice (herbicide resistance) on 4BL near *ph*1 so that they will remain together, either by homologous recombination onto 4BL or by random insertions and cytologically determining which occurred onto 4BL [49]. Thus, while the F_1 and some backcrosses with *Aegilops* could be resistant to herbicides, it is unlikely that the resistance gene could ever integrate into the *Aegilops* genome by homoeologous recombination.

Mitigating Volunteer Weed Establishment Gene Flow by Engineering Hypersensitivity to Herbicides

An interesting tandem construct was demonstrated to work in rice to assure that transgenically glyphosate-resistant rice volunteers cannot survive. This was achieved by spraying the next crop of (non-glyphosate-resistant) rice with the herbicide bentazon. Bentazon is a selective herbicide that can be used in conventional rice, because rice has an enzyme that degrades bentazon to nontoxic products. The transgenic glyphosate-resistant rice contained the glyphosate-resistant gene in tandem with an antisense (reverse direction) form of the gene encoding bentazon resistance [50]. This antisense form suppresses the expression of the bentazon resistance rendering rice to be hypersensitive to bentazon. When bentazon is used, glyphosate-resistant volunteer rice and any hybrids with weedy rice die.

This strategy has been theoretically extended to other crops and other herbicide resistances to develop a seemingly complicated and sophisticated strategy [51]. Still, such strategies can easily be implemented if there is an agreement among farmer groups, chemical producers, biotech and seed companies. The strategy is to have a series of transgenic varieties with opposing metabolic herbicide resistances and hypersensitivities cultured in rotation so that volunteers and hybrids with weedy forms are killed in alternate generations, and weedy forms that did not introgress the transgene are also controlled in each generation. For example, variety 1 contains a gene encoding glyphosate metabolism (glyphosateR) in tandem with the antisense form of the gene degrading glufosinate. Thus, variety 1 is glyphosate resistant and hypersensitive to glufosinate. Variety 2 has a gene encoding glufosinate metabolism (glufosinateR) and an antisense form of the gene encoding glyphosate resistance. Thus variety 2 is glufosinate resistant and is hypersensitive to glyphosate. Thus, when the herbicides and varieties are used in rotation, glyphosate use with variety 1 will kill volunteers of and hybrids with variety 2, as well as the weedy wild type. Glufosinate with variety 2 will kill volunteers and hybrids with variety 1 as well as the wild-type weed [51]. Other mitigator genes can be added in tandem to further preclude gene flow. This type of stacking has the advantage of requiring the use of a single herbicide during each cropping generation.

As complicated as the strategy may sound, it requires only that the herbicide and crop seed be bundled (sold together) and that only a single variety is available each cropping season. Not only does such a strategy deal with gene flow to weedy rice, it also will delay the evolution of both glyphosate and

glufosinate resistances. From past experience with herbicide resistances, such rotations extend the total expected useful lifetime of both herbicides well beyond the sum of expected lifetimes of each, if each had been used as the sole herbicide without rotation.

Implementation of such sustainability extending practices is not unknown even though industry typically cites antitrust laws as preventing joining forces for such strategies. For example, Australian cotton growers joined forces with academic experts on resistance management and industry and decided which insecticides may and may not be used at different times during the growing season to delay the evolution of all resistances [52].

Overcoming Transgenic Herbicide Resistance Once It Has Evolved in Weeds (Science Fiction?)

The following are strategies proposed (for the first time) for controlling herbicide-resistant weeds once they have evolved. The first strategy is an extension of a concept suggested on how to cause insects to commit chemical suicide [53], which was modified to have parasitic *Striga hermonthica* [54], and other outcrossing weeds such as *Lolium* spp. [26] commit chemical suicide. The proposal is as follows: after an outcrossing weed has evolved herbicide resistance, either via gene flow from the crop or by natural means of evolution, the gene(s) responsible must be isolated. The gene(s) in the antisense form is/are inserted into a transposon (a DNA element that can move from one location in the genome to another) that is compatible with the weed, and multiple copies of the transposon are transformed into the weed and seeds bulked up. The weed seeds are sown into a field where resistance is a problem. For 4–6 generations, alternative crops and herbicides are used. It is rare that any herbicide kills more than 95% of weeds. The remaining weeds will interbreed. All offspring of a weed crossing with others bearing multicopies of the transposon will also contain the trait and the trait will quickly spread. If the trait were to be spread by nuclear, Mendelian genetics, only 50% of offspring would bear the trait. Transgenic traits are functionally dominant in plants, so even heterozygous plants with the transgenic override of resistance are now sensitive to the herbicide, and the herbicide again can be used. Because of the antisense, none of the transposon-bearing weeds are now resistant to the original herbicide, and the original transgenic herbicide-resistant crop can be grown again. This strategy is limited to obligate outcrossing weeds, and would be lost when/if the outcrossing species evolved self-compatibility. Transposons normally move genes around a genome, and presumably have moved some transgenes in the crops already commercialized. Thus, it might be hard to find scientific regulatory concerns about such a technology.

Alternatively, the antisense form of the gene overriding resistance can be inserted into a disarmed (no longer pathogenic) systemic virus that is specific to the weed, and the weeds inoculated by virus-coated grit applied by commercial sandblasting equipment. The virus would spread and the weeds would be functionally susceptible to the herbicide. This use of viruses was initially suggested for producing vaccines to animal diseases in fodder crops [26]. Most viruses do not reach generative (sex) cells, which means that every generation of weed would have to receive such an application, as the trait will not be inherited. There should be few regulatory biosafety concerns about the use of a virus that does not insert DNA into generative cells in seed-propagated crops, as the trait will not be inherited through seeds. If a virus can be found that does insert its nucleic acid into generative cells, a combination of the above two strategies could be considered; the antisense gene in a multicopy transposon could be transmitted by such a virus, and herbicide sensitivity would be conferred on the virus/transposon infected weed, but also on all its offspring. Here, there may well be biosafety concerns that must be ascertained and dealt with if indeed this strategy can be determined to be worthwhile.

Future Directions

The present use of transgenic herbicide resistance has proven itself to be non-sustainable for long periods as a stand-alone technology without instituting meaningful strategies to keep these technologies in the farmers' arsenal of weed control options. Similarly and even less sustainable, is the practice of mutating crops to herbicide resistance, where the crops have interbreeding-related weeds in the same fields. Both governments and industry have failed to institute management strategies to sustain such technologies. The lack of

government regulatory intervention is surprising and disturbing. The regulatory systems required management strategies to delay resistance to transgenic Bt insect-resistant crops, a small fraction of the transgenic crops released, but ignored such issues with herbicide-resistant crops, including the deregulation (i.e., permission for commercial cultivation) of transgenic herbicide-resistant oilseed rape, beets, and rice, all crops with interbreeding weeds. Governments have questionable regulatory authority over the non-transgenic herbicide resistances released in rice, wheat, sunflowers, and oilseed rape, all crops with related interbreeding weeds, and a demonstrated ability to lose sustainability. Perhaps, they should assist sustainable agriculture by obtaining such regulatory authority.

The first priority for the future is to learn from the past and rapidly institute strategies to keep the present herbicide resistances useful. Unfortunately, neither industry nor farmers have long-term considerations; this year's profitability is all that seems to matter. Long-term sustainability of profitability is more an interest of governments, and the regulatory regimes must be set up to attain sustainability through requiring innovations. Goals and milestones must be set for instituting management strategies, and then support academia and industry in testing which are the most cost-effective strategies for maintaining long-term sustainability of herbicide-resistant crops, both of transgenic and non-transgenic herbicide-resistant crops. Such crops must be available in the future and are imperative for food security.

Bibliography

Primary Literature

1. Owen M, Dixon P, Shaw D, Weller S, Young B, Wilson R, Jordan D (2010) Sustainability of glyphosate-based weed management: The benchmark study. ISB News Report (http://www.isb.vt.edu/news/2010/Aug10.pdf) August: 1-4
2. Bradshaw LD, Padgette SR, Kimball SL, Wells BH (1997) Perspectives on glyphosate resistance. Weed Technol 11:189–198
3. Gressel J (2002) Molecular biology of weed control. Taylor & Francis, London
4. Franz JE, Mao MK, Sikorski JA (1997) Glyphosate: a unique global herbicide. American Chemical Society, Washington DC
5. James C (2010) Global status of commercialized biotech/GM crops: 2009, The first fourteen years, 1996–2009. ISAAA Brief 41-2009 ISAAA Brief 41-2009 (http://www.isaaa.org/resources/publications/briefs/41/executivesummary/default.asp)
6. Brookes G, Barfoot P (2010) Global impact of biotech crops: Environmental effects, 1996–2008. AgBioForum 13 (1): #6
7. Trigo E, Chudnovsky D, Cap E, López A (2003) The adoption of transgenic crops in Argentine. International Institute for Sustainable Development, Winnepeg
8. Gressel J (2009) Crops with target-site herbicide resistance for *Orobanche* and 3 control. Pest Manag Sci 65:560–565
9. Joel DM, Kleifeld Y, Losner-Goshen D, Herzlinger G, Gressel J (1995) Transgenic crops against parasites. Nature 374:220–221
10. Kanampiu FK, Kabambe V, Massawe C, Jasi L, Friesen D, Ransom JK, Gressel J (2003) Multi-site, multi-season field tests demonstrate that herbicide seed-coating herbicide-resistance maize controls *Striga* spp. and increases yields in several African countries. Crop Prot 22:697–706
11. Kanampiu F, Karaya H, Burnet M, Gressel J (2009) Needs for and effectiveness of slow release herbicide seed treatment *Striga* control formulations for protection against early season crop phytotoxicity. Crop Prot 28:845–853
12. Pfenning M, Palfay G, Guillet T (2008) The Clearfield® technology – A new broad-spectrum post-emergence weed control system for European sunflower growers. J Plant Dis Protect 21:649–653
13. Prostko EP, Grey TL, Davis JW (2009) Imidazolinone-resistant sunflower tolerance to imazapic. Weed Technol 23:188–190
14. Tuinstra MR, Soumana S, Al-Khatib K, Kapran I, Toure A, van Ast A, Bastiaans L, Ochanda NW, Salami I, Kayentao M, Dembele S (2009) Efficacy of herbicide seed treatments for controlling *Striga* infestation of sorghum. Crop Sci 49:923–929
15. Gressel J (2005) Problems in qualifying and quantifying assumptions in plant protection models: resultant simulations can be mistaken by a factor of million. Crop Prot 24:1007–1015
16. Gaines TA, Henry WB, Byrne PF, Westra P, Nissen SJ, Shaner DL (2008) Jointed goatgrass (*Aegilops cylindrica*) by imidazolinone-resistant wheat hybridization under field conditions. Weed Sci 56:32–36
17. Loureiro I, Escorial C, Baudin JMG, Chueca MC (2008) Hybridisation between wheat and *Aegilops geniculata* and hybrid fertility for potential herbicide resistance transfer. Weed Res 48:561–570
18. Loureiro I, Escorial C, Garcia-baudin JM, Chueca C (2009) Hybridization, fertility and herbicide resistance of hybrids between wheat and *Aegilops biuncialis*. Agron Sustain Dev 29:237–245
19. Vaughan DA, Sanchez PL, Ushiki J, Kaga A, Tomooka N (2005) Asian rice and weedy rice – evolutionary perspectives. In: Gressel J (ed) Crop ferality and volunteerism. CRC Press, Boca Raton
20. Gealy DR (2005) Gene movement between rice (*Oryza sativa*) and weedy rice (*Oryza sativa*): a U.S. temperate rice perspective. In: Gressel J (ed) Crop ferality and volunteerism. CRC Press, Boca Raton
21. Valverde BE (2005) The damage by weedy rice – can feral rice remain undetected? In: Gressel J (ed) Crop ferality and volunteerism. CRC Press, Boca Raton
22. Gressel J, Valverde BE (2009) The other, ignored HIV – Highly invasive vegetation. Food Security 1:463–478

23. Ellstrand NC (2003) Dangerous liaisons – when cultivated plants mate with their wild relatives. Johns Hopkins University Press, Baltimore
24. Warwick SI, Stewart CN Jr (2005) Crops come from wild plants: how domestication, transgenes, and linkage together shape ferality. In: Gressel J (ed) Crop ferality and volunteerism. CRC Press, Boca Raton
25. Barnaud A, Trigueros G, McKey D, Joly HI (2008) High outcrossing rates in fields with mixed sorghum landraces: how are landraces maintained? Heredity 101:445–452
26. Gressel J (2008) Genetic glass ceilings: transgenics for crop biodiversity. Johns Hopkins University Press, Baltimore
27. Tesso T, Kapran I, Grenier C, Snow A, Sweeney P, Pedersen J, Marx D, Bothma G, Ejeta G (2008) The potential for crop-to-wild gene flow in sorghum in Ethiopia and Niger: a geographic survey. Crop Sci 48:1425–1431
28. Snow AA, Culley TM, Campbell LG, Sweeney PM, Hegde SG, Ellstrand NC (2010) Long-term persistence of crop alleles in weedy populations of wild radish (*Raphanus raphanistrum*). New Phytol 186:537–548
29. Gressel J (1996) Fewer constraints than proclaimed to the evolution of glyphosate-resistant weeds. Food Secur 8(1):2–5
30. Heap IM (2010) International survey of herbicide-resistant weeds. http://www.weedscience.org/
31. Davis VM, Kruger GR, Stachler JM, Loux MM, Johnson WG (2009) Growth and seed production of horseweed (*Conyza canadensis*) populations resistant to glyphosate, ALS-inhibiting, and multiple (glyphosate plus ALS-inhibiting) herbicides. Weed Sci 57:494–504
32. Valverde BE, Gressel J (2006) Dealing with the evolution and spread of *Sorghum halepense* glyphosate resistance in Argentina. A consultancy report to SENASA available online: http://www.weedscience.org/paper/Johnsongrass%20Glyphosate%20Report.pdf
33. Vila-Aiub MM, Balbi MC, Gundel PE, Ghersa CM, Powles SB (2007) Evolution of glyphosate-resistant Johnsongrass (*Sorghum halepense*) in glyphosate-resistant soybean. Weed Sci 55:566–571
34. Gressel J, Segel L (1990) Negative cross-resistance; a possible key to atrazine resistance management: a call for whole plant data. Z Naturforsch 45c:470–473
35. Owen MDK, Gressel J (2001) Non-traditional concepts of $ynergy for evaluating integrated weed management. In: Hall JC, Hoagland R, Zablotowicz R (eds) Pesticide biotransformations in plants and microorganisms: similarities and divergences. American Chemical Society, Washington DC, pp 376–396
36. Wrubel RP, Gressel J (1994) Are herbicide mixtures useful for delaying the rapid evolution of resistance? A case study. Weed Technol 8:635–648
37. Huang B-Q, Gressel J (1997) Barnyardgrass (*Echinochloa crus-galli*) resistance to both butachlor and thiobencarb in China. Resistant Pest Mgmt 9:5–7
38. Dayan FE, Rimando AM, Pan ZQ, Baerson SR, Gimsing AL, Duke SO (2010) Sorgoleone. Phytochemistry 71:1032–1103
39. Castle LA, Siehl DL, Gorton R, Patten PA, Chen YH, Bertain S, Cho HJ, Duck N, Wong J, Liu D, Lassner MW (2004) Discovery and directed evolution of a glyphosate tolerance gene. Science 304:1151–1154
40. Anonymous (2010) Monsanto completes key regulatory submission for soybeans with dicamba herbicide tolerance trait. http://monsanto.mediaroom.com/index.php?s = 43&item = 863
41. Green JM, Hale T, Pagano MA, Andreassi JL, Gutteridge SA (2009) Response of 98140 corn with *gat4621* and *hra* transgenes to glyphosate and ALS-inhibiting herbicides. Weed Sci 57:142–148
42. Gressel J (1999) Tandem constructs: preventing the rise of superweeds. Trends Biotechnol 17:361–366
43. Al-Ahmad HI, Galili S, Gressel J (2004) Tandem constructs mitigate risks of transgene flow from crops: tobacco as a model. Mol Ecol 13:687–710
44. Al-Ahmad H, Galili S, Gressel J (2005) Poor competitive fitness of transgenically mitigated tobacco in competition with the wild type in a replacement series. Planta 272:372–385
45. Al-Ahmad H, Dwyer J, Moloney MM, Gressel J (2006) Mitigation of establishment of Brassica napus transgenes in volunteers using a tandem construct containing a selectively unfit gene. Plant Biotech J 4:7–21
46. Al-Ahmad H, Gressel J (2006) Mitigation using a tandem construct containing a selectively unfit gene precludes establishment of *Brassica napus* transgenes in hybrids and backcrosses with weedy *Brassica rapa*. Plant Biotech J 4:23–33
47. Rose CW, Millwood MHS, Rao MR, Halfhill MD, Raymer PL, Warwick SI, Al-Ahmad H, Gressel J, Stewart CNJ (2009) Genetic load and transgenic tandem mitigating genes in transgenic *Brassica rapa* (field mustard) × *Brassica napus* (oilseed rape) hybrid populations. BMC Biotechnol 9:93 http://www.biomedcentral.com/1472-6750/1479/1493
48. Weissmann S, Feldman M, Gressel J (2005) Sporadic inter–generic DNA introgression from wheat into wild *Aegilops* spp. Mol Biol Evol 22:2055–2062
49. Weissmann S, Feldman M, Gressel J (2008) Hypothesis: Transgene establishment in wild relatives of wheat can be prevented by utilizing the *Ph*1 gene as a *senso stricto* chaperon to prevent homoeologous recombination. Plant Sci 175: 410–414
50. Lin C, Jun F, Xu X, Te Z, Cheng J, Tu J, Ye G, Shen Z (2008) A built-in strategy for containment of transgenic plants: creation of selectively terminable transgenic rice. PLoS ONE 3(3): e1818
51. Gressel J, Valverde BE (2009) A strategy to provide long-term control of weedy rice while mitigating herbicide resistance transgene flow, and its potential use for other crops with related weeds. Pest Manag Sci 65:723–731
52. Forrester NW (1990) Designing, implementing and servicing an insecticide resistance management strategy. Pestic Sci 28:167–179
53. Grigliatti TA, Pfeifer TA, Meister GA (2001) TAC-TICS: transposon-based insect control systems. In: Vurro M, Gressel J, Butts T, Harman G, Pilgeram A, St-Leger R, Nuss D (eds)

Enhancing biocontrol agents and handling risks. IOS Press, Amsterdam, pp 201–216

54. Gressel J, Levy A (2000) Giving *Striga hermonthica* the DT's. In: Haussmann BIG, Hess DE, Koyama ML, Grivet L, Rattunde HFW, Geiger HH (eds) Breeding for striga resistance in cereals. Margraf Verlag, Weikersheim, pp 207–224

Books and Reviews

Gressel J (2009) Evolving understanding of the evolution of herbicide resistance. Pest Manag Sci 65:1164–1173

Gressel J, Levy AA (2009) Stress, mutators, mutations and stress resistance. In: Pareek A, Sopory SK, Bohnert HJ, Govindjee (eds) Abiotic stress adaptation in plants: physiological, molecular and genomic foundations. Springer, Dordrecht

Gressel J, Segel LA (1978) The paucity of genetic adaptive resistance of plants to herbicides: possible biological reasons and implications. J Theor Biol 75:349–371

LeBaron H, Gressel J (eds) (1982) Herbicide resistance in plants. Wiley, New York, p 449

Nandula VK (ed) (2010) Glyphosate resistance in crops and weeds: history, development, and management. Wiley, New York

Powles SB, Holtum JAM (1994) Herbicide resistance in plants: biology and biochemistry. Lewis, Boca Raton

Powles SB, Shaner D (eds) (2001) Herbicide resistance in world grains. CRC Press, Boca Raton

Valverde BE (2007) Status and management of grass-weed herbicide resistance in Latin America. Weed Technol 21:310–323

Valverde BE, Riches CR, Caseley JC (2000) Prevention and management of herbicide resistant weeds in rice. Cámara de Insumos Agropecuarios, Costa Rica, Internet available: www.weedscience.org/

Sustainable Landscape Design, Urban Forestry and Green Roof Science and Technology, Introduction

Dagmar Haase
Department of Geography, Humboldt University Berlin, Berlin, Germany
Department of Computational Landscape Ecology, Helmholtz Center for Environmental Research – UFZ, Leipzig, Germany

A sustainable landscape is a healthy and resilient landscape that will endure over the long term, which can be achieved by including the five basic principles in landscape management: resource conservation, built development, environmental quality, social equity, and political participation. That means that in sustainable landscapes, ideally, humans and nature represent coevolving systems that interact within the bounds of the geosphere (including biosphere, atmosphere, pedosphere, hydrosphere, etc.) at various temporal and spatial scales and across scales – from the field to the region, or nations, continents, or even globally. The natural functions and ecosystem processes of the sustainable landscape are able to absorb disturbances, retain its basic functions and thus maintain themselves into the future. The need to achieve such sustainable environments in the future should be the driving force changing the way we live and work in the present and future centuries. Climate change and global warming, loss and fragmentation of habitats and biodiversity, decline in water quality and availability, pollution of the atmosphere and large-scale soil sealing, and salinization all point toward a need for behavior change in all sectors of our world. To feed our growing population, extensive agricultural use of the landscape is needed, which contributes to a large extent to some of these aforementioned environmental problems. But also urban landscapes are resource-hungry, requiring significant inputs of energy, water, nutrients, and chemicals while many of our plant selections and practices are unsuited to our environments. The result is all too often lush and green parks and gardens that are thirsty, hungry, deplete the soil, allow invasive plants to escape, use unsustainable materials, contribute to waterway contamination, and provide limited habitat for native fauna. To achieve landscape sustainability and to ensure a healthy future, especially agricultural and urban landscapes need to be more efficient in their use of resources and work with the given ecological and climatic conditions rather than against them.

But how to define sustainability for all the different landscape components mentioned – which dimensions have to be considered? How to measure it? And how should the sustainability of landscapes be evaluated? Which targets have to be set up and which thresholds should not be exceeded? What forms of landscape planning and governance structures exist and how far they refer to the goals of sustainability? And, should sustainability be achieved quasi "gratis" in case population declines? In this section, a range of highly

experienced authors formulate answers to these fundamental questions.

Simon Bell (see entry ► Sustainable Landscapes) introduces the subject of the section: The subject of sustainable landscapes is a complex one because landscape as a concept includes not only the physical structure of the environment but also human perception. This latter, being subjective, means that values of landscape change from person to person, cultural to culture and over time. Thus, compared with a simpler subject such as air quality where there are objective measures of levels of pollutants, for example, what may be a sustainable landscape in one circumstance may not be in another circumstance at another time. This makes the future prediction of sustainable landscapes particularly challenging. Landscapes should be of great concern to most people. Landscapes may have many diverse values. For example, using the common approach of sustainability with the three "pillars," it may have an economic value as scenery for tourism, a social value as the place where we live and an environmental value as the human habitat providing water, food, and sustenance. Some of these values are placed fairly high in Maslow's hierarchy of needs. Therefore, they may not receive a lot of attention in parts of the world where food security, drought, or poverty are significant issues. But elsewhere they are important if not, as yet, satisfactorily taken into account in calculations of sustainability, mainly because measuring and valuing them is seen as to subjective and complicated. The contribution by Simon Bell shows that the subject is worthy of study and that it is an important factor in evaluating overall sustainability. One of the challenges is that the subject lies at the boundary of or overlaps with many other disciplines and that there is a risk of double counting some aspects when indicators of sustainability are chosen, for example. The main field where these values overlap is (landscape) ecology and the concept of ecosystem services.

When thinking about sustainability, it is mainly about how to keep intact nature and environmental resources for either future generation or, more in terms of environmental justice, for other parts of the world. Land use and spatial planning focus on how to minimize negative effects of urban and industrial growth. Set against this context, urban shrinkage represents a new challenge, *Dagmar Haase* argues in her paper (see entry ► Landscape Planning/Design of Shrinking Landscapes). This is true due to the fact that one has to deal with the opposite phenomenon of growth – population decline and accompanying processes of de-densification – which, unemotionally, also asks the same questions as even mentioned for growth: How can land use development be steered in order to ensure quality of life of the population under conditions of decline? How can high-quality and sustainable urban livelihoods be developed? Are there visions for sustainable shrinkage? Resource consumption is a problem particularly in cities due to the concentration of population – that is consumers of environmental goods and ecosystem services. Since some years, more than half of the world population lives in cities. And – what is more – more than 200 cities worldwide, mostly in Europe, Russia, Japan, and the USA, are shrinking: they lose population. Shrinkage and declining population numbers do not mean an automatic decrease of natural resources consumption such as land, energy, or water, because the per capita requirements on environmental resources, ecosystem services, and housing space are increasing. Also in shrinking cities household numbers increase. In consequence, population losses along with rising per capita housing space lead to further land consumption and enlargement of, e.g., transport and infrastructure. Also in shrinking cities sprawling settlement development continues because of specific housing preferences such as single family houses and spacious housing with backdoor garden. Since shrinkage does not follow the logics of growth, there are no receipts for how to sustainably develop or plan a shrinking city. The paper shows that shrinkage appears in many different shapes and argues that there will not be a "one-size-fits-all" or textbook-answer to this question. So doing, the paper addresses the relationship between urban decline, sociodemography, infrastructure, land use, and ecosystems and discusses causes and consequences of shrinkage in the light of sustainability. It ends up with showing how actors in cities react to shrinkage in terms of rethinking their visions, instrumental settings, and strategic planning.

Planning for biodiversity in the city to reconnect humans with nature will definitely be a topic for the twenty-first century which is discussed by *Robbert Snep* and *Philippe Clergeau* (see entry ► Biodiversity in

Cities, Reconnecting Humans with Nature). Worldwide, the diversity of plant and animal life is diminishing at high speed. At the same moment, more and more humans become city dwellers, with both the proportion and absolute number of people living in cities increasing rapidly. An important link between global biodiversity loss and fast urbanization is the enormous ecological foot print by urban dwellers, the huge demand for natural resources as required by the urban life style. Besides, a generally less well-known impact of the global urbanization of human society is the extinction of wildlife experience. People in cities lack frequent and intense human-nature interactions, as compared to our rural history. This leads to a decreased understanding of and support for plant and animal life. This not only negatively impacts biodiversity conservation efforts; it also restricts the long-term abilities of humans to benefit from nature. By promoting urban biodiversity, nature will be enhanced in the direct living and working environment of citizens, enabling humans to reconnect with nature. The entry addresses the opportunities to enhance urban biodiversity and its experience by citizens. The authors illustrate how the city environment is perceived from a wildlife point of view, which is necessary to recognize opportunities to enhance urban biodiversity. Next, they discuss these opportunities one by one, illustrating with examples how to implement them in practice. The authors conclude with an exploration of future possibilities to integrate urban biodiversity conservation opportunities in the broader concept of sustainable city planning, design, and management.

Non-use and shrinkage produce brownfields which appear to be very heterogeneous and thus an experimental field for sustainable urban redevelopment. *Dieter Rink* and *Juliane Matthey* (see entry ► Urban Redevelopment and Quality of Open Spaces) therefore focus on urban redevelopment plans for shrinking cities. Such plans generally proceed on the assumption that an orderly and controlled retreat from extensive development is feasible. Vacated land is to be successively transformed (from the periphery inward) into new parks, woodland, or amenity green space. This is also expected to integrate peripheral settlements better into the surrounding landscape, improve the supply of open space, and contribute to new site qualities in the inner cities. One goal is to establish green corridors that serve both recreational and nature conservation purposes. In shrinking cities, however, redevelopment produces open spaces or brown field sites of various sizes practically everywhere in the urban fabric, smaller sites in inner-city old-housing areas as well as large areas in prefabricated housing estates through systematic demolition and downsizing. Many local authorities engage in scattered downsizing within existing settlements. But this type of urban redevelopment reaches its limits when "holes" steadily multiply and the physical urban fabric disintegrates. Redevelopment and downsizing raise the question of how the design of open and green space can provide a new quality of urban development. The authors see as one of the major challenges for the future is how public funding can best be deployed in handling vast areas of previously developed land within increasingly perforated cities, for example, as succession areas attractive to residents. This paper looks at the solutions already available and what contribution they can make to improving the quality of life in cities.

Martin Volk (see entry ► Landscape Planning for Sustainable Water Usage) deals with landscape planning for sustainable water usage. Extreme events such as floods, droughts, as well as water scarcity and poor water quality have been increasing globally during recent decades. Global change phenomena, increasing population density in some parts of the world, as well as multiple land use of landscapes such as agricultural management, urbanization, and industrialization are some of the main reasons for these problems. Both, the mentioned reasons as well as the resulting environmental consequences, represent some of the world's most pressing problems that occur on different scales – from the field to the region or even globally. In recent decades, integrated river basin and environmental management – including landscape planning – has been introduced as a potential but challenging instrument to tackle these complex transdisciplinary problems around the world. However, several problems still exist before an effective integrated planning and management can be realized. Volk's contribution introduces to these problems and presents contributions to the solution for some of these problems. Among others, promising developments of decision support systems are presented as one future direction

to support sustainable land use planning and water resources management.

Henning Nuissl and *Stefan Siedentop* (see entry ► Landscape Planning for Minimizing Land Consumption) report on another crucial component of landscape sustainability directly related to its use: Land use driven environmental degradation has long been considered a locally scaled phenomenon. Today, the global dimension of land use related environmental change is generally acknowledged by researchers and policy makers. The need to provide a still growing world population with housing, food, fiber, and freshwater accompanied with wasteful land use practices has resulted in a cumulative loss of biologically productive land and ecosystem functions. Moreover, land use practices are directly or indirectly responsible for the chemical degradation of environmental resources and high levels of greenhouse gases. Thus, land use has become a more and more important agent of global change that influences fundamental environmental processes. In their contribution, the authors scrutinize the question that modern land use processes allow humans to increase the short-term supply of material goods but undermine ecosystem services in the long run on regional and global scales.

Within the "built environment" there are lots of potentials more than on green urban areas to change cities into more sustainable places. *Manfred Köhler* (see entry ► Green Roofs, Ecological Functions and ► Green Roof Infrastructures in Urban Areas) argues that, in recent years, there has been a growth in interest in natural green roofs, or eco-roofs, as distinct from roof gardens due to the ecological benefits that may be derived. Roof gardens were traditionally installed in many countries to provide amenity space and for building beautification, in places such as hotels and resorts. The ecological benefits that were derived such as thermal insulation were almost an afterthought. Nowadays, in many instances, natural green roofs are installed to become natural ecosystems in urban areas. The benefits achieved by such installations can be measured not only in the building itself but the surrounding urban area as a whole. Green roofs have been shown to mitigate the urban heat island effect.

Stephan Brenneisen and *Dusty Gedge* (see entry ► Green Roof Planning in Urban Areas) focus in their contribution on green roof planning in cities and urban areas. The authors argue that in the twenty-first century – the century of the (mega) city according to the UN – urban areas will increasingly need to be planned and developed to take in consideration of the ecological and environmental health of the urban clime to ensure cities can cater for people. This is also a pressing matter in as it is recognized that there is a need to adapt cities to the negative effects of climate change. These issues have been central the work of professionals in the field of green roofs over the last 20 years and increasingly the technologies and approaches of green roofs have been shown to have a positive effect on a number of issues facing cities and megacities in terms of ecological and environmental health and in helping cities adapt to climate change as they reduce the urban heat island effect, localized flash floods as well as air and noise pollution and increasing biodiversity in the urban realm. These processes are part of an evolving approach to planning referred variously referred to as green infrastructure or ecosystem services. Urban greening has therefore become an increasing important approach for planners and is likely to be one that will predominate in the future. It took a long time after Le Corbusier's first steps to the implementation of green roofs as an ecological measure to be absorbed into mainstream urban planning. Green roofs became more popular as a part of ecological construction in the 1970s, and in the early 1980s a number of cities implemented nascent strategic planning approaches to encourage the uptake of green roofs. Elsewhere a series of pilot projects were initiated to explore the ideas and approaches to green roofs in urban areas. The main drivers for the implementation of green roofs in the 1970s–1980s research also suggested that green roof provided a broad range of environmental benefits, such as energy savings, reduction in storm water runoff, and overheating, but there was also a recognition that green roofs also promoted health and well-being and were an essentially element in an "ecological" approach to construction.

Stephan Pauleit, Ole Fryd, Antje Backhaus and *Marina Bergen Jensen* discuss in their contribution on ► Green infrastructure and climate change the role of urban planning to mitigate climate change. Since by 2050 two thirds of the world's population will live in cities and, what is more, already today cities of the developed world are a major source of green house

gas emissions, they need to make serious efforts to mitigate climate change. Urban planning can play a major role in this respect by designing compact, low footprint cities. However, climate change will also make a severe impact on cities mostly by intensification of the heat island effect, increase of surface runoff from more frequent and intense rainstorms and by coastal and riverine flooding. Urban planning will play an important role for development and implementation of integrated strategies for climate change mitigation and adaptation. Green infrastructure can assist in adapting cities to climate change by reducing the urban heat island effect and by managing stormwater runoff. Urban greening in form of planting of shade trees and roof greening can also reduce the energy demand for house heating and cooling. Therefore, design of the urban landscape will have a direct influence on mitigating climate change and the impact of climate change on people's livelihoods and assets.

Kjell Nilsson, Cecil Konijnendijk and Anders Busse Nielsen focus in their contribution on urban forestry and its importance for sustainability and human wellfare. Urban forestry has become defined as the art, science and technology of managing trees and forest resources in and around urban communities for the environmental, social, economic and aesthetic benefits trees provide to people. In its broadest sense, urban forestry embraces a multi-managerial system that includes municipal watersheds, wildlife habitats, outdoor recreation opportunities, landscape design, recycling of municipal wastes, tree care in general and the production of wood fibre as a raw material. Urban forestry includes activities carried out in the city centre, suburban areas and the peri-urban or interface area with rural lands. Urban forestry is a new and still developing research field. Growing awareness about the need for more integrated approaches to urban green planning and management, and specific threats to urban tree populations caused by pests and diseases (such as Dutch Elm Disease) led to its emergence in North America during the 1960s. Europe and other parts of the world followed with for example international research networking intensifying during the late 1990s. The concept of urban forestry as encompassing the planning, design, establishment and management of trees and forest stands with amenity values situated in or near urban areas, has become more widely accepted. However, urban forestry is an emerging and still developing field with great potential. Thus, sustainability issues in this emerging field of science and practice are of overall importance and thus found their place in this encyclopedia.

Sustainable Landscapes

Simon Bell
OPENspace Research Centre, Edinburgh College of Art, Edinburgh, UK
Estonian University of Life Sciences, Tartu, Estonia

Article Outline

Glossary
Definition of the Subject and Its Importance
Introduction
Landscape
Place
Personal Construct Theory
Landscape and Time
Landscape as Art
Sustainability and Landscape
Landscape Sensitivity
Visual Sensitivity
Landscape and Visual Capacity
Monitoring Landscape Change
Indicators of Sustainable Landscape
Tools for Evaluating Sustainable Landscapes
Quality of Life and Landscape Change
Sustainable Landscape Planning, Design, Construction, and Management
Future Directions
Bibliography

Glossary

Aesthetics The study of the nature, appreciation and meaning of beauty in the arts, architecture, and landscape.

Beauty The attractive properties of a landscape which occur when a diversity of elements are found together yet are in a harmonious association; the viewer moved emotionally by a scene of beauty.

Ecological aesthetics An approach to aesthetic theory based on the idea that nature is inherently beautiful and that the understandings of the dynamics of nature lead to a richer aesthetic experience.

Landscape A prospect of scenery that can be taken in at a glance from one point of view; an area of land as perceived by people whose character is the result of the action and interaction of natural and/or human factors.

Landscape assessment The process of describing, classifying, and evaluating landscapes.

Landscape character A distinct and recognizable pattern of elements that occur consistently in a particular type of landscape.

Landscape capacity The ability of a landscape to cope with increasing degrees of change without this leading to a change of its essential character.

Landscape design The process of creating a new landscape or modifying an existing one for a combination of practical and aesthetic purposes.

Landscape perception and preference The study of the way people see different landscapes and the reactions they have to them.

Landscape sensitivity The degree to which a given landscape could potentially be affected by possible changes, such as development, which may negatively affect its character.

Landscape value A measure of the different benefits obtained from a landscape. These may be future or potential values as well as those obtained in the present.

Personal construct theory An attempt to explain how people take information about their environment and construct a personal view of this, which becomes normative for them and thus a lens through which they see the world around them.

Place A way of looking at landscape as a location or behavior setting composed of the physical environment, activities, and perceptions.

Place attachment The way people feel connected to a specific location which may arise as a result of many factors, some concerned with the landscape. This may help to give people a sense of identity.

Quality of life The consideration of factors which affect various dimensions of our life and the way people feel. Environmental and aesthetic factors can increase or decrease quality of life.

The sublime An aesthetic sensation which arises when a viewer's senses are swamped by the magnitude of the scale of a landscape that is difficult to comprehend and which seems limitless.

Visual capacity The degree to which a landscape can absorb additional new elements without appearing overloaded.

Visual sensitivity The degree to which different people are likely to be affected by changes in the visual environment as a result of development or landscape change.

Definition of the Subject and Its Importance

The subject of sustainable landscapes is a complex one because landscape as a concept includes not only the physical structure of the environment but also human perception [1]. This latter, being subjective, means that values of landscape change from person to person, cultural to culture, and over time. Thus, compared with a simpler subject such as air quality where there are objective measures of levels of pollutants, for example, what may be a sustainable landscape in one circumstance may not be in another or at one time when compared to another time frame. This makes the future prediction or modeling of sustainable landscapes particularly challenging.

Landscapes should be of great concern to most people and they may have many diverse values. For example, using the common approach of sustainability with the three "pillars," landscape may have an economic value as scenery for tourism; a social value as the place where people live; and an environmental value as the human habitat providing water, food, and sustenance (see Fig. 1). Some of these values are placed fairly high in Maslow's hierarchy of needs [2] and therefore may not receive a lot of attention in parts of the world where food security, drought, or poverty are significant issues. But elsewhere they are important if not, as yet, satisfactorily taken into account in calculations of sustainability, mainly because measuring and valuing them is seen as too subjective and complicated.

This article explores this complex subject and demonstrates that it should be taken into account as seriously as other, more objective measures. It will show that the subject is worthy of study and that it is an important factor in evaluating overall sustainability.

Sustainable Landscapes. Figure 1
This landscape in Wester Ross in Scotland has many values to different people – economic (as a source of income from agriculture, fishing, tourism or forestry) social (as a place to live) aesthetic (it is an attractive scene) and for recreation/tourism (it provides a contrast from everyday urban life and a place to escape from stress (Source: Simon Bell)

One of the challenges is that the subject lies at the boundary of or overlaps with many other disciplines and that there is a risk of double counting some aspects when indicators of sustainability are chosen, for example. The main field where these values overlap is ecology and the concept of ecosystem services.

Introduction

All landscapes, whether urban or rural, mainly natural or intensively managed constantly undergo change. This is normal and cannot be halted, especially when natural geological and ecological processes take place, let alone cultural, economic, and social changes that cause pressures for land use change and development [3]. Throughout the world, land use and landscape change are ever present forces, but they act at different rates and in different ways in different places. Urbanization, leading to urban sprawl, is a widespread phenomenon receiving much attention at the present time and it is a particularly significant process in developing countries – over half the world's populations now live in cities and these cities frequently expand with no planning or organization and create appalling conditions for the life of those forced to live there. In rural areas, which still make up by far the greatest proportion of the land surface, even in densely populated and urbanized areas such as Europe, change is also widespread. In 1995, the European Environmental Agency identified seven factors that have an impact on land use and landscape and which, 15 years later are still present, though to different degrees in different places [4]:

- Intensification of agriculture (Fig. 2)
- Overgrowth of agricultural lands (Fig. 3)
- Urbanization and development of infrastructure (Fig. 4)
- Standardization of building materials and designs (Fig. 5)
- Tourism and recreation (Fig. 6)
- Excavation of mineral resources and establishment of landfill sites (Fig. 7)
- Disappearance of natural biotopes, habitats, and ecosystems, in part as a result of the above factors

The drivers of these changes are social and economic. Social factors include demographic changes, such as lower birth rates and increasing life expectancy leading to an ageing society in developed countries; higher birth rates and increasing life expectancy leading to population pressures in developing countries; migration of people within countries (from rural areas to the cities) or between countries, or from one continent to another. In the case of European and other rural areas, this is tending to lead to rural depopulation, especially by the out-migration of younger people which leaves a declining number of increasingly older people left in the countryside [5]. There may also be countertrends (in developed countries), such as when urban people move back to the countryside, perhaps at retirement, or to live while commuting to the town

Sustainable Landscapes. Figure 2
A landscape in the south west of France near Lectoure, Gers, of intensified agriculture where many older landscape features, especially small woodlands, have been removed and the amount of arable cultivation has increased as a result (Source: Simon Bell)

Sustainable Landscapes. Figure 3
An example of an abandoned field in the Vidzeme region of Latvia where the land is overgrowing with trees and bushes. This is a common sight in the Baltic countries (Source: Simon Bell)

for work, or even to work there (telecommuting). This process is known as "gentrification" of the countryside as people bring urban qualities and expectations with them, which leads to the landscape becoming a place for living in instead of living from. There may even be migration at retirement when people move to countries or regions with better climates and lower living costs, such as Americans from the north-east moving to Florida or British and Dutch moving to Spain [6] (Fig. 8).

Economic changes may drive some of the social changes – such as low farm incomes causing people to seek higher wages in urban areas, or high unemployment leading people to move abroad for work. Economic drivers, such as the need to keep costs down or the need to keep up with technical advances, drive intensification and the use of standardized equipment or infrastructure which results in a reduction of landscape diversity and regional character.

Sustainable Landscapes. Figure 4
Urbanization is proceeding at a fast pace in countries like China. Here in Hangzhou massive areas of multi-story housing are being constructed (Source: Stephan Pauleit)

Sustainable Landscapes. Figure 5
Standardized designs create anonymous landscapes. This housing estate happens to be in a small town in Scotland but the houses could be built in any town or city in the UK (Source: Simon Bell)

Political influences, such as repressive regimes, civil war and unrest and poverty also lead to migration pressures and refugee flows as well as changes to populations where identity with land and landscape may be part of the problem causing the unrest, such as nationalism or religious/cultural competition. All these factors cause changes to land use and landscape, and the movement and displacement of people has significant effects on their attachment to and relationship with landscape.

The two main land-management trends in rural areas are marginalization and intensification which both have an impact on the landscape and its visual- and biodiversity [7]. Marginalization is a feature of developed countries with stable and urbanized populations and may lead to land abandonment as farmland is no longer considered viable to maintain in cultivation and no one wishes to continue managing it (perhaps because the younger people have moved away and there is no one left to manage it) (Fig. 9). This may lead to the loss of cultural landscape elements as traditional features and practices are no longer to be found, such as haymaking or hedge management or the husbandry of local animal breeds. Often it is also traditional knowledge about management, use of local foods and crafts which die out in such circumstances.

Sustainable Landscapes. Figure 6
Tourism development places enormous pressures on the landscape. In the Bavarian Alps ski resorts and associated infrastructure can be significant elements in the scene (Source: Simon Bell)

Sustainable Landscapes. Figure 7
Mineral excavation can affect large tracts of the landscape. Oil shale extraction, Aidu Mine near Kohtla-Nõmme, northern Estonia (Source: Simon Bell)

Intensification is usually accompanied by larger-scale activities in bigger fields, more inputs, such as fertilizer and pesticide, and use of more and larger machinery so that output per employed person is much higher and fewer workers are needed per hectare. Equipment, buildings, and other infrastructure tend to be larger in order to deal with the increased scale. Traditional field patterns, small-scale biodiversity elements, and traditional buildings usually do not fit into the new large-scale patterns of production, so that these tend to disappear. As a result, the landscape becomes homogenized and loses its regional or local identity.

The relative impact of these two processes varies from country to country and region to region according to basic factors, such as terrain, soil type, climate, and distance to markets, so that in the regions with multiple disadvantages marginalization is likely to be greatest and vice versa.

The value of traditional cultural and biodiversity elements in the rural landscape has not gone unrecognized in some regions, and policies for

Sustainable Landscapes. Figure 8
An example of landscape change due to the construction of ex-urban housing developments to meet the demand of international retirement migration from the UK and the Netherlands to Alicante region of Spain (Source Ingo Zasada)

Sustainable Landscapes. Figure 9
A marginalized rural village and landscape in north-east Portugal, in the Montsinho Natural Park, where only old people are left behind (Source: Simon Bell)

conserving important features have increasingly been supported through mechanisms, such as agri-environment schemes, aimed at reducing the intensity of agriculture and protecting or restoring important landscape features in Europe, for example [8].

Putting a historical perspective on the role of change in the rural landscape [9], it can be seen that there have been many examples of major landscape changes, most of which were the result of initiatives by landowners or other powers at the time. A prime example of this is the enclosure movement of England and parts of north-west Europe in the eighteenth and nineteenth centuries which transformed large-scale open landscapes into geometric hedged fields, and in so doing displaced a large proportion of the rural population and caused many of them to move to the towns and cities [10, 11]. The settlement of the American West in the nineteenth century and the division of land using the survey grid not only transformed the landscape but also the population and culture of a huge territory [12]. Collectivization of agriculture in the Soviet Union is another example of major

Sustainable Landscapes. Figure 10
The remains of a collective farm from the Soviet times in Latvia, now collapsed and abandoned. The Baltic countryside is littered with such ruins (Source: Simon Bell)

landscape change undertaken by the power of the time which had massive social consequences (such as famine in Ukraine in the 1930s and deportations of so-called "kulaks" or better-off peasant farmers to Siberia) [13]. Although collectivization has been abandoned, the relics of the infrastructure still litter the countryside of many areas of the former Soviet Union as shown in Fig. 10.

In the development of the discussion on landscape and sustainability, some authors identify two main approaches or "schools" [14]. One is the protection, management, and design of scenic assets, and the other concerns ecosystem services and human well-being [15]. The main profession involved in landscape planning, design, and management, that of landscape architecture, also approaches the subject from two directions: one direction is planning, through the application of processes for evaluating and protecting or managing landscape change in rural areas in order to obtain or maintain scenic and/or cultural benefits while the other direction is the creation of low-impact but socially inclusive design for urban and residential areas. These two aspects need not be mutually exclusive since developments in valued scenic areas may be acceptable only if designed to be low impact.

This entry explores the meaning and understanding of landscape from several perspectives and follows this with consideration of what gives a landscape value and how to describe and define the many facets of value that may exist. This is followed by an assessment of what sustainability in a landscape means and how it can be evaluated and tested. Some examples highlight the possible application of sustainable landscape planning, design, and management at different spatial scales.

Landscape

The concept or definition of landscape has been discussed in many places and means different things in different contexts [3]. The word in English, originating from German and Dutch words such as *landschap* originated in the idea of the land being created or molded. The word landscape itself originates in an old German word *lantscaf*. *Scaf* became the English word "shape" and the German *schaben* or *schaffen*, so that, for example, the current German *Landschaft* means land that has been shaped (by man) [16]. In English the influence of Dutch landscape painting on British art and landscape appreciation has led to the development of the Oxford English Dictionary definition as "a prospect of inland scenery that can be taken in at a glance from one point of view." This is clearly a very visual definition and relates strongly to landscape paintings seen from a single point, but has also become associated with the single viewpoint overlooking a spectacular piece of scenery. In terms of the valuation of special landscapes and the designation of protected scenery, for example, this concept has been

Sustainable Landscapes. Figure 11
A scene of the Grand Tetons seen from the Idaho side of the national park, where the traditional definition of landscape as a prospect of scenery is evident – in this case providing a sense of beauty and possibly the sublime (Source: Simon Bell)

important, so that many of the national parks around the world are in spectacular mountain areas, such as Yosemite in California, the Grand Tetons in Idaho/Wyoming (see Fig. 11) the Rockies in Canada or the Lake District in England.

In other languages, the word for landscape may vary in its origin and the meanings it carries, perhaps deriving from words associated with "land" or with "views." In some cases, it is borrowed from other languages and may or may not carry the original meaning. For example, in French the word for landscape is "paysage," which is derived from the word for land or countryside, "pays," while in Russian the word for landscape when the physical land and its planning are concerned is "landshaft," borrowed from German, but for a landscape painting the word "paysazh" is used, borrowed from French.

This visual definition of landscape in English is also reflected in the literature on aesthetics, where this external, visual experience may be capable of invoking in the observer a sense of beauty or the sublime [3]. The alternative approach, known as the "participatory aesthetic" [3, 17], involves the person experiencing it using more than just the visual senses and being in the landscape, living there, perhaps, or having to travel through it in order to experience it – as it is not visible all at once from a single viewpoint. This tradition suggests that instead of the landscape experience being a special one – the view from the mountaintop – an aesthetic experience is part of the normal, everyday experience of the world around us. Thus, in a country where the countryside is composed of areas of farmland, farmsteads, lakes, rivers, and towns set in a forest, for example, the experience of traveling around, following the winding roads, continuously opens new small-scale, enclosed scenes which quickly change from moment to moment – there are no grand vistas – and frequently provide charming vignettes of the landscape. The same applies to wandering round the winding streets of a medieval city where small squares and glimpses into courtyards provides a rich experience as shown in Fig. 12. If the participatory aesthetic is a viable theory, it makes sense that people living and working in the landscape or visiting it on weekends are sensitive to the changes taking place and are concerned by them. Aesthetic quality of the landscape becomes an important value and not a merely cosmetic, superficial aspect affected by the whims of fashion and taste [3].

The second approach to the definition of landscape is in the ecological literature. In this landscape is primarily a definition of scale [18] somewhere between a region and a site or biotope. The idea of scale relates well to the original definition of landscape as the prospect of scenery – what can be seen from a mountain or hill top is a certain area of land midway in size or scale between a region and a site. The landscape in this definition is composed of the elements of patches and

Sustainable Landscapes. Figure 12
When exploring the winding streets of an old city such as here in Genoa in Italy, all the senses are engaged in the aesthetic experience. As well as the sights there are sounds and smells and the feeling of heat and cool, twisting and turning and the feeling of the pavements under foot (Source: Simon Bell)

corridors of different vegetation or land use, possibly set within a matrix – a land mosaic (see Fig. 13).

Recent approaches have emphasized the ecological landscape as being in a constant state of change – the mosaic patterns being affected by a range of natural and human processes which operate over different time scales [3]. Of particular relevance to the landscape of many countries are the human processes of land abandonment and the natural processes of colonization by forest, or the cutting of the forest and its secondary succession. Both these sets of processes have impacts on the environment – not only for animal habitats but also for the human habitat. Thus, a landscape ecological approach also has to consider the human dimension and cannot only focus on natural aspects – human shaping of the ecosystem has taken place as long as people have been using land, although the rate and scale of human-caused change may be at its greatest and having the most impact today. However, since the ecological aspect is also linked with ecological sustainability and the notion of ecosystem services, this definition and all it implies will not be discussed further in this entry.

The third approach to defining the landscape is in the geographical literature, primarily arising from the field of cultural geography. Here the landscape is seen as the manifestation of all the interactions of people with the land and thus part of the means by which identity (personal, group, national) is created. In this respect landscape is an ideological concept: people have an imagined relationship with land and nature and this provides a lens through which they see themselves and

Sustainable Landscapes. Figure 13
The ecological definition of landscape – a large territory in the Rocky mountains in Colorado with different interconnected section, in this case prairie, forest and alpine montane habitat (Source: Simon Bell)

the world itself [19]. Other writers note that landscapes are both products of culture and also create or recreate culture [20]. It is worth noting how landscape can play a major part in memory and how key landscape elements – rivers, mountains, or forests, for example – are highly symbolic of aspects ranging from nationhood to cultural identity [21]. That people have been shaping landscapes since they evolved from non-human anthropoid apes is not yet completely proven but certainly, since the start of colonization of large parts of the world commencing some 70,000 years ago [22], with the move of anatomically modern humans out of Africa, people have increasingly been major shapers of the landscape. It is no surprise, therefore, that geographers see the landscape first and foremost as a cultural artifact – a cultural landscape, formed by and reflecting back different cultures over time (see Fig. 14). Any landscape is therefore a *palimpsest*, where layers, or at least remnants, of past influences remain to a greater or lesser extent visible and continue to exert an effect on the character of the landscape.

The Council of Europe, in framing the Florence Convention (European Landscape Convention, ELC) chose to define landscape in cultural terms as "an area, as perceived by people, whose character is the result of action and interaction of natural and/or human factors" [1]. This is a very helpful definition not only for practical purposes by being clear and simple but also because it provides a common understanding for those countries which are signatories. The importance of perception in the definition is also significant, not only because it goes back to the first dictionary definition described above, but also because it is through perception that people see and identify themselves in relation to the landscape.

Thus, the landscape can be defined in terms of a combination of natural components, cultural layers, and aesthetic qualities. Landform, soil, drainage, and climate set the scene for natural vegetation potential. Upon this, and frequently acting at the same time, human activities of settlement, forest clearance, agriculture, urban, infrastructural, and industrial development have taken place to a greater or lesser extent (some landscapes remain predominantly natural in influences (see Fig. 15), others dominated by anthropogenic forces). Such human activity may have been planned over large areas and carried out at a single phase or carried out over time by a series of individual or collective actions steered by economics, technology, tradition, and cultural norms, within the limitations of geology, soils, and climate, by generations of farmers and other land managers. The landscape so created or evolved has certain aesthetic qualities; it forms

Sustainable Landscapes. Figure 14
A cultural landscape in the Bordeaux wine-cultivation region in France where human activities contribute as much or more than natural factors to the landscape and its character (Source: Simon Bell)

Sustainable Landscapes. Figure 15
A view of the Grand Canyon National Park where the natural components, are tending to dominate over the cultural ones – more likely to be the case in the USA than in Europe. In this case the forces of erosion have produced an awesome structure which dwarfs human activity (Source: Simon Bell)

a pattern of elements with particular shapes, colors, textures, and so on with a certain sense of unity and diversity. The landscape will also exhibit a certain condition (such as well managed or neglected) and be susceptible to different tendencies for change (such as land abandonment, agricultural intensification, or urban development). What is perceived by an individual is not only a snapshot at a particular time in its evolution, but the person perceiving it will consciously or unconsciously bring their own background knowledge, bibliography, prejudices, and experiences to it and view it in that context [23].

This integrated view of landscape is important for the rest of the discussion presented here. It involves exploring the evolution of the landscape – a particular landscape (or landscapes) within a particular country. It is seen by people from different cultural backgrounds and from different generations, who have many different experiences. They have certain attachments or associations with a given landscape and are sensitive to its condition and how it is likely to change.

Landscape Value

The landscape, using the definition above, has many values to many people – economic (timber and farm produce, mineral extraction, real estate, scenery bringing tourists to an area, etc.); ecological (habitat value for many species, corridor functions, ecosystem services, such as flood mitigation, etc.) and social/cultural/aesthetic/spiritual values (as a place to live, as a place for recreation, as a place with links to a sense of identity, etc.).

Valuation can be assessed using different measures, such as the increase in the value of a property which has an attractive view [24] or other economic approaches; using sets of ecological or quality of life indicators to give relative values of different landscapes or elements within landscapes. Values can also be classified as [25]:

- Use value (where the landscape has a current value for some uses)
- Existence value (where knowing that a beautiful landscape exists even if a person may never visit yet it is considered worth preserving)
- Option value (where there is the possibility for many different uses which may be taken up at some time in the future)
- Bequest value (where the current generation wishes to hand on the landscape in a good condition to the next generation and forgoes a use or option value)

The understanding and calculation of aesthetic value of landscape has been driven by two main schools over the years [26]: expert systems – measuring characteristics and qualities present in scenes, such as the presence or absence of water (see Fig. 16), and trying to be as objective in the measurements of these, relating them to some kind of scale; and perceptual systems – based on preferences of different scenes by different people (e.g., carried out by looking at photographs and rating scenes on a numerical scale). Although questions of visual landscape aesthetics are considered to be highly subjective, involving as they do matters of taste bound up with personal experience, much research has also shown that there is also a lot of similarity in which landscapes people prefer from a range of cultures. This is especially true of "natural" landscapes – mountains, lakes, and so on – though less so for settled landscapes or urban areas [2]. In some ways, the two approaches are coming together by using perceptions of value expressed by different groups to "calibrate" the more measurable or even descriptive aspects, such as key design principles [3, 18].

Cultural landscape values can also be identified using social science techniques, such as individual or

Sustainable Landscapes. Figure 16
A landscape in Glacier National Park in Montana where water forms a significant aspect of the attractiveness of the scene, presenting a perfect reflection of the mountain in the lake. This is one aspect of water's attractiveness (Source: Simon Bell)

group discussions, in order to uncover the extent to which certain self-identified groups associate themselves with a given landscape and what landscape elements or characteristics they mention during such discussions (see section on "Place and Place Attachment" below).

Landscape Character

Under the European Landscape Convention, only part of the approach for looking after landscape is to protect highly valued areas. The rest of the landscape – the great majority in fact, since only small areas are generally designated or protected – should also be managed. This raises the question of what exactly should be managed – certain elements? The patterns of land use? Traditional buildings? Traditional management methods? And what of the changes underway as a result of the different drivers discussed here so far? In order to be as objective as possible, the concept of landscape character has been adopted, especially by government agencies responsible for developing policies and instruments for managing landscapes under the ELC.

In the UK, for example, where this has been developed over many years, landscape character is defined as "a distinct and recognizable pattern of elements that occur consistently in a particular type of landscape" [27]. Particular combinations of geology, landform, soils, vegetation, land use, field patterns, and human settlement create character. Character makes each part of the landscape distinct and gives each its particular sense of place (see Fig. 17). In many countries, some form of inventory of the landscape has been undertaken which provides a baseline for understanding landscape change [28]. As well as topography, land use, settlement patterns, and variations in geology and ecology, the cultural landscape character is informed by historical aspects, traditional house types and location patterns, communication patterns, and specific features, such as churches, castles, unique landform, or historical events and persons.

The term landscape assessment is used for the process of describing, characterizing, and evaluating landscapes. This aims to be as objective as possible in terms of the process and the description, but has to be much more than a mapping exercise. Since the definition of

Sustainable Landscapes. Figure 17
The character of this landscape in Tuscany is formed by the geology, the ecology, the cultivation and settlement layers. Several different kinds of landscape type can be seen within the whole scene (Source: Francisco Fellini)

landscape includes the fact of perception, it is necessary to consider how the landscape appears from within – from viewpoints and from traveling through it – as well as considering other sensory aspects apart from sight, such as sound and smell. Non-physical or "soft" aspects also need to be considered, such as cultural associations. Increasingly, too, there is a need to include the perceptions of local residents and others in the assessment – at least in the valuation part – and this is anticipated in the European Landscape Convention [1].

The result of a landscape character assessment (LCA) is a set of maps defining different areas according to a typology (see Fig. 18) accompanied with a report describing the existing character at the time the LCA was carried out, its condition, the identifiable forces for change, and any planning policies or guidelines that may be suitable for maintaining character.

Place

People frequently identify with a particular place. If a person is asked where they live, they will name a place, not a landscape. A person will say that they are from a place, not a landscape; they may even identify themselves as being from a certain place (a Londoner, a New Yorker, or a Parisian). Thus, when involving people in landscape planning, it is

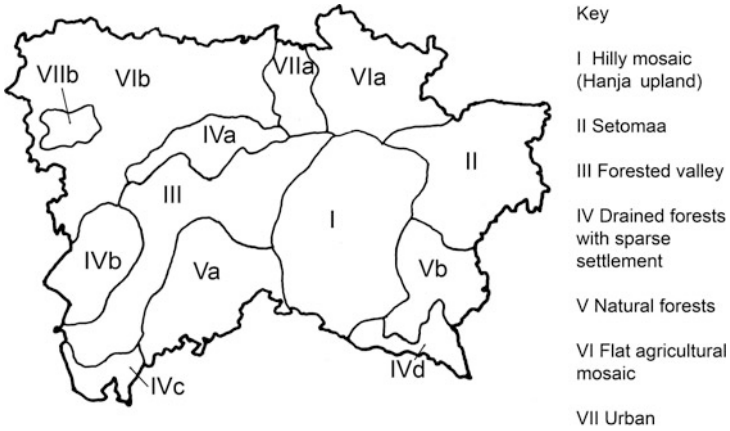

Sustainable Landscapes. Figure 18
An example of a county-level landscape assessment map for Võru Maakond in Estonia. The landscape character areas are fairly broad-brush at this scale (Source: Simon Bell)

best to bear in mind the fact that they think of a place not a landscape. Moreover, people do not tend to think of the physical environment as a separate entity from the social or economic environment, nor separate from the actions they take or the perceptions they hold. However, just because people tend to conflate all these things together and, in an interview or discussion, are often unable to separate them out, it does not mean that it is not important to be able to consider these aspects separately as well as together.

Canter's Theory of Place [29] relies on the concept of "behavior settings," which are described as bounded patterns of human and non-human activity [30]. This theory has been revised and further developed into behavior settings seen as social constructs developed over time [31]. Canter was inspired by both the theory of behavior settings and phenomenology to develop his "psychology of place." In this theory, place is seen as product of physical attributes, human conceptions (perceptions), and activities. A number of studies examining people in landscapes have shown that when people talk about their lives, their perceptions, the physical environment of the place where they live, and the activities they undertake, they are not talking about separate elements but of elements bound in an interactive unit [32]. Thus, Theory of Place enables the planning field to be structured around three attributes: physical environment, activities, and perceptions, with the aim of disentangling the relationships amongst the attributes: for example, when planning deals with an attribute of the physical environment, such as major land-use changes, the interactions between activities, and perceptions with the landscape can be explored.

The meanings particular places hold for people who live in familiar surroundings, especially for a long time, are important for understanding their perceptions and activities during their lives. The places where people live often acquire special emotional significance which in turn creates attachment to that specific place (see Fig. 19). This is because people exist in particular spatial settings, and the emotional connection to a physical location is derived from the meaning given to the location through its role as a setting for experience. A range of thoughts, feelings, beliefs, attitudes, and behaviors are evoked through attachment to place [33].

The concept of place attachment is complex, multifaceted, and approached from many disciplines [34]. Place attachment also depends on interactions, beginning with the premise that all interaction is spatially located, so that place attachment occurs when a particular interaction is accompanied by significant meaning [35]. There are two interdependent components for understanding the feelings a person experiences that binds them to a specific geographic location: the interactional past and the interactional potential of the place. The first component, interactional past, refers to the past experiences or memories associated with the place. The second component, interactional

Sustainable Landscapes. Figure 19
A village in Herefordshire in the UK set among fields. Residents may have lived there all their lives and are likely to have a strong place attachment as a result. (Source: Simon Bell)

potential, is the imagined or anticipated future experiences or expectations associated with the site.

Place attachment often has a special significance for older people [36]. The connection between attachment to place and the unique developmental tasks that accompany the ageing process, such as maintaining a meaningful identity in light of age-related changes, protecting the self against deleterious adjustments due to later life, and maintaining a sense of continuity has been emphasized.

There are two dimensions of place attachment – place dependence and place identity [37, 38]. Place dependence is functional and reflects the importance of a place in providing features and conditions that support specific goals or desired activities for an individual or group. Place identity is more emotional and refers to the symbolic importance of a place as a repository for emotions and relationships that give meaning and purpose to life. Thus, place identity can be considered to be a component of self-identity [39] that enhances self-esteem [40] and increases feelings of belonging to one's community [41, 42].

Personal Construct Theory

The Theory of Place as noted above is a product of environmental psychology and itself is firmly rooted in another important psychological theory, Personal Construct Theory [43]. It is worth discussing briefly because it explains a lot of the way that people's perceptions can be understood. In this theory, people constantly take new experiences and try to organize them into an existing structure based on past experience. The past experience becomes the lens though which new experiences are processed and interpreted. People look at these experiences in terms of similarities and differences and also in terms of significance to them and to others, based on perceptions mediated by their personal constructs. Such constructs may also be shared by social groups. Thus, the data extracted from public participation activities can be evaluated in terms of how these constructs are assembled and to whom they belong. Since people make decisions based on perceptions of what they believe to be a given situation, personal or group constructs become important. A sense of national identity is an example of a personal construct held by a group as is the sense of belonging to a particular village or location. Therefore, all results from any social science research based on asking people about their lives and future intentions must be seen through the lens of Personal Construct Theory. The Theory of Place allows the organization of major factors that make up such

constructs to be identified and made explicit, thus enabling the drivers of behavior or perception to be identified amongst and between groups and individuals.

Landscape and Time

So far the focus of the discussion has been on the fact that a landscape is the product of natural and human processes and experienced by people now, in the present. These processes started a long time past and continue into the future. In order to understand the way landscapes change and their degree of resilience (and therefore one aspect at least of sustainability), it is necessary to be able to consider the time depth associated with a specific landscape.

The identification of distinctive cultural landscapes can be made on the basis of the assessment of the unique combination of elements which set one area apart from another. Since landscapes are always subject to change, they express the way that natural and cultural processes interact with one another over time [9]. Thus, all landscapes are a combination of distinctive patterns which arise as a result of a range of natural and cultural processes, the balance among these over time not only producing the landscapes inherited today but continuing to affect them into the future [3]. Unlike built heritage structures, cultural landscapes can exist both as an artifact and as a system which is a product of these natural, cultural, and social processes.

The time element in any cultural landscape may vary according to several factors, such as the period at which the area was first settled and when humans started to make significant changes, thus leading to greater or lesser time depth being present in different places; the degree to which prehistoric or historical elements have survived in the landscape, perhaps as a result of the materials used in their construction or the degree to which destruction through natural catastrophes, such as earthquakes, or human catastrophes, such as wars, has taken place.

The term *palimpsest* applied to the landscape describes the results of cultural processes which have removed most of the remains of previous eras but left greater or lesser traces behind which can be seen or uncovered and which help to give an area its character and distinctiveness [44] (see Fig. 20). These remains

Sustainable Landscapes. Figure 20
The ancient Roman era theater at Selge in southern Turkey exists within a modern landscape with enormous time depth as a result of many centuries of use of this same landscape together with cultural changes yet long continuity (Source: Simon Bell)

can include physical remains, such as monuments and built structures or field boundaries and ancient trees, but also "ghost" remains, such as legal boundary lines or foundation lines of elements that no longer exist or events that happened there but left no tangible traces.

When developing a strategy to document the time depth of a cultural landscape, it is important to attempt to read it in its context of place and time [45]. Although the concept of landscape is part of the vital and imaginary experiences of a person and is an individual construction, when a community with a distinct culture with roots in the past shares the same values, the identity of a specific landscape becomes a deeper social construction [46]. The time component may therefore play a significant role in the expression of the diversity of shared cultural and natural heritage and form part of the foundation of the sense of identity of particular communities, which needs to be evaluated [47]. A multifaceted/multifunctional perspective of cultural landscapes can be a useful tool for identifying and assessing character using the local and regional historical record that is in part embedded in specific types of physical environment.

Cultural landscapes with significant time depth are frequently more than the sum of artifacts and architectural remains which have survived the long history of

settlement and culture and all the changes that have occurred. However, areas with many archaeological remains may become set aside as special sites, protected as monuments and studied separately without any sense of whether the local people and communities of today have any cultural connection to them [48].

The cultural heritage of landscape can only be acquired by qualified information. Therefore, it is necessary to have tools to read the landscape, its elements and symbols, and its systems and transformations [46]. Technical approaches can be combined with classical historical–geographical methodologies for assessing cultural interfaces within the landscape [49].

In landscape, each man-made feature has its own specific, objective history (in terms of what it is, who made it, when, and for what purpose), whereas human cultures blend stories, myths, and belief with these artifacts to give them meanings which may be different from those originally intended by those who constructed them. Landscapes with a long history of development are therefore more than their physical manifestation – stories, myths, and other associations which have adhered to them over time bring something intangible but no less meaningful to the present time. Since cultural landscapes with a time depth contain so much potential meaning, it is a challenge to identify and interpret the range of aspects that may need to be conserved or managed for the future. This is where the concept of interfaces becomes useful. There are several categories of interface that may be interpreted [49]: those between past and present, between man and nature, between culture and space, and between the spiritual and the visual.

In order to understand time depth, one process that can be used is historic landscape (or land use) assessment [50]. This aims to uncover the different layers of time phases which have affected a specific area, using many different sources such as historic maps and documentary evidence. It can be seen in some ways as a refinement of the landscape character assessment methods described earlier.

Landscape as Art

A further aspect of landscapes and their sustainability is the concept that certain examples can be considered to be living works of art. This classification is attached of numerous examples of historic designed landscape parks and gardens which can be found all over the world. Many of these are associated with specific historical periods and individual designers, with different styles, with major historical persons, and also form part of broader complexes of buildings of historical and architectural merit [51].

Examples such as the palace parks at Versailles, Vaux le Vicomte, or Sceaux in France, constructed in the Baroque style to the order of King Louis XIV by the gardener André Le Notre combine all these factors [52] (see Fig. 21). However, unlike a palace which can be maintained almost indefinitely in its historical and

Sustainable Landscapes. Figure 21
The Baroque gardens at the villa of Sceaux near Paris dating from the same time as Louis XVII and also designed by André Le Nôtre. This is an example of landscape as art (Source: Simon Bell)

original form with suitable conservation techniques, a landscape planted with trees and shrubs and maintained by clipping hedges grows and develops, it suffers from storms and disease and the trees eventually grow old and die. Thus, such places require periodic rejuvenation and careful management, while, at the same time, they may also be developed to reflect the needs and values of the current times.

Thus such landscapes are not only historical artifacts, but they can be considered as much works of art as the buildings, furniture, paintings, and other elements contained within the palace complex located within the park, for example. This adds a different kind of value to a landscape, albeit a relatively limited area territorially (though in some cases still a large area).

Identification and valuation of designed landscapes requires deep knowledge of the historical development of the area over time, but its continued survival depends on knowledge of many techniques of management of living elements [53].

Sustainability and Landscape

From the discussion so far it can be seen that landscape is a complex and multifaceted concept which cannot easily be identified and pinned down in a simple, single model. Since landscape is not only the physical elements which combine in a territory but include, of necessity, many aspects of human perception, the question of defining what sustainability of landscapes really means is also complicated. Since landscapes are always changing and since the very concept of landscape includes change, it becomes difficult to decide what aspects are sustainable and in what way.

From the foregoing discussion it can be seen that landscapes:

- Possess a distinctive character which can be mapped using well-developed techniques
- Are places to which people are attached and which in part at least help to form a sense of identity, but to different people in different ways and at different times
- Possess certain aesthetic qualities which affect quality of life in positive or negative ways depending on how those qualities are manifested and experienced
- Have greater or lesser time depth leading to historical associations and values and which contribute to the aspects described above
- May form living works of art with specific historical and cultural associations

Therefore it is necessary to consider each of these facets as being sensitive to change depending on the nature, rate, type, extent, and the degree of reversibility of change. It is possible to consider three main objectives of landscape management in the context of landscape change pressures:

- Conservation and protection of existing character and values
- Improvement or restoration of the landscape where it may be unattractive, decaying, disturbed, or lacks identity
- Changing the landscape where it is derelict, abandoned, destroyed, or dysfunctional

The aim, taking the lead from the aims of sustainable development from the Brundtland Commission [54], is to retain or enhance the values and functions of a given landscape so that it satisfies the requirements of current generations while safeguarding the options for future generations. In managing change, it is therefore necessary to understand the sensitivities of both physical landscape and people and the capacity of both to cope with potential changes of different types according to the pressures being exerted. In order to do this, it is necessary to understand what makes landscapes and people sensitive to landscape change and how to measure it.

The DPSIR approach (Drivers-Pressures-State-Impact-Response) [55] is commonly used to try to understand how change occurs, and a series of related indicators show the effect of those changes. Applied to landscape, therefore, it is necessary to consider each element of the DPSIR system:

- Drivers: the main drivers of landscape change are demographic change, technological developments, economic cycles, cultural shifts, planning policies, and environmental change. Each of these can be modeled to a certain extent (with greater or lesser degrees of confidence) and can be applied, depending on the models, at different territorial scales. These drivers affect different regions in different ways through the pressures they exert.

- Pressures: the drivers exert pressures on the landscape such as urbanization, spread of urban sprawl, abandonment of remote areas, increased need for transport infrastructure, pollution, change in agricultural techniques, changes in demand for commercial or business land, and construction of technical elements. Such pressures have greater or lesser impacts. People may feel threatened by some or all of these pressures. The pressures change the state of the landscape.
- State: the resulting change in state from that existing before the pressure was applied can be measured and presented using an indicator. Changes in the physical state of the landscape may result in changes to landscape character which may reduce it, strengthen it, or change it (for the better or worse depending on how it is viewed). A particular place may change as a result of urbanization and by an influx of people from elsewhere so that the attachment to that place by the original residents may be weakened, and with it their sense of identity. A cultural landscape which relies on traditional management practices may be lost if modern intensive agriculture takes over or if the area becomes depopulated.
- Impacts: these occur as effects on the landscape and on people. The impact may increase or reduce the attractiveness of a place to live, increase or reduce quality of life, increase or reduce the integrity of a cultural landscape that has survived many centuries. Such impacts need a set of indicators and the calculation of thresholds, so that the degree of impact and the way it affects the sustainability of the landscape can be assessed and remedial measures taken as necessary as part of a planned response.
- Response: the government, government agencies, local authorities, NGOs, or citizen groups and landowners may each seek to control, avoid, prevent, or mitigate the impact by planning or other means and there need to be tools to do so: legal, regulatory, or compensatory, for example, so that any negative effects can be reduced to an acceptable level. Impact assessment undertaken before pressures to develop become actions on the ground is needed, as already exist in many countries (although the mechanisms are currently weak in assessing landscape impact in many places).

Landscape Sensitivity

An important first step in understanding how an expected pressure for development is likely to affect the sustainability of a landscape is to assess its sensitivity. This can be divided into the effect on landscape character, on historical integrity, and on landscape value. Methods of assessing this have been developed for landscape and visual impact assessment as part of the general environmental impact assessment methodology [56].

The potential effect on landscape character depends on the strength and integrity of the landscape likely to be affected by development pressures as well as the scale and nature of the development, and any specific qualities in the landscape which contribute to character and which may be altered. By way of illustrating the potential effect, an example of a development which may be controversial in this respect will be illustrated. Renewable energy is frequently cited as a sustainable technology. Wind turbine developments have to be located in areas where there is plenty of wind, and in the UK, as in many areas of the world, the best sites to be found in hilly or mountainous regions. These often have a strong and wild character into which the presence of large technical elements such as turbines as well as access roads and tracks, power lines, and other features may be considered intrusive and out of place. If the landscape is of relatively small scale, the turbines may appear to dominate it; and if there are many of them, the extent of the landscape affected may be significant (see Fig. 22). Thus, while the sustainability of the renewable energy development may be positive in one regard (energy), it may be considered unsustainable in another regard (landscape). Thus, planning at a strategic level to direct such developments into landscapes with characters which offer greater capacity are likely to help to secure a more sustainable landscape [57].

Effects on historical integrity of a landscape as a result of development pressures will also depend on the nature and scale of the development and the specific historical layers involved. If the landscape can be described as an "archaeological landscape" or one where a complex of remains from specific periods is clearly a dominating factor in its character, then similar effects would apply as for landscape character described above [50]. While, as noted frequently in this paper, the landscape is always changing, current concerns about

Sustainable Landscapes. Figure 22
An example of a windfarm located on a fairly wild moorland in the south of Scotland. Not everyone may think such a development fits into such a landscape (Source: Simon Bell)

change also demand that landscape conservation is practiced wherever appropriate. This is implicit in the ELC [1]. As noted in the introduction, there are several main drivers of change, any or all of which may have an effect on the historical integrity of the landscape. One key change is intensification of agriculture, which may not only remove important ecological elements but also remains which have considerable time depth [4]. These may be field patterns, hedgerows, and old trees, for example. Time depth may also be manifested in strong continuity of cultural traditions such as vernacular buildings in farms and villages which may be replaced by standardized elements which break the sense of time continuity.

The effect on landscape value may be easier to assess because many landscapes have been designated and protected in some way as a result of generally accepted evaluation as a special landscape. In most countries, there are categories of protection of landscapes for scenic reasons (or scenery combined with historical and ecological values). These often have specific legal protection of various degrees of strength. The national parks in the USA were designated for a combination of scenery and public access [58] (see Fig. 23) and are owned by the Federal Government, so that development within them is strictly controlled. However, in many places, development just outside and visible from within is not controlled and leads to negative effects on the landscape. Since the US parks are mainly natural, "unspoilt" landscapes, they have specific qualities which would be vulnerable to many forms of development, although their sheer scale and extent protects them since the effect of peripheral development usually does not penetrate into the core areas. European national parks, such as those found in the UK, are usually cultural landscapes and in part rely for their value as much on cultural elements and ongoing landscape management as they do on their natural scenery [59] (see Fig. 24).

Sustainable Landscapes. Figure 23
Yosemite National Park in California is protected and also highly valued for its spectacular qualities and for the spiritual benefits many people obtain here. It is primarily a natural area, not significantly affected by human activity, although not wholly devoid of it (Source: Simon Bell)

Sustainable Landscapes. Figure 24
The English Lake District National Park combines natural geology and mountainous scenery with human activity cultivation and traditional features (Source: Simon Bell)

In such circumstances, development pressures exists – not least for tourism and recreational infrastructure – but stronger planning controls usually apply and can be used to limit the rate and scale of impact of change. Many people would argue that limited development in this way is necessary to ensure that these landscapes are sustainable in the sense of enabling traditional management practices that led to the character and value of the landscape developing to continue means that they need economic support.

Visual Sensitivity

Since the definition of landscape includes the phase "as perceived by people" [1], any evaluation of sustainability must include the potential negative or positive effects of development pressures on the people who are experiencing the landscape. In the guidance on landscape and visual impact assessment [56], methods of assessing visual sensitivity are described. These generally consider three (sometimes four) factors: the visibility of the likely or proposed development, the numbers of people seeing it and likely to be affected, and the nature of the viewing experience (the fourth factor may be the value of the landscape). Each of these has to be set in the context of the way the development may be viewed.

Using the example of the wind turbine development used earlier, the visibility means the extent over which the development may be visible, radiating out from the site to a distance beyond which it ceases to be visible to the human eye (around 35km) [56]. The visibility may be affected by many factors – intervening hills, vegetation, or structures which may screen the development or parts of it from view. The numbers of people likely to see the development will vary from place to place – in some locations, the population of a whole city may be able to see the development while in others a handful of people may be present in a particular part of the landscape. The visibility from key viewpoints may be modeled using photomontages, for example, as shown in Fig. 25.

The nature of the viewing experience depends on the frequency and the reason for seeing the development. Tourists may be visiting an area in order to obtain a certain type of viewing experience which may not include turbines in their list of desirable features. Long-term residents may be affected by the change to the scene while commuters driving to and fro along a road may not focus on a distant development even though there are large numbers of them visible along a specific route, for example. The context in which the development is seen – the landscape setting, the distance, the relative scale, the lighting conditions, and the character will also have an effect. If the development is seen with a backdrop of wild mountains, it may not be seen as favorably as if the landscape already contains many other technical elements.

Sustainable Landscapes. Figure 25
A photomontage of a windfarm development showing extremely accurately, how it would appear from a specific viewpoint (Source: Margaret McKeen)

The calculation of sensitivity may be a technical exercise based on the factors described above, but this takes no account of how people perceive turbines and whether they see them as negative or positive features in a scene [56]. Turbines may symbolize sustainable development and be seen by some people as positive elements providing evidence of action to protect the environment in general and in the long term, while others may see them more negatively as spoiling the landscape.

Taking the effect of such preferences and perceptions into account in sustainable landscape planning is no easy task because there are many potential stakeholders involved who operate at different spatial scales – local people, regional considerations, national priorities, and so on.

Landscape and Visual Capacity

One approach to strategic sustainable planning of landscape development is the concept of landscape capacity. This means the inherent capability of a given landscape to accept or absorb change without detriment to its character or quality [57]. In some ways, this can be seen as the converse of sensitivity – the higher the sensitivity the lower the capacity, and vice versa. It is not quite that simple because there are factors related to the landscape pattern and structure which may increase or decrease capacity, depending on how they are taken into account. In the example of wind turbines, capacity may depend on aspects, such as landscape scale, the location and position of the development, the number of turbines proposed, and the cumulative effect of several developments in the same landscape.

Visual capacity can be considered in the same way – the visual extent in the scene, the cumulative impact of seeing several separate developments at once, or when traveling along a road for example, as well as the effect of a development (such as of wind turbines) in the background of a scene as opposed to the foreground [57].

In both cases noted above, it is difficult to say whether any landscape which has no examples of a specific development – such as a wind turbine – has any inherent capacity, since such objects are entirely new and alien to the scene. Thus the first step is to introduce the first one, which thus involves a change of state from a landscape with no turbines to one with turbines. After the change of state has occurred, it is more appropriate to consider how many and what configuration of turbines (or any other development) can be added until a tipping point is reached. When the visual impact is considered, this may be different for different people and cannot be calculated by some form of objective expert system, although many authorities would probably like it to be so.

The question of what is a sustainable capacity in a given landscape is therefore a difficult aspect to answer as it is not possible to apply decision rules to

something which depends on many qualitative factors which have to be judged on site or modeled (see section on "Tools for Evaluating Sustainable Landscapes" below).

Monitoring Landscape Change

At the heart of attempting to define and manage a sustainable landscape has to be some kind of process for monitoring the landscape and its change over time. Many examples of monitoring change exist which are based on measuring something which can be mapped [28]. This is useful for some aspects of landscape as it is defined here – changes in vegetation, field boundaries, settlement patterns, or construction of various elements will have an effect on character, for example, although trying to measure this by assessing changes in area of vegetation may not be so directly correlated because plan area may very well not equate with visual area. Since the perceptual aspect of landscape is so important, this must also be taken into account in any monitoring process and qualitatively assessed.

One approach is to use a sampling system. In many landscape (ecological) monitoring systems, such as the UK countryside change program [28], a set of sample areas are visited and their component vegetation and other elements measured and evaluated using a set of criteria. For the landscape, a set of sample viewpoints can fulfill the same function, using panoramic photographs taken at suitable time intervals (the same as for the vegetation or other monitoring) and when linked to mapped information (for which the visible part of the landscape can be identified), the qualitative aspects of the changes can be addressed [60].

Indicators of Sustainable Landscape

According to the DPSIR approach and any method of assessing the effects of change as detected through a combination of map- or photo-based systems, there need to be indicators which show the direction and degree of change in some meaningful way and help to identify when threshold values are approached. Given the subjectivity attached to landscape and the way people may react to change, as well as the perceptual nature of landscape, selection of suitable indicators is by no means an easy task. One attempt has been developed which synthesizes a number of approaches concerning the evaluation of the visual landscape character [61]. This uses nine concepts, and for each concept identifies several dimensions, attributes, and potential indicators. Table 1 summarizes these. The indicators are, in the DPSIR terminology, State indicators, and over time, changes in state could be assessed by them (Fig. 26).

Tools for Evaluating Sustainable Landscapes

There are various technological solutions for evaluating the sustainability of a landscape. These include visualization tools and analytical tools.

Visualization tools range from simple sketches of what a landscape is expected to look like given a certain level of development or the inclusion of certain elements in the landscape, through increasingly sophisticated computer-based or digital graphics which give more realistic or quasi-realistic impression of the appearance of the landscape, to virtual tools which allow the landscape to be modeled in three dimensions and then for the potentially affected population to experience moving around the landscape testing the full impact of where the development can be seen (and heard) [62]. Increasingly, visualizations constructed to specific standards, in order to replicate as closely as possible the viewing experience, have to be provided in support of the assessment of landscape and visual impact. However, static photomontages taken from selected viewpoints are not as helpful as the virtual environment where the potentially affected person has the chance to explore their neighborhood freely and to come to their own conclusions (see Fig. 27), as opposed to the preparation of a technical exercise by professional experts as is the case at present.

Analytical tools include geographic information systems (GIS) used to evaluate, using a system of metrics, the effects of different landscape options or change scenarios and how people respond to them [63]. Such systems can model the visibility of a given landscape from the point of view of the screening effects of landform so that the exact proportion of the landscape likely to be affected is calculated. Metrics need not be only associated with the visual effects but also with habitat effects, drainage, amount of sealed surface, or accessibility from residential areas – aspects which

Sustainable Landscapes. Table 1 Indicators of quality of visual landscape character (Source: [7])

Concept	Dimension	Attribute	Potential indicator
Stewardship	Sense of order, sense of care	Signs of use or abandonment, vegetation succession, condition of elements	Percentage of abandoned land and stage of succession
			Condition of buildings; Areas under positive management
			Length and condition of hedges and walls
			Presence of waste or debris
Coherence	Presence of harmony, unity	Land use, water, pattern	Percentage of land use in natural condition
			Presence and pattern of water
			Repeatability of patterns, colors, textures
Disturbance	Lack of contextual fit, lack of coherence	Disturbed land and disrupted natural areas; construction, infrastructure	Number of disturbing elements
			Percentage area impacted by disturbance
			Visibility of disturbing elements
Historicity	Historical continuity, historical richness	Visible time layers, cultural elements, traditional agricultural patterns and practices	Presence of cultural elements
			Shape and type of linear historical elements
			Age of historical elements
			Number of time layers
			Presence of traditional land use and pattern
Visual scale	Visibility, openness, grain size	Topography, vegetation man-made structures	Viewshed size; Viewshed form
			Depth of view, degree of openness, grain size
Imagebility	Spirit of place/ genius loci, uniqueness, distinctiveness	Spectacular elements, iconic elements, panoramas	Viewpoints
			Presence of spectacular, unique or iconic elements and landmarks
			Presence of water bodies, percentage area of moving water
Complexity	Diversity; variation; complexity of patterns and shapes	Point and linear features, land cover, land form	Number of objects and types
			Evenness index, dominance index
			Diversity indices; Shape diversity
			Size variation indices
			Heterogeneity indices
Naturalness	Intactness, robustness, natural vegetation, lack of human influence	Natural features; structural integrity of vegetation; vegetation/ land-cover type; water; management; patch shape; edge shape	Fractal dimension; vegetation intactness; percentage area with permanent vegetation cover; lack of management; management intensity (type and frequency), naturalism index; degree of wilderness
Ephemera	Seasonal and weather-related changes	Land cover/vegetation; animals; land use (plowing, etc.); water (color reflections and waves); weather	Percentage of land cover with seasonal change
			Presence of animals
			Presence of cyclical farming activities; Percentage area water
			Projected and reflected images; Presence of weather characteristics

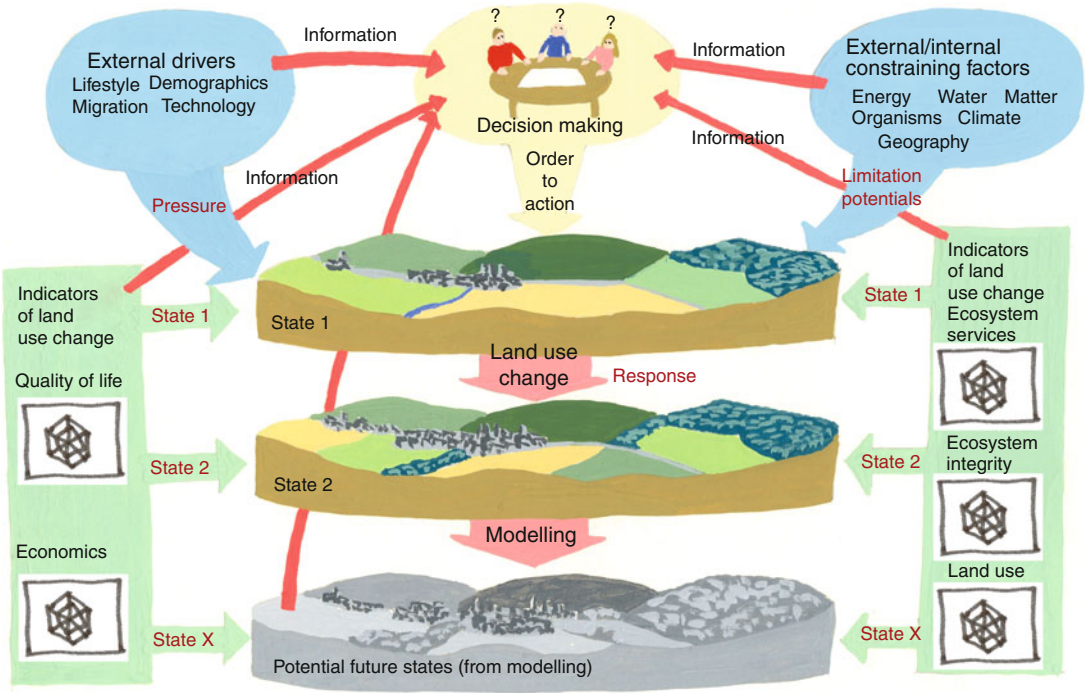

Sustainable Landscapes. Figure 26
A sketch showing how indicators can be used to evaluate differences from one landscape state to another and also to model future potential states. It relates to the DPSIR model (Source: Simon Bell)

Sustainable Landscapes. Figure 27
The Virtual Landscape Theater can be used to simulate the changes to a landscape as experienced by people within the landscape and moving around it (Source: Simon Bell)

have a wider effect on sustainability than the visual/experiential and which may affect the suitability of a plan or design in the wider context of the term.

Quality of Life and Landscape Change

In part, at least, the quality of the landscape affects the quality of life of people living in it or experiencing it. This was realized many years ago by the leading author Nan Fairbrother in her book "New Lives, New Landscapes" where she attempted to define how new urban areas could be designed to increase the quality of life of residents who could move from slum environments in the UK to better housing in a series of new towns [64].

More recently, the concept of quality of life has become popular in many of the large indicator sets for measuring things like sustainable cities, for example [65]. Many of the indicators have nothing to do with landscape – such as the number of teenage pregnancies or adult literacy levels, but some do – such as accessibility of green areas or air quality, for example. These indicators are often measured very crudely and certainly do not take into account the fact that the sensitivity of people may vary for all kinds of reasons. For example, some people prefer to live in city centers where the environment may not be green and where

Sustainable Landscapes. Figure 28
The centre of Manhattan, New York City, may be attractive as a place to live for some people but not for others. Different people belonging to different "tribes" have different views as to whether such a place is suitable for their lifestyle (Source: Simon Bell)

crime levels may be high, but where the life is vibrant and where there is a lot of social and economic activity (see Fig. 28). Young professional adults may be part of this group. Families with young children, however, may prefer suburbs with clean air, lots of green places, and high degrees of safety and security. Yet others may prefer to live in rural areas and are willing to spend long periods commuting into the urban areas for work. Such people belong to different lifestyle groups or, in marketing jargon, "tribes" [66].

As the landscape changes, as the result of various drivers and pressures, the quality of the landscape measured in terms of the indicators noted above, as well as factors such as availability of green space, air quality, noise pollution, safety and security, or convenience of public transport, may lead to a lowering of the perceived quality of life. If people can afford to move house, then the threshold point at which landscape change triggers widespread movement of residents acts as a signal that the landscape is no longer sustainable. Monitoring changes and modeling potential futures as a result of applying the drivers of change can be linked with the way different people are likely to react to different combinations of change and thus to points where quality of life is likely to drop significantly.

Sustainable Landscape Planning, Design, Construction, and Management

The origins of sustainable planning and design can be found in Ian McHarg's seminal work "Design with nature," which advocated looking at many different factors ranging from geology and hydrology to soil and natural vegetation when planning where to locate development, for example [67]. This approach was a pioneer of "sieve mapping" as a tool for evaluating and analyzing the interaction between different layers of information, a task which had to be done manually using overlays at the time (the 1970s), but which is now done using GIS with much more sophistication. The scale at which McHarg worked was mainly at a regional scale, but the methods are also applicable at smaller scales. More recently, the idea of understanding nature, culture, and natural and cultural processes has been developed with an advanced understanding of how these operate, so that the concept of designing with natural and cultural patterns and processes has taken a step forward [3]. One specific area where there have been contentious issues of landscape planning, design, management, and sustainability has been in forests – seen as a renewable resource for many values, but when exploited for timber to the exclusion of everything else has major impacts on ecological, aesthetic, social, and recreational values. Specific methods have been developed to incorporate sustainable design into forestry planning, design, and management [68] (see Fig. 29).

While most of the foregoing has considered the subject of landscape at a fairly large scale and often in the context of landscape planning, at the scale of the design project, sustainability also has to be taken into account. The kind of landscape projects which fall under this category include public parks and green spaces, housing areas, recreation sites (such as in forests or national parks), infrastructure projects, forest landscape design, or restoration of historic parks and gardens.

Aspects to include in sustainable design are concerned with both the process used to develop and create a landscape project, and the elements that comprise the project and its management and maintenance (see Fig. 30). Process aspects may include the role of stakeholders in the preparation of the design brief and objectives, consultation or participation of local people in the development of the design, the contribution of

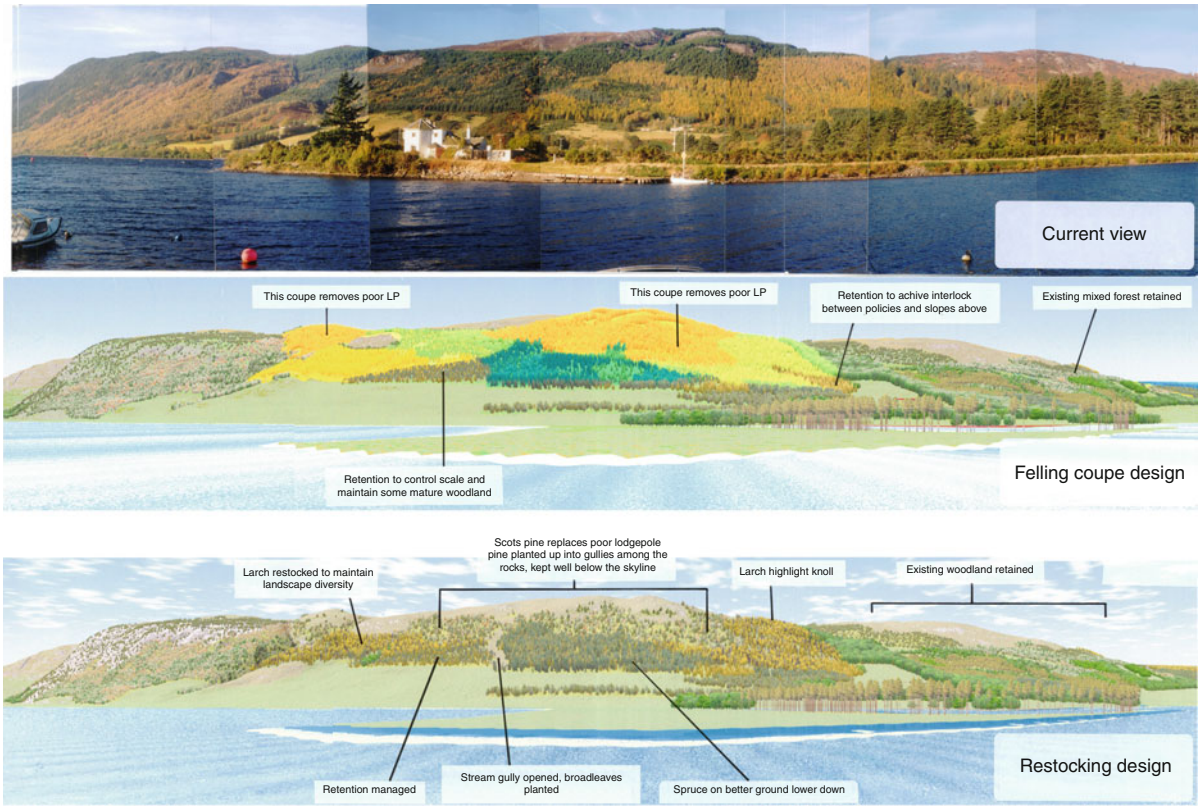

Sustainable Landscapes. Figure 29
An example of large-scale design of a forest in the Highlands of Scotland to show how it will appear in the landscape after certain improvements have been made (for greater sustainability) (Source: Steve Conolly)

the construction and maintenance, as well as the presence of the landscape project to the local economy and the way in which the project takes account of ecological and other environmental issues.

Normally a landscape project of whatever scale sits within a wider environmental, social, and economic context, and so should be evaluated as to how it contributes positively to these over time. Since landscape projects develop and mature over time (a new park is not a finished project but is the start of a process of growth and development which may take decades to mature), their sustainability needs to be considered over the appropriate time frame. The continued involvement of local residents in the way the landscape is managed and possibly modified over time so as to keep contributing the right mix of benefits as the community changes is one aspect; the availability of adequate economic resources to manage the landscape

Sustainable Landscapes. Figure 30
New urban housing in the old docks at Malmö, Sweden, designed to be sustainable in design, construction, use of materials and energy and circulation of water (Source: Simon Bell)

over time so that the investment is not wasted and so that the values continue to flow is another; the maintenance of ecological benefits through the management of the vegetation and habitat elements is also necessary. In places which attract many users, such as outdoor recreation areas within protected landscapes, there may be conflicts with increasing demand from users placing pressure on the natural and financial resources and risking a loss of sustainability [69].

Some landscape projects do not require special funding but are implemented and managed through other means such as in the case of a forest landscape where the activities of forest management, timber harvest, and afforestation are the means by which the design is implemented. In such cases, continual revision and the use of approaches such as "adaptive management" can be applied to ensure continuing sustainability [70].

For those projects where construction and management is undertaken by special contracts – such as the development of a new urban park or a housing area – the use of resources in the construction has to be considered. This includes the use of renewable materials, the use of locally sourced materials, the need for importing topsoil, the need for irrigation and water management for planting areas, the use of local labor in construction, and the life-cycle analysis of materials. At maintenance and management, the use of energy, irrigation, pesticides, machinery, and the longevity of materials should all be considered [71].

Future Directions

As noted in the introduction, landscape in the sense used here – and area of land as perceived by people – the many disciplines interested in this, from landscape architects to environmental psychologists, cultural geographers, or philosophers are constantly exploring new or modified ways of looking at and considering landscape. With the advent of the European Landscape Convention, in Europe at least, the issue will have greater importance and require considerable research from a range of disciplines in order to see its successful implementation. The inspiration of the convention may also have an effect in other regions of the world.

It is also likely that, as the importance of the landscape and outdoor environment increases in terms of its value for human health and well-being, for example, more pressure will be placed on urban green areas and landscapes close to where people live. The evidence base for many of the benefits is not as scientifically rigorous as it might be so this is one area where scientific work is likely to develop [72]. Relating such issues to scales of quality of life which reflect the actual perceptions and values of different societal groups offers further means of linking specific well-being aspects to places and people in a much more sophisticated way.

One major area which has an impact on landscape is the current planning trend to try to make cities more compact in order to reduce the amount of land taken into the urban area and the development of sprawl [73]. While sprawl is a major problem, caused by low-density development on the urban edge associated with transport corridors and ex-urban industry or commerce, there may be negative effects of too much compactness when green space within the urban envelope tends to be squeezed out. Given the importance of green areas within the urban landscape for quality of life and ecosystem services, there is a need to try to ensure that solving one problem does not cause another. This issue is likely to continue as a major one since urban areas are continuing to grow and controls on either sprawl or maintenance of green space are weak in many countries.

Another area where there are likely to be increasing tensions surrounding sustainability is in the effect of sustainable development technologies on the landscape. The example of wind turbine development has been used earlier. While many people advocate the use of renewable energy, other people do not like it to be developed in visually attractive or "natural" landscapes, such as in hilly or mountainous country. Thus, there are two aspects of sustainability in tension with one another. As such developments increasingly affect landscape capacity thresholds, the tensions are only likely to increase.

Participation in planning of the landscape is one important aspect of some approaches to sustainable landscapes and is likely to become more important. This can be tied in with the environmental movement and the various pressures to reduce resource use and to localize more aspects of products and services yielded by the landscape. It also includes the greater involvement of people from different communities in

decisions about the development or protection of local landscapes, especially where they may be many competing demands and perceptions about a place and different degrees of place attachment. A number of tools for public participation exist, but the use of newer technology such as virtual tools, which allow local people to experience different potential landscape futures and to use this for exploring their views and perceptions, is likely to help in resolving such disputes.

Bibliography

Primary Literature

1. Council of Europe (2000) European landscape convention. http://conventions.coe.int/Treaty/en/Treaties/Html/176.htm. Accessed 30 Mar 2010
2. Maslow A (1954) Motivation and need. Harper, New York
3. Bell S (1999) Landscape: pattern, perception and process. E&FN Spon, London
4. European Environmental Agency (1995) European environment: the Dobriš assessment. European Environmental Agency, Copenhagen
5. Bell S, Alves S, Silverinha de Oliveira E, Zuin A (2010) Migration and land use change in Europe: a review. Living Rev Landscape Res 4:2, http://www.livingreviews.org/lrlr-2010-2
6. Zasada I, Alves S, Müller FC, Piorr A, Berges R, Bell S (2010) International retirement migration in the Alicante region, Spain: process, spatial pattern and environmental impacts. J Environ Plann Manage 53(1):125–141
7. Jongman RHG (1996) Ecological and landscape consequences of land use change in Europe. In: Proceedings of the first ECNC seminar on land use change and its ecological consequences, vol. 2, ECNC Publication Series on Man and Nature, Tilburg
8. EU (2005) Overview of agri-environment principles, types, measures, and applications. http://ec.europa.eu/agriculture/publi/reports/agrienv/rep_en.pdf. Accessed 31 Mar 2010
9. Antrop M (2005) Why landscapes of the past are important for the future. Landscape Urban Plann 70:21–34
10. Hoskins A (1955) The making of the English landscape. Hodder and Stoughton, London
11. Rackham O (2000) The history of the countryside. New edition. Phoenix, London
12. Cronon W (1983) Changes in the land. Hill and Wang, New York
13. Bell S, Nikodemus O, Peneze Z, Kruze I (2009) Management of cultural landscapes: what does this mean in the Former Soviet Union: a case study from Latvia. Landscape Res 34(4):425–455
14. Selman P (2008) What do we mean by sustainable landscape? Sustain Science Pract Policy 4(2):23–28
15. Roe M (2007) Landscape and sustainability – an overview. In: Benson J, Roe M (eds) Landscape and sustainability, 2nd edn. Routledge, London, pp 1–15
16. Haber W (2002) Kulturlandschaft zwischen Bild und Wirklichkeit. Sweizerische Akademie der GescheitesundSozialwissenschaften, Berne
17. Berleant A (1982) The aesthetics of environment. Temple University Press, Philadelphia
18. Forman RTT, Godron M (1986) Landscape ecology. Wiley, New York
19. Cosgrove D (1984/1998) Social formation and symbolic landscape. The University of Wisconsin Press, Madison
20. Crang M (1998) Cultural geography. Routledge, London
21. Schama S (1995) Landscape and memory. Alfred A. Knopf, New York
22. Oppenheimer S (2003) Out of Eden. Constable and Robinson, London
23. Bell S (2004) Elements of visual design in the landscape. Spon, Abingdon
24. Tyrväinen L, Miettinen A (2000) Property prices and urban forest amenities. J Environ Econ Manage 39(2):205–223
25. Dziegielewska D (lead author), Tietenberg T, Niggol Seo S (topic editors) (2009) Total economic value. In: Cutler J (ed) Encyclopedia of earth. Environmental Information Coalition, National Council for Science and the Environment), Cleveland, Washington, DC. [First published in the Encyclopedia of Earth 22 Aug 2006; Last revised 28 Aug 2009]. <http://www.eoearth.org/article/Total_economic_value>. Accessed 31 March 2010
26. Daniel T (2001) Whither scenic beauty? Visual landscape quality assessment in the 21st century. Landscape Urban Plann 54(1–4):267–281
27. Countryside Agency and Scottish Natural Heritage (2002) Landscape character assessment – guidance for England and Wales. Countryside Agency, SNH, Battleby, Scotland
28. Countryside survey programme for the UK. http://www.countrysidesurvey.org.uk/index.html. Accessed 31 Mar 2010
29. Canter D (1977) The psychology of place. Architectural, London
30. Barker RG (1968) Ecological psychology: concepts and methods for studying the environment of human behavior. Stanford University Press, Stanford
31. Wicker AW (1979) An introduction to ecological psychology. Cambridge University Press, Cambridge, MA
32. Ward TC, Myers MS (2003) Interviews and questionnaires. In: Bell S (ed) Crossplan: integrated, participatory planning as a tool for rural development. Forestry Commission, Edinburgh
33. Ponzetti JJ (2003) Growing old in rural communities: a visual methodology for studying place attachment. J Rural Community Psychol E6(1):1–11
34. Low SM, Altman I (1992) Place attachment: a conceptual inquiry. In: Altman I, Low SM (eds) Place attachment: human behavior and environment. Plenum, New York, pp 1–12
35. Milligan MJ (1998) Interactional past and potential: the social construction of place attachment. Symbolic Interact 21(1):1–33
36. Rubinstein RL, Parmelee PA (1992) Attachment to place and the representation of the life course by the elderly.

In: Altman I, Low SM (eds) Place attachment: human behavior and environment. Plenum, New York, pp 139–64
37. Williams DR, Patterson ME, Roggenbuck JW, Watson AE (1992) Beyond the commodity metaphor: examining emotional and symbolic attachment to place. Leisure Sci 14:29–46
38. Jorgensen B, Stedman R (2006) A comparative analysis of predictors of sense of place dimensions: attachment to, dependence on, and identification of lake shore properties. J Environ Manage 79:316–327
39. Proshansky HM, Fabian AK, Kaminof R (1983) Place identity: physical world socialization of the self. J Environ Psychol 3:57–83
40. Korpela K (1989) Place-identity as a product of environmental self-regulation. J Environ Psychol 9:241–256
41. Relph E (1976) Place and placelessness. Pion, London
42. Tuan YF (1980) Rootedness versus sense of place. Landscape 24(1):3–8
43. Kelly G (1955) Principles of personal construct psychology, vol I–II. Norton, New York
44. Palimpsest (2010) In Encyclopædia Britannica Online. http://www.britannica.com/EBchecked/topic/439838/palimpsest. Accessed 13 Apr 2010
45. Birnbaum CA (1994) Protecting cultural landscapes planning, treatment and management of historic landscapes. US Department of Interior National Park Service, Technical Preservation Service, Washington, DC, http://www.nps.gov/history/hps/tps/briefs/brief36.htm
46. Farina A (2008) The landscape as a semiotic interface between organisms and resources. Biosemiotics 1:75–83
47. Jones M, Howard P, Olwig KR, Primdahl J, Herlin IS (2007) Multiple interfaces of the European landscape convention. Norsk Geografisk Tidsskrift-Norwegian. J Geogr 61:207–215, ISSN 0029–1951
48. Teutonico JM, Palumbo G (eds) (2002) Management planning for archaeological sites. The Getty Conservation Institute, Los Angeles
49. Palang H, Fry G (2003) Landscape interfaces. In: Palang H, Fry G (eds) Landscape interfaces. cultural heritage in changing landscapes. Kluwer Academic, Dordrecht, pp 1–14
50. Macinnes L (2004) Historical landscape characterization. In: Bishop K, Philips A (eds) Countryside planning: new approaches to management and conservation. Earthscan, London
51. Jellico G, Jellico S (1995) The landscape of man (revised edition). Thames and Hudson, London
52. Berger RW (1985) In the gardens of the Sun King: studies on the Park of Versailles under Louis XIV. Dumbarton Oaks Research Library and Collection, Washington DC
53. Goulty SM (1993) Heritage gardens: care, conservation and management. Routledge, London
54. Our Common Future, Report of the World Commission on Environment and Development, World Commission on Environment and Development (1987) Published as Annex to General Assembly document A/42/427, Development and International Co-operation: Environment 2 Aug 1987
55. European Environment Agency (1999) Environmental indicators: typology and overview. Technical Report No. 25. EEA, Copenhagen
56. Landscape Institute/Institute of Environmental Management and Assessment (2002) Guidelines for landscape and visual impact assessment, 2nd edn. Spon, London
57. Scottish Natural Heritage (2009) Siting and design of windfarms in the landscape version 1. Scottish Natural Heritage, Inverness
58. Everhardt WC (1972) The national park service. Praeger, New York
59. Mair J, Delafons J (2001) The policy origins of Britain's national parks: the Addison Committee 1929–1931. Plann Perspect 16(3):293–309
60. Tapio H (2007) Visuaalinen maisemaseuranta: kulttuurimaiseman muutosten valokuvadokumentointi: kuvat. Taideteollisen korkeakoulun julkaisusarja. A 76. Taideteollinen korkeakoulu. Musta taide, Helsinki
61. Tveit M, Ode A, Fry G (2006) Key concepts in a framework for analysing visual landscape character. Landscape Res 31(3):229–255
62. Macaulay Institute The virtual landscape theatre. http://www.macaulay.ac.uk/landscapes/. Accessed 31 Mar 2010
63. Palmer JF (2004) Using spatial metrics to predict scenic perception in a changing landscape: Dennis, Massachusetts. Landscape Urban Plann 69:201–218
64. Fairbrother N (1970) New lives, new landscapes. Architectural, London
65. European Environment Agency (2009) Ensuring quality of life in European towns and cities. Report No 5/2009. EEA, Copenhagen.
66. Godin S (2008) Tribes: we need you to lead us. Portfolio, New York
67. Mc Harg IL (1967) Design with nature. Wiley, New York
68. Bell S, Apostol D (2008) Designing sustainable forest landscapes. Taylor and Francis, Abingdon
69. Pigram JJJ, Jenkins JM (1999) Outdoor recreation management. Routledge, Abingdon
70. Stankey GH, Clark RN, Bormann BT (2005) Adaptive management of natural resources: theory, concepts, and management institutions. Gen. Tech. Rep. PNW-GTR-654. US Department of Agriculture, Forest Service, Pacific Northwest Research Station, Portland
71. Thompson JW, Sorvig K (2008) Sustainable landscape construction. Island, Washington DC
72. Bell S (2010) A summary of the challenges identified and thoughts on where do we go from here? In: Thompson CW, Aspinall P, Bell S (eds) Challenges for research in landscape and health Routledge, Abingdon, pp 259–278
73. European Environmental Agency (2006) Urban sprawl in Europe. The ignored challenge. Report No 10/2006. EEA, Copenhagen

Books and Reviews

Apostol D, Sinclair M (eds) (2006) Restoring the Pacific Northwest: the art and science of ecological restoration in Cascadia Society for Ecological Restoration. Island, Washington DC

Bell S, Simpson M, Tyrvainen L, Sievanen T, Proebstl U (eds) (2009) European forest recreation and tourism: a handbook. Taylor and Francis, London

Benson J, Roe M (2007) Landscape and sustainability, 2nd edn. Routledge, Abingdon

Berger A (2007) Designing the reclaimed landscape. Routledge, Abingdon

Bishop K, Philips A (2004) Countryside planning: new approaches to management and conservation. Earthscan, London

Brady E (2003) Aesthetics of the natural environment. Edinburgh University Press, Edinburgh

Greem B, Vos W (eds) (2001) Threatened landscapes. Taylor and Francis, Abingdon

McHarg IL (1998) To heal the Earth. Island, Washington DC

Saar M, Palang H (2009) The dimension of place meanings. Living reviews in landscape research 3 downloaded from http://landscaperesearch.livingreviews.org/Articles/. Accessed 31 Mar 2010

Selman P (2006) Planning at the landscape scale. Routledge, Abingdon

Sheppard SRJ, Harshaw WW (2001) Forests and landscapes: linking ecology, sustainability and aesthetics. IUFRO Research Series 6. CABI, Oxford

Uuemaa E, Antrop M, Roosaare J, Riho M, Mander Ü (2008) Landscape metrics and indices: an overview of their use in landscape research. Downloaded from http://landscaperesearch.livingreviews.org/Articles/. Accessed 31 March 2010

Sustainable Productivity, Heat Tolerance for

Anthony E. Hall
Department of Botany and Plant Sciences, University of California Riverside, Quincy, CA, USA

Article Outline

Glossary
Definition of the Subject and Its Importance
Introduction
Climate Change Effects on Crop Plants
Mitigating Effects of Global Warming on Crop Plants
Future Directions
Bibliography

Glossary

C_3 photosynthetic system In which the enzyme rubisco is responsible for the initial fixation of carbon dioxide. All tree and vine crops, all cool-season-adapted annual crops, and most warm-season-adapted annual crops have this photosynthetic system.

C_4 photosynthetic system In which the enzyme PEP carboxylase is responsible for the initial fixation of carbon dioxide. A few tropical grasses (e.g., maize, sorghum, pearl millet, and sugarcane) and a very few warm-season-adapted herbaceous dicotyledonous crops (e.g., grain amaranth) have this photosynthetic system.

CTD Plant canopy temperature depression, the number of degrees Celsius the plant canopy is cooler than air temperature.

FACE Free-air CO_2 enrichment is a system for studying crop responses to elevated [CO_2] under natural open-air field conditions.

Harvest index The ratio of grain yield to total aboveground biomass at harvest.

Heat resistance A cultivar is heat-resistant if it has greater yields of economic product, such as the weight of grain or fruit per unit land area, than standard cultivars in hot environments.

Heat tolerance A cultivar is heat-tolerant if it has a specific process such as germination, vegetative survival, pollination, or fruit set that withstands heat better than the process does in standard cultivars.

Subtropical zones Are where the coldest month has a mean air temperature <18°C, there is a long period (8–12 months) when plants can actively grow (mean monthly air temperatures >10°C), and only occasional frosts occur. This zone is located at low elevations in latitudes between 20° and 30° [26].

Temperate zones Are where there are only 4–7 months when temperatures are high enough for plants to actively grow (mean monthly air temperatures >10°C), and there is a long, cold winter. This zone is located at either high latitudes or at high elevations in more equatorial latitudes [26].

Tropical zones Are where all monthly mean air temperatures are >18°C, and there is no frost and

minimal chilling. This zone is located at low elevations between the Tropic of Cancer and the Tropic of Capricorn [26].

Definition of the Subject and Its Importance

As a consequence of global climate change, air temperatures are predicted to increase by about 4°C during the twenty-first century. Plant physiological and developmental processes respond to temperature by increasing at low temperatures, responding only slightly at optimum temperatures and decreasing at high temperatures. At high temperatures, the processes can become irreversibly damaged. Of particular concern for crop production are the substantial decreases in grain or fruit production caused by experimentally induced increases in air temperature that have been observed in field conditions. In addition, in some zones and years some crop species already are being subjected to temperatures that are above optimal. In a small number of cases, crop cultivars have been bred with developmental and physiological processes that can tolerate a few degrees higher temperature, such that they are heat-resistant and produce more economic yield than standard cultivars in hot environments. Consequently, it is important to determine the circumstances where future breeding of cultivars with heat-tolerant processes, such that they are more heat-resistant than current cultivars, can contribute to the sustainability of crop production during future global warming.

Introduction

During the 1990s, accelerating increases in atmospheric carbon dioxide concentration [CO_2] have occurred leading to the current concentration of 380 ppm and a predicted level greater than 600 ppm by the end of the twenty-first century. As a consequence of the increases in [CO_2] and other gases that absorb infrared radiation, global warming probably already has begun. It has been predicted that temperature increases of about 4°C will take place by the end of the twenty-first century in crop production areas. In some circumstances, these increases in air temperature could result in substantial decreases in economic yield if cultivars, management methods, or crop species are not changed. In contrast, the many crop plants with the C_3 photosynthetic system could exhibit a tendency for increases in photosynthesis and productivity as [CO_2] continues to increase. Consequently, it is important to determine whether elevated [CO_2] can reduce the potentially detrimental effects on productivity of increases in air temperature.

Up to now there has been relatively little emphasis on breeding for heat tolerance in either the public or the private sector but significant progress has been made with a small number of crop species [24]. Breeding the first heat-resistant cultivars by incorporating heat tolerance has taken at least 10 years with annual crop species that are relatively easy to breed. The approach taken has involved incorporating heat tolerance during pollination and seed or fruit set [24]. Breeding heat-resistant cultivars of hard-to-breed perennial species, such as trees or vines, likely would take several decades and many resources. The effects of high temperature, elevated [CO_2], and their interaction on crop plants will be examined. Circumstances where heat-resistant cultivars could help to sustain productivity in the future will be discussed, including consideration of potential negative effects of genes that confer heat tolerance. In addition, circumstances will be described where attempting to incorporate heat tolerance may not be justified and alternative mitigation procedures will be needed.

Climate Change Effects on Crop Plants

Increased Temperature Effects on Crop Plants

From 1950 through 1979, daily minimum temperatures increased more than daily maximum temperatures. However, from 1979 through 2004, there were comparable increases in daily maximum and minimum temperatures [75]. Models predict that daytime and nighttime temperatures will both increase by about 4°C in the twenty-first century. This is important because in some cases high nighttime temperatures have been more damaging to crop productivity than high daytime temperatures [24]. There is some uncertainty with respect to how fast air temperatures may increase and how much they may increase in different parts of the world and seasons of the year.

Higher temperatures can have complex effects on plants. The approach taken in this analysis is to determine: what aspect of temperature is most damaging to productivity (Is it high day temperature or high night

temperature or both and at what stage of development?); what developmental stage or physiological process is most damaged by heat stress; and what extent is economic yield (i.e., grain or fruit yield) decreased when the developmental or physiological process is damaged. Answers to these questions provide the information needed to design efficient programs for breeding heat-resistant plants.

The most reliable method to determine the effects of increases in temperature on productivity is to subject different plots of crop plants growing in the field to increases in temperature. Unfortunately, only a few studies of this type have been conducted. In one of these studies, plots of cowpea that were flowering were enclosed with plastic only during the nighttime hours and a system involving a fan, air-distribution system, heater, and differential thermostat were used to raise the air temperature in the enclosure a fixed number of degrees above ambient air temperature [53]. With this system, daytime conditions on the treated and control plots were not changed, so it is likely that the differences in productivity between the plots were caused by the differences in nighttime temperature. The cowpea plants exhibited a 4.4% decrease in grain yield per degree Celsius increase in nighttime temperature above a threshold daily minimum temperature of 15°C [54]. The lower yields were due to reductions in the proportions of flowers producing pods. In another field study, sorghum exhibited a 28% decrease in grain yield and a 30% decrease in seed number when night temperatures were increased 5°C for 1 week during floret differentiation [17]. When rice plots were subjected to a 4°C increase in temperature both day and night using open-top chambers, there was a decrease in grain yield of 18% [47] due to reductions in spikelet and pollen fertility [45].

Another approach involves growing a crop cultivar with similar management methods in field environments with contrasting thermal regimes. A major problem with correlation studies of this type is that the different field environments also differ with respect to factors other than nighttime temperature, although an attempt was made to minimize these differences in the following examples. When cowpea was grown in four locations in a subtropical zone with contrasting thermal regimes over 2 years a 13.6% decrease in grain yield per degree Celsius increase in average minimum night temperature above a threshold of 16°C between emergence and first flowering was observed [32]. The reduction in productivity was mainly due to reductions in pod set and harvest index (HI is the ratio of grain yield to total shoot biomass). Correlation studies also have been conducted where the productivity of a rice cultivar was examined over 12 years during which time the temperature varied in a tropical zone [60]. In this case, grain yield decreased 10% per degree Celsius increase in minimum night temperature.

A third approach involves studies using glasshouses or growth chambers with artificial lighting systems. While these types of studies can produce information on the mechanisms of heat stress effects because many factors can be kept constant and the studies can be repeated, they tend not to produce reliable data concerning the yield losses due to heat that might occur in field conditions. Studies with cowpea will be discussed because much research on heat-stress effects has been conducted with this crop species and there are indications that some other crop species are affected in a similar manner. Growth chamber studies demonstrated that high night temperatures can reduce pod set of cowpea due to impaired pollination [79], whereas much higher temperatures during the day did not reduce pod set [78]. Artificial pollination studies demonstrated that the female part of the flower, the pistil, was not damaged by high night temperatures [77]. Reciprocal transfers of plants between growth chambers with high or optimal night temperatures demonstrated that the stage of floral development most sensitive to heat stress occurred 9–7 days before anthesis [1]. This stage is after meiosis, which occurs 11 days before anthesis. Damage occurred at the time that the tetrads are released from the microspore mother cell sac [1, 48, 79]. Premature degeneration of the tapetal tissue and lack of endothecium formation were observed which could have been responsible for the low pollen viability, low anther dehiscence, and low pod set under high night temperatures [1]. Tapetal tissue plays an important role in providing nutrients to developing pollen grains and its premature degeneration could thereby stunt pollen development. Based on studies with contrasting cowpea genotypes, Mutters et al. [49] proposed that heat injury during floral development of sensitive cowpea genotypes may be due to reduced translocation of proline from anther walls

and tapetal tissue to developing pollen. Tapetal malfunction has been considered to be the causal mechanism of much of the cytoplasmic and genetic male sterility occurring in plant species [16, 51]. Growth chamber [50] and glasshouse studies [19] have shown that high night temperatures can be more damaging to reproductive development of cowpea under the long days typical of subtropical zones than under the short days that can occur in tropical zones.

Why is pod set in cowpea sensitive to high night temperature while it is not sensitive to much higher temperatures during the day? Growth chamber studies demonstrated that pod set of cowpea is sensitive to heat during a particular time in the night, the last 6 h and not the first 6 h of a 12-h night [48]. The greater sensitivity of pod set to heat under long days was shown to be a phytochrome-mediated effect [50]. Phytochrome-mediated events have a degree of circadian control occurring at a particular time in the 24-h cycle. Mutters and Hall [48] hypothesized that there is a heat-sensitive physiological or developmental process in pollen development that is under circadian control. Natural selection would have favored plants in which this process takes place during the coolest part of the diurnal period, which is the late night and early morning.

As with cowpea, day length also can influence the effect of high temperature on pollination of rice [83]. In addition, glasshouse studies have shown that higher nighttime temperatures that reduced grain yield of rice also reduced percentage of pollen germination and spikelet fertility [46]. Studies in sunlit growth chambers demonstrated, however, that both high day and high night temperature can reduce spikelet fertility in rice [84]. If there is a heat-sensitive process in pollen development that occurs in the coolest period in the 24-h cycle, it could be affected by both late night and early morning temperatures.

From the field and controlled-environment studies, it is apparent that, depending on the crop species, increases in night or day temperature of 4°C during early flowering could cause substantial reductions in fruit or grain yield. The reductions in yield in cowpea and rice appear to have been mainly caused by reduction in pollination. Similar effects have been seen in some other annual crop species including common bean [23]; peanut [72, 73]; tomatoes [59]; pepper [81]; and cotton [70]. The species that appear to be particularly sensitive to high night temperature include: cowpea, common bean, pepper, cotton, sorghum, and possibly rice. Few controlled-environment studies have been conducted of high temperature effects on perennial crops. In one case, for peach, higher temperatures resulted in reduced pollen viability, lack of synchronization in fertilization, reduced fruit set, and reduced fruit yield [52].

Where heat stress is most damaging to economic yield by reducing fruit set and/or seed set, it is a case of the reproductive sink suffering greater damage than the photosynthetic source of carbohydrates. Alternative possibilities for the effects of heat stress include the photosynthetic source suffering significant damage that then reduces economic yield, and cases where both the reproductive sink and the photosynthetic source suffer significant damage.

For Irish potatoes, economic yield may be reduced because of heat-induced reductions in photosynthesis [67]; although initiation of tuberization may be even more sensitive to heat stress than photosynthesis [66]. Grain yield of wheat may be reduced in hot environments because of heat-induced reductions in photosynthesis and stomatal conductance [68]. However, high temperatures during the early floral development can result in infertile pollen and low grain set in wheat [14]. Consequently, reductions in grain yield of wheat in hot environments may be due to both reductions in photosynthesis and damage to reproductive development.

Elevated Atmospheric Carbon Dioxide Concentration [CO_2] Effects

Analyses of air trapped in polar ice indicates that, prior to the year 1800, the [CO_2] fluctuated between 180 and 290 ppm for at least 220,000 years [29]. Since 1800, ice core data indicate increases in [CO_2] from 280 to 315 ppm by 1958. Direct measurements of [CO_2] indicate accelerating increases since 1958 from 315 to 380 ppm by the early 2000s. Predictions indicate [CO_2] could exceed 600 ppm by the end of the twenty-first century.

Plants with the C_4 photosynthetic system evolved during an early period after the [CO_2] became low, and this system represents a specific adaptation to the low [CO_2] environments of the last 200,000 years. The yield

responses of C_4 species to elevated [CO_2] are small, and will not be considered in this analysis. The extent and nature of the evolution of plants with the C_3 photosynthetic system, with respect to low [CO_2], are not known. It is likely that low [CO_2]s over 220,000 years resulted in evolutionary modifications to whole plant processes, such as increases in the ratio of photosynthetic source to carbohydrate sink tissues. Consequently, some C_3 plants may not be well adapted to either future or even present-day levels of [CO_2] due to inadequate investment in sink tissues [30]. Photosynthetic rates of these plants may increase when [CO_2] is increased from the current level of 380 ppm to say 600 ppm but the rates may not increase as much as they would if the whole plant system was adapted to function optimally at a [CO_2] of 600 ppm. Progress during the twenty-first century in increasing the productivity of several C_3 crops through plant breeding was estimated as mainly (77%) resulting from increases in HI with only 23% due to increases in total shoot biomass [22]. This indicates these crop species had an inadequate reproductive sink, for agricultural purposes, and with increasing [CO_2] the reproductive sink may become even more inadequate to support the full photosynthetic potential.

In early studies using controlled-environment enclosures, doubling [CO_2] increased grain yield of various small grain cereals by 32% and various grain legumes by 54% at intermediate temperatures [36]. More recent studies with free-air [CO_2] enrichment (FACE) experiments under field conditions, however, gave grain yield responses to elevated [CO_2] that were about 50% lower than those obtained using enclosures [39]. FACE experiments provide responses that farmers are more likely to get because the crops are grown under natural open-air field conditions. Yield increases in the FACE studies were less than the increases in photosynthesis that occurred with short-term doubling of [CO_2] at the same temperature [3, 61]. A possible explanation for the smaller yield responses to long-term [CO_2] enrichment is the downregulation of photosynthetic capacity that occurred in the FACE experiments [39]. This downregulation has been attributed to feedback mechanisms that operate when the supply of carbohydrates from photosynthesis exceeds sink demands for carbohydrates [3]. Limitations by sink demand were apparent in those FACE experiments where only a small proportion of the increase in photosynthate supply was partitioned to grain [39]. The results of the FACE experiments support the hypothesis that crop plants are not well adapted to the higher [CO_2]s likely to occur by the end of the twenty-first century.

Interactive Effects of Increases in Temperature and [CO_2]

The interactive effects of elevated [CO_2] and higher temperatures on plants are complex [13]. They can be simplified if one separates cases where heat stress limits the reproductive sink from cases in which heat stress limits the photosynthetic source. In many cases, reproductive development is more sensitive to heat stress than overall biomass production resulting in a decrease in HI. For soybean grown under controlled-environment field conditions, HI progressively decreased with increasing temperature under either 330 or 660 ppm [CO_2] and HI was lower with elevated [CO_2] indicating a more severe imbalance between the reproductive sink and the photosynthetic source [6]. Reproductive development of Pima cotton can be so sensitive to high temperatures that the plants do not produce either fruiting branches or bolls [63]. Studies in naturally sunlit, controlled-environment chambers demonstrated that elevated [CO_2] of 700 ppm did not ameliorate this problem [64, 65]. Controlled-environment field studies with rice demonstrated that grain yield decreased 10% per degree Celsius in average temperature above 26°C at [CO_2]s of either 330 or 660 ppm [5]. The decrease in grain yield was mainly due to fewer grains per panicle. High day and high night temperatures can cause decreases in viability of pollen grains at anthesis, increases in floret sterility, and decreases in seed set in rice [84]. Elevated [CO_2] aggravated the heat stress effect on pollen, causing a 1°C decrease in the threshold maximum canopy surface temperature after which the percentage of spikelets having ten or more germinated pollen grains exhibited a precipitous decline [45]. Heat-induced increases in floral sterility may have been responsible for the downregulation of photosynthesis observed in rice under high temperatures and elevated [CO_2] through indirect effects associated with reductions in reproductive sink strength [40].

A study with genotypes that are either heat-tolerant or heat-sensitive during reproductive development has

provided unique insights into the interactive effects of high night temperature and elevated [CO_2]. With high night temperatures, many cowpea genotypes do not produce flowers, while others produce flowers but no pods and the few with total heat tolerance produce flowers and pods [18]. In growth chamber studies with contrasting genotypes in pots under high night temperature, a totally heat-sensitive genotype did not produce any flowers and a partially heat-sensitive genotype did not set any pods under either 350 or 700 ppm [CO_2] [2]. A heat-tolerant genotype had greater pod production under elevated [CO_2] at both high and more optimal night temperatures than a genetically similar cultivar that does not have the heat-tolerance genes [2]. These results indicate that for those many annual crops that are sensitive to heat during reproductive development, incorporating heat tolerance may also enhance their yield responses to elevated [CO_2] over a range of temperatures [29, 30]. This important hypothesis should be more completely tested using other cultivars of cowpea and other crop species.

For cases where the photosynthetic source is particularly sensitive to heat stress, the interactive effects with elevated [CO_2] are less clear. The review of [3] indicates that for C_3 plants, photosynthetic responses to elevated [CO_2] of individual leaves often increased with increasing temperature, up to some maximum temperature, and in some cases biomass responded in the same way. In field studies with wheat using temperature-gradient plastic tunnels, the response of grain yield to elevated [CO_2] of 700 ppm increased from 8% at low seasonal mean temperatures of 10°C to 58% at the highest mean air temperature of 24°C [62]. Other studies with wheat have not exhibited this interactive effect on grain yield of elevated [CO_2] and high temperature [38]. Irish potato responses to elevated [CO_2] of 700 ppm were determined in field canopy chambers maintained at either moderate temperatures or heat-stress temperatures [58]. Tuber yield and total biomass were increased substantially by elevated [CO_2] in the moderate-temperature chambers. In contrast, tuber yields in the heat-stress chambers were very low and there was no effect of elevated [CO_2]. Total biomass production was not affected by the heat-stress treatment. The authors stated that "These results should be viewed as preliminary since they are based on a single growing season and one variety, but they suggest that elevated [CO_2] will not mitigate the negative effects of high-temperature stress on tuberization and yield."

Mitigating Effects of Global Warming on Crop Plants

Circumstances Where Heat-Resistant Cultivars May Help to Sustain Productivity

For some of those annual crops in which reproductive development is particularly sensitive to high temperatures, breeding to incorporate heat tolerance during reproductive development has produced cultivars that are heat-resistant in that they have greater grain or fruit yields than other cultivars in hot environments. Some examples are provided of where breeding heat-resistant cultivars may help to sustain productivity as [CO_2] and temperatures increase including some crop species where heat-resistant cultivars already have been bred, and rice and wheat because of their global importance.

Cowpea and Common Bean Some emphasis is given to cowpea because much has been published on breeding for heat tolerance in this crop. A heat-resistant cowpea cultivar was bred for use during warm seasons in subtropical zones by incorporating heat tolerance during reproductive development [20]. Developing this cultivar required 18 years of breeding. The approach was to take an overall process, heat resistance, that has complex inheritance and divide it into a developmental sequence of simpler heat-tolerant processes which individually were shown to be conferred by one or two major genes [25]. This sequence involved tolerance at the early floral bud stage that conferred the ability to produce flowers under hot long-day conditions; tolerance during pollen development that conferred the ability to set pods under high night temperature; and tolerance during embryo development that conferred the ability to produce large numbers of seeds per pod under high day or high night temperatures. A pedigree breeding program based on this approach and heat-tolerant germplasm are available that would enable additional heat-resistant cowpea cultivars to be bred for use in subtropical zones in about 6 years [28]. The University of California at Riverside has heat-tolerant cowpea lines that are available for use as parents. In breeding for heat resistance,

one of these lines could be crossed with the best available cultivar for the target production zone. Heat tolerance could be incorporated by subjecting a large F_2 generation to a long-day field environment with very high night temperatures (or a glasshouse with very high night temperature and long days) and selecting plants with abundant flower production and pod set. The major gene responsible for heat tolerance during early floral development and the ability to produce flowers is recessive [25], and can be fixed by this selection. A major gene responsible for some of the heat tolerance during pod set is dominant [44]; consequently, selection during additional generations is required to fix this trait. During the fall and winter, one could either select for low leaf-electrolyte-leakage, as a measure of cellular membrane thermostability, to indirectly select for heat tolerance during pod set in the F_3 and F_4 generations in moderate-temperature glasshouses or simply advance two generations using single-seed decent. Many earlier studies have been conducted using leaf-electrolyte-leakage as a measure of cellular membrane thermostability with several crop species [10]. Definitive genetic selection studies with cowpea have demonstrated that low leaf-electrolyte-leakage can be associated with heat tolerance during pod set [71]. Individuals selected for low leaf-electrolyte-leakage under heat stress also tended to have high pod set in hot environments. Individuals selected for high pod set in hot environments also tended to have low leaf-electrolyte-leakage under heat stress. During the next summer, replicate F_5 families could be grown in the extremely hot field nursery (or the glasshouse with very high night temperature) and in parallel nurseries to screen for agronomic traits. Families would be chosen that have abundant flower production, pod set, and number of seed per pod under high night temperature, and suitable agronomic traits in parallel nurseries. The best individual plants would be chosen from within these families. In the following fall and winter, two generations could be advanced in moderate-temperature glasshouses or in a suitable off-season field nursery. While making these generation advances, an adequate quantity of seed should be produced to enable the F_8 lines to be tested for yield and other agronomic traits in several hot, long-day, commercial production environments during the third summer. Potential new cultivars would be selected from these lines and then subjected to one more years yield testing on experiment stations followed by 2 years of yield testing on both experiment stations and farmers' fields.

Most cowpea is produced in tropical zones, such as in the Savanna and Sahelian zones of Africa and in Brazil. Progress has been made in breeding heat-tolerant cowpea cultivars for use in Africa [56, 57]. The approach used involved crossing heat-resistant cowpea parents from the University of California at Riverside with cultivars from Ghana. Selection for heat tolerance during reproductive development was conducted in subtropical long-day environments in California. Final selection for agronomic traits was conducted in northern Ghana. A modified breeding method, however, may be more effective for breeding heat-resistant cowpea cultivars for the tropics than was used for subtropical zones [28]. Heat-resistant African breeding lines could be used as parents and all selection, including that for heat tolerance, should be conducted in Africa. Selection would emphasize ability to set pods and maintenance of large numbers of seeds per pod. Many cowpea cultivars have the ability to produce about 15 ovules per pod, but they rarely produce this many seeds per pod. Under optimal field conditions, the average number of seeds per pod is about 10. In short-day conditions typical of the tropics, heat-sensitive cowpea genotypes produced 50% fewer seeds per pod in a glasshouse with high night temperatures than in a glasshouse with moderate night temperatures [19]. In these studies, several cowpea breeding lines from West Africa were shown to either have high pod set or maintain large numbers of seeds per pod under high night temperatures. These lines could be used as parents to combine heat-tolerance genes and thereby breed cowpea cultivars for Sub-Saharan Africa with greater heat resistance.

Future breeding of heat-resistant cowpea cultivars likely will be done by public plant breeders since as of 2009 there were no significant private breeding programs for cowpea in the world. Some collaborative support for breeding heat-resistant cowpea cultivars can be provided by the University of California at Riverside [31] and the Kano station of the International Institute of Tropical Agriculture in Nigeria. Breeding heat-resistant cowpea cultivars for Africa likely will proceed slowly because national programs have

relatively few resources and other high priorities, such as the need to breed cowpea cultivars with resistance to various pests and diseases.

There are many similarities in the responses to heat of common bean and cowpea [27]. Progress has been made in breeding snap bean types of common beans with heat resistance through incorporating heat tolerance during reproductive development by selecting for high pod set in glasshouses with high night temperatures over two generations [15]. In addition, heat-resistant cultivars of dry bean types of common bean have been bred [7] by selecting for grain yield in hot commercial production environments [8].

Tomato Major contributions to the breeding of heat-resistant tomato cultivars for tropical zones have been made by the Asian Vegetable Research and Development Center in Taiwan [55]. This tomato improvement program gave high priority to incorporating genes for heat tolerance during fruit set. This was achieved by selecting for high fruit set in field nurseries with a sowing date that resulted in strong reductions in fruit set due to heat in sensitive materials. This program has produced open-pollinated and hybrid cultivars with heat resistance, and breeding lines that have been released in at least 32 countries. For subtropical zones, initially, heat-resistant cultivars of tomato were bred by public programs that selected for fruit set in very hot summer field conditions, such as in the Lower Rio Grande Valley in Texas. Subsequently, since the late 1960s, several private breeding programs have been breeding heat-resistant hybrid tomato cultivars for use in the Central Valley of California and elsewhere. For understandable reasons, these private breeding programs have not divulged the methods they have used to incorporate heat tolerance.

Rice A large area of rice is grown in tropical zones at low elevation between the tropics of Cancer and Capricorn. As further warming occurs in this area the major practical solution is to develop heat-resistant rice cultivars. Breeding heat-resistant rice cultivars has received much less attention than breeding for other abiotic stresses [80] and biotic stresses or yield potential. Pollen development, pollination, and spikelet fertility are particularly sensitive to high temperatures. Rice accessions have been discovered that have heat tolerance during flowering, and potentially useful selection criteria have been determined including: flowering earlier in the morning to escape heat; substantial pollen shed (i.e., a large number of pollen grains on the stigma); and high spikelet fertility [80]. Significant research on breeding for heat tolerance in rice has been conducted by the International Rice Research Institute (IRRI) in the past (e.g., [43]). Public rice breeding programs, such as those in China and India, should be able to develop heat-resistant rice cultivars for use in tropical zones by using morphological selection criteria related to pollen and spikelet fertility. National programs in China already have bred heat-sensitive rice lines that are male sterile in hot long-day environments for use in achieving outcrossing in field environments to facilitate the production of hybrid cultivars of rice [83]. All that is needed now is for the national programs in China and elsewhere to select in the opposite direction and breed rice that is not male sterile in hot environments by incorporating greater heat tolerance.

Pima Cotton and Upland Cotton Under high temperatures, cotton plants may not produce fruiting branches or set bolls with Pima cotton being more sensitive to heat stress than upland cotton [37]. Since the early 1960s, selecting for high boll set on low nodes in very hot field conditions has been an important component of the public American Pima cotton breeding program [37]. This program has released a series of six heat-resistant cotton cultivars that have produced progressively higher lint yields under hot field conditions [42]. Surprisingly, these heat-resistant cultivars had progressively higher stomatal conductances as measured in the early afternoon on hot days during peak flowering and fruiting [42]. The authors argued that the adaptive advantage of the higher stomatal conductance appears to be associated with leaf cooling. A tendency to maintain higher stomatal conductances may be even more important in the future since elevated [CO_2] can cause stomata to partially close.

Heat-resistant upland cotton cultivars have been and are being bred for use in subtropical zones by

private breeding programs. Several public programs are breeding heat-resistant cotton cultivars for use in tropical zones [70].

Wheat A large area of wheat is grown in both temperate and subtropical zones. As temperatures increase, some of this production could concentrate in temperate zones; however, heat-resistant wheat cultivars will be useful in many areas as temperatures increase. Due to current farmer interest in growing wheat in hot irrigated conditions, the International Maize and Wheat Improvement Center (CIMMT) has conducted a research program to breed cultivars for this environment. Comparisons of spring wheat cultivars with contrasting heat resistance growing in hot, irrigated environments demonstrated that grain yield was positively correlated with photosynthetic rate and leaf conductance of flag leaves, and canopy temperature depression [68]. Canopy temperature depression (CTD) is the number of degrees Celsius that the crop canopy is cooler than air temperature. Since CTD is dependent on transpiration rate, it provides an alternative to measuring leaf conductance which determines transpiration rate. The CTD is more effective for use in selection in that it can be measured more quickly and covers a larger foliage area than do measurements of leaf conductance. For environments with sunny conditions and a large vapor pressure deficit, CTD was proposed to be a useful trait for selecting for heat tolerance in wheat grown under irrigated conditions that is correlated with higher stomatal conductance and greater photosynthesis [4]. Progress has been made in using measurements of CTD in breeding programs to enhance heat tolerance in spring wheat [69]. In a different approach, studies with genetic lines of wheat that varied in heat resistance demonstrated that low leaf-electrolyte-leakage, as a measure of cellular membrane thermostability, may provide a useful selection criterion for heat resistance in wheat [11]. The authors pointed out, however, that it may only be valuable as a supplemental selection criterion in final breeding stages or as a rough selection tool to reduce a large population into the most likely heat-tolerant core at the early stages of a breeding program. Similarly, selection for CTD may only be useful as a supplemental selection criterion [69]. For a while at least, breeding heat-resistant wheat cultivars likely will mainly depend on empirical selection for grain yield in hot commercial production environments [9].

Do Heat-Tolerance Genes Have Any Negative Effects on Crop Plants?

Genes can have negative as well as positive effects on crop performance due to either pleiotropy, where a single gene has multiple effects, or genetic linkage. One method for evaluating the negative as well as the positive effects of genes is to use backcross breeding to create pairs of near isogenic lines with and without the trait. Ideally this should be done by creating several pairs of lines with different genetic backgrounds to test for potential gene interactions. The performances of the pairs of lines are then compared in contrasting environments to document any positive and negative effects. Six pairs of cowpea lines with differences in heat tolerance during reproductive development have been compared in eight field environments with average night temperatures ranging from being cool to very hot in a subtropical zone [32]. Positive effects were apparent in that the heat-tolerant lines had greater pod set and grain yield than the heat-sensitive lines in the very hot environments. A potential negative effect was detected in that all of the heat-tolerant lines exhibited a progressive dwarfing with increases in night temperature due to shorter main-stem internodes. Performances of the semidwarf heat-tolerant lines and the standard-height heat-sensitive lines were compared at different row spacings with moderate temperatures in a subtropical zone [34]. The semidwarf heat-tolerant lines produced greater grain yields than the standard-height heat-sensitive lines when grown under narrow row spacing and similar grain yields under wide row spacing. In the good growing conditions of these experiments, the semidwarf habit of the heat-tolerant lines appears to be advantageous. In more stressful field conditions and hotter (i.e., tropical zone) environments, the dwarfing would be greater and could seriously reduce the competitiveness of the plants against weeds. The dwarfing associated with heat tolerance may have been due to genetic linkage with the recessive gene that confers heat tolerance during early floral development, and lines are available with heat tolerance during floral development that are not dwarfed [33]. Consequently, it should be possible to

breed heat-tolerant cowpea lines that are not dwarfed. It should be noted, however, that the dwarfing is associated with greater HI [32] and may be responsible for the greater yield response of the heat-tolerant semi-dwarf line to elevated [CO_2] [2].

Potential negative effects of genes may be discovered by theoretical analysis. Heat tolerance during pod set has been associated with low membrane leakage in hot temperatures [71]. Membrane fluidity and function depend on their chemical composition and temperature [76]. Membranes with a chemical composition that is suited to function in hot conditions may not function as well in cool conditions. No evidence for this effect has been reported for cowpea. The heat-tolerant lines had similar grain yields as the heat-sensitive lines in cool field environments [32]. Lines have been bred at the University of California, Riverside that have both chilling tolerance during emergence, associated with low membrane leakage in chilling temperatures [35], and heat tolerance during pod set showing that it is possible to combine these two membrane-dependent traits. In germplasm screening studies, no association was seen between heat tolerance during emergence, chilling tolerance during emergence, and heat tolerance during flowering [21].

Circumstances Where Attempting to Incorporate Heat Tolerance into Cultivars May Not Be Justified and Alternative Mitigation Procedures Will Be Needed

There are many crop species where attempting to incorporate heat tolerance into cultivars may not be effective in sustaining productivity as temperatures increase. Tree and vine crops are difficult to breed using crossing and selection among progeny, and no models are available for incorporating heat tolerance using molecular transgenic methods that have been proven to be effective in enhancing heat resistance.

With crossing and selection, it is necessary to evaluate large numbers of progeny to find individuals that have many of the desired traits. In particular, fruit quality traits are critical for consumer acceptance and must be maintained. This phenotyping takes extensive land area and many years with tree or vine crops.

Much molecular work on heat stress has focused on heat-shock proteins. The classical studies of [82] demonstrated that leaves subjected to high temperatures (50°C) for short periods (15–30 s) tolerated high temperatures (55°C) longer than untreated leaves. Since then there have been many molecular studies of these heat-shock responses that associated them with specific proteins [74]. These proteins have been shown to play a role in enabling seedlings to survive extreme heat shock but they have not been associated with heat tolerance during reproductive development [74]. For example, cowpea genotypes with contrasting heat tolerance during reproductive development [18] have been examined by several laboratories but no differences in heat-shock proteins were detected among them. The heat-shock proteins have not been shown to be useful in enhancing heat resistance, the economic yield of crops in hot environments (e.g., reviews by [12, 76]).

Impacts of future climate changes on some perennial crops in California have been modeled [41]. The authors concluded that climate change in California is very likely to put downward pressure on yields of almonds, walnuts, avocados, and table grapes by 2050; although, they did not include effects of elevated [CO_2] in their analysis. FACE studies with tree species showed an average 28% increase in aboveground biomass production under elevated [CO_2] [39]. Given the long timescales for orchards and vineyards of about 30 years, temperature increases should be considered when selecting perennial cultivars for new plantings. Temperature effects on tree crops can be complex. For example, some deciduous tree crops have a chilling requirement that must be met during the winter to overcome bud dormancy. Insufficient chilling due to warming in winter could result in delayed opening of leaf buds and delayed bloom, and the flowers could be abnormal such that fruit set is reduced [26]. Cultivars of tree crops are available that have smaller chilling requirements but removing an orchard and then replacing it with another cultivar would incur considerable costs since the new orchard would not produce many fruit for several years [41].

Future Directions

For several important annual grain and fruit crops, incorporating heat tolerance during reproductive development by selecting for seed or fruit set under hot conditions can be used to breed heat-resistant cultivars that will help to

sustain productivity as air temperatures increase. These cultivars also may be more responsive to the elevated [CO_2] that will occur in the future. For cases where private plant breeding companies are unlikely to do the necessary breeding, such as with rice and cowpea, more funding and resources should be provided to the public national and international programs that could do this breeding.

For annual crops that produce neither grain nor fruit or for which the main lesion due to heat stress is reduced photosynthetic function, more efficient selection methods could facilitate breeding for heat resistance. More efficient selection methods might be developed if more funds were provided for applied research on heat tolerance in plants. Over the last three decades, relatively little research funding has been devoted to the physiology and genetics of breeding for heat tolerance. In contrast, during this same period, substantial funding has been devoted to molecular studies of heat-shock proteins which, as of 2009, has not produced a documented practical benefit to crop breeding.

For perennial crops, breeding for heat tolerance is extremely difficult. In this case, alternative mitigation methods should be pursued. Predictive methods should be developed and applied to assist farmers to determine when orchards should be removed and what crop and cultivar should be grown instead.

Bibliography

Primary Literature

1. Ahmed FE, Hall AE, DeMason DA (1992) Heat injury during floral development of cowpea (*Vigna unguiculata*, Fabaceae). Am J Bot 79:784–791
2. Ahmed FE, Hall AE, Madore MA (1993) Interactive effects of high temperature and elevated carbon dioxide concentration on cowpea (*Vigna unguiculata* (L.) Walp.). Plant Cell Environ 16:835–842
3. Allen LH (1994) Carbon dioxide increase: direct impacts on crops and indirect effects mediated through anticipated climate changes. In: Boote KJ, Bennett JM, Sinclair TR, Paulsen GM (eds) Physiology and determination of crop yield. Crop Science Society of America, Madison
4. Amani I, Fischer RA, Reynolds MP (1996) Canopy temperature depression associated with yield of irrigated spring wheat cultivars in a hot climate. J Agron Crop Sci 176: 119–129
5. Baker JT, Allen LH (1993) Contrasting crop species response to CO_2 and temperature: rice, soybean and citrus. Vegetatio 104/105:239–260
6. Baker JT, Allen LH, Boote KJ, Jones P, Jones JW (1989) Responses of soybean to air temperature and carbon dioxide concentration. Crop Sci 29:98–105
7. Beaver JS, Miklas PN, Echavez-Badel R (1999) Registration of 'Rosada Nativa' pink bean. Crop Sci 39:1257
8. Beaver JS, Rosas JC, Myers J, Acosta J, Kelly JD, Nchimbi-Msolla S, Misangu R, Bokosi J, Temple S, Arnaud-Santana E, Coyne DP (2003) Contributions of the bean/cowpea CRSP to cultivar and germplasm development in common bean. Field Crops Res 82:87–102
9. Behl RK, Nainawatee HS, Singh KP (1993) High temperature tolerance in wheat. In: Buxton DR, Shibles R, Forsberg RA, Blad BL, Asay KH, Paulsen GM, Wilson RF (eds) International crop science I. Crop Science Society of America, Madison
10. Blum A (1988) Plant breeding for stress environments. CRC, Boca Raton
11. Blum A, Klueva N, Nguyen HT (2001) Wheat thermotolerance is related to yield under heat stress. Euphytica 117:117–123
12. Cheikh N, Miller PR, Kishore G (2000) Role of biotechnology in crop productivity in a changing environment. In: Reddy KR, Hodges HF (eds) Climate change and global crop productivity. CAB International, Wallingford
13. Conroy JP, Seneweera S, Basra AS, Rogers G, Nissen-Wooler B (1994) Influence of rising atmospheric CO_2 concentrations and temperature on growth, yield and grain quality of cereal crops. Aust J Plant Physiol 21:741–758
14. Dawson IA, Wardlaw IF (1989) The tolerance of wheat to high temperatures during reproductive growth. III. Booting to anthesis. Aust J Agric Res 40:965–980
15. Dickson MH (1993) Breeding for heat tolerance in green beans and broccoli. In: Kuo CG (ed) Adaptation of food crops to temperature and water stress. Asian Vegetable Research and Development Center, Shanhua, Publication No 93-410
16. Dundas I, Saxena KB, Byth DE (1981) Microsporogenesis and anther wall development in male-sterile and fertile lines of pigeon pea (*Cajanus cajan* [L.] Millsp.). Euphytica 30:431–435
17. Eastin JD, Castleberry RM, Gerik TJ, Hutquist JH, Mahalakshmi V, Ogunela VB, Rice JR (1983) Physiological aspects of high temperature and water stress. In: Raper CD, Kramer PJ (eds) Crop reactions to water and temperature stresses in humid, temperate climates. Westview Press, Boulder
18. Ehlers JD, Hall AE (1996) Genotypic classification of cowpea based on responses to heat and photoperiod. Crop Sci 36:673–679
19. Ehlers JD, Hall AE (1998) Heat tolerance of contrasting cowpea lines in short and long days. Field Crops Res 55:11–21
20. Ehlers JD, Hall AE, Patel PN, Roberts PA, Matthews WC (2000) Registration of 'California Blackeye 27' cowpea. Crop Sci 40:854–855
21. El-Kholy AS, Hall AE, Mohsen AA (1997) Heat and chilling tolerance during germination and heat tolerance during flowering are not associated in cowpea. Crop Sci 37:456–463

22. Gifford RM (1986) Partitioning of photoassimilate in the development of crop yield. In: Luca WJ, Cronshaw J (eds) Phloem transport. Alan R. Liss, New York
23. Gross Y, Kigel J (1994) Differential sensitivity to high temperatures of stages in the reproductive development of common bean (*Phaseolus vulgaris* L.). Field Crops Res 36:201–212
24. Hall AE (1992) Breeding for heat tolerance. Plant Breed Rev 10:129–168
25. Hall AE (1993) Physiology and breeding for heat tolerance in cowpea, and comparison with other crops. In: Kuo CG (ed) Adaptation of food crops to temperature and water stress. Asian Vegetable Research and Development Center, Shanhua, Publication No 93-410
26. Hall AE (2001) Crop responses to environment. CRC, Boca Raton
27. Hall AE (2004) Comparative ecophysiology of cowpea, common bean and peanut. In: Nguyen HT, Blum A (eds) Physiology and biotechnology integration for plant breeding. Marcel Decker, New York
28. Hall AE (2011) Breeding cowpea for future climates. In: Yadaf S, Redden B, Hatfield JL, Lotze-Campen H, Hall AE (eds) Crop adaptation to climate change. Wiley-Blackwell, Ames
29. Hall AE, Allen LH (1993) Designing cultivars for the climatic conditions of the next century. In: Buxton DR, Shibles R, Forsberg RA, Blad BL, Asay KH, Paulsen GM, Wilson RF (eds) International crop science I. Crop Science Society of America, Madison
30. Hall AE, Ziska LH (2000) Crop breeding strategies for the 21st century. In: Reddy KR, Hodges HF (eds) Climate change and global crop productivity. CAB International, Wallingford
31. Hall AE, Cisse N, Thiaw S, Elawad HOA, Ehlers JD, Ismail AM, Fery RL, Roberts PA, Kitch LW, Murdock LL, Boukar O, Phillips RD, McWatters KH (2003) Development of cowpea cultivars and germplasm by the bean/cowpea CRSP. Field Crops Res 82:103–134
32. Ismail AM, Hall AE (1998) Positive and potential negative effects of heat-tolerance genes in cowpea lines. Crop Sci 38:381–390
33. Ismail AM, Hall AE (1999) Reproductive-stage heat tolerance, leaf membrane thermostability and plant morphology in cowpea. Crop Sci 39:1762–1768
34. Ismail AM, Hall AE (2000) Semidwarf and standard-height cowpea responses to row spacing in different environments. Crop Sci 40:1618–1623
35. Ismail AM, Hall AE, Close TJ (1999) Allelic variation of a dehydrin gene co-segregates with chilling tolerance during seedling emergence. Proc Natl Acad Sci 96:13566–13570
36. Kimball BA (1983) Carbon dioxide and agricultural yield: an assembly and analysis of 430 prior observations. Agron J 75:779–788
37. Kittock DL, Turcotte EL, Hofman WC (1988) Estimation of heat tolerance improvement in recent American Pima cotton cultivars. J Agron Crop Sci 161:305–309
38. Lawlor DW, Mitchell RAC (2000) Crop ecosystems responses to climate change: wheat. In: Reddy KR, Hodges HF (eds) Climate change and global crop productivity. CAB International, Wallingford
39. Leakey ADB, Ainsworth EA, Bernacchi CJ, Rogers A, Long SP, Ort DR (2009) Elevated CO_2 effects on plant carbon, nitrogen, and water relations: six important lessons from FACE. J Exp Bot 60:2859–2876
40. Lin W, Ziska LH, Namuco OS, Bai K (1997) The interaction of high temperature and elevated CO_2 on photosynthetic acclimation of single leaves of rice in situ. Physiol Plant 99:178–184
41. Lobell DB, Field CB, Cahill KN, Bonfils C (2006) Impacts of future climate change on California perennial crop yields: model predictions with climate and crop uncertainties. Agric For Meteor 141:208–218
42. Lu Z, Percy RG, Qualset CO, Zeiger E (1998) Stomatal conductance predicts yields in irrigated Pima cotton and bread wheat grown at high temperatures. J Exp Bot 49:453–460
43. Mackill DJ, Coffman WR (1983) Inheritance of high temperature tolerance and pollen shedding in a rice cross. Z Pflanzenzüchtg 91:61–69
44. Marfo KO, Hall AE (1992) Inheritance of heat tolerance during pod set in cowpea. Crop Sci 32:912–918
45. Matsui T, Namuco OS, Ziska LH, Horie T (1997) Effects of high temperature and CO_2 concentration on spikelet sterility in indica rice. Field Crops Res 51:213–219
46. Mohammed AR, Tarpley L (2009) High nighttime temperatures affect rice productivity through altered pollen germination and spikelet fertility. Agric For Meteor 149:999–1008
47. Moya TB, Ziska LH, Namuco OS, Olszyk D (1998) Growth dynamics and genotypic variation in tropical, field-grown paddy rice (*Oryza sativa* L.) in response to increasing carbon dioxide and temperature. Glob Change Biol 4: 645–656
48. Mutters RG, Hall AE (1992) Reproductive responses of cowpea to high temperatures during different night periods. Crop Sci 32:202–206
49. Mutters RG, Ferreira GR, Hall AE (1989) Proline content of the anthers and pollen of heat-tolerant and heat-sensitive cowpea subjected to different temperatures. Crop Sci 29: 1497–1500
50. Mutters RG, Hall AE, Patel PN (1989) Photoperiod and light quality effects on cowpea floral development at high temperatures. Crop Sci 29:1501–1505
51. Nakishima H, Horner HT, Palmer RG (1984) Histological features of anthers from normal and ms3 mutant soybean. Crop Sci 24:735–739
52. Nava GA, Damalgo GA, Bergamaschi H, Paniz R, Pires dos Santos R, Marodin GAB (2009) Effect of high temperatures in the pre-blooming and blooming periods on ovule formation, pollen grains and yield of 'Granada' peach. Sci Hortic 122:37–44
53. Nielsen CL, Hall AE (1985) Responses of cowpea (*Vigna unguiculata* (L.) Walp.) in the field to high night air temperatures during flowering. I. Thermal regimes of production regions and field experimental system. Field Crops Res 10:167–179

54. Nielsen CL, Hall AE (1985) Responses of cowpea (*Vigna unguiculata* (L.) Walp.) in the field to high night air temperatures during flowering. II. Plant responses. Field Crops Res 10:181–196
55. Opeña RT, Chen JT, Kuo CG, Chen HM (1993) Genetic and physiological aspects of tropical adaptation in tomato. In: Kuo CG (ed) Adaptation of food crops to temperature and water stress. Asian Vegetable Research and Development Center, Shanhua, Publication No 93-410
56. Padi FK, Denwar NN, Kaleem FZ, Salifu AB, Clottey VA, Kombiok J, Haruna M, Hall AE, Marfo KO (2004) Registration of 'Apagbaala' cowpea. Crop Sci 44:1486
57. Padi FK, Denwar NN, Kaleem FZ, Salifu AB, Clottey VA, Kombiok J, Haruna M, Hall AE, Marfo KO (2004) Registration of 'Marfo-Tuya' cowpea. Crop Sci 44:1486–1487
58. Peet MM, Wolfe DW (2000) Crop ecosystem responses to climate change: vegetable crops. In: Reddy KR, Hodges HF (eds) Climate change and global crop productivity. CAB International, Wallingford
59. Peet MM, Sato S, Gardner R (1998) Comparing heat stress on male-fertile and male-sterile tomatoes. Plant Cell Environ 21:225–231
60. Peng S, Huang J, Sheehy JE, Laza RC, Visperas RM, Zhong X, Centeno GS, Kush GS, Cassman KG (2004) Rice yields decline with higher night temperature from global warming. Proc Natl Acad Sci 101:9971–9975
61. Poorter H (1993) Interspecific variation in the growth responses of plants to an elevated ambient CO_2 concentration. Vegetatio 104/105:77–97
62. Rawson HM (1995) Yield responses of two wheat genotypes to carbon dioxide and temperature in field studies using temperature gradient tunnels. Aust J Plant Physiol 22:23–32
63. Reddy KR, Hodges HF, McKinion JM, Wall GW (1992) Temperature effects on Pima cotton growth and development. Agron J 84:237–243
64. Reddy KR, Hodges HF, McKinion JM (1995) Carbon dioxide and temperature effects on Pima cotton development. Agron J 87:820–826
65. Reddy KR, Hodges HF, McKinion JM (1997) A comparison of scenarios for the effect of global climate change on cotton growth and yield. Aust J Plant Physiol 24:707–713
66. Reynolds MP, Ewing EE (1989) Effects of high air and soil temperature stress on growth and tuberization in *Solanum tuberosum*. Ann Bot 64:241–247
67. Reynolds MP, Ewing EE, Owens TG (1990) Photosynthesis at high temperature in tuber-bearing *Solanum* species. Plant Physiol 93:791–797
68. Reynolds MP, Balota M, Delgado MIB, Amani I, Fischer RA (1994) Physiological and morphological traits associated with spring wheat yield under hot, irrigated conditions. Aust J Plant Physiol 21:717–730
69. Reynolds MP, Singh RP, Ibrahim A, Ageeb OAA, Larqué-Saavedra A, Quick JS (1998) Evaluating physiological traits to complement empirical selection for wheat in warm environments. Euphytica 100:85–94
70. Singh RP, Vara Prasad PV, Sunita K, Giri SN, Reddy KR (2007) Influence of high temperature and breeding for heat tolerance in cotton: a review. Adv Agron 93:313–385
71. Thiaw S, Hall AE (2004) Comparison of selection for either leaf-electrolyte-leakage or pod set in enhancing heat tolerance and grain yield of cowpea. Field Crops Res 86: 239–253
72. Vara Prasad PV, Craufurd PQ, Summerfield RJ (1999) Sensitivity of peanut to timing of heat stress during reproductive development. Crop Sci 39:1352–1357
73. Vara Prasad PV, Craufurd PQ, Summerfield RJ (1999) Fruit number in relation to pollen production and viability in groundnut exposed to short periods of heat stress. Ann Bot 84:381–386
74. Vierling E (1991) The roles of heat-shock proteins in plants. Annu Rev Plant Physiol 42:579–620
75. Vose RS, Easterling DR, Gleason B (2005) Maximum and minimum temperature trends for the globe: an update through 2004. Geophys Res Lett 32:L23822
76. Wahid A, Gelani S, Ashraf M, Foolad MR (2007) Heat tolerance in plants: an overview. Environ Exp Bot 61:199–223
77. Warrag MOA, Hall AE (1983) Reproductive responses of cowpea to heat stress: genotypic differences in tolerance to heat at flowering. Crop Sci 23:1088–1092
78. Warrag MOA, Hall AE (1984) Reproductive responses of cowpea (*Vigna unguiculata* (L.) Walp.) to heat stress. I. Responses to soil and day air temperatures. Field Crops Res 8:3–16
79. Warrag MOA, Hall AE (1984) Reproductive responses of cowpea (*Vigna unguiculata* (L.) Walp.) to heat stress. II. Responses to night air temperature. Field Crops Res 8:17–33
80. Wasserman R, Jagadish SVK, Heuer S, Ismail A, Redona E, Serraj R, Singh RK, Howell G, Pathak H, Sumfleth K (2009) Climate change affecting rice production: the physiological and agronomic basis for possible adaptation strategies. Adv Agron 101:59–67
81. Wien HC (1997) Pepper. In: Wien HC (ed) The physiology of vegetable crops. CAB International, Wallingford
82. Yarwood CE (1961) Acquired heat tolerance of leaves to heat. Science 134:941–942
83. Ziguo Z, Hanlai Z (1992) Fertility alteration in photoperiod-sensitive genic male sterile (PGMS) rice in response to photoperiod and temperature. Int Rice Res Newsl 17:7–8
84. Ziska LH, Manalo PA (1996) Increasing night temperature can reduce seed set and potential yield of tropical rice. Aust J Plant Physiol 23:791–794

Websites

Hall AE (2000) Heat stress section in www.plantstress.com

Sustainable Remediation Methods for Metals and Radionuclides

Franz-Georg Simon[1], Tamás Meggyes[2,3]
[1]Department Material and Environment, BAM Federal Institute for Materials Research and Testing, Berlin, Germany
[2]University of Wolverhampton, UK and ICP Hungária, Budapest, Hungary
[3]BAM Federal Institute for Materials Research and Testing, Berlin, Germany

Article Outline

Glossary
Definition of the Subject and Its Importance
Introduction
Groundwater Remediation Using Permeable Reactive Barriers (PRBs)
Construction Methods of Permeable Reactive Barriers
Application of Permeable Reactive Barriers
Combined Chemical and Phytoremediation of Sites Contaminated with Heavy Metals
Electrochemical Remediation
Soil Remediation Based on Natural Processes
Future Directions
Bibliography

Glossary

Biomineralization A process by which living organisms produce minerals.

Chernobyl Ukrainian city site of the largest nuclear power plant accident in history.

Cut-off-wall Underground structure designed to prevent the flow of water.

DART Deep aquifer remediation tool.

Diffusion Movement of ions and molecules from places of higher concentration to places of lower concentration.

Electrochemical remediation Remediation technologies comprising electrochemical transport and transformation methods.

Electrokinetic screens Structures used to prevent radionuclides from diffusing from the polluted area into the environment.

Electromigration Transport of charged ions or ion complexes in solution.

Electroosmosis Movement of liquid relative to a charged stationary surface.

Electrophoresis Movement of charged particles relative to a stationary fluid.

Enhanced electrochemical remediation Use of pH control and additives to improve removal efficiency.

EURT East Urals Radioactive Trail area contaminated due to a nuclear accident.

Natural attenuation (NA) Remediation relying entirely on natural processes.

Permeable reactive barriers Passive in situ treatment zones of reactive material that degrades or immobilizes contaminants as groundwater flows through it.

Phytoremediation Soil remediation using living plants and their associated microorganisms.

Radionuclide or radioisotope An atom with an unstable nucleus whose excess energy is available to be imparted to a newly-created radiation particle within the nucleus or to an atomic electron.

Total material requirement (TMR) Sum of domestic and imported primary natural resources and their hidden flows.

Definition of the Subject and Its Importance

Nearly all materials that support our life originate from the earth's crust, which provides our limited natural resources. The materials must be extracted from the earth, they must be processed to make them suitable for human use. They are employed in all branches of industry, and they produce a number of side products. At the end of their useful life, the residues or wastes must be disposed of. They come into contact with the earth's crust again and may pollute it. Contamination also occurs during their life due to improper handling, storage and use, and depending on their properties, they may pose various degrees of hazard to mankind and the environment. The last two centuries have witnessed an exponential rise in the extent and intensity in the utilization of materials. In some cases, it was realized too late that the situation was moving out of control, which resulted in the impairment to human health and loss of lives. Serious events range from

selling hazardous wastes as fertilizers over spills from chemical facilities polluting major rivers to cyanide pollution due to the breach of a tailings dam in a gold reprocessing facility with nuclear accidents being the most dangerous occurrences.

Sustainability has become the conscientious and future-oriented principle of modern resource management and environmental protection because caring for the future is tantamount to providing manageable and healthy surroundings for ourselves. For the foreseeable future, geotechnical and environmental engineers must therefore be concerned with ensuring a healthy balance between extraction, processing, manufacturing, utilization, recycling, and disposal of materials and products.

Life is impossible without water; our body and those of animals and plants consist overwhelmingly of water. Descriptions of catastrophes show that people can survive without food over several weeks, while the chances of survival without water drop drastically after 3 days. Seventy-one percent of the earth's surface is covered with water and 97% of the earth's water reserves are stored in the oceans. Major shifts in the phase balance (ice, water, vapor) of the earth's water reserves during glacial and interglacial periods resulted in major changes in the area of dry land due to the rise or fall in sea levels. Though it is only a small percentage of the overall amount of water, fresh water is crucial for all living creatures, most specifically man. Our natural drinking water comes from various water bodies: rivers, lakes, and groundwater. In Germany, for instance, about three quarters of drinking water supplies are extracted from groundwater. Soil contaminants very often affect water bodies, which are our drinking water resources; this is why sustainable remediation for metals and radionuclides is of crucial importance for our health and future.

Since it was realized that sites contaminated with metals and radionuclides needed treatment, various remediation methods have been and are being developed. Depending on the size of the contaminated site and urgency of intervention, conventional or recently introduced techniques have been used. Conventional techniques include excavation and removal for treatment of soil and contaminants, or the so-called "pump-and-treat" method, in which contaminated groundwater is removed from the ground by pumping and treated in a treatment plant on the surface. It has the advantage of using proven techniques, is easy to control and the treated groundwater can be reinjected into the ground or discharged in rivers or lakes. Novel methods include permeable reactive barriers, biomineralization, and electrokinetic remediation.

Introduction

The global production of metals has increased tremendously since the last century. From 1950 to 2007 the production of zinc, lead, copper, and nickel grew globally by more than a factor of 4 from 6.3 million tons to 31.7 million tons (see Fig. 1).

The production of metals from resources is always accompanied by environmental impacts [1]. The demand can be covered by production from primary resources like ores, in recycling processes by secondary resources like scrap or by imports. Environmental impact from mining and ore processing arises from waste production (overburden, mine tailings); emission to soil, water, and air; and soil degradation (e.g., by acid mine drainage). The import of refined metals leaves most environmental impact in the origin country. Import of metals has gained significance in the USA for zinc since 1970 and for copper since 2000. Recycling has large relevance in the lead production. More than 70% of lead in the USA comes from secondary resources; in that case mostly from lead acid battery recycling. Metal production from secondary resources in recycling processes has less impact on the environment. The metal concentration in the secondary raw

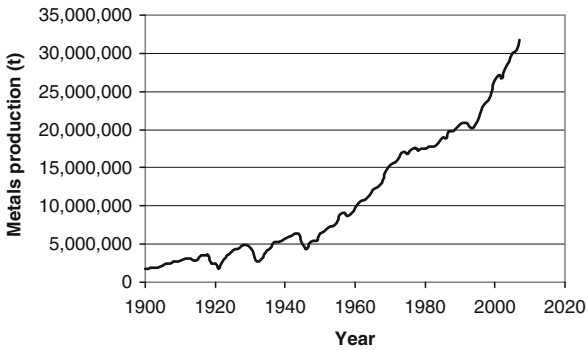

Sustainable Remediation Methods for Metals and Radionuclides. Figure 1
Global production of the four metals zinc, copper, nickel, and lead from 1900 to 2007

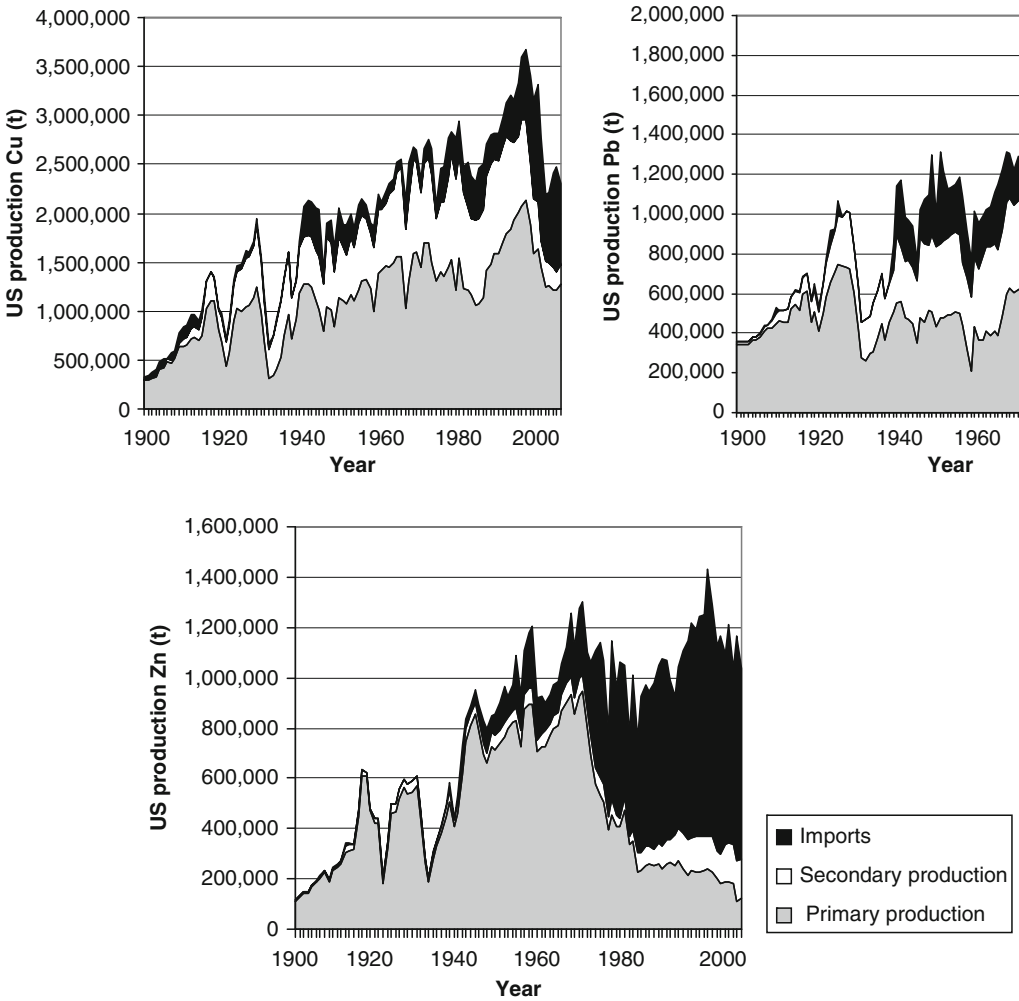

Sustainable Remediation Methods for Metals and Radionuclides. Figure 2
Primary production, secondary production, and imports of copper, lead, and zinc in the USA from 1900 to 2007 (data: www.usgs.gov)

materials is usually higher than in ores and reduction to the elemental form is often not necessary, so that less energy is needed. Figure 2 displays the production patterns for copper, zinc, and lead in the USA from 1990 to 2007.

Mining of natural resources always causes environmental impact such as land use, production of large quantities of waste, destruction of habitat, change in groundwater regime, and quite possibly contamination of soil, water or air [1]. The environmental impact of mining cannot be estimated easily. The concept of Total Material Requirement (TMR) is an attempt to quantify the environmental impact of materials. TMR is the sum of domestic and imported primary natural resources and their hidden flows [2]. Hidden flows are often not considered in environmental analyses because they are attributed with no cost. However, overburden from mining, earth moving for construction, and soil erosion are major sources of ecological damage. From mined minerals to the final products a series of process steps takes place (exploration, mine site development, extraction, milling, washing, concentration, smelting, refining, fabrication), each step is connected to other input flows such as energy or other resources. The hidden flows for metals related to metal ore mining have been investigated by Halada et al. [3]. Table 1 lists

Sustainable Remediation Methods for Metals and Radionuclides. Table 1 TMR of some metals, minerals, and fuels

Material	TMR (t/t material)	Global production (t)	TMR (Mt/year)	Ref.
Sand and gravel	1.18	8,000,000,000	9,440	[5]
Hard coal	2	3,740,000,000	8,826	[5]
Phosphate	34	130,000,000	4,420	[5]
Gold	1,800,000	2,445	4,401	[3]
Crude oil	1.22	3,485,000,000	4,252	[5]
Copper	300	12,900,000	3,870	[3]
Iron	5.1	571,000,000	2,912	[3]
Silver	7,500	160,000	1,200	[3]
Uranium	11,000	45,807	504	[3]
Lead	95	2,980,000	283	[3]
Platinum	1,400,000	178	249	[3]
Aluminum	10	23,900,000	239	[5]

the data for some metals, together with the data for some minerals and fuels. The TMR in the USA in the 1990s was between 80 and 100 t/capita, in the European Union (EU-15) approximately 50 t/capita [4].

Although the TMR concept is widely accepted, there are no economic incentives to reduce TMR because the cost associated with the hidden flows is usually not known. However, such external cost can be calculated from the cost of the remediation of the former German uranium mining sites. In the Western world uranium mining started in 1945 and reached a first maximum in 1957 and a second one in 1977 (see Fig. 3). Production of uranium from mining then decreased because fuel for nuclear power plants was partly manufactured by reprocessing nuclear weapons material. The cumulative global uranium production until 2004 was more than 2.5 million tons with Canada and the USA contributing more than 300,000 t each and Germany more than 200,000 t [6, 7]. The TMR of uranium is 11,000 kg/kg U (see Table 1).

After uranium mining in Germany ended in 1990, remediation began with a focus on controlled flooding of underground mines, water treatment, backfilling of open pit mines; and remediation of mine tailings started [8]. The total cost for the remediation project was estimated to be 6.5 billion euro [9]. So far, 4.2 billion euro has been spent while the project is

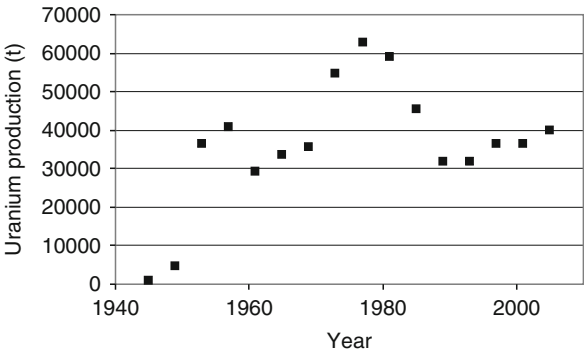

Sustainable Remediation Methods for Metals and Radionuclides. Figure 3
Uranium production in the Western world since 1945

scheduled to end sometime between 2010 and 2015. Based on a total production of 213,809 t of uranium [7] the external costs of uranium mining in Germany can be estimated to be 30 euro/kg U. It should be noted that uranium concentration of German ores was much lower than those of ores exploited today [10]. The market price for uranium is far above this value thus mining of uranium seems to be feasible in such a way that external costs can be covered by the price.

Mineral and metal ores are nonrenewable resources, so that mining finally leads to their exhaustion.

The deposits cannot be regenerated; therefore, a remediation of the environmental damage at mining sites is a basic necessity. Polluting the environment has not been a privilege of our generation alone: even the ancient Greeks managed to pollute land and sea with the waste products of their lead mining, metallurgy, and processing, some 2,000 years ago. But increasing speed in development and industrial revolution multiplied the amounts and types of emissions, and kept adding more complex types of contaminant to the established ones: chemicals, toxic heavy metals, dense nonaqueous phase liquids (DNAPLs), radioactive wastes, etc. In doing so, they have generated a steadily increasing threat to our environment, and our drinking water in particular. In the following sections, remediation processes for soil and groundwater contaminations arising from mining and utilization of metals and radionuclide like uranium are described. A focus is laid on passive in situ methods. Active methods like pump-and-treat are described in detail elsewhere [11].

Groundwater Remediation Using Permeable Reactive Barriers (PRBs)

Soil and groundwater remediation projects often cause high cost due to their large extent and long duration. This is the reason why a number of contaminated sites are not remediated at all. Passive in situ methods offer the advantage that after installation of the system only low operating cost incur and the environment is only disturbed to a small degree [12].

Passive in situ groundwater remediation using permeable reactive barriers (PRBs) is a relatively new and innovative technology with a high potential to significantly reduce the cost of treating contaminated shallow aquifers and, therefore, contribute to the preservation of groundwater resources. A PRB is a subsurface structure situated across the groundwater flow path downstream of a contaminant source (Fig. 4).

The barrier is constructed totally or in part from material that is hydraulically permeable and reacts with the passing groundwater to remove or degrade the contaminants from the groundwater. Processes taking place in the reactive material of the barrier include physical, chemical, or biological contaminant retention or degradation reactions and the reactions of other groundwater constituents with the material. Suitable

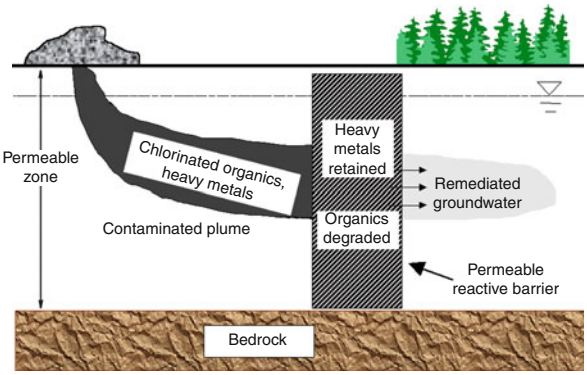

Sustainable Remediation Methods for Metals and Radionuclides. Figure 4
Function of permeable reactive barriers

materials for use as reactive components in PRBs are elemental iron, activated carbon, zeolites, iron oxides/oxyhydrates, phosphates, clay minerals, and others. The most commonly used mechanisms are redox and sorption reactions. The choice of reactive materials and retention mechanisms are dependent on the type of contaminant to be treated by the barrier system.

Permeable reactive barriers are defined by the US Environmental Protection Agency as passive in situ treatment zones of reactive material that degrades or immobilizes contaminants as groundwater flows through it. PRBs are installed as permanent, semipermanent, or replaceable units across the flow path of a contaminant plume. Natural gradients transport contaminants through strategically placed treatment media. The media degrade, sorb, precipitate, or remove chlorinated solvents, metals, radionuclides, and other pollutants. The substantial deviation from common remediation techniques is that the contaminant plume, and not its source, is treated [13].

The concept of PRBs was first developed in North America, with pioneering work conducted at the University of Waterloo in Canada. Initially, the activities including first pilot field tests focussed on "Funnel-and-Gate" systems and abiotic reductive dehalogenation of chlorinates and recalcitrant compounds by elemental iron [14–18]. During the 1990s research activities on PRBs increased significantly, leading to a number of new approaches in terms of PRB design, suitable reactive materials, and target contaminants.

Amongst the first and most widely studied metal compounds treated by PRBs are chromate [19–21] and

uranyl [22–24], which are usually treated by reductive processes using, for example, elemental iron. The use of PRBs for groundwater protection or remediation has also been studied in other fields, for example, the treatment of metals-containing mine waters [25–29]. The treatment of inorganic anions and cations can be grouped into abiotic reduction and immobilization (mostly by elemental iron), biologically mediated reduction and immobilization (bacterial sulfate reduction and precipitation of metals as sulfides), and adsorption and precipitation reactions [20].

The selection of the reactive material to be used in a PRB depends on the type of contaminant and the remediation approach (contaminant removal mechanism). In general, contaminants can be removed from polluted water using the following processes:

- Degradation: Application of chemical or biological reactions that lead to the decomposition of contaminants and the formation of harmless compounds, which are either retained in the barrier or released downstream.
- Precipitation: Immobilization of contaminants by formation of insoluble compounds (minerals), often after first reducing the contaminant to a less soluble species. The immobilized contaminants remain in the barrier material.
- Sorption: Immobilization of contaminants by adsorption or complex formation. The immobilized contaminants remain in the barrier material.

Frequently, groundwater treatment can involve a combination of these processes, which cannot be individually distinguished. Nowadays, the most widely used approaches for PRBs can be grouped into two categories: reductive barriers and sorption barriers. Reductive barriers employ mechanisms that lead to the reduction of the target compound, or parts thereof, to achieve decomposition or immobilization of that compound. Barriers utilizing surface reactions that lead to immobilization of the target contaminants by adsorption, ion exchange, co-precipitation, solid-solution formation, etc., without altering the chemical state of the contaminant are usually termed as sorption barriers.

Two main types of PRB have been used in the field. These are (1) continuous reactive barriers enabling a flow through its full cross section, and (2) "funnel-and-gate" systems [16] in which only special "gates" are permeable to the contaminated groundwater. The continuous PRB configuration is characterized by a single reactive zone installed across the contaminant plume, while the "funnel-and-gate" system consists of an impermeable wall that directs the contaminated plume through one or more permeable gates within the wall (Fig. 5).

The choice between the two configurations depends on the hydrogeological characteristics of the site, the technical applicability of the barrier placement, and the cost of the reactive material. When a high-cost reactive material is used, the "funnel-and-gate" configuration is preferable since the reactive zone requires less material. If a cheap material can be used, it is more profitable to avoid the construction of the impermeable sidewalls by employing a continuous barrier.

Bored-pile cut-off walls can be constructed from secant piles. Holes for adjacent piles are drilled with a time delay ensuring that piles built later cut into the primary piles and establish an intimate contact. Reactive curtains and injected systems create reactive zones with no clear geometric boundaries and have the advantage of easy construction. The reactive material must spread from the boreholes far enough to ensure

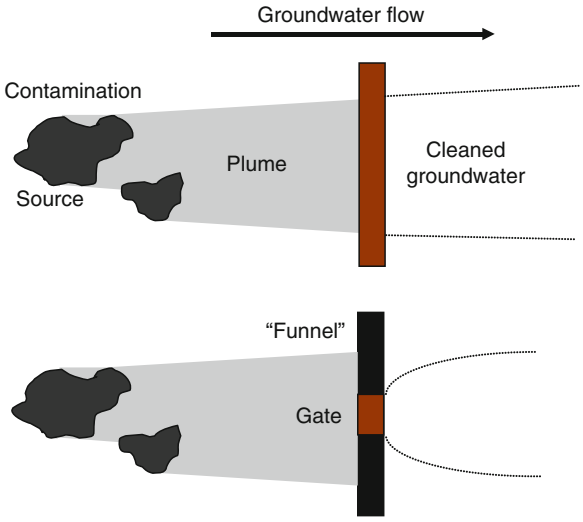

Sustainable Remediation Methods for Metals and Radionuclides. Figure 5
Funnel and gate versus continuous permeable reactive barrier

that parts of the contaminant plume do not escape treatment.

In PRBs, the residence time of the contaminant in the reactive material must be long enough to allow a decrease of the contaminant concentrations down to an acceptable level (the remediation target). For a given contaminant and reactive material the required residence time is a function of the reaction rate and the equilibrium constant. As a PRB is basically a flow-through cell, there is a continual reestablishment of equilibrium (or at least the tendency toward reestablishing equilibrium) as the groundwater passes through the barrier. For example, a given reactive material could reach equilibrium very rapidly with a contaminant, but if the initial concentration is high and the equilibrium constant is low, then a long flow path may be required to reduce the contaminant concentration to an acceptable level. Alternatively, a slow reacting material with a high equilibrium constant may reach an acceptable exit concentration in a relatively short residence time, without ever reaching equilibrium. As a range of factors effect reaction rate, the retention time required to treat the groundwater at a particular site with a specific reactive material should always be determined in a feasibility study (e.g., by column experiments).

Removal of Metals from Groundwater

Cationic metals usually have limited mobility in soil and groundwater with high clay and organic content, high alkalinity, and low permeability [30]. However, complexing agents such as carbonates, hydroxides, sulfates, phosphates, fluorides, and possibly silicates, which are present in natural waters, increase the solubility of metals [31]. Precipitation is a possible reaction for heavy metal contamination to lower the concentrations in the groundwater. Other possibilities are sorption, precipitation subsequent to a chemical reduction or a combination of the different processes.

Precipitation of heavy metals is a commonly used process in wastewater treatment plants. Precipitation is used in the same way in permeable reactive barriers to lower the heavy metal concentrations in groundwater. Chemical precipitation is a process by which a soluble substance is converted into an insoluble form by a reaction with the precipitant. Frequently used precipitants are hydroxides, sulfides, phosphates, and carbonates. The solubility of heavy metal hydroxides, sulfides, and carbonates is pH-dependent. Metal hydroxides exhibit amphoteric behavior, that is, solubility is high both at low pH (removal of hydroxide anions, see Reaction 2, with Me as a generic two-valent heavy metal) and high pH (formation of soluble hydroxo complexes, see Reaction 3). A minimum solubility for most heavy metals is observed between 9 and 11 [32].

$$Me^{2+} + 2OH^- \rightarrow Me(OH)_2(s) \qquad \text{(Reaction 1)}$$

$$Me(OH)_2(s) + 2H^+ \rightarrow Me^{2+} + 2H_2O \qquad \text{(Reaction 2)}$$

$$Me(OH)_2 + OH^- \rightarrow Me(OH)_3^- \qquad \text{(Reaction 3)}$$

A cheap precipitant forming hydroxides is lime [33]. Metal concentrations lower than 1 mg/l, sometimes less than 0.1 mg/l are achievable.

Permeable reactive barriers are systems with low energy consumption and it is therefore important that the precipitates are not changed back by any means to soluble forms. Unlike in wastewater treatment plants, the precipitated material remains in the barrier for the whole period of operation. Spent barrier materials can be replaced by placing the reactive matrix in a double-walled structure with prefabricated elements [34]. Stability of the resulting precipitates is therefore an important issue for the application of precipitation reactions in permeable reactive barriers.

Lead Lead is a major contaminant in solid wastes and soils. Its concentration in drinking water is limited in most countries at very low limits (e.g., in Germany 0.04 mg/l). Lead forms various compounds with low solubility in water. A good example for the formation of very stable precipitates is the reaction of lead ions with hydroxyapatite $Ca_{10}(PO_4)_6(OH)_2$. After dissolution of hydroxyapatite, lead is precipitated as lead hydroxypyromorphite (solubility product log K_{sp} = −62.79 [35, 36]).

$$Ca_{10}(PO_4)_6(OH)_2 + 14H^+ \rightleftharpoons 10Ca^{2+} + 6H_2PO_4 + 2H_2O \qquad \text{(Reaction 4)}$$

$$10Pb^{2+} + 6H_2PO_4 + 2H_2O \rightarrow Pb_{10}(PO_4)_6(OH)_2(s) + 14H^+ \qquad \text{(Reaction 5)}$$

Another reaction type which may control the immobilization of lead with hydroxyapatite is surface adsorption but it was found not feasible by Ma [36]. In the presence of chloride the precipitation of the even more insoluble chloropyromorphite $Pb_{10}(PO_4)_6Cl_2$ is possible [35, 37]. The reaction between heavy metals and apatite is rapid [38] and the resulting precipitates are extremely insoluble. Apatite is therefore suitable as precipitant for permeable reactive barriers.

Chromium Chromium exists in natural waters in the oxidation states +3 and +6. The hexavalent chromium occurs as an oxyanion in the form of CrO_4^- or as $Cr_2O_7^{2-}$. Chromates are more soluble and mobile than Cr(III) compounds. Due to their negative charge these anions are not attracted to negatively charged mineral surfaces [39]. Hexavalent chromium cannot be precipitated as hydroxide. Prior to precipitation, chromium(VI) has to be reduced to chromium(III). The removal of chromium(VI) is performed with sulfide in a single step combining reduction and precipitation (Reaction 6) [32].

$$Cr_2O_7^{2-} + 2FeS + 7H_2O \rightarrow 2Cr(OH)_3 + 2Fe(OH)_3 + 2S + 2OH^- \quad \text{(Reaction 6)}$$

Reduction of chromate with elemental iron has been intensively studied [19, 39, 40]. The overall reaction can be written as:

$$CrO_4^{2-} + Fe^0 + 8H^+ \rightarrow Fe^{3+} + Cr^{3+} + 4H_2O \quad \text{(Reaction 7)}$$

Reaction 7 occurs spontaneously as can be seen in Fig. 6. Couples with lower standard electrode potential reduce couples with higher potential. The stability lines as a function of pH were calculated using the computer program MinteqA2 [35].

In a further step, iron and chromium are precipitated as oxyhydroxides [39].

$$(1-x)Fe^{3+} + xCr^{3+} + 2H_2O \rightarrow Fe_{(1-x)}Cr_xOOH + 3H^+ \quad \text{(Reaction 8)}$$

Remediation of chromium-contaminated groundwater in a subsurface iron reactor system offers the advantage that contaminations arising from chlorinated solvents are treated simultaneously. A successful remediation of a site with such multiple contaminants at a galvanizing plant in Germany was described by Schneider [41].

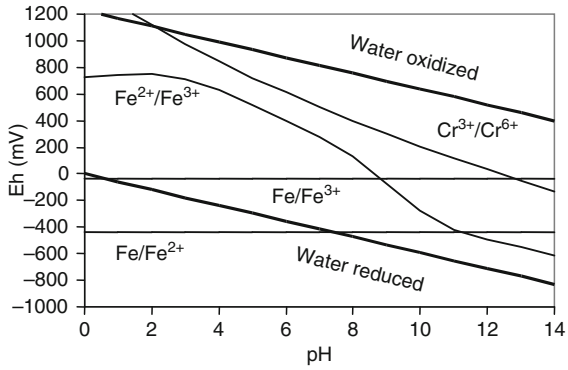

Sustainable Remediation Methods for Metals and Radionuclides. Figure 6
pH-Eh diagram showing the stability fields for water and some iron and chromium species

Uranium Uranium is the heaviest naturally occurring element. All isotopes are radioactive, the half-lives of the two relevant isotopes ^{238}U and ^{235}U are 4.5×10^9 and 7.0×10^8 years, respectively [42]. Uranium present in groundwater, for example, from mine tailings, is dangerous not because of its radioactivity but because of its toxicity as a heavy metal. Based on the German Radiation Protection Act a 0.3-mg/l limit can be calculated from the radiation limit (7.0 Bq/l of the natural mixture of isotopes). Due to its toxicity a limit between 0.02 and 0.002 mg/l is being considered [43].

Uranium occurs mainly in the oxidation states +4 and +6. The hexavalent uranium, that is, the uranyl ion UO_2^{2+} and respective hydroxo- and carbonato-complexes are more mobile than U(IV) compounds, similarly to chromium where Cr(VI) has a higher mobility than Cr(III). The speciation of uranium is a complex system dependent on pH and carbonate concentration as can be seen in Fig. 7 (calculated using MinteqA2 [35]). For more details on the complex uranium solution equilibria see Langmuir [31].

Removal from groundwater is possible by reduction of U(VI) to U(IV) in a reducing environment, for example, by elemental iron [23]:

$$Fe + UO_2^{2+}(aq) \rightarrow Fe^{2+} + UO_2(s) \quad \text{(Reaction 9)}$$

The solubility of uraninite UO_2 is in the range of 10^{-8} mol/l in a pH range between 4 and 14. Below a pH of 4, uranium becomes soluble. A measurement on the dissolution of spent nuclear fuel in deionized water under nonoxidizing conditions provided results in the range of 10^{-9}–10^{-5} mol/l [44]. Under oxidizing conditions where UO_2 can be transformed into the uranyl ion and if complexation reactions can occur, the solubility is enhanced. This can be seen from the pH-Eh diagram of uranium in the presence of carbonate in Fig. 8 (calculated using HSC Chemistry [45]). The reduction of U(VI) to U(IV) by elemental iron is thermodynamically possible over a wide pH range although stronger reducing conditions are needed compared to systems in the absence or with low concentration of carbonate. The stability fields of the U(VI)-carbonate complexes are larger than those of the respective hydroxo-complexes in the absence or at low concentration of carbonate (see dotted line in Fig. 8).

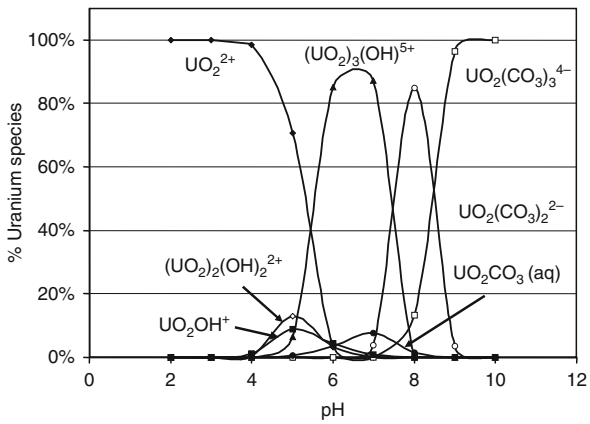

Sustainable Remediation Methods for Metals and Radionuclides. Figure 7
Uranium speciation in aqueous solution with atmospheric CO_2 and total uranium concentration of 5×10^{-6} mol/l

Elemental iron as reactive material for the removal of uranium has already been applied in field experiments [46, 47]. In Hungary, uranium was mined and processed in the southern part of the country, in the Mecsek Mountains, near the city of Pécs. The mined out rock amounted to 46 million tons from which different wastes resulted. Mining activity was terminated at the end of 1997. Rehabilitation of the former industrial sites is in progress. Among different

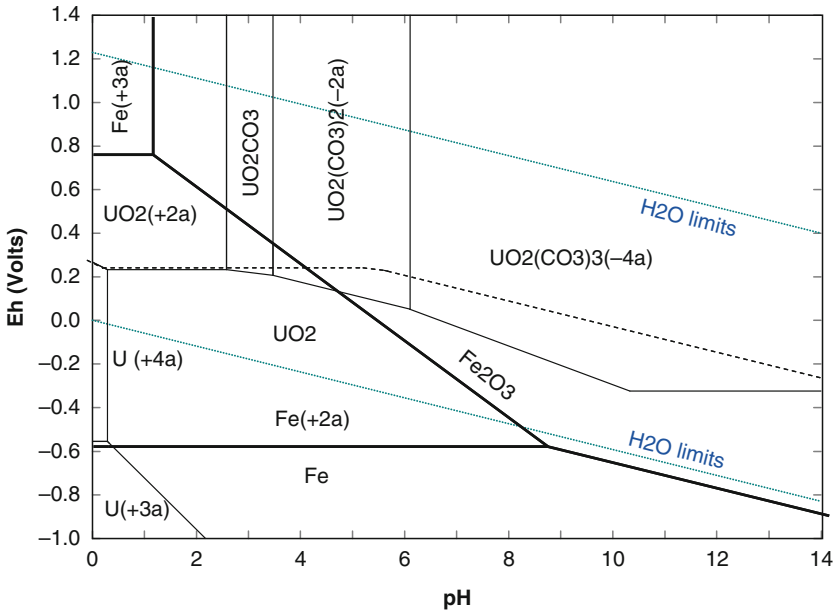

Sustainable Remediation Methods for Metals and Radionuclides. Figure 8
pH-Eh diagram [45] showing the stability fields of uranium species (c = 10^{-6} mol/l) in different oxidation stated in combination with stability filed of elemental iron, Fe^{2+} and Fe^{3+} (*bold lines*). The *dotted line* indicates the stability field of U (VI)-hydroxo complexes in the absence of carbonate

remediation tasks one of the most important issues is the restoration of the quality of groundwater contaminated by seepage from tailings, waste rock piles, and heap leaching residues. A pilot-scale permeable reactive barrier was built at the site near Pécs during the course of the EU project PEREBAR [48] (Fig. 9). The PRB test facility has been in operation since August 2002. The PRB consists of two different zones, zone 1 with a lower content of coarse elemental iron (12% by volume or 0.39 t/m^3, grain size 1–3 mm) and zone 2 with a higher content of fine elemental iron (41% by volume or 1.28 t/m^3, grain size 0.2–3 mm). On both sides (upstream and downstream) sand layers were inserted to distribute water inflow and outflow. The PRB is sealed with clay and geosynthetic clay liners at the bottom and with a geomembrane (high density polyethylene) at both sides and on the top. The design is displayed in Fig. 9. The total mass of elemental iron installed as reactive material was 38 t, from which 5 t was coarser material.

The pilot installation has yielded good removal results for uranium (99%) and is still in operation. Table 2 lists average values for different parameters for the operation period. It can be seen that the pH increased in the PRB by almost 2 units, uranium concentration decreased by at least 95%, TDS was halved and calcium was almost completely removed. The impact of precipitates on the long-term performance of the installation will be investigated in further research.

Monitoring data of the site over a period of 4,500 days (12 years) is shown in Fig. 10. This includes data about the performance of the experimental permeable reactive barrier.

Lowering the uranium concentration without changing the oxidation state is possible by the precipitation of sparingly soluble uranyl phosphates. Addition of phosphate, hydroxyapatite (HAP) or bone char (HAP with a small amount of carbon) to the water may trigger the formation of uranyl phosphate $(UO_2)_3(PO_4)_2$ (log K_{sp} = −49.09 [50]), autunite $Ca(UO_2)_2(PO_4)_2$ (log K_{sp} = −47.28, [50]) or chernikovite $H_2(UO_2)_2(PO_4)_2$ (log K_{sp} = −45.48, [51]). The mechanism of the interaction of uranium with HAP is not yet completely understood. Jeanjean et al. proposed a dissolution-precipitation mechanism [52].

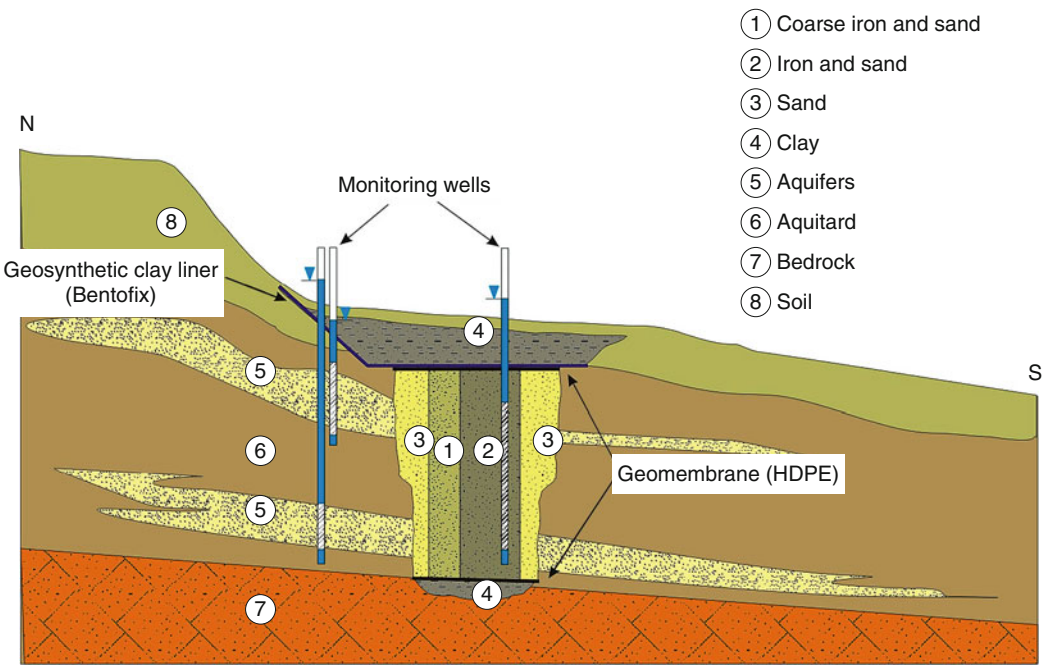

Sustainable Remediation Methods for Metals and Radionuclides. Figure 9
Sketch of the design of the experimental PRB near Pécs [48]

Sustainable Remediation Methods for Metals and Radionuclides. Table 2 Monitoring data of the PRB as of March 22, 2005, after 31 months of operation in the Pécs, Hungary, experimental barrier [48]

Well	Location	pH	EC (μS/cm)	U(VI) (μg/l)	TDS mg/l	Ca (mg/l)	SO_4 (mg/l)	HCO_3 (mg/l)	Fe (mg/l)
PRB-1	Inflow	6.9	1,400	940	1,010	150	320	525	0.002
PRB-10	Zone 1	7.3	1,330	37	937	125	300	275	5.5
PRB-11	Zone 2	8.7	865	10	550	10	185	299	0.03
PRB-14	Outflow	8.7	780	2	540	14	170	268	0.03
PRB-3[a]	Downstream	8.5	420	56	240	5	95	116	0.017

[a]Water is probably diluted by lateral water flow

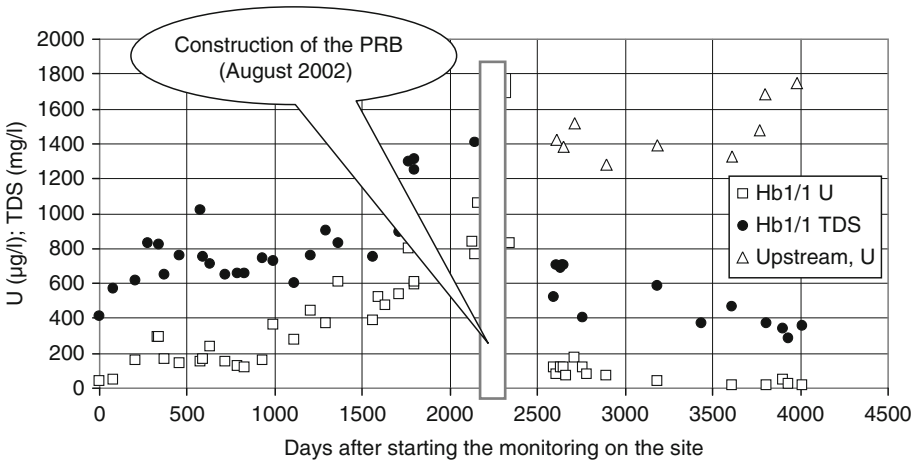

Sustainable Remediation Methods for Metals and Radionuclides. Figure 10
Long-term performance of the permeable reactive barrier near Pécs: uranium concentration and total dissolved solid (TDS) in the observation well Hb1/1 (15 m downstream of the PRB) [49]

With either autunite or chernikovite as the precipitation product the reaction may occur via the sequence displayed below.

$$Ca_5(PO_4)_3OH \rightleftharpoons 5Ca^{2+} + 3PO_4^{3-} + OH^- \quad \text{(Reaction 10)}$$

$$H^+ + OH^- \rightleftharpoons H_2O \quad \text{(Reaction 11)}$$

$$2UO_2^{2+} + Ca^{2+} + 2PO_4^{3-} \rightleftharpoons Ca(UO_2)_2(PO_4)_2 \quad \text{(Reaction 12)}$$

$$2UO_2^{2+} + 2H^+ + 2PO_4^{3-} \rightleftharpoons H_2(UO_2)_2(PO_4)_2 \quad \text{(Reaction 13)}$$

Ion exchange processes (see reaction 14) or surface sorption using HAP (two possible surface groups, reaction 15 and reaction 16) are described by the following equations [53, 54].

$$\equiv Ca^{2+} + UO_2^{2+} \rightleftharpoons \equiv UO_2^{2+} + Ca^{2+} \quad \text{(Reaction 14)}$$

$$\equiv OH + UO_2^{2+} \rightleftharpoons \equiv O - UO_2^{+} + H^+ \quad \text{(Reaction 15)}$$

$$\equiv O_3P - OH^+ + UO_2^{2+} \rightleftharpoons \equiv O_3P - O - UO_2^{2+} + H^+ \quad \text{(Reaction 16)}$$

In the work of Fuller et al. [55] autunite and chernikovite have been identified as solid phases after adding uranyl ions to a saturated solution of hydroxyapatite. Evidence for adsorption of U(VI) to hydroxyapatite surfaces as an inner-sphere complex was found for certain concentration ratios. Similarly uranium phosphates

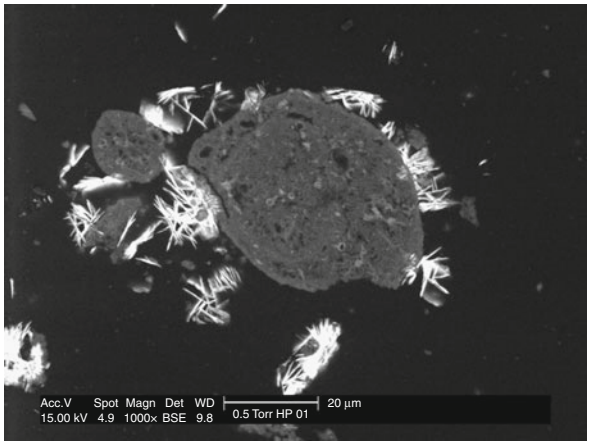

Sustainable Remediation Methods for Metals and Radionuclides. Figure 11
Scanning electron microscopic image recorded in backscatter mode (heavy elements appear bright) from HAP particles with uranium phosphate crystals (verified by the attached EDX system) [56]

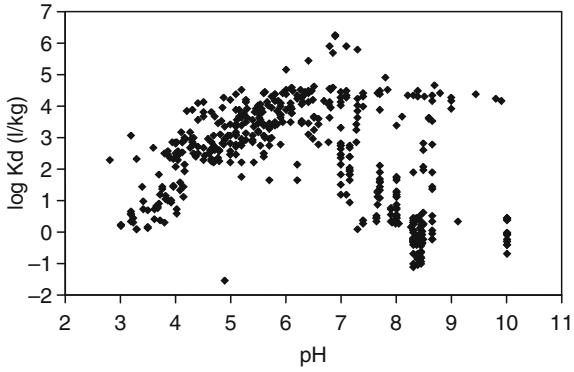

Sustainable Remediation Methods for Metals and Radionuclides. Figure 12
Distribution coefficient K_d of uranium as a function of pH

have been found in laboratory experiments on uranium removal from artificial groundwater [56] (see Fig. 11).

Uranium can also be removed by adsorption on surfaces. Morrison and Spangler [26] have evaluated a range of uranium and molybdenum adsorption tests using a variety of materials. Good removal results have been obtained using lime, hematite, peat, ferric oxyhydroxide, phosphate, and TiO_2, while clays exhibited low sorption potential. Precipitation and adsorption onto a surface are processes that can simultaneously occur in a chemical barrier. Sorption of uranium from groundwater was studied in a series of publications [26, 27, 57]. Surface site complexation can be described by different models with or without electrostatic influence on charged surfaces [35]. With SOH as a notation for a surface site the adsorption reaction of uranium onto ferric oxyhydroxide as sorbent can be written as follows:

$$SOH + UO_2^{2+} + 3H_2O \rightleftarrows SOH - UO_2(OH)_3 + 2H^+ \quad \text{(Reaction 17)}$$

Sorption, rather than precipitation, depends strongly on pH. If several contaminants should be removed from the groundwater an optimum pH for operation of the barrier is needed. This is difficult to achieve for uranium in the presence of molybdenum because the latter is mobile at pH values above 8 while uranium exhibits low mobility [27]. The distribution coefficient K_d of uranium at different pH values in various soils is displayed in Fig. 12 [58]. K_d is defined as the ratio of mass of adsorbate sorbed (mg/kg) to mass of adsorbate in solution (kg/l). High K_d values (l/kg) were derived from adsorption experiments with ferric oxyhydroxide and kaolinite, low values from those with quartz which has low adsorptive properties. The pH dependence arises from surface charge properties of the soil and from the complex aqueous speciation of U(VI).

Sorption onto surfaces and reduction are both possible removal reactions in iron-bearing walls. To which amount and at what efficiency the distinct processes take place was studied in several articles [59–61].

Remediation by Biomineralization

Reducing conditions or conditions leading to precipitation of metals or radionuclides from groundwater can also be established by natural processes, which are in principle similar for all metals and radionuclides. In the following, the sequence is described for uranium [62]. In a first step uranium is associated with organic material (e.g., plants, algae, or microbes). This can occur via adsorption, active cellular uptake, or bioprecipitation. Microorganisms are able to adsorb uranium from solution. For Pseudomonas the distribution coefficient K_d was found to be above 8,000 [63], for *Aspergillus fumigatus* around 10,000 [64]. This is comparable to adsorption on soils at pH values from 5 to 7 (see Fig. 12). Uranium can also be actively taken up into the

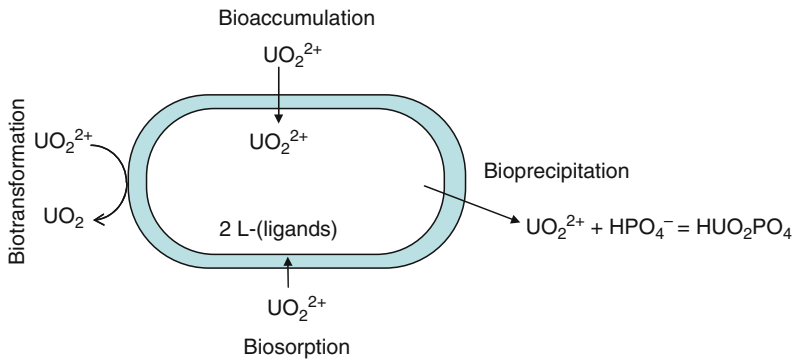

Sustainable Remediation Methods for Metals and Radionuclides. Figure 13
Radionuclide interactions with microorganisms (Adapted from [65])

cells although the radius of uranium is comparably high [65]. Bioprecipitation may take place outside or inside the cells. Sparingly soluble metal hydroxides, carbonates, sulfides, or phosphates may be formed [62]. Then sedimentation of the associated structures occurs. Finally biomineralization takes place by the provision of conditions with low redox potential in the sediments with metal-reducing microbial populations. In these anaerobic sediments, uranium remains stable and no redistribution occurs for millennia [66]. Possible interactions of radionuclides with microorganisms are displayed as summary in Fig. 13.

Construction Methods of Permeable Reactive Barriers

First, cut-off wall construction techniques were applied to permeable reactive barriers with almost no alteration. Single- and two-phase diaphragm walls, bored-pile walls, jet grouting, thin walls, sheet-pile walls, driven cut-off walls, injection, and frozen walls are the most common cut-off wall alternatives. To date, in addition to using cut-off wall construction methods, an increasing number of innovative techniques are being used to construct permeable reactive barriers such as: drilling methods; deep-soil mixing; high-pressure jet technology; injected systems; column and well arrays; deep aquifer remediation tools (DART); and hydraulic fracturing and biobarriers. The main configurations of permeable reactive barriers are:

- Continuous reactive barriers
- Funnel-and-gate systems
- Arrays of wells
- Injected systems

The basic performance requirements for a reactive zone within a PRB are [67–69]:

- Replaceability of the reactive materials
- Higher permeability than the surrounding reservoir
- Stability against fines washed into barriers from the surrounding soil
- Long life-span

The selection of the construction technique mainly depends on site characteristics [70], for example:

- Depth (the most important factor): increasing depth requires more specialized equipment, longer construction times, and is accompanied by higher costs
- Geotechnical considerations: soil/rock strength and presence of obstacles
- Soil excavation: handling and disposal of (contaminated) soil
- Health and safety during construction (entry of personnel into excavations)

The design of PRBs, as with any other technology, should meet the requirements of the best available technique (BAT). In most cases, it may be advantageous to develop a reliable conceptual site model and to perform pumping and treatability tests. The conceptual design report should include the following information [71]:

- The amount and type of any emissions from the remediation scheme and details of any emission control measures

- The volume and quality of any discharge or re-infiltration of treated groundwater
- The power consumption (electricity, fuels, etc.)
- A description of any waste streams generated, and details of their disposal
- Quantification of any material inputs, such as GAC, lime, etc.
- The remediation target levels
- The anticipated overall efficiency
- The anticipated maintenance requirements (man-power, parts)
- The monitoring requirements
- A detailed cost estimate (including the capital costs, construction costs, operating costs, and decommissioning costs)
- A detailed health and safety evaluation of the project

Cut-off Walls

The most commonly used cut-off wall construction methods involve one of the following alternatives [72–74]:

- Trench excavation using supporting fluids capable of solidifying and forming a diaphragm wall (single-phase diaphragm wall) or which – after excavation of the trench – are displaced by another material, which in turn is capable of solidifying (two-phase diaphragm wall)
- Forming a thin slot by driving a beam into the ground, and then consecutively retracting the beam and filling the space with a thick slurry (e.g., thin walls)
- Driving strong elements into the ground (e.g., steel sheet-piles)
- Constructing interlocking boreholes, and backfilling them with concrete to form a wall of interlocking columns
- Injecting or placing reactive materials into the ground in a discontinuous fashion

The most commonly used cut-off wall systems are illustrated in Table 3.

Gate Structures

Gates are the crucial elements of funnel-and-gate systems. A frequently applied gate structure uses sheet-pile boxes in which either the sheet piles are perforated, or suitably arranged gaps provide access for the groundwater. Sheet piles can also be used to separate soil, gravel, reactive material, etc. during placement, and then can be retracted without disturbing the filled-in materials. Large-diameter (a few meters) wells filled with reactive material represent another gate design type.

Reactive Thin Walls

A hollow steel beam is vibrated into the ground to create the space for the wall, and a reactive material is placed into the void as the beam is retracted. The thin-wall technique developed for cut-off walls unites the advantages of slurry trenching and sheet-piling.

Drilling and Deep Soil Mixing

Contiguous circular columns containing reactive material can be installed using either drilling or deep soil mixing [76]. Longer barriers are formed by inserting columns with closely spaced centers. Caisson drills can be used for the drilling, with column diameters of 0.5–2.5 m. Usually, a large circular casing is lowered into the ground, the soil is removed by augers, and the hole is filled with a reactive material.

Jet Technology

High-pressure jets and jet pumps can be used for trench excavation and placement of the reactive material. Both single- and two-phase techniques are viable. A combined jet method involves the use of iron particles both as a reactive material and an abrasive medium in trench excavation. The granulated iron particles can be entrained in high-velocity water jets, which erode the soil or rock.

Well-Based Systems or DART

An array of wells known as the Deep Aquifer Remediation Tool (DART) represents an alternative to continuous barriers [77–79]. This may be helpful at sites where installation of permeable barriers may be impractical for technical or financial reasons. An array of wells can form the gate within a funnel-and-gate system, or serve as a set of in situ reactors, or it can release substances that encourage biological or other processes. An array of wells is essentially

Sustainable Remediation Methods for Metals and Radionuclides. Table 3 Cut-off wall systems [75]

Principle	Cut-off wall system	Soil	Material	Depth (m)	Thickness (m)	Permeability (m/s)	Experience
Excavation of soil and placement of sealing material	Single-phase diaphragm wall	Limited suitability for peat and humic acids	Bentonite-cement mix with or without filler	approx. 35	0.4–1.5	$\leq 1 \times 10^{-10}$	Landfill 30 years
	Two-phase diaphragm wall	Limited suitability for peat and humic acids	Bentonite slurry, soilcrete	>50	0.4–1.5	$< 5 \times 10^{-10}$	Landfill 22 years
	Composite diaphragm wall	Limited suitability for peat and humic acids	Bentonite-cement mix, additional sealers	approx. 30	>0.6	$< 5 \times 10^{-10}$ for cut-off slurry	Landfill 22 years
	Interlocking bored-pile diaphragm wall	No limitation if casing is applied	Soilcrete, concrete	approx. 20	0.6–0.8	$< 5 \times 10^{-10}$	Landfill 15 years
Displacement of soil and installation of sealing material	Thin wall	Suitable for pile driving	Bentonite-cement mix with fillers	18–23	0.05–0.20	$\leq 1 \times 10^{-9}$	Landfill 20 years
	Sheet-pile wall		Steel	15–20	0.01–0.02	–	Contaminated land 20 years
	Driven cut-off wall		Soilcrete, concrete	15–20	>0.4	$\leq 1 \times 10^{-9}$	Contaminated land 20 years
Reducing permeability of soil in place	Injection wall	Injectable	Cement, clay-cement mix, silicate gels	>100	adjustable	$\leq 1 \times 10^{-9}$	Hydraulic and foundation engineering
	Jet grouting, HPI	Very fine-grained	Bentonite-cement mix with and without filler	>100	>0.8	$\leq 1 \times 10^{-10}$	Hydraulic and foundation engineering
	Frozen wall		Liquid nitrogen	>100	>0.8–1.0	–	Civil and mining engineering

a noncontinuous reactive barrier with the advantage that drilling techniques can be used to construct them, allowing lower installation costs and greater depths. The wells filled with reactive materials have lower hydraulic resistance than the surrounding soil, thus the groundwater flow converges toward them. The amount of reactive material required for the wells is much less than for a continuous reactive barrier. It was estimated that the groundwater residence time in a 10-cm-diameter DART ranged from 1.4 h for an outer flow path to 29.3 h through the center of the DART, and this ensured the residence times needed for 99% uranium removal in a metallic-iron PRB in Fry Canyon, Utah [77].

Injected Systems

An injected system without strict geometrical boundaries in terms of a "wall" can control large and deep plumes even if their extent is irregular [78], so it offers a high degree of flexibility. Nevertheless, it is necessary to ensure that the contaminant plume is efficiently treated and that there is no by-pass flow, which may impair the remediation effect. The reactive material cannot be recovered in injected systems, and therefore degradation principles should be preferred. Two main types of injected systems have been developed:

- Injection into existing pores in the ground
- Ground fracturing

Hydraulic Fracturing

Ground fracturing, as used in petroleum engineering to enhance permeability around oil wells, aims at creating an improved zone by cracking the ground under high pressures and pumping sand or similar granular material into the cavity thus created. Using this method within the concept of barrier technology [70, 80], a part of the material filled in may be reactive material intended for pollutant treatment. By using high-energy jets and adjustable outlets, directional fracturing is feasible.

Biobarriers

Subsurface biofilm barriers or biobarriers consist of polymer films and cells of microorganisms, together with captured organic and inorganic particles [81–84]. Biobarriers may selectively plug permeable strata with microbial biomass, thus influencing the hydraulic conductivity. Reduction of the hydraulic conductivity by five orders of magnitude is possible. Biobarrier technology may also be useful as a means of funneling contaminated groundwater through subsurface treatment systems (e.g., funnel-and-gate). Spinnler et al. [85] report on the removal of MTBE (methyl tertiary-butyl ether) and TBA (tertiary-butyl alcohol) contamination using a biobarrier.

Combined PRB–Phytoremediation Systems

Combining reactive barriers with biological techniques may prove efficient for complex pollutants when physical, chemical, and biological effects may be of benefit. For example, phytoremediation and biodegradation can increase the cleanup efficacy of PRBs for creosote, a complex agent used for wood preservation, and consisting of polycyclic aromatic hydrocarbons (PAHs), phenols and nitrogen/sulfur/oxygen heterocyclic aromatics [86].

Biopolymer Trenching

This procedure exhibits similar features to traditional slurry trenching, the main difference being that a biopolymer (e.g., guar gum) is added to the stabilizing suspension [70, 76, 87, 88]. The reactive material can then be placed in the trench using tremie pipes. Following placement, a high-pH enzyme breaker is added to the fluid to break down the remaining biopolymer in the trench.

Application of Permeable Reactive Barriers

The spread of PRB technology is characterized by the fact that by 2005 about 200 reactive barriers had been constructed worldwide – 120 in the USA alone. The development of the technology in Europe can be illustrated by the example of Germany, shown in Table 4. The experimental reactive barrier constructed near Pécs, Hungary is another example of the advance of this groundwater remediation technology (Fig. 9, Table 2).

Combined Chemical and Phytoremediation of Sites Contaminated with Heavy Metals

Combined chemical and phytostabilization proved successful for a diffusely polluted area of an abandoned mining site (contaminated with Zn, Pb, Cd, Cu, and As)

Sustainable Remediation Methods for Metals and Radionuclides. Table 4 Reactive barriers in Germany [89]

Start date	Location	Contaminant	State	Design	Reactor/reactive material	Costs, finances
May 1998	Edenkoben (car parts factory)	Volatile halogenated hydrocarbons (cis-DCE, 1,1,1-TCA, TCE, PCE)	Pilot plant	F&G, 1 gate length 30 m, depth 15 m,	Iron filing, 2 hydr. comm. chambers, passive vertical flow	No data, private
Feb 2001			Operational	F&G, 6 gates length 440 m, depth 15 m		No data, private
June 1998	Rheine (laundry)	Volatile halogenated hydrocarbons (PCE, TCE, cis-DCE)	Pilot plant (R)	Continuous wall, contig. drilled piles (diameter 0.88 m, length 22.5 m	Gray iron granulate – gravel, iron sponge	170,000€, + RUBIN 200,000€
Oct 1998	Tübingen (industrial park)	Volatile halogenated hydrocarbons (TCE, cis-DCE)	Operational (R)	F&G, 3 gates, length 200 m, depth 10 m,	Gray iron granulate in contig. drilled piles	450,000€ private
Oct 1999	Bitterfeld (major chem. ind. area)	Chlorobenzenes, volatile halogenated hydrocarbons, phenols	Pilot plant (S)	5 shafts, suspended steel reactors, depth 24 m, vertical flow	Activated carbon, iron, palladium, microbiology	6,000,000€, state-financed
1999	Kraichgau	Volatile halogenated hydrocarbons	Operational	Cut-off wall, reactor	Activated carbon	No data, private
Jan 2000	Reichenbach (machine factory)	Volatile halogenated hydrocarbons (PCE, TCE, cis-DCE)	Operational	Continuous wall, drilled piles, length 20 m, depth 7 m	Acid condicioned activated carbon	200.000€, private
Jan 2001	Karlsruhe (abandoned gas works)	Polyaromatic hydrocarbons, VC	Operational	F&G, 8 gates length 240 m, depth 17 m,	Activated carbon	3,300,000€, state-financed
Aug 2001	Denkendorf (industrial park)	Volatile halogenated hydrocarbons (PCE, TCE, TCA, cis-DCE, VC)	Operational	D&G, 1 gate shaft + reactor, depth 6 m, vertical flow,drain length 90 m	Activated carbon	No data, private
Sept 2001	Bernau (form. sovjet military laundry)	Volatile halogenated hydrocarbons (high conc. TCE in two layers)	Pilot plant (R)	Special F&G, 18 reactors, closed funnel, acteve water supply	Gray iron granulate, iron, palladium (microbiology and palladium planned)	1,500,000€, 50% state-financed
Sept 2002	Denkendorf (industrial park)	Volatile halogenated hydrocarbons (mainly VC)	Pilot plant (R)	Column experiment in shaft next to activated carbon reactor	Palladium on zeolite, hydrogen	120,000€, state-financed
Jan 2002	Oberursel (industrial park)	Volatile halogenated hydrocarbons	Operational	F&G, 1 gate, length 175 m, depth 4–17 m	Iron	No data, private
Dec 2004	München-Moosach	Polycyclic aromatic hydrocarbons, fenols, BTEX	Operational	In situ reactors in 4 chambers, horiz. drainage and cut-off wall, 1.4 km	Activated carbon	6,000,000€, state-financed

R RUBIN (German Permeable Reactive Barrier Network) project, *S* SAFIRA project, *F&G* funnel and gate

near Gyöngyösoroszi, Northern Hungary [90, 91]. Field experiments using fly ash combined with lime, a grass mixture and two *Sorghum* species were performed. The stabilization of metals was monitored by covering the main pathways, such as leaching by drainage water, plant uptake, and erosion. The experiments proved the efficiency of a fly ash and lime combination together with vegetation (grass is the best) in controlling leaching, erosion, and plant uptake. The amount of toxic metals in the collected drainage water decreased by 85–99%. The toxicity of both water and soil decreased due to the treatment, and healthy vegetation was established on the treated allotments, while no vegetation grew on the untreated control plots.

The effect of redox potential can be advantageously used for soil remediation [92]. Aerobic, anoxic, or anaerobic environment can be created in a reactor or in the soil. Usually, there is high redox potential near the surface; low, but still positive, redox potential in the upper layers of the saturated soil zone; and negative redox potential in the deeper saturated soil layers. Inside ex situ closed reactors and in deeper soil layers, both the aerobic and the anaerobic conditions can be controlled. In open reactors or in the upper layer of the in situ treated soil, aerobic technologies are preferred, whereas in the naturally anaerobic deeper soil layers anaerobic technologies are preferable. Depending on the character of the pollutant, it may be necessary to change the soil's initially anaerobic conditions to aerobic ones or vice versa; exclude the air from an initially aerobic soil; apply alternative electron acceptors to initiate transformation processes: acidic bioleaching of metals from sulfidic ores under aerobic conditions, or stabilization of mercury or other toxic metals in sulfidic form under anaerobic conditions.

Electrochemical Remediation

Technologies used to remediate contaminated soils, sediments, and groundwater based on physicochemical, thermal, and biological principles are often costly, energy-intensive, ineffective, and create adverse environmental impacts [93]. Low permeability and heterogeneities in the layers and contaminant mixtures very often result in poor remediation results. Electrochemical remediation has been found a promising approach in difficult site condition and has been researched worldwide extensively.

To implement an electrochemical technology, first wells are drilled around the contaminated region. Electrodes are installed in the wells and low direct current or low potential gradient is applied to the electrodes [94]. The generated electric field induces several transport, transfer, and transformation processes moving the contaminants to the electrodes where they can be removed. Also, the contaminants may be immobilized or degraded within the contaminated site. Other terms used for electrochemical remediation include electrokinetics, electrokinetic remediation, electroremediation, electroreclamation, etc. If water only is used around the electrodes, the process is called unenhanced electrochemical remediation. Enhanced electrochemical remediation uses conditioning solutions and ion exchange membranes.

Key advantages of electrochemical remediation are:

- Flexibility in terms of choosing ex situ or in situ
- Applicability to low-permeability and heterogeneous layers (clay, silt, loess, etc.)
- Both saturated and unsaturated soils can be treated
- Heavy metals, radionuclides, organic contaminants, and their mixtures can be treated
- It can be integrated into conventional systems

The complex character of the transport, transfer, and transformation processes and the influence of buffer capacity, mineralogy, organic matter content, geochemistry soil-contaminant interactions and heterogeneity on the efficacy require extensive investigations in the design phase. All this is necessary to guarantee successful implementation of electrochemical remediation technologies.

Electrochemical Processes

The fundamental transport mechanisms caused by an electric field are [95]:

- Electromigration (transport of charged ions or ion complexes in solution)
- Electroosmosis (movement of liquid relative to a charged stationary surface)
- Electrophoresis (movement of charged particles relative to a stationary fluid)

Electromigration and electroosmosis occur in fine grained soils, electromigration and electrophoresis are dominant in coarse grained soils.

In addition to mass transport processes, chemical reactions take place at the electrodes. The principal electrode reaction observed is the electrolysis of water. At the anode, water is oxidized and oxygen gas and hydrogen ions are generated:

$$2H_2O \rightarrow O_{2(gas)} + 4H^+{}_{(aq)} + 4e^- \; E^0 = -1.229V \quad \text{(Reaction 18)}$$

At the cathode, water is reduced and hydrogen gas and hydroxide ions are produced:

$$4H_2O + 4e^- \rightarrow 2H_{2(gas)} + 4OH^-{}_{(aq)} \; E^0 = -0.828V \quad \text{(Reaction 19)}$$

This means that acid is produced at the anode, thus pH is reduced and alkaline solution is produced at the cathode, that is, pH is increased. H^+ ions leaving the anode and OH^- ions leaving the cathode change pH of the soil considerably [96].

Electrochemical Transport Processes Electromigration (ionic migration) is the movement of dissolved ionic species in the pore fluid toward the opposite electrode: anions toward the anode and cations toward the cathode [94, 95]. Electromigration is the principal transport process for ionic metals, polar organic molecules, ionic micelles, and colloidal electrolytes including H^+ and OH^- ions. The electromigrative velocity (v_{em}, m/s) can be written as

$$v_{em} = u_i z_i n \tau F E \quad \text{(Eq. 1)}$$

where u_i is the ion mobility in $m^2/(V \cdot s)$, z_i is the ionic valence (dimensionless), n is the porosity (dimensionless), τ is the tortuosity (a dimensionless factor telling how many times longer the actual path of a moving ion is than the straight-line distance between the same two points due to the particle's zigzag motion), F is Faraday's constant its value being 96,487 C/mol electrons (the quantity of electricity equivalent to one mole of electrons, i.e., the product of the Avogadro constant and the charge on an electron in coulombs), E is the electric field strength (V/m). Ionic mobility u_i can be calculated from the Nernst-Einstein-Townsend equation:

$$u_i = \frac{D_i \, |z_i| \, F}{R \, T} \quad \text{(Eq. 2)}$$

where D_i is the molecular diffusion coefficient (m^2/s), R the universal gas constant (8.314 J/K·mol), and T the thermodynamic (absolute) temperature (K).

Electroosmosis. The hydraulic flow due to hydraulic gradient is defined by Darcy's law:

$$q_h = k_h i_h \quad \text{(Eq. 3)}$$

where q_h is the flow rate per unit cross-sectional area in m/s, k_h is the hydraulic conductivity in m/s and i_h the hydraulic gradient, dimensionless. This flow is significant for permeable soils such as sand with a hydraulic conductivity greater than 10^{-5} m/s, but negligible for clays with a hydraulic conductivity of 10^{-8}–10^{-11} m/s.

Electroosmosis is induced by an electric gradient and it is the movement of the pore fluid, which contains dissolved ionic and nonionic species, relative to the stationary soil mass, toward the electrodes. Soil particle surfaces are charged (usually negatively) and cations (positive ions) concentrate within a diffuse double layer adjacent to the particle surface. Due to an electric potential, the locally excess ions migrate in a plane parallel to the particle surface toward the oppositely charged electrode. While migrating, they transfer momentum to the surrounding fluid molecules via viscous forces and produce electroosmotic flow. Electroosmosis is the dominant transport process for dissolved, suspended, or emulsified organic or inorganic contaminants. The Helmholtz-Smoluchowski law gives the electroosmotic velocity as

$$v_{eo} = -\frac{D \, \zeta}{\eta} \, E_z, \quad \text{(Eq. 4)}$$

where v_{eo} is the electroosmotic velocity in m/s, D is the dielectric constant of the fluid in C/(V m), E_z is the applied gradient in V/m, ζ the zeta potential in V, and η is the dynamic viscosity in Pa s. The volumetric flow rate can be written as

$$q_{eo} = n \, A \, \frac{D \, \zeta}{\eta} \, E_z, \quad \text{(Eq. 5)}$$

where n is the porosity, dimensionless and A is the cross-sectional area in m. In practice, the

so-called the electroosmotic permeability coefficient is used:

$$k_{eo} = n \frac{D\,\zeta}{\eta} \qquad \text{(Eq. 6)}$$

giving the flow rate as

$$q_{eo} = k_{eo}\, A\, E_z \qquad \text{(Eq. 7)}$$

where q_{eo} is in m^3/s, k_{eo} in $m^2/(V\ s)$, A in m^2 and E_z in V/m.

In low-permeability regions, electroosmotic flow is significantly greater than flow generated by a hydraulic gradient and it transports dissolved contaminants toward the electrodes. As Eqs. 5–7 indicate, the electroosmotic flow depends on the dielectric constant and viscosity of the pore fluid, the zeta potential (the electric potential between the fixed and mobile parts of the double layer). Zeta potential depends on the type of clay minerals, ionic species, pH, ionic strength, and temperature. Changes in pH due to electrolysis affect the zeta potential and thus the electroosmotic flow. If most parts of the soil are acidified, the direction of electroosmotic flow may be reversed from "anode to cathode" to "cathode to anode." This is called electroendosmosis and it is important to know it in electrokinetic remediation.

Electrophoresis is the transport of charged colloid-sized particles and bound contaminants due to an applied low potential with respect to stationary pore fluid. Mass transport by electrophoresis is negligible in low-permeability systems compared to electromigration and electroosmosis. However, it may become significant or even the dominant transport mechanism for biocolloids (bacteria) and micelles (charged aggregates of molecules or particles).

Diffusion is the movement of contaminant ions and molecules from places of higher concentration to places of lower concentration due to concentration gradient. Ionic mobility of charged species is much higher than the diffusion coefficient; therefore, diffusive transport can often be neglected.

Comparing the different transport processes of metal cations or metal anions, electromigration is the prime mechanism at high concentrations and electroosmosis at low concentrations. Their share to the total mass transport depends on soil type, water content, ion species, and concentration. Hydraulic flow is negligible in silts and low-activity clay compared to electroosmosis. The mass transport of ionic species by electromigration is 10–300 times greater than by electroosmosis. Electroosmosis decreases when pH and zeta potential drop around the end of electrochemical processes.

Electrochemical Mass Transfer Processes The electrolysis reactions (reactions 18 and 19) generate protons (H^+) and hydroxyl ions (OH^-), which migrate toward the oppositely charged electrodes. H^+ is about twice as mobile than OH^-, so protons dominate the system and an acid front moves toward the cathode [94, 96–98]. Where it meets the hydroxyl front moving in the opposite direction, the opposite ions unite and produce water. As a consequence, the soil is divided into two zones with a sudden change in pH: there is a high pH zone around the cathode and a low pH zone around the anode. The actual pH of the soil depends on the transport of the H^+ and OH^- ions and the soil's geochemical properties. First, the soil pH changes both spatially and with respect to time, causing mass transfer between the various phases: solid, precipitate, sorbed, dissolved, and free phase.

Sorption is the partitioning from solution or pore fluid to the solid phase or soil surface. It includes adsorption and ion exchange and depends on the contaminant, soil, and pore fluid. Desorption is the reverse process and is responsible for the release of the contaminants from the solid surface. These processes are affected by the ion migration caused by the electrolysis. The sorption behavior can be determined in batch experiments.

Precipitation and dissolution can significantly influence the removal efficiency. Hydrogen ions encourage acidification and the dissolution of metal hydroxides and carbonates. If the soil has high buffering capacity, this may hinder the migration of hydrogen ions. Hydroxyl ions at the cathode increase pH to 10–12 and this will precipitate heavy metals clogging the soil pores and hindering further contaminant transport. To achieve high removal efficiency, precipitation of metals must be prevented and they must be kept in solution. High pH and low heavy metal concentration may produce negatively charged complexes at the cathode compartment.

Oxidation and reduction are of particular importance for metallic contaminants such as chromium.

Sustainable Remediation Methods for Metals and Radionuclides. Table 5 Heavy metal removal by unenhanced electrochemical remediation [99]

Metal	Origin	Retardant	Time (days)	Removal (%)
As	Gasworks, gold mine, wood preservation	Sorption	125	0–88
Cd	Electroplating, mining, military, wastewater, landfill	High pH	5–48	0–93
Cr	Electroplating, military, wastewater	Cr(III) and Cr(VI) differ	9–85	Difficult 3–64
Cu	Electroplating, military, wastewater, mining		30	Good, 80–99
Hg	Accidental spill		54	Nil
Ni	Electroplating, military		64	Low
Pb	Gasworks, mining paint factory	Soil specific	133	10–98
Zn	Electroplating, mining, military, accumulators		112	Good, 17–99

The trivalent chromium Cr(III) exists in the form of cationic hydroxides, for example, $Cr(OH)_2^+$, and migrates toward the anode. The hexavalent chromium Cr(VI) is present in oxyanions, for example, CrO_4^{2-}, and migrates toward the anode. The valence state of chromium depends on soil properties, reducing and/or oxidizing agents and determines the outcome of electrokinetic remediation. The most important geochemical processes during electrokinetic treatment are:

- Generating pH gradient
- Creating buffering capacity
- Change of zeta potential of soil particle surfaces
- Sorption/desorption
- Complexation
- Redox reactions

Electrochemical Removal of Heavy Metals

Ottosen et al. [99] evaluated a large number of electrochemical removal tests on heavy metals. Ideal soils, often kaolinite, were used to represent low-permeability soils and spiked with a cationic metal (e.g., lead or cadmium) in a specified concentration. Electric potential was applied to the soil sample in an electrokinetic setup. After a certain time, the transport and removal of the metal was determined. Cationic metals existed in soluble ionic form near the anode at a reduced pH and they were transported toward the cathode. However, under unenhanced conditions, they were sorbed or precipitated near the cathode because of high pH due to OH^- coming from the cathode, thus the actual removal result was often minimal. Tests on field soils furnished similar results, all the more as the soils have complex mineralogy, organic content, and buffering capacity. If there is a higher acidic buffering capacity, the soil pH does not decrease near the anode but increases near the cathode. Table 5 shows a brief summary of the conditions and results of unenhanced tests.

To improve metal removal enhanced conditions were applied. They included organic/mineral acids at the cathode to reduce pH, exchange membranes between soil specimen and electrodes to control H^+ and OH^- ion transport and chelating agents to form soluble metal complexes at different pH values. Enhanced tests have shown excellent removal efficiencies. Mercury had to be oxidized first and transformed into ionic form and then it was removed by electromigration. Table 6 shows a brief summary of the conditions and results of enhanced tests.

Removal of Radionuclides

Improper handling of nuclear wastes and spent fuel, activities at nuclear fuel production plants and nuclear waste processing plants, accidents involving nuclear materials, especially those in nuclear reactors, and nuclear weapons tests have caused severe contamination to the soil and groundwater on a number of occasions [100]. Radionuclides may enter the soil and/or groundwater during storage, transport, and use of nuclear fuel and waste. Before being abolished, nuclear tests were a major source of nuclear

Sustainable Remediation Methods for Metals and Radionuclides. Table 6 Heavy metal removal by enhanced electrochemical remediation [99]

Metal	Origin	Enhancement	Time (days)	Removal (%)
As	Gasworks, mining, wood preservation	pH adjustment, HNO_3, Na_2CO_3	6–69	14–90
Cd	Electroplating, metal finishing	Citric acid	10–180	40–92
Cr	Electroplating, wood preservation	pH adjustment, citric acid	7–180	40–98
Cu	Cable production, wood preservation	Ammonia, ammonium nitrate	30	60–95
Hg	Chlor-alkali plant	I_2/I^-, Cl^- addition	182	84–97
Ni	Incinerator sludge, foundry	pH lowering	7–10	52–87
Pb	Leaded petrol, battery manufacture, shooting range	Acetic acid, citric acid, EDTA (ethylenediaminetetra-acetic acid)	10–148	19–96
Zn	Cable production, industrial wastewater	HNO_3, ammonia, ammonium citrate	7–21	25–98

Sustainable Remediation Methods for Metals and Radionuclides. Table 7 Toxicity of radioactive elements [100]

Degree of toxicity	Radioactive element
Extremely high	^{210}Pb, ^{210}Po, ^{226}Ra, ^{228}Th, ^{232}Th, ^{232}U, ^{237}Np, ^{238}Pu, ^{239}Pu, ^{241}Am, ^{242}Cm
High	^{90}Sr, ^{106}Ru, ^{124}Sb, ^{126}I, ^{129}I, ^{144}Ce, ^{170}Tm, ^{210}Bi, ^{223}Ra, ^{224}Ra, ^{227}Th, ^{234}Th, ^{230}U, ^{233}U, ^{234}U, ^{235}U, ^{241}Ru
Medium	^{22}Na, ^{24}Na, ^{32}P, ^{35}S, ^{36}Cl, ^{54}Mn, ^{56}Mn, ^{59}Fe, ^{60}Co, ^{82}Br, ^{89}Sr, ^{90}Y, ^{91}Y, ^{95}Nb, ^{95}Zr, ^{105}Ru, ^{125}Sb, ^{132}I, ^{133}I, ^{134}I, ^{134}Cs, ^{137}Cs, ^{141}Ce, ^{171}Tm, ^{203}Pb, ^{206}Bi, ^{231}Th, ^{239}Np
Moderate	^{14}C, ^{38}Cl, ^{55}Fe, ^{64}Cu, ^{69}Zn, ^{71}Ge, ^{97}Zr, ^{131}Cs, ^{136}Cs
Low	^{3}H

contamination. The most serious contaminations have been caused by the isotopes ^{60}Co, ^{90}Sr, ^{90}Y, ^{106}Ru, ^{137}Cs, ^{144}Ce, ^{147}Pm, ^{238}Pu, ^{239}Pu, ^{240}Pu, and ^{226}Ra. The severity of contamination is largely determined by the toxicity of the radioactive elements involved (Table 7).

Most soil decontamination technologies used are based on flushing soils with various chemicals, chemical leaching, and selective extraction of radionuclides. The main advantage of the new electrokinetic technique is that it can be applied in situ to soils of low filtration ability.

Electrokinetic Localization of Radionuclides Electrokinetic localization aims at preventing further spread of the pollutants and uses protective electrokinetic barriers or screens and techniques to restore the protective function of protective screens.

Electrokinetic Screens Electrokinetic screens are used to prevent radionuclides from diffusing from the polluted area into the environment (groundwater, soil, and other subsurface materials). If the source is a geometrically well-defined body under the surface and is underlain by an impermeable layer (aquitard), an electric field is generated around this body by rows of anode and cathode wells and the field is directed in an oppposite direction to possible radionuclide migration thus forcing the radionuclides toward the center of the contaminated volume. If the contaminated body is on or very close to the surface, for instance, in the form a contaminated pond of radioactive waste, the rows of anode and cathode wells are arranged in an inclined way circularly around the pond so that they make an angle with the surface. This will result in a conical structure beneath the pond forcing migrating pollutants from

both the perimeter and underneath the pond back toward the center. These screens can be applied both at emergency sites and other cases of radioactive pollution.

Electrokinetic Restoration of Protective Screens Clays with high sorption capability usually containing smectite and illite, or other disperse soils such as sand enhanced with oxalic silica-alumina gel can also be used as protective screens as they decrease filtration ability and increase sorption capacity. However, the protective properties of such screens deteriorate with time and the screens accumulate large amounts of radionuclides. Application of electrokinetic technology can improve the sorption characteristics of such screens and can clean them from accumulated radionuclides. Tests were conducted on sand specimens strengthened with oxalic silica-alumina gel and spiked with 3.5 mg/g of ^{88}Sr and the same concentration of ^{133}Cs. Applying an electric field reduced the ^{88}Sr concentration to 1.2 mg/g in the anode zone and increased it to 4.4 mg/g in the cathode zone and 1.8 mg/g for ^{133}Cs in the anode zone and to 4.4 mg/g in the cathode zone. Strontium is most mobile in an acidic medium at pH < 5.5 and its mobility is minimal at $5.5 <$ pH < 7.5 (weakly acidic) and at pH > 7.5 (alkaline).

Cleaning of Soil from Radionuclides after Nuclear Contaminations Using Conventional Techniques Cleaning of soil from radionuclides is a particularly important and demanding task after nuclear accidents of which the most serious ones occurred in the former Soviet Union [101]. They were usually consequences of complex social-political conditions, politically motivated forced weapons production, and absence of proper knowledge and experience in managing radioactive wastes. The severity of a contamination is primarily determined by the presence of long-lived radionuclides, the most important ones being ^{90}Sr ($T_{1/2}$ = 28.1 years), ^{137}Cs ($T_{1/2}$ = 30.17 years), and ^{239}Pu ($T_{1/2}$ = 24,000 years).

1. The Techa River contamination. The "Mayak" Production Plant (near Chelyabinsk, now Ozersk, Eastern Urals) was the first to produce weapons-grade plutonium in the former Soviet Union. The plutonium production needed for the Soviet atomic bomb program generated huge amounts of radioactive wastes whose reduction below the permissible level of 3.7 MBq/l was then not feasible. Therefore, huge amounts of liquid radioactive wastes (110–259 PBq, i.e., 3–7 MCi) were discharged into the Techa-Iset'-Tobol-Irtysh-Ob river system between 1949 and 1956. The amount of radioactive waste accumulated in the Techa River has no equivalent in the world.

The most active discharges were caused by the acetate-fluoride technology used for plutonium extraction. Uranium fission products were responsible for most of the β-activity of wastes, while the long-term contamination was due to ^{90}Sr and ^{137}Cs disposals. The exposure of the population along the river was in the range of several milliSieverts to 4,000 mSv for red bone marrow. In the 1950s and 1960s a scheme of dikes and reservoirs was constructed for restriction and planned elimination of the radionuclides. In the years following the disposal, dietary uptake of ^{90}Sr by humans was very high: ^{90}Sr concentration in milk produced in some villages exceeded the permissible level by 66 times in the early years. Remedial actions implemented included:

1. Technical measures to reduce radioactive concentration
2. Technical and organizational measures to reduce exposure to radiation
3. Measures to control the radiation situation in the coastal region

The use of river water for drinking purposes, fish and farm products was restricted – unfortunately, too late, in some cases 3–4 years after the beginning of the contamination. In 1954–1960 about 7,500 people were evacuated and resettled in other areas. The introduction in the 1970s and the maintenance of a continuous sanitary-protective regime reduced the exposure by 40-fold. Bans for drinking water and free cattle pasturing, food and hay making, and fishing are still in force. Flushing the river bed with larger than normal amounts of noncontaminated water for a couple of months in 2 successive years remained ineffective. Burying the old river bed with new material was considered and rejected as technically unfeasible. Self-healing capacity of nature or natural attenuation such as radioactive decay, redistribution of radionuclides, reduction in radionuclide mobility, and bioavailability proved to be the prime remediation factor. To date, exposure rates are around 0.1 mSv/year, ^{90}Sr

concentration in milk was 18.5 Bq/l in 1968 and 3.7 Bq/liter in 1995, and ^{137}Cs concentration 65.5 Bq/l and 14.0 Bq/l, respectively. Nevertheless the Duma (Russian Parliament) concluded in 2006 that it would not be possible to totally overcome this radioecological problem.

2. The Kyshtym accident [101] also occurred in the Mayak Plutonium Production Plant on 29 September 1957 and was classified category 6 on the 7-point International Nuclear Event Scale (INES) scale. An underground high-activity liquid waste tank exploded (the explosion was equivalent to that of 70–100 t of TNT) emitting a radioactive cloud (740 PBq, i.e., 20 MCi) to a height of 1,000 m. Ninety percent of the contaminant deposited on-site, 10% in the Chelyabinsk, Sverdlovsk, and Tyumen regions creating the so-called East Urals Radioactive Trail (EURT) with an area of 23,000 km, affecting 217 settlements and 270,000 inhabitants and causing at least 200 cases of death from cancer. The affected territory is a chernozem (fertile black soil) area and was used for extensive grain, meat, and milk production. The EURT's boundary was specified by a ^{90}Sr density of 3.7 kBq/m^2. The most seriously contaminated 1,000-km^2 area (105 km by 4.5–6 km, >74 kBq/m^2) was contaminated by ^{144}Ce, ^{144}Pr, ^{95}Zr, ^{95}Nb, ^{90}Sr, ^{90}Y, ^{106}Ru, and ^{106}Rh, where ^{144}Ce uptake by humans through foodstuff and ^{90}Sr in milk were the major contributors to exposure. The exposure dose rate due to external γ-radiation was 200–400 μR/s. Forty years after the accident, the contamination fell by 50-fold, dose rates decreased 4,000 times due to radionuclide decay and vertical migration within the soil, ^{90}Sr uptake via foodstuff dropped by 200–2,000 times. ^{90}Sr uptake by plants is inversely proportional to exchangeable Ca content. The ^{90}Sr concentration is maximum in grass or hay and minimum in potato and root vegetables, while cereal and legume crops are in between. Therefore potatoes, root vegetables, and cereals were cultivated in areas with high ^{90}Sr deposition density, and fodder production and grazing animals in areas with low ^{90}Sr deposition density. ^{90}Sr is mainly deposited in animal bones and the removal rate is very low. However, animal body gives preference to Ca, thus for per unit Ca taken up by the animal, meat was 2.5-fold and milk 10-fold less contaminated compared to fodder. But due to the differences in concentration in different tissues and organs, ^{90}Sr is minimal in muscles, so meat production was found the best option among animal farming practices.

A complex remediation agricultural regime was introduced in the EURT area from spring of 1958. Deep plowing was used to bury the top contaminated layer into sub-arable horizons immediately after radioactive fallout using modernized plows (below 30 cm) and plow-shifters (below 70 cm). This reduced the ^{90}Sr concentration in the arable layer by 80–95% and ^{90}Sr accumulation by 75% in wheat and by 99% in potato. On many small plots the top contaminated layer was removed by bulldozers, graders, and scrapers and buried in special burial facilities. The effect of deep plowing was enhanced by mineral fertilizers, which reduced the ^{90}Sr concentration in the yield by a factor of 10. In addition to reducing ^{90}Sr uptake by plants, plowing immediately after fallout reduced the dose rate of γ-radiation. Processing of raw farm products can effectively contribute to reducing ^{90}Sr concentration: processing milk to butter reduces ^{90}Sr concentration by 20-fold. Conventional processing of grain to flour and grouts reduces ^{90}Sr concentration by two to three times. Starch, alcohol and vegetable oil can be produced practically "clean." In animal products, ^{90}Sr concentration was reduced two to seven times by feeding the animals with potatoes, root vegetables, grain, Ca-rich legume crops, and Ca additives instead of fodders from natural land.

3. The Chernobyl Nuclear Power Plant accident [101] happened on April 26, 1986, and was the largest in the history of nuclear engineering both in terms of radioactivity released and the area affected. The cause of the accident was a flawed reactor design and human failure during a planned reactor stoppage and generator test. The explosion was followed by a fire and the destroyed reactor continued to release radioactivity for 11 days. Table 8 gives an illustration about the extent of contamination.

The total radioactivity released amounted to 5,300 PBq (= 5.3×10^{18} Bq) with ^{137}Cs, ^{134}Cs, ^{90}Sr, and Pu being the chief radionuclides. In the early period after the accident ^{131}I was the dominant contaminant, later on ^{137}Cs, ^{134}Cs, and ^{90}Sr, while ^{137}Cs remained the medium and long-term pollutant. The amount of ^{137}Cs deposited within the Soviet Union was 4.0×10^{16} Bq and ^{137}Cs contamination levels exceeding 37 kBq/m^2 were used to define the limits of the

Sustainable Remediation Methods for Metals and Radionuclides. Table 8 Seriously affected areas and radioactive fallout after the Chernobyl Nuclear Power Plant accident in 1986 (Based on [100])

Country	Polluted area (km) (>1 Ci/km)	Fallout (Ci)
Russia	59,300	520,000
Belorussia	43,500	400,000
Ukraine	37,630	310,000
Sweden	23,440	79,000
Finland	19,000	83,000
Austria	11,800	42,000
Norway	7,180	53,000
Romania	1,200	41,000
Europe	207,500	1,700,000
World		2,100,000

contaminated area, which amounted to 150,000 km^2 (larger than Illinois or Greece). Six million people live in this area in 15,000 settlements and 116,000 people who lived closest to the reactor site were evacuated soon after the accident. Twenty-eight emergency workers died from acute radiation syndrome, 15 patients died from thyroid cancer, and it is roughly estimated that the total number of deaths from cancers caused by Chernobyl may reach 4,000 among the 600,000 people having received the greatest exposures.

The soil cover affected was low-fertility soddy-podzolic soil, sand and sandy loam, and peaty soil. Man-made radionuclides, especially ^{90}Sr and ^{137}Cs, exhibit high mobility in these soils. Thirty percent of the affected region is forest and there are a large number of rivers in the Dnieper catchment area. The key dose-forming radionuclide was ^{137}Cs, which is strongly absorbed by the soil's solid phase. Countermeasures to reduce ^{137}Cs uptake by plants are based on the antagonism in ^{90}Sr and K transport via the trophic chain using potassium saturation, for example, in soil. Unlike ^{90}Sr, ^{137}Cs is evenly distributed in the body and easily removed. In the first 2 months ^{131}I was the main radiological hazard causing an increase in thyroid cancer. Severely contaminated (>1,480 kBq/m^2) agricultural land (200,000 ha) was taken out of use, dairy cattle was banned in the most affected regions. In low-contamination zones the agricultural practice was unchanged, in medium-contamination zones countermeasures were taken and zones highly contaminated were excluded from agricultural use. The countermeasures including deep plowing, mineral fertilizers, and liming managed to reduce ^{137}Cs concentrations in plants by half. Amelioration, plowing, fertilizing, and liming of meadows and pastures reduced ^{137}Cs contents in fodder by 3.6–16.0 times. Ferrocyn compounds were effective in binding ^{137}Cs in the gastrointestinal tract of animals. Processing of milk to milk products was another efficient remedy. Among the water bodies, the cooling pond of the power plant is the most highly contaminated. Dikes, dams, channels, etc., were constructed to limit radionuclide migration in the water bodies – with limited success, though their contribution to dose was low compared to other pathways.

A 30-km restricted zone around the Chernobyl power plant, heavily contaminated with plutonium and transuranic radionuclides, was evacuated and established as a no-access area. Sanitary-hygienic restrictions must be enforced here for tens of years. Though it was suggested to use the area as a long-term storage of radioactive wastes or a natural reserve to quantify long-term radiation effects in the environment, the fate of the abandoned Chernobyl area has not yet been decided.

4. Remediation of the Enewetak Atoll contaminated by nuclear weapons tests [102].

The Enewetak Atoll (Marshall Islands, about half-way between the Philippines and Hawai) is the only nuclear weapons test site where proper cleanup has taken place. The 136 local inhabitants were relocated to the Ujelang Atoll before the tests. The USA conducted 42 nuclear tests on the Atoll from 1948 to 1958. The "Mike" blast in 1952 had an explosive yield of 10.4 Mt, blasted away an island and left a 1-km-diameter crater. The fallout showed ^{244}Pu and ^{246}Pu, and led to the discovery of einsteinium and fermium. The contaminants were fission products, activation products, and fissioned nuclear material, and miscellaneous materials (concrete, metal, cables, buildings, etc.), some of them contaminated. Plutonium activity in the top 2 cm of the soil ranged from 0.4 to 7 mBq/g. The radiological cleanup concentrated on reducing ^{238}Pu, ^{239}Pu, ^{240}Pu, and ^{241}Am in the surface soil on some of the islands. Cleanup and rehabilitation was

implemented between 1977 and 1980. The top layer of soil with a plutonium concentration exceeding 15 Bq/g was removed. 41,600 m^3 contaminated soil was mixed with cement and attapulgite and placed at the bottom of the "Cactus" crater created by one of the blasts. Above the water level, the soil was mixed with cement and compacted to provide a dome shape. Thus communication with subterranean groundwater was prevented. The average transuranic concentration in the soil in the crater was calculated to be 2.4 Bq/g. A committee report in 1982 and an environmental surveillance program concluded that there was no adverse radiological impact on the environment. Checks on the internal radionuclide body content of the repatriated population indicate that there has been no significant radiological health problem.

Electrokinetic Cleaning of Soil from Radionuclides The electrokinetic method is the most efficient cleaning of soil from radionuclides; it can be used with and without flushing, the latter being more efficient. Most regions contaminated with radionuclides contain ^{90}Sr, ^{88}Sr, ^{137}Cs, and ^{133}Cs [100]. Therefore, investigations into electrokinetic cleaning of different soils from sandy loam to clay were focussed on these elements. Electrokinetic tests on ^{88}Sr in sandy loam without flushing showed that the initial Sr concentration of 5 mg/g nearly halved near the anode and increased near the cathode. This shift mainly affected sorbed strontium, dissolved strontium remained largely unchanged. Electrochemical leaching includes electrokinetic removal and flushing by an electrolyte (e.g., [103]). In tests to increase ^{137}Cs and ^{60}Co removal efficiency [104], $CH_3COONa + CH_3COOH$ was added to the soil column and periodically acetic acid was injected into the cathode reservoir to restrain pH increase. The removal of radionuclides was mainly facilitated by electromigration and no precipitate was formed. Twenty-five percent of Cs and 94% of Co was removed in 10 days. In addition, the tests verified the numerical results of the model developed. Korolev et al. performed tests on a sandy loam contaminated with ^{137}Cs from a liquid radioactive waste spill of 80–200 Bq/g activity [103]. They used a three-cell installation (anode, neutral baffle, and cathode) and stainless steel cathodes and platinum-coated titanium anode plates, and pH ≤ 1 was maintained by adding nitric acid. The effect of different anolyte (part of the electrolyte at or near the anode) solutions on the removal in 55 days was: H_2O: 8%, KNO_3: 29% and NH_4NO_3: 47%.

Electrochemical Remediation of Mixed Metal Contaminants

Heavy metals are of great environmental concern due to their persistent character and high toxicity. Unfortunately, sites with mixed metal contaminants are more common than those with single metals only. The main transport mechanisms are: electromigration, electroosmosis, and electrophoresis. The chief parameters affecting transport phenomena and removal efficiency are:

1. Ionic mobility
2. Adsorption capacity
3. Chemical forms of the metals
4. Inhibitory effects

Kim et al. have found that electrokinetic remediation of mixed metals usually yields lower removal efficiency than for individual metals [105]. High concentrations of mixed metal contaminants can be related to transference number, zeta potential, electroosmotic flow, etc. To improve removal efficiency, electrolyte conditioning and electrodialytic remediation have been developed. Electrolyte conditioning enhances the mobility of heavy metals and in doing so encourages their removal from the solid matrix. Enhancing agents such acetic acid, citric acid, EDTA, DTPA, KI, HPCD, H_2SO_4, NaOH, and NaCl have been tested as enhancement solutions and humic acid, ferrous iron, and sulfide as reducing agents for Cr, Ni, Cd removal (e.g., [106]). It has been found that a sequential use of appropriate solutions, rather than a single solution, is beneficial in the removal of multiple metal contaminants, while the mentioned reducing agents have not exhibited any significant effect. Electrodialytic remediation uses ion exchange membranes, which can prevent metal hydroxide precipitation near the cathode region. A cation selective membrane placed in front of the cathode maintains low soil pH, thus heavy metals are unable to precipitate and migrate out of the soil and can be collected in the catholyte. In terms of geometry, circular arrangement was found better. An auxiliary solution cell (ASC) is an innovative device with

a number of small holes in its wall enabling hydroxide ions to move into the ASC and metal contaminants can then be precipitated in the ASC rather than in the cathode electrolyte. Tests on harbor sediments used HCl as a desorbing agent, a solid-to-liquid ratio of 8, dried samples, and a 70-mA current, and yielded a 68–98% removal for Cu, Zn, Pb, and Cd.

Various authors (e.g., [106]) looked into Cr removal when other heavy metals (Ni and Cd) were present and have found that only Cr was often removed. Using tap water as an electrolyte, Cr removal was inefficient. Acetic acid provided a 57% Cr removal efficiency. Using EDTA as an electrolyte, Ni- and Cd-EDTA complexes migrated toward the anode due to their negative charge. NaCl combined with EDTA enabled an as high Cr removal as 79%, possibly due to sustaining current and electroosmotic flow by NaCl; Ni removal was 48% and Cd removal 26%.

Experiments on sewage sludge looked into mobility and removal of Ni, Zn, Cu, As, Cr, and Pb. While Zn removal was 95%, Cu removal 96%, and Ni removal 90%, the efficiency of As removal was rather low: 31%. Alkaline conditions are favorable for As transport toward the anode and for its removal, but high pH causes retardation by enhancing normal electroosmosis toward the cathode. Sodium carbonate, sodium hydroxide, and sodium hypochlorite have been used as enhancing solutions to boost electromigration. However, in the case of kaolinite and mine tailings, high pH and H_2O/KH_2PO_4 and Na_2CO_3/NaOH addition enhanced As removal.

The electrokinetic remediation of Hg is difficult because of its low solubility. The best results in Hg removal were achieved by the oxidation of reduced insoluble Hg(I) to Hg(II) using I_2. This forms an anionic complex and the Hg(II) ions migrate toward the anode. EDTA encouraged heavy metal removal, including Pb by EDTA complex forming. Chloride addition mobilized Hg and increased the removal rate.

The cost of electrokinetic remediation of inorganic contaminants is estimated to be in the range of 115–400 $/m^3 with an average of 200 $/m^3, that is, 90$/t, which is less than excavation and disposal as hazardous waste [107]. Due to the limited number of full-scale electroremediation projects performed, cost estimates are usually based on pilot-scale tests. As the technology matures, confidence is expected to rise and costs should drop.

Integrated Electrokinetic Remediation Technologies

Another advantage of electrokinetic techniques is that they easily can be integrated (coupled) with other technologies promoting their advantageous features by synergistic effects and suppressing their shortcomings [94]. Such integrated technologies include:

- Electrokinetic biobarriers
- Electrolytic reactive barriers
- Electrokinetic-permeable reactive barriers (PRB)
- Electrokinetic-chemical oxidation/reduction
- Electrokinetic-bioremediation
- Electrokinetic-phytoremediation
- Electrokinetic-stabilization
- Electrokinetic-thermal treatment

Most of the integrated methods have been tested for the removal of organic contaminants, but a few of them, especially electrokinetic-permeable reactive barriers, electrokinetic-phytoremediation, and electrokinetic-stabilization, proved efficient for the remediation of sites contaminated with heavy metals. The combined techniques may enhance kinetics of the reactions, eliminate clogging due to mineral precipitation, and increase desorption, thus improving the long-term performance. Another future-oriented aspect is the use of nanomaterials. Research into these coupled technologies is at an early stage and additional work in needed to exploit their potential for remediation.

Soil Remediation Based on Natural Processes

Soil remediation based on natural processes can be classified according to the scale of intervention [108].

Natural attenuation (NA) involves fully natural processes on a contaminated area/site, leading to the reduction of the environmental risk: dispersion, dilution, adsorption, cation- and anion-exchange, filtration and precipitation, volatilization, radioactive decay, chemical or biological stabilization, transformation or destruction of contaminants. No intervention is carried out and, in some cases, not even any monitoring. The only parameters that are required are natural potential and time. However, environmental engineers have to be careful about natural processes, because some of them may actually increase the risk (e.g., accumulation, bioleaching, bioaccumulation, etc.). The main advantage of natural attenuation is its cost-effectiveness,

while its disadvantages are the long time requirement and the limited possibility of influencing the processes.

Monitored natural attenuation (MNA): here natural processes are monitored. If continuous natural risk-reduction takes place, no engineering intervention is necessary. Time is often a limiting factor. If an increase in risk is observed (e.g., if sensitive land uses are endangered by pollution transport, or if there are disadvantageous environmental effects such as high pH, low redox potential, toxic biodegradation products, etc.), then targeted risk-reduction measures may be necessary.

Enhanced natural attenuation (ENA): this involves the intensification of the existing, risk-reducing natural processes by engineering tools. This means that after understanding the complex risk-reducing processes in the soil, engineers should identify the bottlenecks and find the proper engineering tools to eliminate them by changing the environmental parameters, such as pH, redox potential, temperature, or moisture content; or by supplying the soil microflora with nutrients; or by applying additives that are able to change the mobility and bioavailability of the contaminant.

In situ soil remediation itself has two further grades according to the scale of engineering interventions:

1. Working in the contaminated soil volume itself and placing operational tools in it, covering the contaminated soil volume and creating a highly reactive soil volume to treat two- and three-phase soil, groundwater, and/or soil gas. This type of intervention is called "in situ remediation."
2. Using a highly reactive, engineered, permeable volume within the soil, that is, subsurface barriers or zones. The operational tools are placed directly in the engineered volume or its surroundings. This engineered volume is mainly used for the treatment of contaminated groundwater in a flow-through system. Their close relatives are engineered filter-zones for wastewater treatment and man-made wetlands for surface waters.

Ex situ soil remediation is the highest degree of engineering intervention, where the solid soil itself is removed and placed into a vessel-type reactor equipped with all operational tools, where it is treated by process engineering technologies.

Future Directions

Contaminations with radionuclide arose from nuclear weapons testing, accidents, nuclear legacy, and uranium mining and milling. Contaminated sites can be found all over the world. Remediation methods comprise physical, chemical, and biological processes. The limiting factor for remediation is often not the lack of applicable technologies but economic reasons [109]. Therefore, the development of environmentally friendly, economical, and efficient remediation processes is the future challenge for scientists and engineers. There is a need for further research on the mechanisms of passive physicochemical and biological methods. However, the technical feasibility of these processes has already been demonstrated under field and large-scale conditions.

Electrochemical remediation of sites contaminated with metals or radionuclides is a rapidly developing upcoming field of technology. In cases of emergency, conventional methods have to be applied to remediate radionuclide-contaminated areas. They may include removal of the top soil layer; deep plowing; use of mineral fertilizers; discarding products grown on open fields; burying contaminated soil; and creating impermeable repositories for mixtures of contaminated soil, cement, and clay. Permeable reactive barriers have also shown good removal efficiencies for heavy metals and radionuclides. The cleanup of contaminated water bodies, especially river and lake beds, is still an unsolved problem after radioactive contamination. Electrokinetic remediation is based on electromigration, electroosmosis, and electrophoresis, while diffusion is usually insignificant. Their share in the total mass transport depends on soil type, water content, ion species, and concentration. To improve metal removal, enhanced conditions can be applied. They may include organic/mineral acids at the cathode to reduce pH, exchange membranes between soil specimen and electrodes to control H^+ and OH^- ion transport, and chelating agents to form soluble metal complexes. Localization by electrokinetic fences of sites contaminated with radionuclides is another useful treatment technique. Acetic acid and sodium acetate may enhance the removal of ^{137}Cs and ^{60}Co in electrokinetic remediation. When the anolyte is water, removal efficiency is usually low, but the addition of sodium nitrate or ammonium nitrate may increase

^{137}Cs removal considerably. Electrokinetic remediation of mixed metals usually yields lower removal efficiency than for individual metals. Enhancing agents such acetic acid, citric acid, EDTA, DTPA, etc., are helpful in the remediation of mixed metal contaminants as well.

Based on available laboratory results, field application should be encouraged with specific emphasis on [94]:

- Large-scale pilot tests
- Contaminated soils with aged and mixed contaminants
- Extension of the technology to, for example, industrial wastes
- Promotion of analysis based on physicochemical properties, geochemistry, reaction kinetics, equilibrium constants, and transport parameters
- Improvement of cost-efficiency
- Establishing quality control and quality assurance
- More emphasis on sustainability considerations

The application of passive remediation technologies like PRBs and most biological in situ processes require reliable monitoring systems to ensure that remediation goals can be reached. The development of new and innovative sensor systems is, therefore, also indispensable.

Bibliography

Primary Literature

1. Dudka S, Adriano DC (1997) Environmental impacts of metal ore mining and processing: a review. J Environ Qual 26:590–602
2. Adriaanse A, Bringezu S, Hammond A, Moriguchi Y, Rodenburg E, Rogich D, Schütz H (1997) Resource flows: the material basis of industrial economies. World Resource Institute (WRI), Washington, DC
3. Halada K, Ijima K, Katagiri N, Ohkura T (2001) An approximate estimation of total materials requirement of metals. J Jpn Inst Met 65(7):564–570
4. Bringezu S (2002) Towards sustainable resource management in the European union Wuppertal Paper No 121. Wuppertal-institute for climate environment energy, Wuppertal
5. Schmidt-Bleek F (1998) Das MIPS-Konzept. Droemer Knaur, München
6. OECD/NEA (2001) Uranium 2001: resources, production and demand: a joint report by the OECD nuclear energy agency and the international atomic energy agency. OECD Publications, Paris
7. Taylor LE, Brown TJ, Benham AJ, Lusty PAJ, Minchin DJ (2006) World mineral production 2000–04. British Geological Survey. Keyworth, Nottingham
8. Gatzweiler R, Jakubick A, Kiessig G, Paul M, Schreyer J (2002) Flooding strategies for decommisioning of uranium mines – a systems approach. In: Simon FG, Meggyes T, McDonald C (eds) Advanced groundwater remediation – active and passive technologies. Thomas Telford, London
9. Bundesministerium für Wirtschaft und Technologie D (2000) Wismut, Perspektiven durch Sanierung, Brochure
10. Mudd GM, Diesendorf M (2008) Sustainability of uranium mining and milling: toward quantifying resources and eco-efficiency. Environ Sci Technol 42(7):2624–2630
11. Simon FG, Meggyes T, McDonald C (2002) Advanced groundwater remediation – active and passive technologies. Thomas Telford, London
12. Simon FG, Ludwig S, Meggyes T, Stewart DI, Roehl KE (2005) Regulatory and economic aspects. In: Roehl KE, Meggyes T, Simon FG, Stewart DI (eds) Long-term performance of permeable reactive barriers, trace metals and other contaminants in the environment, vol 7. Elsevier, Amsterdam, pp 311–321
13. Schad H, Grathwohl P (1998) Funnel and gate systems for in-situ treatment of contaminated groundwater at former manufactured gas plant sites. In: Burmeier H (ed) Treatment walls and permeable reactive barriers, vol 229. NATO CCMS, Vienna, pp 56–65
14. Gillham RW (1993) Cleaning halogenated contaminants from groundwater. US Patent 5266213, 30 Nov 1993
15. Sivavec TM, Mackenzie PD, Horney DP, Baghel SS (1997) Redox-active selection for permeable reactive barriers. International Conference on Containment Technology, St. Petersburg, USA
16. Starr RC, Cherry JA (1994) In situ remediation of contaminated ground water: the funnel-and-gate system. Ground Water 32(3):465–476
17. Tratnyek PG, Scherer MM, Johnson TL, Matheson LJ (2003) Permeable reactive barriers of iron and other zero-valent metals. In: Tarr MA (ed) Chemical degradation methods for wastes and pollutants. Marcel Dekker, New York
18. Vidic RD, Pohland FG (1996) Treatment walls. Ground-water remediation technologies analysis center. GWTAC, Pittsburgh, PA, Technology evaluation report, TE-96–01
19. Blowes DW, Ptacek CJ (1992) Geochemical remediation of groundwater by permeable reactive walls: removal of chromate by reduction with iron-bearing solids. Subsurface restoration conference, 3rd international conference on groundwater quality research, subsurface restoration conference. Dallas, TX
20. Blowes DW, Ptacek CJ, Benner SG, McRae CWT, Bennett TA, Puls RW (2000) Treatment of inorganic contaminants using permeable reactive barriers. J Contam Hydrol 45:123–137
21. Powell RM, Puls RW, Hightower SK, Clark DA (1995) Corrosive and geochemical mechanisms influencing in situ chromate reduction by metallic iron. 209th American Chemical Society national meeting, Division of Environmental Chemistry conference proceedings vol. 35. Anaheim, CA, pp 784–787
22. Bostick WD, Stevenson RJ, Jarabek RJ, Conca JL (2000) Use of apatite and bone char for the removal of soluble radionuclides

in authentic and simulated DoE groundwater. Adv Environ Res 3(4):488–498
23. Cantrell KJ, Kaplan DI, Wietsma TW (1995) Zero-valent iron for the in situ remediation of selected metals in groundwater. J Hazard Mater 42:201–212
24. Dwyer BP, Marozas DC, Cantrell K, Stewart W (1996) Laboratory and field scale demonstration of reactive barrier systems. Sandia national laboratory, SAND96-2500 – UC-2040
25. Benner SG, Blowes DW, Gould WD, Herbert RB, Ptacek CJ (1999) Geochemistry of a permeable reactive barrier for metals and acid mine drainage. Environ Sci Technol 33(16):2793–2799
26. Morrison SJ, Spangler RR (1992) Extraction of uranium and molybdenum from aqueous solutions: a survey of industrial materials for use in chemical barriers for Uranium mill tailings. Environ Sci Technol 26(10):1922–1931
27. Morrison SJ, Spangler RR (1993) Chemical barriers for controlling groundwater contamination. Environ Prog 12(3):175
28. Naftz DL, Davis JA, Fuller CC, Morrison SJ, Freethey GW, Feltcorn EM, Wilhelm G, Piana MJ, Joye J, Rowland RC (1999) Field demonstration of permeable reactive barriers to control radionuclide and trace-element contamination in groundwater from abandoned mine lands. Toxic substances hydrology program – technical meeting, US geological survey, conference proceedings vol. 1 (99-4018A, contamination from hardrock mining). Charleston, South Carolina, USA, pp 281–288
29. Waybrant KR, Blowes DW, Ptacek CJ (1998) Selection of reactive mixtures for use in permeable reactive walls for treatment of mine drainage. Environ Sci Technol 32(13):1972–1979
30. Fetter CW (1993) Contaminant hydrogeology. Prentice Hall, Upper Saddle River, NJ
31. Langmuir D (1978) Uranium solution-mineral equilibria at low temperatures with applications to sedimentary ore deposits. Geochim Cosmochim Acta 42:547–569
32. Chung NK (1989) Chemical precipitation. In: Freeman HM (ed) Standard handbook of harzadous waste treatment and disposal. McGraw-Hill, New York, pp 7.21–7.32
33. Csővári M, Csicsák J, Földing G (2002) Investigation into calcium-oxide based reactive barriers to attenuate uranium migration. In: Simon FG, Meggyes T, McDonald C (eds) Advanced groundwater remediation – active and passive technologies. Thomas Telford, London, pp 223–235
34. Beitinger E, Fischer W (1994) Permeable treatment bed for use in purifying contaminated ground water streams in situ, Deutsches Patentamt P 4425061.4, WCI Umwelttechnik GmbH
35. Allison JD, Brown DS, Novo-Gradac KJ (1991) MinteqA2/ProdefA2, A geochemical assessment model for environmental systems. US environmental protection agency, database of computer programme, version 3.0. Athens, GA, USA
36. Ma QY, Traina SJ, Logan TJ (1993) In situ Lead immobilization by apatite. Environ Sci Technol 27(9):1803–1810
37. Ma QY, Logan TJ, Traina SJ (1994) Effects of NO^{3-}, Cl^{-}, F^{-}, SO_4^{2-} and CO_3^{2-} on Pb^{2+} immobilization by hydroxyapatite. Environ Sci Technol 28(3):408–418
38. Chen XB, Wright JV (1997) Evaluation of heavy metal remediation on mineral apatite. Water Air Soil Pollut 98:57–78
39. Powell RM, Puls RW, Blowes DW, Vogan JL, Gilham RW, Schultz D, Powell PD, Sivavec T, Landis R (1998) Permeable reactive barrier technologies for contaminant remediation, report, EPA/600/R-98/125. US environmental protection agency, Washington DC,
40. Powell RM, Puls RW, Hightower SK, Sabatini DA (1995) Coupled iron corrosion and chromate reduction: mechanisms for subsurface remediation. Environ Sci Technol 29(8):1913–1922
41. Schneider M (2002) Remediation of chromium contaminated groundwater in subsurface Fe0-reactor systems. In: Simon FG, Meggyes T, McDonald C (eds) Advanced groundwater remediation – active and passive technologies. Thomas Telford, London
42. Seelmann-Eggebert W, Pfennig G, Münzel H, Klewe-Nebenius H (1981) Chart of nuclides. Kernforschungszentrum Karlsruhe
43. Merkel B, Helling C, Falck E, Metzler D, Francis AJ, Hurst S, Kolitsch S (1998) Zusammenfassung Internationale Konferenz. Uranbergbau und Hydrogeologie II. Freiberg, Germany
44. Bickel M, Feinauer D, Mayer K, Möbius S, Wedemeyer H (1996) Uranium, supplement volume C6. In: Fischer D, Huisl W, Stein F (eds) Gmelin handbook of inorganic and organometallic chemistry. Springer-Verlag, Berlin
45. Roine A (2007) HSC chemistry V.6.12. Outotec Research Oy, Finland
46. Csővári M, Berta Z, Csicsák J, Földing G (2005) Mecsek ore, Pécs, Hungary case study. In: Roehl KE, Meggyes T, Simon FG, Stewart DI (eds) Long-term performance of permeable reactive barriers, trace metals and other contaminants in the environment, vol 7. Elsevier, Amsterdam, pp 211–259
47. Naftz DL, Fuller CC, Davis JA, Morrison SJ, Wilkoske C, Piana MJ (2002) Field demonstration of three permeable reactive barriers to control uranium contamination in groundwater, Fry Canyon, Utah. In: Naftz DL, Morrison SJ, Davis JA, Fuller CC (eds) Handbook of groundwater remediation using permeable reactive barriers. Academic, San Diego, pp 402–435
48. Csővári M, Csicsák J, Földing G, Simoncsics G (2005) Experimental iron barrier in Pécs, Hungary case study. In: Roehl KE, Meggyes T, Simon FG, Stewart DI (eds) Long-term performance of permeable reactive barriers, trace metals and other contaminants in the environment, vol 7. Elsevier, Amsterdam, pp 261–281
49. Csővári M (2009) Personal communication
50. Brown D, Potter PE, Wedemeyer H (1981) Uranium, supplement volume C14. In: Keim R (ed), Gmelin handbook of inorganic chemistry. Springer-Verlag, Berlin
51. Grenthe I, Fuger J, Konings RJM, Lemire RJ, Muller AB, Nguyen-Trung C, Wanner H (1992) Chemical thermodynamics of uranium. In: Wanner H, Forest I (eds) Chemical thermodynamics vol. 1. North-Holland Elsevier Science, Amsterdam, p 715
52. Jeanjean J, Rouchaud JC, Tran L, Fedoroff M (1995) Sorption of uranium and other heavy metals on hydroxyapatite. J Radioanal Nucl Chem Lett 201(6):529–539
53. Wu L, Forsling W, Schindler PW (1991) Surface complexation of calcium minerals in aqueous solution, 1. surface protonation at fluorapatite-water interfaces. J Colloid Interface Sci 147(1):178–185

54. Leyva AG, Mearrero J, Smichowski P, Cicerone D (2001) Sorption of antimony onto hydroxyapatite. Environ Sci Technol 35:3669–3675
55. Fuller CC, Bargar JR, Davis JA, Piana MJ (2002) Mechanism of uranium interactions with hydroxyapatite: Implications for groundwater remediation. Environ Sci Technol 36(2):158–165
56. Simon FG, Biermann V, Peplinski B (2008) Uranium removal from groundwater using hydroxyapatite. Appl Geochem 23(8):2137–2145
57. Morrison SJ, Spangler RR, Tripathi VS (1995) Adsorption of uranium(VI) on amorphous ferric oxyhydroxide at high concentrations of dissolved carbon(IV) and sulfur(VI). J Contam Hydrol 17:333–346
58. Office of radiation and indoor air and office of environmental restoration (1999) Review of geochemistry and available Kd values for cadmium, cesium, chromium, lead, plutonium, radon, sStrontium, thorium, tritium and uranium. Understanding variation in partition coefficient, Kd, values, volume II, EPA 402-R-99-004B. US environmental protection agency and US department of energy, Washington, DC, USA
59. Fiedor JN, Bostick WD, Jarabek RJ, Farrell J (1998) Understanding the mechanism of uranium removal from groundwater by zero-valent iron using x-ray photoelectron spectroscopy. Environ Sci Technol 32(10):1466–1473
60. Gu B, Liang L, Dickey MJ, Yin X, Dai S (1998) Reductive precipitation of uranium(VI) by zero-valent iron. Environ Sci Technol 21(21):3366–3373
61. Noubactep C, Meinrath G, Dietrich P, Merkel B (2003) Mitigating uranium in groundwater: prospects and limitations. Environ Sci Technol 37(18):4304–4308
62. Kalin M, Wheeler WN, Meinrath G (2004) The removal of uranium from mining waste water using algal/microbial biomass. J Environ Radioactiv 78(2):151–177
63. Sar P, D'Souza SFD (2001) Biosorptive uranium uptake by a Pseudomaonas strain: characterization and equilibrium studies. J Chem Technol Biotechnol 76:1286–1294
64. Bhainsa KC, D'Souza SFD (1999) Biosorption of uranium (VI) by *Aspergillus fumigatus*. Biotechnol Tech 13:695–699
65. Lloyd JR, Macaskie LE (2002) Biochemical basis of microbe-radionuclide interactions. In: Keith-Roach MJ, Livens FR (eds) Interactions of microorganisms with radionuclides. Elsevier Science, Oxford, pp 313–342
66. Edgington DN, Robbins JA, Colman SM, Orlandini KA, Gustin MP (1996) Uranium-series disequilibrium, sedimentation, diatom frustules, and paleoclimate change in lake Baikal. Earth Planet Sci Lett 142(1-2):29–42
67. Beitinger E (1998) Permeable treatment walls – design, construction and costs, NATO/CCMS pilot study. Evaluation of demonstrated and emerging technologies for the treatment of contaminated land and groundwater (Phase III), 1998 special session. Treatment walls and permeable reactive barriers., vol. 229. North Atlantic treaty organisation, Vienna, Austria, pp 6–16
68. Beitinger E, Bütow E (1997) Konstruktive und herstellungstechnische Anforderungen an unterirdische, durchströmte Reinigungswände zur in-situ Dekontamination. In: Lühr HP (ed) Grundwassersanierung 1997. Erich Schmidt Berlin, pp 342–356
69. Smyth DA, Shikaze SG, Cherry JA (1997) Hydraulic performace of permeable barriers for the in situ treatment of contaminated groundwater. Land Contam Reclamation 5(3):131–137
70. Gavaskar AR (1999) Design and construction techniques for permeable reactive barriers. J Hazard Mater 68:41–71
71. Beitinger E (2002) Engineering and operation of groundwater treatment systems – pump-and-treat versus PRBs. In: Simon FG, Meggyes T, McDonald C (eds) Advanced groundwater remediation – active and passive technologies. Thomas Telford, London
72. Meggyes T, Pye N (1995) Cut-off walls. In: Holzlöhner U, August H, Meggyes T, Brune M (eds) Landfill liner systems. Federal Institute of Materials Research and Testing (BAM), Berlin, Solid and Hazardous Waste Research Unit, The University of Newcastle, Penshaw Press, Sunderland, UK, pp N1–28
73. Meggyes T, Simon FG (2000) Removal of organic and inorganic pollutants from groundwater using permeable reactive barriers. Land Contam Reclamation 8(3):175–187
74. Simon FG, Meggyes T, Tünnermeier T (2002) Groundwater remediation using active and passive processes. In: Simon FG, Meggyes T, McDonald C (eds) Advanced groundwater remediation – active and passive technologies. Thomas Telford, London, pp 3–34
75. Jessberger HL (1992) ITVA Arbeitspapier Dichtwände
76. Day SR, O'Hannesin SF, Marsden L (1999) Geotechnical techniques for the construction of reactive barriers. J Hazard Mater B67:285–297
77. Freethey GW, Naftz DL, Rowland RC, Davis JA (2002) Deep aquifer remediation tools: theory, design, and performance modeling. In: Naftz DL, Morrison SJ, Davis JA, Fuller CC (eds) Handbook of groundwater remediation using permeable reactive barriers. Academic, San Diego, pp 133–161
78. Golder associates Ltd. (1998) Active containment: combined treatment and containment systems. Department of the environment, transport and the regions, London, ISBN 185112 114 5
79. Wilson RD, Mackay DM (1997) Arrays of unpumped wells: an alternative to permeable walls for in situ treatment. Proceedings of international containment technology conference. St. Petersburg, FL, USA, pp 888–894
80. Murdoch L, Slack B, Siegrist B, Vesper S, Meiggs T (1997) Advanced hydraulic fracturing methods to create in situ reactive barriers. International containment technology conference. St. Petersburg, FA, USA, pp 445–451
81. Cunningham A, Warwood B, Sturmann P, Horrigan K, James G, Costerton JW, Hiebert R (1997) Biofilm processes in porous media – practical applications. In: Amy PS, Haldeman DL (eds) The microbiology of the terrestrial deep surface. Lewis, Boca Raton, pp 325–344
82. Cunningham AB, Characklis WG, Abedeen F, Crawford D (1991) Influence of biofilm accumulation on porous media hydrodynamics. Environ Sci Technol 25(7):1305–1311

83. Cunningham AB, Sharp RR, Hiebert R, James G (2003) Subsurface biofilm barriers for the containment and remediation of contaminated groundwater. Biorem J 7(3–4):151–164
84. Sharp RR, Cunningham A (1998) Fundamentals of biobarriers, design, development and activity. Subsurface barrier technology. International Business Communications, Tucson, AZ, USA
85. Spinnler GE, Salanitro JP, Manner PM (2004) In situ remediation of groundwater contaminated with MTBE and TBA using a biobarrier. 1st International symposium on permeable reactive barriers (PRB-Net 2004). Belfast
86. Rasmussen G (2002) Sorption and biodegradation of creosote compounds in permeable reactive barriers. Ph.D. thesis, Agricultural University of Norway
87. Gavaskar A, Gupta N, Sass B, Janosy R, Hicks J (2000) Design guidance for application of permeable reactive barriers for groundwater remediation, Final report. Battelle, Columbus, Ohio
88. Sivavec T, Krug T, Berry-Spark K, Focht R (2002) Performance monitoring of a permeable reactive barrier at the Somersworth, NH landfill superfund site. In: Simon FG, Meggyes T, McDonald C (eds) Advanced groundwater remediation – active and passive technologies. Thomas Telford, London
89. Burmeier H, Birke V, Ebert M, Finkel M, Rosenau D, Schad H (2006) Anwendung von durchströmten Reinigungswänden zur Sanierung von Altlasten. Universität Lüneburg, Fakultät III, Campus Suderburg, Handbuch, BMBF-Vorhaben 0271241
90. Feigl V, Anton A, Fekete F, Gruiz K (2009) Combined chemical and phytostabilization: field application. Land Contam Reclamation 17(3–4):577–584, Special edition by Gruiz K, Meggyes T: Innovative decision-support tools for risk-based environmental management
91. Gruiz K, Molnár M, Fenyvesi É (2009) Verification tool for in situ soil remediation. Land Contam Reclamation 17(3–4):661–684, Special edition by Gruiz K, Meggyes T: Innovative decision-support tools for risk-based environmental management
92. Gruiz K (2009) In situ soil remediation: the reactor approach. Land Contam Reclamation 17(3-4):553–575, Special edition by Gruiz K, Meggyes T: Innovative decision-support tools for risk-based environmental management
93. Sharma HD, Reddy KR (2004) Geoenvironmental engineering – site remediation, waste containment, and emerging waste management technologies. Wiley, Hoboken, NJ
94. Reddy KR, Cameselle C (2009) Electrochemical remediation technologies for polluted soils, sediments and groundwater. Wiley, Hoboken, NJ
95. Gregolec G, Roehl KE, Czurda K (2005) Electrokinetic techniques. In: Roehl KE, Meggyes T, Simon FG, Stewart DI (eds) Long-term performance of permeable reactive barriers, trace metals and other contaminants in the environment, vol 7. Elsevier, Amsterdam, pp 183–209
96. Acar YB, Alshawabkeh AN (1993) Principles of electrokinetic remediation. Environ Sci Technol 27:2638–2647
97. Acar YB, Alshawabkeh AN (1996) Electrokinetic remediation. I: pilot-scale tests with lead-spiked kaolinite. J Geotech Eng 122:173–185
98. Acar YB, Alshawabkeh AN (1996) Electrokinetic remediation. II: theoretical model. J Geotech Eng 122:186–196
99. Ottosen LM, Hansen HK, Jensen PE (2009) Electrochemical removal of heavy metals. In: Reddy KR, Cameselle C (eds) Electrochemical remediation technologies for polluted soils, sediments and groundwater. Wiley, Hoboken, NJ, pp 97–126
100. Korolev VA (2009) Electrochemical removal of radionuclides. In: Reddy KR, Cameselle C (eds) Electrochemical remediation technologies for polluted soils, sediments and groundwater. Wiley, Hoboken, NJ, pp 127–135
101. Alexakhin RM (2009) Remediation of areas contaminated after radiation accidents. In: Voigt G, Fesenko S (eds) Remediation of contaminated environments. Radioactivity in the environment, vol 14. Elsevier, Oxford, pp 177–222
102. Danesi PR (2009) Remediation of sites contaminated by nuclear weapons tests. In: Voigt G, Fesenko S (eds) Remediation of contaminated environments. Radioactivity in the environment, vol 14. Elsevier, Oxford, pp 223–261
103. Korolev VA, Barkhatova YE, Shevtsova EV (2007) Elektrokinetic remediation of radionuclide-contaminated soils. Proceedings of the 6th symposium on Electrokinetic Remediation (EREM-2007). Vigo, Spain, pp 169–170
104. Kim G-N, Oh W-Z, Won H-J, Kim M-G (2003) TRIGA soil decontamination by electrokinetic method. Proceedings of the international conference on radioactive waste management and environmental remediation, ICEM '03. Oxford, UK, pp 1491–1497
105. Kim K-W, Lee K-Y, Kim S-O (2009) Electrokinetic remediation of mixed metal contaminants. In: Voigt G, Fesenko S (eds) Remediation of contaminated environments. Radioactivity in the environment, vol 14. Elsevier, Oxford, pp 287–313
106. Reddy KR, Chinthamreddy S (2004) Enhanced electrokinetic remediation of heavy metals in glacial till soils using different electrolyte solutions. J Environ Eng 130(4):442–455
107. Athmer CJ (2009) Cost estimates for electrokinetic remediation. In: Reddy KR, Cameselle C (eds) Electrochemical remediation technologies for polluted soils, sediments and groundwater. Wiley, Hobooken, NJ, pp 583–587
108. Gruiz K (2009) Soil bioremediation – a bioengineering tool. Land Contam Reclamation 17(3–4):543–551, Special edition by Gruiz K, Meggyes T: Innovative decision-support tools for risk-based environmental management
109. Zhu YG, Chen BD (2009) Principles and technologies for remediation of uranium-contaminated environments. In: Voigt G, Fesenko S (eds) Remediation of contaminated environments. Radioactivity in the environment, vol 14. Elsevier, Oxford, pp 357–374

Books and Reviews

Burmeier H, Birke V, Ebert M, Finkel M, Rosenau D, Schad H (2006) Anwendung von durchströmten Reinigungswänden zur Sanierung von Altlasten. Universität Lüneburg, Fakultät III, Campus Suderburg, Handbuch, BMBF-Vorhaben 0271241

Gavrilescu M, Pavel LV, Cretescu I (2009) Characterization and remediation of soils contaminated with uranium (review). J Hazard Mater 163:475–510

Henderson AD, Demond AH (2007) Long-term performance of zero-valent iron permeable reactive barriers: a critical review. Environ Eng Sci 24:401–423

Naftz DL, Morrison SJ, Davis JA, Fuller CC (2002) Handbook of groundwater remediation using permeable reactive barriers, application to radionuclides, trace metals and nutrients. Academic, San Diego

Nkosi D, Miller G (2002) Breaking new ground – mining, minerals, and sustainable development. International Institute for environment and development and world business council for sustainable development. Earthscan, London

Reddy KR, Cameselle C (2009) Electrochemical remediation technologies for polluted soils, sediments and groundwater. Wiley, Hoboken, NJ

Roehl KE, Meggyes T, Simon FG, Stewart DI (2005) Long-term performance of permeable reactive barriers. In: Nriagu J (ed) Trace metals and other contaminants in the environment, vol 7. Elsevier, Amsterdam

Sharma HD, Reddy KR (2004) Geoenvironmental engineering – site remediation, waste containment, and emerging waste management technologies. Wiley, Hoboken, NJ

Simon FG, Meggyes T, McDonald C (2002) Advanced groundwater remediation – active and passive technologies. Thomas Telford, London

Suthersan S (1996) Remediation engineering: design concepts. Environmental science and engineering series. Lewis, Boca Raton

Voigt G, Fesenko S (2009) Remediation of contaminated environments. In: Baxter MS (ed) Radioactivity in the environment, vol 14. Elsevier, Oxford

Sustainable Remediation: Integrating Risk, Science, and Sustainability Principles

Scott D. Warner[1], Paul W. Hadley[2]
[1]AMEC, Oakland, CA, USA
[2]Department of Toxic Substances Control, California EPA, Sacramento, CA, USA

Article Outline

Glossary
Definition of Subject
Introduction
Science
Risk
Sustainability
Examples of Sustainable Remediation
Summary
Future Directions
Disclaimer
Bibliography

Glossary

Remediation Actions intended to correct a problem, or the implemented solution intended to correct a problem.

Risk The probability of harm.

Risk assessment Formal study and evaluation of risk, often done for contaminated properties and facilities as part of the remediation process.

Sustainability A characteristic of longevity, focusing on social, environmental, and economic factors where conservation of resources is a major objective.

Sustainable remediation Striving to balance the environmental, economic, and social benefits and costs associated with remediation while maintaining a resource conservative approach.

Definition of Subject

The international remediation industry has most recently turned its attention to incorporating sustainability principles and practices into its activities. Great attention is given to developing detailed definitions and quantitative metrics for the social, environmental, and economic aspects of remediation. However, much should be considered and learned from early efforts and influences not only in sustainable remediation but in environmental conservation efforts that appear qualitative in nature but provide observable and real benefit in reducing the actual or potential harm from chemical releases to our environment. The authors discuss some of these early efforts and influences, as well as the benefits of applying sound scientific principles and practices to remediation. These overarching considerations should not be overlooked, as it appears that substantial progress has been made in sustainable remediation even as the remediation industry strives to develop more detailed and quantifiable sustainability metrics.

Introduction

Remediation refers to: (1) actions intended to correct a problem, or (2) the implemented solution intended to correct a problem. Environmental remediation denotes the process and result of removing or lessening the negative impact of pollution or contaminants from environmental media in the subsurface (soil, rock, or groundwater) or above ground (air and surface water). Remediation of contaminated air, land, or water is performed to mitigate risk to human or environmental receptors. If there were no risk, there would likely be little incentive to remedy a situation except for relieving the potential nuisance that may follow such impact. Laws enacted to prevent environmental impact to natural resources, or to clean up pollution, are based on risk of acute or long-term damage to receptors – whether that involves a statistically defensible increase in the development of human cancers, or in the development of aquatic disease or other environmental damage. Regulatory agencies, regardless of jurisdiction, force and oversee remediation measures that are based on meeting the intent of the appropriate legal standard.

Following the enactment of US Federal laws in 1980 with Comprehensive Environmental Response, Compensation, and Liability Act (CERCLA) or Superfund, that focused attention primarily on cleaning up contaminated land and water. Since the early days of Superfund, technology has been used to continuously improve methods to characterize land, groundwater, surface water, and air that have been impacted by contaminants, and to remediate the impacted media. First attempts to clean contaminants from an impacted site primarily relied on removal of the impacted media through gross methods of soil and water removal, for example. Removal actions generally were successful for relatively shallow contaminated soil where urban infrastructure (e.g., buildings, utilities, etc.) did not interfere. As contaminants migrated deeper in the subsurface, or over larger areas, complications in removing all impacted material created conditions that were both extremely expensive to remedy, or were technically impossible to remedy to an appropriate standard within a reasonable time frame.

Regarding impact to groundwater, removal through groundwater pumping often gave a false sense of success, in that early actions appeared to remove substantial volumes of impacted water; however, concentrations of contaminants in groundwater that remained in the subsurface did not lower to legal standards as was initially predicted. In fact, for many sites, contaminants remained in groundwater systems years and decades after groundwater extraction methods were implemented.

Since the early 1990s, remediation methods, particularly for contaminated soil and groundwater, have been focused on removing or destroying as much contaminant as possible using as little resource as possible. That is, methods have been implemented that look to specifically target contaminant reduction in the subsurface without exhuming or extracting the contaminant (so-called in situ methods). This process to use as little energy as possible, or use as little land or other resources to remediate a site, is commonly categorized as being "sustainable" which then mirrors the consideration of "sustainability principles" that have entered many industrial and development processes unrelated to environmental remediation.

Though the term "sustainable" directly refers to a characteristic of longevity, our modern use focuses on conserving, protecting, and balancing ecological resources with human development. Thus, considering remediation, sustainability focuses the practitioner to develop and implement cleanup measures that are not by themselves harmful to ecological resources. (The UK Sustainable remediation Forum (SuRF-UK) www.claire.co.uk/surfuk defines sustainable remediation as "the practice of demonstrating, in terms of environmental, economic and social indicators, that the benefit of undertaking remediation is greater than its impact, and that the optimum remediation solution is selected through the use of a balanced decision-making process.")

Practitioners in the environmental remediation industry have known for some time that the most cost- and technically effective remedies are those that: (1) use scientific principles to accurately characterize the problem to be remedied and (2) are designed using site-specific conditions and objectives, including risk reduction and sustainability enhancement. Considering these concepts, a fully integrated remedy that relies on risk, scientific efficacy, and sustainable principles can be developed. Because sustainability has longevity as its core, the potential for cost-effectiveness also is

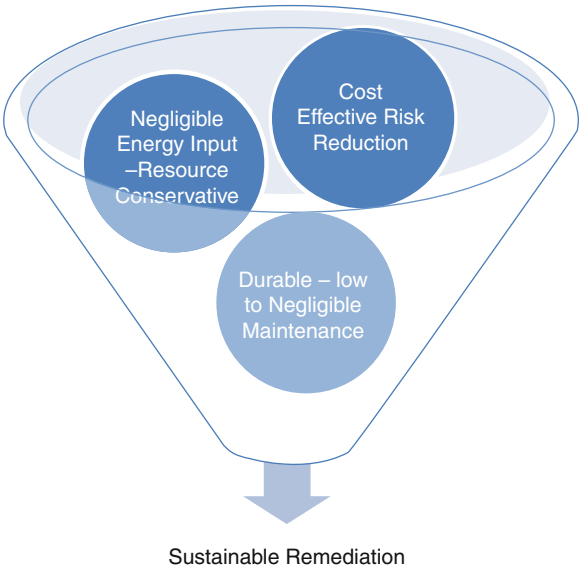

Sustainable Remediation: Integrating Risk, Science, and Sustainability Principles. Figure 1
Components of sustainable remediation

great because for this case, longevity refers to durable and low-maintenance remedies that reduce cost over the life of the project rather than increasing costs with time as what might seem logical for a conventional relationship between time and cost (Fig. 1).

This entry is focused on allowing the reader to better appreciate the benefits of a fully integrated remedy that considers the three pillars of science, risk, and resource conservation in implementing sustainable remediation.

The remainder of this entry is organized to enhance the discussion on various concepts central to applying remediation methods that honor sustainability while using science and risk elements in the method development. This includes presentation of various methods by which "sustainable" remediation can be and has been applied, and resources that are available to assist the designer in developing remediation approaches that incorporate sustainable solutions.

Historical Background

Michael Weinstein, in his 2010 editorial, states that it is impractical to ignore the interactions between managed and natural systems if a sustainable ecosystem is to be maintained [36]. He goes on to note that our focus in this "Age of Humans" – or the Anthrocene – requires us to be better trained in forecasting the consequences of human actions on the natural system if we are to promote a sustainable ecosystem.

This concept has roots that extend far back in time; modern assessments of our requirement to better understand the consequences of our actions extend from Aldo Leopold's treatise on sustainable agriculture in *Sand County Almanac* [15] and Donella Meadows' well-known book of 1972 *The Limits to Growth* [17] to the 1996 development of life cycle analysis (LCA) of remediation approaches as reported to the Ontario Ministry of Environment and Energy (The Ontario Report) [5]. The Ontario Report is remarkable in that it provides one of the earliest recognitions that an LCA of remediation options should include the potential impacts that occur not just at the local scale, but also at regional and global scales from all remediation activities, and not just those activities intended solely to mitigate the site-specific environmental contaminant of concern.

What the early treatment of LCA tells us is the importance of "system boundaries," which essentially is the framework by which a full analysis of life cycle environmental impacts should be made. That is, defining objectives of a project with respect to local site issues, regional secondary items, or larger and less acute global conditions becomes engrained within the sustainability analysis for a remediation project.

Over the next two decades, the concept of sustainability was pushed forward primarily by environmental protection groups through the world. Many of those earlier considerations were established by various United Nations and other global programs. These programs considered economic growth with degradation of resources, population growth with distribution of adequate food and water resources, and even local efforts to increase consumption and use of locally grown and organic products. A 2006 report by the British Broadcasting Company further publicized the critical resource issues of both large and developing countries in North America, Europe, and including India and China did not heed better control and balance over resources and development.

About the time of the BBC report, the Sustainable Remediation Forum (SURF) held its first meeting.

SURF was initiated in the United States to promote the use of sustainable practices during remedial action activities. SURF works to encourage remediation activities that have an objective of balancing economic viability, conserving natural resources and biodiversity, and enhancing the quality of life in surrounding communities. This focus is consistent with the general understanding of sustainability principles, but it applies them to the remediation of contaminated land and water. Just over 20 people attended the first SURF meeting in 2006, but as of this writing the organization has held 17 meetings across the USA, has published several major works and documents in the literature of the remediation industry, and has inspired the creation of several sustainable remediation groups outside the USA.

Although developments in greener design processes in environmental engineering were finding more acceptance in both standard texts (e.g., [18]) and in the later developments of sustainability-based texts on environmental engineering [19], the SURF group in the USA and Europe brought to the forefront the several remediation practices, such as bioremediation, passive in situ treatment, and targeted and focused remediation approaches, that had begun in the mid-1990s and early 2000s but had not been described by sustainability doctrine. These earlier "resource conservative" remedies had effectively reduced the amount of groundwater to be removed (by using hydraulically passive remedies) and the amount of contaminated soil to be excavated. However, the actual sustainable benefits were qualitative in description, rather than quantitative, as is the current trend. The work by SURF to bring these concepts together helped to elevate this consideration in developing remediation plans. Elements of these concepts also are finely exemplified by several case studies that show the incorporation of sustainability principles with environmental engineering education and practice as summarized by Mihelcic and Trotz [20]. Mihelcic and Trotz additionally are effective in pointing out that many practitioners readily understand how their current approaches to projects already fit into the overarching theme of sustainability, while other practitioners find ways to expand their projects to be consistent with sustainability principles once those principles and guidelines are defined and illustrated.

More recently, numerical evaluation tools and models have been established to assist with quantifying the potential sustainable benefits of a remediation action, and to allow comparison of different remedies in terms of resource use (energy, water, air emissions, etc.) for LCAs. Information specific to these tools, which are used both by practitioners and others looking for general comparison methods, however, are not the subject of this entry.

Principle to Application

As the trend in applying sustainability principles to environmental remediation projects continued to progress, the specifics of an application required the creation of accurate objectives, benchmarks, boundaries, and performance metrics. Developing an appropriate remedy relies on first evaluating and qualifying the potential effects that different components from both the contaminant release and potentially the contaminant remedy have on the overall environmental impact of a contaminant release.

The triple bottom line refers to total influence of a remedy with respect to environmental, economic, and social considerations. This concept allows the engineering, regulatory, and public reviewers of a remediation approach to evaluate the positive and negative impacts that a given remedy will promote when implemented, and further provides a method to categorize system boundaries and impacts from acute to chronic.

For this usage, the potential total environmental impact can be negated by the successful implementation of a remedy that is equal, but opposite in impact, to the negative consequences of a contaminant release. However, the remedial success can itself be impacted by conditions that either render it less effective, or add negative impacts (perhaps as unintended consequences) to the remediation attempt. It is possible that no efforts will successfully improve a selected remedy, resulting in the need to select a different and more effective remedy.

Considerable attention is being given to quantifying both the positive and negative (generally unintended) effects of remediation projects as the field of sustainable remediation continues to develop. The aim is to develop approaches for understanding and predicting the positive and negative effects of remediation

projects so that projects of most benefit – as evaluated with regards to both positive and negative effects associated with environmental, economic, and social considerations – are designed and implemented. Researchers and remediation professionals are studying and debating what factors contribute most to the sustainability (or unsustainability) of a remediation project. Their goal is to establish metrics for quantifying those factors, both for evaluating a given project as well as for comparing different projects to one another. With all the various activities that go into a remediation project – from initial sampling and assessment through planning, construction, implementation, and operation and maintenance of a remedy – finding a single metric for directly and simply comparing the impacts of all such activities has proven to be quite a challenge.

The following paragraphs further the relationship among factors of science, risk, and sustainability when considering approaches in environmental remediation. Although sustainable remediation is typically described and discussed as a relatively new and self-contained discipline, it is practiced and implemented in the context of an industry that will continue to co-evolve with developments in science and risk assessment. Implementing the best scientific practices and making decisions most supportable by risk assessments are not typically considered core elements of sustainable remediation. However, the opposite situation – relying on inferior scientific practices and not considering risk – clearly introduces inaccuracy, inefficiency, and ineffectiveness that would be considered by most people as increasing the unsustainability of any remediation project. As such, science, risk, and sustainability are linked when discussing environmental remediation.

Science

Advances in science are inevitable. Many of the activities so common in today's remediation industry were once viewed as breakthroughs. Most prominent in this arena are advances in analytical techniques and instrumentation that have spawned whole programs and technology categories in the remediation industry.

Internet stories and blogs, newspaper articles, and television broadcasts frequently relay the recent detection of a common industrial chemical in the environment, in living creatures, or even in drinking water supplies. Indeed, much of the current remediation industry's focus began in the 1970s when testing of drinking water supplies was expanded beyond common analytes such as nitrate and coliform bacteria, and included industrial chemicals such as trichloroethylene (TCE). With (the then) recently advanced analytical capabilities of the 1970s, industrial chemicals could now be commonly detected in far-flung environments such as the polar ice cap, mammals, fish, soil, and drinking water supplies at parts-per-billion (ppb) levels. Equally important, toxicity testing and analysis for industrial chemicals could also be done or extrapolated to this same analytical region.

While much of the remediation industry was developed in the 1970s as a result of the alarming widespread occurrence of chlorinated solvents in drinking water supplies relying on groundwater, the same pattern played out in a similar fashion as recently as the 1990s. Perchlorate is a compound commonly used in explosives, flares, and solid rocket propellants because of its oxidizing properties. Once viewed as essentially a salt of little or no consequence to public health and the environment, it become a cause or concern because of its potential toxicity. Around that same time, increased analytical capabilities allowed for perchlorate to be detected not just in parts-per-million (ppm) levels, but well down into the ppb range. As had happened some 40 years previously with chlorinated solvents, newspaper and television reports were again alerting the public to the presence of low levels of perchlorate in the environment, in drinking water, and even in foods that constitute a significant portion of a healthy diet.

Along with the detection of perchlorate in drinking water and the food supply came an immediate and intense re-evaluation of its potential toxicity. While a great national debate ensued, eventually state and federal regulatory jurisdictions established regulatory levels for perchlorate in the 1–30 ppb range, roughly three orders of magnitude lower than the historical detection levels.

Advances in analytical techniques have not been limited to the mere detection of individual chemicals. By the 1990s, it was becoming clear that while most scientists had previously considered chlorinated

industrial chemicals to be highly persistent and recalcitrant, even highly chlorinated solvent compounds such as TCE were now observed to be naturally biodegrading at some remediation sites. Indeed, it soon became clear that the presence of two compounds in particular – *cis*-1,2 dichloroethylene (*cis*−1,2–DCE) and vinyl chloride (VC) – were chemical markers of sequential microbial dehalogenation of the parent compound TCE.

The recognition that even TCE could, in some circumstances, be completely degraded by microorganisms to the innocuous end products of carbon dioxide and chloride ion gave rise to a new branch of the remediation industry focused on effecting complete biodegradation of objectionable chemicals, preferably in situ. Commensurate with the growth and development of bioremediation for application to waste sites was an increased opportunity for transfer of biochemical and molecular technologies from other fields of microbiology. Today analytical tools once common only in research laboratories are frequently used to detect, count, and speciate microorganisms capable of carrying out biodegradation. In fact, whereas the remediation industry once labored to merely detect compounds like TCE and its breakdown products, it is now becoming cost-effective to determine the presence of microorganisms, their DNA sequences, and their enzymes capable of carrying out the degradation process. Clearly this reflects a quantum leap in the power and sophistication of analytical techniques and tools available for evaluating waste sites.

While advances in analytical chemistry have clearly fueled the growth and development of the remediation industry, perhaps is the most critical endeavor the struggle to keep up with the need to make sense of all these measurements through application of scientific principles and practices. With increasing analytical power and ease of making measurements, it has become apparent that contaminants in the environment are highly variable in their spatial and temporal distributions. This has given rise to successive or side-by-side measurements of the same medium (typically soil, but also common for groundwater) for the same compound that vary by orders of magnitude. And with that common disparity in nearby measurements has come the conundrum of how to interpret the sampling results.

The variability in measurements commonly made at contaminated sites has long been recognized [6, 14, 21, 26, 31]. One common outcome of this variability is a regulatory response that effectively makes "every sample a site [13]." The consequences of this approach have been shown to possibly result in many orders of magnitude range in determination of risk and in the resulting costs for remediation. In other cases, extremely expensive remediation projects have been undertaken without clear and relevant objectives, typically to disappointing results [23].

So while a clear tenet and foundation of scientific undertakings is to have quantifiable objectives and testable hypotheses, those principles have not always found their way into practice in the remediation industry.

Risk

"Risk" in the remediation industry is generally understood to mean the probability of harm occurring to living organisms associated with exposure to toxic chemicals. Humans are usually the organisms (biological receptors) of most concern associated with waste sites, though in many instances other species are more likely to be exposed and therefore harmed. At remote sites with little human access it is not uncommon that fowl, mammals, or invertebrates rely on the contaminated area as habitat.

The toxic effects of industrial chemicals on biological receptors are known and widely accepted in only a handful of instances. Benzene, for example, and vinyl chloride are widely accepted as potent human carcinogens. However, for the vast majority of chemicals in commerce the potentially toxic effects on humans or most other species are derived by extrapolation of results from laboratory animals, typically mice or rats. As a consequence, not only are there a range of toxic effects that are being estimated by extrapolation, but the levels of exposure at which those effects might be manifest are estimated by extrapolation. Typically toxic effects are induced in laboratory animals at relatively "high" dosages, and then the "low" dosages at which such effects would not have occurred are estimated and then extrapolated to other species. It falls to state and federal regulatory agencies to utilize, develop, or even adopt the results of toxicity testing

and identify the levels of exposure that would lead to regulatory action.

A long history of academic, regulatory, and even industrial testing of chemicals for their toxic effects exists. This history also includes methods by which test results for environmental receptors have been extrapolated and interpreted. The field of contaminated site remediation, however, requires even more challenging extrapolations. Potentially hazardous chemicals in soil and groundwater are likely not presently giving rise to exposure to humans or other biological receptors. However, from well-accepted principles of environmental fate and transport, as well as the remediation industry's firsthand experiences, unmanaged contamination more likely will result in human and general environmental exposure. Thus the "risk assessment process" as applied to contaminated sites relies on projections and predictions of potential exposures to contamination on-site that might occur in the future and, often, at some distance from the current location of the contamination.

The application of the risk assessment process for hazardous waste sites has in many instances become a substantial and expensive undertaking. In light of the variability common in environmental data, the extrapolations from testing on laboratory animals to humans, and the projections and predictions that are part and parcel of the risk assessment process at waste sites, the effort of deciding with any certainty what course of action to take can become quite daunting.

Despite the sometimes overwhelming task of characterizing environmental contamination and making the predictions and projections associated with risk assessments, progress has been made through the development and application of conceptual site models (CSMs). CSMs have been developed for many of the common contamination problems associated with waste sites that can serve to not only guide the characterization efforts but also integrate considerations of risk [1, 8, 16, 24, 28]. Utilization of CSMs for development of site characterization efforts, risk assessment, and even establishment of remediation goals has been a challenge for the remediation industry at large. However, progress has been made on even complex contamination sites of the elements by utilizing a CSM for integrating the complexities of site characterization and the risk assessment process.

Sustainability

The potentially devastating effects of global climate change have been a growing concern for more than a decade. That concern has launched an international focus on managing and reducing the emissions of global warming gases from human sources, particularly those associated with the industrial consumption of fossil fuels.

Concern about global warming has led to the realization that human activity has imposed an important and substantial impact on the earth's resources, many of which are at the point of depletion and even exhaustion. As a result, virtually every segment of modern society has been reviewing its practices with an eye toward reducing not just the emission of global warming gases but also the overall burden on the environment. Virtually every segment of modern society – from governments to families – is at least evaluating how to become more sustainable and less impactful on the environment.

The remediation industry is in a unique situation in that its primary efforts are directed at dealing with the effects of industrial pollution from the beginning. The remediation industry has developed countless approaches and technologies for detecting and then addressing contamination in soil, water, and sediments. Historically, the remediation industry has favored energy-intensive engineered systems that remove and treat contaminants from the impacted media as quickly as possible. Amid growing awareness that these kinds of energy-intensive remediation projects have not often achieved the desired results, and have sometimes had their own unintended environmental impacts, sustainability principles have been brought to the remediation industry relatively recently, primarily by representatives of the industry themselves.

Sustainability, in its broadest context, relies on the precept of balancing the social, environmental, and economic costs and benefits of an undertaking. Sustainable remediation has the same goal [32]. However, sustainable remediation has the additional challenges of characterizing, evaluating, and remediating sometimes highly complex occurrences of environmental contamination, usually including considerations from complicated risk assessments. The sustainable remediation industry must concern itself not only with not

continuing the negative effects of the traditional energy-intensive remediation technologies, but also with addressing the challenges of characterizing and evaluating complex contamination situations in the first place.

The previous sections presented two of the important roles that science has to play in the remediation industry: making environmental measurements and interpreting the results with respect to human health and the environment. The previous sections also illustrated how risk – or more properly, risk assessment – has notable challenges. The first challenge is to identify the unsafe levels of exposure (doses) of toxic chemicals to humans and other biological receptors. The second challenge is to provide an analysis as to how contamination on a particular property might reasonably be expected to result in exposure to humans or other biological receptors. A nexus for integrating these two challenges is the utilization of a CSM, not so much for finding contamination, as it is commonly utilized, but for finding the exposure that might reasonably or realistically occur. At its best a CSM defines the problem to solve and then sets the remediation objectives. As mentioned earlier, the lack of clear remediation objectives is an all too common attribute of unsuccessful remediation projects [23].

Not unlike other remediation projects, sustainable remediation requires that the problem to be solved through remediation be defined initially as quantitative as possible. This can be problematic, even for simple contamination situations [13]. However, with consideration of the environmental impacts of the remedy, a new approach to remediation metrics arises. Where historically an energy-intensive remedy might have been implemented based on the projected time to cleanup and cost, a consideration such as the potential carbon footprint of the remedy might cause one to rethink the overall benefit of that particular cleanup approach.

While still in its inception, sustainable remediation principles are having an effect on how remedies are implemented. Examples of sustainable practices include:

- Using treated groundwater for irrigation purposes instead of the historical approach of discharging the water to a sewer
- Rethinking the benefit of an energy-intensive remediation technology that is emitting tons of carbon dioxide for every few pounds of contaminants removed
- Evaluating the carbon footprint of excavation and redisposal projects along with similar analysis of on-site remedies
- Considering the impact of remediation equipment and activities on sensitive habitat, as was done in the case of the response to the Gulf oil spill [25]

CSMs, in recent practice, have allowed the integration of science and risk assessment to address the challenges inherent in remediation of environmental contamination. In their simplest form, CSMs are pictures of the contamination conditions that pose insignificant risk, and therefore, with an understanding if that condition is exceeded or not, the CSMs give the remediation goals.

With the advent of sustainable remediation as a practice, CSMs can be viewed as being augmented with the analysis of the environmental impacts of the remedy. In the simplest of examples, this can be an analysis of the carbon dioxide emission of various remedies per pound of contaminant removed, along with the projected time to effect a complete remediation. To an extent this would provide a metric (tons of carbon dioxide emitted per pound of contaminant removed) that might give a more complete and balanced view of what remedy might be most environmentally sustainable.

Examples of Sustainable Remediation

Sustainability principles have been incorporated in various projects across the USA for the past 2 decades, although many of these projects were not labeled under "sustainability" which is a more recent phenomenon within the remediation practice. Considering that many examples of sustainable remediation projects typically are not published within the general literature until several years after project implementation, we anticipate that many more examples will be available in written form over the next several years. For highlighting various examples of sustainable remediation, the following examples of sustainability principles being incorporated into a range of cleanup programs and projects are presented below.

SURF 2009

The Sustainable Remediation Forum (SURF) prepared a publication on the application of sustainability principles and practices at remediation projects [32]. SURF, in that publication, identified 42 occurrences where sustainability principles and practices had been incorporated into traditional remediation projects. The projects spanned all ten USEPA Regions.

Many of the 42 projects considered optimization schemes for not only improving performance but for reducing energy-related costs and ancillary environmental impacts. Use of alternative energy sources, selection of in situ remedies to enhance or supplant traditional pump and treat remedies for groundwater, and reliance on institutional controls to allow on-site management of contaminated soils are prominent in the examples given by SURF.

Among the more treatment-oriented projects reported by SURF included permeable barriers for contaminated groundwater and utilization of zero valent iron (ZVI) in combination with clay to treat a chlorinated solvent source zone. Treatment of groundwater and especially the source zones associated with disposal have been major challenges for conventional energy-intensive remediation technologies. A very telling sign is that successful remediation technologies exist for these two highly challenging problems and that these technologies operate passively and far more sustainably than conventional energy-intensive approaches.

SURF 2011

Additional publications from SURF [9] include more examples where sustainability principles and practices have been incorporated. These examples include:

1. *Type of site*: Station site
   Type of analysis: Carbon footprint analysis of existing soil vapor extraction (SVE) system, performing at reduced efficiency after prolonged operation
   Findings/outcome: The SVE system was expending approximately 32 times more fuel than was being removed, creating significant air emissions; the study highlights the importance of looking at whole-systems environmental considerations to avoid disproportionate impacts from remediation versus benefits.
2. *Type of site*: Petroleum contamination
   Type of analysis: Focused sustainability analysis to evaluate greenhouse gas emissions from four alternative remedies to an existing pump-and-treat system, which also included estimates of the time to reach remediation objective for each alternative
   Findings/outcome: Selected a passive aerobic bioremediation approach based on both the time to accomplish remediation and the reduced greenhouse gas emissions for this alternative.
3. *Type of site*: Manufacturing facility with chlorinated solvents in groundwater and intrusion of contamination into nearby surface water and sediments
   Type of analysis: In-depth life cycle assessment (LCA) of greenhouse gases, criteria pollutants, energy demand and marine ecotoxicity of several remedial alternatives
   Findings/outcome: PRBs were selected as the preferred groundwater remedy. Thin-layer sediment placement was selected as a capping mechanism for the nearby contaminated sediments based on the availability of local, clean sediment for that purpose.
4. *Type of site*: Polychlorinated biphenyls (PCBs) in river sediments
   Type of analysis: Compared potential worker fatality for selected sediment remediation alternatives with worker potential risk to human receptors from multiple pathways and exposure scenarios
   Findings/outcome: For this particular project both the risks to workers (up to one incident/fatality per four workers) and human receptors (up to two increased incidents of cancer per hundred persons exposed) were evaluated as "high"; while worker risk and cancer risk are not directly comparable, both are important considerations in development and selection of a remediation strategy.
5. *Type of site*: Lead in soil
   Type of analysis: Consideration of demand for heavy equipment associated with various remedial alternatives and the resulting air emissions from fuel usage

Findings/outcome: Stabilization of impacted soil was the preferred alternative, allowing for disposal of the soil as non-hazardous at a local landfill and avoiding 150,000 miles of truck travel and its associated air emissions.

The examples provided by Holland et al. [9] illustrate the range in approaches to evaluating sustainability. While in some instances an in-depth LCA is undertaken, in other instances relatively straightforward comparison of key parameters – such as miles traveled – is relied upon. As practitioners continue to incorporate sustainability principles and practices into their work, it is hoped that an experience base will develop that allows matching of the appropriate level of analysis with the problem at hand. At this juncture, however, the determination as to how involved a sustainability analysis is warranted is generally left to professional judgment, as well as to the cost considerations associated with sustainability studies.

United States Army Corps of Engineers Interim Guidance on Green and Sustainable Remediation

The United States government is conducting what is undoubtedly the largest collective remediation effort in the world. Vast properties and huge facilities operated over the last 150 years are part of the current cleanup operations to deal with the environmental legacies of past practices that span the entire United States, as well as overseas. Much of the federal cleanup is conducted on current and former military bases and properties. And much of those activities are managed and overseen by the United States Army Corps of Engineers (USACE).

The USACE, in March 2010, provided draft guidance on incorporating green and sustainable practices into cleanup projects [33]. This guidance is significant in many ways. First, because it is primarily intended for use at formerly used defense sites (FUDS) overseen by the USACE, it will find use across the United States as well as abroad. Secondly, because FUDS occur all across the United States and engage the broadest range of state and federal environmental regulatory programs, the green and sustainable remediation practices proposed and enacted through this guidance should engage the entire spectrum of environmental regulatory agencies in the United States. This alone will have a beneficial influence on the remediation industry. The draft Guidance, to that end, includes detail to crosswalk the prevailing regulatory paradigms for cleanup with the principles and practices of green and sustainable remediation.

Lastly, the draft Guidance provides additional thumbnail sketches of projects where green and sustainable principles and practices were incorporated, directs practitioners to quantitative tools for evaluating alternatives, and provides project management aides as well as support for incorporating green and sustainable principles and practices into contracts for cleanup. As such the USACE draft Guidance provides a major impetus and direction for continuing to incorporate sustainable remediation principles and practices into some of the largest remediation efforts in the world.

USEPA Analysis of Facility in East Palo Alto, California

The Romic Environmental Technologies Corporation (Romic) facility is a former hazardous waste management facility in East Palo Alto, California, USA. This site has been the subject of site investigation and remediation activities, most of which occurred prior to the current national interest in green and sustainable remediation. However, because of the detail available on the facility and the environmental cleanup activities, this case provides a comprehensive study opportunity to look in hindsight at the cleanup options considered and implemented.

USEPA [34] considered the footprints of 15 environmental parameters for implementing alternative remedies. The three alternatives considered involved in situ bioremediation, pump and treat, and hybrid implementation of the two alternatives. The footprint contributions include on-site activities, transportation, and non-transportation offsite activities. The USEPA study embraced a life-cycle perspective of the remedial alternatives considered, particularly with regard to off-site activities such as manufacturing of remediation-related materials that would be considered as having environmental footprints "upstream" of the actual remediation project.

A key outcome of the USEPA evaluation was that all of the categories of activities considered – including on-site activities, transportation and

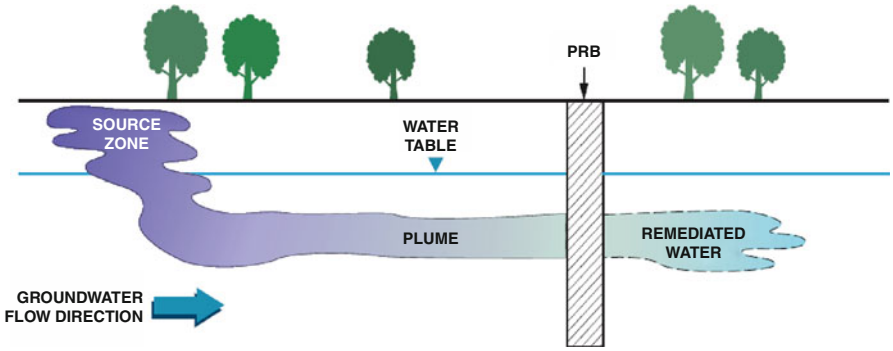

Sustainable Remediation: Integrating Risk, Science, and Sustainability Principles. Figure 2
General concept of a PRB for treating a plume of contaminated groundwater

non-transportation off-site activities – have the potential to contribute significantly to the environmental footprints of cleanup projects. Thus, all types of activities merit evaluation.

The remedial design for the project is considered to have substantially influenced the environmental footprint of a remedy. Combined with the observation that activities "upstream and beyond the fenceline" of a remediation project can contribute significantly to the environmental footprint, there is clear support for the efforts embodied in green and sustainable remediation in looking quite broadly beyond the traditional parameters associated with remedy design that focus primarily on on-site activities and their costs.

Permeable Reactive Barriers

Since the early 1990s, the advent, development, and progression of hydraulically passive in situ remedies for groundwater contamination has created treatment methods that have evolved from being "innovative" to those considered accepted and mature for the treatment of industrial contaminants. The permeable reactive barrier (PRB) technology, which has been the focus of hundreds if not thousands of technical articles and publications (e.g., [10–12, 22, 27, 29, 30]), is considered a "remediation concept" whereby affected groundwater is allowed to flow through, or is routed through, an emplaced subsurface zone of treatment media that has geochemical or biochemical properties appropriate for either destroying, immobilizing, or altering the molecular form of the contaminant sufficiently to render it harmless (Fig. 2).

Early versions of the PRB concept included the use of limestone as a component of reactive media to assist with neutralizing acidic water created from mine tailings piles ([2]; updates for the use of PRBs for mining sites are provided by the Interstate Technology Regulatory Council [ITRC] at: http://www.itrcweb.org/miningwaste-guidance/to_permeable.htm#case_study); the first commercial PRB using granular iron metal was constructed in 1994 to destroy chlorinated aliphatic compounds in groundwater [35] following the development of the technology by researchers at the University of Waterloo [7], and a number of pilot tests of PRBs for treating radioactive constituents in groundwater were attempted in the mid- to late 1990s [22]. Reasonably, it makes sense that since the early 1990s, several hundred pilot tests and a substantial number of full-scale remedies involving the PRB concept have been implemented worldwide, including a recent example at a former US nuclear fuel reprocessing facility [4].

The PRB concept is attractive as a sustainable remediation approach because no groundwater is removed from an aquifer (groundwater flows passively and contaminants migrate advectively through the subsurface treatment system) and no energy is supplied to power pumps or other devices. Over the lifetime of a PRB, which can be decades (the current oldest system is approximately 15 years), water and energy savings are substantial. However, PRBs are constructed systems that do require infrastructure and transportation of

materials which can produce emissions of greenhouse gases and use of recourses. This is where the balance of LSA considerations is important, and consideration of the benefits of the various attributes of risk mitigation with long-term resource conservation, even if short-term resource consumption is required, could be quantified for making an informed decision on implementation of this technology.

The ability to use PRBs, or any other remedy to treat or destroy mobile toxic constituents is dependent on many issues, including cost and constructability, but notably, effective and complete site characterization. Advances in PRB development, particularly in the use of natural materials, and in assessing the effective longevity of PRB materials will continue to develop and provide practitioners with a bevy of new options intended to be highly effective, and highly cost-efficient.

Because this is a passive technology that is not easily adjusted once installed, an accurate conceptual model must be developed and the most important data gaps must be filled before a PRB can be designed. A PRB will fail to meet project objectives, and thus be considered a failure, if it is designed based on data that are incomplete and/or inaccurate. The PRB may not be the correct remedy to select for many contaminant remediation schemes. However, the several decades of experience that the remediation profession has with the PRB technology open up many more potential opportunities for reducing cost, impact, and secondary treatment issues that characterize the difficulty in mitigating contaminant plumes.

Technologies for implementing PRBs will continue to improve and develop (such as injection and deep well PRB installation). The benefits of not having to pump groundwater or supply ongoing energy for treatment will be the primary drivers for the development of such new technologies. We also will find that more natural materials effectively create geochemical conditions that remove a contaminant from the flow field or alter its chemical makeup to less harmful forms. These developments will increase the sustainability of a remediation technology class that, in addition to demonstrated performance characteristics, has the desirable attribute of being passive in nature and, once installed, requires no additional energy inputs for operation.

Summary

Many considerations go into remedial decision making. Some of the key roles of science and risk assessment have been discussed. Other considerations include regulatory requirements, legal constraints, public input, costs, future land use, the availability and reliability of institutional controls, and costs. However, an increasing number of remedies are being evaluated in light of sustainability principles.

The applications of scientific measurements, basic scientific principles, and risk assessment to the practice of environmental remediation have been evolving since the inception of the remediation industry. It is the nature of these fields that they will continue to be developed concerning application to remediation, and breakthroughs will be expected periodically. Similarly, it should be expected that the application of sustainability principles to environmental remediation will continue to evolve, with some breakthroughs occurring from time to time.

Advocates of sustainable remediation are working toward evaluating sustainable practices appropriate and beneficial for environmental remediation. This will include the need to establish metrics that provide a better basis for selection of remedies – metrics that have generally not been sought under the status quo in implementing conventional remediation projects. Even more significantly, those evaluations and sustainability metrics already developed have led to selection of remedies that previously might not even have been considered.

Future Directions

The topic of sustainable remediation has received great attention for more than a decade. As this topic continues to expand – due primarily to a strong need to develop resource conservative, durable, low expense, low footprint, and highly effective remedies for contaminated ground, water and air – the number of opportunities for research and presentation of project examples in the technical literature and at professional conferences is anticipated to grow exponentially. Ideas about sustainable remediation have been and will continue to be linked to the measurements

practitioners make concerning environmental contamination and its consequences. As the technology develops to measure increasingly lower levels of environmental contamination, a tendency that focuses more on the measurements than on the questions they are intended to address may develop but should be discouraged. The authors suggest that advances in scientific practices in remediation should continue concurrently with advances in the practice of sustainable remediation. While acknowledging the challenge that exists in linking the progress in both of these areas, many beneficial linkages will be made through attention to advancing and refining the conceptual site models used to understand environmental contamination and consequences thereof.

Disclaimer

The content and views expressed in this entry are solely those of the authors, and do not reflect the policies or views of the California Department of Toxic Substances Control, AMEC, or any other organization with whom the authors are affiliated.

Bibliography

1. ASTM (2008) Standard guide for developing conceptual site models for contaminated sites, E1689-95, Subcommittee: E47.05, Book of Standards Volume: 11.06
2. Benner SG, Blowes DW, Ptacek CJ (1997) A full-scale porous reactive wall for prevention of acid mine drainage. Ground Water Monit Remed 17(4):99–107
3. British Broadcasting Company (2006) Booming nations threaten earth, BBC News, 12 January
4. Chamberlain J, Michalczak L (2011) Design and installation of a permeable treatment wall at the west valley demonstration project to mitigate expansion of strontium-90 contaminated groundwater – 11138, Waste management symposium Inc, Phoenix, 27 Feb–3 Mar 2011
5. Diamond ML, Page CA, Campbell M, McKenna S (1998) Life cycle framework for contaminated site remediation options: final report. Prepared for Ontario Ministry of Environment and Energy
6. Doctor PG, Gilbert RO (1978) Two studies in variability for soil concentrations: with aliquot size and distance. Selected environmental plutonium research reports of the Nevada Applied Ecology Group (NAEG). Nevada Applied Ecology Group/U.S. Department of Energy, Las Vegas, pp 405–449
7. Gillham RW, O'Hannesin SF (1994) Enhanced degradation of halogenated aliphatics by zero-valent iron. Groundwater 32(6):958–967
8. Hadley PW, Sedman RM (1990) A health-based approach for sampling shallow soils at hazardous waste sites: using the AALsoil contact criterion. Environ Health Perspect 84:203–207
9. Holland K, Lewis R, Tipton K, Karnis S, Dona C, Petrovskis E, Bull L, Taege D, Hook C (2011) Framework for integrating sustainability into remediation projects. Remediation 21(3):7–38
10. Interstate Technology & Regulatory Council (ITRC) (1999a) Regulatory guidance for permeable reactive barriers designed to remediate chlorinated solvents. Interstate Technology Regulatory Council Permeable Reactive Barriers Team, Washington, DC. http://www.itrcweb.org
11. Interstate Technology & Regulatory Council (ITRC) (1999b) Regulatory guidance for permeable reactive barriers designed to remediate inorganics and radionuclide contamination. PRB-3. Interstate Technology & Regulatory Council, Permeable Reactive Barriers Team, Washington, DC. www.itrcweb.org
12. Interstate Technology & Regulatory Council (ITRC) (2005) Permeable reactive barriers: lessons learned/new directions. Interstate Technology Regulatory Council Permeable Reactive Barriers Team, Washington, DC. http://www.itrcweb.org
13. Interstate Technology and Regulatory Council (ITRC) (2008) Use or risk assessment in management of contaminated sites. RISK-2. Interstate Technology and Regulatory Council, Risk Assessment Resources Team, Washington, DC. www.itrcweb.org
14. Jenkins TF, Hewitt AD, Walsh ME, Ranney TA, Ramsey CA, Grant CL, Bjella KL (2005) Representative sampling for energetic compounds at military training ranges. Environ Foren 6:45–55
15. Leopold A (1949) Sand county almanac. Oxford University Press, New York
16. Leu DJ, Hadley PW (1987)The California site mitigation decision tree process – An approach to solving the "how clean should clean be" dilemma. In: Hazardous waste site management: water quality issues, report on a Colloquium Sponsored by the Water Science and Technology Board, National Research Council. National Academy Press, Washington, DC, pp 67–97
17. Meadows DH, Meadows DL, Randers J, Behrens WW III (1972) The limits to growth. Universe Books, New York, pp 205
18. Mihelcic JR (1999) Fundamentals of environmental engineering. Wiley, New York, pp 335
19. Mihelcic JR, Zimmerman JB (2009) Environmental engineering: fundamentals, sustainability, design. Wiley, Hoboken, pp 695
20. Mihelcic JR, Trotz MA (2010) Sustainability and the environmental engineer: implications for education, research, and practice. Environmental Engineer, Winter 2010, American Academy of Environmental Engineers, Annapolis
21. Muegge J, Hadley PW (2009) An evaluation of permeable reactive barrier projects in California. Remed J 20(1):41–57
22. Naftz DL, Morrison SJ, Davis JA, Fuller CC (2002) Handbook of groundwater remediation using permeable reactive barriers, applications to radionuclides, trace metals, and nutrients. Academic, San Diego

23. National Research Council Committee on Source Removal of Contaminants in the Subsurface (NRC) (2004) Contaminants in the subsurface: source zone assessment and remediation. National Academies, Washington, DC
24. Newell CJ, Fahrat SK, Adamson DT, Looney BB (2011) Contaminant plume classification system based on mass discharge. Ground Water (in press)
25. Operational Science Advisory Team (OSAT-2), Gulf Coast Incident Management Team (2011) Summary report for fate and effects of remnant oil in the beach environment. Prepared for LD Stroh, US Coast Guard, Federal On-Scene Coordinator, Deepwater Horizon MC252
26. Ramsey CA, Hewitt AD (2005) A methodology for assessing sample representativeness. Environ Foren 6:71–75
27. Remediation Technologies Development Forum (RTDF), U.S. Environmental Protection Agency (1998) Permeable Reactive Barrier Technologies for Contaminant Remediation. Office of Research and Development, EPA/600/R-98/125
28. Reynolds SD, Hadley PW, Sedman RM (1990) A health-based approach for evaluating soil at depth contaminated by hazardous waste: utilizing the AALsoil contact criterion. Risk Anal 10(4):571–574
29. Roehl KE, Meggyes T, Simon FG, Stewart DI (eds) (2005) Long-term performance of permeable reactive barriers. Elsevier, Amsterdam/London
30. Shoemaker SS, Greiner JF, Gillham RW (1995) Permeable reactive barriers. In: Rumer RR, Mitchell JK (eds) Assessment of barrier containment technologies. International Containment Technology Workshop, Baltimore
31. Schumacher BA, Minnich MM (2000) Extreme short-range variability in VOC-contaminated soils. Environ Sci Technol 34(17):3611–3616
32. Sustainable Remediation Forum (SURF) (2009) Integrating sustainable principles, practices, and metrics into remediation projects. Remed J 19(3) 5–114. Hadley P, Ellis D (eds)
33. United States Army Corps of Engineers (USACE) (2010) Decision framework for incorporation of green and sustainable practices into environmental remediation projects – Interim guidance 10–01. http://www.environmental.usace.army.mil/pdf/IG%2010-01%2003_05_10%20doc.pdf. Accessed 5 Mar 2010
34. United States Environmental Protection Agency (USEPA) (2010) Environmental footprint analysis of three potential remedies – Former Romic Environmental Technologies Corporation Facility East Palo Alto, CA. Final report – 11 May 2010. http://www.clu-in.org/greenremediation/romic/docs/romic_report_rev_051110.pdf
35. Warner SD, Yamane CL, Gallinatti JD, Hankins DA (1998) Considerations for monitoring permeable ground-water treatment walls. J Environ Eng ASCE 124(6):524–529
36. Weinstein M (2010) Sustainability science: the emerging paradigm and the ecology of cities. Sustain Sci Pract Policy 6(1):1–5

Sustainable Smart Grids, Emergence of a Policy Framework

Marilyn A. Brown, Shan Zhou
School of Public Policy, Georgia Institute of Technology, Atlanta, GA, USA

Article Outline

Glossary
Definitions of Smart-Grid Policies and Their Importance
Introduction
Types of Policies to Promote Smart Grids
Smart-Grid Policies of the United States: Federal Efforts
Smart-Grid Policies of the United States: State and Local Efforts
Smart-Grid Policies of the European Union
Smart-Grid Policies of Other Countries
International Collaboration
Future Directions
Conclusion
Bibliography

Glossary

Cost-benefit analysis Cost-benefit analysis is an economic approach to policy evaluation. It measures the timeline of expected costs and benefits associated with policy implementation, discounting future values to produce a net present value. Cost-benefit ratios are also used to evaluate a policy relative to the status quo or an alternative policy formulation.

Demand response Demand response is a means of reducing customer consumption of electricity in response to supply conditions. It is different from energy efficiency, which involves using less electricity to perform a particular task.

Distributed generation Distributed generation involves the production of electricity from many small energy sources (including, for instance, natural gas turbines and solar photovoltaic panels). It is distinct from the prevailing generation of electricity at large centralized facilities.

Feed-in tariffs Feed-in tariffs provide incentives for the generation of renewable electricity. Governments and utilities provide guaranteed purchase contracts for electricity generated from renewables; the particular tariffs may change over time to track the development of technology and cost reduction.

Natural monopoly Natural monopolies occur when economies of scale reduce production costs, such that one firm can produce at lower costs than multiple firms. Many public goods are typically provided by natural monopolies, such as electricity, railway, and water.

Public good A public good is a good that is non-excludable and non-rivalrous. It is costly to keep nonpayers from enjoying a public good, and one's consumption of a public good does not affect another's ability to consume the good. Natural defense and clean air are two examples of public goods.

Renewable electricity standard Renewable electricity standard is a policy target that sets minimum requirement for electricity generated from renewable energy sources.

Renewable energy certificates Renewable energy certificates are tradable energy commodities. One certificate often represents one megawatt-hour of electricity generated from renewable energy.

Time-of-use pricing Time-of-use pricing refers to electricity prices, which change based on time of consumption, such as peak and off-peak periods.

Definitions of Smart-Grid Policies and Their Importance

A smart grid is an electricity network that can (1) cost-efficiently integrate a diverse set of generators, (2) enable consumers to play an active role in managing the demand for electricity, and (3) operate at high levels of power quality and system security [1]. Policies to promote smart grids include net metering tariffs and time-of-use pricing; interconnection and technology standards; subsidies, targets and goals; customer privacy protection laws; and rules governing the ownership of renewable energy credits (Fig. 1).

- Smart grids facilitate the connection and operation of generators of all sizes and technologies. Recent improvements in the cost-effectiveness of distributed generation (DG) have underscored the importance of this ability to interconnect utility-owned DG assets (such as wind and solar farms) as well as customer-owned DG (such as industrial cogeneration facilities and building-integrated photovoltaics). The ability to integrate low-carbon and sustainable energy resources is essential to reducing the environmental impact of electricity supply systems.
- Smart grids also enable consumers to play a part in optimizing the operation of the system by providing them with greater information and options for how they management their energy consumption. With the help of smart-grid technologies and demand response programs, consumers can be motivated to reduce their peak electricity consumption, thereby reducing capital spending for power generation, transmission, and distribution investments [2, 3]. Enduring concerns about oil security combined with recent advances in electric vehicles have created the hope that smart grids could help support the electrification of transportation.
- Through proactive grid management and automated response, smart grids can provide system security and reliability as well as the high levels of power quality needed for increasingly digital economies. The smart grid implementation workshop held by the US Department of Energy (DOE) in 2008 emphasized the ability of smart grids to anticipate and respond to system disturbances in a self-healing manner and to operate resiliently against natural disasters and physical and cyber attack [2].

In sum, smart grids offer the potential to improve the efficiency and affordability of power delivery, mitigate environmental impacts, and reduce oil dependence while maintaining high levels of power system reliability and resilience [1, 4]. These numerous benefits include two critical positive externalities: climate change mitigation and energy security [137]. However, various obstacles inhibit smart grids from gaining rapid and widespread market share. Thus, with the recent introduction of smart-grid technologies has come the emergence of smart-grid policies, which are government interventions designed to protect the public's interest in affordable, dependable, and clean electric power by promoting the deployment of the smart grid.

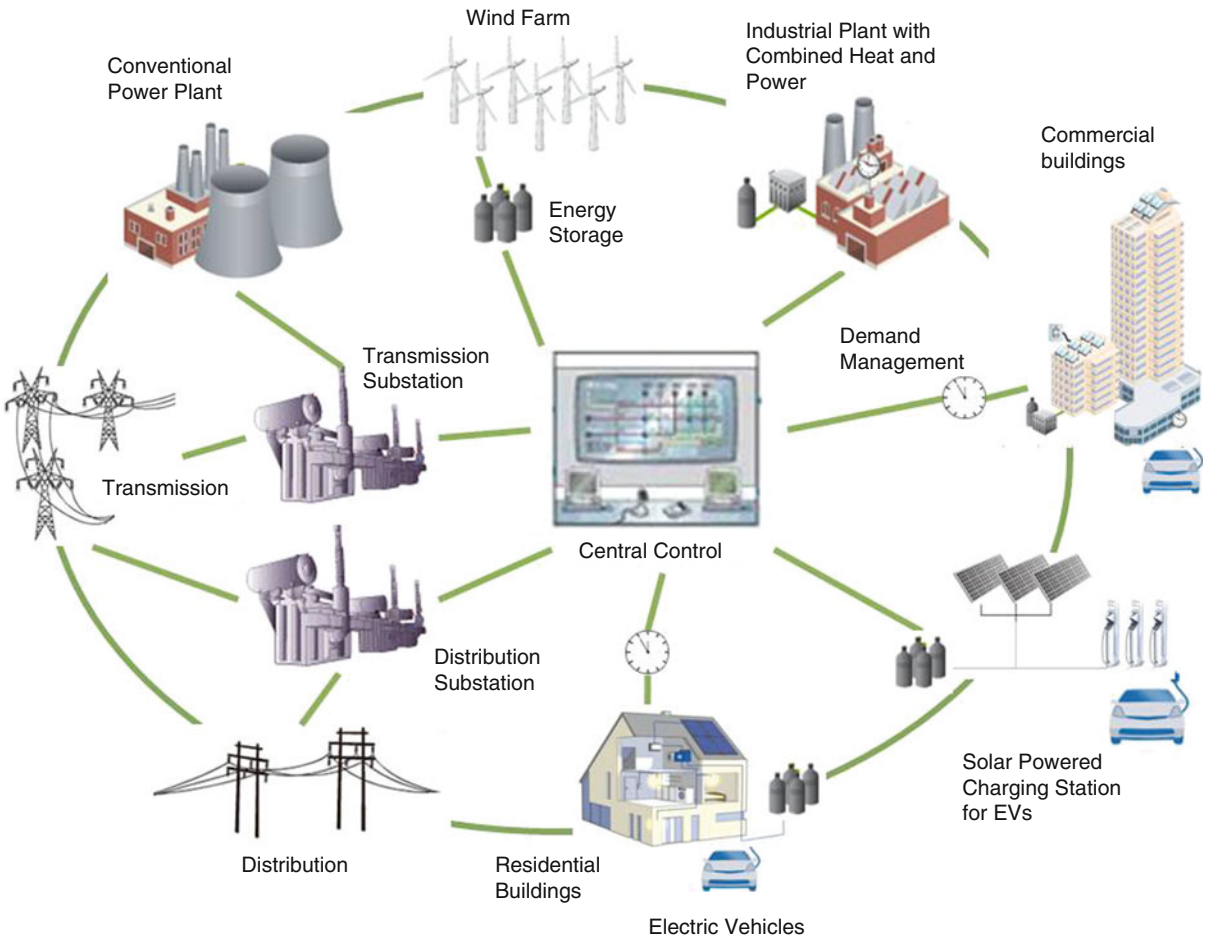

Sustainable Smart Grids, Emergence of a Policy Framework. Figure 1
Smart grid: a vision for the future

Introduction

The electric power infrastructure in most industrialized nations has been designed to support a large, monopolistic, centrally controlled power system. Before 1990, the electricity system in most countries consisted of vertically integrated (generation, transmission, and distribution) monopolies that were highly regulated. The rationale for this system design was the assumption that electricity production is a natural monopoly, where a single firm can produce the total market output at a lower cost than a collection of competing firms. At the transmission stage, the case for natural monopoly and continued regulation remains relatively strong, but the natural monopoly rationale for electricity generation and distribution has been weakened by the introduction of distributed electricity resources and small-scale electricity producers. While local distribution and generation systems in many countries have recently benefited from the introduction of some elements of market competition, the prevailing utility monopoly continues to play a dominant role in the production and distribution of power and generally oppose consumer-owned DG. For this reason, and because of other impediments discussed later in this chapter, smart grids remain an emerging technology.

Vertically integrated power systems have also become increasingly vulnerable to power outages and interruptions. Large-scale blackouts caused by rising electricity peak demand, aging infrastructure, extreme weather conditions, and terrorist attacks produce

significant economic and social costs. For the United States alone, power outages and interruptions cost Americans over $150 billion each year [4]. Outages are more frequent and are affecting an increasing number of people in recent years [4]. The 1987 blackout in Japan caused by high peak demand in the summer affected 2.8 million households [5]. The US–Canadian blackout of August 14, 2003 impacted 50 million people in eight US states and two Canadian provinces, with estimated total costs between $4 and $10 billion [6]. In 2006, 2.5 million customers experienced power outages after Hurricane Katrina hit the US Gulf Coast [7].

These events have stimulated growing public awareness of the need for grid modernization. Transitioning to a smart grid, however, will require implementation of policies to address barriers to smart-grid deployment and to regulate data access and equity concerns.

Technological breakthroughs often precipitate the parallel development of new policy frameworks. This has been the case in the medical profession with stem cell research and cloning, in transportation with the development of commercial space travel and intelligent transportation systems, and in the communications industry with the creation of the Internet and widespread utilization of smart phones. In all of these cases, as with the smart grid, policy frameworks must be created to ensure that the public's interests are protected. Thus, with the recent introduction of smart-grid technologies has come the emergence of new smart-grid policies.

This chapter begins by providing an overview of the barriers that hinder smart-grid deployment, the drivers that motivate it, and the policies that are commonly used to encourage smart-grid investments. Attention then turns to a review of experiences with smart-grid policies beginning with an analysis of US policies and an overview of US stakeholders. To characterize the smart-grid policy initiatives introduced by individual states and utilities, activities of four states are investigated: California, Georgia, New York, and Texas. This chapter also provides some insights into European Union smart-grid policies, with a special focus on Great Britain and Italy. To illustrate the smart-grid policies used in other hemispheres, we also describe policy initiatives in China, Korea, and Japan. This chapter ends with a brief discussion of future directions and conclusions.

Barriers to the Deployment of Smart Grids

Stakeholders worldwide have widely acknowledged the importance of grid modernization. Although many of the technologies needed for smart-grid development are available nowadays, widespread deployment of these technologies is still limited. Effective policies that facilitate the evolution of the electricity grid generally are those that address key barriers to the deployment of smart grids. This section provides a brief description of barriers that have been identified to date.

High Costs. Large upfront cost is one of the greatest challenges to the deployment of smart grids [8]. Like many other green technologies, deployment requires significant initial investment, yet the resulting benefits are not fully realized for many years [3]. Without guaranteed cost-recovery timelines or precedents for smart-grid investment, utilities and policy makers tend to be reluctant to move toward a smart grid [8].

Technical Risks. Implementation of smart grids requires upgrading of the whole electric system. One great technical challenge is to handle the potential impacts of the high-level penetration of new technologies on existing infrastructure [8]. Developing such an integrated system also places demanding requirements on a wide range of technologies, especially advanced metering infrastructure (AMI) technologies and cost-effective energy storage systems [8]. Moreover, from the perspective of policy makers, the uncertainties associated with smart-grid technologies call for highly flexible regulations to guide the path of its development [8].

Regulation and Monopoly Structure. Most of the electricity markets in the world are still operated by natural monopolies. A typical utility business model today is based upon a negotiated rate of return that adequately recovers utilities' capital investments [3]. As their profits are linked with sales, utilities have a financial incentive to maximize the throughput of electricity across their wires; hence they are often reluctant to adopt technologies that improve the efficiency of power supply. Moreover, rate-of-return regulation requires that utility rates are set to provide a "reasonable" return on invested capital, and utilities have to demonstrate the cost-effectiveness of added investments. As many societal benefits associated with smart grids are not fully understood by regulators,

utilities that bear all the cost of smart-grid investments have little incentive to invest in these technologies.

From the consumer's perspective, the current rate design does not reflect the marginal cost of electricity production or the conditions of the wholesale electricity market, which in turn prevents the involvement of the demand side in electricity markets [9]. Without an appropriate pricing mechanism, customers who only receive an end-of-the-month bill tend not to be interested in smart-grid technologies or end-use efficiency [10].

Under current policy schemes, smart-grid technologies face disadvantages when competing conventionally regulated power systems. In order to ensure system reliability, utilities and regulators often pose strict and discriminating rules on interconnection and DG. Incumbent electricity providers and distribution (and transmission) companies have incentives to discourage the deployment of smart grids in light of its potential to increase competition in the electricity market.

There is also a lack of consistency among policies at different levels of governments, which prevents effective collaboration and integration across regions [9]. The development of codes and standards often lags behind the development of smart-grid technologies. More efforts are still needed to create universal standards that promote interoperability and compatibility of smart-grid equipment [9].

Incomplete and Imperfect Information. Many consumers still do not see the benefits of a smart grid, nor do they understand the social and economic costs associated with today's outdated power grid system [9]. Utilities and policy makers could play important roles in the process of defining and communicating the benefits of smart grid to customers [3].

Privacy and Security Concerns. Many technologies that enable the deployment of the smart grid, such as smart meters and sensors, can increase the vulnerability of the grid to cyber attacks [3]. As the number of participants and distributed generators in the electric system increases, so does the complexity of security issues [9]. The tension between protection of consumer privacy and development of smart grid also imposes challenges on privacy protection rules. On the one hand, it is essential for both customers and smart-grid service providers to have access to energy consumption data in order to optimize the use of smart-grid technologies. On the other hand, consumer privacy protection may be in favor of the incumbent utilities that are currently controlling the meters and data, hence create barriers to market entry for new smart grid players [10].

Drivers Toward Smart Grids

Apart from barriers, effective policies must also consider drivers that promote investments in smart grid technologies. Over the past few decades, electricity markets and technologies have experienced rapid growth and development, with increasing focus on reliability. The desire for cleaner air through renewable resources and for oil dependence through electric vehicles also motivates interests in the smart grid.

Increasing Electricity Demand. Global electricity demand is expected to increase by over 150% between 2007 and 2050 under the International Energy Agency (IEA)'s Energy Technology Perspectives 2010 Baseline Scenario [11]. Modeling results show modest increases based on high levels of current demand in developed countries and high growth rates in developing countries such as China and India [11].

Electricity demand also varies across time and seasons. There are usually several peak times during the day while peak loads in a year typically occur in summer and winter (Figs. 2, 3). Due to the rapid development of home appliances and a lack of real-time pricing

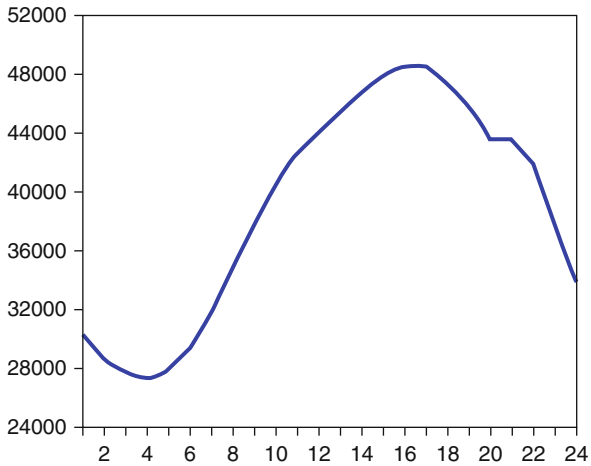

Sustainable Smart Grids, Emergence of a Policy Framework. Figure 2
An example of California load curve in July 2005 (MWh)

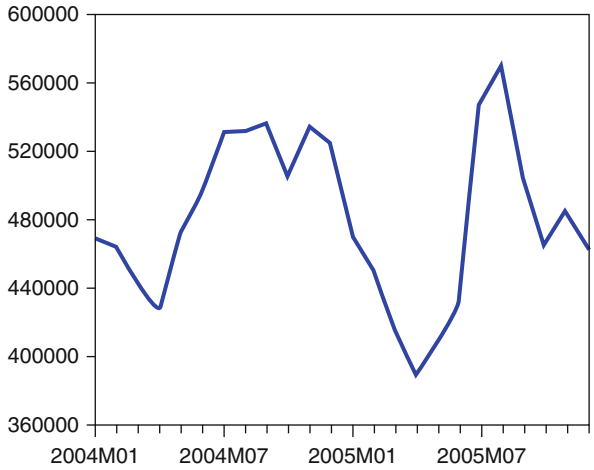

Sustainable Smart Grids, Emergence of a Policy Framework. Figure 3
California average daily demand for electricity (MWh) [13]

signals, peak demand increases steadily over time. Since 1982, growth in peak demand for electricity in the United States has exceeded the growth of transmission system by almost 25% every year [4]; and the US peak demand is expected to grow at an average annual rate of 1.7% between 2009 and 2019 [12]. Rising peak demand stresses the electricity system and requires higher reserve margins for unforeseeable outages. Smart-grid technologies can help reduce demand by enabling time-of-use pricing mechanisms and demand response programs and can improve the efficiency of electricity supply through better integration of renewable DG.

Energy Price Escalation and Electricity Reliability Concerns. Rising petroleum prices have underscored the uncertainties associated with the long-term electricity market. Under EIA's Reference and High Oil Price Scenarios, world oil prices are forecast to increase from $59 per barrel in 2009 to $135 and $210 per barrel, respectively, in 2035 [14]. Many countries are responding to the trend of higher oil prices by increasing electricity generation from more economical sources and reducing the petroleum dependence of their transportation sector.

At the same time, the aging infrastructure has become increasingly vulnerable to power outages and faces challenges associated with the new demands it needs to meet. The electric systems in many developed countries are largely based upon design requirements and technologies developed in the early twentieth century. The huge economic and social losses caused by supply failures have stimulated efforts to enhance the reliability of electricity supply. Electricity is different from other energy commodities as it cannot be stored in a large scale or be traded at the global level [11]. Electricity production and consumption are highly dependent on grid infrastructures, thus must be continually monitored and controlled to prevent widespread electric service interruption. Smart-grid technologies such as sensors and smart meters allow utilities to monitor the grid system based on real-time information, and enable greater use of demand response programs and distributed renewable energy generation.

Climate Change and Clean Air Concerns. Energy-related human activities are a major source of greenhouse gases and air pollutants. In 2009, the electric power sector in the United States emitted 2,160 million metric tons of CO_2, 2,400 and 5,970 thousand metric tons of NO_x and SO_2 [15, 16]. The electric power and transportation sectors were the largest carbon emission sources in 2009, accounting for 39.8% and 34.1%, respectively, of US total emissions [15]. Many countries have set targets for low-carbon and renewable electricity generation to combat climate change, which require extensive changes to the current power systems. A smart grid could exploit the full potential of carbon emissions reduction and air quality improvement in energy sectors, as it encourages low-carbon power generation and transport systems, and can reduce emission in the transmission process.

Deployment of Renewable Power and Electric Vehicles. Efforts to combat climate change have led to a rapid development of environmentally friendly power generation and transportation technologies. As of 2007, 18.4% of world electricity was generated by renewable energy, and the number will increase to 22.7% by 2035 [14]. The transport sector is also undergoing an electrification revolution, which is expected to consume 10% of total electricity by 2050 [11]. As electric vehicles gain market share, it may become difficult for conventional grid infrastructures to provide reliable and stable electricity services [11]. In particular, the intermittency of renewable energy and electric

vehicle charging have to be managed intelligently to avoid supply failures, which provide an excellent opportunity for the deployment of smart grids.

Types of Policies to Promote Smart Grids

This section provides an overview of major smart-grid policies. Current policies address many of the barriers identified above, and are aligned with many key drivers (see Table 1).

Net Metering

Net metering allows customers to use a single meter to measure both the inflow and outflow of electricity, thus enabling them to install and interconnect their own generators with utility grids. With net metering, customers can use the electricity generated from their on-site facilities to offset their electricity consumption and sell excess generation to the utility typically at a retail price, which encourages the deployment of customer-owned distributed energy systems. By allowing utilities to buy back surplus electricity, net metering helps overcome financial barriers faced by distributed renewable facility owners. The buy-back price is determined by utility regulators to reflect the value of electricity delivered to the grid; therefore, it can differ across regions. In some US states, such as California, net surplus compensation policy is closely related to the state's renewable energy policies, as it includes provisions on the ownership of renewable energy credits associated with the purchase of surplus electricity [17].

Additional policy goals for net metering may include diversification of energy sources, improving system reliability, reducing environmental impacts and distribution costs, and stimulating economic development [18]. Net metering has been widely implemented in countries like the United States and Canada. According to the US Energy Policy Act of 2005, all public electric utilities are required to provide net metering service to their customers upon request [19]. As of June 2011, 43 US states have adopted a net metering policy [20].

Net metering usually requires utilities to offer net metering programs to eligible customers and to design a net energy metering tariff scheme to compensate customers for the electricity generated in excess of on-site load. Customer eligibility for net metering programs varies across regions. Eligibility criteria are commonly defined by sectors (e.g., residential, commercial, and industrial), types of renewable resources (e.g., solar, wind, and combined heat and power (CHP)), and generating capacity (e.g., less that 10 KW or up to 1 MW). Net metering rules are often updated by policy makers to meet the needs and priorities of the market. In general, the trend is to increase the system capacity cap, as in the cases in New York and Massachusetts [21] and to broaden the eligible renewable resources.

Interconnection Standards

Interconnection standards establish uniform processes and technical requirements for utilities when connecting DG systems to the electric grid. It allows DG developers to predict costs and time, and ensure the safety and reliability of interconnection processes. Technical requirements often include protocols and standards that guide how generators shall interconnect with the grid, ranging from system capacity limit, the types of qualifying generators, the types of interconnection equipment required for reliability purposes, to the types of eligible generation technologies. Interconnection policy also includes simplified and standard application, connection and operation procedures, which can reduce uncertainties and prevent time delays that customers could encounter when obtaining approval for grid connection. For example, small systems may qualify for a streamlined interconnection process, with fees and application forms specified in the rules.

Interconnection standards have been widely developed and adopted by both governments and nongovernmental organizations. By 2011, 42 US states adopted an interconnection policy [20]. The US Federal Energy Regulatory Commission (FERC) has developed interconnection standard procedures for generators up to 2 MW, generators between 2 and 20 MW, and generators larger than 20 MW that connect to a utility's transmission system [22]. Other organizations such as the National Association of Regulatory Utility Commissioners (NARUC) and the Institute of Electrical and Electronic Engineers (IEEE) have also developed interconnection standards for distributed resources [23, 24].

Sustainable Smart Grids, Emergence of a Policy Framework. Table 1 Smart grid policies to tackle barriers and leverage drivers

Smart grid policies:	Barriers					Drivers			
	High costs	Technical risks	Regulation and monopoly structure	Incomplete and imperfect information	Privacy and security	Increasing electricity demand	Rising energy prices and reliability concerns	Climate change and clean air	Deployment of renewable power and electric vehicles
Net metering	×	×	×			×	×	×	×
Interconnection standards	×	×	×	×	×	×	×	×	×
Dynamic pricing	×		×	×		×	×		×
Smart metering targets			×	×		×	×	×	×
Renewable energy subsidies and regulations	×	×	×			×	×	×	×

Smart Metering Targets

A smart meter is a device that can measure real-time electricity consumption and communicate the information back to the utilities. It usually involves a mix of technologies, including real-time or near real-time sensors, power outage notification, and power quality monitoring. Smart meters, in combination with dynamic pricing, are essential for the promotion of price responsive demand and the success of a smart grid [25]. Smart metering targets have been widely adopted, which often establish smart meter deployment plans for utilities, including the timeline, and the type and number of smart meters to be installed. Sometimes, utilities are required to conduct cost-benefit analysis (CBA) of the proposed smart metering programs.

Demand Response and Dynamic Pricing

Demand response is defined as changes in electric usage by end-use customers from their normal consumption patterns in response to changes in the price of electricity over time, or to incentive payments designed to induce lower electricity use at times of high wholesale market prices or when grid reliability is jeopardized [26]. Many types of demand response programs have been offered by electric utilities and other stakeholders, such as dynamic pricing, peak time rebate, direct load control, and interruptible load. Demand response programs could contribute significantly to peak load reduction. To take the United States as an example, over 500 entities have reported offering demand response programs by 2010, with an estimated demand response resource of more than 58,000 MW (MW), or 7.6% of US peak demand [26].

As one of the most widely implemented demand response programs, dynamic pricing is a market-driven approach to boost demand response in the electricity market. The fundamental idea is to provide accurate price signals to customers and let them decide whether to continue consumption at higher prices or to cut electricity usage during peak times. Under dynamic pricing schemes, utilities charge different rates for electricity based on time, generating cost, and conditions of the grid; hence customers are exposed to some level of electricity price volatility. There are many types of dynamic pricing policies. The most common ones include time-of-use pricing, critical peak pricing, and real-time pricing.

- **Time-of-Use Pricing (TOU)** sets and publishes electricity prices for different time periods in advance. Electricity prices in peak periods are higher than off-peak, which encourages customers to shift electricity consumption to a lower cost period and reduce the peak demand. The rates for each time block are usually adjusted two or three times each year to reflect changes in the wholesale market; however TOU does not address unforeseen weather conditions or equipment failures.
- **Critical Peak Pricing (CPP)** is similar in rate structure to TOU pricing, but it adds one more rate that can vary with the wholesale market. Electricity prices during a limited number of hours of the year, which refer to the "critical peak hours," rise to levels designed to recover the full generation cost, while electricity prices during other times are lower than the critical periods. There can be a number of CPP event days in a year, and utilities usually will notify customers of the events and rates ahead of time.
- **Real-Time Pricing (RTP)** reflects the hourly or an even smaller time-interval marginal cost of electricity, which can be announced at the beginning of the time period or in advance. RTP can capture most of the true variation in the wholesale market, but it gives customers little time to react to price changes [27]. Technology innovations of the last decade have enhanced customers' ability to respond to real-time prices, and eliminated the conflicting issues between greater advanced price notification and more accurate price signals, enabling the greater use of RTP [27].

Compared to flat rate pricing scheme, dynamic pricing is more effective in promoting energy conservation. There is misperception that customers may be averse to dynamic pricing due to the price volatility and the possibility of paying higher bills; some also argue that customers are insensitive to real-time prices [28]. Research has shown that residential customers generally respond to higher electricity prices by reducing consumption, and both TOU and CPP rates could induce reduction in peak demand [29]. There is also empirical evidence that most low-income customers

would save money on their utility bills from dynamic pricing, rather than being negatively affected [30]. Moreover, dynamic pricing may also remove the subsidies embodied in flat rates, which are preserved for social policy reasons but are actually barriers to energy conservation [28].

Enabling dynamic pricing schemes requires the deployment of AMI, which costs from $100 to $200 per meter; however, these costs can be offset by various operational benefits, as well as savings from reduced peak load and avoided capital investment for additional power generation facilities [31]. For instance, the annual long-run benefits associated with a 5% reduction in peak demand in the United States are projected to be $3 billion, representing a discounted present value of $35 billion over a 20-year time horizon [31].

Renewable Energy Subsidies and Regulations

Renewable energy is an essential part of smart grids. Policy makers have developed both financial and regulatory policies to encourage power generation from renewable energy sources, such as feed-in tariffs (FITs) and renewable electricity standards (RES).

FITs are one of the most widely used policy mechanism in the world to encourage the deployment of renewable energy technologies and expansion of renewable energy generation. FITs provide guaranteed long-term purchase agreements for electricity generated from renewable energy sources. Governments usually offer a price for every kilowatt-hour (kWh) of electricity produced based on the types of generation technology, system capacity, and project location. The tariffs might decline over time to track and encourage technology innovation and cost reduction. By 2010, 75 jurisdictions (countries, states, and provinces) have enacted a FIT policy, some of which are developing countries like China, India, Tanzania, and Kenya [32]. FITs create an open and straightforward framework, which not only ensures the long-term stability of revenue from electricity sales, but also reduces risks and overall costs of renewable energy development for society [33]. By 2008, FITs had driven the deployment of 75% of global photovoltaics and 45% of global wind [34].

An RES sets a minimum requirement for the percentage of generation or installed capacity to be provided by renewable energy. Most RES policies require a 5–20% share for renewable energy to be achieved by 2020 and beyond. To achieve RES targets, entities are often allowed to trade renewable energy certificates (RECs), with each certificate representing the certified generation of one unit of renewable energy (typically 1 MWh). As of 2010, RES policies have been implemented by 10 national governments, and 46 state/provincial governments around the world [32].

Other

Many other policies have been designed to address issues in the development process of smart grids, such as consumer protection rules and energy storage policy. Consumer protection rules are particularly important as they create a fair marketplace for both consumers and suppliers [10]. In general, this type of policy includes mandatory disclosure statements and terms and conditions for the contract, which help customers better understand smart grid services. Policy makers also set up rules that regulate the access and usage of customers' personal information and energy consumption data by electric utilities, customers, and third parties. Utilities often have to receive customer consent before releasing the data to a third party.

The inclusion of energy storage systems in grid design and operation can benefit the deployment of smart grid technologies. Related policy issues include cost recovery models of energy storage technologies, incentives to increase private investment, and coherence between energy storage and electric vehicle policies [35]. California is one of the few states that have adopted an energy storage policy. This policy sets up mandatory requirement for developing energy storage systems in the grid. Electric utilities have to procure energy storage systems with a total installed capacity equal or larger than certain percentage of their total peak demand.

Other policies include smart-grid technology standards, customer privacy protection laws, rules governing the ownership of renewable energy credits, smart city policies, and approaches that are tailored to meet the needs of particular regions or market sectors. As shown in Fig. 4, these policies span the geographic scale from the local to the international.

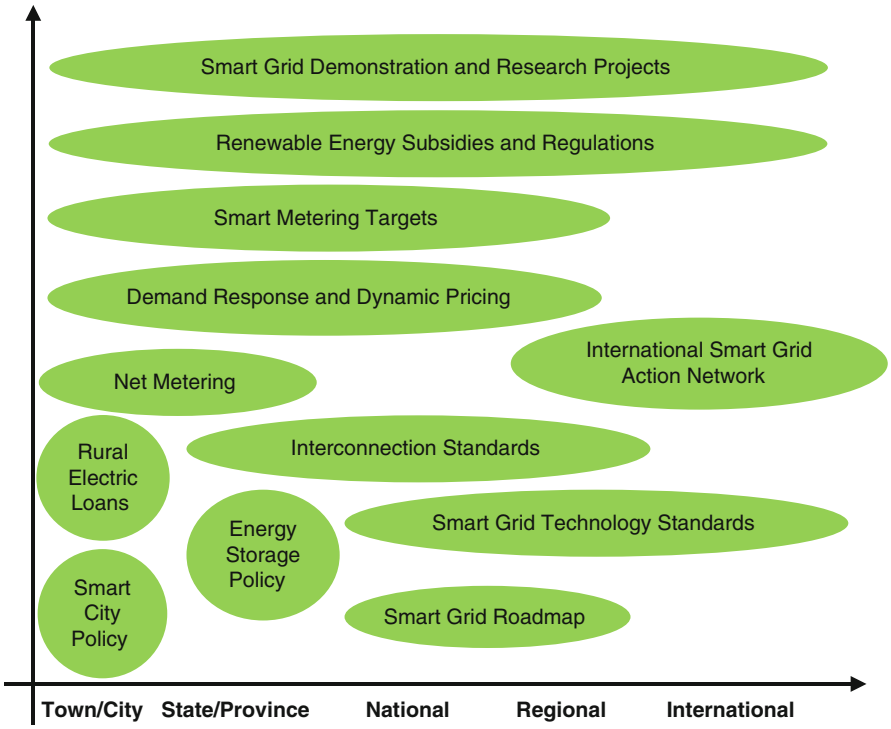

Sustainable Smart Grids, Emergence of a Policy Framework. Figure 4
Smart grid policies: moving from the local to the international scale

Smart-Grid Policies of the United States: Federal Efforts

The United States has been a pioneer in pursuing a low-carbon economy. The government recognizes that a smarter, modernized, and expanded electric system is essential to America's world leadership in a clean-energy future [36]. Development of policies has occurred at both federal and state levels to facilitate the evolution toward a twenty-first-century grid. This section first summarizes major policy efforts of the federal government, and provides a stakeholder analysis of the smart grid policy regime in the United States.

Smart-Grid Legislation and Policy Context

In 2005, Congress passed the Energy Policy Act of 2005, which directs utility regulators to consider time-based pricing and other forms of demand response for their states [19]. Utilities are required to provide each customer a time-based rate schedule and a time-based meter upon customer request [19]. The Energy Independence and Security Act (EISA) of 2007 is the key legislation for modernizing the nation's electricity transmission and distribution system. Title XIII of EISA mandates the Secretary of Energy to establish a smart grid advisory committee and a smart grid task force, to assess the impacts of smart grid deployment, and to take the lead in smart grid technology research, development and demonstration projects [37]. It also requires the National Institute of Standards and Technology (NIST) to develop a smart grid interoperability framework that provides protocols and standards for smart-grid technologies [37]. Under Section 1306 of EISA, a smart grid investment matching grant program was established to provide reimbursement of 20% of qualifying smart-grid investments [37].

The American Recovery and Reinvestment Act (ARRA) of 2009 accelerates the development of smart-grid technologies by appropriating $4.5 billion for electricity delivery and energy reliability modernization efforts [38]. Utilities and other investors can apply stimulus grants to pay up to 50% of the qualifying smart grid technology investments. To date, the Smart Grid

Sustainable Smart Grids, Emergence of a Policy Framework. Table 2 Recovery Act overview [39]

Projects	Total obligations (in million $, 2009)	Number of award recipients
Smart grid investment grant	$3,483	99
Smart grid regional and energy storage demonstration projects	$685	42
Workforce development program	$100	52
Interconnection transmission planning	$80	6
State assistance for recovery act related electricity policies	$49	49
Enhancing state energy assurance	$44	50
Enhancing local government energy assurance	$8	43
Interoperability standards and framework	$12	1

Investment Grant (SGIG) has 99 recipients, with a total public investment amounting to$3.5 billion [39]. Table 2 shows the total obligations and award recipients for the projects authorized by the Recovery Act.

Building on the policy direction set forth in the key legislation, the Federal government published "A Policy Framework for The 21st Century Grid: Enabling Our Secure Energy Future" in June 2011 [36]. This framework identifies and highlights policies that form the nation's overall grid modernization efforts, presenting them within the context of four policy goals: enabling cost-effective smart-grid investments, unlocking the potential for innovation in the electric sector, empowering consumers and enabling them to make informed decisions, and securing the grid [36].

Roles of Government Agencies

The federal government's commitment to grid modernization has spurred efforts of many federal agencies and organizations. DOE is leading the nation's efforts in research, development, and demonstration of smart-grid technologies, and FERC and NIST have been actively engaged in smart-grid technology standard development and implementation. Deployment of smart grids is also closely linked with tasks and missions of many other departments, such as the Environmental Protection Agency's clean energy and climate change initiatives, the Department of Homeland Security and Department of Defense's interest in the security and resiliency of electric grid, and the Department of Commerce's focus on clean energy technology innovation. A summary of responsibilities of major US government agencies is presented in Table 3.

Deployment of smart grids involves a wide array of stakeholders, ranging from electricity utilities, consumers, and manufacturers, to government officials. It is critical to understand the impacts of smart-grid deployment on every stakeholder, and his/her potential influences in smart grid policy-making process. Regulatory framework are expected to take into account the conflicting goals and create aligned incentives for various groups. Table 4 presents a stakeholder analysis for smart-grid policies in the United States.

Smart-Grid Policies of the United States: State and Local Efforts

The scope and pace of smart-grid deployments naturally vary according to the diverse needs, regulatory environments, energy resources, and legacy systems of different states. Decentralized smart-grid deployment efforts provide local flexibility and stimulate experimentation and innovation in policy design and implementation. Thus, it is useful to examine smart-grid policies developed at the state and local level [138]. In this section, four US states are selected for in-depth investigation: California, Georgia, New York, and Texas.

California

California is one of the leading states in the United States driving the deployment of smart-grid technologies. Its policy efforts are discussed in detail in the following section.

- Net Energy Metering Tariffs
  According to Section 2827 of California Public Utilities Code, all electric utilities in California,

Sustainable Smart Grids, Emergence of a Policy Framework. Table 3 Roles of US governmental entities in smart-grid deployment

Agencies	Responsibility
Federal energy regulatory commission (FERC)	Facilitate smart-grid development via its regulations for electricity transmission and wholesale sales: Approve and enforce mandatory reliability standards for bulk power systems Adopt interoperability standards and protocols Provide guidance for the development of smart-grid standards
Department of energy (DOE)	Implement Recovery Act funds for smart-grid deployment Conduct research and development of smart-grid technologies and policies Monitor the progress of smart-grid deployment
Department of agriculture (USDA)	Support grid modernization in rural areas Provide loans for generation, transmission, and distribution of renewable energy
National institute of standards and technology (NIST)	Develop standards for smart-grid technologies Communicate with industry groups to accelerate the adoption of new standards
Smart grid task force	Ensure awareness, coordination and integration of the diverse activities of the federal government related to smart-grid deployment
State public utility commissions	Develop rules to implement state and federal smart grid legislations, such as: Smart-grid standard Dynamic pricing schemes Net metering and interconnection requirements

except the Los Angeles Department of Water and Power, are required to offer net energy metering (NEM) tariffs to customers who install small solar and wind while investor-owned utilities generation facilities are also required to offer NEM tariffs to biogas and fuel cell customer-generators [40]. NEM tariffs are applicable to qualifying facilities (1 MW and less) in residential, commercial, industrial, and agricultural sectors. The cumulative generating capacity of eligible customer-generators is not to exceed 5% of an electric utility's aggregate customer peak demand.

NEM customers can get compensation from utilities for electricity generated in excess of on-site load. Net excess generation will be credited to customers' next bill at the retail rate. By the end of a 12-month period, customers can choose to roll over credit indefinitely or to receive financial compensation for credit at a rate that is determined by the California Public Utility Commission (CPUC). The owner of renewable DG facilities owns the RECs associated with the electricity generated from the facilities, but utilities could receive RECs for the excess electricity that they have compensated the customers.

- Interconnection Standards: Rule 21
  In 1999, the CPUC instituted rulemaking to address interconnection issues [41], becoming one of the first utility commissions to do so. The resulting Rule 21 has been revised continuously to keep consistency with the requirements of the ANSI/IEEE interconnection standards [42]. Rule 21 mandates that DG facilities meet standard interconnection, operating, and metering requirements. Applicants pay an $800 initial review fee and a $600 supplemental review fee before the utility evaluates the interconnection of the generating facility. For generating facilities that cannot be interconnected to a utility's distribution system via simplified interconnection, additional interconnection studies and fees are required. Rule 21 exempts eligible customers for net energy metering under Public Utilities Code Section 2827 from paying for costs associated with application review fees, interconnection studies, and distribution system modifications. However, eligible customers are responsible

Sustainable Smart Grids, Emergence of a Policy Framework. Table 4 Stakeholder analysis of smart grid policies

Stakeholder	Pros	Cons	Dominant position	Potential impact on smart grid deployment
Federal government	Job creation, affordable energy, economic competitiveness, energy security, deployment of clean energy resources, emissions reductions	Costs of smart grid demonstration and research projects; reluctance to pick technology winners	Very favorable	High
State legislatures and utility commissions	Job creation, energy security, deployment of renewable energy, emissions reductions	Cost recovery of smart grid investments, vulnerability to cyber attack	Very favorable to slightly favorable	High
Electric utilities	Reduction in peak load, improved grid stability, improved operational efficiency	Reduction in electricity sales, higher workloads vulnerability to cyber attack	Mixed	High
Smart grid and renewable manufacturers	Increased technology and product sales	None	Very favorable	Medium
Conventional energy companies	None	Reduction in sales of fossil fuels	Unfavorable	High
Environmental groups	Decreased emission of criteria air pollutants and greenhouse gases	None	Very favorable	Medium
Customers	Better energy management, reduced energy bill new products and services	Increased risk of privacy invasion, investment costs	Mixed	Low

for all costs associated with their interconnection facilities.

- Smart Metering Targets
  In 2004, the CPUC directed the three largest investor-owned utilities (IOUs) in California to submit AMI business case analyses and deployment proposals [43]. The three utilities have developed deployment plans for smart meters as part of their smart-grid roadmap and have been given authorization to deploy smart meters throughout their territories (see Table 5). The deployment of smart meters is expected to be completed in 2012, when approximately 12 million electric meters and 5 million natural gas meters will be installed, generating hundreds of millions of dollars in net benefits.
- Smart-Grid Legislation
  California passed Senate Bill (SB) 17 in 2009, which establishes regulatory approaches for the CPUC and utilities to deploy smart-grid technologies. The goal of this bill is to maintain reliable and secure electrical service with infrastructure that can meet future growth in demand, and to achieve other objectives such as the integration of DG resources, demand-side resources, and smart technologies [48]. SB 17 required the CPUC to create a smart grid deployment plan, which laid the groundwork for all IOUs to submit their smart grid deployment plans to the CPUC. The CPUC is also required to conduct impact assessments on relevant state energy initiatives, such as the deployment of AMI, the RES, and greenhouse gas emissions reduction. The bill requires that standards

Sustainable Smart Grids, Emergence of a Policy Framework. Table 5 Deployment of smart meters by California's large utilities [44–47]

	Pacific Gas and Electric Company	San Diego Gas and Electric Company	Southern California Edison Company
Goal	5.1 million electric meters; 4.2 million gas meter modules	1.4 million electric meters; 0.9 gas meter modules	5.3 million electric meters
Total costs	Ratepayer funding for $1.74 billion approved; $466.76 million approved for proposed project upgrade	$572 million approved	$1.63 billion for upgrade requested
Net benefits	$103.9 million	$40–$51 million	$9–$304 million
Deployment timeline	2007–2011	2007–2011	2008–2012

adopted for California be compatible with standards from NIST, FERC, the Gridwise Architecture Council, IEEE, and the North America Electric Reliability Cooperation (NERC). If utilities fail to meet the standards or to present a plan to meet them by the deadline, they will be subject to a penalty.

To facilitate the implementation of SB 17, the CPUC set detailed requirements for utilities' smart-grid deployment plans. Utilities must present a vision of smart grid that is consistent with the legislative initiatives, requiring at least eight topics in their deployment plan, including smart-grid vision statement, deployment baseline, smart-grid strategy, grid security and cyber security strategy, smart-grid roadmap, cost and benefits estimates and metrics [49].

- Customer Privacy Protection Rules
  SB1476 on customer privacy related to AMI became effective in 2010. This bill prohibits utilities from sharing, disclosing, or making accessible to any third party a customer's electrical or gas consumption data [50]. It also requires utilities to protect customers' energy consumption data from unauthorized access, destruction, use, modification, or disclosure, as well as to allow customers to access the data without being required to agree to share their personally identifiable information with a third party [50].
- Dynamic pricing
  The CPUC mandated that dynamic pricing tariff options for all types of customers should be addressed in each utility's comprehensive rate design proceeding application [51]. Furthermore, the CPUC directed each utility "to incorporate default critical peak pricing tariffs for large customers into their next comprehensive rate design proceeding or other appropriate proceeding if directed by the Commission" [52]. In 2010, the CPUC directed the Pacific Gas and Electric Company to implement default and optional critical peak pricing and time-of-use rates (together, referred to as Peak Day Pricing) (see Table 6) [53]. There will be between 9 and 15 Peak Day Pricing event days for each calendar year, and for their first year on a Peak Day Pricing rate scheme, customers will be afforded bill stabilization and can choose to opt out any time [53].

  Southern California Edison Company has also developed several dynamic pricing schemes. It offers voluntary CPP for all its customers, real-time pricing rates to customers with monthly peak demand greater than 500 kW, and agricultural and pumping real time pricing rates to customers who use 70% or more of the electricity for general agricultural purposes, or for general water or sewage pumping [54].
- Energy Storage Bill
  The California State Assembly passed the nation's first energy storage bill (Assembly Bill 2514) in September 2010. This bill mandated utilities to procure new grid-connected energy storage systems [55]. Before October 2013, the CPUC will determine two energy storage procurement targets for utilities to achieve by 2015 and 2020 [55].

Sustainable Smart Grids, Emergence of a Policy Framework. Table 6 Pacific Gas and Electric Company peak day pricing transition plan [53]

Applicable sector	Type of rates	Options
Residential customers with advanced meters	Peak day pricing; non-time-differentiated residential tiered rates	Allows customers to transition to either of the two rates
Large commercial and industrial customers (≥200 kW)	Peak day pricing rates that include time-of-use rates during non-peak day pricing periods	Default; Allows customers to opt out to a time-of-use rate or other time-variant rate
Small and medium commercial and industrial customers (≤200 kW)	Peak day pricing rates that include time-of-use rates during non-peak day pricing periods	Default; Allows customers to opt out to a time-of-use rate or other time-variant rate
Large agricultural customers (≥200 kW)	Peak day pricing rates that include time-of-use rates during non-peak day pricing periods	Default; Allows customers to opt out to a time-of-use rate or other time-variant rate
Small agricultural customers (≤200 kW)	Time of use	Default

- Distributed Generation and Renewable Energy Credits
  Because RECs are critical to the cost-effectiveness of renewable DG facilities, the CPUC has issued several decisions to clarify the participation of renewable DG in the renewable electricity standards. Specifically, "the owner of the renewable DG facilities owns the RECs associated with the generation of electricity from those facilities" [56]. Decision 07-01-018 further states that "utilities will not be counting the output of renewable DG facilities that have received ratepayer incentives toward their renewable portfolio standard obligations." In other words, renewable DG facility owners will retain the RECs produced by their facilities irrespective of whether or not they receive ratepayer funding from programs such as SGIP (see below) or net metering [57].

  The CPUC established the Self-Generation Incentive Program (SGIP) to encourage the development and commercialization of DG technologies. SGIP provides financial incentives to certain entities that install DG (such as micro-turbines, small gas turbines, wind turbines, photovoltaics, fuel cells, and internal combustion engines) to offset some portion of the customer's on-site load (see Table 7) [58]. Due to insufficient funds, the SGIP was terminated in early 2011 [59].

Georgia

Georgia has a broad array of dynamic pricing programs, but relative to California its net metering and interconnection standards are more restrictive. The State also has one of the lowest rates of renewable electricity generation in the country [60].

- Net Metering
  Georgia General Assembly passed the Georgia Cogeneration and Distributed Generation Act of 2001 to encourage private investment in renewable energy [61]. This act requires utilities to provide net metering for all eligible customers. DG facilities are customer-owned and they use photovoltaic systems, wind turbines, and/or fuel cells. The peak generating capacity of eligible systems must be smaller than 10 kW for residential customers and 100 kW for commercial customers. The cumulative generating capacity of net-metered systems is limited to 0.2% of a utility's annual peak demand in the previous year (recall that California's cap was much higher, at 5% of an electric utility's aggregate customer peak demand). Utilities are required to offer bidirectional or single directional metering depending on how the DG facilities are installed. Systems connected on the customer's side of the meter are required to use a bidirectional meter, and any net excess generation will be credited to

Sustainable Smart Grids, Emergence of a Policy Framework. Table 7 Financial incentives and eligibility of the SGIP [57]

Incentive category	Incentive offered	Maximum percentage of project cost (%)	Eligible system size	Eligible technologies
Level 1	$4.50/W	50	30 kW ~1 MW	Photovoltaics; Fuel cells operating on renewable fuel; Wind turbines
Level 2	$2.50/W	40	≤1 MW	Fuel cells operating on nonrenewable fuel and utilizing sufficient waste heat recovery
Level 3	$1.00/W	30	≤1 MW	Microturbines utilizing sufficient waste heat recovery and meeting reliability criteria; Internal combustion engines and small gas turbines, both utilizing sufficient waste heat recovery and meeting reliability criteria

the customer's next bill at tariffs filed with the Georgia Public Service Commission. Systems connected on the utility's side use a single directional meter, and the customer will be charged with a minimum monthly service fee.

In particular, solar photovoltaic generation is encouraged under Georgia's net metering policy scheme. Georgia Power, the dominant utility in the state, operates the Solar Buyback Program, which allows customers to sell electricity produced by solar panels [62]. Georgia Power is responsible for meter installation, but it charges a $3.97 and a $1.31 monthly metering fee, respectively, for single directional metering and bidirectional metering. The solar purchase tariffs are subject to change according to state policies. Through 2010, the Solar Purchase Price was 17 cents per kWh, and the aggregate energy purchases were limited to 2.9 MW. Starting in 2011, solar photovoltaic electricity is purchased at Avoided Solar Cost.

- Interconnection Standards
  The Cogeneration and Distributed Generation Act of 2001 allows certain residential (smaller than 10 kW) and commercial (smaller than 100 kW) facilities that use photovoltaic system, wind turbines, and fuel cells to interconnect and receive net metering tariffs from utilities [61]. This act requires customers to meet applicable interconnection requirements, such as the National Electrical Code, National Electrical Safety Code, and the IEEE standards.
- Smart Metering Targets
  Georgia Power has installed about one million smart meters since 2008, and it plans to provide every customer with a smart meter by the end of 2012 [63]. No additional service charge will be added to customers' energy bill. Few of these smart meters provide real-time information to consumers; they mostly automate the collection of consumption data by the utility.
- Dynamic Pricing
  Georgia Power has been very successful in implementing dynamic pricing programs. An array of dynamic pricing programs is offered to various types of customers, with electricity rates ranging from 1.25 cents per kWh during super off-peak time to 19.29 cents during on-peak hours (see Table 8). For instance, TOU rates are available to residential customers and electric vehicle owners, as well as small, medium, and large businesses. RTP for some customers are based on day-ahead or hour-ahead power supply prices. In 2005, Georgia Power's commercial and industrial real-time pricing programs alone had 1,600 participants, which represented over 5,000 MW of qualifying load [64].

New York

The State of New York was one of the first states to develop standard interconnection requirements, which specified application fees as well as limits to customer costs for interconnection equipment.

Sustainable Smart Grids, Emergence of a Policy Framework. Table 8 Dynamic pricing programs offered by Georgia Power Company [65]

Applicable customers	Type of rates	Electricity rate (cents per kWh)	
Residential	Time-of-use rate	On-peak: 2–7 pm, Mon–Fri, June–Sept	19.29
		Off-peak: all hours not included above	4.36
Plug-in electric vehicle	Time-of-use rate	On-peak: 2–7 pm, Mon–Fri, June–Sept	19.29
		Off-peak: 7 am–11 pm for weekends, holidays, and Oct–May; 7 am–2 pm and 7 pm–11 pm, Mon–Fri, June–Sept	5.83
		Super off-peak: 11 pm–7 am, Mon–Sun for all calendar months	1.25
Small business	Time-of-use rate	On-peak: 2–7 pm, Mon–Fri, June–Sept (not including holidays)	16.17
		Off-peak: all hours not included above	June–Sept: 7.30
			Oct–May: 7.30 for the first 1,500 kWh; 2.79for usage above 1,500 kWh
Medium Business	Time-of-use rate	On-peak: 2–7 pm, Mon–Fri, June–Sept (not including holidays)	11.69
		Shoulder: 12–2:00 pm and 7–9 pm, Mon–Fri, June–Sept (not including holidays)	5.61
		Off-peak: all hours not included above	2.11
Large business	Time-of-use rate	On-peak: 2–7 pm, Mon–Fri, June–Sept (not including holidays)	9.56
		Shoulder: 12–2:00 pm and 7–9 pm, Mon–Fri, June–Sept (not including holidays)	4.32
		Off-peak: all hours not included above	1.51
Customers with a peak 30-min demand larger than 250 kW each month	Real time pricing – day ahead	Hourly prices are determined each day	
Customers with a peak 30-min demand larger than 5,000 kW each month	Real time pricing – hour ahead	Prices are updated each hour, 60 min before becoming effective	

- Net Metering
  New York Public Service Law requires utilities to provide interconnection and net metering for solar, wind, farm waste, micro-CHP, and fuel cell generating facilities [66]. The generating capacity cap varies by technology and sector (see Table 9). The aggregate generating capacity cap for wind was 0.3% of a utility's total electric demand in 2005, and the aggregate generating capacity cap for solar, biogas, micro-CHP, and fuel cell systems combined is set at 1.0% of a utility's 2005 electric demand (this is between the lower value for Georgia and a higher value for California). The New York State Public Service Commission (PSC) and utilities are encouraged to increase the cap for aggregate generating capacity.
- Interconnection Standards
  The New York PSC first developed the Standard Interconnection Requirements (SIR) for DG units in 1999, and has amended it many times [67]. The

Sustainable Smart Grids, Emergence of a Policy Framework. Table 9 Generating capacity cap for eligible distributed facilities in the state of New York [66]

Applicable sector	Solar	Wind	Biogas	Micro-CHP and fuel cells
Residential	25 kW	25 kW	–	10 kW
Nonresidential	2 MW	2 MW	–	–
Farm-based	–	500 kW	1 MW	–

SIR of 2010 contains interconnection and application procedures for distributed facilities 25 kW or less and systems between 25 kW and 2 MW [68]. There is no application fee for applicants proposing to install systems 25 kW or less, but they are responsible for costs of installing the dedicated transformers and other safety equipment if deemed necessary. For systems above 25 kW and up to 2 MW, a nonrefundable $350 application fee is required, and the utility will conduct a preliminary review and a coordinated electric system interconnection review to determine if the proposed facility results in any relay coordination, fault current, and/or voltage regulation problems. The SIR also determines the maximum expense for interconnection equipment that has to be paid by customers. For technical standards, the SIR sets requirements for the design and operation of DG facilities, which are consistent with the IEEE standard 1547.

- Smart Metering Targets
  In an order issued in 1997, the New York PSC views advanced metering as a potential way to develop a robust and competitive retail market [69]. Eligible large commercial and industrial customers were to have the option of owning a Commission-approved meter. Utilities are to provide at least 24 months of customer's energy consumption data at no cost upon a customer request; and they will provide any third party the same data with the customer's approval. This order also states that utilities will invest in smart metering technologies only if it is cost-effective. In 2006, the New York PSC adopted an order to encourage utilities' investment in cost-effective smart metering programs and pilot projects to test various proposals for smart metering deployment [70]. Utilities are also required to file plans and proposals for integrating smart meters into their systems.
- Dynamic Pricing
  In 2005, the New York PSC directed major utilities in the state to accelerate and implement mandatory hourly pricing (MHP) for their largest customers [71]. An order issued in 2006 requires major utilities to develop methods for deriving retail hourly prices, to assess the impacts of MHP, and to submit a report on program implementation [72]. Consolidated Edison Company of New York, Inc. was directed to offer MHP to customers with peak demand greater than 1,500 kW. As of July 2011, this program has been expanded twice and it is now available for customers with peak demand greater than 500 kW [73]. The 2006 order also mandates National Grid to implement MHP for its medium-sized commercial and industrial customers, and requires New York State Electric & Gas Corporation, Rochester Gas and Electric Corporation, and Orange & Rockland Utilities, Inc., to implement MHP for their time-of-use customers at or above 1,000 kW [72]. In 2011, New York PSC approved Rochester Gas & Electric's plan for expanding its MHP program to customers with peak demand greater than 300 kW, which would add an additional 585 MHP customers to this program [74].

Texas

Texas is the only one of the four States examined in this chapter that requires utilities to offer unlimited cumulative generating capacity under their net metering programs.

- Net Metering
  Texas does not have a statewide net metering policy; however, utilities can, but are not required to, compensate customers for electricity that is generated

from distributed renewable resources and sent back to the grid. According to the Public Utility Commission of Texas (PUCT), utilities in Texas are required upon customers' request to provide one or two meters that can separately measure both the inflow and outflow of electricity [75]. Qualifying facilities include distributed renewable generators with a capacity up to 2,000 kW [75]. Beginning in 2009, the PUCT requires each utility to offer qualifying renewable generation facilities that have an aggregate design capacity of 50 kW or less the option of interconnection through a net meter [76]. Excess generation will be purchased by utilities at the avoided cost, and there is no limit on the cumulative generating capacity under the net metering program [76].

Many municipalities and large utilities in Texas have their own net metering programs. For instance, Austin Energy offers a net metering program for renewable energy systems with a generating capacity less than 20 kW [77]. Eligible technologies include solar, wind, geothermal, hydroelectric, wave and tidal energy, biomass, and biomass-based waste products.

- Interconnection Standards
  PUCT rules address the technical and procedural aspects of interconnection of on-site DG facilities [78, 79]. The rules establish interconnection standards that apply to generating facilities with a maximum capacity of 10 MW and connection at a voltage less than 60 kV. In particular, requirements for generators, network interconnection of DG, and control, protection, and safety equipment are specified to ensure safety and reliability of the interconnection. Customers who fail to comply with the standards may be disconnected from the grid. Pre-interconnection studies and fees will be considered based on the characteristics of DG facilities; for instance, customers with DG facilities less than 500 kW that export less than 15% of the total load and contribute less than 25% of the maximum potential short circuit current on a single radial feeder will not be charged with the pre-interconnection study fee [78].

  PUCT also published a Distributed Generation Interconnection Manual to help utilities process interconnection applications. It includes safety and technical requirements of DG installations, applicable rules, application procedures and forms, Texas utility contacts, and equipment pre-certification requirements [80]. Texas utilities are required to evaluate applications based on prespecified criteria, including equipment size and the relative size of the DG system to the feeder load.
- Smart Metering Targets
  Currently, there is no legislation that requires mandatory deployment of smart meters in Texas. However, the state legislature has taken actions to provide more regulatory incentives for smart meter deployment. In 2005, Texas passed House Bill (HB) 2129 to encourage energy saving measures. This bill recognizes the important role that smart meters can play in grid modernization and energy conservation, and encourages the deployment of smart meters by utilities in Texas [81]. It also directs the PUCT to establish a non-bypassable surcharge for a utility to recover reasonable and necessary costs incurred in deploying advanced metering and metering information networks [81]. A subsequent Texas law encourages the development of net metering and advanced meter information networks to allow demand-side energy management and to facilitate demand response initiatives [82].

  Although there is no mandatory smart metering policy, utilities in Texas have been very active in deploying smart meters. The three largest utility companies have all received approval from the PUCT regarding the deployment of smart meters in their territories (see Table 10) [83]. As of August 2010, two million smart meters have been installed, and the total number will reach 6.6 million by the end of 2013. Electric utilities in Texas also established the Smart Meter Texas web portal in 2010, which can provide 15-min energy usage data to retail electric providers and customers with a smart meter [84].
- Customer Privacy Protection Law
  HB2129 sets requirements regarding data security and privacy of smart meters. It states that all meter data, including data used to calculate charges for service, historical load data, and any other proprietary customer information, shall belong to a customer. A customer could allow retail electric

Sustainable Smart Grids, Emergence of a Policy Framework. Table 10 Deployment of smart meters by the three largest utilities in Texas

	Center point	Oncor	AEP Texas
Goal	2.1 million electric meters	3.4 million electric meters	1.1 million electric meters
Achievement as of August 31, 2010	615,518 electric meters	1,251,838 electric meters	78,705 electric meters
Deployment timeline	2009–2012	2008–2012	2009–2013

providers (REPs) to access the data under rules and charges established by the PUCT [81].

- Dynamic Pricing
  A demand response study by FERC found that Texas has the most potential for demand response initiatives, with more than 18 GW expected by 2019 [12]. However, currently there is very little demand response in place, and no mandatory regulations on dynamic pricing. Nevertheless, several electric utility companies offer voluntary dynamic pricing rates. For instance, TOU rate is available for TXU Energy's residential customers who have had smart meters installed at their premises [83]. Participating customers pay 21.9 cent per kWh during summer afternoons (1–6 pm on weekdays from May to October), and 7.9 cent per kWh during off-peak hours.

Smart-Grid Policies of the European Union

The European Union (EU) is the second largest energy market in the world, with over 450 million customers [85]. The objective of European energy policies in the twenty-first century is to achieve a sustainable, competitive, and secure energy supply [86]. Deployment of smart grid forms an essential part of EU's climate change and clean energy initiatives, as it promotes revolution in traditional electricity markets and networks. This section summarizes EU's policies and regulations relating to the deployment of smart-grid technologies. It also examines the smart-grid policy efforts of two EU member countries: Italy and the UK.

Smart-Grid Legislation and Policy Context

- Directive 2001/77/EC
  This Directive requires member states to ensure the transmission and distribution of electricity produced from renewable energy sources without prejudice [87]. Member states are required to publish interconnection standards and rules to facilitate the integration of renewable energy sources into the grid. Transmission and distribution system operators shall provide a comprehensive and detailed estimate of interconnection costs upon customers' request, and publish standard rules regarding the sharing of installation costs.
- Directive 2003/54/EC
  This directive establishes common rules for electricity generation, transmission, distribution, and supply [88]. It mandates member states to publish technical rules and standards governing the interoperability of systems and interconnection activities. Member states are encouraged to implement energy efficiency/demand side management programs to achieve social, economic, and environmental objectives.
- Green Paper on Energy Efficiency or Doing More with Less (2005)
  This Green Paper calls for wide deployment of smart meters and implementation of dynamic pricing programs to promote more economical and rational energy consumption [85]. Policies shall also be designed to encourage the shift from centralized generation to DG.
- Green Paper – A European Strategy for Sustainable, Competitive, and Secure Energy (2006)
  This Green Paper which was published in 2006 emphasizes that Europe has entered into a new energy era [86]. It provides suggestions and options that form the basis of a new energy policy scheme. This document proposes a European grid code that encourages harmonized grid access conditions and allows customers to purchase electricity and gas from suppliers in other member states. It also

suggests that member states develop a plan to increase the interconnection levels between countries.

- Directive 2006/32/EC
  This directive aims to encourage cost-effective and efficient energy consumption in the EU. Member states are required to achieve an energy saving target of 9% by the ninth year of application of this directive. The deployment of appliances and information technologies in residential and commercial sectors will play a significant role in reducing electricity consumption in the future. For instance, this directive recommends intelligent metering systems as one of the eligible energy efficiency improvement measures [89]. Member states are encouraged to subsidize the deployment of improved metering and informative billing.
- Directive 2009/72/EC
  This directive recognizes that innovative pricing formulas, intelligent metering systems, and smart grids are important measures to promote energy efficiency [90]. It mandates member countries to conduct CBA of smart metering programs and requires that 80% of consumers shall be equipped with intelligent metering systems by 2020. This directive also mandates member countries to encourage the development of smart grids to promote decentralized generation and energy conservation.
- Conclusions of the European Council of February 4, 2011
  The Conclusions set the goal of adopting technical standards for electric vehicle charging systems by mid-2011 and for smart grids and meters by the end of 2012 [91].
- Communication "Smart Grid: From Innovation to Deployment"
  This Communication summarizes the current and past policy initiatives that address challenges to smart-grid deployment [92]. Five aspects of government efforts are highlighted: developing common European smart-grid standards, addressing data privacy and security issues, regulatory incentives for smart-grid deployment, smart grids in a competitive retail market in the interest of consumers, and continuous support for innovation and its rapid application.

Smart-Grid Standards

The Conclusions of the European Council of February 4, 2011 confirm that there is an urgent need to adopt European standards for smart grids. To date, the European Commission (EC) has issued three mandates to European Standardization Organizations (ESOs) relating to European standardization policies.

- European Commission Standardization Mandate for Smart Meters (M/441)
  This mandate invites ESOs to develop European standards which will enable interoperability of smart utility meters (electricity, gas, water, and heat) [93].
- European Commission Standardization Mandate for Electric Vehicles (M/468)
  ESOs are requested to develop European standards or to review existing standards to ensure the interoperability and connectivity related to the charging of electric vehicles [94].
- European Commission Standardization Mandate for Smart Grids (M/490)
  This mandate requires ESOs to develop a framework that consists of technical reference architecture, a set of consistent standards and sustainable standardization processes and collaborative tools to enable the continuous standard enhancement and development in the field of smart grids [95].

Government Agencies and Organizations

The EC's Directorate-General for Energy leads the policy development and implementation of energy-related topics, such as smart grids, energy efficiency, security of energy supply, nuclear energy, and renewable energy. Its sub-Directorate B for Security of Supply, Energy Markets & Networks is the most active player in the EU smart grid policy arena. The work of the Directorate-General for Energy is supported by other important government agencies including the Agency for the Cooperation of Energy Regulators (ACER) and the Executive Agency for Competitiveness and Innovation (EACI).

In November 2009, the European Smart Grids Task Force was established to advise the EC on smart-grid policies between 2010 and 2020. It also coordinates and cooperates with other major stakeholders in this area to facilitate smart grids deployment in Europe, including

the Smart Grids European Technology Platform, Smart Grids Forum, and the European Electricity Grids Initiatives (EEGI).

funding mechanisms

The research and development of smart-grid technologies have been receiving financial support from the Framework Program (FPs), the main financial tool through which EU supports research and development activities in a wide range of scientific subjects. The current FP – the Seventh FP (FP7) runs from 2007 to 2013, with a total budget of €50,521 million ($71.5 billion US dollars) [96]. Over the last decade, around €300 million ($424.4 million US dollars) has been spent on smart grid pilot projects [92].

The EC adopted the Recommendation on Mobilizing Information and Communications Technologies to facilitate the transition to an energy-efficient, low-carbon economy in October 2009 [58]. Information and Communications Technologies (ICTs) are seen as important contributors to the achievements of EU's energy and climate goals [97]. Many smart grid projects are funded by the FP-ICT for Energy Efficiency and the Competitiveness and Innovation Framework Program (CIP)-ICT Policy Support Program [98].

- The ADDRESS project
  Active Distribution Network with Full Integration of Demand and Distributed Energy Resources (ADDRESS) is a large-scale project funded by the EC under the seventh FP in the Energy area for the "Smart Energy Networks – Development of Interactive Distribution Energy Networks." The total budget for this project is €16 million ($23 million US dollars), with €9 million ($13 million US dollars) financed by the EC [99]. It is being carried out by a consortium of 25 partners from 11 European countries between 2008 and 2012, under the coordination of one of the largest utilities in Europe – Enel Distribuzione. Partners include universities, research institutes, distribution and transmission network operators, energy supply and retail companies, electric equipment manufacturers, home appliance manufacturers and consultants, and ICT providers and electric equipment manufacturers. The goal of this project is to enable the participation of small and medium customers in the electric market, and finally realize the vision of the European Smart Grids Technology Platform – developing a network that is flexible, reliable, accessible, and economic.

Smart-Grid Policies in Italy and the UK

- Italy
  In line with the provisions of Directive 2009/28/EC, the Italian government issued the "Italian National Renewable Energy Action Plan" in June 2010. The plan provides measures to encourage the modernization of transmission and distribution networks, the integrated management of various generation systems and loads (including electric vehicles), and power generation from renewable sources [100].

  The Interregional Operational Plan for Renewable Energy Sources and Energy Saving was approved by the EC in December 2007, with the aim to "increase the ratio of load supplied by renewable and the energy efficiency, promoting the local development opportunities in four Italian Southern regions: Campania, Puglia, Calabria, Sicilia" [101]. A total of €1.6 billion ($2.3 billion US dollars) was allocated to the program for the period of 2007–2013, with €803 million ($1.23 billion US dollars) provided by the European Regional Development Fund (ERDF) [101]. One focus of this program is to improve the infrastructure of transmission networks to promote renewable energy sources and CHP generation, which receives €100 million funding from ERDF and Italian state funds [100]. In this context, the Ministry of Economic Development and Enel Distribuzione together launched a €77 million "Smart Medium Voltage Networks" project in southern Italy to make the medium voltage distribution networks more favorable to photovoltaic systems with installed capacity between 100 kW and 1 MW [100]. The Italian utility regulator (Autoritàper l' Energia Elettricaedil Gas) has awarded eight tariff-based financial projects on active medium voltage networks, to demonstrate at-scale advanced network management and automation solutions necessary to integrate DG [102].

Italy has one of the largest and most extensive smart metering programs in the world. Enel Distribuzione, the largest power company in Italy and the second listed utility by installed capacity in Europe, has already completed the installation of smart meters in its electrical distribution system. Thirty-two million customers can have access to more efficient and flexible services brought by smart meters, such as the hourly based tariff system introduced in 2005 [103]. The company has plans to install smart meters for its gas distribution grid, and extend the smart metering system to its distribution grids in Spain, where 13 million smart meters will be installed during the period 2010–2015 [103]. Enel Distribuzione also launched the E-mobility Italy program in three Italian cities: Rome, Milan, and Pisa in 2008 [104]. The program will deliver 100 electric vehicles to selected drivers in the three cities, and build 400 intelligent electric vehicle recharging stations.

- United Kingdom

  The renewable target for the UK is to generate 15% of its energy from renewables by 2020, which requires 30% of its electricity to come from renewables by that time [105]. The British government issued the Carbon Plan in 2011, which sets a firm, long-term and legally binding framework to cut emissions by at least 34% by 2020 and 80% by 2050 – below the 1990 baseline [106]. The British government sees smart grids as an effective approach to meet challenges of energy security and climate change, as well as to achieve a low-carbon economy. In the Carbon Plan, smart metering is identified as a way for energy efficiency improvements, as it can change consumer behavior.

  Under Sections 88–91 of the 2008 Energy Act, the Secretary of State is allowed to modify energy distribution and supply licenses to force the license holders to install or facilitate the installation of smart meters [107]. This Act also introduces the FITs for low-carbon electricity generation facilities with a generating capacity less than 5 MW. Eligible technologies include biomass, biofuels, fuel cells, photovoltaics, waves and tides, wind, solar power, geothermal sources, and CHP systems with a capacity of 50 kW or less.

  The Energy Bill 2010–2011, together with its provisions for the new "Green Deal," was first introduced in December 2010. It aims to facilitate the country's energy efficiency improvements by providing financial incentives to householders, private landlords, and businesses [108]. Smart metering is an essential part of the Green Deal.

  In July 2010, the Department of Energy and Climate Change (DECC) and Office of the Gas and Electricity Markets (Ofgem) published the "Smart Metering Implementation Program: Prospectus" which sets out detailed proposals for the delivery of smart and advanced meters to all homes and small businesses in Great Britain. This prospectus sets design requirements, central communications, data management, and the rollout plan for the deployment of smart meters, and it seeks responses from the public on a number of questions [109].

  DECC and Ofgem jointly published the government's response to the Smart Meter Prospectus in March 2011 [110]. According to this document, suppliers are required to provide smart meters to smaller nondomestic sectors, and both smart meters and in-home display (IHD) will be provided to domestic customers. Smart meter equipment and devices will have to meet the technical standards in the Functional Requirements Catalog, which was published alongside this document. With respect to privacy protection, customers will be able to choose how their consumption data is used and by whom, except where data is required for regulatory purposes. The British government expects full rollout of smart metering by 2019. It is estimated that over 50 million electricity and gas meters will be installed, with a total financial investment of over £11 billion ($17.6 billion US dollars) and a net benefit of more than £7 billion ($11.2 billion US dollars) [110]. However, a report published by the National Audit Office concludes that there is a high level of uncertainty with regard to the extent to which smart meters will bring changes in customers' energy consumption patterns [111]. It recommends DECC and Ofgem to develop benefits realization plans and customer engagement strategy to minimize the potential risk.

Smart-Grid Policies of Other Countries

Japan

The electricity supply in Japan is highly reliable with a power failure time per year/per household of only 16 minutes compared to 162 minutes in the U.S. [112]. However, Japan aims to reduce carbon emissions by 30% by 2030 compared to the 1990 level [113]. Renewable energy and energy efficiency are expected to play an important role in achieving this goal. Thus, smart-grid investments are needed.

Japan's deployment approach is slightly different from other countries. Smart-grid deployment is seen as creating an opportunity for Japanese industries to gain competitiveness in the global market. The concept of "smart community," which refers to a new, intelligent, and sustainable way of living, not only stimulates changes in the electricity market, but also motivates innovations in automobiles, telecommunications, and home appliances industries.

The Ministry of Economy, Trade and Industry of Japan (METI) is the major government agency responsible for smart-grid development. Its objectives are to enable further integration of renewable energy, facilitate the development of electric vehicles and the charging infrastructure, and create new services using smart meters and ICT networks [114]. In 2009, the METI invested over $73 million on three demonstration projects: Remote Island Smart Grid Project, Smart Charge Project, and Smart House Project. Technologies that were tested include battery storage, electric vehicle charging system, residential photovoltaics, fuel cells, and demand response appliances. In 2010, the METI launched four large-scale smart community pilot projects in Kansai Science City, Yokohama City, Kitakyushu City, and Toyota City [115]. The primary goal of these projects is to develop Community Energy Management Systems, which are a combination of technologies including smart meters, home energy management systems, building and energy management systems, electric vehicles, photovoltaics, and batteries. Four smart community demonstration projects located in the State of New Mexico (US), Hawaii (US), Lyon (France), and Malaga (Spain) have also been carried out by the New Energy and Industrial Technology Development Organization (NEDO), an administrative branch of the METI [116]. These projects aim to prepare for the large-scale introduction of renewable energy, power storage, and electrical vehicle management systems.

There have been increasing cooperation and collaboration between Japan's public and private sectors in the deployment of smart grids. For instance, the Japan Smart Community Alliance established by NEDO in 2010 provides a platform for the participation of a wide range of stakeholders, including industries, electric utilities, government agencies, and research institutes [117]. Toshiba Corporation, Tokyo Electric Corporation, and the Tokyo Electric Power Company are also working together to launch a venture into the commercialization of smart meters [118]. The large-scale deployment of smart meters will start from 2013, and the goal is to have smart meters installed in all households across Tokyo Electric Power's service area.

Another challenge faced by Japan is energy security, as over 90% of energy consumed by Japan is imported. The Japanese government's goal is to have 70% of its electricity generated from zero-emission sources, and almost double its energy independence by 2030 [113]. In order to achieve this target, the government is developing a FIT scheme to purchase renewable energy generated in Japan. The "New Purchase System for Photovoltaic Electricity" was launched on November 1, 2009 [119]. Surplus electricity generated from solar photovoltaics is purchased at ¥48/kWh ($0.59/kWh) for residential sector, and ¥24/kWh ($0.30/kWh) for industries, businesses, and schools. The buyback prices will decrease each year based on the innovation and price trends of solar photovoltaic technologies.

The Republic of Korea

The electric system of the Republic of Korea is more reliable and efficient compared to many other developed countries [120]. However, the country is highly dependent on imported petroleum and liquefied natural gas. It imports over 90% of the total energy consumed, and has only 2.7% produced from renewable energy sources [121]. The greenhouse gases emissions of Korea also are expected to increase more rapidly than many other developed countries: by 2035, its carbon emissions will increase 35% from the 2002

base line, compared to less than 15% for all the OECD countries [121]. Although as a non-Annex I Party, Korea does not have obligations to reduce carbon emissions under the Kyoto Protocol, the Korean government sets a voluntary goal of reducing its greenhouse gas emissions by 30% below the business-as-usual case by 2020 [121]. Reducing the nation's energy dependence and carbon intensity is one of the top priorities of the Korean government.

The deployment of smart-grid technologies has started since 2005. Korea launched the Power IT National Program in order to develop digital, environmental-friendly and intelligent electric power devices and systems, and advance Korean electric power and electrical industries [122]. Ten projects were selected for systematic implementation, including development of energy management systems, intelligent transmission and distribution networks, advanced substation automation systems, power equipment monitoring systems, power line communication ubiquitous technology, power semiconductor, and consumer portal systems.

In August 2008, President Lee Myung-bak announced "Korea's National Strategy for Green Growth," which proposes a total investment of 107 trillion won (US $101 billion) between 2009 and 2013 [121]. The deployment of smart-grid technologies is a key part of this five-year plan. Among the 27 core green technologies listed in the national plan, more than one third is related to the development of smart grid and smart cities.

The Korea government has announced the "Smart Grid Road Map 2030" as a key step to build a low-carbon, green growth economy in the long run [123]. The roadmap will be implemented in five sectors: smart power grid, smart consumers, smart transportation, smart renewables, and smart electricity services. By 2030, a nationwide smart grid and 27,140 power charge stations for electric vehicles will be built; and the penetration rate of smart meters and AMI will reach 100% by 2020. Besides, Korea will have 11% of its energy from renewables, and achieve a maximum of 10% power reduction by 2030. The annual blackout time per household will be reduced from 15 min in 2012 to 9 min in 2030, and the power transmission and distribution loss rate will decrease from 3.9% in 2012 to 3.0% in 2030. A total of 27.5 trillion won ($25.85 billion US dollars) will be allocated for the technology development and infrastructure construction in this plan, which is expected to generate 50,000 new jobs every year and reduce a total of 230 million tons of greenhouse gases by 2030.

As a first step to implement the Road Map, the Korean government started a pilot program on Jeju Island in June 2009, which consists of a fully integrated smart grid system for 6,000 households, wind farms, and four distribution lines [124]. A total of $50 million public funds and $150 million private funds will be invested between 2009 and 2013. More than 100 companies from automobile, renewable, power, telecommunication, and home appliance industries participate in the program.

The People's Republic of China

Since the 1980s, China's energy consumption has been growing at an unprecedented rate due to the rapid development of its economy. Between 1990 and 2010, its electricity generation increased from 621.2 to 4206.5 Terawatt-hours (TWh) [125]. The nation's annual growth rate of electricity demand exceeded 10% in 2001 and reached 15% in 2003, exceeding the projected growth rate of 6% [126]. The country has experienced several power outages since 2005, and the shortfall in electricity has started to hurt China's economy [126]. In order to meet the increasing demand and secure economic growth, the Chinese government has increased its investment in electric infrastructure. In recent years, China also aims to make the transition from a traditional manufacturing economy to a high-tech and high value-added manufacturing and service economy. The new energy industry and transport system are two key sectors that receive government support.

In May 2009, the State Grid Corporation of China announced the plan for developing a national wide "strong and smart grid" in China by 2020 [127]. The Ultra High Voltage (UHV) transmission and highly efficient distribution transformer, which enable the expansion of transmission and distribution capacity and reduce loss are the key technologies to be developed and deployed. This plan shows that deployment of smart grids in China can be quite different from the rest of the world, especially from the developed

countries. It focuses more on the transmission side than the distribution side, due to the fact that major power generation sources in China, such as coal and hydropower are located in remote areas, and there are huge disparities among power generation in different regions. Other reasons for the focus on transmission might be the relatively primitive structure at the distribution ends, and the unique asset ownership and management structure of utilities and electric markets [128].

The Amendment of the Renewable Energy Law (2009) urges utilities to develop and apply smart grid and energy storage technologies to improve grid operation and management, and facilitate the interconnection of distributed renewable energy [129]. The Chinese government also supports the construction of independent renewable micro-grids in areas not covered by power grids. Promoting the development of clean energy and smart grids is among the top priorities of the government, as noted in the 12th Five-Year Plan that became effective on March 14, 2011 [130–132].

The 12th Five-Year Plan sets separate targets for energy intensity (16% reduction by 2015), non-fossil fuel energy (11.4% of the total primary energy consumption by 2015), and carbon emissions per unit Gross Domestic Product (GDP) (17% reduction by 2015) [132]. Smart grids and clean energy technologies are seen as effective approaches to achieve these targets. New energy industry (nuclear, wind, solar, biomass, and smart grids) and new energy vehicle industry (plug-in hybrid vehicles and electric vehicles) are identified as two of the seven strategic emerging industries that would receive financial and regulatory support from the government. By 2015, several long-distance UHV transmission lines and 200,000 km of transmission lines (333 kV and above) will be constructed. The Plan also proposes the "Rural Electricity Supply Project" to upgrade the rural electric grid and meet the increasing demand of the rural areas. Some of the targets include: developing 1,000 photovoltaics demonstration villages, 200 green energy counties, 300 hydropower and rural electrification counties, and 10,000 MW small hydropower. Between 2011 and 2015, China will invest 286 billion yuan ($44 billion US dollars) in smart-grid deployment [133].

Countries are in different stages of smart-grid deployment. Smart-grid policies are often designed to address the needs and challenges faced by countries. Table 11 summarizes the energy and climate change targets of the five nations and regions, as well as the drivers and focuses of their smart-grid policies.

International Collaboration

The SmartGrids European Technology Platform was established in 2004, with an aim to enhance the level of coherence between the European, national, and regional efforts addressing smart grids. One important role of this platform is to cooperate with other countries, especially North America and Japan, to ensure international development paths for smart grids are complementary and consistent with the development of commercial products [134].

The IEA Implementing Agreement on Electricity Networks Analysis, Research and Development (ENARD) was developed by 14 IEA member countries in July 2006. Its mission is to provide comprehensive and unbiased information, data, and advice to key stakeholders and policymakers of the issues relating to current and anticipated developments in electricity transmission and distribution networks [135]. Some of the work programs that are closely linked to smart grids include Annex II (DG system integration), Annex III (infrastructure asset management), and Annex IV (transmission system issues). ENARD is currently focusing its activities within the IEA member countries; however, it is open to participation by non-IEA member countries, private sectors, and nongovernmental organizations.

Established in April 2010, the Global Smart Grid Federation (GSGF) brings together the key smart grid stakeholders around the world, such as US GridWise Alliance, Smart Grid Australia, Smart Grid Canada, Smart Grid Ireland, Korean Smart Grid Association, India Smart Grid Forum, and the Japan Smart Community Alliance [136]. Its goals are to facilitate the collaboration of governments and nongovernmental organizations, to support the development of smart-grid technologies and foster knowledge sharing. The International Smart Grid Action Network (ISGAN) was launched at the first Clean Energy Ministerial in Washington, D.C. in July 2010 to accelerate the development of smart-grid technologies at the global level. ISGAN focuses on five principal areas including policy, standards, and regulation; finance and business

Sustainable Smart Grids, Emergence of a Policy Framework. Table 11 National targets, policy drivers and focuses by country

	Targets			
	Carbon reduction	Renewable energy (share of total primary energy supply)	Policy drivers	Policy focuses
USA	17% below 2005 level by 2020	Varies across states: CA – 33% by 2020 TX – 5,880 MW by 2020 NY – 29% by 2015 GA – no target	Power system reliability; Renewable energy and energy efficiency; Economic revitalization	Technical and operational standards; Smart meters; Dynamic pricing and demand response programs
EU	20% below 1990 level by 2020	20% by 2020	Renewable energy and energy efficiency; Carbon emissions reduction	Technical and operational standards; Smart meters
Japan	30% below 1990 by 2030	13% by 2030	Energy security; Carbon emissions reduction; Enhancing competitiveness of domestic industries	Smart community; Solar photovoltaic generation
Korea	30% below BAU by 2020	11% by 2030	Energy security; Carbon emissions reduction; Enhancing competitiveness of domestic industries	Smart power grid; Smart consumers; Smart transportation; Smart renewables; Smart electricity services
China	Carbon intensity: 17% below 2011 by 2015	11.4% by 2015	Economic development; Reducing power generation disparities between regions; Reducing energy/carbon intensity; Strategic economic restructuring	Ultrahigh voltage (UHV) regional transmission; Upgrading and modernizing urban and rural electric grid

models; technology and systems development; user and consumer engagement; and workforce skills and knowledge [137]. It includes four projects: the global smart grid inventory, smart grid case studies, benefit-cost analyses, and toolkits and synthesis of insights for decision makers.

Future Directions

As the interoperability of technologies is essential for a large-scale and integrated deployment of smart grids, development of standards at the national and global level will be particularly important in the future. Establishment of lead agencies to coordinate efforts at various levels of governments would facilitate the standardization process, as well as address the cyber security issue across all sectors.

The electric power industry is facing tremendous opportunities and becoming increasingly important in the new emerging low-carbon economy. The costs required for a full deployment of the smart grid are large. Currently, government is still the key player in smart grid investments. This suggests the need for a policy framework that attracts private capital investment, especially from renewable project developers and communication and information technology companies.

A competitive electricity market that encourages variable business models could enhance the flexibility of the electricity system and support an increasing

penetration of renewable generation technologies. Reforming the rate design mechanisms that are currently discouraging utilities' investment in advanced technologies, and ensuring that costs and benefits are shared among all stakeholders are also important future directions. Regulatory changes that remove barriers to a competitive energy market could also optimize overall operations and costs, hence increasing the net social benefits from smart grids.

As the deployment of smart grids progresses, demand response and DG may significantly reduce peak demand and make some generation facilities redundant. This requires sophisticated resource planning and CBA at the early stages of smart-grid deployment. Smart grid customer policies, such as dynamic pricing and customer protection, are highly dependent on the understanding of customer behavior. New policies should be developed based on social science studies on consumer feedback and behavior changes in response to smart grid technologies and regulations.

Collaboration on smart-grid standards and experience sharing of demonstration projects can reduce repetition and overlap in smart-grid deployment efforts. Sharing best practices can be particularly beneficial to those developing countries, where electricity infrastructure is expanding rapidly.

Conclusion

This entry underscores the novelty of emerging smart-grid policies. Along with the recent introduction of smart-grid technologies has emerged a new generation of regulations and fiscal policies to ensure that the public's interests are protected.

Access to real-time metered data is illustrative of the new issues requiring public regulation. States are beginning to set requirements regarding data security and privacy of smart meters. Texas, for example, has determined that all meter data, including data used to calculate charges for service, historical load data, and any other proprietary customer information, will belong to a customer; however, customers can allow retail electric providers to access the data under rules and charges established by the Public Utility Commission of Texas.

The ownership of renewable energy credits from customer-owned renewable facilities is another issue that is only now being clarified. The issue is important because RECs have significant economic value, and clear rules and regulations regarding their ownership could help reduce confusion and uncertainties associated with smart-grid investment. This policy issue is also contentious as it involves the design and consideration of several policy regimes, including renewable electricity standards, net metering, interconnection policies, and utility subsidies for renewable projects.

As is typical of emerging policies designed to address issues associated with technological innovations, there is great variability in the goals and the design of smart-grid policies.

- For example, while most states have net metering and interconnection standards, the specifics of these policies vary widely. Due to different preferences in promoting renewable technologies, eligible technologies and customer types vary across net metering and interconnection standards. The application and evaluation procedures for net metering and interconnection also reflect variations in grid safety and reliability concerns.
- Numerous different types of dynamic pricing rates have emerged over the past decade. As might be expected, different pricing regimes have gained prominence in different market segments. Most often, pilot projects have been first launched by large industrial customers, followed by commercial and large nonresidential customers. Variability among dynamic pricing rates also reflects the differences in the policy goals of cost recovery and demand response programs. In general, opt-out options and bill stabilization measures are provided for customer protection. Outreach and education activities are often conducted to increase public awareness of dynamic rates.
- There also is a wide array of policies to support DG-especially renewables. (More limited efforts have addressed the deployment of fuel cells and CHP systems.) Both regulatory policies and financial incentives are widely used to support DG investments. For example, 29 states have implemented a renewable electricity standard [20]. Financial incentive range from FITs to production tax credits, investment tax credits, and loans. To date, 34 states provide loan programs and 24 states provide tax credits for renewables [20].

Despite this wide-ranging policy variability, some policy principles are emerging:

- Cost estimation and allocation are critical, as they could facilitate investment in new smart grid infrastructures. Policies have also been designed to set up cost-sharing rules between the private and public sector, and sometimes, costs are allocated to all customers that benefit from the project. Government subsidies are often used to constrain interconnection costs to affordable levels. For instance, eligible customers for net metering in California are exempted from fees charged by the government, and pay only the costs associated with their interconnection facilities.
- CBA and evaluation metrics are becoming essential, and some government agencies are beginning to require the collection of such information. In some cases, government agencies will invest in smart metering technologies and will subsidize smart-grid investments only if planning and evaluation data show that the subsidies generate more benefits than costs.

Evidence from the past decade suggests that the rapid and widespread deployment of smart-grid technologies will not occur without supporting policies. This review of emerging smart-grid policies in the United States, European Union, Japan, Korea, and China suggests that considerable progress has been made to develop effective policy frameworks. Nevertheless, further advances are needed to harmonize policies across nations, states, and localities, and to learn from recent experiences with this new generation of electric grid technologies [138].

Bibliography

Primary Literature

1. The European Smart Grid Task Force (2010) Task Force Smart Grids – vision and work programme
2. U.S. Department of Energy (2008) Metrics for measuring progress toward implementation of the smart grid: results of the breakout session discussions at the Smart Grid Implementation Workshop, Washington, DC
3. The Electricity Advisory Committee (2008) Smart grid: enabler of the new energy economy, U.S. Department of Energy, Washington, DC
4. U.S. Department of Energy (2008) The smart grid: an introduction. Washington, DC
5. Kurita A, Sakurai T (1988) The power system failure on 23 July 1987 in Tokyo. Paper presented at the 27th IEEE Conference on Decision and Control, Austin, TX
6. U.S.-Canada Power System Outage Task Force (2004) Final report on the 14 August 2003 blackout in the United States and Canada: causes and recommendations. U.S. Department of Energy/Ministry of Natural Resources, Washington, DC; Ottawa, Canada
7. The White House (2006) The federal response to hurricane Katrina: lessons learned. http://library.stmarytx.edu/acadlib/edocs/katrinawh.pdf
8. U.S. Department of Energy (2009) Smart grid system report. Washington, DC
9. National Energy Technology Laboratory (2007) The NETL modern grid initiative powering our 21st-century economy: barriers to achieving the modern grid. U.S. Department of Energy, Washington, DC
10. Brown A, Salter R (2010) Smart grid issues in state law and regulation. Galvin Electricity Initiative
11. International Energy Agency (2010) Energy technology perspectives 2010. OECD/IEA, Paris
12. The Brattle Group, Freeman Sullivan & Co. and Global Energy Partners, LLC (2009) A national assessment of demand response potential. Federal energy regulatory commission staff report. Federal Energy Regulatory Commission, Washington, DC
13. Tseng P (2007) Modeling regional electricity generation. U.S. Energy Information Administration, Washington, DC
14. U.S. Energy Information Administration (2010) International energy outlook 2010. Washington, DC
15. U.S. Energy Information Administration (2011) Emissions of greenhouse gases in the U.S. Retrieved 23 June 2011, from http://www.eia.gov/environment/emissions/ghg_report/ghg_overview.cfm
16. U.S. Energy Information Administration (2010) Electric power industry 2009: year in review. Retrieved 23 June 2011, from http://www.eia.gov/cneaf/electricity/epa/epa_sum.html
17. California Public Utilities Commission (2011) Net Surplus Compensation. Retrieved 21 June 2011, from http://www.cpuc.ca.gov/PUC/energy/DistGen/netsurplus.htm
18. California Public Utilities Commission Energy Division (2005) Update on determining the costs and benefits of California's Net Metering Program as required by Assembly Bill 58
19. Public Law 109–58: Energy Policy Act of 2005. (119 Stat. 594; Date: 8/8/2005). Text from: United States Public Laws. Available from: ProQuest® Congressional; Accessed 23 May 2011
20. Database of State Incentives for Renewables & Efficiency (2011) Summary maps. Retrieved 20 June 2011, from http://www.dsireusa.org/summarymaps/index.cfm?ee=1&RE=1
21. Doris E, Busche S et al (2009) Net Metering Policy Development in Minnesota: Overview of Trends in Nationwide Policy Development and Implications of Increasing the Eligible

System Size Cap. National Renewable Energy Laboratory, Golden, CO
22. Federal Energy Regulatory Commission (2006) Generator Interconnection. Retrieved 21 June 2011, from http://www.ferc.gov/industries/electric/indus-act/gi.asp
23. National Association of Regulatory Utility Commissioners (2003) Model interconnection procedures and agreement for small distributed generation resources. U.S. Dept. of Energy, Washington, DC
24. Institute of Electrical and Electronic Engineers Standards Association (2010) 1547 series of interconnection standards. Retrieved 21 June 2011, from http://grouper.ieee.org/groups/scc21/dr_shared/
25. Brown MA, Chandler J et al (2009) Making homes part of the climate solution: policy options to promote energy efficiency. Oak Ridge National Laboratory, Oak Ridge, TN
26. Federal Energy Regulatory Commission (2011) Assessment of demand response and advanced metering staff report. Washington, DC
27. Borenstein S, Jaske M et al (2002) Dynamic pricing, advanced metering and demand response in electricity markets. The Center for the Study of Energy Markets (CSEM) working paper series. University of California Energy Institute, Berkeley, CA
28. Faruqui A, Hledik R (2009) Transitioning to dynamic pricing. The Brattle Group, San Francisco, CA
29. Faruqui A, Sergici S (2009) Household response to dynamic pricing of electricity – a survey of the experimental evidence. The Brattle Group, San Francisco, CA
30. Faruqui A, Palmer J (2011) Dynamic pricing of electricity and its discontents. The Brattle Group, San Francisco, CA
31. Faruqui A, Hledik R et al (2007) The power of five percent: how dynamic pricing can save $35 billion in electricity costs. The Brattle Group, San Francisco, CA
32. Renewable Energy Policy Network for the 21st Century (REN21) (2011) Renewables 2010 global status report. REN21 Secretariat, Paris
33. Couture TD, Cory K et al (2010) A policymaker's guide to feed-in tariff policy design. National Renewable Energy Laboratory, U.S. Department of Energy, Golden, CO
34. DB Climate Change Advisors (2010) GET FiT program: global energy transfer feed-in tariffs for developing countries, Deutsche Bank Group
35. KEMA (2009) Electricity storage: policy issues. Retrieved 13 Jul 2011, from http://www.kema.com/Images/KEMA%20Energy%20Storage%20Policy%20Briefing.pdf
36. Executive Office of the President of the United States (2011) A policy framework for the 21st century grid: enabling our secure energy future. Executive Office of the President of the United States, Washington, DC
37. Public Law 110–140: Energy Independence and Security Act of 2007. (121 Stat. 1492; Date: 12/19/2007). Text from: United States Public Laws. Available from: ProQuest® Congressional; Accessed 3 June 2011
38. Public Law 111–5: American Recovery and Reinvestment Act of 2009. (123 Stat. 115; Date: 02/17/2009). Text from: United States Public Laws. Available from: ProQuest® Congressional; Accessed 6 June 2011
39. U. S. Department of Energy (2011) American Recovery & Reinvestment Act – Recovery Act Overview. Retrieved 21 June 2011, from http://www.oe.energy.gov/american_recovery_reinvestment_act.htm
40. California Public Utilities Commission (1995) California Public Utilities Code Section 2827
41. The Public Utilities Commission of the State of California (1999) Order instituting rulemaking into distributed generation
42. California Public Utilities Commission (2006) Rule 21 model rule draft to implement D.05-08-013
43. California Public Utilities Commission (2004) Administrative law judge and assigned commissioner's ruling adopting a business case analysis framework for advanced metering infrastructure. California Public Utilities Commission. Rulemaking 02-06-001
44. California Public Utilities Commission (2006) Final opinion authorizing Pacific Gas And Electric Company to deploy advanced metering infrastructure. Decision 06-07-027
45. California Public Utilities Commission (2009) Decision on Pacific Gas and Electric Company's Proposed Upgrade to the Smart Meter Program. Decision 09-03-026
46. California Public Utilities Commission (2007) Opinion approving settlement on San Diego Gas & Electric Company's advanced metering infrastructure project. Decision 07-04-043
47. California Public Utilities Commission (2008) Decision approving settlement on Southern California Edison Company advanced metering infrastructure deployment. Decision 08-09-039
48. California Public Utilities Commission (2009) An act to add Chapter 4 (commencing with Section 8360) to Division 4.1 of the Public Utilities Code, relating to electricity. Senate Bill No. 17
49. California Public Utilities Commission (2010) Decision adopting requirements for smart grid deployment plans pursuant to Senate Bill 17 (PADILLA), Chapter 327, Statutes of 2009. Decision 10-06-047
50. California Public Utilities Commission (2010) An act to add Chapter 5 (commencing with Section 8380) to Division 4.1 of, and to repeal Section 393 of, the Public Utilities Code, relating to public utilities. SB 1476
51. California Public Utilities Commission (2005) Decision closing this rulemaking and identifying future activities related to demand response. Decision 05-11-009
52. California Public Utilities Commission (2006) Decision adopting default critical peak pricing for 2007. Decision 06-05-038
53. California Public Utilities Commission (2010) Decision on peak day pricing for Pacific Gas and Electric Company. Decision 10-02-032
54. Southern California Edison (2010) Demand Response Programs. Retrieved 27 June 2011, from http://asset.sce.com/Documents/Shared/100818_Demand_Response_Program_Guide.pdf

55. California Public Utilities Commission (2010) An act to amend Section 9620 of, and to add Chapter 7.7 (commencing with Section 2835) to Part 2 of Division 1 of, the Public Utilities Code, relating to energy. AB 2514
56. California Public Utilities Commission (2005) Opinion clarifying participation of renewable distributed generation in the renewable portfolio standards program. Decision 05-05-011
57. California Public Utilities Commission (2007) Opinion adopting methods to determine the renewable energy credits from renewable distributed generation. Decision 07-01-018
58. California Public Utilities Commission (2001) Interim Opinion: Implementation of Public Utlities Code Section 399.15(b), Paragraphs 4–7; load control and distributed generation initiatives. Decision 01-03-073
59. California Public Utilities Commission (2011) Assigned commissioner's ruling directing temporary suspension of accepting customer reservation requests under the self-generation incentive program. In: Proceeding R10-05-004, San Francisco
60. Brown MA, Gumerman E, Baek Y, Wang J, Morris C, Wang Yu (2011) Renewable energy in the South. Southeast Energy Efficiency Alliance, Atlanta, GA. Retrieved 29 June 2011, from http://www.seealliance.org/PDFs/RENEWABLE%20ENERGY%20IN%20THE%20SOUTH.pdf
61. Georgia General Assembly (2001) The Georgia Cogeneration and Distributed Generation Act of 2001. Senate Bill 93
62. Georgia Power (2011) Electric service tariff: renewable and nonrenewable resources schedule: RNR-7. Retrieved 29 June 2011, from http://www.georgiapower.com/pricing/pdf/11.10_RNR-7.pdf
63. Georgia Power (2011) Your meter is about to get smarter. Retrieved 29 June 2011, from http://www.georgiapower.com/residential/smartmeter.asp
64. Charles J, Black Energy Economics (2011) Dynamic Pricing Evaluation for Washington. National Association of Regulatory Utility Commissioners (NARUC) Grants & Research Department
65. Georgia Power (2011) Business pricing – Georgia power. Retrieved 29 June 2011, from http://georgiapower.com/pricing/gpc_rates.asp
66. State of New York Public Service Commission (1997). New York Consolidated Laws, Public Service Law, Article 4. Provisions Relating to Gas and Electrical Corporations; Regulation of Price of Gas and Electricity. NY CLS Pub Ser § 66-j & 66-l
67. State of New York Public Service Commission (1999) Opinion and oder adopting standard interconnection requirements for distributed generation units. Case 94-E-0952
68. New York State Public Service Commission (2010) New York state standardized interconnection requirements and application process for new distributed generators 2 MW or less connected in parallel with utility distribution systems
69. State of New York Public Service Commission (1997) Opinion and order establishing regulatory policies for competitive metering. Opinion No. 97-13.Case 94-E-0952
70. State of New York Public Service Commission (2006) Order relating to electric and gas metering services. Case 94-E-0952, Case 00-E-0165, Case 02-M-0514
71. State of New York Public Service Commission (2005) Order instituting further proceedings and requiring the filling of draft tariffs. Case 03-E-0641
72. State of New York Public Service Commission (2006) Order denying petitions for rehearing and clarification in part and adopting mandatory hourly pricing requirements. Case 03-E-0641
73. Consolidated Edison Company of New York, I (2009) Mandatory hourly pricing (MHP) program. Retrieved 1 Jul 2011, from http://www.coned.com/escos/news/ESCONewsletters/2009/ESCO%20Newsletter_2009-23.pdf
74. State of New York Public Service Commission (2011) CASE 09-E-0717 proceeding on motion of the commission as to the rates, charges, rules and regulation of rochester gas and electric corporation for electric service: plan for implementation of expansion of mandatory hourly pricing
75. Public Utility Commission of Texas (2008) Chapter 25. Substantive rules applicable to electric service providers – metering for distributed renewable generation. § 25.213
76. Public Utility Commission of Texas (2009). Chapter 25. Substantive rules applicable to electric service providers – arrangements between qualifying facilities and electric utilities. §25.242 (h)
77. Austin Energy (2010) Distributed generation from renewable resources rider. Retrieved 13 Jul 2011, from http://www.austinenergy.com/About%20Us/Rates/distributedGenerationFromRenewableSources.htm
78. Public Utility Commission of Texas (2001) Chapter 25. Substantive rules applicable to electric service providers – §25.211 interconnection of on-site distributed generation (DG). §25.211
79. Public Utility Commission of Texas (1999) Chapter 25. Substantive Rules applicable to electric service providers – §25.212 Technical requirements for interconnection and parallel operation of on-site distributed generation. §25.212
80. Public Utility Commission of Texas (2002) Distributed generation interconnection manual
81. Public Utility Commission of Texas (2005) An act relating to energy-saving measures that reduce the emission of air contaminants. H.B. No. 2129
82. Public Utility Commission of Texas (2007) An act relating to energy demand, energy load, energy efficiency incentives, energy programs, and energy performance measures. H.B. No. 3693
83. Public Utility Commission of Texas (2010) Report to the 82nd Texas legislature: a report on advanced metering as required by House Bill 2129, Austin
84. Smart Meter Texas (2011) Frequently Asked Questions. Retrieved 28 June 2011, from https://www.smartmetertexas.com/CAP/public/learn_more/learn_more_ faq.html#a2
85. Commission of the European Communities (2005) Green paper on energy efficiency or doing more with less. COM (2005) 265 final, Brussels

86. Commission of the European Communities (2006) Green paper: a european strategy for sustainable, competitive and secure energy. COM(2006) 105 final, Brussels
87. The European Parliament and the Council of the European Union (2001) Directive 2011/77/EC of the European Parliament and of the Council of 27 September 2001 on the promotion of electricity produced from renewable energy sources in the internal electricity market. OJ L 283/33, Official Journal of the European Communities
88. The European Parliament and the Council of the European Union (2003) Directive 2003/54/EC of the European Parliament and of the Council of 26June 2003concerning common rules for the internal market in electricity and repealing Directive 96/92/EC.OJ L 176/37, Official Journal of the European Communities
89. The European Parliament and the Council of the European Union (2006) Directive 2006/32/EC of the European Parliament and of the Council on energy end-use efficiency and energy services and repealing Council Directive 93/76/EEC. The European Parliament and the Council of the European Union, Official Journal of the European Union. OJ L 114/64, Official Journal of the European Communities
90. The European Parliament and the Council of the European Union (2009) Directive 2009/72/EC of the European Parliament and of the Council of 13 July 2009 concerning common rules for the internal market in electricity and repealing Directive 2003/54/EC. The European Parliament and the Council of the European Union, Official Journal of the European Union. OJ L211/55, Official Journal of the European Communities
91. General Secretariat of the Council (2011) European Council 4 February 2011-conclusions, Brussels
92. European Commission (2011) Communication from the Commission to the European Parliament, The Council, The European Economic and Social Committee and the Committee of the Regions: smart grids: from innovation to deployment. COM (2011) 202 Final
93. European Commission (2009) Standardization mandate to CEN, CENELEC and ETSI in the field of measuring instruments for the development of an open architecture for utility meters involving communication protocols enabling interoperability, M/441 EN. European Commission, Brussels
94. European Commission (2010) Standardization Mandate to CEN, CENELEC and ETSI concerning the charging of electric vehicles, M/468 EN. European Commission, Brussels
95. European Commission (2011) Standardization mandate to European Standardization Organizations (ESOs) to support European Smart Grid Deployment, M/490. European Commission-Directorate General for Energy, Brussels
96. European Commission (2011) Understand FP7. Retrieved 5 Jul 2011, from http://cordis.europa.eu/fp7/faq_en.html
97. The Commission of the European Communities (2009) Commission recommendation of 9.10.2009 on mobilising information and communications technologies to facilitate the transition to an energy-efficient, low-carbon economy. Sec (2009)1315, Sec(2009)1316. Commission of the European Communities, Brussels
98. European Commission (2011) ICT for sustainable growth. Retrieved 6 June 2011, from http://cordis.europa.eu/fp7/ict/sustainable-growth/energy_en.html#smartgrids
99. ADDRESS (2011) Towards the smart grids of the future. Retrieved 5 Jul 2011, from http://www.addressfp7.org/
100. Italian Ministry for Economic Development (2010) Italian National Renewable Energy Action Plan
101. European Commission (2007) Development Programmes - Operational Programme Renewable Energy and Energy Efficiency. Retrieved 5 Jul 2011, from http://ec.europa.eu/regional_policy/country/prordn/details_new.cfm?gv_PAY=BG&gv_reg=ALL&gv_PGM=1040&gv_defL=4&LAN=7
102. International Energy Agency (2011) Technology roadmap – smart grids. OECD/IEA, Paris
103. Enel (2011) Smart metering system. Retrieved 5 Jul 2011, from http://www.enel.com/en-GB/innovation/project_technology/zero_emission_life/smart_networks/smart_meters.aspx?it=0
104. Enel Distribuzione (2011) E-mobility. Retrieved 5 Jul 2011, from http://www.enel.com/en-GB/innovation/project_technology/zero_emission_life/mobile_sustainability/e-mobility.aspx?it=-2
105. Redpoint Energy and Trilemma UK (2010) Electricity market reform analysis of policy options
106. HM Government (2011) Carbon plan. Department of Energy and Climate Change
107. UK Parliament (2008) Energy Act 2008
108. The UK Parliament (2011) Energy Bill [HL] 2010–11. Retrieved 5 Jul 2011, from http://services.parliament.uk/bills/2010-11/energyhl.html
109. Department of Energy and Climate Change and Office of the Gas and Electricity Markets (2010) Smart metering implementation programme: prospectus
110. Department of Energy and Climate Change and Office of the Gas and Electricity Markets (2011) Smart metering implementation programme: response to prospectus consultation
111. National Audit Office (2011) Department of Energy and Climate Change: preparations for the roll-out of smart meters, London
112. Nakanishi H (2010) Japan's Approaches to Smart Community. Technical regulations, standards and conformity assessment policy division. Ministry of Economy, Trade and Industry, Japan
113. Ministry of Economy, Trade and Industry, Japan (2010) The strategic energy plan of Japan. Retrieved 6 Jul 2011, from http://www.meti.go.jp/english/press/data/pdf/20100618_08a.pdf
114. Ito S (2009) Japan's initiative on smart grid – a proposal of nature grid. Information Economy Division, Ministry of Economy Trade and Industry (METI)
115. Ministry of Economy, Trade and Industry, Japan (2010) Announcement of master plans for the demonstration of next-generation energy and social systems. Retrieved 6 Jul 2011, from http://www.meti.go.jp/english/press/data/20100811_01.html

116. New Energy and Industrial Technology Development Organization (2011) NEDO projects – news list (2011). Retrieved 9 June 2011, from http://www.nedo.go.jp/english/archives2011_index.html
117. Japan Smart Community Alliance (2010) What's JSCA. Retrieved 5 Jul 2011, from https://www.smart-japan.org/english/tabid/103/Default.aspx
118. Yogasingam A (2009) Toshiba partners with two companies to commercialize smart meters, EE Times
119. Ministry of Economy, Trade and Industry, Japan (2009) The new purchase system for photovoltaic electricity will be launched 1 Nov 2009. Retrieved 7 Jul 2011, from http://www.meti.go.jp/english/press/data/20090831_02.html
120. Bae H, Wheelock C (2010) Smart grid in Korea-smart power grid, consumers, transportation, renewable energy, and electricity service: market analysis and forecasts, PikeResearch
121. United Nations Environment Programme (UNEP) (2010) Overview of the Republic of Korea's National Strategy for Green Growth
122. Ministry of Knowledge Economy and Korea Smart Grid Institute (2005) 10 Power IT Projects. Retrieved 7 Jul 2011, from http://www.smartgrid.or.kr/Ebook/10POWER_IT_PROJECTS.PDF
123. Ministry of Knowledge Economy and Korea Smart Grid Institute (2010) Korea's smart grid roadmap 2030: laying the foundation for low carbon, green growth by 2030. Retrieved 7 Jul 2011, from http://www.greentechmedia.com/images/wysiwyg/News/SG-Road-Map.pdf
124. Korea Smart Grid Institute (2010) Korea's Jeju smart grid test-bed overview. Retrieved 9 June 2011, from http://www.smartgrid.or.kr/10eng3-1.php
125. BP (2011) BP Statistical Review of World Energy June 2011. Retrieved 12 Jul 2011, from http://www.bp.com/sectionbodycopy.do?categoryId=7500&contentId=7068481
126. Austin A (2005) Energy and power in China: domestic regulation and foreign policy. The Foregin Policy Centre, London
127. State Grid Corporation of China (2011) The acceleration of smart grids. Retrieved 5 Jul 2011, from http://www.sgcc.com.cn/ztzl/newzndw/cyfz/03/243983.shtml
128. Li J (2009) From strong to smart: the Chinese smart grid and its relation with the globe, Asia energy platform
129. The National People's Congress Standing Committee (2009) Renewable Energy Law of the People's Republic of China (Amended)
130. Xinhua News Agency (2010) Report on the work of the government of China 2010, Beijing
131. Xinhua News Agency (2011) Report on the work of the government of China 2011, Beijing
132. Xinhua News Agency (2011) The 12th five-year plan for National Economy and Social Development of the People's Republic of China, Beijing. Retrieved 2 Jul 2011, from http://www.gov.cn/2011lh/content_1825838.htm
133. Smart Grid China Summit (2011) China's leading smart grid gathering for interaction and knowledge sharing. Retrieved 10 Jul 2011, from http://www.smartgridchinasummit.com/smartgrid/
134. Directorate-General for Research (2006) European smart grids technology platform -vision and strategy for Europe's electricity networks of the future, Brussels
135. Baker JN (2011) International energy agency implementing agreement on electricity networks analysis, research and development: programme of work. International Energy Agency
136. Global Smart Grid Federation (2011) About the global smart grid federation. Retrieved 1 Jul 2011, from http://www.globalsmartgridfederation.org/about.html
137. The International Smart Grid Action Network (2011) Fact sheet: international smart grid action network. Retrieved 2 Jul 2011, from http://www.cleanenergyministerial.org/pdfs/factsheets/CEM2_Fact_Sheet_ISGAN_07April2011.pdf
138. Brown MA, Sovacool BK (2011) Climate change and global energy security: technology and policy options. MIT Press, Cambridge, MS

Books and Reviews

Gellings CW (2009) The smart grid: enabling energy efficiency and demand response. Fairmont, Lilburn, GA

Heffner G (2011) Smart grid – smart customer policy needs. An IEA paper submitted to the Energy Efficiency Working Party. International Energy Agency, Paris

Willrich M (2009) Electricity transmission policy for America: enabling a smart grid, end-to-end. Energy innovation working paper series, Massachusetts Institute of Technology

Sustainable Transportation

Mehrdad Ehsani
Department of Electrical and Computer Engineering, Texas A&M University, College Station, TX, USA

Article Outline

Glossary
Definition of the Subject
Introduction
Sustainable Transportation: Definition
Sustainable Transportation: Solutions
Sustainable Transportation: Types of Vehicles and Technologies
Bibliography

Glossary

Conventional vehicle A vehicle with an internal combustion engine alone.

Electric vehicle A vehicle with an electric motor and a battery bank for propulsion.

Hybrid vehicle A vehicle having a combination of internal combustion engine and electric motor for propulsion.

Hydrocarbons Organic fuels consisting mainly of hydrogen and carbon atoms from fossil or other sources.

Sustainable Compatible with long-term life on earth.

Transportation Vehicle and fuel technology complex.

Definition of the Subject

Sustainable transportation, as used in this entry, refers to vehicle and fuel technologies whose availability and environmental impacts are compatible with sustained life and economic development on the planet. The sustainable vehicle technologies focus on the fuel efficiency, operation, environmental impact, and availability of the raw materials for fabrication. The sustainable fuel technologies focus on long-term availability and environmental impact. These two foci are intimately coupled and make sustainable transportation highly multidisciplinary.

Introduction

The development of internal combustion engine (ICE) vehicles, especially automobiles, is one of the greatest achievements of modern technology. Automobiles have made great contributions to the growth of modern society by satisfying many of its needs for mobility in everyday life. The rapid development of the automotive industry, unlike that of any other industry, has prompted the progress of human society from a primitive one to a highly developed industrial society. However, the large number of automobiles in use around the world has caused and continues to cause serious problems for the environment and human life. Air pollution, global warming, and the rapid depletion of the Earth's petroleum resources are now problems of paramount concern [1]. Around the world, there were about 900 million cars and light trucks on the road in 2009; they burn over 260 billion gallons of gasoline and diesel fuel yearly [2, 3]. These numbers are increasing rapidly. According to the *Wall Street Journal*, there could be one billion cars on the road by 2020; Forrester Research puts the number at 1.2 billion but it could be higher [4]. According to the Institute for the Analysis of Global Security, world oil consumption will grow by 60% between now and 2020, with India and China leading the charge (China is predicted to overtake the United States as the world's biggest car market in 20 years; India could follow 10 years later) [4].

Air Pollution

At present, all vehicles rely on the combustion of hydrocarbon fuels to derive the energy necessary for their propulsion. Combustion is a reaction between the fuel and the air that releases heat and combustion products. The heat is converted to mechanical power by an engine and the combustion products are released to the atmosphere. A hydrocarbon is a chemical compound with molecules made up of carbon and hydrogen atoms. Ideally, the combustion of a hydrocarbon yields only carbon dioxide and water, which do not harm the environment. Indeed, green plants "digest" carbon dioxide by photosynthesis. Carbon dioxide is a necessary ingredient in vegetal life. Animals do not suffer from breathing carbon dioxide unless its concentration in air is such that oxygen is almost absent.

Actually, the combustion of hydrocarbon fuel in combustion engines is never ideal. Besides carbon dioxide and water, the combustion products contain a certain amount of nitrogen oxides (NO_x), carbon monoxides (CO), and unburned hydrocarbons (HC), all of which are toxic to human health.

Nitrogen Oxides Nitrogen oxides (NO_x) result from the reaction between nitrogen in the air and oxygen. Theoretically, nitrogen is an inert gas. However, the high temperatures and pressures in engines create favorable conditions for the formation of nitrogen oxides. Temperature is by far the most important parameter in nitrogen oxide formation. The most commonly found nitrogen oxide is the nitric oxide (NO), although small amounts of nitric dioxide (NO_2) and traces of nitrous oxide (N_2O) are present.

Once released in the atmosphere, NO reacts with oxygen to form NO_2. This is later decomposed by the sun's ultraviolet radiation back to NO and highly reactive oxygen atoms that attack the membranes of living cells. Nitrogen dioxide is partly responsible for smog; its brownish color makes smog visible. It also reacts with atmospheric water to form nitric acid (HNO_3), which dilutes in rain. This phenomenon is referred to as "acid rain" and is responsible for the destruction of forests in industrialized countries [1]. Acid rain also contributes to the degradation of historical monuments made of marble [1].

Carbon Monoxide Carbon monoxide results from the incomplete combustion of hydrocarbons due to a lack of oxygen [1]. It is a poison to humans and animals that breathe it. Once carbon monoxide reaches the blood cells, it fixes to the hemoglobin in place of oxygen, thus diminishing the quantity of oxygen that reaches the organs and reducing the physical and mental abilities of the affected living beings [1]. Dizziness is the first symptom of carbon monoxide poisoning, which can rapidly lead to death. Carbon monoxide binds more strongly to hemoglobin than oxygen. The bonds are so strong that normal body functions cannot break them. Persons intoxicated by carbon monoxide must be treated in pressurized chambers, where the pressure makes carbon monoxide–hemoglobin bonds easier to break.

Unburned Hydrocarbons Unburned hydrocarbons are a result of the incomplete combustion of hydrocarbons [1, 2]. Depending on their nature, unburned hydrocarbons may be harmful to living beings [2]. Some of these unburned hydrocarbons may be direct poisons or carcinogenic chemicals such as particulates, benzene, or others. Unburned hydrocarbons are also responsible for smog: the sun's ultraviolet radiations interact with the unburned hydrocarbons and NO in the atmosphere to form ozone and other products. Ozone is a molecule formed of three oxygen atoms. It is colorless but very dangerous, and poisons as it attacks the membranes of living cells, thus causing them to age prematurely or die. Toddlers, older people, and asthmatic humans suffer greatly from exposure to high ozone concentrations. Annually, deaths from high ozone peaks in polluted cities are reported [3].

Other Pollutants Impurities in fuels result in the emission of pollutants. The major impurity is sulfur which is mostly found in diesel and jet fuel, but also in gasoline and natural gas [1]. The combustion of sulfur (or sulfur compounds such as hydrogen sulfide) with oxygen releases sulfur oxides (SO_x). Sulfur dioxide (SO_2) is the major product of this combustion. Upon contact with air, it forms sulfur trioxide, which later reacts with water to form sulfuric acid, a major component of acid rains. It should be noted that sulfur oxide emissions originate from transportation sources but also largely from the combustion of coal in power plants and steel factories. In addition, there is debate over the exact contribution of natural sources such as volcanoes.

Petroleum companies add chemical compounds to their fuels in order to improve the performances or lifetime of engines [1]. Tetraethyl lead, often referred to simply as "lead," was used to improve the knock resistance of gasoline and therefore allow better engine performance. However, the combustion of this chemical releases lead metal, which is responsible for a neurological disease called "saturnism." Its use is now forbidden in most developed countries and it has been replaced by other chemicals [1].

Global Warming

Global warming is a result of the "greenhouse effect" induced by the presence of carbon dioxide and other gases, such as methane, in the atmosphere. These gases trap the sun's infrared radiation reflected by the ground, thus retaining the energy in the atmosphere and increasing the temperature. An increased Earth temperature results in major ecological damages to its ecosystems and in many natural disasters that affect human populations [2].

Among the ecological damages induced by global warming, the disappearance of some endangered species is a concern because it destabilizes the natural resources that feed some populations. There are also concerns about the migration of some species from warm seas to previously colder northern seas, where they can potentially destroy indigenous species and the economies that live off those species. This may be happening in the Mediterranean Sea, where barracudas from the Red Sea have been observed.

Natural disasters command our attention more than ecological disasters because of the amplitude of the damages they cause. Global warming is believed to have induced a meteorological phenomenon such as "El Nino," which disturbs the South Pacific region and regularly causes tornadoes, inundations, and dryness. The melting of the polar icecaps, another major result of global warming, raises the sea level and can cause the permanent inundation of coastal regions, and sometimes of entire countries.

Carbon dioxide is the result of the combustion of hydrocarbons and coal. Transportation accounts for a large share (32% from 1980 to 1999) of carbon dioxide emissions. The distribution of carbon dioxide emissions is shown in Fig. 1 [4].

Figure 2 shows the trend in carbon dioxide emissions. The transportation sector is clearly now the major contributor of carbon dioxide emissions. It should be noted that developing countries are rapidly increasing their transportation sector, and these countries represent a very large share of the world population. Further discussion is provided in the next subsection.

The large amounts of carbon dioxide released in the atmosphere by human activities are believed to be largely responsible for the increase in global Earth temperature observed during the last decades (Fig. 3). It is important to note that carbon dioxide is indeed digested by plants and sequestrated by the oceans in the form of carbonates. However, these natural assimilation processes are limited and cannot assimilate all of the emitted carbon dioxide, resulting in an accumulation of carbon dioxide in the atmosphere.

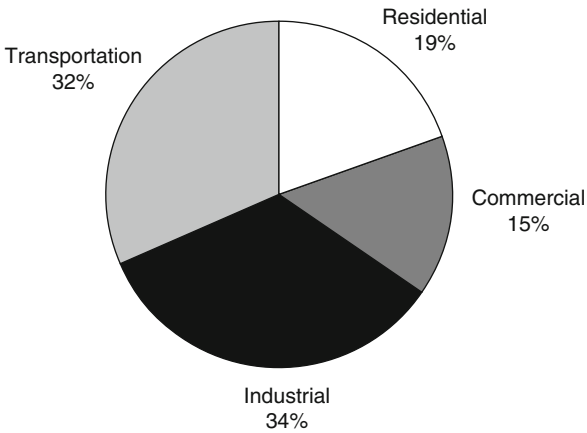

Sustainable Transportation. Figure 1
Carbon dioxide emission distribution from 1980 to 1999

Petroleum Resources

The vast majority of fuels for transportation are liquid fuels originating from petroleum. Petroleum is a fossil fuel, resulting from the decomposition of living matters that were imprisoned millions of years ago (Ordovician, 600–400 million years ago) in geologically stable layers. The process is roughly the following: the living matters (mostly plants) die and are slowly covered by sediments. Over time, these accumulating sediments form thick layers, and transform to rock. The living matters are trapped in a closed space, where they encounter high pressures and temperatures, and slowly transform into either hydrocarbons or coal, depending on their nature. This process took millions of years to accomplish. This is what makes the Earth's resources in fossil fuels finite.

The proved reserves are "those quantities that geological and engineering information indicates with reasonable certainty can be recovered in the future from known reservoirs under existing economic and operating conditions" [5]. Therefore, they do not constitute an indicator of the Earth's total reserves.

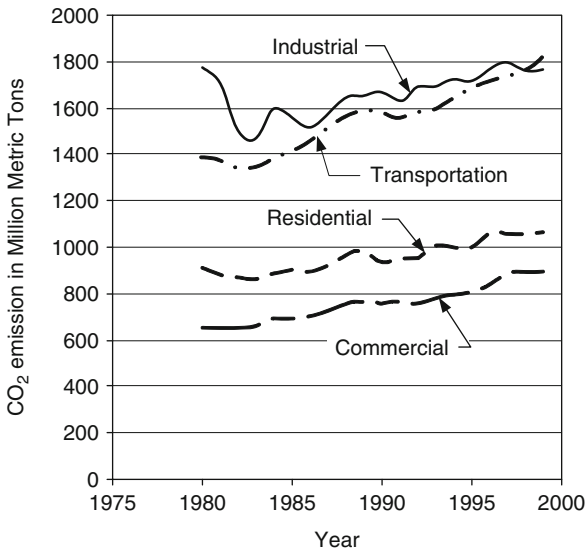

Sustainable Transportation. Figure 2
Evolution of CO_2 emission

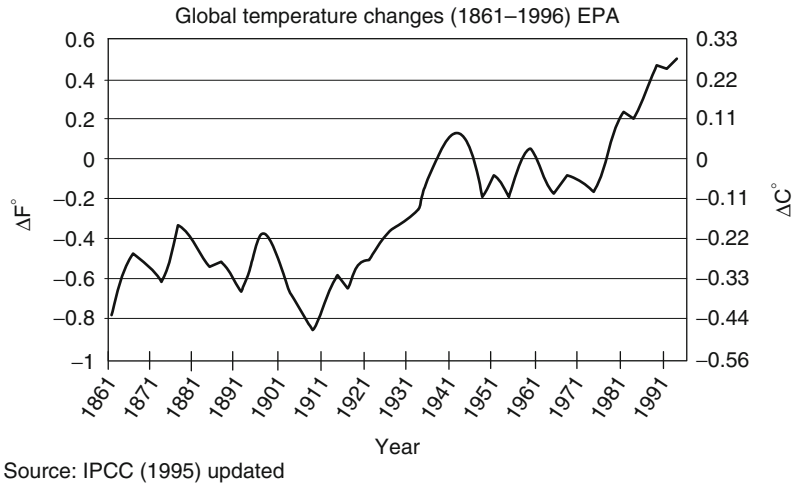

Sustainable Transportation. Figure 3
Global earth atmospheric temperature

The proved reserves, as they are given in the British Petroleum 2001 estimate [5], are given in billion tones in Table 1. The R/P ratio is the number of years that the proved reserves would last if the production were to continue at its current level. This ratio is also given in Table 1 for each region [5].

The oil extracted nowadays is the easily extractable oil that lies close to the surface, in regions where the climate does not pose major problems. It is believed that far more oil lies underneath the crust of the Earth in such regions like Siberia, or the American and Canadian Arctic. In these regions, the climate and ecological concerns are major obstacles to extracting or prospecting for oil. The estimation of the total Earth's reserves is a difficult task for political and technical reasons. A 2000 estimation of the undiscovered oil resources by the US Geological Survey is given in Table 2 [6].

Although the R/P ratio does not include future discoveries, it is significant. Indeed, it is based on proved reserves, which are easily accessible to this day. The amount of future oil discoveries is hypothetical, and the newly discovered oil will not be easily accessible. The R/P ratio is also based on the hypothesis that the production will remain constant. It is obvious, however, that consumption (and therefore the production) is increasing yearly to keep up with the growth of developed and developing economies. Consumption is likely to increase in gigantic proportions with the rapid development of some largely populated countries, particularly in the Asia Pacific region. The plot of Fig. 4 shows the trend in oil consumption over the last 20 years [7]. Oil consumption is given in 1,000 barrels per day (one barrel is about 8 metric tons).

Sustainable Transportation. Table 1 Proved petroleum reserves in 2000

Region	Proved reserves in 2000 in billion tons	R/P ratio
North America	8.5	13.8
South and Central America	13.6	39
Europe	2.5	7.7
Africa	10	26.8
Middle East	92.5	83.6
Former USSR	9.0	22.7
Asia Pacific	6.0	15.9
Total world	142.1	39.9

Despite the drop in oil consumption for Eastern Europe and the former USSR, the world trend is clearly increasing, as shown in Fig. 5. The fastest growing region is Asia Pacific, where most of the world's population lives. An explosion in oil consumption is to be expected, with a proportional increase in pollutant emissions and CO_2 emissions.

Sustainable Transportation. Table 2 US Geological Survey estimate of undiscovered oil in 2000

Region	Undiscovered oil in 2000 in billion tons
North America	19.8
South and Central American	14.9
Europe	3.0
Sub-Saharan Africa and Antarctic	9.7
Middle East and North Africa	31.2
Former USSR	15.7
Asia Pacific	4.0
World (potential growth)	98.3 (91.5)

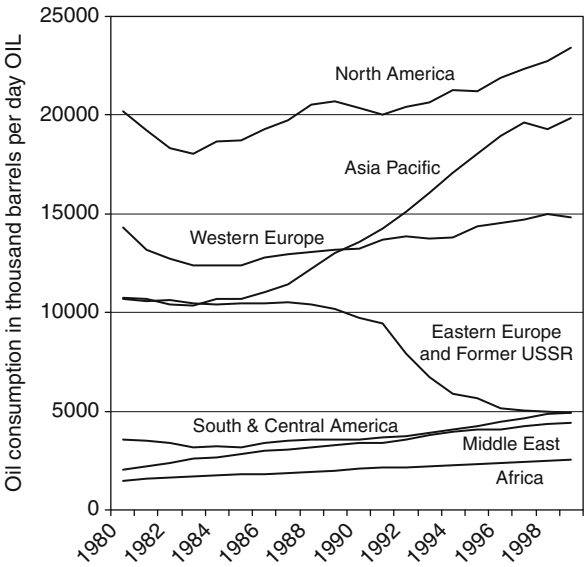

Sustainable Transportation. Figure 4 Oil consumption per region

Induced Costs

The problems associated with the frenetic combustion of fossil fuels are many: pollution, global warming, and foreseeable exhaustion of resources, among others. Although difficult to estimate, the costs associated with these problems are huge and indirect [8], and may be financial, human, or both.

Costs induced by pollution include, but are not limited to, health expenses, the cost of replanting forests devastated by acid rain, and the cost of cleaning and fixing monuments corroded by acid rain. Health expenses probably represent the largest share of these costs, especially in developed countries with socialized medicine or health-insured populations.

Costs associated with global warming are difficult to assess. They may include the cost of damages caused by hurricanes, lost crops due to dryness, damaged properties due to floods, and international aid to relieve the affected populations. The amount is potentially huge.

Most of the petroleum-producing countries are not the largest petroleum-consuming countries. Most of the production is located in the Middle East, while most of the consumption is located in Europe, North America, and Asia Pacific. As a result, consumers have to import their oil and depend on the producing countries. This issue is particularly sensitive in the Middle East, where political turmoil affected the oil delivery to Western countries in 1973 and 1977. The Gulf War, Iran-Iraq war, and the constant surveillance of the area by the United States and allied forces come at a cost that is both human and financial. The dependency of Western economies upon a fluctuating oil supply is potentially expensive. Indeed, a shortage in oil supply causes a serious slowdown of the economy, resulting in damaged perishable goods, lost business opportunities, and the eventual impossibility to run businesses.

In searching for a solution to the problems associated with oil consumption, one has to take into account those induced costs. This is difficult because the cost is not necessarily asserted where it is generated. Many of the induced costs cannot be counted in asserting the benefits of an eventual solution. The solution to these problems will have to be economically sustainable and commercially viable without government subsidies in order to sustain itself in the long run. Nevertheless, it remains clear that any solution to these problems – even if it is only a partial solution – will indeed result in cost savings, which will benefit the payers.

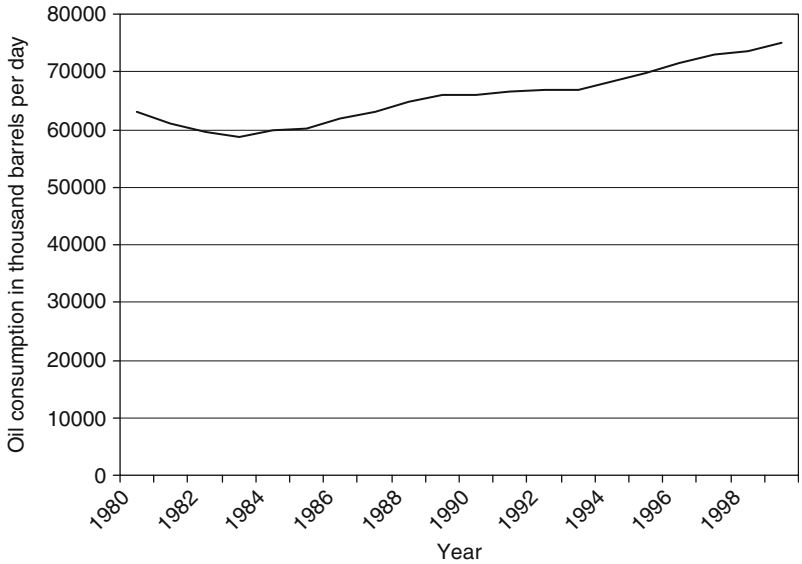

Sustainable Transportation. Figure 5
World oil consumption

Importance of Different Transportation Development Strategies to Future Oil Supply

The number of years that oil resources of the Earth can support our oil supply completely depends on the new discovery of oil reserves and cumulative oil production (as well as cumulative oil consumption). Historical data show that the new discovery of oil reserves grows slowly. On the other hand, the consumption shows high growth rate, as shown in Fig. 6. If oil discovery and consumption follow the current trends, the world oil resource will be used up by about 2038 [9, 10].

It is becoming more and more difficult to discover new reserves of petroleum under the Earth. The cost of exploring new oil fields is becoming higher and higher. It is believed that the scenario of the oil supply will not change much if the consumption rate cannot be significantly reduced.

As shown in Fig. 7, the transportation sector is the primary user of petroleum, consuming 49% of the oil used in the world in 1997. The patterns of consumption of industrialized and developing countries are quite different, however. In the heat and power segments of the markets in industrialized countries, nonpetroleum energy sources were able to compete with and substitute for oil throughout the 1980s; and by 1990, oil consumption in other sectors was less than in the transportation sector.

Most of the gains in worldwide oil use occur in the transportation sector. Of the total increase (11.4 million barrels per day) projected for the industrialized countries from 1997 to 2020, 10.7 million barrels per day are attributed to the transportation sector, where few alternatives are economical until late in the forecast.

In the developing countries, the transportation sector also shows the fastest projected growth in petroleum consumption, promising to rise nearly to the level of non-transportation energy use by 2020. In the developing world, however, unlike in industrialized countries, oil use for purposes other than transportation is projected to contribute 42% of the total increase in petroleum consumption. The growth in non-transportation petroleum consumption in developing countries is caused in part by the substitution of petroleum products for noncommercial fuels (such as wood burning for home heating and cooking).

Improving the fuel economy of vehicles has crucial impact on the oil supply. So far, the most promising technologies are hybrid-electric vehicles and fuel cell vehicles. Hybrid vehicles, using current internal

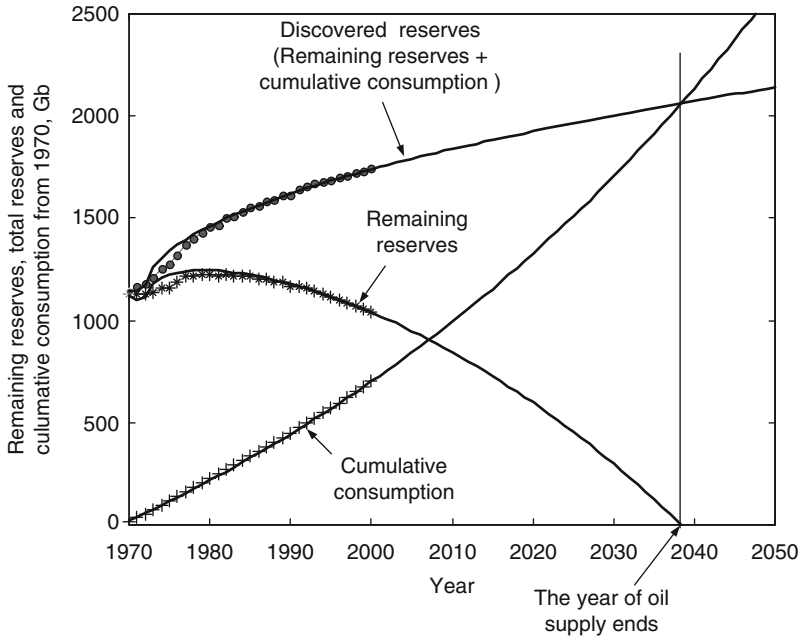

Sustainable Transportation. Figure 6
World oil discovery, remaining reserves, and cumulative consumption

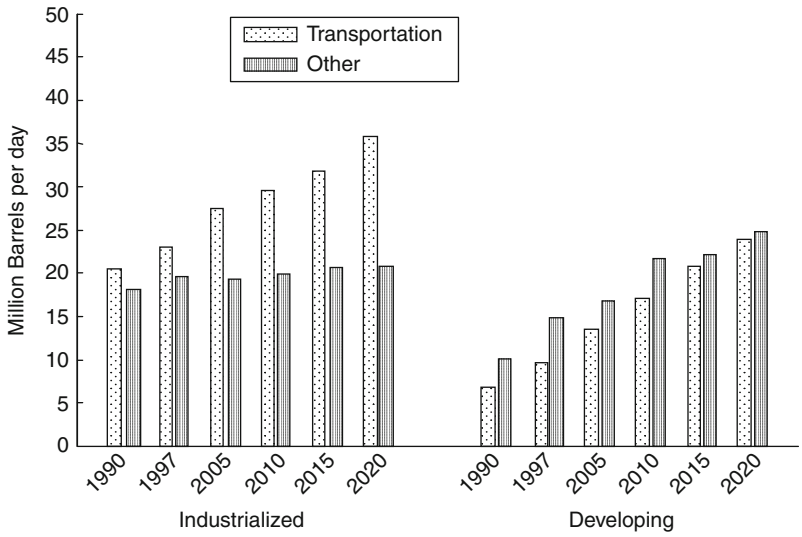

Sustainable Transportation. Figure 7
World oil consumption

combustion engines (ICEs) as their primary power source and batteries/electric motor as the peaking power source, have much higher operation efficiency than those powered by ICE alone. The hardware and software of this technology are almost ready for industrial manufacturing. On the other hand, fuel cell vehicles, which are potentially more efficient and cleaner than hybrid-electric vehicles, are still in

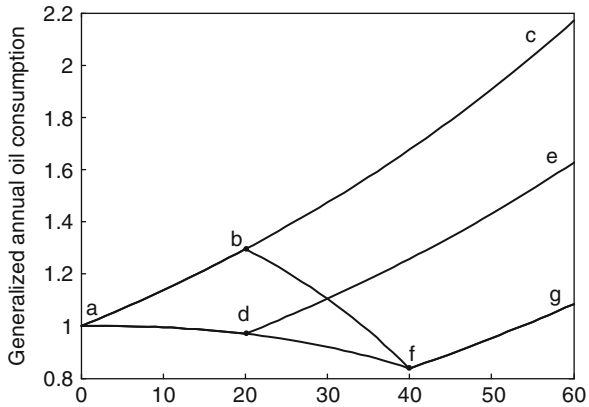

Sustainable Transportation. Figure 8
Comparison of the annual fuel consumption between different development strategies of the next-generation vehicles

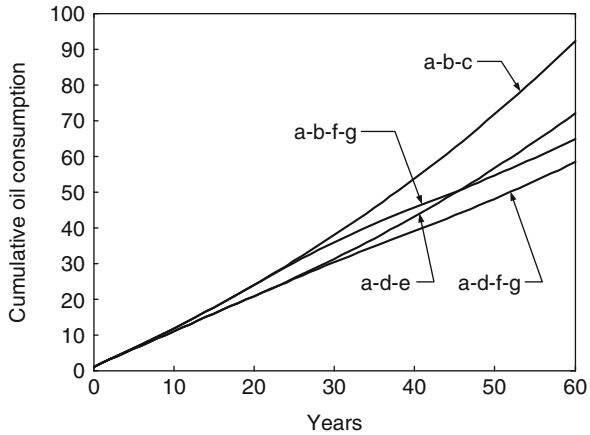

Sustainable Transportation. Figure 9
Comparison of the cumulative fuel consumption between different development strategies of the next-generation vehicles

the laboratory stage and it will take a long time to overcome technical hurdles for commercialization.

Figure 8 shows the generalized annual fuel consumptions of different development strategies of next-generation vehicles. Curve *a-b-c* represents the annual fuel consumption trend of current vehicles, which is assumed to have a 1.3% annual growth rate. This annual growth rate is assumed to be the annual growth rate of the total vehicle number. Curve *a-d-e* represents a development strategy in which conventional vehicles gradually become hybrid vehicles during the first 20 years, and after 20 years, all the vehicles will be hybrid vehicles. In this strategy, it is assumed that the hybrid vehicle is 25% more efficient than a current conventional vehicle (25% less fuel consumption). Curve *a-b-f-g* represents a strategy in which, in the first 20 years, fuel cell vehicles are in a developing stage while current conventional vehicles are still on the market. In the second 20 years, the fuel cell vehicles will gradually go to market, starting from point b and becoming totally fuel cell powered at point f. In this strategy, it is assumed that 50% less fuel will be consumed by fuel cell vehicles than that by current conventional vehicles. Curve *a-d-f-g* represents the strategy that the vehicles become hybrid in the first 20 years, and fuel cell powered in the second 20 years.

Cumulative oil consumption is more meaningful because it involves the annual consumption and the time effect, and is directly associated with the reduction of oil reserves as shown in Fig. 6. Figure 9 shows the scenario of generalized cumulative oil consumptions of the development strategies mentioned above. Although fuel cell vehicles are more efficient than hybrid vehicles, the cumulative fuel consumption by strategy *a-b-f-g* (a fuel cell vehicle in the second 20 years) is higher than strategy *a-d-e* (a hybrid vehicle in the first 20 years) within 45 years, due to the time effect. From Fig. 8, it is clear that strategy *a-d-f-g* (a hybrid vehicle in the first 20 years and a fuel cell vehicle in the second 20 years) is the best. Figures 6 and 9 reveal another important fact: Fuel cell vehicles should not rely on oil products because of the difficulty of future oil supply 45 years later. Thus, the best development strategy of next-generation transportation would be to commercialize hybrid-electric vehicles immediately, and at the same time, do the best to commercialize nonpetroleum fuel cell vehicles as soon as possible.

Sustainable Transportation: Definition

In the opinion of some, urban transport systems based around the automobile have proved unsustainable, consuming excessive energy, affecting the health of populations, and delivering a declining level of service despite increasing investments. The sustainable transport movement focuses on solutions to these problems [5]. The term "sustainable transport" came into use as a logical follow-on from sustainable

development, and is used to describe modes of transport, and systems of transport planning, which are consistent with wider concerns of sustainability.

Sustainable transport systems make a positive contribution to the environmental, social, and economic sustainability of the communities they serve. There are many definitions of the sustainable transport, and of the related terms sustainable transportation and sustainable mobility. One such definition, from the European Union Council of Ministers of Transport, defines a sustainable transportation system as one that:

- Allows the basic access and development needs of individuals, companies, and society to be met safely and in a manner consistent with human and ecosystem health, and promotes equity within and between successive generations
- Is affordable, operates fairly and efficiently, offers a choice of transport mode, and supports a competitive economy, as well as balanced regional development
- Limits emissions and waste within the planet's ability to absorb them, uses renewable resources at or below their rates of generation, and uses nonrenewable resources at or below the rates of development of renewable substitutes, while minimizing the impact on the use of land and the generation of noise [6]

Sustainable Transportation: Solutions

There is a need to develop and accelerate the use of clean and efficient vehicle technologies, as well as renewable fuels, which together could dramatically reduce the demand for petroleum products [7]. This can be done in the following ways:

- Development of hybrid-electric and plug-in hybrid-electric vehicles can provide significant improvement in fuel economy and petroleum displacement.
- Researchers are looking to make batteries more affordable and recyclable, as well as enhance battery range, performance, and life.
- Alternative fuels (ethanol blends, biodiesel, hydrogen, electricity, propane, and compressed natural gas) can reduce oil consumption.
- Reducing vehicle weight directly improves vehicle efficiency and fuel economy, and can potentially reduce vehicle operating costs. The introduction of cost-effective, high-strength materials can significantly reduce vehicle weight without compromising safety.
- Improved combustion technologies and optimized fuel systems can improve near- and mid-term fuel efficiency.

Sustainable Transportation: Types of Vehicles and Technologies

There are three main types of vehicles: combustion, hybrid, and electric vehicles. The combustion vehicle is one in which the only source of power comes from using an internal combustion engine (ICE). The hybrid vehicle or hybrid-electric vehicle (HEV) is composed of the combination of an electric motor and a combustion engine for propulsion, as where the electric vehicle (EV) only uses one or more electric motors for propulsion.

Conventional Combustion Vehicles

A vast majority of current transportation vehicles use ICEs for propulsion. The ICE is a power plant in which the power for propulsion comes from the combustion of a fuel with an oxidizer within a chamber [8]. The fuel typically used for this process is petrol or gasoline which is derived from fossil fuels. This liquid hydrocarbon fuel has a high energy density (approximately 34.2 MJ/L), therefore giving the ICE a high power-to-weight ratio. From these key advantages over other types of vehicles also come the disadvantages of increased air pollution from exhaust emissions, an average efficiency of 18–20%, and the continuing use of fuel and production of emissions during times of no movement. ICEs are typically classified by the fuel they use:

- Petroleum: Gasoline, diesel, liquefied petroleum gas (LPG), compressed natural gas, jet fuel, etc.
- Coal: Methanol, gasoline, and diesel made from carbon using the Fischer-Tropsch process
- Biofuels and vegoils: Biobutanol, biodiesel, bioethanol, biomethanol, biogas, peanut oil, etc.

A specific type of ICE that is becoming popular in the transportation market is the flex-fuel vehicle (FFV). FFVs are an alternative fuel vehicle with an internal combustion engine designed to operate on more than one fuel, usually gasoline blended with either ethanol or methanol fuel, and stored in the same tank [10]. Flex-fuel engines are capable of burning any proportion of the resulting blend in the combustion chamber as fuel injection and spark timing are adjusted automatically according to the actual blend detected by electronic sensors. Like conventional gasoline vehicles, FFVs have a single fuel tank, fuel system, and engine. The most common commercially available FFV in the world market is the ethanol FFV, with around 18 million automobiles and light duty trucks on the roads by 2009, and concentrated in four markets, Brazil (9.3 million), United States (around 8 million), Canada (600,000), and Europe (181,458 led by Sweden).

The FFV's fuel economy on E85 (85% ethanol, 15% gasoline) is somewhat less than when operating on gasoline alone, but has lower greenhouse gas emissions than that of the gasoline-operated ICE. Using the GREET model (greenhouse gases, regulated emissions, and energy use in transportation), Argonne National Laboratory indicates in "Ethanol, The Complete Energy Lifecycle Picture" that greenhouse gas emissions are reduced approximately 15% when ethanol produced from corn is used. Using E85 also reduces CO_2 emissions and provides significant reductions in emissions of many harmful toxins, including benzene, a known human carcinogen. However, E85 also increases emissions of acetaldehyde – a toxic pollutant. Additional testing is being completed to expand the understanding of the emissions impacts of E85 [1].

The operating fuel economy of a vehicle depends on a number of factors, which include: fuel consumption characteristics of the engine, gear number and ratios, vehicle resistance, vehicle speed, and operating conditions. The fuel economy of an ICE is usually evaluated by the amount of fuel per kWh energy output, which is referred to as the specific fuel consumption (g/kWh). The fuel consumption is quite different from one operating point to another, shown in Fig. 10. Vehicle fuel economy can be calculated by finding the load power and the specific fuel consumption for the engine.

The engine power output is always equal to the resistance power of the vehicle, that is:

$$P_e = \frac{V}{\eta_t}\left(F_f + F_w + F_g + M_v \delta \frac{dV}{dt}\right)$$

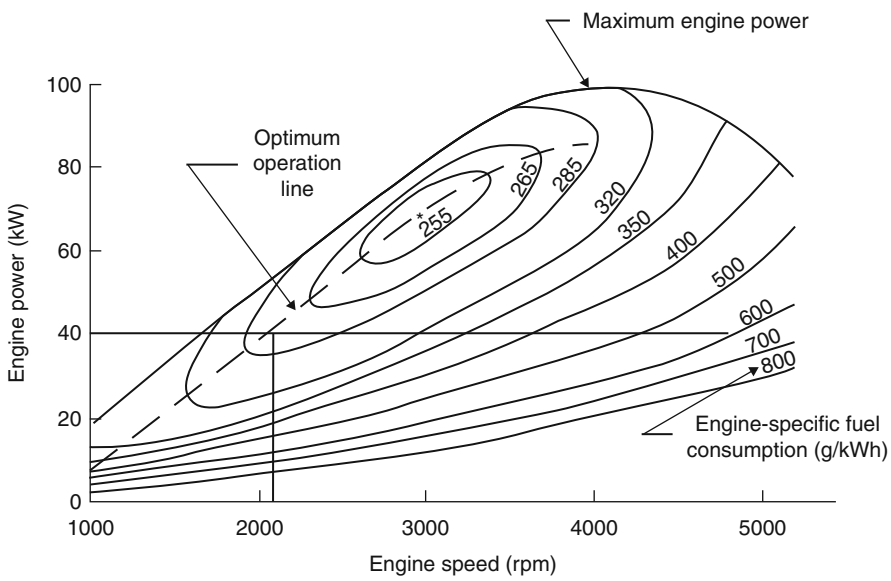

Sustainable Transportation. Figure 10
Fuel economy characteristics of a typical gasoline engine

The engine speed, related to vehicle speed and gear ratio can be expressed as:

$$N_e = \frac{30 V i_g i_0}{\pi r_d}$$

After the engine power and speed are determined, the value of the specific fuel consumption, g_e, can be found from Fig. 10. The time rate of fuel consumption can be calculated by:

$$Q_{fr} = \frac{P_e g_e}{1000 \gamma_f}(1/h),$$

where g_e is the specific fuel consumption of the engine in g/kWh and γ_f is the mass density of the fuel in kg/L. The total fuel consumption within a total distance, S, at a constant cruising speed, V, is obtained by:

$$Q_S = \frac{P_e g_e}{1000 \gamma_f} \frac{S}{V}$$

At high speeds, the fuel consumption increases because the aerodynamic resistance power increases with the speed cubed. The fuel economy of the vehicle can be enhanced due to the reduced engine speed at a given vehicle speed and increased gear ratio and can be seen in Fig. 11.

Figure 12 indicates that the engine has a much lower operating efficiency in low gear than in high gear. For this reason, the fuel economy of a vehicle can be improved with a higher gear transmission or a continuously variable transmission.

It should be noted that because of the complexity of vehicle operation in the real world, fuel consumption at

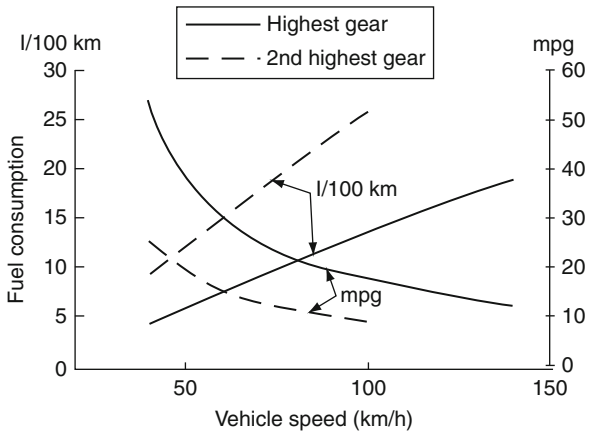

Sustainable Transportation. Figure 11
Fuel economy characteristics of a typical vehicle at constant speed

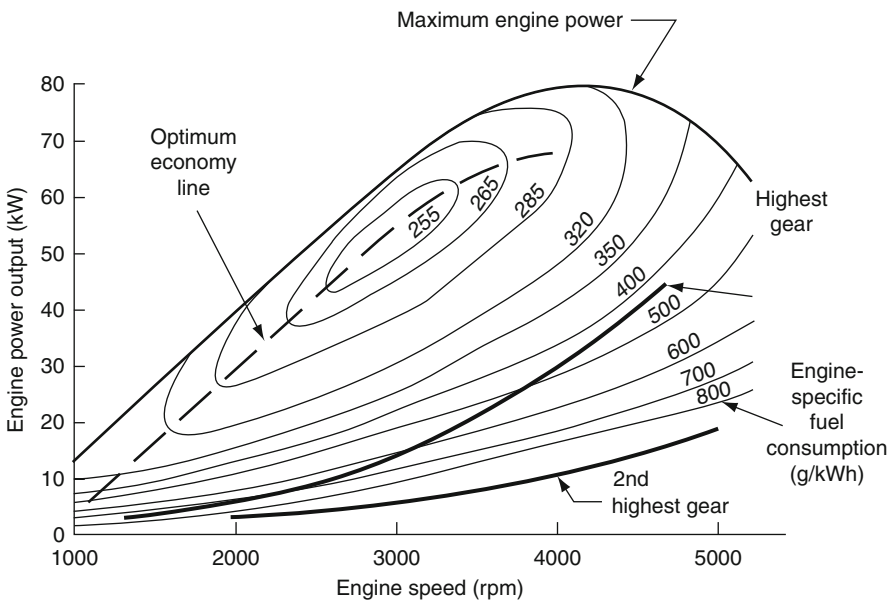

Sustainable Transportation. Figure 12
Operating point of an ICE at constant speed with highest gear and second highest gear

constant speed cannot accurately represent fuel consumption for a vehicle under real driving conditions. Various drive cycles have been developed to simulate real driving conditions. The drive cycles are usually represented by the speed of the vehicle along with the relative driving time. To calculate fuel consumption in a drive cycle, the total fuel consumption can be obtained by the summation of fuel consumption in each time interval, Δt_i:

$$Q_{tc} = \sum_i \frac{P_{ei} g_{ei}}{1000 \gamma_f} \Delta t_i,$$

where P_{ei} is the average power of the engine in the i_{th} time interval in kW, g_{ei} is the average specific fuel consumption of the engine in the i_{th} time interval in g/kWh, and Δt_i is the i_{th} time interval in hours. Figures 13, 14, and 15 show the EPA FTP75 urban and highway drive cycles, fuel economy for urban drive cycle, and fuel economy for highway drive cycle, respectively. From these one can see the typical operating points and fuel consumption for this particular drive cycle.

Conventional vehicles with ICEs provide good performance and long driving range by utilizing the high energy-density advantages of petroleum fuels. However, conventional ICE vehicles bear the disadvantages of poor fuel economy and environmental pollution. The main reasons for their poor fuel economy are as follows:

- Engine fuel efficiency characteristics mismatched with the real operation requirements
- The dissipation of vehicle kinetic energy during braking especially while operating in urban areas
- Low efficiency of hydraulic torque converter in the transmission of current automobiles in stop-and-go driving patterns

The effort to improve the fuel economy of vehicles has been an ongoing process in the automobile industry. This can be done in various ways: reducing vehicle resistance, improving ICE operating efficiency, and properly matching transmission and advanced drive trains. The use of light materials and advanced manufacturing technologies can reduce the weight of vehicles and in turn reduce the rolling resistance and internal resistance during acceleration. This will reduce the demanded power from the ICE. The use of advanced materials in tire production is another important method of reducing the rolling resistance of vehicles. By introducing a flow-shaped body style with a smooth surface, the aerodynamic resistance can be reduced causing an improvement in fuel economy at higher speeds. Proper construction of the transmission, good lubrication, and proper adjustment and tightening of moving parts in the transmission can help

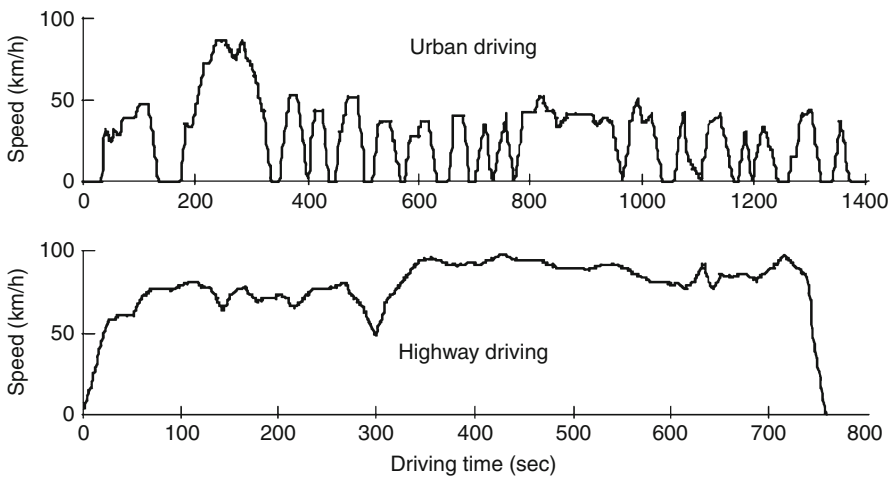

Sustainable Transportation. Figure 13
EPA FTP75 urban and highway drive cycles

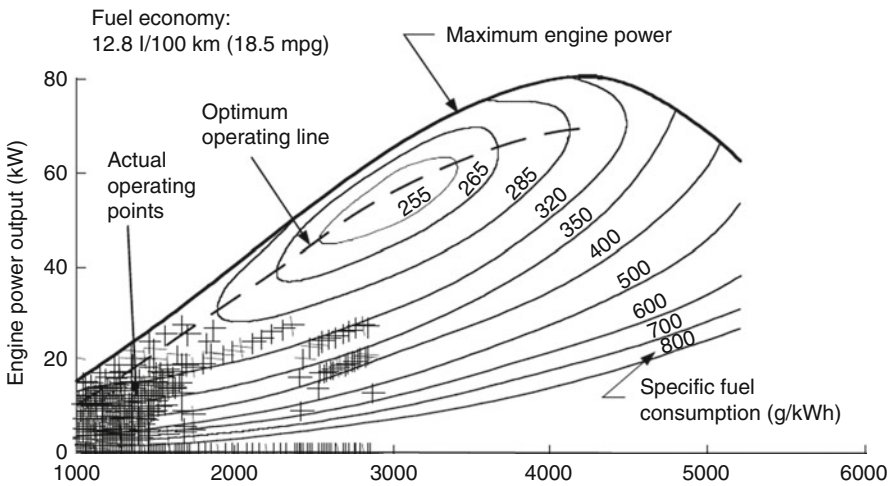

Sustainable Transportation. Figure 14
Fuel economy and engine operating points for EPA FTP75 urban and highway drive cycle overlapped on engine fuel consumption characteristics map

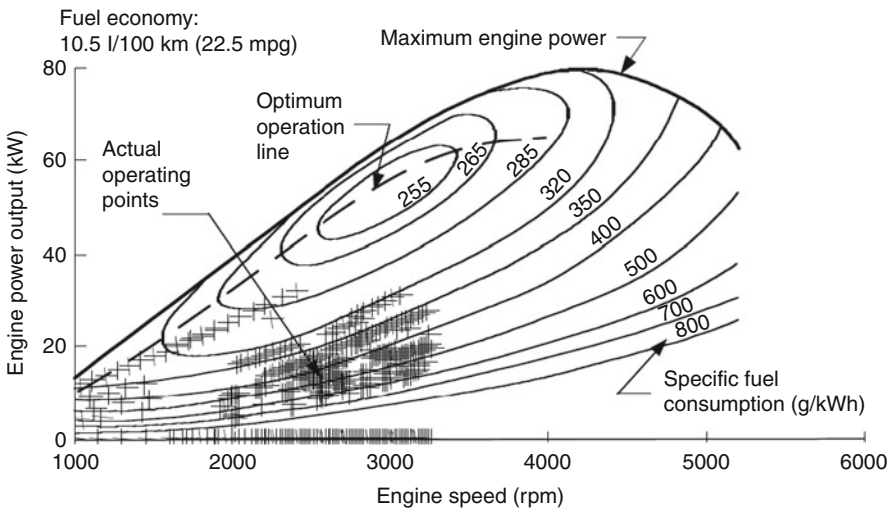

Sustainable Transportation. Figure 15
Fuel economy and engine operating points for EPA FTP75 highway drive cycle overlapped on engine fuel consumption characteristics map

improve the transmission efficiency. The parameters of the transmission, especially the gear number and gear ratios, have considerable influence on the operating fuel economy as described previously. In the design of the transmission, the parameters should be constructed such that the engine will operate close to its fuel optimum region. Improving engine operation efficiency has the potential to contribute to the improvement of vehicle fuel economy. There are many effective advanced techniques, such as accurate air/fuel ratio control with computer-controlled fuel injection, high thermal isolated materials for reducing thermal loss, varying ignition-timing techniques, active controlled valve and port, etc. Advanced drive trains developed

in recent years, such as new power plants, various hybrid drive trains, etc., may greatly improve the fuel economy of vehicles. Fuel cells have higher efficiency and lower emissions than conventional internal combustion engines. Hybridization of a conventional combustion engine with an advanced electric motor drive may greatly enhance the overall efficiency of vehicles.

Hybrid-Electric Vehicles

A hybrid-electric vehicle, HEV, is one that has two or more energy sources and energy converters. In this case the HEV has an electrical energy source (batteries and electric motor) and a mechanical energy source (ICE). Base power for the HEV may be provided by the ICE, a Stirling engine, fuel cell, etc. The design of the base power source, ICE or fuel cell, for the HEV will be much smaller than that of a single power train design because the base power source does not have to be designed to provide the dynamic power. The dynamic power is to be provided by the second energy source, most commonly, electrochemical batteries and electric motors. The dynamic power may also be provided by an electric motor powered by ultracapacitors, flywheels (mechanical batteries), and their combinations. Some advantages and disadvantages of HEVs are shown in Fig. 16. The currently available HEVs are the Toyota Prius, Honda Insight, Ford Escape, and Chevrolet Volt.

Conventional vehicles with ICEs provide good performance and long operating range by utilizing the high energy-density advantages of petroleum fuels. However, conventional ICE vehicles bear the disadvantages of poor fuel economy and environmental pollution. Battery-powered electric vehicles (EV), on the other hand, possess some advantages over conventional ICE vehicles, such as high energy efficiency and zero environmental pollution. However, the performance, especially the operation range per battery charge, is far less competitive than ICE vehicles, due to the lower energy content of the batteries vs. the energy content of gasoline. HEVs have the advantages of both ICE vehicles and EVs and overcome each of their individual disadvantages.

The architecture of a hybrid vehicle is loosely defined as the connection between the components that define the energy flow routes and control ports. There are three types of HEVs:

- Parallel: The gas tank supplies fuel for the ICE and the batteries provide power to the motor. Both power the transmission, which provides propulsion for the vehicle.
- Series: The ICE does not directly propel the vehicle but instead turns a generator, which sends power to either the motor or the batteries.
- Series–parallel: It has the flexibility to operate in either a series or parallel mode.

The series drive train is fully independent when decoupled from the driven wheels, Fig. 17. Therefore, it can be operated at any point on its torque – speed characteristic map, and can potentially be operated solely within its maximum efficiency region. Because electric motors have near-ideal torque – speed characteristics for traction – they do not need a multi-gear transmission. Therefore, their construction is greatly simplified and the cost is reduced. Furthermore, instead of using one motor and a differential gear, two motors may be used, each powering a single

Sustainable Transportation. Figure 16
Advantages/disadvantages of HEVs

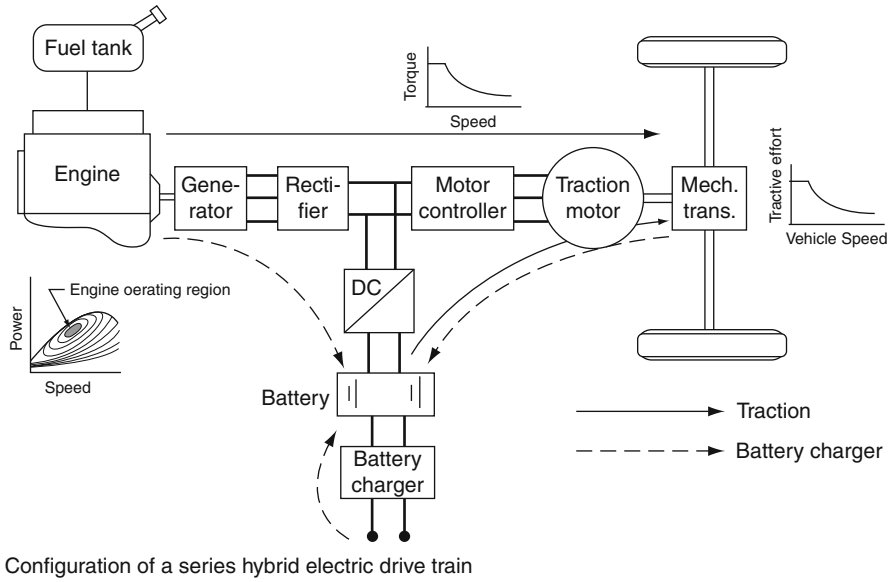

Sustainable Transportation. Figure 17
Series HEV configuration

wheel. This provides speed decoupling between the two wheels like a differential but also acts as a limited slip differential for traction control purposes. Simple control strategies may be used as a result of the mechanical decoupling provided by the electrical transmission. A disadvantage of the Series HEV is that the energy from the engine is converted twice (mechanical to electrical in the generator and electrical to mechanical in the traction motor). The inefficiencies of the generator and traction motor add up and the losses may be significant. Also, the generator adds additional weight and cost to the vehicle. Since the traction motor is the only power plant for propulsion it must be designed to meet the maximum requirements for performance.

A parallel hybrid drive train is a drive train in which the engine supplies its power mechanically to the wheels like in a conventional ICE-powered vehicle, Fig. 18. It is assisted by an electric motor that is mechanically coupled to the transmission. The mechanical coupling of parallel hybrids may be a torque or speed mechanical coupling leaving room for several types of configurations. The torque coupling adds the torques of the engine and the electric motor together or splits the engine torque into two parts: propelling and battery charging. If a multi-gear transmission is used, the performance and overall efficiency of the drive train may be superior to other designs, because two multi-gear transmissions provide more opportunities for both the engine and electric traction system (electric machine and batteries) to operate in their optimum region. This design also provides great flexibility in the design of the engine and electric motor characteristics. The multi-gear transmission also adds complexity to the drive train, which may not be desired. The main advantage of the hybrid drive train with speed coupling is that the speeds of the two power plants are decoupled; therefore, the speed of both power plants can be chosen freely. This advantage is important to power plants such as the Stirling engine and the gas turbine engine, in which their efficiencies are sensitive to speed and less sensitive to torque. Also, the electric machines and the eventual differential gear system occupy considerable space and may reduce the available passenger and luggage space.

Another subtype added to the hybrid market is the plug-in hybrid-electric vehicle (PHEV), Fig. 19. The PHEV is usually an ICE – electric (parallel or series) hybrid with increased energy storage capacity (usually Li-ion batteries). It may be connected to the utility grid after driving to avoid charging using the ICE. The sudden push for this architecture stems

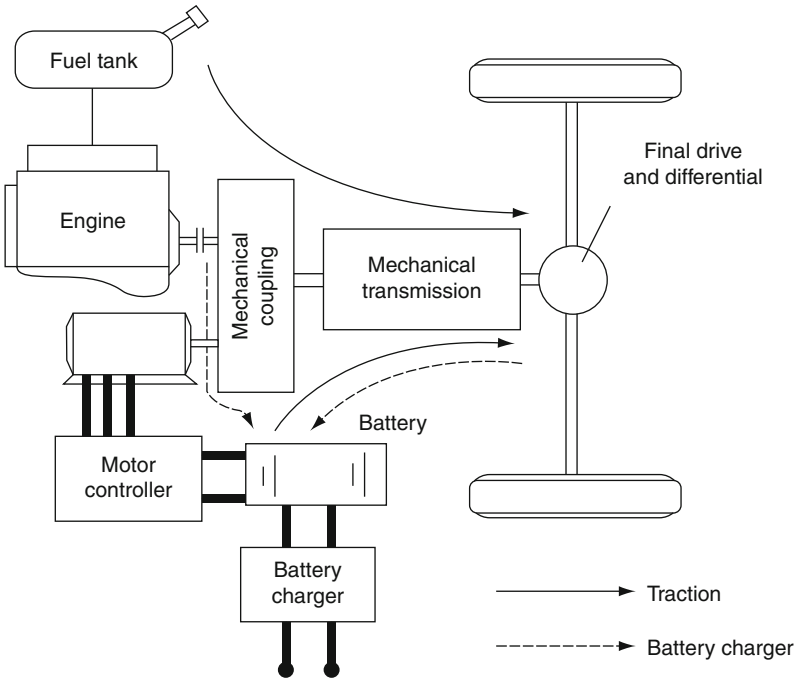

Configuration of a Parallel hybrid electric drive train

Sustainable Transportation. Figure 18
Parallel HEV configuration

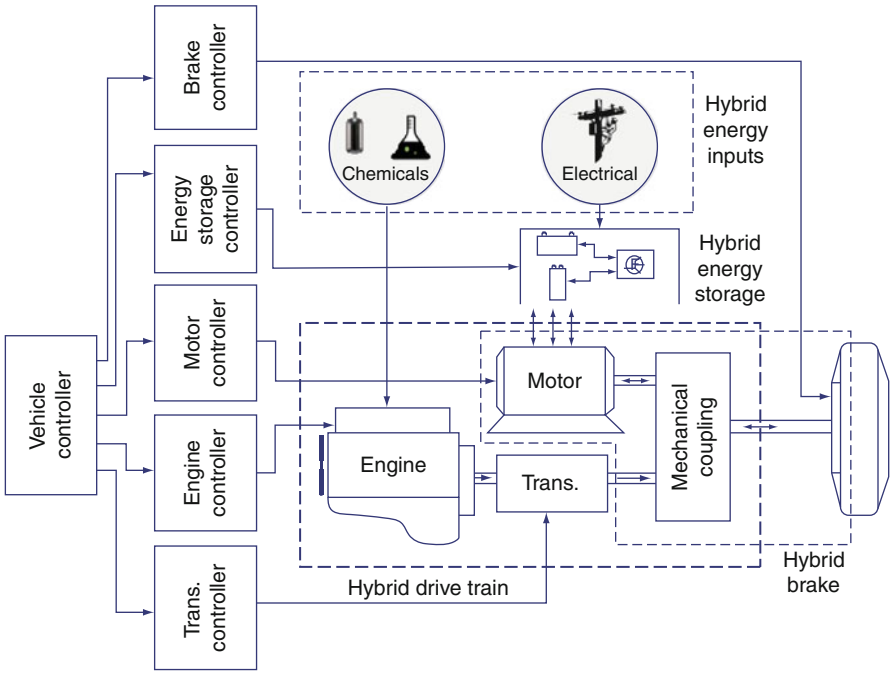

Sustainable Transportation. Figure 19
PHEV configuration

from the fact that the advantages of the battery-powered EV and the charge-sustained HEV are combined. The biggest advantage of this is that one can charge the batteries from the utility grid as opposed to using fuel and the ICE. As of 2007, most plug-in hybrid conversions of conventional hybrids utilize the series–parallel architecture. PHEVs use no fossil fuel during their all-electric range and produce lower greenhouse gas emissions if their batteries are charged from renewable electricity. In most cases these vehicles will be charged by a fossil fuel–based generating plant, causing the emissions to be shifted to the generating plants, making them localized points of pollution. PHEVs also eliminate the problem of "range anxiety" associated with all-electric vehicles, because the combustion engine works as a backup when the batteries are depleted. Other benefits include improved national energy security, fewer fill-ups at the filling station, convenience of home recharging, and the opportunity to provide emergency backup power in the home. Some of the issues that surround the PHEV are design and trade-offs against battery life, capacity, heat dissipation, weight, costs, and safety. Another major hurdle to overcome is the introduction of new infrastructure to accommodate these vehicles. Even if this infrastructure is installed, the issue of utilization may affect the electric grid if the vehicles are charged during peak hours.

The major component of HEVs, PHEVs, and EVs is the energy storage system. This technology represents one of the critical barriers to the development and marketing of cost-competitive HEVs and PHEVs [9]. The energy storage requirements for these two types of vehicles are somewhat different. HEVs require energy storage devices that can deliver high power pulses. For HEV applications, the goal is to develop cells that provide peak power of 1,000 W/kg or greater, have a cycle life of at least 300,000 shallow cycles, and have a calendar life of 15 years. PHEVs require devices that can both store significant energy and deliver high power pulses. PHEVs will require batteries that can deliver significant energy (several kWh) for several thousand discharge cycles from an almost full charge to a lower state of charge. It has been suggested that a PHEV battery would operate in a charge-depleting hybrid mode from about 90% of full charge to about 25% of full charge. Once the battery reaches this lower state of charge, it will function in a manner similar to the battery in an HEV and must be able to sustain 200,000–300,000 shallow, high power cycles with a 15-year calendar life. The specific energy (Wh/kg) of most current batteries is not sufficient to meet the weight and volume goals for PHEVs.

Electric Vehicles

Electric vehicles (EVs) use an electric motor for traction, and chemical batteries, fuel cells, ultracapacitors, and/or flywheels for their corresponding energy sources. A typical configuration is shown in Fig. 20. The drive train consists of three major subsystems: electric motor, energy source, and auxiliary components. EVs produce zero emissions during propulsion, do not use any petroleum onboard, have a high efficiency, and have a quiet and smooth operation. The major issue with EVs is the energy and power density of the batteries.

The overall system design of EVs is based on the type of market the designer is looking to enter into. Each market has different performance criteria and some are shown below:

- On-road personal transportation: Speed, comfort, load capacity, and range
- Service vehicle (mail): Speed, acceleration, and range
- City taxi: High speed, high acceleration, and range
- Trucks: Speed, acceleration, high load capacity, and range
- Off-road vehicles: High gradeability, high load capacity, and range

Each of these designs has to be designed around the energy storage component. This component energy density will determine the number of units necessary to fulfill the most important design criteria of all for EVs, the range. All of these performance criteria are related to the power of the drive train and the energy stored in the energy storage component. For EV drive train design, proper motor power rating and transmission parameters are the primary considerations to meet the performance specification (acceleration time, maximum speed, and gradeability). The design of all these parameters depends mostly on the speed–power (torque) characteristics of the traction motor, shown in Fig. 21.

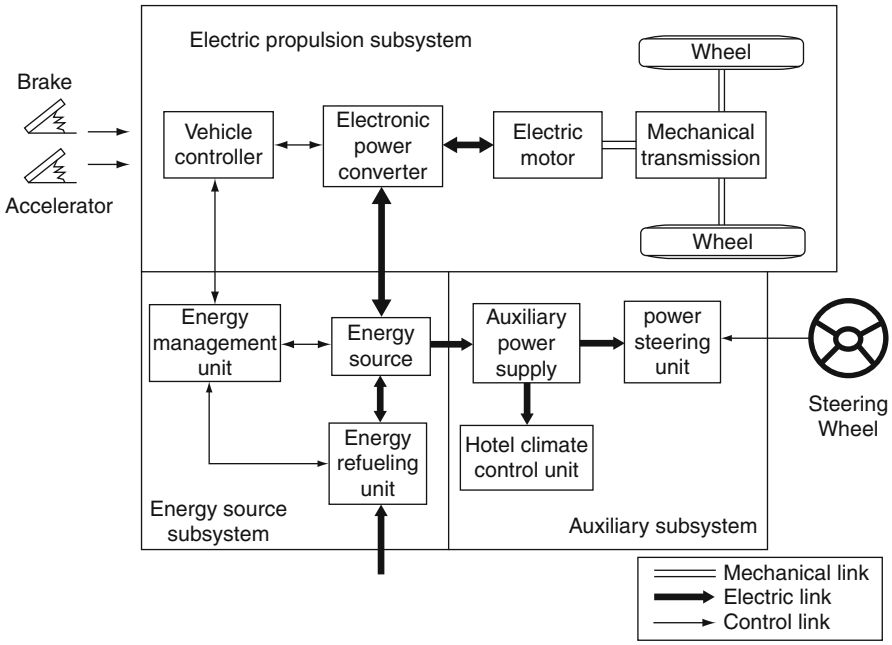

Sustainable Transportation. Figure 20
Typical EV configuration

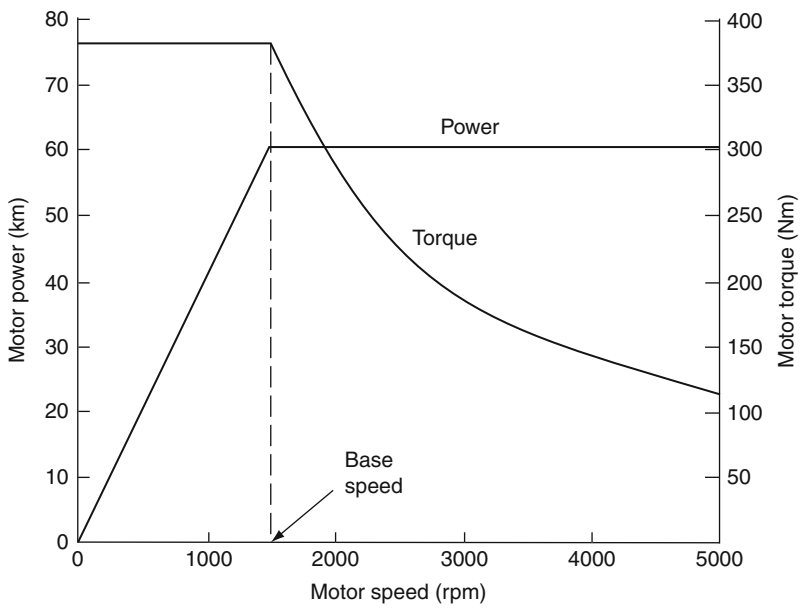

Sustainable Transportation. Figure 21
Typical variable speed electric motor characteristics

Fuel cell vehicles (FCVs) look like conventional vehicles from the outside, but inside they contain technologically advanced components not found in today's vehicles. The most obvious difference is the fuel cell stack that converts hydrogen gas stored onboard with oxygen from the air into electricity to drive the electric motor that propels the vehicle. A well to wheel energy analysis, Fig. 22, performed for DOE shows the typical efficiency of this process. Fuel cells are electrochemical devices that convert chemical energy in fuels into electrical energy directly, promising power generation with high efficiency and low environmental impact [2]. Yet the biggest issue is the onboard storage of hydrogen and how to get the hydrogen onboard safely. Though fuel cells could, in principle, process a wide variety of fuels and oxidants, of most interest today are those fuel cells that use common fuels (or their derivatives) or hydrogen as a reductant, and ambient air as the oxidant.

Most fuel cell power systems are comprised of three main components: unit cells, stacks, and balance of plant components. The unit cell is where the electrochemical reaction takes place. If you string numerous of these unit cells together you get what is called a fuel cell stack. The unit cells are combined by electrically connecting the cells to construct the desired electrical output capacity. The balance of plant components are used to provide feedstream conditioning (including a fuel processor if needed), thermal management, and electric power conditioning among other ancillary and interface functions.

In a typical fuel cell, fuel is fed continuously to the anode (negative electrode) and an oxidant (often oxygen from air) is fed continuously to the cathode (positive electrode). The electrochemical reactions take place at the electrodes to produce an electric current through the electrolyte, while driving a complementary electric current that performs work on the load. Although a fuel cell is similar to a typical battery in many ways, it differs in several respects. The battery is an energy storage device in which all the energy available is stored within the battery itself (at least the reductant). The battery will cease to produce electrical energy when the chemical reactants are consumed (i.e., discharged). A fuel cell, on the other hand, is an energy conversion device to which fuel and oxidant are

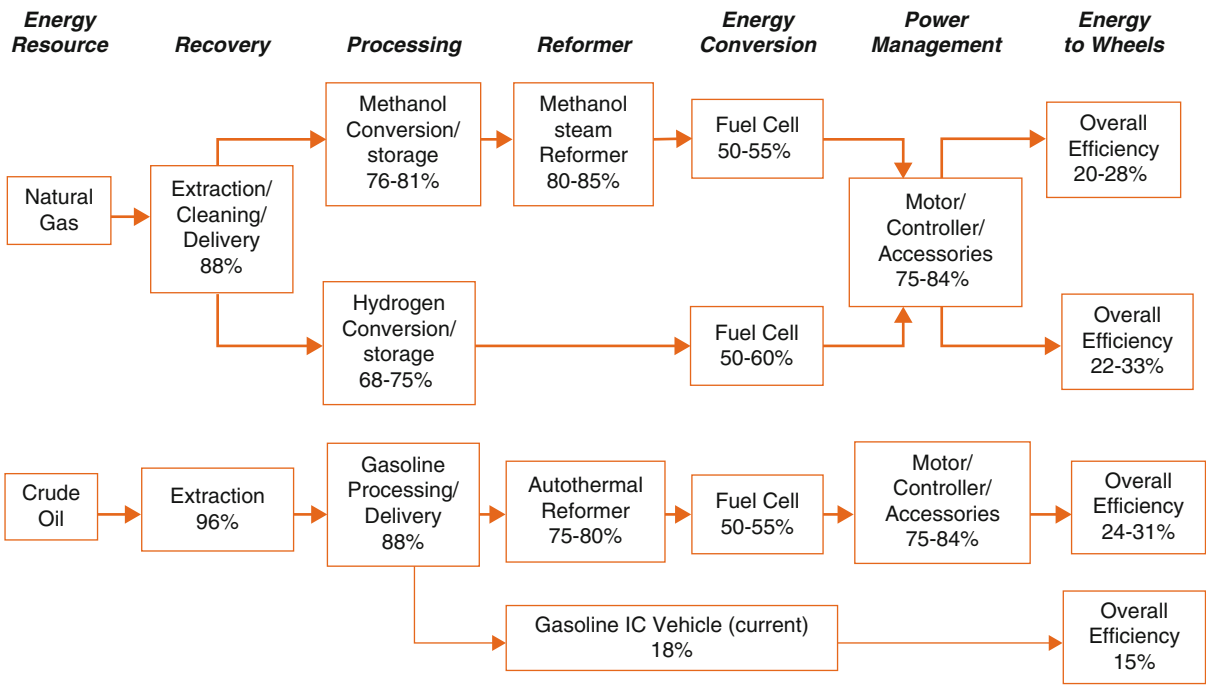

Sustainable Transportation. Figure 22
"Well to wheel" efficiency for various vehicle scenarios

Sustainable Transportation. Table 3 Summary of major differences of fuel cell types

	PEFC	AFC	PAFC	MCFC	SOFC
Electrolyte	Hydrated polymeric ion exchange membranes	Mobilized or immobilized potassium hydroxide in asbestos matrix	Immobilized liquid phosphoric acid in SiC	Immobilized liquid molten carbonate in $LiAlO_2$	Perovskites (ceramics)
Electrodes	Carbon	Transition metals	Carbon	Nickel and nickel oxide	Perovskite and perovskite/metal cermet
Catalyst	Platinum	Platinum	Platinum	Electrode material	Electrode material
Interconnect	Carbon or metal	Metal	Graphite	Stainless steel or nickel	Nickel, ceramic, or steel
Operating temperature	40–80°C	65–220°C	205°C	650°C	600–1,000°C
Charge carrier	H^+	OH^-	H^+	$CO3^-$	O^-
External reformer for hydrocarbon fuels	Yes	Yes	Yes	No, for some fuels	No, for some fuels and cell designs
External shift conversion of CO to hydrogen	Yes, plus purification to remove trace CO	Yes, plus purification to remove CO and CO_2	Yes	No	No
Prime cell components	Carbon based	Carbon based	Graphite based	Stainless based	Ceramic
Product water management	Evaporative	Evaporative	Evaporative	Gaseous product	Gaseous product
Product heat management	Process gas + liquid cooling medium	Process gas + electrolyte circulation	Process gas + liquid cooling medium or steam generation	Internal reforming + process gas	Internal reforming + process gas

supplied continuously. In principle, the fuel cell produces power for as long as fuel is supplied [2]. Table 3 shows typical fuel cell types and materials and operating characteristics.

In parallel with the classification by electrolyte, some fuel cells are classified by the type of fuel used. Direct alcohol fuel cells (DAFC) or, more commonly, direct methanol fuel cells (DMFC) use alcohol without reforming. Mostly, this refers to a PEFC-type fuel cell in which methanol or another alcohol is used directly, mainly for portable applications. Direct carbon fuel cells (DCFC) use solid carbon (presumably a fuel derived from coal, pet-coke, or biomass) directly in the anode, without an intermediate gasification step. Concepts with solid oxide, molten carbonate, and alkaline electrolytes are all under development. The thermodynamics of the reactions in a DCFC allow very high efficiency conversion. Therefore, if the technology can be developed into practical systems, it could ultimately have a significant impact on coal-based power generation. The most common is the hydrogen fuel cell which uses hydrogen as its fuel and oxygen (usually from air) as its oxidant.

Battery electric vehicles (BEVs) are propelled by an electric motor (or motors) powered by rechargeable battery packs. BEVs are becoming more and more attractive with the advancement of new battery technology (Li-ion) that have higher power and energy density (i.e., greater possible acceleration and more range with less batteries) and higher oil prices [11]. Electric motors have several advantages over internal combustion engines (ICEs). For example, electric motors convert 75% of the chemical energy from the batteries to power the wheels as where the ICE can only convert 20% of the energy stored in gasoline. EVs emit no tailpipe pollutants, although the power plant producing the electricity may emit them. If the electricity used to charge the EV comes from renewable then there would be no air pollutants. Using electricity as the propulsion fuel would reduce energy dependence on fossil fuels. Electric motors provide quiet, smooth operation and stronger acceleration and require less maintenance than ICEs.

EVs face significant battery-related challenges in the areas of driving range, recharge time, battery cost, and size and weight. The typical driving range for current EVs are about 100–200 miles before needing to be recharged as where typical gasoline vehicles can go well over 300 miles before refueling. This could possibly be overcome by setting up more charging stations, but in order to fully recharge the battery, it can take anywhere from 4 to 8 h. Even a "quick charge" to 80% can take up to 30 min. Also the cost of these batteries is relatively expensive and may need replacement one or more times over the life of the vehicle. The amount and weight of these batteries has improved over the years, but they still take up a significant amount of vehicle space depending on the type of performance that the battery pack was designed.

Bibliography

1. U.S DOE, Office of the Energy Efficiency and Renewable Energy (2010) DOE/GO-102010-3002
2. EG&G Technical Services Inc for DOE (2004) Fuel cell handbook, 7th edn
3. http://en.wikipedia.org/wiki/Automobiles
4. Oliver R (2007) All about: hybrid transportation. CNN.com/world business. 16 Sep 2007
5. http://en.wikipedia.org/wiki/Sustainable_transport
6. Todd Litman, Sustainable transportation and TDM online TDM encyclopedia. http://www.vtpi.org/tdm/tdm67.htm
7. Department of Energy: Vehicle Technologies Program, Advancing new vehicle technologies and fuels. www.vehicles.energy.gov
8. http://en.wikipedia.org/wiki/Internal_combustion_engine
9. http://www.science.energy.gov/sbir/solicitations/Energy_Storage
10. http://en.wikipedia.org/wiki/Flexible-fuel_vehicle
11. http://en.wikipedia.org/wiki/Battery_electric_vehicle
12. Brill M, Dorau T Life-cycle Analysis. ICF International
13. http://www.gdrc.org/uem/lca/life-cycle.html
14. Cohn R (1994) Electric vehicle life-cycle analysis. Master of Science thesis, MIT
15. Samaras C, Meisterling K (2008) Life-cycle assessment of greenhouse gas emissions from plug in hybrid vehicles. Environ Sci Technol 42:3170–3176
16. ISO 14040, International Standards Organization (2006)
17. Meier P (2002) Life-cycle assessment of electricity generation systems and applications for climate change policy analysis. PhD dissertation, University Wisconsin-Madison
18. Ehsani Y et al (2010) In: Ehsani M, Gao Y, Gay SE, Emadi A (eds) Modern electric, hybrid electric, and fuel cell vehicles – Fundamentals, theory, and design, 2nd edn. Boca Raton, CRC Press

Sustainable Vehicle Fuels, Well-to-Wheel Analysis

Amgad Elgowainy, Michael Wang
Center for Transportation Research, Argonne National Laboratory, Argonne, IL, USA

Article Outline

Glossary
Definition of the Subject
Introduction
Biofuel Pathways
Hydrogen Pathways with Fuel-Cell Vehicles
Electricity Pathways with Phevs and Bevs
Future Directions
Bibliography

Glossary

All-electric range (AER) The driving range of a plug-in hybrid electric vehicle (PHEV) in charge-depleting (CD) mode.

Battery-powered electric vehicle (BEV) A vehicle that stores electricity in rechargeable battery packs and uses an electric motor instead of an internal combustion engine for propulsion.

Biofuels Liquid fuels (such as ethanol and biodiesel) that are derived from bio-feedstock sources such as corn, cellulosic biomass, and soybeans.

Charge depleting (CD) In charge-depleting mode, PHEV uses the electricity in the battery pack to propel the vehicle until the battery reaches a defined minimum state of charge, at which the battery is considered depleted.

Charge sustaining (CS) In charge-sustaining mode, PHEV uses the onboard fuel and internal combustion engines to propel the vehicle and to sustain the state of charge of the battery pack.

Fuel-cell vehicle (FCV) A vehicle that converts hydrogen to electricity by using fuel cells, which powers an electric motor to propel the vehicle.

Greenhouse gases (GHGs) Gases in the atmosphere, such as carbon dioxide, nitrogen oxides, and methane, that absorb and trap solar radiation in the infrared frequency range, thus elevating the temperature of the atmosphere in a process similar to the greenhouse concept.

Hybrid electric vehicle (HEV) A vehicle that combines an internal combustion engine (ICE) with a battery and an electric motor to propel the vehicle and achieve improved fuel economy.

Internal combustion engine vehicle (ICEV) A vehicle that uses an internal combustion engine (ICE) to propel the vehicle.

Plug-in hybrid electric vehicle (PHEV) A hybrid electric vehicle with a rechargeable battery, which can be charged from a wall outlet that is connected to the electrical grid.

Pump-to-wheels (PTW) Represents the vehicle's operation stage of the fuel cycle.

Well-to-pump (WTP) Represents the fuel cycle stage that incorporates the feedstock and fuel production and processing, as well as fuel delivery or energy transmission.

Well-to-wheels (WTW) Represents the combined well-to-pump and pump-to-wheels stages of the fuel cycle.

Definition of the Subject

As the global population and economy continue to grow, so, too, will the demand for energy. The transportation sector has been relying solely on petroleum, consuming more than 50% of the global world oil production [1]. In terms of demand, the United States is the top oil-importing country. Two major issues facing the transportation sector in the United States – and other major countries as well – are energy security and environmental sustainability. Improvements in the energy efficiency of vehicles and the substitution of petroleum fuels with alternative fuels can help slow the growth in the demand for petroleum oil and mitigate the increase in greenhouse gas emissions associated with the use of petroleum. Biofuels, hydrogen, and electricity are being promoted as alternatives to petroleum, and their use may help cut greenhouse gas emissions. Although using biofuels in vehicles produces greenhouse gas emissions, using hydrogen and electricity as vehicle fuels produces no such emissions. Such use of fuel in vehicles to power the wheels is known as the *pump-to-wheels* (PTW) stage of the fuel cycle. On the other hand, the production of biofuels results in sequestration of CO_2 from the atmosphere during the growth of the bio-feedstock sources, while hydrogen production and electricity generation result in greenhouse gas emissions because they are mostly produced from fossil sources. Such fuel production from the primary feedstock sources, along with the associated transportation and distribution activities, is known as the *well-to-pump* (WTP) stage of the fuel cycle. Combining the WTP stage with the PTW stage provides a *well-to-wheels* (WTW) metric that facilitates the comparison of alternative fuels from an environmental sustainability perspective on a common basis.

The terms WTW, fuel cycle, cradle-to-grave, and life cycle are used interchangeably in the literature for life-cycle assessments. However, the term WTW is more pertinent to transportation fuels for use in vehicles. Figure 1 shows a schematic of the WTW stages for fuel use in vehicles. This chapter highlights the key stages and factors that impact the WTW results of using biofuels, hydrogen, and electricity and examines the potential reduction of WTW energy use and greenhouse gas emissions associated with using biofuels in internal combustion engine vehicles (ICEVs), hydrogen in fuel-cell vehicles, and electricity in plug-in hybrid electric vehicles (PHEVs) and battery-powered electric vehicles (BEVs), in comparison to using gasoline in ICEVs.

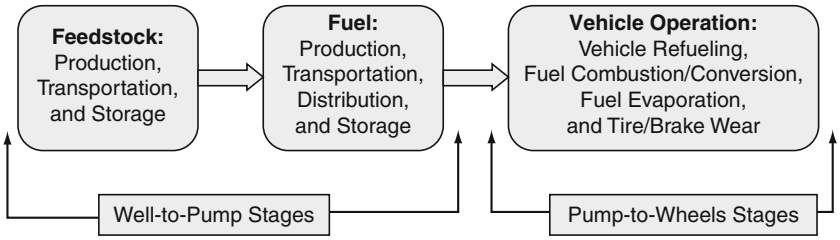

Sustainable Vehicle Fuels, Well-to-Wheel Analysis. Figure 1
WTW stages of alternative fuel and vehicle systems

Introduction

In 1990, the world consumed 366×10^9 GJ of energy; in 2006, this total consumption was increased by 36% to 499×10^9 GJ. As the world economy and population continue to grow, total energy use worldwide is projected to increase to 716×10^9 GJ by 2030, which is a 44% increase over consumption in 2006 [1]. Figure 2 shows the contribution of different types of primary energy to the total energy consumption worldwide. Of the five primary types of energy, oil accounts for the largest share, coal the second largest, and natural gas the third largest. In 1990, worldwide, oil accounted for 39% of total energy use, coal for 26%, and natural gas for 22%. In 2030, the shares are projected to be 32, 28, and 23% for oil, coal, and natural gas, respectively.

The transportation sector is the largest oil-consuming sector worldwide. In 2005, the transportation sector consumed 52% of total worldwide oil production. In 2030, the transportation sector is projected to consume 58% of that total. In the United States, the transportation sector already accounts for approximately two-thirds of oil consumption. More significantly, the US transportation sector relies solely on oil (over 95% of transportation energy is from oil). The transportation sector is the major contributor to the fast growth of worldwide demand for oil. One issue under debate is whether the world will run out of oil and, if so, when. What is not under debate is the geographic distribution of oil resources and oil demand – both are undoubtedly unbalanced.

Figure 3 shows the geographic distribution of the proved world oil reserve as of the end of 2007 [2]. This oil reserve distribution results in concentrated oil production in a few regions. In 2005, total world oil production was 82 million barrels a day (MM b/d). In 2030, oil production is projected to be 103 MM b/d [1]. Of the total production, the 13 members of the Organization of the Petroleum Exporting Countries (OPEC) produced 35.3 MM b/d in 2005 and are projected to produce 47.7 MM b/d in 2030. Other non-OPEC countries (including Russia, Latin American countries, non-OPEC African countries, and Caspian area countries) produced 18 MM b/d in 2005 and may produce 31.3 MM b/d in 2030. These countries together produced 53.3 MM b/d in 2005 and will produce 79 MM b/d in 2030, accounting for 65% and 77% of total production in 2005 and 2030, respectively. To help put oil production in the context of consumption, Figure 4 shows the geographic distribution of world oil consumption in 2005 and 2030 [1]. The geographic mismatch between oil production and oil consumption has prompted major oil-consuming countries to pursue policies of achieving energy independence by reducing the amount of oil imported, especially when oil prices rose to 140 US dollars a barrel in the summer of 2007.

In addition to the oil production-consumption issue, the effect of using oil on the environment is an ongoing concern. More specifically, global greenhouse gas emissions have grown from 28.7 gigatonnes (Gt) of CO_2 equivalents (CO_2-eq) in 1970 to 49 Gt in 2004, which is a 70% increase in 34 years [3]. With a business-as-usual scenario, the Intergovernmental Panel on Climate Change (IPCC) projects that global greenhouse gas emissions could increase by up to 36.7 Gt of CO_2-eq between 2000 and 2030. On the other hand, stabilization of global atmospheric CO_2 concentration at 490–590 ppm requires reduction of global greenhouse gas emissions in 2050 by as much as 60% relative

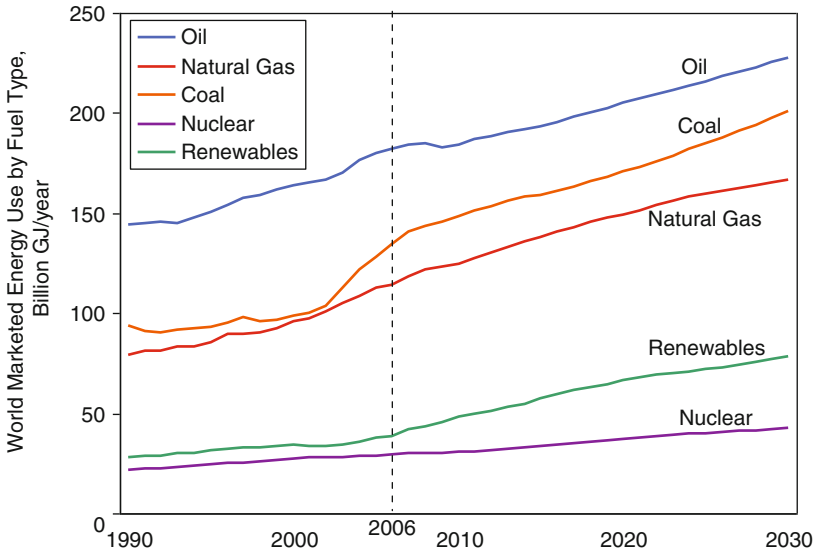

Sustainable Vehicle Fuels, Well-to-Wheel Analysis. Figure 2
Shares of primary energy types to the total world energy consumption [1]

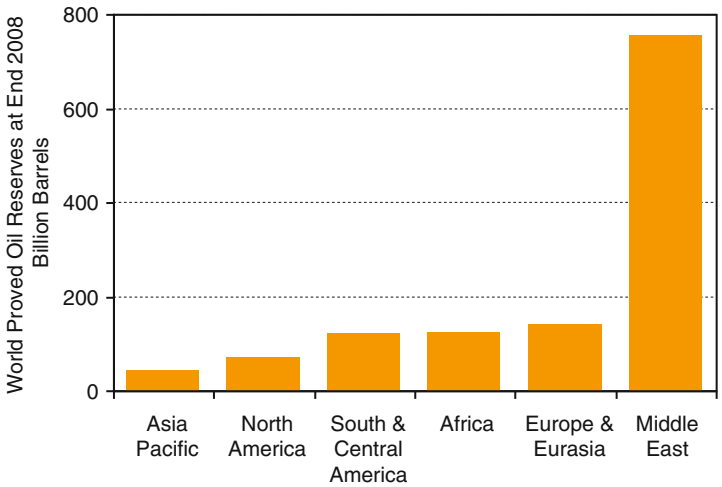

Sustainable Vehicle Fuels, Well-to-Wheel Analysis. Figure 3
Geographic distribution of world proved oil reserve [2]

to the 2000 global greenhouse gas emissions, which is an enormous global challenge. In 2004, the global transportation sector alone emitted 6.3 Gt of CO_2-eq. While the global transportation sector accounts for only 13% of total global emissions of greenhouse gases, it accounts for 23% of global energy-related greenhouse gas emissions [3]. In developed countries such as the United States, the transportation sector contributes 26% of total greenhouse gas emissions and more than 33% of energy-related greenhouse gas emissions [4]. Global transportation greenhouse gas emissions could increase to 9.1 Gt by 2030 and 12 Gt by 2050.

As a result of concerns about energy security and greenhouse gas emissions associated with the transportation sector, many nations have mandated higher

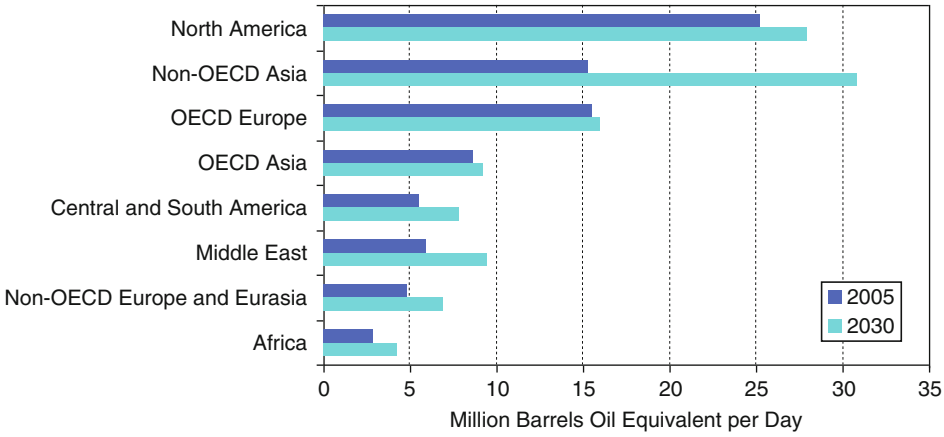

Sustainable Vehicle Fuels, Well-to-Wheel Analysis. Figure 4
Geographic distribution of world oil consumption [1] (OECD is Organization for Economic Cooperation and Development)

standards for vehicle's fuel economy and are exploring the use of alternative fuels in order to contain growth in the demand for petroleum oil and mitigate the projected increase in greenhouse gas emissions.

In the United States, biofuels, hydrogen, and electricity have been promoted for their potential to help reduce petroleum use and greenhouse gas emissions. In general, they can be produced regionally and locally from various sources to provide fuels for motor vehicle use. While electricity and most biofuels can be delivered to energy storage devices in vehicles by using the existing delivery infrastructure, the use of hydrogen requires the development of a delivery and refueling infrastructure before large commercial deployment of fuel-cell vehicles can be realized.

For the WTW analysis of alternative vehicle technologies powered by biofuels, hydrogen, and electricity, the Greenhouse gases, Regulated Emissions, and Energy use in Transportation (GREET) model, developed by Argonne National Laboratory, has been employed to estimate the energy use and greenhouse gas emissions associated with the production, transportation, and consumption of these alternative fuels [5]. The energy and emissions accounting starts from the primary energy source (well) and ends with the vehicle's operation stage (wheels).

The following sections present the important stages, results, and key issues associated with the WTW stages of biofuels, hydrogen, and electricity as alternative transportation fuels.

Biofuel Pathways

The carbon in biofuels is from the air during biomass growth – thus, biofuels have the potential to reduce greenhouse gas emissions significantly. However, the life cycle of biofuel contains such activities as fertilizer production, farming, biofuel production, and biofuel combustion, which may consume fossil energy and produce greenhouse gas emissions. Life-cycle analysis (LCA) has been conducted to examine biofuel energy and environmental effects, and its methodologies have advanced in the past 20 years. In the early years of examining biofuels, the so-called energy balance (energy contained in biofuels minus fossil energy consumed to make them through the whole life cycle) was estimated for biofuels, especially for corn-based ethanol [6, 7]. LCA models have been developed since the early 1990s, and detailed LCAs have been conducted to examine the energy benefits of using biofuels and their emission effects on the environment – especially corn based and cellulosic ethanol in comparison to petroleum fuels [5, 8, 9]. While LCA results of biofuels have generally shown energy and greenhouse gas benefits of biofuels relative to petroleum fuels, the magnitude of the benefits is determined by the types of feedstocks and production technologies. In addition, LCA results are influenced heavily by decisions in LCAs regarding the system boundary of a given analysis and the method of dealing with coproducts of biofuels, among many other factors. The current focus of evaluations of the effects of using biofuel on energy and

environmental is on indirect effects, such as land-use changes from biofuel production, and on other environmental sustainability issues, such as water consumption, biodiversity, and soil erosion, among many others [10–12].

At present, two major biofuels are produced worldwide: ethanol and biodiesel. Ethanol is used in spark-ignition engines (or gasoline engines) from low-level blends, such as E10 (10% of ethanol and 90% gasoline by volume), to high-level blends, such as E85 in the United States and E100 (pure ethanol) in Brazil. While low-level ethanol blends can be used in gasoline vehicles without vehicle modifications, use of high-level blends requires modifying gasoline vehicles to make so-called dedicated ethanol vehicles, as was done in Brazil in the 1970s to late 1990s, or to make flexible-fuel vehicles (FFVs), as in the United States and currently in Brazil. Ethanol is usually transported separately to distribution centers where it is blended with gasoline.

Pure biodiesel (B100) can be used in compression-ignition engines (diesel engines). However, there are issues associated with the use of pure or a higher percentage of biodiesel in a blend with petroleum diesel. Using B100 requires modifying diesel vehicles in addition to meeting special storage requirements to ensure fuel stability. In most cases, and with adequate biodiesel fuel quality, biodiesel blends with petroleum diesel of up to 20% by volume (B20) can be used in diesel vehicles without vehicle modifications.

Ethanol is currently produced from the fermentation of starches and sugars in corn, sugarcane, cassava, wheat, sugar beets, and other crops. In the United States, which is the largest producer of ethanol, ethanol has been produced from corn since 1980. In Brazil, sugarcane ethanol has been produced for almost 100 years. Recently, China and Southeast Asia began to produce fuel ethanol from cassava (China also produces a significant amount of corn ethanol). In Europe, ethanol is produced from corn, wheat, and sugar beets. Cellulosic biomass, such as crop residues (e.g., corn stover), forest residues, and energy crops (e.g., switchgrass [SWG]), is being considered for producing cellulosic ethanol.

Biodiesel is produced from vegetable oils and animal fats via a transesterification process. In the United States, biodiesel is produced from soybeans. In Europe, biodiesel is produced primarily from rapeseeds. In Southeast Asia (particularly in Malaysia), biodiesel is produced from palm oil.

Besides the fermentation and transesterification processes, there are many other technology paths available for producing biofuels. For example, cellulosic biomass can be gasified to produce synthetic gas (syngas). Syngas can be then used to produce Fischer-Tropsch (FT) diesel via the FT synthesis process or ethanol via fermentation of syngas. Renewable hydrocarbon fuels (such as gasoline and diesel) could be produced from vegetable oils and animal fats via the hydrogenation process. Cellulosic biomass can also be pyrolyzed to produce a bio-oil. The bio-oil can then be used to produce gasoline and diesel. Butanol, a fuel with higher volumetric energy content than ethanol, could be produced from sugars via fermentation processes. Recently, interest has heightened in producing hydrocarbon fuels from algae.

Biofuel Life-Cycle Analysis System Boundary

Figure 5 shows the life-cycle analysis boundary defined for the corn ethanol pathway in GREET. For other biofuel cycles, the boundary is defined in similar ways. In particular, the corn ethanol life cycle includes fertilizer manufacture, corn farming, ethanol production, and ethanol use in vehicles. All transportation activities involved in moving goods from one location to another (such as corn movement from farms to ethanol plants) are included. Coproduct distillers' grains and solubles (DGS) and their emission effects are also included in the life-cycle analysis. Most recently, potential direct and indirect land use changes associated with large-scale corn ethanol production have begun to be included as well.

An LCA of biofuels is usually compared to an LCA of such baseline fuels as petroleum gasoline and diesel, and so the life-cycle system boundary needs to be defined for gasoline and diesel. To make the comparison between biofuels and petroleum fuels valid, the system boundary between them needs to be defined as consistently as possible. Figure 6 shows the LCA system boundary usually defined for petroleum gasoline and diesel.

As Fig. 6 shows, the life cycle of petroleum fuels begins with petroleum recovery in oil fields and ends

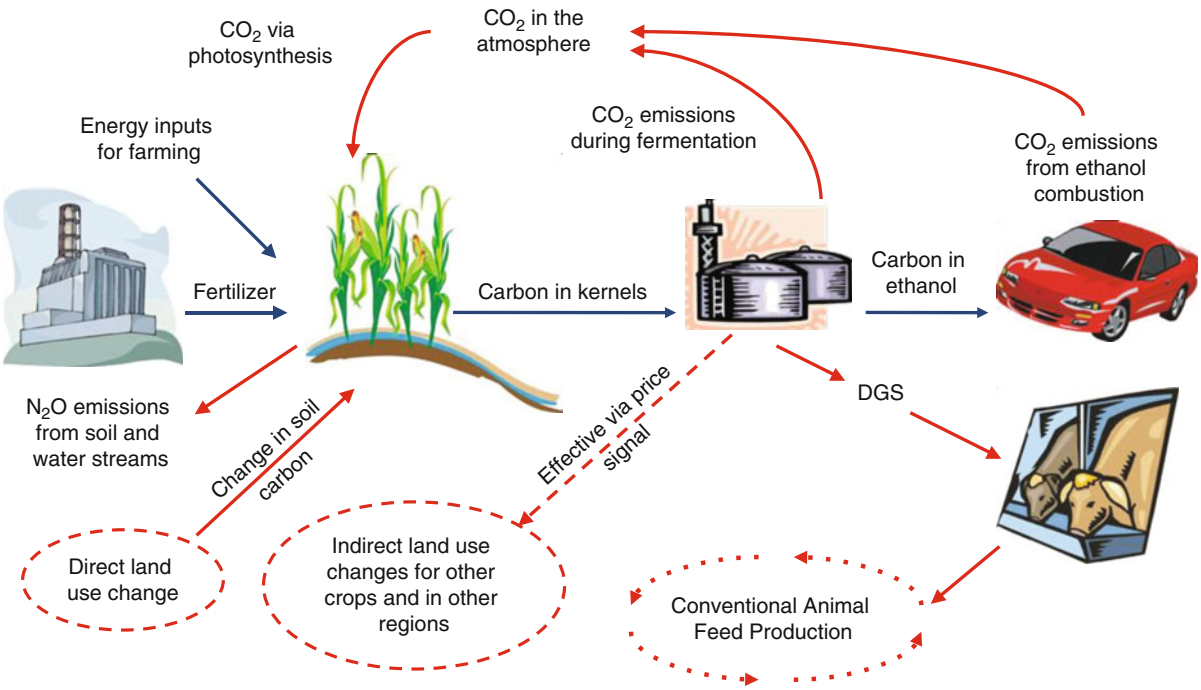

Sustainable Vehicle Fuels, Well-to-Wheel Analysis. Figure 5
Life-cycle analysis system boundary for corn-based ethanol

with gasoline and diesel combustion in motor vehicles. Besides production-related activities, all transportation-related activities to move goods from one location to another (such as crude oil from oil fields to petroleum refineries) are included. Again, infrastructure-related activities (such as construction of drilling rigs and petroleum refineries) are not included in the LCA of petroleum gasoline and diesel. Oil exploration, which occurs well before oil recovery, is also usually not included in petroleum fuel LCAs. Recently, attempts began to be made to include such indirect effects for petroleum life cycle as military operations to secure access to Middle East oil [13].

Life-Cycle Energy Use and Greenhouse Gas Emission Results of Key Biofuel Pathways

Corn and Cellulosic Ethanol Since the beginning of the US corn ethanol program in 1980, production of US corn ethanol has risen to 13 billion gallons in 2010 [14]. The US 2007 Energy Independence and Security Act established a goal to produce 15 billion gallons per year of corn ethanol by 2015. The corn ethanol industry expanded quickly to reach that goal.

Historically, corn ethanol has been produced from both dry and wet milling plants with different front-end milling technologies and with different coproducts. Wet milling plants were built in large sizes and with the flexibility of producing multiple coproducts, but they required significant capital investments. Dry milling plants initially were built in small sizes and with a single coproduct (i.e., DGS) and required lower capital investments. Since 2000, all newly built corn ethanol plants in the United States have been dry milling plants. Recently, the size of dry milling plants has approached that of wet milling plants. Some of the newly built dry milling plants produce more than 100 million gallons of ethanol per year.

Corn ethanol plants require a large amount of steam for fermentation and distillation. Natural gas (NG) is the primary process fuel, and coal is used in wet milling plants to generate steam. On average, 80–90% of US corn ethanol capacity is fueled with NG and the remaining 10–20% with coal.

Since the beginning of the US corn ethanol program, the energy use intensity of corn ethanol plants has been reduced from more than 19.5 mega Joules (MJ)

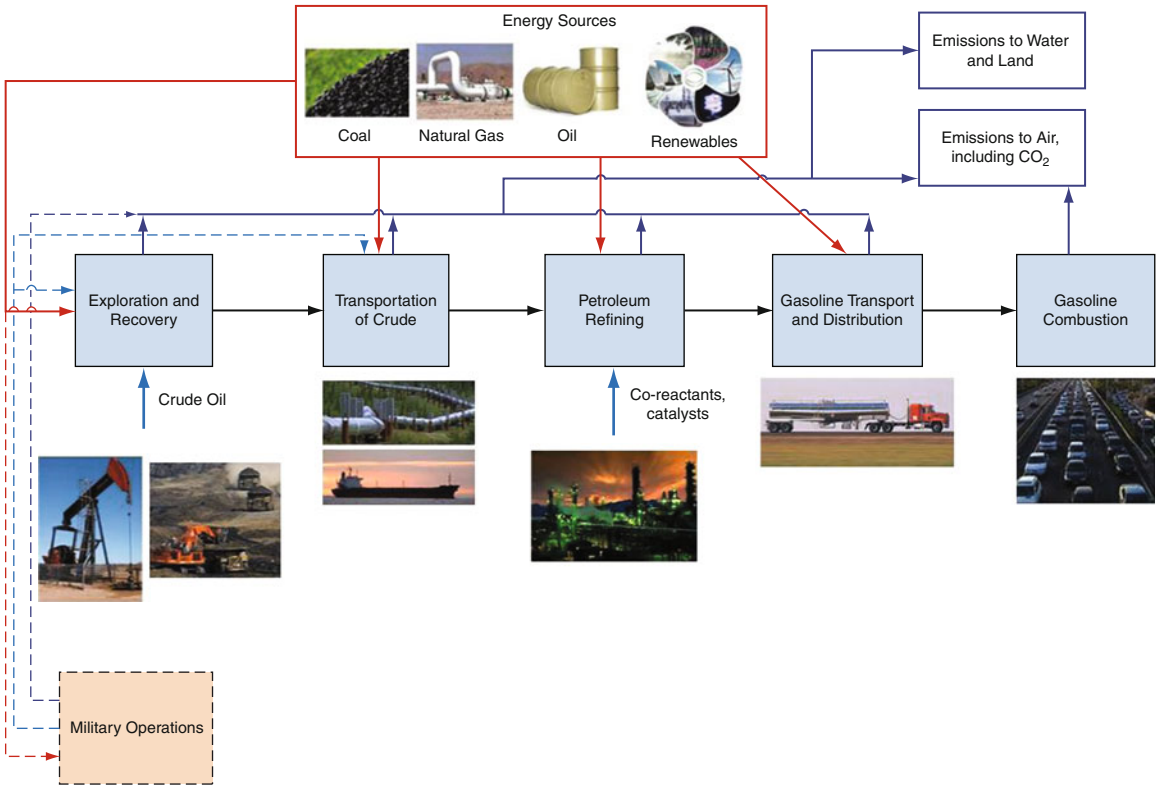

Sustainable Vehicle Fuels, Well-to-Wheel Analysis. Figure 6
Life-cycle analysis system boundary for petroleum gasoline and diesel

per liter (70,000 British thermal units [Btu] per gallon) of ethanol [6] to less than 8.4 MJ (30,000 Btu) [15]. This greater than 57% reduction in energy intensity has been achieved by high ethanol yield, increased production of wet DGS in lieu of dry DGS, and better process designs, all of which were driven by the economics of ethanol plant operation.

Corn farming requires large amounts of nitrogen fertilizer and fuels, although since the 1970s, usage intensities for chemicals and fuels associated with US corn farming have been reduced significantly. For example, US corn productivity in terms of corn yield per unit of fertilizer input to farms has increased by 88% between 1970 and 2005 [15]. This was accomplished by a continuous increase in corn yield per unit of land without a corresponding increase in fertilizer use. Mainly because the corn yield per unit of land was increased, farming energy use per unit of corn yielded was reduced by 50% between 1996 and 2005, according to the three most recent farming energy expenditure surveys conducted by the US Department of Agriculture.

Figure 7 shows shares of greenhouse gas emissions by key activities for corn ethanol. Ethanol plants are by far the largest source of greenhouse gas emissions. N_2O emissions from nitrogen fertilizer nitrification and denitrification in cornfields (and with a small amount of CO_2 emissions from lime in cornfields) are the second largest source of greenhouse gas emissions. Greenhouse gas emissions from nitrogen fertilizer and other chemical plants (such as phosphorous fertilizer, potash fertilizer, and lime) and from farming energy consumption are significant contributors as well.

Various cellulosic biomass feedstocks could be used for ethanol production, including crop residues, such as corn stover, wheat straw, and rice straw; forest residues; dedicated energy crops, such as switchgrass, miscanthus, willow trees, and hybrid poplars; and municipal solid wastes. The LCAs of cellulosic ethanol that have been completed at Argonne National

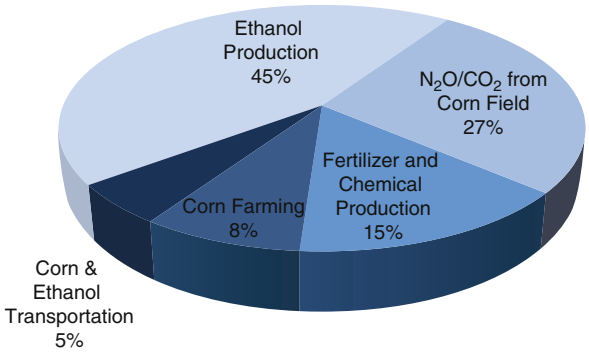

Sustainable Vehicle Fuels, Well-to-Wheel Analysis. Figure 7
Shares of greenhouse gas emission sources for corn ethanol

Laboratory include ethanol from corn stover, forest residues, and switchgrass.

Wu et al. examined these cellulosic ethanol pathways [16]. Corn stover is usually left in cornfields for soil protection and as a nutrient supplement for the next growing season. Extensive research has been done to examine how much stover can be removed from cornfields without causing soil quality to deteriorate. Within the LCA context, the operation of collecting and transporting corn stover from fields to cellulosic ethanol plants needs to be taken into account. In addition, the nutrients removed from cornfields as corn stover is removed need to be supplemented during the next season for growing crops. These factors were considered in Argonne's LCA for the corn stover-to-ethanol pathway. As for the forest residue-to-ethanol pathway, major activities for this pathway include stumping, collecting, and transporting forest wastes from fields to ethanol plants. In fact, the amount of diesel fuel used for these activities could be significant [16].

Switchgrass can be farmed as a dedicated energy crop. Managed switchgrass farms may require fertilizer applications in order to maintain a desirable yield per unit of land, although the amount of fertilizer used is less for switchgrass farming than for corn farming. Also, if switchgr*ass farming occurs in arid regions* (*such as the US Pacific Northwest*), *irrigation* may be also required. If switchgrass is grown on marginal land or unmanaged prairie land, the growth of switchgrass could, indeed, help increase soil carbon content, resulting in additional greenhouse gas emission reductions.

In ethanol plants, cellulosic biomass undergoes a pretreatment process so that cellulose and hemicellulose can be broken down into simple sugars for hydrolysis and further fermentation. The lignin portion of the biomass cannot be fermented. Because of its high energy content, lignin can be used as a process fuel in cellulosic ethanol plants to provide the needed steam. In fact, mass balance calculations indicate that the amount of lignin available in cellulosic ethanol plants can exceed the amount of lignin needed for steam generation. Combined heat and power systems are proposed to generate both steam and electricity in cellulosic ethanol plants. Some of the generated electricity can be exported to the electric grid to displace conventional electric power generation, which offers additional reductions in greenhouse gas emissions.

Figure 8 shows life-cycle CO_2-eq emissions of greenhouse gases for six types of corn ethanol, and three types of cellulosic ethanol. Here, the effects of corn ethanol on greenhouse gas emissions include emissions from direct and indirect changes in land use changes, which are subject to great uncertainties (see section Direct and Indirect Land Use Changes). Corn ethanol plants using coal do not offer greenhouse gas emissions reductions. Average wet milling plants (with 73% of process fuel being natural gas) offer moderate reductions in greenhouse gas emissions. The lower greenhouse gas emissions benefits associated with wet milling ethanol are the result of higher energy use in wet milling plants and lower emission credits with wet milling coproducts (the system boundary expansion method has been used to estimate emission credits of ethanol's coproducts). On the other hand, dry milling plants (except those using coal) offer significant greenhouse gas emissions reductions, especially when wet DGS is produced and a significant amount of energy use can be avoided. On the other hand, the three types of cellulosic ethanol offer large reductions in greenhouse gas emissions because the steam required in cellulosic ethanol plants is generated with lignin of biomass and electricity is exported to displace conventional electricity generation [15].

Sugarcane Ethanol Wang et al. evaluated the potential reduction in greenhouse gas emissions associated

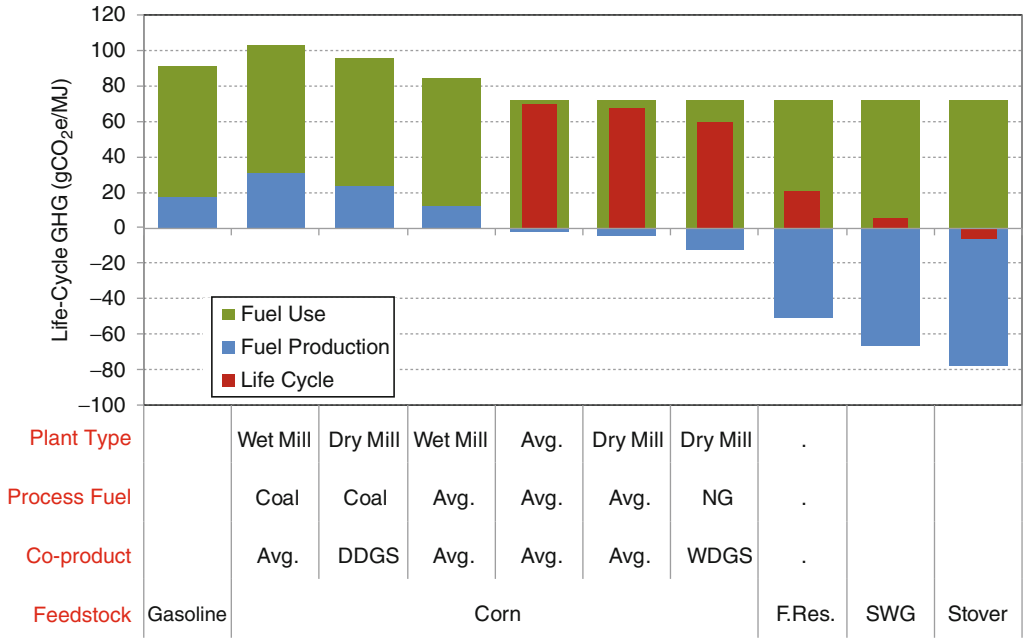

Sustainable Vehicle Fuels, Well-to-Wheel Analysis. Figure 8
Life-cycle greenhouse gas emissions of petroleum gasoline, corn ethanol, and cellulosic ethanol (g CO_2-eq per MJ)

with Brazilian sugarcane ethanol used in both Brazil and the United States [17]. Similarly, Loarie et al. evaluated sugarcane ethanol production and use in Brazil [18].

The sugarcane-to-ethanol cycle includes fertilizer manufacture, sugarcane farming, ethanol production, and ethanol use in vehicles. Traditionally, sugarcane is harvested by laborers, comprising the so-called manual harvest with open-field burning. Brazil is on a trend to replace manual harvests with mechanical harvests using farming machinery. Brazilian sugarcane mills produce ethanol and sugar. The split between the two products depends on market demand and prices of both. Bagasse, the leftover material after juice extraction, is burned in sugar mills to generate steam and power. A significant amount of electricity is exported from sugar mills. Figure 9 shows the system boundary for an LCA of sugarcane ethanol in the GREET model.

Figure 10 shows the shares of greenhouse gas emissions by key activities of the sugarcane ethanol life cycle. CH_4 and N_2O emissions from open-field burning in sugarcane plantations alone are responsible for 25% of total greenhouse gas emissions for sugarcane ethanol. Overall, the five major contributors to sugarcane ethanol greenhouse gas emissions are open-field burning, N_2O emissions from sugarcane fields, fertilizer production, greenhouse gas emissions from sugarcane ethanol transportation, and farming energy consumption. Sugarcane ethanol plants generate the least amount of greenhouse gas emissions since combustion of bagasse for steam and power generation returns CO_2 untaken during sugarcane plant growth back to the air. Using sugarcane ethanol achieves reductions in greenhouse gas emissions of 75–80%, which is similar to the reductions in greenhouse gas emissions associated with using cellulosic ethanol.

Biodiesel and Renewable Diesel from Soybeans

Biodiesel is produced from seed oils or animal fats via the transesterification process. In the United States, most biodiesel is produced from soybean oil. The production volume of biodiesel in the United States increased dramatically between 2000 and 2008 [19]. However, since then, US biodiesel production declined because of high soybean feedstock costs, limited biodiesel demand in the United States, and the EU's policy restriction of biodiesel import from the United States. It remains to be seen if these conditions will change.

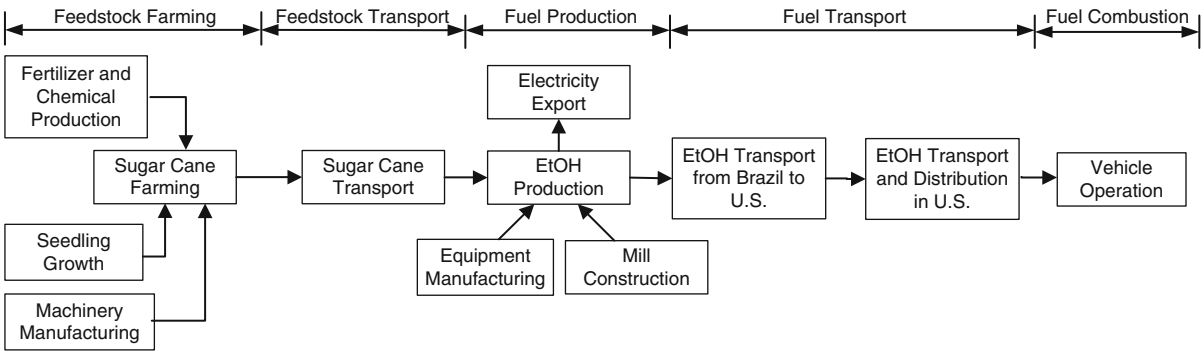

Sustainable Vehicle Fuels, Well-to-Wheel Analysis. Figure 9
Life-cycle analysis system boundary of sugarcane ethanol life-cycle analysis

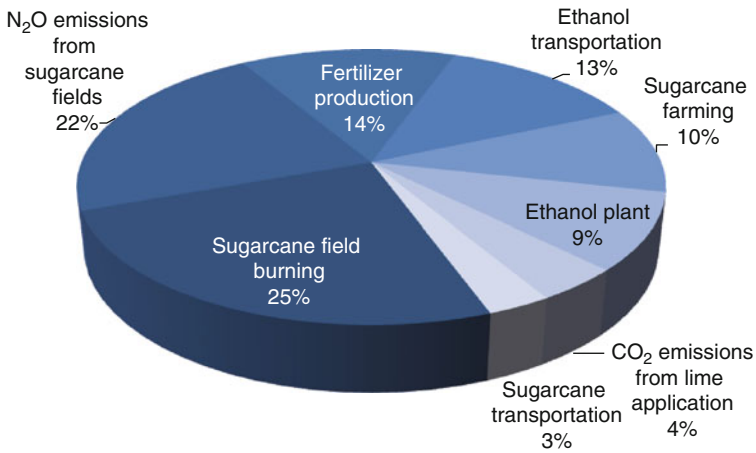

Sustainable Vehicle Fuels, Well-to-Wheel Analysis. Figure 10
Shares of greenhouse gas emissions by key activities of the sugarcane ethanol life cycle (*Notes*: Two renewable diesel production technologies [the Canadian SuperCetane and the U.S. UOP technologies] are presented: The four bars for each fuel group represent four methods of dealing with coproducts of biodiesel and renewable diesel)

New process technologies based on hydrogenation to convert seed oils and animal fats to renewable diesel with properties similar to those of petroleum diesel fuels have recently emerged [20]. Huo et al. conducted an LCA of soybean-based biodiesel and renewable diesel in the United States. Soybean farming in the US Midwest is usually rotated with corn farming [20]. Because the soybean plant's legume has the ability to fix nitrogen in the soil, soybean farming requires much less nitrogen fertilizer than corn farming does, which helps increase the energy and emission benefits of soybean-based biodiesel and renewable diesel.

Before production of biodiesel or renewable diesel, soybeans are crushed to separate soy meals and soy oil. Soy meals are a high-value animal feed product. On a mass basis, 82% of soybeans end up in soy meals and the remaining 18% in soy oil. Soy oil is then used to produce biodiesel or renewable diesel.

In biodiesel plants, glycerin, a specialty chemical, is produced together with biodiesel. On a mass basis, 82% of soy oil ends up in biodiesel and 18% in glycerin. In renewable diesel plants, fuel gas, heavy oils, and propane are also produced.

Figure 11 presents LCA results of reductions in greenhouse gas emissions associated with the use of

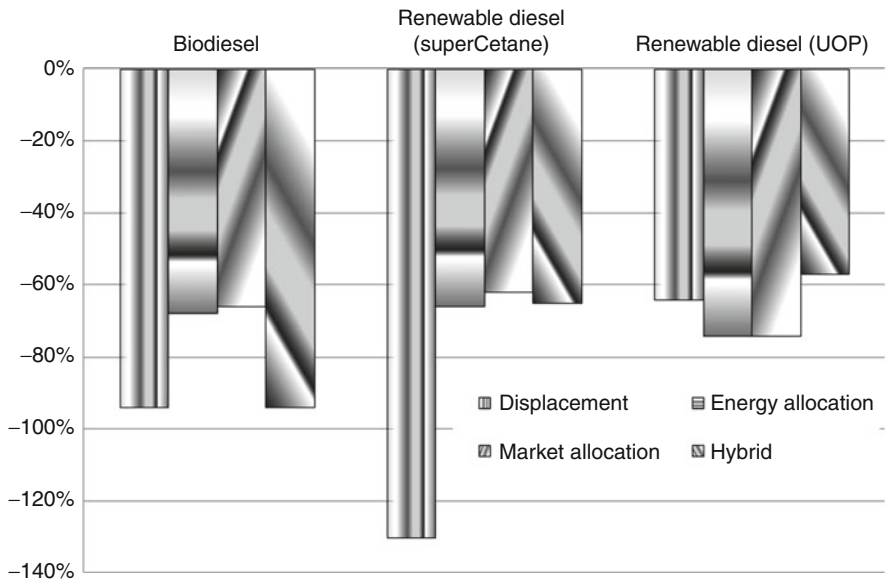

Sustainable Vehicle Fuels, Well-to-Wheel Analysis. Figure 11
Reductions in greenhouse gas emissions associated with soybean-based biodiesel and renewable diesel (relative to petroleum diesel, on a per-unit energy basis) [20]

biodiesel and renewable diesel. In general, biodiesel and renewable diesel can reduce greenhouse gas emissions by more than 60% relative to petroleum diesel. As the chart shows, the methods used in LCAs to address coproducts have a significant effect on LCA results for biodiesel and renewable diesel.

Outstanding Issues of Biofuel Life-Cycle Analysis

This section presents three outstanding issues that are in debate and that can significantly affect LCA results for biofuels.

Direct and Indirect Land-Use Changes Although the land-use change issue for biofuels was not new, Searchinger et al. were the first to develop quantitative results for this issue and advocated against certain types of biofuel on the basis of their results [10]. Conceptually, the production of biofuels will require that biomass feedstocks are grown on land. Growth of a given feedstock on a piece of land changes the original land use pattern of that piece of land. This land-use change is referred to as a *direct land-use change*. Direct land use changes are identifiable and measureable since such changes can be directly observed and attributed to biofuel production. On the other hand, use of agricultural commodities (such as corn) causes an imbalance between supply and demand of agricultural commodities, which can trigger increases in commodity prices. The price increase signal can have ripple effects, causing cultivation of additional land for growing agricultural commodities somewhere in the world. This land-use change is referred as to an *indirect land use change*. As one can expect, indirect land use changes are supposed to be caused by increased commodity prices. Indirect land use changes may be simulated with computable general equilibrium (CGE) models to take into account all interrelationships among all economic sectors and activities via the price elasticity of commodities. Searchinger et al. used the FAPRI (Food and Agricultural Policy Research Institute) model (which is a partial, not general, equilibrium model) to develop estimates of direct and indirect land use changes [10]. The GTAP (Global Trade Analysis Project) model developed by Purdue University is a general equilibrium model that has been used by several organizations to address land-use change issues.

After publication of the Searchinger study, the simulation and data problems of that study were identified, as were the problems of land-use change modeling by

CGE models in general. Major efforts have been made to expand and upgrade these models to better simulate land-use change issues for biofuels [21–24].

Carbon emissions (carbon sequestration, in some cases) from land-use changes are determined by using changes in aboveground biomass and belowground biomass and soil carbon contents of different types of land cover. Even though data sources regarding these are available, they are not comprehensive enough to cover all major types of land cover in different global regions. Often, scarce data from a small set of regions are applied to different global regions [25]. In addition, soil carbon content data cover only a shallow depth of soil (such as the top 30 cm). Adequate, comprehensive data on aboveground biomass, belowground biomass, and soil carbon content will require considerable effort to collect and accumulate for use.

Coproduct Treatment in Biofuel Life-Cycle Analyses

As the results in Fig. 11 for biodiesel and renewable diesel show, the results of LCA for biofuels can vary significantly, depending on the method selected in dealing with biofuel coproducts.

Wang et al. examined methodologies for dealing with coproducts in biofuel LCAs [26]. They explored five methods. First, with the mass-based allocation method, energy and emission burdens of a given biofuel pathway are allocated among all products according to their mass output shares. This allocation method is based on the presumption that energy use and emissions are somewhat related to the amount of mass processed. This method is widely used in LCAs of consumer products and embedded in some generic LCA models. The method is applicable as long as all products are used for their mass values (e.g., a kilogram of steel for use). However, this method becomes problematic when products have distinctly different uses. For example, in the cases of sugarcane ethanol and cellulosic ethanol production, electricity is coproduced but cannot be allocated by mass.

Second, with the energy-content-based method, the energy and emission burdens of a given fuel production pathway are allocated among products according to their share of energy output. The energy outputs of all products are calculated by using the amount of products and their energy content (usually heating content of the products). This method is applicable where most of the products, if not all, are used for their energy content. The method becomes problematic when products have distinctly different uses. For example, starch-based ethanol plants produce ethanol and animal feeds. Even though animal feeds have energy content, they are used because of their significant nutritional values, not their heating values, which are on par with conventional animal feeds (such as corn and soybean meal).

Third, the market-value-based method allocates energy and emission burdens based on economic revenue shares of individual products. The economic revenue of a given product is calculated from the product yield of a given pathway and the price of the product. Economists generally advocate use of this method. In fact, some LCA applications of general equilibrium models adopt this method. This method assumes that activities and decisions are driven by economics, and thus burdens should be disbursed according to economic benefits. One unique advantage of this method is that it normalizes all products to a common basis – their economic values. However, in practice, this method is subject to great fluctuations in product prices.

Fourth, the process-purpose-based method estimates energy use and emissions of individual processes in a fuel production facility. The energy use and emissions of a given process are allocated to a given product if the purpose of that process is solely for the production of the given product. An example is the dryer in a corn ethanol plant. The dryer is installed to dry DGS. Thus, energy use and emissions from the dryer operation are allocated to DGS. However, in many cases, individual processes in a facility may produce multiple products, creating a need to allocate energy and emissions of a given process among all products from the process. Furthermore, this method requires energy and emission data at the process level, not at the facility level, which may not be available to researchers for many biofuel facilities. Even if the process-purpose-based method is applied to a given facility, the activities upstream of the facility still need to be allocated. For example, this method can be used to allocate energy use and emissions of corn ethanol plants between ethanol and DGS. But the allocation of energy use and emissions of corn farming between ethanol and DGS still needs to be decided. This decision, in turn, might be based on the mass-, energy-content-, or market-based method.

Fifth, with the displacement method (also called the "system boundary expansion method"), the products that are to be displaced by nonfuel coproducts are determined first. Energy and emission burdens of producing the otherwise displaced products are then estimated. The estimated energy and emission burdens are credits that are subtracted from the total energy and emission burdens of the biofuel production cycle. While the displacement method is generally advocated for LCAs, its implementation poses some major challenges. The method requires conducting LCAs for the conventional products that will be displaced, which could be time- and resource-intensive. Another major problem with the displacement method is that when nonfuel products are a large share of the total output, the method generates distorted LCA results for fuels [26].

Whether a given method can be uniformly and blindly recommended for LCA studies is far from settled. Consistency of coproduct method choices for evaluation of different biofuel production pathways may not serve the purpose of providing reliable LCA results well. Transparency of LCA methods is important in LCA studies, and sensitive cases with multiple coproduct methods may be warranted in LCA studies where coproducts can significantly impact study outcomes.

Other Environmental Sustainability Issues Environmental sustainability issues of biofuel production and utilization are now an important topic. Such issues include freshwater consumption for feedstock growth and biofuel production, effects on soil erosion of growing certain feedstocks, implications of feedstock growth on biodiversity, and effects of producing and using biofuels on air pollution and its health-related effects. So far, these issues have not been addressed systematically on the life-cycle basis. Nonetheless, such issues as freshwater consumption were estimated by examining key (but not all) stages of the biofuel life cycle. In addition, some of the issues (such as biodiversity) are difficult to address quantitatively. Eventually, these issues should be addressed along the entire life cycle of biofuels (i.e., all stages of the life cycle should be considered). More importantly, these issues should be addressed on a comparative basis so that biofuels can be compared with baseline petroleum gasoline and diesel for relative environmental sustainability implications.

Wu et al. recently estimated the consumptive water requirements of ethanol and gasoline production [12]. For biofuel production, the key determinants are feedstock and the amount of irrigation water needed to generate reasonable yields. For gasoline production, the key determinants are the characteristics of individual oil reservoirs, the recovery technology used, and the degree of produced water recycling. On average, corn ethanol production tends to consume more water on a life-cycle basis than does cellulosic ethanol production. Net water use for cellulosic ethanol production is comparable to that of gasoline. Biofuels production exhibits significant regional differences in water use. Consumptive water use for corn ethanol production varies significantly in the major US corn-growing regions. Producing a liter of corn ethanol can consume as little as 10 or as much as 324 L of water, depending on the amount of irrigation water used for corn growing. On average, more than half of US corn ethanol is produced at a water use rate of 10 L of water per liter of ethanol. Switchgrass-based cellulosic ethanol production, when the switchgrass is grown in its native habitat in the United States, can consume from 1.9 to 9.8 L of water per liter of cellulosic ethanol, depending on process technology. In comparison, net water use to produce a liter of gasoline varies from less than 3 L to nearly 7 L.

Hydrogen Pathways with Fuel-Cell Vehicles

Hydrogen is a clean fuel that can be converted into electricity with high efficiency in fuel cells to power electric motors for vehicle propulsion. Using hydrogen in FCVs produces no tailpipe emissions. Furthermore, hydrogen can be produced from diverse feedstock sources, including nonfossil and renewable sources. This mitigates the risk of future dependence on a single source of fuels to satisfy the transportation needs, as is the case with the current global dependence on petroleum fuels.

Fuel-cell vehicles (FCVs) are being promoted primarily because of their high efficiency that is not limited by Carnot theoretical heat engine efficiency and because of their zero or near-zero emissions. Governments and private industries are actively investigating

market barriers and vehicle and fuel infrastructure constraints so that the introduction of FCVs will be successful when the technology is ready for the mass market. FCVs are based on proton exchange membrane (PEM) technology of fuel cells, which requires hydrogen as a fuel. The PEM fuel cell generates electricity from the hydrogen fuel through an electrochemical conversion process and stores the generated electricity in a battery. The battery then powers an electric motor to propel the vehicle.

The delivery infrastructure for large-scale deployment of FCVs is not in place. This represents a major challenge to a large-scale commercialization of FCVs. Another challenge for hydrogen FCV technology is storing a sufficient amount of hydrogen aboard the vehicle in a practical amount of space for an acceptable vehicle range and at a reasonable cost. A variety of hydrogen storage technologies are being researched and developed. These include physical storage approaches – modest-pressure gas (350 bar), high-pressure gas (700 bar), and cryo-compressed hydrogen storage – as well as material-based storage systems. Material approaches include metal hydrides; sorbents, such as carbon and metal organic frameworks (MOFs); and chemical hydrides. The storage system technology directly impacts the WTW energy efficiency, greenhouse gas emissions, and costs of hydrogen and fuel-cell vehicles [27].

Although hydrogen-powered FCVs offer zero vehicular emissions, production of hydrogen – such as from natural gas (NG) or grid electricity as hydrogen is being currently produced – can generate a significant amount of emissions and suffer significant energy penalty. Such energy penalty and emissions are accounted for in the WTP stage of the fuel cycle as explained earlier.

Hydrogen Fuel-Cycle Pathways

Central Hydrogen Production Via Steam Methane Reforming Steam methane reforming (SMR) is a process in which high-temperature steam (700–1,000°C) is used to produce hydrogen from natural gas. In the first stage of the process, methane reacts with steam in an endothermic reaction under 3–25-bar pressure in the presence of a catalyst to produce hydrogen, carbon monoxide, and a relatively small amount of carbon dioxide. Subsequently, the carbon monoxide and steam are reacted by using a catalyst to produce carbon dioxide and more hydrogen. Carbon dioxide and other impurities are typically removed from the gas stream by using pressure swing adsorption (PSA), leaving essentially pure hydrogen. The efficiency range of hydrogen production via SMR is between 68% and 75% [28].

Central Hydrogen Production Via Wind Energy The desire to minimize greenhouse gas emissions associated with hydrogen production for FCVs is likely to increase interest in producing hydrogen via the electrolysis of water by using renewably generated electricity. Wind power has entered the mainstream utility market because currently available government incentives make it competitive with conventional alternatives. Without a major breakthrough or shift in incentives, wind is likely to remain the lowest-cost source of renewable electricity. Production of hydrogen from wind power helps alleviate the intermittent problem of wind power. An annual average wind speed greater than 6 m/s (13 mph) is required for utility-scale wind power plants. Producing 1 kg of gaseous hydrogen approximately requires 50 kWh of electricity, while the lower heating value (LHV) of hydrogen is 33.3 kWh/kg. In such case, the electrolyzer efficiency is 67% [29].

Distributed Hydrogen Production Via Electrolysis Hydrogen can be produced at the refueling station by electrolysis of water with grid electricity. Because electricity transmission and distribution infrastructure is already in place throughout most countries, this production option helps avoid long-distance transportation of hydrogen from central production locations. However, if hydrogen is produced via electrolysis at refueling stations for the large-scale FCV market, a large amount of electricity could be required. In such case, electricity distribution lines to refueling stations will probably need to be upgraded to allow sufficient power for hydrogen production. The energy use and the greenhouse gas emissions associated with hydrogen production depend on the electrolyzer's efficiency and the technologies used for grid power generation, respectively. The electrolyzer efficiency ranges from 67% to 76% [28].

Compression of Hydrogen Hydrogen compression is needed for pipeline delivery, for loading into tube trailers, and for dispensing into FCVs. The power demand of a compressor can be reduced by maintaining the gas temperatures as low as possible. Thus, low compression power can be achieved through multistage compression with intercooling between stages. Considering the thermodynamic properties of hydrogen, and with isentropic efficiencies in the range of 60–80%, the allowable pressure rise per stage of compression is in the range of 2.0–2.5. For such pressure ratios and with intercooling, stage outlet temperatures are low enough that perfect gas relationships adjusted with compressibility factor provide a reasonable estimate of compression power requirements as follow:

$$\text{Power} = (\mathrm{Z})(\dot{\mathrm{m}})(R)(\mathrm{T})(\mathrm{n})\left(\frac{1}{\eta}\right)\left(\frac{\mathrm{k}}{\mathrm{k}-1}\right) \times \left[\left(\frac{\mathrm{P}_{\mathrm{outlet}}}{\mathrm{P}_{\mathrm{inlet}}}\right)^{\left(\frac{\mathrm{k}-1}{\mathrm{nk}}\right)} - 1\right],$$

where Z is the mean compressibility factor
m is the mass flow rate
R is the universal gas constant
T is the inlet gas temperature
n is the number of stages
η is the isentropic efficiency of compression
k is the ratio of specific heats
$\mathrm{P}_{\mathrm{outlet}}$ is the compressor discharge pressure and
$\mathrm{P}_{\mathrm{inlet}}$ is the compressor inlet pressure

The equation assumes the intercooler outlet temperatures are equal to the ambient temperature [30]. The greenhouse gas emissions associated with compression of hydrogen depend on the compression pressure ratio and efficiency, as well as the technologies used to generate the electricity for compression.

Liquefaction of Hydrogen One of the most efficient methods to package hydrogen molecules at high energy density for transportation and storage purposes is to liquefy hydrogen after its production. Liquefaction includes gas compression, cooling with water, and precooling with liquid nitrogen to drop the hydrogen below its inversion temperature (200 K). However, liquefying hydrogen requires cooling to temperatures below 20 K. Cooling to that temperature requires significant electrical energy use at approximately 10–13 kWh per kg of hydrogen. It is estimated, however, that advanced liquefaction plants could reduce electrical energy requirements to 8 kWh/kg [30]. The greenhouse gas emissions associated with liquefying hydrogen depend on the liquefier efficiency and the technologies used to generate the electricity required for liquefaction. Once liquefied, hydrogen can be efficiently transported, stored, and dispensed into FCVs in liquid, cryo-compressed, or gaseous form. However, liquid hydrogen is subject to significant boil-off losses if stored for a long period. Because of these losses, liquid hydrogen pathways generally consume more energy and produce more emissions than gaseous hydrogen pathways.

Hydrogen Consumption by FCVs

The key parameter determining the hydrogen consumption by FCVs is the vehicle's fuel economy. The testing of the fuel economy of the first- and second-generation FCVs, through the Department of Energy (DOE)'s Controlled Hydrogen Fleet and Infrastructure Validation and Demonstration Project, resulted in an adjusted fuel-economy range of 42–57 miles/kg hydrogen for the four teams for first-generation vehicles, as compared to 43–58 miles/kg for second-generation vehicles [31]. More recently, FCVs produced by Honda and Toyota achieved fuel economies at 60 mi/kg and 70 mi/kg, respectively. The fuel economy of FCVs depends greatly on the fuel cell system and electric motor efficiencies. The DOE targets a peak efficiency of 60% for fuel cells, which has already been demonstrated by many FCV OEMs. Currently, most of the research is focused on reducing the cost of the fuel cell system.

Hydrogen Delivery and Storage in FCVs

The transition to hydrogen-powered vehicles requires the development of hydrogen infrastructure, including refueling stations. Distributing hydrogen depends on how it is packaged for dispensing into hydrogen vehicles. Packaging affects not only density (weight/volume) but also the operation of potential delivery modes and onboard storage, a problem that has been called the "grand challenge" of the hydrogen economy. Energy-dense packaging is a critical issue for hydrogen

fuel and was a major focus of the DOE's hydrogen and fuel cells initiative [44]. Although high-pressure gaseous storage is currently closest to meeting the DOE goal of 8 wt.% hydrogen, other storage technologies are also being investigated (e.g., metal hydrides, carbon nanostructures, and carriers like methanol or other hydrogen-rich chemicals). Depending on the success of these efforts, hydrogen could be delivered as a high-pressure gas, as a cryogenic liquid, or at standard temperature and pressure via a solid or liquid carrier. The associated energy use associated with each mode of delivery/dispensing could be quite different [32].

Among the options that are being used and proposed for onboard hydrogen storage in FCVs are 350-bar and 700-bar gaseous storage, as well as supercritical cryo-compressed storage of hydrogen. The 350-bar gaseous storage option requires less energy for hydrogen compression into the vehicle's tank, but it results in low energy density and reduced vehicle travel range between refills. The 700-bar gaseous storage option improves the vehicle's travel range but requires higher compression energy, in addition to cooling to −40°C to attain a fill rate comparable to that of current gasoline vehicles (approximately at 1.6 kg/min). The compression energy requirements for 350-bar and 700-bar gaseous dispensing options are 2 kWh/kg and 3 kWh/kg, respectively. The cooling to −40°C results in an additional 0.25 kWh per kg of hydrogen for the 700-bar dispensing option. The cryo-compressed option requires delivering hydrogen in liquid form, which incurs a large energy penalty at the liquefaction plant, as discussed earlier. Currently, most OEMs are favoring the 700-bar storage option.

WTW Results of Hydrogen Fcvs

Figure 12 shows the reduction in the WTW total energy use for various hydrogen production pathways relative to the conventional gasoline ICE vehicle pathway. These energy use results reflect the WTP energy use and the fuel economy of FCVs. The reduction in the total energy use is directly proportional to the WTW efficiency of the pathway. Central production of hydrogen from natural gas via steam methane reforming with 350-bar dispensing provides a reduction in total energy of 39% compared to the conventional gasoline pathway. The reduction is attributed mainly to the high efficiency of fuel cells, which results in a fuel economy ratio of 2.3 relative to the baseline gasoline's vehicle fuel economy. The reduction in total energy for the same production pathway drops to 36% with the 700-bar dispensing option because of the additional compression and cooling requirements, as discussed earlier. If liquefaction is used to facilitate high-energy-density packaging for more cost-effective delivery and improved FCV travel range, the reduction in total energy for the natural gas SMR pathway fades to 7%, relative to baseline gasoline vehicles. This reduction is due to the high energy use associated with the liquefaction process. Central production of hydrogen via

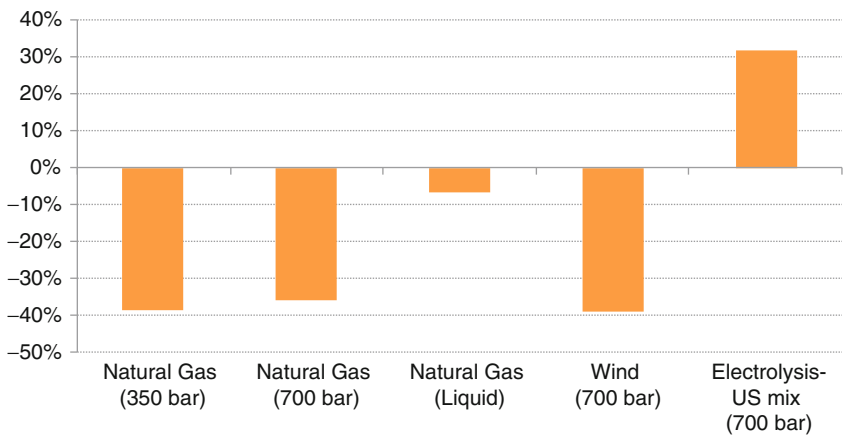

Sustainable Vehicle Fuels, Well-to-Wheel Analysis. Figure 12
Reduction in WTW total energy (relative to gasoline) for various hydrogen production pathways

electrolysis using electricity from renewable sources, such as wind, results in a reduction in total energy similar to that of the natural gas SMR pathway at 39%. For the wind-to-hydrogen pathway, the accounting of energy use starts with the energy in electricity because the wind power is available in abundance and will be lost if not utilized. Therefore, the conversion efficiency of wind power to electricity impacts the economics rather than the sustainability of such conversion. However, when hydrogen is produced via electrolysis at distributed locations (i.e., at a refueling station), it uses electricity from the grid. Considering the US grid mix with a combined fossil energy efficiency of 40%, an electrolyzer efficiency of 71%, and a compression efficiency of 91%, the WTW total energy use for this pathway exceeds that of the baseline gasoline by 32%, as shown in Figure 12.

Figure 13 shows the reduction in the WTW petroleum energy use for various hydrogen production pathways relative to a conventional gasoline ICEV pathway. All hydrogen production pathways virtually eliminate the dependence on petroleum fuels for vehicle operation. The WTW efficiency of the pathways implied in Fig. 12 does not impact the degree of petroleum reduction simply because the feedstock sources in these pathways are nonpetroleum, except for a small share of electricity power generation (2%) in the US mix that is produced from residual oil.

Figure 14 shows the reduction in the WTW greenhouse gas emissions for various hydrogen production pathways relative to a conventional gasoline ICEV pathway. The reduction in greenhouse gas emissions shows a trend similar to the reduction in total energy in Fig. 12, but with renewable sources (i.e., wind) exhibiting significantly more reductions in greenhouse gas emissions compared to fossil sources of hydrogen production (i.e., natural gas) and the US grid mix. While natural gas SMR production pathway provides reductions in WTW greenhouse gas emissions of 49% and 46% for the 350-bar and 700-bar dispensing options, respectively, the wind pathway provides a reduction of 89% in greenhouse gas emissions relative to the baseline gasoline pathway. Hydrogen production via electrolysis using the US average grid mix results in a 40% increase in greenhouse gas emissions relative to gasoline, mainly because of the low WTP efficiency for this pathway and the high dependence of the US grid on fossil sources – especially coal – for power generation.

Hydrogen Life-Cycle Analysis Issues and Uncertainties

The production and delivery of hydrogen for dispensing in FCVs may result in significant energy penalty and greenhouse gas emissions for some pathways. Natural gas is currently being used for commercial production of hydrogen. While natural gas is the least carbon intensive option among all fossil fuels and is abundant at a lower cost than petroleum fuels on a

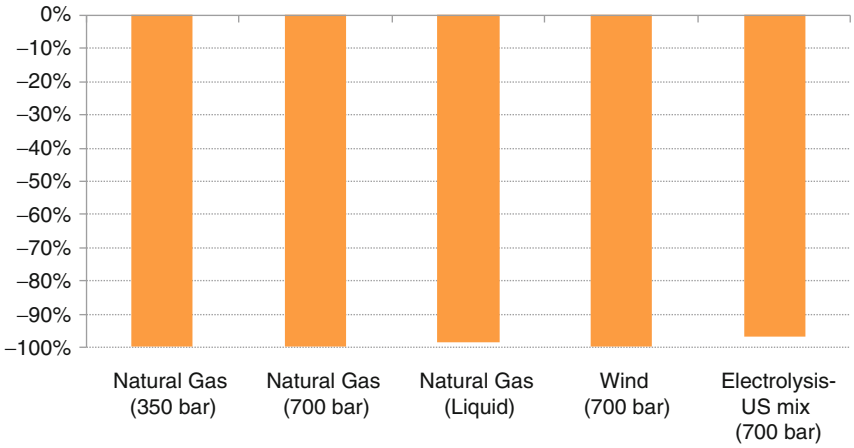

Sustainable Vehicle Fuels, Well-to-Wheel Analysis. Figure 13
WTW petroleum reduction (relative to gasoline) for various hydrogen production pathways

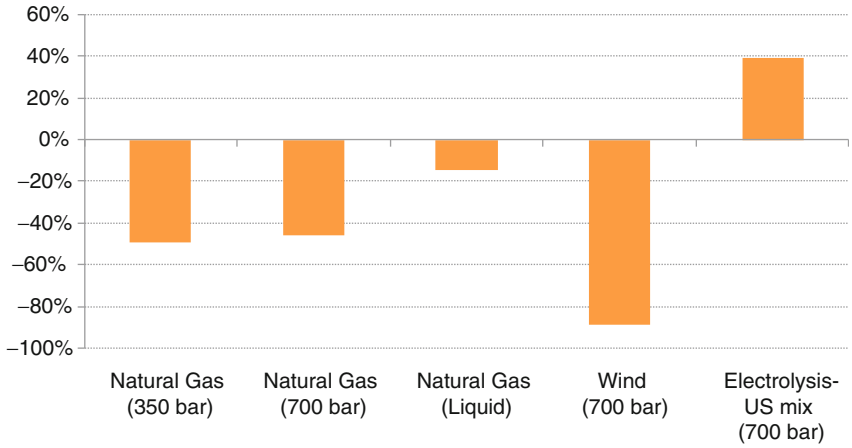

Sustainable Vehicle Fuels, Well-to-Wheel Analysis. Figure 14
WTW reductions in greenhouse gas emissions (relative to gasoline) for various hydrogen production pathways

per-unit-energy basis, its potential for greenhouse gas emissions reduction by producing hydrogen for FCVs is limited to less than 40% relative to gasoline ICEVs. Furthermore, packaging hydrogen at high energy density through the increased compression to 700 bar and cooling, or through liquefaction, further reduces the efficiency of the hydrogen's WTW pathway and its potential greenhouse gas emissions benefits. Distributed production of hydrogen via electrolysis at refueling sites would rely on the local generation mix of electricity. If the electricity is generated from such fossil sources as coal or natural gas, the resulting WTW efficiency and greenhouse gas emissions of the hydrogen via electrolysis pathway will be worse than those of the baseline gasoline ICEVs. However, producing hydrogen from nonfossil sources (such as wind electricity) reduces the greenhouse gas emissions significantly compared to gasoline. Further technological advances in the production of hydrogen from nonfossil sources, as well as developing a viable delivery infrastructure and improving FCV onboard storage technologies, are needed to facilitate a meaningful reduction of greenhouse gas emissions relative to today's gasoline ICEVs.

Electricity Pathways with Phevs and Bevs

Electricity can be used in PHEVs and BEVs. Since US electricity production is largely independent of petroleum fuel use, PHEVs and BEVs have been touted for their potential to reduce petroleum use and greenhouse gas emissions through gains in efficiency and use of electricity. The PHEV category can cover a wide variety of options with respect to technical attributes, such as the battery chemistry, the amount of grid electricity that can be stored in the battery, and the powertrain and fuel choices. In addition, the driving behavior of consumers could also significantly affect the energy use and the greenhouse gas effects of PHEVs. The magnitude of energy and greenhouse gas emission benefits of PHEVs and BEVs is affected by the type of electricity generation used for the vehicle's recharging and the vehicle's energy efficiency.

Many LCA studies have been completed for PHEVs and BEVs, as well as for conventional gasoline ICEVs and gasoline hybrid electric vehicles (HEVs) [33–38]. These studies concurred that the battery operation (also known as charge-depleting [CD] operation) of PHEVs and BEVs reduces petroleum use since the electricity generation in the United States (as in most of the world's large economies) is powered by nonpetroleum fuels. However, these studies produced mixed results when estimating the greenhouse gas emissions of PHEVs and BEVs. These results are attributed to the difference in the assumptions associated with efficiencies of vehicle powertrains, on-road adjustment factor for fuel and electricity consumption, and electricity generation mix and efficiencies.

PHEVs are similar to regular HEVs, except that PHEVs employ a bigger battery, which is recharged

through a wall outlet by drawing electricity from the grid. They have the potential to reduce the transportation system's dependence on petroleum and the emissions of greenhouse gases by using off-peak excess electricity-generation capacity and increasing the vehicle's energy efficiency. The reduction in petroleum use by PHEVs increases with a corresponding increase in their electric range, which is proportional to the size of the battery employed. Gains in fuel economy by PHEVs and BEVs relative to conventional vehicles are another key factor determining their benefits in terms of energy use and greenhouse gas emissions.

While all previous studies predicted significant reductions in petroleum energy with the use of PHEVs and BEVs, they predicted mixed results for greenhouse gas emissions from these vehicles. For example, some studies estimated that PHEVs and BEVs (recharging from the US average mix) generate fewer greenhouse gas emissions than gasoline ICE vehicles, but they generate greenhouse gas emissions equal to (or more) than those of gasoline HEVs [33–35]. In contrast, other studies estimated that PHEVs operating in CD mode can outperform HEVs in terms of reductions in greenhouse gas emissions if 75% or more of the required electricity is generated from natural gas combined-cycle (NGCC) [36] and produce lower greenhouse gas emissions, even with coal-based electricity, compared with gasoline ICE vehicles [38]. A recent study by Argonne National Laboratory conducted detailed dispatch modeling simulations in different US utility service areas with different charging scenarios for PHEVs and explored "real-world" driving energy use for PHEVs vs. gasoline vehicles [38]. The key factors impacting the WTW analysis of PHEVs and BEVs and the findings of the Argonne study are discussed next.

PHEV Fuel-Cycle Pathways

Since a PHEV consumes fuel and electricity, its pathway consists of two parallel paths for these two energy sources. The fuel path includes the recovery of the feedstock (e.g., crude), the transportation of the feedstock, the production of the fuel (e.g., refining of crude to gasoline), and the transportation of the fuel to the pump. The electricity path includes the recovery, processing, and transportation of the fuel used for electricity generation (e.g., natural gas, coal, and uranium), the technology used for electric power generation (e.g., steam power plant, natural gas combustion turbine), the transmission of the electricity to the wall outlet, and the charging of the vehicle's battery. The fuel and electricity production and transmission represent the WTP stage of the pathway, while the vehicle's consumption of fuel and electricity represents the PTW stage.

A PHEV charges the battery to a high state of charge (SOC) (e.g., 90%). Then, the vehicle operates in a CD mode by using the stored electricity in the battery until it reaches a low SOC (e.g., 30%). Once the battery reaches the low SOC threshold, the PHEV operates in a charge-sustaining (CS) mode, which is similar to the operation of regular HEVs [39]. This operation strategy allows the vehicle to operate as a zero-emission vehicle in CD operation. However, battery cost and PHEV performance requirements have led automakers to consider a "blended" CD mode, through which the engine is intermittently turned on, resulting in an increase in the CD range by utilizing the electric powertrain and the engine simultaneously (blended operation).

Fuel and Electricity Consumption by PHEVs

Since the automotive industry has yet to produce PHEVs and BEVs, the fuel and electricity consumption of PHEVs and BEVs are estimated by employing vehicle simulation models, such as Argonne's Powertrain System Analysis Toolkit (PSAT). PSAT can simulate different vehicle configurations through a standard or custom driving cycle to produce the fuel consumption by these vehicle technologies. PHEV designs in the Argonne study covered PHEV10 (i.e., 10 miles of electric range), PHEV20, PHEV30, and PHEV40. The higher electric range the vehicle has, the less petroleum fuel the vehicle will need to consume. Nevertheless, increased electric range requires a bigger battery, resulting in increased cost and weight of the vehicle. The high cost of batteries led vehicle designers to explore ways to extend the electric range through a "blended" operation of the engine with the electric motor. However, the intermittent operation of the engine in blended mode has the potential to create bursts of emissions when the engine comes on, making

it necessary to develop modifications of the emissions control systems in order to meet emissions standards. The blended operation of the engine and the electric motor extends the vehicle's electric range significantly while allowing for more efficient utilization of the battery.

One major complication associated with PHEVs is how to rate these vehicles with respect to their electricity and fuel consumption. The EPA develops on-road fuel economy estimates that appear on the window stickers of all new cars and light trucks sold in the United States [40]. The purpose of the fuel economy label is to assist consumers in comparing the fuel economy of different vehicles as they make their purchase decision [41]. However, the current methodology for rating fuel economy is not adaptable to rating PHEVs because of electricity consumption and intermittent engine use in blended CD operation. Furthermore, fuel economy expressed as miles per gallon (MPG) leads customers to falsely believe that the amount of gasoline consumed by an automobile decreases as a linear function of a car's MPG [42]. The actual relationship is curvilinear, as shown in Fig. 15. The figure shows that a 10-mpg improvement at lower fuel economy produces much higher fuel consumption savings compared to the same improvement at higher fuel economy. For example, increasing fuel economy from 10 to 20 mpg results in savings of 5 gal over 100 miles of traveling distance, while an equivalent increase from 40 to 50 mpg results in savings of a mere 0.5 gal over the same traveling distance. Critics of fuel economy labeling argue that representing fuel efficiency in terms of amount of gasoline consumed for a given distance (e.g., gallons per 100 miles), which is commonly used outside of the United States, would make the benefits of greater fuel efficiency more transparent [42]. More recently, the New York State Senate passed a bill requiring state car dealers to post a chart converting MPG to gallons per 1,000 miles (the average monthly driving distance) in 5-mpg increments. The bill has to clear the State Assembly before it could be signed into law. Reporting gallons per 100 miles for fuel consumption and kWh per 100 miles for electricity consumption on the window sticker of PHEVs could be easily converted to the cost per 100 miles since the prices per gallon of gasoline and per kWh of electricity are usually known in the locality surrounding the customer traveling. Table 1 shows the fuel and electricity consumption of gasoline ICEVs, HEVs, and PHEVs, as well as BEVs based on recent analysis by Argonne [38].

PHEV Electric Demand (Load) Profiles and Electricity Generation Mix for Battery Recharging

PHEVs will draw electric energy from the electric grid. The extent of electricity demand can be estimated by examining patterns of vehicle usage and estimating the potential number of PHEVs that will be plugged in. The daily electricity demands for various PHEVs can be estimated by analyzing the following four factors:

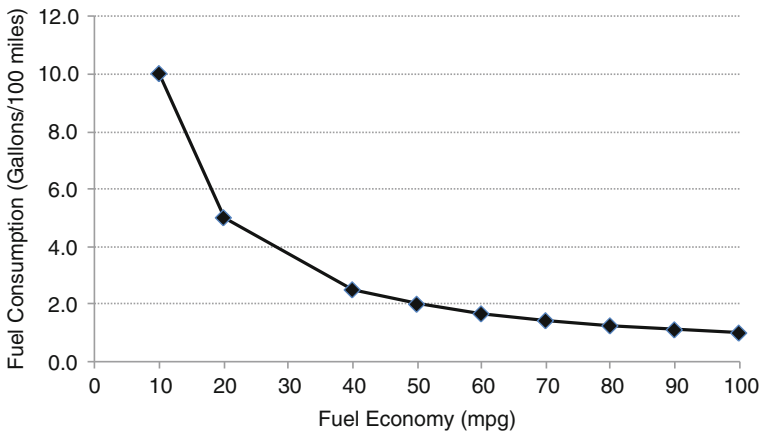

Sustainable Vehicle Fuels, Well-to-Wheel Analysis. Figure 15
Relationship between fuel economy and fuel consumption

Sustainable Vehicle Fuels, Well-to-Wheel Analysis. Table 1 Fuel and electricity consumption for alternative gasoline vehicle technologies

			PHEV10		PHEV20		PHEV30		PHEV40		BEV
	ICEV	HEV	CD	CS	CD	CS	CD	CS	CD	CS	CD
Gallons per 100 miles	3.52	2.41	1.35	2.24	1.24	2.25	0.28	2.91	0.16	2.94	N/A
kWh per 100 miles	N/A	N/A	22.6	N/A	22.1	N/A	38.7	N/A	39.0	N/A	40.4

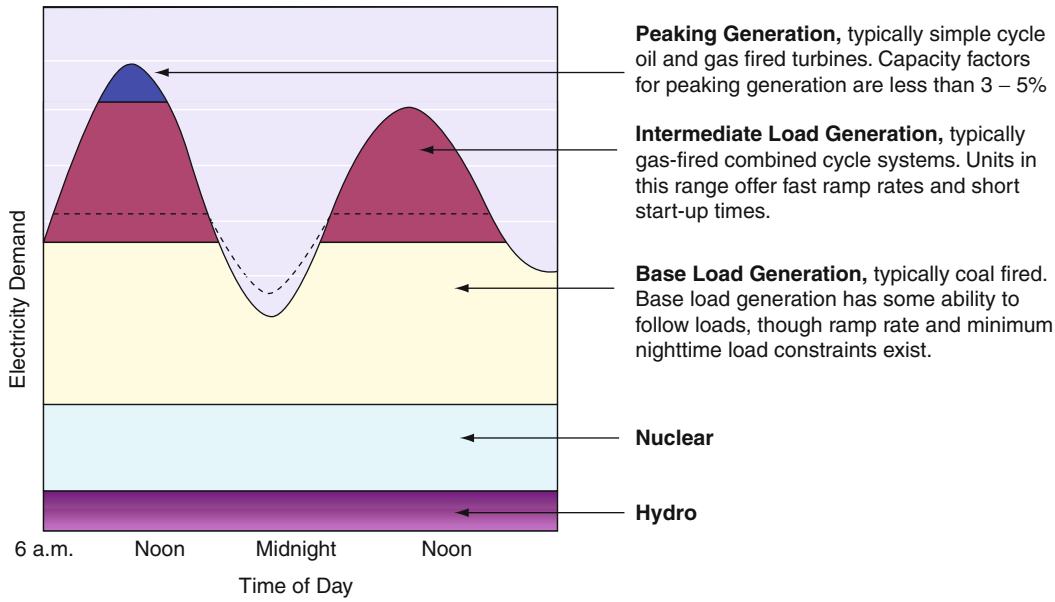

Sustainable Vehicle Fuels, Well-to-Wheel Analysis. Figure 16
Typical summer electric load profile and dispatch scheme for many U.S. utilities [43]

(1) daily vehicle usage, (2) pattern of vehicle arrival at home at the end of the last trip, (3) number of PHEVs of different electric ranges that will be plugged in each day, and (4) amount of electric power that will be drawn by each PHEV and the time required for charging. For estimating electricity demand by PHEVs, the number of PHEVs that will be on road in a given year needs to be estimated.

Once the PHEV load profile is established, a dispatch model simulating the electric power generation and transmission system in a utility area can predict the marginal electricity generation mix dispatched for battery recharging in that area. The marginal electricity generation mix for battery recharging is a major factor impacting the WTW results of PHEVs and BEVs.

The generation mix at the time of charging is a strong function of the time of day, time of year, geographic region, vehicle and charger design, base and vehicular load growth patterns, and the associated generation expansion in the years before the charging event of interest.

Figure 16, developed by Shelby and Mui, is an illustration of the diurnal peaks of demand for a hypothetical summer day [43]. Sharp summer peaks are caused by the demand for air-conditioning, although such peaks typically occur in the late afternoon and early evening. However, demand is at a minimum overnight when businesses are closed, lights are off, and air-conditioning load is at its lowest. As the demand for electricity increases, additional generating units are dispatched to meet the load. When

a PHEV charger is activated, it causes additional load on the marginal generator (i.e., the last unit brought on line). When that unit reaches full capacity, another unit is brought on line as the marginal unit, and so forth. Therefore, when a large number of PHEVs are added to a system, several additional generation units may be required to meet the charging load. Consequently, the energy use and emissions of those units are allocated to the PHEV charging load. In an extensive interconnected region, transmission constraints can develop so that several geographically separated generating units must operate at part load to meet an increasing demand.

Seasonal load variations also affect the mix of units brought on line to meet the PHEV charging demand. High summer electric loads are typical for most of the United States, reflecting power demand for air-conditioning. Electric heating loads tend to increase off-peak demands and may compete with the off-peak charging of PHEVs during the winter season.

The vehicle design characteristic with the greatest influence on PHEV charging load is battery capacity, which is related to the electric range and weight of the vehicle. It is most commonly assumed that the charger will operate at normal household power levels, typically 110 V and no more than 20 A. A sport utility vehicle (SUV) type of PHEV may require larger batteries than a compact or sedan type of PHEV. To charge these batteries in a reasonable length of time, more charging current is required. Higher charging current could be accomplished with a charger operating on 220 V at 30 A. Single-phase, 220-V service is available to all residential customers, but such service typically will require professional installation of additional circuit breakers, lines, and a dedicated outlet. The benefit of reduced charging time comes at an additional cost of the higher demand.

The inventory of units available for PHEV charging is slowly changing as old units are retired or are refitted with new environmental controls and as new units are constructed in anticipation of increasing demand. Also, existing units may change place in the dispatch order as they age or as new plants come on line. Although commercial introduction of PHEVs is expected in 2010, the demand for PHEV charging will not likely be substantial for a long time because of the low fleet turnover rate (approximately 7–8% per year in the United States).

Planning to expand generation must take into account both the extent of likely demand growth and the daily and seasonal dynamic structure of the projected demand. Relatively constant loads are best served by large base-load units with low fuel and variable costs. Daily peak loads may best be served by units with low fixed (investment) costs, such as gas turbines. However, lower fuel-cost options, including hydro, will be applied to peak loads if capacity is available. The generation mix applied at a specific time is predicted by dispatch models. The dispatch models match available capacity to the dynamic load by using cost, emissions, or other criteria to optimize the system. Dispatch models also take reliability and scheduled plant outages into consideration.

Combining Charge-Depletion and Charge-Sustaining WTW Results for Phevs

To combine the fuel and electricity pathways together for PHEVs, PHEV miles with electricity vs. with fuels must be estimated. The split depends on daily miles driven by individual drivers and the electric ranges of different PHEVs. With national daily mile distribution, Figure 17 shows the miles that could be driven with electricity for given electric ranges of PHEVs on the basis of US national household travel survey data [38].

WTW Results of PHEVs and BEVs

Figure 18 shows the WTW results of gasoline PHEVs, in addition to gasoline ICEVs, gasoline regular HEVs, and BEVs. The implication of the electricity generation mix resides in the carbon intensity of the used fuel and the efficiency of the generation technology. The energy use associated with electricity generation and greenhouse gas emissions increase progressively as the marginal mix becomes less efficient and dominated by coal or residual oil. PHEVs recharging from NGCC generation produce greenhouse gas emissions comparable to or less than those of regular HEVs, while PHEVs recharging from coal-based power generation produce greenhouse gas emissions comparable to or slightly

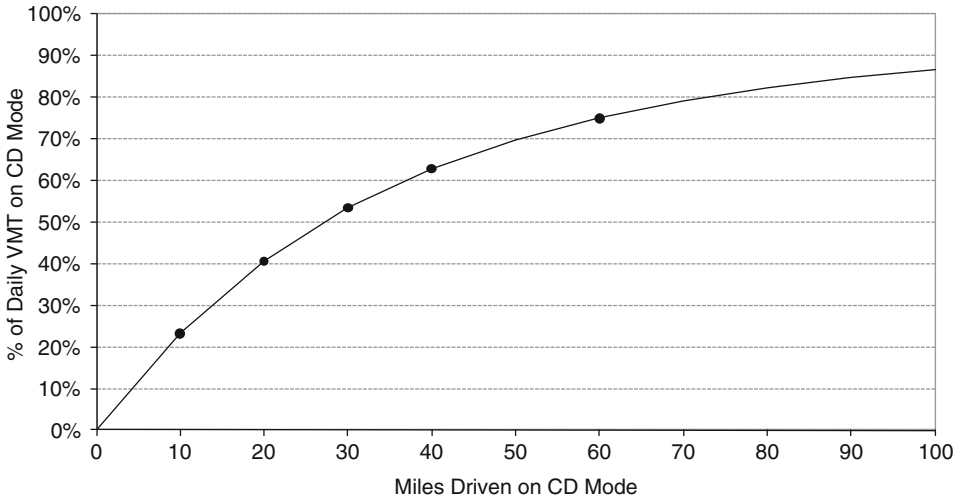

Sustainable Vehicle Fuels, Well-to-Wheel Analysis. Figure 17
Percentage of daily VMT available for substitution by a PHEV in CD mode [38]

higher than those of ICEVs. Usually, more petroleum savings and greater reductions in greenhouse gas emissions are realized with an increase in a vehicle's electric range when the generation mix is independent of oil. Furthermore, when the charging of PHEV occurs from a low-carbon generation mix (e.g., NGCC) or from a renewable source, PHEVs with high electric ranges provide significantly more petroleum savings and reductions in greenhouse gas emissions. BEVs extend the savings in petroleum energy and greenhouse gas emissions further and represent the upper limit in potential benefits from PHEVs.

Electric Drive Technology Life-Cycle Analysis Issues and Uncertainties

Electricity and Fuel Consumption of PHEVs Two main factors impact the electricity and fuel consumption of PHEVs: (1) vehicle configuration and (2) driving conditions. The vehicle configuration could assume a variety of power ratings for the battery, engine, and electric motor, as well as a variety of control strategies used in these powertrain components. Driving conditions include driver aggressiveness, extent of air-conditioning use, and cold-weather operation. Other uncertainties include the rate of technological advancement in the critical components of each vehicle technology (e.g., batteries and chargers), which affects the efficiency of battery charging and discharging. Such uncertainties impact fuel and electricity consumption during vehicle operation, which, in turn, impacts the WTW results.

Electricity Generation Mix for Recharging PHEVs Generation expansion planning, which optimizes changes to the generator inventory, is a complex process that takes into account load growth projections, the technical performance characteristics of current and future generator options, and known and potential changes in regulations. Existing and evolving policies aimed at reduction of electricity demand, greenhouse gas emissions, and other criteria pollutants (e.g., Energy Efficiency Resource Standard [EERS] and Renewable Portfolio Standard [RPS] in many states, mercury regulations, and Clean Air Interstate Rule [CAIR]) impact the economics and ultimately the retirement of existing generation technologies, as well as the selection of future generation technologies. The final inventory in one or two decades, or more in the future, would likely be substantially different under these constraints than it would be in a business-as-usual case. Generation expansion may also be influenced by the PHEV charging demand itself, and this charging demand is likely to increase along with

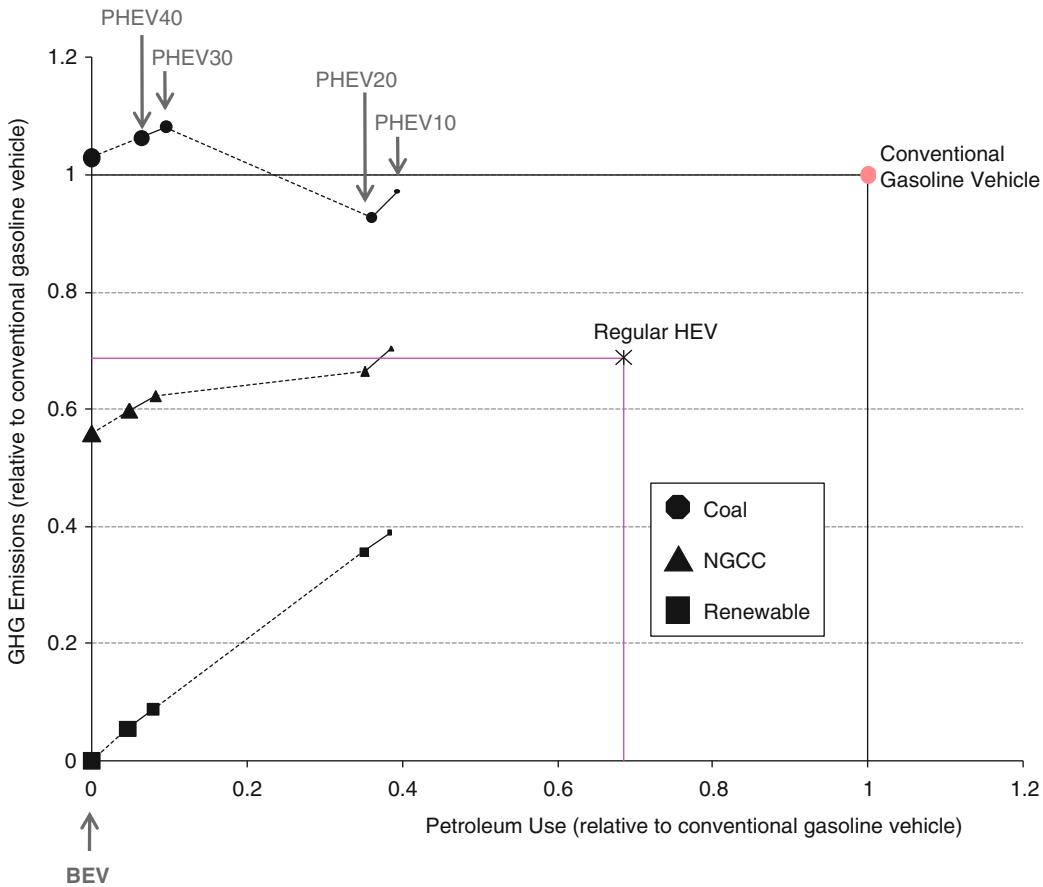

Sustainable Vehicle Fuels, Well-to-Wheel Analysis. Figure 18
WTW petroleum use and greenhouse gas emissions for CD operation of gasoline vehicles (conventional, HEVs, PHEVs, and BEVs)

a general increase in transportation energy demand. Thus, projections of generation expansion become linked to projections of transportation demand. Such transportation demand is determined by many uncertain factors, which include the number of PHEVs and BEVs that will be on the road in a given region during a given year, the number of charges per vehicle per day, the time of day for each charging event, and the rate at which charging occurs.

Share of National Vehicle Miles Traveled (VMT) Powered by Electricity The "share of miles electrified," which directly impacts petroleum energy savings, depends on many factors with considerable uncertainty. Adoption of PHEVs will be slow because of low vehicle-fleet turnover rate. Furthermore, not everyone will purchase PHEVs because they will likely complement, rather than displace, HEVs. Also, PHEVs will vary in terms of their electric range capabilities and will have different configurations of the electric machine, battery, and engine. The nominal electric range will not be realized because of variations in driving conditions, driver characteristics, accessory use, and other parameters. The various control strategies for utilizing the engine and the electric motor could result in a myriad of VMT shares in CD operation. Batteries may be charged more than once per day and may not be fully discharged before recharging. Such factors impact the share of miles electrified, which determines the percentage of petroleum displacement, and impact the

PHEV load profile, which determines the marginal generation mix and the corresponding greenhouse gas emissions profile of PHEV in different regions.

Future Directions

In the 2007 US Energy Independence and Security Act, the US Congress established goals of producing 15 billion gallons of corn-based ethanol a year by 2015 and additional 21 billion gallons of advanced biofuels a year by 2022. In 2010, 13 billion gallons of corn ethanol were already produced. The United States is on the way to exceed the goal of 15 billion gallons of corn ethanol by 2015, despite the current debate whether corn ethanol incentive offered by the federal government should continue or not. On the other hand, the US government has invested through R&D, grants, and loans in developing and building cellulosic ethanol plants. It is anticipated that some cellulosic ethanol plants will be in operation in the next few years with significant amount of cellulosic ethanol to be produced. At present, the E10 market (10% ethanol blended into gasoline) is facing an ethanol demand saturation point (the so-called blending wall issue). The US EPA recently determined that ethanol blends higher than E10 could be used in gasoline vehicles that were produced after 2000. This finding addresses the blending wall issue for the near future. In the long term, flexible-fuel vehicles (FFVs) using ethanol up to E85 can expand the ethanol market. In addition, new biofuel R&D efforts are being made to develop technologies that produce gasoline- or diesel-like liquid biofuels (the so-called drop-in fuels). Drop-in fuels based on such biofuel technologies as pyrolysis and gasification, among other technologies, can overcome the fuels infrastructure and vehicles incomparability problems related to ethanol. Finally, public and private R&D efforts are being made to develop algae-based biofuels. Algae have a significantly high theoretically yield, between 10 and 100 times more fuel per unit area than other biofuel crops, and can be grown without affecting fresh water resources. The key R&D stages for algae-based fuels include algae growth, algae drying, algal oil extraction, and biofuel production. The key challenges to producing algae-based fuels include the capturing and transportation of CO_2 to the algae farm, the drying of the algae, and the high investment cost.

Many countries developed plans to commercialize fuel-cell vehicles. Initiated in 2010, the H_2 Mobility is a commercialization plan for hydrogen fuel-cell vehicles in Europe, which aims at identifying cost-effective funding mechanisms to deploy hydrogen infrastructure and FCVs, and to accelerate vehicles' market transformation in Europe. The stakeholders in Europe joined efforts to build up a hydrogen fueling infrastructure and establish Germany as lead market for FCVs in Europe. Similarly, stakeholders in Japan announced an initiative to introduce FCVs in the Japanese market and to develop a hydrogen supply infrastructure starting with 100 hydrogen refueling stations by 2015. California developed a plan for the deployment of hydrogen FCVs and refueling stations. The plan called for the development of 40 refueling stations statewide in anticipation of 50,000 FCVs planned for deployment by major car manufacturers in California by 2017. The deployment of FCVs in California will partially satisfy the zero-emission vehicle (ZEV) mandate, which aims at meeting California's mobile source emission reduction goals by requiring large automakers to produce certain percentages of zero-emission vehicles for sale in California. Since 2003, the US DOE has been funding a research and development program for fuel cells with a goal of achieving 60% peak efficiency for PEM fuel cells at a cost of \$30/kW and a durability of 5,000 h of operation. While the PEM fuel cells achieved the efficiency and durability targets, the cost target has yet to be attained, mainly because of the expensive platinum that is being used as a catalyst. R&D efforts are underway to develop catalysts for PEM fuel cells using less expensive materials such as doped carbon nanotubes. The US DOE is also funding R&D efforts to ultimately achieve onboard storage targets of 2.5 and 2.3 kWh of hydrogen per kg and per liter of FCV's storage system, respectively, as well as a traveling range of 300 miles. DOE has also set a pretax cost target in the range of \$2 to \$4 per kg of delivered hydrogen to be competitive with gasoline ICEVs on a cost-per-mile basis over the vehicle's life. Gas and energy companies are exploring ways to produce and deliver hydrogen at a competitive cost while satisfying the vehicle's onboard storage requirements and fill rate protocols.

In 2008, President Obama stated his goal of putting one million electric vehicles on the road by 2015. To reach that goal, $2.4 billion was allocated in the Recovery Act investment to support research and development of electric vehicles. Additionally, The US government initiated a tax credit of $7,500 per electric vehicle (some states such as California offer additional credits) as an incentive for purchasing BEVs and PHEVs. The US Department of Energy (DOE) developed an extensive energy storage R&D program with the goal of developing a battery that could power a vehicle 300 miles on a single charge at a cost of $300/kWh, a durability of 15 years, and an energy density of 150 Wh per kg of the battery system. While great progress has been made in advanced battery technology, these targets have yet to be achieved or verified. Meanwhile, automakers are developing vehicles that are lighter in weight with aerodynamic designs to decrease the required battery capacity for a given vehicle's range. Furthermore, the US federal government as well as many US state governments have enacted policies and provided incentives to encourage electric power generation from renewable sources such as wind, solar, and geothermal. Other countries such as Canada and Germany provide tax credits for wind generation, with guaranteed grid access at prices above average electricity prices. This will reduce the impact of electrifying the transportation system on the environment. The US government is also providing funds to support building of electric vehicle infrastructure and accelerate the installation of charging stations. To manage the added electricity demand created by electric vehicles, the US DOE supports the development of the smart grid concept, which involves upgrading the existing electric grid to employ real-time, two-way communication technologies that allow consumers to connect directly with their electricity providers.

Bibliography

1. Energy Information Administration, the U.S. Department of Energy (2009) International energy outlook 2009. DOE/EIA-0484, Washington, DC
2. BP Statistical review of world energy (2009) British Petroleum, London
3. Intergovernmental Panel on Climate Change (2007) Climate change 2007: mitigation: technical summary, working group III report. Cambridge University Press, Cambridge
4. U.S. Environmental Protection Agency (2008) Inventory of U.S. greenhouse gas emissions and sinks: 1990–2006. Washington DC
5. Wang MQ (1996) Development and use of the GREET model to estimate fuel-cycle energy use and emissions of various transportation technologies and fuels. ANL/ESD-31. Center for Transportation Research, Argonne National Laboratory, Argonne, IL
6. Chambers RS, Herendeen RA, Joyce JJ, Penner PS (1979) Gasohol: does it or doesn't it produce positive net energy? Science 206:789–795
7. Pimentel D, Patzek TW (2005) Ethanol production using corn, switchgrass, and wood. Biodiesel production using soybean and sunflower. Nat Res Res 14:65–76
8. Delucchi MA (1991) Emissions of greenhouse gases from use of transportation fuels and electricity, vol. 1. ANL/ESD/TM-22. Center for Transportation Research, Argonne National Laboratory, Argonne, IL
9. Wang MQ, Saricks C, Wu M (1997) Fuel-cycle fossil energy use and greenhouse gas emissions of fuel ethanol produced from U.S. Midwest corn. Prepared for Illinois Department of Commerce and Community Affairs by Center for Transportation Research, Argonne National Laboratory, Argonne, IL
10. Searchinger T, Heimlich R, Houghton RA, Dong F, Elobeid A, Fabiosa J, Tokgoz S, Hayes D, Yu TH (2008) Use of U.S. croplands for biofuels increases greenhouse gases through emissions from land use change. Science 319(5867):1235–1238
11. Kim H, Kim S, Dale B (2009) Biofuels, land use change, and greenhouse gas emissions: some unexplored variables. Environ Sci Technol 43:961–967
12. Wu M, Mintz M, Wang M, Arora S (2009) Consumptive water use in the production of ethanol and petroleum gasoline. Environ Manage 44:981–997
13. Liska AJ, Yang HS, Bremer VR, Klopfenstein TJ, Walters DT, Erickson GE, Cassman KG (2009) Improvements in life-cycle energy efficiency and greenhouse gas emissions of corn-ethanol. J Ind Ecol 13:58–74
14. Renewable Fuels Association (2011) 2011 ethanol industry outlook: growing innovation. Washington DC
15. Wang M, Han J, Haq Z, Tyner WE, Wu M, Elgowainy A (2011) Energy and greenhouse gas emission effects of corn and cellulosic ethanol with technology improvements and land use changes. Biomass Bioenergy 35:1885–1896
16. Wu M, Wang M, Huo H (2006) Fuel-cycle assessment of selected bioethanol production pathways in the United States. ANL/ESD/06-7. Center for Transportation Research, Argonne National Laboratory, Argonne, IL
17. Wang M, Wu M, Huo H, Liu J (2008) Well-to-wheels energy use and greenhouse gas emissions of Brazilian sugarcane ethanol production simulated by using the GREET model. Int Sugar J 110(1317):527–545

18. Loarie SR, Lobell DB, Asner GP, Mu Q, Field CB (2011) Direct impacts on local climate of sugar-cane expansion in Brazil. Nat Clim Change Lett 1:105–109. doi:10.1038/NCLIMATE1067
19. National Biodiesel Board (2009) Estimated U.S. biodiesel production. http://www.biodiesel.org/pdf_files/fuelfactsheets/Production_Graph_Slide.pdf. Accessed 3 March 2009
20. Huo H, Wang M, Bloyd C, Putsche V (2008) Life-cycle assessment of energy and greenhouse gas effects of soybean-derived biodiesel and renewable fuels. ANL/ESD/08-2. Center for Transportation Research, Argonne National Laboratory, Argonne, IL
21. CARB (California Air Resources Board) (2009) Proposed regulation for implementing low carbon, volume1, staff report: initial statement of reasons, Sacramento, CA
22. EPA (U.S. Environmental Protection Agency) (2010) Regulations of fuels and fuels additives: changes to renewable fuel standard program; final rule, Federal Register March 26, vol 5, No 58, pp14670–14904
23. Hertel TW, Golub AA, Jones AD, O'Hare M, Plevin RJ, Kammen DM (2010) Effects of US maize ethanol in global land use and greenhouse gas emissions: estimating market-mediated responses. Bioscience 60:223–231
24. Tyner WE, Taheripour F, Zhuang Q, Birur D, Baldos U (2010) Land use changes and consequent CO2 emissions due to US corn ethanol production: A comprehensive analysis, Department of Agricultural Economics, Purdue University, Indiana
25. IPCC (Intergovernmental Panel on Climate Change) (2006) 2006 IPCC guidelines for national greenhouse gas inventory: vol 4 — agriculture, forestry, and other land use. Hayama, Japan
26. Wang M, Huo H, Arora S (2010) Methodologies of dealing with coproducts of biofuels in life-cycle analysis and consequent results within the U.S. context. Energy Policy. doi:10.1016/j.enpol.2010.03.052
27. Paster MP et al (2011) Hydrogen storage technology options for fuel cell vehicles: Well-to-wheel costs, energy efficiencies, and greenhouse gas emissions, Int J Hydrogen Energy, doi:10.1016/j.ijhydene.2011.07.056
28. Wang M (2002) Fuel choices for fuel-cell vehicles: well-to-wheels energy and emission impacts. J Power Sources 112:307–321
29. Elgowainy A, Marianne Mintz M, Steward D, Sozinova O, Brown D, Gardiner M (2010) Liquid hydrogen production and delivery from a dedicated wind power plant. Center for Transportation Research, Argonne National Laboratory, Argonne, IL
30. Chen TP, Paster M, Gardiner M, Elgowainy A, Ringer M, Kelly B, Lasher S, McKenney K (2008) Hydrogen delivery infrastructure options analysis: Task 2, appendix B, http://www1.eere.energy.gov/hydrogenandfuelcells/pdfs/delivery_infrastructure_analysis.pdf. Accessed on 31 Aug 2011
31. Wipke K, Sprik S, Kurtz J, Ramsden T (2010) Learning demonstration interim progress report. Technical Report NREL/TP-560-49129. NREL, CO
32. Mintz M, Gillette J, Elgowainy A, Paster M, Ringer M, Brown D, Li J (2006) A hydrogen delivery scenario analysis model to analyze hydrogen distribution options: HDSAM, Paper No. 06–3085, Transportation Research Record series, TRB
33. Kromer MA, Heywood JB (2007) Electric powertrains: opportunities and challenges in the U.S. light-duty vehicle fleet. Publication No. LFEE 2007–03 RP, May 2007. Massachusetts Institute of Technology (MIT), Cambridge MA
34. Thomas CE (2009) Cost-benefit analyses of alternative light-duty transportation options for the 21st century. National Hydrogen Association Conference, Columbia, SC, 31 March 2009
35. National Research Council (2009) Transitions to alternative transportation technologies — plug-in hybrid electric vehicles. The National Academies Press, Washington DC. ISBN 0-309-14851-0
36. Passier G, Conte FV, Smets S, Badin F, Brouwer A, Alaküla M, Santini D, Alexander M (2007) Status overview of hybrid and electric vehicle technology. MON-RPT-033-DTS-2007-02955, Final Report Phase III, Annex VII, IA-HEV, IEA, TNO Report. Delft, Netherlands. IEA, 6 Dec 2007
37. Electric Power Research Institute and Natural Resources Defense Council (2007) Environmental assessment of plug-in hybrid electric vehicles. Vol 1: Nationwide greenhouse gas emissions. EPRI Report# 1015325, July 2007. EPRI, USA
38. Elgowainy A, Han J, Poch L, Wang M, Vyas A, Mahalik M, Rousseau A (2010) Well-to-wheels analysis of energy use and greenhouse gas emissions of plug-in hybrid electric vehicles. ANL/ESD/10-1. Center for Transportation Research, Argonne National Laboratory, Argonne, IL
39. Shidore N, Bohn T, Duoba M, Lohse-Busch H, Sharer P (2007) PHEV 'all electric range' and fuel economy in charge sustaining mode for low SOC operation of the JCS VL41M Li-ion battery using battery HIL. In: Proceedings of the electric vehicle symposium 23, Anaheim, CA, 2–5 December 2007
40. U.S. Environmental Protection Agency (2006) Fuel economy labeling of motor vehicle revisions to improve calculation of fuel economy estimates, Final Technical Support Document, EPA420-R-06-017, Dec 2006
41. Walsh K (2009) Comments on proposed rulemaking to establish light duty vehicle greenhouse gas emission standards and corporate average fuel economy standards. Fisker Automotive, Inc. Anaheim CA, 3 Dec 2009
42. Larrick RP, Soll JB (2008) ECONOMICS: the MPG illusion, policy forum. Science 320(5883):1593–1594
43. Shelby M, Mui S (2007) Plug-in hybrids: a scenario analysis. Presented at the 86th Annual Meeting of the Transportation Research Board, Washington, DC, 22 Jan 2007
44. U.S. Department of Energy, Office of Hydrogen, Fuel Cells and Infrastructure Technologies (2007) Multiyear Research, Development and Demonstration Plan. http://www1.eere.energy.gov/hydrogenandfuelcells/mypp/. Accessed on 31 Aug 2011

Sustainable Water Treatment Using Nanofiltration and Tight Ultrafiltration Membranes

Jaeweon Cho[1], Juan Antonio López Ramínez[2], H. K. Shon[3], Kiho Park[4], Minho Park[4]
[1]Gwangju Institute Science and Technology (GIST), Department of Environmental Science and Engineering, Natural Organic Matter Lab, Gwangju, Korea
[2]Departamento de Tecnologias del Medio Ambiente, Centro Andaluz Superior de Estudios Marinos, CASEM, Universidad de Cádiz, Cadiz, Spain
[3]School of Civil and Environmental Engineering, University of Technology, Sydney, Broadway, NSW, Australia
[4]Environment & Energy Research Team, Daewoo Institute of Construction Technology, Suwon, Gyeonggi-do, South Korea

Article Outline

Glossary
Definition of the Subject
Introduction
Performance Aspect
Fouling Aspect
Future Directions
Conclusion
Acknowledgments
Bibliography

Glossary

Effective MWCO The MWCO of a membrane, with respect to specific (either nonionic or ionic) compounds.

Molecular weight cutoff (MWCO) of a membrane (absolute MWCO) The molecular weight of nonionic compounds that can be removed by 90% by the membrane.

Nanofiltration (NF) membrane Membrane of which the MWCO ranges between approximately 150–1,000 Da and for which solute transmission through the membrane pores is governed by convection over diffusion (this differentiates NF from reverse osmosis (RO) membranes).

Tight ultrafiltration (UF) membrane Membrane of which the MWCO ranges between approximately 1,000–10,000 Da and is generally used to remove macromolecular types of contaminants, including protein and polysaccharides.

Definition of the Subject

Research and application results regarding nanofiltration (NF) and tight ultrafiltration (UF) were reviewed to obtain useful information that can reveal existing limitations when applied to both drinking water and wastewater reclamation treatment processes. These limitations can be categorized as affecting membrane performance, with respect to micropollutants or taste/odor controls, as well as fouling with organics, inorganics, and microorganisms. Membrane filtration includes not only physical (i.e., size exclusion based on pore size of membrane) but also chemical (both electrostatic and hydrophobic interactions) processes; thus, it is believed that all problems and limitations in membrane filtration areas should be based on both physical and chemical theories and ideas. Also, supporting technologies such as protocols and methodologies for water quality analyses and membrane fouling indices are suggested through this review.

Introduction

The content of this chapter is designed to give engineers, researchers, and students an insight into membrane filtration. The topic is addressed using the knowledge and understanding of membranes and their application in the treatment of contaminated water. In this chapter, relatively high-pressure membrane filtration methods are referred to, including those using nanofiltration (NF) and tight ultrafiltration (UF) membranes. Recently, nanofiltration membranes are increasingly being considered as an option for advanced water and wastewater reclamation treatments. This use is particularly evident in the case of micropollutant controls, including pharmaceuticals, endocrine disrupting chemicals, and personal care products [1–3], as well as taste and odor controls [4]. However, one single process cannot be applied to all contaminants. For example, there are even problems with reverse osmosis (RO) membranes, such as high costs and fouling. As such, fundamental to the proper design of membranes, is the

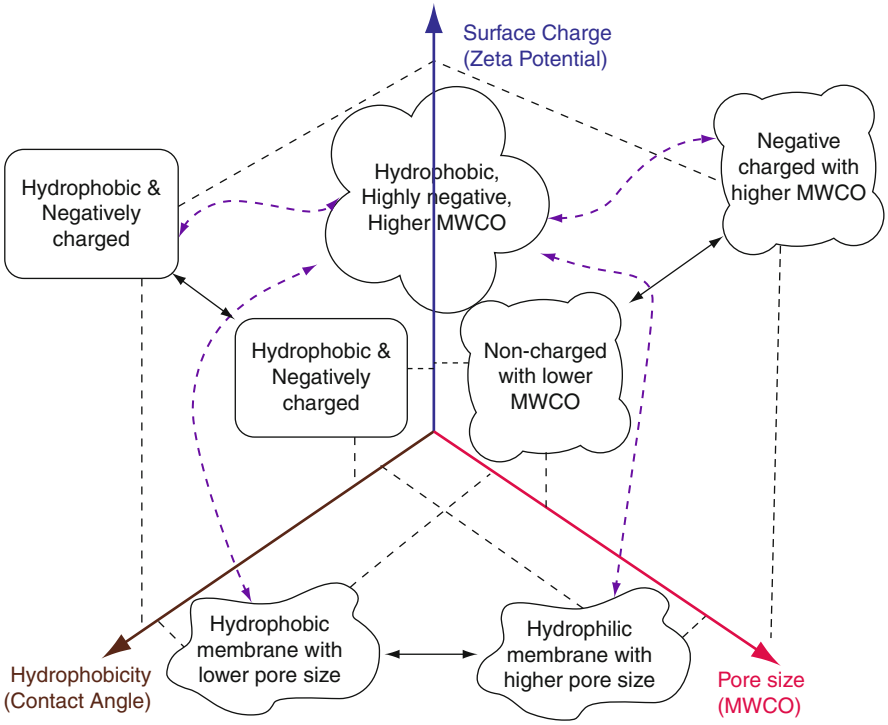

Sustainable Water Treatment Using Nanofiltration and Tight Ultrafiltration Membranes. Figure 1
Conceptual figure of membrane properties, using three different parameters, including surface charge, hydrophobicity, and pore size, as measured through zeta potential, contact angle, and molecular weight cutoff (MWCO), respectively. Depending upon the water quality conditions, e.g., natural organic matter (NOM) characteristics, hydrophobic (or hydrophilic)/negatively charged (or less-charged)/lower (or higher) pore size membranes may be selected in order to maximize membrane performance and to minimize fouling

understanding of membrane filtration itself, especially in relation to hydrodynamics and the mass transport of various contaminants, in addition to developing a deeper understanding of the chemical interactions between contaminants and membranes.

When initiating water treatment projects, both the membranes and water qualities need to be characterized. Based on these characterizations, both membrane performance and problematic fouling can then be predicted, using one – or a combination – of various membrane mechanisms, including physical size exclusion, electrostatic interactions, and hydrophobic interactions. Membrane properties include pore size distribution, surface charge (in terms of zeta potential), and surface hydrophobicity (through roughness and contact angle) [5–7]. A summary of the membrane properties that may be helpful when selecting appropriate membranes for specific contaminants, based on different physical and chemical characteristics, is depicted in Fig. 1.

This review was performed in an attempt to provide useful facts and guidelines for membranes used in advanced water and wastewater reclamation treatments, based on papers already published. As a researcher with nearly 15 years experience in the membrane filtration area, even though technologies and their applications for actual plants have progressed (cases and projects have increased in number and aspects), a fundamental understanding of core concepts and their application is still lacking. For instance, as of this writing, there is no fouling index except that based on the silt density index (SDI) and no reasonable water quality parameters or indices capable of evaluating both raw and membrane-treated water, with more appropriate sensors. Through this review, the aim is to deliver a clarification of existing problems and

limitations and to then visualize potential solutions and steps to be taken in the near future to improve sustainable water treatment plans.

Performance Aspect

Membrane performance is generally determined by pore size, as most membrane filtration systems utilize a physical barrier. Based on this concept, size (or molecular weight, in daltons), for which 90% of a nonionic molecule (such as polyethylene glycols) can be removed by the corresponding membrane, can be defined as the molecular weight cutoff (MWCO). However, as membranes have an electrostatic potential on their surfaces, determined by its zeta potential, they can induce electrostatic interactions with ionized molecules; charges likely induce charge repulsion, resulting in a reduced (i.e., lowered) MWCO, though hydrodynamic conditions can also influence the membrane MWCO, via diffusional phenomena. Generally, membrane manufacturers provide an absolute MWCO, as determined without consideration of the electrostatic interactions, hydrodynamic conditions, and diffusional phenomena. As such, actual users are recommended to determine (or at least consider) the modified (effective) MWCO [5].

Concentration Polarization

Based on the number of membranes available, there is a need to inquire as to which membrane is best for a specific case and how it can be most effectively operated. Indeed, one may have to answer to this question when dealing with problems and various projects; otherwise, one may select an inappropriate membrane that would provide less water production and/or poorer performance. To this end, the concentration polarization is the first thing to understand in order to predict membrane performance, with regard to both contaminant removal and fouling. Concentration polarization is defined as an increased concentration of contaminants near the membrane surface resulting from many different phenomena, such as the transport of the contaminants and interactions between the contaminants and the membrane surface. Concentration polarization can be described, as shown in Fig. 2, along with the equation

$$J/k = \ln\left[\left(C_m - C_p\right)/\left(C_B - C_p\right)\right],$$

where J (cm/s) is the flux through the membrane, k (cm/s) is the mass transfer coefficient, and C_m, C_B, and C_p are the solute concentrations of the layer near the membrane surface, bulk solution, and treated sample, respectively.

The concentration polarization equation has two significant implications: (1) flux is not connected to the transmembrane pressure, and (2) the ratio of J/k affects the concentration C_m. Please recall that J (↓) is the water flux toward the membrane surface and k (↑) is the mass transfer coefficient that has the same dimension as J and of which the direction is opposite to J. Here, J (flux, cm/s) can be calculated by dividing the flow rate through the membrane by the area of the membrane, and k (mass transfer coefficient of the contaminant, cm/s) can be determined via the Sherwood relationship equation [8]. As k is a major factor influencing the membrane performance, with respect to contaminant removal and fouling, k values have to be calculated based on equations suitable for specific molecules of interest in the test cases, instead of simply using a general equation of k for salts, as provided in other references. It is understood that if the transmembrane pressure increases, J increases. And, the mass transfer coefficient (k) can be controlled by varying the cross-flow velocity; if the cross-flow velocity increases, k increases, and vice versa [8], which indicates that the increased k value promotes the shear-based back diffusion of solutes away from the membrane surface.

Based on the theory of concentration polarization, the subsequent adoption of this concept to an actual membrane filtration process is also important. For this task, it is important to understand solute transport through the membrane pores, which is indirectly (based on the k) related to the concentration polarization [9]. During this conceptual and practical consideration, practical definitions between reverse osmosis (RO) and nanofiltration (NF) membranes can also be differentiated (Fig. 3).

Hydrodynamic Consideration

The effects of J/k (from the concentration polarization equation) ratio on membrane performance have been demonstrated in a number of previous papers [10–12]. From aspects of J/k described in the previous

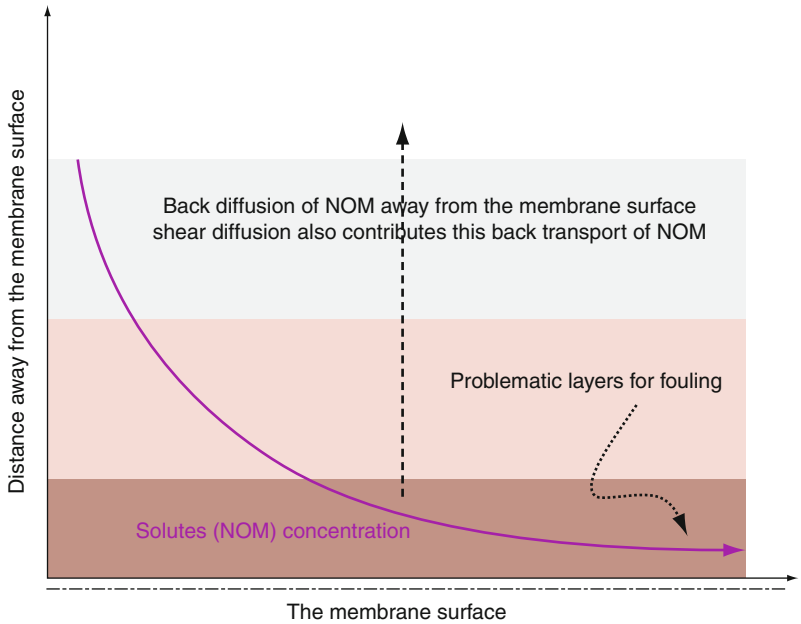

Sustainable Water Treatment Using Nanofiltration and Tight Ultrafiltration Membranes. Figure 2
Concentration polarization: Near the membrane surface, the solute concentration substantially increases, resulting in both a severe flux decline and irreversible membrane fouling. More solute moving toward the membrane surface results in higher concentration polarization, with the other conditions being the same. However, the concentration difference induces back diffusion of NOM to the upper direction, which can thereby reduce the concentration polarization; this back diffusion can also be promoted by shear-induced diffusion resulting from the cross-flow velocity (i.e., concept of mass transfer coefficient (k))

section pertaining to the concentration polarization, under convection dominant conditions, higher and lower J/k ratios can respectively induce lowered and enhanced membrane removal rates, even for the same contaminants [5, 11]. With data obtained from different water samples, containing relatively hydrophilic versus hydrophobic organic matters, the same membrane provided different rates of dissolved organic carbon (DOC) removal, with different J/k ratios, even for the same water sample; a higher J/k ratio resulted in a decrease in removal, which was more severe with the hydrophilic than the hydrophobic DOC. With the relatively hydrophobic DOC, negatively charged UF membranes could provide a higher DOC rejection than expected, based on the J/k ratio – it is thought here that electrostatic interactions might overcome inherent hydrodynamic effects (Fig. 4).

Membranes can also provide different effective MWCO values for different water sources. Thus, the MWCO for a membrane is expected to have many different values, in addition to the absolute value that is generally provided by the manufacturers; a lower MWCO implies a high potential to remove corresponding contaminants, under specific filtration conditions [5]. With varying J/k ratio values, a corresponding change in the removal of organic matters can be seen, i.e., a higher (lower) J/k induces lowered (enhanced) MWCO values for a membrane for the same concentration of organic matter (Table 1).

Electrostatic Interaction

Among various membrane performance mechanisms used to effectively remove contaminants, electrostatic interaction may be the most important for achieving sustainable water production, depending on the combination of given membranes and water. Note that the size exclusion for a membrane is relatively difficult to change for a given MWCO. As such, much higher removal efficiencies for a charged membrane can be

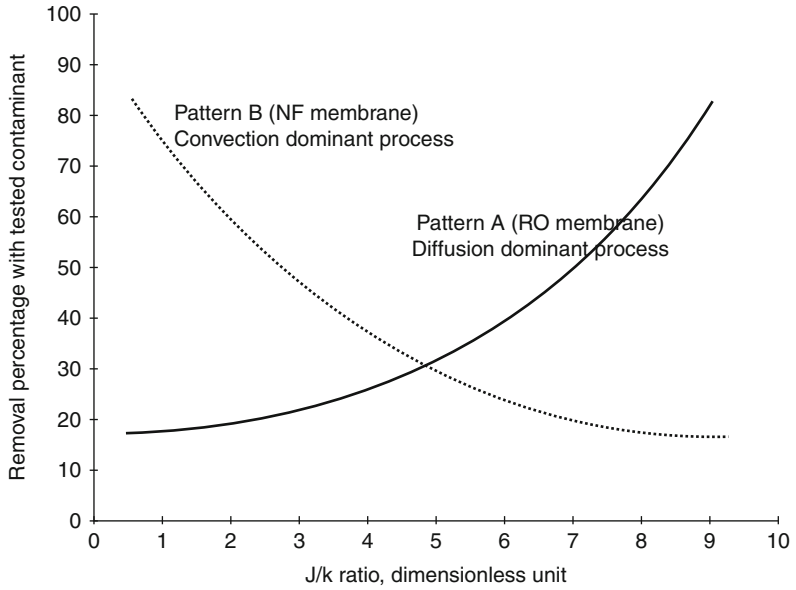

Sustainable Water Treatment Using Nanofiltration and Tight Ultrafiltration Membranes. Figure 3
Two removal patterns of solutes (e.g., NOM) with membranes. Pattern A: as J/k increases (with k fixed), contaminant removal also increases, which indicates that the solute transport is not affected by water transport through the membrane pores. This is defined as the diffusion transport of the solute through the membrane pores. This transport occurs mostly in RO membranes, such as in those used in the desalination process. Pattern B: as J/k increases (with k fixed), contaminant removal decreases, as the contaminants (solutes) transmit through the pores together with water, which can be defined as convection transport. This form of transport occurs in loose types of membranes, such as in NF, UF, and MF membranes

obtained using likely charged molecules and ions, than based on its fixed absolute MWCO value [13] (Fig. 5).

Through this figure, one can easily imagine that the same membrane (e.g., negatively charged UF membrane) gives a much lower MWCO value for the hydrophobic NOM than for the hydrophilic NOM, as previously discussed in the hydrodynamic section of the membrane performance [5, 13]. Once again, one should define the MWCO using both the absolute (determined with noncharged molecules) and effective (determined with actual contaminants) values. For new studies and/or actual treatment plant projects, effective MWCO values for candidate membranes and source water of interest are recommended to be decided, prior to pilot tests, along with the final decision of membrane selection.

Typical Applications

Micropollutants Control Micropollutants can be defined as organic substances presented in waters of interest, with respect to both human health and ecological risk perspectives, having trace levels ranging from picograms per liter to a few nanograms per liter. To this end, pharmaceuticals and endocrine disrupting chemicals (EDCs) may be categorized as typical micropollutants. And even though the toxicity issue is beyond the scope of this paper, the difference between the level of wastewater/natural aquatic/drinking water and toxicological effect concentrations needs to be understood. Typically, their levels of lethality, growth prevention, and even no-observed-effect (generally in the range of mg/L), as determined using specific fish, bacteria, daphnia, algae, and other aquatic organisms, seem much higher than even those of wastewater effluents (generally in the range of ng/L or μg/L) [14–16]. However, Kim et al. [17] reported very low predicted no-effect concentrations for some pharmaceuticals (such as sulfamethoxazole, acetaminophen, and carbamazepine), as determined using bacterium, which are close to normal concentrations of wastewater effluents and even drinking source waters.

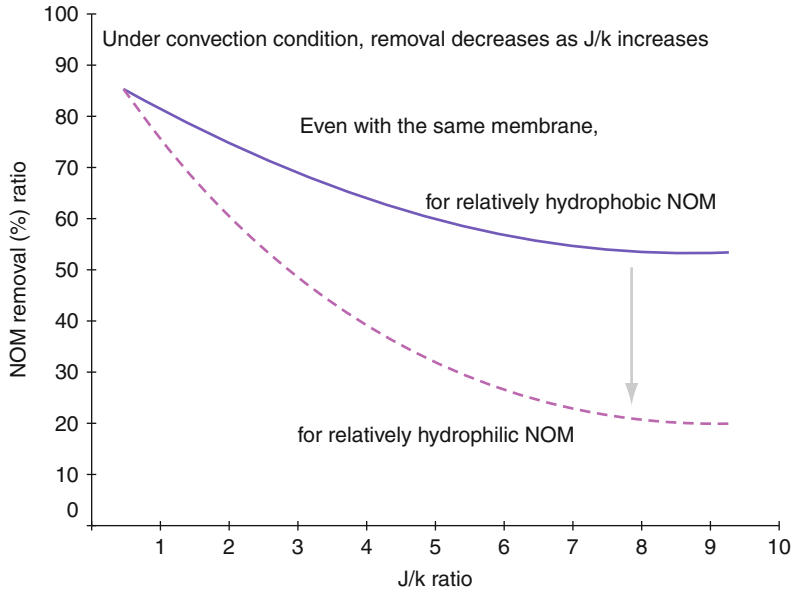

Sustainable Water Treatment Using Nanofiltration and Tight Ultrafiltration Membranes. Figure 4 According to the concentration polarization and NOM transmissions, under convection-dominant NOM transmission conditions, NOM removal decreases as J/k ratio increases. Thus, if the transmembrane pressure is increased to obtain more flux, removal performance will have to be sacrificed. However, the decrease is not as severe for relatively hydrophobic NOM compared to relatively hydrophilic NOM

Sustainable Water Treatment Using Nanofiltration and Tight Ultrafiltration Membranes. Table 1 Effects of the J/k ratio on the removal potential and effective MWCO, based on the same membrane and contaminant

J/k	Removal	Effective MWCO
Higher	Lowered	Higher
Lower	Enhanced	Lower

Micropollutant removal was also extensively investigated for various treatment processes, including oxidation, coagulation, adsorption, and membrane filtration [3, 18]. Chlorination was found to be effective for controlling most EDCs and some pharmaceuticals. For the two classical advanced treatment processes (ozonation and activated carbon adsorption), they were very effective in removal, though there were distinctive patterns. The removal efficiencies of micropollutants increase as corresponding octanol water coefficients (K_{ow}) increase with powered activated carbon (PAC), with exceptions for compounds having pK_a values lower than ~6.0, which means that negatively ionized compounds have difficulty being adsorbed. It was found that removals by ozonation were substantially low for micropollutants having symmetric structures (such as meprobamate and iopromide) compared to other micropollutants; NF membranes were identified as being the most effective for controlling almost all micropollutants, except for tri (2-chloroethyl) phosphate (TCEP) [2, 3]. From the studies in Korea, US, and Spain, there was difficulty in controlling for TCEP using various NF membranes with an MWCO lower than the TCEP molecular weight; thus, it seems that the effective removal of TCEP remains as a primary obstacle to more extensive NF membrane applications (Fig. 6).

Wastewater Reclamation NF membranes have been identified as an effective process for wastewater effluents (treated by MBR in our studies) to provide reusable water with a fairly high water quality, in terms of DOC, TN, and micropollutant levels, as reported in previous works [2, 19]. As was discussed, only TCEP seems not to be effectively removed by NF membrane applications, as almost all other contaminants were

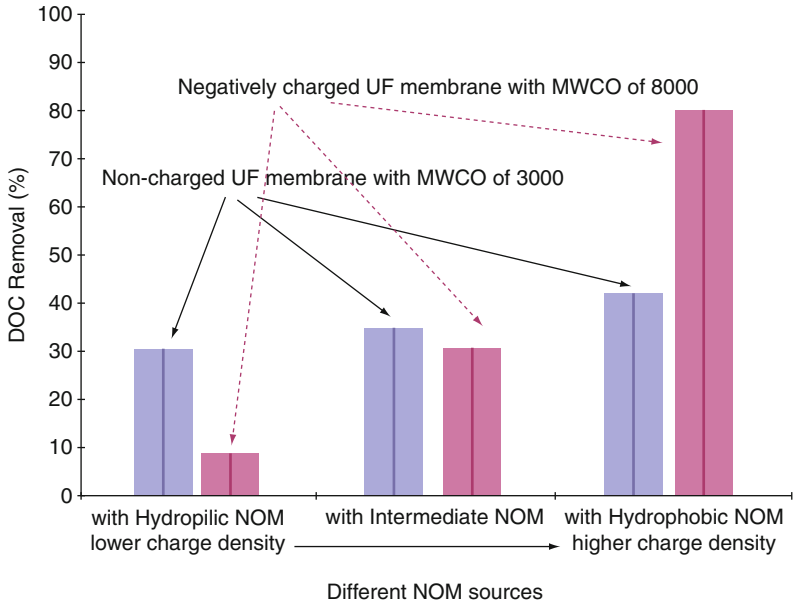

Sustainable Water Treatment Using Nanofiltration and Tight Ultrafiltration Membranes. Figure 5
Charged UF membranes, with a lower MWCO than the noncharged UF membrane, can more effectively remove relatively hydrophobic NOM than the noncharged UF membrane, even though it exhibits a lower removal efficiency for relatively hydrophilic NOM (conceptually redrawn from Fig. 9 of Cho et al. [13])

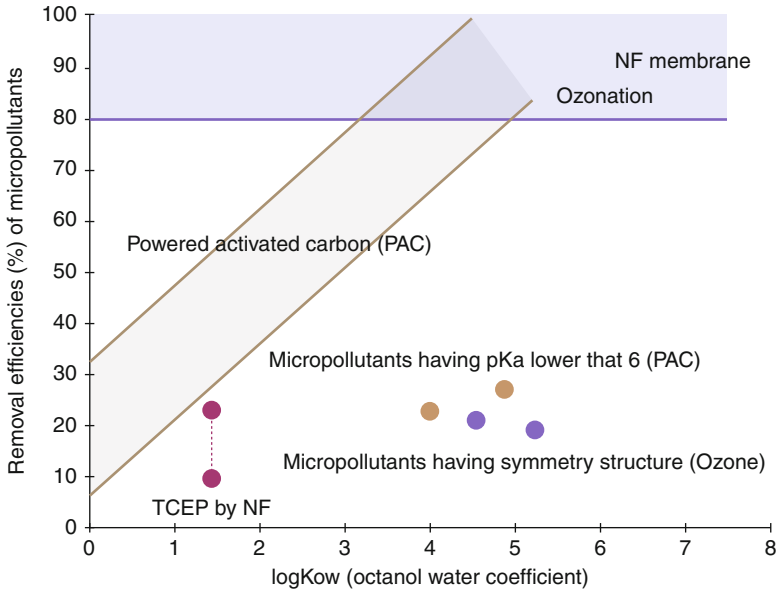

Sustainable Water Treatment Using Nanofiltration and Tight Ultrafiltration Membranes. Figure 6
Conceptual patterns of the removal efficiency of micropollutants by powered activated carbon (PAC), ozonation, and NF membrane; this figure is conceptually redrawn using the data shown in Westerhoff et al. [3], Kim et al. [2], and based on our other experiences

successfully controlled after NF application. For example, DOC levels were lower than ~0.3 mgC/L, of which performance is close to that of the loose RO membrane. Nitrogen as ammonia was not efficiently controlled by the NF membrane tested, but the nitrate formed after being nitrified in MBR was successfully removed. The NF membrane even controlled most heavy metals and ions to a fairly high extent. As such, it seems that NF membranes are capable of replacing RO membranes in terms of providing sustainable and economic water production in areas except for desalination. Thus, the combination of MBR followed by NF or RO membrane processes has been recognized and should be considered the most potential choice for future applications.

Taste and Odor Control One of most frequently encountered problems in drinking water treatments pertains to taste and odor control, which does not have a single best option for compliance. Taste and odor compounds are known to originate from algal metabolites (geosmin, 2-MIB (2-methylisoborneol)), halogenoanisoles (2,4,6-trichloroanisole, 2,4,6-tribromoanisole), and halogenophenols (2-chlorophenol, 2,6-dibromophenol), of which odor threshold concentrations range from 20 pg/L (2,4,6-tribromoanisole) to 88 ng/L (2-chlorophenol). Ozonation, UF membranes, and activated carbon processes have been used in attempts to efficiently solve these problems, though lack the required robustness and reliability to comply with all potential compounds causing foul taste and odor [4, 20]. Indeed, to our knowledge, cases of exclusively using full-scale NF membrane processes for taste and odor problems are very rare or do not exist. Our experiences with pilot-scale NF membrane process for taste and odor compound controls revealed that NF was to some extent very efficient, but it did not provide complete control of all problematic compounds; removal efficiencies varied with different compounds (e.g., geosmin was more easily removed than 2-MIB) and also depended on NF membrane materials (meta-phenylene diamine (MPD) versus piperazine-based), operating condition (in terms of J/k ratio), and operating duration (for ~1 year), among other factors.

Biodegradable Organic Matter Control NF membranes are well known to effectively control NOM to minimize formation of chlorine-based disinfection by-products (DBPs), such as trihalomethanes (THM) and haloacetic acids (HAA) [21]. However, once NF membranes are built in treatment plants, DBP minimization is no longer a concern as the quality of the treated water is fairly high, with a total organic carbon (TOC) of generally less than 0.3–0.4 mgC/l. Meanwhile, control of biodegradable organic carbons, as identified with respect to biodegradable organic carbon (BDOC) and/or assimilable organic carbon (AOC), must be considered in order to monitor the stability of treated water prior to discharging into a distribution system [6, 21]; even the efficiency of NOM removal by various NF membranes is consistently high (~80–90%), with respect to DOC, but those with respect to BDOC and AOC vary depending on the membrane used. In particular, the removal efficiencies of both BDOC and AOC are not important; instead, levels of treated water are used as indicative measures, from a biostability point of view. However, it is yet uncertain as to what sufficiently low BDOC and AOC levels should be in order to prevent microbial regrowth in the distribution system, as organic water quality conditions are different in different water sources, and protocols of measuring BDOC (using acclimated sand bioreactor) and AOC (using NOX and P17 bacteria) also depend upon many varying conditions.

Fouling Aspect

Once fouling occurs, flux substantially decreases; thus, clean water can no longer be produced. Understanding fouling phenomena enables us to minimize fouling and the subsequent flux decline, and to properly clean the fouled membrane and recover the flux decline [13, 22]. Membranes are fouled by organic matter, inorganics (such as calcium precipitates, oxidized manganese), as well as microorganisms and their extracellular substances. It is still not certain whether either hydrophobic or hydrophilic organic matter dominantly fouls NF and tight UF membranes; fouling depends on membrane properties such as the surface charge, material, and surface morphology; however, hydrophilic polysaccharide-like substances significantly fouled most tested NF and tight UF membranes, as based on our studies [10, 13, 23, 24]. In addition, for relatively hydrophobic membranes, hydrophobic organic matter

could also foul membranes, especially under high calcium level conditions, which can be explained by using electrostatic interaction mechanisms [25–27].

Similar to the performance aspect, fouling is also affected by hydrodynamic conditions such as the J/k ratio; even though the same UF membrane was evaluated with the same water, the UF membrane provided very different flux decline patterns from different J/k ratios [10]. Even with the same UF membrane for the same water source, the degree of flux decline substantially decreases at the lower J/k ratio, with enhancement of NOM removal (Fig. 7). As previously discussed, a lower J/k ratio can be achieved by increasing the cross-flow velocity, calculated by the Sherwood relation, with a fixed flux (J). For this reason, it is recommended that plant design engineers consider pump capacity in order to provide a sufficient flow rate into the membrane module, which can then produce a high cross-flow velocity.

Effective and timely cleaning of fouled membranes is important to sustainably produce water; cleaning strategies should be based on the characteristics of foulants, which are obtained from cleaning steps with either clean water or chemical solutions. Generally, caustic (followed by acidic) cleaning is efficient for organic foulants, whereas acidic solutions have to be applied to membranes that control hardness or are exposed to water having a high manganese concentration; otherwise, membranes may experience severe clogging problems with corresponding precipitations and/or coatings. In water containing relatively high levels of manganese, preoxidation (i.e., prechlorination) should not be applied to prevent coating of the oxidized manganese precipitate on the membrane surface. Microorganism growth on the membrane surface may also be critical depending upon the water quality; thus, periodic disinfection is needed, based on a careful selection of dosage and disinfectant (i.e., chlorine) concentration, which may deteriorate the membrane backbone structure, such as the polyamide chain of typical NF membranes (Fig. 8).

Organic Fouling

As previously discussed, there is still controversy pertaining as to whether either hydrophobic (humic) or hydrophilic (nonhumic) organic substances dominantly foul the membrane surface. Most results depend

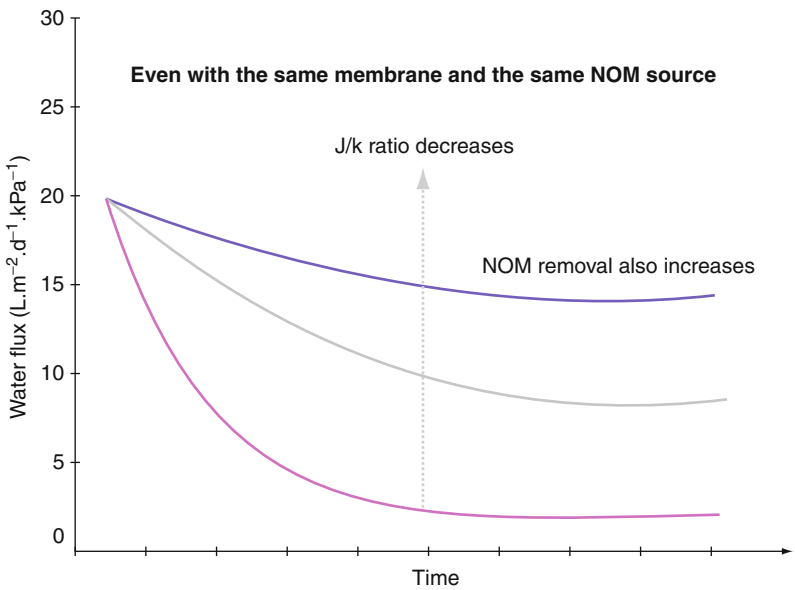

Sustainable Water Treatment Using Nanofiltration and Tight Ultrafiltration Membranes. Figure 7
Flux decline can be minimized under a lowered J/k ratio condition, even with the same membrane and the same NOM source combination, which can be achieved by increasing the cross-flow velocity, using a fixed water flux through the membrane surface (conceptually redrawn from Fig. 8 in [10])

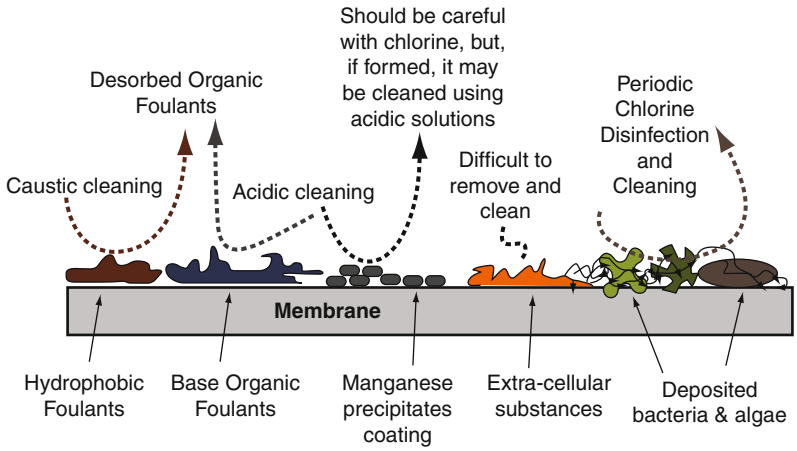

Sustainable Water Treatment Using Nanofiltration and Tight Ultrafiltration Membranes. Figure 8
Conceptual figure showing strategies for cleaning membranes fouled with organics (hydrophobic versus hydrophilic compounds, or probably humic versus nonhumic substances), inorganic precipitates, extracellular substances, and microorganisms

upon the conditions of feedwater characteristics and membrane properties; thus, it is safer to open all the possibility with whole types of foulants. Colloidal organic matter (COM), another important portion of the range of organic matter, is recognized as being able to severely foul both hydrophobic and hydrophilic membrane surfaces and is not easy to desorb with acidic or basic cleaning solutions. COM is known to originate from fractured cells of microorganisms [24, 28–30].

Characteristics of organic foulants on membrane surfaces were found to be significantly influenced by the relative hydrophobicity or hydrophilicity of NOM in the feedwater [10]. However, hydrophobic portions in the organic foulants were less than those in the feedwater, which means that hydrophilic (both hydrophilic and transphilic, based on analyses using XAD-8/4 resin fractionation) foulants highly contributed to the flux decline and fouling. When mass analyses of foulants desorbed by either acidic or basic solutions were conducted, nonionic hydrophilic organic foulant portions still remained as irreversible foulants; thus, the hydrophilic foulants are believed to be more important. This supposition was supported by the foulants measured by Fourier transform infrared (FTIR) spectroscopy, especially based on the peaks around 1,000 cm^{-1}, which correspond to the peaks for carbohydrates and/or polysaccharide-like substances ([23]). It is also that that potential COM foulants also have FTIR peaks around 1,000 cm^{-1}, and these can be isolated using a dialysis bag membrane having an MWCO of 2,000–4,000 Da [30].

Biofouling

Microbial organisms themselves may be foulants as well, in addition to their extracellular substances; fouling depends on the feedwater source and which types of microorganisms preferentially foul specific membranes. This research area deserves to be studied more intensively with many different source waters and membranes. One case study performed by our group, using a surface water source, revealed that poly(vinylidene difluoride) (PVDF) membranes predominantly had alpha proteobacteria on their surface over other beta and gamma proteobacteria, as identified using a 16S rRNA gene clone library method, which is probably due to the relatively clean and oligotrophic drinking water source [31].

Potential Organic Fouling Index

The silt density index (SDI) is a typical membrane fouling index for desalination; however, there has yet to be a definitive index developed for organic membrane fouling for both drinking water and wastewater reclamation treatments. Or, as one single index may

not be a robust membrane index for water treatment for all different water qualities, there may be a need to develop many potential indices for different membrane categories (i.e., NF versus tight UF), which also depend on different organic matter characteristics. There has been an attempt to develop new concepts for organic fouling indices, especially using NOM; for this, the size of NOM in the units of nanometers, instead of molecular weight (in daltons), was determined using an asymmetric flow field-flow fractionation (FFF) equipped with the membrane of interest to demonstrate organic fouling. Using this size concept and additional statistical analyses, a new organic fouling index that can be obtained by using a flow FFF equipped with the membrane of interest and a specified water source [32, 33] was proposed. Note that even though the fouling index using the flow FFF is not easy to obtain, combining the specific membrane and feedwater of interest related to the fouling index is the primary advantage of this method, compared to the use of other indirect methodologies, like SDI. Another attempt was then taken to determine the fouling index of microorganisms, once again with membranes of interest, using the flow FFF [34]. Again, both the size and shape of microorganisms are likely factors that influence depositions on the membrane surface.

Future Directions

As previously discussed, an organic fouling index is needed in order to effectively and correctly predict fouling behavior and potential foulants, for both drinking water and wastewater reclamation processes. Microorganisms themselves also deserve to be studied, with respect to membrane biofouling.

Attempts should be taken to develop new membrane materials for less fouling, higher performance (better removal and greater permeability), and greater chemical resistance (especially to chlorine).

It seems necessary that a water quality index be introduced as a representative for all other micropollutants; complicated and precise measurement techniques cannot be easily conducted for all projects. Thus, a water quality index may help to efficiently evaluate different water qualities, with respect to micropollutants, and also assist in the design of appropriate membrane processes, including membrane types, materials, and suitable pre- and posttreatment processes.

Similarly, the TOC alone seems insufficient for representing all qualities of membrane-treated waters, with respect to the regulations required, biostability in the distribution system, and DBP formation potential, among others. Thus, new water quality parameters and corresponding measurement protocols still need to be developed.

Taste and odor control by NF membranes also need further development, such as information pertaining to best membrane types (pore size, material), operating conditions, and combination with pre- or posttreatment processes, etc.

The design, operation, and cleaning of membrane processes for drinking water or wastewater reclamation treatments frequently require the use of modeling, based on either numerical methods or empirical equations or conceptual analytic tools, which need related parameters to be selected, such as mass transfer and/or diffusion coefficients of contaminants of interest (e.g., what equations are needed to calculate the diffusion coefficient of a certain NOM?).

Guidelines for membrane cleaning strategies are needed for different projects in drinking water (such as DBP, taste and odor, micropollutants controls) and wastewater reclamation treatments.

This research may be further extended to another growing membrane desalination technique, i.e., forward osmosis (FO) or membrane distillation (MD). All of these indices, water quality problems and issues, and membrane fouling and cleaning issues can be studied for both emerging membrane technologies. It will help us to set all operating standards for FO and MD operation well ahead of time.

Conclusion

A clear revelation of problems and limitations in water treatment processes with NF and tight UF membranes is the major objective of this review. It is known that the completion of this clarification in one review paper is not possible; however, it can at least be illustrated that membrane applications certainly have the potential to be used for sustainable water production if properly used, and, at the same time, what problems are present when used, with some limitations, can be understood.

The same difficulties have been repeatedly experienced in membrane applications, without resolution and/or correction, over the last 15 years; there continues to be a serious lack of information pertaining to membranes for use in projects, with only the MWCO and simple permeability information available. The aim of this entry is to add to the general body of knowledge to improve both membrane itself and by supporting technologies used in water quality analyses, in addition to process operation and maintenance and other related areas.

Acknowledgments

The paper work was conducted during the sabbatical year (2011) of the corresponding author while residing in Spain, which was supported by the Gwangju Institute of Science and Technology, Korea, and the Universidad de Cadiz, Spain, and in part by the National Research Lab (NOM, ROA-2007-000-20055-0) and Daewoo Projects, Korea.

Bibliography

1. Benotti MJ, Trenholm RA, Vanderford BJ, Holady JC, Stanford BD, Snyder S (2009) Pharmaceuticals and endocrine disrupting compounds in U.S. drinking water. Environ Sci Technol 43(3):597–603
2. Kim SD, Cho J, Kim In S, Vanerford BJ, Snyder SA (2007) Occurrence and removal of pharmaceuticals and endocrine disruptors in South Korean surface, drinking, and waste waters. Water Res 41:1013–1021
3. Westerhoff P, Yoon Y, Snyder S, Wert E (2005) Fate of endocrine-disruptor, pharmaceutical, and personal care product chemicals during simulated drinking water treatment processes. Environ Sci Technol 39:6649–6663
4. Park N, Lee Y, Lee S, Cho J (2007) Removal of taste and odor model compound (2,4,6-trichloroanisole) by tight ultrafiltration membranes. Desalination 212:28–36
5. Lee S, Park G, Amy G, Hong S-K, Moon S-H, Lee D-H, Cho J (2002) Determination of membrane pore size distribution using the fractional rejection of nonionic and charged macromolecules. J Membr Sci 201:191–201
6. Park N, Kwon B, Sun M, Ahn H, Kim C, Kwoak C, Lee D, Chae S, Hyung H, Cho J (2005) Application of various membranes to remove NOM typically occurring in Korea with respect to DBP, AOC and transport parameters. Desalination 178:161–169
7. Shim Y, Lee H-J, Lee S, Moon S-H, Cho J (2002) Effects of natural organic matter and ionic species on membrane surface charge. Environ Sci Technol 36:3864–3871
8. Lee S, Amy G, Cho J (2004) Applicability of Sherwood correlations for natural organic matter (NOM) transport in nanofiltration (NF) membranes. J Membr Sci 240:49–65
9. Lee S, Moon J, Yim S-K, Moon S-H, Cho J (2002) The relationship between flux decline of NF membranes with NOM transport characteristics: convection versus diffusion. Desalination 147:237–241
10. Cho J, Amy G, Pellegrino J (2000) Membrane filtration of natural organic matter: comparison of flux decline, NOM rejection, and foulants during filtration with three UF membranes. Desalination 127:283–298
11. Cho J, Sohn J, Choi H, Kim In S, Amy G (2002) Effects of molecular weight cutoff, f/k ratio (a hydrodynamic condition), and hydrophobic interactions on natural organic matter rejection and fouling in membranes. J Water Supply Res Technol AQUA 51(2):109–123
12. Park N, Cho J (2008) Natural organic matter diffusivity for transport characterizations in nanofiltration and ultrafiltration membranes. J Membr Sci 315:133–140
13. Cho J, Amy G, Pellegrino J (2000) Membrane filtration of natural organic matter: factors and mechanisms affecting rejection and flux decline with charged ultrafiltration (UF) membrane. J Membr Sci 164:89–110
14. Fent K, Weston AA, Caminada D (2006) Review: ecotoxicology of human pharmaceuticals. Aquat Toxicol 76:122–159
15. Kostich MS, Lazorchak JM (2008) Risks to aquatic organisms posed by human pharmaceutical use. Sci Total Environ 389:329–339
16. Laenge R, Steger-Hartmann T, Schweinfurth H (2006) The environmental risk assessment of human pharmaceuticals in the overall EU regulatory affairs process. Regul Toxicol Pharmacol 45:223–228
17. Kim Y, Choi K, Jung J, Park S, Kim P-G, Park J (2007) Aquatic toxicity of acetaminophen, carbamazepine, cimetidine, diltiazem and six major sulfonamides, and their potential ecological risks in Korea. Environ Int 33:370–375
18. Snyder SA, Westerhoff P, Yoon Y, Sedlak DL (2003) Pharmaceuticals, personal care products, and endocrine disruptors in water: implications for the water industry. Environ Eng Sci 20(5):449–469
19. Chon K, Lee S, Chon K, Hussain AA, Cho J (2010) Developing organic fouling indices of microfiltration and nanofiltration membranes for wastewater reclamation. Desalin Water Treat 18:61–70
20. Baudin I, Campos C, Laine JM (2001) Removal of organic matter by the PAC-UF process: first two years of a full-scale application. Water Sci Technol Water Supply 1(4):253–263
21. Kwon B, Lee S, Cho J, Ahn H, Lee D, Shin HS (2005) Biodegradability, DBP formation, and membrane fouling potential of natural organic matter: characterization and controllability. Environ Sci Technol 39:732–739
22. Lee H, Amy G, Cho J, Yoon Y, Moon S-H, Kim In S (2001) Cleaning strategies for flux recovery of an ultrafiltration membrane fouled by natural organic matter. Water Res 35(14):3301–3308
23. Cho J, Amy G, Pellegrino J, Yoon Y (1998) Characterization of clean and natural organic matter (NOM) fouled NF and UF membranes, and foulants characterization. Desalination 118:101–108

24. Park N, Kwon B, Kim In S, Cho J (2005) Biofouling potential of various NF membranes with respect to bacteria and their soluble microbial products (SMP): characterization, flux decline, and transport phenomena. J Membr Sci 258:43–54
25. Braghetta A, DiGiano FA, Ball WP (1997) Nanofiltration of natural organic matter: pH and ionic strength effects. J Environ Eng ASCE 123(7):628–641
26. Hong S, Elimelech M (1997) Chemical and physical aspects of natural organic matter (NOM) fouling of nanofiltration membranes. J Membr Sci 132:159–181
27. Jucker C, Clark MM (1994) Adsorption of aquatic humic substances on hydrophobic ultrafiltration membranes. J Membr Sci 97:37–52
28. Jang N, Ren X, Kim G, Ahn C, Cho J, Kim IS (2007) Characteristics of soluble microbial products and extracellular polymeric substances in the membrane bioreactor for water reuse. Desalination 202:90–98
29. Kwon B, Park N, Cho J (2005) Effect of algae on fouling and efficiency of UF membranes. Desalination 179:203–214
30. Park N, Kwon B, Kim S-D, Cho J (2006) Characterizations of the colloidal and microbial organic matters with respect to membrane foulants. J Membr Sci 275:29–36
31. Chon K, Chon K, Chang J-S, Oh H, Lee E, Cho J (2009) Technical note: community of bacteria attached on the PVDF MF membrane surface fouled from drinking water treatment, in Seoul, Korea. Drink Water Eng Sci 2:35–39
32. Moon J, Kim S-H, Cho J (2006) Characterization of natural organic matter as nano particle using flow field-flow fractionation. Colloid Surf A Physicochem Eng Asp 287:232–236
33. Moon J, Lee S, Song J-H, Cho J (2010) Membrane fouling indicator of effluent organic matter with nanofiltration for wastewater reclamation, as obtained from flow field-flow fractionation. Sep Purif 73:164–172
34. Lee E, Shon HK, Cho J (2010) Biofouling characteristics using flow field-flow fractionation: effect of bacteria and membrane properties. Bioresour Technol 101:1487–1493

Switched Reluctance Motor Drives for Propulsion and Regenerative Braking in EV and HEV

Mehrdad Ehsani
Department of Electrical & Computer Engineering, Texas A&M University, College Station, TX, USA

Article Outline

Glossary
Definition of the Subject
Introduction
Advantage of the Extended Constant Power Range for Propulsion
Extended Constant Power Range for Regenerative Braking
Switched Reluctance Motor Drive for Extended Constant Power Operation
Future Directions
Bibliography

Glossary

Drive cycle A profile of vehicle speed versus time

Extended constant power range Operation of the electric motor beyond its rated speed by attempting to keep its power constant

Power electronic converter The electronic circuit for controlling voltages and currents for power control

Regenerative braking The use of electric machine as generator for vehicle braking force

Switched reluctance motor A form of variable reluctance motor with discrete air gap magnetic fluxes and currents

X factor The ratio of maximum to rated motor speeds

Definition of the Subject

Electric and hybrid electric vehicles (EV and HEV) are considered an essential element of sustainable energy and transportation complex. This is mainly due to their high efficiency and low emissions. The specific technology and characteristics of the traction motor are essential for the performance and efficiency of the EV and HEV. Various motor technologies have been considered and used in EV and HEV drives over the past 100 years. This choice was mainly governed by the available motor and electronic controls available at the time and also on the deeper understanding of the nature of electrical vehicle traction. The historical progression of the traction motor technologies has roughly been dc motors, induction motors, and lately, permanent magnet motors.

This article introduces a new basis for the selection of vehicle traction motor technology. On this basis, the modern switched reluctance motor drive technology is shown to be very attractive for future EV and HEV applications.

Introduction

Electric and hybrid electric vehicles are attractive as candidates for sustainable transportation. This is mainly due to their high efficiency and low emission. In EV and HEV, the *electric motor* is used for both *propulsion* and *regenerative braking*. Therefore, the selection of an electric motor for the EV and HEV should be based on both its propulsion and regenerative braking characteristics.

Various motor technologies have been considered and used in EV and HEV drives over the past 100 years. This choice was mainly governed by the available motor and electronic control technologies at the time and also on the understanding of the nature of electrical vehicle traction. The historical progression of the traction motor technologies has roughly been dc motors, induction motors, and lately, permanent magnet motors.

Vehicle dynamics, such as initial acceleration, indicates the power rating of the propulsion motor. It has been shown by our research group that a motor with an *extended speed range* at *constant power*can minimize the power rating of the propulsion system for achieving the same acceleration performance [1]. Furthermore, a motor with an extended *constant power range* can also recover more *kinetic energy* during regenerative braking. Therefore, a motor with extended constant power speed range is advantageous for EV and HEV traction application.

For the above reasons, the *switched reluctance motor (SRM)* is considered a promising candidate for traction in EV and HEV. In addition to having a *wide speed range*, especially at constant power, these motors have a rugged and low-cost structure, reliable drive power converter topology, and high efficiency over a wide range of speed. However, in order to obtain an extended constant power range, the SRM must be especially designed. Special control design will then meet the requirements for recovering most of the kinetic energy during regenerative braking.

This article introduces the concept of extended speed range at constant power and its benefit in vehicle traction application. Then, the advantage of switched reluctance motor for meeting the required extended speed range is introduced.

Advantage of the Extended Constant Power Range for Propulsion

The initial vehicle acceleration requirement is the main determinant of the power rating of the propulsion system. A *traction motor* with constant power over an extended speed range will result in the minimal power rating of the propulsion system for a specified *initial acceleration*. This has been proven by our group at Texas A&M University and is shown in [1] and briefly reviewed in this section.

Figure 1 illustrates a typical *torque-speed characteristic* of any electric motor. In this figure, V_{rm}, V_{rv}, and V_{max} represent the rated speed of the motor, the rated speed of the vehicle, and the maximum speed of the vehicle, respectively. When the vehicle accelerates from zero to V_{rv} (for example, 100 km/h or 60 mph), the maximum traction force on the driven wheels, F_m, is limited to a constant design value up to speed V_{rm}. Above this speed, the maximum traction force is limited by P_m/V, where F_m and P_m represent the maximum traction force and power of the motor, respectively.

It can be shown that the motor power rating can be represented by:

$$Pm = \frac{m}{2t_f}\left(V_{rm}{}^2 + V_{rv}{}^2\right) \tag{1}$$

where m stands for vehicle speed.

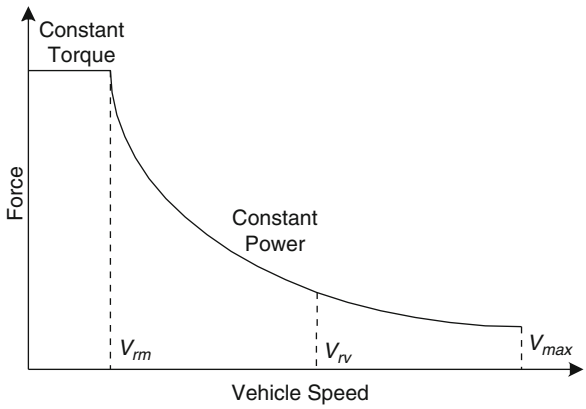

Switched Reluctance Motor Drives for Propulsion and Regenerative Braking in EV and HEV. Figure 1 Torque-speed characteristic of the electric motor in terms of traction force and vehicle speed

Minimizing this motor power with the design value, V_{rm} means

$$\partial P_m / \partial V_{rm} = 0 \quad (2)$$

Therefore,

$$V_{rm} = 0 \quad (3)$$

Equation 3 indicates that the power rating of the propulsion system will be minimized for a given design specification of going from standstill to V_{rv} in t_f seconds. This means that the motor runs entirely in constant power regime. However, it is physically impossible to run a motor entirely in the constant power range, from zero speed to its maximum speed. Therefore, a motor with a long speed range in constant power is preferred for minimizing the power rating of the propulsion system.

Here a realistic vehicle example to illustrate the point is given. The parameters of the vehicle are shown in Table 1.

Different traction motor technologies, with different ratios of maximum speed to rated speed, V_{max}/V_{rm} (referred to as the X factor), are used for accelerating the above vehicle from standstill to 100 km/h (62.5 mph) in 15 s. Ratios of 2:1, 3:1, 4:1, 5:1, and 6:1 are considered. The required motor and vehicle drive train power ratings for each motor are shown in Table 2.

Extended Constant Power Range for Regenerative Braking

In EV and HEV, when the electric braking system can provide high enough braking force, the mechanical braking is not used, and all the kinetic energy can be recovered by *regenerative braking*. Otherwise, the mechanical braking system has to be added to provide enough braking force on the wheels. Thus, some kinetic energy is dissipated in the form of heat (Fig. 2).

To find the optimal motor torque-speed characteristic for braking, the required braking force distribution of the above vehicle at different speeds is studied on a standard vehicle drive cycle called US06 (combined, high-speed, and high-acceleration driving cycle) and is plotted in Fig. 3. The torque-speed characteristics of motors with different *X factors* that are capable of accelerating the vehicle from standstill to 100 km/h in 15 s are also plotted in Fig. 3.

Figure 3 shows that more *braking force* is used at low speeds and less braking force is used at high speed on this drive cycle. Figure 3 also shows that when the X factor is less than 4:1, the motor cannot provide enough braking force at low speeds. Therefore, more mechanical braking has to be used to slow down the vehicle, and more kinetic energy is lost in the form of heat. In this example, when the X factor is higher than 4:1, the motor can provide adequate braking force at both low and high speeds. Therefore, more of the kinetic energy can be recovered by regenerative braking. Figure 4 shows the kinetic energy that is not recovered for each motor X factor.

To obtain the required extended constant power range, a multi-gear transmission may be used in combination with a motor with a narrow constant power range. An example of a motor technology with limited constant power range is the permanent magnet motor. However, the multi-gear transmission complicates the structure and lowers the efficiency of the propulsion system. Further, if automatic transmission is used, the poor efficiency of the hydraulic torque converter further aggravates the power efficiency of the vehicle traction system.

Switched Reluctance Motor Drives for Propulsion and Regenerative Braking in EV and HEV. Table 1 Parameters of the studied vehicle

Vehicle mass (kg)	1,500
Radius of the wheel (m)	0.2794
Aerodynamic drag coefficient	0.3
Rolling resistance coefficient	0.009
Front area (m^2)	2.0
Air density (kg/m^3)	1.225

Switched Reluctance Motor Drives for Propulsion and Regenerative Braking in EV and HEV. Table 2 Required power ratings of the propulsion system versus the X factor of the motor for achieving the same acceleration

X ratio	2:1	3:1	4:1	5:1	6:1
Power rating (kW)	90	66	57.8	54	52.3

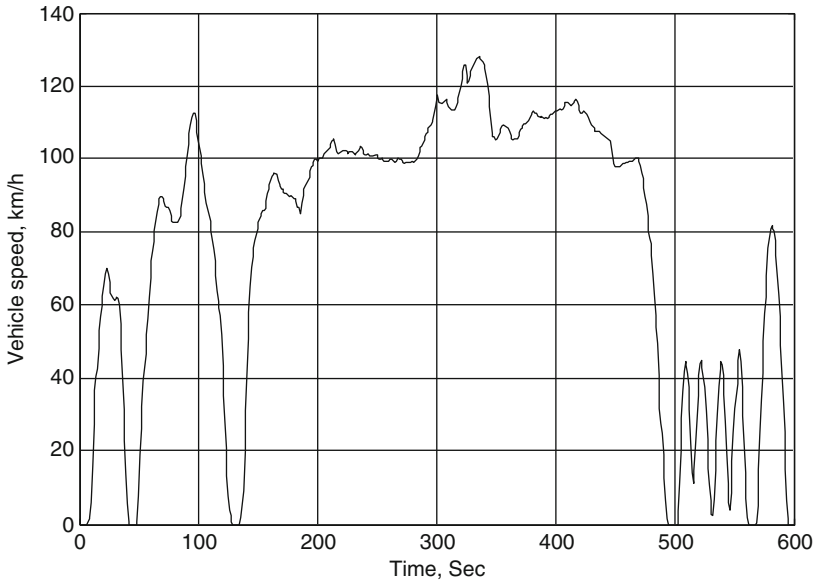

Switched Reluctance Motor Drives for Propulsion and Regenerative Braking in EV and HEV. Figure 2
Vehicle speed variation in US06 drive cycle

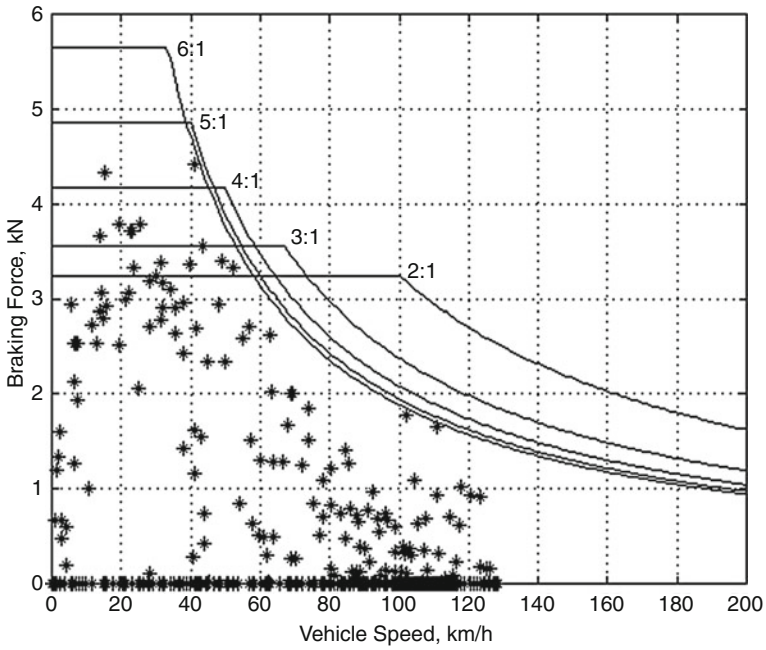

Switched Reluctance Motor Drives for Propulsion and Regenerative Braking in EV and HEV. Figure 3
Braking force distribution at different speeds in US06 drive cycle and the braking force-speed profile of the motors with different X factors capable of achieving the same initial acceleration

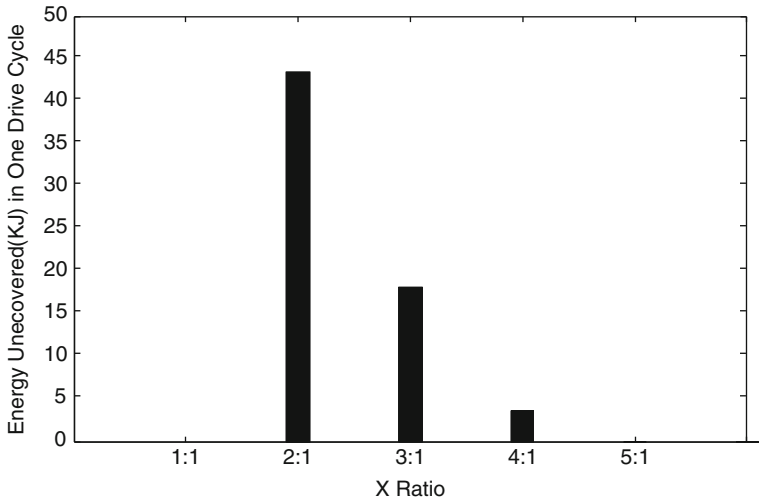

Switched Reluctance Motor Drives for Propulsion and Regenerative Braking in EV and HEV. Figure 4
Energy not recovered in one drive cycle by motors with different X factors

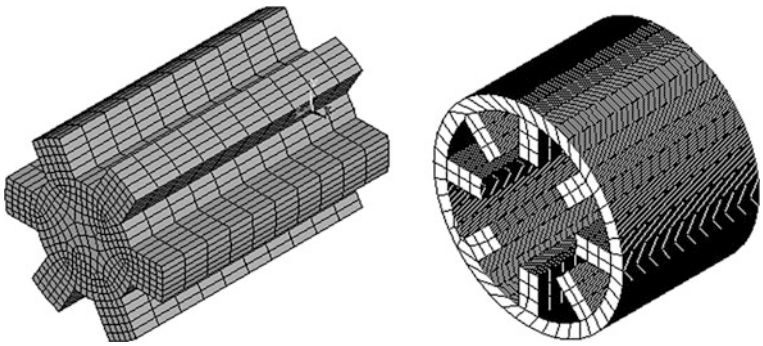

Switched Reluctance Motor Drives for Propulsion and Regenerative Braking in EV and HEV. Figure 5
Cross sections of rotor and stator of a 4-phase 8/6 SRM

Switched Reluctance Motor Drive for Extended Constant Power Operation

The switched reluctance motor can more easily have the necessary extended constant power range without the need for a multi-gear transmission. Therefore, the SRM is an attractive candidate for the traction motor in EV and HEV.

Mechanical Structure of SRM

The switched reluctance motor has salient poles both on the stator and rotor. It has concentrated windings on the stator and no winding on the rotor. In Fig. 5, cross sections of stator and rotor of a 4-phase 8/6 SRM is shown. The geometries of a few other types of SRM are shown in Fig. 6.

Electrical Structure of SRM

Figure 7 shows one common structure of the *power electronic converter*connected to a 4-phase SRM. Each leg of the converter drives one phase of the SRM in a sequential manner, based on the instantaneous position of the rotor.

Figure 8 shows the ideal phase inductance, current, and torque of the SRM. Positive (*motoring*)

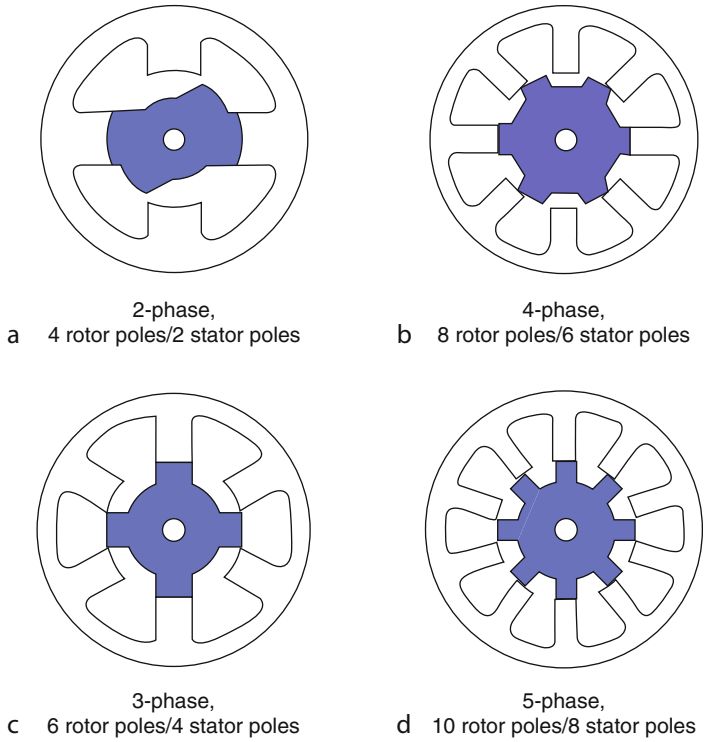

Switched Reluctance Motor Drives for Propulsion and Regenerative Braking in EV and HEV. Figure 6
Geometries of various switched reluctance motors

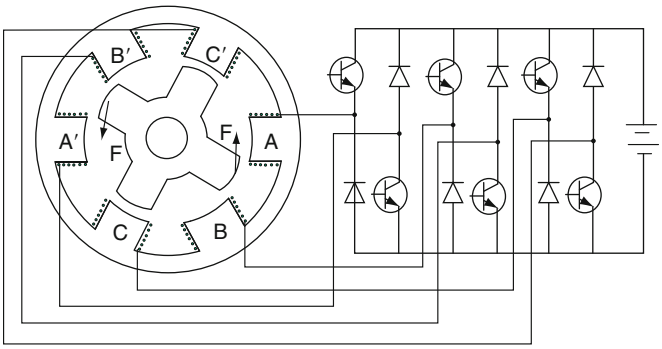

Switched Reluctance Motor Drives for Propulsion and Regenerative Braking in EV and HEV. Figure 7
Construction of SRM drive

torque is produced if the phase is excited when the phase inductance is increasing as the rotor rotates. Negative (*generating*) torque is produced if the phase is excited when the phase inductance is dropping as the rotor moves. This implies that the position information is necessary for control of the SRM drive.

SRM can inherently operate with extremely long constant power range. This long constant power range makes SRM highly favorable for vehicle traction application. In addition, recently developed full speed *sensorless* control technology will make SRM a more attractive candidate for military vehicle traction application [2–8].

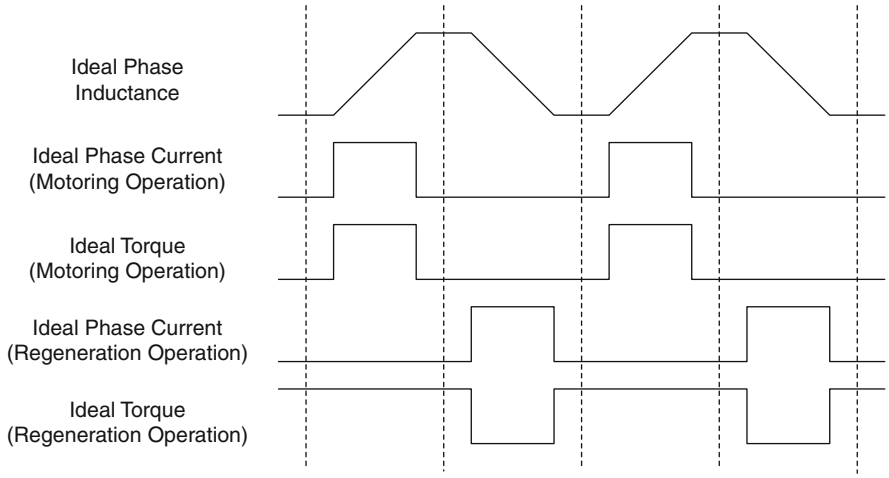

Switched Reluctance Motor Drives for Propulsion and Regenerative Braking in EV and HEV. Figure 8
Idealized inductance, current, and torque profiles of the SRM

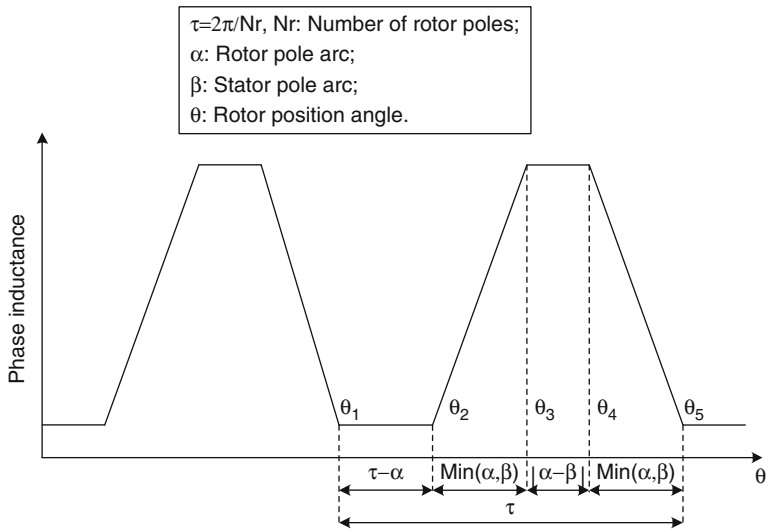

Switched Reluctance Motor Drives for Propulsion and Regenerative Braking in EV and HEV. Figure 9
Inductance profile of the SRM

Figure 9 shows the details of phase inductance versus rotor position angle of the SRM. By properly choosing small pole arcs, large air gap at unaligned position, and small air gap at aligned position, one can make the inductance profile of the SRM have a large dead zone at the unaligned position while making the SRM able to provide the required rated power. In vehicle traction application, this large dead zone in the inductance profile enables large phase advancing control of SRM so that enough phase current, hence enough torque, can be built in the SRM when the rotor speed is above the base speed. Some examples of the traction SRM drive for achieving extended constant power speed range are presented in [9].

The steep SRM inductance slope, shown in Fig. 9, can be used to produce a high electric torque both in propulsion and regenerative braking operation. In regenerative braking operation, when the motor

speed is below the base speed, the phase current can be easily adjusted to produce the required braking torque. One can find the relation between the phase current and the electric torque with an artificial neural network using the data obtained from numerical simulation. Neural networks can be used to find the relation between the turn-off rotor position and the phase current amplitude and torque using the data obtained from numerical simulation. This neural-network-based SRM control strategy for regenerative braking in EV and HEV is presented in [10].

Future Directions

The advantage of the motor with an extended constant power speed range for both propulsion and regenerative braking operation in electric and hybrid electric vehicle applications was presented. The switched reluctance motor is an attractive candidate for the traction motor of EV and HEV due to its inherent capability of having an extended constant power range, with proper design and control. The basic design and control strategies of the SRM drive for achieving the extended constant power range in both propulsion and regenerative braking operation were also presented in this article.

At the present, the SRM technology suffers from a few drawbacks. The most important of these is the dearth of manufacturers and suppliers. The others are the inherent noise and vibrations that these motors produce. However, these problems have been shown to be surmountable.

In time, rare earth permanent magnets, used in permanent magnet motors, will become more scarce and expensive, and the advantages of the SRM for traction will become better understood by the vehicle designers and manufacturers. This may lead to the evolution of EV and HEV traction motor technology to switched reluctance motors.

Bibliography

1. Ehsani M, Rahman KM, Toliyat HA (1997) Propulsion system design of electric and hybrid vehicles. IEEE Trans Ind Electron 44(1):19–27
2. Ehsani M (1990) Position sensor elimination technique for the switched reluctance motor drive, US Patent 5072166
3. Ehsani M (1994) Phase and amplitude modulation techniques for rotor position sensing in switched reluctance motors, US Patent No. 5,291,115
4. Ehsani M, Husain I, Mahajan S, Ramani KR (1994) New modulation encoding techniques for indirect rotor position sensing in switched reluctance motors. IEEE Trans Ind Appl 30(1):85–91
5. Dunlop GR, Marvelly JD (1987) Evaluation of a self commuted switched reluctance motor. In: Proceeding of 1987 electric energy conference, Adelaide, pp 317–320
6. Ehsani M, Husain I (1992) Rotor position sensing in switched reluctance motor drives by measuring mutually induced voltages. In Conference Record of 1992 IEEE Industry Application Society Annual Meeting, vol 1, Houston, pp 422–429
7. Lumsdaine A, Lang JH (1990) State observer for variable reluctance motors. IEEE Trans Ind Electron 37(2):133–142
8. Bass JT, Ehsani M, Miller TJE (1987) Simplified electronics for torque control of sensorless switched reluctance motor. IEEE Trans Ind Electron 34(2)
9. Rahman KM, Fahimi B, Suresh G, Rajarathnam AV, Ehsani M (2000) Advantages of switched reluctance motor applications to EV and HEV: design and control issues. IEEE Trans Ind Appl 36(1):111–121
10. Gao H, Gao Y, Ehsani M (2001) A neural network based SRM control strategy for regenerative braking in EV and HEV. To be presented in IEEE International Electric Machine Design and Control Conference 2001, Massachusetts, Cambridge, June 2001
11. Ehsani M, Gao Y, Butler KL (1999) Application of electrically peaking hybrid (ELPH) propulsion system to a full-size passenger car with simulated design verification. IEEE Trans Veh Technol 48(6):1779–1787
12. Ehsani M et al. (2001) Design issues of the switched reluctance motor drive for propulsion and regenerative braking in EV and HEV. In: Proceedings of the SAE-FTT'01, Costa Mesa
13. Gao Y, Rahman KM, Ehsani M (1997) Parametric design of the drive train of an electrically peaking hybrid (ELPH) vehicle, SAE International SP-1234, Paper No. 970294
14. Gao Y, Chen L, Ehsani M (1999) Investigation of the effectiveness of regenerative braking for EV and HEV. SAE International SP-1466, Paper No. 1999-01-2910, August 1999

T

Thermal Energy Storage

Rainer Tamme, Doerte Laing, Wolf-Dieter Steinmann, Thomas Bauer
Institute of Technical Thermodynamics, German Aerospace Center, Stuttgart, Germany

Article Outline

Glossary
Definition of the Subject
Introduction
Principles of Sensible Heat Storage
Principles of Latent Heat Storage
Principles of Chemical Heat Storage
Thermal Energy Storage for Concentrated Solar Power
Future Directions
Bibliography

Glossary

Latent heat storage Is connected with a phase transformation of the storage materials (phase change materials – PCM), typically changing their physical phase from solid to liquid and vice versa. The phase change is always coupled with the absorption or release of heat and occurs at a constant temperature. Thus, the heat added or released cannot be sensed and appears to be latent. Stored energy is equivalent to the heat (enthalpy) for melting and freezing.

Sensible heat storage Results in an increase or decrease of the storage material temperature stored energy is proportional to the temperature difference of the used materials.

Thermochemical heat storage Is based on reversible thermochemical reactions. The energy is stored in the form of chemical compounds created by an endothermic reaction and it is recovered again by recombining the compounds in an exothermic reaction. The heat stored and released is equivalent to the heat (enthalpy) of reaction.

Definition of the Subject

Thermal energy storage (TES) is a key element for effective and increased utilization of solar energy in the sectors heating and cooling, process heat, and power generation. Solar thermal energy shows seasonally (summer–winter), daily (day–night), and hourly (clouds) flux variations which does not enable a solar system to provide heat or thermal power according to the demand profile of specific users. Strategies to overcome this problem are to operate in hybrid (solar + fossil) mode and/or to use TES. By integrated TES solar thermal system shows significant benefits:

- Solar contribution is increased, allows operation during times of no solar radiation.
- Rapid flux variations can be compensated (avoid strong gradients for connected components, e.g., piping, heat exchanger, boiler, turbines, etc.) which increase lifetime of components.
- Surplus energy can be used and does not need to be dumped.
- Size of subsequent components, e.g., evaporator, condenser, boiler, turbines, can be reduced.
- Allows improved thermal management of the solar system (e.g., increased start-up time, accurate preheating of solar steam cycle).
- Can be used to cover peak demand.

Introduction

A characteristic of thermal energy storage systems is that they are diversified with respect to temperature, power level, and heat transfer fluids and that each application is characterized by its specific operation parameters. This requires the understanding of a broad portfolio of storage designs, media, and methods.

Robert A. Meyers (ed.), *Encyclopedia of Sustainability Science and Technology*, DOI 10.1007/978-1-4419-0851-3,
© Springer Science+Business Media, LLC 2012

Heat – in the physical sense – is a form of energy and can be stored in various ways and for many different applications. *Low-temperature heat* is stored for heating, ventilation and air-conditioning (HVAC), and domestic hot water supply, and *high-temperature heat* for industrial processes and solar thermal power plants. Thermal energy storage can be classified according to the heat storage mechanism in sensible heat storage, latent heat storage, and thermochemical heat storage. For the different storage mechanisms, Fig. 1 shows the working temperature and the relation between energy density and maturity.

Each storage concept has its best suited materials and these may occur in different physical phases: as solids, liquids, or via phase change. For example, the volumetric and gravimetric energy densities of the materials have a decisive impact on the capacity of the storage system. The thermal conductivity of the materials is important for the charge and discharge power of the storage system. Furthermore, small density changes versus temperature minimize thermomechanical stress phenomena. A decisive criterion of a heat storage medium is its price and the costs that arise upon its utilization. Long life and a high cycling stability are prerequisites for economic application, i.e., at a price competitive with existing storage facilities.

The charge and discharge powers of sensible and latent heat storage systems are determined mainly by heat transfer processes. For thermochemical storage, mass and heat transfer processes are the dominating physical effects.

The heat of the carrier fluid may be either transferred *directly* to the storage material as, for example, in a dry pebble bed with air flow, or a heat exchanger may be required as in a solar domestic hot water store where the water–antifreeze mixture flowing through a solar collector has to be separated from the hot water for consumption (*indirect* concept). Other aspects of selecting a heat storage material may be operational advantages in energy supply systems or a larger flexibility in application. A survey of heat storage media is given in Fig. 2.

Principles of Sensible Heat Storage

Sensible heat always results in an increase or decrease of the material temperature. All materials have a capability of absorbing and storing heat due to the fact that they

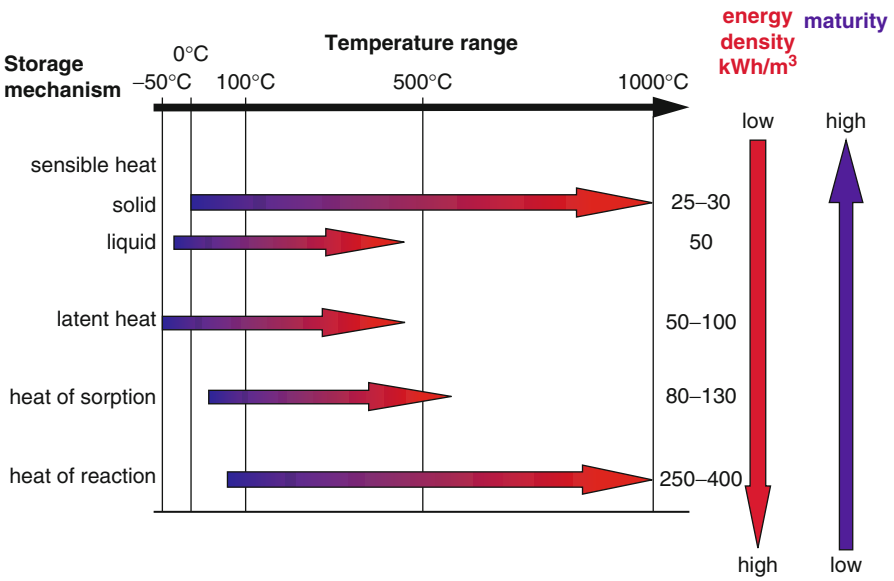

Thermal Energy Storage. Figure 1
Thermal energy storage mechanism, its working temperature, and correlation to energy density and status of technical maturity

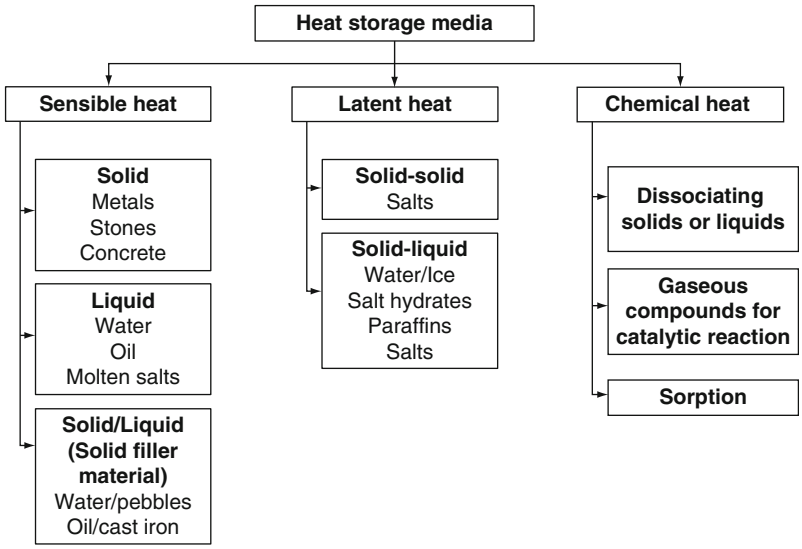

Thermal Energy Storage. Figure 2
Overview of heat storage media with examples

have a mass m and a specific heat capacity c_p at constant pressure. For a temperature difference $\Delta T = T_2 - T_1$ this heat (or enthalpy) amounts to

$$Q_{sensible} = m \cdot c_p \cdot (T_2 - T_1) \quad (1)$$

T_2 denotes the material temperature at the end of the heat absorbing (charging) process and T_1 at the beginning of this process. This heat is released in the respective discharging process.

In Table 1 some characteristic materials are listed together with their thermophysical properties. It needs to be considered, that some material values, such as graphite, are strongly temperature dependent. Also, for example, impurities in metals cause a drop in the thermal conductivity values. Equation 2 defines the thermal diffusivity a, where λ is the thermal conductivity and ρ the density. Equation 3 gives the definition of the heat diffusivity b.

$$a = \frac{\lambda}{\rho \cdot c_p} \quad (2)$$

$$b = \sqrt{\lambda \cdot \rho \cdot c_p} \quad (3)$$

Metals and graphite are best suited for quick charging and discharging (high thermal diffusivity a) and for a large amount of heat stored in a given time (high heat diffusivity b). Other solid materials such as stones are much less advantageous; their respective values are smaller by an order of magnitude.

Liquids offer the advantage of a possible use as both storage medium and heat transfer fluid. The most widely applied media, in this respect, are water and thermal oil.

Solid Storage Materials

Solid materials can be utilized in a wide temperature range and heated up to very high temperature (e.g., refractory bricks in Cowper regenerators to 1,000°C). Solids are often chemically inert and have a low vapor pressure. In addition, the containment can often be simpler compared to systems based on liquids. Solid storage materials can be classified as metals and nonmetals.

Natural materials in the form of rocks and pebbles are abundant and cheap. For low temperatures, rock and soil can be used as ground storage. For high temperatures, the thermomechanical stability of the solids is important. Here, rocks such as granite, basalt, and quartzite, as well as pebbles can have suitable properties.

Of the manufactured solid materials, various ceramics are widely used as heat storage materials. In the low-temperature range, bricks act as a buffer

Thermal Energy Storage. Table 1 Thermophysical properties of media for sensible heat storage

Material	T, °C	ρ, (kg/m^3)	c_p, (kJ/[kg·K])	λ, (W/[m·K])	$10^6 \times a$, (m^2/s)	$10^{-3} \times b$, (J/[m^{2}Ks$^{1/2}$])
Solids						
Aluminum 99.99%	20	2,700	0.945	238.4	93.3	24.66
Copper (commercial)	20	8,300	0.419	372	107	35.97
Iron	20	7,850	0.465	59.3	16.3	14.7
Lead	20	11,340	0.131	35.25	23.6	7.24
Brick (dry)	20	1,800	0.84	0.50	0.33	0.87
Concrete (aggregates)	20	2,200	0.72	1.45	0.94	1.52
Granite	20	2,750	0.89	2.9	1.18	2.67
Graphite	20	2,200	0.61	155	120	14.41
Limestone	20	2,500	0.74	2.2	1.19	2.02
Sandstone	20	2,200	0.71	1.8	1.15	1.68
Slag	20	2,700	0.84	0.57	0.25	1.13
Sodium chloride	20	2,165	0.86	6.5	3.5	3.5
Soil (clay)	20	1,450	0.88	1.28	1.0	1.28
Soil (gravelly)	20	2,040	1.84	0.59	0.16	1.49
Liquids						
Molten salt (K-$NaNO_3$)	230	1,950	1.57	0.50	0.16	1.24
Paraffin (liquid)	20	900	2.13	0.26	0.14	0.71
Silicone oil (AK250)	25	970	1.465	0.168	0.118	0.49
Sodium	100	927	1.385	85.84	66.85	10.50
Transformer oil	60	842	2.09	0.122	0.069	0.46
Water	20	998	4.183	0.598	0.142	1.58

for the climatization of buildings. At higher temperatures, refractory bricks based on oxides (silica, alumina, magnesia, and iron oxide – feolite), carbonates (e.g., magnesite), and their mixtures are commercially utilized in applications such as Cowper regenerators, night-storage heaters, and tiled stoves.

For high temperatures, concrete is another attractive sensible heat storage material, because of its low cost due to inexpensive aggregates, the availability throughout the world and the available and simple processing route via casting. Figure 3 shows a concrete storage unit which can operate up to 400°C [1, 2].

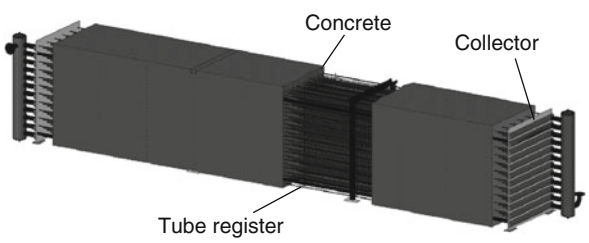

Thermal Energy Storage. Figure 3 Schematic layout of a concrete storage module showing the main elements: tube register, concrete storage material, and heat transfer fluid collector

Typically, metals exhibit higher thermal conductivities but are less attractive from an economic point of view compared to nonmetals. This high conductivity is advantageous in terms of a fast charge and discharge process of the storage system. High conductivity metals, such as aluminum and copper, can be used in electronics as a heat sink and for thermal management. *Cast iron* is an alternative material with a high thermal conductivity and volumetric heat capacity (energy density). It is used for high-temperature storage together with oil as heat carrier.

The heat transfer concept of storage systems using solid materials is usually based on an additional fluid as a heat carrier (e.g., water, steam, air, oil, molten salt) for the charge and discharge process. The heat carrier fluid may be operated either in direct contact (e.g., Cowper regenerators in the high-temperature glass and steel industry) or indirect contact (e.g., via a tubular heat exchanger) with the solid storage material.

Direct contact design is realized as a packed bed of solid particles in a container, such as a pebble bed or a rock pile, or in a more defined arrangement such as a regular array of checker bricks. Heat has to be carried to or from such stores by a heat carrier such as air or water. These beds provide a large surface area for heat transfer in their dispersed materials; the internal heat losses are only small because the particles have little surface contact to surrounding particles and thus, little conduction losses. For low temperatures, reduced insulation around the storage container is sufficient when air – with a small thermal conductivity – is used as a heat carrier and fills the gaps between the particles. Such particle beds, however, cause a large pressure drop in the fluid flow. This has to be compensated by pumps or compressors. Another drawback is the large storage volume required. Conveniently, this is provided in underground installations.

As the solid storage materials are in direct contact with the fluid heat carriers, properties of the solids have to be taken into account which affect fluid flow and heat transfer, such as particle and container size, mechanical durability against abrasion, and thermal cycling and hygroscopy.

The thermal stratification (see section "Liquid Storage Materials") is well maintained in a heat store, because natural convection in the heat carrier is suppressed and internal heat conduction is low, because of the aforementioned reasons. The combination of hollow bricks and air has been known as hypocaust-heating systems since antiquity. Water-flooded pebble beds are known as artificial aquifers.

In some cases the direct contact of heat carrier and storage material is not economic or feasible, for example, if the heat carrier is pressurized (e.g., steam) or incompatible with the storage medium. In this case, a design with indirect contact of carrier and storage medium can be utilized. The previous shown example of a high-temperature concrete storage using a steel tube register with pressurized water, steam, or oil as heat carrier (Fig. 3) represents this case [1, 2].

Liquid Storage Materials

The most widely used liquid for thermal storage is water. Water has the following advantages:

1. It is abundant and inexpensive.
2. It has a relatively high heat diffusivity ($b = 1.58 \times 10^3$ Jm^{-2} K^{-1} s$^{-1/2}$) and a relatively low thermal (temperature) diffusivity ($a = 0.142 \times 10^{-6}$ m^2/s), which is an advantage for thermal stratification within a hot-water storage tank.
3. It can be easily stored in all kinds of containers.
4. The control of water flow systems is highly flexible and is often state of the art.
5. Water can be directly used without heat exchangers; it is easy to handle, nontoxic, and noncombustible.
6. It is easily mixable with additives (antifreeze, anticorrosive).

Water has also some disadvantages, which can be summarized as follows:

1. It only provides a limited operation range between 0°C (freezing) and 100°C (boiling).
2. It is corrosive.
3. It has high vapor pressures ($p > 5$ bar) at temperatures >155°C.

The vapor pressure can be reduced when mixtures of water with other chemicals are applied; e.g., a mixture of 50% H_2O and 50% NaOH can be used

up to 140°C without a pressure vessel. The liquid material storage approach can be realized as a single tank or a two-tank concept consisting of two individual tanks at different temperature and fluid level. In a single tank, hot and cold media require thermal stratification to reduce losses.

Thermal stratification in heat storage vessels is desired, because the value of high temperature heat is maintained in the upper part of the vessel, while low-temperature fluid (as backflow from a heat consumer) can still be stored in the lower part of the vessel. The temperature distribution within a storage vessel varies with time. Due to transient internal heat conduction, the stratification is destroyed in the course of time, even in very well insulated vessels.

Applications of Water Storages for Solar Energy Storage tanks for hot water are used in industry and dwellings. They come in sizes of 0.1 m^3 (domestic hot water storage) to 12,000 m^3 (solar-assisted district heating). The most recent development is "solar combination stores" of about 0.5 m^3 which serve for both domestic hot water supply and house heating.

Water is commonly used also in large thermal stores, both as storage medium and heat transfer fluid. In large stores (e.g., seasonal stores for solar energy), the storage capacity can be turned over only once or – at the most – three times a year. Such a small energy turnover makes the stored heat expensive unless the storage container is inexpensive.

A technical/economical boundary for *steel tanks* is a size of around 100,000 m^3. For *ground containers,* the waterproof liner may create problems (e.g., tightness after welding, perforation by stones): plastic liners and stainless steel liners are used. These large containers are built of concrete and they are fully or partly buried in the ground. Their capacity is approximately 80 kWh/m^3. In summer, hot water is fed to the water layers on top and cold water withdrawn from the bottom; in winter, hot water is withdrawn from the top layers and cold water referred at the bottom.

In so-called *ground stores* low-temperature heat is stored in soil or pebbles. The storage medium in such cases is a mixture of water and solid particles. Density ϱ and specific heat capacity c of these mixtures can be obtained from the mixing laws. The thermal conductivity λ depends strongly on the composition of the mixture. Although some mathematical equations exist in the literature, reliable data for λ depend on measurements. Heat is usually exchanged with the ground by tubes containing a circulating carrier fluid, mostly water. These tubes may be placed close to the surface (0.5–1 m below) in a meandering arrangement or spirally wound in horizontal ditches. For large stores (more than 10,000 m^3 water equivalent storage capacity), vertical holes are drilled for the heat exchanger tubes.

In some areas, geology allows for a so-called *aquifer store*. This requires a permeable layer of soil (pebbles or sand) enclosed between horizontal layers of impermeable material (clay). Under such advantageous conditions, two fountains can be drilled some distance apart from each other and hot water can be inserted in summer and withdrawn in winter. Problems can arise from minerals dissolving in the water and precipitating on tubes and heat exchangers.

So-called *man-made aquifers* are built in sizes of 10,000 m^3; the ground excavations are filled with pebbles and water and sealed by plastic sheets. In all cases where mixtures of water and solid material are used for heat storage, the storage volume has to be larger than in the case of pure water. Rough data for the different types are given in Table 2.

Large-scale solar thermal storage in water is possible in *solar ponds*. These ponds act both as solar collector and as storage. In this concept the water itself is used as an insulator. The convection in the water can be suppressed by different methods. One common method is to utilize a density gradient which corresponds to a salt concentration gradient.

Molten Salt For temperatures above 100°C, molten salts are attractive candidates for sensible heat storage.

Thermal Energy Storage. Table 2 Storage volume of different storage media compared to pure water for 1 m water equivalent and 60 kWh capacity at $\Delta T = 50$ K

Storage media	Storage volume
Hot water storage	1 m^3
Pebble – water storage	1.3–2 m^3
Aquifer storage	2–3 m^3
Borehole storage	4–5 m^3

The major advantages of molten salts are low costs, high thermal stabilities, and low vapor pressures. The low vapor pressure results in storage designs without pressurized vessels. Also, many salts can be operated in air contact without significant degradation. In general there is experience with molten salts from a number of industrial applications related to heat treatment, thermochemical reactions, and heat transfer. For solar thermal power plants, large-scale two-tank storage systems with a capacity of several ten thousand tons have been built (see section "Indirect Storage in Liquid Media"). Typically, a non-eutectic salt mixture of 60 wt.% sodium nitrate and 40 wt.% potassium nitrate is utilized. The eutectic mixture has a melting temperature of 222°C and the thermal stability limit is at about 550°C. One major difficulty with molten salts is unwanted freezing during operation. Hence, often additional heating systems are required.

Further Liquid Storage Materials Oil is a common heat transfer fluid and has also been used as a liquid storage material. For example, mineral oil can be used at ambient pressures up to about 300°C. Synthetic oils are thermally stable up to around 400°C, but at higher temperatures they have to be pressurized which is often uneconomic.

For media other than water, the liquid storage material often creates the predominate cost of the entire storage system. In these cases low-cost solid filler material can replace the more expensive liquid storage material (e.g., cast iron in oil, molten salt thermocline designs).

Principles of Latent Heat Storage

Materials for the storage of latent heat are also named phase change materials (PCM), because of the fact that they change their physical phase from solid to liquid and vice versa [3–13]. The phase change is always coupled with the absorption of heat when the solid melts – heat of melting – and a heat release when the liquid solidifies. The phase change occurs at the melting temperature Tm. At that temperature, these materials melt when heat is added, but do not exhibit a rise in temperature. Thus, the heat added cannot be sensed and appears to be latent.

A change of one crystalline form into another without a physical phase change may also be considered as storage of latent heat. The phase change of salt hydrates is considered a solid–liquid transformation. The solid hydrate crystals release their water of crystallization at a certain temperature (or a temperature range) and the anhydrous salt dissolves in this water. This process is reversed when heat is withdrawn. The heat (or enthalpy at p = const.) stored with a phase change amounts to

$$q_{latent} = \Delta h_m \tag{4}$$

where Δh_m is the latent heat (enthalpy) of melting. When a material is heated from an initial temperature T_1 to the melting temperature T_m and the melt is further heated to T_2, the total heat stored is

$$\begin{aligned} Q_{\text{total}} &= Q_{\text{sensible},solid} + Q_{\text{latent}} + Q_{\text{sensible},liquid} \\ &= q_{\text{total}} \cdot m \end{aligned} \tag{5}$$

or using (1), (4), and (5):

$$\begin{aligned} Q_{\text{total}} &= m \cdot c_{p,solid}(T_m - T_1) + m \cdot \Delta h_m \\ &\quad + m \cdot c_{p,liquid}(T_2 - T_m) \end{aligned} \tag{6}$$

The specific heat capacity of the solid phase is $c_{p,solid}$ and of the liquid phase $c_{p,liquid}$.

The heat of fusion (or heat of melting) is much greater than the sensible heat. Therefore, phase change materials have a larger volumetric energy storage capacity than sensible storage materials, if smaller temperature intervals are considered. A further advantage of PCMs is the absorption and the release of heat at a constant temperature; this melting temperature is material-specific and the material can be selected accordingly.

In most cases the heat of the solid–liquid phase change is utilized. The heat of solid–solid phase changes (rearrangement of crystalline forms) is typical smaller compared to the heat of melting and solidification. Although enthalpies are large, the liquid–gas phase change is not utilized for latent heat storage due to the large volume of the gas phase.

Latent heat storage materials should be inexpensive and be characterized by:

1. A large phase-change enthalpy and a high density
2. A large thermal diffusivity in the solid and liquid phase
3. Thermal stability and cycle stability with a low vapor pressure

4. Little or no subcooling during freezing and little or no supersaturation during melting
5. A low thermal expansion, i.e., low volume change during melting

They should neither exhibit segregation (e.g., like Glauber's salt), nor be poisonous, flammable, or form explosive phases. They should not be corrosive, or react with materials in contact, such as containment, heat exchanger, and heat transfer enhancement structure. Various phase change materials are listed together with their thermophysical properties in Table 3. Thermophysical properties are not always available and their values may differ among different literature sources. Impurities in the substances can change the properties considerably. The table presents only characteristic materials; many more are found in literature.

Thermal Energy Storage. Table 3 Thermophysical properties of solid to liquid phase-change materials. The values are related to the solid (s) and liquid (l) phase below and above the respective melting point

Salt system	T (°C)	H (J/g)	λ_s (W/mK)	λ_l (W/mK)	$C_{p,s}$ (J/gK)	$C_{p,l}$ (J/gK)	ρ_l (g/cm^3)	$\Delta V/V_s$ (%)
Ice and salt hydrates								
H_2O	0	334	2.3	0.56	2.10	4.22	1.00	−8.3
$KF{\cdot}4H_2O$	19	230	n.a.	n.a.	1.8	2.4	1.46	n.a.
$CaCl_2{\cdot}6H_2O$	30	180	1.1	0.5	1.4	2.1–2.3	1.56	13
$Na_2SO_4{\cdot}10H_2O$	32	250	0.5	n.a.	1.9	3.3	1.41	4
$Na_2HPO_4{\cdot}12H_2O$	35	280	0.5	0.5	1.5–1.7	2.0–3.2	1.44	5
$Na(CH_3COO){\cdot}3H_2O$	58	250	0.7	0.4	2.1	3.0	1.28	13
Pure metals								
Na	98	113	122	87	1.36	1.38	0.93	2.8
Zn	419	112	100	50	0.45	0.48	6.76	1.9
Al	660	397	211	91	1.18	1.18	2.38	7.5
Anhydrous salts and their mixtures (Composition in weight%)								
KNO_3–$LiNO_3$ (67–33)	133	170	n.a.	n.a.	n.a.	n.a.	1.9	14
KNO_3–$NaNO_2$–$NaNO_3$ (53–40–7)	142	80	0.5	0.5	1.3	1.6	1.98	4
$LiNO_3$–$NaNO_3$ (49–51)	194	265	n.a.	0.5	n.a.	n.a.	1.9	13
KNO_3–$NaNO_3$ (54–46)	222	100	n.a.	0.5	1.4	1.5	1.95	5
$LiNO_3$	254	360	1.4	0.6	1.8	1.6–2.0	1.78	22
$NaNO_2$	270	180	0.7–1.3	0.5–0.7	n.a.	1.6–1.8	1.81	17
$NaNO_3$	306	175	0.6	0.51	1.66	1.66	1.91	11
NaOH	322	210	0.9	0.8	2.0	2.1	2.13	16
KNO_3	337	100	n.a.	0.4–0.5	1.4	1.3–1.4	1.87–1.89	3
NaCl–KCl–$MgCl_2$ (24.5–20.5–55)	393	240	1,0	n.a.	1,0	1,0	1.8	n.a.
K_2CO_3–Li_2CO_3–Na_2CO_3 (35–32–33)	397	275	n.a.	n.a.	1.7	1.6	1.90	17
K_2CO_3–Li_2CO_3 (65–35)	505	345	n.a.	n.a.	1.3–1.8	1.8–2.3	1.96	10

Cold Storage (0°C and Below)

For refrigeration below 0°C, ice slurries using a solution of water–salt (brine) and water–glycol can be utilized. Applications are industrial processes and space cooling. Within the solution fine solid crystals are suspended. A major advantage of the slurries is that they can be pumped. Hence, they can act as both the heat carrier and the heat storage medium. The slurry has the advantage of a larger heat capacity compared to the solution.

For space cooling, latent heat water–ice storage systems are commercially available. These systems utilize different heat transfer concepts. In the ice-on-coil design the ice grows around the heat exchanger tubes. Another concept utilizes spherical capsules filled with the PCM water/ice (macroencapsulation). These capsules are surrounded by the heat transfer fluid. Both, coils and capsules are commonly made of polymers such as polyethylene. At this stage, alternative direct contact heat transfer concepts to reduce costs of the heat exchanger or the capsules are examined but have not evolved commercially. Another very old concept is the use of natural ice (or snow) as a seasonal storage to supply cold in summer. Nowadays, there is an interest in the cooling of buildings and many snow storage demonstration plants have been built. For the transportation of food, beverage, and other products, smaller insulated boxes with encapsulated ice modules are commonly used.

Low-Temperature Storage (0–120°C)

Salt Hydrates Many salt hydrates are sufficiently inexpensive; they are only little corrosive and slightly toxic. They exhibit only small changes in volume during phase change and have a relatively high heat of fusion (compared to organic compounds) at low melting temperature. Salt hydrates are of the chemical form $X(Y)_i \cdot n\ H_2O$ with $X(Y)_i$ representing an inorganic compound. When the salt hydrate is heated to its transition temperature, one of the following reactions will take place:

$$X(Y)_i \cdot nH_2O \rightarrow X(Y)_i + nH_2O \quad (7)$$

$$X(Y)_i \cdot nH_2O \rightarrow X(Y)_i \cdot oH_2O + (n - o)H_2O \quad (8)$$

At the melting point, the hydrate crystals split up into either anhydrous salt and water (7) or into a hydrate with a lower number of water molecules and water (8). Several salt hydrates have two major drawbacks for thermal storage: They suffer from incongruent melting and supercooling.

Incongruent melting occurs when not enough water of crystallization is released during thawing and the anhydrous salt cannot completely dissolve. The solid residual part settles at the bottom of the container due to its higher density. In the reverse process (during recrystallization), some fraction of the precipitated solid is unable to come into contact with the water necessary for its recrystallization. Thus, the useful heat of fusion reduces after several charge–discharge cycles. Incongruent melting can be prevented by:

1. Addition of a thickening agent which holds the anhydrous solid part in suspension and prevents its settling
2. Stirring, vibrating, or rotating the material
3. Addition of excess water
4. Encapsulation of the material (e.g., in plastics, as metallic containers may be corroded)

Supercooling occurs during cooling (heat discharge) when no sufficient nucleation sites are available. The crystallization does not take place at the melting point; the liquid is cooled below that point and the stored heat is not discharged at the expected melting temperature, but at some arbitrary temperature. In some cases it might happen that the stored heat cannot be withdrawn, because the temperature difference between the subcooled melt and the required fluid temperature is not high enough. Supercooling can be prevented by addition of small quantities of a nucleating agent with a crystal structure similar to that of the salt.

Paraffins Paraffins are waxy solids at room temperature. Their melting points and heat of fusion increase with molar mass. Compounds in the series $C_{14}H_{30}$–$C_{40}H_{82}$ have melting points in the range 6–80°C. They are advantageous storage materials for the following reasons:

1. They are widely available and inexpensive.
2. Noncorrosive and nontoxic.
3. Chemically stable, with a low density.
4. Phase transformation is rapid.
5. Supercooling is negligible.

But they show the following drawbacks:

1. Low volumetric energy density (compared to salt hydrates).
2. Change in volume during melting by about 10%.
3. Low thermal conductivity and diffusivity.
4. No distinct melting point, because cheap technical paraffins used for thermal storage are mixtures of many compounds.
5. Not compatible with plastics.
6. They are flammable.

Applications for Solar Heating and Cooling

There are several commercial PCM products without a heat carrier fluid (passive systems) [10]. In these applications the PCM increases the heat capacity of the system and the PCM stabilizes the temperature of the system. Commercial PCM products are available in the areas of insulated transport containers (e.g., medical applications), the thermal management of electronic equipment, electric heating systems (e.g., floor heating), and human body comfort (e.g., pocket heater, clothes). Another area of commercial products is the space cooling of buildings. In particular in lightweight buildings with a low thermal mass, the PCM can reduce temperature fluctuation and cut peak temperatures. There are different ways to insert the PCM in the building. They include the additional use of boards and panels, such as gypsum plasterboard with microencapsulated paraffin and aluminum bags filled with salt hydrates. Another option is the integration of the PCM into the building material, such as plaster and concrete containing microencapsulated PCM.

For the heating and cooling of buildings, PCM systems with a heat carrier fluid, commonly water and air, have been researched [10]. The advantage of these active systems is that they have a higher heat transfer rate (or shorter charge/discharge time) compared to passive systems. For buildings, the discharge of the PCM at night is a key issue. Cooling of the PCM in the building can be achieved by a cold forced convection stream of night air which passes the PCM unit. The PCM systems can be located in the floor, ceiling, wall, or ventilation channels. In some cases the outside air is too warm at night and cooling with night air cannot be utilized. In this situation, water or brine as a heat carrier fluid and alternative cold sources can be used. The cold can be from natural sources (e.g., groundwater and soil) or from artificial sources (e.g., absorption chiller). Typically, the water or brine flows through capillary tubes within the PCM panels or boards. The replacement of conventional hot water storage systems, mainly for space heating and tap water in households, is also of research interest. Typical storage temperatures range from 40°C to 70°C. The heat transfer is usually limited by the low thermal conductivity of the PCMs. Heat transfer designs include mainly indirect contact concepts (e.g., heat exchanger tubes with and without fins, as well as encapsulated-PCM in the water), but also other concepts (direct contact concepts, PCM slurries).

High-Temperature PCM Storage (Above 120°C)

For the temperature range above 120°C, organic PCMs have been proposed. Their critical aspects have been not fully assessed. They include the long-term thermal stability, the reactivity with air oxygen, and the high vapor pressure. Some disadvantages can be overcome if hermetically sealed storage systems are utilized.

The thermal stability of inorganic materials is inherently higher. For temperatures from 120°C to 1,000°C, inorganic anhydrous salts can be utilized. There are solid–solid and solid–liquid phase transitions of anhydrous salts which can be used. The cations are mainly alkali (e.g., Li, Na, K) and alkaline earth (e.g., Ca, Mg) metals. Anions which are considered include nitrates, nitrites, hydroxides, bromides, carbonates, chlorides, sulfates, and fluorides. Many anhydrous salts are miscible and this results in a large variety of potential single salts and salt mixtures (binary and ternary systems). Table 3 shows selected examples of PCMs. For temperatures up to 350°C, in particular alkali metal nitrates and nitrites and their mixtures are suitable PCMs, if requirements such as handling and steel compatibility are taken into account [11].

In the temperature range 120–320°C, steam storage systems based on PCMs have been developed. These systems utilize a fine parallel pipe heat exchanger which is integrated into the PCM (Fig. 4). During the charging process, the steam condenses inside the pipes and the PCM melts. During discharging, the solidifying PCM releases heat, the water evaporates inside the pipes, and steam is generated. Applications of these

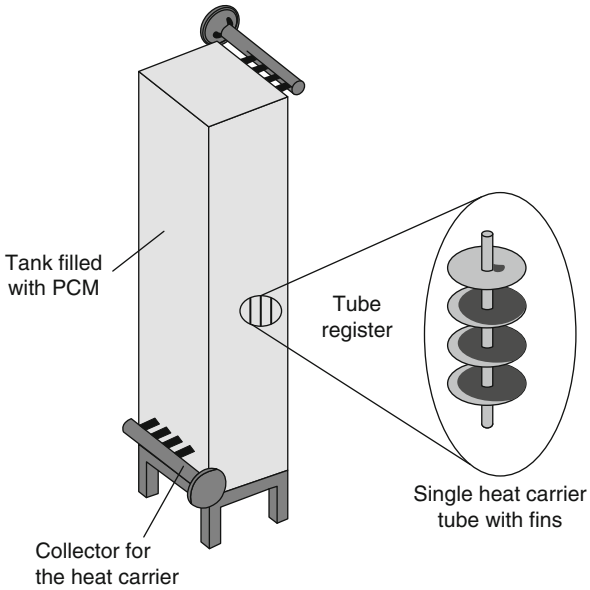

Thermal Energy Storage. Figure 4
Schematic drawing of a PCM storage module with integrated fins for enhanced heat transfer

steam storage systems include the areas of solar thermal power generation, industrial process heat utilization, and combined heat and power generation [12, 13].

Heat Transfer Concepts and Composites

The thermal conductivity of the PCM affects significantly the power density and the heat transfer design of the system. The power density of the storage systems corresponds to the melting and solidification time of the PCM. A typical design is a tubular heat exchanger integrated into the storage material and many applications require melting and solidification times in the order of hours. As can be seen in Table 3, the thermal conductivity of all common PCMs are lower than 1 W/(m.K). These conditions result in a storage design with a large number of heat exchanger tubes and this design is often not economic. Hence, cost-effective storage systems require the development of concepts that compensate this low thermal heat conductivity.

A number of heat transfer enhancement concepts has been proposed [12, 13]. The thermal conductivity can be enhanced by using composite materials, where the properties of a high latent heat of a PCM and a good thermal conductivity of an additive are combined. An aspect of interest is the form stability of the composites without phase separation after several melting and solidification cycles. For low-temperature applications (<100°C), paraffin/graphite composites have been successfully demonstrated. Other approaches aim for an extended heat transfer area between the heat carrier and the PCM. This can be achieved by the encapsulation of the PCM. The capsules provide a large heat transfer area for the surrounding heat carrier fluid (e.g., water or air). Another demonstrated approach is the utilization of finned heat carrier tubes to increase heat transfer. Other conductive structures inserted in the PCM have been also examined.

Principles of Chemical Heat Storage

Reversible thermochemical reactions can be used for storing thermal energy [9, 14]. The energy is stored in the form of chemical compounds created by an endothermic reaction and it is recovered again by recombining the compounds in an exothermic reaction. The heat stored and released is equivalent to the heat (enthalpy) of reaction.

The enthalpy of reaction, generally, is much larger than the enthalpy of transition (in latent heat storage) or the sensible heat stored over a reasonable temperature span. The storage density (based on solid mass or volume) is much larger for thermochemical storage materials than for latent or sensible heat storage materials. Table 4 shows materials for the storage of chemical heat, their temperature of reaction, and their heat of reaction related to the educt reactant. The determination of the volumetric energy density of the system Δh_{sys} shows that storage of gaseous reaction products at 50 bar results in a low Δh_{sys} compared to the volumetric energy density of the educt $\Delta h_{r,educt}$. On the other hand, storage of liquid (or liquefied) reaction products or utilization of atmospheric gases (e.g., O_2) leads to a high volumetric energy density of the system Δh_{sys}.

The reversible reactions suitable for heat storage can be classified into thermal dissociation reactions and catalytic reactions.

Gas–Solid Dissociation Reactions

Certain solid or liquid compounds can undergo dissociation reactions when they are heated. A gas is released

Thermal Energy Storage. Table 4 Temperature and heat of reaction of materials for thermochemical heat storage

Material	T_r (1 bar) (°C)	$\Delta h_{r,educt}$ (kJ/mol)	$\Delta h_{r,educt}$ (KWh/t)	$\Delta h_{r,educt}$[a] (KWh/m^3)	Δh_{sys}[a,b] (KWh/m^3)
Hydroxides					
$Mg(OH)_2 \leftrightarrow MgO + H_2O$	268	78	372	442	323
$Ca(OH)_2 \leftrightarrow CaO + H_2O$	521	100	373	410	324
$Ba(OH)_2 \leftrightarrow BaO + H_2O$					
Ammonium salt					
$NH_4HSO_4 \leftrightarrow NH_3 + H_2 + SO_3$	467	337	813	727	136
Salt hydrates					
$MgSO_4{\cdot}7H_2O \leftrightarrow MgSO_4 + 7H_2O$	122	411	463	389	272
$CaCl_2{\cdot}2H_2O \leftrightarrow CaCl_2{\cdot}H_2O + H_2O$	174	48	91	84	75
$CuSO_4{\cdot}5H_2O \leftrightarrow CuSO_4{\cdot}H_2O + 4H_2O$	104	226	251	287	216
$CuSO4{\cdot}H_2O \leftrightarrow CuSO_4 + H_2O$	205	73	114	163	142
Peroxide salts					
$BaO_2 \leftrightarrow BaO + ½O_2$	782	75	123	305	66
$KO_2 \leftrightarrow ½\ K_2O + ¾\ O_2$	668	101	395	423	64
Carbonates					
$CaCO_3 \leftrightarrow CaO + CO_2$	896	167	463	626	113
$BaCO_3 \leftrightarrow BaO + CO_2$	1,497	212	298	661	139
Metal hydrides					
$MgH_2 \leftrightarrow Mg + H_2$	293	79	834	605	41
$Mg_2NiH_4 \leftrightarrow Mg_2Ni + 2\ H_2$	253	128	319	–	–
Catalytic reactions					
$NH_3 \leftrightarrow 1/2\ N_2 + 3/2\ H_2$	195	49	799	546	21
$SO_3 \leftrightarrow SO_2 + 1/2\ O_2$	767	98	340	678	82
Reforming					
$CH_4 + H_2O \leftrightarrow CO + 3\ H_2$	687	205	1,672	n/a	23
$CH_4 + CO_2 \leftrightarrow 2CO + 2\ H_2$	687	247	1,143	n/a	24

The pressure vessel and other system components are not included
[a]Solids: assumed is a powder with 50% pore volume.
Liquids (stored below 50 bar): H_2O, NH_3, SO_3, SO_2.
Gases stored at 50 bar: H_2, O_2, CO_2, O_2, CO
[b]The volumetric energy density of the system Δh_{sys} is based on the volume of the reactant and products.

while the depleted solid or liquid remains in the reactor (endothermic reaction, i.e., *charging of the store*). The reverse reaction will occur spontaneously if the equilibrium is changed by a temperature decrease or a pressure increase. Therefore, the dissociation products have to be separated and stored individually. For *discharge*, in the exothermic reaction, the gas is recombined with the solid or liquid.

In general there are various types of gas–solid reaction systems that can be used for thermochemical energy storage. Among them are:

- Dehydration of metal salt hydrates (application in the range of 40–260°C)
- Dehydrogenation of metal hydrides (application in the range of 80–400°C)
- Dehydration of metal hydroxides (application in the range of 250–800°C)
- Decarboxylation of metal carbonates (application in the range of 100–950°C)
- Thermal deoxygenation of metal oxides (application in the range of 600–1,000°C)

The dissociation of calcium hydroxide ($Ca(OH)_2 \leftrightarrow CaO + H_2O$) has been investigated and reversibility of the reaction could be proven with a reaction enthalpy of 100 kJ/mol and an equilibrium temperature of 521°C at 1 bar. DLR is investigating this reaction system since several years, as especially its temperature range as well as the low material costs and its availability show promising potential for later large-scale application in solar trough power plants [15]. Complete reversibility as well as cycling stability could be shown by thermal analysis.

Concerning central air receivers, a recent project led by General Atomics in cooperation with DLR explores the experimental feasibility of using different multivalent solid oxides for high-temperature thermochemical heat storage [16]. One of the identified promising candidates for such a thermochemical storage system is based on manganese oxide redox reactions [17, 18]: $6\,Mn_2O_3 \leftrightarrow 4\,Mn_3O_4 + O_2$. This step is thermodynamically favorable at relevant temperatures for application with a central air receiver and has a reaction enthalpy of 31.8 kJ per mol of Mn_2O_3.

Catalytic Reactions

These are usually gas – gas reactions. A catalyst is required to obtain high reaction rates. The reaction products are transported in a pipeline from the charging source to the consumer (discharging sink). This system is called chemical heat pipeline or chemical heat pipe.

Thermochemical storage by heterogeneously catalyzed gas phase reactions has been demonstrated for the catalytic dissociation of ammonia in a 15 kW solar reactor by the Australian National University where solar heat is used to dissociate NH_3 into nitrogen and hydrogen [19]. The stored heat is retrieved by recombination of N_2 and H_2 to form ammonia. A closed thermochemical cycle for solar-driven methane reforming was successfully tested in a directly irradiated solar reformer in 280 kW scale in a joint project between the Weizmann Institute in Israel and DLR [20]. The main drawback of the approach of heterogeneously catalyzed gas phase reactions is the requirement to separate, compress, and store gases thus adding to the cost and complexity of the process.

Thermal Energy Storage for Concentrated Solar Power

Regarding electric grid and quality of bulk power supply, it is the ability to provide dispatch on demand that makes solar thermal power stand out from other renewable energy technologies like PV or wind. Thermal energy storage systems store excess thermal heat collected by the solar field (Fig. 5). Storage systems, alone or in combination with some fossil fuel backup, keep the plant running under full-load conditions. Improvements on operational flexibility and energy dispatchability by thermal storage and hybridization are identified as key technology objectives for R&D development. The capability of storing high-temperature thermal energy leads to economically

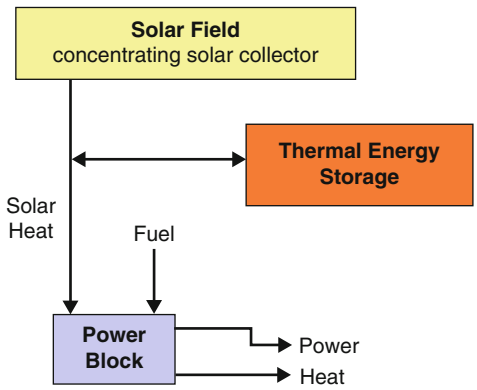

Thermal Energy Storage. Figure 5
Basic layout of a solar thermal power plant with integrated thermal energy storage

competitive design options, since only the solar part of the plant has to be oversized. This solar thermal power plant feature is tremendously relevant, since penetration of solar energy into the bulk electricity market is possible only when substitution of intermediate-load power plants of about 4,000–5,000 h/year is achieved.

From a technical point of view, the storage must have high energy density, good heat transfer between the heat transfer fluid (HTF) and the storage medium, mechanically and chemically stable storage media, compatibility between the heat exchanger, heat transfer fluid and storage medium, complete reversibility, and minimum thermal losses. In a TES system, heat can be stored in the form of sensible, latent, or thermochemical energy.

The option to integrate cost-effective storage systems directly into the facilities represents a significant advantage of solar thermal power plants over other concepts using renewable energy sources. Storage capacity allows not only demand-oriented electricity generation, by compensating fluctuation in solar insolation caused by cloud passing. Storage units facilitate the control of systems using concentrated solar power. Storage systems support the adaptation of power cycles or industrial processes, permitting usually only slow thermal transients, to the energy flow provided by the solar collectors, which can show very fast variations since only the direct irradiation is used.

Only in the first of the early solar thermal power plants built between 1985 to 1991 in the USA, storage capacity was integrated. The focus in this initial phase was mainly on the development of collector components. Many of the commercial solar thermal power plants being developed or under construction in Spain include storage capacity. In order to minimize financial risk, the most mature storage technologies (molten salt storage or steam accumulators) were chosen for these facilities. In parallel, research activities aiming at increased efficiency, reduced investment costs, and extended operation temperature range have been initiated.

Classification of Thermal Storage Systems

Concentrated solar heat is used for electricity generation and process heat applications. While the maximum temperature of the working fluid strongly depends on the application, the minimum temperature usually exceeds 100°C. Consequently, liquid water at atmospheric pressure cannot be used as storage medium; experiences from low-temperature systems intended for heating and cooling cannot be applied. For medium- and high-temperature thermal energy storage various basic concepts have been suggested. These concepts can be described by various technical criteria. Among these the most important are:

- Thermal power provided during the discharging process, power transferred during the charging process
- Capacity of the storage unit, i.e., total energy provided during the discharge process
- Temperature of heat provided during the discharge, maximum temperature accepted during charging process
- Frequency of charging/discharging cycles
- Reaction time needed to provide nominal load
- Thermal losses, parasitic power needed during charging/discharging process
- Exergetic efficiency

The multitude of criteria makes a direct comparison of storage systems difficult. Values like thermal power or temperature might also be time-dependent for certain storage concepts. Storage units must be adapted both to the energy source (solar collectors) and the consumer (thermal process). Since different types of solar collectors can be combined with various thermal processes, the resulting systems show specific requirements regarding the integration of a storage unit. Consequently, a general rating identification of the most promising concept is not possible; the selection depends on the specific application.

Thermal Energy Storage Concepts

This survey focuses on storage systems operated at temperatures exceeding 100°C and intended for applications requiring thermal power between 100 kW (solar process heat application) and several hundreds of MW (solar thermal electricity). Basic concepts proposed for such applications can be divided into systems applying a direct storage of the working fluid used in the solar collector and indirect systems transferring energy to a separate storage medium as shown in Fig. 6 [21, 22]. The simplest concept uses an additional volume of hot working fluid to store energy. This concept is usually

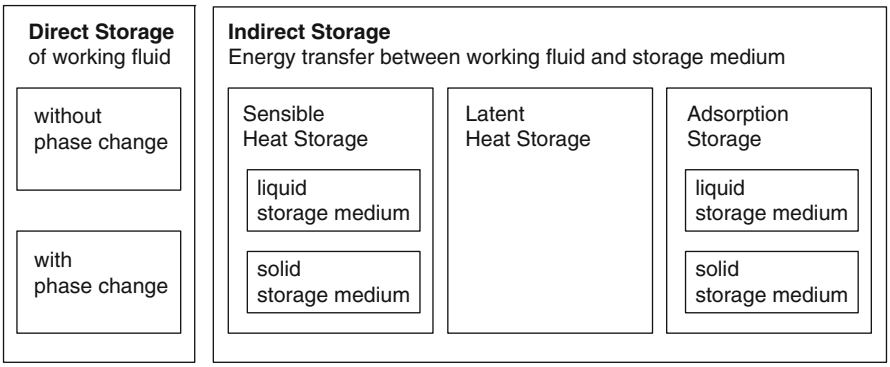

Thermal Energy Storage. Figure 6
Basic storage concepts under consideration for systems using concentrated solar power

only cost-effective if storage is possible at atmospheric pressure, the partial pressure of the working fluid at storage temperature should be low. In a modification of this concept, the working fluid undergoes a phase change during the charging/discharging process.

Many working fluids cannot be directly stored; the energy must be transferred to a separate storage medium. Dependent on the physical principle used for changing the energy content of the storage material, sensible heat storage can be distinguished from latent heat energy storage and adsorption concepts. While indirect sensible storage has already reached commercial status, latent heat storage has recently reached pre-commercial status. Various latent heat storage materials showing different melting points can be composed to form a cascaded system. Sensible heat storage systems and latent heat storage systems can also be combined to benefit from the specific advantages of both concepts. In addition to the aforementioned concepts, sorption systems using energy changes related to adsorption/desorption processes are considered for energy storage, but for temperatures relevant for concentrated solar power an application seems not to be imminent. This is also true for chemical storage concepts, where questions concerning reversibility and efficiency have to be clarified.

Direct Storage of Liquid Working Fluid

The various storage concepts show different states of maturity. Due to cheap fossil fuel available as backup source and limited requirements concerning dispatchability, the extent of storage capacity integrated in early commercial solar thermal facilities was limited. For the initial installations, concepts based on a direct storage were preferred representing a low-risk approach demanding limited development effort. The cost efficiency of storage concepts is strongly related to the frequency of charging/discharging cycles. The focus is currently on systems compensating transients caused by clouds and on systems for daily charging/discharging system. Seasonal storage is not considered to be cost-effective within the near future.

Among the nine parabolic trough power plants SEGS I- SEGS IX built in California between 1985 and 1991, only SEGS-I was equipped with a storage unit allowing the operation of the 14 MW_{el} plant for about 3 h (Fig. 7) [23]. In contrast to the later SEGS-plants, SEGS-I uses a mineral oil as heat transfer medium in the solar collectors, which is significantly cheaper than the synthetic VP1 oil applied in the other SEGS plants. The relatively low-cost mineral oil allowed the direct storage in an additional volume of hot heat transfer fluid. This approach is not cost-effective with VP1 not only due to the higher costs of the heat transfer fluid: At 400°C VP1 requires a pressure of about 11 bar, so a pressure vessel is needed for storage. In SEGS-I about 3,260 m^3 mineral oil were stored in the hot tank at a temperature of 307°C. The storage system was damaged by a fire in 1999.

The second example for large-scale direct energy storage is the Solar Two central receiver power plant

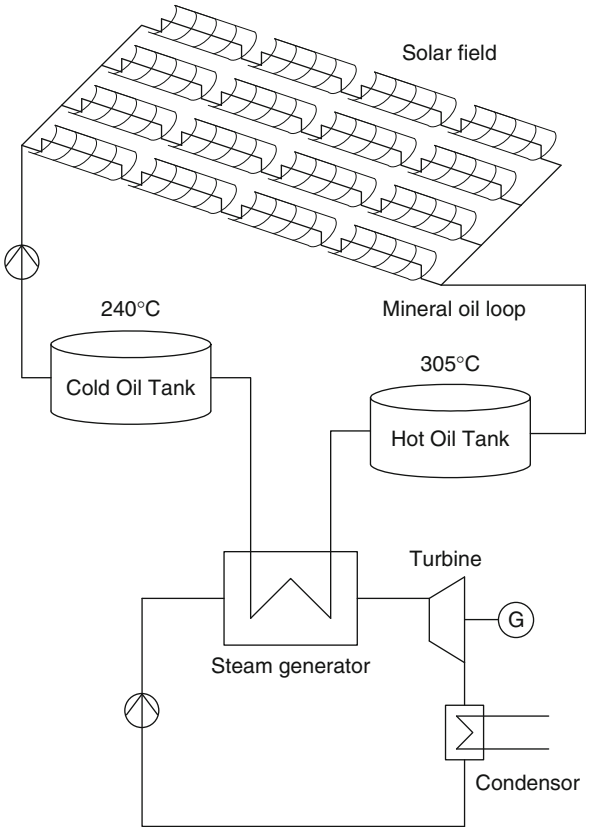

Thermal Energy Storage. Figure 7
Simplified scheme of SEGS-I parabolic trough plant with direct storage of heat transfer fluid

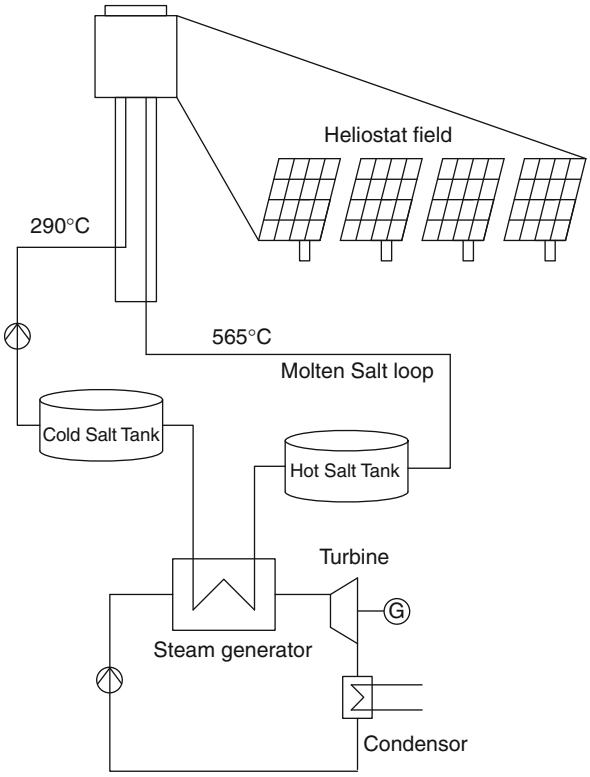

Thermal Energy Storage. Figure 8
Simplified scheme of Solar Two power plant with central receiver and direct storage of molten salt used as heat transfer fluid

using molten salt as a heat transfer fluid (Fig. 8). This demonstration power plant was erected in 1994 on basis of the Solar One facility and was operated until 1999. The maximum electrical power was 11 MW, the two-tank storage system with a total volume of about 1,700 m^3 had an inventory of 1,400 t of a mixture of molten sodium nitrate (60% by weight) and potassium nitrate (40% by weight). The thermal capacity of the storage system operated between 565°C and 290°C was 107 MWh, allowing the operation of the turbine for 3 h [24].

Direct Storage with Phase Change (Steam Accumulators)

While today's application of energy storage in the process industry is still limited, almost the complete existing capacity is based on steam accumulator technology. Here, the unique thermal storage ability of liquid water is applied by using pressure vessels as storage tanks (Fig. 9). Steam accumulators are charged by condensation of steam fed into the pressurized liquid volume [25, 26]. Since the pressure vessel is filled with saturated liquid water, the pressure increases during the charging process. During the discharge process the pressure in the storage vessel is decreased and saturated steam is extracted. The storage capacity corresponds to the variation of sensible energy of the liquid volume during the discharging process. Since the water in the volume is in the saturation state, a change in temperature is correlated to a change of pressure of the saturated steam provided during the discharge process. While a larger decrease of pressure is advantageous regarding the volumetric storage capacity, the acceptable pressure

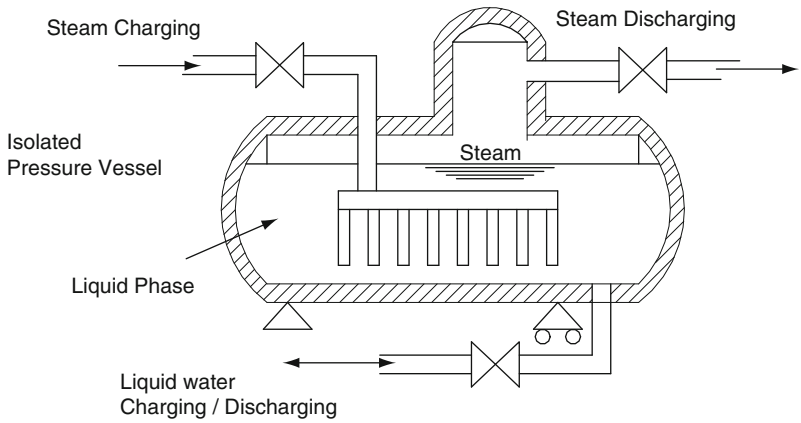

Thermal Energy Storage. Figure 9
Scheme of a steam accumulator

variation might be limited by efficiency considerations. Due to the logarithmic correlation between saturation pressure and saturation temperature, the absolute reduction of the pressure during the discharge process is increased at higher pressure levels to provide the same energy. The cost-effective capacity of steam accumulators is limited by the size of pressure vessel. Due to the short reaction time this concept can be used as buffer storage to compensate cloud passing or to support other storage concepts, which show a larger storage capacity and require a longer start-up procedure.

The PS10 central receiver power plant, representing the first European commercial solar thermal power plant starting operation in 2007, uses a steam accumulator for compensation of cloud transients. Four tanks with a total storage capacity of 20 MWh enable a 50% load operation of the 11 MW_{el} for about 50 min. The storage system is charged with saturated steam at 45 bar; during the discharge process saturated steam is provided at variable pressure.

Indirect Storage Concepts

Direct storage is not a cost-effective solution for all working fluids used in solar absorbers. Synthetic heat transfer oil is used to operate the parabolic troughs at temperatures up to 400°C, but this heat transfer fluid is too expensive for direct storage. Superheated steam and hot air show a very low volumetric energy density, so direct storage in pressure vessels is not practical. Storage systems for these working fluids use a separate storage medium. Pressurized working fluids (synthetic oil, steam) utilize a heat exchanger to transfer the energy between working fluid and storage medium. Efficient indirect energy storage demands the minimization of the temperature difference between the heat transfer fluid and the storage medium. Since both single-phase fluids (e.g., thermal oil, air, molten salt) and two-phase fluids (e.g., steam) are used as heat transfer medium in the solar collectors, the corresponding storage systems use either single-phase storage media (sensible heat storage) or two-phase storage materials (phase change materials, PCM). It is difficult to compare single phase and two phase storage systems on a component level. The storage performance depends on the integration in the overall process. Hence, it is recommended to compare single phase and two phase approaches on a system level. In contrast to low-temperature heating applications, the higher volumetric energy density of PCM systems is usually not relevant as criterion for concentrating solar systems, since necessary space is only of minor importance.

In all indirect storage concepts the maximum temperature of the working fluid is lower during the discharge process than during the charging process due to the unavoidable necessary temperature difference between working fluid and storage material. The minimization of this decrease and cost-effective design of the heat exchanger is a central issue for all indirect storage concepts.

Indirect Storage in Solid Media Sensible heat storage in solid media requires the integration of a heat exchanger into the storage material. While capacity-related costs play an important role in the selection of storage media, other requirements result from the integration of the heat exchanger, since the investment for the tubes and manifolds represents a significant share of total costs. The optimization of the geometry of the heat exchanger is essential for a cost-effective storage system. The thermal heat conductivity and the volumetric storage capacity of the storage material determine the needed surface area of the heat exchanger. Additional aspects are the thermal expansion rate of the storage material, which should be similar to the material used for the heat exchanger to limit thermal stress. The storage material should show a high cycling stability. Considering the various selection criteria, high temperature resistant concrete was identified as promising storage material [1]. Table 5 shows some of the relevant properties.

The storage capacity of sensible storage systems depends on the temperature variation during the charging process: figures for capacity-specific costs for the storage material require the definition of the temperature variation in the storage material during the discharge process. This value is also slightly influenced by the temperature range, since the specific heat capacity is temperature dependent.

During recent years, concrete storage systems intended for parabolic trough power plants using synthetic oil as heat transfer fluid have been developed. This storage unit is operated between 290°C and 390°C with daily charging/discharging cycle (Fig. 10). For this application, a parallel tube heat exchanger design using a concrete with quartz aggregates and a low level of binder made of blast furnace and flue ash is considered to be the most cost-effective solution. In order to increase the thermal conductivity, several alternative material options have been examined. Additives included metal splinters and graphite powder. So far, these approaches did not show an economic advantage. The integration of heat transfer enhancement structures within the concrete block has also been researched. It was found that the additional costs outweigh the benefit of this approach.

The optimization of the operation strategy offers an option for improving the efficiency of a solid medium storage. If the mass flow rate through the storage and the inlet temperature is kept constant during the charging process, the temperature at the outlet of the storage unit increases dependent on the charging state. Usually, this temperature is limited to avoid damaging of the absorbers. Consequently, the charging must be stopped, the capacity of the storage unit cannot be utilized completely. By applying modular storage units, the usable storage capacity can be increased. An improved adaptation of the storage to the demands of the power cycle during the discharging process results in a further increase of the usable capacity [2].

A test module with a capacity of 350 kWh was connected to parabolic trough collectors of the Plataforma Solar de Almeria and operated successfully during summer 2003. Long-term stability of the concrete storage approach was proven by operation of an enhanced storage module from 2008 to 2010 (Fig. 11). While these test units were operated with synthetic oil as heat transfer medium, concrete storage is also considered for application with superheated steam. A second-generation concrete storage module with a capacity of about 300 kWh is being built and tested for operation with steam at 100 bar and 500°C [27].

Thermal Energy Storage. Table 5 Properties of high-temperature concrete used for sensible heat storage

Density at 370°C (kg/m^3)	2,250
Specific heat capacity at 370°C (J/kgK)	1,100
Thermal conductivity at 370°C (W/mK)	1.3
Coefficient of thermal expansion at 370°C (10^{-6}/K)	11.6
Capacity (kWh/m^3·K)	0.68
Capacity specific costs ($/kWh) (only storage material, ΔT = 100 K)	1.8

Indirect Storage in Liquid Media Indirect storage in liquid media allows the separation of storage medium and heat exchanger; the size of the heat exchanger is only determined by the necessary power and not by the capacity of the storage unit. Since the area-specific power density is higher, using liquid storage media usually requires smaller heat exchangers than using

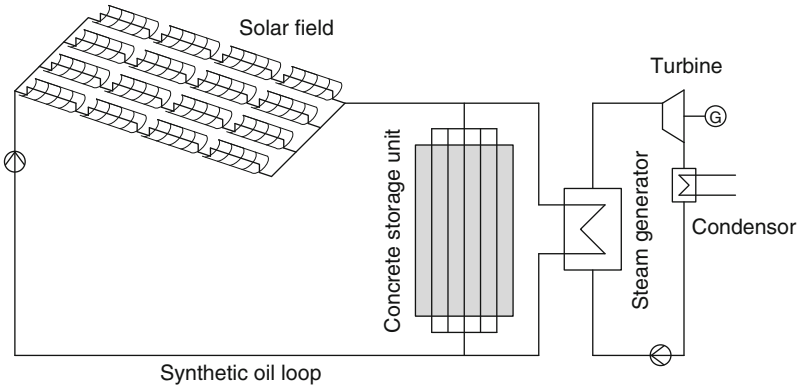

Thermal Energy Storage. Figure 10
Simplified scheme of a parabolic trough power plant with integrated concrete storage

Thermal Energy Storage. Figure 11
Photo of a concrete storage module during long-term testing

solid storage media with embedded heat exchanger. A significant advantage of liquid media storage is the simple operation strategy, because the temperature can easily be kept constant during the discharge process.

Table 6 shows the relevant properties for some potential liquid storage media. Regarding costs, safety aspects, and thermal stability within the relevant temperature range, nitrate salts and nitrite salts are the preferred candidate fluids for liquid energy storage. The application of these salts requires the consideration of the lower temperature limit defined by the melting temperature and the maximum temperature limit resulting from thermal stability. Freezing must be prevented in the piping, the heat exchanger, and in the storage tanks.

The advantage of using molten salt storage systems is the availability of experiences from the Solar Two project. Since this concept is considered as already proven, it was selected for the Andasol power plants using parabolic trough technology [28]. The schematic layout of the plant is shown in Fig. 12.

At present, the two-tank molten salt storage is the only commercially available concept for large thermal capacities being suitable for solar thermal power plants. In the Andasol I plant 28,500 t of molten salt (60 wt.% NaNO3, 40 wt.% KNO3) are stored in two tanks with a total volume of 32,600 m^3 and are operated between 385°C and 290°C. It presents a 7.5 h storage system providing energy to generate 50 MW electrical power. Plant operation was started in 2009 [29]. Based on the favorable experience with the Andasol storage systems, the molten salt storage approach is applied to Andasol II and III plants as well to further parabolic trough plants in Spain. Detailed characteristics and experience with the two-tank system are well documented [29, 30].

Limitations of molten salt storage are high costs of the storage media, the high melting point of molten salts that lead to the need for freeze protection and risk of corrosion. Figure 13 shows the main expense fractions. This shows that the salt inventory and the tanks have significant cost-reduction potentials.

However, specific storage costs can be reduced considerably, when the storage is implemented in systems with larger temperature differences, as the

Thermal Energy Storage. Table 6 Data for media considered for liquid storage of sensible heat

	Application range (°C)	Specific heat capacity (J/(kgK))	Density (kg/m^3)	Capacity (kWh/m^{3}K)	Specific costs – only storage material ($/kWh) (ΔT = 100 K)
KNO3–NaNO3(eu)	222–540	1,400	2,000	0.77	12.5
KNO3–NaNO2–NaNO3(eu)	142–540	1,400	2,000	0.77	22.5
Mineral oil	0–320	2,900	700	0.56	42
Synthetic oil (pressurized)	20–400	2,450	750	0.68	58

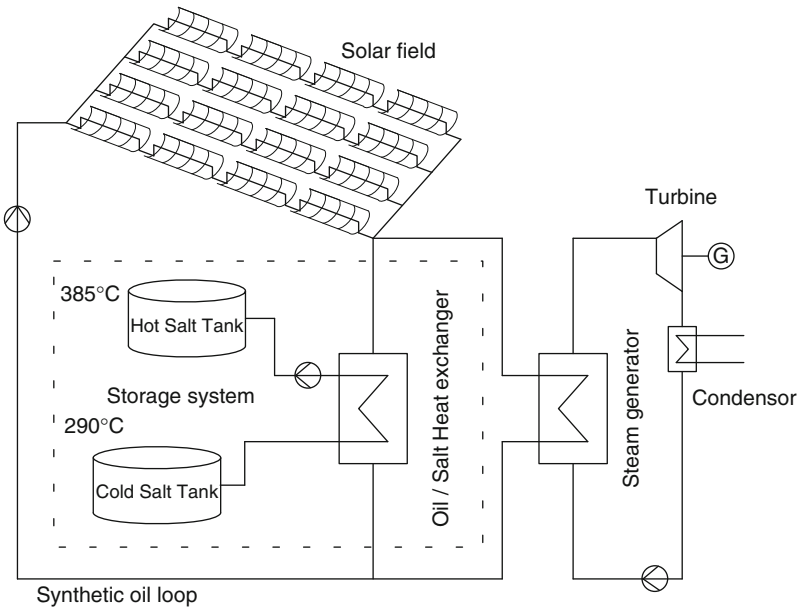

Thermal Energy Storage. Figure 12
Simplified scheme of a parabolic trough power plant with indirect storage system using molten salt

capacity of a molten salt storage is directly proportional to the temperature difference between the hot and the cold tank. In this context, the commercial solar tower power plant Gemasolar in Andalusia, Spain is an example. The construction of the plant was completed in 2010 and the start of operation is scheduled for 2011 [31]. In this power plant, the first commercial direct two-tank system will be realized.

Indirect Storage with Phase Change Materials
Phase change materials (PCM) are used for energy storage with little temperature variations of the storage material. Most PCM systems use the energy associated with melting or solidification processes. This energy is transferred at nearly constant temperature, characteristic energy densities of storage materials are in the range of 50–200 kJ/kg. This latent heat corresponds to a change of sensible energy resulting from a temperature change of 100–150°C for a typical storage material. While PCM systems usually show a higher complexity than sensible heat storage units, they are preferred for systems using steam in absorbers, since during the isothermal condensation and evaporation processes the temperature difference between steam and storage material can be kept small (Figs. 14, 15).

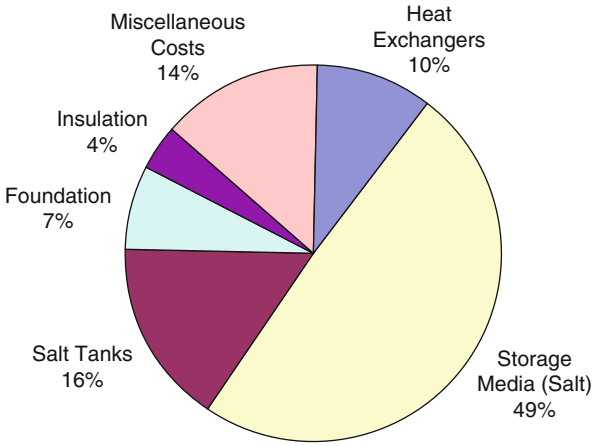

Thermal Energy Storage. Figure 13
Distribution of investment costs for an indirect two-tank storage system [28]

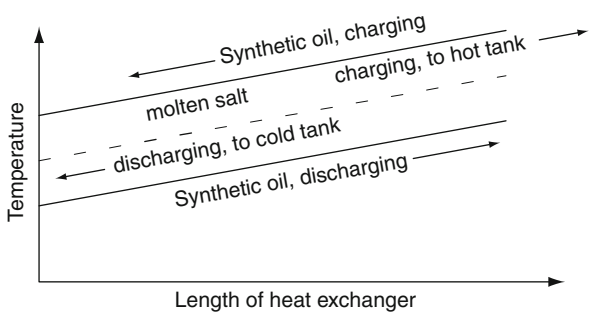

Thermal Energy Storage. Figure 14
Heat transfer in an indirect storage system using synthetic oil as heat transfer fluid and molten salt as storage medium

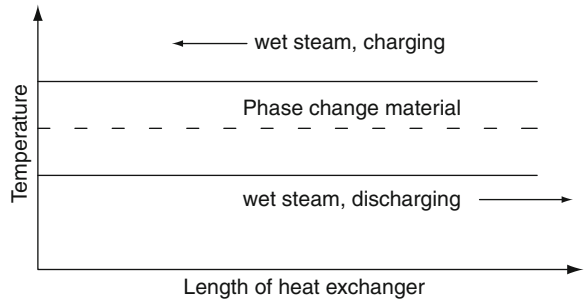

Thermal Energy Storage. Figure 15
Heat transfer in an indirect storage system using saturated steam as heat transfer fluid and PCM as storage medium

Thermal Energy Storage. Table 7 Selected materials with melting temperatures in the range relevant for solar thermal power plants and solar process heat applications using steam

Storage media	Melting temperature (°C)	Capacity-specific costs ($/kWh) only material, only latent heat	Heat conductivity (W/[m K])
Tin	232	900	60
Lead	327	150	35
Nitrate/ nitrite salts	130–350	20	0.5

A first selection of candidate storage materials results from the melting temperature, which should be adapted to the specific process. In systems using steam as working fluid, the melting temperature should be close to the saturation temperature resulting from the operation pressure. For concentrating solar systems with operation pressures in the range 1–120 bar, the required melting temperatures are between 100°C and 325°C. Tables 3 and 7 show selected materials with melting temperatures in this range.

With respect to costs, nitrate and nitrite salts and their mixtures are considered to be the most promising candidate materials for PCM storage. These salts can be applied either as pure substances or as (eutectic) mixture of two or more components. While a large number of systems have been suggested as PCM [32], due to aspects like environmental compatibility, hygroscopicity, or cycling stability, a limited number of substances are considered to be of practical use; three examples are shown in Table 8.

The relatively poor thermal conductance represents the major drawback of these salts. This is the dominant problem complicating the implementation of cost-effective PCM systems due to low volumetric power density. PCM systems exceeding temperatures of 100°C have long been limited to lab-scale experiments. If a heat exchanger is embedded in the storage volume, pure PCM requires a very large heat transfer area resulting in high investment costs. The successful demonstration of direct steam generation

Thermal Energy Storage. Table 8 Properties of selected nitrate salts as PCM

Storage media	Melting temperature (°C)	Heat of fusion (kJ/kg)	Density (kg/m^3)	Capacity latent heat (kWh/m^3)	Costs ($/kWh) only material, only latent heat
KNO_3–$NaNO_3$(eu)	222	100	2,000	55	17.5
KNO_3–$NaNO_2$–$NaNO_3$(eu)	142	60	2,000	33	52.5
$NaNO_3$	306	175	1,900	96	9.5

in parabolic troughs gave rise to an increased demand for PCM storage. The focus of the research activities during the last years [13] were directed to:

- Macro-encapsulation of PCM in small containers stored in pressurized steam volume
- Composite materials made of PCM and an additional material showing high thermal conductivity (e.g., graphite)
- Integration of heat transfer structures into the storage volume to enhance the heat transfer within the PCM

The integration of an internal heat transfer structure has been identified as the most promising concept. The so-called Sandwich concept uses thin plates arranged perpendicular to the axis of tubes of a parallel pipe heat exchanger embedded in the PCM volume. Candidate plate materials are expanded graphite showing a high thermal conductivity (>150 W/(mK)) or metals.

A pilot storage for solar plants with direct steam generation was designed and constructed using sodium nitrate ($NaNO_3$) with a melting temperature of 306°C as the phase change material. The PCM storage module uses the sandwich design with aluminum fins to reach the required high heat transfer rates and accordingly the required charge and discharge times. After successful testing of the lab-scale storage, the design was scaled up to about 14 t of salt with a latent heat capacity of approx. 700 kWh and adapted to the design parameters of the water/steam test loop (128 bar, 400°C) [33]. A picture of the PCM module is shown in Fig. 16. In contrast to previous test modules, the tube register is arranged vertically. As the sodium nitrate experiences a volume increase of approx. 10% during melting, an excess volume is provided for the liquid phase at the top of the storage. It needs to be ensured that there are open paths for the fluid to expand into this volume, which is accomplished by the vertical position of the tubes, where the salt melts first. Pressure losses

Thermal Energy Storage. Figure 16
Photo of a 700 kWh $NaNO_3$ PCM pilot storage with internal recirculation equipment

through the PCM storage module are very low, as the fluid flows through many parallel pipes of ca. 7 m length, resulting in low flow velocities.

In charging mode, steam with a temperature slightly above saturation properties (typically ~107 bar, ~320°C) is routed into the PCM module where it condenses. The flow direction during charging is from top to bottom so that the condensate is removed by gravity. A condensate drain assures that the medium leaves the module only in liquid form. The module is expected to be able to condense the full mass flow of 0.8 kg/s that the test loop can provide.

For discharging, the tube register of the PCM module is flooded with liquid water at a temperature just below saturation properties (typically ~81 bar, ~295°C). The saturated steam produced by the module during discharge is dried in a steam separator (spherical drum on the tower to the left of the insulated PCM module in Fig. 16). The liquid water from the steam separator is recirculated either by natural recirculation or by a pump. During discharge, the flow direction is from bottom to top.

If superheated steam is generated in the solar collectors, both single phase (preheating, superheating) and two-phase (evaporation) heat transfer takes place. The corresponding storage system must allow both sensible and isothermal storage to be efficient. The conceptual layout of such modular storage system for storage and generation of superheated steam is shown in Fig. 17.

Regenerator Storage for Solar Central Receiver Plants

Central receiver power plants using air as a heat transfer medium offer the potential to particularly cost-effective solutions with high conversion efficiencies [34–36]. Also, the suitable heat storage technology – regenerator storage based on directly heated solid media – has a simple setup, is applicable to highest temperatures and has best prospects for a deployment in large installations [37, 38]. These aspects indicate good opportunities for a near-term commercialization.

However, for a successful market introduction, efficient and up-scalable solutions for the heat storage are a prerequisite. Storage regenerators are well suited to the needs, but need further investigations to clarify open questions concerning design and materials. Though first concepts have been looked at in the early 1990s, the status of this storage application is still at an early stage.

Initial designs and tests for atmospheric receivers have been carried out by the German TSA consortium.

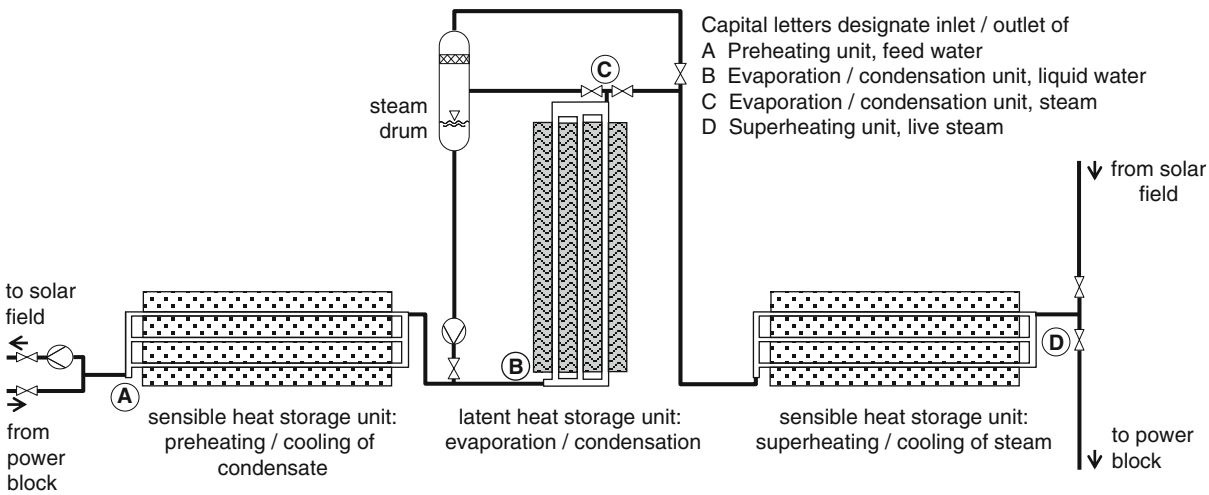

Thermal Energy Storage. Figure 17
Overview of a modular thermal energy storage system for DSG combining sensible and latent heat storage

For that purpose, a test facility, including a thermal storage, was erected in Spain in 1991. However, rather than aspects of storage design, the system demonstration was in the focus of work. The storage was based on a packed bed of aluminum oxide in spherical shape, providing a thermal capacity of about 1 MWh. Though fully functional, this concept turns out not to allow a direct scale-up to commercial size: high costs for the high-purity aluminum oxide and increased thermally induced mechanical loads during cyclic operation represent the main barriers.

The heat storage of the recently commissioned solar tower plant in Jülich, Germany uses refractory in a stacked arrangement and therefore avoids such mechanical issues [39]. The Solar Power Tower Jülich is an experimental central receiver plant, inaugurated in 2009 to serve the needs of a further development of this technology. Erection and operation of the plant are accompanied by a research program with the objective to cover remaining uncertainties of design and operation and to further promote the development of the technology toward a commercial deployment [39, 40]. As a part of this work program also heat storage operation and design are addressed.

The plant uses an open volumetric receiver technology. In its primary cycle, air at atmospheric pressure is heated up to temperatures of about 700°C. This solar heat then powers a steam generator, producing steam at 100 bars and 500°C and driving a 1.5 MW_{el} turbine-generator set. In parallel to the steam generator and receiver, the heat storage is integrated into the power cycle, see Fig. 18 below. It is implemented as an air-cooled regenerator storage, an installation that is still unique in this application.

The design of the storage was derived from industrial applications of thermal exhaust air purification. These RTO (regenerative thermal oxidizer) systems are applied to purify air from volatile organic compounds through an exothermic process taking place inside a regenerator's heat exchanging ceramic inventory at temperatures up to 1,100°C. The storage is located within the plant's tower. It extends over two stories, close to the locations of receiver and steam generator.

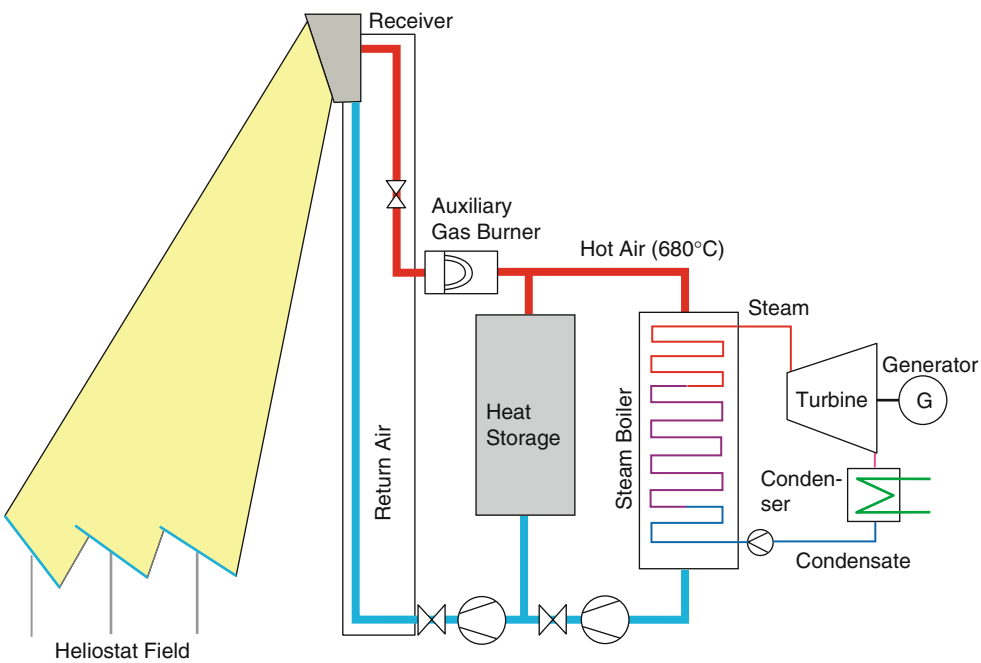

Thermal Energy Storage. Figure 18
Schematic plant layout of solar power tower with integrated regenerator storage

At rated operation conditions, the storage system is cycled between 120°C and 680°C and supplies a storage capacity of almost 9 MWh. Further technical specifications include data for the discharge heat rate, discharge duration, and permissible outlet temperature variations as summarized in Table 9.

During charge operation the hot air from the receiver enters the storage's dome and flows downward through the storage chambers, forming a moving temperature profile as typically found in regenerator storage. Reversing the flow direction through the storage starts discharge operation and supplies heat to the steam generator's air loop.

Thermal Energy Storage. Table 9 Specifications of an air-cooled regenerator storage

Inlet temperature (charge/discharge)	680°C/120°C
Outlet temperature (charge/discharge)	680–640°C/120–150°C
Charge mass flow	9.4 kg/s
Discharge heat rate	5.7 MW_{th}
Full load discharge period	1.5 h
Pressure loss	<1,500 Pa

Full functionality of the storage subsystem was confirmed during a test campaign performed in 2010: Standstill operation shows that thermal losses are kept at a low level (Fig. 19). Cycling operation at high heat rates levels could be performed as expected for charge and discharge operation. The successful installation and testing experience is considered an important step toward a further development of this storage technology. Present results support the view that the technology represents a promising basis for up-scaled implementations in solar applications and beyond.

On that way, further aspects need to be addressed. This includes a better understanding of internal air flow and flow distribution, design improvements in terms of heat transfer, losses, and cost efficiency, as well as the investigation of alternatives for the inventory arrangement, including packed beds and the potential for higher operation temperatures [40, 41].

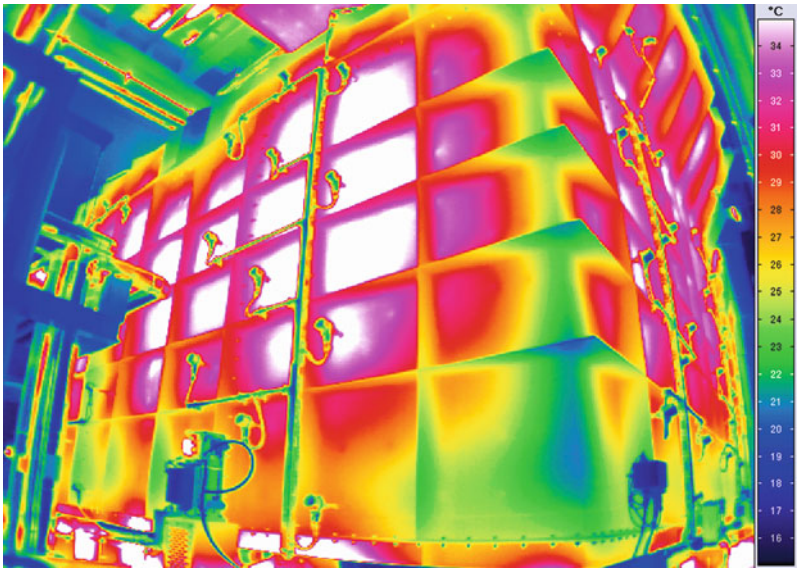

Thermal Energy Storage. Figure 19
Infrared image of the lateral storage surface during standstill

Future Directions

Current research topics are aiming at the development of advanced thermal energy storage systems having the capability to reduce the investment cost. New approaches are covering heat transfer fluids and storage materials with superior thermophysical properties as well as new concepts for improved heat transfer and storage design. Examples are:

- Binary and ternary liquid salts systems with low freezing point but thermal stability beyond 600°C
- Low-cost filler materials to replace expensive salt systems
- Thermally stable nanomaterials to improve thermophysical properties of liquids
- PCM materials with thermal conductivity beyond 10 W/mK
- New heat transfer concepts to decouple the functions of storage capacity and loading power
- Sensible heat storage with fluidized solid particles
- Adjustment of thermochemical heat storage for high-temperature application

Most of these approaches are still in the laboratory scale and need to be validated and proven for up-scaling to commercial scale. From the results important impact toward more efficient, reliable, and economic thermal energy storage systems can be expected.

Bibliography

1. Laing D, Steinmann W-D, Tamme R, Richter C (2006) Solid media thermal storage for parabolic trough power plants. Sol Energ 80:1283–1289
2. Laing D, Steinmann W-D, Fiß M, Tamme R, Brand T, Bahl C (2008) Solid media thermal storage development and analysis of modular storage operation concepts for parabolic trough power plants. J Sol Energ Eng 130:011006-1/5
3. Goldstein M (1961) Some physical chemical aspects of heat storage. In: U.N. Conference on new sources of energy, Rome, vol 35, pp 5–7
4. Telkes M (1974) Solar energy storage. ASHRAE J 16:38–44
5. Altmann M, Yeh H, Lorsch HG (1973) Conservation and better utilization of electric power by means of thermal energy storage and solar heating. Final summary report, NSF/RANN/SE/G/27976/PR 73/5, University of Pennsylvania
6. Lorsch HG (1974) Thermal energy storage. Final report, NSF/RANN/74–021C
7. Carlson B, Stymme H, Wettermark G (1978) Storage of low-temperature heat in salt-hydrate melts – calcium chloride hexahydrate. Swedish Council for Building. Research D 12
8. Ozawa T et al (1980) Screening of latent heat thermal energy storage materials by using evaluated thermodynamic data. In: 7th Codata international conference, Kyoto
9. Mar RW (1980) Material science issues encountered during the development of thermochemical concepts. In: Murr LE (ed) Solar materials science. Academic, London
10. Mehling H, Cabeza LF (2008) Heat and cold storage with PCM – an up to date introduction into basics and applications. Springer, Heidelberg
11. Bauer T, Laing D, Steinmann WD, Kröner U, Tamme R (2008) Screening of phase change materials for process heat applications in the temperature range 120 to 250°C. In: Proceedings of Eurosun, Lisbon, 7–10 Oct 2008
12. Tamme R, Bauer T, Buschle J, Laing D, Müller-Steinhagen H, Steinmann W-D (2008) Latent heat storage above 1208 C for applications in the industrial process heat sector and solar power generation. Int J Energ Res 32:264–271
13. Steinmann W-D, Tamme R (2008) Latent heat storage for solar steam systems. J Sol Energ Eng 130:011004-1/5
14. Wenthworth WE, Chen F (1976) Simple thermal decomposition reactions for storage of solar thermal energy. Sol Energ 18:205–214
15. Schaube F, Wörner A, Tamme R (2010) High temperature thermo-chemical heat storage for CSP using gas-solid reactions, Proceedings of SolarPACES 2010, Perpignan
16. Wong B, Brown L, Schaube F, Tamme R, Sattler C (2010) Oxide based thermochemical heat storage, Proceedings of SolarPACES 2010, Perpignan
17. Stobbe ER, de Boer BA, Geus JW (1999) The reduction and oxidation behaviour of manganese oxides. Catal Today 47:161–167
18. Zaki MI et al (1998) Thermochemistry of manganese oxides in reactive gas atmospheres: Probing catalytic MnOx compositions in the atmosphere of CO+O2. Thermochimica Acta 311: 97–103
19. Lovegrove K et al (2004) Developing ammonia based thermochemical energy storage for dish power plants. Sol Energ 76:331–337
20. Buck R et al (1994) Development of a volumetric receiver-reactor for solar methane reforming. J Sol Energ Eng 116: 73–78
21. Beckmann G, Gilli PV (1984) Thermal energy storage. Springer, Berlin
22. Dinter F, Geyer M, Tamme R (1990) Thermal energy storage for commercial applications. Springer, Berlin
23. Herrmann U, Kearney D (2002) Survey of thermal energy storage for parabolic trough power plants. J Sol Energ Eng 124:145–152
24. Pacheco JE (2002) Final test and evaluation results from the solar two project. Sandia National Laboratories, SAND2002–0120

25. Goldstern W (1970) Steam storage installation. Pergamon Press, Oxford
26. Steinmann WD, Eck M (2006) Buffer storage for direct steam generation. Sol Energ 80:1277–1282, Elsevier
27. Laing D, Bahl C, Fiß M (2010) Commisioning of a thermal energy storage system for direct steam generation. In: Proceedings. SolarPACES 2010, Perpignan, 21–24 Sep 2010
28. Kelly B, Kearney D (2006) Thermal storage commercial plant design study for a 2-tank indirect molten salt system. NREL/SR-550-40166
29. Relloso S, Delgado E (2009) Experience with molten salt thermal storage in a commercial parabolic trough plant. In: Proceedings of the SolarPACES 2009, Berlin
30. Kolb GJ (2010) Evaluation of annual performance of 2-tank and thermocline thermal storage system for trough plants. In: Proceedings of the SolarPACES 2010, Perpignan
31. Online newspaper library of Torresol Energy (2011) The innovative Gemasolar plant will be the main project of Torresol Energy at WFES 2011. Press release 11.01.2011. http://www.torresolenergy.com/TORRESOL/Press/torresol-takes-part-wfes-2011. Accessed 14 Mar 2011
32. Janz GJ et al (1979) Physical properties data compilation relevant to energy storage II. Molten salts: data on single and multi-component salt systems. NSRDS-National Standard Reference Data System
33. Laing D, Bahl C, Bauer T, Lehmann D, Steinmann W-D (2010) Thermal energy storage for direct steam generation. Sol Energ 85:627–633
34. Romero M et al (2002) An update on solar central receiver systems, projects, and technologies. ASME J Sol Energ Eng 124:98–108
35. Pitz-Paal R et al (2005) European concentrated solar thermal road-mapping (ECOSTAR): roadmap document. SES-CT-2003-502578
36. Price H (2002) Assessment of parabolic trough and power tower solar technology cost and performance forecasts. Sargent & Lundy, NREL/SR-550-34440
37. Haeger M et al (1994) Phoebus technology program solar air receiver (TSA). Operational experiences with the experimental set-up of a 2.5 MWth volumetric air receiver (TSA) at the plataforma solar de Almería. PSA-TR02/94
38. Fricker HW (2004) Regenerative thermal storage in atmospheric air system solar power plants. Energy 29:871–881
39. Zunft S, Hänel M, Krüger M, Dreissigacker V, Göhring F, Wahl E (2010) Jülich solar power tower – Experimental evaluation of the storage subsystem and performance calculations. In: Proceedings of the SolarPACES 2010 conference (SolarPACES 2010), Perpignan, 21–24 Sep 2010
40. Zunft S, Hänel M, Krüger M, Dreißigacker V (2009) High-temperature heat storage for air-cooled solar central receiver plants: a design study. In: Proceedings of the SolarPACES 2009, Berlin, 15–18 Sep 2009
41. Dreißigacker V, Müller-Steinhagen H, Zunft S (2010) Thermo-mechanical analysis of packed beds for large-scale storage of high temperature heat. Heat Mass Transf 46:1199–1207

Thermal Treatment of Waste: Key Element for Sustainable Waste Management

Paul H. Brunner
Institute for Water Quality, Resource and Waste Management, Vienna University of Technology, Vienna, Austria

Article Outline

Glossary
Definition of the Subject and Its Importance
Introduction
Today's Material Turnover Results in Large Volumes of Waste Requiring Appropriate "Final Sinks"
Goals of Waste Management and of Thermal Waste Treatment
Thermal Waste Treatment for Environmental Protection
The Contribution of Thermal Waste Treatment to Resource Conservation
Future Directions
Bibliography

Glossary

Atmophilic Characterizing an element that concentrates in the atmosphere.

Dioxin Short for di-benzo-dioxine, often substituted with various chlorine atoms such as 2,3,7,8-tetrachlorodibenzo-p-dioxin (TCDD).

Di-benzo-furan Dioxin with one of the two oxygen atoms replaced by a carbon–carbon bond.

PVC Polyvinylchloride

Transfer coefficient k_{Xi} Coefficient describing the partitioning of an element X among "i" products of incineration.

SEA Statistical entropy analysis (see Waste-to Energy (WTE): Decreasing the Entropy of Solid Wastes and Increasing Metal Recovery in this volume).

MSW Municipal solid waste, representing mixed waste that is collected by a given collection system. Since, in addition, other collection systems for recycling might be present too (paper, glass, metals etc.), MSW from different regions with different collection systems might vary even if consumption patterns are identical.

Definition of the Subject and Its Importance

Thermal treatment of waste is not an isolated process: It is part of waste management, energy supply, resource management, and environmental protection. It is linked to economic activities and requires financial, material, and human resources. Without thermal waste treatment, waste management cannot reach its goals. In fact, waste-to-energy (or incineration as it is called commonly in Europe) reduces significantly environmental pollution by persistent organic substances and, also, by some inorganic elements such as heavy metals. Hence, it is important to point out the contribution of waste incineration to sustainable waste management, and to show the potential and limitations of this technology in a broader view. This is even more relevant since the material turnover of modern societies has increased dramatically during the last century, making it necessary to apply powerful and safe technologies both at the front and back end of the material system.

Introduction

Waste management is an integral part of materials management. It serves as an important interface between the so-called anthroposphere (the man-made sphere or technosphere) and the environment [1]. Waste management ensures that harmful substances do not cross this border and that useful materials and energy are cycled back to the anthroposphere. In order to take effective and efficient measures in waste management, a certain knowledge of the material metabolism of the anthroposphere is necessary. A striking example is forecasting of waste generation: When the buildings stock and age distribution, plus certain economic parameters of a region, are known, the generation of construction wastes can be predicted. As another example, when the consumption, stocks, and lifetime of plastic materials are known, the amount and composition of plastic wastes to be treated by recycling and waste disposal can be easily assessed.

Also, in the case of hazardous substances, it is important to have a minimum knowledge of the anthroposphere: Which are the significant sources of heavy metals such as cadmium, lead, and mercury in wastes, and when and how legislation – such as a ban on mercury in batteries – can effect waste composition? Due to progress in science and technology, the anthropogenic metabolism is constantly changing, with new materials being introduced and increasing complexity of everyday goods. It is therefore necessary to look at the anthroposphere as a dynamic organism with rapidly varying flows (years) and slowly varying stocks (decades). This is also reflected in the amounts and composition of the generated wastes.

Hence, this entry starts with an overview of the material flows and stocks of the most important activities of the metabolism of the anthroposphere, emphasizing changes over time. It then focuses on the goals of waste management and points out the contribution of thermal treatment to waste management. While the focus is on municipal solid waste (MSW) and MSW combustion with energy recovery, most insights can be applied to the thermal treatment of other types of wastes. In particular, the goals of waste incineration, which are explicitly discussed in section "Goals of Waste Management and of Thermal Waste Treatment", are the same for all wastes.

The main objective of this entry is to point out that waste incineration is an indispensable constituent of every modern waste management system, because of the variety and complexity of materials used in the anthroposphere: While certain fractions can be recycled, there still remain large amounts of useless and hazardous materials that have to be converted into minerals by means of thermal treatment of the MSW.

Today's Material Turnover Results in Large Volumes of Waste Requiring Appropriate "Final Sinks"

The activity "to clean," defined as the separation of the "wanted" from the "unwanted," is a basic human need [1]. All organisms have to take up and excrete materials as a consequence of their metabolism. The food, drinks, and air consumed annually by human beings is about 6 Mg per capita; the resulting output amounts to about 1 Mg per capita of feces and urine and 5 Mg per capita of gas. This so-called physiological metabolism has been basically the same over thousands of years. Even with dietary habits evolving over time and representing differences in culture and economic development, the basic human mass flow is comparatively constant. However, the composition of this mass flow can change substantially, e.g., as

has been observed for the consumption of animal protein in affluent countries.

In addition to the physiological metabolism, modern man depends on the so-called anthropogenic or man-made metabolism. This includes the total material turnover of all goods necessary to sustain a modern standard of living. With the evolution from hunters and gatherers to today's service-oriented affluent societies, the material turnover of men has increased dramatically. Table 1 presents the per capita flows associated with the essential activities of humanity, in prehistoric and modern times. For the activities "to nourish," "to clean," and "to reside," only flows and stocks within private households are shown; the activity "to transport and communicate" also includes the fraction of materials used outside the household, such as roads and other infrastructure.

"To nourish" includes storage, preparation, and consumption of food, beverages, and air. "To clean" stands for the separation of wanted and unwanted goods in households and includes all cleaning processes such as laundry, dish washing, bathroom, vacuum cleaning, etc. The main material used is water mostly as a conveyor belt for dirt, feces, and urine. Materials included in "to reside and work" are mainly fuel (oil, gas, coal, and wood) and construction materials used to protect and shelter humans from the environment. The same materials are instrumental for the activity "to transport and communicate," comprising the transport of persons, goods, information, and energy by individual and public transport media on roads, rails, water, and airways, as well as cables, computers, and satellites.

While the total material turnover has increased by more than one order of magnitude, there has been little change in the "to nourish" activity while the activity "to clean" has experienced an extraordinary increase in mass flows, from less than 0.1 Mg to 60 Mg per capita per year. The same enormous increase has been experienced in the activities "to reside and work" and "to transport and communicate." In modern societies, the activity "to clean" implies the biggest material turnover. Due to the consumption of 60 Mg water per capita annually, modern households and cities experience a healthy environment, with no threats any more from waterborne diseases. The other side of the coin is the large amount of water and wastewater that have to be managed. It becomes evident that for the functioning of modern cities, wastewater management of 60 Mg per capita is more demanding than solid waste management of "only" 2.7 Mg per capita per year (Table 2).

Table 2 below shows the large material stocks that have been accumulated in order to fulfill human requirements. The growth of these stocks is impressive: If present growth rates continue in the future, the anthropogenic stock will double in about 100 years. However, it is doubtful that such a future growth is a realistic assumption. It has to be kept in mind that these activities serve human needs. While a certain material turnover supports human welfare and prosperity, too high a stock may become a heavy burden in terms of resource and financial requirements for maintenance, renewal, and upgrading. It is not known yet if there is an optimum size of anthropogenic stock beyond which the societal benefit becomes marginal or even negative.

Thermal Treatment of Waste: Key Element for Sustainable Waste Management. Table 1 Turnover and stock of materials for prehistoric and modern men (Data from [1])

	Material flows (Mg/capita/year)		Material stocks (Mg/capita/year)		Annual change in material stock (Mg/capita/year)	
Activity	Prehistoric	Modern	Prehistoric	Modern	Prehistoric	Modern
"To nourish"	5.6	5.7	0	<0.1	0	+ <0.1
"To clean"	<0.1	60	0	0.1	0	+ <0.1
"To reside and work"	<0.1	10	<0.1	100	0	+ 1
"To transport and communicate"	0	10	0	160	0	+ 2
Total	6	86	<0.1	260	~0	+ 3

Thermal Treatment of Waste: Key Element for Sustainable Waste Management. Table 2 Input, output, stocks, and stock changes of the most important activities of humanity, in Mg per capita per year [1]

Activity	Input	Output			Stock
		Wastewater	Off-gas	Solid residues	
"To nourish"	5.7	0.9	4.7	0.1	<0.1
"To clean"	60	60	0	0.02	0.1
"To reside and work"	10	0	7.6	1	100 + 1
"To transport and communicate"	10	0	6	1.6	160 + 2
Total	86	61	19	2.7	260 + 3

The data in Table 2 also shows implications relevant for waste management: The solid output of human activities in private households amounts to 2.7 Mg per capita annually. Another 3 Mg per capita are accumulated in anthropogenic stocks. In the future, when these 3 Mg per capita per year have reached the end of their life, they will become wastes. Therefore, it is clear that the amount of wastes to be managed will increase considerably in the future. This is particularly the case for wastes from construction and infrastructure. New measures to reduce the generation of wastes will not much influence the existing material stocks that inevitably will become wastes to be managed.

Table 2 shows the mass flows of materials used in various human activities. However, the quality of the materials used must also be considered. Today's consumer products and long lifetime goods (infrastructure, buildings) are highly complex mixtures of innumerable individual substances. These material combinations allow new and better functions of products, prolong the lifetime of goods, and improve their economic and environmental performance. Since 1939, the world production of chemicals has increased 400-fold, reaching close to 500 million Mg in 2010. As of this date, there are about 7 million known chemical substances. Close to 70,000 are produced for regular use in the industrial, agriculture, and service sector and of these, 5–10% are considered hazardous and about 200 are known to be carcinogenic.

Historically, the materials used were mainly of geogenic (stone, gravel, sand) and biogenic (wood, cotton, and other biomass) origin. Today, while stones, gravel, and sand are still used widely, most products contain metals and synthetic, fossil-based organic substances. As a consequence, during the last three centuries, wastes produced have changed from harmless geogenic and biomass materials to complex blends of degradable as well as persistent, man-made organic and inorganic materials. While in preindustrial times, hygienic problems associated with waste and waste water were of primary relevance, today's challenge has shifted: The biggest threat for men and environment from modern material turnover and resulting wastes are risks emanating from inappropriate handling of hazardous substances.

Thus, for modern anthropogenic metabolism, waste management must play a key role in

- Redirecting the huge amount of materials used by modern men back into a useful cycle (recycling)
- Providing facilities to safely dispose of the hazardous substances that are leaving the consumption process (safe disposal)
- Informing the manufacturing process regarding the use of substances and design of products (design for recycling and disposal)

In particular – since all materials extracted from the earth and the biosphere, or synthesized by humans, will turn into waste at one point – waste management must provide final sinks for these materials [2]. A "sink" stands for a process that receives waste materials and emissions from human habitat. The most important and powerful sink is the atmosphere which is a perfect conveyor belt for gaseous substances. Next comes the hydrosphere that collects salts and organic substances by rainwater in watersheds and transfers them into rivers that convey them to the sea. The soil also acts also as a sink for landfilled wastes, when sewage sludge

is applied to soil, and for airborne dust particles that settle on land.

Substances may be transported from one sink to another. Over long time periods, speciation of substances in soils, lakes, sediments, or landfills can change significantly due to natural as well as anthropogenic impacts, e.g., by means of eutrophication, acidification, or a shift in redox conditions. In addition to biogeochemical reactions, geological processes such as erosion, weathering, seismic activities, and landslides can relocate substances from one sink to another. Therefore, a sink such as a landfill may not be a long-term sink from a geological perspective.

Sustainable waste management requires that waste-derived problems are solved here and now, and that they are not deferred and passed on to the next generations. Thus, a so-called final sink is defined as a place on the planet where substances have residence times of over 10,000 years. This ensures that the resulting emissions are small and that the fate of a substance is more or less under control. Final sinks are, for instance, underground salt mines, ocean sediments, places on the ground where sedimentation prevails over erosion, etc.

For organic substances, there is a second category of final sinks. In contrast to passive natural final sinks, active "final sink" reactions transform organic substances rapidly into other substances, such as metabolites. In the case of mineralization, the end products are carbon dioxide, water, and –depending on the composition of the initial material – other products such as hydrochloric acid or sulfates. From the point of view of organic substances, such active final sinks represent the last step in the lifetime of a substance. Mineralization is the ultimate method to dispose of hazardous organic substances; it is thus a necessary element of every waste management system.

For affluent societies with a high material turnover, it is necessary to have appropriate final sinks for all substances. The search for ultimate sinks has a long tradition and has not reached its goal as yet [3]. The need for final sinks is well documented by current challenges such as climate change, or the ozone hole, both of which are manifestations of inadequate final sinks. The utilization of fossil carbon overloads carbon sinks, resulting in the rise of concentrations of carbon dioxide and methane in the atmosphere. Also, production, use, and emissions of certain chlorinated and fluorinated carbohydrates (CFCs) have resulted in high concentrations of CFCs in the sink stratosphere, depleting the ozone layer and creating the so-called ozone hole.

Goals of Waste Management and of Thermal Waste Treatment

The first goal of waste management has been and still is the *protection of human health and life*. While in affluent countries with well-developed waste management systems this has become a matter of course, in many less developed countries this is still the chief objective for establishing waste management. In parallel to this goal, and also linked to it since human health depends on a sound environment, stands the *protection of the environment*.

The second goal of waste management is *resource conservation*: conservation of materials, energy, and land. This objective becomes the more important with higher material turnover and population density, with megacities as hotspots of resource use and resulting wastes. There are two main benefits from the pursuit of this goal: Recycling enhances the availability of resources and significantly reduces environmental pollution by reducing the need for primary production that in general represents the most polluting step in the life cycle of a product.

The third goal represents more of a framework for sustainable waste management: The practice of waste management shall *not cause any burden for future generations*. Landfilling that produces long-term emissions requiring treatment and control for several centuries [4] does not comply with this objective. What is needed are final storage landfills that have very small emissions even for long time periods (thousands of years). Landfills can only become final sinks for substances when wastes are pretreated and organic compounds are completely mineralized, before landfilling. Recycling of wastes containing hazardous substances without removing the harmful constituents such as heavily stabilized plastic materials also poses a burden for future generations.

Concerning neighboring countries, wastes should be exported *only* when the receiving country is able to manage wastes as well as its constituents in a safe, responsible, and resource-conserving way (cf. Basel Convention [5]).

The means to reach these goals are manifold. In the nineteenth century, "collection and transport of wastes out of town as fast as possible" was the main principle of waste management. Today, sophisticated logistic systems, high-tech mechanical sorting processes, mature and efficient recycling concepts are state of the art in many affluent countries. On the other side, for emerging economies, the economic situation does not allow to apply sophisticated waste treatment processes such as sorting, incineration, or mechanical-biological treatment.

It should be kept in mind that most societies spend between 0.2% and 0.4% of their GDP for waste management [6]. Thus, in a wealthy region with a GDP above US $ 30.000 per capita, people are willing and can afford to spend about US$100 per capita annually for waste management. This enables the region to implement modern waste management systems including waste-to-energy. By contrast, in an emerging economy with a per capita GDP below US$3.000, the financial resources available for waste management are less than 10 US$ per capita and year. It is clear that for this sum, it is neither possible to construct nor to operate an MSW incinerator. Hence, subsidizing the investment of an MSW incinerator or any other expensive treatment technology in an emerging economy is not an appropriate means to solve waste management problems.

The goals of MSW incineration are congruent with, but more specific than, the goals of waste management and can be summarized as follows:

Protection of Humans and the Environment

Disinfection: The original objective of waste incineration is still one of the main – but often forgotten – goals and advantages of modern incineration. No other waste treatment process such as landfilling or composting has a similar hygienic effect. The high temperature and long residence time in modern incinerators guarantees complete destruction of all microorganisms. Thus, incinerators are a necessary final sink for all those materials that are biologically contaminated. This is especially important for high-density megacities, where the outbreak of diseases can have disastrous consequences. A particular case is represented by hospital wastes that require special attention due to their high concentration of pathogenic organisms. Such materials demand special care for delivery, storage, and feeding. Thus, they need to be packaged and handled with special care when they are co-combusted with MSW, or they are treated in specialized furnaces. In case of an outbreak of contagious diseases, it is of great value to have incinerators at hand that are designed to safely dispose of biologically contaminated materials.

Complete oxidation: A main goal of incineration is to completely mineralize organic substances to CO_2, H_2O, and other inorganic compounds. As discussed in the previous section, thousands of tons of hazardous organic substances are produced in industry, utilized by consumers, and collected by waste management. The hazardous materials that are built into consumer products and investment goods can neither be recycled nor composted or landfilled because of their persistent and toxic properties. They need to be broken down by thermal treatment at elevated temperatures, with sufficient oxygen supply and at long enough residence times to completely destroy any organic material. If special care is taken, "de novo" synthesis of trace organic substances in the furnace and subsequent boiler and flue gas cleaning can be minimized, and the overall conversion rate for total organic carbon to carbon dioxide and carbonates (bottom ash and APC residue) is close to 99%. The remaining carbon in the WTE bottom ash has been found to consist of 19–38% organic carbon, 33–62% of elemental carbon, and 10–38% of inorganic carbon [7] (Fig. 1).

Emissions compatible with environmental standards: The first goal of waste incineration is to protect the environment from pathogenic organisms, hazardous organic chemicals, and heavy metals and other toxic substances. As will be discussed in section "Goals of Waste Management and of Thermal Waste Treatment", state-of-the-art incineration has reached this goal. Table 3 presents the example of cadmium on a regional scale: Let us consider a region of 250 km^2 with a population of 100,000, each producing about 400 kg of MSW per year containing 10 mg Cd/kg MSW. Table 3 shows the increase of Cd in the regional soil, assuming that all emitted Cd settles in the region (such a hypothesis is justified if the region is surrounded by similar regions that import the same amount of Cd as they are exporting). Cadmium is chosen here because in the 1970s, this volatile heavy metal was recognized as the most significant pollutant emitted by MSW

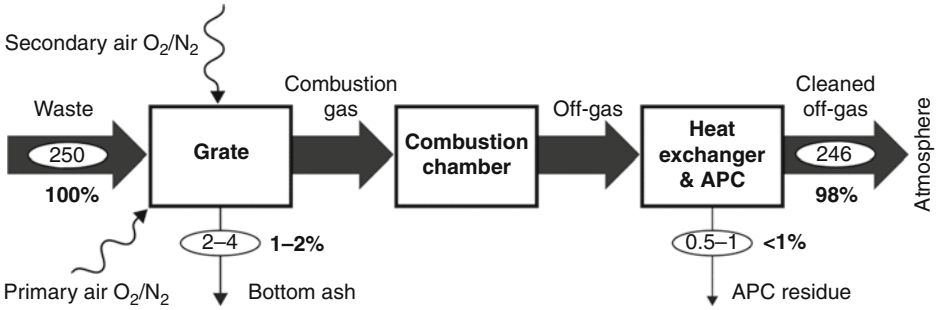

Thermal Treatment of Waste: Key Element for Sustainable Waste Management. Figure 1
Flow of carbon through an MSW incinerator: Carbon is effectively oxidized to CO_2; the small amounts of carbon in bottom ash and APC residue are mostly inorganic carbon

Thermal Treatment of Waste: Key Element for Sustainable Waste Management. Table 3 Contribution of modern waste-to-energy plants to cadmium loading of soils

Transfer coefficient, $k_{Cd\ cleaned\ off\text{-}gas}$	Emission, mg Cd/Nm^3 of stack gas	Cd flow to soil in 1,000 years, mg Cd/m^2
0.1	0.2	200
0.01	0.02	20
0.001	0.002	2
best available technology		
0.0005	0.001	1
Geogenic background concentration in soils:		90 mg/m^3

incinerators at that time [9, 10]. The fraction of input Cd that is emitted in the stack gas after the Air Pollution Control (APC) system is expressed by the transfer coefficient. It should be noted that state-of-the-art incinerators operate at transfer coefficients for cadmium of less than 0.0005; as shown in Table 3, emissions from such incinerators are insignificant when compared to other sources, and their contribution to geogenic values of cadmium is low even when long time periods are considered (Table 3).

Concentration of hazardous substances: As shown in Fig. 2, thermal treatment processes have the power to concentrate or deplete elements in the various incineration products. Atmophilic metals with comparatively high vapor pressures and low boiling points, such as mercury, cadmium, tin, zinc, antimony and lead, are preferentially transferred from the combustion grate to the gas phase. During gas cooling, the metal vapors condense on available surfaces which are in general provided by the large number of small particles formed by incineration. These particles, overproportionally loaded with atmophilic metals, are removed from the process gas stream by electrostatic precipitators or fabric filters, yielding a filter residue that is highly concentrated in useful but also toxic heavy metals. The overall accumulation effect is remarkable: Starting with 1 Mg (i.e., 1 t) of MSW containing 10 mg of Cd, an MSW incinerator produces about 20–30 kg of APC residue containing 360 mg Cd/kg.

The concentration in the APC residue (also called "fly ash") during the incineration process occurs only with atmophilic metals and chemical compounds with a high vapor pressure, such as metal chlorides. Metals and metal compounds with low volatility such as iron, chromium, titanium, and cobalt accumulate rather in the bottom ash. Due to the different behavior of various metals, it will never be possible to direct all useful, or all hazardous, materials to one particular fraction of incineration products. However, the partitioning described above allows the recovery of some metals from the bottom ash and some from the APC residue.

Immobilization: Bottom ash and APC residues contain soluble compounds such as chlorides, nitrates, or sulfates of metals. Thus, a main concern is the long-term mobility of heavy metals. Due to the individual partitioning of substances, the solubility of bottom ash and APC residue is not the same. Volatile metals and soluble chlorides are mostly transferred to the fly ash product; the bottom ash contains more oxides, and

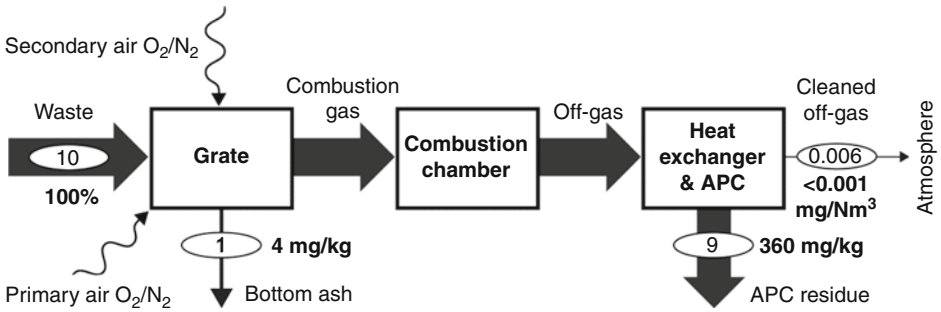

Thermal Treatment of Waste: Key Element for Sustainable Waste Management. Figure 2
Flow of cadmium through an MSW incinerator; the concentration of cadmium in APC residues increases 40-fold from 10 mg Cd/kg in MSW to 360 mg Cd/kg; the cadmium concentration in bottom ash is 2.5 times lower than in MSW

some sulfates that are less soluble. Both products react with water and air (O_2, CO_2), and are by no means in a thermodynamic equilibrium when exposed to the environment. The long-term mobility of heavy metals in bottom ash depends on pH and thus on the acid-neutralizing capacity [8]. Bottom ash appears to be predominantly buffered by calcium minerals. Under alkaline conditions, calcium hydroxides/silicates and CaCO3 can dissolve. In neutral-to-acidic conditions, silicate dissolution becomes increasingly relevant. Basic calcium hydroxide/silicate components are likely to be neutralized by CO_2 or silica. The solution chemistry of the APC residues is similarly controlled by pH. Thus, solidification by cement stabilization or other treatment requires careful control of pH conditions, anticipating the future fate of the landfilled material (leaching and environmental conditions).

Resource Conservation

Volume reduction: This is particularly for large cities where landfill space close to waste producers is rare. Incineration decreases the mass of MSW by 70–75% and the volume by 90%. Thus, the lifetime of landfills can be reduced at least by a factor of 4. If materials are further recovered from bottom ash, it is feasible to reduce the required volume for ash disposal to less than 10% of the volume required for landfilling of untreated MSW.

Energy recovery: While initially the recovery of heat was more directed toward the protection of the air pollution control (APC) devices, most of today's MSW incinerators are well embedded in regional electricity grids and, sometimes, are also linked to district heating networks. In 2009, MSW incinerators across Europe had an annual capacity of 73×10^6 Mg and supplied 30 TWh of electricity and 55 TWh of heat. The share of waste-derived energy in Europe amounts to less than 1% of total energy demand. About 50% of energy derived from MSW combustion originates from renewable sources, such as wood, paper, and biomass. The contribution of MSW incinerators to renewable energy supply in Europe totals about 4%.

Recovery of materials: The products of incineration contain not only hazardous substances but also valuable resources. The recovery of iron from the bottom ash has a long tradition; also, the reuse of bottom ash as construction material has been practiced for hundred years by now (although with limited success). Today, it seems feasible and economically attractive to recover more metals, such as copper, aluminum, and others. Also, the enriched concentration of atmophilic metals in filter ashes potentially opens the possibility to recover metals such as cadmium, zinc, antimony, and others from APC residues. The main objective must be to enrich valuable constituents in highly concentrated small fractions by optimizing the thermqal treatment process and, also, to divert those elements that reduce the effectiveness of recovery to a small fraction that can be landfilled. The ideal of zero solid incineration residues to landfill will be difficult to reach, considering that the intricate composition of bottom and filter ash reflects the complex mixture of nearly all elements of the periodic table that are present in MSW.

In view of the goals of waste management and of incineration, what is the contribution of waste

incineration to attaining the goals of waste management? In particular, what is the main contribution of MSW incineration for the protection of humans and the environment, and for resource conservation? These questions will be discussed in the following section.

Thermal Waste Treatment for Environmental Protection

In addition to fulfilling the goals of recycling, waste management must also provide a solution for those materials that cannot be recycled. This applies in particular to the large amount of hazardous substances that are used today in modern products such as biocides, flame retardants, heavy metals, nanoparticles, etc. Mechanical or biochemical treatment such as sorting combined with composting or anaerobic digestion can neither decompose nor eliminate these substances. The key role of thermal treatment is to completely mineralize organic substances, and to control inorganic substances by concentration. At present, no other waste treatment process is available that fulfills this task at the same proven reliability, cost-effectiveness, and environmental soundness.

Toward the end of the nineteenth century, waste incineration was introduced as a means to prevent pollution. The first plants were been built in England and Germany, as an alternative to waste disposal on agricultural land that spoiled valuable farmlands with disease-spreading microorganisms. These incinerators, directed toward the first goal of waste management, did have a stack but they were not equipped with APC systems and did not recover the chemical energy contained in MSW. Their sole purpose was to prevent the application of MSW on valuable farmland by reducing volume and mass. It is interesting to note that the bottom ash of some of these early incineration plants was used as a construction material as far back as the beginning of the twentieth century. Unfortunately, there are no records as to why this practice was abandoned later; it is likely that the bricks made at that early time from incinerator ash did not fulfill their purpose in the long run.

The next step of development was the introduction of simple filters for the removal of particulates, and of energy recovery. Both went hand in hand, since even simple filter systems require the cooling of flue gas temperatures. Municipal incinerator plants built in the late 1960s were already equipped with sophisticated energy recovery (combined district heating with electricity production), but the air pollution control devices removed only coarse particulate matter (legal standards at that time were around 150 mg of dust per Nm^3 off-gas). Waste incineration got a boost during the oil crisis of 1973 when fuel prices skyrocketed. Shortly after, the first groundbreaking studies on heavy metals in incinerator off-gas appeared in the scientific literature [9, 10]. This had little effect until the 1980s when – under heavy pressure from an informed public and legislation in countries like Switzerland, Denmark, and Sweden – the waste-to-energy industry developed highly efficient APC pollution control devices.

Today, emissions from state-of-the-art waste incinerators are among the lowest of all industrial power plants. Thanks to technological advancements that were inconceivable in the 1970s, modern municipal solid waste incinerators can beat most stringent existing regulations easily, for some parameters even by orders of magnitude. Figure 3 summarizes the reduction emissions from municipal solid waste incineration from 1930 to 1970 and 1995. The graph stops at 1995 because the highly advanced state of the art of APC of 1995 has not changed much since then; further improvements have focused on energy efficiency, cost-effectiveness, and reliability.

Particulate matter and lead have been reduced by about four orders of magnitude, and most other heavy metals and dioxins by three orders of magnitude. Also, hydrochloric acid and sulfur oxides have been drastically eliminated, and only for nitrogen oxides the reduction was somewhat moderate. The increase in HCl and dioxins in the 1970s was due to the introduction of PVC that made up about 1% of the mass of MSW.

Table 4 shows that today – in contrast to some earlier publications – the share of MSW incineration for total dioxin emissions is insignificant. Of course this applies only for countries employing BAT (in the USA: MACT) incineration, such as Austria, Germany, Japan, the Netherlands, Singapore, Sweden, Switzerland, and the USA.

In view of the objectives of waste management, it is important to point out the pollution potential by burning household waste in private stoves. This practice might appear attractive in areas with high penetration of solid fuel household furnaces. Such furnaces, designed to

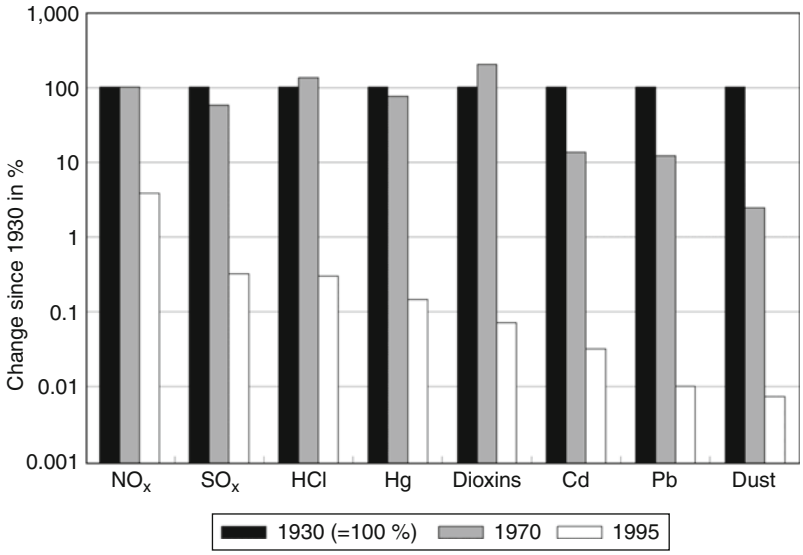

Thermal Treatment of Waste: Key Element for Sustainable Waste Management. Figure 3
Development of emissions from municipal solid waste incineration from 1930 to 1995 on a concentration base (mass per volume of off-gas)

Thermal Treatment of Waste: Key Element for Sustainable Waste Management. Table 4 Contribution of MSW incineration to national dioxin/furan load in Germany and Austria (calculation is based on data from [11] and [12], assuming that all MSW generated is incinerated)

Country	Total emissions of PCDD/PCDF (g TEQ/year)	Share of MSW incineration	
		g TEQ/year	%
Germany	800–1,200	5.5	0.5–0.7
Austria	50–320	0.53	0.2–1.1

produce heat without generating greenhouse gases, are becoming increasingly popular, and are sometimes even subsidized by authorities. With increasing fuel costs, some waste will eventually be used as a fuel for such furnaces, resulting in severe air pollution.

Figure 3 can be used to compare emission values of today's MSW incinerators (emissions of 1995) and household furnaces (emissions of 1970). It is striking that even if only 1% of all waste is incinerated in household furnaces, the emission load of dioxins and particulates will be much larger than for state-of-the-art MSW incineration. It is important to convey this message to the general public that aims at reducing greenhouse gases by burning waste-derived products in their heating systems.

MSW is more important as a carrier of heavy metals than as an energy carrier (Fig. 4). Thus, it is important to stress that incineration is first of all a process that protects the environment from harmful organic and inorganic substances. The generation of useful energy is an added value, but not the main purpose. This is important when it comes to the disposal or use of bottom ash and filter ash. If a posttreatment of incineration residues such as concentration, solidification, or immobilization requires energy, this should not be weighed against the benefit of protecting the environment from harmful substances. After all, the turnover of energy in waste management is marginal when compared to total energy demand. Today, the challenge of producing incineration residues that have "final storage quality" has been recognized and is in focus of research and development. While treated bottom ash is close to final storage quality, in Germany and some other countries, the APC residues are disposed of in underground salt mines where the risk of water contact and thus mobilization is exceptionally small.

In terms of greenhouse gas reduction, incineration has a double advantage: Since about 50% of MSW is of

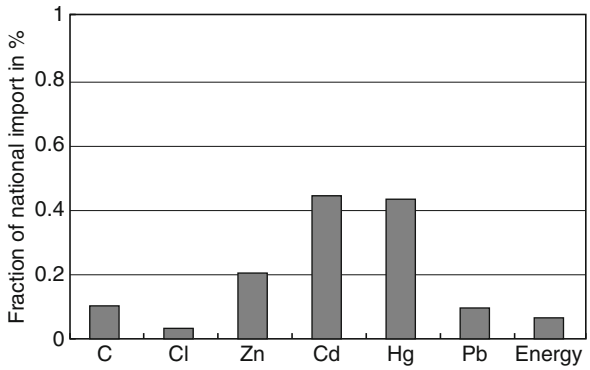

Thermal Treatment of Waste: Key Element for Sustainable Waste Management. Figure 4
Fraction of selected substances and energy contained in MSW compared to national import flow: the case of Switzerland 1990–2000

biogenic origin [13], it contributes also to the reduction of greenhouse gases by replacing fossil fuel derived energy. Also, in contrast to composting producing "cold" CO_2 or landfilling with limited gas recovery, the organic carbon is not released as unproductive CO_2 and CH_4 to the atmosphere but is used to produce electricity and/or heat.

The Contribution of Thermal Waste Treatment to Resource Conservation

As a result of advanced APC technologies, MSW incinerators have become marginal polluters of air, water, and soil when compared to other high-temperature industrial processes. At the same time, as waste-to-energy capacity increases, the amount of solid incineration products, in particular APC residues, is also

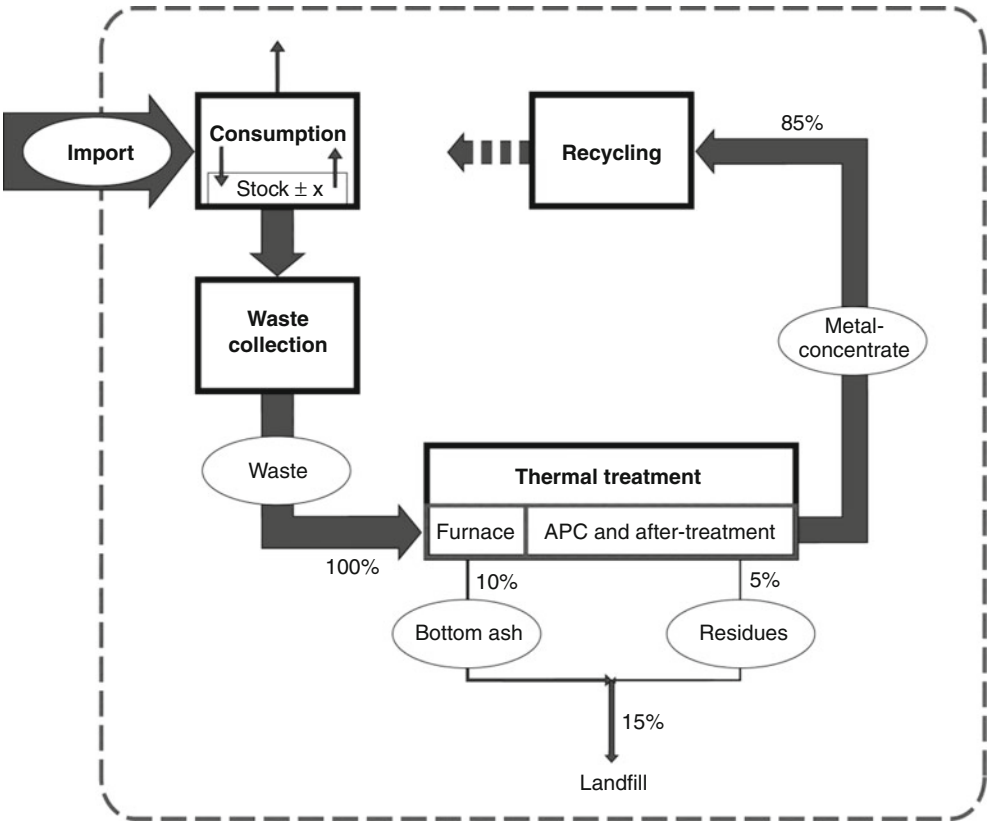

Thermal Treatment of Waste: Key Element for Sustainable Waste Management. Figure 5
Recovery of atmophilic metals from APC residues allows substantial recycling of particular metals such as cadmium, zinc, tin, and antimony. Taking into account that MSW contains nearly half of the national import of Cd, about 40% of this metal used could be recycled by recovery from the APC residues of MSW incineration

increasing and poses a new challenge. In the future, main emphasis will be laid on beneficial use and/or disposal of the solid products of incineration, namely, bottom ash and APC residues. Both materials comprise considerable amounts of valuable substances in concentrated form. While iron scrap in bottom ash is already routinely collected and economically recycled, current research focuses more on the reclamation of aluminum, copper, and other nonferrous metals. It appears that substantial amounts can be recovered at competitive costs. The goal will be to separate those materials that are clean enough and well suited for construction purposes (stones, sand, concrete, and other residues from construction materials).

Certain atmophilic heavy metals such as cadmium are highly enriched in APC residues. Therefore, this material presents not only a risk but also an opportunity for resource recovery. About 50% of the national import of Cd ends up finally in MSW and similar wastes that are suitable for MSW incineration (Fig. 4). Roughly 80% of the Cd entering an incinerator leaves the plant as APC residue (the partitioning between bottom ash and APC residues depends upon incineration design, operating conditions, and waste composition, e.g., Cd in batteries or in plastic additives). Therefore, as shown in Fig. 5, nearly half of the Cd used in a region can be recovered from the APC residue of waste-to-energy plants within the region. Similar material recovery is possible for other atmophilic metals such as Zn, Pb, Sn, and Sb. However, for most of these other metals, the ratio of metal in MSW to national imports is less than 50% (Fig. 4).

Future Directions

The potential of MSW incineration for improving waste management is not yet fully exploited. The following outlook summarizes some of the ideas that have been presented recently, again listed in the order of: first, health and environmental protection and, second, resource recovery.

While average emissions are exceptionally low, some emission peaks can be discerned when short-term time series are analyzed. Mitigation measures such as waste pretreatment, in situ homogenization, or alternative thermal treatment technologies should be examined. Since new materials such as nanoparticles and rare metals are penetrating the market, the fate of these new substances during combustion as well as in residues resulting from incineration needs to be investigated.

MSW incinerators can also be used as tools to monitor MSW composition. On one hand, biogenic carbon can be distinguished from fossil carbon. As stated earlier, incineration contributes toward the reduction of greenhouse gas emissions. Several methods exist to measure the biogenic fraction of CO_2 in the off-gas of incineration with good accuracy [13]. In order to take advantage of the greenhouse gas reduction potential of MSW incineration, incinerators should be included in emission trading schemes.

Incinerators can also be used for cost-effective routine analysis of elemental waste composition. For this purpose, an initial mass balance for the determination of transfer coefficients is made. It is then followed by identifying those incineration products that are the main carrier of certain substances, such as stack gas for carbon, scrubber water for chlorine, APC residue dust for cadmium and antimony, and bottom ash for aluminum and iron. On the basis of the transfer coefficients, the selected elements can be easily determined by measuring the concentration in a well-accessible incineration product of known mass flow, such as the APC residue [14]. The main advantage of this method for waste analysis is that the incinerator acts as a large homogenizer. Consequently, sample size and frequency can be much smaller as compared to direct characterization of the MSW and the results will be more reliable than those from classical waste analysis.

Concerning resource recovery, large-scale research programs have been started in order to recover additional resources from bottom ash [15]. So far, these studies of sophisticated mechanical separation processes point out that many more valuable substances can be extracted from bottom ash. Some of the proponents go as far as to state that, in the future, separate collection of some waste fractions will become obsolete due to the new possibilities of recovering selected substances from incineration products [16].

Concerning APC residues, new concepts are still in the visionary phase. Since these materials make up only a small fraction of the initial MSW (2–3%), it seems feasible to collect them for central treatment at a few regional centers, e.g., serving a population of 10 million.

The resulting amount of 100.000 Mg of APC residue would represent a resource base that would allow for economic recovery of certain metals.

In the future, new methods will be required for evaluation of waste management scenarios. The present LCA approach is not well suited to assessing long-term challenges such as landfill emissions during the next five centuries, or multiple recycling of hazardous substances in recovery schemes. New evaluation criteria such as the statistical entropy analysis SEA [17] (see contribution by Rechberger in this volume) or the final sink approach [18] represent additional means for an objective appraisal of MSW incineration.

MSW incineration has gone a long way from simple combustion to sophisticated waste-to-energy (WTE). It will certainly keep on advancing in the future. In order to conquer and penetrate new markets, it will be necessary to decrease costs of investment, operation, and maintenance. The art will be to deliver the same performance regarding environmental protection, resource conservation, and reliability at lower costs. Considering that waste incineration is now a mature business, with decades of solid and successful experience, this new goal seems feasible. It will ensure that a larger percentage of the global population can enjoy the benefits of this key waste treatment technology.

Bibliography

1. Baccini P, Brunner PH (in press) Metabolism of the anthroposphere – analysis, evaluation and design. MIT Press, Cambridge, MA
2. Brunner PH (2004) Material flow analysis and the ultimate sink. J Ind Ecol 8(3):4–7
3. Tarr AJ (1997) The search for the ultimate sink – urban pollution in historical perspective. The University of Akron Press, Akron
4. Belevi H, Baccini P (1989) Long-term behavior of municipal solid waste landfills. Waste Manage Res 7(1):43–56
5. Basel Convention (1992) Retrieved 27 Jan 2011from http://www.basel.int/
6. Brunner PH, Fellner J (2007) Setting priorities for waste management strategies in developing countries. Waste Manage Res 25:234–240
7. van Zomerena A, Comans RNJ (2009) Carbon speciation in municipal solid waste incinerator (MSWI) bottom ash in relation to facilitated metal leaching. Waste Manage 29(7):2059–2064
8. Johnson CA, Brandenberger S, Baccini P (1995) Acid neutralizing capacity of municipal waste incinerator bottom ash. Environ Sci Technol 29(1):142–147
9. Greenberg RR, Zoller WH, Gordon GE (1978) Composition and size distribution of particles released in refuse incineration. Environ Sci Technol 12:566–573
10. Greenberg RR, Gordon GE, Zoller WH, Jacho RB, Neundorf DW, Yost KJ (1978) Composition of particles emitted from the Nicosia municipal incinerator. Environ Sci Technol 12:1329–1332
11. Orthofer R, Vesely A (1990) Abschätzung von toxischen Emissionen (PCDD, PCDF, PAH, BaP) aus Verbrennungsprozessen in Österreich (Estimation of toxic emissions (PCDD, PCDF, PAH, BaP) from combustion processes in Austria), Seibersdorf Research Report OEFZS 4554
12. Wintermeyer D, Rotard W (1994) Dioxin Emissionen in der BRD – Versuch einer Bilanzierung. Staub Reinhaltung Luft 54: 81–86
13. Fellner J, Cencic O, Rechberger H (2007) A new method to determine the ratio of electricity production from fossil and biogenic sources in waste-to-energy plants. Environ Sci Technol 41(7):2579–2586
14. Morf L, Brunner PH (1998) The MSW Incinerator as a monitoring tool for waste management. Environ Sci Technol 32(12): 1825–1831
15. ZAR (2011) Stiftung zentrum für nachhaltige ressourcen- und abfallnutzung. Retrieved 31 Jan 2011 from http://www.zar-ch.ch/
16. Bunge R (2008) Metalle aus Abfall: geld stinkt nicht, Innovationsworkshop IPEK 02/2008 University of Applied Sciences Rapperswil, Switzerland
17. Rechberger H, Brunner PH (2002) A new, entropy based method to support waste and resource management decisions. Environ Sci Technol 34(4):809–816
18. Döberl G, Brunner PH (2004) Substances and their final sinks – a new indicator for monitoring sustainability. Symposium indicators for evaluating sustainable development – the ecological dimension, Berlin, Germany, 1–2 Nov 2004

3D Pose Estimation of Vehicles Using Stereo Camera

Björn Barrois[1], Christian Wöhler[2]
[1]EvoBus GmbH, Neu-Ulm, Germany
[2]Image Analysis Group, Dortmund University of Technology, Dortmund, Germany

Article Outline

Glossary
Definition of the Subject
Introduction and State of the Art
Discussion
A System for Stereo-Based 3D Pose Estimation of Vehicles

Experimental Evaluation
Summary and Conclusion
Future Directions
Bibliography

Glossary

3D Pose estimation Estimation of the translational and rotational degrees of freedom of an object, usually corresponding to its position in 3D space and its orientation angles. For articulated objects additional, internal degrees of freedom are estimated.

Driver assistance system A system which helps the driver of a car in specific traffic situations in order to increase safety.

Iterative closest point (ICP) algorithm An algorithm which finds a set of translation and rotation parameters fitting a measured point cloud to a model.

Optical flow The optical flow vector denotes the motion in image space of the projection of a scene point between two subsequent images of a sequence.

Quaternion Number system which extends the system of complex numbers. In computer vision and computer graphics, quaternions are used for the efficient representation of rotations.

Scene flow Vector field describing the 3D scene points visible in the image and their current motion in 3D space. Projecting the scene flow into the image plane yields the optical flow.

Stereo vision 3D reconstruction of a scene based on a pair of images.

Yaw angle Angle measuring the rotation of a vehicle around its vertical axis.

Yaw rate Temporal derivative of the yaw angle.

Definition of the Subject

For advanced driver assistance systems, the 3D poses and motion states of oncoming and intersecting vehicles represent important information. This work describes methods for 3D vehicle pose estimation based on a motion-attributed 3D point cloud generated. First, stereo and optical flow information is computed for the investigated scene. A four-dimensional clustering approach separates the static from the moving objects in the scene. The iterative closest point algorithm (ICP) estimates the vehicle pose using a cuboid as a weak vehicle model. Classical ICP optimization is based on the Euclidean distance metric. Its computational efficiency can be significantly increased by applying a quaternion-based optimization scheme. In vehicle-based small-baseline stereo systems, it is favorable to use a polar distance metric which especially takes into account the error distribution of the stereo measurement process. To derive the pose parameters and simultaneously their temporal derivatives, i.e., the motion state of the vehicle, from two subsequent stereo image pairs in order to avoid a temporal filtering stage, a model-based scene flow method is applied. Here, 3D points on the object surface are reprojected into the stereo images and similarities between image windows extracted around the reprojected points are maximized. An experimental evaluation is performed on seven different real-world sequences, where different stereo algorithms, baseline distances, distance metrics, and optimization algorithms are examined. The results show that the proposed polar distance metric yields a higher accuracy especially for the estimation of the yaw angle of a vehicle than the common Euclidean distance metric, especially when using pixel-accurate stereo points. The model-based scene flow approach yields a refined 3D pose estimation along with the instantaneous motion state of the vehicle.

Introduction and State of the Art

Some approaches for detection of obstacles around the ego-vehicle can be found in the literature, but the existence of an obstacle is not enough information to evaluate the situation entirely. The knowledge about pose and motion of oncoming and intersecting vehicles is important to avoid accidents. Especially at intersections, analysis of the behavior of other road users is important to help the driver to pass through the intersection in a safe and comfortable manner. Furthermore, pose information is important for the recognition and prediction of driving maneuvers and the analysis of complex traffic situations involving several traffic participants. This section provides an overview of the state of the art in the field of vehicle pose estimation, where approaches relying on different sensor concepts are discussed.

Systems Based on Monocular Images

A system for segmentation and detection of vehicles using a monocular camera system is described in [1], where a vehicle model defined by seven parameters is used. The position of the vehicle is determined by taking into account the symmetry of the edges in the image, the shape of the model, and the shadow of the vehicle. An evaluation of this approach is not available.

In [2] a Kalman filter–based system for tracking vehicles in front of the ego-vehicle is presented. The contours of other vehicle candidates are extracted using a Hough transform and circumscribed by a bounding box. Furthermore, a classifier determines if the bounding box corresponds to a vehicle or a background pattern. A 3D model is used for tracking the vehicles in 3D space, where the measurement is interpreted as the projection of the 3D model into the 2D image plane, which yields the 3D position of the vehicle. System evaluation is performed based on radar data, where an accuracy of the distance estimation of the image-based approach of better than 1 m at a distance of 60 m is achieved.

Early methods for vehicle detection in the field of traffic surveillance are proposed in [3–5]. These approaches are based on observing a road intersection with a fixed camera. The vehicles are represented by polyhedral models which are adapted to the edges extracted from the images. A 3D scene model provides information about free space and possible occlusions. An illumination model is used to suppress the influence of shadows on the pose estimation. To obtain a prediction of the motion behavior, a description of the possible motion patterns based on a physical model is used. The vehicle is tracked across the sequence using optical flow analysis combined with an extended Kalman filter.

Systems Based on Sensor Fusion

A system consisting of a camera and a radar sensor is used in [6] to detect traffic participants. The advantages of the two sensors (high lateral resolution of the camera, high accuracy of the distances and radial velocities measured by the radar sensor) are used to estimate the position of vehicles driving ahead of the ego-vehicle. The distance is measured based on radar information while the lateral extension of the object is inferred from the camera image. The evaluation of the system is restricted to the accuracy of the estimated bounding box in the image.

The combination of a monocular color camera and a radar sensor is proposed in [7]. Shadows, rear lights, line segments, and symmetric features are extracted from the image and combined with the radar information in a low-level fusion step. A subsequent post-processing step aims for removing false detections and determining the vehicle positions. An evaluation of the metric accuracy of the system is not available.

A laser scanner and a video camera are used in [8] to estimate the pose, size, and velocity of vehicles. The detection and 3D pose estimation of vehicles is obtained based on the laser scanner data. Relying on the pose estimation result, rectified side views of the detected vehicles are constructed, which are in turn used by a cascade classifier to distinguish vehicles in front of the ego-vehicle from background patterns. The evaluation in [8] is limited to the classification performance of the system, while the geometric detection accuracy is not examined.

Similarly, a combination of a laser scanner and a camera is used in [9] for the recognition of objects in traffic scenes. This approach is based on sensor fusion relying on vehicle-specific features extracted from both sensors. Besides the application of autonomously following the vehicle driving ahead, traffic jam and road intersection scenarios are examined. It is shown that the proposed system is able to track vehicles even in the presence of high accelerations.

Stereo Camera Systems

The early approach to stereo-based vehicle detection described in [10] relies on a stereo camera system with a relatively long baseline approximately corresponding to the width of the ego-vehicle. Vehicles driving behind the ego-vehicle are extracted from the 3D point cloud, and a Kalman filter is applied, where the highway scenario is addressed specifically. Due to the long baseline, an estimation of the vehicle position is possible for distances of 100 m and more.

Stereo information and optical flow data are combined in [11] to determine the position and the velocity of vehicles. The 3D points and the extracted optical flow field are processed simultaneously by an extended

Kalman filter framework. Objects are inferred from the scene along with their velocities using a clustering technique. A considerable settling time of the temporal filtering stage is observed. The accuracy of the proposed method is not evaluated.

A fairly complex system relying on 3D scene reconstruction based on the fusion of structure from motion data and stereo vision is described in [12]. A detection step yields the objects present in the scene along with their approximate orientation in discrete steps and an assignment to different object classes using the approach introduced in [13]. The results are reliable in a depth range between 15 and 30 m. The pose of the objects is not compared to ground truth data.

A stereo camera is used in [14] to detect vehicles driving ahead and estimate their distance to the ego-vehicle. In a first step, a stereo-based 3D reconstruction of the scene is performed. A symmetry analysis extracts rear views of vehicles from one of the camera images, and a bounding box is computed. The vehicle is then tracked in the 2D image space and associated with the 3D data in a separate step.

Stereo analysis based on affine warping is used in [15] to detect obstacles ahead of the ego-vehicle. The image of the left camera is warped and mapped onto the image of the right camera using affine warping and edge comparison. Dynamic programming estimates a boundary between the road surface and obstacles on the road. However, the orientations of the obstacles are not estimated.

In [16], a stereo camera system is used for several applications, e.g., the detection and tracking of vehicles and pedestrians. An occupancy grid distinguishing between free and occupied regions in front of the vehicle is created using the 3D points of an initial stereo analysis to detect objects in front of the car. Once an object is found, its size, aspect ratio, and orientation are used to find a corresponding model in an object model database. The most suitable 3D model from the database is projected into the image and fitted to the image of the object using chamfer matching. The distance up to which this approach yields reliable results is about 35 m. No evaluation of the pose estimation accuracy is given.

The approach introduced in [17] uses a sparse scene flow field which is established by a point-wise Kalman filter–based integration of stereo and optical flow information. An extended Kalman filter tracks the point cluster representing the vehicle. The resulting motion-attributed 3D point cloud is segmented according to their position and motion state, where the independently moving parts of the scene are regarded as objects. The objects are tracked using a second, object-specific Kalman filter stage. An explicit vehicle model is not utilized, but the size of the vehicle is estimated based on the size of the point cloud. The proposed system is evaluated on synthetically rendered image sequences. The settling time of the Kalman filter framework typically amounts to about 25 frames (cf. also [11]). An extension of this approach is proposed in [18], where the observed object trajectories are analyzed by a particle filter stage in order to obtain a prediction of the vehicle motion for time intervals of several seconds. Example images and pose estimation results are shown in Fig. 1.

Three approaches to the adaptation of a temporal filtering stage are discussed in [19] for vehicle tracking based on stereo information. Specifically, an interacting multiple model (IMM), a maximum likelihood estimation of the filter parameters based on the yaw rate, and an extended model taking into account the yaw acceleration are discussed. The proposed tracking approaches are evaluated using synthetically generated images as well as 3D point clouds synthetically generated based on real trajectories of the vehicle center. On these data sets, the positional accuracy of the system amounts to 0.1–0.2 m and the accuracy of the filtered yaw rate to about 2–6° per second.

Discussion

In many state-of-the-art systems, the orientation angle of the vehicle remains undetermined or needs to be inferred from the specific application scenario, e.g., when vehicles driving ahead of the ego-vehicle are detected. Other systems estimate the orientation angle by a temporal filtering stage, which has the disadvantage of delays occurring due to the finite settling time. For an accurate prediction of the motion behavior the direct measurement of the vehicle orientation is essential. Furthermore, metric evaluations of the estimated poses in comparison to independently determined real-world reference data can hardly be found in the existing literature, such that it is difficult or impossible to

3D Pose Estimation of Vehicles Using Stereo Camera. Figure 1
Tracking results obtained with the stereo-based method described in [17, 18] for an oncoming vehicle first detected at 48 m distance. The predicted driving path indicating curve radius and velocity for the next second and the tracked 3D points are shown as well as a bounding box indicating the object pose (from [18])

compare different existing approaches with respect to measurement accuracy.

A general disadvantage of systems using monocular cameras is the low accuracy of the resulting distance measurements, while systems relying on sensor fusion require a considerable instrumental and calibration effort. In principle, a laser scanner is a sensor which is well suited for measuring the 3D pose of vehicles due to its high lateral resolution and distance accuracy, but laser scanners still tend to be too expensive for commercial automotive systems. Hence, stereo cameras are a promising cost-efficient alternative as they provide both a high lateral resolution and a reasonable accuracy of the measured distances in ranges relevant for typical traffic scenarios.

A System for Stereo-Based 3D Pose Estimation of Vehicles

This section describes approaches for 3D pose estimation of vehicles at high accuracy without relying on temporal filtering. A tracking-by-detection approach is performed where the pose estimation is performed individually for each frame. First, the input images from a calibrated camera system are rectified to standard geometry with epipolar lines parallel to the image rows. A sparse scene flow field is computed to obtain reliable depth information combined with motion information about the investigated scene, where three different algorithm combinations are used to compute a sparse incomplete scene flow field, i.e., a motion-attributed 3D point cloud. Separate objects are extracted by clustering, where each point is defined by three spatial coordinates and one or two velocity coordinates. The 3D points associated with the object are used by an iterative closest point (ICP) method to determine the object pose, where the classical Euclidean distance or a polar distance metric can be used. In a last step, a model-based scene flow stage yields a refined estimation of the pose parameters and their instantaneous temporal derivatives.

Extraction of Depth and Motion

Spacetime Stereo (adopted from [20] and [36]) The spacetime stereo algorithm is based on local intensity modeling and yields 3D points with the associated motion component parallel to the epipolar lines [20]. Image regions corresponding to a sufficiently high vertical intensity gradient are extracted in the left and right camera image, and their local spatiotemporal neighborhood is modeled by the model function $h(\vec{P}, u, v, t)$ where u and v denote the pixel coordinates, t the time coordinate in a spatiotemporal region of interest, and $\vec{P}$ the vector of function parameters:

$$h(\vec{P}, u, v, t) = p_1(v, t)\ tanh\ [p_2(v,\ t)u + p_3(v, t)] + p_4(v, t) \tag{1}$$

The tanh function approximates the shape of an ideal edge blurred by the optical system. The functions $p_i(v, t)$ are polynomials in v and t of (in principle) arbitrary order. In the experiments described in section "Experimental Evaluation," linear polynomials were used. Correspondence analysis is then based on a comparison of the modeled edges in the left and the right image in terms of the sum of squared differences (SSD). The SSD values on each epipolar line are analyzed, where different constraints can be taken into account: uniqueness, ordering, or the minimum weighted matching constraint [21]. Analysis of the model function parameters yields the velocity component along the epipolar line and sub-pixel-accurate disparity values. An example of the intensity profile of an observed moving edge versus a moving edge modeled according to Eq. 1 is shown in Fig. 2.

Feature-Based Stereo and Optical Flow (adopted from [36]) The utilized feature-based method for computing stereo and optical flow is based on local features to obtain a representation of the investigated scene [22]. The features are established in both images (left and right camera or current and previous time step), then the comparison is performed using a hash table technique. This approach provides a fast implementation of the algorithm. The correspondences have pixel accuracy, which is a disadvantage in comparison with the other regarded stereo algorithms. The combination of the stereo and optical flow results yields 3D points associated with the motion parallel to the image plane.

Correlation Stereo and Feature-Based Optical Flow (adopted from [36]) The combination of correlation-based stereo with the feature-based optical flow technique yields optical flow and more precise depth information in video real time. The correlation-based stereo method performs a SSD comparison of left and right image patches [23]. An interest operator (Prewitt filter) is used to separate reliable from unreliable depth information. The combination yields 3D points with two-dimensional motion vectors.

Clustering

This section provides an extended description of the clustering technique outlined in [36]. An initial segmentation of the attributed 3D point cloud extracted with any of the sparse scene flow techniques (cf. Fig. 3a) is obtained by means of a graph-based unsupervised clustering technique [24] in a space of 4, 5, or 6 dimensions spanned by the three spatial coordinates and the extracted velocity components of the

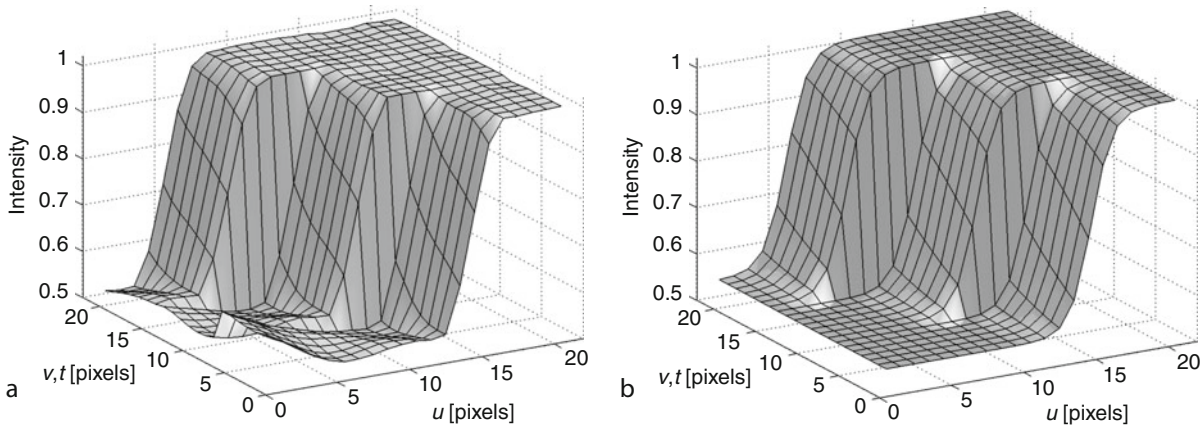

3D Pose Estimation of Vehicles Using Stereo Camera. Figure 2
(**a**) Spatiotemporal intensity profile of a moving edge, measured over a time interval of three time steps. The size of the spatiotemporal matching window is 21 × 7 × 3 pixels. For visualization, the (v, t) axis is divided such that each time step comprises an interval of seven pixels. (**b**) Modeling result according to Eq. 1 (from [37])

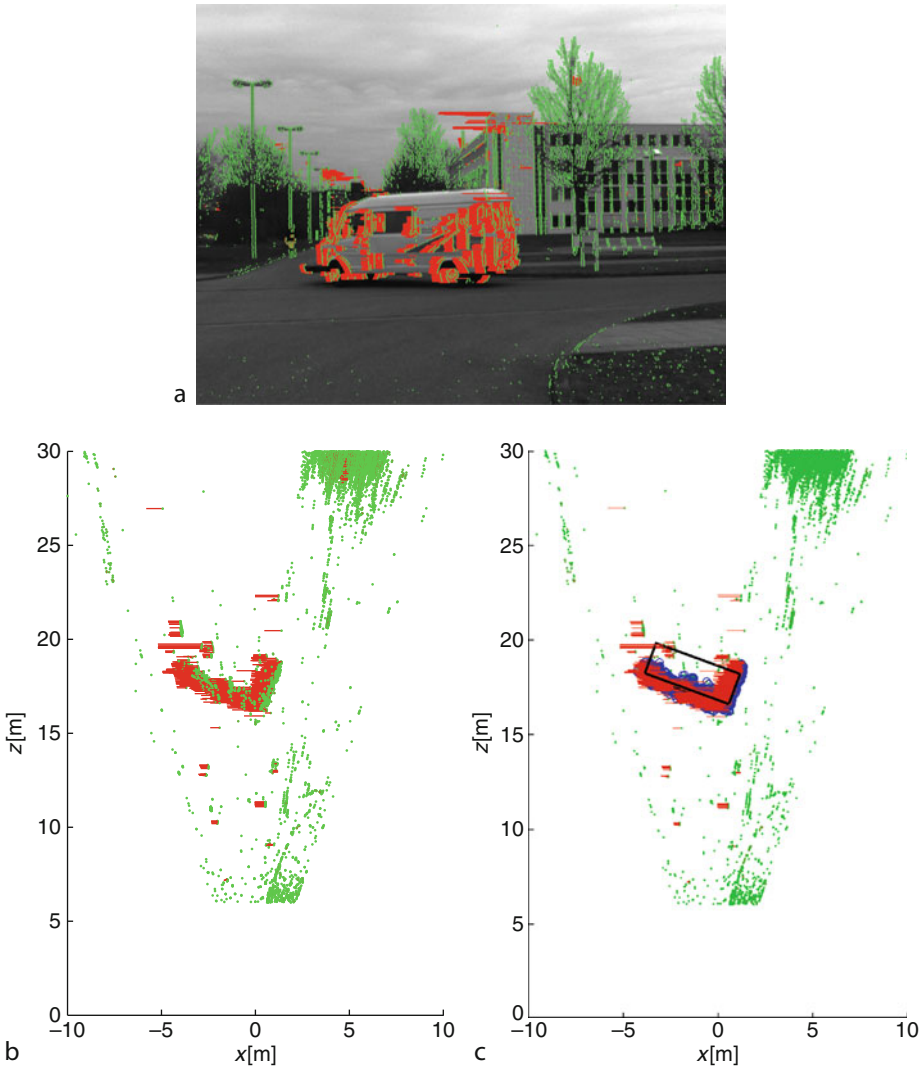

3D Pose Estimation of Vehicles Using Stereo Camera. Figure 3
Example of an incomplete sparse scene flow field. (**a**) Original image with projected 3D points (*green*) and associated motion vectors (*red*). (**b**) Bird's-eye view of the same scene. (**c**) Clustered points belonging to the vehicle (*blue*) together with the adapted model (*black*) (adapted from [36])

3D points [25]. This clustering stage generates a scene-dependent number of clusters, essentially separating the moving object from the (stationary or differently moving) background.

To avoid the need for a parameter that weights spatial against velocity coordinates, the graph-based method in [24] is used which takes into account the spatial and velocity coordinates separately. Accordingly, for two scene flow points

$$\vec{P}_1 = \begin{pmatrix} x_1 \\ y_1 \\ z_1 \\ \dot{x}_1 \\ \dot{y}_1 \\ \dot{z}_1 \end{pmatrix} \quad \text{and} \quad \vec{P}_2 = \begin{pmatrix} x_2 \\ y_2 \\ z_2 \\ \dot{x}_2 \\ \dot{y}_2 \\ \dot{z}_2 \end{pmatrix}, \tag{2}$$

the distance measure $\vec{\delta} = (\delta_e,\ \delta_v)^T$ of the clustering algorithm is a vector with two components given by

$$\delta_e = \sqrt{(x_1 - x_2)^2 + (y_1 - y_2)^2 + (z_1 - z_2)^2}$$
$$\delta_v = \sqrt{(\dot{x}_1 - \dot{x}_2)^2 + (\dot{y}_1 - \dot{y}_2)^2 + (\dot{z}_1 - \dot{z}_2)^2}. \quad (3)$$

The clustering approach is based on two thresholds θ_e (for the spatial distance) and θ_v (for differences in velocity). Two scene flow points can be assigned to the same cluster if $\delta_e < \theta_e$ and $\delta_v < \theta_v$. Hence, it is not necessary to combine the different features into a single scalar value as it would be necessary for classical clustering approaches such as the *k*-means algorithm [26].

The method in [24] relies on a graph-based technique to establish clusters, where the scene flow points are regarded as the nodes and the distances between them as the edges of the graph. The points are sorted according to the norms of their associated velocities, and the resulting sorted list $S = \{\vec{P}_1, \ldots, \vec{P}_n\}$ is traversed completely. For each point $\vec{P}_i = (x_i, y_i, z_i, \dot{x}_i, \dot{y}_i, \dot{z}_i,)^T$ with $i = 1, \ldots, n$ its distances according to Eq. 3 to the subsequent points in the sorted list are computed. If the velocity distance δ_v to one of the subsequent points falls below the threshold θ_v, the search is terminated. If $\delta_e < \theta_e$ and $\delta_v < \theta_v$, the two points are assigned to the same cluster. Once the complete sorted list has been traversed, indices are assigned to the clusters based on a recursive algorithm.

Important advantages of this clustering algorithm in the context of vehicle detection are its high computational efficiency, its simple parameterization, and the fact that the overall number of clusters does not need to be known in advance. The nontrivial problem of appropriately weighting spatial against velocity coordinates does not occur. Since only velocity differences between neighboring points are regarded, the algorithm avoids a decomposition of rotating objects such as turning vehicles into different clusters – as a result of the velocity components varying continuously along the object axis, such a decomposition would occur for many classical clustering approaches which rely on single scalar distance metrics.

Pose Estimation Based on the ICP Algorithm

The outline in this section of the ICP algorithm is adopted from [25] and [36]; it is extended by the description of a computationally efficient quaternion-based optimization approach. A classical method to register a point cloud to a geometric object model is the iterative closest point (ICP) algorithm introduced in [27]. Given an initial estimate of the object pose, the pose parameters are updated by minimizing the mean squared distance between the scene points and the model, and the point assignment is repeated accordingly. This procedure is applied in an iterative manner. As a result, the algorithm yields the three-dimensional object pose. In [27], this method is applied to the registration of point sets, curves, and surfaces. However, the approach can only be used in situations where all scene points belong to the object as it is a pose estimation rather than a scene segmentation technique.

In the ICP algorithm proposed in [28], the scene points as well as the object model are represented as sets of chained points. During each iteration step, the pose parameters are updated, and at the same time some scene points are assigned to the object model while others are rejected, based on the distance to the object and the similarity of the tangent directions of the scene and model curves. Thus, outliers in the point cloud data are automatically rejected, and the algorithm is robust with respect to disappearing and reappearing object parts as well as partial occlusions. As a result, the algorithm yields the subset of scene points belonging to the object, i.e., a scene segmentation, along with the object pose.

Euclidean Distance Metric (adopted from [36]) For pose estimation of vehicles, a cuboid is utilized as a weak geometric model representing several vehicle types. An initial pose is estimated based on the centroid and the first principal component of the vehicle point cloud. Afterward, the ICP algorithm fits the geometric model to the point cloud. Thus, the translational pose parameters t_x and t_z and the yaw angle θ are updated by minimizing the mean squared distance between the scene points and the model. The distance d_i is the perpendicular between the visible model side and the 3D point in Euclidean space (cf. Fig. 4a), where $\vec{p}_i$ denotes the 3D point and $\vec{p}_{m_i}$ the corresponding point on the model plane:

$$d_i(t_x, t_z, \theta) = \| \vec{p}_i - \vec{p}_{m_i} \| . \quad (4)$$

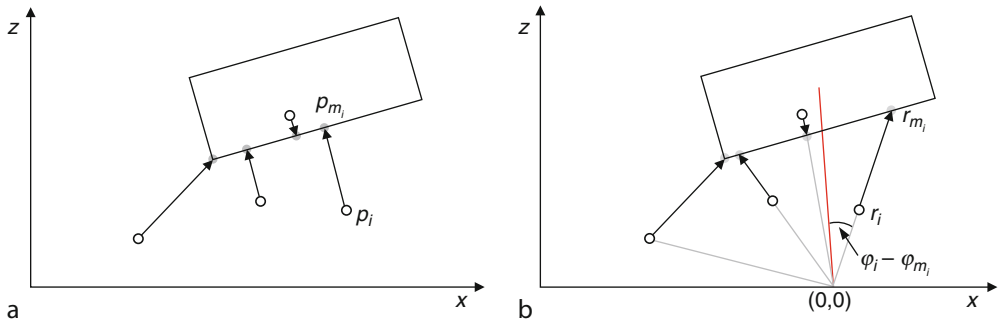

3D Pose Estimation of Vehicles Using Stereo Camera. Figure 4
Illustration of the Euclidean and the polar distance metric

To obtain the vehicle pose, a nonlinear minimization of the error function with respect to the pose parameters t_x, t_z, and θ is performed using the Levenberg–Marquardt algorithm or the Downhill Simplex algorithm [29].

Quaternion-Based Optimization A closed-form solution for the problem of relative orientation between two point clouds with known correspondences is proposed in [30], where quaternions are used for direct parameter estimation. A quaternion $\dot{q}$ is defined by four real numbers q_a, q_b, q_c, and q_d according to

$$\dot{q} = q_a + iq_b + jq_c + kq_d. \tag{5}$$

The last three summands in Eq. 5 can be seen as three "imaginary parts" analogous to the imaginary part of a complex number [31]. Similar to complex numbers, it is $i^2 = j^2 = k^2 = -1$. Unit quaternions are quaternions of norm 1, i.e., $\| \dot{q} \| = 1$. Quaternions allow a much more efficient representation of rotations in 3D space than classical rotation matrices, especially when several rotations are performed subsequently. Calculation rules for quaternions are described in [31].

The measured 3D point cloud is denoted by $\{\vec{w}_{p_i}\}$, the set of corresponding model points by $\{\vec{w}_{m_i}\}$, where $i = 1, \ldots, n$ with n as the number of measured 3D points. Subtraction of the centroids yields the zero-mean transformed 3D point clouds $\left\{\vec{w}'_{p_i}\right\}$ and $\left\{\vec{w}'_{m_i}\right\}$. It is shown in [30] that the determination of the transformation (translation and rotation) between two point clouds requires the determination of the unit quaternion $\dot{q}$ which maximizes the expression

$$\sum_{i=1}^{n} \left(\dot{q}\dot{w}'_{p_i}\dot{q}*\right) \dot{w}'_{m_i} \tag{6}$$

Applying the calculation rules for quaternions to expression (6) yields

$$\dot{q}^T \; N \; \dot{q} \tag{7}$$

to be maximized with respect to $\dot{q}$, where

$$N = \sum_{i=1}^{n} R_{p_i}^T R_{m_i}. \tag{8}$$

In Eq. 8, the matrices R_{p_i} and R_{m_i} are given by

$$R_{p_i} = \begin{pmatrix} 0 & -x'_{p_i} & -y'_{p_i} & -z'_{p_i} \\ x'_{p_i} & 0 & z'_{p_i} & -y'_{p_i} \\ y'_{p_i} & -z'_{p_i} & 0 & x'_{p_i} \\ z'_{p_i} & y'_{p_i} & -x'_{p_i} & 0 \end{pmatrix}$$
$$R_{m_i} = \begin{pmatrix} 0 & -x'_{m_i} & -y'_{m_i} & -z'_{m_i} \\ x'_{m_i} & 0 & z'_{m_i} & -y'_{m_i} \\ y'_{m_i} & -z'_{m_i} & 0 & x'_{m_i} \\ z'_{m_i} & y'_{m_i} & -x'_{m_i} & 0 \end{pmatrix}. \tag{9}$$

The unit quaternion $\dot{q}$ that maximizes expression (8) is then given by the eigenvector $\vec{e}_{\max}$ corresponding to the largest eigenvalue of N. The characteristic polynomial is of degree 4 and can therefore be solved analytically. Based on $\dot{q} = \vec{e}_{\max} = (q_0, q_x, q_y, q_z)^T$, the rotation matrix between the 3D point clouds $\left\{\vec{w}'_{p_i}\right\}$ and $\left\{\vec{w}'_{m_i}\right\}$ is given by

$$R = \begin{pmatrix} q_0^2 + q_x^2 + q_y^2 - q_z^2 & 2(q_x q_y - q_0 q_z) & 2(q_x q_z + q_0 q_y) \\ 2(q_y q_x + q_0 q_z) & q_0^2 - q_x^2 + q_y^2 - q_z^2 & 2(q_y q_z + q_0 q_x) \\ 2(q_z q_x + q_0 q_y) & 2(q_z q_y + q_0 q_x) & q_0^2 - q_x^2 - q_y^2 + q_z^2 \end{pmatrix}. \tag{10}$$

This analytical approach is computationally highly efficient. For noisy data, however, it suffers from a low robustness as it inherently yields a solution defined by the least-mean-squared Euclidean distance between the points, which is strongly influenced by outliers. Furthermore, when an object model defined by planes is used, the point-to-plane matching can only be performed once before determining the transformation.

As a consequence, it is favorable to combine the analytical optimization technique according to [30] with the ICP approach in order to obtain an algorithm which is faster than the nonlinear optimization scheme but also robust with respect to outliers. The initial pose is again determined based on the centroid and the first principal component of the point cluster representing the moving object. In a first step, point-to-plane matching is performed to obtain the closest point $\vec{p}_{m_i}$ on the model surface for each 3D point $\vec{p}_i$, where the Euclidean distance between $\vec{p}_i$ and $\vec{p}_{m_i}$ is denoted by $d_i = \| \vec{p}_i - \vec{p}_{m_i} \|$. The previously described quaternion-based technique according to [30] yields an analytical solution for the rotation and translation parameters between the 3D point cloud and the cloud of corresponding points on the model surface by minimizing the mean-squared Euclidean distance.

To "imitate" the behavior of an M-estimator in the quaternion-based optimization scheme, each point is weighted with the fair weighting function $w_f\left(d_i^{(0)}\right)$ prior to the optimization procedure, where $d_i^{(0)}$ is the initial Euclidean distance of the i-th 3D point from the model surface. The fair weighting function is given by

$$w_f(x) = \frac{1}{1 + \frac{|x|}{c}} \tag{11}$$

with c as a user-defined parameter. The corresponding error function E_{quat} then amounts to

$$E_{\text{quat}} = \sum_{i=1}^{N} \left[\| \vec{p}_i - \vec{p}_{m_i} \| \, w_f\left(d_i^{(0)}\right) \right]^2. \tag{12}$$

Once the pose refinement step has been performed, remaining outliers are eliminated from the point cloud. The quaternion-based optimization procedure is iterated once or twice, where the points are reweighted according to Eq. 12 for each iteration. The behavior of the quaternion-based optimization is similar to that of a direct nonlinear minimization of the Euclidean distances with an M-estimator error function as long as the pose refinement determined by that operation is small.

For the real-world data regarded in section "Experimental Evaluation" a general observation is that if the original, unweighted 3D points are used in the quaternion-based optimization scheme, the resulting pose accuracy strongly degrades especially for the yaw angle. The computation time of the quaternion-based optimization scheme is about 40 times lower than that of the nonlinear ICP methods (cf. section "Computational Efficiency").

Polar Distance Metric (adopted from [36]) The ICP algorithm with the Euclidean metric does not take into account the properties of the stereo measurement process. When reconstructing 3D points from two cameras, the relation between the disparity and the depth is nonlinear. This results in a low accuracy for points which are far away from the camera, while points close to the camera have a higher accuracy. The noise of the point positions is neither Gaussian nor symmetric. The Euclidean metric used in the standard ICP assumes at least a symmetric error distribution of the measurements. To overcome this problem one might think of transforming the geometric model into disparity space (pixel coordinates and disparities), which may be very complex depending on the model. It is thus preferable to use a distance metric which takes into account the nonlinearity of the measurement error.

The 3D points are represented in polar coordinates (cf. Fig. 4b) on the xz plane, where the distance is $r(x, y, z) = \sqrt{x^2 + y^2 + z^2}$ and the polar angle amounts to $\varphi = \arctan(x/z)$. Assuming an ideal pinhole camera model, the pixel coordinates (u, v) can be transformed into the 3D coordinates according to $u/f = x/z$ and $v/f = y/z$, where f denotes the camera constant measured in pixel units. Assuming a standard epipolar geometry, the depth coordinate z can be calculated by $z = bf/d$, where b is the baseline distance in meters and d the disparity in pixels. Using these

equations, the distance to the camera $r(u, v, d)$ is given by

$$r(u, v, d) = \sqrt{\left(\frac{bu}{d}\right)^2 + \left(\frac{bv}{d}\right)^2 + \left(\frac{bf}{d}\right)^2}. \quad (13)$$

An error calculation based on the total differential dr is used to analyze the relations of the depth measurement process:

$$dr = \frac{\partial r}{\partial u} du + \frac{\partial r}{\partial v} dv + \frac{\partial r}{\partial d} dd \quad (14)$$

Converting these terms into three-dimensional world coordinate expressions results in the following relations:

$$\begin{aligned} \frac{\partial r}{\partial u} &= \frac{x}{f}\frac{z}{r} \\ \frac{\partial r}{\partial v} &= \frac{y}{f}\frac{z}{r} \\ \frac{\partial r}{\partial d} &= \frac{z^3}{bfr}. \end{aligned} \quad (15)$$

The term z/r is smaller than or equal to 1. The terms x/f, y/f, and z/f all have the same order of magnitude. The measurement errors du and dv of the pixel coordinates u, v, and the disparity measurement error dd are of the order 0.1–1 pixels and independent of z and r. In our scenario, one can assume that $z/b \gg 1$, whereby the measurement error dr largely depends on the disparity error dd. Accordingly, dr is approximately proportional to z^2.

Hence, this error analysis yields the result that the normalized measurement error dr/z^2 has an approximately Gaussian distribution. The error distribution of the polar angle φ is also approximately of Gaussian shape. This results in an error function E for the model fit which consists of an error term regarding the distance of a 3D point to the model and a second error term regarding the polar angle difference, combined by the weight factor λ:

$$E(\{r_i\}, \{z_i\}, \{\varphi_i\}) = \sum_{i=1}^{N} \left[E_r^2(r_i, z_i) + \lambda E_\varphi^2(\varphi_i)\right]. \quad (16)$$

The first error term E_r only depends on distances from the camera, where r_i is the distance of the object point i to the camera and r_{m_i} the distance to the camera of the intersection point of the same line of sight with the model:

$$E_r(r_i, z_i) = \frac{r_i - r_{m_i}}{z_i^2}. \quad (17)$$

The second error term E_φ only depends on the polar angles:

$$E_\varphi(\varphi_i) = \frac{\varphi_i - \varphi_M}{2}(1 + \tanh|\alpha(|\varphi_i - \varphi_M| - \beta)|). \quad (18)$$

The hyperbolic tangent enforces continuity of the angular error function and is required for the convergence behavior of the optimization. The value φ_M denotes the polar angle of the center point of the model. The parameter β corresponds to about half the angular width of the model projected into the image plane, whereas α is a user-defined parameter which influences the optimization behavior. Error function (16) can be minimized in the same manner as the error function involving the Euclidean metric using a nonlinear optimization method.

Computational Efficiency For the ICP approaches described in sections "Euclidean Distance Metric" and "Polar Distance Metric" involving standard nonlinear minimization techniques, the repeatedly performed point-to-plane matching and distance evaluation may lead to a significant computational burden of the ICP algorithm with polar coordinates. The C++ implementation requires about 1 ms computation time on a single 2 GHz core for 100 points, where the computation time increases linearly with the number of points. In the application scenario of section "Experimental Evaluation," the object is typically represented by 200–400 points. The computational efficiency of the quaternion-based optimization scheme (cf. section "Quaternion-Based Optimization") is about 40 times higher than that of the nonlinear ICP methods.

Model-Based Scene Flow

In this section, a temporal extension of the concept of model-based stereo is described, which is termed model-based scene flow. This method aims for a computation of the 3D pose of the object and an instantaneous estimation of its temporal derivative using two subsequent stereo image pairs, thus avoiding

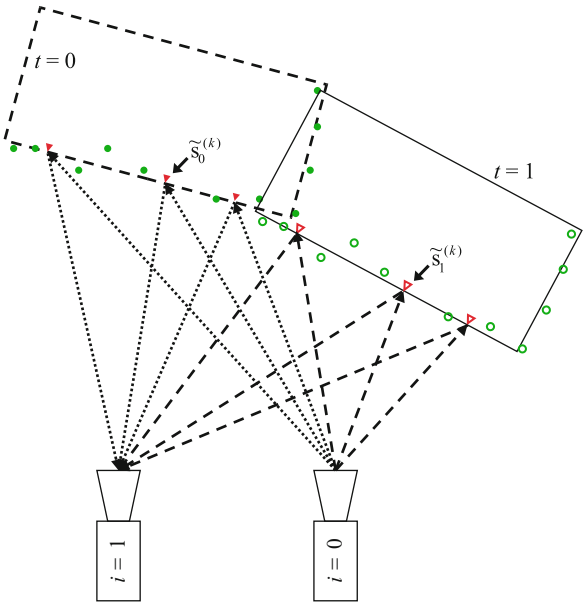

3D Pose Estimation of Vehicles Using Stereo Camera. Figure 5
Principle of model-based scene flow. *Circles*: 3D points, *triangles*: corresponding points on the model surface

a temporal filtering stage. To initialize the lateral velocity $\dot{t}_x$ of the vehicle, information provided by the optical flow field of the right camera is used. The velocity $\dot{t}_z$ along the depth axis and the yaw rate $\dot{\theta}$ are initially unknown, such that their values are initialized by zero.

The basic idea of model-based scene flow estimation is to use the model surface together with the pose parameters and their temporal derivatives to obtain the homographies that determine image points corresponding to each other in all four images. Pose and motion parameters are used to connect images taken at the same time by different cameras and images acquired at different times, respectively (cf. Fig. 5). Image windows of predefined size around the K reprojected points are extracted from the four images (cf. Fig. 6). Each of the four images I_{it} is identified by two indices i and t, where the right image is denoted by the index $i = 0$ and the left image by $i = 1$, while the previous time step is denoted by the index $t = 0$ and the current time step by $t = 1$.

The 3D model is assumed to be composed of planes, which is always the case for tessellated models

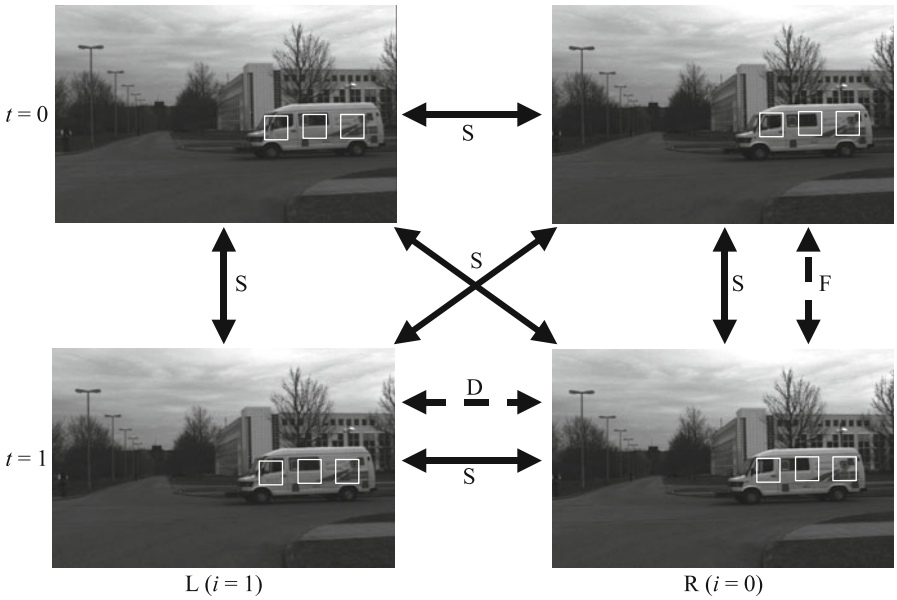

3D Pose Estimation of Vehicles Using Stereo Camera. Figure 6
Determination of optical flow (F), disparity (D), and scene flow (S)

like the cuboid used in section "Experimental Evaluation." The projective vector $\tilde{q}_{i't'}^{(k)}$ of the pixel coordinates of window k in image i' at time step t' is obtained from the corresponding projective vector $\tilde{q}_{it}^{(k)}$ in image i at time step t by the homography ${}_{it}^{i't'}H^{(k)}$ induced by the model plane on which the center of window k is located. It is thus

$$\tilde{q}_{i't'}^{(k)} = {}_{it}^{i't'}H^{(k)}\,\tilde{q}_{it}^{(k)} \tag{19}$$

with $k = 1, \ldots, K$. The homography ${}_{it}^{i't'}H^{(k)}$ depends on the known extrinsic and intrinsic camera parameters and on the pose at time steps t and t' of the model plane on which patch k is located, which follows from the 3D pose parameters of the object and their temporal derivatives.

A detailed description of the concept of the homography induced by a plane is given in [32]. Effectively, the determination of the homography ${}_{it}^{i't'}H^{(k)}$ between the views of camera i at time step t and camera i' at time step t' relies on the following procedure (cf. Fig. 5): The first step is the computation of the intersection point $\tilde{s}_t^{(k)}$, at time step t between the ray that belongs to the image point $\tilde{q}_{i't'}^{(k)}$ and the model plane at time step t on which the center of window k is located. If $t \neq t'$, the point $\tilde{s}_t^{(k)}$, which is a 3D point in the scene, has to be adjusted according to the object motion between the time steps t and t', resulting in the point $\tilde{s}_{t'}^{(k)}$. This adjustment consists of a rotation and a translation readily inferred from the temporal derivatives of the pose parameters. If $t = t'$, $\tilde{s}_{t'}^{(k)} = \tilde{s}_t^{(k)}$. The point $\tilde{s}_{t'}^{(k)}$, is then projected into camera i', resulting in the corresponding image point $\tilde{q}_{i't'}^{(k)}$.

The error function E_{msf} minimized by the model-based scene flow algorithm consists of the sum over the six pairwise similarity measures between the projected image patches according to

$$E_{msf} = \sum_{k,i,t,i'\neq i,t'\neq t} S\left(I_{it}\left(\tilde{q}_{it}^{(k)}\right),\ I_{i't'}\left(\tilde{q}_{i't'}^{(k)}\right)\right) \tag{20}$$

where S denotes the similarity measure, $I_{it}\left(\tilde{q}_{it}^{(k)}\right)$ the window around the point $\tilde{q}_{it}^{(k)}$ in image i at time step t, and $I_{i't'}\left(\tilde{q}_{i't'}^{(k)}\right)$ the corresponding window in image i' at time step t', warped by the homography ${}_{it}^{i't'}H^{(k)}$. Warping is required to account for the difference in perspective between the views.

The zero-mean sum of squared differences (SSD) and the normalized cross-correlation coefficient (NCC) are used as the similarity measure S. A Sobel edge detector is used as an interest operator to select windows which display a significant amount of contrast. The parameters describing the 3D pose and its temporal derivatives are obtained by minimizing (SSD) or maximizing (NCC) Eq. (20) using the Gauss–Newton algorithm. If only one stereo image pair is regarded, optimization of Eq. 20 yields a pose estimation according to the concept of model-based stereo.

The computational efficiency of the model-based scene flow is typically comparable to that of the ICP approach with classical optimization (i.e., without quaternions) as described in sections "Euclidean Distance Metric" and "Polar Distance Metric."

Experimental Evaluation

This section presents an evaluation of the ICP-based approach and the model-based scene flow stage. It partially draws upon the description in [36]. Three color cameras with a resolution of 1,034 × 776 pixels were used for image acquisition. The cameras were mounted side by side at different displacements, resulting in three different baseline distances b of 0.102, 0.228, and 0.380 m. The frame rate of the sequences is about 14 fps. The color information is only used for ground truth calculation, whereas for the stereo algorithms the images were converted to grayscale. Several colored markers have been attached to the vehicle, and a color classifier was used to extract the markers in the images. Afterward, the corner positions in each image were estimated by a highly accurate corner detector [33] at sub-pixel accuracy. The corner positions were used for bundle adjustment to compute the three-dimensional world coordinates of each corner point. Four markers were attached to each side of the vehicle, such that the corresponding plane is overdetermined. The colored markers hardly display a contrast in the grayscale images and therefore do not generate additional 3D points or optical flow vectors.

The system performs a frame-by-frame 3D pose estimation without any temporal filtering (tracking by detection). The 3D point cloud is clustered to obtain

the scene part which represents the vehicle. The first principal component of this point cloud is used to initialize the angular pose parameter.

A set of seven different scenes, each of which was recorded with three different stereo baseline distances, is used. These sequences display a moving vehicle on a road crossing in typical intersection situations, either passing straight through the intersection or turning left or right at different velocities, where the distance of the object from the camera amounts to 15–30 m. (The images and reference data are publicly available at http://aiweb.techfak.uni-bielefeld.de/content/vehicle-pose-data-set.) The evaluation is based on two geometric indicators: the yaw angle difference between the true yaw angle and the pose estimation result and the mean distance of the ground truth points to the corresponding model planes. The differences are visualized using error bars denoting the median of the full sequence and the 25% and the 75% quantiles, respectively.

For the images rectified to standard stereo geometry, the effective principal distance amounts to $f = 1{,}350$ pixels, such that $bf = 307.8$ m pixel for the medium baseline distance of $b = 0.228$ m. According to [33], the difference between two checkerboard corner positions (i.e., a disparity value) can be measured with an accuracy (here corresponding to one-half of the difference between the 25% and the 75% quantiles) of $\Delta d = 0.032$ pixels. At a typical object distance from the camera of $z_0 = 20$ m, the disparity thus amounts to $d_0 = bf/z_0 = 15.39$ pixels, resulting in a depth difference accuracy of $\sqrt{2}[bf/d_0 - bf/(d_0 + \Delta d)] = 0.059$ m (cf. law of error propagation). The distance in the scene between the pairs of markers attached to the frontal and the rear part of the vehicle amounts to about 3 m, such that the

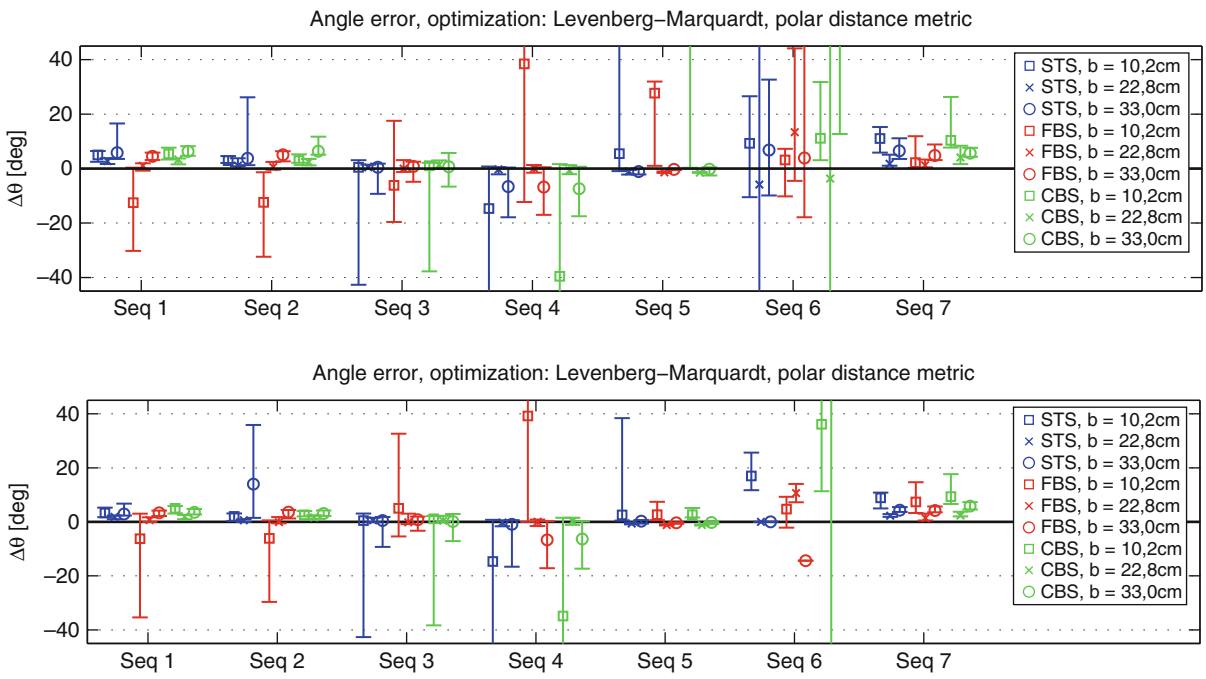

3D Pose Estimation of Vehicles Using Stereo Camera. Figure 7
Dependence of the yaw angle error (denoted by $\Delta\theta$) on the stereo baseline; Levenberg–Marquardt optimization, polar distance metric. *Upper diagram*: all images; *lower diagram*: rear views excluded. Blue color denotes the spacetime stereo technique (STS), red color the feature-based stereo (FBS), and green color the correlation-based stereo (CBS). The small baseline is marked by squares, the intermediate baseline by crosses, and the large baseline by circles. The intermediate baseline distance is most favorable with respect to the yaw angle error

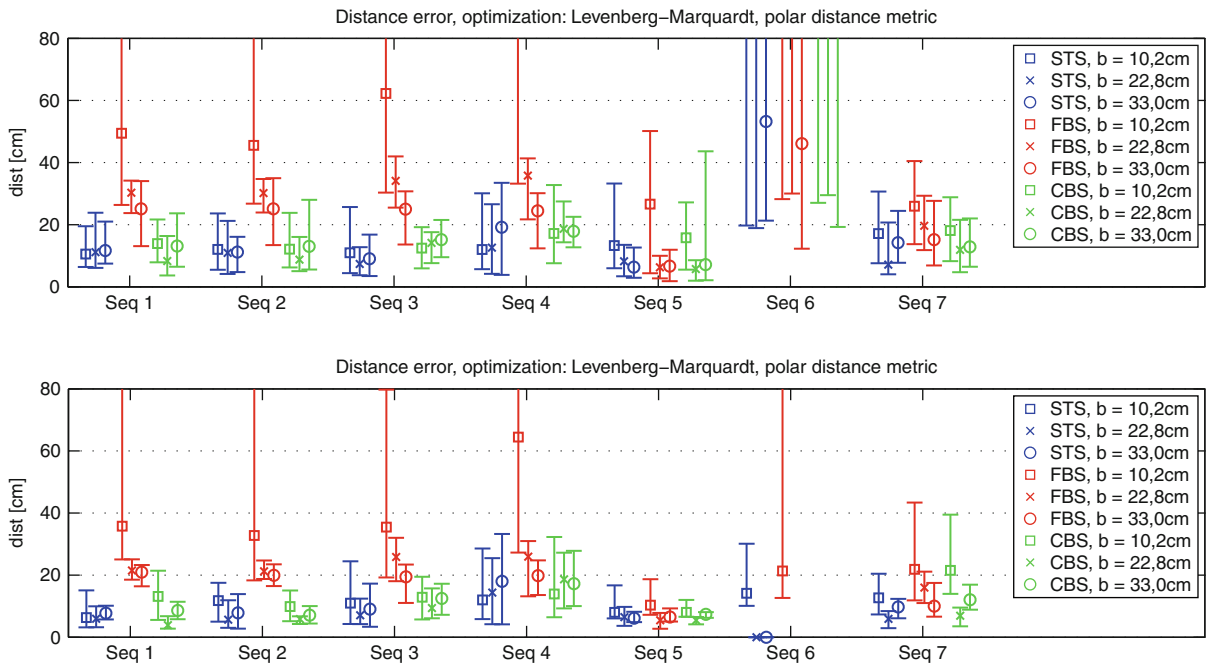

3D Pose Estimation of Vehicles Using Stereo Camera. Figure 8

Dependence of the distance error on the stereo baseline; Levenberg–Marquardt optimization, polar distance metric. *Upper diagram*: all images; *lower diagram*: rear views excluded. Colors and markers as in Fig. 7

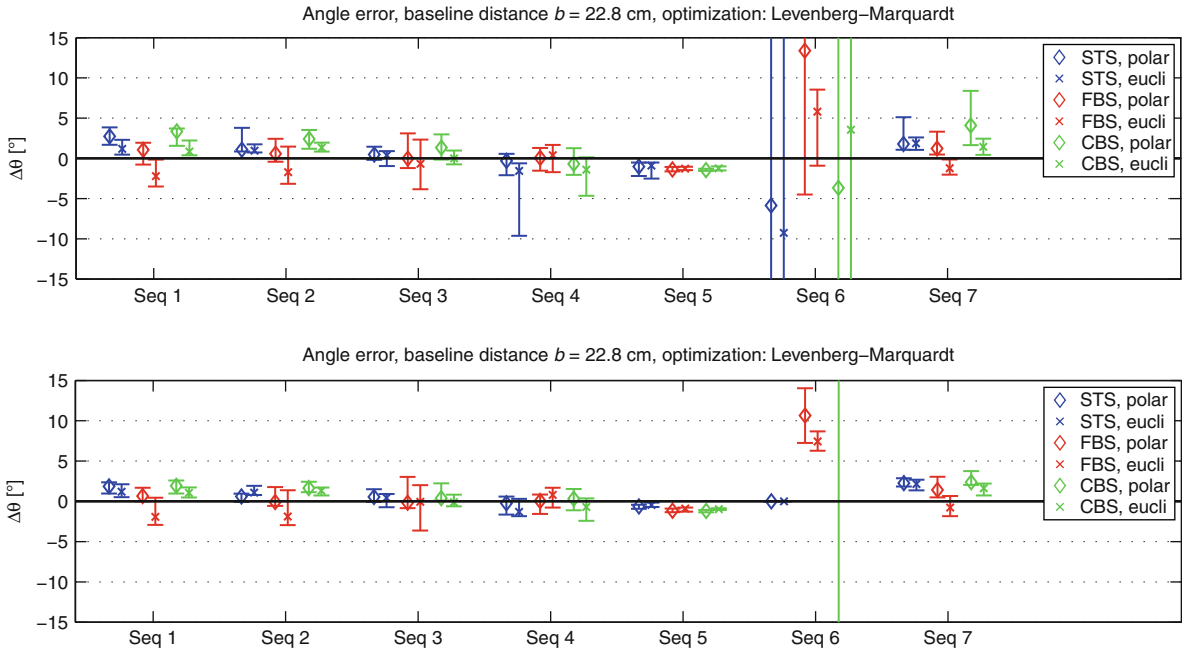

3D Pose Estimation of Vehicles Using Stereo Camera. Figure 9

Dependence of the yaw angle error (denoted by $\Delta\theta$) on the stereo algorithm; Levenberg–Marquardt optimization, intermediate stereo baseline. *Upper diagram*: all images; *lower diagram*: rear views excluded. The colors (blue, red, and green) denote the stereo algorithm, while diamonds represent the polar metric and stars the Euclidean metric

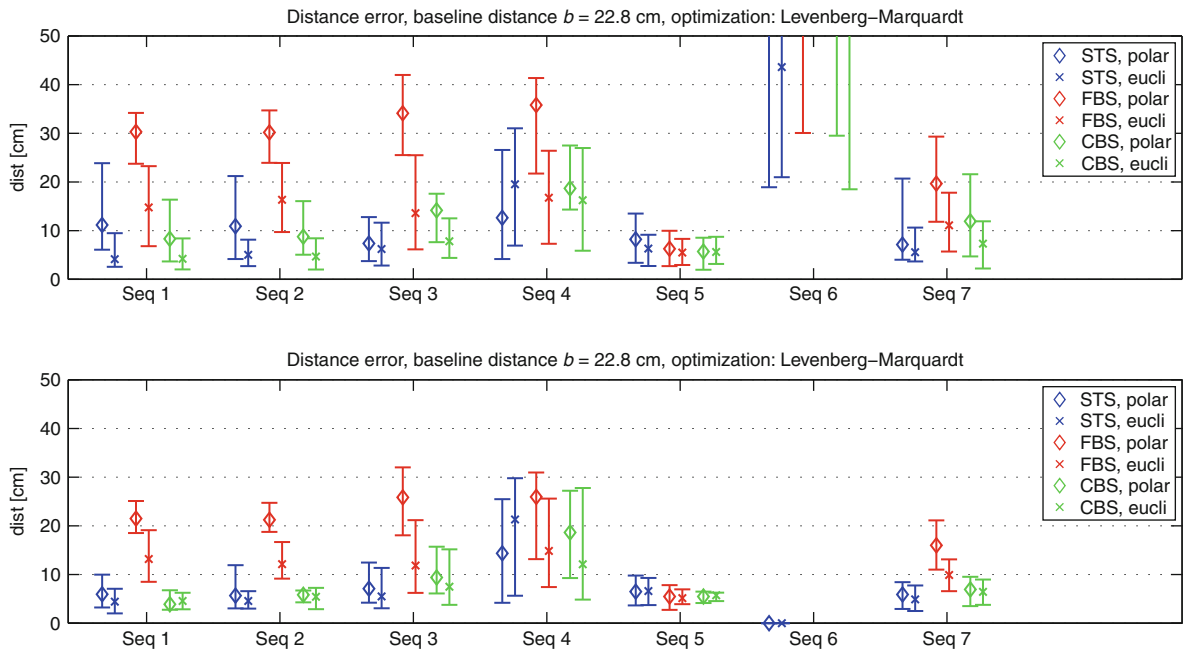

3D Pose Estimation of Vehicles Using Stereo Camera. Figure 10

Dependence of the distance error on the stereo algorithm; Levenberg–Marquardt optimization, intermediate stereo baseline. *Upper diagram*: all images; *lower diagram*: rear views excluded. Colors and markers as in Fig. 9

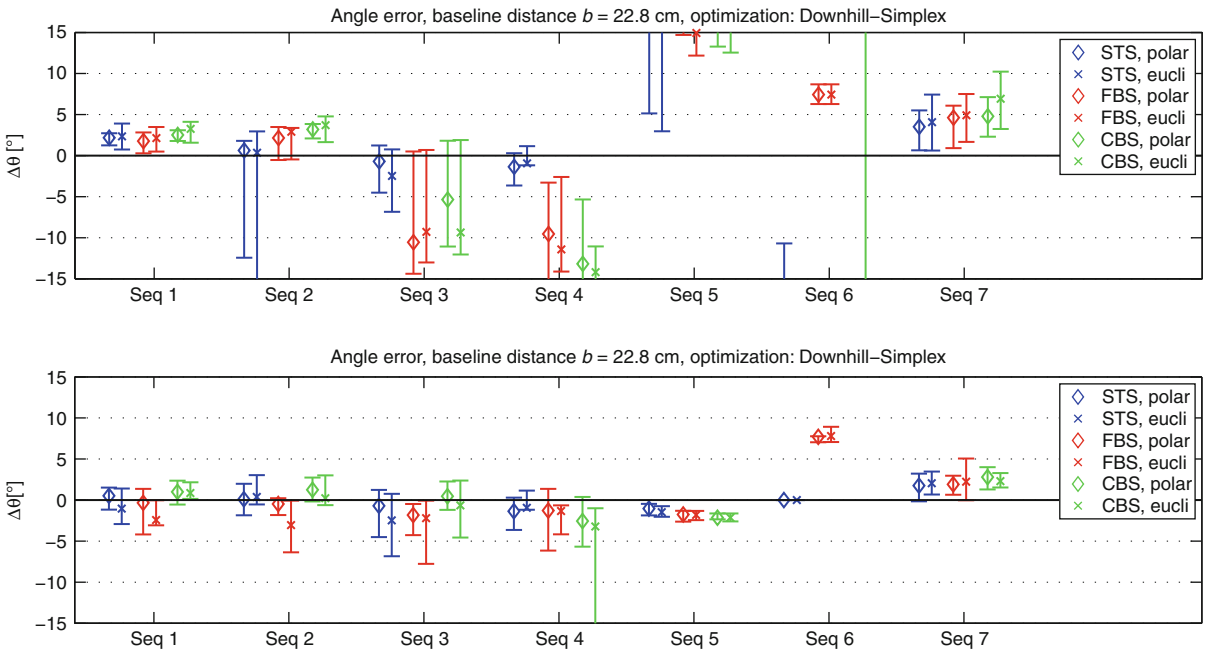

3D Pose Estimation of Vehicles Using Stereo Camera. Figure 11

Yaw angle error for Downhill Simplex optimization, intermediate stereo baseline. *Upper diagram*: all images; *lower diagram*: rear views excluded. Colors and markers as in Fig. 9

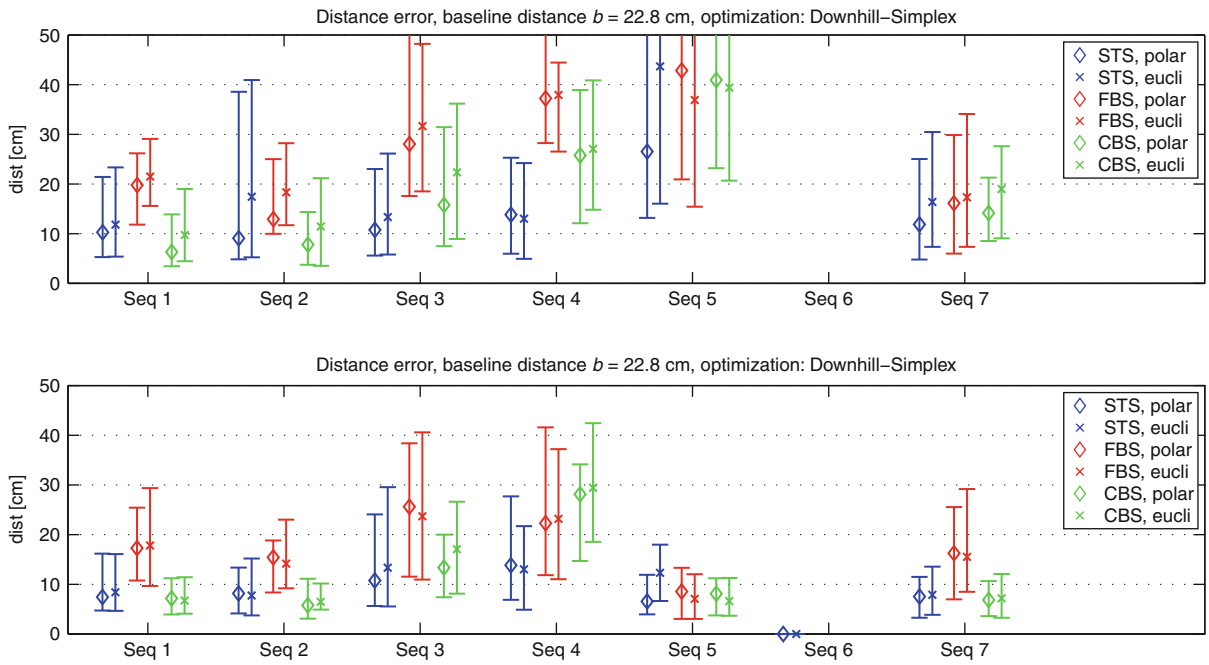

3D Pose Estimation of Vehicles Using Stereo Camera. Figure 12
Distance error for Downhill Simplex optimization, intermediate stereo baseline. *Upper diagram*: all images; *lower diagram*: rear views excluded. Colors and markers as in Fig. 9

lowest accuracy of the yaw angle, which occurs when the vehicle is observed laterally, corresponds to 1.1°. The absolute depth and yaw angle errors are proportional to z_0^2.

Evaluation of the ICP-Based 3D Pose Estimation

This section provides an evaluation of the ICP-based approach with respect to the influence of the baseline distance of the stereo camera system, the employed stereo algorithm, the distance metric, and the optimization algorithm used for minimizing the error function with respect to the pose parameters. In Figs. 7–12, the median values and 25% and 75% quantiles of the deviations of the inferred pose parameters from their ground truth values are determined (1) based on all images of each sequence (upper diagram) and (2) based on all images in which the extension of the 3D point cloud in x direction is at least 20% larger than the vehicle width (lower diagram). The second evaluation has been added because the pose estimation result is expected to be rather unreliable for frontal and rear views of the vehicle due to the resulting small number of 3D points on its longer side.

Baseline Distance (adopted from [36]) The first part of the evaluation analyzes the different baseline distances of the sequences. Figure 7 shows the yaw angle error and Fig. 8 the distance error for the three different baseline distances for all seven sequences using the three different stereo approaches described. The comparison between the different baseline distances shows that the smallest baseline is not sufficient for our application. Especially for vehicles turning left or right in front of the camera (sequences 3 and 4) the errors are large. The largest baseline also produces larger errors, since due to the large camera displacement and the resulting parallax effects the stereo algorithms produce a smaller number of correct correspondences.

Stereo Algorithm (adopted from [36]) To evaluate the different stereo algorithms, tracking results are

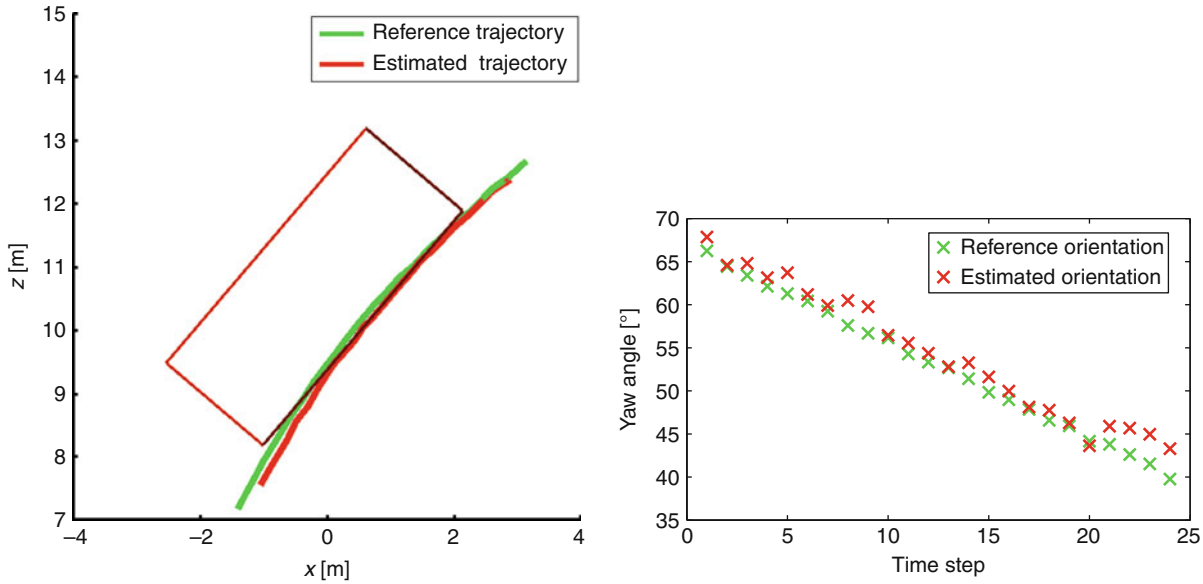

3D Pose Estimation of Vehicles Using Stereo Camera. Figure 13
Left: Trajectory for sequence S5 with the vehicle model drawn for one time step, depicting the position of the center of the lateral model surface. *Right*: Behavior of the yaw angle for the same sequence

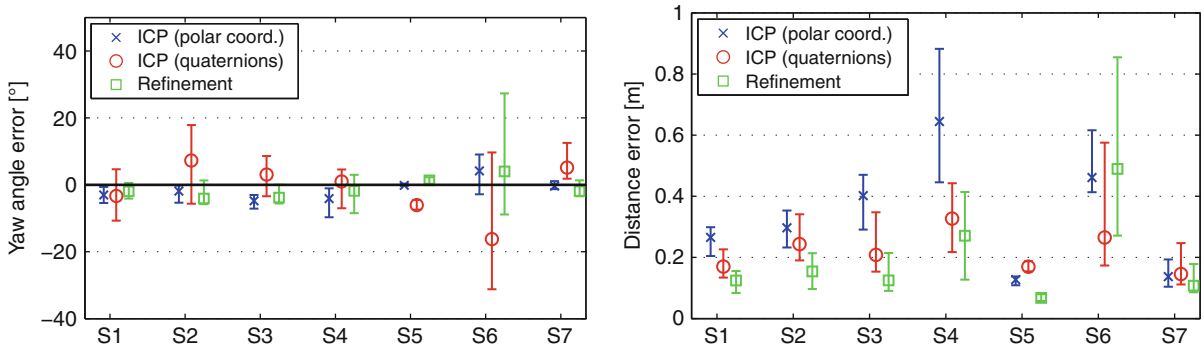

3D Pose Estimation of Vehicles Using Stereo Camera. Figure 14
Yaw angle error (*left*) and distance error (*right*). Symbols denote the median values and error bars the 25% and 75% quantiles. "Refinement" denotes the result of model-based scene flow

computed for all sequences with the intermediate baseline distance and the Levenberg–Marquardt algorithm. Figures 9 and 10 show the results of the different stereo algorithms, where both distance metrics (Euclidean and polar) are evaluated. The results for the yaw angle error show that the difference between the pixel accurate feature-based stereo and the other two algorithms with sub-pixel accuracy is negligible. The results are similar for all three stereo algorithms. However, regarding the vehicle position, a difference between pixel and sub-pixel accuracy is noticeable. The distances of the feature-based stereo results show an up to three times higher error for sequences 1, 2, and 3. No significant difference between the spacetime stereo and the correlation-based stereo can be found.

Distance Metric (adopted from [36]) Figures 9 and 10 show the pose estimation errors for the two distance

metrics. For the position error both metrics have a similar performance, whereas the polar distance metric produces a smaller yaw angle error for most sequences. The computation time for the polar metric is the same as for the Euclidean metric.

Optimization Algorithm (adopted from [36]) The results of the Downhill Simplex optimization are shown in Fig. 11 for the yaw angle error and in Fig. 12 for the error of the average distance between the ground truth points and the corresponding model planes. The yaw angle errors are all higher for the Downhill Simplex algorithm. Considering that the number of function calls of the Levenberg–Marquardt algorithm is of the same order of magnitude (about 100 function calls) as for the Downhill Simplex algorithm with a better pose estimation accuracy, the Levenberg–Marquardt algorithm appears to be preferable. The distance errors show a similar behavior.

Evaluation of the Model-Based Scene Flow Stage

For the evaluation of the model-based scene flow stage, an initial pose is computed using the quaternion-based ICP algorithm according to section "Quaternion-Based Optimization." The stereo baseline is set to $b = 0.228$ m, corresponding to the configuration which turned out to yield the most accurate pose estimation results according to section "Evaluation of the ICP-Based 3D Pose Estimation." Figure 13 depicts an example trajectory and the estimated yaw angle for sequence S5. The reference trajectory is obtained using the average position of the four colored markers. The estimated trajectory is generated based on the center of the corresponding model surface.

The reference data for the temporal pose derivatives are obtained by numerical differentiation of the pose reference data with respect to time. Since the resulting yaw rate is too noisy to provide sufficiently reliable reference values, a fourth-order polynomial fitted to the differentiated yaw angle reference values is used as reference data for the yaw rate. In Figs. 14 and 15, the deviations between the estimated pose parameters and their temporal derivatives and the corresponding reference values are visualized by error bars denoting the median over the sequence and the 25% and the 75% quantiles, respectively. The model-based scene flow method is always initialized with the result of the quaternion-based ICP approach.

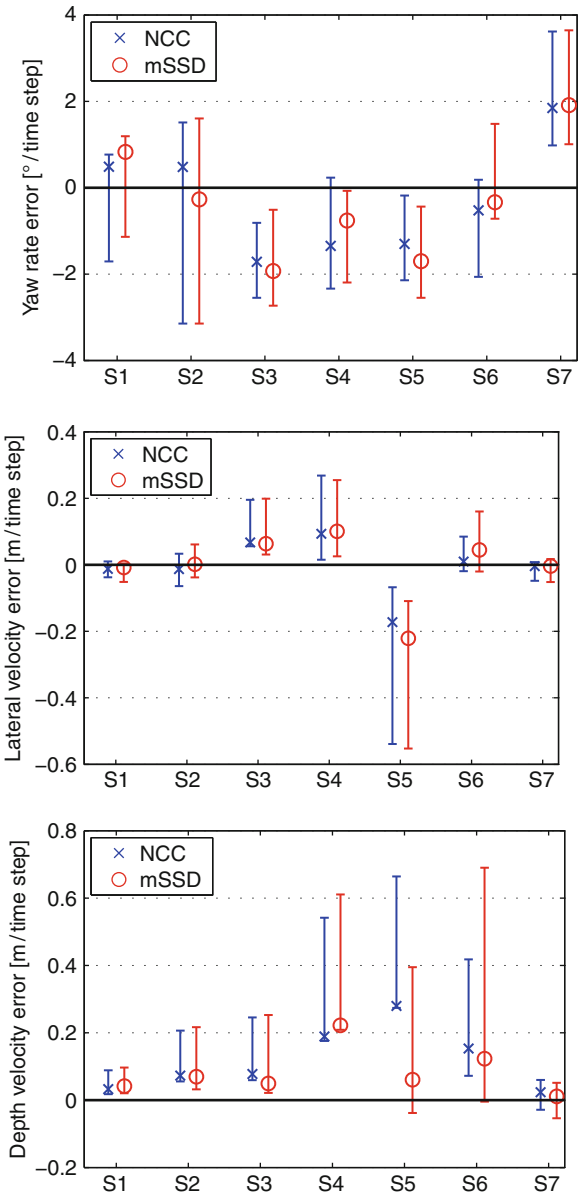

3D Pose Estimation of Vehicles Using Stereo Camera. Figure 15
Error of the yaw rate (*top*), horizontal velocity (*middle*), and the velocity along the depth axis (*bottom*). Symbols denote the median values and error bars the 25% and 75% quantiles

The average yaw angle accuracy of the nonlinear ICP approach with polar coordinates is about three

3D Pose Estimation of Vehicles Using Stereo Camera. Figure 16
Example sequence showing a passenger car turning right

times higher than that of the quaternion-based solution, i.e., 2.4° ± 2.1° versus 4.3° ± 6.3° (cf. Fig. 14, top). The average yaw angle error of the model-based scene flow method amounts to 1.8° ± 3.4°. The fairly large error interval is mainly caused by the high uncertainty observed for sequence S6 while the errors are comparable to those of the nonlinear ICP approach for all other sequences. The average positional error of the quaternion-based ICP is lower by one third than that of the nonlinear ICP (0.21 ± 0.07 m vs. 0.31 ± 0.08 m); the model-based scene flow method yields a comparable average error value of 0.19 ± 0.11 m (cf. median values in Fig. 14, bottom).

The accuracy of the yaw rate estimated with the model-based scene flow approach, averaged over all test sequences, corresponds to 1.2° ± 1.3° per time step (cf. Fig. 15). The average horizontal velocity error amounts to 0.06 ± 0.07 m per time step, while the average error of the velocity component along the depth axis is somewhat higher and corresponds to 0.11 ± 0.09 m per time step. For the model-based scene flow method, the evaluation results do not show significant differences between the zero-mean SSD and the NCC similarity measures. Comparably large errors mainly occur for sequences S4, S5, and S6, where in most images the object is far away from the camera ($z \approx 30$ m) and only its rear side is visible.

As a further example, a short image sequence of 1.5 s length is regarded, showing a passenger car performing a turning maneuver (cf. Fig. 16). The image size amounts to 640 × 480 pixels, the frame rate is 12 fps, and the baseline distance corresponds to 0.3 m. In the regarded traffic setting, no photogrammetric markers could be attached to the vehicle and thus no reference data are available. The position (t_x, t_z) and the yaw angle θ determined with the model-based scene flow method illustrate that the vehicle moves laterally from the right to the left, approaches the camera, and performs a rotation by about 25°, corresponding to an average yaw rate of about 1.4° per time step (cf. Fig. 17). The measurements of the instantaneous yaw rate $\dot{\theta}$ are somewhat noisy but consistently indicate a value slightly decreasing from about 1.5 to 1.0° per time step. The measured instantaneous lateral velocity $\dot{t}_x$ of 0.14–0.18 m per time step is consistent with the behavior of the lateral position t_x over time. The measurements of the depth velocity $\dot{t}_z$ are rather noisy but illustrate that the model-based scene flow method is able to instantaneously detect small velocity components along the depth axis of only a few centimeters per time step, corresponding to less than a percent of the depth itself. At the end of the sequence, the depth velocities are close to zero since the vehicle moves more laterally with respect to the camera than at the beginning.

Summary and Conclusion

This study has described and evaluated approaches for three-dimensional pose estimation of vehicles using a stereo camera. After computation of stereo and optical flow information, a graph-based clustering stage in the space spanned by the spatial and velocity coordinates separates the static from the moving objects in the scene. An iterative closest point algorithm (ICP) estimates the vehicle pose using a cuboid as a weak vehicle model. A classical nonlinear optimization and a computationally efficient quaternion-based analytical

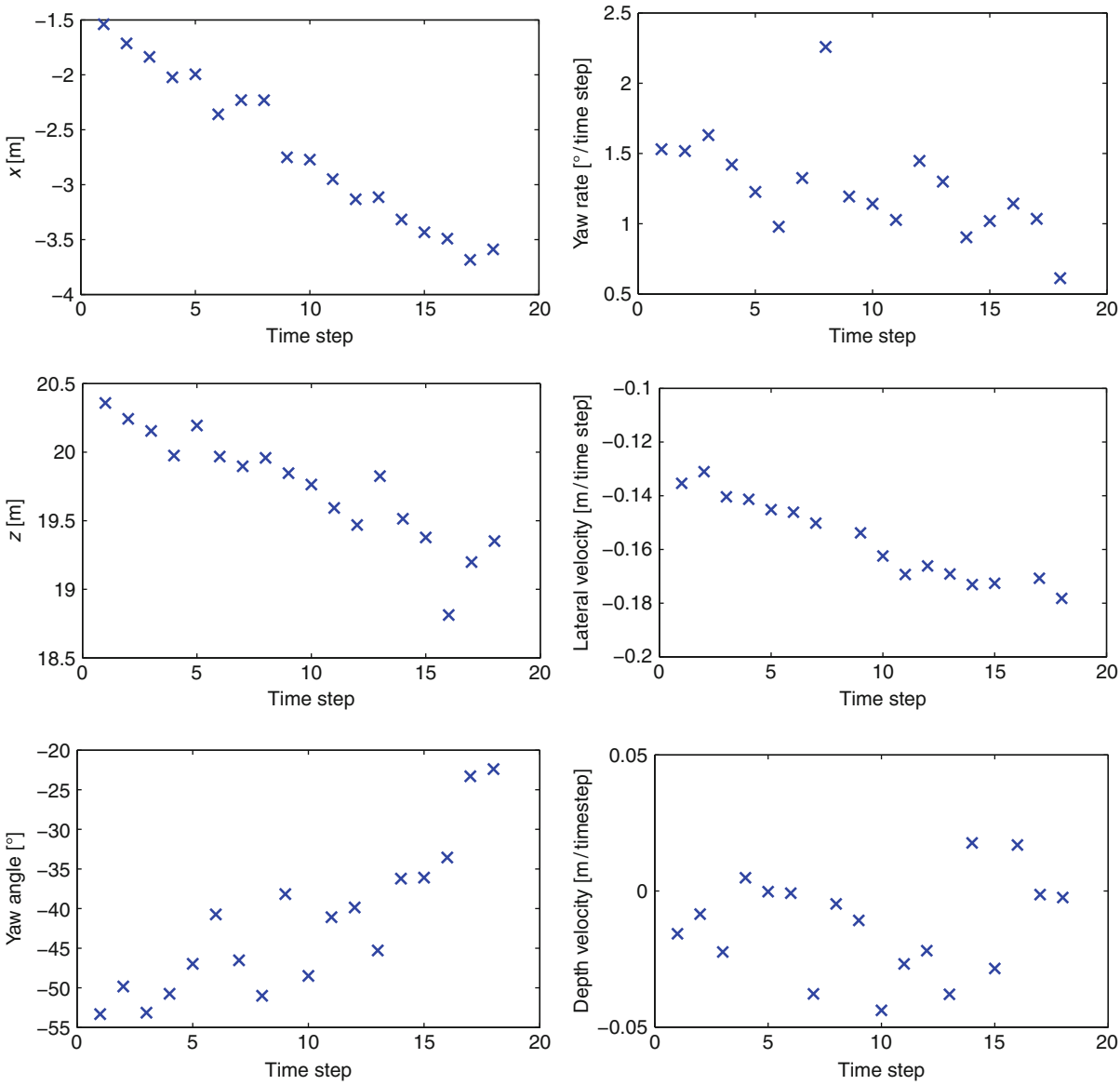

3D Pose Estimation of Vehicles Using Stereo Camera. Figure 17
Pose parameters and their temporal derivatives estimated with the model-based scene flow method for the image sequence shown in Fig. 16

approach relying on the Euclidean distance metric have been compared to a distance metric based on polar coordinates which takes into account the properties of the stereo measurement process. The tracking-by-detection approach has been employed, such that no temporal filtering (e.g., Kalman filtering) has been applied. The algorithm has been evaluated on seven different real-world sequences with respect to different stereo algorithms, baselines, distance metrics, and optimization algorithms. The first part of the evaluation has regarded all images of all sequences, while in a second part the images in which the vehicle is oriented longitudinally with respect to the camera have been excluded. For most of the sequences, the pose

estimation yields reliable results for about 90% of the time steps. Only in sequence S6 the vehicle drives nearly parallel to the z axis, leading to a small projected extension of the 3D point cloud in x direction, resulting in unreliable pose estimation results for more than 90% of the frames of that sequence.

Furthermore, a method for model-based estimation of 3D pose parameters and their instantaneous temporal derivatives has been examined in the context of moving vehicle detection. The quaternion-based ICP algorithm has been used for initialization. Pose refinement and estimation of the temporal pose derivatives are again performed without relying on temporal filtering, using a model-based scene flow method where 3D points on the object surface are reprojected into pairs of stereo images acquired at subsequent time steps and similarities between image windows extracted around the reprojected points are maximized.

The evaluation shows that for obstacles in a range between 10 and 30 m ahead of the ego-vehicle, the intermediate baseline distance of 0.228 m is preferable. In that scenario a sub-pixel accurate stereo algorithm yields up to three times higher distance accuracies when compared to a pixel accurate algorithm. To minimize the point distances in the ICP algorithm, the Levenberg–Marquardt algorithm yields better accuracies than the Downhill Simplex optimization while the number of function calls is comparable. The proposed polar distance metric is preferable to the Euclidean distance metric as for most sequences it yields a higher accuracy of the estimated yaw angle, especially for the pixel accurate stereo algorithm. If this most favorable configuration is employed, the pose estimation yields yaw angle errors typically smaller than 3° and absolute distance errors of about 0.1 m, corresponding to relative distance errors around 0.5%. For the model-based scene flow method, the yaw angle and positional errors are similar. The accuracy of the estimated instantaneous yaw rate is about 1° per time step, while the accuracies of the lateral velocity and the velocity along the depth axis are both of the order of 0.1 m per time step.

These evaluation results indicate that the described methods for image-based 3D pose estimation of vehicles yield useful information for driver assistance systems in which instantaneous knowledge about the position and motion direction of vehicles is of essential importance.

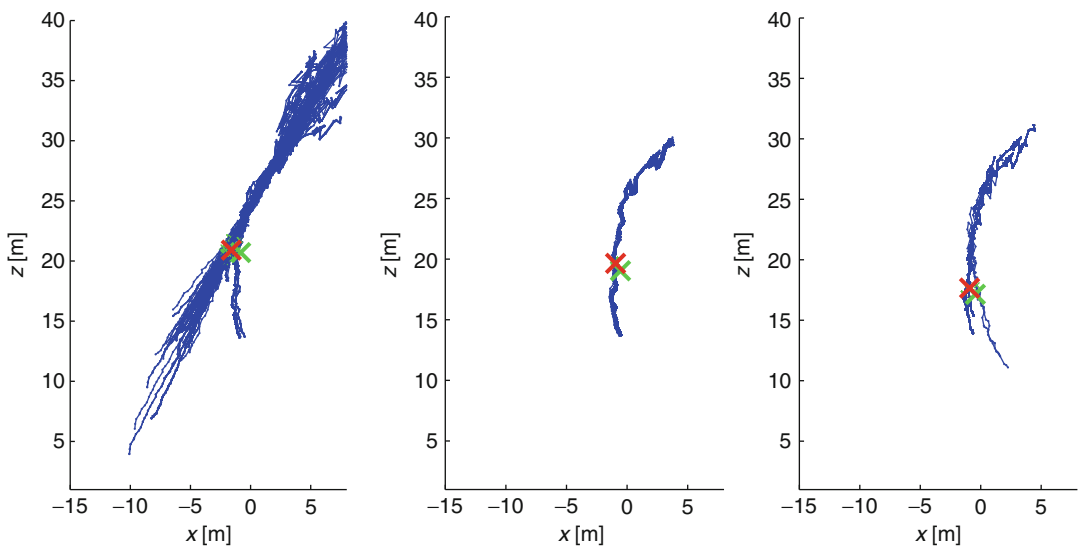

3D Pose Estimation of Vehicles Using Stereo Camera. Figure 18
Particles (*blue*) for a vehicle driving across a roundabout (time $t = 0.0$ s, 0.1 s, 0.3 s, *left to right*) as obtained with the particle filter method described in [34]. The estimated vehicle position (*red*) is compared with the true position (*green*) (from [34])

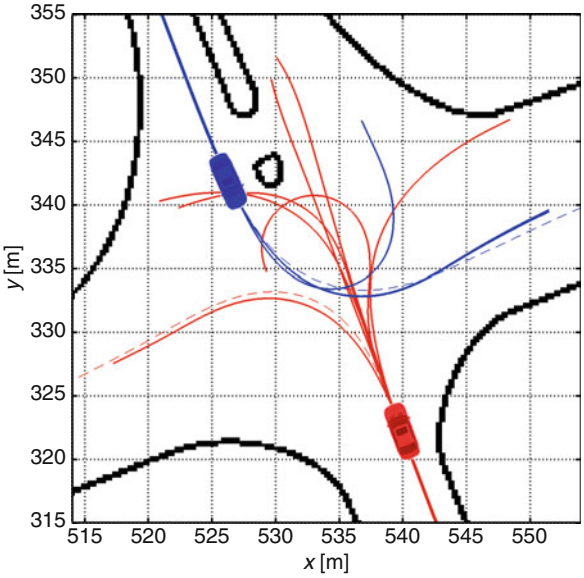

3D Pose Estimation of Vehicles Using Stereo Camera. Figure 19
Example of an early stage of a situation in which both vehicles are turning left (cf. [35]). The future positions (ground truth) of the vehicles are represented by the dashed lines, while the solid lines represent the predictions (from [35])

Future Directions

In driver assistance systems for complex traffic scenarios such as road intersections or roundabouts in the urban environment, highly dynamical motion patterns need to be predicted several seconds into the future. Such predictions may serve for the recognition of driving maneuvers or the analysis of situations involving several vehicles with respect to the possible occurrence of collisions.

As an example of ongoing work in this field, the object position is predicted in [34] based on a Bayesian framework in which the probability distribution of the motion hypotheses is represented by a set of measured example trajectories (particles) rather than motion models. These particles are propagated over time using a particle filter [18, 34]. The measurement noise is inherent in the example trajectories and therefore does not need to be modeled. An example result is shown in Fig. 18. Effectively, this method avoids using simple motion models by cognitive prediction of motion patterns based on a large data base of known motion behaviors.

A further step is the recognition and prediction of situations involving two or more vehicles based on their 3D poses simultaneously acquired over time. Recent work [35] focuses on the recognition of situations involving two vehicles at road intersections. For each vehicle, a set of possible future motion trajectories is predicted several seconds ahead by the trajectory particle filter using a motion database (cf. Fig. 19). An interaction model based on the mutual visibility of the vehicles and the assumption that the drivers will attempt to avoid a collision is used to assign probabilities to possible future situations (cf. Fig. 19), allowing a classification of the situation by a probabilistic framework.

These short descriptions of research activities in the fields of cognitive motion prediction, maneuver recognition, and situation classification illustrate possible future directions of the evolution of driver assistance systems. Fundamentally relying on 3D pose estimation results, such systems will anticipate the behavior of the traffic participants and predict their positions, motion patterns, individual intentions, and mutual interactions.

Bibliography

1. Collado JM, Hilario C, de la Escalera A, Armingol JM (2004) Model based vehicle detection for intelligent vehicles. In: Proceedings of the IEEE intelligent vehicles symposium, Parma, pp 572–577
2. Dellaert F, Thorpe CE (1997) Robust car tracking using kalman filtering and Bayesian templates. In: Proceedings of the conference on intelligent transportation systems, Boston
3. Koller D, Danilidis K, Nagel H-H (1993) Model-based object tracking in monocular image sequences of road traffic scenes. Int J Comput Vision 10(3):257–281
4. Kollnig H, Nagel H-H (1997) 3D pose estimation by directly matching polyhedral models to gray value gradients. Int J Comput Vision 23(3):283–302
5. Haag M, Nagel H-H (1999) Combination of edge element and optical flow estimates for 3D model-based vehicle tracking in traffic image sequences. Int J Comput Vis 35(3):295–319
6. Kato T, Ninomiya Y, Masaki I (2002) An obstacle detection method by fusion of radar and motion stereo. IEEE Trans Intell Transp Syst 3(3):182–188

7. Steux B, Laurgeau C, Salesse L, Wautier D (2002) Fade: a vehicle detection and tracking system featuring monocular color vision and radar data fusion. Proceedings of the IEEE Intell Vehicle Symp 2:632–639
8. Wender S, Dietmayer K (2007) 3D vehicle detection using a laser scanner and a video camera. In: Proceedings of the sixth European congress on ITS in Europe, Aalborg
9. Kaempchen N (2007) Feature-level fusion of laser scanner and video data for advanced driver assistance systems. PhD thesis, Faculty of Engineering and Computer Science, Ulm University
10. Knöppel C, Regensburger U, Schanz A, Michaelis B (2000) Robuste Erkennung von Straßenfahrzeugen im Rückraumbereich eines Straßenfahrzeuges. In: Proceedings of the 22nd DAGM symposium. Springer, Heidelberg, pp 35–42
11. Dang T, Hoffmann C, Stiller C (2002) Fusing optical flow and stereo disparity for object tracking. In: Proceedings of the IEEE international conference on intelligent transportation systems, Singapore
12. Leibe B, Cornelis N, Cornelis K, van Gool L (2006) Integrating recognition and reconstruction for cognitive traffic scene analysis from a moving vehicle. In: Proceedings of the 28th DAGM annual pattern recognition symposium. Springer, Heidelberg, pp 192–201
13. Leibe B, Schiele B (2004) Scale-invariant object categorization using a scale-adaptive mean-shift search. In: Proceedings of the 26th DAGM annual pattern recognition symposium. Springer, Heidelberg, pp 145–153
14. Toulminet G, Bertozzi M, Mousset S, Bensrhair A, Broggi A (2006) Vehicle detection by means of stereo vision-based obstacles features extraction and monocular pattern analysis. IEEE Trans Image Process 15(8):2364–2375
15. Kubota S, Nakano T, Okamoto Y (2007) A global optimization algorithm for realtime on-board stereo obstacle detection systems. In: Proceedings of the IEEE intelligent vehicles symposium, Istanbul, pp 7–12
16. Nedevschi S, Danescu R, Marita T, Oniga F, Pocol C, Sobol S, Tomiuc C, Vancea C, Meinecke MM, Graf T, To TB, Obojski MA (2007) A sensor for urban driving assistance systems based on dense stereovision. In: Proceedings of the IEEE intelligent vehicles symposium, Istanbul, pp 276–283
17. Barth A, Franke U (2008) Where will the oncoming vehicle be the next second? In: Proceedings of the IEEE intelligent vehicles symposium, Eindhoven
18. Hermes C, Barth A, Wöhler C, Kummert F (2009) Object motion analysis and prediction in stereo image sequences. In: Proceedings of the Oldenburger 3D-Tage, Oldenburg
19. Barth A, Siegemund J, Franke U, Förstner W (2009) Simultaneous estimation of pose and motion at highly dynamic turn maneuvers. In: Proceedings of the 31st DAGM symposium, Springer, Heidelberg, pp 262–271
20. Schmidt J, Wöhler C, Krüger L, Gövert T, Hermes C (2007) 3D scene segmentation and object tracking in multiocular image sequences. In: Proceedings of the fifth international conference on computer vision systems, Bielefeld. http://biecoll.ub.uni-bielefeld.de/volltexte/2007/29/
21. Fielding G, Kam M (1997) Applying the Hungarian method to stereo matching. In: Proceedings of the IEEE conference on decision and control, San Diego, pp 549–558
22. Stein F (2004) Efficient computation of optical flow using the census transform. In: Proceedings of DAGM annual pattern recognition symposium, Tuebingen, pp 79–86
23. Franke U, Joos A (2000) Real-time stereo vision for urban traffic scene understanding. In: Proceedings of the IEEE intelligent vehicles symposium, Dearborn, pp 273–278
24. Bock HH (1974) Automatische Klassifikation. Vandenhoeck & Ruprecht, Göttingen
25. Barrois B, Wöhler C (2008) Spatio-temporal 3D pose estimation of objects in stereo images. In: Proceedings of the sixth international conference on computer vision systems, vol 5008, Lecture notes in computer science. Springer, Heidelberg, pp 507–516
26. Duda RO, Hart PE, Stork DG (2000) Pattern classification, 2nd edn. Wiley, New York
27. Besl PJ, McKay ND (1992) A method for registration of 3-d shapes. IEEE Trans Pattern Anal Mach Intell 14(2):239–256
28. Zhang Z (1992) Iterative point matching for registration of free-form curves. IN-RIA, Technical Report. ftp://ftp.inria.fr/INRIA/publication/publi-ps-gz/RR/RR-1658.ps.gz
29. Press WH, Teukolsky SA, Vetterling WT, Flannery BP (1992) Numerical recipes in C: the art of scientific computing. Cambridge University Press, New Delhi
30. Horn BKP (1987) Closed-form solution of absolute orientation using unit quaternions. J Opt Soc Am A 4(4):629–642
31. Hamilton WR (1866) Elements of quaternions. Longmans, Green, London
32. Hartley R, Zisserman A (2003) Multiple view geometry in computer vision, 2nd edn. Cambridge University Press, Cambridge
33. Krüger L, Wöhler C (2011) Accurate chequerboard corner localisation for camera calibration and scene reconstruction. Pattern Recognit Lett (to appear)
34. Hermes C, Einhaus J, Hahn M, Wöhler C, Kummert F (2010) vehicle tracking and motion prediction in complex urban scenarios. In: Proceedings of the IEEE intelligent vehicles symposium, San Diego
35. Käfer E, Hermes C, Wöhler C, Ritter H, Kummert F (2010) Recognition of situation classes at road intersections. In: Proceedings of the IEEE international conference on robotics and automation, Anchorage
36. Barrois B, Hristova S, Wöhler C, Kummert F, Hermes C (2009) 3D pose estimation of vehicles using a stereo camera. In: Proceedings of the IEEE intelligent vehicles symposium, Xi'an
37. Wöhler C (2009) 3D computer vision. Springer-Verlag, Berlin/Heidelberg

Tidal Energy

Ian G. Bryden
Head of Institute for Energy Systems, School of Engineering, The University of Edinburgh, Edinburgh, UK

Article Outline

Glossary
Definition of the Subject
Introduction
The Tides
Harnessing the Energy in the Tides
Future Directions
Bibliography

Glossary

Barrage An artificial barrier, usually constructed across an estuary, designed to maintain different water levels on either side.

Ebb tide The stage of a tide in which the water depth is reducing.

Flood tide The stage of a tide in which the water depth is increasing.

Neap tide Smaller fortnightly tides falling between the spring tides.

Spring tide Large fortnightly tides, resulting from the Earth, Sun, and Moon being approximately in line.

Tidal basin The area of water behind a tidal barrage.

Tidal currents Water currents resulting from tidal action.

Tidal stream A tidal current which has been accelerated as a result of the natural geography.

Tides The response of the world's seas and oceans to the influences of the Moon and the Sun relative to the Earth.

Turbine A mechanical system in which energy in a moving fluid is transferred to a rotating system.

Definition of the Subject

Tidal energy, as interpreted in this essay, is considered to be the artificial extraction of energy from: either the rise or fall of the sea surface under the influence of tides or the extraction of energy from tidally driven currents. The associated theoretical energy resources are considerable on a global scale, but the geographic conditions necessary for significant tidal ranges, or current velocities, do tend to be restricted to a relatively small number of sites worldwide. Some of the most attractive tidal range sites, however, such as the Severn Estuary, between England and Wales, and the Bay of Fundy in Canada possess very considerable energy flux densities. Similarly, the most energetic tidal currents, such as in the Pentland Firth, to the north of the Scottish mainland, would also appear to offer major prospects for development.

Although there has been considerable progress in recent years toward the commercial exploitation of the tides for energy, the use of tidal energy is not new. Tide "mills" were used in northern France and southern England as far back as the late Roman era but were most prolific during medieval times. Tidal waters turned water wheels to drive cereal grinding apparatus in areas with few rapidly flowing rivers. The Eling Tide Mill, for example, is still operational, largely as an educational and tourist facility, and is a very early example of tidal entrainment, represented by a barrage positioned to interfere with natural tidal flows. Entrainment is a more general term than "barrage" and encompasses alternative techniques such as lagoons. In the twentieth and twenty-first centuries, tides have been seriously reexamined as sources of energy to power industry and commerce.

Introduction

Despite the installation of a major tidal energy plant at La Rance, France, in the 1960s, research and development throughout the 1970s and 1980s was largely restricted to university laboratories, with little commercial involvement. Interest in the use of the tides for the generation of electricity has increased significantly, however, in the last 20 years. From the early 1990s to the present day, governments have started, once again, to consider the tides as a potential source of energy and industry has seen prospects for profitable development. Governmental interest has largely been driven by concerns over long-term energy security and climate change. The deployment of strategic tidal capacity remains, however, a significant challenge,

which will require significant effort and resolve if the expectations of politicians and industrialist are to be achieved by 2020 and beyond.

The Tides

Explaining the existence of tides, using Newton's theories of gravitation and the mechanics of motion, represented a major step toward understanding the universe around us. The "equilibrium tidal theory," which is sometimes known as "the Newtonian theory of tides," gives a partial description of tidal behavior for an abstract water covered planet Earth and is outlined in most introductory texts on oceanography [1]. In effect, the tides represent a marine manifestation of energy fluxes present in the Earth–Moon–Sun system. These fluxes are complicated by the presence of land masses, which can result in local enhancement of the energy fluxes, where conditions are appropriate. The Bristol Channel between England and Wales and the Bay of Fundy in Canada are two noteworthy examples, which possess exceptionally high tidal ranges.

Although tides and tidal influences can be predicted centuries in advance because of the essentially mechanistic effects which drive them, the sea surface is also subject to weather-related effects of which waves are the most obvious. In addition, pressure effects and wind-driven currents will be superimposed upon tidal effects. These can, however, now be forecast over periods of hours and days from meteorological information.

Harnessing the Energy in the Tides

Approaches to Exploitation

There are two approaches to harnessing energy from tides:

- The first is to exploit the rise and fall of the sea level through entrainment. This includes "traditional" barrage methods as well and tidal lagoons and fences.
- The second approach involves harnessing local tidal currents using technology reminiscent of wind turbines.

Tidal Barrages

Principles and History Sites of particular interest include the Bay of Fundy in Canada, which has a mean tidal range of 10 m, the Severn Estuary between England and Wales, with a mean tidal range of 8 m, and the Rance Estuary in Northern France, with a mean range of 7 m. A tidal barrage power plant has been operating at La Rance in Brittany since 1966 [2]. This plant is capable of generating 240 MW and incorporates a road crossing of the estuary. It has recently undergone a major 10-year refurbishment program.

Barrages have also been constructed at Annapolis Royal in Nova Scotia (18 MW), the Bay of Kislaya, near Murmansk (400 kW), and at Jangxia Creek in the East China Sea (500 kW) [3]. Schemes have been proposed for the Bay of Fundy and for the Severn Estuary but have never been built.

The prospect of generating electricity in the Severn Estuary has excited engineers and planners since the end of the nineteenth century, even before there was a significant demand for electricity! A serious proposal for an 800-MW generation scheme was made in 1925 [4], and this particular option continued to be examined seriously into the 1950s. Although the UK government has recently been considering options for the commercial development of the Severn Estuary, this has now been rejected for the foreseeable future.

In South Korea, the Sihwa Lake Tidal Power Plant was completed in 2010 with a preliminary capacity of 254 MW and has replaced La Rance as the largest tidal entrainment system. The plant uses ten 25.4 MW submerged bulb turbines. Unlike La Rance, the plant operates in flood rather than ebb mode in order to minimize some very specific environmental effects in the site.

Tidal barrages can operate in a variety of modes. These can be broken down initially into single basin schemes and multiple basin schemes. The simplest of these are the single basin schemes:

Single-Basin Tidal Barrage Schemes These require a single barrage across an estuary, as shown in Fig. 1. There are three different methods of generating electricity with a single basin. All involve a combination of sluices which, when open, allow water to flow relatively freely through the barrage and/or gated turbines, which generate electricity when required.

Ebb Generation: Electricity is generated only during the ebb tide. During the flood tide, water is allowed to flow freely through sluices into the barrage.

At high tide, the sluices are closed and water retained behind the barrage. When the water outside the barrage has fallen sufficiently to establish a significant head between the basin and the open water, the basin water is allowed to flow out though low head turbines and to generate electricity. The system behavior can be considered in phases. These are represented in Fig. 2 to show the periods of generation within the tidal cycle.

Typically the water will only be allowed to flow through the turbines once the head is approximately half the tidal range. This method will generate electricity for, at most, 40% of the tidal range.

Flood Generation: The sluices and turbine gates are initially kept closed during the flood tide to allow the water level to build up outside of the barrage, as shown in Fig. 3. As with ebb generation, once a sufficient head has been established, the turbine gates will be opened and water can flow into the basin generating electricity.

This approach is generally viewed less favorably than the ebb method, as keeping a tidal basin at low tide for extended periods might have detrimental effects on the environment and shipping. However, the special circumstances in the Korean Sihwa project have made flood mode the preferred option.

Two-Way Generation: It is possible, in principle, to generate electricity in both ebb and flood. Unfortunately, computer models do not generally suggest a major increase in the energy production. In addition, there would be further costs associated with requirements for either two-way turbines or a double set to handle the two-way flow. Advantages include, however, reduced periods with no generation and peak power would be lower, allowing reduction in generator costs.

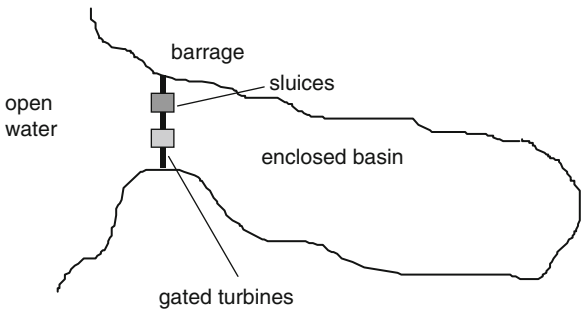

Tidal Energy. Figure 1
Hypothetical tidal barrage configuration

Double Basin Systems Single basin systems can only ever deliver energy during the parts of the tidal cycle. Double basin systems, as shown schematically in Fig. 4, might allow energy storage and enhanced control over output power levels.

The main basin might behave like conventional ebb or flood generation single basin system. Some of the electricity generated could be used to pump water to and from the second basin to ensure a more robust generation capability.

It is not likely that multiple basin systems will become popular, as low head turbines are unlikely to be sufficiently efficient to allow economic storage of energy.

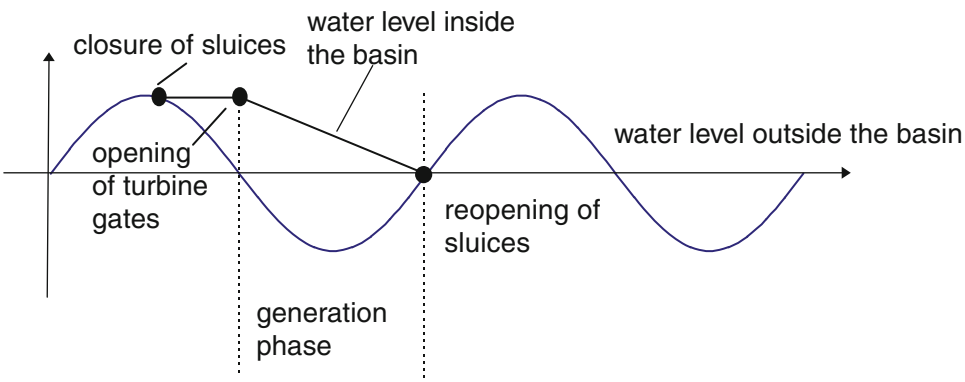

Tidal Energy. Figure 2
Water levels in an ebb generation scheme

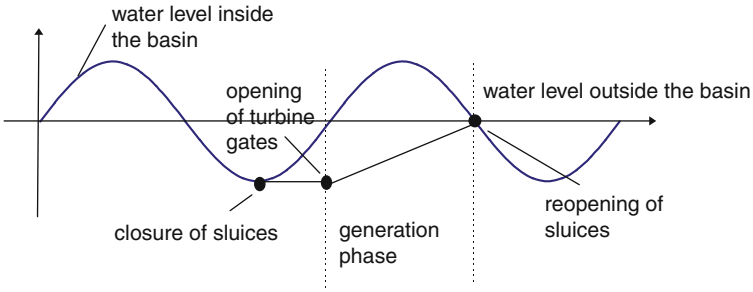

Tidal Energy. Figure 3
Water levels in a flood generation scheme

The overall efficiency of such low head storage is unlikely to exceed 30%. Conventional pump storage systems, with overall efficiencies exceeding 70%, are more attractive, especially as they are proven technology.

Possible Sites for Future Tidal Barrage Developments Worldwide there are numerous sites which might be technically suitable for development, although whether the resource can be developed economically is yet to be conclusively determined [3]. These include, and this is not a definitive list:

Site	Mean tidal range (m)	Barrage length (m)	Estimated annual energy production (GWh)
Severn Estuary (UK)	7.0	17,000	12,900
Solway Firth (UK)	5.5	30,000	10,050
Bay of Fundy (Canada)	11.7	8,000	11,700
Gulf of Cambay (India)	6.1	25,000	16,400

Tidal Lagoons

Tidal barrage developments are likely to cause significant environmental change. Whether this would be acceptable would depend upon the individual development circumstances. Ebb generation will, for example, result in raised mean water levels. A barrage will also cause obstruction to shipping and other maritime activities, which will have an effect on the local economy.

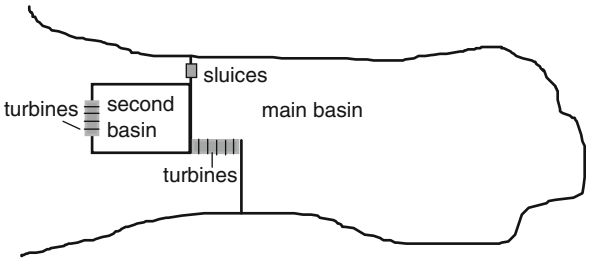

Tidal Energy. Figure 4
Hypothetical two basin system

Artificial lagoons [5] have been proposed as alternatives to barrages. The principal advantage is that the coastline, including the intertidal zone, would be largely unaffected. Careful positioning of the lagoon could also ensure that shipping routes would be unaffected. Although preliminary studies suggest that costs might be competitive with other sources of renewable energy, there has not yet been any in-depth peer-reviewed comparative assessment of the tidal lagoon concept.

Tidal Current Technology

Principles and History The development of a barrage or lagoon would represent a substantial investment of time and money. Many planners and engineers favor the development of tidal current systems, which could be developed incrementally. Indeed,

the progressive development of a local tidal current resource might allow subsequent advances in technology, or understanding of the resource, to be incorporated at later stages. The most significant early attempt to prove the practicality of tidal current power was conducted in Loch Linnhe in the Scottish West Highlands in the early 1990s [6]. This used a turbine held mid-water by cables, which stretched from a seabed anchor to a floating barge.

In 2000, a large floating device (the ENERMAR project [7]) was tested in the Strait of Messina between Sicily and the Italian mainland. Between May 2003 and October 2009, Marine Current Turbines (MCT) Ltd [8]. of Bristol, England, demonstrated a 300-KW pillar-mounted prototype system called SeaFlow in the Bristol Channel.

Figure 5 shows the SeaFlow system with its nacelle raised into the "maintenance position." This system, having completed its test program, has now been decommissioned.

The Canadian Clean Current project involved the testing of a ducted horizontal axis machine at Race Rock between July and September 2006, before being removed in May 2007 and subsequently reinstalled after modification in October 2008.

MCT installed their commercial scale prototype, SeaGen, in Strangford Narrows in Northern Ireland in 2008. Although having some similarities with SeaFlow, it is equipped with two rotors and has a rated capacity of 1.2 MW. An artist's impression is shown in Fig. 6, and the operational system is shown in Fig. 7.

In Norway, the Hammerfest Strom system [9] demonstrated between 2003 and 2007 that a 300-KW pillar-mounted horizontal axis systems could operate in a fjord environment. The company now has ongoing plans for a larger 1-MW system, which it is intended to be available for commercial installation from 2012.

In the USA, Verdant Power Ltd. successfully demonstrated an array of six 5-m-diameter horizontal axis tidal turbines in New York's East River from 2006–2008 [10]. The company now has detailed plans for a substantially larger development, using larger, more advanced technology.

Tidal Energy. Figure 5
SeaFlow with the nacelle raised

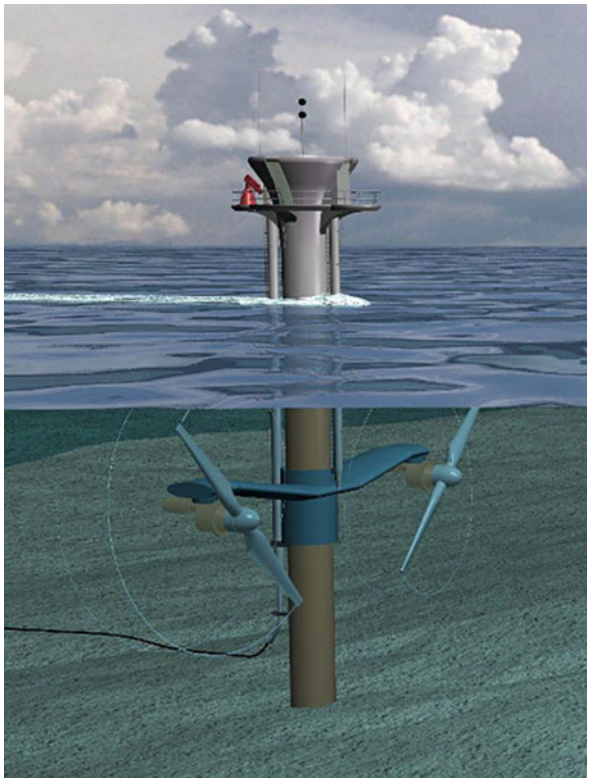

Tidal Energy. Figure 6
Artist's impression of SeaGen

Tidal Energy. Figure 7
Photograph of SeaGen in operation

In 2007, The European Marine Energy Centre [11], which was established in 2004 to allow the testing of full-scale marine energy technology in a robust and transparent manner, became fully equipped for the testing of tidal, as well as wave energy technology. The tidal test berths are located off the south-western tip of the island of Eday, in an area known as the Fall of Warness. The facility offers five tidal berths at depths ranging from 25 to 50 m in an area 2 km across and approximately 3.5 km in length. Each berth has a dedicated cable connecting back to the local grid. At the time of writing, there is one fully operational device [12] installed.

This is operated by Open Hydro Ltd. and is a novel annular turbine system held by twin vertical pillars. The system can be seen in its maintenance position in Fig. 8. The company has also been testing a novel barge-based installation system which could significantly lower costs.

There are presently two additional devices in the process of being installed at EMEC. The first, shown in Fig. 9, has been developed by Tidal Generation Ltd. (TGL) and the second by Atlantis Power Ltd. Although EMEC was the world's first dedicated marine energy testing center, there are now ambitious developments elsewhere in the world, notably in Canada, where FORCE (Fundy Ocean Research Centre for Energy) is developing a significant test capability.

The physics of the conversion of energy from tidal currents is superficially very similar to the conversion of kinetic energy in the wind. Many devices have, therefore, a resemblance to wind turbines. There is, however, no total agreement on the form and geometry of the technology itself. Wind systems are generally horizontal axis rotating turbines with the axis of rotation parallel to the direction of flow. Many tidal developers also favor this approach, as can be seen in the images of prototype systems. Vertical axis systems, in which the axis of rotation is perpendicular to the direction of flow, have not, however, been rejected. ENEMAR, for example, used a vertical axis turbine.

Energy Available in Tidal Currents It is usual in renewable energy to consider the theoretical, technical, and practical resource. The theoretical resource is that

Tidal Energy. Figure 8
The Open Hydro System installed at EMEC

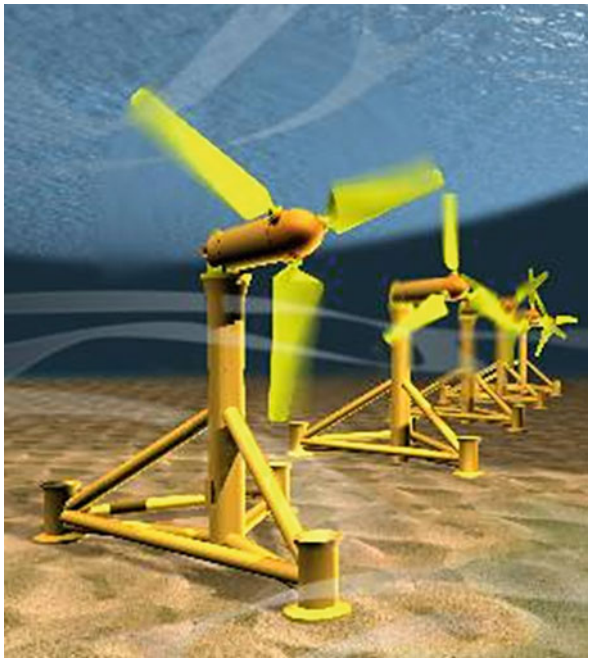

Tidal Energy. Figure 9
Artist's impression of the TGL Ltd. system being installed at EMEC

which could in principle be extracted, without consideration of technology or constraints. The "technical" resource is what could be exploited using reasonably available technology. The "practical" resource is what could be exploited after consideration of external constraints, competing use (shipping lanes, etc.) and environmental sensitivity.

It is tempting to draw analogies between wind power and tidal current power when assessing the resource. In both, it is possible to calculate the kinetic energy carried by a moving fluid and to relate this to a kinetic energy flux density. This, however, represents only part of the energy flux in a current: Energy is dissipated through "friction" between the water and boundaries; the surface of the sea in current will not be in level, and there will be changes in the potential energy of the water as it flows across a site. Generally, the potential energy changes and the frictional dispersion will exceed the kinetic flux!

Any serious analysis of the development potential of a tidal site should also consider the temporal and spatial complexity of the flow and the impact of extraction on the flow patterns. This will generally involve

numerical modeling of both the tides and the technology to allow assessment of the impact for proposed extraction scenarios, which will require high quality tidal/hydraulic data.

The "theoretical" resource will be difficult to identify for all but the simplest environments. It will usually be easier to estimate the "practical" resource by identifying what would be acceptable changes in the flow environment and using numerical methods to determine how much energy could be extracted without exceeding these limits. Individual prospective tidal sites, either estuaries or high-flow-speed areas, need site-dependent consideration. This makes the production of high-level resource assessments very difficult. Knowledge of the processes is now sufficient, however, to allow robust estimates of the practical resource at a selected site, provided sufficiently detailed data is available.

Development Options for Tidal Currents Tidal devices operate in a very different environment from onshore wind turbines, with specific problems associated with installation, survivability, and maintenance. These will need to be solved before true commercial exploitation can be achieved. Development options often involve the use of dedicated installation and maintenance vessels, which suggests that tidal currents might only be economically exploited in large sites, justifying the use of expensive infrastructures.

Many industrial, commercial, and public bodies have suggested that there is a high degree of synergy between a prospective tidal current generation industry and the offshore oil and gas industry. This offers the prospect of a new industry developing in partnership with the petroleum sector, which could, perhaps, result in accelerated development.

Tides are essentially predictable as they derive from astronomic processes, as discussed earlier in this article. Wind power systems are dependent upon random atmospheric processes and can be difficult to integrate into strategic electricity distribution networks. The predictability of the tides might make such integration much easier.

Prototype devices are now available but there are still issues to be resolved before commercial exploitation, for example: there is only limited understanding of how devices will operate in arrays, although working theories are becoming available; turbulence may also be a problem as extreme fluctuations often exceeding 10% of the time averaged mean have been measured [13]. System designs must accommodate this; similarly, tidal devices will be exposed to waves, and this will also pose design challenges, if the systems are to be robust.

Such gaps in understanding should not, however, prevent ongoing deployment of technology, provided that developers are aware of the constraints that knowledge gaps impose and recognize that they themselves are part of the research process, which will ultimately allow cost-effective exploitation of the tidal current resource.

Future Directions

In a future in which energy costs are likely to rise, assuming that low-cost nuclear fusion or other long-term alternatives do not make unexpectedly early arrivals, tidal barrage schemes could prove to be major providers of strategic energy in the mid-twenty-first century and beyond, although the recent decision by the UK Government not to proceed with the development of a Severn barrage has disappointed many. The technology for tidal barrage systems is already available, and there is no doubt, given the experience at La Rance, that the resource is substantial and available. Ongoing development of the Korean resource also suggests that future development elsewhere in the world is possible. The Bay of Fundy remains a tantalizing option for a future in which energy costs are likely to rise considerably in real terms.

It is likely that tidal current systems will continue to be developed. The first truly commercial developments should appear this decade if progress continues. Tidal current systems may not have the strategic potential of barrage systems, but, in the short term at least, they do offer opportunities for supplying energy in rural coastal and island communities. In the longer term, massive sites such as the Pentland Firth could become strategically important. In November 2008, The Crown Estate, which owns the seabed in the Firth, invited proposals for the development of sites in the firth and surrounding waters [14]. Leases have now been granted for 1.6 GW of installed capacity, covering both wave and tidal current development. Of this, some 1.2 GW is intended to be tidal.

Bibliography

1. Bearman G (ed) (1997) Waves, tides and shallow water processes. The Open University, Milton Keynes
2. Banal M, Bichon A (1981) Tidal energy in France. The Rance tidal power station-some results after 15 years in operation. In: Proceedings of the second international symposium on wave and tidal energy, Cambridge
3. Boyle G (ed) (1996) Renewable energy. The Open University, Milton Keynes
4. "Severn Barrage Scheme", Hansard, 4th February 1926
5. www.tidalelectric.com
6. www.itpower.co.uk/ResearchDevelopment.htm
7. www.pontediarchimede.com
8. www.marineturbines.com
9. www.tidevannsenergi.com
10. www.verdantpower.com
11. www.emec.org.uk
12. www.openhydro.com
13. Norris J, Bryden I (2007) The European marine energy centre (EMEC): facilities and resources. Proc Inst Civil Eng 160(2): 51–58. doi:10.1680/ener.2007.160.2.51
14. www.thecrownestate.co.uk/newscontent/92-round-1-pentland-firth.htm

Topographic Solar Radiation Modeling for Environmental Applications

Hofierka Jaroslav
Department of Geography and Regional Development, University of Presov, Presov, Slovakia

Article Outline

Glossary
Definition of the Subject
Introduction
Modeling Topographic Effects on Solar Radiation
Computing Clear-Sky Radiation
Computing Real-Sky Radiation
The r.sun Solar Radiation Model
Computing Spatially Distributed Solar Radiation Databases
Future Directions
Acknowledgments
Bibliography

Glossary

Geographic information system (GIS) Any information system that is used to collect, store, process, and present geographic information. In a narrow sense it means a specific application software dealing with geographic information. In a broader sense, it includes software, hardware, data, and people.

Digital elevation model (DEM) A digital representation of the land surface expressing a spatial distribution of elevations. It can be represented by a raster or vector data model.

Topography A study of Earth's surface geometry. It is also known as geomorphometry, a science of quantitative land surface analysis. The land surface (relief, terrain) is characterized by a set of morphometric parameters including slope, aspect, curvatures, and other more complex parameters.

Solar radiation database A set of digital maps representing a spatial and temporal distribution of solar radiation and related meteorological data over a specific region.

Clear-sky radiation Solar radiation under clear-sky atmospheric conditions. The extraterrestrial solar radiation is attenuated only by air mass with atmospheric gases and aerosols.

Real-sky radiation Solar radiation under real-sky conditions, that is, including the cloudiness.

Linke turbidity factor A measure of solar beam radiation attenuation caused by water vapor and aerosol particles in the atmosphere.

Raster A GIS data model representing geographic phenomena as arrays of cells that store attribute values.

Viewshed A graph showing the angular distribution of sky visibility and obstruction at the location. It is calculated from a DEM by searching in a specified set of directions around the location.

Definition of the Subject

Solar radiation exhibits strong spatial and temporal variations influenced by many factors. For example, basic patterns of seasonal and daily variations given by astronomic factors are modified by actual atmospheric conditions influencing absorption, scattering, and solar radiation spectrum. Such data offer some basic information about the available solar radiation. However,

patterns at regional and local scales may significantly deviate from these general trends. Large land surface features may cause strong local radiation gradients, thus inducing specific microclimate and hydrological conditions. Consequently, in mountainous regions, topography plays a critical role in the spatial distribution of solar radiation incident on the surface.

Currently available solar radiation databases derived from ground or satellite measurements contain data with an insufficient level of detail that in most cases do not represent adequately the spatial variability in solar radiation caused by topographic factors. To account for this variability, topographic solar radiation models, often integrated with geographic information systems (GIS), have been developed. Topographic factors are derived from digital elevation models (DEMs) representing the land surface. Higher spatial resolutions in DEMs bring the necessary level of detail in local estimates of solar radiation and its components incident on the surface. Moreover, topographic models are capable of providing estimates of solar radiation and related solar parameters at various time horizons and periods necessary for many environmental applications.

Introduction

Solar radiation incident at any location on the Earth's surface is the result of complex interactions of energy between the atmosphere and land or ocean surfaces. On a global scale, the latitudinal gradients of radiation are caused by the Earth's geometry and its rotation and revolution around the Sun. At regional and local scales over land, surface heterogeneities constitute the major factor modifying the spatial distribution of radiation. Spatial variabilities in land surface elevation, slope (inclination), aspect (orientation), and shadows cast by terrain features create strong local gradients that modify the global radiation field.

Spatial and temporal variations in incoming solar radiation determine the patterns and dynamics of many environmental phenomena (e.g., air and soil temperature, water balance, snow melting, photosynthesis, evapotranspiration, or biomass production) with a direct impact on the natural distribution of certain plants. Therefore, this spatial variability should be taken into account when studying the surface energy balance or when preparing the localization of production crops (from agriculture or forestry). Moreover, high-resolution spatially distributed solar radiation data are also desired for solar energy applications, including building design, landscape architecture, photovoltaics (PV), or remote sensing.

At present, a number of solar radiation databases are available, such as NASA's SSE (http://eosweb.larc.nasa.gov/sse/), the European Solar Radiation Atlas [1], MeteoNorm [2], Satel-Light [3], SOLEMI (http://www.solemi.com/), HelioClim-2 (http://www.helioclim.net/), RETScreen (http://www.retscreen.net/), PVGIS [4], or 3TIER (http://www.3tier.com/). These databases were developed from ground radiation measurements, satellite images with interpolation techniques, and solar radiation models. They provide various solar radiation data and other related information helpful in global and regional studies. However, the spatial resolution of these databases is usually not sufficient for local studies. For example, the typical spatial resolution of global/regional solar databases that are derived from the Meteosat second-generation meteorological satellites is 1–5 km. Local solar radiation studies with topographic effects require higher spatial resolutions (less than 1 km). The spatial distribution of solar radiation in mountainous regions is strongly influenced by topography, which cannot be captured by satellite-based estimates nor by sparse ground measurements using radiometers.

The importance of topographic distribution of solar radiation in hydrological and biological processes has long been known (e.g., [5–11]). In the northern hemisphere, south-facing slopes generally receive more solar radiation than northern slopes, and therefore have a different heat and water balance regime. Areas frequently shaded by terrain features (e.g., bottoms of deep valleys) exhibit different microclimate profiles than open space areas. To account for this variability, topographic solar models have been created and often integrated with geographical information systems (GIS). Such models provide rapid, cost-efficient, and accurate estimates of solar radiation over large regions, while considering slope inclination, aspect, and shadowing effects. Coupling radiation models with both GIS and image processing systems improves their ability to use various environmental data and to be combined with other environmental models.

Significant progress has been made toward developing solar radiation models in the last 2 decades [12]. One of the first GIS-based solar radiation models was SolarFlux [12, 13] developed for the Arc/Info GIS system commercialized by ESRI. A series of solar radiation algorithms were also implemented in the Genasys GIS using AML scripts [14]. To describe the underlining radiative processes, these models use rather simple empirical formulas and parameters that are spatially averaged (lumped) and therefore not suitable for assessments over large areas.

More advanced methods for ecological and biological applications are implemented in Solar Analyst, developed as an ArcView GIS extension [15]. In the preprocessing phase, the model generates an upward-looking hemispherical viewshed based on a digital elevation model (DEM). The solar model is suitable for local-scale studies. It is not flexible enough for calculations of atmospheric transmissivity or diffuse fraction of the total irradiance, since it only allows very limited settings for the available parameters, using either data from the nearest weather stations or just typical values. This makes its use too simplistic over large areas, with progressive deterioration of accuracy as the study area increases.

The SRAD model [16, 17] was designed to evaluate a complex set of short-wave and long-wave solar radiation interactions between the Earth's surface and atmosphere. Although based on a simplified representation of the underlying physics, the main solar radiation factors are considered and the model is able to characterize the spatial variability in landscape processes. However, it is specifically designed for the modeling of topo- and meso-scale processes, so that the calculation of solar radiation over large areas is also limited.

The *r.sun* solar radiation model has been developed by Hofierka [18] for the open-source environment of GRASS GIS [19]. The improved version of the model, later developed by Šúri and Hofierka [20], models all three components of solar radiation under both clear-sky and real-sky atmospheric conditions. The model has been successfully used in a wide range of applications including PV electricity production [4, 21].

Modeling Topographic Effects on Solar Radiation

Solar radiation is a sum of three components: beam radiation incoming directly from the Sun, diffuse radiation from the sky (available even under overcast conditions), as well as radiation diffusively reflected from nearby terrain features. This reflected component exists only in non-flat areas. The local variation in solar radiation incident at the surface is determined by two major factors: topography and cloudiness. Topography affects the distribution of solar radiation fluxes via several topographic attributes: elevation, slope, aspect, and terrain features creating shadows. In the northern hemisphere, for example, south-facing inclined surfaces at high latitudes may receive a higher amount of solar radiation than flat areas.

Slope and aspect of the land surface modify the incident beam, diffuse, and ground-reflected components. These two parameters influence the spatial-temporal patterns of the radiation field over hilly terrain. The influence of slope and aspect is more pronounced under clear-sky (sunny) weather than under cloudy conditions, when diffuse radiation dominates. Shadows cast by neighboring terrain features may substantially reduce the amount of available radiation especially at low solar altitudes. Elevation affects the attenuation of radiation through the total optical thickness of the atmosphere. At high elevation, due to a lower optical thickness, the attenuation from atmospheric gases and aerosols is less pronounced, so that the incident radiation's magnitude is higher than at low elevation. Similar issues, albeit even more complex, exist when trying to simulate the radiation field over urban fabrics, due to the added complexity of rapid spatial variations in ground albedo, interreflections between buildings, complex shading issues, and additional attenuation due to pollution.

Most radiometric stations are equipped with sensors that measure global horizontal radiation, sometimes diffuse horizontal radiation, and more rarely direct normal radiation. If both the global and diffuse components are measured, the direct normal component can be calculated using the actual Sun altitude over the horizon, which can be calculated from time, date, and location coordinates. Similarly, the radiation incident on slopes can be estimated from global and diffuse radiation data, provided the ratio of global radiation on a slope to that on a horizontal surface is known [22]. Because there is usually a very sparse spatial coverage of meteorological stations measuring solar radiation, it is generally very useful to estimate the solar radiation components locally incident on the surface using a topographical

solar radiation model. Such a model may provide more accurate estimates than satellites especially in mountainous regions with strong topographic effects.

Digital Elevation Models

The most common digital representation of the land surface is via a DEM. In DEMs, elevations can be regularly spaced in the form of grids (a raster-based data model) or irregularly spaced as triangulated irregular networks (TINs). The cell of the grid (a minimal area with a unique value of elevation) defines the spatial resolution of the raster-based DEM. The DEMs based on the TIN data model are characterized by triangles with variable sizes.

DEMs are used to calculate slopes and aspects, and ultimately the amount of solar radiation incident at the surface. In mountainous regions, shadows cast by terrain features can greatly attenuate the available radiation, so that a shadowing analysis is necessary. However, the accuracy of such an analysis is very sensitive to the DEM's resolution. For applications at a global scale, solar radiation calculated with a spatial resolution of 10–40 km or more provides only overall information, which is not compatible with a detailed shadowing analysis. For resolutions of 1–5 km or better, the shadowing analysis should be considered, especially in mountainous or urban regions. In very local studies with DEMs at resolutions of hundreds to tenths of meters, the data accuracy strongly affects the shadowing analysis. In such cases, DEMs preserving the features of surface extremes (e.g., tops of the mountains, saddles, ridges, or bottoms of valleys) should be used rather than smoothed data. Moreover, digital surface models (DSM) that also include specific sun-obstructing features of the surface (e.g., forest, urban constructions, etc.) can be used. In the topographic modeling of solar radiation, DSMs are preferred because they better represent features casting shadows at lower solar altitudes. More information on DEMs, DSMs, data sources, production techniques, and quality issues can be found elsewhere, for example, [16, 23, 24].

Computing Clear-Sky Radiation

The Sun's position in the sky relative to the position of a point of interest at the surface is a key parameter in topographic solar radiation models. Basic solar geometry is defined by a set of solar parameters including latitude and longitude of the location, time, and solar declination. Then the position of the Sun in the sky with respect to a horizontal surface can be expressed by two coordinates: the solar altitude, h_0, defined as the angle between the solar beam and the horizontal surface, and the solar azimuth, A_0, defined as the horizontal angle between the Sun and the local meridian (Fig. 1).

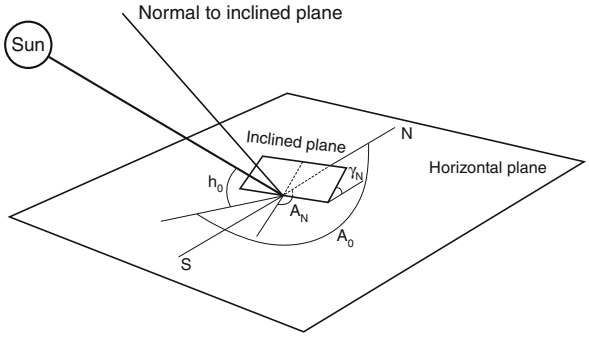

Topographic Solar Radiation Modeling for Environmental Applications. Figure 1
Geometry of the solar beam

The following description is for the solar topographic model that derived from the research by Šúri and Hofierka [20], which also resulted in the *r.sun* solar radiation model for the open-source environment of GRASS GIS [19]. Whereas the calculation of the beam component is quite straightforward, the main difference between all topographic models is in the treatment of the diffuse component [25]. This component depends on climate and regional surface conditions, and it is often the largest source of estimation error. The equations used in the *r.sun* model are based on the research conducted for the European Solar Radiation Atlas project [1, 26] and reflect European climate conditions. The ground-reflected radiation usually contributes only several percent to the overall global radiation on inclined surfaces and therefore is ignored by most models. However, larger contributions of this component may exist in mountains, especially in snow conditions. Nevertheless, the *r.sun* model takes also into account this component via simple equations that are adequate for most applications.

Beam Radiation

The beam irradiance on inclined surfaces, B_{ic} (W/m^2), is calculated as follows:

$$B_{ic} = B_{0c} \sin \delta_{exp} \quad (1)$$

or

$$B_{ic} = B_{hc} \sin \delta_{exp} / \sin h_0 \quad (2)$$

where B_{0c} is the beam irradiance normal to the solar beam (W/m^2), B_{hc} is the beam irradiance on horizontal surfaces (W/m^2), δ_{exp} is the solar incidence angle measured between the Sun and the inclined surface, and h_0 is the solar altitude.

If the inclined surface is defined by slope γ_N and aspect A_N, then the solar incidence angle δ_{exp} is defined as [27, 28]:

$$\sin \delta_{exp} = C'_{31} \cos (T - \lambda') + C'_{33} \quad (3)$$

where

$$C'_{31} = \cos \varphi' \cos \delta, C'_{33} = \sin \varphi' \sin \delta \quad (4)$$

and

$$\sin \varphi' = -\cos \varphi \sin \gamma_N \cos A_N + \sin \varphi \cos \gamma_N \quad (5)$$

$$\tan \lambda' = -(\sin \gamma_N \sin A_N)/(\sin \varphi \sin \gamma_N \cos A_N + \cos \varphi \cos \gamma_N)$$

The hour angle T (rad) is calculated from the local solar time, t, expressed in decimal hours on the 24-h clock as:

$$T = 0.261799(t - 12) \quad (6)$$

The Sun's position given by the solar altitude h_0 and the solar azimuth A_0 is calculated as follows [27, 28]:

$$\sin h_0 = C_{31} \cos T + C_{33} \quad (7)$$

$$\cos A_0 = (C_{11} \cos T + C_{13}) / \left((C_{22} \sin T)^2 + (C_{11} \cos T + C_{13})^2 \right)^{1/2}$$

where

$$C_{11} = \sin \varphi \cos \delta, C_{13} = -\cos \varphi \sin \delta,$$
$$C_{22} = \cos \delta, C_{31} = \cos \varphi \cos \delta, C_{33} = \sin \varphi \sin \delta \quad (8)$$

The hour angle of the time of sunrise/sunset over the horizontal plane, $T_h^{r,s}$, is defined as:

$$\cos T_h^{r,s} = -C_{33}/C_{31}. \quad (9)$$

The hour angle of the time of sunrise/sunset over the inclined surface, $T_i^{r,s}$, can be calculated by analogy:

$$\cos(T_i^{r,s} - \lambda') = -C'_{33}/C'_{31} \quad (10)$$

The value of the solar declination δ (rad) valid for a specified day can be found in astronomical handbooks or computed using one of the appropriate approximation formulas (see, e.g., [22, 29]).

The beam irradiance normal to the solar beam is attenuated by the cloudless atmosphere and calculated as:

$$B_{0c} = G_0 e^{-RmL} \quad (11)$$

where G_0 is the extraterrestrial irradiance normal to the solar beam (W/m^2) and the term RmL denotes the attenuation factor representing the Rayleigh optical thickness for a relative optical air mass m. The atmospheric turbidity is expressed by the Linke turbidity factor.

The beam irradiance on a horizontal surface B_{hc} (W/m^2) is given by the following expression:

$$B_{hc} = B_{0c} \sin h_0 \quad (12)$$

where h_0 is the solar altitude angle given by Eq. 7.

Diffuse Radiation

Calculations of diffuse radiation are always prone to some degree of approximation. Diffuse radiation depends on solar geometry, local topography, and atmosphere constituents causing absorption and scattering (e.g., clouds, particulates, aerosols). Diffuse radiation is anisotropic, that is, it varies over the sky depending on direction. Modeling anisotropy is a complex task, which would require knowledge of the amount of sky visible at a point (i.e., a sky-view factor) and of rapidly changing clouds at any instant. To simplify the task, it is often assumed that diffuse radiation is isotropic, which means that the diffuse sky radiance is constant over all directions. This can be a viable solution especially for long-term modeling.

Due to its complexity, the diffuse irradiance incident on the horizontal is usually obtained from

empirical models that have at least regional validity. The clear-sky diffuse radiation component of the *r.sun* solar radiation model presented here is based on the European Solar Radiation Atlas project [1].

The diffuse irradiance on a horizontal surface, D_{hc} (W/m^2) is estimated as the product of three terms: G_0, a diffuse transmission function, Tn, dependent only on the Linke turbidity factor L, and a diffuse solar altitude function, F_d, dependent only on solar altitude h_0 [1]:

$$D_{hc} = G_0 Tn(L) F_d(h_0) \tag{13}$$

$F_d(h_0)$ reduces to 1 for a vertically overhead Sun. The product G_0 Tn(L) then estimates the theoretical diffuse irradiance on the horizontal surface for the air-mass 2 Linke turbidity factor. The following second-order polynomial expression is used [1]:

$$Tn(L) = -0.015843 + 0.030543L + 0.0003797L^2. \tag{14}$$

The solar altitude function is evaluated using the expression:

$$F_d(h_0) = A_1 + A_2 \sinh_0 + A_3 \sin^2 h_0 \tag{15}$$

where the values of the coefficients A_1, A_2, and A_3 depend only on the Linke turbidity L.

The clear-sky diffuse irradiance on an inclined surface, D_{ic} (W/m^2) is estimated separately for sunlit, potentially sunlit, and shadowed surfaces. The exact expressions for these cases can be found in [30].

Ground-Reflected Radiation

The ground-reflected component of solar radiation is usually quite small (e.g., several percents of global radiation). It depends on topography and ground reflectance. The reflectance of the land surface is expressed via ground albedo. In flat areas, the ground reflected radiation is almost nonexistent; however, it may become significant in mountainous areas and higher latitudes with lower altitudes of the Sun and frequent presence of snow. Under such circumstances, the usual approach of considering the ground albedo as constant may lead to incorrect results. A good estimate of the albedo of all surrounding surfaces is a prerequisite to obtain correct results, particularly in calculations of the energy balance of vegetation, amount of transpiration, and energy interception [22]. However, estimating the albedo value is not easy. Usually, tabulated (constant) values are used for typical land cover classes. In reality, the albedo may exhibit temporal variations due to ground cover and vegetation changes, variations in the soil's moisture content, periodic snow cover, etc. For example, Muneer [22] presents typical values of albedo for natural surfaces and ground or vegetation covers. In general, the values range from 0.15 to 0.30, but snow-covered ground could reach 0.9. Surface reflectance maps are generally derived from satellite spectral observations (e.g., [31–34]). Then these maps can be used to obtain the net solar radiation [32] over a large area. Spatial and temporal resolutions of the reflectance maps determine the accuracy of estimates. A higher spatial resolution of land cover maps may provide better spatial accuracy, whereas satellite spectral observation provides better estimates of temporal variations.

In the *r.sun* model, estimates of the clear-sky ground reflected radiation for inclined surfaces (R_i) rely on the isotropic assumption. The ground-reflected clear-sky diffuse irradiance received on inclined surfaces (W/m^2) in the absence of shading is proportional to the global horizontal irradiance, G_{hc}, mean ground albedo, ρ_g, and a fraction of the ground viewed by the inclined surface, $r_g(\gamma_N)$ [22]:

$$R_i = \rho_g G_{hc} r_g(\gamma_N) \tag{16}$$

where

$$r_g(\gamma_N) = (1 - \cos\gamma_N)/2 \tag{17}$$

and the global irradiance on the horizontal surface, G_{hc} (W/m^2) is given as a sum of its beam and diffuse component:

$$G_{hc} = B_{hc} + D_{hc}. \tag{18}$$

Computing Real-Sky Radiation

To properly estimate the real-sky irradiance, overcast and partially cloudy conditions must also be taken into account. However, human meteorological cloudiness observations are usually prone to subjective errors and do not sufficiently describe the physical nature or spatial and temporal patterns

of different types of cloud cover. The overcast irradiance (diffuse only) is calculated from clear-sky raster maps by application of a transmittance factor that parameterizes the attenuation of cloud cover. Examples of explicit calculations of this parameter can be found in [35, 36]. A simpler parameter, called the clear-sky index, can be used to calculate real-sky radiation for horizontal and inclined surfaces [20].

For the assessment of global radiation on a horizontal surface under overcast conditions, G_h, the clear-sky values, G_{hc}, are multiplied by the clear-sky index, k_c [3, 37, 38]:

$$G_h = G_{hc} k_c. \tag{19}$$

Index k_c represents the atmospheric transmission expressed as a ratio between the global horizontal irradiance under overcast and clear-sky conditions. For a set of ground meteorological stations, the clear-sky index can be calculated from the measured global irradiance, G_{hs}, and the computed values of clear-sky global radiation, G_{hc}:

$$k_c = G_{hs}/G_{hc}. \tag{20}$$

Alternatively, k_c can be derived from other sources of climatological data (e.g., cloudiness [39]). The raster maps of k_c must then be derived by spatial interpolation. The k_c index can also be calculated directly from modeled shortwave surface irradiance predictions derived from satellite data. The latter method is based on the similarity between the planetary albedo recorded by spaceborne radiometers and the surface radiant flux [3, 37, 40].

To evaluate the overcast global irradiance for inclined surfaces, G_i, the beam, diffuse, and reflected components are calculated similar to clear-sky equations by just substituting B_{hc} for B_h and D_{hc} for D_h. To compute D_h and B_h, the clear-sky index k_c has to be treated separately, as follows [20]:

$$D_h = D_{hc} k^d{}_c \tag{21}$$

$$B_h = B_{hc} k^b{}_c.$$

The diffuse fraction, or ratio of diffuse to global radiation D_h/G, is a strong function of cloudiness, and therefore is markedly different under clear and overcast skies. In Europe, the diffuse ratio typically varies between 0.3 and 1.0 [40]. The underlying physical processes are quite complicated, and usually represented only by empirical equations [1, 39]. However, for many meteorological stations where the global irradiance, G_{hs}, is measured, the diffuse component, D_{hs}, is either measured or calculated from cloudiness, sunshine, or other climatological data. The raster map of D_{hs}/G_{hs} can be derived from such point values by spatial interpolation. Consecutively, the raster maps of diffuse and beam components of the clear-sky index can be computed as follows [20]:

$$D_h = G_h D_{hs}/G_{hs} \tag{22}$$

$$B_h = G_h - D_h$$

$$k^d{}_c = D_h/D_{hc} \tag{23}$$

$$k^b{}_c = B_h/B_{hc}$$

where subscript s is meant to distinguish data measured at meteorological stations (B_{hs} and D_{hs}) from the estimated values of B_h and D_h.

The r.sun Solar Radiation Model

The methodology described above has been applied to the *r.sun* solar radiation model within the open-source environment of GRASS GIS [18, 20, 41]. GRASS GIS is a free, open-source software that warrants users, developers, and researchers free access to the source code and ways to further improve it [19]. The *r.sun* module of GRASS GIS can be used for any geographical region and time to assess the solar radiation field, and evaluate the irradiance incident on any elemental surface. It has been also successfully applied to assessments of PV electricity production at regional and local scales [4, 20, 24]. A detailed description of the module can be found in [19] and in the GRASS GIS online manual (http://grass.osgeo.org/).

The *r.sun* model estimates the beam, diffuse, and reflected components of clear-sky radiation after taking into account the attenuation of extraterrestrial radiation by air-mass effects and atmosphere turbidity. The real-sky radiation is approximated from the latter results using the clear-sky index, which represents the attenuation of clear-sky radiation by cloudiness. The clear-sky index map is usually derived from ground radiation measurements by interpolation or from

satellite-based predictions. Calculations of the irradiance incident on inclined planes require the estimation of the beam and diffuse components of global horizontal radiation. Similar to the clear-sky index, the ratio of diffuse and global radiation can be derived by interpolating ground-based data or by models based on satellite data.

In summary, the *r.sun* module has the following key features [24]:

- It is a raster-based GIS program with spatially variable input and output data. Alternatively, selected parameters can be set as constants.
- It is a free, open-source program with available source code for further improvement.
- It provides all components of clear-sky and real-sky solar radiation for irradiation (Wh/m^2) and irradiance values (W/m^2).
- Its calculations can be performed assuming solar or civil time.
- It is scalable to various spatial resolutions and region sizes. Memory management and code optimization allows the use of high-resolution data.
- Integration with the open-source environment of GRASS GIS provides other GIS tools for processing the input and output data directly within a single computing environment.

The *r.sun* module works in two modes. *Mode 1* is for instantaneous calculations, for which raster-based maps of solar irradiance (W/m^2) and solar incident angles (degrees) are obtained. In *mode 2*, the raster-based maps provide daily sums of solar irradiation (Wh/m^2) and daily direct-sun duration (min). These are computed from the integration of irradiance values (derived in mode 1) that are calculated at a user-selected time step from sunrise to sunset. If such option is also selected, the computation can account for sky obstructions (shadowing) by local terrain features. These two modes can be used separately or in combination to provide estimates of incident radiation for any desired time step or interval. This is done by incorporating Unix shell scripts (e.g., in the Linux operating system).

Recently, the *r.sun* module has been supplemented by other GRASS GIS modules to help prepare spatially distributed solar databases [42]. For example, *r.sunyear* calculates the optimal tilt of south oriented planes in order to maximize the collectable daily or annual irradiation with 1° precision. This module provides the optimized tilt of the collector plane, as well as the corresponding global irradiation values including the beam, diffuse, and reflected components.

The most computationally demanding part of topographic solar radiation modeling is the analysis of land surface shadows. To calculate shadows, the internal procedure of the *r.sun* module can be used. Alternatively, for large-size grids, the more efficient *r.horizon* module is preferable. The output of this module is a grid representing the elevation angles between the horizontal and the apparent horizon for any specified direction. Series of such grids describing the horizon angles over all directions (with a specified azimuthal step, usually between 3.75° and 15°) can then be used as the input to the *r.sun* module, thus simplifying its internal procedure. Both the *r.horizon* module and the internal shadowing algorithm of the *r.sun* module consider the curvature of the Earth and the angular distortions caused by various cartographic projections.

Computing Spatially Distributed Solar Radiation Databases

Solar radiation parameters are essential to many environmental processes and human activities. Thus it is important to determine with a sufficient spatial and temporal accuracy the amount of solar radiation intercepted by any point on the Earth's surface. Radiation data are usually available from selected ground meteorological stations operating under the auspices of the World Meteorological Organization (WMO). Such data can be retrieved from the World Radiation Data Centre (WRDC). The archives of the WRDC are available online (http://wrdc-mgo.nrel.gov and http://wrdc.mgo.rssi.ru/). However, such data do not cover areas between the measurement stations. In most cases, only global irradiation is available in these archives. Models must therefore be used to estimate the beam and diffuse components. This can be done by using additional meteorological data, such as cloud cover, the turbidity factor, and air temperature.

Currently, there are several satellites whose cloud data can be used to evaluate global radiation at regional or global scales. Various international and national

programs provide satellite-derived solar radiation maps, but their spatial resolution is usually coarse (5–300 km). Among such global initiatives, the International Satellite Cloud Climatology Project (ISCCP) and related programs such as NASA's Surface Solar Energy (SSE) are worth noting [43].

In several regions, digital solar atlases on CD or DVD have been developed to meet the increasing demand for accurate solar radiation data. These atlases are often supplemented by software to compute other parameters of interest and provide a graphical user interface to the maps. For example, the MeteoNorm software (http://www.meteonorm.com) contains various solar radiation or climatological data and software tools to perform spatial interpolations and estimate the irradiance on inclined surfaces. Another example is the European Solar Radiation Atlas [1] covering the European continent.

Currently, new web-based services provide new possibilities for solar radiation applications. For example, the SoDa Web service (http://www.soda-is.com) provides an integrated access to several online databases with a wide range of applications [43]. Other examples are the National Renewable Energy Laboratory (NREL) site (http://rredc.nrel.gov/solar), the RETScreen project (http://www.retscreen.net), the 3Tier web service (http://www.3tier.com), or the PVGIS site for PV assessments (http://re.jrc.ec.europa.eu/pvgis/).

These solar radiation databases provide basic solar radiation maps, such as mean daily values of global horizontal, direct normal, or diffuse horizontal radiation. Thus, the user with interests in the spatial distribution of solar radiation over land must use additional calculations and models to assess the effective solar irradiance/irradiation that is incident on tilted surfaces.

Recently, Hofierka and Cebecauer [24, 44] have developed the national solar radiation database for Slovakia with a spatial resolution of 100 m. This also includes topographic solar radiation maps suitable for environmental applications. The solar radiation database has been derived using the *r.sun* model described above, and additional solar radiation algorithms. The raster-based solar radiation database consists of 12 monthly mean and one annual mean of daily sums of global irradiation on a horizontal plane under real-sky and clear-sky conditions, spatially distributed values of optimum inclination angle of a plane maximizing the solar radiation collection (e.g., for solar energy applications) and monthly means of real-sky global irradiation for optimally inclined planes. Moreover, several other raster-based maps were prepared, including the beam, diffuse, and reflected components of global irradiation, Linke turbidity coefficients, ratios of diffuse and global irradiation on a horizontal plane, ratios of global irradiation on optimally inclined and horizontal planes, as well as the underlying DEM.

Input Data

The data used in this study were derived from the existing data sources and then further processed in GRASS GIS and by the *r.sun* solar radiation model. The input dataset included a 100-m resolution DEM, measured values of global and diffuse radiation from 22 ground meteorological stations, and monthly maps of Linke turbidity coefficient.

As mentioned earlier, the essential input for topographic solar radiation modeling is a proper DEM. The spatial resolution of raster-based DEMs significantly affects the accuracy of modeling and spatial patterns of solar irradiation. The DEM used for the Slovakia database was based on the SRTM data from the C-band SAR interferometry instrument [45] acquired during an Endeavour space shuttle mission that took place in 2001. These data cover approximately 80% of the total Earth surface. In the northern hemisphere, the data covers all areas up to 60° latitude. The original resolution of the data is 1 arcsec (≈30 m). For areas outside the USA, only the coarser 3-arcsec data are freely available (http://srtm.usgs.gov/), which still determine an excellent resolution (≈90 m). The horizontal and vertical accuracy of the data is sufficient for most solar applications, even at local scales. In this study, the 3-arcsec data available in the WGS84 geographic coordinate system were reprojected and resampled to 100-m resolution (Fig. 2). To accurately take into account the shadowing effects of surrounding terrain, a 50-km strip of DEM behind the state border of Slovakia was also included. The detailed daily analysis of shadows on large grids throughout a year means very high computing demands, which can be minimized by the *r.horizon* module. A set of 96 data layers representing horizon angles with an azimuthal angle step of 3.75° were precomputed using this module.

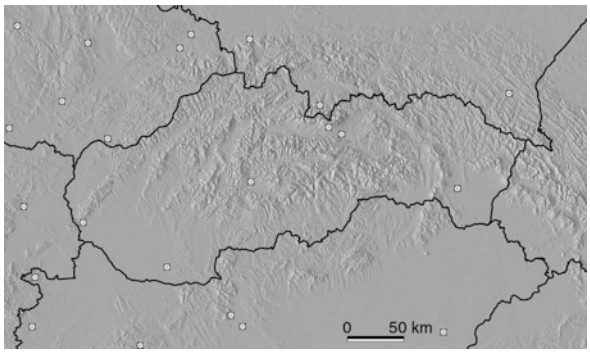

Topographic Solar Radiation Modeling for Environmental Applications. Figure 2
Ground meteorological stations measuring solar radiation and DEM derived from the SRTM data

This considerably accelerated calculations in the *r.sun* module [44].

Ground meteorological stations measuring solar radiation and other related meteorological parameters (e.g., turbidity, cloudiness, etc.) are usually sparse and unevenly distributed. In most cases, their spacing is such that the spatial variability in solar radiation cannot be accurately derived. In Slovakia, only six meteorological stations measuring global solar radiation are available. To use the maximum possible information, these stations have been supplemented by another set of 16 nearby meteorological stations in neighboring countries, for a total of 22 stations used in this study (Fig. 2). The measurement of global and diffuse solar radiation is needed to assess the ratio of real-sky and clear-sky radiation represented by the clear-sky index and its beam and diffuse components. These are necessary in order to derive the real-sky radiation on inclined surfaces.

To prepare spatially distributed input data derived from measured or modeled solar radiation data, interpolation techniques are frequently used, such as splines, weighted averages, or kriging (see, e.g., [46–48]). However, a low spatial density of meteorological stations measuring solar radiation still requires a sophisticated interpolation approach, such as co-kriging [49, 50] or multivariate splines [20, 51], in order to include additional variables and useful information from a DEM or satellite images, and effectively improve the quality of interpolation. Using this approach, Šúri et al. [4] have prepared a PVGIS database (http://re.jrc.ec.europa.eu/pvgis/) with 1-km spatial resolution, which contains a comprehensive set of various solar radiation data. This includes the *r.sun* input parameters for Europe, which also covers the territory of Slovakia. The beam and diffuse clear-sky index components were derived from the monthly means of global and diffuse radiation measured at many meteorological stations (including the 22 stations considered in the Slovakia study) during the 1981–1990 period [1], and from clear-sky global irradiations computed using the *r.sun* model [4]. The input data for this study included the beam and diffuse clear-sky index components and Linke turbidity grid maps taken from the PVGIS database, which were all resampled to 100-m resolution using the *r.resamp.rst* interpolation resampling module in GRASS GIS. The original maps of monthly Linke turbidity factor were obtained from a global database [52] at their original spatial resolution of 5′ (≈8 km). The estimation of turbidity is still prone to large uncertainties and affects the accuracy of clear-sky radiation maps, particularly those for the beam and diffuse components.

The monthly mean clear-sky index and diffuse fraction were interpolated using the *v.vol.rst* module in GRASS GIS, which is based on a tri-variate version of the Regularized Spline with Tension method [19]. Finally, the elevation variable was represented by the 100-m DEM derived from the SRTM data, thus enhancing the resolution and accuracy of interpolation in mountainous regions.

Calculation Procedure

The solar database represented by the final maps in Figs. 3–6 was computed by the *r.sun* module with the help of the above-mentioned GRASS GIS modules in three major steps [20]:

1. Computation of global clear-sky irradiation on a horizontal plane
2. Calculation of global real-sky irradiation on a horizontal plane and its beam and diffuse components using the beam and diffuse clear-sky index components
3. Computation of the optimal inclination of the south-oriented plane to maximize the annual irradiation yield using the *r.sunyear* module, and computation of irradiation for optimally inclined planes

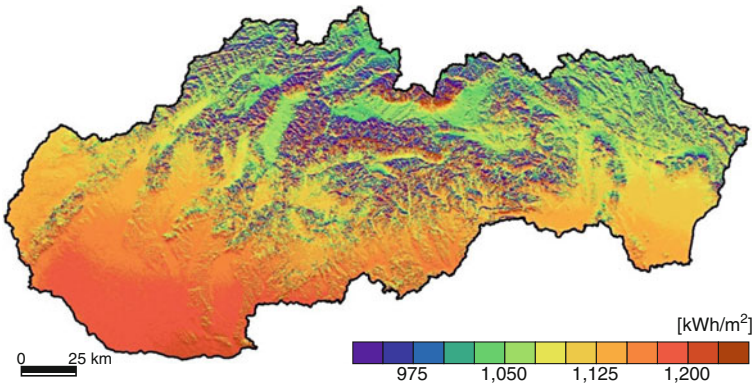

Topographic Solar Radiation Modeling for Environmental Applications. Figure 3
Annual real-sky global solar irradiation incident on the ground surface in Slovakia

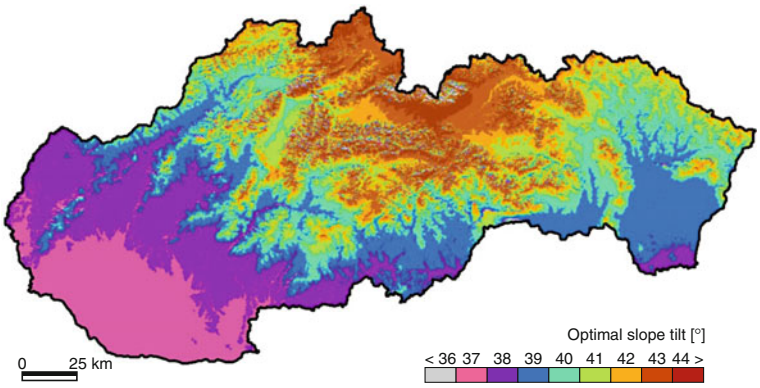

Topographic Solar Radiation Modeling for Environmental Applications. Figure 4
Optimal slope tilt maximizing the annual solar input in Slovakia

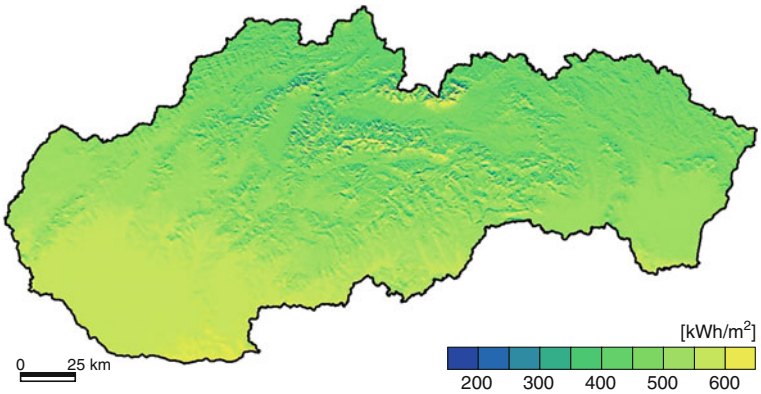

Topographic Solar Radiation Modeling for Environmental Applications. Figure 5
Annual real-sky beam solar irradiation

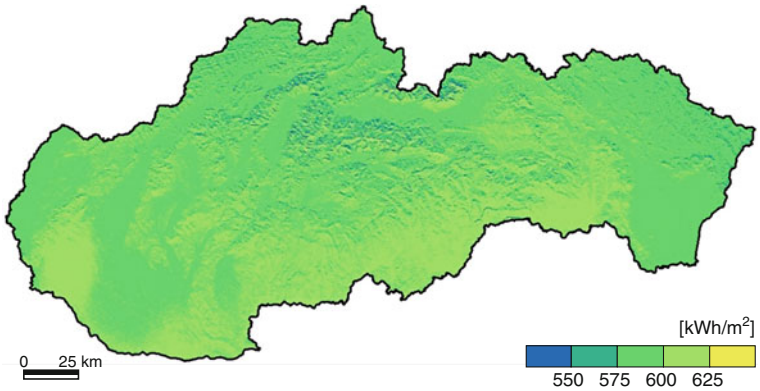

Topographic Solar Radiation Modeling for Environmental Applications. Figure 6
Annual real-sky diffuse solar irradiation

All databases were derived in the form of spatially distributed raster-based maps representing monthly and annual means of daily sums of irradiation in kWh/m^2. The long-term mean values were determined by the input data, that is, long-term monthly means of the clear-sky index and of the Linke turbidity coefficient. Although these important inputs have a coarse time resolution, the use of a high-resolution DEM provides the capability to better model the daily and seasonal dynamics of solar radiation. Values of slope and aspect were calculated from the SRTM DEM using the *r.slope.aspect* module. Calculations were performed for the median day of each month, taken as the effective average day. An integration time step of 15 min was used to obtain daily sums of irradiation. A shell-scripting technique in GRASS GIS was used to calculate monthly values of irradiation using the *r.sun* module in *mode 2*.

The resulting spatial maps of solar radiation consist of:

1. Monthly means of global irradiation including all components for clear and real skies on a horizontal plane
2. Monthly means of global irradiation including all components for real-sky incident at the land surface
3. Irradiance values incident at the land surface in 15-min steps for March, June, September, and December

The monthly means were subsequently summed up to get annual values.

The quality of outputs from any topographic solar radiation model reflects that of the source data and of the solar radiation methodology. A high-resolution DEM improves the accuracy of topography factors (absolute air mass and shadowing). The real-sky irradiation results are more influenced by the lack of representative ground-based measurements reflecting local variations and dynamics of cloudiness. In the Slovakia case, ground-based measurements were spatially interpolated using a sophisticated tri-variate interpolation method that can make the local variability of irradiation dependent on topography [20, 51].

The overall accuracy of the database represented by monthly and annual values of irradiation was assessed using basic statistics, the relative mean bias error (rMBE), and relative root mean squared error (rRMSE). The rMBE measures the overall bias. For the six available radiometric stations in Slovakia, it reached 3.1% and 2.7% for the monthly and annual real-sky global irradiations on a horizontal plane, respectively. The rRMSE, which is more a measure of random errors, was a bit higher – approaching 5.9% and 4.2% for the monthly and annual irradiations, respectively [24].

For Slovakia, the mean annual real-sky global irradiation incident on the surface (Fig. 3) averages from 925 kWh/m^2 on northern slopes and bottoms of valleys to 1,250 kWh/m^2 on southern slopes of mountains, with locally higher values. Interestingly, these southern slopes have a higher solar input than horizontal areas in the southern part of the country (1,150–1,200 kWh/m^2). The optimal slope tilt maximizing the annual solar irradiation

input is in the range of 36–44°, that is, slightly less than latitude (Fig. 4). This confirms the findings by Gueymard [53] for the US territory. The optimal slope tilt was calculated using the *r.sunyear* module that iteratively calculates the optimal slope tilt using the *r.sun* model [54]. The values of optimal slope tilt also explain why south-oriented, steeper slopes at higher latitudes may receive more radiation than horizontal areas at lower latitudes. Figure 4 also indicates that the spatial variability in global radiation incident on the ground is quite high in Slovakia, with mountainous areas exhibiting the strongest gradients, as could be expected.

Figure 5 shows the mean annual real-sky beam irradiation incident on the ground surface in Slovakia. This component is the most sensitive to changes in land surface geometry, especially under lower solar altitudes due to the occurrence of shadows. Mountains also often trigger a local increase in cloudiness, thus attenuating the beam radiation component. The mean annual beam irradiation varies from 100 kWh/m^2 on northern slopes and valley bottoms to 650 kWh/m^2 on southern slopes and flat areas.

Diffuse radiation (Fig. 6) is the second most important component of global radiation. The amount of diffuse radiation is directly affected by the clear-sky index and to a lesser extent by topography. The *r.sun* model considers the terrain's slope, but not the indirect, sky blocking effect of the neighboring terrain on diffuse radiation. The mean annual diffuse irradiation varies only slightly from 500 kWh/m^2 on northern slopes and valley bottoms to 650 kWh/m^2 on southern slopes and higher elevations. Over flat areas, an intermediate value of ≈600 kWh/m^2 per year is typical. The spatial variability in diffuse irradiation is lower than in beam irradiation, since the influence of shading effects on this component is weaker.

Reflected radiation (Fig. 7) has the lowest share in global radiation, as could be expected. It exists only in non-flat areas, and reaches the highest values in mountains. The mean annual reflected irradiation is from

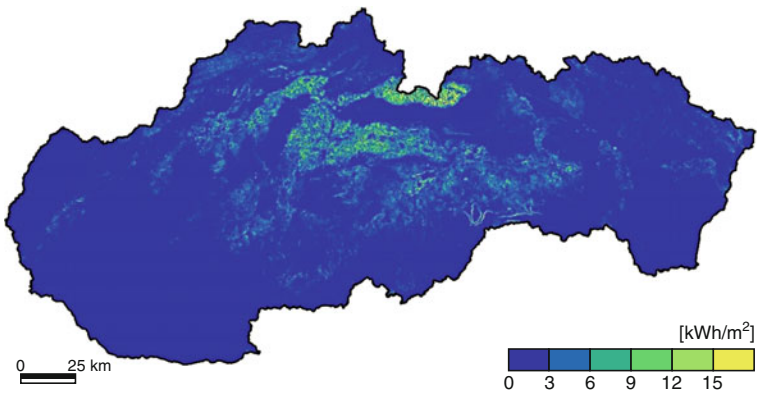

Topographic Solar Radiation Modeling for Environmental Applications. Figure 7
Annual real-sky reflected solar irradiation

Topographic Solar Radiation Modeling for Environmental Applications. Table 1 Mean, minimal, and maximal daily global irradiation incident on the ground surface in Slovakia (kWh/m^2)

Daily irradiation (kWh/m^2)	Month												
	1	2	3	4	5	6	7	8	9	10	11	12	Year
Mean	0.9	1.6	2.7	3.9	4.8	5.0	5.3	4.4	3.2	2.2	1.1	0.7	3.0
Minimum	0.3	0.6	1.0	1.3	1.8	2.0	2.0	1.5	1.0	0.7	0.5	0.3	1.1
Maximum	2.3	3.2	4.1	4.7	5.5	5.8	6.1	5.3	4.4	3.5	2.3	1.7	3.9

0 kWh/m^2 in flat areas to 18 kWh/m^2 on steep slopes in mountains. The seasonal variability in albedo was not considered.

The seasonal variability in mean daily global irradiation over Slovakia is presented in Table 1. This variability is quite high due to the relatively high latitude (47°–49°). During the summer months (June to August), the mean daily irradiation is about 5.5 times higher than during the winter months (December to February). The highest seasonal variability and differences can be found on northern slopes (up to seven times), in contrast to southern slopes where differences are only ≈2.5 times. This seasonal variability is caused by topographic effects that are increased during winter when solar altitudes are lower and hence frequent shadows are cast by terrain features.

Future Directions

Topographic solar radiation models are increasingly available for various environmental applications. However, due to their complexity and input data requirements, they still lack some features that could improve the accuracy of the modeling results. While clear-sky beam component is well defined and easily calculated, the diffuse component is prone to approximations, even under clear-sky conditions. Thus the anisotropic character of diffuse radiation is often approximated by the isotropic assumption. The problem is even more complex under real-sky conditions. Spatial and temporal variability caused by clouds can overwhelm the topographic variability [12].

The long-term values of real-sky radiation incident at the land surface can be well approximated using ground-based or satellite-based measurements. The ground-based data are usually sparsely and unevenly distributed and therefore more advanced techniques of spatial interpolation might be necessary. The advanced interpolation and disaggregation techniques can be used to assess the real-sky radiation with higher spatial resolutions and topographic effects. However, the short-term changes away from weather stations lack adequate modeling tools. The satellite-based data are evenly distributed, however, often spatially averaged (smoothed) and therefore less accurate in mountainous areas. Still, topographic models and elevation data can be used to disaggregate satellite data in areas with strong topographic effects, and thus increase the accuracy of estimates [55].

Recently, the *r.sun* topographic solar radiation model has been successfully applied to assessments of roof potential for solar energy applications in urban areas [21]. However, the analysis is limited to 2-D surfaces (roofs) and cannot be applied to vertical facades. Therefore, future improvements of topographic solar radiation models should also include extension to 3-D modeling for vertical surfaces including complex urban areas and overlapping plant canopies.

Acknowledgments

This work was supported by the Ministry of Education of the Slovak Republic under Grant VEGA 1/0355/09.

Bibliography

1. Scharmer K, Greif J (2000) The European Solar Radiation Atlas, vol 2, Database and Exploitation Software. Paris. Presses de l'École des Mines de Paris, France
2. Remund J, Kunz S, Lang R (1999) METEONORM: global meteorological database for solar energy and applied climatology, Solar Engineering Handbook, version 4.0. Meteotest, Bern
3. Hammer A, Heinemann D, Westerhellweg A, Ineichen P, Olseth JA, Skartveit A, Dumortier D, Fontoynont M, Wald L, Beyer HG, Reise Ch, Roche L, Page J (1998) Derivation of daylight and solar irradiance data from satellite observations. In: Proceedings of the 9th conference on satellite meteorology and oceanography, Paris, May 1998, pp 747–750
4. Šúri M, Huld TA, Dunlop ED (2005) PVGIS: a web-based solar radiation database for the calculation of PV potential in Europe. Int J Sustainable Energy 24:55–67
5. Cottle HJ (1932) Vegetation on north and south slopes of mountains in south-western Texas. Ecology 13:121–134
6. Wilson RG (1970) Topographic Influences on a Forest Microclimate. McGill University, Montreal, Canada
7. Halverson HG, Smith JL (1979) Solar radiation as a forest management tool: a primer of principles and application, General technical report PSW-33. The Forest Service of the US Department of Agriculture, Berkeley
8. Dozier J (1980) A clear-sky spectral solar radiation model for snow-covered mountainous terrain. Water Resour Res 16:709–718
9. Gates DM (1980) Biophysical ecology. Springer, New York, pp 96–146
10. Moore ID, Grayson RB, Ladson AR (1991) Digital terrain modelling: a review of hydrological, geomorphological and biological applications. Hydrol Process 11:47–54

11. Fu P, Rich PM (2000) A geometric solar radiation model with applications in agriculture and forestry. Comput Electron Agric 37:25–35
12. Dubayah R, Rich PM (1995) Topographic solar radiation models for GIS. Int J Geogr Inf Syst 9:405–413
13. Hetrick WA, Rich PM, Barnes FJ, Weiss SB (1993) GIS-based solar radiation flux models, American society for photogrammetry and remote sensing technical papers, vol 3, GIS photogrammetry and modeling. Wiley, New York, pp 132–143
14. Kumar L, Skidmore AK, Knowles E (1997) Modeling topographic variation in solar radiation in a GIS environment. Int J Geogr Inf Sci 11:475–497
15. Fu P, Rich PM (2000) The solar analyst 1.0 user Manual. Helios Environmental Modeling Institute, Lawrence, KS
16. Wilson JP, Gallant JC (2000) Secondary topographic attributes. In: Wilson JP, Gallant JC (eds) Terrain analysis; principles and applications. Wiley, New York, pp 87–132
17. McKenney DW, Mackey BG, Zavitz BL (1999) Calibration and sensitivity analysis of a spatially-distributed solar radiation model. Int J Geogr Inf Sci 13:49–65
18. Hofierka J (1997) Direct solar radiation modelling within an open GIS environment. In: Proceedings of the joint European GI conference, Vienna, pp 575–584
19. Neteler M, Mitasova H (2004) Open Source GIS: a GRASS GIS approach, 2nd edn. Kluwer, Boston
20. Šúri M, Hofierka J (2004) A new GIS-based solar radiation model and its application to photovoltaic assessments. Trans GIS 8:175–190
21. Hofierka J, Kaňuk J (2009) Assessment of photovoltaic potential in urban areas using open-source solar radiation tools. Renewable Energy 34:2206–2214
22. Muneer T (2004) Solar radiation and daylight models. Elsevier, Amsterdam
23. Hengl T, Reuter HI (2009) Geomorphometry: concepts, software, applications, vol 33, Developments in Soil Science. Elsevier, Amsterdam
24. Hofierka J, Cebecauer T (2008) Spatially distributed assessment of solar resources for energy applications in Slovakia. Acta Facultatis Studiorum Humanitatis et Naturae Universitatis Prešoviensis. Prírodné vedy Folia Geogr 12:97–114
25. Perez R, Seals R, Ineichen P, Steward R, Menicucci D (1987) A new simplified version of the Perez diffuse irradiance model for tilted surfaces. Sol Energy 39:221–231
26. Rigollier Ch, Bauer O, Wald L (2000) On the clear sky model of the ESRA – European Solar radiation Atlas – with respect to the Heliosat method. Sol Energy 68:33–48
27. Krcho J (1990) Morfometrická analýza a digitálne modely georeliéfu. Bratislava, Veda (in Slovak)
28. Jenčo M (1992) Distribúcia priameho slnečného žiarenia na reoreliéfe a jej modelovanie pomocou komplexného digitálneho modelu reliéfu. Geografický časopis 44:342–355 (in Slovak)
29. Gruter JW (1984) Radiation nomenclature. 2nd solar energy programme of the CEC, Project F, Solar radiation data. CEC, Brussels
30. Muneer T (1990) Solar radiation model for Europe. Build Serv Eng Res Technol 11:153–163
31. Brest CL, Goward SN (1987) Deriving surface albedo measurements from narrow band satellite data. Intl J Remote Sens 8:351–367
32. Dubayah R (1992) Estimating net solar radiation using Landsat Thematic Mapper and digital elevation data. Water Resour Res 28:2469–2484
33. Duguay CR, LeDrew EF (1992) Estimating surface reflectance and Albedo from LANDSAT-5 thematic mapper over rugged terrain. Photogramm Eng Remote Sens 57:551–558
34. Dubayah R, Loechel S (1997) Modeling topographic solar radiation using GOES data. J Appl Meteorol 36:141–154
35. Becker S (2001) Calculation of direct solar and diffuse radiation in Israel. Int J Climatol 21:1561–1576
36. Kitler R, Mikler J (1986) Základy využívania slnečného žiarenia. Bratislava, Veda (in Slovak)
37. Beyer HG, Costanzo C, Heinemann D (1996) Modifications of the Heliosat procedure for irradiance estimates from satellite images. Sol Energy 56:207–212
38. Rigollier Ch, Lefèvre M, Wald L (2001) Heliosat version 2, integration and exploitation of networked solar radiation databases for environment monitoring (SoDa), European commission project no. IST-1999-122245, report. http://www.helioclim.org/publications/heliosat2_d3.2.pdf. Accessed 14 December 2010
39. Kasten F, Czeplak G (1980) Solar and terrestrial radiation dependent on the amount and type of cloud. Sol Energy 24:177–189
40. Cano D, Monget JM, Albuisson M, Guillard H, Regas N, Wald L (1986) A method for the determination of the global solar radiation from meteorological satellite data. Sol Energy 37:31–39
41. Hofierka J, Šúri M (2002) The solar radiation model for Open source GIS: implementation and applications. In: Ciolli M, Zatelli P (eds) Proceedings of the open source free software GIS – GRASS users conference, Trento, Italy, 11–13 Sept 2002, CD-ROM
42. Šúri M, Huld TA, Dunlop ED, Ossenbrink HA (2007) Potential of solar electricity generation in the European Union member states and candidate countries. Sol Energy 81:1295–1305
43. Wald L (2006) Available databases, products and services. In: Dunlop ED, Wald L, Šúri M (eds) Solar energy resources management for electricity generation from local level to global scale. Nova Science Publishers, New York, pp 29–41
44. Hofierka J, Cebecauer T (2007) Priestorová a časová distribúcia slnečného žiarenia na georeliéfe Slovenska. In: Střelcová K, Škvarenina J, Blaženec M (eds) Bioclimatology and natural hazards, CD-ROM proceedings of the international scientific conference, Polana nad Detvou, Slovak Bioclimatological Society, Technical University Zvolen (in Slovak), Slovakia, 17–20 Sept 2007
45. Zyl JJ (2001) The shuttle radar topography mission (SRTM): a breakthrough in remote sensing of topography. Acta Astronaut 48:559–565
46. Hutchinson MF, Booth TH, McMahon LP, Nin HA (1984) Estimating monthly mean values of daily total solar radiation for Australia. Sol Energy 32:277–290
47. Hulme M, Conway D, Jones PD, Jiang T, Barrow EM, Turney C (1995) A 1961-1990 climatology for Europe for climate

change modelling and impact applications. Int J Climatol 15:1333–64
48. Zelenka A, Czeplak G, D'Agostino V, Josefson W, Maxwell E, Perez R (1992) Techniques for Supplementing Solar Radiation Network Data, Technical Report, International Energy Agency, # IEA-SHCP-9D-1. Swiss Meteorological Institute, Switzerland
49. D'Agostino V, Zelenka A (1992) Supplementing solar radiation network data by co-kriging with satellite images. Int J Climatol 12:749–761
50. Beyer HG, Czeplak G, Terzenbach U, Wald L (1997) Assessment of the method used to construct clearness index maps for the new European solar radiation atlas (ESRA). Sol Energy 61:389–397
51. Hofierka J, Parajka P, Mitasova M, Mitas L (2002) Multivariate interpolation of precipitation using regularized spline with tension. Trans GIS 6:135–150
52. Remund J, Wald L, Lefèvre M, Ranchin T, Page J (2003) Worldwide linke turbidity information. In: Proceedings of ISES solar world congress on solar energy for a sustainable future, Göteborg, Sweden, 14–20 June 2003
53. Gueymard CA (2008) Fixed or tracking solar collectors? Helping the decision process with the solar resource enhancement factor. In: Proceedings of optical modeling and measurements for solar energy systems II conference, SPIE, vol 7046, San Diego
54. Šúri M, Huld TA, Dunlop ED, Hofierka J (2007) Solar resource modelling for energy applications. In: Peckham RJ, Jordan G (eds) Digital terrain modelling, development and applications in a policy support environment, Series lecture notes in geoinformation and cartography. Springer, Heidelberg, pp 259–273
55. Ruiz-Arias JA, Cebecauer T, Tovar-Pescador J, Šúri M (2010) Spatial disaggregation of satellite-derived irradiance using a high-resolution digital elevation model. Sol Energy 84:1644–1657

Toxic Chemical Risks

Edward A. Laws
Louisiana State University, School of the Coast and Environment, Baton Rouge, LA, USA

Article Outline

Glossary
Definition of the Subject
Introduction
Lifestyle-Associated Exposure to Toxic Chemicals
Exposure to Toxic Chemicals in the Home
Future Directions
Bibliography

Glossary

Alkaloid A colorless, complex, and bitter organic base containing nitrogen and usually oxygen that is often physiologically active.

Analgesic Painkiller.

Apoptosis A genetically directed process of cell self-destruction that eliminates DNA-damaged, superfluous, or unwanted cells.

Cold turkey Cold flashes with goose bumps, one of the symptoms associated with withdrawal from a drug to which a person has become addicted.

Dopamine A neurotransmitter in the brain that plays an important role, inter alia, in behavior and reward.

Opioid A chemical that binds to and activates the opioid receptors in the nervous system and gastrointestinal tract; includes both natural opiates (derived from opium) and synthetic drugs possessing narcotic properties similar to opiates but not derived from opium.

Secondhand smoke Smoke inhaled by a nonsmoker and consisting of mainstream smoke (smoke exhaled by a smoker) and sidestream smoke (smoke from the end of a lighted cigarette, pipe, or cigar).

Teratogenic Causing developmental malformations.

Definition of the Subject

At the present time there are approximately 100,000 chemicals in the environment, with an additional 500–1,000 added each year. Although not all these chemicals are toxic, merely keeping up-to-date information on the possible toxicity of so many compounds is a prodigious task. Federal agencies such as the Environmental Protection Agency (EPA), Food and Drug Administration (FDA), and Consumer Product Safety Commission (CPSC) are responsible for establishing rules and guidelines that ensure, insofar as possible, that risks associated with exposure to toxic chemicals are within acceptable limits. Legislation such as the Clean Air Act, originally passed in 1963, and Clean Water Act, a 1977 amendment to the 1972 Federal Water Pollution Control Act, have done much to advance the cause of environmental safety. Ironically perhaps, in the United States the primary sources of exposure to toxic chemicals and poisons are related to lifestyle issues, including in particular smoking, drinking (alcohol), use/abuse of pharmaceutical and

recreational drugs, and obesity. Most incidents of poisoning occur in the home, where unintentional exposure to toxic chemicals is often the result of ignorance and/or carelessness. Education and public awareness have therefore become important components of the effort to address the issue of exposure to toxic chemicals in the United States.

Introduction

On the first day of class students in an honors section of an introductory environmental science class at Louisiana State University were asked to answer a series of multiple-choice questions to determine how much they knew about the subject before taking the course. One of the questions asked (Dr. Vince Wilson, personal communication):

The statement, "Water can be a poison," is an example of

1. No agent has a single effect
2. The water quality of the Baton Rouge Public Water System
3. Dose makes the poison
4. A sensitive population
5. Toxicology is an empirical science

The correct answer is "dose makes the poison," the translation of a statement made in German by the sixteenth century physician Paracelsus. It underscores the fact that many substances commonly considered to be toxic are presumably harmless if the dose or degree of exposure is sufficiently small. This line of reasoning underlies the concept of an acceptable daily intake (ADI), for example, of food additives and contaminants [1, p. 2]. The ADI is a dose of the substance that would be expected to be associated with no appreciable adverse health effects if administered over the lifetime of a healthy person. On the other hand, consumption of too much of an otherwise benign substance can have serious health consequences. Water intoxication, for example, is a potentially fatal condition that occurs when consumption of too much water causes an abnormal balance of electrolytes in the body.

In judging the risk associated with exposure to toxic chemicals, one must consider the duration of exposure as well as the dose. In toxicology the distinction is typically made between short-term or acute exposure and long-term or chronic exposure. Experimentally acute and chronic exposures are defined to be exposures lasting up to 14 days and greater than 1 year, respectively, with "intermediate exposure" used to characterize exposures lasting 14 days to 1 year [2]. These definitions are arbitrary, and in practice exposure times may vary continuously from seconds to an entire lifetime.

Alcohol consumption is a good example of an issue linked to exposure time. In most states in the United States, a person is considered to be intoxicated if his/her blood alcohol content exceeds 0.08%. Consumption of alcohol can have fatal consequences if the blood alcohol content approaches ~0.40%. Death results from alcohol's depressant effect on vital areas of the brain that control consciousness, respiration, and heart rate. To provide some context to these numbers, a person weighing ~100 pounds (45 kg) who consumed the contents of two 12-ounce cans of beer (5% alcohol content) over a short timeframe (~30–40 min) would likely have a blood alcohol content of ~0.10% (i.e., above the legal limit for driving) and a blood alcohol content of ~0.40% (i.e., potentially lethal) if he/she consumed eight 12-ounce cans of beer over the same timeframe. On the other hand, a 150-pound (68 kg) person who consumed the same quantities of beer over the same timeframe would likely have blood alcohol levels of only ~0.06% (i.e., below the legal limit for driving) and 0.25% (intoxicated and perhaps experiencing serious side effects, but probably not life-threatening), respectively. Incidentally, the tendency of people to vomit when they have had too much to drink is a natural defense mechanism and allows the body to rid itself of alcohol that has not already been absorbed into the bloodstream. Unfortunately this defense mechanism is not infallible. When some people have had too much to drink they lose consciousness and never recover, either because of the effect of the alcohol on their brain or because they choke on their own vomit and are unable to clear their air passages.

The effects of consuming 12-ounce cans of beer are very different if the timeframe is longer. If a 100-pound person consumed one 12-ounce can of beer per day for 8 days, for example, his/her blood alcohol level would probably never rise to more than 0.05%, below the legal limit for driving and far below the level associated with potentially fatal effects.

Perhaps surprisingly, most (~90%) exposures to toxic chemicals occur in the home and involve everyday household items. Not surprisingly, most exposures (85–90%) are accidents, although some are intentional (e.g., suicides). With the notable exception of cigarette smoke, about 75% of cases in the United States involve ingestion of a poison (as opposed, e.g., to inhalation of a toxin or exposure via dermal contact), and, with the exception of alcohol consumption, over half the cases involve children under the age of six. Interestingly, the greatest public health problems associated with exposure to toxic chemicals involve lifestyle decisions as opposed, for example, to living downwind or downstream from an obvious source of pollution.

Lifestyle-Associated Exposure to Toxic Chemicals

Smoking

In the United States and many other countries, by far the single greatest source of exposure to toxic chemicals is tobacco smoke, primarily the result of cigarette smoking. Cigarette smoke contains several hundred toxins, of which 44, the so-called Hoffmann analytes [3–5], are believed to be most relevant to smoking-related health effects [6]. These include the following:

- Ammonia (NH_3): Nicotine, which is the addictive component of cigarettes, exists in two forms, bound and free. The free form of nicotine vaporizes more readily, and from the vapor phase is rapidly absorbed by the lungs and transported by the bloodstream to the brain. Adding ammonia to cigarettes facilitates the conversion of bound to free nicotine and thereby enhances the pleasurable effects associated with secretion of dopamine by brain neurons that have been stimulated either directly or indirectly by nicotine. Ammonia is also a toxic gas that can damage the respiratory system when it combines with water to form ammonium hydroxide:

  $$NH_3 + H_2O \rightarrow NH_4OH$$

  NH_4OH is highly alkaline and corrosive. Exposure to NH_4OH is associated with coughing, sore throat, shortness of breath, and a burning sensation, all of which may be associated with smoking.
- Arsenic (As): Arsenic is a well-known toxin that has been used in pesticides for more than 1,000 years. The most commonly used formulation has been lead arsenate, which was used extensively for control of insect pests until the end of World War II, when more effective synthetic organic insecticides became available. However, it is estimated that smokers breathe in between 0.8 and 2.4 μg of As per pack of cigarettes [7] due to continued use of arsenic-containing pesticides by tobacco growers. The toxicity of As is related to its disruptive effects on a wide variety of metabolic processes leading to, inter alia, oxidative stress, lactic acidosis, anemia, central nervous system dysfunction, and apparent thiamine deficiency.
- Benzene (C_6H_6): Benzene, a human carcinogen and known cause of leukemia, is found in cigarette smoke, which is believed to account for about half of human exposure. Chronic exposure to benzene can result in a variety of health problems including anemia, leukemia, and adverse effects on the immune system [8, 9].
- Benzo[a]pyrene ($C_{20}H_{12}$): Benzo[a]pyrene is a five-ring polycyclic aromatic hydrocarbon formed by the fusion of a benzene ring with pyrene. It is found in all smoke associated with the combustion of organic matter, including tobacco leaves. Metabolites of benzo[a]pyrene have been shown to be mutagenic and are highly carcinogenic [10]. Amounts of benzo[a]pyrene in cigarettes range from ~3 to 30 ng per cigarette and are roughly in proportion to declared tar values [11]. The carcinogenic effects of benzo[a]pyrene are associated with binding of its diol epoxide metabolites to the tumor suppressor protein P53, which normally functions as a cell cycle regulator. Damage to P53 is related to more than half of all human cancers and to an even higher percentage of lung cancers [12, 13].
- Cadmium (Cd): In general leafy vegetables such as lettuce and spinach contain high levels of cadmium, which they accumulate from the soil. This is a natural phenomenon, and tobacco leaves are no exception. A cigarette smoker will typically take in about 3.0 μg of Cd per pack, of which 25% will be absorbed [14]. Chronic exposure to Cd is associated with kidney and liver damage, and in severe cases to softening of the bones [15]. Smokers typically have about twice the body burden of Cd as nonsmokers [16, 17].

- Carbon monoxide (CO): Carbon monoxide is a colorless, odorless gas that results from the combustion of organic matter with inadequate amounts of oxygen. The concentration of CO in the air inhaled with cigarette smoke is about 2%, of which ~85% is absorbed [18, 19]. A person smoking 20 cigarettes per day (the minimum number of cigarettes per pack in the United States is 20) would be expected to absorb ~200 mg of CO [20], considerably higher than the maximum of 24 mg d^{-1} that can be safely tolerated [18]. The adverse effects of CO exposure are typically associated with its tendency to bind to hemoglobin and hence to interfere with the ability of hemoglobin to absorb and transport oxygen. Ironically, the affinity between CO and hemoglobin is about 230 times greater than the affinity between O_2 and hemoglobin [21, 22]. Additional adverse effects may be caused by the tendency of CO to bind to myoglobin, a protein that binds iron and oxygen in muscle tissues, and to cytochrome oxidase, an enzyme in the respiratory electron transport chain.
- Formaldehyde (CH_2O): Formaldehyde is a colorless but pungent gas found in cigarette smoke as a result of the pyrolysis of saccharides used as tobacco ingredients [23–25]. It is carcinogenic [26–29] and causes damage to the lungs when inhaled [30, 31]. The amount of formaldehyde inhaled in cigarette smoke is closely correlated with the tar content of the cigarette and ranges as high as 40–50 μg per cigarette [20]. Estimated exposure levels in the oral cavity during smoking range as high as 115 parts per million (ppm), which is considerably higher than the Occupational Safety and Health Administration (OSHA) short-term (15 min) exposure limit (STEL) of 2 ppm.
- Hydrogen cyanide (HCN): Hydrogen cyanide is a colorless, poisonous gas that was used as a genocidal agent by the Nazis during World War II. A byproduct of burning tobacco, HCN is found in cigarette smoke in amounts sufficient to produce exposures of 144–351 μg per cigarette [6, 32]. To put this number in context, the STEL for HCN is 4.7 ppm in the air one breathes. An average person inhales about 11 m^3 of air per day or 115 L in 15 min. If the air contained 4.7 ppm HCN vapor, the person would be inhaling about 0.54 mL or 22 μmol of HCN vapor in 15 min (this calculation assumes that HCN vapor behaves like an ideal gas and that the temperature is 25 °C or 77 °F). Twenty-two micromoles of HCN have a mass of 594 μg. Thus smoking 2–4 cigarettes in 15 min would very likely lead to the inhalation of a quantity of HCN greater than the OHSA short-term exposure limit for this toxic gas. Headache, nausea, and vertigo are symptoms associated with chronic exposure to HCN [33].
- Nicotine ($C_{10}H_{14}N_2$): Nicotine is an alkaloid that is responsible for the addictive nature of tobacco use. However, it has also been implicated in DNA damage, oxidative stress, and inhibition of apoptosis [34, 35]. The latter effect could be a factor in the etiology of smoking-associated cancer of the lungs and oral cavity, that is, inhibition of programmed cell death may allow the multiplication of "chemically initiated cells" [35]. Doses of nicotine associated with cigarette smoking are highly correlated with the tar content of cigarettes and range as high as 1.0–1.2 mg per cigarette [20].
- TSNAs: This acronym stands for tobacco-specific N-nitrosamines, a category that includes four compounds linked to smoking-related cancers: (1) N′-nitrosonornicotine (NNN), (2) 4-methyl-N-nitrosamino-1-(3-pyridyl)-1-butanone (NNK), (3) N-nitrosoanatabine (NAT), and (4) N-nitrosoanabasine (NAB). Together with the polycyclic aromatic hydrocarbons (e.g., benzo[a]pyrene) these are among the most potent cancer-causing agents in cigarette smoke [36–38]. NNN, NNK, and NNAL, for example, cause cancer in mice, rats, and hamsters [36]. The TSNAs are produced during tobacco processing and smoking and are derived from nicotine and minor tobacco alkaloids. A variety of experimental studies have demonstrated that TSNAs are in fact procarcinogens, that is, agents that require metabolic activation before they become carcinogenic. Their activation involves α-hydroxylation to form unstable α-hydroxynitrosamines, which then decompose to diazohydroxides that react with cellular components, including DNA and hemoglobin. There is good evidence that TSNAs contribute to the increased risk for cancer (1) of the upper digestive tract among tobacco chewers and (2) of lung cancer, especially pulmonary adenocarcinoma, in smokers [36].

Considering the large number of toxic compounds in cigarette smoke, including in particular those implicated in causing cancer, it should come as no surprise that smoking is associated with a considerable health risk. Approximately 440,000 people die each year in the United States as a result of cigarette smoking, including approximately 50,000 who die from exposure to secondhand smoke. The combined death toll accounts for almost 20% of all deaths in the United States annually (the death rate in the United States is about 2.4 million people per year) and exceeds all deaths associated with alcohol, AIDS, car accidents, illegal drugs, murders, and suicides combined [39]. The lifespan of smokers is about 14 years shorter than that of nonsmokers [40]. Statistics compiled by the Centers for Disease Control (CDC) indicate that persons who smoke increase their risk of dying from bronchitis and emphysema roughly tenfold. Men and women who smoke increase their risk of dying from lung cancer by more than a factor of 22 and by nearly a factor of 12, respectively [39]. In the United States, cigarette smoking is estimated to be responsible for $193 billion in annual health-related economic losses (this figure includes $96 billion in direct medical costs and another ~$97 billion in lost productivity), a figure that translates to about $10.47 in economic costs per pack of cigarettes sold [41].

The good news is that smoking in the United States is on the decline. The percentage of adults who smoke has declined more-or-less monotonically from a high of 42.4% in 1965 to 20.6% in 2008–2009 (Fig. 1). The percentage of high school students who smoke has declined even more rapidly, from a high of 36% in 1997 to 19.5% in 2009 [42].

The pattern evident in Fig. 1 reflects increasing public awareness of the health risks associated with cigarette smoking and, in recent years, an effort by the federal government to reduce tobacco-related diseases and deaths. The National Tobacco Control Program (NTCP), created by the CDC in 1999, provides funding and technical support to state and territorial health departments with the following goals:

- Prevent initiation of smoking by youth.
- Promote quitting among both adults and youth.

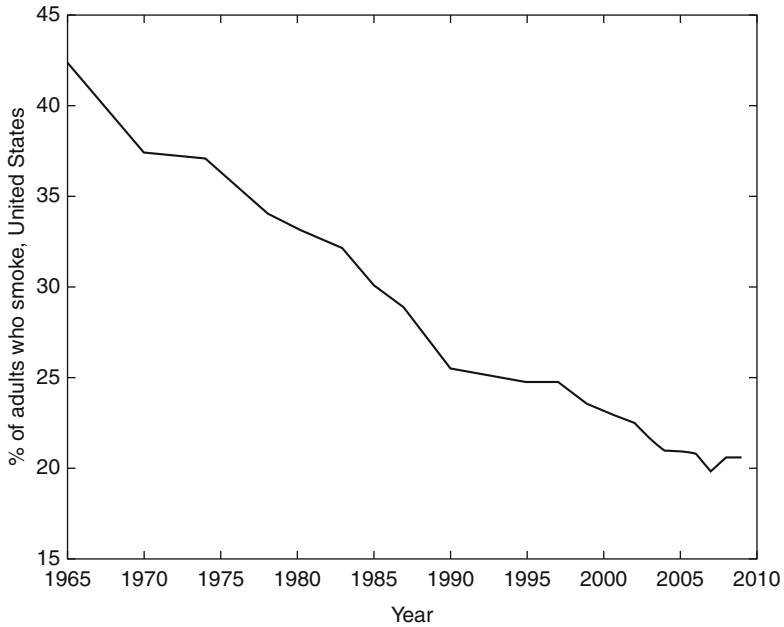

Toxic Chemical Risks. Figure 1
Percentage of adults in the United States who smoke [42]

- Eliminate exposure to secondhand smoke.
- Identify and eliminate disparities among population groups.

More information about the program is available at the NTCP Web site:
http://www.cdc.gov/tobacco/tobacco_control_programs/ntcp/index.htm

Alcohol Consumption

Alcohol is probably the oldest drug used by human beings, with commercial production of wine traceable to as early as 1,500 B.C. [43]. The alcohol in question is ethanol (ethyl alcohol), which is produced by the fermentation of sugar via the overall reaction:

$$C_6H_{12}O_6 \rightarrow 2C_2H_5OH + 2CO_2$$
$$\text{sugar} \rightarrow \text{ethanol} + \text{carbon dioxide}$$

The pleasurable effects of ethanol are associated with its effects on the brain. From the digestive tract ethanol rapidly passes to the blood stream and from there to all parts of the body, including the brain. Ethanol depresses the membrane responsiveness of all neurons in the body, which explains the slower reaction time and sedative effects associated with ethanol consumption. Ethanol also helps to increase the release of dopamine by brain neurons, which results in artificial feelings of pleasure. This interference with normal brain functionality eventually causes the brain to reduce dopamine activity, leading over time to a greatly reduced ability to experience pleasure by normal means. This in turn leads to alcohol addiction.

In addition to being addictive, ethanol is also toxic. In fact, it is routinely used as an antiseptic because it kills bacterial cells. At a sufficiently high concentration it will kill virtually any cell. Even doses typical of recreational consumption of alcoholic beverages lead to a loss of a small number of cells in the brain and liver. If repeated often enough, this can lead to health problems, for example, hepatic cirrhosis and cancers. The fact that the ethanol content of wine is about 10%, for example, is no accident. The yeasts that typically mediate the fermentation process in winemaking die if the ethanol content of the product exceeds about 12%.

The organ primarily responsible for eliminating ethanol from the human body is the liver, where ethanol is converted to acetaldehyde via the enzyme alcohol dehydrogenase:

$$2C_2H_5OH + O_2 \rightarrow 2C_2H_4O + 2H_2O$$
$$\text{ethanol} + O_2 \rightarrow \text{acetaldehyde} + H_2O$$

This does not solve the toxicity problem, however, because acetaldehyde itself is toxic and is responsible for many of the symptoms associated with hangover. In the liver, acetaldehyde is converted to acetic acid ($C_2H_4O_2$) via acetaldehyde dehydrogenase. Simplistically:

$$2C_2H_4O + O_2 \rightarrow 2C_2H_4O_2$$
$$\text{acetaldehyde} + O_2 \rightarrow \text{acetic acid}$$

Problem solved? The answer is yes if a person consumes ethanol infrequently enough, but as noted in the introduction to this chapter, the dose makes the poison. Serious health problems can arise if a person consumes ethanol too frequently over a long period of time. Health problems associated with such long-term ethanol consumption include the following [44]:

- Liver damage: Alcoholic hepatitis, cirrhosis of the liver, and cancer of the liver can all result from chronic ethanol consumption. Alcoholic hepatitis is an inflammation of the liver caused by excessive ethanol consumption. Cirrhosis of the liver is caused by a gradual deterioration of the functionality of the liver and is characterized by replacement of normal liver tissue by scar tissue.
- Brain damage: There are a variety of symptoms here, including impaired judgment, vision, and coordination (leading in some cases to accidents), cell death (leading to dementia and in some cases to paralysis), and in cases of acute overdoses, coma and death.
- Impacts on the reproductive system: Here again, there are many symptoms, including impotence due to hormone imbalances, birth defects caused by mutations of egg or sperm cells, fetal alcohol syndrome (damage to the fetus associated with the fact that ethanol passes from the mother's bloodstream across the placenta to the fetus), teratogenic effects, and breast cancer.

- Damage to the digestive tract: Impacts include inflammation and cancer of the throat, esophagus, stomach, pancreas, small intestine, and colon.

The greatest risks from ethanol consumption are associated with the development of a condition called alcoholism. Simplistically, this is a condition that develops when a person's brain has been sufficiently altered by ethanol consumption that the person must drink to feel normal. The result is compulsive drinking. Failure to drink leads to serious withdrawal symptoms that include nausea, sweating, shakiness, anxiety, and in a small percentage of cases, to a condition called delirium tremens, which can be fatal. Most people who become alcoholics and subsequently stop drinking do so only with assistance.

How many people are alcoholics? About 10% of Americans are estimated to have "an alcohol problem" and 7.7% "abuse alcohol or are alcoholic" [45]. Thirty-eight percent of American families report a "history of alcoholism" [46].

The costs associated with alcoholism in terms of lives, human health, and societal impacts are very large. In the United States, more than 100,000 people die annually as a result of excessive alcohol consumption. This is about 4% of the annual death rate in the United States. The specific causes of death include, inter alia, drunken driving, cirrhosis of the liver, cancer, and stroke. In the case of drunken driving, many victims are not themselves alcoholics but instead are innocent bystanders. Roughly half of all homicides, 40% of assaults, and one-third of all fatal car accidents, suicides, and hospital admissions in the United States are alcohol related. The economic costs associated with alcohol abuse and alcoholism in the United States are roughly $230 billion per year, almost 80% more than the costs related to all other addictive drugs combined [45, 47].

Most people who drink are not alcoholics. In the United States, roughly 44% of adults (18 years and older) consume an average of at least one drink per month, including 60% of persons 21–34 years of age, 46% for adults aged 60–64, and 33% of persons 65 or older [48]. Clearly only a small fraction of persons who consume ethanol become alcoholics. The risk of becoming an alcoholic is to some extent a function of genetics. Alcoholism runs in families [49, 50]. But the risk of becoming an alcoholic is also a function of one's environment, including peer pressure, the influence of family and friends, and the ease with which one can obtain alcohol [48].

Drug Abuse/Misuse

In the last 30 years, the number of deaths associated with unintentional drug overdoses has increased dramatically in the United States (Fig. 2). Most of the increase has not been due to the use of illegal drugs such as cocaine and heroin but rather due to misuse/abuse of prescription painkillers (analgesics) that are opioids (Fig. 3). Opiates are compounds derived from opium poppies and include morphine and codeine. Opioid analgesics are synthetic or semisynthetic analogues of opiates and include oxycodone (e.g., OxyContin®), hydrocodone (e.g., Vicodin®), propoxyphene (e.g., Darvon®), and hydromorphone (e.g., Dilaudid®) [51].

Naively one might assume that deaths associated with opioid analgesics are primarily linked to little children getting into medicine cabinets or old people mixing up their pills, but that is not the case. According to Paulozzi [53], the trend in opioid-related deaths apparent in Fig. 3 is due to the increasing use of "prescription drugs, especially opioid painkillers,

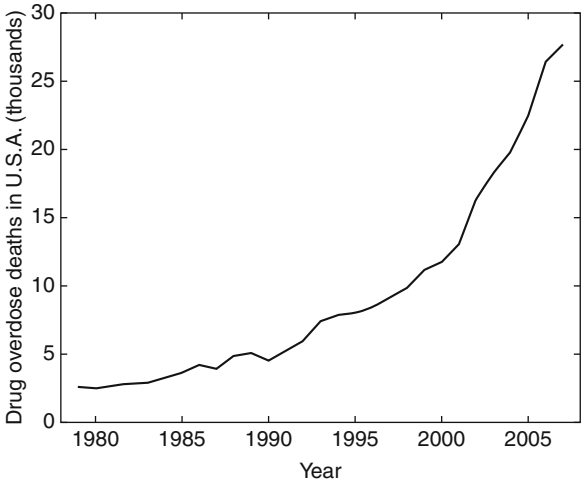

Toxic Chemical Risks. Figure 2
Number of deaths per year in the United States associated with unintentional drug overdoses [52]

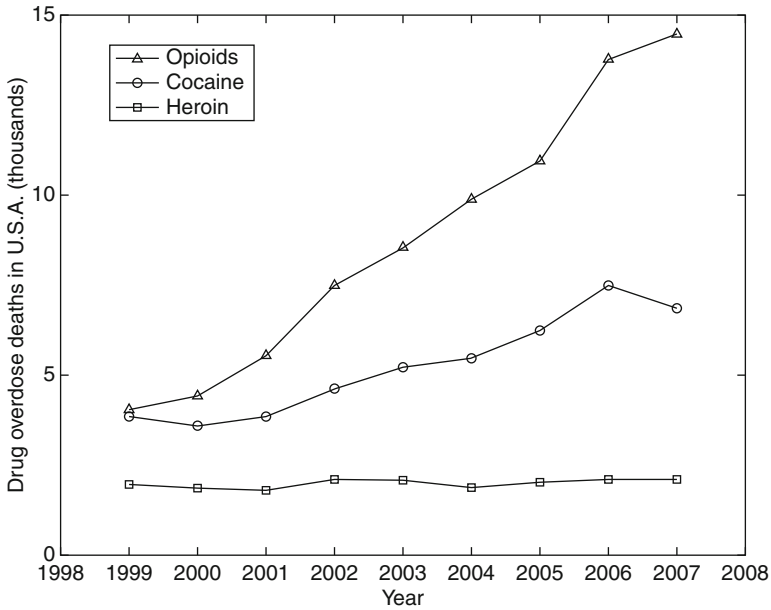

Toxic Chemical Risks. Figure 3

Number of deaths per year in the United States associated with unintentional overdoses of opioids, cocaine, and heroin [54, 55]

among people during the working years of life." A high percentage of the people who die have a history of drug abuse, and many have no prescription for the drug. Mixing of prescription drugs with illegal drugs is common, and "some alter the prescription drugs by crushing and snorting them or dissolving and injecting them" [53].

The problems associated with the use of opioid analgesics are an excellent example of the adage that the dose makes the poison. When used as prescribed, opioid analgesics can be very effective painkillers. They bind to specific proteins (opioid receptors) in the brain, spinal cord, and gastrointestinal tract, and in this way they can block the transmission of pain signals to the brain.

There are side effects associated with opioid/opiate use. One is suppression of coughing, which is why codeine, for example, is incorporated into a number of cough syrups and cold remedies. Another is constipation, which explains why loperamide, an opioid derived from piperdine, is used to treat diarrhea. More insidious side effects include drowsiness and a feeling of euphoria. The former is associated with the lethal effects of an opioid overdose, which leads to a suppression of breathing and may ultimately cause respiratory failure. The latter effect is responsible for the abuse and compulsive use of opioids. Persons addicted to opioids experience withdrawal symptoms if use of the drugs is reduced or stopped. These symptoms include muscle and bone pain, insomnia, diarrhea, vomiting, involuntary leg movements, and cold flashes with goose bumps (i.e., cold turkey). Interestingly, the synthetic opioid methadone blocks the effects of other opioids (including heroin), eliminates withdrawal symptoms, relieves drug craving, and has been used for decades to treat opioid addicts [56]. Fortunately, properly supervised use of opioid analgesics seldom results in clinical addiction.

Cocaine is an illegal drug and one of the most addictive of all stimulants. Derived from the coca bush, cocaine is marketed "on the street" in two forms: a water-soluble hydrochloride salt and a water-insoluble cocaine base. A cocaine user can either inject the water-soluble form with a hypodermic needle or snort (i.e., inhale) the hydrochloride salt powder through the nose, where it is readily absorbed through nasal tissues into the bloodstream. The base form is processed to produce a substance known as crack that

can be smoked. The term "crack" comes from the crackling sound heard when the mixture is smoked. Once it has entered the blood stream, cocaine travels to the brain, where it produces a euphoric effect that is responsible for its popularity and addictive properties. In a nutshell, cocaine causes dopamine to accumulate at nerve synapses (small gaps between two neurons) in the brain and thereby heightens the pleasurable sensations associated with dopamine secretion. Rather than stimulating the secretion of dopamine by a neuron, the mechanism involves blockage of the natural process by which dopamine is recycled from the synapse to the neuron by specialized proteins called dopamine transporters.

The pleasurable effects of cocaine appear rapidly but are of short duration. When cocaine is absorbed rapidly via either injection or smoking, the effects are intense but dissipate after 5–10 min. Snorting is associated with a delayed response that is less intense but persists for 15–30 min [57].

In addition to the general euphoric sensation associated with cocaine use, there are other psychological effects. Users feel mentally alert, talkative, and energetic and temporarily may feel less need for sleeping and eating. Physiological effects include constricted blood vessels and an increase in body temperature, pulse, and blood pressure. Medical complications arising from the physiological effects of cocaine include the following [57]:

- Cardiovascular effects: arrhythmias (heart rhythm disturbances), heart attacks
- Neurological effects: strokes, seizures, headaches, coma
- Gastrointestinal complications: abdominal pain, nausea

Deaths associated with cocaine use are typically associated respiratory failures preceded by cardiac arrest or seizures. In addition, there is an even greater danger associated with the use of cocaine during alcohol consumption. Alcohol and cocaine together are the most common two-drug combination responsible for drug-related deaths [57].

Clearly there is a very significant risk associated with cocaine abuse, and with the exception of its very limited use as a topical anesthetic in nasal and lacrimal duct surgery, it is associated with no beneficial applications. Moreover, there are presently no medications approved by the Food and Drug Administration (FDA) to treat cocaine addiction. In 2007, cocaine abuse accounted for 13% of all admissions to drug abuse treatment programs in the United States, and a majority of those cocaine addicts were abusing multiple drugs [57]. Treatment of cocaine addiction is a complex process, not only because of the frequent problem of multiple-drug abuse but also because of the complex biological (e.g., changes in the brain), social, familial, and environmental problems that must typically be addressed in the treatment process. Flynn et al. [58] examined the factors that contributed to long-term recovery from cocaine dependence of 708 patients from 45 treatment programs in the United States and concluded that only 33% of the sample were "highly favorable" at follow-up. The major reasons cited for improvements were "motivations to change, positive influences of family, strength from religion and spirituality, and help from drug treatment."

Given the highly addictive nature of cocaine, the absence of approved medications for treatment of addiction, and the mixed success of treatment programs, Benjamin Franklin's observation that "an ounce of prevention is worth a pound of cure" applies (Franklin's comment was advice related to fighting fires; he founded Philadelphia's Union Fire Company). The good news is that use of cocaine by teenagers has been declining in the United States since roughly 1997 (Fig. 4). This decline, however, has followed a period of increase during the 1990s. It is apparent from Fig. 4 that the percentage of US teenagers who use cocaine is little different now than in 1990.

Heroin is the most abused and the most rapidly acting of the natural opiates. It is obtained by the acetylation of the two hydroxyl groups of morphine with acetyl chloride, that is, the two –OH groups are replaced with $–OCOCH_3$ groups (Fig. 5). This modification makes heroin much less soluble in water than morphine but allows it to pass the blood-brain barrier much more rapidly than morphine. Interestingly, once inside the brain, heroin is converted to morphine and then rapidly binds to opioid receptors [60], leading to a surge of pleasurable sensation known as a "rush."

Heroin may be injected, sniffed/snorted, or smoked. Intravenous injection is very common because

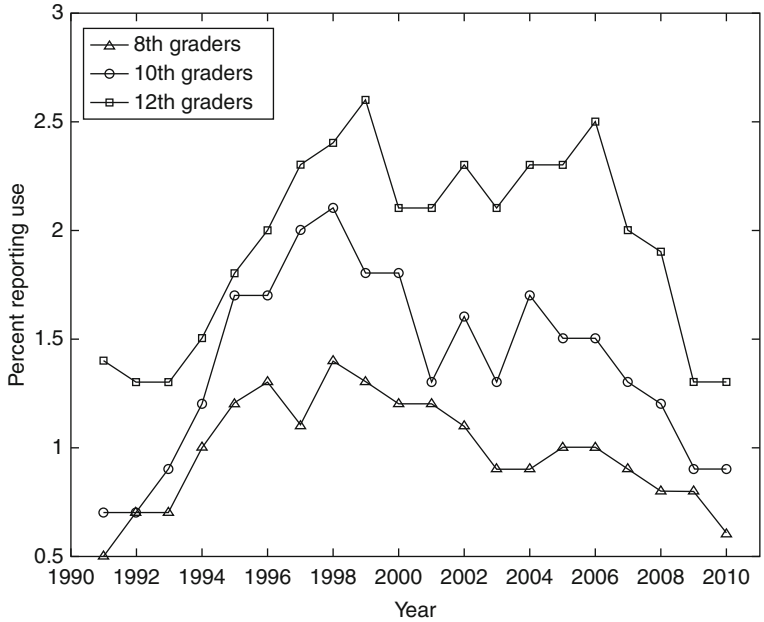

Toxic Chemical Risks. Figure 4
Trends in a 30-day prevalence of cocaine abuse among 8th, 10th, and 12th graders [59]

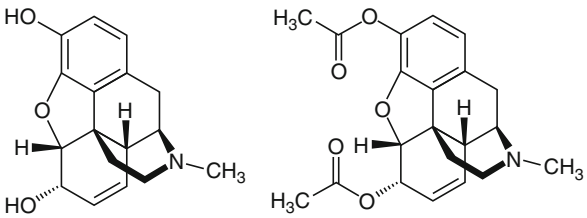

Toxic Chemical Risks. Figure 5
Structures of morphine (*left*) [61] and heroin (*right*) [62]

it provides the most rapid (less than 10 s) onset of euphoria. It is not uncommon for a heroin abuser to inject up to four times per day. Feelings of euphoria follow intramuscular injection and sniffing/snorting by 5–8 and 10–15 min, respectively [60]. Heroin is addictive regardless of how it is administered.

The risks associated with heroin addiction are numerous. For persons who inject, sharing of needles can lead to some of the most serious consequences: infection with hepatitis B and C, HIV, and other blood-borne viruses. Thirty-six percent of AIDS cases and an estimated 70–80% of the 35,000 new hepatitis C infections that occur in the United States each year are attributable to injection drug use [62, 63].

Then there are the effects of the heroin itself. After the initial rush, heroin users typically feel drowsy for several hours. Cardiac function and breathing slow, and in cases of overdose may slow to the point of death. On the street heroin is typically "cut" with other drugs or with substances such as sugar, starch, or powdered milk. As a result, users of street heroin are often unsure of the purity of the drug they are using. This uncertainty can easily lead to overdoses.

Chronic heroin injection can lead to a variety of medical problems, including scarred and/or collapsed veins, bacterial infections, and liver or kidney disease [62]. In addition to these physiological effects, heroin addicts gradually spend more and more of their time and energy obtaining and using heroin. "Once they are addicted, the heroin abuser's primary purpose in life becomes seeking and using drugs" [62]. Withdrawal symptoms include restlessness, muscle and bone pain, insomnia, diarrhea, vomiting, involuntary leg movements, and the aforementioned cold turkey effects. These typically begin to manifest themselves within 1–2 days after the last dose of heroin and subside within 1 week, although in some cases they last for many months [62].

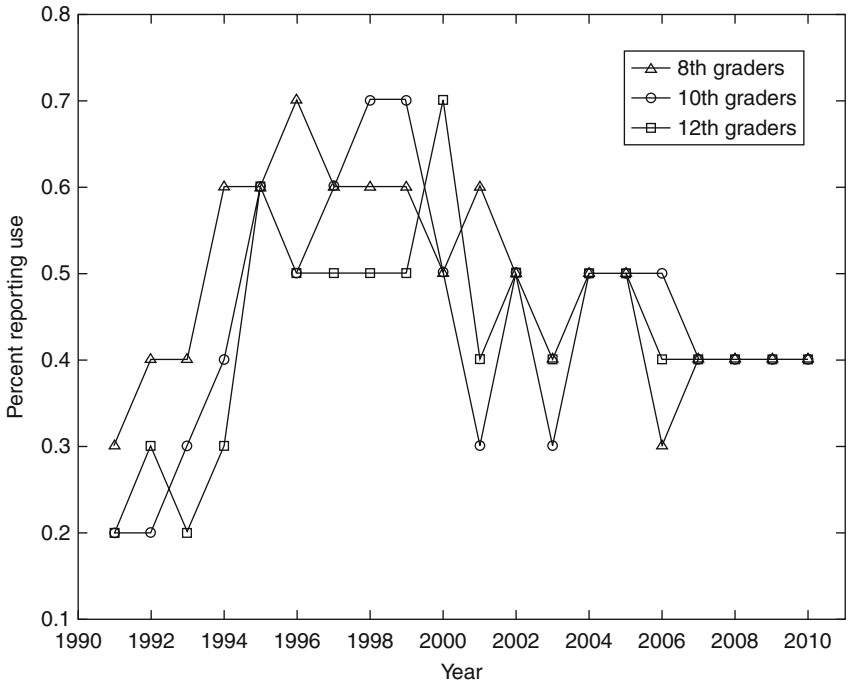

Toxic Chemical Risks. Figure 6
Trends in 30-day prevalence of heroin abuse among 8th, 10th, and 12th graders [59]

The good news is that there are a variety of effective treatments available for heroin addiction. As already noted, methadone effectively blocks the effects of heroin and has been used successfully to treat heroin addicts for decades. When properly used methadone is not intoxicating or sedating, it may be used safely for as long as 10 years or more. It is taken orally and suppresses withdrawal symptoms for 24–36 h. Very importantly, it relieves the craving for heroin, which is a major cause of relapse. A more recent development has been the use of buprenorphine, a semisynthetic opioid, for the same purpose. Use of buprenorphine is associated with less risk of addiction and can be prescribed in the privacy of a doctor's office. Another treatment, a combination of buprenorphine and naloxone (Suboxone®), is designed to minimize the possibility of abuse [62].

According to a 2003 survey of drug use in the United States [64], roughly 3.7 million people had used heroin at least once in their lives, 119,000 had used heroin within the previous month, and 314,000 had used heroin within the previous year. The number of deaths attributable to heroin use in the United States has been constant for the last 20 years (Fig. 3) and has averaged about 2,000 per year. The fraction of teenagers who abuse heroin has been constant since ~2000 (Fig. 6) and is higher now than in the early 1990s. Thus heroin abuse and addiction continue to be serious problems in the United States.

Obesity

Food is perhaps the quintessential example of a substance for which the dose makes the poison. Most people do not think of food as a poison, but obesity is a serious problem in the United States and a disease formally recognized by the Centers for Disease Control and Prevention.

For a number of years public health agencies have used a metric called the body mass index (BMI) to determine whether a person's weight is normal or not.

If a person's weight and height are quantified in pounds and inches, respectively, the BMI is determined from the following equation:

$$\mathrm{BMI} = 703\,\frac{\mathrm{weight}}{\mathrm{height}^2}$$

Thus, for example, a person whose height is 70.3 in. and whose weight is 140.6 pounds would have a BMI of 20. As a rule of thumb, a person is categorized as follows based on his/her BMI:

- Underweight: <18.5
- Normal: 18.5–25.0
- Overweight: 25.0–30.0
- Obese: 30.0–40.0
- Extremely obese: >40.0

These are somewhat arbitrary definitions and in individual cases should be interpreted with the understanding that what is normal for one person may not be normal for another. With that caveat, the BMI index has proven very useful for assessing the general health of a population relative to the issue of obesity.

The average weight of adults in the United States has been slowly increasing since 1960 (Fig. 7, upper left). The average weight of both men and women increased by ~25 pounds between 1960 and 2000. Interestingly, there was no change in the percentage of adults in the overweight category (Fig. 7, upper right), but there were rather dramatic increases in the percentages of adults characterized as obese (Fig. 7, lower left) and extremely obese (Fig. 7, lower right).

At the present time roughly 100 million adults in the United States are overweight or obese. Obesity substantially increases a person's risk of the following [67]:

- Morbidity from hypertension
- Dyslipidemia (abnormal amounts of lipids such as cholesterol and fat in the blood)

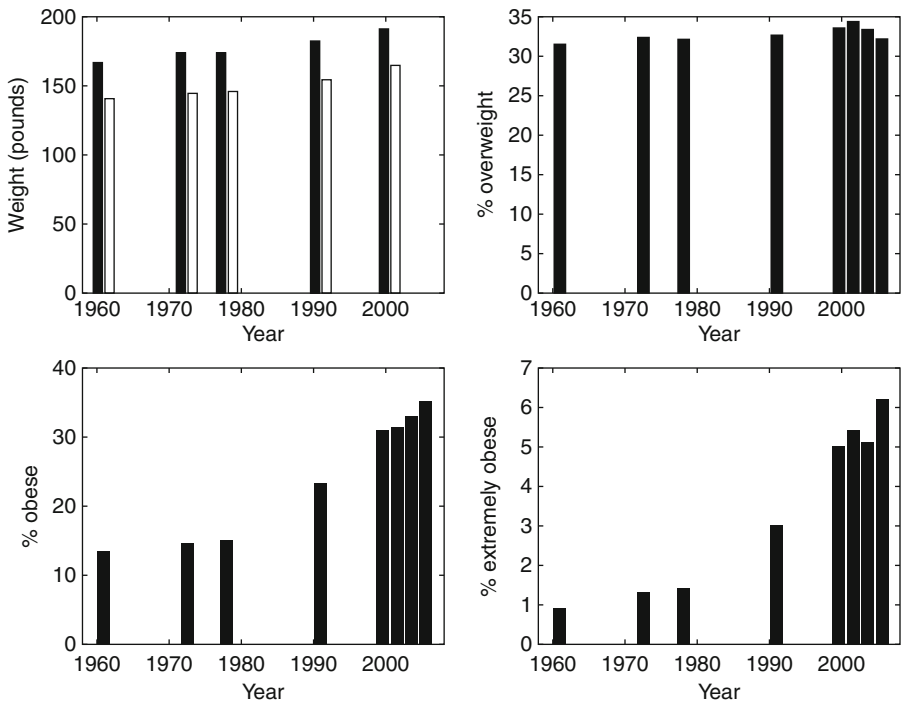

Toxic Chemical Risks. Figure 7

Metrics of US adults 20–74 years old with respect to weight. *Upper left*: Average weight of adult males (■) and females (□). *Upper right*: Percentage of adults with BMIs of 25–30. *Lower left*: Percentage of adults with BMIs of 30–40. *Lower right*: Percentage of adults with BMIs greater than 40 [65, 66]

- Type II diabetes (adult-onset diabetes)
- Coronary heart disease
- Stroke
- Gallbladder disease
- Osteoarthritis (degenerative joint disease)
- Sleep apnea (abnormal pauses or abnormally low breathing during sleep)
- Respiratory problems
- Endometrial (lining of the uterus), breast, prostate, and colon cancers
- Social stigmatization and discrimination

While there is no question that obesity significantly increases a person's risk of developing a number of potentially serious health problems, there is less agreement about what to do about obesity. The number of diet/exercise books in a typical bookstore is a good indication of the uncertainty associated with treatment of this disease. Guidelines recommended by the National Heart, Lung, and Blood Institute include the following:

- Goals
  - Initial target of weight loss should be 10%. If successful, further weight loss may be attempted.
  - Initial rate of weight loss should be 1–2 pounds per week for up to 6 months.
- Methods
  - Dietary therapy
    - Low-calorie diets with reduced fat content.
    - Reducing fat without reducing calories is futile.
    - Target caloric reduction should be 500–1,000 kcal per day.
  - Physical activity
    - The target here is at least 30 min of moderate-intensity physical activity on most, and preferably all, days of the week. Although physical activity will not be the primary determinant of weight loss, it will increase cardiorespiratory fitness and may decrease abdominal fat and help with maintenance of weight loss.
  - Behavior therapy
    - This translates to identifying ways to motivate the person who is trying to lose weight.
  - Pharmacotherapy
    - This is the use of FDA-approved drugs and is only recommended if their use is supervised and their efficacy assessed by a physician.
  - Weight loss surgery
    - This is only recommended in cases of clinically severe obesity when less invasive methods have failed and the patient is at high risk for obesity-associated morbidity or mortality.

Finally, there is the issue of weight loss maintenance. As with other lifestyle-related risks, the tendency to become obese can be a chronic problem that requires a lifetime of vigilance to overcome. The most effective strategy is a combination of dietary therapy, physical activity, and behavior therapy [67].

Exposure to Toxic Chemicals in the Home

Lead

Of all the toxic chemicals to which humans are exposed, lead has perhaps the longest history of exposure and today impacts the health of the greatest number of people. Lead is mined primarily from deposits of the mineral galena, or lead sulfide (PbS). Since metallic lead can be separated from PbS by heating at low temperatures easily achieved by burning wood or charcoal, it was not difficult for early civilizations to extract lead. The overall reaction is:

$$PbS + O_2 \rightarrow SO_2 + Pb$$

From written and archeological evidence, it is known that lead was used by the Egyptians as long ago as 1500 BC. The Romans used lead extensively to line their aqueducts and water mains, and both the Greeks and Romans used lead to line cooking vessels, since bronze pots tend to give food a bitter taste [68]. At least one author has suggested that endemic lead poisoning caused by the consumption of contaminated food and drink contributed significantly to the fall of the Roman Empire [69]. The use of lead or lead salts to sweeten wine was common in Europe after the ninth century, and associated outbreaks of lead poisoning were not infrequent. In colonial America lead poisoning was also a problem, mainly due to the use of lead

condensing tubes for distilling rum and the use of earthenware with a high lead content [68].

For obvious reasons, the principal uses of lead today are of an industrial rather than culinary nature. By far the major use, accounting for 87% of total lead consumption in the United States, is the production of batteries. However, lead batteries have never been a major source of human exposure to lead. During much of the twentieth century by far the most important source of human exposure was the use of lead in gasoline. Although leaded gasoline is no longer sold in the United States, lead was used extensively in the United States as a gasoline additive for roughly 60 years. This practice dates back to 1923, when tetraethyl lead was first introduced as an antiknock additive. This use was suspended during part of 1925 and 1926 pending the establishment of safety standards for its manufacture and handling, but after the spring of 1926 lead additives were commonly used in most gasoline sold in the Unites States and throughout the world. Beginning in 1960, organic alkyl lead compounds were blended into gasoline along with tetraethyl lead to further improve antiknock characteristics, and the additives were subsequently referred to as lead alkyls rather than just tetraethyl lead [68]. As of 1973, the lead content of gasoline sold in the United States averaged about 0.58 g/L.

Because of concern over pollution of the environment with lead, in 1974 the Environmental Protection Agency (EPA) requested a phasedown in the use of lead alkyls in gasoline to 0.45 g/L on January 1, 1975, and to 0.13 g/L as of January 1, 1979. In December 1974, however, the US Circuit Court of Appeals in Washington ruled against the EPA, stating that evidence did not support the EPA contention that automobile emissions contributed significantly to blood lead levels, and that the EPA regulation was arbitrary and capricious.

Since that time the legal status of gasoline lead additives has changed significantly. This change has resulted partly from the requirement for exhaust emission control devices on automobiles. The devices function poorly if at all when lead is present in the exhaust fumes, since the lead poisons the catalyst, which is designed to help oxidize unburned hydrocarbons. Furthermore, there is increasing awareness of the danger of environmental lead pollution due to the use of leaded gasoline. Since July 1, 1977, all new cars sold in the United States have been required to run on unleaded gas, defined as gasoline containing less than 0.013 g/L lead. Finally, the government required that the lead content of leaded gasoline be reduced to 0.13 g/L by July 1, 1985, and to 0.10 g/L by January 1, 1986. The result of these regulations was a tenfold decline in the use of lead in gasoline in the United States between the early 1970s and 1986. Leaded gasoline is now completely phased out in the United States. European countries began slowly phasing out leaded gasoline in the 1980s and mandated elimination in the 1990s. Leaded gasoline was phased out in sub-Saharan Africa by 2006 [70]. China banned the sale of leaded gasoline in 2000, although production by clandestine factories for use in older vehicles continued until at least 2004 [71].

The decline in the blood lead levels of people in the United States during the phaseout of leaded gasoline (Fig. 8) is provocative considering the Circuit Court of Appeals 1974 ruling that evidence did not support the EPA's contention that automobile emissions contributed significantly to blood lead levels. During the period 1976–1980, blood lead levels declined in almost direct proportion to the use of leaded gasoline, suggesting that automobile emissions not only were contributing significantly to blood lead levels, but were in fact the dominant contributors.

Why all the concern about lead? With respect to toxicology, lead is a general metabolic poison. The pathological effects are varied, but in general reflect the tendency of lead to interact with proteins and hence to damage tissue and interfere with the proper functioning of enzymes [68]. Lead is known to inhibit active transport mechanisms involving ATP, to depress the activity of the enzyme cholinesterase, to suppress cellular oxidation–reduction reactions, and to inhibit protein synthesis [68]. Lead poisoning is also associated with the following problems:

- Anemia: Lead is known to disrupt several enzymes involved in the production of heme, a constituent of hemoglobin and various other respiratory pigments, and has been shown to interfere with the uptake of iron by red blood cells. Anemia associated with lead poisoning is undoubtedly caused in part by these effects. There is also evidence, however,

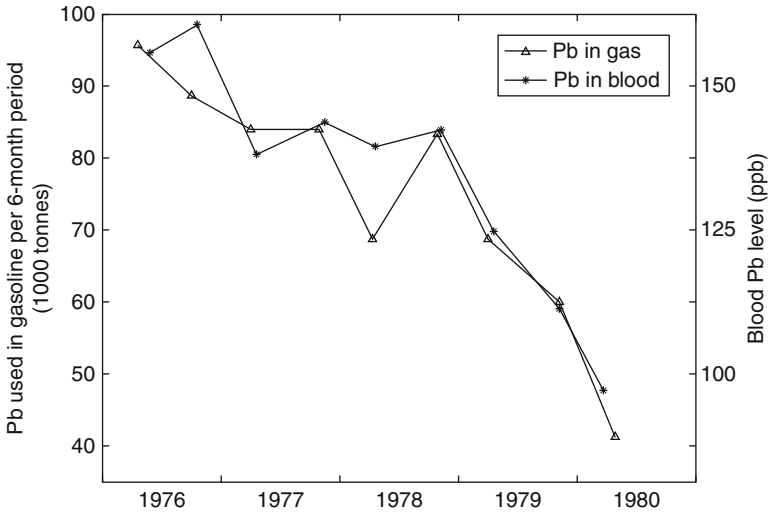

Toxic Chemical Risks. Figure 8
Change in blood lead levels during phaseout of leaded gasoline in the United States [72]

that lead causes a shortening of the life of red blood cells, probably due to disruption of the red cell membrane [68].

- Damage to the Central Nervous System (CNS): Damage to both the peripheral and central nervous system, including the brain, may be caused by a degeneration of nerve fibers and interference with the permeability of capillaries in the brain due to lead intoxication. The exact mechanism responsible for these effects is not known, and indeed several factors, including enzyme inhibition and tissue damage, may be involved [68]. The CNS effects mainly impact children under 5 years of age, since lead does not pass the blood-brain barrier as easily in adults. Asymptomatic exposure to low doses of lead in young children (toddlers) can lead to permanent decreases in IQ.
- Kidney Damage: Kidney damage characterized by atrophy of the renal tubules is a well-established effect of lead poisoning. The damage is associated with elevated levels of amino acids, sugar, and phosphate in the urine [68]. Gout caused by kidney damage has also been associated with lead poisoning, the consumption of illicitly distilled whiskey (moonshine) being a common cause. Concentrations of lead in moonshine often exceed 10 ppm due to the use of lead in the distillation apparatus [73]. Waldron and Stöfen [68] cite one example of a hospital in which 37 of 43 cases of gout admitted in 1967 were caused by the consumption of lead-contaminated liquor.
- Effects on Children and Reproduction: From the standpoint of human health, the greatest danger of lead poisoning is undoubtedly to young children, particularly those living in urban areas. Neurological damage caused by the poisoning of such children may be permanent and can result in impaired physical as well as mental development. Even the unborn fetus is not protected from the effects of lead poisoning. There is evidence that the brain of the fetus is much more sensitive to lead poisoning than the brain of the infant or young child, and lead has repeatedly been shown to cause birth defects in experimental animals [73]. Although there is little information to indicate that lead has a teratogenic effect on humans, exposure of pregnant women to lead can induce miscarriages and stillbirths [68].

Most of the body burden of lead is found in the bones, and although the lead content of bones can now be assayed using noninvasive x-ray fluorescence techniques [74], historically it has been much more practical to relate health effects on living persons to the level of lead in the blood, PbB. Table 1 summarizes the lowest PbB levels associated with various health effects as summarized by the EPA [73] and CDC [75].

Toxic Chemical Risks. Table 1 Lowest PbB levels associated with health effects in humans

Lead in blood ($\mu g\ L^{-1}$)	Effect	Population group
100	ALA-d inhibition	Children and adults
	Adverse effects on intelligence, hearing, and growth	Children
100–150	Interference with vitamin D metabolism	Children
150–200	Protoporphyrin elevation in red blood cells	Women and children
250–300	Protoporphyrin elevation in red blood cells	Adult males
400	Increased urinary ALA excretion	Children and adults
400	Anemia	Children
400	Coproporphyrin elevation	Adults and children
500	Anemia	Adults
500–600	Cognitive deficits	Children
500–600	Peripheral neuropathies	Adults and children
800–1,000	Encephalopathic symptoms	Children
1,000–1,200	Encephalopathic symptoms	Adults

PbB levels as low as 100 $\mu g\ L^{-1}$ do not cause distinctive symptoms, but are associated with decreased intelligence and impaired neurobehavioral development, decreased stature or growth, decreased hearing acuity, and decreased ability to maintain a steady posture. The activity of δ-aminolaevulinic acid dehydratase (ALA-d), an enzyme involved in heme metabolism, is also adversely affected at a PbB level of 100 $\mu g\ L^{-1}$. Interference with vitamin D metabolism occurs at PbB levels of 100–150 $\mu g\ L^{-1}$, and increased concentrations of protoporphyrin, a substrate needed for heme synthesis, and ALA begin to appear in red blood cells and urine, respectively, at slightly higher PbB levels. Actual decreases in hemoglobin, somewhat loosely referred to in Table 1 as anemia, occur at PbB levels of about 400–500 $\mu g\ L^{-1}$. Based on this evidence, the Centers for Disease Control have concluded that children's PbB levels should not exceed 100 $\mu g\ L^{-1}$ [75].

Unfortunately a great many children as well as adults in the United States have PbB levels greater than 100 $\mu g\ L^{-1}$. For example, a study of urban children in seven different US cities between 1967 and 1970 revealed that about 29% had blood levels over 400 $\mu g\ L^{-1}$, and almost 9% had blood lead levels over 500 $\mu g\ L^{-1}$ [68]. A blood lead level of 500–800 $\mu g\ L^{-1}$ is considered to be the threshold level of classical lead poisoning [76]. At the present time in the United States ~250,000 children less than 6 years old have blood lead levels exceeding 100 $\mu g\ L^{-1}$ [77].

Now that leaded gasoline has been phased out, the principal sources of exposure to lead are deteriorating lead-based paint, lead-contaminated dust, and lead-contaminated residential soil [78]. Of these three, the historical use of lead-based paint has proven to be the most problematic. Lead was used for many years in paints as a pigment, and in oil paints lead naphthenate is used as a drying agent. In 1918, 40% of all painters were estimated to have symptoms of lead poisoning because of their contact with such paint [79]. The most serious problem associated with the use of lead in paints, however, has been the poisoning of small children who eat paint chips or teethe on windowsills or other surfaces that have been painted with lead-based paints. Dust from deteriorating paint may also contaminate windowsills, carpets, furniture, and toys and be ingested by children who touch the dust and subsequently put their fingers in their mouths. Between 1954 and 1967, a total of 2,038 children were treated for lead poisoning in New York City alone, and of these 128 died [79]. On January 1, 1973, the Food and Drug Administration (FDA) banned the use of paint containing over 0.5% lead on residential surfaces accessible to children [68], and effective February 27, 1978, paint containing over 0.06% lead was banned as hazardous for use in residences, schools, hospitals, parks, playgrounds, and public buildings under the aegis of the Consumer Product Safety Act. The only exceptions specifically written into the 1977 legislation were paints and coatings for motor vehicles and boats. The problem of poisoning from lead-based paints remains a serious public health problem, however, because many older buildings contain lead-based paints. A 1988 Public Health Service report revealed that 52% of American homes

had layers of lead-based paint on their walls and woodwork [74]. Today lead poisoning is the number one environmental health risk for children in the United States, and 80% of lead poisonings are caused by lead-based paint in homes and apartments built before 1978 [80].

Naively one might assume that simply painting over lead-based paint would solve the problem, but according to the EPA, that is "not enough" [78].

> ► To permanently remove lead hazards, you must hire a certified lead "abatement" contractor. Abatement (or permanent hazard elimination) methods include removing, sealing, or enclosing lead-based paint with special materials.... Always hire a person with special training for correcting lead problems – someone who knows how to do this work safely and has the proper equipment to clean up thoroughly [78].

Short of having the lead-based paint removed by a certified contractor, people who find themselves living in housing units painted with lead-based paint are advised to take the following steps [78]:

- If you rent, notify your landlord of peeling or chipping paint.
- Clean up paint chips immediately.
- Clean floors, window frames, windowsills, and other surfaces weekly. Use a mop, sponge, or paper towel with warm water and a general all-purpose cleaner or a cleaner made specifically for lead. Thoroughly rinse sponges and mop heads after cleaning dirty or dusty areas.
- Wash children's hands often, especially before they eat and before nap time and bedtime.
- Keep play areas clean. Wash bottles, pacifiers, toys, and stuffed animals regularly.
- Keep children from chewing windowsills or other painted surfaces.
- Clean or remove shoes before entering your home to avoid tracking in lead from soil.

Other Chemicals

Almost 90% of all poison exposures occur in the home, and after lead there is a rather long list of toxic chemicals to which people have been exposed, in most (~87%) cases unintentionally. Seventy-five percent of poison exposures involve ingestion of a toxic substance, and children less than 6 years old are the victims in roughly half the incidents, although they account for only 2% of the poison fatalities. In almost 40% of the cases involving children, cosmetics and personal care products, cleaning compounds, analgesics, and plants (e.g., holly berries and mistletoe berries) are the source of the toxin(s). Although adults account for a small percentage of poison exposures, they account for more than 75% of all fatalities related to poison exposure [81]. The following examples illustrate several facets of the poison exposure problem.

1. Antibacterials found in many cosmetic and personal care products: Triclosan is a chlorinated organic bactericide used in soaps, deodorants, toothpastes, shaving creams, mouthwashes, and cleaning supplies and is infused in consumer products such as kitchen utensils, toys, bedding, socks, and trash bags [82]. Its use for 40 years has been regulated by three different federal agencies, the FDA, EPA, and Consumer Product Safety Commission. Remarkably, the FDA has been working on the development of rules for the use of triclosan for much of that time but has yet to promulgate any [83]. Japan and Canada, on the other hand, have banned triclosan in consumer products.

   What is the problem? Concerns about the effects of triclosan on human health are related to several issues. First, several studies have linked triclosan to allergic reactions in children [84–87]. Second, triclosan reacts with chlorine in water to produce chloroform, which the EPA classifies as a probable human carcinogen, and smaller amounts of other chlorinated compounds that, in the presence of sunlight, are converted to dioxin [88–91], some forms of which are highly toxic and very potent endocrine disruptors. So widespread is the use of triclosan that it has been found in the urine of 75% of people tested by the CDC [83] and even in human breast milk [92, 93].

   Given this information, one might wonder why the US government has not taken some action to restrict the use of triclosan, but there is another side to the story. In commenting on the presence of triclosan in breast milk, Dayan [92], for example,

concludes, "There is no evidence to indicate that the presence of a miniscule amount of triclosan in breast milk presents a risk to babies," and while it is true that triclosan reacts with chlorine in tap water to produce chloroform, the concentrations of chloroform reported in the study by Rule et al. [94] were smaller than the amounts often present in chlorinated drinking water [82]. With respect to allergic reactions, Campbell and Zirwas [86] acknowledge that, "Several cases of contact dermatitis secondary to triclosan have been reported" but that, "Allergy to triclosan-based products is uncommon," and Schena et al. [85], in a study of patients with chronic eczema, concluded, "Triclosan is well tolerated and has a very low sensitizing potential even in high-risk patients affected by eczema."

There is no question that very large numbers of people (arguably almost everyone) in the United States are exposed to triclosan, but is there a health risk associated with exposure to this chemical? It seems that the jury is still out on this question. And would the health risk of bacterial infection be heightened if use of triclosan were banned? Remarkably, a study carried out by the University of Michigan concluded, "Washing hands with an antibacterial soap was no more effective in preventing infectious illness than plain soap. Moreover, antibacterial soaps at formulations sold to the public do not remove any more bacteria from the hands during washing than plain soaps" [95].

2. Dangerous mixtures of household chemicals: Without realizing the danger, people sometimes mix bleach with ammonia. The resulting chemical reactions can produce a real witches' brew of toxic gases. Bleach is just a dilute (typically 6%) aqueous solution of sodium hypochlorite (NaOCl). Ammonia (NH_3) is a gas, and when dissolved in water exists as a mixture of the dissolved gas and ammonium ion (NH_4^+). When roughly equal amounts of bleach and ammonia are combined the following reaction occurs:

$$2NaOCl + 2NH_3 \rightarrow 2NaONH_3 + Cl_2$$

Chlorine gas, Cl_2, is a highly corrosive gas that can do serious damage to the lungs, nasal passages, and trachea when inhaled. It was used as a chemical weapon during World War I and by Nazi Germany in World War II. When more bleach is added than ammonia the following reaction occurs:

$$3NaOCl + NH_3 \rightarrow 3NaOH + NCl_3$$

NaOH is a very strong base and caustic to soft tissue. NCl_3, nitrogen trichloride, is highly toxic and sufficiently volatile that it is likely to explode in the face of the unsuspecting chemical mixer. And finally, if ammonia is added in excess of the amount of bleach, the following series of reactions may occur:

$$NH_3 + NaOCl \rightarrow +NaOH + NH_2Cl$$
$$NH_3 + NH_2Cl + NaOH \rightarrow N_2H_4 + NaCl + H_2O$$
$$2NH_2Cl + N_2H_4 \rightarrow 2NH_4Cl + N_2$$

The third reaction is very exothermic (releases a large amount of heat) and typically leads to an explosion.

Another common mistake is to mix bleach with either toilet bowl cleaners or vinegar. People presumably do this because they think mixing the two will produce a better cleaner and disinfectant. In both cases, one of the products is Cl_2, which, as already noted, is a very toxic gas. Mixing bleach and toilet bowl cleaner, which contains hydrochloric acid (HCl), leads to the following reaction:

$$NaOCl + HCl \rightarrow Cl_2 + NaOH$$

Mixing bleach with vinegar, which contains acetic acid (CH_3CO_2H), leads to the following reaction:

$$2NaOCl + 2CH_3CO_2H \rightarrow Cl_2 + 2H_2O + 2CH_3CO_2^- + 2Na^+$$

In either case, the result could be very painful and possibly fatal for the unwary mixer of chemicals.

Future Directions

Given the fact that most exposures to toxic chemicals are associated with lifestyle issues, it is provocative to ask what lies ahead. Clearly the prevalence of smoking has been on the decline in the Unites States, and if the trend apparent in Fig. 1 is extrapolated another 50 years, only a small percentage of adults will be smoking by that time. The risks associated with smoking are well established. The challenges to reducing the societal

costs associated with smoking now lie in the realms of education and social science. How far the percentage of smokers can be reduced through education and public awareness efforts is unclear at this time.

The risks associated with alcohol consumption are also well defined, and because alcohol consumption is much more socially acceptable than smoking, it is unlikely that the costs associated with drinking will be substantially reduced in the years ahead.

Abuse of drugs is a major public health problem whose solution, if there is one, will lie in the realm of education and social science. Despite the best efforts of law enforcement agencies, it is apparent that if people want illegal drugs, they will get them, and if they want prescription drugs without a prescription, that can happen too. The solution will require reducing the desire/need for the artificial euphoria associated with use of drugs such as opioids, cocaine, and heroin. Drug abuse is a difficult and complex problem, and particularly in the case of opioids (Fig 3) with no apparent resolution in sight.

Obesity is a serious problem in the United States, and awareness of the magnitude of the problem has been slow to emerge. Trends in recent years (Fig. 7) are not encouraging. Education and public awareness of the costs of obesity will help, but much of the underlying problem is the simple fact that people like to eat.

Lead has been historically and remains today a major environmental pollutant. The phasing out of leaded gasoline has been a very positive step, but now there is the legacy of the many homes and apartments that were painted with lead-based paint prior to 1978. Eventually these will be taken out of service, but the process has been slow because of the cost and hazards associated with renovating interiors painted with lead-based paint.

Numerous unintentional exposures to toxic chemicals occur in and around the home. Improved education and public awareness of the hazards of certain chemicals can help reduce the frequency of these exposures. The presence of potential toxins in consumer products is an issue that must be addressed by government agencies such as the FDA, EPA, and Consumer Product Safety Commission. In some cases a judgment must be made between the benefits and the risks. In the United States, 35,000–40,000 people die in automobile accidents each year, but there is no movement to take cars off the roads. While the benefits and costs associated with automobile use are arguably well defined, such is not the case with triclosan, for which both the benefits and risks are in dispute.

Bibliography

Primary Literature

1. WHO (1987) Principles for the safety assessment of food additives and contaminants in food. WHO Press, Geneva
2. CDC (2009) Glossary of terms. http://www.atsdr.cdc.gov/glossary.html. Accessed 16 Mar, 2011
3. Hoffmann D, Hoffmann I (2001) The changing cigarette: chemical studies and bioassays. In: Burns DM, Benowitz NL (eds) Risks associated with smoking cigarettes with low machine-measured yields of tar and nicotine. U.S. Department of Health and Human Services, Public Health Service, National Institutes of Health, National Cancer Institute, Washington, DC, pp 159–191
4. Hoffmann D, Hoffmann I (1998) Tobacco smoke components. Beitr Tabakforsch Int 18:49–52
5. Hoffmann D, Hoffmann I, El-Bayoumy K (2001) The less harmful cigarette: a controversial issue. A tribute to Ernst L. Wynder. Chem Res Toxicol 14(7):767–790
6. Baker RR, da Silva JRP, Smith G (2004) The effect of tobacco ingredients on smoke chemistry. Part I: Flavourings and additives. Food Chem Toxicol 42:S3–S37
7. Staff (1990) Proposed identification of inorganic arsenic as a toxic air contaminant. California Air Resources Board and Department of Health Services, Sacramento
8. Korte JE, Hertz-Picciotto I, Schulz MR, Ball LM, Duell EJ (2000) The contribution of benzene to smoking-induced leukemia. Environ Health Perspect 108(4):333–339
9. Staff (2004) The health consequences of smoking: a report of the surgeon general. Centers for Disease Control and Prevention, Atlanta, GA
10. Denissenko MF, Pao A, Tang MS, Pfeifer GP (1996) Preferential formation of benzo a pyrene adducts at lung cancer mutational hotspots in P53. Science 274(5286):430–432
11. Kaiserman MJ, Rickert WS (1992) Carcinogens in tobacco-smoke – benzo a pyrene from Canadian cigarettes and cigarette tobacco. Am J Public Health 82(7):1023–1026
12. Greenblatt MS, Bennett WP, Hollstein M, Harris CC (1994) Mutations in the P53 tumor-suppressor gene – clues to cancer etiology and molecular pathogenesis. Cancer Res 54(18):4855–4878
13. Lane DP (1992) Cancer – P53, guardian of the genome. Nature 358(6381):15–16
14. EPA (1980) Ambient water quality for cadmium. EPA 440/5-80-025, Washington, DC
15. Kasuya M et al (1992) Water pollution by cadmium and the onset of Itai-Itai disease. Water Sci Technol 25(11):149–156
16. Olsson IM et al (2002) Cadmium in blood and urine – Impact of sex, age, dietary intake, iron status, and former smoking – Association of renal effects. Environ Health Perspect 110(12): 1185–1190

17. Paschal DC et al (2000) Exposure of the US population aged 6 years and older to cadmium: 1988–1994. Arch Environ Contam Toxicol 38(3):377–383
18. Bokhoven C, Niessen HJ (1961) Amounts of oxides of nitrogen and carbon monoxide In cigarette smoke, with and without inhalation. Nature 192(480):458
19. Kaufman DW, Helmrich SP, Rosenberg L, Miettinen OS, Shapiro S (1983) Nicotine and carbon-monoxide content of cigarette-smoke and the risk of myocardial-infarction in young men. N Engl J Med 308(8):409–413
20. Counts ME, Hsu FS, Laffoon SW, Dwyer RW, Cox RH (2004) Mainstream smoke constituent yields and predicting relationships from a worldwide market sample of cigarette brands: ISO smoking conditions. Regul Toxicol Pharmacol 39(2):111–134
21. Bateman DN (2003) Carbon monoxide. Medicine 31(10): 41–42
22. Townsend CL, Maynard RL (2002) Effects on health of prolonged exposure to low concentrations of carbon monoxide. Occup Environ Med 59(10):708–711
23. Baker RR (2006) The generation of formaldehyde in cigarettes – overview and recent experiments. Food Chem Toxicol 44(11):1799–1822
24. Baker RR, Coburn S, Liu C (2006) The pyrolytic formation of formaldehyde from sugars and tobacco. J Anal Appl Pyrol 77(1):12–21
25. Li S, Banyasz JL, Parrish ME, Lyons-Hart J, Shafer KH (2002) Formaldehyde in the gas phase of mainstream cigarette smoke. J Anal Appl Pyrol 65(2):137–145
26. Albert RE et al (1982) Gaseous formaldehyde and hydrogen-chloride induction of nasal cancer in the rat. J Natl Cancer Inst 68(4):597–603
27. Blair A, Saracci R, Stewart PA, Hayes RB, Shy C (1990) Epidemiologic evidence on the relationship between formaldehyde exposure and cancer. Scand J Work Environ Health 16(6): 381–393
28. Casanova M, Morgan KT, Gross EA, Moss OR, Heck HD (1994) DNA-protein cross-links and cell replication at specific sites in the nose of F344 rats exposed subchronically to formaldehyde. Fundam Appl Toxicol 23(4):525–536
29. Olsen JH et al (1984) Occupational formaldehyde exposure and increased nasal cancer risk in man. Int J Cancer 34(5): 639–644
30. Horvath EP, Anderson H, Pierce WE, Hanrahan L, Wendlick JD (1988) Effects of formaldehyde on the mucous-membranes and lungs – a study of an industrial-population. JAMA 259(5):701–707
31. Liteplo RG, Meek ME (2003) Inhaled formaldehyde: exposure estimation, hazard characterization, and exposure-response analysis. J Toxicol Environ Health B Crit Rev 6(1):85–114
32. Rodgman A, Perfetti TA (2008) The chemical components of tobacco and tobacco smoke. CRC Press, Boca Raton, 1840 pp
33. Hathaway GJ, Proctor NH, Hughes JP, Fischman ML (1991) Proctor and Hughes' chemical hazards of the workplace. Van Nostrand Reinhold, New York, NY
34. Argentin G, Cicchetti R (2004) Genotoxic and antiapoptotic effect of nicotine on human gingival fibroblasts. Toxicol Sci 79(1):75–81
35. Campain JA (2004) Nicotine: potentially a multifunctional carcinogen? Toxicol Sci 79(1):1–3
36. Hoffmann D, Brunnemann KD, Prokopczyk B, Djordjevic MV (1994) Tobacco-specific N-nitrosamines and areca-derived N-nitrosamines – chemistry, biochemistry, carcinogenicity, and relevance to humans. J Toxicol Environ Health 41(1):1–52
37. Pfeifer GP et al (2002) Tobacco smoke carcinogens, DNA damage and p53 mutations in smoking-associated cancers. Oncogene 21(48):7435–7451
38. Hoffmann D, Hoffmann I (1997) The changing cigarette, 1950–1995. J Toxicol Environ Health 50(4):307–364
39. CDC (2011) Toll of tobacco in the United States. University of Pennsylvania Center for Interdisciplinary Research on Nicotine Addiction, Philadelphia, PA. http://www.med.upenn.edu/cirna/pdf/USA_Figures.pdf. Accessed 26 Apr 2011
40. CDC (2011) Annual smoking-attributable mortality, years of potential life lost, and economic costs – United States, 1995–1999. http://www.cdc.gov/tobacco/data_statistics/mmwrs/byyear/2002/mm5114a2/highlights.htm. Accessed 6 Mar 2011
41. CDC (2011) Economic facts about U.S. tobacco production and use. http://www.cdc.gov/tobacco/data_statistics/fact_sheets/economics/econ_facts/#costs. Accessed 7 Mar 2011
42. CDC (2011) Trends in current cigarette smoking among high school students and adults, united states, 1965–2009. Centers for Disease Control and Prevention, Atlanta, GA. http://www.cdc.gov/tobacco/data_statistics/tables/trends/cig_smoking/index.htm. Accessed 26 Apr 2011
43. Courtwright DT (2001) Forces of habit: drugs and the making of the modern world. Harvard University Press, Cambridge, MA
44. Lord JL et al (1987) Coming to grips with alcoholism. US News World Rep 103(22):57–62
45. Anonymous (2011) Alcohol abuse statistics. http://www.about-alcohol-abuse.com/Alcohol_Abuse_Statistics.html. Accessed 8 Mar 2011
46. Harford TC (1992) Family history of alcoholism in the United-States – prevalence and demographic characteristics. Br J Addict 87(6):931–935
47. Anonymous (2010) The party's over. Nature 468 (7323):475
48. Anonymous (2011) Alcoholism. http://www.addiction-help-line.com/alcohol_addiction.html. Accessed 9 Mar 2011
49. Anthenelli RM, Schuckit MA (1993) Affective and anxiety disorders and alcohol and drug dependence: diagnosis and treatment. J Addict Disord 12:73–87
50. Goodwin DW (1985) Alcoholism and genetics – the sins of the fathers. Arch Gen Psychiatry 42(2):171–174
51. Paulozzi LJ, Ryan GW (2006) Opioid analgesics and rates of fatal drug poisoning in the United States. Am J Prev Med 31(6):506–511
52. CDC (2011) CDC WONDER. http://wonder.cdc.gov/. Accessed 11 Mar 2011

53. Paulozzi LJ (2008) Trends in unintentional drug overdose deaths. http://www.hhs.gov/asl/testify/2008/03/t20080312b.html. Accessed 11 Mar 2011
54. Warner ME, Chen LH, Makuc DM (2009) Increase in fatal poisonings involving opioid analgesics in the United States, 1999–2006. Centers for Disease Control and Prevention, Atlanta, GA
55. CDC (2011) Unintentional drug poisoning in the United States. http://www.cdc.gov/HomeandRecreationalSafety/pdf/poison-issue-brief.pdf. Accessed 11 Mar 2011
56. Anonymous (2011) Opioids. http://www.drug-addiction.com/opioids.htm. Accessed 11 Mar 2011
57. NIDA (2010) Cocaine: abuse and addiction. U.S. Department of Health and Human Services, National Institutes of Health, Research Triangle Park, NC
58. Flynn PM, Joe GW, Broome KM, Simpson DD, Brown BS (2003) Looking back on cocaine dependence: reasons for recovery. Am J Addict 12(5):398–411
59. Johnston LD, O'Malley PM, Bachman JG, Schulenberg JE (2010) Marijuana use is rising; ecstasy use is beginning to rise; and alcohol use is declining among U.S. teens. http://www.monitoringthefuture.org. Accessed 11 Mar 2011
60. NIDA (2005) Heroin abuse and addiction. U.S. Department of Health and Human Services, National Institutes of Health, Research Triangle Park, NC
61. Anoonymous (2011) Morphine. http://en.wikipedia.org/wiki/Morphine. Accessed 12 Mar 2011
62. Anonymous (2011) Heroin. http://en.wikipedia.org/wiki/Heroin. Accessed 12 Mar 2011
63. CDC (2002) Drug-associated HIV transmission continues in the United States. Centers for Disease Control and Prevention, Atlanta, GA
64. Anonymous (2004) Results from the 2003 national survey on drug use and health: national findings. Office of Applied Studies, Research Triangle Park, NC
65. NCHS (2008) Prevalence of overweight, obesity and extreme obesity among adults: United States, trends 1976-80 through 2005–2006. National Center for Health Statistics, Hyattsville, MD
66. NCHS (2004) Mean body weight, height, and body mass index, United States 1960–2002. National Center for Health Statistics, Hyattsville, MD
67. NHLBI (1998) Clinical guidelines on the identification, evaluation, and treatment of overweight and obesity in adults. National Heart, Lung, and Blood Institute, Research Triangle Park, NC
68. Waldron HA, Stöfen D (1974) Sub-clinical lead poisoning. Academic, New York
69. Gilfillan SC (1965) Lead poisoning and the fall of Rome. J Occup Environ Med 7(2):53–60
70. IPIECA (2010) Leaded gasoline phase-out. http://www.ipieca.org/topic/operations-and-fuels/leaded-gasoline-phase-out. Accessed 12 Mar 2011
71. Mcdonald J (2007) China's lead problems go beyond toys. http://www.usatoday.com/money/economy/2007-08-15-3066711946_x.htm. Accessed 12 Mar 2011
72. Annest JL (1983) Trends in the blood lead levels of the U.S. population. In: Rutter M, Jones RR (eds) Lead versus health. John Wiley and Sons, Chichester and New York, pp 33–58
73. EPA (1980) Ambient water quality for lead. EPA-440/4-80-057. Environmental Protection Agency, Washington, DC
74. Blackman A (1991) Controlling a childhood menace. Time 137(8):68–69
75. CDC (1991) Preventing lead poisoning in young children. Centers for Disease Control and Prevention, Atlanta, GA
76. Patterson CC (1965) Contaminated and natural lead environments and man. Arch Environ Health 11:344–360
77. CDC (2011) Lead. http://www.cdc.gov/nceh/lead/. Accessed 13 Mar 2011
78. EPA (2011) Lead in paint, dust, and soil. http://www.epa.gov/lead/. Accessed 12 Mar 2011
79. Craig PP, Berlin E (1971) The air of poverty. Environment 13(5):2–9
80. Anonymous (2011) Frequently asked questions. http://www.leadpro.com/faq.html. Accessed 12 Mar 2011
81. Litovitz TL et al (2001) 2000 annual report of the American association of poison control centers toxic exposure surveillance system. Am J Emerg Med 19(5):337–395
82. Anonymous (2011) Triclosan. http://en.wikipedia.org/wiki/Triclosan. Accessed 13 Mar 2011
83. Layton L (2010) FDA says studies on triclosan, used in sanitizers and soaps, raise concerns. http://www.washingtonpost.com/wp-dyn/content/article/2010/04/07/AR2010040704621.html. Accessed 13 Mar 2011
84. Wong CSM, Beck MH (2001) Allergic contact dermatitis from triclosan in antibacterial handwashes. Contact Dermat 45(5):307–307
85. Schena D, Papagrigoraki A, Girolomoni G (2008) Sensitizing potential of triclosan and triclosan-based skin care products in patients with chronic eczema. Dermatol Ther 21: S35–S38
86. Campbell L, Zirwas MJ (2006) Triclosan. Dermatitis 17(4): 204–207
87. Bhutani T, Jacob SE (2009) Triclosan: a potential allergen in suture-line allergic contact dermatitis. Dermatol Surg 35(5): 888–889
88. Mezcua M et al (2004) Evidence of 2,7/2,8-dibenzodichloro-p-dioxin as a photodegradation product of triclosan in water and wastewater samples. Anal Chim Acta 524(1–2):241–247
89. Latch DE et al (2005) Aqueous photochemistry of triclosan: Formation of 2,4-dichlorophenol, 2,8-dichlorodibenzo-p-dioxin, and oligomerization products. Environ Toxicol Chem 24(3):517–525
90. Latch DE, Packer JL, Arnold WA, McNeill K (2003) Photochemical conversion of triclosan to 2,8-dichlorodibenzo-p-dioxin in aqueous solution. J Photochem Photobiol A Chem 158(1): 63–66
91. Aranami K, Readman JW (2007) Photolytic degradation of triclosan in freshwater and seawater. Chemosphere 66(6): 1052–1056

92. Dayan AD (2007) Risk assessment of triclosan Irgasan (R) in human breast milk. Food Chem Toxicol 45(1): 125–129
93. Allmyr M, Adolfsson-Erici M, McLachlan MS, Sandborgh-Englund G (2006) Triclosan in plasma and milk from Swedish nursing mothers and their exposure via personal care products. Sci Total Environ 372(1):87–93
94. Rule KL, Ebbett VR, Vikesland PJ (2005) Formation of chloroform and chlorinated organics by free-chlorine-mediated oxidation of triclosan. Environ Sci Technol 39(9):3176–3185
95. Anonymous (2007) Plain soap as effective as antibacterial but without the risk. http://www.physorg.com/news106418144.html. Accessed 14 Mar 2011

Books and Reviews

Higgins TE, Sachdev JA, Engleman SA (2010) Toxic chemicals: risk prevention through use reduction. CRC Press, Boca Raton

Nielsen E, Ostergaard G, Larsen JC (2008) Toxicological risk assessment of chemicals: a practical guide. Informa Healthcare, London

Penningroth S (2010) Essentials of toxic chemical risk: science and society. CRC Press, Boca Raton

Richardson ML (ed) (1996) Risk reduction: chemicals and energy into the 21st century. Taylor and Francis, London

Toxic Organic Chemicals

Simanga Gama[1], Jon A. Arnot[2], Don Mackay[1]
[1]Canadian Centre for Environmental Modelling and Chemistry, Trent University, Peterborough, ON, Canada
[2]Department of Physical and Environmental Sciences, University of Toronto Scarborough, Toronto, ON, Canada

Article Outline

Glossary
Definition of the Subject
Introduction
Properties and Characteristics of Toxic Organic Chemicals
The Stockholm Convention on Persistent Organic Pollutants (POPs)
Chemical Classes
Conclusions
Future Directions
Bibliography

Glossary

Bioaccumulation The phenomenon similar to bioconcentration but including uptake from food as well as uptake from the ambient environment. This is expressed as a bioaccumulation factor (BAF) and generally applies to organisms in the environment. The BAF is the steady-state ratio of the chemical concentration in the organism to that in the environment.

Bioconcentration The phenomenon by which an organism, such as a fish, absorbs chemical from its ambient environment of water or air by respiratory uptake and/or dermal absorption. The steady-state ratio of the chemical concentration in the organism to the chemical concentration in its ambient environment of water or air is the bioconcentration factor, (BCF) and the BCF is usually measured in a laboratory test.

Biomagnification The ratio of the chemical concentration in the predator to that of the prey.

Hazard The inherent toxic potency of a chemical, usually expressed as the quantity or concentration of the substance necessary to elicit a defined adverse effect in the organism.

Mass Balance Model A mathematical description of the fate and transport of a chemical in the environment, usually in the form of a computer program. The model provides a complete accounting of all processes experienced by the chemical and is used to estimate environmental concentrations, persistence, and exposures. Models may also be used to forecast future changes in concentrations as a result of actions to reduce contamination.

Persistence The average time that a discharged chemical survives in the environment before it is degraded into another substance or substances. It may be expressed as a "half-life" by analogy to radioactive substances or as a residence time.

Risk The likelihood that there will be an adverse effect as a result of exposure to the chemical. Risk thus depends both on toxic potency (hazard) and the prevailing exposure.

Toxicity The phenomenon by which a chemical substance elicits an adverse effect on an exposed organism. The effect may be death (lethality) or a less severe effect such as a failure to reproduce, an increased vulnerability to predation or significant behavioral changes.

Definition of the Subject

Organic chemicals play an invaluable role in the modern lifestyle. They include pharmaceuticals, pesticides, plastics, fuels, solvents, explosives, surface coatings, adhesives, disinfectants, and fire retardants. From the perspective of conservation and sustainability, the preferred strategy is to use chemicals such that they perform their desired function, cause no unintended adverse effects, and hence leave no legacy of contamination. This is a fundamental component in the move toward "green chemistry" which also strives to reduce resource depletion, energy use, ozone depletion, and interference with natural biogeochemical cycles. Of the over 50 million chemicals that have been characterized, most are organic compounds. Some 100,000 are commercially produced in quantities large enough to raise concerns that they may become present in the environment in sufficient quantities and at sufficient concentrations to cause risks to the well-being of humans or other organisms. As a response to this concern, most regulatory agencies have listed chemicals of national concern, a typical number being in the hundreds to thousands. These "toxic organic chemicals" merit regulatory scrutiny and possible controls over synthesis and use. At the international level, the Stockholm Convention has listed over 20 substances as worthy of regulation or even bans. Most of these are synthetic chlorinated organic substances, but some naturally occurring and inadvertently produced substances are also of concern. In this entry, the chemical attributes or properties of these substances are described and criteria that dictate the level of concern about hazard and risk to environmental and human health are outlined. Selected classes of organic chemicals are then discussed in more detail.

Introduction

A consensus has emerged among the scientific and regulatory communities that it is a combination of properties of chemical substances that dictates their designation as "toxic organic substances" and thus the need for their regulation. The result has been the identification of classes of chemicals as persistent organic pollutants (POPs) and persistent bioaccumulative and toxics (PBTs) and those that undergo long-range transport (LRT) on a global scale. Although numerical criteria have been developed for certain key chemical properties such as toxicity and persistence, it is apparent that there is a continuum of properties, thus there is no clear demarcation between for example, PBTs and non-PBTs. There are varying degrees of PBT-like character among "toxic organic chemicals." It can be justifiably argued that all chemical substances are toxic if the administered dose or exposure is sufficient, that is, as stated over 500 years ago by Paracelsus, "it is the dose that makes the poison." Accordingly, there is no clear demarcation between toxic and nontoxic substances: the demarcation must be on the basis of both potency as a toxic agent and the exposure experienced in the environment. The regulatory focus must be on ensuring the principles of sustainability and conservation by reducing exposure.

It is important to discriminate between the terms hazard and risk, since these terms are often wrongly used interchangeably. Hazard reflects the inherent properties of the chemical such as its toxic potency, regardless of the actual exposure. Risk reflects the probability of adverse effects as a function of both hazard and the actual exposure. A highly hazardous substance may pose a low risk and vice versa.

Properties and Characteristics of Toxic Organic Chemicals

Organic chemicals tend to fall into distinct classes based on their molecular structure, an example being the alcohols of increasing carbon chain length, methanol, ethanol, propanol, butanol, etc. There is often a systematic change in properties such as boiling point or vapor pressure in such homologous series. This feature is invaluable in that interpolation and modest extrapolation of properties is often possible. This is formalized in linear free energy relationships (LFER) and is exploited in the development of quantitative structure activity (or property) relationships (QSARs and QSPRs) that are widely used for property estimation purposes. As quantum chemical molecular

modeling computation methods become more reliable and accessible, it is clear that the key properties of chemical substances are amenable to a priori estimation from molecular structure.

A key LFER arises from a systematic increase in halogenation of a parent organic substance. For example, the series benzene, chlorobenzene, dichlorobenzene to hexachlorobenzene displays consistent changes in properties such as a decrease in vapor pressure and aqueous solubilities. This also occurs with bromine and to an extent with fluorine substitution and with increased methylation, for example, benzene, toluene, xylene, etc. These systematic property changes are exploited when later reviewing the properties of groups of chemicals such as the polychlorinated biphenyls (PCBs). The key properties as discussed by Mackay et al. [1] are addressed below.

Molecular structure and molar mass (g/mol) are obvious fundamental properties that reflect the constituent elements (molar mass) and their location in the chemical (molecular structure). It is necessary to discriminate between isomers – chemicals comprised of the same elements but with different structural or spatial patterns. For example, the four stereoisomers of hexachlorocyclohexane (HCH) are comprised of the exact same elements (six carbon, six chlorine, and six hydrogen atoms) contained in the same general structure (a cyclic ring of six carbon atoms, each with a bond to a chlorine and a hydrogen atom), but with different three-dimensional spatial patterns of these bonds. The seemingly minor differences in HCH isomer structure result in significant differences in toxicity.

Melting point and boiling point dictate the state of the pure chemical at atmospheric temperatures and pressure as either solids, liquids, or gases.

Chemical solubility and partitioning: the tendency of a substance to partition from its pure state into the atmosphere, water, and octanol, is expressed, respectively, as the saturation vapor pressure, aqueous solubility, and solubility in octanol. These properties are useful but are not always measurable. For example, the solubility of ethanol in water is not measurable because of miscibility. Octanol is widely accepted as a surrogate phase for partitioning into lipids (fats) in biota and for natural organic matter (OM) and organic carbon (OC) in soils and sediments. Since saturation conditions for organic chemicals rarely exist in the environment, it is more convenient to use ratios of these three solubilities, that is, the three partition coefficients or ratios of concentrations, K_{AW} (air–water), K_{OW} (octanol–water), and K_{OA} (octanol–air). Clearly only two of these are independent since K_{OA} is K_{OW}/K_{AW}. The air–water partition coefficient K_{AW} is $H/S^S{}_W$ or $(P^S/RT)/S^S{}_W$ where P^S is the saturation vapor pressure (Pa), R is the gas constant (8.314 Pa m^3/mol K), T is absolute temperature (K), $S^S{}_W$ is the solubility in water (mol/m^3), H is the Henry's law constant (Pa m^3/mol) and is $P^S/S^S{}_W$. For most environmental purposes, K_{OW} is assumed to be equivalent to the lipid–water partition coefficient. K_{OW} is also used to estimate partitioning to organic carbon from water (K_{OC}) as approximately 0.35 K_{OW} plus or minus a factor of three [2].

The K_{AW}, K_{OW}, K_{OA} properties thus largely dictate the equilibrium partitioning characteristics of the chemicals between air, water, soils, and sediments that contain organic carbon as well as biota in terms of their lipid content. A chemical space diagram provides a convenient depiction of these properties as plots of either log K_{AW} versus log K_{OW}, (in which case the constant log K_{OA} values lie on a diagonal), or as log K_{AW} versus log K_{OA}, with log K_{OW} values lying on a diagonal. Figure 1 is such a plot and shows the points corresponding to the series of chemicals representing particular chemical classes. For example, points for 1,1′-(2,2,2-trichloroethylidene)bis 4-chloro-benzene (DDT), benzo(a)pyrene, and PCBs are plotted showing the wide variation in partitioning properties which translate into differences in environmental fate. On this plot are lines corresponding to various estimated mass percentage partitioning between air, water, and octanol phases for an assumed volumetric proportion of these phases.

These simple relationships apply only if the molecule does not dissociate or ionize as applies to organic acids such as phenols at high pH and organic bases such as amines at low pH. For these substances, knowledge of the dissociation constant pK_A and the prevailing pH is essential.

Reactivity, expressed as a rate constant or half-life, is an essential property because it determines the persistence, that is, the residence time of the chemical in the environment. Persistence is important because to a first approximation the quantity of the chemical residing in the environment (kg) and hence the

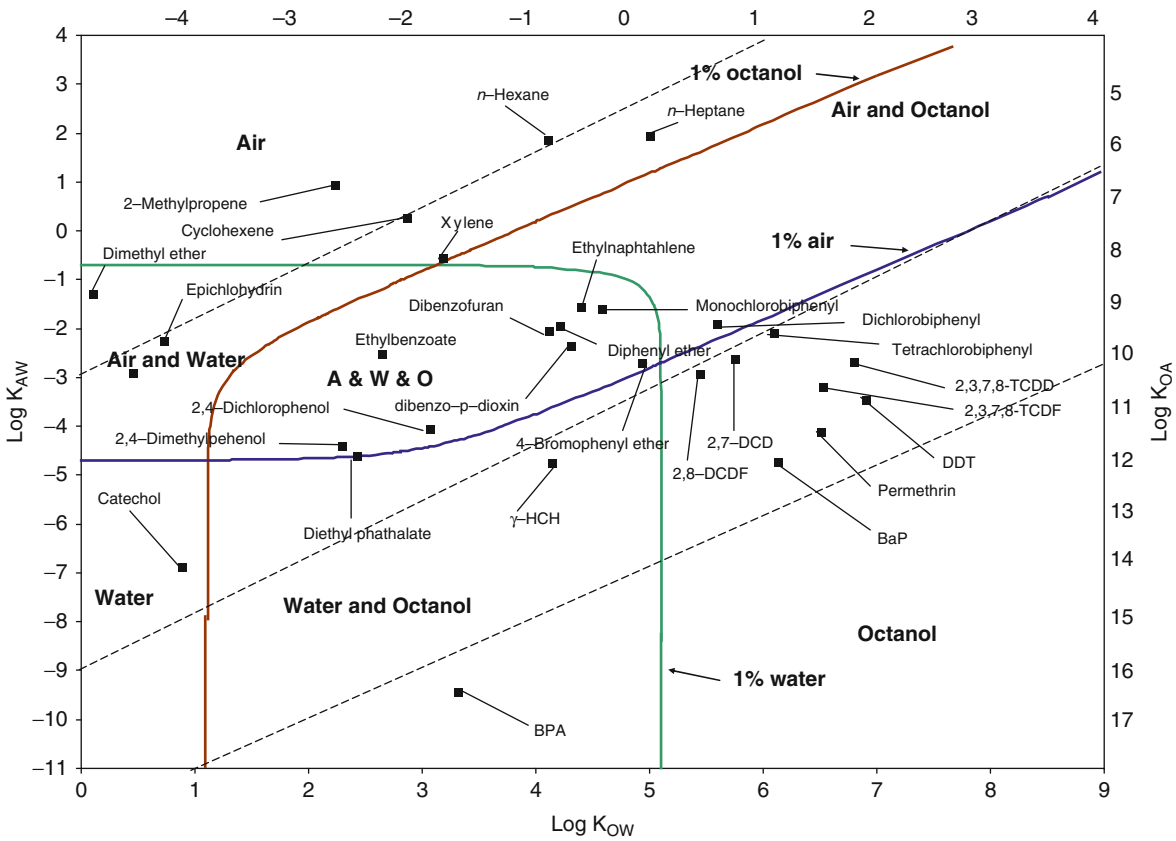

Toxic Organic Chemicals. Figure 1

Chemical space plot of the air–water partition coefficient (log K_{AW}) versus the octanol–water partition coefficient (log K_{OW}) showing positions of chemical classes on the three media of air, water, and octanol. Octanol serves as a surrogate for organic matter in soils and sediments. Constant log K_{OA} values form the dashed diagonals on this plot of 1, 6, and 10 (from top to bottom) since log K_{OA} is log K_{OW}−log K_{AW}. The heavy lines represent 1% partitioning into each medium

concentrations that exert toxicity (kg/m^3) are proportional to the discharge rate of chemical to the environment (kg/h) and to the chemical's residence time (h). Chemicals usually react following second-order kinetics

$$\text{Rate} = k_2 C_C C_R = k_1 C_C = 0.693 C_C / t_{1/2}$$

where k_2 is a second-order rate constant, C_C is chemical concentration, and C_R is the concentration of a reacting species such as hydroxyl radicals in the atmosphere [3]. It is often convenient to lump k_2 and C_R as a first-order rate constant k_1 (h^{-1}) but this assumes that C_R and k_2 are constant. In reality, both vary spatially and temporally, thus the half-life $t_{1/2}$ is also expected to vary. Despite this variability, persistence is such an important property that it is necessary to provide estimates of half-lives of the chemical for all relevant media to which the chemical partitions. Some literature and databases exist on the half-lives of well-studied priority chemicals in air, water, soils, sediments, and in biota by metabolic conversions or biotransformation [1, 4–6]. There is, however, a paucity of data for other substances including "emerging" contaminants. The most common mechanisms are reaction with oxidizing species such as hydroxyl radicals, hydrolysis, photolysis (direct and indirect), biodegradation by microorganisms, and biotransformation in animals and plants.

Regulatory agencies have set half-life criteria for specific environmental media (for example, 60 days in water and 2 days in the atmosphere) [7]; however, in addition to medium-specific half-lives, the overall or

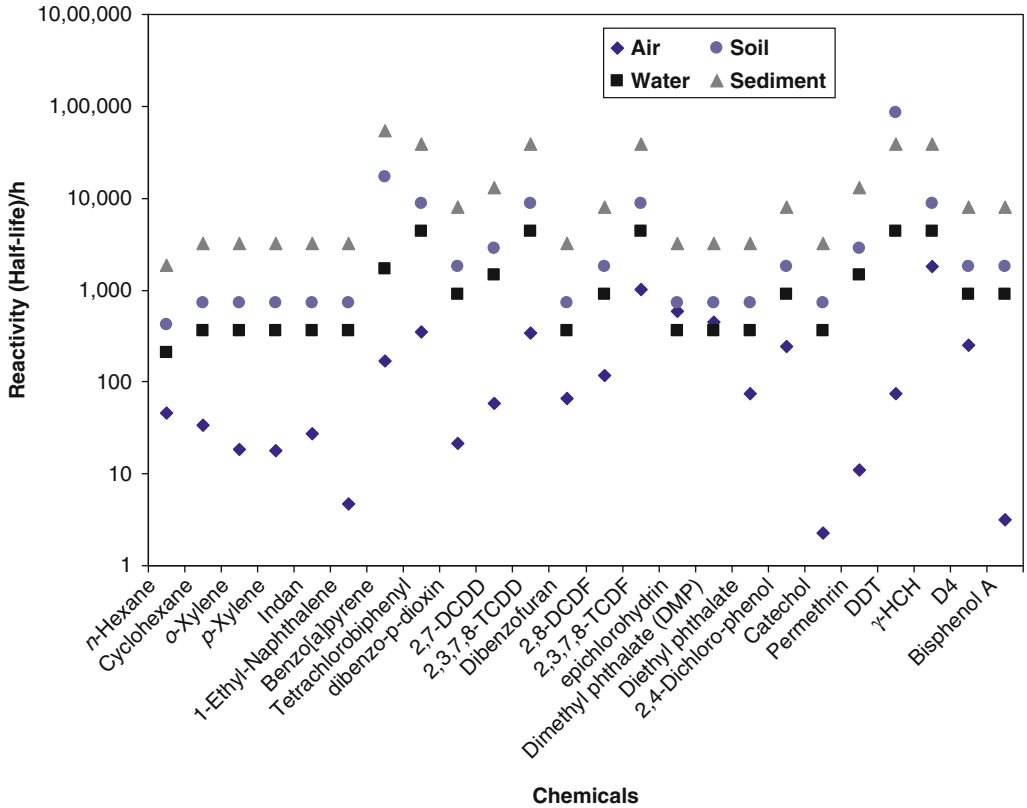

Toxic Organic Chemicals. Figure 2
Estimated half-lives (hours) of selected chemicals in air, water, soil, and sediment [6]

average persistence of a chemical in the environment is also important and is controlled by the relative quantities of chemical in each medium [8]. The relative quantities in each environmental medium, often referred to as the environmental fate and distribution, are largely a function of the partitioning properties of the chemical and the composition of the environment. In principle, the overall reaction rate constant (k_{OV}) is the weighted mean of the rate constants, the weighting being done according to the proportions in each medium. Computer programs such as the OECD Tool [9] are used to perform such calculations and yield an "overall persistence." This quantity is essential in any assessment of sustainability because the year-to-year carryover of a chemical is controlled by overall persistence. In principle, an overall persistence ($P_{OV} = 0.693/k_{OV}$) of say 2 years implies that an appreciable fraction of the chemical discharged in year 1 will remain after 5 or more years. Indeed, this is the most important single property of an organic chemical, hence their designation as persistent organic pollutants (POPs) [10]. See also the discussion by Gouin et al. [11], Mackay [12] and Scheringer [13]. Figure 2 illustrates the variation in reactivity of a selection of chemicals in each medium.

Potential for long-range transport (LRT) in air or oceans is increasingly recognized as a cause for concern because the adverse effects may be experienced at locations remote from the source [13]. Obvious regions of concern are the Arctic and Antarctic where local biota may be unacceptably contaminated and used as food by mammals including humans. Multimedia mass balance models have been developed that predict the influence of a chemical's environmental phase distribution on its ability to be transported over long distances [14]. Persistence, and hence reactivity, of the chemical in air influences its potential to be transported over long distances in air. Multimedia models currently used to estimate LRT parameter include Globo-POP [15], RAIDAR [16], and the

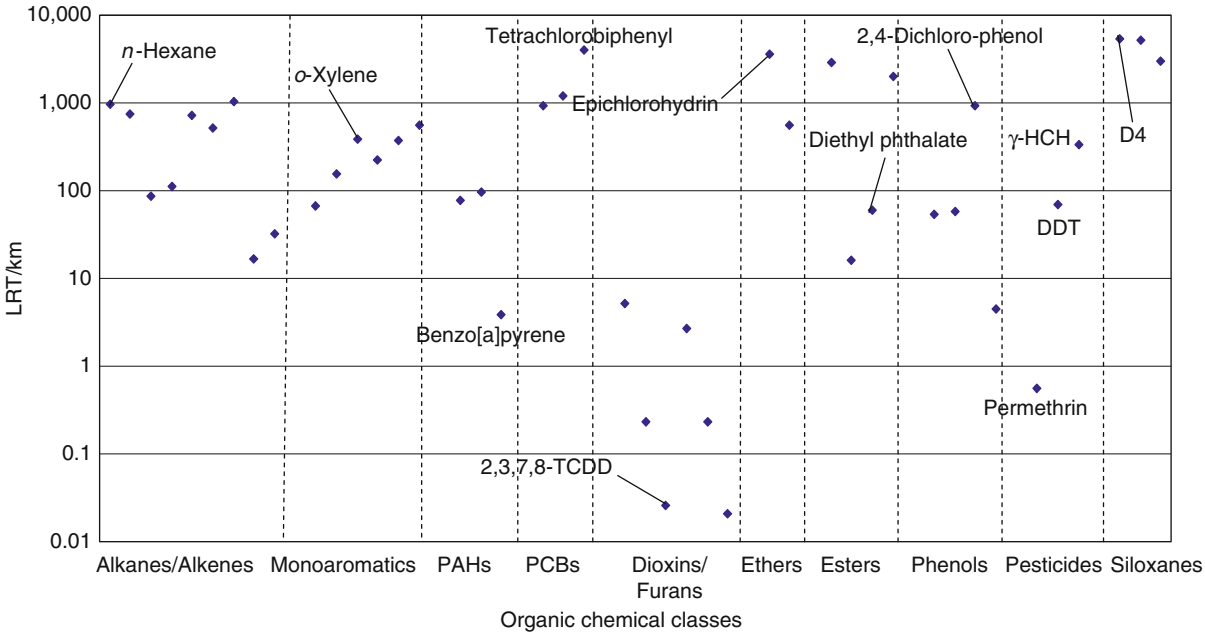

Toxic Organic Chemicals. Figure 3

Long-range transport (LRT; km) in air estimated by Level II fate calculations using the RAIDAR 1.00 model [16]. The chemicals are categorized into general classes

OECD Tool [9]. The models simulate LRT by incorporating the chemical partitioning properties discussed above. More complex global atmospheric and oceanic circulation models have also been used to simulate and forecast the global cycling of chemicals, for example, Guglielmo et al. [17].

Figure 3 shows the variation in long-range transport potential as calculated by the RAIDAR model for a selection of substances.

Bioaccumulation/Bioconcentration and Toxicity

Bioaccumulation refers to the tendency for an organic chemical to partition into biota from their surrounding environment. The bioconcentration factor (BCF) is a metric of bioaccumulation and is the steady-state ratio of the chemical concentration in an organism, such as a fish, to the chemical concentration in an environmental medium, such as water. The BCF is usually measured in a laboratory test and does not include exposures to chemical from dietary sources. Bioaccumulation includes chemical uptake from the environment, that is, bioconcentration, and from food. Biomagnification refers to the increase in chemical concentration from prey to predator [18].

Chemical hydrophobicity, as characterized by K_{OW}, plays a large role in determining the BCF and the toxicity of the chemical as measured in aquatic tests for fish. Hydrophobic organic chemicals bioconcentrate in aquatic organisms as a result of the chemical partitioning from the water into the lipids of the organism. Prolonged bioconcentration of the chemical may induce toxicity by, for example, disrupting the integrity of the lipid bilayer of cell membranes, that is, baseline narcotic mode-of-toxic action. Indeed, the bioaccumulation process results in the transport of chemical from external media, where there are generally no sites for toxic action, into the organism, where there are sites for toxic action [19]. Figure 4 illustrates the fundamental role of partitioning (or bioconcentration) on aquatic toxicity when the parameters for the BCF (L/kg) and toxicity in fish (LC50; mg/L) are plotted as functions of K_{OW}. Bioconcentration and aquatic toxicity (expressed as 1/LC50) both increase with K_{OW} and the slopes of the two relationships are almost identical. Chemicals with log K_{OW} greater than 5 include polycyclic aromatic hydrocarbons (PAHs), many pesticides, chlorinated furans and dioxins, and polychlorinated biphenyls (PCBs) which are implicated as being both toxic and persistent. Chemicals

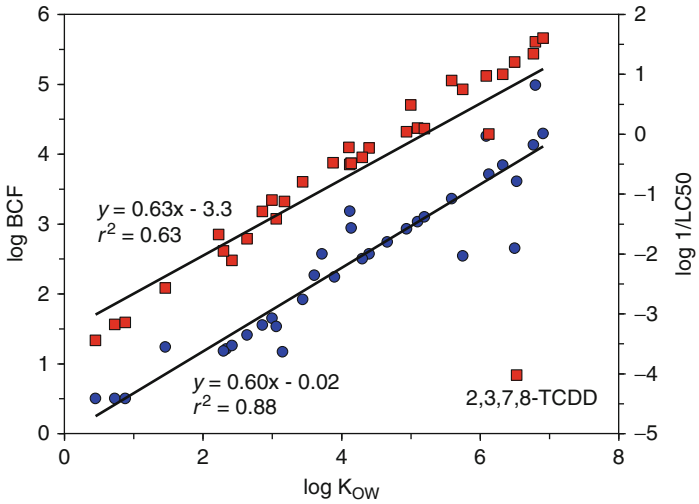

Toxic Organic Chemicals. Figure 4
Plot of bioconcentration factors (BCF; L/kg, *blue circles*) in fish and 14-day aquatic toxicity estimates for fish (1/LC50; L/mg, *red squares*) of selected organic chemicals as a function of chemical hydrophobicity (K_{OW}) [6]

that are highly toxic, such as 2,3,7,8-tetrachlorodibenzo-*p*-dioxin (2,3,7,8-TCDD), and that have modes of action that are more specific than baseline narcosis will typically fall well below the 1/LC50 regression line.

The Stockholm Convention on Persistent Organic Pollutants (POPs)

The Stockholm Convention is an international agreement designed to limit the use of chemicals that are persistent, bioaccumulative, and subject to long-range transport on a continental or global scale such that they cause significant adverse effects (toxicity) in regions distant from where they are used or manufactured [10]. The initial group comprised of 12 substances or classes was colloquially designated the "dirty dozen." In recent years, other substances have been added. Table 1 lists these substances. It is noteworthy that many are chlorinated hydrocarbons, the reason being that chlorination impacts stability and hence persistence to the molecule.

Chemical Classes

A brief description of some chemical classes is given and provides references for further reading. Molecular structures for selected chemicals in each class are also provided.

Alkanes and Alkenes

The alkanes are present in fuels and generally exhibit low solubilities in water, which when coupled with their relatively high vapor pressures results in relatively high air–water partition coefficients (K_{AW}). Values of K_{OW} are high and increase with carbon number, for example, *n*-hexane has a log K_{OW} value of 4.11 while the higher molecular weight *n*-heptane has a log K_{OW} value of 5.0 [1]. Half-lives in air and water are relatively short (approximately 40 and 200 h in air and water) [1, 3]. The corresponding unsaturated hydrocarbons or alkenes are more soluble in water, have lower K_{AW} and K_{OW} values and are more reactive, especially in air in which half-lives may be only a few hours. They are thus implicated in the formation of photochemical smog due to the presence of the double bond which renders them susceptible to oxidation by hydroxyl radical. This class of chemicals predominantly partitions to air as indicated in Fig. 1.

The halogenated (primarily chlorinated) alkanes are less flammable and are thus valuable solvents but they have longer half-lives and are more environmentally persistent, especially in soils and ground water. They are more hydrophobic than the parent alkanes as a result of their lower solubility in water. Of particular environmental concern are the chlorinated C_2 alkanes and alkenes such as trichloroethylene that are

Toxic Organic Chemicals. Table 1 Chemicals listed under the Stockholm Convention or under review as of 2010; these chemicals are categorized under Annex A (Elimination), Annex B (Restriction), or Annex C (Unintentional production)

Initial 12 chemicals (i.e., "Dirty Dozen")	
Aldrin (Annex A)	Pesticide
Chlordane (Annex A)	Pesticide
DDT (Annex B)	Pesticide
Dieldrin (Annex A)	Pesticide
Endrin (Annex A)	Pesticide
Heptachlor (Annex A)	Pesticide
Hexachlorobenzene (Annex A, C)	Industrial chemical
Mirex (Annex A)	Pesticide
Toxaphene (Annex A)	Pesticide
Polychlorinated biphenyls (Annex A, C)	Industrial chemical and flame retardant
Polychlorinated dibenzo-*p*-dioxins (Annex C)	By-product
Polychlorinated dibenzofurans (Annex C)	By-product
Recently listed chemicals	
α-hexachlorocyclohexane (Annex A)	Pesticide, by-product
β-hexachlorocyclohexane (Annex A)	Pesticide, by-product
γ-hexachlorocyclohexane (Annex A)	Pesticide
Chlordecone (Annex A)	Pesticide
Hexabromobiphenyl (Annex A)	Industrial chemical and flame retardant
Pentachlorobenzene (Annex A, C)	Pesticide, industrial chemical
Perfluorooctane sulfonic acid, its salts and perfluorooctane sulfonyl fluoride (Annex B)	
Polybrominated diphenyl ethers (Annex A)	Industrial chemical
Tetra, pentabromodiphenyl ether (Commercial penta)	
hexa- and heptabromodiphenyl ether (Commercial octa)	

Toxic Organic Chemicals. Table 1 (Continued)

Chemicals under review as of 2010	
Endosulfan (Annex F)	Insecticide
Hexabromocyclododecane (Annex E)	Flame retardant
Short-chained chlorinated paraffins (Annex E)	Used in pressure lubricants in metal industry. Also used in sealers, glue coatings in building industry, and in leather and rubber treatments.

widely used as solvents and have become frequent groundwater contaminants. The chlorinated long- and short-chain paraffin compounds have many uses, notably as cutting oils.

The cycloalkanes are similar in properties to the alkanes. The fully chlorinated cyclohexanes are of concern because of their persistence, volatility, and potential for long-range transport. The pesticide lindane (γ-hexachlorocyclohexane or γ-HCH) and its isomers α-HCH and β-HCH have been distributed globally by transport in air and ocean currents. Uses of these chemicals are now limited. Brominated cyclohexanes that are used as fire retardants are also persistent and bioaccumulative.

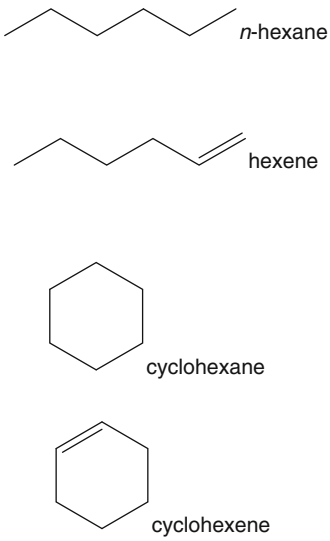

Mono-aromatics

The mono-aromatics, for example, benzene, toluene, and the isomers of xylene, are significant components of fuels and are important chemical intermediates. They have higher solubilities in water than the corresponding cycloalkanes and they are relatively volatile and reactive in air contributing to photochemical smog [3]. Mono-aromatics such as xylene partition mostly to air as indicated in Fig. 1, while higher molecular weight aromatics such as polyaromatic hydrocarbons (e.g., 1-ethyl naphthalene) have lower volatilities and water solubilities. Chlorination results in increased persistence and hydrophobicity (K_{OW}). Hexachlorobenzene is very persistent and has become globally distributed by atmospheric transport and is banned under the Stockholm Convention.

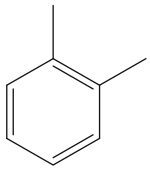

o-xylene

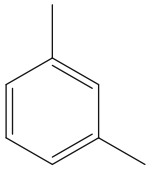

m-xylene

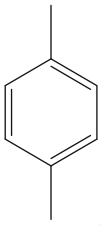

p-xylene

Polyaromatic Hydrocarbons (PAHs)

Fusion of a number of benzene rings results in an important series of PAHs such as the 2-ring naphthalene, 3-ring phenanthrene, 4-ring pyrene, and 5-ring benzo-a-pyrene (BaP). These substances are formed along with smoke and soot during incomplete combustion. They are hydrophobic, relatively involatile, and are regarded as particularly toxic. BaP is a well-studied human carcinogen. The primary environmental concern is human inhalation in the vicinity of combustion sources. Chlorinated naphthalenes are used as PCB substitutes and are hydrophobic and persistent. Chlorination of PAHs increases their hydrophobicity and stability, and decreases their water solubility and volatility. For further reading, see Haritash and Kaushik [20], Mastral and Callen [21], and Wilson and Jones [22].

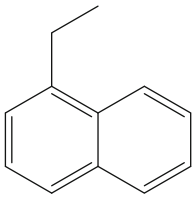

1-ethyl-naphthalene

Polychlorinated Biphenyls (PCBs)

Polychlorinated biphenyls (PCBs) are a class of stable synthetic organic chemicals consisting of 209 possible congeners. PCBs are used industrially as dielectric fluids in capacitors and transformers but also as flame retardants, inks, sealants, and plasticizers. The stability of the C–Cl covalent bond makes these chemicals more persistent in the environment. Most biodegradation reactions involve oxidation or reduction of substrate chemicals. PCBs are also resistant to oxidation, making them resistant to biodegradation. As one of the most notorious toxic organics they have been banned under the Stockholm Convention, but large quantities remain in use and they are widespread in distribution. PCBs are associated with adverse health effects in many fish, marine mammal, and avian species. For instance, levels of PCBs above 20 mg/kg in the blubber of whales and seals have been linked to thyroid, immune, and reproductive disruption [23, 24]. PCBs are predicted to partition to octanol more than air and water, but they are sufficiently volatile to be subject to atmospheric transport. For further reading, see also Fox et al. [25], Hoffman et al. [26], Borga et al. [27], Aken et al. [28], Van den Berg et al. [29], and Domingo and Bocio [30].

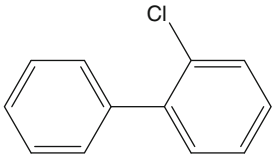

2-chlorobiphenyl

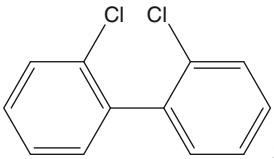

2,2'-dichlorobiphenyl

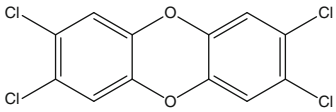

2,3,7,8-tetrachlorodibenzo-*p*-dioxin

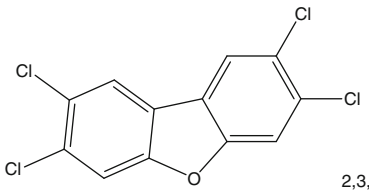

2,3,7,8-tetrachlorodibenzofuran

Dioxins and Furans

Non-chlorinated dioxins and furans such as dibenzo-dioxin and dibenzo-furan, respectively, are relatively water soluble and volatile as indicated in Fig. 1 and they can partition to all three media. Chlorinated dioxins and furans are by-products of industrial processes and naturally occurring, and are categorized as being unintentionally produced under Annex C of the Stockholm Convention [10]. Chlorination of dioxins and furans results in increased hydrophobicity, lower water solubilities, and lower volatilities, as demonstrated in Fig. 1 where chloro-furans and chloro-dioxins such as 2,8-dichlorodibenzo-furan (2,8-DCDF), 2,7-dichlorodibenzo-dioxin (2,7-DCDD), respectively, are regarded as partitioning largely to octanol, that is, organic phases. Increased chlorination further increases their hydrophobicity as indicated with 2,3,7,8-TCDD and 2,3,7,8-TCDF. A notable congener is 2,3,7,8-tetrachlorodibenzo-p-dioxin (2,3,7,8-TCDD), which is a very potent and persistent toxicant, indeed one of the most toxic organic chemicals known. See also Lohmann and Jones [31], Aberg et al. [32], Van den Berg et al. [29], and Domingo and Bocio [30].

Ethers

Of more recent environmental concern are certain halogenated ethers such as polybrominated diphenyl ethers (PBDEs). PBDEs are used as fire retardants and are added to a wide variety of commercial and household products. For example, PBDEs are added to polyurethane foam and used in upholstered furniture to reduce their flammability [33]. Commercial pentabromodiphenyl ether, which is mainly composed of tetrabromodiphenyl ether and pentabromodiphenyl ether, is categorized as a persistent organic pollutant and has recently been banned under the Stockholm Convention [10]. Because of their low water solubility, relatively high log K_{OW}, low log K_{AW}, and low vapor pressure, in the environment they partition primarily to sediments and soils. Their persistence in soil and sediments can result in accumulation in the environment and in food webs. Short non-brominated ethers such as dimethyl ether (a common laboratory solvent) are highly soluble, have a high vapor pressure and low log K_{OW} (see Fig. 1), and are less persistent. See also Vonderheide et al. [34], Wang et al. [35], and de Wit et al. [36].

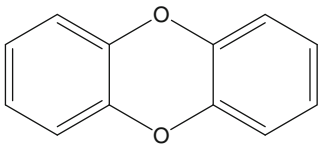

dibenzo-*p*-dioxin

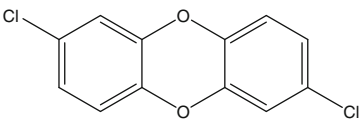

2,7-dichlorodibenzo-*p*-dioxin

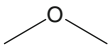

dimethyl ether

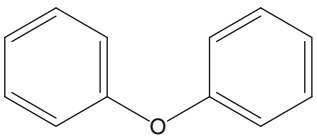

diphenyl ether

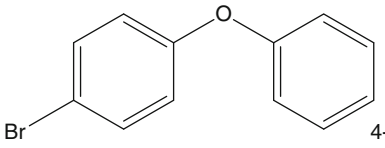

4-bromodiphenyl ether

Esters

Esters are a product of a condensation reaction between alcohols and carboxylic acids. Esters of low molecular weight are relatively volatile and are components of fragrances. Notably among the esters of environmental concern are the phthalate acid esters (PAEs). These commercial chemicals have been used in a wide range of products namely; household electronics, building materials, insecticides and pharmaceutical products. These compounds are found worldwide in oceans, groundwater, sediment, and the atmosphere [37, 38]. Examples of PAEs include dimethyl phthalate (DMP) and diethyl phthalate (DEP).

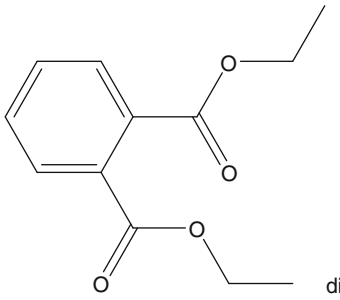

diethyl phthalate

Phenols

Phenols are derivatives of benzene possessing a hydroxyl (−OH) group. They are used as reagents in the manufacture of dyes, drugs, fungicides, and pesticides and in chemical and paper industries. Sources of emissions of phenolic waste to the environment are from petroleum refineries, industrial plants, mine discharges, and through general uses in products containing resins and paints. The hydroxyl group can dissociate into a phenolate and hydrogen ions imparting acidity and relatively high solubility in water [39]. Substituted phenols such as chlorinated and methylated (2, 4-dichlorophenol, pentachlorophenol (PCP) and 2, 4-dimethylphenol) are more susceptible to dissociation and are more acidic and toxic. PCP has been widely used as a wood preservative, while phenol was one of the first medical disinfectants. Catechol is a unique phenol with two hydroxyl groups and is implicated in affecting the human nerve center system, inhibits DNA replication, and leads to chromosomal aberration [40]. Derivatives of catechol include the toxic agents in poison ivy and poison oak.

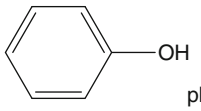

phenol

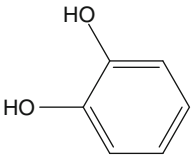

catechol

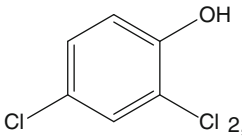

2,4-dichlorophenol

Pesticides

Pesticides are designed to have properties that enable them to reach and impact the target organism or pest including insects, rodents, and vegetation. Effectiveness is increased by persistence, but this can result in nonselective toxicity to other non-targeted organisms including birds and humans. They may have a greater potential to contaminate a wide range of environmental media. Many of the original pesticides were organochlorine (OC) compounds which are now either banned or highly restricted under the Stockholm Convention [10]. Many OCs are relatively volatile; thus, evaporation is an important loss process for pesticides from the areas where they are applied initially, they then move to the atmosphere and eventually get transported through air to remote areas. Notable among the OCs are DDT and its related compounds DDE and DDD, and lindane (γ-HCH). Permethrin, a synthetic pyrethroid insecticide used

worldwide to control a broad range of insect pests such as mosquitoes, is also highly hydrophobic and partitions in the environment in a manner similar to DDT. OC pesticides have been largely replaced by organophosphates, pyrethroids, and other substances that are less persistent, but often more potent toxicants. For further reading on pesticides, especially on their global distribution, see Weber et al. [41], Hoferkamp et al. [42], Li and Macdonald [43], and Muir and de Wit [44].

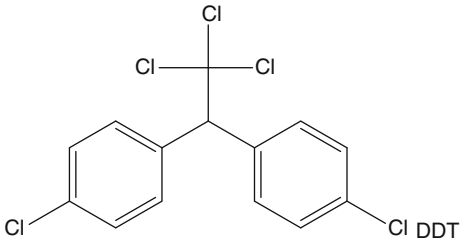

DDT

Personal Care, Indoor, and Household Products

Most organic substances in personal care and household products can impact humans directly in the home and they may enter the environment through sewage wastes (down the drain releases) or by direct releases to air. Included in this group are detergents, fragrances, flame retardants, additives to plastics, and indoor pesticides and solvents. An example is the class of cyclic siloxanes whose backbone is formed of repeated oxygen and silicon atoms with methyl groups attached. These compounds are components of toiletries such as antiperspirants, soaps, and shampoos and are used in many other "household" products including textiles, paints, sealants, lubricants, and nonmedicinal ingredients in pharmaceuticals. They are relatively nontoxic but they can be quite persistent [45]. They are highly volatile with large K_{AW} values and hence predominantly partition to air as illustrated in Fig. 1. Bisphenol A (BPA) (2,2-bis(4-hydroxyphenyl) propane) has been used often in the production of hard plastic (polycarbonate) bottles and metal-based food and beverage can liners in the past few decades. BPA is regarded as an endocrine-disrupting chemical (EDC) [46]. Regulatory agencies have recently expressed serious concerns about the potential effects of BPA on the brain and prostate gland in fetuses, infants, and young children and some have banned the sale and importation of baby bottles containing BPA [47]. A variety of other organic substances are emitted from various indoor sources, including office equipment such as printers [48].

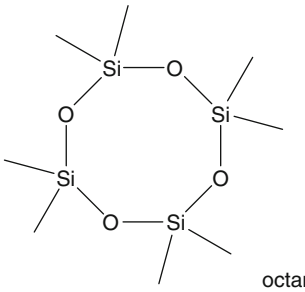

octamethylcyclotetrasiloxane (D4)

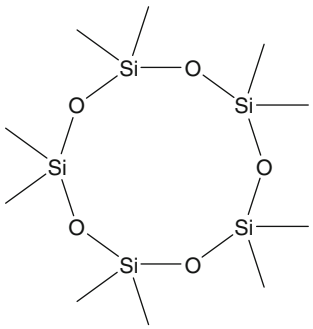

decamethylcyclopentasiloxane (D5)

Conclusions

There is a wide range of organic chemicals that have the potential to be toxic with a multitude of uses and with properties that vary greatly resulting in a diversity of environmental behavior characteristics and exposure routes. Management of these substances presents a considerable challenge to governments and industries. Mistakes have been made in the past by synthesizing and dispersing substances such as DDT and PCBs that have proven to be persistent, bioaccumulative, toxic and have become globally distributed. There is optimism that such mistakes can be avoided in the future if there is an adequate understanding of the factors that dictate environmental partitioning, fate, exposure, and toxicity. Effort is now being devoted to searching for new toxic organics by advance knowledge of their

structural and property characteristics [49–51]. It is increasingly possible to estimate the critical chemical properties from molecular structure and assess environmental fate and transport quantitatively using mass balance models that can be validated using monitoring data. If this information can be exploited in advance of commercial distribution, it should be possible to enjoy the many benefits of synthetic organic chemicals without the adverse effects that have been, and are being experienced, from uses that do not satisfy the principles of conservation and sustainability.

Future Directions

The effective future management of toxic organic chemicals in the environment can be improved by a number of scientific and regulatory actions. There is a need for better information on the production, uses and rates of discharge of chemicals, both nationally and internationally. Improved methods of estimating chemical properties from molecular structure are desirable including partitioning, degradability, and toxicity. These improvements could enhance the assessment of chemical fate and possible effects by industry, thus avoiding repetition of past mistakes. Undoubtedly, there are as yet unidentified toxic organic substances, thus there is an incentive to improve techniques and sensitivity of chemical analyses and monitoring of environmental media. As a complement to these monitoring efforts there is a need to further develop, apply, and validate the use of computer models that predict environmental fate and effects. Finally there is a strong incentive to increase the effectiveness of regulatory programs, both nationally and internationally by incorporating the emerging scientific advances and providing a holistic and transparent evaluation of risk to the public and the ecosystem. Ultimately it is an informed public that is the best guarantee that society will maintain and enhance actions to improve sustainability and conservation.

Bibliography

1. Mackay D, Shiu WY, Ma KC (2000) Physical-chemical Properties and Environmental Fate Handbook. Chapman and Hall CRCnetBASE, CRC Press LLC, Boca Raton
2. Seth R, Mackay D, Muncke J (1999) Estimating the organic carbon partition coefficient and its variability for hydrophobic chemicals. Environ Sci Technol 33(14): 2390–2394
3. Atkinson R, Arey J, Aschmann SM (2008) Atmospheric chemistry of alkanes: review and recent developments. Atmos Environ 42(23):5859–5871
4. Howard PH, Boethling RS, Jarvis WF, Meylan WM, Michalenko EM (1991) Handbook of Environmental Degradation Rates. Lewis Publishers, Chelsea
5. Arnot JA, Mackay D, Parkerton TF, Bonnell M (2008) A database of fish biotransformation rates for organic chemicals. Environ Toxicol Chem 27(11):2263–2270
6. U.S. EPA (2009) Exposure assessment tools and models, estimation programs interface (EPI) suite, ver. 4.0. U.S. Environmental Protection Agency, Exposure Assessment Branch, Washington, DC
7. Government of Canada, Persistence and Bioaccumulation Regulations. Canada Gazette Part II March 29, 2000
8. Webster E, Mackay D, Wania F (1998) Evaluating environmental persistence. Environ Toxicol Chem 17:2148–2158
9. Wegmann F, Cavin L, MacLeod M, Scheringer M, Hungerbühler K (2009) The OECD software tool for screening chemicals for persistence and long-range transport potential. Environ Modell Softw 24(2):228–237
10. UNEP (2001) Final Act of the Conference of Plenipotentiaries on the Stockholm Convention on Persistent Organic Pollutants. In: United Nations Environment Program, Geneva, Switzerland, p 44
11. Gouin T, Mackay D, Webster E, Wania F (2000) Screening chemicals for persistence in the environment. Environ Sci Technol 34(5):881–884
12. Mackay D, McCarthy LS, MacLeod M (2001) On the validity of classifying chemicals for persistence, bioaccumulation, toxicity and potential for long-range transport. Environ Toxicol Chem 20(7):1491–1498
13. Scheringer M (2002) Persistence and Spatial Range of Environmental Chemicals. Wiley-VCH, Weinheim
14. Wania F (2003) Assessing the potential of persistent organic chemicals for long-range transport and accumulation in polar regions. Environ Sci Technol 37(7):1344–1351
15. Wania F, Mackay D (1995) A global distribution model for persistent organic-chemicals. Sci Total Environ 161: 211–232
16. Arnot JA, Mackay D, Webster E, Southwood JM (2006) Screening level risk assessment model for chemical fate and effects in the environment. Environ Sci Technol 40(7):2316–2323
17. Guglielmo F, Lammel G, Maier-Reimer E (2009) Global environmental cycling of γ-HCH and DDT in the 1980s – a study using a coupled atmosphere and ocean general circulation model. Chemosphere 76(11):1509–1517
18. Gobas FAPC, Morrison HA (2000) Bioconcentration and Biomagnification in the Aquatic Environment. In: Boethling RS, Mackay D (eds) Handbook of Property Estimation Methods for Chemicals: Environmental and Health Sciences. CRC Press, Boca Raton

19. McCarty LS, Mackay D (1993) Enhancing ecotoxicological modeling and assessment: body residues and modes of toxic action. Environ Sci Technol 27(9):1719–1728
20. Haritash AK, Kaushik CP (2009) Biodegradation aspects of polycyclic aromatic hydrocarbons (PAHs): a review. J Hazard Mater 169(1–3):1–15
21. Mastral AM, Callen MS (2000) A review on polycyclic aromatic hydrocarbon (PAH) emissions from energy generation. Environ Sci Technol 34(15):3051–3057
22. Wilson SC, Jones KC (1993) Bioremediation of soil contaminated with polynuclear aromatic hydrocarbons (PAHs): a review. Environ Pollut 81(3):229–249
23. Kannan K, Blankenship AL, Jones PD, Giesy JP (2000) Toxicity reference values for the toxic effects of polychlorinated biphenyls to aquatic mammals. Hum Ecol Risk Assess 6:181–201
24. Hornbuckle K, Robertson L (2010) Polychlorinated Biphenyls (PCBs): sources, exposures, toxicities. Environ Sci Technol 44(8):2749–2751
25. Fox GA, Weseloh DV, Kubiak TJ, Erdman TC (1991) Reproductive outcomes in colonial fish-eating birds – a biomarker for developmental toxicants in Great-Lakes food-chains .1. Historical and ecotoxicological perspectives. J Great Lakes Res 17(2):153–157
26. Hoffman DJ, Rice CP, Kubiak TJ (1996) PCBs and dioxins in birds. In: Beyer WN, Heinz GH, Redmon-Norwood AW (eds) Environmental Contaminants in Wildlife: Interpreting Tissue Concentrations. Lewis Publishers, Boca Raton, pp 165–207
27. Borga K, Fisk AT, Hargrave B, Hoekstra PF, Swackhamer D, Muir DCG (2005) Bioaccumulation factors for PCBs revisited. Environ Sci Technol 39(12):4523–4532
28. Aken BV, Correa PA, Schnoor JL (2009) Phytoremediation of polychlorinated biphenyls: new trends and promises. Environ Sci Technol 44(8):2767–2776
29. Van den Berg M, Birnbaum LS, Bosveld ATC, Brunstrom B, Cook P, Feeley M, Giesy JP, Hanberg A, Hasegawa R, Kennedy SW, Kubiak T, Larsen JC, van Leeuwen FXR, Liem AKD, Nolt C, Peterson RE, Poellinger L, Safe S, Schrenk D, Tillitt DE, Tysklind M, Younes M, Waern F, Zacharewski T (1998) Toxic equivalency factors (TEFs) for PCBs, PCDDs PCDFs for humans and wildlife. Environ Health Perspect 106(12):775–792
30. Domingo JL, Bocio A (2007) Levels of PCDD/PCDFs and PCBs in edible marine species and human intake: a literature review. Environ Int 33(3):397–405
31. Lohmann R, Jones KC (1998) Dioxins and furans in air and deposition – a review of levels, behavior and process. Sci Total Environ 219:53–81
32. Aberg A, MacLeod M, Wiberg K (2008) Physical-chemical property data for dibenzo-*p*-dioxin (DD), dibenzofuran (DF), and chlorinated DD/Fs: a critical review and recommended values. J Phys Chem Ref Data 37(4):1997–2008
33. Hites RA (2004) Polybrominated diphenyl ethers in the environment and in people: a meta-analysis of concentrations. Environ Sci Technol 38(4):945–956
34. Vonderheide AP, Mueller KE, Meija J, Welsh GL (2008) Polybrominated diphenyl ethers: causes for concern and knowledge gaps regarding environmental distribution, fate and toxicity. Sci Total Environ 400(1–3):425–436
35. Wang Y, Jiang G, Lam PKS, Li A (2007) Polybrominated diphenyl ethers in the East Asian environment: a critical review. Environ Int 33(7):963–973
36. de Wit CA, Herzke D, Vorkamp K (2010) Brominated flame retardants in the Arctic environment – trends and new candidates. Sci Total Environ 408(15):2885–2918
37. Staples CA, Peterson DR, Parkerton TF, Adams WJ (1997) The environmental fate of phthalate esters: a literature review. Chemosphere 35(4):667–749
38. Peijenburg WJGM, Struis J (2006) Occurrence of phthalate esters in the environment of the Netherlands. Ecotoxicol Environ Saf 63:204–215
39. Shiu W, Ma K-C, Varhanickova D, Mackay D (1994) Chlorophenols and alkylphenols: a review and correlation of environmentally relevant properties and fate in an evaluative environment. Chemosphere 29(6):1155–1224
40. Topping DC, Bernard LG, O'Donoghue JL, English JC (2007) Hydroquinone: acute and subchronic toxicity studies with emphasis on neurobehavioral and nephrotoxic effects. Food Chem Toxicol 45:70–78
41. Weber J, Halsall CJ, Muir D, Teixeira C, Small J, Solomon K, Hermanson M, Bidleman T (2010) Endosulfan, a global pesticide: a review of its fate in the environment and occurrence in the Arctic. Sci Total Environ 408: 2966–2984
42. Hoferkamp L, Hermanson MH, Muir DCG (2010) Current use pesticides in Arctic media; 2000–2007. Sci Total Environ 408(15):2985–2994
43. Li YF, Macdonald RW (2005) Sources and pathways of selected organochlorine pesticides to the Arctic and the effect of pathway divergence on trends in biota: a review. Sci Total Environ 342(1–3):87–106
44. Muir DCG, de Wit CA (2010) Trends of legacy and new persistent organic pollutants in the circumpolar arctic: overview, conclusions, and recommendations. Sci Total Environ 408:3044–3051
45. Graiver D, Farminer KW, Narayan R (2003) A review of the fate and effects of silicones in the environment. J Polym Environ 11(4):129–136
46. Hiroi T, Okada K, Imaoka S, Osada M, Funae Y (2006) Bisphenol A binds to protein disulfide isomerase and inhibits its enzymatic and hormone-binding activities. Endocrinology 147:2773–2780
47. Meeker JD, Calafat AM, Hauser R (2010) Urinary bisphenol A concentrations in relation to serum thyroid and reproductive hormone levels in men from an infertility clinic. Environ Sci Technol 44(4):1458–1463
48. Destaillats H, Maddalena RL, Singer BC, Hodgson AT, McKone TE (2008) Indoor pollutants emitted by office equipment: a review of reported data and information needs. Atmos Environ 42(7):1371–1388

49. Brown TN, Wania F (2008) Screening chemicals for the potential to be persistent organic pollutants: a case study of arctic contaminants. Environ Sci Technol 42(14): 5202–5209
50. Howard PH, Muir DCG (2010) Identifying new persistent and bioaccumulative organics among chemicals in commerce. Environ Sci Technol 44(7):2277–2285
51. Muir DCG, Howard PH (2006) Are there other persistent organic pollutants? A challenge for environmental chemists. Environ Sci Technol 40(23):7157–7166

Transgene Expression in Plants, Control of

Sylvie De Buck[1], Annelies De Paepe[2], Ann Depicker[3]
[1]Department of Plant Biotechnology and Genetics, Ghent University, Ghent, Belgium
[2]Department of Plant Systems Biology, Flanders Institute for Biotechnology VIB, Ghent, Belgium
[3]UGent Vakgroep Plantenbiotechnologie en Genetica, VIB Plant Systems Biology Department, Ghent University, Ghent, Belgium

Article Outline

Glossary
Definition of the Subject
Introduction
Generation of Transgenic Plants by *Agrobacterium*-Mediated Transformation or Direct Gene Transfer
Transgene Loci Can Be Either Simple or Complex
Regulatory Sequences Have a Major Impact on Transgene Expression and Expression Variability
The Influence of the Integration Position on Transgene Expression
Correlation Between T-DNA Locus Structure and Homology-Based Silencing
Control of Gene Expression by the Generation of Single-Copy Transformants
Use of Gene Silencing Mutants to Overcome Transgene Expression Variability
Future Directions
Acknowledgments
Bibliography

Glossary

CRE/*loxP* A site-specific recombination system in which the CRE recombinase catalyzes recombination between *loxP* sequences. A *loxP* sequence is 34 bp long and consists of two inverted repeats of 13 bp and one spacer region of 8 bp. The orientation of the *loxP* sequence is determined by the spacer region.

Inverted T-DNA repeat Repeat obtained from the integration of two T-DNA copies at one genetic locus, but with one T-DNA integrated in inverted orientation compared to the other.

Position effect Influence of the position of a gene in the genome upon its expression.

Posttranscriptional gene silencing (PTGS) Silencing mechanism leading to the sequence-specific degradation of target mRNAs and sequence-specific suppression of translation.

Single-copy transformant Transgenic plant harboring only one copy of the introduced DNA segment.

Transcriptional gene silencing (TGS) Silencing mechanism that targets homologous DNA sequences in the promoter, suppressing transcription and correlating with promoter sequence methylation.

Transfer DNA (T-DNA) The DNA fragment that is delineated by the right and left border repeats and is transferred from *Agrobacterium* to the plant cell by the type-IV secretion system.

Transgene expression variability Variability that is higher in a population of transformants than expected based on gene dosage effects.

Transgenic plant Plant harboring one or more external DNA segments that had been introduced and stabilized by integration into the plant genome. The foreign DNA is transferred to the plant cell via *Agrobacterium*-mediated transformation or direct gene transfer.

Definition of the Subject

To define the subject in relation to the title, we would like to emphasize that most of the results and conclusions described below were obtained in the model plants *Arabidopsis thaliana* and *Nicotiana tabacum* after *Agrobacterium*-mediated transformation, and in

a limited number of crops, such as wheat, rice, and soybean, after direct gene transfer. Additionally, most of the transgenes described below are transcriptional fusions with the 35S promoter from the cauliflower mosaic virus. Indeed, to obtain transgenic plants with high and constitutive expression of a transgene, the 35S promoter is commonly used. This 35S promoter is very powerful, because it generally leads to constitutively high transcript and protein levels of the transgene in most dicot plants and is not greatly influenced by environmental conditions or tissue types. However, over the years, it became clear that 35S-driven transgene expression is very variable in the different transformants of a transgenic plant population with the same construct. For most analyzed overexpression constructs containing this 35S promoter, more than a 100-fold difference in protein accumulation levels has been observed. Approximately 20% of the transformants have high recombinant protein accumulation levels, but approximately 80% display an intermediate or low and unstable transgene expression. Additionally, high-expression transformants often segregate progeny plants with low recombinant protein accumulation levels. Thus, it is imperative that for scientific analysis and applications, the variability of 35S-driven transgenes is known in different transformants and generations. In this contribution, the possible causes of variation in transgene expression in a population of transgenic plants are discussed and several approaches to diminish the variability are reviewed.

Introduction

From the mid-1980s on, transgenic plants were generated by adding one or more genes to a plant's genome. Transformation was usually achieved with gold-particle bombardment or through the gene transfer process via *Agrobacterium tumefaciens*, a soil bacterium carrying an engineered T-DNA vector. The inserted gene sequence, known as the transgene, can be derived from any living prokaryotic or eukaryotic organism. Transgenic plants were originally engineered to address specific scientific questions and to investigate the plant biology in general. However, the ability to create transgenic plants also opened the way to manipulate crop plants for better characteristics, such as increased yield, enhanced quality, pest or disease resistance, superior tolerance to heat, cold, and drought, and nutritional improvement. In addition, transformation of plants allows molecular farming of many limiting components, such as proteins, metabolites, fatty acids, and bioenergy precursors.

To generate transgenic plants, transformation methods had to be explored and ameliorated. Furthermore, the vectors and expression cassettes for controlled integration and expression of the introduced transgenes had to be worked out. Once the *Agrobacterium*-based system for T-DNA transfer had been unraveled, the simple view was that a particular T-DNA sequence could be constructed to be integrated as a single copy into the plant genome. However, it turned out that transformants quite often integrate two to ten T-DNA copies at one locus or dispersed over several loci [1]. Moreover, the transferred DNA is integrated randomly and, thus, every transformant containing the same transgene differs regarding the integration site and the transgene copy number [2]. Concerning transgene expression, in principle, it is very straightforward to combine particular gene-controlling elements with a coding sequence of interest to obtain a predictable level of transgene expression. The most frequently used promoter elements are the promoter of the nopaline synthase gene (pNOS), driving weak and constitutive expression of the downstream transcribed sequence, and the promoter of the cauliflower virus 35S transcript (p35S), driving in general at least 20-fold higher expression levels. Whereas the majority of transformants with transgenes controlled by the pNOS promoter display the same mRNA level, independent transgenic lines generated with a p35S-controlled transgene construct show variable transgene expression with more than 100-fold difference in recombinant protein levels. In the latter case, frequently the recombinant protein accumulation levels in the different transformants are distributed bimodally [3]. Low p35S transgene expression occurs regularly in transgenic lines with multiple T-DNA copies, particularly when they are integrated into inverted orientation. As a consequence, the transgenes are transcribed convergently [4]. However, also single T-DNA copies can result in low or even no transgene expression [5]. Originally, the mean of recombinant protein accumulation levels in different transformants was considered to represent the expression strength of a particular

transgene construct. Afterward, it was realized that the class of transformants with high transgene expression correlated better with the transgene expression capacity [6], implying that all transformants with intermediate and low transgene expression have controlling mechanisms that result in transgene suppression or transgene silencing.

A first and visually dramatic example of transgene silencing was found in plants that overexpressed gene constructs coding for pigment production in wild-type petunia (*Petunia hybrida*) with purple flowers [7, 8]. Contrary to their expectations, the flowers of the transgenic petunia exhibited reduced and variable instead of increased pigmentation. As both the expression of endogenes and transgenes were suppressed, this phenomenon was called cosuppression [7, 8]. Later on, the transgene silencing mechanisms were divided into three groups [9]. One group harbors the transgene silencing events based on position effects and heterochromatization. As transgenes integrate randomly, different transformants contain the transgene at a different chromosomal position and nearby located chromatin-controlling elements, enhancers and silencers, are expected to influence the activity of the integrated gene. The other two groups of silencing mechanisms operate via homology between the silencer sequences and the target silenced genes, do not depend on position, and exert their effects *in trans* [9, 10]. Transcriptional silencing (TGS) refers to the silencing process that suppresses transcription of the silenced genes based on homology in the silencer locus-containing promoter region. TGS functions at the level of prevention of transcription initiation of the silenced genes; is often accompanied with concomitant DNA methylation, altered histone modifications, and heterochromatin formation; and is stably inherited through meiosis and mitosis [11]. In contrast, post-transcriptional gene silencing (PTGS) needs homology in the transcribed region, results in specific transcript degradation and/or specific repression of translational initiation, and resets through sexual propagation [10, 12].

Here, different parameters that influence transgene expression in plants are described: (1) the transformation process, which results in plants with transgene loci that can be either simple or complex; (2) the different regulatory sequences used in the transgene expression construct; (3) the position of the integrated transgene into the plant genome; and (4) the correlation between repeat structures and transgene silencing. Several approaches to minimize the transgene expression variability are discussed: (1) the resolution of complex integration loci by the CRE/*loxP* recombination process, (2) site-specific or site-directed integration, and (3) the use of gene silencing mutants to create a population of transgenic plants with high and stable transgene expression.

Generation of Transgenic Plants by *Agrobacterium*-Mediated Transformation or Direct Gene Transfer

Agrobacterium-mediated transformation is the most widely used method to generate transgenic plants [13, 14], although direct transformation methods are still very important for certain crop plants (see below). During *Agrobacterium* transformation, the transferred DNA (T-DNA), delineated by the right border (RB) and left border (LB) repeats, is integrated into the plant genome by illegitimate recombination. Overall, approximately one half of the transformants contains only one T-DNA copy and the other half multiple T-DNAs (two to ten), integrated at one or several independent loci [2, 15].

The T-DNA integrates at random in any chromosome [2] (Fig. 1) and is as efficient in all five chromosomes of *Arabidopsis thaliana* as in intergenic and intragenic sequences and in exons and introns (Fig. 1) [16, 17]. With promoterless selectable markers and consecutive selection on those markers, many transformants could be recovered, indicating that T-DNAs frequently integrate in transcriptionally active regions [18, 19], but in the absence of transcriptional activation selection, many transformants integrated the T-DNA between genes and in repetitive DNA. Under nonselective conditions, silent T-DNA insertions were found in heterochromatic regions, centromeres, telomeres, and rDNA repeats [20, 21]. T-DNA integration is accompanied with small deletions of the plant target DNA and/or T-DNA ends. Very often, microhomology of 2–10 bp is observed between the plant pre-insertion site and the T-DNA ends, suggesting that T-DNA integration occurs via the nonhomology-dependent double-stranded break repair [2, 15, 22].

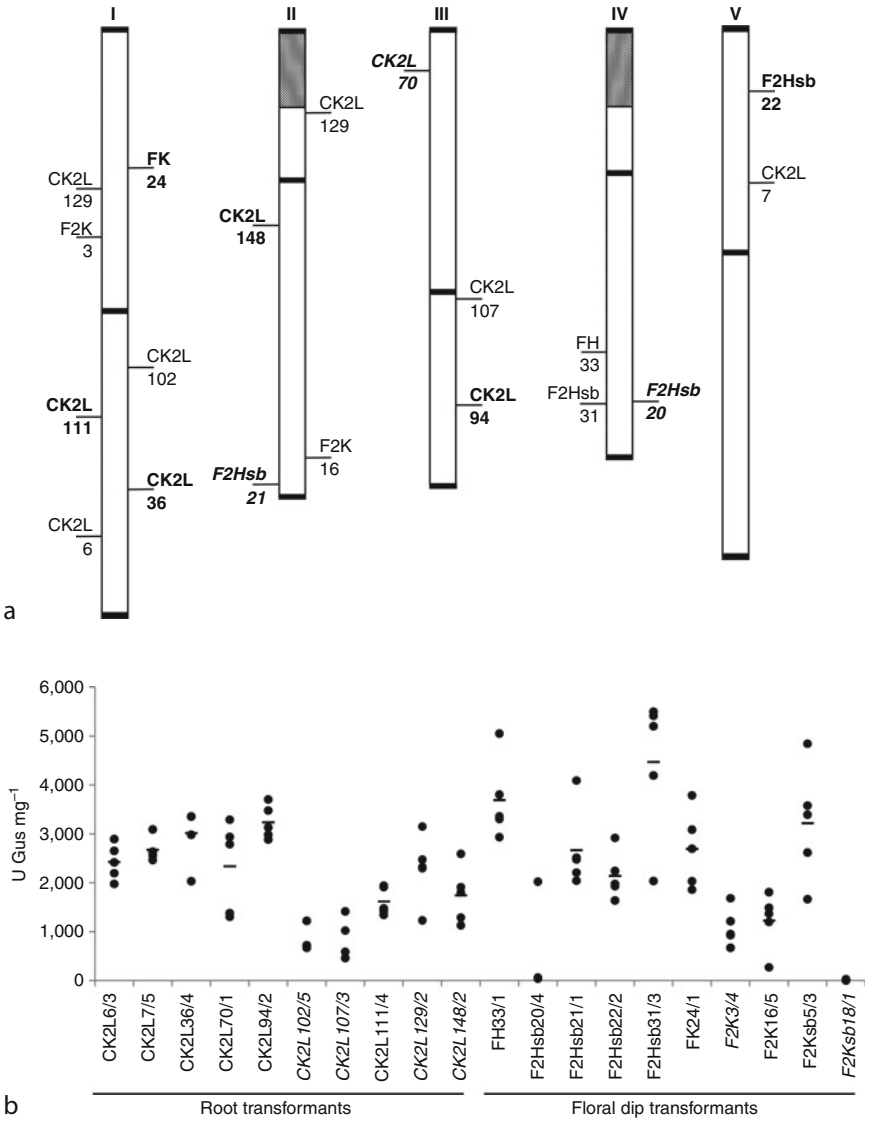

Transgene Expression in Plants, Control of. Figure 1

Random integration of single-copy T-DNAs into the *Arabidopsis* genome and the similar GUS activity levels yielded by single-copy 35S-*GUS* transgenes in the different transformants (Adapted from [17]). (**a**) Distribution of 18 single-copy T-DNA transformants on the five chromosomes of the *Arabidopsis* genome. In nine transformants, the T-DNA is integrated into an intergenic region and nine in a transcribed annotated gene (indicated in *bold*). Of these nine intragenic inserted T-DNAs, six were integrated into an exon and three into an intron (indicated in *italics*). Centromeres and telomeres are indicated in *vertical black boxes* and rDNA repeats in *gray boxes*. For transformant CK2L129, the LB and RB regions were fused to sequences of chromosomes 1 and 2. (**b**) GUS activity analysis in the T2 generation of 20 different single-copy T-DNA transformants. GUS activity was measured in the leaves of five 6-week-old seedlings per transformant (represented as a *dot*). All transformants were homozygous for the T-DNA insertion, except for the transformants indicated in *italics*. The average GUS activity level in the five seedlings of the homozygous transformants is marked by a *line*. The intra-transformant variability in GUS activity was as high as the inter-transformant variability, except for two transformants without detectable GUS activity. GUS activity levels are given as units GUS mg^{-1} of total soluble protein. For transformants F2Ksb5 and F2Ksb18, the integration position into the genome could not be determined (see **a**)

In theory, only the T-DNA, delineated by the LB and RB, is transferred to the plant cell, but in many plants, vector backbone sequences are transferred and integrated into the genome as well [23–26]. Two mechanisms might account for this vector backbone transfer. First, the LB repeat could mistakenly be recognized as initiation site for T-strand production and, as such, result in the transfer of vector backbone sequences. Second, the consequence of inefficient recognition of the LB repeat might be read-through from the T-DNA into the vector sequences [23, 27]. Both mechanisms can be distinguished by analyzing whether or not the LB T-DNA sequences are directly linked to the vector sequences. The vector backbone transfer and integration is seemingly not influenced by the plant species, the explant type used for transformation, the T-DNA vector replicon type, or the selection [25]. Molecular DNA blot and polymerase chain reaction analyses revealed that the vector backbone sequences were mostly linked to both the LB and RB T-DNAs. In fact, the complete vector backbone sequence was integrated between two in tandem oriented T-DNAs, emphasizing the importance of the second mechanism in which the integration of complete vector backbone sequences results from a conjugative transfer initiated at the RB, followed by copying of the T-DNA, the vector, and again a T-DNA from a circular template due to read-through of consecutively the LB and RB [25]. Furthermore, the results demonstrated that neither the RB nor the LB was efficiently recognized as termination and initiation sites, respectively [25]. Additional evidence that the surrounding regions of the border repeats are important for the recognition of the repeat as initiation or termination site was obtained from hybrid border regions. In the absence of the surrounding border regions, the LB repeat was not recognized as T-DNA termination site; addition of the natural LB inner region and occurrence of both the octopine and nopaline LB regions with their repeats, improved the correct recognition of the LB repeat when compared to an LB with only the LB outer region [26].

A number of agronomically important plant species are still recalcitrant for *Agrobacterium*-mediated transformation and are, therefore, transformed with direct gene transfer methods, such as particle bombardment or biolistics, electroporation, and polyethylene glycol transformation [28]. A disadvantage of these techniques is that transformants tend to have multiple transgene copies integrated as a concatemeric array at one locus, and contain inverted repeats [29–33]. However, several approaches have been described to circumvent this problem (see below).

Transgene Loci Can Be Either Simple or Complex

Upon *Agrobacterium*-mediated transformation, a significant number of transformants contain a single-copy T-DNA insert, but, dependent on the transformation method used, a high percentage of transformants contain multiple T-DNAs integrated into the plant host genome. These multiple T-DNA copies are mostly clustered in one genetic locus, but they can also be present in two or more loci. Multiple T-DNAs integrated at one genetic locus are organized as direct and/or inverted repeats of the T-DNA segment. Complex T-DNA loci were found in many plant species, such as *Arabidopsis*, tobacco (*Nicotiana tabacum*), petunia, and potato (*Solanum tuberosum*) [34–38]. As direct and inverted T-DNA repeats were not found in the bacteria, they are believed to be formed in the plant cell prior to or during the T-DNA integration [34, 35, 39, 40].

Two models have been proposed for the formation of multicopy T-DNA loci upon *Agrobacterium*-mediated transformation: the replication and the ligation models [38]. In the replication model, the repeats originate from a single T-DNA copy that is replicated after introduction in the plant cell and before or during integration into the genome. This hypothesis is favored because all T-DNAs involved in repeat structures had analogous breakpoints in a restriction analysis and because three identical T-DNA copies were observed after transformation with a library of T-DNAs containing different promoters [38, 41, 42]. However, cotransformation experiments with different T-DNAs originating from different agrobacteria gave, with a similar frequency, rise to T-DNA loci with different T-DNAs in direct or inverted orientation [1, 34, 35, 43–46]. As these T-DNA structures cannot be formed by replication, but only by ligation of the cotransformed T-DNA copies before or during integration [34, 35], the ligation model postulates that repeats originate from extrachromosomal ligation of two or more individual T-DNAs prior to or during integration into the genome [34] and even that repeat structures are formed by the cointegration of

several T-strand intermediates in one target site rather than by ligation of T-strands [39]. In any case, T-DNA inverted repeats about the RB, an integration structure that is frequently observed upon *Agrobacterium*-mediated transformation, can only be formed after duplication of the transferred single-stranded T-DNAs. Sequence analysis of T-DNA junctions revealed that, during the formation of T-DNA repeat structures, end-to-end ligation of double-stranded T-DNAs occurs especially between right T-DNA ends, whereas recombination based on microhomology regions and insertions of filler DNA was more frequent at LB junctions [22, 35]. None of the sequenced T-DNA/T-DNA junctions contained plant DNA, suggesting that T-DNA recombination and ligation occurred in the majority of cases before integration [35].

Analysis of which parameter determined the structure and complexity of the transgene locus indicated a possible correlation with either the used *Agrobacterium* strain, the titer, or the physiology of the bacterial inocula, bacterial vectors, plant species, or ecotype, but overall no clear picture was obtained [1, 34, 38, 44, 47, 48]. Single-copy T-DNA insertions were found predominantly upon *Arabidopsis* root transformation, whereas multiple insertions, especially organized in T-DNA repeat structures over the RB occurred in transformants generated by leaf disc transformation [48]. However, this was not found in root and leaf disc transformants in an independent experiment (M. De Neve and A. Depicker, unpublished results), indicating that other parameters had to be involved. Nevertheless, a detailed study revealed that the structure of the T-DNA integration locus is especially determined by the transformed target cell [1, 48]. Whereas 20 years ago, *Agrobacterium*-mediated transformation of *Arabidopsis* was achieved mainly by in vitro tissue explant methods, such as root transformation [49], nowadays floral dip is commonly used [50], but the obtained T-DNA copy number in transformants obtained after both transformation methods varies much. To analyze whether this difference was due to cotransformation frequencies or to replication in the plant cell, several floral dip and root transformations were done with mixtures of *Agrobacterium* strains, each carrying one or two different T-DNA vectors, allowing to trace back the origin of complex T-DNA loci [1]. Although the cotransformation frequencies of T-DNAs originating from different agrobacteria after floral dip and root transformation were comparable, and the frequencies of T-DNA originating from one bacterium only slightly higher than those after floral dip transformation, the T-DNA copy numbers in the transformants differed completely. Upon floral dip transformation, on average T-DNA copies were integrated at one genetic locus versus one to three after root transformation [1]. The cotransformation frequencies might explain the T-DNA copy number in most root transformants, but not in floral dip transformants. Therefore, it was postulated that T-DNA replication of a single T-strand occurs in the plant cell before or during T-DNA integration and that its frequency is much higher upon floral dip than upon root transformation [1]. Because the same *Agrobacterium* strains had been used in both transformation methods, not the bacterium but the type of target cell determined the complexity of the T-DNA pattern [1].

In general, transformants obtained after direct gene transfer contain more transgene copies than after *Agrobacterium*-mediated transformation [30–32]. In maize (*Zea mays*), comparison of transgene copy numbers and RNA expression levels upon transformation via direct gene transfer and *Agrobacterium*-mediated transformation revealed that more than 90% of the transformants obtained after *Agrobacterium*-mediated transformation harbored fewer than three T-DNA copies, while most of the transformants obtained after particle bombardment contained more than three copies [32], of which some of the transformants contained as many as 100 copies of the transgene [32]. Another observation was that the transformants obtained after *Agrobacterium*-mediated transformation displayed a higher transgene expression than after particle bombardment. Besides the expected positive correlation between transgene copy number and transgene expression, frequently a negative correlation between gene dosage and transgene expression was observed (see below) [51].

Recent research revealed that more single-copy integrants could be obtained by particle bombardment when a limited quantity of DNA was used for bombardment [52, 53]. A decrease in DNA from 1.5 to 2.5 ng per shot resulted in an increase of single-copy transformants from 30% to 70% [52, 53]. The 10% reduction in transformation efficiency was more than

compensated by the more efficient screening for single-copy transformants [53]. Additionally, complex integration patterns could also be avoided when cassette DNA, harboring a promoter, a coding region and a 3′ end region, instead of whole plasmids were used for bombardment [52, 54–56].

Regulatory Sequences Have a Major Impact on Transgene Expression and Expression Variability

To obtain transformants with high and stable transgene expression, the construct should be designed carefully because several sequences might have a great impact on the transgene expression and expression variability. Especially, the selected promoter that drives the transgene expression will determine the accumulation levels of the transgene transcript and, indirectly, of the transgene-encoded protein. Since the beginning of chimeric gene constructions, plant scientists predominantly chose the 35S promoter of the cauliflower mosaic virus as a strong and constitutive promoter to overexpress a coding sequence of interest [57] and for the promoters of the nopaline (pNOS) and octopine (pOCS) synthase-encoding genes, as weak promoters, for instance to drive the selectable marker genes in dicots.

The strength of the 35S promoter increases when upstream activator sequences are added [58], but as a consequence, single-copy transgenes driven by a 35S promoter with two upstream activator regions are more prone to gene silencing [59–61]. In general, silencing frequency correlates positively with the promoter strength [61–64]. Indeed, silencing did not occur frequently when a weak pNOS promoter was used [62], whereas the 35S promoter is very prone to transgene silencing, most probably because the high expression leads to transgene RNA accumulation levels above a certain threshold that triggers RNA degradation [65]. Strikingly, promoters do not only influence the levels, but also the variability of expression in a population of independently transformed plants with the same transgene [66]. Transformation of *Arabidopsis* plants with a p35S-*β-glucuronidase* (*GUS*) construct resulted in a bimodal expression pattern, with more than 80% of the primary transformants showing a very low and less than 20% a high GUS accumulation [3, 66]. The mannopine synthase promoter (pMAS) yielded gene expression levels that were only slightly lower than those of the 35S promoter, but the variation in transgene expression was at least eightfold lower [66]. The bimodal character of the p35S promoter versus the normal distribution of the pMAS-driven gene expression suggests that silencing phenomena occur less frequently in plants transformed with pMAS than with p35S.

Not only the promoter, but also the codon usage might play a role in determining the transcript stability and/or translation efficiency. For *Arabidopsis*, highly expressed endogenous genes seem to contain a C at the third codon position, whereas genes with low expression levels have predominantly a T in that position [67]. By adapting codon usage in the green fluorescent protein (GFP)-encoding gene toward a higher proportion of codons with a C or a G in the third position, more highly *GFP*-expressing plants were generated [68]. Additionally, the nature of the coding sequence and the sequence composition seem to be important parameters in determining the transcript accumulation and/or threshold above which silencing is initiated [62, 69]. The transcript levels of the three reporter genes *GUS*, *GFP*, and streptomycin phosphotransferase (*SPT*) controlled by the same p35S, varied, reflecting the expected dissimilar transcript stability and turnover for different sequences. Furthermore, other effects also determined the transcript accumulation because the steady-state transgene transcript levels in transformants containing two copies of the *GUS* transgene were lower than in those carrying only one copy, while in transformants with two copies of the *SPT* or the *GFP* genes, the levels were higher than those with only one of the respective genes. The transcript length and GC content of the coding sequences were unlikely to be primary determinants for the gene-specific threshold for the silencing trigger [69]. Indeed, although the *GFP* and *SPT* transgenes have almost identical transcript lengths and similar GC content, silencing was activated at a different copy number. Silencing of *GUS* expression was already observed in plants with three P35S-*GUS* copies, while *GFP* and *SPT* expression were only reduced in plants carrying five or more 35S-*GFP* and nine or more 35S-*SPT* copies.

In tobacco plants, different 5′ leader sequences were modulated by P35S-driven expression [6].

A 31-nucleotide random leader stimulated translation 20- and 100-fold compared to the nine- and four-nucleotide synthetic leaders, respectively. However, the 30-nucleotide satellite tobacco necrosis virus leader and both the 79-nucleotide tobacco mosaic virus (TMV) and the plant chlorophyll *a/b*-binding protein (66-Cab22L) leaders were approximately two- to threefold and fivefold stronger than this 31-nucleotide random leader, respectively [6]. On the contrary, the 5′-untranslated regions (5′ UTRs) of MAS and TMV did not influence the transgene expression variability [66]. Similarly, also four terminators (tMAS, tNOS, tG7, and tOCS) were analyzed for their effect on transgene expression, but none affected levels and variability [66]. That especially certain combinations of different elements can lead to high and stable transgene expression was clearly demonstrated [70]. The combination of the strong *ß-phaseolin* promoter, with the 5′ and 3′ regulatory sequences of the *arceline 5-I* gene and efficient endoplasmic reticulum-targeting signals boosted the expression of an antibody fragment to 36% of the total soluble protein in *Arabidopsis* seeds. Furthermore, the variation in transgene expression was very low [70].

A significantly increased level of transgene expression can be observed for particular intron-containing transgenes when compared to their respective intronless constructs. This phenomenon, designated "intron-mediated enhancement," has been demonstrated both in monocots and dicots [71–74]. The ability of an intron to enhance transgene expression depends on the sequence and position of the intron within the transgene [72, 75]. Generally, stimulation of mRNA accumulation decreases with increasing distance of the intron from the promoter and its effect is greatly diminished or entirely lost when the intron is placed in the 3′ UTR [71, 75]. The mechanism of intron-mediated enhancement is largely unknown, but has been postulated to be due to an increased accumulation of mRNA, enhanced transcript stability, and/or an enhanced translation [71, 72, 74, 76].

The effect of matrix attachment regions (MARs) on transgene expression levels and stability is still unclear and contradictory results have been obtained [66, 77–79]. In some studies, MARs significantly increased the average protein accumulation levels in transgenic plants and reduced the transgene expression variability [80–83]. For instance, the chicken lysozyme MAR (chiMAR) reduced the expression variability by seven- to eightfold in transgenic potato [83], whereas this chiMAR had no influence on the transgene expression levels and variability in *Arabidopsis* transformants, unless the gene silencing mutants were used as genetic background for transformation [3, 66, 78, 84]. The lack of positive effect of the MARs was caused neither by the transformation method, nor by the plant species used for transformation, because this chiMAR did not influence the *Arabidopsis* transformants obtained after root or floral dip transformation and the tobacco transformants [78]. Moreover, a tobacco-derived MAR sequence had no positive effect on transgene expression in the *Arabidopsis* wild-type Columbia-0 transformants [78].

The Influence of the Integration Position on Transgene Expression

Although the presence of multiple transgene copies, especially in inverted orientation, is the major trigger to induce transgene silencing (see below), also single-copy plants can show variation in transgene expression and undergo transgene silencing [5, 17, 60, 85–88]. Two general explanations for the inactivation of single-copy transgenes have been proposed that are not mutually exclusive: recognition of a transgene as foreign DNA and subsequent TGS and neighborhood of spreading heterochromatin domains. In the first explanation for position effects, transgenes might be recognized as nonself sequences, and especially the difference in GC content of the transgene versus the flanking sequences might induce chromatin changes and epigenetic variation [12, 89]. Indeed, a single copy of the GC-rich *A1* gene from maize became specifically methylated in transgenic petunia (*Petunia hybrida*), while the homolog of gerbera (*Gerbera hybrida*), with a GC content similar to that of petunia, remained unmethylated [89, 90]. In the second explanation, position effects result from heterochromatization of the transgene integrated close to heterochromatin domains, which is similar to the position effect variegation, extensively studied in fruit fly (*Drosophila melanogaster*). Thus, also in plants, the chromosomal position of a transgene is expected to cause variability in transgene expression [9, 91]. In petunia, single-copy transgenes were strongly silenced

when they were integrated into a highly repetitive region [5]. Likewise, two single-copy transformants were identified with unstable transgene expression that were integrated into intercalary and paracentromeric locations [85], while the two stably expressing loci were integrated into the vicinity of telomeres and flanked at least on one side by plant DNA with AT-rich regions. However, the number of examined cases is limited and T-DNA insertion into heterochromatic regions has been demonstrated not to be necessarily associated with transgene silencing [16].

To determine whether the integration position had a major effect on transgene expression variability, a large transformant population had been screened for single-copy T-DNA transformants and the transgene accumulation levels were compared [17]. Twenty single-copy transformants were selected based on antibiotic resistance marker expression and in all of them the T-DNA integration was characterized at the sequence level in the *Arabidopsis* genome (Fig. 1a). In 18 of the 20 transformants, the p35S-driven *GUS* expression was high and stable in two subsequent generations. Furthermore, the GUS activity levels in these 18 different transformants could be considered as similar, because the intra-transformant variability was as high as the inter-transformant variability (Fig. 1b). Integration into an intergenic or genic region and into an exon or intron did not result in differential transgene expression (Fig. 1) and, additionally, integration into a gene in sense or antisense orientation had no influence on the transgene expression, indicating that overlapping transcription from the endogene and transgene did not induce transgene silencing in *Arabidopsis* [17].

Another hypothesis was that transgene expression might be reduced by the absence of MAR sequences near the T-DNA integration site or by the presence of neighboring highly methylated sequences [92, 93]. However, no general correlation with these factors was observed [17]. There has also been some debate on the influence of vector backbone sequences, cointegrated into the plant genome on transgene expression. In a first report based on the observation that two unstably expressed loci harbored binary vector sequences directly contiguous to the right T-DNA border, whereas two stably expressed loci contained no vector backbone sequences, vector sequences were postulated to trigger TGS [85]. Later, several studies showed that the integration of vector sequences, even with a GC content strongly diverged from that of the plant genome, had no negative influence on transgene expression [17, 94, 95].

In general, one can conclude that in *Arabidopsis*, the integration position of single-copy T-DNAs does not strongly influence transgene expression [17, 62, 94], but one should take care not to extrapolate this finding too far. The *Arabidopsis* genome is small (125 Mb) and has a low amount of heterochromatic DNA, while the genome of *Drosophila*, in which position effect variegation is often observed, is comparable in size, but consists for one third of centric heterochromatin [96]. Also, one should be aware that all the above-described observations were based on transformants that were selected on the expression of one selectable marker on the same T-DNA, implying that silenced heterochromatic T-DNA insertions were not recovered. Indeed, an increased number of T-DNA integrations into heterochromatic regions were found without selection in *Arabidopsis* [20, 21]. Apparently, the kanamycin selection had failed to identify approximately 30% of all integration events, because the expression of the selectable marker was absent or very low [21]. Analysis revealed that not PTGS, but TGS, caused this discrepancy in transformation efficiency. Furthermore, the integration sites of the lines with silenced transgenes mapped to heterochromatic regions, including telomeres, centromeres, and rDNA repeats [20, 21], which are regions that are significantly underrepresented in T-DNA integration studies with transformants identified by selection [21].

Nevertheless, the holy grail of plant biotechnology is to integrate the transgenes into the plant genome via homologous recombination. Indeed, in contrast to yeast and the moss *Physcomitrella patens*, the frequency of transgene integration via homologous integration is extremely low. When compared to random integration, targeted integration of a transgene into the homologous sequence of the plant genome occurs in the range from 0.01% to 0.1% [97, 98]. Several approaches, with variable success, have already been applied to detect gene targeting events among the random integration events: (1) application of gene-specific selection or screening for the target genes; (2) use of positive–negative selection and, hence, reduction of the transformants with randomly integrated transgenes; and (3) overexpression of

genes involved in homologous recombination in yeast, such as the *RAD54* gene [99–101]. Additionally, induction of double-stranded breaks in the genome has been reported to result in an increased targeted integration frequency [102, 103]. Nowadays, these double-stranded breaks are produced by zinc finger nucleases (ZFNs) [104–106]. These ZFNs are synthetic restriction enzymes that can be specifically designed to cleave virtually any long stretch of double-stranded DNA sequence [107]. A defective *GUS:NPTII* reporter gene, carrying a recognition site for ZFN and integrated at various chromosomal sites in ten different tobacco lines, was restored via homologous recombination in 10% of the transformed protoplasts, regardless of the chromosomal position of the reporter gene [105]. Approximately 20% of the *GUS:NPTII* reporter gene was repaired solely with homologous recombination, but the other events still contained additional DNA insertions and deletions [105]. Moreover, ZFNs are probably a promising tool to efficiently achieve targeted integration into plants. Once this procedure is optimized, plants with high, stable, and predictable accumulation levels of important heterologous proteins might be obtained with an increased frequency.

Correlation Between T-DNA Locus Structure and Homology-Based Silencing

Based on the gene dosage rationale, screening for transgenic plants with multiple transgene copies might be predicted to result in plants with high transgene expression. A direct correlation between transgene copy number and expression level has indeed been reported [51, 62]. However, also the inverse correlation is observed with p35S-driven transgenes inserted as convergently transcribed inverted repeats: the reproduction of the expression of the inverted repeat transgene copies is much lower than that of a single-copy transgene [51, 108].

Increased Transgene Dosage Can Result in PTGS

Below a certain number of identical p35S-driven transgenes, gene copy number and expression correlated positively [62]. Transgene expression seemed stable and high over all generations analyzed and a comparable expression level was obtained for all independent lines harboring the same copy number of a certain transgene. However, once above a certain copy number, gene silencing occurred, implying that silencing was triggered by threshold concentrations of either transgene transcript or another product of transgene expression (Fig. 2) [62]. In many reports, the correlation between high transgene copy number and transgene expression was negative: the higher the copy number, the lower the expression level per gene copy [59, 61, 109]. Not the copy number per se, but especially the arrangement of the transgene copies in one genetic locus, seemed responsible for the low transgene expression. Indeed, as described above, multiple T-DNAs at one genetic locus are frequently integrated as a direct or an inverted repeat (Fig. 2) [1, 34, 35].

Several other examples show a correlation between transgene silencing and the presence of tandem repeats, which might be linked to exceeding the mRNA threshold level above which PTGS is initiated (Fig. 2) [59, 110, 111]. The same is true for transgene loci that are not silenced under hemizygous, but become silenced under homozygous conditions, as, for instance, in tobacco and *Arabidopsis* [60, 87, 112, 113].

Convergent Transcription from Inverted T-DNA Repeat Structures Is a Strong Trigger for PTGS

Invariably, convergently transcribed 35S-driven transgenes from invertedly repeated T-DNAs are posttranscriptionally silenced to a level that is only 1% or less of the single-copy transgene (Fig. 2) [4, 51, 59, 61, 108, 113–118]. Additionally, invertedly repeated transgenes can very efficiently silence *in trans* homologous sequences located elsewhere in the genome [51, 108, 117, 119]. This direct correlation between invertedly repeated trangenes and transgene silencing has been demonstrated experimentally by the deletion of one of the transgenes from the inverted repeat that released transgene silencing and a 100-fold increase in expression [108]. Indeed, in two parental lines, harboring two invertedly repeated 35S-driven *GUS* genes, the GUS activity was low and both the coding sequences and the center of the inverted repeat were densely methylated. Homologous transgenes at other chromosomal positions were silenced *in trans* by the inverted repeat silencer locus [108, 118]. Removal of one of the *GUS* copies from this silencer locus by the CRE recombinase resulted in all cases in constitutively

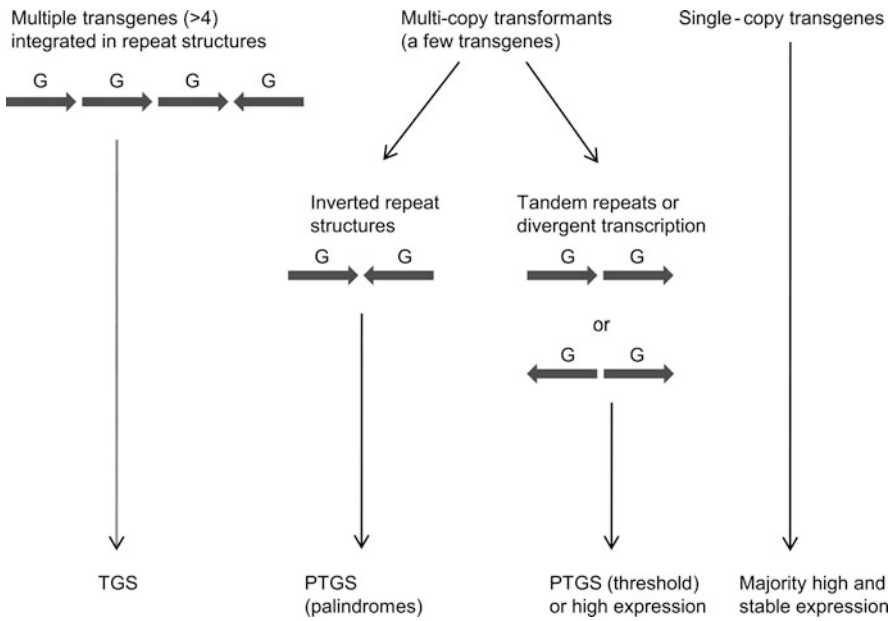

Transgene Expression in Plants, Control of. Figure 2
Relation between locus structure and the expression of a p35S-driven transgene. Upon transformation, both single-copy and multicopy transformants are generated. Both single-copy plants and plants with multiple T-DNAs arranged in tandem repeat or in repeats giving rise to transgene divergent transcription generally display high and stable transgene expression. Plants carrying convergently transcribed transgenes show low transgene expression as a result of PTGS, whereas plants harboring multiple transgenes integrated into a concatemeric array frequently result in TGS. Abbreviations: *G* gene, *TGS* transcriptional gene silencing, *PTGS* posttranscriptional gene silencing

high *GUS* expression, a significant decrease in methylation and lack of *in trans* silencing capacity [108, 118]. Strikingly, the spacer region in-between the two invertedly repeated transgenes seemed to determine the efficiency of transgene silencing. The presence of an 826-bp non-repetitive spacer region in-between the invertedly repeated transgenes strongly decreased the degree and the stability of silencing [108], but in another system, inverted repeats interrupted by a non-palindromic spacer region varying from 500 bp to 1,022 bp still gave efficient silencing [120].

Multiple T-DNA Copies at One Locus Tend to Become Transcriptionally Silenced After Several Generations

Multiple T-DNA repeats not only induce PTGS, but also TGS. Induction of TGS occurs especially when a concatemeric array or inverted repeats of transgenes are formed and when different genes are regulated by the same promoter [119, 121–124]. The 271 locus, consisting of multiple T-DNAs with an antisense nitrite reductase driven by the 35S promoter, is transcriptionally silenced and is also able to very efficiently *in trans* silence another single-copy p35S-driven transgene [119]. Transgene expression is seemingly less stable over sexually than over vegetatively propagated generations [125]. Indeed, expression of the sulfur-rich sunflower (*Helianthus annuus*) seed albumin (*SSA*) and the phosphinothricin (*BAR*) genes, all driven by p35S, progressively decreased in transgenic clover (*Trifolium subterraneum*) [122]. The expression of both genes was stable until the T3 generation, but in the T7 generation, all plants were completely susceptible to the herbicide and the mean level of the SSA protein was much lower than those observed in the T3 generation. This progressive decrease in expression correlated with the reduced transcription level of both genes and strong CpG methylation in the promoter [122]. Not only the strong 35S promoter, but also the weak pNOS can

trigger TGS. The H2 locus, a locus harboring six copies of pNOS, all transcriptionally silenced loci, strongly methylated the promoter regions [121]. Also, transcription of an inverted repeat of pNOS could trigger TGS and methylation of pNOS *in trans*, and this progressively decreased through generations [124].

How to Prevent Transgene Silencing?

To prevent transgene silencing, single-copy transgene inserts should be screened (see below) and inclusion of identical sequences in different transgene constructs should be avoided [126]. Even a homology of 90 bp in the promoter region can be sufficient to trigger TGS [119]. Additionally, the use of multiple identical 3′ end regions can result in low transgene expression levels. A homology of 239 nucleotides in the 3′ UTR is sufficient to be recognized efficiently by the homology-based RNA degradation machinery [117] and also a homology of approximately 204 nucleotides in the 3′ UTR is enough for a single-copy transgene to activate the *in trans* silencing of another transgene with the same 3′ UTR [113]. Also designing transgenes without any inverted repeat is important to guarantee high and stable expression. Indeed, upon transcription of these inverted repeats, hairpin structures and double-stranded RNA are formed initiating transgene silencing [127]. Almost complete cosuppression of an endogenous gene in tomato (*Solanum esculentum*) was obtained after transformation with a homologous transgene construct that harbored two upstream inverted repeats in the 5′ UTR.

Control of Gene Expression by the Generation of Single-Copy Transformants

As mentioned above, transformants obtained after *Agrobacterium*-mediated gene transfer often contain multiple T-DNA copies in direct or inverted orientations, and the frequency of single-copy transformants is rather low [1, 17]. Because screening for single-copy T-DNA transformants strongly enriches for transformants with stable and high transgene expression [17], single-copy transformants need to be identified in a large pool of plants. Currently, conventional, but time-consuming and labor-intensive methods, such as DNA gel blot analysis and T-DNA fingerprinting are used [128]. Recently, transformation technologies and vectors have been developed to increase the frequency of single-copy transformants during or after transformation with site-specific recombination.

Generation of Single-Copy Transformants by Resolution of Complex Integration Loci by Site-Specific Recombination

A T-DNA construct, harboring site-specific *loxP* recombination sites, was designed to reduce complex T-DNA loci into a single T-DNA insert (Fig. 3a) [129]. This T-DNA harbored two invertedly oriented *loxP* recombination sites inside and immediately adjacent to the left and right T-DNA border ends [129]. Recombination between the outermost *loxP* sequences in direct orientation should resolve multiple copies into a single T-DNA copy, regardless of the number and orientation of the *loxP*-derived T-DNA copies inserted at one locus.

In a first approach, seven *Arabidopsis* transformants with multiple T-DNA inserts on a single locus were crossed with a homozygous *CRE*-expressing line [129]. In three hybrids, the complex T-DNA locus was reduced efficiently to a single-copy locus and in two of them, the resolution of the inverted repeat locus was accompanied by an at least tenfold-enhanced and stable transgene expression (Fig. 3a–d). In the progeny plants, only the simplified T-DNA locus was detected upon segregation of the *CRE* recombinase gene, proving that excision took place in the progenitor cells of the gametes (Fig. 3b and c) [129]. Unfortunately, in four of the seven transformants, the complex T-DNA locus could not be resolved by CRE-mediated transformation to a single T-DNA copy, although some rearrangements occurred as demonstrated on DNA gel blots. Strikingly, these complex T-DNA loci that were not resolved, had variable expression levels in different progeny plants with the same complex locus, implying some epigenetic imprints imposed by the interaction with the CRE recombinase. Possible reasons for the lack of resolution in these transformants might be deletion of the most extreme *loxP* sequences, too low CRE activity, or inaccessibility of the *loxP* sequences due to heterochromatinization of the complex locus [129]. Indeed, a correlation between the efficiency of CRE-mediated recombination and the CRE mRNA levels had been demonstrated [130].

In a second approach, the T-DNA vector with oppositely oriented *loxP* sequences was transformed into

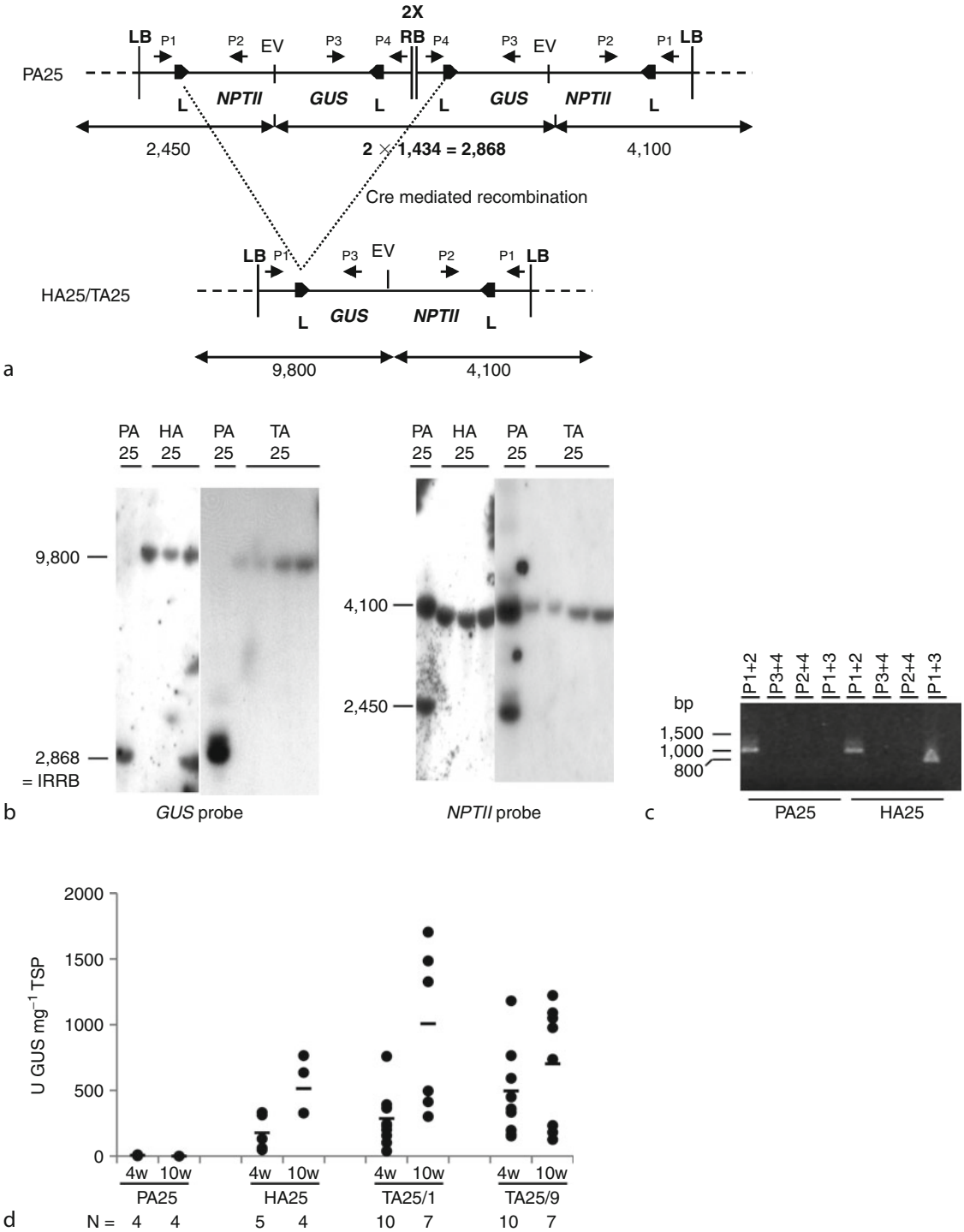

Transgene Expression in Plants, Control of. Figure 3 (Continued)

T

CRE-expressing *Arabidopsis* plants [88] and 55% of the primary transformants were single-copy T-DNA plants versus only 15% in control plants. Most of the single-copy transformants in *CRE*-expressing background (70%) displayed a continuous somatic inversion of the DNA fragment between the two inverted *loxP* sequences. To avoid this phenomenon, a new T-DNA vector, harboring only one *loxP* sequence adjacent to the LB or RB, was transformed in a *CRE*-expressing plant and up to 70% of the transformants were single copy. As resolution to single-copy plants is only efficient when the outermost *loxP* sites are in direct orientation, inverted T-DNA repeats might be mostly internal to multiple T-DNA copy arrays and they rarely occur at the ends after floral dip transformation in *Arabidopsis* [88]. Most single-copy transformants, obtained with both T-DNA vectors, displayed high and stable transgene expression. Strikingly however, the transgene expression in the majority of multicopy CRE transformants was stable and uniform, suggesting that the CRE recombinase prevented also the generation of inverted T-DNA repeats or modified the chromatin structure of the locus, so that it became less sensitive for gene silencing [88]. In both strategies, the *CRE* expression cassette is still present after resolution of the complex T-DNA locus, which can be a disadvantage, because, except for *Arabidopsis*, high *CRE* expression can result in severe growth phenotypes and reduced fertility in some plant species [131]. To avoid this drawback, *loxP*-containing T-DNAs could be transformed into hemizygous *CRE*-expressing plants, with 25% of the transformed progenies without *CRE* expression cassette as a consequence [88]. Also backcrossing of a homozygous *CRE*-expressing line with a wild-type plant would result in transformants without the *CRE*-containing T-DNA. Alternatively, the CRE recombinase protein could also be transiently introduced into the plant cell nucleus. Vergunst et al. [132] developed a VirB/D4-dependent translocation system in which the CRE recombinase was fused with the VIRE2 or VIRF proteins of *A. tumefaciens*. Together with the VIR proteins, the CRE recombinase was transferred to the plant cell and site-specific recombination took place. This recombination did not require any transferred DNA [132], but the question remains whether this CRE recombinase activity would be high enough to mediate complex T-DNA loci resolution and to transfer the CRE recombinase very efficiciently.

Transgene Expression in Plants, Control of. Figure 3

Single-copy T-DNA transformants with high and stable transgene expression as a result of CRE/*loxP* recombination-mediated resolution (Adapted from [129]). (**a**) Schematic representation of the CRE/*loxP*-mediated resolution of a complex locus to a single T-DNA (not on scale). Parental (P) plant PA25 contained two T-DNAs in inverted orientation. After the plant DNA was digested with the *EcoR*V (EV) enzyme, a fragment of 2,868 bp after hybridization with the *GUS* probe is indicative for the inverted T-DNA repeat about the RB, while two T-DNA/plant junctions of 2,450 bp and 4,100 bp were observed after hybridization with the *NPTII* probe, revealing the left T-DNA/plant DNA junctions. The hybrid (H) HA25 was obtained after crossing the parental plant with a *CRE*-expressing plant. CRE/*loxP*-mediated resolution between the two outermost *loxP* sites resulted in a new T-DNA harboring two LB regions in HA25 and the F2 progeny plants TA25. The primers P1, P2, P3, and P4 are indicated, showing homology with the LB region, the *GUS*-coding sequence, the *NPTII* coding sequence, and the RB region, respectively. (**b**) DNA gel blot analysis on *EcoR*V-digested DNA of PA25, HA25, and TA25. After CRE/*loxP*-mediated resolution, only one original LB-T-DNA/plant junction fragment was detected after hybridization with the *NPTII* probe fragment. Additionally, as expected, one new T-DNA/plant junction was observed after hybridization with the *GUS* probe. (**c**) Polymerase chain reaction (PCR) analysis on PA25 and HA25 transformants to identify the newly formed T-DNA configurations. Primer combination P1+2 amplified an LB/NPTII junction of 1,142 bp; primer combination P1+3 amplified an LB/GUS junction of 914 bp (*arrow 2*). With primer P4, no PCR fragment was obtained in PA25, because no inverted repeats could be amplified by PCR. Upon CRE/*loxP*-mediated resolution, the RB inverted palindrome was deleted, and only PCR products with the LB region of primer P1 were obtained. (**d**) GUS activity analysis in leaves of 4- and 10-week-old PA25, HA25, and TA25 seedlings. The measurements and the mean are indicated by *dots* and *line*, respectively. GUS activity levels are given as units GUS mg^{-1} of total soluble protein. The number (*N*) of the analyzed seedlings is indicated

Simplification of complex T-DNA loci was also observed by Verweire et al. [133]. To ultimately develop a T-DNA vector that generates homozygous marker-free transgenic *Arabidopsis* plants without the need of additional transformation rounds or crosses, a germline-specific auto-excision vector was designed that harbored both the selectable marker and the *CRE* expression cassette between two *lox*P sequences in direct repeat. Additionally, the *CRE* recombinase was driven by the germline-specific 2.2-kb promoter fragment of the *SOLO DANCERS* gene, which is active in both the male and female meiocytes of *Arabidopsis*. In this manner, the transgenic plants become genetically programmed so that the marker gene is lost after the initial selection of the primary transformants. Surprisingly, not only marker-free homozygous progenies were obtained very efficiently, but also the locus structure in these progeny plants was simplified [133].

A similar approach to resolve complex transgene loci had been developed previously for the generation of single-copy transgenic wheat plants after direct gene transfer. In this case, the selectable marker was removed simultaneously with the resolution of the complex locus [134]. The transformation vector consisted of a transgene flanked by two *lox511* sites, a mutant variant of the wild-type *loxP* sequence, in inverted orientation. Additionally, the selectable marker gene was flanked by two wild-type *loxP* recombination sites in the same orientation. Two correct and independent recombination reactions could take place, because *lox511* and *loxP* did not recombine, with transformants with a marker-free, single-copy insertion of the transgene in the plant genome as a consequence. Crossing of four wheat transformants, harboring a multicopy locus, with a *CRE*-expressing wheat transformant, resulted in 62/72 F2 plants with a single-copy, marker-free, transgene locus [134]. Because the resolved locus still contained two *lox511* sites in inverted orientation, the CRE recombinase could still mediate inversion of the transgene between these two sites. Therefore, all F1 plants were chimeric for the inversion and harbored both transgene orientations.

To avoid crossing with a *CRE*-expressing plant, the transgene, flanked by the oppositely oriented *loxP* sites in maize cells, was cobombarded with a *CRE*-expressing construct [135]. This cotransformation resulted in 85% primary transformants harboring one or two copies of the introduced gene, of which 38% harbored a single copy. Of these single-copy plants, 60% lacked also the recombinase gene, because during cobombardment a molar ratio of 3:1 transgene to CRE construct was used. In this manner, an overall efficiency of 23% of plants with only one copy of the transgene construct was obtained [135]. This cotransformation strategy requires that the selectable marker is retained in the primary transformants. However, a strategy with two different recombination systems and two different selectable markers could result in the integration of one transgene without the incorporation of additional unneeded DNA in the transgenic plant [135].

Besides the use of the CRE/*loxP* recombination system to obtain efficiently single-copy transformants, other strategies have been proposed and evaluated. A site-specific recombination strategy was described in which two sets of directly repeated FLP recognition target (FRT) sites [136] flanked a "to-be-removed" (TBR) region. The FRT sites flanking one TBR are inverted in relation to the sites flanking the other TBR. Each TBR can be excised independently, because only recombination between directly repeated FRT sites can cause excision. Furthermore, one site-specific recombinase reaction could simultaneously induce double excisions, resulting in the resolution of complex T-DNA loci. Indeed, the progenies of 70% of the *Arabidopsis* transformants harbored only one or two copies of the transgene, while 40% contained only one T-DNA copy. This frequency of transformants with a simple T-DNA integration pattern is significantly higher than the 5–20% single-copy transformants normally obtained after floral dip transformation [1, 17]. Most interestingly, the reduced copy number was also strongly associated with increased expression [137].

Generation of Single-Copy Transformants by Site-Specific or Site-Directed Integration

Besides the use of site-specific recombination to resolve complex transgene loci into simple loci before, during or after integration, this site-specific recombination system can also be applied to produce plants with a simple integration pattern through site-specific integration [86, 138–141]. In addition, with this technology, transgenes can be targeted to a specific preselected chromosomal site

to eliminate variation in gene expression. The strategy to obtain single-copy transformants via site-specific integration consists of two transformation rounds. In the first round, a target line is generated, harboring a target *lox* site between the promoter and the *CRE* gene. In the second transformation, the vector carrying the gene of interest and two *lox* sites is introduced into the target line. When the gene of interest is integrated into the *lox* site of the target line, the expression of the recombinase gene is stopped. Site-specific gene integration in plants has been described with various DNA delivery methods, such as polyethylene glycol-mediated tobacco protoplast transformation [86], *Agrobacterium*-mediated transformation of *Arabidopsis* [138], and biolistic-mediated transformation of rice [139, 141]. After *Agrobacterium*-mediated transformation, the frequency of *CRE*-mediated gene integration was very low (approximately 2%) compared to the DNA delivery via direct gene transfer, probably because the transferred DNA during *Agrobacterium* transformation is single stranded, which is not a substrate for the CRE recombinase [139, 140].

By combining site-specific gene integration with gene expression analysis, the absolute level of transgene expression could be shown to vary up to tenfold, depending on the target site in the tobacco genome, indicating that the chromosome position can affect the level of transgene expression [86]. Additionally, despite the identical integration pattern, half of the transgenic tobacco lines showed the expected expression of the transgene and the other half very low *GUS* expression. This low *GUS* expression was due to transgene silencing, because it was correlated with DNA methylation and low transcript levels. Furthermore, this DNA methylation was specific for the newly introduced DNA sequences. Also in independent experiments, regenerants could be divided also upon site-directed integration in two categories: the single-copy lines that contained one site-specific insert without additional sequence integration and multicopy lines in which, besides the site-specific integration, additional transgene copies were integrated into the plant genome [140, 141]. The transgene expression of the single-copy rice transformants was high and stable and the variation was lower than that of the multicopy lines. In approximately half of the multicopy lines, expression of the site-specific integrated transgene could be reactivated and stabilized when the illegitimate integrated inserts were segregated away. In the remaining half, the expression could not be restored, because the random integrations were genetically linked to the site-specific integration event [141].

A site-directed integration system for *Agrobacterium*-mediated transformation of tobacco was developed in which a single transgene copy could be integrated precisely into a predefined target locus by recombinase-mediated cassette exchange (RMCE) [142]. In the RMCE-based site-directed integration strategy that uses the R-RS system from *Zygosaccharomyces rouxii*, a single-copy of the target cassette, surrounded by two oppositely oriented RS sites, is randomly integrated into the plant genome. The exchange cassette contains the selectable marker gene and the gene of interest between two opposite RS sites, and the recombinase gene, the selectable marker gene, and the gene of interest between directly oriented RS sites. This third RS site excluded random integration events. The recombinase will catalyze a double crossover between the two RS sites, replacing the target cassette by the exchange cassette and removing the recombinase gene. Expression analysis revealed that the obtained site-specific recombined plants from the same target line had approximately the same transgene expression level and less transgene expression variability than the random-integration transgenic plants and no transgene silencing [142]. Strikingly, transgenes in the same direction at the same target locus had the same level of activity, in contrast to transgenes in different directions, indicating that the surrounding genome DNA sequence outside the target locus might affect the activity of the gene. Also after direct gene transfer of soybean (*Glycine max*), site-specific integration via RMCE occurred efficiently and stable transgene expression was stable [143].

Another approach to obtain single-copy transgenic lines is the "Agrolistic" method, in which the advantages of *Agrobacterium*-mediated transformation and biolistics were combined [144, 145]. The *VIRD* genes were cobombarded with the T-DNA borders, flanking the introduced transgene. Approximately, 20% of the transformed tobacco calli contained only the T-DNA with correctly processed border sequences and no integrated vector backbone sequences [144], whereas

10–35% of transgenic maize calli contained one to two transgene copies. The addition of *VIRE2* genes even doubled this transformation efficiency [145]. Finally, the application of niacimide, a product that reduces recombination of extrachromosomal molecules, resulted in the generation of single-copy transformants in wheat with an efficiency of 8% [146].

Use of Gene Silencing Mutants to Overcome Transgene Expression Variability

Variation in transgene expression in a population of plants is frequently due to PTGS of the transgenes. Several genes are involved in PTGS and mutant screens revealed that the RNA-dependent RNA polymerase (RDRP6, SGS2) is essential for PTGS to occur [147, 148]. Therefore, a logical approach to overcome PTGS in a population of transgenic plants was to generate transformants in an *rdr6* mutant background, impaired in PTGS [3, 84]. Introduction of p35S-*GUS* or p35S-*GFP* transgenes into the *Arabidopsis sgs*2 and *sgs*3 mutants (two different alleles of *RDR6*) resulted in stable and high expression of these transgenes in 100% of the transformants analyzed [3], while, similarly, the outcome of introduction of a cyclin-dependent kinase inhibitor 6 gene under the control of p35S was a clear overexpression phenotype, typical for high expression of the kinase inhibitor, in all transformants. Also the transgene expression in transformants with convergent transcription of invertedly repeated T-DNAs was high. Interestingly, immediate transgene silencing in the F1 progeny plants occurred by backcrossing of these high-expressing transformants containing an inverted repeat T-DNA locus with a wild-type nontransformed plant. This observation clearly demonstrates that RDRP6 is required for the generation of double-stranded RNA, also from inverted repeat loci, and that not the read-through transcripts from the convergently transcribed genes generate the double-stranded RNA, as is widely believed. Similar results were obtained when the transgenes were driven by the pCAS promoter, a strong constitutive promoter derived from the cassava vein mosaic virus [149]. On the contrary, expression variability was not significantly reduced in the plants transformed with *sgs*2 and *sgs*3 when the transgenes were under control of the hybrid pOMA1 promoter, a hybrid promoter consisting of parts of the pMAS and pOCS, which might be too weak to trigger PTGS [3], in contrast to the strong p35S and pCAS. When the T-DNA constructs were flanked by MARs of the chicken lysozyme gene, the GUS activity was boosted fivefold and 12-fold in *sgs*2 and *sgs*3 background, respectively, in contrast to the wild-type background, making this PTGS-MAR expression system very attractive for the production of heterologous proteins in plants [3, 84].

Future Directions

The ultimate aim is to generate transgenic plants with a predictable, well-controlled, and stable transgene expression over many generations. As described above, to achieve this goal, many parameters should be taken into account. Most importantly, the transgene construct should be optimally designed: a suitable promoter should be selected that drives transgene expression in the desired way, multiple homologous sequences should be avoided in the transgene construct, and foreign unnecessary DNA should be as much as possible prevented to be integrated into the plant genome. Until now, the transgene construct was integrated via illegitimate recombination, but recent reports on site-specific integration let one assume that targeted integration via ZFNs will soon become feasible routinely [105]. At the same time, this method will enrich for single-copy transformants ensuring stable transgene expression. Importantly, the majority of the above-described observations and conclusions are all based on genes driven by the strong constitutive p35S. Therefore, it is perfectly conceivable that all these observations are typical for this promoter, but cannot be extrapolated to other promoters. In the future, the use of strong plant promoters instead of the 35S promoter in transgene constructs might be a big improvement to obtain controllable and stable high transgene expression. Indeed, in general, plant promoter–gene fusions show limited quantitative and qualitative variations in transgene expression in different transformants. Analysis of the expression profile of the *ARCELIN-5* regulatory sequences in *Arabidopsis* seeds revealed that, surprisingly, the *Arabidopsis* seeds accumulated ARCELIN-5, an abundant protein found in common bean (*Phaseolus vulgaris*), to 15% of the total soluble protein content [150]. All transformants

had low plant-to-plant variation and even in plants harboring a complex T-DNA integration pattern, with invertedly and directly repeated T-DNAs, the transgene expression was high and stable [150]. Similar results were found for genes driven by the *ß-PHASEOLIN* promoter of common bean [70].

However, to really control transgene expression in plants, the underlying triggers that initiate PTGS and TGS have to be understood in much more detail. Do all plant promoters give less variation in transgene expression compared to viral and bacterial promoters? Do plant promoters also induce silencing and with which frequency? Intriguingly, why do certain loci with multiple p35S-driven transgene copies provoke silencing and why others not? Silencing is often triggered when gene expression rises above a certain threshold, but what is the nature of this threshold and how is the threshold measured? Can transcript levels be increased by the insertion of particular stabilizing elements? To answer all these questions, an integrated approach will have to be followed, including the use of well-designed transgene constructs differing only in a single transgene element in combination with different mutants. Molecular characterization of the transgene locus, the transcript steady state and turnover levels, and the translation efficiency should allow to unravel the network of gene expression control and identify the most important master elements. The ultimate goal is to be able to construct transgenes with a predefined expression pattern in a reliable way.

Acknowledgments

The authors thank Martine De Cock for help with the manuscript. This work was supported in part by grants from the European Union BIOTECH program (QLRT-2000-00078) with additional cofinancing from the Flemish Community, the "Bijzonder Onderzoeksfonds" of Ghent University (BOF 01111400), and the Research Foundation-Flanders (no. G.021106).

Bibliography

1. De Buck S, Podevin N, Nolf J, Jacobs A, Depicker A (2009) The T-DNA integration pattern in *Arabidopsis* transformants is highly determined by the transformed target cell. Plant J 60:134–145
2. Windels P, De Buck S, Depicker A (2008) *Agrobacterium tumefaciens*-mediated transformation: patterns of T-DNA integration into the host genome. In: Tzfira T, Citovsky V (eds) *Agrobacterium*: from biology to biotechnology. Springer, New York, pp 441–481
3. Butaye KMJ, Goderis IJWM, Wouters PFJ, Pues JM-TG, Delauré SL, Broekaert WF, Depicker A, Cammue BPA, De Bolle MFC (2004) Stable high-level transgene expression in *Arabidopsis thaliana* using gene silencing mutants and matrix attachment regions. Plant J 39:440–449
4. Muskens MWM, Vissers APA, Mol JNM, Kooter JM (2000) Role of inverted DNA repeats in transcriptional and post-transcriptional gene silencing. Plant Mol Biol 43:243–260
5. Pröls F, Meyer P (1992) The methylation pattern of chromosomal integration regions influence gene activity of transferred DNA in *Petunia hybrida*. Plant J 2:465–475
6. De Loose M, Danthinne X, Van Bockstaele E, Van Montagu M, Depicker A (1995) Different 5′ leader sequences modulate β-glucuronidase accumulation levels in transgenic *Nicotiana tabacum* plants. Euphytica 85:209–216
7. Napoli C, Lemieux C, Jorgensen R (1990) Introduction of a chimeric chalcone synthase gene into petunia results in reversible co-suppression of homologous genes *in trans*. Plant Cell 2:279–289
8. van der Krol AR, Mur LA, Beld M, Mol JNM, Stuitje AR (1990) Flavonoid genes in petunia: addition of a limited number of gene copies may lead to a suppression of gene expression. Plant Cell 2:291–299
9. Depicker A, Van Montagu M (1997) Post-transcriptional gene silencing in plants. Curr Opin Cell Biol 9:373–382
10. Frizzi A, Huang S (2010) Tapping RNA silencing pathways for plant biotechnology. Plant Biotechnol J 8:655–677
11. Vaucheret H, Fagard M (2001) Transcriptional gene silencing in plants: targets, inducers and regulators. Trends Genet 17:29–35
12. Matzke AJM, Matzke MA (1998) Position effects and epigenetic silencing of plant transgenes. Curr Opin Plant Biol 1:142–148
13. Tzfira T, Citovsky V (2006) *Agrobacterium*-mediated genetic transformation of plants: biology and biotechnology. Curr Opin Biotechnol 17:147–154
14. Banta LM, Montenegro M (2008) *Agrobacterium* and plant biotechnology. In: Tzfira T, Citovsky V (eds) *Agrobacterium*: from biology to biotechnology. Springer, New York, pp 73–148
15. Tzfira T, Li J, Lacroix B, Citovsky V (2004) *Agrobacterium* T-DNA integration: molecules and models. Trends Genet 20:375–383
16. Forsbach A, Schubert D, Lechtenberg B, Gils M, Schmidt R (2003) A comprehensive characterization of single-copy T-DNA insertions in the *Arabidopsis thaliana* genome. Plant Mol Biol 52:161–176
17. De Buck S, Windels P, De Loose M, Depicker A (2004) Single-copy T-DNAs integrated at different positions in the *Arabidopsis* genome display uniform and comparable β-glucuronidase accumulation levels. Cell Mol Life Sci 61:2632–2645

18. Koncz C, Martini N, Mayerhofer R, Koncz-Kalman Z, Körber H, Redei GP, Schell J (1989) High-frequency T-DNA-mediated gene tagging in plants. Proc Natl Acad Sci USA 86:8467–8471
19. Herman L, Jacobs A, Van Montagu M, Depicker A (1990) Plant chromosome/marker gene fusion assay for study of normal and truncated T-DNA integration events. Mol Gen Genet 224:248–256
20. Kim S-I, Veena GSB (2007) Genome-wide analysis of *Agrobacterium* T-DNA integration sites in the *Arabidopsis* genome generated under non-selective conditions. Plant J 51:779–791
21. Francis KE, Spiker S (2005) Identification of *Arabidopsis thaliana* transformants without selection reveals a high occurrence of silenced T-DNA integrations. Plant J 41:464–477
22. Windels P, De Buck S, Van Bockstaele E, De Loose M, Depicker A (2003) T-DNA integration in *Arabidopsis* chromosomes: presence and origin of filler DNA sequences. Plant Physiol 133:2061–2068
23. Wenck A, Czakó M, Kanevski I, Márton L (1997) Frequent collinear long transfer of DNA inclusive of the whole binary vector during *Agrobacterium*-mediated transformation. Plant Mol Biol 34:913–922
24. Kononov ME, Bassuner B, Gelvin SB (1997) Integration of T-DNA binary vector 'backbone' sequences into the tobacco genome: evidence for multiple complex patterns of integration. Plant J 11:945–957
25. De Buck S, De Wilde C, Van Montagu M, Depicker A (2000) T-DNA vector backbone sequences are frequently integrated into the genome of transgenic plants obtained by *Agrobacterium*-mediated transformation. Mol Breed 6:459–468
26. Podevin N, De Buck S, De Wilde C, Depicker A (2006) Insights into recognition of the T-DNA border repeats as termination sites for T-strand synthesis by *Agrobacterium tumefaciens*. Transgenic Res 15:557–571
27. van der Graaff E, den Dulk-Ras A, Hooykaas PJJ (1996) Deviating T-DNA transfer from *Agrobacterium tumefaciens* to plants. Plant Mol Biol 31:677–681
28. Barcelo P, Lazzeri PA (1998) Direct gene transfer: chemical, electrical and physical methds. In: Lindsey K (ed) Transgenic plant research. Harwood Academic Publishers, Amsterdam, pp 35–55
29. Kohli A, Leech M, Vain P, Laurie DA, Christou P (1998) Transgene organization in rice engineered through direct DNA transfer supports a two-phase integration mechanism mediated by the establishment of integration hot spots. Proc Natl Acad Sci USA 95:7203–7208
30. Zhao ZY, Gu W, Cai T, Tagliani LA, Hondred D, Bond D, Krell S, Rudert ML, Bruce WB, Pierce DA (1998) Molecular analysis of T0 plants transformed by *Agrobacterium* and comparison of *Agrobacterium*-mediated transformation with bombardment transformation in maize. Maize Genet Coop Newsletter 72:34–37
31. Dai S, Zheng P, Marmey P, Zhang S, Tian W, Chen S, Beachy RN, Fauquet C (2001) Comparative analysis of transgenic rice plants obtained by *Agrobacterium*-mediated transformation and particle bombardement. Mol Breed 7:25–33
32. Shou H, Frame BR, Whitham SA, Wang K (2004) Assessment of transgenic maize events produced by particle bombardment or *Agrobacterium*-mediated transformation. Mol Breed 13:201–208
33. Altpeter F, Baisakh N, Beachy R, Bock R, Capell T, Christou P, Daniell H, Datta K, Dix PJ, Fauquet C, Huang N, Kohli A, Mooibroek H, Nicholson L, Nguyen TH, Nugent G, Raemakers K, Romano A, Somers DA, Stoger E, Taylor N, Visser R (2005) Particle bombardment and the genetic enhancement of crops: myths and realities. Mol Breed 15:305–327
34. De Neve M, De Buck S, Jacobs A, Van Montagu M, Depicker A (1997) T-DNA integration patterns in co-transformed plant cells suggest that T-DNA repeats originate from co-integration of separate T-DNAs. Plant J 11:15–29
35. De Buck S, Jacobs A, Van Montagu M, Depicker A (1999) The DNA sequences of T-DNA junctions suggest that complex T-DNA loci are formed by a recombination process resembling T-DNA integration. Plant J 20:295–304
36. Cluster PD, O'Dell M, Metzlaff M, Flavell RB (1996) Details of T-DNA structural organization from a transgenic Petunia population exhibiting co-suppression. Plant Mol Biol 32:1197–1203
37. Wolters A-MA, Trindade LM, Jacobsen E, Visser RGF (1998) Fluorescence *in situ* hybridization on extended DNA fibres as a tool to analyse complex T-DNA loci in potato. Plant J 13:837–847
38. Jorgensen R, Snyder C, Jones JDG (1987) T-DNA is organized predominantly in inverted repeat structures in plants transformed with *Agrobacterium tumefaciens* C58 derivatives. Mol Gen Genet 207:471–477
39. Krizkova L, Hrouda M (1998) Direct repeats of T-DNA integrated in tobacco chromosome: characterization of junction regions. Plant J 16:673–680
40. Kumar S, Fladung M (2000) Transgene repeats in aspen: molecular characterisation suggests simultaneous integration of independent T-DNAs into receptive hotspots in the host genome. Mol Gen Genet 264:20–28
41. Van Lijsebettens M, Inzé D, Schell J, Van Montagu M (1986) Transformed cell clones as a tool to study T-DNA integration mediated by *Agrobacterium tumefaciens*. J Mol Biol 188:129–145
42. Herman LMF, Van Montagu M, Depicker AG (1986) Isolation of tobacco DNA segments with plant promoter activity. Mol Cell Biol 6:4486–4492
43. Depicker A, Herman L, Jacobs A, Schell J, Van Montagu M (1985) Frequencies of simultaneous transformation with different T-DNAs and their relevance to the *Agrobacterium*/plant cell interaction. Mol Gen Genet 201:477–484
44. De Block M, Debrouwer D (1991) Two T-DNA's co-transformed into *Brassica napus* by a double *Agrobacterium tumefaciens*

infection are mainly integrated at the same locus. Theor Appl Genet 82:257–263
45. Poirier Y, Ventre G, Nawrath C (2000) High-frequency linkage of co-expressing T-DNA in transgenic *Arabidopsis thaliana* transformed by vacuum-infiltration of *Agrobacterium tumefaciens*. Theor Appl Genet 100:487–493
46. Radchuk VV, Van DT, Klocke E (2005) Multiple gene co-integration in *Arabidopsis thaliana* predominantly occurs in the same genetic locus after simultaneous in planta transformation with distinct *Agrobacterium tumefaciens* strains. Plant Sci 168:1515–1523
47. Nam J, Matthysse AG, Gelvin SB (1997) Differences in susceptibility of Arabidopsis ecotypes to crown gall disease may result from a deficiency in T-DNA integration. Plant Cell 9:317–333
48. Grevelding C, Fantes V, Kemper E, Schell J, Masterson R (1993) Single-copy T-DNA insertions in *Arabidopsis* are the predominant form of integration in root-derived transgenics, whereas multiple insertions are found in leaf discs. Plant Mol Biol 23:847–860
49. Valvekens D, Van Montagu M, Van Lijsebettens M (1988) *Agrobacterium tumefaciens*-mediated transformation of *Arabidopsis thaliana* root explants by using kanamycin selection. Proc Natl Acad Sci USA 85:5536–5540
50. Clough SJ, Bent AF (1998) Floral dip: a simplified method for *Agrobacterium*-mediated transformation of *Arabidopsis thaliana*. Plant J 16:735–743
51. Hobbs SLA, Warkentin TD, DeLong CMO (1993) Transgene copy number can be positively or negatively associated with transgene expression. Plant Mol Biol 21:17–26
52. Shiva Prakash N, Bhojaraja R, Shivbachan SK, Hari Priya GG, Nagraj TK, Prasad V, Srikanth Babu V, Jayaprakash TL, Dasgupta S, Spencer TM, Boddupalli RS (2009) Marker-free transgenic corn plant production through co-bombardement. Plant Cell Rep 28:1655–1668
53. Lowe BA, Shiva Prakash N, Way M, Mann MT, Spencer TM, Boddupalli RS (2009) Enhanced single copy integration events in corn via particle bombardment using low quantities of DNA. Transgenic Res 18:831–840
54. Loc TN, Tinjuangjun P, Gatehouse AMR, Christou P, Gatehouse AJ (2002) Linear transgene constructs lacking vector backbone sequences generate transgenic rice plants which accumulate higher levels of proteins conferring insect resistance. Mol Breed 9:231–244
55. Yao Q, Cong L, Chang JL, Li KX, Yang GX, He GY (2006) Low copy number gene transfer and stable expression in a commercial wheat cultivar via particle bombardment. J Exp Bot 57:3737–3746
56. Fu X, Duc LT, Fontana S, Bong BB, Tinjuangjun P, Sudhakar D, Twyman RM, Christou P, Kohli A (2000) Linear transgene constructs lacking vector backbone sequences generate low-copy-number transgenic plants with simple integration patterns. Transgenic Res 9:11–19
57. Odell JT, Nagy F, Chua N-H (1985) Identification of DNA sequences required for activity of the cauliflower mosaic virus 35S promoter. Nature 313:810–812
58. Fang R-X, Nagy F, Sivasubramaniam S, Chua N-H (1989) Multiple *cis* regulatory elements for maximal expression of the cauliflower mosaic virus 35S promoter in transgenic plants. Plant Cell 1:141–150
59. Jorgensen RA, Cluster PD, English J, Que Q, Napoli CA (1996) Chalcone synthase cosuppression phenotypes in petunia flowers: comparison of sense vs. antisense constructs and single-copy vs. complex T-DNA sequences. Plant Mol Biol 31:957–973
60. Elmayan T, Vaucheret H (1996) Expression of single copies of a strongly expressed *35S* transgene can be silenced post-transcriptionally. Plant J 9:787–797
61. Que Q, Wang H-Y, English JJ, Jorgensen RA (1997) The frequency and degree of cosuppression by sense chalcone synthase transgenes are dependent on transgene promoter strength and are reduced by premature nonsense codons in the transgene coding sequence. Plant Cell 9: 1357–1368
62. Lechtenberg B, Schubert D, Forsbach A, Gils M, Schmidt R (2003) Neither inverted repeat T-DNA configurations nor arrangements of tandemly repeated transgenes are sufficient to trigger transgene silencing. Plant J 34:507–517
63. Marjanac G, Karimi M, Naudts M, Beeckman T, Depicker A, De Buck S (2009) Gene silencing induced by hairpin or inverted repeated sense transgenes varies among promoters and cell types. New Phytol 184:851–864
64. Chuang C-F, Meyerowitz EM (2000) Specific and heritable genetic interference by double-stranded RNA in *Arabidopsis thaliana*. Proc Natl Acad Sci USA 97:4985–4990
65. Vaucheret H, Elmayan T, Thierry D, van der Geest A, Hall T, Conner AJ, Mlynarova L, Nap J-P (1998) Flank matrix attachment regions (MARs) from chicken, bean, yeast or tobacco do not prevent homology-dependent *trans*-silencing in transgenic tobacco plants. Mol Gen Genet 259:388–392
66. De Bolle MFC, Butaye KMJ, Coucke WJW, Goderis IJWM, Wouters PFJ, van Boxel N, Broekaert WF, Cammue BPA (2003) Analysis of the influence of promoter elements and a matrix attachment region on the inter-individual variation of transgene expression in populations of *Arabidopsis thaliana*. Plant Sci 165:169–179
67. Mathé C, Peresetsky A, Déhais P, Van Montagu M, Rouzé P (1999) Classification of *Arabidopsis thaliana* gene sequences: clustering of coding sequences into two groups according to codon usage improves gene prediction. J Mol Biol 285:1977–1991
68. Rouwendal GJA, Mendes O, Wolbert EJH, de Boer AD (1997) Enhanced expression in tobacco of the gene encoding green fluorescent protein by modification of its codon usage. Plant Mol Biol 33:989–999
69. Schubert D, Lechtenberg B, Forsbach A, Gils M, Bahadur S, Schmidt R (2004) Silencing in Arabidopsis T-DNA transformants: the predominant role of a gene-specific RNA sensing mechanism versus position effects. Plant Cell 16:2561–2572

70. De Jaeger G, Scheffer S, Jacobs A, Zambre M, Zobell O, Goossens A, Depicker A, Angenon G (2002) Boosting heterologous protein production in transgenic dicotyledonous seeds using *Phaseolus vulgaris* regulatory sequences. Nat Biotechnol 20:1265–1268
71. Mascarenhas D, Mettler IJ, Pierce DA, Lowe HW (1990) Intron-mediated enhancement of heterologous gene expression in maize. Plant Mol Biol 15:913–920
72. Bourdon V, Harvey A, Lonsdale DM (2001) Introns and their positions affect the translational activity of mRNA in plant cells. EMBO Rep 2:394–398
73. Rose AB, Elfersi T, Parra G, Korf I (2008) Promoter-proximal introns in *Arabidopsis thaliana* are enriched in dispersed signals that elevate gene expression. Plant Cell 20: 543–551
74. Barlett JG, Snape JW, Harwood WA (2009) Intron-mediated enhancement as a method for increasing transgene expression levels in barley. Plant Biotechnol J 7: 856–866
75. Rose AB (2004) The effect of intron location on intron-mediated enhancement of gene expression in *Arabidopsis*. Plant J 40:744–751
76. Tanaka A, Mita S, Ohta S, Kyozuka J, Shimamoto K, Nakamura K (1990) Enhancement of foreign gene expression by a dicot intron in rice but not in tobacco is correlated with an increased level of mRNA and an efficient splicing of the intron. Nucleic Acids Res 18:6767–6770
77. Allen GC, Spiker S, Thompson WF (2000) Use of matrix attachment regions (MARs) to minimize transgene silencing. Plant Mol Biol 43:361–376
78. De Bolle MFC, Butaye KMJ, Goderis IJWM, Wouters PFJ, Jacobs A, Delauré SL, Depicker A, Cammue BPA (2007) The influence of matrix attachment regions on transgene expression in *Arabidopsis thaliana* wild type and gene silencing mutants. Plant Mol Biol 63:533–543
79. Butaye KMJ, Cammue BPA, Delauré SL, De Bolle MFC (2005) Approaches to minimize variation of transgene expression in plants. Mol Breed 16:79–91
80. Petersen K, Leah R, Knudsen S, Cameron-Mills V (2002) Matrix attachment regions (MARs) enhance transformation frequencies and reduce variance of transgene expression of barley. Plant Mol Biol 49:45–58
81. Ülker B, Allen GC, Thompson WF, Spiker S, Weissinger AK (1999) A tobacco matrix attachment region reduces the loss of transgene expression in the progeny of transgenic tobacco plants. Plant J 18:253–263
82. Vain P, Worland B, Kohli A, Snape JW, Christou P, Allen GC, Thompson WF (1999) Matrix attachment regions increase transgene expression levels and stability in transgenic rice plants and their progeny. Plant J 18: 233–242
83. Mlynárová L, Jansen RC, Conner AJ, Stiekema WJ, Nap J-P (1995) The MAR-mediated reduction in position effect can be uncoupled from copy number-dependent expression in transgenic plants. Plant Cell 7:599–609
84. Sels J, Delauré SL, Aerts AM, Proost P, Cammue BPA, De Bolle MFC (2007) Use of a PTGS-MAR expression system for efficient in planta production of bioactive *Arabidopsis thaliana* plant defensins. Transgenic Res 16:531–538
85. Iglesias VA, Moscone EA, Papp I, Neuhuber F, Michalowski S, Phelan T, Spiker S, Matzke M, Matzke AJM (1997) Molecular and cytogenetic analyses of stably and unstably expressed transgene loci in tobacco. Plant Cell 9:1251–1264
86. Day CD, Lee E, Kobayashi J, Holappa LD, Albert H, Ow DW (2000) Transgene integration into the same chromosome location can produce alleles that express at a predictable level, or alleles that are differentially silenced. Genes Dev 14:2869–2880
87. De Wilde C, Podevin N, Windels P, Depicker A (2001) Silencing of antibody genes in plants with single-copy transgene inserts as a result of gene dosage effects. Mol Genet Genomics 265:647–653
88. De Paepe A, De Buck S, Hoorelbeke K, Nolf J, Peck I, Depicker A (2009) High frequency of single-copy T-DNA transformants by floral dip in *CRE*-expressing *Arabidopsis* plants. Plant J 59: 517–527
89. Meyer P, Heidmann I (1994) Epigenetic variants of a transgenic petunia line show hypermethylation in transgene DNA: an indication for specific recognition of foreign DNA in transgenic plants. Mol Gen Genet 243:390–399
90. Elomaa P, Helariutta Y, Griesbach RJ, Kotilainen M, Seppänen P, Teeri TH (1995) Transgene inactivation in *Petunia hybrida* is influenced by the properties of the foreign gene. Mol Gen Genet 248:649–656
91. Peach C, Velten J (1991) Transgene expression variability (position effect) of CAT and GUS reporter genes driven by linked divergent T-DNA promoters. Plant Mol Biol 17:49–60
92. Meyer P, Heidmann I, Niedenhof I (1993) Differences in DNA-methylation are associated with a paramutation phenomenon in transgenic petunia. Plant J 4:89–100
93. Holmes-Davis R, Comai L (1998) Nuclear matrix attachment regions and plant gene expression. Trends Plant Sci 3: 91–97
94. Meza TJ, Stangeland B, Mercy IS, Skårn M, Nymoen DA, Berg A, Butenko MA, Håkelien A-M, Haslekås C, Meza-Zepeda LA, Aalen RB (2002) Analyses of single-copy *Arabidopsis* T-DNA-transformed lines show that the presence of vector backbone sequences, short inverted repeats and DNA methylation is not sufficient or necessary for the induction of transgene silencing. Nucleic Acids Res 30:4556–4566
95. Kunz C, Narangajavana J, Jakowitsch J, Park Y-D, Delon TR, Kovarik A, Koukaková B, van der Winden J, Moscone E, Aufsatz W, Mette MF, Matzke M, Matzke AJM (2003) Studies on the effects of a flanking repetitive sequence on the expression of single-copy transgenes in *Nicotiana sylvestris* and in *N. sylvestris-N. tomentosiformis* hybrids. Plant Mol Biol 52: 203–215

96. Adams MD, Celniker SE, Holt RA, Evans CA, Gocayne JD, Amanatides PG, Scherer SE, Li PW, Hoskins RA, Galle RF, George RA, Lewis SE, Richards S, Ashburner M, Henderson SN, Sutton GG, Wortman JR, Yandell MD, Zhang Q, Chen LX, Brandon RC, Rogers Y-HC, Blazej RG, Champe M, Pfeiffer BD, Wan KH, Doyle C, Baxter EG, Helt G, Nelson CR, Gabor Miklos GL, Abril JF, Agbayani A, An H-J, Andrews-Pfannkoch C, Baldwin D, Ballew RM, Basu A, Baxendale J, Bayraktaroglu L, Beasley EM, Beeson KY, Benos PV, Berman BP, Bhandari D, Bolshakov S, Borkova D, Botchan MR, Bouck J, Brokstein P, Brottier P, Burtis KC, Busam DA, Butler H, Cadieu E, Center A, Chandra I, Cherry JM, Cawley S, Dahlke C, Davenport LB, Davies P, de Pablos B, Delcher A, Deng Z, Deslattes May A, Dew I, Dietz SM, Dodson K, Doup LE, Downes M, Dugan-Rocha S, Dunkov BC, Dunn P, Durbin KJ, Evangelista CC, Ferraz C, Ferriera S, Fleischmann W, Fosler C, Gabrielian AE, Garg NS, Gelbart WM, Glasser K, Glodek A, Gong F, Gorrell JH, Gu Z, Guan P, Harris M, Harris NL, Harvey D, Heiman TJ, Hernandez JR, Houck J, Hostin D, Houston KA, Howland TJ, Wei M-H, Ibegwam X, Jalali M, Kalush F, Karpen GH, Ke Z, Kennison JA, Ketchum KA, Kimmel BE, Kodira CD, Kraft C, Kravitz S, Kulp D, Lai Z, Lasko P, Lei Y, Levitsky AA, Li J, Li Z, Liang Y, Lin X, Liu X, Mattei B, McIntosh TC, McLeod MP, McPherson D, Merkulov G, Milshina NV, Mobarry C, Morris J, Moshrefi A, Mount SM, Moy M, Murphy B, Murphy L, Muzny DM, Nelson DL, Nelson DR, Nelson KA, Nixon K, Nusskern DR, Pacleb JM, Palazzolo M, Pittman GS, Pan S, Pollard J, Puri V, Reese MG, Reinert K, Remington K, Saunders RDC, Scheeler F, Shen H, Shue BC, Sidén-Kiamos I, Simpson M, Skupski MP, Smith T, Spier E, Spradling AC, Stapleton M, Strong R, Sun E, Svirskas R, Tector C, Turner R, Venter E, Wang AH, Wang X, Wang Z-Y, Wassarman DA, Weinstock GM, Weissenbach J, Williams SM, Woodage T, Worley KC, Wu D, Yang S, Yao QA, Ye J, Yeh R-F, Zaveri JS, Zhan M, Zhang G, Zhao Q, Zheng L, Zheng XH, Zhong FN, Zhong W, Zhou X, Zhu S, Zhu X, Smith HO, Gibbs RA, Myers EW, Rubin GM, Venter JC (2000) The genome sequence of *Drosophila melanogaster*. Science 287:2185–2195
97. Puchta H (2002) Gene replacement by homologous recombination in plants. Plant Mol Biol 48:173–182
98. Hanin M, Paszkowski J (2003) Plant genome modification by homologous recombination. Curr Opin Plant Biol 6:157–162
99. Hanin M, Volrath S, Bogucki A, Briker M, Ward E, Paszkowski J (2001) Gene targeting in *Arabidopsis*. Plant J 28:671–677
100. Shaked H, Melamed-Bessudo C, Levy AA (2005) High-frequency gene targeting in *Arabidopsis* plants expressing the yeast *RAD54* gene. Proc Natl Acad Sci USA 102: 12265–12269
101. Terada R, Johzuka-Hisatomi Y, Saitoh M, Asao H, Iida S (2007) Gene targeting by homologous recombination as a biotechnological tool for rice functional genomics. Plant Physiol 144:846–856
102. Salomon S, Puchta H (1998) Capture of genomic and T-DNA sequences during double-strand break repair in somatic plant cells. EMBO J 17:6086–6095
103. Tzfira T, Frankman LR, Vaidya M, Citovsky V (2003) Site-specific integration of *Agrobacterium tumefaciens* T-DNA via double-stranded intermediates. Plant Physiol 133: 1011–1023
104. Lloyd A, Plaisier CL, Carroll D, Drews GN (2005) Targeted mutagenesis using zinc-finger nucleases in *Arabidopsis*. Proc Natl Acad Sci USA 102:2232–2237
105. Wright DA, Townsend JA, Winfrey RJ Jr, Irwin PA, Rajagopal J, Lonosky PM, Hall BD, Jondle MD, Voytas DF (2005) High-frequency homologous recombination in plants mediated by zinc-finger nucleases. Plant J 44:693–705
106. Cai CQ, Doyon Y, Ainley WM, Miller JC, DeKelver RC, Moehle EA, Rock JM, Lee Y-L, Garrison R, Schulenberg L, Blue R, Worden A, Baker L, Faraji F, Zhang L, Holmes MC, Rebar EJ, Collingwood TN, Rubin-Wilson B, Gregory PD, Urnov FD, Petolino JF (2009) Targeted transgene integration in plant cells using designed zinc finger nucleases. Plant Mol Biol 69:699–709
107. Carroll D, Morton JJ, Beumer KJ, Segal DJ (2006) Design, construction and *in vitro* testing of zinc finger nucleases. Nat Protoc 1:1329–1341
108. De Buck S, Van Montagu M, Depicker A (2001) Transgene silencing of invertedly repeated transgenes is released upon deletion of one of the transgenes involved. Plant Mol Biol 46:433–445
109. Hobbs SLA, Kpodar P, DeLong CMO (1990) The effect of T-DNA copy number, position and methylation on reporter gene expression in tobacco transformants. Plant Mol Biol 15:851–864
110. Assaad FF, Tucker KL, Signer ER (1993) Epigenetic repeat-induced gene silencing (RIGS) in *Arabidopsis*. Plant Mol Biol 22:1067–1085
111. Sijen T, Wellink J, Hiriart J-B, van Kammen A (1996) RNA-mediated virus resistance: role of repeated transgenes and delineation of targeted regions. Plant Cell 8: 2277–2294
112. de Carvalho F, Gheysen G, Kushnir S, Van Montagu M, Inzé D, Castresana C (1992) Suppression of β-1, 3-glucanase transgene expression in homozygous plants. EMBO J 11:2595–2602
113. De Neve M, De Buck S, De Wilde C, Van Houdt H, Strobbe I, Jacobs A, Van Montagu M, Depicker A (1999) Gene silencing results in instability of antibody production in transgenic plants. Mol Gen Genet 260:582–592
114. Ingelbrecht I, Van Houdt H, Van Montagu M, Depicker A (1994) Posttranscriptional silencing of reporter transgenes in tobacco correlates with DNA methylation. Proc Natl Acad Sci USA 91:10502–10506
115. Stam M, de Bruin R, Kenter S, van der Hoorn RAL, van Blokland R, Mol JNM, Kooter JM (1997) Post-transcriptional silencing of chalcone synthase in *Petunia* by inverted transgene repeats. Plant J 12:63–82
116. Jones JDG, Gilbert DE, Grady KL, Jorgensen RA (1987) T-DNA structure and gene expression in petunia plants transformed by *Agrobacterium tumefaciens* C58 derivatives. Mol Gen Genet 207:478–485

117. Van Houdt H, Kova_ík A, Van Montagu M, Depicker A (2000) Cross-talk between posttranscriptionally silenced neomycin phosphotransferase II transgenes. FEBS Lett 467:41–46
118. De Buck S, Depicker A (2001) Disruption of their palindromic arrangement leads to selective loss of DNA methylation in inversely repeated *gus* transgenes in Arabidopsis. Mol Genet Genomics 265:1060–1068
119. Vaucheret H (1993) Identification of a general silencer for 19S and 35S promoters in a transgenic tobacco plant: 90 bp of homology in the promoter sequence are sufficient for trans-inactivation. CR Acad Sci Paris, Life Sci 316:1471–1483
120. Hutvágner G, Mlynárová L, Nap J-P (2000) Detailed characterization of the posttranscriptional gene-silencing-related small RNA in a GUS gene-silenced tobacco. RNA 6:1445–1454
121. Matzke AJM, Neuhuber F, Park Y-D, Ambros PF, Matzke MA (1994) Homology-dependent gene silencing in transgenic plants: epistatic silencing loci contain multiple copies of methylated transgenes. Mol Gen Genet 244:219–229
122. Hagan ND, Spencer D, Moore AE, Higgins TJV (2003) Changes in methylation during progressive transcriptional silencing in transgenic subterranean clover. Plant Biotechnol J 1:479–490
123. Meza TJ, Enerly E, Børud B, Larsen F, Mandal A, Aalen RB, Jakobsen KS (2002) A human CpG island randomly inserted into a plant genome is protected from methylation. Transgenic Res 11:133–142
124. Fischer U, Kuhlmann M, Pecinka A, Schmidt R, Mette MF (2008) Local DNA features affect RNA-directed transcriptional gene silencing and DNA methylation. Plant J 53:1–10
125. Brunner AM, Li J, DiFazio SP, Shevchenko O, Montgomery BE, Mohamed R, Wei H, Ma C, Elias AA, VanWormer K, Strauss SH (2007) Genetic containment of forest plantations. Tree Genet Genomes 3:75–100
126. De Wilde C, Van Houdt H, De Buck S, Angenon G, De Jaeger G, Depicker A (2000) Plants as bioreactors for protein production: avoiding the problem of transgene silencing. Plant Mol Biol 43:347–359
127. Hamilton AJ, Brown S, Yuanhai H, Ishizuka M, Lowe A, Alpuche Solis A-G, Grierson D (1998) A transgene with repeated DNA causes high frequency, post-transcriptional suppression of ACC-oxidase gene expression in tomato. Plant J 15:737–746
128. De Buck S, Depicker A (2004) Gene expression and level of expression. In: Christou P, Klee H (eds) Handbook of plant biotechnology, vol 1. Wiley, Chichester, pp 331–345
129. De Buck S, Peck I, De Wilde C, Marjanac G, Nolf J, De Paepe A, Depicker A (2007) Generation of single-copy T-DNA transformants in *Arabidopsis* by the CRE/*loxP* recombination-mediated resolution system. Plant Physiol 145:1171–1182
130. Marjanac G, De Paepe A, Peck I, Jacobs A, De Buck S, Depicker A (2008) Evaluation of CRE-mediated excision approaches in *Arabidopsis thaliana*. Transgenic Res 17:239–250
131. Coppoolse ER, de Vroomen MJ, Roelofs D, Smit J, van Gennip F, Hersmus BJM, Nijkamp HJJ, van Haaren MJJ (2003) Cre recombinase expression can result in phenotypic aberrations in plants. Plant Mol Biol 51:263–279
132. Vergunst AC, Schrammeijer B, den Dulk-Ras A, de Vlaam CMT, Regensburg-Tuïnk TJG, Hooykaas PJJ (2000) VirB/D4-dependent protein translocation from *Agrobacterium* into plant cells. Science 290:979–982
133. Verweire D, Verleyen K, De Buck S, Claeys M, Angenon G (2007) Marker-free transgenic plants through genetically programmed auto-excision. Plant Physiol 145:1220–1231
134. Srivastava V, Anderson OD, Ow DW (1999) Single-copy transgenic wheat generated through the resolution of complex integration patterns. Proc Natl Acad Sci USA 96:11117–11121
135. Srivastava V, Ow DW (2001) Single-copy primary transformants of maize obtained through the co-introduction of a recombinase-expressing construct. Plant Mol Biol 46:561–566
136. Kilby NJ, Davies GJ, Snaith MR, Murray JAH (1995) FLP recombinase in transgenic plants: constitutive activity in stably transformed tobacco and generation of marked cell clones in *Arabidopsis*. Plant J 8:637–652
137. Kumar S, Thompson WF (2009) Simultaneous excision of two transgene flanking sequences and resolution of complex integration loci. Plant Mol Biol 69:23–32
138. Vergunst AC, Jansen LET, Hooykaas PJJ (1998) Site-specific integration of *Agrobacterium* T-DNA in *Arabidopsis thaliana* mediated by Cre recombinase. Nucleic Acids Res 26: 2729–2734
139. Srivastava V, Ow DW (2001) Biolistic mediated site-specific integration in rice. Mol Breed 8:345–349
140. Srivastava V, Ow DW (2004) Marker-free site-specific gene integration in plants. Trends Biotechnol 22:627–629
141. Chawla R, Ariza-Nieto M, Wilson AJ, Moore SK, Srivastava V (2006) Transgene expression produced by biolistic-mediated, site-specific gene integration is consistently inherited by the subsequent generations. Plant Biotechnol J 4:209–218
142. Nanto K, Sato K, Katayama Y, Ebinuma H (2009) Expression of a transgene exchanged by the recombinase-mediated cassette exchange (RMCE) method in plants. Plant Cell Rep 28:777–785
143. Li Z, Xing A, Moon BP, McCardell RP, Mills K, Falco SC (2009) Site-specific integration of transgenes in soybean via recombinase-mediated DNA cassette exchange. Plant Physiol 151:1087–1095
144. Hansen G, Chilton M-D (1996) "Agrolistic" transformation of plant cells: integration of T-strands generated *in planta*. Proc Natl Acad Sci USA 93:14978–14983
145. Hansen G, Shillito RD, Chilton M-D (1997) T-strand integration in maize protoplasts after codelivery of a T-DNA substrate and virulence genes. Proc Natl Acad Sci USA 94:11726–11730

146. De Block M, Debrouwer D, Moens T (1997) The development of a nuclear male sterility system in wheat. Expression of the barnase gene under the control of tapetum specific promoters. Theor Appl Genet 95:125–131
147. Dalmay T, Hamilton A, Rudd S, Angell S, Baulcombe DC (2000) An RNA-dependent RNA polymerase gene in *Arabidopsis* is required for posttranscriptional gene silencing mediated by a transgene but not by a virus. Cell 101:543–553
148. Mourrain P, Béclin C, Elmayan T, Feuerbach F, Godon C, Morel J-B, Jouette D, Lacombe A-M, Nikic S, Picault N, Rémoué K, Sanial M, Vo T-A, Vaucheret H (2000) *Arabidopsis SGS2* and *SGS3* genes are required for posttranscriptional gene silencing and natural virus resistance. Cell 101:533–542
149. Verdaguer B, de Kochko A, Beachy RN, Fauquet C (1996) Isolation and expression in transgenic tobacco and rice plants of the cassava vein mosaic virus (CVMV) promoter. Plant Mol Biol 31:1129–1139
150. Goossens A, Dillen W, De Clercq J, Van Montagu M, Angenon G (1999) The *arcelin-5* gene of *Phaseolus vulgaris* directs high seed-specific expression in transgenic *Phaseolus acutifolius* and *Arabidopsis* plants. Plant Physiol 120: 1095–1104

Transgenic Crops Resistant to Fungal, Bacterial and Viral Pathogens

Tennant Paula[1], Fuchs Marc[2]
[1]Department of Life Sciences, University of the West Indies, Mona, Kingston, WI, Jamaica
[2]Department of Plant Pathology and Plant-Microbe Biology, Cornell University, New York State Agricultural Experiment Station, Geneva, NY, USA

Article Outline

Glossary
Definition of the Subject
Introduction
Transgenic Resistance to Fungal Pathogens
Transgenic Resistance to Bacterial Pathogens
Transgenic Resistance to Viral Pathogens
Status of Commercialized Disease Resistant Transgenic Crops
Conclusions
Future Directions
Bibliography

Glossary

Bacterium A unicellular, prokaryotic microorganism with a wide range of shapes that is surrounded by a lipid membrane and a cell wall made of peptidoglycan, and has few intracellular structures, no nucleus but a single circular chromosome located in the cytoplasm and reproduces by binary fission.

Fungus A eukaryotic organism such as a yeast or a mold, with cell walls that contain glucans and chitin, membrane-bound nuclei with chromosomes and cytoplasmic organelles, soluble carbohydrates, and storage compounds, and exhibits enormous diversity in life cycle strategies, morphologies, and ecologies.

Pathogen An infectious agent that causes disease to its host.

Pathogenicity The capacity of a pathogen to cause disease.

Pathogenicity factors Products encoded by a pathogen that are crucial for the establishment of disease, e.g., proteins involved in the attachment of the pathogen to the plant surface or penetration and colonization of the host.

Resistance The reaction of a host to a pathogen that derives from preformed defenses and/or defense responses induced following infection.

Systemic acquired resistance (SAR) A mechanism of induced defense that acts nonspecifically throughout the plant, is associated with the accumulation of pathogenesis-related proteins and requires the signal molecule, salicylic acid.

Transgenic plant A plant that results from the application of recombinant DNA and plant tissue culture technologies.

Virus A small obligate parasite that utilizes the cellular metabolic pathways of its host organism to replicate its genes which are made up of deoxyribonucleic or ribonucleic acid and are encapsidated in a protein coat.

Definition of the Subject

Loss of crops due to fungal, bacterial, and viral diseases can have a large impact on human food supplies and local economies, as well as on the social stability of rural communities. It is conservatively estimated that diseases, insects, and weeds together cause 30–40% loss of all crops worldwide [1]. Annual losses worldwide

due to plant diseases are estimated to ~14% of total losses and about $220 billion. In addition, the need for measures to control diseases limits the acreage of land available for cultivation, restricts the crops that can be grown in fields already contaminated with certain pathogens and necessitates the use of agrochemicals for treating seeds, fumigating soils, spraying plants, and applying fruit postharvest treatments. Such control measures add to the cost of food production and toxic chemicals can be harmful to human health and the environment [1].

Since the beginning of agriculture, crop plants have been domesticated and improved for various traits such as increased yield, improved nutritious composition, enhanced disease resistance, and tolerance to abiotic factors, among others. The selection and use of resistant crop cultivars is the most efficient and most environmentally friendly strategy to mitigate the impact of fungal, bacterial, and viral diseases. Resistance to pathogens can be achieved by application of disease-suppressing cultural practices, use of plant defense-promoting substances, deployment of biological agents antagonistic to the pathogens that cause disease, agrochemicals, conventional breeding strategies, and genetic engineering [1]. The need for controlling plant diseases effectively is not only a major challenge, but also a necessity to reduce food losses while improving food quality and safeguarding the environment.

The advent of molecular genetics and plant transformation, in combination with an increased understanding of pathogen–host interactions, has opened new avenues for the development of disease-resistant crops through genetic engineering. Research groups from academia and industry created the first transgenic plants in the early 1980s [2–5]. These early transgenic plants were laboratory specimens (tobacco, petunia, and sunflower). Subsequent research developed transgenic plants, including horticultural crops, with useful traits such as disease resistance. Transgenic crops resistant to fungal, bacterial, and viral diseases were created following extensive research. The first disease-resistant transgenic crop, i.e., a virus-resistant transgenic summer squash, was deregulated in the USA in 1994. Several cultivars derived from the deregulated transgenic summer squash lines were commercialized in the USA in 1996 [6]. The adoption rate of virus-resistant transgenic summer squash has been increasing steadily since the initial releases. Other commercially available virus-resistant transgenic crops include papaya in the USA, and sweet pepper and tomato in the People's Republic of China. Transgenic crops resistant to fungal and bacterial diseases have been developed and evaluated under field conditions. However, in spite of remarkable progress, their development and release lags behind virus-resistant transgenic crops.

Introduction

Plants provide microorganisms, including viruses, with a diversity of habitats [7]. Ensuing interactions are either detrimental or beneficial and are classified as neutralism, commensalism, synergism, mutualism, amensalism, or parasitism. It is the latter association that has been a major challenge to crop production for centuries.

In the parasitic interaction, an organism lives within the plant host or on its outer surfaces and obtains its nutrients from the latter [1]. The removal of nutrients often affects normal growth and development of the plant and may be associated with pathogenicity. Virus infections commonly result in the inhibition of plant growth as well as the development of undesirable morphological changes and decreased yield [8]. Unlike fungal and bacterial pathogens, viruses induce disease in plant hosts primarily by utilizing cellular components and disrupting cellular processes. Fungi are responsible for diseases referred to as blight, gray mold, bunts, powdery, and downy mildews. These microbes have evolved at least three strategies that lead to less-than-healthy plants; enzymes that breakdown the plant cell wall and cuticle, toxins that either reduce the activity of the host cells or inhibit it completely, and plant-specific hormones that interfere with the hormonal equilibrium of the plant cell [9]. Bacterial pathogens cause pre- and post-harvest diseases that are characterized by cankers, galls, wilts, spotting of leaves, and stem or fruit rots of various vegetable and fruit crops. The invasion of healthy plant tissue through a wound or an area of dead or dying tissue is generally followed by the initiation of infection, which is similar to that of fungi, and is associated with the breakdown of cell walls, the production of toxins, exo-polysaccharides or proteins that mimic plant hormones.

Plant diseases, whether initiated by viruses, bacteria, or fungi, are of paramount importance because of the destruction they cause to plants and plant products. The effects not only threaten crop productivity and reduce farmers' net income, but also the food supply, and by extension, the economies of rural areas and even countries [10]. Zadoks and Schein [11] differentiate between primary and secondary losses and direct and indirect losses. Primary losses refer to those sustained because of plant disease (before or after harvest) in yield or wages, while secondary losses are losses of future production capacity. On the other hand, losses in quality, quantity, and production capacity, and socioeconomic losses are classified as direct and indirect losses, respectively.

Disease control efforts to date have focused on various crop husbandry techniques including crop rotation, and the avoidance of spread of infested soil and pathogen-carrying plant materials. The most widely used management strategy is the application of agrochemicals, particularly against fungal pathogens. Chemical protection against bacterial pathogens is not as evolved as that against fungi, and is not applicable to viruses. The most widely used methods against bacterial diseases primarily center on phytosanitary practices, harvesting techniques, and storage conditions, and eventually on the use of antibiotics. However, the intensive use of agrochemicals has led to the development of resistance in various microbial populations and in some cases the chemicals are no longer used because of their high toxicity or problems with persistence in the soil. Nowadays, the focus is on strategies that allow for crop production with minimal use of agrochemicals. The most effective strategy to mitigate the impact of diseases on agriculture involves breeding-resistant crop cultivars. The majority of the cultivars available today have been generated through the classical method of hybridization [12] and the introgression of genes responsible for resistance. Resistant plants ward off pathogen attack by an innate immunity of each cell, systemic signals emanating from infection sites and a suite of cellular responses that follow the activation of the gene for resistance. However, there are many pathogens for which no effective sources of disease resistance have been identified. Technologies such as genetic engineering and gene transfer methods offer an alternative means for the development of disease resistant cultivars. In contrast to conventional breeding which involves the random mixing of the tens of thousands of genes present in both the resistant and susceptible plant, the latter technology allows the transfer of only the resistance gene to the susceptible plant and the preservation of its valuable economic traits. Moreover, the genetic sources for disease resistance are not limited to closely related plant species. During the last decade, considerable progress has been made in the development of virus resistant transgenic plants, while the development of fungal- and bacterial-resistant transgenic plants has lagged behind.

This chapter examines the different strategies devised for the development of resistance to fungal, bacterial, and viral diseases through genetic engineering. A description of the genes employed to confer resistance against given pathogens and the mechanisms underlying engineered resistance are provided. Emphasis will be on horticultural crops and the recent applications of transgenic resistance to agriculture. Factors affecting the development, release, and adoption of transgenic crops with resistance to fungal, bacterial, and viral diseases will be identified and discussed. The final sections offer overall conclusions, cover the impending direction of the development of transgenic disease resistance and some reflection on the impact of transgenic crops resistant to fungi, bacteria, and viruses in terms of effective disease management, mitigation of disease impact on agriculture, improved production of quality food, and better preservation of the environment.

Transgenic Resistance to Fungal Pathogens

Plants have evolved a complex pathogen defense system that is driven by tight balances between the induction of specific defense pathways and cell death. Much progress has recently been made in identifying and understanding a number of the genes and gene products involved in these defenses as well as the signaling pathways. The findings have prompted the development of a variety of strategies for producing fungus-resistant transgenic plants that are based on the manipulation of the plant's innate defense system, the production of antifungal proteins or the neutralization of fungal pathogenicity factors.

The earliest strategy employed in the development of resistance against fungal pathogens involved the

enhancement of the plant's natural defenses through the overexpression of pathogenesis-related proteins (PR- proteins). PR- proteins form part of the general resistance mechanism in plants, that is, systemic acquired resistance (SAR), which is induced by necrotizing pathogens or by treatment with chemicals such as salicylic acid. Initial studies on the development of fungus-resistant transgenic plants examined the effects of expressing a single PR-protein gene in transgenic plants, while later studies looked at the co-expression of combinations thereof, in an attempt to improve on the levels of resistance, to target a wider spectrum of fungal pathogens and to provide longer-term protection.

In 1991, Broglie and coworkers [13] reported on the first fungus-resistant transgenic plants. Transgenic tobacco and rapeseed plants, transformed with a chitinase gene isolated from bean, exhibited enhanced resistance against the soil-borne fungus, *Rhizoctonia solani*. Presumably, expression of the chitinase transgene played a dual role in protecting against infection; that is, the enzyme inhibited growth of the pathogen by cell wall digestion and the released pathogen-borne elicitors induced additional defense reactions in the plants. Following the first pioneering work of Broglie et al. [13], Lorito et al. [14] showed that an endochitinase gene (*ThEn-42*) from the mycoparasitic fungus, *Trichoderma harzianum*, conferred similar resistance to the fungal pathogens, *Alternaria alternata, A. solani, Botrytis cinerea*, and *Rhizoctonia solani* in transgenic tobacco and potato (cv. 'Desiree'). The effectiveness of glucanase, another PR-protein, in transgenic plants was demonstrated in banana transformed with β-1, 3 glucanase from soybean. Increased protection was observed when transgenic banana was infected with *Fusarium oxysporum* f. sp. *cubense* [15]. Further, the combinatorial expression of two chitinase genes [16] or chitinase and glucanase genes was found to give increased levels of protection than the expression of the PR-proteins in single transformants [17]. Subsequent strategies employed the co-expression of transgenes encoding differently acting antifungal proteins with similar results. For example, ÓBrian et al. [18] confirmed protection against *Rhizoctonia solani* in transgenic tobacco carrying three barley proteins; chitinase, β-1, 3 glucanase, and plant ribosome-inactivating protein (RIP). While the first two enzymes targeted the cell wall of the pathogen, RIP targeted and inactivated fungal ribsomes. RIPs possess N-glycosidase activity and catalyze the removal of an adenine residue from the 28S rRNA, thus inhibiting protein elongation.

Another emerging strategy against fungal pathogens involves the use of genes encoding small cysteine-rich antifungal proteins. These proteins play a role in the plant's innate defense mechanism and include thionins, defensins, and lipid transfer proteins.

The antimicrobial activities of thionins are well known, particularly those found in barley. Antimicrobial action, most likely based on the induction of membrane permeabilization resulting in cell disruption and death, is not limited to fungi and these proteins are effective against bacteria and oomycetes. Given this growth inhibition activity, transgenic plants overexpressing thionins have been generated to provide fungal resistance. Epple et al. [19] overexpressed an endogenous endothionin *Thi2.1* gene in *Arabidopsis thaliana* and observed enhanced resistance against *Fusarium oxysporum* f. sp. *matthiolae*. Similar levels of resistance were obtained with *Thi2.1* transgenic tomato against bacterial and Fusarium wilt [20].

Other small cysteine- rich proteins referred to as defensins are increasingly becoming recognized as candidates of defense transgenes. Defensins were originally called γ-thionins due to similarities to *a*- and *b*-thionins, but it was later shown that the former proteins shared appreciable structural and functional commonalities to insect and mammalian defensins, hence the name change. As with thionins, the mechanism of action has yet to be confirmed. However there is strong evidence of the induction of ion fluxes across the plasma membranes of living fungal hyphae followed by interactions with glycosylceramides at the fungal cell surface. Expression of single-protein defensin gene constructs has been deployed in transgenic plants as well as cleavable, chimeric polyprotein constructs in an attempt to increase expression levels in planta and to introduce broad-spectrum resistance. The constitutive expression of a mustard defensin conferred resistance to *Fusarium moniliforme* and *Phytophthora parasitica* pv. *nicotianae* in tobacco and *Pheaoisariopsis personata* and *Cercospora arachidicola*, which jointly cause late leaf spot disease in peanuts [21]. François et al. [22] engineered a polyprotein construct using defensin genes *DmAMP1*

from *Dahlia merckii* seeds and *Rs-AFP2* from *Raphanus sativus* seeds. The genes were joined by a linker peptide obtained from *Impatiens balsamina* seeds [22] and used for the transformation of *Arabidopsis*. Antifungal activity was obtained against *Fusarium culmorum* in in vitro assays using purified fractions from extracellular fluids of the transgenic plants.

Lipid transfer proteins (LTPs) are the third group of small cysteine-rich antifungal proteins (ca. 10 KDa) found in higher plants. As the name implies, LTPs are involved in shuttling phospholipids and other fatty acid groups between cell membranes and bind acyl chains; culminating in membrane permeabilization and a direct cytotoxic effect on fungal cells. Constitutive expression of pepper (cv. Habanero) LTPs, *CALTPI*, and *CALTPII*, in tobacco conferred enhanced resistance to *Phytophthora nicotianae* and the bacterial pathogen, *Pseudomonas syringae* pv. *tabaci* [23]. When a wheat LTP (*Ltp3F1*) was linked with a chitinase gene from barley (*chi2*) and transformed into carrots, reduced disease symptoms against necrotrophic foliar fungal pathogens, *Alternaria radicicola* and *Botrytis cinerea*, were obtained; 95% for *Botrytis* and 90% for *Alternaria* infection compared to 40–50% for single-gene transformants [24].

Phytoalexins are another group of plant secondary metabolites with primarily antifungal activity that have been exploited in the development of fungus-resistant transgenic plants. These metabolites are of low molecular weight (ca. <1,000 Da) and are synthesized or accumulated in response to infection or stress related to infection. Resveratrol is the best studied phytoalexin of grapevine that is synthesized from the precursors, malonyl-CoA and *p*-coumaroyl-CoA, by the action of stilbene synthase. Apparently, the accumulation of resveratrol upon infection triggers the synthesis of a fungal phenol oxidase that results in self-intoxication through the conversion of resveratrol to a more toxic dimmer, viniferin. Grapevine stilbene synthase transformation of tomato and papaya [25] introduced increased protection against *Botrytis cinerea* and *Phytophthora palmivora,* respectively. However, in other cases, e.g., strawberry, increased resistance was not obtained [26].

Increased evidence in recent years indicate the possibility of achieving improved resistance in transgenic plants expressing transcription factors that participate in the regulation of plant defense responses. Five major families of plant transcription factors have been described; basic region/leucine zipper motif (bZIP), zinc finger motif WRKY, MYB, ethylene-responsive element binding proteins (EREBP), and homeodomain proteins. Transcription factors play a crucial role in the transmission of pathogen-derived defense signals. They are involved either in the activation or suppression of downstream defense gene expression or the regulation of cross-talk between different signaling pathways. Presumably the mode of action is by binding promoter elements (W-box) of SAR gene promoters. Thus, the strategy is particularly attractive as the constitutive expression of a transcription factor may also modify the expression of all genes under its regulation. Solano et al. [27] engineered transgenic *Arabidopsis* plants with the ethylene-response-factor 1 (*ERF1*), an early ethylene-response gene that is regulated by the ethylene-insensitive gene EIN3 and, which in turn, regulates the expression of several pathogen responsive genes. The transgenic plants showed a clear reduction in *Botrytis cinerea* infection, with 40–70% of plants remaining symptomless after challenge and never developing macroscopic or microscopic necrosis. *ERF1* also mediated *Arabidopsis* resistance against the soil borne fungi, *Fusarium oxysporum* sp. *conglutinans* and *F. oxysporum* f. sp. *lycopersici* [28]. An ERF transcription factor (*GbERF2*) gene derived from cotton enhanced the resistance of transgenic tobacco to fungal infection by *Alternaria longipes* [29]. The accumulation of *GbERF2* transcripts along with transcripts of PR-proteins, such as *PR-1b*, *PR2*, and *PR4*, were detected.

Rather than using strategies based on the overexpression of PR-proteins or transcription factors that are induced during SAR for enhanced fungal resistance, other researchers have examined the effects of the constitutive expression of signaling molecules that play an important role in the induction of defense proteins. Components of the elicitor-receptor system were used to generate these transgenic plants. The system, explained by the gene-of gene-model, is the major line of plant defense against pathogens. Essentially, a pathogen protein encoded by an avirulence gene (*Avr*) is recognized by a plant protein encoded by a resistance gene (*R*), resulting in the activation of a number of defense mechanisms including the

hypersensitive reaction and the restriction of the pathogen at the site of infection. Thus resistance against fungal pathogens carrying a particular *Avr* gene is introduced via the transfer of the corresponding *R* gene from a resistant plant to a susceptible plant. The success and durability of the strategy correlates strongly on the ability of the *R* gene product to recognize *Avr* proteins secreted by most if not all of the races of the pathogen. During the last decade, several sequences of *R* genes have been characterized into five classes according to their functional domains. Three classes contain leucine-rich repeats. The most common class encodes proteins with an amino-terminal nucleotide-binding site (NBS) and a carboxy-terminal leucine-rich repeat (LRR) and confers resistance against nematodes, sucking insects, viruses, bacteria, oomycetes, and fungi. The proof of concept has been conducted with the model system, tobacco, as well as various economic crops. Rice plants transgenic for the *R* gene alleles, *Pi9*, *Pi2*, and *Piz*, against the rice blast fungus, *Magnaporthe grisea,* were reported highly resistant to 43 isolates collected from 13 countries [30]. In flax, three alleles of the flax rust resistance gene, *L* (*L2*, *L6*, and *L10*) when transformed into a highly susceptible rust cultivar, unequivocally demonstrated resistance against strains of pathogen (*Melampsora lini*) with the corresponding *Avr* gene [31]. Increased resistance was also obtained when transgenic tobacco transformed with the same three flax genes was challenged with two pathogens of tobacco. Increased resistance was conferred against *Cercospora nicotianae* and the oomycete, *Phytophthora parasitica* pv. *nicotianae* in *L6* transgenics and one *L10* transgenic plant [32]. Resistance was attributed to the constitutive expression of defense genes rather than recognition of the pathogens by the *L6* gene product. Of note, the *L6* transgenic plants exhibited a stunted phenotype.

Another arm of the plants' innate defense that is being investigated is that of RNA silencing. Accumulating evidence suggests the involvement of small interfering RNAs (siRNAs) and microRNAs (miRNAs) in the response to fungal pathogens. The involvement of plant siRNAs, short, noncoding RNAs between 20 and 24 nucleotides (nt) in length, have been implicated in the defense against viruses, and more recently bacterial pathogens, and is discussed in a later section of the chapter. miRNAs comprise the 21-nt class of siRNAs and short-interfering RNAs comprise the 24- nt class of siRNAs. Work with pine and the canker- forming rust fungus, *Cronartium quercuum* f. sp. fusiforme, identified 82 putative miRNA targets, including NBS-LRR proteins, receptor-like kinases, laccases, and MYB transcription factors, which are most likely associated with disease responses that restrict fungal growth [33]. Ellendorff et al. [34] showed that RNA silencing plays a role in the defense against *Verticillium* in *Arabidopsis*, but the siRNA involved were not identified. Further research into the targets and processes will invariably have broad implications in potentiating basal defenses against fungal phytopathogens.

Other strategies have explored the development of enhanced resistance through the expression of gene products that target components of the arsenal of the fungus. One approach employed the transformation a susceptible cultivar with sequences encoding polygalacturonase inhibiting proteins (PGIPs). PGIPs, proteins structurally related to several resistance gene products, are expressed in the cell wall of a number of plants and belong to a superfamily of LRR proteins, suggesting involvement in pathogen recognition. These proteins inhibit the activity of fungal endo-polygalacturonases presumably by binding at either the substrate binding site or the underside of the endo-polygalacturonase. The resulting oligogalacturonides induce a range of defense responses. *Arabidopsis* plants overexpressing *PGIP* isolated from pear showed decreases in disease symptoms produced by *Botrytis cinerea* [35]. Similarly, transgenic wheat accumulating bean PGIP developed smaller lesions when challenged with the necrotropic fungus, *Bipolaris sorokiniana* [36]. In earlier studies with transgenic tomato carrying a PGIP transgene isolated from bean, enhanced resistance against *Fusarium oxysporum* f. sp. *lycopersici, Botrytis cinerea,* and *Alternaria solani* was not obtained [37].

Another component of the arsenal that some fungi (e.g., *Sclerotinia sclerotiorum*) use to infect plants that is regarded as a pathogenicity factor is oxalate. Oxalic acid apparently assists in initiating infection through acidification, which facilitates cell wall–degrading enzyme activity, through pH-mediated tissue damage, or via the sequestration of calcium ions. Evidence for the utility of hydrogen peroxide–generating enzymes in protective plant responses was provided by the expression of oxalate oxidase, which catalyzes the degradation

of oxalic acid to produce carbon dioxide and hydrogen peroxide (H_2O_2). Essentially increased H_2O_2 production limits the growth of the invading pathogen in planta and triggers the activation of a range of defense responses. Sunflower and tomato transformed with a wheat oxalate oxidase gene exhibited increased resistance to *Sclerotinia sclerotiorum* [38, 39]. Potato (cv. Bintje) and poplar expressing the same gene showed increased resistance to *S. musiva* [40] and the oomycete, *Phytophthora infestans* [41], respectively.

Transgenic Resistance to Bacterial Pathogens

Knowledge of bacteria–host interactions, in particular of the mechanisms of pathogenesis, and efforts to bolster plant defense mechanisms, has provided a strong basis for implementing transgenic approaches for bacterial disease management. Several strategies aiming at the lysis or prevention of bacterial growth have been investigated based on the use of bacterial-resistance genes, avirulence genes, expression of antibacterial peptides that act as bactericidal or bacteriolytic agents, and the application of the concept of pathogen-derived resistance. The latter describes the use of genetic elements from a pathogen's own genome to confer resistance in an otherwise susceptible host via genetic engineering [42].

Members of the NBS-LRR class of disease *R* genes have been employed to provide effective protection against bacteria when transferred into new species. Transformation of a susceptible rice cultivar with the resistance gene *Xa21* that was isolated from a resistant rice line and characterized by positional sequencing and functional genetics conferred resistance to *Xanthomonas oryzae* [43]. Field tests of *Xa21* transgenic rice have shown satisfactory results in the Philippines, India, and the People's Republic of China [44], but deregulation of transgenic *Xa21* rice is still pending. It should be noted that hybrid rice containing *Xa21* was developed by conventional breeding [45]. Similarly, *Xa1* provided resistance to *Xanthomonas oryzae* pv. *oryzae* in transgenic rice [46]. Rice expressing an *R*-gene from maize were resistant against *Xanthomonas oryzae* pv. *oryzicola* [47]. Also, *Bs2* of pepper confers resistance to *Xanthommonas campestris* pv. *vesicatoria* in transgenic tomato [48]. Tomato plants expressing *Pto* showed resistance to *Pseudomonas syringae* pv. *tomato* and *Xanthomonas campestris* pv. *versicatoria* [49]. The transgenic approach based on *R*-genes circumvents tedious crosses and backcrosses of conventional breeding as well as linkages to undesired traits.

Another approach to confer resistance to bacterial diseases is based on the use of lytic peptides from insects that form pores in bacterial membranes. For example, cecropins are bactericidal peptides from the giant silk moth, *Hyalophora cecropia*, which interact with bacterial membranes and form transient ion channels. The peptides are active against a wide range of plant pathogenic bacteria including *Erwinia carotovora*, *E. amylovora*, *Pseudomonas syringae*, *Ralstonia solanacearum*, and *Xanthomonas campestris*. Native, mutant (SB37 and MB39) or synthetic polypeptides (Shiva-1 and D4E1) that are designed for increased activity have been used for engineered resistance against bacterial diseases. Infection caused by *Erwinia carotovora* sp. *atroseptica* is reduced in transgenic potato expressing the Shiva-1 and SB-37 lytic peptide analogs [50]. Transgenic apple trees expressing SB-37 showed increased resistance to *E. amylovora* in field tests [51]. Poplar expressing D4E1 had more resistance to *Agrobacterium tumefaciens* and *Xanthomonas populi* than control nontransformed trees [52, 53]. Attacin is another small protein from the giant silk moth with antibacterial activity that inhibits synthesis of the outer bacterial membrane. Transgenic potato attacin expression has enhanced resistance to *Erwinia carotovora* sp. *atrospetica* [50]. Attacin [54] as well as lactoferrin [55] provide enhanced resistance against *Erwinia amylovora* in pear. Similarly, transgenic apple expression of the attacin E gene exhibit enhanced resistance to *Erwinia amylovora* [56] even under field conditions [57].

Lysozymes from various sources have been exploited in the development of transgenic resistance against bacterial diseases. Lysozymes are ubiquitous bacteriolytic enzymes that cleave the murein layer of bacterial petidoglycan, resulting in a weakening of the bacterial cell wall. A chimeric bacteriophage T4 lysozyme fused to a plant signal peptide reduces the susceptibility of transgenic potato plants to *Erwinia carotovora* spp. *atroseptica* [58]. Transgenic apple trees with the bacteriophage T4 lysozyme exhibited significant resistance to fire blight infection [59] and the bovine lysozyme isozyme was shown to confer

resistance to *Xanthomonas campestris* in tomato, rice, and potato [60].

Tachyplesin, an antibacterial peptide isolated from the horseshoe crab (*Tachypleus tridentatus*), reduces the incidence of rubber rot caused by *E. carotovora* in transgenic potato [61].

Reactive oxygen species play important roles in various defense responses of plants, including pathogen infection. A prolonged local oxidative burst is one of the earliest events correlated with plant resistance at the site of pathogen invasion; see the previous section for detailed information on the role of oxalate oxidase in plant defense responses. Transgenic potato tubers expressing a glucose oxidase from *Aspergillus niger* for the production of large amounts of hydrogen peroxidase exhibit strong resistance to *Erwinia carotovora* [62].

Many bacteria control virulence factor expression by a cell-to-cell communication system referred to as quorum sensing. Disruption of bacterial quorum sensing has been proposed as a disease management strategy and several techniques with the potential to disrupt quorum sensing have been investigated. The enzyme *N*-acyl homoserine lactone (AHL)-lactonase (AiiA) isolated from the soil-borne *Bacillus* sp. 240B1, which catalyzes the degradation of AHL and attenuates symptoms caused by plant pathogens by degrading the quorum-sensing autoinducer AHL of the soft rot pathogen, *Erwinia carotovora*, induces enhanced resistance in transgenic potato [63].

Several pathovars of *Pseudomonas syringae* produce extracellular toxins that often increase their virulence toward plants. Phaseolotoxin is one such example. Phaseolotoxin is a modified tripeptide that inhibits the plant enzyme, ornithine carbamoyl transferase (OCTase), and is produced by the *P. syringae* pvs. *phaseolicola* and *actinidiae* as well as by a single strain of *P. syringae* pv. syringae, CFBP3388. Transgenic bean expressing *argK* that codes for a phaseolotoxin-insensitive OCTase show resistance to *Pseudomonas syringae* pv. *phaseolicola* [64].

An example of pathogen-derived resistance against a bacterial disease, crown gall, is reported by Krastanova et al. [65]. Based on an earlier report on the use of a truncated virE2 gene construct lacking the 215 C-terminal amino acids to confer resistance to grown gall disease in tobacco [66], these authors used a truncated form of *virD2* from *Agrobacterium tumefaciens* strains C58 and A6, and *Agrobacerium vitis* strain CG450 to engineer resistance to crown gall disease in transgenic grape rootstocks. Resistant lines show a substantial reduction in tumoreginicity and develop very small sized galls [65].

Other researchers used a different approach against the soil-borne bacterium, *Agrobacterium tumefaciens,* that utilized oncogenes of the phytopathogen. *Agrobacterium tumefaciens* possesses several oncogenes (e.g., *iaaM* and *ipt*) that trigger de novo synthesis of auxins and cytokinins to generate tumors following horizontal gene transfer into the plant genome. By expressing two self-complementary RNA constructs designed to initiate RNA interference (RNAi) of the *iaaM* and *ipt* oncogenes of *A. tumefaciens*, resistance to crown gall disease development was achieved in transgenic tomato plants. Transformed tomato lines display between 0.0% and 24.2% tumorigenesis, whereas controls averaged 100% tumorigenesis following stem inoculation with various strains of *A. tumefaciens* [67]. This mechanism of resistance is based on RNA silencing rather than the highly specific receptor–ligand-binding interactions characteristic of traditional plant resistance genes.

Manipulation of the plant's innate defense signaling pathways offers an alternative approach to conferring resistance against bacterial diseases by controlling a large number of induced genes either directly or indirectly. The nonexpressor of PR genes, *NPR1*, is a key regulatory gene of the salicylic acid-mediated systemic acquired resistance in *Arabidodpsis thaliana.* Moreover, *NPR1* plays a key role in ethylene and jasmonic acid signaling pathways that are involved in induced systemic resistance. Plants expressing *AtNPR1* are resistant to bacterial, fungal, and viral pathogens [68–70]. Similarly, transgenic carrots expressing *AtNPR1* are resistant to *Xanthomonas hortorum* as well as to fungal pathogens [71] and transgenic tomato plants expressing *AtNPR1* show enhanced resistance to *Ralstonia solanacearum* and to a lesser extent *to Xanthomonas campestris* [68]. When introduced into rice, *AtNPR1* confers resistance to the bacterial pathogen, *Xanthomonas oryzae* pv. *oryzae* [72]. Overexpression of the rice *AtNPR1* homolog, *OsNPR1*, also enhances resistance to *X. oryzae* pv. *oryzae* in rice [73] and overexpression of an apple

NPRI confers increased resistance to *Erwinia amylovora* in transgenic apple cultivar 'Galaxy' and transgenic apple rootstock M26 [74].

The involvement of endogenous siRNA and miRNAs in mediating the triggering of defense mechanisms against bacteria is an area of considerable interest. In spite of tremendous progress at identifying and sequencing siRNAs and miRNAs, information available on the involvement of endogenous small RNAs at mediating defense regulation is scarce. One miRNA (miR393) was recently shown to contribute to basal defense against bacteria by targeting auxin-signaling components [75]. Agorio and Vera [76] characterized an *Arabidopsis* ocp (overexpressor of cationic peroxidase) mutant that overexpresses the H_2O_2-responsive Ep5C promoter. The ocp11 mutant exhibits enhanced disease susceptibility to several virulent and avirulent *Pseudomonas syringae* strains. OCP11 was cloned and found to encode ARGONAUTE4 (AGO4), a component of the pathway that mediates the transcriptional gene silencing associated with siRNA. The mutant allele, ago4–1, was examined and found to be compromised in resistance to *P. syringae* [76]. This work provided insight into the involvement of small RNA gene silencing pathways in resistance to bacterial pathogens. Silencing the expression of key genes involved in pathogen–host interactions and disease susceptibility is opening new avenues for bacterial disease management.

Transgenic Resistance to Viral Pathogens

Transgenic resistance generally complements conventional breeding methodologies for the development of virus-resistant crops; however, the approach devised to engineer resistance against viral diseases differs from strategies employed in engineering resistance against fungal and bacterial diseases. This is due to the fact that viruses utilize cellular organelles and metabolic pathways for their replication. As such, they interfere with the basic functions in a living cell, unlike fungi and bacteria, which produce specialized reproductive structures or reproduce by binary fission. The approach to engineering resistance to viral diseases in crops essentially consists of activating anti-viral pathways of a natural, innate, and potent defense mechanism against viruses called RNA silencing [77–82].

Prior to the discovery of RNA silencing in the late 1990s and early 2000s, the concept of PDR [42] was commonly applied to engineering resistance against viral diseases. Initially, the viral coat protein gene was the preferred construct used to confer resistance to viruses in plants. However, it soon became apparent that almost any sequence derived from a viral genome, i.e., coat protein gene, movement protein gene, proteinase gene, RNA-dependent RNA polymerase gene, 5′ and 3′ noncoding regions, satellite RNA, defective interfering RNA, could provide resistance. Validated first in tobacco plants expressing the coat protein gene of *Tobacco mosaic virus* (TMV) [83], PDR was subsequently applied to horticultural crops for engineered resistance against viral diseases. In the first field trial of transgenic plants engineered for virus resistance, tomato plants expressing the coat protein gene of TMV were evaluated for resistance to mechanical inoculation by TMV [84]. Only 5% of the transgenic plants were symptomatic at the end of the trial compared with 99% of the nontransformed control plants. This study indicated that overexpression of the coat protein gene provided practical control of TMV under field conditions. Also, inoculated transgenic and uninoculated nontransformed plants had identical fruit yield, indicating that the transformation process and expression of the TMV coat protein gene did not alter the horticultural performance of the transgenic tomato plants.

The efficiency of viral genes at conferring resistance against vector-mediated virus transmission was first shown with cucumber plants engineered for resistance to *Cucumber mosaic virus* (CMV). Plants expressing the coat protein gene of CMV showed a significantly reduced incidence of CMV and a lower percentage of symptomatic plants than nontransformed control plants following CMV inoculation via aphid vectors [85]. In these studies, mechanically inoculated cucumber plants dispersed throughout the field provided reliable sources of inoculum for natural aphid populations to vector CMV. This approach coupled with the fact that field trials were established at a time of abundant endemic aphid flights caused sufficient disease pressure to make inferences about disease progress, resistance, and yield [85]. Subsequently, many other studies have confirmed the usefulness of engineered resistance at providing practical control of aphid-transmitted virus diseases [6].

PDR offers unique solutions to infection by multiple viruses, for example, by co-engineering and co-transferring genes from several viruses into a single host plant. The usefulness of multiple viral genes to control mixed virus infections was demonstrated early on with potato plants expressing the coat protein genes of *Potato virus X* (PVX) and *Potato virus Y* (PVY) [86, 87]. Potato line 303 was highly resistant to infections by PVX and PVY in the field [87]. Later, summer squash plants expressing coat protein gene constructs of CMV, *Zucchini yellow mosaic virus* (ZYMV) and/or *Watermelon mosaic virus* (WMV) were engineered for resistance to single viruses or combinations of these three viruses [88]. Among summer squash engineered for multiple virus resistance, line ZW-20 expressing the coat protein genes of ZYMV and WMV was highly resistant, regardless of whether the infections were initiated by mechanical inoculations or mediated by aphid vectors [88, 89]. Similarly, transgenic line CZW-3 expressing the coat protein genes of CMV, ZYMV, and WMV was highly resistant to mixed infections by these three viruses following aphid transmission [88, 90].

Following the initial discovery by Powell Abel et al. [83], the viral coat protein gene from various viruses was introduced into numerous economically important crop species with the aim of achieving resistance. It was initially believed that resistance was provided by the viral protein itself via a mechanism involving excess plant-expressed coat protein that interfered with the uncoating step in viral replication [91]. However, it soon became apparent that resistance could be achieved in transgenic plants producing low or undetectable levels of coat protein [92]. The mechanism underlying the engineered resistance involved degradation of the transgene-derived mRNA into small fragments in a sequence-specific manner. This phenomenon was subsequently referred to as RNA silencing [78–82]. This antiviral plant defense mechanism is initiated by double stranded RNA (dsRNA) structures that are identical to the RNA to be degraded [93]. Silencing is associated with the production of 21–24 nt duplexes called small interfering RNAs (siRNAs) [94, 95]. The siRNAs are produced from dsRNA precursors by an endonuclease known as Dicer and become incorporated and converted to single stranded RNAs (ssRNAs) in an Argonaute-containing-RNA-induced silencing complex (RISC) that targets RNA for cleavage [80, 82, 96, 97].

RNA silencing is an innate and potent plant response to virus infection and a natural example of the concept of PDR that has provided new and unprecedented insights into virus–host interactions. Several approaches have been used to express dsRNA cognate to viral RNA for activation of RNA silencing. Expressing sense and antisense viral genes or inverted repeat viral genes to express hairpin RNAs (hpRNA) for the formation of duplex RNA are some of the most recent strategies used to engineer resistance against viruses [81]. For example, intron-spliced hairpin RNA (ihpRNA), ihpRNA overhang, and ihpRNA spacer were evaluated for resistance to PVY [98, 99]. The ihpRNA was found to be the most efficient construct to conferring resistance to PVY with 90% of the plants exhibiting RNA silencing [99]. The same strategy based on the use of highly conserved genetic segments of several viruses into a single transgene construct achieved multiple virus resistance [100].

Artificial plant micro RNAs (amiRNAs) have been used also to engineer virus resistance in plants. The *Arabidopsis thaliana* pre-miR159a precursor was used to generate two amiRNAs^{159} (amiR-P69^{159} and amiR-HC-Pro^{159}) with sequences complementary to *Turnip yellow mosaic virus* (TYMV) and *Turnip mosaic virus* (TuMV), respectively [101]. The amiR-P69159 was designed to target the viral suppressor P69 of TYMV while amiR-HC-Pro^{159} targeted the viral suppressor HC-Pro of TuMV. Transgenic plants carrying both transgenes expressed the corresponding amiRNAs and showed specific resistance to TYMV and TuMV. Low temperatures had no substantial effect on miRNA accumulation [101]. Similarly, the miR171 of *Nicotiana benthamiana* was used to target the 2b gene of CMV and confer resistance to CMV [102]. Although very promising, amiRNAs have not been used yet in crops for virus resistance.

Strategies other than PDR and RNA silencing have also been applied to confer resistance to viral diseases in plants. Peptides or protein microdomains designed to block protein-binding sites have been used. For example, peptide aptamers designed to microdomains of the nucleoprotein of *Tomato spotted wilt virus* (TSWV) that interact with one of the N-protein homomultimerization domains confer resistance to TSWV and

other tospoviruses in *Nicotiana* species [103]. Similarly, antibody-based resistance has been investigated as an innovative strategy to confer virus resistance in plants. Hybridoma-derived single-chain variable antibody fragments (scFv) were engineered for resistance to various viruses in model plants [104–108]. A number of plant proteins with antiviral activity have been identified and exploited for engineered resistance to viruses in plants. A class of proteins termed ribosome-inactivating proteins [109], protease inhibitors (cystatins) [110], and the interferon-regulated 2–5A system [111, 112] were used successfully to confer virus resistance.

Status of Commercialized Disease Resistant Transgenic Crops

Since the early studies of Powell Abel and coworkers [83], numerous cereal, vegetable, legume, flower, forage, turf, and fruit crops expressing virus-derived gene constructs have been created [6]. Many have been tested under field conditions and shown to be highly resistant to virus infections. Among the transgenic crops produced and evaluated in the field, two lines of transgenic summer squash, i.e., line ZW-20 resistant to ZYMV and WMV, and line CZW-3 resistant to ZYMV, WMV, and CMV [88], and papaya resistant to PRSV [113] have been deregulated and released for commercial use in the USA. Summer squash line ZW-20 received exemption status in 1994 and was the first disease-resistant transgenic crop to be commercialized. Summer squash line CZW-3 was deregulated and commercialized in 1996. Five transgenic zucchini cultivars and six transgenic straightneck or crookneck yellow squash cultivars derived from lines ZW-20 and CZW-3 were developed by conventional breeding. Their adoption is increasing steadily since their initial release in 1996. In 2006, the adoption rate was estimated to 22% (3,250 ha) across the country with an average rate of 70% in New Jersey and 20% in Florida, Georgia, and South Carolina [114]. Papaya expressing the coat protein gene of PRSV was deregulated and commercialized in Hawaii in 1998. PRSV is a major limiting factor to papaya production in Hawaii and around the world. After extensive testing, PRSV-resistant papaya was released in 1998 as devastation caused by the virus reached record proportions in the archipelago's main production region [113]. The impact of PRSV-resistant papaya on the papaya industry in Hawaii is evidenced by its rapid adoption rate. In 2000, the first wave of transgenic papaya bore fruit on more than 42% of the total acreage, and by 2009, transgenic papaya cultivars were planted on more than 90% of the total papaya land in Hawaii (780 of 866 total hectares) ([114], D. Gonsalves, personal communication October 2009).

Tomato and sweet pepper resistant to CMV and papaya resistant to PRSV are also released in the People's Republic of China [115, 116]. Limited, if any, information is available on their adoption rate. Two virus-resistant potato lines were deregulated also in 1998 and 2000 in the USA. After failed attempts to create a potato line resistant to *Potato leafroll virus* (PLRV) by coat protein gene expression, lines expressing a PLRV replicase gene were created, field tested, deregulated, and commercialized [117]. Resistance to PLRV was stacked with the coat protein gene of PVY. Many growers in the Pacific Northwest, Midwest USA and Canada are growing virus-resistant transgenic potato, and a breakdown in resistance has not been reported, neither any detrimental impact on the environmental or human health. Nonetheless, virus-resistant potato was withdrawn from the market after the 2001 growing season due to the reluctance of large processors and exporters to adopt these products [117].

Although not released yet, the transgenic plum cultivar 'Honeysweet' resistant to *Plum pox virus* (PPV) and another PRSV-resistant papaya are under consideration for deregulation in the USA. Plum trees expressing a coat protein gene of PPV are highly resistant to PPV infection [118–121]. The US Department of Agriculture (USDA) Animal and Plant Health Inspection Service (APHIS) granted this plum cultivar deregulated status [122] and the Food and Drug Administration (FDA) has deemed a premarket review of the 'Honeysweet' unnecessary. Presently, the Environmental Protection Agency (EPA) is examining deregulation petitions for 'Honeysweet'. Papaya line X17-2 is also being considered for deregulation in the United States. Line X17-2 differs from the previously deregulated Hawaiian papaya in that it expresses the coat protein gene of a Florida isolate of PRSV and is suitable for cultivation in Florida [123]. APHIS and

FDA granted X17-2-deregulated status and EPA is presently reviewing a deregulation petition [124].

Despite considerable progress in identifying genes that confer resistance against fungal and bacterial pathogens and testing their efficacy in transgenic plants under greenhouse conditions, it appears that the challenge is to translate the results to an effect in the field under continuous pathogen pressure. A search of the field testing release permit database in the USA reveals over 25 applications for field testing fungus-resistant transgenic soybean, corn, grape, strawberry, tobacco, lettuce, wheat, and American elm between 1993 and 2009. Both single traits such as resistance to Dutch Elm disease, ear mold, or downy mildew, were assessed as well as multiple traits against *Botrytis cinerea*, bacterial pathogens, nematodes, abiotic tolerance, glyphosate tolerance, and altered nutritional properties (oil and seed composition). Based on the FAO Biotechnology in Developing Countries Database (FAO-BioDeC), field trials have been conducted in South Africa with transgenic strawberry expressing a phytoalexin synthesis gene and transgenic cotton with resistance to *Verticillium* and *Fusarium* in China. A few countries in Latin America, namely, Argentina, Brazil, and Cuba, are working on transgenic fungal resistance in tropical fruit trees, with some results already in the field. Apart from small projects in China, Thailand, and Pakistan addressing potato and wheat wilt, tomato wilt, and blight in rice, far fewer initiatives have been devoted to the development of transgenic cultivars with resistance against bacterial diseases.

To date, no transgenic cultivar with fungal or bacterial resistance has been released into commerce. The outcomes of field experiments have been variable and not in all cases is the resistance observed in the greenhouse extended to the field [125, 126]. In general, the constitutive expression of antimicrobial proteins in the transgenic host appears to confer partial resistance against these pathogens or increased tolerance at best, rather than absolute resistance. It is also clear that the resistance is limited to a few pathogens. The findings of Punja and Raharjo [127] further suggest that the levels of resistance in transgenic plants are influenced by interactions between endogenous and transgene defense compounds. These authors showed that transgenic carrots carrying a chitinase gene from tobacco exhibited enhanced resistance against *Botrytis cinera*, *Rhizoctonia solani*, and *Sclerotium rolfsii*. However, the transgenic plants reacted similarly to *Alternaria radicini* and *Thielaviopsis basicola* as nontransgenic carrots. Further, improved resistance was not obtained against the same sleuth of pathogens and transgenic carrots expressing a chitinase gene from petunia. Indistinguishable disease reactions to *A. cucumerina, B. cinera, Collectotrichum lagenarium*, and *R. solani* were observed with transgenic and nontransgenic cucumber plants transformed with the chitinase gene from three sources, tobacco and petunia, as above, as well as bean.

Conclusions

Plant diseases caused by fungi, bacteria, and viruses are responsible for enormous losses in cultivated crops worldwide. Disease management relies on prevention, cultural practices, biological control, use of chemical pesticides and insecticides, antibiotic sprays, and selection of host resistant genotypes. These approaches have had limited success in the prevention or cure of diseases. Moreover, the frequent use of biocides, especially in subtherapeutic doses, is leading to the rapid development of resistance in certain fungi and bacteria. In addition, preventing fungal infection not only helps in combating yield losses but also keeps crops free of toxic compounds that are produced by some pathogenic fungi and referred to as mycotoxins. These compounds can affect the immune system and disrupt hormone balances or can be carcinogenic. Therefore, there is an urgent need to develop alternative ways to control infections caused by fungal, bacterial, and viral pathogens in agriculture.

The incorporation of specific disease-resistant traits in plants through genetic engineering offers a means to prevent disease-associated losses. For viruses, the concept of PDR [42] provided unique opportunities for innovative solutions to control virus diseases by developing resistant crops expressing genetic elements derived from a virus's own genome. Thirty years after the inception of PDR, various transgenic crops have been engineered for virus resistance and virus-resistant papaya, summer squash, sweet pepper, and tomato have been deregulated and released commercially. Applying the concept of PDR and the antiviral pathways of RNA silencing provides unique opportunities for developing virus-resistant crops and implementing

efficient and environmentally sound management approaches to mitigate the impact of viral diseases. Based on the tremendous progress, the prospects of further advancing this innovative technology for practical control of virus diseases are very promising.

Engineered resistance to fungal and bacterial diseases is more complex than engineered resistance to viral diseases. This is due to the complex nature of fungi and bacteria, as well as complex interactions with their hosts. Therefore, in spite of remarkable progress and promising reports from greenhouse evaluations and field tests, no cultivar with engineered resistance to fungi and bacteria have been deregulated yet or commercially released. The fact that transgenic crops with resistance to fungi or bacteria might not have provided equivalent levels of plant protection compared to conventional management strategies in practice could account for the reluctance to deliver transgenic plans or seeds to growers. Also, the degree of resistance to fungal and bacterial diseases achieved so far might be of limited practical use for disease management. However, new insights into pathogen–host interactions and the application of siRNA and microRNA technologies will undoubtedly identify new targets and open new horizons for the management of fungal and bacterial diseases.

Future Directions

Transgenic virus resistance is undoubtedly the most advanced of the applications of biotechnology for the management of plant pathogens. There is the documented safe release of virus-resistant transgenic crops over the past 14 years in the USA, in addition to a significant amount of evidence that these crops have little to no detrimental impact on animal health and the environment beyond those of conventional agricultural crops [6]. Given the discovery and elucidation of the antiviral pathways of RNA silencing, various new approaches have been used to develop transgenes more likely to stimulate RNA silencing via the design of transgenes that will form dsRNA structures in planta. These approaches seemingly have an advantage over a full-length coat protein gene in the sense orientation as they are generally unable to produce a functional protein, thus alleviating concerns arising from the presence of the coat protein in plant material. Some nonviral sources of virus resistance, such as host resistance genes and the silencing of host genes that are necessary for viral replication [81] have also been investigated and could theoretically alleviate concerns about synergism, recombination, and transencapsidation. Work with transcription factors, in particular the ERF subfamily transcription, provided evidence of increased resistance to bacterial, fungal, and viral pathogens as well as abiotic stress via overexpression of the soybean *GmERF3* transcription factor in tobacco [128]. The mechanism of the effect remains unknown; it is likely that a range of effects such as elevated antioxidant capacity, induced expression of chitinases, or antimicrobial compounds in *GmERF3* transgenic plants and the suppression of viral spread as a consequence of the reduced virus propagation are responsible. The commercial potential of these technologies remain largely undiscussed and untested.

On the other hand, engineering resistance to fungal and bacterial diseases has proven more recalcitrant. Whereas crops engineered for resistance against viral pathogens are in the market, no commercial transgenic product with enhanced resistance against fungal or bacterial diseases is currently available. These organisms have developed numerous survival strategies and more complex interactions with the plant host. As a result, it has proven more difficult to engineer resistance against these pathogens; far beyond designing a simple defense strategy involving the use of a single gene.

Strides in deciphering the siRNAs that are induced or repressed in response to pathogen attack will invariably contribute to new technologies for the development of transgenic resistance against fungal and bacterial pathogens. Microarray analysis with more wild-type plants and RNA-silencing mutants should reveal the relationship between the physiological processes and the associated disease-resistant phenotype. In the interim, the use of stacks or pyramids of *R* genes either from self or non-host plant species is perhaps the best approach available for the development of transgenic resistance against these pathogens. Presumably, this strategy would not affect resistance to nontarget pathogens while providing durable and broad-spectrum resistance and not interfering with the tight controls of the plants' defense systems. But the full potential of *R* gene expression to provide wide range resistance cannot be realized as long as its use is

clouded by controversy over what it does and how well it works. The major limitation of the use of *R* genes in the development of transgenic resistance lies in the durability of the resistance, which is driven by the highly specific recognition of the elicitor molecule of the pathogen. Pathogens are usually able to overcome *R* gene–mediated recognition through the accumulation of mutations or through the loss of the elicitor gene [129, 130]. Moreover, not in all cases is resistance obtained after transfer to species that are not closely related [32]. Although a plethora of data is available on the identity of genes and gene products involved in plant resistance, knowledge of pathogenesis is relatively primitive. Continued sequencing of crop plant genomes as well as pathogen genome analysis will invariably lead to decoding of the functions of various defense genes as well as pathways and the isolation of more *R* genes. With this knowledge, the precise manipulation of *R* genes to permit binding to proteins of pathogens and the activation of defense responses will be possible, and facilitate the design of synthetic *R* genes with desired specificities. For example, work with 13 alleles (*L*, *L1* to *L11*, and *LH*) from the *L* locus from flax suggests a role for the TIR region and LRR region of L proteins in the flax–flax rust interaction [131]. Most of the sequence variation between the three resistance genes, *Pi9, Pi2, and Piz*, is confined to the LRR domains, indicating that this domain plays a major role in determination of *Magnaporthe grisea* resistance specificities [30]. Further, Jia et al. [132] provided evidence that a single amino acid change in the *Pi-ta* LRD (leucine rich domain) or the *AVR-Pita*$_{176}$ protease motif disrupted interaction between the two and subsequent a loss of resistance against *M. grisea*, the etiological agent of rice blast disease. As more data become available on the structural information and on the interactions between resistance proteins and pathogen ligands, the tweaking of *R* gene domains to accommodate resistance of pathogens infecting distantly related crop species will be likely possible. Moreover, this could be extended to antimicrobial proteins that target components of the pathogen's arsenal, e.g., PGIP. Manipulation of their primary structure and hence determinants of specificity could theoretically generate novel recognition specificities.

Multiple races and range in plant hosts are major issues facing the development of durable disease resistance against fungal and bacterial pathogens. Moreover, in some instances, the expression of enhanced resistance is accompanied by reduced growth or altered morphology or development, given that the plant has been reprogrammed into defense mode. Precise control of transgene expression is thus pivotal; restricted expression at the site of infection and quick induction is crucial as well as a quick response to a wide variety of pathogens [133]. One option is to use pathogen-inducible promoters. Given that the available pathogen-inducible promoters show some patterns of background expression, trancriptomics will play an important role in the identification of more suitable promoters. Work with *Arabidopsis* has already identified potential candidates [134], as have investigations into synthetic promoters combining *cis* elements (W box and GCC-like box) that are conserved across species for restricted expression exclusively at the site of attempted pathogen invasion [135]. Other approaches are considering defensin promoters [136], while others have utilized tissue-specific promoters with some success [137]. The endogenous endothionin *Thi2.1* gene in *Arabidopsis thaliana* gene in tomato under the control of a fruit-inactive promoter (RB7) provided significant levels of enhanced resistance to bacterial and Fusarium wilt [137]. More recently, one study targeted the expression of the PR-protein in leaf trichomes, the preferential port for plant colonization by fungi. The gene encoding an exo α-1, 3-glucanase from *Trichoderma harzianum* was fused to the ATP promoter that confers high expression levels in trichome cells and transferred to *Arabidopsis* [138]. Increased resistance was obtained against *Botrytis cinerea* in needle-wounded and spray assays with transgenic plants. Up to 20% fewer total leaf infections were observed.

In summary, transgenic resistance against viral, fungal, and bacterial pathogens is being addressed on many fronts. The challenge is to develop durable, broad-spectrum resistance, given the diversity of strategies that pathogens deploy and their ability to rapidly adapt. Clearly, an integrated approach based on the knowledge of the defense system of the plant, the arsenal of the pathogen to cause disease and the key genes involved in pathogenesis is required for the design of effective transgenic management strategies. To date, tremendous progress has been made for viruses. Encouraging results have been obtained for

various fungi and bacteria. The prospects of further advancing transgenic crops for practical control of fungal, bacterial, and viral diseases are very promising.

Bibliography

Primary Literature

1. Agrios G (2005) Plant pathology, 5th edn. Elsevier/Academic, San Diego, CA
2. Herrera-Estrella L, Depicker A, van Montagu M, Schell S (1983) Expression of chimaeric genes transferred into plant cells using a Ti-plasmid-derived vector. Nature 303:209–213
3. Bevan MW, Flavell RB, Chilton MD (1983) A chimaeric antibiotic resistance gene as a selectable marker for plant cell transformation. Nature 304:184–187
4. Fraley RT, Rogers SG, Horsch RB, Sanders PR, Flick JS, Adams SP, Bittner ML, Brand LA, Fink CL, Fry JS, Galluppi GR, Goldberg SB, Hoffmann NL, Woo SC (1983) Expression of bacterial genes in plant cells. Proc Natl Acad Sci USA 80:4803–4807
5. Murai N, Sutton DW, Murray MG, Slightom JL, Merlo DJ, Reichert NA, Sengupta-Gopalan C, Stock CA, Barker RF, Kemp JD, Hall TC (1983) Phaseolin gene from bean is expressed after transfer to sunflower via tumor-inducing plasmid vectors. Science 222:476–482
6. Fuchs M, Gonsalves D (2007) Safety of virus-resistant transgenic plants two decades after their introduction: lessons from realistic field risk assessment studies. Annu Rev Phytopathol 45:173–202
7. Lindow SE, Hecht-Poinar EI, Elliot VJ (eds) (2002) Phyllosphere microbiology. American Phytopathological Society, St. Paul, MN
8. Matthews R (1973) Induction of disease by viruses, with special reference to *Turnip yellow mosaic virus*. Annu Rev Phytopathol 11:147–168
9. Struck C (2006) Infection strategies of plant parasitic fungi. In: Cooke BM, Gareth Jones D, Kaye B (eds) The epidemiology of plant diseases. Springer, Netherlands, pp 117–137
10. Oerke EC (2006) Crop losses to pests. J Agric Sci 144:31–43
11. Zadoks JC, Schein RD (1979) Epidemiology and plant disease management. Oxford Press, New York
12. Scorza R (2003) Breeding and molecular genetics. In: Auxt Baugher T, Singha S (eds) Concise encyclopedia of temperate tree fruit. The Haworth Press Inc, Binghamton, NY
13. Broglie K, Chet I, Holliday M, Cressman R, Biddle P, Knowlton S, Mauvais CJ, Broglie R (1991) Transgenic plants with enhanced resistance to the fungal pathogen *Rhizoctonia solani*. Science 254:1194–1197
14. Lorito M, Woo SL, Garcia Fernandez I, Colucci G, Harman G, Pintor-Toros J, Filippone E, Muccifora S, Lawrence C, Zoina A, Tuzun S, Scala F (1998) Genes from mycoparasitic fungi as a source for improving plant resistance to fungal pathogens. Proc Natl Acad Sci USA 95:12734–12739
15. Maziah M, Sariah M, Sreeramanan S (2007) Transgenic banana rastali (AAB) with b 1, 3-glucanase gene for tolerance to fusarium wilt race 1 disease via *Agrobacterium*-mediated transformation system. Plant Pathol J 6:271–282
16. Bolar JP, Norelli JL, Harman GE, Brown SK, Aldwinckle HS (2001) Synergistic activity of endochitinase and exochitinase from *Trichoderma atroviride* (*T. harzianum*) against the pathogenic fungus (*Venturia inaequalis*) in transgenic apple plants. Trans Res 10:533–543
17. Anand A, Zhou T, Trick H, Gill B, Bocku W, Muthukrishnan S (2003) Greenhouse and field testing of transgenic wheat plants stably expressing genes for thaumatin-like protein, chitinase and glucanase against *Fusarium graminearum*. J Exp Bot 54:1101–1111
18. ÓBrien PA, MacNish GC, Milton NM (2001) Transgenic tobacco plants show different resistance to *Rhizoctonia solani* AG 4 and AG 8. Aust Plant Pathol 30:221–225
19. Epple P, Apel K, Bohlmann H (1997) Overexpression of an endogenous thionin enhances resistance of *Arabidopsis* against *Fusarrium oxysporum*. Plant Cell 9:509–520
20. Chan Y, Prasad V, Sanjaya C, Chen K, Liu P, Chan M, Cheng C (2005) Transgenic tomato plants expressing an *Arabidopsis* thionin (*Thi2.1*) driven by fruit-inactive promoter battle against phytopathogenic attack. Planta 221:386–393
21. Anuradha TS, Divya K, Jami SK, Kirto PB (2008) Transgenic tobacco and peanut plants expressing a mustard defensin show resistance to fungal pathogens. Plant Cell Rep 27:1777–1786
22. François I, De Bolle M, Dwyer G, Goderis I, Woutors P, Verhaert P, Proost P, Schaaper W, Cammue B, Broekaert W (2002) Transgenic expression in *Arabidopsis* of a polyprotein construct leading to production of two different antimicrobial proteins. Plant Physiol 128:1346–1358
23. Sarowar S, Kim J, Deok Kim K, Kook Hwang B, Han Ok S, Sheop Shin J (2009) Overexpression of lipid transfer protein (LTP) genes enhances resistance to plant pathogens and LTP functions in long-distance systemic signaling in tobacco. Plant Cell Rep 28:419–427
24. Jayaraj J, Punja Z (2007) Combined expression of chitinase and lipid transfer protein genes in transgenic carrot plants enhances resistance to foliar fungal pathogens. Plant Cell Rep 26:1539–1546
25. Zhu YJ, Tang CS, Moore P (2005) Increased disease resistance in papaya by transforming a pathogen-inducible stilbene synthase gene. Acta Hort 692:107–114
26. Hanhineva K, Kokko H, Rogachev I, Aharoni A, Karenlampi S (2009) Stilbene synthase gene transfer caused alterations in the phenylpropanoid metabolism of transgenic strawberry (*Fragaria ananassa*). J Exp Bot 60:2093–2106
27. Solano R, Stepanova A, Chao QM, Ecker JR (1998) Nuclear events in ethylene signaling: a transcriptional cascade mediated by ETHYLENE-INSENSITIVE3 and ETHYLENERESPONSE-FACTOR1. Gene Dev 12:3703–3714
28. Berrocal-Lobo M, Molina A (2004) ETHYLENE RESPONSE FACTOR 1 mediates *Arabidopsis* resistance to the soil-borne

fungus *Fusarium oxysporum*. Mol Plant-Microbe Interact 17:763–770
29. Zuo K, Qin J, Zhao J, Ling H, Zhang L, Cao Y, Tang K (2007) Over-expression *GbERF2* transcription factor in tobacco enhances brown spots disease resistance by activating expression of downstream genes. Gene 391:80–90
30. Qu S, Liu G, Zhou B, Bellizzi M, Zeng L, Dai L, Han B, Wang GL (2006) The broad-spectrum blast resistance gene *Pi9* encodes a nucleotide binding site-leucine-rich repeat protein and is a member of a multigene family in rice. Genet 172:1901–1914
31. Ellis J, Dodds P, Lawrence G (2007) Flax rust resistance gene specificity is based on direct resistance-avirulence protein interactions. Annu Rev Phytopathol 45:289–306
32. Frost D, Way H, Howles P, Luck J, Manners J, Hardham A, Finnegan J, Ellis J (2004) Tobacco transgenic for the flax rust resistance gene *L* expresses allele-specific activation of defense responses. Mol Plant-Microbe Interact 17:224–232
33. Lu SF, Sun YH, Amerson H, Chiang VL (2007) MicroRNAs in loblolly pine (*Pinus taeda* L.) and their association with fusiform rust gall development. Plant J 51:1077–1098
34. Ellendorff U, Fradin EF, de Jonge R, Thomma BP (2009) RNA silencing is required for *Arabidopsis* defence against *Verticillium* wilt disease. J Exp Bot 60:591–602
35. Powell AL, Van Kan J, Ten Have A, Visser J, Greve LC, Bennett AB, Labavitch JM (2000) Transgenic expression of pear PGIP in tomato limits fungal colonization. Mol Plant-Microbe Interact 13:942–950
36. Janni M, Sella L, Favaron F, Blechl A, De Lorenzo G, D'Ovidio R (2008) The expression of a bean PGIP in transgenic wheat confers increased resistance to the fungal pathogen *Bipolaris sorokiniana*. Mol Plant-Microbe Interact 21:171–178
37. Desiderio A, Aracri B, Leckie F, Mattei B, Salvi G, Tigelaar H, Van Roekel JS, Baulcombe DC, Melchers LS, De Lorenzo G, Cervone F (1997) Polygalacturonase-inhibiting proteins (PGIPs) with different specificities are expressed in *Phaseolus vulgaris*. Mol Plant-Microbe Interact 10:852–860
38. Hu X, Bidney DL, Yalpani N, Duvick JP, Crasta O, Folkerts O, Lu G (2003) Overexpression of a gene encoding hydrogen peroxide-generating oxalate oxidase evokes defense responses in sunflower. Plant Physiol 133:170–181
39. Walz A, Zingen-Sell I, Loeffer M, Sauer M (2008) Expression of an oxalate oxidase gene in tomato and severity of disease caused by *Botrytis cinerea* and *Sclerotinia sclerotiorum*. Plant Pathol 57:453–458
40. Liang H, Zheng J, Duan XY, Sheng BQ, Jia SG, Wang DW, Ouyang JW, Li JY, Li LC, Tian WZ, Hain R, Jia X (2000) A transgenic wheat with a stilbene synthase gene resistant to powdery mildew obtained by biolistic method. Chin Sci Bull 45:634–638
41. Schneider M, Droz E, Malnoe P, Chatot C, Bonnel E, Metrauz J (2002) Transgenic potato plants expressing oxalate oxidase have increased resistance to oomycete and bacterial pathogens. Potato Res 45:177–185
42. Sanford JC, Johnston SA (1985) The concept of parasite-derived resistance-deriving resistance genes from the parasite's own genome. J Theor Biol 113:395–405
43. Wang GL, Song WY, Ruan DL, Sideris S, Ronald PC (1996) The cloned gene, Xa21, confers resistance to multiple *Xanthamonas oryzae* pv. *oryzae* isolates in transgenic pants. Mol Plant-Microbe Interact 9:850–855
44. Datta SK (2004) Rice biotechnology: a need for developing countries. AgBioForum 7:31–35
45. Zhang J, Li X, Jiang G, Xu Y, He Y (2006) Pyramiding of Xa7 and Xa21 for the improvement of disease resistance to bacterial blight in hybrid rice. Plant Breed 125:600–605
46. Yoshimura S, Yamanouchi U, Katayose Y, Toki S, Wang ZX, Kono I, Kurata N, Yano M, Iwata N, Sasaki T (1998) Expression of *Xa1*, a bacterial blight-resistance gene in rice, is induced by bacterial inoculation. Proc Natl Acad Sci USA 95:1663–1668
47. Zhao BY, Lin XH, Poland J, Trick H, Leach J, Hulbert S (2005) From the covers: A maize resistance gene functions against bacterial streak disease in rice. Proc Natl Acad Sci USA 102:15383–15388
48. Tai TH, Dahlbeck D, Clark ET, Gajiwala P, Pasion R, Whalen MC, Stall RE, Staskawicz BJ (1999) Expression of the Bs2 pepper gene confers resistance to bacterial spot disease in tomato. Proc Natl Acad Sci USA 23:14153–14158
49. Mysore KS, D'Ascenzo MD, He X, Martin G (2003) Overexpression of the disease resistance gene *Pto* in tomato induces gene expression changes similar to immune responses in human and fruitfly. Plant Physiol 132:1901–1912
50. Arce P, Moreno M, Gutierrez M, Gebauer M, Dell'Orto P, Torres H, Acuna I, Oliger P, Venegas A, Jordana X, Kalazich J, Hluigue L (1999) Enhanced resistance to bacteria infection by *Erwinia carotovora* subsp. *atroseptica* in transgenic potato plants expression the attacin or the cecropin SB-37 gemes. Am J Potato Res 76:169–177
51. Norelli JL, Mills JZ, Jensen LA, Momol MT, Ko K, Aldwinckle HS (1998) Genetic engineering of apple for increased resistance to fire blight. Acta Hort 484:541–546
52. Mentag R, Luckevich M, Morency MJ, Seguin A (2003) Bacterial disease resistance of transgenic hybrid poplar expressing the synthetic antimicrobial peptide D4E1. Tree Physiol 23:405–411
53. Montesinos E (2007) Antimicrobial peptides and plant disease control. FEMS Microbiol Lett 270:1–11
54. Reynoird JP, Mourgues F, Norelli J, Aldwinckle HS, Brisset MN, Chevreau E (1999) First evidence for improved resistance to fire blight in transgenic pear expressing the *attacin* E gene from *Hyalophora cecropia*. Plant Sci 149:23–31
55. Malnoy M, Venissse JS, Brisset MN, Chevreau E (2003) Expression of bovine lactoferrin cDNA confers resistance to *Erwinia amylovora* in transgenic pear. Mol Breed 12:231–244
56. Norelli JL, Mills JZ, Momol MT, Aldwinckle HS (1999) effect of cecropin-like transgenes on fire blight resistance of apple. Acta Hort 489:273–278

57. Ko K, Norelli JL, Reynoird JP, Boresjza-Wysocka E, Brown SK, Aldwinckle HS (2000) Effect of untranslated leader sequence of AMV RNA 4 and signal peptide of pathogenesis-related protein 1b on attacin gene expression, and resistance to fire blight in transgenic apple. Biotech Lett 22:373–381
58. Düring K, Porsch P, Fladung M, Lörz H (1993) Transgenic potato plants resistant to the phytopathogenic bacterium *Erwinia carotovora*. Plant J 3:587–598
59. Ko K (1999) Attacin and T4 lysozyme transgenic 'Galazy' apple. Regulation of transgene expression and plant resistance to fire blight (*Erwinia amylovora*). PhD dissertation, Cornell University, New York
60. Mirkov TE, Fitzmaurice LC (1995) Protection of plants against plant pathogens. US Patent No 5422108
61. Allefs JJHM, de Jong ER, Florack DEA, Hoogendoors J, Stiekema WJ (1996) *Erwinia* soft rot resistance of potato cultivars expressing antimicrobial peptide tachyplesin. Mol Breed 2: 97–105
62. Wu G, Shortl BJ, Lawrence EB, Levine EB, Fitzsimmons KC, Shah DM (1995) Disease resistance conferred by expression of a gene encoding H_2O_2-generating glucose oxidase in transgenic potato plants. Plant Cell 7:1357–1368
63. Dong YH, Wang L, Xu JL, Zhang HB, Zhang XF, Zhang LH (2001) Quenching quorum-sensing-dependent bacterial infection by an *N*-acyl homoserine lactonase. Nature 411:813–817
64. Herrera-Estrella L, Simpson J (1995) Genetically engineered resistance to bacterial and fungal pathogens. World J Microbiol Biotechnol 11:383–392
65. Krastanova SV, Sekiya M, Holden MR, Xue B, Pang S-Z, Momol EA, Gonsalves D, Burr TJ (2010) Transformation of grape rootstocks with a truncated *Agrobacterium* virE2 gene confers resistance to crown gall disease. Trans Res 19:949–958
66. Citovsky V, Warnick D, Zambryski P (1994) Nuclear import of *Agrobacterium* VirD2 and VirE2 proteins in maize and tobacco. Proc Natl Acad Sci USA 91:3210–3214
67. Escobar MA, Civerolo EL, Summerfelt KR, Dandekar AM (2001) RNAi-mediated oncogene silencing confers resistance to crown gall tumorigenesis. Proc Natl Acad Sci USA 98:13437–13442
68. Lin WC, Lu CF, Wu JW, Cheng ML, Lin YM, Yang NS, Black L, Green SK, Wang JF, Cheng CP (2004) Transgenic tomato plants expressing the Arabidopsis NPR1 gene display enhanced resistance to a spectrum of fungal and bacterial diseases. Trans Res 13:567–581
69. Makandar R, Essig JS, Schapaugh MA, Trick HN, Shah J (2006) Genetically engineered resistance to Fusarium head blight in wheat by expression of Arabidopsis NPR1. Mol Plant Microbe Interact 19:123–129
70. Meur G, Budatha M, Srinivasan T, Kumar KRR, Gupta AD, Kirti PB (2008) Constitutive expression of Arabidopsis NPR1 confers enhanced resistance to the early instars of *Spodoptera litura* in transgenic tobacco. Physiol Plant 133:765–775
71. Wally O, Jayaraj J, Punja ZK (2009) Broad-spectrum disease resistance to necrotrophic and biotrophic pathogens in transgenic carrots (*Daucus carota* L.) expressing an Arabidopsis *NPR1* gene. Planta 231:131–141
72. Chen MS, Fitzgerald HA, Yadav RC, Canlas PE, Dong XN, Ronald PC (2001) Evidence for a disease-resistance pathway in rice similar to the NPR1-mediated signaling pathway in Arabidopsis. Plant J 27:101–113
73. Chen M, Fitzgerald HA, Canlas PE, Navarre DA, Ronald PC (2005) Overexpression of a rice NPR1 homolog leads to constitutive activation of defense response and hypersensitivity to light. Mol Plant-Microbe Interact 18:511–520
74. Malnoy M, Jin Q, Borjsze-Wysocka EE, He SY, Aldwinckle HS (2007) Overexpression of the apple MpNPR1 gene confers increased disease resistance in *Malus* x *domestica*. Mol Plant-Microbe Interact 20:1568–1580
75. Navarro L, Dunoyer P, Jay F, Arnold B, Dharmasiri N, Estelle M, Voinnet O, Jones JD (2006) A plant miRNA contributes to antibacterial resistance by repressing auxin signaling. Science 312:436–439
76. Agorio A, Vera P (2007) ARGONAUTE4 is required for resistance to *Pseudomonas syringae* in *Arabidopsis*. Plant Cell 19:3778–3790
77. Baulcombe D (2007) Amplified silencing. Science 315:199–200
78. Eamens A, Wang M-B, Smith NA, Waterhouse PM (2008) RNA silencing in plants: yesterday, today and tomorrow. Plant Physiol 147:456–468
79. Lin S-S, Henriques R, Wu H-W, Niu Q-W, Yeh S-D, Chua N-H (2007) Strategies and mechanisms of plant virus resistance. Plant Biotech Rep 1:125–134
80. Obbart DJ, Gordon KH, Buck AH, Jiggins FM (2009) The evolution of RNAi as a defence against viruses and transposable elements. Phil Trans R Soc B 364:99–115
81. Prins M, Laimer M, Noris E, Schubert J, Wassenegger M, Tepfer M (2008) Strategies for antiviral resistance in transgenic plants. Mol Plant Pathol 9:73–83
82. Voinnet O (2008) Post-transcriptional RNA silencing in plant-microbe interactions: a touch of robustness and versatility. Curr Opin Plant Biol 11:464–470
83. Powell Abel P, Nelson RS, De B, Hoffman N, Rogers SG, Fraley RT, Beachy RN (1986) Delay of disease development in transgenic plants that express the tobacco mosaic virus coat protein gene. Science 232:738–743
84. Nelson RS, McCormick SM, Delannay X, Dube P, Layton J, Anderson EJ, Kaniewskia M, Proksch RK, Horsch RB, Rogers SG, Fraley RT, Beachy RN (1988) Virus tolerance, plant growth and field performance of transgenic tomato plants expressing coat protein from tobacco mosaic virus. Bio/Technology 6:403–409
85. Gonsalves D, Chee P, Provvidenti R, Seem R, Slightom JL (1992) Comparison of coat protein-mediated and genetically-derived resistance in cucumbers to infection by *Cucumber mosaic virus* under field conditions with natural challenge inoculations by vectors. Bio/Technology 10:1562–1570
86. Lawson C, Kaniewski W, Haley L, Rozman R, Newell C, Sanders P, Tumer N (1990) Engineering resistance to mixed virus infection in a commercial potato cultivar: resistance of *Potato virus X* and *Potato virus Y* in transgenic Russet Burbank. Bio/Technology 8:127–134

87. Kaniewski W, Lawson C, Sammons B, Haley L, Hart J, Delannay X, Tumer N (1990) Field resistance of transgenic Russet Burbank potato to effects of infection by *Potato virus X* and *Potato virus Y*. Bio/Technology 8:750–754
88. Tricoli DM, Carney KJ, Russell PF, McMaster JR, Groff DW, Hadden KC, Himmel PT, Hubbard JP, Boeshore ML, Quemada HD (1995) Field evaluation of transgenic squash containing single or multiple virus coat protein gene constructs for resistance to *Cucumber mosaic virus*, *Watermelon mosaic virus 2*, and *Zucchini yellow mosaic virus*. Bio/Technology 13:1458–1465
89. Fuchs M, Gonsalves D (1995) Resistance of transgenic squash Pavo ZW-20 expressing the coat protein genes of zucchini yellow mosaic virus and watermelon mosaic virus 2 to mixed infections by both potyviruses. Bio/Technology 13:1466–1473
90. Fuchs M, Tricoli DM, McMaster JR, Carney KJ, Schesser M, McFerson JR, Gonsalves D (1998) Comparative virus resistance and fruit yield of transgenic squash with single and multiple coat protein genes. Plant Dis 82:1350–1356
91. Lindbo JA, Dougherty WG (2005) Plant Pathology and RNAi: a brief history. Annu Rev Phytopathol 43:191–204
92. Lindbo JA, Silva-Rosales L, Proebsting WM, Dougherty WG (1993) Induction of a highly specific antiviral state in transgenic plants: implications for regulation of gene expression and virus resistance. Plant Cell 5:1749–1759
93. Waterhouse PM, Graham MW, Wang MB (1998) Virus resistance and gene silencing in plants can be induced by simultaneous expression of sense and antisense RNA. Proc Natl Acad Sci USA 95:13959–13964
94. Hamilton AJ, Baulcombe DC (1999) A species of small antisense RNA in post-transcriptional gene silencing in plants. Science 286:950–952
95. Hamilton AJ, Voinnet O, Chappell L, Baulcombe DC (2002) Two classes of short interfering RNA in RNA silencing. EMBO J 21:4671–4679
96. Deleris A, Gallego-Bartolome J, Bao J, Kasschau KD, Carrington JC, Voinnet O (2006) Hierarchical action and inhibition of plant dicer-like proteins in antiviral defense. Science 313:68–71
97. Hannon GJ (2002) RNA interference. Nature 418:244–251
98. Smith NA, Singh SP, Wang M-B, Stoutjesdijk P, Green A, Waterhouse PM (2000) Total silencing by intron-spliced hairpin RNAs. Nature 407:319–320
99. Wesley V, Helliwell CA, Smith NA, Wang MB, Rouse DT, Liu Q, Gooding PS, Singh SP, Abbott D, Stoutjesdijk PA, Robinson SP, Gleave AP, Green AG, Waterhouse PM (2001) Construct design for efficient, effective and high-throughput gene silencing in plants. Plant J 27:581–590
100. Bucher E, Lohuis D, van Poppel PMJA, Geerts-Dimitriadou C, Goldbach R, Prins M (2006) Multiple virus resistance at a frequency using a single transgene construct. J Gen Virol 87:3697–3701
101. Niu Q-W, Lin S-S, Reyes JL, Chen K-C, Wu H-W, Yeh S-D, Chua N-H (2006) Expression of artificial microRNAs in transgenic *Arabidopsis thaliana* confers virus resistance. Nat Biotechnol 11:1420–1428
102. Qu F, Ye X, Morris TJ (2008) Arabidopsis DRB4, AGO1, AGO7, and RDR6 participate in a DCL4-initiated antiviral RNA silencing pathway negatively regulated by DCL1. Proc Natl Acad Sci USA 105:14732–14737
103. Rudolph C, Schreier PH, Uhrig JF (2003) Peptide-mediated broad-spectrum plant resistance to tospoviruses. Proc Natl Acad Sci USA 100:4429–4434
104. Boonrod K, Galetzka D, Nagy PD, Conrad U, Krczal G (2004) Single-chain antibodies against a plant viral RNA-dependent RNA polymerase confer virus resistance. Nat Biotechnol 22:856–862
105. Nölke G, Fischer R, Shillberg S (2004) Antibody-based pathogen resistance in plants. J Plant Pathol 86:5–17
106. Nölke R, Cobanov P, Uhde-Holzem K, Reustle G, Fischer R, Shillberg S (2009) *Grapevine fanleaf virus* (GFLV)-specific antibodies confer GFLV and *Arabis mosaic virus* (ArMV) resistance in *Nicotiana benthamiana*. Mol Plant Pathol 10:41–49
107. Schillberg S, Zimmermann S, Findlay K, Fischer R (2000) Plasma membrane display of anti-viral single chain Fv fragments confers resistance to *Tobacco mosaic virus*. Mol Breed 6:317–326
108. Tavladoraki P, Benvenuto E, Trinca S, De Martinis D, Cattaneo A, Galeffi P (1993) Transgenic plants expressing a functional single-chain Fv antibody are specifically protected from virus attack. Nature 366:469–472
109. Lodge JK, Kaniweski WK, Tumer NE (1993) Broad-spectrum virus resistance in transgenic plants expressing pokeweed antiviral protein. Proc Natl Acad Sci USA 90:7089–7093
110. Gutierrez-Campos R, Torres-Acosta JA, Saucedo-Arias LJ, Gomez-Lim MA (1999) The use of cysteine proteinase inhibitors to engineer resistance against potyviruses in transgenic tobacco plants. Nat Biotechnol 17:1223–1226
111. Mitra A, Higgins DW, Langenberg WG, Nie H, Sengupta DN, Silverman RH (1996) A mammalian 2–5A system functions as an antiviral pathway in transgenic plants. Proc Natl Acad Sci USA 93:6780–6785
112. Ogawa T, Hori T, Ishida I (1996) Virus-induced cell death in plants expressing the mammalian 2′, 5′, oligoadenylate system. Nat Biotechnol 14:1566–1569
113. Gonsalves D (1998) Control of *Papaya ringspot virus* in papaya: a case study. Annu Rev Phytopathol 36:415–437
114. Johnson SR, Strom S, Grillo K (2007) Quantification of the impacts on US agriculture of biotechnology-derived crops planted in 2006. National Center for Food and Agriculture policy. http://www.ncfap.org
115. James C (2010) Global status of commercialized biotech/GM crops. The first thirteen years, 1996 to 2008. http://www.isaaa.org/resources/publications/briefs/39/executivesummary/default.html
116. Stone R (2008) China plans $3.5 billion GM crops initiative. Science 321:1279
117. Kaniewski WK, Thomas PE (2004) The potato story. Agric Biol Forum 7:41–46

118. Capote N, Pérez-Panadés J, Monzó C, Carbonell E, Urbaneja A, Scorza R, Ravelonandro M, Cambra M (2007) Assessment of the diversity and dynamics of *Plum pox virus* and aphid populations in transgenic European plums under Mediterranean conditions. Trans Res 17:367–377
119. Hily JM, Scorza R, Malinowski T, Zawadzka B, Ravelonandro M (2004) Stability of gene silencing-based resistance to *Plum pox virus* in transgenic plum (*Prunus domestica* L.) under field conditions. Transgenic Res 5:427–436
120. Malinowski T, Cambra M, Capote N, Zawadzka B, Gorris MT, Ravelonandro M (2006) Field trials of plum clones transformed with the *Plum pox virus* coat protein (PPV-CP) gene. Plant Dis 90:1012–1018
121. Zagrai I, Capote N, Ravelonandro M, Ravelonandro M, Cambra M, Zagrai L, Scorza R (2008) *Plum pox virus* silencing of C5 transgeic plums is stable uner challenge inoculation with heterologous viruses. J Plant Pathol 90:S1.63–S1.71
122. Bech R (2007) Finding of no significant impact and decision notice. Determination of nonregulated status for C5 plum resistant to plum pox virus. Animal and Plant Health Inspection Service. http://www.aphis.usda.gov/brs/aphisdocs2/04_26401p_com.pdf
123. Davis MJ (2004) Petition for Determination of Nonregulated status for the X17-2 line of papaya: A *Papaya ringspot virus*-resistant papaya. Animal and Plant Health Inspection Service. http://www.aphis.usda.gov/brs/aphisdocs/04_33701p.pdf
124. Shea K (2009) University of Florida; determination of nonregulated status for papaya genetically engineered for resistance to the *Papaya ringspot virus*. Animal and Plant Health Inspection Service. Fed Regist 74:45163–45164. http://edocket.access.gpo.gov/2009/pdf/E9-21092.pdf
125. Anand A, Zhou T, Trick HN, Gill BS, Bockus WW, Muthukrishnan S (2003) Greenhouse and field testing of transgenic wheat plants stably expressing genes for thaumatin-like protein, chitinase and glucanase against *Fusarium graminearum*. J Exp Bot 54:1101–1111
126. Chenault K, Melouk H, Payton M (2005) Field reaction to *Sclerotinia* blight among transgenic peanut lines containing antifungal genes. Crop Sci 45:511–515
127. Punja Z, Raharjo S (1996) Response of transgenic cucumber and carrot plants expressing different chitinase enzymes to inoculation with fungal pathogens. Plant Dis 80:999–1005
128. Zhang G, Chen M, Li L, Xu Z, Chen X, Jiaming Guo J, Youzhi M (2009) Overexpression of the soybean *GmERF3* gene, an AP2/ERF type transcription factor for increased tolerances to salt, drought, and diseases in transgenic tobacco. J Exp Bot 60:3781–3796
129. Joosten MH, Cozijnsen TJ, De Wit PJ (1994) Host resistance to fungal tomato pathogen lost by a single base pair change in an avirulence gene. Nature 367:384–386
130. Gassmann W, Dahlbeck D, Chesnokova O, Minsavage G, Jones J, Stakawicz B (2000) Molecular evolution of virulence in natural field strains of *Xanthomonas campestris* pv. *vesicatoria*. J Bacteriol 182:7053–7059
131. Ellis JG, Lawrence GJ, Luck JE, Dodds PN (1999) Identification of regions in alleles of the flax rust resistance gene *L* that determine differences in gene-for-gene specificity. Plant Cell 11:495–506
132. Jia Y, McAdams S, Bryan E, Hershey H, Valent B (2000) Direct interaction of the resistance gene and avirulence gene products confers rice blast resistance. EMBO J 14: 4004–4014
133. Gurr SJ, Rushton PJ (2005) Engineering plants with increased disease resistance: how are we going to express it? Trends Biotechnol 23:283–290
134. Eulgen T (2005) Regulation of the *Arabidopsis* defence transcriptome. Trends Plant Sci 10:71–78
135. Rushton P, Reinstädler A, Lipka V, Lippok B, Somssich I (2002) Synthetic plant promoters containing defined regulatory elements provide novel insights into pathogen- and wound-induced signaling. Plant Cell 14:749–762
136. Kovalchuk N, Li M, Wittek F, Reid N, Singh R, Shirley N, Ismagul A, Eliby S, Johnson A, Milligan A, Hrmova M, Langridge P, Lopato S (2010) Defensin promoters as potential tools for engineering disease resistance in cereal grains. Plant Biotechnol J 8:47–64
137. Chan Y, Prasad V, Sanjaya K, Chen K, Liu P, Chan M, Cheng C (2005) Transgenic tomato plants expressing an *Arabidopsis* thionin (*Thi2.1*) driven by fruit-inactive promoter battle against phytopathogenic attack. Planta 221:386–393
138. Calo L, Garcia I, Gotor C, Romero LC (2006) Leaf hairs influence phytopathogenic fungus infection and confer an increased resistance when expressing a Trichoderma a-1, 3-glucanase. J Exp Bot 57:3911–3920

Books and Reviews

Charkowski AO (2007) Potential disease control strategies revealed by genome sequencing and functional genetics of plant pathogenic bacteria. In: Punja ZK, De Boer SH, Sanfaçon H (eds) Biotechnology and plant disease management. CAB International, Cambridge, MA, pp 402–497

Csroba T, Pantaleo V, Burgyán J (2009) RNA silencing: an antiviral mechanism. In: Loebenstein G, Carr JP (eds) Advances in virus research, vol 75, natural and engineered resistance to plant viruses. Academic, San Diego, CA, pp 35–72

Diaz-Pendón JA, Ding S-W (2008) Direct and indirect roles of viral suppressors of RNA silencing in pathogenesis. Annu Rev Phytopathol 46:303–326

Knox RE, Clarke FR (2007) Molecular breeding approaches for enhanced resistance against fungal pathogens. In: Punja ZK, De Boer SH, Sanfaçon H (eds) Biotechnology and plant disease management. CAB International, Cambridge, MA, pp 321–357

Misra S, Bhargava A (2007) Application of cationic antimicrobial peptides for management of plant diseases. In: Punja ZK, De Boer SH, Sanfaçon H (eds) Biotechnology and plant disease management. CAB International, Cambridge, MA, pp 301–320

Rommens CM, Kishore GM (2000) Exploiting the full potential of disease-resistance genes for agricultural use. Curr Opin Biotechnol 11:120–125
Ruiz-Ferrer V, Voinnet O (2009) Roles of plant small RNAs in biotic stress responses. Annu Rev Plant Biol 60:485–510
Stuiver MH (2006) Engineering fungal resistance in crops. In: Halford N (ed) Plant biotechnology: current and future applications of genetically modified crops. Wiley, West Sussex, England, pp 225–239
Stuiver MH, Custers JH (2000) Engineering disease resistance in plants. Nature 411:865–868
Suzuki JY, Tripathi S, Gonsalves D (2007) Virus-resistant transgenic papaya: commercial development and regulatory and environmental issues. In: Punja ZK, De Boer SH, Sanfaçon H (eds) Biotechnology and plant disease management. CAB International, Cambridge, MA, pp 436–461
Xing T (2007) Signal transduction pathways and disease resistant genes and their applications to fungal disease control. In: Punja ZK, De Boer SH, Sanfaçon H (eds) Biotechnology and plant disease management. CAB International, Cambridge, MA, pp 1–15
Yang CH, Yang S (2007) Modulating quorum sensing and type III secretion systems in bacterial plant pathogens for disease management. In: Punja ZK, De Boer SH, Sanfaçon H (eds) Biotechnology and plant disease management. CAB International, Cambridge, MA, pp 16–57

Transgenic Crops, Environmental Impact

Angharad M. R. Gatehouse[1], Martin G. Edwards[1], Natalie Ferry[1,2], Micheal D. K. Owen[3]
[1]School of Biology, Newcastle Institute for Research on Sustainability, Newcastle University, Newcastle upon Tyne, UK
[2]School of Environment and Life Sciences, University of Salford, Salford, UK
[3]Department of Agronomy, Iowa State University, Ames, IA, USA

Article Outline

Glossary
Definition of the Subject
Introduction
Insect-Resistant Transgenic Crops
Herbicide-Tolerant/Resistant Transgenic Crops
Environmental Impact of Transgenic Crops
Future Directions
Conclusion
Bibliography

Glossary

***Bt*-expressing transgenic crops**
Insect resistance crops
Novel mechanisms for insect resistance
Herbicide-tolerant transgenic crops
Food security
Sustainability
Risk assessment
Environmental impact
Impact on beneficial insects
Gene flow

Definition of the Subject

Agriculture is the production of food and commodities through farming. Since its dawn some 10,000 years ago, humankind has had an ever increasing impact on the environment. With the increasing intensification of agriculture, particularly during the twentieth century, this impact has become even more pronounced, often with undesirable or unacceptable consequences, including water pollution, soil erosion, and loss of habitat, often accompanied by a loss of biodiversity. Pests, particularly weedy plants, demonstrate a remarkable ability to adapt to agricultural production systems. The practice of growing monocultures, typically used in intensive agriculture, increases the number of pests; these are currently predominantly controlled through use of pesticides. However, with increasing exposure to pesticides, many pest populations are evolving resistance to these compounds. An additional problem encountered with many pesticides, and particularly insecticides, is their non-target effects on beneficial insects. Transgenic crops expressing genes conferring either resistance to insect pests and/or herbicides are becoming increasingly more widely grown. However, in many parts of the world, before such crops are commercialized, they have to be assessed for their potential environmental impact which measures the impact they will have on non-target species and their ability to outcompete native species. Environmental risk assessments cover both the transgenic crop

concerned and the potential impacted environment. The assessment process includes evaluation of the characteristics of the crop and its effect and stability in the environment, combined with ecological characteristics of the environment in which the introduction will take place. The assessment also includes unintended consequences that could result from the insertion of the new gene. For all transgenic crops, the direct and indirect effects they have on non-target organisms must be considered. Furthermore, issues relating to potential gene flow to other non-transgenic cultivars and/or wild near-relatives also must be addressed.

Introduction

Food security figures are high on both the political and social agenda [1]. This is not surprising given that the global population increased fourfold during the last century, with current estimates suggesting that it will reach approximately 9.2 billion by 2050 (Fig. 1). However, this increase has primarily been seen in the developing regions of the world, with population remaining relatively static in the developed world. As expected, it is those countries least able that need to significantly increase food production, with an estimated increase in productivity of 300% for Africa and 80% for Latin America; even so, it is estimated that North America will need to increase productivity by some 30% [2]. Without an increase in "farm productivity," this required increase in food production equates to an additional 1.6 billion hectares of arable land by 2050, a scenario that is becoming increasingly less sustainable or, indeed, achievable. An immediate priority for agriculture is thus to achieve increased crop yields in a sustainable and cost-effective way in order to avoid a Malthusian disaster.

The concept of utilizing a transgenic (biotech) approach was realized in the mid-1990s with the commercial introduction of genetically modified crops. In 2009, it was estimated that some 14 million farmers planted 134 million hectares (330 million acres) of biotech crops in 25 countries, representing a 7% increase over the preceding year [3]. Interestingly, 90% of these farmers were small and resource-poor farmers from developing countries. In economic terms, the global market value for biotech crops in 2009 was US$10.5 billion; this figure represents 20%

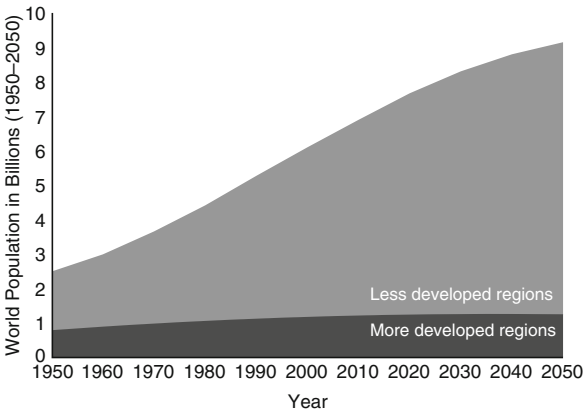

Transgenic Crops, Environmental Impact. Figure 1 Project world population increase from 1950 to 2050 showing an overall fourfold increase in population. During this period, population growth in the more developed regions of the world are predicted to remain moderately static

of the US$52.2 billion global crop protection market and 30% of US$34 billion commercial seed market. Of this US$10.5 billion biotech crop market, approximately 50% was accounted for by biotech maize, with soybean, cotton, and canola (oilseed rape) accounting for 37.2%, 10.5%, and 3%, respectively.

Although transgenic crops have only been available since the 1990s, they have dramatically changed the face of world agriculture and are likely to represent the most rapidly adopted technology in agriculture [4]. This trend is largely attributed to one herbicide, glyphosate (*N*-(phosphonomethyl)glycine), and crops that are genetically modified to have selectivity (resistance) to the glyphosate when the herbicide is applied topically to them. However, many new transgenic crops have been introduced that include multiple transgenic traits, thus providing greater value to agriculture. The reported increased economic profitability attributable to transgenic crops is a major factor that provides the impetus for the increasing adoption of these crops worldwide, both in developing as well as industrialized nations [5]. Despite their benefits, not least in increasing crop yield in a more sustainable and environmentally benign way compared to intensive agriculture (Tables 1 [6] and 2 [6–20]), neither the technology, nor the crops, are universally perceived as of benefit to humankind. There are fears that all

Transgenic Crops, Environmental Impact. Table 1 Average farm level agronomic and economic effects of *Bt* crops

Country	Insecticide reduction (%)	Increase in effective yield (%)	Increase in gross margin (US$/ha)
	Bt cotton	*Bt cotton*	*Bt cotton*
Argentina	47	33	23
Australia	48	0	66
China	65	24	470
India	41	37	135
Mexico	77	9	295
South Africa	33	22	91
USA	36	10	58
	Bt maize	*Bt maize*	*Bt maize*
Argentina	0	9	20
Philippines	5	34	53
South Africa	10	11	42
Spain	63	6	70
USA	8	5	12

Source: Zilberman et al. (2010) [6] (Courtesy of *Choices* and the Agricultural & Applied Economics Association)

Transgenic Crops, Environmental Impact. Table 2 Summary of primary studies on the effects of herbicide-tolerant (HT) crops on yields

Crop/Reference	Data source	Effect on yields
Herbicide-tolerant soybeans		
[7]	Experiments	Same
[8]	Experiments	Increase
[9]	Experiments	Increase
[10]	Survey	Increase
[11]	Survey	Small increase
[12]	Survey	Small decrease
[13]	Survey	Same
[14]	Survey	Increase
[15]	Survey	Same
Herbicide-tolerant cotton		
[16]	Experiments	Same
[17]	Experiments	Same
[18]	Experiments	Same
[19]	Experiments	Same
[20]	Survey	Increase

Source: Zilberman et al. (2010) [6] (Courtesy of *Choices* and the Agricultural & Applied Economics Association)

questions of risk attributable to the wide-scale growing of such crops have not been adequately addressed, or perhaps even identified [21]. While many of these fears may be unfounded, public debate concerning potential environmental and public health risks is crucial.

This chapter will provide a brief overview of first-generation transgenic crops. Specifically, it will discuss the environmental impact of the wide-scale growing of such crops both in terms of their potential non-target effects and the potential for gene flow.

Insect-Resistant Transgenic Crops

Insect-resistant transgenic crops, also known as Biotech crops, were first commercialized in the USA during the mid-1990s with the introduction of genetically modified corn (maize), potato, and cotton plants expressing genes encoding the entomocidal δ-endotoxin from *Bacillus thuringiensis* (*Bt*; also known as crystal/Cry proteins). In terms of *Bt*-expressing maize and cotton, the current market is estimated at US$2.3 billion and US$0.9 billion, respectively. Detailed knowledge on the mode of action of these Cry proteins is not only essential to optimize their efficacy against target insects, but also to predict the potential for non-target effects on beneficial insects. On ingestion, *Bt* toxins are solubilized in the midgut where they are proteolytically cleaved at the N-terminal to a 65–70-kDa truncated (active) form. The active molecules then exert their pathological effects by binding to a specific receptor (s) in the midgut epithelial cells and insert into the membrane where they form pores, this results in cell

death by colloid osmotic lysis, followed by death of the insect [22]. In most commercial crop varieties, these Cry proteins are expressed in the active form and as such differ from those used in biopesticide formulations where the Cry proteins are present as protoxins.

Early commercial varieties of insect-resistant transgenic crops expressed single crystal (Cry) proteins with specific activity against lepidopteran pests as illustrated by Bollgard® cotton expressing Cry1Ac developed by Monsanto and Attribute® maize expressing Cry1Ab developed by Syngenta. Subsequently, other lepidopteran-active *Bt* toxins, such as Cry1F and Cry2Ab2, were introduced, and often presented as pyramided genes in a single variety (Widestrike® cotton expressing both Cry1F + Cry1Ac developed by Dow Agrosciences and Bollgard II® cotton expressing Cry1Ac + Cry2Ab2 developed by Monsanto). Transgenic crops, particularly maize, expressing Cry3 proteins to protect against coleopteran pests such as chrysomelid root-worms have also been commercialized (e.g., Monsanto's Yieldgard Rootworm® maize expressing Cry3Bb1, Dow Agrosciences' Herculex RW® maize expressing Cry34Ab1 and Cry35Ab1, stacked with a HT gene, and Syngenta's Agrisure RW® maize expressing a modified version of Cry3A). In 2009, SmartStax, a novel biotech maize containing eight different genes for insect and herbicide resistance, was granted approval in the USA. Furthermore, Syngenta has recently launched Agrisure Viptera trait-stacked corn, the first commercially available variety to exploit a non-cry *Bt* protein (Vip3) for the provision of multiple pest resistance. In China, *Bt* cotton cultivars expressing Cry1Ac together with a modified cowpea trypsin inhibitor (CpTI) were commercially released in 2000 [23], and in 2005, accounted for approximately 15% of the cotton crop [24]. The major reason for co-expressing *Bt* and CpTI in cotton was to reduce the likelihood of the insects becoming resistant to this cultivar, thus extending its effective life.

While it is clear that *Bt*-expressing crops have made a significant beneficial impact to global agriculture, not least in terms of pest reduction, improved quality, and increased yield (Table 1 [6]), it is also becoming increasingly evident that there is a need to develop alternative strategies, not least because of the potential for pest populations to evolve resistance [25], and to the lack of effective control of homopteran pests. Recently, crops expressing vegetative insecticidal proteins (VIPs) have been commercialized (see above). However, alternative approaches based on the use of plant-derived or animal-derived genes, including those from insects (such as those encoding immunosuppressive proteins), are being investigated and developed. More recently, the potential to identify and exploit endogenous resistance genes using functional genomics and the use of RNAi are actively being investigated [26–30]. However, if these novel approaches are to play a useful role in crop protection, it is desirable that they do not have a negative impact on beneficial organisms at higher trophic levels since this would inevitably affect agro-ecosystem function. This is equally true for *Bt*-expressing crops.

Herbicide-Tolerant/Resistant Transgenic Crops

From the first commercialization of transgenic crops, to date, herbicide tolerance has consistently been the dominant trait and, as a consequence of its rapid and widespread adoption, has made an immeasurable change to global agriculture. In 2009, herbicide tolerance deployed in soybean, maize (corn), canola (oilseed rape), cotton, sugarbeet, and alfalfa occupied 62% (83.6 million hectares) of the global biotech area of 134 million hectares. Furthermore, in 2009, the stacked double and triple traits occupied an area of 28.7 million hectares (equivalent to 21% of global biotech crop area), much larger than the insect-resistant varieties which occupied 21.7 million hectares (15%). Interestingly, stacked trait products and herbicide-tolerant products grew at the same rate of 6%, while insect resistance as a trait grew at 14% [31].

While there are a number of herbicide-tolerant transgenic crops that have been developed to several herbicides with different modes of phytotoxic action, the primary influence in world agriculture is glyphosate [32, 33]. This preference for glyphosate is based on (1) the target site, (2) the ability of this compound to translocate in plants, and (3) the inability of plants to rapidly detoxify it. Glyphosate controls weeds by inhibiting 5-enolpyruvylshikimate-3-phosphate synthase (EPSPS; EC 2.5.1.19), a key enzyme in the shikimate biosynthetic pathway which is necessary for the production of the aromatic amino acids, auxin, phytoalexins, folic acid, lignin, plastoquinones, and many other secondary plant

products. Over 30% of the carbon fixed by plants may pass through this pathway. Inhibition of EPSPS by glyphosate deregulates the pathway, leading to even more carbon flowing through the pathway with accumulation of shikimate and shikimate-3-phosphate. Up to 16% of the plant's dry matter can accumulate as shikimate. Glyphosate occupies the binding site on EPSPS for phosphoenolpyruvate, a substrate of EPSPS, by mimicking an intermediate state of the enzyme-substrate complex. There are two forms of EPSPS in nature, EPSPS I, which is found in plants, fungi, and most bacteria, and is sensitive to glyphosate. The second form is EPSP II, which is found in glyphosate-resistant bacteria and is not inhibited by glyphosate. It is thus the gene encoding an EPSPS II that has been used to genetically engineer crops to confer resistance/tolerance to this particular herbicide [34].

Environmental Impact of Transgenic Crops

The adoption of transgenic crops, and in particular herbicide-tolerant crops, has resulted in significant changes in agronomic practices. Many clear benefits to both the grower and consumer can be identified with transgenic crops that are currently grown, not least in the often significant increases in productivity accompanied by reductions in synthetic pesticide usage (Tables 1 [6] and 2 [7–20, 35–37]), thus making transgenic crops more environmentally sustainable. Despite the fact that such crops have now been commercialized for some 15 years, alongside these benefits, concerns are still being expressed as to their safety, particularly in terms of their impact on human health and the environment. It is imperative that these concerns are addressed in a scientifically sound and appropriate manner. Thus, assessing the environmental consequences of transgenic crops is an important prerequisite to their commercialization.

In many regions of the world, regulatory frameworks are in place to ensure that all pre-commercial transgenic crops are evaluated for potential impacts on human health, animal health, and the environment according to established standards of risk assessment and current scientific knowledge, prior to authorizations for import or planting being granted. The environmental risk assessment for such crops follows the same fundamental principles as other risk assessment schemes, i.e., risk is a function of hazard and exposure. However, one of the main differences that sets risk assessment of transgenic crops apart from other risk assessment procedures is that it is highly dependent on the crop and the introduced trait; hence, a case-by-case approach is required [38].

Impact of Insect-Resistant Transgenic Crops on Beneficial Insects

For any technology to be acceptable to the public at large, the perceived benefits have to outweigh any potential/perceived risk – this requirement is equally true for transgenic crops [39]. Common to all transgenic crops currently grown, general environmental concerns relate to the potential for horizontal gene transfer, gene flow, and invasiveness to occur both in managed and natural environments. However, in the case of insect-resistant transgenic crops, perhaps, the greatest concerns relate to their non-target effects and, in particular, their effects on beneficial insects such as natural enemies (predators and parasitoids) and pollinators.

An important consideration is the likelihood of exposure of the transgene product to the non-target insect, and indeed the different routes of exposure. The most obvious exposure route for non-target herbivores is through direct ingestion of plant material, although this will be influenced by the mode of insect feeding and spatial and temporal expression patterns of the transgene product within the plant. While exposure to pollinators is via the nectar and pollen, exposure routes to natural enemies are more diverse. Although many predators and parasitoids, particularly in the adult stage, are facultative herbivores and thus can be exposed to transgene products directly from consuming plant tissues (pollen, nectar), the larval stages are more likely to be exposed from consuming insects that have themselves fed on plant tissues where the transgene product has been expressed and accumulated. It is pertinent to point out that in some cases, particularly when the host is a sap-sucking insect such as aphids, that the natural enemy is rarely exposed to the transgene product; however, the scenario is quite different when the host is a chewing insect, in which case the likelihood of the natural enemy being exposed is very high.

Impact on Natural Enemies Agro-ecosystems consist of complex trophic interactions, with many aspects of the physiology, ecology, and behavior of the organisms present being governed by interactions with organisms from the same or different trophic levels. Since plants are the basis of these food webs on which all organisms at higher trophic levels depend, and since herbivorous insect species at the second trophic level have an important position in food webs, together with the fact that approximately 50% of all insect species are plant feeders, the potential for exposure to non-targets, either directly (bi-trophic) or indirectly (tri-trophic), is high. This is particularly true for predators and parasitoids which play an important role in suppressing insect pest populations both in the field and under specialized cultivation systems. Because of this important role and because expression of transgenes that confer enhanced levels of resistance to insect pests is of particular relevance (since they are aimed at manipulating the biology of organisms in a different trophic level to that of the plant), these beneficial insects have been the focus of numerous major studies to evaluate the non-target effects of transgenic crops. The nature of these investigations has been very varied ranging from detailed studies at the molecular/biochemical level under controlled environmental conditions, to glasshouse trials using deliberately infested plants and released natural enemies, to effects at the population level in the field. Further, they have involved delivering the transgene product both in artificial diet and *in planta* and either directly (at the bi-trophic level) or via a tri-trophic (plant-pest-natural enemy) interaction. Recent studies relating to both the effects of *Bt*-expressing crops and crops expressing molecules still under development are summarized in Tables 3 [40–72] and 4 [50, 51, 73–102] for predators and parasitoids, respectively.

As mentioned above, prior to their commercialization, all transgenic crops have to undergo rigorous risk assessment. However, despite a global commodities market, the risk assessment process itself varies from region to region, as does the non-target organisms selected for testing. Obviously, the latter will vary depending upon geographical and climatic regions; however, there are concerns that there should be greater uniformity in the species selected; these should at least be representative of the major ecosystem functions. In an attempt to address this short-coming, Romeis et al. [103] have recently refined the 3-tier risk assessment to evaluate potential adverse impacts of insect-resistant transgenic crops on non-target arthropods, with specific recommendations for early-tier laboratory studies used in the risk assessment process. Although this risk assessment protocol has been primarily developed for crops expressing *Bt* toxins, the concepts put forward apply to other arthropod-active proteins. Typically, the risk assessment follows a tiered approach that starts with laboratory studies under worst-case exposure conditions; such studies have a high ability to detect adverse effects on non-target species, if present. Clear guidance on how such data are produced in laboratory studies assists the product developer and risk assessors. The need for a high level of reproducibility and clearly defined risk hypotheses contribute to the robustness of, and confidence in, the environmental risk assessments of transgenic plants. Further, these authors emphasized that confidence in the results of early-tier laboratory studies is a precondition for the acceptance of data across regulatory jurisdictions and should encourage agencies to share useful information and thus avoid redundant testing. When evaluating potential risks of a given technology, it is important to use relevant comparators. This holds true for risk assessment of transgenic crops. Few studies have actually been designed to directly compare recombinant DNA technology with conventional pest control strategies, although recent studies by Mulligan et al. [68, 69] directly compared the non-target effects of the synthetic pesticide cypermethrin with oilseed rape plants expressing a cysteine protease inhibitor against two predators. While neither form of pest control treatment negatively affected the carabid, the effects of the transgenic crop on the lacewing were significantly lower than with the commonly used pesticide.

Recent studies have performed meta-analyses on a modified public database [104] to synthesize current knowledge about the effects of *Bt* cotton, maize, and potato on the abundance and interactions of arthropod non-target functional guilds [105]. Overall, they show no uniform effects of *Bt* cotton, maize, and potato on the functional guilds of non-target arthropods. In fact, use of and type of insecticides influenced the magnitude and direction of effects; and insecticide effects were much larger than those of *Bt* crops. Similarly,

Transgenic Crops, Environmental Impact. Table 3 Impacts of transgenic crops and transgene products on predators

Protein [1]	Transgenic plant or diet	Pest	Natural enemy	Effects on natural enemy	Reference
Bt	Corn (Cry1Ab)	Direct feeding (pollen)	Several (Coleoptera, Heteroptera, Neuroptera)	No effects on predators in both laboratory and field experiments	[40]
	Corn (Cry3Bb1)	*Diabrotica* spp. (Col: Chrysomelidae)	Several (Araneae, Carabidae, Staphylinidae)	No consistent negative effect	[41]
	Corn (Cry1Ab)	*Ostrinia nubilalis*; *Spodoptera littoralis* (Lep: Noctuidae)	*Caladenia carnea*	*Bt*-fed prey increased predator mortality and development times	[42]
		S. littoralis	*C. carnea*	Negative effects, as observed previously, determined to be due to reduced prey quality	[43]
		Tetranychus urticae (Acari)	*Stethorus punctillum* (Col: Coccinellidae)	No effects in both laboratory and field experiments	[44]
		Direct feeding (pollen)	Spiders (Araneae)		[45, 46]
	Corn (Cry3Bb1)	*Rhopalosiphum maidis* (Hom: Aphididae)	*Coleomegilla maculate* (Col.: Coccinellidae)	No effects when fed non-target aphid prey	[47]
	Corn (VIP3A + Cry1Ab)	Lepidoptera pests	Several (13 arthropod orders)	Large-scale study showed no negative effects of stacked traits over conventional corn	[48]
	Cotton (Cy1Ac)	*Aphis gossypii* (Hem. Aphididae)	*Chrysopa pallens* (Neu: Chrysopidae)	No effect	[49]
	Cotton (Cry1Ac)	Several	Predators (several)	Minor reductions in predator density in the field	[50, 51]
	Cotton (Cry1Ac/ Cry2Ab)	Lepidopterous pests		Predator numbers similar or higher in *Bt* cotton field plots	[52,53]
	Cotton (Cry1Ac)	*Spodoptera exigua*, *Helicoverpa zea* (Lep: Noctuidae)	*Geocoris punctipes* (Het: Lygaeidae)	No effects in field experiments	[54]
		S. exigua	*Podisus maculiventris*	No effects	[55]
		Lepidopterous pests	*C. carnea*; *Orius tristicolor* (Het: Anthocoridae)	No effects in field experiments	[56]
	Potato (Cry3Aa)	*Leptinotarsa decemlineata*	Several heteropteran predators and spiders	No effect of predator densities in the field	[57]

Transgenic Crops, Environmental Impact. Table 3 (Continued)

Protein [1]	Transgenic plant or diet	Pest	Natural enemy	Effects on natural enemy	Reference
	Potato (Cry3Aa)	*L. decemlineata*	Coleoptera, Araneae	No effects on field pitfall trap capture numbers	[58]
	Potato (Cry3)	*Myzus persicae*	*Hippodamia convergens* (Col: Coccinellidae)	No effect	[59]
	Potato (Cry3A)	Lep. Hem.	Several (Heteroptera)	No effects on development time	[60]
	Potato		*Harmonia axyridis*, *Nebria brevicollis*	No effects	[61]
CpTI	Injected prey	*L. oleracea*	*P. maculiventris* (Het: Pentatomidae)	Reduced growth of predators	[62]
	Potato		*P. maculiventris*	No effects	[62]
	Strawberry	*Otiorhynchus sulcatus* (Col: Curculionidae)	Carabids and others	Field abundance not affected	[63]
HvCPI-1 C68 → G	Potato	*L. decemlineata*	*P. maculiventris*	No effect	[64]
		S. littoralis			[64]
MTI-2	Oilseed rape	*Plutella xylostella*	*Pterostichus madidus* (Col: Carabidae)	No effects on reproductive fitness; female weight gain reduced at first but compensated for later	[65]
Aprotinin (bovine pancreatic or bovine spleen trypsin inhibitor) (BPTI/BSTI)	Diet	*Helicoverpa armigera*	*Harpalus affinis* (Col: Carabidae)	Beetles consumed less prey after 24 h of exposure to inhibitor-fed prey	[66]
BPTI/BSTI		*H. armigera*	*Nebria brevicollis* (Col: Carabidae)	Transient minor changes in adult beetle weights	[67]
OCI		Direct feeding	*C. carnea*	No effect via contaminated pollen	[68]
	Oilseed rape	*Deroceras reticulatum* (Mollusca)	*Pterostichus melanarius* (Col. Carabidae)	No effects on beetle mortality, weight gain, or food consumption	[69]
	Oilseed rape	*P. xylostella* (Lep: Plutellidae)	*H. axyridis*	No effect on survival or development of ladybird	[70]
	Potato	*L. decemlineata* (Colorado potato beetle)	*Perillus bioculatus* (Het: Pentatomidae)	No effects	[71]
Soybean trypsin inhibitor (SBTI)	Diet	Direct feeding	*C. carnea*		[72]

Transgenic Crops, Environmental Impact. Table 4 Impacts of transgenic crops and transgene products on parasitoids

Protein [1]	Transgenic plant or diet	Pest	Natural enemy	Effects on natural enemy	Reference
Bt	Corn (Cry1Ab)	*Chilo partellus* (Lep: Crambidae)	*Diaeretiella rapae* (Hym: Braconidae)	Reduced survival due to host mortality, smaller cocoons and adults	[73]
	Corn (Cry1Ab) (field)	*Ostrinia nubilalis* (Lep: Crambidae)	*Macrocentrus cingulum* (Hym: Braconidae)	Reductions of 29–60% is numbers of wasps found in the field	[74]
	Corn (Cry1Ab)	*Spodoptera frugiperda* (Lep: Noctuidae)	*Campoletis sonorensis* (Hym: Ichneumonidae)	Wasps were significantly smaller when developing in *Bt*-fed hosts	[75]
		Eoreuma loftini (Lep: Pyralidae)	*Parallorhogas pyralophagus* (Hym: Braconidae)	Various aspects of parasitoid biology (not all) negatively affected	[76]
	Cotton (Cry1Ac)	*Helicoverpa armigera* (Lep: Noctuidae)	*Microplitis mediator* (Hym: Braconidae)	Wasp survival and development negatively affected	[77, 78]
		Pseudoplusia includens (Lep: Noctuidae)	*Cotesia marginiventris* (Hym: Braconidae), *Copidosoma floridanum* (Hym: Encyrtidae)	Development times for both wasp species negatively affected. Adult longevity for *C. marginiventris* reduced	[79]
	Cotton (Cry1Ac) (field)	Hemipteran pests	Aphelinid parasitoids	Small reduction of parasitoid population density relative to non-*Bt* cotton	[50, 51]
	Diet (Cry1Ac)	*Spodoptera litura/H. armigera* (Lep: Noctuidae)	*Meteorus pulchricornis* (Hym: braconidae); *Cotesia kazak* (Hym: Braconidae)	Survival of both unaffected in *Bt*-fed *S. litura. M.pulchricornis* negatively affected by *Bt* –fed *H. armigera*	[80]
	Oilseed rape (Cry1Ac)	*Plutella xylostella* (Lep: Plutellidae)	*Cotesia plutellae* (Hym: Braconidae)	No effect when *Bt*-resistant hosts were parasitized	[81]
	Broccoli	*P. xylostella*	*Diadegma insulare* (Hym: Ichneumonidae)	No effect on parasitoid when exposed by *Bt*-resistant hosts	[82]
	Pine (Cry1Ac)	*Pseudocoremia suavis* (Lep: Geometridae)	*M. pulchricornis*	No effect on parasitoid developmental parameters	[83]
	Diet (Cry9Aa)	*Galleria mellonella* (Lep: Gelechiidae)	*Exorista larvarum* (Dip: Tachinidae)	No effect on fly parasitoid when exposed to facticious *Bt*-fed hosts	[84]
	Tobacco (Cry1Ab) (field)	*Heliothis virescens* (Lep. Noctuidae)	*C. sonorensis*	Rates of parasitism increased	[85]
CpTI	Diet or potato	*Lacanobia. oleracea* (Lep: Noctuidae)	*Eulophus pennicornis* (Hym: Eulophidae)	Fewer hosts parasitized, no effects on parasitoids	[86]

Transgenic Crops, Environmental Impact. Table 4 (Continued)

Protein [1]	Transgenic plant or diet	Pest	Natural enemy	Effects on natural enemy	Reference
CpTI	Diet	Direct feeding (adult wasps)	*E. pennicornis*	No effects	[87]
CpTI and *Bt*	Cotton	*H. armigera*	*Microplitis mediator* (Hym: Braconidae)	No greater effects than with *Bt*-cotton	[78]
	Cotton pollen	Direct feeding	*Trichogramma chilonis* (Hym: Trichogrammatidae)	No adverse effects due to CpTI	[88]
OC1	Diet	*Macrosiphum euphorbiae* (Hom: Aphididae)	*Aphelinus abdominalis* (Hym: Braconidae)	Parasitoid fitness impaired	[89]
	Potato	*M. euphorbiae*	*Aphidius nigripes* (Hym: Braconidae)	Wasp size and fecundity increased on OC1 line	[90]
	Oilseed rape	*Myzus persicae* (Hom: Aphididae)	*Diaeretiella rapae* (Hym: Braconidae)	No consistent effects on adult wasp emergence and sex ratio; no effects on control of aphids	[91]
OC1 IΔD86 (for nematode control)	Potato (field)	*M. euphorbiae*, *M. persicae*	*Aphidius ervi* (Hym: Braconidae)	No effects on percent parasitism, adult wasp emergence, parasitoid communities more diverse on GM plants	[92]
Con A	Diet	Direct feeding	*E. pennicornis*	Higher doses reduced adult longevity and reproductive fitness	[87], [93]
GNA		*M. euphorbiae*	*A. abdominalis*	No effect via host feeding on aphids Reduced size and longevity of adults when exposed via host	[94, 95]
		Direct feeding (adult wasps)	*Aphidius colemani* (Hym: Braconidae)	Higher doses reduced adult longevity	[96]
	Honeydew	Direct feeding (adult wasps)	*A. ervi*	Indirect negative affect potentially due to altered honeydew composition	[97]
	Potato/diet	*M. persicae*	*A. ervi*	No effects via potato, dose-dependent effects on development via diet	[94, 95]
	Sucrose diet	Direct feeding	*Cotesia glomerata* (Hym: Braconidae)	Higher doses reduced longevity	[96]
	Diet/ Sugarcane	*Diatraea saccharalis* (sugarcane borer)	*Cotesia flavipes* (Hym: Braconidae)	Small negative effects on parasitism. No effects on host location of prey or parasitism	[98, 99]
	Potato/Diet	*L. oleracea*	*E. pennicornis*	No effect on parasitism success	[100]
	Diet	Direct feeding		Reduced adult longevity and reproductive fitness	[87], [93]

Transgenic Crops, Environmental Impact. Table 4 (Continued)

Protein [1]	Transgenic plant or diet	Pest	Natural enemy	Effects on natural enemy	Reference
	Host diet/host injection	*L. oleracea*	*E. pennicornis*	Negative effects on the survival of parasitoid larvae	[93]
	Sugarcane	*E. loftini*	*P. pyralophagus*	Reduced size and longevity of adult wasps	[101]
	Tomato/ potato/diet	*L. oleracea*	*Meteorus gyrator* (Hym: Braconidae)	No effects	[102]
	Sucrose diet	Direct feeding (adult wasps)	*Trichogramma brassicae* (Hym: Trichogrammatidae)	Antifeedant; high dose reduced longevity	[96]

Duan et al. [106] performed meta-analyses comparing results for non-target invertebrates exposed to *Bacillus thuringiensis* (*Bt*) Cry proteins in laboratory studies with results derived from independent field studies examining effects on the abundance of non-target invertebrates. In this case, the findings support the assumption that laboratory studies of transgenic insecticidal crops show effects that are either consistent with, or more conservative than, those found in field studies.

In combination with robust field data [107], the evidence strongly supports *Bt* crops as an environmentally neutral technology, especially in comparison to insecticides. These findings are thus in agreement with those of Mulligan et al. [68, 69].

Impact on Pollinators Many of the world's crops depend on insects for pollination and it is critically important that agricultural biotechnology does not disrupt this essential "ecosystem service" – as such, pollinators are critical to agriculture, in addition to their vital role in helping maintain biodiversity. Thus, representative pollinators form an important part of the risk assessment process and much of what has been stated for natural enemies applies to these species too. In common with natural enemies, transgenic plants can impact on pollinators in two ways, either directly (via the transgenic plant itself posing a hazard to the pollinator), or indirectly (via the use of a transgenic crop affecting other ecological requirements of the pollinator). Of the extensive field trials carried out to date with either *Bt*-expressing crops, or HT transgenic crops, no deleterious effects on pollinators have been reported [108]. Furthermore, results from the many studies carried out to date on transgenic plants still under development suggest that only a few of the lectins and protease inhibitors tested could present dose-dependent hazards to bees, and then only if expressed in the pollen at sufficiently high levels; most current promoters used, albeit constitutive promoters, only express at very low levels, if at all, in the pollen.

In addition to evaluating the potential impacts of transgenic crops on pollinator species, it is also important to address issues relating to the ability of these species to collect and transport pollen between transgenic and non-transgenic crops, i.e., their role in pollen dispersal and hence gene flow. Recombinant proteins are usually expressed at low levels in the pollen of transgenic plants due to the use of specific "constitutive" promoters in the gene constructs. However, the transgenes themselves are present in DNA contained in the pollen, and therefore may be transferred to other related plants via the activities of the pollinator species.

Impact of Herbicide-Tolerant Transgenic Crops

The wide-scale growing of glyphosate-tolerant crops has resulted in an increase in glyphosate usage at the expense of other herbicides [4, 109–111]. However, despite this increase in glyphosate use, overall, the use of HT crops has resulted, overall, in a significant reduction in pesticides. This has been accompanied by a reduction in tillage which has an additional benefit

of reducing the use of petroleum-based fuels as well as an implicit gain in time-use efficiency by growers [112]. Furthermore, HT crops have dramatically changed the crop cultivars selected by growers and has hastened the development of new transgenic crops for commercial distribution worldwide [32, 113].

Weed control based on HT crops is efficient and cost effective and provides considerable savings in terms of both time and labor [114]. However, despite this and other obvious benefits of the technology (see above), there is much opposition in some quarters to these crops – possibly more so than for insect-resistant transgenic crops. One of the reasons for this opposition stems from a lack of effective communication and understanding between the general public and the scientific and agricultural communities [21, 115]. Designing a risk assessment to test specific questions to also address societal concerns may help address this issue since it would provide an opportunity for society to participate in the regulatory decisions affecting HT crops [116]. It is possible that a major part of the concern expressed about HT crops is that the technology is associated with herbicide use, which in itself is perceived as risky by the public sector [117]. The mode of action of glyphosate is well understood and in fact was one of the first commercially successful herbicides to have an identified enzymatic site of action in plants. The selective and specific interaction of glyphosate with EPSPS accounts for its potent herbicidal properties and low toxicity to other life forms; as such, this will significantly reduce the potential for direct non-target effects and should negate many of these concerns.

Despite their undoubted success and major contribution to global agriculture, potential risks associated with the technology must be assessed, not least in terms of the increased use of glyphosate [112, 118–121]. However, this apart, the primary environmental risk associated with HT crops relates to their impact on weed population shifts, whether expressed as the rise in economic prominence of a new weedy species or the evolution of glyphosate-tolerant weed biotypes. This position is supported by the herbicide resistance risk analysis which suggests that glyphosate-based systems are at high risk of selecting for glyphosate-tolerant weeds [122], although not all research supports this view point [123].

Impact on Biodiversity Agriculture itself has had a major impact on biodiversity, often manifested in a marked decline in the abundance of species [124–126]. While it is suggested that the ecosystem effects of HT crops have been minimal [127], the indirect impact of these crops on the agro-ecosystem, particularly as a result of changes in tillage and weed management tactics, is important [128]. There is conflicting evidence in the literature with some reports suggesting an increase in species diversity in HT-based systems while other reports suggest a reduction [129–133]. These apparent contradictions may be due to the fact that effects are often specific to the crop in question and dependent on the different weed management tactics used for HT crops compared to non-transgenic crops [134, 135]. For example, deployment of HT crops was shown to have a negative impact on butterfly population densities as an indirect effect of good weed control, reflecting a lack of nectar availability [136]. In contrast, little effect was observed for bees, gastropods, and other invertebrates. Furthermore, the effects of such crops on the soil biota were found to be negligible [132]. Thus, there appears to be both favorable and unfavorable data on the effects of HT crops on biological diversity [32]. The critical consideration is that these effects are highly dependent on specific crop and management tactics. It is likely that any unfavorable effect on biological diversity could be ameliorated by subtle manipulation of the HT-based system.

Gene Flow Another pervasive problem with HT crops is their coexistence with non-GM crops. Three important considerations have to be addressed: (1) introgression of the trait via pollen (pollen drift); (2) containment of plant products during the production year (grain segregation); and (3) volunteer HT plants in following years [115]. While HT crops and their non-transgenic counterparts can, and do, coexist, and while grain segregation and controlling volunteers is feasible [115, 137], controlling/preventing introgression of the HT trait via pollen movement in open-pollinated crops such as maize is considerably more difficult [138–141]. A number of factors affect the success of maize pollen movement and subsequent pollination, and generally, the greater the distance between the pollen source and donor, the less likely is the introgression of the transgenic trait [139, 140].

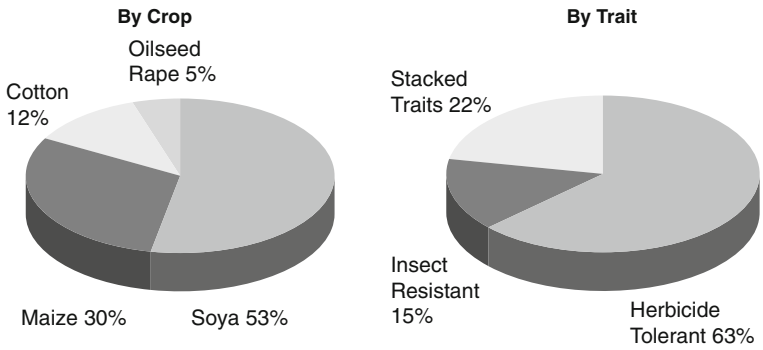

Transgenic Crops, Environmental Impact. Figure 2
Global status of biotech crops for 2008

Given the tolerance levels established for some transgenic traits in non-transgenic crops, the isolation distances required to mitigate the risks of gene flow may be too great to be realistic in commercial maize production systems [142]. Other open-pollinated crops have also been scrutinized with significant legal ramification [143–146]. However, because of the possibility of "contamination" as a consequence of gene flow, many countries require buffer zones between fields growing transgenic crops and their non-transgenic counter parts; the size of these buffer zones will vary, depending upon a number of different factors including the crop itself. It is suggested that the issues of the coexistence of such crops with non-transgenic crops will continue to be a concern as long as there are economic differences between the crop cultivar types [147–149].

Future Directions

The major traits currently commercialized predominantly confer resistance to biotic stress, with herbicide-tolerant (HT) crops occupying the market share (Fig. 2). In 2009, SmartStax, a novel biotech maize containing eight different genes for insect and herbicide resistance, was approved for commercialization in the USA. These so-called first-generation transgenic crops, expressing improved agricultural traits are often perceived as being of benefit to the grower rather than to the consumer *per se*. Although the seed is more expensive, such crops lower the costs of production by reducing inputs of machinery, fuel, and chemical pesticides. In addition, due to more effective pest control, crop yields are often higher (Tables 1 [6] and 2 [7–20]). However, it is important to appreciate the environmental and health benefits of growing these first-generation transgenic crops, many of which are associated with reduced spraying of highly toxic chemical insecticides and herbicides. In terms of environmental benefits, these include controlling farm runoff that otherwise pollutes water systems and reduced mechanical weeding, so reducing loss of topsoil [150], while the major health benefits are a consequence of reduced pesticide exposure for farmers and rural laborers, and lower pesticide residues for consumers.

In addition to transgenic crops with increased tolerance to biotic stress, drought-tolerant maize is expected to be deployed in the USA in 2012 and sub-Saharan Africa in 2017. Other transgenic crops on the horizon include adoption of Golden Rice by the Philippines in 2012 and Bangladesh and India before 2015. Other smaller hectarage crops are also expected to be approved by 2015, including potatoes with pest and/or disease resistance, sugarcane with quality and agronomic traits, and disease-resistant bananas [3]. Interestingly, wheat remains the last major staple crop without approved biotech traits. However, political will for the crop is growing globally and many authorities suggest that China may be the first country to approve biotech wheat as early as 5 years from now.

As the science develops, so does the technology, but irrespective of which particular generation of transgenic crops is being considered, their environmental impact is of prime importance. Any risk assessment

process must thus keep pace with the changing technology and the development of novel crops expressing novel traits.

Conclusion

Although one of the major concerns of recombinant DNA technology relates to its impact on non-target organisms, and thus on biodiversity, these fears have not, in the main, been realized, although there have been some well-publicized cases to the contrary. Concern over the potential for *Bt*-expressing maize to have negative effects on the Monarch Butterfly (*Danaus plexippus*) population was voiced following the publication of lab-based studies that demonstrated that unrealistically high levels of pollen from such plants had a deleterious effect [151]. However, subsequent large-scale field trials demonstrated this not to be the case, one factor being that when the maize was in flower, the Monarchs were not present [152–157]. Thus, in this instance, while the potential hazard was high, exposure was negligible resulting in effectively zero risk. Other examples include reports of initial studies concerning toxicity of *Bt* maize–fed hosts toward the predator *Chrysoperla carnae* (the green lacewing) via a tri-trophic interaction [42]. However, subsequent studies demonstrated that *Bt* Cry1Ab was not toxic to the larvae but that the effects reported were mediated by prey quality [158]. Studies of this type emphasize the need not only to place them within an ecological context, but also to use appropriate comparators in the risk assessment process. Studies such as those carried out by Hilbeck [42] and colleagues emphasize the importance of scientific rigor and the need for demonstration of "cause and effect."

While numerous studies have now been carried out to evaluate the environmental safety of transgenic crops on beneficial insects such as natural enemies that play an important role in biological control and pollinators, in the vast majority of cases, few negative effects have actually been demonstrated. Interestingly, in the majority of cases studied to date regarding natural enemies, it is apparent that the predator/parasitoid is often able to avoid the toxic effects of the different insecticidal proteins being expressed, despite exposure at physiologically relevant levels. Further, there is evidence that the transgene product is diluted as it passes through the different trophic levels. For pollinators, this lack of toxicity is attributed to lack of receptors, in the case of *Bt*, and lack of exposure when expressed in the transgenic plant.

In addition to their potential impact on biodiversity, other environmental concerns relating to the deployment of transgenic crops are the potential for gene flow, particularly in the case of HT crops. However, the potential for gene flow is highly dependent upon the plant species [159]. Gene flow in crops can occur via pollen and via seed, the latter potentially affecting agriculture temporally and on a much larger scale than gene flow attributable to pollen [160]; in general, it is acknowledged that the risks of unintended trait movement are difficult to assess [161]. It is, however, important to point out that gene flow is no different in transgenic crops than in non-transgenic cultivars and that gene flow from transgenic crops is a reality [162]. To expect compliance of zero gene flow is neither reasonable nor realistic, and an acceptable tolerance must be established for the coexistence of transgenic crops with their non-transgenic counterparts.

Bibliography

1. Royal Society Policy Document 11/09 (2009) Reaping the benefits: science and the sustainable intensification of global agriculture. Royal Society, London
2. FAO (2000) Agriculture: Towards 2015/30. Technical interim report, April. Economic and social department. Rome, Italy
3. James C (2008) Global status of commercialized biotech/GM crops: 2008. The First Thirteen Years, 1996 to 2008. ISAAA Brief 39-2008: Executive Summary. ISAAA, New York
4. Service RF (2007b) A growing threat down on the farm. Science 316:1114–1117
5. Meyer B (2008) Biotech crops gaining favor around the globe. Learfield Communications, Inc., Jefferson City
6. Zilberman D, Sexton SE, Marra M, Fernandez-Cornejo J (2010) The economic impact of genetically engineered crops. http://www.choicesmagazine.org/
7. Delannay X, Bauman TT, Beighley DH, Buettner MJ, Coble HD, DeFelice MS, Derting CW, Diedrick TJ, Griffin JL, Hagood ES, Hancock FG, Hart SE, LaVallee BJ, Loux MM, Lueschen WE, Matson KW, Moots CK, Murdock E, Nickell AD, Owen MDK, Paschall EH II, Prochaska LM, Raymond PJ, Reynolds DB, Rhodes WK, Roeth FW, Sprankle PL, Tarochionc LJ, Tinius CN, Walker RH, Wax LM, Weigelt HD, Padgette SR (1995) Yield evaluation of a glyphosate-tolerant soybean line after treatment with glyphosate. Crop Sci 35:1461–1467

8. Roberts RK, Pendergrass R, Hayes RM (1998) Farm-level economic analysis of roundup ReadyTM soybeans. Paper presented at the Southern Agricultural Economics Association meeting, Little Rock, 1–4 Feb 1998
9. Arnold JC, Shaw DR, Medlin CR (1998) Roundup ReadyTM programs versus conventional programs: efficacy, varietal performance, and economics. Proc South Weed Sci Soc 51: 272–273
10. Marra M, Carlson G, Hubbell B (1998) Economic impacts of the first crop biotechnologies. Available at http://www.ag.econ.ncsu.edu/faculty/marra/firstcrop/imp001.gif
11. Fernandez-Cornejo J, Klotz-Ingram C, Jans S (2002) Farm-level effects of adopting herbicide-tolerant soybeans in the USA. J Agric Appl Econ 34:149–163
12. Duffy M (2001) Who benefits from biotechnology? Paper presented at the American Seed Trade Association meeting. Chicago, 5–7 Dec 2001
13. Marra MC (2004) Review of the economic and environmental impacts of agbiotech: a global perspective. AgBioForum 6:144–145, Nicholas GK (ed)
14. Bernard JC, Pesek JD Jr, Fan C C (2004) Delaware farmers adoption of GE soybeans in a time of uncertain U.S. adoption. Agribus Int J 20:81–94
15. Qaim M, Traxler G (2005) Roundup Ready soybean in Argentina: farm level and aggregate welfare effects. Agric Econ 32:73–86
16. Vencill WK (1996) Weed management systems utilizing herbicide-resistant cotton. Proceedings of the Beltwide Cotton Conferences Cotton Weed Science Research Conference 2:1532–1533
17. Keeling W, Dotray P, Jones C, Sunderland S (1996) Roundup^{TM} ready cotton: a potential new weed management tool for the Texas high plains. Proceedings of the Beltwide Cotton Conferences Cotton Weed Science Research Conference 2:1529
18. Goldman IL (1998) From out of old fields comes all this new corn: An historical perspective on heterosis in plant improvement. Concepts and breeding of heterosis in crop plants. Book series: CSSA Special Publications Issue: 25, pp 1–12
19. Culpepper AS, York AC (1998) Weed management in glyphosate-tolerant cotton. J Cotton Sci 4:174–185
20. Fernandez-Cornejo J, Klotz-Ingram C, Jans S (2000) Farm-level effects of adopting genetically engineered crops in the USA. In: Lesser WL (ed) Transitions in agrobiotech: economics of strategy and policy. Food Marketing Research Center, University of Connecticut and Department of Research Economics, University of Massachusetts, pp 57–72
21. Krayer von Krauss MP, Casman EA, Small MJ (2004) Elicitation of expert judgments of uncertainty in the risk assessment of herbicide-tolerant oilseed crops. Risk Anal 24:1515–1527
22. de Maagd RA, Bravo A, Crickmore N (2001) How *Bacillus thuringiensis* has evolved specific toxins to colonize the insect world. Trends Genet 17:193–199
23. Song XX, Wang SM (2001) Status and evaluation on the expression of cotton varieties in the production in China in the past 20 years. Cotton Sci 13:315–320
24. He KL, Wang ZY, Zhang YJ (2009) Monitoring *Bt* resistance in the field: China as a case study. In: Ferry N, Gatehouse AMR (eds) Environmental impact of genetically modified crops. Wallingford, CAB International, pp 344–359, Chap 16
25. Tabashnik BE, Carrié Y (2009) Insect resistance to genetically modified crops. In: Ferry N, Gatehouse AMR (eds) Environmental impact of genetically modified crops. CAB International, Wallingford, pp 74–100, Chap 5
26. Christou P, Capell T, Kohli A, Gatehouse JA, Gatehouse AMR (2006) Recent developments and future prospects in insect pest control in transgenic crops. Trends Plant Sci 11:302–308
27. Gatehouse JA (2002) Plant resistance towards insect herbivores: a dynamic interaction. New Phytol 156:145–169
28. Gatehouse JA (2008) Biotechnological prospects for engineering insect-resistant plants. Plant Physiol 146: 881–887
29. Malone LA, Gatehouse AMR, Barratt BIP (2008) Beyond Bt: alternative strategies for insect-resistant crops. In: Romeis J, Shelton T, Kennedy G (eds) Integration of insect-resistant genetically modified crops within integrated pest management programs, Series on Progress in Biological Control. Springer, New York
30. Price DR, Gatehouse JA (2008) RNAi-mediated crop protection against insects. Trends Biotechnol 26:393–400
31. James C (2009) Global status of commercialized biotech/GM crops: 2009. ISAAA Brief No. 41. ISAAA: Ithaca
32. Duke SO (2005) Taking stock of herbicide-resistant crops ten years after introduction. Pest Manag Sci 61:211–218
33. Duke SO, Powles SB (2008) Glyphosate: a once-in-a-century herbicide. Pest Manag Sci 64:319–325
34. Mazur S, Falco C (1989) The development of herbicide resistant crops. Annu Rev Plant Physiol Plant Mol Biol 40:441–470
35. Betz FS, Hammond BG, Fuchs RL (2000) Safety and advantages of *Bacillus thuringiensis*-protected plants to control insect pests. Regul Toxicol Pharmacol 32:156–173
36. Cattaneo MG, Yafuso C, Schmidt C, Huang CY, Rahman M, Olson C, Ellers-Kirk C, Orr BJ, Marsh SE, Antilla L, Dutilleu P, Carriere Y (2006) Farm-scale evaluation of the impacts of transgenic cotton on biodiversity, pesticide use, and yield. Proc Natl Acad Sci USA 103:7571–7576
37. Thies JE, Devare MH (2007) An ecological assessment of transgenic crops. J Dev Stud 43:97–129
38. Tencalla FG, Nickson TE, Garcia-Alonso M (2009) Environmental risk assessment. In: Ferry N, Gatehouse AMR (eds) Environmental impact of genetically modified crops. CAB International, Wallingford, pp 61–73, Chap 4
39. Waltz E (2009) Battlefield. Nature 461:27–32
40. Pilcher CD, Obrycki JJ, Rice ME, Lewis LC (1997) Preimaginal development, survival, and field abundance of insect predators on transgenic *Bacillus thuringiensis* corn. Environ Entomol 26:446–454

41. Bhatti MA, Duan J, Head G, Jiang CJ, Mckee MJ, Nickson TE, Pilcher CL, Pilcher CD (2005) Field evaluation of the impact of corn rootworm (Coleoptera: Chrysomelidae)-protected Bt corn on ground-dwelling invertebrates. Environ Entomol 34:1325–1335
42. Hilbeck A, Baumgartner M, Fried PM, Bigler F (1998) Effects of transgenic *Bacillus thuringiensis* corn-fed prey on mortality and development time of immature *Chrysoperla carnea* (Neuroptera: Chrysopidae). Environ Entomol 27: 480–487
43. Dutton A, Klein H, Romeis J, Bigler F (2002) Uptake of Bt-toxin by herbivores feeding on transgenic maize and consequences for the predator *Chrysoperla carnea*. Ecol Entomol 27:441–447
44. Alvarez-Alfageme F, Ferry N, Castanera P, Ortego F, Gatehouse AMR (2008) Prey mediated effects of Bt maize on fitness and digestive physiology of the red spider mite predator *Stethorus punctillum* Weise (Coleoptera: Coccinellidae). Transgenic Res 17:943–954
45. Ludy C, Lang A (2006) A 3-year field-scale monitoring of foliage-dwelling spiders (Araneae) in transgenic Bt maize fields and adjacent field margins. Biol Control 38:314–324
46. Ludy C, Lang A (2006) Bt maize pollen exposure and impact on the garden spider, *Araneus diadematus*. Entomol Exp Appl 118:145–156
47. Lundgren JG, Wiedenmann RN (2005) Tritrophic interactions among Bt (CryMb1) corn, aphid prey, and the predator *Coleomegilla maculata* (Coleoptera: Coccinellidae). Environ Entomol 34:1621–1625
48. Dively GP (2005) Impact of transgenic VIP3a x Cry1ab lepidopteran-resistant field corn on the nontarget arthropod community. Environ Entomol 34:1267–1291
49. Guo JY, Wan FH, Dong L, Lovei GL, Han ZJ (2008) Tri-trophic interactions between *Bt* cotton, the herbivore *Aphis gossypii* Glover (Homoptera: Aphididae), and the predator *Chrysopa pallens* (Rambur) (Neuroptera: Chrysopidae). Environ Entomol 37:263–270
50. Naranjo SE (2005) Long-term assessment of the effects of transgenic *Bt* cotton on the abundance of nontarget arthropod natural enemies. Environ Entomol 34: 1193–1210
51. Naranjo SE (2005) Long-term assessment of the effects of transgenic Bt cotton on the function of the natural enemy community. Environ Entomol 34:1211–1223
52. Hagerty AM, Kilpatrick AL, Turnipseed SG, Sullivan MJ, Bridges WC (2005) Predaceous arthropods and lepidopteran pests on conventional, Bollgard, and Bollgard II cotton under untreated and disrupted conditions. Environ Entomol 34:105–114
53. Head G, Moar M, Eubanks M, Freeman B, Ruberson J, Hagerty A, Turnipseed S (2005) A multiyear, large-scale comparison of arthropod populations on commercially managed *Bt* and non-*Bt* cotton fields. Environ Entomol 34:1257–1266
54. Torres JB, Ruberson JR (2006) Interactions of *Bt*-cotton and the omnivorous big-eyed bug *Geocoris punctipes* (Say), a key predator in cotton fields. Biol Control 39:47–57
55. Torres JB, Ruberson JR (2008) Interactions of *Bacillus thuringiensis* Cry1Ac toxin in genetically engineered cotton with predatory heteropterans. Transgenic Res 17:345–354
56. Sisterson M, Biggs RW, Manhardt NM, Carriere Y, Dennehy TJ, Tabashnik BE (2007) Effects of transgenic Bt cotton on insecticide use and abundance of two generalist predators. Entomol Exp Appl 124:305–311
57. Reed GL, Jensen AS, Riebe J, Head G, Duan JJ (2001) Transgenic Bt potato and conventional insecticides for Colorado potato beetle management: comparative efficacy and non-target impacts. Entomol Exp Appl 100: 89–100
58. Duan JJ, Head G, Jensen A, Reed G (2004) Effects of transgenic *Bacillus thuringiensis* potato and conventional insecticides for Colorado potato beetle (Coleoptera: Chrysomelidae) management on the abundance of ground-dwelling arthropods in Oregon potato ecosystems. Environ Entomol 33:275–281
59. Dogan EB, Berry RE, Reed GL, Rossignol PA (1996) Biological parameters of convergent lady beetle (Coleoptera: Coccinellidae) feeding on aphids (Homoptera: Aphididae) on transgenic potato. J Econ Entomol 89:1105–1108
60. Armer CA, Berry RE, Kogan M (2000) Longevity of phytophagous heteropteran predators feeding on transgenic Bt-potato plants. Entomol Exp Appl 95:329–333
61. Ferry N, Mulligan EA, Majerus MEN, Gatehouse AMR (2007) Bitrophic and tritrophic effects of Bt Cry3A transgenic potato on beneficial, non-target, beetles. Transgenic Res 16:795–812
62. Bell HA, Down RE, Fitches EC, Edwards JP, Gatehouse AMR (2003) Impact of genetically modified potato expressing plant-derived insect resistance genes on the predatory bug *Podisus maculiventris*. Biocontrol Sci Technol 13:729–742
63. Graham J, Gordon SC, Smith K, McNicol RJ, McNicol JW (2002) The effect of the cowpea trypspin inhibitor in strawberry on damage by vine weevil under field conditions. J Hortic Sci Biotechnol 77:33–40
64. Alvarez-Alfageme F, Martinez M, Pascual-Ruiz S, Castanera P, Diaz I, Ortego F (2007) Effects of potato plants expressing a barley cystatin on the predatory bug *Podisus maculiventris* via herbivorous prey feeding on the plant. Transgenic Res 16:1–13
65. Ferry N, Jouanin L, Ceci LR, Mulligan EA, Emami K, Gatehouse JA, Gatehouse AMR (2005) Impact of oilseed rape expressing the insecticidal serine protease inhibitor, mustard trypsin inhibitor-2 on the beneficial predator *Pterostichus madidus*. Mol Ecol 14:337–349
66. Jørgensen HB, Lövei GL (1999) Tri-trophic effect on predator feeding: consumption by the carabid *Harpalus affinis* of *Heliothis armigera* caterpillars fed on proteinase inhibitor-containing diet. Entomol Exp Appl 93:113–116

67. Burgess EPJ, Malone LA, Christeller JT, Lester MT, Murray C, Philip BA, Phung MM, Tregidga EL (2002) Avidin expressed in transgenic tobacco leaves confers resistance to two noctuid pests, *Helicoverpa armigera* and *Spodoptera litura*. Transgenic Res 11:185–198
68. Mulligan EA, Ferry N, Jouanin L, Romeis J, Gatehouse AMR (2010) Characterisation of adult green lacewing (*Chrysoperla carnea*) digestive physiology: comparison of the impact of genetically modified crops and conventional pest control. Pest Manag Sci 66(3):325–336
69. Mulligan EA, Ferry N, Jouanin L, Walters K, Port GR, Gatehouse AMR (2006) Comparing the impact of conventional pesticide and use of a transgenic pest-resistant crop on the beneficial carabid beetle *Pterostichus melanarius*. Pest Manag Sci 62:999–1012
70. Ferry N, Raemaekers RJM, Majerus MEN, Jouanin L, Port G, Gatehouse JA, Gatehouse AMR (2003) Impact of oilseed rape expressing the insecticidal cysteine protease inhibitor oryzacystatin on the beneficial predator *Harmonia axyridis* (Multicolored Asian Ladybeetle). Mol Ecol 12:493–504
71. Bouchard E, Cloutier C, Michaud D (2003) Oryzacystatin I expressed in transgenic potato induces digestive compensation in an insect natural predator via its herbivorous prey feeding on the plant. Mol Ecol 12:2439–2446
72. Lawo NC, Romeis J (2008) Assessing the utilization of a carbohydrate food source and the impact of insecticidal proteins on larvae of the green lacewing, *Chrysoperla carnea*. Biol Control 44:389–398
73. Prutz G, Dettner K (2004) Effect of Bt corn leaf suspension on food consumption by *Chilo partellus* and life history parameters of its parasitoid *Cotesia flavipes* under laboratory conditions. Entomol Exp Appl 111:179–187
74. Pilcher CD, Rice ME, Obrycki JJ (2005) Impact of transgenic *Bacillus thuringiensis* corn and crop phenology on five nontarget arthropods. Environ Entomol 34:1302–1316
75. Sanders CJ, Pell JK, Poppy GM, Raybould A, Garcia-Alonso M, Schuler TH (2007) Host-plant mediated effects of transgenic maize on the insect parasitoid *Campoletis sonorensis* (Hymenoptera: Ichneumonidae). Biol Control 40: 362–369
76. Bernal JS, Griset JG, Gillogly PO (2002) Impacts of developing on Bt maize-intoxicated hosts on fitness parameters of a stem borer parasitoid. J Entomol Sci 37:27–40
77. Liu XX, Zhang QW, Xu BL, Li JC (2006) Effects of Cry1Ac toxin of *Bacillus thuringiensis* and nuclear polyhedrosis virus of *Helicoverpa armigera* (Hübner) (Lepidoptera: Noctuidae) on larval mortality and pupation. Pest Manag Sci 62:729–737
78. Liu XX, Zhang QW, Zhao JZ, Cai QN, Xu HL, Li JC (2005) Effects of the Cry1Ac toxin of *Bacillus thuringiensis* on *Microplitis mediator*, a parasitoid of the cotton bollworm, *Helicoverpa armigera*. Entomol Exp Appl 114:205–213
79. Baur ME, Boethel DJ (2003) Effect of Bt-cotton expressing Cry1A(c) on the survival and fecundity of two hymenopteran parasitoids (Braconidae, Encyrtidae) in the laboratory. Biol Control 26:325–332
80. Walker GP, Cameron PJ, MacDonald FM, Madhusudhan VV, Wallace AR (2007) Impacts of *Bacillus thuringiensis* toxins on parasitoids (Hymenoptera: Braconidae) of *Spodoptera litura* and *Helicoverpa armigera* (Lepidoptera: Noctuidae). Biol Control 40:142–151
81. Schuler TH, Denholm I, Clark SJ, Stewart CN, Poppy GM (2004) Effects of Bt plants on the development and survival of the parasitoid *Cotesia plutellae* (Hymenoptera: Braconidae) in susceptible and Bt-resistant larvae of the diamondback moth, *Plutella xylostella* (Lepidoptera: Plutellidae). J Insect Physiol 50:435–443
82. Chen M, Zhao JZ, Collins HL, Earle ED, Cao J, Shelton AM (2008) A critical assessment of the effects of Bt transgenic plants on parasitoids. PLoS ONE 3:1–7
83. Barraclough EI, Burgess EPJ, Philip BA, Wohlers MW, Malone LA (2009) Tritrophic impacts of Bt-expressing transgenic pine on the parasitoid *Meteorus pulchricornis* (Hymenoptera: Braconidae) via its host *Pseudocoremia suavis* (Lepidoptera: Geometridae). Biol Control 49:192–199
84. Marchetti E, Alberghini S, Battisti A, Squartini A, Baronio P, Dindo ML (2009) Effects of conventional and transgenic *Bacillus thuringiensis galleriae* toxin on *Exorista larvarum* (Diptera: Tachinidae), a parasitoid of forest defoliating Lepidoptera. Biol Control Sci Technol 19: 463–473
85. Johnson MT, Gould F (1992) Interaction of genetically engineered host plant resistance and natural enemies of *Heliothis virescens* (Lepidoptera: Noctuidae) in tobacco. Environ Entomol 21:586–597
86. Bell HA, Fitches EC, Down RE, Ford L, Marris GC, Edwards JP, Gatehouse JA, Gatehouse AMR (2001) Effect of dietary cowpea trypsin inhibitor (CpTI) on the growth and development of the tomato moth *Lacanobia oleracea* (Lepidoptera: Noctuidae) and on the success of the gregarious ectoparasitoid *Eulophus pennicornis* (Hymenoptera: Eulophidae). Pest Manag Sci 57:57–65
87. Bell HA, Kirkbride-Smith AE, Marris GC, Edwards JP, Gatehouse AMR (2004) Oral toxicity and impact on fecundity of three insecticidal proteins on the gregarious ectoparasitoid *Eulophus pennicornis* (Hymenoptera: Eulophidae). Agric Forest Entomol 6:215–222
88. Geng JH, Shen ZR, Song K, Zheng L (2006) Effect of pollen of regular cotton and transgenic Bt plus CpTI cotton on the survival and reproduction of the parasitoid wasp *Trichogramma chilonis* (Hymenoptera: Trichogrammatidae) in the laboratory. Environ Entomol 35:1661–1668
89. Azzouz H, Cherqui A, Campan EDM, Rahbe Y, Duport G, Jouanin L, Kaiser L, Giordanengo P (2005) Effects of plant protease inhibitors, oryzacystatin I and soybean Bowman-Birk inhibitor, on the aphid *Macrosiphum euphorbiae* (Homoptera, Aphididae) and its parasitoid *Aphelinus abdominalis* (Hymenoptera, Aphelinidae). J Insect Physiol 51:75–86

90. Ashouri A, Michaud D, Cloutier C (2001) Recombinant and classically selected factors of potato plant resistance to the Colorado potato beetle, *Leptinotarsa decemlineata*, variously affect the potato aphid parasitoid *Aphidius nigripes*. Biocontrol 46:401–418
91. Schuler TH, Denholm I, Jouanin L, Clark SJ, Clark AJ, Poppy GM (2001) Population-scale laboratory studies of the effect of transgenic plants on nontarget insects. Mol Ecol 10:1845–1853
92. Cowgill SE, Danks C, Atkinson HJ (2004) Multitrophic interactions involving genetically modified potatoes, nontarget aphids, natural enemies and hyperparasitoids. Mol Ecol 13:639–647
93. Wakefield ME, Bell HA, Gatehouse AMR (2010) Longevity and fecundity of *Eulophus pennicornis*, an ectoparasitoid of the tomato moth *Lacanobia oleracea*, is affected by nutritional state and diet quality. Agric Forest Entomol 12:19–27
94. Couty A, de la Vina G, Clark SJ, Kaiser L, Pham-Delegue MH, Poppy GM (2001) Direct and indirect sublethal effects of *Galanthus nivalis* agglutinin (GNA) on the development of a potato-aphid parasitoid, *Aphelinus abdominalis* (Hymenoptera: Aphelinidae). J Insect Physiol 47:553–561
95. Couty A, Poppy GM (2001) Does host-feeding on GNA-intoxicated aphids by *Aphelinus abdominalis* affect their longevity and/or fecundity? Entomol Exp Appl 100: 331–337
96. Romeis J, Babendreier D, Wackers FL (2003) Consumption of snowdrop lectin (*Galanthus nivalis* agglutinin) causes direct effects on adult parasitic wasps. Oecologia 134: 528–536
97. Hogervorst PAM, Wackers FL, Woodring J, Romeis J (2009) Snowdrop lectin (*Galanthus nivalis* agglutinin) in aphid honeydew negatively affects survival of a honeydew- consuming parasitoid. Agric Forest Entomol 11:161–173
98. Setamou M, Bernal JS, Legaspi JC, Mirkov TE (2002) Effects of snowdrop lectin (*Galanthus nivalis* agglutinin) expressed in transgenic sugarcane on fitness of *Cotesia flavipes* (Hymenoptera: Braconidae), a parasitoid of the nontarget pest *Diatraea saccharalis* (Lepidoptera: Crambidae). Ann Entomol Soc Am 95:75–83
99. Setamou M, Bernal JS, Legaspi JC, Mirkov TE, Legaspi BC (2002) Evaluation of lectin-expressing transgenic sugarcane against stalkborers (Lepidoptera: Pyralidae): Effects on life history parameters. J Econ Entomol 95:469–477
100. Bell HA, Fitches EC, Down RE, Marris GC, Edwards JP, Gatehouse JA, Gatehouse AMR (1999) The effect of snowdrop lectin (GNA) delivered via artificial diet and transgenic plants on *Eulophus pennicornis* (Hymenoptera: Eulophidae), a parasitoid of the tomato moth *Lacanobia oleracea* (Lepidoptera: Noctuidae). J Insect Physiol 45:983–991
101. Tomov BW, Bernal JS, Vinson SB (2003) Impacts of transgenic sugarcane expressing GNA lectin on parasitism of Mexican rice borer by *Parallorhogas pyralophagus* (Marsh) (Hymenoptera: Braconidae). Environ Entomol 32:866–872
102. Wakefield ME, Bell HA, Fitches EC, Edwards JP, Gatehouse AMR (2006) Effects of *Galanthus nivalis* agglutinin (GNA) expressed in tomato leaves on larvae of the tomato moth *Lacanobia oleracea* (Lepidoptera: Noctuidae) and the effect of GNA on the development of the endoparasitoid *Meteorus gyrator* (Hymenoptera: Braconidae). Bull Entomol Res 96:43–52
103. Romeis J, Hellmich RL, Candolfi MP, Carstens K, De Schrijver A, Gatehouse AMR, Herman RA, Huesing, JE, McLean MA, Raybould A, Shelton AM, Waggoner A (2010) Recommendations for the design of laboratory studies on non-target arthropods for risk assessment of genetically engineered plants. Transgenic Res 1–22
104. Marvier M, McCreedy C, Regetz J, Kareiva P (2007) A meta-analysis of effects of Bt cotton and maize on nontarget invertebrates. Science 316:1475–1477
105. Wolfenbarger LL, Naranjo SE, Lundgren JG, Bitzer RJ, Watrud LS (2008) Bt crop effects on functional guilds of non-target arthropods: a meta-analysis. PLoS ONE 3(5):e2118. doi:10.1371/journal.pone.0002118
106. Duan JJ, Lundgren JG, Naranjo S, Marvier M (2010) Extrapolating non-target risk of *Bt* crops from laboratory to field. Biol Lett 23(6):74–77
107. Sanvido O, Romeis J, Bigler F (2007) Ecological impacts of genetically modified crops: Ten years of field research and commercial cultivation. In: Green Gene Technology: Research in an Area of Social Conflict, vol 107. Advances in Biochemical Engineering/Biotechnology. Springer-Verlag Berlin, Berlin, pp 235–278
108. Malone MA, Burgess EPJ (2009) Impact of genetically modified crops on pollinators. In: Ferry N, Gatehouse AMR (eds) Environmental impact of genetically modified crops. CAB International, Wallingford, pp 199–224
109. Young BG (2006) Changes in herbicide use patterns and production practices resulting from glyphosate-resistant crops. Weed Technol 20:301–307
110. Service RF (2007) Glyphosate – the conservationist's friend? Science 316:1116–1117
111. Foresman C, Glasgow L (2008) US grower perceptions and experiences with glyphosate-resistant weeds. Pest Manag Sci 64:388–391
112. Sankula S (2006) Quantification of the impacts on US agriculture of biotechnology-derived crops planted in 2005. Executive Summary. National Center for Food and Agricultural Policy, Washington, DC
113. Dill GM, CaJacob CA, Padgette SR (2008) Glyphosate-resistant crops: adoption, use and future considerations. Pest Manag Sci 64:326–331
114. Gianessi LP, Reigner NP (2007) The value of herbicides in U.S. crop production. Weed Technol 21:559–566
115. Owen MDK (2005) Maize and soybeans – controllable volunteerism without ferality. In: Gressel J (ed) Crop ferality and volunteerism. CRC, Boca Raton, pp 149–165
116. Johnson KL, Raybould AF, Hudson MD, Poppy GM (2006) How does scientific risk assessment of GM crops fit within the wider risk analysis? Trends Plant Sci 12:1–5

117. Madsen KH, Sandoe P (2005) Ethical reflections on herbicide-resistant crops. Pest Manag Sci 61:318–325
118. Dill GM (2005) Glyphosate-resistant crops; history, status and future. Pest Manag Sci 61:219–224
119. Gianessi LP (2005) Economic and herbicide use impacts of glyphosate-resistant crops. Pest Manag Sci 61:241–245
120. Rissler J, Mellon M (1996) The ecological risks of engineered organisms. MIT, Cambridge
121. Altieri MA (2000) The ecological impacts of transgenic crops on agroecosystem health. Agroecology in action. University of California: Berkeley
122. Vidal RA, Trezzi MM, De Prado R, Ruiz-Santaella JP, Vial-Aiub M (2007) Glyphosate resistant biotypes of wild poinsettia (*Euphorbia heterophylla* L.) and its risk analysis on glyphosate-resistant soybeans. J Food Agric Environ 5:265–269
123. Werth JA, Preston C, Taylor IN, Charles GW, Roberts GN, Baker J (2008) Managing the risk of glyphosate resistance in Australian glyphosate-resistant cotton production systems. Pest Manag Sci 64:417–421
124. Krebs JR, Wilson JD, Bradbury RB, Siriwardena GM (1999) The second Silent Spring? Nature 400:611–612
125. Schutte G (2003) Herbicide resistance: Promises and prospects of biodiversity for European agriculture. Agric Hum Values 20:217–230
126. Benton TG (2007) Managing farming's footprint on biodiversity. Science 315:341–342
127. Davis LC (2006) Genetic engineering, ecosystem change, and agriculture: an update. Biotechnol Mol Biol Rev 1:87–102
128. Norris RF (2005) Ecological bases of interactions between weeds and organisms in other pest categories. Weed Sci 53:909–913
129. Scursoni J, Peterson D, Forcella F, Gunsolus J, Arnold RB, Owen M, Smeda OR, Vidrine R (2001) Weed diversity in glyphosate-tolerant soybean from Minnesota to Louisiana. In: Hartzler RG (ed) CD-ROM Computer File. North Central Weed Science Society, Champaign, Milwaukee
130. Bitzer RJ, Buckelew LD, Pedigo LP (2002) Effects of transgenic herbicide-resistant soybean varieties and systems on surface-active springtails (Entognatha: Collembola). Environ Entomol 31:449–461
131. Freckleton RP, Stephens PA, Sutherland WJ, Watkinson AR (2004) Amelioration of biodiversity impacts of genetically modified crops: predicting transient versus long-term effects. Proc R Soc Biol 271:325–331
132. Cerdeira AL, Duke SO (2006) The current status and environmental impacts of glyphosate-resistant crops: a review. J Environ Qual 35:1633–1658
133. Scursoni JA, Forcella F, Gunsolus J (2007) Weed escapes and delayed emergence in glyphosate-resistant soybean. Crop Protect 26:212–218
134. Heard MS, Hawes C, Champion GT, Clark SJ, Firbank LG, Haughton AJ, Parish AM, Perry JN, Rothery JN, Scott P, Skellern RJ, Squire MP, Hill GR (2003) Weeds in fields with contrasting conventional and genetically modified herbicide-tolerant crops. I. Effects on abundance and diversity. Philos Trans R Soc Lond B 358:1819–1832
135. Heard MS, Clark SJ, Rothery P, Perry JN, Bohan DA, Brooks DR, Champion GT, Dewar AM, Hawes C, Haughton AJ, May MJ, Scott RJ, Stuart RS, Squire GR, Firbank LG (2006) Effects of successive seasons of genetically modified herbicide-tolerant maize cropping on weeds and invertebrates. Ann Appl Biol 149:249–254
136. Roy DB, Bohan DA, Haughton AJ, Hill MO, Osborne JL, Clark SJ, Perry JN, Rothery P, Scott RJ, Brooks DR, Champion GT, Hawes C, Heard MS, Firbank LG (2003) Invertebrates and vegetation of field margins adjacent to crops subject to contrasting herbicide regimes in the Farm Scale Evaluations of genetically modified herbicide-tolerant crops. Philos Trans R Soc Lond B 358:1879–1898
137. Owen MDK (2000) Current use of transgenic herbicide-resistant soybean and corn in the USA. Crop Prot 19: 765–771
138. Luan V, Figueroa SJ, Baltazar MB, Gomez MR, Townsend LR, Schoper JB (2001) Maize pollen longevity and distance isolation requirements for effective pollen control. Crop Sci 41:1551–1557
139. Palmer RG, Gai J, Sun H, Burton JW (2001) Production and evaluation of hybrid soybean. In: Janick J (ed) Plant breeding reviews. Wiley, New York, pp 263–308
140. Westgate ME, Lizaso J, Batchelor W (2003) Quantitative relationship between pollen shed density and grain yield in maize. Crop Sci 43:934–942
141. Abud SPI, Moreira MS, Farias Neto CT, Vianna AL, Andrade GR, Nunes SRM, Guerzoni J, Monteiro RA, Assuncao PMFO, Rech MS, Aragao EL (2004) Distance of flow in transgenic BROO-69515 and the non transgenic soybean in the Cerrado Region, Brasil. In: Moscardi F, Hoffmann-Campo CB, Saraiva OF, Galerani PR, Krzyzanowski FC, Carrao-Panizzi MC (eds) VII World Soybean Research Conference. Brasilian Agricultural Research Corporation, Foz do Iguassu, Brazil, pp 110–111
142. Matus-Cadiz PH, Horak MJ, Blomquist LK (2004) Gene flow in wheat at the field scale. Crop Sci 44:718–727
143. Charles D (2007) U.S. courts say transgenic crops need tighter scrutiny. Science 315:1069
144. Fisher L (2007) Growers continue to grow and use Roundup Ready alfalfa but Monsanto Company is disappointed with preliminary injunction affecting purchase and planting. http://www.monsanto.com Accessed 8 March 2007
145. Harriman P (2007) Roundup Ready concerns land alfalfa seed in court. http://4.26.159.139/static/news/NEWSID_8242.php. Accessed 8 March 2007
146. Weise E (2007) Effect of genetically engineered alfalfa cultivate a debate, USA Today. http://www.columbia.org/pdf_files/centerforfoodsafety20.pdf. Accessed 08 December 2010
147. Hurburgh JCR (2000) The GMO controversy and grain handling for 2000. GMO and Grain, Iowa State University, Ames
148. Hurburgh JCR (2003) Constraints for isolation and traceability of grains. Iowa State University, Ames

149. Ginder RG (2001) Channelling, identity preservation and the value chain: Lessons from the recent problems with starlink corn, Staff General Research Papers, Iowa State University, Department of Economics, http://econpapers.repec.org/RePEc:isu:genres:11480
150. Qaim M (2010) The benefits of genetically modified crops—and the costs of inefficient regulation. Resources for the future. www.rff.org/Publications/WPC/Pages/The-Benefits-of-Genetically-Modified-Crops-and-the-Costs-of-Inefficient-Regulation.aspx
151. Losey JE, Rayor LS, Carter ME (1999) Transgenic pollen harms monarch larvae. Nature 399:214
152. Stanley-Horn DE, Dively GP, Hellmich RL, Mattila HR, Sears MK, Rose R, Jesse LCH, Losey JE, Obrycki JJ, Lewis L (2001) Assessing the impact of Cry1Ab-expressing corn pollen on monarch butterfly larvae in field studies. Proc Natl Acad Sci USA 98:11931–11936
153. Zangerl AR, McKenna D, Wraight CL, Carroll M, Ficarello P, Warner R, Berenbaum MR (2001) Effects of exposure to event 176 *Bacillus thuringiensis* corn pollen on monarch and black swallowtail caterpillars under field conditions. Proc Natl Acad Sci USA 98:11908–11912
154. Pleasants JM, Hellmich RL, Dively GP, Sears MK, Stanley-Horn DE, Mattila HR, Foster JE, Clark P, Jones GD (2001) Corn pollen deposition on milkweeds in and near cornfields. Proc Natl Acad Sci USA 98:11919–11924
155. Oberhauser KS, Prysby MD, Mattila HR, Stanley-Horn DE, Sears MK, Dively G, Olson E, Pleasants JM, Lam WKF, Hellmich RL (2001) Temporal and spatial overlap between monarch larvae and corn pollen. Proc Natl Acad Sci USA 98: 11913–11918
156. Sears MK, Hellmich RL, Stanley-Horn DE, Oberhauser KS, Pleasants JM, Mattila HR, Siegfried BD, Dively GP (2001) Impact of *Bt* corn pollen on monarch butterfly populations: a risk assessment. Proc Natl Acad Sci USA 98:11937–11942
157. Gatehouse AMR, Ferry N, Raemaekers RJM (2002) The case of the monarch butterfly: a verdict is returned. Trends Genet 18:249–251
158. Obrist LB, Dutton A, Romeis J, Bigler F (2006) Biological activity of Cry1Ab toxin expressed by Bt maize following ingestion by herbivorous arthropods and exposure of the predator *Chrysoperla carnea*. Biocontrol 51:31–48
159. Ellstand NC (2003) Current knowledge of gene flow in plants: implications for transgene flow. Philos Trans R Soc Lond B 358:1163–1170
160. Hall LM, Good A, Beckie HJ, Warwick SI (2003) Gene flow in herbicide-resistant canola (*Brassica napus*): the *Canadian experience*. In: Lelley T, Balazs E, Tepfer M (eds) Ecological impact of GMO dissemination in agroecosystems. Facultas Verlagsun Buchhandels AG, Austria, pp 57–66
161. Clark EA (2006) Environmental risks of genetic engineering. Euphytica 148:47–60
162. Mallory-Smith C, Zapiola M (2008) Gene flow from glyphosate-resistant crops. Pest Manag Sci 64:428–440

Transgenic Crops, Next Generation

Martina Newell-McGloughlin
Department of Plant Pathology, University of California Davis, Davis, CA, USA

Article Outline

Glossary
Definition of the Subject
Introduction
Progress to Date
The Next Generation
Barriers to Introduction
Future Directions
Bibliography

Glossary

Abiotic stress External (nonliving) factors which can cause harmful effects to plants, such as soil conditions, drought, and extreme temperatures.

Acclimatization Adaptation of an organism to a new environment.

Adaptation In the evolutionary sense, some heritable feature of an individual's phenotype that improves its chances of survival and reproduction in the existing environment.

Additive genetic variance Genetic variance associated with the average effects of substituting one allele for another.

Agronomic performance/trait Pertains to practices of agricultural production and its costs and the management of crop land. Examples of agronomic traits include yield, input requirements, stress tolerance.

Agrobacterium tumefaciens A bacterium normally responsible for causing crown gall disease in a variety of plants. A plasmid has been isolated from this bacterium that is useful in plant genetic engineering. This plasmid, called the Ti plasmid, has been modified so that it does not cause disease but can carry foreign DNA into susceptible plant cells.

Aldolase An enzyme, not subject to allosteric regulation, that catalyzes in a reversible reaction the

cleavage of fructose 1,6-biphosphate to form dihydroxyacetone phosphate and glyceraldehyde 3-phosphate. The enzyme catalyzing the fourth reaction in the glycolytic pathway, which splits a monosaccharide into two 3-carbon units.

Allele Any of several alternative forms of a given gene.

Allele frequency Often called gene frequency. A measure of how common an allele is in a population the proportion of all alleles at one gene locus that are of one specific type in a population.

Allelic exclusion A process whereby only one immunoglobulin light chain and one heavy chain gene are transcribed in any one cell; the other genes are repressed.

Allogenic Of the same species, but with a different genotype.

Allopolyploid Polyploid produced by the hybridization of two species.

Allopolyploid Plants Plants having more than two sets of haploid chromosomes inherited from different species.

Allosteric Regulation Regulation of an enzyme's activity by binding of a small molecule at a site that does not overlap the active site region.

Anabolic The part of metabolism that is concerned with synthetic reactions.

Aneuploid Having a chromosome number that is not an exact multiple of the haploid number, caused by one chromosome set being incomplete or chromosomes being present in extra numbers.

Aneuploidy The condition of a cell or an organism that has additions or deletions of a small number of whole chromosomes from the expected balanced diploid number of chromosomes.

Antibiotic Chemical substance formed as a metabolic by-product in bacteria or fungi and used to treat bacterial infections. Antibiotics can be produced naturally, using microorganisms, or synthetically.

Antibody A protein produced by the immune system in response to an antigen (a molecule that is perceived to be foreign). Antibodies bind specifically to their target antigen to help the immune system destroy the foreign entity.

Antinutrients Substances that act in direct competition with or otherwise inhibit or interfere with the use or absorption of a nutrient.

Antisense RNA RNA produced by copying and reversing a portion of an RNA-encoding DNA, usually including a protein-specifying region, and placing it next to a transcription-control sequence. This cassette can be delivered to the target cell, resulting in genetic transformation and production of RNA that is complementary to the RNA that is produced from the original, not reversed, DNA segment. This complementary, or antisense, RNA is able to bind to the complementary sequences of the target RNA, resulting in the inhibition of expression of the target gene.

Antiserum Blood serum containing specific antibodies against an antigen. Antisera are used to confer passive immunity to diseases and as analytical and preparative reagents for antigens, for example, to determine potential allergenicity.

Avirulent Unable to cause disease.

Bacillus thuringiensis (Bt) A naturally occurring microorganism which produces a toxin protein that only kills organisms with alkalineing stomachs, such as insect larvae. As and when delivered as a part of the whole killed organism, this toxin protein has been used for biological control for decades. The genetic information that encodes the toxin protein was identified and was moved into plants to make them insect tolerant.

Bioconversion Chemical restructuring of raw materials by using a biocatalyst.

Biodegradable Capable of being broken down by the action of microorganisms, usually by microorganisms and under conditions generally in the environment.

Bioinformatics The discipline encompassing the development and utilization of computational facilities to store, analyze, and interpret biological data.

Biomass The totality of biological matter in a given area. As commonly used in biotechnology, it refers to the use of cellulose, a renewable resource, for the production of chemicals that can be used to generate energy or as alternative feedstocks for the chemical industry to reduce dependence on nonrenewable fossil fuels.

Bioprocess A process in which living cells, or components thereof, are used to produce a desired end product.

Biosynthesis Production of a chemical by a living organism.

Biotechnology Development of products by a biological process. Production may be carried out by using intact organisms, such as yeasts and bacteria, or by using natural substances (e.g., enzymes) from organisms.

Biosynthetic The formation of complex compounds from simple substances by living organisms.

Biotic Stress Living organisms which can harm plants, such as viruses, fungi, and bacteria, and harmful insects. (See Abiotic stress).

Callus A cluster of undifferentiated plant cells that can, for some species, be induced to form the whole plant.

Calvin Cycle A series of enzymatic reactions, occurring during photosynthesis, in which glucose is synthesized from carbon dioxide.

Catalyst An agent (such as an enzyme or a metallic complex) that facilitates a reaction but is not itself changed at the completion of the reaction.

Catabolic The part of metabolism that is concerned with degradation reactions.

Chloroplast A chlorophyll-containing photosynthetic organelle, found in eukaryotic cells that can harness light energy.

Cistron A length of chromosomal DNA representing the smallest functional unit of heredity, essentially identical to a gene.

Clone A group of genes, cells, or organisms derived from a common ancestor. Because there is no combining of genetic material (as in sexual reproduction), the members of the clone are genetically identical or nearly identical to the parent.

Codon A sequence of three nucleotide bases that in the process of protein synthesis specifies an amino acid or provides a signal to stop or start protein synthesis (translation).

Coenzyme An organic compound that is necessary for the functioning of an enzyme.Coenzymes are smaller than the enzymes themselves and may be tightly or loosely attached to the enzyme protein molecule.

Cofactor A nonprotein substance required for certain enzymes to function. Cofactors can be coenzymes or metallic ions.

Comparative genomics The comparison of genome structure and function across different species for further understanding of biological mechanisms and evolutionary processes.

Composition analysis The determination of the concentration of compounds in a plant. Compounds that are commonly quantified are proteins, fats, carbohydrates, minerals, vitamins, amino acids, fatty acids, and antinutrients.

Conventional breeding Breeding of plants carried out by controlled transfer of pollen from one plant to another followed by selection of progeny through multiple generations for a desirable phenotype. This method has also often included irradiation or mutation of plants or seeds to induce extra variation in the donor material.

Complementary DNA (cDNA) DNA synthesized from an expressed messenger RNA through a process known as reverse transcription. This type of DNA is used for cloning or as a DNA probe for locating specific genes in DNA hybridization studies.

Coumarins White vanilla-scented crystalline esters used in perfumes and flavorings and as an anticoagulant. Formula: C9H6O2.

Crossbreeding Interbreeding (of animals or plants) using parents of different races, varieties, breeds, etc.

Cyto- A prefix referring to cell or cell plasm.

Cytokines Intercellular signals, usually protein or glycoprotein, involved in the regulation of cellular proliferation and function.

Diet A specific allowance or selection of food or feed that a person or animal regularly consumes.

Diploid A cell with two complete sets of chromosomes. Cf. Haploid.

DNA sequencing Technologies through which the order of base pairs in a DNA molecule can be determined.

Enzyme A protein catalyst that facilitates specific chemical or metabolic reactions necessary for cell growth and reproduction. Cf Catalyst.

Epigenetics The study of changes in gene expression caused by mechanisms other than changes in the underlying DNA sequence – hence the name epi- (Greek: επί- over, above, outer) -genetics. Examples of such changes might be DNA methylation or

histone deacetylation, both of which serve to suppress gene expression without altering the sequence of the silenced genes.

Event The term used to describe a plant and its offspring that contain a specific insertion of DNA. Such events will be distinguishable from other events by their unique site of integration of the introduced DNA.

Exposure assessment The qualitative and/or quantitative evaluation of the likely exposure to biological, chemical, and physical agents via different sources.

Feedstock The raw material used in chemical or biological processes.

Flavonoids Any of a group of organic compounds that occur as pigments in fruit and flowers.

Food additive Any substance not normally consumed as a food by itself and not normally used as a typical ingredient of food, whether or not it has nutritive value, the intentional addition of which to a food for a technological (including organoleptic) purpose in the manufacture, processing, preparation, treatment, packing, packaging, transport, or holding of such food results, or may be expected to result (directly or indirectly), in it or its by-products becoming a component of or otherwise affecting the characteristics of such foods. The term does not include "contaminants" or substances added to food for maintaining or improving nutritional qualities.

Fructan A type of polymer of fructose, present in certain fruits.

Functional foods The Institute of Medicine's Food and Nutrition Board defined functional foods as "any food or food ingredient that may provide a health benefit beyond the traditional nutrients it contains."

Functional genomics The development and implementation of technologies to characterize the mechanisms through which genes and their products function and interact with each other and with the environment. The science that is usually applied to the studies of gene and the expression (mRNA) of usually large numbers of genes simultaneously.

Gene expression The process through which a gene is activated at particular time and place so that its functional product is produced.

Gene flow The exchange of genetic traits between populations by movement of individuals, gametes, or spores. It involves the spread of new variants among different populations through dispersal.

Gene silencing (See RNAi) A method usually performed by the expression of an mRNA of complementary or the same nucleotide sequence in a cell such that the expression of the mRNA causes the downregulation of the protein which is being targeted.

Gene transfer The transfer of genes to an organism. Usually used in terms of transfer of a gene to an organism other that the original organism, through the tools of biotechnology.

Gene A segment of chromosome that encodes the necessary regulatory and sequence information to direct the synthesis of a protein or RNA product. (*See also* Operator Regulatory g. Structural g. Suppressor g).

Gene mapping Determination of the relative locations of genes on a chromosome.

Gene sequencing Determination of the sequence of nucleotide bases in a strand of DNA.

Genetic engineering A technology used to alter the genetic material of living cells in order to make them capable of producing new substances or performing new functions.

Genetic map A Map showing the positions of genetic markers along the length of a chromosome relative to each other (genetic map) or in absolute distances from each other (physical map).

Genome The total hereditary material of a cell, comprising the entire chromosomal set found in each nucleus of a given species.

Genomics Science that studies the genomes (i.e., the complete genetic information) of living beings. This commonly entails the analysis of DNA sequence data and the identification of genes.

Genotype Genetic makeup of an individual or group. Cf. Phenotype.

Germplasm The total genetic variability, represented by germ cells or seeds, available within a particular population of organisms.

Gene pool The total genetic information contained within a given population.

Glycoalkaloid toxins Steroid-like compounds produced by plant members of the botanical family Solanaceae, most notably "solanine" present in potato tubers.

Golden rice In 1999, Swiss and German scientists announced the development of a genetically engineered rice crop that produces beta-carotene, a substance which the body converts to vitamin A. This improved nutrient rice was developed to treat individuals suffering from vitamin A deficiency, a condition that afflicts millions of people in developing countries, especially children and pregnant women.

Haploid A cell with half the usual number of chromosomes, or only one chromosome set. Sex cells are haploid. Cf. Diploid.

Hazard characterization The qualitative and/or quantitative evaluation of the nature of the adverse health effects associated with biological, chemical, and physical agents. For chemical agents, a dose-response assessment should be performed if the data are obtainable.

Hazard identification The identification of biological, chemical, and physical agents capable of causing adverse health or environmental effects.

Hazard A biological, chemical, or physical agent, or condition, with the potential to cause an adverse health or environmental effect.

Hereditary Capable of being transferred as genetic information from parent cells to progeny.

Heterozygote With respect to a particular gene at a defined chromosomal locus, a heterozygote has a different allelic form of the gene on each of the two homologous chromosomes.

Homologous Corresponding or alike in structure, position, or origin.

Homologous recombination Rearrangement of related DNA sequences on a different molecule by crossing over in a region of identical sequence.

Homozygote With respect to a particular gene at a defined chromosomal locus, a homozygote has the same allelic form of the gene on each of the two homologous chromosomes.

Hormone A chemical that acts as a messenger or stimulatory signal, relaying instructions to stop or start certain physiological activities. Hormones are synthesized in one type of cell and then released to direct the function of other cell types.

Horizontal gene transfer Transmission of DNA between species, involving close contact between the donor's DNA and the recipient, uptake of DNA by the recipient, and stable incorporation of the DNA into the recipient's genome.

Host A cell or organism used for growth of a virus, plasmid, or other form of foreign DNA, or for the production of cloned substances.

Hybridization Production of offspring, or hybrids, from genetically dissimilar parents. The process can be used to produce hybrid plants (by cross-breeding two different varieties) or hybridomas (hybrid cells formed by fusing two unlike cells, used in producing monoclonal antibodies). The term is also used to refer to the binding of complementary strands of DNA or RNA.

Hybrid The offspring of two parents differing in at least one genetic characteristic (trait). Also, a heteroduplex DNA or DNA-RNA molecule.

Identity preservation The segregation of one crop type from another at every stage from production and processing to distribution. This process is usually performed through audits and site visits and provides independent third-party verification of the segregation.

Immunoassay Technique for identifying substances based on the use of antibodies.

Immunogen Any substance that can elicit an immune response, especially specific antibody production. An immunogen that reacts with the elicited antibody may be called an antigen.

Inbred Progeny produced as a result of inbreeding.

Inducer A molecule or substance that increases the rate of enzyme synthesis, usually by blocking the action of the corresponding repressor.

Inserted DNA The segment of DNA that is introduced into the chromosome, plasmid, or other vectors using recombinant DNA techniques.

Introgressed Backcrossing of hybrids of two plant populations to introduce new genes into a wild population.

Inulins A fructose polysaccharide present in the tubers and rhizomes of some plants. Formula: $(C_6H_{10}O_5)_n$.

In vitro Literally, "in glass." Performed in a test tube or other laboratory apparatus.

In vivo In the living organism.

Invertase activity Enzyme activity occurring in the intestinal juice of animals and in yeasts, that hydrolyses sucrose to glucose and fructose.

Isoflavones Water-soluble chemicals, also known as phytoestrogens, found in many plants and so named because they cause effects in the mammalian body somewhat similar to those of estrogen. The most investigated natural isoflavones, genistein and daidzen, are found in soy products and the herb red clover.

Knock in Replacement of a gene by a mutant version of the same gene using homologous recombination.

Knock out Inactivation of a gene by homologous recombination following transfection with a suitable DNA construct.

Linkage The tendency for certain genes to be inherited together due to their physical proximity on the chromosome.

Locus (Plural loci) The position of a gene, DNA marker, or genetic marker on a chromosome. (See gene locus).

Macronutrient Any substance, such as carbon, hydrogen, or oxygen, that is required in large amounts for healthy growth and development.

Marker Any genetic element (locus, allele, DNA sequence, or chromosome feature) which can be readily detected by phenotype, cytological or molecular techniques, and used to follow a chromosome or chromosomal segment during genetic analysis.

Marker assisted selection or marker aided selection (MAS) A process whereby a marker (morphological, biochemical, or one based on DNA/RNA variation) is used for indirect selection of a genetic determinant or determinants of a trait of interest (i.e., productivity, disease resistance, abiotic stress tolerance, and/or quality). This process is used in plant and animal breeding.

Mass spectrometry Analytical technique by which compounds in a vacuum compartment are ionized, eventually fragmented, accelerated, and detected based upon the mass-dependent behavior of the ionized compounds or their fragments in response to the application of a magnetic or electric field in a vacuum.

Messenger RNA (mRNA) Nucleic acid that carries instructions to a ribosome for the synthesis of a particular protein.

Metabolism All biochemical activities carried out by an organism to maintain life.

Metabolite A substance produced during or taking part in metabolism.

Metabolomics "Open-ended" analytical techniques that generate profiles of the metabolites, that is, chemical substances within a biological sample. Commonly differences between profiles of different (groups of) samples are determined and the identity of the associated metabolites elucidated. Contrary to targeted analysis, these techniques are indiscriminate in that they do not require prior knowledge of every single substance that is present.

Microarray A microscopic, ordered array of nucleic acids, proteins, small molecules, cells, or other substances that enables parallel analysis of complex biochemical samples. There are many different types of microarrays both from a biological and production system perspective. The generic terms "DNA array," "GeneChipTM," or "hybridization array" are used to refer broadly to all types of oligonucleotide-based arrays. The two most common are cDNA arrays and genomic arrays. cDNA array: A microarray composed of grid of nucleic acid molecules of known composition linked to a solid substrate, which can be probed with total messenger RNA from a cell or tissue to reveal changes in gene expression relative to a control sample.

Micronutrient Any substance, such as a vitamin or trace element, essential for healthy growth and development but required only in minute amounts.

Mini-chromosome Contains only centromeres and telomeres with little additional DNA. This provides the ability to accept multiple genes coding for stacked traits. They are particularly useful because they allow scientists to add numerous genes onto one mini-chromosome and manipulate those genes easily because they are all in one place.

mRNA Messenger RNA.

Multigenic Of hereditary characteristics one that is specified by several genes.

Mutant A cell that manifests new characteristics due to a change in its DNA.

Mutation A structural change in a DNA sequence resulting from uncorrected errors during DNA replication.

Mutation Breeding Genetic change caused by natural phenomena or by use of mutagens. Stable mutations in genes are passed on to offspring unstable mutations are not.

Nitrogen fixation A biological process (usually associated with plants) whereby certain bacteria convert nitrogen in the air to ammonia, thus forming a nutrient essential for growth.

Nucleic acid Large molecules, generally found in the cell nucleus and/or cytoplasm, that are made up of nucleotide bases. The two kinds of nucleic acid are DNA and RNA.

Nucleotides The building blocks of nucleic acids. Each nucleotide is composed of sugar, phosphate, and one of four nitrogen bases. If the sugar is ribose, the nucleotide is termed a "ribonucleotide," whereas deoxyribonucleotides have deoxyribose as the sugar component (i.e., adenine, cytosine, guanine, and thymine in the case of DNA). The sequence of the nucleotides within the nucleic acid determines, for example, the amino acid sequence of an encoded protein.

Nucleus In eukaryotic cells, the centrally located organelle that encloses most of the chromosomes. Minor amounts of chromosomal substance DNA are found in some other organelles, most notably the mitochondria and the chloroplasts.

Nutritionally improved Improving the quantity, ratio, and/or bioavailability of essential macro- and micronutrients and other compounds for which the clinical and epidemiological evidence is clear that they play a significant role in the maintenance of optimal health and are limiting in diets.

Nutraceutical The term was coined by the Foundation for Innovation in Medicine in 1991 and is defined as "any substance that may be considered a food or part of a food and provides medical or health benefits, including the prevention and treatment of disease."

Organoleptic Able to perceive a sensory stimulus such as taste.

Operon Sequence of genes responsible for synthesizing the enzymes needed for biosynthesis of a molecule. An operon is controlled by an operator gene and a repressor gene.

Pathogen Disease-causing organism.

Peptide Two or more amino acids joined by a linkage called a peptide bond.

Pesticide Any substance intended for preventing, destroying, attracting, repelling, or controlling any pest including unwanted species of plants or animals during the production, storage, transport, distribution and processing of food, agricultural commodities, or animal feeds, or which may be administered to animals for the control of ectoparasites. The term includes substances intended for use as a plant-growth regulator, defoliant, desiccant, fruit-thinning agent, or sprouting inhibitor, and substances applied to crops either before or after harvest to protect the commodity from deterioration during storage and transport. The term normally excludes fertilizers, plant and animal nutrients, food additives, and animal drugs.

Phenotype Observable characteristics, resulting from interaction between an organism's genetic makeup and the environment. Cf. Genotype

Phenylpropanoids Especially the derivatives of the cinnamyl alcohols and of cinnamic acids, isolated from medicinal plants due to the interest as the source for the preparation of the remedies.

Photosynthesis Conversion by plants of light energy into chemical energy, which is then used to support the plants' biological processes.

Phytate (phytic acid) A phosphorus-containing compound in the outer husks of cereal grains that, in addition to limiting the bioavailability of phosphorous itself, binds with minerals and inhibits their absorption.

Phytochemicals Small molecule chemicals unique to plants and plant products.

Plasmid Circular extrachromosomal DNA molecules present in bacteria and yeast. Plasmids replicate autonomously each time the organism, a bacterium, divides and are transmitted to the daughter cells. DNA segments are commonly cloned using plasmid vectors.

Plasticity The quality of being plastic or able to be molded, changed.

Plastid Any of various small particles in the cytoplasm of the cells of plants and some animals that contain pigments (see chromoplast), starch, oil, protein, etc.

Pleiotropic Genes or mutations that result in the production of multiple effects at the phenotypic level. It is the consequence of the fact that biochemical pathways starting from different genes intersect in many places, inhibiting, deflecting, and variously modifying each other. Introduced genes may also insert into sites that effect phenotypic changes other than the one desired.

Polyclonal Derived from different types of cells.

Polymer A long molecule of repeated subunits.

Polypeptide Long chain of amino acids joined by peptide bonds. *Post-Transcriptional Gene Silencing* Post-transcriptional gene silencing (PTGS) is a sequence-specific RNA degradation system designed to act as an antiviral defense mechanism. A form of PTGS triggered by transgenic DNA, called co-suppression, was initially described in plants and a related phenomenon, termed quelling, was later observed in the filamentous fungus *Neurospora crassa*.

Posttranscriptional modification A series of processes through which protein molecules are biochemically modified within a cell following their synthesis by translation of messenger RNA. A protein may undergo a complex series of modifications in different cellular compartments before its final functional form is produced.

Profiling Creation of indiscriminate patterns of the substances within a sample with the aid of analytical techniques, such as functional genomics, proteomics, and metabolomics. The identity of the compounds detectable within the pattern need not be known.

Promoter A DNA sequence that is located near or even partially within encoding nucleotide sequences and which controls gene expression. Promoters are required for binding of RNA polymerase to initiate transcription.

Protein Proteins are biological effector molecules encoded by an organism's genome. A protein consists of one or more polypeptide chains of amino acid subunits. The functional action of a protein depends on its three-dimensional structure, which is determined by its amino acid composition and any posttranscriptional modifications.

Proteomics The development and application of techniques used to investigate the protein products of the genome and how they interact to determine biological functions. This is an "Open ended" analytical technique that generates profiles of the proteins within a biological sample. The technique is commonly used to find differences between profiles of different (groups of) samples are and determined and the identity of the associated proteins elucidated. Contrary to targeted analysis, these techniques are indiscriminate in that they do not require prior knowledge of every single substance protein present that is analyzed beforehand.

Protoplast fusion The fusion of two plant protoplasts that each consists of the living parts of a cell, including the protoplasm and cell membrane but not the vacuoles or the cell wall.

Protoplast The cellular material that remains after the cell wall has been removed. A plant cell from which the cell wall has been removed by mechanical or enzymatic means. Protoplasts can be prepared from primary tissues of most plant organs as well as from cultured plant cells.

Quantitative trait loci The locations of genes that together govern a multigenic trait, such as yield or fruit mass.

Recombinant DNA Any DNA molecule formed by joining DNA segments from different sources (not necessarily different organisms). This may also be a strand of DNA synthesized in the laboratory by splicing together selected parts of DNA strands from different organic species, or by adding a selected part to an existing DNA strand.

Regeneration Laboratory technique for forming a new plant from a clump of plant cells.

Regulatory gene A gene that acts to control the protein-synthesizing activity of other genes.

Regulatory sequence A DNA sequence to which specific proteins bind to activate or repress the expression of a gene.

Replication Reproduction or duplication, as of an exact copy of a strand of DNA.

Rhizobium A class of microorganisms that converts atmospheric nitrogen into a form that plants can utilize for growth. Species of this microorganism grow symbiotically on the roots of certain legumes such as peas, beans, and alfalfa.

Ribonucleic acid (RNA) A molecule similar to DNA that functions primarily to decode the instructions for protein synthesis that are carried by genes. (*See also* Messenger RNA Transfer RNA).

Ribosome A cellular component, containing protein and RNA, that is involved in protein sythesis.

Ribozyme Any of the RNA molecules possessing catalytic activity and acting as biological catalysts.

Risk A function of the probability of an adverse health effect and the severity of that effect, consequential to a hazard(s).

Risk analysis A process consisting of three components: risk assessment, risk management, and risk communication.

Risk assessment A scientific process consisting of the following steps: (1) hazard identification, (2) hazard characterization, (3) exposure assessment, and (4) risk characterization.

Risk characterization The qualitative and/or quantitative estimation, including attendant uncertainties, of the probability of occurrence and severity of known or potential adverse health effects in a given population based on hazard identification, hazard characterization, and exposure assessment.

Risk communication The interactive exchange of information and opinions throughout the risk analysis process concerning hazards and risks, risk-related factors, and risk perceptions, among risk assessors, risk managers, population, industry, the academic community, and other parties, including the explanation of risk assessment findings and the basis of risk management decisions.

Risk management The process, distinct from risk assessment, of weighing policy alternatives, in consultation with all interested parties, considering risk assessment and other factors relevant for the health protection of population and for the promotion of fair practices, and if needed, selecting appropriate prevention and control options.

RNAi RNA Interference (RNAi), a term coined by Fire et al. in 1998, is a phenomenon whereby small double-stranded RNA (referred as small interference RNA or siRNA) can induce efficient sequence-specific silence of gene expression.

SAFOTEST EU project on new methods for the safety testing of transgenic food.

Scale-up Transition from small-scale production to production of large industrial quantities.

Secondary metabolites Chemical substances within a biological organism sample that are not necessary for, or concerned with, primary cellular functions. Examples of secondary metabolites are Secondary metabolism proceeds by modification of the primary metabolites of photosynthesis, respiration, etc., by four main pathways. The malonate/polyketide pathway leads to the production of fatty acids and naphthoquinones. The mevalonate/isoprenoid pathway leads to the various terpenes (such as menthol), carotenoids and steroids. The shikimate pathway leads to aromatic amino acids and the phenolics and the final group of metabolites is a nonspecific mix of amino-acid derivatives including the and alkaloids (such as solanine) and others of mixed biogenesis.

Selectable marker A gene, often encoding resistance to an antibiotic or an herbicide, introduced into a group of cells to allow identification of those cells that contain the gene of interest from the cells that do not. Selectable markers are used in genetic engineering to facilitate identification of cells that have incorporated another desirable trait that is not easy to identify in individual cells.

Selective breeding Making deliberate crosses or matings of organisms so the offspring will have particular desired characteristics derived from one or both of the parents.

Selective medium Nutrient material constituted such that it will support the growth of specific organisms while inhibiting the growth of others.

Sequence homology The measurable likeness degree of identity or similarity between two nucleotides or amino acid sequences.

Sera-binding tests Immunological assays that evaluate for the presence of antigen-specific IgE in blood serum obtained from individuals allergic to food,

pollen, or other environmental antigens. Sera-binding tests include assays such as western blotting, ELISA, ELISA-inhibition, RAST, and RAST-inhibition techniques.

Shikimate pathway Pathway in microorganisms and plants involved in the biosynthesis of the aromatic amino acid family (phenylalanine, tyrosine, tryptophan) with a requirement for chorismate as well as shikimate. Secondary metabolites such as lignin, pigments, UV light protectants, phenolic redox molecules, and other aromatic compounds, such as folic acid and ubiquinone, are postscript products of the shikimate pathway.

Signal transduction The molecular pathways mechanism through which a cell senses changes in its external environment and changes its gene expression patterns in response.

Signal sequence The N-terminal sequence of a secreted protein, which is required for transport through the cell membrane.

Small interfering RNA (siRNA) Small Interfering RNA (siRNA) is 21–23-nt double-stranded RNA molecules. It guides the cleavage and degradation of its cognate RNA.

Site-specific recombination A crossover event, such as the integration of phage lambda, that requires homology of only a very short region and uses an enzyme specific for that recombination. Recombination occurring between two specific sequences that need not be homologous, mediated by a specific recombination system.

Somaclonal selection Epigenetic or genetic changes, sometimes expressed as a new trait, resulting from in vitro culture of higher plant cells. Somatic (vegetative nonsexual) plant cells can be propagated in vitro in an appropriate nutrient medium. The cells which multiply by division of the parent somatic cells are called somaclones and, theoretically, should be genetically identical with the parent. In fact this process occasionally in vitro cell culture of somatic cells, whether from a leaf, a stem, a root, a shoot, or a cotyledon, frequently generates cell plants which are significantly different, epigenetically and/or genetically, from the parent in a stable fashion and such progenies are called somaclonal variants and may provide a useful source of genetic variation.

Stilbenes A colorless or slightly yellow crystalline water-insoluble unsaturated hydrocarbon used in the manufacture of dyes trans-1,2-diphenylethene. Formula: C6H5CH:CHC6H5. It forms the backbone structure of several compounds with estrogenic activity. Trans-3,4′,5-trihydroxy-stilbene also known as resveratrol, has been found in some experiments to inhibit cell mutations, and stimulate at least one enzyme that can inactivate certain carcinogens, and may contribute to a low incidence of cardiovascular disease.

Structural gene A gene that codes for a protein, such as an enzyme.

Substantial equivalence In the report of the 1996 FAO/WHO Expert Consultation, substantial equivalence was identified as being "established by a demonstration that the characteristics assessed for the genetically modified organism, or the specific food product derived therefrom, are equivalent to the same characteristics of the conventional comparator. The levels and variation for characteristics in the genetically modified organism must be within the natural range of variation for those characteristics considered in the comparator and be based upon an appropriate analysis of data." In the Codex Guideline for the Conduct of Food Safety Assessment of Foods Derived from Recombinant-DNA Plants (2003), the concept of substantial equivalence is described as "a key step in the safety assessment process. However, it is not a safety assessment in itself rather it represents the starting point which is used to structure the safety assessment of a new food relative to its conventional counterpart. This concept is used to identify similarities and differences between the new food and its conventional counterpart. It aids in the identification of potential safety and nutritional issues and is considered the most appropriate strategy to date for safety assessment of foods derived from recombinant-DNA plants. The safety assessment carried out in this way does not imply absolute safety of the new product; rather it focuses on assessing the safety of any identified differences so that the safety of the new product can be considered relative to its conventional counterpart."

Substrate Material acted on by an enzyme.

Synteny All loci on one chromosome are said to be syntenic (literally on the same ribbon). Loci may appear to be unlinked by conventional genetic tests for linkage but still be syntenic.

Systems biology A biology-based interdisciplinary study field that focuses on complex interactions in biological systems claiming that it uses a new perspective (holism instead of reduction). Particularly, from year 2000 onward, the term is used widely in the biosciences, and in a variety of contexts. An often stated ambition of systems biology is the modeling and discovery of emergent properties, properties of a system whose theoretical description is only possible using techniques which fall under the remit of systems biology.

Tannins Any of a class of yellowish or brownish solid compounds found in many plants and used as tanning agents, mordants, medical astringents, etc. Tannins are derivatives of gallic acid with the empirical formula $C_{76}H_{52}O_{46}$.

T-DNA The segment of the Ti plasmid of *A. tumefaciens* that is transferred to the plant genome following natural infection.

Ti Plasmid A plasmid containing the gene(s) responsible for inducing plant tumor formation transfer of genes from *A. tumefaciens* to plant cells.

Tissue culture In vitro growth in nutrient medium of cells isolated from tissue.

Traditional breeding Modification of plants and animals through selective breeding. Practices used in traditional plant breeding may include aspects of biotechnology such as tissue culture and mutational breeding.

Transcription The process through which a gene is expressed to generate a complementary messenger RNA molecule. Synthesis of messenger (or any other) RNA on a DNA template.

Transcription activator–like effector nucleases (TALENs) Transcription activator–like effector (TALE) proteins from Xanthomonasare nucleases that cleave unique genomic sequences in living cells and can be used for targeted gene editing and mutagenesis.

Transcriptome The total messenger RNA expressed in a cell or tissue at a given point in time.

Transgene A gene from one source that has been incorporated into the genome of another organism.

Transgenic plant A fertile plant that carries an introduced gene(s) in its germ line.

Transformation Change in the genetic structure of an organism by the incorporation of foreign DNA.

Transgenic organism An organism formed by the insertion of foreign genetic material into the germ line cells of organisms. Recombinant DNA techniques are commonly used to produce transgenic organisms.

Translation Process by which the information on a messenger RNA molecule is used to direct the synthesis of a protein.

Transmissible spongiform encephalopathy A disease that can be transmitted from one animal to another and will produce changes in the brain that appear similar to a sponge (i.e., some of the cells are clear when seen down the microscope).

Transposon A segment of DNA that can move around and be inserted at several sites in the genome of a cell possibly altering expression. The first to be described was the Ac/Ds system in maize shown by McClintock to cause unstable mutations.

Trypsin inhibitors Antinutrient proteins present in plants such as soybeans that inhibit the digestive enzyme, trypsin if not inactivated by heating or other processing methods.

Unintended effect An effect that was not the purpose of the genetic modification or mutation. An unintended effect may be either predictable or unpredictable, based on the knowledge of, among other things, the function of the introduced DNA and of the native DNA affected by the genetic modification. A predicted unintended effect would be, for example, variations in metabolic intermediates and endpoints, and an unpredicted effect might be turning on of unknown endogenous genes.

Variety A subdivision of a species for taxonomic classification also referred to as a "cultivar." A variety is a group of individual plants that is uniform, stable, and distinct genetically from other groups of individuals in the same species.

Virulence Ability to infect or cause disease.

Virus A submicroscopic organism that contains genetic information but cannot reproduce by itself. To replicate, it must invade another cell and use parts of that cell's reproductive machinery.

Wildtype The form of an organism that occurs most frequently in nature.

Definition of the Subject

New and innovative techniques will be required to improve the efficiency of the global agriculture sector to ensure an ample supply of healthy food. To confound this situation the inequity between the affluent and developing countries will continue to grow and only a handful of technologies are sufficiently scale neutral to help with redressing this imbalance. Biotechnology is one such technology which offers efficient and cost-effective means to produce a diverse array of novel, value-added products and tools. The first generation of biotechnology products commercialized were crops focusing largely on input agronomic traits whose value was often opaque to consumers. The coming generations of crop plants can be grouped into four broad areas each presenting what, on the surface, may appear as unique challenges and opportunities. The present and future focus is on continuing improvement of agronomic traits such as yield and abiotic stress resistance in addition to the biotic stress tolerance of the present generation; crop plants as biomass feedstocks for biofuels and "bio-synthetics"; value-added output traits such as improved nutrition and food functionality; and plants as production factories for therapeutics and industrial products. From a consumer perspective the focus on value-added traits, especially improved nutrition, is undoubtedly one of the areas of greatest interest.

Introduction

During the coming decades, food and agricultural production systems will need to be significantly enhanced to respond to a number of remarkable changes, such as a growing world population; increasing international competition; globalization; shifts to increased meat consumption in developing countries and rising consumer demands for improved food quality, safety, health enhancement, and convenience. The 2008 World Bank Development Report emphasized that "Agriculture is a vital development tool for achieving the Millennium Development Goals that call for halving by 2015 the share of people suffering from extreme poverty and hunger [1]." The Report notes that three out of every four people in developing countries live in rural areas and most of them depend directly or indirectly on agriculture for their livelihoods. It recognizes that overcoming abject poverty cannot be achieved in sub-Saharan Africa without a revolution in agricultural productivity for resource-poor farmers in Africa, many of whom are women.

New and innovative techniques will be required to ensure that this revolution produces an ample supply of nutritious food by improving the efficiency of the global agriculture sector. Innovation is essential for sustaining and enhancing agricultural productivity. This involves new, science-based products and processes that contribute reliable methods for improving quality, productivity, and environmental sustainability. Biotechnology has introduced a new dimension to such innovation, offering efficient and cost-effective means to produce a diverse array of novel, value-added products and tools. It has the potential to improve qualitative and quantitative aspects of food, feed, fiber, and biofuel production; reduce the dependency of agriculture on chemicals and fossil fuels; diminish overcultivation and erosion; and lower the cost of raw materials, all in an environmentally sustainable manner. Commercialization of the first generation of products of recombinant DNA technology was another facet in a long history of human intervention in nature for agricultural and food production purposes. As such, the same parameters of risk-based assessment should apply. Commercialization of products must be undertaken within a regulatory framework that ensures adequate protection of the consumer, the environment, and alternate production systems while not stymieing innovation.

In a world whose population is increasing disproportionally in disadvantaged regions, it is hard to envisage feeding and sustaining these numbers in a livable environment without the use of biotechnology. From 1800 onward, more food was simply produced by plowing up virgin land and forest. The land area used for farming increased about fivefold up to the middle of the twentieth century in step with population

increases. The Green Revolution put a brake on this expansion, increasing yields threefold with limited need for further expansion. Since 1950, the proportion of the land devoted to farming has barely increased, even though the world population doubled over the same period. At least half the available good quality soil is currently used for agriculture, with the remainder under tropical forests. Coupling this with the ever diminishing nonrenewable resources and the compounding effects of climate change on the limitation of land usage leads to an obvious dilemma. Unless a second Green Revolution is carried out, increasing yield but limiting it to land currently used for farming, there will be further deterioration of natural habitats and biodiversity that may threaten more than our lifestyles.

During the most recent global food crisis in 2008 which was erroneously laid disproportionately on the shoulders of biofuel production, most especially grain ethanol, the Gates Foundation announced $306 million in grants to boost agricultural yields in the developing world, with nearly $165 million to replenish depleted soils in Africa. As noted by US News and World reports these efforts are not without controversy as they charge that critics consider that western philanthropists are violating African "food sovereignty" and promoting American at the expense of peasant farmers who are knowledgeable about local practices [2]. But local practices have yielded scarcity. A farmer in India grows three to four times as much food on the same amount of land as a farmer in Africa; a farmer in China, roughly seven times as much.

As noted, the FAO reports that global demand for food could easily double over the period 2000–2050, with a two-and-a-half- threefold increase in the poorest countries [2]. They found that biotechnology and genetic engineering of crops hold great promise for agriculture in developing countries. The report noted that more than 70% of the world's poor still live in rural areas and depend directly on agriculture for their survival. The WHO estimates that 800 million people worldwide suffer from malnutrition. It is difficult to imagine a promising alternative to biotechnology and industrial agriculture that will sustain such numbers without catastrophic consequences. As far back as 2004 the Economic and Social Council of the United Nations (ECOSOC) noted that most developing countries are unlikely to meet the Millennium Development Goals without a clear political commitment to making science and technology among top priorities in their development agenda [3]. FAO members called for strengthening efforts in maximizing the benefits and minimizing the potential adverse consequences of biotechnology, through the Committee on Agriculture, the Council and the Conference, the development of a multidisciplinary, cross-sectoral program. In response, the Biotechnology Applications in Food and Agriculture, Forestry and Fisheries Priority Area for Interdisciplinary Action (Biotech-PAIA) was established and an Inter-Departmental Working Group on Biotechnology was set up to oversee its planning and implementation [4]. And prior to that the US National Academy of Sciences, joined by six other academies from around the world (Royal Society of London, Third World Academy of Sciences, and National Academies of Brazil, China, India, and Mexico) issued a report in 2000 declaring that biotechnology should be used to increase the production of main food staples, improve the efficiency of production, reduce the environmental impact of agriculture, and provide access to food for small-scale farmers [5]. Agricultural research of all forms holds an important key to meeting their needs, as the FAO noted biotechnology can speed up conventional breeding programs and may offer solutions where conventional methods fail. This is a positive outcome for consumers and the environment.

Progress to Date

Modifications of crop plants can be organized into two broad-based non-mutually exclusive categories: those that benefit the producer and those that benefit the consumer. Modifications that protect the crop from either biotic or abiotic stress (biotic stress being damage by predators such as insects and nematodes and disease agents such as viruses, fungi, bacteria, and weeds, and abiotic stress in the form of drought, cold, heat, and poor soils), or increase in total crop yield benefit the producer and are called "input traits." The majority of modified crops in commercial use fit in this group. Scientists have just begun to tap the large potential of biotechnology to produce varieties of plants that confer a wide spectrum of advantages to consumers. These varieties are modified with "output traits."

Developing and commercializing plants with these improved traits involves overcoming a variety of technical, regulatory, and perception challenges inherent in perceived and real challenges of complex modifications. Both the panoply of traditional plant breeding tools and modern biotechnology-based techniques will be required to produce plants with the desired quality traits. In addition to the older gene transfer technology where mostly single genes were modified, newer techniques such as the use of RNA interference to manipulate endogenous genes and especially the use of transcription factors to modulate whole suites of genes and metabolic networks will become increasingly important tools in the effort to introduce valuable traits. The later approach is already a major focus in multigenic and quantitative traits such as developing stress tolerance crops and modifying paths for improving nutritional characteristics.

Since the first biotech crop was commercialized in 1996, genetically modified (GM) crops are now grown commercially by 15.4 million farmers in 29 countries on 366 million acres [6] (Fig. 1). More than half of the 63 countries engaged in biotech research, development, and production are developing countries. While North America still leads with US acreage accounting for about 45% of the total acreage worldwide, nevertheless, 19 of the 29 countries are developing countries and of the 15.4 million farmers that grew these crops, a full 14.4 million (90%) are resource-poor LDC farmers. The most recent countries to join this group were, in 2009, South America (Uruguay, Paraguay, and Bolivia) and Africa (Egypt and Burkina Fosa) and in 2010, three countries planted approved biotech crops for the first time and Germany resumed planting. Pakistan planted Bt cotton, as did Myanmar, and notably Sweden, the first Scandinavian country to plant a biotech crop, planted "Amflora," a potato with high amylase starch for industrial applications. Germany also resumed adoption of biotech crops by planting "Amflora" for a net gain of four countries in 2010 [6]. The first generation of such crops focused largely on input agronomic traits, and the next generation will focus more on value-added output traits. In the next decade, some studies estimate, the global value of biotech crops will increase nearly fivefold to $210 billion [7].

Agricultural biotechnology has helped farmers around the world boost their productivity and grow crops in more ecologically healthy fields while allowing much more efficient use of resources. This technology allows reduced tillage, which cuts down on greenhouse gas emissions, water runoff, machinery use, and soil erosion. Meanwhile, the benefits experienced by larger-scale farmers in both industrialized nations and lesser-developed countries are already considerable [6]. Research by Brookes and Barfoot [8, 9] shows in the first 11 years of GM crop cultivation that global net farm income increased by $33.8 billion since 1996; the environmental footprint associated with pesticide use was reduced by 15.4%; and there was a reduction in carbon dioxide emissions in 2006 equivalent to taking nearly 6.6 million cars off the road for a year.

An earlier study by researchers at Denmark's National Environmental Research Institute (NERI) monitored the fields of conventional and glyphosate-tolerant sugar beet. They found that the GM plots supported more plant species and insects than the conventional plots, thus providing more food for birds, and other types of wildlife use of transgenic crops increased biodiversity compared to traditional herbicide treatments [10]. Proper measurements in the UK indicate that no-till, (directly compared with plowed organic fields on the same farm and using the same farmer) uses only one third fossil fuel, uses land much more efficiently, reduces nitrate (and pesticide) runoff by at least half, and increases soil carbon which is lost when plowed. In addition, bird territories are orders of magnitude higher, soil erosion almost vanishes, and soil invertebrates such as earthworms soar in numbers, as do predatory arthropods to keep pests down. Organic fields in the UK see a threefold rise in weeds on conversion that necessitates use of the plow [11].

Therefore, reduced-till agriculture means healthier soil, with reduced erosion and far less carbon dioxide release. Soil carbon sequestration will be an important part of any international strategy to mitigate the increase in atmospheric CO_2 concentrations. By adopting more sustainable management practices, agriculture may play a large part in enhancing soil carbon sequestration across the globe. One way is by reducing the amount of conventional tillage, after long-term tillage soil carbon stocks are depleted. In general, cultivation is not a sustainable practice. It is energy intensive and exposes soil to wind and water erosion.

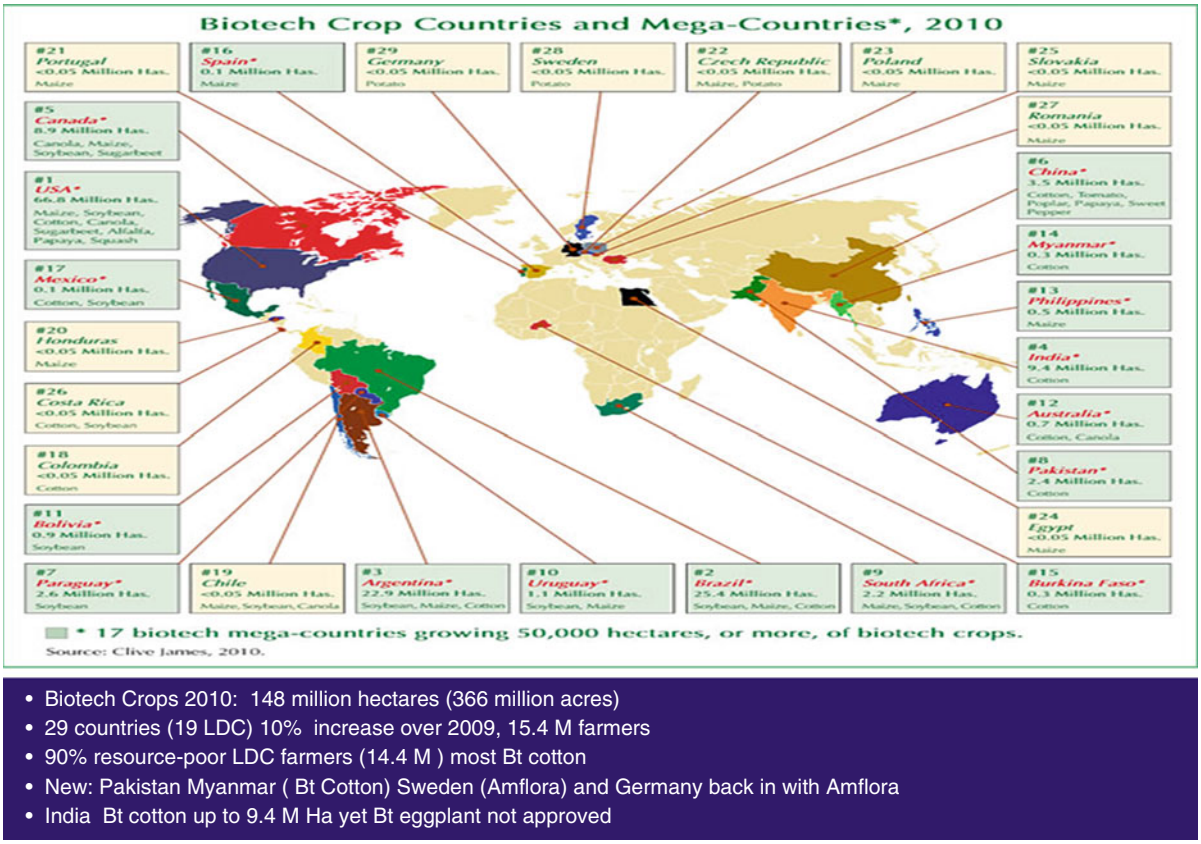

- Biotech Crops 2010: 148 million hectares (366 million acres)
- 29 countries (19 LDC) 10% increase over 2009, 15.4 M farmers
- 90% resource-poor LDC farmers (14.4 M) most Bt cotton
- New: Pakistan Myanmar (Bt Cotton) Sweden (Amflora) and Germany back in with Amflora
- India Bt cotton up to 9.4 M Ha yet Bt eggplant not approved

Transgenic Crops, Next Generation. Figure 1
Global map of biotech crop countries and mega-countries in 2010

It allows rain to compact the soil and increases the oxygen content thus allowing organic matter to oxidize away. In turn, lower organic matter in the soil allows more compaction and more nutrient loss. Additionally in warmer and drier climates, evaporative water loss may be reduced as residue remains on the soil surface creating a wetter and cooler soil microclimate.

The Brooks and Barfoot study indicates that pesticide use fell by over 286 million kg (−7.8%: equivalent to about 40% of the annual volume of pesticide-active ingredient applied to arable crops in the European Union). Less spraying means fewer tractor passes, contributing to lower carbon dioxide emissions. Insect-resistant maize also has a collateral effect – less insect damage results in much less infection by fungal molds which reduces mycotoxins that are known health risks causing such problems as liver cancer to humans and animals. Bt corn resulted in a 90% reduction in mycotoxin fungal fumonisins [12]. In addition to the obvious health benefits, the total US economic benefit is estimated to be approximately $23million annually [6]. The only "natural" way to control those fungi is the use of copper sulfate which has one of the highest toxic hazard ratings of acceptable pesticides and selects for antibiotic-resistant bacteria in the soil.

A 2005 paper from the Royal Society suggests that intensive high-yield farming on less land is better for wildlife than "wildlife-friendly" less-efficient farming [13]. They provide convincing evidence that without yield increase, land use will double by 2050 and that this effect will be especially significant in developing countries where, without greater productivity China and India will need four times the land area to support

their expanding populations. They show that in Latin America, where increased productivity was achieved, there was a significant decrease in deforestation; those producers with greatest yield increase had lower land use.

While North America remains the epicenter for cutting edge GM research, other regions, namely, China are emerging as contenders on the global stage. Agricultural science is now China's fastest-growing research field with China's share of global publications in agricultural science growing from 1.5% in 1999 to 5% in 2008 [6]. China's early experience with Bt cotton demonstrated the direct and indirect benefits of its investment in plant biotechnology research and product development. In 2002, Bt cotton was grown in 2.1 million hectares by around five million farmers. At that time the average Bt cotton farmer had reduced pesticide sprayings for the Asian bollworm from 20 to 6 times per year, reduced applications by 59–80% compared to conventional cotton (assessed in 3 years of use), and produced a kilogram of cotton for 28% less cost than the farmer using non-Bt varieties. Net revenues increased by 357–549 USD/ha compared to conventional cotton (assessed in 3 years of use) [14]. Ultimately, however, it is the social benefits from reducing exposure to insecticides and saving lives which is the real payoff.

The demand for productivity-enhancing technologies by farmers and for cost savings by consumers, the rate of increase in research investments, and success with Bt cotton suggest that products from China's research program will 1 day become widespread inside China. Indeed China is emerging as one of the trendsetters in the adoption of novel traits as more recently China is setting the pace for new approvals, with Bt rice and phytase maize approved on November 27, 2009. Rice is the principal staple for much of the world and maize is the largest animal feed source. Bt rice has the potential to increase yields up to 8%, decrease pesticide use by 80% (17 kg/ha), and generate US$4 billion in benefits annually [6]. The phytase approval is a major step forward in approvals as it is the first since the FLAVR SAVR tomato focusing on a "quality" trait. However, it is far more than this, both literally and figuratively since this single trait addresses several issues from nutritional to environmental as expanded on later.

The first GM crop to be released for commercial cultivation in India was Bt cotton, developed by the Maharashtra Seed Company (Mahyco) in partnership with Monsanto. The approval, which was given in 2002, came after several years of field trials following the biosafety procedures laid down by the government. Three cotton hybrids were granted permission for field sowing in six states for 3 years. For the first season, farmer demand for Bt cotton seed was very high; it is estimated that 44,500 ha of certified Bt cotton were planted by nearly 55,000 farmers. However, the initial events thrived in regions that resembled the area in which they were originally developed but did not perform as well in growing regions with disparate climate challenges. It was not until the trait was introgressed into locally adapted varieties that Bt cotton thrived in all growing regions. Between 2005 and 2006 the biggest impact of this approach was realized. From 3 Bt cotton hybrids in 2002 to 62 in 2006 the rapid deployment of Bt cotton hybrids based on different agro-climatic conditions resulted in decreased insecticide sprays by 39%, and increased yield of 31%, resulting in increased profit per hectare of 88% or $ 250. Over this period of rapid deployment the average cotton yields increased from 308 to 450 kg/ha of lint (of this increase 50% could be attributed to Bt technology). Over the same period raw cotton exports rose from 0.9 million bales in 2005 to 4.7 million in 2006 and had achieved 5.9 million by 2007 [15]. By 2009, 5.6 million resource-poor farmers in India planted 8.4 million hectares of Bt cotton, equivalent to 87% of the 9.6 million hectare national cotton crop. The increase from 50,000 ha when Bt cotton was first commercialized in 2002 to 8.4 million hectares in 2009 represents an unprecedented 168-fold increase in 8 years. Between 2002 and 2008, Bt cotton generated economic benefits for farmers valued at US $5.1 billion, halved insecticide requirements, contributed to the doubling of yield and transformed India from a cotton importer to a major exporter. Choudary contends that the deployment of Bt cotton over the last 8 years has resulted in India becoming the number one exporter of cotton globally as well as the second largest cotton producer in the world [15].

However, despite the success of Bt cotton the expected successful commercialization of Bt eggplant never materialized as an effective opposition managed to scupper its approval. Bt eggplant, or brinjal as it is

referred to in India, was found to be effective against fruit and shoot borer (FSB), with 98% insect mortality in shoots and 100% in fruits compared to less than 30% mortality in non-Bt counterparts. The multi-location research trials confirmed that Bt brinjal required, on average, 77% less insecticides than non-Bt counterparts for control of FSB, and 42% less for the control of all insect pests of brinjal. The benefits of Bt brinjal translate to an average increase of 116% in marketable fruits over conventional hybrids, and 166% increase over popular open-pollinated varieties [16]. Furthermore, the significant decrease in insecticide usage reduced the farmers' exposure to insecticides and resulted in a substantial decline in pesticide residues on brinjal fruits. Scientists have estimated that Bt brinjal will deliver farmers a net economic benefit ranging from $330 to $397 per acre with national benefits to India exceeding $400 million per year. However in February, 2010, the environmental minister announced a 6-month moratorium citing that "There is no overriding food security argument for Bt brinjal. Our objective is to restore public confidence and trust in Bt brinjal" [17], clearly articulating the fact that the decision was not based on scientific analysis or risk assessment.

A number of other multi-institutional projects have also been launched, including the development of transgenic plants for resistance to geminiviruses in cotton, mungbean, and tomato, resistance to rice tungro disease, development of a nutritionally enhanced potato with a balanced amino acid composition, and development of molecular methods for heterosis breeding. Other transgenic crops that are awaiting approval for commercial cultivation include transgenic herbicide-tolerant mustard hybrids and nutritionally enhanced potato varieties. However, despite the resounding success of Bt cotton, given the experience with Bt brinjal it is difficult to be optimistic about the prospects for commercialization of food crops.

A somewhat similar but even more insidious situation was experienced by Egypt. In 2008, Egypt became the first country in the Arab world (and only one of three in Africa) to commercialize biotech crops by planting 700 ha of Bt yellow maize. The variety commercialized, Ajeeb-YG, is a cross between MON 810 and an Egyptian maize variety with resistance to three corn borer pests. The reason that the amount was so low can in part be attributed to political pressure from their EU market.

The Next Generation

The vast majority of products approved to date are in the area of agronomic traits, most specifically biotic stress. The principal focus in the immediate future will remain on agronomic traits especially the area of pest control but with an increasing interest in abiotic stress tolerance which is gaining prominence as external pressures from climate change to land use change.

On the biotic stress tolerance side the focus is expanding to multi-tiered control systems. This in theory serves a double advantage, primarily expanding the effectiveness of the broad-based resistance events but also allowing more effective management of the resistance trait since there is less selective pressure when genes are stacked. SmartStax, an eight-trait event developed through collaboration between Monsanto and Dow takes advantage of multiple modes of insect protection and herbicide tolerance against above and below ground insects and provides broad herbicide tolerance, including Yieldgard VT Triple (Monsanto), Herculex Xtra (Dow), Roundup Ready 2 (Monsanto), and Liberty Link (Dow). It is currently available for corn, but cotton, soybean, and specialty crop variations are to be released [18]. It is estimated that this should require only 5% refuge acres as opposed to the 20% mandated for older technologies to mitigate against pest tolerance [15].

On the second area of agronomic traits, namely abiotic stress, there is a meta-issue that overlays much of the individual efforts, which is climate change. This poses a real challenge in terms of available agricultural land and freshwater use. Apart from the obvious effects of climate change, the decline of crop yields, ocean acidification, poor nutrition and abiotic stress, population displacement, and threatened ecosystems are effects underlined by the Stern Report [19] as potential consequences of climate change. In addition there are also broader, more systemic effects of drought beyond food insecurity such as decreased household income, the loss of assets due to slaughter of livestock, health threats due to the lack of water for hygiene and household uses, environmental degradation, and less-sustainable land management.

These effects should be considered in the light of growing population levels. In order to feed the overall population, the world will have to double its rate of agricultural production over the next 25 years, despite having already quadrupled it in the last 50 years. Severe drought accounts for half the world's food emergencies annually [1]. In 2003, the World Food Program spent US$565 million in response to drought in sub-Saharan Africa (SSA). In this context, solutions must be developed to adapt crops to the existing but also evolving conditions, such as marginal soils or harsher conditions such as cold, heat, drought, and salinity. The agriculture sector is both a contributor and provider of potential solutions to this phenomenon. It impacts two of the principal components of climate change greenhouse gases and water. Agriculture is a major source of the former emissions. Practices – such as deforestation, cattle feedlots, and fertilizer use – currently account for about 25% of greenhouse gas emissions. When broken down this amounts to 14% of carbon dioxide emission, 48% of methane, and 52% of nitrous oxide emissions [19]. In addition, this sector uses a significant amount of available freshwater – approximately 70% of the water currently consumed by humans is used in agriculture – and this is likely to increase as temperatures rise.

Given the potential impacts of climate change on the range and extent of agricultural productivity and the impact of agriculture practices itself on global warming, techniques should play a substantial part in mitigating against climate change. Green biotechnology offers a set of tools which can help producers limit greenhouse gas emissions as well as adapting their agricultural techniques to shifting climates. The three major contributions of green biotechnology to the mitigation of the impact of climate change are greenhouse gas reduction, crop adaptation (environmental stress, changing niches) and protection, and yield increase in less desirable and marginal soils.

On the first of these issues greenhouse gas reduction in addition to carbon dioxide agriculture contributes two of the other major gases indeed one of them nitrous oxide has a global warming potential of about 300 times that of carbon dioxide. In addition, nitrous oxides stay in the atmosphere for a considerable period. Nitrous oxide is produced through bacterial degradation of applied nitrogen fertilizer. In addition, fertilizer can contribute to eutrophication at ground level so its reduction is desirable on several levels. However, nitrogen is essential for crop production since it is quantitatively the most essential nutrient for plants and a major factor limiting crop productivity. One of the critical steps limiting the efficient use of nitrogen is the ability of plants to acquire it from applied fertilizer. Therefore, the development of crop plants that absorb and use nitrogen more efficiently can serve both the plant and the environment. Arcadia Biosciences of Davis, CA, developed nitrogen-efficient crops by introducing a barley AlaAT (alanine aminotransferase) into both rice and canola. Arcadia's Nitrogen Use Efficiency (NUE) technology produces plants with yields that are equivalent to conventional varieties but which require significantly less nitrogen fertilizer because the AlaAT gene allows more efficient use. Compared with controls, transgenic plants also demonstrated significant changes in key metabolites and total nitrogen content, confirming increased nitrogen uptake efficiency. This technology has the potential to reduce the amount of nitrogen fertilizer that is lost by farmers every year due to leaching into the air, soil, and waterways. In addition to environmental pressures, nitrogen costs can represent a significant portion of a farmer's input costs and can significantly impact farmer profitability. Farmers spend $60 billion annually for 150 million tons of fertilizer [20]. The technology has been licensed to Dupont for maize and Monsanto for application in canola.

The second area where green technology can help in a changing climate is crop adaptation to environmental stress and changing niches. Under stress plants will divert energy into survival instead of producing biomass and reproduction, so addressing this impact should have substantial effect on yield. In addition, improved stress tolerance allows expanded growing season especially earlier planting and further reduces yield variability and grower financial risk. The most critical of these stresses is water. One of the most effective methods of addressing water limitation problems, namely, irrigation, unfortunately is also one of the major causes of arable land degradation. It is estimated that 24.7 million acres of farmland worldwide is lost each year due to salinity build up resulting from over irrigation. In fact crops are now limited by salinity on 40% of the world's irrigated land (25% of the USA).

To address the extreme end of irrigation impact Eduardo Blumwald at UC Davis used AtNHX1, the most abundant vacuolar Na+/H+ antiporter in Arabidopsis thaliana which mediates the transport of Na+ and K+ into the vacuole. By overexpressing this vacuolar Na+/H+ antiporter, transgenic tomatoes were able to grow, flower, and produce fruit in the presence of 200 mM sodium chloride [21]. Arcadia Biosciences had now introduced this gene into economically important crops.

Even at a more moderate level of impact it is estimated that about 70–80 million acres in USA suffer yield losses due to moderate water stress. The most critical time for water stress is near-pollination and flowering where yields with or without irrigation can vary by up to 100%. This effect is clearly demonstrable in dry land production where yields can be cut in half in the absence of irrigation. At this time about 15% of US maize acres are irrigated. Given the negative effective and cost of irrigation it is estimated 20 million acres in USA would benefit from a drought tolerance gene that gives a 10% yield increase. It would also allow shifting of high-value crops into production on more marginal land.

One of the first commercialized products to have included a "yield gene" is Monsanto's second generation Roundup Ready 2 Yield® Soybeans which include not only the glyphosate-tolerant trait but also that which was developed using extensive gene mapping to identify specific DNA regions that segregated with yield increase. It is a perfect example of the power of combining recombinant DNA technology with genomics tools. The company claims that following 4 years of field trials across six US states showed 7–11% higher yields, compared to the first generation of Roundup Ready soybeans. At the National Technical Biosafety Committee (CTNBio) meeting in Brazil in August 2010, the committee approved the Bt enhanced version of this product for planting in Brazil [18].

As noted transcription factors are some of the most versatile tools being employed in developing stress-tolerant plants. One of the most versatile classes of transcription factors in so far as environmental response is concerned is the DREB (dehydration-responsive element binding protein) transcription factors which are involved in the biotic stress signaling pathway and can activate as many as 12 resistant functional genes relying on DREmembers of cis regulation under adverse conditions, for instance, rd29, cor15, and rd17, cause proline content to rise so as to enable plants to improve in many resistances such as drought, freezing, and salt tolerance. It has been possible to engineer stress tolerance in transgenic plants by manipulating the expression of DREBs [22]. One isolated from Arabidopsis has improved drought tolerance increasing productivity by at least twofold during severe water stress. In Monsanto field trials using this approach, maize yields have increased underwater stress by up to 30% [22].

Other approaches include modification of individual genes involved in stress response and cell signaling. For example, drought-tolerant canola engineered to reduce the levels of PARP [poly(ADP-ribose) polymerase], a key stress-related protein in many organisms, shows relative yield increases of up to +44% compared to control varieties. A subset of the transcription factors homeodomain leucine zipper proteins (HDZip) play a role in regulating adaptation responses including developmental adjustment to environmental cues such as water stress in plants [23]. One of these effectors is abscisic acid (ABA), an important plant regulator controlling many environmental responses including stomata movement which is itself modulated by the DREB elements. Some work is being done on modifying HDZip directly and others are working indirectly, for example, down regulating farnesyltransferase, a signaling system in the production of abscisic acid and stomata control, which results in stomata closure and water retention.

Investigators are also working on modifying basic acid to enhance the tolerance of plants to water-deficit by delaying the drought-induced leaf senescence and abscission during the stress episode. Using tobacco plants expressing an isopentenyltransferase (IPT) gene under the control of a stress- and maturation-induced promoter (PSARK) it was shown that delayed drought-induced leaf senescence resulted in remarkable drought-tolerant phenotypes, as well as minimal yield loss when plants were watered with only 30% of the water used under controlled conditions [24]. This is now being introduced into rice among other crops. This work is being done in conjunction with Arcadia Biosciences. In addition, Bayer CropScience, Pioneer Hi-Bred, BASF and Dow among others are conducting research on maize, cotton, canola, and rice, to develop a new generation of stress-tolerant, high-performance

crop varieties. Clearly stress-tolerant traits are of paramount importance in LDCs especially sub-Saharan Africa and Asia. Major efforts are already underway on this front. The partnership, known as Water Efficient Maize for Africa (WEMA), was formed in response to a growing call by African farmers, leaders, and scientists to address the devastating effects of drought on small-scale farmers. Frequent drought leads to crop failure, hunger, and poverty. Climate change can only aggravate this situation [25].

On the other end of the spectrum of climate change impact is flooding due to changing rain patterns and rising sea levels. This is already a major cause of rice crop loss. It is estimated that four million tons of rice are lost every year because of flooding which is sufficient to feed 30 million people. Rice is not grown in flooded fields through necessity but rather to control weeds, however, most rice varieties die after more than 3 days of complete submergence. Researchers know of at least one rice variety FR13A that can tolerate flooding for longer periods, but conventional breeding failed to create an event that was acceptable to farmers. The Ronald laboratory at UC Davis cloned the submergence tolerance (Sub1) locus from this resistance variety using a map-based cloning approach. The Sub1 locus encodes three putative transcription regulators one of which increases dramatically in response to oxygen deprivation in sub1 seedlings, whereas Sub1C levels decrease. Transgenic lines over-expressing the Sub1A-1 gene have been introgressed into a submergence-intolerant line and display-enhanced submergence tolerance [26].

There is also some research in the final abiotic stress focus area, namely, expansion of crops into and increased yield in less desirable and marginal soils. For example, a gene that produces citric acid in roots can protect plants from soils contaminated with aluminum as it binds to the contaminant preventing uptake by the root system [27]. Genes such as these can allow crops to be cultivated in hostile soils and temperatures increasing geographic range while reducing potential impact on fragile ecosystems.

While exciting and very relevant, research in abiotic stress tolerance is still an input trait. The first generation of biotechnology crops focused largely on those input agronomic traits; the next generation will focus more on value-added output traits. This will include identifying and isolating genes and metabolites that will make possible the enhancement of valuable traits, with some of the later compounds being produced in mass quantities for niche markets. Two of the more promising markets are improved nutrition including nutraceuticals, or so-called functional foods, and plants developed as bioreactors (production factories) for the commercial-level production of valuable proteins and compounds, a field known as plant molecular farming [28]_ENREF_24.

While the correlative link between food and health, beyond meeting basic nutrition requirements, has only been unequivocally proven in a number of cases, a growing body of evidence indicates that food components can influence physiological processes at all stages of life [29]. Nutrition intervention from a functionality perspective has a personal dimension. Determining individual response is at least as complex a challenge as the task of increasing or decreasing the amount of a specific protein, fatty acid, or other components of the plant itself. There is also evidence that early food regimes can effect later life health, for example, some children that survived famine conditions in certain regions of Africa grew into adults battling obesity and related problems presumably due to the selective advantage of the thrifty gene in their early food-stressed environment becoming a hazard during more abundant times especially if later diets are calorie-dense.

Functional foods are defined as any modified food or food ingredient that may provide a health benefit beyond the traditional nutrients it contains. Scientific evidence is accumulating to support the role of phytochemicals and functional foods in the prevention and treatment of disease. Functional food components are of increasing interest in the prevention and/or treatment of a number of the leading causes of death including but not limited to cancer, diabetes, cardiovascular disease, and hypertension. Many food components are known to influence the expression of both structural genes and transcription factors in humans. Examples of these phytochemicals are listed in Table 2. The large diversity of phytochemicals suggests that the potential impact of phytochemicals and functional foods on human and animal health is worth examining as targets of biotechnology efforts. Developing plants

with improved quality traits involves overcoming a variety of technical challenges inherent to metabolic engineering programs. Both traditional plant breeding and biotechnology techniques are needed to produce plants carrying the desired quality traits [29] (Table 1).

From a health perspective, plant components of dietary interest can be broadly divided into four main categories, which can be further broken down into positive and negative attributions for human nutrition, macronutrients (proteins, carbohydrates, lipids [oils], and fiber), micronutrients (vitamins, minerals, phytochemicals), anti-nutrients (substances such as phytate that limit bioavailability of nutrients), allergens, intolerances, and toxins [29]. Developing and commercializing plants with these improved traits involves overcoming a variety of technical, regulatory, and perception challenges inherent in perceived and real challenges of complex modifications. Both the panoply of traditional plant breeding tools and modern biotechnology-based techniques will be required to produce plants with the desired quality traits. Table 2 presents examples of crops that have already been genetically modified with macro- and micronutrient traits that may provide nutritional benefits.

In addition to functional foods, this area has the potential to address both nutrition and environmental impact. A good example of this is the addition of transgenic phytase enzymes to crops to reduce the need to add phosphate to feed [6]. Most of the phosphate is added to counteract the non-bioavailability of phosphorus in phytic acid and the sequestering effect of phytic acid on uptake of divalent mineral ions such as iron, calcium, and zinc. Unfortunately excess phosphate is excreted causing major environmental impact through eutrophication and fish kills in regions with intense pig and poultry farming [28, 29]. In addition, in humans, such mineral deficiencies due to phytate binding are estimated to afflict two to three billion people, primarily in the developing world. Several studies have shown that Aspergillus-derived phytases can be produced in large quantities in a range of plants including cereals with clear-cut positive effects on phytate degradation, and phosphate and mineral bioavailability in animal-feeding trials [104]. It is thus conceivable that genetic engineering of staples for increased phytase expression could have potential for improving iron and zinc bioavailability alleviating the need for supplementation in all monogastrics and consequent reduction in polluting runoff in non-ruminant animals [105]. As noted earlier China has led the way in the approval of this "output trait" in Maize being the first country to approve commercialization in November 2009 [6]. Continuing improvements in molecular and genomic technologies are contributing to the acceleration of such product development. One estimate states that foods that are used for functional purposes made up 10% of the $503 billion total US retail food market [106].

In addition to being a source of nutrition, plants have been a valuable wellspring of therapeutics for centuries. During the past decade, however, intensive research has focused on expanding this source through rDNA biotechnology and essentially using plants and animals as living factories for the commercial production of vaccines, therapeutics, and other valuable products such as industrial enzymes and biosynthetic feedstocks [28].

More pressingly, with the increasing costs in economic and environmental terms of our dependency on fossil fuels, biotechnology offers innovative means to improve plant material for biomass conversion and enzymes to do the converting. There are two principal classes of biofuels: bio-alcohol (initially bio-ethanol but with increasing interest in higher-energy alcohols such as bio-butanol) and bio-diesel.

The first generation of biofuels was fermented from easy sources of simple sugars such as sugarcane and simple polymers primarily from grain starch. This source of bio-ethanol is unsustainable on many levels including the fact that its sources compete with food and especially feed grains for markets, land, and water. The focus for second generation bio-alcohols is mostly on complex polymers, primarily cellulosic ethanols and what are being termed third generation bio-alcohols such as bio-butanol [107]. From a biotechnology perspective work is being carried out on the biomass component focusing on increased production in such sources as switchgrass and miscanthus by among other things modifying photoperiodicity genes to switch energy to vegetative tissue production and improved biomass conversion by such approaches as reducing lignin composition and incorporating self-activating enzyme digestion upon harvesting. On the enzyme component companies including

Transgenic Crops, Next Generation. Table 1 Examples of crops in research with nutritionally improved traits[a]

Trait	Crop (trait detail)	References
Protein and amino acids		
Protein quality and level	Bahiagrass (protein↑)	Luciani and Wofford [30]
	Canola (amino acid composition)	Roesler et al. [31]
	Maize (amino acid composition; protein↑)	Cromwell et al. 1969, [32], Yang et al. [33], O'Quinn et al. [34], Young et al. [35]
	Potato (amino acid composition; protein↑)	Chakraborty et al. [36], Li et al. [37], Yu and Ao [38], Atanassov et al. [39]
	Rice (protein↑; amino acid)	Katsube et al. [40]
	Soybean (amino acid balance)	Rapp [41]; Dinkins et al. [42]
	Sweet Potato (protein↑)	Prakash and Jaynes [43]
	Wheat (protein↑)	Uauy et al. [44]
Essential amino acids	Canola (lysine↑)	Falco et al. [45]
	Lupin (methionine↑)	White et al. [46]
	Maize (lysine↑; methionine↑)	Agbios 2006, Lai [47]
	Potato (methionine↑)	Zeh et al. [48]
	Sorghum (lysine↑)	Zhao et al. 2003
	Soybean (lysine↑; tryptophan↑)	Falco et al. [45], Galili et al. [49]
Oils and fatty acids		
	Canola (lauric acid↑; γ-linolenic acid↑; + ω-3 fatty acids; 8:0 and 10:0 fatty acids↑; lauric + myristic acid↑; oleic acid↑)	Del Vecchio [50], Froman [51], James et al. [52], Ursin [53], Dehesh et al. 1996, Agbios 2006, Roesler et al. [31]
	Cotton (oleic acid↑; oleic acid + stearic acid↑)	Chapman et al. [54], Liu et al. [55]
	Linseed (+ ω-3 and -6 fatty acids)	Abbadi et al. [56]
	Maize (oil↑)	Young et al. [35]
	Oil Palm (oleic acid↑ or stearic acid↑; oleic acid↑ + palmitic acid↓)	Parveez [57], Jalani et al. [58]
	Rice (α-linolenic acid↑)	Anai et al. [59]
	Soybean (oleic acid↑; γ-linolenic acid↑)	Kinney [60], Reddy and Thomas [61]
	Safflower (γ Linoleic Acid GLA↑)	Arcadia [62]
Carbohydrates		
Fructans	Chicory, (fructan↑; fructan modification)	Smeekens [63], Sprenger et al. [64], Sevenier et al. [65]
	Maize (fructan↑)	Caimi et al. [66]
	Potato (fructan↑)	Hellwege et al. [67]
	Sugar beet (fructan↑)	Smeekens [63]
Frustose, Raffinose, Stachyose	Soybean	Hartwig et al. [68]

Transgenic Crops, Next Generation. Table 1 (Continued)

Trait	Crop (trait detail)	References
Inulin	Potato (inulin↑)	Hellwege et al. [69]
Starch	Rice (amylase ↑)	Chiang et al. [70], Schwall et al. [71]
Micronutrients and functional Metabolites		
Vitamins and Carotenoids	Canola (vitamin E↑)	Shintani and DellaPenna [72]
	Maize (vitamin E↑; vitamin C↑; beta-carotene↑; folate↑)	Rocheford et al. [73], Cahoon et al. [74], Chen et al. [75], Naqvi et al. [76]
	Mustard (+β-carotene)	Shewmaker et al. [77]
	Potato (β-carotene and lutein↑)	Ducreux et al. [78]
	Rice (+β-carotene)	Ye et al. [79]
	Strawberry (vitamin C↑)	Agius et al. [80]
	Tomato (folate↑; phytoene and β-carotene↑; lycopene↑; provitamin A↑)	Della Penna 2007, Diaz de la Garza et al. [81], Enfissi et al. [82] Mehta et al. 2002, Fraser et al. [83], Rosati et al. [84]
Functional secondary metabolites	Apple (+stilbenes)	Szankowski et al. [85]
	Alfalfa (+resveratrol)	Hipskind and Paiva [86]
	Kiwi (+resveratrol)	Kobayashi et al. [87]
	Maize (flavonoids↑)	Yu et al. [88]
	Potato (anthocyanin and alkaloid glycoside↓; solanin↓)	Lukaszewicz et al. [89]
	Rice (flavonoids↑; +resveratrol)	Shin et al. 2006, Stark-Lorenzen et al. [90]
	Soybean (flavonoids↑)	Yu et al. [91]
	Tomato (+resveratrol; chlorogenic acid↑; flavonoids↑; stilbene↑anthocyanins↑)	Giovinazzo et al. [92], Niggeweg et al. [93], Muir et al. [94], Rosati et al. [84], Gonzali et al. [95]
	Wheat (caffeic and ferulic acids↑; +resveratrol)	UPI [96]
Mineral availabilities	Alfalfa (phytase↑)	Austin-Phillips et al. [97]
	Lettuce (iron↑)	Goto et al. [98]
	Rice (iron↑)	Lucca et al. [99]
	Maize(phytase↑, ferritin↑)	Drakakaki et al. [100], Han [101]
	Soybean (phytase↑)	Denbow et al. [102]
	Wheat (phytase↑)	Brinch-Pedersen et al. [103]

[a]Excludes protein/starch functionality, shelf life, taste/aesthetics, fiber quality and allergen reduction traits. Modified from Newell-McGloughlin [29] (25)

Novozymes (Davis, CA) and Danisco (Palo Alto, CA) are making considerable strides in improving the effectiveness, specificity, and cost of cellulosic enzymes and increasing the conversion range especially for the more difficult pentose sugars such as xylose. Protein engineers are taking a synthetic biology approach with recent progress in engineering more stable and effective enzymes such as cellobiohydrolases by researchers at Caltech [108] and completely novel metabolic pathways by the Berkeley company, Amyris [109].

Transgenic Crops, Next Generation. Table 2 Examples of plant components with suggested functionality[a]

Class/components	Source[b]	Potential Health Benefits
Carotenoids		
Alpha-carotene	Carrots	Neutralizes free radicals that may cause damage to cells
Beta-carotene	Various fruits, vegetables	Neutralizes free radicals
Lutein	Green vegetables	Contributes to maintenance of healthy vision
Lycopene	Tomatoes and tomato products (ketchup, sauces)	May reduce risk of prostate cancer
Zeaxanthin	Eggs, citrus, maize	Contributes to the maintenance of healthy vision
Dietary fiber		
Insoluble fiber	Wheat bran	May reduce risk of breast and/or colon cancer
Beta glucan[c]	Oats	May reduce risk of cardiovascular disease (CVD)
Soluble fiber[c]	Psyllium	May reduce risk of CVD
Whole grains[c]	Cereal grains	May reduce risk of CVD
Collagen Hydrolysate	Gelatin	May help improve some symptoms associated with osteoarthritis
Fatty acids		
Omega-3 fatty acids – DHA/EPA	Tuna; fish and marine oils	May reduce risk of CVD and improve mental, visual functions
Conjugated linoleic acid (CLA)	Cheese, meat products	May improve body composition, may decrease risk of certain cancers
Gamma linolenic acid	Borage, evening primrose	May reduce inflammation risk of cancer, CVD disease and improve body composition
Flavonoids		
Anthocyanidins: cyanidin	Berries	Neutralize free radicals, may reduce risk of cancer
Hydroxycinnamates	Wheat	Antioxidant-like activities, may reduce risk of degenerative diseases
Flavanols: catechins, tannins	Tea (green, catechins), (black, tannins)	Neutralize free radicals, may reduce risk of cancer
Flavanones	Citrus	Neutralize free radicals, may reduce risk of cancer
Flavones: quercetin	Fruits/vegetables	Neutralize free radicals, may reduce risk of cancer
Glucosinolates, indoles, isothiocyanates		
Sulphoraphane	Cruciferous vegetables (broccoli, kale), horseradish	Neutralizes free radicals, may reduce risk of cancer
Phenolics		
Stilbenes – resveratrol	Grapes	May reduce risk of degenerative diseases; heart disease; cancer. May have longevity effect
Caffeic acid, ferulic acid	Fruits, vegetables, citrus	Antioxidant-like activities; may reduce risk of degenerative diseases; heart disease, eye disease
Epicatechin	Cacao	Antioxidant-like activities; may reduce risk of degenerative diseases; heart disease

Transgenic Crops, Next Generation. Table 2 (Continued)

Class/components	Source[b]	Potential Health Benefits
Plant stanols/sterols		
Stanol/sterol ester[c]	Maize, soy, wheat, wood oils	May reduce risk of coronary heart disease (CHD) by lowering blood cholesterol levels
Prebiotic/probiotics		
Fructans, inulins, fructo-oligosaccharides (FOS)	Jerusalem artichokes, shallots, onion powder	May improve gastrointestinal health
Lactobacillus	Yogurt, other dairy	May improve gastrointestinal health
Saponins	Soybeans, soy foods, soy protein-containing foods	May lower LDL cholesterol; contains anticancer enzymes
Soybean protein	Soybeans and soy-based foods	25 g/day may reduce risk of heart disease.
Phytoestrogens		
Isoflavones – daidzein, genistein	Soybeans and soy-based foods	May reduce menopause symptoms, such as hot flashes, reduce osteoporosis, CVD
Lignans	Flax, rye, vegetables	May protect against heart disease and some cancers; may lower LDL cholesterol, total cholesterol, and triglycerides
Sulfides/thiols		
Diallyl sulfide	Onions, garlic, olives, leeks, scallions	May lower LDL cholesterol, helps to maintain healthy immune system
Allyl methyl trisulfide, dithiolthiones	Cruciferous vegetables	May lower LDL cholesterol, helps to maintain healthy immune system
Tannins		
Proanthocyanidins	Cranberries, cranberry products, cocoa, chocolate, black tea	May improve urinary tract health May reduce risk of CVD, and high blood pressure

[a]Examples are not an all-inclusive list

[b]US Food and Drug Administration approved health claim established for component. Modified from Newell-McGloughlin [29] (25)

Biodiesel is defined by the National Biodiesel Board as a mono-alkyl ester. It is basically vegetable oil or animal fat–based diesel fuel consisting of long-chain alkyl (methyl, propyl, or ethyl) esters. Biodiesel is typically made via a trans-esterification process reacting lipids (vegetable oil, animal fat) with an alcohol.

Biodiesel per se can be used by standard diesel engines and is therefore qualitatively distinct from the vegetable, animal, and other waste oils used to fuel-converted diesel engines. Biodiesel can be used alone, or blended with petrodiesel. Biodiesel has better lubricating properties and much higher cetane ratings than today's lower sulfur diesel fuels but is still not economical as an alternate stand-alone fuel. Although still carbon-based, it is suggested by some that in terms of biofuels the algal biodiesel approach is much more sustainable than either the cellulosic or other land-based sources with DOE claiming that algae fuel yields have not yet been accurately determined, but DOE is reported as saying that algae yield 30 times more energy per acre than land crops such as soybeans [110].

From a biotechnology perspective the main focus for expanding interest in this area is increasing lipid production and modifying lipid composition for optimum performance. Work is being done to modify algae for increased production of desirable medium chain fatty acids (MCFA) which abrogates the requirement for cracking and isomerizing of long chain fatty acids (LCFAs).

The advantages of MCFAs over LCFAs are high energy density, low fuel viscosity, low flash point, and low freezing point. The real issue with algal production systems is the scale-up step for commercial-level production where contamination, dewetting, and lipid isolation are still economically prohibitive. In February 2010, the Defense Advanced Research Projects Agency announced that the US military was about to begin large-scale production of jet fuel from algal pond isolates [111].

Barriers to Introduction

Most of the crops approved to date do appear to support the notion that the deregulation process is prohibitive for any but well-financed companies whose focus is primarily on the large commodity crops as just discussed. Worldwide there is clear asymmetry and lack of consensus in regulatory systems [112]. This discourages research on anything but the most mundane of crops and traits and is a real disincentive to creative research. For all intent and purposes there is just one trait from a public institution that has successfully traversed the regulatory minefields and been translated into a commercially viable commodity and that is the viral coat protein protection system initially developed for the papaya ringspot virus pandemic in Hawaii. This crop, papaya is a major tropical fruit crop in the Asian region. However, production in many Asian countries is set back by the prevalence of the PRSV disease as well as post-harvest losses. The PRSV-resistant papaya, based on RNAi suppression of the coat protein expression, literally saved the $17 M economy in Hawaii and is of significant importance in Taiwan and other SE Asian countries. Coat protein-based resistance is a demonstration of what is known as post-transcriptional gene silencing (PTGS). RNA interference (RNAi) in animals and basal eukaryotes, quelling in fungi, and PTGS in plants are examples of a broad family of phenomena collectively called RNA silencing. This system has now been applied to many species. A 5-year effort to combat plum pox virus disease through PTGS resistance paid off. In 1990, USDA/Agricultural Research Service (ARS) scientists began their efforts with a papaya ringspot virus coat protein gene obtained from Dennis Gonsalves [113]. This gene shows 70% homology to the plum pox gene and has been used to control other viruses similarly related to papaya ringspot. However, irrespective of the mechanism, it is important that resistance based on a single gene is managed well and alternate control mechanisms are introduced to reduce pressure on the development of viral resistance. Other approaches include expression of the RNA replicating enzymes of the virus, expression of satellite RNA, replicating RNA molecules that are molecular parasites of the virus, or the use of protease inhibitors to interfere with processing of the viral proteins.

While translation of biotech research into value-added products for producers and consumers is a challenge in the USA, it is exponentially more difficult in LDCs [112]. A problem facing Africa in particular is the lack of a dynamic private sector to take technologies to the farmer. It has also been estimated that regulatory costs might exceed the costs of research and experimentation needed to develop a given GM crop, which is a major problem in releasing such crops to the market. A way to reduce the costs of generating food and environmental safety data is to develop regional "centers of excellence" with complementary facilities where food safety testing can be done reliably and regulatory costs could be reduced. The economic gains from using genetically modified crop technology in sub-Saharan Africa (SSA) are potentially large according to the World Bank Group [114]. The results suggest that the welfare gains are potentially very large, especially from golden rice and nutritionally enhanced GM wheat, and that those benefits are diminished only slightly by the presence of the de facto European Union's current ban on imports of GM foods.

The authors used the global economy-wide computable general equilibrium model known as GTAP. They specifically noted that if SSA countries impose bans on GM crop imports in deference to EU market demand for non-GM products, the domestic consumer loss net of that protectionism boost to SSA farmers would be more than the small gain derived from greater market access to the EU.

Problems cited for the slow passage of GM crops from experimental, to trial, to commercial stage especially in LDCs include the lack of capacity to negotiate licenses to use genes and research techniques patented by others, especially for crops with export potential [28]. In addition, there are difficulties in meeting

regulatory requirements and a lack of effective public commercialization modalities and working extension networks. Biosafety and IPR regulations still have to be enforced in many countries for an effective and safe use of genetically engineered crops, especially if their production is meant for the export market.

Scientific, civic, and religious opinion leaders from all over the world have expressed support for the value of this technology. Florence Wambugu (CEO, Africa Harvest Biotech Foundation International, Kenya) states that the great potential of biotechnology to increase agriculture in Africa lies in its "packaged technology in the seed," which ensures technology benefits without changing local cultural practices [115]. For example, over 120 million children worldwide are deficient in vitamin A. In the late 1990s, Potrykus [108] group engineered rice to accumulate provitamin A (b-carotene). Incorporation of this trait into rice cultivars and widespread distribution of this "packaged technology in the seed" could prevent one to two million deaths each year. She observes that in the past, many foreign donors funded high-input projects, which have not been sustainable because they have failed to address social and economic issues such as changes in cultural practice [115]. In concurrence with this, Ismail Serageldin, former Chairman of the CGIAR (Consultative Group on International Agricultural Research) noted that, a priori, biotechnology could contribute to food security by helping to promote sustainable agriculture centered on smallholder farmers in developing countries [104].

US Consumer attitudes also tend to be relatively positive on the whole about agricultural biotechnology. In a 2010 IFIC survey, consumers were determined to be largely familiar with the term "biotechnology" [116]: More than two thirds of consumers (69%) have read or heard at least "a little" about the concept. Half (51%) of consumers say they are favorable toward farmers using biotechnology to grow more crops that would help meet food demand. In addition, significantly more consumers this year (28% vs. 23% in 2008) believe foods produced through biotechnology are available in the supermarket today, although this figure is still relatively low. Certain benefits of biotechnology are found to resonate better with consumers than others. These tend to be consumer-facing qualities such as improved health or better taste. For example, the majority of consumers say they are somewhat or very likely to purchase foods produced through biotechnology to provide more healthful fats like Omega-3 s (76%), to avoid trans fat (74%), and to make foods taste better/fresher (67%). This is consistent from 2008. Additionally, more than three quarters (77%) of consumers say they would be likely to purchase foods produced through biotechnology for their ability to reduce pesticide use, and 73% of consumers said they would be likely to purchase bread, crackers, cookies, cereal, or pasta made with flour from wheat that had been modified by biotechnology to use less land, water, and/or pesticides. Of the 18% who would like to see additional information on the FDA label, only 3% mentioned anything about biotechnology.

But what of the context in which these crops are grown? Can all cropping systems co-exist in harmony? According to Brookes and Barfoot, [8, 117] it is important to determine the relative importance of different crop production systems based on planted area, production, and economic value to the region in question. The issue is what, if any, are the economic consequences of adventitious presence of material from one crop system within another based on the notion that farmers should be able to cultivate freely the crops of their choice using whichever production system works best in any given context (GM, conventional, or organic). It is never a food or environmental safety issue but rather a production and marketing matter. The heart of the issue is assessing the likelihood of adventitious presence of material from one production system affecting another and the potential impacts. This requires consistency when dealing with adventitious presence of any unwanted material including, but most definitely not limited to, biotech-derived material. Adventitious presence is simply the unintended incidence of something other than the desired crop such as small quantities of weed seeds, seeds from other crops, dirt, insects, or foreign material (e.g., stones). It is unrealistic to expect 100% purity for any crops, or products derived therefrom, so thresholds that are consistent across all materials should be set and should not discriminate (e.g., thresholds for adventitious presence of biotech material should be the same as applied to thresholds for other unwanted material and vice versa). All measures should be proportionate, non-discriminatory, and science-based.

The issue of economic liability provisions that compensate growers for adventitious presence of biotech material is often raised [117]. Historically, worldwide the market has adequately addressed economic liability issues relating to the adventitious presence of unwanted material in any agricultural crop. For example, for certified seed the onus is on the producers, who require isolation from undesired pollination for the purity of their product, to insure such purity; this is not their neighbor's problem. By extension the onus is on growers of any specialty crops to take action to protect the purity of their crops since these are self-imposed standards for and by that market. Growers who have themselves chosen a more stringent standard than that established in EU legislation should not expect their neighbors to bear the special management costs of meeting that self-imposed standard; to do so would reverse fundamental freedoms of economic activity and would establish a dangerous precedent. To allow specialty operators to formulate unrealistic standards for GM in their own produce would impose impossibly high standards on neighbors and would effectively impose a ban on the choice of other producers. Such growers usually are rewarded by higher prices and niche markets for taking such actions. Their neighbors enjoy no such advantage.

Existing legislation in North America and the EU is more than adequate to protect all grower and consumer interests but if new regulations were considered to address economic liability provisions for any negative economic consequences of adventitious presence of unwanted material, the same principle should apply to all farmers regardless of their chosen production methods. On equity grounds, biotech growers should have equal access to compensation for adventitious presence of material from conventional or organic crops (such as fungal contamination) as conventional and organic producers have from biotech growers. No one sector should be able to unfairly prohibit another – access and choice work both ways. All co-existence measures should be based on legal, practical, and scientific realities and not on commercial or niche marketing objectives. Where unintended presence has occurred on a number of occasions to date such as the presence of minute levels of Bayer Crop Sciences–regulated material LLRICE 604 found in Clearfield 131 (CL131) rice seed in 2007 and Mycogen's event "32" in maize in 2008, the agencies cooperated and determined that these events did not prove any risk as they carried similar constructs to those already having achieved non-regulated status.

According to Brookes and Barfoot, [8, 117] biotech crops co-exist successfully with conventional and organic crops in North America (where, as noted, biotech crops account for the majority of acreage of important arable crops like soybeans, cotton, and maize) Spain, and more recently the Czech Republic. The market has developed practical, proportionate, and workable coexistence measures without new regulations or indeed any government intervention. Where isolated instances of adventitious presence of biotech material have been found in conventional or organic crops these have usually been caused by inadequate implementation of good coexistence practices (e.g., inefficient segregation of crops in storage and transport, nonuse of tested, certified seed). Under civil liability (i.e., tort damages) and for intellectual property infringement (except for the unauthorized StarLink), there have been no lawsuits brought by any parties for adventitious presence. Every case brought by a seed company for infringement has involved a claim that the farmer charged with infringement was an intentional infringer (i.e., adventitious presence was not the issue). And, to date, each of these cases was upheld by the courts. Indeed, all except one notable exception in North America has conceded to this claim. The exception is Percy Schmeiser who famously was found by a number of courts to have infringed Monsanto's glyphosate-tolerant patent by deliberately spraying and subsequently saving seeds from resistant sport canola plants found growing near his property. He initially claimed adventitious contamination but upon losing all the way to the Canadian Supreme court he changed tact to try to take advantage of Canadian patent law which prohibits patenting of higher organisms. While the court upheld this they determined that the construct within the plant was subject to IP protection and so Schmeiser was found to have infringed a patentable article under Canadian law.

Virtually all EU member states have transcribed EU Directive 2001/18 and implement EU regulations on traceability and labeling. Within the EU, provision has been made for a de minimis threshold for unavoidable presence of GMOs but no actual threshold has been set.

Therefore, the default state of the 0.9% on labeling and traceability is the one enforced. In the USA, organic products cannot be (legally) downgraded or the producer decertified by unintentional presence when all required measures and best practices are adhered to and no producer has been so impacted to date [118].

Going forward there are four major stanchions to the furtherance of co-existence and all of them are incumbent on cooperation.

1. Monitoring: Verify the models and predictions about cost, isolation standards, and generally to learn how the farming community copes with the requirements for keeping the product streams separated.
2. Dialog: Strategy development takes place in a dialog between the scientific and technical community and all relevant stakeholders. (The Czech Republic [119].)
3. Stewardship: Stewardship programs should take into account the interests of both GM and non-GM farmers. Existing product stewardship programs for non-GM crops in farming should be a starting point for developing stewardship schemes for GM crops.
4. Research: The scientific community should be encouraged to fill the knowledge gaps that have been identified. Projects are needed to validate models and guidelines, including long-term studies. Building up mechanistic, probabilistic, and predictive models of gene flow etc. Methods for restricting gene flow by eliminating the fertility of pollen or seeds (apomixis, cytoplasmic male sterility, plastid transformation, Genetic Use Restriction Technology (GURT), etc.).

The World Trade Organization ruled in 2006 that a 6-year European ban on genetically engineered crops violates international trade. The three-person panel issued its decision ruling in favor of the three countries, USA, Canada, and Argentina, on a large majority of the 25 crops under dispute in the case while issuing mixed rulings on a few crops. The panel also ruled in favor of challenging national bans on specific biotech crops issued by Austria, France, Germany, Greece, Italy, and Luxembourg. The EU had argued that it did not have a moratorium but that it just took more time to weigh the possible risks to health and the environment posed by genetically engineered foods. It said it needed to take a "precautionary" approach to regulation, which is different from what it called Washington's "laissez-faire" stance.

The trade organization panel appears not to have challenged Europe's regulatory process for biotech crops. Rather, it said Europe failed to follow its own procedures, resulting in undue delay of decisions. Interestingly one of the most comprehensive assessments on the technology was conducted by EU scientists. An EU Commission Report [120] that summarized biosafety research of 400 scientific teams from all original 15 EU countries conducted over 15 years stated that research on biotechnology-derived plants and products so far developed and marketed, following usual risk assessment procedures, has not shown any new risks to human health or the environment beyond the usual uncertainties of conventional plant breeding. Indeed, the use of more precise technology and the greater regulatory scrutiny probably make them even safer than conventional plants and foods. If there are unforeseen environmental effects – none have appeared as yet – these should be rapidly detected by existing monitoring systems. This analysis was repeated in a 2008 EU Joint Research Centre (JRC) Report commissioned by Members of the European Parliament (MEPs) conducted by world experts including the European Food Safety Authority (EFSA), the World Health Organization (WHO), and others [120]. Their report concluded that there is no evidence that genetically modified foods have any harmful effects; a declaration signed by over 3,500 scientists including 25 Nobel Laureates reiterates this position [28].

Future Directions

As agriculture must adapt to rapidly changing needs and growing conditions it is important to become more effective at producing more or less with limited resources and only the tools of biotechnology will allow us to bypass physiological and environmental limitations to produce sufficient food, feed, fuels, and fiber on ever diminishing arable land to meet ever increasing demand. The challenges going forward are foremost technical as one strives to modify qualitative as opposed to quantitative traits and intricates metabolic pathways and

networks as opposed to single genes; the scientific hurdles to achieve these aims are not trivial. However, with the tools now coming online in the fields of genomics, proteomics, metabolmics, and bioinformatics, there is the potential to make major modifications to introgress desirable traits. For example, tools such as next generation sequencing, RNA interference (RNAi), transcription factors (Tfs), transcription activator-like effector nucleases (TALENs), mini-chromosomes, combinatorial transformation, epigenetic modification, network engineering, and systems biology will allow us to apply both reductive and holistic approaches to identify, modify, introgress, and subsequently and simultaneously study the expression and interaction of transgenes on tens of thousands of endogenous genes in elite germplasm backgrounds. With these newly evolving tools, one is beginning to dissect the global effects of metabolic engineering on metabolites, enzyme activities, and fluxes. With rapidly emerging technologies, the increase in our understanding of and ability to manipulate plant metabolism during the coming decades should place plant researchers in the position of being able to modify crop traits to respond to the diversity of needs from minimizing environmental impact to optimizing productivity and quality output.

Non-technical limitations include intellectual property restrictions which may limit translation of public research if not managed judiciously; secondly, liability concerns over abuse or misuse of constructs; thirdly prohibitive and asymmetric biosafety regimes and finally public acceptance. The latter two in many ways are the most insidious of limitations as they have little basis in rational process and thus are difficult to redress effectively – the last in particular is often predicated on how much of the former is perceived to be of concern, and how positions are presented by the opposing factions. It is often easier to appeal to emotion and self-fear than it is to present reasoned and judicious scientific rational for basing risk analysis. Indeed the actual commercialization of biotech products may have little to do with technical limitations and more to do with these external constraints primarily the process of regulatory approval. The flagship of improved nutritional varieties, namely, beta carotene–enhanced rice commonly referred to as golden rice, despite being under consideration since the late 1990s and subject to a barrage of risk assessments is unlikely to be approved until 2012 at the earliest. Ingo Potrykus, the developer, says an unreasonable amount of testing has been required without scientific justification. In a recent *Nature* article [121], he lays the blame largely on the regulatory process which he considers excessive observing that unjustified and impractical legal requirements are preventing genetically engineered crops from saving millions from starvation and malnutrition.

In the final analysis, resources are finite and true sustainability can come only from an enlightened philosophy that promotes the development of resource-enhancing technologies. Antithetically, those who claim to be the stalwarts of sustainability are, on occasion, the very ones who oppose the development and application of those tools that can help to insure such sustainability. The only sure way to insure food security and protect the planet's resources is not to settle into the complacency of maintaining the status quo but to engage in continual, constructive change based on scientific knowledge. Thus, if one is to be accountable to posterity it is not just the choice but one's duty to promote and apply responsible science and technology in all endeavors.

Bibliography

1. World Bank (2007) Agriculture for development, overview. World Bank, Washington, DC
2. Lavelle M, Garber K (2008) Eight ways to fix the global food crisis US news and world reports. Posted 9 May 2008. http://www.climos.com/news/articles/8waysto.htm
3. F. W. F. a. A. O. o. t. U. N. W. H. (2004) The state of food and agriculture 2003-2004, agricultural biotechnology, meeting the needs of the poor? vol 35. Food and Agriculture Organization of the United Nations, Rome, pp 1–209
4. Economic and Social Council: Commission on Science and Technology for Development (2004) Resolution 2004/68. Science and Technology for Development. Council, E. a. S
5. Agbioworld (2000) Seven scientific academies support GM crops reproduced from The Times (London), 12 July 2000. http://www.agbioworld.org/biotech-info/topics/dev-world/academies.html
6. James C (2011) Global status of commercialized biotech/GM Crops: 2010. ISAAA briefs 42-2010. ISAAA, Ithaca. http://www.isaaa.org/resources/publications/briefs/42/executivesummary/default.asp
7. Ghadar F, Spindler H (2005) Industrial management the growth of biotechnology (Global tectonics: Part 1). http://www.entrepreneur.com/tradejournals/article/135568229.html
8. Brooks G, Barfoot P (2008) Co-existence of GM and Non-GM arable crops: the Non-GM and organic context in the EU. PG Economics, Dorchester

9. Brooks G, Barfoot P (2005) The global economic and environmental impact – The first nine years 1996–2004. AgBioForum 8:187–196
10. Elmegaard N, Pedersen MB (2001) Flora and fauna in Roundup tolerant fodder beet fields. National Environment Research Institute, Technical Report No. 349, p 40
11. Trewavas A (2001) Urban myths of organic farming. Nature 410:409–410
12. Folcher L, Delos M, Marengue E, Jarry M, Weissenberger A, Eychenne N, Regnault-Roger C (2010) Lower mycotoxin levels in Bt maize grain. Agron Sustain Dev 30(4):711–719
13. Green RE, Cornell SJ, Scharlemann JP, Balmford A (2005) Farming and the fate of wild nature. Science 307:550–555
14. Huang J, Rozelle S, Pray C, Wang Q (2002) Plant biotechnology in China. Science 295:674–676
15. Choudhary B, Gaur K (2010) BT cotton in India: a country profile. ISAAA, Ithaca
16. Choudhary B, Gaur K (2008) The development and regulation of BT brinjal in India (Eggplant/Aubergine). ISAAA Brief No. 38, Ithaca
17. Bricknel T (2010) India delays BT brinjal decision. Fruitnet.com
18. Monsanto (2010) Insect protected roundup ready 2 yield soybeans achieve important milestone toward commercialization in Brazil
19. Stern N (2006) Review on the economics of climate change. HM Treasury, London
20. Svoboda E (2008) The future of farming is in nitrogen efficiency fast company. Posted 1 Oct 2008. http://www.fastcompany.com/magazine/129/seed-money.html
21. Sottosanto JB, Saranga Y, Blumwald E (2007) Impact of AtNHX1, a vacuolar Na+/H+ antiporter, upon gene expression during short- and long-term salt stress in Arabidopsis thaliana. BMC Plant Biol 7:18
22. Agarwal PK, Agarwal P, Reddy MK, Sopory SK (2006) Role of DREB transcription factors in abiotic and biotic stress tolerance in plants. Plant Cell Rep 25:1263–1274
23. Deng X, Phillips J, Brautigam A, Engstrom P, Johannesson H, Ouwerkerk PB, Ruberti I, Salinas J, Vera P, Iannacone R, Meijer AH, Bartels D (2006) A homeodomain leucine zipper gene from Craterostigma plantagineum regulates abscisic acid responsive gene expression and physiological responses. Plant Mol Biol 61:469–489
24. Rivero RM, Shulaev V, Blumwald E (2009) Cytokinin-dependent photorespiration and the protection of photosynthesis during water deficit. Plant Physiol 150:1530–1540
25. Foundation AAT (2007) Combining breeding and biotechnology to develop water efficient maize for Africa (WEMA)
26. Jung KH, Seo YS, Walia H, Cao P, Fukao T, Canlas PE, Amonpant F, Bailey-Serres J, Ronald PC (2010) The submergence tolerance regulator Sub1A mediates stress-responsive expression of AP2/ERF transcription factors. Plant Physiol 152:1674–1692
27. Lopez-Bucio J, Nieto-Jacobo MF, Ramirez-Rodriguez VV, Herrera-Estrella L (2000) Organic acid metabolism in plants: from adaptive physiology to transgenic varieties for cultivation in extreme soils. Plant Sci 160:1–13
28. Newell-McGloughlin M (2006) "Functional foods" and biopharmaceuticals: the next generation of the gm revolution. American Enterprise Institute, Washington, DC, pp 163–178
29. Newell-McGloughlin M (2008) Nutritionally improved agricultural crops. Plant Physiol 147:939–953
30. Luciani G, Wofford DS (2005) Over-expression of a soybean vegetative storage protein gene in Bahiagrass (Paspalumnotatum var. Flugge). http://www.ufgi.ufl.edu/Symposium/FG2005program_rev.pdf
31. Roesler K et al (1997) Targeting of the Arabidopsis homomeric acetyl-coenzymeA carboxylase to plastids of rapeseeds. Plant Physiol 113:75–81
32. Cromwell GL et al (1967) Nutritional value of opaque-2 corn for swine. J Anim Sci 26:1325–1331
33. Yang SH et al (2002) Expression of a synthetic porcine alpha-lactalbumingene in the kernels of transgenic maize. Transgenic Res 11:11–20
34. O'Quinn PR et al (2000) Nutritional value of a genetically improved highlysine, high-oil corn for young pigs. J Anim Sci 78:2144–2149
35. Young TE et al (2004) Senescence-induced expression of cytokinin reverses pistil abortion during maize flower development. Plant J 38:910–922
36. Chakraborty S et al (2000) Increased nutritive value of transgenic potato by expressing a nonallergenic seed albumin gene from Amaranthushypochondriacus. Proc Natl Acad Sci USA 97:3724–3729
37. Li LLS et al (2001) Increase of sulphur-containing amino acids in transgenicpotato with 10 kuzein gene from maize. Chin Sci Bull 46:482–484
38. Yu J, Ao G (1997) Expression of 10 kDa sulfur-rich prolamin gene of rice inpotato. Acta Bot Sin 39:329–334
39. Atanassov ABA et al (2004) To reach the poor – results from the ISNAR-IFPRINext Harvest study on genetically modified crops, public research, and policyimplications. EPTD discussion paper – Environment and Production Technology Division, International Food Policy Research Institute, Washington, DC
40. Katsube T et al (1999) Accumulation of soybean glycinin and its assembly withthe glutelins in rice. Plant Physiol 120:1063–1074
41. Rapp W (2002) Development of soybeans with improved amino acid composition. In: 93 rd AOCS annual meeting and expo. American Oil Chemists' Society Press, Montreal, pp 79–86
42. Dinkins RDRM et al (2001) Increased sulfur amino acids in soybean plantsoverexpressing the maize 15 kDazein protein. In Vitro Cell Dev Biol Plant 37:742–747
43. Prakash CS, Jaynes J (2000) Increasing the protein content in sweet potato using a synthetic storage protein gene. Abstr Papers Am Chem Soc 219:U36
44. Uauy C et al (2006) Gene regulating senescence improves grain protein, zinc, and iron content in wheat. Science 314:1298–1301

45. Falco SC et al (1995) Transgenic canola and soybean seeds with increased lysine. Biotechnology 13:577–582, New York
46. White CLTL et al (2001) Increased efficiency of wool growth and live weightgain in Merino sheep fed transgenic lupin seed containing sunflower albumin.J. Sci. Food Agric 81:147–154
47. Lai JS (2002) Increasing maize seed methionine by mRNA stability. Plant J 30:395–402
48. Zeh M et al (2001) Antisense inhibition of threonine synthase leads to highmethionine content in transgenic potato plants. Plant Physiol 127:792–802
49. Galili G et al (2002) Genetic, molecular, and genomic approaches to improvethe value of plant foods and feeds. Crit Rev Plant Sci 21:167–204
50. Del Vecchio A (1996) High-laurate canola. How Calgene's program began, where it's headed. INFORM Int News Fats Oils Relat Mater 7:230–243
51. Froman B (2002) Genetic modification of oils for improved health benefits:production of long chain omega-3 fatty acids in plants. Abstr Papers Am Chem Soc 223:U35
52. James MJ et al (2003) Metabolism of stearidonic acid in human subjects:comparison with the metabolism of other n-3 fatty acids. Am J Clin Nutr 77:1140–1145
53. Ursin VM (2003) Modification of plant lipids for human health: development of functional land-based omega-3 fatty acids. J Nutr 133:4271–4274
54. Chapman KDA-BS et al (2001) Transgenic cotton plants with increased seedoleic acid content. J Am Oil Chem Soc 78:941–947
55. Liu Q et al (2002) High-oleic and high-stearic cottonseed oils: nutritionally improved cooking oils developed using gene silencing. J Am Coll Nutr 21(3 suppl):205S–211S
56. Abbadi ADF et al (2004) Biosynthesis of very-long-chain polyunsaturatedfatty acids in transgenic oilseeds: constraints on their accumulation. Plant Cell 16:2734–2748
57. Parveez G (2003) Novel products from transgenic oil palm. AgBiotechNet 5:1–8
58. Jalani BSCS et al (1997) Improvement of palm oil through breeding andbiotechnology. J Am Oil Chem Soc 74:1451–1455
59. Anai T et al (2003) Improvement of rice (Oryza sativa L.) seed oil qualitythrough introduction of a soybean microsomal omega-3 fatty acid desaturasegene. Plant Cell Rep 21:988–992
60. Kinney AJ (1998) Designer oils: the high oleic acid soybean. In: Roller SHS (ed) Genetic modification in the food industry: a strategy for food quality improvement. Blackie Academic and Professional, Oxford
61. Reddy AS, Thomas TL (1996) Expression of a cyanobacterial delta 6-desaturase gene results in gamma-linolenic acid production in transgenicplants. Nat Biotechnol 14:639–642
62. Arcadia Biosciences (2008) Arcadia biosciences and bioriginal food and science corp. Enter strategic alliance to market high GLA safflower oil. *Business Wire*. http://findarticles.com/p/articles/mi_m0EIN/is_2008_Feb_22/ai_n24320185/
63. Smeekens S (1997) Engineering plant metabolism. Trends Plant Sci 2:286–287
64. Sprenger N et al (1997) Fructan synthesis in transgenic tobacco and chicoryplants expressing barley sucrose: fructan 6-fructosyltransferase. FEBS Lett 400:355–358
65. Sevenier R et al (1998) High level fructan accumulation in a transgenic sugarbeet. Nat Biotechnol 16:843–846
66. Caimi PG et al (1996) Fructan accumulation and sucrose metabolism intransgenic maize endosperm expressing a Bacillus amyloliquefaciens SacB gene. Plant Physiol 110:355–363
67. Hellwege EM et al (1997) Transgenic potato tubers accumulate high levels of1-kestose and nystose: functional identification of a sucrose 1-fructosyltransferase of artichoke (Cynarascolymus) blossom discs. Plant J 12:1057–1065
68. Hartwig E et al (1997) Seed protein and its relationship to soluble sugars insoybeans. Crop Sci 37:770–773
69. Hellwege EM et al (2000) Transgenic potato (Solanumtuberosum) tubers synthesize the full spectrum of inulin molecules naturally occurring in globeartichoke (Cynarascolymus) roots. Proc Natl Acad Sci USA 97:8699–8704
70. Chiang CYF et al (2005) Expression of a bi-functional and thermostableamylopullulanase in transgenic rice seeds leads to autohydrolysis and alteredcomposition of starch. Mol Breed 15:125–143
71. Schwall GP et al (2000) Production of very-high-amylose potato starch byinhibition of SBE A and B. Nat Biotechnol 18:551–554
72. Shintani D, DellaPenna D (1998) Elevating the vitamin E content ofplants through metabolic engineering. Science 282:2098–2100
73. Rocheford TR et al (2002) Enhancement of vitamin E levels in corn. J Am Coll Nutr 21(3 suppl):191S–198S
74. Cahoon EB et al (2003) Metabolic redesign of vitamin E biosynthesis in plantsfor tocotrienol production and increased antioxidant content. Nat Biotechnol 21:1082–1087
75. Chen Z et al (2003) Increasing vitamin C content of plants through enhancedascorbate recycling. Proc Natl Acad Sci USA 100:3525–3530
76. Naqvi S et al (2009) Transgenic multivitamin corn through biofortification ofendosperm with three vitamins representing three distinct metabolic pathways. Proc Nat Acad Sci USA 106:7762–7767
77. Shewmaker CK et al (1999) Seed-specific overexpression of phytoenesynthase: increase in carotenoids and other metabolic effects. Plant J 20:401–412
78. Ducreux LJ et al (2005) Metabolic engineering of high carotenoid potatotubers containing enhanced levels of beta-carotene and lutein. J Exp Bot 56:81–89
79. Ye X et al (2000) Engineering the provitamin A (beta-carotene) biosynthetic pathway into (carotenoid-free) rice endosperm. Science 287:303–305
80. Agius F et al (2003) Engineering increased vitamin C levels in plants byoverexpression of a D-galacturonic acid reductase. Nat Biotechnol 21:177–181
81. Diaz de la Garza R et al (2004) Folatebiofortification in tomatoes byengineering the pteridine branch of folate synthesis. Proc Natl Acad Sci USA 101:13720–13725

82. Enfissi EM et al (2005) Metabolic engineering of the mevalonate and nonmevalonateisopentenyldiphosphate-forming pathways for the production of health-promoting isoprenoids in tomato. Plant Biotechnol J 3:17–27
83. Fraser PDRS et al (2001) Elevation of carotenoids in tomato by geneticmanipulation. J Sci Food Agric 81:822–827
84. Rosati C et al (2000) Metabolic engineering of beta-carotene and lycopenecontent in tomato fruit. Plant J 24:413–419
85. Szankowski I et al (2003) Transformation of apple (MalusdomesticaBorkh.)with the stilbene synthase gene from grapevine (Vitisvinifera L.) and a PGIPgene from kiwi (Actinidiadeliciosa). Plant Cell Rep 22:141–149
86. Hipskind JD, Paiva NL (2000) Constitutive accumulation of aresveratrol-glucoside in transgenic alfalfa increases resistance to Phomamedicaginis. Mol Plant Microbe Interact 13:551–562
87. Kobayashi SDC et al (2000) Kiwifruits (Actinidiadeliciosa) transformed with aVitisstilbene synthase gene produce piceid (resveratrol-glucoside). Plant Cell Rep 19:904–910
88. Yu O et al (2000) Production of the isoflavonesgenistein and daidzein in nonlegumedicot and monocot tissues. Plant Physiol 124:781–794
89. Lukaszewicz M et al (2004) Antioxidant capacity manipulation in transgenicpotato tuber by changes in phenolic compounds content. J Agric Food Chem 52:1526–1533
90. Stark-Lorenzen PNB et al (1997) Transfer of a grapevine stilbene synthasegene to rice (Oryza sativa L.). Plant Cell Rep 16:668–673
91. Yu O et al (2003) Metabolic engineering to increase isoflavone biosynthesis insoybean seed. Phytochemistry 63:753–763
92. Giovinazzo G et al (2005) Antioxidant metabolite profiles in tomato fruitconstitutively expressing the grapevine stilbene synthase gene. Plant Biotechnol J 3:57–69
93. Niggeweg R et al (2004) Engineering plants with increased levels of theantioxidant chlorogenic acid. Nat Biotechnol 22:746–754
94. Muir SR et al (2001) Overexpression of petunia chalconeisomerase in tomatoresults in fruit containing increased levels of flavonols. Nat Biotechnol 19:470–474
95. Gonzali S et al (2009) Purple as a tomato: towards high anthocyanin tomatoes. Trends Plant Sci 14:237–241
96. UPI (2002) Wheat inhibits colon cancer. United Press International, Washington, DC
97. Austin-Phillips SBE et al (1999) Production of industrial and animal feed enzymes in transgenic Alfalfa. http://www.molecularfarming.com/nonmedical.html
98. Goto F et al (2000) Iron accumulation and enhanced growth in transgeniclettuce plants expressing the iron-binding protein ferritin. Theor Appl Genet 100:658–664
99. Lucca P et al (2002) Fighting iron deficiency anemia with iron-rich rice. J Am Coll Nutr 21(3 suppl):184S–190S
100. Drakakaki G et al (2005) Endosperm-specific co-expression of recombinant soybean ferritin and Aspergillusphytase in maize results in significant increases in the levels of bioavailable iron. Plant Mol Biol 59:869–880
101. Han G (2009) Origin agritech announces final approval of world's first genetically modified phytase corn. http://www.allbusiness.com/science-technology/biology-biotechnology-genetic/13453842-1.html
102. Denbow DM et al (1998) Soybeans transformed with a fungal phytasegene improve phosphorus availability for broilers. Poult Sci 77:878–881
103. Brinch-Pedersen H et al (2000) Generation of transgenic wheat (Triticumaestivum L.) for constitutive accumulation of an Aspergillusphytase. Mol Breed 6:195–206
104. Zhang ZB, Kornegay ET, Radcliffe JS, Wilson JH, Veit HP (2000) Comparison of phytase from genetically engineered Aspergillus and canola in weanling pig diets. J Anim Sci 78:2868–2878
105. Lucca P, Hurrell R, Potrykus I (2002) Fighting iron deficiency anemia with iron-rich rice. J Am Coll Nutr 21:184S
106. Newell-McGloughlin M (2006) A Retrospective prospective perspective on agricultural biotechnology ten years on. J Commer Biotechnol 12(1):20–27
107. Programme UNE (2009) Towards sustainable production and use of resources: assessing biofuels, United Nations Environment
108. Heinzelman P, Snow CD, Wu I, Nguyen C, Villalobos A, Govindarajan S, Minshull J, Arnold FH (2009) A family of thermostable fungal cellulases created by structure-guided recombination. Proc Natl Acad Sci USA A106:5610–5615
109. Ritch E (2008) Microbes drive new Amyris biodiesel plant. Cleantech Group, San Francisco
110. Hartman E (2008) A promising oil alternative: algae energy. The Washington Post
111. Goldenberg S (2010) Algae to solve the Pentagon's jet fuel problem. The Guardian, London
112. Newell-McGloughlin M (2002) Ten reasons why biotechnology will be important to the developing world. AgBioWorld 2(3 and 4)
113. Gonsalves D (1998) Control of papaya ringspot virus in papaya: a case study. Annu Rev Phytopathol 36:415–437
114. Anderson K, Jackson LA (2005) Some implications of GM food technology policies for Sub-Saharan Africa. J Afr Econ 14(3):385–410
115. Wambugu F (1999) Why Africa needs agricultural biotech. Nature 400:15–16
116. Council IFI (2010) Consumer perceptions of food technology. Cogent Research of Cambridge, Massachusetts for the International Food Information Council, Cambridge
117. Brookes G, Barfoot P (2004) Co-existence of GM and non-GM arable crops: the non-GM and organic context in the EU. PG Economics, Dorchester
118. Kershen D (2006) Legal liability issues in agricultural biotechnology. http://www.nationalaglawcenter.org/assets/articles/kershen_biotech.pdf
119. Křístková M (2008) Principles of co-existence. Department of Agriculture, The Czech Republic. http://www.mzp.cz/www/webdav_biosafety.nsf/biosafety/pdf/coexistence.pdf

120. Council EUJR (2008) Scientific and technical contribution to the development of an overall health strategy in the area of GMOs
121. Potrykus I (2010) Regulation must be revolutionized. Nature 466:561
122. Boettiger S, Alvarez S, Getting better technologies to the poor. A public intellectual property resource
123. Potrykus I (1999) Vitamin-A and iron-enriched rices may hold key to combating blindness and malnutrition: a biotechnology advance. Nat Biotechnol 17:37
124. Report EC (2001) GMO research in perspective
125. Agbios (2008) GM crop database. Agbios. http://www.agbios.com/dbase.php?action=ShowForm
126. Zhao ZYGK et al (2002) Nutritionally improved transgenic sorghum. PlantBiotechnology 2002 and beyond. In: Proceedings of the 10th IAPTC&B congress, Orlando, 23–28 June 2002
127. Glei M et al (2006) Both wheat (Triticumaestivum) bran arabinoxylans and gutflora-mediated fermentation products protect human colon cells fromgenotoxic activities of 4-hydroxynonenal and hydrogen peroxide. J Agric Food Chem 54:2088–2095

Transgenic Crops, Risk Assessment and Regulatory Framework in the European Union

Yann Devos[1], Wendy Craig[2], Joachim Schiemann[3]
[1]GMO Unit, European Food Safety Authority (EFSA), Parma, Italy
[2]Biosafety Unit, International Centre for Genetic Engineering and Biotechnology (ICGEB), Trieste, Italy
[3]Julius Kühn Institute (JKI), Federal Research Centre for Cultivated Plants, Institute for Biosafety of Genetically Modified Plants, Quedlinburg, Germany

Article Outline

Glossary
Definition of the Subject
Introduction
Regulatory Oversight of GM Plants and Their Derived Food and Feed Products
The Cartagena Protocol on Biosafety
Process-Based Versus Product-Based Approach
Regulatory Framework for GMOs in the EU
Risk Assessment Principles
Risk Assessment Concepts and Approaches
Future Directions
Acknowledgments
Bibliography

Glossary

Biodiversity Biodiversity is the quantity and variability among living organisms within species (genetic diversity), between species and between ecosystems. Biodiversity is not itself an ecosystem service, but underpins the supply of services. The value placed on biodiversity for its own sake is captured under the cultural ecosystem service called "ethical values" (according to the Economics of Ecosystems and Biodiversity report [1]).

Deliberate release Any intentional introduction into the environment of a genetically modified organism (GMO) or a combination of GMOs for which no specific containment measures are used to limit their contact with, and to provide a high level of safety for, the general population and the environment (according to Directive 2001/18/EC on the deliberate release into the environment of GMOs [2]).

Ecosystem An ecosystem is a dynamic complex of plant, animal, and microorganism communities and their non-living environment interacting as a functional unit. Examples of ecosystems include rainforests, grasslands, urban parks, and cultivated farmlands. Ecosystems can be relatively undisturbed by humans, such as virgin rainforests, or can be modified by human activity (according to the Economics of Ecosystems and Biodiversity report [1]).

Ecosystem services Ecosystem services are the benefits that people obtain from ecosystems. Examples include food, freshwater, timber, climate regulation, protection from natural hazards, erosion control, pharmaceutical ingredients, and recreation (according to the Economics of Ecosystems and Biodiversity report [1]).

Environmental harm Environmental harm can be defined as a measurable adverse change in a natural resource or measurable impairment of a natural resource service which may occur directly or indirectly (according to Directive 2004/35/EC on environmental liability [3]).

Genetically modified/transgenic organisms Organisms, such as plants, animals, and microorganisms (with the exception of human beings), in which the genetic material (DNA) has been altered in such

a way that does not occur naturally by mating and/or natural recombination (according to Directive 2001/18/EC on the deliberate release into the environment of GMOs [2]).

Living modified organism Any living organism that possesses a novel combination of genetic material obtained through the use of modern biotechnology (according to the Cartagena Protocol on Biosafety [4]).

Modern biotechnology The application of (1) *in vitro* nucleic acid techniques, including recombinant deoxyribonucleic acid (DNA) and direct introduction of nucleic acid into cells or organelles, or (2) fusion of cells beyond the taxonomic family, that overcome natural physiological reproductive or recombination barriers and that are not techniques used in traditional breeding and selection (according to the Cartagena Protocol on Biosafety [4]).

Organism Any biological entity capable of replication or of transferring genetic material (according to Directive 2001/18/EC on the deliberate release into the environment of GMOs [2]).

Placing on the market Making available to third parties, whether in return for payment or free of charge (according to Directive 2001/18/EC on the deliberate release into the environment of GMOs [2]).

Risk assessment Process of evaluation of risk, including the identification of scientific uncertainties, of the likelihood and severity of an adverse effect(s) or event(s) occurring to human and animal health or the environment following exposure under defined conditions to a risk source(s). A risk assessment comprises problem formulation (or hazard identification), hazard characterization, exposure characterization, and risk characterization (according to [5]).

Definition of the Subject

This contribution describes the risk assessment principles and the regulatory framework for transgenic (genetically modified (GM)) crops in the European Union (EU).

While the global cropping area of GM crops reached 148 million hectares in 2010, the total area cultivated with GM crops in the EU was less than 100,000 ha. Most GM crops are thus cultivated outside the EU, but might subsequently be imported and eventually further processed in the EU, mostly for animal feed purposes.

It is globally accepted that agro-food biotechnology could contribute to achieving the objectives (conservation of biological diversity, sustainable use of its components, fair and equitable sharing of the benefits arising out of the utilization of genetic resources) laid down in the Convention on Biological Diversity, if developed and used with adequate safety measures for both the environment and human health. Generally, the safety measures are embedded in process- or product-based regulatory framework. The EU regulatory framework is process-based, precautionary, and includes mandatory labeling and traceability requirements for GM crops and their derived food and feed products. During its development, the EU regulatory system has become increasingly more stringent.

GM crops and their derived food and feed products are generally subject to a risk analysis before they can be commercialized. In the EU, the risk analysis consists of three components: risk assessment, risk management, and risk communication. In risk assessment, potential adverse impacts associated with a specific activity are scientifically characterized on a case-by-case basis, while in risk management, policy alternatives to accept, minimize, or reduce the characterized risks are weighed and, if needed, appropriate prevention and control options are selected. Risk management is functionally and temporally separate from risk assessment in order to reduce any conflict of interest and to protect the scientific integrity of risk assessment. Risk communication is defined as an interactive exchange of information and opinions on risk throughout risk analysis, between risk assessors, risk managers, and other interested parties.

When analyzing potential risks, it is important to bear in mind that the real choice is not between GM crops that are inherently risky and traditionally bred ones that are completely safe. The cultivation of existing crops and those with novel traits (including GM crops) will have both positive and negative consequences. To fully acknowledge the overall outcome of adopting specific crops, and to assess and manage more

effectively the environmental footprint of agriculture as a whole, the conclusion is that broader and more balanced legislative oversight is needed in the EU.

Introduction

The global cropping area of GM crops (including soya bean, maize, cotton, oilseed rape, and sugar beet) has consistently increased each year since they were first commercially cultivated in 1996. While the global cropping area of GM crops reached 148 million hectares in 2010, the total area under GM cultivation in the European Union (EU) was approximately 91,400 ha [6]. Most approved GM crops worldwide are thus currently cultivated outside the EU, but might subsequently be imported and eventually further processed in the EU, mostly for animal feed purposes.

The disparity in adoption rates of GM crops between the EU and the rest of the world is generally attributed both to societal and political opposition toward agro-food biotechnology, and to complex regulatory approval procedures in the EU [7, 8]. In the mid-1990s, the advent of GM crops aroused strong societal concerns [9–12]. Fostered by several highly publicized and successive food safety crises (e.g., bovine spongiform encephalopathy, dioxins, emergence of pathogens such as *Escherichia coli* 0157), public suspicion toward regulatory authorities, scientists and technocratic decision making grew [13]. The media, which was explicitly involved in framing public perception and societal image-building of agro-food biotechnology [14, 15], exacerbated the social amplification of risk [16]. In the late 1990s, increasing societal and political opposition contributed to a *de facto* moratorium on new GM crop market approvals. This was adopted at a meeting of the EU Council of environmental Ministers in June 1999, where five EU Member States indicated that they would oppose any new approvals pending a revision of the legislation [17]. The moratorium did not have a formal status and did not revoke pre-1999 approvals of GM crops or food products, nor did it officially prevent new approvals of GM food products. However, the moratorium was *de facto* effective since a sufficient number of Member States ensured a blocking majority of the legislative process [18]. As a consequence, several GM crop market applications remained blocked in the EU regulatory system for over a decade.

From 1999 onward, policy makers started to continuously revise the legal conditions under which GM crops and derived food and feed products were to be allowed to be used in the EU, in order to slow down further erosion of public and market confidence (reviewed in [10]). These various legal and institutional reforms, although leading to the upheaval of the *de facto* moratorium in 2004 and a regulatory regime that imposes the most stringent criteria for their approval worldwide (cf., WTO dispute between the US and EU), did not dissipate societal concerns. As Gaskell et al. [19] put it "the new regulatory frame appears to have done little to allay the European public's anxieties about agro-food biotechnology," and "the years of controversy have led many people in Europe to believe that anything that has to do with GM food is undesirable". Member States continue to raise safety objections during the approval process for the placing on the market of GM crops. While the new EU regulatory system should guarantee a harmonized and science-based process, none of the GM plant market applications that were positively evaluated by the EU authority responsible for providing advice on the safety of GMOs, the European Food Safety Authority (EFSA), have attained the necessary qualified majority (neither in favor nor against the approval of GMOs) from the relevant regulatory committees or the Council of Ministers, both for exhibiting substantial abstentions in voting [18, 20]. In most cases, the European Commission has adopted favorable decisions that are not endorsed by a qualified majority of Member States, whereas in other cases, decisions are still pending.

In response to the European Commission approvals for the marketing of GM crops, several Member States invoked national safeguard measures to provisionally restrict or prohibit the use and/or sale of approved GMOs in their territory. Even though EFSA concluded that, in terms of risk to human and animal health and the environment, no new scientific evidence had been presented that would invalidate former risk assessments, the Council of Ministers rejected the proposals of the European Commission to repeal invoked safeguard measures. To reduce the recourse of Member States to safeguard measures and to facilitate the decision making process, the European Commission

proposed in July 2010 to confer to Member States the freedom to allow, restrict, or ban the cultivation of GMOs on part or all of their territory [21, 22]. In addition, the European Commission issued a new Recommendation on coexistence of GM crops with conventional and/or organic crops [23] that replaces the previous recommendation from 2003. Whether these proposals will help to unlock the European legal gridlock is debatable. The European Parliament and Council are expected to discuss the proposals, with a view to legal implementation, in the autumn of 2010 [24]. However, several Member States have already notified the European Commission of their intention to prohibit the cultivation of the Amflora® starch potato, which was approved for cultivation in March 2010. It was the first EU approval for cultivation of a GM crop in the past decade. This approval has garnered considerable public controversy [25] and is illustrative of the lasting skeptical and/or ambivalent attitude of the European society toward agro-food biotechnology.

Regulatory Oversight of GM Plants and Their Derived Food and Feed Products

Heightened global awareness and concern over accelerating environmental degradation during the latter quarter of the twentieth century resulted in a desire by the international community to push the protection of the environment higher up the political agenda. These efforts came to fruition in 1992 when the Convention on Biological Diversity (CBD) came into force. Its objectives include "the conservation of biological diversity, the sustainable use of its components and the fair and equitable sharing of the benefits arising out of the utilization of genetic resources" [26]. During the elaboration of the Convention, negotiators recognized that biotechnology could contribute to achieving these objectives, if developed and used with adequate safety measures for both the environment and human health. Accordingly, procedures were developed to address the safe transfer, handling, and use of any LMO (used interchangeable with GMO in this contribution) resulting from biotechnology that may have an adverse effect on the conservation and sustainable use of biological diversity (Article 19.3, CBD). These procedures formed the Cartagena Protocol on Biosafety (CPB; 4), which came into force in 2003 and has 160 signatory countries to date (October 2010). Parties lacking a cohesive biosafety policy undertook, or are currently undertaking, a number of initiatives to put a national framework in place in order to comply with the CPB.

This period of heightened political activity in environmental protection has coincided with a concomitant rise in GM crop cultivation. The number of countries opting to grow GM crops has increased steadily from 6 in 1996, the first year of commercialization, to 18 in 2003 and 25 in 2009 [27]. Among the top 10 GM crop-growing countries by area, the USA, Argentina, Canada, Uruguay, and Australia are currently not Parties to the CPB. At the same time, many developing countries that have ratified the CPB are still in the process of elaborating a regulatory framework governing the import or cultivation of GM crops. This has led to the current situation where different strategies and standards have been adopted at the national level, caused by the different infrastructures available in developed and developing countries, and has resulted in much confusion and difficulty in harmonizing environment and trade agreements and regulations.

The Cartagena Protocol on Biosafety

The CPB has been the primary driving force behind many countries establishing national biosafety regulatory systems for GM crops and animals. Attempts have been made under the CPB, as an international legally binding treaty, to set forth the scientific and legal boundaries for those systems, and establish a minimum set of rules and procedures to "ensure an adequate level of protection to avoid or minimize potential adverse effects on the conservation and sustainable use of biological diversity, taking into account human health". The CPB also sets minimum standards for regulating certain aspects concerning the safe transfer, handling, and use of LMOs [28].

The necessary set of techniques to produce GMOs has been defined not only by the CPB, but also by other relevant international treaties, guidelines, and standards, including the Principles for the Risk Analysis of Foods Derived from Modern Biotechnology [29], and the International Standards for Phytosanitary Measures [30]. The application of modern biotechnology allows the intentional crossing of natural breeding

barriers, the underlying molecular processes of which are qualified as sufficiently "new" so that they and the resulting organisms can be patented as inventions.

In many countries, the terms "genetically modified organism," "genetically engineered organism," and "transgenic organism" are widely used, including in domestic legislation, to describe LMOs covered by the CPB [31]. Different countries therefore have biosafety regulations to guide the development of GM crops. Such regulations are key to ensuring the environmental and human safety of GMOs and give the public confidence in GM products [28].

Although the CPB covers all LMOs, it primarily addresses two particular uses of LMOs: [1] those that will be intentionally introduced into the environment and [2] those used for food, feed, or processing (FFP). For LMOs used for other purposes, such as LMOs used in the laboratory, the Protocol leaves any regulation to the discretion of the individual country. The CPB also does not cover products derived from LMOs, such as processed foods that have ingredients that came from LMOs.

To ensure the safe transfer, handling, and use of LMOs, the CPB sets up two separate procedures. The first time that an LMO is to be intentionally introduced into the environment, the CPB sets up an Advanced Informed Agreement (AIA) procedure (Article 7). This procedure requires that an exporter of an LMO provides a notice with detailed information about the LMO to the importing country (Article 8). The importing country then reviews the information, conducts a risk assessment, and decides, based on the risk assessment results, whether to approve or reject the LMO (Articles 10 and 15). In deciding whether to accept the LMO, the importing country can invoke risk management measures to address issues that arise from the risk assessment (Article 16). The importing country also can err on the side of precaution (discussed below) and not approve an LMO if there is insufficient information to adequately assess its particular potential risks (Article 10 [6]).

The second procedure set up by the CPB is for LMOs for FFP (such as maize, soya bean, wheat, or other grains that will be fed to humans or animals). For these LMOs, the AIA procedure is not required (Article 11). Instead, the CPB establishes a simpler system which reflects the decreased likelihood that these LMOs will affect the biodiversity of the exporting country. Before the LMO can be exported to another country, the safety decision in the exporting country is communicated to other countries through the Biosafety Clearing-House (BCH; http://bch.cbd.int/). A country may require prior consent, however, under its domestic regulatory framework, as long as that requirement has been posted on the Biosafety Clearing-House (Article 11).

The CPB also contains numerous other provisions that complement the review procedures for LMOs discussed above and address issues important to a uniform and comprehensive biosafety regulatory process. There are provisions on reviewing decisions for new information (Article 12), simplified procedures for certain LMOs that do not present risks (Article 13) and emergency procedures for unintentional releases of LMOs (Article 17). The CPB also addresses issues such as public awareness and participation (Article 23), and what to do about confidential information (Article 21). Thus, the Protocol attempts to establish a complete and comprehensive set of procedures and legal obligations to assess and manage the potential risks of LMOs on biological diversity, also taking into account risks to human health.

While proponents of modern biotechnology state that no new risks are associated with GMOs, others feel that the new methods of producing organisms might be associated with new risks. Premarket procedures have therefore been established by many regulatory authorities around the world, and are applied to assess how the organisms may behave and evolve in the environment, and how they may interact with other species. The CPB sets forth the information about an LMO that is needed before it is released into the environment or used for FFP. Annexes I and II contain detailed lists on the major categories of information needed to assess the potential risks of an LMO. They provide models which a national biosafety regulatory system can use as standard data requirements. Of course, individual countries may add to the list of required information, depending on particular environment issues within their country or if they choose to address other risk areas (such as food safety or socioeconomic concerns).

The CPB also attempts to explain what a scientific risk assessment of an LMO should entail. Annex III sets forth the objective of the risk assessment, what the risk assessment will be used for, the general principles that the risk assessment must follow, the methodology of the risk assessment, and particular points to consider when assessing the potential risks of an LMO. The Annex provides a clear explanation to interested parties about what is expected in the risk assessment, what will guide the risk assessment, and how it will be used. Therefore, the Protocol's Annexes attempts to provide sufficient information and details so that countries which adopt those provisions will establish harmonized and standardized procedures that will be transparent and understandable.

Precaution and the CPB

Based on the reaffirmation of the precautionary approach contained in Principle 15 of the Rio Declaration on Environment and Development (1992), Articles 10 (para. 6) and 11 (para. 8) of the CPB both state that

- "Lack of scientific certainty due to insufficient relevant scientific information and knowledge regarding the extent of the potential adverse effects of a living modified organism on the conservation and sustainable use of biological diversity in the Party of import, taking also into account risks to human health, shall not prevent that Party from taking a decision, as appropriate, with regard to the import of the living modified organism . . .. in order to avoid or minimize such potential adverse effects".

However, ever since the CPB came into force, government regulators and their technical experts, political activists, and GM product developers have debated this inclusion of the precautionary approach. Disagreements have raged over whether such an approach is a useful tool for managing the risks of biotechnology and its products. Resolving these disputes is made difficult by the lack of a formal, established definition, making it unclear exactly what it means in practical terms and what it requires of governments and innovators. Therefore, governments may act at their discretion to restrict or ban products or activities even before obtaining proof that a harm is imminent, although no obligation to do so seems to be implied in the CPB. This had led opponents of such actions to argue that conversely, such decisions can also jeopardize human health and the environment at large, for example, during the severe food shortage of 2002 in Southern Africa when food aid shipments containing transgenic maize were rejected on the basis of potential harm. Until clarity is forthcoming, this will remain fertile ground for dispute and open for possible abuse.

Process-Based Versus Product-Based Approach

In Europe, as in all Parties of the CPB, a *process-based* regulatory system governs the regulation of GMOs, as the techniques used for their production were considered new and raised specific safety concerns. A GMO is thus mainly characterized by the technique used to produce it, and is defined as an organism in which the genetic material has been altered in a way that does not occur naturally by crossing and/or natural recombination [2]. Directive 2001/18/EC, on the deliberate release of GMOs into the environment, provides a list of techniques in Annexes IA and IB that: (1) result in genetic modification; (2) are not considered to result in genetic modification; or that (3) result in genetic modification, but yield organisms that are excluded from the scope of the Directive [2, 32]. Production techniques falling under the EU GMO definition are:

- Recombinant nucleic acid techniques involving the formation of new combinations of genetic material by the insertion of nucleic acid molecules produced by whatever means outside an organism, into any virus, bacterial plasmid, or other vector system and their incorporation into a host organism in which they do not naturally occur but in which they are capable of continued propagation
- Techniques involving the direct introduction into an organism of heritable material prepared outside the organism including microinjection, macroinjection, and microencapsulation
- Cell fusion (including protoplast fusion) or hybridization techniques where live cells with new combinations of heritable genetic material are formed through the fusion of two or more cells by means of methods that do not occur naturally

In vitro fertilization, natural transformation processes (e.g., conjugation, transduction, transformation), and polyploidy induction are not considered to result in genetic modification and are, therefore, currently excluded from the GMO definition. Techniques of genetic modification yielding organisms that currently are excluded from the GMO definition are mutagenesis and cell fusion of plant cells of organisms which can exchange genetic material through "traditional" production techniques [2].

In the USA and Canada, a *product-based* regulatory approach is followed for the regulation of GMOs [33–35]. Legislation focuses on the risks of products, and not the techniques of production, as genetic modification *per se* is not considered inherently risky. Because the focus is on novel traits or attributes introduced into a plant, rather than the method of production, both plants and their derived food and feed products are regulated under the existing regulatory system.

Whether legal regimes using production techniques instead of the product itself as a trigger for regulatory oversight provide the best framework for an adequate safety assessment of GMOs is at best debatable. On the one hand, it is questionable whether newly developed crop improvement techniques will outgrow the current EU GMO legislation [36, 37]. On the other hand, it is not intuitively obvious why conventionally bred plants and their derived products are not subject to a similar safety assessment as those obtained through genetic modification [38, 39] or, conversely, why GM plants are regulated more strictly than conventionally bred ones in the EU [40, 41]. With techno-scientific advances and innovations, the knowledge about plant genes and their regulation and functions has increased, while new plant production techniques have emerged to induce or select desired plant characteristics, such as RNA interference and oligonucleotide-mediated mutagenesis (see, e.g., [32, 42–44]). These new techniques may challenge the current regulatory definition of a GMO, because it is not always clear whether the products obtained through these techniques would be captured by, or excluded from, the EU GMO definition [36]. The current EU regulation is therefore heavily reliant upon the need to regularly update the list of techniques and their possible uses; otherwise, it runs the risk of quickly becoming obsolete, as the rate of innovation and advances in the field of biotechnology marches on. In addition, the ability to detect products of such emerging technologies will be severely challenged, and as such, there will need to be a greater emphasis placed on traceability mechanisms for this approach to be practically regulated. In recognition of this, EU Member States and the European Commission are considering recent developments in plant breeding and are discussing if the current EU legalization appropriately covers these new techniques and their application, and whether they should be subject to regulatory requirements. Recently, in an answer to a parliamentary question, the European Commission stated that a specific working group of external experts has been put in place to determine which of the newly developed plant production techniques would result in genetic modification and would thus be captured by, or excluded from, the EU GMO definition (cf., Parliamentary question P-6606/07 2008).

Regulatory Framework for GMOs in the EU

The EU has the most stringent and wide-ranging regulations on GM products and commodities in the world. Their development can be traced back to the aforementioned food safety incidences in the mid-1990s that affected European consumer confidence in government regulatory agencies and agribusiness groups. These concerns have developed to include a negative view of GM products and of the companies that develop and market these products. Furthermore, the ongoing maintenance of trade barriers against agricultural imports in general has resulted in strong political pressure to regulate GM products [45].

The EU regulatory approach is precautionary, process-related, and includes mandatory labeling and traceability requirements for food and feed crops, unprocessed or processed. Only non-food GM products (unseeded), such as textile or other industrial products, are not subject to any requirement.

EU legislation is adopted through a system of interactions between the three main EU institutions: the European Parliament; the Council of the European Union (i.e., representatives of all the EU Member States at the ministerial level); and the European Commission. In most cases, the European

Commission initiates legislative proposals that are decided jointly by the Council and the European Parliament; the most common legislative measures are Regulations (acts that are binding in their entirety and are immediately applicable throughout the EU) and Directives (acts that require the modification or establishment of national measures, generally for harmonization purposes). Legislation pertaining to GMOs in the EU is further elaborated below.

Contained Use and Deliberate Release Directives

In the early 1990s, two European Directives for the use of GMOs were adopted: to ensure the protection of human and animal health and the environment; to guarantee consumers' freedom of choice without misleading consumers/users; and to create an internal market that makes the free movement of GMOs possible within the EU without unequal competition and impediments between and within Member States. Directive 90/219/EEC, which has since been amended by Directive 98/81/EEC, regulated the contained use of GM microorganisms, while Directive 90/220/EEC regulated the deliberate release of GMOs into the environment, covering both the release for research purposes (part B) and for commercial use as or in products (part C). This triad reflects the stepwise process GM crops go through, beginning with experiments under contained use (e.g., laboratory, greenhouse), through experimental release, up to the placing on the market. According to the step-by-step principle, the containment of GMOs can be reduced and the scale of release increased gradually, if assessment of earlier steps indicated that the next step can be taken.

Novel Food Regulation

On 15 May 1997, Regulation (EC) No 258/97 – the so-called *Novel Food Regulation* – removed food products derived from GM plants from the scope of Directive 90/220/EEC on the deliberate release of GMOs into the environment. The new regulation covered risk assessment procedures and the marketing and labeling of all types of novel foods, including those produced by new plant production techniques such as genetic engineering, as well as food without a history of safe use in the EU. Under the Novel Food Regulation, the safety assessment of GM food was based on the principle of *substantial equivalence* between the GM food and its traditionally cultivated non-GM counterpart. The non-GM counterpart was generally taken to have a history of safe use, allowing it to serve as baseline in the comparison of its chemical composition and phenotypic characteristics to those of GM food [46–48].

According to the *labeling provisions* of the Novel Food Regulation, labeling was not required when a GM raw material had been treated technically in such a way that neither the new DNA, nor the protein could be detected in the end product. Since May 1997, processed oil from GM oilseed rape, maize, and cotton, and processed food and food ingredients derived from GM maize have been notified as being substantially equivalent and thus approved for human consumption under the simplified procedure of the Novel Food Regulation. Moreover, labeling did not apply to food already used for human consumption in the EU prior to the establishment of the Novel Food Regulation. Food already marketed, such as GTS40-3-2 soya bean and Bt176 maize, were not considered as novel. With the adoption of Regulations (EC) No 1813/97 and 1139/98, the labeling of GTS40-3-2 soya bean and Bt176 maize foodstuffs also became compulsory. From that moment on, the label literally had to contain the words "produced from GM soya bean" or "produced from GM maize" when the new protein or transgene was detectable in the end product intended for consumption. A final product needed no label when a GM raw material had been technically treated in such a way that neither the new protein nor the transgene could be detected (e.g., hydrolyzed soya bean proteins, refined oils). With Regulation (EC) No 50/2000, the labeling provisions were extended to additives and flavorings that have been genetically modified or that have been produced from a GMO.

Revised Deliberate Release Directive

On 17 October 2002, Directive 2001/18/EC replaced (the older) Directive 90/220/EEC. With it (1) the precautionary principle was explicitly adopted as a guide; (2) risk assessment criteria were broadened to include direct, indirect, immediate, delayed, and cumulative long-term adverse effects; (3) post-market environmental monitoring (PMEM) became compulsory;

(4) the need for a common methodology for the environmental risk assessment was established; (5) the requirement of reexamination of risk assessment and management conclusions in light of new scientific evidence was strengthened by limiting the duration of market consents to a maximum of ten years; (6) specific considerations related to the use of antibiotic resistance marker genes were introduced; (7) existing labeling provisions applying to GM food were extended to all marketed products containing GMOs; (8) the general concept of traceability at all stages of commercialization was introduced; (9) transparency in the decision making process was increased; (10) consultation of the public became mandatory in the approval procedure; (11) the possibility to consult an ethics committee was confirmed; and (12) the implementation of national cultivation registers was required, recording the locations where GM plants have been grown for experimental purposes.

General Food Law and Establishment of the European Food Safety Authority

Adding to Directive 2001/18/EC, Regulation (EC) No 178/2002 – the so-called *General Food Law* – laid down general principles of food law and procedures in food and feed safety. It defines food and feed and other agricultural inputs at the level of primary production, as well as hazard, risk, risk analysis, risk assessment, risk management, and risk communication. Furthermore, the General Food Law sets food and feed safety requirements in order to determine whether any food or feed may be injurious to human and animal health. With this Regulation, the application of the precautionary principle was further extended to risk analysis of all food and feed in the EU, whether of GM-origin or not.

In response to a multiple wave of food crises that caused considerable public concern in Europe about food safety and the ability of regulatory authorities to fully protect consumers, the *European Food Safety Authority* (EFSA) was created as a European-wide risk assessment body. EFSA is tasked: (1) to provide science-based advice at the request of the European Commission on any matter within its mission, or in the framework of Community legislation; (2) to issue scientific advice on its own initiative; and (3) to issue advice upon request of the European Parliament or a Member State on matters falling within its mission (Article 29 of the General Food Law). By providing "independent, objective, and transparent" science-based advice, EFSA aims to ensure a high level of consumer protection and to restore and maintain confidence in the EU food supply.

EFSA has ten Scientific Panels addressing food safety issues in the different sectors of food and feed production, and a Scientific Committee. The EFSA Scientific Panel on Genetically Modified Organisms (EFSA GMO Panel) consists of 21 scientific experts from European research institutes, universities, or risk assessment bodies. The EFSA GMO Panel issues: (1) *scientific opinions* on the safety of GMO market approval dossiers and on national safeguard clauses invoked by Member States; and (2) produces *guidelines* for the risk assessment of GMOs upon request of the European Commission in the framework of Directive 2001/18/EC and Regulation (EC) No 1829/2003. These guidelines provide assistance to those preparing and presenting GMO market applications, by describing principles, concepts, data requirements, and issues to be considered in the frame of risk assessment. So far, the following guidances have been issued:

- Guidance document for the risk assessment of GM plants and derived food and feed (issued in 2004; published in 2006; revised in 2008 and 2011)
- Guidance document for the risk assessment of GM microorganisms and their derived products intended for food and feed use (issued in 2006; revised in 2011)
- Guidance document for the renewal of authorizations of existing GMO products (issued in 2006)
- Guidance document for the risk assessment of GM plants containing stacked transformation events (issued in 2007; replaced by the latest revision of the Guidance document for the risk assessment of GM plants and derived food and feed, see above)
- Guidance for the risk assessment of GM plants used for non-food or non-feed purposes (issued in 2009)
- Guidance on the environmental risk assessment of GM plants (issued in 2010)
- Guidance on selection of comparators for the risk assessment of GM plants (issued in 2011)
- Guidance on the PMEM of GM plants (issued in 2011)

Scientific opinions and reports are also issued on specific risk assessment issues regarding food, feed, and environmental safety related to GMOs, such as: the safety of antibiotic resistance marker genes; the use of animal feeding trials for testing of whole GM food and feed; the statistical analysis of results of field trials; the evaluation of GM plants cultivated for non-food/feed purposes; PMEM; statistical considerations for the safety evaluation of GMOs; and the assessment of allergenicity of GM foods. A scientific opinion on the environmental risk assessment of non-target organisms exposed to GM plants was recently adopted, as well as a scientific opinion on the annual PMEM report on the cultivation of maize MON810 in 2009. The EFSA GMO Panel is continuously considering new scientific information and recent developments in the field of GMO risk assessment, and as such, it has undertaken several initiatives to incorporate them into its operational procedures (see [49, 50] for further details).

GM Food and Feed Regulation

Issued on 18 April 2004, Regulation (EC) No 1829/2003 on GM food and feed covers the commercialization and risk assessment of GM food and feed, such as food/feed containing or consisting of, food/feed produced from, and food/feed containing ingredients produced from GMOs, as well as seed or other plant-propagating material. Prior to this date, approvals for human food use were required under the Novel Food Regulation, whereas feed use was assessed under Directive 2001/18/EC and its predecessor. The amended approval procedure is centralized around EFSA and based on a "*one door – one key*" approach whereby all commercial uses can be covered in the same GM plant market approval dossier. Moreover, it also introduces the need for a GM crop market application to cover both food and feed uses, as it avoids market approval for a single use in case a product is likely to be used for both purposes (e.g., [51]). In response to the heated debates that challenged the "principle of substantial equivalence," the principle was demoted to a "comparative analysis" in the GM Food and Feed Regulation. The safety assessment of GM food and feed remains based on a comparative analysis in which the non-GM counterpart serves as baseline. However, it requires more evidence of safety than before. Since the principle of "substantial equivalence" was intensely criticized by various actors, it was no longer interpreted as the endpoint of risk assessment, but rather as the starting point. Whether GM food is subject to further safety assessment depends on the identified similarities and differences between the GM food and its non-GM counterpart: (1) if substantial equivalence is established, the need for further testing is to be investigated on a case-by-case basis; (2) if substantial equivalence is established, except for a single or few specific traits of GM crops, further tests must be done focusing on these traits in order to assess their potential impact on human and animal health; and (3) if neither partial nor total substantial equivalence is established, the wholesomeness of the food product is to be assessed. In the same line of arguments, the simplified authorization procedure was abandoned under the GM Food and Feed Regulation.

Approval Procedures for placing GM crops on the Market

Procedures for approval of GM crops in the EU follow comitology rules that involve different actors such as the European Commission, EFSA, the Regulatory Committee of Member States representatives under Directive 2001/18/EC, the Standing Committee on the Food Chain and Animal Health (SCFCAH) under Regulation (EC) 1829/2003, and the Councils of Ministers. In principle, the delegation of powers to the European Commission along with the supervision of the European Commission's use of these powers through committees composed of Member States representatives is considered a convenient mechanism. It enables efficient decision making, engenders a close and cooperative working relationship between the European Commission and Member States, and maintains a degree of control over the process by Member States [20]. The voting system is based on the number of votes designated to each of the 27 Member States and is proportional to their percentage of the EU population. A qualified majority should be at least 74% of the total votes (255) *and* 14 Member States *and* 62% of the EU population; a blocking minority is at least 26% of the votes [91] *or* 14 Member States *or* >38% of the EU population [18].

Approved GM products can move freely throughout all EU Member States in conformity with any

conditions set out in the approval, and enter into the public register of GM food and feed (Community Register: http://ec.europa.eu/food/dyna/gm_register/index_en.cfm). Authorizations are valid throughout the EU, have a maximum duration of ten years, and can be renewed.

Approval Procedure Under Directive 2001/18/EC Under Directive 2001/18/EC, the approval procedure for placing a GMO on the market involves all Member States, the European Commission, and possibly EFSA (see Fig. 1). The GM crop market application is first submitted to the National Competent Authority of a Member State. Upon receipt of the application, the National Competent Authority issues a risk assessment report that may be favorable or unfavorable regarding market approval of the GMO under consideration. In the event of a favorable opinion, the Member State informs the other Member States via the European Commission. The other Member States and the European Commission examine the risk assessment report and may pose observations and objections.

If there are no objections by other Member States or by the European Commission, the National Competent Authority that carried out the original risk assessment approves the placing on the market of the product, and issues a final approval permitting the marketing of the GMO within the Community.

If objections are raised, the procedure provides for a conciliation phase among the Member States, the European Commission, and the applicant in order to resolve the outstanding questions. In case objections are maintained at the end of the conciliation phase, a Decision is taken at EU level. The European Commission first asks the scientific opinion of the EFSA GMO Panel on the safety of the GMO in question. In the case of EFSA issuing a positive opinion, the European Commission presents a Draft Decision to the Regulatory Committee under Directive 2001/18/EC for an opinion. If the Regulatory Committee gives a favorable opinion by qualified majority, the European Commission adopts the Decision. If not, the Draft Decision is submitted to the Council of Ministers for adoption or rejection by qualified majority. If the Council does not act within three months, the European Commission adopts the draft Decision.

Approval Procedure Under the GM Food and Feed Regulation Under the GM food and feed Regulation, a GM crop market application is submitted to the National Competent Authority of a Member State, which forwards it to EFSA. If the application covers the use of seeds or other plant-propagating material for cultivation, EFSA asks a National Competent Authority under Directive 2001/18/EC to perform the environmental risk assessment that will be considered by EFSA during its final assessment (see e.g., [52]).

From the receipt of a valid GM crop market application, EFSA endeavors to deliver its scientific opinion within a time limit of six months. This time limit can be extended if EFSA or the Commission's Community Reference Laboratory seeks supplementary information from the applicant. Within three months after receiving EFSA's scientific opinion, the European Commission submits a Draft Decision to the SCFCAH. If SCFCAH gives a favorable opinion by qualified majority, the European Commission adopts the Decision. If not, the Draft Decision is submitted to the Council of Ministers for adoption or rejection by qualified majority. If the Council does not act within three months or does not obtain a qualifying majority for adoption or rejection of the Commission Draft Decision, the European Commission adopts the Decision (see Fig. 1).

Labeling and Traceability Regulation

Regulation (EC) No 1830/2003 on the labeling and traceability of GM food and feed complements, clarifies, and makes operational some of the labeling and traceability objectives of previous legislation. This Regulation extended labeling provisions to feed, seed, bulk products, food that are delivered as such to the final consumers or mass caterers, and to products in which GMO-derived DNA or protein (e.g., refined oils) is no longer detectable. These requirements go further than previously, because the use of genetic modification in itself is now sufficient to justify labeling. The label must be shown in a clearly visible, legible, and indelible manner, and must contain the reference "genetically modified," "produced from genetically modified" or "contains genetically modified." When a GM food or feed is different from its conventional counterpart, the label must also provide information about any characteristic or property that renders it different. When there

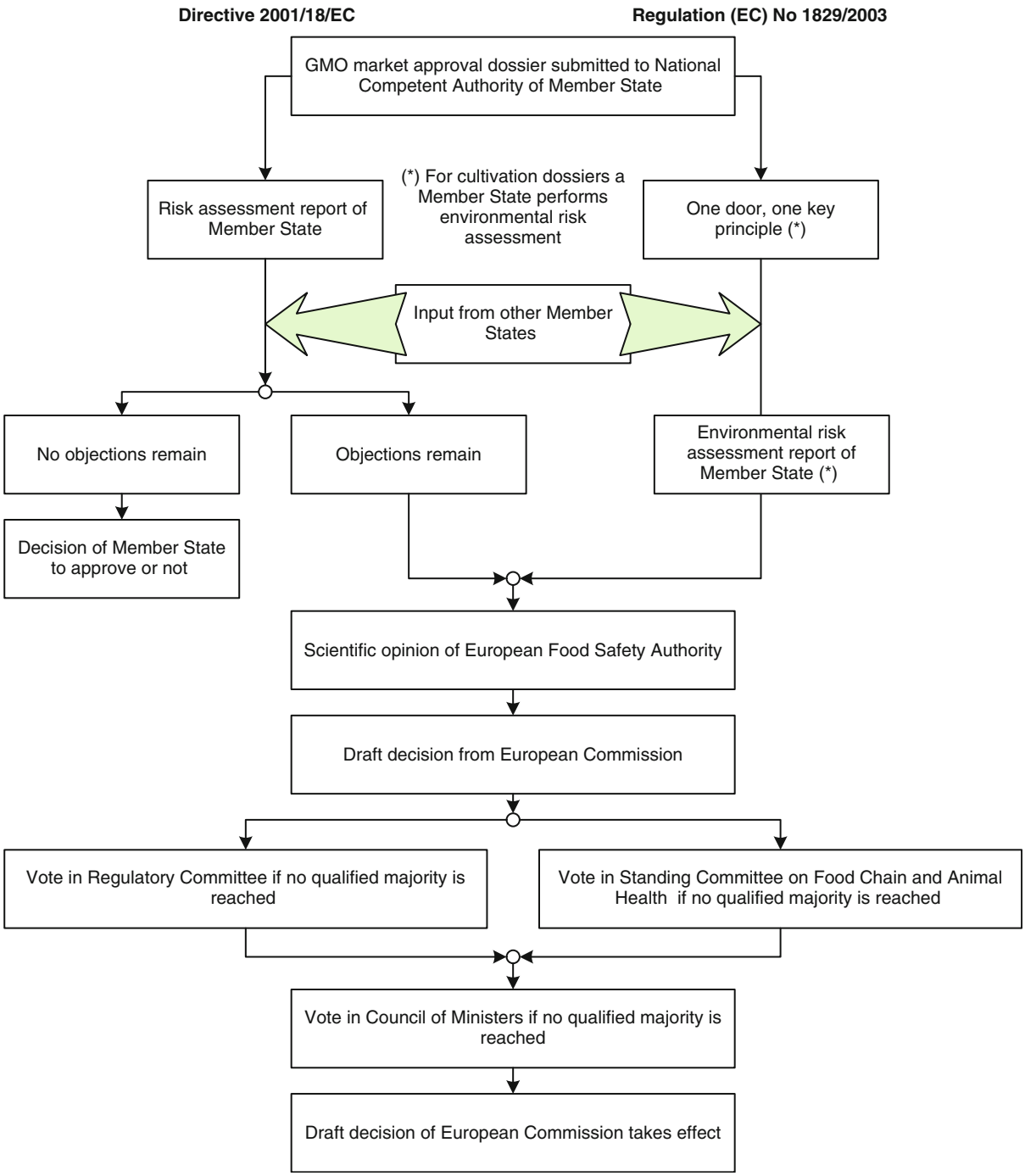

Transgenic Crops, Risk Assessment and Regulatory Framework in the European Union. Figure 1
Approval procedure for placing GM crops on the EU market under Directive 2001/18/EC and Regulation (EC) No 1829/2003 (Figure adapted from EFSA (Parma, Italy) and GHK Consulting Ltd (London, UK))

is no conventional counterpart, the label must contain appropriate information about the nature and characteristics of the GM food or feed. Any characteristic or property that gives rise to ethical or even religious concerns also has to be mentioned. Products being produced with the help of GMOs – rather than actually made out of them – do not require labeling. As such, meat, eggs, milk, and dairy products from animals fed GM crops fall outside the remit of labeling provisions. Since substances assisting in food production, carrier substances, or culture media for microorganisms are not considered foods, their labeling is not considered necessary.

Labeling Thresholds

Tolerance thresholds for the unintentional or technically unavoidable presence of approved GM material in non-GM products were established in the EU. A tolerance threshold refers to the maximum admixture level for GMO content under which the comingled product does not have to be labeled as containing a GMO. It is often argued that there is no scientific justification for the established thresholds. Since GM crops and derived food and feed products are declared safe before marketing, thresholds do not relate to safety or health issues. However, thresholds reflect a balance between differently framed societal concerns and requests and technical capabilities. The translation of labeling thresholds in practice still entails enormous technical and scientific challenges.

Regulation (EC) No 49/2000 set the labeling threshold for the adventitious GMO presence in non-GM food at 1% of the food ingredient. The GM Food and Feed Regulation decreased the tolerance threshold to 0.9%, and extended it to feed and products intended for direct processing. There is zero tolerance in the EU concerning unapproved GM plant events, unless they had previously received a favorable scientific risk assessment for marketing from EFSA and a detection method is publicly available. In the latter case, a threshold of 0.5% may be applied transitionally. A threshold has yet to be defined for seeds as discussions have remained at an impasse. Possible thresholds that will be proposed for seeds will be established at levels such that the GMO content of 0.9% can be guaranteed in food, feed, or crops. Proposals made by the Scientific Committee on Plants in 2001 ranged between 0.3% for cross-pollinating crops, and 0.5% for self-pollinating and vegetatively propagated crops [53]. As no such thresholds have been established to date, any seed lot containing authorized GM seed for cultivation in the EU has to be labeled as containing GM material.

Organic growers principally aim at keeping their products free from any GM material. Regulation (EC) No 1804/1999 on organic production of agricultural products states that the use of GMOs is not compatible with the organic production method. The Regulation, however, foresees a *de minimis* tolerance threshold for the unavoidable presence of GM material in organic products. It was thus anticipated that organic producers would opt for a tolerance threshold ranging between the limit of quantification of a DNA analysis (0.1%) and the tolerance threshold for food and feed products (0.9%). In a press release published on 21 December 2005 (IP/05/1679), the European Commission emphasized that an organic product with an adventitious content of GM material below 0.9% could still be labeled as organic. On 12 June 2007, this point of view was confirmed at a meeting of the EU agriculture ministers, where political agreement was reached on a new Regulation on organic production and labeling (IP/07/807). However, in its recent recommendation on guidelines for the development of national coexistence measures to avoid the unintended presence of GMOs in conventional and organic crops [23], the European Commission allows Member States to aim at levels of unintended GMO presence that are *lower* than the 0.9% labeling threshold in certain cases. It stated that

- "The potential loss of income for organic and some conventional producers (e.g., certain food producers) may be due to the presence of GMO traces at levels lower than 0.9%. In those cases, and in the interest of protecting particular types of production, concerned Member States may define measures that aim at reaching levels of presence of GMOs in other crops lower than 0.9%".

In this respect, the European Commission referred to Member States that have developed national standards for different types of "GM-free labeling" [23]. Since the organic sector advocates that GM crops are not

compatible with organic farming [54, 55], they will seek to establish the limit of DNA quantification analysis as the basis to determine the tolerance threshold in organic products.

Coexistence

In order to provide a high degree of consumers' choice in the EU, a coexistence policy was adopted to maintain different agricultural production systems. It specifically aimed to enable the side-by-side development of different cropping systems without excluding any agricultural option. In this way, farmers would maintain their ability to make a practical choice between conventional, organic, and GM crops. Since coexistence only applies to approved GM crops that were judged to be safe before their market entry [56], safety issues fall outside the remit of coexistence [57–59].

The European Commission recognized that completely avoiding the unintentional presence of GM material in non-GM products is difficult in the agricultural context [23, 60]. As agriculture is an open system, a certain amount of adventitious mixing is unavoidable. Various sources have been identified that could contribute to on-farm adventitious mixing between GM and non-GM crops (Fig. 2): (1) the use of impure seed [61, 62]; (2) cross-fertilization due to pollen flow between neighboring fields [63–65]; (3) the occurrence of volunteer plants originating from seeds and/or vegetative plant parts from previous GM crops [66–69]; (4) mixing of plant material in machinery during sowing, harvest, and/or postharvest operations [51]; and – to a lesser extent – (5) cross-fertilization from certain sexually compatible wild relatives and feral plants [70–72]. As completely avoiding admixing is difficult in the agricultural context, tolerance thresholds were established for the unintentional or technically unavoidable presence of approved GM material in non-GM products. If the content of GM material in a non-GM product exceeds the established tolerance threshold of 0.9%, the product has to be labeled as containing GM material, which may affect its market acceptability.

According to Article 43 of the GM Food and Feed Regulation, Member States are empowered to take appropriate measures to avoid the unintentional presence of GM material in other products. There are principally two strategies Member States have established, or are developing, to warrant coexistence of different cropping systems: *ex ante* regulations; and *ex post* liability schemes [23, 73–75]. Regulations are considered *ex ante* if they have to be followed by GM

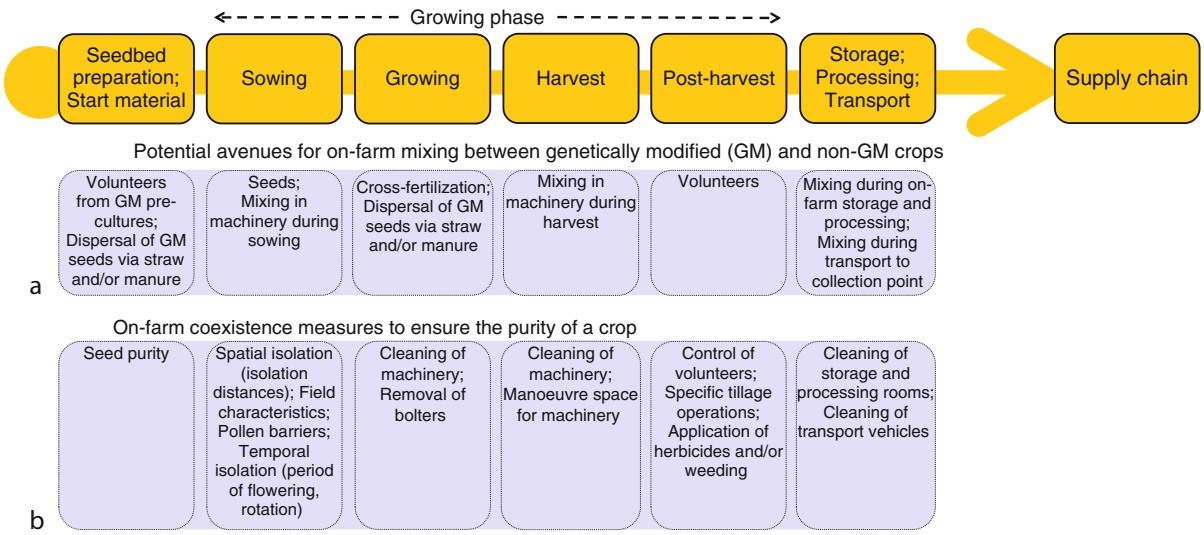

Transgenic Crops, Risk Assessment and Regulatory Framework in the European Union. Figure 2
(**a**) Potential avenues for on-farm adventitious mixing between GM and non-GM crops and (**b**) on-farm coexistence measures to ensure the purity of a crop during the production process (Figure reprinted from [59])

crop adopters while growing GM crops. *Ex ante* regulations prescribe preventive on-farm measures that should ensure that tolerance thresholds are not exceeded in neighboring non-GM agricultural production systems. Contrary to *ex ante* coexistence regulations, *ex post* liability schemes are backward looking: they cover questions of liability and the requirement to redress the incurred economic harm once adventitious mixing in a non-GM product has occurred after the cultivation of GM crops [59].

For decades, seed production regulations have specified statutory segregation measures (so-called identity preservation measures) between seed crops and conventional crop production of the same species to maximize varietal seed purity. Apart from seed production, experience with identity preservation systems is also available from the cultivation of different crop types grown for different uses [76]. Several of the proposed measures to ensure varietal seed and crop purity can be applied within the context of coexistence to limit the adventitious content of GM material in seeds and plant products. These measures include: (1) the use of certified seed; (2) spatially isolating fields of the same crop; (3) implementing pollen barriers around fields; (4) scheduling different sowing and flowering periods; (5) limiting carryover of GM volunteers into the following crop through the extension of cropping intervals; (6) cleaning agricultural machinery and transport vehicles of seed remnants; (7) controlling volunteers and wild relatives; (8) applying effective postharvest tillage operations; (9) retaining records of field history; and (10) the voluntary clustering of fields (Fig. 2). If Member States can demonstrate that the aforementioned preventive coexistence measures are not sufficient to achieve the desirable levels of purity, the European Commission gives those Member States the possibility "to exclude GMO cultivation from large areas of their territory" [23].

The European Coexistence Bureau (ECoB) recently issued a report on best practices to ensure the coexistence between maize cropping systems. Based on a comprehensive assessment of data generated in field experiments, commercial cultivation of GM maize, as well as modeling exercises under European environmental conditions, the report describes best management practices that can be put in place for each potential source of admixture [77]. It is important to realize that the level of containment needed to ensure coexistence will mainly be driven by the established tolerance thresholds: the lower the tolerance threshold, the stricter the on-farm measures needed to meet labeling requirements. Apart from defining the level of containment needed, tolerance thresholds also determine the level of GM material that initiates the need to redress economic harm due to adventitious mixing. The adventitious presence of GM material above the tolerance threshold set out in EU legislation triggers the need for the product that was intended to be a non-GM product, to be labeled as containing GMOs. In other words, the product has to be labeled as containing GMOs only in cases when the established threshold is exceeded. According to the European Commission,

- "The presence of GM material in food and feed has an economic effect only when it exceeds the 0.9% labelling thresholds", but as mentioned previously, "Member States can aim at levels of unintended GMO presence that are lowerthan the 0.9% labelling threshold in cases where the potential loss of income of organic and some conventional producers may be due to the presence of GMO traces at levels lower than 0.9%" [23].

In its Communication to the Council and the European Parliament from 2003, the European Commission has clearly emphasized that coexistence measures should not go beyond what is necessary to ensure that the unintentional presence of GM material in non-GM products remains below established labeling thresholds, and thus should be proportionate to the objective that is pursued. This point was reiterated in its 2010 coexistence recommendation [23], in which the European Commission stated that

- "Coexistence measures should avoid any necessary burden for farmers, seed producers, cooperatives and other operators associated with any production type". Moreover, it argued that "the choice of measures should take into account the regional and local constraints and characteristics, such as the shape and size of fields in a region, the fragmentation and geographical dispersion of fields belonging to individual farms and regional farm management practices".

While some Member States have taken this advice into account for most conventional producers, others

decided to propose or adopt measures that aim at keeping the amount of GM material present in conventional products as low as possible. In some cases, proposed measures, such as large and fixed isolation distances between fields of GM and conventional crops, appear to entail greater efforts for GM growers than necessary, which raises questions about the proportionality of these measures. Several authors have argued that wide and fixed isolation distances, as currently proposed by several Member States, fail to satisfy several challenges [58, 59, 78–85]. First, they are excessive from a scientific point of view; second, they are difficult to implement in practice; third, they are inconsistent with regional heterogeneity of farming; and fourth, they are not proportional to the economic incentives for coexistence. To enable regionally and economically proportionate coexistence, policy makers should allow integrating flexibility in *ex ante* coexistence regulations. This might be achieved by allowing plural coexistence measures that are adaptable to local farming and cropping conditions, and that are negotiable amongst farmers. Computer-based decision support tools may thereby play a crucial role in the future case-by-case-based coexistence approach, as they allow the prediction of achievable levels of coexistence between neighboring maize fields under various conditions. One caveat here is that policy makers may be reluctant to adopt such a case-by-case coexistence approach because of the difficulties of implementation.

Risk Assessment Principles

Interplay of Risk Assessment, Risk Management, and Risk Communication

GMOs and their derived food and feed products are generally subject to a risk analysis before they can be commercialized [49, 86]. In the EU, the risk analysis consists of three components: risk assessment, risk management, and risk communication (Fig. 3). In risk assessment, potential adverse impacts associated with

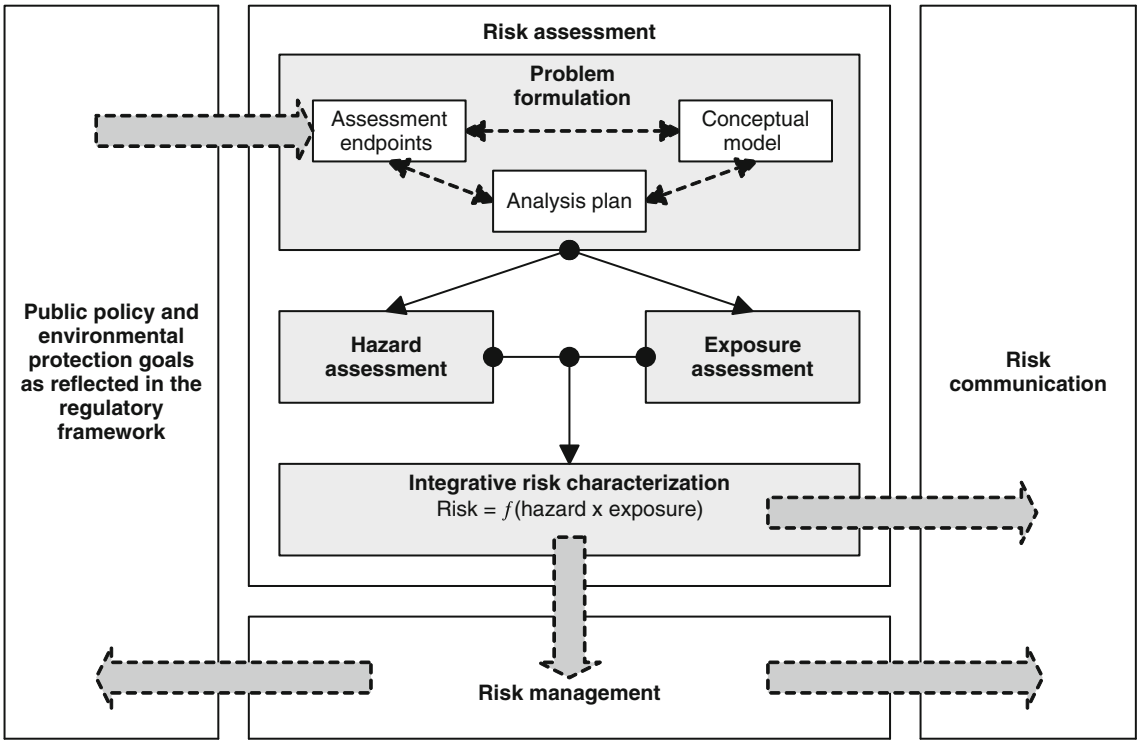

Transgenic Crops, Risk Assessment and Regulatory Framework in the European Union. Figure 3
Risk analysis: The diagram depicts the main components of risk analysis, together with the successive steps comprising the environmental risk assessment of GM plants (Figure reprinted from [50])

a specific activity are scientifically characterized on a case-by-case basis, while in risk management, policy alternatives to accept, minimize, or reduce the characterized risks are weighed and, if needed, appropriate prevention and control options are selected. Because risk managers and regulators rely on risk assessments to make an informed decision on whether or not to approve a certain use of a GM plant, it should explain clearly what assumptions have been made during the risk assessment, and what is the nature and magnitude of uncertainties associated with the characterized risks. The decision whether a certain risk is acceptable and/or tolerable under a particular set of conditions is not part of the risk assessment itself, but part of the wider risk analysis, as this choice is not only based on scientific criteria, but also involves political, social, cultural, and economic considerations. Risk management is also functionally and temporally separate from risk assessment in order to reduce any conflict of interest and to protect the scientific integrity of risk assessment [5]. Risk communication is defined as an interactive exchange of information and opinions on risk throughout risk analysis, between risk assessors, risk managers, and other interested parties. It includes the explanation of risk assessment findings and of the basis upon which risk management decisions are made [87].

Even though there are considerable differences in regulatory requirements for GM crops between countries, environmental priorities (including the preservation of biodiversity) as well as risk terminology, most risk assessments of GM crops follow a science-based assessment process that estimates the level of risk through comparison with a non-GM counterpart [49, 88]. In addition, regulatory requirements involve the consideration of a range of issues relevant to the overall risk assessment in order to determine the impact of the GM crop on human/animal health and the environment relative to the non-GM crop, and thus its relative safety [89, 90]. Some of these elements are discussed in the next sections.

Risk Assessment Methodology and Terminology

Despite the considerable variation among risk assessment frameworks for GM plants, risk assessment generally comprises several sequential steps: (1) problem formulation as a critical first step (including hazard identification); (2) hazard characterization, that examines potential hazards and their magnitude; (3) exposure characterization, that covers levels and likelihood of exposure; and (4) integrative risk characterization, in which the magnitude of consequences and the likelihood of occurrence are integrated (Fig. 3). In the EU, the guidance notes supplementing Annex II of Directive 2001/18/EC on the principles for the environmental risk assessment requires the definition of mitigation measures as a fifth step in the environmental risk assessment in order to manage identified risks. These mitigation measures aim to reduce the identified risks associated with GMO deployment to an acceptable level and should consider defined areas of uncertainty. Accordingly, any proposed mitigation measure is considered for the evaluation of the overall risk of GMO deployment.

Various single risk assessment studies have postulated dire risks when all they have done is characterized either a hazard associated with the use of GM crops, or an exposure to the GM crop without demonstrating whether this exposure is hazardous [5]. These studies confuse hazard or exposure with risk. In this way, they only allow speculative conclusions and contribute to uncertainties in the environmental risk assessment process. Moreover, it is important to distinguish risk from hazard, as the terms have different meanings. The term hazard is associated with the potential of an agent or situation to cause adverse effects or harm. It refers to an inherent property of that agent or situation. Risk is recognized as a function of the probability and severity (magnitude) of an adverse effect occurring to human and animal health or the environment, following exposure to a hazard under defined conditions. Without hazard, there can be no harm and thus no risk.

Problem Formulation (Including Scoping and Planning)

In order to identify the areas of greatest concern or uncertainty related to risks, each risk assessment begins with the identification and formulation of the problem, usually in the context of regulatory decision making [91]. In this respect, the most important questions to be solved and meriting detailed risk characterization are identified [92].

Problem formulation involves: (1) the identification of characteristics of the GM crop capable of

causing potential adverse effects to the environment (hazards) together with (2) the identification of pathways of exposure through which the GM crop may adversely affect the environment. This process comprises a qualitative description of the nature of potential adverse effects and its potential triggers, as well as of plausible exposure pathways to the GM crop that might result in environmental harm. Problem formulation also involves: (3) the definition of assessment endpoints, which are explicit and unambiguous targets for protection extracted from legislation and public policy goals; and (4) outlining specific hypotheses to guide the generation and evaluation of data in the subsequent successive risk assessment steps. It involves the development of a methodology – through a conceptual model and analysis plan – that will help to direct the risk characterization and to produce information that will be relevant for regulatory decision making [92–96]. In this way, problem formulation helps to make the risk assessment process comprehensive and transparent by summarizing existing scientific knowledge and explicitly stating the assumptions and principles underlying the risk assessment. Information considered in problem formulation, comprising existing knowledge of the GM crop and its interactions with the receiving environment, takes many forms. It includes published scientific literature, expert opinions, and research data. Data generated to characterize the GM crop during product development by applicants, and subsequently submitted to regulatory authorities as part of GM crop market application also provide an important source of information considered in the frame of problem formulation. Data to support problem formulation can derive from molecular, compositional, and agronomic/phenotypic analyses performed during GM crop development. Information of this type is frequently available in advance of the environmental risk assessment in order to characterize the GM crop [97–101]. If the level and quality of the available information is high, then the risk assessment can reduce the number of risk hypotheses that need to be tested for risk characterization [94, 95].

Hazard Identification: Characterization of the GM Crop Problem formulation starts with the precise characterization of the GM crop in order to identify potential hazards. This is usually achieved through a comparative safety assessment. A comparison of the characteristics of the GM plant with those of its non-GM counterpart enables the identification of similarities and differences between the two. It enables the characterization of intended differences that were the target of the genetic modification, as well as the identification of unintended differences that may lead to harm [97–101]. The identification of differences in problem formulation is considered of primary importance, because it will direct the subsequent course of actions in the risk assessment [92, 102]. While some differences may be deemed irrelevant to the assessment, others may be meaningful in terms of posing harm to the environment or to human and animal health. Should meaningful differences be identified, the risk that they pose must be evaluated, together with those of the intended modifications, such that an evaluation of their possible biological/ecological relevance can be made (requiring them to be directly linked to those aspects of the environment that are legally protected from harm – see below).

From Protection Goals to Assessment Endpoints A crucial step in problem formulation is to identify aspects of the environment (e.g., valued entity, ecosystem service/function) that need to be protected from harm according to protection goals set out in existing EU legislation, and to translate those into concrete measurable phenomena. Risk assessors need to know *what* to protect, *where* to protect it, and over *what time period*. Usually, aspects of the environment to be protected can be divided into two discrete but interconnected categories: the protection of biodiversity (biodiversity conservation), and the protection of functions/services provided by ecosystems. Ecosystem *services* are distinct from ecosystem *functions* by virtue of the fact that humans, rather than other species, benefit directly from these natural assets and processes. The benefits to humans are many and varied; however, those ecosystem services relevant in an agricultural context include food and feed production, pollination, pest regulation, decomposition of organic matter, soil nutrient cycling, soil structure and formation, water regulation and purification, and cultural services (such as aesthetic value and recreation). The precise relationship between biotic and abiotic processes and the ecosystem functions they drive

is an area of considerable scientific debate. Some species contribute to ecosystem functioning in ways that are unique and hence their addition or loss from a community would cause detectable changes in functioning. Most ecosystems, however, exhibit functional redundancy, where several species are able to perform the same critical function. These species are at least partly substitutable and their loss can be compensated for by other species.

The challenge to problem formulation is that, in EU legislation, protection goals are general concepts that are defined in broad terms, which often are too vague to be scientifically useful in the frame of environmental risk assessments of GM crops. Moreover, a broad array and diversity of protection goals are mentioned in EU legislation. The resultant interpretation is that everything should be protected, everywhere, all of the time. However, to be useful in terms of ecological risks and decision making, it is important that general and broadly defined protection goals are translated into concise and concrete measurable assessment endpoints. If the protection of biodiversity is a public policy goal, then a typical assessment endpoint can be the abundance and species richness of certain groups of organisms at a relevant life stage within a landscape or region over a specific time period [102]. Assessment endpoints represent aspects of the environment to be protected and that can be assessed: they are defined by the valued attribute and/or function (e.g., control of arthropod pest populations) of an ecological entity (e.g., arthropod natural enemies) that could be affected adversely by the GM crop and that requires protection from harm [103]. It is not an abstract goal such as ecosystem health or sustainability, but a real, operationally definable property of an aspect of the environment that reflects management or protection goals laid down in EU legislation. Because arthropod natural enemies fulfill relevant ecological services by contributing to the natural regulation of arthropod pest populations within crop fields, they can be identified as the entity to be preserved; similarly, the biological control functions they perform can be identified as the attribute/function (e.g., [104]). It is important that assessment endpoints are defined as far as possible using measurable criteria relevant to the case under study, such that any change in these endpoints can be readily identified. Moreover, assessment endpoints should ideally be selected based on: relevancy to the protection goal; ecological relevance; susceptibility to the potential stressor; and practicality [105].

Once assessment endpoints have been set, the level of environmental protection to be maintained, or the environmental quality to be preserved, needs to be defined. This process includes establishing the *harmful effect* and both the *spatial* and the *temporal scales* relevant for the ecological entity and its attribute/function to be preserved (Table 1). The harmful effect describes to what extent the environmental quality should be preserved (or above what threshold a difference between the GM crop and its appropriate comparator may lead to harm and would be considered a disturbance in environmental quality). For the conservation of biodiversity, a relevant decrease in abundance of protected or valued species can be seen as a harmful change. Similarly, for ecosystem services, a relevant disturbance in ecological function can be seen as a harmful change [106]. The spatial and temporal scales are the habitats in which, and the period during which, environmental quality should be preserved, respectively [104, 107].

Conceptual Model: Exposure Profiles and Hypotheses The conceptual model describes the consequential exposure scenario of how harm to the assessment endpoint may arise from GM crop deployment and allows for a characterization of risks. Key relationships are described: between the GM crop and the valued entity to be protected from harm; pathways of exposure through which the GM crop may affect the valued entity either directly or indirectly (= exposure profile); and any potential impact of the GM crop to the environment [92, 96]. The conceptual model includes available information on: the nature of the stressor; its intended uses; reasonable exposure profiles; and potential responses of the assessment endpoint as a result of exposure. It can take an array of forms, from the simplest of statements to complex flowcharts and diagrams.

Environmental pathways and levels of exposure will vary depending upon the intended uses of a GM crop, such as import, processing, food, feed, and/or cultivation. In the case where the use of GM plants does not include cultivation in the EU, problem formulation will consider exposure: (1) via accidental release of propagules, such as seeds of the imported commodity spilled into the

Transgenic Crops, Risk Assessment and Regulatory Framework in the European Union. Table 1 Criteria to operationalise protection goals[a]

Criterion	Measurable variable
Ecological entity	Species of conservation concern; ecosystem service
Attribute	Abundance; ecological function
Unit of protection	Individual; population; community; functional group; assemblage; guild
Harmful effect	Relevant decrease in abundance; relevant disturbance in ecological function
Spatial scale of effect	Field; field margin; other agricultural land; non-agricultural habitats; landscape
Temporal scale of effect	Generations; days; weeks; months; seasons; years

[a]Table adapted from the stakeholders' workshop "Protection goals for environmental risk assessment of pesticides: what and where to protect?" organized by the EFSA Panel on Plant Protection Products and their Residues (PPR) (http://www.efsa.europa.eu/en/scdocs/scdoc/1672.htm); see also [108, 134]

environment during transportation and processing, potentially leading to sporadic feral GM plants; (2) indirect exposure through manure and feces from the gastrointestinal tracts of animals mainly fed the GM crop; and/or (3) manure or organic plant matter either imported as a fertilizer or soil amendment or derived from other byproducts of industrial processes. In the case where the GM crop use includes cultivation in the EU, problem formulation will consider exposure resulting from the expected cultivation in the receiving environment.

A well-structured conceptual model in which the components of the system are detailed will allow the identification and formulation of relevant hypotheses that arise from the consideration of potentially significant risks. These hypotheses are necessary to make assumptions and predictions about how a stressor or identified difference in the GM plant could affect and pose harm to an assessment endpoint [94, 95]. Importantly, within the analysis phase, hypotheses amenable to testing and corroboration are defined [92] which further guide the methodological approach taken to evaluate the magnitude of harm [92, 102].

Analysis Plan: Statistical Considerations and Experimental Design The last step of problem formulation comprises an analysis plan in which decisions are made about the most appropriate way to measure the response of each assessment endpoint to GM crop deployment. In this planning phase, approaches are delineated for the generation and evaluation of requisite data, in order to test hypotheses formulated in the conceptual model. Reasonable scenarios are placed in an analysis plan by describing and selecting: (1) the various measures to be used (measurement endpoints) in the assessment and subsequent risk characterization; and (2) the description of methods and criteria for measurement.

The measurement endpoints, derived directly from the assessment endpoints, define the indicator of change that will actually be recorded as part of a comparative risk assessment study [107], and usually constitute estimates of *exposure* or *hazard*. Measures of exposure cover properties of the GM crop and are described in terms of the route, frequency, duration, and intensity of exposure relative to the valued entity [92], while measures of hazard represent the measurable change to the valued entity in response to a changed attribute (e.g., transgenic protein) of the GM crop to which it is exposed [107]. Measures of hazard may be an acute lethal concentration resulting in the death of 50% of the organisms tested (LC_{50}), or a chronic *no observable adverse effect level* (NOAEL) measured for the valued entity [92]. How exposure measurement relates to the hazard measurement is described in the risk formulation.

Once specific measurement endpoints are chosen and given a priority, appropriate methods and criteria of measurement are selected and described in the analysis plan [93]. This includes information on: studies to be conducted; the appropriate tier for analysis; the design of protocols; and statistical power [96, 102, 106, 107, 109, 110]. The selection and prioritizing of measures to be used and testing needed enable the allocation of appropriate human and financial resources [111], so that only essential data for risk characterization are collected [94].

It is important to realize that for practical reasons not all potentially exposed non-target organisms can be tested for regulatory purposes [102]. Therefore, it is necessary to select an appropriate subset of species that

can be tested effectively under laboratory conditions [102], or that are available in sufficient numbers in the field to give statistically meaningful results [96, 112–115]. This selection of species is based on several criteria, comprising: ecological relevance of the species; the likely exposure of the species to the GM crop; species susceptibility to known or potential stressors; the anthropocentric value of the species; and species testability [96, 102, 113, 116]. The environmental risk assessment may also consider species with special aesthetic or cultural values, or species of conservation importance and that are classified as threatened or endangered, although these are unlikely to be tested directly but substituted by a surrogate species in tests. The number and type of species that are to be tested will depend upon the hypotheses generated during the conceptual model.

Once assessment and measurement endpoints have been set and approaches have been delineated for the generation and evaluation of requisite data to test hypotheses formulated during problem formulation, the level of environmental change that constitutes harm is to be set through *limits of concern*. These limits of concern define the minimum relevant ecological effect that is deemed of sufficient magnitude to cause harm, and is therefore biologically significant. Limits of concern are directly related to the type of studies that are to be performed either in the laboratory or in the (semi)-field. For laboratory studies, limits of concern are conservative trigger values which, if exceeded, will indicate potential risks and the need for exposure assessments and determination of field scale effects. For field studies, the lower limit, which corresponds for example to a decrease in the abundance of a particular species in the presence of the GM plant relative to that for its appropriate comparator, will usually be defined by the threshold effect deemed to be of just sufficient magnitude to cause environmental harm [106]. Knowing in advance what effect size is to be determined is crucial, as this information will enable to design the study in a way that it has sufficient statistical power to detect the anticipated effect. Limits of concern are estimated from literature data, modelling, and existing knowledge, and may be based on political, social, cultural and economic considerations. To define the minimum relevant ecological effect that is deemed biologically significant and that is deemed of sufficient magnitude to cause harm, it is important that (sets of) limits of concern for each assessment endpoint are set. Usually, the lower limit, which corresponds for example to a decrease in the abundance of a particular species in the presence of the GM crop relative to that for the non-GM counterpart, will be defined by the threshold effect that was deemed to be of just sufficient magnitude to cause environmental harm [106]. If these limits are exceeded, then detailed quantitative modeling of exposure may be required to scale up effects at the field level, both temporally and spatially. For studies in environment(s) that are controlled, the limits of concern will usually be trigger values which, if exceeded, will either lead to conclusions on risks or the need for further assessment in field [106]. Limits of concern can be defined by, for example, literature data, modeling, existing knowledge and policy goals. Ideally, these limits should be set by risk managers, as they will describe the extent of impact tolerated on a protection goal resulting from GM crop market approvals.

Conclusion Problem formulation is the crucial starting point for risk assessments, as it enables a structured, logical approach to detecting potential risks. Having a properly constructed analysis plan based on a conceptual model that is clearly linked to assessment endpoints helps to guide the collection of data that are relevant to investigating the possible safety of a GM crop. Moreover, it helps the risk assessment process to be comprehensive (by summarizing existing knowledge of the system under study) and transparent (by explicitly stating significant assumptions underlying the risk assessment, and ultimately regulatory decision making). In contrast, poor problem formulation can lead to the collection of data that are either unnecessary, superfluous, or irrelevant, diverting time and efforts from the more serious of the identified risks, thereby slowing down the procedure and increasing associated costs [90, 92, 94, 95, 117].

Risk Assessment Concepts and Approaches

Several concepts and approaches are considered during the risk assessment of GM crops. Risk assessment of GM crops: (1) is science-based, where quantitative information is available, and uses qualitative

information in the form of expert judgment; (2) uses a comparative approach; (3) is case specific; (4) is iterative and, in a transparent manner, examines previous conclusions in light of new information; and (5) follows a tiered approach.

Science-Based Assessment

The evaluation of potential adverse effects is based on scientific and technical data, and on common methodology for the identification, gathering, and interpretation of relevant data.

Comparative Safety Assessment and Familiarity Concept

The risk assessment strategy for GM crops seeks to use appropriate methods to compare a GM crop with its non-GM counterpart. The importance of risks posed by a GM crop is placed in the context of risks posed by its non-GM counterpart. A two-step approach is followed, starting with the identification of possible differences between the GM and non-GM counterpart (= proof of difference); which is then followed by the assessment of the environmental and food/feed consequences of any identified differences (= proof of equivalence) (see [106] for further details). The proof of difference approach verifies whether the GM crop is different from its non-GM counterpart, and may lead to the characterization of a potential risk depending on the type of the identified difference, and the extent and pattern of its exposure. The proof of equivalence approach aims to verify whether the GM crop is equivalent to its non-GM counterpart within bounds defined by so-called limits of concern. The two approaches are complementary: statistically significant differences may point to biological changes caused by the genetic modification, but these may or may not be relevant from the viewpoint of environmental harm [106, 118].

For the *food/feed safety assessment*, the equivalence test involves a comparison of the GM crop with a selection of non-GM counterparts, such as commercial varieties, aiming to identify any values of the GM crop that lie within the range of values from natural variation (i.e., observed among the set of non-GM counterparts included in the trial). The underlying assumption is that traditionally bred plants have a history of safe use for the consumer or animals and the environment, and familiarity for the consumer. For the *environmental risk assessment*, conventional cropping systems are not characterized as having a history of safe use, therefore, a near-isogenic conventional counterpart is used to identify any differences with the GM crop which might result in environmental harm. However, in any agricultural system, environmental impact critically depends upon crop management practices, such as the application of pesticides, environmental stewardship, and any mitigation measures adopted. Hence, the characterization of management regimes is an integral part of the definition of whatever comparator is chosen for the environmental risk assessment of GM crops [106].

The concept of familiarity is based on the fact that most GM crops are developed from more traditionally bred crops, the biology of which is well known. The knowledge about the non-GM crop, gained through experience over time, can therefore be used in a risk assessment to establish differences associated with the genetic modification and the subsequent management of the GM crop. According to the Organisation for Economic Co-operation and Development (OECD), familiarity is derived from the knowledge and experience available from conducting a risk analysis prior to the scale-up of any new crop variety in a particular environment, and from previous GM crop market applications for similar constructs and traits in similar or different crops [119]. However, it is important to bear in mind that familiarity is not an endpoint in risk assessment and does not necessarily equate to safety. If differences between the GM crop and its appropriate comparator have been identified, it needs to be determined whether these differences have any significance for the assessment endpoint under consideration.

The comparative safety assessment is usually based on data from three different sources: molecular, compositional, and agronomic/phenotypic analyses. The molecular characterization includes a precise characterization of the inserted DNA, information on which genes are expressed in the GM crop, and evidence that no detectable unintended effects have occurred because of the insertion [86]. Agronomic, phenotypic, and compositional data collected from field trials carried

out in a range of agricultural environments that are typical of the place where the crop is grown will highlight whether the GM crop is equivalent in its functional properties to the non-GM counterpart and, in particular, how stable they are from year to year and across environments.

Molecular Characterization In an environmental risk assessment, molecular characterization data can be used to test the hypothesis that the inserted DNA does not disrupt endogenous plant genes, or trigger the production of new proteins/metabolites (other than the intended ones). If any endogenous plant genes were disrupted, rearranged, or overexpressed, these differences would be considered as unintended effects of the genetic modification, and would be further assessed to determine the biological significance thereof. A variety of data and information is therefore necessary as no individual test can detect all possible unintended effects or identify, with certainty, those relevant to human health or environmental impact. Specifically, detailed information is usually required on: the source of the donor DNA; the transformation method; the organization of the inserted DNA at the insertion site(s); and on the expression and stability of the insert. Information concerning vector construction and the transformation method employed, as well as on all known gene regulatory elements and coding sequences is also relevant. Many authorities require the modification system to be mapped to a degree consistent with available technology, usually to the level of base sequence. An evaluation of whether the transgenes behave similarly to endogenous plant genes in their stability and inheritance between generations is also carried out. Hence, a risk assessment would have to be conducted to determine whether any detected unintended effects could result in potential adverse effects on human or animal health and the environment [100, 101]. Notably, insertional effects (intended or otherwise) are related to the specific transformation event, and not to the function of the inserted transgene; therefore, as with random mutation, most unintended changes caused by deliberate insertions of genetic material will be, at best, neutral to the plant. It is extremely rare for a significant improvement in ecological fitness or substantial compositional changes to result [120].

Compositional Analysis Compositional analyses enable the determination of any differences in key components as a result of the genetic modification, and to test the hypothesis that no difference in key component concentrations exists between the GM crop and its non-GM counterpart. Compositional data are generated in field trials carried out in several locations throughout the intended area of cultivation of the crop. In these field trials, the GM crop is grown alongside its appropriate comparator, and samples are taken. Parameters are selected that are typical for the crop that is assessed, and that are representative of the main metabolic pathways. Significant changes in these parameters are expected to be indicative of more fundamental changes in the crop that requires further evaluation [121]. The lack of statistically significant differences in the concentration of multiple analytes is a strong indication that the genetic modification has not introduced new constituents, nor harmful unintended changes. However, should statistically significant differences be detected, a harmful change is not necessarily indicated: should the different concentration of a specific analyte in the GM crop be within the range known for the crop, then it can be considered biologically insignificant, otherwise they will constitute "unintended identified" differences that require consideration in the risk assessment [100, 101].

Agronomic and Phenotypic Characterization Information on agronomic and phenotypic characteristics is obtained from multi-location agronomic field trials representative of different environments where the GM crop may be grown. To assess the agronomic performance of the GM crop, a sound understanding of the biology of the crop is required, as well as its relationship with the environment in which it is to be released. A variety of plant characteristics, such as plant vigor, growth habit, yield, crop quality, insect and disease susceptibility, fertility, dispersal mechanisms, and endogenous toxins, are recorded and any differences in the GM crop identified, which could potentially cause it to become a weed of agricultural or natural habitats, or otherwise interact differently than the non-GM counterpart in the environment. If there are no significant differences in characteristics associated with survival, growth, and reproduction, then it is likely that the genetic modification did not

alter the persistence, invasiveness or gene flow potential of the GM crop. If significant differences are identified, the values obtained in the GM crop will be assessed for their biological relevance by comparing them with the range of values known for (non-GM) commercial varieties [98–101].

Case-by-Case Principle

No two environmental risk assessments are the same, as each is dependent upon a range of variables found when considering: both the source and target environments; the biological and ecological characteristics of the GM crop; the scale and frequency of the proposed deliberate release; and the interactions amongst them [97, 122]. It is obvious that each range of variables will also differ between risk assessments, and thus a case-by-case approach is taken. In this way, the required information for the environmental risk assessment may vary depending on: the plant species under consideration; its intended use; and potential receiving environments, taking into account specific cultivation requirements and the presence of GM crops already in the environment.

Iterative and Adaptive

It is recognized that an environmental risk assessment is framed within the scientific knowledge available at the time it is conducted, and that regulatory decisions are made in this context. The environmental risk assessment has to take into account uncertainty at various levels, and which may arise from: limitations in the data (e.g., limited exposure data); gaps in the effect database; the limitation of the test systems and measurement endpoints selected; inadequacy of study designs; and the uncertainties in extrapolating between species. Scientific uncertainty may also arise from differing interpretations of existing data or the lack of some relevant data. Uncertainty may relate to qualitative or quantitative elements of the analysis [106]. Although it may be impossible to identify all the uncertainties present, the assessment should include a description of the types of uncertainties encountered and considered during the different risk assessment steps. Their relative importance and influence on the assessment outcome should also be described. Under current EU legislation, a high precision in environmental risk assessments becomes near impossible to achieve, as the identification of any areas of uncertainty which relate to areas outside current knowledge and the limited scope of the assessment is a mandatory requirement, for example, the impact of large-scale exposure of different environments from GM crop cultivation, the impact of exposure over long periods of time, and any cumulative long-term effects.

PMEM, which became mandatory under current EU legislation, aims to identify possible unanticipated adverse effects on human health or the environment which could arise directly or indirectly from GM crops. It also allows for the collection of additional data during the cultivation phase. The scientific knowledge obtained during the monitoring of GM crops, along with experiences gained from their cultivation and any other new knowledge (generated through biosafety research), provides valuable information to risk assessors to update environmental risk assessments and reduce any remaining uncertainties. In the EU, the objectives of a monitoring plan according to Annex VII of Directive 2001/18/EC are: (1) to confirm that any assumption regarding the occurrence and impact of potential adverse effects of the GMO, or its use, in the environmental risk assessment are correct; and (2) to identify the occurrence of adverse effects of the GMO, or its use, on human or animal health or the environment which were not anticipated in the environmental risk assessment. A PMEM plan of GM crops is mandatory in all market approval dossiers submitted under Directive 2001/18/EC and the GM Food and Feed Regulation.

In the EU, PMEM is composed of *case-specific monitoring* and *general surveillance*. Case-specific monitoring is not obligatory, but may be required to verify risk assessment assumptions and conclusions, whereas a general surveillance plan, as part of a GM crop market application, is a legal obligation. Due to different objectives between case-specific monitoring and general surveillance, their underlying concepts differ [123]. Case-specific monitoring enables the determination of whether, and to what extent, anticipated adverse effects occur during GM crop deployment, and thus to relate observed changes to specific causes. It is mainly triggered by scientific uncertainties that were identified

in the environmental risk assessment. Therefore, a hypothesis is established that can be tested on the basis of newly collected monitoring data ("bottom-up approach"). In general surveillance, by contrast, the general status of the environment that is associated with the GM crop deployment is monitored without any preconceived hypothesis in order to detect any possible effects that were not anticipated in the environmental risk assessment, or that are long term and cumulative. Should any such effects be observed, they are studied in more detail to determine whether the effect is adverse and whether it is associated with the use of a GM crop [87]. General surveillance data can originate from various sources: (1) farm questionnaires; (2) existing surveillance networks (such as plant health surveys, soil surveys, ecological and environmental observations); (3) scientific literature; (4) industry stewardship programs; and (5) alert issues. Questionnaires for farmers form a useful part of general surveillance, as this tool enables the reporting of any observations of effects linked with GM crop cultivation: farm questionnaires use first-hand observations and rely on farmers' knowledge and experience of their local agricultural environments, comparative crop performance and other factors that may influence events on their land [124]. With this tool, monitoring focuses mainly on the cultivation area of GM crops and its surroundings, which is relevant to protection goals such as sustainable agriculture, soil function, or plant health. Aspects of biodiversity, however, are only addressed indirectly (such as the adoption of conservation/no-till practices, rotation regimes, biological control failures) and may not be sufficiently resolved [125]. Therefore, additional sources of information should be considered in the frame of general surveillance. Moreover, farm questionnaires should include different combinations and mixtures of GM crops that may be grown in sequence or rotation in fields [126]. Directive 2001/18/EC proposes to make use of established routine surveillance networks. EU Member States have various networks in place – some of which have a long history of data collection – that may be helpful in the context of general surveillance of GM crops. The networks involved in routine surveillance offer recognized expertise in a specific domain and have the tools to capture information on important environmental aspects over a large geographical area. However, networks fully meeting all the needs of GM crop monitoring are limited: most do not always provide data of relevance to monitoring the impacts of GM crop cultivation [125, 127]. Concern has been raised, predominantly outside of the EU, however, that in the absence of a valid hypothesis, PMEM for undefined hypothetical adverse effects from a GM crop is not feasible, and adds nothing to the premarket testing results, while potentially undermining confidence in the overall safety assessment process [128].

Risk assessments undertaken in the EU are always iterative, in the sense that regulatory decisions are temporary, reversible, and adaptable in light of new information that becomes available. Under Directive 2001/18/EC, the requirement of reexamination has been strengthened by limiting the duration of any market consent to a maximum period of ten years.

Tiered Approach

An environmental risk assessment is generally conducted in a tiered manner, where information collected in lower tiers directs the extent and nature of any experimentation conducted in higher tiers (Fig. 4). Thereby, hazards are evaluated within different tiers that progress from worst-case scenario conditions, framed in highly controlled laboratory environments, to more realistic conditions in the field [87, 97, 102, 122, 129–131]. Usually, three tiers is the norm, comprising of experimental tests under controlled conditions (tier 1: laboratory tests where test organisms are exposed to a high level of the newly expressed protein as pure protein; tier 2: laboratory tests where test organisms are exposed to refined, more realistic, levels of the newly expressed protein as pure protein or plant material); and (semi-)field tests (tier 3). Within each tier, all relevant data are gathered in order to determine whether there is sufficient information to conclude the risk assessment at that tier. The conclusion can only be made if any residual uncertainty has been defined, otherwise additional investigations to generate further data at a higher tier (s) are designed and undertaken to do so [102]. In the case that no reliable risk conclusions can be drawn, decision making can consider whether risk management measures (tier 4) should be put in place to reduce the overall risk. It is important that throughout the

assessment, the problem being addressed (tier 0) remains appropriate and is revised, if necessary.

Lower-tier tests serve to identify and test potential hazards under worst-case scenario conditions and thus involve conservative assumptions, acknowledging that the likelihood of detecting any potential adverse effects of the GM crop or its products on target and nontarget biota increases directly with increasing (usually excessive) levels of exposure. These studies are conducted under controlled laboratory or growth room conditions in order to: quantify effects in relation to known exposure levels; to provide high levels of replication and control; and to increase the statistical power for testing the established hypotheses. Effects of the GM crop on indirectly exposed organisms, that is, those that are one or two steps removed in the food chain (e.g., predators and parasites of primary phytophagous or plant pathogenic organisms), are generally assessed in the second tier, which is also generally conducted under controlled laboratory, growth room or glasshouse conditions in order to measure effects in relation to known exposure levels [87]. If no hazards are identified and the GM crop is not different from the appropriate comparator, the tested product may be regarded as safe, and no further testing at a higher tier deemed necessary.

However, should potential hazards be detected in early-tier tests or if unacceptable uncertainties concerning possible hazards remain, additional information is required to confirm whether the observed effect might still be detected at more realistic rates and routes of exposure [87, 97, 102, 131]. Progression to larger-scale experiments in higher tiers aims to provide increasingly refined estimates of exposure. Field trials are then established in which the cultivation of the GM crop is conducted with greater environmental realism and thus relevance. As such, actual levels of exposure of different biota can be quantified. In comparison with the appropriate comparator and its management, likely ecological adverse effects due to the GM plant and its management can be determined. While higher-tier studies offer greater environmental relevance, they may have lower statistical power due to the higher variability of environmental conditions (e.g., climate) that can mask effects generated by the GM crop or its product [131]. In exceptional cases, higher-tier studies may be conducted at an initial stage when early-tier tests are not possible or

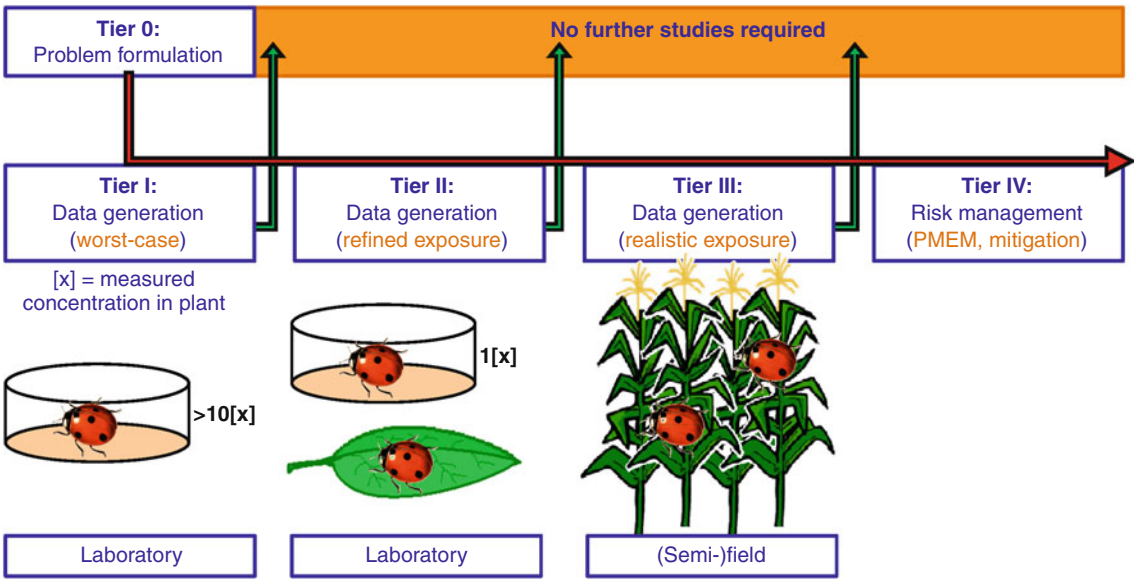

Transgenic Crops, Risk Assessment and Regulatory Framework in the European Union. Figure 4
Tiered approach to non-target organism testing (Figure adapted from [97])

meaningful. As such, many risk assessments are conducted in a tiered manner, meaning that risk assessment studies increase in complexity depending upon the findings at each level of assessment [91]. In cases where uncertainty about the risk remains after higher-tier studies, one can always return to lower tiers to conduct additional studies [102].

The tiered approach is consistent with the iterative or adaptive nature of risk assessment where conclusions are reviewed when new information is obtained. Uncertainty in risk assessment is reduced because each tier is guided by results obtained in the previous tier, and specific, testable, and relevant hypotheses are formulated based on these data [87, 97, 102, 122, 131].

Future Directions

Since one of the main objectives of the EU GMO regulatory framework is to ensure a high level of protection of human and animal health and the environment, the focus is on the assessment of risks. Whether GM crops fulfill wider socioeconomic and ecological aspirations is not considered explicitly. However, when analyzing potential risks, it is important to bear in mind that the real choice is not between GM crops that are inherently risky and traditionally bred ones that are completely safe. Both existing crops and those with novel traits (including GM crops) will have both positive and negative attributes [56]. To fully acknowledge the overall consequences of adopting specific crops, and to assess and manage more effectively the environmental footprint of agriculture as a whole, it has been suggested that broader and more balanced legislative oversight is needed in the EU [132, 133]. At the EFSA scientific colloquium on challenges and approaches for the environmental risk assessment of GM plants [133], the discussion group on broadening the scope of the environmental risk assessment provided the following recommendations:

- A paradigm shift would be required to change from risk assessment as it is currently practiced, to a more sophisticated assessment which balances risks and benefits: (i) The focus on only GM crops defies scientific evidence. In the longer term, risk assessors could develop an alternative approach on a scientific basis. 'Novelty' is one option. (ii) The status quo, in which risk assessment is interpreted very narrowly in terms of adverse impacts, is not sustainable, and perceptions of the quality of environmental risk assessments suffer as a result. A framework for the future is required. (iii) There is a need to build decision support tools for the risk assessors to better consider impacts of whole farming systems.

The assessment of GM crops has intersected with a wider debate about sustainable agriculture in the EU, blurring any distinctions between environmental, agricultural, and socioeconomic issues. A sustainability assessment may be helpful in recovering public and market confidence, as it integrates larger societal concerns. It enables to define and integrate the underlying values at stake, trade possible risks against benefits, compare technological alternatives, evaluate the usefulness of GM crops, and to assess a whole agricultural system. In this way, it may promote finding a better balance between agricultural production and biodiversity, and evolve toward a socially more robust risk analysis, in which sustainable development is the goal.

While such an integral sustainability assessment certainly will not make things easier and might be an unachievable ideal, it may offer a helpful framing of the debate about multiple controversial aspects. Social, ecological, and economic considerations (such as ensuring social equity and cohesion, a high level of environmental protection, and economic prosperity) that have too often been treated in isolation could then be brought together and explored in a holistic and long-term perspective. Preferences for certain options would no longer be advanced independently of the broader, more complex agricultural and societal context. Likewise, underlying values at stake and normative perspectives fueling the debate might be brought to light.

Disclaimer

Opinions and views expressed in this entry are strictly those of the authors, and may not necessarily represent those of the organizations where the authors are currently employed.

Acknowledgments

The authors wish to thank Salvatore Arpaia, Detlef Bartsch, Adinda De Schrijver, Matty Demont, Achim Gathmann, Rosemary Hails, Jozsef Kiss, Antoine

Messéan, Karin Nienstedt, Joe Perry, Dirk Reheul, Olivier Sanvido, and Jeremy Sweet for inspiring discussions that helped to develop this entry.

Bibliography

1. EC (2008) The Economics of Ecosystems and Biodiversity – Interim Report 2008. http://ec.europa.eu/environment/nature/biodiversity/economics
2. EC (2001) Directive 2001/18/EC of the European Parliament and of the Council of 12 March 2001 on the deliberate release into the environment of genetically modified organisms and repealing Council Directive 90/220/EEC. Off J Eur Communities L106:1–39
3. EC (2004) Directive 2004/35/EC of the European Parliament and of the Council of 21 April 2004 on environmental liability with regard to the prevention and remedying of environmental damage. Off J Eur Communities L143:56–75
4. Secretariat of the CBD (2000) Cartagena protocol on biosafety to the convention on biological diversity: text and annexes. Secretariat of the Convention on Biological Diversity (CBD), Montreal, Canada. http://www.cbd.int/doc/legal/cartagena-protocol-en.pdf
5. Johnson KL, Raybould AF, Hudson MD, Poppy GM (2007) How does scientific risk assessment of GM crops fit within the wider risk analysis? Trends Plant Sci 12:1–5
6. James C (2010) Global status of commercialized biotech/GM crops: 2010. Highlights of ISAAA briefs No 42, Ithaca, New York
7. Chapotin SM, Wolt JD (2007) Genetically modified crops for the bioeconomy: meeting public and regulatory expectations. Transgenic Res 16:675–688
8. Herring RJ (2008) Opposition to transgenic technologies: ideology, interests and collective action frames. Nat Rev 9:458–463
9. Levidow L, Carr S, Wield D (2005) European Union regulation of agribiotechnology: precautionary links between science, expertise and policy. Sci Public Policy 32:261–276
10. Devos Y, Reheul D, De Waele D, Van Speybroeck L (2006) The interplay between societal concerns and the regulatory frame on GM crops in the European Union. Environ Biosaf Res 5:127–149
11. Devos Y, Maeseele P, Reheul D, Van Speybroeck L, De Waele D (2008) Ethics in the societal debate on genetically modified organisms: a (re)quest for *Sense* and *Sensibility*. J Agric Environ Ethics 21:29–61
12. Levidow L, Carr S (2007) GM crops on trial: technological development as a real world experiment. Futures 39:408–431
13. Lofstedt RE (2006) How can we make food risk communication better: where are we and where are we going? J Risk Res 9:869–890
14. Marks LA, Kalaitzandonakes N, Wilkins L, Zakharova L (2007) Mass media framing of biotechnology news. Public Underst Sci 16:183–203
15. Maeseele PA, Schuurman D (2008) Biotechnology and the popular press in Northern Belgium. Sci Commun 29:435–471
16. Kasperson RE, Kasperson JX (1996) The social amplification and attenuation of risk. Ann Am Acad Polit Soc Sci 545:95–105
17. Winickoff D, Jasanoff S, Busch L, Grove-White R, Wynne B (2005) Adjudicating the GM food wars: science, risk, and democracy in world trade law. Yale J Int Law 30:81–123
18. Kuiper HA, Davies HV (2010) The SAFE FOODS risk analysis framework suitable for GMOs? Food Control. doi:10.1016/j.foodcont.2010.02.011
19. Gaskell G, Allansdottir A, Allum N, Corchero C, Fischler C, Hampel J, Jackson J, Kronberger N, Mejlgaard N, Revuelta G, Schreiner C, Stares S, Torgersen H, Wagner W (2006) Europeans and Biotechnology in 2005: Patterns and Trends, Eurobarometer 64.3. http://ec.europa.eu/research/press/2006/pdf/pr1906_eb_64_3_final_report-may2006_en.pdf
20. Christiansen T, Polak J (2009) Comitology between political decision-making and technocratic governance: regulating GMOs in the European Union. Eipascope Bull 1:5–11
21. EC (2010) Proposal for a Regulation of the European Parliament and of the Council amending Directive 2001/18/EC as regards the possibility for the Member States to restrict or prohibit the cultivation of GMOs in their territory. http://ec.europa.eu/food/food/biotechnology/docs/proposal_en.pdf
22. EC (2010) Communication from the Commission to the European Parliament, the Council, the Economics and Social Committee and the Committee of the Regions on the freedom for Member States to decide on the cultivation of genetically modified crops. http://ec.europa.eu/food/food/biotechnology/docs/communication_en.pdf
23. EC (2010) Commission Recommendation of 13 July 2010 on guidelines for the development of national co-existence measures to avoid the unintended presence of GMOs in conventional and organic crops. http://ec.europa.eu/food/food/biotechnology/docs/new_recommendation_en.pdf
24. Chipman A (2010) Fears over Europe's GM crop plan. Nature 466:542–543
25. Ryffel GU (2010) Making the most of GM potatoes. Nat Biotechnol 28:318
26. Secretariat of the CBD (1992) Convention on biological diversity. Secretariat of the Convention on Biological Diversity (CBD), Montreal, Canada. http://www.biodiv.org/doc/legal/cbd-en.pdf
27. James C (2009) Global status of commercialized biotech/GM crops: 2009. ISAAA Brief No. 41. ISAAA, Ithaca
28. Jaffe G (2004) Regulating transgenic crops: a comparative analysis of different regulatory processes. Transgenic Res 13:5–19
29. FAO/WHO (2000) Safety aspects of genetically modified foods of plant origin. A joint FAO/WHO consultation on foods derived from biotechnology, Geneva, Switzerland, 29 May–2 June 2000. World Health Organization, Geneva
30. Secretariat of the IPPC (2005) Pest risk analysis for quarantine pests, including analysis of environmental risks and living modified organisms. International Standards for Phytosanitary

Measures (ISPM) No. 11. Secretariat of the International Plant Protection Convention (IPPC), Food and Agriculture Organization of the United Nations, Rome, Italy. ftp://ftp.fao.org/docrep/fao/008/y5874e/y5874e00.pdf
31. Mackenzie R, Burhenne-Guilmin F, La Vina AGM, Werksman JD (2003) An explanatory guide to the Cartagena protocol on biosafety. In cooperation with Ascencio A, Kinderlerer J, Kummer K, Tapper R. IUCN, Gland, Switzerland and Cambridge, UK. www.cbd.int/doc/books/2003/B-01669.pdf
32. Breyer D, Herman P, Brandenburger A, Gheysen G, Remaut E, Soumillion P, Van Doorsselaere J, Custers R, Pauwels K, Sneyers M, Reheul D (2009) Commentary: Genetic modification through oligonucleotide-mediated mutagenesis. A GMO regulatory challenge? Environ Biosaf Res 8:57–64
33. Macdonald P, Yarrow S (2003) Regulation of Bt crops in Canada. J Invertebr Pathol 83:93–99
34. McHughen A, Smyth S (2008) US regulatory system for genetically modified [genetically modified organisms (GMO), rDNA or transgenic] crop cultivars. Plant Biotechnol J 6:2–12
35. Smyth S, McHughen A (2008) Regulating innovative crops technologies in Canada: the case of regulation genetically modified crops. Plant Biotechnol J 6:213–225
36. COGEM (2006) New techniques in plant biotechnology. COGEM Report CGM/061024-02. http://www.cogem.net/ContentFiles/CGM061024-02%20new%20techniques%20in%20plantbiotechnology.pdf
37. Morris SH, Spillane C (2008) GM directive deficiencies in the European Union. EMBO Rep 9:500–504
38. Batista R, Saibo N, Lourenço T, Oliveira MM (2008) Microarray analyses reveal that plant mutagenesis may induce more transcriptomic changes than transgene insertion. Proc Natl Acad Sci USA 105:3640–3645
39. Kok EJ, Keijer J, Kleter GA, Kuiper HA (2008) Comparative safety assessment of plant-derived foods. Regul Toxicol Pharmacol 50:98–113
40. Bradford KJ, Van Deynze A, Gutterson N, Parrott W, Strauss SH (2005) Regulating transgenic crops sensibly: lessons from plant breeding, biotechnology and genomics. Nat Biotechnol 23:439–444
41. Morris SH (2007) EU biotech crop regulations and environmental risk: a case of the emperor's new clothes? Trends Biotechnol 25:2–6
42. Jacobsen E, Schouten HJ (2007) Cisgenesis strongly improves introgression breeding and induced translocation breeding of plants. Trends Biotechnol 25:219–223
43. Rommens CM, Haring MA, Swords K, Davies HV, Belknap WR (2007) The intragenic approach as a new extension to traditional plant breeding. Trends Plant Sci 12:397–403
44. COGEM (2009) Novel plant breeding techniques – consequences of new genetic modification-based plant breeding techniques in comparison to conventional plant breeding, report 2009-02. http://www.cogem.net/ContentFiles/Microsoft%20Word%20-%20New%20plant%20breeding%20techniques%20definitieve%20versie.pdf
45. Foster M, Berry P, Hogan J (2003) Market access issues for GM products. Australian Bureau of Agricultural and Resource Economics (ABARE) eReport 03.13, Canberra, Australia. http://abareonlineshop.com/PdfFiles/PC12559.pdf
46. Kuiper HA, Kleter GA, Noteborn HPJM, Kok EJ (2002) Substantial equivalence – an appropriate paradigm for the safety assessment of genetically modified food. Toxicology 181–182:427–431
47. Kok EJ, Kuiper HA (2003) Comparative safety assessment for biotech crops. Trends Biotechnol 21:439–444
48. König A, Cockburn A, Crevel RWR, Debruyne E, Grafstroem R, Hammerling U, Kimber I, Knudsen I, Kuiper HA, Peijnenburg AACM, Penninks AH, Poulsen M, Schauzu M, Wal JM (2004) Assessment of the safety of foods derived from genetically modified (GM) crops. Food Chem Toxicol 42:1047–1088
49. Paoletti C, Flamm E, Yan W, Meek S, Renckens S, Fellous M, Kuiper H (2008) GMO risk assessment around the world: some examples. Trends Food Sci Technol 19:S66–S74
50. Devos Y, Lheureux K, Schiemann J (2010) Regulatory oversight and safety assessment of plants with novel traits. In: Kempken F, Jung C (eds) Genetic modification of plants – agriculture, horticulture & forestry, Series: Biotechnology in Agriculture and Forestry, vol 64. Springer, Berlin, pp 553–574
51. Demeke T, Perry DJ, Scowcroft WR (2006) Adventitious presence of GMOs: scientific overview for Canadian grains. Can J Plant Sci 86:1–23
52. Lheureux K, Mestdagh S, Devos Y (2008) Collaboration between the EFSA GMO Panel and national EU competent authorities for the environmental risk assessment of GM crop cultivation applications. J Consum Prot Food Saf 3(S2):51
53. SCP (2001) Opinion of the Scientific Committee on Plants concerning the adventitious presence of GM seeds in conventional seeds. http://ec.europa.eu/comm/food/fs/sc/scp/out93_gmo_en.pdf
54. Verhoog H, Matze M, Lammerts Van Bueren E, Baars T (2003) The role of the concept of the natural (naturalness) in organic farming. J Agric Environ Ethics 16:29–49
55. Altieri MA (2005) The myth of coexistence: why transgenic crops are not compatible with agroecologically based systems of production. Bull Sci Technol Soc 25:1–11
56. Sanvido O, Romeis J, Bigler F (2007) Ecological impacts of genetically modified crops: ten years of field research and commercial cultivation. Adv Biochem Eng Biotechnol 107:235–278
57. Schiemann J (2003) Co-existence of genetically modified crops with conventional and organic farming. Environ Biosaf Res 2:213–217
58. Devos Y, Demont M, Sanvido O (2008) Coexistence in the EU–return of the moratorium on GM crops? Nat Biotechnol 26:1223–1225
59. Devos Y, Demont M, Dillen K, Reheul D, Kaiser M, Sanvido O (2009) Coexistence of genetically modified (GM) and non-GM crops in the European Union. Agron Sustain Dev 29:11–30

60. EC (2003) Commission Recommendation of 23 July 2003 on guidelines for the development of national strategies and best practices to ensure the coexistence of genetically modified crops with conventional and organic farming. Off J Eur Communities L189:36–47
61. Friesen LF, Nelson AG, Van Acker RC (2003) Evidence of contamination of pedigreed canola (*Brassica napus*) seedlots in western Canada with genetically modified herbicide resistance traits. Agron J 95:1342–1347
62. Jørgensen T, Hauser TP, Jørgensen RB (2007) Adventitious presence of other varieties in oilseed rape (*Brassica napus*) from seed banks and certified seed. Seed Sci Res 17:115–125
63. Devos Y, Reheul D, De Schrijver A (2005) The co-existence between transgenic and non-transgenic maize in the European Union: a focus on pollen flow and cross-fertilization. Environ Biosaf Res 4:71–87
64. Hüsken A, Dietz-Pfeilstetter A (2007) Pollen-mediated intraspecific gene flow from herbicide resistant oilseed rape (*Brassica napus* L.). Transgenic Res 16:557–569
65. Sanvido O, Widmer F, Winzeler M, Streit B, Szerencsits E, Bigler F (2008) Definition and feasibility of isolation distances for transgenic maize. Transgenic Res 17:317–355
66. Devos Y, Reheul D, De Schrijver A, Cors F, Moens W (2004) Management of transgenic herbicide-tolerant oilseed rape in Europe: a case study on minimizing vertical gene flow. Environ Biosaf Res 3:135–148
67. Lutman PJW, Berry K, Payne RW, Simpson E, Sweet JB, Champion GT, May MJ, Wightman P, Walker K, Lainsbury M (2005) Persistence of seeds from crops of conventional and herbicide tolerant oilseed rape (*Brassica napus*). Proc R Soc Lond B 272:1909–1915
68. Messéan A, Sausse C, Gasquez J, Darmency H (2007) Occurrence of genetically modified oilseed rape seeds in the harvests of subsequent conventional oilseed rape over time. Eur J Agron 27:115–122
69. Gruber S, Colbach N, Barbottin A, Pekrun C (2008) Post-harvest gene escape and approaches for minimizing it. CAB Rev Perspect Agric Vet Sci Nutr Nat Resour 3:1–17
70. Jørgensen RB (2007) Oilseed rape: co-existence and gene flow from wild species. Adv Bot Res 45:451–464
71. Knispel AL, McLachlan S, Van Acker R, Friesen LF (2008) Gene flow and multiple herbicide resistance in escaped canola populations. Weed Sci 56:72–80
72. Pivard S, Adamczyk K, Lecomte J, Lavigne C, Bouvier A, Deville A, Gouyon PH, Huet S (2008) Where do the feral oilseed rape populations come from? A large-scale study of their possible origin in a farmland area. J Appl Ecol 45:476–485
73. Beckmann V, Soregaroli C, Wesseler J (2006) Coexistence rules and regulations in the European Union. Am J Agric Econ 88:1193–1199
74. EC (2006) Report on the implementation of national measures on the co-existence of genetically modified crops with conventional and organic farming, European Commission. http://ec.europa.eu/agriculture/coexistence/sec313_en.pdf
75. Koch BA (2007) Liability and compensation schemes for damage resulting from the presence of genetically modified organisms in non-GM crops. http://ec.europa.eu/agriculture/analysis/external/liability_gmo/full_text_en.pdf
76. Sundstrom F, Williams J, Van Deynze A, Bradford KJ (2002) Identity preservation of agricultural commodities. ANR Publication No. 8077, University of California
77. Czarnak-Klos M, Rodríguez-Cerezo E (2010) Best practice documents for coexistence of genetically modified crops with conventional and organic farming. 1. Maize crop production. European Coexistence Bureau (ECoB) report. http://ecob.jrc.ec.europa.eu/documents/Maize.pdf
78. Demont M, Devos Y (2008) Regulating coexistence of GM and non-GM crops without jeopardizing economic incentives. Trends Biotechnol 26:353–358
79. Demont M, Daems W, Dillen K, Mathijs E, Sausse C, Tollens E (2008) Regulating coexistence in Europe: Beware of the domino-effect! Ecol Econ 64:683–689
80. Demont M, Dillen K, Daems W, Sausse C, Tollens E, Mathijs E (2009) On the proportionality of EU spatial *ex ante* coexistence regulations. Food Pol 34:508–518
81. Demont M, Devos Y, Sanvido O (2010) Towards flexible coexistence regulations for GM crops in the EU. EuroChoices 9:18–24
82. Demont M, Dillen K, Daems W, Sausse C, Tollens E, Mathijs E (2010) On the proportionality of EU spatial *ex ante* coexistence regulations: Reply. Food Pol 35:183–184
83. Beckmann V, Soregaroli C, Wesseler J (2010) *Ex-ante* regulation and *ex-post* liability under uncertainty and irreversibility: governing the coexistence of GM crops. Econ 4, http://www.economics-ejournal.org/economics/journalarticles/2010-9
84. Ramessar K, Capell T, Twyman RM, Christou P (2010) Going to ridiculous lengths: European coexistence regulations for GM crops. Nat Biotechnol 28:133–136
85. Riesgo L, Areal FJ, Sanvido O, Rodríguez-Cerezo E (2010) Distances needed to limit cross-fertilization between GM and conventional maize in Europe. Nat Biotechnol 28:780–782
86. Craig W, Tepfer M (2007) Introduction to the safety/risk assessment of GM crops. J Agric Invest 5:36–42
87. EFSA (2006) Guidance document of the scientific panel on genetically modified organisms for the risk assessment of genetically modified plants and derived food and feed. EFSA J 99:1–100
88. Hill RA (2005) Conceptualizing risk assessment methodology for genetically modified organisms. Environ Biosaf Res 4:67–70
89. Conner AJ, Glare TR, Nap J-P (2003) The release of genetically modified crops into the environment. Part II: overview of ecological risk assessment. Plant J 33:19–46
90. Craig W, Tepfer M, Degrassi G, Ripandelli D (2008) An overview of general features of risk assessment of genetically modified crops. Euphytica 164:853–880
91. Hill RA, Sendashonga C (2003) General principles for risk assessment of living modified organisms: lessons from chemical risk assessment. Environ Biosaf Res 2:81–88

92. Wolt JD, Keese P, Raybould A, Fitzpatrick JW, Burachik M, Gray A, Olin SS, Schiemann J, Sears M, Wu F (2010) Problem formulation in the environmental risk assessment for genetically modified plants. Transgenic Res 19:425–436
93. EPA (1998) Guidelines for ecological risk assessment. EPA/630/R095/002F, US EPA risk assessment forum. US Environmental Protection Agency, Washington DC. http://cfpub.epa.gov/ncea/raf/recordisplay.cfm?deid=12460
94. Raybould A (2006) Problem formulation and hypothesis testing for environmental risk assessments of genetically modified crops. Environ Biosaf Res 5:119–125
95. Raybould A (2007) Ecological versus ecotoxicological methods for assessing the environmental risks of transgenic crops. Plant Sci 173:589–602
96. Romeis J, Hellmich RL, Candolfi MP, Carstens K, De Schrijver A, Gatehouse AMR, Herman RA, Huesing JE, McLean MA, Raybould A, Shelton AM, Waggoner A (2010) Recommendations for the design of laboratory studies on non-target arthropods for risk assessment of genetically engineered plants. Transgenic Res. doi:10.1007/s11248-010-9446-x
97. Garcia-Alonso M, Jacobs E, Raybould A, Nickson TE, Sowig P, Willekens H, Van der Kouwe P, Layton R, Amijee F, Fuentes AM, Tencalla F (2006) A tiered system for assessing the risk of genetically modified plants to non-target organisms. Environ Biosaf Res 5:57–65
98. Horak MJ, Rosenbaum EW, Woodrum CL, Martens AB, Mery RF, Cothren JT, Burns JA, Nickson TE, Pester TA, Jiang C, Hart JL, Sammons B (2007) Characterization of roundup ready flex cotton, 'MON 88913', for use in ecological risk assessment: Evaluation of seed germination, vegetative and reproductive growth, and ecological interactions. Crop Sci 47:268–277
99. Nickson TE (2008) Planning environmental risk assessment for genetically modified crops: problem formulation for stress-tolerant crops. Plant Physiol 147:494–502
100. Garcia-Alonso M (2010) Current challenges in environmental risk assessment: The assessment of unintended effects of GM crops on non-target organisms. IOBC/wprs Bull 52:57–63
101. Raybould A, Tuttle A, Shore S, Stone T (2010) Environmental risk assessment for transgenic crops producing output trait enzymes. Transgenic Res 19:595–609
102. Romeis J, Bartsch D, Bigler F, Candolfi MP, Gielkens MMC, Hartley SE, Hellmich RL, Huesing JE, Jepson PC, Layton R, Quemada H, Raybould A, Rose RI, Schiemann J, Sears MK, Shelton AM, Sweet J, Vaituzis Z, Wolt JD (2008) Assessment of risk of insect-resistant transgenic crops to nontarget arthropods. Nat Biotechnol 26:203–208
103. Suter GW (2000) Generic assessment endpoints are needed for ecological risk assessment. Risk Anal 20:173–178
104. Sanvido O, Romeis J, Bigler F (2009) An approach for post-market monitoring of potential environmental effects of Bt-maize expressing Cry1Ab on natural enemies. J Appl Entomol 133:236–248
105. Suter GW (2007) Ecological risk assessment, 2nd edn. CRC Press, Boca Raton, p 643
106. Perry JN, ter Braak CJF, Dixon PM, Duan JJ, Hails RS, Huesken A, Lavielle A, Marvier M, Scardi M, Schmidt K, Tothmeresz B, Schaarschmidt F, van der Voet H (2009) Statistical aspects of environmental risk assessment of GM plants for effects on non-target organisms. Environ Biosaf Res 8:65–78
107. Storkey J, Bohan DA, Haughton AJ, Champion GT, Perry JN, Poppy GM, Woiwod IP (2008) Providing the evidence base for environmental risk assessments of novel farm management practices. Environ Sci Policy 11:579–587
108. EFSA (2010) EFSA Panel on Plant Protection Products and their Residues (PPR); Scientific Opinion on the development of specific protection goal options for environmental risk assessment of pesticides, in particular in relation to the revision of the Guidance Documents on Aquatic and Terrestrial Ecotoxicology (SANCO/3268/2001 and SANCO/10329/2002). EFSA J 1821, 1-55. http://www.efsa.europa.eu/en/scdocs/doc/1821.pdf
109. Marvier M (2002) Improving risk assessment for nontarget safety of transgenic crops. Ecol Appl 12: 1119–1124
110. Lövei GL, Arpaia S (2005) The impact of transgenic plants on natural enemies: a critical review of laboratory studies. Entomol Exp Appl 114:1–14
111. Qi A, Perry JN, Pidgeon JD, Haylock LA, Brooks DR (2008) Cost-efficacy in measuring farmland biodiversity – lessons from the farm scale evaluations of genetically modified herbicide-tolerant crops. Ann Appl Biol 152: 93–101
112. Gathmann A, Wirooks L, Hothhorn LA, Bartsch D, Schuphan I (2006) Impact of Bt-maize pollen (MON810) on lepidopteran larvae living on accompanying weeds. Mol Ecol 15: 2677–2685
113. Todd JH, Ramankutty P, Barraclough EI, Malone LA (2008) A screening method for prioritizing non-target invertebrates for improved biosafety testing of transgenic crops. Environ Biosaf Res 7:35–56
114. Aviron S, Sanvido O, Romeis J, Herzog F, Bigler F (2009) Case-specific monitoring of butterflies to determine potential effects of transgenic *Bt*-maize in Switzerland. Agric Ecosyst Environ 131:137–144
115. Rauschen R, Schultheis E, Pagel-Wieder S, Schuphan I, Eber S (2009) Impact of Bt-corn MON88017 in comparison to three conventional lines on *Trigonotylus caelestialium* (Kirkaldy) (Heteroptera: Miridae) field densities. Transgenic Res 18:203–214
116. Andow DA, Lövei GL, Arpaia S (2006) Ecological risk assessment for Bt crops. Nat Biotechnol 24:749–751
117. Raybould A (2010) Reducing uncertainty in regulatory decision-making for transgenic crops. More ecological research or clearer environmental risk assessment? GM Crops 1:1–7

118. EFSA (2010) Scientific opinion of the scientific panel on genetically modified organisms on statistical considerations for the safety evaluation of GMOs. EFSA J 1250:1–59
119. OECD (1993) Safety evaluation of foods derived by modern biotechnology, concepts and principles. Organization for Economic Co-operation and Development, Paris. ISBN 92-64-13859-5
120. Petersen W, Umbeck P, Hokanson K, Halsey M (2005) Biosafety considerations for selectable and scorable markers in cassava (*Manihot esculenta* Crantz) biotechnology. Environ Biosaf Res 4:89–102
121. Aumaitre A, Aulrich K, Chesson A, Flachowsky G, Piva G (2002) New feeds from genetically modified plants: substantial equivalence, nutritional equivalence, digestibility, and safety for animals and the food chain. Livest Prod Sci 74:223–238
122. Andow DA, Zwahlen C (2006) Assessing environmental risks of transgenic plants. Ecol Lett 9:196–214
123. Sanvido O, Widmer F, Winzeler M, Bigler F (2005) A conceptual framework for the design of environmental post-market monitoring of genetically modified plants. Environ Biosaf Res 4:13–27
124. Schmidt K, Wilhelm R, Schmidtke J, Beissner L, Mönkemeyer W, Böttinger P, Sweet J, Schiemann J (2008) Farm questionnaires for monitoring genetically modified crops: a case study using GM maize. Environ Biosaf Res 7:163–179
125. Wilhelm R, Sanvido O, Castanera P, Schmidt K, Schiemann J (2009) Monitoring the commercial cultivation of *Bt* maize in Europe – conclusions and recommendations for future monitoring practice. Environ Biosaf Res 8:219–225
126. Sweet JB (2008) General surveillance of multiple transgenic events. J Verbr Lebensm 3:12
127. Graef F, De Schrijver A, Murray A (2008) GMO monitoring data coordination and harmonisation at EU level – outcomes of the European Commission Working Group on Guidance Notes supplementing Annex VII of Directive 2001/18/EC. J Verbr Lebensm 3:17–20
128. ILSI Task Force (2004) Nutritional and safety assessments of foods and feeds nutritionally improved through biotechnology. Task Force of the International Life Science Institute (ILSI) International Food Biotechnology Committee. Compr Rev Food Sci Food Saf 3:35–104
129. Dutton A, Romeis J, Bigler F (2003) Assessing the risks of insect resistant transgenic plants on entomophagous arthropods: Bt-maize expressing Cry1Ab as a case study. BioControl 48:611–636
130. Wilkinson MJ, Sweet J, Poppy GM (2003) Risk assessment of GM plants: avoiding gridlock? Trends Plant Sci 8:208–212
131. Bartsch D, Gathmann A, Saeglitz C, Sinha A (2008) Field testing of transgenic plants. In: Stewart CN Jr (ed) Plant biotechnology and genetic principles, techniques, and applications. Wiley, London, pp 311–323
132. ACRE (2007) Managing the footprint of agriculture: towards a comparative assessment of risks and benefits for novel agricultural systems. DEFRA, London. http://www.defra.gov.uk/environment/acre/fsewiderissues/pdf/acre-wi-final.pdf
133. EFSA (2008) Environmental risk assessment of genetically modified plants – challenges and approaches. EFSA Scientific Colloquium Series 8, June 2007. European Food Safety Authority, Brussels. http://www.efsa.europa.eu/en/colloquiareports/colloquiagmoera.htm
134. Sanvido O, Romeis J, Gathmann A, Gielkens M, Raybould A, Bigler F (2011) Evaluating environmental risks of genetically modified crops – ecological harm criteria for regulatory decision-making. Environment & Science Policy, doi:10.1016/j.envsci.2011.08.006

Transgenic Fishes: Applications, State of the Art, and Risk Concerns

Eric M. Hallerman
Department of Fisheries and Wildlife Sciences, Virginia Polytechnic Institute and State University, Blacksburg, VA, USA

Article Outline

Glossary
Definition of the Subject
Introduction
Ecological Risk Assessment for Transgenic Fish in the Accessible Ecosystem
Risk Management
Future Directions: Transgenic Fish Considered Within the Sustainability Paradigm
Bibliography

Glossary

Accessible ecosystem The aquatic environment immediately accessible to an organism were it to escape from the research or culture facility, and more distant habitats in the contiguous environment into which the organism or its offspring reasonably may be expected to disperse.

Confinement A system of physical, chemical, biological, and operations management measures used to contain a transgenic fish within an experimental or culture facility or to prevent its establishment in the accessible ecosystem upon escape or release.

Direct effects (or impacts) Effects of a transgenic fish on an (other) organism(s) in the accessible

ecosystem, which are effected through mechanisms involving biotic factors. Examples would include but not be limited to reproduction with or predation upon or competition with members of the same or other species.

Environmental effects (or impacts) Consequences of an experiment or of aquaculture that might include, but are not limited to, changes in the structure, function, or resiliency of the accessible ecosystem; changes in the gene pool of populations resident in the accessible ecosystem; or decline in the abundance of a population of threatened, endangered, or special concern species in the accessible ecosystem.

Harm A perturbation resulting in negative impact to a population or species.

Hazard An agent or process that has the potential to produce harm.

Indirect effects (or impacts) Effects of a transgenic fish on (an) other organism(s) in the accessible ecosystem that are effected through mechanisms involving abiotic factors or additional species. Examples would include, but not be limited to, modification of the physical environment, affecting its suitability as habitat for other species and cascading effects of altered trophic function upon the aquatic community.

Introgression The incorporation of genes from one species into the gene pool of another; alternatively, breeding of a transgenic individual with wild-type individuals, leading to introduction and persistence of the transgene in the wild gene pool.

Novel trait Expression of a compound not normally found in the species, e.g., an antifreeze polypeptide in Atlantic salmon; alternatively, expression of a compound normally found in the species, but under novel gene regulation; for example, expression of a growth hormone gene under the transcriptional control of a promoter element not normally associated with the gene.

Risk The likelihood of harm resulting from exposure to a hazard.

Transgene An artificial DNA molecule containing a structural gene whose expression would confer a novel trait upon its host. The transgene would contain a regulatory element to control its expression in the host and an element signaling the point at which transcription would terminate and a poly-A tail added to the messenger RNA transcript.

Definition of the Subject

A transgenic fish or shellfish bears within its chromosomal DNA a gene construct – that is, a transgene, a gene whose expression is under novel regulation – that was introduced by human intervention. A variety of methods may be utilized to introduce foreign DNA into the genome of fishes [1]. Microinjection of a DNA vector into the cytoplasm of a fertilized egg was the first [2, 3] and remains the most commonly used method for producing founders of a transgenic line. Electroporation, the application of short electrical pulses to make the cell membrane permeable and thereby permit entry of DNA vectors into fertilized fish eggs, has been used to produce transgenic fishes [4, 5]. Electroporation also has been used to introduce DNA vectors into sperm, which in turn was utilized to fertilize eggs to produce transgenic founders [6]. A variation of the "gene gun" method, which involves bombardment of fertilized eggs with DNA-coated microprojectiles, was demonstrated using medaka, or rice fish, a model species [7]. Retroviruses [8] and transposable elements [9] have been modified to carry genes of interest and, using the ability of these elements to insert themselves into the genome of a host, to insert foreign DNA into zebrafish chromosomes.

Because they have large eggs, high fecundity, and external fertilization and development, fishes provide excellent systems for gene transfer. By introducing a major gene whose expression is under novel regulation, biotechnologists can achieve dramatic impacts upon valued phenotypes. Since the mid-1980s when the first transgenic fish were produced [2, 3], gene transfer studies have been conducted using over 35 species [1]. Following the demonstration of the concept [10], a variety of transgenic zebrafish, medaka, and other fishes have been developed as experimental models for biomedical research [11–13]. Many transgenic lines have been developed for potential use in aquaculture (see below), targeting growth rate enhancement and a variety of other production-related traits. Similarly, several sport fishes (e.g., northern pike [14]) have been transformed with growth hormone

genes in order to increase growth rate, aggressiveness, or ultimate size. Transgenic zebrafish expressing fluorescent proteins have been marketed as novel aquarium pets [15]. Transgenic lines have been developed for biomonitoring of chemicals in the aquatic environment [16–18].

Because they express novel traits, transgenic fish may prove attractive for aquaculture, fisheries management, or other applications. While production of transgenic fishes may prove profitable, there are broader and longer-term questions regarding whether such use would prove ecologically, economically, and socially sustainable. Because most transgenic fish lines have been produced for purposes of aquaculture, this contribution focuses upon sustainability of transgenic fishes intended for food production.

Transgenic Fishes: Applications, State of the Art, and Risk Concerns. Figure 1
A coho salmon expressing a salmon growth hormone transgene (*above*) exhibited growth that was dramatically greater than that of a same-aged, non-transgenic full-sibling (*below*) (Courtesy: R.H. Devlin)

Introduction

As world population increases, so also does its demand for fisheries products. However, since 1985, the total harvest from capture fisheries has fluctuated at approximately 90 million metric tons (MMT) [19], suggesting that capture fisheries are at or above maximum sustainable yields [20]. Since 1970, the contribution of aquaculture to world supplies of fisheries products has grown from approximately 5 MMT to over 50 MMT annually. Against this background, it is clear that the projected growth in demand for fisheries products can be met only through growth in production from aquaculture. The historical and projected growth in aquaculture raises the question of whether aquaculture is sustainable as currently practiced. First raised by the environmental community [21], the question then was critically examined by the aquaculture community itself [22]. Academic and commercial aquaculturists now are working to define and achieve sustainability [23–25]. Among key innovations so driven are changes in aquaculture feeds to decrease the content of scarce fish meal and oil [26, 27] and selective breeding to develop stocks of fish adapted to utilizing such feeds [28, 29]. There is increasing emphasis among aquaculturists on producing fishes that are herbivores or omnivores rather than carnivores. Within this broader context, whether transgenic fishes would contribute to the sustainability of aquaculture depends upon the host fish, the transgene, the confinement system in which the fish are raised, and any impacts that might follow should transgenic fish escape or be introduced into the accessible environment.

Traits targeted by transgenesis. A number of different traits have been targeted for genetic improvement via transgenesis. Growth hormone (GH) genes have been introduced into over a dozen aquaculture species to increase growth rate. Noteworthy examples where growth was increased several-fold relative to wild-type include Atlantic salmon [30, 31], coho salmon [32, Fig. 1], Nile tilapia [33], common carp [34], and rohu carp [35]. The most notable example of growth enhancement is that of mud loach, for which up to 35-fold growth rate enhancement was observed [36]. Antifreeze protein genes from Arctic or Antarctic fishes have been transferred to increase the tolerance of species sensitive to freezing in marine waters chilled to below the freezing point of fish flesh (e.g., Atlantic salmon [37]). Genes for bactericidal compounds have been introduced to heighten nonspecific disease resistance of cultured fishes (e.g., cecropin in channel catfish [38] and human lactoferrin in grass carp [39, 40]). The major storage form for phosphorus in grain is phytate, which is largely indigestible and has antinutritional properties; following demonstration that medaka transgenic for a microbial phytase gene exhibited improved phytate utilization [41], phytase also was transferred into tilapia [42]. Transgenic

approaches have been proposed for reproductive confinement of fish [43] (see also below), including expression of an antisense DNA complementary to the gonadotropin-releasing hormone transcript [44] and a "sterile-feral" *zBMP2* construct that blocks a critical developmental gene unless a repressor compound is applied to the animal in captivity [45]. When a key biochemical pathway is disrupted by lack of one enzyme, the function of that pathway can be restored by the expression of a transgene; for example, a rat L-gulono-γ-lactone oxidase transgene was introduced into rainbow trout in an attempt to complete the biosynthetic pathway for L-ascorbic acid [46]. While not exhaustive, these examples illustrate the scope of efforts to genetically improve cultured stocks of fishes using gene transfer methodologies.

Most transgenic lines described above have not been subject to the generations of breeding needed to develop a homozygous line stably expressing the transgene. However, development of some GH-transgenic lines is well advanced and efforts to commercialize them are ongoing. A/F protein, producers of GH-transgenic Atlantic salmon, have petitioned the US Food and Drug Administration for approval to market eggs of transgenic Atlantic salmon to commercial aquaculture producers [31]. The Cuban government is considering a request for production of GH-transgenic tilapia [47]. Marketing of a GH-transgenic common carp line is under consideration by the Chinese government [48]. With the prospect of improved production efficiency, it is not surprising that some aquaculturists want to produce GH-transgenic fish commercially. Commercialization of transgenic fishes, however, poses ecological, food safety, regulatory, and animal welfare concerns [49–52].

Confinement systems. Many different fish culture systems are in commercial use. Closed recirculating systems hold fish in indoor tanks and the water is treated in filtration systems; the associated expenses are such that only high-value species can be produced economically. Raceways are long, narrow outdoor tanks, with water from a spring routed through the system once and then discharged; rainbow trout are commonly reared in raceways. Ponds, which may have discharge to a nearby stream or river, are used to produce many species including tilapias and catfishes. Marine netpens, mesh cages suspended in bays or fjords, are used to produce Atlantic salmon, coho salmon, Atlantic cod, and other species. Ocean ranching involves release of juvenile salmon, trout, or charr into the ocean, to be collected later upon their return to spawn as adults. Clearly, these different types of culture systems vary in terms of their production economics and in their ability to reliably confine fishes.

Entry of cultured fish into the accessible ecosystem. Most commercial aquaculture operations have a routine, often significant escape of fish. Escapes can occur through equipment failures, during handling or transport operations, through predator intrusion into facilities, as a result of storms, or by other mechanisms. In particular, escapes of salmon and trout from marine net-pen facilities are common, ranging from minor incidents where a few fish escape to massive escapes. In the native range of Atlantic salmon, an estimated two million farmed salmon escape each year into the North Atlantic [53]. Outside the native range, millions of Atlantic salmon have escaped on the west coasts of North [54] and South America [55]. Although salmon farm operators are attempting to prevent escapes by upgrading confinement systems, installing predator deterrent devices, and other actions, it still must be assumed that escapes will occur [56].

Escape of cultured fish into the accessible ecosystem and interaction with local intraspecific and interspecific populations is a well-documented environmental concern [57–61]. The potential ecological and genetic interactions between cultured and wild fish have raised concern about the viability of affected wild stocks. Ecological concerns focus upon competition for space and food resources and direct predation [62]. Genetic concerns include the potential breakdown of locally adapted traits through interbreeding and introgression and range up to replacement of native stocks by cultured stocks [63]. Such concerns are posed by the prospect of producing transgenic fish in aquaculture, with the additional unknown posed by possible effects of the transgene. Because of the prospect of escape of cultured transgenic fish, we must consider not only the benefits of transgenic fish to aquaculture, but also any ecological and genetic hazards that they pose. Hazards posed by transgenic fish were first inferred on the basis of ecological principles [64–67], and then supported by empirical studies.

Ecological Risk Assessment for Transgenic Fish in the Accessible Ecosystem

Ecological risk assessment for transgenic organisms should be based upon case-by-case assessment of the host species, transgene construct, transgene integration site within the genome, and receiving ecosystem [49, 64, 68, 69]. Because most fishes do not have a long history of domestication, many cultured stocks retain the ability to survive and reproduce in the accessible ecosystem. Hence, consideration of ecological risk and genetic hazards posed by transgenic fish that might escape from a culture facility is appropriate.

Consideration of harms posed by transgenic fish must be based on an understanding of key concepts underlying the science and practice of risk analysis [49]. In this context, a *harm* is defined as a perturbation resulting in negative impacts to a species. A *hazard* is defined as an *agent or process* that has the potential to produce harm. A *risk* is defined as the *likelihood* of harm resulting from exposure to the hazard. Risk, R, is estimated as the product of the probability of exposure, $P(E)$, and the conditional probability of harm given that exposure has occurred, $P(H|E)$. That is, $R = P(E) \times P(H|E)$. The steps in risk analysis, then, are to: (1) identify potential harms; (2) identify hazards that might lead to harms; (3) define what exposure means for an aquaculture stock and assess the likelihood of exposure, $P(E)$; (4) quantify the likelihood of harm given that exposure has occurred, $P(H|E)$; and (5) multiply the resulting probabilities to yield a quantitative estimate of risk.

Exact probabilities of risk may prove difficult or impossible to determine for all types of possible ecological or genetic harm. Indeed, it is unlikely that all possible harms would be known *a priori*, particularly with respect to any indirect effects. Hence, it may be necessary – based on current knowledge of population genetics, population dynamics, receiving ecological communities, and experience with cultured stocks – to classify levels of concern regarding likely ecological and genetic impacts posed by cultured stocks into *qualitative* categories ranging from low to high.

Potential harms. Harms potentially posed by transgenic fishes would be the outcome of a chain of events occurring after escape or release from a culture system. Examples of harms that potentially might be realized by transgenic fishes entering or becoming established in an accessible ecosystem [49, 64–66] would include decline in abundance of loss of a native species. A locally adapted natural population could be replaced with a transgenic population or experience introgression of the transgene, decreasing the degree of local adaptation. Changes in ecosystem structure or function could result in decreased fisheries production or in ecosystem resiliency in the face of further ecological stressors.

Ecological hazards. Ecological hazards that could lead to harms becoming realized are posed to a range of species with which a transgenic fish might interact in the accessible ecosystem. Ecological hazards include the possibility of heightened predation or competition, as well as alteration of population or community dynamics due to activities of the transgenic fish. Examples from empirical studies illustrate some of these potential ecological hazards.

Several studies have focused on Atlantic salmon expressing a GH transgene. In order to support their rapid growth, these transgenic salmon have significantly faster routine metabolic rates and growth rates than domesticated and wild individuals of equal mass, and therefore require more energy to sustain body function [70, 71]. GH-transgenic salmon must consume food at a more rapid rate than control salmon. Abrahams and Sutterlin [72] observed behavior of size-matched transgenic and control salmon in experiments where fish could feed in safety or in the presence of the predator. Growth-enhanced transgenic fish were significantly more willing to risk exposure to a predator in order to gain access to food, and exhibited increased feeding rate and average speed of movement. However, transgenic fish reduced their exposure to predators in response to increases in the magnitude of risk, suggesting that their more active behavior may not necessarily lead to increased susceptibility to predation.

Devlin et al. [73] compared the intake of contested food pellets by size-matched pairs of one control (1 year older non-transgenic) and one transgenic coho salmon. The transgenic fish consumed 2.5 times more contested pellets than controls. Overall, transgenic fish consumed 2.9 times more pellets than non-transgenic controls, indicating high feeding motivation of transgenics throughout the feeding trials. In subsequent experiments, at low levels of food availability,

dominant, generally transgenic individuals dominated acquisition of food resources [74]. Further, when food availability was low, populations containing transgenics crashed, while in contrast, groups containing only non-transgenic salmon exhibited 72% survival and increase of population biomass. Hence, genotype-by-environment interactions affect ecological risk assessment. Sundstrom et al. [75] exposed GH transgenic and wild coho salmon fry to a live predator in a naturalized experimental stream tank under conditions of high and low food abundance. In both cases, mortality rates of transgenic fry were significantly higher than those of wild fry.

Ecological hazards posed by transgenic fish are not limited to salmonid species. Duan et al. [76] observed food consumption, frequency of movement, and feeding hierarchy in transgenic and size-matched control common carp under conditions of limited food supply. Transgenic fish consumed 1.9 times as many pellets, moved 73% more frequently, and exhibited a higher standing in the feeding hierarchy, but did not realize their higher growth potential. The authors concluded that elevated ability to compete for limited food resources could be advantageous to transgenic carp after escape into the accessible ecosystem.

These and other empirical findings to date tend to support the competitive ability of GH-transgenic fishes with conspecifics, and suggest the likelihood that ecological harms could become realized should large numbers of GH transgenics escape from culture or a transgenic population become established. Clearly, not all possible ecological interactions have been considered experimentally. Ecological hazards posed by transgenic fish expressing other sorts of transgenes, for example, a phytase gene that could confer ability to effectively utilize a broader range of foods, have not yet been examined empirically.

Given the range of interacting species and accessible ecosystems, and given the temporal and spatial variation of ecosystems, it is difficult to predict the ecological outcome should transgenic fish escape from aquaculture operations and enter accessible ecosystems. Devlin et al. [77] review methodologies to assess potential ecosystem effects of transgenic fish before they enter unconfined environments, outlining a strategy for identifying the most important data and discussing methods for obtaining them. Key issues include characterization of the accessible ecosystem, phenotypic characterization of the transgenic fish, experimentation appropriate for relating the transgenic phenotype and ecological impacts, and recognizing and accounting for sources of uncertainty.

Genetic hazards. Although reproductive confinement methodologies such as sterilization by triploidy or transgenesis have been proposed to minimize reproductive interaction between transgenic and wild fish (see below), to date these technologies have not been demonstrated to be completely effective [78]. Should transgenic fish be reproductively fertile, they potentially could interbreed with natural populations. Genetic or evolutionary impacts that could be realized would depend on the fitness of novel genotypes in the wild. There may be cases where fitness relative to the wild type is high, posing introgression of transgenes into natural populations. There may also be cases where maladaptive traits would be introduced into native populations, posing a hazard to the demographic viability of the receiving population. Empirical studies illustrate possible genetic hazards to wild populations of fish.

Considering the possible impact of introgression of transgenes into wild populations, Devlin et al. [79] examined growth enhancement due to expression of a GH transgene in both wild and selectively bred commercial rainbow trout strains and showed that the effect of expression of the transgene varied among the respective strains. Transgenic wild-strain rainbow trout retained the slender body morphology of the wild-type strain, but their final size at maturity was increased by transgenesis. Both domestic and wild-strain trout had reduced viability, and in the case of the domestic strain, all transgenic individuals died before sexual maturation. The greatest response to expression of the transgene was in hybrids of a wild and domesticated strain.

Devlin et al. [80] compared the reproductive performance of transgenic and non-transgenic coho salmon. GH-transgenic fish showed precocious smoltification and onset of sexual maturation but no increase of adult body size, indicating compression of the normal life history. However, strong genotype-by-environment interactions were shown for the effects of transgenesis and culture environment. Bessey et al. [81]

found no differences in gamete quality or in vitro offspring production. The transgenic fish were able to breed successfully in the absence of competition, but at a significantly lower level than hatchery fish (i.e., fish reared artificially as young and then released to complete their life history naturally). When in direct competition with hatchery fish, however, the transgenic coho salmon were competitively and reproductively inferior to the point where they had little or no success.

Models have been developed to predict the outcome of introgression of a transgene into a wild population, notably for cases where expression of the transgene differentially affects various components of fitness. Muir and Howard [82] developed a deterministic model that predicted that under certain conditions, a transgene introduced into a natural population by a small number of transgenic fish would spread as a result of enhanced mating advantage enjoyed by larger individuals, but the reduced viability of offspring would cause eventual local extinction of populations. The predicted time to extinction of a wild population would be a function of the mating advantage of transgenic males relative to that of wild-type males and the relative viability of transgenic offspring. Muir and Howard [83] subsequently considered a transgenic organism's fitness components (juvenile viability, adult viability, age at sexual maturity, female fecundity, male fertility, and mating advantage), using various combinations of fitness component values in addition to empirically derived estimates for medaka, a model species, to parameterize and run the model. For a wide range of parameter values, the model predicted that transgenes could spread through populations despite high juvenile viability costs if there were sufficiently high positive effects on other fitness components. Sensitivity analyses showed that transgene effects on age at sexual maturity would have the greatest effect on transgene frequency, followed by juvenile viability, mating advantage, female fecundity, and male fertility, with the least impact due to changes in adult viability. Extinction hazards also could be posed when the transgene: (1) increases male mating success but reduces adult viability; (2) increases adult viability but reduces male fertility; or (3) increases both male mating success and adult viability, but reduces male fertility [84]. Using a different approach, Hedrick [85] developed a deterministic model for invasion of transgenes into natural populations and showed that if a transgene gives rise to a male mating advantage and a general viability disadvantage, then the conditions for its invasion of a natural population are very broad. More specifically, for two-thirds of the possible combinations of mating and viability parameters, the transgene increased in frequency. In addition, the demographic viability of the natural population was reduced, increasing the probability of extinction of the natural population.

Kapuscinski et al. [86] presented a step-by-step method for assessing risk posed by gene flow and possible introgression of a transgene into a wild population (Fig. 2) considering probabilities of escape of a transgenic fish from confinement, encountering wild-type mates, reproducing, and the young surviving to transit the transgene to future generations. Currently, our empirical knowledge of genetic hazards posed by production of transgenic fish and shellfish and their associated risks is limited. Ecological risk assessments are ongoing for GH-transgenic coho and Atlantic salmon, as well as other transgenic fishes, including both model species and aquaculture species. Many critical experiments aimed at estimating fitness parameters [67, 83] have yet to be conducted.

Risk Management

Many key inputs for a quantitative ecological risk assessment currently are unknown. Further, many key aspects of risk assessment are difficult or impossible to address, given the spatial and temporal variability of ecosystems and the adaptive ability of populations. Under at least some circumstances, escaped transgenics could negatively impact accessible ecosystems and populations; hence, should a producer or oversight body determine that production of a transgenic stock poses harm to a population in the accessible ecosystem, the consideration then turns to managing the associated risk. From the viewpoint of ecological sustainability, risk might be managed by producing transgenic fish only under conditions of confinement. In some contexts, production of transgenic fish might go forward only under conditions of strict confinement aimed at ensuring no escape of transgenic fish into the accessible ecosystem.

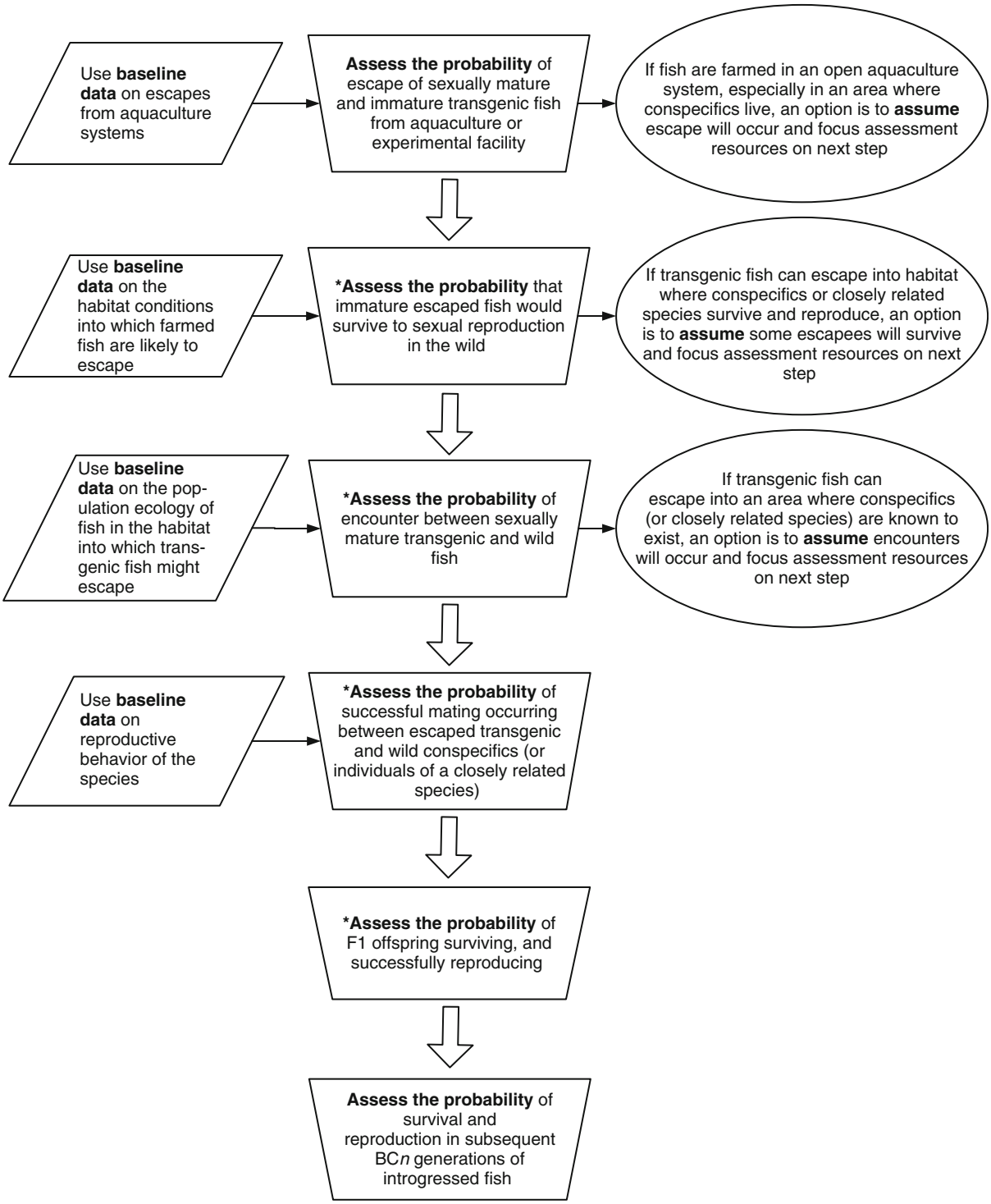

Transgenic Fishes: Applications, State of the Art, and Risk Concerns. Figure 2
A pathway for conducting an assessment of the risk of gene flow posed by a transgenic fish (From [86]). *Asterisks* denote assessment steps that require empirical information on traits exhibited by the transgenic fish

Risk management is the design, selection, and implementation of a program of actions to minimize risk. In the context of formal risk analysis, it becomes clear that the best approach for minimizing the likelihood of harm being realized is to minimize exposure to the hazard. Three non-mutually exclusive approaches include: (1) physically confining the cultured stock on aquaculture facilities, (2) reproductively confining cultured stocks, and (3) operations management. Management of risks posed by transgenic fishes has been considered for experimental [87] and commercial production systems [88].

Physical confinement. Physical confinement of cultured aquatic organisms will require a combination of measures in order to prove effective [87, 88]. Context is key; the ease or difficulty of managing risk will depend greatly on the geographic location of an aquaculture facility. Sites subject to flooding, violent storms, or wave action are poorly suited for confinement of production stocks. Virtually all physical confinement systems will include barriers to escape of cultured organisms from the culture site, including mechanical or physical/chemical barriers. Mechanical barriers are structures that physically hold back cultured organisms from escaping the project site. Examples include stationary or moving screens, (e.g., floor drains, standpipe screens), tank covers, filters (e.g., gravel traps), grinders or pumps, and French drains. A French drain is a filter for screening effluent from an aquaculture facility that contains gravel and geotextiles through which even small life-stages cannot pass. Physical or chemical barriers use manipulation of physical (e.g., elevation of temperature) or chemical (e.g., administration of chlorine) attributes of effluent water to induce 100% mortality of any escaped organisms before they can reach the accessible ecosystem. The set of barriers must prevent escape of the hardest-to-retain life-stage held at the aquaculture operation, usually the smallest life-stage. Because no barrier is 100% effective at all times, for effective physical confinement, each possible escape path from the aquaculture facility would have redundant barriers to escape of cultured organisms. Barriers also must prevent access of predators that can carry cultured organisms off-site (e.g., avian predators) or damage ponds (e.g., muskrats), allowing escape of cultured organisms.

Reproductive confinement. A key element of many risk management strategies is reproductive confinement, especially for cases where physical confinement alone is unlikely to prove effective. Two approaches, culture of monosex or sterile stocks, might be applied singly or in combination.

Procedures have been developed for producing monosex stocks of fish through direct, hormone-mediated sex reversal and indirectly by sex reversal, followed by progeny testing and selection of broodstock that yield monosex offspring. For example, production of all-female rainbow trout [89] and all-male Nile tilapia [90] stocks comprise growing segments of the respective aquaculture sectors. Production of monosex stocks may provide an acceptable high level of reproductive confinement in contexts where transgenic escapees have no possibility of encountering prospective mates in the accessible ecosystem. Production of monosex stocks will not provide reliable reproductive confinement if there is a population of the same species or of a closely related species with which escaped transgenics may hybridize in the accessible ecosystem. Further, for monosex production to provide reliable confinement, sex ratios would have to be absolutely monosex, an outcome which has not generally been achieved in commercial production [88].

Reproductive confinement also might be achieved through chromosome set manipulation. Fishes can be produced that have three, instead of the usual two chromosome sets. Such fish are said to be triploid, and are reproductively sterile because they produce gametes with unusual numbers of chromosomes. Should their eggs or sperm give rise to an embryo, the unmatched chromosomes would disrupt normal embryogenesis, leading to death of the embryo. All-triploid stocks can be produced most reliably by the crossing of diploid and tetraploid broodstock, although lack of tetraploid broodstock precludes the approach for many species. Alternatively, triploid stocks can be produced by *de novo* induction. *De novo* triploidy induction is not always 100% effective and, hence, triploid broods will have to be screened to determine whether they are indeed all-triploid [78]. This extra handling and screening add to the cost of seed-stock production.

Other approaches for reproductive confinement may become available in the future, including the possibility of reversible sterility through transgenesis. A transgene that produces antisense gonadotropin-releasing hormone

appears to cause sterility in male transgenic rainbow trout [44], but does not seem fully effective in females [91]. Use of a similar approach in tilapia sometimes greatly reduced fertility, but at other times was ineffective in both sexes (N. Maclean, quoted in [45]). Thresher et al. [45] developed a transgene that renders the host sterile, allowing normal development only if a repressor compound is applied during a particular life-history stage. The authors demonstrated its effectiveness in founder-generation transgenic zebrafish, channel catfish, and Pacific oyster. Definitive demonstration of this "sterile-feral" approach would require successful trials in homozygous transgenic lines and demonstration of the effectiveness of the repressor under commercial aquaculture conditions. Wang and Van Eenennaam [43] reviewed developing transgenic approaches to reproductive confinement of transgenic fishes, in addition to the approaches above also considering gonad-specific transgene excision. They suggested that slow progress in development of transgenic reproductive confinement systems is attributable to limited fundamental knowledge of possible gene targets to inactivate in order to induce sterility, preclude gondal development, or disrupt embryogenesis, as well as difficulties in implementing such highly technical approaches in vivo.

Operations management. Operations management is a key, though often overlooked, aspect of a confinement system [87, 88]. Measures are needed to: (1) ensure that normal activities of workers at the aquaculture operation are consistent with the goal of effective confinement, (2) prevent unauthorized human access to the site, and (3) ensure regular inspection and maintenance of physical confinement systems. Effective supervision of project personnel is critical for operations management.

Operations management also must consider biosecurity after cultured organisms are removed purposefully from the culture site, that is, harvested and transported through the marketing process. For biosecurity purposes, it would be best if only dead fish were sent to market. This is counter to marketing practices in many developing countries, where live sales prevail. Live sale is a known route for introductions of nonindigenous species, and exemplified by recent introduction and establishment of snakeheads in the USA [92].

Effective risk management calls for combinations of confinements. Combinations of risk management measures are advisable so that failure of any one measure will not necessarily lead to escape of confined stocks [87, 88]. It is infeasible to anticipate the best combination of risk management measures for every possible case. Differences in species, production traits, receiving ecosystems, and culture systems will affect the case-by-case determination of appropriate risk management measures.

Future Directions: Transgenic Fish Considered Within the Sustainability Paradigm

Interactive decision-making framework. Recognizing that sustainability has ecological, economic, and social dimensions, what conditions would have to be met for aquaculture production of transgenic fish to prove sustainable? The range of issues posed by a proposed utilization of transgenic fish in aquaculture might best be considered within in a three-stage, interactive framework involving a range of stakeholders [93, 94] (Fig. 3). Involvement of the full range of stakeholders would bring all existing knowledge into the deliberative process, make the process transparent to stakeholders, enhance the understanding and acceptance of the outcome of risk analysis, and promote social acceptance of the technology. Stage I of the process involves identifying the problem at hand, engaging stakeholders, identifying possible technical solutions to the problem at hand, and identifying potential harms, risk pathways, and assessment methods. Stage II of the process is risk assessment, leading to estimating the likelihood that harm will become realized should the proposed production of transgenic fish go forward. Upon estimation of that risk, a decision would be faced as to whether the risk is acceptable. If it proves acceptable, the decision may be made to go forward. If the level of risk proves unacceptably high, risk management measures would be identified and residual risk quantified, and the decision of whether to go forward would again be considered. Should the proposed action be implemented, genetic, ecological, and social outcomes should be monitored. As discussed below, because all potential harms and associated pathways cannot be known and precisely predicted *a priori*, it will be necessary to update the risk analysis as knowledge accumulates using an adaptive management approach [95, 96].

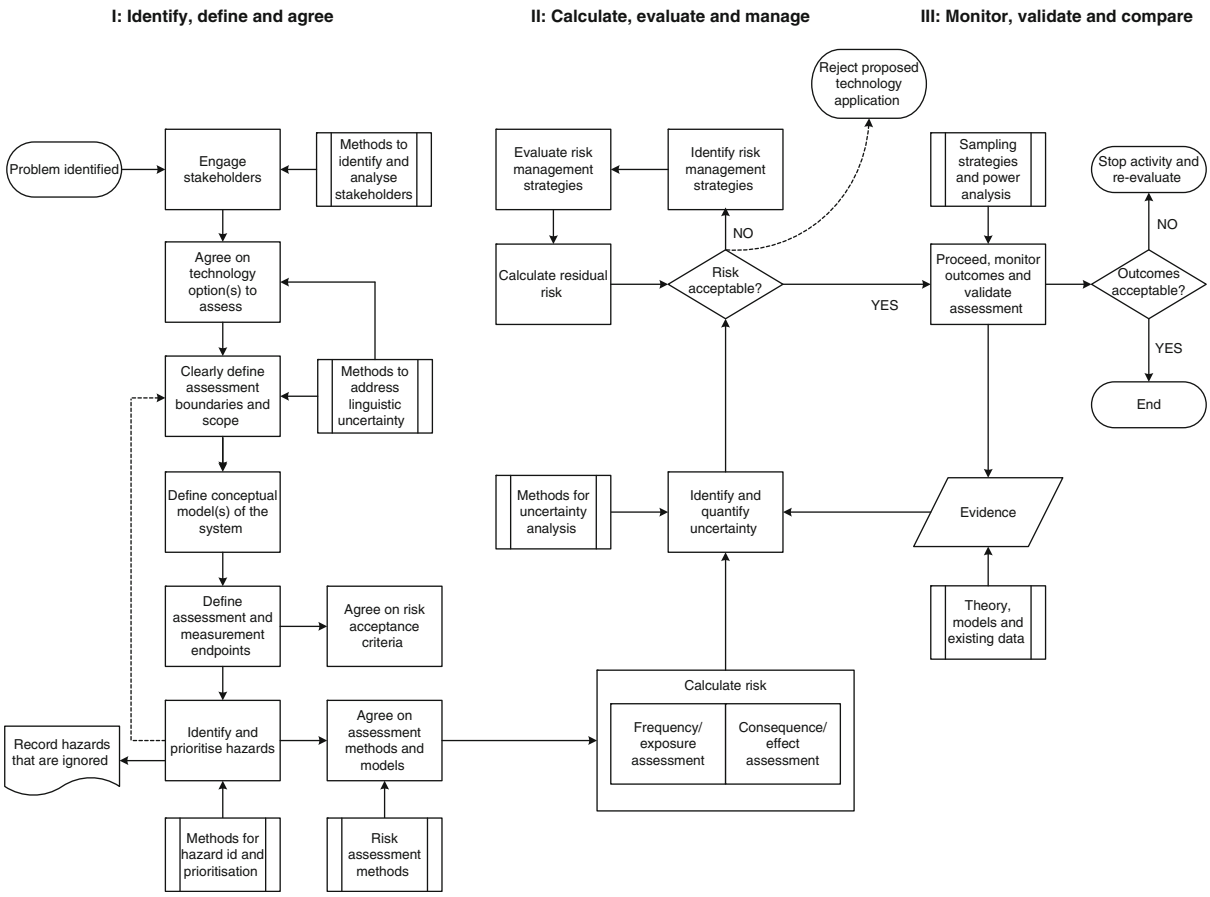

Transgenic Fishes: Applications, State of the Art, and Risk Concerns. Figure 3
Overview of a framework for environmental risk assessment of a transgenic fish embedded within a larger social context (From [94]). The framework has three stages. In the first stage, participants agree of an assessment option, define the scope of the assessment, agree on conceptual models, identify assessment and measurement end points, and agree upon a list of prioritized hazards. In the second stage, the risks and uncertainties associated with these hazards are assessed, risks are compared to predetermined acceptance criteria, and where necessary, risk management strategies are identified and evaluated. In the third stage, predictions of the risk assessment are compared with empirical findings, generating data used to reexamine uncertainty in the risk assessment

Trade-offs of benefits and risks. The prospect of producing transgenic fishes in aquaculture poses a mix of benefits and risks that would affect the assessment of whether such production would promote ecological, economic, and social sustainability within the decision-making framework. Consideration of several examples will illustrate how trade-offs among benefits and risks will affect the assessment of sustainability.

Benefits and hazards posed by GH transgenics have been considered empirically, and some of the associated risks have been quantified. GH-transgenic fish exhibit rapid growth and perhaps also improved feed conversion ratio, promoting production efficiencies in terms of more efficient utilization of inputs, including facilities, labor, and feedstuffs. However, as noted above, risk assessment research to date suggests a considerable likelihood of ecological or genetic impacts should GH transgenics escape into accessible ecosystems. This risk can be managed by adoption of an appropriate suite of risk management measures (see above). Risk management will have attendant costs, decreasing profitability by some as-yet unquantified

amount. Some segments of society are opposed to production of transgenic organisms [97], affecting the social aspect of whether this first wave of transgenic fishes will prove widely marketable and socially sustainable.

Empirical evaluations of both benefits and risks are yet to be conducted for other lines of transgenic fishes that may be considered for commercial production. Trade-offs among benefits and hazards may be anticipated. For example, as noted above, production of fish expressing a phytase transgene would take advantage of their ability to more efficiently utilize seed meals, increasing feed conversion efficiency and reducing the discharge of unutilized phosphorus from feed, decreasing eutrophication of waters in culture facilities and in waters receiving aquaculture discharges [41]. However, ability to efficiently utilize a wider range of natural foods might render escaped transgenic fish more competitive in accessible ecosystems. In particular, phytase-transgenic tilapia [42] might become even more competitive than wild-type tilapia, which are already recognized as invasive in a range of ecosystems in tropical and subtropical regions [98]. While effective confinement might be achievable in well-managed commercial operations, it likely cannot be achieved on subsistence farms, greatly influencing the assessment of whether phytase-transgenic tilapia would promote sustainability in developing countries.

As noted above, several transgenic fish lines have been produced for use as biomonitors [16–18] for detection of waterborne mutagens that would trigger expression of readily detected marker compounds in the fish. Such fishes would be exposed to such compounds by holding them in confinements in the waterbody of interest or by transporting the water to a confined fish-holding system. The benefits of long-term, integrative monitoring of water quality are clear. Any risks that might flow from the possibility of a nonindigenous species being used, escaping, and becoming naturalized in the waterbody at issue could be managed by use of effective confinement or by use of a species that cannot become established in the accessible ecosystem, for example, a tropical species sensitive to winter temperatures in the temperate zone.

These examples indicate how trade-offs of economic benefits and ecological risks, adoption of risk management measures, and ecological and social context interact to affect the sustainability of transgenic fishes for aquaculture and other applications. Explicit consideration of benefit and ecological risk, and hopefully also ecological, economic, and social aspects of sustainability would accompany societal consideration of whether and how to go forward with commercial production of transgenic fishes.

Oversight of production of transgenic fishes. The decision of whether and under what conditions production of transgenic fish would go forward will largely be made at the national level. As noted above, at least three countries – the USA, Cuba, and the People's Republic of China – are considering applications for commercial production of transgenic fish. The USA, Canada, the European Union, and Norway have regulatory systems in place for oversight of aquaculture biotechnology. Under Article 21 of the United Nations Convention on Environment and Development and the subsequent Cartagena Protocol, signatories commit to developing and implementing policies for oversight of biotechnology. Consequently, many countries – for example, Cuba, Thailand, and the People's Republic of China [99] – are in the process of developing and implementing policy and staffing government offices that would be utilized to consider applications for production of transgenic fish.

Adaptive and proactive management. Many critical unknowns complicate risk assessment and risk management for transgenic aquaculture stocks. The adaptive management approach is based on recognition that knowledge of the environmental and social systems into which the aquaculture stocks would enter is *always* incomplete. Hence, management should evolve as knowledge of these systems increases [96]. Management cannot adapt if realized by a single passage through transgenesis and breeding, decision of whether and how to produce the transgenic stocks, and implementation of the distribution and production process. Instead, adaptive management would include risk assessment for candidate areas for distribution, incorporation of risk management into the production program, and capacity building as appropriate to meet program goals. Once transgenic stocks are distributed, culture operations and receiving ecosystems would be monitored for indicators of ecological and social conditions [96, 100]. Should monitoring indicate

that economic and social benefits are being realized without ecological harms occurring, then few if any adjustments to program implementation are required. However, should monitoring indicate that production of cultured stocks is *not* contributing to nutritional and economic well-being or that the stocks are escaping and impacting accessible ecosystems, then it will prove necessary to redefine goals, revise implementation, and continue monitoring.

The issue of whether and under what conditions transgenic fish would promote sustainability of aquaculture has been raised largely after research and development on the first wave of transgenic fish lines was well advanced, after proponents have applied for regulatory approval for commercial production. Kapuscinski et al. [101] proposed a proactive "safety-first" approach in which an early, prospective risk assessment would be conducted in order to guide planning and implementation of measures to prevent or minimize risk as development of a transgenic line progresses. Transgene constructs would be designed for safety. Gene transfer scientists would strive for better control of copy number, genomic insertion site, and control of expression of the trangene, contributing to better-controlled modification of phenotype. Transgenic lines would be evaluated for stability of transgenic expression and transmission. Development of inducible expression of transgenes would reduce risk should transgenic fish escape into the environment. Improvements in confinement also would reduce risk posed by aquaculture production of transgenic fishes.

Applications of transgenic fishes, the science of risk assessment, the practice of risk management, and public policies for oversight of biotechnology are all in development. The degree to which production of transgenic fishes ultimately will prove sustainable will depend upon many societal decisions of whether and under what conditions to utilize transgenic technology in aquaculture.

Bibliography

Primary Literature

1. Zbikowska HM (2003) Fish can be first – advances in fish transgenesis for commercial applications. Transgenic Res 12:379–389
2. Zhu Z, Li G, He L, Chen S (1985) Novel gene transfer into the fertilized eggs of goldfish (*Carassius auratus* L. 1758). Z Angew Ichthyol 1:31–34
3. Chourrout D, Guyomard R, Houdebine L-M (1986) High efficiency gene transfer in rainbow trout (*Salmo gairdneri* Rich.) by microinjection into egg cytoplasm. Aquaculture 51:143–150
4. Inoue K, Yamashita S, Hata J, Kabeno K, Asada S, Nagahisa E, Fujita T (1990) Electroporation as a new technique for producing transgenic fish. Cell Diff Dev 29:123–128
5. Powers DA, Hereford I, Cole T, Chen TT, Lin CM, Kight K, Creech K, Dunham R (1992) Electroporation: a method for transferring genes into the gamete of zebrafish (*Brachiodanio rerio*), channel catfish (*Ictalurus punctatus*), and common carp (*Cyprinus carpio*). Mol Mar Biol Biotechnol 1:301–308
6. Muller F, Ivics Z, Erdelyi F, Papp T, Varadi I, Horvath L, Maclean N (1992) Introducing foreign genes into fish eggs with electoporated sperm as a carrier. Mol Mar Biol Biotechnol 1:276–281
7. Yamauchi M, Kinoshita M, Sasanuma M, Tsuji S, Terada M, Morimyo M, Ishikawa Y (2000) Introduction of a foreign gene into medakafish using the particle gun method. J Exp Zool 287:285–293
8. Ivics Z, Izsvak Z, Hackett PB (1993) Enhanced incorporation of transgenic DNA into zebrafish chromosomes by a retroviral integration protein. Mol Mar Biol Biotechnol 2:166–173
9. Izsvak Z, Ivics Z, Plasterk RH (2000) Sleeping beauty, a wide host-range transposon vector for genetic transformation in vertebrates. J Mol Biol 302:93–102
10. Stuart GW, McMurray JV, Westerfield M (1988) Replication, integration, and stable germ-line transmission of foreign sequences injected into early zebrafish embryos. Development 103:403–412
11. Dodd A, Curtis PM, Williams LC, Love DR (2000) Zebrafish: bridging the gaps between development and disease. Hum Mol Genet 9:2443–2449
12. Dooley K, Zon LI (2000) Zebrafish: a model system for the study of human disease. Curr Opin Genet Dev 10:252–256
13. Ward AC, Lieschke GJ (2002) The zebrafish as a model system for human disease. Front Biosci 7:827–833
14. Gross ML, Schneider JF, Moav N, Alvarez C, Myster SH, Liu Z, Hew C, Hallerman EM, Hackett PB, Guise KS, Faras AJ, Kapuscinski AR (1992) Molecular analysis and growth evaluation of northern pike (*Esox lucius*) microinjected with growth hormone genes. Aquaculture 103:253–273
15. Hallerman EM (2004) GloFish, the first GM animal commercialized, profits amid controversy. ISB (Information Systems for Biotechnology) news report, June 2004. www.isb.vt.edu/news/2004/artspdf/june0405.pdf, accessed November 22, 2010
16. Winn RN, Norris MB, Brayer KJ, Torres C, Muller SL (2000) Detections of mutations in transgenic fish carrying a bacteriophage λ cII transgene target. Proc Nat Acad Sci USA 97:12655–12660
17. Amanuma K, Takeda H, Amanuma H, Aoki Y (2000) Transgenic zebrafish for detecting mutations caused by compounds in aquatic environments. Nat Biotechnol 18:62–65

18. Carvan MJ III, Dalton TP, Stuart GW, Nebert DW (2000) Transgenic zebrafish as sentinels for aquatic pollution. Ann NY Acad Sci 919:133–147
19. Food and Agriculture Organization of the United Nations (2009) State of world fisheries and aquaculture. Fisheries and Aquaculture Department, FAO, Rome. http://www.fao.org, accessed October 30, 2009
20. Myers RA, Worm B (2003) Rapid worldwide depletion of predatory fish communities. Nature 423:280–283
21. Goldburg R, Triplett T (1997) Murky waters: environmental effects of aquaculture in the United States. Environmental Defense Fund, New York, p 198. www.edf.documents/490_AQUA.pdf, accessed November 22, 2010
22. Black KD (2001) Environmental impacts of aquaculture. CRC, Boca Raton, p 214
23. Bardach JE (ed) (1997) Sustainable aquaculture. Wiley, New York, p 251
24. Svennevig N, Reinertsen H, New M (eds) (1999) Sustainable aquaculture: food for the future? Balkema Publishers, Rotterdam, p 348
25. Jana BB, Webster CD (eds) (2003) Sustainable aquaculture: global perspectives. Haworth, New York, p 365
26. Gomes EF, Rema P, Kaushik SJ (1995) Replacement of fish meal by plant proteins in the diet of rainbow trout (*Oncorhynchus mykiss*): digestibility and growth performance. Aquaculture 130:177–186
27. Gatlin DM III, Barrows FT, Brown P, Dabrowski K, Gaylord TG, Hardy RW, Herman E, Hu G, Krogdahl A, Nelson R, Overturf K, Rust M, Sealey W, Skonberg D, Souza EJ, Stone D, Wilson R, Wurtele E (2007) Expanding the utilization of sustainable plant produce in aquafeed: a review. Aquacult Res 38: 551–579
28. Pierce LR, Palti Y, Silverstein JT, Barrows FT, Hallerman EM, Parsons JE (2008) Family growth response to fishmeal and plant-based diets shows genotype x diet interaction in rainbow trout (*Oncorhynchus mykiss*). Aquaculture 278:37–42
29. Dupont-Nivet M, Medale F, Leonard J, LeGuillou S, Tiquet F, Quillet E, Geurden I (2009) Evidence of genotype-diet interactions in the response of rainbow trout (*Oncorhynchus mykiss*) clones to a diet with or without fishmeal at early growth. Aquaculture 295:15–21
30. Du SJ, Gong ZY, Fletcher GL, Shears MA, King MJ, Idler DR, Hew CL (1992) Growth enhancement in transgenic Atlantic salmon by the use of an all-fish chimeric growth hormone gene construct. Biotechnology 10:176–181
31. Fletcher GL, Shears MA, Yaskowiak ES, King MJ, Goddard SV (2004) Gene transfer: potential to enhance the genome of Atlantic salmon for aquaculture. Aust J Exp Agric 44: 1095–1100
32. Devlin RH, Yesaki TY, Biagi CA, Donaldson EM, Swanson P, Chan WK (1994) Extraordinary salmon growth. Nature 371:209–210
33. Rahman MA, Ronyai A, Engidaw BZ, Jauncey K, Hwang GL, Smith A, Roderick E, Penman D, Varadi L, Maclean N (2001) Growth and nutritional trials on transgenic Nile tilapia containing an exogenous fish growth hormone gene. J Fish Biol 59:62–78
34. Hinits Y, Moav B (1999) Growth performance studies in transgenic *Cyprinus carpio*. Aquaculture 173:285–296
35. Venugopal T, Anathy V, Kirankumar S, Pandian TJ (2004) Growth enhancement and food conversion efficiency of transgenic fish, *Labeo rohita*. J Exp Biol 301A:477–490
36. Nam YK, Noh JK, Cho YS, Cho HJ, Cho KN, Kim CG, Kim DS (2001) Dramatically accelerated growth and extraordinary gigantism of transgenic mud loach *Misgurnus mizolepis*. Transgenic Res 10:353–362
37. Hew CL, Poon R, Xiong F, Gauthier S, Shears M, King M, Davies P, Fletcher G (1999) Liver-specific and seasonal expression of transgenic Atlantic salmon harboring the winter flounder antifreeze protein gene. Transgenic Res 8:405–414
38. Dunham RA, Warr GW, Nichols A, Duncan PL, Argue B, Middleton D, Kucuktas H (2002) Enhanced bacterial disease resistance of transgenic channel catfish *Ictalurus punctatus* possessing cecropin genes. Mar Biotechnol 4:338–344
39. Zhong J, Wang Y, Zhu Z (2002) Introduction of the human lactoferrin gene into grass carp (*Ctenopharyngodon idellus*) to increase resistance against GCH virus. Aquaculture 214: 93–101
40. Mao W, Wang Y, Wang W, Wu B, Feng J, Zhu Z (2004) Enhanced resistance to *Aeromonas hydrophila* infection and enhanced phagocytic activities in human lactoferrin-transgenic grass carp (*Ctenopharyngodon idellus*). Aquaculture 242:93–103
41. Hostetler HA, Collodi P, Devlin RH, Muir WM (2005) Improved phytate phosphorus utilization by Japanese medaka transgenic for the *Aspergillus niger* phytase gene. Zebrafish 2:19–31
42. Kemeh H (2004) Development of phytase transgenic Nile tilapia. Ph.D. dissertation, Purdue University, West Lafayette. www.docs.lib.purdue.edu, accessed October 30, 2009
43. Wong AC, Van Eenennaam AL (2008) Transgenic approaches for the reproductive containment of genetically engineered fish. Aquaculture 275:1–12
44. Uzbekova S, Chyb J, Ferrierre F, Bailhache T, Prunet P, Alestrom P, Breton B (2000) Transgenic rainbow trout expressed sGnRH-antisense RNA under the control of sGnRH promoter of Atlantic salmon. J Mol Endocrinol 25:337–350
45. Thresher R, Grewe P, Patil J, Whyhard S, Templeton M, Chaimongkol A, Hardy C, Hinds L, Dunham R (2009) Development of repressible sterility to prevent the establishment of feral populations of exotic and genetically modified animals. Aquaculture 290:104–109
46. Krasnov A, Pitkanen TI, Molsa H (1999) Gene transfer for targeted modification of salmonid fish metabolism. Genet Anal 15:115–119
47. Guillen I, Berlanga J, Valenzuela CM, Morales A, Toledo J, Estrada MP, Puentes P, Hayes O, LaFuente J (1999) Safety evaluation of transgenic tilapia with accelerated growth. Mar Biotechnol 1:2–14
48. Wu G, Sun Y, Zhu Z (2003) Growth hormone gene transfer in common carp. Aquat Living Resour 16:416–420

49. National Research Council (2002) Animal biotechnology: science-based concerns. National Academy, Washington, DC, p 179. http://www.nap.org, accessed November 22, 2010
50. Pew Initiative on Food and Biotechnology (2003) Future fish: issues in science and regulation of transgenic fish. www.pewtrusts.org/our_work_report_detail.aspx?id.33350, accessed November 22, 2010
51. Food and Agriculture Organization of the United Nations and World Health Organization (2004) Safety assessment of foods derived from genetically modified animals, including fish. FAO food and nutrition paper 79, FAO, Rome
52. Hallerman EM, McLean E, Fleming IA (2006) Effects of growth hormone transgenes on the behavior and welfare of aquacultured fishes: a review identifying research needs. Appl Anim Behav Sci 104:265–294
53. Schiermeier Q (2003) Fish farms' threat to salmon stocks exposed. Nature 425:753
54. Volpe J, Taylor E, Rimmer D, Glickman B (2000) Evidence of natural reproduction of aquaculture-escaped Atlantic salmon in a coastal British Columbia River. Conserv Biol 14:899–903
55. Soto D, Jara F, Moreno C (2001) Escaped salmon in the inner seas, southern Chile: facing ecological and social conflicts. Ecol Appl 11:1750–1762
56. Council on Environmental Quality and Office of Science and Technology Policy (2000) Case study no. 1: growth-enhanced salmon. http://www.ostp.gov/what'snew/casestudies, accessed January 20, 2000
57. Schramm HL Jr, Piper RG (eds) (1995) Uses and effects of cultured fishes in aquatic ecosystems. In: American fisheries society symposium 15, American Fisheries Society, Bethesda
58. McGinnnity P, Prodohl P, Ferguson A, Hynes R, Maoilieidigh NO, Baker N, Cotter D, O'Hea B, Cooke D, Rogan G, Taggart J, Cross T (2003) Fitness reduction and potential extinction of wild populations of Atlantic salmon, *Salmo salar*, as a result of interactions with escaped farmed salmon. Proc R Soc Lond B 270:2443–2450
59. Fleming IA, Hindar K, Mjølnerød IB, Jonsson B, Balstad T, Lamberg A (2000) Lifetime success and interactions of farm salmon invading a native population. Proc R Soc Lond B 267:1517–1523
60. Nickum, MJ, Mazik PM, Nickum JG, MacKinlay DD (eds). (2004) Propagated fish in resource management. In: American fisheries society symposium 44, American Fisheries Society, Bethesda, MD
61. Verspoor E, Stradmeyer L, Nielsen JL (eds) (2007) The Atlantic salmon: genetics, conservation, and management. Blackwell, Oxford
62. Gross M (1998) One species with two biologies: Atlantic salmon (*Salmo salar*) in the wild and in aquaculture. Can J Fish Aquat Sci 55:131–144
63. Saegrov H, Hindar K, Kalas S, Lura H (1997) Escaped farmed Atlantic salmon replace the original salmon stock in the River Vosso, western Norway. ICES J Mar Sci 54:1166–1172
64. Kapuscinski AR, Hallerman EM (1990) Transgenic fish and public policy. Anticipating environmental impacts of transgenic fish. Fisheries 15(1):2–11
65. Kapuscinski AR, Hallerman EM (1991) Implications of introduction of transgenic fish into natural ecosystems. Can J Fish Aquat Sci 48(Suppl 1):99–107
66. Hallerman EM, Kapuscinski AR (1992) Ecological implications of using transgenic fishes in aquaculture. ICES Mar Sci Symp 194:56–66
67. Hallerman EM, Kapuscinski AR (1993) Potential impacts of transgenic and genetically manipulated fish on wild populations: addressing the uncertainties through field testing. In: Cloud JG, Thorgaard GH (eds) Genetic conservation of salmonid fishes. Plenum, New York, pp 93–112
68. Tiedje JM, Colwell RK, Grossman YL, Hodson RE, Lenski RE, Mack RN, Regal PJ (1989) The planned introduction of genetically engineered organisms: ecological considerations and recommendations. Ecology 70:298–315
69. Snow A, Andow D, Gepts P, Hallerman E, Powers A, Tiedje J, Wolfenbarger L (2005) Ecological risks and benefits associated with the environmental release of GMOs. Ecol Appl 15:377–404
70. Stevens ED, Sutterlin A, Cook T (1998) Respiratory metabolism and swimming performance in growth hormone transgenic Atlantic salmon. Can J Fish Aquat Sci 55:2028–2035
71. Cook JT, McNiven MA, Sutterlin AM (2000) Metabolic rate of pre-smolt growth-enhanced transgenic Atlantic salmon (*Salmo salar*). Aquaculture 188:33–45
72. Abrahams MV, Sutterlin A (1999) The foraging and antipredator behavior of growth-enhanced transgenic Atlantic salmon. Anim Behav 58:933–942
73. Devlin RH, Johnsson JI, Smailus DE, Biagi CA, Johnsson E, Bjornsson BT (1999) Increased ability to compete for food by growth hormone transgenic coho salmon (*Oncorhynchus kisutch* Walbaum). Aquacult Res 30:1–4
74. Devlin RH, Biagi CA, Yesaki TY (2004) Growth viability and genetic characteristics of GH transgenic coho salmon strains. Aquaculture 236:607–632
75. Sundstrom LF, Lohmus M, Johnsson JI, Devlin RH (2004) Growth hormone transgenic salmon pay for growth potential with increased predation mortality. Proc R Soc Lond B 271:S350–S352
76. Duan M, Zhang T, Hu W, Sundstrom LF, Wang Y, Li Z, Zhu Z (2009) Elevated ability to compete for limited food resources by "all-fish" growth hormone transgenic common carp (*Cyprinus carpio* L.). J Fish Biol 75:1459–1469
77. Devlin RH, Sundstrom LF, Johnsson JI, Flaming IA, Hayes KR, Ojwang WO, Bamaradeniya C, Zakaria-Ismail M (2007) Assessing ecological effects of transgenic fish prior to entry into nature. In: Kapuscinski AR, Hayes KR, Li S, Dana G, Hallerman EM, Schei PJ (eds) Environmental risk assessment of genetically modified organisms, vol 3, Methodologies for transgenic fish. CAB International, Wallingford, Oxfordshire, pp 151–187
78. National Research Council (2004) Biological confinement of genetically engineered organisms. National Academy, Washington, DC, p 255. http://www.nap.org, accessed November 22, 2010
79. Devlin RH, Biagi CA, Yesaki TY, Smailus DE, Byatt JC (2001) A growth-hormone transgene boosts the size of wild but not domesticated trout. Nature 409:781–782

80. Devlin RH, D'Andrade M, Uh M, Biagi CA (2004) Population effects of growth hormone transgenic coho salmon depend on food availability and genotype by environment interactions. Proc Nat Acad Sci USA 101: 9303–9308
81. Bessey C, Devlin RH, Liley NR, Biagi CA (2004) Reproductive performance of growth-enhanced transgenic coho salmon. Trans Am Fish Soc 133:1205–1220
82. Muir WM, Howard RD (1999) Possible ecological risks of transgenic organism release when transgenes affect mating success: sexual selection and the Trojan gene hypothesis. Proc Nat Acad Sci USA 96:13853–13856
83. Muir WM, Howard RD (2001) Fitness components and ecological risks of transgenic release: a model using Japanese medaka (*Oryzias latipes*). Am Nat 158:1–16
84. Muir WM, Howard RD (2002) Assessment of the possible ecological risks and hazards of transgenic fish with implications for other sexually reproducing organisms. Transgenic Res 11:101–114
85. Hedrick PW (2001) Invasion of transgenes from salmon or other genetically modified organisms into natural populations. Can J Fish Aquat Sci 58:841–844
86. Kapuscinski AR, Hard JJ, Paulson KM, Neira R, Ponniah A, Kamonrat W, Mwanja W, Fleming IA, Gallardo J, Devlin RH, Tresiak J (2007) Approaches to assessing gene flow. In: Kapuscinski AR, Hayes KR, Li S, Dana G, Hallerman EM, Schei PJ (eds) Environmental risk assessment of genetically modified organisms, vol 3, Methodologies for transgenic fish. CAB International, Wallingford, Oxfordshire, pp 112–150
87. Agricultural Biotechnology Research Advisory Committee – US Department of Agriculture (1995) Performance standards for safely conducting research with genetically modified fish and shellfish. http://www.isb.vt.edu/perfstands, accessed October 30, 2009
88. Mair GC, Nam YK, Solar II (2007) Risk management: reducing risk through confinement of transgenic fish. In: Kapuscinski AR, Hayes KR, Li S, Dana G, Hallerman EM, Schei PJ (eds) Environmental risk assessment of genetically modified organisms, vol 3, Methodologies for transgenic fish. CAB International, Wallingford, Oxfordshire, pp 209–238
89. Bye VJ, Lincoln RF (1986) Commercial methods for the control of sexual maturation of rainbow trout (*Salmo gairdneri*). Aquaculture 57:299–309
90. Mair GC, Abucay JS, Skibinski DOF, Abella TA, Beardmore JA (1997) Genetic manipulation of the sex ratio for large scale production of all-male tilapia *Oreochromis niloticus* L. Can J Fish Aquat Sci 54:396–404
91. Dunham RA (2004) Aquaculture and fisheries biotechnology: genetic approaches. CABI, UK, p 372
92. Dolin EJ (2003) Snake head: a fish out of water. Smithsonian Books, Washington, DC
93. Kapuscinski AR, Li S, Hayes K, Dana G, Hallerman E, Schei P (eds) (2007) Environmental risk assessment of genetically modified organisms, vol 3, Methodologies for transgenic fish. CABI Publishers, Wallingford, Oxfordshire
94. Hayes KR, Kapuscinski AR, Dana G, Li S, Devlin RH (2007) Introduction to environmental risk assessment for transgenic fish. In: Kapuscinski AR, Hayes KR, Li S, Dana G, Hallerman EM, Schei PJ (eds) Environmental risk assessment of genetically modified organisms, vol 3, Methodologies for transgenic fish. CAB International, Wallingford, Oxfordshire, pp 1–28
95. National Research Council (1996) Understanding risk: informing decisions in a democratic society. National Academy, Washington, DC
96. Kapuscinski, AR, Nega T, Hallerman EM (1999) Adaptive biosafety assessment and management regimes for aquatic genetically modified organisms in the environment. In: Pullin RSV, Bartley DM, Kooiman J (eds) Towards policies for conservation and sustainable use of aquatic genetic resources. In: ICLARM (International Center for Living Aquatic Resources Management) conference proceedings 59, pp 225–251
97. Rollin BE (1995) The Frankenstein syndrome: ethical and social issues in the genetic engineering of animals. Cambridge University Press, Cambridge, UK
98. Moreau J (1983) A review of introductions of tilapia in open waters of Africa, their influence on ecology and fisheries. In: Fishelson L, Yaron Z (eds) International symposium on tilapia in aquaculture, Tel Aviv University Press, Nazareth, Israel, May 8–13 1983, pp 77–85
99. Nelson KC, Basiao Z, Cooper AM, Dey M, Foniciella D, Lorenzo Hernandez M, Kunawasen S, Leelapatra W, Li S, Ratner BD, Toledo MI (2007) Problem formulation and options assessment: science-guided deliberation in environmental risk assessment of transgenic fish. In: Kapuscinski AR, Hayes KR, Li S, Dana G, Hallerman EM, Schei PJ (eds) Environmental risk assessment of genetically modified organisms, vol 3, Methodologies for transgenic fish. CAB International, Wallingford, Oxfordshire, pp 29–60
100. Senenan W, Hard JJ, Alcivar-Warren A, Trisak J, Zakaria-Ismail M, Lorenzo Hernandez M (2007) Risk management: post-approval monitoring and remediation. In: Kapuscinski AR, Hayes KR, Li S, Dana G, Hallerman EM, Schei PJ (eds) Environmental risk assessment of genetically modified organisms, vol 3, Methodologies for transgenic fish. CAB International, Wallingford, Oxfordshire, pp 239–271
101. Kapuscinski AR, Goodman RM, Hann SD, Jacobs LR, Pullins EE, Johnson CS, Kinsey JD, Krall RL, La Vina A, Mellon M, Ruttan V (2003) Making "safety first" a reality for biotechnology products. Nature Biotech 21:599–601

Books and Reviews

Beaumont AR, Hoare K (2003) Biotechnology and genetics in fisheries and aquaculture. Blackwell, Oxford, p 158

Bondad-Reantaso MG, Arthur JR, Subasinghe RP (eds) (2008) Understanding and applying risk analysis in aquaculture. FAO fisheries technical paper, no 519. FAO, Rome

Devlin RH, Sundstrom LF, Muir WM (2006) Interface of biotechnology and ecology for environmental risk assessments of transgenic fishes. Trends Biotechnol 24:89–97
Ennion SJ, Goldspink G (eds) (1996) Gene expression and manipulation in aquatic organisms. Cambridge University Press, Cambridge, UK, p 214
Hew CL, Fletcher GL (eds) (1992) Transgenic fish. World Scientific Publishing Co., Singapore
Hew CL, Fletcher GL (2001) The role of aquatic biotechnology in aquaculture. Aquaculture 197:191–204
Iyengar A, Muller F, Maclean N (1996) Regulation and expression of transgenes in fish – a review. Transgenic Res 5:147–166
Maclean N, Laight RJ (2000) The application of gene manipulation to aquaculture. Aquaculture 85:1–20
McLean E, Devlin RH (2000) Application of biotechnology to enhance growth of salmonids and other fish. In: Fingerman M, Nagabhushanam R (eds) Recent advances in marine biotechnology, vol 4, Aquaculture, Part B: Fishes. Science Publishers, Enfield, pp 17–55
Mench JA (1999) Ethics, animal welfare and transgenic farm animals. In: Murray JD, Anderson GB, Oberbauer AM, McGloghlin MM (eds) Transgenic animals in agriculture. CABI International, Wallingford, pp 251–268
Millar K, Tomkins S (2007) Ethical analysis of the use of GM fish: emerging issues for aquaculture. J Agr Environ Ethic 20:437–453
Organization for Economic Cooperation and Development (1995) Environmental impacts of aquatic biotechnology. OECD, Paris
Rasmussen RS, Morrisey MT (2007) Biotechnology in aquaculture: transgenics and polyploidy. Comp Rev Food Sci Food Safety 6:2–16

Transgenic Livestock for Food Production, Introduction

C. Bruce A. Whitelaw
The Roslin Institute and Royal (Dick) School of Veterinary Studies, Division of Developmental Biology, University of Edinburgh, Scotland, UK

Our societies currently face many big challenges: how to feed the increasing world population, how to balance the competing demands for land and water, how to mitigate climate change, and how to maintain healthy lifestyle into old age. Among other technologies, the animal genetic revolution offers several strategies to mitigate these challenges and provide benefit for mankind. While achieving this, we need to maintain and where appropriate increase the welfare and existence of animals we use in agriculture and biomedicine. Transgenic technologies, the ability to add or transfer or change the genetic makeup of an animal, can contribute. In the following ten entries, this premise is presented in detail. Why the entries were selected and how they complement each other while giving an overview of the field of transgenic animal biotechnology is described below.

The cornerstone of biological research is the ability to experimentally alter gene activity. In this way, the functional importance of a gene can be studied. This can be achieved indirectly through altering the environment of cells or organisms, for example, adding specific nutrients to a culture condition or infecting with a pathogen. Alternatively, direct manipulation can be achieved through genetic engineering. This section focuses on the later strategy which includes gene addition, gene removal (or inactivation), or gene alteration. To illustrate this, gene addition might be appropriate where an enhanced functionality is required such as food utilization, while gene inactivation would be appropriate if the aim was to remove a food allergen. Both have been successfully applied to animals and this is likely to be so going forward. In addition, as methodology becomes more sophisticated and the ability to directly alter a given gene sequence, this strategy will see more and more application; for example, where gene diversity is identified that could be applied to engineer altered metabolism or reduce disease susceptibility.

Although initially performed in bacteria, researchers quickly developed the tools to genetically modify animals. First in mice at the end of the 1970s, then livestock in the following decade, in parallel strategies for altering the germ line in fish and birds were developed. Researchers have developed strategies which enable precise spatial and temporal changes to target gene activity. Many consider transgenic or genetic modification (GM) methods (► Transgenics: Alternative Gene Transfer Methods) as part of the technical continuum that is available to animal breeders. As such, GM or transgenic animal technology would simply represent new methodology alongside the more established tools as artificial insemination and embryo transfer. These new animal reproductive tools include somatic cloning and in vitro embryo production, and when combined with the emerging molecular genetic tools provide powerful new opportunities for livestock breeding.

The first transgenic livestock were reported in 1985. Since these early days of this technology, there has been

a steady increase in the availability of tools available (► Transgenic Livestock Technologies) for this form of assisted reproduction in animals. Some developments have been heralded as breakthroughs only to quickly drop out of favor while others have received limited use. Recently, reagents based on precisely targeted enzymatic cleavage of the genome that in addition to strategies such as gene knockdown provide the animal geneticist with both efficient and sophisticated methods with which to generate transgenic animals.

Perhaps one of the most consequential scientific advances of recent years was the technical breakthrough that produced "Dolly" the sheep at the Roslin Institute. This animal was produced by nuclear transfer (also termed SCNT, somatic cell nuclear transfer), or as it is commonly referred to as cloning. Animal cloning involves the replacement of the genetic material found in an unfertilized egg with that from a donor cell's genetic material. SCNT reflects considerable scientific thinking and offers the experimental biologist considerable insights into the functional reprogramming of cellular function in addition to details of cellular subcomponent roles in normal cell activity (► Livestock Somatic Cell Nuclear Transfer). In addition to being a valuable aspect of research in its own right, SCNT can be combined with genetic engineering tools to precisely modify the genome of mammals (► Nuclear Transfer to Produce Transgenic Mammals). This combination offers exciting commercial opportunities across the fields of agriculture and animal breeding, to the biomedical arena and novel biotechnological processes.

Transgenic technologies are not restricted to mammals. Due to its use in food production and as an experimental organism in scientific research, the chicken is the most widely used bird species for experimental development of avian transgenic technologies (► Avian Specific Transgenesis). Perhaps the most exiting recent advance is that of precise gene modification in special avian cells called primordial stem cells. These new tools offer strategies for the production of transgenic birds other than the chicken. As such, this is an area currently experiencing rapid development and many expect it will be in birds that GM technologies will be first successfully exploited to produce animals that have enhanced resistance to infectious pathogens.

Although it can be argued that technically transgenic technology is most advanced for mammals, and currently developing quickest for birds, it is considered very likely that the first commercial application of transgenic animals that will enter the food chain will be in fish (► Transgenic Fishes: Applications, State of the Art, and Risk Concerns). Fish that grow faster are providing the first test of the regulatory systems while providing the focus for much debate on broader and longer-term questions regarding whether such use would prove ecologically, economically, and socially sustainable. There is also considerable effort being directed at the development of transgenic strategies to combat disease in fish populations, and the technology can be equally applied to food fish as to sport fish.

As the world population increases there is an increasing demand for food including both plant and animal products. The demand for meat and milk are increasing at a faster rate than for plant products because of increased wealth in developing countries. Animal products represent a concentrated protein and vitamin source which complements cereal and other vegetable proteins. Intensification of livestock production to satisfy the demand is exacerbating the deleterious impact of intensive animal agriculture on the environment and new approaches are needed to reduce the impact. Transgenic animals that have a smaller environmental footprint, increased productivity brought about by enhancing aspects of agriculturally important traits can contribute to this societal challenge. For this potential to be realized an active dialogue between all stakeholders is required to achieve ethically accepted sustainable future animal production.

The animals we all recognize in farms today are the result of many centuries of domestication. The driving force for this has largely come from man's desire for meat. This single process has shaped the rural landscape we all recognize today. It is therefore not surprising that animal breeders look to transgenic strategies to enhance the traditional animal breeding traits including food production (► Transgenic Livestock, Enhanced Nutritional Quality in). The focus now is not on quantity but on quality, while reflecting the rapid industrialization of our world and the associate increase in affluence experienced by many (but not all) of our communities. Food choice is now considered alongside sustainability. Animal welfare is paramount while still recognizing that many of the world

population live in poverty with starvation a constant threat. Transgenic technologies offer the potential of quick solutions to the production of food products with enhanced specific nutritional characteristics from animals. The goal is healthier and safer food. However, this potential will only be realized with consumer acceptance in GM technology.

Two specific examples of traditional breeding traits that transgenic technology may provide innovative solutions are worthy of specific attention. The first is that of animal fertility (► Transgenic Technologies and Increased Livestock Fertility). Reproductive efficiency of domestic animals is critical to the sustainability of modern livestock industries. With various indicators of reducing fertility now appearing in our farms it is timely to consider innovative approaches to halt this decline. Aspects under investigation include increasing litter size in livestock or egg-laying capacity in poultry. More radically this technology could be applied to reduce the limitations associated with seasonal breeding.

The second topic that is attracting considerable interest in both the scientific research community and in the animal breeding industry is that of animals that are less susceptible to the ravages and distress of disease (► Disease-Resistant Transgenic Animals). Offering both enhanced animal welfare and economic advantages this field is both fast moving and innovative, building much on the genomic revolution which is in turn constructed from the strong discipline of genetics. With huge impact on global animal health and the associated impact of zoonotic disease in man, this is an area which offers huge benefit to man and animal alike.

The simultaneous need for more food as the world population expands and that of limiting both short-term and longer-term environmental consequences is a huge challenge for man. Increased animal productivity could directly compromising our environment. Transgenic technology through providing animals that have a smaller environmental footprint (► Transgenic Livestock, Decreasing Environmental Impact of) could form an important part of the compromise that is inevitable if we are to provide sufficient food for our increasing human needs. Under development are projects aiming to reduce manure output and decrease greenhouse gas production. It is argued that the food security agenda being promoted by many governments will lead to greater acceptance of transgenic animals, following the slow but every increasing presence and consumption of transgenic plant products.

Transgenic animals present a dilemma for us. This technology offers rapid change with the promise of economic benefit, enhanced food security and better animal welfare. Yet transgenic technologies directly challenge many ethical aspects of thinking (► Transgenic Livestock, Ethical Concerns and Debate). Central to the process of acceptance is a conscious dialogue between all stakeholders – to build up a generally acceptable stance on what is good with respect to the ethical limits of human use of animals.

At the time of writing, there are no transgenic livestock in production – with faster growing fish being the closest and disease resistant birds being the most exciting. By the time of reading, this may well have changed – or be close to such a scenario. Agricultural advances have been enormously successful in providing an inexpensive supply of high-quality and safe foods. The new advance of transgenesis is likely to continue this trend providing some of the solutions to tomorrow's agricultural challenges. Governmental and industrial financial support – ideally in equal measures – is needed to achieve this. Equally important is the public dialogue to expose the benefits this technology can offer all stakeholders in our diverse world society.

Transgenic Livestock Technologies

Cesare Galli[1,2], Andrea Perota[1], Giovanna Lazzari[1], Franco Lucchini[3]
[1]Avantea, Laboratorio di Tecnologie della Riproduzione, Cremona, Italy
[2]Clinical Veterinary Department, University of Bologna, Italy
[3]Centro Ricerche Biotecnologiche, Università Cattolica del Sacro Cuore, Cremona, Italy

Article Outline

Glossary
Definition of the Subject
Introduction
Assisted Reproduction Techniques

Techniques for Genetic Engineering
Transferring the DNA into the Cell
Emerging Technologies
Future Directions
Acknowledgments
Bibliography

Glossary

Genetic engineering Recombinant DNA technology, gene manipulation including experimental manipulation of genetic material for industrial or medical use.

Germ cells Cells able to give rise to a functional gamete in multicellular animals.

Assisted reproduction The medical and laboratory processes used to reproduce the steps necessary to generate a newborn starting from gametes and or embryos.

IVF In Vitro Fertilization, the laboratory process in which a mammalian egg is fertilized outside the body and then put back inside to grow into a new individual.

ICSI Intra Cytoplasmic Sperm Injection, a procedure by which a spermatozoa is injected directly into the cytoplasm thus overcoming artificially the natural barriers of the oocyte.

SCNT Somatic Cell Nuclear Transfer, a technique that generates genomic copies of any given individual animal by replacing inside an oocyte its genome with the genome taken from somatic cells of a donor animal.

iPS cells Induced Pluripotent Stem cells, somatic cells that have been turned into pluripotent stem cells by the overexpression of pluripotency genes like OCT4, Nanog, Sox3, and Klf4.

Preimplantation embryo Following fertilization, the mammalian one-cell embryo (*zygote*) is still enclosed into the transparent proteic shell of the oocytes (*Zona pellucida*). During the journey along the oviduct it repeatedly cleaves to form an aggregate of smaller cells (*Morula Stage)* and finally develops an inner cavity (*Blastocyst stage*). Once in the uterus, the expanded blastocyst hatches breaking the zona pellucida and begins the implantation on the endometrium.

Chimerism The status of an organism made up by cells of different genotypes (like in the mythological monster *Chimera*). Chimeras derive from the aggregation of two different embryos of the same specie or from two different specie closely related (e.g., sheep and goat).

Mosaicism The cells of the organism own the same background genotype but are diverse in carrying or not a single mutation (or transgene). Such different cells may show a "patchy" distribution within tissues (like in a mosaic).

cDNA (complementary DNA) is a sequence of DNA obtained by reverse transcription of the mRNA (messenger RNA). It retains the whole information for coding the protein, but lacks the introns originally present in the chromosomal gene.

Zinc finger nuclease Recombinant enzyme able to bind a specific sequence of DNA and to "cut" it, generating a Double Strand Break (DSB). It is composed by an artificial DNA binding domain (a polypeptide with a repeat of regions each folded around a zinc ion, to evoke the idea of the fingers) linked to a bacterial nuclease domain, capable to hydrolyze the phosphate bond of the DNA.

Transposon A mobile genetic element able to transpose, that is, to excide itself from one site of the genome and to integrate in a different site. It does not move from one cell to another.

Retroviruses A class of viruses with a RNA genome, able to bind specific receptor on the target cell, to enter across the cell membrane and to transcribe its RNA in a DNA copy by means of its own RNA-dependent DNA polymerase (reverse transcriptase). Specific sequences promote the integration of the viral DNA into the genome of the host.

AAV A defective virus, with a small, single-stranded DNA genome, belonging to the family of Parvoviridae. AAV is able to replicate only in case of concomitant presence of an active adenovirus in the same cell. AAV can often integrate a double-stranded form of its DNA into the genome of the host.

Recombinase A family of enzymes able to exchange stretches of DNA among different molecules. Recombinases like CRE, coded by the genome of bacteriophage P1 (a virus parasiting a bacterium),

recognize specific sequences as target of their activity. In the presence of such Recombination Recognition Sites, phagic recombinase is able to insert and excide the viral genome from the bacterial chromosome.

siRNA Silencer RNA or short interfering RNA are small synthetic RNA molecules able to trigger the degradation of a target messenger RNA bearing the same sequence. This results in a posttranscriptional inhibition of gene expression. SiRNA complexes derive from the processing of artificial shRNAs (short hairpin RNA) bearing a secondary double-stranded structure that is subsequently processed by the endogenous cell machinery. RNA-mediated inhibition of gene expression, also known as RNA-interference, is naturally observed in most eukaryotes and relies on a specific pathway involving specific endoribonucleases and endogenous micro-RNA (miRNAs) genes.

Definition of the Subject

Recombinant DNA technology and gene transfer were set about 40 years ago and since then have provided powerful tools for the production of biological molecules, the development of new varieties of crops, and for generating key animal models in biomedical research.

Following the synthesis of recombinant insulin, many other pharmacological proteins have been produced by expressing heterologous genes in microorganisms, plants, and animals.

The application of gene transfer or "transgenesis" to animals has been developed mainly in mouse, while its use for generating transgenic livestock has encountered unanticipated resistances originated by social, economical and technical consideration. Apart from public concern and social consideration about the release of Genetically Engineered (GE) products in the market and GE animals into the environment, which will not be discussed in this chapter, the development of transgenic livestock has been slow due to the technical difficulties faced in transferring this technology from mouse to large domestic animals and by the initial discouraging results, outlining the difficulties in obtaining the expected effect upon a genetic modification.

This review will survey the scientific advancement making the generation of GE swine and ruminants more accessible in the last few years, positively influencing the technical and, as a consequence, the economical issues related to their development.

Introduction

Genetic mutations and equally engineering (GE) of living organisms are part of biological processes that are inherited through reproduction across generations. Such events provide the genetic variability that is at the core of evolution of the species and ensure its survival both in plants and animal kingdoms. The understanding of the biology at the basis of such physiological events, the discovery of the mechanisms and the molecules involved has allowed the investigators to exploit and adapt such tools for the artificial modification of the genome of living organisms from virus and bacteria to mammals including primates. These developments that led to definitions and guidelines of what is now called DNA recombinant technology can be traced back to 1975 to the Asilomar Conference where the scientific community met to discuss potential hazard and regulation. DNA recombinant technology had the potential to be taken from bacteria and viruses to plants and animals with, at the time, unknown biological consequences and biosafety concerns. It was not too long in fact that the first GE mammals were produced [1, 2]. Palmiter's results were dramatic in the sense that the mouse engineered to express the rat growth hormone grew to the size double that of the normal mice, thus opening the door to the application of such technologies in livestock, as stated in the abstract "This approach has implications for studying the biological effects of growth hormone, as a way to accelerate animal growth, as a model for gigantism, as a means of correcting genetic disease, and as a method of farming valuable gene products".

Since then, GE technology in mammals has been developed mainly in the laboratory mouse to study development and disease processes for research and clinical purposes with the ability to manipulate any given gene of the mouse genome. The developments in livestock immediately followed [3]; however it soon became evident that it was only the beginning and to reach such objective it was a difficult task and more knowledge was required. Beside the know-how required to engineer the genome, to make those modifications into the animals inherited through generations, it is necessary

to operate during the early stages of embryonic development or on the germ cells to be able to have all the cells originating from the embryo GE. This is the reason why the developments of assisted reproduction techniques have been crucial for the generation of transgenic animals, especially in livestock where the access in vivo to preimplantation embryos is more complex, expensive, and cumbersome than in the mouse. It can be stated that the developments in transgenic livestock have been set by the development of assisted reproduction techniques like oocyte in vitro maturation and fertilization, intracytoplasmic sperm injection, embryo culture, and somatic cell nuclear transfer (SCNT).

The injection of recombinant DNA into the pronucleus of the zygote has been the first technique used to generate GE livestock. This required a large supply of zygotes that can be easily generated in mice in vivo but are very expensive or sometimes impossible to obtain from the donor females of larger animals because of the costs involved and the low efficiency (only 1–5% of the injected embryos result in transgenic offspring).

Nevertheless, first studies on sheep and pigs involved the use of in vivo produced zygotes, adapting the protocols already set for the mouse [1, 3–5]. On the other hand, the generation of transgenic calves was not practically manageable by this route and could only be achieved [6] using in vitro maturation and fertilization of oocytes collected at the slaughterhouse [7] where large numbers can be generated at a low cost without the use of live animals.

Besides the classical microinjection procedure, alternative approaches have been developed to bring exogenous DNA into the nucleus of the embryo. Embryonic stem cells are largely used in the mouse to generate transgenic animals. They can be replicated in culture for a long period without losing their pluripotency, that is, their ability to take part in the formation of a developing embryo. Thanks to this peculiar behavior, they can be GE to obtain cell clones bearing specific modification of the genome. Such cells can be introduced in the early embryo where they participate in the development of a chimeric organism and eventually integrate into the germ line [8]. This approach has opened the way to the development of the so-called gene targeting, allowing the generation of transgenic mice bearing specific mutations, including disruption of specific genes (knock-out) or insertion of new coding sequences in specific loci (knock-in). ES cells are not yet available in livestock, therefore this route is not yet practicable [9].

An alternative approach has been disclosed by the development of somatic cell nuclear transfer (SCNT) technology, currently the preferred route to make transgenic livestock [10]. Somatic cells may be GE, even by gene targeting, and then used for SCNT. Although SCNT is not very efficient, all the animals obtained carry the selected mutation that has been introduced in the somatic cells subsequently used for nuclear transfer.

In addition, alternative approaches have been developed to generate transgenic animals like the infection with an engineered retrovirus of in vitro cultured preimplantation embryos or the injection of a sperm together with the desired recombinant DNA vector during intracytoplasmic sperm injection (ICSI).

In the following paragraphs, the developments in assisted reproduction technologies that have made GE of livestock possible will be described, then the methods currently used, and finally emerging technologies that promise to make GE simpler, more precise, and reliable.

Assisted Reproduction Techniques

Reproduction is the key biological function that is exploited to make a GE animal. Other approaches can be used, however, if the procedures do not target the germ line or the very early embryo then the genetic modification will not be inherited by the offspring and will be lost in the following generation. This is why the transgene has to be introduced either in the gametes or in an embryo at the very early stage of development, ideally when the embryo it is at the one-cell stage. Therefore, mastering assisted reproduction techniques is the key for the successful generation of GE mammals including livestock (Fig. 1).

Male Germ Line

Male germ cells are located in the testis. In the testis, all stages of development are found from spermatogonial stem cells to mature spermatozoa. Spermatogonia can be collected through a biopsy, cultured in vitro [11] and when are reintroduced in the testis they can give

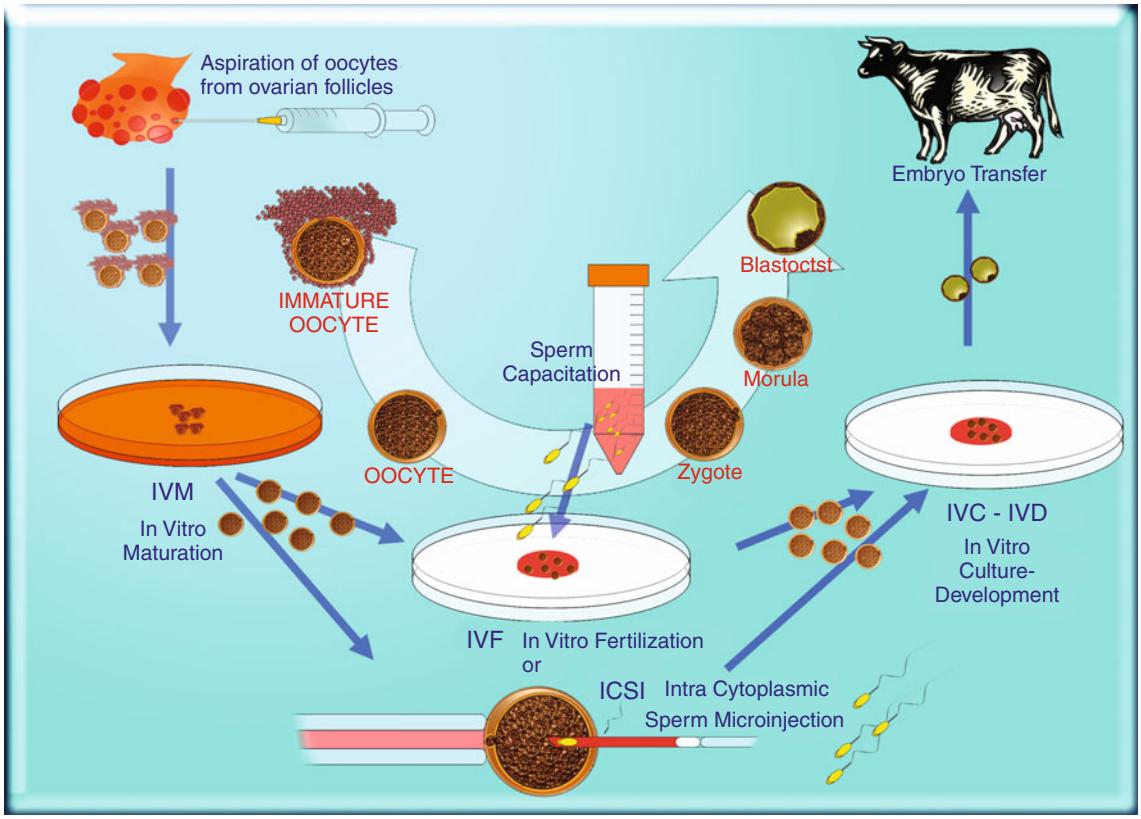

Transgenic Livestock Technologies. Figure 1
Summary of Reproductive Technologies (*in counterclockwise*) Ovarian immature oocytes are recovered from ovaries at slaughterhouse, matured in vitro by culturing in a specific medium, fertilized in vitro by co-incubation with capacitated spermatozoa or microinjected with a spermatozoa with a glass micropipette.The resulting zygotes are cultured in vitro until developed to blastocyst stage and finally transferred to the uterus of a synchronized recipient female by a surgical or a nonsurgical procedure depending on the species

rise to functional spermatozoa [12, 13]. During in vitro culture, spermatogonial stem cells can be GE and later transplanted back to the testis to restore spermatogenesis [14]. More easily from sexually mature animals, spermatozoa are recovered from the ejaculate, extended with appropriate diluents, and stored for fresh insemination or cryopreserved for later use. This is a well-established technique in livestock for use in artificial insemination. Spermatogenesis continues after puberty throughout the life of the animals producing an unlimited amount of spermatozoa. In an alternative route, prior to artificial insemination, spermatozoa can be exposed to the transgene in vitro. Spermatozoa can bind DNA and then convey it inside the oocyte at the time of fertilization [15]. Although the technique is not always reproducible [16], in this simple way some success in making GE livestock has been reported [94–96].

Female Germ Line and the Embryo

In mammals, primordial follicles, the functional unit that contains the female germ cell, exist on the ovaries but only a tiny proportion of the oocytes are effectively generating a progeny while almost all of the remaining are lost during lifetime through atresia. For many years, several investigators isolated and investigated the biology of intact primordial follicles in rodents [17] and finally grew them successfully in culture [18]. This task

proved much more difficult in large animals with bigger ovaries having a lot of connective tissue [19]. Successful development with the birth of live calves, albeit at a low rate, was later obtained by culturing bovine oocytes from more advanced (secondary) follicles [20]. The culture requirements for growing a complex tridimensional structure, such as an ovarian follicle, are so complex that the only progress that has been made is the culture in vivo of thin slices of the ovary following transplantation in humans where this now has a potential application in patients undergoing certain therapies [21].

From the late 1970s, it became clear that also in farm animals it was possible to exploit the oocyte reservoir present in antral follicles from the ovaries of slaughtered animals. Oocytes present in antral follicles have completed the growth phase and they are ready for maturation and fertilization [22, 23]. Initially, successful development was obtained by maturing the oocytes inside the follicles [24]. The subsequent understanding of the crucial role of the surrounding follicular/cumulus cells during the initial phases of maturation [25] lead to the development of a coculture system for in vitro maturation of extrafollicular oocytes obtaining a high proportion of such oocytes developing into live lambs after in vivo transfer [26]. After the successful achievement of in vitro maturation in sheep, the work was expanded investigating in the sheep the effects of gonadotropins [27], and to the cow [28–31] but also to the pig [32] and to the horse [33] and other species as well. Immature oocytes can also be recovered with the ovum pick-up technique in live donor females of different livestock species like cattle [34–36], buffaloes [37], and horses [38]. The development of in vitro maturation is today an irreplaceable, cost-effective and reliable source of mature oocytes for the production of embryos in vitro following in vitro fertilization and the various biotechnological applications connected to it.

Following the seminal work done in laboratory animals [39] in vitro fertilization (IVF) is well developed in farm animal species. Following the birth of the first IVF calf derived from in vivo matured oocytes [40] significant advancements were obtained in IVF when heparin was used as capacitating agent for bull sperm [41]. At about the same time, IVF became a reality in other large species except the horse where the success has been only exceptional and only one foal has been reported as the result of IVF. The horse eventually benefited of the development of intracytoplasmic sperm injection (ICSI) in humans [42]. The use of ICSI has been very efficient as a way to circumvent failure of in vitro fertilization with a high degree of efficiency [23], not matched in other farm animals like cattle [43, 44], sheep [45], or pigs [46] where the efficiency of ICSI for embryo production is lower as compared to IVF and, therefore, this technique is not used for routine practical application. But this is in fact the way to introduce together with the sperm also the DNA vector required to make the genetic modification [47]. In pigs on the other hand, IVF is characterized by a high incidence of polispermy that compromises embryonic development. This problem has been overcome in part by improving the quality of in vitro matured oocytes rather than effectively changing IVF conditions.

The immediate goal of increasing the efficiency of in vitro embryo production (IVP) especially in cattle has been the initial driving force of applied research in this field. However, it became soon obvious that merely counting the number of blastocysts was not an accurate measure of the quality of the overall procedure and of the viability of the embryos [48]. For many years, these constraints on the culture of viable cattle embryos in vitro were overcome by using in vivo culture in the oviduct of sheep [7]. In particular, a major concern after in vitro culture of IVF embryos was caused by the description of the so-called Large Offspring Syndrome (LOS), first in sheep and then in cattle [49]. The use of serum supplementation and coculture were later recognized as the primary cause of LOS. Later on, an extensive field study [50] demonstrated that the incidence of LOS was greatly reduced using a SOF (Synthetic Oviductal Fluid) [51]-based formulation or similar formulations of the embryo culture media. These findings clearly indicated that in vitro culture can alter development at very early stage and that the Large Offspring Syndrome is correlated to abnormally advanced embryonic growth and gene expression pattern already at very early stages [52]. Nevertheless the in vitro fertilization and preimplantation embryo culture in vitro allow to generate the number of zygotes required either for DNA microinjection or for virus infection, procedures that would otherwise not be

possible or be very difficult for livestock using in vivo produced zygotes from superovulated donors as it is done in laboratory mice.

Nuclear Transfer and Cloning

Somatic cell nuclear transfer, better known as cloning, is a technique that allows the generation of individuals with the same genome; thus technically speaking, cloned animals carry the same genome of the donor cell used for the SCNT process, thus they are like twins between themselves and twins of the animal who donated the somatic cell. The genome comes from the nucleus of a cell that can be taken from an embryo, a fetus, or an animal. The nucleus has to be placed into a mature oocyte, as outlined above whose chromosomes are removed before hand. The nuclear transfer step reconstructs an embryo, with its entire genome originating from the cell's nucleus that will subsequently develop like any other embryo conceived by fertilization albeit at a lower efficiency. Cloning by nuclear transfer that brought to the birth of Dolly the sheep [10] is a milestone achievement that has attracted the attention of the general public toward farm animal embryo technologies. This is one of the best examples where the search of new reproductive techniques in farm animals has also provided basic knowledge not previously obtained in laboratory animals. The fundamental work of cloning by nuclear transfer was done in amphybia [53] in the 1960s, however, significant advancements of the technology were achieved with embryo cloning of farm animals [54] when matured oocytes, instead of zygotes, became the recipients of the donor nuclei. Ten years later, it was again farm animals that, with somatic cell nuclear transfer, gave a major contribution to the basic understanding of cell reprogramming and epigenetic control of mammalian development, opening a new era in cell biology. The success with which different mammals were cloned was directly correlated to the availability of good quality mature oocytes and good quality embryos either after in vivo or in vitro culture. Then, it was merely a combination of already available technologies of gamete and embryo manipulation that lead to success and, for example, in the horse it was not until such technologies were developed that cloning was achieved in a consistent and reproducible way [55, 56]. In the last 10 years, the efficiency of somatic cell nuclear transfer as a whole has not improved much and its practical application is limited to the production of animals that have high added value like breeding stock [56–58] or for generating transgenic founder animals when nuclear transfer is combined with genetic engineering of somatic cells [59–62].

Understanding the constraints of nuclear transfer and developing the concept of reprogramming of fully differentiated somatic cells and the derivation of stem cells from cloned embryos [63, 64] for potential biotechnology and therapeutic applications, has fostered the idea of reprogramming differentiated cells in vitro directly without the need of the oocyte. A set of four genes has been demonstrated to be at the core of pluripotency and when transfected to somatic cells gave rise to induced pluripotent stem cells (iPS cells) [65]. These cells, of somatic origin, are extraordinary because they carry most of the properties of embryonic stem cells derived from the early embryo and represent a major breakthrough to overcome the limitation of embryonic stem cells derivation in humans and livestock.

Once the molecular basis of pluripotency will be fully understood, it will be a major step forward that is expected to lead to advances in nuclear transfer technology and cloning of farm animals for agricultural and biomedical applications on a larger, solid basis.

Embryonic Stem Cells

Embryonic stem cells (ES cells) are pluripotent cells that originate from the early embryo either from the inner cell mass or from the early epiblast. ES cells are cultured and expanded in vitro in undifferentiated conditions, can be GE if necessary, and when reintroduced in the embryos can give rise to any cell type including the germ line, except trophoblast. This is why they are defined as pluripotent and not totipotent cells which is a feature of gametes, zygotes, and early cleavage stages blastomeres only. Today, mouse ES cells technology is the principal route to make GE offspring [8].

The derivation of farm animal ES cells, equivalent to those described for the mouse, has not been reported yet (therefore this route for GE is not available at present in livestock species but it might be so in the near future). However, over the years, from 1981 when mouse ES cells were first discovered [66, 67], many laboratories have

attempted ES cell derivation mainly from cattle, pig, and sheep embryos [9, 68]. The original mouse approach has been extensively used and finally proven, with no doubt, unsuccessful although a few reports have been published on the derivation of so-called ES-like cells [69]. However, the stemness (pluripotency) of these cells appeared to be very limited and most likely they represent trophoblastic cells given their epithelial nature, loss of OCT4 expression, and limited differentiation potential [68–70]. The prominent tendency for neural differentiation often observed when attempting ES cell derivation from large animals is another challenge, but it represents an interesting and robust in vitro model for the study of early neurulation events in mammals [64].

In light of all the published reports and observations, it appears that the search for ES cells in farm animals should abandon the original mouse procedure and pay more attention to the recent findings for ES derivation in mouse and humans based on different signaling pathways and/or specific small molecules inhibitors. Advances in mouse and, more recently, in human ES cells culture have demonstrated that a number of different culture conditions can support pluripotency of embryo-derived stem cells. Mouse ES cells can be grown not only in serum-supplemented cultures with LIF and feeders but also in serum-free and feeder-free culture by the addition of BMP molecules. This second method has been developed following the finding that mouse ES cells grown in serum-supplemented medium and LIF can be differentiated in neuroectodermal cells by serum and LIF withdrawal [71]. The role of BMP molecules is to counteract and block the induction of neural differentiation and fix the undifferentiated state in a clever balance between conflicting inductive signaling pathways [71]. Along the same lines, a novel approach for ES derivation in the mouse has been developed on the rationale that the undifferentiated state can be maintained in culture by simply shielding the pluripotent cells of the embryos from endogenous pro-differentiation FGF4 signaling. This method is based on the use of specific inhibitors of the FGF signaling cascade in association with GSK3 inhibitors, the latter acting by improving cell viability. Both mouse and, remarkably for the first time, also rat ES cells have been obtained by inhibition of differentiation signaling introducing the concept that ES cells represent a ground-state pluripotency capable of self-renewing providing that differentiation signals are blocked [72, 73].

Other protocols, based on the stimulation of the nodal-activin signaling pathways, have been shown to maintain the undifferentiated proliferation of human ES cells and mouse epiblast stem cells (EpiSCs). The latter are a type of pluripotent embryo-derived stem cells derived from the egg cylinder as compared to ES cells that derive from inner cell mass or very early epiblast cells. Interestingly, mouse EpiSCs have been shown to be very similar to human ES cells in morphology, growth factors requirement, and gene expression [74, 75] while mouse ES cells differ considerably from human ES in culture requirements for the maintenance of the undifferentiated state, growth rate, and response to inductive signals. Another important difference between mouse ES cells and EpiSCs is the fact that only the former are capable of giving rise to chimeric offspring following blastocyst injection. A recent publication has reported the first success in the derivation of pig EpiSCs [76] and represents a significant step forward toward understanding the requirements for maintaining pluripotency of cultured epiblast cells from farm animal embryos.

In an applied perspective, embryonic stem cells in farm animals are important for several reasons but the most relevant is to provide a method to introduce precise genetic modification into animals by homologous recombination in ES cells [60] followed by blastocyst injection for chimera derivation and breeding, or by somatic cell nuclear transfer. A second important objective is to provide large animal models in which the ES cell technology can be tested for tissue-specific differentiation [77] and cell therapy of various tissues and organs.

Techniques for Genetic Engineering

The meaning commonly given to the term "transgenic" or "GE-" animal, indicate an individual bearing an exogenous fragment of DNA integrated in its genome and transmitting such modification to its descendant through a Mendelian fashion. Therefore, situations like "somatic transgenesis" will not be taken into consideration, where the genetic modification is limited to somatic tissues e.g., in case of gene-therapy protocols applied to adult individuals) or "episomal transgenesis", where the exogenous DNA is present inside the cell nucleus but as an autonomous

replicating entity, whose stability and replication are separated from those of host's chromosomes.

The natural processes driving the integration of a transgene into the chomosomes of the host cell are mediated by a set of enzymatic function related to the DNA-repair pathways. The enzymes involved in these pathways are responsible of repairing the host's DNA molecule in case of double strand break (DSB). The resolution of a DSB inside the cell nucleus may follow two alternative pathways, catalyzed by different enzymes. The first and more common process involves the Non-Homologous End Joining (NHEJ) pathway, where the free ends of DNA generated by the DSB are relinked together. The exogenous DNA introduced in the nucleus may be recruited during this process and integrated between the endogenous arms of a broken chromosome. The integration of a transgene through the NHEJ pathway causes its random positioning into the genome of the host and the frequent integration of multiple copies of the transgene in the same locus, end by end. Both the random integration site and the generation of a multiple-copy array can influence the expression of the transgene in an unpredictable way. The alternative enzymatic machinery available in the cell for repairing DSBs is the Homologous Recombination (HR) pathway. It relies on the availability of a full copy of the broken molecule to provide a one-strand template to restore the original DNA sequence. This enzymatic activity is principally evident during gametogenesis (when it is involved in crossing over between sister chromosomes) and maintains higher level during early embryonic development compared to somatic adult cells.

A transgene may be integrated by HR if it carries a region of homology with the target region in the host genome with the advantage of driving the insertion of the transgene in a specific locus and as a single copy. Nevertheless, this event is still rare compared to random integration by NHEJ. Even in ES cells, that retains a significant HR activity, the event of a targeted insertion of a transgene by HR is two to four orders of magnitude less frequent compared to its random integration.

For this reason, the process of gene targeting through natural HR can be performed only on cell cultures, where a large number of integration events can be generated and the cells carrying the desired event can be selected and isolated. The obvious next step to generate a transgenic animal is the capability of turning these cells into new individuals. In mouse, this has be accomplished by performing gene targeting in ES cells, that are able upon being introduced in a host embryo, to take part to the generation of a chimeric animal including part of its germ line and, as a consequence to pass the acquired mutation to its offspring [78]. As functional pluripotent ES cells have never been obtained from species different than the mouse, the possibility of performing gene targeting has been limited to this species until in 1996 Ian Wilmut and colleagues disclosed the way toward mammalian cloning by SCNT [79].

By then, even though somatic cells retain lower HR activity compared to ES cells, the option of performing gene targeting in this cells and to derive a whole animal from their genome has been demonstrated in swine, ovine, and bovine.

Since the generation of the first transgenic large animals by pronuclear microinjection, including transgenic pigs [3], major advances have been made, mainly by use of assisted reproductive technologies [80] as described earlier. Depending on the purpose of the genetic modification, the approach to transgenesis may aim to the random or the targeted integration of the transgene. In both cases, the obvious but sometime underscored consideration is that the final aim of the process is not only to insert a transgene into the genome, but also its proper *expression*. The hard track toward this is the result of intermediate steps, including (Fig. 2):

1. *Accurate design of the transgene*, involving the selection of the desired gene, its regulatory sequences, and all the additional sequences able to drive its integration and the expression of the desired phenotype in the right tissue at the right time
2. *Introduction of the DNA across the cell membrane* of the embryo or of the cell to be used in nuclear transfer
3. *Integration of the new DNA sequence into the genome*. This step may be mediated only by the endogenous NHEJ or HR pathways but, in some cases, a customized integration of the transgene may be artificially induced by the activity of exogenous recombinases or endonucleases specifically introduced into the cell

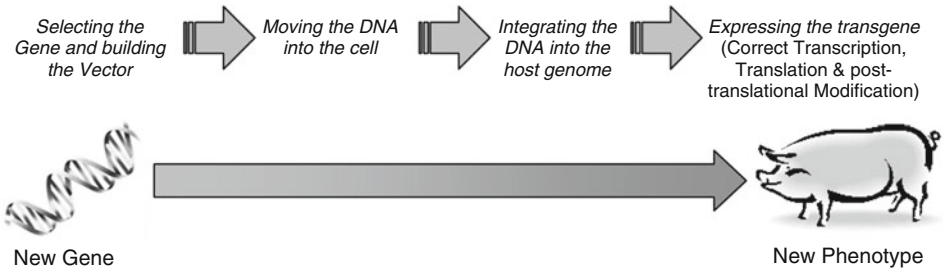

Transgenic Livestock Technologies. Figure 2
Steps in obtaining a functional transgenic animal. The definition of transgenic is commonly associated with an organism bearing a new piece of DNA, but the true goal of the procedure is obtaining an animal expressing a new gene according to a desired pattern, that is, showing a new phenotype. Anticipating the final expression pattern of a transgene is still the weaker step in this technology (From [141])

4. *Correct expression of the transgene* is dependent on the good implementation of all of the previously described phases and on a bit of luck. It is usually necessary to producing a large number of different integration events (i.e., embryos or cell clones) to allow the identification and the selection of the best performing, that will be used to generate and expand the desired transgenic line.

During the last years, the toolbox of the genetic engineer has expanded with new instruments allowing a better control on each of the described steps and an overall improvement on the whole procedure. Moreover, some genetic manipulation procedures initially available only for mice, have become concrete even for livestock.

Choosing the Gene and Assembling the Vector

Once the gene to be transferred has been identified, several alternative options are available to generate a transgenic vector (Fig. 3). The coding sequence of the gene itself may be used as cDNA, as genomic sequence (including introns) or as a minigene (a fusion of cDNA and genomic sequences of the same gene). The presence of one or more introns into the transgene, triggering the splicing process, is a major factor improving the transport of mRNA through the nuclear membrane and the effective expression of the exogenous gene [81, 82]. The regulatory sequences to be included into the transgene are chosen according to the need. The original promoter and enhancers may be conserved to drive the gene according to its original expression pattern, alternatively, heterologous promoters may be used to trigger a different tissue-specific or an ubiquitous expression. In case the gene has to be driven by its original regulatory sequences, the selected genomic fragment should be as large as possible to maximize the chance of a correct expression [83]. Indeed, if a gene has to be transferred from one species to another where the same regulatory signals are recognized, increasing the dimension of the fragment to be transferred allows to including not only the original promoter, but also distal enhancers and chromosomal modifiers [84, 85]. On the other hand, the large size of such DNA molecules influences the choice of the technique required for their introduction into the cell, due to the care required to purify and handle large and fragile DNA molecules. Although microinjection allows the introduction of such big molecules, larger than 100 Kbp, the efficiency of the procedure greatly decreases with the increase of DNA size and a significant part of the resulting transgenic animals integrates only fragmented transgenes, due to shearing of DNA during injection and/or its enzymatic degradation before going into the chromosome. To improve the transfer of large DNA fragment into the genome, specific procedures have been developed, like the ICSI-mediated Gene Transfer (see below). Besides the selection of the gene and its regulatory sequences, additional features may be inserted into the transgenic vector. In case the transgene has to be introduced in cultured cells, it is often required the insertion of a selection

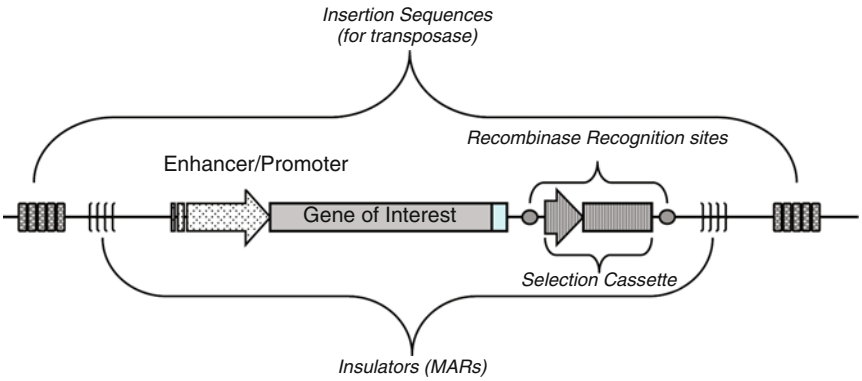

Transgenic Livestock Technologies. Figure 3
Generic structure of a transgenic vector. Beside the expression cassette for the Gene of interest (promoter, CDS and polyA site), additional sequences may be useful to increase the integration frequency of the vector (transposon-derived IS) or to support its regular expression (Insulators). Some features, like drug-resistance genes, are required for isolating cell clones but their persistence in the resulting transgenic organism is undesirable. They can be ablated by means of exogenous recombinases (From [141])

cassette, providing resistance to a specific xenobiotic. As the integration of the vector in the genome of the cell is quite a rare event, the addition of a xenobiotic to the culture medium allows to grow only the transformed cell, that become resistant to it, and to eliminate the rest of the culture.

On the other hand, as the residual presence of this cassette in the transgenic animal may be deleterious or undesired, such cassette may be "floxed" (flanked by lox sites) for a subsequent removal through transient expression of Cre recombinase [86] (see further below).

Random integration of the transgene into the genome is recognized as the main source of variability in the expression of the exogenous genes, due to the influence of flanking genomic regions that may affect the expression pattern of the transgene or "switch it off" by epigenetic silencing. To avoid this behavior, insulator sequences may be inserted to shield the transgene from the influence of the chromosomal location [87–90]. Such insulators, called Matrix Attachment Regions (MARs), bend the transgene in a single transcriptional domain bound by its ends to the nuclear matrix. Additional features of the DNA construct can confer to the vector the behavior of a transposon, being recognized by a transposase that can be cotransferred or transiently co-expressed with the gene during gene transfer. This strategy will be described further below.

Transferring the DNA into the Cell

Pronuclear Microinjection

Pronuclear microinjection is now less commonly used in livestock, having been largely replaced by more efficient and less expensive techniques, after the demonstration of the possibility of cloning mammalians by nuclear transfer [10, 91]. Previously, microinjection was considered the most reliable technique to generate transgenic large animals, albeit inefficient and quite expensive in large animals. In vivo production of zygotes provides very viable embryos, but is an expensive approach. The data reported by Krimperfort concerning the generation of the first transgenic calf in 1991, starting from in vitro produced embryos, evidenced the huge effort made in generating this animal.

Two thousand four hundred and seventy (2,470) oocytes were matured and fertilized in vitro to give 1154 zygotes that underwent microinjection; among them, only 129 developed and were transferred in 99 recipient cows. Twenty one (21) calves were born, only two of which were bearing the transgene. One of them died at birth. The other, a male called Herman, grew to adulthood and was mated, because its transgene, coding for human lactoferrin, was designed to be active into the mammary gland of transgenic cows. Sadly, the expression of this gene in the milk of Herman's daughters was extremely low, making the whole project useless. At the

time, the cost of the whole procedure for producing such transgenic bull was estimated around 500,000 dollars.

Different factors may affect the expression of microinjected transgenes, considering that they integrate in random sites of the host genome. The disadvantage compared to what happens for gene transfer in cultured cells, in detecting the transgene integration ahead of embryo transfer, although possible, is not practically convenient following pronuclear microinjection, let alone the assessment of its expression. For this reason, most of the animals resulting from microinjection protocols are non-transgenic (Fig. 4).

Last but not least, obtaining embryos bearing targeted transgene integration, until recently, was considered nearly impossible by this approach. DNA integration upon standard microinjection is achieved mostly via NHEJ, resulting in a random positioning of the transgene into the genome and a consequent unpredictable effect of the flanking regulatory elements on the expression of the transgene itself. Recent advances in enzymatic engineering has demonstrated the possibility to overcome this limit obtaining the targeted integration of a transgene by means of Zinc Finger Nucleases [92] as discussed below.

Sperm-Mediated Gene Transfer (SMGT)

In 1989, Lavitrano and colleagues reported a new approach to generate transgenic mice based on pre-incubation of spermatozoa with exogenous DNA followed by in vitro fertilization [15]. This unconventional approach was accepted with skepticism by many scientists working in the field of transgenesis [16, 93]. In spite of that, other authors reported success in

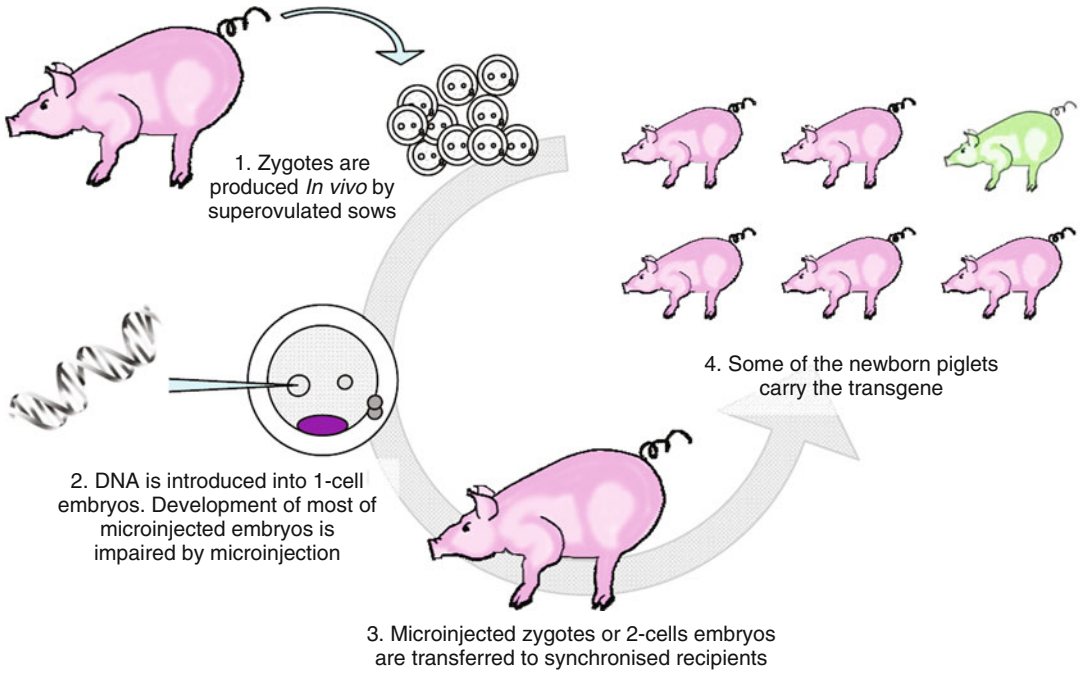

Transgenic Livestock Technologies. Figure 4
Transgenic production by pronuclear microinjection One-cell embryos are recovered from superovulated females. Such zygotes shows high viability but their production in vivo is somewhat expensive. Embryos are centrifuged to reveal pronuclei and DNA is microinjected into one of them. Microinjection of DNA affects embryo viability. Surviving embryos are transferred in synchronized sows. The proportion of transferred microinjected embryos developing to viable offspring is low and variable, moreover only small fraction of them carries the transgene. The pattern of expression is unpredictable. The overall efficiency of this procedure in terms of living transgenic/microinjected embryos usually ranges from 1% to 4% (From [141])

obtaining transgenic animals by variations of SMGT protocol [94, 95]. After few years, the same technique was adapted to the production of transgenic pigs bearing a hDAF transgene [94–96]. The benefits of this technique, compared to pronuclear microinjection, are low cost and ease of use. Nevertheless, the insertion is still random and the transgene can be rearranged, thus affecting the expression levels. The long-term expression of the transgene remains controversial [97].

ICSI-Mediated Gene Transfer (ICSI-MGT)

ICSI-mediated gene transfer is a technique sharing some analogies with SMGT and microinjection, where both the transgene and the sperm head are introduced with a micropipette into the cytoplasm of the oocyte [47]. In mice, ICSI-MGT is more efficient than standard microinjection and can be particularly effective when a large construct (ranging from 100 kb to more than 0.5–1 Mb, i.e., YAC, BAC, microchromosome) has to be transferred [98]. Together with the use of polyamines to condense DNA, the large size of the micropipette used for injecting the sperm head preserves DNA integrity minimizing mechanical shearing.

Although assisted reproductive technologies (Fig. 1) in pig still suffer some limits, possibly due to specific requirements in embryo culture conditions yet to be defined, some researchers succeeded in producing transgenic pigs by co-incubating sperm with a DNA vector and microinjecting the spermatozoa directly into the ooplasm. After the transfer of 702 embryos into 5 gilts, 2 out of 35 fetuses recovered were transgenic. In vivo production of zygotes provides very viable embryos, but is an expensive approach and requires the use of animals. Nevertheless, this is the preferred source of embryos for this procedure, because microinjection by itself heavily impairs the subsequent embryonic development and decreases the number of newborns following embryo transfer [99].

Viral-Mediated Transgenesis

During their life cycle, retroviruses are able to enter the cytoplasmic membrane of a target cell by binding specific receptor, to reach the nucleus and to retrotranscribe a DNA molecule using their RNA genome as a template. This DNA molecule will often integrate into the host genome.

Mimicking such behavior, retroviral-derived vectors have been engineered to carry a specific transgene to be integrated into the target genome, but lack the genes required for completing their replicative cycle. Such retroviral vectors, initially developed to target somatic cells for human gene therapy, can also infect preimplantation embryos, providing that the zona pellucida is removed or at least breached, since it is a barrier to the viruses. The retrovirus integrates its complementary DNA into the genome of the embryo. The cell cycle of the infected cell may be susceptible or not to integration depending on the origin of the selected viral vector. For this reason, early trials with retroviral vectors resulted in mosaic animals, due to the failure of these vectors to enter the genome during one-cell stage but only during subsequent embryo divisions. A more recent generation of viral vectors is based on the structure of lentiviruses like HIV. Lentiviral gene transfer is extremely efficient, with 80–100% of the animals being born transgenic after oocyte or embryo, or somatic cell culture infection@ [100]. Lentiviruses have been used in a variety of experiments to transduce cells with various transgenes. These experiments include siRNA knock-down for stem cells and for somatic cells, and nuclear transfer (see below) for generating desired modifications. Lentiviral transgenesis is one of the main techniques currently proposed for somatic gene therapy. Such approach is associated with known risks and observed limits. During clinical trials, retroviral transgenesis has been associated with oncogene activation by insertional mutagenesis [101, 102]. To reduce this risk, the interest of the researchers is moving toward replication-deficient vectors [103]. An additional concern about the use of lentiviral vectors is their possible recombination with latent wild retrovirus to generate unpredictable infectious or mobile particles. Among virus-derived vectors, lentiviral (LV) have the property of infecting cells both during replication and in quiescent phase. During lentiviral-mediated transgenesis, the use of some drugs like cytokines or proteasome inhibitors can increase LV gene transfer [60, 104]. Santoni de Sio and colleagues [104] have shown that human hematopoietic stem cells (HSCs) can be transduced to high efficiency by a short exposure to LVs in the presence of SCF, TPO, IL-6, and Flt3L. Moreover, it was shown that the proteasome restricts LV transduction in HSCs and that using the

reversible peptide–aldehyde proteasome inhibitor MG132 and the peptide-boronate inhibitor PS-341 during the LV-GFP transduction period, there is a substantial drug-dose-dependent increase in the frequency of transgene expressing cells and in their mean fluorescence intensity [104].

The use of lentiviral vectors for transgenesis results in a significant degree of mosaicism among transgenic newborns, due to the possible multiplicity of integration events during the first cleavages of the embryo [105]. Even though lentiviral vectors enter as a single copy into their insertion site, their integration mechanism is very efficient, frequently resulting in multiple copies integrated in different part of the genome and in a complex pattern of transmission to the offspring [105]. Due to their random positioning into the chromosomes, lentiviral vectors may still undergo epigenetic silencing by methylation [106]. Another class of effective vectors for transgenesis was derived from the adeno-associated virus (AAV). AAV-derived vectors have the advantage to cross the cell membrane delivering single stranded DNA molecules straight to the nucleus. Some adeno-associated viruses are peculiar in their behavior of targeting specific integration site in the host genome [107]. Adenoviral ssDNA shows a high effectiveness in integrating into the host genome through homologous recombination, even in somatic cells [108, 109]. Recently, Rogers et al. produced a CFTR-null pig using AAV-mediated gene targeting and SCNT [110, 111]. These authors generated a pig with both null (knock-out) and ΔF508 (knock-in) modifications. Gene targeting using the AAV approach has resulted in a very efficient strategy for obtaining knock-out of the CFTR gene that is not expressed in fibroblasts.

Somatic Cell Nuclear Transfer

Somatic cell nuclear transfer (SCNT) has become the leading tool for generating animals from GE somatic cells (Fig. 5). SCNT works better in pigs than in other large animals [112, 113]. A recent innovation to make the technique user-friendly is the zona-free system. After zona removal, enucleation can be performed with a micropipette, for subsequent zona-free fusion, activation, and culture [113, 114], or by cutting the cytoplasts for handmade cloning [115, 116]. Major limitations are represented by the lack of embryonic stem cell (ESC) technologies. Somatic cells are currently being used in the procedures, but they have a limited life span, thus restricting the time the cells can be cultured in vitro for genetic engineering. Fibroblasts (both from fetal and adult origin) have a fine life span and can undergo a maximum of 40–50 population doubling in vitro while maintaining a normal kariotype. Such number of population doublings allow only for a round of cell transfection followed by drug selection to identify a clonal cell population with the desired modification. In fact by the time this has been achieved, the cells have spent most of their proliferative capacity and have to be used for SCNT before they reach complete senescence. So, the use of fibroblasts limits this approach to one modification in vitro at the time since they would not survive a second round of transfection. After SCNT, the fibroblasts are rejuvenated and have fully restored their proliferative capacity. At this point, cloned fetuses are recovered to establish a new fibroblast cell line that can be then subjected to a new round of genetic modification. This process can be repeated several times with apparently no adverse effects [59]; however it requires time and animals. Relating to this topic, recent reports describe the derivation of induced pluripotent stem cells (iPSC) from pig fibroblasts [117–119], however the objective is still far since culture conditions to maintain livestock embryonic stem cells are not known (further discussed below). The opportunity of performing the whole genetic engineering on cell cultured in vitro and finally transferring the manipulated genome to the enucleated oocytes allows selection for gene targeting events, both for *knocking out* an unwanted gene or for *knocking in* a transgene in a predetermined reliable position, guaranteeing its best expression.

A similar model, implementing the 1,3 galactosiltransferase knockout in pigs was developed by Takahagi and colleagues that knocked out the first allele of this gene in porcine fetal fibroblast already expressing hDAF and N-AcetylglucosaminylTransferase -III (GNT-III) [120]. In a further step, the authors selected cultures for spontaneous null mutations of the second allele occurring in vitro, and used these cells for nuclear transfer. In this way, the resulting cloned pigs were transgenic for hDAF and GNT-III on a 1,3 galactosiltransferase null background [121].

SCNT technology overcomes many limitations of previous procedures, making possible the gene targeting

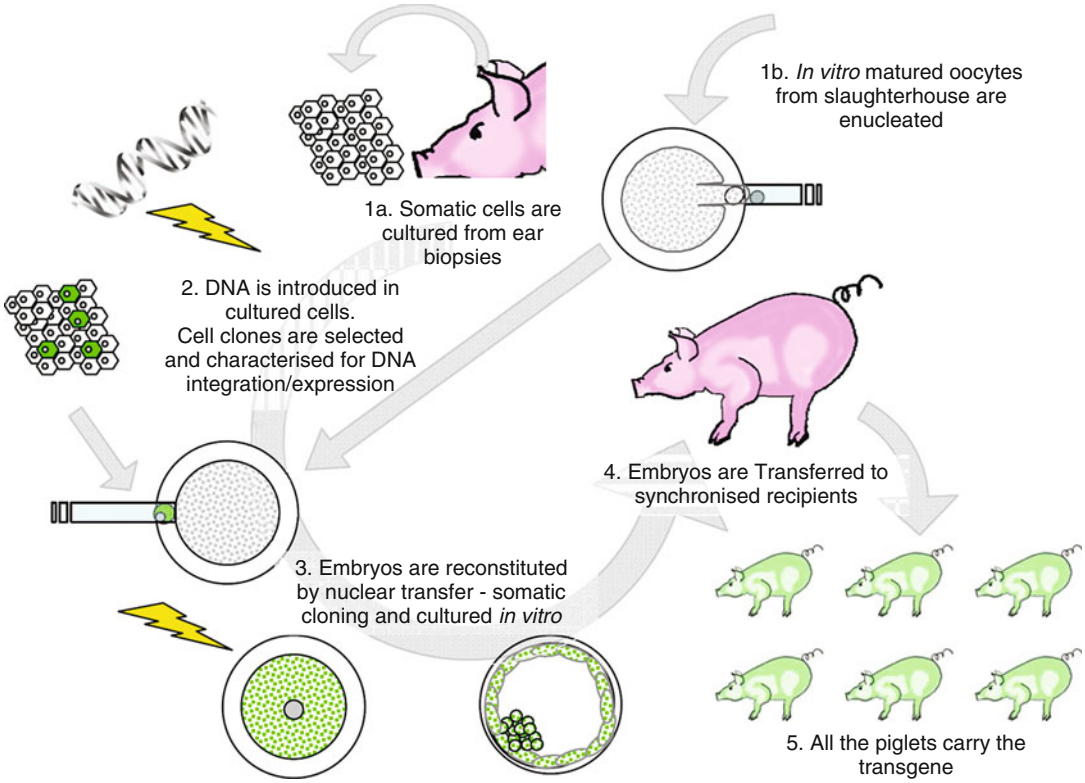

Transgenic Livestock Technologies. Figure 5

Transgenic production by SCNT. The transgene is transferred into the genome of cultured fibroblasts. Transgenic cell clones are isolated and characterized. This first step is relatively inexpensive. A more accurate prediction of the transgene expression is possible. Next, embryos are reconstituted by SCNT, cultured and transferred in synchronized sows. Although the viability of cloned embryos is variable but usually poor, all of the resulting newborns are transgenic (From [141])

approach to livestock genome and providing a less expensive way to perform genetic engineering. Indeed, most of the cost and the efforts related to transgenic technology applied to large animal are derived from housing animals, preparation for embryo transfer up to the birth and weaning of the newborn animals.

The opportunity of using cell clones fully characterized in term of transgene integration and expression, guaranteeing 100% of transgenics among born animals, greatly increases the efficiency of the protocol and drops the costs when an ubiquitous or inducible promoter is used and the expression is maintained in subsequent generations through germ line development (Fig. 6) [112]. On the other hand, SCNT is not the final solution for every problem, as most of the matter concerning the proper activity of the transgenes, with regard to its temporal and tissue-specific expression, still needs to be completed on the whole animal. Possible improvements to overcome these problems are offered by recent advances in genetic engineering.

Emerging Technologies

Several new technologies becoming available may be of great benefit in the future to make GE large animals.

Induced Pluripotent Stem Cells (iPS Cells)

In 2006, a breakthrough study [65] demonstrated that viral transduction of a handful of genes (Oct4, Sox2, Klf4, and c-Myc) can reprogram mouse embryonic fibroblasts into ES cell-like cells which carry all the molecular features of true embryo-derived ES cells

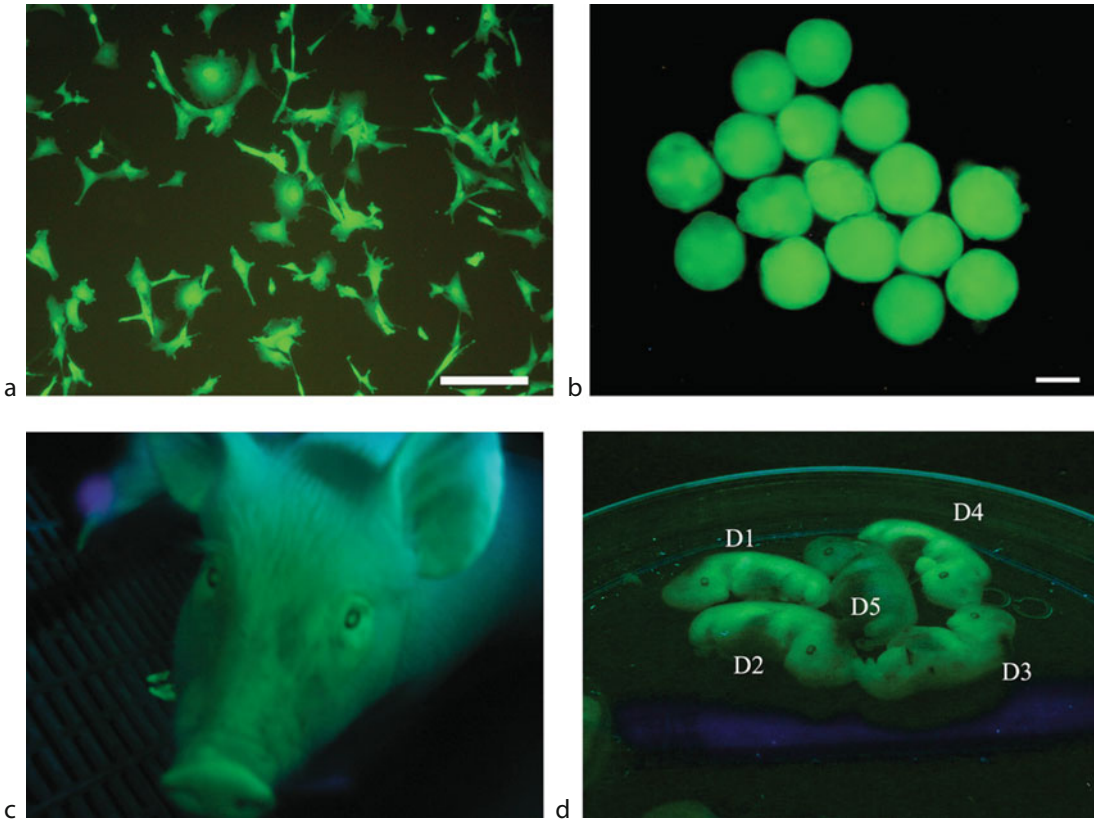

Transgenic Livestock Technologies. Figure 6
Successful selection of GFP transgenic cells and transmission through the germline of the transgene to the next generation. Clonal fibroblasts selected for high expression of GFP (**a**), GFP expression in embryos after SCNT (**b**) and in the resulting animal (**c**). Fetuses obtained after breeding the GFP boar to a wild type sow (**d**). Fetus D1, D2, D3, D4 are transgenic and express the same high level of GFP of the original boar, D5 is a wild type fetus negative for GFP (From [141])

including the ability to give rise to germ line chimeras. The following year the generation of human iPS cells was achieved [122, 123] using slightly modified transduction methods and set of genes. Since then, several groups have contributed to the field with new combinations of reprogramming genes, cell types, and viral and nonviral delivery systems. More recently, the addition of small molecules acting on chromatin structure, such as valproic acid, a histone deacetylase inhibitor has allowed further progress by showing that only Oct4 and Sox2 are required for reprogramming of human fibroblasts [124]. Several other small molecules acting on chromatin or on specific signaling pathways have been investigated to improve the efficiency and safety of iPS cells technology (see as review [125]). In large animals, attempts to derive iPS cells have been made resulting in a few reports about induced reprogramming of pig fibroblasts [117–119]. Although promising data have been presented, the evidence of full reprogramming, measured by sustained activation of endogenous genes and silencing of reprogramming genes, has not been achieved. Most likely, the lack of robust procedures for the establishment embryo-derived ES cells in large animals represents a major limit also for the development of the iPS cells technology. More detailed knowledge on the role of pluripotency genes in the early embryo is needed to advance the field of induced pluripotency not only in the mouse [126] but also in large animal species.

Enzymatic Engineering

Transposons Transposons, called also "jumping genes" are mobile genetic elements; class II transposons are small segments of DNA able to move across the genome of a cell from one region to another, by means of the action of enzymes (transposase) encoded within the transposon itself or supplied in trans by another source (Fig. 7). Transposons have been found in many living organism, from bacteria to plants and animals. The simplest autonomous replicating transposons in vertebrates, like those belonging to TC1/Mariner class, are composed by two inverted terminal repeat flanking a sequence coding for a specific transposase. Although the movement of transposons across different

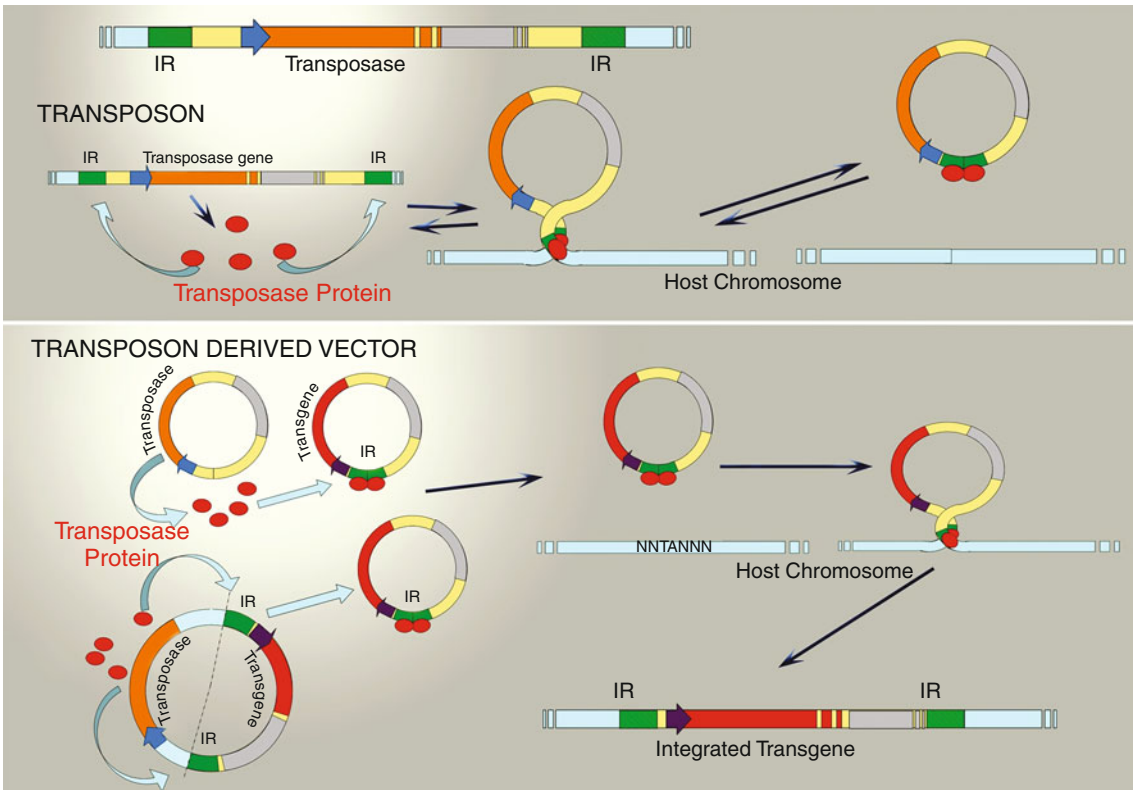

Transgenic Livestock Technologies. Figure 7
Integrative vectors based on Transposon signals *Top*: Natural occurring DNA-transposons consists of a common minimal structure represented by a gene coding for a specific transposase (TP) and two terminal inverted repeats (IRs). Following the expression of the gene, its product is able to bind to the inverted repeats, inducing the circularization and the excision of the complete DNA segment surrounded by IRs. Depending on the type of transposon, excision can leave small footprint in the chromosome or restore the exact original sequence. Following excision, the circular transposon, still bound to transposase, can integrate in a new site of the genome. In presence of transposase, both the excision and the integration of the transposon are catalyzed. Some transposons, like PiggyBac, prefers transcriptionally active genomic region for their integration. *Bottom*: A Transposon-derived vector is represented by a transgene flanked by a pair of IRs, but lacking the transposase CDS between them.The integration of this vector can be obtained with high efficiency by expressing the specific transposase *in trans* – on a different vector (**a**) – or *in cis* – on the same vector but by a cassette located outside the IRs-delimited portion (**b**). The transiently expressed exogenous transposase promotes the integrative cycle of the vector but, due to the absence of a stable source of protein, the integration of the vector is irreversible (From [141])

organism does not seem to be a common capability, philogenetic studies strongly suggest that "jumps" of transposons across species have happened during evolution [127]. Modified transposons, like "Sleeping Beauty" and "PiggyBac" have been largely used for precise and efficient delivery of DNA expression cassettes in vertebrate cells. Sleeping Beauty (SB) belongs to the TC1/Mariner class of transposons and these transposases require a TA dinucleotide base pair as integration site, a sequence that is duplicated during the integration process. The SB transposon system consists of two components: (1) a defective transposon, made up by gene of interest flanked by inverted repeats (IRs) but lacking the transposase gene, and (2) a source of transposase. During transposition, the SB transposase recognizes the ends of the IRs and excises the transposon from the delivered plasmid DNA inserting it in to another DNA site.

In a recent study, it was shown that co-transfection of PEGE cells with Sleeping Beauty (SB), Passport (PP) Tol2 and PiggyBac (PB), with their corresponding transposase expression constructs, resulted respectively in 13.5-, 5-, 21-, and 28-fold increases over transfection without transposase [128]. In addition to increasing the efficiency of integration, transposase-mediated transgenesis precisely integrates a single copy of the transposon into one or more locations in the genome, avoiding transgene concatemerization that can cause shutdown of gene expression.

Cre/LoxP Recombinases The integration site of a transgene strongly influences its expression pattern. To overcome the gamble of a random integration, it is possible to target the insertion of the transgene to a transcriptionally active location of the genome, avoiding the risks of both silencing the transgene and disrupting an endogenous gene (insertional mutagenesis).

One possible strategy to obtain this goal is the use of phage recombinases like Cre or FLP that catalyze a conservative DNA recombination event between two short recombinase recognition sites (RRS), loxP and FRT (Fig. 8), respectively. Such enzymes, used by bacteriophages during their infection cycle, allows the excision or inversion of the DNA between two RRSs, depending on their orientation [128]. The artificial modification of the sequences of the parental RRSs has allowed to develop the so-called Recombinase-Mediated Cassette exchange (RMCE), a protocol to modify a specific locus in the genome after an initial "tagging" by the introduction of a pair of incompatible RRSs [129]. In this way, (1) a cell line is modified by inserting a RRS-flanked reporter gene in different random position, (2) the deriving clones are screened to select the one presenting the best integration site, and (3) the gene of interest can be exchanged with the reporter to assure its proper expression. A predictable modification of the genome may be realized by driving the process of DNA repair through homologous recombination (gene targeting). This process, largely used in mouse ES cells, allows the interruption of endogenous sequences (knock-out) or the insertion of new genes (knock-in) in a specific locus [130, 131]. Unfortunately, the HR pathway is much less efficient in somatic cells like fibroblasts, making this procedure much harder, in particular for genes that are inactive in the target cell type not allowing the use of gene-trap (promoterless) approaches.

Zinc Finger Nucleases (ZFNs) Zinc finger nucleases (ZFNs) show promise in improving the efficiency of gene targeting by introducing DNA double-strand breaks in target genes, which then stimulate the cell's endogenous HR machinery. Zing finger nucleases are hybrid proteins containing an array of zinc-finger DNA-binding domain and a FokI endonuclease domain (Fig. 9). The DNA zinc-finger domains are designed to recognize a specific sequence, inducing a double stranded break in the target site. Such break promotes a local DNA repair activity that is efficiently accomplished by HR if a template with homologous sequence is provided. Many studies have been developed in human and mouse cells [60, 132]. A recent paper demonstrates the possibility of generating transgenic rats by pronuclear microinjection of specific ZFN expression vectors together with a gene targeting construct [92].

An additional requirement in developing transgenic livestock is the need of expressing multiple transgenes in a coordinate pattern in the same animal. As previously noted, protocol bringing to random integration of multiple transgenes, often result in similarly random level of expression, with some

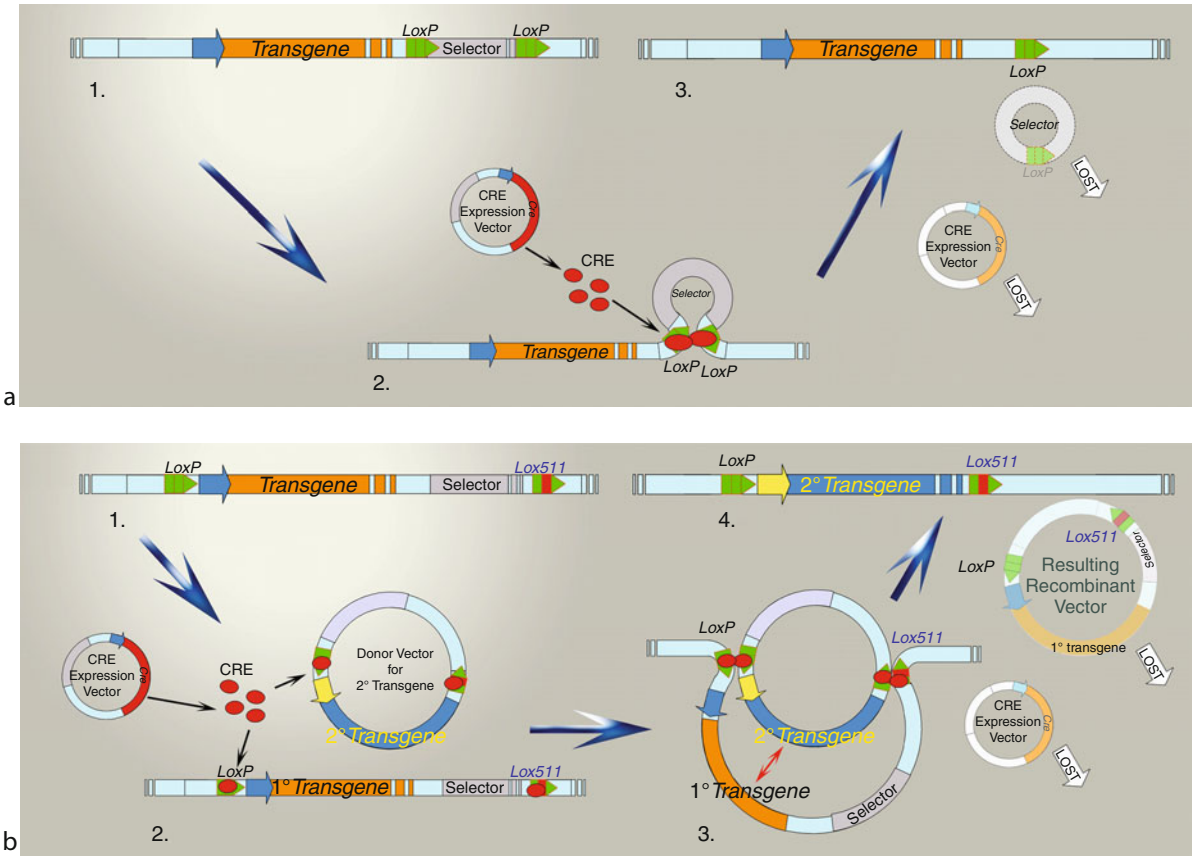

Transgenic Livestock Technologies. Figure 8

Targeted rearrangement of an integrated transgene by Cre recombinase. (**a**) Homologous Lox sites in the same orientation allows the excision of the enclosed region when Cre is expressed (**b**) Heterologous Lox sites do not allow excision but promote RMCE (Recombinase Mediated Cassette Exchange) if a vector bearing a Lox-flanked transgene is introduced together with CRE

transgenes working and some other not. A strategy to speed multiple transgene integration is represented by recent adaptation of the 2A system from foot and mouth disease virus (FMDV) to mammalian transgenic technology [133, 134]. In this system, the open reading frame (ORF) consists of multiple individual cDNAs separated by sequences encoding 2A and furin cleavage sites. A single complex mRNA is produced and translated into a single polypeptide that is cleaved into individual exogenous proteins at the 2A sites.

siRNA In cells transfected with siRNA vectors, targeted mRNAs are degraded by endonuclease activity and the amount of protein translated may be reduced by over 95%, thus resulting in a significant knock-down and is an alternative approach to achieving more complex and difficult knock-outs (KO). This technique is particularly useful when more than one copy of the endogenous gene is present and the usual KO approach is not feasible. This is indeed the case of pathogens like porcine endogenous retrovirus (PERV) [135–137]; for example, "knock-down" of PERV expression has been shown in transgenic pigs expressing siRNA corresponding to the viral pol2 sequence [138]. This approach could even be of interest in generating transgenic animals resistant to specific viral pathogens, by steady expression of virus-inhibiting siRNA molecules in their cells.

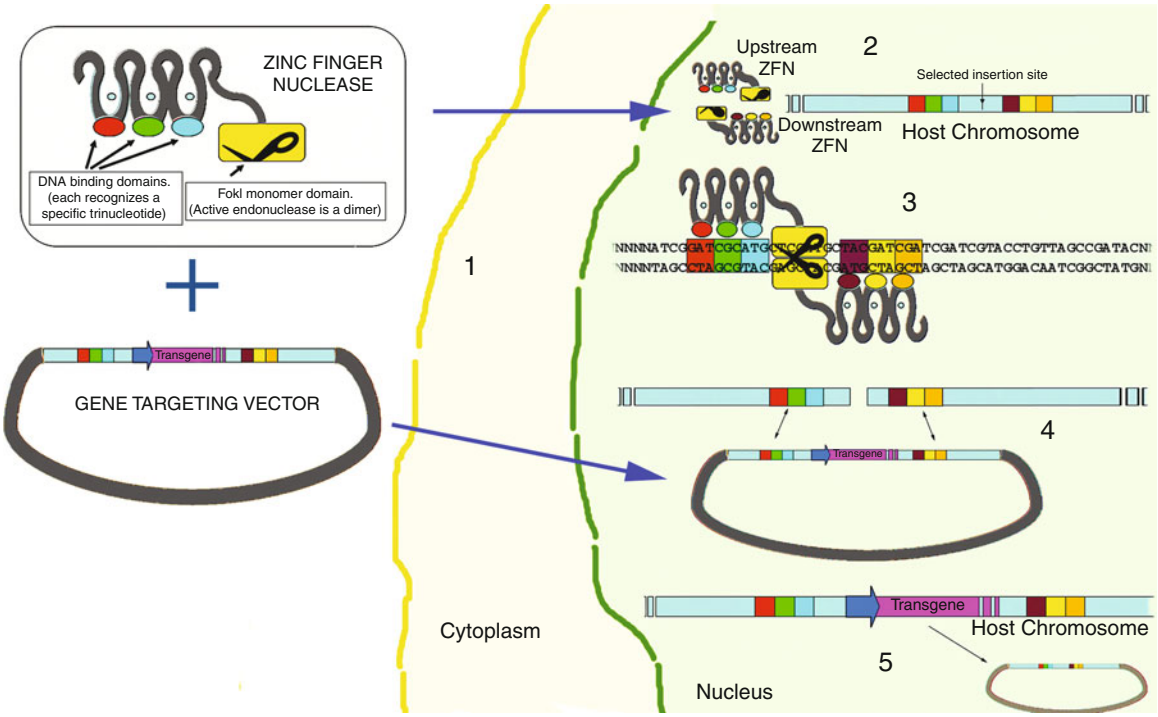

Transgenic Livestock Technologies. Figure 9
Homologous Recombination via Zinc Finger Nucleases (ZFNs) 1. A gene targeting DNA vector is prepared, where the transgene is flanked by DNA sequences homologous to the target locus. In different vectors, two ZFNs are designed, each coding for a specific DNA binding region and a FokI endonuclease monomeric domain. The two sequences recognized by the ZFNs are positioned upstream and downstream the selected insertion site in the target locus. The ZFN is introduced into the cell by microinjection, electroporation or transfection of a DNA expression vector or of a mRNA transcript. 2. The mRNAs are translated in two Zinc Finger Proteins. Each "finger" motif of the ZFN recognizes a sequence of three nucleotide (in this example, three "fingers" recognize a 9 bp target). A single ZFN binding to the DNA does not produce any effect. 3. When both the ZFN bind the DNA at the right distance, FokI domains can dimerize and produce a Double Strand Break in the target site. 4. DNA repair on the DSB can proceed through the NHEJ pathway, but, due to the availability of homologous sequences provided by the targeting vector, can also follow the route of Homologous Recombination 5. By Homologous Recombination, the transgene is introduced into the target site. The endogenous allele and the vector backbone sequences are lost (From [141])

Future Directions

The GE of livestock is slowly making progress toward possible applications both is science and industry. SCNT has been the major advancement in this field for the last 25 years. Nevertheless, many are the issues that need to be addressed to make GE of livestock robust, reproducible, and affordable. Assisted reproduction techniques are continuously improved and refined, however, the availability of true embryonic stem cells is still the one of the limiting factors for precise GE and the recent report of alternative sources like iPS cells have yet to prove their value for this purpose and it might take a long time before they become a reality. The designing of more effective DNA delivery vectors relies on the sequence of the genome. In livestock, this is lagging behind that of the human or mouse, therefore, it is not always possible to translate discoveries made in those species to livestock unless genomic information are generated by homology and partial sequencing. The ability to target the insertion of the transgene into a locus on a chromosome to assure

its expression also through generations would be a significant advancement since today few of the GE livestock expresses the inserted transgene at the level desired and the expression is often not stable.

The ability to target specific genes either by knockout through HR or knockdown by siRNA, will make it possible to develop functional genomics (i.e., understanding the function of a particular gene) in mammalian species closer to the human other than the mouse and to generate large animal models of human diseases, especially for those diseases that the mouse model has failed to reproduce the human phenotype [110, 139]. Animal models are required both to understand the pathogenesis of a disease, to develop and test possible new therapeutic approaches to it. Biotechnological application of GE animals again for biomedical application include the field of xenotransplantation, i.e., the possibility to transplant tissues and organs from one species (usually the pig) to humans [140, 141]. This requires multiple GE to make pig organs accepted by the human immune system. Another biotech application is the GE of livestock to express antibodies or proteins that have a therapeutic use in human cancer or other diseases [59] in sufficient quantities and affordable costs that would not otherwise be possible by other means.

Although the biomedical field is the more advanced and more receptive for this new technology, there are also potential applications in agriculture for breeding and selection of livestock. Proof of principle have been already obtained for increasing yield in cheese production [62] or better quality pork meat [142] as well as for disease resistance [61, 138].

GE of livestock is an expanding area of research with great potential for applications in the biomedical, biotechnology, and agricultural fields. This technology provides a tremendous potential to select and breed animals with specific genetic makeup much faster than by conventional breeding schemes; however, this will be possible when full understanding of the underlying biological mechanisms will be known.

Acknowledgments

Grant support was received from EU Xenome Project (LSHB-CT-2006-037377), EU PluriSys (n°223485), EU ESNATS (n° 201619), Regione Lombardia and Cariplo Foundation (NOBEL).

Bibliography

1. Gordon JW, Scangos GA, Plotkin DJ, Barbosa JA, Ruddle FH (1980) Genetic transformation of mouse embryos by microinjection of purified DNA. Proc Natl Acad Sci USA 77:7380–7384
2. Palmiter RD, Brinster RL, Hammer RE, Trumbauer ME, Rosenfeld MG, Birnberg NC, Evans RM (1982) Dramatic growth of mice that develop from eggs microinjected with metallothionein-growth hormone fusion genes. Nature 300:611–615
3. Hammer RE, Pursel VG, Rexroad CE Jr, Wall RJ, Bolt DJ, Ebert KM, Palmiter RD, Brinster RL (1985) Production of transgenic rabbits, sheep and pigs by microinjection. Nature 315:680–683
4. Simons PJ, Wilmut IA, Clark J, Archibald AL, Bishop JO, Lathe R (1988) Gene transfer into sheep. Biotechnology 6:179–183
5. Wall RJ, Pursel VG, Shamay A, McKnight RA, Pittius CW, Hennighausen L (1991) High-level synthesis of a heterologous milk protein in the mammary glands of transgenic swine. Proc Natl Acad Sci USA 88:1696–1700
6. Krimpenfort P, Rademakers A, Eyestone W, van der Schans A, van den Broek S, Kooiman P, Kootwijk E, Platenburg G, Pieper F, Strijker R (1991) Generation of transgenic dairy cattle using 'in vitro' embryo production. Bio/technology (Nature Publishing Company) 9:844–847
7. Galli C, Lazzari G (1996) Practical aspects of IVM/IVF n cattle. Anim Reprod Sci 42:371–379
8. Capecchi MR (1989) Altering the genome by homologous recombination. Science 244:1288–1292
9. Galli C, Lazzari G, Flechon JE, Moor RM (1994) Embryonic stem cells in farm animals. Zygote 2:385–389
10. Wilmut I, Schnieke AE, McWhir J, Kind AJ, Campbell KH (1997) Viable offspring derived from fetal and adult mammalian cells. Nature 385:810–813
11. Brinster RL (2007) Male germline stem cells: from mice to men. Science 316:404–405
12. Brinster RL, Zimmermann JW (1994) Spermatogenesis following male germ-cell transplantation. Proc Natl Acad Sci USA 91:11298–11302
13. Dobrinski I (2008) Male germ cell transplantation. Reprod Domest Anim 43(Suppl 2):288–294
14. Brinster RL (2002) Germline stem cell transplantation and transgenesis. Science 296:2174–2176
15. Lavitrano M, Camaioni A, Fazio VM, Dolci S, Farace MG, Spadafora C (1989) Sperm cells as vectors for introducing foreign DNA into eggs: genetic transformation of mice. Cell 57:717–723
16. Brinster RL, Sandgren EP, Behringer RR, Palmiter RD (1989) No simple solution for making transgenic mice. Cell 59:239–241
17. Roy SK, Greenwald GS (1985) An enzymatic method for dissociation of intact follicles from the hamster ovary: histological and quantitative aspects. Biol Reprod 32:203–215
18. Eppig JJ, O'Brien MJ (1996) Development in vitro of mouse oocytes from primordial follicles. Biol Reprod 54:197–207
19. Lazzari G, Galli C, Moor RM (1994) Functional changes in the somatic and germinal compartments during follicle growth in pigs. Anim Reprod Sci 35:119–130

20. Miyano T, Manabe N (2007) Oocyte growth and acquisition of meiotic competence. Soc Reprod Fertil Suppl 63:531–538
21. Meirow D, Levron J, Eldar-Geva T, Hardan I, Fridman E, Yemini Z, Dor J (2007) Monitoring the ovaries after autotransplantation of cryopreserved ovarian tissue: endocrine studies, in vitro fertilization cycles, and live birth. Fertil Steril 87:418 e417–418 e415
22. Galli C, Moor RM (1991) Development of immature bovine oocytes into viable embryos in vitro. Bull 'Association Anat 228:67–71
23. Galli C, Colleoni S, Duchi R, Lagutina I, Lazzari G (2007) Developmental competence of equine oocytes and embryos obtained by in vitro procedures ranging from in vitro maturation and ICSI to embryo culture, cryopreservation and somatic cell nuclear transfer. Anim Reprod Sci 98:39–55
24. Moor RM, Trounson AO (1977) Hormonal and follicular factors affecting maturation of sheep oocytes in vitro and their subsequent developmental capacity. J Reprod Fertil 49:101–109
25. Moor RM, Osborn JC, Cran DG, Walters DE (1981) Selective effect of gonadotrophins on cell coupling, nuclear maturation and protein synthesis in mammalian oocytes. J Embryol Exp Morphol 61:347–365
26. Staigmiller R, Moor R (1984) Effect of follicle cells on the maturation and developmental competence of ovine oocytes matured outside the follicle. Gamete Res 9:221–229
27. Galli C, Moor RM (1991) Gonadotrophin requirements for the in vitro maturation of sheep oocytes and their subsequent embryonic development. Theriogenology 35:1083–1093
28. Carolan C, Monaghan P, Gallagher M, Gordon I (1994) Effect of recovery method on yield of bovine oocytes per ovary and their developmental competence after maturation, fertilization and culture in vitro. Theriogenology 41:1061–1068
29. Lu K, Polge C. A summary of two-year's results in large scale in vitro bovine embryo production. Proc 12th Inter. Cong. Animal Reproduction, The Hague 1992:1315–1317
30. Goto K, Kajihara Y, Kosaka S, Koba M, Nakanishi Y, Ogawa K (1988) Pregnancies after co-culture of cumulus cells with bovine embryos derived from in-vitro fertilization of in-vitro matured follicular oocytes. J Reprod Fertil 83:753–758
31. Xu KP, Greve T, Callesen H, Hyttel P (1987) Pregnancy resulting from cattle oocytes matured and fertilized in vitro. J Reprod Fertil 81:501–504
32. Moor RM, Mattioli M, Ding J, Nagai T (1990) Maturation of pig oocytes in vivo and in vitro. J Reprod Fertil Suppl 40:197–210
33. Zhang JJ, Boyle MS, Allen WR, Galli C (1989) Recent studies on in vivo fertilization of in vitro matured horse oocytes. Equine Vet J 8:101–104
34. Galli C, Crotti G, Notari C, Turini P, Duchi R, Lazzari G (2001) Embryo production by ovum pick up from live donors. Theriogenology 55:1341–1357
35. Pieterse MC, Vos PL, Kruip TA, Wurth YA, van Beneden TH, Willemse AH, Taverne MA (1991) Transvaginal ultrasound guided follicular aspiration of bovine oocytes. Theriogenology 35:857–862
36. Hasler JF, Henderson WB, Hurtgen PJ, Jin ZQ, McCauley AD, Mower SA, Neely B, Shuey LS, Stokes JE, Trimmer SA (1995) Production, freezing and transfer of bovine IVF embryos and subsequent calving results. Theriogenology 43:141–152
37. Galli C, Duchi R, Crotti G, Lazzari G (1998) Embryo production by Ovum Pick Up in Water Buffalo. Theriogenology 49:400
38. Galli C, Crotti G, Turini P, Duchi R, Mari G, Zavaglia G, Duchamp G, Daels P, Lazzari G (2002) Frozen- thawed embryos produced by Ovum Pick Up of immature oocytes and ICSI are capable to establish pregnancies in the horse. Theriogenology 58:705–708
39. Yanagimachi R, Chang MC (1964) In Vitro Fertilization of Golden Hamster Ova. J Exp Zool 156:361–375
40. Brackett BG, Bousquet D, Boice ML, Donawick WJ, Evans JF, Dressel MA (1982) Normal development following in vitro fertilization in the cow. Biol Reprod 27:147–158
41. Parrish JJ, Susko-Parrish JL, Leibfried-Rutledge ML, Critser ES, Eyestone WH, First NL (1986) Bovine in vitro fertilization with frozen-thawed semen. Theriogenology 25:591–600
42. Palermo G, Joris H, Devroey P, Van Steirteghem AC (1992) Pregnancies after intracytoplasmic injection of single spermatozoon into an oocyte. Lancet 340:17–18
43. Goto K, Yanagita K (1995) Normality of calves obtained by intracytoplasmic sperm injection. Hum Reprod 10:1554
44. Galli C, Vassiliev I, Lagutina I, Galli A, Lazzari G (2003) Bovine embryo development following ICSI: effect of activation, sperm capacitation and pre-treatment with dithiothreitol. Theriogenology 60:1467–1480
45. Catt SL, Catt JW, Gomez MC, Maxwell WM, Evans G (1996) Birth of a male lamb derived from an in vitro matured oocyte fertilised by intracytoplasmic injection of a single presumptive male sperm. Vet Rec 139:494–495
46. Kolbe T, Holtz W (2000) Birth of a piglet derived from an oocyte fertilized by intracytoplasmic sperm injection (ICSI). Anim Reprod Sci 64:97–101
47. Perry AC, Wakayama T, Kishikawa H, Kasai T, Okabe M, Toyoda Y, Yanagimachi R (1999) Mammalian transgenesis by intracytoplasmic sperm injection. Science 284:1180–1183
48. Gandolfi F, Moor RM (1987) Stimulation of early embryonic development in the sheep by co-culture with oviduct epithelial cells. J Reprod Fertil 81:23–28
49. Young LE, Sinclair KD, Wilmut I (1998) Large offspring syndrome in cattle and sheep. Rev Reprod 3:155–163
50. van Wagtendonk-de Leeuw AM, Mullaart E, de Roos AP, Merton JS, den Daas JH, Kemp B, de Ruigh L (2000) Effects of different reproduction techniques: AI MOET or IVP, on health and welfare of bovine offspring. Theriogenology 53:575–597
51. Tervit HR, Whittingham DG, Rowson LE (1972) Successful culture in vitro of sheep and cattle ova. J Reprod Fertil 30:493–497
52. Lazzari G, Wrenzycki C, Herrmann D, Duchi R, Kruip T, Niemann H, Galli C (2002) Cellular and molecular deviations in bovine in vitro-produced embryos are related to the large offspring syndrome. Biol Reprod 67:767–775

53. Gurdon JB (2006) From nuclear transfer to nuclear reprogramming: the reversal of cell differentiation. Annu Rev Cell Dev Biol 22:1–22
54. Willadsen SM (1986) Nuclear transplantation in sheep embryos. Nature 320:63–65
55. Galli C, Lagutina I, Crotti G, Colleoni S, Turini P, Ponderato N, Duchi R, Lazzari G (2003) Pregnancy: a cloned horse born to its dam twin. Nature 424:635
56. Lagutina I, Lazzari G, Duchi R, Colleoni S, Ponderato N, Turini P, Crotti G, Galli C (2005) Somatic cell nuclear transfer in horses: effect of oocyte morphology, embryo reconstruction method and donor cell type. Reproduction 130:559–567
57. Galli C, Duchi R, Moor RM, Lazzari G (1999) Mammalian leukocytes contain all the genetic information necessary for the development of a new individual. Cloning 1:161–170
58. Galli C, Duchi R, Crotti G, Turini P, Ponderato N, Colleoni S, Lagutina I, Lazzari G (2003) Bovine embryo technologies. Theriogenology 59:599–616
59. Kuroiwa Y, Kasinathan P, Matsushita H, Sathiyaselan J, Sullivan EJ, Kakitani M, Tomizuka K, Ishida I, Robl JM (2004) Sequential targeting of the genes encoding immunoglobulin-mu and prion protein in cattle. Nat Genet 36:775–780
60. Lombardo A, Genovese P, Beausejour CM, Colleoni S, Lee YL, Kim KA, Ando D, Urnov FD, Galli C, Gregory PD, Holmes MC, Naldini L (2007) Gene editing in human stem cells using zinc finger nucleases and integrase-defective lentiviral vector delivery. Nat Biotechnol 25:1298–1306
61. Wall RJ, Powell AM, Paape MJ, Kerr DE, Bannerman DD, Pursel VG, Wells KD, Talbot N, Hawk HW (2005) Genetically enhanced cows resist intramammary Staphylococcus aureus infection. Nat Biotechnol 23:445–451
62. Brophy B, Smolenski G, Wheeler T, Wells D, L'Huillier P, Laible G (2003) Cloned transgenic cattle produce milk with higher levels of beta-casein and kappa-casein. Nat Biotechnol 21:157–162
63. Wakayama T, Tabar V, Rodriguez I, Perry AC, Studer L, Mombaerts P (2001) Differentiation of embryonic stem cell lines generated from adult somatic cells by nuclear transfer. Science 292:740–743
64. Lazzari G, Colleoni S, Giannelli SG, Brunetti D, Colombo E, Lagutina I, Galli C, Broccoli V (2006) Direct derivation of neural rosettes from cloned bovine blastocysts: a model of early neurulation events and neural crest specification in vitro. Stem Cells 24:2514–2521
65. Takahashi K, Yamanaka S (2006) Induction of pluripotent stem cells from mouse embryonic and adult fibroblast cultures by defined factors. Cell 126:663–676
66. Evans MJ, Kaufman MH (1981) Establishment in culture of pluripotential cells from mouse embryos. Nature 292:154–156
67. Martin GR (1981) Isolation of a pluripotent cell line from early mouse embryos cultured in medium conditioned by teratocarcinoma stem cells. Proc Natl Acad Sci USA 78:7634–7638
68. Keefer CL, Pant D, Blomberg L, Talbot NC (2007) Challenges and prospects for the establishment of embryonic stem cell lines of domesticated ungulates. Anim Reprod Sci 98:147–168
69. Notarianni E, Galli C, Laurie S, Moor RM, Evans MJ (1991) Derivation of pluripotent, embryonic cell lines from the pig and sheep. J Reprod Fertil Suppl 43:255–260
70. Iwasaki S, Campbell KH, Galli C, Akiyama K (2000) Production of live calves derived from embryonic stem-like cells aggregated with tetraploid embryos. Biol Reprod 62: 470–475
71. Ying QL, Stavridis M, Griffiths D, Li M, Smith A (2003) Conversion of embryonic stem cells into neuroectodermal precursors in adherent monoculture. Nat Biotechnol 21: 183–186
72. Ying QL, Wray J, Nichols J, Batlle-Morera L, Doble B, Woodgett J, Cohen P, Smith A (2008) The ground state of embryonic stem cell self-renewal. Nature 453:519–523
73. Buehr M, Meek S, Blair K, Yang J, Ure J, Silva J, McLay R, Hall J, Ying QL, Smith A (2008) Capture of authentic embryonic stem cells from rat blastocysts. Cell 135:1287–1298
74. Tesar PJ, Chenoweth JG, Brook FA, Davies TJ, Evans EP, Mack DL, Gardner RL, McKay RD (2007) New cell lines from mouse epiblast share defining features with human embryonic stem cells. Nature 448:196–199
75. Brons IG, Smithers LE, Trotter MW, Rugg-Gunn P, Sun B, de Chuva Sousa Lopes SM, Howlett SK, Clarkson A, Ahrlund-Richter L, Pedersen RA, Vallier L (2007) Derivation of pluripotent epiblast stem cells from mammalian embryos. Nature 448:191–195
76. Alberio R, Croxall N, Allegrucci C. Pig Epiblast Stem Cells Depend on Activin/Nodal Signaling for Pluripotency and Self Renewal. Stem Cells Dev 2010.
77. Brown BD, Gentner B, Cantore A, Colleoni S, Amendola M, Zingale A, Baccarini A, Lazzari G, Galli C, Naldini L (2007) Endogenous microRNA can be broadly exploited to regulate transgene expression according to tissue, lineage and differentiation state. Nat Biotechnol 25:1457–1467
78. Mansour SL, Thomas KR, Capecchi MR (1988) Disruption of the proto-oncogene int-2 in mouse embryo-derived stem cells: a general strategy for targeting mutations to non-selectable genes. Nature 336:348–352
79. Campbell KH, McWhir J, Ritchie WA, Wilmut I (1996) Sheep cloned by nuclear transfer from a cultured cell line. Nature 380:64–66
80. Galli C, Lazzari G (2008) The manipulation of gametes and embryos in farm animals. Reprod Domest Anim 43(Suppl 2):1–7
81. Brinster RL, Allen JM, Behringer RR, Gelinas RE, Palmiter RD (1988) Introns increase transcriptional efficiency in transgenic mice. Proc Natl Acad Sci USA 85:836–840
82. Palmiter RD, Sandgren EP, Avarbock MR, Allen DD, Brinster RL (1991) Heterologous introns can enhance expression of transgenes in mice. Proc Natl Acad Sci USA 88:478–482
83. Schedl A, Montoliu L, Kelsey G, Schutz G (1993) A yeast artificial chromosome covering the tyrosinase gene confers copy number-dependent expression in transgenic mice. Nature 362:258–261
84. Giraldo P, Montoliu L (2001) Size matters: use of YACs, BACs and PACs in transgenic animals. Transgenic Res 10:83–103

85. Van Keuren ML, Gavrilina GB, Filipiak WE, Zeidler MG, Saunders TL (2009) Generating transgenic mice from bacterial artificial chromosomes: transgenesis efficiency, integration and expression outcomes. Transgenic Res 18:769–785
86. Sauer B, Henderson N (1990) Targeted insertion of exogenous DNA into the eukaryotic genome by the Cre recombinase. New Biol 2:441–449
87. Allen GC, Spiker S, Thompson WF (2005) Transgene integration: use of matrix attachment regions. Meth Molecular Biology Clifton N J 286:313–326
88. Harraghy N, Gaussin A, Mermod N (2008) Sustained transgene expression using MAR elements. Curr Gene Ther 8:353–366
89. McKnight RA, Shamay A, Sankaran L, Wall RJ, Hennighausen L (1992) Matrix-attachment regions can impart position-independent regulation of a tissue-specific gene in transgenic mice. Proc Natl Acad Sci USA 89:6943–6947
90. McKnight RA, Spencer M, Wall RJ, Hennighausen L (1996) Severe position effects imposed on a 1 kb mouse whey acidic protein gene promoter are overcome by heterologous matrix attachment regions. Mol Reprod Dev 44:179–184
91. Polejaeva IA, Chen SH, Vaught TD, Page RL, Mullins J, Ball S, Dai Y, Boone J, Walker S, Ayares DL, Colman A, Campbell KH (2000) Cloned pigs produced by nuclear transfer from adult somatic cells. Nature 407:86–90
92. Geurts AM, Cost GJ, Freyvert Y, Zeitler B, Miller JC, Choi VM, Jenkins SS, Wood A, Cui X, Meng X, Vincent A, Lam S, Michalkiewicz M, Schilling R, Foeckler J, Kalloway S, Weiler H, Menoret S, Anegon I, Davis GD, Zhang L, Rebar EJ, Gregory PD, Urnov FD, Jacob HJ, Buelow R (2009) Knockout rats via embryo microinjection of zinc-finger nucleases. Science 325:433
93. Dickson D (1989) "Dangerous" liaisons in cell biology. Science 244:1539–1540
94. Chang K, Qian J, Jiang M, Liu YH, Wu MC, Chen CD, Lai CK, Lo HL, Hsiao CT, Brown L, Bolen J Jr, Huang HI, Ho PY, Shih PY, Yao CW, Lin WJ, Chen CH, Wu FY, Lin YJ, Xu J, Wang K (2002) Effective generation of transgenic pigs and mice by linker based sperm-mediated gene transfer. BMC Biotechnol 2:5
95. Shen W, Li L, Pan Q, Min L, Dong H, Deng J (2006) Efficient and simple production of transgenic mice and rabbits using the new DMSO-sperm mediated exogenous DNA transfer method. Mol Reprod Dev 73:589–594
96. Lavitrano M, Bacci ML, Forni M, Lazzereschi D, Di Stefano C, Fioretti D, Giancotti P, Marfe G, Pucci L, Renzi L, Wang H, Stoppacciaro A, Stassi G, Sargiacomo M, Sinibaldi P, Turchi V, Giovannoni R, Della Casa G, Seren E, Rossi G (2002) Efficient production by sperm-mediated gene transfer of human decay accelerating factor (hDAF) transgenic pigs for xenotransplantation. Proc Natl Acad Sci USA 99:14230–14235
97. Wu Z, Li Z, Yang J (2008) Transient transgene transmission to piglets by intrauterine insemination of spermatozoa incubated with DNA fragments. Mol Reprod Dev 75:26–32
98. Moreira PN, Perez-Crespo M, Ramirez MA, Pozueta J, Montoliu L, Gutierrez-Adan A (2007) Effect of transgene concentration, flanking matrix attachment regions, and RecA-coating on the efficiency of mouse transgenesis mediated by intracytoplasmic sperm injection. Biol Reprod 76:336–343
99. Kurome M, Ueda H, Tomii R, Naruse K, Nagashima H (2006) Production of transgenic-clone pigs by the combination of ICSI-mediated gene transfer with somatic cell nuclear transfer. Transgenic Res 15:229–240
100. Whitelaw CB, Radcliffe PA, Ritchie WA, Carlisle A, Ellard FM, Pena RN, Rowe J, Clark AJ, King TJ, Mitrophanous KA (2004) Efficient generation of transgenic pigs using equine infectious anaemia virus (EIAV) derived vector. FEBS Lett 571:233–236
101. Hacein-Bey-Abina S, Garrigue A, Wang GP, Soulier J, Lim A, Morillon E, Clappier E, Caccavelli L, Delabesse E, Beldjord K, Asnafi V, MacIntyre E, Dal Cortivo L, Radford I, Brousse N, Sigaux F, Moshous D, Hauer J, Borkhardt A, Belohradsky BH, Wintergerst U, Velez MC, Leiva L, Sorensen R, Wulffraat N, Blanche S, Bushman FD, Fischer A, Cavazzana-Calvo M (2008) Insertional oncogenesis in 4 patients after retrovirus-mediated gene therapy of\ SCID-X1. J Clin Invest 118: 3132–3142
102. Howe SJ, Mansour MR, Schwarzwaelder K, Bartholomae C, Hubank M, Kempski H, Brugman MH, Pike-Overzet K, Chatters SJ, de Ridder D, Gilmour KC, Adams S, Thornhill SI, Parsley KL, Staal FJ, Gale RE, Linch DC, Bayford J, Brown L, Quaye M, Kinnon C, Ancliff P, Webb DK, Schmidt M, von Kalle C, Gaspar HB, Thrasher AJ (2008) Insertional mutagenesis combined with acquired somatic mutations causes\ leukemogenesis following gene therapy of SCID-X1 patients. J Clin Invest 118:3143–3150
103. Romano G (2009) An update on gene therapy programs. Drug News Perspect 22:435–440
104. de Sio FR Santoni, Gritti A, Cascio P, Neri M, Sampaolesi M, Galli C, Luban J, Naldini L (2008) Lentiviral vector gene transfer is limited by the proteasome at postentry steps in various types of stem cells. Stem Cells 26:2142–2152
105. Chan AW, Chong KY, Martinovich C, Simerly C, Schatten G (2001) Transgenic monkeys produced by retroviral gene transfer into mature oocytes. Science 291:309–312
106. Hofmann A, Kessler B, Ewerling S, Kabermann A, Brem G, Wolf E, Pfeifer A (2006) Epigenetic regulation of lentiviral transgene vectors in a large animal model. Mol Ther 13:59–66
107. Henckaerts E, Dutheil N, Zeltner N, Kattman S, Kohlbrenner E, Ward P, Clement N, Rebollo P, Kennedy M, Keller GM, Linden RM (2009) Site-specific integration of adeno-associated virus involves partial duplication of the target locus. Proc Natl Acad Sci USA 106:7571–7576
108. Miller DG, Wang PR, Petek LM, Hirata RK, Sands MS, Russell DW (2006) Gene targeting in vivo by adeno-associated virus vectors. Nat Biotechnol 24:1022–1026

109. Russell DW, Hirata RK (1998) Human gene targeting by viral vectors. Nat Genet 18:325–330
110. Rogers CS, Stoltz DA, Meyerholz DK, Ostedgaard LS, Rokhlina T, Taft PJ, Rogan MP, Pezzulo AA, Karp PH, Itani OA, Kabel AC, Wohlford-Lenane CL, Davis GJ, Hanfland RA, Smith TL, Samuel M, Wax D, Murphy CN, Rieke A, Whitworth K, Uc A, Starner TD, Brogden KA, Shilyansky J, McCray PB Jr, Zabner J, Prather RS, Welsh MJ (2008) Disruption of the CFTR gene produces a model of cystic fibrosis in newborn pigs. Science 321:1837–1841
111. Rogers CS, Hao Y, Rokhlina T, Samuel M, Stoltz DA, Li Y, Petroff E, Vermeer DW, Kabel AC, Yan Z, Spate L, Wax D, Murphy CN, Rieke A, Whitworth K, Linville ML, Korte SW, Engelhardt JF, Welsh MJ, Prather RS (2008) Production of CFTR-null and CFTR-DeltaF508 heterozygous pigs by adeno-associated virus-mediated gene targeting and somatic cell nuclear transfer. J Clin Invest 118:1571–1577
112. Brunetti D, Perota A, Lagutina I, Colleoni S, Duchi R, Calabrese F, Seveso M, Cozzi E, Lazzari G, Lucchini F, Galli C (2008) Transgene expression of green fluorescent protein and germ line transmission in cloned pigs derived from in vitro transfected adult fibroblasts. Cloning Stem Cells 10(4):409–420
113. Lagutina I, Lazzari G, Duchi R, Turini P, Tessaro I, Brunetti D, Colleoni S, Crotti G, Galli C (2007) Comparative aspects of somatic cell nuclear transfer with conventional and zona-free method in cattle, horse, pig and sheep. Theriogenology 67:90–98
114. Lagutina I, Lazzari G, Galli C (2006) Birth of cloned pigs from zona-free nuclear transfer blastocysts developed in vitro before transfer. Cloning Stem Cells 8:283–293
115. Kragh PM, Du Y, Corydon TJ, Purup S, Bolund L, Vajta G (2005) Efficient in vitro production of porcine blastocysts by hand-made cloning with a combined electrical and chemical activation. Theriogenology 64:1536–1545
116. Vajta G, Kragh PM, Mtango NR, Callesen H (2005) Hand-made cloning approach: potentials and limitations. Reprod Fertil Dev 17:97–112
117. Esteban MA, Xu J, Yang J, Peng M, Qin D, Li W, Jiang Z, Chen J, Deng K, Zhong M, Cai J, Lai L, Pei D (2009) Generation of induced pluripotent stem cell lines from Tibetan miniature pig. J Biol Chem 284:17634–17640
118. Ezashi T, Telugu BP, Alexenko AP, Sachdev S, Sinha S, Roberts RM (2009) Derivation of induced pluripotent stem cells from pig somatic cells. Proc Natl Acad Sci USA 106:10993–10998
119. Wu Z, Chen J, Ren J, Bao L, Liao J, Cui C, Rao L, Li H, Gu Y, Dai H, Zhu H, Teng X, Cheng L, Xiao L (2009) Generation of pig induced pluripotent stem cells with a drug-inducible system. J Mol Cell Biol 1:46–54
120. Takahagi Y, Fujimura T, Miyagawa S, Nagashima H, Shigehisa T, Shirakura R, Murakami H (2005) Production of alpha 1, 3-galactosyltransferase gene knockout pigs expressing both human decay-accelerating factor and N-acetylglucosaminyltransferase III. Mol Reprod Dev 71: 331–338
121. Fujimura T, Takahagi Y, Shigehisa T, Nagashima H, Miyagawa S, Shirakura R, Murakami H (2008) Production of alpha 1, 3-galactosyltransferase gene-deficient pigs by somatic cell nuclear transfer: a novel selection method for gal alpha 1, 3-Gal antigen-deficient cells. Mol Reprod Dev 75:1372–1378
122. Takahashi K, Tanabe K, Ohnuki M, Narita M, Ichisaka T, Tomoda K, Yamanaka S (2007) Induction of pluripotent stem cells from adult human fibroblasts by defined factors. Cell 131:861–872
123. Yu J, Vodyanik MA, Smuga-Otto K, Antosiewicz-Bourget J, Frane JL, Tian S, Nie J, Jonsdottir GA, Ruotti V, Stewart R, Slukvin II, Thomson JA (2007) Induced pluripotent stem cell lines derived from human somatic cells. Science 318:1917–1920
124. Huangfu D, Osafune K, Maehr R, Guo W, Eijkelenboom A, Chen S, Muhlestein W, Melton DA (2008) Induction of pluripotent stem cells from primary human fibroblasts with only Oct4 and Sox2. Nat Biotechnol 26:1269–1275
125. Feng B, Ng JH, Heng JC, Ng HH (2009) Molecules that promote or enhance reprogramming of somatic cells to induced pluripotent stem cells. Cell Stem Cell 4:301–312
126. Ralston A, Rossant J (2010) The genetics of induced pluripotency. Reproduction 139:35–44
127. Bartolome C, Bello X, Maside X (2009) Widespread evidence for horizontal transfer of transposable elements across Drosophila genomes. Genome Biol 10:R22
128. Clark KJ, Carlson DF, Foster LK, Kong BW, Foster DN, Fahrenkrug SC (2007) Enzymatic engineering of the porcine genome with transposons and recombinases. BMC Biotechnol 7:42
129. Araki K, Araki M, Yamamura K (2002) Site-directed integration of the cre gene mediated by Cre recombinase using a combination of mutant lox sites. Nucleic Acids Res 30:e103
130. Irion S, Luche H, Gadue P, Fehling HJ, Kennedy M, Keller G (2007) Identification and targeting of the ROSA26 locus in human embryonic stem cells. Nat Biotechnol 25:1477–1482
131. Nyabi O, Naessens M, Haigh K, Gembarska A, Goossens S, Maetens M, De Clercq S, Drogat B, Haenebalcke L, Bartunkova S, De Vos I, De Craene B, Karimi M, Berx G, Nagy A, Hilson P, Marine JC, Haigh JJ (2009) Efficient mouse transgenesis using Gateway-compatible ROSA26 locus targeting\ vectors and F1 hybrid ES cells. Nucleic Acids Res 37:e55
132. Porteus MH (2006) Mammalian gene targeting with designed zinc finger nucleases. Mol Ther 13:438–446
133. d'Apice AJ, Cowan PJ (2008) Gene-modified pigs. Xenotransplantation 15:87–90
134. Fang J, Qian JJ, Yi S, Harding TC, Tu GH, VanRoey M, Jooss K (2005) Stable antibody expression at therapeutic levels using the 2A peptide. Nat Biotechnol 23: 584–590

135. Bartosch B, Stefanidis D, Myers R, Weiss R, Patience C, Takeuchi Y (2004) Evidence and consequence of porcine endogenous retrovirus recombination. J Virol 78:13880–13890
136. Moalic Y, Felix H, Takeuchi Y, Jestin A, Blanchard Y (2009) Genome areas with high gene density and CpG island neighborhood strongly attract porcine endogenous retrovirus for integration and favor the formation of hot spots. J Virol 83:1920–1929
137. Takeuchi Y, Patience C, Magre S, Weiss RA, Banerjee PT, Le Tissier P, Stoye JP (1998) Host range and interference studies of three classes of pig endogenous retrovirus. J Virol 72:9986–9991
138. Dieckhoff B, Petersen B, Kues WA, Kurth R, Niemann H, Denner J (2008) Knockdown of porcine endogenous retrovirus (PERV) expression by PERV-specific shRNA in transgenic pigs. Xenotransplantation 15:36–45
139. Kragh PM, Nielsen AL, Li J, Du Y, Lin L, Schmidt M, Bogh IB, Holm IE, Jakobsen JE, Johansen MG, Purup S, Bolund L, Vajta G, Jorgensen AL (2009) Hemizygous minipigs produced by random gene insertion and handmade cloning express the Alzheimer's disease-causing dominant mutation APPsw. Transgenic Res 18:545–558
140. Petersen B, Carnwath JW, Niemann H (2009) The perspectives for porcine-to-human xenografts. Comp Immunol Microbiol Infect Dis 32:91–105
141. Galli C, Perota A, Brunetti D, Lagutina I, Lazzari G, Lucchini F (2010) Genetic engineering including superseding microinjection: new ways to make GM pigs. Xenotransplantation 17(6):397–410
142. Lai L, Kang JX, Li R, Wang J, Witt WT, Yong HY, Hao Y, Wax DM, Murphy CN, Rieke A, Samuel M, Linville ML, Korte SW, Evans RW, Starzl TE, Prather RS, Dai Y (2006) Generation of cloned transgenic pigs rich in omega-3 fatty acids. Nat Biotechnol 24:435–436

Books

Gordon IR (2003) Laboratory production of cattle embryos, vol Series No. 27, 2nd edn, Biotechnology in agriculture. CAB International, Wallingford

Gordon I (2004) Reproductive technologies in farm animals. CAB International, Wallingford. ISBN 0 85199 862 3

Hafez B, Hafez ESE (2000) Reproduction in farm animals, 7th ed. Lippincott Williams & Wilkins. ISBN 0-683-30577-8

Monk M (1987) Mammalian development, a practical approach. In: Rickwood D, Hames BD (eds) The practical approach series. IRL Press Ltd, Oxford/Washington, DC

Nagy A (2003) Manipulating the mouse embryo : a laboratory manual. Cold Spring Harbor Laboratory Press, Cold Spring Harbor. ISBN: 0879695749 0879695919

Robertson E (1987) Teratocarcinoma and embryonic stem cells, a practical approach. In: Rickwood D, Hames BD (eds) The practical approach series. IRL Press Ltd, Oxford/Washington, DC

Transgenic Livestock, Decreasing Environmental Impact of

Serguei P. Golovan[1], Cecil W. Forsberg[2]
[1]Department of Animal and Food Science, University of Delaware, Newark, DE, USA
[2]Department of Molecular and Cellular Biology, University of Guelph, Guelph, ON, Canada

Article Outline

Glossary
Definition of the Subject
Introduction
Future Directions
Bibliography

Glossary

Arabinoxylan A polymeric backbone of β(1,4) linked xylose residues with attached C(O)-2,3-linked arabinose residues that is found mainly in cereal grains. It becomes highly viscous when dissolved in the gastrointestinal tract and is not digested by monogastric animals.

Eutrophication A process where water bodies receive excess nutrients especially as phosphorus or nitrogen that stimulate excessive plant and algal growth resulting in reduced water quality.

β-Glucan A polymer found primarily in cereal grains consisting of β (1,3:1,4) linked glucose residues that becomes viscous on solubilization in the gastrointestinal tract and is not digested by monogastric animals.

Glycanase Any enzyme that catalyzes the hydrolysis of a glycan, which includes glucanases and xylanases of all types.

Phytase Any type of phosphatase enzyme that catalyzes the hydrolysis of phytic acid releasing phosphate molecules.

Phytic Acid Inositol hexakisphosphate (or phytate when in the salt form) is the principle storage form of phosphorus in many plants. It accounts for 50–80% of the total phosphorus present and is poorly digested by monogastric animals.

Definition of the Subject

As the world population increases, there is an increasing demand for food including both plant and animal products. The demand for meat and milk are increasing at a faster rate than for plant products because of increased wealth in developing countries. Intensification of livestock production to satisfy the demand is exacerbating the deleterious impact of intensive animal agriculture on the environment and new approaches are needed to reduce the impact. One approach is through the development of transgenic animals that have a smaller environmental footprint. At present there are no transgenic livestock in production. Transgenic livestock that have reduced environmental impact have been developed, but most proposed strategies are at the early stages of development. Physiological modifications that would reduce the impact of livestock include changes to improve feed utilization, increase growth and increase disease resistance, reduce manure output, and decrease greenhouse gas production. Obviously an essential factor is that the changes in physiology of the transgenic animal must have no deleterious effect on health, welfare, performance, and the environment.

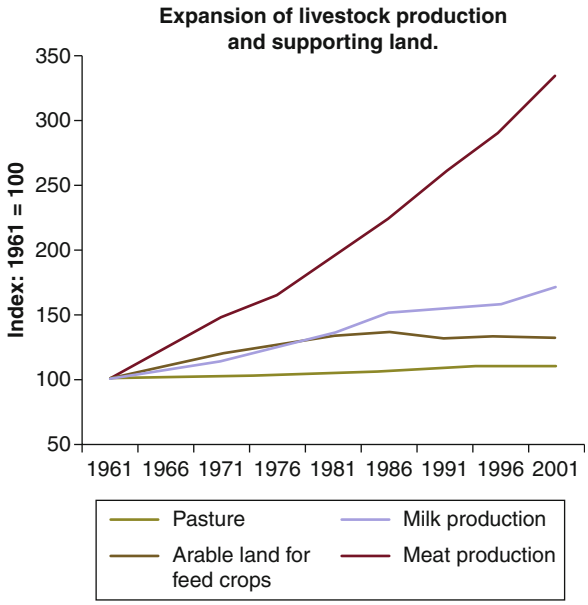

Steinfeld H, Gerber P PNAS 2010;107:18237–18238

Transgenic Livestock, Decreasing Environmental Impact of. Figure 1
Global expansion of livestock production and supporting land

Introduction

Environmental Impact of Livestock

Demand projections point to increases of global meat consumption of 68% and of global milk consumption of 57% of the 2000 base period by 2030 [26, 83]. While agriculture could be considered a "green" industry which uses solar energy to produce food and fiber for human use, it has also become a serious threat to global ecological systems. Currently forest losses in tropical countries is largely due to conversion to agricultural land to increase global grazing and cropland dedicated to the production of feed that already amounts to approximately 70% of all agricultural land [84]. The trends are illustrated by Fig. 1. Livestock production is a major cause of greenhouse gas production, particularly methane production, and as well is a major source of pollution due to the extensive use of pesticides, antibiotics, and nutrients (nitrogen, phosphorus, and minerals) that result in increased eutrophication with deterioration in water quality in many countries [87]. The major *challenge for animal agriculture in this century is to sustain and increase meat and milk production without further degrading the environment.*

Production of meat from monogastric animals, mainly swine and poultry, has increased 103% over the period from 1987 to 2007 compared to ruminant meat production that increased by 28% [27]. The shift to monogastric species and continued productivity gains have the potential to reduce environmental impact per unit of animal production in the future, but with overall production increasing, serious pollution concerns remain. The issues and options in addressing the environmental consequences of a growing livestock sector are clearly enunciated in a paper by Gerber et al. [30].

Selective breeding of animals has greatly improved commercial performance of livestock and is especially useful for improvement of *multi-gene traits.* Yet, selective breeding is a slow process, depending on the rate of animal reproduction and can only operate on alleles and genes present in animal population with little control over what to express, where, when, and how

much. Continuous selection for a particular trait may result in decreased genetic variability in the locus and decrease ability for further selection. For example, only a few proven bulls produce the majority of offspring in the world Holstein populations and similar reduced breed diversity in US swine and poultry is a cause for concern [56]. It is also difficult to introduce beneficial alleles from rare breeds into existing commercial population because it leads to decreased performance for economically important traits. In contrast, animal genetic engineering allows precise introduction of new alleles from rare breeds, novel genes from evolutionary distant species, or even completely artificial genes with control of the time, place, and amount of gene expression in an animal. Furthermore, a transgenic animal is a self-replicating high-tech animal – it might be expensive to produce but it is cheap to propagate.

Reducing the impact on the environment through animal transgenesis can take many forms (Table 1), for example, improving the overall feed digestion by the animal or reducing the excretion of a specific nutrient such as phosphorus. More subtle means of improving the efficiency of animal production could include enhanced disease resistance or even improving the nutritional quality of the meat since it would increase the product value.

Swine

Growth and Improved Digestion The first transgenic food animal developed that exhibited a trait consistent with a reduced environmental footprint was the transgenic line of pigs developed by Pursel and colleagues [64]. These pigs contained an increased level of bovine growth hormone that gave rise to an 18% increase in feed efficiency and an 11–14% increase in growth rate (Table 1). These improvements obviously decreased manure production per unit of body weight gain. Unfortunately, the pigs exhibited lameness, stress susceptibility, gastric ulcers, and other

Transgenic Livestock, Decreasing Environmental Impact of. Table 1 Genetic modifications in livestock to improve overall performance and reduce environmental impact

Species	Trait	Protein/RNA; Transgene	Reference
Pig	Phosphorus metabolism	Phytase; PSP-APPA	[33]
Pig	Increased growth	Growth hormone; hMTpGH	[57]
Pig	Increased growth	Insulin-like growth factor; (mMT-HIGF-1)	[65]
Pig	Increased lactose in milk	α-lactalbumin; bovine α-lactalbumin	[90]
Pig	Influenza resistance	Mx protein; mMx1-Mx	[53]
Pig, Cattle	Disease resistance	IgA; mouse a and ***x*** chains	[46]
Cattle	Avoids spontaneous prion occurrence	Knockout vectors pBPrP(H)KOneo; pBPrP(H)KOpuro	[73]
Cattle	*Staphylococcus aureus* resistance	Lysostaphin; β-lactoglobulin promoter linked to lysostaphin, neomycin resistance, and GFP	[88]
Cattle	Mastitis resistance	Human lactoferrin in milk	[79]
Goat	Reduced mastitis and healthier kids	Human lysozyme; A_{s1}-casein promoter-hLZcDNA	[38]
Sheep	Visna virus envelope	Visna LTR-env	[14]
Sheep	Ovine prion locus	Homologous recombination	[21]
Sheep	Increased growth	Ovine growth hormone; metallothionein promoter	[1]
Chicken	Influenza virus resistance	Chicken U6 promoter; cRNA binding site influenza virus polymerase	[49]

health problems that negated the unique improvements observed, but the study documented that the problem was due to overproduced growth hormone. In a separate study by Nottle et al. [57], the level of growth hormone was controlled by using an inducible promoter, a modified human metallothionein promoter fused to the cDNA sequence for the porcine growth hormone. They documented improved growth of founder animals as compared to non-transgenic littermates, but the study was not carried beyond litter mates. Later, Pursel and colleagues [63] developed transgenic pigs that expressed insulin-like growth factor I (IGF-I) to determine whether directing the expression of IGF-I specifically to striated muscle would enhance lean muscle growth in pigs. However, they observed only a decreased daily rate of fat accretion in the transgenic pigs as compared to the rate in the unmodified pigs. This may be explained by the observation that transgenic modification of a trait that has already undergone intensive selection through traditional breeding and is a metabolic process with multiple effects can have unexpected and in some cases deleterious outcomes [22].

A different approach to enhancing growth rate of pigs was achieved by the introduction of the bovine α-lactalbumin gene into pigs. Sows containing the α-lactalbumin gene produce an increased concentration of lactose in milk during the early lactation that increases the growth rates of piglets [55, 90]. This novel transgenic modification improves efficiency of production by either allowing earlier weaning or more robust piglets at weaning.

Phosphorus is a key nutrient for all living things. At the same time, phosphorus mining damages the environment, and phosphorus-induced eutrophication leads to harmful algal blooms, decreased biodiversity, and changes in species composition. In addition, the global supply of mined phosphorus is running out and some estimate that within 30–40 years there will not be sufficient phosphorus to meet agricultural demand [16, 76]. Manure is a valuable organic fertilizer, but the high phosphorus (P) concentration in relation to the nitrogen (N) content is problematic. A desirable N/P ratio for plant growth is 6.0 for an increment in yield, [42]. This ratio is derived by using the N and P concentrations after losses due to volatilization, which is primarily an N loss. In contrast, the N/P values for manure from pigs, dairy cattle, and poultry are approximately 0.96, 2.6, and 1.7, respectively. Therefore manures from pigs, dairy cattle, and poultry are 6.3, 2.3, and 3.4-fold enriched in phosphorus in relation to nitrogen utilized by cereal grain crops. This documents the doubly serious impact of excess P relative to N in the manure for land spreading. To decrease phosphorus-induced eutrophication caused by the high phosphorus content of pig manure and to reduce the need for supplemental phosphorus in the diet, Golovan and colleagues [33] developed transgenic pigs expressing an *Escherichia coli* phytase driven by the mouse parotid secretory protein promoter that gave rise to phytase production in the salivary glands (Fig. 2). Phytase, secreted by the parotid gland in the saliva, mixes with the incoming food particles during chewing and hydrolyzes phytate in the acidic environment of the stomach-releasing phosphate that is readily absorbed in the small intestine. Since the dietary phosphorus requirement of the transgenic pigs can be satisfied by the cereal grain diet without inclusion of either supplemental P or supplemental microbial phytase, there is an overall decrease in P excretion in the feces and urine that will enter the environment [33]. A line of these phytase pigs currently in the eighth generation exhibited salivary phytase activities at a levels similar to that of the founding transgenic pig, and excrete 30–65% less phosphorus in the manure depending upon the stage of growth and diet consumed. Trials have documented that the phytase pigs have similar reproductive characteristics, health, and growth rates to that of conventional pigs (Forsberg, unpublished data). The pig parotid secretory protein promoter was also tested [95], but the salivary phytase production in mice was not as efficient as that described by Golovan et al. [32] for the mouse PSP promoter. It would be very instructive to assess the efficacy of the pig PSP promoter driving phytase synthesis in the pig.

Cereal grains and plant protein supplements have an imbalance of amino acids with an excess of nonessential amino acids and lesser amounts of the essential amino acids lysine methionine and threonine [58]. This imbalance results in high excretion of nitrogen from nonessential amino acids, and the swine ammonia emission metric (kg livestock^{-1}) is higher than either beef or dairy cattle [10]. Ammonia emissions are substantially reduced by inclusion in the diet of

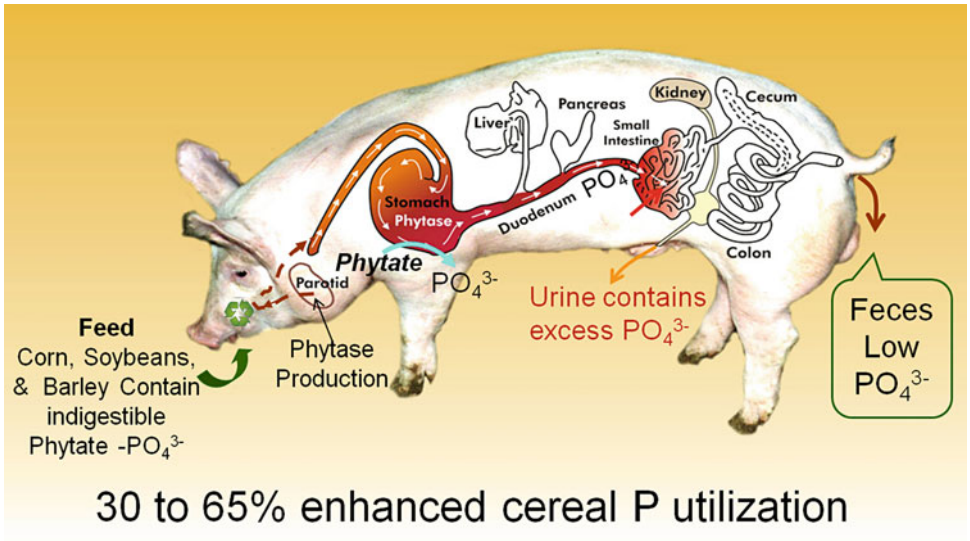

Transgenic Livestock, Decreasing Environmental Impact of. Figure 2
High phytate feed consumption by the Enviropig™

essential amino acids lysine, methionine, and threonine. Endowing pigs with the selected ability to synthesize essential amino acids in the appropriate proportions would decrease the need for protein supplements and would also decrease the excretion of ammonia arising from degradation of nonessential amino acids. To test this thesis, Rees and Hay [71] genetically modified mouse 3T3 cells by the introduction of a chimeric gene containing the coding regions of the *E. coli* gene for aspartokinaseI/homoserine dehydrogenase I and the *Corynebacterium glutamicum* gene for aspartic semialdehyde dehydrogenase subcloned into a Simian virus 40 based mammalian expression vector. These cells produced homoserine. By transfecting these cells with the plasmid pSVthrB/c containing genes coding for homoserine kinase and threonine synthase, the modified cell line expressed the complete pathway for the synthesis of threonine from aspartic acid, and the cell line no longer had a growth requirement for threonine. Therefore, by using the appropriate promoters with these genes it should be possible to produce genetically modified pigs/animals with the innate endogenous capacity to synthesis the essential amino acid threonine. The introduction of genes for the endogenous synthesis of methionine and lysine would be highly beneficial; unfortunately, the development of transgenes appropriately regulated to make each biosynthetic pathway function in tissues will be a daunting task because methionine synthesis requires four additional genes coding for enzymes that convert of homoserine to methionine. Lysine synthesis would require as many as nine genes coding for enzymes in the pathway beginning with aspartic acid (http://www.genome.jp/kegg/pathway/map/map00300). Alternatively, it might be possible to improve utilization of essential amino acids present in feed by increasing ileal digestibility (phytase, cellulase), absorption from gut (amino acid transporters), or even by increasing proportion of gut microorganisms responsible for synthesis of the essential amino acids by developing selective attachment receptors or by suppression of competitors using antimicrobial proteins.

Cereal grains and plant protein supplements contain indigestible structural carbohydrate components including β-glucan and arabinoxylan that are not digested by nonruminant species and are mainly excreted in the manure. It has been shown that supplementation of the diet with exogenous β-glucanase and xylanase improves growth of the piglets [23]. However, supplementation of grower diets with glycanase enzymes has given mixed results. In a study by Nyachoti et al. [59] no beneficial effect was observed by the inclusion of glycanase while Ji et al. [40] observed a distinct beneficial effect on digestion.

The beneficial effect of supplemental glucanase was the basis for testing whether this class of enzymes can be expressed in animals to enhance digestion. To test this hypothesis a transgene composed of the mouse pancreas–specific amylase 2.2 promoter and the associated signal sequence was linked to the *Bacillus subtilis* endoglucanase with a 3′polyadenylation sequence. The transgene was introduced into mice by pronuclear microinjection. Offspring containing the transgene expressed the endoglucanase gene in the pancreas and secreted the truncated, but active glucanase into the small intestine [96]. Ohnishi et al. [60] showed that overexpression of the Rab3D upregulated amylase secretion from the pancreatic acini of transgenic mice; therefore it is possible this technique could be used to further enhance glycanase synthesis and secretion from the pancreas into the small intestine. Together with a report by Hall et al. [35] describing the transgenic expression of a *Clostridium thermocellum* thermostable glucanase in the pancreas of the mouse using an elastase promoter/enhancer, these studies show the feasibility of expressing hydrolase genes in the gastrointestinal tracts of livestock.

Health Status Health is a major issue in livestock production documented by the deleterious economic impacts [72] of current and emerging swine zoonoses [82]. Strategies to improve resistance of swine to viral diseases such as foot-and-mouth disease, influenza, and porcine reproductive and respiratory syndrome which depend on host cellular machinery include antisense, decoys, ribozyme, and RNA interference [47, 92]. Recent work on the control of the African swine fever virus through the use of RNA interference may soon show success [41]. To provide resistance against a broad range of bacteria and some viruses, Cheung et al. [11] introduced into mice the porcine protegrin-1 using the cytomegalovirus promoter. Protegrin is an antimicrobial peptide that targets both gram-negative and gram-positive bacteria as well as enveloped viruses. They showed increased resistance to the swine pathogen *Actinobacillus suis*. This protein normally is expressed in neutrophils, and the intent in this study was to assess the effect of more general expression that would affect the bacteria at an earlier stage in the infection. Introduction of this construct into pigs and subsequent testing will be very informative since subclinical infections in pigs are a major cause of poorer feed efficiency in many environments.

Ruminants

Enhanced Digestion No transgenic ruminants have been reported that have a reduced impact on the environment through enhanced growth characteristics or reduced nutrient excretion. However, it was shown that feeding phytase and cellulases to lactating dairy cows resulted in reduced fecal excretion of dry matter, neutral detergent fiber, and acid detergent fiber, and reduced nitrogen and phosphorus in feces [43]. The beneficial effect of supplemental enzymes was found despite the presence of 101 distinct ruminal microbial phytases [37] and 27,755 putative carbohydrate-active genes, many of which presumably code for ruminal plant cell wall degrading enzymes [36]. Because added phytase enhances phosphorus utilization, transgenic expression of a phytase in the salivary glands of the cow using a promoter such as the indigenous salivary Bsp30a protein promoter [66, 91] would seem to be a possible strategy since Bsp30a is produced at a high concentration in saliva. No information is available on the Bsp30a promoter at this time; therefore background work would be necessary before testing this hypothesis.

Whether there would be interest in exploring the salivary production of glycanases in ruminants is questionable since variable results have been obtained by supplementation of diets with cellulases [5, 6, 62].

Methane from livestock accounts for approximately 37% of the methane produced by human-related activities, and the single largest source being enteric fermentation, mainly in ruminant livestock [30]. To reduce methane production in cattle, one option proposed was to generate transgenic cattle that produce salivary antibodies against rumen methanogens which subsequently bind to and inhibit their action in the rumen [44]. The same authors also identified the prophage φ-mru that is able to lyse methanogen cells. Secretion of anti-methanogenic proteins in the saliva would seem feasible from a physiological perspective as there are several strong salivary promoters [91]. However, before such experiments are undertaken it obviously would

be prudent to conduct feeding trials and testing for effects on the methanogenic population and to monitor the effect on the animal.

Health Disease is an ongoing drag on the efficiency in the production of ruminant animals [72]. Mastitis has a serious impact on milk production by ruminants [4]. To eliminate the deleterious effect of mastitis in dairy cows, Wall et al. [88] expressed lysostaphin in the milk. This antimicrobial protein enhanced the resistance to *Staphylococcus aureus* and provisionally could help maintain high milk production as a consequence of reduced mastitis if the genetic modification were accepted for commercial production. In a similar vein Maga et al. [51] demonstrated that human lysozyme expressed in the mammary gland of transgenic dairy goats inhibited the growth of bacteria that cause mastitis and this occurs without an effect on health or performance [38]. In a different approach Simojoki et al. [80] genetically modified dairy cows to secrete human lactoferrin in the milk. Again, it enhanced resistance to mastitis infections. Other avenues to improved performance could be through prion knockouts [73] and developing resistance to viruses (infectious bovine rhinotracheitis, bovine respiratory syncytial viruses, parainfluenza, bovine viral diarrhea, rabies, and foot-and-mouth disease) through the application of an RNA interference-based approach [47].

Poultry

Enhanced Digestion Inclusion of phytase, glucanase, and xylanase in the poultry diet enhances feed digestibility. Phytase was shown to enhance availability of phosphorus and other minerals, and in addition, to enhance amino acid digestibility [18]. The chicken is reported to have a weak endogenous magnesium-stimulated phytase activity associated with the intestinal brush boarder [50], but apparently contributes little to overall phytate digestion. Initial work has been done to develop a secretory competent form of the enzyme with higher activity for expression in poultry [12], although no further work has been reported. Use of the salivary glands of poultry as a site for transgenic phytase production is a possibility since these glands have been identified [61, 75]. However, based on the low amylase activity of the salivary glands reported for both chickens and turkeys [39], it is questionable whether a suitable promoter is available and a sufficient capacity for synthesis is possible to provide the quantity of enzyme necessary. Another possible site for secretion of hydrolytic enzymes is in the proventriculus using the chitinase promoter [85]; however, this would initially require the cloning and characterization of the promoter. Introduction of any transgene probably would involve use of either a combinatorial cis-regulatory element [77] or a lentiviral vector [49].

Arabinoxylanases alleviate viscosity-induced diffusion constraints associated with diets containing wheat, rye, barley, and triticale. Glucanases have a similar effect digesting β-glucans present and small amounts of amorphous cellulose. These glycanases were shown to enhance the amino acid digestibility [18]. The positive action of these feed enzymes opens the possibility for genetic modification.

Health Subclinical disease in poultry dramatically increases the environmental impact of the birds. For example, subclinical necrotic enteritis in broiler chickens results in a 12% reduction in body weight and an 11% decrease in feed utilization efficiency [81]. Other subclinical diseases undoubtedly have a similar impact; therefore, improving health substantively reduced the environmental footprint of poultry. The application of interference-based gene silencing may be an effective strategy for control of Marek's disease, infectious bursal disease, avian leucosis, Rous sarcoma virus, and avian influenza [47]. The report by Lyall et al. [49] on the production of transgenic chickens resistant to avian influenza viruses is an excellent example of the use of RNA interference to reduce mortalities of producing birds.

Issues with Expression of Novel Hydrolases in the Gastrointestinal Tract

Novel gene products that either have been expressed in the gastrointestinal tract of mammals, or that may be considered for expression are summarized in Table 2. Many phytases have been characterized and considered as potential feed enzymes [67], although only three phytases are illustrated as examples, the *E. coli* phytase expressed in the Enviropig™, the Avian phytase and the rat phytase, the only phytases so far identified in

Transgenic Livestock, Decreasing Environmental Impact of. Table 2 Enzymes with some criteria suitable for gastrointestinal expression

Source	Catalytic properties	Mol. Wt.	pH Opt and Min/Max	Temp (°C) Max Act.	Sp.Act. U/mg^{-1} min^{-1}	Protease resistance
E. coli [31]	Phytase/acid phosphatase	44,708 Da	Opt 4.5/2.5–3	60	2,326/712	Pepsin resistant and trypsin sensitive
			Min 2.0			
			Max 10			
Avian histidine phosphatase [74], [12]	Acid phosphatase/phytase	53,000 and 55,000 Da	4.5-7.5	Assay 40	0.5	?
Rat [94]	Phytase and alkaline phosphatase	70,000 and 90,000 Da	Phytase – 7.5	Assay 37	5.6	?
			Phosphatase – 10.4			
Bacillus [70]	Bifunctional phytase/ endoglucanase	73,000 Da	Phytase – 7	55	Phytase – 8	?
			Endoglucanase – 6		Endoglucanase – 10	
			Range 4.0 – 8.0			
F. succinogenes [89]	1,3-1,4-β-glucanase	27,957 Da	Opt 6–8	50	10,800	?
			Min 4.0			
Bisporus sp. [48]	1,3-1,4-β-glucanase	48,000 Da after deglycosylation	Opt 5.0	60	4,040	Pepsin and trypsin resistant
			Range 1–8			
Alicyclobacillus sp. [2]	Endo-β-1,4-glucanase	48,000 Da	Opt 2.6	65	5,032	Pepsin and trypsin resistant
			Range 1.8–7.6			
Alicyclobacillus sp. [3]	Endo-β-1,4-glucanase	60,000 Da	3.4	60	?	Pepsin and trypsin resistant
			Range 1.2–8.2			
Aspergillus niger [45]	Endo-β-1,4-xylanase	23,000 Da	Opt 5.5	50	3,881	?
N. patriciarum [93]	Endo-β-1,4-xylanase	26,000 Da	Opt 6.0	60	5,000	?
Phialophora. Sp. G5 [97]	Endo- β-1,4-xylanase	55,000 Da	Opt 4.0	70	351	Pepsin and trypsin resistant
			Range			
Paenibacillus sp. Strain E18 [78]	Bifunctional Endo-β-1,4-xylanase/1,3-1,4-β-glucanase	39,000 Da	Opt 6.5–9.0	50	Oat spelt xylan-358	?
					Barley-β-glucan-133	
C. thermocellum/Geobacillus thermophilus [24]	Chimeric xylanase-arabinofuranosidase	97,000 Da	Opt 6.0	65		?

mammals, but has low activity. A variety of xylanases and glucanases are listed. It includes high-activity glucanases and xylanases, bifunctional xylanase/glucanase enzymes where the same catalytic domain hydrolyzes both substrates and chimeric enzymes. The chimeric enzymes can have any combination of catalytic domains, for example, phytase and endoglucanase, xylanase and glucanase, or other combinations of domains. The bifunctional and chimeric enzymes have the advantage of providing multiple activities in one protein, which has the advantage of using a single promoter.

There are a variety of factors that need to be considered when deciding upon promoter(s) and gene(s) for expression in the alimentary tract of animals. Ideally the introduced transgene should impose the minimal metabolic load with minimal interference of existing physiological and biochemical pathways of the host.

Transgene (protein or RNA):

1. Preferably the transformation of interest should be performed by a single molecule. If more than one protein/RNA is involved it may be possible to design the transgene which express multiple transgenes (see below).
2. The transgene must code for a low molecular mass stable protein with a high specific activity, and targeted to the correct compartment.
3. Cryptic posttranslational modification sites are often present in proteins isolated from non-mammalian species and must be removed if activity/stability is affected (i.e., lysostaphin glycosylation).
4. The pH and temperature optima should correspond closely to that of the site of action which would be pH 2–5 if it should be active in the stomach/proventriculus, or pH 5–8 if secreted into the small intestine where it would be active [13, 20, 34].
5. The enzyme must be resistant to proteases: pepsin if expressed in the stomach, or resistant to tryptic enzymes if expressed and active in the small intestine. If the enzyme were expressed in the salivary glands for activity in the small intestine then it would need to be both pepsin and trypsin resistant, stable at low pH, and highly active at neutral pH.
6. Preferably the enzyme should be isolated from the organism with a Generally Recognized As Safe (GRAS) status and have no significant homology to allergenic, pathogenic, or toxic proteins. It is also preferable that it not exhibit any similarity to known allergens, and it would even be useful to eliminate possible glycosylation sites to avoid the development of an allergenic nature [15].

Regulatory elements:

1. Promoter should be tightly controlled allowing expression of the transgene only in desired tissue at the desired time and at a specific level. Strong ubiquitous promoters commonly used for transgenic work are undesirable as they often result in transgene toxicity and undesirable side effects. An interesting observation in plants was that repetitious use of the same promoter did not lead to transcriptional silencing [54], and this may also apply to mammals.
2. Gene-specific regulatory sequences (5′ and 3′ UTR, polyA, introns, Kozak start sequence, etc.) should be used to optimize the transcription and translation of transgene.
3. The codon usage should be modified to correspond closely to that of highly expressed proteins within the biosynthetic tissue [9, 28].
4. Insulators and locus control regions (LCR), such as the chicken P-globin locus, should be used to isolate transgene from effect of neighboring chromatin and stabilize the expression level across multiple generations [8].

Multi-gene Expression

The obvious path for the development of transgenic animals is the expression of multiple genes to further enhance the value of an animal. Regulatory agencies undoubtedly will have a preference for the expression by multiple novel genes in an animal produced by crosses of "previously approved" animals with a single transgene to avoid confusion that could result from the interaction of transgenic traits. Whether these will require a further regulatory submission remains to be determined. Since it will be desirable to develop lines of transgenic livestock homozygous for multiple novel traits, a new approach will be needed to eliminate numerous crosses and continued testing for the presence of each gene. The approved transgenes could also be introduced into new

breeds/species by cotransformation, or sequential transformation of established transgenic lines in the same species. Cotransformation could be done with unlinked constructs using different promoters when different ratios of protein products are required. Multiple transgenes can also be housed on a mammalian artificial chromosome. In cases where the same proportion of the protein product is needed, multicistronic constructs with multiple internal *ribosome* entry site (IRES), or even as a single translation product in which individual proteins are separated by cellular protease sites, *could be used* [52].

A proven strategy for multi-transgenic animal production is to use the recent adaptation of the 2A system from foot-and-mouth disease virus [20, 25]. With this approach the open reading frame consists of multiple individual cDNAs separated by sequences encoding 2A and furin cleavage sites. A single complex mRNA is produced and translated into a single complex polypeptide that is spontaneously cleaved into individual exogenous proteins at the 2A sites in the endoplasmic reticulum. This results in equimolar ratios of each of the individual transgenic proteins emerging from the Golgi. This expression system has been demonstrated to produce transgenic animals with up to four transgenes being expressed from a single transcript [86].

Sequential introduction of transgenes would benefit from establishing transgene locus which allows high and stable expression and into which multiple transgenes can be introduced and removed as necessary using site-specific recombination technologies such as Cre/lox, Flp/frt, φC31 integrase, or Gateway systems [7].

A refinement to further speed up the production of homozygous populations is through the application for flow cytometry [29]. Flow cytometric separation of X and Y chromosome-bearing spermatozoa has been demonstrated to be effective in cattle and pigs and resulted in the birth of healthy offspring of the predetermined gender [68, 69].

Future Directions

Intensive selection by current breeding practices have developed livestock that are growing and producing near their physiological upper limits, and any further improvements may enhance stress leading to disease susceptibility. Reduction in the environmental footprint of livestock will come through: identification and elimination of bottlenecks in metabolic and physiological pathways, introduction of novel traits that enable the digestion of dietary components previously not digested (e.g., phytate, glycans), through the introduction of novel metabolic pathways for synthesis of essential nutrients (e.g., amino acids), and through enhanced disease resistance. These novel transgenic animals will only be accepted by farmers if they are as robust as the currently available conventional livestock. Furthermore, these new genetically engineered animals will only enter the human food chain once consumers are satisfied that the meat products are absolutely safe, since they have the choice between conventional and transgenic products. Therefore, the central issue is the confidence consumers have in the national regulatory system. With the expected increase in human population and increasing environmental constraints, greater acceptance of transgenic animals is anticipated in line with the acceptance of transgenic plant products.

Bibliography

1. Adams NR, Briegel JR, Ward KA (2002) The impact of a transgene for ovine growth hormone on the performance of two breeds of sheep. J Anim Sci 80:2325–2333
2. Bai Y, Wang J, Zhang Z, Shi P, Luo H, Huang H, Feng Y, Yao B (2010a) Extremely acidic β−1,4-glucanase, CelA4, from thermoacidophilic *Alicyclobacillus* sp. A4 with high protease resistance and potential as a pig feed additive. J Agric Food Chem 58:1970–1975
3. Bai Y, Wang J, Zhang Z, Shi P, Luo H, Huang H, Luo C, Yao B (2010b) Expression of an extremely acidic β-1,4-glucanase from thermoacidophilic *Alicyclobacillus* sp. A4 in *Pichia pastoris* is improved by truncating the gene sequence. Microb Cell Fact 9:33
4. Barkema HW, Green MJ, Bradley AJ, Zadoks RN (2009) Invited review: the role of contagious disease in udder health. J Dairy Sci 92:4717–4729
5. Beauchemin KA, Colombatto D, Morgavi DP (2004a) A rationale for the development of feed enzyme products for ruminants. Can J Anim Sci 84:23–36
6. Beauchemin KA, Colombatto D, Morgavi DP, Yang WZ, Rode LM (2004b) Mode of action of exogenous cell wall degrading enzymes for ruminants. Can J Anim Sci 84:13–22
7. Brown WRA, Lee NCO, Xu Z, Smith MCM (2011) Serine recombinases as tools for genome engineering. Methods 53:372–379
8. Bulger M, Groudine M (2010) Enhancers: the abundance and function of regulatory sequences beyond promoters. Dev Biol 339:250–257

9. Cannarrozzi G, Schraudolph NN, Faty M, von Rohr RP, Friberg MT, Roth AC, Gonnet P, Gonnet G, Barral Y (2010) A role for codon order in translation dynamics. Cell 141:355–367
10. Carew R (2010) Ammonia emissions from livestock industries in Canada: feasibility of abatement strategies. Environ Pollut 158:2618–2626
11. Cheung QC, Turner PV, Song C, Wu D, Cai HY, Macinnes JI, Li J (2008) Enhanced resistance to bacterial infection in protegrin-1 transgenic mice. Antimicrob Agents Chemother 52:1812–1819
12. Cho J, Choi K, Darden T, Reynolds PR, Petitte JN, Shears SB (2006) Avian multiple inositol polyphosphate phosphatase is an active phytase that can be engineered to help ameliorate the planet's "phosphate crisis". J Biotechnol 126:248–259
13. Clemens ET, Stevens CE, Southworth M (1975) Sites of organic acid production and pattern of digesta movement in the gastrointestinal tract of swine. J Nutr 105:759–768
14. Clements JE, Wall RJ, Narayan O, Hauer D, Schoborg R, Sheffer D, Powell A, Carruth LM, Zink MC, Rexroad CE (1994) Development of transgenic sheep that express the Visna virus envelope gene. Virology 200:370–380
15. CODEX 2008 Report of the seventh session of the Codex*Ad Hoc* intergovernmental task force on foods derived from biotechnology. http://www.codexalimentarius. net/web/archives.jsp?year = 08
16. Cordell D, Drangert JO, White S (2009) The story of phosphorus: global food security and food for thought. Glob Environ Change 19:292–305
17. Cowieson AJ, Bedford MR, Selle PH, Ravindran V (2009) Phytate and microbial phytase: implications for endogenous nitrogen losses and nutrient availability. World's Poult Sci J 65:401–417
18. Cowieson AJ, Bedford MR, Ravindran V (2010) Interactions between xylanase and glucanase in maize-soy-based diets for broilers. Brit Poult Sci 51:246–257
19. Dahlke F, Ribeiro AML, Kessler AM, Lima AR, Maiorka A (2003) Effects of corn particle size and physical form of the diet on the gastrointestinal structures of broiler chickens. Braz J Poult Sci 5:61–67
20. D'Apice AJ, Cowan PJ (2008) Gene-modified pigs. Xenotransplantation 15:87–90
21. Denning C, Burl S, Ainslie A, Bracken J, Dinnyes A, Fletcher J, King T, Ritchie M, Ritchie WA, Rollo M, de Sousa P, Travers A, Wilmut I, Clark AJ (2001) Deletion of the α(1,3)galactosyl transferase (*GGTA1*) gene and the prion protein (*PrP*) gene in sheep. Nat Biotechnol 19:559–562
22. Devlin RH, Sakhrani D, Tymchuk WE, Rise ML, Goh B (2009) Domestication and growth hormone transgenesis cause similar changes in gene expression in coho salmon (Oncorhynchus kisutch). Proc Natl Acad Sci USA 106:3047–3052
23. Fan CL, Han XY, Xu ZR, Wang LJ, Shi LR (2009) Effects of β-glucanase and xylanase supplementation on gastrointestinal digestive enzyme activities of weaned piglets fed a barley-based diet. J Anim Physiol Anim Nutr 93:271–276
24. Fan Z, Wagschal K, Lee CC, Kong Q, Shen KA, Maiti IB, Yuan L (2009) The construction and characterization of two xylan-degrading chimeric enzymes. Biotechnol Bioeng 102:684–692
25. Fang J, Qian JJ, Yi S, Harding TC, Tu GH, VanRoey M, Jooss K (2005) Stable antibody expression at therapeutic levels using the 2A peptide. Nat Biotechnol 23:584–590
26. Food and Agriculture Organization (2006) World agriculture: towards 2030/2050-interim report. Food and Agriculture Organization, Rome
27. Food and Agriculture Organization (2009) State of food and agriculture – Livestock in the balance. Food and Agriculture Organization, Rome
28. Fredrick K, Ibba M (2010) How the sequence of a gene can tune its translation. Cell 141:227–229
29. Garner DL (2006) Flow cytometric sexing of mammalian sperm. Theriogenology 65:943–957
30. Gerber PJ, Vellinga TV, Steinfeld H (2010) Issues and options in addressing the environmental consequences of livestock sector's growth. Meat Sci 84:244–247
31. Golovan S, Wang G, Zhang J, Forsberg CW (2000) Characterization and overproduction of the *Escherichia coli appA* encoded bifunctional enzyme which exhibits both phytase and acid phosphatase activities. Can J Microbiol 46:59–71
32. Golovan SP, Hayes MA, Phillips JP, Forsberg CW (2001) Transgenic mice expressing bacterial phytase as a model for phosphorus pollution control. Nat Biotechnol 19:429–433
33. Golovan SP, Meidinger RG, Ajakaiye A, Cottrill M, Wiederkehr MZ, Barney D, Plante C, Pollard J, Fan MZ, Hayes MA, Laursen J, Hjorth JP, Hacker RR, Phillips JP, Forsberg CW (2001) Pigs expressing salivary phytase produce low phosphorus manure. Nat Biotechnol 19:741–745
34. Guinotte F, Gautron J, Soumarmon A, Robert JC, Peranzi G, Nys Y (1993) Gastric acid secretion in the chicken: effect of histamine H_2 antagonists and H+/K(+)-ATPase inhibitors on gastro-intestinal pH and of sexual maturity calcium carbonate level and particle size on proventricular H+/K + ATPase activity. Comp Biochem Physiol Comp Physiol 106:319–327
35. Hall J, Ali S, Surani MA, Hazlewood GP, Clark AJ, Simons JP, Hirst BH, Gilbert HJ (1993) Manipulation of the repertoire of digestive enzymes secreted into the gastrointestinal tract of transgenic mice. Nat Biotechnol 11:376–379
36. Hess M, Sczyrba A, Egan R, Kim TW, Chokhawala H, Schroth G, Luo S, Clark DS, Chen F, Zhang T, Mackie RI, Pennacchio LA, Tringe SG, Visel A, Woyke T, Wang Z, Rubin EM (2011) Metagenomic discovery of biomass-degrading genes and genomes from cow rumen. Science 331:463–467
37. Huang H, Zhang R, Fu D, Luo J, Li Z, Luo H, Shi P, Yang P, Diao Q, Yao B (2011) Diversity, abundance and characterization of ruminal cysteine phytases suggest their important role in phytate degradation. Environ Microbiol 13:747–757
38. Jackson KA, Berg JM, Murray JD, Maga EA (2010) Evaluating the fitness of human lysozyme transgenic dairy goats: growth and reproductive traits. Transgenic Res 19:977–986

39. Jerrett SA, Goodge WR (1973) Evidence for amylase in avian salivary glands. J Morphol 139:27–45
40. Ji F, Casper DP, Brown PK, Spangler DA, Haydon KD, Pettigrew JE (2008) Effects of dietary supplementation of an enzyme blend on the ileal and fecal digestibility of nutrients in growing pigs. J Anim Sci 86:1533–1543
41. Keita D, Heath L, Albina E (2010) Control of African swine fever virus replication by small interfering RNA targeting the A151R and VP72 genes. Antivir Ther 15:727–736
42. Kellogg RL, Lander CH, Moffitt DC, Gollehon N (2000) Manure nutrients relative to the capacity of cropland and pastureland to assimilate nutrients: spatial and temporal trends for the United States. http://www.nrcs. usda. gov/technical/NRI/pubs/manntr. html 1–140
43. Knowlton KF, Taylor MS, Hill SR, Cobb C, Wilson KF (2007) Manure nutrient excretion by lactating cows fed exogenous phytase and cellulase. J Dairy Sci 90:4356–4360
44. Leahy SC, Kelly WJ, Altermann E, Ronimus RS, Yeoman CJ, Pacheco DM, Li D, Kong Z, McTavish S, Sang C, Lambie SC, Janssen PH, Dey D, Attwood GT (2010) The genome sequence of the rumen methanogen *Methanobrevibacter ruminantium* reveals new possibilities for controlling ruminant methane emissions. PLoS One 5:e8926
45. Levasseur A, Asther M, Record E (2005) Overproduction and characterization of xylanase B from *Asperguillus niger*. Can J Microbiol 51:177–183
46. Lo D, Pursel V, Linton PJ, Sandgren E, Behringer R, Rexroad C, Palmiter RD, Brinster RL (1991) Expression of mouse IgA by transgenic mice, pigs and sheep. Eur J Immunol 21:1001–1006
47. Long CR, Tessanne KJ, Golding MC (2010) Applications of RNA interference-based gene silencing in animal agriculture. Reprod Fertil Dev 22:47–58
48. Luo H, Yang J, Yang P, Li J, Huang H, Shi P, Bai Y, Wang Y, Fan Y, Yao B (2010) Gene cloning and expression of a new acidic family 7 endo-β-1,3-1,4-glucanase from the acidophilic fungus *Bispora* sp. MEY-1. Appl Microbiol Biotechnol 85:1015–1023
49. Lyall J, Irvine RM, Sherman A, McKinley TJ, Néñz A, Purdie A, Outtrim L, Brown IH, Rolleston-Smith G, Sang H, Tiley L (2011) Suppression of Avian influenza transmission in genetically modified chickens. Science 331:223–226
50. Maenz DD, Classen HL (1998) Phytase activity in the small intestinal brush border membrane of the chicken. Poult Sci 77:557–563
51. Maga EA, Cullor JS, Smith W, Anderson GB, Murray JD (2006) Human lysozyme expressed in the mammary gland of transgenic dairy goats can inhibit the growth of bacteria that cause mastitis and the cold-spoilage of milk. Foodborne Pathog Dis 3:384–392
52. Martinez-Salas E (1999) Internal ribosome entry site biology and its use in expression vectors. Curr Opin Biotechnol 10:458–464
53. Muller M, Brem G (1994) Transgenic strategies to increase disease resistance in livestock. Reprod Fertil Dev 6: 605–613
54. Naqvi S, Farre G, Sanahuja G, Capell T, Zhu C, Christou P (2010) When more is better: multigene engineering in plants. Trends Plant Sci 15:48–56
55. Noble MS, Rodriguez-Zas S, Cook JB, Bleck GT, Hurley WL, Wheeler MB (2002) Lactational performance of first-parity transgenic gilts expressing bovine α-lactalbumin in their milk. J Anim Sci 80:1090–1096
56. Notter DR (1999) The importance of genetic diversity in livestock populations of the future. J Anim Sci 77:61–69
57. Nottle MB, Nagashima H, Verma PJ, Du ZT, Grupen CG, McIlfatrick SM, Ashman RJ, Harding MP, Giannakis C, Wigley PL, Lyons IG, Harrison DT, Luxford BG, Campbell RG, Crawford RJ, Robins AJ (1999) Production and analysis of transgenic pigs containing a metallothionein porcine growth hormone gene construct. In: Transgenic animals in agriculture. Commonwealth Agriculture Bureau International, London, pp 145–156
58. NRC (1998) Nutrient requirements of swine. National Academy Press, Washington, DC
59. Nyachoti CM, Arntfield SD, Guenter W, Cenkowski S, Opapeju FO (2006) Effect of micronized pea and enzyme supplementation on nutrient utilization and manure output in growing pigs. J Anim Sci 84:2150–2156
60. Ohnishi H, Samuelson LC, Yule DI, Ernst SA, Williams JA (1997) Overexpression of Rab3D enhances regulated amylase secretion from pancreatic acini of transgenic mice. J Clin Invest 100:3044–3052
61. Olmedo LA, Samar ME, Avila RE, de Crosa MG, Dettin L (2000) Avian minor salivary glands: an ultrastructural study of the secretory granules in mucous and seromucous cells. Acta Odontol Latinoam 13:87–99
62. Peters A, Lebzien P, Meyer U, Borchert U, Bulang M, Flachowsky G (2010) Effect of exogenous fibrolytic enzymes on ruminal fermentation and nutrient digestion in dairy cows. Arch Anim Nutr 64:221–237
63. Pursel VG, Pinkert CA, Miller KF, Bolt DJ, Campbell RG, Palmiter RD, Brinster RL, Hammer RE (1989) Genetic engineering of livestock. Science 244:1281–1287
64. Pursel VG, Wall RJ, Michell AD, Elsasser TH, Solomon MB, Coleman ME, DeMayo F, Schwartz RJ (1999) Transgenic animals in agriculture. In: Expression of insulin-like growth factor-1 in skeletal muscle of transgenic swine. CABI Publishing, New York, pp 131–144
65. Pursel VG, Mitchell AD, Bee G, Elsasser TH, McMurtry JP, Wall RJ, Coleman ME, Schwartz RJ (2004) Growth and tissue accretion rates of swine expressing an insulin-like growth factor I transgene. Anim Biotechnol 15:33–45
66. Rajan GH, Morris CA, Carruthers VR, Wilkins RJ, Wheeler TT (1996) The relative abundance of a salivary protein, bSP30, is correlated with susceptibility to bloat in cattle herds selected for high or low bloat susceptibility. Anim Genet 27:407–414
67. Rao DECS, Rao KV, Reddy TP, Reddy VD (2009) Molecular characterization, physicochemical properties, known and potential applications of phytases: an overview. Crit Rev Biotechnol 29:182–198

68. Rath D, Johnson LA (2008) Application and commercialization of flow cytometrically sex-sorted semen. Reprod Domest Anim 43(Suppl 2):338–346
69. Rath D, Ruiz S, Sieg B (2003) Birth of female piglets following intrauterine insemination of a sow using flow cytometrically sexed boar semen. Vet Rec 152:400–401
70. Reddy VA, Venu K, Rao DE, Rao KV, Reddy VD (2009) Chimeric gene construct coding for bi-functional enzyme endowed with endoglucanase and phytase activities. Arch Microbiol 191:171–175
71. Rees WD, Hay SM (1995) The biosynthesis of threonine by mammalian cells: expression of a complete bacterial biosynthetic pathway in an animal cell. Biochem J 309(Pt 3):999–1007
72. Rich KM, Perry BD (2010) The economic and poverty impacts of animal diseases in developing countries: New roles, new demands for economics and epidemiology. Prev Vet Med 97:1–8
73. Richt JA, Kasinathan P, Hamir AN, Castilla J, Sathiyaseelan T, Vargas F, Sathiyaseelan J, Wu H, Matsushita H, Koster J, Kato S, Ishida I, Soto C, Robl JM, Kuroiwa Y (2007) Production of cattle lacking prion protein. Nat Biotechnol 25:132–138
74. Romano PR, Wang J, O'Keefe RJ, Puzas JE, Rosier RN, Reynolds PR (1998) HiPER1, a phosphatase of the endoplasmic reticulum with a role in chondrocyte maturation. J Cell Sci 111:803–813
75. Samar ME, Avila RE, Esteban FJ, Olmedo L, Dettin L, Massone A, Pedrosa JA, Peinado MA (2002) Histochemical and ultrastructural study of the chicken salivary palatine glands. Acta Histochem 104:199–207
76. Schröder JJ, Smit AL, Cordell D, Rosemarin A (2011) Improved phosphorus use efficiency in agriculture: a key requirement for its sustainable use. Chemosphere 84(6):822–831
77. Seo HW, Kim TM, Choi JW, Han BK, Song G, Han JY (2010) Evaluation of combinatorial cis-regulatory elements for stable gene expression in chicken cells. BMC Biotechnol 10:69
78. Shi P, Tian J, Yuan T, Liu X, Huang H, Bai Y, Yang P, Chen X, Wu N, Yao B (2010) *Paenibacillus* sp. strain E18 bifunctional xylanase-glucanase with a single catalytic domain. Appl Environ Microbiol 76:3620–3624
79. Simojoki H, Orro T, Taponen S, Pyorala S (2009) Host response in bovine mastitis experimentally induced with *Staphylococcus chromogenes*. Vet Microbiol 134:95–99
80. Simojoki H, Hyvonen P, Orro T, Pyorala S (2010) High concentration of human lactoferrin in milk of rhLf-transgenic cows relieves signs of bovine experimental Staphylococcus chromogenes intramammary infection. Vet Immunol Immunopathol 136:265–271
81. Skinner JT, Bauer S, Young V, Pauling G, Wilson J (2010) An economic analysis of the impact of subclinical (mild) necrotic enteritis in broiler chickens. Avian Dis 54:1237–1240
82. Smith TC, Harper AL, Nair R, Wardyn SE, Hanson BM, Ferguson DD, Dressler AE (2011) Emerging swine zoonoses. Vector Borne Zoonotic Dis 11:1–10
83. Steinfeld H, Gerber P (2010) Livestock production and the global environment: consume less or produce better? Proc Natl Acad Sci USA 107:18237–18238
84. Steinfeld H, Gerber P, Wassenaar T, Castel V, Rosales M, de Hann C (2006) Livestock's long shadow – Evnironmental issues and options. FAO, Rome
85. Suzuki M, Fujimoto W, Goto M, Morimatsu M, Syuto B, Iwanaga T (2002) Cellular expression of gut chitinase mRNA in the gastrointestinal tract of mice and chickens. J Histochem Cytochem 50:1081–1089
86. Szymczak AL, Workman CJ, Wang Y, Vignali KM, Dilioglou S, Vanin EF, Vignali DA (2004) Correction of multi-gene deficiency in vivo using a single 'self-cleaving' 2A peptide-based retroviral vector. Nat Biotechnol 22:589–594
87. Tilman D, Fargione J, Wolff B, D'Antonio C, Dobson A, Howarth R, Schindler D, Schlesinger WH, Simberloff D, Swackhamer D (2001) Forecasting agriculturally driven global environmental changes. Science 292:281–284
88. Wall RJ, Powell AM, Paape MJ, Kerr DE, Bannerman DD, Pursel VG, Wells K, Talbot N, Hawk HW (2005) Genetically enhanced cows resist intramammary *Staphylococcus aureus* infection. Nat Biotechnol 23:445–451
89. Wen TN, Chen JL, Lee SH, Yang NS, Shyur LF (2005) A truncated *Fibrobacter succinogenes* 1,3-1,4-β-D-glucanase with improved enzymatic activity and thermotolerance. Biochemistry 44: 9197–9205
90. Wheeler MB, Bleck GT, Donovan SM (2001) Transgenic alteration of sow milk to improve piglet growth and health. Reprod Suppl 58:313–324
91. Wheeler TT, Hood K, Oden K, McCracken J, Morris CA (2003) Bovine parotid secretory protein: structure, expression and relatedness to other BPI (bactericidal/permeability-increasing protein)-like proteins. Biochem Soc Trans 31:781–784
92. Wise TG, Schafer DS, Lowenthal JW, Doran TJ (2008) The use of RNAi and transgenics to develop viral disease resistant livestock. Dev Biol (Basel) 132:377–382
93. Xue GP, Denman SE, Glassop D, Johnson JS, Dierens LM, Gobius KS, Aylward JH (1995) Modification of a xylanase cDNA isolated from an anaerobic fungus *Neocallimastix patriciarum* for high-level expression in *Escherichia coli*. J Biotechnol 38:269–277
94. Yang W-J, Matsuda Y, Sano S, Masutani H, Nakagawa H (1991) Purification and characterization of phytase from rat intestinal mucosa. Biochim Biophys Acta 1075:75–82
95. Yin HF, Fan BL, Yang B, Liu YF, Luo J, Tian XH, Li N (2006) Cloning of pig parotid secretory protein gene upstream promoter and the establishment of a transgenic mouse model expressing bacterial phytase for agricultural phosphorus pollution control. J Anim Sci 84:513–519
96. Zhang JX, Meidinger R, Forsberg CW, Krell PJ, Phillips JP (1999) Expression and processing of a bacterial endoglucanase in transgenic mice. Arch Biochem Biophys 367:317–321
97. Zhang F, Shi P, Bai Y, Luo H, Yuan T, Huang H, Yang P, Miao L, Yao B (2011) An acid and highly thermostable xylanase from *Phialophora* sp. G5. Appl Microbiol Biotechnol 89:1851–1858

Transgenic Livestock, Enhanced Nutritional Quality in

Götz Laible
AgResearch, Ruakura Research Centre, Hamilton, New Zealand

Article Outline

Glossary
Definition of the Subject and Its Importance
Introduction
Milk with Enhanced Nutritional Qualities
Meat with Enhanced Nutritional Qualities
Safer Food from Livestock with Enhanced Health Characteristics
Future Directions
Bibliography

Glossary

Antimicrobial A substance with the ability to kill microbes.

Bacteriolytic Causing the lysis of bacteria.

Bacteriostatic Term to describe a substance that inhibits bacterial growth.

Casein micelle Protein particle consisting of aggregated casein proteins in colloidal suspension.

Circadian rhythm A daily cycle controlling the biological processes in living organisms.

Dominant-negative molecule A mutant molecule capable of interacting with the wild-type form to produce an inactive complex.

Endogenous Internally derived or synthesized.

Endopeptidase Proteolytic enzyme that can only break peptide bonds within the molecule but not at the termini.

Gastrointestinal Term referring to the digestive tract.

Genome Entirety of an organism's hereditary information.

Glycomacropeptide κ-casein-derived peptide released by rennet during cheese manufacture.

Homologous recombination Exchange of genetic material between two DNA fragments by crossing over in a region with sequence homology.

In vitro Experimental procedure conducted artificially.

Knockdown Attenuation of gene function usually resulting in diminished amount of synthesis of the protein that the gene encodes.

Knockin Integration of a new gene which replaces an endogenous gene.

Knockout Functional disruption of a specific gene of an organism commonly achieved by a partial or complete deletion of the gene sequence.

Pathogen/pathogenic Infectious agent/disease causing.

Phenotype/phenotypic A measurable characteristic of an animal such as hair color growth rate, or degree of carcass marbling. These traits are the product of genetics and the environment.

Phenylketonuria Genetic disorder in which the essential amino acid phenylalanine cannot be metabolized potentially causing mental retardation.

Pleiotropic effects The phenomena of a single gene having influences on multiple traits.

Prion An infectious protein particle.

Promoter A regulatory DNA sequence that controls the transcription of a particular gene.

RNA interference A sequence-specific gene-silencing process in which double-stranded RNAs trigger the destruction of specific RNAs.

Somatic cell count Quantification of somatic cells found in milk as an indicator for the quality of the milk.

Transgene An exogenous gene introduced into the genome of another organism.

Transgenic An animal plant or microbe whose genetic material has been altered using an artificial process.

Unsaturated (saturated) fatty acids Fatty acid molecules with (no) double bonds.

Whey Liquid that remains after separation of the solid fraction when cheese is made.

Definition of the Subject and Its Importance

Since the domestication of animals several millennia ago, which enabled the transition from hunter-gatherer to farming communities, humans have shaped livestock according to specific needs for food, both in quantity and quality. Industrialization and rapid population growths prompted immense changes to farming systems, human lifestyle, and food choices, and is predicted to result in drastic climate changes within

a relative short time period. Thus, current food production systems face new challenges in this rapidly changing world, in particular demands for safe and healthier food to address modern health concerns and the desire for longevity. In the past, traditional breeding and selection schemes have been invaluable for the incremental improvement of food animals. However, the process is slow and undirected and is not well suited for enhancing specific nutritional characteristics. The relatively new transgenic technology offers the potential for enhancing existing or introducing entirely novel characteristics at unprecedented rates and magnitudes and could provide substantial benefits for consumers in the form of healthier and safer food. Nevertheless, the complexity of food production traits should not be underestimated. The accurate modification of the appropriate gene(s) to generate desired phenotypes able to deliver enhanced food products remains challenging and requires careful testing and evaluation. Despite the unrivaled opportunities for innovative functional foods and the progress realized with transgenic crops, lack of acceptance due to concerns associated with the technological novelty of transgenic livestock has so far greatly limited even the research-driven evaluation of new concepts aimed at food applications.

Introduction

Livestock animals are farmed for human food production and are a primary source of dietary proteins, lipids, carbohydrates, vitamins, and minerals from milk and meat. The development of efficient farming production systems has played a crucial role to satisfy the elementary requirement for a stable food source to meet the daily nutritional needs of a multibillion human population. While milk and meat represent in general, a high-quality food source for humans, the effects of modernization and associated substantial changes to the farming systems and lifestyle of people create new challenges for providing a healthy diet of high nutritional quality. The increased understanding of how human nutritional requirements relate to health and longevity provides new opportunities to optimize the nutritional quality of food products and thus improve human health and well-being. Animal fat, which is an ingredient of all animal food products, can serve as an example to illustrate this correlation. They are relatively high in saturated fats (which have been strongly associated with cardiovascular and coronary heart disease), but low in beneficial, unsaturated fats. Thus, higher levels of unsaturated fats and lower levels of saturated fats would improve the nutritional quality of animal-derived food products. Efforts to increase the ratio of unsaturated to saturated fat have received considerable attention. However, attempts to alter the composition of milk and meat to improve its nutritional quality by conventional breeding and selection strategies have proved to be difficult. Traditional breeding and marker-assisted selection schemes are limited to the random combination of some but not all superior allelic gene variants existing within the gene pool of the livestock species. In contrast, transgenic animal technology allows for a more targeted approach with the prospect to introduce specific genes which are known to impact on defined phenotypic traits to enhance existing characteristics. Unlike traditional breeding and selection, the genetic improvement of livestock by genetic engineering is not restricted by the species barrier and can utilize the gene pool of other species to introduce entirely novel and unique characteristics. Moreover, transgenic technology is a versatile platform technology that can employ additive strategies to introduce a new gene function (gain of function), delete gene functions (knockout, loss of function), replace an endogenous gene function with a different one (knockin, exchange of function), or precisely control when and where the genetic alteration is applied (inducible gene expression and conditional knockout). Thus, it holds great promise as a new tool that can deliver solutions for many of the problems concerning the efficient production of high-quality foods from animals.

Despite mounting lifestyle-related health problems, food security, and environmental pressures which need to be urgently addressed, negative public perception, ethical concerns, regulatory uncertainties, and an associated reluctance to fund this line of research have been major factors that have so far greatly limited the international research efforts to evaluate the potential of the transgenic technology for enhancing food production of livestock. While transgenic plants have been commercialized since 1996 [1], transgenic livestock applications for

food production have so far been restricted to a few proof-of-concept studies that aim to improve the nutritional quality of milk and meat and will be outlined in detail in the following sections.

Milk with Enhanced Nutritional Qualities

Milk is an important food with high protein content. The protein fraction determines many of the functional properties and provides opportunities for nutritional enhancement through additional health benefits, increased food safety, and improved processing properties for dairy food manufacture.

One approach has been the introduction of new antimicrobial properties into milk, to provide passive immunity to consumers. Lyzozyme (LZ) is a naturally occurring antimicrobial protein, present in milk, saliva, and tears of mammals, where it forms part of the defense system against bacterial infections. However, it is found at three orders of magnitude higher concentration in human milk as compared to dairy milk. The introduction of an expression construct for human LZ resulted in LZ levels in the milk of the transgenic goats equivalent to about 68% of the level found in human milk [2]. The consumption of the human LZ-containing goat milk by pigs exerted beneficial effects and improved their gastrointestinal health [3, 4]. Although the milk has not been tested in humans, the promising results suggest similar gastrointestinal benefits could be possible for humans. In addition, the elevated LZ levels increased general food safety properties of the milk by reducing the bacterial growth that causes cold-spoilage thus prolonging its shelf life. Following a similar strategy, recombinant human lactoferrin (LF) has been overexpressed in the milk of dairy cattle [5]. LF is a minor milk protein with antimicrobial and anti-inflammatory properties, which can support the innate defense mechanisms. Although bovine LF has similar functions, it is present in milk at very low levels. Its human counterpart has been fully adapted to human requirements during evolution and is expected to be better suited for human health applications, in particular, at elevated levels. The transgenic cows were shown to produce milk that contains human LF at concentrations much higher than the natural level of bovine LF. These new characteristics indicate that this functional food might offer new health benefits such as increased protection against infections and healthier intestinal microflora. A conceptually related approach aims to boost the immune system through food-mediated delivery of neutralizing monoclonal antibodies to target specific pathogenic microorganisms of the digestive tract. Thus, consumption of antibody-enriched milk could provide instant protection from infections which severely affect those with increased susceptibility, including the elderly, infants, and patients with illnesses. Proof-of-concept studies in mice successfully demonstrated the potential of this approach. The expression of high antibody levels in milk was able to confer complete protection for the suckling young when challenged with an otherwise lethal dose of virus [6]. Whether the health-enhancing attributes of the functional proteins described above can indeed be realized as food-mediated health benefits in humans is presently unknown and still needs to be assessed.

Although milk from dairy cows is a very common human food, it is known to trigger allergic reactions in some people, a phenomenon that is particularly problematic in infants. Not present in human milk, β-lactoglobulin has been identified as a major whey protein in the milk of dairy species and is thought to be a major allergen in the milk of cows. Reduction of this allergenic protein in dairy milk would make it more amenable for susceptible individuals. This could be achieved by either the disruption of the β-lactoglobulin gene using homologous recombination, often referred to as knockout, or the specific knockdown of its expression by RNA interference (RNAi). However, gene knockouts, a standard approach for the functional characterization of genes in mice, proved to be difficult in farm animals due to low recombination efficiencies in primary livestock cells. Thus RNAi technology might provide a more straightforward approach to unravel the role of β-lactoglobulin and reduce the allergenicity of cow's milk.

Altering the milk composition by altering the levels and ratios of the main endogenous milk proteins has been suggested to enhance the nutritional quality of milk and its processing characteristics, including increased heat stability, calcium content, and cheese manufacture [7, 8]. A drastic change of milk composition has been achieved recently with the introduction of additional β- and κ-casein genes in transgenic cattle [9]. The milk derived from these cows showed a two- to

threefold increase in κ-casein and a minor change for β-casein. These changes affected the physical appearance of the milk, which showed a distinctive color change from ordinary white to yellow for the modified milk [10]. Because κ-casein is located on the surface of the casein micelles, any increase in κ-casein is expected to reduce the size of the casein micelles [11]. The reduced size of the micelles affects the light scattering properties and is thought to be the reason for the observed color change in the high κ-casein milk [10]. Although the effects on the processing characteristics of this novel milk still remain to be determined, trial cheese production resulted in cheese with increased levels of essential amino acids and beneficial minerals and thus improved nutritional quality.

Furthermore, due to the higher κ-casein content, this speciality milk is an improved source of κ-casein-derived bioactive peptides [12] such as glycomacropeptide (GMP) which has been associated with a wide range of health-promoting activities including protection against toxins, bacteria, and viruses, suppression of gastrointestinal inflammation, and modulation of the immune system [13]. GMP is one of the few naturally occurring proteins that lacks the amino acid phenylalanine, which makes it a safe source of dietary protein for people suffering from the genetic disorder phenylketonuria (PKU). They cannot metabolize phenylalanine, and normally need to avoid high-protein foods such as dairy products to prevent the detrimental accumulation of phenylalanine metabolites.

An extension to this, highlighting the unique ability of the transgenic technology to provide novel foods tailored for specific dietary requirements, is the development of transgenic rabbits that produce a milk protein suitable as dietary replacement for PKU sufferers [14].

The carbohydrate component of dairy milk has been another target for modifying milk composition to improve health attributes. The milk sugar lactose causes intestinal disorders in lactose-intolerant people who lack adequate intestinal lactose-hydrolyzing enzyme activity to sufficiently digest lactose after milk consumption [15]. Two strategies to reduce the milk sugar lactose content were evaluated in transgenic mouse models which could provide an elegant alternative to expensive postharvest milk processing. The complete disruption of the expression of α-lactalbumin, an essential component of the lactose synthetase complex, resulted in lactose-free milk [16]. However, because lactose is the main osmotic regulator of milk secretion, it strongly affected production and secretion of the milk, which was highly concentrated and the transgenic mice were unable to sustain lactation. In comparison to the knockout strategy, knockdown of α-lactalbumin expression through RNAi could offer better control, to achieve an acceptable reduction of the lactose and water content of milk, without impacting on its vital attributes. Thus, it might provide an opportunity to reduce the lactose content and at the same time significantly lower transportation costs of liquid milk.

A more successful approach addressing lactose intolerance, which cleverly dissected the issues of osmolarity and lactose levels, targeted the expression of a mammalian lactose hydrolyzing enzyme to the mammary gland [17]. Milk lactose was reduced by 50–85% without affecting osmolarity, due to the conversion of the produced lactose into the osmotically active monosaccharides, glucose, and galactose. Although the transgenic mouse results are promising, and it was speculated that a similar reduction of lactose in bovine milk could ameliorate lactose intolerance, they can only provide an indication due to substantial species-specific differences in milk composition. So far, this approach has not been transferred to livestock and still awaits verification of its merit in dairy cows.

Beside protein and sugar, fat is another important nutritional component of milk which has a significant impact on human health and provides opportunities for the improvement of dairy products. Animal fats are very rich in saturated fatty acids (SFA) which are considered "unhealthy" and have been associated with cardiovascular and coronary heart disease. A major focus is therefore to decrease the unhealthy fats in favor of the healthier unsaturated fats. This would have the added benefit of decreasing the hardness of milk fat resulting in softer butter, with improved spreadability. As the majority of the long-chain fatty acids in milk fat and in particular unsaturated fatty acids (UFAs) originate from food sources, an effective approach to improve milk fat composition might be to tailor the diet of dairy cows through the use of particular forage species or feed additives [18, 19]. Transgenic technology on the other hand provides the ability of a more directed approach, by modulating endogenous

enzymes involved in lipid metabolism. The mammary gland-specific expression in transgenic goats of the rat stearoyl-CoA desaturase (SCD), an enzyme involved in converting SFAs into mono-UFAs, resulted in an increase of mono-UFAs and decreased levels of medium chain SFAs [20]. However, this beneficial change in the milk fat composition was only transient in this particular study. It was most prominent in early lactation which was thought to be a consequence of high instability of the SCD-encoding mRNA and the resulting low expression levels.

Another concept has been to lower the total fat content by disrupting acetyl-coenzyme A carboxylase to prevent de novo fatty acid synthesis in the mammary gland, which accounts for about 50% of the milk fat [7]. While low-fat liquid milk is desirable from a consumer perspective, for the cow it could reduce the feed energy requirements and improve body condition which is likely to translate into lower milk production costs and improved conception rates during early lactation.

A more extreme variation of the concept of adjusting the activity of endogenous enzymes involved in lipid metabolism is the introduction of novel enzymatic activities normally not found in mammals. This can provide livestock animals with the ability to endogenously synthesize essential poly-UFAs (PUFA) and transform their food products into enriched sources. As a result, food products derived from these animals could offer a range of additional PUFA-specific health benefits such as reduced risk for the development of coronary heart disease and a healthy immune system [21]. This strategy was first tested in transgenic mice with the introduction of the fat-1 gene encoding the Caenorhabditis elegans n-3 fatty acid desaturase, an enzyme activity that is absent in vertebrates and renders transgenic animals capable of producing omega-3 FAs through conversion of dietary derived n-6 FAs. Omega-3 is a class of beneficial n-3 PUFAs that is associated with a lower risk of morbidity and mortality from atherosclerosis and coronary heart disease. Milk-specific expression of the desaturase in transgenic mice resulted in elevated levels of long-chain n-3 PUFAs and a concomitant decrease in n-6 PUFAs, although this was most pronounced in phospholipids which are a minor fraction of milk fat, and to a lesser degree in the milk triacylglycerides [22]. Pups consuming the n-3 PUFA enriched milk accumulated the n-3 PUFA docohexaenoic acid in their brains, a compound which has been associated with cognitive performance [23]. The constitutive expression using a humanized fat-1 gene resulted in essentially similar qualitative changes of the n-3 and n-6 PUFAs in milk but at a higher magnitude [24]. So far, the concept has been transferred to pigs but not to any of the dairy species. Unfortunately, changes to the milk fat composition were not investigated in these pigs because the main focus for the study was on the fat content of meat and will be discussed in the next section.

Meat with Enhanced Nutritional Qualities

The introduction of a novel FA desaturase activity to genetically complement mammals with the ability to endogenously synthesize essential PUFA and improve the nutritional characteristics of meat was pioneered in a transgenic mouse model mentioned in the previous section [24]. Mice were engineered by integrating a humanized version of the fat-1 gene into their genomes. Expression of the Caenorhabditis elegans n-3 FA desaturase in these transgenic mice resulted in muscles that were highly enriched in the beneficial omega-3 FAs. While all organs and tissues of the transgenic mice showed a marked reduction of the n-6 to n-3 FA ratio, the effect was greatest for skeletal muscle where the ratio dropped from a value of ~50 for conventional mice to close to 1 for transgenic mice. Considering the health concerns associated with the typically high n-6 to n-3 ratio of Western diets, consumption of food products from omega-3 enriched livestock may provide an opportunity to improve diets. When the approach was recently applied to pigs, the constitutive expression of the fat-1 transgene essentially replicated these results with tail samples from the transgenic pigs found to be highly enriched in omega-3 FAs, in particular for two of the most potent n-3 FAs mainly found in fish [25]. Although, the nutritional consequences still need to be investigated in greater detail, transgenic food animals enriched in omega-3 FAs may provide a more economical, safe, and sustainable means to

fortify meat than the current practice of feeding animals with fish meal and satisfy the growing demand for omega-3 fatty acids in human nutrition [26].

Following a similar concept, pigs were engineered for the endogenous production of the essential PUFA linoleic acid by introducing the FAD2 gene encoding the Δ12 FA desaturase from spinach [27]. Expression of the plant desaturase was selectively targeted to adipocytes and resulted in transgenic pigs showing a 20% increase in linoleic acid content of their white adipose tissue. These results further substantiate the prospect for improving the fatty acid composition of domestic animals through transgenic technology. Meat produced by transgenic pigs could ultimately provide an alternative source for essential FAs, which may ameliorate lifestyle-related health concerns.

Early transgenic livestock studies were mainly focused on modifying body composition for enhanced meat production by stimulating muscle growth via the introduction of genes for growth factors such as growth hormone (GH) or insulin-like growth factor I (IGF-I), a concept that has been highly successful in proof-of-concept studies in transgenic mice [28–31]. Although pigs responded with remarkable growth enhancement following the administration of exogenous GH [32], the initial studies with transgenic GH pigs [33] and sheep [34, 35] were disappointing. The transgenic animals achieved only slightly increased growth rates and were plagued by a range of deleterious side effects due to high systemic GH levels. These were a consequence of poor regulatory control of the transgene activity [33, 36]. Targeting the transgene expression to skeletal muscle [37] or applying conditional expression strategies with the ability to switch it on or off [38] essentially overcame the problem of generating adverse health effects in the transgenic animals and resulted in more desirable effects on growth rate and body composition. Pigs engineered for the tissue-specific expression of human IGF-I in skeletal muscle produced approximately 10% more carcass lean tissue and 20% less total carcass fat. Unexpectedly, the effects showed a strong gender bias with the body composition of transgenic males remaining comparable to conventional boars [37]. Transgenic sheep overexpressing ovine GH, controlled by a zinc-inducible promoter, grew significantly faster, and had a leaner body composition [39]. However, the transgenic sheep had higher parasite fecal egg counts, a potential indication of a compromised immune system.

The modest success of improving growth characteristics in sheep and pigs with growth factor-encoding transgenes is in complete contrast to what has been achieved with GH-enhanced transgenic fish using all piscine DNA constructs [40–43]. In the majority of fish species, the GH transgene resulted in dramatic growth acceleration with up to 35-fold increased growth rates in transgenic loach and salmonids and produced fish that reach double the normal body size in half the normal time [44]. However, some of these growth-enhanced fish showed undesirable pleiotropic effects such as altered skin color, modified skull shape, decreased fertility, and decreased viability. Intriguingly, the astounding growth phenotypes were only achievable in wild fish and could not be replicated in domesticated fish [45]. This may indicate that there is a biological ceiling for further growth enhancement by GH in highly selected domesticated animals, which could explain why the approach achieved only slightly accelerated growth rates in transgenic GH pigs and sheep. Thus, for livestock, the approach, at least in its current form, appears unlikely to deliver on its promise to substantially increase meat production which has to be achieved without adversely impacting on the health of the transgenic animals. The only beneficial outcome realized was some nutritional enhancement through the production of leaner meat, which may provide new leads to further improve the nutritional quality of meat.

A promising alternative strategy to boost growth performance with the prospect of greater control might be the direct manipulation of key regulators of skeletal muscle development. Myostatin is a crucial negative regulator of muscle growth, whose function was revealed with a mouse knockout model which showed two to three times the muscle mass of wild-type mice [46]. These mice closely resembled the double-muscling phenotype of some cattle breeds characterized by a 20% increase in muscle mass associated with a reduction in fat tissue. Analysis of the myostatin gene revealed that these breeds are carriers of natural mutations that result in loss of myostatin function as the underlying cause for the double-muscle phenotype in cattle [47, 48]. The bulkier conformation of these animals is, however,

causing major calving difficulties in these breeds, which are associated with significant welfare concerns. Transgenic technology provides the possibility to avoid these concerns by restricting the effects on the myostatin pathway to only postnatal stages of major muscle growth. The feasibility of such an approach was already demonstrated with a conditional myostatin knockout in mice resulting in postnatal disruption of the myostatin gene and comparable increase in muscle mass to a constitutive knockout [49]. However, additive strategies to interfere with the myostatin pathway including the expression of dominant-negative molecules [50, 51] or RNAi [52, 53] might offer even more flexibility with the ability to control the degree of increased muscle mass. Using site-specific recombination techniques, transgenic mice were generated with a muscle-specific expression cassette for a dominant-negative myostatin pro-domain integrated into the male-specific Y-chromosome [54]. Males of these lines showed a 5–20% increase in skeletal muscle mass; because females do not have a Y-chromosome, all females were non-transgenic and not affected in their growth characteristics. Combined with a postnatal or inducible expression strategy, interference with myostatin function targeted to males only could improve the efficiency of current cattle production systems with the concomitant production of bulls with superior meat production ability and elite dairy cows.

Safer Food from Livestock with Enhanced Health Characteristics

Any improvement to the health status of food animals has an immediate positive effect on food safety, which ultimately will lead to safer food products of superior quality. Moreover, healthier livestock would deliver a whole range of additional beneficial attributes, including improved animal welfare, reduced reliance on animal remedies, reduced risk for disease transmission to humans, and improved reproductive performance and production. While conventional breeding programs with the aim of reducing susceptibility of livestock to pests and diseases have not been very successful, the prospect of complementing traditional disease control measures with transgenic technology is particularly appealing, because it provides new, targeted strategies for improved disease control and animal health [55, 56].

One of the most costly diseases in agriculture is a bacterial infection of the mammary gland known as mastitis. The disease causes a significant reduction of milk yields and renders the milk produced by infected cows unsuitable and unsafe for human consumption. In its nonclinical appearance, the main indicator is a high somatic cell count in milk. Mastitis, however, has the potential to severely affect the health of infected animals and can cause death or require euthanasia on animal welfare grounds. In dairy cattle, about one third of clinical mastitis cases are caused by Staphylococcus aureus infection, a pathogen which, due to its ability of intracellular survival, is particularly difficult to control with conventional antibiotic therapies. Transgenic technology can provide alternative mastitis prevention strategies and in one such approach, the expression of a bacteriolytic enzyme in mammary gland cells, has already been evaluated.

Lysostaphin is a bacterial enzyme with endopeptidase activity that cleaves crucial cell wall components of staphylococci resulting in the lysis of the bacteria. Its potential as an effective antimicrobial agent for the treatment of mastitis was first demonstrated in a mouse model where the mammary-specific expression of lysostaphin conferred a protective effect against Staphylococcus aureus infections [57]. Recently, the concept has been successfully extended to cattle. The transgenic cows, which produced lysostaphin in their milk, recapitulated the mouse results and showed a high degree of protection when challenged with the pathogen [58].

Two other proteins with antimicrobial properties, LF and LZ have long been suggested as strong candidates to confer resistance of mastitis in cattle [59]. Although conceptually similar to the lysostaphin approach, cows overexpressing the antimicrobial protein human LF in their milk appeared to gain no improved protection against mastitis when challenged with an Escherichia coli strain isolated from cows with clinical mastitis [60]. This was rather unexpected, considering that these transgenic cows produced much greater levels of human LF in milk compared to the milk enriched with lysostaphin. Serving as a model for dairy cattle, human LZ has been expressed in the mammary gland of goats [2]. The potent bacteriostatic properties of the milk produced by these goats against two mastitis causing bacteria strongly suggests that human LZ might be another excellent candidate for conferring resistance to mastitis [61].

Particularly, in light of the human LF results, direct experimental validation of the protective potential will be required to determine the effectiveness of human LZ in preventing mastitis.

A different concept to introduce disease-resistant properties into livestock attempts to strengthen the immune system through the expression of pathogen-specific antibodies and thus providing instant immunity without prior exposure to this particular pathogen. The first studies in livestock involved the expression of mouse monoclonal antibodies in transgenic rabbits, sheep, and pigs but were met with little success because of unexpected problems to express fully functional antibodies [62, 63].

An extension of this approach has been the targeted production of viral-neutralizing monoclonal antibodies in milk, to provide passive immunity and protection from viral infections, which can severely affect suckling neonates. A mouse model expressing a coronavirus specific monoclonal antibody in milk demonstrated that the sustained production of high antibody levels throughout lactation could successfully neutralize the viral infectivity [64]. Moreover, in a similar study, suckling young were challenged with a lethal dose of murine hepatitis virus (MHV). Ingestion of MHV-specific antibody-enriched milk produced by the transgenic mice induced full protection against the viral infection in the pups [6].

The disruption of the virus entry mechanism proved to be an equally potent strategy. Transgenic mice engineered for the expression of a soluble form of a porcine herpes virus receptor, gained effectively full resistance against pseudorabies virus (PRV) infections [65]. Furthermore, the transgenic mice displayed superior protection levels compared to mice vaccinated with an attenuated PRV strain, demonstrating that this transgenic approach may offer superior efficiency for the control of pseudorabies in livestock [66].

The introduction of a specific disease resistance gene MX1 from mouse, known to confer resistance to influenza viruses in mice was another approach evaluated for its potential to protect livestock animals from viral infections. Similar to other pioneering studies prior to the mid-1990s, difficulties to adequately control Mx1 expression in transgenic pigs hampered the approach, which ultimately failed to achieve viral protection in pigs [67]. For now, the real potential of this approach remains unknown but the identification of antiviral Mx alleles from livestock species [68–70] and new tools for the improved control of transgene expression levels, such as the recently developed auto-regulative tetracycline-responsive expression cassette [71], may encourage a reevaluation of MX alleles for their potential to confer disease resistance in domesticated animals.

Rather than attempting to provide additional protective attributes, transgenic technology also enables the direct targeting of endogenous genes implicated in disease pathways. Such a concept has been applied to produce livestock animals which are resistant to the fatal neurodegenerative prion diseases or transmissible spongiform encephalopathies. This family of diseases, which include scrapie and the "mad cow disease" bovine spongiform encephalopathy, or BSE for short, is characterized by an accumulation of a misfolded isoform of the cellular prion protein (PrP) that acts as a novel infectious agent. Proof-of-concept studies in the mouse [72, 73], either introduction of mutated prion protein genes [74], gene knockout [75–77], or RNAi-mediated knockdown of PrP expression [78] demonstrated the possibility to produce animals that are resistant to prion diseases. Resistant livestock, certain to be free of such diseases would eliminate the risk for potential transmission of the disease to humans and provide additional safeguards for the food chain. However, some mouse studies raised concerns that the loss of the normal cellular function of PrP may adversely affect the animals by interfering with the circadian rhythm [79], synaptic functions [80, 81], learning [82], or loss of movement coordination [83]. When these findings were further investigated, the underlying molecular cause was not the loss of PrP function but an interference with the expression pattern of an adjacent gene as a result of only partially deleting the PrP locus [84–86].

Initial studies in sheep [75] and goats [77] indicated that animals heterozygous for the PrP knockout display, at least in young animals, a normal phenotype. These findings could now be confirmed with homozygous knockout cattle with deletions of the entire PrP gene [87]. In vitro assays with brain tissue homogenates derived from these PrP deficient cattle demonstrated resistance to prion propagation while the cattle were apparently normal in all aspects analyzed.

The recent development of RNAi technology, based on the expression of a short RNA molecule that can interfere with the activity of a specific target gene offers new opportunities to directly attack pathogens by disrupting their lifecycles. It is particularly attractive as an antiviral strategy, where RNAi can be used to target viral transcripts and suppress viral infection [88]. Because RNAi is a sequence-specific process, it will only affect the virus but not the host animal. Validated by the successful application of RNAi to control viral diseases in mouse model systems [89–91], the concept is applicable to a wide range of significant pathogens such as the RNA viruses that constitute over two thirds of the Office International Des Epizooties (OIE) list-A pathogens [88]. Recent outbreaks of viral diseases in farmed animals with immense socioeconomic and animal welfare costs such as foot and mouth disease or with the risk to cross the species barrier into humans such as Severe Acute Respiratory Syndrome (SARS), avian influenza and swine flu highlight the importance for improving current intervention strategies. Several studies are presently undertaken to evaluate the effectiveness of RNAi-mediated viral resistance in domesticated animals including chickens, pigs, cattle, sheep, and horses.

Future Directions

Transgenic livestock technology has made tremendous progress since its humble beginnings in 1985 [92]. Poor control of the transgene activity presented a main problem in early studies. Today, it is possible to integrate a transgene into a specific site of the genome and provide accurate control from the endogenous regulatory sequence elements. In addition, molecular switches have been developed which enable to switch the expression of a transgene on or off and can be combined to form sophisticated gene control networks [93]. In parallel, the understanding of how gene function relates to phenotypes is rapidly growing and has been further accelerated with the sequencing of the genomes of livestock species [94–96]. Thus, the application of transgenic technology to improve food production holds much promise for the future. Yet, transgenic technology should not be seen in isolation and as sole answer to all questions. The greatest benefit will result from combining transgenic strategies with other effective technologies. At present, however, most consumers consider transgenic technology for food applications as risky and unsafe and thus not acceptable [97]. While this may be predominantly driven by a general unease about an unfamiliar new technology, it had profound effects on politicians, regulators, and research investors and has largely prevented its application. With the mounting pressure on food safety and security, food and lifestyle-related health problems in the context of the rapidly increasing population and a changing climate, calls are becoming louder that this promising technology can no longer be ignored [98]. To gain consumer acceptance, it will be crucial to engage into an open dialog with the public that balances perceived against real risks. Only if a robust risk benefit assessment forms the bases for a decision on the acceptability of food-producing transgenic livestock will there be a chance to realize the benefits of the technology.

Bibliography

Primary Literature

1. James C (2009) Global status of commercialized biotech/GM crops: 2009. ISAAA Brief No. 41. ISAAA, Ithaca, NY
2. Maga EA, Shoemaker CF, Rowe JD, BonDurant RH et al (2006) Production and processing of milk from transgenic goats expressing human lysozyme in the mammary gland. J Dairy Sci 89:518–524
3. Brundige DR, Maga EA, Klasing KC, Murray JD (2008) Lysozyme transgenic goats' milk influences gastrointestinal morphology in young pigs. J Nutr 138:921–926
4. Brundige DR, Maga EA, Klasing KC, Murray JD (2010) Consumption of pasteurized human lysozyme transgenic goats' milk alters serum metabolite profile in young pigs. Transgenic Res 19:563–574
5. van Berkel PH, Welling MM, Geerts M, van Veen HA et al (2002) Large scale production of recombinant human lactoferrin in the milk of transgenic cows. Nat Biotechnol 20:484–487
6. Kolb AF, Pewe L, Webster J, Perlman S et al (2001) Virus-neutralizing monoclonal antibody expressed in milk of transgenic mice provides full protection against virus-induced encephalitis. J Virol 75:2803–2809
7. Wall RJ, Kerr DE, Bondioli KR (1997) Transgenic dairy cattle: genetic engineering on a large scale. J Dairy Sci 80:2213–2224
8. Zuelke KA (1998) Transgenic modification of cows milk for value-added processing. Reprod Fertil Dev 10:671–676

9. Brophy B, Smolenski G, Wheeler T, Wells D et al (2003) Cloned transgenic cattle produce milk with higher levels of beta-casein and kappa-casein. Nat Biotechnol 21:157–162
10. Laible G, Brophy B, Knighton D, Wells DN (2007) Compositional analysis of dairy products derived from clones and cloned transgenic cattle. Theriogenology 67:166–177
11. Farrell HM, Malin EL, Brown EM, Qi PX (2006) Casein micelle structure: what can be learned from milk synthesis and structural biology? Curr Opin Coll Interface Sci 11:135–147
12. Clare DA, Swaisgood HE (2000) Bioactive milk peptides: a prospectus. J Dairy Sci 83:1187–1195
13. Brody EP (2000) Biological activities of bovine glycomacropeptide. Br J Nutr 84(suppl 1):S39–S46
14. Baranyi M, Hiripi L, Szabo L, Catunda AP et al (2007) Isolation and some effects of functional, low-phenylalanine kappa-casein expressed in the milk of transgenic rabbits. J Biotechnol 128:383–392
15. Sahi T (1994) Genetics and epidemiology of adult-type hypolactasia. Scand J Gastroenterol Suppl 202:7–20
16. Stinnakre MG, Vilotte JL, Soulier S, Mercier JC (1994) Creation and phenotypic analysis of alpha-lactalbumin-deficient mice. Proc Natl Acad Sci USA 91:6544–6548
17. Jost B, Vilotte JL, Duluc I, Rodeau JL et al (1999) Production of low-lactose milk by ectopic expression of intestinal lactase in the mouse mammary gland. Nat Biotechnol 17:160–164
18. Kay JK, Roche JR, Kolver ES, Thomson NA et al (2005) A comparison between feeding systems (pasture and TMR) and the effect of vitamin E supplementation on plasma and milk fatty acid profiles in dairy cows. J Dairy Res 72:322–332
19. Palmquist DL, Beaulieu AD, Barbano DM (1993) Feed and animal factors influencing milk fat composition. J Dairy Sci 76:1753–1771
20. Reh WA, Maga EA, Collette NM, Moyer A et al (2004) Hot topic: using a stearoyl-CoA desaturase transgene to alter milk fatty acid composition. J Dairy Sci 87:3510–3514
21. Simopoulos AP (1999) Essential fatty acids in health and chronic disease. Am J Clin Nutr 70:560S–569S
22. Kao BT, Lewis KA, DePeters EJ, Van Eenennaam AL (2006) Endogenous production and elevated levels of long-chain n-3 fatty acids in the milk of transgenic mice. J Dairy Sci 89:3195–3201
23. McCann JC, Ames BN (2005) Is docosahexaenoic acid, an n-3 long-chain polyunsaturated fatty acid, required for development of normal brain function? An overview of evidence from cognitive and behavioral tests in humans and animals. Am J Clin Nutr 82:281–295
24. Kang JX, Wang JD, Wu L, Kang ZB (2004) Transgenic mice – Fat-1 mice convert n-6 to n-3 fatty acids. Nature 427:504
25. Lai L, Kang JX, Li R, Wang J et al (2006) Generation of cloned transgenic pigs rich in omega-3 fatty acids. Nat Biotechnol 24:435–436
26. Kang JX, Leaf A (2007) Why the omega-3 piggy should go to market. Nat Biotechnol 25:505
27. Saeki K, Matsumoto K, Kinoshita M, Suzuki I et al (2004) Functional expression of a Delta12 fatty acid desaturase gene from spinach in transgenic pigs. Proc Natl Acad Sci USA 101:6361–6366
28. Hammer RE, Brinster RL, Rosenfeld MG, Evans RM et al (1985) Expression of human growth hormone-releasing factor in transgenic mice results in increased somatic growth. Nature 315:413–416
29. Mathews LS, Hammer RE, Behringer RR, D'Ercole AJ et al (1988) Growth enhancement of transgenic mice expressing human insulin-like growth factor I. Endocrinology 123: 2827–2833
30. Palmiter RD, Brinster RL, Hammer RE, Trumbauer ME et al (1982) Dramatic growth of mice that develop from eggs microinjected with metallothionein-growth hormone fusion genes. Nature 300:611–615
31. Palmiter RD, Norstedt G, Gelinas RE, Hammer RE et al (1983) Metallothionein-human GH fusion genes stimulate growth of mice. Science 222:809–814
32. Chung CS, Etherton TD, Wiggins JP (1985) Stimulation of swine growth by porcine growth hormone. J Anim Sci 60:118–130
33. Pursel VG, Pinkert CA, Miller KF, Bolt DJ et al (1989) Genetic engineering of livestock. Science 244:1281–1288
34. Murray JD, Nancarrow CD, Marshall JT, Hazelton IG et al (1989) Production of transgenic merino sheep by microinjection of ovine metallothionein-ovine growth hormone fusion genes. Reprod Fertil Dev 1:147–155
35. Rexroad CE Jr, Hammer RE, Bolt DJ, Mayo KE et al (1989) Production of transgenic sheep with growth-regulating genes. Mol Reprod Dev 1:164–169
36. Pursel VG, Rexroad CE Jr (1993) Recent progress in the transgenic modification of swine and sheep. Mol Reprod Dev 36:251–254
37. Pursel VG, Wall RJ, Mitchell AD, Elasser TH et al (1999) Expression of insulin-like growth factor-1 in skeletal muscle of transgenic swine. In: Murray JD, Anderson GB, Oberbauer AM, McGloughlin MM (eds) Transgenic animals in agriculture. CABI, Oxon, UK, pp 131–144
38. Nottle MB, Nagashima H, Verma PJ, Du ZT et al (1999) Production and analysis of transgenic pigs containing a metallothionein porcine growth hormone gene construct. In: Murray JD, Anderson GB, Oberbauer AM, McGloughlin MM (eds) Transgenic animals in agriculture. CABI, Oxon, UK, pp 145–156
39. Adams NR, Briegel JR, Ward KA (2002) The impact of a transgene for ovine growth hormone on the performance of two breeds of sheep. J Anim Sci 80:2325–2333
40. Devlin RH, Yesaki YT, Biagi CA, Donaldson EM et al (1994) Extraordinary salmon growth. Nature 371:209–210
41. Du SJ, Gong Z, Fletcher GL, Shears MA et al (1992) Growth enhancement in transgenic Atlantic salmon by the use of an

"all fish" chimeric growth hormone gene construct. Biotechnology 10:176–181
42. Nam Y, Noh J, Cho Y, Cho H et al (2001) Dramatically accelerated growth and extraordinary gigantism of transgenic mud loach Misgurnus mizolepis. Transgenic Res 10:353–362
43. Rahman MA, Maclean N (1999) Growth performance of transgenic tilapia containing an exogenous piscine growth hormone gene. In: McAndrew B, Penman D, Hulata G (eds) Aquaculture 173:1/4, 333–346. 34 ref
44. Zbikowska HM (2003) Fish can be first-advances in fish transgenesis for commercial applications. Transgenic Res 12:379–389
45. Devlin RH, Biagi CA, Yesaki TY, Smailus DE et al (2001) Growth of domesticated transgenic fish. Nature 409:781–782
46. McPherron AC, Lawler AM, Lee SJ (1997) Regulation of skeletal muscle mass in mice by a new TGF-beta superfamily member. Nature 387:83–90
47. Kambadur R, Sharma M, Smith TP, Bass JJ (1997) Mutations in myostatin (GDF8) in double-muscled Belgian Blue and Piedmontese cattle. Genome Res 7:910–916
48. McPherron AC, Lee S-J (1997) Double muscling in cattle during to mutations in the myostatin gene. Proc Natl Acad Sci USA 94:12457–12461
49. Grobet L, Pirottin D, Farnir F, Poncelet D et al (2003) Modulating skeletal muscle mass by postnatal, muscle-specific inactivation of the myostatin gene. Genesis 35:227–238
50. Lee S-J, Reed LA, Davies MV, Girgenrath S et al (2005) Regulation of muscle growth by multiple ligands signaling through activin type II receptors. PNAS 102:18117–18122
51. Yang J, Ratovitski T, Brady J, Solomon M et al (2001) Expression of myostatin pro domain results in muscular transgenic mice. Mol Reprod Dev 60:351–361
52. Jain H, Singh S, Kadam M, Sarkhel BC (2010) Knockdown of the myostatin gene by RNA interference in caprine fibroblast cells. J Biotechnol 145:99–102
53. Magee TR, Artaza JN, Ferrini MG, Vernet D et al (2006) Myostatin short interfering hairpin RNA gene transfer increases skeletal muscle mass. J Gene Med 8:1171–1181
54. Pirottin D, Grobet L, Adamantidis A, Farnir F et al (2005) Transgenic engineering of male-specific muscular hypertrophy. Proc Natl Acad Sci USA 102:6413–6418
55. Muller M, Brem G (1998) Transgenic approaches to the increase of disease resistance in farm animals. Revue Scientifique Et Technique (International Office Of Epizootics) 17:365–378
56. Whitelaw CB, Sang HM (2005) Disease-resistant genetically modified animals. Rev Sci Tech 24:275–283
57. Kerr DE, Plaut K, Bramley AJ, Williamson CM et al (2001) Lysostaphin expression in mammary glands confers protection against staphylococcal infection in transgenic mice. Nat Biotechnol 19:66–70
58. Wall RJ, Powell AM, Paape MJ, Kerr DE et al (2005) Genetically enhanced cows resist intramammary Staphylococcus aureus infection. Nat Biotechnol 23:445–451
59. Seyfert HM, Henke M, Interthal H, Klussmann U et al (1996) Defining candidate genes for mastitis resistance in cattle: The role of lactoferrin and lysozyme. J Anim Breed Genet 113:269–276
60. Hyvonen P, Suojala L, Orro T, Haaranen J et al (2006) Transgenic cows that produce recombinant human lactoferrin in milk are not protected from experimental Escherichia coli intramammary infection. Infect Immun 74:6206–6212
61. Maga EA, Cullor JS, Smith W, Anderson GB et al (2006) Human lysozyme expressed in the mammary gland of transgenic dairy goats can inhibit the growth of bacteria that cause mastitis and the cold-spoilage of milk. Foodborne Pathog Dis 3:384–392
62. Lo D, Pursel V, Linton PJ, Sandgren E et al (1991) Expression of Mouse Iga by transgenic mice pigs And sheep. Eur J Immunol 21:1001–1006
63. Weidle UH, Lenz H, Brem G (1991) Genes encoding a mouse monoclonal antibody are expressed in transgenic mice, rabbits and pigs. Gene 98:185
64. Castilla J, Pintado B, Sola I, Sanchez-Morgado JM et al (1998) Engineering passive immunity in transgenic mice secreting virus-neutralizing antibodies in milk. Nat Biotechnol 16:349–354
65. Ono E, Amagai K, Taharaguchi S, Tomioka Y et al (2004) Transgenic mice expressing a soluble form of porcine nectin-1/herpesvirus entry mediator C as a model for pseudorabies-resistant livestock. Proc Natl Acad Sci USA 101:16150–16155
66. Ono E, Tomioka Y, Taharaguchi S, Cherel P (2006) Comparison of protection levels against pseudorabies virus infection of transgenic mice expressing a soluble form of porcine nectin-1/HveC and vaccinated mice. Vet Microbiol 114:327–330
67. Mueller M, Brenig B, Winnacker E-L, Brem G (1992) Transgenic pigs carry cDNA copies encoding the murine Mx1 protein which confers resistance to influenza virus infection. Gene 121:263–270
68. Asano A, Ko JH, Morozumi T, Hamashima N et al (2002) Polymorphisms and the antiviral property of porcine Mx1 protein. J Vet Med Sci 64:1085–1089
69. Baise E, Pire G, Leroy M, Gerardin J et al (2004) Conditional expression of Type I interferon-induced bovine Mx1 GTPase in a stable transgenic vero cell line interferes with replication of vesicular stomatitis virus. J Interferon Cytokine Res 24:513–521
70. Leroy M, Pire G, Baise E, Desmecht D (2006) Expression of the interferon-alpha/beta-inducible bovine Mx1 dynamin interferes with replication of rabies virus. Neurobiol Dis 21:515
71. Kues WA, Schwinzer R, Wirth D, Verhoeyen E et al (2006) Epigenetic silencing and tissue independent expression of

a novel tetracycline inducible system in double-transgenic pigs. FASEB J 20:1200–1202
72. Bueler H, Aguzzi A, Sailer A, Greiner RA et al (1993) Mice devoid of PrP are resistant to scrapie. Cell 73:1339–1347
73. Perrier V, Kaneko K, Safar J, Vergara J et al (2002) Dominant-negative inhibition of prion replication in transgenic mice. Proc Natl Acad Sci USA 99:13079–13084
74. Cyranoski D (2003) Koreans rustle up madness-resistant cows. Nature 426:743
75. Denning C, Burl S, Ainslie A, Bracken J et al (2001) Deletion of the alpha(1, 3)galactosyl transferase (GGTA1) gene and the prion protein (PrP) gene in sheep. Nat Biotechnol 19:559–562
76. Kuroiwa Y, Kasinathan P, Matsushita H, Sathiyaselan J et al (2004) Sequential targeting of the genes encoding immunoglobulin-mu and prion protein in cattle. Nat Genet 36:775–780
77. Yu G, Chen J, Yu H, Liu S et al (2006) Functional disruption of the prion protein gene in cloned goats. J Gen Virol 87:1019–1027
78. Golding MC, Long CR, Carmell MA, Hannon GJ et al (2006) Suppression of prion protein in livestock by RNA interference. Proc Natl Acad Sci USA 103:5285–5290
79. Tobler I, Gaus SE, Deboer T, Achermann P et al (1996) Altered circadian activity rhythms and sleep in mice devoid of prion protein. Nature 380:639
80. Collinge J, Whittington MA, Sidle KCL, Smith CJ et al (1994) Prion protein is necessary for normal synaptic function. Nature 370:295
81. Mallucci GR, Ratte S, Asante EA, Linehan J (2002) Post-natal knockout of prion protein alters hippocampal CA1 properties, but does not result in neurodegeneration. [erratum appears in EMBO J 2002 Mar 1;21(5):1240]. EMBO J 21:202–210
82. Criado JR, Sanchez-Alavez M, Conti B, Giacchino JL et al (2005) Mice devoid of prion protein have cognitive deficits that are rescued by reconstitution of PrP in neurons. Neurobiol Dis 19:255
83. Sakaguchi S, Katamine S, Nishida N, Moriuchi R et al (1996) Loss of cerebellar Purkinje cells in aged mice homozygous for a disrupted PrP gene. Nature 380:528
84. Li A, Sakaguchi S, Atarashi R, Roy BC et al (2000) Identification of a novel gene encoding a PrP-like protein expressed as chimeric transcripts fused to PrP exon 1/2 in ataxic mouse line with a disrupted PrP gene. Cell Mol Neurobiol 20: 553–567
85. Moore RC, Lee IY, Silverman GL, Harrison PM et al (1999) Ataxia in prion protein (PrP)-deficient mice is associated with upregulation of the novel PrP-like protein doppel. J Mol Biol 292:797
86. Rossi D, Cozzio A, Flechsig E, Klein MA et al (2001) Onset of ataxia and Purkinje cell loss in PrP null mice inversely correlated with Dpl level in brain. EMBO J 20:694–702
87. Richt JA, Kasinathan P, Hamir AN, Castilla J et al (2007) Production of cattle lacking prion protein. Nat Biotechnol 25:132
88. Clark J, Whitelaw B (2003) A future for transgenic livestock. Nat Rev Genet 4:825–833
89. Carmona S, Ely A, Crowther C, Moolla N et al (2006) Effective inhibition of HBV replication in vivo by anti-HBx short hairpin RNAs. Mol Ther 13:411–421
90. McCaffrey AP, Nakai H, Pandey K, Huang Z et al (2003) Inhibition of hepatitis B virus in mice by RNA interference. Nat Biotechnol 21:639–644
91. Tompkins SM, Lo CY, Tumpey TM, Epstein SL (2004) Protection against lethal influenza virus challenge by RNA interference in vivo. Proc Natl Acad Sci USA 101:8682–8686
92. Hammer RE, Pursel VG, Rexroad CE Jr, Wall RJ et al (1985) Production of transgenic rabbits, sheep and pigs by microinjection. Nature 315:680–683
93. Greber D, Fussenegger M (2007) Mammalian synthetic biology: engineering of sophisticated gene networks. J Biotechnol 130:329–345
94. Amaral AJ, Megens HJ, Kerstens HH, Heuven HC et al (2009) Application of massive parallel sequencing to whole genome SNP discovery in the porcine genome. BMC Genomics 10:374
95. Elsik CG, Tellam RL, Worley KC, Gibbs RA et al (2009) The genome sequence of taurine cattle: a window to ruminant biology and evolution. Science 324:522–528
96. Wallis JW, Aerts J, Groenen MA, Crooijmans RP et al (2004) A physical map of the chicken genome. Nature 432:761–764
97. Pardo R, Engelhard M, Hagen K, Jorgensen RB et al (2009) The role of means and goals in technology acceptance. A differentiated landscape of public perceptions of pharming. EMBO Rep 10:1069–1075
98. Fedoroff NV, Battisti DS, Beachy RN, Cooper PJ et al (2010) Radically rethinking agriculture for the 21st century. Science 327:833–834

Books and Reviews

Council for Agricultural Science and Technology (CAST) (2003) Biotechnology in animal agriculture: an overview. Issue Paper 23. CAST, Ames, Lowa

Council for Agricultural Science and Technology (CAST) (2009) Animal productivity and genetic diversity: cloned and transgenic animals. Issue Paper 43. CAST, Ames, Lowa

Gottlieb S, Wheeler MB (2008) Genetically engineered animals and public health: compelling benefits for health care, nutrition, the environment and animal welfare. www.bio.org/foodag/animals/ge_animal_benefits.pdf

Heller KJ (2006) Genetically engineered food: methods and detection. Wiley-VHC, Weinheim

Jimenez-Flores R, Richardson T (1988) Genetic engineering of the caseins to modify the behavior of milk during processing: a review. J Dairy Sci 71:2640–2654

Swain DL, Charmley E, Steel JW, Coffey SG (2007) Redesigning animal agriculture: the challenge for the 21st century. CABI, Wallingford, UK

Transgenic Livestock, Ethical Concerns and Debate

Mickey Gjerris[1], Reinhard Huber[2], Jesper Lassen[1], I Anna S. Olsson[2], Peter Sandøe[1]
[1]Danish Centre for Bioethics and Risk Assessment, Institute of Food and Resource Economics, University of Copenhagen, Frederiksberg, Denmark
[2]Laboratory Animal Science Group, IBMC – Instituto de Biologia Molecular e Celular, Universidade do Porto, Porto, Portugal

Article Outline

Glossary
Definition of the Subject
Introduction
Science and Applications
Public Perceptions of Transgenic Technologies
The Ethical Issues
Public Discussions
Future Directions
Bibliography

Glossary

Animal bioreactor Transgenic animal that produces recombinant proteins in its milk, egg white, blood, urine, or seminal plasma.

Antibody Protein produced as part of the immune reaction to render harmless a foreign substance (e.g., bacteria) entering the body of an organism.

Cloning (a) Production of exact copies (clones) of a gene/genes (gene cloning). The DNA strand containing the gene of interest is cut into suitably sized pieces (fragmentation) and the gene of interest is linked to a piece of DNA (cloning vector). This vector is then introduced into cells (transfection) which are cultured in vitro and then screened for the presence of the gene of interest. (b) Production of genetically identical organisms by somatic cell nuclear transfer (SCNT). It involves the introduction of the nucleus of a somatic cell from the organism to be cloned into an enucleated egg cell. The resulting cell divides after activation (application of electric shock) into an embryo which may then be implanted into a surrogate mother (reproductive cloning) or used to establish a tissue culture (therapeutic cloning).

Embryonic germ cell Pluripotent stem cells derived from early germ cells with properties similar to embryonic stem cells.

Embryonic stem cell Cell derived from an early embryo that is not differentiated by itself but may divide either to form (a) other stem cells or (b) cells that differentiate into specialized cell types.

Gene copy number Genes naturally exist in varying number of copies in the genome. In relation to genetic modification, gene copy number refers to the number of copies of a transgene that integrate into the host genome.

Gene expression The assembly of a product (mainly protein) based on the information coded in a gene.

Gene targeting The modification of a certain endogenous gene of an organism based on homologous recombination.

Germ cell Cell that produces gametes (egg cells in females, sperm in males).

Heterozygous Organism/cell in which the two chromosomes in a pair contain different alleles (alternative forms of a gene) at a given locus. The dominant allele will determine the phenotype.

Homologous recombination The exchange of genetic information between two similar or identical strands of DNA (often during meiosis, i.e., the formation of gametes). This process is used for the introduction of DNA sequences into the genome of organisms by gene targeting.

Homozygous Organism/cell in which the two chromosomes in a pair contain identical alleles (alternative forms of a gene) at a given locus. The alleles may either be dominant or recessive.

Hemizygous Organism/cell with only the given allele present at the given locus of only one of the chromosomes in a pair.

Knockout The replacement of a functioning endogenous gene with an inoperable version.

Lentiviruses Viruses that are able to infect both dividing and nondividing cells and are therefore used as tools as vectors for gene delivery.

Marker-assisted selection Method allowing the selection of breeding animals based on their genotype rather than their phenotype. Regions of the genome

that control certain production traits are mapped and DNA markers that control production traits are identified. Animals whose genome contains the desired markers are selected for further breeding.

Motivation The internal state of an animal which makes it behave in a certain way; the overall summation of all internal and external factors affecting decision-making.

Pronucleus The nucleus of either a sperm (male p.) or an egg (female p.) cell before their fusion inside the egg cell in the process of fertilization. At pronuclear microinjection, the DNA containing the transgene is injected into one of the pronuclei which fuse. After implantation of the egg into a female, the resulting embryo develops into a hemizygous transgenic animal which must be bred to obtain homozygous transgenic animals.

Recombinant protein Proteins that are expressed based on recombinant DNA (rDNA). rDNA is obtained by genetic engineering techniques, i.e., the ´artificial´ combination of information contained in the transgene and in the host genome.

Somatic nuclear cell transfer See Cloning.

Subjective experience Conscious mental state, an experience that the individual is aware of.

Viral vector Virus-based vehicle to introduce genetic information into cells making use of the capacity of viruses to transfer their genome into the cells they infect. For transgenesis purposes, they are rendered replication-deficient to avoid replication once the transfer of the genetic information of interest into the cell has taken place.

Definition of the Subject

Humans have been able to manipulate the genomes of livestock through selective breeding for centuries; however, direct intervention has become possible only through the development of transgenic technology over the past 3 decades. So far, genetically modified animals have mainly been developed for basic research and biomedicine, but they are slowly beginning to enter the agricultural production system. In this article, livestock is defined to be all species used within the agricultural and aquacultural system. Note that such animals can be genetically modified for use within basic and medical research as well.

Most people would readily agree that there is a difference between what humans *can* do and what they *ought* to do. Equally, most people would happily acknowledge that it is good to do the morally right thing. However, the harmony usually ends there, because although it is easy to agree that a good thing should be promoted, it is often hard to reach consensus on what that good thing is, how it can be promoted, and to what extent the end justifies the means. There may also be disagreement over what counts as a bad outcome or about whether there are acts which are wrong in themselves. As soon as questions as these are discussed whether in private or in public, people are engaging in an ethical discussion – a discussion in which the aim is to reach agreement on what is good and bad and what is right and wrong.

Such ethical discussions have closely shadowed developments within biotechnology over the past 30 years. A range of applications of biotechnology to animals, including reproductive technologies, genetic modification, and cloning, has prompted concern about the ethical limits of human use of animals. It is probably an understatement to say that discussion has so far led to no consensus in the public sphere, but it would also be an overstatement to say that the debate has led to unanimous agreement. What *has* emerged, among other things, is a clearer understanding of the basic ethical assumptions driving the different viewpoints, together with greater attention to the ethical duties of humans toward animals.

The technological challenge of animal biotechnology is: What *can* be done? This question is closely followed by the question: What *ought* to be done? As with any other human activity, this question needs to be answered if decisions on what to do are to be made. That is both the blessing and the curse of being an ethical creature equipped with a conscience. Humans cannot just act and use the possibilities that lie before them; they have to take responsibility for the values that are promoted through their choices. At the same time, there are huge disagreements about what the relationship between *can do* and *ought to do* in the area of transgenic animals is. One of the consequences of this is that ethics cannot be pursued as a mere afterthought to the technology or as something of concern only to opponents of the technology.

The subject of this article is the ethical concerns about transgenic livestock. While the strict scientific definition of "transgenesis" implies that genetic material is transferred between species [1, 2], the term is often used interchangeably with genetic modification to cover a wider range of techniques in which the animal genome is manipulated – e.g., including the inactivation of genes. For livestock applications, transgenesis proper is the predominant kind of genetic modification, and so, in this chapter, "transgenic" is used only to refer to the transfer between species. Examples of genetic modification will be used additionally to clarify important points. The goal is to make the different areas of concern that arise in the ethical debates transparent, and to discuss different ways of approaching a public dialogue on these matters.

Introduction

Gene technology and other forms of modern biotechnology have given rise to ethical controversies since they were first introduced in the early 1980s. This has led to a growing awareness among both scientists and politicians that successful implementation of biotechnology in democratic and pluralistic societies requires ethical concerns to be discussed and taken seriously. Numerous and extensive attempts have thus been made over the past 3 decades to engage stakeholders and the public in general in discussion of the ethical aspects of biotechnology.

Already, the earliest transgenic animals in the 1980s were the subject of controversy [3–6]. However, it was probably with the creation of the cloned sheep Dolly in 1997 that animal biotechnology became widely known to the public in the industrialized world [7]. Looking at both studies of public opinion on the subject and the ethical literature, one can see that the concerns here can be divided into distinct groups. Some relate to possible impacts on humans, either through health-related risks, environmental consequences, or socio-economic changes. Some revolve around the possible conflicts arising from the possibility of patenting living beings. Others revolve around animal welfare, and different concepts of that, while the last group expresses more general concerns about the (un)naturalness of the technologies, and possible violations of the integrity of the animal species. One discussion that arches over all of these issues and has been an important determinant in framing the ethical debate as a whole focuses on how best to regulate the area.

Sociological studies have revealed public skepticism about transgenic animals. Considerations of risk, usefulness, animal welfare, and other moral values play a substantial role in the public evaluation of the technologies. Based to some extent on these studies, many attempts have been made to engage the public and stakeholders such as scientists, politicians, legislators, industry, animal welfare organizations, consumers, and others in society-wide discussions of how the new technologies can be implemented in a way that will be acceptable for a majority of citizens. Whether or not these attempts have been successful obviously depends on the criteria of success applied. What can be said, however, is that they have not led to general agreement about the development and use of transgenic animals.

In this area of ethical thinking and public discourse, it is necessary to be aware of the open-ended nature of the discussion. From a scientific point of view, there is a world of difference between a knockout pig that has had a gene disabled to better serve as a organ donor for humans (xenotransplantation) [8] and a goat that has had a human gene inserted that expresses itself in the mammary glands thus enabling human proteins to be harvested from the milk [9]. But from the point of view of the nonexpert, these differences might seem ethically unimportant if the concern in play is the possible violation of the species' integrity.

There is also a tendency among experts to look primarily at methods, or techniques, when evaluating biotechnology, whereas members of the public often bring in considerations of usefulness as well. Ethical discussions thus differ from technical discussions, and it is necessary to critically evaluate the amount of scientific knowledge and expertise needed within different layers of the ethical discussion. Obviously, science and scientific thinking cannot be left out of ethical discussions of science and its technical applications, but neither should their importance be overstressed [10].

Similarly, it can be problematic if the subject of the ethical discussion becomes too narrow. There is a tendency in the current research environment for ethics to follow natural science into increasingly specialized fields where it becomes difficult to include other areas of science with similar concerns. But at

the level of ethical concerns, it is sometimes helpful to discuss transgenic livestock together with, for example, other issues relating to modern intensive animal production [11]. Thus the concerns that people have about transgenic livestock may to a large extent be about taking an already problematic development even further.

As a prerequisite to any ethical debate about transgenic livestock, it is of course necessary to make it clear what the subject of the discussion is, and what areas of application are involved. This ensures an informed debate in which misunderstandings resulting from unclarity are avoided.

Science and Applications

From Early Research to Maturing Technology

Humans have manipulated the genetic makeup of livestock through the process of domestication for thousands of years. Scientifically based farm animal breeding began in the early twentieth century, and, particularly since the 1950s, it has had a profound effect on most livestock species. Various modern biotechnologies – particularly reproductive technologies – have gradually been adopted since the 1980s.

A comparatively recent technology in this process of development is genetic engineering/modification; this emerged in the 1980s and has evolved considerably since. Genetic modification involves the direct manipulation of the genome of a group of founder animals, unlike traditional breeding, where animals are selected on the basis of their phenotype and then mated in order to approach a certain breeding goal gradually. There is a degree of vagueness in the definition of the techniques used to generate genetically modified organisms. Genetic modification, in the broadest sense, has been defined as an "altering of the genetic material in that [the GM] organism in a way that does not occur naturally by mating or natural recombination or both" [12]; this covers a wide array of technologies.

Genetic modification and transgenesis are sometimes used synonymously, but the term "transgenesis" is often defined more narrowly to apply to just one aspect of genetic modification: transgenic animals carry foreign genetic information (i.e., information from another species) and transmit this information to their progeny, because the transgene is integrated in the germ cells of the animal [1]. Genetic modification may involve further modification of the genome (moving, deleting, multiplying, modifying genes) within an organism – e.g., the creation of knockout animals. Creating a knockout animal involves the targeted inactivation of a gene. In this process, the protein usually produced as a consequence of the genetic information in question is no longer produced. This is achieved by replacing an active gene with an inactive version, thus preventing the gene in question from being expressed [13]. Knockout applications are common in mice used for fundamental and biomedical research; however, in livestock species, transgenesis is the most common form of genetic modification, although even here, knockout applications do exist (e.g., mini-pigs which have had genes knocked out in connection with xenotransplantation research) [14].

The main projected advantages of transgenesis over established breeding techniques include the possibility of introducing genes that do not exist in the genome of the parents (outside the species), and the opportunity to target desirable traits without coselecting genetically coupled undesirable ones. The foreign gene is introduced in early stage embryos (first cell stage) or in cells that participate later in the complete development of the animal [13]. These embryos develop into transgenic founder animals, which can then be used in further breeding. Regardless of the particular method used, the main steps in producing transgenic animals are as follows [15]:

- Identifying the trait of interest and localizing the corresponding gene in the donor species genome
- Multiplying the gene through cloning
- Production of a suitable construct for gene transfer
- Gene transfer
- Proof of integration of the foreign gene
- Proof of expression of the foreign gene in the host animal
- Demonstrating that offspring of founder animals inherit the foreign gene
- Selective breeding to diffuse the foreign gene into the relevant population of animals

Some of the technology to create transgenic livestock is based on methods developed for use in mice: the first transgenic mammals created by pronuclear microinjection in 1980 were mice [16]. This method

was adapted in 1985 to create the first transgenic livestock (rabbits, sheep, pigs) [17].

In further developing the technologies, researchers have tried to address technical limitations, and to develop alternatives to pronuclear injection with improved efficiency (i.e., proportion of newborn animals carrying the transgene), predictability, and control of gene expression. Predictability refers to where in the host genome the transgene is integrated. When technologies in which the integration site is random are used, there may be unexpected expression patterns as a result of interference with the host genome. Technologies allowing targeted integration increase predictability by giving greater control of gene expression. Whether or not the number of copies can be controlled is also relevant, as copy number influences the level and stability of transgene expression [18].

Table 1 provides an overview of the most prominent methods of transgenesis, noting the availability for different species as well as the predictability, efficiency, and feasibility.

There are however several practical obstacles to routine production of transgenic livestock [21]. The efficiency of the methods used was very low in the beginning, and although progress has been made here, transgenesis still cannot compete with other methods used for the genetic improvement of livestock (e.g., selective breeding in combination with artificial insemination and marker-assisted selection) on cost efficiency, practicality, and public/political acceptance. Furthermore, many traits of interest in livestock are controlled by more than one gene and are therefore difficult to improve by transgenesis. The introduction of transgenesis in livestock breeding is further complicated by the fact that, typically at any rate, very few transgenic animals are generated in the first generation. This makes diffusion into a breeding population without corresponding inbreeding depression difficult. It also means that, since the phenotypic uniformity of transgenic offspring is often limited, the evaluation of gene expression in transgenic livestock would require a large number of animals.

Fish have been popular models for research into transgenesis as they are easy to maintain/handle and highly fertile. They have easily manipulable, large eggs, which are fertilized and develop externally; fish species also usually tolerate genetic manipulation well during early development (unlike, say, rats). The most

Transgenic Livestock, Ethical Concerns and Debate. Table 1 Summary of existing transgenic approaches (Adapted from [19, 20])

Transgenic method	Availability	Integration site(s)[a]	Number of copies per site	Efficiency[b]/ technical difficulty	Note
Microinjection	Most mammals[c]	Random	Variable	Low/medium	First method
Somatic cell nuclear transfer	Most mammals	Can be determined	Often single copy	Low/high	>1997
Lentivirus-based	Most mammals	Random and multiple	Single copy	High/low	Late 1990s
Sperm manipulation	Most mammals[c]	Random	Variable	Moderate/low	Successful application in few laboratories so far
ES/EG[d] cells	Mice and rats, not (yet) available in livestock	Predetermined	Often single copy	Low/NA[e]	Recently successful in Chicken (EG [91])

[a]Determination of the site of integration or random integration in the genome
[b]Arbitrary scale: low, <5%; moderate, >5%; high, >80%
[c]All mammals tested so far
[d]Embryonic stem/Embryonic Germ
[e]Not Applicable as not used in livestock (so far)

common technique used for gene transfer is still pronuclear microinjection but, as with other livestock species, research into increased efficiency has led to the development/adaptation of new methods, including electroporation (i.e., improving the permeability of the cell membrane for DNA macromolecules by applying short electric pulses), sperm-mediated gene transfer, direct gene transfer into tissues of adult fish (via intramuscular injection of DNA or "gene gun delivery"), and the use of viral vectors [22–24].

Risks are attached to the technology, naturally, and sometimes these are unpredictable. They include the occurrence of undesirable effects of transgene expression, which should be addressed in food safety assessment schemes (like in other emerging novel foods). In particular, safety assessment should be performed regarding toxic/antinutritional effects, allergenic potential, bioactivity (e.g., hormones active *post* consumption) [25]. For a thorough discussion of different risks associated with transgenic livestock, please see "The Ethical Issuessection ."

Applications of Genetic Modification to Livestock

Several explorations of potential applications of genetic modification to livestock species have been published [1, 20, 26–29], and agricultural purposes have been examined in particular [2, 30]. The authors of these studies usually distinguish between biomedical and agricultural applications. The basis of this distinction seems to be that applications in the agricultural domain facilitate the direct consumption of products from transgenic animals/their offspring by humans, while in the biomedical field, applications target human health via the development of pharmaceuticals, antibodies, transferable organs/tissues, or by studies into basic biological processes and disease mechanisms. There are products for direct consumption, such as functional foods, which however may fall into both categories [31].

The history of R&D here shows that – apart from scientific interest in basic biological questions – transgenic livestock research has undergone changes of focus and has followed funding and fashion. In this process, biomedical applications such as xenotransplantation, animals as "bioreactors" and disease models, and among agricultural applications the "Enviropig®" have emerged.

Initial developments in transgenic farm animals focused on the improvement of one of the classical production-related traits: growth [17]. The animals involved have become popularly known as "Beltsville pigs." Ever since, there have been reports of procedures involving transgenesis for specific problems with, and questions about, livestock production (for a recent review [2]).

There have been attempts to use the technologies to improve animal health and disease resistance. There are various ways of achieving this, including passive immunization of young animals against viruses through antibody expression in milk and improvement of early growth and/or viability in piglets through increased sow milk yield when overexpressing bovine alpha-lactalbumin. Food quality and the improved usability of animal products for human consumption (e.g., the expression of human lactoferrin in milk to obtain positive effects on the immune system, reduction of lactose to circumvent intolerance, carcass and meat composition alteration toward leaner meat, and meat with higher content of omega-3 fatty acids) can also be mentioned in this context. Another production-related application aims at diminishing the "ecological footprint" of industrial pig production: this involves the expression of a bacterial phytase gene in the saliva of pigs which leads to reduced phosphorous excretion.

Moving to the broader and related area of genetic modification, gene knockout has been employed in efforts to induce disease resistance (prion diseases) [1]; it has also been used to create pigs that do not express alpha 1,3 GT in an attempt to overcome organ rejection after xenotransplantation.

Apart from its applications in biomedicine and basic biological research, transgenic technology has been used in fish to improve production parameters such as growth and food conversion, adaptation to cold environments (lowering the freezing point of body fluids through the expression of antifreeze proteins), disease resistance and prevention of the introduction of transgenes into wild populations (sterility). As with land farm animals, in 1985, the very first successful application of transgenic technology reported in fish aimed at increased growth by introducing a gene for human growth hormone (to be expressed, in this case, in goldfish). For an extensive review of applications see [24].

In a relatively recent review paper, tentative projections as to when various applications of transgenic livestock will be applied in the field are made [20]. Most of the biomedical and agricultural applications projected by Niemann and colleagues to be introduced some time beyond 2005 are still at the research stage in 2010; and, of the applications listed, only recombinant pharmaceutical proteins have actually reached the market: in 2006 the European Commission, and in 2009 the FDA in the USA, gave approval for the drug ATryn® (a recombinant form of human antithrombin, an agent that prevents blood-clotting) to be produced in the milk of transgenic goats for pharmaceutical markets. Growth-enhanced transgenic fish are often presented as the most promising candidate for the introduction of transgenic animals for food production [23, 32].

Future Perspectives

The idea of using transgenic animals in food production is controversial not only with the public, but also within the scientific community. The success of transgenic livestock for agricultural purposes has failed to meet initial expectations not least as a result of its practical limitations as compared with other breeding tools [1].

Scientists differ considerably in their assessments of the impact transgenic livestock will have on animal agriculture, and in the time-frame within which this impact will unfold. These attitudes also reflect opinions about the usefulness and feasibility of the technology; in general, biomedical applications usually meet with more optimism than agricultural applications. The following excerpts from relevant publications that can be seen in Table 2 illustrate the range of views:

Animal biotechnology is embedded in a social context and therefore affected by general trends in the societies in which it unfolds. This also means that one should be neither excessively optimistic about altruistic motives behind the technology nor excessively suspicious about possible egoistic and narrow motives. In general, one should bear in mind – when listening to all the problems that the technology might solve and how soon it will revolutionize human lives – that in western capitalist society, the worlds of research and business, science and technology, and knowledge-building and knowledge-using, have converged. Scientists are not necessarily independent and altruistic, but human beings working in a marketplace like everybody else. They are, in other words, stakeholders. A certain amount of sound skepticism in evaluating the claims they make is therefore probably not going to be wasted [33].

It must at the same time be remembered that the potential of the technology is enormous and the range of applications almost endless – in theory, at any rate. But as the last 25–30 years have shown, it is a long way from having an idea to making it work. Sometimes, it seems that the more that is learned through science, the more it is realized how little is known, because the world in general, and molecular biology specifically, turns out to be much more complicated than initially believed [34]. When trying to assess the potential applications of transgenic livestock, there is, therefore, a large and inescapable uncertainty.

Public Perceptions of Transgenic Technologies

This section describes public perceptions of transgenic animals. As a point of departure, it should be noted that while experts, in the nature of their profession, tend to assess transgenic animals as an isolated phenomenon, the public often see these animals within a wider context. Thus most lay persons will see transgenic animals as parts of modern biotechnology. Respecting this, this section first places public perceptions of transgenic animals within a wider context of other applications of biotechnology within the agricultural and medical fields; and, second, present various aspects of the public perceptions of transgenic animals. Another aspect of the contextuality of public perceptions is the fact that perceptions should be interpreted, or understood, in the particular context in which they arise. Perceptions reflect deeper rooted cultural and/or religious values as well as passing material settings – and so they will vary with continents, countries, and religions. The following descriptions examine public attitudes in both Europe and North America, but the main focus is on Europe.

Accounts of public perceptions have two main empirical sources: qualitative interview studies or quantitative surveys. The former, which involve group interviews or individual interviews, are effective at delivering a deeper insight into the arguments and values behind specific views, but as a result of the

Transgenic Livestock, Ethical Concerns and Debate. Table 2 Examples of scientists' views on impact of transgenic livestock and relevant time frame

	Impact	Time frame
Optimistic/clear-cut predictions	"Transgenic technology allows for the stable introduction of exogenous genetic information into livestock genomes. With its ability to enhance existing or introduce entirely novel characteristics at unprecedented magnitude and speed, this emerging technology is expected to have a profound impact on the genetic improvement of livestock in the future." [2] "The overwhelming challenge to agriculture in the next century will be to feed a huge population while creating and maintaining sustainable agricultural systems. Biotechnology, including transgenic livestock, will play a key role in meeting this challenge by allowing greater precision in resource use and product design." [30]	"Sixteen years ago, transgenic animal technology was invented, and, since then, an industry has formed to exploit that technology. In the next 16 years, products created by that technology will likely be in the hands of consumers." [26]
Moderate optimism/"some time in the future"	"New methods for modifying the genome will underpin a resurgence of research using transgenic livestock. This will not only increase our understanding of basic biology in commercial species, but might also lead to the generation of animals that are more resistant to infectious disease." [1]	"We anticipate that in the near future, genetically modified animals will play a significant role in the biomedical field but that agricultural applications will develop more slowly due to the complexity of many economically important traits and to current resistance to the concept of engineered farm animals." [15] "While various transgenic concepts for the genetic improvement of livestock animals for agriculture are being evaluated the integration of this technology into practical farming systems remains some distance in the future." [2]
Critical/uncertain about time-frame	"It is not clear at all that the benefits that genetic engineering has produced hitherto compensate the potential risks of widely using these products in animal production. Putting the question in a crude way: Are we risking our health for a 5% of the benefits in milk production? Should we use transgenic pigs for a 33% less manure spread? In general, every advance of molecular genetics has been received with high expectations in the field of animal production, but the consequent application, if any, has been much more modest." [1]	"Over the past few years several commercial ventures have withdrawn from transgenic biopharming for various, usually financial, reasons. So, even though much of the groundwork has been doneit is unclear what the future holds for this use [agricultural applications] of transgenic livestock. [. . .] It will take both a better understanding of the genomes of livestock, with the anticipated increase in candidate genes to choose from, and a major practical success before transgenic technology seriously challenges genetic improvement of livestock through selection for most conventional traits." [1] "When a procedure is challenged for some present reason, it is not uncommon to argue that in the future all these problems will be solved. [. . .] In the opinion of the author of this paper, the general attitude towards genetic engineering in domestic livestock should be reconsidered." [21]

limited number of participants, the interviews give a poor picture of the representation and structure of perceptions across the public at large. Quantitative surveys, by contrast, often involve 1,000 or more respondents. Their strength, as a tool, lies in the ability to produce a picture of the distribution of perceptions within a population in a country or a region.

One of the most frequently cited sources of information about public perceptions of new biotechnologies is the Eurobarometer surveys. These have been carried out regularly and simultaneously in all EU-member countries, since 1989. Since the Eurobarometers contain a number of core questions which, with small variations, have been included in all surveys, they provide real insight into the longitudinal development of public perceptions of modern biotechnology in Europe. As a supplement – but indeed not as systematically and regularly – interview studies have been carried out. These, however, are often designed to study a specific aspect of modern biotechnology, and this aspect, or topic, is seldom transgenic animals.

Perceptions of Transgenic Animals as an Application of Modern Biotechnology

A number of interesting findings emerge in the Eurobarometer surveys [35–38]. First, the surveys demonstrate that the new biotechnologies are not assessed and rejected, or accepted, en bloc; rather the public makes a balanced judgment about different applications by weighing the relevant pros and cons. One distinct result of the surveys has been the finding that if these pros and cons are categorized as matters of risk, usefulness, and moral concerns, both risks and utilities are important, but moral concerns has a veto-like character [39].

Second, the studies show that perceptions depend on the type of application. Relatively speaking, applications within the medical domain are generally accepted, whereas food-related applications are viewed with considerably more skepticism. Qualitative studies have demonstrated that this differentiation between applications is linked to the kinds of usefulness provided by the different applications [40, 41]. Thus more acceptable applications are seen as useful, in a societal sense, in virtue of their potential contribution to, for example, the alleviation of hunger, human suffering, or environmental problems. The less acceptable applications, by contrast, are generally useful only in an economic way or to the individual.

Within this general picture, it has been found in North America as well as in Europe that applications including transgenic animals tend to be approached with skepticism [41, 42]. In the 1996 and 2002 Eurobarometers, for example, transgenic animals produced for xenotransplantation were, together with GM foods and GM crops, assessed as one of the least acceptable of seven applications [37, 43]. Despite the fact that xenotransplantation belongs to the medical area it is viewed with some skepticism by the public. One explanation of this may be another somewhat consistent finding. This is the existence of an "organism scale" – something not only indicated by the Eurobarometers, but also found in interview studies [41, 42, 44]. On this scale, acceptance is related to the distance (as it were) between the genetically manipulated organism and humans. Apes and some other mammals are located at the top of the scale, and plants and microorganisms are at the bottom. Thus the fact that the use of transgenic animals in xenotransplantation involve organisms (animals) located toward the top of the scale may contribute to the public skepticism.

Perceptions of Transgenic Animals

This section provides more details about the specific concerns present in public perceptions of transgenic animals. The presentation is structured using the now common distinction between risks, usefulness, and ethics/other moral concerns.

Transgenic Animals as a Risk In the sociology of risk, the concept of risk most often refers to any side effect of an action, practice, or technology [45]. Here, however, public perceptions of risks of transgenic animals follow the convention within studies of biotechnology, where risks are solely understood as the (unwanted) consequences for human health and the environment.

The data on transgenic animals as a risk is somewhat limited. Eurobarometer surveys include perceptions of risk related to transgenic animals in 1996 (xenotransplants and research animals) and again in 2002 (xenotransplants). In 1996 as well as in 2002,

almost 60% of the respondents to some extent agreed that the use of transgenic animals in xenotransplantation was risky [43, 46]. It is, however, impossible to determine whether this relatively high perception of risk refers to xenotransplantation as a strategy or to the transgenic animals themselves. The fact that 60% also regarded the less complex question of transgenic research animals as risky in 1996, however, indicates a considerable concern about the risks.

A qualitative study carried out in Denmark in 2002 gives an indication of the worries lying behind this risk perception [44]. First, it was found, during the exploratory interviews, that human health problems arising from the consumption of meat from transgenic or otherwise manipulated animals were not prominent issues. In discussions of GM foods in general, it transpired that there were no particular short-term concerns, mainly because people trusted the authorities and their risk assessments – but also that, by contrast, in the long run, there was some skepticism, partly because participants were not sure if the experts could foresee the long-term risks to human health. Here, references were made to the BSE crisis, which was taken to have demonstrated experts' inability to predict health consequences. In this context, some also raised concerns about the fact that the natural order of things is challenged through the use of modern biotechnologies. This natural, or god-given, order is seen as incorporating an inherent safety mechanism that is bypassed by the use of genetic technology.

Other interview studies have found similarly low levels of concern about the risks associated with the use of transgenic animals in xenotransplantation [47]. The environmental risks also seem to be considered low: essentially, it is believed that it is possible to prevent transgenic animals (unlike microorganisms and plants) from escaping and spreading their genes.

Transgenic Animals and Usefulness As noted above usefulness has several aspects: societal, individual/self-interested, and economic. Within this spectrum, the Eurobarometer surveys aim to determine the level of perceived societal usefulness by asking how useful for society the respondents find different applications. Results show that in both 1996 and 2002, about 60% of the Europeans surveyed judged xenotransplantation useful to society, and in 1996, a somewhat smaller proportion (52%) found transgenic research animals useful. It should be stressed, however, that both applications fall within the medical area, which is known to be generally more acceptable. The interviews in Denmark confirmed this general picture, sometimes pointing to the purpose (e.g., fighting obesity) being noble, but the strategy (e.g., transgenic leaner meat from pigs) wrong, since there are well known and less controversial alternatives (e.g., obesity-curbing diets) that should be pursued first. Interview participants, however, often found themselves trapped in a dilemma between the highly valued principle that transgenic animals must serve a societal purpose, and their own interests; and sometimes this resulted in pragmatic acceptance of applications in their own interest, despite their principled rejection of the same applications.

Transgenic Animals and Other Moral Concerns In most other situations where the human use of animals is on the agenda, animal welfare is a major theme. It is striking that there is little evidence that welfare, conceived of, in the narrow sense, involving a direct effect on the well-being of the animals, is important in public perceptions of transgenic animals. In interview studies this aspect seems to be conspicuous by its absence. Instead, participants raise questions about animal integrity, or about what can be justified with regard to human treatment of animals [39, 44] – a finding that by and large is confirmed by an OECD review from 2008 [48]. In particular, the question of integrity seems to be important in the assessment of transgenic animals, and to contribute to the establishment of the ethical limits to the degree of manipulation that can be exercised over other living beings. Rather than providing final answers to the question of where such limits should be drawn, qualitative studies allow the public to voice questions such as: "Is human life worth more than that of an animal? (. . .) Which is more morally acceptable: waiting for a 17-year-old motorcyclist to die or using a pig as a 'spare parts bin'" [39].

Despite such statements, in which animals are valued as such, a zoo-sociological classification [49] can, it seems, be discerned in the few studies of public perceptions of animal biotechnology. According to this classification of animals, there are different limits to what you can do to different species of animal.

The classification seems to reflect the idea that the closer an animal resembles humans, the better are the reasons (or the greater the usefulness) required to justify manipulating it. Hence, fish are not as important as cows, and cows are less important than primates.

The Ethical Issues

In this section, the ethical concerns typically raised in published discussions of animal biotechnology and in debates in the public sphere will be analyzed. The concerns will be organized into three main categories: risks to humans, risks to animals, and other moral concerns. In this way, the section follows the findings of the sociological studies and can be seen as an attempt to provide an ethical analysis of the values underlying public perceptions of biotechnology at the same time as being an assessment of the kinds of risk the development of transgenic animals present.

It is important to realize that ethical categories do not come out of the blue. The fact that many discussions of transgenic animals center on risks is no coincidence; it reflects the fact that the regulation of biotechnology is cantered on risks, as was mentioned earlier. There are differences in the way biotechnology is regulated in different parts of the world. However, the various regulatory regimes governing transgenic livestock more or less share the following requirements: (1) the livestock must not present a risk to the environment; (2) nor may it present a risk to human health; and (3) nor may it present a risk to animal health. If these three requirements are fulfilled, there is, in most regulatory regimes, no legitimate reason to set up limits to the development and use of transgenic livestock. In light of this regulatory situation, it is no wonder that discussions of transgenic livestock, like discussions regarding other forms of biotechnology, take risk issues as their starting point.

Risks to Humans

The risks to humans are uncontroversial in the sense that everybody involved in the discussion acknowledges that, to the extent that the technology presents serious risks to humans, this is a serious matter. Following the literature on the subject, it can be said that with regard to human health and the environment, transgenic technology so far does not seem to carry significant risks to humans, whereas the socio-economic impact of the technology on such matters as food prices, agricultural production systems, and financial interests are much harder to assess.

Health Risks to humans are most often equated with the risks to human health presented by products from transgenic animals consumed as medicine or food. Only a very limited amount of research has been done in this area, since very few products have been developed. There is, however, a substantial literature on what risks should be taken into consideration when such products are evaluated. In the medical area, it is recommended that the risk assessment should follow the conventional testing of newly developed drugs. In the food area, risks arising from the modification of proteins, allergenicity, toxicology and nutritional value, and so on, will be important parameters [50].

One concern relates to the possibility that the genes transferred might cause allergic reactions in people. If a gene from a plant is transferred into an animal and that gene is responsible for the production of a protein that makes some people allergic to the plant, then that gene could very well make the same people allergic to the meat and/or milk from the animal. There are clearly ways of avoiding the most obvious problems here – by choosing genes that are not known to produce allergenic proteins, or by labeling all products from transgenic animals. But the whole area of food allergy is scientifically complicated, with many unknowns. Basically, it would seem that the risks in this area can be managed, but for each potential product careful consideration will have to be given to the question which genes should be used for modifying which animals [51].

Another issue of importance is whether the physical composition of the food product will change and thus possibly alter the nutritional value of the product. This result could be intentional or unintentional. One might attempt to genetically modify an animal to change the nutritional value of its meat and milk. It could be the amount or composition of fat in pigs, as in the case of the omega-3 pig [52] or the amount of lactoferrin in milk [53]. In such cases, it would be necessary to evaluate how these changes might affect human health in comparison with traditional products. But the changes could be unintended. Thus they might be caused by changes in genes that are not directly linked

to the nutritional value of an animal. Molecular biology is a very complex science that tells that genes are interconnected and seldom work alone. What happens to one gene can have effects elsewhere. Thus changes in genes related, for instance, to the environmental impact of an animal might have unintended side effects in that they also affect its nutritional value. Furthermore, less than perfect methods of gene transfer could also lead to unintended genetic changes. Only through effective testing and control procedures can such problems be countered in a responsible way. As no genetically modified animals have been approved for the agricultural market yet, and since only few have been developed and tested, it is very hard to say precisely how large a risk this is. It should be clear, however, that this issue will need to be addressed on a case-by-case basis. It will depend on the gene inserted and the animal modified, and it will, in all likelihood, be impossible to say anything general about the matter.

One area of biomedicine where it can be foreseen that the technology presents serious risks to humans has attracted attention. This is the xenotransplantation of pig organs. The worry is that dormant viruses in the pig genome could be transferred to humans through the organs and then "awaken" in the new environment in the human host organism, giving rise to a newly emergent disease against which humans have no natural defense. Notorious examples of emergent diseases transferred from animals to humans are the Spanish Flu, AIDS, and Avian Influenza. In the worst-case scenario just one xenotransplantation "gone wrong" could cause a pandemic [54]. The degree of scientific uncertainty here is rather high, as is generally the case in newly emerged fields of research. However, putting problems raised by the transplantation of live tissue from one species to another to one side, at present, the risks to human health presented by transgenic animals seem to be manageable.

The Environment Some of the ethical concerns connected with transgenic livestock relate particularly to the environment. One such concern is that the animals might escape and breed with wild populations, thus spreading their genes in an uncontrollable way. The most cited example here is that of transgenic fish – e.g., salmon with genetic alterations allowing faster growth. The concerns in this area can either be about the indirect consequences this might have for humans (in this case, economic losses to the fishing industry if transgenic fish cause havoc in the wild-living species that are already under pressure from intense fishing), or direct concerns for the animals and the wider ecosystem [51, 55]. With the exception of fish, individual animals produced by biotechnological methods are rather easy to confine, and this makes it less likely that they will be a hazard for the environment. But here, as with most other concerns discussed so far, it will be necessary to evaluate the animals case by case to estimate the risks: in this case, by trying to anticipate how the animals will interact with the environment and whether this will be a threat to human interests.

Other Concerns for Risks to Human Interests Other concerns focus on the socio-economic changes transgenic animals could bring about, especially if they are ever integrated on a large scale into farming and food production. As the technology is not yet developed, let alone introduced, in this area, it is very hard to guess what will happen. But concerns that the technologies will strengthen the movement toward large-scale farming and could deepen the divide between the developed and the developing world are not unrealistic – witness what usually happens when new technology is introduced and what has happened within the sphere of plant biotechnology. For further discussion of these concerns about the impact of biotechnology on agriculture in general [10].

Another kind of concern for humans that is sometimes raised is that the continuing reification or commodification of nature, where nature is seen exclusively as a resource to be used by humans, will harden human ethical sensitivity in general, thus ultimately causing ethical problems between humans as well. This kind of argument has been laid against the unethical use of animals since the dawn of western philosophy – as, for instance, in the work of Thomas Aquinas (*c.* 1225–1274). The key idea is that by being harsh to animals, humans may end up being harsh to their fellow humans. This idea is closely connected to concerns that humans, by turning what is strange and unknown into biological factories, lose an important part of what it is to be a living being that shares the world with other living beings, thus diminishing the human world [56].

In addition to these concerns, it is often suggested that if the applications of biotechnology are accepted on animals, there might be a gradual change of views on these applications and in the end their use on humans would be found acceptable. In this "slippery slope argument" the problem is not the production of transgenic animals in itself (point A), which is seen as ethically acceptable, but the production of transgenic human beings (point B), which is seen as unacceptable and claimed to be at the bottom of an inescapable slide down a moral slope. Thus point A should be avoided, although it is perfectly acceptable in itself, because it automatically leads to point B: a place that it is in no way desirable to be at.

Risks to Animal Welfare

Transgenic technologies used on livestock may cause welfare problems for the animals. As genetic modification means, by definition, the generation of animals of a genotype and phenotype not presently existing, during research and development, it is necessary to make predictions about the health and welfare of these animals, based on what is known about the gene itself and on previous experience with the technology. Genetically modified animals have so far mainly been used in biological research and as disease models. Usually, the goal of modification is to produce animals that either under- or overexpress certain genes, or which express a mutated, disease-causing human gene. In all of these cases, body function in the organism is in some way disrupted. Although the severity varies, welfare problems often accompany these disruptions.

The situation is different with transgenic livestock. Here, there is no *formal* conflict between the objective of the research and the health of the animals: ideally, animals functioning as bioreactors or xenotransplantation donors, as well as transgenic animals in food production, should be healthy. But this is not always the case, and harmful side effects may arise. For example, the "Beltsville pigs" involved in the earliest experiments suffered from extensive health and welfare problems (stress susceptibility, with only marginal improvement of the desired trait, namely growth [57]).

The problems here may arise at different stages in the development of transgenic animals: the in vitro technologies used at the beginning of the process may have a negative impact on early development by disturbing early gene expression. The site of transgene integration is also relevant, as insertional mutations may lead to the loss of host gene function in the "affected" region. This risk is more frequent with those technologies where there is no control over where the transgene integrates. However, it is primarily a problem at the research stage: as such animals are not desirable as so-called "founder animals" for diffusion of the transgene into a wider population, other individuals will be selected for further breeding.

Finally, the level, and the developmental and temporal control of their expression, may mean that proteins, which are the products of transgene expression, cause problems in transgenic animal [58]. Welfare problems deriving from the activity of the transgene itself will affect much larger numbers of animals, because these problems will accompany the gene as it spreads in the population. This could be the case, for example, if animals are engineered to improve production, and if the greater production results in more prevalent production-related diseases.

Systematic welfare assessment schemes in transgenic livestock are still lacking, even though recommendations on this matter were published almost 10 years ago [58] and have been updated more recently [59]. Conclusions about the welfare of transgenic livestock have often been based, not on comprehensive studies, but rather on small-scale, or anecdotal, reports leading scientists to state, for example, that the transgenic animals "have shown no obvious abnormal phenotype" [60], are "apparently normal" [2], or "developed normally" [20].

Welfare Assessment The requirements of welfare assessment schemes in experimental design should reflect the numbers of affected animals at different stages of a transgenic program (first time generation, an increasing number of animals, and establishment of the production herds). In the early stages, with low numbers, predictions of the welfare of the animals will mostly be based on previous experience with the transgene/gene product, if available, in other species (mice); anecdotal information will be essential. As animal numbers increase quantitative research comparing groups of transgenic and control (nontransgenic) animals should be performed. With the establishment of

production herds it will not be possible to monitor the individual animal; therefore, surveillance and sampling of welfare-relevant effects of transgenesis will become more important [59].

Which aspects of the welfare of transgenic animals are assessed will depend to some extent on how animal welfare is defined. Animal welfare scientists typically base their evaluations on the clinical health and subjective experiences of animals [61]. Often, the subjective experience of animals is taken to be expressed in what animals choose. Recently, this approach has been summarized as follows: "Good welfare is defined as animals being healthy and having what they want" [62].

A broader, and complementary, perspective also includes the animal's opportunity to engage in essential species-specific behavior [61, 63, 64]. This broader perspective is related to an even wider set of concerns about animal biotechnology wherein, the anxiety is not that the technology poses risks to animal welfare, but that it violates animal integrity and basic concepts of naturalness. This will be further discussed in section "Naturalness and Integrity".

The Narrow and the Broad Perspective on Animal Welfare From the narrow perspective defined above, a transgenic application is problematic only if it gives rise to health problems or negative subjective experiences. From the broader perspective, the question of animal welfare is also about the extent to which the animal is allowed to fulfill its species-specific potential. The broader perspective thus points to an additional group of considerations that has to be taken into account when reflecting on animal welfare. It should be noted that the two perspectives are not mutually exclusive. Equally, they will often deliver similar recommendations.

Nevertheless, the two kinds of consideration can, on occasion, be difficult to reconcile in practice; and in that eventuality, it becomes important to clarify what kind of perspective is in play. This can be illustrated with two examples.

First, the battery cage in which laying hens are prevented from performing a range of highly motivated behaviors emerged early on as one of the most emblematic issues in the discussion of farm animal welfare. Following many years of intense debate, accompanied by research to develop and evaluate alternative approaches, policy makers have decided to outlaw this housing system, which will be phased out in the EU by the end of 2012. However, if the problem is defined as the frustration of highly motivated behaviors, an alternative (though as yet hypothetical) solution would be to change the birds, so that they become content with the limited life in a battery cage. From a narrow perspective, there is no ethical objection to denying the animal the opportunity to behave as a bird would do in nature (as battery cage egg production does) as long as this does not negatively affect the subjective welfare of the animals, i.e., lead to negative experiences [64]. Therefore, if birds could be caused to lack motivations other than those that could be satisfied in the cage, this would be a good thing to do from the narrow perspective; it would reduce animal suffering in what is, of course, a highly profitable housing system [65, 66].

For the foreseeable future, this seems to be an academic discussion, as the technology is not, as yet, able to produce such animals – if it ever will be. To begin with, the trait to modify would have a complex genetic background, since the objective must be an animal in which one has eradicated all motivations other than those that can be satisfied in a battery cage. Second, it will be a difficult challenge to ensure that one is indeed modifying the animal into one with a restricted set of motivations rather than an animal that reacts passively, or even with apathy, to adverse conditions [67].

From the broader animal welfare perspective, on the other hand, the very idea that hens should be designed to cope well with battery cages raises serious worries and questions about the natural life of chickens, and about the experiences that constitute such a life. Thus even if it is technically possible, this kind of manipulation is highly questionable from the broader perspective.

If the battery cage case was hypothetical, the blind hen case represents a real situation. A Canadian scientist involved in poultry breeding has bred a blind egg-laying hen [68]. The blindness was thus not inflicted on living chickens, but congenital. According to the researchers, blind hens would be at less risk from feather-pecking and cannibalism, these being welfare problems typically found within free-range production systems. Again, from a narrow welfare perspective, this would seem to be a welcome solution to a rather serious welfare problem.

From the broader perspective, both the notion of deliberately breeding chickens that have such limited potential as to be content with life in a battery cage and the aim of breeding blind hens to solve production problems in the agricultural sector are seen as ethically problematic in ways that might outweigh the advantages of these ideas as perceived from the narrow perspective. Something just seems to be amiss when you deliberately create an animal with less potential than normal [69], whether or not the animal has negative experiences as a result. From this perspective, the task is not to change the animals to fit within the limits of the production system, but to adapt the production system to accommodate the needs of the animals. Implicit in this version of the broader perspective is a certain respect for the natural state of the animal.

It should be said, however, that another version of the broader perspective takes a slightly different view. While agreeing that the natural behavior of the animal is to be respected, the advocate of this view does not consider the natural behavior of the animal to be something static. Just as domesticated animals have been bred to be better adapted to housing in confinement in the past, animals today can be bred, either conventionally or through genetic modification, to be better adapted for modern-day production systems. Thus the fact that one can alter the nature of an animal by genetic modification does not constitute an ethical problem as long as one respects the nature that the animal ends up with [65, 66].

Whether animal welfare is seen from the narrow or one of the broader perspectives, the difference between traditional breeding technologies and the new biotechnological tools seems to be more of a quantitative difference in the potential of applications and associated welfare problems than a qualitative difference that creates entirely new welfare issues. The novelty or technological nature of the changes does not in itself introduce new concerns.

Other Ethical Concerns

From the concerns regarding species-specific behavior within the broader perspective, there is a connection to other concerns that are most often treated outside the discussion of animal welfare. These are concerns about the perceived unnaturalness of the technology and possible violations of the integrity of the animals. Rather than being related to the individual animals themselves, these have to do with a more abstract and wider human perception of what an animal is. They can be said to fall within the scope of animal ethics, but outside the scope of animal welfare.

Naturalness and Integrity Technologies involving the genetic modification of animals are often labeled "unnatural" [44, 70]. As discussed previously, there might be differences in the more technical details over how unnatural the animals are in scientific terms. An animal that has had a gene inserted from another species that it would not be able to share genes with is normally seen as more unnatural than an animal which has had an extra gene from its own species inserted. But it is often argued that from a scientific perspective, this is just a matter of degree and not something requiring the label "unnatural" to be placed on products with which it is associated. There seems to be no qualitative differences between what is going on in traditional breeding and modern biotechnologies. The one follows almost logically from the other, and to label one of them "unnatural" would be to label the other likewise [71]. However, not everyone agrees with this conclusion. It has been argued that the fact that traditional breeding methods are already accepted by at least most of the public, does not necessarily mean that the next, much more advanced, step is also acceptable [72]. The growing attention to the welfare of animals produced through transgenic technologies might even serve as reason to look back on already established, and hitherto innocent, methods of animal breeding with critical eyes [34].

Another criticism of the term "unnatural" is that, although it is intuitively compelling, the normative impact of naturalness suffers from three inherent ambiguities when applied to domesticated animals. First of all, it is almost impossible to point to a stage in the development of such animals that would constitute their natural state and thus be the developmental point that should be respected [64]. Second, even without human interference, animals evolve to adapt to changing environments. Claiming that it is unnatural to change the genomes of animals can therefore, from a scientific point of view, be seen as saying that nature is unnatural. Finally, it needs to be explained why it is

assumed that what is natural is also ethically good. Cancer, earthquakes, and influenza are naturally occurring phenomena, but very few would, for that reason, deem them to be ethically good. For reasons such as these, the notion of naturalness is very often rejected as unclear and insignificant to the ethical debate [73].

These criticisms are very relevant. However, they might be seen as utterly failing to address the fundamental issues at stake in ethical debate about unnaturalness. There seem to be two different viewpoints from which the technologies can be discussed. As Anne Chapman has pointed out, the debate around unnaturalness and biotechnology tends to operate with only two very distinct concepts of nature. Nature is seen either as everything there is (leaving nothing to be unnatural) or as everything that is untouched by humans (in which case all things touched by human activity become unnatural). What is lacking is a middle ground that takes into account the fact that, from an everyday perspective, most people experience the naturalness of things as a gradually developing quality: things can be more or less natural [74]. This difference can very well be expressed in terms of the degree of control that humans exercise over natural processes. Here, it becomes obvious that although the genetic inheritance of animals is changed both through conventional breeding and through transgenic technologies, the latter, being more powerful, are more unnatural.

This understanding of the difference between natural and unnatural as being determined basically by the extent of human control can also be used as an interpretative key that helps to clarify the concerns underlying the claim that transgenic technologies violate the *integrity* of animals.

There are several definitions of the concept of animal integrity available, yet it seems that the notion still eludes clear understanding. The word is derived from the Latin "integer" meaning *wholeness, completed, untouched, unharmed.* Rutger and Heeger [75] define animal integrity as the "wholeness and intactness of the animal and its species-specific balance, as well as the capacity to sustain itself in an environment suitable to the species." De Vries [76] interprets this definition as one mainly aiming at physical, biological, or genetic wholeness. To a large extent, violations of animal integrity will therefore also violate the welfare of the animal [77]; and they will do so irrespective of whether animal welfare is understood from the narrow or one of the broad perspectives.

What is of special interest here, however, is whether practices that do not produce ill health, negative mental states in the animal, or prevent the animal from performing its species-specific behavior can also be seen as violation of integrity. An example, already discussed above, would be breeding animals that fits the production systems better rather than developing housing systems that satisfy the existing behavioral needs of the animals [66]. Again, one might consider changes of composition in dairy cow milk to mimic the content of human milk [78].

The debate about what integrity is, and why it is relevant, mimics the debate about naturalness in important ways. The concept of integrity is often (as in the definition proposed by Rutger and Heeger [75]) tied tightly to biological, empirical features such as behavior, the possession of an unaltered genome, and so on. The concept is then often criticized and questioned, since it makes it unclear why the integrity is especially violated through biotechnology [79].

The notion of integrity is perhaps better understood as one expressing the ethical reservations some experience when animals are commodified to an extent where the distinction between unnatural and natural breaks down, or where the power humans exercise on the animal leaves the animal as nothing more than a resource to fulfill human needs. Integrity is thus something that is experienced directly, but something also that shows up when there is a violation of it [80]. It is experienced in a phenomenological understanding of the animal – not reducing it to an object for examination or a resource to be developed, but affirming the notion of it as another "flesh-of-the-world" entity [81] sharing a "more-than-human-lifeworld" [56] with humans and all the other members of the biotic community. The claim is then that the integrity of the animal is present at this level of experience as the "completeness" of the animal before humans show up with their ability to change animals into something that can satisfy human needs. Self-evidently, an animal can be killed, but life cannot be breathen back into it. In essence, integrity is the experience that the animal is whole, complete, full, finished, when humans encounter it. Humans cannot add to it, only take away [82].

When developed along these lines, the concept of integrity loses it biological foundations and thus becomes impossible to assess from a scientific point of view. Some will probably find that the prescientific nature of the concept disqualifies it automatically; others might find that by interpreting integrity as a "zone of untouchableness" given by the sheer existence of the animal, the moral concerns about interfering in the lives of animals can be seen to make sense, even if they go beyond the animal's welfare interests.

Respect for Autonomy As has already been mentioned, current legislation in most countries is set up to permit transgenic livestock only if this does not pose a risk to the environment and to the animals' health; and to ensure that products originating from transgenic livestock will be allowed to enter the food chain only if they pose no risk to human health. As should be clear from the above analysis, a number of reasons why people might be skeptical about transgenic livestock can be described, and some of these will go beyond what is captured by legislation. First, some people will assess risks differently from the experts giving advice to the authorities. Second, some people will have a wider notion of what counts as a risk than that embedded in the legislation. Finally, third, some people may have moral concerns that go beyond the risk paradigm as shown earlier.

In light of this, one can ask to what extent people should have choice when they buy animal-based products. According to current legislation in the US, there is no requirement to label products derived from GM animals, whereas current EU legislation requires such products to be labeled. Here, then there will be room for a genuine ethical disagreement about whether consumers have the right to be told about the origin of animal products – and retain this right whether or not the products pose a risk. Those opposed to mandatory labeling will typically argue that such labeling may cause unfounded fears in consumers, whereas those in favor of it may argue that consumers ought to have the right to choose for themselves in line with what matters to them; and opinion polls seem to show that many consumers want to know whether or not food products are genetically modified [83].

Public Discussions

The advent of modern biotechnologies, and subsequent ethical debate, has been closely followed by a number of stakeholders: researchers, the biotech industry, politicians devising the legislative framework, NGOs within the areas of environmentalism, animal welfare, animal rights, and so forth. From the outset, it has been clear that the technologies raise ethical issues and that it is necessary to debate these. Equally, after the controversies surrounding the introduction of GM crops and products based on these crops in Europe in the 1990s, it became glaringly apparent that there was widespread skepticism about biotechnology, and that it would be necessary to create some kind of dialogue between stakeholders in the public sphere.

In this section, it is discussed how different motivations for entering this dialogue shape the dialogue itself and the subjects that are deemed relevant within it. As should be apparent from the analysis of ethical concerns provided above, it is not a shortage of subjects to talk about that characterizes the area. As in the section on public perceptions of transgenic animals, it has been necessary to widen the scope and look at the issue at a more general level to capture the trends in the discussions. There is, however, little reason to doubt that ethical discussion of the issues raised by transgenic animals will follow the pattern seen so far in adjacent technologies.

Public Participation and Dialogue

Today "dialogue with the public" is almost a mantra within the biotech community – a community that can be said to consist of all stakeholders, from the most jubilant adherents of the technologies to the most fundamentalist skeptics. The idea of public participation in the preparation of policies for emerging technologies such as biotechnology is very widely accepted. But whereas the general idea of public participation and the concept of dialogue are almost universal within the western world, the content of these notions is far from self-evident [84].

Quite what is meant by "public participation" can, generally speaking, be said to be decided by the reasons for supporting such participation in the first place. There seems to be a continuum from, on the one hand, those who support public participation because

it is a way of assuring the public of some sort of democratic or semi-democratic influence, to those who see public participation as a way of merely legitimizing the technologies in the eyes of the public. In the first case, the goal is to live up to democratic ideals of some sort without influencing the result of the participation. In the second, the point is to get the technologies accepted [85].

The influence of the goal of the public participation on the structure of the debate can most easily be seen when the concept of *dialogue* is considered. There seem to be three different understandings of the concept of dialogue in ethical discussions of biotechnology today. One is (1) a specific variety of (so to speak) *monological* dialogue. This assumes that widespread skepticism about biotechnology is based on the public's lack of knowledge and understanding of the technologies. The remedy to this is therefore knowledge transfer from the sphere of science to the public. As soon as public has been educated the skepticism will disappear.

This way of thinking, sometimes labeled "the knowledge deficit model" [86], is very widespread in the scientific community. One noteworthy example of it can be found in the report *Why clone farm animals? Goals, motives, assumptions, values and concerns among European scientists working with cloning of farm animals* [87]. Here, a group of scientists working on cloning are interviewed about the technology and various aspects of it. All say that it is very important to establish a dialogue with the public about the technology, but when directly asked what subjects would be suited for such a dialogue, they invariably answer that the public should be provided with information about the technology.

The largest problem with the knowledge deficit model is that, although it continues to thrive within the scientific community, it has been refuted in sociological studies of the public perceptions of biotechnology. What happens when citizens are provided with information about the science and possible applications is that they form an opinion about it; but there is no evidence to suggest that knowledge in general erases skepticism [44].

(2) A second form of dialogue is as monological as the first, but the exchange moves in the opposite direction – it is the public rather than the scientists now doing all the talking. Here, the task is to examine public attitudes to biotechnological applications and figure out which will be socially acceptable. The goal is thus to ensure that the technologies pursued will not end up in the same situation as the GMOs in Europe in the 1990s. Very often, the two monological kinds of dialogue are combined, so that consumer preferences and consumer education go hand-in-hand in an attempt to produce social acceptance for the development of the technologies [85].

(3) The third concept of dialogue in the current debate sees dialogue as a way of balancing two very important considerations. One consideration is to respect the other person, whether it is a single person, a group of stakeholders, or society at large. The other is to take responsibility for one's own views of the world and attempt to do what one sincerely believes to be in the best interest of the other (whoever that may be). A classic example of this conflict can be found in the relationship between the physician and the patient. The ethical duty for the physician is to avoid taking all responsibility from the patient (paternalism as tyranny) and yet not leave the patient on his own in trying to decide upon different methods of treatment in the mistaken belief that the task of a physician is just to provide neutral information and at all costs respect the patient's right to self-determinacy (autonomy as denial of responsibility).

The concept of dialogue implies that there are two or more opinions about something, and that the people holding these opinions are willing to discuss them, holding a small window open in the back of their minds to the possibility that they may be wrong. A dialogue where it is from the outset decided that only one part of the dialogue (and that is usually the other part) could end up changing their minds is no dialogue, but could better be described as a caricature of energetic and zealous religious proselytizing.

When promoting public participation in the debates about such things as transgenic animals, it is important to realize that this is always done with a specific goal in mind – and that this goal will always influence the way the dialogue is structured. Similarly, the motivation for entering the dialogue in the first place will influence views on what questions are relevant and who should participate. These differences are also visible within different cultures where, for example, the role of the scientists and nonexperts in the

debates are understood very differently, just as the purpose of the whole exercise is understood quite differently [88].

Possible Goals of Ethical Dialogues

Motivation for entering ethical discussion of biotechnology in general and transgenic livestock in particular varies from stakeholder to stakeholder, although it is probably safe to say that all stakeholders enter the discussion because they think that the information they can bring will convince others of their viewpoints [73]. But besides the urge to win the argument, there are other and more realistic goals of ethical dialogue, and these could provide reasons for entering in the first place.

The first reason is enlightenment or clarification. Ethical debates are where humans meet and exchange their views. This gives the involved parties a chance to explain their views and listen to the explanations of others. Thus the areas of disagreement and the values that underlie them can both be clarified. This need not lead to agreement, of course; it will only do so if some of the disagreements turn out to be based on misunderstandings either of the viewpoints of the opponent or the facts of the issue. But it can lead to a better understanding of the opponent's viewpoints; and that is valuable in itself. It is valuable, first and foremost, because understanding is itself valuable, and second, because it is easier to find areas of consensus and compromise if you have an understanding of the viewpoints of others rather than just finding them irrational or blind to the ethical dimensions of the issue. Understanding why someone has certain opinions makes it easier to respect him or her, and it can create an environment around the debate that makes it easier to move on to the next step [89].

The second possible result of ethical debates is that the decisions eventually reached are socially robust. A socially robust decision is here understood as a decision that seeks to include widely held concerns about a technology while at the same time allowing it to progress in areas that are of significant benefit to society. As mentioned earlier in section "Public Perceptions of Transgenic Technologies," it is apparent from sociological studies that, in biotechnology, there are two scales of importance. One is the scale of organism, the other a scale of applications. The simpler the organism, the more acceptable the technologies become; and the more the application of the technology addresses issues like health, the environment, and aid to the developing world, the more acceptable it becomes [44]. Thus using transgenic technologies to produce livestock that will benefit medical research will, in all likelihood, be more socially acceptable than producing livestock that can improve productivity in agriculture.

By targeting on areas of need, developments in transgenic livestock would therefore be less problematic than they would be if the focus was on areas of economic gain. A socially robust development process will mean that certain applications are left aside in order to gain broad societal acceptance of the progress of the technologies [90].

Future Directions

The technology to produce transgenic animals is here to stay. The genie cannot be put back in the bottle. And as the technology is further developed and refined, it will, in all likelihood, become more and more economically feasible and sustainable to produce animals through these technologies. But the ethical problems will not disappear either. The issue of animal welfare as seen from a narrow perspective will continue to play a role, as will the issues around possible negative impacts on human health and the environment. Even when more data on these risks become available, it should be obvious from the discussion of GM crops that the risk evaluation will continue to be an area of controversy for many years to come.

Discussion of the socio-economic impact of the technologies will intensify. If the animals enter the agricultural sector and the food production chain, there is reason to expect that they will only strengthen the current trends within agriculture, where ever larger units with animals dominate production in a highly technological environment. This will inevitably give rise to ethical debate – but probably debate of a sort that is already taking place about how the agricultural production system should function. In the areas of naturalness and integrity, ethical disagreement will continue to flourish, especially if animals are produced for applications that are not generally regarded as important to society.

All in all, then, it is safe to say that ethical debate about transgenic livestock, and about the development of the technology, will continue to play a significant role in the future. As research and technology development becomes more and more reliant on private funding, it will be necessary to show that the development of transgenic animals will pay off investors. Finally, there is no doubt that the area will continue to be a political and ideological battle scene. It will therefore be necessary to apply methods of public participation that include many viewpoints. These methods should help to ensure socially robust development in a technology, for which the potential to create social and ethical conflicts seem as large as the technological potential.

Bibliography

1. Clark J, Whitelaw B (2003) A future for transgenic livestock. Nat Rev Genet 4:825–833
2. Laible G (2009) Enhancing livestock through genetic engineering – recent advances and future prospects. Comp Immunol Microbiol Infect Dis 32:123–137
3. Lacy WB, Lacy LR, Busch L (1988) Agricultural biotechnology research: practices, consequences, and policy recommendations. Agric Hum Values 5(3):3–14
4. Baile CA, Krestel-Rickert DH (1988) Will society permit the potential of genetic engineering to advance the frontiers of biology? J Anim Sci 66:2125–2130
5. Fox MV (1989) Genetic engineering and animal welfare. Appl Anim Behav Sci 22(2):105–113
6. Gavora JS, Lister EE (1989) Practical and ethical considerations of agricultural research assistance for the third world. J Agric Environ Ethics 2(4):307–322
7. Wilmut I, Schnieke AE, McWhir J, Kind AJ, Campbell KH (1997) Viable offspring derived from fetal and adult mammalian cells. Nature 385:810–813
8. Cooper DKC, Dorling A, Pierson RN III, Rees M, Seebach J, Yazer M, Ohdan H, Awwad M, Ayares D (2007) [Alpha]1, 3-galactosyltransferase gene-knockout pigs for xenotransplantation: where do we go from here? Transplantation 84(1):1–7
9. Kling J (2009) First US approval for a transgenic animal drug. Nat Biotechnol 27:302–304
10. Thompson PB (1997) Food biotechnology in ethical perspective. Blackie Academic & Professional, London
11. Gamborg C, Gjerris M (2009) The price of responsibility. In: Gjerris M, Gamborg C, Olesen JE, Wolf J (eds) Earth on fire. Climate change from a philosophical and ethical perspective. University of Copenhagen, Copenhagen, Open access. Available at www.earthonfire.foi.dk
12. European Commission (2001) Directive 2001/18/EC of the European Parliament and of the Council of 12 March 2001 on the deliberate release into the environment of genetically modified organisms and repealing Council Directive 90/220/EEC – Commission Declaration. European Commission, Brussels
13. Houdebine LM (2009) Methods to generate transgenic animals. In: Engelhard M, Hagen K, Boysen M (eds) Genetic engineering in livestock: new applications and interdisciplinary perspectives. Springer-Verlag, Berlin, pp 31–48
14. Lai L, Kolber-Simonds D, Park KW, Cheong HT, Greenstein JL, Im GS, Samuel M, Bonk A, Rieke A, Day BN, Murphy CN, Carter DB, Hawley RJ, Prather RS (2002) Production of α-1,3-galactosyltransferase knockout pigs by nuclear transfer cloning. Science 295(5557):1089–1092
15. Niemann H, Kues W, Carnwath JW (2007) Transgenic farm animals: current status and perspectives for agriculture and biomedicine. In: Engelhard M, Hagen K, Boysen M (eds) Symposium on new application of livestock genetic engineering. Springer-Verlag, Berlin, pp 1–30
16. Gordon JW, Scangos GA, Plotkin DJ, Barbosa JA, Ruddle FH (1980) Genetic transformation of mouse embryos by microinjection of purified DNA. Proc Natl Acad Sci USA Biol Sci 77:7380–7384
17. Hammer RE, Pursel VG, Rexroad CE, Wall R, Bolt DJ, Ebert KM, Palmiter RD, Brinster RL (1985) Production of transgenic rabbits, sheep and pigs by microinjection. Nature 315:680–683
18. Kong QR, Wu ML, Huan YJ, Zhang L, Liu HY, Bou G, Luo YB, Mu YS, Liu ZH (2009) Transgene expression is associated with copy number and cytomegalovirus promoter methylation in transgenic pigs. PLoS ONE 4:10
19. Le Provost F, Lillico S, Passet B, Young R, Whitelaw B, Vilotte JL (2009) Zinc finger nuclease technology heralds a new era in mammalian transgenesis. Trends Biotechnol 28:134–141
20. Niemann H, Kues W, Carnwath JW (2005) Transgenic farm animals: present and future. Rev Sci Tech 24(1):285–298
21. Blasco A (2008) The role of genetic engineering in livestock production. Livest Sci 113:191–201
22. Foresti F (2000) Biotechnology and fish culture. Hydrobiologia 420:45–47
23. Zbikowska HM (2003) Fish can be first – advances in fish transgenesis for commercial applications. Transgenic Res 12:379–389
24. Rasmussen RS, Morrissey MT (2007) Biotechnology in aquaculture: transgenics and polyploidy. Compr Rev Food Sci Food Saf 6:2–16
25. Kelly L (2005) The safety assessment of foods from transgenic and cloned animals using the comparative approach. Rev Sci Tech 24:61–74
26. Wall RJ (1996) Transgenic livestock: progress and prospects for the future. Theriogenology 45(1):57–68
27. Wolf E, Schernthaner W, Zakhartchenko V, Prelle K, Stojkovic M, Brem G (2000) Transgenic technology in farm animals – progress and perspectives. Exp Physiol 85:615–625
28. Niemann H, Kues WA (2003) Application of transgenesis in livestock for agriculture and biomedicine. Anim Reprod Sci 79:291–317
29. Wheeler MB (2007) Agricultural applications for transgenic livestock. Trends Biotechnol 25:204–210

30. Bremel RD, Homan EJ, Howard TH (2001) Current and future promises of transgenesis for agricultural livestock in a global marketplace. J Dairy Sci 84:E1–E8
31. Prather RS (2006) Cloned transgenic heart-healthy pork? Transgenic Res 15:405–407
32. Hallerman EM, McLean E, Fleming IA (2007) Effects of growth hormone transgenes on the behaviour and welfare of aquacultured fishes: a review identifying research needs. Appl Anim Behav Sci 104:265–294
33. Nightingale P, Martin P (2004) The myth of the biotech revolution. Trends Biotechnol 22(1):564–569
34. Gjerris M, Olsson A, Sandøe P (2006) Animal biotechnology and animal welfare. In: Council of Europe (ed) Ethical eye – animal welfare. Council of Europe, Strasbourg, pp 8–110
35. Durant J, Bauer J, Gaskell G (1998) Biotechnology in the public sphere. Science Museum, London
36. Gaskell G, Bauer M (2002) Biotechnology 1996–2000: the years of controversy. Science Museum, London
37. Gaskell G, Allum N, Stares S (2003) Europeans and biotechnology in 2002. Eurobarometer 58.0
38. Gaskell G, Allansdottir A, Allum N, Corchero C, Fischler C, Hampel J, Jackson J, Kronberger N, Mejlgaard N, Revuelta G, Schreiner C, Stares S, Torgersen H, Wagner W (2006) Europeans and biotechnology in 2005: patterns and trends. Eurobarometer 64.3
39. Wagner W, Kronberger N, Allum N, Cheveigné de S, Diego C, Gaskell G, Heinßen M, Midden CJH, Ødegaard M, Öhman S, Rizzo B, Rusanen T, Stathopoulou A (2002) Pandora's genes – images of genes and nature. In: Bauer MW, Gaskell G (eds) Biotechnology. The making of a global controversy. Cambridge University Press, Cambridge, pp 244–276
40. Lassen J, Jamison A (2006) Genetic technologies meet the public: the discourses of concern. Sci Technol Hum Values 31(1):8–28
41. Einsiedel EF (2005) Public perceptions of transgenic animals. Rev Sci Tech 24(1):149–157
42. Frewer LJ, Howard C, Shepherd R (1997) Public concerns in the United Kingdom about general and specific applications of genetic engineering: risk, benefit, and ethics. Sci Technol Hum Values 22(1):98–124
43. Gaskell G, Bauer MW, Durant J (1998) Public perceptions of biotechnology in 1996: eurobarometer 46.1. In: Durant J, Bauer MW, Gaskell G (eds) Biotechnology in the public sphere. A European sourcebook. Science Museum, London, pp 189–214
44. Lassen J, Gjerris M, Sandøe P (2006) After dolly – ethical limits to the use of biotechnology on farm animals. Theriogenology 65:992–1004
45. Beck U (1992) Risk society. Towards a new modernity. Sage, London
46. European Commission (2002) Eurobarometer 58.0. European Commission
47. Dahl K, Sandøe P, Johnsen PF, Lassen J, Hansen AK (2003) Outline of a risk assessment: the welfare of future xeno-donor pigs. Anim Welfare 12:219–237
48. Rigaud N (2008) Biotechnology: ethical and social debates. OECD, Paris
49. Arluke A, Sanders CR (1996) Regarding animals. Temple University Press, Philadelphia
50. National Research Council and Institute of Medicine of the National Academies (2004) Safety of genetically engineered foods. Approaches to assessing unintended health effects. National Academy of Science, Washington
51. The Royal Society of Canada (2001) Elements of precaution: recommendations for the regulation of food biotechnology in Canada. An expert panel report on the future of food biotechnology. The Royal Society of Canada, Ottawa
52. Lai L, Jing X, Kang X, Li R, Wang J, Witt WT, Yong HY, Hao Y, Wax DM, Murphy CN, Rieke A, Samuel M, Linville ML, Korte SW, Evans RW, Starz TE, Prather RS, Dai Y (2006) Generation of cloned transgenic pigs rich in omega-3 fatty acids. Nat Biotechnol 24:435–436
53. Wall RJ, Kerr DE, Bondioli KR (1997) Transgenic dairy cattle: genetic engineering on a large scale. J Dairy Sci 80(9):2213–2224
54. Fishman JA, Patience C (2004) Xenotransplantation: infectious risks revisited. Am J Transplant 2004(4):1383–1390
55. PEW Initiative on Food and Biotechnology (2003) Future fish. Issues in science and regulation of transgenic fish. PEW Initiative on Food and Biotechnology, Washington
56. Abram D (1996) The spell of the sensuous. Vintage Books, New York
57. Pursel VG, Pinkert CA, Miller KF, Bolt DJ, Campbell RG, Palmiter RD, Brinster RL, Hammer RE (1989) Genetic engineering of livestock. Science 244:1281–1288
58. Van Reenen CG, Meuwissen THE, Hopster H, Oldenbroek K, Kruip TAM, Blokhuis HJ (2001) Transgenesis may affect farm animal welfare: a case for systematic risk assessment. J Anim Sci 79:1763–1779
59. Van Reenen CG (2007) Assessing the welfare of transgenic farm animals. In: Engelhard M, Hagen K, Boysen M (eds) Symposium on new application of livestock genetic engineering. Springer-Verlag, Berlin, pp 119–143
60. Wheeler MB (2002) Production of transgenic livestock: promise fulfilled. In: Sixth international workshop on the biology of lactation in farm animals, Quebec, 2002. American Society of Animal Science, pp 32–37
61. Duncan IJH, Fraser D (1997) Understanding animal welfare. In: Appleby MC, Hughes BO (eds) Animal welfare. CAB International, Wallingford, pp 19–31
62. Dawkins MS (2004) Using behavior to assess welfare. Anim Welfare 13:3–7
63. Fraser D, Weary DM, Pajor EA, Milligan BN (1997) A scientific conception of animal welfare that reflects ethical concerns. Anim Welfare 6:187–205
64. Appleby MC, Sandøe P (2002) Philosophical debate on the nature of well-being: implications for animal welfare. Anim Welfare 11(3):283–294
65. Rollin BE (1995) Frankenstein syndrome: ethical and social issues in the genetic engineering of animals. Cambridge University Press, Cambridge

66. Shriver A (2009) Knocking out pain in livestock: can technology succeed where morality has stalled? Neuroethics 2(3):115–124
67. D'Eath RB, Conington J, Lawrence AB, Olsson IAS, Sandøe P (2010) Breeding for behavioural change in farm animals: practical, economic and ethical considerations. Anim Welfare 19(5):17–27
68. Ali A, Cheng KM (1985) Early egg production in genetically blind (rc/rc) chickens in comparison with sighted (Rc+/rc) controls. Poult Sci 64(5):789–794
69. Lassen J, Sandøe P, Forkman B (2006) Happy pigs are dirty! – conflicting perspectives on animal welfare. Livest Sci 103(3):221–230
70. Verhoog H (2003) Naturalness and the genetic modification of animals. Trends Biotechnol 21(7):294–297
71. Sandøe P, Holtug N, Simonsen HB (1996) Ethical limits to domestication. J Agric Environ Ethics 19(5):469–493
72. Task Group on Public Perceptions of Biotechnology (1999) Ethical aspects of agricultural biotechnology. European Federation of Biotechnology, Den Haag
73. Reiss MJ, Straughan R (2000) Improving nature. The science and ethics of genetic engineering. Cambridge University Press, Cambridge
74. Chapman A (2005) Genetic engineering: the unnatural argument. Techné 9(2):81–93
75. Rutger B, Heeger R (1999) Inherent worth and respect for animal integrity. In: Dol M, van Vlissingen MF, Kasanmoentalib S, Visser T, Zwart H (eds) Recognizing the intrinsic value of nature. Van Gorcum, Assen, pp 41–53
76. De Vries R (2006) Genetic engineering and the integrity of animals. J Agric Environ Ethics 19(5):469–493
77. Vorstenbosch J (1993) The concept of integrity. Its significance for the ethical discussion on biotechnology and animals. Livest Prod Sci 36:109–112
78. Gottlieb S, Wheeler MD (2008) Genetically engineered animals and public health: compelling benefits for health care, nutrition, the environment, and animal welfare. BIO – The Biotehnology Organisation, Washington
79. Bovenkerk B, Brom FWA, Van Den Bergh BJ (2002) Brave new birds: the use of 'animal integrity' in animal ethics. Hastings Cent Rep 32:16–22
80. Cooper DE (1998) Intervention, humility and animal integrity. In: Holland A, Johnson A (eds) Animal biotechnology and ethics. Chapman & Hall, London, pp 145–155
81. Merleau-Ponty M (1969) The visible and the invisible. Northwestern University Press, Evanston
82. Løgstrup KE (1995) Vidde og prægnans. Sprogfilosofiske betragtninger. Metafysik I. 2. udg. Gyldendal, København
83. Roosen J, Lusk JL, Fox JA (2001) Consumer demand for and attitudes toward alternative beef labeling strategies in France, Germany, and the UK. Agribusiness 19(1):77–90
84. Nielsen AP, Lassen J, Sandøe P (2004) Involving the public – participatory methods and democratic ideals. Glob Bioeth 17:191–201
85. Gjerris M (2008) The three teachings of biotechnology. In: David K, Thompson P (eds) What can nanotechnology learn from biotechnology? Elsevier, Burlington, pp 91–106
86. Bauer MW, Bonfadelli H (2002) Controversy, media coverage and public knowledge. In: Bauer MW, Gaskell G (eds) Biotechnology. The making of a global controversy. Cambridge University Press, Cambridge, pp 149–175
87. Meyer G (2005) Why clone farm animals? Goals, motives, assumptions, values and concerns among European scientists working with cloning of farm animals, Project report 8. Danish Centre for Bioethics and Risk Assessment, Frederiksberg
88. Nielsen AP, Lassen J, Sandøe P (2007) Democracy at its best? The consensus conference in a cross-national perspective. J Agric Environ Ethics 20:13–35
89. Gjerris M (2009) This is not a hammer – on ethics and technology. In: Bedau M, Parke E (eds) Our future with protocells: the social and ethical implications of the creation of living technology. MIT Press, Boston, pp 291–306
90. Gjerris M, Sandøe P (2006) Farm animal cloning: the role of the concept of animal integrity in debating and regulating the technology. In: Kaiser M, Lien ME (eds) Ethics and the politics of food: preprints of the 6. Congress of the European Society for Agricultural and Food Ethics. Academic, Wageningen, pp 320–324
91. van de Lavoir MC, Mather-Love C, Leighton P, Diamond JH, Heyer BS, Roberts R, Zhu L, Winters-Digiacinto P, Kerchner A, Gessaro T, Swanberg S, Delany ME, Etches RJ (2006) High-grade transgenic somatic chimeras from chicken embryonic stem cells. Mech Dev 123:31–41

Transgenic Technologies and Increased Livestock Fertility

F. Xavier Donadeu, Cheryl J. Ashworth
The Roslin Institute and Royal (Dick) School of Veterinary Studies, University of Edinburgh, Scotland, UK

Article Outline

Glossary
Definition of the Subject and Its Importance
Introduction
The Problem of Low Fertility in Modern Livestock
The Need and Potential of Transgenic Technologies to Improve Reproductive Performance of Livestock Species
Potential Targets for Transgenic Improvement of Livestock Fertility
Future Directions
Bibliography

Glossary

Bone morphogenetic proteins (BMPs) Group of molecules belonging to the transforming growth factor family that were initially discovered by their ability to induce the formation of bone and cartilage. BMPs provide pivotal morphogenetic signals orchestrating tissue architecture throughout the body.

Calving The act of delivering a calf at the end of normal bovine pregnancy.

Energy balance In reference to animal physiology, it is the relation between energy intake from nutrient consumption and energy expenditure to maintain body functions.

Estrus The stage of the estrous cycle when a female is sexually receptive and during which ovulation occurs.

Fertility The ability to produce healthy offspring.

First-service conception rate Refers to the percentage of animals in a herd that become pregnant upon insemination on the first estrous cycle after parturition.

Genetic selection/selective breeding The process of breeding animals or plants with the goal of enhancing particular genetic traits.

Heterozygous Refers to an individual having two different alleles for a given trait.

Homozygous Refers to an individual having identical paternally and maternally inherited alleles for a given trait.

Knockin Integration of a new gene which replaces an endogenous gene.

Knockout Functional disruption of a specific gene of an organism, commonly achieved by a partial or complete deletion of the gene sequence.

Livestock Domesticated animals raised to produce commodities such as food, fiber and labor.

Mutation A change in the DNA sequence of a gene which can result in changes in the sequence and function of the encoded protein.

Ovarian follicle The structural and functional unit in the ovary within which an oocyte grows and matures until it is expelled during ovulation.

Ovulation The process by which mature ovarian follicles rupture under the influence of luteinizing hormone to release an oocyte into the oviduct.

Phenotype/phenotypic A measurable characteristic of an animal such as hair color or growth rate, and which is the product of genetics and the environment.

Point mutation A mutation involving a single nucleotide base pair in a DNA sequence.

Production trait A genetically determined characteristic of an individual of a livestock species which relates to its capacity to provide a certain product (milk, meat, fiber, eggs, work) which contributes directly to the value of the animal for the farmer.

Promoter A regulatory DNA sequence that controls the transcription of a particular gene.

Reproductive performance The productivity of an animal or herd in terms of offspring produced.

Reproductive/breeding efficiency Related to the capacity of an individual to successfully carry out all reproductive processes from gamete formation to fertilization, establishment of pregnancy and delivery of healthy offspring.

Seasonal reproduction Refers to the dependence of reproductive activity on seasonal factors, most notably changes in day length, in certain species.

Single nucleotide polymorphism DNA sequence variations involving alteration of a single nucleotide in a genome sequence.

Transgene An exogenous gene introduced into the genome of another organism.

Transgenic An animal, plant or microbe whose genetic material has been altered using an artificial process.

Zinc finger nucleases (ZFNs) Synthetic proteins consisting of an engineered DNA-binding motif characterized by multiple finger-like protrusions (finger domain) and which has been fused to the cleavage domain of the *FokI* restriction endonuclease. ZFNs can be used to induce double-stranded breaks in specific DNA sequences and thereby promote site-specific homologous recombination and targeted manipulation of genomic loci in a variety of different cell types.

Definition of the Subject and Its Importance

The possibility of using transgenic technology to promote desirable traits, including enhanced reproductive efficiency, in livestock species has attracted

considerable interest since transgenic animals were first produced. Almost 20 years ago McEvoy and associates [1] proposed that transgenic technologies could be used to increase reproductive output in food producing animals by increasing litter size in livestock or egg-laying capacity in poultry, and by reducing the limitations associated with seasonal breeding. During the intervening 2 decades, the uptake of transgenic technologies in livestock production has been limited because of technical, regulatory and ethical constraints [2]. However, the availability of novel technologies, such as Zinc finger nucleases (ZFNs) [3], which allow for greater precision and control, together with a growing need to increase livestock productivity to meet the requirements of a growing world population will likely help to realize current aspirations on use of transgenesis in animal reproduction. The application of transgenic technologies in laboratory animals has been invaluable in considerably furthering our understanding of numerous reproductive processes including gonad development and function [4–6], oogenesis and early embryogenesis [7, 8], and trophoblast gene function [9, 10], and through this increased understanding will lead to new strategies to improve reproductive efficiency of livestock species.

Introduction

Reproductive efficiency of domestic animals is critical to the sustainability of modern livestock industries. Thousands of years of domestication led to changes in the reproductive physiology of animals, for example, a dramatic reduction in the influence of season on reproduction in cattle and pigs. During modern times, intensification of farming systems coupled with the implementation of programs of genetic improvement aimed at selection for specific (non-reproductive) productivity traits had further effects on reproductive physiology often with negative consequences to breeding efficiency, with ultimately an impact on the overall productivity and sustainability of livestock industries. Meeting the increasing world demands for animal products will require increased production of healthy offspring from livestock while coping with a decrease in the availability of natural resources to maintain these animals. Achieving this within a reasonable time frame will require the use of strategies alternative, or in addition, to traditional breeding and genetic selection. This entry will describe current limitations in reproductive performance of livestock. The potential and limitations of transgenic technologies to address such problems will then be described and specific illustrative examples will be provided.

The Problem of Low Fertility in Modern Livestock

At its 2009 World Food Summit, the United Nations Food and Agricultural Organization recognized that agricultural output will need to increase by 70% by 2050 in order to feed the world's population which is expected to exceed 9 billion in this timeframe (FAO 2009, ftp://ftp.fao.org/docrep/fao/Meeting/018/k6050e.pdf). A significant portion of that output will be derived from the demand for animal protein, especially in developing countries as they become more affluent. Considering increasing production constrains derived from climate change and competing demands on resources, the key target for the future of livestock production will be to maximize the number of offspring produced by each female animal that are also fit for purpose. This will involve three challenges, namely, to increase the numbers of offspring that a female can produce, to optimize the in utero conditions under which fetuses develop so to maximize development of appropriate phenotypes, and to bias offspring sex to reflect animal usage. Meeting these challenges will require continued advances of traditional methods and approaches, such as husbandry and genetics, as well as the broad uptake of newer and emerging biotechnological solutions such as transgenesis.

An important point to be made is that these challenges will need to be accomplished in the face of a persistent decrease in livestock fertility associated with modern farming systems in western countries, particularly affecting the dairy, pig and chicken meat industries [11–13]. In these animals, specific production traits (milk, meat) have been genetically selected at the expense of a reduction in non-selected traits such as fertility. In many cases an even more important contribution to low fertility in modern livestock herds has resulted from industry consolidation into fewer, larger production units which are managed intensively toward the primary objective of maximal economic gain.

A clear example of this is the dairy cattle industry, where a steady increase in milk productivity over the past few decades has been associated with a progressive decline in fertility to current first-service conception rates below 40%, resulting in extended calving intervals and premature culling [11, 14, 15]. According to the UK's Dairy Science Forum (2008), poor fertility in dairy herds is estimated to cost to the UK industry alone above £300 million a year, in addition to being a major welfare issue. Under current management schemes, to maximize milk production cows need to conceive soon after parturition so that the interval between lactations is minimized and a target of one-calf-a-year can be achieved. This requires timely restoration of gonadotropin secretion and ovarian activity after calving, together with adequate uterine clearance and repair, if successful follicle maturation and ovulation followed by fertilization and establishment of pregnancy is to take place by about 90–100 days [16, 17]. However, dairy cattle have been selected to efficiently partition nutrients toward milk [18] production thus creating a state of negative energy balance after parturition where reinitiation of high milk production will occur preferentially to restoration of reproductive function conducive to establishment of pregnancy [19].

Even more profound effects on reproductive activity in cattle but also in other livestock [20–22] are derived from suboptimal management of animals under intensive farming conditions including under nutrition, stress and general poor health reflected, for example, in a high incidence of lameness and mastitis, two major conditions associated with low reproductive performance of dairy cattle [11, 14]. Repeated calving itself poses an enormous risk to sustained reproductive performance because of the incidence of parturition-related or postpartum complications (e.g., dystocia, retained fetal membranes, endometritis). Poor management, together with suboptimal ovarian function during postpartum, also leads to poor estrus detection in large herds of dairy cows and other livestock leading to a dramatic decrease in the efficiency of artificial insemination-based programs [23]. Finally, several other factors can have a large impact on overall female health including subclinical infections and environmental factors such as heat stress which has direct effects on follicle development, oocyte quality and embryo development [24, 25].

Poor management is a primary cause of low reproductive performance of livestock in developing countries. As an example, the domestic buffalo constitutes an essential farming resource to millions of families in developing countries, particularly Asia. This species has been traditionally regarded as having low reproductive efficiency, including late attainment of puberty, a seasonal pattern of reproduction, poor expression of estrus, low conception rates and long calving intervals. To a large extent, these characteristics can be attributed to environmental and managerial factors including the absence of a year-round nutrient supply, harsh environmental conditions and suboptimal human intervention [26, 27]. Different studies have shown that buffalo fertility can improve considerably by exercising proper management and feeding and that this can be enhanced by genetic selection [27, 28].

In some instances, the problem is not a lack of nutrients but over nutrition. This is the case in the broiler chicken, in which overfeeding of growth-selected animals results in excessive recruitment of ovarian follicles leading to simultaneous ovulation of multiple follicles. This alters the timing of egg laying and results in poor eggshell quality [29]. This problem has been addressed by nutrient restriction of animals which is necessary to achieve reasonable levels of egg production. This is a significant production and welfare issue as nutrient-restricted broiler breeders show clear evidence of physiological stress as well as an increased incidence of abnormal behaviors, among other problems [30].

Limitations on the reproductive performance of livestock can also be imposed by naturally evolved traits. This is the case in sheep, goats and horses, in which ovulatory activity is restricted to certain periods of the year to ensure that offspring are born at a time when food resources are plentiful [31]. Another example is the inability to selectively breed for the desired gender for a given production trait (for example females only for milk and males only for meat production) which within livestock industries leads to considerable waste and welfare concerns due to the need to cull the less useful gender.

The Need and Potential of Transgenic Technologies to Improve Reproductive Performance of Livestock Species

As outlined above, declining fertility trends in livestock can be partially reversed by improved management. This may include pharmacological control of reproductive function which, although effective in the short term, is nonetheless expensive and has limited benefits as not all animals respond adequately to hormone treatments, particularly if these are not associated with improvements in more basic aspects of management [32–34].

Interventions aimed at increasing general herd health and welfare and reducing stress can be very effective in substantially improving fertility, particularly if they include close monitoring of the reproductive status of individual animals. Optimal implementation of such measures, however, can be costly and in some cases may not be feasible and/or economically viable, particularly in developing countries.

Optimum nutrition is also an important aspect of good management, particularly as it relates to prevention of low energy balance during postpartum and other critical reproductive states [15, 19]. It has been shown that the extent to which reproductive performance can be increased through nutrition is limited [35] and that a given diet can have different effects on different aspects of reproduction, as exemplified by the administration of diets which stimulate plasma insulin levels in postpartum cattle [36]. Such diets can effectively stimulate follicle development but at the same time have negative effects on the oocyte, justifying the need for carefully tailoring diet composition to specific reproductive functions if optimum fertility is to be achieved.

Although selection of livestock for certain production traits has been associated with a loss of fertility, studies with dairy cattle have shown that this loss can be reversed, through genome-wide selection on multiple traits, without completely compromising milk production [35]. However, eliminating the fertility problem in livestock through genetics would require that reproductive traits be included as a significant component of selection indexes and the desired outcome may not be achieved in decades. Alternatively, genetic gain could be aimed at reducing the impact of poor fertility on productivity, for example, by selecting for extended lactation periods in dairy cattle [14], although in many instances this may not be economically feasible. In addition, it is unlikely that existing genetic variation in modern livestock lines will continue to generate the rate of gain obtained in the past. On that note, the use of transgenic technology to induce modifications in selected genes followed by conventional breeding and selection would offer an attractive alternative to effectively introduce desirable fertility traits in livestock, particularly in cattle and sheep which have long generation times and small offspring numbers.

Transgenic approaches have been used in livestock for the purposes of increasing productivity, conferring disease resistance and increasing environmental sustainability [2]. Similar approaches could be used to increase fertility (Fig. 1). These could be aimed at improving reproductive function directly (for example, by removing genes that naturally suppress ovulation) or indirectly (for example, by improving energy utilization by reproductive tissues) or at facilitating reproductive management of livestock (for example, by inserting reporter genes that could facilitate estrus detection or early pregnancy diagnosis). To achieve this, gene knockin or knockout approaches could be used to modify whole genes or large portions of these genes. Alternatively, novel ZFN technology allows for targeted or untargeted gene mutagenesis to be induced to selectively modify gene function in animals [37–39]. This approach would be more likely to be accepted by the public than the insertion of foreign genes into livestock genomes and it could also provide more predictable results, particularly if natural or induced mutations of the gene(s) of interest already existed in the same or a different species.

Successful application of transgenesis in livestock fertility will ultimately require a more thorough understanding of reproductive physiology in these species. Transgenic studies aimed at targeting fertility genes in livestock have not been reported and therefore potential gene targets would have to be obtained from data on naturally occurring mutations or single nucleotide polymorphisms associated with fertility, or from results of experimental gene targeting in rodents, which can already provide a substantial list of

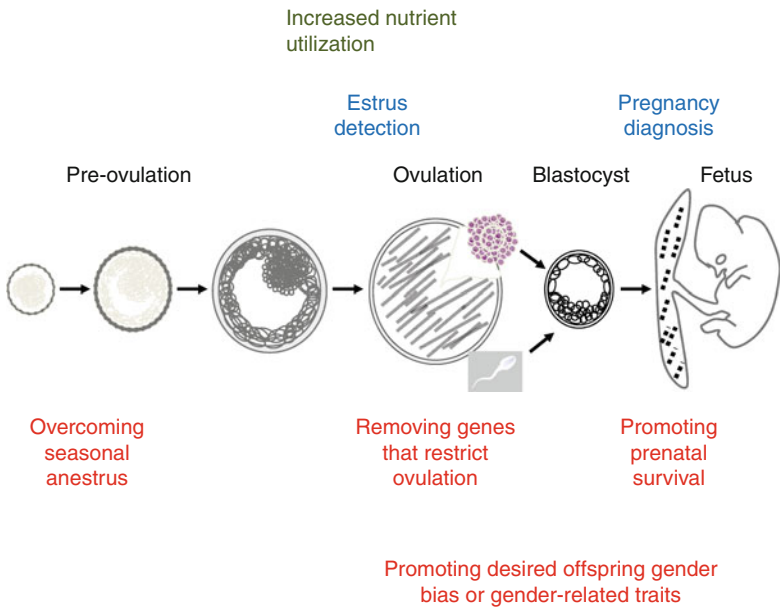

Transgenic Technologies and Increased Livestock Fertility. Figure 1
Schematic diagram showing stages of the reproductive process where transgenic technologies could impact. The examples presented include strategies to directly improve reproductive function (in *red*), to indirectly favor reproductive success (in *green*), or to facilitate reproductive management (in *blue*)

candidate genes [40]. It must be stressed that, because of significant species differences, considerable caution should be used when attempting to extrapolate results from genetically modified mice into other species. A clear example of this is the failure of genetic deficiencies in bone morphogenetic protein (BMP) 15 or growth differentiation factor (GDF) 9, which are naturally associated with multiple ovulation in sheep, to increase the ovulatory response in mice [41]. In addition, it is essential to remember that most reproductive traits are controlled by several genes acting in concert and they may not therefore be easily altered by targeting a single gene. Finally, genetic modification in mice can reportedly be associated with a reduction of fertility in vitro [42], an observation that would need to be properly addressed.

The choice of a particular gene modification aimed at improving livestock fertility would need to be based on different considerations. Optimally, a gene should be targeted only in a specific cell type or organ of interest. This could be achieved with the use of cell-specific gene promoters to drive the targeting event. Choosing a gene target with naturally restricted expression, if possible restricted to the cell type of interest, would be technically simpler and more efficient. In addition, small-scale mutagenesis rather than whole gene replacement or insertion of a new gene would be preferred to achieve the desired phenotype effects. This is now possible with remarkable efficiency in rodents and pigs by using ZFN technology [37–39]. Lastly, the intended mutation would optimally exist naturally and have been characterized thus allowing more accurate prediction of the phenotype in transgenic offspring.

Potential Targets for Transgenic Improvement of Livestock Fertility

Among the genes that could be targeted to increase fertility in livestock, certain members of the BMP family meet all three criteria described above for an optimum target. In this section, these genes will be first considered in detail followed by brief reference to others that could be targeted to improve different aspects of reproduction.

Natural mutations in the BMP ligands, BMP15 and GDF9, and in the BMP receptor type 1B (BMPR1B)

have been described in different breeds of high prolificacy sheep and some of them have been characterized in detail [43, 44]. Five different point mutations were identified in BMP15 (*FecX* locus) and one in each of GDF9 (*FecG*) and BMPR1B (*FecB*). These mutations led in each case to reduced production of biologically active protein and/or altered protein signaling. Homozygosis for either BMP15 or GDF9 mutations is associated with infertility due to disruption of early ovarian follicle development, whereas heterozygous animals show natural higher ovulatory rates than wild types (about 3–4 vs 2 follicles per ovulation). The BMPR1B mutation in sheep is also associated with a higher ovulation rate in heterozygous animals, but in this case homozygous animals not only are fertile but they display an even larger positive effect on ovulation rate ($\geq$5 follicles per ovulation). Expression of BMP15 and GDF9, but not BMR1B, is mostly restricted to the oocyte. For both BMP15 and GDF9 mutations, the different ovarian phenotypes observed in homozygous and heterozygous animals are thought to largely reflect the role of these growth factors in promoting cellular proliferation during early stages of follicular development and in preventing premature maturation of late stage follicles, respectively (Fig. 2) [43, 45]. In heterozygotes for either mutation, reduced growth factor levels reportedly lead to increased responsiveness to the gonadotropin, follicle-stimulating hormone, and premature acquisition of responsiveness to luteinizing hormone, by granulosa cells of developing follicles which facilitates follicle maturation leading to the recruitment of an increased number of ovulatory follicles [43]. This phenomenon could be exploited using transgenesis to increase ovulatory rate not only in other sheep breeds but also in monovular species such as cattle. Evidence from immunization studies indicates that, as in sheep, altering the levels of BMP15 and/or GDF in cattle has clear effects on follicle development and ovulation rate [46]. Based on this and other information on the biological role of BMP15 and GDF9 in the bovine ovary [47], as well as on the phenotype described in mutant sheep, it can be predicted that similar mutations in BMP15 and/or GDF9 in cattle would result in animals with increased follicular sensitivity to gonadotropins and therefore a reduced gonadotropin dependence for follicle maturation. This change would provide a clear physiological

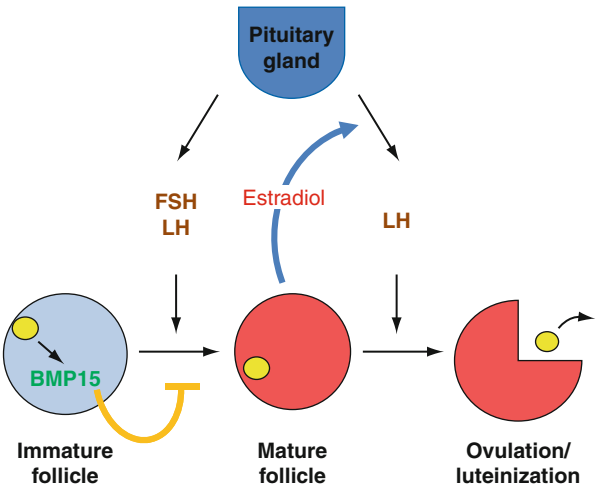

Transgenic Technologies and Increased Livestock Fertility. Figure 2
Schematic of the physiological control of ovarian follicle maturation by pituitary gonadotropins and oocyte-derived BMP ligands. For simplicity, only BMP15 is shown. During normal estrous cycles, systemic gonadotropin levels stimulate follicle maturation leading to the production of estradiol which will eventually trigger a surge in pituitary LH release and ovulation followed by luteinization of follicular cells. Current evidence from ruminants indicates that BMP15 restricts the maturation-promoting effects of gonadotropins thus preventing the development of an excessive number of preovulatory follicles and early ovulation and/or luteinization. It is proposed that transgenically altering the levels of BMP15 in cattle would counteract the relative deficiency in gonadotropin levels during the postpartum period leading to early ovulation. *FSH* Follicle-stimulating hormone, *LH* Luteinizing hormone, *BMP15* Bone morphogenetic protein 15

advantage during situations, such as the early lactation period, when energy demands for reproduction cannot be fully met resulting in insufficient gonadotropin stimulation that prevents normal follicle maturation and restoration of ovulatory activity [16, 48]. As a result, ovulatory activity would be predictably restored early after parturition providing an opportunity for reduced calving intervals. It is very important to consider, however, that for the increased incidence of ovulation in such transgenic cattle to effectively lead to an increase in reproductive efficiency, it would have to be associated with the implementation of

measures to ensure adequate oocyte quality and uterine health, so that pregnancy could be successfully established and maintained. An increased frequency of twining would be likely in the transgenic cattle lines which, although not desirable in certain situations, could still be exploited by the cattle industry to increase productivity. In addition to the natural mutations considered here, there are other high prolificacy phenotypes identified in sheep which do not seem to be associated with the BMP system [49]; identification of the specific genes involved will provide additional targets for manipulation of fertility in livestock.

Aside from the BMP system, there is evidence in livestock to indicate that the estrogen receptor (ESR) could be targeted to increase prolificacy. In pigs, there are associations between litter size and several genes including the ESR, prolactin receptor (PPLR), and retinol-binding protein (RBP) genes [50]. Rothschild and associates [51] found a *Pvull* polymorphism in intron 9 of *ESR1* in prolific Chinese Meishan pigs and commercial Large White populations. Among the Pvull genotype sows homozygous for the desired allele had larger litters at birth with more live born piglets. Introduction of a mutated or polymorphic ESR gene could therefore be used to increase litter size in several pig breeds.

The use of transgenesis has also been proposed to address gender inefficiency in livestock industries [2]. More precisely, it was suggested that genes involved in the production of functional sperm [52] or sex determination [6] and that have been successfully targeted in mice and birds could be used as targets for transgenic alteration of sex ratios in livestock. For example, the gene, *DMRT1* (doublesex and mab-3-related transcription factor 1), is implicated in male gonad development in vertebrates and its knockdown using RNA interference in early chicken embryos resulted in gonadal feminization of genetically male embryos leading to partial sex reversal [6]. An alternative approach to address gender inefficiency would be, rather than trying to alter the natural gender ratio, to transgenically enhance specific production traits in a gender-specific manner. As an example, in an attempt to produce transgenic animals with muscular hypertrophy similar to "double-muscling" which results from naturally occurring loss-of-function myostatin *(MSTN)* mutations in cattle [53], Georges and associates [54] targeted trans-inactivators of *Mstn* on the Y chromosome of mice. The resulting transgenic males showed a 5–20% increase in skeletal muscle mass. The authors suggested the use of this approach in dairy cattle to produce breeds with combined beef and dairy abilities [54].

Finally, targeting of a number of other aspects of reproductive physiology through transgenesis may be desirable to address specific causes of reduced fertility. This could be done for example to improve prenatal survival in different species by increasing the expression of known luteotrophic and antiluteolytic conceptus signals which would be expected to reduce embryo mortality and thereby improve pregnancy rate [55], or to reduce seasonal constraints on reproduction by targeting the neuroendocrine pathways involved [56] to generate transgenic small ruminants capable of year-round breeding in temperate latitudes.

Future Directions

Since first reported over 30 years ago [57], the use of transgenic technologies in mice has been extremely useful in unraveling genetic mechanisms, including reproductive processes. Although since then the application of such technologies in other species including livestock has encountered numerous roadblocks, considerable technical improvements have been made which now allow specific and precise gene targeting in vivo [38, 39]. The vast potential of transgenic technologies in livestock has been extensively demonstrated by the successful targeting of many production-related traits in ruminants, cattle and sheep [2]. Although there has been public reluctance toward the use of such technologies in food-producing animals, technical advances allowing the production of safer foods from transgenic animals together with mounting social pressures demanding an increase in the availability of animal products for a growing world population will likely change this, and recent FDA approval of a genetically modified salmon [58] is a good indication of such change already happening. Although attempts at transgenically increasing livestock fertility have not been reported, transgenic technologies hold particular promise in that regard, both in terms of reversing current decreasing fertility trends and alleviating natural fertility constraints of livestock, two aspects that have a profound impact on overall industry

productivity and efficiency, and which is set to become increasingly important as demands for higher livestock productivity continue to increase. Studies in livestock species to increase understanding of their reproductive processes and to develop further refined gene targeting technologies will be key in bringing the realization of such promise much closer.

Bibliography

1. McEvoy TG, Robinson JJ, Sreenan JM (1992) A role for transgenic animals in food production? Trends Food Sci Technol 3(11):294–302
2. Fahrenkrug SC, Blake A, Carlson DF, Doran T, Van Eenennaam A, Faber D, Galli C, Gao Q, Hackett PB, Li N, Maga EA, Muir WM, Murray JD, Shi D, Stotish R, Sullivan E, Taylor JF, Walton M, Wheeler M, Whitelaw B, Glenn BP (2010) Precision genetics for complex objectives in animal agriculture. J Anim Sci 88(7):2530–2539
3. Cathomen T, Keith Joung J (2008) Zinc-finger nucleases: the next generation emerges. Mol Ther 16(7):1200–1207
4. Matzuk MM, DeMayo FJ, Hadsell LA, Kumar TR (2003) Overexpression of human chorionic gonadotropin causes multiple reproductive defects in transgenic mice. Biol Reprod 69(1):338–346
5. Rulli SB, Ahtiainen P, Makela S, Toppari J, Poutanen M, Huhtaniemi I (2003) Elevated steroidogenesis, defective reproductive organs, and infertility in transgenic male mice overexpressing human chorionic gonadotropin. Endocrinology 144(11):4980–4990
6. Smith CA, Roeszler KN, Ohnesorg T, Cummins DM, Farlie PG, Doran TJ, Sinclair AH (2009) The avian Z-linked gene DMRT1 is required for male sex determination in the chicken. Nature 461(7261):267–271
7. Yan C, Elvin JA, Lin Y-N, Hadsell LA, Wang J, DeMayo FJ, Matzuk MM (2006) Regulation of growth differentiation factor 9 expression in oocytes in vivo: a key role of the E-box. Biol Reprod 74(6):999–1006
8. Huang X, Andreu-Vieyra CV, Wang M, Cooney AJ, Matzuk MM, Zhang P (2009) Preimplantation mouse embryos depend on inhibitory phosphorylation of separase to prevent chromosome missegregation. Mol Cell Biol 29(6):1498–1505
9. Okada Y, Ueshin Y, Isotani A, Saito-Fujita T, Nakashima H, Kimura K, Mizoguchi A, Oh-hora M, Mori Y, Ogata M, Oshima RG, Okabe M, Ikawa M (2007) Complementation of placental defects and embryonic lethality by trophoblast-specific lentiviral gene transfer. Nat Biotechnol 25(2):233–237
10. Morioka Y, Isotani A, Oshima RG, Okabe M, Ikawa M (2009) Placenta-specific gene activation and inactivation using integrase-defective lentiviral vectors with the Cre/LoxP system. Genesis 47(12):793–798
11. Lucy MC (2001) Reproductive loss in high-producing dairy cattle: where will it end? J Dairy Sci 84(6):1277–1293
12. Young B, Dewey CE, Friendship RM (2010) Management factors associated with farrowing rate in commercial sow herds in Ontario. Can Vet J 51(2):185–189
13. Julian RJ (2005) Production and growth related disorders and other metabolic diseases of poultry – a review. Vet J 169(3): 350–369
14. Dobson H, Smith RF, Royal MD, Knight CH, Sheldon IM (2007) The high producing dairy cow and its reproductive performance. Reprod Domest Anim 42(Suppl 2):17–23
15. Chagas LM, Bass JJ, Blache D, Burke CR, Kay JK, Lindsay DR, Lucy MC, Martin GB, Meier S, Rhodes FM, Roche JR, Thatcher WW, Webb R (2007) Invited review: new perspectives on the roles of nutrition and metabolic priorities in the subfertility of high-producing dairy cows. J Dairy Sci 90(9):4022–4032
16. Crowe M (2008) Resumption of ovarian cyclicity in postpartum beef and dairy cows. Reprod Domest Anim 43(s5): 20–28
17. Sheldon IM, Cronin J, Goetze L, Donofrio G, Schuberth H-J (2009) Defining postpartum uterine disease and the mechanisms of infection and immunity in the female reproductive tract in cattle. Biol Reprod 81(6):1025–1032
18. Yan T, Mayne CS, Keady TWJ, Agnew RE (2006) Effects of dairy cow genotype with two planes of nutrition on energy partitioning between milk and body tissue. J Dairy Sci 89(3):1031–1042
19. Wathes DC, Fenwick M, Cheng Z, Bourne N, Llewellyn S, Morris DG, Kenny D, Murphy J, Fitzpatrick R (2007) Influence of negative energy balance on cyclicity and fertility in the high producing dairy cow. Theriogenology 68:S232–S241
20. von Borell E, Dobson H, Prunier A (2007) Stress, behaviour and reproductive performance in female cattle and pigs. Horm Behav 52(1):130–138
21. Moberg GP (1991) How behavioral stress disrupts the endocrine control of reproduction in domestic animals. J Dairy Sci 74(1):304–311
22. Reynolds LP, Borowicz PP, Caton JS, Vonnahme KA, Luther JS, Hammer CJ, Maddock Carlin KR, Grazul-Bilska AT, Redmer DA (2010) Developmental programming: the concept, large animal models, and the key role of uteroplacental vascular development. J Anim Sci 88(13 electronic suppl):E61–E72
23. Roelofs J, López-Gatius F, Hunter RHF, van Eerdenburg FJCM, Hanzen C (2010) When is a cow in estrus? Clinical and practical aspects. Theriogenology 74(3):327–344
24. Hansen PJ, Aréchiga CF (1999) Strategies for managing reproduction in the heat-stressed dairy cow. J Anim Sci 77(E-Suppl 2): 36–50
25. Roth Z (2008) Heat stress, the follicle, and its enclosed oocyte: mechanisms and potential strategies to improve fertility in dairy cows. Reprod Domest Anim 43:238–244
26. Perera B (2008) Reproduction in domestic buffalo. Reprod Domest Anim 43:200–206
27. Presicce GA (2007) Reproduction in the water buffalo. Reprod Domest Anim 42:24–32
28. Baruselli PS, Reis EL, Marques MO, Nasser LF, Bó GA (2004) The use of hormonal treatments to improve reproductive

performance of anestrous beef cattle in tropical climates. Anim Reprod Sci 82:479–486
29. Renema R, Robinson F, Proudman J, Newcombe M, McKay R (1999) Effects of body weight and feed allocation during sexual maturation in broiler breeder hens. 2. Ovarian morphology and plasma hormone profiles. Poult Sci 78(5):629–639
30. Mench JA (2002) Broiler breeders: feed restriction and welfare. World Poult Sci J 58:23–29
31. Donadeu FX, Watson ED (2007) Seasonal changes in ovarian activity: lessons learnt from the horse. Anim Reprod Sci 100 (3–4):225–242
32. Thatcher WW, Moreira F, Santos JEP, Mattos RC, Lopes FL, Pancarci SM, Risco CA (2001) Effects of hormonal treatments on reproductive performance and embryo production. Theriogenology 55(1):75–89
33. Bó GA, Baruselli PS, Chesta PM, Martins CM (2006) The timing of ovulation and insemination schedules in superstimulated cattle. Theriogenology 65(1):89–101
34. De Rensis F, López-Gatius F, García-Ispierto I, Techakumpu M (2010) Clinical use of human chorionic gonadotropin in dairy cows: an update. Theriogenology 73(8):1001–1008
35. Coleman J, Pierce KM, Berry DP, Brennan A, Horan B (2009) The influence of genetic selection and feed system on the reproductive performance of spring-calving dairy cows within future pasture-based production systems. J Dairy Sci 92(10): 5258–5269
36. Garnsworthy PC, Fouladi-Nashta AA, Mann GE, Sinclair KD, Webb R (2009) Effect of dietary-induced changes in plasma insulin concentrations during the early post partum period on pregnancy rate in dairy cows. Reproduction 137(4):759–768
37. Cui X, Ji D, Fisher DA, Wu Y, Briner DM, Weinstein EJ (2011) Targeted integration in rat and mouse embryos with zinc-finger nucleases. Nat Biotechnol 29(1):64–67
38. Whyte JJ, Zhao J, Wells KD, Samuel MS, Whitworth KM, Walters EM, Laughlin MH, Prather RS (2011) Gene targeting with zinc finger nucleases to produce cloned eGFP knockout pigs. Mol Reprod Dev 78(1):2
39. Yang D, Yang H, Li W, Zhao B, Ouyang Z, Liu Z, Zhao Y, Fan N, Song J, Tian J, Li F, Zhang J, Chang L, Pei D, Chen YE, Lai L (2011) Generation of PPAR[gamma] mono-allelic knockout pigs via zinc-finger nucleases and nuclear transfer cloning. Cell Res 21(6):979–982
40. Roy A, Matzuk MM (2006) Deconstructing mammalian reproduction: using knockouts to define fertility pathways. Reproduction 131(2):207–219
41. Yan C, Wang P, DeMayo J, DeMayo FJ, Elvin JA, Carino C, Prasad SV, Skinner SS, Dunbar BS, Dube JL, Celeste AJ, Matzuk MM (2001) Synergistic roles of bone morphogenetic protein 15 and growth differentiation factor 9 in ovarian function. Mol Endocrinol 15(6):854–866
42. Vasudevan K, Raber J, Sztein J (2010) Fertility comparison between wild type and transgenic mice by in vitro fertilization. Transgenic Res 19(4):587–594
43. McNatty KP, Smith P, Moore LG, Reader K, Lun S, Hanrahan JP, Groome NP, Laitinen M, Ritvos O, Juengel JL (2005) Oocyte-expressed genes affecting ovulation rate. Mol Cell Endocrinol 234(1–2):57–66
44. Souza CJH, GonzÃ¡lez-Bulnes A, Campbell BK, McNeilly AS, Baird DT (2004) Mechanisms of action of the principal prolific genes and their application to sheep production. Reprod Fertil Dev 16(4):395–401
45. Shimasaki S, Moore RK, Otsuka F, Erickson GF (2004) The bone morphogenetic protein system in mammalian reproduction. Endocr Rev 25(1):72–101
46. Juengel JL, Hudson NL, Berg M, Hamel K, Smith P, Lawrence SB, Whiting L, McNatty KP (2009) Effects of active immunization against growth differentiation factor 9 and/or bone morphogenetic protein 15 on ovarian function in cattle. Reproduction 138(1):107–114
47. Knight PG, Glister C (2006) TGF-{beta} superfamily members and ovarian follicle development. Reproduction 132(2):191–206
48. Yavas Y, Wallon JS (2000) Induction of ovulation in postpartum suckled beef cows: a review. Theriogenology 54(1):1–23
49. Juengel JL, O'Connell AR, French MC, Proctor LE, Wheeler R, Farquhar PA, Dodds KG, Galloway SM, Johnstone PD, Davis GH (2011) Identification of a line of sheep carrying a putative autosomal gene increasing ovulation rate in sheep that does not appear to interact with mutations in the TGFB superfamily. Biol Reprod 85(1):113–120
50. Onteru SK, Ross JW, Rothschild MF (2009) The role of gene discovery, QTL analyses and gene expression in reproductive traits in the pig. Soc Reprod Fertil Suppl 66:87–102
51. Rothschild M, Jacobson C, Vaske D, Tuggle C, Wang L, Short T, Eckardt G, Sasaki S, Vincent A, McLaren D, Southwood O, van der Steen H, Mileham A, Plastow G (1996) The estrogen receptor locus is associated with a major gene influencing litter size in pigs. Proc Natl Acad Sci USA 93(1):201–205
52. Véron N, Bauer H, Weiße AY, Lüder G, Werber M, Herrmann BG (2009) Retention of gene products in syncytial spermatids promotes non-Mendelian inheritance as revealed by the t complex responder. Genes Dev 23(23):2705–2710
53. Kambadur R, Sharma M, Smith TPL, Bass JJ (1997) Mutations in myostatin (GDF8) in Double-Muscled Belgian Blue and Piedmontese Cattle. Genome Res 7(9):910–915
54. Pirottin D, Grobet L, Adamantidis A, Farnir F, Herens C, Schrøder HD, Georges M (2005) Transgenic engineering of male-specific muscular hypertrophy. Proc Natl Acad Sci USA 102(18):6413–6418
55. Bazer FW, Wu G, Spencer TE, Johnson GA, Burghardt RC, Bayless K (2010) Novel pathways for implantation and establishment and maintenance of pregnancy in mammals. Mol Hum Reprod 16(3):135–152
56. Dardente H, Wyse CA, Birnie MJ, Dupré SM, Loudon ASI, Lincoln GA, Hazlerigg DG (2010) A molecular switch for photoperiod responsiveness in mammals. Curr Biol 20(24):2193–2198
57. Gordon J, Ruddle F (1981) Integration and stable germ line transmission of genes injected into mouse pronuclei. Science 214(4526):1244–1246
58. Fox JL (2010) Transgenic salmon inches toward finish line. Nat Biotechnol 28(11):1141–1142

Transgenics: Alternative Gene Transfer Methods

Louis-Marie Houdebine
Biologie du Développement et Reproduction, Institut National de le Recherche Agronomique, Jouy en Josas, France

Article Outline

Glossary
Definition of the Subject
Introduction
Methods of Gene Transfer
Future Directions
Bibliography

Glossary

Animal cloning Non-sexual reproduction of an animal by transfer of a nucleus from a differentiated cell into the cytoplasm of an enucleated oocyte; SCNT (somatic cell nuclear transfer): cloning using a somatic cell as nuclear donor.

Chimeric animal Animal containing cells from two animals; chimeras are obtained by transferring embryonic cells from an animal into a recipient embryo; the chimera gametes contain the genome from one of the two embryos.

Hybrid Animal resulting from the sexual reproduction of parents from different breeds (intraspecies hybrid) or parents from different species (interspecies hybrid).

Knockdown Inhibition of the expression of a gene at the mRNA level by a siRNA.

Knockin Targeted integration of a gene by homologous recombination.

Knockout Inactivation of a gene by homologous recombination.

Lentiviral vector Gene construction able to integrate a foreign gene into a genome via an infection mechanism.

Meganuclease Endonuclease that is able to cut both strands of DNA and enhance the efficiency of homologous recombination.

Pluripotent cell Cell that is able to participate in the development of all the organs; lines of pluripotent cells can be established from early embryos (ES: embryonic stem cells) or from somatic cells (iPS: induced pluripotent cells) obtained by the transfer of genes responsible for the pluripotency of embryonic cells.

siRNA Small interfering RNA (also known as RNAi) that is able to inactivate specifically an mRNA by its degradation or by the reversible inhibition of its translation; siRNAs are generated by the degradation of long double-stranded RNAs, by the transcription of micro-RNA genes, by the transcription of gene constructions coding for shRNAs (small hairpin RNAs), or by chemical synthesis.

Transgenesis Experimental transfer of an isolated gene (or a DNA fragment of any origin) to animal cells making the transmission of the genetic modification to progeny by sexual reproduction possible. The animals harboring the foreign genes are known as transgenic animals, transgenics, GM animals (genetically modified animals), rDNA animals (recombinant DNA animals), or GE animals (genetically engineered animals).

Zinc finger nuclease (ZFN) Engineered nucleases that are able to cleave both strands of genomic DNA in specific sites. ZFNs as meganucleases are able to induce a DNA repair and a local mutation equivalent to a knockout in the absence of foreign DNA or targeted gene integration at a high efficiency in the presence of a homologous recombination vector.

Definition of the Subject

Various techniques and mainly gene cloning, genome sequencing as well as transcriptomics provide researchers with an increasing number of genes. In order to know the role of the genes and the mechanisms of their regulation, it is mandatory to reintroduce them into their natural complex environment, cells, and animals. Transgenesis has thus become a major tool for biologists, and presently, at least 90% of GM animals are generated for basic studies. Transgenesis is not only a tool for research; it is also more and more extensively used for various biotechnological projects in the traditional fields of biology applications: medicine and agriculture.

The information provided by the understanding of the biological functions of humans and animals may

give clue for the design of new treatments for patients and selection of farm animals, respectively. Transgenesis has thus become a key tool for the creation of animal models for the study of human diseases. These studies may even provide researchers with genetic markers for diagnosis and genetic selection. The newly identified and studied genes may be used to produce small quantity of the corresponding recombinant proteins to establish relations between their structure and their activity. Very large quantity of recombinant proteins of pharmaceutical interest may also be produced in milk or egg white of transgenic animals. Pig cells and organs may in principle be genetically modified to become tolerated by patients. Some newly identified genes may as well be transferred to farm animal to improve production as it is already the case in plants [112](Fig. 1).

The available techniques make it possible the addition of exogenous genes and the elimination of genetic information in various animal genomes. Several more and more sophisticated tools allow also a fine-tuning of transgene expression. Although the generation of transgenic animals is no more a bottleneck for their different use, it remains laborious and costly especially in large animals. Some improvements of the methods are required and in course. The methods of gene transfer are closely linked to the reproduction techniques and to the aim of the projects. These methods, which include the construction of the genes to be transferred and which are adapted to the different animal species are described in the present chapter.

Introduction

By essence, living organisms are in permanent evolution. This phenomenon is relatively slow, and it was probably not perceived by humans until they invented agriculture and breeding. The control of plant and animal reproduction made the empirical genetic selection possible which provided to human communities all their essential food products, pets, and ornamental plants. This led to the generation of profoundly genetically modified organisms. Carrots, tomatoes, silkworm, some dogs, etc. are unable to survive without the assistance of humans.

The discovery of the Mendel laws allowed an improvement of the genetic selection. Yet, this selection remained based on spontaneous, thus random and unknown, mutations. During the first half of the last century, it appeared necessary and possible to increase the number of random mutations to enlarge the choice of the genetically modified organisms corresponding to

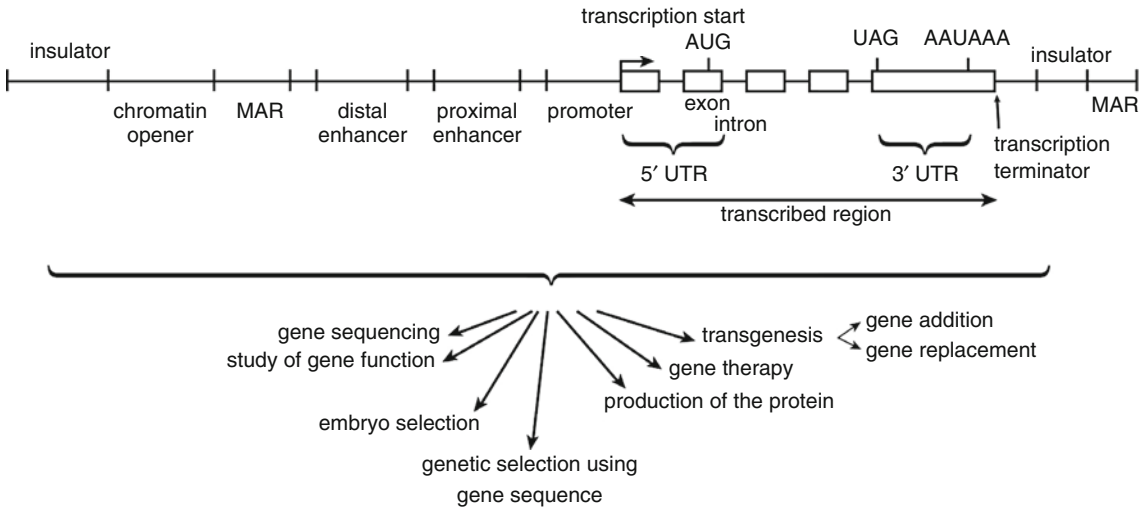

Transgenics: Alternative Gene Transfer Methods. Figure 1
The different uses of isolated genes. Transgenesis, which includes random and targeted gene addition as well as specific gene inactivation and replacement is an essential tool for gene study and for biotechnological applications

the expectations of experimenters, farmers, and breeders. This was achieved by using chemical mutagens and by generating multiple intraspecies and interspecies hybrids. One of the most impressive examples is the creation of a new cereal, triticale, which results from an artificial crossing between wheat and rye. This new plant is currently a source of feed.

All these methods are imprecise as they induce multiple unknown mutations in addition to those which are expected. One of the problems of conventional genetic selection, either to create models or to improve production, is that the selected genes are unknown and that a large number of genes also unknown are co-selected with the genes of interest (Fig. 2). Yet, these approaches were globally highly beneficial for humans. They also show that the plasticity of living organisms is high and that humans have empirically learned to manipulate them successfully with limited undesirable side effects. The discovery of DNA and genes opened wide avenues for research and biotechnological applications. Indeed, the manipulation of isolated and known genes makes it possible more diverse and better controlled genetic modifications (Fig. 2).

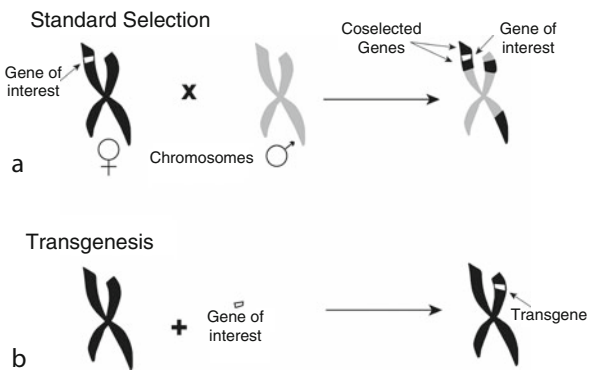

Transgenics: Alternative Gene Transfer Methods. Figure 2
(**a**) Conventional genetic selection relies on the random chromosome rearrangement during sexual reproduction and, thus, to the random distribution of the different gene versions in offspring. The gene of interest responsible for the expression of a valuable genetic trait, and which is selected, is then unknown and the process implies the co-selection of a number of unknown potentially deleterious genes surrounding the gene of interest.
(**b**) Selection by gene transfer offers the possibility to add (or delete) a single gene having a known function into a living organism. This gene may be of various origins and may be optimized before being transferred

The introduction of isolated genes into cells has become a common practise in the 1970s of the last century, soon after the emergence of the genetic engineering techniques. It represented a great progress for the understanding of gene functions and mechanisms of action. This technique is still widely used, and it started being complemented in 1980 and 1983 by gene transfer into animals and plants, respectively, to generate lines of genetically modified organisms, also known as transgenic animals and plants.

The first transgenic animals, mice, were obtained by microinjecting the genes into one of the nuclei (pronuclei) of 1-day embryos [31]. This method could be extrapolated successfully to three other mammals (rabbits, pigs, and sheep) in 1985 [32], but it soon appeared that other methods had to be implemented for some species. Transgenesis is presently carried out essentially for basic research in only a few species: a mammal (mice), an insect (drosophila), fish (medaka and zebra fish), and a worm (*Caenorhabditis elegans*). Some farm animals (rabbits, pigs, chicken, sheep, goat, and cow) are being used for specific studies, which cannot be performed for biological reasons with laboratory animals. Essentially, the products from some farm animals are expected to be improved by transgenesis in addition to classical genetic selection in the coming decades.

Several techniques to generate transgenic animals have made considerable progress in the past decade: (1) direct gene transfer into embryos either by microinjection of DNA, transposons, or lentiviral vectors or via sperm incubated with DNA and transferred to oocytes by ICSI (intracytoplasmic sperm injection), (2) via intermediate cells in which the gene modifications have been achieved and further used to generate animals harboring the foreign DNA sequence; these cells are either pluripotent cells that are able to give birth to chimeric transgenic animals ES (embryonic stem cells) in mice as well as iPS (induced pluripotent cells obtained after dedifferentiation of somatic cells) potentially in most species or somatic cells used for generating transgenic clones (Fig. 3).

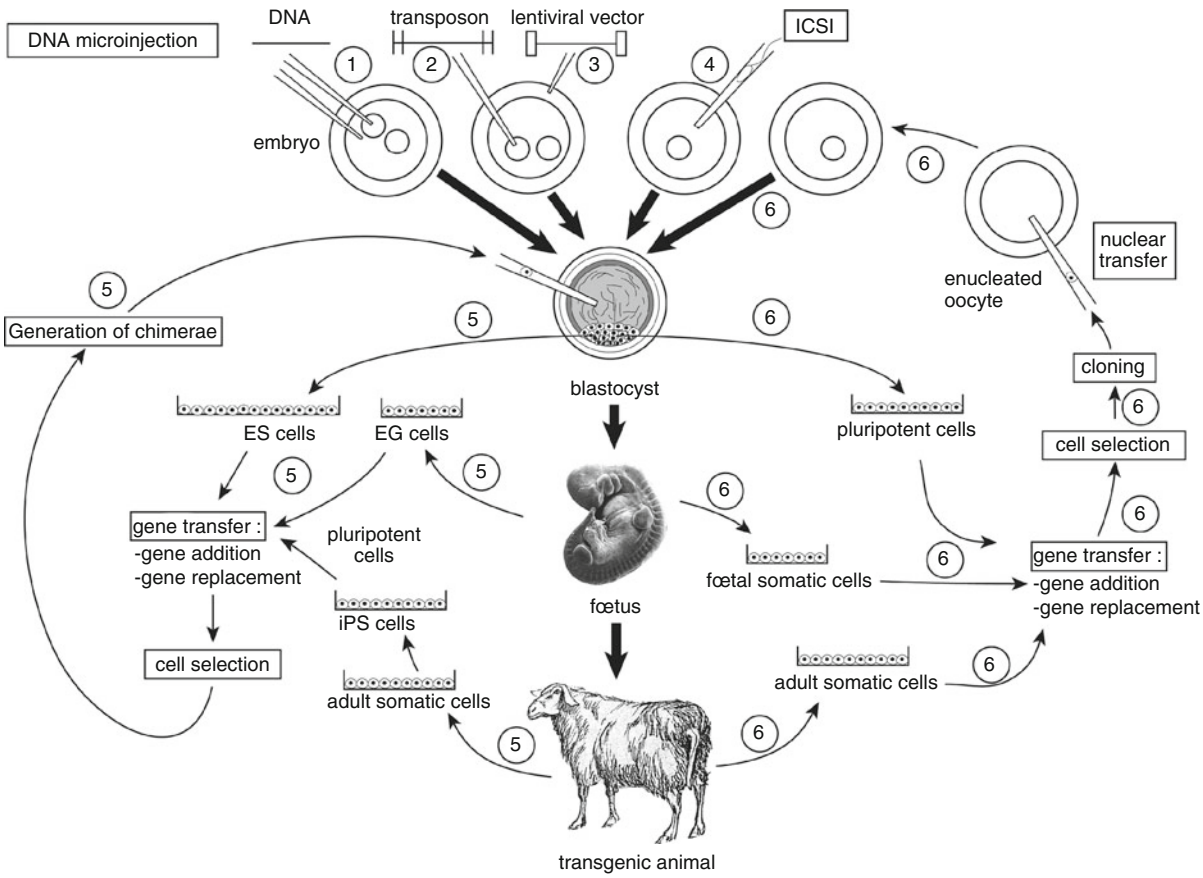

Transgenics: Alternative Gene Transfer Methods. Figure 3
Different methods to generate transgenic animals: (1) DNA transfer via direct microinjection into pronucleus or cytoplasm of embryo; (2) DNA transfer via a transposon: The foreign gene is introduced into the transposon, which is injected into a pronucleus; (3) DNA transfer via a lentiviral vector: The gene of interest introduced in a lentiviral vector is injected between the zona pellucida and membrane of the oocyte or the embryo; (4) DNA transfer via sperm: Sperm is incubated with the foreign gene and injected into the oocyte cytoplasm for fertilization by ICSI (intracytoplamic sperm injection); (5) DNA transfer via pluripotent or multipotent cells: The foreign gene is introduced into pluripotent cell lines (ES, embryonic stem cells: lines established from early embryo or iPS: cells obtained after dedifferentiation of somatic cells) or into multipotent cell lines (EG, gonad cells lines established from primordial germ cells of fetal gonads); the pluripotent cells containing the foreign gene are injected into an early embryo to generate chimeric animals harboring the foreign gene DNA; the multipotent EG cells containing the foreign gene are injected into embryos to generate gametes harboring the transgene; in both cases, the transgene is transmitted to progeny; (6) DNA transfer via cloning: The foreign gene is transferred into a somatic cell, the nucleus of which is introduced into the cytoplasm of an enucleated oocyte to generate a transgenic clone. Methods 1, 2, 3, and 4 allow random gene addition whereas methods 5 and 6 allow random gene addition and targeted gene integration via homologous recombination for gene addition or gene replacement including gene knockout and knockin

Another problem emerged rapidly. The very first transgenes were expressed, and they were able, in some cases, to induce some phenotypic modifications in animals. The first example was the giant mice obtained in 1982 [71] by overexpressing growth hormone genes. It also appeared that the expression of the transgenes was often not satisfactory and not easily controlled. This was clearly due to the insufficient knowledge of the

mechanisms controlling gene expression. Thus, for years, only empirical gene constructions having sometimes limited efficiency were used. The strategy of researchers was and often still is to generate several lines of transgenic mice (or other species) and to keep only those in which the transgene is expressed as expected. This strategy appeared insufficient when costly large transgenic animals were to be used and when finely tuned transgene expression was needed. Different methods to express transgenes in a well-controlled manner were found: (1) gene targeting by homologous recombination [8] improved or not by a genomic DNA cleavage locally induced by engineered meganucleases or zinc finger nucleases, leading either to gene knockin or knockout by a gene replacement as well as by NHEJ (non-homologous end joining), (2) conditional knockout using Cre recombinase gene controlled by exogenous inducers such as doxycycline and a engineered Cre recombinase activated by 4-hydroxy tamoxifen, (3) inactivation of mRNA by knockdown with siRNA derived from transgenes coding for shRNA or miRNA, (4) overexpression of negative transdominant proteins inactivating the genes at the protein level.

The failure of transgene expression raised fundamental questions on gene mechanism of action to experimenters. This is particularly the case for the discovery of remote regulatory elements globally known as insulators. Indeed, as opposed to bacteria, yeast, and plants, essential transcription regulators are spread over long genomic DNA regions in animals and, namely, in higher vertebrates [53]. Interestingly, answers were given to some of these questions, thanks to transgenesis and transgenesis efficiency was improved, thanks to these discoveries. Despite very significant improvement of several transgenesis methods, the efficiency of gene transfer and the control of transgene expression remain limiting factors for the optimal use of transgenic animals for research as well as for biotechnological applications. Important improvements of these methods are in course. The more efficient of gene targeting via the action of meganucleases and zinc finger endonucleases is a case in point.

Methods of Gene Transfer

Gene Transfer into Cells

Spontaneous gene transfer into cells occurs only marginally. Different techniques are being used to reach this goal. A group of techniques relies on artificial physicochemical or mechanical processes whereas another group utilizes natural mechanisms of gene transfer, essentially infection. Transfection implies the association of DNA with molecules, which have the capacity to bind cell plasma membrane and to internalize the complex into the cytoplasm. The endocytosis process includes the transfer of the internalized material into lysosomes where it is processed or degraded. A proportion of non-degraded DNA is more or less randomly recombined. A part of the DNA is then transferred to the nucleus, and the genes it contains may be transiently transcribed. When cells do not divide, the DNA may stay several days in the nucleus. During cell division, most part of the foreign DNA is degraded and in a small percentage of cells, the foreign DNA becomes integrated into the host genome either randomly or in a targeted manner according to the sequence of the transferred DNA. A number of molecules are available, and new ones are regularly proposed to enhance the efficiency of cell transfection. These molecules may increase the endocytotic process according to the cell type, diminish the degradation of DNA, favor the transfer of DNA or the nucleus, or be less cytotoxic.

An alternative to transfection is electroporation. The method consists of incubating cells in the presence of DNA and to submit them to pulses of electric field, which generate transient pores in plasma membrane allowing the uptake of DNA. This technique is relatively efficient according to the cell type to obtain stable cells harboring a foreign gene, but many cells do not survive after the electric pulses. The fate of DNA in cells is essentially similar to this following transfection.

It is possible to select the cells in which the foreign DNA is stably integrated into the genome. To reach easily this goal, one popular way consists of co-transfecting a selection gene with the gene of interest. The selection gene may be independent of the gene of interest. Random recombination may then associate the two genes in the same DNA fragment, making the selection of the cells harboring the two co-integrated genes possible. Alternatively, the selection gene may have been associated to the gene of interest in a specific construction. The co-integration of the two genes is then more frequent, and the selection of the cells harboring the gene of interest is easier.

One possible drawback of this protocol is that the selection gene remains present in the cell.

The most efficient classical way to transfer gene into cells is the direct DNA microinjection in the cytoplasm or the nucleus. This method is relatively laborious, requires specific material, and a specific training. Moreover, gene transfer can then be achieved only in a limited number of cells.

Natural mechanisms of gene transfer are being implemented to transfer foreign DNA into cells. Some molecules are naturally able to transfer DNA from the outside of the cells to their nucleus. Lactoferrin was shown to have this property, but this mechanism seems insufficiently efficient to be used. The natural capacity of viruses to transfer their genes into cells by infection mechanisms has been retained to design viral vectors carrying the foreign genes. Such vectors have been studied and used during the last two decades with limited success for gene therapy. A few types of viruses have been retained to be used for gene therapy and those which transfer their genes into the cell genome are being implemented to generate transgenic animals. These vectors rely on the use of retroviral genomes, which must be integrated into the infected cells to be replicated and able to synthesize infectious viral particles.

Gene Transfer into Embryo

To generate transgenic animals, the foreign gene must be present and integrated into the genome of the embryos at the one-cell stage to allow its transmission into all the cells of the animal or at least of their gametes. The simplest theoretical way to reach this goal is to transfer the foreign gene directly into the embryo. In practice, this strategy is not always efficient. Indeed, embryos are rare and costly cells especially in large farm animals. In species in which gametes are very abundant, the direct gene transfer using biolistics has met success in fish and marine invertebrates [63] and insects [18]. In practice, this method consists of incubating DNA with gold or platinum. The DNA-coated particles are then launched through the membrane of the embryos.

Hence, only the highly efficient methods of gene transfer may be successful in these conditions even if only random gene integration is needed. The targeted integration of foreign DNA is a rare event as it is based on a homologous recombination between the host gene and the vector. In these situations, even the most efficient classical techniques of gene transfer are unable to induce a gene targeting at an acceptable rate.

The genetic modifications must then be achieved in cultured cells, which must have the capacity to participate in the development of the embryos and be able to transmit the genetic modification to progeny. Pluripotent cells (ES cells or iPS) may, in the best cases, participate in the generation of chimeric animals in which a significant proportion of the gametes harbor the foreign DNA. Particular multipotent cells, the primordial germ cells (EG cells) in birds can participate in the formation of genetically modified gametes and in the generation of transgenic animals. The animal cloning technique is another possibility. The genetic modification is then performed in somatic cells that are further used to generate transgenic clones by nuclear transfer.

These different methods to generate transgenic animals are schematically represented in Fig. 3.

Mechanisms of Gene Integration

Random Integration The foreign DNA introduced into the cytoplasm by any method recombines according to a random process, leading to the formation of multimers known as concatemers including gene rearrangement and mutations. The different copies of the gene are then organized in head to tail or in tandem. When the foreign DNA is introduced directly into the nucleus (essentially by microinjection), a polymerization also occurs but following a process of homologous recombination generating concatemers organized essentially in tandem with limited mutations and rearrangements. The integration of foreign DNA fragment into a genome may occur by two different mechanisms. The most frequent process is considered as leading to a random integration. Targeted integration is much less frequent.

In both cases, the foreign DNA is progressively degraded by the cell. This includes the action of exonucleases, which generate randomly single-stranded sequences in both ends of the foreign DNA. These sequences can recognize complementary regions in the genome, leading to the formation of hybrids. During the cellular DNA replication, these abnormal

structures are corrected by the repair mechanisms of the cell. This leads to the elimination of the foreign DNA or to its integration in the genome [3] (Fig. 4). This process implementing a heterologous recombination is considered as random since the recognition of the host DNA site depends on the action of the exonucleases. The different lines of transgenic animals obtained in this way are thus all different from each other. They contain variable copy number of the transgene integrated each time at a different site. The integration of the foreign gene may damage locally the host DNA. Moreover, the transgene is then frequently submitted to the unpredictable and unknown effects of the transcription regulatory elements located in its vicinity. The regulatory elements of the transgene may also alter the transcription of the host genes in its vicinity.

The integration of the foreign DNA by these methods is thus not controlled but likely not completely random as it occurs more frequently in regions containing genes and thus having an open chromatin structure, favoring the access of the foreign DNA to the host DNA. The integration site may be known by sequencing the flanking regions of the transgene.

A systematic study revealed that transgenic mice heterozygous for the transgene show rarely abnormalities. On the contrary, the homozygous mice appear

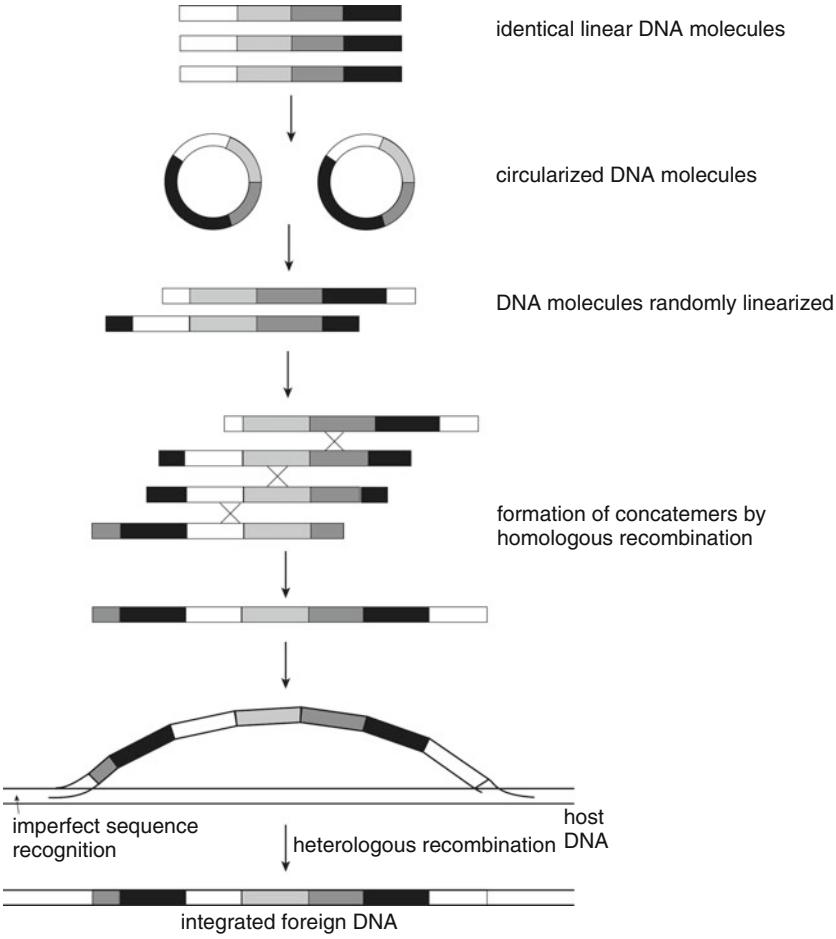

Transgenics: Alternative Gene Transfer Methods. Figure 4
Mechanism of random DNA integration. The ends of the foreign DNA are partially digested generating single-stranded sequences, which randomly recognize complementary host DNA sequences and provoke the integration of the foreign DNA

altered in a proportion as high as 3–10%, suggesting that the uncontrolled integration of the foreign DNA is often mutagenic [103, 104].

Targeted Integration To avoid the side effects of the random integration, it is possible to target the integration of the foreign gene using homologous recombination. This mechanism is based on the recognition between a genome sequence and the sequence of the exogenous DNA. This recognition leads to the formation of hybrid and finally by the precise replacement of the endogenous gene by the exogenous DNA (Fig. 5). Homologous recombination exists in all living organisms. It is implemented to repair mutated genes using the other allele as a matrix, to redistribute the regions of homologous chromosomes during the formation of gametes, and to generate functional antibody genes from parent genes. Homologous recombination is routinely used to genetically modify bacteria and yeast. Homologous recombination is a rare event corresponding to about 0.1–1% of the heterologous recombination. It is therefore not implemented directly in early embryos but in intermediate cells further used to generate transgenic animals.

Homologous recombination allows in practice the replacement of a given gene by an exogenous DNA fragment. Several applications of this approach are possible: (1) the replacement of a gene by a non-functional DNA sequence, leading to the inactivation of the targeted gene known as gene knockout (Fig. 5), (2) the targeting of a foreign gene into a given region of the genome or the replacement of an allele by another allele known as knockin.

DNA Microinjection

About 1,000 copies of the isolated foreign gene contained in 1–2 pl may be injected into one of the pronuclei of 1-day mammal embryos. This method implies a superovulation of the females followed by a mating with a male to obtain an optimum number of embryos. The resulting one-cell embryos are collected the next day and microinjected with DNA. The embryos are then transferred to hormonally prepared recipient females using surgery operations. The yield of this method in mice is of 1–3 of transgenics for 100 microinjected and transferred embryos. This rate is relatively low, and this is due to a large extent to the fact that only 50% of the embryos survive after the microinjection. This is clearly due to the mutagenic effect of DNA as the survival of embryos is high when the buffer without DNA is injected. In fact, 1,000 copies of the gene correspond to a very large excess of DNA in the cell, making the multiple random deleterious

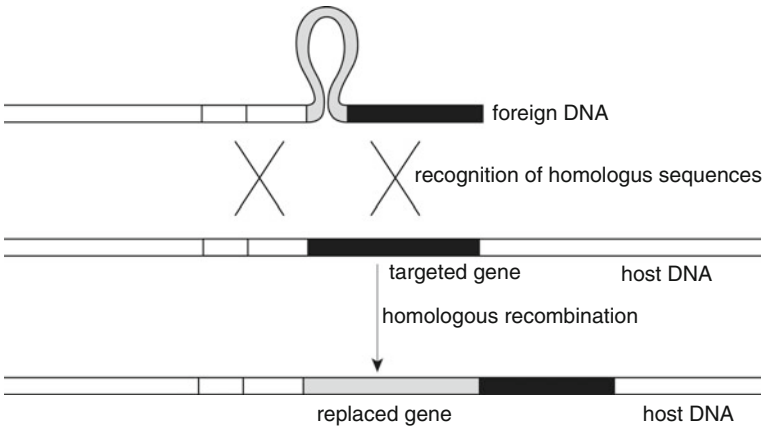

Transgenics: Alternative Gene Transfer Methods. Figure 5
Mechanism of targeted integration. An exogenous DNA having a sequence of several kb similar to that of a host gene may replace the host gene using a homologous recombination process. If a non-homologous sequence is surrounded by two homologous sequences, the two independent homologous recombinations direct the integration of the non-homologous sequence, leading to the knockout of the targeted gene

integrations and genome rearrangements depicted above possible. Despite its drawback and the fact that it is laborious, this technique is still the most frequently used in mice and rabbits. The efficiency of DNA microinjection is lower in all the other mammalian species and very low in ruminants. This is not due to the difficulty to inject DNA but to the fact that the mechanism of integration is for unknown reasons much less efficient in some species.

The DNA microinjection in pronuclei gives birth to at least 30% of mice mosaic for the transgene. The transgene is then not present in all the cells of the transgenic founder. This is due to the fact that the integration of the foreign DNA occurs sometimes not in the first cell but later at the two- or four-cell stage. The transmission of the transgene from these founders appears not to respect the Mendel law. The transmission rate is due to the fact that the transgene is not present in all the gametes. At the next generation, the proportion of transgenics is Mendelian [24]. About 1% of transgenic founders do not transmit their transgene as the mosaicism is very high and the transgene is rare or non-existent in gametes.

In non-mammalian species, the pronuclei cannot be visualized as the embryo is embedded in an abundant and opaque vitellus. High amounts of DNA (millions of copies in a few nanoliters) must then be injected into the cytoplasm of the one-cell embryos. This relatively simple technique is efficient in several fish species [42, 56] but highly inefficient in chicken, in Xenopus, in some fish, and in insects. For unknown reasons, the integration of the foreign DNA thus does not occur in some species. In lower vertebrates and invertebrates, the embryo DNA and the foreign DNA are replicated very rapidly. The foreign DNA is then highly amplified leading to multiple independent integrations occurring during the first days of embryo development in the same animals. The resulting transgenic animals are often very mosaic making it difficult their use. Several reproduction cycles allow a segregation of the different transgenes until the animals contain a single integration site.

In a *C. elegans*, direct DNA injection into gonad syncytium leads to the generation of transgenics with a good yield [98].

Gene constructs bordered by I-Sce1 sites have been used to generate transgenic fish. The plasmids were previously cut by the I-Sce1, and the fraction was injected without any previous DNA purification. Unexpectedly, this protocol markedly increased the yield of transgenesis. Interestingly, the same observation was made in Xenopus. The mechanism improving transgenesis is not known [97]. The I-Sce1 might protect DNA against degradation, favor DNA transfer to the nucleus, or directly stimulate the integration mechanism.

Microinjection is therefore a good technique but insufficient in some species. Additional methods have been found and are still under study.

Detection of the transgene and examination of its integrity can be achieved using Southern blotting or PCR using multiple primers corresponding to various regions of the transgene. Zygocity of the transgene may be evaluated by quantitative PCR [69] or in situ hybridization.

Use of Transposons

Transposons are short genomic DNA regions, which are replicated and randomly integrated into the same genome. The number of a given transposon is thus increasing until the cell blocks this process to protect itself from the degradation of its genome. Foreign genes can be introduced into transposons in vitro. The recombinant transposons may then be microinjected into 1-day embryos as it is for DNA. A transposon contains a gene coding for an integrase specific of this type of transposon and required for the integration of the transposon. The integrase gene is bordered by two inverted terminal repeat regions (ITR) required for the transposon integration. The addition of the foreign DNA implies the elimination of the integrase gene. This makes space for the foreign DNA, and it also prevents the recombinant transposon to disseminate in the genome. To allow the integration of the recombinant transposon, the integrase protein or a gene construction directing the synthesis of the integrase must be co-injected with the recombinant transposon (Fig. 6). The foreign gene thus becomes integrated into the embryos with a yield of about 1%. Essentially, all the transgenic insects are generated by using transposons as vectors [43, 95]. Transposons also proved efficient to generate transgenic fish, chicken, and mammals [22, 23]. The transposons used for transgenesis

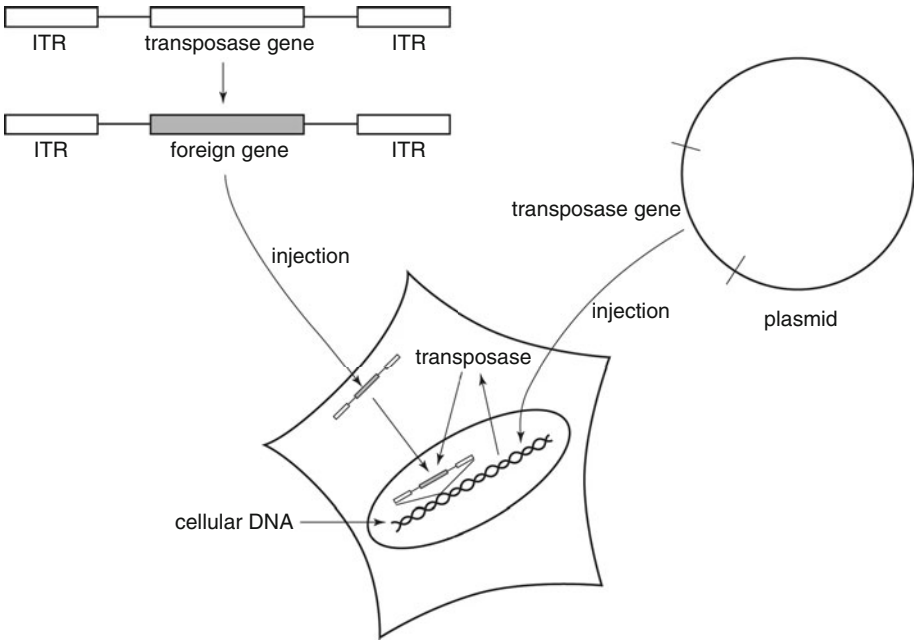

Transgenics: Alternative Gene Transfer Methods. Figure 6
Gene transfer using a transposon. The integrase gene of a transposon is replaced by the gene of interest between the two ITR (inverted terminal repeats) required with the integrase for an efficient integration. Integrase or a gene coding for this protein must be injected with the transposon to allow its integration

are chosen or engineered to be unable to disseminate in the host genome under the action of the integrase of endogenous transposons. Transposons are therefore efficient and safe tools, but they can harbor no more than 2–3 kb of foreign DNA.

Transposons are being used with ICSI giving a high transgenensis rate [64].

Efficient transposons started being used to disseminate in genomes after the addition of the corresponding integrase into cells. This leads to multiple random integrations of the transposon providing researchers with insertional mutants. A correlation may then be established between a biological alteration of the animals and the nature of the gene inactivated by the presence of the transposon within the gene [22].

Use of Lentiviral Vectors

Retroviruses have not the capacity to autoreplicate, and they must be integrated stably into the genome of the cells they infected to replicate. This explains why up to 1% of animal genomes contain degenerated retroviral genes. This property of retroviruses is implemented to integrate foreign genes in cells, in animals, and in patient's somatic cells. For this purpose, the viral genes are removed from the genome of lentiviruses (a category of retroviruses) and replaced by the genes of interest. Viral particles are then prepared and used to transfer the foreign genes into oocytes or one-cell embryos (Fig. 7). Retroviral vectors have been studied and used during the last two decades for gene therapy. Important improvements of these vectors have markedly enhanced their efficiency. Vectors using ALV (avian leucosis virus) studied two decades ago proved poorly efficient to generate transgenic chicken [4, 83].

The lentiviruses have the advantage over the common retroviruses to be able to infect and transfer their genes in quiescent as well as in multiplying cells. The majority of the retrovirus genomes need a cell multiplication including a transient degradation of the nuclear membrane to reach chromatin and integrate into the cell genome. On the contrary, lentiviral viruses contain proteins carrying their genome to the nucleus in quiescent as well as in multiplying cells.

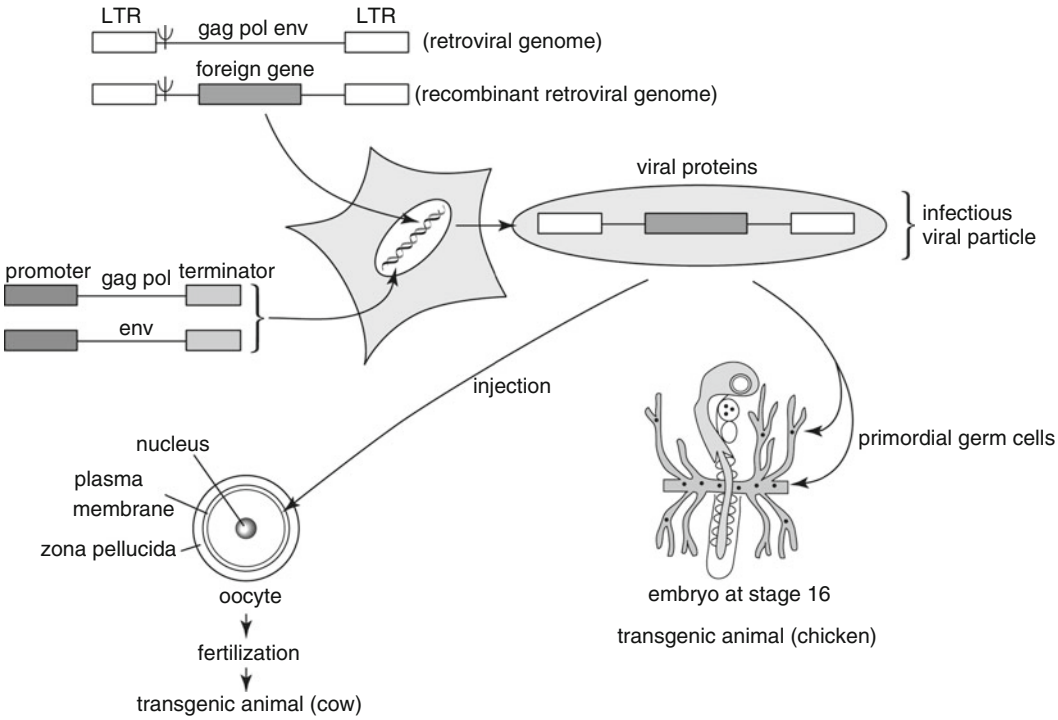

Transgenics: Alternative Gene Transfer Methods. Figure 7
Gene transfer using lentiviral vectors. The pathogenic genes are removed from the HIV genome and replaced by the gene of interest. The gene construction is transfected into trans-complementing cells synthesizing the essential HIV proteins required for the formation of infectious recombinant particles. The particles secreted from the cells in the culture medium are injected between the zona pellucida and the membrane of the cell embryos or of oocytes or within the fetal gonad in chicken. The infection is followed by an efficient integration of the gene of interest

EIAV (equine infectious anemia virus) proved that it is able to generate transgenic chicken [60]. Presently, the most frequently used lentiviral vector derives from the HIV (human immunodeficiency virus) genome. The natural envelope protein of the HIV, which recognizes specific receptors on the plasma membrane to induce infection has been replaced by the envelope of vesicular somatitis virus, which is not a retrovirus. This envelope recognizes the phospholipids of plasma membrane, making the infection of essentially all cell types possible. The particles containing this envelope are stable, and they can be concentrated and administered at a high concentration into embryos or oocytes. For unknown reasons, lentiviral vectors have to be injected in cow oocytes rather than in one-cell embryos to transfer their genes.

Safe experimental conditions have been defined to use the lentiviral vectors. This method proved very highly efficient in several species including mammals [74, 78] and birds [11, 52, 86]. Up to 90% of transgenic animals may be obtained. This results from the fact that with high viral particle concentration, multiple independent integrations take place in the embryo genome. These integrations may occur later than the first cell stage giving birth to mosaic animals. The selection of lines harboring a single integration is preferable, but it may take a very long time in farm animals. Reducing the concentration of viral particles reduces the yield of transgenics but also the multiple integrations.

Trangenes transferred by lentiviral vectors are reputed not to become silent on the contrary to transgenes transferred by plasmidic constructions. This may be due in part to the fact that one or several integrated copies are active whereas others have been silenced. Lentiviral proved to be efficient tools to express transgenes coding for siRNAs [99].

Interestingly, siRNA could induce specific gene knockdown in rat [19, 35]. This observation is important as the classical tools to induce gene knockout (ES cells and cloning) are not available in this species. Lentiviral harboring foreign genes driven by cell-specific promoters may direct the expression of the transgenes in the targeted cells specifically [86]. The use of lentiviral vectors is limited by the fact that they cannot harbor more than 8 kb of foreign DNA. Special constructions must also sometimes be prepared to reduce the influence of the viral enhancers on the transgene promoter.

In mammals, the lentiviral vectors are injected between the zona pellucida and the cell membrane of one-cell embryos or oocytes. The efficiency of lentiviral vectors may be enhanced by injecting envelope-free constructions into cell cytoplasm [108].

The preparation of lentiviral particles carrying foreign genes is routinely achieved by academic and private structures at a moderate price. This possibility is particularly attractive for laboratories, which do not need a frequent use of this tool.

Use of ICSI

Foreign DNA must not necessarily be introduced into one-cell embryos. In principle, it can be as well injected in gametes before fertilization. DNA microinjection into oocytes proved inefficient, and this approach was soon abandoned. Using sperm is another possibility based on the assumption that foreign DNA cannot integrate into the genome as in this cell DNA is embedded in protamines and not able to replicate. Sperm was rather postulated to bind DNA in its surface and carry it into the oocyte during fertilization.

More than a decade ago, it was shown that sperm incubated in the presence of DNA before being used for fertilization was able to transfer the foreign gene into the oocyte and generate transgenic mice. This approach proved capable of generating transgenic mice, sheep, chicken, fish, and pigs [45, 109]. However, this method appeared difficult to use as DNA was frequently degraded [91]. The seminal plasma contains high DNAse activity, which degrades the gene and only rearranged fragments of the foreign genes were generally found in the transgenic animals. An appropriate sperm washing is required to prevent DNA degradation. For no clear reasons, not all the ejaculates can lead to a success of the method. Transgenic mice and rabbits were obtained by incubating sperm with DNA in the presence of DMSO (dimethylsulfoxide) and by using conventional in vitro fertilization [87].

The method has been greatly improved by using ICSI (intracytoplasmic Sperm Injection). This technique, which consists of injecting sperm into the cytoplasm of oocytes is currently used for in vitro fertilization in humans. To transfer genes, sperms from which plasma membrane has been damaged by freezing and thawing or with a mild treatment by non-polar detergents were incubated in the presence of the gene of interest and further used for fertilization by ICSI. The ICSI approach started being implemented in Xenopus a decade ago as all the other methods failed [59]. This method proved efficient in mice [65, 88] and pigs [109]. Transposon use and ICSI may be combined to increase the yield of transgenesis [64, 88].

ICSI is therefore an excellent method to generate transgenic animals on condition that ICSI is possible in the considered species. One advantage of ICSI is that both long and short DNA fragments of DNA may be used sucessfully. DNA rearrangements may occur during ICSI especially when long DNA fragments are used. Another advantage is that foreign DNA is integrated mostly at the first cell stage of embryos. This reduces the number of animals being mosaic for the transgene.

Use of Episomal Vectors

The methods described above to transfer foreign genes rely on the integration of the DNA into the host genome. Another theoretical possibility is the use of episomal vectors capable of autoreplicating in host cells independently of the genomic DNA and transferred to daughter cells. Fragments of chromosomes are being used for particular projects, requiring the transfer of very long DNA fragments [44]. These chromosomal vectors are not of an easy use, and they carry a number of genes in addition to the gene of interest. These extra genes may interfere with the transgene or with the whole organism of the host.

Another possibility consists of using vectors, which derive from viruses having the capacity to replicate in animal cells and to be transferred to daughter cells. Herpes viruses are naturally stably maintained as autonomous circular minichromosome at a low copy

number in animal cells. Foreign genes can be introduced into Herpes viral vectors and be maintained during cell division. This kind of vectors is generally species specific. This greatly reduces their potential use as well-known Herpes viruses are not available for all animal species.

Episomal vectors not based on the use of viral elements are available. Such a vector proved highly efficient to transfer foreign genes into pig embryo using ICSI [58]. This vector was maintained without any selection pressure in the cells of the early developing embryos but seemingly not later. These vectors are therefore excellent tools to study transgene effect during early embryo development. Hence, until now, only the integration of foreign DNA into the host genome makes it possible the generation of stable lines of transgenic animals.

A theoretical safety problem raised by the use of episomal vectors is that it could be transmitted to other cells mechanically and thus independently of any infectious process. However, this event is expected to occur very rarely. More likely, non-integrated DNA is more available to recombine with homologous sequences in the host genome, leading to mutations, chromosome rearrangement, or integration.

Use of Intermediate Cells

Use of Pluripotent Cells In some situations, the efficiency of the genetic modification is too low to be achieved by the methods described above. This is particularly the case for gene targeting. One possibility to circumvent this problem is to genetically modify pluripotent cells that are further used to participate in the development of living organisms. Pluripotent cells have the capacity to participate in the development of all the organs including gametes.

Pluripotent cells exist in the early embryos (morula and blastocysts), and they are known as ES cells (embryonic stem cells). The pluripotent cells can be cultured, genetically modified, selected and transferred into morula or blastocysts. These cells participate in the development of the embryo to give birth to chimeric transgenic animals (Fig. 3). This means that the organs of the animals, including sexual cells, derive from the genetically modified cells or from the recipient embryo. A proportion of the offsprings from these chimeric animals harbor the genetic modification if they derive from the transplanted cells.

The first ES cells implemented to genetically modify animals (mice) were used at the end of the 1980s. For unknown reasons, commonly used ES cell lines have been established only in two mouse lines and mainly in the 129/Sv strain. In other lines and species, the ES cells lose their pluripotency. They can give birth to animals, which are still chimeric but have no more the capacity to transmit the genetic modification to their offspring. In practice, this complicates sometimes the use of the knockout mice. Indeed, in a number of cases, the gene knockout should be obtained in a genetic background very different from that of the 129/Sv strain. Successive crossings allow the mutation to be transferred in the strain in which the biological function in question may be optimally studied.

After sustained efforts for two decades, authentic rat ES cell lines have been established [7, 2, 49–51]. This breakthrough relies on the use of small molecules added into the culture medium. These molecules control essential genes required for the maintenance of pluripotency. They replace proteins like LIF, which are commonly used for mouse ES cells but are not successful in other species.

Recent experiments have shown that the transfer of three genes, normally expressed in pluripotent cells, into somatic cells can dedifferentiate these organ cells into pluripotent cells known as iPS (induced pluripotent cells) and almost similar to ES cells [68, 72, 93, 105]. Interestingly, small molecules can mimic and replace Kfl4 gene, which is one of the genes required to transform somatic cells into pluripotent cells [55]. These experiments open avenues for cell therapy and gene therapy [76]. The approach known as therapeutic cloning and based on the capacity of cloning (SCNT) to dedifferentiate somatic cells into totipotent cells further differentiated in vitro into pluripotent cells has become virtually no more strictly necessary. iPS cells can potentially be obtained in different species by this method. Similarly, iPS cells might be implemented for transgenesis in species in which ES cells are not available (Fig. 3). Cow and pig iPS cells have been obtained and are currently under study.

Use of Primordial Germ Cells and Testis Stem Cells Experiments carried out a few years ago showed that

chicken primordial germ cells (PGC) can be isolated and cultured in conditions maintaining their multipotency giving stable cell lines known as EG cells (embryonic gonad cells). Foreign genes can be transferred into EG cells, which can be implanted into recipient embryos and participate in gonad development. In practice, the EG cells, which contain the gene of interest and a selection gene are cloned, amplified, and injected into an early embryo in which the majority of the cells have been destroyed by irradiation. This gives the best chance to the EG cells to colonize the embryo and to give birth to transgenic showing a high degree of chimerism and thus transmitting their transgene to progeny with a high yield. This approach has greatly simplified the generation of transgenic chicken [33, 101].

Testicular cells, which are sperm precursors can be isolated, cultured, genetically modified, more or less differentiated in vitro, and transplanted into recipient testis to give functional sperms that are able to generate transgenic animals by fertilization. Alternatively, sperm cell precursors may be genetically modified in situ using viral vectors [33, 41, 46, 48, 94]. These methods are still under study, and they are not currently used to generate transgenic animals.

Use of Cloning

The birth of Dolly, the sheep, demonstrated that the genome of somatic cells can be reprogrammed after being introduced into an enucleated oocyte. This generates a pseudo-embryo capable, with a relatively low yield, of giving birth to clones of the cell donor. This technique was initially designed to improve transgenesis efficiency in farm animals. This approach is likely to be used to accelerate genetic selection, but its only real application is presently transgenesis [81, 85]. The principle of this method is described in Fig. 3, and this topic is the matter of another chapter. Genes are transferred into somatic cells, which are then used to generate transgenic clones. This method has become the most frequently used for big farm animals as it simplifies the task of experimenters and enhances the rate of transgenic animals. Recently published important data have shown that the cloning technique does not provoke mutations in the clones [67].

Gene Construction

Random Integration A problem, which has not been completely solved is the reliability of transgene expression [36–38]. In the early 1980s, the first experiments to generate transgenic mice revealed that transgenes were often not working as expected. In a number of cases, the expression of the transgenes was very weak and not strictly specific to the promoter associated with the foreign gene. In a few cases, it was demonstrated that the ectopic expression of the transgenes was due to the presence of genomic enhancers in the vicinity of the integrated foreign DNA. The frequent transgene silencing was thought to be induced by the integration of the foreign genes near genomic silencers. These putative silencers were rarely identified suggesting that the ectopic transgene expression and their silencing could be not symmetrical phenomena. It was also proved that the level of transgene expression was generally not a function of the integrated copy number. In a number of cases, the expression level appeared even lower when the number of integrated copies was higher. A striking demonstration was given by the experiment in which the human β-globin gene was bordered by two LoxP sequences and integrated into mouse genome as several copies in tandem. The transgene remained silent in these mice but was reactivated in their offspring in which the copy number was reduced to one by the action of the Cre recombinase [26].

After about one decade, it appeared that this was due to chromatin position effects suggesting that the transgenes were recognized as foreign sequences by some unknown cellular mechanisms. One of the most surprising data was that a genomic DNA sequence containing the whole human β-globin gene including its promoter region allowing the gene to be expressed as expected in cultured red blood cells remained silent in transgenic mice. This discrepancy suggested that the transgene silencing occurred more in vivo than in cultured cells and that this phenomenon could take place during the early phase of embryo development. A hypothesis was also that the genomic DNA sequence contained the whole β-globin gene and some but not all the transcription regulators. A confrontation of the very low expression level in patients suffering from β-thalassemia and the structure of their DNA in the genomic β-globin gene region revealed that, in some

cases, the gene and its promoter were normal but that some remote genome regions were missing. This suggested that these regions could be the putative regulators missing in transgenic mice. An association of these regions with the β-globin gene allowed the later to be highly expressed in transgenic mice. The extensive study of the β-globin gene locus in several species revealed that remote regulatory elements are present on both side of the locus. These elements bind transcription factors specifically present in differentiated red blood cells, and they form a transcription complex known as a hub in the vicinity of the promoter through a looping process (Fig. 8) ([20, 21]). This type of mechanism seems to be common to many if not all genes in vertebrates and similarly also in invertebrates.

These observations may explain at least in part why traditionally constructed transgenes are so often poorly active and they suggest using long genomic DNA fragments contained in BAC (bacterial artificial chromosome) vectors to promote transgene expression [53]. The implementation of the long DNA fragments may be laborious as they are sensitive to mechanical degradation [100, 102]. The long DNA fragments can be transferred using microinjection, ICSI, gene targeting, or via intermediate cells. The failure of transgene activity is likely due to multiple reasons, which still complicate the construction of vectors allowing an efficient and reliable expression of transgenes. The optimized conditions to use long DNA fragments as vectors are described in a recent paper [102].

Nucleotidic Composition of the Vectors Integrated retroviral sequences and transposons are inactivated by a cytosine methylation of the CpG motifs and the local formation of condensed chromatin (heterochromatin) in which histones are deacetylated and methylated in some sites. Transgenes seem to be inactivated by similar mechanisms. Many of the vertebrate genes contain CpG islets in their regulatory regions, which contribute to their expression. Some of the CpG motifs belong to the binding site of the transcription factor Sp1, which is present not only in the promoter region of the gene but also sometimes in the first introns. An exceedingly large number CpG motif in vectors induces transgene silencing. The replacement of some of the GC-rich regions by AT-rich regions improves transgene expression. MARs (matrix-attached region) are frequently found in the vicinity of genes, and they bind DNA to the nuclear matrix locally. MARs are generally AT rich, and they have been added into vectors to tentatively improve transgene expression. This approach met variable success. The *Escherichia coli* β-galactosidase gene is rich in

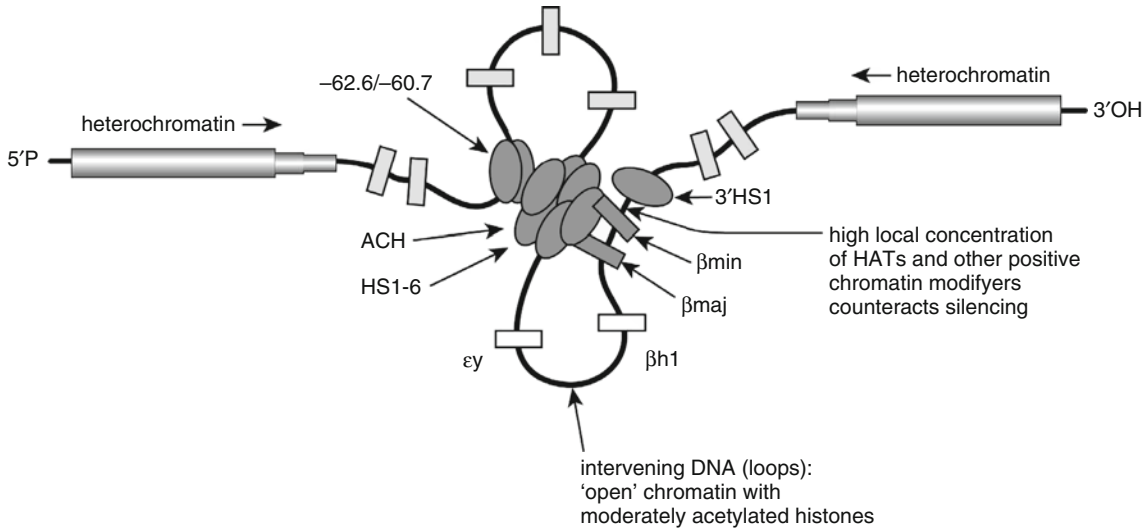

Transgenics: Alternative Gene Transfer Methods. Figure 8
Mechanism of action of remote transcription enhancers. The formation of loops allows the various regulatory factors to be in close vicinity and generate an active transcription complex

CpG, and it is known to be a potent transgene silencer. This silencing potency proved to be markedly reduced as the number of CpG was diminished [17, 34]. The coding sequences of a transgene may thus be obtained by chemical synthesis to replace a part of the CpG-rich codons by others without modifying the sequence of the corresponding protein.

Use of Insulators In order to improve the expression of transgenes, it is possible to use large genomic DNA fragments (50–250 kb) expected to contain all the regulatory elements of the gene of interest [53]. It implies only the isolation and characterization of BACs (bacterial artificial chromosome) from a bank. Linearized or circular BACs may be used as such if the expression of the gene(s) they contain is wanted [102]. One drawback of using BACs is that they often contain several genes. The BACs thus transfer all these genes potentially generating unknown and unwanted interactions with the animals. If needed, these genes may be inactivated in BACs by performing short deletions, for example, of the cap region, using homologous recombination in bacteria.

An attractive approach consists of using BACs as vectors harboring the foreign genes. The foreign DNA sequence must be introduced into the BAC using homologous recombination in bacteria. It is important to note that the transgenes driven by BACs rarely work in an ideal fashion, if only this concept has a real meaning. Long genomic DNA fragments are expected to suppress the position effects, which is not often fully the case. Indeed, it is clear that the variegated expression, which characterizes the conventional transgenes is less or even much less frequent in animals harboring BAC vectors. A higher proportion of animals expressing the transgenes is generally found with BAC than with plasmid vectors. Yet, the different lines harboring BACs vectors usually do not express the transgenes at an identical level for a given number of integrated copies. Similarly, it has been rarely reported that the expression of the transgenes was strictly a function of the copy number of the integrated BACs. This means that the BACs provide transgenes with essential elements for their expression but they remain often not fully able to suppress the position effects. This disappointing observation may not be surprising from a theoretical point of view. Indeed, a locus has been constructed during evolution to express in an appropriate manner the genes it contains. This implies that these genes are protected against deleterious positions effects in their natural chromatin environment. They have no theoretical reasons to be independent of the position effect in all their integration sites. Some BACs may contain all the elements providing transgenes with a complete independence of the integration site. If not, a BAC vector may still contain enough regulatory elements improving significantly transgene expression to justify its use.

A more sophisticated approach could consist of using as vectors containing not all the DNA sequence of BACs but only the major elements involved in the control of gene and transgene expression. This implies that these regulatory elements have been identified, characterized, and introduced into mini-BACs or even plasmids. An example of this is a major regulatory region of the genes present in mammalian β-globin locus, which is located upstream within the locus of olfactory receptor genes [21]. The study of the remote genomic regulatory elements is still in infancy. Apart from the technical difficulty to study them is the fact that each gene or gene cluster seems to have used available genomic sequences to design specific mechanisms allowing a satisfactory expression. Some of these regulatory elements have an unexpected structure. Examples are SINE B2 and Alu sequences or some active tRNA genes, which are essential regulators for neighbor genes [54].

The notion of boundary elements and insulators is essential to understand how unrelated genes can be expressed in a specific manner without being under the dependency of the neighbor gene regulators. This situation is clearly often not encountered for transgenes suggesting that the constructs commonly used do not contains the natural insulators. Insulator activity has been found in the LCR (locus control region) of the chicken β-globin locus. This activity was identified in a 300 bp fragment, which proved its ability to block in a specific sense the action of an enhancer when added between this enhancer and a promoter directing the expression of a reporter gene. The enhancer blocker was mediated by the binding of the regulatory protein CTCF to a specific DNA sequence. The CTCF element has now been found in the boundary region of several other genes. This type of elements, known as enhancer-blocking

insulators, cannot be assimilated to silencers as the former act only when they are located between an enhancer and a promoter. Moreover, the enhancer-blocking insulators often show unidirectional action.

This 300-bp region of the chicken β-globin locus was found later to contain another sequence known as a chromatin opener. Chromatin openers are regulators capable of maintaining a local euchromatin configuration favoring the expression of the neighbor gene by preventing the local formation of condensed chromatin (heterochromatin) [27]. The elements having this function are known as barrier insulators [27]. The barrier insulators cannot be assimilated to enhancers as their effect does not occur during transient foreign gene expression in transfected cells. The region locus known as 5'HS4 and containing the 300-bp sequence can improve the expression of a number of unrelated transgenes in mammals [29, 92]. However, the potency of the 5'HS4 element remains generally insufficient to express transgenes in a fully satisfactory manner.

In the mean time, the presence of AT-rich MARs within the genomic region required for the expression of a gene suggested that these sequences were essential remote regulators. This hypothesis was not confirmed [90].

Optimization of the Transcribed Region The 5′UTR (untranslated region) must have less GC sequences stabilizing double-stranded hairpin structures, which do not favor ribosome migration to the initiation codon. The AUG initiation codon must preferably be in the Kozak consensus sequence GCCA/GCCAUGG to optimize translation initiation. The natural 5′UTR of the gene of interest may contain sequences regulating translation. It may be then useful not to keep this region and replace it by a short (not less than 80 nucleotides) AT-rich 5′UTR region from gene known to be efficiently translated in many cell types or in the targeted cells of the animals. Some mRNAs encode proteins, which are not naturally secreted. Peptide signals may be added to their cDNA.

A transgene must contain at least one intron, which is required to favor the transfer of the mRNA to the cytoplasm. The first intron of many genes contains sites, which bind transcription factors and they may favor transgene expression. The intron excision is dependent upon several signals comprising consensus sequences in both splicing sites (CAG GUA/GAGUA/UGGG in 5′ and CAG G. . .GAA/G. . .GAA/G. . .in 3′), namely, a CU-rich region immediately upstream of the 3′splicing site and a BPS site (branched point sequence) U/CNCUGAC at about 30 nucleotides upstream of the 3′splicing site and upon splicing enhancers [61]. The second intron of the rabbit β-globin gene is considered as efficient to express transgenes in mammals. The intron(s) must preferably be put before the coding region. If an intron is added after the translated region, the 5′splicing site must be located not more than 50 nucleotides from the termination codon to avoid the activation of the NMD (nonsense-mediated decay), which degrades the mRNA [10].

The cDNA and other regions of the vectors may preferably be chemically synthesized. This allows reducing the number of CpG motifs, to choose the best codons, to eliminate cryptic 3′or 5′splicing sites and sequences known to prevent transcription or translation.

The 3′UTR region of a number of mRNA contains signals for mRNA translation and stability. A number of mRNAs have an AU-rich region with the AUUUA motif in their 3′UTR. These mRNAs have a short half-life controlled by the cell cycle (Beelman and Parker 1995). The fortuitous presence of such sequences must be searched and eliminated to prevent a poor transgene expression. Some mRNAs contain translation regulators acting by the binding of proteins favoring the recycling of ribosomes by binding to the 5′UTR. CU-rich regions in the 3′UTR enhance the stability of the mRNAs, and they may be added in the vectors downstream of the cDNAs. Stabilizing sequence can be taken in the 3′UTR of the human or bovine genes and of the α-globin gene, which also contain efficient transcription terminators [13]. Some proteins are anchored to the plasma membrane by a GPI structure (glycophosphatidylinositol). A protein normally not anchored in this way acquires this property by adding in the 3′end of the cDNA the peptide, allowing the addition of GPI. Micro-RNAs (miRNA), the role of which was recently discovered, inhibit specifically the translation of an mRNA after forming a hybrid with its 3′UTR. The presence of target sequence for a miRNA may unduly inhibit the expression of a transgene. This target sequence should then be deleted.

Targeted Integration The techniques described above lead to uncontrolled but not strictly random gene integration. Foreign DNA is preferentially integrated into gene-rich genome regions, and its location can be precisely identified. A foreign DNA fragment can recombine very precisely with a genomic DNA region containing a similar sequence. This natural mechanism known as homologous recombination makes the precise replacement of a gene by another possible. An active gene may thus be replaced by an inactive version, leading precisely to an inactivation of the targeted gene (gene knockout).

The targeted gene may as well be replaced by an active gene (gene knockin). This technique allows therefore a better controlled transgenesis reducing possible damage of the genomic DNA at the integration site and frequent side effects of the genes located in the vicinity of the transgene on the expression of the transgene. Two mouse genomic loci are currently being used as foreign gene knockin. One is the HPRT locus [6] and the other is Rosa 26 locus [110]. The genes of these loci are known to be expressed constitutively, and they were supposed to be bordered by regulators able to drive the expression of transgenes in a reliable manner. In practice, a number of transgenes appeared to be expressed as expected when integrated in these loci. Interestingly, also the expression of the transgenes added in these loci remained specific to the promoter linked to the foreign genes. The two loci thus appear to maintain an open chromatin configuration, favoring the expression of the transgenes irrespective of their composition.

Yet, this approach remains limited by the fact that the homologous recombination required for gene targeting is a rare event. The targeted integrations by homologous recombination of a foreign DNA represent 0.1–1% of the total integrations. The cells in which targeted integration occurred must be selected and used to generate a transgenic animal. The formation of chimeric embryos using pluripotent cells, multipotent cells, or the cloning technique is presently required to obtain a targeted integration.

Meganucleases were discovered in yeast about two decades ago, and it was shown that they participate in intron generation. These enzymes recognize sites as long as 18 nucleotides leaving negligible chance to cleave mammalian genomic DNA. About 80 natural meganucleases have been identified so far. It was observed later than one of these meganucleases I-Sce1 induces chromosome recombination in mammalian cells and this was attributed to the fact that meganucleases cleave both DNA strands [14]. Such breaks stimulate DNA repair mechanism. It was also shown that I-Sce1 amplifies the rate of homologous recombination [15] and consequently gene replacement in mammalian cells [16]. The DNA sequences recognized by natural meganucleases must then be added to the genome of animals either at targeted sites by homologous recombination or at random sites. To circumvent this problem, hundreds of engineered meganucleases each recognizing a specific genomic DNA sites have been obtained making a local cleavage of DNA and gene targeting possible [25].

Multiple engineered zinc finger nucleases (ZFN) have also been obtained. Each of these enzymes has the capacity to cut one DNA strand at a unique genomic DNA site. To mimic natural meganucleases and cut locally both DNA strands, two ZFN each recognizing a DNA strand at neighbor sites are needed [75]. Engineered meganucleases and engineered zinc finger nucleases, thus, make it possible gene targeting at multiple sites of the genome. This method, which is being developed to improve the efficiency and the precision of gene therapy for humans can be applied to target the integration of foreign DNA into experimental animals. Interestingly, when the recombination vector is not added with the meganuclease or the ZFN, the genomic DNA repair takes place spontaneously but often with alteration of the sequence. This process known as NHEJ (non-homologous end joining) corresponds to a knockout (Fig. 9) [84, 106]. This mechanism is efficient, and it allowed a knockout in one cell fish and rat embryos after the injection of engineered meganucleases [28, 107]. This method can be considered as a transgenesis without transgene. This inclines to think that gene targeting might be achieved directly in mammal embryos by injecting an engineered meganuclease or ZFN with or without a homologous recombination vector.

In the same line, the bacterial enzyme phiC31, which is an integrase, recognizes several sites in various animal genomes and allows the efficient integration of foreign genes at the targeted sites. Several other recombination systems rely on the use of integrases such as Cre and Flp, which recognize specific sites of about

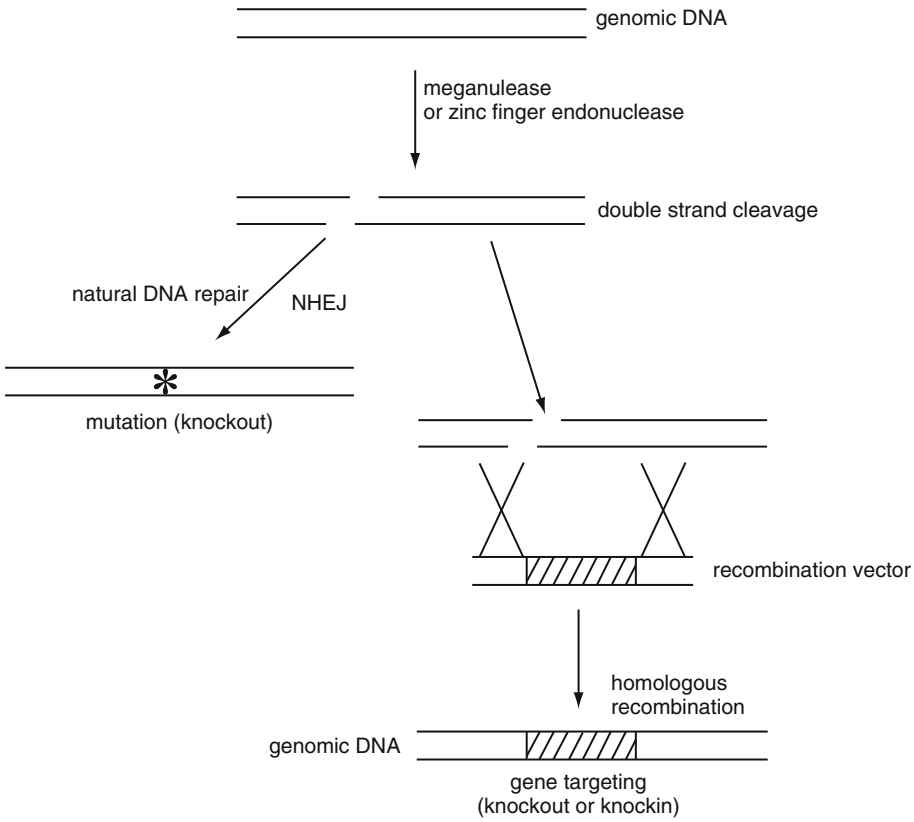

Transgenics: Alternative Gene Transfer Methods. Figure 9
Engineered meganucleases or ZFN (zinc finger nucleases) induce a targeted local cleavage of both genomic DNA strands. In the absence of recombination vector, the DNA is repaired leading to frequent local mutations and to a knockout. In the presence of a recombination vector, the foreign gene is integrated into the targeted site with a high efficiency

30 nucleotides (LoxP and FRT, respectively), which must be added to the animal genome. In practice, deletion of the integrated foreign DNA has more chance to occur than integration. Mutated LoxP and FRT sequences capable of promoting integration but not deletion must be used. This approach is known as RMCE (Recombinase-mediated Cassette Exchange) [1]. These systems are more often used to delete a DNA region previously bordered by the LoxP or the FRT sequences.

The Co-expression of Several Cistrons It is sometimes necessary to express two or even three genes in the same transgenic animals. The co-injection of several independent vectors makes the generation of up to 80% of the animals harboring the two or three genes, which are co-integrated at the same site possible. An alternative consists of using IRES (internal ribosome entry site). Such sequences exist in the 5′UTR of many mRNAs, the translation of which is controlled by these sequences, which bind specific cellular inducible proteins. Such sequences may be added between two cistrons and allow their simultaneous translation from a single vector. The addition of the IRES 80 nucleotides after the termination codon of the first cistron may contribute to favor the expression of the second cistron [39]. It should be kept in mind that IRES represents a family of sequences acting by different mechanisms, which are only partly known.

Gene Inactivation (Knockdown) with Interfering RNAs Long double-stranded RNAs are randomly cut into 19–21 nucleotide fragments known as siRNA (small interfering RNA) or RNAi. One of the two

strands of the siRNA is kept and targeted to an mRNA having a complementary sequence. This induces the degradation of the mRNA or the reversible inhibition of its translation. In practise, a synthetic gene containing the targeted 19–21 nucleotide sequence followed a short random sequence and by the targeted sequence in the opposite orientation is linked to a promoter acting with RNA polymerase III (usually U6 or H1 gene promoters). The RNAs synthesized by such vectors form a 19–21 nucleotide double-stranded RNA known as shRNAs (short hairpin RNA) and are processed in cells to generate active siRNAs. An appropriate expression of siRNA genes in transgenic animals can be obtained when they are introduced into lentiviral vectors [99].

The recent discovery of the role of micro-RNAs has increased the possibility to use interfering RNAs. Micro-RNAs are encoded by short genes expressed under the control of RNA polymerase II promoters. Their primary products are transformed into siRNAs. Alternatively, the sequence coding for a micro-RNA and even several micro-RNAs in tandem may be inserted into introns without any promoter. The promoter of the gene or transgene thus drives transcription of the micro-RNA genes and the intron degradation releases micro-RNA precursors, which are processed in the nucleus and the cytoplasm, generating active siRNAs (Ripoll et al. unpublished data). The mature miRNAs, which are fully complementary to the targeted mRNA induce degradation of this mRNA. The miRNAs, which are only partially complementary to the targeted mRNA and which recognize a sequence located in the 3′UTR (3′untranslated region) of the mRNA inhibit translation of this mRNA without inducing its degradation. The possibility known as knockdown to generate transgenic animals expressing siRNAs preventing specifically the expression of a gene by degrading the corresponding mRNA or inhibiting its translation has opened avenues for the control of gene expression in vivo. The application of the siRNA approach raises specific problems in animals. Long double-stranded RNAs induce interferons and some unspecific immune reactions [89]. On the other hand, siRNAs are not autoamplified in higher animals and this reduces their potency. Vectors to express miRNA gene are available, but simple shRNA genes are not easily expressed in transgenic animals using conventional vectors. Moreover, siRNAs may off-target mRNAs and generate deleterious side effects.

Several programs based on empirical data indicate the putative optimal shRNA sequences that are able to generate siRNA strands complementary to the mRNAs. A very important point is to choose a target region of the mRNA, which is not in double-stranded structure and thus accessible to the siRNA. Banks of shRNA genes in lentiviral vectors are available for the mRNAs of different species. It remains that most of the siRNAs do not inhibit the targeted gene to more than 70–80%, which may be insufficient to obtain some relevant animal models. It is tempting to use vectors expressing the shRNA genes at a relatively high level. This may not lead to any significant increase of the inhibition and to an off-targeting, which may be detrimental or even lethal for the animals [89]. In fact, it seems that a well-targeted siRNA can be highly active even at a low concentration. It appears, therefore, to be of paramount importance to select the shRNA capable of inhibiting strongly the targeted mRNA even at a low concentration in cell systems before generating transgenic animals [79].

Use of Transdominant Negative Proteins The action of a gene can be blocked at the protein level by expressing specific inhibitors such as antibodies recognizing the protein of interest [66]. Alternatively, transdominant negative proteins acting as decoys may be used. Transgenic mice mimicking type II diabetes were obtained by overexpressing a mutated insulin receptor still capable of binding the hormone but not of transducing its message [9]. Similarly, overexpression of pseudorabies virus receptor in transgenic mice protects these animals against Aujeszky disease [70].

Genetic Ablation Destroying specifically given cell types in animals may reveal their role in organogenesis. This can be achieved by expressing genes coding for toxins. The challenge is then to express quite specifically the transgenes. Different systems are implemented for this purpose [12, 82]. They rely on two-step mechanisms, which reduce the risk of ectopic expression of the toxin genes.

Control of Transgenes by Exogenous Inducers All the vectors described above and used to express

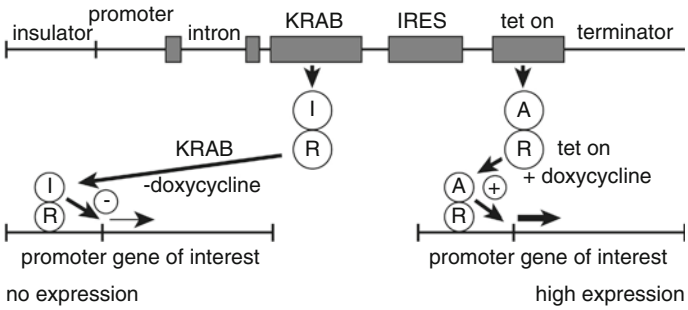

Transgenics: Alternative Gene Transfer Methods. Figure 10
The control of transgene expression may be controlled by an exogenous inducer. In the absence of the inducer (doxycycline), the transcription enhancer (Tet on) is not bound to DNA and it does not stimulate transcription whereas the transcription inhibitor (KRAB) is bound to DNA and reduces the background expression of the gene of interest. In the presence of doxycycline, the reverse is true and the gene of interest is activated

transgenes contain promoters, which are naturally active in the cells of the transgenic animals. This implies that the transgenes are regulated by the natural inducers of the host genes. The induction of a transgene may then coincide with the unwanted stimulation of a number of host genes. Artificial promoters containing regulatory elements from both animal genes and bacterial genes have been designed. The resulting promoters are active in animal cells but controlled by substances active in bacteria but not in animals. The most popular system is based on the use the bacterial tetracycline repressor gene. In practise, the transgene becomes reversibly activated only when tetracycline or doxycycline is administered to the animals. Various mutants are available making it possible either the induction of the transgene or its inhibition by the addition of the exogenous inducer. A number of similar systems are available and currently used in transgenic animals with a good success [30, 57]. In order to reduce the background expression of the transgene in the absence of the exogenous inducers, the alternative expression of a transcription repressor as KRAB and of an inducer as Tet-on system may be implemented (Fig. 10). These tools, which require the transfer of several genes offer virtually the possibility to express a transgene precisely in a given cell type and at a given moment.

Gene Deletion Conventional homologous recombination makes it possible gene deletion known as knock-out. Another possibility consists of using the Cre-LoxP

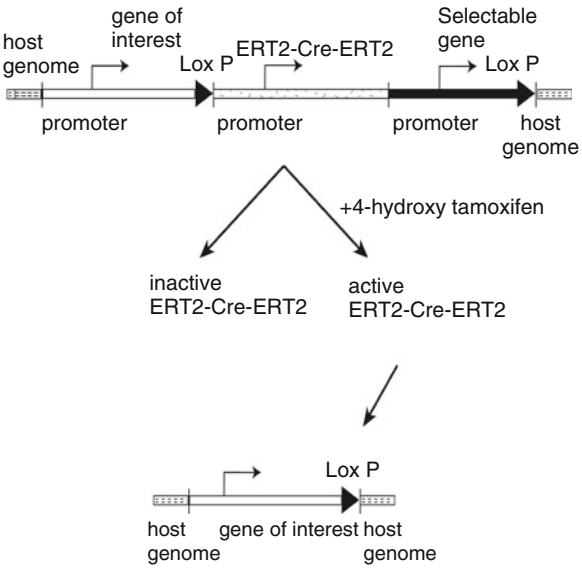

Transgenics: Alternative Gene Transfer Methods. Figure 11
Activation of Cre recombinase and selectable gene elimination by 4-hydroxy tamoxifen. The Cre recombinase gene expression may be under the control of the Tet-on system itself under the control of a cell-specific promoter. The fusion protein Cre recombinase–mutated estrogen receptor is active only in the presence 4-hydroxy tamoxifen. The elimination of the DNA region bordered by LoxP sequences is thus sharply controlled. The selection gene and the Cre recombinase may thus be eliminated from transgenic animals at any stage of their life

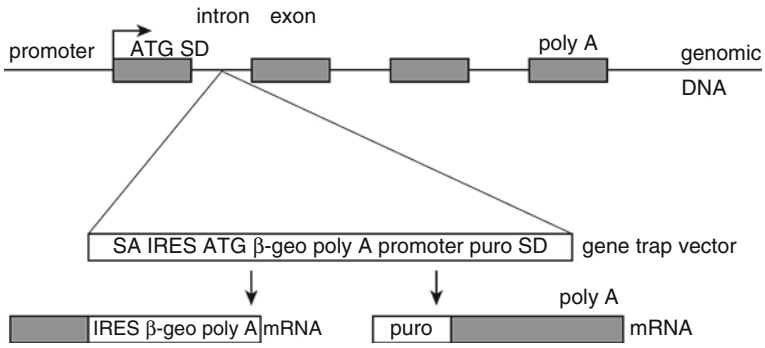

Transgenics: Alternative Gene Transfer Methods. Figure 12
Schematic representation of a gene trapping vector. The vector is randomly integrated into the genome of cells that are able to generate transgenic animals (Fig. 3). The β-geo gene is a fusion of the β-galactosidase gene, giving a blue color to cells, and neomycin resistance gene, giving a resistance to geneticin. The vector contains also the puromycin resistance gene, splicing acceptor sites, no promoter, and no transcription terminator. The β-geo selection gene is expressed only when it was integrated into a functional gene. The inactivated gene may be identified by sequencing the genomic DNA flanking the integrated vector. A correlation between the inactivated gene and an altered biological function of the animal may be established

or Flp-FRT systems. A LoxP sequence must first be added to both ends of the fragment to delete. The presence of the Cre recombinase will then recombine the two LoxP sites, leading to a deletion of the DNA fragment located between the LoxP regions. This makes it possible the elimination of a selection gene. The same approach allows the specific and controlled deletion of an inhibitory DNA region, leading to the activation of the gene located in its vicinity. The Cre recombinase may be synthesized by the corresponding gene under the direction of a cell-specific promoter including promoters under the control of doxycycline. Another level of control can be obtained by using an engineered Cre recombinase, which becomes reversibly active in the presence of an estrogen analogue, 4-hydroxy tamoxifen (Fig. 11) [62]. This offers the advantage of having the active Cre recombinase for short periods of time. This prevents the non-specific action of the Cre recombinase, which can recognize cryptic sites in the host genome and induce illegitimate recombination damaging the host DNA. This tool is appropriate to delete genes for resistance to antibiotics.

Vectors for Gene Trapping The identification of genes involved in a given biological function is an essential step to understand the role of the genes particularly those responsible for human diseases. One possibility is to use vectors for the trapping of active genes. One such vector is described in Fig. 12. Other vectors are shown in the chapter of a book [36]. New tools make it possible random gene knockout in genomes by inserting foreign DNA sequences using transposons [22] or lentiviral vectors. Banks of siRNA genes in lentiviral vectors can also be used to knock-down genes. The inhibited genes can thus be identified and correlations with altered biological functions in the animals become possible.

Future Directions

During the coming decade, transgenesis in animals is expected to be as intensively or even more used than presently. One of the trends is to refine the different tools for basic research as for the different applications. The time when transgenic mice were prepared in a blind manner by microinjecting simple gene constructions is getting over. The recent and very significant improvement of the gene transfer techniques should make several animal species less marginal in the transgenesis field. The number of transgenic models for basic research is being extended to a larger number of species, namely to rats, chicken, Xenopus,

and even cow [47, 80, 96]. The sequencing of an increasing number of genomes, including different mouse strains and even different individuals, will contribute to extend the use of animal transgenesis.

The proportion of transgenic animals used for basic research, including the models for the study of human diseases, is currently very high. This proportion should change but moderately in favor of applications in the food domain and also in the pharmaceutical field including the production of pig cells and organs for patients and the production of recombinant pharmaceutical proteins. Indeed, the production of pig cells and organs is making significant progress but it remains unpredictable when and if the transplantation of pig cells and organs will become a tangible reality as many problems remain to be solved [73].

The production of pharmaceutical proteins in milk and egg white has become a realistic approach as the techniques have reached sufficient maturity even if the production of each protein is a challenge. Yet, this application of transgenesis is coming more slowly than anticipated. For complex reasons not clearly related to the efficiency of the technique or to biosafety guidelines, the pharmaceutical companies remain more or less reluctant to start using animals to obtain pharmaceutical proteins. Companies may consider that their profit is presently higher with the production of recombinant proteins in conventional fermentors harboring animal cell lines, even or because this system generates a shortage of medicaments for patients. A recent multiauthor book is a survey of all the aspects of this technique including the ethical considerations [77].

Whatever happens, the application of transgenic animals for food production should become a reality in the coming decade. The increasing knowledge of alleles in farm animals and of a variety of other possible transgenes should give more space to the use of transgenesis to improve animal production. The recent achievement of the cow genome sequencing will contribute to using cattle alleles more extensively. It remains that the generation of relevant transgenic founders and their extensive use in breeding will be slower than in plants due to the high cost of transgenesis and the time required for the dissemination of their genomes in herds. The poor acceptability of biotechnology particularly in the EU is another hurdle.

The recent progress of several techniques of gene transfer are becoming more popular in laboratories and companies and therefore should be pursued. DNA microinjection into embryos will still be used in the species in which it is efficient. Lentiviral vectors are more and more frequently used, and this trend should become still stronger as the preparation of efficient and safe lentiviral particles has become a standard technique. Other viral vectors could be implemented in future. One candidate is AAV (adeno-associated virus). This virus is spontaneously integrated into cell genomes as lentiviruses. AAV vectors are used with some success for gene therapy in humans [111]. One of its advantages over lentiviruses is that they can harbor longer DNA fragments. Viral vectors might prove attractive for some applications in breeding. It is indeed conceivable to introduce massively foreign genes only into somatic cells. Examples are fish or more generally the animals, which swim or fly and can disseminate in environment. Growth hormone genes transferred into a sufficient number of salmon somatic cells might have the same biological effect on growth than the corresponding transgene without any risk of its dissemination in oceans.

More and more transposons are found and engineered to be able to generate efficiently and in a safe manner a variety of transgenic animals. One of the challenges of modern biology is to decipher the mechanisms involved between given genetic information and the expression of a physiological function. The systematic random integration of transposons and also of lentiviral vectors into the genome of cells able to participate in the development of transgenic animals is expected to generate banks of cells and animals in which physiological disorders can be connected to the genes interrupted by the vectors. This approach is similar to that of generating banks of animals having genes inactivated by knockout or knockdown. Several animal and data banks are available: EMMA in EU, Jackson Laboratory in USA, IMSR (International Mouse Strain Resource), ISTT (International Society for Transgenic Technologies) www.transtechsociety.org, [40], private companies (namely Charles River) as well as academic and private structures for the generation of transgenic mice, rats, and rabbits.

Gene transfer using ICSI has met a great success in mice and a few other species. It is simpler and more

efficient than conventional DNA injection. A broader implementation of this technique is presently limited by the fact that ICSI independently of transgenesis is still possible in only a small number of species. This situation is essentially due to the fact that researchers have not yet acquired this knowledge. The principle of ICSI is common to all species, but the manipulation of oocytes and sperm needs specific training. ICSI should thus be used more intensively in the near future in mice and extended to other species. The possible combination of ICSI and transposons as well as of envelope-free lentiviral particles might contribute to enhance gene transfer efficiency.

A trend is clearly to perform the genetic modifications not directly in embryos but rather in intermediate cells further used to generate transgenic animals. The long-term success of mouse ES cells to target gene transfer via the generation of chimeric animals is expected to be rapidly extended to the use of rat ES cells and iPS cells in different species, which are able to generate chimeric animals as ES cells. Progress must be made before iPS cells are used for transgenesis. This is being achieved as iPS cells are extensively studied since they are expected to be a major tool for cell therapy and gene therapy in humans. The techniques to generate iPS cells from somatic cells must be adapted to each species. An important recent progress is the possibility of dedifferentiating somatic cells no more by transferring the three identified key genes but by introducing the corresponding mRNAs, which are unstable by essence and thus leave no genetic information in the iPS cells. It is conceivable to transfer the three genes able to generate iPS cells into embryonic cells to obtain more easily ES cells. Indeed, cultured ES cells are known to quickly lose their pluripotency in most mouse lines and essentially in all other species but rats. ES cells from a number of species might become a reality in this way. The preliminary success, which made it possible the use of small molecules in culture medium instead of proteins to generate pluripotent cells from embryos or somatic cells is very encouraging. It suggests that the generation and the use of pluripotent cells in multiple species might become a relatively easy task. This would facilitate markedly the genetic modification of animal genomes. A more speculative reasoning is to postulate that the complete dedifferentiation of somatic cells into totipotent cells will be possible some day by the transfer of genes or chemical inducers, which remain to be found. Cloning and transgenesis as well as their coupling and related ethical problems would be considerably simplified.

Cloning by SCNT proved that it is possible to make the random and targeted gene transfer. The popularization of this technique is likely, but it depends on improvement of the technique. Indeed, clones are often if not always epigenetically modified leading to a limited efficiency, to a reduced welfare of the animals, and potentially to health problems. Significant improvement has been achieved in 10 years, and a better control of cloning should occur in the coming years.

The construction of vectors making it possible a reliable and well-controlled expression of the transgenes will be progressively improved by the empirical use of BAC containing long genomic DNA fragments with the majority of the remote transcription regulators. The use of long genomic DNA fragments as vectors is expected to become more and more frequent but to remain empirical for some time. Most likely, an increasing number of BAC vectors containing regulatory elements for the expression of transgenes in the different cells types will become available. Despite the higher difficulty to manipulate BAC rather than plasmids constructs, researchers will prefer in a number of cases to invest a part of their time in the construction of BAC vectors to tentatively obtain better transgenic models. Rapid progress is being made on the description of chromatin structure and activity. Gene study is more and more performed at the level of a locus and not only of a given gene. This will provide researchers with well-identified chromatin regulators, which will be used to design compact vectors containing these regulators capable of optimizing transgene expression.

Gene targeting is essential to obtain relevant transgenic models. The demonstration that a local cleavage of DNA by natural or engineered meganucleases or by engineered zinc finger nuclease considerably increases the efficiency of homologous recombination is of major importance for basic and applied research particularly for projects involving transgenesis. Gene knockin and knockout are expected to become much more efficient, up to the point perhaps to be possible directly in one-cell embryos and not only via intermediate cells.

The demonstration that DNA cleavage by zinc finger nuclease in the absence of recombination vectors is followed by an imperfect DNA repair (NHEJ), which in a significant proportion of cases leads to a mutation, thus to a gene knockout. The fact that gene knockout by NHEJ could be obtained directly in fish embryos opens new avenues as this protocol does not require any more the laborious gene knockout by homologous recombination. Hundreds of engineered zinc fingers have been designed to recognize specific sites in different genomes. This number should increase rapidly in the coming years. A particularly fascinating point is that NHEJ as well as conventional knockout and knockin might be applied not only to genes proper but also to their genomic regulators. This would allow the study of the regulators of various loci without implementing the laborious manipulation of BACs.

The discovery of siRNA has rapidly been followed by the generation of gene knockdown in plants. The same did not occur in animals. The use of long double-stranded RNA induces deleterious side effects in animals. The availability of lentiviral vector banks harboring genes coding for shRNAs makes gene knockdown easier in animals. The efficiency of this approach remains limited by the insufficient knowledge on the mechanisms of RNA interference. Progress has been made to empirically design siRNA having a high and specific inhibitory effect on gene expression. An important parameter is now taken into consideration. It is known that the sequence of the siRNA determines the choice of the strand, which will target the mRNA of interest and its capacity to inactivate this mRNA. It now clear that the local structure of the mRNA is essential to make the access of the siRNA possible. Additional progress is expected in this field, and it should facilitate gene knockdown in transgenic animals.

Using constructs in which the transgene is under the control of exogenous inducers like doxycycline is a reality. Sophisticated systems reducing the background expression of the transgene expression in the absence of the inducers are currently used. The possibility of using these systems to create relevant transgenic models is expected to be more and more frequently used. Improvement of these techniques is likely by finding additional inducers.

It is essential to be able to knock out genes in chosen cells and at defined period of the animal life. This conditional knockout implies the used of the Cre/LoxP or similar systems. The conditional expression of the Cre recombinase and its conditional activation by 4-hydroxy tamoxifen offer a great flexibility. Improvement of these systems is possible. A more extensive use of these systems, which give satisfaction to researchers will be done in the coming years.

Transgenesis techniques are thus making important progress for the generation of transgenic animals as for the fine control of transgene expression. The available tools and those in development are expected to be adapted to the systematic study of multiple genes required for the development of integrative biology.

Bibliography

Primary Literature

1. Baer A, Bode J (2001) Coping with kinetic and thermodynamic barriers: RMCE, an efficient strategy for the targeted integration of transgenes. Curr Opin Biotechnol 12:473–448
2. Baker M (2009) Authentic rat embryonic stem cells. Nat Rep Stem Cells. doi:10.1038/stemcells 2009.11
3. Bishop JO (1997) Chromosomal insertion of foreign DNA. In: Houdebine LM (ed) Transgenic animal generation and use. Harwood Academic Publishers, Amsterdam, pp 219–224
4. Bosselman RA, Hsu RY, Boggs T, Hu S, Bruszewski J, Ou S, Kozar L, Martin F, Green C, Jacobsen F, Nicolson M, Schultz JA, Semon KM, Rishell W, Stewart RG (1989) Germline transmission of exogenous genes in the chicken. Science 243:533–535
5. Bronson SK, Smithies O (1994) Altering mice by homologous recombination using embryonic stem cells. J Biol Chem 269:27155–27158
6. Bronson SK, Plaehn EG, Kluckman KD, Hagaman JR, Maeda N, Smithies O (1996) Single-copy transgenic mice with chosen-site integration. Proc Natl Acad Sci USA 93:9067–9072
7. Buehr M, Meek S, Blair K, Yang J, Ure J, Silva J, McLay R, Hall J, Ying QL, Smith A (2008) Capture of authentic embryonic stem cells from rat blastocysts. Cell 135:1287–1298
8. Capecchi MR (1989) Altering the genome by homologous recombination. Science 244:1288–1292
9. Chang PY, Benecke H, Le Marchand-Brustel Y, Lawitts J, Moller DE (1994) Expression of a dominant-negative mutant human insulin receptor in the muscle of transgenic mice. J Biol Chem 269:16034–16040
10. Chang YF, Imam JS, Wilkinson M (2007) The nonsense-mediated decay RNA surveillance pathway. Annu Rev Biochem 76:51–74
11. Chapman SC, Lawson A, Macarthur WC, Wiese RJ, Loechel RH, Burgos-Trinidad M, Wakefield JK, Ramabhadran R, Mauch TJ, Schoenwolf GC (2005) Ubiquitous GFP expression in transgenic chickens using a lentiviral vector. Development 132:935–940

12. Chen YT, Levasseur R, Vaishnav S, Karsenty G, Bradley A (2004) Bigenic Cre/loxP, puDeltatk conditional genetic ablation. Nucleic Acids Res 32:e161
13. Chkheidze AN, Lyakhov DL, Makeyev AV, Morales J, Kong J, Liebhaber SA (1999) Assembly of the α-globin mRNA stability complex reflects binary interaction between the pyrimidine-rich 3′ untranslated region determinant and poly(C) binding protein α CP. Mol Cell Biol 19:4572–4581
14. Choulika A, Perrin A, Dujon B, Nicolas JF (1994) The yeast I-Sce I meganuclease induces site-directed chromosomal recombination in mammalian cells. C R Acad Sci 317:1013–1019
15. Choulika A, Perrin A, Dujon B, Nicolas JF (1995) Induction of homologous recombination in mammalian cells using the I-Sce I system of Saccharomyces cerevisiae. Mol Cell Biol 15:1968–1973
16. Cohen-Tannoudji M, Robine S, Choulika A, Babinet C, Louvard D, Jaisser F (1998) I-Sce I-induced gene replacement at a natural locus in embryonic stem cells. Mol Cell Biol 18:1444–1448
17. Cohen-Tannoudji M, Babinet C, Morello D (2000) Lac Z and ubiquitously expressed genes: should divorce be pronounced? Transgenic Res 9:233–235
18. Couble P (1997) The biolistic. In: Houdebine LM (ed) Transgenic animal generation and use. Harwood Academic Publishers, Amsterdam, pp 209–213
19. Dann CT (2007) New technology for an old favorite: lentiviral transgenesis and RNAi in rats. Transgenic Res 16:571–580
20. de Laat W, Grosveld F (2003) Spatial organization of gene expression: the active chromatin hub. Chromosome Res 11:447–459
21. de Laat W, Klous P, Kooren J, Noordermeer D, Palstra RJ, Simonis M, Splinter E, Grosveld F (2008) Three-dimensional organization of gene expression in erythroid cells. Curr Top Dev Biol 82:117–139
22. Ding S, Wu X, Li G, Han M, Zhuang Y, Xu T (2005) Efficient transposition of the piggyBac (PB) transposon in mammalian cells and mice. Cell 122:473–483
23. Dupuy AJ, Clark K, Carlson CM, Fritz S, Davidson AE, Markley KM, Finley K, Fletcher CF, Ekker SC, Hackett PB, Horn S, Largaespada DA (2002) Mammalian germ-line transgenesis by transposition. Proc Natl Acad Sci USA 99:4495–4499
24. Echelard Y (1997) Genetic mosaicism in the generation of transgenic mice. In: Houdebine LM (ed) Transgenic animal generation and use. Harwood Academic Publishers, Amsterdam, pp 233–225
25. Epinat JC, Arnould S, Chames P, Rochaix P, Desfontaines D, Puzin C, Patin A, Zanghellini A, Paques F, Lacroix E (2003) A novel engineered meganuclease induces homologous recombination in yeast and mammalian cells. Nucleic Acids Res 31:2952–2962
26. Garrick D, Fiering S, Martin DI, Whitelaw E (1998) Repeat-induced gene silencing in mammals. Nat Genet 18:56–59
27. Gaszner M, Felsenfeld G (2006) Insulators: exploiting transcriptional and epigenetic mechanisms. Nat Rev Genet 7:703–713
28. Geurts AM, Cost GJ, Freyvert Y, Zeitler B, Miller JC, Choi VM, Jenkins SS, Wood A, Cui X, Meng X, Vincent A, Lam S, Michalkiewicz M, Schilling R, Foeckler J, Kalloway S, Weiler H, Ménoret S, Anegon I, Davis GD, Zhang L, Rebar EJ, Gregory PD, Urnov FD, Jacob HJ, Buelow R (2009) Knockout rats via embryo microinjection of zinc-finger nucleases. Science 325:433
29. Giraldo P, Rival-Gervier S, Houdebine LM, Montoliu L (2003) The potential benefits of insulators on heterogonous constructs in transgenic. Transgenic Res 12:751–755
30. Gitzinger M, Kemmer C, El-Baba MD, Weber W, Fussenegger M (2009) Controlling transgene expression in subcutaneous implants using a skin lotion containing the apple metabolite phloretin. Proc Natl Acad Sci USA 106:10638–10643
31. Gordon JW, Scangos GA, Plotkin DJ et al (1980) Genetic transformation of mouse embryos by microinjection of purified DNA. Proc Natl Acad Sci USA 77:7380–7384
32. Hammer RE, Pursel VG, Rexroad CE et al (1985) Production of transgenic rabbits, sheep and pigs by microinjection. Nature 315:680–683
33. Han JY (2009) Germ cells and transgenic chicken. Comp Immunol Microbiol Infect Dis 32:61–80
34. Henry I, Forlani S, Vaillant S, Muschler J, Choulika A, Nicolas JF (1999) LagoZ and LagZ, 2 genes depleted of CpG dinucleotides, derived from the LacZ gene for the study of epigenetic control. C R Acad Sci III 322:1061–1070
35. Herold MJ, van den Brandt J, Seibler J, Reichardt HM (2008) Inducible and reversible gene silencing by stable integration of an shRNA-encoding lentivirus in transgenic rats. Proc Natl Acad Sci USA 105:18507–18512
36. Houdebine LM (2003) Animal transgenesis and cloning. Wiley, Chichester, 250 pp
37. Houdebine LM (2007) Transgenic animal models and target validation. Methods Mol Biol 360:163–202
38. Houdebine LM (2009) Methods to generate transgenic animals in ethics of science and technology assessment. Springer-Verlag, Heildelberg/Berlin/New York, pp 31–48
39. Houdebine LM, Attal J (1999) Internal ribosome entry sites (IRESs): reality and use. Transgenic Res 8:157–177
40. Jerchow B (2009) Transgenic technology meeting 2008 in Toronto, Canada: a meeting report. Transgenic Res. doi:10.1007/s11248-008-9238-8
41. Kalina J, Senigl F, Micáková A, Mucksová J, Blazkova J, Yan H, Poplstein M, Hejnar J, Trefil P (2007) Retrovirus-mediated in vitro gene transfer into chicken male germ line cells. Reproduction 134:445–453
42. Kapuscinski AR, Hayes KR, Li S, Dana G (2007) Environmental risk assessment of genetically modified organisms, vol. 3 Methodologies for transgenic fish. Series eds. Hallerman EM (Guest) and Schei PJ. CAB International, Oxford, pp 304
43. Kayser K (1997) Gene transfer in Drosophila melanogaster. In: Houdebine LM (ed) Transgenic animal generation and use. Harwood Academic Publishers, Amsterdam, pp 133–137
44. Kuroiwa Y, Kasinathan P, Choi YJ, Naeem R, Tomizuka K, Sullivan EJ, Knott JG, Duteau A, Goldsby RA, Osborne BA, Ishida I, Robl JM (2002) Cloned transchromosomic calves producing human immunoglobulin. Nat Biotechnol 20: 889–894

45. Lavitrano M, Bacci ML, Forni M, Lazzereschi D, Di Stefano C, Fioretti D, Giancotti P, Marfe G, Pucci L, Renzi L, Wang H, Stoppacciaro A, Stassi G, Sargiacomo M, Sinibaldi P, Turchi V, Giovannoni R, Della Casa G, Seren E, Rossi G (2002) Efficient production by sperm-mediated gene transfer of human decay accelerating factor (hDAF) transgenic pigs for xenotransplantation. Proc Natl Acad Sci USA 99:14230–14235
46. Lee YM, Jung JG, Kim JN, Park TS, Kim TM, Shin SS, Kang DK, Lim JM, Han JY (2006) A testis-mediated germline chimera production based on transfer of chicken testicular cells directly into heterologous testes. Biol Reprod 75:380–386
47. Lewin HA (2009) It's a Bull's Market. Research on domesticated livestock heralds new advances in evolutionary biology, animal breeding, and animal models for human diseases. Science 324:478–479
48. Li BC, Sun GB, Sun HC, Xu Q, Gao B, Zhou GY, Zhao WM, Wu XS, Bao WB, Yu F, Wang KH, Chen GH (2007) Efficient generation of transgenic chickens using the spermatogonial stem cells in vivo and ex vivo transfection. Reproduction 134: 445–453
49. Li P, Tong C, Mehrian-Shai R, Jia L, Wu N, Yan Y, Maxson RE, Schulze EN, Song H, Hsieh CL, Pera MF, Ying QL (2008) Germline competent embryonic stem cells derived from rat blastocysts. Cell 135:1299–1310
50. Li W, Wei W, Zhu S, Zhu J, Shi Y, Lin T, Hao E, Hayek A, Deng H, Ding S (2009) Generation of rat and human induced pluripotent stem cells by combining genetic reprogramming and chemical inhibitors. Cell Stem Cell 4:16–19
51. Liao J, Cui C, Chen S, Ren J, Chen J, Gao Y, Li H, Jia N, Cheng L, Xiao H, Xiao L (2008) Generation of induced pluripotent stem cell lines from adult rat cells. Cell Stem Cell 4:11–15
52. Lillico SG, Sherman A, McGrew MJ, Robertson CD, Smith J, Haslam C, Barnard P, Radcliffe PA, Mitrophanous A, Elliot EA, Sang HM (2007) Oviduct-specific expression of two therapeutic proteins in transgenic hens. Proc Natl Acad Sci USA 104:1771–1776
53. Long X, Miano JM (2007) Remote control of gene expression. J Biol Chem 282:15941–15945
54. Lunyak VV, Prefontaine GG, Núñez E, Cramer T, Ju BG, Ohgi KA, Hutt K, Roy R, García-Díaz A, Zhu X, Yung Y, Montoliu L, Glass CK, Rosenfeld MG (2007) Developmentally regulated activation of a SINE B2 repeat as a domain boundary in organogenesis. Science 317:248–251
55. Lyssiotis CA, Foreman RK, Staerk J, Garcia M, Mathur D, Markoulaki S, Hanna J, Lairson LL, Charette BD, Bouchez LC, Bollong M, Kunick C, Brinker A, Cho CY, Schultz PG, Jaenisch R (2009) Reprogramming of murine fibroblasts to induced pluripotent stem cells with chemical complementation of Klf4. Proc Natl Acad Sci USA 106:8912–8917
56. Maclean N (2003) Genetically modified fish and their effects on food quality and human health and nutrition. Trends Food Sci Technol 14:242–252
57. Malphettes L, Fussenegger M (2006) Improved transgene expression fine-tuning in mammalian cells using a novel transcription-translation network. J Biotechnol 124:732–746
58. Manzini S, Vargiolu A, Stehle IM, Bacci ML, Cerrito MG, Giovannoni R, Zannoni A, Bianco MR, Forni M, Donini P, Papa M, Lipps HJ, Lavitrano M (2006) Genetically modified pigs produced with a nonviral episomal vector. Proc Natl Acad Sci USA 103:17672–17677
59. Marsh-Armstrong N, Huang H, Berry DL, Brown DD (1999) Germ-line transmission of transgenes in Xenopus laevis. Proc Natl Acad Sci USA 96:14389–14393
60. McGrew MJ, Sherman A, Ellard FM, Lillico SG, Gilhooley HJ, Kingsman AJ, Mitrophanous KA, Sang H (2004) Efficient production of transgenic chickens using lentiviral vectors. EMBO Rep 5:728–733
61. Mersch B, Gepperth A, Suhai Sand Hotz-Wagenblatt A (2008) Automatic detection of exonic splicing enhancers (ESEs) using SVMs. BMC Bioinform 9:369. doi:10.1186/1471-2105-9-369
62. Metzger D, Chambon P (2001) Site- and time-specific gene targeting in the mouse. Methods 24:71–80
63. Mialhe E, Boulo V, Cadoret JP, Cedeno V, Rousseau C, Motte E, Gendreau S, Bachère E (1997) Gene transfer technology in marine invertebrates. In: Houdebine LM (ed) Transgenic animal generation and use. Harwood Academic Publishers, Amsterdam, pp 151–155
64. Moisyadi S, Kaminski JM, Yanagimachi R (2009) Use of intracytoplasmic sperm injection (ICSI) to generate transgenic animals. Comp Immunol Microbiol Infect Dis 32:47–60
65. Moreira PN, Pozueta J, Pérez-Crespo M, Valdivieso F, Gutiérrez-Adán A, Montoliu L (2007) Improving the generation of genomic-type transgenic mice by ICSI. Transgenic Res 16:163–168
66. Müller M (2000) Increasing disease resistance in transgenic domestic. In: Toutant JP, Balazs E (eds) Molecular farming. Institute National de la Recherche Agronomique, Paris, pp 87–98
67. Murphey P, Yamazaki Y, McMahan CA, Walter CA, Yanagimachi R, McCarrey JR (2009) Epigenetic regulation of genetic integrity is reprogrammed during cloning. Proc Natl Acad Sci USA 106:4731–4735
68. Nakagawa M, Koyanagi M, Tanabe K, Takahashi K, Ichisaka T, Aoi T, Okita K, Mochiduki Y, Takizawa N, Yamanaka S (2008) Generation of induced pluripotent stem cells without Myc from mouse and human fibroblasts. Nat Biotechnol 26: 101–110
69. Notini AJ, Li R, Western PS, Sinclair AH, White SJ (2009) Rapid and reliable determination of transgene zygosity in mice by multiplex ligation-dependent probe amplification. Transgenic Res. 18:987–991
70. Ono E, Amagai K, Taharaguchi S, Tomioka Y, Yoshino S, Watanabe Y, Cherel P, Houdebine LM, Adam M, Eloit M, Inobe M, Uede T (2004) Transgenic mice expressing a soluble form of porcine nectin-1/herpesvirus entry mediator C as a model for pseudorabies-resistant livestock. Proc Natl Acad Sci USA 101:16150–16155
71. Palmiter RD, Brinster RE, Trumbauer ME, Rosenfeld MG, Birnberg NC, Evans RM (1982) Dramatic growth of mice that develop from eggs microinjected with metallothionein-growth hormone fusion genes. Nature 300:611–615

72. Pera MF, Hasegawa K (2008) Simpler and safer cell reprogramming. Nat Biotechnol 26:59–60
73. Petersen B, Carnwath W, Niemann H (2009) The perspectives for porcine-to-human xenografts. Comp Immunol Microbiol Infect Dis 32:61–80
74. Pfeifer A (2006) Lentiviral transgenesis – a versatile tool for basic research and gene therapy. Curr Gene Ther 6: 535–542
75. Porteus MF, Carroll D (2005) Gene targeting using zinc finger nucleases. Nat Biotechnol 23:967–973
76. Rao M (2007) Scalable human ES culture for therapeutic use: propagation, differentiation, genetic modification and regulatory issues. Gene Ther 15:82–88
77. Rehbinder E, Engelhard M, Hagen K, Jorgensen RB, Pardo-Avellaneda R, Schnieke A, Thiele F (2009) Pharming. Promises and risks of biopharmaceuticals derived from genetically modified plants and animals. Ethics of Science and Technology Assessment Vol 35. Springer-Verlag, Berlin/Heidelberg
78. Ritchie WA, Neil C, King T, Whitelaw CB (2007) Transgenic embryos and mice produced from low titre lentiviral vectors. Transgenic Res 16:661–664
79. RNAi: Multi-author review (2009) Nature 457:7228
80. Roberts RM, Smith GW, Bazer FW, Cibelli J, Seidel GE Jr, Bauman DE, Reynolds LP, Ireland JJ (2009) Farm animal research in crisis. Science 324:468–469
81. Robl JM, Wang Z, Kasinathan P, Kuroiwa Y (2007) Transgenic animal production and animal biotechnology. Theriogenology 67:127–133
82. Saito M, Iwawaki T, Taya C, Yonekawa H, Noda M, Inui Y, Mekada E, Kimata Y, Tsuru A, Kohno K (2001) Diphtheria toxin receptor-mediated conditional and targeted cell ablation in transgenic mice. Nat Biotechnol 19:746–750
83. Salter DW, Smith EJ, Hughes SH, Wright SE, Crittenden LB (1987) Transgenic chickens: insertion of retroviral genes into the chicken germ line. Virology 157:236–240
84. Santiago Y, Chan E, Liu PQ et al (2008) Targeted gene knockout in mammalian cells by using engineered zinc-finger nucleases. Proc Natl Acad Sci USA 105:5809–5814
85. Schnieke AE, Kind AJ, Ritchie WA, Mycock K, Scott AR, Ritchie M, Wilmut I, Colman A, Campbell KH (1997) Human factor IX transgenic sheep produced by transfer of nuclei from transfected fetal fibroblasts. Science 278:2130–2133
86. Scott BB, Lois C (2005) Generation of tissue-specific transgenic birds with lentiviral vectors. Proc Natl Acad Sci USA 102:16443–16447
87. Shen W, Li L, Pan Q, Min L, Dong H, Deng J (2006) Efficient and simple production of transgenic mice and rabbits using the new DMSO-sperm mediated exogenous DNA transfer method. Mol Reprod Dev 73:589–594
88. Shinohara ET, Kaminski JM, Segal DJ, Pelczar P, Kolhe R, Ryan T, Coates CJ, Fraser MJ, Handler AM, Yanagimachi R, Moisyadi S (2007) Active integration: new strategies for transgenesis. Transgenic Res 16:333–339
89. Sioud M (2006) Innate sensing of self and non-self RNAs by toll-like receptors. Trends Mol Med 12:167–176
90. Sippel AE, Saueressig H, Hubler MC, Faust N, Bonifer C (1997) Insulation of transgenes from chromosomal position effects. In: Houdebine LM (ed) Transgenic animal generation and use. Harwood Academic Publishers, Amsterdam, pp 257–266
91. Smith K, Spadafora C (2005) Sperm mediated gene transfer: applications and implications. BioEssays 27:551–562
92. Taboit-Dameron F, Malassagne B, Viglietta C, Puissant C, Leroux-Coyau M, Chéreau C, Attal J, Weill B, Houdebine LM (1999) Association of the 5'HS4 sequence of the chicken beta-globin locus control region with human EF1-alpha gene promoter induces ubiquitous and high expression of human CD55 and CD59 cDNAs in transgenic rabbits. Transgenic Res 8:223–235
93. Takahashi K, Tanabe K, Ohnuki M, Narita M, Ichisaka T, Tomoda K, Yamanaka S (2007) Induction of pluripotent stem cells from adult human fibroblasts by defined factors. Cell 131:861–872
94. Takehashi M, Kanatsu-Shinohara M, Inoue K, Ogonuki N, Miki H, Toyokuni S, Ogura A, Shinohara T (2007) Adenovirus-mediated gene delivery into mouse spermatogonial stem cells. Proc Natl Acad Sci USA 104:2596–2601
95. Tamura T, Thibert C, Royer C, Kanda T, Abraham E, Kamba M, Komoto N, Thomas JL, Mauchamp B, Chavancy G, Shirk P, Fraser M, Prudhomme JC, Couble P (2000) Germline transformation of the silkworm Bombyx mori L. using a piggyBac transposon-derived vector. Nat Biotechnol 1:81–84
96. The Bovine Genome Sequencing and Analysis Consortium, Elsik CG, Tellam RL, Worley KC (2009) The genome sequence of taurine cattle: a window to ruminant biology and evolution. Science 324:522–528
97. Thermes V, Grabher C, Ristoratore F, Bourrat F, Choulika A, Wittbrodt J, Joly JS (2002) I-SceI meganuclease mediates highly efficient transgenesis in fish. Mech Dev 118:91–98
98. Thierry-Mieg D, Naert K, Bonnerot C (1997) Genetic transformation of *Caenorhabditis elegans*. In: Houdebine LM (ed) Transgenic animal generation and use. Harwood Academic Publishers, Amsterdam, pp 137–151
99. Tiscornia G, Singer O, Ikawa M, Verma IM (2003) A general method for gene knockdown in mice by using lentiviral vectors expressing small interfering RNA. Proc Natl Acad Sci USA 100:1844–1848
100. Umland T, Montoliu L, Schütz G (1997) The use of yeast artificial chromosomes for transgenesis. In: Houdebine LM (ed) Transgenic animal generation and use. Harwood Academic Publishers, Amsterdam, pp 289–298
101. Van de Lavoir MC, Diamond JH, Leighton PA, Mather-Love C, Heyer BS, Bradshaw R, Kerchner A, Hooi LT, Gessara TM, Swanberg SE, Delany ME, Etches RJ (2006) Germline transmission of genetically modified primordial germ cells. Nature 441:766–769
102. Van Keuren ML, Gavrilina GB, Filipiak WE, Zeidler MG, Saunders TL (2009) Generating transgenic mice from bacterial artificial chromosomes: transgenesis efficiency, integration and expression outcomes. Transgenic Res. doi 10.1007/s11248-009-9271-2
103. Van Reenen CG (2009) Assessing the welfare of transgenic farm animals. In Ethics of science and technology

assessment. Springer-Verlag, Heildelberg/Berlin/New York, pp 119–143
104. Van Reenen CG, Meuwissen THE, Hopster H, Oldenbroek K, Kruip TH, Blokhuis HJ (2001) Transgenesis may affect farm animal welfare: a case for systemic risk assessment. J Anim Sci 79:1763–1769
105. Wernig M, Meissner A, Foreman R, Brambrink T, Ku M, Hochedlinger K, Bernstein BE, Jaenisch R (2007) In vitro reprogramming of fibroblasts into a pluripotent ES-cell-like state. Nature 448:318–324
106. Wilson JH (2008) Knockout punches with a fistful of zinc fingers. Proc Natl Acad Sci USA 105:5653–5654
107. Woods IG, Schier AF (2008) Targeted mutagenesis in zebrafish. Nat Biotechnol 26:650–651
108. Yang SH, Agca Y, Cheng PH, Yang JJ, Agca C, Wing Sang Chan A (2007) Enhanced transgenesis by intracytoplasmic injection of envelope-free lentivirus. Genesis 45:177–183
109. Yong HY, Hao Y, Lai L, Li R, Murphy CN, Rieke A, Wax D, Samuel M, Prather RS (2006) Production of a transgenic piglet by a sperm injection technique in which no chemical or physical treatments were used for oocytes or sperm. Mol Reprod Dev 73:595–599
110. Zambrowicz BP, Imamoto A, Fiering S, Herzenberg LA, Kerr WG, Soriano P (1997) Disruption of overlapping transcripts in the ROSA beta geo 26 gene trap strain leads to widespread expression of beta-galactosidase in mouse embryos and hematopoietic cells. Proc Natl Acad Sci USA 94:3789–3794

Books and Reviews

Honaramooz A, Megee S, Zeng W, Destrempes MM, Overton SA, Luo J, Galantino-Homer H, Modelski M, Chen F, Blash S, Melican DT, Gavin WG, Ayres S, Yang F, Wang PJ, Echelard Y, Dobrinski I (2008) Adeno-associated virus (AAV)–mediated transduction of male germ line stem cells results in transgene transmission after germ cell transplantation. FASEB J 22:374–382

Niemann H, Kues W, Carnwath JW (2009) Methods to generate transgenic animals in ethics of science and technology assessment, vol. 34. Springer-Verlag, Heildelberg/Berlin/New York, pp 1–30

Transit-Oriented Development and Land Use

Robert Cervero
Department of City and Regional Planning, University of California, Berkeley, CA, USA

Article Outline

Glossary
Definition of the Subject
Introduction
The Scope of TOD
Bus-Based TOD: Bogotá and Curitiba
America's TOD Success Story: Arlington County, Virginia
The Transportation and Environmental Benefits of TOD
TOD and Ridership at the Workplace
TOD and Parking
TOD Implementation Tools
Central-City Redevelopment Around Streetcar Lines
The Challenges of Mixed-Use TODs
Financing TODs
Future Directions
Bibliography

Glossary

Bus rapid transit High-quality bus services that mimic some of the mobility benefits of exclusive-guideway rail transit services but at a fraction of the cost, including busways, dedicated-lane services, and buses that operate with special features like signal prioritization and queue-jumper lanes at busy intersections.

Joint development Development activities on or near a transit agency's property that generates revenue and ridership benefits.

Public transportation Common-carrier forms of mass transportation available as a mobility service to the general populous, including heavy rail, light rail, and bus transit.

Self selection Willful decisions of residents to move into particular neighborhoods for lifestyle reasons and thereby have a bearing on travel behavior.

Smart growth Compact, mixed-use urban development that encourages alternatives to automobile travel, including transit usage, and that promotes environmental conservation and which can include, but is not limited to, transit-oriented development.

Transit value capture Securing profits from increases in land values conferred by public transit investments to help finance capital costs, including fixed guideways, rolling stock, and neighborhood improvements.

Definition of the Subject

Transit-oriented development, or TOD, is a term used to describe the physical integration and linkage of

public transportation investments and urban land development at or near a station. TOD typically takes the form of compact, mixed land-use development with high-quality pedestrian environments that is concentrated around rail transit nodes [1]. TODs can also occur around the stations and stops of busways and bus services that operate on exclusive, dedicated lanes, often referred to as Bus Rapid Transit (BRT).

The chief objective of TOD is to encourage larger shares of motorized trips to be taken by public transportation and as a result to reduce traffic congestion and improve environmental conditions, including air quality (since the private automobile is the primary source of ozone, carbon monoxide, and particulate matter emissions in many cities of the world). Secondary objectives of TOD might include revitalizing a long-distressed urban district, encouraging the production of more affordable housing and curbing the consumption of agricultural land and open space.

Introduction

TOD is often viewed as an antidote to car-dependent sprawl. By attracting a mix of residences, businesses, shops, and civic activities within a quarter-mile walking distance of an urban railway station, proponents argue that TOD can draw people to transit and thus relieve traffic congestion, improve air quality, and contribute toward climate stabilization. The station and its immediate surroundings can also serve as the hub of a community – a focal point for organizing the regeneration of stagnant neighborhoods and in the case of greenfields, the design and construction of new ones. Thus TOD is championed for both its environmental and its place-making benefits. Of course, the two are not unrelated. Traffic-snarled districts hardly make attractive, livable places. And as discussed later, places that are conducive to transit riding can help free-up traffic jams.

TOD has gained popularity in the United States, the world's most car-dependent country, for three key reasons. One, it is arguably the most cogent, understandable form of "smart growth." Citizens, politicians, and city-planners alike understand that if there is a logical place to concentrate urban growth, it is in and around transit stations. Second, demographic and lifestyle trends are working in favor of TOD. Living around transit stations appeals to growing numbers of Americans, like childless couples, Generation X'ers, and empty-nesters who value convenience and access to high-quality transit and who place a premium on being in a walkable community with urban amenities. Recent studies have rated TOD as a top real estate investment, estimating that as many as one- third of newly formed households in rail-served US metropolitan areas are receptive to transit-oriented living [2]. For many, TOD residency is a quality-of-life issue. As one study put it, "TODs are all about creating choice for people, about housing, lifestyle and travel"[3]. Third, more and more public policy initiatives favor TODs. As the federal, state, and local government levels, funding programs and incentives in the form of regulatory relief are favoring public and private invests in and around transit stations.

The Scope of TOD

A national study in the United States found that in 2003 about 100 of the nation's 3,300 fixed rail transit stations, or around 3%, could be considered TODs – in the sense all had a mix of land uses, embodied urban designs that created safe and attractive walking environments, and met minimum density thresholds (at least 12 dwelling units and 50 workers per net acre of land) [4]. Far more common than TODs, however, are what have been called "Transit adjacent developments," or TADs. TADs comprise buildings that are near transit stops but fail to induce residents, workers, and shoppers to patronize transit because of their designs and physical orientations. A mid-rise office building with standard parking supplies whose main entrance faces away from the nearby train station, forcing patrons to take a round-about path, is more TAD than TOD. By one definition, TAD is "physically near transit (but) fails to capitalize upon this proximity. . .(It) lacks any functional connectivity to transit – whether in terms of land-use composition, means of station access, or site design" [5].

The trade-off between creating a TOD versus a TAD reflects the inherent conflict between the transit station as "nodes" versus "places." On the one hand, stations are logistical nodes wherein cars, buses, taxis, delivery trucks, pedestrians, and cyclist converge for accessing transit and allowing intermodal transfers. On the other

hand, stations and their environs are places for creating or rebuilding community hubs. Whenever the logistical needs of a station win out, the resulting road designs and parking layouts often detract from the quality of walking, creating more of a TAD than a TOD. This has often been the case in and around suburban rail transit stations in the United States.

On the global stage, TOD is most fully developed in Europe, and in particular Scandinavia. In cities like Copenhagen, Denmark, and Stockholm, Sweden, corridors for channeling overspill growth from the urban centers were identified and reserved early in the planning process, and rail infrastructure was built, often in advance of demand, to steer growth along desired growth axes [6]. As importantly, greenbelt wedges set aside as agricultural preserves, open space, and natural habitats were also designated and accordingly major infrastructure was directed away from these districts. In the case of Stockholm, the last half-century of strategic regional planning has given rise to a regional settlement and commutation pattern that has substantially lowered car-dependency in middle-income suburbs. Stockholm planners focused on creating jobs-housing balance along rail-served axial corridors. This in turn has produced directional-flow balances. During peak hours, 55% of commuters are typically traveling in one direction on trains and 45% are heading in the other direction [6]. Moreover, Stockholm's transit modal share is nearly twice that found in bigger rail-served European cities like Berlin and even higher than inner London's market share. In fact, Stockholm is one of the few places where automobility appears to be receding. Between 1980 and 1990, it was the only city in a sample of 37 global cities that registered a per capita decline in car use – a drop off of 229 annual kilometers of travel per person [7].

Bus-Based TOD: Bogotá and Curitiba

While rail-based TODs are most prevalent worldwide, in good part because rail transit delivers the most regional accessibility benefits and thus are attractive to private investors, in recent time TODs are also taking form along Bus Rapid Transit (BRT) corridors. Many medium-sized global cities are looking to BRT as the most affordable form of high-performance public transit investment. BRT aims to achieve the speed and performance advantages of grade-separated services at a fraction of the cost by cleverly using bus-based approaches. Among its key features are: exclusivity, notably physical segregation; seamless (same-level) transfers; advanced bus technology: clean fuels, lightweight materials, low floors, advanced communications, docking systems; supportive armature: signal priorities, bus turnouts, curb realignments, automated vehicle location (AVL) systems, automated routing and dispatching; and expeditious fare collection and boarding: off-vehicle payment, smart cards. Two noteworthy international experiences with BOT and TOD, both in Latin America, are Curitiba, Brazil and Bogotá, Colombia.

The environmental benefits of balancing urban growth along bus-served linear axes and aggressively pursuing a "transit first" policy are underscored by experiences in Curitiba, Brazil. Curitiba, widely viewed as one of the world's most sustainable, well-managed metropolises, is also one of the most accessible – a product of some 40 years of carefully integrating urbanization and transportation improvements. By emphasizing planning for people rather than cars, Curitiba has evolved along well-defined radial axes that are intensively served by dedicated busways. Along some corridors, streams of double-articulated buses haul 16,000 passengers per hour, comparable to what much pricier Metrorail systems carry. A design element used to enhance accessibility in Curitiba is the "trinary" – three parallel roadways with compatible land uses. An important benefit of mixed land uses and transit service levels along these corridors, besides phenomenally high ridership rates, has been balanced, bi-directional flows, ensuring efficient use of available bus capacity, just as in the case of Stockholm. On a per capita basis, Curitiba is one of Brazil's wealthiest city yet it averages considerably more transit trips than much bigger Rio de Janeiro and São Paulo [6]. It also boasts the cleanest air among any Brazilian city over 1 million inhabitants, despite being a provincial capital with a sizable industrial sector. The strong, workable nexus that exists between Curitiba's bus-based transit system and its mixed-use linear settlement pattern deserves most of the credit.

Bogotá, the Andean capital of Colombia, has gained global recognition for its highly efficient and productive bus rapid transit (BRT) system. For a city of

7.5 million inhabitants facing civil conflict and deep economic problems, Bogotá's emergence as one of the world's most sustainable metropolises is all the more remarkable. In the late 1990s, Bogotá began operating a high-speed, high-capacity bus system, called Transmilenio, building upon Curitiba's successes with dedicated busways. A big difference, however, is that Curitiba relies principally upon circular, crosstown bus routes to interconnect radial busways. Outside of downtown, relatively little was invested in pedestrian and bikeway improvements. Bogotá, on the other hand, actively embraced pedestrian and bicycle access.

The 42-km, 3-line Transmilenio busway is the centerpiece of Bogotá's vast bus network. (The dedicated system will eventually expand to 22 lines covering 391 km.) Bus lanes are situated in boulevard medians, with weather protected, attractively designed stations spaced every 500 m or so. Because of dual carriageways that enable buses to overtake each other and high-level platforms that allow expeditious boardings and alightings, Transmilenio has a throughput of some 35,000 persons per direction per hour, a number that matches that of many Metrorail system. Some one million passengers ride Transmilenio buses each weekday, three times the ridership of two rail lines in Medellin, Colombia (achieved at less than one-fifth of the Medellin Metro's construction costs) and according to one study providing for a social rate of return of 61% [8].

Particularly important to the transitway has been Bogotá's attention to pedestrian and bicycle access, in the form of "green connectors." Perpendicular and grade-separated pedways and bikeways connect some of the poorest barrios and informal housing settlements (with highly transit-dependent populations) to the busways. Other innovative features of Bogotá's sustainable transport program include license-plate rationing, parking management, and car-free districting. Bogotá is an extraordinary example of matching infrastructure "hardware" with public-policy "software." The city boasts Latin America's most extensive network of cycleways (250 km), the world's longest pedestrian corridor (17 km), and the planet's biggest Car Free Day (covering an entire city of 35,000 ha).

While Bogotá's Transmilenio system has not dramatically altered the cityscape to date, at least when compared to places like Curitiba, research shows that commercial properties have reaped benefits from proximity to busway stations. A hedonic price- model analysis found a monthly rental discount of 1.87% for every additional 0.1 km from a BRT station, all else being equal [9]. This suggests a pent-up market demand for the accessibility benefits conferred by high-quality bus-based transit in cities of developing countries. A more recent analysis found that land-value capitalization increased as Transmilenio expanded into new neighborhood, revealing the network benefits of adding regional connectivity to the system [10].

As with many successful transit investments, it has been the attention to design details, matched by good macro-scale planning, that has contributed to Tranmilenio's success [11]. Car parking is mainly limited to the end stations of the Transmilenio busway. Nearly half of the 57 intermediate stations are served by skywalks/pedestrian overpasses. A phalanx of sidewalks and bikeways feed into all stations, most embellished by vegetative landscaping. Some two dozen civic plazas, pocket parks, and recreational facilities lie within a half kilometer of busway stops. Today, an estimated 45% of Transmilenio users reach stations by foot or bicycle [11].

America's TOD Success Story: Arlington County, Virginia

No place in the United States has witnessed more mid-to-high rise, mixed-use development along a rail corridor over the past three decades than Arlington County, Virginia [4]. This 26 square mile county just south of the nation's capital has experienced a tremendous increase in building activity since Washington Metrorail's 1978 opening: more 25 million square feet of office space, 4+ million square feet of retail space, some 25,000 mixed-income dwelling units, and over 6,500 hotel rooms. Of the nearly 190,000 people today living in Arlington County, in the early 2000s, 26% resided within a Metrorail-served corridor (roughly a one-quarter mile walkshed of stations), even though these corridors comprised only 8% of county land area. If the development added to these two corridors had been built at suburban density standards, such as in neighboring Fairfax County, Virginia, seven times as much land area would have been required [4].

Arlington County's TODs have hardly been the result of good fortune or happenstance.

The transformation of once-rural Arlington County into a showcase of compact, mixed-use TOD has been the product of ambitious, laser-focused station-area planning and investment. Prior to Metrorail's arrival, Arlington County planners understood that high-performance transit provided an unprecedented opportunity to shape future growth and proceeded to introduce various strategies – targeted infrastructure improvements, incentive zoning, development proffers, and permissive and as-of-right zoning – to entice private investments around stations. After preparing countywide and station-area plans on desired land-use outcomes, density and setback configurations, and circulation systems, zoning classifications were changed and developments that complied with these classifications could proceed unencumbered. The ability of complying developers to create TODs "as-of-right" was particularly important for it meant developers could line up capital, secure loans, incur upfront costs, and phase-in construction without the fear of local government "changing its mind." Another key factor was the decision not to align Arlington County's Metrorail rail corridor in the median of Interstate-66, thus suppressing development potential. Instead, County officials persuaded the region's transit authority to align the corridor in the traditional urban centers to help jump-start the process of urban regeneration.

The pay-off of concentrated growth along rail corridors is revealed in Arlington County's transit ridership statistics. The County today boasts one of the highest percentages of transit use in the Washington, DC. region, with nearly 40% of Metrorail corridor residents commuting to work by public transit [4]. An important outcome of promoting mixed-use development along Arlington County's rail corridors has been balanced jobs and housing growth which in turn has produced balanced two-way travel flows. Counts of station entries and exits in Arlington County were nearly equal during peak hours as well as the off-peak. During the morning rush hours, many of the county's Metrorail stations are both trip origins and destinations, meaning trains and buses are full in both directions. The presence of so much retail-entertainment-hotel activities along the County's Metrorail corridors has further filled trains and buses during the midday and on weekends. Arlington County averages higher shares of transit boardings and alightings at its stations in off-peak hours than other jurisdiction in the region with the exception of downtown Washington, DC.

The Transportation and Environmental Benefits of TOD

The litmus test for whether TOD yields environmental and other societal benefits is the degree to which it increases transit ridership, and in particular draws former motorists into trains and buses. Past research in the United States shows that neighborhoods designed according to TOD principles are associated with lower car ownership rates [4, 12], appreciably higher transit modal splits for commuting [13, 14], and fewer vehicle trips per day [15]. In California, surveys show that residents who live near a transit station use transit for their commutes at a rate four to five times higher than residents of the same region who don't live near stations [14]. This pattern has held steady over time. In the case of the Pleasant Hill station of the Bay Area Rapid Transit (BART) system in the San Francisco-Oakland region, for instance, 47% of station-area residents took transit to work in 1993 [13]. Ten years later, in 2003, the share was 44% [14].

While TODs bump up the shares of residents' trips by transit, more important to many observers – particularly traffic engineers and elected officials – is the impact on local traffic conditions. A recent study of 17 TOD projects in five US metropolitan areas (Philadelphia, Northeast New Jersey, Washington, DC, Portland, and the San Francisco Bay Area) uncovered evidence of "vehicle trip de-generation" [15]. Over a typical weekday period, TOD housing projects in these five regions averaged 44% fewer daily vehicle trips than that estimated by the *Trip Generation* manual of the Institute of Transportation Engineers (ITE), which is widely used as the reference manual for gauging traffic impacts of new projects. During peak hours, transit-oriented housing projects generated one-half the typical number of vehicle trips per dwelling unit.

The higher transit use and lower trip generation rates among station-area residents are largely a product of what economists call "self selection." People who prefer to take a train to work – whether to avoid the stress of fighting traffic or to have time to read a newspaper en route to work – purposely choose to

live near a rail stop, that is, they are predisposed to transit commuting; they are not "converted" to transit use simply because of where they live. Residing near transit is thus a lifestyle choice. A recent study estimated that around 40% of the ridership bonus attributed to TOD is due to self selection [16].

While TODs generate fewer trips per dwelling unit, this does not necessarily mean they reduce local traffic congestion. Indeed, often the opposite holds which poses a fundamental dilemma – not only for TODs but for all urban developments that increase average densities. Invariably, because not all TOD residents take transit, denser development will congest the nearby road intersections during peak periods. Experiences show that in settings like the United States, where the majority of households own cars, a given percentage increase in density (dwelling units per acre) will not be matched a similar percentage decline in car trips per acre, meaning that car-traffic densities invariably rise. Thus in the near term, even if it is well served by transit, dense development translates into more traffic congestion. Not-in-my-backyard (NIMBY) opposition to higher density has stopped TOD plans around a number of middle-income neighborhoods served by the heavy-rail BART system in the San Francisco East Bay, mainly through building height restrictions. Over the past 20 years, some 2,400 new households have located within a 5-min walk to the Pleasant Hill BART station. Once a critical mass of TOD residents forms, they create neighborhood associations which, among other things, stop efforts to add more development. In Pleasant Hill, plans to build a massive entertainment complex, with a 20-screen IMAX movie theater, were scuttled due to neighborhood backlash. The lesson is clear: do not expect to transform middle-income, stable neighborhoods with large-scale infill projects, because residents have the political might to stop such proposals every step of the way. More acceptable are TOD proposals for transitional neighborhoods, redevelopment districts, or greenfields with few people around to oppose new development. Also, large-scale, regional trip generators that bring outsiders to neighborhoods made up of professional-class residents will rarely be embraced by residentially dominated TODs. Only local- and neighborhood-serving land uses will be welcomed in such settings.

The downside of preventing new growth around transit stations is that the development will end up elsewhere and most likely increase vehicle miles traveled (VMT) – the strongest single correlate of greenhouse gas emissions (GHG), air pollution, and energy consumption in the transport sector. Like toothpaste in a tube, if development is squeezed from one area, it simply gets redistributed elsewhere. Shifting growth from TOD to AOD (automobile-oriented development) can reduce local traffic congestion at the cost of environmental degradation for a region at large.

It can be argued that there is good and bad congestion, just like good and bad cholesterol. Congestion caused by TOD, many urbanologist would contend, is, for the most part, good. There is no avoiding the fact that denser areas have denser traffic. Dense cities with world-class rail systems, like Paris and London, are often more traffic-choked than sprawling cities. Yet these dense cities are also attractive places to live, work, and visit. Congestion is part of the territory of being an active, vibrant place. TOD, moreover, offers a relief valve to congestion. In a TOD, it is easier to predict when and where congestion will occur, and it is easier to avoid that congestion, e.g., one can hop on a train or ride a bike.

TOD and Ridership at the Workplace

While TOD planning and design has traditionally focused on residential development, unless nonresidential destinations are also served by high-quality transit, few TOD residents opt for rail or bus travel. Studies show that TOD workplaces also yield ridership dividends, though not because of self-selection but rather proximity and convenience [17]. Parking policies and designs are particularly important determinants of whether those working in TODs ride transit or not.

A study of workers in 10 office buildings near suburban rail stations in California found, on average, 19% of commute trips were by public transit, with considerable variation [14, 16]. Other factors, however, weighed heavily on whether TOD workers commuted by transit. This is reflected by the logit-model results in Fig. 1. The figures show the likelihood that TOD workers in California commuted by transit as a function of parking supplies, employer assistance with transit costs, and frequency of feeder bus services. With 25 feeder

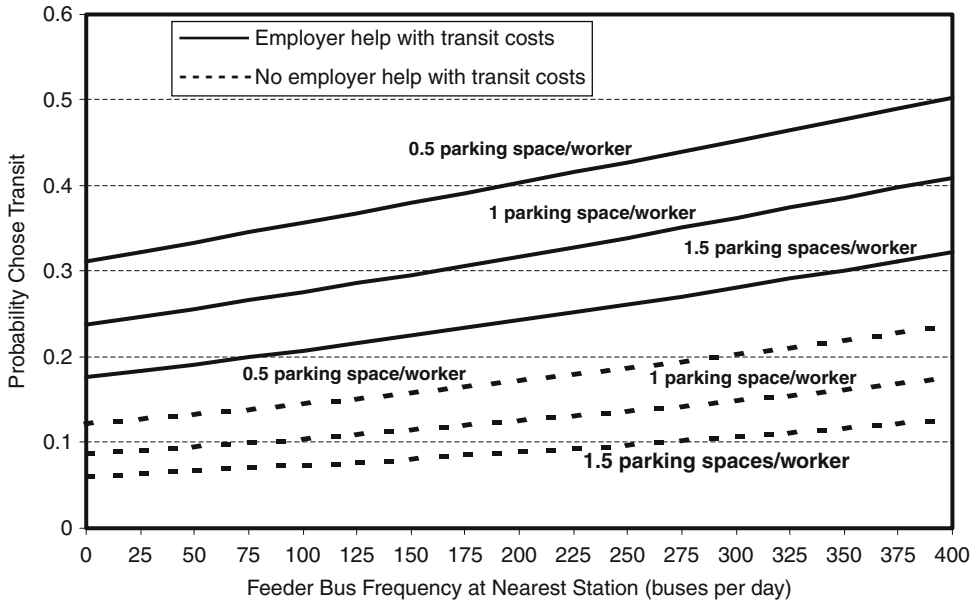

Transit-Oriented Development and Land Use. Figure 1
Influences of employer policies and feeder bus frequencies on transit commuting among office workers in California

buses per day, an office setting with 50% more parking spaces than workers, and no employer help with transit costs, the model predicts that just 8% of office workers near a rail station will commute by transit. At the other extreme, for a worker heading to a station with 400 daily feeder buses who work for an employer who provides transit-pass assistance and provides one parking space for every two workers, the likelihood that he or she will commute by transit is 50%. Over the range of feeder bus frequencies, the differential in transit commuting probabilities is 30–40% depending on how generous employers are in promoting transit (i.e., minimal parking and help with transit costs) or in accommodating the automobile (i.e., ample parking and no help with transit costs). Clearly, successful TODs are far more than physical design challenges: the policy "software" that accompanies the built-design "hardware" matters tremendously.

TOD and Parking

Critics charge that many large-scale housing projects near urban rail stations are "over-parked" – more parking is provided than is needed [18]. Excessive parking can drive up the cost of housing, consume valuable land near transit, and impose such environmental costs as increased impervious surface areas (that contribute to urban heat-island effects and stream-water pollution from oily run-offs). As noted, transit stations are thought to offer "location efficiency," enabling residents to get by with fewer cars than they might otherwise own. Yet lenders and planners often insist that code-standard parking be provided in station areas regardless. This can drive up the cost of station-area housing, thus defeating the purpose of promoting affordable housing construction near major transit stops.

A recent study raises some questions whether suburban TODs indeed average less parking, at least in the United States [15]. In the case of Portland, Oregon, while average vehicle trip generation rates of TOD projects were 41% below ITE rates, the average use of parking spaces was only 11% less. The parking occupancy at three of the 15 surveyed TOD projects in Portland was actually higher than that predicted by the ITE *Parking Generation* manual. In the San Francisco Bay Area, owning and parking a car was even more of a necessity. There, TOD parking rates were equivalent to ITE's standard of 1.2 spaces per unit. For all seven TOD housing projects surveyed

near the Fremont BART station, parking levels were actually higher than the ITE rates – as much as 40% above.

What might explain high parking rates combined with high transit ridership rates for TODs? One factor may be that most cities do not reduce the parking requirements for TODs which in turn induces car ownership. One survey of TODs in California found no reduction in cities' parking requirements at seven of the 11 sites studied [17]. Planners appear to assume that more transit will not reduce parking demand, and they may be right. In most suburban TODs, many residents still need access to a car. They just do not use them as much. But like most suburbanites, they still need a car to get to most non-work destinations – the vast majority of which are located away from rail stops. While transit-oriented housing might mean that more trip *origins* are near rail stops, as long as most *destinations* are not, TOD residents will still own cars and use them for shopping, going out to eat, and the like.

The fact that some suburban TODs encourage transit riding yet fail to prompt residents to reduce car ownership suggests that TODs might be a natural setting for carsharing. A study of City CarShare members in San Francisco found that 4 years into the program, 29% of carshare members had gotten rid of one or more of their cars and 63% lived in zero-vehicle households [18]. Putting shared-cars in and around TODs could relieve many households from owning a second car or a vehicle altogether. Through a combination of proximity advantages and lifestyle predispositions, living near transit can *de*-generate vehicle trips. And with the option of carsharing, it might reduce parking demands as well. This has been the case in cities like Zurich, Switzerland. Zurich, for example, has the second highest per capita transit use in the world (over 600 transit trips per capita per year) and the highest per capita carsharing participation anywhere (7% of households are members of Mobility Carsharing Switzerland) [6]. And in spite of having one of the world's highest per capita incomes (on a purchasing power parity basis), only one out of three households has an off-street parking space. Zurich also has the highest commercial real estate prices in Europe (along Bahnhoffstrasse) and according to the management consulting firm, Arthur D. Little, ranks number one in quality of life among global cities [6]. In Zurich, world-class transit, carsharing, parking limits, and prosperity go hand-in-hand.

Another policy response might be the introduction of more flexibility in parking policies for housing near rail stops. Flexibility can be in the form of enabling projects to provide below-code parking levels when justified, e.g., compact projects with short, direct walking connections to transit and perhaps on-site retail establishments. Flexible parking standards provide latitude in providing the optimal number of parking spaces [19]. Flexibility can also take the form of unbundling the cost of providing parking from the cost of building (or renting) housing [20]. This would allow developers to better scale the amount of parking provided to what each tenant or homeowner is willing to pay for each car owned, i.e., let the market demand, rather than a possibly out-dated government fiat, determine supply. And flexibility can be in the form of allowing TOD tenants to choose deeply discounted transit passes for frequent riders instead of a 300 square foot parking space.

TOD Implementation Tools

Moving from the theory to the practice of TOD is often fraught with difficulties, especially in car-dependent countries like the United States. A national survey of urban planners in US cities with TODs cast light on the kinds of implementation tools being used to leverage TOD [4]. Most prominent has been zoning, usually in the form of overlays. Overlay zones are frequently introduced on an interim basis to head-off auto-oriented uses that might compromise a TOD and to specify desired land uses as of right, such as housing and convenience shops. For urban TODs, densities of 20–30 dwelling units per residential acre and floor area ratios (i.e., building area divided by land area) of 1.0 and above are not uncommon. Some of the more progressive TOD zoning districts, such as those found in Portland, Oregon, Seattle, San Diego, and Denver, also lower requirements for car parking and sometimes even for bicycles. The city of San Diego, for instance, recommends parking reductions as high as 15% for urban TODs.

Besides zoning, other tools frequently used in the United States to encourage TOD include: funding for station-area planning and ancillary capital

improvements; density bonuses, sometimes used to encourage affordable housing; and relaxation of parking standards. Next in the order of frequency of usage have been land-based tools, like land purchases on the open market (for land-banking and potential "deal-making") and assistance with land assemblage. For the most part, redevelopment agencies have applied these tools, meaning their role in leveraging TOD has been mainly limited to economically depressed or blighted neighborhood settings. Because of the higher risk involved, redevelopment tools have often been accompanied by other funding sources, sometimes with a dozen or more participants involved in the process.

Central-City Redevelopment Around Streetcar Lines

A good example of successfully using zoning tools and financial incentives to leverage central-city redevelopment in a transit corridor is the Pearl District in downtown Portland, Oregon. The Pearl District is the most dramatic transformation of downtown Portland in the last 20 years. Once home to a large artist community and an "incubator" for start-up businesses in abandoned warehouses, the Pearl District is now an emerging mixed-use neighborhood of upscale loft housing, parks, art galleries, boutiques, cafes, and restaurants. Since 2001, more than 1,700 condominiums and apartments have been built. Moreover, 55% of all development in downtown Portland has been within a block of the streetcar service since its opening [21].

A major catalyst to the transformation of the Pearl District was the construction of the Portland Streetcar, the first modern streetcar system to be built in the United States. The streetcar has been equal parts housing and transportation tool, as streetcar construction was explicitly linked to high-density development via density bonuses and an innovative developer agreement. As a result of this agreement, the average density of the District is now 120 housing units per acre, the highest in the city. Moreover, properties near the streetcar line more closely approach permissible densities than properties situated farther away [21].

Tax incentives were introduced to moderate possible gentrification effects of streetcar-induced redevelopment. Many affordable housing projects in Portland receive 10-year property tax abatements if they are within walking distance of a rail line. While the abatements are loosely related to projected price levels and affordability, their primary purpose is to ensure denser development (as specified in the developer agreement) than the market would otherwise support.

Residents in the Pearl District fit the demographic profile found in other Portland area TODs – childless, and either young people seeking smaller lofts, older professionals looking for an urban lifestyle with little upkeep ("downsizing boomers"), or retiring seniors. This variety of homeowner types has contributed to the depth of the market.

The Challenges of Mixed-Use TODs

As dense, mixed-use forms of development, many of the barriers to TOD are generic to all forms of compact growth – not-in-my-backyard (NIMBY) resistance, higher risks and costs, and institutional inertia. Still, some of the barriers to smart growth are more pronounced when it comes to TOD. Mixed-use development is one of them. Mixed land uses, a signature feature of TODs, pose a host of difficulties not only in terms of design but also in lining up funding, investors, and contractors. Planners sometimes impose a design template of ground-floor retail and upper-level housing or offices, i.e., vertical mixing – on any and all development proposals within a TOD. Mixed-use projects are much trickier to design, finance, and sometimes lease than single-use ones [12]. Finding the right formula for mixed land uses can be every bit as difficult as rationalizing parking policies. Vertical mixing is particularly problematic. Quite often, the ground-level retail component of mixed-use TODs suffer the most, in part because they are poorly laid out. Ground-floor retail, for example, is doomed to fail unless it opens onto a street with busy foot traffic and convenient car access. Mixed housing-retail projects also pose unique design challenges. Ground-floor retail needs greater floor-to-floor height (typically 15–18 ft) to be marketable, compared with the 8–10 ft between residential floors. This means the entire ground floor, including multifamily areas, must have higher ceilings, which increases project costs. Ground-floor restaurants pose problems such as where to put the exhaust shafts for kitchens. The exact size and location of restaurant

space may not be known until leases are signed. Designers must thus allow exhaust shafts to be put in several potential locations, which can reduce net leasable space. And ground-floor restaurants might be unappealing to upper-level residences seeking quiet and privacy in the evening. Local governments need to be sensitive to these issues and focus more on achieving a desired land-use mix within a transit station area as opposed to individual parcels, i.e., pursue "horizontal" neighborhood-scale mixes versus "vertical" within-building mixes.

Financing TODs

For TODs to take form, there must be money to pay not only for transit infrastructure, like stations and parking, but also the armature – civic squares, streetscape enhancements, pocket parks, expanded trunkline sewage and piped water capacity – that surrounds a TOD station. Joint development is the form of value capture that has been most widely used to finance America's most successful TODs. Under this approach, a public transit agency partners with a private developer to build a real-estate project on land or air rights owned by the transit agency itself. In return, the transit agency receives either revenue (i.e., revenue sharing) or passes on part or all of the costs of rail-station and ancillary construction (i.e., cost sharing). Among the most common forms of revenue-sharing schemes are land leases, air-rights development, and station interface or connection-fee programs. Cost-sharing schemes include sharing construction expenses, incentive-based programs that produce benefits for private financing (e.g., density bonuses), and joint use of equipment like ventilation systems.

As a value capture tool for transit, joint development has the most appeal in settings where a significant amount of land is available to a transit agency, preferably purchased on the open market at a fairly low cost (which usually means prior to formal announcement of a new railway project). This has been the case in Hong Kong where the city's transit operator, MTR Corporation, obtains more than half of its revenue from ancillary real-estate property development [22]. To the degree joint development is limited to a geographically restricted area, such as one or two small parcels owned by a transit agency, it fails to capture value from a broader area benefiting from new transit services.

Another common way to leverage and fund TODs, especially in the United States, has been Tax Increment Financing, or TIF. Under this scheme, incremental increases in property tax revenues are channeled back into a district to help revitalize distressed neighborhoods. TIF has been used extensively to encourage TOD in many parts of the United States. In the city of Chicago, half of the 129 TIF districts in 2003 contained a railway station [4]. The state of Pennsylvania applies TIF in Transit Revitalization Investment Districts (TRIDs) to promote economic development and TOD. A criticism of TIF is it diverts tax dollars that would otherwise accrue to a city's general treasury and as thus creates a privileged (i.e., subsidized) zone. Such equity concerns have limited the application of TIFs to much of the developing world.

Some TODs have relied on impact fees as their chief source of funding. These are charges assessed on new development to defray the cost of expanding and extended public services. In 1981, the city of San Francisco, California introduced a Transit Impact Development Fee (TIDF) levied against new downtown office buildings to produce income for operating and maintaining the city's MUNI transit network, comprising light rail, diesel bus, trolley bus, and cable-car services. TIDF revenues produce around $10 million annually. Broward County, Florida, has a Transit Oriented Concurrency system that similarly generates income for transit operations by levying a fixed fee on new development. This program covers around 30% of annual bus-transit operating and capital costs for the county [23]. Because limiting impact fees to new development only can deter investments in all but the healthiest real-estate markets and inflates the cost of housing, it has been applied on a limited basis outside of the United States. In the developing world, exactions are more common wherein developers cover the cost of expanding infrastructure (e.g., water and sewer trunkline capacities) to serve a site.

Future Directions

TODs are a type "smart growth" and sustainable urbanism that have tremendous growth potential due to both supportive public policies and market forces.

Global experiences show that the integration of public transport and land use can yield appreciable sustainability benefits that redound to both the private and public sectors. In many settings, developers know they can earn handsome profits building, leasing, and selling TODs. As long as traffic congestion continues to worsen in TODs and demographic trends continue to shift in the direction of smaller, non-traditional households, there will always be a market demand for TODs. However, forward-looking and pro-active public-sector strategic planning will always be a necessity as well if sustainable and cost-effective TODs are to take form. In many automobile-reliant cities of the world, TODs often take the form of a few nodes, or islands, in a sea of auto-oriented development. Unless there are enough TODs, linearly aligned along natural travel corridors to create a critical mass, few transit ridership (and correspondingly auto-reducing) benefits will accrue. That is, there need to be enough origin–destination combinations formed by TODs in non-downtown settings to draw enough motorists into the trains and buses so as to put an appreciable dent in car traffic. Otherwise, stand-alone TODs can very much backfire by creating dense nodes in otherwise auto-oriented settings so as to increase traffic congestion along roads feeding into transit stations.

What is likely on the horizon for particularly progressive-minded cities might be the emergence of "Green TODs." Green TOD is a marriage of TOD and Green Urbanism. This combination is, potentially, a potent elixir. TOD works on the VMT-reduction side of shrinking a city's carbon footprint. Green Urbanism reduces emissions and waste from stationary sources, in the form of green architecture and sustainable community designs. In combination they can deliver energy self-sufficiency and zero-waste living. Renewable energy might come from solar and wind as well bio-fuels created from human waste and other byproducts. Recycling and reuse of materials, community gardens, and low-impact building materials further reduce the carbon footprint of Green TODs (Table 1).

Transit-Oriented Development and Land Use. Table 1
Forms of emission reductions form green TODs

TOD	Green urbanism
Mobile sources • *Transit design*: World-class transit (trunk and distribution) Station as hub • *Non-motorized access*: (bike paths, pedways) • *Bikesharing/carsharing* • *Minimal parking*: (reduced land consumption, building massing, and impervious surfaces) • *Compact, mixed uses*	Stationary sources • *Energy self-sufficient*: (renewably powered – solar, wind turbines) • *Zero-waste*: (recycle, reuse, methane digesters, rainwater collection for irrigation, and gray water use) • *Community gardens*: (compost, canopies) • *Buildings*: Green roofs Orientation (optimal temperatures) Materials (recycled, low impact)

Synergies would like accrue from combining TOD and Green Urbanism. The higher community densities needed to fill the trains and buses that serve TODs at the same time reduce heating and cooling expenses from the embedded energy savings of shared-wall construction. Smart electric grids generated by photovoltaic panels and wind turbines designed as canopies above stations might also power light-rail cars, plug-in hybrids, and electric buses. Additionally, the compact, mixed-use pattern of development around rail stations can support walking, biking, and the use of limited range private vehicles to reach relatively nearby destinations, thus helping to grow such infant-industries as electric vehicles. One could imagine a future of hydrogen-fueling and electric-battery swap depots in a green community focused on a rail node and for which the destinations of many travelers are close by.

Hammarby Sjöstad, a brownfield redevelopment in the city of Stockholm, is an example, *par excellence*, of marrying of TOD and green urbanism. The combination of railway services, carsharing, and bike-sharing has dramatically reduced vehicle-kilometers traveled of Hammarby's residents and correspondingly greenhouse gas emissions and energy consumption. In 2008, 25% of trips by Hammarby's residents were by bicycle or walking and 52% were by transit, much higher than regional averages [24]. Carbon dioxide emission from private cars was 52% less for households in Hammarby Sjöstad than in planned communities of similar income structure in the suburbs of Stockholm [24]. And the design of an energy self-sufficient and low-waste community has further shrunk the project's environmental footprint.

Today, residents of Hammerby Sjöstad produce 50% of the power they need by turning recycled wastewater and domestic waste into heating, cooling, and electricity.

The future of TOD, worldwide, is undeniably bright. As long as urban ills like traffic congestion and air pollution – and global concerns like oil dependency and climate change – persist or worsen, TOD will be embraced as a desirable form of urbanism. Rapid urbanization, combined with equally rapid urban and inter-city rapid rail construction, in countries like China could mean more TODs find particular acceptance in former third-world countries that are rapidly industrializing and modernizing.

Bibliography

1. Cervero R (2008) Transit-oriented development in America: strategies, issues, policy directions. In: Haas T (ed) New urbanism and beyond: designing cities for the future. Rizzoli, New York, pp 124–129
2. Renne J (2009) From transit-adjacent to transit-oriented development. Local Environ 14(1):1–15
3. Urban Land Institute, San Francisco (2008) Bay area TOD marketplace. Urban Land Institute, San Francisco, p 1
4. Cervero R et al (2004) Transit oriented development in America: experiences, challenges, and prospects. TCRP report 102. National Academy Press, Washington
5. Cervero R, Ferrell C, Murpy S (2002) Transit-oriented development and joint development in the United States: a literature review, research results digest number 52. Transportation Research Board, Washington
6. Cervero R (1998) The transit metropolis: a global inquiry. Island Press, Washington
7. Kenworthy J, Laube L (1999) An international sourcebook of automobile dependence in cities: 1960–1990. University of Colorado Press, Boulder
8. Consejo Nacional de Politica Económica y Social (2000) Sistema de Servicio Publico Urbano de Transporte Masivo de Pasajeros de Bogotá. Departamento Nacional de Planeación, Documento No. 3093
9. Targa F, Rodriquez D (2004) Analysis of Bogotá's bus rapid transit system and its impact on land development. Carolina Plann J Winter:26–36
10. Rodriquez D, Mojica C (2009) Capitalization of BRT network expansions effects into prices of non-expansion areas. Transp Research Part A 43(5):561–575
11. Cervero R, Sarmiento O, Jacoby E, Gomez L, Neiman A (2009) Influences of built environments on walking and cycling: lessons from Bogotá. Int J Sustain Transp 3:203–226
12. Dunphy R, Cervero R, Dock F, McAvey M, Porter D, Swenson C (2004) Developing around transit: strategies and solutions that work. Urban Land Institute, Washington
13. Cervero R (1994) Transit-based housing in California: evidence on ridership impacts. Transp Policy 1(3):174–183
14. Lund H, Willson R, Cervero R (2006) A re-evaluation of travel behavior in California TODs. J Arch Plann Res 23(3):247–263
15. Cervero R, Arrington G (2008) Vehicle trip reduction impacts of transit-oriented housing. J Public Transp 11(3):1–17
16. Cervero R (2007) Transit oriented development's ridership bonus: a product of self selection and public policies. Environ Plann A 39:2068–2085
17. Bernick M, Cervero R (1997) Transit villages for the 21st century. McGraw-Hill, New York
18. Daisa J (2004) Traffic, parking, and transit oriented development. In: Dittmar H, Ohland G (eds) The new transit town: best practices in transit-oriented development. Island Press, Washington, pp 114–129
19. Cervero R, Golub A, Nee B (2007) City carShare: longer-term travel-demand and car ownership impacts. Transp Res Rec 199:70–80
20. Dunphy R, Myerson D, Pawlukiewicz M (2004) Chapter 7: Ten principles for developing around transit. In: Dunphy R et al (eds) Developing around transit: strategies and solutions that work. Urban Land Institute, Washington
21. Shoup D (2005) The high cost of free parking. Planner's Press, Chicago
22. Cervero R, Murakami J (2009) Rail + property development in Hong Kong: experiences and extensions. Urban Stud 46(10):2019–2043
23. Fogarty N, Eaton N, Belzer D, Ohland G (2008) Capturing the value of transit. Center for Transit Oriented Development, Oakland
24. Brick K (2008) Summary report: follow-up of environment impact in Hammarby Sjöstad. Grontmij AB, Stockholm

Transmission Blackouts: Risk, Causes, and Mitigation

Damir Novosel
Quanta Technology, LLC, Raleigh, NC, USA

Article Outline

Glossary
Definition of the Subject and Its Importance
Introduction
Grid Development History
Challenges in Taming the Grid from Wide-Area Blackouts
History and Examples
Pre-outage Conditions and Risks for Blackouts

Symptoms of Blackouts
Power System Modeling and Analysis
How Disturbances Turn into Blackouts
Blackout Prevention
System Integrity Protection Schemes
System Restoration
Future Directions
Conclusions
Acknowledgment
Bibliography

Glossary

DOE Department of Energy
EMS Energy Management System
FACTS Flexible AC Transmission System
FERC Federal Energy Regulatory Commission
GPS Global Positioning Satellite
ISO Independent System Operator
NERC North American Reliability Council
PDC Phasor Data Concentrator
PMU Phasor Measurement Unit
RAS Remedial Action Scheme
TSO Transmission System Operator
SCADA Supervisory Control and Data Acquisition
SIPS System Integrity Protection Scheme
UCTE Union for the Coordination of Transmission of Electricity
WAMPAC Wide Area Monitoring, Protection, and Control
WECC Western Electricity Coordinating Council

Definition of the Subject and Its Importance

Power system blackouts result in complete interruption of electricity supply to all consumers in a large area. While it may be possible to trace a blackout's beginning to a single incident (e.g., transmission line sagging into a tree), cascading outages are the result of multiple low-probability events occurring in unanticipated or unintended sequence. The likelihood of power system disturbances escalating into a large-scale cascading outage increases when the grid is already under stress.

Blackouts may look like bad luck, but they are result of how the grid is managed. Statistically, a sequence of low-probability contingencies with complex interactions causing a blackout may not happen often but will eventually take place unless measures are taken to prevent it. Presently, some of the grids around the world (e.g., parts of the North American grid) may be susceptible to blackouts as aging and insufficient grid infrastructure may not be adequate to accommodate grid changes, such as renewable generation resources and load growth. Deployment of "Smart Grid" monitoring, control, and protection devices, software tools, and telecommunication infrastructure helps better manage the grid, but does not replace investments in the infrastructure.

Although large-scale blackouts are very low-probability events, they carry immense costs for customers and society in general as well as for power companies. It is easy to misjudge the risks and costs of such extreme cases.

Although widespread outages cannot be completely prevented, their occurrence can be reduced, propagation (size) and consequences arrested, and restoration sped up. In last couple of decades, power systems around the world have been more stressed as the capacity reserves and system margins have been reduced resulting in more blackouts with huge costs to the society.

Introduction

Wide-area electrical blackouts have raised many questions about the specifics of such events and the vulnerability of interconnected power systems [1–4]. Power systems are complex interconnected machines with many components operating in harmony when the system is balanced. When a problem occurs in part of the system, the impact of the trouble may cause to the system losing its balance momentarily. In most cases, the system is immediately isolated and shortly after recovers with no further propagation observed outside of the immediate area.

Exchange of information stemming from the recent worldwide blackout findings and "smart grid" technology innovations shed new lights on the current conditions and needs of power systems. Examination of the root causes, the resulting effects on neighboring systems, and implementation of proven solutions to help prevent propagation of such large-scale events should help in designing and operating reliable "smart grid" and power delivery infrastructures for today and in the

future. Power system professionals can take in consideration the costly lessons of the past, maintain a library of historical lessons about "What and Why it Happened" for the generations to come, and act as catalysts to achieve desired level of power system reliability.

The high cost and the need for extensive mitigation strategies against grid congestions, combined with this type of probabilistic assessments, have led into risk management not focusing on appropriate, cost-effective mitigation actions. From a broader prospective, a misconception may be formed about the grid reliability or its exposure to large-scale outages every so often. It is easy to misjudge the risk of such extreme cases. (Risk is the product of the cost and associated probability, and both factors are very hard to assess accurately.) The high costs of extensive mitigation strategies (e.g., building new transmission lines), combined with inaccurate probabilistic assessments ("blackouts will not happen in my system"), have led to inadequate risk management practices, including not focusing on cost-effective prevention and mitigation initiatives. Such initiatives can provide value through avoidance of huge blackout costs. The following stakeholders benefit from outage/blackout avoidance:

- The society/ratepayers. For example, society costs for August 14, 2003 blackout in the USA and Canada and for August 2006 WECC blackout were estimated at $7B and $1B, respectively.
- The electric utilities, ISOs, generation producers, etc. Costs of service restoration, undelivered energy, cost of litigation, and the negative impact on stock price.

Understanding the complexities of the interconnected power grid, need for proper planning, good maintenance, and sound operating practices are the key to deliver electric power to modern day necessities and prevent the problems of tomorrow's grids. This article offers practical insight on risks and leading causes of widespread blackouts and how best to prevent them to achieve higher levels of grid reliability.

Grid Development History

In the 1930s, electrical power was delivered to consumers around the world by individual, not connected electrical systems. Regional systems have been created next to make power systems more robust and delivery more reliable. The original function of the interconnected systems was to form the backbone for the security of supply and to reach its required high reliability level at reasonable costs. In the 1950s, the power system professionals foresaw the importance of further improving delivery of reliable electricity to consumers. The grid systems have been developed to assure mutual assistance between transmission system participants and/or national subsystems including common use of reserve capacities to optimize the use of energy resources by allowing exchanges between the systems.

Thus, a strategy of interconnecting neighboring systems to improve reliability and security margins became a reality around the world. Coordinated rules for the mutual support of interconnected systems were defined and adopted by the power pool members between power systems, including interconnections among countries (e.g., UCTE in Europe). Since the late 1970s, the electrical transnational infrastructures were exploited more and more for energy exchanges that took advantage of the different production costs of electricity in the various nations or interconnected grids in order to deliver lower cost energy and achieve maximum profits. However, the bulk power system was not originally engineered to transfer large amounts of power between neighboring systems over long ranges but to enable neighboring utilities to support each other during stressed conditions.

In recent years, deregulated energy concepts have created additional burden on the system for using the same conductor for additional capacity increasing already high transfers as new generation sources (including renewable energy) are brought on-line to meet the demand. The high level of power exchanges in today's energy market is technically being provided outside of the scope of the original system design. The higher demand, coupled by low level investments in technology and infrastructure upgrades and capacity increase, has led the Control Area operators to run the system close to the edge, as close to the limits as permitted by the reliability criteria and, sometimes, beyond the limits. At the same time, our increased respect and awareness for the environment and the "Not in My Backyard" sentiments have made it difficult

to site transmission lines or major local generation sources, especially in the more densely populated areas, where load is heavy. These difficulties make the system expansions expensive and difficult, and offer new challenges to deliver reliable power.

Recently, major investments have been made worldwide in "smart grid" technologies, e.g., US DOE investment grants. Major motivation for Transmission "smart grid" is in preventing blackouts using Wide Area Monitoring Protection and Control (WAMPAC) technologies, such as synchronized measurements using GPS signals.

There are still isolated power systems around the world (e.g., island networks). Unlike interconnected grids, those power systems do not have flexibility to get help from the neighboring systems to optimally balance generation and load, both during normal and stressed conditions. Those systems are more vulnerable to generation and transmission system outage and require long-term, coordinated planning and investments in the complete electrical grid infrastructure to achieve reliable and cost-effective grid operation and maintenance.

Challenges in Taming the Grid from Wide-Area Blackouts

Evolutions in technology continue to improve all aspects of our lives from precision surgical equipment for use in highly critical operations, to automatic banking anytime of the day, electric rail systems to reduce emissions, and to our home appliances. Many of the technological innovations have been achieved in recent quarter century and have readily found their way in our daily lives. The modern day amenities and our respect for the environment have also increased our dependency on energy, hence, our expectations for uninterrupted reliable power. However, the demand for availability of power for many of these modern day equipment has not been systematically and uniformly considered. Modern technology is the catalyst driving power delivery demanding grid reliability, and the marked increased dependency on availability has raised the bar on human expectation.

Some of the electrical power systems that experienced blackout in last decade (e.g., North America, Europe) are among the most reliable systems worldwide. However, they are subject to a host of challenges – aging infrastructures, renewable and distributed energy integration, transmission and distribution grid expansion to meet the growing load demand and transfer renewable energy to load centers, etc. Figure 1 shows impact of the 2003 blackout on supplying power to the consumers (before and after the blackout).

After some major blackouts worldwide in the last 2 decades, utilities have hardened their electrical systems, and regulatory organizations (e.g., NERC and FERC and state regulators in the USA) have focused on

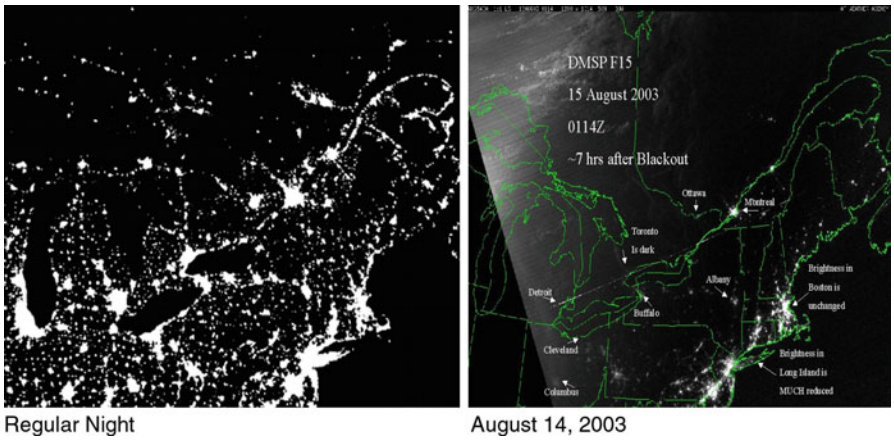

Transmission Blackouts: Risk, Causes, and Mitigation. Figure 1
Effects of August 14, 2003 blackout in North America

defining and enforcing reliability standards. This has resulted in better planned, operated, and maintained grid. However, one of the challenges facing the electric industry today is the balance between reliability, economics, environmental, and other public purpose objectives to optimize transmission and distribution resources to meet the demand. Resources and transmission adequacy are necessary components of a reliable and economic supply. Though the reliability and market economics are driven by different policies and incentives, they cannot be separated when the objective is reliability and availability. Today, grid planning in the regional and interregional environment faces an extremely difficult task given the challenge to achieve resource adequacy in today's restructured industry, where market economics, local concerns, and renewable energy resources often derive the decision for generation facility siting remote from major load centers. Equally difficult is planning for an adequate transmission system when the location of future generation facilities is uncertain and the lead time for transmission construction is very long (just the permitting process may take several years).

It is more important than ever to find ways to project transmission and distribution growth, solutions to deploy, and criteria to be applied to guide prudent investment decision. Some of the key areas to address are the following:

- Integration of renewable energy – As renewable resources (e.g., wind and solar) are located far from the load centers, additional stress was put on the system, causing higher vulnerability to outages.
- Price for reliability – Costs and risks transmission owners and customers are willing to assume. The power industry is accustomed to optimize investments and evaluate return on investments based primarily on financial aspects of trading energy and serving load within certain reliability criteria. This is often done without considering financial aspects of unavailable energy (undue service interruptions) due to low reliability and slow restoration that incurs significant costs to the society. This is an incomplete financial model that results in suboptimal investment strategies.
- Large regional geographic areas should be included in the scope of transmission planning and decision-making. However, when assets need to be built, it is not easy to identify true beneficiaries and how costs are to be shared.
- Quick restoration – As it may not be possible to completely avoid outages, it is required with today's technology to reduce power restoration.

Electricity is the key resource for our society; however, strategic planning (regional and national) requires additional priority to improve system reliability.

History and Examples

Within the last decade, the number of wide-area outages has rapidly increased (blackouts in north-east USA and Canada, western USA, Brazil, Italy, Sweden, Denmark, England, India, Malaysia, Australia, New Zealand, Greece, etc.) affecting over 300 million customers worldwide. As the likelihood of low-probability events escalating into a cascading outage increases when the grid is already under stress due to preexisting conditions, one can conclude that power grids are more prone to disturbances than ever.

History has showed that both unscheduled and scheduled (regular maintenance) outages have affected power system's balanced operation hence signifying the grid complexity during managed conditions [1, 2, 5–7]. In the case of the August 1996 North America disturbance that affected 12 million people [5], a series of equipment were being removed for maintenance in parts of the Western grid when the weather was moderate, yet these pieces of equipment were needed to support transfers in other parts of the Western grid, which was experiencing extremely high temperatures.

Analysis of the 2003 incident in the north-eastern part of the USA [6], which affected 50 million people, revealed that a series of cascading events over the course of several hours, rather than a single instantaneous problem, initiated the major disturbance phenomenon that toppled the large part of the US Eastern Interconnection. The blackout itself was preceded by scheduled generation outages and line tripping caused by overgrown trees in the right-of-way. It was accompanied by failures of EMS/SCADA alarm systems, which prevented operators from diagnosing problems. The initial line disconnection caused another 345 kV line to overload and sag into a tree, resulting in

remaining 345 kV lines to disconnect. Underlying 135 kV lines overloaded and disconnected, followed by tripping of generating units, causing a part of the system to go black. A lack of communication and coordination between utilities and ISOs involved exacerbated the problem. The grid was restored in 1–2 days (depending on the area affected and ability to get generators back on line).

The September 2003 disturbance in the connected European grid affected 57 million people. Several 220–400 kV lines were out of service for maintenance reasons prior to the event occurrence. Italian grid was importing 6 GW from the rest of the grid. One of the 380 kV lines disconnected due a tree contact. The parallel line overloaded, and although the import was reduced, it was not enough to prevent sagging into a tree and disconnecting. Other lines to Italy overloaded and tripped, resulting in isolating Italian grid 12 s after the loss of the second line. During those 12 s, low voltage in northern Italy caused generators to disconnect. Other countries tripped generation (app. 6.7 GW). In summary, 2.5 min after islanding, Italy goes black separated from the rest of the grid. However, unlike the blackout in the USA, it took only 5–9 h to restore the power to major cities. Main reasons are for faster restoration was type of generation that was able to get back on line faster and accompanying restoration processes (e.g., so-called black-start capabilities allowing fast generation reconnection).

The most severe disturbance in the history of UCTE considering number of Transmission System Operators (TSOs) involved happened in October 2006 [7] when system separated in three islands. Following were key reasons for the disturbance:

- N-1 criterion (planning criteria so that a single equipment outage does not create a system disturbance) was not fulfilled as wind generation was not adequately predicted. Large wind storms increased production in northern Germany.
- Inappropriate inter-TSO coordination and training. The time of the planned line outage was changed, and new conditions were not checked.
- Uncoordinated protection settings on both sides of the critical line.
- Uncoordinated operation of wind generators.
- Inadequate coordination of restoration.

All the above blackouts included combination of phenomena such as line overloads, voltage and angular instability, and system separation. Those blackouts have served as catalysts in propelling the power industry toward analyzing blackouts and finding solutions to prevent such occurrences. The 1994–1996 blackouts in the western part of North America resulted in formation of investigating teams which ultimately made a combined list of 130 conclusions and 54 recommendations [7]. The August 14, 2003 investigating teams identified 60 recommendations (14 by North American Reliability Council, or NERC, and 46 by the US Canadian Task Force) [6]. The Union for the Coordination of Transmission of Electricity (UCTE) identified 14 observations for the September 28, 2003 outage, very similar to those identified for the outages in North America that happened just a month before. Although major improvements have been accomplished after the blackouts in corresponding grids, the similarities in findings among those blackouts prove that if recommendations had been used among grids, the impacts of the outages could have been minimized [4].

By some accounts [8]:

- These kinds of outages are consistent with historical statistics, and they will continue to happen. Some may compare blackouts to events such as long-term weather forecasting (hurricane and mudslides) or to natural disasters such as earthquakes as being difficult to predict and/or to prevent.
- The more immediate problem may be the industry's investment of less than 0.5% in R&D, one of the lowest rates for any industrial sector.
- A power system is composed of hundreds of thousands of pieces of equipment from bulk autotransformers, high-voltage transmission systems, to a light bulb. It has been suggested that one could not get a computer big enough to model a complex system as, for example, the Eastern Interconnection and perform the planning studies.
- Large blackouts occur because the grid isn't forcefully engineered to prevent them. Purposely weakening the grid can reduce large blackouts but would increase the frequency of smaller ones.

Chifong Thomas, formerly transmission planning engineer from Pacific Gas and Electric Co. points out that if large blackouts occur anyways, as they are hard

to predict as earthquakes, then nothing anyone could do would make any difference. This contradicts the premise that industry underinvestment in R&D is the immediate problem. If the first premise is true, the second one is irrelevant. She also points out that if the grid planning is done comprehensively and correctly, then operators with proper training should have time to respond to contingencies and/or to limit the impacts of the contingency.

Dr. Mayer Sasson, principal advisor of Electric Markets Policy Group at Consolidated Edison Co. of New York, highlights the vulnerability of the interconnected grid by pointing out that it may take only one member of a control area to be operating outside of the reliability limits for any reason, including unintentionally, to cause a cascading outage that can quickly propagate to neighboring interconnected system control areas. This underscores the criticality of complying with mandatory reliability rules.

Dr. Bogdan Kasztenny, power system protection and control application manager at Schweitzer Engineering Laboratories, raises the important issue of human factor involvement in the last few critical hours before any major event. "Even in a poorly designed and under-invested system, operators could sometimes salvage an event that seems to be disastrous, or collapse an otherwise quite secure situation in a strong and reliable system. It is not so with earthquakes. Power systems are man-made creations run by humans. Operational procedures, availability and accuracy of real-time information, adequate training including dry runs on simulators are technical means that improve response of the operators."

Kasztenny emphasizes that the power system is a complex generating, transmitting, and distributing system for a medium that cannot be stored, or buffered, in the reality of very limited redundancy. This makes it quite different from the banking, phone, or similar systems. Other systems are subject to brownouts. However, the power system must balance the medium under physical constraints and is therefore subject to collapse if the constraints are violated.

Pre-outage Conditions and Risks for Blackouts

The grid is a tremendously complex system, and the interconnections that allow us to benefit from higher reliability and lower costs also cause the domino failures experienced in many parts of the world in recent years. Although there is a tendency to point at one or two significant events as the main reasons for triggering cascading outages, major blackouts are typically caused by a sequence of low-probability multiple contingencies with complex interactions. The three "Ts" – Trees, Tools, and Training – have been identified as the leading focus areas to prevent widespread outages not caused by natural events. However, disturbances have occurred following extremely low-probability successive unscheduled equipment outages beyond planning criteria. There have also been cases of system disturbances caused by scheduled equipment outages when the electrical system has not been adjusted, for continued safe operation, prior to the equipment being removed. Low-probability sequential outages are also not anticipated by system operators, thus rendering the power system more susceptible to wide-area blackouts. As the chain of events at various locations in the interconnected grid unfolds, operators cannot act quickly enough to mitigate the fast developing disturbances.

Power systems are engineered to allow for reliable power delivery in the absence of one, two, or more major pieces of equipment such as lines, transformers, or bulk generation, commonly referred to as contingency conditions. For example, after the 2003 blackout in North America, North American Electric Reliability Council (NERC) set forth the reliability standards and performance requirements that are enforced by audits. However, the complexity of the grid operation makes it difficult to study the permutation of contingency conditions that would lead to perfect reliability at reasonable cost. Accurate sequence of events is difficult to predict, as there is practically an infinite number of operating contingencies. With system changes, e.g., independent power producers selling power to remote regions, load growth, new equipment installations that cause significant changes in power flow to name a few, these contingencies may significantly differ from the expectations of the original system planners and engineers.

The likelihood of power system disturbances escalating into a large-scale blackouts increases when the grid is already under stress due to preconditions. Those preconditions are summarized as follows:

- Congested grid with tight operating margins
  - Not building lines or generation as fast as required, exacerbated by difficulty in identifying business models to recover costs, and a cumbersome permitting process
  - Not well-planned wholesale merchant transactions with scheduled transactions not changed to allow for transmission relief when required
- System stress caused by intermittent renewable energy and/or suboptimal operating practices
- Insufficient reactive support where and when required to maintain required voltage levels
  - Adequate dynamic reactive power is required close to the load as reactive power cannot be transferred over long distances
- Uncoordinated planning between transmission and generation
  - Inadequate system reserve, such as generation spinning reserve
- Inadequate planning/operation studies
  - No routine use of an effective contingency analysis tool
  - Uncoordinated interregional transmission planning
- Aging infrastructure, prone to failures, accompanied by insufficient level of investment in maintaining the grid
  - It is more and more difficult to isolate and remove equipment for maintenance
- Both scheduled and uncoordinated maintenance
- Lack of system and component knowledge (e.g., system operator not aware of line loading margins)
- Inadequate right-of-way maintenance or environmental policies versus right-of-way vegetation management
- Weather (high temperatures; wind, thunderstorm, fog, etc.)
- Regulatory uncertainty
- Inadequate Automatic Warning, Protection, and Control Systems

In general, combination of various factors makes power systems more susceptible to disturbances.

Symptoms of Blackouts

It is the cascading events that cause disturbances to propagate and turn into blackouts. System is stressed and as system and equipment faults occur, the chain of events starts. For example, some generators and/or lines are out for maintenance, line trips due to a fault. Other lines get overloaded, and another line gets in contact with a tree and trips. There is a hidden failure in the protection system (e.g., outdated settings or HW failures) that causes another line or generator to trip. At that stage, power system is faced with overloaded equipment, voltage instability, transient instability, and/or small signal instability. If fast actions (e.g., load shedding, system separation) are not taken, system cascades into a blackout.

Evaluation of disturbances shows that protection systems have been involved in 70% of the blackout events [9]. For example, distance relays trip on overload and/or low-voltage sensitive or ground overcurrent relays trip on high unbalance during high load. Inadequate or faulty alarm and monitoring equipment, communications, and real-time information processing can further exacerbate disturbances in the system. Either information is not available or operators are flooded with alarms, so they cannot make proper decisions fast.

Human error and slow operator response are major contributing factors for cascading outages. As a disturbance develops, operators in various regions are faced with the questions "is the best course of actions to sacrifice own load, cut interties, or get support from neighbors?," "should we help or should we separate?." Important aspect in designing connected power systems is that individual systems should not allow cascading outages to spread throughout the system.

There are a number of other contributing factors that allow a blackout to spread, including lack of coordinated response among control areas. If each region focuses primarily on its own transmission system, the total connected system may not be reliable. As it is very difficult for operators to decide on best actions during a fast developing disturbance, it is desirable to take automated actions before system separates or to separate it in a controllable manner.

Generally, disturbance propagation involves a combination of several phenomena:

- Equipment tripping due to faults or overloads (e.g., transmission lines and transformers). These events

may cause other equipment to get overloaded, creating a cascading event contributing further to system-wide outages.

- Power system islanding (frequency instability) when power system separates. Islands are formed, with an imbalance between generation and load, causing the frequency to deviate from the nominal value, leading to additional equipment tripping.
- Loss of synchronous operation among generators (angular or out-of-step instability) and small signal instability that may cause self-exciting inter-area oscillations if not damped.
- Voltage instability/collapse problems that usually occur when the power transfer is increased and voltage support is inadequate because local resources have been displaced by remote resources without the proper installation of needed transmission lines or voltage support devices in the "right" locations.

Table 1 shows the types of wide-area disturbances likely to occur in two different types of interconnected power grids, namely, meshed network versus an interconnected transmission system of narrow corridors consisting of extensive generation tied to the interconnection [10]. One star indicates that those phenomena did not affect a particular grid configuration in the past, but have affected modern grids. Two stars indicate major phenomena in a particular grid configuration.

The characteristics of the power system influencing the types of mitigation methods have been described in a variety of literature [1–4, 9–13]. The relative time of action for different type of events, from normal to extreme, varies depending on the type and speed of the disturbance and the need for coordination. Example of the time line for different type of events is shown in Fig. 2.

Deployment of a well-coordinated overall defense plan to prevent blackouts requires implementation and coordination of various schemes and actions, spanning different time periods. When events can be controlled to result in gradual shutdown of the available resources rather than permitting them to cascade, their impact could be minimized. A practical approach to identifying stressed system conditions, which are symptomatic of cascading, is feasible. This can be done by defining and modeling the power system parameters considered for reliable operation such as voltage, frequency, or phase angle at critical locations. Such findings can then be implemented through investments in Hardware equipment and Software tools that help manage the grid more effectively.

Transmission Blackouts: Risk, Causes, and Mitigation. Table 1 Types of wide-area events for different transmission systems

System config.	Densely meshed power system with dispersed generation and load		Lightly meshed transmission systems with localized generation and load	
Events	Located in a large interconnection	Not interconnected or by far the largest partner	Located in a large interconnection	Not interconnected or by far the largest partner
Overloads	**	**	*	*
Frequency instability	*	**	*	**
Voltage instability	*	*	**	**
Transient angle instability	*	*	**	**
Small signal stability	*	*	*	*

*Phenomena did not affect a particular grid configuration in the past, but have affected modern grids

**Major phenomena in a particular grid configuration

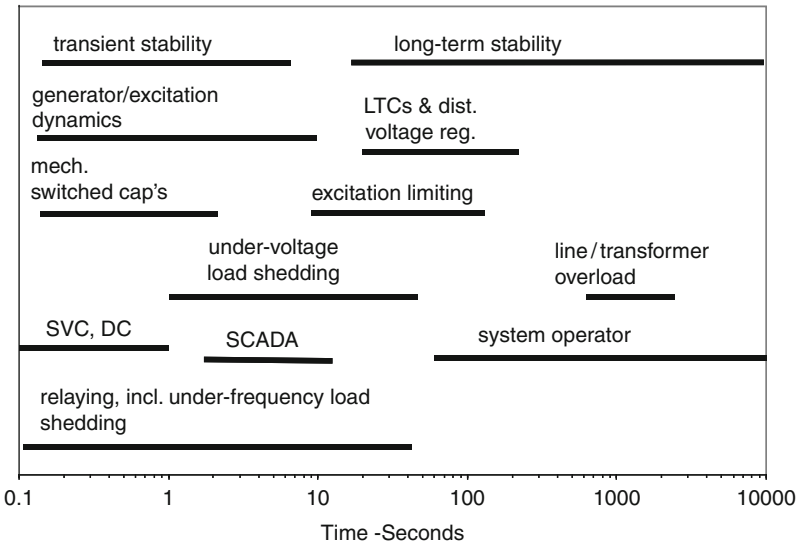

Transmission Blackouts: Risk, Causes, and Mitigation. Figure 2
Some time frame factors of power system dynamics

Power System Modeling and Analysis

Electrical grids have been characterized as the most widespread interconnected, complex, dynamic systems made by humans. A power system carries tremendous amount of electricity that all depend on. Although blackouts are difficult to predict and prevent, the notion that it is not possible to simulate the grid behavior, to identify and address most vulnerabilities, is not accurate.

Carson Taylor, power system simulation expert (formerly with Bonneville Power Administration), confirms that today's technology allows for detailed modeling of complex power systems. Taylor emphasizes that the Eastern Interconnection has been simulated in great detail with 40,000+ bus models. Simulations with 100,000+ models are feasible. Feasibility increases with IT advancements. Computation is not a large problem. Computation is scalable by parallel computation on multiple servers; cases can be farmed out to the multiple servers. Simultaneous processing method is used for energy management system dynamic security assessment.

Professor Göran Andersson, Eidgenössische Technische Hochschule (ETH) University in Zurich and a noted expert in power system dynamics, concurs with Taylor and brings up an important issue that the challenge is not technical, i.e., modeling or computer capacity related; rather it is the data management and proper interpretation. Professor Andersson also underlines that the "Statistical methods can give some information and insight concerning the sizes and frequencies of blackouts, which is of value. However, the problem is the calibration of the frequency scale, since this requires a detailed modeling of the interactions. The statistical insights, however, do not provide to any large extent the guidance to avoid blackouts to the power system professionals operating the systems. In terms of modeling, the details of the system and the interactions between different components and subsystems are indispensable."

Both Andersson and Taylor emphasize that best practice is to continually improve and update models and compare simulations with real power system response. This is not unique for power systems and is continuously being done in the industry and academia. In addition, much progress has been made over the years, and even if predictions from simulations are problematic, efforts to model, simulate, and validate performance provide invaluable insight for a reliable power system operation.

In conclusion, the power grid can be modeled and studied; however, as there is an infinite number of

contingencies that can occur and the current state is not precisely known, it is not possible to exactly predict disturbance propagation far in the future. However, innovations in power system tools from planning, to monitoring, to operation are strategies that would help in meeting the challenges of the twenty-first century expectations in reliable power delivery.

How Disturbances Turn into Blackouts

It has been demonstrated time and again that wide-area blackouts are caused by operation of the interconnected power system outside of the operating limits or for operating conditions that have not been thoroughly studied. As described by Vahid Madani, principal engineer at PG&E, one of the ways to understand the challenges of power delivery is to liken it to driving the highways via motor vehicle. As motor vehicle operators, most of us have experienced a wide variety of unplanned difficulties and challenges slowing down our travels. In many ways, widespread outages have similar characteristics as a highway traffic gridlock. Some of the key aspects of traffic jams include the following:

- Not enough lanes to accommodate the growing demand.
- As one or two lanes are closed, the traffic flow is significantly impacted, and in the most severe case, it causes a complete highway shutdown. A circumstance out of control of those not involved with the accident, yet they are stuck (blackout).
- A properly designed system would include major alternate freeways that are easily accessed through proper detours to minimize impact from the gridlocks.
- Repair of the old highways may not be enough to solve traffic congestion. At times prudent investments in building new traffic lanes, or completely new thruways, and innovative traffic control systems are needed.

Dr. Daniel Karlsson, system analysis and protection expert from Sweden, also compares the expansion of highway traffic with an expansion of the power grid as both have grown from minor systems to extremely important infrastructures in the same time period and both continue to grow. However, he points out that the public accepts a much higher degree of failures (e.g., people seriously injured or worse) due to automobile traffic than they accept a widespread power outage, demonstrating the important role of electricity in our daily lives and hence the criticality of reliable power delivery.

- Karlsson brings up a historical perspective to explain how the large interconnected power systems of today have been formed due to constant demands on capacity, economy, and reliability. He points out that initial power systems were small grids with low capacity and low reliability. Extensions emerged as dictated by capacity needs. To improve reliability of the individual systems by allowing support from the neighbors, these systems were interconnected. New phenomena appeared, such as transient instability, resulting in studies and actions to counteract them. Complex powerful power systems introduced new transmission capacity problems and actions to counteract them (series capacitors inserted in the transmission line, shunt capacitors and reactors, automatic tap changers to control transformer voltage, etc.). This consequently brought new phenomena like sub-synchronous resonance and voltage instability and, again, a need for new studies and equipment, such as Flexible AC Transmission Systems (FACTS), High Voltage DC (HVDC) links. Dr. Karlsson emphasizes that the complexity of the present power system, and factors such as environmental and rights of way, governmental, cost-to-benefit evaluation for large scale investments will derive us to maximize the use of current assets without truly addressing the rising demand for new infrastructure. This trend will continue to challenge the industry with new technology and actions: superconductivity, energy storage, micro-grid, etc.

There is also a strong relation between system size and reliability. In the ever growing demand to be supported by the power system, our industry tends to push the limits challenging the reliability with a question, "where is the edge?" This is particularly true in many places such as North America, where the expansion efforts are not growing as much, or as rapidly as, the grid is being utilized.

It is noted that weakening or splitting the grid on purpose during normal operation is not a sound alternative, as this strategy would make a full circle for the

grid. For example, by operating the power grid in separate islands, one could easily weaken the power system. That would effectively mean coming back to the original design of the small grid with low capacity. Separating the grid into islands would also impact deregulation, e.g., each DG would be selling power to its own neighborhood. The small utility will soon need occasional support for reserve margin, voltage, and reactive margins from neighboring systems, hence, back to the interconnected grid. The solution is not in separating the grid into islands, rather to resolve transmission problems to mitigate potential for widespread cascading outages.

Chifong Thomas dismisses the argument that large blackouts occur because planning engineers spend too much time preventing small blackouts. She argues that this theory ignores the fundamental fact that large blackouts start out as small problems that do not by themselves necessarily lead to blackouts. They lead to blackouts when small problems are not corrected in time.

Professor Vijay Vittal, Iowa State University, corroborates that the impact of such severe system failures could be mitigated by several approaches such as use of corrective controls or performing more effective analysis closer to real time.

The effective way to minimize disturbance propagation is to truly understand the common causes and design the appropriate solutions. The system needs to be addressed as a whole, implementing various planning, operations, maintenance, and regulatory measures in a coordinated way.

A possibility to prevent propagation of the disturbance throughout interconnected grid, but not weaken the grid during normal operation, is to design the interconnected power system to allow for intentional separation into stable islands or interrupt small amounts of load only when the system experiences major disturbances. As operators may not be able to act fast enough to take into account all data related to the on-line state of the system, separation actions should be done automatically. System Integrity Protection Schemes (SIPS) are wide-area automatic schemes that are designed to detect abnormal system conditions and initiate pre-planned automatic and corrective actions based on system studies [10–13]. They are also referred to as Special Protection Schemes (SPS), or Remedial Action Schemes (RAS). They detect abnormal wide-area system conditions and trigger automatic actions to restore acceptable system performance. The initiating factor in implementing significant number of SIPS in the western part of the USA (WECC) has been to better protect the system against multiple contingencies, particularly after the 1994 and 1996 blackouts [7]. Designing the grid with appropriate measures for voltage control and advance warning systems such as wide-area protection and control would allow for both strong interconnected grids during normal operation (to make system more reliable and secure) and creation of predetermined islands only when necessary.

In conclusion, instead of weakening the grid, power industry needs to address deregulation as one important aspect in understanding the underlying causes of system-wide outages. The bulk power system was often not originally designed to transfer large amounts of power between neighboring systems. Individual power systems were interconnected to improve electrical network reliability by enabling neighboring utilities to support each other during stressed conditions. In recent years, deregulation has imposed additional requirements of high transfers from new generation sources to the load areas. At the same time, public pressures and the "Not in My Backyard" sentiment make it difficult to site transmission lines or major local generation sources, especially in the more densely populated heavy load areas, making the system expansion very expensive and difficult. In addition, recent disturbances have, more and more, been accompanied by voltage stability problems.

In summary, following are the main reasons for disturbances to turn into blackouts:

- Inability to prevent sequential tripping due to overloads, power swings, and voltage fluctuations
- Inadequate or faulty EMS/SCADA system (incl. alarm burst) – need for reliable alarm filtering, proper visualization, and analysis tools
- Protection miss-operation or unnecessary actions
  - Incorrect settings, e.g., impedance-based protective devices tripping on overloads (NERC developed regulations after the 2003 blackout to address it)
  - Hidden failures: uncovered application design flows or HW failures

  - Inadequate design, e.g., application of impedance-based protective devices without the out-of-step blocking
- Inability of operators to prevent further propagation of the fast-developing disturbance
- Lack of coordinated response during developing disturbances, e.g., joint procedures between ISOs to deal with the problem quickly and effectively
- Generators tripping too early – generator tripping to be coordinated with the rest of the system

Blackout Prevention

The alarming increase in the number of major blackouts requires exploring new frontiers in deployment of well-defined and coordinated overall plans (planning, operations, and maintenance). As analysis of recent disturbances reveals some common threads among them, the conclusion is that propagation can be arrested and impact of disturbances reduced if knowledge gained is properly utilized [1–4].

The best way to minimize wide-area power system disturbances is to understand the leading causes. Study of blackout history in the past decade shows that in each case the reliability standards have been violated in some form or fashion demonstrating the priority for more stringent compliance enforcement of the standards, necessity to invest wisely in new transmission facilities that expand the reliability parameters of the grid in the "right" areas, new grid monitoring technologies, and especially the tools that help us make it simpler to manage the day-to-day operation.

Electric reliability and efficiency are affected by four segments of the electricity value chain: generation, transmission, distribution, and end use. Satisfactory system performance requires investments in all these segments of the system. Increasing supply without improving transmission and distribution infrastructure in the right locations, for example, may actually lead to more serious reliability issues.

The retirement and replacement of transmission equipment at the end of its useful life will be another important remedy for increasing failure rates and potential outages in the future. Aside from the aging infrastructure concerns, the transmission grid must be upgraded and expanded to continue to meet the growing demands. For example, high-voltage power electronic devices allow more precise and rapid switching to improve system control and to help increase the level of power transfer that can be accommodated by the existing grid. Distributed energy technologies, if properly applied, could also play a role in relieving power flow demands on the transmission networks. In conclusion, while the new investments shall certainly include some new transmission lines, it will also encompass power delivery technologies such as series capacitors, single-phase operation of transmission lines, FACTS, HVDC links, energy storage, superconducting materials, and micro-grids.

The legislative and governmental commitments to build infrastructure, compliance with reliability requirements, and state, regional, and interregional plans are required to achieve the sustainable grid. Measure such as computerized control and data acquisition, phase-shifting transformers, coordination mechanisms, and electronic data exchange between operators are also some alternatives that improve the capability of the existing infrastructure and allow for a more robust power exchange.

Furthermore, reliable power system performance requires a balance of many critical components such as adequate reserve real and reactive power margins, reliable real-time telemetry and status monitoring, real-time state estimation, properly set, maintained, coordinated, and tuned protection and control systems, etc. Academic, industry, and governmental initiatives are required to set and enforce the standards for voltage control and reactive power practice, to improve system modeling and validation process, to enhance operator-training curriculum, and to assure that operators are assigned responsibility to take actions to prevent disturbance propagation.

In terms of modeling, quantitative analysis is needed to validate models of generators, turbines, and the associated controls to match actual system oscillations and damping. Likewise, dynamic loading or stability impact on protection devices (designed to operate for faulted conditions, e.g., tree contact) should be considered, and routine protection coordination studies using accurate model should be regularly performed. There are also concerns associated with protection and control application and settings when short-term market conditions for power transfers stress the equipment resulting in a risk of equipment outage.

Tools that improve real-time system monitoring, evaluation, visibility, security, congestion tracking, control, visualization, and information sharing about grid conditions over a wide region will allow operators to manage the grid more reliably on a day-to-day basis as well as in emergencies. Poorly recognized dynamic constraints can unnecessarily narrow operating limits and endanger reliability. Real-time security analysis tools are becoming increasingly critical for daily operation to visualize critical stability boundaries and to determine stability operating limits based on actual conditions.

Finally, the recent large-scale generation trips and remedial action responses have provided some very good benchmarks for combined small and large-scale analysis. Reexamination of traditional planning, operating, system design, protection applications, and device settings will help improve system response to slow or limit the spread of cascading outages. The frequency and varying impact levels of worldwide blackouts have provided the power industry with opportunities and supporting information to:

- Study the complex power system phenomenon to minimize propagation for future system-wide events using accurate and user friendly tools
- Validate the system studies against actual power system performance and governor modeling data
- Environmental and political factors limiting new addition of generation and transmission capabilities. Highlight the needed support for regulatory measures to ease wise grid expansions, grid reinforcements, and well-established and measured reliability enforcement process
- Operating capacity reserves and margins for transmission flows must remain available to allow system adjustments during unintended multiple contingency conditions. Enforce reliability requirements, for example, Planning Standards for Normal and Emergency Conditions
- Visit existing operating practices and real-time data exchange policies among control areas
- Make use of enhance maintenance practices and asset management tools
- Timely deploy Special Integrity Protection Schemes (SIPSs) to prevent spreading of the disturbance

Furthermore, protection systems are usually involved in major wide-area disturbances, sometimes preventing further propagation, and sometimes contributing to the spread of the disturbances [14]. A very important lesson is that the design and operation of conventional protection and control schemes have to be scrutinized assuming stressed conditions. Improvements to existing protection systems can help prevent cascading and minimize the impact and number of wide-area disturbances. In general, a protection system should operate only for its designed conditions. Preventing further disturbance propagation should be achieved by designing and setting protection, and control schemes do not miss-operate during major disturbance conditions. However, some experiences include relay operations that prevented further cascading by tripping on system conditions for which they were not designed.

Some key opportunities for improvement include coordinated adaptive protection and control systems and wide-area monitoring with advance warning systems, as elements of WAMPAC. The advance technology today promotes the concept of the "smart grid" – an integrated, electronically controlled power system that will offer unprecedented flexibility and functionality, and improve system reliability. The concept of the smart power delivery system includes automated capabilities to recognize problems, find solutions, and optimize the performance of the system.

In summary, corrective and preventive actions to avoid wide-area blackouts are the following:

- Provide operator with:
  - Tools to measure, monitor, assess, and predict both system performance and the performance of market participants
  - Training, incl. coordinated approach among control areas and use of dispatch training simulators
- Improve monitoring and diagnostics and control center performance
  - Availability of critical functions needs to be 99.99%
  - Assure adequate exchange of information between neighboring control centers
  - Secure real-time operating limits on a daily basis
  - Shared and consistent rating information required
- Use dynamic line ratings ambient temperature, wind, pre-contingency loading, etc., to better understand what the actual system margins are

- Better utilize available and standby generation in the area; implement black-start capabilities
- Improved maintenance and condition assessment of aging infrastructure
- Improve vegetation management
- Accurate generator, dynamic load, and reactive support device models, including renewable generation models
- Advanced algorithms and programs to assist the operator, such as "faster than real-time simulations"
- Protection coordination studies across regions and in coordination with equipment control and protection
  - Study and review protection designs on a regular basis, as system conditions change
  - Assure planned relay operation (e.g., distance relays not to trip on out-of-step and overload; ground overcurrent relays not to trip on high unbalance during high load, coordinated zone 3 operation, etc.)
  - Avoid hidden failures by adequate testing of not only individual relays but also overall relay applications
  - Increase the security of protection design in the areas vulnerable to blackouts
- Deploy Wide Area Monitoring, Protection, and Control (WAMPAC) systems to improve grid visibility and initiate corresponding actions

In conclusion, it is important to take a balanced approach to fixing the system as a whole by implementing various planning, operations, and maintenance measures and weighing the costs, performance impacts, and risks associated with each measure. One needs to evaluate how to operate and maintain the power system for the years to come to meet defined reliability objectives. There is no silver bullet solution to preventing blackouts, but there are general measures than can and should be taken to minimize impact of wide-area disturbances.

Each entity needs to focus on further process improvement, standardization, and better asset utilization, all parts of overall asset management strategy. This is the key to increased reliability and to protecting investments. Prudent capital investment in power system infrastructure has to be based on stringent cost-benefit analysis to optimize investments. For example, increase in generation ("conventional" or renewable energy) has to be planned in conjunction with strengthening the transmission grid. Holistic, multi-year system planning is required to achieve efficient, reliable, and cost-effective grid. In addition, independent certification of technical systems and business processes can be an important element of assuring that proper actions are taken, processes implemented, and investments made.

System Integrity Protection Schemes

Examples of large blackouts in the past decade have shown that the risk of large blackouts is no longer acceptable and can lead to very large and unexpected social and financial consequences. Reduction of the risk of large system-wide disturbances and blackouts requires that system protection function be approached with the assistance of modern technologies in support of preserving system integrity under adverse conditions.

These schemes, defined as System Integrity Protection Schemes (SIPS) [10–13], are installed to protect the integrity of the power system or strategic portions thereof, as opposed to conventional protection systems that are dedicated to a specific power system element. The SIPS encompasses Special Protection System (SPS), Remedial Action Schemes (RAS), as well as other system integrity schemes such as Underfrequency, Undervoltage, Out-of-Step, etc. These schemes provide reasonable countermeasures to slow and/or stop cascading outages caused by extreme contingencies.

SIPS goal is to prevent propagation of disturbances for severe system emergencies caused by unplanned operating conditions and ensure system security. They stabilize the power system for equipment outages, N-2 (two key elements out of service) or beyond by:

- Preventing cascading overloading of the lines and transformers
- Arresting voltage decline
- Initiating pre-planned separation of the power system

Advanced detection and control strategies through the concept of SIPS offer a cohesive management of the

disturbances. With the increased availability of advanced computer, communication, and measurement technologies, more "intelligent" equipment can be used at the local level to improve the overall response. Traditional dependant contingency/event-based systems could be enhanced to include power system response based algorithms with proper local supervisions for security.

The IEEE Power System Relaying Committee has developed a worldwide survey on SIPS [12]. Figure 3 shows a summary of the overall SIPS purpose classification. The numbers of SIPS performing similar types of functions have been grouped to indicate the total number of SIPS types. For each type of SIPS scheme, the number of schemes serving a similar purpose has been indicated, with the following classification:

1. Essential: Prevent cascading outages
2. Increased Security: Minimize area affected by undesirable conditions
3. Increased Power Flow Capability: To extend transmission system rating without adding new transmission facilities or to delay enhancement of transmission networks
4. Important: Avoid difficult operating conditions
5. Normal: A better functioning of the network

Note that almost all classifications are evenly distributed (with exception of "Important" which is at 8%). The approximate even distribution of classifications of SIPS highlights the important role of SIPS in grid reliability and how SIPS are integrated part of the grid development worldwide.

It is clear from Fig. 3 that the application of SIPS has become a component of a comprehensive total grid operation and protection philosophy. The fact that 22% of the entries are applications to address "normal" system conditions demonstrates that SIPS are no longer applied solely for system security purposes. In fact, close examination of Fig. 3 reveals SIPS applications can be viewed as two major categories:

- *Operational system improvement* (49% with three components: 19% Increased Power Flow, 8% Important, plus 22% Normal)
- *System security* (51% with two components, 22% Essential plus 29% for Increased Security) which at one time was the primary intent of SIPS

Figure 4 shows the intent of the various types of SIPS. The fact that voltage instability is the most often addressed phenomenon confirms that systems are now more complex than ever. The voltage stability phenomenon was firstly discovered at the beginning of 1980s as systems were getting more complex. The information in Fig. 4 correlates with the classifications in Fig. 3, demonstrating that worldwide SIPS are integrated components of various aspects of grid operation.

System Restoration

Another critical step in minimizing the impact of widespread blackouts is the need for effective and fast power system restoration. Returning equipment to service followed by quick restoration of power to the users is of paramount importance and can significantly minimize consequences of further outages.

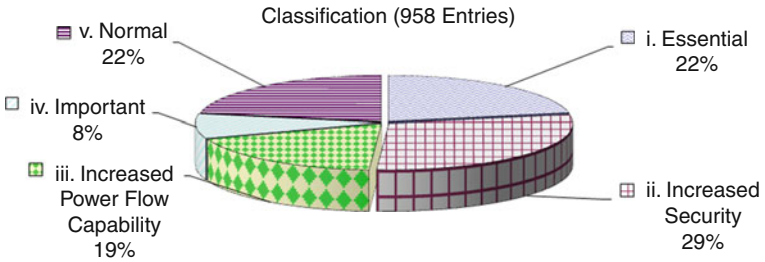

Transmission Blackouts: Risk, Causes, and Mitigation. Figure 3
SIPS classification

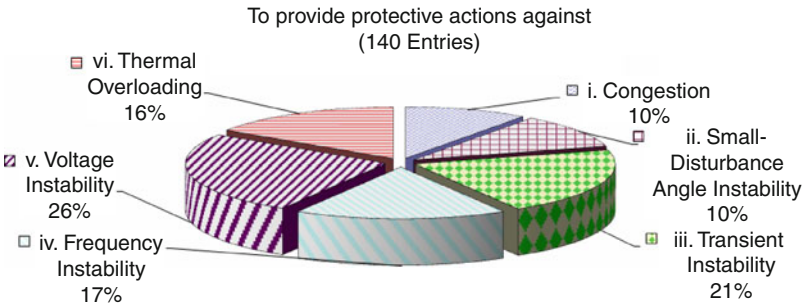

Transmission Blackouts: Risk, Causes, and Mitigation. Figure 4
SIPS purpose

Today's technology can be used to our advantage for intelligent restoration. Some of the key elements for responsive restoration are the following:

- Well-defined procedures that require overall coordination within the restoring area, as well as with the neighboring electric networks.
- Reliable and efficient restoration software tools significantly aid operators and area coordinators to execute operating procedures and to make proper decisions. This tool is a part of EMS/SCADA system that provides voltage, frequency, excitation, outage status, and other data.
- Regular training sessions to assure effectiveness of the process. These sessions should include practice drill scenarios. The drill scenarios should incorporate any regional reliability or governmental policy requirements. For example, there may be a time delay requirement for load restoration after bulk power system has returned to service, to allow the system to stabilize. There may also be critical loads, which must be given higher priority in restoration.
- Substations need to be manned to open breakers or switches to clear re-energization pathways and establish ability to control load restoration.

Today's technology allows us to propel in designing schemes to aid in quick restoration. Even if advanced tools and procedures are in place to speed up restoration, there are limits on how fast the system can be restored depending on the type and distribution of generation. After the August 14, 2003 blackout in North America, it took considerable time to restore generation. Some of the units did not have capabilities to be put in service immediately (black-start capabilities), and some units required longer time to be put on-line with full power (e.g., nuclear units due to security and steam turbines due to allowable ramp-up rates). Also of equal consideration is the type of load served, the system configuration, and the effects of connecting the load back to the network (Cold Load Pickup or Hot Load Pickup affects end user restoration time). While most of the cities have been restored in 5–9 h during the Italian blackout in September 2003, it took over a day to restore power back to Detroit and New York. Göran Andersson points out that in the recent Swedish-Danish blackout, the 400 kV grid was restored within 2 h, most customers were connected within 4 h, and the last customer reconnected within 6 h.

Mayer Sasson explains the slower pace for load restoration experienced in New York. The low-voltage network loads in New York City and Manhattan area are a highly meshed network system that affords a very high degree of reliability against localized outages. However, under blackout conditions, when a network is to be restored, the network is isolated into 100–200 MW portions that need to be re-energized at a time, requiring a time-consuming and careful process such that the inrush does not provide a set back to the restoration effort.

As discussed before, by designing the power system to transfer power across large distances and not providing enough reactive power close to the load or building the accompanying transmission lines may have detrimental effects on power system operation. Similarly, designing the power system not considering the effects on restoration efforts may have detrimental effects on the speed of restoration. In conclusion,

restoration time and system security could be significantly improved by planning of the generation mix and location considering not only market factors but incorporating value of reliable operation and faster restoration in the financial model. This approach would result in optimal, long-term investment strategies.

Future Directions

As the power grids worldwide have become more complex and are operated closer to the operating limits, applications of Wide Area Monitoring, Protection, and Control (WAMPAC) systems have become necessary to better manage the grid reliability and performance security [15]. Control areas within the interconnected grids or among countries are recognizing that bulk power systems should be treated as one system and power system professionals are challenged to upgrade the system with technologies that makes the task of grid control manageable. New technologies such as synchronized measurements have advanced to support commercial WAMPAC deployment so that implementation of various applications is both possible and warranted, representing prudent investment.

Although large-scale demonstrations of using this technology are reported around the world, full-fledged productized systems have just started to be deployed. In the USA, those initiatives have been driven by transmission "smart grid" investments supported by DOE stimulus grants and NERC. WAMPAC systems using synchronized measurements have some unique deployment challenges as they require engagement of multiple users with diverse requirements and varying needs. Such large-scale systems not only offer a lot of promising reliability and financial benefits but also push the boundaries of conventional grid operations.

Synchronized measurement applications, using GPS synchronized Phasor Measurement Units (PMUs), offer large reliability and financial benefits for customers/society and the electrical grid when implemented across the interconnected grid. As measurements are reported 20–60 times per second, PMUs are well suited to track grid dynamics in real time. Compared to current EMS monitoring tools that use

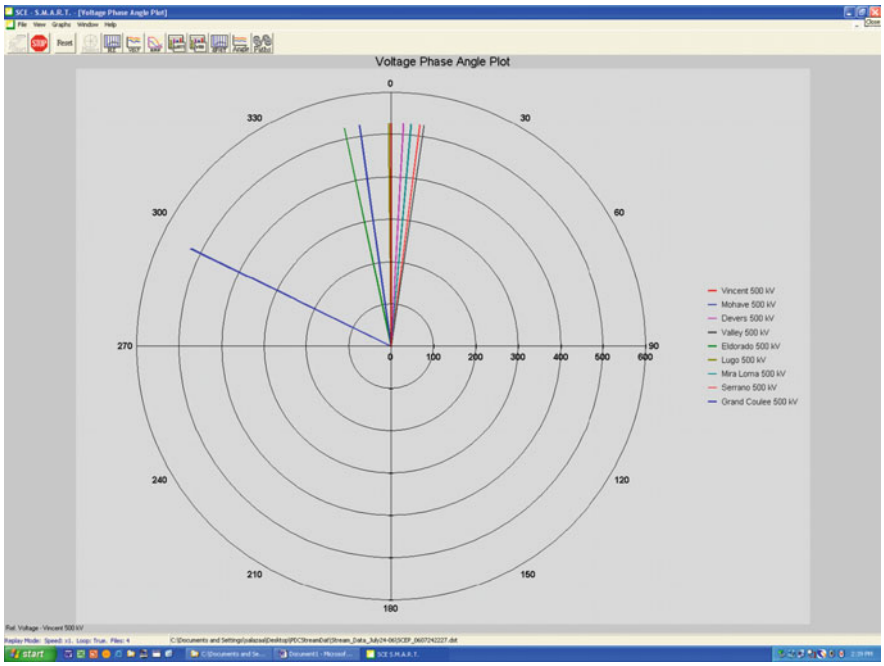

Transmission Blackouts: Risk, Causes, and Mitigation. Figure 5
Key system voltage angles – WECC disturbance on July 24, 2006

information from state estimation and SCADA over several second intervals, time-synchronized PMUs introduce the possibility of directly measuring the system state instead of estimating it based on system models and telemetry data. If implemented properly, the technology also allows for providing data integrity validation without added cost. This technology is instrumental for:

- Improving WAMPAC in real time including applications such as early warning systems, SIPS, detection and analysis of system stability, etc., and enabling faster system restoration
- Faster and more accurate analysis of vast number of data during transient events
- Validation and development of power system models

All of the above helps with avoidance and analysis of outages that may have extreme manifestation in blackouts. Due to its accuracy and wide-area coverage, synchronized measurement technology is a paradigm shift enabling unique tracking of power system dynamics. Synchronized measurement applications enable true early warning systems to detect conditions that lead to catastrophic events, help with restoration, and improve the quality of data for event analysis.

The display shown in Fig. 5 is a dynamic angle display during the disturbance in the western part of the USA in 2006. Those types of displays are used both for post-disturbance analysis and as an operational tool to help during the disturbance.

The conceptual WAMPAC system has interesting parallels with the human nervous system. Figure 6 shows the simplest concept of a WAMPAC system that

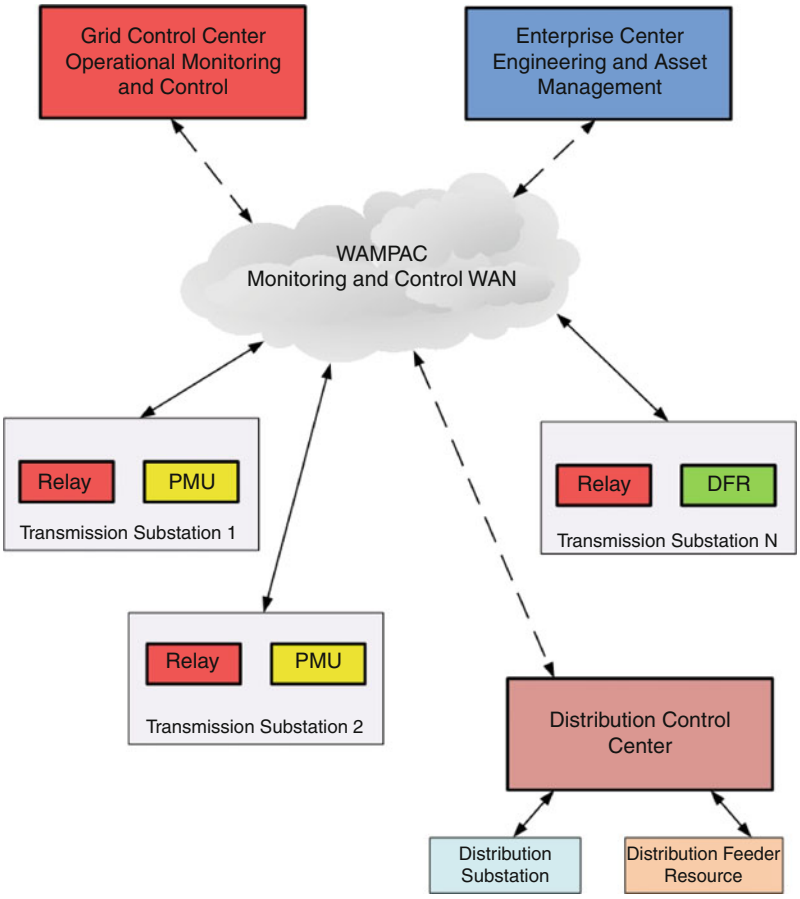

Transmission Blackouts: Risk, Causes, and Mitigation. Figure 6
Basic conceptual WAMPAC system

spans a complete utility transmission system, or even an entire unified operating region. This conceptual description focuses on likely future implementations, without concern of integrating today's persistent but obsolescent components like independent SCADA RTUs. WAMPAC is in fact ultimately capable of absorbing all of the functions of today's SCADA and EMS, including not only measurement and control but also state estimation and real-time contingency analysis.

In summary, Wide Area Monitoring, Protection, and Control (WAMPAC) is a must for transmission smart grid as it is necessary to increase probability to prevent blackouts by improving following applications [15]:

- Data analysis and visualization – Significant benefits are achieved with the ability to analyze events much faster in a synchronized fashion on-line or post-mortem.
- System reliability improvement by preventing cascading outages due to voltage, angular, and frequency instability, thermal overloads, and low frequency oscillations – These applications result in huge societal benefits.
- System operations and planning, improved modeling – Synchronized measurement enables paradigm shift with high reporting rates not available with any other technology and in developing accurate power system models.
- Market operations: Congestion Management and Locational Marginal Pricing – These applications enable large financial benefits by better grid utilization.

With today's technology, it is possible to tie all the monitoring, control, and protection devices together through an information network. The key to a successful solution is fast detection, fast and powerful control devices, communication system, and smart algorithms.

Conclusions

Power system is very complex and human-made. Our industry needs to keep planning, operating, and maintaining it as efficient and as reliable as possible, including preventing blackouts. There is a general understanding of blackouts caused by natural disasters (earthquake, hurricanes, etc.). However, system-wide outages created by humans and/or not arrested due to suboptimal design should be easier to prevent. Analysis of large disturbances reveals some common threads among them, leading to the following conclusions:

- Need to understand the symptoms and root causes of the major disturbances and learn from the past blackouts.
- The power grid should not be operated under system conditions that have not been studied.
- Implement specific solutions to reduce the likelihood and propagation of outages.
- Restoration time could be reduced.

In summary, although it is not possible to avoid multiple contingency initiated blackouts, the probability, size, and impact of wide-area blackouts could be reduced and the propagation stopped.

Although electrical industry (utilities, ISOs, generation owners, regulators, universities, etc.) takes major initiatives after blackouts (such as investments in "smart grid" technologies), grids around the world always face host of new and old challenges. Applying a patchwork of individual measures to manage the grid is not sufficient. It is necessary to take a balanced approach to fixing the system as a whole by implementing a well-defined and coordinated overall strategy including various planning, operations, maintenance, and regulatory measures, weighing the costs, performance, and risks associated with each measure. It is important to always envision how power system should operate 10–30 years in the future; then design and overhaul it with this forward-looking approach.

Within the context of this approach, specific solutions to reduce the likelihood of outages can be addressed – because once the overall causes of wide-area disturbances are minimized, the smaller contributing factors are easier to handle, further diminishing the incidence of failures. The advent of advancements in information technology (IT), innovations in power system monitoring, and deployment of advance warning systems enables tools to arrest the grid from wide-area blackouts and meet the expectations for reliable power delivery. For example, while investing in strengthening the electrical grid infrastructure, such as rebuilding T&D grid and installing new generation and controls (e.g., reactive power devices, FACTS, HVDC), could not be replaced, "smart grid" WAMPAC

deployment is necessary and cost-effective way to improve grid reliability. Under normal conditions, and with sufficient automatic supports, operators are able to adequately control power system operation. However, the speed and complexity of disturbance phenomena makes control of the grid more suited to automated WAMPAC systems to respond to fast developing and complex disturbances.

Acknowledgment

The author expresses appreciation to the following Distinguished Industry Experts for their contributions and guidance: Göran Andersson, Miroslav Begovic, Daniel Karlsson, Bogdan Kasztenny, Mayer Sasson, Carlson Taylor, Chifong Thomas, Vijay Vittal, Jim Thorp, and Eric Udren. Special appreciation and recognition is extended to the Distinguished Expert Vahid Madani, whose ideas and work have been instrumental for the completeness of this chapter.

Bibliography

Primary Literature

1. Novosel D, Begovic M, Madani V (2004) Shedding light on blackouts. IEEE Power and Energy Magazine, Jan/Feb 2004 (lead article)
2. Madani V, Novosel D (2005) Getting a grip on the grid. IEEE Spectrum, pp 42–47 December 2005. Also, Taming the Power Grid in www.spectrum.ieee.org
3. Novosel D, Madani V (2006) Blackout Prevention. In: Yearbook of Science and Technology, McGraw Hill, pp 34–38
4. Madani V, Novosel D, Apostolov A, Corsi S (2004) Innovative solutions for preventing wide area disturbance propagation. In: IREP symposium, Cortina d'Ampezzo, Italy, Aug 2004
5. WECC (1996) Western system coordinating council disturbance report for the power system outage that occurred on the western interconnection. www.NERC.com
6. U.S.-Canada Power System Outage Task Force (2004) Final Report on the August 14, 2003 Blackout in the United States and Canada: Causes and Recommendations. www.FERC.gov, April 2004
7. UCTE (2007) System disturbance on 4 Nov 2006. http://www.ucte.com
8. Fairley P (2004) Unruly power grid. IEEE Spectrum 41(8):22–27
9. Horowitz SH, Phadke AG (2003) Boosting immunity to blackouts. IEEE Power and Energy Magazine, Sept/Oct 2003
10. CIGRE WG C2.02.24 (2007) Defense plan against extreme contingencies. ELECTRA, pp 46–61, Apr 2007
11. Horowitz S, Novosel D, Madani V, Adamiak M (2008) System-wide protection. IEEE Power and Energy Magazine, Sept/Oct 2008
12. Madani V, Novosel D, Begovic M, Adamiak M (2008) Application considerations in system integrity protection schemes (SIPS). GE Protection and Control Magazine, pp 25–30, May 2008
13. Madani V, Novosel D, Horowitz S, Adamiak M, Amantegui J, Karlsson D, Imai S, Apostolov A (2010) IEEE PSRC report on global industry experiences with system integrity protection schemes (SIPS). IEEE Trans PWRD 25(4):2143–2155
14. Novosel D, Bartok G, Henneberg G, Mysore P, Tziouvaras D, Ward S (2010) IEEE PSRC report on performance of relaying during wide-area stressed conditions. IEEE Trans PWRD 25(1):3–16
15. Novosel D, Madani V, Bhargava B, Vu K, Cole J (2008) Dawn of the grid synchronization. IEEE Power and Energy Magazine, vol 6, Jan/Feb 2008, pp 49–60

Books and Reviews

Kundur P (1994) Power system stability and control. McGraw-Hill, New York

Massoud Amin S, Wollenberg BF (2005) Toward a smart grid. IEEE Power and Energy Magazine, Sept–Oct 2005

Phadke AG, Thorp JS (2008) Synchronized phasor measurements and their applications. Springer, New York

Taylor CW (1999) Improving grid behavior. IEEE Spectrum 36:40–45

Transport and Fate of Chemicals in the Environment, Introduction

John S. Gulliver
St. Anthony Falls Laboratory, Department of Civil Engineering, University of Minnesota, Minneapolis, MN, USA

Article Outline

Glossary
Introduction
Transport Processes
Chemical Fate
The Importance of Mixing
Resistance to Transport
Conclusion
Future Directions
Bibliography

Glossary

Concentration The quantity of a compound or chemical per unit volume, unit mass, or unit mole, where

1 mole = 6.02×10^{23} molecules of the chemical or compound. In this text, concentration in mass or moles per volume of water, mass per mass of solid, and moles per mole of gas will be discussed, depending upon the media of interest.

Convection The movement of a constituent with the movement of the fluid.

Density Total mass per unit volume.

Diffusion The spreading of fluid constituents through the motion inherent to atoms and molecules.

Diffusion coefficient A coefficient that describes the tendency of molecules to spread a constituent mass.

Dilution The mixing of a more concentrated solution with one that is less concentrated. The adage "The solution to pollution is dilution" is still used, sometimes appropriately, for many pollution and mitigation processes.

Kinematic viscosity The fluid viscosity divided by the fluid density, resulting in units that are similar to a diffusion coefficient, or length squared per time.

Turbulent diffusion The mixing of chemicals by turbulence, such that a turbulent diffusion coefficient can be defined separately from the temporal mean convection.

Introduction

Estimating the fate and transport of chemicals released into the environment is an interesting and challenging task. The environment can rarely be approximated as well mixed, and the chemicals in the environment often are not close to equilibrium. Thus, chemical fate and transport in the environment requires a background in the physics of fluid flow and transport, chemical thermodynamics, chemical kinetics, and the biology that interacts with all of these processes. The goal is to follow chemicals as they move, diffuse, and disperse through the environment. These chemicals will inevitably react to form other chemicals, in a manner that approaches, but rarely achieves, a local equilibrium. Many times, these reactions are biologically mediated, with a rate of reaction that more closely relates to an organism being hungry, or not hungry, than to first-order kinetics.

The global environment is large, on the chemical fate and transport scale. Individuals attempt to apply the mathematics of diffusion to the atmosphere, lakes, rivers, groundwater, and the ocean, depending on the system for which the material is most applicable, and to transfer between these systems. Volatilization of a compound from a water body, condensation of a compound from the air, and adsorption of a compound from a fluid onto a solid are all interfacial transport processes. Thus, the fate and transport of chemicals in the environmental media of earth, water, and the atmosphere will be the topic. Contributions in this section will first attempt to formulate fate and transport problems such that they can be solved, regardless of the media or of the transport process, through the mathematics of diffusion (see chapters on ► Chemicals in the Environment, Diffusive Transport; ► Chemicals in the Environment, Dispersive Transport; ► Chemicals in the Environment, Turbulent Transport; ► Toxic Organic Chemicals; ► Transport in the Environment). Applications of these principals to specific media and between media will then be described (see chapters on ► Transport with Jets and Plumes of Chemicals in the Environment; ► Atmosphere-Water Exchange; ► Sediment–Water Interfaces, Chemical Flux at; ► River Fate and Transport; ► Lake and Reservoir Fate and Transport of Chemicals; ► Oceanic Fate and Transport of Chemicals; and ► Subsurface Fate and Transport of Chemicals).

Transport Processes

A transport process, as used herein, is one that moves chemicals and other properties of the fluid through the environment. *Diffusion* of chemicals is one transport process, which is always present. It is a spreading process, which cannot be reversed (without the involvement of another media such as in reverse osmosis). *Convection or advection* is the transport of chemicals from one place to another by fluid flow. The convection and diffusion of a chemical cloud, as represented in Fig. 1, is the movement of the cloud and spreading of the cloud over time.

Turbulent diffusion is actually a form of advection, but the turbulent eddies tend to mix fluid with a random characteristic similar to that of the diffusion process, when viewed from enough distance. The representation given in Fig. 1 could also be used to represent convection and turbulent diffusion, except that the pace of turbulent diffusion is normally more than one

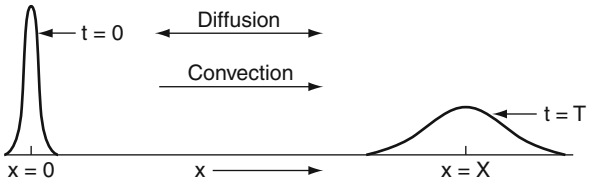

Transport and Fate of Chemicals in the Environment, Introduction. Figure 1
Illustration of convection and diffusion of a chemical cloud along the x-space coordinate (*x*-axis) [2]

order of magnitude greater than diffusion. This higher pace of turbulent diffusion means that diffusion and turbulent diffusion do not normally need to be considered together because they can be seen as parallel rate processes, and one has a much different time and distance scale than the other. If two parallel processes occur simultaneously, and one is much faster than the other, the second process can normally be ignored. This is discussed further in this section.

Dispersion is the combination of a nonuniform velocity profile and either diffusion or turbulent diffusion to spread the chemical longitudinally or laterally. Dispersion is something very different than either diffusion or turbulent diffusion because the velocity profile must be nonuniform for dispersion to occur. The longitudinal dispersion of a pipe flow is illustrated in Fig. 2. While there is diffusion of the chemical, the nonuniform velocity profile creates a dispersion that is much greater than would occur with diffusion alone. The other important difference is that *dispersion reflects the spreading of a cross-sectional mean concentration*, while diffusion represents the spreading of a local concentration. In some contexts, typically in atmospheric applications, turbulent diffusion is also considered to be a form of dispersion. This is only a semantic difference, and herein, the differentiation will continue to be between turbulent diffusion and the dispersion of a mean concentration.

Interfacial transfer is the transport of a chemical across an interface. The most studied form of interfacial transfer is absorption and volatilization, or condensation and evaporation, which is the transport of a chemical across the air–water interface. Another form of interfacial transfer would be adsorption and desorption, generally from water or air to the surface of a particle of soil, sediment, or dust. Illustration of both of these forms of interfacial transfer will be given later in this section.

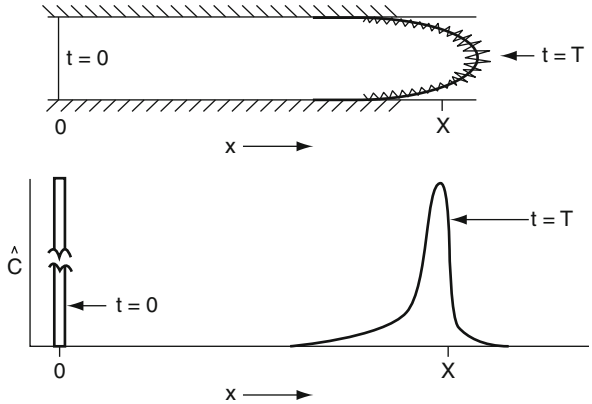

Transport and Fate of Chemicals in the Environment, Introduction. Figure 2
Illustration of longitudinal dispersion of a tracer "plane" at t = 0 to a dispersed "cloud" at *t* = *T*. is the cross-sectional mean concentration [2]

Finally, there is *multiphase transport*, which is the transport of more than one phase, usually partially mixed in some fashion. The settling of particles in water or air, the fall of drops, and the rise of bubbles in water are all examples of multiphase transport. Figure 3 illustrates three flow fields that represent multiphase transport.

Mass transport problems are solved with the *diffusion equation*, often represented as

$$\underbrace{\frac{\partial C}{\partial t}}_{1} + \underbrace{u\frac{\partial C}{\partial x} + v\frac{\partial C}{\partial y} + w\frac{\partial C}{\partial z}}_{2} = \underbrace{D\left[\frac{\partial^2 C}{\partial x^2} + \frac{\partial^2 C}{\partial y^2} + \frac{\partial^2 C}{\partial y^2} + \frac{\partial^2 C}{\partial z^2}\right]}_{3} + \underbrace{S}_{4} \tag{1}$$

where C is the concentration of a chemical; t is time; u, v, and w represent the temporal mean velocity in the x, y, and z directions, respectively; and D represents a diffusion coefficient. The first term (1) on the far left of Eq.1 represents the rate of accumulation of chemical concentration. The second terms (2) represent the mean convection of the chemical. The third terms (3) to the right of the equal sign represent either diffusion or turbulent diffusion of chemical. The fourth term (4) represents the multitude of reactions that are possible in a fluid in environmental media.

Chemical Fate

Chemical fate is the eventual short-term or long-term disposition of chemicals, usually to another

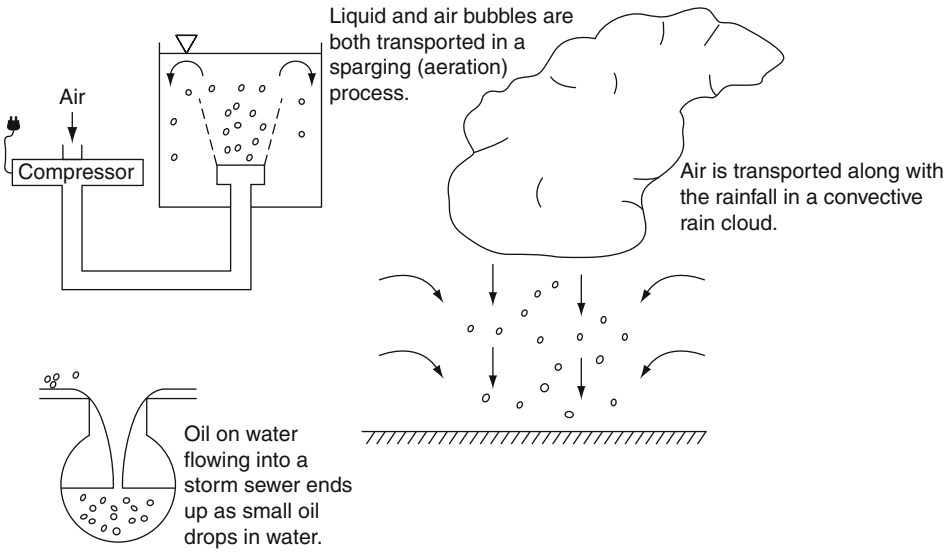

Transport and Fate of Chemicals in the Environment, Introduction. Figure 3
Illustration of sparged multiphase transport. In these two cases, air bubbles create a water flow, and rain drops create an airflow. The oil drops and rain drops create an airflow. The oil drops do not have a significant rise or fall velocity in water and are simply transported [2]

chemical or storage. Some examples that fit the concept of short-term and long-term fate are given in Table 1. If a polychlorinated biphenyl (PCB) compound is in groundwater, the media is soil and water. The "short-term" fate will be that the PCB will primarily adsorb to the soil. The "long-term" fate is that the chemical will desorb, when the PCB-laden water has left, and eventually be bioremediated by microbacteria looking for carbon sources. If this PCB is in the atmosphere, it will be adsorbed primarily to aerosols and particles in the short-term, while its long-term fate will probably be photocatalyzed degradation.

There are as many examples of short-term and long-term fate as there are chemical–media combinations. An important consideration for this topic is whether one is interested in short-term or long-term fate. This is often a question to be answered by toxicologists because it is the most toxic forms of a chemical that are of most interest.

Transport and Fate of Chemicals in the Environment, Introduction. Table 1 Examples of short-term and long-term fate

Chemical	Media	Short-term fate	Long-term fate
PCB	Soil and water	Adsorbed to soil	Bioremediated degradation
PCB	Atmosphere	Adsorbed to aerosols	Photocatalyzed degradation
CO_2	Water	Reactions to carbonate and bicarbonate	Photosynthesis to oxygen and biomass
Benzene	Water	Adsorbed to suspended particles	Bioremediated degradation
Ammonia	Soil and water	Reaction to ammonium	Bioremediated degradation to N_2

The Importance of Mixing

Mixing is a rate-related parameter in that most rates of reaction or transport are dependent upon mixing in environmental systems. When mixing is dominant (the slowest process), the first-order rate equation can be described as

$$\text{Rate of process} = \text{Mixing parameter} \times \text{Difference from equilibrium} \quad (2)$$

Thus, two items are needed to compute the rate of the process: the equilibrium concentrations for all species involved and the mixing rate parameter. A common example would be dissolved oxygen concentration in aquatic ecosystems.

One of the most common chemicals of concern in water bodies is oxygen. Without sufficient oxygen, the biota would be changed because the "desirable" organisms in the water body require oxygen to live. The rate of oxygen transfer between the atmosphere and a water body is therefore important to the health of the aquatic biota. For air-water oxygen transfer, Eq. 2 can be formulated as

$$\frac{dM}{dt} = K_L A\left(\frac{C_a}{H} - C\right) \quad (3)$$

where dM/dt is the rate of mass transfer into the water, K_L is a bulk oxygen transfer coefficient, A is the surface area for transfer, C_a is the concentration of oxygen in the air, H is a coefficient that partitions oxygen between the air and water at equilibrium (called Henry's Law constant for liquids and gas equilibrium), and C is the concentration of oxygen in the water. Air is 20.8% oxygen, so the concentration of oxygen in the atmosphere is determined primarily by atmospheric pressure. Henry's Law constant for oxygen is a function of pressure as well as temperature. Thus, the equilibrium concentration of oxygen is influenced by the thermodynamic variables pressure and temperature. The rate parameter is $K_L A$, which has units of volume/second. The difference from equilibrium partitioning is represented by $C_a/H - C$. It is C that is typically needed to bring as close to equilibrium with the atmosphere as possible, and the means to do it is by having a large dM/dt. This usually means a large $K_L A$ because it would be difficult to alter either C_a or H in the atmosphere. While the surface area is often established by the boundary conditions, K_L is determined by the turbulence and diffusion coefficient (i.e., mixing) close to the water surface and represents the rate of mixing per unit surface area. Thus, the primary variable that can be changed in order to increase dM/dt is the mixing parameter represented by K_L. Some further examples of mixing rate and equilibrium parameters in environmental processes are given in Table 2.

Resistance to Transport

An important concept for environmental transport is *resistance*. That is, the inverse of a rate parameter is a resistance to chemical transport, or in equation form:

$$\frac{1}{\text{Rate parameter}} = \text{Resistance to chemical transport} = R \quad (4)$$

Figure 4 gives an example of the adsorption of a compound to suspended sediment, modeled as two resistances in series. At first, the compound is dissolved in water. For successful adsorption, the compound must be transported to the sorption sites on the surface of the sediment. The inverse of this transport rate can also be considered as a resistance to transport, R_1. Then, the compound, upon reaching the surface of the suspended sediment, must find a sorption site for adsorption. This second rate parameter is more related to surface chemistry than to diffusive transport, and is considered as a second resistance, R_2, that acts in series to the first resistance. The second resistance cannot occur without crossing the first resistance of transport to the sorption site, so they must occur in series.

Now, if R_1 is much greater than R_2, it can be assumed that R_2 is zero without compromising the accuracy of the rate calculation. In electric circuits, two resistances applied in series are simply added together in calculating the line resistance. The same is true for resistance to chemical transport. If R_1 is 1,000 resistance units and R_2 is 1 resistance unit, R_2 can be ignored and still be within 99.9% of the correct answer.

Another example is the air–water transfer of a compound, illustrated in Fig. 5. This example will be used to explain volatile and nonvolatile compounds. There is resistance to transport on both sides of the interface, regardless of whether the compound is classified as volatile or nonvolatile. The resistance to transport in the liquid phase is given as $R_L = 1/K_L$. If chemical transfer is being described through an equation like Eq. 3, the resistance to transfer in the gas phase is given as $R_G = 1/(HK_G)$. The equilibrium constant is

Transport and Fate of Chemicals in the Environment, Introduction. Table 2 Examples of important mixing rate and equilibrium parameters in environmental processes

Process	Mixing-rate-related parameter	Equilibrium parameter
1. Treatment processes		
Coagulation/flocculation	Size of coagulation and flocculation basins and proper mixing (residence time)	Dose of coagulants (alum)
Softening	Design of softening tank to increase mixing	Dose of softening agent (lime)
Settling	Design of settling basin to reduce mixing	$\rightarrow 0$
Chlorination	Design of chlorination and dechlorination chambers for proper mixing and res. time	Dose of chlorine
Filtration	Size of filter bed	Length of time before backflushing
2. Surface waters		
Oxygen transfer	Diffusion and turbulent mixing	Atmospheric O_2 conc. Henry's Law constant
Volatilization of pollutants	Diffusion and turbulent mixing	$\rightarrow 0$
Toxic spills	Diffusion and turbulent mixing	Spill–water equilibrium
Internal loading of nutrients	Hypolimnetic mixing	O_2 concentration in hypolimnion
Sorption onto suspended sediments	Turbulent mixing exposes chemicals to sediment	Sediment–water partitioning
3. Atmosphere		
Greenhouse gases (CO_2, CH_4)	Turbulent mixing	Atmospheric concentrations
Volatilization of spills	Turbulent mixing and dispersion	$\rightarrow 0$
Aerosols	Turbulent mixing, dispersion, and settling	None
4. Groundwater and sediments		
Spills	Advection and dispersion	$\rightarrow 0$
O_2	Diffusion and advection	Atmospheric conc. of O_2
Sorption of soil	Advection and diffusion	Equilibrium soil–water partitioning

in the R_G equation because the equivalent waterside concentrations are being used to represent the concentration difference from equilibrium, and the gas phase resistance needs to be a resistance to an equivalent water concentration.

The gas phase and the liquid phase resistances are applied in series. In general, gas film coefficients are roughly two orders of magnitude greater than liquid film coefficients. It is also true that Henry's Law constant, H, varies over many orders of magnitude as the transported compounds are varied. Nitrogen gas, for example, has a Henry's Law constant of approximately 15, using mass concentrations. The herbicide, atrazine, has a Henry's Law constant of 3×10^{-6}. Thus, the ratio R_G/R_L would vary by seven orders of magnitude between nitrogen gas and atrazine.

If these orders of magnitude are put into a series resistance equation,

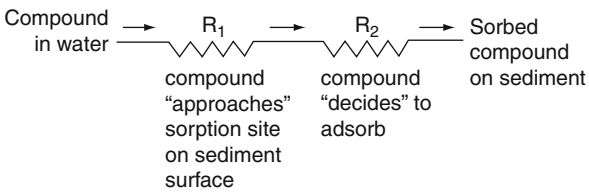

Transport and Fate of Chemicals in the Environment, Introduction. Figure 4
Adsorption analogy to two resistors in a series: adsorption of an organic compound to sediment [2]

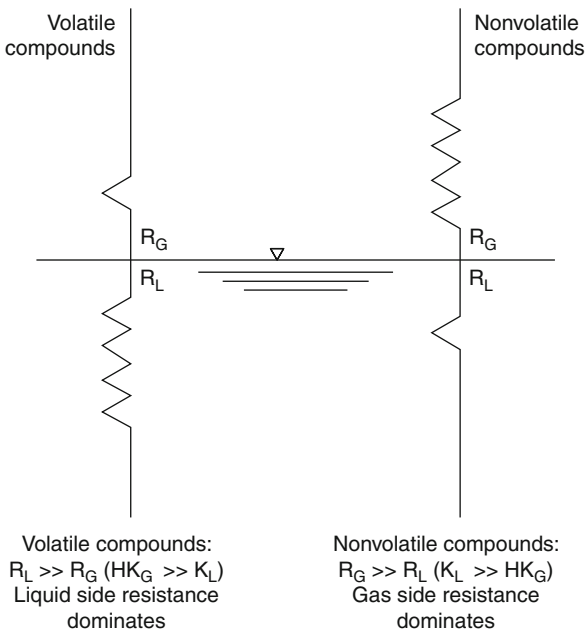

Transport and Fate of Chemicals in the Environment, Introduction. Figure 5
Air–water transfer analogy to two resistors in a series [2]

$$R = R_L + R_G = \frac{1}{K_L} + \frac{1}{HK_G} \tag{5}$$

Due to the Henry's Law constants, it can be seen that for nitrogen gas, $R \cong R_L$, and for atrazine, $R \cong R_G$. If a typical ratio of $K_G/K_L \sim 100$ is applied, $R_G = R_L$ when $H = 0.01$.

Now, the mass transfer between phases is given as

$$\frac{dM}{dt} = \frac{A}{R}\left(\frac{C_a}{H} - C\right) \tag{6}$$

or

$$\frac{dM}{dt} = \frac{A}{1/K_L + 1/HK_G}\left(\frac{C_a}{H} - C\right) \tag{7}$$

Nitrogen gas would be a volatile compound because the equilibrium is strongly to the gas phase, and there is little gas phase resistance to its transfer, i.e., $1/K_L \gg 1/(HK_G)$. For that reason, N_2 is generally called a gas, as are many other volatile compounds such as methane, oxygen, and propane.

Atrazine, on the other hand, would be a nonvolatile compound, $1/(HK_G) \gg 1/K_L$, because equilibrium is strongly to the liquid phase due to the small Henry's Law constant. There is also a strong gas phase resistance to the transfer. Atrazine was manufactured to remain in the liquid phase, where it will act as a herbicide, rather than in the gas phase, where the farm personnel will be breathing this toxic chemical. If you were going to pick a nonionic compound that is not made by humans from the list of those that are gas or liquid in our environment, a good guess is that it would be a volatile or semivolatile compound. There are only a few environmental compounds that are nonvolatile. Remarkably, one of them is water. While the atmosphere may be as much as 3% water, the water bodies in the world are very close to 100% water. The equilibrium is strongly to the liquid side, due to a large equilibrium-partitioning constant.

One theme of this discussion can now be stated as follows: when transport processes occur in series, it is the slower transport processes that are important for chemical transport calculations because the *resistance* to transport is large, just as the large resistors of a series in an electronic circuit are the most important.

Now is the time for the second theme: when transport processes *occur in parallel*, the fast transport process with the low resistance dominates. The result is the opposite of resistances in series. Figure 6 illustrates this concept with the transport of a compound from a water body to a sorption site on a solid. In the bulk solution, there is diffusion and turbulent diffusion occurring simultaneously. Transport can occur due to either process, so there are two different paths that may be followed, without the need of the other path. These transport processes are operating in parallel, and the faster transport process will transport most of the

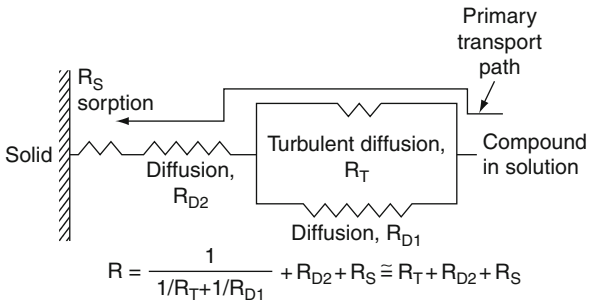

Transport and Fate of Chemicals in the Environment, Introduction. Figure 6
Transport to a sorption site and the resistor analogy [2]

compound. The analogy to electronic circuits applies in this case as well. Beginning with a compound in solution in Fig. 6, there are two parallel transport paths, each with a resistance to transfer. Most of the compound will be transported through the path with the least resistance. Many times, the path with the greater resistance can be ignored because the quantity of compound transported through this path is very small. When the compound comes close to the solid, however, the turbulent diffusion dissipates because eddies become so small that they are dissipated by the viscous action of the water. Now, one is back to one transport path, with the act of sorption and diffusion acting in series. Thus, the slowest transport path once again becomes the important process.

The overall resistance to the sorption process illustrated in Fig. 6 can be written as follows:

$$R = \frac{1}{1/R_T + 1/R_{D1}} + R_{D2} + R_S \cong R_T + R_{D2} + R_S \tag{8}$$

where R_T, R_{D1}, R_{D2}, and R_S are the resistances to turbulent transport, diffusive transport in the bulk of the fluid, diffusive transport near the solid surface, and adsorption, respectively. It can be seen that, in Fig. 6 and Eq. 8, the resistance due to diffusion in the bulk of the fluid can be neglected because turbulent diffusion is a parallel path. The resistance due to diffusion only needs to be considered when there is no parallel path for turbulent diffusion, such as very near the surface of the solid. Thus, R_{D1} can be ignored, but not R_{D2}.

Conclusion

In this chapter, some of the topics that will be covered and applied in the other chapters of the section have been introduced, where the physics of mass transport are essential. These and similar engineering concepts will be revisited throughout the first half of this volume, in an attempt to develop models in the environmental fate and transport of chemicals that are close to realistic, but can be solved, even if that solution is approximate.

Future Directions

Global climate change is a topic for the present and future because society has only begun to assess and tackle the causes, implications, and remediation of the new Anthropocene [1]. There are global warming gases (CO_2 and CH_4) and global cooling gases (refrigerants) that are transported between the oceans and the atmosphere and could be transported between the atmosphere and the earth (carbon sequestration). These global transport rates are not quick, so we humans will be dealing with transport to a greater extent in the future. On a more local scale, urbanization is creating nonsource pollution of water and the atmosphere that is increasing. Roads, parking lots, and rooftops are often directly connected to lakes and rivers through storm sewers, and the pollution of urban activities is not insubstantial. This will be a bigger concern as discovery about this source of pollution occurs. Finally, the nitrogen of various forms released from agricultural activities continues to create hypoxic (dead) zones when the rivers have transported this nutrient to the oceans. The nitrification–denitrification processes as organic nitrogen is decomposed to ammonia, utilized by aerobic bacteria to make nitrites and nitrates, and finally converted by anaerobic bacteria to nitrogen gas occurring in streams and rivers add an interesting complexity to the fate and transport calculations.

Bibliography

1. Ellis E (2011) A man-made world. The Economist London, UK, 26 May 2011
2. Gulliver JS (2007) Introduction to chemical transport in the environment. Cambridge University Press, Cambridge, UK

Transport in the Environment

John S. Gulliver
St. Anthony Falls Laboratory, Department of Civil Engineering, University of Minnesota, Minneapolis, MN, USA

Article Outline

Glossary
Definition of Transport in the Environment
Introduction
Development of the Diffusion Equation
Adsorption and Desorption in Sediments and Soils
Example Applications of the Diffusion Equation
Conclusion
Future Directions
Bibliography

Glossary

Adsorption The process of dissolved chemicals sticking to a solid.

Convection The movement of a constituent with movement of the fluid.

Desorption The detachment of a chemical from a solid.

Diffusion The spreading of fluid constituents through the motion inherent to atoms and molecules.

Diffusion coefficient A coefficient that describes the tendency of molecules to spread a constituent mass.

Dirac delta An impulse of a given quantity (mass) that occurs over an infinitely short time or space.

Kinematic viscosity The fluid viscosity divided by the fluid density, resulting in units that are similar to a diffusion coefficient, or length squared per time.

Laminar flow Flow that has no turbulent eddies, where the fluid flows in laminas and diffusion creates the mixing of the fluid.

Retardation factor A divisor that indicates the slowing of chemical movement through a media due to adsorption.

Reynolds number The ratio of inertial to viscous forces, resulting in a meaningful velocity times a meaningful distance divided by kinematic viscosity.

Definition of Transport in the Environment

In this section various solution techniques for the convection-diffusion equation are reviewed, which is generally defined as the mass transport equation with diffusive terms. These techniques will be applied to chemical transport solutions in sediments. There are also a number of applications to chemical transport in biofilms. There are many other applications of the convection-diffusion equation, but they require more background with regard to the physics of mixing processes, which will be addressed in later sections of the volume.

Introduction

What is *mass (or chemical) transport*? It is the transport of a solute (the dissolved chemical) in a solvent (everything else). The solute is the dissolvee and the solvent is the dissolver. There are liquids that are generally classified as solvents because they typically play that role in industry. Some examples would be degreasing and dry-cleaning solvents, such as trichloroethylene (TCE). In environmental applications, these "solvents" are the solutes, and water or air is usually the solvent. In fact, when neither water nor air are the solvents, a general term "nonaqueous phase liquid," or NAPL, is applied. NAPL is defined as a liquid that is not water, which could be composed of any number of compounds.

The substance being transported can either be dissolved (part of the same phase as the solvent) or particulate substances. The diffusion equation will also be discussed by considering mass conservation in a fixed control volume. The mass conservation equation can be written as:

$$\begin{aligned} &\textit{Flux rate IN} - \textit{Flux rate OUT} + \textit{Rate of} \\ &(\textit{Sources} - \textit{Sinks}) = \textit{Rate of Accumulation} \end{aligned} \tag{1}$$

Now that there is our mass conservation equation, it must be decided which control volume would be the most convenient for our applications. The control volumes used most for this type of mass balance are given in Fig. 1. The general control volume, given in Fig. 1a, is used for descriptive purposes, to maintain generality. It is rare that one works with something that approximates such a contorted control volume. The control volumes that are used in practice are given

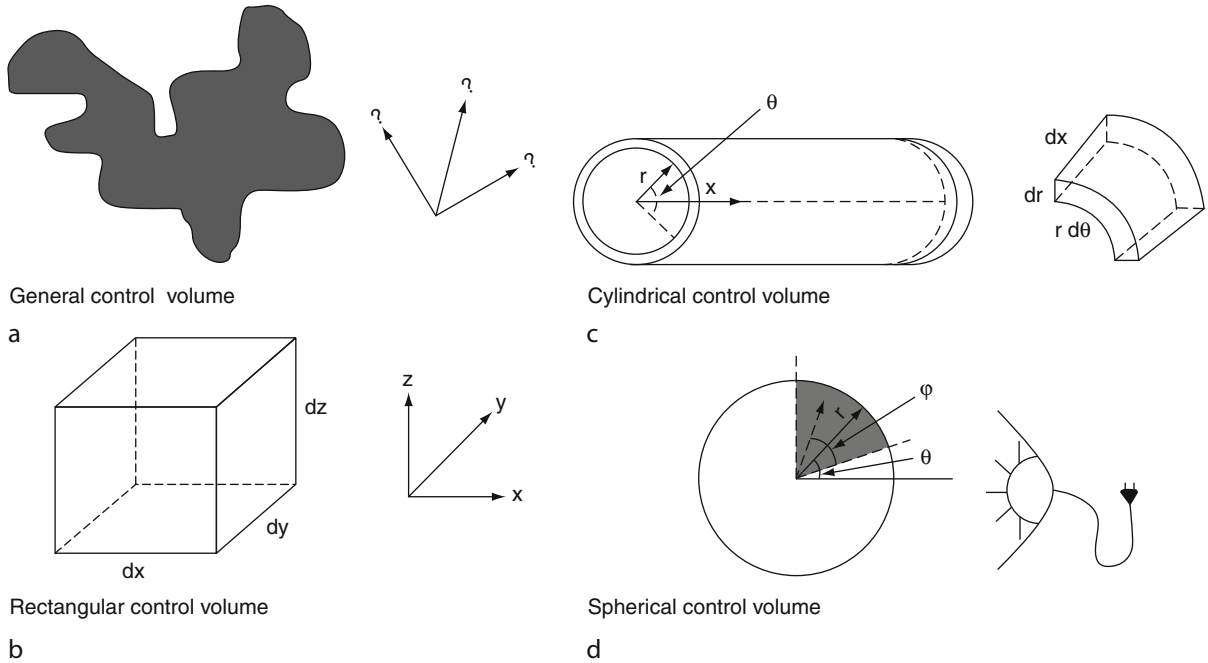

Transport in the Environment. Figure 1
Common control volumes found in engineering texts and (for the latter three) used in solving the diffusion equation. (From [1])

in Figs. 1b, c, and d. For the environmental applications of chemical transport, the rectangular control volume, Fig. 1b, has proven to be the most useful. The cylindrical control volume, Fig. 1c, is used to make pipe or tube flow problems easier to solve, and the spherical control volume, Fig. 1d, is often helpful when dealing with transport in and around particles or drops. For this control volume, it is convenient to imagine a light being shined along the axis, which casts a shadow of the vector on to a plane normal to the light. The φ angle is measured from the reference axis to the shadow in this plane.

A rectangular control volume will be used for the development of our mass conservation (diffusion) equation.

Development of the Diffusion Equation

The diffusion equation will be developed by considering each term in Eq. 1 separately. In addition, the flux terms will be divided into diffusive and convective flux rates.

Diffusive Flux Rate

The molecules of a fluid "at rest" are still moving because of their internal energy. They are vibrating. In a solid, the molecules are held in a lattice. In a gas or liquid, they are not, so they move around because of this vibration. Since the molecules are vibrating in all directions, the movement appears to be random. Diffusive fluxes are described by Fick's law [9], given in the section by Dr. Cussler on diffusion. For this purpose, let us consider one side of our control volume, normal to the x-axis, with an area A_x, shown in Fig. 2. Fick's law describes the diffusive flux rate as:

$$\text{Diffusive flux rate (g/s)} = -\mathrm{D}\,(\mathrm{m}^2/\mathrm{s})\,\frac{\partial C}{\partial x}\,(\mathrm{g/m}^4)\,A_x(m^2) \tag{2}$$

where C is concentration of the solute (tracer), D is the diffusion coefficient of the solute in the solvent (water), which relates to how fast how and far the tracer molecules are moving to and fro, and $\partial C/\partial x$ is the gradient of concentration with respect to x, or the slope of C

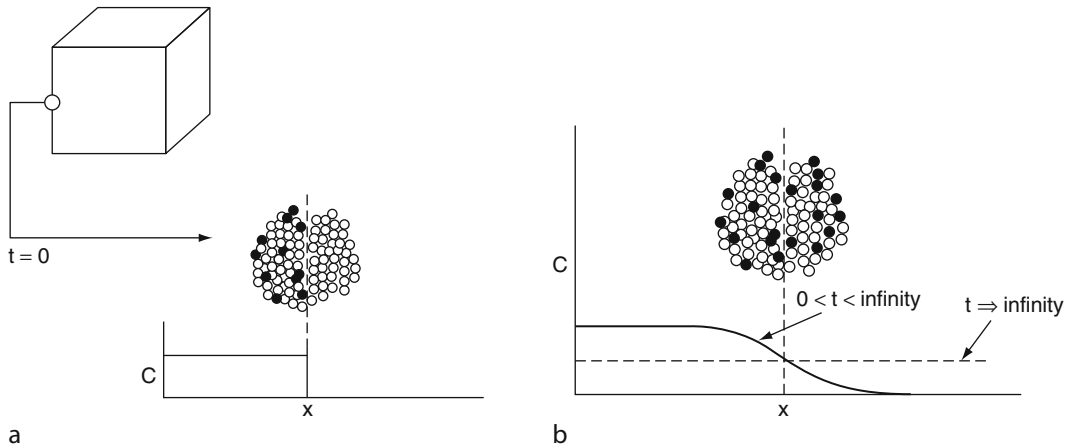

Transport in the Environment. Figure 2
Illustration of net diffusive flux through one side of the rectangular control volume. (From [1])

with x, as shown in Fig. 2. Thus, the diffusive flux rate depends upon the diffusion coefficient and the *gradient* of concentration with distance.

Convective Flux

The convective flux rate into our control volume is simply the chemical mass carried in by convection. If the same box of Fig. 2 is considered, except with a velocity component u in the x-direction, the convective flux rate into the box from the left-hand side is:

$$\text{Convective flux rate (g/s)} = \text{Velocity component normal to surface (m/s)} \times \text{Surface area (m}^2\text{)} \times \text{Concentration (g/m}^3\text{)} \tag{3}$$

or

$$\text{Convective flux rate} = uA_xC \tag{4}$$

where u is the component of velocity in the x-direction and A_x is the surface area normal to the x-axis on that side of the box. All six sides of our box would have a convective flux rate through them, just as they would have a diffusive flux.

Rate of Accumulation

The rate of accumulation is the change of chemical mass per unit time, or:

$$\text{Rate of accumulation (g/s)} = \mathcal{V}(\text{m}^3)\frac{\partial C}{\partial t}(\text{g/m}^3/\text{s}) \tag{5}$$

where $\mathcal{V}$ is the volume of our box.

Source and Sink Rates

The solute chemical can appear or disappear through chemical reaction. In addition, interfacial transfer is often integrated over the control volume and considered as a source or sink throughout the control volume. This type of pseudo-reaction can be of significant help in solving chemical transport problems when averages over a larger control volume, such as cross-sectional mean concentrations, are being computed. For both cases (chemical reactions and pseudo-reactions), the source and sink rates are given as:

$$\text{Source} - \text{sink rate (g/s)} = S\,(\text{g/m}^3/\text{s})\mathcal{V}(\text{m}^3) \tag{6}$$

where S is the net source/sink rate per unit volume. The particular reactions that a given chemical is likely to undergo will determine the form of S used in Eq. 6. These are listed in Table 1. The source/sink term could be a combination of two or more of these reactions. For convenience in determining analytical solutions to the diffusion equation, most source/sink terms are approximated as either a first-order or zero-order reaction.

Transport in the Environment. Table 1 Common source and sink terms used in the convection-diffusion equation

Source/sink name	Equation	Units of constant
Zero order	$S = k_o$	k_o – g/m^3-s
First order	$S = k_1 C$	$k_1 = S^{-1}$
Second order	$S = k_2 C^2$	k_2-m^3/g-s
Independent variable	$S = k_{1i} P^a$	k_{1i} – s^{-1}
	$S = k_{2i} PC^b$	k_{2i} – m^3/g-s
Monod kinetics[c]	$S = \frac{\mu_m C}{k_c + C} P$	μ_m = maximum growth rate (s^{-1})
		k_c = half-saturation coefficient (g/m^3)

[a]If P is nearly constant, then k_{1i} can be provided as a zero-order term
[b]Often called second order
[c]Common for biologically mediated reactions

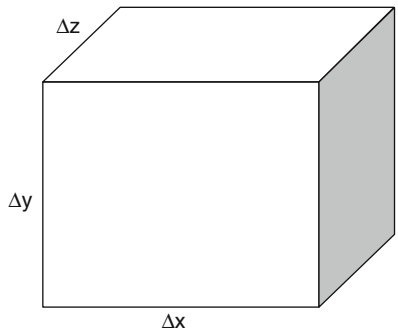

Transport in the Environment. Figure 3 Dimension of the rectangular control volume

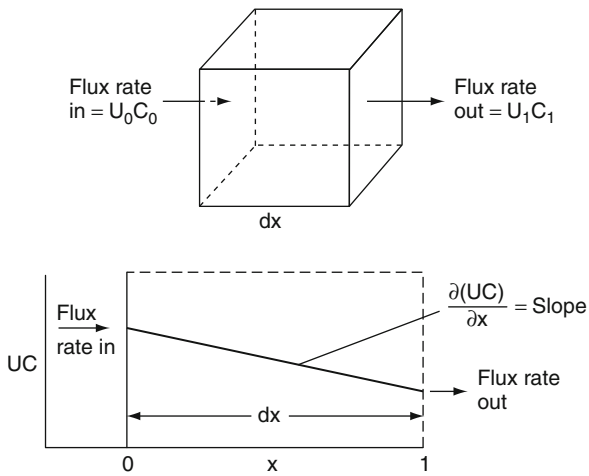

Transport in the Environment. Figure 4 Illustration of the x-component of mass flux rate into and out of the rectangular control volume. (From [1])

Mass Balance on Control Volume

A mass balance on one compound in our box is based upon the principle that whatever comes in must do one of three things: be accumulated in the box, flux out of another side, or react in the source/sink terms. If it seems simple, it is.

We will begin by assigning lengths to the sides of our box of dx, dy, and dz, as shown in Fig. 3. Then, for simplicity in this mass balance, we will arbitrarily designate the flux as positive in the $+x$-direction, $+y$-direction, and $+z$-direction. The x-direction flux, so designated, is illustrated in Fig. 4. Then, the two flux terms in Eq. 1 become:

$$\text{Flux rate in} + \text{Difference in flux rate} = \text{Flux rate out} \tag{7}$$

or, because a *difference* can be equated to a *gradient times the distance over which the gradient is applied*:

$$\text{Flux rate out} - \text{Flux rate in} = \text{Gradient in flux rate} \times \text{Distance} \tag{8}$$

Equation 8 can thus be applied along each spatial component as:

$$\text{Flux rate}(\text{out} - \text{in})_x = \frac{\partial}{\partial x}(\text{flux rate})\,dx \tag{9a}$$

$$\text{Flux rate}(\text{out} - \text{in})_y = \frac{\partial}{\partial y}(\text{flux rate})\,dy \tag{9b}$$

$$\text{Flux rate}(\text{out} - \text{in})_z = \frac{\partial}{\partial z}(\text{flux rate})\,dz \tag{9c}$$

Convective flux rates. The convective and diffusive flux rates are dealt with separately. They will eventually be separated in the final diffusion equation, and it is convenient to make that break now. The x-component of the convective flux rate is equal to the x-component

of velocity times the concentration times the area of our box normal to the x-axis. Therefore, in terms of convective flux rates, Eq. 9a becomes:

$$\text{Convective flux rate}(\text{out}-\text{in})_x = \frac{\partial}{\partial x}(u\,C\,A_x)dx = \frac{\partial}{\partial x}(u\,C)dx\,dy\,dz \tag{10a}$$

Because the normal area, $Ax = dy\ dz$, of our box does not change with x, it can be pulled out of the partial with respect to x. This is done in the second part of Eq. 10a. The same can be done with the y- and z-components of the convective flux rate:

$$\text{Convective flux rate}\,(\text{out}-\text{in})_y = \frac{\partial}{\partial y}(v\,C\,A_y)dy = \frac{\partial}{\partial y}(v\,C)\,dx\,dy\,dz \tag{10b}$$

$$\text{Convective flux rate}\,(\text{out}-\text{in})_z = \frac{\partial}{\partial y}(w\,C\,A_z)dz = \frac{\partial}{\partial z}(w\,C)dx\,dy\,dz \tag{10c}$$

Finally, adding Eqs. 10a, 10b, and 10c results in the total net convective flux rate.

$$\text{Net convective flux rate} = \left[\frac{\partial}{\partial x}(u\,C)+\frac{\partial}{\partial y}(vC)+\frac{\partial}{\partial z}(wC)\right]dx\,dy\,dz \tag{11}$$

Diffusive flux rates. For net diffusive flux rate in the x-direction, Eq. 9a becomes:

$$\text{Diffusive flux rate}(\text{out}-\text{in})_x = \frac{\partial}{\partial x}\left(-D\frac{\partial C}{\partial x}A_x\right)dx = \frac{\partial}{\partial x}\left(-D\frac{\partial C}{\partial x}\right)dx\,dy\,dz \tag{12a}$$

The y- and z-directions give a result similar to Eq. 12a:

$$\text{Diffusive flux rate}\,(\text{out}-\text{in})_y = \frac{\partial}{\partial y}\left(-D\frac{\partial C}{\partial y}A_y\right)dy = \frac{\partial}{\partial y}\left(-D\frac{\partial C}{\partial y}\right)dx\ dy\ dz \tag{12b}$$

$$\text{Diffusive flux rate}\,(\text{out}-\text{in})_z = \frac{\partial}{\partial z}\left(-D\frac{\partial C}{\partial z}A_z\right)dz = \frac{\partial}{\partial z}\left(-D\frac{\partial C}{\partial z}\right)dx\ dy\ dz \tag{12c}$$

Finally, Eqs. 12a, 12b, and 12c can be added to write an equation describing the net diffusive flux rate (out–in) out of the control volume:

$$\text{Net diffusive flux rate} = -\left[\frac{\partial}{\partial x}\left(D\frac{\partial C}{\partial x}\right)+\frac{\partial}{\partial y}\left(D\frac{\partial C}{\partial y}\right)+\frac{\partial}{\partial z}\left(D\frac{\partial C}{\partial z}\right)\right]dx\,dy\,dz \tag{13}$$

The diffusion coefficient is often not a function of distance, such that Eq. 13 can be further simplified by putting the constant value diffusion coefficient in front of the partial derivative. However, we will also be substituting turbulent diffusion and dispersion coefficients for D when appropriate to certain applications, and they are not always constant in all directions. We will therefore leave the diffusion coefficient inside the brackets for now.

Control volume mass balance. Now Eqs. 1, 5, 6, 11, and 13 can be combined into a mass balance on our box for Cartesian coordinates. After dividing by $\forall = dx\,dy\,dz$ and moving the diffusive flux terms to the right-hand side, this mass balance is:

$$\frac{\partial C}{\partial t}+\frac{\partial}{\partial x}(uC)+\frac{\partial}{\partial y}(vC)+\frac{\partial}{\partial z}(wC) = \left[\frac{\partial}{\partial x}\left(D\frac{\partial C}{\partial x}\right)+\frac{\partial}{\partial y}\left(D\frac{\partial C}{\partial y}\right)+\frac{\partial}{\partial z}\left(D\frac{\partial C}{\partial z}\right)\right]+S \tag{14}$$

When working with a computational transport code, there is little reason to further simplify Eq. 14. One primary objective of this section, however, is to

develop approximate analytical solutions to environmental transport problems, and we will normally be assuming that diffusivity is not a function of position, or x, y, and z. The convective transport terms can be expanded with the chain rule of partial differentiation:

$$\frac{\partial}{\partial x}(uC) = u\frac{\partial C}{\partial x} + C\frac{\partial u}{\partial x} \tag{15a}$$

$$\frac{\partial}{\partial y}(vC) = v\frac{\partial C}{\partial y} + C\frac{\partial v}{\partial y} \tag{15b}$$

$$\frac{\partial}{\partial z}(wC) = w\frac{\partial C}{\partial z} + C\frac{\partial w}{\partial z} \tag{15c}$$

This may not seem like much help, because we have expanded three terms into six. However, if the flow is assumed to be incompressible, a derivation given in fluid mechanics texts (the continuity equation) is:

$$\rho\left(\frac{\partial u}{\partial x} + \frac{\partial v}{\partial y} + \frac{\partial w}{\partial z}\right) = 0 \tag{16}$$

where ρ is the density of the fluid. Since Eqs. 15a, b, and c are added together in the mass balance equation, the incompressible assumption means that the terms on the far right-hand side of these equations will sum to zero, or:

$$\frac{\partial}{\partial x}(uC) + \frac{\partial}{\partial y}(vC) + \frac{\partial}{\partial z}(wC) = u\frac{\partial C}{\partial x} + v\frac{\partial C}{\partial y} + w\frac{\partial C}{\partial z} \tag{17}$$

The incompressible flow assumption is most always accurate for water in environmental applications, and is often a good assumption for air. Air flow is close to incompressible as long as the Mach number (flow velocity/speed of sound) is below 0.3. A Mach number of 0.3 corresponds to an air flow velocity of approximately 110 m/s.

Equation 14 then becomes

$$\frac{\partial C}{\partial t} + u\frac{\partial C}{\partial x} + v\frac{\partial C}{\partial y} + w\frac{\partial C}{\partial z} = D\left(\frac{\partial^2 C}{\partial x^2} + \frac{\partial^2 C}{\partial y^2} + \frac{\partial^2 C}{\partial z^2}\right) + S \tag{18}$$

The only assumptions made in developing Eq. 18 are (1) that diffusivity does not change with spatial coordinate and (2) incompressible flow. Equation 18 will be further simplified in order to develop analytical solutions for mass transport problems. In some cases, all that needs to be done is orient the flow direction so that it corresponds with one of the coordinate axes. There would then be only one convection term.

Adsorption and Desorption in Sediments and Soils

Sorption relates to a compound sticking to the surface of a particle. Adsorption relates to the process of compound attachment to a particle surface, and desorption relates to the process of detachment. Sorption processes will now be reviewed because there are many compounds that are sorptive and subject to spills. Then the solutions of the diffusion equation can be examined as they apply to highly sorptive compounds.

Environmental chemicals are generally classified by the Greek terms hydrophilic (likes water) and hydrophobic (hates water). Water is a polar molecule, in that it has two hydrogen atoms on one side, and an oxygen atom on the other. Solutes with a polarity or charge, therefore, will have water molecules surrounding them with the tendency to have the proper charge of atom adjacent to the solute. Most amides and alcohols are strongly polar, and also soluble in water. These are generally hydrophilic compounds. Other organic compounds with larger molecular weights, especially with aromatic rings, are generally nonpolar and are classified as hydrophobic compounds. It makes sense that these hydrophobic compounds would adsorb to the nonpolar organic material in the sediments or soils. There are handbooks [7] that can be used to estimate the chemical thermodynamics of a water-particle system.

How can sorption be handled in our transport equation? For particles that are not transported with the flow field, like sediments and groundwater flow, we are interested in the water concentrations. The sorbed portion of the compound is not in the solute phase, and should not be considered in the transport equation except when transfer of the compound between the water and particles occur. Adsorption would then be a sink of the compound and desorption would be a source.

Let us assign S_p to be the mass of chemical sorbed to particles per mass of solids contained in our control volume, and C to be the concentration of the compound in solution. Then, the source term in the

diffusion equation is equal to the rate of change of mass due to adsorption and desorption per unit volume, or:

$$S = \frac{\rho_b}{\varepsilon}\frac{\partial S_p}{\partial t} \tag{19}$$

where ρ_b is the bulk density of the solid (mass of solid/volume of fluid and solid), ε is the porosity of the media (volume of fluid/volume of fluid and solid), and $\partial S_p/\partial t$ is the rate of sorption relative to the mass of solid (mass adsorbed/mass of solid/time). If the sorption rate is negative, desorption is occurring. The units of S in Eq. 19 are mass adsorbed/volume of fluid/time. This is similar to the units for the $\partial C/\partial t$ term, which are a change of mass/volume of fluid/time.

The source term in Eq. 19 requires a separate differential equation for S_p, which would incorporate the concentration of the compound in solution. There would thus be two equations that need to be solved simultaneously. However, most sorption rates are high, relative to the transport rates in sediments and soil. Thus, *local equilibrium in adsorption and desorption is often a good assumption*. It also simplifies the solution to a transport problem considerably. If that assumption is made, S_p changes in proportion to C alone, or:

$$S_p = S_p(C) \tag{20}$$

and

$$\frac{\partial S_p}{\partial t} = \frac{\partial S_p}{\partial C}\frac{\partial C}{\partial t} \tag{21}$$

Now, if Eq. 21 is substituted into 19, we get:

$$S = \frac{\rho_b}{\varepsilon}\frac{\partial S_p}{\partial C}\frac{\partial C}{\partial t} \tag{22}$$

The $\partial S_p/\partial C$ term can be found from the equilibrium relationship of Freundlich isotherms, expressed as:

$$S_p = K_d\, C^{\beta} \tag{23}$$

where K_d is an equilibrium-partitioning coefficient between the fluid and sorption to the solid and β is a coefficient fit to measured data. Then,

$$\frac{\partial S_p}{\partial C} = \beta\, K_d\, C^{\beta-1} \tag{24}$$

At the lower concentrations normally found in the environment, $\beta = 1$ is a valid assumption. Then Eq. 24 becomes

$$\frac{\partial S_p}{\partial C} = K_d\,(\beta = 1) \tag{25}$$

Substituting Eq. 25 into 22 now results in a source term that no longer contains the variable S_p, and keeps the partial differential equation (PDE) of our mass balance linear:

$$S = \frac{\rho_b}{\varepsilon}\, K_d \frac{\partial C}{\partial t} \tag{26}$$

Now, if Eq. 26 is substituted into our mass transport Eqs. 15a–c for the source term, the result is a PDE where the only dependent variable is C:

$$\begin{aligned}\frac{\partial C}{\partial t} + u\frac{\partial C}{\partial x} + v\frac{\partial C}{\partial y} + w\frac{\partial C}{\partial z} \\ = D\left(\frac{\partial^2 C}{\partial x^2} + \frac{\partial^2 C}{\partial y^2} + \frac{\partial^2 C}{\partial z^2}\right) - \frac{\rho_b}{\varepsilon}K_d\frac{\partial C}{\partial t}\end{aligned} \tag{27}$$

or

$$\begin{aligned}\left(1 + \frac{\rho_b}{\varepsilon}K_d\right)\frac{\partial C}{\partial t} + u\frac{\partial C}{\partial x} + v\frac{\partial C}{\partial y} + w\frac{\partial C}{\partial z} \\ = D\left(\frac{\partial^2 C}{\partial x^2} + \frac{\partial^2 C}{\partial y^2} + \frac{\partial^2 C}{\partial z^2}\right)\end{aligned} \tag{28}$$

If we divide Eq. 28 by the term $(1 + K_d\rho_b/\varepsilon)$, we can see that all convective and diffusive transport is *retarded* by equilibrium adsorption and desorption. Thus, a *retardation factor* is defined:

$$R = \text{retardation factor} = 1 + K_d\rho_b/\varepsilon \tag{29}$$

and Eq. 28 becomes:

$$\begin{aligned}\frac{\partial C}{\partial t} + \frac{u}{R}\frac{\partial C}{\partial x} + \frac{v}{R}\frac{\partial C}{\partial y} + \frac{w}{R}\frac{\partial C}{\partial z} \\ = \frac{D}{R}\left(\frac{\partial^2 C}{\partial x^2} + \frac{\partial^2 C}{\partial y^2} + \frac{\partial^2 C}{\partial z^2}\right)\end{aligned} \tag{30}$$

Equation 30 indicates that as long as it can be assumed that the sorption rates are fast compared to our transport rates and the equilibrium partitioning is linearly related to concentration, the retardation factor can utilize and simply convert all of the transport terms through dividing by R. Thus, if there is a spill into the groundwater table that is highly hydrophobic, it would

transport through the soil more slowly than one which is hydrophilic. Both the convective and the diffusive flux would be "retarded" for the hydrophobic compound. If both hydrophilic and hydrophobic compounds are contained in the spill, the hydrophilic compound would show up first at a downstream location. The similarity to the manner in which a chromatographic column separates compounds is not fortuitous, because the column is separating compounds through their sorption to the column's media.

Determination of K_d from octanol-water partitioning coefficient. There have been a number of empirical equations developed to determine the water-solid partitioning coefficient, K_d [7]. These are primarily for the many organic chemicals that exist in the environment, usually due to human impacts. Many of them use the octanol-water partitioning coefficient for the compound as an indicator of hydrophobicity. Octanol is a relatively insoluble organic compound. Since most organic compounds tend to adsorb to the organic portion of the particles, a hydrophobic organic compound placed in an octanol-water solution will tend toward the octanol. The ratio of concentration in the octanol over concentration in the water will indicate the degree of the hydrophobicity. It is a straightforward and relatively easy measurement to make, so most organic compounds of interest in the environment have an octanol-water partitioning coefficient that has been measured.

Karikhoff et al. [2] developed a simple empirical equation for equilibrium partitioning of organic compounds that will be used in this text (other equations are given in Lehman et al. [7]):

$$K_d = \beta f K_{ow} \tag{31}$$

where K_{ow} is the dimensionless octanol-water partitioning coefficient, f is the fraction of soil that is organic matter (usually from zero in sand to 0.01 in sandy soil to 0.10 in muck), and β is an empirical coefficient, estimated by Karikhoff to be 0.41 cm^3/g. It is generally the organic matter in the medium to which organic compounds adsorb, hence the use of organic fraction.

The other parameters required to compute a retardation coefficient are the bulk density, ρ_b, and the porosity of the media, ε. The bulk density of the water and soil is typically 1.6–2.1 g/cm^3. The porosity of the soil or sediments is typically 0.2–0.4. Thus ρ_b/ε is typically between 4 and 10 g/cm^3.

Example Applications of the Diffusion Equation

The first application of the diffusive is transport of oxygen into lake sediments and the use of oxygen by the bacteria to result in a steady-state oxygen concentration profile.

Example 1: Steady O_2 concentration profile in lake sediments (steady-state solution with a first-order sink). Given a concentration, C_o, in the overlying water, and a first-order sink of oxygen in the sediments, develop an equation to describe the dissolved oxygen concentration profile in the sediments (Fig. 5).

Assume:

- Steady: $\frac{\partial}{\partial t} \Rightarrow 0$
- No flow: $u, v, w \Rightarrow 0$
- Small horizontal variation: $\frac{\partial^2 C}{\partial z^2} >> \frac{\partial^2 C}{\partial x^2}, \frac{\partial^2 C}{\partial y^2}$
- No sorption: $R = 1$ (accurate for O_2 in sediments)
- First-order sink: $S = -kC$, where k is a rate constant

Then, the diffusive mass transport Eqs. 15a–c becomes:

$$0 = D\frac{\partial^2 C}{\partial z^2} - kC$$

or, since $C = C(z)$

$$0 = D\frac{d^2 C}{\partial z^2} - kC$$

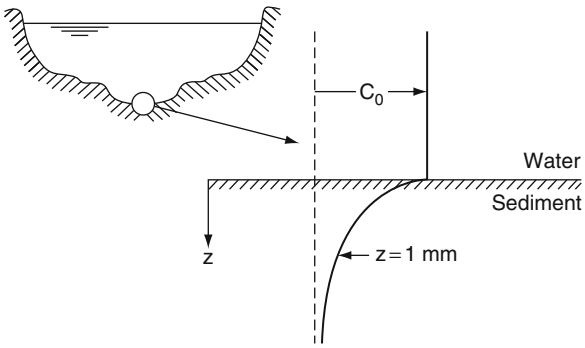

Transport in the Environment. Figure 5
Illustration of dissolved oxygen profile in lake sediments. (From [1])

A solution to this equation requires two boundary conditions because it is a second-order equation. These two are:

B.C.#1: @ $z = 0$, $C = C_{;0}$
B.C.#2: @ $z \to \infty$, $C \Rightarrow 0$

This solution may be achieved by: (1) separating variables and integrating or (2) solving the equation as a second-order, linear ordinary differential equation (ODE). The latter will be used since the solution technique is more general.

1. Assign λ to be the $\frac{d}{dz}$ operator. Then, the equation becomes

$$\left(\lambda^2 - \frac{k}{D}\right) C = 0$$

2. Solve for λ

$$\lambda = \pm\sqrt{k/D}$$

3. The solution, developed in texts on solving ordinary differential equations [6], is

$$C = \beta_1 e^{\lambda_1 z} + \beta_2 e^{\lambda_1 z} \quad \lambda_1 = +\sqrt{k/D}$$

$$\lambda_2 = -\sqrt{k/D}$$

4. β_1 and β_2 are determined from boundary conditions

Apply B.C. #2:

$$C = 0 = \beta_1\, e^{\sqrt{k/D}\infty} + \beta_2\, e^{-\sqrt{k/D}\infty}$$

This is only possible if $\beta_1 = 0$. Apply B.C. #1:

$$C_0 = 0 + \beta_2 e^{-0} = \beta_2$$

Thus, the solution is:

$$C = C_o\, \mathrm{e}^{-\sqrt{k/D}z}$$

which is plotted in Fig. 6.

At steady state, the oxygen profile is a balance between diffusion from the sediment surface and bacterial use of oxygen in the sediments. If the sediments are mostly sand, the depth of the layer with oxygen can be 10 cm or more. If the sediments have a substantial organic content (like a mud), the aerobic layer (>0.1 g/m^3 oxygen concentration) can be less than 1 mm.

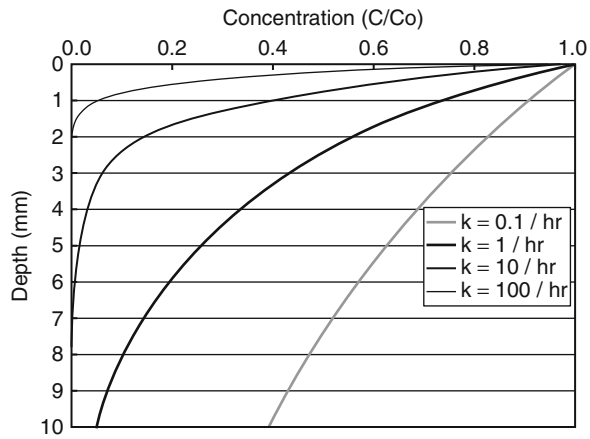

Transport in the Environment. Figure 6
Solution to Example 1

Example 2: Unsteady dissolution of a highly soluble pollutant* (Herbicides, Pesticides, Ammonia, Alcohols, etc.) *into groundwater (unsteady, one-dimensional solution with pulse boundary conditions). A tanker truck carrying a highly soluble compound in Mississippi tried to avoid an armadillo at night, ran off the interstate at a high speed, turned over in the drainage ditch, and spilled a soluble compound. The compound has infiltrated into the ground, and much of it has reached and temporarily spread out over the groundwater table, as illustrated in Fig 7. As part of a spill response team, you need to estimate the groundwater contamination. Predict concentrations over time in the groundwater table.

The mass transport equation for this example is:

$$\frac{\partial C}{\partial t} + u\frac{\partial C}{\partial x} + v\frac{\partial C}{dy} + w\frac{\partial C}{\partial z} = D\left(\frac{\partial^2 C}{\partial x^2} + \frac{\partial^2 C}{\partial y^2} + \frac{\partial^2 C}{\partial z^2}\right) + S$$

Assume:

1. Minimal horizontal variations

$$0 \cong \frac{\partial C}{\partial x} = \frac{\partial^2 C}{\partial x^2} \cong \frac{\partial C}{\partial y} \cong \frac{\partial^2 C}{\partial y^2}$$

2. No flow in the vertical direction, $w = 0$
3. No reactions, including adsorption and desorption, such that $S = 0$.

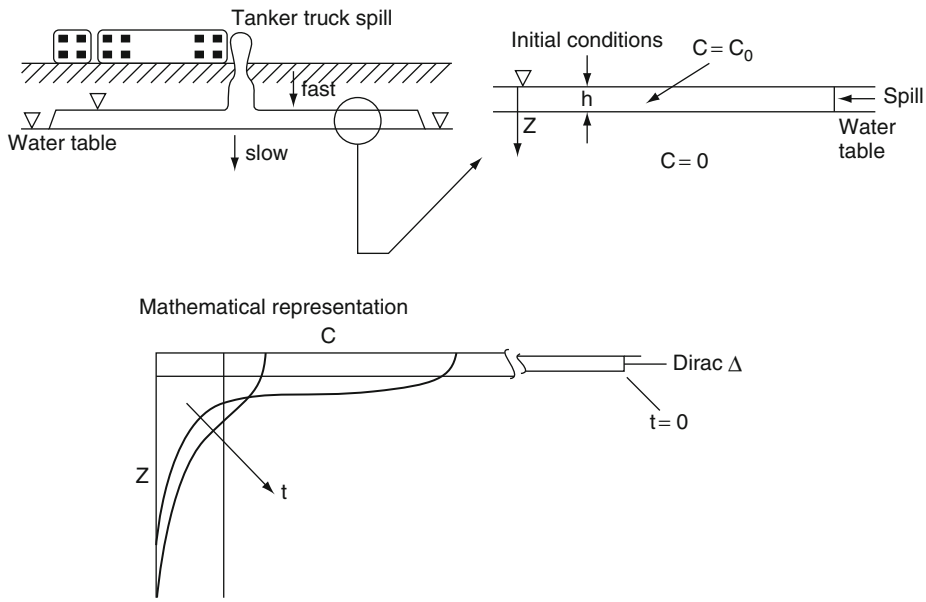

Transport in the Environment. Figure 7
Illustration of the tanker truck spill. (From [1])

Then with these three assumptions, the governing equation becomes:

$$\frac{\partial C}{\partial t} = D\,\frac{\partial^2 C}{\partial z^2}$$

The initial conditions will be simulated with these boundary conditions:

1. The mass of chemical is assumed to be spread instantaneously across a very thin layer at $t = 0$ (a Dirac delta in z and t). At $z = 0^+$, $t = 0$, the total mass = M and the total surface area is A.
2. At $z \Rightarrow \infty$, $C \Rightarrow 0$.

The above equation, with boundary conditions (1) and (2), has the solution:

$$C = \frac{2\,M/A}{\sqrt{4\,\pi\,Dt}}\,e^{-z^2/4\,Dt}$$

What does the solution look like? The solution can be made dimensionless by assuming that the initial thickness of the spill layer is Δh. Then, a new variable $z = k\,\Delta h$ will be used in assigning:

$$\eta = \frac{\Delta h}{\sqrt{4Dt}}$$

with

$$C^* = \frac{CA\,\Delta h}{2\,M}$$

Substituting these equations into the solution gives:

$$C^* = \frac{\eta}{\sqrt{\pi}}\,e^{-(k\eta)^2}$$

which is plotted versus depth at various times in Fig. 8. The concentration at $z = 0$ decreases as the initial mass is diffused. At low values of time, the concentration at and close to $z = 0$ is strongly dependent upon the Δh chosen. At larger times and deeper depths, however, this dependency decreases, and the solution becomes independent of Δh.

It is interesting to note that the solution is very similar to a Gaussian probability distribution, with the following relationship for $P(z)$:

$$P(z) = \frac{1}{\sigma\sqrt{2\pi}}\,e^{-(z-z_m)^2/2\sigma^2}$$

where z_m is the depth of the maximum concentration (or the center of concentration mass).

Comparing the probability distribution and the solution to this problem, we can see that:

$$2\,\sigma^2 \Leftrightarrow 4\,Dt$$

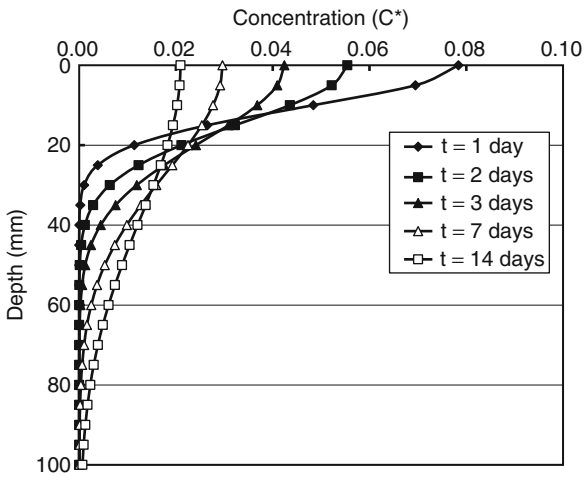

Transport in the Environment. Figure 8
Solution to the tanker truck spill illustrating groundwater concentration versus distance at various times. $\Delta h = 2$ mm, $D = 6 \times 10^{-4}$ mm^2/s

or:

$$D = \sigma^2/2t$$

Note that if we measure σ, we can determine D.

Example 3*: *Dichlorobenzene concentration in lake sediments due to a plating facility discharge (solution to a concentration front). Sometimes the boundary conditions can be approximated as a step in concentration. This difference in boundary conditions changes the solution from one which is related to pulse boundaries (known mass release) to one resulting from a concentration front with a known concentration at one boundary.

For many years, a plating facility for a telecommunications company let their rinse waters flow into an adjacent lake. The compounds used in their rinse included dichlorobenzene, which is a semi-volatile compound that also has a fairly high tendency to adsorb to organic compounds in the sediments. Within a few years of the plating facility opening, the dichlorobenzene concentration reached a steady-state value in the lake waters as illustrated in Fig. 9. Estimate the buildup of dichlorobenzene in the sediments during the 50 years since the facility opened until it stopped discharging its untreated waste water.

Assumptions:

1. Biodegradation is small. $\therefore$ S $\Rightarrow$ 0 except for sorption.
2. Variation in x and y are small

$$\frac{\partial^2 C}{\partial x^2}, \frac{\partial^2 C}{\partial y^2} << \frac{\partial^2 C}{\partial z^2}$$

3. No flow in sediments under lake: $u = v = w = 0$
4. $D \cong 6 \times 10^{-10}$ m^2/s
5. $\frac{\rho_b}{\varepsilon} = 6.3 \;\Rightarrow\; R = 1 + \frac{\rho_b}{\varepsilon} K_d = 96$

Then the diffusion equation for the sediments becomes:

$$\frac{\partial C}{\partial t} = \frac{D}{R}\frac{\partial^2 C}{\partial z^2}$$

with boundary conditions:

(a) $t > 0$, $z = 0$; $C = C_0$
(b) $t = 0$, $z \neq 0$; $C = 0$

There are three known techniques to solve this governing equation:

Laplace transforms, Fourier transforms, and change of variables, which incorporates both luck and skill. We will use change of variables:

Assign $\eta = \frac{z}{\sqrt{4\,Dt/R}}$

$$\frac{\partial C}{\partial t} = \frac{\partial C}{\partial \eta}\frac{\partial \eta}{\partial t} = \frac{-1}{4}\frac{z}{\sqrt{Dt/Rt}}\frac{\partial C}{\partial \eta} = \frac{-\eta}{2t}\frac{\partial C}{\partial \eta}$$

$$\frac{\partial C}{\partial z} = \frac{\partial C}{\partial \eta}\frac{\partial \eta}{\partial z} = \frac{1}{2\sqrt{Dt/R}}\frac{\partial C}{\partial \eta}$$

$$\frac{\partial^2 C}{\partial z^2} = \frac{\partial}{\partial \eta}\left(\frac{\partial C}{\partial z}\right)\frac{\partial \eta}{\partial z} = \frac{R}{4Dt}\frac{\partial^2 C}{\partial \eta^2}$$

Then the governing equation becomes:

$$\frac{-\eta}{2t}\frac{\partial C}{\partial \eta} + \frac{D}{R}\left(\frac{R}{4Dt}\frac{\partial^2 C}{\partial \eta^2}\right) = 0$$

or

$$\frac{d^2 C}{d\eta^2} + 2\eta\frac{dC}{d\eta} = 0 \qquad (32)$$

This equation may be written as: $\frac{dC'}{d\eta} + 2\eta C' = 0$

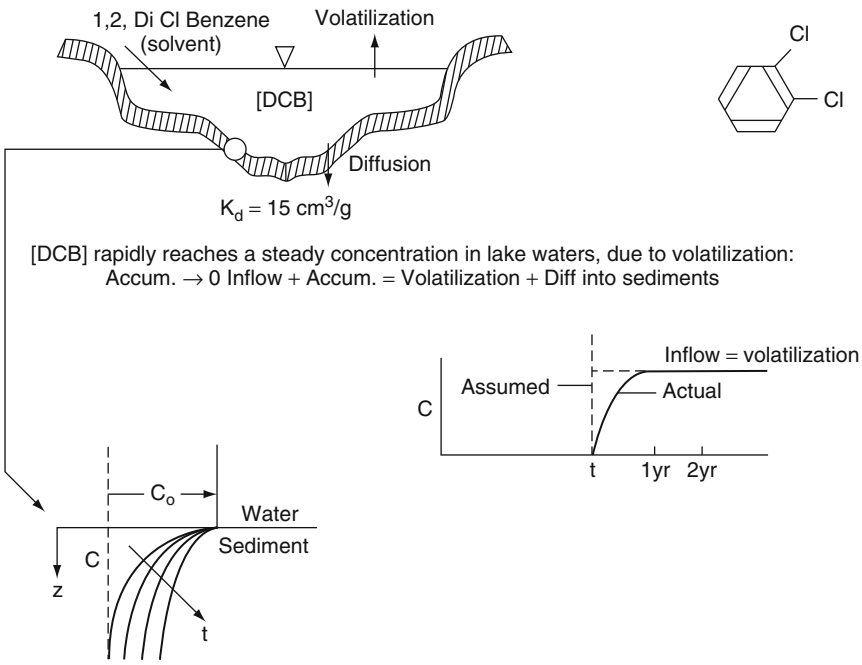

Transport in the Environment. Figure 9
Illustration of concentration front moving down into the sediments of a lake. (From [1])

where $C' = \frac{dC}{d\eta}$ or

$$\frac{1}{C'}\, dC' = -2\eta\ d\eta$$

We can integrate this:

$$\ell n\, C' = -\eta^2 + \beta_o$$

or

$$C' = e^{\beta o}\, e^{-\eta^2} = \beta_1\, e^{-\eta^2}$$

Now integrate again:

$$C = \beta_1 \int_0^{\eta} e^{-\eta^2} d\eta + \beta_2 \Rightarrow \beta_1 \int_0^{\eta} e^{-\phi^2} d\phi + \beta_2$$

Now, note that the error function is given as:

$$erf\ (\eta) = \frac{2}{\sqrt{\pi}} \int_0^{\eta} e^{-\phi^2} d\phi$$

and the complementary error function is erfc(η) = 1−erf(η). Values of the error function and complimentary error function for various values of η may be found in an Internet search. The error function is designed such that erf(∞) = 1, erfc(∞) = 0, erf(0) = 0, and erfc (0) = 1. The solution may therefore be written as:

$$C = \beta_1\ erf\ (\eta) + \beta_2$$

Now we need to determine our boundary conditions in terms of η:

1. $t > 0, z = 0, \quad \eta = 0, \quad C = C_0$
2. $t = 0, z = 0, \quad \eta = \infty, \quad C = 0$

Checking other boundary conditions:
$t \to \infty, \quad \eta \Rightarrow 0, \quad C = C_0$
$z \to \infty, \quad \eta \Rightarrow \infty, \quad C = 0$

Now, at $\eta = 0$, $C = C_0$, thus:

$$C_0 = \beta_1 0 + \beta_2$$

or

$$\beta_2 = C_0$$

At $\eta = \infty$, $C = 0$

$$0 = \beta_1 1 + C_0$$

or

$$\beta_1 = -C_0$$

Then, our solution is:

$$C = C_0\left(1 - erf\left(\frac{z}{\sqrt{4\,Dt/R}}\right)\right) = C_0\,erfc(\eta) \quad (33)$$

which is illustrated in Fig. 10.

We will now apply Eq. 33 to estimate the dichlorobenzene penetration versus time from spillage. The results are given in Table 2, which gives the interstitial dichlorobenzene concentrations.

The total concentration (TDCB(z)) includes compound adsorbed to the sediments.

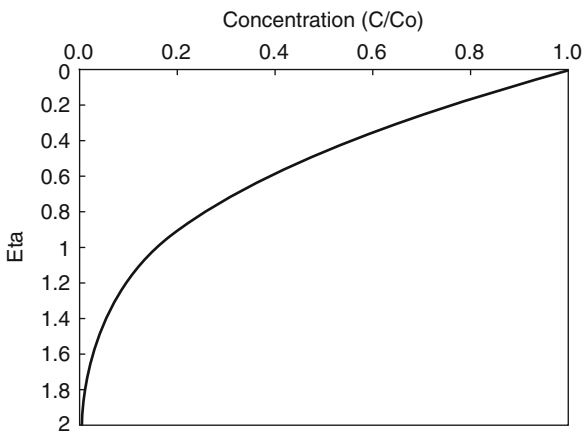

Transport in the Environment. Figure 10
Illustration of the effect of the change of variables used in Example 3. Eta = η

Transport in the Environment. Table 2 Penetration of dichlorobenzene into the sediment over time

Time, z	1 year, C/C_0	4 years, C/C_0	10 years, C/C_0	50 years, C/C_0
1 mm	0.96	0.98	0.988	0.994
1 cm	0.62	0.803	0.87	0.94
10 cm	0	0.015	0.11	0.48
20 cm	0	0	0.01	0.16
30 cm	0	0	0	0.03
100 cm	0	0	0	0

$$TDCB(z) = C(z) + (1-\varepsilon)\rho_s S$$

where ε = porosity

$1-\varepsilon$ = % by volume sediment $\cong$ 0.6
ρ_s = density of sediment $\cong$ 2.5 g/cm^3
S = concentration of sorbed compound (g DCB/g sediment)

Since $S = K_d\,C_1$, the above equation becomes:

$$\begin{aligned} TDCB(z) &= C(z)(1 + (1-\varepsilon)\,\rho_s K_d) \\ &= C(z)(1 + 0.6(2.5\text{g/cm}^3)(15\text{cm}^3/\text{g}) \end{aligned}$$

or

$$TDCB = 23.5\,C(z)$$

Thus, the total dichlorobenzene per volume of sediment and water would be 23.5 times the concentrations given in Table 2.

Conclusion

The purpose of this section of the volume is to introduce the reader to the equations and mathematics used in developing approximate solutions (due to simplified boundary conditions) to convection-diffusion processes. One may say that, with computational capabilities, there is no longer any need to develop these approximate solutions. However, these approximate solutions are useful in the following manners:

1. A quick, back of the envelope solution is always much quicker and more reliable than a computational solution. Computational solutions require substantial time to develop and are often wrong until they are fully vetted.
2. A computational solution always requires vetting, which means that a computational solution is compared to an analytical solution, hopefully in a similar condition with simplified boundary conditions. This means that some analytical solution is always needed, and as close to the real simulation as possible, to make sure that the computational solution is doing what the user desires.
3. Developing analytical solutions are an excellent means of getting a feel for solutions to the convection-diffusion equations. It is a knowledge-building practice that is difficult to surpass.

Note that the examples given in this section do not include any with convection. That is because convection in the environment most always includes either turbulence (surface waters and the atmosphere) or dispersion (groundwater). These will be dealt with in other sections.

Future Directions

Most of the future directions with regard to transport in the environment (without turbulent transport) will involve transport across interfaces, such as the air–water and solid–fluid interfaces. While research has been conducted on describing the predominant transport mechanisms for these two cases (McCready et al. [8], [3–5]), there is more to be done. An especially vexing problem is transport in the vadose zone of soils (unsaturated zone). The multiplicity of three interfaces, air, water, and soil, and the heterogeneities in the soil make this a complex problem to handle in a deterministic manner. However, meaningful relationships for an effective diffusion coefficient still need to be developed.

Bibliography

Primary Literature

1. Gulliver JS (2007) An introduction to chemical transport in the environment. Cambridge University Press, Cambridge
2. Karikhoff SW, Brown DS, Scott TA (1979) Sorption of hydrophobic pollutants on natural sediments. Water Res 13:241
3. Brunley BH, Jirka GH (1987) Near-surface turbulence in a grid-stirred tank. J Fluid Mech 183:235–263
4. Campbell JA, Hanratty TJ (1982) Mass transfer between a turbulent fluid and a solid boundary: linear theory. AICHE J 28:988
5. Janzen J, Jirka H, Jirka G, Schulz H, Gulliver JS (2010) Estimation of mass transfer velocity based on measured turbulence parameters. Am Inst Chem Eng J 56(8):2005–2017
6. Kreyszig E (1982) Advanced engineering mathematics, 4th edn. Wiley, New York
7. Lehman WJ, Reehl WF, Rosenblatt DH (1990) Handbook of chemical property estimation. American Chemical Society, Washington, DC
8. McCready MA, Vassiliadou E, Hanratty T (1986) Computer simulation of turbulent mass transfer at a mobile interface. AICHEJ 32(7):1108
9. Fick AE (1855) Ueber Diffusion, Annelen der Physik 170(1):59–86

Books and Reviews

Crank J (1975) The mathematics of diffusion, 2nd edn. Oxford University Press, Oxford

Cussler EL (1997) Diffusion: mass transfer in fluid systems, 2nd edn. Cambridge University Press, Cambridge

Transport with Jets and Plumes of Chemicals in the Environment

Wenming Zhang, Nallamuthu Rajaratnam, David Z. Zhu

Department of Civil and Environmental Engineering, University of Alberta, Edmonton, AB, Canada

Article Outline

Glossary
Definition of the Subject and Its Importance
Introduction
Turbulent Jets and Plumes in Stagnant Environment
Effect of Boundaries on Jets and Plumes
Multiphase Jets and Plumes
Future Directions
Bibliography

Glossary

Bubbly jet The jet produced by injecting gas-liquid mixture into a liquid.

Buoyant jet The plume with momentum or jet with buoyancy.

Circular jet The jet produced through a nozzle with a circular cross section.

Diffuser The device which has multiple nozzles to quickly mix the discharged substances (e.g., effluent or air) with the surrounding ambient fluid.

Jet The flow generated by the release of momentum usually through a nozzle or slot.

Jet in coflow The jet discharged in the direction of a flowing ambient fluid.

Jet in crossflow The jet discharged at an oblique angle to a flowing ambient fluid.

Plane jet Also called "slot jet" or "two-dimensional jet", the jet produced through a slender slot.

Plume The flow generated by the release of buoyancy.

Surface jet The jet discharged at (or near) the surface of an ambient fluid.

Slurry jet The jet produced by injecting solid-liquid mixture into a liquid.

Wall jet The jet discharged tangentially or at a certain angle to a solid boundary (wall).

Definition of the Subject and Its Importance

Jets and plumes are common in our environment. Some examples of jets are: wastewater discharged from an outfall, emission from an aircraft or vehicle, and the eruption of volcano. Some examples of plumes are: the smoke from a chimney stack or cigarette, the thermal plumes from a fire, municipal wastewater or hot water discharged in deep water, and oil spill from sea bed. One of the most important features of jets or plumes is its ability of entraining ambient fluid to achieve self-dilution. This greatly triggers our interests to study jets and plumes. This book chapter is a review of the studies on turbulent jets and plumes, with a focus on the transport of conservative pollutants.

Introduction

The earliest experimental study of turbulent jets appears to be the work of Trupel on circular jets in 1915 [1]. Förthmann performed an experimental study of plane turbulent jets in 1934 and his work also considered plane turbulent wall jets [23]. The results of these investigations showed the similarity of the velocity profiles at different distances from the sources of the jets. These studies were followed by the extensive investigations of Hinze and Zijnen [28] on circular jets and Albertson et al. [4] for plane and circular jets. Turbulence characteristics of plane jets were studied by Heskestad [27] for plane jets and Wygnanski and Fielder [105] for circular jets. Theoretical solutions for plane jets were developed by Tollmien in 1926 for plane jets and by Goertler in 1942 for circular jets [73]. Numerical studies of turbulent jets followed, starting with the work of Rodi and Spalding [82]. Abramovich [1], Rajaratnam [73], and Fischer et al. [21] provided comprehensive treatment of jets.

Turner [97] provides an introduction to study turbulent plumes in his book on *Buoyancy Effects in Fluids*. Rouse et al. [84] performed an experimental study of plane and circular plumes wherein they found that the velocity and density defect profiles were similar if proper scales were chosen for velocity, width, and density defect. Morton et al. [58] published an integral study of plumes, wherein the concept of entrainment coefficient was introduced. Since then numerous studies have been conducted on turbulent plumes and forced turbulent plumes (buoyant jets). These studies have been summarized in Chen and Rodi [15] and Lee and Chu [45]. Turbulent jets and plumes have been studied extensively not only because these flows are very interesting but also that they are of considerable practical importance in the fields of hydraulic, mechanical, aeronautical, environmental, and chemical engineering and many other fields.

This book chapter will first review the most classic and well-established theories on simple jets or plumes in stagnant water, and then consider effects of boundaries including: the bed (wall) and the surface of ambient fluid; coflowing and cross-flowing ambient fluid; and the interaction of neighboring jets in the case of multiple jets. Next, two kind of multiphase jets and plumes – bubbly jets and plumes, and slurry jets and plumes – will be briefly introduced. Multiphase jets and plumes are much more complicated compared to the single-phase ones, but have gained more interest in recent years because of their wide applications. Finally, some directions for future researches will be highlighted.

Turbulent Jets and Plumes in Stagnant Environment

In this section, the focus is on the transport of conservative pollutants in a steady-state turbulent jet or plume issuing from a simple (plane or circular) nozzle into stagnant ambient fluid of large extent. Such jets or plumes are called simple jets or simple plumes. Theories in this area have been well established. Close to the nozzle exit, there is a wedge-like or cone-like region termed "potential core" where the width of initial velocity distribution decays to a point. The length of the potential core is very short, about $10.4b_0$ for a plane jet where b_0 is the half slot width, or $6.2d_0$ for a circular jet where d_0 is the nozzle diameter [45]. Therefore, for practical purposes, our attention will be limited on the flow beyond the potential core, i.e., in the "fully developed flow" region (see Fig. 1).

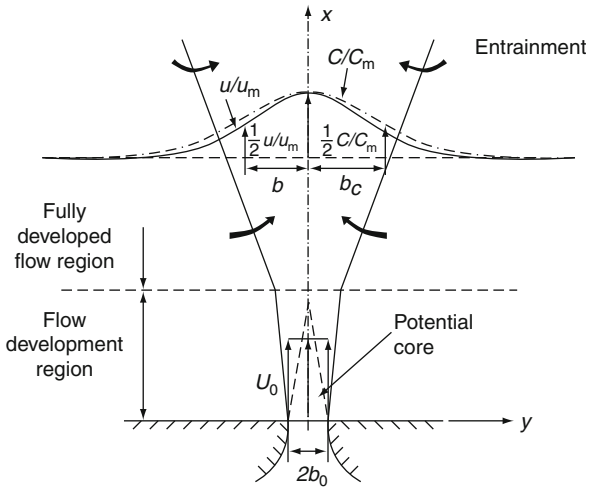

Transport with Jets and Plumes of Chemicals in the Environment. Figure 1
Schematic of a simple plane jet (for circular jet, replace $2b_0$ by d_0 and y by r)

The reader who is interested in flow development region may refer to Rajaratnam [73].

Simple Jets

The integral method is the most common method for analyzing simple jets or plumes. The following is a brief introduction on this method. For a plane jet as shown in Fig. 1, the Reynolds-averaged Navier-Stokes equation in x direction, continuity equation, and pollutant conservation equation, respectively, can be simplified as [73]:

$$u\frac{\partial u}{\partial x} + v\frac{\partial u}{\partial y} = \frac{1}{\rho}\frac{\partial \tau}{\partial y} \tag{1}$$

$$\frac{\partial u}{\partial x} + \frac{\partial v}{\partial y} = 0 \tag{2}$$

$$\frac{\partial uC}{\partial x} + \frac{\partial vC}{\partial y} = \varepsilon\frac{\partial^2 C}{\partial y^2} \tag{3}$$

where u and v are the time-averaged velocities in x and y directions, respectively; C is the pollutant concentration; ρ is the density of the fluid; τ is the turbulent shear stress and ε is the mean value of turbulent diffusion coefficient. After multiplying Eq. 1 by ρ and then integrating from $y = 0$ to $y = \infty$, Eq. 1 becomes:

$$\frac{d}{dx}\int_o^\infty \rho u^2\, dy = 0 \tag{4}$$

Equation 4 states that the jet momentum flux at different x-sections is conserved. Using Eq. 2 and integrating the first term of Eq. 2 from $y = 0$ to $y = \infty$, we have:

$$\frac{dq_x}{dx} = \frac{d}{dx}\int_0^\infty u\, dy = -v_{y=\infty} \tag{5}$$

where q_x is the jet volume flux per unit slot length. The entrainment hypothesis assumes that the entrainment velocity $v_e = v_{y=\infty} = -\alpha_e u_m$, where α_e is called the jet entrainment coefficient, u_m is jet centerline (maximum) velocity, and the negative sign indicates the ambient fluid is entrained into the jet. Equation 5 says that the jet volume flux increases with traveling distance x due to the entrainment of ambient fluid, which explains the ability of jet in diluting pollutants. Similarly, integrating Eq. 3 from $y = 0$ to $y = \infty$, we have:

$$\frac{d}{dx}\int_0^\infty uC\, dy = 0 \tag{6}$$

Equation 6 states that the mass fluxes of pollutants at different x-sections are conserved if the chemical or biological reactions of pollutants are not considered.

Numerous laboratory experiments and numerical simulations have confirmed that beyond the potential core, the jet velocity or concentration exhibits self-similarity. The most widely used expression for such similarity is the Gaussian distribution, which represents laboratory data satisfactorily:

$$\frac{u}{u_m} = \exp\left[-k_1\left(\frac{y}{b}\right)^2\right] \tag{7}$$

$$\frac{C}{C_m} = \exp\left[-k_1\left(\frac{y}{k_2 b}\right)^2\right] \tag{8}$$

where C_m is the jet time-averaged centerline (maximum) concentration, b is the jet velocity half-width where the velocity is 50% (if $k_1 = 0.693$, refer to Fig. 1) or 37% (if $k_1 = 1$) of u_m, $k_2 b$ defines the jet concentration half-width where the concentration is 50% or 37% of C_m, and k_2 is the ratio of concentration half-width to velocity half-width. Using Eqs. 4–8, the analytical solutions for plane jets can be derived, as shown in Table 1. The coefficients of the solutions are mainly determined from experimental results and integrations.

Transport with Jets and Plumes of Chemicals in the Environment. Table 1 Summary of mean properties of simple plane jet and circular jet

Parameter	Plane jet	Circular jet
Maximum (centerline) concentration C_m	$\frac{C_m}{C_0} = \frac{\alpha_1}{\sqrt{\frac{x}{b_0}}}$, where α_1 = 3.37 in [21], 3.45 in [74], 3.21 in [45]	$\frac{C_m}{C_0} = \frac{\alpha_1}{\frac{x}{d_0}}$, where α_1 = 4.96 in [21], 5.34 in [74], 5.26 in [45]
Cross-sectional average concentration C_{avg}	$\frac{C_m}{C_{avg}} = \alpha_2$, where α_2 = 1.2 in [21], 1.25 in [45]	$\frac{C_m}{C_{avg}} = \alpha_2$, where α_2 = 1.4 in [21], 1.76 in [74], 1.68 in [45]
Maximum (centerline) velocity u_m	$\frac{u_m}{U_0} = \frac{\alpha_3}{\sqrt{\frac{x}{b_0}}}$, where α_3 = 3.50 in [73], 3.41 in [21], 3.65 in [45]	$\frac{u_m}{U_0} = \frac{\alpha_3}{\frac{x}{d_0}}$, where α_3 = 6.3 in [73], 6.2 in [21] and [45], 6.13 in [74]
Velocity half-width b[a]	$b = \alpha_4 x$, where α_4 = 0.10 in [73], 0.116 in [21], 0.097 in [74], 0.12 in [45]	$b = \alpha_4 x$, where α_4 = 0.10 in [73], 0.107 in [21], 0.096 in [74], 0.114 in [45]
Concentration half-width b_C[a]	$\frac{b_C}{b} = \alpha_5$, where α_5 = 1.35 in [21] and [45], 1.17 in [74]	$\frac{b_C}{b} = \alpha_5$, where α_5 = 1.19 in [21], 1.17 in [74], 1.2 in [45]
Entrainment coefficient α_e	α_e = 0.053 in [73] and [45]	α_e = 0.026 in [73], 0.028 in [74], 0.057 in [45]

Source: [21, 45, 73, 74].
[a]In [21] and [45], b (or b_C) is defined as where the velocity (or concentration) is 37% of u_m (or C_m); while in others, defined as 50% of u_m (or C_m).

Using the same procedures as above, the equations of momentum flux, volume flux, and pollutant mass flux for a circular jet can be derived. These equations suggest that the jet momentum flux at any x-section is conserved and the jet volume flux across any x-section increases with traveling distance due to the entrainment of ambient fluid. Although the entrainment causes the pollutant to get diluted within the jet core, the mass flux of any conservative pollutant at any x-section is conserved. The solutions of these equations for circular jets are summarized in Table 1.

Simple Plumes

A plume is produced from a steady discharge of a fluid whose motion is controlled by its buoyancy, with negligible effect of initial momentum. First, a plane plume of density ρ_0 issued into a stagnant unstratified ambient fluid of density ρ_a is considered. It is assumed that $\frac{\Delta\rho_0}{\rho_a} \ll 1$ (true for most practical cases), where the initial density defect $\Delta\rho_0 = \rho_a - \rho_0$. After some manipulation, it can be shown that the Reynolds-averaged Navier-Stokes equation in x direction becomes:

$$u\frac{\partial u}{\partial x} + v\frac{\partial u}{\partial y} = \frac{1}{\rho_a}\frac{\partial \tau}{\partial y} + g\frac{\Delta\rho}{\rho_a} \tag{9}$$

where $\Delta\rho = \rho_a - \rho$ and ρ is the plume density. For a plane plume, the continuity equation and pollutant conservation equation can be simplified in the same form as for a plane jet (Eqs. 2 and 3).

Using the integral method, Eq. 9 can be reduced to:

$$\frac{d}{dx}\int_0^\infty \rho u^2 dy = \int_0^\infty g\Delta\rho dy \tag{10}$$

Equation 10 says that axial momentum flux increases in x direction, and the increase rate is equal to the buoyancy per unit length (in x direction) of the plume. For a plane plume, the continuity equation and pollutant conservation equation can be reduced the same as Eqs. 5 and 6. Equation 5 states that the volume flux of a plume increases due to the entrainment of ambient fluid, and Eq. 6 states that although the concentration of pollutant decreases, its total mass flux is conserved. Note that C in Eq. 6 can be also interpreted as $g\Delta\rho$, and then Eq. 6 becomes the integral form of buoyancy conservation equation.

Experimental results show that: similarly as for jets, the plume velocity or concentration also exhibit self-similarity and the Gaussian distribution can well describe it. Using the Gaussian profiles (Eqs. 7 and 8), the analytical solutions for a plane plume can be

derived as shown in Table 2. The coefficients differ slightly in different references as they are determined using the results of different experiments. Here, to constitute the solutions, an useful dimensionless parameter is indroduced – the densimetric Froude number at the slot exit $F_0 = \frac{U_0}{\sqrt{g\left(\frac{\Delta\rho}{\rho_a}\right)b_0}}$ (for circular plume, $F_0 = \frac{U_0}{\sqrt{g\left(\frac{\Delta\rho}{\rho_a}\right)d_0}}$).

For a circular plume, the Reynolds-averaged Navier-Stokes equations, continuity equation and pollutant conservation equation, can be simplified, and the integral method can be used to obtain their integral forms of the equations. These equations indicate that the momentum flux in the plume increases with axial (x) direction, and the increase rate is equal to the buoyant force per unit axial length; the volume flux in the plume increases due to the entrainment of ambient fluid; and the pollutant mass flux (or the flux of density defect) remains invariant in the axial direction. The analytical solutions for a circular plume are also presented in Table 2. The constants in these equations change slightly in different references where different experimental results were used.

Buoyant Jets

For a buoyant jet, the initial momentum flux cannot be neglected. Near the nozzle (slot) exit, it is expected that the buoyant flow will be like a jet; after some distance from the exit where the increase of momentum flux is much larger than the initial momentum flux, the buoyant flow will behave like a plume. For a plane buoyant jet, based on dimensional analysis, a characteristic length scale to judge whether the buoyant flow behaves like a jet or plume may be defined as:

$$L_M = \frac{M_0}{B_0^{\frac{2}{3}}} \tag{11}$$

where the initial specific momentum flux $M_0 = qU_0$; the initial specific buoyancy flux $B_0 = qg\frac{\Delta\rho_0}{\rho_a}$. If the jet centerline trajectory $l \ll l_M$, the buoyant jet can be treated as a pure jet and the simple jet equations can

Transport with Jets and Plumes of Chemicals in the Environment. Table 2 Summary of mean properties of plane plume and circular plume

Parameter	Plane plume	Circular plume
Maximum (centerline) concentration C_m or density defect $\Delta\rho_m$	$\frac{C_m}{C_0} = \frac{\Delta\rho_m}{\Delta\rho_0} = \frac{\alpha_1 F_0^{\frac{2}{3}}}{x/b_0}$, where $F_0 = \frac{U_0}{\sqrt{g\frac{\Delta\rho}{\rho_a}b_0}}$, α_1 = 3.78 in [21], 3.84 in [74], 4.25 in [45]	$\frac{C_m}{C_0} = \frac{\Delta\rho_m}{\Delta\rho_0} = \frac{\alpha_1 F_0^{\frac{2}{3}}}{\left(\frac{x}{d_0}\right)^{\frac{5}{3}}}$, where $F_0 = \frac{U_0}{\sqrt{g\frac{\Delta\rho}{\rho_a}d_0}}$, α_1 = 7.75 in [21], 7.83 or 9.37 in (from different methods in Ref. [74]), 8.90 in [45]
Cross-sectional average concentration C_{avg}	$\frac{C_m}{C_{avg}} = \alpha_2$, where α_2 = 1.32 in [74], 1.25 in [45]	$\frac{C_m}{C_{avg}} = \alpha_2$, where α_2 = 1.40 in [21], 1.70 in [45]
Maximum (centerline) velocity u_m	$\frac{u_m}{u_0} = \frac{\alpha_3}{F_0^{\frac{2}{3}}}$, where α_3 = 2.09 in [21], 2.52 in [74], 2.85 in [45]	$\frac{u_m}{U_0} = \frac{\alpha_3}{F_0^{\frac{2}{3}}\left(\frac{x}{d_0}\right)^{\frac{1}{3}}}$, where α_3 = 4.34 in [21], 4.00 or 4.33 in (from different methods in Ref. [74]), 4.35 in [45]
Velocity half-width b[a]	$b = \alpha_4 x$, where α_4 = 0.116 in [21] and [45], 0.128 in [74]	$b = \alpha_4 x$, where α_4 = 0.100 in [21], 0.085 in [74], 0.105 in [45]
Concentration half-width b_C[a]	$b_C/b. = \alpha_5$, where α_5 =1.35 in [21] and [45], 1.17 in [74]	$b_C/b = \alpha_5$, where α_5 =1.20 in [21], 1.16 in [74], 1.19 in [45]
Entrainment coefficient α_e	α_e = 0.136 in [74], 0.103 in [45]	α_e = 0.047 in [74], 0.088 in [45]

Source: [21, 45, 74].

[a]In [21] and [45], b (or b_C) is defined as where the velocity (or concentration) is 37% of u_m (or C_m); while in [74], defined as 50% of u_m (or C_m).

be used; if $l \gg l_M$, it can be treated as a pure plume and the simple plume equations are valid. Buoyant jets will be plume-like beyond $\frac{l}{l_M} \geq 4 \sim 5$ [41, 65].

Characteristic length scale of jet/plume can only roughly help us calculate the evolution of a buoyant jet. The Reynolds equations, continuity equation and pollutant mass conservation equations can be simplified and the integral method can be used to obtain the analytical solutions. For a plane buoyant jet, the integral forms of the momentum, continuity, pollutant mass (or buoyancy) conservation equations are the same as Eqs. 10, 5 and 6, respectively. Here, for a buoyant jet, the integral form of energy equation needs to be introduced (as a result of multiplying Eq. 9 by u and integrating from $y = 0$ to $y = \infty$):

$$\frac{d}{dx}\int_0^\infty \frac{\rho u^2}{2} u dy = -\int_0^\infty \tau \frac{\partial u}{\partial y} dy + \int_0^\infty g\Delta\rho u\, dy \tag{12}$$

Equation 12 states that the flux of kinetic energy in the jet plume is decreased by turbulence production (first term in the right hand side of Eq. 12) and increased by the work done by buoyancy (second term in the right hand side).

The Gaussian type self-similarity equations are still valid for plane buoyant jets. Using Eqs. 7 and 8, as well as the experimental results on the jet spreading rate $\frac{db}{dx}$ and on the ratio of the concentration half-width to the velocity half-width $\frac{b_C}{b}$, and after some mathematical manipulations, the solutions for a plane buoyant jet can be obtained as shown in Table 3. It is interesting to note that in Table 3, the jet centerline concentration or velocity equation are composed of two parts, corresponding to two limits (pure jet-like or pure plume-like conditions).

The characteristic length scale for a buoyant circular jet or plume is:

$$L_M = \frac{M_0^{\frac{3}{4}}}{B_0^{\frac{1}{2}}} \tag{13}$$

Similarly, for a buoyant circular jet, the integral equations of the momentum, continuity, pollutant mass (or buoyancy) conservation, and kinetic energy can be obtained. Using the Gaussian distribution for jet velocity or concentration and some experimental data, the analytical solutions for buoyant circular jets are shown in Table 3.

Effect of Boundaries on Jets and Plumes

In this section, the effect of different types of boundaries on jets and plumes will be considered, including the solid bed (wall), the free surface of ambient fluid, the coflowing or crossflowing ambient fluid, and the neighboring jets in the case of multiple jets.

Wall Jets

Wall jets are the jets discharged tangentially or at certain angles to a solid boundary (wall) (see Fig. 2). A simple case is first considered: a plane jet discharged tangentially to a smooth flat plate in deep still ambient fluid of the same kind. For turbulent plane wall jets with high Reynolds numbers ($R_0 = \frac{U_0 b_0}{\nu} = 10^4 \sim 10^5$, where ν is the kinematic viscosity of the fluid) at the slot exit, the length of the potential core will be $(6.1 \sim 6.7)b_0$ [73], which is in the same range as for simple jets. As expected, experiments show that, near the wall, there exists a thin layer (boundary layer) where the jet velocity increases from zero at the wall to a maximum velocity u_m; above the boundary layer (named free mixing region), the jet velocity decreases from u_m to zero at some large distance y from the wall. Similarly as for simple jets, the jet width may be defined as where the jet velocity is 50% (or 37%) of u_m and $\frac{\partial u}{\partial y} < 0$ (i.e., in the free mixing region). In the boundary layer region, the boundary layer theories may be used to further divide this region into two or three sub-layers: in the sub-layer very close to the wall, the velocity distribution is linear with y; some distance away from the wall, the velocity distribution can be described by the logarithmic law [87]. For the velocity distributions of the entire wall jet, after some distance (about $20b_0$) from the slot exit, they exhibit self-similarity [23, 99]. Verhoff [99] proposed an empirical equation which agreed well with the experimental data:

$$\frac{u}{u_m} = 1.48\left(\frac{y}{b}\right)^{\frac{1}{7}}\left[1 - \mathrm{erf}\left(0.68\frac{y}{b}\right)\right] \tag{14}$$

Using the equations of motion and the integral method, the following results could be obtained for plane wall jets: $u_m \propto x^{-\frac{1}{2}}$; $b \propto x$. The detailed results are listed in Table 4. To study the effect of wall roughness on wall jets, readers may refer to Rajaratnam [72], Tachie et al. [95], Dey et al. [19], and Rostamy et al. [83]. To study the jets impinging on walls, readers

Transport with Jets and Plumes of Chemicals in the Environment. Table 3 Summary of mean properties of turbulent buoyant jet

Parameter	Plane buoyant jet	Circular buoyant jet
Characteristic length for jet/plume L_M	$L_M = \frac{M_0}{B_0^{\frac{2}{3}}}$	$L_M = \frac{M_0^{\frac{3}{4}}}{B_0^{\frac{1}{2}}}$
Maximum (centerline) concentration C_m or density defect $\Delta\rho_m$	$\frac{C_m}{C_0} = \frac{\Delta\rho_m}{\Delta\rho_0} = \frac{\alpha_{11}}{\left[\frac{\alpha_{12}}{F_0^2} + \frac{\alpha_{13}}{\left(\frac{x}{b_0}\right)^{\frac{3}{2}}}\right]^{\frac{1}{3}}} \frac{1}{\left(\frac{x}{b_0}\right)}$, where $F_0 = \frac{U_0}{\sqrt{g\frac{\Delta\rho}{\rho_a} b_0}}$, $\alpha_{11} = 12.75$, $\alpha_{12} = 21.19$, $\alpha_{13} = 50.0$ in [74]	$\frac{C_m}{C_0} = \frac{\Delta\rho_m}{\Delta\rho_0} = \frac{\alpha_{11}}{\left[\frac{\alpha_{12}}{F_0^2}\left(\frac{x}{d_0}\right)^5 + \alpha_{13}\left(\frac{x}{d_0}\right)^3\right]^{\frac{1}{3}}}$, where $\alpha_{11} = 100$, $\alpha_{12} = 1{,}920$, $\alpha_{13} = 6{,}720$ in [74]
Cross-sectional average concentration C_{avg}	$\frac{C_m}{C_{avg}} = \sqrt{1 + \frac{1}{k_2^2}} = 1.24$, where $k_2 = \frac{b_C}{b} = 1.35$ in [45]	$\frac{C_m}{C_{avg}} = 1.80$ in [74] $\frac{C_m}{C_{avg}} = 1 + \frac{1}{k_2^2} = 1.69$, where $k_2 = \frac{b_C}{b} = 1.2$ in [45]
Maximum (centerline) velocity u_m	$\frac{u_m}{U_0} = \left[\frac{\alpha_{31}}{F_0^2} + \frac{\alpha_{32}}{\left(\frac{x}{b_0}\right)^{\frac{3}{2}}}\right]^{\frac{1}{3}}$, where $\alpha_{31} = 21.2$, $\alpha_{32} = 50.7$ in [74]	$\frac{u_m}{U_0} = \left[\frac{\alpha_{31}}{F_0^2\left(\frac{x}{d_0}\right)} + \frac{\alpha_{32}}{\left(\frac{x}{d_0}\right)^3}\right]^{\frac{1}{3}}$, where $\alpha_{31} = 64.75$, $\alpha_{32} = 223.25$ in [74]
Velocity half-width b	$b = \alpha_4 x$, where $\alpha_4 = 0.097$ in [74]	$b = \alpha_4 x$, where $\alpha_4 = 0.097$ in [74]
Concentration half-width b_C	$\frac{b_C}{b} = \alpha_5$, where $\alpha_5 = 1.18$ in [74]	$\frac{b_C}{b} = \alpha_5$, where $\alpha_5 = 1.16$ in [74]
Entrainment Coefficient α_e	$\alpha_e = \alpha_{ej} + \frac{\alpha_{61}(\alpha_{ep} - \alpha_{ej})}{\alpha_{61} + \frac{\alpha_{62}F_0^2}{\left(\frac{x}{b_0}\right)^{\frac{3}{2}}}}$, where α_{ej} and α_{ep} are the entrainment coefficients for the plane jet and plume, respectively, $\alpha_{61} = 17.1$, $\alpha_{62} = 41.4$ in [74]	$\alpha_e = \alpha_{ej} + \frac{\alpha_{61}}{\alpha_{62} + \frac{\alpha_{63}F_0^3}{\left(\frac{x}{d_0}\right)^3}}$, where $\alpha_{61} = 0.44$, $\alpha_{62} = 20.74$, $\alpha_{63} = 2.38$ in [74]

Source: [45, 74].

may refer to Beltaos and Rajaratnam [10], Rajaratnam [73], and Chan et al. [14].

For non-buoyant circular wall jets (herein termed "bluff wall jet" to include semicircular and rectangular wall jets with aspect ratio not very different from unity; the properties of bluff jets are not very different from those of circular jets), a number of studies have been conducted: square wall jets by Sforza and Herbst [88], circular wall jets by Newman et al. [61], bluff (including square, rectangular, circular, elliptic, and equilateral triangular) wall jets by Rajaratnam and Pani [77], square wall jets by Lübcke et al. [53], and circular wall jets by Agelin-Chaab [3]. These experiments show that after some distance from the potential core, the velocity distributions both in the vertical central plane and in the horizontal plane (see Fig. 2) are self-similar. From similarity analysis on the equations of motion or from dimensional analysis, the following results can be obtained for bluff wall jets: $u_m \propto x^{-1}$; $b_y \propto x$; $b_z \propto x$ [73]. Experimental results support these predictions, and the results are listed in Table 4.

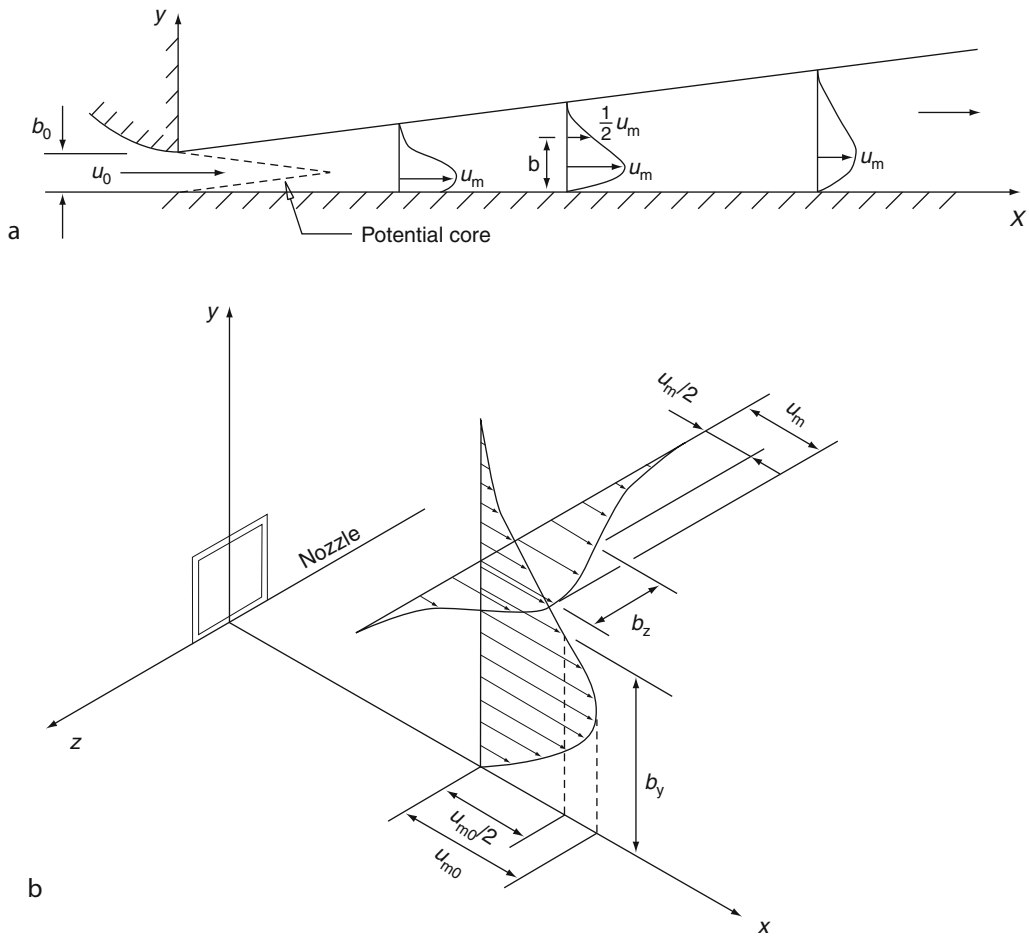

Transport with Jets and Plumes of Chemicals in the Environment. Figure 2
Schematic of (**a**) plane and (**b**) bluff wall jets

Surface Jets

A surface jet can be produced by discharging a fluid at the surface of an ambient fluid (see Fig. 3). One typical example is the surface discharge of heated water from a power plant through either an open-channel or a pipe into an ocean, a lake, or river. Rivers flowing into lakes, reservoirs, and oceans and storm water discharges into rivers may be also viewed as surface jets. In this section, our attention will be limited in the region from the end of the jet potential core to the end of the near field (where the mixing is still dominated by the jet momentum and buoyancy). The length of the near field is in the order of $100\sqrt{A_0}$, where A_0 is the cross-sectional area of the flow at discharge [74]. For the mixing in the far field (where the turbulence in rivers, lakes, or oceans dominates further mixing), readers can refer to Fischer et al. [21] and Rutherford [85].

Non-buoyant plane surface jets in stagnant water are now considered. Equations 1–8 for plane submerged jets also work for plane surface jets. Using the integral method and some mathematical manipulations, some useful results can be obtained: $u_m \propto x^{-\frac{1}{2}}$; $b \propto x$; $c_m \propto x^{-\frac{1}{2}}$, which are in the same form as those for plane submerged jets (Table 1). Experiments on plane surface jets were conducted by Chu and Vanvari [16], Rajaratnam and Humphries [76], and others. The experimental results are listed in Table 5. The results confirm that essentially a plane surface jet is quite similar to half of the corresponding plane submerged jets, but with slightly different coefficients. For example,

Transport with Jets and Plumes of Chemicals in the Environment. Table 4 Summary of mean properties of plane wall jet and bluff wall jet

Parameter	Plane wall jet	Bluff wall jet
Maximum (centerline) concentration C_m		
Cross-sectional average concentration C_{avg}	$\frac{C_{avg}}{C_0} = \frac{\alpha_1}{\frac{x}{b_0}}$, where α_1 = 4.032 in [73]	
Maximum (centerline) velocity u_m	$\frac{u_m}{U_0} = \frac{\alpha_3}{\sqrt{\frac{x}{b_0}}}$, where α_3 = 3.50 in [78] & [73]	
Velocity half-width b	$b = \alpha_4 x$, where α_4 = 0.068 in [73]; $\frac{db}{dx}$ = 0.073 in [44]	$\frac{b_y}{d_0} = 0.90 + \alpha_{41}\frac{x}{h}$ $\frac{b_z}{B} = \alpha_{42}\frac{x}{B} - 1.25$ where α_{41} =0.045, α_{42} =0.20, B is the nozzle (horizontal) width in [77] & [73]; $\frac{db_y}{dx} = 0.048$ and $\frac{db_z}{dx} = 0.26$ in [44]
Concentration half-width b_C		
Entrainment Coefficient α_e	α_e = 0.035 in [73]	

Source: [44, 73, 77, 78].

the jet spreading rate of plane surface jets $\frac{db}{dx} = 0.07$, smaller than the value of 0.10 for plane submerged jets.

Next, non-buoyant bluff surface jets in stagnant water are considered. From the experiments of Rajaratnam and Humphries [76], the Gaussian function describes the velocity distributions well both in vertical (half-Gaussian) and transverse directions, unless there is excess wave generation at the water surface (in this case u_m occurs some distance below the water surface). Using the integral method, it can be shown that: $u_m \propto x^{-1}$;$b_z \propto x$; $b_y \propto x$, which are in the same forms as for circular submerged jets. Rajaratnam and Humphries' experimental results show that the jet spreading rate in the transverse direction $\frac{db_z}{dx} = 0.09$, twice of that in the vertical direction $\frac{db_y}{dx} = 0.044$. The phenomenon of the several times faster transverse spreading has also been observed in the studies of Anthony and Willmarth [6], Gholamreza-kashi et al. [24], and Cuthbertson and Davies [18]. These studies further found that there exists a thin layer (called "surface current") at the free surface, which exhibits even faster transverse spreading compared to that below the layer. Comparing Table 5 with Table 4, one may find that surface jets are somehow similar to wall jets, e.g., they both spread faster in the horizontal direction than in the vertical direction due to the boundary constraint in the vertical direction, and they have similar forms of jet equations.

For the surface discharges such as heated water into rivers or wastewater into the oceans, the effect of buoyancy needs to be considered. Experimental results have indicated that the behavior of buoyant surface jets is mainly controlled by three parameters: the Richardson number at the outfall, $Ri_0 = gd_0\Delta\rho_0/(\rho_a U_0^2)$; the depth (thickness) of the surface jet, d_0 (or b_0 for a plane jet); and the depth of the surface stratified layer formed at the end of the near field of the surface jet, $\overline{b_\infty}$. For a buoyant surface jet with a fixed Ri_0, depending on the value of $\frac{d_0}{\overline{b_\infty}}$, there could be four possible hydraulic phenomena: a surface jet, a surface (density) jump at the outfall, a surface jet followed by a surface jump, or a drowned jump. Rajaratnam and Subramanyan [79] presented a graph to distinguish which of the four possibilities may happen for a plane buoyant surface jet. For the case of a pure plane

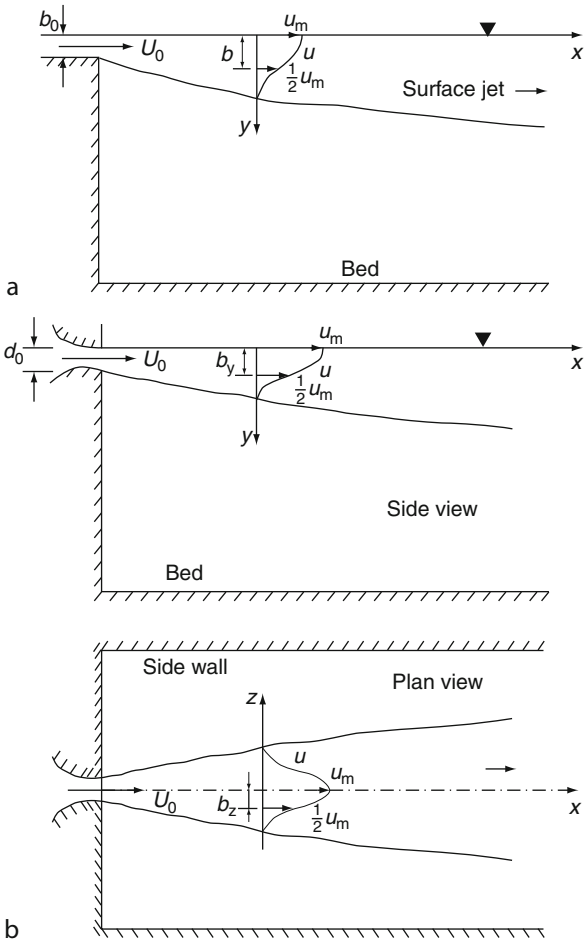

Transport with Jets and Plumes of Chemicals in the Environment. Figure 3
Schematic of (**a**) plane and (**b**) bluff surface jets

buoyant surface jet (without any jump), the experiments of Rajaratnam and Subramanyan [79] show that: initially the jet spreading rate $\frac{db}{dx}$ follows the equation of the plane non-buoyant surface jet, but after some longitudinal distance, the spreading rate slows down, and eventually the jet thickness approaches a constant. In other words, generally the buoyancy effect constrains the spreading of a plane surface jet. Their results also indicate that $\frac{u}{u_m}$ is self-similar at different x-sections; however, these self-similarities can no longer be described by the Gaussian distribution and seem to be related with Ri_0. The results of Chu and Vanvari [16] reveal that the entrainment coefficient α_e of a plane buoyant surface jet decreases continuously with the increase of bulk Ri (defined as $\frac{U_0 d_0 g \Delta\rho_0}{\rho_a u_m^3}$) with x; and α_e equals to zero when Ri increases to 0.2.

For bluff buoyant surface jets, a number of experiments have shown that the jet behavior is strongly affected by Ri_0 at the outfall. For convenience, bluff surface jets may be classified into two classes, the small Ri_0 class ($Ri_0 \leq 0.1$) and the large Ri_0 class ($Ri_0 > 0.1$). From a number of experiments, the common findings for the two classes are that the vertical velocity profile $u(y)$ in the center-plane and the transverse (across the jet) velocity profile $u(z)$ just below the water surface are self-similar, and the self-similarities can be well described by half-Gaussian or Gaussian distribution. Using the similarity analysis of the simplified equations of motion, the following relations can be obtained: for the small Ri_0 class, $u_m \propto x^{-1}$, $C_m \propto x^{-1}$, $b_y \propto x$, $b_z \propto x$; and for the large Ri_0 class, $u_m \propto x^{-\frac{1}{3}}$, $C_m \propto x^{-\frac{2}{3}}$, $b_y =$ constant, $b_z \propto x$. The detailed results are listed in Table 6.

Jets and Plumes in Coflow

Similarly as solid bed or free surface of ambient fluid, coflowing or crossflowing ambient fluid itself can be viewed as some sort of boundary affecting jet behaviors. When jets are discharged in the direction of flowing ambient fluids, this is the problem of jets in coflow (Fig. 4). Extensive experimental and numerical studies show that beyond the potential core, the jet concentration and the jet excess velocity relative to the ambient velocity exhibit self-similarity. The self-similarity may be described by the Gaussian distribution, exponent function, or cosine expression [45, 73]. In the following, plane jets in uniform coflow will be briefly introduced, followed by circular jets.

For coflowing plane jets, the integral form of equation of motion is:

$$\frac{d}{dx}\int_0^\infty \rho u \Delta u dy = 0 \tag{15}$$

where $\Delta u = u - U_a$, the jet excess velocity. Equation 15 states that the excess momentum flux is conserved in x direction. Using Eq. 15 and similarity analysis, Rajaratnam [73] obtained the following asymptotic relations: for the strong jet region (i.e., $\frac{\Delta u_m}{U_a} \gg 1$), $\Delta u_m \propto x^{-\frac{1}{2}}$ and $b \propto x$; and for the weak jet region (i.e., $\frac{\Delta u_m}{U_a} \ll 1$), $\Delta u_m \propto x^{-\frac{1}{2}}$ and $b \propto x^{\frac{1}{2}}$. Based on the

Transport with Jets and Plumes of Chemicals in the Environment. Table 5 Summary of mean properties of non-buoyant plane surface jet and bluff surface jet

Parameter	Non-buoyant plane surface jet	Non-buoyant bluff surface jet
Maximum (centerline) concentration C_m		
Cross-sectional average concentration C_{avg}		
Maximum (centerline) velocity u_m	$\frac{u_m}{U_0} = \frac{\alpha_3}{\sqrt{\frac{x}{b_0}}}$, where α_3 = 3.1 in [76]	$\frac{u_m}{U_0} = \frac{\alpha_3}{x/d_0}$, where α_3 = 13 in [24]
Velocity half-width b	$\frac{db}{dx} = \alpha_4$, where α_4 = 0.07 in [74] & [76]	In transverse direction: $db_z/dx = \alpha_{41}$ In vertical direction: $db_y/dx = \alpha_{42}$ where α_{41} = 0.09 in [74] & [76], 0.12 (below the free surface) and 0.22 (at the free surface) in [24]; and α_{42} = 0.044 in [74] & [76], 0.025 in [24]
Concentration half-width b_C	$b_C/b = \alpha_5$, where α_5 = 1.15 in [74]	
Entrainment coefficient α_e	α_e = 0.037 in [74]	

Source: [24, 73, 74, 76].

experimental results in the literature, Rajaratnam [73] derived that:

$$\frac{\Delta u_m}{\sqrt{U_0(U_0 - U_a)}} = \frac{3.41}{\sqrt{\frac{x}{b_0}}} \tag{16}$$

$$\frac{b}{b_0} = 0.118\frac{x}{b_0}\frac{1}{1 + \frac{0.41}{\sqrt{\alpha(\alpha-1)}}\sqrt{\frac{x}{b_0}}} \tag{17}$$

where $\alpha = \frac{U_o}{U_a}$, the ratio of jet exit velocity to ambient velocity. Note that Rajaratnam [73] also summarized other more complex forms of equations for Δu_m and b, which were derived by Patel [68] and Pande and Rajaratnam [62].

For circular jets in coflow, the integral momentum equation can be derived:

$$\frac{d}{dx}\int_0^\infty \rho 2\pi r u \Delta u dr = 0 \tag{18}$$

which says that the jet excess momentum is conserved in axial direction. Using Eq. 18 and similarity analysis on the equations of motion, Rajaratnam [73] presented the following asymptotic relations: for the strong jet region (i.e., $\frac{\Delta u_m}{U_a} \gg 1$), $\Delta u_m \propto x^{-1}$ and $b \propto x$; for the weak jet region (i.e., $\frac{\Delta u_m}{U_a} \ll 1$), $\Delta u_m \propto x^{-\frac{2}{3}}$ and $b \propto x^{\frac{1}{3}}$. Pande and Rajaratnam [62] proposed a complex expression for Δu_m. Lee and Chu [45] also derived asymptotic solutions for circular jets in coflow: for the strong jet region, the jet solution is assumed to be the same as in stagnant water (see Table 1); for the weak jet region,

$$\frac{\Delta u_m}{U_a} = 2.14\left(\frac{x}{l_m{}^*}\right)^{-\frac{2}{3}} \tag{19}$$

$$\frac{b}{l_m{}^*} = 0.385\left(\frac{x}{l_m{}^*}\right)^{\frac{1}{3}} \tag{20}$$

where $l_m{}^*$ is the excess momentum length scale defined as $\frac{M_{e0}^{1/2}}{U_a}$; $M_{e0} = (U_0 - U_a)\frac{U_0 \pi d_0{}^2}{4}$, the jet specific excess momentum at discharge.

To completely model circular jets in coflow, Lee and Chu [45] formulated an integral model based on a Lagrangian jet spreading hypothesis:

$$U^{*2} + U^* - \frac{1}{\pi B^{*2}} = 0 \tag{21}$$

Transport with Jets and Plumes of Chemicals in the Environment. Table 6 Summary of Mean properties of buoyant plane surface jet and bluff surface jet

Parameter	Buoyant plane surface jet	Buoyant bluff surface jet with $Ri_0 \leq 0.1$	Buoyant bluff surface jet with $Ri_0 > 0.1$
Maximum (centerline) concentration C_m			$\frac{C_m}{C_0} = \frac{\alpha_1}{\left(\frac{x}{\sqrt{A_0}}\right)^{\frac{2}{3}}}$, where α_1 = 2.83 in [74]
Cross-sectional average concentration C_{avg}			
Maximum (centerline) velocity u_m	$\frac{u}{u_m}$ exhibits self-similarity, but cannot be well described by Gaussian profile, as $\frac{u}{u_m} \approx 0$ at $\frac{y}{b} \approx 1.4$ [79]	$\frac{u_m}{U_0} = \frac{\alpha_3 Ri_0^{\frac{1}{10}}}{\sqrt{\frac{x}{A_0}}}$, where α_3 = 15.3 in [74] & [75]	$\frac{u_m}{U_0} = \frac{\alpha_3}{\left(\frac{x}{\sqrt{A_0}} - 5.0\right)^{1/3}}$, where α_3 = 1.25 in [74]
Velocity half-width b	First $\frac{b}{b_0}$ increases linearly as non-buoyant surface jet to some point $\frac{x}{b_0}$ (the location depends on Ri_0); then the increase rate $\frac{db}{dx}$ decreases nonlinearly, finally approaches asymptotically a horizontal line [79].	$\frac{db_y}{dx} = \alpha_{41}$ $\frac{db_z}{dx} = \alpha_{42}$ where α_{41} decreases with Ri_0 (α_{41} = 0.044 for Ri_0 =0, 0.02 for Ri_0 =0.038, 0 for Ri_0 =0.09); α_{42} increases with Ri_0 in [74] & [75]	$\frac{b_{y*}}{d_0} = \frac{\alpha_{41}}{Ri_0^{1/8}}$ $\frac{b_z}{\sqrt{A_0}} = \alpha_{42}\left(\frac{x}{\sqrt{A_0}} + 2.0\right)$ where b_{y*} is the average of b_y which changes slightly with y; α_{41} =0.29 in [63], 0.26 in [74]; α_{42} =0.54 in [74]
Concentration half-width b_C		$\frac{b_{yC}}{b_y} = \alpha_{51}$ $\frac{b_{zC}}{b_z} = \alpha_{52}$ where α_{51} = 1.0 in [74] & [75] and α_{52} = 1.15 in [74]	$\frac{b_{yC}}{b_y} = \alpha_{51}$ $\frac{b_{zC}}{b_z} = \alpha_{52}$ where α_{51} = 1.12 in [63] & [74]; and α_{52} = 1.9 in [63], 1.6 in [74]
Entrainment coefficient α_e	α_e decreases from about 0.04 to 0 when Ri increases from 0 (non-buoyant plane surface jet) to 0.2 [16]		

Source: [16, 63, 74, 75, 79].

$$\frac{dB^*}{dx} = \beta_s \frac{U^*}{1 + U^*} \tag{22}$$

where $U^* = \frac{\Delta U}{U_a}$; $B^* = \frac{B}{l_m^*}$; ΔU and B are, respectively, the excess velocity and half of the width of the top-hat profile (instead of the Gaussian profile) of an equivalent jet, which carries the same mass flow and excess momentum flux as the actual jet; and $\beta_s = \frac{dB}{dx}$ in stagnant water. It can be proved that $\Delta U = \frac{\Delta u_m}{2}$ and $B = \sqrt{2}b$, where Δu_m and b are, respectively, the maximum excess velocity and 37% half-width for the Gaussian profile. From Eqs. 21 and 22, ΔU and B can be solved. The actual jet centerline dilution can be obtained:

$$S_c = \frac{C_0}{C_m} = \frac{\lambda^2 \pi B^2 \left(U_a + \frac{2}{1+\lambda^2}\Delta U\right)}{2{Q_0}^2} \tag{23}$$

where Q_0 and C_0 are the initial jet discharge and concentration, respectively; λ is the ratio of concentration half-width to velocity half-width using the Gaussian profile ($\lambda \approx 1.2$). The modeling results of Lee and

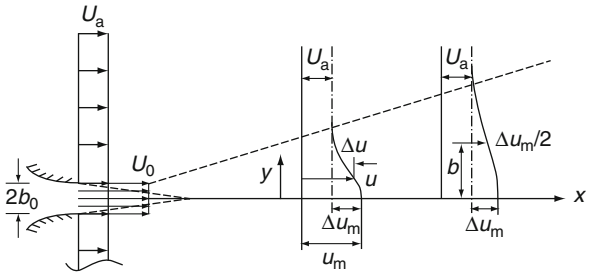

Transport with Jets and Plumes of Chemicals in the Environment. Figure 4
Schematic of plane jets in coflow (for circular jets, replace $2b_0$ by d_0 and y by r)

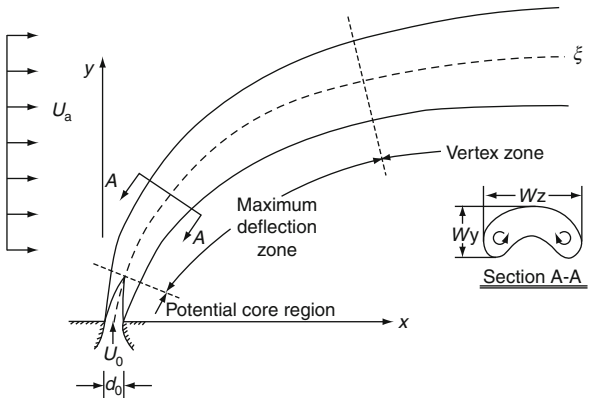

Transport with Jets and Plumes of Chemicals in the Environment. Figure 5
Schematic of jets in crossflow

Chu [45] reveal that the centerline dilution of a circular jet in coflow is only slightly smaller than that in stagnant water; and the centerline excess velocity decays in a similar way as in stagnant water.

Jets and Plumes in Crossflow

Now consider a non-buoyant circular jet discharged at an oblique angle (not 0 or 180 degree) to a flowing ambient fluid. In fact, most outfalls or diffusers in oceans or rivers discharge effluents as jets in crossflow, as the jet (effluent) dilution can be considerably enhanced even in a weak crossflow [45, 73]. Jets in crossflow have been studied extensively by Abramovich [1], Rajaratnam [73], Fischer et al. [21], Wright [102, 103], Andreopoulos [5], Hodgson and Rajaratnam [29], Margason [54], Smith and Mungal [91], Lee and Chu [45], Huang et al. [31], Kikkert et al. [38], and others. According to these studies, the evolution of jets in crossflow can be divided into three regions: the potential core region, the maximum deflection region, and the vortex region (see Fig. 5). The length of the potential core has been found to be mostly controlled by the relative strength of the jet compared to the crossflow ($\alpha = \frac{U_0}{U_a}$), and typically in the range of 2–6d_0 which is smaller than that of a free jet [70].

Beyond the potential core region, the jet would be largely deflected due to the stagnation pressure exerted by the free stream and the entrainment of ambient fluid (and thus horizontal momentum). Jet deflection probably is the most distinct feature in crossflow. After the maximum deflection region, the jet would be gradually parallel to the direction of ambient flow. Laboratory experiments [1, 29, 45] and numerical simulations [45] have found that after some distance beyond the potential core, the jet cross section would be like a kidney shape with a pair of two counter-rotating vortices (see Fig. 5). The vortex pair significantly entrains ambient fluid in the form of tornado vortices into the jet [45], which explains the considerable enhancement of jet dilution in crossflow. The concentrations at the centers of the two vortices have been found to be about 1.1–1.6 times of the jet centerline concentration [29, 45].

For non-buoyant jets in crossflow, it is common to analyze them in three regions: the momentum dominated near field (MDNF), the momentum dominated far field (MDFF), and the transition between MDNF and MDFF. If the jet trajectory $\xi \ll l_m$, where l_m is defined as:

$$l_m = \frac{M_{v0}^{\frac{1}{2}}}{U_a} \tag{24}$$

and M_{v0} is the vertical momentum at the exit, then the jet is in MDNF, where the effect of jet momentum is much stronger than that of the ambient crossflow. In MDNF, the classic equations for jets in stagnant ambient fluid are approximately valid. If $\xi \gg l_m$, the jet is in MDFF, where the effect of ambient crossflow is dominant over the jet momentum. In MDFF, the jet properties can be studied with physical and numerical models. Fischer et al. [21] used dimensional analysis to find the asymptotic formulas for MDNF and MDFF.

Lee and Chu [45] studied the jets in MDFF based on the analogy to advected line puffs. Using length-scale analysis and numerical models, they proposed the formulas which can represent satisfactorily the experimental results:

$$\frac{y_c}{l_m} = 1.56\left(\frac{x}{l_m}\right)^{\frac{1}{3}} \tag{25}$$

$$b_{vc} = 0.28 y_c \tag{26}$$

$$S_c = 0.46\frac{U_a {y_c}^2}{Q_0} \tag{27}$$

where y_c is the vertical location of the centerline concentration, b_{vc} is the vertical centerline half-width defined by 37% of the centerline concentration and S_c is the centerline dilution.

The most common jet discharge angle in crossflow is 90 degree, i.e., jets are discharged at right angle to the ambient crossflow. Rajaratnam [73] summarized the early studies in 1950s to 1970s that mostly focused on jet trajectories. Hodgson and Rajaratnam [29] conducted detailed laboratory experiments on circular jets at right angle to crossflow and proposed the following equations:

$$S_c = 1.09\left(\frac{\alpha x}{d_0}\right)^{0.56} \tag{28}$$

$$\frac{y_c}{\alpha d_0} = 1.46\left(\frac{x}{\alpha d_0}\right)^{0.26} \tag{29}$$

$$\frac{W_z}{\alpha d_0} = 1.20\left(\frac{x}{\alpha d_0}\right)^{0.29} \tag{30}$$

$$\frac{W_y}{\alpha d_0} = 0.78\left(\frac{x}{\alpha d_0}\right)^{0.37} \tag{31}$$

where W_z and W_y are the jet width and thickness (see Fig. 5). Equations 28–31 have also been validated by a field experiment in the Lesser Slave River, Canada. Hodgson and Rajaratnam's equations are mainly derived based on the experiments conducted in the range of $\frac{x}{\alpha d_0} = 1 \sim 1,000$. It is interesting to note that Hodgson and Rajaratnam's expressions fit the experimental data satisfactorily both in MDNF, MDFF, and the transition between the two.

Now consider a circular plume in crossflow. Similarly as l_m, a length scale l_b needs to be defined to compare the relative strength of plume buoyancy with crossflow:

$$l_b = \frac{B_0}{{U_a}^3} \tag{32}$$

If the jet trajectory $\xi \ll l_b$, then the plume is in the buoyancy dominated near field (BDNF) where the effect of buoyancy is dominant over crossflow; if $\xi \gg l_b$, then plume is in the buoyancy dominated far field (BDFF) where the effect of crossflow is more pronounced than the buoyancy. In BDNF, the plume is essentially vertical and only slightly advected, thus the equations for plumes in stagnant fluid are approximately valid. Similarly as jets in crossflow, after some distance from the nozzle, the plume cross section will become a kidney shape that is made up of a vortex pair, and the concentration at the centers of the vortices have been found to be 1.4–1.7 times of the plume centerline concentration. In BDFF, the plume bends over and finally approaches the ambient flow direction. The analysis on the plume properties in BDFF relies on experiments or numerical models. Based on the equations of motion and the use of similarity solutions, Fischer et al. [21] derived asymptotic formulas for the BDNF and BDFF. As the plume in the BDFF behaves similarly as the advected line thermal, Lee and Chu [45] used numerical models to obtain the plume characteristics. The predictions are comparable to experimental results. The formulas Lee and Chu derived are:

$$\frac{y_c}{l_b} = 1.3\left(\frac{x}{l_b}\right)^{\frac{2}{3}} \tag{33}$$

$$b_{vc} = 0.4 y_c \tag{34}$$

$$S_c = 0.46\frac{U_a {y_c}^2}{Q_0} \tag{35}$$

Note Eq. 35 for BDFF is exactly in the same form as the equation for MDFF.

Now consider the case of a circular buoyant jet in crossflow. In this case, the relative strengths of buoyancy, momentum, and crossflow need to be considered. If $l_b \ll l_m$, then the jet would in sequence experience in MDNF, MDFF, and BDFF; if $l_b \gg l_m$, then the sequence would be MDNF, BDNF, and BDFF [21, 43, 45]. Equations should be selected carefully according to the studied location of the jet (e.g., in MDNF or MDFF or BDNF or BDFF). The transitions between

MDNF and MDFF and between BDNF and BDFF are better treated using numerical models [45].

For jets directed at an oblique angle to crossflow, the reader may refer to Platten and Keffer [69] and Kikkert et al. [38]. For plane jets and plume in crossflow, the reader may refer to Girshovich [25], Jones and Wille [36], Kalita et al. [37], and Huang et al. [31].

Multiple Jets

Effluents may be discharged via single port outfalls or multiport diffusers. Multiport diffusers are commonly used given their fast mixing and diluting ability and thus less adverse impacts on the environment. The jets issuing from the ports of a multiport diffuser are usually viewed as multiple jets. The characteristics of multiple jets are primarily determined by the arrangements of multiport diffusers. Generally, multiport diffusers can be classified into three categories: unidirectional diffuser (where net horizontal momentum flux is imparted perpendicular to diffuser line), staged diffuser (where net horizontal momentum flux is imparted parallel to the diffuser line), and alternating diffuser (where no net horizontal momentum flux is imparted) [20]. Figure 6 illustrates one typical example of a unidirectional diffuser. It is expected that different types of diffusers have significantly different jet mixing and spreading properties.

Studies on multiple jets (or diffusers) have been reported extensively in the past decades ([2, 21, 32, 34, 35, 39, 40, 45, 46, 94, 96, 100, 107], etc.). Most of these studies focused on the deep water ambient condition (e.g., in oceans and lakes), and limited studies dealt with the shallow water condition (e.g., in rivers). In this section, only the deep water condition will be considered. Theoretically, multiple jets in sequence experience: the individual free jet zone (where jets has no effect on each other), the jet merging zone (where the interaction between jets are strong), and the two-dimenstional zone thereafter [66, 107] (see Fig. 7). In practice, multiple jets are usually simplified as one line momentum source, neglecting the interactions between individual jets that are complex and not well understood [35, 46].

In the previous sections, some basic characteristics of three-dimensional free jets and two-dimentional (plane) jets have been introduced; hence, in the following, the studies on the merging process of unidirectional non-buoyant circular jets will be briefly summarized. As yet, only limited studies on jet merging have been reported [30, 40, 64, 71, 100]. To calculate the concentration or velocity field in the jet merging

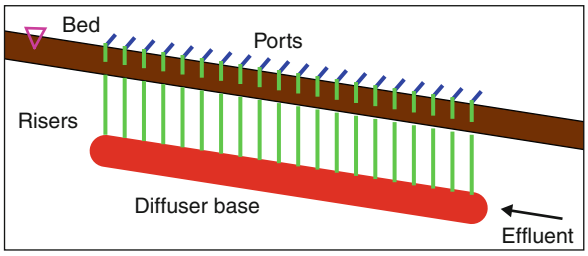

Transport with Jets and Plumes of Chemicals in the Environment. Figure 6
An example of a unidirectional diffuser

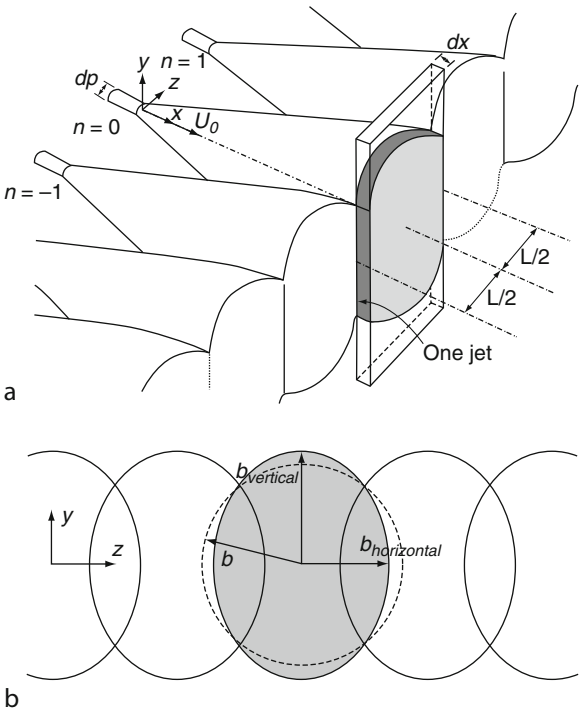

Transport with Jets and Plumes of Chemicals in the Environment. Figure 7
(**a**) Schematic of multiple merging jets, with the indication of (**b**) jet cross-section deformation (Modified from [100])

process, the most widely used method is superposition. However, as the momentum equation is nonlinear, simple superposition of individual jets would overestimate the jet velocity. Knystautas [40] studied the velocity field of merging jets in still ambient fluid and showed that the jet velocity can be modeled by superposing the momentum (u^2) of individual jets (based on Reichardt's hypothesis). Hodgson et al. [30] reported the following equation for the velocity field of the merging jets in still water:

$$u^2 = \sum_{i=-n}^{i=+n} u_i{}^2 = u_m{}^2 \sum_{i=-n}^{i=+n} \exp\left[-150\left(\frac{z-iL}{x}\right)^2\right] \tag{36}$$

where $(2n + 1)$ is the number of jets; the centerline velocity of each individual jet $u_m = \frac{6.13 U_0 d_0}{x}$; L is the distance between the centers of neighboring jets; z is the transverse distance from the central jet axis. Hodgson et al. [30] extended the Reichardt's hypothesis on lateral transport of momentum to the lateral transport of pollutant, and showed that uC is additive. After solving the velocity field from Eq. 36, the pollutant concentration field can be obtained from Eq. 37:

$$uC = \sum_{i=-n}^{i=+n} u_i C_i = u_m C_m \sum_{i=-n}^{i=+n} \exp\left[-130\left(\frac{z-iL}{x}\right)^2\right] \tag{37}$$

where the centerline concentration of each individual jet $C_m = \frac{5.34 C_0 d_0}{x}$. Hodgson's experimental results validated the use of Eqs. 36 and 37.

Hodgson et al. [30] revealed some basic physics in the jet merging, where the jet spreading rate $\frac{db}{dx}$ and the ratio of the jet concentration half-width to the velocity half-width $\frac{b_C}{b}$ are both assumed to be constant during merging. Wang and Davidson [100] developed a similar model for jet merging in stagnant ambient fluid, but allows the change of $\frac{db}{dx}$ and $\frac{b_C}{b}$ during merging, as well as the change of these parameters in horizontal (the jet merging) plane and vertical (the free entrainment) plane. Theoretical analysis and experimental data indicate that the jet merging in stagnant ambient fluid occurs at $4.5 < \frac{x}{L} < 12$. Note that in Wang and Davidson [100], the start of merging refers to the location where the jet interaction begins to influence the bulk properties of the central jet, which is beyond the location where the physical jet boundaries start intersecting. By studying their experimental data and that of Knystautas [40], Wang and Davidson [100] found that, during the jet merging, the jet spreading rate $\frac{db}{dx}$ (or $\frac{db_C}{dx}$) increases by 30% in the vertical plane, while it decreases by a similar amount in the horizontal plane; the ratio of velocity half-width in the vertical plane to that in the horizontal plane $\frac{b_{\text{vertical}}}{b_{\text{horizontal}}}$ increases from 1 to 1.5 during merging; and the ratio of concentration half-widths $\frac{b_{C,\text{vertical}}}{b_{C,\text{horizontal}}}$ increases from 1 to 1.8. Obviously, the jet merging process constrains the jet spreading and thus dilution in the jet merging plane, while accelerates them in the free entrainment plane. This phenomenon is similar to the boundary effects found in wall jets or surface jets.

In recent years, researchers started to study the jet merging in coflow [64, 71]. Pun et al. [71] developed a multiple-point hybrid model for merging jets in coflow, which combines a length-scale model and an Eulerian-integral model. The model allows multiple transition points for each parameter (jet velocity, spread and dilution), instead of a single transition point for all these parameters. The multiple-point hybrid model is shown to be able to significantly reduce transition errors during merging compared to the single-point model, and predicts favorable results compared to the integral solution. Pani et al. [64] developed a model based on Reichardt's hypothesis for multiple coflowing jets. Instead of momentum (u^2) is additive in stagnant water, Pani et al. showed that the excess momentum ($u\Delta u$) is additive in coflow and follows Gaussian distribution. Using the method of superposition and a generalized spreading hypothesis, Pani et al. presented the equations for predicting the velocity field and centerline dilution downstream of multiple circular jets in coflow, which appeared to agree with the experimental data.

Multiphase Jets and Plumes

In this section, two kind of multiphase jets and plumes will be introduced: bubbly jets and plumes and slurry jets and plumes, which have wide engineering applications.

Bubbly Jets and Plumes

Bubbly jets are produced by injecting gas-liquid mixtures into liquids, while bubble plumes are

produced by injecting gases into liquids. Bubble plumes and bubbly jets are widely used to achieve artificial aeration, circulation and mixing in confined reactors, aeration tanks, polluted water bodies, ice-covered rivers, and deep stratified lakes and reservoirs [48, 86, 101, 104]. Such kind of gas-liquid two-phase flow is also common in some hydraulic structures, e.g., the super-gas saturation downstream of hydro-power dams. So far, most of the early studies were conducted in confined setups, where the sizes and geometry of the setup further complicates the characteristics of bubbly jets and plumes [51]. In this section, the studies in stagnant water of relatively large setup will be introduced and then the case with flowing ambient fluid will be considered.

For two-phase flows, the dissolving of the gas phase into the liquid phase can be derived from Fick's law of diffusion as [60]:

$$\frac{dC}{dt} = K_L a(C_s - C) \tag{38}$$

where C is the dissolved gas (e.g., oxygen) concentration in the liquid, C_S is the saturation dissolved gas concentration, t is the time, K_L is the mass transfer coefficient, and a is the gas-liquid interfacial area per unit liquid volume (also named the specific interfacial area). From Eq. 38, the gas transfer rate is mainly controlled by K_L and a, which differ significantly in different setups. Previous studies [9, 59] have shown that these two parameters are greatly influenced by bubble size. Bubble size depends on a number of factors: nozzle sizes and types, initial gas volume fractions, the solubility and mass transfer ability of the gas, turbulence intensity and flow structure of the ambient liquid, impurities and surfactants in the ambient liquid, etc. [17, 49–52]. Lima Neto et al. [50] proposed a criterion to judge the sizes and shapes of the bubbles produced by injecting a mixture of air and water into water: if the nozzle Reynolds number $\mathrm{Re} = \frac{U_{w0} d_0}{\nu_w} < 8000$ (where U_{w0} is the superficial water velocity based on the water discharge at the nozzle and nozzle diameter d_0), then large and irregular bubbles will be produced; if $Re \geq 8{,}000$, smaller and uniform bubbles will be produced. A decrease in gas discharge or an increase in liquid discharge will decrease the bubble size [50, 52, 98].

Now consider the vertical injection of a pure gas into a pure stagnant liquid. The bubbles produced at the orifice will coalescence/breakup and rise, inducing ambient liquid entrained into the bubble core and the dissolving of the gas into the ambient. Lima Neto et al. [49] studied air injection into still water with six different nozzles (single orifice, multiple orifices, and airstone), and found that the water entrained into the bubble core under different initial air discharges Q_a and nozzle types can be described as a function of Q_a and vertical distance from the nozzles.

For a vertical bubbly jet in stagnant liquid, Milgram [56], Brevik and Kristainsen [12], and Lima Neto et al. [50] reported that the bubble area typically only occupies 50–90% of the bubbly jet in the radial direction. Lima Neto et al. [50] studied bubbly jets produced by injecting a mixture of air-water into stagnant water and found that the more uniform and smaller the bubble sizes, the wider the bubble core can spread in the radial direction; within the bubbly jets, the radial distributions of the time-averaged bubble concentration (void fraction) and water velocity of the mean flow can be well described by Gaussian distributions, similarly as for single-phase jets or plumes; and $\mathrm{d}b/\mathrm{d}x$ of the bubbly jets is close to that of the pure water jet.

Although the existence of bubbles seems not to change the Gaussian profiles, the entrainment of the ambient into the bubbly jets is significantly enhanced. Milgram [56], Socolofsky and Adams [92], Brevik and Kristainsen [12], and Lima Neto et al. [50] reported the entrainment coefficient of bubbly jets is in the range of 0.03–0.15, much larger than the values of pure jets or plumes. The additional entrainment probably associates with the bubble wakes [47] and additional liquid turbulence caused by interactions of the bubbles and their wakes [50]. At a specific height of the centerline of a bubbly jet, Lima Neto et al. [50] compared the liquid volume flux Q_w of the bubbly jet with that of a pure water jet with the same nozzle diameter and water flow rate:

$$\frac{Q_w}{Q_{w(C_0=0)}} = 1 + 6.426 \times 10^6 \left(\frac{C_0}{\mathrm{Re}}\right)^{\frac{3}{2}} \tag{39}$$

where the initial gas volume fraction $C_0 = \frac{Q_{a0}}{(Q_{a0}+Q_{w0})}$; Q_{a0} and Q_{w0} are the initial volumetric flow rates of air and water, respectively. It is expected that the average

dilution of a bubbly jet is larger than that of a pure jet due to the additional entrainment of ambient water as shown in the second term of the the right hand side of Eq. 39.

For a bubbly jet injected horizontally into a stagnant liquid, there are only limited experimental studies [22, 52, 57, 98]. Lima Neto et al. [52] studied the injection of air-water mixtures into a water tank of relatively large size and reported that: first, the bubbly jet comes out of the nozzle as a whole quasi-horizontal bubbly jet where bubble breakup/coalescence occurs and only a few bubbles escape from the bubbly jet and rise vertically due to buoyancy; then, there follows a separation zone where the quasi-vertical bubble plume partially separates from the water jet (when the initial gas volume fraction $C_0 < 0.15$, the bubble plume will completely separate from the water jet); finally, the bubble plume continues rising and the water jet impinges the water surface and becomes surface jet. In Lima Neto et al. [52], the length and width of the bubble plume as well as the centerline trajectories of the bubble plume and water jet were also proposed in dimensionless forms.

For bubbly jets, bubble properties and mean liquid flow could be non-dimensionalized as functions of the initial gas volume fraction and nozzle Reynolds number for the vertical injection or as functions of the initial gas volume fraction and nozzle densimetric Froude number for the horizontal injection [50, 52]. The variation of bubble properties and mean liquid flow along the jet centerline and across the jet needs further studies. For bubble plume modeling, the reader may refer to Bravo et al. [11] and others.

Crossflow will exert significant effects on bubbly jets or bubble plumes, of which the most distinguishing one is the possibility of separation of bubble plumes (named generally as dispersed phases) from the entrained ambient fluids (continuous phases) [92]. So far, very limited studies have been reported on bubbly jets or bubble plumes in crossflow. Socolofsky and Adams [92] conducted laboratory experiments on bubble plumes produced by injecting air, air and oil, as well as air and alcohol in uniform crossflow. In weak crossflow, the separation between the bubble plumes and the entrained fluid does not occur before the plumes reach the surface. While in strong crossflow, the separation is significant and the separation height h_s can be given by an empirical relation:

$$h_s = \frac{5.1 B_0}{\left(U_a u_s^{2.4}\right)^{0.88}} \tag{40}$$

where U_a is the horizontal crossflow velocity; u_s is the bubble slip (terminal rise) velocity; $B_0 = Q_0 g'$; Q_0 is the discharge of the plume fluid; $g' = \frac{(\rho_a - \rho_p)g}{\rho_a}$; ρ_a is the ambient density of water; and ρ_p is the density of the plume fluid. Socolofsky and Adams also reported that before h_s, the plumes can be treated as single-phase plumes; after h_s, the bubble plumes follow the trajectory of the vector sum of u_s and U_a (i.e., the bubble plumes rise in a linear line), and the separated entrained fluid behaves like a momentum jet (the momentum is gained by the acceleration of bubbles before the separation).

Slurry Jets and Plumes

Slurry jets are produced by injecting a mixture of liquid phase and solid phase (such as sand or clay particles). Slurry jets have wide applications in pumping industrial (e.g., mining or petroleum) tailings into settling tanks, dredging and land reclamation, discharging storm water and industrial waters that have solid particles, etc. A number of experimental and numerical studies in this area have been reported [7, 13, 26, 33, 55, 67, 90]. Usually, two injection ways were used, vertically upward and vertically downward. In the following, the main focus will be on the vertically downward injection of slurry jets into stagnant ambient fluids. Compared to single-phase jets, the adding of the solid phase will change the properties of the flow [89].

Previous experiments have indicated that the velocity and concentration of the solid phase across slurry jets follow self-similar Gaussian distributions [26, 33, 90]. In the slurry jets with dilute solid particles, Jiang et al. [33] reported that the velocity and concentration of the liquid phase also exhibit self-similar Gaussian profiles. However, this may not be valid for the slurry jets with high concentration solid particles.

The spreading of the solid phase has been found to increase linearly along the axial direction [13, 26, 55]. Brush [13] reported that the spreading rate of the velocity of the solid phase $\frac{db_s}{dx}$ depended on the particle size. Mazurek et al. [55] confirmed this by photographic measurements on sand jets, and further generalized the spreading as a function of the initial

densimetric Froude number of the solid particle. Recently, Hall et al. [26] conducted detailed experiments on pure sand jets and sand-water slurry jets in stagnant water. With the densimetric Froude number at the nozzle exit ($F_0 = \frac{U_0}{\sqrt{\frac{gd_0(\rho_s-\rho_w)}{\rho_w}}}$ where U_0 is the initial velocity of the sand particle from a nozzle of diameter d_0 and ρ_s is sand density) in the range of $2 \sim 6$, $\frac{db_s}{dx}$ measured $0.087 \sim 0.109$, not very different from that of single-phase jets in stagnant fluids. The difference lies in the ratio of concentration to velocity spreading rates of the solid phase ($\frac{b_{s,C}}{b_s}$). Hall et al. [26] reported that, for sand jets and slurry jets with high F_0 ($F_0 \approx 6$), $\frac{b_{s,C}}{b_s} = 0.86 \sim 0.92$, which means the sand concentration spreads slower than the velocity; and for slurry jets with low F_0 ($F_0 \approx 2$), $\frac{b_{s,C}}{b_s} \approx 1.0$ which means they have almost equal spreading rates. This finding is contrary to the classic single-phase jet theory, which states that the concentration scale spreads faster than the velocity scale ($\frac{b_C}{b} \approx 1.2$).

Similar as single-phase jets, along the axial direction of slurry jets, the velocity and concentration of both solid phase and liquid phase decay rapidly. According to Hall et al. [26], beyond the potential core (about $2.9\, d_0\, F_0^{\frac{2}{5}}$), the axial concentration of the solid phase can be well described by:

$$\frac{C_m}{C_0} = \frac{17.12}{\left(\frac{x}{d_0 F_0^{\frac{2}{5}}}\right)^{\frac{5}{3}} + 11.39} \tag{41}$$

In Eq. 41, the $-5/3$ power relation is very similar to that of single-phase plume (Table 2), as Eq. 41 was established in the region at $x > 5L_M$ where the buoyant slurry jet behaved like a slurry plume [65]. Similar $-5/3$ power relation was also built for the sand concentration in sand jets. For both sand jets and slurry jets, the axial velocity of the solid phase was found to decrease rapidly and then reach a final plateau region. Generally, before the plateau region, the axial velocity of the solid phase in slurry jets can be well represented by:

$$\frac{u_m F_0}{U_0} = \frac{1.63}{\left(\frac{x}{d_0 F_0}\right)^{\frac{1}{3}} + 0.56} \tag{42}$$

Similar as Eq. 42, for sand jets, before reaching the velocity plateau region, the axial sand velocity was also found to follow the $-1/3$ power relation, which is very similar to that of single-phase plumes (Table 2). The terminal (settling) centerline velocity of the solid phase was found in the range of $0.32 \sim 0.43$ m/s, which is larger than the settling velocity of 0.033 m/s for individual solid particles. The larger terminal velocity probably can be attributed to the interactions between solid particles, i.e., the wake of previous solid particles tends to decrease the drag forces for the following particles.

For the studies dealing with particle interactions, the reader may refer to Lain and Garcia [42], Tamburello and Amitay [93], and Yan et al. [106]. For the effect of solid particle size on velocity distribution, concentration profile and turbulent properties, the reader may refer to Azimi et al. [8]. For vertically upward slurry jets, the reader may refer to Jiang et al. [33].

Future Directions

Some of the basic characteristics of a variety of jets and plumes have been reviewed, including simple jets and plumes, buoyant jets, surface jets, wall jets, jets and plumes in coflow and crossflow, multiple jets, bubbly jets and plumes, and slurry jets and plumes. The turbulence and turbulence structures in these flows have not been discussed. Interested readers may refer to the works of Heskestad [27], Wygnanski and Fielder [105], and Launder and Rodi [44]. Also, the behaviors of jets and plumes in stratified environment have not been considered. The readers may refer to the works of Morton et al. [58], Turner [97], and Roberts et al. [80, 81]. To facilitate the applications of jets and plumes theories, software packages have been developed. The USEPA-supported CORMIX is perhaps the most commonly used expert system for dealing with environmental problems involving jets and plumes. Other models are VISJET and Visual Plume. In addition to the simple jets and plumes, all the other varieties of jets and plumes are still currently under active studies. This constitutes the general tone for the future research. Herein, some of key areas are listed as follows:

- Physics and models of bubbly jets, and their application in aeration and mixing of ponds, lakes, and wastewater treatment plants

- Physics and models of slurry jets, and their industrial applications
- Physics and models of three phase jets and plumes, especially oil-water-gas plumes produced by oil spills in oceans
- Physics and models of jets and plumes in stratified environment
- Development, improvement, and validation of computational fluid dynamics (CFD) modeling (such as direct numerical modeling (DNS); large eddy simulation (LES); k-epsilon modeling; and others).

Bibliography

Primary Literature

1. Abramovich GN (1963) The theory of turbulent jets. MIT Press, Cambridge, MA, 671 p
2. Adams EE (1982) Dilution analysis for unidirectional diffusers. ASCE J Hydraul Div 108(HY3):327–342
3. Agelin-Chaab M (2010) Experimental study of three-dimensional offset jets and wall jets. Ph.D. thesis, Department of Mechanical and Manufacturing Engineering, University of Manitoba, Winnipeg
4. Albertson ML, Dai YB, Jensen RA, Rouse H (1950) Diffusion of submerged jets. Trans ASCE 115:639–697
5. Andreopoulos J (1985) On the structure of jets in a crossflow. J Fluid Mech 157:163–197
6. Anthony DG, Willmarth WW (1992) Turbulence measurements in a round jet beneath a free surface. J Fluid Mech 243:699–720
7. Awaya Y, Fujisaki K, Matsunaga K (1985) Transition in the behavior of sediment laden vertical buoyant jet. J Hydrosci Hydr Eng 3(1):63–74
8. Azimi AH, Zhu DZ, Rajaratnam N (2010) Effect of particle size on the characteristics of sand jets in water. J Eng Mech (in press)
9. Barnhart EL (1969) Transfer of oxygen in aqueous solutions. J Sanit Eng Div 95(3):645–661
10. Beltaos S, Rajaratnam N (1972) Plane turbulent impinging jets. J Hydr Res 11:29–59
11. Bravo HR, Gulliver JS, Hondzo M (2007) Development of a commercial code-based two-fluid model for bubble plumes. Environ Modell Softw 22(4):536–547
12. Brevik I, Kristiansen Ø (2002) The flow in and around air bubble plumes. Int J Multiph Flow 28:617–634
13. Brush LMJ (1962) Exploratory study of sediment diffusion. J Geophys Res 67(4):1427–1433
14. Chan T, Zhou Y, Liu M, Leung C (2003) Mean flow and turbulent measurements of the impingement wall jet on a semi-circular convex surface. Exp Fluids 34(1):140–149
15. Chen CJ, Rodi W (1980) Vertical turbulent buoyant jets – a review of experimental data. Pergamon, Oxford. 83 p
16. Chu VH, Vanvari MR (1976) Experimental study of turbulent stratified shearing flow. J Hydraul Div ASCE 102(6):691–706
17. Clift R, Grace JR, Weber ME (1978) Bubbles, drops, and particles. Academic, New York, 380 p
18. Cuthbertson AJS, Davies PA (2008) Deposition from particle-laden, round, turbulent, horizontal, buoyant jets in stationary and coflowing receiving fluids. J Hydraul Eng 134(4): 390–402
19. Dey S, Nath TK, Bose SK (2010) Fully rough submerged plane wall-jets. J Hydro Environ Res 4(4):301–316
20. Doneker RL, Jirka GH (2007) CORMIX user manual – a hydrodynamic mixing zone model and decision support system for pollutant discharges into surface waters. U.S. EPA-823-K-07-001, pp 1–236
21. Fischer HB, List EJ, Imberger J, Brooks NH (1979) Mixing in inland and coastal waters. Academic, New York, 483 p
22. Fonade C, Doubrovine N, Maranges C, Morchain J (2001) Influence of a transverse flowrate on the oxygen transfer performance in heterogeneous aeration: case of hydro-ejectors. Water Res 35(14):3429–3435
23. Förthmann E (1936) Turbulent jet expansion. English translation N.A.C.A. TM-789. (Original paper in German, 1934. Ing. Archiv., 5)
24. Gholamreza-kashi S, Martinuzzi RJ, Baddour RE (2007) Mean flow field of a nonbuoyant rectangular surface jet. J Hydraul Eng 133(2):234–239
25. Girshovich TA (1966) Theoretical and experimental study of a plane turbulent jet in a crossflow. Fluid Dyn 9:84–86
26. Hall N, Elenany M, Zhu DZ, Rajaratnam N (2010) Experimental study of sand and slurry jets in water. J Hydraul Eng 136(10):727–738
27. Heskestad G (1965) Hot-wire measurements in a plane turbulent jet. Trans ASME J Appl Mech 32:1–14
28. Hinze JO, Van Der Hegge Zijnen BG (1949) Transfer of heat and matter in the turbulent mixing zone of an axially symmetrical jet. Appl Sci Res A1:435–461
29. Hodgson JE, Rajaratnam N (1992) An experimental study of jet dilution in crossflows. Can J Civ Eng 19:733–743
30. Hodgson JE, Moawad AK, Rajaratnam N (1999) Concentration field of multiple circular turbulent jets. J Hydr Res 37(2):249–256
31. Huang JF, Davidson MJ, Nokes RI (2005) Two-dimensional and line jets in a weak cross-flow. J Hydr Res 43(4):390–398
32. Huang H, Fergen RE, Rroni JR, Tsai JJ (1996) Probabilistic analysis of ocean outfall mixing zones. J Environ Eng 122(5):359–367
33. Jiang JS, Law AWK, Cheng NS (2005) Two-phase analysis of vertical sediment-laden jets. J Eng Mech 131(3):308–318
34. Jirka GH, Akar PJ (1991) Hydrodynamic classification of submerged multiport-diffuser discharges. J Hydr Eng 117(9):1113–1128
35. Jirka GH, Harleman DRF (1973) The mechanics of submerged multiport diffuser for buoyant discharges in shallow water. R.M. Parsons Laboratory Report, Massachusetts Institute of Technology, Boston

36. Jones WP, Wille M (1996) Large-eddy simulation of a plane jet in a cross-flow. Int J Heat Fluid Flow 17:296–306
37. Kalita K, Dewan A, Dass AK (2002) Predication of turbulent plane jet in crossflow. Numer Heat Transfer A 41:101–111
38. Kikkert GA, Davidson MJ, Nokes RI (2009) A jet at an oblique angle to a cross-flow. J Hydro Env Res 3(2):69–76
39. Kim DG, Seo IW (2000) Modeling the mixing of heated water discharged from a submerged multiport diffuser. J Hydraul Res 38(4):259–269
40. Knystautas R (1964) The turbulent jet from a series of holes in Line. Aeronaut Q 15:1–28
41. Kotsovinos NE, List EJ (1977) Plane turbulent buoyant jet. Part I. Integral properties. J Fluid Mech 81:25–44
42. Lain S, Garcia J (2006) Study of four-way coupling on turbulent particle-laden jet flows. Chem Eng Sci 61:6775–6785
43. Lam KM, Lee WY, Chan CHC, Lee JHW (2006) Global behaviors of a round buoyant jet in a counterflow. J Hydr Eng 132(6):589–604
44. Launder BE, Rodi W (1983) The turbulent wall jet - measurement and modeling. Ann Rev Fluid Mech 15:429–459
45. Lee JHW, Chu VH (2003) Turbulent jets and plumes – a lagrangian approach. Kluwer, Norwell, 390 p
46. Lee JHW, Jirka GH (1980) Multiport diffuser as line source of momentum in shallow water. Water Resour Res 16(4): 695–708
47. Leitch AM, Baines WD (1989) Liquid volume flux in a weak bubble plume. J Fluid Mech 205:77–98
48. Lima Neto IE, Zhu DZ, Rajaratnam N, Yu T, Spafford M, McEachern P (2007) Dissolved oxygen downstream of an effluent outfall in an ice-cover river: natural and artificial aeration. J Env Eng 133(11):1051–1060
49. Lima Neto IE, Zhu DZ, Rajaratnam N (2008) Air injection in water with different nozzles. J Environ Eng 134(4):283–294
50. Lima Neto IE, Zhu DZ, Rajaratnam N (2008) Bubbly jets in stagnant water. Int J Multiph Flow 34(12):1130–1141
51. Lima Neto IE, Zhu DZ, Rajaratnam N (2008) Effect of tank size and geometry on the flow induced by circular bubble plumes and water jets. J Hydr Eng 134(6):833–842
52. Lima Neto IE, Zhu DZ, Rajaratnam N (2008) Horizontal injection of gas-liquid mixtures in a water tank. J Hydr Eng 134(12):1722–1731
53. Lübcke HM, Rung Th, Thiele F (2003) Predication of the spreading mechanism of 3D turbulent wall jets with explicit Reynolds-stress closures. Int J Heat Fluid Flow 24: 434–443
54. Margason RJ (1993) Fifty years of jet in cross flow research. Computational and experimental assessment of jets in cross flow. AGARD, Report CP-534
55. Mazurek KA, Christison K, Rajaratnam N (2002) Turbulent sand jet in water. J Hydr Res 40(4):527–530
56. Milgram H (1983) Mean flow in round bubble plumes. J Fluid Mech 133:345–376
57. Morchain J, Moranges C, Fonade C (2000) CFD modeling of a two-phase jet aerator under influence of a crossflow. Water Res 34(13):3460–3472
58. Morton BR, Taylor GI, Turner JS (1956) Turbulent gravitational convection from maintained and instantaneous sources. Proc R Soc Lond A 234:1–23
59. Motarjemi M, Jameson GJ (1978) Mass transfer from very small bubbles – the optimum bubble size for aeration. Chem Eng Sci 33(11):1415–1423
60. Mueller JA, Boyle WC, Pöpel HJ (2002) Aeration: principles and practice. CRC Press, New York
61. Newman BG, Patel RP, Savage SB, Tjio HK (1972) Three-dimensional wall jet originating from a circular orifice. Aeronaut Quart 23:188–200
62. Pande BBL, Rajaratnam N (1979) Turbulent jets in co-flowing streams. ASCE J Eng Mech 105:1025–1038
63. Pande BBL, Rajaratnam N (1977) An experimental study of bluff buoyant turbulent surface jets. J Hydr Res 15(3): 261–275
64. Pani BS, Lee JHW, Lai ACH (2009) Application of Reichardt's hypothesis for multiple coflowing jets. J Hydro-environ Res 3(3):121–128
65. Papanicolaou PN, List EJ (1988) Investigations of round vertical turbulent buoyant jets. J Fluid Mech 195:341–391
66. Parr AD, Sayre WW (1979) Multiple jets in shallow flowing receiving waters. ASCE J Hydraul Div 105(HY11):1357–1374
67. Parthasarathy RN, Faeth GM (1987) Structure of particle laden turbulent water jets in still water. Int J Multiph Flow 13(5):699–716
68. Patel RP (1971) Turbulent jets and wall jets in uniform streaming flow. Aeronaut Q 22:311–326
69. Platten JL, Keffer JF (1971) Deflected Turbulent Jet Flows. Trans ASME J Appl Mech 38E(4):756–758
70. Pratte BD, Baines WD (1967) Profiles of the round turbulent jets in a cross flow. J Hydr Div ASCE 92:53–64
71. Pun KL, Davidson MJ, Wang HJ (2000) Merging jets in a co-flowing ambient fluid – a hybrid approach. J Hydraul Res 38(2):105–114
72. Rajaratnam N (1967) Plane turbulent wall jets on rough boundaries. Water Power 49:149–242
73. Rajaratnam N (1976) Turbulent jets. Elsevier Scientific, Amsterdam, 304 p
74. Rajaratnam N (1984) Turbulent jets and plumes, Lecture Notes, University of Alberta, Edmonton, Canada
75. Rajaratnam N (1985) An experimental study of bluff surface discharges with small Richardson number. J Hydraul Res 23(1):47–55
76. Rajaratnam N, Humphries JA (1984) Turbulent non-buoyant surface jets. J Hydraul Res 22(2):103–105
77. Rajaratnam N, Pani BS (1974) Three-dimensional turbulent wall jets. Proc ASCE J Hydraul Div 100:69–83
78. Rajaratnam N, Subramanya K (1967) Diffusion of rectangular wall jets in wide channels. J Hydraul Res 5:281–294
79. Rajaratnam N, Subramanyan S (1985) Plane turbulent buoyant surface jets and jumps. J Hydraul Res 23(2):131–146
80. Roberts PJW, Snyder WH, Baumgartner DJ (1989) Ocean outfalls I: Submerged waste field formation. J Hydraul Eng 115(HY1):1–25

81. Roberts PJW, Snyder WH, Baumgartner DJ (1989) Ocean outfalls II: Spatial evolution of submerged waste field. J Hydraul Eng 115(HY1):26–48
82. Rodi W, Spalding DB (1970) A two-parameter model of turbulence and its application to free jets. Wärme Stoffübertragung 3:85–95
83. Rostamy N, Bergstrom D, Sumner D (2010) An experimental study of a turbulent wall jet on smooth and rough surfaces. In: Nickels TB (ed) IUTAM symposium on the physics of wall-bounded turbulent flows on rough walls, Cambridge, UK
84. Rouse H, Yih CS, Humphreys HW (1952) Gravitational convection from a boundary source. Tellus 4:201–210
85. Rutherford JC (1994) River mixing. Wiley, West Sussex, 347 p
86. Schierholz EL, Gulliver JS, Wilhelms SC, Henneman HE (2006) Gas transfer from air diffusers. Water Res 40(5):1018–1026
87. Schlichting H, Gersten K (2000) Boundary layer theory. Springer, Berlin Heidelberg, 801 p
88. Sforza PM, Herbst G (1970) A study of three-dimensional incompressible turbulent wall jets. Am Inst Aeronaut Astron J 8:276–283
89. Sheen HJ, Jou BH, Lee YT (1994) Effect of particle size on a two-phase turbulent jet. Exp Therm Fluid Sci 8: 315–327
90. Singansetti SR (1966) Diffusion of sediment in submerged jet. J Hydraul Div 92(2):153–168
91. Smith SH, Mungal MG (1998) Mixing, structure and scaling of the jet in crossflow. J Fluid Mech 357:83–122
92. Socolofsky SA, Adams EE (2002) Multi-phase plumes in uniform and stratified crossflow. J Hydraul Res 40(6): 661–672
93. Tamburello DA, Amitay M (2008) Active manipulation of a particle laden jet. Int J Multiph Flow 34:829–851
94. Tang HS, Paik J, Sotiropoulos F, Khangaonkar T (2008) Three-dimensional numerical modeling of initial mixing of thermal discharges at real-life configurations. J Hydraul Eng 134(9):1210–1224
95. Tachie MF, Balachandar R, Bergstrom DJ (2004) Roughness effects on turbulent plane wall jets in an open channel. Exp Fluid 37(2):281–292
96. Tian X, Roberts PJW, Daviero GJ (2004) Marine wastewater discharges from multiport diffuser. II: unstratified flowing water. J Hydraul Eng 130(12):1147–1155
97. Turner JS (1973) Buoyancy effects in fluids. Cambridge University Press, Cambridge, 367 p
98. Varley J (1995) Submerged gas-liquid jets: bubble size prediction. Chem Eng Sci 50(5):901–905
99. Verhoff A (1963) The two-dimensional turbulent wall jet with and without an external stream. Report 626, Princeton University
100. Wang HJ, Davidson MJ (2003) Jet interaction in a still ambient fluid. J Hydraul Eng 129(5):349–357
101. Whipple WJ, Yu SL (1970) Instream aerators for polluted rivers. J Sanit Eng Div 96(5):1153–1165
102. Wright SJ (1977) Mean behavior of buoyant jet in a crossflow. J Hydraul Div ASCE 103(HY5):499–513
103. Wright SJ (1984) Buoyant jets in density-stratified crossflow. J Hydraul Eng ASCE 110(5):643–656
104. Wüest A, Brooks NH, Imboden DM (1992) Bubble plume modeling for lake restoration. Water Resour Res 28(12):3235–3250
105. Wygnanski I, Fielder H (1969) Some measurements in the self-preserving jet. J Fluid Mech 38:577–612
106. Yan J, Luo K, Fan J, Tsuji Y, Cen K (2008) Direct numerical simulation of particle dispersion in a turbulent jet considering inter-particle collisions. Int J Multiph Flow 34: 723–733
107. Zhang W, Zhu DZ (2011) Near-field mixing downstream of a multiport diffuser in a shallow river. J Environ Eng 137(4): 230–240

Books and Reviews

Cheremisinoff NP (ed) (1986) Encyclopedia of fluid mechanics, vol 2, Dynamics of single-fluid flow and mixing. Gulf, Houston, 1505 p

Cheremisinoff NP (ed) (1986) Encyclopedia of fluid mechanics, vol 3, Gas-liquid flow. Gulf, Houston, 1535 p

Cheremisinoff NP (ed) (1993) Encyclopedia of fluid mechanics, vol 2, Advances in multiphase flow. Gulf, Houston, 674 p

Davies PA, Valente Neves MJ (eds) (1994) Recent research advances in the fluid mechanics of turbulent jets and plumes. Kluwer, Dordrecht, 514 p

Fay JA (1973) Buoyant plumes and wakes. Ann Rev Fluid Mech 5:151–160

Jirka GH (2004) Integral model for turbulent buoyant jets in unbounded stratified flow. Part 1: single round jet. Environ Fluid Mech 4:1–56

Jirka GH (2006) Integral model for turbulent buoyant jets in unbounded stratified flow. Part 2: plane jet dynamics resulting from multiport diffuser jets. Environ Fluid Mech 6:43–100

List EJ (1982) Turbulent jets and plumes. Ann Rev Fluid Mech 14:189–212

Philip AA (1997) Jets, plumes and mixing at the coast. In: Allen PA (ed) Earth surface processes. Blackwell, Oxford, pp 241–266, Chapter 7

Rodi W (1982) Turbulent buoyant jets and plumes. Pergamon, Oxford, 184 p

Rubin H, Atkinson J (2001) Environmental fluid mechanics. Marcel Dekker, New York, 728 p

Shen HH, Cheng AHD, Wang KH, Teng MH, Liu CCK (eds) (2002) Environmental fluid mechanics theories and applications. ASCE, Reston, 467 p

Wood AW (2010) Turbulent plumes in nature. Ann Rev Fluid Mech 42:391–412

Wood IR, Bell RG, Wilkinson DL (eds) (1993) Ocean disposal of wastewater. World Scientific, Singapore, 425 p

Tritium in the Environment

Philip A. Davis[1], Dan C. Galeriu[2]
[1]AECL, Chalk River, ON, Canada
[2]Life and Environmental Physics Department, "Horia Hulubei" Institute for Physics and Nuclear Engineering, Bucharest-Magurele, Romania

Article Outline

Glossary
Definition of the Subject
Introduction
Properties and Species of Tritium
Behavior of Tritium in the Environment
Concentrations in Background Areas
Long-Term Average Concentrations Due to Routine Releases
Time-Dependent Concentrations Due to Acute Releases
Model Validation and Uncertainty
Future Directions
Appendix A
Bibliography

Glossary

Buried tritium Tritium in exchangeable positions in large biomolecules in the dry matter of environmental materials that is not removed by rinsing with tritium-free water

Deposition The process by which airborne contaminants are transferred from the atmosphere to the underlying surface (soil, plants, or water bodies)

Dose The amount of energy absorbed in the body, or in an organ or tissue of the body, due to exposure to ionizing radiation, multiplied by a weighting factor to account for the degree of biological damage inflicted by the type of radiation in question

Evapotranspiration The sum of evaporation (the movement of water to the air from sources such as the soil and water bodies) and plant transpiration (the movement of water within a plant and its subsequent loss as vapor to the air through stomata in the leaves)

Isotope One of two or more forms of an element differing from each other in atomic weight and in nuclear but not chemical properties

Isotopic effects Physical and chemical effects in plant and animal processes that arise due to differences in mass of different isotopes of the same element

Organically bound tritium (OBT) Carbon-bound and buried tritium formed in living systems through natural environmental or biological processes from HTO

Specific activity The amount of activity of a radioactive element per unit amount of the stable form of the element (Bq ^{3}H/kg ^{1}H in the case of tritium)

Translocation The movement of a contaminant from one part of a plant or animal to another part

Tritium A radioactive isotope of hydrogen with one proton and two neutrons

Tritiated water (HTO) Water (or water vapor) in which a hydrogen atom is replaced by a tritium atom in some molecules

Definition of the Subject

Tritium is a radioactive isotope of hydrogen that can be released to the environment in small amounts during routine operation of nuclear facilities, and in higher amounts during some types of accidents. Tritium atoms exchange readily with hydrogen atoms in all environmental materials, including water. This means that tritium moves rapidly through the environment and enters the human body via inhalation of contaminated air and ingestion of contaminated food products. Once inside the body, tritium can be a constituent atom in any given water molecule and organic compound, imparting high local doses to cells that are radiosensitive. The study of environmental tritium is the study of the processes governing the behavior, transfer, and concentration of tritium in air, soil, plants, animals, and water bodies following releases to air and water. The understanding gained from such work is used to develop the ability to accurately estimate the dose to humans exposed to environmental tritium.

Introduction

Tritium (^{3}H) is a radioactive isotope of hydrogen (^{1}H). It forms naturally in the upper atmosphere from the interaction of the neutrons in cosmic radiation with nitrogen and oxygen [1]. Very small amounts of natural tritium also arise from neutron capture by lithium in

rocks of the earth's crust. Anthropogenic sources of tritium include nuclear weapons testing, military production, fuel reprocessing plants, the manufacture of tritium lights, and medical and academic research that uses tritium as a radioactive label. Of more relevance in the present context, tritium is also produced during the operation of nuclear power reactors. All reactors control the fission process using neutron absorbers such as boron or lithium, which yield helium and tritium under neutron flux. Pressurized heavy water reactors have another route of tritium production, namely, the interaction of neutrons with the deuterium of the heavy water in the moderator and primary heat transport systems. Fusion reactors, in which tritium is the fuel, represent a future potential source of the isotope.

Nuclear reactors, either fission or fusion, are likely to play a major role in energy generation in a sustainable economy. This implies that small amounts of tritium will continue to be released routinely to air and water, and that larger releases are possible under accident conditions. Once in the environment, tritium is very mobile and can be effectively incorporated into biological systems, including the human body, where it can impart a significant dose to radiosensitive cells. The environmental behavior of tritium must be understood to estimate these doses, and to minimize risks to the environment and humans.

This entry reviews the current state of knowledge of environmental tritium. The properties of tritium and its chemical forms are discussed first, followed by a qualitative description of its behavior in terrestrial and aquatic systems. Quantitative sections on tritium concentrations in background areas and in the vicinity of routine and accidental releases are presented next from both observational and modeling points of view. The validity of environmental tritium models and the uncertainties in their predictions are discussed. This entry concludes with the identification of the main knowledge gaps and a discussion of future directions in environmental tritium research. Tritium dosimetry and human health effects are not covered here, but are addressed in the entry by Bundy et al. in this Encyclopedia.

Properties and Species of Tritium

The tritium nucleus contains one proton and two neutrons; the hydrogen nucleus also contains one proton but no neutrons. Tritium decays to ^{3}He by emitting a beta particle (electron) and neutrino from one of its neutrons. The energy range of the beta particle is from 0 to 18.6 keV with an average energy of 5.69 keV. The radioactive half-life of tritium is 12.26 years.

Tritium readily exchanges with hydrogen and so is found in the multiplicity of environmental materials in which hydrogen occurs. The electrical configuration and chemical properties of tritium and hydrogen are similar but the two isotopes show small differences in some physical phenomena and some chemical reaction rates due to the difference in their atomic masses. Moreover, the presence of the β-decay energy associated with tritium provides the activation energy for some chemical reactions. Reactions involving tritium can occur at lower temperatures than those involving hydrogen.

Tritium is emitted to the environment from nuclear facilities in two main chemical forms: tritiated water (HTO) and tritiated hydrogen gas (HT). HTO dominates releases from fission reactors and from most existing tritium-handling facilities, and is the form most commonly found in the environment. HTO released to the atmosphere mixes with air moisture and exchanges with water pools in soil, plants, and animals. Exposure pathways to humans include inhalation, absorption through the skin, and food ingestion. HTO released with liquid effluents contaminates the receiving water body and is taken up by aquatic organisms [2]. Humans are exposed when they drink contaminated water and eat contaminated fish.

Plants and animals incorporate a fraction of their HTO content into organic compounds in isotopic-exchange or enzyme-catalyzed reactions [3, 4]. In exchange reactions, tritium bonds to oxygen, sulfur, phosphorus, or nitrogen atoms in the form of hydroxides, thiols, phosphides, and amines, respectively. Conventionally, this is termed exchangeable organically bound tritium (OBT). Exchangeable OBT is in equilibrium with the HTO in the plant or animal in question, and behaves as HTO in all respects. In enzyme-catalyzed reactions, tritium bonds to carbon chains of organic molecules. This is usually termed non-exchangeable OBT. This is the form of tritium that remains in dry biomatter that has been repeatedly washed with tritium-free water. Tritium so bound is more strongly attached than exchangeable tritium and

has longer retention times; such bonds are only dissolved during catabolic reactions.

Plant HTO is involved in the formation of OBT through various metabolic processes, primarily photosynthesis, that use plant water. OBT is formed in plant leaves but can be translocated to the edible parts of the plant and taken up by animals and humans through the food chain. Metabolic processes in aquatic plants also result in the formation of OBT, which is transferred to higher consumers in the ecosystem through ingestion. OBT taken into the body is broken down into more basic biological building blocks and then rebuilt into organic material in the body. About 50% of ingested OBT is converted to HTO during this process. In contrast, most ingested HTO remains as HTO in the body.

A small fraction of the tritium emitted by fission reactors is in the form of tritiated hydrogen gas. HT is not of radiological concern in itself since it is only weakly absorbed by the body and imparts a very low dose. However, HT released to the atmosphere diffuses into soil pore spaces, where it is oxidized to HTO by microorganisms containing the hydrogenase enzyme [5]. Some of the HTO so formed is taken up by plants and some is emitted to the atmosphere. Thus all of the exposure pathways discussed above for atmospheric HTO releases, including the formation and ingestion of OBT, are relevant for HT releases as well. The dose consequences of an atmospheric HT release are determined entirely by the HTO formed in the soil and its subsequent environmental behavior. Because HT is insoluble in water, there is no need to consider liquid HT releases.

Tritium can also be released to the environment in organic forms such as tritiated methane, tritiated pump oil, or tritiated pharmaceuticals. These tritiated organics can be inhaled and ingested, since they can be taken up to a limited extent by plants. They generally make a very small contribution to the total tritium dose to members of the public, but exceptions can occur for large releases [6].

Specific activity concepts are useful in understanding environmental tritium behavior. Specific activity (SA) is defined as the radioisotope activity per unit mass of the stable element (Bq ^{3}H/kg ^{1}H in the case of tritium). Because tritium atoms exchange so rapidly with hydrogen in aqueous parts of the environment (including the water of living organisms), the behavior of tritium mimics that of hydrogen in physical and biological processes. In particular, the flux of tritium from one environmental compartment to another is determined by the flux of hydrogen. If two compartments with different specific activities are allowed to come into equilibrium, the resulting SA of both compartments (which is determined by the total tritium and total hydrogen contents of the compartments) will be equal, with a value that lies between the two initial SAs. This implies that there can be no bioaccumulation of HTO in the environment. Tritium differs from most other radionuclides in this respect. For example, the cesium concentration in fish can exceed the cesium concentration in the water in which the fish swim, but this is not the case for HTO.

In theory, the SA model applies to OBT as well as to HTO, and it does in practice when long-term average concentrations are considered in a system where OBT is formed metabolically from HTO. However, the long biological half-life of OBT relative to that of HTO occasionally results in the apparent violation of SA concepts. The OBT concentration in a plant exposed periodically to an airborne HTO plume will be higher than the atmospheric HTO concentration when the plume is not present. Similarly, OBT concentrations will exceed HTO concentrations in organisms if the OBT appears through direct incorporation of tritated organic material with high SA. For example, the OBT/HTO ratios measured in fish from Cardiff Bay in the UK are high because the fish ingest tritiated organics released to the water column from a nearby pharmaceutical plant [6]. These are not examples of the bioaccumulation of tritium, but rather the manifestation of the mismatch in the biological half-lives of HTO and OBT. These ideas are discussed elaborately in section "Nonequilibrium Conditions."

Tritium specific activity can be formulated in terms of the tritium concentration in water (in Bq L^{-1}) rather than the ratio of tritium activity to the mass of hydrogen in a given compartment. There is a one-to-one correspondence between these two quantities and it is the concentration in water that is normally measured. In the case of OBT, the concentration in Bq L^{-1} is determined as the activity in the water equivalent of the dry matter (the water produced by complete combustion of the dry material).

The low energy of the tritium beta particle means that the radiation cannot penetrate human skin. Thus, tritium does not impart an external dose from deposited radioactivity or immersion in contaminated air. Tritium can cause damage to organisms only if taken into the body through inhalation, ingestion, or absorption through the skin. Once inside the body, tritium can be a constituent atom in any given water molecule and organic compound. HTO and exchangeable OBT are retained in the body with a biological half-life of approximately 10 days. HT can dissolve in the blood but is exhaled within a few minutes. Doses from the inhalation of HT are therefore about 25,000 times lower than doses from inhaled HTO. On the other hand, non-exchangeable OBT has a biological half-life of about 40 days and imparts a dose that is more than twice that of HTO. Since the tritium atoms in non-exchangeable OBT are fixed in place, the subcellular location of a given atom is of importance in determining the effects of its beta decay, and high absorbed doses can occur locally in cells that are radiosensitive [7]. Furthermore, because of its low initial energy and short range, the average density of ionization produced by the passage of a tritium beta particle is higher than that for a moderate/high energy particle.

More information on tritium dosimetry and the dose consequences of tritium releases to the environment can be found in the entry by Bundy et al. in this Encyclopedia.

Behavior of Tritium in the Environment

Hydrogen is ubiquitous in the environment and is part of many chemical compounds, including water and most organic materials. As an isotope of hydrogen, tritium enters freely into these compounds and its movement through the environment can be inferred from the cycling of hydrogen. As a result, tritium is unique among radionuclides in a number of respects:

- In aqueous systems, tritium moves as a nonreactive, non-absorbed constituent with the bulk water flow. Accordingly, the environmental transport of tritium is governed in large part by local and global hydrologic cycles.
- As a gas, tritium moves in response to its own vapor pressure gradient and can, under some circumstances, move against the water vapor flux.
- Tritium deposited from the atmosphere to soil and plants is readily recycled back to the atmosphere via evapotranspiration, forming a secondary airborne plume.
- The processes responsible for tritium transfer have timescales as short as minutes. Tritium can be rapidly taken up by organisms but just as rapidly lost. As a result, tritium transfer is highly dependent upon the environmental conditions prevailing at the time and place of release and the time of measurement.
- Tritium can be effectively incorporated into biological systems, including the human body, as organically bound tritium.
- Although tritium is three times heavier than hydrogen, it usually occurs as part of larger molecules. Therefore, isotopic effects, although present, are not important in environmental tritium transport, except in OBT formation.
- Tritium is transferred through the environment and through food chains without bioaccumulation in any compartment.

These unique features must be taken into account in understanding the environmental transport of tritium and in estimating the radiological consequences of releases to the environment.

Cycling of HTO Among Air, Soil, and Vegetation

On release to the atmosphere, HTO is advected by the mean wind and diffused by turbulent eddies in the same way as other radionuclides. A receptor close to a tritium source does not experience steady air concentrations even if the release rate is constant and continuous. Changes in wind speed, stability, and particularly wind direction induce changes in air concentrations on hourly timescales.

HTO can be lost from the atmosphere by wet or dry deposition to soil, plants, or surface water. As a vapor, HTO can diffuse directly into the soil pore space and into the leaf stomates [8, 9]. This deposition rate is driven by the gradient between the concentration of HTO in the atmosphere and in the air within the pore space or within the sub-stomatal cavities. HTO deposition can occur even when the water vapor flux is upward, as long as the HTO partial pressure gradient is downward. This happens, for example, when an

airborne plume passes over a relatively uncontaminated surface on a clear summer day when evapotranspiration is in progress [10]. The deposition rate depends on the diffusion resistances [11] that the tritium molecules encounter in passing from the air to the underlying surface. These include the aerodynamic resistance of the atmosphere, the boundary layer resistance of the laminar sub-layer close to the plant or soil surface, and the stomatal and surface resistances of the plant and soil matrix, respectively.

HTO is also lost from the air to underlying surfaces by wet deposition. HTO molecules diffuse through the air and through the surface of individual raindrops or snowflakes and are carried to the ground with the precipitation. The amount of washout depends on the diffusion resistances and on the concentration of HTO in air moisture (C_{am}). The HTO concentration in precipitation is usually less than C_{am} because the precipitation, which is initially uncontaminated as it starts its fall, does not come into equilibrium with air moisture in the small amount of time needed to pass through the plume.

When the wind blows the plume away from a receptor that previously experienced a period of deposition, the HTO partial pressure gradient and the diffusive flux will immediately reverse direction and HTO will be rapidly lost from soil and plants to the atmosphere by evapotranspiration. The rate of loss is determined by the HTO gradient and the aerodynamic, boundary layer, stomatal, and surface resistances discussed above in connection with deposition. In these circumstances, the soil and plants represent a ground-level area source that generates a secondary airborne HTO plume.

The rate of HTO reemission from soils depends strongly on the HTO distribution with depth that resulted from earlier deposition. The distribution determines the initial availability of HTO at the soil surface and the subsequent resupply from deeper layers by diffusion and advection. The tritium profile in soil following short-term dry deposition of HTO takes the form of an error function with a scaling length of less than 1 cm [12]. Most of the tritium remains near the soil surface and reemission occurs quickly once the airborne plume has passed. In contrast, the profile resulting from wet deposition tends to be fairly uniform with depth since rain and any tritium it contains is able to penetrate to lower levels of the soil. In this case, reemission occurs slowly because relatively small amounts of HTO are found near the surface and because the high soil water content retards upward HTO diffusion from lower layers.

Because tritium deposited under dry conditions tends to be quickly reemitted when the plume moves off a given location, the persistent HTO inventory in soil arises largely through wet deposition. Tritium not returned to the atmosphere by evaporation moves through the soil by vapor transport or by the mass flow of liquid water. Vapor transport occurs by diffusion through the air-filled pores at a rate determined by the HTO concentration gradient and is usually important only in dry soils. The mass flow mechanism is common to other radionuclides but is more efficient for tritium, which undergoes no retardation and moves at essentially the same rate as water under the influence of gravity and capillary forces. Tritium is lost from the soil by drainage and root uptake, the latter mechanism depending on the rooting depth of the vegetation. The HTO concentration in soil water depends on all of the processes discussed above as well as on the soil water content. The soil concentration tends to be lower than C_{am} because precipitation, which is the primary source of soil HTO, has a concentration lower than C_{am}.

Over long time periods in humid climates, tritiated water moves gradually downward through the soil profile as it is displaced by subsequent precipitation. It eventually passes below the root zone where it may enter regional groundwater systems. It is then lost to the local biosphere unless the aquifer discharges to a surface water body or is tapped by a well.

Tritium is carried from the soil into plant roots with the bulk water flow driven by transpiration. The tritium concentration in the transpiration stream is a weighted average of the concentrations in the soil layers from which the water is drawn. The HTO concentration in leaves is determined by the concentration in the transpiration stream, by the uptake or loss of tritium by vapor diffusion through the stomata, and by the volume of water in the plant. Under steady conditions, the concentration in the plant lies between that of the soil and air with a magnitude that depends on the atmospheric humidity and the air/leaf temperature difference [13]. Concentrations in fruit tend to be lower than concentrations in foliage due to a slower

water turnover rate in fruit. Concentrations in root crops are also low since these crops draw a relatively greater fraction of their water from the soil than they do from the air.

Plant concentrations do not remain static during the night even though little transpiration occurs and the diffusion resistance is high because the stomata are closed. Experiments suggest that tritium continues to be taken up by the plant leaves during the night, although at a lower rate than during the day [14, 15].

HTO concentrations in air, plants, and soil at a given location near a tritium source are in a highly dynamic state [16]. When the atmospheric plume is present, air concentrations are high, plant concentrations build up rapidly and then level off, and surface soil concentrations increase steadily. When the atmospheric plume moves off, air concentrations decrease abruptly but remain measurable because of reemission of deposited tritium. Similarly, plant concentrations drop off rapidly to levels that reflect concentrations in the transpiration stream. Surface soil concentrations also decrease quickly, although concentrations at deeper levels change only slowly with time. The cycle repeats when the wind brings the plume back over the location in question. In general, concentrations in any one part of the system are not in equilibrium with concentrations in any other part at any time, as they should according to specific activity concepts. This can create problems in interpreting tritium field measurements, particularly when sampling in the various compartments is done at different times and/or over different averaging periods. For example, the HTO concentration in vegetation can be much lower than the air concentration (if the plant sample is taken just after the airborne plume reaches the site) or much higher (if the sample is taken just after the plume moves off the site). These are not examples of isotopic effects or tritium bioaccumulation, but simply artifacts of measurements made in a transient system.

Organically Bound Tritium Formation in Plants

Photosynthesis is the most important process of tritium incorporation into organic compounds during daylight hours. Non-exchangeable OBT formed by photosynthesis in green plants appears initially in carbohydrates [3]. Subsequent polymerization results in the incorporation of OBT in such complex molecules as polysaccharides (starch and cellulose), proteins, lipids, and nucleic acids. The amount of OBT produced depends on a large number of environmental factors and plant parameters including light levels, oxygen and carbon dioxide concentrations, temperature, air circulation, and water supply, all of which show considerable diurnal and seasonal variations. OBT concentrations are reduced by slow conversion back to HTO by maintenance respiration and, following an acute exposure, by subsequent plant growth. NCRP [17] reports a biological half-life of non-exchangeable OBT in plants of about 25 days, but this value includes the effects of growth dilution. OBT makes up a few percent of the total tritium activity in most plants but up to 90% in grains, which have a high organic content.

OBT can also be produced in the dark, although at rates 3–10 times lower than those resulting from photosynthesis [14, 15, 18, 19]. The processes involve the metabolic turnover and synthesis of organic compounds such as proteins, oils, alkaloids, and vitamins using the energy of respiration. Plant tissue is dynamic, breaking down, and rebuilding continuously, and tritium atoms from HTO can be incorporated into non-exchangeable sites during the rebuilding phase.

OBT is formed only in the green parts of plants, but can be translocated to roots, stems, and edible fruits. The compounds formed by photosynthesis at the beginning of the vegetative period (including those containing OBT) are used primarily for growth of leaves, stems, and roots. Later in the growing season, usually after flowering, most of the assimilates are used in the development of fruits and tubers. The amount of OBT appearing in edible plant parts is therefore greatest if the exposure to atmospheric tritium occurs after flowering [20]. Diabate and Strack [21] observed that the major factor influencing translocation is the growth stage of the plant, while light conditions do not play a significant role.

The large difference in mass between hydrogen and tritium gives rise to significant isotopic effects in OBT formation. Tritium is discriminated against in the cleavage of the O–H bond of tritiated water during photosynthesis, so that less tritium than hydrogen is incorporated into organic molecules. In contrast, once fixed to carbon, tritium is cleft more slowly than C–H bonds. The net result is an OBT concentration that is

20–40% lower than the HTO concentration in the water to which the plant is exposed [22, 23].

Recently, Baumgärtner, and Donhärl [24] and Baumgärtner [25] identified another form of OBT, called buried tritium, which is defined as the tritium in exchangeable positions in large biomolecules in dry matter that is not removed by rinsing with tritium-free water. Such tritium is not carbon bound but is simply folded into large molecules that are not accessible for exchange with tritium-free water. Buried tritium contributes to the concentration in the traditional experimental determination of OBT but it quickly exchanges with hydrogen atoms in the body and acts as HTO rather than OBT following ingestion. The rapid increase in plant OBT concentrations observed in the first few hours following acute HTO exposure in some experiments may be evidence of buried tritium forming by exchange through non-metabolic processes [15].

The nature of OBT was debated by the Tritium and Carbon-14 Working Group of the International Atomic Energy Agency's EMRAS (Environmental Modeling for Radiation Safety) program [26], which settled on the following definition: "OBT is carbon-bound and buried tritium formed in living systems through natural environmental or biological processes from HTO. Other types of organic tritium (e.g. tritiated methane, tritiated pump oil, radiochemicals and so on) should be called tritiated organics, which can exist in any chemical or physical form." This definition was clarified through a number of notes, and the full definition is given in Appendix A.

The EMRAS definition is consistent with the quantity measured in the traditional analytical determination of OBT, namely the tritium concentration in the combustion water produced by the oxidation of dry matter that has been washed with tritium-free water [27]. The definition was deliberately chosen to maintain this connection in order to preserve the meaning of past analyses and current analytical techniques. The definition does not include non-exchangeable OBT but does include buried tritium. It also distinguishes between organically bound tritium that is formed in the environment and tritiated organics, which are produced through industrial processes.

The concept and significance of buried tritium is still under debate. Baumgärtner and Donhärl [24] and Baumgärtner [25] suggest that buried tritium makes up 50% or more of what is traditionally measured as OBT. Lower fractions, typically 5% and at most 20%, have been reported elsewhere [26]. In the face of this discrepancy, the question remains open pending new experimental data. If buried tritium is a reality and behaves as non-exchangeable OBT in the body, OBT doses may be overestimated by present OBT measurements.

Uptake by Terrestrial Animals

Tritium is taken into the bodies of animals (including human beings) through inhalation and ingestion of food and water [28, 29]. Uptake also occurs by absorption through the skin, which is a minor pathway for animals with their thick skins. Losses occur through respiration, sweating, excretion, and (in the case of cows) milking. Tritium concentrations in the body depend on rates of uptake and loss, and on concentrations in the air, drinking water, and food taken in by the animal. These concentrations may vary widely since animals are mobile and may draw their air, food, and water from different parts of the environment.

HTO diffuses freely and rapidly across all cell membranes and equilibrates with body fluids within minutes. When exposure stops, the HTO concentration in the body decreases with a biological half-life of 3–10 days for the vast majority of the tritium, which behaves as HTO in the body water [30], and a half-life of 40 days for the small amount incorporated as OBT into body dry matter [31]. These timescales suggest that tritium concentrations in animals fluctuate over time but do not follow day-to-day changes of concentrations in their environment.

Non-exchangeable OBT in the body arises principally from assimilation of ingested OBT in foods [32]. As much as 50% of the OBT in food fed to animals appears as OBT in the animal itself, attached to biochemical compounds such as amino acids, sugars, protein, starches, lipids, and cell structural materials. A small fraction (<5%) of HTO taken into the body is irreversibly incorporated into organic molecules through the enzymatic reactions involved in carbohydrate metabolism [33]. Twenty times more OBT is incorporated into milk fat and casein after OBT ingestion than after HTO intake [30, 34]. The extent of incorporation depends on the length of exposure and

the metabolic activity, which differs from organ to organ. Thus, OBT can be localized in the body in a relatively small number of cells and at relatively high concentrations. Fats and proteins retain more of their OBT during digestion than do carbohydrates. However, most OBT ingested with food is metabolically oxidized to HTO during digestion and assimilation and enters the compartment of free body water.

OBT has a longer retention time than tritiated water in animals. When exposure stops, OBT is lost slowly from the body as a result of metabolic oxidation to HTO, which is then excreted. The biological half-life of this process is variable. van den Hoek et al. [34] measured values ranging from 60 to 330 days, whereas Galeriu et al. [35] suggest values of 88 days for cows, 75 days for calves, >100 days for pigs, and >190 days for goats. Hill and Johnson [36] reviewed OBT retention half-lives for humans and found values ranging from 20 to 226 days. Based on studies in which adult rats were fed dried flounder containing OBT, Hodgson et al. [31] proposed that 70% of the tritium in humans would be excreted with a 10-day half time and 30% with a 100-day half time. The biological half-life varies with the type of molecule (carbohydrate, protein, or lipid) since different molecules have significantly different metabolic turnover rates. The half-lives for animals reflect protein and lipid metabolism and are longer than half-lives for plants, which are composed primarily of carbohydrates [37, 38]. The constant synthesis of organic compounds in dairy cows during milk production results in the continuous formation of OBT, which is excreted in milk, urine, and feces at a rate only slightly slower than that of HTO.

Conversion of HT to HTO

Small amounts of tritiated hydrogen are released from heavy water reactors and larger amounts from tritium recovery facilities. HT is biologically inert, and direct exposure results in very low radiological doses. However, HT can diffuse into the soil and be converted to HTO by enzyme-mediated reactions. The converted HT is subsequently transported as HTO, which dominates doses from an HT release. Therefore, deposition and conversion are the only HT-specific processes that need to be explicitly considered in assessing the consequences of an HT release.

The oxidation of HT in the soil is mediated by hydrogenase, an enzyme that exists freely or in association with many bacteria of various taxonomic groups, in many eucaryotic algae, in some protozoan microorganisms, and in several mosses [39, 40]. Hydrogenase is able to break the bonds in the HT molecule and then oxidize it to tritiated water. Oxidation rates are independent of soil particle composition, organic content, pH, or chemical properties [41]. The number of HT-oxidizing organisms decreases with depth in the soil [5] but is sufficiently great to provide biological reaction sites for all HT molecules at all depths. Thus the rate of deposition is usually not limited by the number or activity of conversion sites, since the soil has the capacity to convert to HTO essentially all the HT that diffuses into it. Rather, the rate is governed by processes that control access of HT to the reaction sites on pore walls. These processes include diffusion both into the soil and within the pore air, both of which are affected by soil water content, which is the most influential variable determining deposition rate. The water content controls the available air-filled pore space and thus the rate of HT diffusion within the soil. Water content also affects the degree to which soil particles are covered by water films, which restrict access of the relatively insoluble HT to reaction sites located on soil particle surfaces. The HT deposition rate therefore decreases with increasing soil water content.

HT deposition rates also decrease rapidly as soil moisture drops below 3% [42]. Biological activity is diminished in extremely dry soils, and in this case, HT deposition is limited by the reduced number of conversion sites. In temperate regions, however, surface soil water contents typically exceed 4% and oxidation capacity is not an issue except during prolonged dry spells. Oxidation activity and HT deposition rate also decrease as soil temperatures drop below freezing [43], although some seasonal variability may be due to changes in soil moisture content rather than to variations in temperature. Organic content affects available pore space and pore size distribution and thus can influence diffusion and HT deposition rate [5]. Soils with vegetation cover show higher deposition rates than bare soils, suggesting that root systems enhance soil porosity (and hence diffusion) and increase microbial activity.

The combined effects of diffusion and microbial oxidation result in an HTO profile that decreases

exponentially with depth in the soil [44]. The depth at which the HTO concentration drops to 1/e of its value at the surface (the scaling length) is typically between about 1.5 and 3.0 cm, which implies that most of the HT is oxidized within the top 6 cm of the soil. The diffusion rate of HT in soil is faster than that of HTO, resulting in a lower surface concentration and a deeper profile. The initial reemission rate for HT deposition is therefore about three times lower than it is in the case of an HTO source. For an HT release, the secondary airborne HTO plume appears immediately, even in the presence of the initial HT cloud, because the HTO concentration gradient is always directed upward.

The HT deposition rate is usually expressed quantitatively as a deposition velocity (v_d), defined as the HT deposition flux per unit horizontal area of soil divided by the concentration of HT in air. Numerous experiments have demonstrated that the deposition velocity of HT to soil is usually in the range 10^{-4} to 10^{-3} m s^{-1} for soils of typical water content under nonfreezing conditions. Deposition velocities decrease with increasing water content and colder temperatures, dropping to about 10^{-5} m s^{-1} for very wet or frozen soils. Good agreement exists between data obtained using chambers in the laboratory [45, 46], chambers in the field [43, 44, 47], and measurements made in the open environment [48–50]. Local inhomogeneities in soil conditions and vegetation cover can result in a tenfold variation in v_d within a natural field.

HT can be taken up and converted to HTO by foliage [40, 51], and gas-phase oxidation can occur in the atmosphere [52], but the amount of HTO produced by either of these processes is insignificant compared to the amount generated in the soil. Biological conversion of HT may proceed relatively rapidly within at least some types of soil litter, with deposition velocities in the lower range of those to soil [53, 54].

Aquatic Processes

Tritium released to a surface water body is transported by the mass flow of the receiving waters and its concentration is determined by dilution, dispersion, and evaporation. Of these processes, the only one not experienced by most other radionuclides is evaporation, but this can have a large influence on HTO concentrations in some systems [55]. Because fresh water systems vary widely in their characteristics, concentrations depend strongly on the properties of the specific site. An aquatic receptor close to a tritium source may not experience steady water concentrations even if the release rate is constant and continuous. Changes in stratification, current speed, and (in lakes and oceans) current direction may cause water concentrations to fluctuate on daily timescales. Moreover, fish may experience changing water concentrations as they pass into and out of the tritium plume during their movements through the water body.

Most aquatic organisms are totally immersed in water and have high water exchange rates. Uptake of HTO is therefore very quick, and concentrations in tissue become equal to water concentrations within minutes or hours [56, 57].

The process of OBT formation is much the same in aquatic plants as it is in terrestrial plants. Exchangeable and non-exchangeable OBT are formed through photosynthesis during the day and through a variety of metabolic processes in the dark. The OBT can be translocated from its place of formation to storage organs in the plant, and is degraded to HTO through respiration. Isotopic effects also play a role in determining OBT concentrations. A small fraction of the HTO taken in by aquatic animals is converted to OBT in anabolic processes. Metabolic processes in the animal depend on water temperature, and seasonal effects should be taken into account in estimating OBT formation [58]. Fish metabolism slows down appreciably when the fish growth rate becomes less than 10% of the optimum growth rate, which occurs for water temperatures below 6–8°C. Elimination of OBT from fish tissues is relatively rapid for small fish, with biological half-lives in the range of 5–25 days [56, 59]. Data for larger fish are missing but longer values are expected.

Tritium reaches the oceans via direct release, via discharge from rivers and groundwaters, and via deposition from the atmosphere. It quickly spreads through the surface mixed layer, which is about 100-m thick, and is reduced to very low concentrations by the huge water volumes available for dilution [60]. Exchange with deeper layers is slow and any tritium transported downward joins oceanic circulation and decays away before the water reappears on the surface. Little is lost to the atmosphere since the low water concentrations mean that the diffusion gradient is usually directed

downward and deposition is favored over evaporation. Marine organisms take up tritium in the same way that fresh water organisms do, but concentrations are extremely low.

Environmental Tritium Concentrations

All of the environmental transport processes discussed above operate regardless of whether the tritium source is short-term or continuous, local or global. However, the resulting environmental concentrations depend very much on these factors. The following three sections discuss environmental tritium concentrations in background areas, near continuous sources, and near time-dependent sources, respectively.

Concentrations in Background Areas

In the present context, a background area is an area remote from local tritium-handling facilities. The only significant tritium sources in such areas are those that operate on global scales. These include cosmogenic production, neutron capture by lithium in rocks, and the residue of fallout from atmospheric nuclear weapons testing in the late 1950s and early 1960s. All of these sources together result in global background tritium concentrations of about 2–3 Bq L^{-1} in air moisture, precipitation, surface waters, and the aqueous phase of living organisms [1]. This is an extremely low abundance, corresponding to roughly 1 tritium atom in 10^{17} hydrogen atoms. Because of the large spatial scale of sources in background areas, concentrations tend to be constant in time and space and are independent of the averaging time used to measure them.

Long-Term Average Concentrations Due to Routine Releases

Nuclear power reactors, fuel reprocessing plants, and tritium light factories all routinely release small amounts of tritium on a continuous, or quasi-continuous, basis. A receptor close to such a source does not experience steady air concentrations even if the release rate is constant. Changes in meteorological conditions, particularly wind direction, induce changes in air concentrations on hourly timescales. However, it is not instantaneous concentrations that are of interest for routine releases since the doses they impart are very low. Rather it is the long-term average concentrations, which are used to ensure that annual dose limits are not exceeded, and which are generally steady from year to year. Thus, measurement programs and models for predicting environmental concentrations around continuous sources are generally designed to generate annual average values. Concentrations can be 10–100 times higher than background levels at the exclusion zone of tritium-handling facilities, and higher still closer to specific sources. Concentrations due to atmospheric releases of HTO, atmospheric releases of HT, and aquatic releases of HTO are discussed in turn below.

Atmospheric Releases of HTO

Observations Long-term average concentrations in the various environmental compartments at a given location near a continuous atmospheric tritium source are in equilibrium, but are not equal. Concentrations in precipitation are lower than those in air moisture because precipitation, which is initially uncontaminated, usually does not come into equilibrium with air moisture in the small amount of time needed to fall through the airborne plume. Concentrations in soil are similar to those in precipitation since the persistent HTO inventory in soil arises largely through wet deposition. Observations of long-term average concentrations in air moisture (C_{am}) and soil water (C_{sw}) suggest that values of the ratio C_{sw}/C_{am} lie in the range 0.1–0.4 [61–63]. The value depends upon a number of local factors, notably the frequency with which rain falls when the airborne plume is present at the site of interest.

Plants take up tritium from both air moisture and soil water. The relative contribution of these compartments to the tritium concentration in the plant depends on the relative humidity (RH) of the atmosphere [13, 64]. When RH = 1, the transpiration stream shuts down and no soil tritium is carried to the leaves. In this case, the tritium in the leaves is due entirely to transfer from the air via diffusion through the stomates, and the leaf concentration comes into equilibrium with the concentration in air moisture. As the humidity drops, transpiration brings low concentration water up to the leaves, diluting the input from

the air. In the limit RH = 0 (a physically impossible situation), there is no HTO in the air and no transfer from air to leaf, and the plant concentration equals the concentration in the transpiration stream. The long-term average value of RH in temperate climates is about 75% and the plant HTO concentration lies closer to the concentration in air moisture than to that in soil water.

The relative contribution of air moisture and soil water to the tritium concentration in the plant also depends on the part of the plant under consideration. The partitioning in terms of relative humidity applies specifically to plant leaves that, under normal circumstances, draw the majority of their tritium from the air. The balance changes for fruit, tubers, or root crops, which draw a larger fraction of their tritium from the soil [65]. The concentration in tubers and root crops is close to that in soil water. The concentration in fruit water is intermediate between the concentration in leaves and soil water.

Observations of long-term average tritium concentrations in air moisture and plant water (C_{pw}) show that values of the ratio C_{pw}/C_{am} exhibit considerable scatter, with a mean of 0.68 for leafy and non-leafy vegetables [66]. Lower values apply to root crops and fruit, which draw more of their water from the soil.

Since most plant dry matter is formed in the presence of water, the plant OBT concentration is similar to the HTO concentration. However, due to the larger mass of tritium compared to hydrogen, isotopic fractionation results in an OBT specific activity that is lower than that for HTO [22]. The presence of exchangeable hydrogen in the plant combustion water also contributes to the relatively low dry weight concentration.

Because HTO and OBT have very different formation and clearance times in plants (a few hours and several weeks, respectively), and because tritium concentrations in air vary rapidly in time due to fluctuations in meteorological conditions, it is difficult to obtain reliable estimates of the long-term OBT/HTO ratio from field data. The most dependable values come from controlled laboratory experiments, where the plant is exposed to an HTO concentration that is held constant or monitored continuously. Table 1 summarizes literature values of OBT/HTO ratios obtained under controlled conditions. Although the number of data points is small, all values are less than 1, with a mean of 0.54 for the crops considered (maize, barley, and alfalfa).

Tritium in the Environment. Table 1 Empirical values of the OBT/HTO ratio in plants obtained under controlled laboratory conditions

Plant type	OBT/HTO ratio	Reference
Maize	0.51[a] ± 0.03 0.66 ± 0.01	[23] [67]
Barley	0.42[a] ± 0.01 0.55 ± 0.01	[23] [67]
Alfalfa	0.58[a] ± 0.02	[22]
Mean	0.54 ± 0.09	

[a]The concentrations measured in these experiments as "OBT" consisted of both exchangeable and non-exchangeable organically bound tritium. To eliminate the contribution of exchangeable OBT, the OBT/HTO ratios reported in the publications were corrected by subtracting 0.22, which represents the proportion of exchangeable hydrogen in the total hydrogen of the samples [68].

Concentrations in animal products reflect the concentrations in the drinking water and various foods that make up their diet. Animal concentrations are generally lower than concentrations in air or plants for two reasons. First, some food products may be imported from sites remote from the source and be uncontaminated. Second, the tritium inventory is diluted by drinking water, which is usually drawn from a large water body with mainly uncontaminated input.

Models Most models designed to calculate long-term average tritium concentrations avoid the explicit simulation of the individual transport processes and short-term dynamics that are characteristic of environmental tritium behavior. To take these factors into account would require large amounts of computing time and site-specific data, and would result in large uncertainties in the predicted concentrations. Instead, it is customary to use simpler models that describe the integrated response of the system, and for which appropriate generic data exist. These models have traditionally been based on the specific activity approach, in which tritium is assumed to mix with hydrogen in a source compartment, resulting in a certain SA.

Any organism drawing hydrogen from this compartment draws tritium in proportion, and attains the same SA as the source compartment. If the organism draws hydrogen (and tritium) from more than one compartment, the SA in the organism is a weighted average of the specific activities in these compartments.

The general mathematical expression of this approach is given in Eq. 1. The specific activity SA_j in a compartment j that draws an element S from N other compartments is given by:

$$SA_j = \frac{A_j}{S_j} = \frac{\sum_{i=1}^{N} f_i \cdot D_{Fi} \cdot A_i}{\sum_{i=1}^{N} f_i \cdot S_i} \quad (1)$$

In Eq. 1, A_i is the concentration of the active form of the element in compartment i (Bq kg^{-1}), S_i is the concentration of the stable form (g kg^{-1}), and f_i is the flux of S from compartment i to compartment j (g d^{-1}). D_F is an isotopic discrimination factor that is introduced to allow for the possibility that the stable and active forms may have significantly different masses and therefore different transfer rates between compartments. The concentration of the radioisotope in compartment j is found by multiplying SA_j by the concentration of the stable element in the compartment.

For an atmospheric release of HTO, it is the concentration in air moisture C_{am} (Bq L^{-1}) that drives the transfer of tritium in the environment. The tritium concentration in air (C_a, Bq m^{-3} air) is related to C_{am} through the atmospheric absolute humidity q (kg m^{-3}):

$$C_a = q\, C_{am} \quad (2)$$

The value of C_a is generally known, either through measurement or through calculations involving an atmospheric dispersion model such as the sector-averaged Gaussian plume model. Care should be taken in choosing the air concentration used to drive the model. Plants take up tritium through their leaves primarily during daylight hours in the growing season, and air concentrations used to model this process should be based on meteorological data for this period. On the other hand, concentrations in soil and surface water should reflect annual average air concentrations, since deposition occurs throughout the day and throughout the year.

In its simplest form, the SA model assumes that the tritium concentration in all environmental compartments (including man) is equal to the tritium concentration in air moisture at the location of interest [69]. However, as discussed above, the tritium concentration in the environment is usually less than that in air, as isotopic exchange with relatively uncontaminated water pools results in progressive dilution of the tritium in compartments farther along the exposure pathways. The net effect of these dilutions is a dose that is a factor two to three lower than that predicted on the assumption of full specific activity equilibrium in all compartments.

There are a number of ways to obtain more realistic estimates of long-term average concentrations in the environment. In the simplest of these, concentrations in soil and plants can be deduced directly from the concentration in air moisture using observed values of the ratios C_{sw}/C_{am} and C_{pw}/C_{am}. Similarly, the OBT concentration in plants can be obtained from the plant HTO concentration and the observed OBT/HTO ratio. This approach will give reasonably good estimates at sites where meteorological conditions, soil properties and plant species are similar to those at the sites where the ratios were observed, but may not perform as well otherwise.

A number of more detailed models have been proposed for calculating steady-state concentrations in the various environmental compartments. In a common approach to estimating soil water concentrations, the amount of HTO deposited (ω_w, Bq m^{-2}) in the course of one rainfall event that lasts Δt s is first calculated from

$$\omega_w = \Lambda Q \exp\,(-\Lambda\, x/u)\Delta t/(x\, u\, \Delta\theta), \quad (3)$$

where Λ is the washout coefficient (s^{-1}), Q is the release rate (Bq s^{-1}), x is the downwind distance from source to receptor (m), u is the wind speed (m s^{-1}), and $\Delta\theta$ is the angular width of the sector (radians), assuming that a sector-averaged dispersion model has been used to calculate air concentrations. The total amount of activity deposited per year is found by summing the amounts deposited during each rainfall occurring in that year. Soil concentrations are calculated by dividing ω_w by the annual precipitation. Only HTO that is

deposited with precipitation is assumed to be retained in the soil since dry-deposited HTO is quickly reemitted to the atmosphere by evaporation.

Belot [61] proposed a more complex model for soil water concentrations that accounts for the contributions of both wet and dry deposition:

$$C_{sw} = \frac{v_d\, C_a + F_w}{v_e\, \rho_s + I_r} \tag{4}$$

Here v_d is the exchange velocity of HTO from air to soil (m s^{-1}), F_w is the average flux density of tritium wet deposition (Bq m^{-2} s^{-1}), v_e is the exchange velocity from soil to air (m s^{-1}), ρ_s is the water concentration in air saturated at the soil surface temperature (L m^{-3}), and I_r is the infiltration rate of water through the root zone (L m^{-2} s^{-1}).

Many modelers calculate plant HTO concentration using a model proposed by Murphy [13], which explicitly considers contributions from both air and soil:

$$C_{pw} = [RHC_{am} + (1 - RH)C_{sw}]/\gamma, \tag{5}$$

where $\gamma = 0.909$ is the ratio of the H_2O vapor pressure to that of HTO. In deriving Eq. 5, it has been assumed that the temperature of the air, soil surface, and leaf are the same; that the mass of plant water is constant over time; and that the HTO concentration in soil water at the soil surface is equal to the concentration in root water. OBT concentrations in plants are generally calculated by assuming that the specific activity in the organic material is equal to the specific activity in the aqueous phase multiplied by an isotopic discrimination factor. More detailed OBT models would require the simulation of photosynthesis, which is too complex for inclusion in a long-term average model.

HTO concentrations in animal products (C_{aw}; Bq L^{-1}) are usually calculated using a specific activity approach, in which the animal's total daily tritium intake from ingestion and inhalation is mixed into the total daily amount of water taken in [66, 70, 71]:

$$C_{aw} = f_{fw} C_{pw} + f_{fdm} C_{OBT} + f_{dw} C_{dw} + f_{in} C_{am}. \tag{6}$$

Here C_{OBT} (Bq L^{-1}) is the OBT concentration in plant combustion water, C_{dw} (Bq L^{-1}) is the tritium concentration in drinking water and f_{fw}, f_{fdm}, f_{dw}, and f_{in} are the fractions of the total water intake contributed by water in the aqueous part of food, water in the dry matter of food, drinking water, and inhalation (including skin absorption), respectively. These fractions can be readily estimated from the diet of the animal, and so can be changed to represent different species and climates. The HTO concentration in drinking water is not easy to determine since the water could come from a surface water body of any size or from a well. Since water concentrations due to an atmospheric release are likely to be small, C_{dw} is generally set to an arbitrarily small fraction (<0.1) of C_{am}. OBT concentrations are calculated on the assumption that the specific activity in the organic material equals the specific activity in the aqueous phase, apart from isotopic effects.

Galeriu et al. [72, 73] have recently developed a metabolic approach to calculating HTO and OBT concentrations in animal products. The model explicitly takes into account transfers from HTO in the diet to HTO and OBT in the product, and from OBT in the diet to HTO and OBT in the product. The output of the model is expressed as the ratio of the concentration in the animal product to the concentration in its feed, drinking water, and inhaled air. Separate ratios are determined for HTO and OBT intakes. The model involves a number of animal and plant properties, which can be varied to reflect a given species, diet, production rate, agricultural practice, or climate.

Detailed descriptions of models that calculate long-term average tritium concentrations in the environment due to chronic atmospheric releases of HTO can be found in [62, 66, 70, 71].

Atmospheric Releases of HT

Observations As noted above, HT released to the atmosphere is not itself of radiological concern. However, HT diffuses into soil pore spaces where it is oxidized to HTO by microorganisms. Some of the HTO so formed is taken up by plants through their roots with transpiration water, and some is emitted to the atmosphere. This HTO is available for uptake by animals and humans through inhalation and ingestion. Doses from an atmospheric release of HT are determined entirely by the HTO formed in the soil.

There are very few observations of environmental HTO concentrations arising from the release of HT. Most HT sources also emit HTO directly to the atmosphere, which masks the HTO formed in the environment from the HT. The only reliable data come from an

Tritium in the Environment. Table 2 Geometric means (GM) and geometric standard deviations (GSD) for lognormal distributions for the HTO/HT ratios for air moisture, soil water, and plant water

Compartment	GM (Bq L^{-1} HTO)/(Bq m^{-3} HT)	GSD
Air moisture	4	1.5
Soil water	6	1.5
Plant water	6	1.5

experiment carried out at Chalk River Laboratories (CRL) in 1994, in which an agricultural plot was continuously exposed to elevated levels of HT in air over a 12-day period [50, 74]. HTO concentrations in air, soil, and plants increased rapidly at the beginning of the release but leveled off toward the end, at which point the system was at or near steady state. The data were analyzed in terms of the steady-state ratios of HTO in air moisture to HT in air, HTO in soil water to HT in air, and HTO in plant water to HT in air [75]. The geometric means and geometric standard deviations of these ratios are shown in Table 2. The value of the air ratio in units of Bq m^{-3} HTO per Bq m^{-3} HT was 0.045.

The values of the ratios showed no dependence on downwind distance or the frequency with which the wind blew toward the receptor. The value of the plant ratio was found to apply to all plant types since the data did not show any significant difference among leafy vegetables, tubers, and fruit crops. The values of the ratios may not be directly applicable at other nuclear sites where soils are significantly different than those at CRL in terms of the properties that control HT deposition and oxidation (water content, porosity, and distribution of microorganisms).

Models The measured HTO/HT ratios explicitly account for the processes of HT deposition to soil, conversion of HT to HTO in the soil, reemission of the HTO to the atmosphere, and uptake of the HTO by plants. Thus they provide a simple way to estimate the HTO concentrations in air, soil, and plants, assuming that the HT concentration in air is known through measurement or modeling. This is the approach taken in almost all models for calculating long-term average concentrations for continuous HT sources [62, 66, 76]. The use of the ratios avoids the need to simulate the transfer processes explicitly, which is not warranted in this type of model. Once the HTO concentrations are known, the remainder of the HT model (formation of organically bound tritium in plants, transfer to animals and humans) is the same as that for HTO. The direct transfer of HT to plants, animals, or water bodies is insignificant.

Aquatic Releases of HTO

Observations Most aquatic organisms are totally immersed in water and have high water exchange rates. Therefore, in water bodies receiving continuous input, concentrations in plant and animal tissues are in equilibrium with water concentrations. For example, in a study of a small Canadian shield lake chronically contaminated with tritium, Kim et al. [2] found that submerged plants, and the submerged parts of emergent plants, had the same concentration as the local water, whether they were rooted in the sediments or not. In the emergent parts of plants such as cattails, the HTO concentration was the average of the water and air concentrations. The HTO concentrations in fish and benthic organisms were the same as the concentration in the water and food that they accessed. Concentrations in the top few centimeters of sediment water were similar to those in the water column itself.

Because aquatic plants are immersed in an environment of uniform HTO concentration, the OBT concentration in their combustion water is the same as their HTO concentration apart from an isotopic discrimination factor, which must be determined empirically for steady-state conditions. Kirchmann et al. [77] showed that the specific activity of tritium in the organic material of aquatic plants such as algae reached 0.8 of that in the surrounding water. Lower values (0.5 for submerged plants and 0.7 for emergent plants) have been found in other studies [2, 56].

The OBT concentration in aquatic animals is also the same as the HTO concentration, reduced by a discrimination factor D_F that takes account of isotopic effects arising both in the fish and in different components of its food and water intakes. Because HTO and OBT have very different biological half-lives in aquatic animals, and because the animals can encounter different tritium concentrations as they move through their water body, it is difficult to obtain reliable estimates of D_F from animals collected in the

Tritium in the Environment. Table 3 Values of the isotopic discrimination factor for fish (D_F) obtained under equilibrium conditions

Fish type	D_F	Reference
Bullhead (catfish)	0.77	[2]
Pike	0.84	[2]
Bass	1.30[a]	[78]
Bluegill	0.97[a] 0.49[a]	[79] [80]
Largemouth bass	0.41[a]	[80]
Mosquito fish	0.34[a] 0.67[a]	[80] [81]
Carp	0.60[a]	[82]
Mean	0.66	

[a]The concentrations measured in these experiments as "OBT" consisted of both exchangeable and non-exchangeable organically bound tritium. To eliminate the contribution of exchangeable OBT, the OBT/HTO ratios reported in the publications were corrected by subtracting 0.2, which represents the proportion of exchangeable hydrogen in the total hydrogen of the samples [59].

wild. More dependable values can be obtained if the animal lives its entire life in an environment where the HTO concentration does not change, or if it is exposed over a long period of time to contaminated food and water in a controlled setting. Values of D_F obtained under such conditions show a mean of 0.66 (Table 3).

Models HTO concentrations in water following chronic release to a surface water body can be calculated using standard aquatic dispersion models [83, 84]. Under the assumption of full specific activity equilibrium in all aquatic compartments, the HTO concentrations in aquatic plants and animals are both equal to the concentration in water.

Given the similarities in the processes responsible for OBT formation in terrestrial and aquatic plants, the model for OBT concentrations in aquatic plants is the same as that for terrestrial species. Accordingly, the OBT concentration in the combustion water is calculated as the product of the plant water concentration and a discrimination factor that accounts for isotopic effects in dry matter production. The plant water concentration used in these calculations should be the concentration in the above-water part of the plant for emergent plants and in the submerged part otherwise. The model for OBT concentrations in aquatic animals takes the same form as the plant model, with a discrimination factor appropriate for animals.

Nonequilibrium Conditions

OBT/HTO ratios in terrestrial plants collected in the field near continuous tritium sources often show values greater than 1 [85–89], in apparent violation of specific activity concepts. There are a number of explanations for this, one being the significantly different formation and clearance times of HTO and OBT in plants. An HTO measurement at a single point in time reflects the instantaneous HTO concentration at that time, but a single OBT measurement reflects an integrated value over the month or two prior to sampling. If an airborne tritium plume is present when the samples are taken, the HTO concentration will be larger than the OBT concentration and the ratio will be less than 1. If the plume is not present, the HTO concentration will be less than the OBT concentration, and the ratio will be greater than 1. Since winds typically blow in any one direction at most 20% of the time at a given site, it is likely that a tritium plume will not be present at a particular sampling time, so that ratios greater than 1 will be seen more frequently than ratios less than 1.

Different translocation patterns for HTO and OBT [65], and possibly direct incorporation into plant cells of volatile tritiated organic compounds such as formaldehyde, are other mechanisms that could lead to OBT/HTO ratios greater than 1. Diurnal effects, and measurements made when the plant is under heat or water stress, may also contribute to large values of the ratio.

Large OBT/HTO ratios have also been observed in the aquatic environment. Jean-Baptiste et al. [90] found elevated tritium concentrations in fish, plants, and sediments both upstream and downstream of a nuclear generating station on the Rhone River in France. HTO concentrations in the organisms were in equilibrium with the river water, but non-exchangeable OBT levels in fish, plants, and sediments exceeded the levels in water by factors of 3, 100, and 10,000, respectively. This apparent enrichment in the organic phase was postulated to arise from the release to the river of

fine particles of tritiated compounds used in luminous paints in a clock factory further upstream. This would explain the preferential accumulation observed in sediments due to the settling of the particles in the riverbed, and to a lesser extent on plants leaves and in fish that ingest the plants. Alternatively, the large sediment concentrations may be due to the sorption of tritium from an aqueous source to organic-rich sediment grains [91].

A similar situation recently occurred in Wales, where non-exchangeable OBT concentrations in mussels and benthic fish in Cardiff Bay were found to be 1,000 times higher than the HTO concentration in the seawater. These very high concentrations were believed to arise through direct ingestion by the animals of a variety of tritiated compounds that were released to the bay in bioavailable form from a radiopharmaceutical plant [6, 92, 93]. The selective uptake of dissolved organic tritium by primitive aquatic organisms is well documented [94–96].

The above observations do not suggest that plants and animals accumulate OBT after chronic HTO exposure in either terrestrial or aquatic environments. Rather, these and similar cases represent nonequilibrium conditions for which specific activity concepts do not apply. OBT/HTO ratios less than 1 can be expected only in cases in which the OBT is formed through metabolic processes involving HTO, and in which the averaging time of the HTO and OBT concentrations is the same. However, OBT/HTO ratios measured in 22 plant samples at Thunder Bay, Ontario, which is remote from all tritium sources, varied between 3.5 and 6.2 [97]. Similarly, Baumgärtner [25] reported the accumulation of tritium in biomolecules of plants grown in tritiated water. These results are presently unexplained, but it is emphasized that OBT/HTO ratios obtained in systems where equilibrium conditions are clearly in effect are consistently less than 1 (Table 1).

Time-Dependent Concentrations Due to Acute Releases

Acute tritium releases take many forms. Accidents at nuclear power reactors or fuel reprocessing plants can result in the release of various amounts of tritium over various time intervals. Release rates generally are highly time-dependent. Livestock may undergo a step change in their dietary tritium if they are turned out on contaminated pasture after eating stored food for some time. The environmental consequences of a given acute tritium release are also scenario-specific, depending on the meteorological conditions in effect at the time of the release and shortly thereafter, and on the properties of the soils, plants, and animals that are exposed. Concentrations can be high enough in some very low probability scenarios to require protective actions to avoid human health effects.

The interest in acute releases is usually in the time-dependent environmental concentrations that result, with particular emphasis on maximum and time-integrated values. It is often difficult to obtain reliable estimates of these quantities given the unexpected nature of accidents and the typically short time available for response. As a result, almost all the reliable information on environmental tritium concentrations following a dynamic HTO release comes from controlled experiments that typically focus on a single environmental compartment (soil, plant, or animal). Since the effects of dynamic releases are difficult to generalize, they are illustrated here through a number of case studies.

Atmospheric Releases of HTO

Observations *Short-Term Exposure of Soybeans to Elevated Levels of HTO in Air:* In a series of experiments carried out by the Korean Atomic Energy Research Institute, potted soybean plants at various stages of growth were exposed for 1 h to elevated levels of tritium in a glove box [26]. The soil in the pots was covered by vinyl paper to prevent tritium from depositing to the soil, so that the air-to-leaf transfer process could be studied in isolation. Following exposure, the plants were removed from the glove box and cultivated as usual outdoors. Samples of the plant leaves, stems, shells, and seeds were taken at various times after the exposure and measured for their HTO and OBT concentrations.

Figure 1 shows the HTO concentration in the leaves and stems of a plant exposed before its pods had started to form. The observed plant concentrations have been normalized by the average HTO concentration in air moisture in the glove box during the exposure. At the

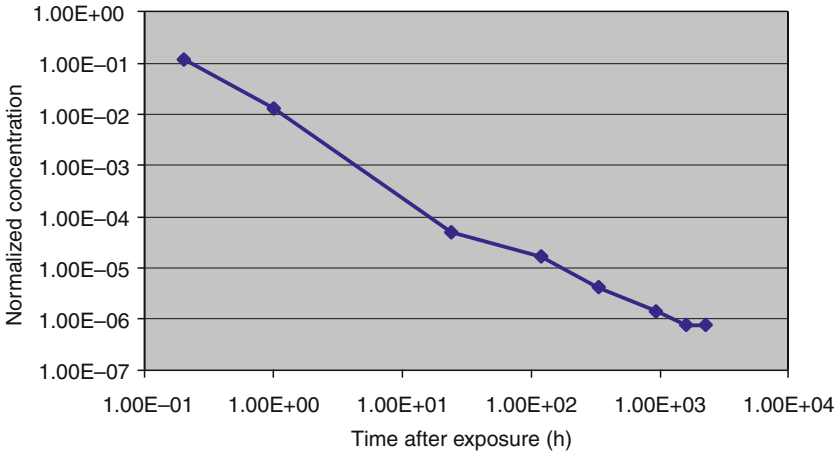

Tritium in the Environment. Figure 1
Normalized HTO concentration in soybean leaves and stems as a function of time after exposure

time of the first measurement, which was made 12 min after the exposure ended, the plant concentration was about 12% of the air moisture concentration. Higher values were probably achieved immediately after the exposure ended. The plant concentration dropped off by a factor of 10 in the first hour to a value just over 1% of the air moisture concentration. It continued to drop until the last two measurement points, at which time it leveled off at a value equal to the background concentration at the site. Other experiments involving plants at different growth stages showed the same general patterns but somewhat different dynamics, suggesting that tritium behavior in plants depends on the timing of the exposure relative to the growth stage. Differences in the results may also have been caused by differences in the growth rates of the plants and differences in the meteorological conditions they experienced after the exposure.

A number of exposure experiments similar to those described above have been carried out at night [14, 15]. The data show the same general features as the daytime experiments, with an increase in plant concentration during exposure and a decrease once the exposure ends. However, the rates of uptake and loss are lower at night than during the day, as are the maximum concentrations reached in the plant.

Exposure of a Sow to an OBT-Contaminated Diet: In an experiment carried out at SCK-CEN in Belgium, a pregnant sow of the Belgische Landras strain, weighing about 180 kg, was given feed contaminated with OBT for 84 days before delivery [26]. The food had an average concentration of 577 Bq g^{-1} dry weight and was composed of a mixture of milk powder, potato powder, and dried algae. As the pregnancy progressed, the amount of food given to the sow increased. Throughout the period, the animal had free access to water but intake was not monitored. Concentrations of total tritium (HTO plus OBT) in urine and OBT in fecal dry matter were measured every week for 10 weeks.

The results of the experiment are shown in Fig. 2. The OBT concentration in feces was much greater than the total tritium concentration in urine over the entire study period. This was expected since the tritium was administered as OBT. The fecal concentration increased rapidly in the first week of the study as the dietary OBT entered the sow's gastrointestinal tract and began to be excreted. The concentration continued to rise until the sixth week of the study and then dropped off slightly. The fecal concentration actually exceeded the dietary concentration. In the labeling process, the OBT became associated with the indigestible fraction of the feed at a higher concentration than the average for the feed as a whole, and it was the indigestible fraction that appeared as feces. The total tritium concentration in urine increased quickly at the beginning of the study, reaching a value of 57 Bq ml^{-1} at the end of the first week. This rose to about 100 Bq ml^{-1} by the end

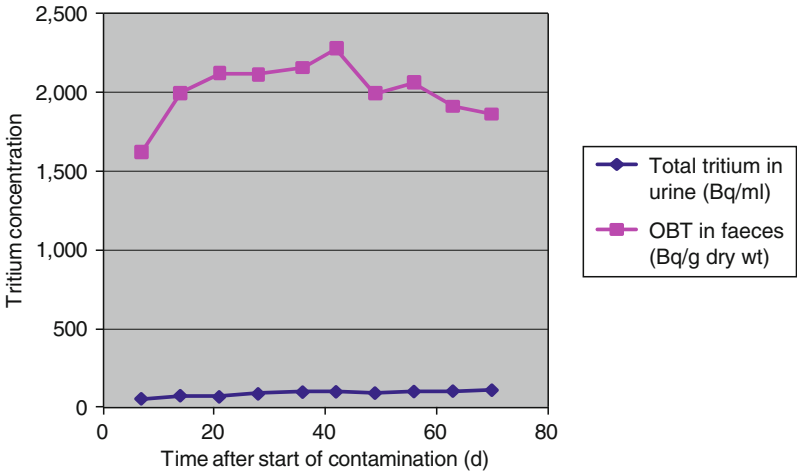

Tritium in the Environment. Figure 2
Tritium concentrations in urine and feces as a function of time after the start of contamination

of the fifth week, and stayed fairly steady thereafter. HTO made up the majority of the total tritium, and arose from the breakdown of the ingested OBT during digestion. The initial rapid rise in concentration followed by a more gradual approach to steady state is typical of situations in which an environmental compartment or organism undergoes a step increase in its tritium exposure.

Models *Dynamic Compartment Models:* Models for treating the dynamic release of tritium to the environment are commonly of two types: compartment models [98–100] and process-oriented models [101–103]. The compartment models extend specific activity concepts from steady-state to dynamic conditions by considering the ratios of active-to-stable fluxes between compartments rather than the ratios of active-to-stable concentrations in the compartments. These models are formulated as a system of linear, first-order differential equations, each of which describes the change in concentration in a given compartment as the difference between inputs and losses. The simplest models have only two compartments (one organic for the whole body and one aqueous for body water) whereas more complex models can have many more. Compartment models do not simulate processes explicitly but describe them using bulk transfer coefficients, or rate constants. Thus, the key factor in the reliability of these models is the availability of good data on which to base the rate constants. The required values are derived from data on the hydrological cycle or experimental data on tritium transfer in the environment. The latter might include tritium inventories and fluxes in a given compartment or tritium turnover times in the compartment. Biological halftimes are imposed from a simple mass balance of body water (for HTO) and carbon (for OBT).

Process-Oriented Models: Process-oriented models explicitly simulate the processes responsible for tritium transfer within and between compartments. They generally determine air concentrations using a two-step approach. In the first step, the concentration in the primary plume arising from direct release to the atmosphere is calculated using an atmospheric dispersion model. In the second step, the contribution due to reemission is taken into account using an area source approach in which the contaminated surface is divided into a number of cells. The total amount of HTO released from each cell is assumed to come from a point source in the center of the cell. Downwind concentrations due to a given cell are calculated using a dispersion model in which the plume is subject to initial widening to reflect the crosswind dimension of the cell. The total air concentration due to reemission is found by summing the contributions from each cell.

In most process-oriented models, the transfer of HTO between air and soil is modeled using an exchange velocity, v_{ex}^{s} (m s^{-1}), which is based on a resistance approach:

$$v_{ex}^{s} = (r_a + r_b + r_s)^{-1}. \quad (7)$$

Here r_a, r_b, and r_s are the HTO resistances to transfer through the air to the surroundings of the soil, through the laminar boundary layer just above the soil surface, and through the soil surface to deeper layers, respectively. All of the resistances are calculated from local data on soil properties and prevailing meteorological conditions.

Wet deposition of HTO to soil is usually calculated using a washout coefficient that depends on precipitation intensity, although more complex models are available [104]. The total tritium activity deposited by wet and dry processes on the soil is mixed into the soil water content to calculate the HTO concentration in the soil. The soil water content is determined from precipitation, evapotranspiration, and transport between layers due to matric forces. Transport is calculated using Darcy's equation [105] with appropriate values for the hydraulic conductivity and suction tension. The equations are solved numerically for each of n soil layers, where n is chosen to provide a balance between the accuracy of the model predictions and computational time.

In most process-oriented models, the transfer of HTO between air and plant is treated as a diffusion process and calculated as the product of the exchange velocity for plants, v_{ex}^{p}, and the HTO vapor pressure gradient between air and plant water [8, 64]. Time-dependent HTO concentrations in the plant are calculated from

$$dC_{pw}/dt = v_{ex}^{p}\left(C_a - \gamma\, q_s\, C_{pw}\right)/m_w, \quad (8)$$

where q_s (kg m^{-3}) is the absolute humidity of air saturated at leaf temperature (assumed equal to air temperature) and m_w is the mass of vegetation water per unit ground surface area (kg m^{-2}). The exchange velocity for plants, v_{ex}^{p}, is given by an equation similar to Eq. 7 but with the soil resistance replaced by a stomatal resistance, which describes transfer through the leaf epidermis into the plant. The stomatal resistance can be decreased to reflect increased uptake when the plant leaves are wet from precipitation, or increased to model reduced uptake at night. Equation 8 can be used to estimate plant water concentrations when the HTO flux is from air to plant (when an airborne plume is present) or from plant to air (when the air is uncontaminated).

Equation 8 can be modified to account for the contribution of soil water to the plant concentration by adding a term $T\,C_{rz}/m_w$ to the right-hand side of the equation. Here C_{rz} (Bq L^{-1}) is the average HTO concentration in root zone soil water and T is the flux of water from the surface due to transpiration, which is given by

$$T = v_{ex}^{p}(q_s - q) \quad (9)$$

The reemission of HTO from soil and plants to the atmosphere can be coupled to the evapotranspiration process [106]. The flux of reemitted HTO from soil to air (Bq m^{-2} s^{-1}) is given by

$$F_s = -v_{ex}^{s}(C_a - q\,C_r), \quad (10)$$

where C_r (Bq L^{-1}) is the HTO concentration in soil water near the soil surface. Similarly, the flux of reemitted HTO from plant to air is given by

$$F_p = -v_{ex}^{p}\left(C_a - q\,C_{pw}\right), \quad (11)$$

F_s and F_p provide the source terms for calculating air concentrations due to reemission from soil and plants, respectively.

Plant growth and OBT formation in process-oriented models are treated using a photosynthesis model. The net photosynthesis rate is estimated from incoming solar radiation, atmospheric humidity, air temperature, soil water content, and properties of the plant canopy. The buildup of organic material is based on the amount of CO_2 assimilation [107, 108]. OBT formation is assumed to depend on the rate of organic matter production and the HTO concentration in the plant water. Some models assume that OBT can form at night. This process is generally modeled very simply by setting the nighttime formation rate to a fraction of the daytime rate, since the processes responsible for OBT formation in the dark are not well known. OBT in the green parts of plants is allowed to slowly decompose to HTO; the loss rate from grain and tubers is slower still. The plant OBT concentration is also diluted over time

by new, relatively uncontaminated dry matter that forms after the airborne plume has passed.

Galeriu et al. [109] recently proposed a process-oriented, dynamic animal model that can be applied to all mammals, both wild and domesticated. The model is based on energy need and directly relates the organic matter turnover rate to the net metabolic energy turnover rate. The relationship between these two quantities is applied both at the whole body level and at organ levels. The model requires the net energy from food as input rather than the gross energy, which is used in digestion as well as metabolism. The link between gross energy and metabolized net energy is dependent on the type of animal, its source of energy, and how it has adapted to that source.

The model includes a body water compartment to account for HTO and exchangeable OBT. The principal organic compartments were selected after considering their relevance to the food chain, radiation protection, and biological importance. Organs with high metabolic rates, including the brain and the walls of gastrointestinal organs, are combined in a viscera compartment. Blood is separated into red blood cells and blood plasma, which is the vector for the transfer of metabolites. Simplified intake compartments are included for the dynamics of their contents. Transfers from the organic compartments to blood plasma are given by the relative metabolic rate, whereas the reverse transfers are assessed using stable element mass balance.

Tritium is assumed to enter the body through the diet and is mostly absorbed from the small intestine. The dry matter intake is partitioned into a metabolizable fraction, which is associated primarily with non-exchangeable OBT and transferred to blood plasma, and an excreted fraction, which is associated with exchangeable OBT. Of the metabolizable fraction, only a part is transformed into the net input of energy and matter, the rest being lost through respiration or passed to body water.

The exchangeable fraction in the metabolizable diet is directly transferred to the body water compartment. The amount of HTO converted to OBT is calculated using a transfer rate from body water to blood plasma that is based on the fraction of organically bound hydrogen in the body derived from exchangeable hydrogen (0.25–0.35) and the assumption of mass balance in an equilibrium situation. Other losses from the water compartment are assessed using a transfer rate based on the intake of hydrogen in drinking water, food, and respiration water.

For laboratory and some farm animals, all inputs for this model are available from the literature on animal metabolism, nutrition, and body composition. The model has recently been expanded to predict tritium dynamics in chicken broilers and eggs [110].

Time-dependent tritium concentrations in process-oriented models are calculated on relatively short time steps that vary in length from a few seconds to 1 h. Modeling of tritium transport on this scale requires large amounts of computer time and is not practical for calculating doses weeks or months after a short-term release. Moreover, detailed modeling beyond a few days is not necessary since adequate predictions can be obtained using simpler models and longer time steps. Accordingly, process-oriented models are used only for the first 100 h or so following a release. At longer times, dynamic compartment models running on daily time steps are used.

Atmospheric Releases of HT

Observations *Short-Term HT Release Experiments:* The time-dependent behavior of tritium in the environment following a short-term HT release to the atmosphere has been observed in two acute release experiments, one carried out in France in 1986 [111–113] and one in Canada in 1987 [114, 115]. In the French experiment, a total of 256 TBq of HT was released over a 2-min period from a 40-m high stack beginning at 13:12 in the afternoon. The wind speed was moderate (3.5 m s^{-1}) during the release and the sky was clear. The surrounding environment consisted of cultivated fields, meadows, and small, forested areas. The soil was characterized as a silty-clay loam of fine texture. A variety of tritium measurements were carried out at a point 800 m from the stack and on two crosswind sampling lines 1,000 and 2,500 m downwind.

In the Canadian experiment, 3.54 TBq of HT were released over a 30-min period from a height of 1 m beginning at 15:20 in the afternoon. The wind was light (2.25 m s^{-1}) during the release and the weather was fair. The soil was a very fine sandy to silty loam with 2–3% organic material in the top 22 cm. The study area was vegetated with common grasses, herbs, mosses,

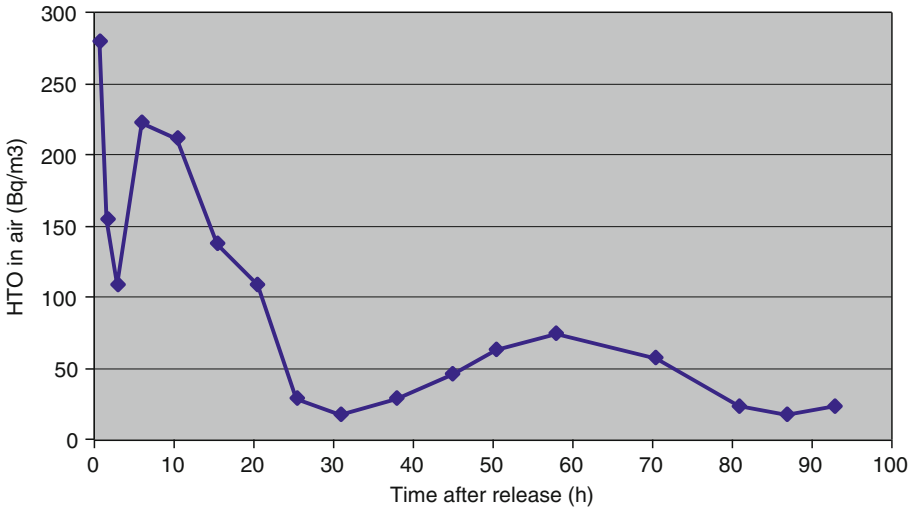

Tritium in the Environment. Figure 3
HTO concentrations in air for the 4-day period following the HT release in France

and large-toothed aspen saplings. Tritium concentrations were measured at various distances between 5 and 400 m from the source.

Figure 3 shows the HTO concentrations in air for the French experiment. The concentrations were measured 5 cm above ground level at a downwind distance of 800 m over the 4 days following the release, at intervals ranging from 30 min to 15 h. High HTO concentrations were observed immediately after the release as the HT was converted to HTO by microorganisms in the soil and reemitted to the atmosphere. The HTO concentrations dropped off quickly over the first 3 h as the wind carried the resuspended plume away from the sampling site, but recovered at hour 6 as the wind returned to the site. Concentrations subsequently showed an overall decrease, with occasional fluctuations depending on meteorological conditions. The Canadian results showed the same general tendencies, with a rapid buildup of HTO followed by fluctuating concentrations superimposed on a gradual downward trend.

Models The few models capable of simulating the buildup of HTO in the environment following an HT release to air are all process-oriented models. For example, in the ETMOD code [103], diffusion of HT into the soil and its subsequent oxidation is described by a first-order reaction and diffusion model based on Fick's law [105]. The reaction coefficient for oxidation is expressed in terms of a deposition velocity, which is given by the resistance approach (Eq. 7). All deposited HT is assumed transformed into HTO. Once the soil HTO concentration is known, the rate of HTO reemission to the atmosphere is calculated using Eq. 10. HTO air concentrations due to reemission are then determined by breaking the contaminated surface into a number of cells, using a dispersion model to calculate the air concentration at the location of interest due to each cell, and summing over all cells. The ability to model reemission is crucial for an HT release, where there is no direct airborne HTO plume. Once the air concentration is known, concentrations in plants can be determined using Eq. 8.

Aquatic Releases of HTO

Observations *Concentrations in Mussels Following an Abrupt Increase in Ambient Tritium Levels:* In an experiment carried out at Chalk River Laboratories (CRL) of AECL [57], freshwater Barnes mussels (*Elliptio complanata*) were transplanted from an area in the Ottawa River with background tritium concentrations (<10 Bq L^{-1}) to Perch Lake, a small lake on CRL property that has elevated tritium concentrations ($\sim$4,500 Bq L^{-1}). The mussels, which were all about 14–15 years old, were placed in cages at the sediment-to-water interface at a depth of approximately 0.4 m in

an area of the lake where many mussels are found naturally. Each cage was filled with 5–10 cm of sandy surface sediments originating from the area surrounding the cages, a depth that enabled mussels to position themselves in an upright position with their siphons pointed upward. Following transplantation, the mussels were sampled on an expanding time step over the course of an 86-day period. The HTO and OBT concentrations were measured in the soft tissue of each mussel sample to follow the buildup of tritium in the animals over time.

The HTO concentration in the mussels increased very quickly over time, becoming essentially identical to the water concentration within 2 h of transplantation. The OBT concentration also increased rapidly in this period, but more slowly than the HTO concentration, reaching about 25% of the water concentration after 2 h (Fig. 4). The OBT concentration continued to increase thereafter, but at a slower rate, attaining about 50% of the water concentration 40 days after transplantation. Unexpectedly, the concentration dropped by a factor of 2 between this time and the last sampling point 84 days after transplantation. This may be due to the reproductive behavior of the animals. Mussel gonads and embryos grow rapidly in midsummer and may have incorporated tritium at a faster rate than other tissues. Release of the larvae and sperm into the water column between mid-August (when the second last mussel sample was taken) and early October (when the last sample was taken) may have caused the decline in the OBT concentration in the mussels.

Models Dynamic compartment models are usually used to simulate tritium transfer in aquatic systems subject to short-term releases. Transfers between compartments are based on published rates of tritium uptake and loss by aquatic plants and animals. Plants assimilate HTO from the water column and, for rooted plants, from sediments; animals also take up HTO from these sources and additionally from the food chain. However, the water column is by far the dominant source and HTO concentrations in plants and animals can usually be expressed in terms of the time-dependent water concentration. A single compartment representing the aqueous phase in the plant or animal is usually sufficient for this purpose. For aquatic systems subject to an increase in water concentration from an initial value of C_w^i to a final value of C_w^f, the HTO concentration (C_{HTO}) in plants and animals is given by

$$C_{HTO} = C_w^i + C_w^f[1 - \exp(-k_u t)] \quad (12)$$

Here k_u is the rate at which tritium is taken up by the plant or animal from the water column. If the water concentration decreases to zero from a value of C_w^f, the time-dependent HTO concentration varies as

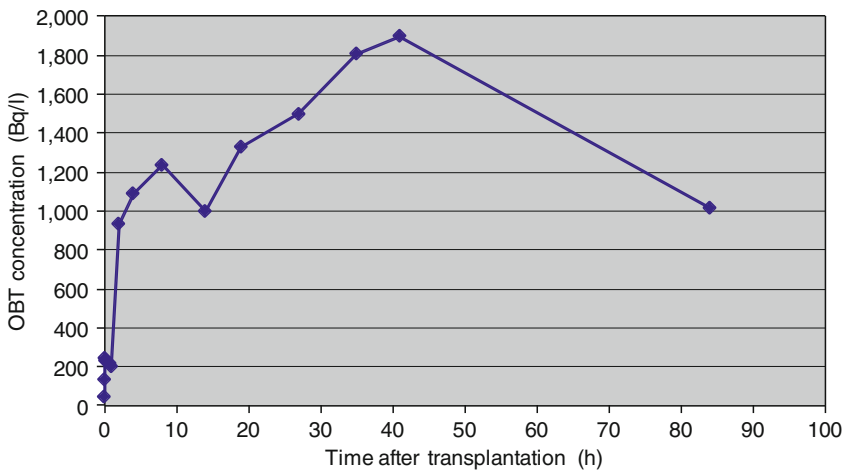

Tritium in the Environment. Figure 4
OBT concentration in mussels as a function of time after transplantation

$$C_{HTO} = C_w^f \exp(-k_l t), \quad (13)$$

where k_l is the rate at which tritium is lost from the organism. The rate constants k_u and k_l may be different for uptake and loss and for plants and animals, but they typically have values greater than 2 or 3 h^{-1}, implying that the HTO concentration in plants and animals comes into equilibrium with the new water concentrations in minutes or hours.

The basic mechanism of OBT formation in aquatic plants, as in terrestrial plants, is photosynthesis. Heling and Galeriu [116] proposed the following equation for the OBT concentration in phytoplankton (C_{OBT}^p):

$$\frac{dC_{OBT}^p}{dt} = 0.4 \cdot \mu \cdot f_D \cdot C_W - \mu \cdot C_{OBT}^p \quad (14)$$

Here f_D is the dry mass fraction of the phytoplankton and μ is their growth rate, which depends on light levels, water temperature, and the amount of waterborne nutrients.

For aquatic animals, OBT is formed by the metabolization of HTO in the body and by the direct incorporation of OBT taken in with food. The OBT concentration in the animal (C_{OBT}^p) is given by [117]:

$$\frac{dC_{OBT}^a}{dt} = \alpha\ C_f(t) + \beta\ C_w(t) - \kappa\ C_{OBT}^a \quad (15)$$

Here C_f is the OBT concentration in the animal's food, α is the transfer coefficient from HTO in water to OBT in the animal, β is the transfer coefficient from OBT in food to OBT in the animal, and κ is the loss rate of OBT from the animal.

The values of α, β, κ, and C_f all depend on the type of aquatic animal in question. The key parameter is κ, the OBT biological loss rate, which reflects both the growth rate of the animal and metabolic losses by respiration, and depends on animal mass, daily consumption rate, water temperature, and net assimilation efficiency. For zooplankton, values of κ range from 0.19 to 0.7 d^{-1}, with an average of 0.3 d^{-1}. Mollusks and crustaceans show large variability and must be considered case by case [118]. For mollusks with a weight near 1 g, κ ~0.02 d^{-1}; this decreases to 0.005 d^{-1} at about 30 g. An average value for crustaceans is 0.007 d^{-1}. A special example is the mussel *Mytilus edulis*, which is taken as a reference animal for radioprotection purposes. Based on experimental data on respiration, the OBT loss rate (at 10°C) decreases from 0.012 to 0.006 d^{-1} as the fresh weight increases from 5 to 80 g. Similarly, κ differs by a factor of 3 for different mussel species of similar mass. For small fish, κ is in the range 0.03–0.14 d^{-1}. Data for larger fish are missing but smaller values are expected. The large range for κ demonstrates the need to choose a value specific to the animal in question in each modeling application.

For some aquatic animals such as mussels, the predictions of models with a single OBT compartment are often not in satisfactory agreement with observations. For these animals, the experimental data can be better reproduced by multi-compartment models. For example, the single OBT compartment can be broken down into two, one with a fast OBT loss rate and one with a slow rate. Alternatively, a separate compartment representing stomach contents can be added to the model to account for OBT associated with food that had not yet been digested.

Model Validation and Uncertainty

Environmental transport models are only representations of reality, and their predictions must be validated before they can be used with confidence. Most testing of environmental tritium models has taken place in international model validation programs such as BIOMOVS II (Biosphere Model Validation Study Phase II [119]), BIOMASS (Biosphere Model Assessment [61]), EMRAS (Environmental Modeling for Radiation Safety [26]), and EMRAS II (Environmental Modeling for Radiation Safety Phase II [120]), each of which included a working group on tritium. In each program, the validity of the participating models was determined by comparing their predictions with data obtained in laboratory or field studies, or with the predictions of other models. The test scenarios covered terrestrial and aquatic ecosystems and steady-state and dynamic conditions.

For most scenarios, the predictions of the various models tended to bracket the observations, suggesting that, in an average sense, the models reflect a good conceptual understanding of the environmental transport of tritium. However, the predictions of any given model differed from the observations by a factor of 2 for scenarios involving continuous releases, and by a factor of 10 or more for short-term releases.

In particular, the dynamics of OBT concentrations in plants and animals were poorly reproduced in scenarios involving short-term releases.

Galeriu et al. [109] tested the dynamic animal model described above with experimental data. In most cases, the model gave predictions that lay within a factor of 2 of the observations. An exception occurred for sheep fed a single intake of tritium-labeled glucose and acetate. In this case, the model predictions were a factor of 3–4 lower than the observations. This may have been due to the specific labeled compounds used in the study, which may not have mimicked items in the real diet. Alternatively, it may have been caused by the inability of the model to simulate the specifics of ruminant digestion of compounds in the diet. The predictions of tritium concentrations in bioassay media (urine and blood) after various intakes were of special interest, because these can be used in dosimetry. The model performed well in predicting OBT concentrations in blood after an HTO intake, but for a single OBT intake the model failed to predict OBT concentrations during the first few days. This reflects the simplified model assumption of a single metabolic pool (and a single transfer rate) for organs.

Participants in the various model validation programs also estimated the uncertainties in their predictions. For HTO endpoints in steady-state scenarios, these were roughly consistent with a 95% confidence interval (97.5th percentile divided by the 2.5th percentile) of a factor 3–4. Uncertainties were slightly higher for OBT concentrations, since the uncertainties in OBT include those for HTO plus additional ones specific to OBT itself. For scenarios involving short-term releases, the 95% confidence intervals on HTO concentrations were about a factor of 10 shortly after exposure, and larger at later times. The confidence intervals were generally smaller for OBT than for HTO, reflecting the fact that, for dynamic scenarios, HTO varies rapidly over time whereas OBT integrates.

These results are consistent with a formal uncertainty analysis of the UFOTRI code, a dynamic, process-oriented model for simulating the environmental transfer of tritium following an accidental release [121]. The calculations were carried out for a scenario involving a short-term release of HTO to the atmosphere over an agricultural area. The 95% confidence interval was estimated to cover a factor of 10 for HTO concentrations in plant leaves and a factor of 4 for OBT concentrations in edible plant parts at harvest. These estimates reflect the uncertainty due to parameter values only and do not include uncertainties due to model structure. The uncertainties were largest for concentrations predicted immediately after exposure and decreased slightly thereafter.

The uncertainties in the models can be reduced by

- Ensuring that the air concentrations used to drive the models are of high quality and match the resolution and averaging requirements of the scenario
- Incorporating as much site-specific information as possible on land use, local soil properties, and predominant crop cultivars and animal breeds
- Basing all sub-models on the physical approaches available for the disciplines in question. For example, knowledge from the agricultural sciences should be used to improve models for crop growth, photosynthesis, translocation, and so on. Recent progress in understanding environmental hydrogen cycling should also be considered
- Recognizing and accounting for any unusual experimental conditions (water stress, an uncommon cultivar or breed) in the model application
- Using suitable spatial and temporal averaging in the models. Predicted OBT concentrations in plants and animals should be based on air concentrations averaged over the month or two prior to sampling
- Using realistic plant and animal growth models in the calculations
- Incorporating changing meteorological and environmental conditions in the models in a dynamic way
- Developing a standard conceptual model for accidental releases (an ongoing project in the EMRAS II program)

Future Directions

Future experimental work on tritium transfer in the environment should focus on the processes that are most poorly understood, namely:

- Plant uptake of HTO at night and when it is raining
- OBT formation in plants at night
- Translocation of OBT to fruit and roots
- Isotopic discrimination

- Tritium behavior in soils following deposition, including deposition of HT and conversion to HTO
- Tritium behavior in winter, including washout by snow, dry deposition to snow, and the fate of tritium in the snow pack
- The uptake and metabolism of tritium by animals

In addition, further experimental work is needed to confirm and explain previous observations in the following two areas:

- The large OBT/HTO ratios that have been observed in soils, plants and fish under conditions that are ostensibly at equilibrium
- The existence and magnitude of buried tritium

Environmental tritium models should be modified to reflect the knowledge gained through new experimental work in the areas discussed above. In addition, steady-state models for chronic releases should be revised to account for the fact that fluctuations in release rates and meteorological conditions result in a state of quasi-equilibrium in the environment, rather than the complete equilibrium assumed by the models. A rigorous sensitivity analysis of dynamic models for a variety of scenarios would be useful in establishing priorities for future work.

Finally, the uncertainty in the measurement of OBT concentrations in environmental samples, especially at low levels, is large. Certified reference materials and standard analytical procedures are needed to reduce this uncertainty and provide more confidence in the measurements.

Further work along the lines suggested above will result in better understanding of tritium behavior and concentrations in the environment, and an improved ability to estimate doses due to exposure to tritium released to air or water.

Appendix A

Definition of Organically Bound Tritium (OBT) Proposed by the EMRAS Tritium and C-14 Working Group

Definition OBT is carbon-bound and buried tritium formed in living systems through natural environmental or biological processes from HTO (or HT via HTO). Other types of organic tritium (e.g., tritiated methane, tritiated pump oil, and radiochemicals) should be called tritiated organics, which can exist in any chemical or physical form.

Notes

1. Buried tritium is tritium that occupies exchangeable positions in large biomolecules in dry matter but that is not removed by rinsing with tritium-free water. Buried tritium therefore contributes to the OBT concentration in the traditional experimental determination of OBT. It is analogous to buried hydrogen in biochemistry.
2. OBT should not include tritium bound to sulfur, nitrogen, or oxygen (exchangeable OBT) that can be removed by washing with tritium-free water. This fraction depends strongly on the HTO concentration in effect at the time of sampling and can exchange with water vapor during analysis. Inclusion of the exchangeable fraction would lead to measurements that are highly variable and difficult to interpret.
3. From an analytical perspective, OBT is the activity in dry biomatter that is not exchangeable with water. In measuring OBT concentrations, exchangeable OBT should first be removed by moderately drying the sample without decomposing the organic molecules, washing the residue repeatedly with tritium-free water, and then drying the material again. The OBT concentration can then be determined as the tritium activity in the dry sample. This is generally done by combusting the sample and determining the activity in the combustion water by liquid scintillation counting, or by analyzing the sample by He-3 mass spectrometry. There are no generally accepted standard techniques for measuring OBT and the methods used should be documented when reporting results.
4. In the washing process, exchangeable tritium nuclei are removed and replaced by hydrogen nuclei, but exchangeable hydrogen nuclei are simply replaced by other hydrogen nuclei. Thus, measurements of OBT do not reflect the specific activity of the non-exchangeable hydrogen. This specific activity can be estimated by dividing the measured concentration by the fraction of hydrogen nuclei in the dry sample that are non-exchangeable. For example, this

fraction has been empirically determined to be 0.78 for leaf tissues, but different values may apply for other plant or animal materials. Care must be taken in comparing model predictions and experimental data that the same quantity (OBT concentration or specific activity of non-exchangeable hydrogen nuclei) is being considered.

5. OBT concentrations should be reported in units of Bq L^{-1} of combustion water. This is the fundamental unit that can be converted, if necessary, to the specific activity of the non-exchangeable hydrogen nuclei. Use of Bq L^{-1} makes it easy to compare concentrations in different media and to determine whether specific activity is depleted, preserved, or enriched when tritium is transferred from one compartment to another.
6. OBT refers to organic tritium formed from HTO by natural processes in living organisms, or in materials such as soils or lake sediments that are derived from living material. Put another way, OBT is that organic tritium found in a normal diet that imparts a dose consistent with the ICRP ingestion dose coefficient for OBT. All other types of organic tritium, no matter how they form or how they appear in the environment, should be called tritiated organics and assigned their own dose coefficient for purposes of dose calculation.

Bibliography

Primary Literature

1. Okada S, Momoshima N (1993) Overview of tritium: characteristics, sources, and problems. Health Phys 65:595–609
2. Kim SB, Workman WJG, Davis PA, Yankovich T (2004) Tritium concentrations in the Perch Lake aquatic ecosystem. AECL Report CTD-03700-ENA-003. Chalk River Laboratories, Chalk River
3. Diabate S, Strack S (1993) Organically bound tritium. Health Phys 65:698–712
4. Belot Y (1986) Tritium in plants: a review. Radiat Prot Dosim 16:101–105
5. Dunstall TG, Ogram GL, Spencer FS (1985) Elemental tritium deposition and conversion in the terrestrial environment. Fusion Technol 8:2551–2556
6. Williams JL, Russ RM, McCubbin D, Knowles JF (2001) An overview of tritium behaviour in the Severn Estuary (UK). J Radiol Prot 21:337–344
7. Fairlie I (1992) Tritium: the overlooked nuclear hazard. Ecologist 22:228–232
8. Belot Y, Ganthier K, Camus H, Caput C (1979) Prediction of the flux of tritiated water from the air to plant leaves. Health Phys 37:575
9. Garland JA (1979) Transfer of tritiated water vapour to and from land surfaces. In: Behaviour of tritium in the environment, IAEA-SM-232/74, Vienna, pp 349–358
10. Täschner M, Bunnenberg C, Camus H, Belot Y (1995) Investigations and modeling of tritium re-emission from soil. Fusion Technol 28:976–981
11. Hicks BB, Baldocchi DD, Meyers TP, Hosker JR, Matt DR (1987) A preliminary multiple resistance routine for deriving dry deposition velocities from measured quantities. Water Air Soil Pollut 36:311–330
12. Feinhals J, Bunnenberg C (1988) Laboratory investigations of HTO deposition to soils. Fusion Technol 14:1253
13. Murphy CE Jr (1984) The relationship between tritiated water activities in air, vegetation and soil under steady-state conditions. Health Phys 47:635–639
14. Atarashi M, Amano H, Ichimasa M, Ichimasa Y (1998) Deposition of D_2O from air to plant and soil during an experiment of D_2O vapor release into a vinyl house. Fusion Eng Des 42:133–140
15. Strack S, Diabate S, Raskob W (2005) Organically bound tritium in plants: insights gained by long-term experience in experimental and modeling research. Fusion Sci Technol 48:767–770
16. Murphy CE Jr (1993) Tritium transport and cycling in the environment. Health Phys 65:683–697
17. NCRP (1979) Tritium in the environment. National Commission on Radiation Protection report no. 62, Bethesda
18. Moses V, Calvin M (1959) Photosynthesis studies with tritiated water. Biochim Biophys Acta 33:297–312
19. Thompson RG, Nelson CD (1971) Photosynthetic assimilation and translocation of ^{3}H- and ^{14}C-organic compounds after ^{3}HHO and $^{14}CO_2$ were simultaneously offered to a primary leaf of soybean. Can J Bot 49:757–766
20. Indeka L (1981) Incorporation of tritiated water from the atmosphere into aqueous and organic components of plants. In: Jaworowski Z (ed) Biological incorporation of tritium. Final report to the United States Environmental Protection Agency concerning research contract no. 05-536-3, CLOR-115/D, pp 21–27
21. Diabate S, Strack S (1997) Organically bound tritium in wheat after short-term exposure to atmospheric tritium under laboratory conditions. J Environ Radioactiv 36:157–175
22. McFarlane JC (1976) Tritium fractionation in plants. Environ Exp Bot 16:9–14
23. Garland JA, Ameen M (1979) Incorporation of tritium in grain plants. Health Phys 36:35–38
24. Baumgärtner F, Donhärl W (2004) Non-exchangeable organically bound tritium (OBT): its real nature. Anal Bioanal Chem 379:204–209
25. Baumgärtner F (2005) Accumulative tritium transfer from water into biosystems. Fusion Sci Technol 48:787–790
26. IAEA (2010) Modeling the environmental transfer of tritium and carbon-14 to biota and man. Final report, Tritium and

Carbon-14 Working Group, IAEA EMRAS Program. International Atomic Energy Agency, Vienna
27. Ware A, Allott RW (1999) Review of methods for the analysis of total tritium and organically bound tritium. National Compliance Assessment Service technical report NCAS/TR/99/003
28. Robertson JS (1973) Tritium turnover rates in mammals. In: Moghissi AA, Carver MW (eds) Tritium. Messenger Graphics, Phoenix, pp 322–326
29. van den Hoek J, Kirchmann R, Juan NB (1979) Transfer and incorporation of tritium in mammals. In: Behaviour of tritium in the environment. International Atomic Energy Agency, Vienna, pp 433–444, IAEA-SM-232/74
30. van den Hoek J, ten Have MHJ, Gerber GB (1983) The metabolism of tritium and water in the lactating dairy cow. Health Phys 44:127–133
31. Hodgson A, Scott JE, Fell TP, Harrison JD (2005) Dose from the consumption of Cardiff Bay flounder containing organically bound tritium. J Radiol Prot 25:149–159
32. NCAS (2001) Potential for bio-accumulation of organically bound tritium in the environment: review of monitoring data. National Compliance Assessment Service technical report NCAS/TR/2000/026
33. Kirchmann R, Charles P, van Bruwaene R, Remy J, Koch G, van den Hoek J (1977) Distribution of tritium in the different organs of calves and pigs after ingestion of various tritiated feeds. Curr Top Radiat Res Quart 12:291–312
34. van den Hoek J, ten Have MHJ, Gerber GB, Kirchmann R (1985) The transfer of tritium-labeled organic material from grass into cow's milk. Radiat Res 103:105–113
35. Galeriu D, Beresford NA, Takeda H, Melintescu A, Crout NMJ (2003) Towards a model for the dynamic transfer of tritium and carbon in mammals. Radiat Prot Dosim 105:387–390
36. Hill RL, Johnson JR (1993) Metabolism and dosimetry of tritium. Health Phys 65:628–647
37. Rudran K (1988) Significance of in vivo organic binding of tritium following intake of tritiated water. Radiat Prot Dosim 25:5–13
38. CERRIE (2004) Tritium: properties, metabolism and dosimetry. Committee Examining Radiation Risks of Internal Emitters, London
39. Friedrich B, Schwartz E (1993) Molecular biology and hydrogen utilization in aerobic chemolithotrophs. Annu Rev Microbiol 47:351
40. Ichimasa Y, Ichimasa M, Jiang H, Katsuno K (1995) In vitro determination of HT oxidation activity and tritium concentration in soil and vegetation during chronic HT release experiment at Chalk River. Fusion Technol 28:877–882
41. McFarlane JC, Rogers RD, Bradley DV (1978) Environmental tritium oxidation in surface soil. Environ Sci Technol 12: 590–593
42. Bunnenberg C, Feinhals J, Wiener B (1986) Differences in the behaviour of HTO and H_2O in soil after condensation from the atmosphere and conversion of HT to HTO and OBT in soil relative to moisture content and pore volume. Radiat Prot Dosim 14:83–87
43. Spencer FS, Vereecken-Sheehan L (1994) HTO relationships between air, soil and vegetation and seasonal dependence of HTO deposition to soil. Ontario Hydro report A-NBP-94-36-K, Toronto
44. Dunstall TG, Ogram GL (1991) Diffusion and biological oxidation as component processes regulating the deposition of tritiated hydrogen to soils. Ontario Hydro report 90-235-K, Toronto
45. Fallon RD (1982) Influences of pH, temperature and moisture on gaseous tritium uptake in surface soils. Appl Environ Microbiol 44:171–178
46. Förstel H (1986) Uptake of elementary tritium by the soil. Radiat Prot Dosim 16:75–81
47. Garland JA, Cox LC (1980) The absorption of tritium gas by English soils, plants and the sea. Water Air Soil Pollut 14: 103–114
48. Sweet CW, Murphy CE Jr (1981) Oxidation of molecular tritium by intact soils. Environ Sci Technol 15:1485–1487
49. Wiener B, Täschner M, Bunnenberg C (1988) Tritium pathways in the atmosphere-soil system after a HT release. Niedersaechsisches Institut fuer Radiooekologie (NIR), Hannover
50. Davis PA, Workman WJG, Amiro BD, Spencer FS, Noguchi H, Amano H, Ichimasa Y, Ichimasa M (1995) Overview of the 1994 chronic HT release experiment at Chalk River. Fusion Technol 28:840–845
51. Brown RM, Ogram GL, Spencer FS (1990) Oxidation and dispersion of HT in the environment: the August 1986 field experiment at Chalk River. Health Phys 58:171–181
52. Conrad R (1988) Biogeochemistry and ecophysiology of atmospheric CO and H_2. Adv Microb Ecol 10:231–283
53. Spencer FS, Dunstall TG (1986) Molecular tritium conversion in vegetation, litter and soil. Radiat Prot Dosim 16:89–93
54. Sweet CW, Murphy CE Jr (1984) Tritium deposition in pine trees and soil from atmospheric releases of molecular tritium. Environ Sci Technol 18:358–361
55. Horton JH, Corey JC, Wallace RM (1971) Tritium loss from water exposed to the atmosphere. Environ Sci Technol 5:338–343
56. Blaylock BG, Hoffman FO, Frank ML (1986) Tritium in the aquatic environment. Radiat Prot Dosim 16:65–71
57. Yankovich TL, Kim SB, Baumgärtner F, Galeriu D, Melintescu A, Miyamoto K, Saito M, Siclet F, Davis PA (2010) Measured and modeled tritium concentrations in freshwater Barnes mussels (Elliptio complanata) exposed to an abrupt increase in ambient tritium levels. J Environ Radioact (in press)
58. Galeriu D, Takeda H, Melintescu A, Trivedi A (2005) Energy metabolism and human dosimetry of tritium. Fusion Sci Technol 48:795–798
59. Rodgers DW (1992) Tritium dynamics in juvenile rainbow trout, Salmo gairdneri. Health Phys 63:331–337
60. Ostlund HG, Fine RA (1979) Oceanic distribution and transport of tritium. In: Behaviour of tritium in the environment. International Atomic Energy Agency, Vienna, pp 301–311, IAEA-SM-232/74

61. IAEA (2003) Modeling the environmental transport of tritium in the vicinity of long-term atmospheric and sub-surface sources. BIOMASS-3. International Atomic Energy Agency, Vienna
62. IAEA (2010) Handbook of parameter values for the prediction of radionuclide transfer in terrestrial and freshwater environments. Technical report series no. 472. International Atomic Energy Agency, Vienna
63. Davis PA, Kotzer TG, Workman WJG (2002) Environmental tritium concentrations due to continuous atmospheric sources. Fusion Sci Technol 41:453–457
64. Melintescu A, Galeriu D (2005) A versatile model for tritium transfer from atmosphere to plant and soil. Radioprotection 40(Suppl 1):S437–S442
65. Spencer FS (1984) Tritiated water uptake kinetics in tissue-free water and organically bound fractions of tomato plants. Ontario Hydro Research Division, Toronto, Report No. 84-69-K
66. CSA (2009) Guidelines for calculating derived release limits for radioactive material in airborne and liquid effluents for normal operation of nuclear facilities. Canadian Standard Association Standard N288.1
67. Kim M-A, Baumgärtner F (1994) Equilibrium and non-equilibrium partition of tritium between organics and tissue water of different biological systems. Appl Radiat Isot 45:353–360
68. Guenot J, Belot Y (1984) Assimilation of ^{3}H in photosynthesizing leaves exposed to HTO. Health Phys 47:849–855
69. Evans AG (1969) New dose estimates from chronic tritium exposures. Health Phys 16:57–63
70. Raskob W (1994) Description of NORMTRI: a computer program for assessing the off-site consequences from air-borne releases of tritium during normal operation of nuclear facilities. Kernforschungszentrum Karlsruhe, Karlsruhe, Report KfK-5364
71. Peterson S-R, Davis PA (2002) Tritium doses from chronic atmospheric releases: a new approach proposed for regulatory compliance. Health Phys 82:213–225
72. Galeriu D, Crout NMJ, Melintescu A, Beresford NA, Peterson S-R, Van Hess M (2001) Metabolic derivation of tritium transfer factors in animal products. Radiat Environ Biophys 40:325–334
73. Galeriu D, Melintescu A, Takeda H (2007) Risk from tritium exposure. IRPA Regional Congress for Central and Eastern Europe, Brasov. www.irpa2007romania.com
74. Davis PA, Galeriu DC, Spencer FS, Amiro BD (1995) Evolution of HTO concentrations in soil, vegetation and air during an experimental chronic HT release. Fusion Technol 28:833–839
75. Davis PA, Bickel GA (2000) Environmental HTO/HT ratios arising from a chronic atmospheric HT release. In: Proceedings of the international workshop on the environmental behavior and biological effects of tritium, Osaka
76. Neil BCJ (1991) An environmental pathway model for chronic emissions of tritiated hydrogen gas. Ontario Hydro report HSD-ST-91-21, Toronto
77. Kirchmann R, Bonotto S, Soman SD, Krishnamoorthy TM, Iyengar TS, Moghissi AA (1979) Transfer and incorporation of tritium in aquatic organisms. In: Behaviour of tritium in the environment. International Atomic Energy Agency, Vienna, IAEA-SM-232/96
78. Eaton D, Murphy CE Jr (1992) Tritium uptake by fish in a small stream. Westinghouse Savannah River Company report WRSC-TR-92-193-Rev 1, Aiken
79. Elwood JW (1971) Tritium behaviour in fish from a chronically contaminated lake. In: Proceedings of the 3rd national symposium on radioecology, Oak Ridge, 10–12 May 1971, pp 435–439
80. Blaylock BG, Frank ML (1979) Distribution of tritium in a chronically contaminated lake. In: Behaviour of tritium in the environment. International Atomic Energy Agency, Vienna, p 711, IAEA-SM-232/74
81. Patzer RG, Moghissi AA, McNelis DN (1973) Accumulation of tritium in various species of fish reared in tritiated water. In: Symposium on environmental behaviour of radionuclides released in the nuclear industry, Aix-en-Provence. International Atomic Energy Agency, Vienna, p 403
82. Strand JA, Templeton WL, Olson PA (1976) Fixation and long-term accumulation of tritium from tritiated water in an experimental aquatic environment. In: Watson JS, Wiffen FW (eds) Radiation effects and tritium technology for fusion reactors. Gatlinburg, TN, pp III-77–95
83. NCRP (1996) Screening models for releases of radionuclides to atmosphere, surface water, and ground. Report number 123, National Council on Radiation Protection and Measurements, Bethesda
84. Bird GA, Stephenson M, Cornett RJ (1993) The surface water model for the assessment of Canada's nuclear fuel waste management concept. Waste Manage 13:153–170
85. Koenig LA, Fark S, Hempelman S, Langguth KG, Paglioisa G, Papadopoulos D, Strack S (1987) Untersuchungen zum transport von tritium in der umvelt. Kernforschungs-zentrum Karlsruhe, Karlsruhe, Report KfK 4131
86. Hisamatsu S, Takizawa Y, Itoh M, Ueno K, Katsumata T, Sakanoue M (1989) Further study on fallout ^{3}H ingestion in Akita, Japan. Health Phys 57:559–563
87. Takashima Y, Momoshima N, Kaji T (1989) High specific activity of organically bound tritium in pine needles and search for its cause in the environment. In: Tritium radiobiology and health physics. Institute of Plasma Physics, Nagoya, pp 46–58, Report No. IPPY-REV-3
88. Brown RM (1988) Assessment of the significance of organically bound tritium in environmental materials. Atomic Energy Control Board report no. INFO-0283, Ottawa
89. Pointurier F, Baglan N, Alanic G, Chiappini R (2003) Determination of organically bound tritium background level in biological samples from a wide area in the south-west of France. J Environ Radioactiv 68:171–189
90. Jean-Baptiste P, Baumier D, Fourre E, Dapoigny A, Clavel B (2007) The distribution of tritium in the terrestrial and aquatic environments of the Creys-Malville nuclear power plant (2002–2005). J Environ Radioactiv 94:107–118
91. Turner A, Millward GE, Stemp M (2009) Distribution of tritium in estuarine waters: The role of organic matter. J Environ Radioactiv 100:890–895

92. McCubbin D, Leonard KS, Bailey TA, Williams J, Tossell P (2001) Incorporation of organic tritium (^{3}H) by marine organisms and sediment in the Severn estuary/Bristol channel (UK). Mar Pollut Bull 42:852–863
93. Environmental Agency (2001) Potential for bio-accumulation of organically bound tritium in the environment: review of monitoring data. National Compliance Assessment Service technical report, NCAS/TR/2000/026
94. Strack S, Kistner G, Emeis C (1979) Incorporation of tritium into plancktonic algae in a continuous culture under dynamic equilibrium. In: Behaviour of tritium in the environment. International Atomic Energy Agency, Vienna, p 219, STI/PUB/498
95. Strack S, Bonotto S, Kirchmann R (1980) Radioactive contamination of the marine environment: uptake and distribution of H^3 in Dunaliella bioculatas. Helgoländer Meeresunters 33:153–163
96. Strack S, Kirchmann R, Luttke A, Bonoto S (1983) Selective accumulation of organically bound tritium in the marine unicelular algae Dunaliella bioculatas and Acetabularia mediterranea. Int J Appl Radiat Isot 34:865–869
97. Kim SB (2010) Unpublished data. AECL, Chalk River Laboratories, Chalk River
98. Smith GM, Robinson PC, Stenhouse MJ (1995) H-3 foodchain modelling following short-term release to atmosphere. Report IE3947-1, version 2.0, Intera Information Technologies, Henley-on-Thames
99. Higgins NA, Shaw PV, Haywood SM, Jones JA (1996) TRIF, a dynamic model for predicting the transfer of tritium through the terrestrial foodchain. National Radiological Protection Board report, NRPB-R278
100. Watkins BM, Robinson PC, Smith GM (1998) Update of models for assessing short-term atmospheric releases of C-14 and tritium in the light of new information and experimental data. Ministry of Agriculture Fisheries and Food, London, Report MAFF-5044-1
101. Raskob W (1993) Description of the new version 4.0 of the tritium model UFOTRI including user guide. Kernforschungszentrum Kalsruhe, Karlsruhe, Report KfK-5194
102. Russell SB, Ogram GL (1992) ETMOD: a new environmental tritium model. Fusion Technol 21:645–650
103. Thompson JW, Kennedy JA, Lina JM (1992) ETMOD software quality assurance documentation, vol I. CFFTP P-9205/CFFTP-03421 (577), Canadian Fusion Fuels Technology Project, Toronto
104. Atanassov D, Galeriu D (2010) Rain scavenging of tritiated water vapour: a numerical Eulerian stationary model. J Environ Res (submitted)
105. Kirkham D, Powers WL (1972) Advanced soil physics. Wiley-Interscience, New York
106. Brutsaert WH (1982) Evaporation into the atmosphere. D. Reidel, Dordrecht
107. Goudriaan J (1986) A simple and fast numerical method for the computation of daily totals of crop photosynthesis. Agric For Meteorol 38:249–254
108. Sellers PJ (1985) Canopy reflectance, photosynthesis and transpiration. Int J Remote Sens 6:1335–1372
109. Galeriu D, Melintescu A, Beresford NA, Takeda H, Crout NMJ (2009) The dynamic transfer of ^{3}H and ^{14}C in mammals – a proposed generic model. Radiat Environ Biophys 48:29–45
110. Melintescu A, Galeriu D (2010) Energy metabolism used as a tool to model the transfer of ^{14}C and ^{3}H in animals. Radiat Environ Biophys (submitted)
111. Paillard Ph, Calando JP, Clerc H, Gros R, Belot Y (1988) Tritium release experiment in France: Results concerning HT/HTO conversion in the air and soil. Fusion Technol 14: 1226–1230
112. Djerassi H, Gulden W (1988) Overview of the tritium release experiment in France. Fusion Technol 14:1216–1221
113. Wiener B, Täschner M, Bunnenberg C (1988) HTO re-emission from soil after HT deposition and dose consequences of HT releases. Fusion Technol 14:1247–1252
114. Burnham CD, Brown RM, Ogram GL, Spencer FS (1988) An overview of experiments at Chalk River on HT dispersion in the environment. Fusion Technol 14:1159–1164
115. Russell SB, Ogram GL (1988) Modelling elemental tritium deposition, conversion and re-emission using Ontario Hydro's tritium dispersion code. Fusion Technol 14: 1193–1198
116. Heling R, Galeriu D (2002) Modification of LAKECO-B for ^{3}H. NRG report P20874/02.55114/I, Arnhem
117. Galeriu D, Heling R, Melintescu A (2005) The dynamics of tritium- including OBT- in the aquatic food chain. Fusion Sci Technol 48:779–782
118. Melintescu A (2009) Modelling the tritium impact on the environment. Seminar held at Universidad Politecnica de Madrid, Department of Nuclear Engineering, Madrid. http://www.din.upm.es/drupal/files/Conf-Tritium-AMelintescu.pdf
119. Barry PJ, Watkins BM, Belot Y, Davis PA, Edlund O, Galeriu D, Raskob W, Russell S, Togawa O (1998) Intercomparison of model predictions of tritium concentrations in soil and foods following acute airborne HTO exposure. J Environ Radioactiv 42:191–207
120. IAEA (2010) Environmental modeling for radiation safety – phase II (EMRAS II). http://www-ns.iaea.org/projects/emras/emras2/default.htm
121. Galeriu DC, Davis PA, Chouhan S, Raskob W (1995) Uncertainty and sensitivity analysis for the environmental tritium code UFOTRI. Fusion Technol 28:853–858

Books and Reviews

Moghissi AA, Carver MW (eds) (1973) Tritium. Messenger Graphics, Phoenix

IAEA (1979) Behaviour of tritium in the environment. International Atomic Energy Agency, Vienna, IAEA-SM-232/74

(1993) Health Phys 65, Special issue on the environmental behaviour and dosimetry of tritium

(1997) J Environ Radioactiv 36, Special issue on environmental tritium

Tritium, Health Effects and Dosimetry

Kevin Bundy, Bertrand Thériault, Rachel Lane, Julie Burtt, Patsy Thompson
Directorate of Environmental and Radiation Protection and Assessment, Canadian Nuclear Safety Commission, Ottawa, ON, Canada

Article Outline

Glossary
Definition of the Subject
Introduction
Physical, Chemical, and Radioactive Properties of Tritium
Adverse Health Effects Due to Tritium
Relative Biological Effectiveness
Future Directions
Abbreviations
Bibliography

Glossary

Absorbed dose The energy deposited by ionizing radiation to a suitably small volume of matter divided by the mass of that volume. Unit gray, symbol Gy.

Beta particles High-energy negatively charged electrons or positively charged positrons that are ejected by radioactive (unstable) elements as they decay. A beta particle is identical in mass and charge to an electron. Beta particles are relatively small and can be stopped, for example, by a sheet of aluminum a few millimeters thick.

Biokinetic model A mathematical description of the behavior of radionuclides in the metabolic processes of cells, tissues, organs, and organisms. It is most frequently used to describe distribution of radionuclides among tissues and excretion.

Biological half-life Of a given radionuclide, the time required for the activity to decrease, by biological clearance, to half of its original activity.

Carcinogen Any agent, such as a chemical or a form of radiation that can cause cancer.

Chromosome Structure composed of a very long DNA molecule and associated proteins that carries part (or all) of the hereditary information of an organism.

Chromosome aberrations Damage to chromosomes resulting in dicentric chromosomes, centric chromosomes, acentric rings, or terminal deletions.

Chronic exposure Exposure persisting in time. The adjective "chronic" relates only to the duration of exposure, and does not imply anything about the magnitude of the doses involved. Normally used to refer to exposures persisting from days to many years.

Deterministic effects Changes in cells and tissues that are certain to occur after an acute dose of radiation (in excess of a threshold value of at least 1,000 mSv), below which the radiation effect is not detected. The severity of health effects – such as skin reddening, burns, and hair loss – increase with the radiation dose received.

DNA Deoxyribonucleic acid is the molecular compound in the nucleus of a cell that forms the blueprint for the structure and function of the cell. DNA has a three-dimensional structure in which two DNA chains are held together by hydrogen bonding between the bases, forming a helix.

Dose A general term for a measure of the energy deposited by radiation in a unit mass. See the more specific terms absorbed dose, equivalent dose, effective dose, and collective dose.

Dose and dose rate effectiveness factor (DDREF) The ratio between the risk per unit effective dose for high doses and dose rates and low doses and dose rates.

Dose mean lineal energies The average or mean energy that is released by the radiant particle along its path. This value is then used to calculate the absorbed dose in Gray.

Dose rate A dose delivered over any unit of time (e.g., an annual dose is technically a dose rate).

Dosimetric model (1) For intakes of radionuclides into the body, a model that estimates the dose in various organs and tissues per disintegration of a radionuclide in a specified source organ (site of deposition or transit in the body). (2) For external exposure, model that estimates the dose rate in organs and tissues per unit activity concentration of a radionuclide in an environmental medium.

Dosimetry A scientific subspecialty in radiation protection and medical physics that focuses on

calculating the internal and external doses from ionizing radiation.

Gray (Gy) Radiation damage is dependent on the absorption of radiation energy and is approximately proportional to the concentration of absorbed energy in tissue. The gray is the SI unit of absorbed radiation dose corresponding to the absorption of 1 Joule (J) of radiation energy per kilogram of material. For gamma and beta radiations, the gray is numerically equal to the sievert.

Hematopoietic Any developmental series of cells that derives from hematopoietic stem cells and results in the production of mature blood cells.

Hereditary effect A radiation induced health effect that occurs in a descendent of the exposed person.

In vitro Latin for "within the glass," a term used to describe experiments that are performed not in a living organism but in a controlled environment, such as in a test tube or Petri dish.

In vivo Latin for "within the living," a term used to describe experiments using a whole, living organism as opposed to a partial or dead organism, or an in vitro controlled environment.

Internal emitter A radioactive substance that has entered the body through ingestion, inhalation, or absorption.

Isotropic effect The difference in physical properties and chemical reactivity due to the difference in mass between isotopes of the same element.

Linear energy transfer A measure of energy deposited over a distance as the energy is transferred from radiation to the exposed matter. A high value of linear energy transfer indicates that energy is deposited within a small distance (i.e., Joules μm^{-1}).

Oocyte The developing egg. It is usually a large and immobile cell.

Oogenesis Formation and maturation of oocytes in the ovary.

Orthovoltage x-rays X-rays produced by x-ray tubes operating at voltages in the 200–500 kVp range (i.e., the peak voltage), and thus possessing energy up to 200–500 keV, although there is a spectrum of energies with a peak much less than the peak tube voltage.

Relative biological effectiveness (RBE) A relative measure of the effectiveness of different radiation types in inducing a specified health effect. It is expressed as the inverse ratio of the absorbed doses of two different radiation types, the denominator being the reference radiation that would produce the same degree of a defined biological end point.

Stochastic effects A term used to group radiation induced health effects that have a statistical risk, such as cancer or inheritable diseases. For these diseases, the probability of their occurrence increases proportionally to the radiation dose received: the lower the dose, the lower the probability of occurrence. However, at no time, even for high doses, is it certain that cancer or genetic damage will result.

Teratogenic Substances or agents that can interfere with normal embryonic development.

Tritium A radioactive isotope of the element hydrogen (symbol T or ^{3}H). The nucleus of tritium (sometimes called a triton) contains one proton and two neutrons. Tritium atoms can replace hydrogen atoms in water molecules to form tritiated water (HTO), in organic molecules to form organically bound tritium (OBT), in air to form tritiated gas (HT). Tritium also exists in many other compounds such as tritiated hydrocarbons, tritiated particulates, tritiated thymidine, and metal tritides (tritium bearing metals).

X-ray Ionizing electromagnetic radiation emitted by an atom when it has been bombarded with electrons. X-rays differ from gamma rays in that they are emitted from the orbiting electrons, not the nucleus, and they have a much wider energy range, or spectra. A "soft X-ray" is one of low energy, generally below 100 keV.

Definition of the Subject

Tritium is a radioactive isotope of hydrogen that is produced both naturally and by man-made activities such as nuclear power plants. As a hydrogen isotope, a tritium atom behaves in the same physical and chemical manner as hydrogen atoms and so it can become part of water molecules and organic molecules. In these forms, tritium is very mobile and can enter biological systems and has the potential to damage living cells.

The biological damage caused by tritium radiation is the same as that from other radiations, but properties such as being an internal risk, being a very weak beta emitter, and being part of organic molecules

distinguish its effects from that of other radiations such as x-rays and gamma rays.

Tritium is also distinguished in that it is one of the most studied radioisotopes with respect to causing biological effects. This contribution reviews what is known of the biological effects of tritium, how its radiation compares in effectiveness with other radiations, and how the dose of tritium is assessed in humans.

This present report is an abridged version of the CNSC report "Health Effects, Dosimetry and Radiological Protection of Tritium" which was published in March 2010 and is available at http://nuclearsafety.gc.ca.

Introduction

Tritium (T or H-3), hydrogen's only radioactive isotope, can exist in several forms including tritiated water (HTO), tritiated gas (HT), and organically bound tritium (OBT). The emitted beta particle from tritium has a relatively low mean energy causing it to have a very short range in dry air. It can be absorbed by sheets of plastic, glass, or metal and cannot penetrate the dead layers of skin. Adverse health effects from tritium beta radiation therefore can only occur if inhaled, ingested, or absorbed into the body through the skin in large quantities. Once taken into the body, the beta particle possesses sufficient energy to ionize atoms and molecules.

This present report is an abridged version of the Canadian Nuclear Safety Commission's report "Health Effects, Dosimetry and Radiological Protection of Tritium" which was published in March 2010 as part of the CNSC's Tritium Studies Project. This 3-year research and information-gathering project was initiated as a result of questions raised during a public hearing related to the licensing of a tritium facility. The goal of the research was to expand the body of knowledge on tritium and to further enhance regulatory oversight of tritium-related activities in Canada.

The objective of this report is to provide an overview of the current knowledge of what is known about the adverse health effects from tritium radiation. To understand why tritium poses a health risk, a basis of tritium's physical, chemical, and radiological properties is required and is provided in section "Physical, Chemical, and Radioactive Properties of Tritium." This includes an introduction to the organic forms of tritium collectively known as OBT.

The section on "Adverse Health Effects due to Tritium" discusses the adverse health effects from tritium of which there are two main types: deterministic and stochastic. The discussion is primarily devoted to laboratory studies, but a brief overview of relevant human epidemiological studies is provided as well as a review of what is known about the biological effects of OBT. In addition, section "Non-radiological Effects of Tritium" discusses the theoretical effects from tritium that are caused not by its radiation, but instead by the form it changes into after disintegration.

The effectiveness of a particular radiation producing a specific biological effect is often determined through comparison to the dose required to produce the same effect by a standard radiation such as gamma rays. This is conventionally referred to as the "relative biological effectiveness" (RBE). The section on "Relative Biological Effectiveness" gives an overview of a number of studies that have measured the RBE of tritium beta radiation and offers a possible explanation in section "RBE Literature Reviews and Experimental Studies" on why tritium has a higher RBE than other radiations with much higher energies.

Finally the section on Dosimetry and Biokinetics provides a review of the biological modeling which describes how tritium and OBT behave in the body and how the resultant dose from that distribution is calculated. This includes discussions of intakes by inhalation, ingestion, and skin absorption and dose models for pregnancy and nursing.

Physical, Chemical, and Radioactive Properties of Tritium

Hydrogen, the simplest and most common element, has three isotopes:

- Protium (H-1), which contains only a proton in its nucleus and is by far the most common hydrogen isotope
- Deuterium (H-2), which contains a proton and a neutron
- Tritium (H-3), which has a proton and two neutrons, and is hydrogen's only radioactive isotope

Tritium is produced:

- Naturally through various interactions of cosmic rays and atoms in the atmosphere – the principal one being the neutron irradiation of nitrogen
- As a by-product of the operation of nuclear and research reactors including the capture of a fission neutron by a deuterium atom or neutron capture by Boron-10 and Lithium-6

Radioactive Properties

Tritium decays to a stable form of helium by emitting an electron from its nucleus (beta radiation) and an antineutrino (see Fig. 1):

It has a radioactive half-life of 12.3 years and a specific activity of 3.56×10^{14} Bq/g. The emitted beta particle has a mean energy of 5.7 keV and a maximum energy of 18.6 keV. Despite this very low energy, these particles possess sufficient energy to ionize atoms and molecules. Due to its very low energy, tritium's beta radiation has a very short range (approximately 6 mm) in dry air; is completely absorbed by sheets of plastic, glass, or metal; and cannot penetrate dead layers of skin. However, this beta radiation can pose a health risk if tritium is taken into the body. The maximum range of a tritium beta particle is approximately 6 μm in living tissue [1], compared to typical cells (or cell nuclei) that have diameters from about 7–30 μm (nuclei of about 6–15 μm) [2].

Chemical Forms and Properties

Tritium is almost chemically identical to the other hydrogen isotopes and can exist in several chemical forms including: HTO, HT, and OBT.

Tritiated Water The most common form of tritium is HTO, where a tritium atom replaces a hydrogen atom in water (H_2O) to form HTO. HTO has the same chemical properties as water and is also odorless and colorless. Water with a tritium activity of 1 Bq/L contains less than 1 tritium atom per 100,000 million, million (1 in 10^{17}) molecules. The majority of tritium in the atmosphere is in the form of HTO and can be transferred to humans by inhalation, skin absorption (liquid and vapor) [3, 4], or ingestion of drinking water or food [5, 6]. HTO exposure is generally the most important consideration in assessing dose, since HTO quickly reaches equilibrium with water in the body and is distributed uniformly to all soft tissues. The International Commission on Radiological Protection (ICRP) [5] recommended that internalized HTO be assumed to be completely and instantaneously absorbed and distributed uniformly with all body water. As a result, the concentration in sweat, sputum, urine, blood, perspiration, and exhaled water vapor is taken to be the same [7]. HTO is excreted via urine, feces, sweat, and breath [8].

$$^{3}H \rightarrow {}^{3}He + e^{-} + \nu_e$$

Tritium, Health Effects and Dosimetry. Figure 1 Decay formula for tritium

Tritiated Gas HT is formed when a tritium atom replaces a hydrogen atom to form a tritium–hydrogen bond. In its elemental form, HT is an invisible, odorless gas chemically identical to hydrogen gas. HT is relatively inert in biological systems and has a very low uptake into body fluids and tissues [7]. The main exposure pathways of HT include inhalation or skin contact with HT-contaminated surfaces. Releases from tritium processing facilities (such as self-luminous light manufactures, tritium recovery facilities, and nuclear fuel processing facilities) represent the primary source of exposure to HT. HT can be oxidized in the atmosphere to HTO. If deposited on the ground, it is converted to HTO through microbial agents near the soil surface [9].

Organically Bound Tritium Following an intake of tritium (typically in the form of HTO) by plants or animals, a fraction of the tritium can become incorporated into organic molecules such as carbohydrates, fats, or proteins and is termed organically bound tritium (OBT; [note that OBT is an acronym that stands for organically bound tritium and is not a chemical formula such as HT and HTO]). Within the body, OBT can become incorporated into various compounds such as amino acids, sugars, and structural materials such as collagen [10, 11]. OBT can also enter the body directly by ingestion of tritiated food, by inhalation of volatile organic vapors or aerosols, or it can be formed in vivo from tritium that is present in the general body

pools after exposure to other tritium-containing compounds [12]. If the tritium atom is attached to a carbon atom in an enzymatically catalyzed reaction, it is essentially fixed to that molecule until the molecule is metabolized. Conversely, tritium atoms bonded to oxygen, sulfur, nitrogen, or phosphorous atoms will readily exchange with hydrogen atoms in the surrounding cellular water and are therefore considered as an exchangeable tritium compound [12]. While both forms can be regarded as OBT, it is the nonexchangeable carbon-bound tritium that exhibits longer retention time in the body characteristic of organic molecules. Tritium–hydrogen exchange reactions occur in organic molecules with chemical groups such as nitrogen monohydride (NH), hydroxyl (OH), and thiol (SH). Nonexchangeable tritium is incorporated into more stable bonds with carbon atoms by enzyme catalyzed reactions [12].

Adverse Health Effects due to Tritium

Tritium beta radiation does not penetrate the dead outer layer of the skin. Therefore, tritium only poses a health risk if inhaled, ingested, or absorbed into the body through the skin in large quantities. If the chemical form is HTO, it will not collect in any specific tissue or organ but will distribute itself uniformly throughout the body. If it is part of an organic molecule, it may be incorporated into specific molecules or tissues. Generally speaking, the proximity of tritium to key molecules – principally deoxyribonucleic acid (DNA) – will determine the importance of the damage it will inflict when it undergoes nuclear transformation and emits a beta particle. Since HTO and most forms of OBT are assumed to be uniformly distributed in body tissues and cells, one would expect intakes of tritium to result in radiation effects similar to that of whole-body exposures from other types of low-linear energy transfer (LET) radiation, such as x-rays and gamma rays. Of course, the severity of the damage would vary according to differences in the RBE of the different radiations as well as to dose and dose rate effects.

An exception to these direct interactions is a phenomenon known as the "bystander effect," where nonirradiated cells exhibit the same symptoms as nearby irradiated cells. This has been demonstrated in many studies [13], using primarily alpha particle and photon irradiation but the effect has also been demonstrated in a study using tritium [14]. Most of the studies have been conducted in vitro, but the bystander effect has been observed in a limited number of in vivo studies and it is thought to be due to an unidentified chemical messenger. What is known is that the bystander effect occurs at the cellular level of biological damage and any damage induced by it will have already been accounted for in dose–response assessments.

As with all other forms of ionizing radiation, adverse health effects from tritium exposure can be classified as deterministic or stochastic.

- Deterministic effects:
  - Occur within relatively short time frames after exceeding a dose threshold
  - There is an increase in severity (e.g., cataracts, skin reddening) as dose increases
- Stochastic effects (cancer and hereditary effects):
  - Are assumed not to have dose thresholds
  - Have a greater probability of occurring as dose increases

Sections "Deterministic Effects" and "Stochastic Effects" review several studies looking at deterministic and stochastic effects, respectively. The review of deterministic effects includes lethality (death), teratogenicity (birth defects), and reproductive effects. The review of stochastic effects includes carcinogenicity (cancer) and hereditary effects. Section "Human Epidemiology" reviews epidemiological studies on workers and in the public that have been exposed to tritium.

Note that the conversion of an intake of tritium in becquerels to a dose is dependent on a number of factors such as the assumed turnover rate, or biological half life, of body water. This factor can differ by a factor of two or more between studies and consequently, the final calculated dose for the same tritium intake may also vary by a similar factor. Where no dose information is given, or if the cited literature was dated (e.g., 1950s), the doses were calculated for this review. The dose calculations assumed an HTO half-life in mice of 1.2 days which is consistent with that of Rodgers [15] and Richmond et al. [16].

Deterministic Effects

Lethality Brues et al. [17] demonstrated the lethality of tritium by inducing death in mice by administering

one-time tritium injections of 0.126–8.4 GBq. The researchers reported a lethal dose ($LD_{50/30}$) that would kill 50% of the population within 30 days of 37 MBq/g of body weight (BW). Their mice had an average weight of 20 g, which translates to an initial intake of about 1.11 GBq. Brues et al. [17] calculated the dose from this intake to be about 1,000 "reps" (older unit, equal to about 9 Gy). Using modern dosimetry calculations, it appears that a dose of 37 MBq/g BW gives a dose of around 6 Gy, due to difference in assumed water biological half-lives. Furchner [18] determined a $LD_{50/30}$ value of 8 Gy, by a single injection of about 24 MBq to female mice, but again, this translates to a dose of about 4 Gy with newer biological half-life. Yokoro et al. [19] (see also Yamamoto et al. [20]) found a $LD_{50/30}$ of about 8 Gy from a single injection of 0.56 GBq in one strain of mice and 0.93 GBq injection in another.

Yamamoto et al. [20] investigated chronic intakes of HTO that would be lethal in mice by continuously administered HTO. They found that the concentration of tritium reached a plateau in organs and blood after about 7 days. A typical time of 2 weeks for hematopoietic death occurred following intakes of drinking water with tritium concentrations from 148 to 592 GBq/L. The lowest total dose inducing death was 11 Gy at a drinking water concentration of 148 GBq/L. All observed deaths were due to hematopoietic failure.

Although details are vague, tritium was reported to be the cause of death of two workers in 1953 in Chelyabinsk-40 (now Ozyorsk) Russia. Doses were estimated at 10–12 Gy, indicative of massive intakes [21, 22].

In summary:

- The radiation dose from tritium necessary to cause death in mice is slightly greater than an acute external irradiation by x-rays or gamma rays, with a tritium $LD_{50/30}$ of about 6–9 Gy. This corresponds to an acute intake in the order of 1 GBq or a chronic dose of about 11 Gy (~0.5 GBq) when tritium is orally administered.
- An unusual finding was that hematopoietic death prevailed over the gastrointestinal syndrome following the exposure to radiation from tritium. The latter would have occurred if a similar dose had been given with gamma or x-rays [20].

Teratogenic Effects Teratogenic effects occur when an agent interferes with the development of an embryo or a fetus in utero. Teratogenic effects are not hereditary; that is, they are not passed on to future generations. In general, a tissue's sensitivity to radiation is directly proportional to the rate of proliferation of its cells. Therefore, a fetus that is rapidly developing from an embryo is expected to be more sensitive to radiation than an infant, child, or adult. This inference is supported by the results of experiments in animal models and by experience with human populations exposed to doses of radiation above 100 mSv (for example, medical exposures, atomic bomb survivors). Radiation's most significant harmful effects to the human fetus include mental retardation, delayed intrauterine growth, and childhood cancers (such as leukemia) [23, 24].

Straume and Carsten [25] reviewed current literature looking at tritium exposure during fetal development. They pointed out that some fetal cells rapidly divide during certain stages of development and differentiate to form organs and tissues while others such as neurons or oocytes involve very little or no further cell proliferation. Consequently, tritium that is incorporated into "long-lived" molecules (becoming OBT) could result in large integrated doses over the lifetime of the cells, since the tritium would not be diluted by further cell proliferation. The dose from tritium incorporated into molecules such as DNA and histones of rapidly dividing cells was small compared to the dose from HTO as observed by Commerford et al. [26]. Conversely, for long-lived cells, the dose from tritium incorporated into DNA and histones could exceed that from HTO. This was also discussed in some depth by the Advisory Group on Ionizing Radiation (AGIR) reporting to the UK Health Protection Agency [27] and will be presented in the following discussion on reproductive effects. The AGIR [27] concluded that tritium could be incorporated during pregnancy into the DNA of fetal oocytes and remain there until fertilization decades later; however, it also concluded that DNA is not a stable molecule and that there is a turnover of its molecules over time. The net radiological impact of this phenomenon is unclear, but would be related to dose and the amount of tritium deposited within the DNA of the long-lived cells. To be deposited within DNA, tritium would have to be bound to

a specific organic molecule (such as a nucleic acid) that could become part of a DNA molecule. All OBT compounds represent a fraction (∼13%) [28] of the total tritium in the environment, but OBT molecules could be any one of the thousands of different types of organic molecules. It is therefore reasonable to expect that a low number of OBT compounds are used to build DNA. The section of the report on reproductive effects (see section "Reproductive Effects") discusses this phenomenon in more detail.

Dekaban [29] first summarized radiation-induced teratogenic effects in humans when he reported developmental effects due to medical x-ray treatments in the 1920s and early 1930s, when radiation was widely used to treat many diseases. The report evaluated a group of children who were exposed in utero to radiation when their mothers had pelvic x-ray exposures. Doses of 200–300 R (∼2–3 Gy) consistently induced fetal damage. The following were the most frequent anomalies identified in children who were irradiated during intrauterine life: (1) small size at birth and markedly stunted growth, (2) microcephaly, (3) mental retardation, (4) microphthalmus, (5) pigmentary degeneration of the retina, (6) genital and skeletal malformations, and (7) cataracts. However, Mulvihill et al. [30] later reported that these effects depend on gestational age and that other case reports of radiotherapy during pregnancy showed that anomalies did not always develop.

Zamenhof and Van Marthans [31] studied how five generations of rats were affected by pre- and postnatal exposure to HTO. Female rats were given HTO (111 MBq/L) beginning in adolescence and throughout pregnancy. This exposure to tritium did not produce any signs of radiation illness or increase in cataract formations in the mothers. The courses and outcomes of pregnancy were also normal, but 60% of the newborn rats exhibited hematomas, edemas, and subdural hemorrhages. None of these effects lasted beyond 30 days of age.

A study by Laskey et al. [32] maintained rats on activities of 0.37–370 kBq HTO/mL of body water from conception of the first generation until delivery of the second generation. The corresponding dose rates were 0.03–30 milligray per day (mGy/day). An exposure to 370 MBq/L of body water resulted in a 30% weight reduction of the testes in the first generation of adult males, but there was no impairment of growth or reproductive ability. The following were noted in the second generation of newborns: a relative reduction of brain weights at exposures of 3.7–370 MBq/L (0.3–30 mGy/day); a decrease in BW at 37 MBq/L (3 mGy/day) and 370 MBq/L (30 mGy/day); a decrease in litter size and an increase in resorption at 370 MBq/L (30 mGy/day). In their discussion, Laskey et al. [32] noted that similar effects had not been observed in other studies with comparable doses of Cobalt-60 gamma radiation. Laskey et al. [32] did not observe litter size effects or resorption either at or below 37 MBq/L (∼3 mGy/day), although higher dose rates showed statistically significant reductions in the weights of both male and female rats.

Bursian et al. [33] looked at effects on rats continuously exposed to HTO concentrations of 0, 37, 370, and 3,700 Bq/mL from conception to birth. The in utero exposure to doses as low as 0.66 Gy (370 MBq/L) produced measurable and persistent decreases in brain weight and increases in norepinephrine concentrations at 21 and 45 days postnatal. No differences from controls were observed in the rate of turnover or the concentrations of dopamine, acetylcholinesterase, or monoamine oxidase; although it is unclear what effects would have occurred at different concentrations.

In an experiment by Jones et al. [34], drinking water containing HTO was given to pregnant squirrel monkeys at levels ranging from 16 to 1,000 times the "permissible level for human consumption." No effects in newborn progeny were seen in terms of BW, body dimensions, organ weights, hematological patterns, the histology of organs, or tissues, with the exception of the ovaries. Dobson et al. [35, 36] found a decrease in the number of immature oocytes at the highest doses.

In summary, tritium radiation-induced teratogenic effects have been demonstrated in laboratory studies and are consistent with similar effects from external photon radiation. Teratogenic effects in animal studies start to occur at doses of about 0.4–0.6 Gy from chronic intakes of HTO.

Reproductive Effects Reproductive organs and tissues in both males and females are among the most radiosensitive tissues, with mature gametes being the most sensitive cells. In the male, spermatogenesis is a proliferative and continuous process, where sperm

originate from spermatogonial stem cells and undergo many developmental stages, from the primordial germ cell to the mature spermatozoa. This process continues throughout adult life and due to continual replenishment, testes are among the most radiosensitive tissues.

In the female, germ cells are called oocytes. They are produced in the ovary and give rise to the ovum (egg), which can be fertilized. Oocyte formation (oogenesis) occurs in the female during fetal life, with primary oocytes produced in the ovaries of the fetus by the fifth month of pregnancy. About seven million primary oocytes are initially produced but only about 400,000 remain by puberty. The oocyte development process includes several stages of maturation, from the production of oogonia from primitive germ cells to development of primary oocytes and formation of definitive oocytes at puberty.

Effects in the Female Since tritium distributes itself throughout the body, it can be taken up by a developing oocyte and incorporated in its DNA. Tritium incorporated into oocyte DNA could theoretically irradiate the oocytes over a period of 30 or more years. Because oocytes do not divide until fertilized, there is little turnover of the DNA molecules which implies that the biological half-life of the tritium imbedded in oocyte DNA could approach the radioactive half-life of tritium, 12.3 years. The AGIR [27] points out that while a biological process gradually exchanges all the components of DNA molecules – including that of tritium-labeled DNA – it would take 50 years to replace 2–5% of a cell's genome (DNA). Therefore, most of the tritium incorporated in an oocyte will remain there for its whole life.

Straume and Carsten [25] reviewed tritium effects on oocytes, reporting that most of the information on radiosensitivity in humans came from autopsies of women who had been exposed to substantial doses of external radiation [37], and from fertility histories of women exposed to radiation from therapy or atomic bombs [38–40]. In all cases, the data were for adult women.

Available data for human females suggest that in adult women, maturing and mature oocytes are more sensitive than immature ones. This is in contrast with observations of mice, whose immature oocytes are by far the most sensitive to radiation killing – about 100 times more sensitive than matures ones [41]. In women, an exposure of 2.5–6 Gy will lead to permanent sterility (effect on resting oocytes) [42, 43]. The threshold for temporary effects on fertility appears to be at least 0.6 Gy of acute x-rays and 1.5 Gy for protracted or fractionated low-LET radiations [42].

In studies on both mice and rats, Satow [44, 45] looked at tritium effectiveness in killing oocytes. While the study primarily examined the RBE of tritium, significant oocyte reabsorbtion was found at HTO intakes of 0.17 MBq/g of BW, corresponding to a total dose of 39 mGy [41].

To assess the risk that tritium radiation would damage oocyte DNA, the AGIR [27] modeled the dose and hereditary risk in a critical group of pregnant women, who consumed an annual total of 24 kg of tritium-contaminated flounder from Cardiff Bay. It was assumed that the flounder had a tritium concentration of 50 kBq/kg, which implies that the critical group ingested 1,200 kBq of OBT per year. At this rate of intake, the tritium in the body would reach an equilibrium concentration of 175 kBq. The model estimated that approximately 4% of oocytes could experience a tritium disintegration within the next 30 years following intake and that the frequency of severe hereditary effects resulting from this would be expected to be around 1 in 1,000,000 (10^{-6}). This is comparable to the 3–4% rate of spontaneous birth defects that are observable and inheritable.

Overall, female reproductive systems – and principally those of mice – appear to suffer the greatest adverse health effects from tritium exposure. As Baker [41] reports, the mouse oocyte is about 100 times more radiosensitive than the human oocyte; therefore doses that affect mice oocytes would not be expected to affect human ones.

Effects in the Male Unlike oocytes, spermatagonia are continuously produced from stem cells throughout adult life. Like all tissues that are rapidly replaced, there are certain germ-cell stages that are highly sensitive to cell killing by ionizing radiation. Experiments in mice have shown that the most sensitive cells are the type A and B spermatagonia, which can be reduced by 50% by doses of only about 0.3 Gy of acute x-rays [46, 47] (as reported in Straume and Carsten [25]). The spermatid and spermatozoa stages are much less sensitive

than the spermatogonia stage [48]. Lambert [49] found a 27% reduction of mouse spermatagonia that were injected with tritiated thymidine (3HDtr) at a dose of 185 kBq/g of body mass and with HTO at a dose of 2,220 kBq/g of body mass (dose to the nucleus of 84 mGy and 49 mGy, respectively).

Although the results are from a single individual, UNSCEAR [40] reported temporary sterility after doses of only 0.15 Gy of acute x-rays and permanent sterility after acute doses of 3–5 Gy. Chronic exposure studies in dogs demonstrate that x-ray dose rates of 1–2 mGy/day do not impair sperm production [43]. If this data were transposed to humans it would imply that the threshold for reduced sperm production in the adult male may be in the order of 10 mGy/day. For continuous exposure, this would add up to 3–4 Gy/year [25]. A dose of 10 mGy/day due to tritium would require an intake of about 500 MBq/day.

Stochastic Effects

Carcinogenicity Carcinogenicity is the ability of a radiological, chemical, or biological agent to produce cancer. Ionizing radiation was one of the first such agents observed to induce cancer from its early uses in the 1900s. Many of the first researchers were unaware of the risk that radiation presented and succumbed to radiation-induced cancer. The study of populations exposed to radiation, such as the atomic bomb survivors, medical patients, and nuclear energy workers, has provided the basis of our current radiation dose limits. Most of the populations studied were those exposed to external radiation, such as x-rays, gamma rays, or neutrons. Risks to humans from exposure to internal emitters are largely limited to uranium miners exposed to radon progeny, radium dial painters, and patients injected with thorotrast [50]. While epidemiological studies are ongoing, to date no human studies have ever demonstrated tritium-induced cancer (see the section on human epidemiology).

Due to a lack of direct experimental evidence, the cancer risk posed by internal emitters to humans has largely been derived from populations that received high, external exposures such as those in the Japanese atomic bomb survivors Life Span Study [51]. Many studies have looked at the incidence of cancer among laboratory animals exposed to gamma radiation and x-rays. While it did not involve exposures to tritium, one of the most comprehensive studies on the effects of radiation was done by Tanaka et al. [52], who looked at cause of death and neoplasia in 4,000 mice exposed to Cesium-137 gamma rays at 21, 1.1, and 0.05 mGy/day. Equal numbers of male and female mice were exposed for approximately 400 days with resultant doses of 8,000, 400, and 20 mGy. Compared to the nonirradiated controls, there was a significantly higher frequency of myeloid leukemia in males, of soft tissue neoplasms and malignant granulosa cell tumors in females, and of hemangiosarcoma in both sexes exposed to 21 mGy/day (8 Gy cumulative dose). The number of multiple primary neoplasms per mouse was also significantly increased in mice irradiated at 21 mGy/day. Both sexes exposed to 21 mGy/day had significantly shorter life spans than control groups, but only the females had significant shorter life spans when exposed to 1.1 mGy/day (0.4 Gy). Females exposed to 0.05 mGy/day (0.02 Gy cumulative dose) also had a shorter average life span by about 8 days, but this was not statistically significant.

Many laboratory studies on animals have clearly demonstrated that tritium can induce cancer, although this has not been studied as extensively as gamma and x-ray exposures.

In Yamamoto et al. [53], HTO was administered to mice in drinking water at concentrations that ranged from 9.25 GBq/L (0.240 Gy/day) to 0.37 GBq/L (0.010 Gy/day). Female mice maintained on this drinking water survived for more than 150 days, but 70–80% of them developed tumors. In the range from 1.85 to 9.25 GBq/L of HTO (0.048–0.240 Gy/day), the main cause of death was thymic lymphoma. However, at 0.925 GBq/L (0.024 Gy/day), the incidence of thymic lymphoma was lower, while tumor incidence was greater. In addition, tumor types became more diverse at lower concentrations of HTO. The latent period of tumor development was shorter and the life-shortening effect was more marked in this tritium beta irradiation study than in other studies that used x-ray or gamma irradiation. However, Yamamoto et al. [53] did not attempt to estimate the RBE of the tritium exposure.

Yamamoto et al. [54] administered tritiated drinking water to mice throughout their lives, resulting in dose rates of 0.2, 0.9, and 3.6 mGy/day. The thymic

lymphoma dose–response curve started to increase exponentially at about 0.9 mGy/day, giving a threshold at about 12 mGy/day (although there was no significant difference from controls at 0.9 mGy/day). The group receiving 3.6 mGy/day had significantly shortened life spans compared to controls, while the other groups did not. Increases in BW were noted for the animals that received lower dose rates (0.9 mGy/day). Yamamoto et al. [54] concluded that the threshold dose rate for tumor induction by HTO is around 12 mGy/day, and that the threshold dose rate for Cobalt-60 gamma irradiation is higher than that for tritium beta irradiation.

Gragtmans et al. [55] estimated the RBE of tritium beta radiation to induce tumors in the breast tissue of rats. Incidence of mammary tumors over time was compared to that of controls in a rat strain where these tumors occur naturally. Tritium was injected intraperitoneally at concentrations of 45–370 MBq/100 g BW followed by four additional injections at 2-day intervals, producing doses of 0.46, 0.92, 1.63, and 3.85 Gy. The reference radiation was 200 kVp x-rays delivered over 10 days in doses of 0.29, 0.57, 1.1, and 2.0 Gy. There was early onset of the tumors at 150 days posttreatment for all irradiations when compared to controls. Since these animals would naturally develop mammary tumors, the irradiation likely decreased the onset time of the tumor but did not necessarily increase the overall incidence. Therefore, some care must be taken when interpreting the results.

Johnson et al. [56] estimated lifetime incidence of myeloid leukemia in seven groups of ~750 mice given single injections of HTO of 90, 180, or 270 MBq each, corresponding to doses of 0.85, 1.86, and 3.04 Gy. The incidence of myeloid leukemia increased from 0.13% (control) to 6–8% (treated) with apparent excesses at the lowest doses. The calculated RBE for tritium beta rays was 1.0 ± 0.5 to 1.3 ± 0.3 (best estimate 1.2 ± 0.3) using chronic x-ray exposure as the reference radiation. The Johnson et al. [56] study primarily aimed to determine an RBE for tritium using myeloid leukemia as an endpoint and not necessarily as a measure of the induction of myeloid leukemia and other cancers. Therefore, while they reported on the incidence of other cancers, they did not determine the lowest dose of incidence. Other cancers such as reticulum cell sarcoma did occur, but usually at doses of 2 Gy or higher. Indeed, for some types of cancer, incidence appeared lower than in controls in both the tritium and x-ray irradiated animals, but no tests for significance were done to verify this.

Seyama et al. [57] examined the cumulative incidence of tumors in mice over different exposure regimes for tritium beta irradiation, neutrons, Cobalt-60, and Cesium-137 gamma radiation. Mice were injected with HTO intraperitoneally at concentrations of 0.14, 0.28, 0.56, and 0.74 GBq, giving doses of 1.97, 3.95, 7.90, and 10.53 Gy, respectively. At 400 days, tumor incidence was 4%, 8%, 18%, and 24% respectively, but by 500 days, incidences differed little among the groups. This indicated that even the lowest dose (1.97 Gy) was sufficient to elicit the same incidence of tumors, with higher doses simply accelerating the onset. Increased incidence of T-cell lymphoma was also induced with 4 weekly injections of similar doses. Increased tumor incidence over controls was seen in the ovary, liver, lung, mammary glands, and uterus. There were also high incidences of lymphoma and leukemia.

Balonov et al. [58] summarized Russian studies that exposed mice and rats to tritium. One of the studies reported [59] exposed mice through continuous HTO ingestion of 37–1,850 kBq/g/day, which delivered doses of 1.2–2.8 Gy. Damage to DNA was only observed at the end of the intake period in animals with the greatest intake. DNA repair was also found to be slower in this group compared to the controls. The data presented by Balonov et al. [58] showed that tritium induced many types of tumors, including leukemia and solid cancers, in mice and rats.

A literature review by Straume [60] analyzed the risks, including cancer, of exposure to tritium radiation. Because cancer risk information due to tritium radiation was not available for humans, cancer risk estimates for tritium were derived from human populations exposed to gamma and x-ray radiation and from experimental animal studies. Straume [60] used a Monte Carlo sampling program to generate frequency distributions of excess cancer mortality from chronic, low-level exposure to HTO. He used frequency distributions for dose rate effectiveness factors from 1 to 12 (based upon animal studies), with a central value of the RBE for tritium between 2 and 3 and a range of 0–4.5. His analysis produced a skewed risk distribution with a 50th-percentile risk per

milligray of 81×10^{-6} with a 90% confidence range of $38–185 \times 10^{-6}$ per milligray. This value is comparable to radiation risk estimates of ICRP [61], BEIR [43], and UNSCEAR [62] which are 50×10^{-6}, 79×10^{-6}, and $70–110 \times 10^{-6}$ per milligray, respectively.

Although the above studies demonstrate that tritium's beta radiation is carcinogenic, it remains uncertain at what dose tritium will induce cancer. The lowest dose observed to induce cancer in mice is in the range of about 1 mGy/day. The work by Straume [60] perhaps gives the greatest insight into tritium-induced carcinogenesis and corroborates the risk factors presented by ICRP [61], BEIR [43], and UNSCEAR [62].

Hereditary Effects It is theoretically possible that damage to the chromosomes in oocytes or spermatagonia may be mutagenic and therefore carried forward in subsequent generations. However, the latest ICRP recommendations [63] maintain that "there continues to be no direct evidence that exposure of parents to radiation leads to excess heritable disease in offspring." Nevertheless, based upon animal experiment results, the ICRP estimates a genetic risk of about 0.2%/Gy for up to the second generation (grandchildren). For low-LET radiation, the ICRP value for the probability of severe hereditary effects is 0.5%/Gy, based on extrapolation from male mouse data.

The United Nations Scientific Committee on the Effects of Atomic Radiation (UNSCEAR) [64] estimated genetic risks:

1. To a population sustaining low-LET, low-dose, or chronic irradiation exposure generation after generation
2. To a population that sustains low-LET, low-dose, or chronic irradiation to one generation only

In the first case, the total genetic detriment was estimated to be ~0.41–0.64% risk per parental Gy per million progeny above baseline (background incidence) to the first generation and ~0.53–0.91% risk per Gy per million progeny above baseline to the second generation.

In the second case, the total genetic detriment was again estimated to be ~0.41–0.64% risk per Gy per million progeny above baseline to the first generation. However, because only the first generation had received the continuous radiation exposure, the risk in the second generation dropped to 0.16–0.43% risk per Gy per million progeny above baseline.

As for the applicability of these risk estimates to tritium radiation, Straume and Carsten [25] noted that the genetic effects observed for other low-LET radiations were also present following exposure to tritium, either from HTO or from OBT. By grouping RBE studies with genetic endpoints (such as chromosome aberrations and mutations in mice), they determined that the RBE ranged from 1 to 3, with the higher values associated with low doses and low-dose rates (due largely to the curvilinear response of the reference radiation).

Therefore, it could be concluded that if gamma rays were the reference radiation, then the genetic risk estimates from UNSCEAR and the ICRP could be doubled for the risk posed by tritium exposure. It should be noted, however, that this conclusion is based upon animal studies and that genetic effects in humans due to radiation exposure have never been observed to date.

Adverse Health Effects of Organically Bound Tritium Some of the tritium released into the environment will naturally bind with organic molecules, either through enzymatically catalyzed reactions where a hydrogen atom is replaced by a tritium atom or through natural exchange reactions. If the tritium atom is attached to a carbon atom in an enzymatically catalyzed reaction, it is essentially fixed to that molecule until the molecule is metabolized. Conversely, tritium atoms bonded to oxygen, sulfur, nitrogen, or phosphorous atoms will readily exchange with hydrogen atoms in the surrounding cellular water and are therefore considered as an exchangeable tritium compound [12]. Both nonexchangeable and exchangeable compounds are referred to as OBT. However, the nonexchangeable tritium will exhibit retention times determined by the metabolism of the molecules concerned, while the exchangeable tritium will be indistinguishable in its retention from that of HTO in cellular water.

OBT is a general term applying to a large group of compounds, where tritium is bound to organic molecules, including tritiated sugars, polysaccharides, lipids (fats), proteins, and DNA precursors. The extent of cellular injury caused by an OBT molecule depends largely upon where it is incorporated into a cell and if

it is there long enough for the tritium atom to decay. Tritiated DNA precursors, such as ^{3}HTdR, are theoretically more efficient at causing cellular injury since they form part of the basic building block of a DNA strand. On the other hand, tritiated molecules that are more remote from DNA in the cell such as a tritiated fat molecule or a tritiated amino acid in a structural protein should pose a lesser risk.

Lambert [49] studied the effects of HTO and ^{3}HTdR on rat spermatagonia and determined an RBE of 1.3 for ^{3}HTdR and 2.3 for HTO. He pointed out that these values should be viewed with caution due to uncertainty on several factors, such as the time of death of the spermatagonia and the amount of tritium that induced it.

One of the few studies looking at effects of tritiated amino acids and nucleosides was done by Furuno-Fukushi et al. [65] where they treated mouse lymphocytic leukemia cells for 50 h with ^{3}HTdR, lysine, arginine, leucine, and aspartic acid. Doses ranged from approximately 50 mGy to 800 Gy (as interpreted from graphical data). Cell survival decreased linearly for all compounds with effects greatest for thymidine, followed by arginine, lysine, leucine, and aspartic acid; similar results were found for cell mutation frequencies. The concentrations for detectable cell killing and mutagenesis ranged from less than 37 MBq/L for ^{3}HTdR, 37–370 MBq/L for tritiated amino acids and 18.5–185 MBq/mL for HTO. Furuno-Fukushi et al. [65] compared the cell killing results of a previous study that examined the effects of HTO and gamma rays at similar doses and dose rates [66]; calculated RBEs of 2.9, 2.6, and 5.9 for mutation induction relative to low-dose rate gamma rays for HTO; tritiated amino acids and tritiated thymidine, respectively. However, the use of nonconcurrent reference radiation controls places some doubt on these results. They also reported that the tritiated amino acids were distributed homogenously within the cell, as is the case for HTO.

Wang et al. [67] examined the effects of OBT on cultured mouse embryonic mid brain cells using ^{3}HTdR, uridine, arginine, and glutamic acid. The cells were exposed to different concentrations of the tritiated compounds over a 20-hour period. Assays of cell proliferation and differentiation and DNA and protein content were conducted. To determine the RBE, cultures of cells were also exposed to 150 kVp x-rays at 0.5 Gy/min as the reference radiation. Calculated RBEs were in the range of 4.6–8.7 with the largest being for ^{3}HTdR. The study was heavily criticized by Trivedi et al. [68] who pointed out various shortcomings; for example, the reference radiation was over a much shorter period than the tritium exposure, cell cultures were handled improperly, and the data analysis was missing information.

In their review of the available studies on OBT, Straume and Carsten [25] concluded that the RBE of tritium is slightly larger than that of HTO when it is bound to amino acids, and is about 2 times higher when bound to nuclear bases like thymidine.

In summary, while many studies have examined how OBT is partitioned within the body and within the cell, studies specifically looking at health effects due to OBT are limited. Those that are available indicate that most organic compounds have about the same RBE as HTO, since they are distributed throughout cells and do not lead to preferential irradiation of the nucleus. Incorporation of ^{3}HTdR, however, can lead to concentration of tritium in the nucleus, resulting in RBE values of about twice that of HTO, calculated on the basis of average cell/tissue dose. With the exception of DNA precursors, it can be concluded that the greater effect of OBT relative to HTO is due to longer retention times, and proportionately greater dose per Bq intake, rather than differences in RBE (see sections "Adverse Health Effects due to Tritium" and "Relative Biological Effectiveness").

Occupational and public doses due to exposures to OBT would arise from a mixture of tritiated compounds, including amino acids, sugars, fats, nucleic acids, and polysaccharides (in the case of public doses). There are some special instances where specific OBT compounds such as ^{3}HTdR would be used (for example, laboratory studies), but these would be under strictly controlled conditions to limit intakes. There are two relevant studies on this subject:

- Steel and Lamerton [69] measured tritium activity in several different organs in juvenile rats after an injection of ^{3}HTdR. The greatest uptakes of ^{3}HTdR were in the bone marrow, the testis and the lungs. The lungs retained the ^{3}HTdR the longest, although at much lower concentrations than found in the bone marrow. The time for tritium activity to be

reduced to half the initial amount ranged from 1 day for the colon to 25 days for the testis, although the retention period changed over the course of the experiment (up to 56 days) likely due to the reuse of the ^{3}HTdR.

- Lambert and Clifton [70] showed that only about 2% of ingested ^{3}HTdR is incorporated into DNA.

Human Epidemiology All of the studies mentioned previously have been under controlled, laboratory conditions and there are no significant studies of biota exposed to tritium under environmental settings. There have, however, been a number of human epidemiological studies that offer some insight on environmental exposures.

Epidemiological studies have formed the basis for attributing human health risks to radiation exposure. Studies of the Japanese atomic bomb survivors (Preston et al. [71–73]), patients treated with radiation (Boice et al. [74, 75]; Weiss et al. [76, 77]; Howe [78]; Howe and McLaughlin [79]; Little et al. [80]; Little and Boice [81]), and radiation exposed workers (Lubin et al. [82]; Cardis et al. [83]; Cardis et al. [84, 85] have been assessed to estimate radiation risk coefficients (ICRP [61]; BEIR [24]; UNSCEAR [13, 51]. Unfortunately, there is little data specific to tritium. In epidemiological studies where tritium exposures exist, workers were also exposed to other radiations, particularly external gamma irradiation. Tritium specific exposures are often lacking from these assessments.

Several ecological studies of members of the public living in the vicinity of nuclear facilities assessed the relationship between the community's health (such as incidence and mortality rates of childhood leukemia, non-Hodgkin's lymphoma, birth defects, and other health indicators) and the average environmental releases from, or residential proximity to, a facility. There were no individual estimates of tritium exposure (or other risk factors) in these studies. No inference of the health effects from tritium can be made because of the limitations of such ecological studies [13]. Given the extremely low levels of radiation exposures from the facilities [86–91] adverse health effects would be highly unlikely.

The recent German KKiK case–control studies by Spix et al. [92] and Kaatsch et al. [93] of childhood leukemia have raised significant attention. There were no such results in France [94] or Britain [95], and Grosche [96] observed that the trend in risk decreased over time, which could indicate some agent being involved, for which the prevalence is reduced over time. Grosche et al. [89] found no indication that tritium discharges from the Krümmel NPP were involved in any excess of childhood leukemia found nearby. Currently, there is no support for a causal relationship between any chemical or physical risk factor and the observed risk of childhood leukemia among children younger than 5 years of age living within 5 km of German NPPs (SSK [97]). The observed risk remains unexplained, however, it should be noted that clusters of childhood cancers, including leukemia, have been observed where no nuclear facilities exist.

The cohort studies of radiation workers provide the best available information on the risk of tritium exposure. However, few studies have direct information on tritium exposure, and fewer still directly assess the health effects of tritium exposure alone. The studies of Beral et al. [98], Cragle et al. [99], Johnson et al. [100], Zablotska et al. [101], Schubauer-Berrigan et al. [102], and Richardson and Wing [103] assessed health effects with tritium doses in combination with other (film-badge) doses. Thus, it is difficult to assess the component of risk associated specifically with tritium; especially since the tritium contribution to total dose was generally very small compared to other sources of radiation exposure. Hazelton et al. [104], for example, noted that whole-body tritium exposures were generally small in comparison to gamma exposures and that the dose–response for tritium in a restricted analysis was not statistically significant. The lack of an excess risk found from total occupational radiation dose, and the small contribution of tritium to the total dose, implies that any risk from tritium would be negligible [105].

The United Kingdom Committee Examining Radiation Risk from Internal Emitters (CERRIE) [106] report recognized an elevated health risk at moderate and high levels of internal exposure. However, at low levels any increase in risk may be undetectable and there is no clear evidence that current radiation risk estimates are radically underestimated. The AGIR [27] review of epidemiological studies of exposure to tritium concluded that the available epidemiological literature of environmental and occupational tritium exposures do

not provide enough detail to estimate risks from tritium exposure and recommended an international collaborative study of nuclear workers. The UK's Health Protection Agency [27] and the ICRP [107] supported the AGIR conclusions and recommendations.

In summary, while there has been a number of epidemiological studies conducted which have included tritium exposure, no definitive conclusions can be drawn as to effects to humans at current exposure levels. However, the lack of an excess risk from total occupational radiation dose and the small contribution from tritium to the total dose implies that any risk from tritium alone would be negligible.

Nonradiological Effects of Tritium

Transmutation Transmutation is the conversion of one element to another through radioactive decay. When tritium undergoes decay, it becomes Helium-3 (^{3}He), a stable, inert gas. As a different element, it no longer holds the chemical properties of a hydrogen isotope, which could lead to detrimental consequences in addition to those caused by the radiation. For example, if a tritium atom is bound to a DNA molecule when it decays, most of the kinetic energy will accompany the beta radiation as it is ejected from the nucleus, but some energy will provide a "kickback" to the ^{3}He atom as recoil energy. Kacena [108] determined that the recoil energy is too small (about 3 eV) to cause ionization of the DNA molecule on its own. However, the resultant ^{3}He atom would then be attached to a carbon atom with a very weak bond. This bond would tend to break leading to a free helium atom and possibly an ionized DNA molecule. The ionized DNA molecule may then be repaired, or if irreparable, lead to permanent DNA damage.

Myers and Johnson [109] performed a comprehensive review of transmutation effects. They pointed out that the degree of damage caused by transmutation of tritium to a helium atom could theoretically vary significantly, depending on the position of the tritium atom in specific DNA nucleotides. The studies also covered several test systems from the S13 virus, two strains of the bacterium *Escherichia coli*, *Drosophila melanogaster* (fruit fly), and cultured mammalian cells. Based on the position of the tritium on the nucleic acid, varying degrees of damage were noted – in one case, by a factor of 500 in the S13 virus. However, it should be noted that the S13 virus only has a single strand of DNA and therefore does not have the repair capacity of higher organisms. In summary, Myers and Johnson [109] argued that it would be highly conservative to assume that the mutations observed in lower organisms would be detectable in mammalian cells, and that the number of detectable mutations in mammals (resulting from transmutation) would not likely exceed 5%.

Carsten [1] discussed the possibility that such effects would be manifested in humans after ingesting HTO or OBT as food. He suggested that the risk was small enough to pose no significant hazard, primarily because only 2% of the DNA hydrogen is located at the 5-position of the cytosine ring; therefore, damage would be minimal. In their review, Feinendegen and Bond [110] reached the same conclusion: "the effects of intracellular tritium are overwhelmingly due to beta irradiation of the nucleus" and "transmutation effects do not produce a measurable effect."

In any event, if DNA damage did occur from transmutation, it is unlikely that it could be discerned from radiation-induced damage and would be accounted for in the RBE. The AGIR [27] drew a similar conclusion.

Isotopic Effect of Tritium With two additional neutrons, a tritium atom has approximately three times the mass of a conventional hydrogen atom (protium). While chemically equivalent to hydrogen, tritium has slightly different physical properties due to its increased mass. Diabaté and Strack [12] noted that reaction rates decreased as atomic mass increased, causing a significant isotopic effect. Therefore, in reactions with HTO as a precursor, regular hydrogen would be preferentially used (instead of tritium) due to its lower atomic mass. However, as pointed out by the AGIR [27], any effects due to isotopic differences would be accounted for in the determination of RBE values.

Conclusion on Adverse Health Effects

Laboratory studies have demonstrated that tritium induces lethality, teratogenicity, genetic (chromosome aberrations), and reproductive effects. Tritium has also been shown to induce and promote cancer in mice under experimental conditions. Table 1 summarizes the studies reviewed in this report, although one should be careful when comparing the endpoints and the

Tritium, Health Effects and Dosimetry. Table 1 Overview of studies showing lowest concentration or administered dose of tritium to produce an adverse effect

Study	Means of exposure	Test animals	Parameter	Lowest concentration or administered dose to show effect	Dose (when available)
Lethality					
Brues et al. [17]	Single injection of HTO	Mice	$LD_{50/30}$	0.037 GBq/g body weight (BW) (~1.5 GBq total dose)	9 Gy (~6 Gy[a])
Yokoro et al. [19]	Single injection of HTO	Mice	Lowest dose	0.37 GBq	~5 Gy
Yokoro et al. [19]	Single injection of HTO	Mice	$LD_{50/30}$	0.56–0.93 GBq	~8–13 Gy
Furchner [18]	Single injection of HTO	Mice	$LD_{50/30}$	0.024 GBq	8 Gy (~ 4 Gy[a])
Yamamoto et al. [20]	Ingestion of HTO	Mice	Lowest dose	1.37 GBq	11.1 Gy
Teratogenic effects					
Zamenhof and Van Marthans [31]	Ingestion of HTO	Mice	No observed effects in mothers, temporary effects in offspring	111 MBq/L	N/A
Laskey et al. [32]	Ingestion of HTO	Mice	Lowest dose reduced brain weight	3.7 MBq/L	0.00003 Gy/day
Bursian et al. [33]	Ingestion of HTO	Mice	Reduced brain weight and neural hormones	370 MBq/L	0.66 Gy
Jones et al. [34]	Ingestion of HTO	Squirrel monkeys	Oocyte reduction, no other noted effects	111 MBq/L	N/A
Reproductive effects					
Satow et al. [44, 45]	Injection of HTO	Mice	Oocyte reduction	0.17 MBq/g BW	0.035 Gy
Lambert [49]	Injection of ^{3}HTdR	Mice	Reduction of spermatogonia	185 kBq/g BW	0.084 Gy (to cell nucleus)
Lambert [49]	Injection of HTO	Mice	Reduction of spermatogonia	2.22 MBq/g BW	0.049 Gy (to cell nucleus)
Carcinogenicity					
Yamamoto et al. [53]	Ingestion of HTO	Mice	Thymic lymphoma	1.85 GBq/L	0.048 Gy/day
Yamamoto et al. [53]	Ingestion of HTO	Mice	Solid tumors	0.925 GBq/L	0.024 Gy/day
Yamamoto et al. [54]	Ingestion of HTO	Mice	Thymic lymphoma	0.463 GBq/L	0.012 Gy/day
Gragtmans et al. [55]	Injection of HTO	Rats	Early onset of mammary tumor	0.45 MBq/g BW	0.46 Gy
Johnson et al. [56]	Injection of HTO	Mice	Myeloid leukemia	90 MBq	0.85 Gy
Seyama et al. [57]	Injection of HTO	Mice	Tumors	140 MBq	1.97 Gy
Mushkacheva et al. [59]	Ingestion of HTO	Mice	DNA damage	37 kBq/g/day	1.2 Gy

[a]Estimated for this report using a biological half life of water of 1.2 days

different dose regimes (injection or ingestion), especially with respect to the mouse oocyte. Generally, doses above 0.5 GBq and radiation doses of 0.5 Gy are needed to induce an adverse health effect. The exception to this, as discussed earlier, is the mouse reproductive system, whose oocytes are about 100 times more radiosensitive than that of humans.

Because it is ionizing radiation, the tritium beta particle would also be expected to induce hereditary and reproductive effects. This is in line with an equivalent dose of gamma or x-ray radiation, although no studies were found to support this hypothesis. Similarly, noncancer effects such as cardiovascular disease could also be expected as a result of radiation exposures to doses exceeding 0.5 Gy. Not surprisingly, the doses resulting from the amount of tritium needed to cause these effects are essentially the same as doses of other types of ionizing radiation (gamma and x-ray) when the RBE and dose protraction are taken into account. Current risk estimates for tritium therefore appear to be appropriate.

In general, the greater biological effectiveness of OBT relative to HTO appears to be related to longer retention times, rather than to differences in RBE. DNA precursors are the exception, where preferential irradiation of the nucleus can give higher RBE values, expressed in terms of average cell dose. However, OBT concentrations in the environment are generally low and the compounds that pose the greatest risk (such as ^{3}HTdR) are not expected to approach concentrations anywhere near those that pose a significant risk.

Nonradiological effects from tritium such as transmutation and isotopic effects are unlikely, but if they do occur, it would not be possible to distinguish their effects from those of radiation. Therefore, they are taken into account in risk estimates and do not require special consideration.

Relative Biological Effectiveness

In radiation biology, absorbed dose refers to the amount of radiation energy deposited within a unit mass, typically tissue or individual cells. However, it is clear that the deposited energy alone does not dictate the amount of biological damage and that other factors like the type of radiation and the chemical form of the radioisotope play a role. To equate absorbed doses from different radiations, and thus permit the use of a single unit of dose for radiation protection purposes, the effectiveness of the radiations must be quantified. Quantification requires a strict comparison of the effects of the radiation of interest with those effects caused by a standard or reference radiation. The ratio of the response of the two radiation types is termed the RBE.

With respect to tritium beta radiation, the selection of the reference radiation makes a significant difference in the resultant RBE. In addition, Little and Lambert [111] and the AGIR [27] point out that the dose from the reference radiation must be delivered in the same fashion as that of the tritium irradiation, which implies a chronic exposure with an exponential decay if the concentration of the tritium in the body is not maintained at a constant value.

To further complicate matters, the response of the tissue or organ being irradiated may not be linear for the radiation of interest or the reference radiation. Straume and Carsten [25] discuss this at some length, indicating that the RBE can vary significantly with changes in dose rate and radiation quality (LET). Therefore, for radiation protection purposes, it is desirable to assess the RBE for doses and dose rates that are comparable to those received in environmental and occupational settings. However, as the AGIR [27] points out, the dose response curve for acute doses of low-LET reference radiation is often curvilinear in relation to the response of radiations with higher LET (such as tritium's beta radiation). Studies at these lower doses give a maximum RBE value, which would be more appropriate for occupational and environmental exposures. This is referred to as the RBE_{MAX} or RBE_{M}.

There have been many experimental determinations of the RBE for tritium radiation, using various biological endpoints, both in vitro and in vivo, and using gamma and x-rays as the reference radiations. In vivo (Latin for "within the living") implies that the living tissue of an entire living animal is used in the study. In vitro (Latin for "within the glass") is the general designation given to experimental studies done on tissues or cells outside of the body; for example, in a Petri dish.

Several reviews of these studies have been conducted, some of them critical, that have highlighted

errors or omissions in the work that might have affected the RBE determination. These too are briefly reviewed in the following section.

RBE Literature Reviews and Experimental Studies

Straume and Carsten [25] identified 12 published RBE studies for HTO compared with orthovoltage (200–500 kVp) x-rays and 21 RBE studies for HTO compared with gamma rays from Cesium-137 or Cobalt-60. Combining these studies, they calculated an arithmetic mean RBE value of 1.8 using x-rays as the reference radiation and 2.3 relative to gamma rays. They commented that their estimates were based upon studies that used radiation delivered at doses and dose rates higher than those generally received by radiation workers and members of the public; therefore, their estimated RBE values could have been lower than the actual RBE values than should be used for human risk assessment.

The Little and Lambert [111] critique of the Straume and Carsten [25] review pointed out that Straume and Carsten [25] included a number of studies that did not have adequate concurrent external (x-ray or gamma ray) radiation-exposed groups (e.g., Prosser et al. [112]; Carsten and Commerford [113]; Russell et al. [114]; and Furuno-Fukushi et al. [65]). In addition, some of the other calculations of RBE conducted by Straume and Carsten [25] (for example, the tritium experiments of Prosser et al. [112]) combined with the Cobalt-60 experiments of Lloyd et al. [115] were based on nonconcurrent experiments.

The AGIR report [27] discusses the RBE of tritium radiation as well as track-structure considerations, the relationship between the RBE and the dose and dose rate effectiveness factor (DDREF), the use of different reference radiations, and experimental studies. The biokinetic models of HTO and OBT were discussed through an examination of the current ICRP models, a review of the key information underlying those models, a discussion of more recent models, and the special aspects of DNA precursors. There was also a detailed review of reproductive effects in the female, especially on oocyte formation and fertilization.

The AGIR authors critically reviewed several papers that estimated the tritium RBE value under different experimental regimes. Twenty-four studies were divided into in vivo and in vitro experiments, and subdivided as either chronic or acute irradiation regimes. To be classified as a chronic irradiation, the external irradiation dose rate had to be comparable to the tritium exposure. The biological endpoints of the tritium studies included carcinogenesis, chromosomal aberration, cell death, and others. With one exception, they only included papers published in peer reviewed journals or conference proceedings; the exception being an article by Chopra and Heddle [116], which they included because of the well-conducted experiments and data analysis.

The AGIR made the following conclusions regarding the tritium RBE value:

1. Various theoretical and experimental studies of radiation of LET similar to that of tritium beta particles led to the general expectation of an RBE value for tritium of at least 2 compared with gamma radiation.
2. Neither transmutation effects nor isotopic discrimination associated with tritium appear likely to have major effects, but any effect would be in the direction of tending to increase the observed RBE value.
3. Experimentally determined RBE values can vary significantly depending on the choice of reference radiation. It was recommended that high-energy gamma rays should be the preferred choice for reporting RBE values. Where lower energy x-rays and gamma rays were used as the standard, an appropriate adjustment should be taken into account when discussing the results. In addition, the reference radiation used should be adequately described and include anything, such as filtration, that would modify the energy spectrum.
4. Interpretation of RBE experiments was complicated by dose rates that were rarely comparable and by reference radiation that may have been more effective than hard gamma rays.
5. In a wide variety of cellular and genetic studies, RBE values for HTO have generally been observed in the range from 1 to 2 when compared with orthovoltage x-rays, and in the range from 2 to 3 when compared with gamma rays.
6. For developmental endpoints, the RBE values for HTO were similar to those obtained from cellular and genetic studies.

7. Whole animal carcinogenesis studies yielded RBE values with central estimates generally in the range of 0.8–2.5 (x-rays and gamma rays as the reference radiations). However, the AGIR had several reservations with these studies. In particular, in some of the studies the frequency of cancers appears to have been saturated or nearly saturated at the lowest doses employed (about 1 Sv), so the slope of the dose–response curve was above the relevant dose levels – which represent the area of interest for radiation protection purposes.
8. The AGIR considered the most likely RBE value relative to chronically delivered hard gamma rays was between 2 and 3 and considered a value of 2 most appropriate. This was based largely on an analysis of the available experimental data with rounding and biophysical considerations. Fractional values were not considered appropriate.

In addition to the above, the most significant recommendation of the AGIR report was related to the use of a provisional value of 2 for the radiation weighting factor (w_R) for tritium until an internationally agreed value becomes available.

Little and Lambert [111] used the RBE estimates from the acceptable studies to compute an aggregate "best linear unbiased estimate (inverse-variance weighted) of the RBE" and the 95% confidence limit of the RBE estimates. Their definition of the RBE was based upon the ratio of the initial slopes (i.e., lower doses) of the tritium and gamma (or x-ray) dose–response curves which was roughly equivalent to the standard definition of the RBE_M.

In their summary of the carcinogenesis studies, Little and Lambert [111] indicated that the overall aggregate results imply RBE values with a central estimate in the range of 1.2–2.5 and 97.5 upper percentile of no more than 3.0. The three studies that used chronic x-rays and chronic gamma irradiation yielded an aggregate RBE value of 1.19 (95% confidence interval (CI): 0.88–1.49) and 2.49 (95% CI: 2.00–2.98), respectively.

Little and Lambert [111] stated that they doubted the in vivo cancer data in the studies. Nevertheless, their estimates of RBE in relation to late health effects (such as cancer) were derived by combining the in vivo cancer data estimates for endpoints for other than cell survival (and related endpoints) to yield an aggregate RBE of 2.19 (95% CI: 2.04–2.33) and 1.17 (95% CI: 0.96–1.39) when using chronic gamma rays and chronic x-rays, respectively, as the reference radiation.

The term "radiation effectiveness factor" (REF) was used by Kocher et al. [117] to represent the biological effectiveness of a radiation dose for the purpose of estimating cancer risks and probability of causation in identified individuals. This differs from an RBE in that the REF applies strictly to the results of specific radiobiological studies under controlled conditions. Also, the REFs for induction of cancers in humans developed in this work were expressed as both a central estimate (median) and a subjective probability distribution (95% confidence levels) to represent their uncertainty.

Part of the work by Kocher et al. [117] estimated the RBE_M for tritium beta particles, where M represents the maximum value. Estimates of the RBE_M were taken from Tables 1–3 of Straume and Carsten [25] where three of five studies, using chronic exposure to x-rays, had a central estimate of 2–3 for RBE_M. They further reasoned that "if a nominal biological effectiveness of X-rays relative to high-energy gamma rays of 2 is assumed on the basis of the probability distribution of REF_L for orthovoltage X-rays . . ., those data suggest that RBE_M for ^3H beta particles relative to gamma rays delivered chronically could be as high as about 4–6." Based on this reasoning, their REF_L for "electrons less than 15 keV had a 50th percentile value of 2.4 and a 95% confidence interval of 1.2–5.0."

The *Canadian Environmental Protection Act*, 1999 (Environment Canada [118]) requires the federal Ministers of the Environment and of Health to prepare and publish a Priority Substances List (PSL) that identifies

Tritium, Health Effects and Dosimetry. Table 2 Track average LET in water for various radiations based on a cut-off energy, Δ, of 100 eV (based on ICRU [119])

Radiation	$\bar{L}_{\Delta,T}$(keV/μm)
Cobalt-60 gamma radiation (1,173 and 1,332 keV)	0.22
200 kVp x-rays	1.7
Tritium beta radiation (mean 5.7 keV)	4.7
50 kVp x-rays	6.3

Tritium, Health Effects and Dosimetry. Table 3 ICRP Publication 67 – [127]-Parameters describing the distribution and retention of tritium after acute intakes of tritiated water

Age	Distribution (%)		Biological half-life (days)	
	HTO component	OBT component	HTO component	OBT component
3 months	97	3	3.0	8
1 year	97	3	3.5	15
5 years	97	3	4.6	19
10 years	97	3	5.7	26
15 years	97	3	7.9	32
Adult	97	3	10.0	40

substances, including chemicals, groups of chemicals, effluents, and wastes, that may be harmful to the environment or constitute a danger to human health. In complying with the Act, the Ministries of Environment Canada and Health Canada undertook an assessment of the impact on nonhuman biota from the releases of radionuclides from nuclear facilities (Environment Canada/Health Canada [118]). Tritium was included in the review since it is released to the environment from the operation of CANDU nuclear power reactors. Although nonhuman biota were the primary focus, much of the review included studies looking at the effects of tritium on mammals and so is relevant to this report. Reproductive effects of tritium exposure were of special interest, since reproductive organs are one of the most radiosensitive tissues and reproductive failure could affect biota populations. The report looked at many studies and reviews to determine what the investigators called an "ecodosimetry weighting factor." They reported the results of nine studies looking at reproductive effects of tritium in mammals and fish, which gave tritium radiation RBE values from 1.7 to 3.8 (the highest value was due to reduction in fish egg fertilization). The report also "gamma normalized" (multiplied the RBE by 2, using x-rays as a reference to make the value comparable to a gamma radiation reference) the RBE value of spermhead survival reported by Lambert [49], giving an estimated RBE of 4.8. These RBE values were compared to those of Straume and Carsten [25], resulting in an "ecodosimetry weighting factor" of 3 for tritium radiation for ecotoxicological risk assessment purposes.

Electron Energy and Ionization Path Lengths: Why Tritium Radiation Is More Effective Than Gamma Radiation The experimental evidence seen in this and other reviews provides a convincing argument that the RBE for tritium radiation is greater than that of 200–250 kVp x-rays and Cobalt-60 or Cesium-137 gamma radiation.

The amount of energy lost per unit distance is referred to as the linear energy transfer (LET), often expressed in units of keV/μm. Interactions between radiation and molecules will cause ionization in some of the molecules. Electromagnetic radiation, such as gamma rays and x-rays has a much lower LET than alpha particles. As Table 2 indicates (International Commission on Radiological Units and Measurements ICRU [119]), low-energy photons and electrons release more energy per micrometer than higher energy photons. However, the lower energy photons release much less total energy and travel much shorter distances than their higher energy counterparts.

Photons (gamma rays and x-rays) act indirectly and the type of interaction is energy related, causing molecular ionization through photon absorption (photoelectric and pair production) or scattering events (Compton interactions). Particle radiation, such as tritium's beta radiation, can damage key molecules like DNA through both direct and indirect interaction. This damage occurs from the production of free radicals (e.g., hydroxyl) caused by the ionization of water molecules – which may, in turn, damage DNA.

The most significant cellular damage caused by radiation is breakage of the DNA molecular chain. DNA is a double helix, meaning there are two

corresponding and linked molecular chains containing corresponding nucleic acids. Radiation-induced DNA damage usually results in damage to the base molecules; single strand breaks (SSBs), double strand breaks (DSBs), DNA-protein cross-links, or a combination of some or all of these. The degree of damage is related to the density of the radiation track. A large deposition of energy within a DNA molecule may cause a cluster of damage. If the damage is great, then it may not be fully reparable and can cause cell death or permanent chromosome damage.

Nikjoo and Goodhead [120] suggested that the most significant biological effects are caused by sizeable clusters of energy deposition and that the net biological effect increases with the severity of the initial damage. Most of this type of damage is thought to be due to low energy secondary electrons that are produced as the radiation slows down. They concluded by stating that the lower energy electrons are more effective than higher energy ones (for example, greater than 100 keV) in producing complex damage and that this was observed in experiments with ultrasoft x-rays.

Another important aspect is the location of the tritium atom when it disintegrates. HTO will be relatively evenly distributed throughout tissues and cells. On the other hand, OBT may be incorporated into important molecules such as DNA. The release of a beta particle from that position has a greater probability of causing damage than an HTO molecule in the cellular fluid, for example. With respect to the impact of OBT, Chen [120] used a Monte Carlo code to generate simulated tracks in order to compare the dose mean linear energies (keV/μm) for HTO and OBT molecules in spherical regions with diameters of 10 nm to 2 μm. The results indicated that a mean linear energy for OBT was a factor of 1.7 higher than for HTO, using the assumption that the extent of the increase would depend on the OBT molecule's location within the cell.

Computational models appear to confirm that the higher RBE of tritium, as well as that of other low-energy radiation, is at least partly due to the high-LET and correspondingly short path length of tritium beta particles. The relatively large deposition of energy within a very small volume induces SSBs and DSBs and also causes complex damage that may not be reparable. When the tritium is incorporated into DNA, there is a higher probability of biological damage.

Summary

The RBE provides a referenced correction factor for comparing the effects of different radiations, giving direction for the development of a universal measurement of dose, the sievert (Sv). Much of the discussion in this report and those of others, such as the AGIR [27] and Straume and Carsten [25], has centered upon an appropriate single value for the RBE of tritium. Although there have been more than 50 different estimates of this value, it is clear considerable variation exists. This, combined with uncertainty in radiobiological data, makes it difficult to select one value. The choice of a reference radiation accounts for much of this variability, due to the difference in the RBE of x-rays and higher energy gamma rays. Other factors contributing to the observed range include:

- Differences in radiosensitivity of tissues, organs, and organisms
- Different biological endpoints
- Variation in DDREFs
- Dosimetry
- Choice of in vitro or in vivo test systems

For occupational and public exposures, the most relevant endpoint is radiogenic cancer, (particularly radiation delivered at occupational or slightly greater levels), but there are very few studies at occupational dose levels, since most experiments use more than 1 Gy. However, overwhelming evidence supports an RBE for tritium of at least 2 when pooling the data from all studies, including those examining the most relevant endpoints, which were reviewed in this report. Given the range of observed values, an RBE of at least 2 for tritium beta particles should be seen as a general indication of the greater effectiveness of these particles versus low-LET radiation. This would apply to cancer induction in humans in the absence of better experimental data and specifically, any tritium-specific epidemiological data.

Dosimetry and Biokinetics

Calculating the committed effective dose received as a result of taking tritium into the body is done in two steps. First, a model describing the behavior of the tritiated compound taken into the body is used to predict where the tritium will go in the body and the rate at

which it will be removed from the body. Such a model is known as a biokinetic model. Second, a dosimetric model is used to calculate how much tritium will decay while it is in the various organs and tissues of the body and how much of the energy from the beta particles it emits during decay will be absorbed by the body. This allows us to calculate the dose resulting from the intake of tritium. Because tritium is removed gradually from the body after an intake, the committed effective dose takes into account the dose received for 50 years following the intake of a radionuclide into the body.

Since the energy carried by tritium beta radiation is of short range, all of its energy is absorbed in the tissues and organs in which the tritium atoms are located. This describes the dosimetric model for tritium. The biokinetic model for tritium is more complex and depends on the type of tritiated compound taken into the body.

This section presents the main biokinetic models used for calculating dose as a result of taking tritium compounds into the body, either by inhalation, ingestion, or absorption through the skin. In particular, it presents the tritium biokinetic models recommended by the International Commission on Radiological Protection (ICRP) and the basis for these models. Other models are also considered, which take into account types of exposures that are not considered by the ICRP models or give a more accurate description of the biokinetics of certain tritiated compounds. Examples of applications of the tritium dosimetric model are also provided by presenting dose coefficients calculated with the biokinetic models discussed.

Overview of Current ICRP Models for Tritiated Water and Organically Bound Tritium

Tritium may enter the body by inhalation, absorption through skin, and ingestion. The first two are the most frequent forms of intake in the workplace, while all three routes of intake can contribute to exposures to members of the public. Skin contact with tritium-contaminated surfaces, such as metal and glass, has been shown to result in the formation of OBT in the body. Skin contact is therefore considered as a different mode of intake compared to the absorption of HTO through skin, and has also been shown to be a route of intake in the workplace [7].

The fate of tritium once taken into the body is determined mostly by its chemical form in the external environment. One can expect to find HTO in most workplaces and environmental media where tritium is present. In most OBT compounds, tritium that is bound to oxygen, nitrogen, phosphorus, or sulfur will exchange freely with hydrogen in water. Therefore, it has the same metabolism and distribution in the body as HTO and is called the exchangeable bound tritium fraction. Tritium bound to carbon will not exchange with hydrogen in water. Tritium in such C–H bonds is known as nonexchangeable bound tritium. In general, considerations of the biokinetics of OBT refer to the nonexchangeable component that exhibits retention times determined by carbon turnover rather than HTO kinetics.

Tritiated compounds may also exist in particulate forms, such as airborne particles that contain tritium. The retention and clearance of these particulates in the respiratory tract depend on several factors, for example, the particle's size and chemical composition. For the purpose of dose assessment, tritium absorbed into blood after tritiated particulates have been inhaled is treated as HTO after it has left the lungs [122–125]. Although tritium beta rays are partially self-attenuated within the particle, the dose to the lower lung – from particles that slowly dissolve – can be up to two orders of magnitude higher than that from the same activity of inhaled HTO [126].

The tritiated compounds are therefore categorized according to the metabolic model that best describes their dynamics after uptake. Two primary metabolic models, which are discussed in this section, are used to estimate the dose from tritiated compounds:

- *The HTO model*, which is used to estimate the dose resulting from intakes of HTO or other tritiated compounds that partially convert to HTO after being taken into the body
- *The OBT model*, used to estimate the dose resulting from intakes of various tritiated organic compounds (nonexchangeable bound tritium)

A third model, which applies to tritium absorbed through the skin from HT-contaminated surfaces, is also described. Finally, the biokinetics of tritiated compounds in relation to pregnancy and to nursing is discussed in this section.

Internal Dosimetry of Tritiated Compounds Using the ICRP HTO Model

The ICRP Model for the Inhalation and Ingestion of Tritiated Water The ICRP HTO model [127], illustrated in Fig. 2, is used to assess doses for:

- Intakes of HTO
- HTO formed following intakes as HT
- Tritiated hydrocarbon vapors and gases
- Tritiated particulates

For intakes as HTO, the model assumes instantaneous translocation to blood. It is further assumed that HTO is transferred from the blood, with a biological half-life of 6 h and then distributed uniformly throughout the body. The model assumes that 97% of tritium taken in remains as HTO once distributed, while 3% is converted to OBT. In adults, HTO is retained with a biological half-life of 10 days, and OBT is retained with the biological half-life of carbon, which is 40 days. HTO is assumed to be distributed uniformly throughout the 42 L of body water. The assumed partitioning between HTO and OBT after acute intakes of HTO in various age groups, as well as corresponding biological half-lives, is given in Table 3 [128].

The model used to derive the committed effective dose per unit intake (dose coefficient) to adults resulting from the intake of HTO, as recommended by the ICRP [125, 128] and is based on Fig. 2. This model considers the ICRP's recommendations for radiation weighting factors as well as tissue weighting factors. The committed effective dose per unit intake is

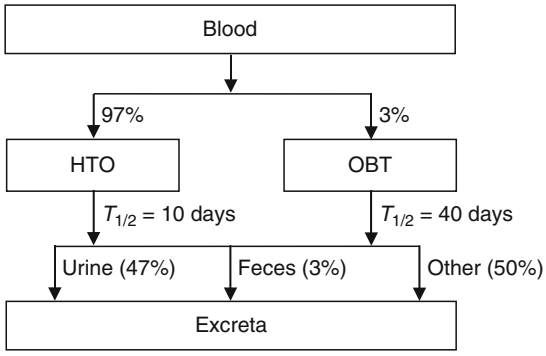

Tritium, Health Effects and Dosimetry. Figure 2 ICRP Publication 71 – [125]-Model for the biokinetics of tritiated water

the computed effective dose received up to 50 years following a single intake for adults and up to 70 years for intakes by infants and children. The value for intakes of HTO by adults computed by the ICRP is 1.8×10^{-11} Sv/Bq. A slightly different dose coefficient, 2.0×10^{-11} Sv/Bq, was recommended by Health Canada and the Canadian Nuclear Safety Commission [129, 130] and incorporated in past regulatory documents [131]. The ICRP dose coefficient is based on the assumption that dose from HTO is received by 68.8 kg of tissue, which includes several kilograms of noncellular bone. This value was derived from the total body mass of 70 kg minus the masses of the contents of the gastrointestinal tract (1,005 g), urinary bladder (102 g), and of the gall bladder (62 g) [5]. Because the relevant dose is that to the nucleus of sensitive cells from contained HTO, the Atomic Energy Control Board (now the Canadian Nuclear Safety Commission) recommended using a dose coefficient of 2.0×10^{-11} Sv/Bq to assess the dose resulting from intakes of HTO. This recommendation considered dose received by 63 kg of soft tissue: a mass equal to the mass of the total body (70 kg), minus the skeleton mass (10 kg). Because the latter includes radiosensitive marrow, the mass of the marrow (3 kg) must be included in the dose calculation. The dose coefficient of 2.0×10^{-11} Sv/Bq considered dose to a mass of 70 kg − 10 kg + 3 kg = 63 kg [5]. Furthermore, the dose coefficient recommended by the Federal Provincial Working Group on Bioassay and In Vivo Monitoring [129], 2.0×10^{-11} Sv/Bq, assumed that 97.8% of tritium entering the body as HTO remained as HTO, with a biological half-life of 9.7 days, while 2.2% was converted to OBT and was retained with a biological half-life of 48.5 days [132].

More recently, the ICRP model for HTO [128] was used to calculate the dose to 68.8 kg of soft tissue, with corrections using the updated values of 10.5 kg for skeleton mass and 3.65 kg for marrow mass [133]. The resulting dose coefficient was 2.0×10^{-11} Sv/Bq, a value that the CNSC continues to recommend and use [130].

The contribution of the OBT fraction to dose in the ICRP's HTO model has been shown to be about 10% [132, 134]. This has been verified to be adequate for dose estimates under both acute and chronic intakes [135, 136].

Absorption of HTO Through Skin HTO is also known to be absorbed through skin from the vapor phase or the liquid phase, i.e., by immersion [3, 4, 137]. The ICRP [125] addresses HTO intake via skin absorption by reference to Osborne [137], Hill and Johnson [7], and Myers and Johnson [109], the latter being a literature review. About 1% of HTO activity per m^3 in air is taken to be absorbed through the skin per minute. This results in absorption through the skin contributing about one third of the total HTO intake for a given HTO concentration in air when the exposed individual is active during exposure (breathing in more air than when at rest). Using the same assumptions, the amount of HTO absorbed through the skin in a given time is about equal to the amount inhaled in the same period of time when the exposed individual is at rest during exposure.

ICRP Model for the Inhalation of Elemental Tritium Gas Following inhalation of elemental tritium gas (HT), a small fraction (about 0.01%) [138] of the inhaled activity is dissolved in body fluids and then oxidized to HTO. The latter is the predominant contributor to dose. HT gas is not significantly absorbed through the skin and does not readily convert to HTO on the skin. Irradiation of the lungs from inhaled HT gas does not significantly increase the committed effective dose [139] because of the short range in tissue of this tritium beta particle (see Section The Inhalation of Elemental Tritium Gas). The dose coefficient for the inhalation of HT gas is therefore taken to be 0.01% of that used for the inhalation of HTO.

Tritiated Hydrocarbons Various forms of tritiated hydrocarbons have been identified. Tritiated methane (CTH_3) is the only such tritiated compound for which the ICRP recommends a dose coefficient based on the HTO model. CTH_3 is known to form as a result of microbial degradation within tritiated waste. About 1% of inhaled CTH_3 is assumed to be converted to HTO [140]. The dose coefficient for CTH_3 is therefore 1% of that for HTO. The HTO model is not recommended for interpreting bioassay data collected following an intake of CTH_3; the use of workplace or environmental data is more appropriate. The ICRP approach is considered to give a conservative dose coefficient [140].

Summary of Dose Coefficients Based on the ICRP HTO Model Table 4 presents the ICRP's recommended dose coefficients for tritiated particulates, as well as for other tritiated compounds [141].

Table 5 illustrates the effect of age on the dose per unit intake for the inhalation of HTO and compares these dose coefficients to the value for adults.

Internal Dosimetry of Tritiated Compounds Using the ICRP OBT Model

Figure 3 illustrates the ICRP model [125, 127] used to assess doses that result from the intake of unspecified

Tritium, Health Effects and Dosimetry. Table 4 ICRP Publication 72. [141]. Dose coefficients based on the ICRP HTO model for various tritiated compounds, modes of intake and age groups

Tritiated compound	Mode of intake	Dose coefficient (Sv/Bq)	
		Infants (1 year old)	Adults
HTO[a]	Inhalation	4.8×10^{-11}	1.8×10^{-11}
HTO	Ingestion	4.8×10^{-11}	1.8×10^{-11}
HT	Inhalation	4.8×10^{-11}	1.8×10^{-15}
CTH_3	Inhalation	4.8×10^{-13}	1.8×10^{-13}
Type F particulates[b]	Inhalation	2.0×10^{-11}	6.2×10^{-12}
Type M particulates[b]	Inhalation	2.7×10^{-10}	4.5×10^{-11}
Type S particulates[b]	Inhalation	1.0×10^{-9}	2.6×10^{-10}

[a]The dose from the inhalation of HTO does not include absorption through the skin and should be increased by a factor of 1.5 in order to account for it

[b]Dose coefficients shown for particulates of 1 μm activity median aerodynamic diameter (AMAD)

organic forms of OBT. It assumes that OBT, once taken into the body, is translocated to blood completely and instantaneously and then distributed uniformly throughout body tissues. In the absence of specific information on the inhaled organic compound, it is assumed that tritium absorbed to blood will behave as it does after ingestion (i.e., that 50% is retained as OBT in body tissues and that 50% is catabolized to HTO) and that its turnover time will be similar to those of water.

It is assumed that tritium inhaled as organic compounds is absorbed to blood instantaneously and is transferred from blood with a biological half-life of 6 h, with 50% retained as OBT in body tissues and 50% catabolized to HTO [142].

Data on the metabolic processes and retention of nonbiological tritiated organic compounds (such as tritiated oils and solvents) following inhalation are scarce [7]. These compounds are therefore not considered further in this section.

Tritiated organic compounds in the diet may include tritiated proteins, fats, and carbohydrates. The ICRP model for the ingestion of OBT [127] is intended to represent normal dietary content of these different forms. The model was developed in the absence of good information about the specific proportions of OBT in components of the human diet and how tritium is incorporated into organic molecules in body tissues.

In this model, it is assumed that all ingested tritiated organic compounds are completely absorbed from the gastrointestinal tract to blood, after which the tritium from these compounds is uniformly distributed in tissue. In reality, the distribution of tritium in the various tissues will depend on the chemical form of the tritium and the metabolic activity of the individual tissue.

Experimental studies of the relative incorporation of tritium into OBT in body tissues following intakes of HTO and OBT suggest that about 9–45% of tritium from dietary OBT is incorporated into body OBT. The ICRP OBT model therefore conservatively assumes that after tritium is absorbed from blood (in adults), further to ingestion as OBT:

- Fifty percent of tritium will follow the metabolic behavior of carbon, having a biological half-life of 40 days.
- Fifty percent of tritium will behave as HTO, having a biological half-life of 10 days.

Tritium, Health Effects and Dosimetry. Table 5 ICRP Publication 72 [141]. Dose coefficients for HTO inhalation for various age groups

Age	Dose coefficient (Sv/Bq)	Ratio of dose coefficient to that of adult
3 months	6.4×10^{-11}	3.6
1 year	4.8×10^{-11}	2.7
5 years	3.1×10^{-11}	1.7
10 years	2.3×10^{-11}	1.3
15 years	1.8×10^{-11}	1.0
Adult	1.8×10^{-11}	1.0

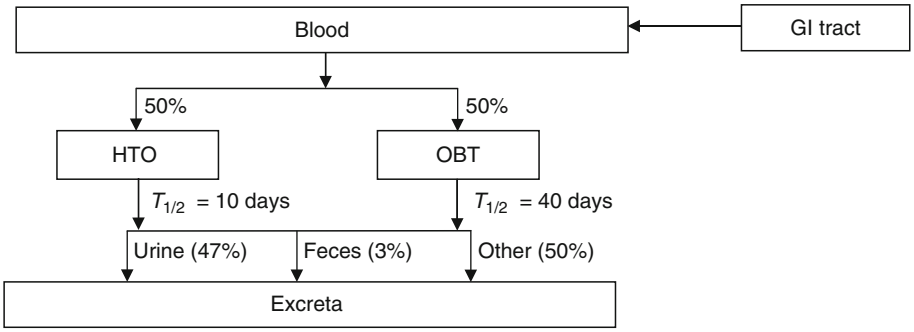

Tritium, Health Effects and Dosimetry. Figure 3
ICRP Publication 71 – [124]-Model for the biokinetics of organically bound tritium

Tritium, Health Effects and Dosimetry. Table 6 ICRP Publication 67 [128]. Partitioning between HTO and OBT after dietary intakes of OBT

Age	Distribution (%)		Biological half-life (days)	
	HTO component	OBT component	HTO component	OBT component
3 months	50	50	3.0	8
1 year	50	50	3.5	15
5 years	50	50	4.6	19
10 years	50	50	5.7	26
15 years	50	50	7.9	32
Adult	50	50	10.0	40

It should be noted that less than 10% of OBT in diet is excreted in the form of OBT in urine (mostly in the form of urea), and ~3% OBT is excreted in feces.

Table 6 gives the assumed partitioning between HTO and OBT and corresponding biological half-lives, after dietary intakes of OBT in various age groups [128]. The ICRP's recommended dose coefficients for OBT are shown in Table 7 [141]. Table 8 shows the effect of age on dose per unit intake for the ingestion of OBT.

Tritium, Health Effects and Dosimetry. Table 7 ICRP Publication 72 [141]. Dose coefficients based on the ICRP OBT model for various modes of intake and age groups

Tritiated compound	Mode of intake	Dose coefficient (Sv/Bq)	
		Infants (1 year old)	Adults
OBT	Inhalation	1.1×10^{-10}	4.1×10^{-11}
OBT	Ingestion	1.2×10^{-10}	4.2×10^{-11}

Tritium, Health Effects and Dosimetry. Table 8 ICRP Publication 72 [141]. Dose coefficients for OBT ingestion for various age groups

Age	Dose coefficient (Sv/Bq)	Ratio of dose coefficient to that of adult
3 months	1.2×10^{-10}	2.9
1 year	1.2×10^{-10}	2.9
5 years	7.3×10^{-11}	1.7
10 years	5.7×10^{-11}	1.4
15 years	4.2×10^{-11}	1.0
Adult	4.2×10^{-11}	1.0

Intakes of Tritium in Relation to Pregnancy and Nursing

Pregnancy and Tritium Intake The ICRP [142] has provided biokinetic and dosimetric models and dose coefficients for the embryo, the fetus, and the newborn as a result of intakes of radionuclides by the mother.

In prenatal dosimetry, the term "embryo" refers to the developing offspring up to the end of week 8 of pregnancy, including the initial stages of growth up to the end of organogenesis. At this time, the embryo weighs less than about 10 g. During this stage, the dose to the fetus is assumed to be the same as that to the uterus wall.

The term "fetus" refers to the developing offspring after week 8 of pregnancy. During this stage of pregnancy, doses to fetal organs and tissues are calculated using biokinetic models that describe tritium behavior in the fetus itself, as this behavior will differ from the assumed tritium behavior in the mother. For the ICRP [142] report, models that take into account existing relevant biokinetic data were developed to calculate dose to offspring. Data collected from studies in animals, and in humans where available, and were used as the basis for biokinetic models for the transfer of radionuclides to the fetus. These data also provide a basis for the relative concentrations of radionuclides averaged for the whole body of the fetus (C_F) and the mother (C_M). The ratios of C_F:C_M are mainly taken

Tritium, Health Effects and Dosimetry. Table 9 ICRP Publication 88 [142]. Selected prenatal and infant dose coefficients

Tritiated compound type and mode of intake	Prenatal dose coefficients (Sv/Bq)		Dose coefficients for 3 month old (Sv/Bq)
	Acute maternal intakes[a]	Chronic maternal intakes[b]	
HTO inhalation	3.6×10^{-11}	3.1×10^{-11}	6.4×10^{-11}
HTO ingestion	3.6×10^{-11}	3.1×10^{-11}	6.4×10^{-11}
OBT ingestion	7.6×10^{-11}	6.3×10^{-11}	1.2×10^{-10}

[a]Values are for acute intakes at the end of week 10 of pregnancy. Acute intakes occurring at other times yield lower dose coefficients
[b]Chronic intake begins at start of pregnancy and lasts for the duration of the pregnancy

from studies presenting data at short times postintake. The ICRP [142] report conservatively assumed that the recommended C_F:C_M ratios applied to the time of intake and remained constant throughout pregnancy.

The ICRP [142] report presents dose coefficients for both chronic and acute maternal intakes by inhalation or ingestion. Acute intakes from 6 months before conception until the end of week 35 of pregnancy are considered. The report also provides chronic intakes lasting from 5 years or 1 year before conception until the time of conception, as well as chronic intakes lasting for the duration of the pregnancy. Effective doses to the offspring until birth, per unit intake by the mother, are presented, along with total committed effective doses to the offspring up to age 70, including doses resulting from radionuclides retained by the offspring at birth and doses received in utero.

HTO rapidly crosses the placenta after it is inhaled or ingested by the mother. Dose to the fetus resulting from such intakes depends on the water content of the fetus over the course of its development. As gestation progresses, water content decreases, while amounts of protein, fat, and minerals increase. The percentage of total body water decreases from about 93–95% at week 6 of pregnancy to 70–72% at birth. For comparison, the percentage of total body water in a nonpregnant woman is about 50%. While maternal total body water content is known to increase during pregnancy, studies disagree on the absolute values of total body water content. This disagreement is related to data on fetal body water content and the derivation of the amniotic fluid volume. However, calculations have shown that the maternal biological half-life of HTO varies from about 10 days at the start of pregnancy to about 12 days at term. This variation in the biological half-life does not significantly affect the ICRP fetal dose coefficients for HTO [142].

Until week 8 of pregnancy, the dose to the embryo is taken to be equal to that of the uterus. This dose is proportional to the concentration of HTO in maternal body water. For dose to the fetus (after week 8), the HTO concentration in fetal body water is taken to be equal to that in the mother.

Using an average body water content of 80% for the fetus and 50% for the mother, the ICRP uses a C_F:C_M ratio of 1.6 for HTO dose coefficients. This C_F:C_M ratio of 1.6 is applied to both the HTO and OBT components for intakes of OBT. Fetal tritium is assumed to be uniformly distributed throughout all tissues. Following birth, the biokinetic model for the 3-month-old [127] is used to assess dose to the newborn. Table 9 presents selected prenatal dose coefficients with comparisons to dose coefficients for the 3-month-old.

These dose coefficients are greater than other chronic dose coefficients tabulated by the ICRP [142], namely for chronic intakes starting 5 years and 1 year before pregnancy and lasting until the start of pregnancy.

Nursing and Tritium Intake The ICRP [143] has recommended dose coefficients for newborns from intakes of radionuclides in maternal milk resulting from maternal intakes. As with prenatal doses, acute and chronic intakes by the mother are considered for intakes by both ingestion and inhalation. Nursing is assumed to continue for 6 months after birth, and ingestion dose coefficients for infants are applied [128]. Maternal intakes during pregnancy and during

Tritium, Health Effects and Dosimetry. Table 10 ICRP Publication 95 [143]. Selected nursing infant dose coefficients

Tritiated compound type and mode of intake	Dose coefficient (Sv/Bq)	
	Acute maternal intakes[a]	Chronic maternal intakes[b]
HTO inhalation	2.2×10^{-11}	2.0×10^{-11}
HTO ingestion	2.2×10^{-11}	2.0×10^{-11}
OBT ingestion	3.5×10^{-11}	3.0×10^{-11}

[a]Values are based on acute maternal intake at 1 week after birth
[b]Acute intakes occurring at other times yield lower dose coefficients

lactation are also considered. The ICRP's approach estimates the activity of radionuclides transferred to milk as a function of maternal intake for various intake scenarios (acute or chronic intake regimes, and for various maternal intake times relative to birth).

The HTO and OBT models described in previously were modified by the ICRP [143] to account for transfer to milk. The rate of OBT transfer to milk was taken to be that of carbon. The ICRP [143] presented dose coefficients based on the assumptions of 6 feeds per day and an average daily intake by the infant of 0.8 L. Table 10 shows selected dose coefficients for doses to nursing infants resulting from maternal intakes of tritium.

Review of Currently Available Information about the Biokinetics of Tritiated Compounds

Dosimetry of Tritiated Compounds Using the HTO Model The parameters in the ICRP's HTO biokinetic model described above include the water and carbon biological half-lives and the HTO/OBT partitioning coefficients. The bases for biological half-lives and the HTO/OBT partitioning coefficients are discussed below.

Several studies have examined the biological half-life of HTO in adults. Butler and Leroy [144] found this parameter to vary with water intake (decreasing with increasing water intake rate), ambient temperature (decreasing with increasing ambient temperature), and age (decreasing with increasing age in adults). In this study, 310 cases of HTO intakes showed the biological half-life to vary from about 4 to 18 days, with a mean of 9.5 days. Other studies used fewer cases, but showed similar results for HTO [7]: from 6 days for eight cases [145] to 12 days for five cases [146]. The ICRP's HTO model adopted a biological half-life of 10 days for adults.

The biological half-life of 40 days that is used for the OBT compartment in body tissues is based on carbon turnover in the body. This was derived from the ratio of the Reference Man [5] carbon body content (16 kg) to the daily carbon intake (0.3 kg per day) and yields a biological half-life for carbon (0.693×16 kg/0.3 kg/day = 37 days). The calculated value of 37 days was rounded to 40 days in the ICRP model.

Some studies have also reported a longer lived component, which represents retained tritium that has a biological half-life greater than water or that of carbon in the HTO model. Such a component contributes to the committed effective dose and may influence how bioassay data are interpreted. Example results from such studies are shown in Table 11. In general, OBT in compartment 3 has a long biological half-life relative to the half-life of 40 days used in the ICRP model for OBT. OBT in this long-lived compartment represents less than 1% of total OBT. Taylor [157] has taken this long-lived compartment into account in HTO modeling. This is discussed further later in this section.

The partitioning of HTO and OBT after intakes of tritium as HT was examined by Takeda and Kasida [158] as part of a study of the biokinetics of HTO in rats. These investigators found that "initially, the ratio of tissue-bound tritium to total tritium was about 3% in the kidney and 1–5% in other tissues." Based on this study, the ICRP model assumes that 3% of initial HTO intakes are partitioned to OBT. Other investigators have found values of less than 1%; for example, Snyder et al. [149] reported a value of 0.4%, based on a single human exposure case. A study of an unplanned acute HTO intake incident involving eight male workers suggested a long-term component (average $T_{½}$ of 74 $\pm$18 days), which accounted for 0.5%$\pm$0.2% of the initial HTO intake [156]. Balonov et al. [146] also reported a long-term component partitioning fraction of 0.5% for a human subject (compared to 3% in the ICRP HTO model).

Tritium, Health Effects and Dosimetry. Table 11 Selected tritium retention half-lives in humans following intakes of tritiated water

Study	Number of cases	Biological half-life (days)		
		Compartment 1 (body water)	Compartment 2 (organically bound)	Compartment 3 (organically bound)
Pinson and Langham [3]	9	11.3		
Foy et al. [147]	10	5–11 (mean: 7.5)		
Wylie et al. [148]	7	6.4–12.1 (mean: 8.5)		
Butler and Leroy [144]	310	4–18 (mean: 9.5)		
Osborne [137]	30	6.4–14.4 (mean: 10.5)		
Snyder et al. [149]	1	8.7	34	
Sanders and Reinig [150]	1	6.1[a]	23	344
Minder [151]	1		10–30	139–230
Lambert et al. [152]	1	9.1[b]	36	
Moghissi et al. [153][c]	2		21 and 33	280 and 2,020[d]
Moghissi et al. [154][e]	3		21 and 26	280 and 550 350 ± 190[f]
Bennet [155]		8.7	30	550
Balonov et al. [146]		12	39–76	
Rudran [145]	8	3.3–7.7 (mean: 6.0)	30.8–131 (mean: 81.7)	
Trivedi et al. [156]	8	6.2–12.8[g] (mean: 8.4)	58–104 (mean: 74 ± 18)	

[a]Oral diuretic administered from days 3 to 35 postintake
[b]HT/HTO acute intake
[c]Data for two tritium luminous dial painters collected 6–10 months after termination of employment
[d]Long-term behaviour of the data in one subject is attributed to seasonal effects, as described by Pinson [3]
[e]Based on additional data from subjects used in Moghissi et al. [153]
[f]Data for a third subject, which was introduced in this study
[g]During the initial period when the exposed individuals increased fluid intakes, for 1 month postintake, the biological half-life varied from 5.0 to 8.1 days with a mean of 6.3 days

More recently, a three-compartment model was developed to assess HTO excretion data from the limited human data that have been published [157]. A three-component exponential function was derived to represent the urinary excretion data from these studies. However, it was noted that results showed reasonably wide variations, both in observed biological half-lives and in proportions of total tritium entering

Tritium, Health Effects and Dosimetry. Table 12 Parameters for the HTO model recommended by Taylor [157]

Model component	Distribution (%)	Biological half-life (days)
HTO	99	10
OBT[a]	0.98	40
OBT[b]	0.02	350

[a]Short-term OBT compartment
[b]Long-term OBT compartment

the compartments (OBT), which turn over more slowly [157]. The model parameters are shown in Table 12. The resulting dose per unit intake of HTO by adults, based on this model, is 1.7×10^{-11} Sv/Bq. The current ICRP dose coefficient for HTO is 1.8×10^{-11} Sv/Bq [139]. This change would not be relevant for routine monitoring situations, where the dose is estimated by interpolating the tritium concentration in body water, between tritium-in-urine measurements taken frequently (for instance, every 2 weeks).

This latter method of dose estimation is independent of the time between intake and submission of a urine sample for tritium-in-urine measurement. Worker monitoring programs based on urine bioassay are typically used for routine monitoring when tritium doses are not significant, typically in cases that involve less than a few millisievert per year. Also, these programs are designed so that urine samples are submitted frequently enough to ensure accurate dose estimates. The method currently used to estimate doses from measurements of the concentration of tritium in urine has been described [129]. Workers' tritium-in-urine concentration is determined using liquid scintillation analysis. Linear interpolation is carried out between successive bioassay results, in order to calculate the workers' effective dose received between urine samples. Doses received during each annual monitoring period are summed to obtain the annual dose. The committed effective dose, resulting from intakes of tritium during the year, but received during the following year (as a result of tritium retention in the body) is also calculated by multiplying the year's last bioassay sample result by a committed dose factor [129, 131].

Taylor's model would be relevant for special bioassay monitoring following unplanned significant intakes of HTO, where individual monitoring may extend several weeks postintake and when the individual has been removed from work that might result in further intakes of tritium.

Absorption of HTO Through Skin The absorption of tritium through skin from either the vapor phase or the liquid phase has been investigated by various authors, such as Pinson and Langham [3], DeLong et al. [4], and Osborne [137]. DeLong et al. [4] exposed mice, rats, and human adult volunteers (all males) to HTO vapor in air. Animals were sacrificed following exposure and urine samples were collected from human subjects for 48 h after the end of exposure. Water absorption rates, calculated from measurements of tritium in blood and total body water, suggest a lag in the distribution of the absorbed water. Absorption of tritium through the skin was the same when skin was covered with a cloth (cotton) as when it was not covered. The rate of water absorption was also found to be proportional to water vapor pressure. This suggests a single diffusion mechanism for percutaneous absorption. The data also suggests that the rate of percutaneous absorption of tritium from HTO in air is about the same as the rate of pulmonary absorption from the same atmosphere.

Pinson and Langham [3] exposed human subjects' forearm skin to HTO in the form of vapor as well as water. When exposed to HTO vapor, the average absorption rate was 0.018 mg/cm^2/min, compared with exposure to HTO in the liquid phase, where the absorption rate through skin was 0.04–0.065 mg/cm^2/min. The average absorption rate when exposed to HTO vapor was larger than could be accounted for by diffusion due to vapor pressure alone. A faster rate of uptake during short exposures was explained by a blotter effect (the ability of a material to draw a liquid into it). The study also found that the skin absorption rate increased with increasing skin temperature. As with DeLong [4], Pinson and Langham [3] found that "the quantity of HTO entering the body through the total skin, when exposed to an atmosphere containing a given activity per unit volume, would be about equal to that entering through the lungs."

Osborne [137] exposed volunteers (whole-body exposure) to HTO in air and measured tritium in urine. As with Pinson and Langham [3], Osborne

found a correlation between skin absorption rate and skin temperature. Overall, skin absorption rates were found to be similar to those reported by Pinson and Langham [3]. Osborne [137] also reported that the total skin intake rate assumed by the ICRP at that time [159] was twice the average intake rate observed. The assumption used in ICRP [159] was that the amount of tritium absorbed through the skin was equal to the amount inhaled. The assumption now is that the amount of tritium absorbed through the skin is half the amount inhaled.

The Inhalation of Elemental Tritium Gas The ICRP [134] recommended basing HT inhalation dose primarily on exposure of the lung, as opposed to exposure of the skin. Oxidation of HT to HTO in vivo was not considered at that time. The ICRP's Derived Air Concentration (DAC) [134] is calculated such that a typical worker breathing air, with a constant concentration of a specified radionuclide equal to the derived air concentration (DAC) for an entire working year, would receive a committed effective dose of 50 mSv. It should be noted the DAC is now based on a committed effective dose of 20 mSv. The DAC recommended at that time by the ICRP for HT was 2×10^{10} Bq/m^3 compared with that for HTO, which was 8×10^5 Bq/m^3.

A small fraction of inhaled elemental tritium gas is converted to HTO in the body. The absorption of HT through skin appears to be negligible and it does not convert to HTO on contact with skin [7]. Compared to HTO, HT is slightly soluble in body fluids and has a much lower uptake into biological systems. After inhalation, most HT is exhaled, but a small fraction is dissolved in body fluids and then oxidized to HTO by bacteria in the GI tract [160]. This is the only known biological site of HT oxidation [160].

The studies of Pinson and Laugham [3] and Peterman et al. [138] indicate that exposure to HT results in the excretion of HTO in urine, and that HTO formed from the oxidation of HT is retained in the body and excreted with the usual biological half-life of about 10 days. About 0.01% of HT gas inhaled by human volunteers was converted to HTO in the body [138].

Using HT and HTO biokinetic models proposed by Peterman et al. [138], in parallel with human volunteer HT inhalation data, it was concluded at the time that the committed effective dose from inhaled HT was dominated by two roughly equal contributors: dose to lungs resulting from HT in inhaled air and dose from HTO formed by the oxidation of HT.

The ICRP has since recommended [139, 161] a revised dose coefficient for inhalation of HT gas. This stems from two sources: the work by Peterman et al. [138], described above, and the ICRP's revision of the human respiratory tract model – in particular, consideration of human respiratory tract morphology. The short range of tritium beta particles (6 μm in tissue) is such that most of the energy is not deposited in target cells of the respiratory tract. The average cell depth of these cells' nuclei ranges from about 10 to 50 μm in the extrathoracic, bronchial, and bronchiolar regions of the respiratory tract [139]. In the current ICRP [139] model of the respiratory tract, tritium beta particles are taken to deliver dose only in the alveolar-interstitial (AI) region after inhalation of HT. As discussed by Trivedi and Gentner [162], the nuclei of target cells within the AI region are at depths of less than 10 μm and can be assumed to receive some dose from HT.

The lung dose rate calculated with the ICRP Publication 66 model [139] is about one third of the mean lung dose rate calculated with the ICRP Publication 30 [134] model. As a result, the effective dose per unit intake resulting from oxidized HT is several times higher than that due to the direct irradiation of the lungs by HT gas.

The revised ICRP HT dose coefficient, 1.8×10^{-15} Sv/Bq, is 10,000 times less than the coefficient for HTO [161]. This dose coefficient includes only the oxidation of HT into HTO, and not direct irradiation of the lungs by HT gas in air. The latter might increase the committed effective dose by about 20%. In cases where the dose is predominantly due to HT, exposure of the lungs should be taken into account.

It also follows from the above that the committed effective dose resulting from HT inhalation can be estimated using measurements of HTO concentration in urine [162].

An upper limit on the lung dose resulting from HT gas in the lungs can be calculated from HTO-in-urine measurements. However, this upper bound assumes that the entire intake occurred as HT. Some or all of the HTO in urine may have actually resulted from the

inhalation of HTO. Calculated in this manner, the contribution of lung dose to the committed effective dose is most likely overestimated, unless the HT to HTO ratio in air is known [162]. Consequently, when workers are exposed to both HTO and HT, the main contributor to dose is HTO and doses are not significant, it is adequate to calculate their dose from measurements of HTO in urine, without calculating an upper bound to lung dose from HT. When the dose is significant (e.g., more than a few millisievert for workers or close to the dose limit for members of the public), and due mainly to HT, exposure of the lungs should be taken into account by increasing the HT dose coefficient by 20%.

Intake Resulting from Skin Contact with Tritium-Gas-Contaminated Surfaces Studies have examined the behavior of tritium in the body as a result of skin contact with HT-contaminated metal surfaces (HT dissolves in most materials). These studies found that OBT from such skin contact exposures [163] is excreted in urine. In turn, the type of tritiated compound produced in the body as a result of the skin's contact with tritium will determine the resulting committed effective dose.

Elemental tritium gas and HTO are known to sorb to surfaces. There is negligible absorption of airborne elemental tritium gas through skin, but exposure of skin to tritium-gas-contaminated surfaces has been shown to result in the absorption of tritium – both as HTO and OBT [163]. When metal surfaces contaminated with tritium gas were applied to the inside forearm of four human volunteers, urinary excretion of tritium was found to reach a maximum rate about 24 h after exposure. In each subject, the excretion of total tritium at the peak time was about 20 times the amount of HTO excreted; that is, 5% of the tritium urinary excretion rate at the time of maximum excretion rate was due to HTO. The remaining tritium (that was not HTO) was determined to be organically bound. One to three weeks after the exposure, the rate of total tritium excreted was the same as that of HTO. Following intake via this route, up to 50% of the excreted OBT has been found to be excreted via urine following a biological half-life of about 1–2 days, and the rest of the OBT following a biological half-life of 0.1–0.2 days. HTO formed as a result of such skin exposure to HT-contaminated surfaces has been found to be excreted in urine with a biological half-life of about 14 days.

About 0.5% of the tritium initially sorbed to the surface to which the volunteers were exposed was absorbed as HTO, and about 0.3% was absorbed as OBT. The results did not depend on the type of material, as long as the surface adsorbed tritium gas (similar results were obtained for various types of metals and for glass). In addition, the amount of tritium absorbed was found to be independent of the duration of exposure. The effective dose resulting from such intakes of tritium was estimated to range from 8.7×10^{-12} to 9.7×10^{-12} Sv/Bq absorbed [164].

Ingestion of Organically Bound Tritium While HTO distributes reasonably uniformly throughout body tissues, OBT formed in body tissues after intakes of OBT will be distributed among tissues according to their relative metabolic activities. OBT distribution will also depend on the chemical nature of the compound ingested. However, greater uptake by tissues with higher metabolic activity will generally be associated with shorter retention times, because of higher turnover. The nonuniform distribution of OBT is discussed in this section.

Experimental evidence indicates that, after an intake of OBT, about 9 times more tritium is bound to organic compounds in major tissues, compared with intakes of HTO [10]. Takeda and Kasida [158] also found that following HTO intakes in animals, 1–5% of tritium became incorporated in organic constituents of tissues. Therefore, 9–45% of tritium taken in as OBT would be expected to be incorporated in organic molecules in tissue. The ICRP's assumption that 50% of tritium remains as OBT after an intake of OBT stems from this reasoning.

The ICRP's HTO and OBT models [127] therefore predict that 17 times more tritium (50% vs 3%) will be incorporated as OBT following an acute OBT intake, compared to an HTO intake over a period of time (chronic intake). This is consistent with experimental results of Moghissi et al. [153], Rochalska and Szot [10], Sanders and Reinig [150], Snyder et al. [158], and Takeda and Kasida[149], which indicate ratios ranging from 3 to 20. It should be noted that the ICRP's OBT model predicts 43 times more OBT in

the body than does the Taylor [157] HTO model. However, Rodgers [15] found a ratio of about 12, suggesting that the current ICRP HTO model more accurately predicts the amount of OBT in the body from chronic intakes of HTO than does Taylor's HTO model.

The relative amounts of tritium incorporated into OBT following chronic intakes of HTO and OBT can be estimated from results of the study by Rodgers [15]. This study, carried out using mice, involved chronic intakes of HTO, OBT, or both for 56 days. At 56 days after the start of chronic intakes, the amounts of HTO and OBT in the mice would have been at steady state. The levels of OBT and HTO in the mice were then examined for about 1 month after the chronic exposure ended.

In the case of mice exposed to HTO only, the OBT concentration in tissues was about 22% of the HTO concentration. The ICRP HTO model [127] predicts this value to be about 12% at steady state, while the Taylor [157] model predicts this value to be about 5%.

In the case of mice exposed to OBT only, the OBT concentration in tissues was about a factor of 6 greater than the HTO concentration. This compared to the factor of 4 predicted by the ICRP OBT model [127].

This study also found that the amount of OBT in tissues resulting from OBT intake was about 12 times greater than the amount of OBT in tissues resulting from HTO intakes, which is in close agreement with the results from Rochalska and Szot [10]. Although the ICRP models appear to underestimate the amounts of OBT retained in the body in some cases of chronic intakes, they predict that the dose attributable to OBT, from intakes of OBT, is 10 times greater than the dose from OBT from intakes of HTO. This is in agreement with Rodgers' findings. Overall, it can be concluded that these studies are generally consistent and that the ICRP model does not underestimate dose.

Rogers [15] observed that after chronic exposure had ended, OBT was lost from the mice at a rate best described by a two-compartment model, with about 40% of OBT being cleared rapidly (with half-lives of 2.0–3.2 days in mice), and the remaining OBT being cleared much more slowly (with half-lives of 24–30 days in mice). The faster-clearing compartment's rate constant was not significantly different from those associated with HTO clearance from mice. Rogers attributed this faster-clearing compartment to loosely bound or exchangeable OBT. The slower-clearing compartment was due to nonexchangeable OBT.

Rodgers [15] also found that when exposed to HTO only, the HTO in the mice contributed more than 95% of the total tritium dose during the chronic exposure. In the case of mice exposed to OBT only, the study found that about 50% of the total dose was attributable to OBT in tissue (in adult humans, the HTO:OBT dose ratio follows the ratio of the half-lives; 10 days:40 days). However, after the end of chronic intake, due to the longer biological half-life of OBT, the total dose resulting from OBT (in the case of mice exposed to OBT only) was about one order of magnitude greater than that of mice exposed to HTO only. This dominance of the dose attributable to OBT began after the end of chronic intake, as HTO cleared faster than OBT. The latter is consistent with predictions of the ICRP's OBT model; that is, a dose from OBT that is one order of magnitude greater after the end of chronic intake.

In order to relate the study by Rodgers [15] to human dietary intakes of tritium, a study by Trivedi et al. [135] is worthy of consideration. OBT:HTO ratios greater than 1 have been observed in some foods grown near environmental sources of tritium. The range of the OBT:HTO ratio in dietary intakes varies according to many factors, such as diet and atmospheric conditions. A study of doses received by a population residing near a nuclear facility showed that OBT contributes about 16% of the total tritium dose from all sources of tritium exposure [165]. In this case, the average OBT:HTO ratio in food items consumed by these individuals was 0.04. This value was mainly influenced by the proportion of food that was not locally grown, but that was imported into the study region. From this information, Trivedi and Gentner [162] concluded that "unless the population living near tritium facilities consumes locally grown food items for a large proportion of the year (an uncommon situation around Canadian CANDU stations), dietary intake of OBT has only minor contributions to dose."

There are some uncertainties associated with OBT metabolism as described by the ICRP's OBT model, particularly the retention of OBT in children and the effect of organ growth on OBT retention. Also, the relative depositions of OBT in various organs and tissues are not fully known for all age groups. This implies

there is no age-dependent biokinetic model for dietary intakes of OBT that accounts for age-related physiological and anatomical variations. HTO turnover in the human body is well established, but measurement data for tritium turnover in organic compounds are limited, particularly for long-term biokinetic components.

Animal studies have shown a nonuniform distribution of OBT among soft tissues of the body. Also, within a single organ, tritium is distributed nonuniformly among the various organic molecules [127]. However, other than for the special case of DNA precursors it appears that any nonuniformity of distribution within cells will be small, and in any case will be reflected in RBE values.

Several studies have investigated the distribution of OBT within cells and the bodies of test animals. These have helped produce dosimetry models of energy deposition within cells. The section on "Electron Energy and Ionization Path Lengths: Why Tritium Radiation Is More Effective Than Gamma Radiation" provides more details on dosimetry aspects, but the work by Chen [121] warrants discussion here as it estimates an RBE for tritium. Chen [121] ran a Monte Carlo simulation of beta radiation energy tracts from tritium bound to radiosensitive sites with varying spherical diameters (10 nm to 2 μm) and compared this to the energy distribution of HTO that was homogeneously distributed throughout the body. As expected, the "dose mean linear energies" of OBT were higher than that of the HTO by a factor of 1.7, which was close to the value found by Straume and Carsten [25]. However, as the AGIR [27] points out, "the extent of any increase will depend on the extent that OBT does preferentially localize within critical targets"; that is, if the OBT were homogenously distributed, then the added effect would be much lower.

About 70% of the hydrogen in the human body is in the exchangeable form, with about 95% of this hydrogen forming water molecules. Nonexchangeable hydrogen forms covalent bonds with carbon, and is found in components such as protein, lipids, and carbohydrates. Several factors determine the distribution of OBT in the body resulting from tritium in the diet. These include the ratio of OBT to HTO in the dietary items; daily intakes of carbohydrates, fats, and proteins; oxidation rates of the dietary constituents; the gut absorption factors for organic precursors (namely monosaccharides, fatty acids, and amino acids); the retention of organic precursors; and HTO and OBT excretion rates [166].

Physiological models of OBT biokinetics have been proposed by Richardson [167], Richardson and Dunford [168], and Melintescu et al. [22]. They provide sex-differentiated biokinetics and dose coefficients for males and females. Richardson et al. [169] present sex differences in dose coefficients based on the ICRP model, which stem from a daily carbon intake rate that differs between females (228 g carbon) and males (303 g carbon). The resulting biological half-life of carbon is 51 days for female adults and 40 days for male adults. Richardson and Dunford [168] consider the differing water and organic contents of tissues and organs, as well as differing biokinetics for their organic components, as presented in the non-ICRP "HCNO Model" [168]. Table 13 shows dose per unit intake values for adults from these studies and the values as published by the ICRP for its HTO and OBT models. It can be seen that dose coefficients from the various

Tritium, Health Effects and Dosimetry. Table 13 Adult dose coefficients from physiologically based OBT biokinetic models

Biokinetic model	Dose coefficient (Sv/Bq)
Ingestion of HTO	
ICRP 72 [141]	1.8×10^{-11}
Richardson et al. [161]	1.8×10^{-11} (males)
	2.2×10^{-11} (females)
Melintescu et al. [22]	1.6×10^{-11} (males)
	2.3×10^{-11} (females)
Ingestion of OBT	
ICRP 72 [141]	4.2×10^{-11}
Richardson et al. [166]	4.2×10^{-11} (males)
	6.1×10^{-11} (females)
Richardson [167]	7.6×10^{-11} (adults, PNM model)
Richardson and Dunford [168]	7.4×10^{-11}[a]
Melintescu et al. [22]	4.7×10^{-11} (males) 7.0×10^{-11} (females)

[a]For "Reference Man" diet [5]

studies in Table 13 are within a factor of 2 of the ICRP [141] values, with the highest one from Richardson and Dunford [168]. It should be noted that Richardson and Dunford [168] also provide dose coefficients for tritiated nutrients, with the highest value for tritiated protein at 8.4×10^{-11} Sv/Bq, which is twice the ICRP [141] value for OBT.

Richardson et al. [166] conducted a literature review of studies on OBT exposure and found that there exists a significant amount of information on intakes of tritiated food from animal experiments, but very little data from human intakes. The review also found there is sparse information on the exchangeable and nonexchangeable forms of OBT in diet. This, in turn, may have introduced uncertainties in current dosimetric models for tritium in the diet. Based on this literature review, Richardson [167] proposed a biokinetic model based on the overall catabolic reactions of foodstuffs, the Principal Nutrient Metabolic (PNM) model. This model accounts for the nonuniform deposition of OBT in tissues and organs, but, as with the ICRP model, does not include compartments representing the long-term retention of structural proteins and fat as adipose tissue.

It can be seen from Table 13 that taking gender differences into account increases the dose coefficient by up to about 25% for HTO and up to 50% for OBT. Accounting for the nonuniform distribution of OBT increases the dose by up to 80%.

Biokinetics of Tritiated DNA Precursors Tritium may be incorporated into DNA or RNA for the purpose of experiments studying cell kinetics. This section examines the biokinetics of such compounds. The nucleic acid precursors thymidine and deoxycytidine are most commonly labeled with tritium for this purpose. Uridine and adenine are most commonly labeled with tritium for work involving RNA [27].

After tritiated thymidine (^{3}HTdR) is administered to humans or animals, it is incorporated into DNA during the synthesis stage of the cell cycle. Following ingestion of ^{3}HTdR, about 2% of the tritium is incorporated into DNA [49], and the remainder appears as HTO. Tritiated thymidine is available for only a short time after intake and primarily for uptake by rapidly cycling cells such as bone marrow or gut. Chronic exposure to ^{3}HTdR will also label slowly cycling cells. Hence, the rate of turnover of these cells will determine the retention rate of this tritium.

The NCRP [8] examined the dose resulting from ingestion of ^{3}HTdR based on considerations that are mainly theoretical. In the case of acute intakes by ingestion, it was concluded that tritium ingested as thymidine is 8.6 times more hazardous than that ingested as HTO. It also suggests this may need revision as more precise data on stem cells and ^{3}HTdR distribution and incorporation rates become available. Conclusions regarding chronic intakes are similar. In the cases of other tritium-labeled DNA and RNA precursors, the recommendation is to apply exposure limits for ^{3}HTdR until more data on the radiation effects of these other compounds become available. ^{3}HTdR is unstable above $-4°$C and therefore may degrade once released into the environment.

The NCRP [8] states

- Because DNA is metabolically stable, in contrast to RNA, label bound to RNA precursor will be distributed, as a function of time, with increasing preference to DNA. Hence, for cells with a long lifespan, it is finally the rate of cellular proliferation that defines the biological half-life of the radionuclide incorporated in the cell nucleus, irrespective of whether it was initially bound to RNA or DNA. On this basis, the dose to the stem cell nucleus from ^{3}H-thymidine is about 50 times higher than from the same amount administered as ^{3}HOH

Furthermore, the same report states

- it appears justified to estimate the long-term hazard from labeled RNA precursors . . . to be not larger than that from the same amount of equally labeled thymidine. Until more experimental evidence is available, late hazards from labeled RNA precursors should be considered similar to those from equally labeled thymidine

Komatsu et al. [170] examined the dose resulting from tritium bound to DNA, as a result of ingesting HTO and OBT. These investigators fed HTO and food to mice for 22 days. Equilibrium was reached by the 16th day of chronic intake. In the group of mice fed tritiated food, the highest ratio of OBT to HTO was found to be 2.2 in the liver. Liver DNA was found to have a lower specific activity than that of liver OBT. This was attributed to tritiated DNA containing little, if any, exchangeable OBT,

which has a high specific activity. Comparing the specific activities of DNA-bound tritium in both groups of mice (those fed HTO and those fed tritiated food) the specific activity of DNA-bound tritium in the tritiated food group was found to be 4.6 times that of the HTO group. The study also suggests that the ratio of the specific activity of DNA-bound tritium to HTO may be higher in embryos than in adults.

Tritium bound to DNA was found to contribute little (less than 1%) to the total dose as a result of chronic exposure to either HTO or food. The total doses for both exposure groups were found to be similar for chronic intakes. In the case of acute intakes of HTO, DNA-bound tritium was found to contribute about 20% to the total dose from intakes of HTO and about 40% to the total dose from intakes of tritiated food. The total dose resulting from the ingestion of tritiated food was found to be about double that from the ingestion of HTO.

More recently, Melintescu et al. [22] reported that tritium can be strongly bound in the hydration shell, mostly in DNA. This tritium, referred to as buried tritium, represents about 5% of the OBT concentration in plants and 20% of that in fish. Buried tritium contributes to the total dose resulting from tritium intake. Melintescu et al. [22] report that effects due to buried tritium are included in the assessment of the RBE and radiation weighting factor, so dose from buried tritium does not need to be added to the total tritium dose calculation.

Arguments have been presented suggesting that tritiated DNA and histone precursors present a significantly greater risk than that resulting from HTO [171, 172]. The author indicates such tritiated compounds may be 1,000–5,000 times more effective than HTO because of their heterogeneous distribution in the body. The author attributes this mainly to the short range of tritium's beta particles, which causes their energy to be deposited in the cell nucleus. The authors also note that it remains to be proven that no significant risk exists from tritium bound to DNA as a result of releases of HTO to the environment (from HTO taken up by plants and animals, converted into OBT by these plants or animals, ingested by humans and incorporated into human cell nuclei).

Bridges [173, 174] responded to both articles by Müller [171, 172] by stating that the approximate 1,000-fold difference in effects is based on units of activity (such as becquerels) in the medium, rather than in terms of the dose to the cell or the nucleus. Also, the work referred to by Müller was carried out on in vitro systems, while in vivo results are quite different. Almost all ingested thymidine is broken down in the gut, and there is evidence that the effectiveness of ^{3}HTdR in adult mammals is only slightly greater than that expected from HTO. Furthermore, free ^{3}HTdR is unstable in the environment and therefore unlikely to be a source of exposure to tritiated thymidine. Available information indicates that the amount of tritium incorporated into DNA in in vivo systems is too small to cause the RBE to increase.

Summary and Conclusions

While current ICRP models for intake of HTO, HT, and OBT are reasonably consistent with experimental results, further work related to HT and OBT biokinetics is suggested in this section.

HTO behavior is well understood, and the current ICRP model appears to accurately predict HTO body burden and urinary excretion. The ICRP is considering adopting a revised biokinetic model for HTO [157]. Although the Taylor [157] model for HTO has a dose coefficient similar to that of the current ICRP model, it treats OBT differently by considering the long-term retention of tritium. It has been proposed that the ICRP adopt the Taylor Mode. However, given the variation in the limited data on which the Taylor model was based, it would be beneficial to assess it against further human data. Moreover, it would be of interest to compare the Taylor model's predicted contribution of OBT to dose with the work of Trivedi et al. [135, 136], which studied OBT contribution to dose in actual human HTO exposure cases. Finally, the Taylor model applies only to adults; an expansion to various age groups is needed to satisfy the requirements of public dose assessments.

When elemental tritium gas is inhaled, the dose to the cells of the respiratory tract's AI region should be considered when the exposure is predominantly to HT.

The ICRP's OBT model appears to be generally consistent with experimental results. However, it does not account for the differentiated deposition of OBT between various organs and tissues. The use of

physiologically based OBT models, such as the one proposed by Richardson and Dunford [168], should be encouraged when significant doses are expected (such as in nonroutine or accidental exposures). The validation and incorporation of these models in computer codes would facilitate their use in OBT dose assessments. Furthermore, it would be valuable to expand this type of model to include age dependency for all age groups, including the nursing infant.

The NCRP [8] presented a review and interpretation of data on the distribution of radionuclides incorporated in genetic material. A review of recent work on this topic would allow this information to be updated. Finally, Komatsu et al. [170] concluded that the total dose resulting from the ingestion of tritiated food is about twice that from the ingestion of HTO. This suggests that current OBT dose coefficients account for the binding of tritium to DNA.

Future Directions

Tritium is a significant by-product from nuclear reactors that use heavy water as a neutron moderator. Tritium releases from such plants form the largest contribution to radiation dose from nonnatural sources to biota in the environment and to members of the public.

While the biological effects of tritium have likely been studied more than that of any other radionuclide, some uncertainty still remains with respect to effects at lower doses. This has consequences both in radiological protection of humans and the environment. As illustrated in this report, the outcome of most concern at low doses is that of stochastic effects such as cancer and possibly hereditary effects.

The study of stochastic effects is challenging due to limitations in conventional animal models (e.g., short life spans). These studies are especially important because there is little information known about the RBE of tritium radiation when the endpoints are statistically based, such as cancer. Newer breeds of laboratory animals, such as those more susceptible to some cancers, may aid in meeting those challenges. Also, advances in molecular biology may provide answers at the cellular level.

Furthermore, questions still remain on the effectiveness of various OBT compounds as well as how they behave within the body. For example, a tritiated fat molecule will have a much longer residency within the body, but its radiological consequence would be much less than a tritiated DNA precursor with a much shorter biological residency. Therefore, more work is needed in first identifying how the various OBT compounds are partitioned within the body and then to understand the radiological consequences.

Similarly, epidemiological studies of humans occupationally exposed to tritium may yield some information on health effects. To date, such studies are complicated by small numbers in exposed populations or confounding factors such as concurrent exposures to other radiations or chemical carcinogens. An international effort involving the grouping of populations would be required to attain suitable statistical power.

Abbreviations

AECL	Atomic Energy Canada Limited
AGIR	Advisory Group on Ionizing Radiation
AI	Alveolar-interstitial
BEIR	Biological Effects of Ionizing radiation
BW	Body weight
C_F	Concentration fetus
C_M	Concentration mother
CANDU	Canadian deuterium uranium
CERRIE	Committee Examining Radiation Risk from Internal Emitters
CI	Confidence interval
CNSC	Canadian Nuclear Safety Commission
CTH_3	Tritiated methane
DAC	Derived air concentration
DDREF	Dose and dose rate effectiveness factor
DNA	Deoxyribonucleic acid
GI	Gastro-intestinal
H_2O	Chemical symbol for water, also seen as HOH
HCNO	Hydrogen carbon nitrogen oxygen
HSE	Health and Safety Executive
HT	Tritiated gas
^{3}HTdR	Tritiated thymidine
HTO	Tritiated water
ICRP	International Commission on Radiological Protection
ICRU	International Commission on Radiological Units and Measurements
LD	Lethal dose

$LD_{50/30}$	Lethal dose that kills 50% of the population in 30 days
LDEF	Low dose effectiveness factor
LET	Linear energy transfer
N	Number
NCRP	National Council on Radiation Protection
NGS	Nuclear generating station
NPP	Nuclear power plant
OBT	Organically bound tritium
OH	Hydroxyl
OPG	Ontario Power Generation
OR	Odds ratio
PNM	Principal nutrient metabolic
PSL	Priority substance list
PWR	Pressurized water reactor
Q	Quality factor
RBE	Relative biological effectiveness
$RBE_{MAX/M}$	Maximum relative biological effectiveness
REF	Radiation effectiveness factor
RR	Relative risk
SMR	Standardized mortality ratio
SSB	Single strand break
SSK	German Commission on Radiological Protection
Type F,M,S	Type fast, medium, slow, absorption rates
UK	United Kingdom
UKAEA	United Kingdom Atomic Energy Authority
UNSCEAR	United Nations Scientific Committee on the Effects of Atomic Radiation
w_R	Radiation weighting factor
w_T	Tissue weighting factor
χ^2	Chi squared

Units

Bq: becquerel
cm: centimeter
d: day
g: gram
GBq: gigabecquerel
Gy: gray
h: hour
kBq: kilobecquerel
keV: kiloelectron volts
kg: kilogram
km^2: kilometer squared
kV: kilovolt
kVcp: kilovolt constant potential
kVp: kilovolt peak
L: liter
MBq: megabequerel
m: meter
m^2: meter squared
m^3: meter cubed
mGy: milligray
mL: milliliter
mm: millimeter
mSv: millisievert
R: röntgen
Sv: sievert
μSv: microsievert
μm: micrometer
y: year

Bibliography

1. Carsten AL (1979) Tritium in the environment: isotopic effects and transmutation. In: Lett JT, Adler H (eds) Advances in radiation biology. Academic, New York
2. Virsik RP, Schäfer CH, Harder D (1980) Chromosome aberrations induced in human lymphocytes by ultrasoft Al_K and C_K X-rays. Int J Radiat Biol 38(5):545–557
3. Pinson EA, Langham WH (1957) Physiology and toxicology of tritium in Man. J Appl Physiol 10:108–126
4. DeLong CW, Thompson RC, Kornberg HA (1954) Percutaneous absorption of tritium oxide. Am J Roentgenol Radium Ther Nucl Med 71:1038–1045
5. International Commission on Radiological Protection (ICRP) (1975) Report of the task group on reference man. ICRP Publication 23. Pergamon, New York
6. Belloni P, Clemente GF, Di Piero S, Ingrao G (1983) Tritium levels in blood and urine samples of the members of the Italian general population and some exposed subjects. Radiat Prot Dosim 4:109–113
7. Hill RL, Johnson JR (1993) Metabolism and dosimetry of tritium. Health Phys 65(6):628–647
8. National Council on Radiation Protection and Measurements (NCRP) (1979) Tritium and other radionuclide labelled organic compounds incorporated into genetic material. Report No. 63 U.S. NCRP, Washington, DC
9. Amano H, Atarashi M, Noguchi H, Yokoyama S (1995) Formation of organically bound tritium in plants during the 1994 chronic HT release experiment at Chalk River. Fusion Technol 28:814–820
10. Rochalska M, Szot Z (1977) The incorporation of organically-bound tritium of food into some organs of the rat. Int J Radiat Biol 31(4):391–395

11. Saito M, Ishida MR (1989) Dose-modification factor for accumulated dose to cell nucleus due to protein-bound H-3. Health Phys 56:869–874
12. Diabaté S, Strack S (1993) Organically bound tritium. Health Phys 65(6):698–712
13. United Nations Scientific Committee on the Effects of Atomic Radiation (UNSCEAR) (2008) United Nations. Effects of ionizing radiation. Volume II, Annex C – Non-targeted and delayed effects of exposure to ionizing radiation. 2006 Report to the General Assembly, with scientific annexes. United Nations, New York
14. Persaud R, Zhou H, Baker SE, Hei TK, Hall EJ (2005) Assessment of low linear energy transfer radiation-induced bystander mutagenesis in a three-dimensional culture model. Cancer Res 65:9876–9882
15. Rodgers DW (1992) Tritium dynamics in mice exposed to tritiated water and diet. Health Phys 63:331–337
16. Richmond CR, Langham WH, Trujillo TT (1962) Comparative metabolism of tritiated water by mammals. J Cell Comp Physiol 59:45–53
17. Brues AM, Stroud AN, Rietz L (1952) Toxicity of tritium oxide to mice. Proc Soc Exp Biol Med 79(1):174–176
18. Furchner JE (1957) Relative biological effectiveness of tritium beta-particles and cobalt 60 gamma-rays measured by lethality in CF1 mice. Radiat Res 6:483–490
19. Yokoro K, Yamamoto O, Seyama T, Kinomura A (1986) Acute and chronic effects of tritiated water in mice with special reference to its carcinogenicity: an interim report. Radiat Prot Dosim 16:165–168
20. Yamamoto O, Yokoro T, Seyama A, Kinomura T (1990) HTO oral administration in mice. I: threshold dose rate for haematopoietic death. Int J Radiat Biol 57(3):543–549
21. Soloviev V, Ilyin LA, Baranov AE et al (2001) In: Gusev IA, Guskova AK, Mettler FA (eds) Medical management of radiation accidents, 2nd edn. CRC Press, Boca Raton, pp 46 and 158
22. Melintescu A, Galeriu D, Takeda H (2007) Reassessment of tritium dose coefficients for the general public. Radiat Prot Dosim 127(1–4):153–157
23. National Research Council (NRC) (1980) The effects on populations of exposure to low levels of ionizing radiation. The committee on the biological effects of ionizing radiations (BEIR III). The National Academies Press, Washington, DC
24. National Research Council (NRC) (2006) Health Risks from exposure to low levels of ionizing radiation: BEIR VII Phase 2. Board on radiation effects research. The committee on the biological effects of ionizing radiations (BEIR). The National Academies Press, Washington, DC
25. Straume T, Carsten AL (1993) Tritium radiobiology and relative biological effectiveness. Health Phys 65(6):657–672
26. Commerford SL, Carsten AL, Cronkite EP (1982) The turnover of tritium in cell nuclei, chromatin, DNA, and histone. Radiat Res 92:521–529
27. Health Protection Agency (HPA) (2007) Review of risks from tritium with particular attention to tritiated water and organic compounds containing tritium. Report of AGIR subgroup on tritium risks, UK advisory group on ionizing radiation. http://www.hpa.org.uk/radiation/advisory_groups/agir/index.htm
28. Brown RM (1995) The measurement of tritium in Canadian food items. Atomic Energy Control Board (now the Canadian Nuclear Safety Commission) AECB INFO 0499. Atomic Energy Control Board, Ottawa
29. Dekaban AS (1968) Abnormalities in children exposed to x-radiation during various stages of gestation: tentative timetable of radiation injury to the human fetus. Int J Nucl Med 9(9):471–477
30. Mulvihill JJ, Harvey EB, Boice JD Jr, Chakravarti A, Miller RW (1991) Normal findings 52 years after in utero radiation exposure. Lancet 338(8776):1202–1203
31. Zamenhof S, van Martheus E (1979) The effects of chronic ingestion of tritiated water on the prenatal brain development. Radiat Res 77:117–127
32. Laskey JW, Pamsh JL, Cahill DF (1973) Some effects of lifetime parental exposure to low levels of tritium on the F2 generation. Radiat Res 56(17):1–179
33. Bursian SJ, Cahill DF, Laskey JW, Parker LN (1975) Some aspects of brain neurochemistry after intrauterine exposure to tritium. Int J Radiat Biol Relat Stud Phys Chem Med 27(5):455–461
34. Jones DC, Krebs JS, Sasmore DP, Mitoma C (1980) Evaluation of neonatal squirrel monkeys receiving tritiated water throughout gestation. Radiat Res 83(3):592–606
35. Dobson RL, Cooper MF (1974) Tritium toxicity: effects of low-level ^{3}HOH exposure on developing female germ cells in the mouse. Radiat Res 58:91–100
36. Dobson RL, Kwan TC (1976) The RBE of tritium radiation measured in mouse oocytes: increase at low exposure levels. Radiat Res 66:615–625
37. Lushbaugh CC, Ricks RC (1972) Some cytokinetic and histopathologic considerations of irradiated male and female gonadal tissues. In: Vaeth JM (ed) Frontiers of radiation therapy and oncology, vol 6. Karger, Basel, pp 228–248
38. Lushbaugh CC, Casarett GW (1976) The effects of gonadal irradiation in clinical radiation therapy: a review. Cancer 37(2 Suppl):1111–1125
39. Baker TG, Neal P (1977) Action of ionizing radiations on the mammalian ovary. In: Zuckerman S, Weir BJ (eds) The ovary, vol 3. Academic, New York
40. United Nations Scientific Committee on the effects of ionising radiation (UNSCEAR) (1982) Ionising radiation: sources and biological effects, Vienna
41. Baker TG (1971) Comparative aspects of the effects of radiation during oogenesis. Mutat Res 11:9–22
42. International Commission on Radiological Protection (ICRP) (1984) A compilation of the major concepts and quantities in use by the ICRP. ICRP Publication 42. Ann ICRP 14(4). Pergamon, New York
43. National Research Council (NRC) (1990) Health risks from exposure to low levels of ionizing radiation. The committee on the biological effects of ionizing radiations BEIR V. National Academies Press, Washington, DC

44. Satow Y, Hori H, Lee J-Y, Ohtaki M, Sawada S, Nakamura N, Okada S (1989) Effect of tritiated water on female germ cells: mouse oocytes killing and RBE. Int J Radiat Biol 56(3):293–299
45. Satow Y, Hori H, Lee J-Y (1989) Teratogenic effect of fission neutron and tritium water on rat embryo. J UOEH 11(Suppl):416–431
46. Oakberg EF (1955) Sensitivity and time of degeneration of spermatogenic cells irradiated in various stages of maturation in the mouse. Radiat Res 2:369–391
47. Oakberg EF (1959) Initial depletion and subsequent recovery of spermatogonia of the mouse after 20 R of gamma rays and 100, 300, and 600 R of x-rays. Radiat Res 11:700–719
48. Oakberg EF, Clark E (1964) Species comparison of radiation response of the gonads. In: Carlson WD, Gaffner FX (eds) Effects of ionizing radiation on the reproductive system. Pergamon, Oxford, pp 11–24
49. Lambert BE (1969) Cytological damage produced in the mouse testes by tritiated thymidine, tritiated water and X-rays. Health Phys 17:547–557
50. National Research Council (NRC) (1988) Health risks of radon and other internally deposited alpha-emitters. The committee on the biological effects of ionizing radiations (BEIR IV). National Academy Press, Washington, DC
51. United Nations Scientific Committee on the Effects of Atomic Radiation (UNSCEAR) (2000) United Nations. Sources and effects of ionizing radiation, vol I: sources; vol II: effects. Report to the General Assembly, with scientific annexes. United Nations sales publication E.00.IX.3 and E.00.IX.4. United Nations, New York
52. Tanaka IB, Tanaka S, Ichinohe K, Matsushita S, Matsumoto T, Otsu H, Oghiso Y, Sato F (2007) Cause of death and neoplasia in mice continuously exposed to very low dose rates of gamma rays. Radiat Res 167(4):417–437
53. Yamamoto O, Seyama T, Jo T, Terato H, Saito T, Kinomura A (1995) Oral administration of tritiated water (HTO) in mouse. II. tumour development: I/II/III. Int J Radiat Biol 68(1):47–54
54. Yamamoto O, Seyama T, Itoh H, Fujimoto N (1998) Oral administration of tritiated water (HTO) in mouse. III: low dose-rate irradiation and threshold dose-rate for radiation risk. Int J Radiat Biol 73(5):535–541
55. Gragtmans NJ, Myers DK, Johnson JR, Jones AR, Johnson LD (1984) Occurrence of mammary tumors in rats after exposure to tritium beta rays and 200 kVp x-rays. Radiat Res 99(3): 636–650
56. Johnson JR, Myers DK, Jackson JS, Dunford DW, Gragtmans NJ, Wyatt HM, Jones AR, Percy DH (1995) Relative biological effectiveness of tritium for induction of myeloid leukemia in CBA/H mice. Radiat Res 144(1):82–89
57. Seyama T, Yamamoto O, Kinomura A, Yokoro K (1991) Carcinogenic effects of tritiated water (HTO) in mice: in comparison to those of neutrons and gamma-rays. J Radiat Res 32(Supp 2):132–142
58. Balonov MI, Muksinova KN, Mushkacheva GS (1993) Tritium radiobiological effects in mammals: review of experiments in the last decade in Russia. Health Phys 65(6):713–726
59. Mushkacheva GS, Rusinova GG, Muskinova KN, Lemberg VK, Shorokhova VB, Revina VS, Uryadnitskaya TI (1992) In: Buldakov L (ed) Genetic structures and tritium. Energoatomizdat, Moscow (in Russian)
60. Straume T (1993) Tritium risk assessment. Health Phys 65(6):673–682
61. International Commission on Radiological Protection (ICRP) (1991) 1990 recommendations of the international commission on radiological protection. ICRP Publication 60, Ann ICRP 21(1-3):1–201. Pergamon, Oxford
62. United Nations Scientific Committee on the effects of ionising radiation (UNSCEAR) (1988) Sources, effects and risks of ionizing radiation, Vienna
63. International Commission on Radiological Protection (ICRP) (2007) Recommendations of the ICRP. IRCP Publication 103. Ann ICRP 37(2–4). Pergamon, Oxford
64. United Nations Scientific Committee on the Effects of Atomic Radiation (UNSCEAR) (2001) Hereditary effects of radiation. Report to the General Assembly, with Scientific Annex. United Nations, New York
65. Furuno-Fukushi I, Ueno AM, Matsudaira H (1987) Cell killing and mutation to 6-thioguanine resistance after exposure to tritiated amino acids and tritiated thymidine in cultured mammalian cells (L5178Y). Radiat Res 110:428–438
66. Ueno AM, Furuno-Fukushi I, Matsudaira H (1982) Induction cell killing, micronuclei, and mutation to 6-thioguanine resistance after exposure to low-dose-rate γ rays and tritiated water in cultured mammalian cells (L5178Y). Radiat Res 91:447–456
67. Wang B, Watanabe K, Yamada T, Takeshi S, Shima A (1996) Effects of beta radiation from organically bound tritium on cultured mouse embryonic mid brain cells. Health Phys 71(6):915–921
68. Trivedi A, Morrison DP, Gentner NE (1997) Relative biological effectiveness for organically bound tritium. Health Phys 73(2):397–398
69. Steel GG, Lamerton LF (1965) The turnover of tritium from thymidine in tissues of the rat. Exp Cell Res 37:117–123
70. Lambert BE, Clifton RJ (1968) Radiation doses resulting from the ingestion of tritiated thymidine by the rat. Health Phys 15:3–9
71. Preston DL, Shimizu Y, Pierce DA, Suyama A, Mabuchi K (2003) Studies of mortality of atomic bomb survivors. Report 13: solid cancer and noncancer disease mortality: 1950–1997. Radiat Res 160:381–407
72. Preston DL, Pierce DA, Shimizu Y, Cullings HM, Fujita S, Funamoto S, Kodama K (2004) Effect of recent changes in atomic bomb survivor dosimetry on cancer mortality risk estimates. Radiat Res 162:377–389
73. Preston DL, Ron E, Tokuoka S, Funamoto S, Nishi N, Soda M, Mabuchi K, Kodama K (2007) Solid cancer incidence in atomic bomb survivors: 1958–1998. Radiat Res 168(1):1–64
74. Boice JD Jr, Day NE, Andersen A, Brinton LA, Brown R, Choi NW, Clarke EA, Coleman MP et al (1985) Second cancers following radiation treatment for cervical cancer. An international

collaboration among cancer registries. J Natl Cancer Inst 74: 955–975
75. Boice JD Jr, Engholm G, Kleinerman RA, Blettner M, Stovall M, Lisco H, Moloney WC et al (1988) Radiation dose and second cancer risk in patients treated for cancer of the cervix. Radiat Res 116:3–55
76. Weiss HA, Darby SC, Doll R (1994) Cancer mortality following X-ray treatment for ankylosing spondylitis. Int J Cancer 59:327–338
77. Weiss HA, Darby SC, Fearn T, Doll R (1995) Leukemia mortality after X-ray treatment for ankylosing spondylitis. Radiat Res 142:1–11
78. Howe GR (1995) Lung cancer mortality between 1950 and 1987 after exposure to fractionated moderate-dose-rate ionizing radiation in the Canadian fluoroscopy cohort study and a comparison with lung cancer mortality in the atomic bomb survivors study. Radiat Res 142:295–304
79. Howe GR, McLaughlin J (1996) Breast cancer mortality between 1950 and 1987 after exposure to fractionated moderate-dose-rate ionizing radiation in the Canadian fluoroscopy cohort study and a comparison with breast cancer mortality in the atomic bomb survivors study. Radiat Res 145:694–707
80. Little MP, Weiss HA, Boice JD Jr, Darby SC, Day NE, Muirhead CR (1999) Risks of in Japanese atomic bomb survivors, in women treated for cervical cancer, and in patients treated for ankylosing spondylitis. Radiat Res 152(3):280–292
81. Little MP, Boice JD Jr (1999) Comparison of breast cancer incidence in the Massachusetts tuberculosis fluoroscopy cohort and in the Japanese atomic bomb survivors. Radiat Res 151:218–224
82. Lubin JH, Boice JD Jr, Edling C, Hornung RW, Howe GR, Kunz E et al (1995) Lung cancer in radon-exposed miners and estimation of risk from indoor exposure. J Natl Cancer Inst 87(11):817–827
83. Cardis E, Gilbert ES, Carpenter L, Howe G, Kato I, Armstrong BK, Beral V, Cowper G, Douglas A, Fix J, Fry SA, Kaldor J, Lave C, Salmon L, Smith PG, Voelz GL, Wiggs LD (1995) Effects of low doses and low dose rates of external ionizing radiation: cancer mortality among nuclear industry workers in three countries. Radiat Res 142:117–132
84. Cardis E, Vrijheid M, Blettner M, Gilbert E, Hakama M, Hill C, Howe G, Kaldor J, Muirhead CR, Schubauer-Berigan M, Yoshimura T, Bermann F, Cowper G, Fix J, Hacker C, Heinmiller B, Marshall M, Thierry-Chef I, Utterback D, Ahn YO, Amoros E, Ashmore P, Auvinen A, Bae JM, Solano JB, Biau A, Combalot E, Deboodt P, Diez Sacristan A, Eklof M, Engels H, Engholm G, Gulis G, Habib R, Holan K, Hyvonen H, Kerekes A, Kurtinaitis J, Malker H, Martuzzi M, Mastauskas A, Monnet A, Moser M, Pearce MS, Richardson DB, Rodriguez-Artalejo F, Rogel A, Tardy H, Telle-Lamberton M, Turai I, Usel M, Veress K (2005) Risk of cancer after low doses of ionising radiation: retrospective cohort study in 15 countries. Br Med J 331(7508):77
85. Cardis E, Vrijheid M, Blettner M, Gilbert E, Hakama M, Hill C, Howe G, Kaldor J, Muirhead CR et al (2007) The 15 country collaborative study of cancer risk among radiation workers in the nuclear industry: estimates of radiation-related cancer risks. Radiat Res 167(4):396–416
86. Canadian Nuclear Safety Commission (2009) Tritium releases and dose consequences in Canada in 2006. Part of the tritium studies project INFO-0793
87. Durham Region Health Department (2007) Radiation and health in Durham region. Durham Region Health Department, Oshawa
88. Evrard A-S, Hemon D, Morin A, Laurier D, Tirmarche M, Backe J-C, Cartier M, Clavel J (2006) Childhood leukaemia incidence around French nuclear installations using geographic zoning based on gaseous discharge dose estimates. Br J Cancer 94(9):1342–1347
89. Grosche B, Lackland D, Mohr L, Dunbar J, Nicholas J, Burkart W, Hoel D (1999) Leukaemia in the vicinity of two tritium-releasing nuclear facilities: a comparison of the Kruemmel Site, Germany, and the Savannah River Site, South Carolina, USA. J Radiol Prot 19:243–252
90. Jablon S, Hrubec Z, Boice JD Jr (1991) Cancer in populations living near nuclear facilities. A survey of mortality nationwide and incidence in two states. J Am Med Assoc 265(11):1403–1408
91. Sever LE, Hessol NA, Gilbert ES, McIntyre JM (1988) The prevalence at birth of congenital malformations in communities near the Hanford site. Am J Epidemiol 127(2):243–254
92. Spix C, Schmiedel S, Kaatsch P, Schulze-Rath R, Blettner M (2008) Case-control study on childhood cancer in the vicinity of nuclear power plants in Germany 1980–2003. Eur J Cancer 44(2):275–284
93. Kaatsch P, Spix C, Schulze-Rath R, Schmiedel S, Blettner M (2008) Leukaemia in young children in the vicinity of German nuclear power plants. Int J Cancer 122(4):721–726
94. Laurier D, Hemon D, Clavel J (2008) Childhood leukaemia incidence below the age of 5 years near French nuclear power plants. J Res Pract 28:401–403
95. Bithell JF, Keegan TJ, Kroll ME, Murphy FG, Vincent TJ (2008) Childhood leukaemia near British nuclear installations: methodological issues and recent results. Radiat Prot Dosim 132(2):191–197
96. Grosche B (2008) The "Kinderkrebs in der umgerbung von kernkraftwerken" study: results put into perspective. Radiat Prot Dosim 132(2):198–201
97. SSK (German Radiological Protection Commission) (2008) Assessment of the "Epidemiological Study on Childhood Cancer in the Vicinity of Nuclear Power Plants" (KiKK Study): position of the commission on radiological protection (SSK). SSK, Bonn
98. Beral V, Fraser P, Carpenter L, Booth M, Brown A, Rose G (1988) Mortality of employees of the atomic weapons establishment, 1951–82. Br Med J 297:757–770
99. Cragle DL, Watkins JP, Robertson-DeMers K (1998) Mortality among workers at the Savannah River nuclear fuels production facility. In: ASA 1998 proceedings of the section on statistics in epidemiology. American Statistical Association, Alexandria, pp 83–87. http://www.orau.gov/ehsd/EpiProceedings-jj-9-30-98.doc

100. Johnson P, Atkinson WD, Nicholls JL (1999) Updated analysis of mortality in workers at UK atomic weapons establishments. In: Proceedings of the SRP sixth international symposium: achievements & challenges: advancing radiation protection into the 21st century, Southport
101. Zablotska LB, Ashmore JP, Howe GR (2004) Analysis of mortality among Canadian nuclear power industry workers after chronic low-dose exposure to ionizing radiation. Radiat Res 161:633–641
102. Schubauer-Berrigan MK, Daniels RD, Fleming DA, Markey AM, Couch JR, Ahrenholz SH, Burphy JS, Anderson JL, Tseng C-Y (2007) Risk of chronic myeloid and acute leukemia mortality after exposure to ionizing radiation among workers at four U.S. nuclear weapons facilities and a nuclear naval shipyard. Radiat Res 167:222–232
103. Richardson DB, Wing S (2007) Leukemia mortality among workers at the Savannah River Site. Am J Epidemiol 166(9):1015–1022
104. Hazelton WD, Suresh MH, Curtis SB, Zielinski JM, Ashmore PJ, Krewski D (2006) Biologically based analysis of lung cancer incidence in a large Canadian occupational cohort with low-dose ionizing radiation exposure, and comparison with Japanese atomic bomb survivors. J Toxicol Environ Health A 69:1013–1038
105. Laurier D, Grosche B, Hall P (2002) Risk of childhood leukemia in the vicinity of nuclear installations – findings and recent controversies. Acta Oncol 41(1):14–24
106. Committee Examining Radiation Risks of Internal Emitters (CERRIE) (2004) Final report [downloaded 20 October 2004]. http://www.cerrie.org/report/
107. Cox R, Menzel H-G, Preston J (2008) Invited editorial: internal dosimetry and tritium – the ICRP position. J Res Pract 28(2):131–135
108. Kacena V (1967) Chemical effects of decay of incorporated radioisotopes. In: Proceedings of the conference on biological effects of transmutation and decay of incorporated radioisotopes. IAEA, Vienna, pp 199–214
109. Myers DK, Johnson JR (1991) Toxicity and dosimetry of tritium: a review. Atomic Energy Control Board (now the Canadian Nuclear Safety Commission), Ottawa; Advisory Committee on Radiological Protection; INFO-0377
110. Feinendegen LE, Bond VP (1971) Transmutation versus beta irradiation in the pathological effects of tritium decay. In: Moghissi AA, Carter MW (eds) Tritium. Messenger Graphics, Nevada, pp 221–232
111. Little MP, Lambert BE (2008) Systematic review of experimental studies of relative biological effectiveness of tritium. Radiat Environ Biophys 47(1):71–93
112. Prosser JS, Lloyd DC, Edwards AA, Stather JW (1983) The induction of chromosome aberrations in human lymphocytes by exposure to tritiated water. Radiat Prot Dosim 4(1):21–26
113. Carsten AL, Commerford SL (1976) Dominant lethal mutations in mice resulting from chronic tritiated water (HTO) ingestion. Radiat Res 66:609–614
114. Russell WL, Cumming RB, Kelly EM, Phipps EL (1979) Induction of specific-locus mutations in the mouse by tritiated water. In: Behaviour of tritium in the environment. In: Proceedings of a symposium on the behaviour of tritium in the environment, 16 Oct 1978, San Francisco, IAEA-SM-232/85. IAEA, Vienna, pp 489–497
115. Lloyd DC, Purrott RJ, Dolphin GW, Bolton D, Edwards AA (1975) The relationship between chromosome aberrations and low LET radiation dose to human lymphocytes. Int J Radiat Biol 28:75–90
116. Chopra C, Heddle JA (1988) Cytogenetic measurements of the relative biological effectiveness of tritium. Report INFO-0287. Atomic Energy Control Board (now the Canadian Nuclear Safety Commission), Ottawa
117. Kocher DC, Apostoaei AI, Hoffman FO (2005) Radiation effectiveness factors for use in calculating probability of causation of radiogenic cancers. Health Phys 89(1):3–32
118. Environment Canada (EC), Health Canada (HC) (PSL2) (2003) Releases of radionuclides from nuclear facilities (impact on non-human biota). Canadian Environmental Protection Act, 1999, Priority substances list assessment report. Environment Canada, Ottawa
119. International Commission on Radiation Units and Measurements (ICRU) (1970) Linear energy transfer. ICRU Report 16, Bethesda
120. Nikjoo H, Goodhead DT (1991) Track structure analysis illustrating the prominent role of low energy electrons in radiobiological effects of low-LET radiations. Phys Med Biol 36:229–238
121. Chen J (2006) Radiation quality of tritium. Radiat Prot Dosim 122(1–4):546–548
122. Cheng YS, Snipes MB, Kropf RF, Jow HN (1995) Radiation dosimetry of metal tritides. Health Phys 68(Suppl 6):S53
123. Cheng YS, Snipes MB, Wang Y, Jow HN (1999) Biokinetics and dosimetry of titanium tritide particulates in the lung. Health Phys 76(2):120–128
124. Cheng YS, Zhou Y, Wang Y, Inkret WC, Wermer JR, Joseph R (2002) Dose estimate of inhaled hafnium tritide using the ICRP 66 lung model. Health Phys 82(6):817–824
125. International Commission on Radiological Protection (ICRP) (1995) Age-dependent doses to members of the public from intakes of radionuclides: part 4, inhalation dose coefficients. Publication 71, 25(3–4). Pergamon, Oxford
126. Richardson RB, Hong A (2001) Dose to lung from inhaled tritiated particles. Health Phys 81(3):313–324
127. International Commission on Radiological Protection (ICRP) (1989) Age-dependent doses to members of the public from intake of radionuclides: part 1. ICRP Publication 56. Ann ICRP 20(2). Pergamon, Oxford
128. International Commission on Radiological Protection (ICRP) (1993) Age-dependent doses to members of the public from intake of radionuclides: part 2. ICRP Publication 67. Ann ICRP 23(3/4). Pergamon, Oxford
129. Health and Welfare Canada (1983) Bioassay guideline 2 – guidelines for tritium bioassay, Report of the working group

on bioassay and in vivo monitoring criteria, Environmental Health Directorate, 83-EHD-87
130. Canadian Nuclear Safety Commission (2005) Radiobioassay and dose assessment for intakes of tritium, Report of the CNSC working group on internal dosimetry, RPS-0182B, Radiation Index
131. Atomic Energy Control Board (now the Canadian Nuclear Safety Commission) (1987) The determination of effective doses from the intake of tritiated water. Regulatory Policy Statement R-100
132. Johnson JR (1982) The estimation of the effective dose equivalent from tritiated water exposures using tritium concentrations in urine. Radiat Prot Dosim 2:245–247
133. International Commission on Radiological Protection (ICRP) (1995) Basic anatomical and physiological data for use in radiological protection: the skeleton. Publication 70, 25(2). Pergamon, Oxford
134. International Commission on Radiological Protection (ICRP) (1979–1982) Limits for intakes of radionuclides by workers, ICRP Publication 30, Part 1 (and Supplement), Part 2 (and Supplement), Part 3 (and Supplements A and B), and Index, prepared by Committee 2, adopted by the Commission in July 1978, Annals of the ICRP. Pergamon, New York
135. Trivedi A, Galeriu D, Richardson RB (1997) Dose contribution from metabolized organically bound tritium after acute tritiated water intakes in humans. Health Phys 73(4):579–586
136. Trivedi A, Galeriu D, Lamothe ES (2000) Dose contribution from metabolized OBT after chronic tritiated water intakes in humans. Health Phys 78(1):2–7
137. Osborne RV (1966) Absorption of tritiated water by people. Health Phys 12:1527–1537
138. Peterman BF, Johnson JR, McElroy RGC (1985) HT/HTO conversion in mammals. Fusion Technol 8:2557–2563
139. International Commission on Radiological Protection (ICRP) (1994) Human respiratory tract model for radiological protection. Publication 66, 24(1–3). Pergamon, Oxford
140. Phipps AM, Kendall GW, Fell TP, Harrison JD (1990) Doses from radioactive methane. Radiat Prot Dosim 30:191–195
141. International Commission on Radiological Protection (ICRP) (1996) Age-dependent doses to members of the public from intake of radionuclides: part 5. ICRP Publication 72. Ann ICRP 26(1). Pergamon, Oxford
142. International Commission on Radiological Protection (ICRP) (2001) Doses to the embryo and fetus from intakes of radionuclides by the mother. Publication 88, 31(1–3). Pergamon, Oxford
143. International Commission on Radiological Protection (ICRP) (2004) Doses to infants from ingestion of radionuclides in mothers' milk. ICRP Publication 95, 34(3–4). Pergamon, Oxford
144. Butler HC, Leroy JH (1965) Observation of biological half-life of tritium. Health Phys 11:283–285
145. Rudran K (1988) Significance of in vivo organic binding of tritium following intake of tritiated water. Radiat Prot Dosim 25(1):5–13
146. Balonov MI, Dolgirev EI, Likhtarev IA (1974) Exchange kinetics and dosimetry of tritium oxide in man for different routes of administration. Health Phys 27(4):367–375
147. Foy JM, Schneiden H (1960) Estimation of total body water (virtual tritium space) in the rat, cat, rabbit, guinea-pig and man, and of the biological half-life of tritium in man. J Physiol 154:169–176
148. Wylie KF, Bigler WA, Grove GR (1963) Biological half-life of tritium. Health Phys 9:911–914
149. Snyder WS, Fish BR, Bernard SR, Ford MR, Muir JR (1968) Urinary excretion of tritium following exposure of man to HTO – a two exponential model. Phys Med Biol 13: 547–559
150. Sanders SM Jr, Reinig WC (1968) Assessment of tritium in man. In: Diagnosis and treatment of deposited radionuclides. Excerpta Medica Foundation, Amsterdam, pp 534–542
151. Minder W (1969) Internal contamination with tritium. Strahlentherapie 137:700–704
152. Lambert BE, Sharp HBA, Dawson KB (1971) An accidental intake of tritiated water. Am Ind Hyg Assoc J 32:682–686
153. Moghissi AA, Carter MW, Lieberman R (1971) Long-term evaluation of the biological half-life of tritium. Health Phys 21:57–60
154. Moghissi AA, Carter MW, Lieberman R (1972) Further studies on the long-term evaluation of the biological half-life of tritium. Health Phys 23:805–806
155. Bennet BG (1972) The radiation dose due to acute intake of tritium in man. USAEC Report, HASL-253
156. Trivedi A, Richardson RB, Galeriu D (1994) Dose from organically bound tritium after an acute tritiated water intake in humans. Atomic Energy Control Board (Canada) Research Report INFO-0598
157. Taylor DM (2003) A biokinetic model for predicting the retention of ^{3}H in the human body after intakes of tritiated water. Radiat Prot Dosim 105:225–228
158. Takeda H, Kasida Y (1979) Biological behavior of tritium after administration of tritiated water in the Rat. J Radiat Res 20:174–185
159. International Commission on Radiological Protection (ICRP) (1959) Recommendations of the international commission on radiological protection: report of committee II. ICRP Publication 2. Pergamon, London
160. Ichimasa Y, Ichimasa M, Shiba T, Oda M, Akita Y (1986) Fixation of tritium gas by rats. Radiat Prot Dosim 16:127–130
161. International Commission on Radiological Protection (ICRP) (1994) Dose coefficients for intakes of radionuclides by workers. Publication 68, 24(4). Pergamon, Oxford
162. Trivedi A, Gentner NE (1999) Dosimetry and health effects of tritium, AECL RC-2243. AECL, Chalk River
163. Eakins JD, Hutchinson WP, Lally AE (1975) The radiological hazard from tritium sorbed on metal surfaces. Health Phys 28(3):213–224
164. Johnson JR, Dunford DW (1985) Dosimetric models of ^{3}H from skin absorption following contact with T2-contaminated surfaces. Health Phys 48(1):110–113

165. Trivedi A, Cornett RJ, Galeriu D, Workman W, Brown RM (1997) Daily tritium intakes by people living near a heavy-water research reactor facility: dosimetric significance. AECL-11648, COG-96-333-I
166. Richardson RB, Trivedi A, Greenstock CL (1998) Dosimetry of organically bound tritium derived from diet – phase 1. AECB RSP-068
167. Richardson RB (2001) Dosimetry of organically bound tritium derived from diet – phase 2. Report to the Canadian nuclear safety commission, Contract no. 87055-8-5044/001/SS
168. Richardson R, Dunford DW (2003) A biochemical-based model for the dosimetry of dietary organically bound tritium. Health Phys 85(5):523–538
169. Richardson RB, Dunford DW, Peterson SR (2001) Influence of gender differences in the carbon pool on dose factors for intakes of tritium and ^{14}C-labelled compounds. Health Phys 81(3):302–312
170. Komatsu K, Okamura Y, Sakamoto K (1990) Radiation dose to mouse liver cells from ingestion of tritiated food and water. Health Phys 58:625–629
171. Müller WU (2008) Comment on the invited editorial 'effectiveness of tritium beta particles'. J Res Pract 28:249–252
172. Müller WU (2008) Reply to the reply to comment on the invited editorial 'effectiveness of tritium beta particles'. J Res Pract 28:423–426
173. Bridges BA (2008) Reply to comment on the invited editorial 'effectiveness of tritium beta particles'. J Res Pract 28:249–252
174. Bridges BA (2008) A further reply. J Res Pract 28:423–426

Tropical Health and Sustainability

J. Kevin Baird
Eijkman–Oxford Clinical Research Unit, Jalan Diponegoro, Jakarta, Indonesia
Centre for Tropical Medicine, Nuffield Department of Medicine, University of Oxford, Oxford, UK

Article Outline

Glossary
Definition of the Subject and Its Importance
Introduction
Forging Tools
Providing Tools
Diagnostics Are Critical
Insecticides Are Critical
Drug Delivery
The Vaccine Development Gambit
R&D Investment
Sustainable S&T in Tropical Health
Southern Scientific and Technological Development
Future Directions
Acknowledgments
Bibliography

Glossary

ACT Artemisinin-combined therapies, a large class of paired drugs that represent the front-line treatments for malaria globally.

BCMS Board for the Coordination of Malaria Studies, a US government entity established during World War II and later dissolved to coordinate management of the development of new antimalarial therapies.

BMGF Bill & Melinda Gates Foundation.

CFR Case fatality rate, the percentage of patients with a given clinical condition not surviving.

DDT Pesticide ((1,1,1-trichloro-2,2-di(4-chlorophenyl) ethane)), once often used in IRS applications.

G6PD Glucose-6-phosphate dehydrogenase, an inherited deficiency of which causes patients to be vulnerable to mild to severe drug-induced acute intravascular hemolysis.

GFATM Global Fund for AIDS, Tuberculosis and Malaria, a consortium of International donors committing resources to those health issues.

GMEC Global Malaria Eradication Campaign of the 1950s and 1960s.

GMP Good manufacturing practice, a high standard of manufacturing certified by experts.

IRS Indoor residual spraying, in malaria control the practice of spraying the interior walls of homes with insecticide in order to attack mosquitoes that feed on humans.

ITN Insecticide-treated net, or a net that covers a bed at night to protect sleeping people from mosquito bites and malaria infection.

Malaria Infection by protozoan parasites (*Plasmodium* species) carried by mosquitoes, often serious and fatal.

MMV Medicines for Malaria Venture, a public-private partnership committed to developing and licensing new antimalarials therapies.

North/south Generally characterizes global geographic divide between so-called developed and developing nations.

R&D Research and development, deliberate, systematic application of S&T in striving toward specific understanding or objectives.

RDT Rapid diagnostic test, an immunochromatographic, point-of-care kit used at village level to diagnose pathogens (malaria) at low cost.

S&T Science and technology, techniques for expanding understanding of the physical universe.

Sustainability Technologies or systems that operate effectively in the absence of long-term external financial or technical assistance.

Tropical health Health issues specific to the tropical zones, especially endemic infectious diseases and underdeveloped healthcare delivery.

WHO World Health Organization.

WRAIR The Walter Reed Army Institute of Research in Washington, DC, where development of antimalarials by the US government has been supported.

Definition of the Subject and Its Importance

Tropical health may be considered relevant to the range of human maladies that occur either predominantly in the tropics or become exacerbated by poorly resourced healthcare delivery systems typical of many nations in the tropics. More often, it is both of those factors, as with malaria. Sustainability implies the introduction of novel interventions aimed at mitigating the burdens and risks of such maladies by improving or replacing existing instruments that may be inadequate or suboptimal. Sustainability further implies a design of those instruments amenable to the capacities of those left to use them, following the inevitable retreat of sponsors and their fiscal and technical resources. Further, the instrument must prove effective in mitigating the problem at which it aims. The research and development (R&D) of sustainable technologies against tropical infections represents a relentlessly urgent task, often linked to preventable deaths in very substantial numbers.

The limited ability of underdeveloped healthcare systems to implement many or most new health technologies greatly compounds the difficulty of achieving sustainability. New science and technology (S&T) must be adapted to settings often completely alien to its developers, both in terms of ability to satisfactorily apply it and its suitability in achieving desired impacts. The subject of tropical health and sustainability is thus concerned with the gap between new technological tools and the ability of tropical healthcare systems to leverage them in improving human health. Further, the intended tools may be poorly conceived as a consequence of fundamental misunderstanding of the problem and, even with appropriate implementation, contribute little to real progress against it.

These distinct gaps, such as the poor grasp of the health problem on one side and of new technologies on the other, may be historically viewed along a North/South geographic divide. The nations that industrialized in the nineteenth century and led the scientific and technological revolution of the twentieth century were predominantly above the Tropic of Cancer. Below that divide, most nations remained largely agrarian and relatively less developed as far as S&T were concerned. Today, many nations of that South are often characterized as developing or resource limited and nations of the North, of course also continuously developing, are characterized as developed or resource rich. The North still commands global scientific and technological superiority, at least within the context of how the North views that critical field of human endeavor. Sustainable S&T in tropical health thus typically refer to tools developed in the North but put to practical and effective use in the South.

The importance of tropical health and sustainability lies in both the Northern and Southern perspectives of what this subject may mean in practice. In the North it implies applying a formidable suite of S&T capacities in improving Southern health. The Southern perspective may focus upon broad improvement of healthcare delivery by any means and not necessarily by the application of what may be poorly understood or even unknown Northern technologies. This perspective may be misconstrued in the North as the larger part of the problem, that is, a lack of awareness of the possibilities of Northern technology. This in turn leads the North to assume leadership roles in applying their R&D capacities to Southern health problems. Poor grasp of those health challenges may instead be the larger part of S&T sustainability failures in addressing them. This entry explores that problematic paradigm and alternatives to it.

Introduction

The frontiers of science and technology (S&T) represent increasingly expensive investments in a future

driven by expanding complexity and sophistication of research and development (R&D) systems. Nations endowed with the fiscal and technical wherewithal for such investments have historically dominated important scientific and technological progress. Moreover, these advances have often been driven by conspicuous national self-interest, for example, geopolitical competition with the Soviet Union catalyzed the US National Aeronautics & Space Administration into a technology behemoth. The US Department of Defense may be described in the same terms. Quite distinct from military superiority, nations also recognize the extraordinary economic potential of S&T, and it is increasingly linked to the political and economic security of nations. Contemporary reviews of national S&T agendas express this explicitly [1, 2]. The advancement of other nations in S&T may be construed as a threat by the empowering of potential economic competitors or even political or military rivals. One nation or group of nations may be inherently reluctant to promote the advancement of the S&T capacities of other nations.

Northern nations certainly acknowledge the vital importance of improving the global human condition and they do not lack in humanitarian compassion and generosity. Vast resources and technical know-how have flowed from North to South in the hope of alleviating endemic human suffering in much of the tropics. According to the Organization for Economic Development and Assistance, $104 billion was donated to developing countries by developed countries in 2007 (http://www.oecd.org/dataoecd/47/25/41724314.pdf). About $6 billion of that figure went to the health sector (in 2006), and recipient governments expended three times that amount from their own coffers for the same purpose [3]. However, very few of these resources are applied to advancing Southern or Northern health S&T/R&D per se – these funds almost invariably go to the application of proven rather than experimental technological solutions to human health problems. The North aims to apply proven technologies against Southern health problems through the broad aid schema. These funds and their application in the business of improving Southern health may be thought of as downstream from the S&T/R&D capacities aimed at improving the efficacy of these interventions.

In the S&T context of this encyclopedia, focus may be given to those R&D capacities and their effectiveness in real support of the downstream application of interventions against human health problems. This entry further focuses on a single important health issue, malaria, as an example of how Northern S&T works on a serious Southern health problem. The relatively vast sums available for malaria R&D (a recent development) likely create dynamics distinct from neglected tropical diseases like leishmaniasis, trypanosomiasis, filariasis, and many others. However, "neglected" may remain an appropriate term for malaria despite the funds being expended on it. An important question is the efficacy or impact of those funds in creating technologies that contribute to solving the problem.

Malaria causes very high burdens of morbidity and mortality, in addition to significantly stunting economic development [4]. At least hundreds of thousands perish each year and hundreds of millions suffer debilitating illness [5, 6]. In the tropical South, such burdens have remained entrenched despite the emergence of modern medications against the parasite and insecticides against the mosquito vectors over 90 years ago [7]. Malaria is preventable, treatable, and its cycle of transmission may be permanently broken with available S&T. This is known with certainty. Why then does malaria remain such an enormous human problem? This question strikes at core key issues in tropical health sustainability in the context of North-South R&D collaboration.

In 2011, a consortium of organizations funded by the Bill & Melinda Gates Foundation (BMGF) published an enormously informative and useful summary of global malaria R&D activities and financing (Fig. 1), predominantly for the period 2004–2009 [8]. The perspective taken in this entry reaches further back, to the Northern commitment to and later abandonment of malaria as an S&T endeavor between 1900 and 1965. The modern era of malaria R&D began around 1980 when Northern laboratories began applying fast-breaking biotechnological methodologies in earnest. These broader views provide insights on North-South S&T dynamics and a means of assessing the strengths and weaknesses historically embedded within them.

Forging Tools

The analogy of endemic malaria as a craftsman's problem to be worked by applying the range of tools in

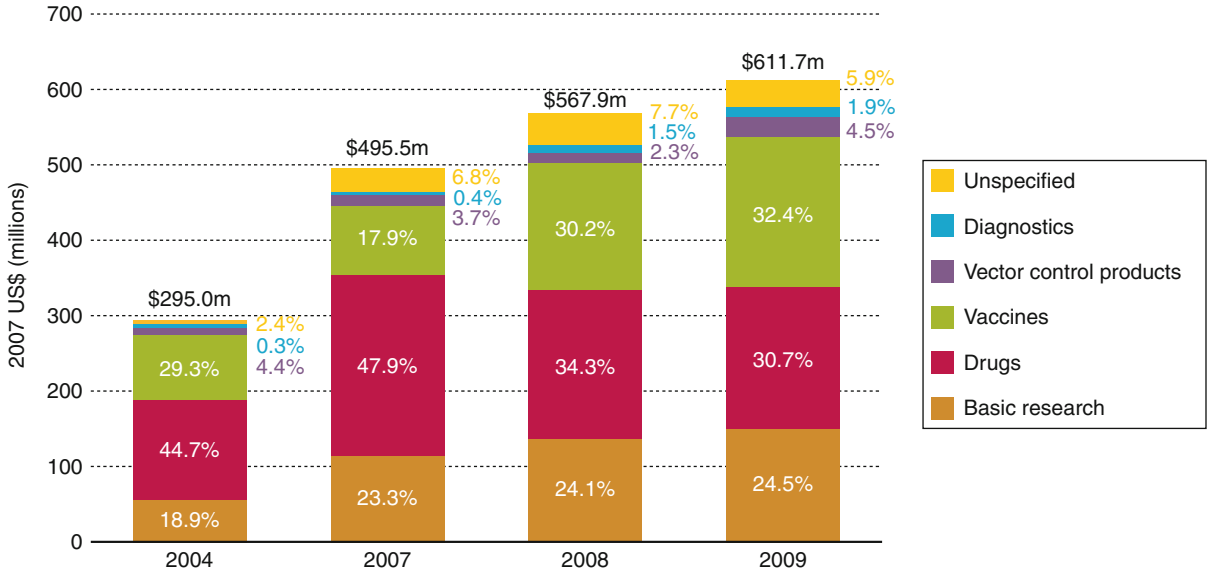

Tropical Health and Sustainability. Figure 1
Global malaria R&D spending (Taken from reference [8] with permission of the Malaria Vaccine Initiative)

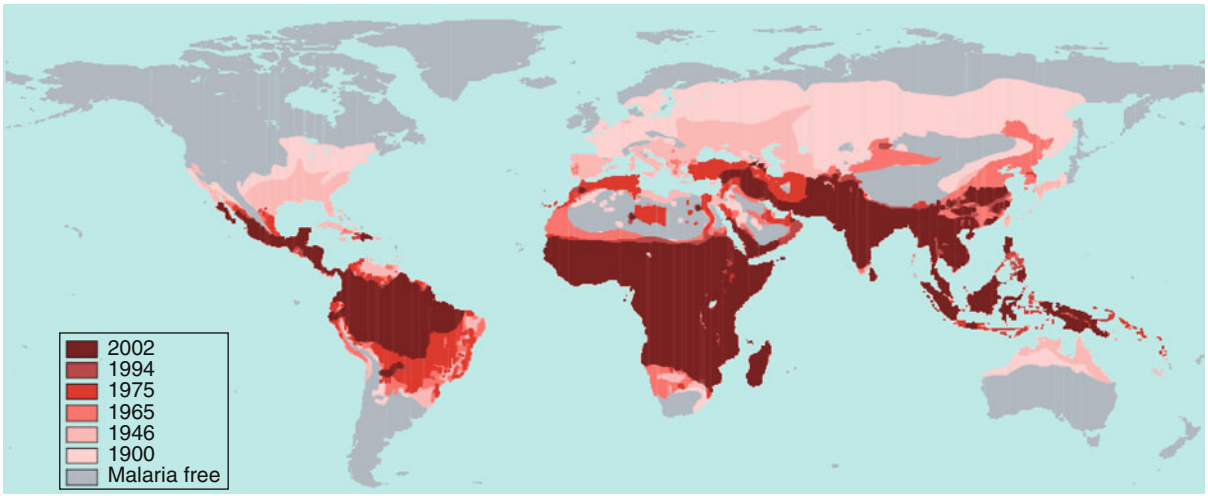

Tropical Health and Sustainability. Figure 2
The retreat of malaria to current endemic bounds since 1900 (Taken from reference [9] with permission of the authors and publishers)

a toolbox provides a useful conceptualization of human management of that problem. The craftsman's finished project may be thought of as a void once occupied with the human misery caused by malaria. The analogy finds further usefulness in recognizing the craftsman as representing the governments and institutions in endemic zones doing the physical work of crafting that project. They pick up the tools and use them. In the first half of the twentieth century, the Northern craftsman designed and forged the tools in his toolbox. As may be seen by the retreat of malaria between 1900 and 1965 [9] (Fig. 2), this approach produced effective outcomes. Malaria disappeared from the North and began to be thought of as an exclusively Southern

disease. The retreat of malaria involved complex dynamics [7], especially economic, but its initiation only after science generated sufficient understanding and tools makes compelling argument for the vital efficacy of S&T in achieving such gains.

A glance at where malaria remains entrenched today reveals where that early Northern toolbox has proved inadequate to the task of elimination. Experts will see determinants of that failure according to their respective area of expertise. The biologist will point to the tropical climate as especially conducive to the transmission of malaria parasites by their anopheline mosquito definitive hosts. The medic will highlight inadequate healthcare systems. The economist will blame the relatively impoverished condition of the nations composing the malaria belt. Sociologists and politicians will note armed conflict and poor or unstable systems of governance dotted across that belt. And each expert would be partly correct. All of these issues contribute to the contemporary intransigence of endemic malaria in the tropics and even some temperate zones, despite the long availability of technologies adequate to the problem elsewhere. Northern R&D strives to outfit the Southern craftsman with an improved toolbox that may overcome these factors.

The Northern R&D community engaging malaria sees itself as the designer and forger of those tools. Historic Northern dominance in S&T and inarguably superior standing in R&D capacities relative to those of the South, logically lead to the assumption of this role. Northern laboratories engaging the malaria problem express this role explicitly. As one example among a wide range of Northern R&D institutions, the following comes from the US National Institutes of Health, National Institute for Allergy & Infectious Diseases (NIAID) 2008 publication, "NIAID Research Agenda for Malaria," and the section headed, "Malaria Prevention & Control Strategies" [10]: "*To reverse the trend toward rising malaria prevalence and its return to countries where it had been eliminated, new drugs, diagnostics, and vector management tools, as well as effective vaccines, are urgently needed. There also is an acute need to understand the factors that favor the effective use of new interventions and of prevention and control interventions already available. To develop both new products and a more complete understanding of factors that assure their effective introduction and use, public-private partnerships are essential.*" The message also comes across in the 2011 "Staying the Course?" monograph [8]: "*. . . investment in malaria R&D would create new tools that would more rapidly decrease the malaria burden. . ..*"

The presumed superior usefulness of those Northern tools to the task at hand, as opposed to those that could possibly be developed by the Southern craftsman himself, may be rationally challenged. However, Southern R&D capacity today cannot match that in the North and long-term investment in Southern S&T as an alternative approach has been, and continues to be, trumped by the often expressed sentiment, most recently in the malaria R&D monograph [8], that: "*Providing slow and inadequate funding over the next five to six years will not only delay the time when donors can begin to reduce their malaria R&D funding but – more importantly – will unnecessarily delay saving millions of lives in the developing world.*" The unspoken corollary is the humanitarian urgency in fighting malaria renders the long and difficult work of building Southern R&D capacity strategically irrelevant. Northern R&D strategizes a solution for global malaria upon what is effectively faith in its ability to deliver definitive solutions in the short term.

The contemporary position of an organization called the Multilateral Initiative on Malaria (MIM) supports this assessment. MIM was formed for the specific purpose of creating malaria R&D capacities in Africa. The malaria R&D monograph [8] devotes a single sentence to the organization and offers no insight on its funding levels, despite the rich details on funding embedded throughout the book. MIM's funding page on its website (www.mimalaria.org) was blank in July 2011. It may be surmised from other numbers provided in the monograph that the MIM budget was perhaps about $1.4 million dollars in 2009 (it is also unclear where that funding originated) [8]. It may thus be seen that of the $612 million dollars allocated to malaria R&D in 2009, 0.2% of that was committed to building Southern malaria R&D capacity, and only in Africa. At least within the Northern R&D agenda expressed in that monograph, standing Northern R&D capacity and the urgency of lives lost seems to preclude meaningful investment in long-term transfer of R&D capacities southward.

Providing Tools

If Northern R&D is to be the designated driver of tool design and delivery to the Southern craftsman, an assessment of its performance in this role may be instructive and useful. Performance evaluations look backward rather than forward, even though ultimately aimed at better performance in the future. Assessments of possible or hoped-for performance add little to the utility of such evaluations. Useful evaluation of R&D performance thus demands suspension of its primary focus, the future. How has the Northern R&D posture of the past delivered upon a future represented by today? What lessons may be gathered from that experience and applied in a strategic sense to better performance in reaching a planned and sustainable future?

The primary tools of malaria control today are rapid diagnostic tests (RDTs), artemisinin-combined therapies (ACTs), insecticide-treated bed nets (ITNs), and, increasingly, indoor residual insecticide spraying (IRS) [11]. None of these tools emerged from mainstream contemporary Northern malaria R&D imperatives or programs (Table 1). RDTs and ITNs were almost entirely commercially developed, and IRS represents an almost abandoned and recently rediscovered tool developed almost a century ago. The vital artemisinin component of ACTs came from the Chinese Army, and the concept and promise of ACTs emerged in the late 1980s and early 1990s from individuals (particularly Prof. Nicholas White at Mahidol University in Thailand) and private industry (Novartis began codeveloping an ACT with public Chinese partners in 1990) rather than any Northern R&D agenda impelling them in that direction [12]. Up to the present day, with the exception of drugs, the other three vital tools in the standing malaria control toolbox represent the two most severely underfunded avenues of the malaria R&D agenda: diagnostics (1% of funding) and mosquito vector-based interventions (4% of funding) [8].

The proposed strategy to deal with this underfunding is to hold all other areas (basic, drugs, vaccines) stable and to reserve the hoped-for 2% increases in annual funding to those neglected avenues [8]. In short, the expressed strategy is to give those two areas, currently funded at $30 million, an incremental (and hoped-for) increase of about $12 million per year. If this report represents Northern S&T consensus (it does not purport to do so), nothing in basic, drugs, or vaccines research may be sacrificed beyond the savings of achieved targets (and those go to offer relief to donors). The Northern toolmaker's investment preferences seem to reflect optimism for delivery of more practical and useful tools than diagnosis and warding off mosquitoes. Drugs and vaccines (and the basic research that ultimately drives those two avenues) command the Northern R&D agenda at 89% of expenditures between 2004 and 2009 [8]. Has the toolmaker gotten this balance right?

Another legitimate question may be, "Who is this toolmaker?" There is no formal body that gathers and determines the direction and magnitude of malaria

Tropical Health and Sustainability. Table 1 The malaria control toolbox 2011

Tools	State of the art	Era developed	Sector developed	Utility
Diagnosis of infection	Immunochromatographic cassettes	1990s	Private	Limited
Diagnosis of G6PD deficiency	NADP + reduction assays	1960s	Private	Poor
Therapy against acute attack	ACTs	1990s	Private	Good
Therapy against relapse	Primaquine	1940s	US Army	Poor
Therapy against transmission	Primaquine	1940s	US Army	Poor
Medical insecticides	Pyrethroids, carbamates, organophosphates	1970s	Private	Poor
Insecticide treated nets	Long-lasting pyrethroid impregnated nets	1990s	Private	Limited

R&D funding decisions. The malaria R&D monograph [8] is simply a summary of where investments have been made and by whom. The data are presented for the expressed purpose of guiding those bringing fiscal resources to the malaria R&D table. Thus, the people embedded in funding organizations and having the responsibility of distributing those funds constitute the toolmaker and his collective resources – money, ideas, expertise, a plan, and the will to achieve it.

In 2009, $612 million was expended on malaria R&D. The $99 million from this figure expended by biotechnological firms may be discounted because the funds do not set anyone else's research agenda – they overwhelmingly fund their own R&D imperatives and operations [8]. Two thirds of the remaining $513 million came from the BMGF ($184 million), the US NIH ($116 million), and the US Department of Defense ($38 million). Three European donors followed with a collective $77 million (European Commission, Wellcome Trust, UK Medical Research Council). The balance of $98 million came from a variety of other donors. Decision makers in R&D funding among these organizations, collectively and proportionally, embody the major global malaria toolmaker.

Diagnostics Are Critical

Malaria in the real world is poorly understood by most in the North. The terminology "real world" captures the sum of complex medical, scientific, ecological, social, economic, and political determinants of endemic transmission and disease. It also expresses real (evidence-based) versus imagined (supposition-based) understanding of the character of entrenched endemic malaria. Strategists look at malaria in terms of the burdens of morbidity and mortality imposed by each of the five species of plasmodia routinely infecting humans. This entry considers only two of those species, *Plasmodium falciparum* (cause of falciparum malaria) and *Plasmodium vivax* (cause of vivax malaria) because these likely represent the vast majority of the global malaria burden.

Estimating Burden of Morbidity

Few in the North appreciate the great distance between the real malaria case numbers and those reported by Ministries of Health (MoH) and globally summarized by the World Health Organization (WHO) each year [13]. The crucial importance of that distance is even less appreciated as a key determinant of S&T sustainability failures against endemic malaria. It reflects not just incomplete understanding of the magnitude of those burdens [6, 14], but also what ultimately drives the unseen and unknown burdens in place and time, that is, in the real world. This vulnerability is driven by unsustainable S&T for the diagnosis of malaria in endemic zones.

Data from Indonesia, to be considered typical among endemic nations, illustrate unsustainable diagnostic S&T and the consequences of the failure to mobilize a nearly adequate R&D response to it. In 2008, WHO reported between 1.4 and 1.8 million annual malaria cases in Indonesia during the years 2000–2006. In 2009, they modified estimates for the same years to between 1.3 and 3.0 million. These were based on confirmed cases reported to them by the Indonesian authorities ranging from 0.22 to 0.44 million per year [13, 15]. The differences in those numbers reflect suppositions regarding the efficiency of Indonesian diagnosis and reporting systems. Studies by the Malaria Atlas Project (MAP) based upon prevalence surveys and Bayesian statistical modeling, estimated 12 million clinical attacks by falciparum malaria alone [16]. Capture of laboratory-confirmed and reported cases of malaria reflected by the numbers provided by MoH implies a roughly 10% case diagnosis rate by the WHO estimates of total cases. That rate drops to less than 1% using the MAP case estimate which excludes vivax malaria. By either estimate, despite the order of magnitude difference between them, the majority of malaria cases in Indonesia go undiagnosed and unreported [17].

The Ministry of Health of Indonesia, like almost all others, reserves therapy with ACTs to cases having a confirmed diagnosis, and all others receive ineffective chloroquine or sulfadoxine/pyrimethamine because there are few practical options [18]. They do so under the rules of the Global Fund for AIDS, Tuberculosis, and Malaria (GFATM) – the donor paying the bill for most ACTs in Indonesia. GFATM reasonably does not wish to have precious ACTs wasted for any given febrile illness. It may be appreciated that this enormous problem is not a challenge of better drugs, but better

diagnosis. Failure to deliver diagnostic services and reporting directly causes most malaria in endemic zones to go undiagnosed, unreported, and not treated.

Estimating Burden of Mortality

Reports and estimates of malaria mortality rates in Indonesia also range freely across several decimal places. The Government of Indonesia's Central Bureau of Statistics conducted national Household Health Surveys in 1995 and 2001, and estimated 30,000–38,000 deaths due to malaria had occurred in each of those years [17]. In 2001, the WHO reported 68 deaths caused by malaria in Indonesia [15]. This reported number was 494 in 2006, and WHO estimated the number to be closer to 3,000 deaths [15]. A recent study in India challenged the government's estimates of malaria mortality at 15,000 deaths in 2008 [19]. Investigators conducted verbal autopsies (interviewing surviving family members of people lost to premature death on the clinical nature of the fatal illness), using a rigorous sampling methodology to represent the broader population. They analyzed 122,000 deaths during 2001–2003, and their findings led to an estimate of 205,000 deaths annually from malaria, and death by malaria carried a 1.8% risk by age 70. They found that 86% of deaths caused by malaria did not occur in any healthcare facility, and thus went unreported. Verbal autopsy methodologies of course come with uncertainties, but it may be that fewer than 1 in 10–100 or more deaths caused by malaria are reported from endemic zones. Unsustainable S&T for diagnosis and reporting explain these dangerous gaps in understanding mortality burdens and their demographic/geographic distributions.

The species of plasmodia responsible for death cannot be ascertained in verbal autopsy, but it is now known that in India specifically, *P. vivax* at least occasionally and perhaps routinely causes death in malaria patients [20–23]. The same has been found in other regions [24–31]. Long known as "benign tertian malaria," such reports of fatal vivax malaria have been met with appropriate, albeit stubborn skepticism in malariology circles. The conventional view has been that only the "malignant tertian malaria" of *P. falciparum* routinely causes the range of life-threatening syndromes linked to malaria.

Benign Tertian Malaria Fallacy

Careful study of the genesis of the term "benign tertian malaria" in the late 1800s and the clinical experience with malaria therapy of neurosyphilis in the 1920s and 1930s provides important insights on the contemporary view of vivax malaria as an insignificant contributor to global malaria mortality. The notion of benign and malignant malarias had been well known long before Laveran's discovery of the plasmodia in 1880 [32]. After broad acceptance of species identity between *P. falciparum* and *P. vivax* at around 1890, a few elite clinical study centers in Europe and America sought to reconcile taxonomic identity to those clinical classifications of malaria. As pointed out by Kitchen in 1949 [33], taxonomic identity should have been the frame of reference rather than ambiguous and confused clinical classifications. As early as 1901, a pathologist in New York City describing autopsy findings of a fatal case of vivax malaria challenged the certainty of *P. vivax* as a benign infection [34]. He wrote, "*While the statement of the Italian authorities has long held true that no autopsy in a case of malaria with infection by the large tertian parasite, as the infection is never fatal, the present case requires modification of that view. . ..*"

The advent of malaria for therapy of neurosyphilis in the 1920s added substantial depth to the understanding of clinical course and taxonomic identity. Despite contemporary views by some that vivax malaria in those patients did not cause severe or threatening disease [35], death caused by vivax malaria carried consistent and apparently strain-specific risks ranging from 3% to 15% case fatality rates (CFR). At treatment centers across the USA, the CFR was extraordinarily consistent at 3–6% after therapy had been optimized [36–41]. Prior to both learning to screen out poor candidates for treatment and gaining expertise in successful clinical management, the CFR had been between 15% and 30%. At least one series of fatal treatments had been followed by autopsy studies that confirmed malaria as the cause of death (rather than any underlying disease, including neurosyphilis) in at least half of the patients [40]. Most physicians reporting these experiences expressed the conviction that malaria had killed most of their nonsurviving patients. Nicol [42] wrote in 1932, "*One must acknowledge that, though in a few cases death is caused by*

intercurrent disease, malaria, if not directly responsible, must be regarded as a contributing factor; in most cases the malaria itself is the cause." It should be recalled that in that era unsuccessful therapy of neurosyphilis would almost always end in death for the patient. This fact, and the only 35% efficacy of malaria therapy against the disease under the best of circumstances [42], explains the aggressive and extreme treatment. More severe and punishing repeated malaria paroxysms (episodic extreme chills and spiking fevers) improved the odds of successful therapy. Nicol [42] closed the above-cited quotation with, "*Risks, however, must be taken in treating a disease which, if untreated, proves fatal.*"

Clinics in the UK usually used the Madagascar strain of *P. vivax* and this strain for treatment of neurosyphilis typically killed 10–14% of patients [43]. Clinics in the Netherlands used a local strain of *P. vivax* that carried a 0% CFR, but had very low therapeutic efficacy against neurosyphilis. A switch to the Madagascar strain improved efficacy but came with an 8% CFR [44]. One clinic in the UK evaluated *P. falciparum* for therapy and reported a 4% CFR [45]. It may thus be appreciated that most strains of vivax malaria, permitted to follow a severe course of infection, may threaten life in at least 5% of patients. Contemporary studies in hospitals report CFR among patients classified as having severe illness at between 5% and 10%, a rate roughly equal to that among patients with severe falciparum malaria in the same hospitals.

The chapter on clinical vivax malaria penned by S.F. Kitchen [33] in the classic 1949 text on malaria does not deal directly with the neurosyphilis mortality data. The author describes some controversy on the issue of severe and fatal vivax malaria but dismisses it as implausible largely on the basis of this parasite rarely causing hyperparasitemia – a well-known risk factor for death in falciparum malaria and the basis of its "malignant tertian malaria" moniker. Relatively low parasitemia is routinely documented in contemporary reports of severe and fatal disease in vivax malaria, and this may reflect an unknown pathogenesis distinct from falciparum malaria. The seemingly nonthreatening low parasitemias of vivax malaria may have deceived earlier workers. Indeed, Kitchen [33] wrote, "*...present knowledge concerning the provocative potentialities of low-grade parasitemias does not permit denial of the possibility that the presence of the Plasmodium [vivax], even in very small numbers, may serve as an incitant of entirely foreign conditions...*." Today it is known, for example, that *P. vivax* is physiologically capable of accessing the bone marrow [46] and is sometimes found in that tissue [47].

Although further studies are required to gauge the burden of severe morbidity and mortality of vivax relative to falciparum malaria in endemic zones, the infection is certainly not benign. Regardless of relative burden, the persistent view of vivax malaria as a benign entity may be considered incompatible with available evidence and probably dangerous to patients and populations living with this threat.

Vivax Malaria and Global Malaria Burden

The long-engrained notion that only *P. falciparum* kills profoundly shapes how the global malaria problem is perceived as a whole and, ultimately, strategized to deal with. A statement very similar to this may be found in popular, peer-reviewed, and authoritative technical media [48–50], "80% of cases and 90% of the world's deaths caused by malaria occur in Africa." Vivax malaria is relatively rare in sub-Saharan Africa as a consequence of the almost universal inherited absence of a molecule called Duffy factor on the surface of red blood cells which *P. vivax* requires for invasion. Thus, the dominance of *P. falciparum* on that continent, and the relative dominance of *P. vivax* elsewhere (along with the presumption of its benign nature) largely accounts for that popular supposition. As the severe morbidity in vivax malaria and very high estimated all malaria mortality data from India and elsewhere suggest [19–31], the assertion is scientifically unsound and perhaps likely to be a gross distortion of malaria as it occurs in the real world.

The statement likely overstates the relative burden of falciparum malaria and simply dismisses the contribution of vivax malaria to the global burden of morbidity and mortality. Hay and colleagues [16] estimated African clinical attacks of falciparum malaria accounted for 60% of the global burden of that species. Almost all of the remaining estimated attacks by falciparum malaria occurred in Central, South, and Southeast Asia, where the substantial burden of vivax

malaria, yet to be reliably estimated, also occurs [51]. The number of clinical attacks caused by *P. vivax* is estimated between 100 and 400 million [9]. As has been explained, the mortality burden imposed by this parasite (and very likely by *P. falciparum* as well) may be described as unknown. Adding the lower end of the vivax malaria morbidity range to the global falciparum clinical attack numbers for 2007 of Hay et al. [16] suggests at least 50% of the global burden of clinical attacks by any species occurs in Central, South, and Southeast Asia.

If careful study confirms heavy burdens of morbidity and mortality caused by endemic vivax malaria in Asia and elsewhere, the response to this threat would largely be limited to chemotherapies no longer likely to work (chloroquine), another that never worked effectively in the first place (primaquine), or others untried against this species. This hypothetical scenario contains an uncontestable core fact: the burden of morbidity or mortality of vivax malaria anywhere it occurs is not known. And yet, Northern science up to 2011 remains almost wholly focused on falciparum malaria, especially in an African context. Research on *P. vivax* between 2007 and 2009 accounted for only 3.1% of R&D funding [8]. There may be serious consequences to this possible miscalculation driven by unsustainable S&T for the diagnosis of malaria in endemic zones.

Proven resistance to the first-line treatment of acute vivax malaria, chloroquine, now occurs across the Indonesian archipelago, at sites through the Mekong region, and cases have been reported from the Indian subcontinent [52]. Another drug, primaquine, must also be administered to prevent further attacks caused by dormant forms in the liver. The efficacy of that drug has not been unambiguously measured since the 1950s. The hemolytic toxicity of primaquine in glucose-6-phosphate dehydrogenase (G6PD) deficient patients – so prevalent in endemic zones (5–25%) – coupled with the failure to field sustainable diagnostic S&T for that disorder, likely drives therapeutic effectiveness of primaquine close to null in endemic zones [53, 54]. There are no standardized means of assessing the efficacy of these drugs against this parasite, and no mechanisms of activity against the parasite or of resistance to the drugs are known. Worse still, the standing drug development paradigm, designed for and largely serving the fielding of drugs against the acute attack of falciparum malaria, is very poorly suited for fielding new therapies for radical cure of vivax malaria [55].

RDTs Have Limited Utility

Several dozen commercially available immunochromatographic RDTs for malaria compete for the large volume of global sales. Most of these kits perform very well in specific settings, but in others they completely fail to meet operational requirements. Ideally, the kit is used for the diagnosis of malaria in acutely ill patients in endemic zones lacking access to a definitive microscopic diagnosis of malaria by Giemsa-stained blood film. When falciparum malaria is the offending agent and parasitemia is higher than 200 parasites/μL, sensitivity and specificity each come in at well above 90% in most kits. Below that threshold, sensitivity falls precipitously. In vivax malaria, the corresponding threshold is about 500 parasites/μL for most kits [56]. The threshold of parasitemia causing illness in nonimmune patients falls far below both of those diagnostic thresholds for RDTs [57]. Also, cross-sectional surveys in endemic zones typically show median parasitemia levels at or below those thresholds, especially for vivax malaria [58, 59]. Thus, RDTs are not suitable for diagnosis in nonimmune patients or for detection of parasitemia among asymptomatic residents of endemic zones.

Asymptomatic carriers of malaria represent the rule rather than the exception in almost all endemic zones. These infections almost universally present very low levels of parasitemia far beyond the diagnostic reach of RDTs [59]. Cross-sectional surveys in Cambodia employing ultrasensitive polymerase chain reaction (PCR) diagnostics revealed that only about half of those positives were also positive by expert microscopy, and far fewer by RDT. Thus, elimination strategies must consider mass administration of drugs in populations having very low levels of endemic malaria, as a consequence of diagnostics, inadequate to the task of finding and treating the few infected people [60]. Current RDT technology leaves wide diagnostic gaps in endemic zones.

Diagnostics R&D Performance Evaluation

The failure to develop sustainable diagnostic and reporting S&T for endemic zones may have distorted

the view of global malaria with possibly serious consequences. By the nearly complete neglect of unrecognized heavily burdened regions [61] and a heavily burdening species [62, 63], one may have been lured, by diagnostic blindness, into a position of profound strategic weakness. Assuming that vivax malaria indeed kills with some regularity in India and elsewhere, it may be reasonable to assert that one does not have even the barest grasp of malaria in the real world, that is, it is not known how many acute attacks kill how many people, where, or by which parasite, much less who is most vulnerable and why. Poor diagnostics is the reason and the Northern R&D toolmaker appears unable to prioritize that task (1% of R&D funding [8]).

Insecticides Are Critical

Since the discovery in 1880 by Alphonse Laveran that plasmodia cause malaria, and of their transmission by anopheline mosquitoes by Ronald Ross in 1898, malariologists have fiercely argued strategies of control focused upon treatment versus interventions aimed at the anopheline vectors. In the early 1900s, Robert Koch championed the former, and Ross the latter [64]. Both applied their concepts in the field (Koch with quinine in New Guinea, and Ross with crude anti-mosquito measures in West Africa) with almost no success. However, key successes in the era that followed, along with the discovery of dichlorodiphenyltrichloroethane (DDT), ensured the dominance of mosquito vector control in the global malaria eradication effort undertaken during the 1950s and 1960s and, later, misplaced disillusionment with that strategy.

Abandonment of a Proven Tool

Between 1904 and 1914, William Crawford Gorgas effectively attacked the mosquito vectors of the yellow fever and malaria in Panama that had decisively dashed the French efforts of the 1880s to build a canal [65]. Watson in British Malaya (today Malaysia) tamed malaria on economically important plantations by deliberate and highly specific environmental modifications aimed at the behavior of the local anopheline vector. His approach, called species sanitation, was successfully applied by Dutch and Indonesian malariologists in the Netherlands East Indies of the 1920s and 1930s [66]. In the same period, William Soper successfully eliminated from Brazil the imported and terribly efficient African mosquito vector of malaria, *Anopheles gambiae* [67]. Mueller discovered DDT in Germany at about the same time, and the US military brought it to bear as a defensive weapon against malaria and other insect vector-borne diseases during and immediately after the Second World War.

The technological stage was thus set in the late 1940s for the conception and strategic design of an ambitious effort to eradicate malaria through the 1950s and 1960s. The USA pushed and largely financed the WHO-led Global Malaria Eradication Campaign (GMEC), which was essentially an attack upon anophelines using principally DDT. The role of another product liberated from wartime Germany, the extraordinarily safe and effective treatment for acute malaria called chloroquine [68], was secondary or a mop-up in that strategy.

DDT exploited a behavior of anophelines – most species go indoors at night, feed upon sleeping people and, heavily laden with a blood meal, rest upon interior walls. DDT applied to those walls provided an opportunity for lethal contact with insecticide even many months after its application. Indoor residual insecticide spraying, or IRS, proved remarkably effective in malaria control in almost every setting. Global malaria numbers in the era of its systematic application plummeted, except in most of Africa where IRS was not applied in earnest for want of the logistical infrastructure to do so. In India, for example, over 800,000 deaths due to malaria each year fell to, reportedly, none [69]. Malaria transmission ceased in most of the Caribbean and was sharply curtailed all across Central and South America. Endemic malaria disappeared from Southern Europe, North Africa, Japan, Taiwan, the Korean peninsula, and most of Java [70].

Northern agriculture effectively derailed the success of DDT by hijacking the medically important product. The aerial spraying of DDT across many millions of square miles of croplands resulted in vast quantities of this very stable compound being introduced into the environment at disastrous cost. In 1971 in the USA alone, the year before such practice was legally banned, 14 million pounds of DDT was used in the agricultural sector [71]. The practice harmed beneficial insect populations and accumulated dangerously in higher

predators, even those above the Arctic Circle. Theft of a medically important instrument by Northern agriculture spilled southward. The onset of resistance to DDT by anopheline mosquitoes may have been driven by agricultural applications. In the late 1960s, as many of these problems were coming fully to light, the GMEC formally collapsed [72].

Adopting Impractical Tools

Northern agricultural insecticide industries turned to their S&T engines to solve the problem of the loss of DDT with viable alternatives. They required insecticides only stable long enough for the quick work of killing crop pests. Three classes of insecticides emerged to dominate that market: organophosphates, carbamates, and pyrethroids. These short-lived compounds, their costs, along with relatively high toxicity or noxious character make them poorly suited for IRS. Nonetheless, in the decades that followed, and up to the present day, Southern IRS against malaria and other vector-borne diseases of the tropics has depended upon these insecticides developed and licensed for Northern agricultural practices [73]. The impracticality of the new insecticides contributed to the broad contraction or collapse of IRS programs in the endemic tropics [74]. Those products stand as clear examples of the sometime very poor fit of Northern S&T imperatives and products to Southern health problems.

Cost-effective, safe, and practical long-lasting insecticides sprayed inside homes were nowhere in that Northern R&D agenda for the simple reason that Northern homes were not being invaded by insects carrying life-threatening infections.

Revitalizing IRS

Roberts and colleagues [75] documented quantitative insights on the health costs incurred by Northern aversion to DDT especially, and IRS in general. A science- and public health-led campaign narrowly averted a 2001 effort to ban DDT for any use anywhere in the world [76]. The aversion to DDT, borne of its reckless agricultural application, irrationally inhibited endorsement or support to Southern IRS operations for decades. In 2007, WHO reversed its long-standing recommendation against IRS in areas of stable transmission and today recommends DDT for such operations [77]. In that reversal, WHO expressed, "*DDT is still needed and used for vector control simply because there is no alternative of both equivalent efficacy and operational feasibility. . ..*" The reason for that simple truth is clear: Northern insecticides R&D abandoned the task of medical insecticides 60 years ago and there has been no Southern R&D capacity to pick it up.

Northern sociopolitical aversion to IRS has at long last diminished to greater support and emphasis on this vital tool in the control toolbox. In late 2009, for example, USAID advertised a US$130 million grant for support of IRS operations in Tanzania. However, unleashing such resources to apply poorly suited short-lived insecticides may greatly dampen efficiency and impact. A recent study described a microencapsulated organophosphate insecticide (chlorpyrifos methyl, Dow Agrosciences) with >90% activity persisting at least 9 months when used in experimental IRS [78]. This work, and the growing realization of the threat of resistance to both pyrethroids and DDT [79, 80], emphasizes the need for much more R&D on insecticides.

Reliance upon Northern agricultural S&T for medically useful insecticides should be acknowledged as at least inefficient and perhaps impractical. The discovery and development of medical insecticides should not be simply incidental to agricultural pesticides. The malaria R&D monograph [8], however, points hopefully to Northern industrial pesticide firms as a means of supplementing the pitifully small amounts of funding committed to insecticides.

Insecticides R&D Performance Evaluation

Northern R&D on discovery of medically important insecticides for use in IRS or ITNs has been nascent since the discovery of DDT in the 1930s. This failure, viewed in light of the enormous impact of DDT against malaria in the middle of the twentieth century, may be considered the most conspicuous of all Northern R&D failures on global malaria. The stubborn and irrational Northern aversion to insecticide tools for malaria control may at last be waning, but R&D investment in earnest exploration of improving these tools remain grossly inadequate. Hopefully, however, the BMGF expressed interest in spatial repellency of some compounds by making a substantial investment in a proof-of-concept trial in Indonesia in 2009 (JKB is

an investigator in that effort), and their Grand Challenges funding scheme invested in mosquito attractant/repellant molecule discovery. Agricultural insecticide developers apply algorithms of chemical lethality and exclude compounds on the basis of repellant characteristics that would diminish opportunities for lethal contact with an insecticide product. If spatial repellency proves effective in risk reduction in endemic zones, it would reopen the universe of chemical exploration possibilities with development algorithms wholly distinct from insecticides. Perhaps not coincident with its operational efficacy in the past century, DDT happens to be one of the most effective compounds known in eliciting avoidance behavior in anopheline mosquitoes [81].

Drug Delivery

Humanity always needs new and better anti-infective drugs – diverse microbial populations mount their formidable Darwinian defenses that make old drugs useless, and new infections emerge. The commercial pharmaceutical industries of the North generate streams of new therapies in a fiercely competitive market environment that sharply hones the science and technologies (and regulatory prowess) of surviving companies. The prospect of profit drives and sustains this superb and very expensive engine of biotechnological innovation. However, at least several major multinational pharmaceutical firms have stepped into the malaria R&D arena with fairly substantial investments. During 2007–2009, they brought 14% of the $1.68 billion R&D investment (including work on vaccines), but kept this funding almost entirely internal [8]. Industry also frequently participates in antimalarial drug development through donor-funded product development partnerships (PDPs) like the Medicines for Malaria Venture (MMV) funded by BMGF, Wellcome Trust, WHO, and others. PDPs spent $114 million donor funds on malaria R&D in 2009. Private enterprises (both major multinationals and small to medium businesses) and academic or other not-for-profit institutions divided that pie in roughly equal halves [8].

State of the Art

Understanding these investments and the dynamics driving them requires a brief look at the class of therapies called the ACTs. The artemisinin family of drugs (artemisinin, artesunate, artemether, arte-ether, and dihydro-artemisinin), all rapidly excreted, combines with another typically slowly excreted antimalarial drug (mefloquine, piperaquine, lumefantrine, pyronaridine, or others) to both improve efficacy and protect the artemisinins against onset of parasite resistance to them [12]. ACTs today are manufactured commercially at many factories scattered across Southeast and South Asia, the Middle East, and Africa. These companies produce dozens of ACTs in as many formulations and means of packaging. The artemisinins have no patent protections, nor do the majority of drugs partnered with them. These products also share other important characteristics: almost none have been produced by the standards of Good Manufacturing Practice (GMP) as applied and certified by regulators, and few have co-formulated the components, preferring instead to package them together as separate pills. Few of these manufacturers possess the resources or influence to press for the aggressive arrest and prosecution of counterfeiters of their products. Collectively, these important flaws permit patients to take medication inadequate for cure and thereby expose each therapeutic agent to real risk of onset of resistance.

The GFATM will not fund ACT products of unproven quality. Therapies must be approved by WHO, and such approval includes certified compliance to GMP [82]. In effect, the availability of ACTs to Southern governments hinges upon access to GMP product. One strategy at work with GFATM funding policy is to push inferior drugs out of the marketplace with the superior drugs simply by making them at least as affordable. Thus, GMP product emerges as a key determinant of success in this strategy. In the 13 years of its existence, MMV has fielded two such ACTs (Coartem™, Novartis; Coarsucam™, Sanofi Aventis). Two others approach registration in 2011 (Euartesim™, Sigma Tau; and Pyramax®, Shin Poong).

Even as GMP co-formulated ACTs now approach closer to broader reality, resistance to ACTs has emerged in the Mekong region [83] where commercially driven monotherapy with artesunate and counterfeiting has been rampant [84]. Expansion of this problem into the rest of South and Southeast Asia, and ultimately Africa (as occurred with previous antimalarials), would constitute a global health catastrophe because currently there are no therapeutic

replacements [85]. This problem could possibly have been averted by early use of GMP, co-formulated ACTs, and aggressive, commercially driven protection against counterfeiting. The neglect of malaria chemotherapy as a whole by Northern pharmaceutical S&T, and also by malaria institutional R&D stalwarts during the second half of the 1900s, today has the South precariously near persistent, untreatable, and unbeatable endemic malaria. How did such neglect arise? Addressing this question requires examination of the genesis and content of the chemotherapeutics toolbox of 1965.

Chemotherapeutics Accomplishment: 1900–1965

Assessment of current strategy for delivery of drugs, as summarized above, requires consideration of where Northern S&T left off when it effectively abandoned the problem of malaria chemotherapy in 1965 as a mission accomplished. Examining malaria R&D capacities and imperatives in the preceding half century provides essential understanding of that turning point.

Scientific chemotherapy of malaria emerged in the organic chemistry crucible of the German aniline dye industry in the closing years of the 1800s. Screening for activity against parasites in bird models of malaria, the German laboratories of I.G. Farben during the 1920s and 1930s discovered many active classes and compounds [86]. The two most important were the 4- and 8-aminoquinolines, and focus upon them during the frenetic war-spurred search for better therapies in the 1940s delivered what were to be considered the ultimate antimalarial drugs.

Chemotherapy of malaria in 1940–1941 remained overwhelmingly dominated by quinine. The few synthetic antimalarial drugs in the market fared poorly due to unpleasant or even dangerous side effects. The German chemotherapists had superior drugs coming and plotted to unhinge the Dutch monopoly on chemotherapy of malaria manifest by their control of 95% of the world trade in quinine [87]. The following year, the Nazis occupied Holland and the Imperial Japanese armed forces occupied Java and Sumatra, where virtually all Dutch quinine originated. Axis powers denied the Allied forces access to the only drug then widely used to treat malaria.

The Allies understood the coming warfare would be conducted where malaria posed a serious threat. Endemic malaria loomed ominously in the Western Pacific especially, and their worst fears were soon realized: the first offensive ground combat involving American troops in that war was at Guadalcanal in the Solomon Islands in mid-1942; those troops suffered malaria attack rates of 1,700/1,000 man-years [88]. When the US Army Americal Division was evacuated from Guadalcanal to nonmalarious Fiji, their chemoprophylaxis was withdrawn and they suffered attack rates by *P. vivax* of 3,700/1,000 man-years [89].

The US Government mobilized to solve their serious malaria problem. The malariologists enlisted in the effort, and their sponsors, viewed success in their endeavors as directly impacting the likelihood and speed of military victory, especially in the Pacific [90]. The Board for the Coordination of Malaria Studies (BCMS), managed from within the US National Science Foundation, oversaw the evaluation of over 14,000 potential drugs from discovery to clinical trials in dozens of laboratories and clinics around the USA, Australia, and Britain. Their top priority was *P. vivax* because it accounted for five of every six cases among Allied troops. The Allies quickly mobilized production of a synthetic antimalarial (lifting it from the German S&T machine that generated it) called atabrine (also called mepacrine or quinacrine) and put it to work for both prophylaxis and treatment [91]. This hasty solution, however, had serious drawbacks. The skin of troops adhering to atabrine prophylaxis turned a distinct yellow hue and compliance had to be strictly enforced. More importantly, atabrine had an unexpected and dangerous interaction with the only drug then available against relapse, pamaquine.

Pamaquine was the first synthetic antimalarial licensed and marketed for therapy against malaria (as Plasmochin). This 8-aminoquinoline compound exerted excellent activity against the then poorly understood phenomenon of relapse in vivax malaria. Its activity against the sexual stages responsible for infecting mosquitoes was also known. Following its distribution in the 1920s, however, it earned the reputation of being sometimes an exceptionally dangerous drug [92]. As is well known today, the 8-aminoquinolines as a class exhibit potentially lethal toxicity in patients with an inherited deficiency of glucose-6-phosphate dehydrogenase (G6PD). Unwitting administration to many such patients caused

fatalities [92] and the drug never saw widespread use. The Allies, however, facing their serious relapse problems in the Pacific theater of World War II, mobilized pamaquine to that zone and serious toxicity problems followed [93, 94]. The BCMS issued a classified report in early 1943 demonstrating that when atabrine (but not quinine) was administered with pamaquine, plasma levels of the latter elevated tenfold. An already dangerous drug to some became a dangerous drug to all, and in mid-1943 the US Surgeon General ordered it withdrawn as therapy against relapse (although it could still be used, and was, in lower doses against transmission) [95]. The Allies were effectively forced to surrender to their serious relapse problem.

The BCMS resolved to address this problem. They screened several hundred candidate 8-aminoquinolines for toxicity in rats and monkeys and sent 24 drugs to clinical trials in prisoner volunteers in the USA. That screening had critically important limitations, but the BCMS in its haste to deliver a replacement therapy accepted those acknowledged shortcomings. The screening for antimalarial activity of those compounds in birds, for example, was understood to be nearly irrelevant and the developers largely ignored those data [90]. Efficacy could only be ascertained against clinical relapse in humans. Knowing the 8-aminoquinolines to be uniquely effective against clinical relapse as a class, and relatively toxic, the screening became a search for the least toxic 8-aminoquinoline without a means of screening for efficacy before evaluation in clinical trials. By almost any contemporary standard of science, this search for a replacement therapy for pamaquine may be characterized as incomplete and barely adequate. The product thus discovered reflected these qualities.

The superior candidate drug to emerge from this program was primaquine. It exhibited a slightly higher therapeutic index than pamaquine, and its anticipated toxicity (acute intravascular hemolysis) in subjects with G6PD deficiency, discovery of which occurred in that clinical development program, was confirmed [96]. As the Korean War unfolded during the early 1950s primaquine saw wide application with good therapeutic results. Chloroquine had been registered as therapy of choice against acute attacks of vivax malaria in 1946 [97]. These two companion drugs thus became therapy of choice for radical cure (meaning complete cure) against vivax malaria, and it remains today as the only such therapy with that licensed therapeutic indication.

As the American war in Vietnam loomed in the early 1960s, further clinical work on chloroquine and primaquine provided products useful to that military effort. The Americans developed methods of treatment and prophylaxis using these drugs that would not threaten the safety of its many G6PD deficient troops (the abnormality did not excuse them from eligibility for conscription and the US Army chose to not screen against it). They discovered that the most common African variant of G6PD deficiency (A-) could safely tolerate weekly doses of the drug over 8 weeks, as opposed to the relatively threatening daily dosing of 14 days. Remarkably, the efficacy of primaquine against relapse appeared to rest wholly upon total dose with almost no regard to schedule of that dosing; the same total dose of primaquine against *Plasmodium cynomolgi* in rhesus macaques – a superb model of vivax relapse – showed equally good efficacy when administered as a single dose, or multiple doses over weeks [98]. US military medicine thus delivered the "C-P" pill for protection of their troops against both acute attacks (with a weekly dose of 300 mg chloroquine) and relapse (with a weekly dose of 45 mg primaquine in the same tablet). As an added therapeutic bonus, it was shown that single 45 mg doses of primaquine in the company of chloroquine effectively killed the infectivity of the sexual stages responsible for malaria transmission [99, 100].

Thus, in the mid-1960s, corresponding with the nadir of global malaria in the wake of the GMEC, Northern S&T effectively abandoned malaria chemotherapy as a mission accomplished. That mission may be appreciated as having been driven by the threat of malaria to troops engaged in warfare in the tropics. The technically flawed and partial explorations that had been conducted nonetheless provided products suited to those Northern requirements and further or better explorations seemed pointless. The South would live with those chemotherapeutic solutions for the coming decades, and still does.

Chemotherapeutics Limbo: 1965–1995

The malaria chemotherapeutics status quo in 1965 and the reluctance of S&T in the North over the ensuing

30 years to effectively engage the problem leaves us where we stand today – poorly equipped to deal with the malaria problem of the South in a physical and strategic sense. An examination of the management of the highest chemotherapeutic priority – treating the acute attack – during this era, and our response to it, provides useful historic insights.

As has been described, the Northern R&D engine delivered chloroquine and primaquine around 1950 as the primary workhorse drugs for global malaria. Resistance to chloroquine by falciparum malaria emerged in the late 1950s and early 1960s. By the 1980s the problem had consolidated globally and new therapies trickled out of the few Northern laboratories engaged in chemotherapeutic discovery and development. Alternatively, older and less ideal drugs developed during the effort of the 1940s and 1950s were dusted off and put to work, for example, sufladoxine-pyrimethamine, proguanil, and others. However, resistance to those therapies emerged with astonishing speed and thoroughness [101]. Quinine combined with antibiotics like tetracycline or doxycycline then, in that crisis setting, found application against chloroquine-resistant falciparum malaria. Oral quinine, however, may be one of the most impractical therapies: it requires three doses daily for 7 days and causes a wide range of very unpleasant side effects; a syndrome called cinchonism that often deranges compliance to therapy.

Very few genuinely new therapies emerged during that era, most of them emanating from the US Army program at the Walter Reed Army Institute of Research (WRAIR) [102]. That program developed and fielded mefloquine (Lariam™) by the mid-1980s and it found broad application for chemoprophylaxis. However, patent protection, perceptions of its poor tolerability in many people, along with the emergence of resistance to it in areas of Southeast Asia, limited its broader application in almost all endemic zones. More recently, however, it has been partnered with an artemisinin, especially in the Mekong region, but not from GMP manufacturers. This exposes the drug to risk of poor manufacture and counterfeiting, and the packaging as separate pills risks poor compliance and onset of resistance to both artemisinin and mefloquine components. One co-formulated artesunate-mefloquine therapy has been registered in Brazil and other Latin American countries through the Drugs for Neglected Diseases Initiative. Nonetheless, mefloquine may be considered a minor contribution to the toolbox against global malaria.

The other genuinely new therapy to emerge at the tail end of the same era (and with roots in WRAIR), atovaquone-proguanil (Malarone™) followed a similar path to global malaria irrelevance. Glaxo-Wellcome (later to become GlaxoSmithKline (GSK)) took up the cause of developing this drug for the prevention and treatment of malaria during the early 1990s. Their rapid success in registering it for these indications reflects both corporate determination and skill, and superior chemotherapeutic properties: very safe and well tolerated, highly effective against acute attacks of all the malarias (including multidrug resistant falciparum malaria), co-formulated, and available as a GMP product. The single known serious problem with this drug at the time, its relatively high cost, seemed to exclude it from the global malaria toolbox. GSK, however, generously aimed to see this extraordinary therapy put to work. In cooperation with various government and nongovernment partners, they created the Malarone Donation Program with the expressed aim of providing a million treatments with this drug annually at no cost to the end users [103]. However, flaws in this strategy would undo that program.

Evidence emerged that a single point mutation in *P. falciparum* caused it to be completely and irreversibly resistant to atovoquone + proguanil [104]. Malariologists worried that its broad application would quickly result in its loss, and perhaps other important drugs via cross-resistance [105]. The donation program coped with this potential danger by setting down very strict criteria for its clinical use. Consequently, at pilot sites in Kenya, only 0.68% of malaria patients received the treatment and that minority were among the least likely to suffer a fatal outcome [106]. Hence, mortality rates among the vastly excluded majority were not affected by the intervention. African authors of that "lessons learned" report [106] explained that new drugs were not the imperative; poor access to any drug drove transmission and high mortality. The complex social and political process that drove the donation program to pilot implementation in Africa excluded African voices wholly at first and later invited them but suppressed

their dissenting views [107]. The Northern voice and conviction that this new tool required implementation in the South, along with their fiscal authority and influence, dominated the strategic consensus. Despite valiant and conspicuously generous efforts by GSK to contribute to the global malaria problem with this drug, the drug plays a very minor role in malaria treatment and control in endemic zones.

Northern S&T between 1965 and 1995 effectively failed to yield a solution for the highest chemotherapeutic imperative in endemic zones: treatment of the acute attack. At Southern clinics around the globe in the 1990s and well into the 2000s patients were still being treated with drugs invented half a century earlier. These drugs were less safe and effective than chloroquine in the heyday of its efficacy, and a cost in human lives was rapidly accumulating [108]. This is when the contemporary efforts to field ACTs as front-line therapies, already described, at last took root and continue today. Treating the acute attack, one of several chemotherapeutic challenges with malaria, may be far less an S&T challenge than finding it, diagnosing it, and reporting it. Assuming that the diagnostics S&T challenge is met, have the chemotherapeutic tools that are needed to capitalize on the accurate identification of the infected person been assembled? Northern R&D obsession with the acute attack unfortunately comes with neglect of the other possibly useful drugs for managing endemic malaria at that critical time/place interface when the parasites meet the range of chemotherapeutic instruments aimed at them.

Chemotherapeutics Neglect

The chemotherapy of malaria consists of five distinct compartments, treatment of acute attack (using blood schizontocidal agents) being one. The other compartments include: drugs aimed against the dormant stages in liver, called hypnozoites, responsible for relapse (using hypnozoitocides); drugs aimed against active stages in the liver, called tissue schizonts, that lead to acute attacks (using tissue schizontocides); drugs affecting the sexual stages in blood, called gametocytes, responsible for infection of biting mosquitoes and transmission of malaria (using gametocytocides); and drugs that prevent the development of parasites in the mosquito gut (called sporontocides). Figure 3 illustrates these compartments.

The blood schizontocidal antimalarials constitute the vast majority of antimalarial drugs in use today. These drugs, with few exceptions and when taken as directed, exert therapeutic activity only in that compartment. A few exhibit minor or limited activity elsewhere, for example, atovaquone may act as a tissue schizontocide against falciparum but not vivax malaria; chloroquine kills the gametoctyes of vivax but not falciparum malaria; and the artemisinins will kill gametocytes of falciparum malaria but not if already mature. One drug in clinical use today remarkably exhibits therapeutic activity in all of these compartments. That drug is primaquine, and despite its extraordinary dexterity in killing a wide range of morphologically and physiologically distinct forms of parasites (including across species), it is a tool of very limited utility in the global malaria toolbox. This is a consequence of both failing to tame its sometimes dangerous side effects and to develop practical means of gauging its therapeutic efficacies.

G6PD Deficiency The hemolytic toxicity of primaquine, and the absence of a Northern R&D response to the problem, largely explains its very limited utility in endemic zones. Sustained daily dosing with primaquine (15 or 30 mg daily for 14 days) poses a potentially lethal threat to patients with some variants of G6PD deficiency [109]. The US Army developers of primaquine, however, effectively solved this problem by discovery of both the nonlethal threat of daily dosing in African-American soldiers with the A- variant of the deficiency, and by fielding the perfectly safe (in A- variants) and efficacious single weekly dose of 45 mg for 8 weeks [110]. The diagnosis of G6PD deficiency requires a cold chain for shipping and storage of reagents, specialized skills and equipment: micropipettors, water bath, test tubes, and ultraviolet lamp, for example. This poses little technical challenge to care providers in the North, but in the endemic zones of the South such laboratory capacities are very rare. The providers who most often see malaria must chance potentially serious harm or choose not to prescribe the drug. G6PD deficiency and the unsustainable nature of that diagnosis in endemic zones (as it has been for 50 years) render primaquine almost wholly ineffective as a therapy to prevent relapse.

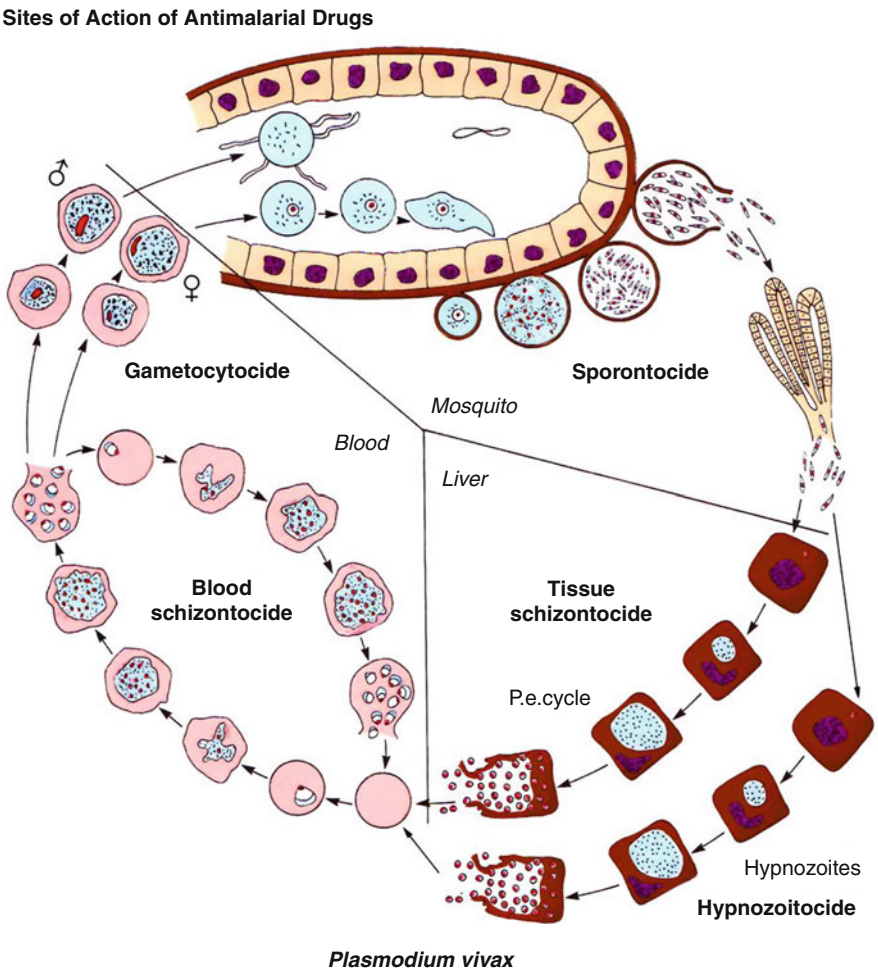

Tropical Health and Sustainability. Figure 3
Life cycle of *P. vivax* and chemotherapeutic compartments. The life cycle of *P. falciparum* would be essentially similar to this with the lone exception of the hypnozoite shunt in the cycle, which that parasite lacks (Taken from reference [53] with the permission of the American Society of Microbiology. Figure by Prof. Wallace Peters with artwork by Ms. Andrea Darlow)

Development of a point-of-care diagnostic device for G6PD deficiency would substantially mitigate this problem. The US Army recently supported the development of such a tool in order to improve the safety and effectiveness of an experimental replacement for primaquine, another hemolytic 8-aminoquinoline called Tafenoquine [111]. The product of that effort, however, can only be used reliably at temperatures below 25°C [112]. Another commercial company in the USA (AccessBio©, New Jersey) independently took up the point-of-care challenge and has a product in research and development that is simple, inexpensive, and heat-stable. That kit has performed well in initial field evaluations in Cambodia [113]. AccessBio© initiated this R&D effort with no support or guidance from mainstream malaria R&D funders, and WHO provided the funding for that evaluation (JKB is an investigator on that effort).

Primaquine suited Northern settings and requirements, and adapting it to safe use in Southern settings has never been an R&D imperative. Among the many dozens of G6PD deficiency variants, the primaquine sensitivity phenotype has been characterized in only three geographic settings (African A-, Mediterranean

B-, and, only recently, Mahidol from Thailand). These variants represent mild, severe, and moderate primaquine sensitivity phenotypes, respectively. Although residual G6PD enzyme activity has been characterized in most variants, its use as a surrogate for the primaquine sensitivity phenotype is a supposition not supported with clinical evidence. WHO has long recommended a single 45 mg dose without screening for G6PD deficiency, but largely upon the (inadequate) safety evidence from the USA that involved healthy African-American volunteers having the mild A- variant of this disorder [94]. However, in a very limited series of studies in the USA and Italy, a single 45 mg dose caused acute intravascular hemolysis of 25% of red blood cells in otherwise healthy volunteers having the Mediterranean B- variant (severe primaquine sensitivity) [114, 115]. Safe dosing in one variant may not hold for others.

Gametocytocide Poor understanding of primaquine sensitivity phenotypes creates very serious practical problems in malaria control. This may be most appreciated by the application of a single 45 mg dose of primaquine as a gametocytocide against falciparum malaria [116]. A 25% hemolysis in an acutely ill and already anemic patient may contribute significantly to onset of life-threatening complications. Remarkably, the safety of primaquine gametocytocidal therapy in patients with malaria, much less G6PD deficiency variants of any type, has not been systematically carried out. Limited recent studies from Africa suggest a significant threat to malaria patient safety [117, 118]. Countries aiming to apply the 45 mg dose of primaquine as a supplement to their control or elimination strategies must first demonstrate safety among the variants of G6PD deficiency occurring in their areas of operations. In 2011, the WHO undertook sponsorship of such studies in Cambodia using its own relatively meager R&D funding resources (JKB is an investigator on that effort).

The safety and efficacy of primaquine as a gametocytocide in falciparum malaria were evaluated with chloroquine therapy for the acute attack over 50 years ago [99, 100]. Chloroquine is no longer used in this capacity, and no clinical evaluation of the safety and efficacy of primaquine as a gametocytocide when administered with any ACT has occurred. The artemisinins exert activity against immature gametocytes and could possibly yield a lower and less threatening optimal dose of primaquine. Northern R&D, however, expresses no agenda for clinical research on primaquine for any therapeutic indication.

The most conspicuous neglect of the gametocytocidal compartment has been the failure to conduct a systematic chemical survey of compounds for this activity. Northern S&T obsession with the acute attack and neglect of other avenues to address the problem of endemic malaria may be most evident in this line of investigation. An examination of the fairly extensive body of work on gametocytocidal properties of chemotherapeutic agents reveals that almost all such evaluations have been conducted on drugs with proven therapeutic activity against the asexual blood stages causing acute malaria [119]. Killing gametocytes has apparently been thought of strictly as a therapeutic bonus to treatment of the acute attack. The possibility of a safe, effective, and perhaps already widely available drug at low cost providing a means to effectively arrest transmission has not been explored. Northern S&T could have, with relative technical ease, conducted such explorations over 35 years ago. A 2011 call for proposals for such work from BMGF represents a welcome sign of dawning realization of the importance and enormous promise of this approach.

Hypnozoitocide The primary therapeutic application of primaquine, as a hypnozoitocide, offers further evidence of Northern R&D inability to respond effectively to Southern problems with critical tools in its chemotherapeutics toolbox. Although primaquine has been the only therapeutic agent against relapse for the past 60 years, almost no research of its mechanisms of activity against the hypnozoites has been carried out. There is no understanding of its therapeutic target, much less which of its many metabolites may be most active. Resistance to primaquine by hypnozoites almost certainly occurs, but there is no validated means of confirming that phenotype and complete ignorance of the corresponding genotypes. Simply observing responses to therapy does not adequately address that problem because parasitemia occurring weeks to months after treatment may represent either therapeutic failure (relapse despite therapy) or simply a new infection. No means of distinguishing those events by

molecular genotyping has been established, largely due to the biological complexity imposed by the hypnozoite [120]. Unambiguous estimates of primaquine efficacy thus require the absence of risk of reinfection. Such studies have not been done since the development of primaquine in experimentally challenged American prisoners in the 1940s and 1950s [121]. Consequently, there is almost no grasp of the therapeutic efficacy of the only drug against relapse in vivax malaria anywhere it occurs. Primaquine may already have been lost to resistance and there is no validated means of evaluating that possibility.

Chemotherapeutics Performance Evaluation

Over the past six decades, through periods of ebbing and flowing fiscal support, Northern R&D has focused available energies and resources, and still does, on the acute attack of falciparum malaria. The almost complete neglect all other forms of chemotherapy currently in the toolbox of the Southern craftsman working the problem now imperils successful elimination goals. And we were warned as L.T. Coggeshall [122] wrote in 1952, "*The greatest misconceptions about the treatment of malaria, especially in the past, has arisen from the fact that too many considered it a single disease. Malaria is not a disease – it is a variety of diseases.*" There are therapies for one of the malarias and, effectively, almost none for the others. One key element of this neglect has been the failure to adapt *P. vivax* to continuous in vitro cultivation in Northern laboratories as occurred with *P. falciparum* in the 1970s [123]. Setting aside the improbability of adequate R&D investment in achieving that feat for *P. vivax*, this failure does not excuse Northern R&D from dealing with this parasite. While it is true the problem limits Northern laboratories from effectively engaging the problem in the North, transfer of the required R&D capacities southward stands as an obvious but inadequately funded solution. In this and other issues of chemotherapeutics neglect outlined here, it remains unclear whether the 3.1% share of malaria R&D spending on *P. vivax* [8], and perhaps even less on gametocytocidal therapies, is the cause or effect of their neglect. Either way, "inadequate" effectively describes Northern R&D performance in these vital pieces of the malaria control toolbox. In a chemotherapeutics sense, the Southern craftsman trying to disassemble endemic malaria may be thought of as equipped with a fixed-gauge wrench for nuts of many gauges.

The Vaccine Development Gambit

In 2011, a phase III clinical trial of a malaria vaccine called RTS, S in 15,640 children aged up to 17 months is underway at 11 study sites in Africa [124]. This bold and expensive effort reflects the enormous technical and fiscal challenges in malaria vaccine development. It also expresses the Northern determination to produce this particular tool despite the extraordinary gamble of resources and will.

The leading edge biotechnology-driven effort to develop vaccines against malaria has been an epic, contentious, and, thus far anticlimactic journey of 30 years [125]. The modern effort to engineer a protein subunit vaccine began in earnest and with a great deal of optimism in the early 1980s with emergent recombinant DNA technology swinging open a very promising door. Having genetically engineered bacteria to produce malaria proteins in kilogram quantities seemed a means of conquering malaria with relative ease. Instead, through a long series of preclinical and clinical R&D efforts around the globe, *P. falciparum* has consistently shrugged off the eloquently derived antibodies and T-cells arrayed against it [125–127].

The steepness of the R&D challenge in vaccination stems from the failure to adequately understand the enormously complex immune response provoked by malaria. That response varies terrifically across variables like age, history of exposure, intensity of exposure, and host and parasite genetics [128]. The dawn of the scientific understanding of immunity to malaria began in 1899 when Robert Koch visited Dutch colleagues at what would become the Eijkman Institute in Batavia on the island of Java in the East Indies. Koch noticed that densities and frequencies of parasitemia declined sharply with age at heavily endemic Ambarawa in central Java, whereas at much less endemic Sukabumi in western Java those values remained relatively level across ages. Koch surmised that heavy exposure to infection, over a period of many years, imbued protection against high levels of parasitemia and attendant disease (see citations

in [128]). The same pattern has been consistently observed over the decades and naturally acquired immunity has been considered the cumulative product of chronic and heavy exposure to infection. Immunologists envision the human immune system "learning" the antigenic repertoire of the parasite by repeated exposures and eventually, at around adolescence, mastering it [129].

Likewise, vaccinologists viewed their challenge as one of "teaching" that immune response by exposure to the proper parasite antigen or set of antigens. Though very simply expressed, this characterizes the malaria vaccine development strategy. Accepting the supposition that very young children in heavily endemic Africa constitute the majority of deaths due to malaria, the expressed R&D priority of vaccinating them is sensible. This demographic group is indeed vulnerable, exceedingly so compared to their parents. Adult Africans in heavily endemic areas, though almost constantly infected, very rarely suffer even minor illness (unless pregnant, especially for the first time). The susceptibility of their children to anemia, cerebral malaria, pulmonary complications, and other life-threatening syndromes stands in stark contrast [130]. They seem to have not "learned" to tame this infection and the appropriately "instructive" vaccine would mitigate their losses to malaria. This simplistic concept suffers logical pitfalls, however, evident with closer examination of the dynamics at work between those very young hosts and the parasites invading them.

A single episode of malaria in a nonimmune traveler, left untreated for too long, very often threatens rapid devolution into a life-threatening event. African children, on the other hand, experience about six to eight new infections each year in many endemic zones. Over 95% of them survive this rigorous challenge and go on to become malaria-hardy adults. This survival, surely impacted by access to therapy, nutrition, genetics, and probably many other factors, must also reflect successful immunological management of the always-present threat of sliding into lethal complications [128]. The loss of some of these children to malaria begins to less resemble a failure to "learn" a specific immune response from its parasite instructor, but more like an intrinsic failure to mount the appropriate immune response that permitted survival among almost all others in their cohort. And yet, vaccine R&D remains focused on parasite antigens rather than the intrinsic basis for success versus failure in what amounts to a 95% efficacious vaccination by the parasite itself. There is almost no understanding of what constitutes an appropriate versus inappropriate immune response to natural infection and the determinants of that life versus death turning of events. This gap in understanding extends to responses to experimental vaccines.

The consequences of such poor understanding may be found embedded in the process of malaria vaccine development and it imposes extraordinary financial risk. Unlike drug development, where compounds may be rejected or pushed forward on the basis of unambiguous laboratory determinations of activity against the parasite, malaria vaccine developers possess no such tool of discernment. No single immune response or set of responses has been shown to reliably predict protection in the infected human at any age or history of exposure, much less specifically infants and small children chronically exposed to infection. Vaccine candidates advance (or do not) through development algorithms on the basis of rational suppositions about protection in humans. Immunogenicity in terms of specific humoral or cellular targets, for example, may be the basis of development decisions even though those responses may have no evidence-validated role or compelling and consistent correlation with achieved protection in humans. Phase I and II trials in healthy nonimmune European or American adults for vaccines aimed at African infants and effectively already immune children compounds this problem. These generally acknowledged pitfalls [8] effectively defer credible vaccine development decisions to phase II and III trials. The vaccine RTS,S, now in phase III trials, was invented in 1987, tested in humans in 1992, evaluated in Africans in 1995, and evaluated in small numbers of African children between 2004 and 2007. The inadequate understanding of immunity to malaria as it occurs in the real world imposes a vaccine development paradigm resembling a roulette wheel with each turn of it coming with decades of work and many millions of dollars. Surely only repeated success could sustain such a development paradigm, and yet it is one having 30 years of failure. What sustains it?

R&D Investment

Today, malaria vaccine proponents glare over their fiscal parapets at their antimalarial drug development competitors vying for the same large share of malaria R&D resources. Each points to the failings and shortcomings of the other in making their cases for funding before donors and sponsors. The vaccines camp usually, albeit narrowly, wins the resources contest (Fig. 1). The reasons for the consistency of this large investment, despite decades of frustration, perhaps reflect how we perceive the malaria problem and, arguably, national self-interest in S&T capacity, agility, and economic spin-off.

Malaria vaccine development has and continues to probe the very far leading edges of contemporary and potentially industrial biotechnological immunology [131]. Beginning in earnest in the 1980s, the best and brightest were generously resourced and engaged in a globally important scientific endeavor. Northern laboratories blossomed and hummed with activity [127]. The US and European biotechnology industries enjoyed many technological and economic spin-offs from the effort. One of the malaria vaccine biotechnology pioneers, Wayne T. Hockmeyer, retired from the US Army in the late 1980s and went directly on to found Molecular Vaccines Inc. (later renamed MedImmune), a biotechnology concern purchased by AstraZeneca in 2007 for $15.2 billion. The vaccines industry saw and participated in proofs-of-concept of novel approaches to vaccine development like DNA vaccines and arrays of sophisticated adjuvants. In short, over 30 years of malaria vaccine development produced many scientific, technological, and economic dividends without delivering, yet, a licensed vaccine.

This is the nature of science, where exploration leads to unexpected destinations. Simply having a technical problem and the wherewithal to address it is key to S&T success even without directly solving the primary problem. The nature of funding in malaria vaccine development illustrates the linkage between S&T capacity and national S&T self-interest. The laboratories that executed malaria vaccine development work were supported by the nations where the laboratories were located, with few minor exceptions. American-funded efforts went primarily to American laboratories, as was true of European efforts, and even one bold effort in Colombia [132] was funded by that government. What is likely at work is the irresistible drive to reap the peripheral benefits of S&T endeavors within borders. No nation in the endemic zones, save the valiant Colombian example, undertook vaccine discovery and development. That may be due to a lack of fiscal resources, standing technical capacity, and an available technologically endowed workforce. But those determinants themselves provide grim reflection of the unwillingness of Northern nations, collectively, to make substantial direct investment in S&T foundations in the South.

It may be argued that the North harvests S&T/R&D dividends derived from a Southern problem – and reasonably counter-argued that the investments are their own and, because of standing capacities, the less costly and speediest avenue to solving the problem. The Northern R&D posture would be supportable if it delivered the most useful tools, but it has not and does not seem strategically positioned to do so. Northern R&D engaging the malaria problem yields tremendous and important advances in S&T, but it historically exhibits very limited abilities in delivery of practical and useful tools that significantly impact malaria as a global health problem.

Sustainable S&T in Tropical Health

Northern R&D remains the technological fulcrum for the public health lever against Southern infections, and this may be an important contributor to stymied and perhaps unsustainable progress. Gordon Harrison wrote in his 1978 history of malaria [64] of the failure of the global eradication effort in the prior decade, "*Failure so universal, so apparently ineluctable, must be trying to tell us something. The lesson could be of course that we have proved incompetent warriors. It could also be that we have misconstrued the problem.*" The failure of Northern R&D agendas to field relevant tools against endemic Southern malaria must also be trying to tell us something. Bench malaria science of Northern S&T is a powerful engine of scientific discovery and human progress engaged in the fight against malaria, and the aim here is not to demean those earnest endeavors by compassionate and dedicated people. The aim is to spark reconsideration of reliance solely upon that engine for practical solutions.

Southern scientists may be criticized for having abandoned the field to Northern scientists, but this is unjust and self-serving of the critic. As the Malarone Donation Program already described illustrates, Northern bias, imperatives, and fiscal influence may displace Southern voice and initiative out of the strategic equation. This is where the Northern perception of a lack of Southern awareness of useful technologies plays in the unhelpful assumption of Northern leadership on decisions regarding tools intended for Southern use. In the Malarone example, Northern science perceived a powerful new drug available at no cost, whereas African stakeholders perceived a futile intervention not addressing the real problem. Southern scientists put up futile active and passive resistance to the program because the proposed intervention deflected alternatives and the prospect of progress. The report of Shretta et al. [110] documents this history and should be studied by Northern scientists engaging the malaria problem.

What the Southern scientists pointed to was not the drug, but the availability of diagnosis and treatment where most deadly malaria occurred [109, 110]. It may be that Northern S&T perceives such a problem as one it is not particularly suited to engage. In other words, the problem seems practical rather than technological, at least in how the North perceives its technology imperatives. The Northern perception may be that problems that do not engage the suite of Northern technology assets need not involve them. That may be, but their technological imperatives and financial resources tend to suffocate alternative approaches by Southern scientists co-opted into a Northern R&D agenda.

Malaria vaccines represent the primary Northern S&T answer, or at least hope, to solve lethal malaria at isolated sites all across the global endemic belt. Vaccination in lieu of very hard to sustain diagnosis and treatment services seems the ideal solution. Vaccines have pushed the burden of morbidity and mortality due to infections to the lowest point in all of human history, and such a track record is hard to argue against. However, one may forcefully argue that hope is a poor offensive strategy against entrenched malaria. Determination, will, resources, and faith in the success of vaccines may be defied by the unfolding of an unknowable future. Preparing for possible failure of vaccines neither endorses nor ensures it, and responsibly envisioning a future without vaccines prudently commands attention to alternative technological approaches. Putting the development of those approaches into Southern hands may be the surest means of success with most appropriate technologies providing sustainable solutions.

Southern Scientific and Technological Development

This entry has emphasized the problems with Southern reliance upon Northern technological innovation to diminish preventable endemic infectious disease burdens. A South empowered with indigenous S&T capacities would likely generate more effective instruments that more quickly lift those burdens. Such capacity would likewise, as it did in the North, spin off substantial economic benefits that indirectly drive endemic diseases down and health up. Achieving this would require deliberate action by those nations of the North capable of delivering such capacities, and the foresight to see very significant short-term losses recovered many times over in the longer term.

It may be argued, despite the MIM example already discussed, that the North already invests in the development of S&T capacities of the South. Each year many Southern scientists receive academic and technological training in the North with generous support from Northern sponsors in the government, academia, and private sectors. This approach, however, may be unlikely to yield real capacities in Southern S&T. Many of these students acquire skill sets that cannot be applied in their home nations. There are few institutions with the technological capacities of the Northern universities they attend. These students typically either remain in the North as valued technologically skilled immigrants, or they go home and assume positions that do not hone and deepen their technological abilities. Many of the latter subsequently relocate to developed nations selfishly promoting immigration policies designed specifically to lure them away [133]. The promise of advanced S&T training for Southern scientists in the North rings hollow without Southern R&D institutions where those skills may be put to effective work.

The key may be establishing S&T "nurseries" in the South having specific technological suites and focused objectives. In the example of malaria, few could argue against the potential direct and indirect benefits of an institution committed wholly to the development of medically useful insecticides or repellants, or another dedicated to a thorough chemical exploration of potential therapeutic agents aimed solely at sexual blood stages and arresting malaria transmission. The production of GMP malaria vaccines would nurture a commercial industrial biotechnological base capable of expansion to other vaccine-preventable illnesses and pharmaceuticals. S&T sustainability successes standing today in the South offer examples.

The Eijkman Institute for Molecular Biology in Jakarta, Indonesia is named after the Dutch scientist who discovered vitamin B as the cause and cure of beriberi with work executed largely in that city between 1886 and 1925. Christiaan Eijkman was awarded the Nobel Prize in 1929 for the discovery of vitamins [134]. During this heyday, the institute employed both Dutch and Indonesian scientists functioning as full peers heading their own avenues of biomedical research of tropical infections. The war in the Pacific saw the Dutch scientists arrested and imprisoned. The Indonesian scientists carried on with the work of the institute largely without direct interference from the Japanese forces. Tragically, however, an occupier suspicious of intellectual elites executed many Indonesian doctors and medical scientists [135]. The director of the Eijkman Institute in 1944, Achmad Mochtar, offered a false confession of the murder of 900 Indonesian slave laborers by sabotage of a vaccine administered to them. He did this in exchange for the liberty of almost the entire Indonesian technical staff of the Eijkman Institute being held in prison and brutally tortured. In July 1945, the occupiers executed Mochtar. This event, and the bloody war for independence from the Netherlands that immediately followed, effectively destroyed the institute and it formally closed in 1965 [136].

In 1990, the dynamic then Minister of Science and Technology (later to become the third President of Indonesia), B.J. Habibie, devoted considerable government resources and his formidable force of personality to reopen the institute as a nursery for biotechnological innovation. He segregated it from the ministerial hierarchies in order to protect it from the political vagaries of the Indonesian federal system. The laboratory became a semiautonomous institutional appendage to his ministry. Habibie, himself a product of the European Airbus Industrie S&T engine, sought an Indonesian scientist immersed, tried, and tested in the culture of Northern S&T. He found and recruited Prof. Sangkot Marzuki, then a tenured and highly productive cellular and molecular biologist at Monash University in Australia. The fledgling laboratory in Jakarta received generous support from the government until the economic collapse and political turmoil of 1998. The laboratory nonetheless survived by its own scientific and technological wits, becoming a largely self-sustaining research institution through the conduct of work paid for by competitive, merit-driven grants. Their focus on molecular biology endows them today with sophisticated gene sequencing and analysis capacities. Those are being leveraged to attract funding for specific work on discrete pathogens endemic to Indonesia, in addition to a variety of human genetic, wildlife conservation, and even criminal law enforcement molecular biological problems.

The primary point with this example is that young Indonesian scientists, whether trained at home or abroad, have a stable institution where they may sharpen their skills with ever-steeper technological challenges under the mentorship of both senior Indonesian scientists and their foreign partners. The scientists in the institute are not government employees and their salaries are thus neither guaranteed nor constrained. They are able to commit fully to the S&T mission, with the certain understanding that secure employment demands scientific productivity and overcoming stiff competition from other labs engaged in similar work around the world. More importantly, consistent success provides a career of advancement in abilities, responsibilities, and compensation reflective of such success.

Almost all scientists today manage their professional lives in this way, no matter where they happen to live. Doing science at the leading edge is a hard-earned privilege reserved for those able to demonstrate the ability to contribute to the furthering of that edge. Instilling this understanding, and providing places where sustained success is possible and deliberately nurtured, substantially furthers the S&T capacity of the Republic of Indonesia as a whole. It is not the

S&T per se that makes this possible; it is the institute, its foundations, and its culture of uncompromising scientific excellence. B.J. Habibie and the leadership of the Eijkman Institute understood this and achieved it.

That institute is certainly not the only example of significant progress in the deliberate long-term commitment to the systematic nurturing of Southern S&T capacities. The Pasteur Institutes around the world provide excellent nurseries for local S&T, as do the laboratories funded by the Wellcome Trust in Kenya, Tanzania, Thailand, and Vietnam. Indeed, the former Pasteur Institute (founded in 1896) at Bandung, West Java, created most of the vaccines used in Southeast Asia prior to the Second World War, and the foundations of that investment remain today in the same physical location occupied by the government-owned industry that produces most of Indonesia's vaccines. Not coincidentally, Indonesia's vibrant and lucrative pharmaceutical manufacturing industries surround that facility. Bringing S&T capacities southward obviously has and can provide sustainable S&T and R&D enterprises and their biotechnological industrial spin-offs.

The North must overcome its impatience and evidently misplaced self-confidence in its ability to effectively engage Southern health problems. S&T is the key to successfully resolving those burdens, but probably not as practiced in the North. Supplanting Southern S&T into the leadership role of R&D aimed at its infectious disease burdens should be deliberately planned, financed, and executed.

Future Directions

The certain failures and likely strategic missteps by Northern S&T put forth in this entry aim at dispassionate and rational reflection on the means of addressing Southern health problems in the S&T/R&D arena. Accepting Northern R&D agendas as poorly suited to the task, despite the humanitarian urgency, brings appropriate and useful focus to mitigating deficiencies in Southern R&D capacities. Resisting the fiscal and temporal expediencies that push R&D capacities and agendas northward may prove the surest means of sustainable and substantial gains in tropical health. Placing durable R&D capacities in the South as a primary rather than tangential benefit of fruitful North-South S&T collaboration generally characterizes a direction aiming at that envisioned future.

Southern scientists have much to learn from their Northern counterparts, especially those in positions of institutional leadership of R&D endeavors. The intensely competitive leading edge of S&T requires institutional foundations that create and reward healthy scientific competitiveness. Northern R&D laboratories that fail to compete quickly vanish, and the cruel Darwinian-like forces that shape effective Northern R&D must also be brought to bear on Southern R&D enterprises – their vitality and sustainability requires it. Transfer of those R&D survival skills is perhaps where Northern S&T may be put to most effective use in the South. And the task of transfer should not be viewed as passive, as by example, but direct and deliberate participation in the building of those skills and capacities in Southern R&D enterprises. Acknowledging limited Southern S&T capacities as the core impediment to improving Southern health, rather than possible or hoped for tools emanating from Northern S&T, naturally leads in that direction.

Such a course requires strategic thinking, long-term commitment, flexibility, and inspired international cooperation and trust from both North and South partners undertaking it. Northern investment ought to aim at institutional R&D competitiveness rather than the R&D agenda itself. Logically, however, this inevitably leads to establishing successful R&D endeavors of a specific goal-oriented nature. Scientific productivity would be engrained in any rational North-South institutional R&D capacity-building cooperative endeavor. In short, success in the core institutional capacity-building objective necessarily carries with it R&D success and rewards for both partners. An effective win-win formula ensures their mutual R&D survival, and therefore commitment to the endeavor. Perhaps most importantly, the Northern partner would not be bringing to the partnership a predetermined R&D agenda. That would be decided between the partners and the sponsor of their endeavor.

That third party in this envisioned collaboration, the sponsor, represents the primary challenge in realizing it. At least in the realm of malaria R&D today, that sponsor is most likely to be an American funding agency with what it views as clear product- or knowledge-development paths and technical milestones to accomplish in achieving success, that is,

fielding a product that it decided would be useful. The Northern obsession with the development of products of its conception for Southern health progress should be acknowledged as a significant impediment and tempered if not abandoned.

The assumption of Southern R&D leadership on Southern health issues would require many years of determined will and real reform on both sides of the Tropic of Cancer to achieve and sustain. It may require pragmatic lessening of the faith Northern R&D exhibits in its ability to deliver solutions in the short term. Southern awareness of the intensely competitive nature of biomedical R&D should rise to a level consistent with firm commitment to that very difficult course. Southern R&D enterprises must not depend wholly upon funding from noncompetitive sources, and gauge their own relevance upon the objective evidence of competitive survival.

Southern public and private donors also need to participate and engage R&D endeavors managed by Southern institutions. Northern dominance of the R&D agenda in part stems from the reluctance of Southern donors to make these investments and thus bring that voice and influence to discussion and consensus. Their absence becomes ever more conspicuous with the booming economies of East, South East, and South Asia in comparison to the now troubled Northern economies. Establishing stable and sustainable R&D enterprises in the South may imbue such donors with the confidence and even self-interest to make such investments. Northern investments in Southern R&D should at least be matched by Southern governments and donors positioned to contribute. The South desperately requires humanitarian visionaries and champions, as in the models of Sir Henry Wellcome, Bill and Melinda Gates, Warren Buffett, and others in the North, to generously and intelligently unleash available capital upon very serious tropical health challenges.

North-South S&T/R&D cooperation on tropical health, after all, aims at lifting the mingled burdens of endemic diseases and poverty in the South. Northeast Asia largely achieved this feat over the past 50 years and today is the mercantile engine of the global economy. Brazil in South America has made large strides in health and trade and with it drives a substantial portion of the North American economy. Healthy people liberated from the pursuit of survival assume the pursuit of happiness that drives modern economies. They become educated, economically creative, and productive, selling to each other the accoutrements of easier and more fulfilling lives. Acknowledging North-South S&T/R&D parity as a key element in such progress moves far broader development agendas rapidly forward. Success in these endeavors may ultimately remove the conceptual utility of dividing the world into these two disparate spheres.

Acknowledgments

JKB is supported by the Wellcome Trust grant #B9RJIXO. Prof. Jeremy Farrar, Dr. Simon Hay, and Dr. Trevor Jones provided helpful reviews of the manuscript.

Bibliography

Primary Literature

1. Galama T, Hosek J (2008) U.S. competitiveness in science and technology. RAND Corporation, Santa Monica
2. Committee on Ensuring the Best Presidential and Federal Advisory Committee Science and Technology Appointments, National Academy of Sciences, National Academy of Engineering, Institute of Medicine (2005) Science and technology in the national interest: ensuring the best presidential and federal advisory committee science and technology appointments. The National Academies Press, Washington, DC, p 208
3. Lu C, Schneider MT, Gubbins P, Leach-Kemon K, Jamison D, Murray CJL (2010) Public financing of health in developing countries: a cross-national systematic analysis. Lancet 375:1375–1387
4. Sachs J, Malaney P (2002) The economic and social burden of malaria. Nature 415:680–685
5. WHO (2010) World malaria report 2010. WHO, Geneva
6. Hay SI, Okiro EA, Gething PW et al (2010) Estimating the global clinical burden of *Plasmodium falciparum* malaria in 2007. PLoS Med 7:e1000290
7. Gething PW, Smith DL, Patil AP, Tatem AJ, Snow RW, Hay SI (2010) Climate change and the global malaria recession. Nature 465:342–345
8. PATH (2011) Staying the course? Malaria research and development in a time of economic uncertainty. PATH, Seattle
9. Hay SI, Guerra CA, Tatem AJ, Noor AM, Snow RW (2004) The global distribution and population at risk of malaria: past, present, and future. Lancet Inf Dis 4:327–336
10. NIH (2008) NIAID agenda for malaria, Bethesda, Maryland
11. WHO (2008) Global Malaria Action Plan, Geneva
12. Nosten F, Luxemburger C, ter Kuile FO, Woodrow C, Eh JP, Chonsuphajaisddhi T, White NJ (1994) Treatment of

multi-drug resistant *Plasmodium falciparum* with a 3-day artesunate-mefloquine combination. J Infect Dis 170:971–977
13. WHO (2008) World malaria report. WHO, Geneva
14. Snow RW, Guerra CA, Noor AM, Myint HY, Hay SI (2005) The global distribution of clinical episodes of *Plasmodium falciparum* malaria. Nature 434:214–217
15. WHO (2009) World malaria report. WHO, Geneva
16. Hay SI, Okira EA, Gething PW, Patil AP, Tatem AJ, Guerra CA, Snow RW (2010) Estimating the global clinical burden of *Plasmodium falciparum* malaria in 2007. PLoS Med 6:e1000290
17. Elyazar I, Hay SI, Baird JK (2011) Malaria distribution, prevalence, drug resistance and control in Indonesia. Adv Parasitol 74:41–175
18. Harijanto PN (2010) Malaria treatment using artemisinin in Indonesia. Acta Med Indones 42:51–56
19. Dhingra N, Jha P, Sharma VP et al (2010) Adult and child malaria mortality in India. Lancet 376:1768–1774
20. Kochar DK, Saxena V, Singh N et al (2005) *Plasmodium vivax* malaria. Emerg Inf Dis 11:132–134
21. Kochar DK, Tanwar GS, Khatri PC et al (2010) Clinical features of children hospitalized with malaria - a study from Bikaner, Northwest India. Am J Trop Med Hyg 83:981–989
22. Srivastava S, Ahmad S, Shirazi N, Verma SK, Puri P (2011) Retrospective analysis of vivax malaria patients presenting to tertiary care referral centre of Uttarakhand. Acta Trop 117:82–85
23. Sharma A, Khanduri U (2009) How benign is benign tertian malaria? J Vector Borne Dis 46:141–144
24. Barcus MJ, Basri H, Picarima H et al (2007) Demographic risk factors for severe and fatal vivax and falciparum malaria among hospital admissions in northeastern Indonesian Papua. Am J Trop Med Hyg 77:984–991
25. Genton B, D'Acremont V, Rare L et al (2008) *Plasmodium vivax* and mixed infections are associated with severe malaria in children: a prospective cohort study from Papua New Guinea. PLoS Med 5:e127
26. Tjitra E, Anstey NM, Sugiarto P et al (2008) Multidrug-resistant *Plasmodium vivax* associated with severe and fatal malaria: a prospective study in Papua, Indonesia. PLoS Med 5:e128
27. Andrade BB, Reis-Filho A, Souza-Neto SM et al (2010) Severe *Plasmodium vivax* malaria exhibits marked inflammatory imbalance. Malar J 9:13
28. Beg MA, Khan R, Baig SM et al (2002) Cerebral involvement in benign tertian malaria. Am J Trop Med Hyg 67:230–232
29. Lomar AV, Vidal JE, Lomar FP et al (2005) Acute respiratory distress syndrome due to vivax malaria: case report and literature review. Braz J Infect Dis 9:425–430
30. Lawn SD, Krishna S, Jarvis JN, Joet T, Macallan DC (2003) Case reports: pernicious complications of benign vivax malaria. Trans R Soc Trop Med Hyg 97:551–553
31. Spudick JM, Garcia LS, Graham DM, Haake DA (2005) Diagnostic and therapeutic pitfalls associated with primaquine-tolerant *Plasmodium vivax*. J Clin Microbiol 43:978–981
32. Sternberg GM (1884) Malaria and malarial diseases. Wood, New York, p 329
33. Kitchen SF (1949) Vivax malaria. In: Boyd MF (ed) Malariology, vol II. W.B. Saunders, Philadelphia
34. Ewing J (1902) Contribution to the pathological anatomy of malarial fever. J Exp Med 6:119–180
35. Bassat Q, Alonso P (2011) Defying malaria: fathoming severe *Plasmodium vivax* disease. Nat Med 17:48–49
36. Eldridge WW et al (1925) Treatment of paresis: results of inoculation with the organism of benign tertian malaria. JAMA 84:1097–1101
37. Ferraro A et al (1927) The malaria treatment of general paresis. J Nerv Ment Dis 65:225–239
38. Freeman W, Eldridge WW, Hall RW (1934) Malaria treatment of dementia paralytica: results in 205 cases after five to eleven years. South Med J 27:122–126
39. O'Leary PA, Welsh AL (1933) Treatment of neurosyphilis with malaria: observations on nine hundred and eighty-four cases in the last nine years. JAMA 101:498–501
40. Fong TCC (1937) A study of the mortality rate and complications following therapeutic malaria. South Med J 30:1084–1088
41. Krauss W (1932) Analysis of reports of 8,354 cases of IMPF-malaria. South Med J 27:537–541
42. Nicol WD (1932) A review of seven year's malarial therapy in general paralysis. J Ment Sci 78:843–866
43. James SP, Nicol WD, Shute PG (1936) Clinical and parasitological observations on induced malaria. Proc R Soc Med 29:27–42
44. Verhave JP (2010) personal communication
45. James SP, Nicol WD, Shute PG (1932) A study of induced malignant tertian malaria. Proc R Soc Med 25:37–52
46. Handayani S, Chiu DT, Tjitra E et al (2009) High deformability of *Plasmodium vivax*-infected red blood cells under microfluidic conditions. J Infect Dis 199:445–450
47. O'Donnell J, Goldman JM, Wagner K et al (1998) Donor-derived *Plasmodium vivax* infection following volunteer unrelated bone marrow transplantation. Bone Marrow Transplant 21:313–314
48. Finkel M (2007) Bedlam in the blood: malaria. National Geographic, July 2007, pp 32–67
49. UN Millennium Project (2005) Coming to grips with malaria in the new millennium. Earthscan, London, p 129
50. US CDC (2011) Grand rounds: the opportunity for and challenges to malaria eradication. MMWR 60:476–480
51. Guerra CA, Howes RE, Patil AP et al (2010) The international limits and population at risk of *Plasmodium vivax* malaria in 2009. PLoS Negl Trop Dis 8:e774
52. Baird JK (2004) Resistance to chloroquine by *Plasmodium vivax*. Antimicrob Agents Chemother 48:4075–4083
53. Baird JK (2009) Resistance to therapies for *Plasmodium vivax*. Clin Microbiol Rev 22:508–534
54. Baird JK (2005) Effectiveness of antimalarial drugs. N Engl J Med 352:1565–1577
55. Baird JK (2011) Resistance to chloroquine unhinges vivax malaria therapeutics. Antimicrob Agents Chemother 55:1827–1830

56. WHO (2009) Rapid diagnostic test performance: results of WHO product testing of malaria RDTs: round 1 (2008). WHO, Geneva
57. Epstein J, Rao S, Williams F et al (2007) Safety and clinical outcome of experimental challenge of human volunteers with *Plasmodium falciparum*-infected mosquitoes: an update. J Infect Dis 196:145–154
58. Syafruddin D, Krisin, Asih P et al (2009) Seasonal prevalence of malaria in West Sumba district, Indonesia. Malar J 8:8
59. Harris I, Sharrock WW, Bain LM et al (2010) A large proportion of asymptomatic Plasmodium infections with low and sub-microscopic parasite densities in the low transmission setting of Temotu Province, Solomon Islands: challenges for malaria diagnostics in an elimination setting. Malar J 9:254
60. WHO (2011) Consideration of mass drug administration for the containment of artemisinin resistant malaria in the Greater Mekong Sub-Region. Report of a consensus meeting, 27–28 Sept 2010, Geneva
61. Snow RW, Guerra CA, Mutheu JJ, Hay SI (2008) International funding for malaria control in relation to populations at risk of stable *Plasmodium falciparum* transmission. PLoS Med 5: e142
62. Price RN, Tjitra E, Guerra CA et al (2007) Vivax malaria: neglected and not benign. Am J Trop Med Hyg 77(suppl 6):79–87
63. Baird JK (2007) Neglect of vivax malaria. Parasitol Today 23:533–539
64. Harrison G (1978) Mosquitoes, malaria and man: a history of the hostilities since 1880. John Murray, London, p 314
65. McCullough D (1978) The path between the seas: the creation of the Panama Canal 1870–1914. Simon & Schuster, New York, p 698
66. Takken W, Snellen WB, Verhave JP, Knols BGJ, Atmoswedjono S (1990) Envirnmental measures for malaria control in Indonesia – an historical review on species sanitation, Wageningen Agricultural University Papers 90-7, p 167
67. Killeen GF (2003) Following Soper's footsteps: northeast Brazil 63 years after eradication of *Anopheles gambiae*. Lancet Infect Dis 3:663–666
68. Coatney GR (1963) Pitfalls in a discovery: the chronicle of chloroquine. Am J Trop Med Hyg 12:121–128
69. Sharma VP (1996) Re-emergence of malaria in India. Indian J Med Res 103:26–45
70. Baird JK (2000) Resurgent malaria at the millennium: control strategies in crisis. Drugs 59:719–743
71. Gianessi LP, Puffer CA (1992) Reregistration of minor pesticides: some observations and implications. In: USDA (ed) Inputs situation and outlook report. USDA, Washington, DC, pp 52–60
72. Packard RM (1998) 'No other logical choice': global malaria eradication and the politics of international health in the post-war era. Parassitologica 40:217–229
73. WHO (2006) Pesticides and their application for the control of vectors and pests of public health importance, 6th edn. Department of Control of Neglected Tropical Diseases, WHO Pesticide evaluation scheme (WHOPES), Geneva, p 125
74. Roberts DR, Manguin S, Mouchet J (2000) DDT house spraying and re-emerging malaria. Lancet 356:330–332
75. Roberts DR, Laughlin LL, Hsheih P, Legters LJ (1997) DDT, global strategies, and a malaria control crisis in South America. Emerg Inf Dis 3:295–302
76. Attaran A, Maharaj R (2000) Ethical debate: doctoring malaria badly; the global campaign to ban DDT. BMJ 321:1403–1405
77. WHO (2007) Position statement: the use of DDT in malaria vector control. Global Malaria Program, Geneva
78. N'Guessan R, Boko P, Odjo A, Chabi J, Akogbeto M, Rowland M (2010) Control of pyrethroid and DDT-resistant *Anopheles gambiae* by application of indoor residual spraying or mosquito nets treated with a long-lasting organophosphate insecticide, chlorpyriphos-methyl. Malar J 9:44
79. Protopopoff N, Verhaeghen K, Van Borel W et al (2008) A significant increase in kdr in *Anopheles gambiae* is associated with an intensive vector control intervention in Burundi highlands. Trop Med Int Health 13:1479–1487
80. Czeher C, Labbo R, Arzika I, Duchemin JB (2008) Evidence of increasing Leu-Phe knockdown resistance mutation in *Anopheles gambiae* from Niger following a nationwide long-lasting insecticide-treated nets implementation. Malar J 7:189
81. Grieco JP, Achee NL, Chareonviriyaphap T et al (2007) A new classification system for the actions of IRS chemicals traditionally used for malaria control. PLoS One 2(8):156–167
82. The Global Fund to Fight AIDS, Tuberculosis and Malaria. Global Fund Policy on Quality Assurance for Pharmaceutical Products: procurement of single and limited source pharmaceuticals. Tenth Board Meeting, Geneva, 21–22 Apr 2005, GF-B10-9, Annex 4, p 47
83. Carrara VI, Zwang J, Ashley EA et al (2009) Changes in the treatment responses to artesunate-mefloquine on the northwestern border of Thailand during 13 years of continuous deployment. PLoS One 4:e4551
84. Dundorp AM, Newton PN, Mayxay M et al (2004) Fake antimalarials in Southeast Asia are a major impediment to malaria control: multinational cross-sectional survey on the prevalence of fake antimalarials. Trop Med Int Health 9:1241–1246
85. White NJ (2010) Artemisinin resistance – the clock is ticking. Lancet 376:2051–2052
86. Field JW (1938) Notes on the chemotherapy of malaria. Bulletin from the Institute for Medical Research, Federated Malay States 2:63–81
87. Fiammetta R (2003) The miraculous fever tree: malaria and the quest for a cure that changed the world. Harper Collins, New York
88. Joy RJT (1999) Malaria in American troops in the South and Southwest Pacific in World War II. Med Hist 43:192–207
89. Downs WG, Harper PA, Lisansky ET (1947) Malaria and other insect-borne diseases in the South Pacific Campaign, 1942–1945. II. Epidemiology of insect-borne diseases in Army troops. Am J Trop Med 27:69–89
90. Shannon JA (1946) Chemotherapy of malaria. Bull NY Acad Med 22:345–357

91. Slater LB (2009) War and disease: biomedical research on malaria in the 20th century (Critical issues in health and medicine). Rutgers University Press, New Brunswick, p 272
92. Brosius OT (1927) Section II. Plasmochin in malaria. In: Sixteenth Annual Report. Medical Department, United Fruit Company, Boston, pp 26–81
93. Board for the Coordination of Malaria Studies (1943) Results of study of plasmochin toxicity: cases occurring in large scale use of the drug for suppression and treatment of malaria. Malaria Report No.290. Archive of the National Academy of Sciences, Washington, DC
94. Board for the Coordination of Malaria Studies (1943) Study of the curative action of plasmochin in vivax malaria: studies in Army and Navy installations. Malaria Report No. 358. Archive of the National Academy of Sciences, Washington, DC
95. Office of the Surgeon General (1943) The drug treatment of malaria, suppressive and clinical. Circular letter No. 153. JAMA 123:205–208
96. Carson PE, Flanagan CL, Ickes CE, Alving AS (1956) Enzymatic deficiency in primaquine-sensitive erythrocytes. Science 14:103–139
97. Most H et al (1946) Chloroquine for treatment of aute attacks of vivax malaria. JAMA 131:963–967
98. Schmidt LH et al (1977) Radical cure of infections with *Plasmodium cynomolgi*: a function of total 8-aminoquinoline dose. Am J Trop Med Hyg 26:1116–1128
99. Burgess RW, Bray RS (1961) The effect of a single dose of primaquine on gametocytes, gametogony and sporogony of *Laverania falciparum*. Bull World Health Organ 24:451–456
100. Rieckmann KH, McNamara JV, Frischer H, Stockert TA, Carson PE, Powell RD (1968) Gametocytocidal and sporontocidal effects of primaquine and of sulfadiazine with pyrimethamine in a chloroquine-resistant strain of *Plasmodium falciparum*. Bull World Health Organ 38:625–632
101. Peters W (1987) Chemotherapy and drug resistance in malaria, 2nd edn. Academic, London, p 1100
102. Ockenhouse CF, Magill A, Smith D, Milhous W (2005) History of US military contributions to the study of malaria. Mil Med 170(Suppl 1):12–16
103. Oyediran AB, Heisler M (1999) Malarone donation program. J Travel Med 6(Suppl 1):28–30
104. Korsinczky M, Chen N, Kotecka B, Saul A, Rieckmann K, Chen Q (2000) Mutations in *Plasmodium falciparum* cytochrome b that are associated with atovaquone resistance are located at a putative drug-binding site. Antimicrob Agents Chemother 44:2100–2108
105. Ringwald P, Basco LK (1998) Malarone-donation programme in Africa. Lancet 351:673–674
106. Oyediran AB, Ddumba EM, Ochola SA, Lucas AO, Koporc K, Dowdle WR (2002) A private-public partnership for malaria control: lessons learned from the Malarone Donation Programme. Bull World Health Organ 80:817–821
107. Shretta R, Walt G, Brugha R, Snow RW (2001) A political analysis of corporate drug donation: the example of Malarone in Kenya. Health Policy Plan 16:161–170
108. Attaran A, Barnes KI, Curtis C et al (2004) WHO, the Global Fund, and medical malpractice in malaria treatment. Lancet 363:237–240
109. Cappelini MD, Fiorelli G (2008) Glucose-6-phosphate dehydrogenase deficiency. Lancet 371:64–74
110. Alving AS, Johnson CF, Tarlov AR, Brewer GJ, Kellermeyer RW, Carso PE (1960) Mitigation of the hemolytic effect of primaquine and enhancement of its action against exoerythrocytic forms of the Chesson strain of *Plasmodium vivax* by intermittent regimens of drug administration. Bull World Health Organ 22:621–631
111. Crockett M, Kain KC (2007) Tafenoquine: a promising new antimalarial agent. Expert Opin Investig Drugs 16:705–715
112. Tinley KE, Loughlin AM, Jepson A, Barnett ED (2010) Evaluation of a qualitative enzyme chromatographic test for glucose-6-phosphate dehydrogenase deficiency. Am J Trop Med Hyg 82:210–214
113. Khim S, Nguon C, Guillard B, Socheat D, Chy S, Sum S, Nhem S, Bouchier C, Tichit M, Christophel E, Taylor R, Baird JK, Menard D (2011) Performance of the CareStart G6PD deficiency screening test. PLoS One (in press)
114. Pannacciulli I, Tizianello A, Ajmar F, Salvidio E (1965) The course of experimentally induced hemolytic anemia in a primaquine-sensitive Caucasian: a case study. Blood 25:92–95
115. George GN, Sears DA, McCurdy PR, Conrad ME (1967) Primaquine sensitivity in Caucasians: hemolytic reactions induced by primaquine in G6PD deficient subjects. J Lab Clin Med 70:80–93
116. Baird JK, Surjadjaja S (2011) Consideration of ethics in primaquine therapy against malaria transmission. Trends Parasitol 27:11–16
117. Shekalaghe S, Drakely C, Gosling R et al (2007) Primaquine clears submicroscopic *Plasmodium falciparum* gametocytes that persist after treatment with sulphadoxine-pyrimethamine and artesunate. PLoS One 2:e1023
118. Shekalaghe SA, ter Braak R, Daou M et al (2010) In Tanzania, hemolysis after a single dose of primaquine coadministered with an artemisinin is not restricted to glucose-6-phosphate dehydrogenase deficient (G6PD A-) individuals. Antimicrob Agents Chemother 54:1762–1768
119. Butcher GA (1997) Antimalarial drugs and the mosquito transmission of Plasmodium. Int J Parasitol 27:975–987
120. Imwong M, Snounou G, Purkittayakamee S et al (2007) Relapses of *Plasmodium vivax* infection usually result from activation of heterologous hypnozoites. J Infect Dis 195:927–933
121. Baird JK, Hoffman SL (2004) Primaquine therapy for malaria. Clin Infect Dis 39:1659–1667
122. Coggeshall LT (1952) The treatment of malaria. Am J Trop Med Hyg 1:124–131
123. Trager W, Jensen JB (1976) Human parasites in continuous culture. Science 193:673–675
124. Malaria Vaccine Initiative (2011) Fact sheet: the RTS, S malaria vaccine candidate, Mar 2011, Washington, DC

125. Sherman IW (2009) The elusive malaria vaccine: miracle or mirage? American Society for Microbiology, Washington, DC, p 391
126. Committee on US Military Malaria Vaccine Research (2006) Battling malaria: strengthening the U.S. military vaccine program. National Academies Press, Washington, DC, p 144
127. Desowitz RS (1993) The malaria capers: tales of parasites and people. W.W. Norton, New York, p 288
128. Doolan DL, Dobano C, Baird JK (2009) Acquired immunity to malaria. Clin Microbiol Rev 22:13–36
129. Hviid L (2005) Naturally acquired immunity to *Plasmodium falciparum* in Africa. Acta Trop 95:270–275
130. Marsh K, Forster D, Waruiru C et al (1995) Indicators of life-threatening malaria in African children. N Engl J Med 72:334–336
131. Crompton PD, Pierce SK, Miller LH (2010) Advances and challenges in malaria vaccine development. J Clin Invest 120:4168–4178
132. Graves PM, Gelband H (2009) Vaccines for preventing malaria (SPf66). Cochrane Libr 2:1–30
133. Carrington WJ, Deragiache E (1999) How extensive is the brain drain? Finance Dev 36:46–49
134. Carpenter KJ (2000) Beriberi, white rice and vitamin B: a disease, a cause and a cure. University of California Press, Berkeley, p 296
135. Post P, Frederick WH, Heidebrink I, Sato S (eds) (2009) The encyclopedia of Indonesia in World War II. Brill, Leiden, Netherlands, p 710
136. Stone R (2010) Righting a 65-year-old wrong. Science 329:30–31

Books and Reviews

Feacham GA, Phillips AA, Targett GA (eds) (2009) Shrinking the malaria map: a prospectus on malaria elimination. University of California San Francisco, Global Health Group, San Francisco, p 187

Lobo L (2010) Malaria in the social context: a study in western India. Routledge, New Delhi, p 213

Packard RM (2007) The making of a tropical disease: a short history of malaria. The Johns Hopkins University Press, Baltimore, p 320

Shah S (2011) The fever: how malaria has ruled humankind for 500,000 years. Picador, New York, p 320

Sherman IW (2010) Magic bullets to conquer malaria: from quinine to qinghaosu. American Society for Microbiology Press, Washington, DC, p 298

Snowden F (2006) The conquest of malaria: Italy, 1900–1962. Yale University Press, New Haven, p 304

Winther PC (2005) Anglo-European science and the rhetoric of empire: malaria, opium and British rule in India 1756–1895. Lexington Books, New York, p 450

Yip K-C (ed) (2009) Disease, colonialism and the state: malaria in modern East Asian history. Hong Kong University Press, Hong Kong, p 161

True Color Night Vision Video Systems in Intelligent Vehicles

Dirk Hertel
Quincy, MA, USA

Article Outline

Glossary
Definition of the Subject and Its Importance
Introduction
The Automotive Imaging Application
Human Perception of the Automotive Imaging Environment
The Automotive Imaging Environment
Extending the Dynamic Range
Extending Spectral Sensitivity into NIR
Adding Color Differentiation to VIS + NIR-Sensitive Imager
Visual Representation of the VIS + NIR Color Information
Conclusion
Future Directions
Bibliography

Glossary

Automotive night vision A technical system to enhance human night vision in situations where visibility is limited or challenging to the human visual system, for example in situations where the range of distances illuminated by headlights is shorter than the safe braking distance or in situations where the human eye may be too slow to adapt to sudden changes in brightness. It requires an effective human–machine interface, for example, a visual display to make available to the driver real-time additional visual information.

CMOS image sensor An active-pixel image sensor (APS) consisting of an integrated circuit with an array of light-sensitive cells (pixels) and manufactured using complementary metal–oxide–semiconductor (CMOS) technology. Each pixel combines a photodetector with an active amplifier that may perform additional functions such as controlling the pixel response to light and extending the pixel's dynamic range.

Driver assistance system (DAS) A technical system to assist the driver in the task of driving, especially in situations where the human sensory system (visual, auditory) or human attention might fail to recognize a dangerous situation, or when the human response time in the perceptual-motor task of recognizing a dangerous situation then using vehicle controls to take corrective action may be too slow to avoid an accident.

Dynamic range Dynamic range is the ratio between the largest and smallest possible signal values of a changeable quantity such as light. For image sensors and cameras, dynamic range refers to input radiance or luminance signals and is defined as the ratio between the maximum and minimum signals where a camera can simultaneously capture detail carried by small signal variations.

Electromagnetic spectrum, visible (VIS) and near-infrared (NIR) The human eye can detect the visible (VIS) portion of the electromagnetic spectrum ranging from wavelengths of about 380 to 730 nm. Infrared is electromagnetic radiation with longer wavelengths than visual, with NIR denoting the shortest wavelengths of the IR-spectrum between 700 and 1,400 nm.

Wide dynamic range (WDR) Also referred to as high dynamic range (HDR), it covers a family of techniques to extend the dynamic range of image sensors beyond that of an image sensor with a linear relationship between input radiance and digital output signal.

Definition of the Subject and Its Importance

Vision-based driver assistance aims to increase traffic safety at night by enhancing human night vision in situations where visibility is limited or challenging to the human visual system. The night vision cameras described sense the near-infrared radiation of the car's own headlights to extend the range of forward vision, while, at the same time, discriminating traffic-relevant colors of signal lights and signage. Adaptive wide-dynamic-range image sensor technology ensures that scene detail in both deep shadow and bright highlight is captured even in situations where the human eye may be blinded or too slow to adapt to sudden changes in brightness. The information from the near-infrared and visible spectrum is combined into natural-looking color images and communicated to the driver via on-board visual displays to enable recognition of the traffic situation.

Introduction

Since the late 1990s, there has been research into driver assistance systems employing sensors to perceive the automotive environment and utilize their outputs to create warning and vehicle control signals. Vision-based systems are of particular importance because more than 90% of driving decisions and actions are based on vision. Although the human visual system (HVS) is able to adapt to a vast range of lighting conditions, the rate of visual adaptation is often outpaced by the rate of change in lighting conditions while driving, for example when passing blinding headlights at night. Camera-based vision systems have the capability to aid the driver in critical situations by more rapidly adapting to changes in brightness and intra-scene dynamic range. They may also extend spectral sensitivity into the NIR to utilize the invisible portion of the headlight spectrum or can additionally employ NIR-only headlights that can be used in high-beam mode without blinding other drivers. Since the visual channel has the highest capacity of information transfer compared to other senses, image displays are used as human–machine interface to communicate information to the driver. However, the displayed image must be of sufficient quality to meet minimum requirements of usefulness so that scene objects can be seen, and of naturalness so that scene objects can be instantly recognized. For example, displayed objects with too little contrast will be overlooked while objects with unnatural grayscale and color appearance or distorted perspective may not be recognized in a timely fashion.

Although the majority of research on driver assistance systems focuses on image processing to interpret the information delivered by image sensors, comparatively little attention is given to the task of capturing scene detail. Since the camera forms the first link in the image information processing chain, its performance is critical; if the intra-scene dynamic range, the ratio of the brightest to darkest information-carrying intensity, exceeds the dynamic range of the

image sensor, then scene detail will be lost and cannot be recovered by image processing.

A model-based methodology is one that:

- Characterizes the automotive imaging environment (photospace) as wide dynamic range (WDR)
- Defines incremental signal-to-noise ratio (iSNR) as the criterion for reliably capturing WDR scene detail
- Uses the inherent sensitivity of silicon-based image sensors to utilize scene information carried by NIR radiation
- Separates color and NIR information in the image sensor and WDR image signal processing
- Defines the principles for combining luminance information from the visual and NIR spectral ranges with traffic-relevant color information into a natural and useful image for visual display

The Automotive Imaging Application

Reduced visibility at night substantially increases the risk of traffic accidents caused by misjudgment of dark roadways or failure to recognize the presence of pedestrians and obstacles. If an accident does occur, passive safety systems such as seat belts and airbags can reduce the percentage of fatalities to the vehicle's occupant, but only to a limited degree [1]. Any further reduction of traffic fatalities requires the use of active driver assistance systems.

Driver Assistance

Driver assistance can be classified into comfort systems and safety systems. These systems employ sensors that take measurements of the automotive environment, interpret the signals delivered by the sensors, generate warning signals, and, if the driver takes no action, even take over vehicle controls. The distinction between comfort and safety is fluid; parking guidance makes parallel parking more comfortable but also enhances safety by detecting persons and objects not visible to the driver. As an example of active safety, lane-keeping systems analyze sensor signals to determine if the vehicle is leaving the lane or roadway, then generate warning signals and in case of driver inaction steering signals. Other examples are lane-change assistance with blind-spot monitoring, collision avoidance, and driver-drowsiness monitoring.

Vision-Based Driver Assistance Vision-based driver assistance has a high potential of increasing traffic safety. First, more than 90% of the information that is critical for making driving decisions comes through the visual channel. Second, conditions that impair the flow of visual information have a significant impact on traffic safety. Nighttime driving is twice as risky as daytime driving, even though the volume of traffic is often less at night. Nighttime accidents tend to be more severe, with a disproportionate increase of fatalities compared to the volume of traffic. Nighttime accidents more often involve pedestrians or cyclists. The illumination of the roadway may be inadequate. For example, dipped headlights stretch over a fixed range of about 180 ft, but the safe braking distance increases with speed exceeding the visibility range at speeds greater than 30 mph [2].

Video-based driver assistance systems provide additional image information in situations where visibility is poor (night vision) or obstructed (side or rear vision). Applications range from driver assistance with forward and rear view images displayed on a dashboard screen to active safety systems where the video footage is analyzed by software that can issue warnings or trigger vehicle controls. On the front-end of these systems are video cameras that must capture scene details reliably under all circumstances.

Requirements of Vision Systems for Driver Assistance The basic requirements for a vision-based driver assistance system are image quality and reliability.

Image Quality Image quality can be defined as "the degree to which the image can be successfully exploited by the observer" [3]. An image of "high" quality should satisfy three criteria: genuineness, usefulness, and naturalness (GUN-model).

- Genuineness is described as the degree of apparent similarity of the reproduced image and its viewing environment with the external reference, that is, the original image and environment. Genuineness is related to fidelity, for example between a painting and its photographic reproduction.
- Usefulness is how relevant the reproduced image and environment are to the observer and the task activity. Usefulness is related to the discriminability of objects in the image, for example obstacles on a dark roadway.

- Naturalness is described as the degree of apparent similarity between the reproduced image and environment and the viewer's internal references, that is, memory prototypes. It is related to recognizability of objects in the image, for example whether the obstacles on a dark roadway are pedestrians or deer.

Night vision systems for driver assistance do not require genuineness, but they do require both usefulness and naturalness. Color and near-infrared (NIR) can supply important additional information that increases the usefulness of a night vision image, though NIR sensitivity may affect color saturation and thus reduce the naturalness of displayed images (section "Adding Color Differentiation to VIS + NIR-Sensitive Imager").

Image information that is interpreted by software has to fulfill the criterion of usefulness. Image information displayed for viewing has to be natural so that it can be interpreted instantly. An unnatural image requires effort by the interpreter and thus can distract, for example, false colors, inverted grayscale (thermal images), or distorted perspective (extreme fisheye).

Reliability The main difference between photography and automotive imaging is that the former is in most cases controlled by a conscious subject – the photographer – who selects the frame, knows what is in the scene, and can avoid extremes (strong light sources). However, when a camera is fixed in a vehicle, frame selection and content are arbitrarily determined by vehicle position, so intra-scene dynamic range may include, for example, approaching headlights, glare from other vehicles, tunnel entrances or exits, or solar glare. Image detail provides information about the objects in the real world, such as their location, shape, size, brightness, and color. If the dynamic range of a camera is too narrow to accommodate the intra-scene dynamic range, important object details will be missing from the corresponding image. Once lost by capture failure, these details can never be recreated with image post-processing [4, 5].

Conclusion: Model-Based Approach The design of automotive vision systems is governed by performance versus cost trade-offs. Therefore, it is important that the design is based on a clear understanding of the nonnegotiable performance thresholds such as sensitivity, signal-to-noise ratio, and dynamic range. A model-based design can quantitatively define and meet the performance requirements of automotive night vision. This includes models of human color night vision, the automotive night vision environment (photospace), and detection of scene detail (signal-to-noise ratio).

Human Perception of the Automotive Imaging Environment

The human visual system (HVS) is able to adapt to a vast range of natural and artificial lighting conditions. The mechanisms of adaptation are complex and include the combined responses of iris, lens, retinal photoreceptors, plus processing in the retina and visual cortex.

Day and Night Vision

Viewing the environment from a fast moving vehicle means that the driver's visual system must adapt to a visual environment that changes more rapidly than for a pedestrian or stationary observer. Under daylight conditions, such changes requiring instant adaptation include driving into the deep shadow of a bridge or tunnel, emerging from deep shadow into bright daylight, and solar glare. At night, the most challenging situation occurs immediately after passing the blindingly bright headlights of oncoming vehicles and having to adapt to the comparatively dark roadway ahead. These examples illustrate that adaptation of the HVS to instantly changing stimuli is the most critical issue in the automotive environment.

However, the models describing human day and night vision refer to steady states of global adaptation to defined ranges of light levels and characterize the responses of the two types of retinal sensors, rods and cones, to these light levels. Three distinct adaptation states of the human eye have been identified: photopic, mesopic, and scotopic.

- Photopic vision in bright light is dominated by cone receptors of relatively low sensitivity that provide full color at high acuity, which is highest at a central foveal field of about 2°. The spectral sensitivity function for photopic vision is measured as the

combined response of the long-, medium-, and short-wavelength-sensitive cones and standardized as the photopic luminous efficiency function $V(\lambda)$ with peak sensitivity at 555 nm (yellowish green).

- Scotopic vision, at very low light levels, relies on highly sensitive rods that provide only a monochrome image with poor acuity at the center of the field of vision but increased acuity toward the periphery. The peak of the scotopic luminous efficiency function $V'(\lambda)$ is at 510 nm, shifted toward bluish green, the so-called Purkinje-shift.
- Mesopic vision is a transition phase between photopic and scotopic vision that is invoked at luminance levels below 10 cd/m^2 and above 0.01 cd/m^2. The mesopic luminous efficiency function has not yet been standardized. Proposals range from a simple weighted average of the photopic and scotopic sensitivity functions to more complex chromatic models that weigh the contributions from the individual cones and yield sensitivity functions with two or three peaks [6]. Mesopic vision thus represents a balance between photopic and scotopic vision where the response of monochrome and color receptors will depend not only on overall light level but also on the scene-dependent local distribution of brightness on the retina. For example, the response within those areas of the retina that are stimulated by bright colored traffic lights is still cone-dominated while the response of retinal areas that are stimulated by dark background objects is rod-dominated.

Due to the presence of artificial lights in the automotive environment at night, the eye's adaptation never quite reaches the scotopic state but remains between or in the photopic and mesopic states. Color vision in very dark scenes is restricted to bright colored lights (traffic, tail, and brake lights), retroreflective signage, and surfaces brightly illuminated by headlights and streetlights. As these are relatively small and isolated by a dark background, they are referred to as "unrelated colors" [7]. Thus, relevant traffic lights are perceived as colored, but most dark objects (foliage, pedestrian's clothes) are perceived as monochrome.

Although the simultaneous dynamic range of the human eye, also known as the instantaneous sensitivity window, is limited to about 10,000:1, adaptation enables the HVS to adapt over time to a much wider range of luminance levels (Fig. 5). The rate of adaptation of the HVS to changing light levels is critical to traffic safety. Adaptation works with two time constants: fast (transient) adaptation occurs within seconds whereas slow adaptation happens on a much longer timescale, ranging from several minutes up to three quarters of an hour. Fast adaptation is the instant reaction to a sudden change in brightness, for example tunnel entry or exit, and vision is impaired until adaptation is achieved, usually after 1–2 s. Therefore, fast adaptation is of utmost importance in the performance of the HVS during driving. The rate of slow adaptation depends on the direction (dark takes longer than bright adaptation) and the light levels before and after adaptation. For example, the brighter the initial light level and the darker the final light level, the more time is required for slow dark adaptation. Headlight glare from oncoming vehicles constantly interrupts the process of dark adaptation.

Challenges to the Human Visual System

Driving under night conditions is very stressful to the HVS. First, the range of luminance levels is extremely large, ranging from blinding oncoming headlights to dark objects beyond the cone of one's own headlights. The constant change in peak brightness and position of the highlights puts the eye under the constant strain of global and local adaptation so that the retina is constantly registering either photopic or mesopic brightness levels. Color vision is restricted to bright lights and brightly illuminated objects whose position in the field of vision changes rapidly and constantly. The rate of change in stimuli will almost always exceed the rate of transient (fast) adaptation. Visual night driving performance can be evaluated by the responses to three visual subtasks that are defined by questions and evaluated by corresponding parameters: "Can it be seen?" (contrast threshold), "How quickly?" (reaction time), and "What is it?" (recognition threshold) [6]. The ability of the HVS to fulfill these tasks decreases with age (Table 1). The most serious aspect of age-related visual deterioration is the slowing of transient adaptation, making it more likely that the driver is "blind" immediately after sudden changes of brightness. At night, headlight glare can lead to the

phenomenon of "black holes," a temporary inability to perceive dark background detail after blinding. Although all drivers experience black holes, older drivers take longer to recover vision after the experience. Many societies have an increasing proportion of older drivers, so the implications of this issue are ever greater.

True Color Night Vision Video Systems in Intelligent Vehicles. Table 1 Visual impact of aging on human vision performance

Parameter	Effect of aging	Visual impact
Sensitivity	Decreases	Less light reaches retina
Color perception	Deteriorates	Loss of blue sensitivity
Rate of dark adaptation	Slows	"Black holes"
Glare	Increases	Loss of dynamic range
Contrast sensitivity	Decreases	Loss of detail
Peripheral vision	Decreases	Restricted

The simulation in Fig. 1 illustrates the loss of sensitivity and shift in color vision due to yellowing with age.

Conclusion: Producing Natural Images Under Mesopic Conditions

Night vision images displayed for the driver have to be rendered "naturally" so that traffic-relevant objects can be quickly seen and recognized. This requires that illuminated dark details such as pedestrians are rendered as a sufficiently bright monochrome image while "unrelated color" objects such as traffic lights are rendered with their correct hue and sufficient saturation (Fig. 2). In other words, the best compromise is to reconstruct a good luminance image then add those

True Color Night Vision Video Systems in Intelligent Vehicles. Figure 1 Simulated change in night color vision with age (**a**) 20, (**b**) 60, and (**c**) 70 [42]

True Color Night Vision Video Systems in Intelligent Vehicles. Figure 2
Same scene showing (**a**) related color at daytime and (**b**) unrelated color at nighttime [8]

unrelated colors that are relevant to the traffic scene. This way, the automotive vision system will mimic the mesopic state of the HVS, but with two key improvements. First, as adaptation to sudden changes in light levels is almost instantaneous, the driver is provided with visual information by the safety system in situations where the HVS adapts slowly. Second, the displayed luminance image is brighter and more detailed at a wider field of view in comparison to the corresponding rod-based HVS perception of the dark background. Although color cameras do not experience a shift in spectral sensitivity akin to the Purkinje shift, image processing algorithms (such as white balancing) still have to be applied to correct color shifts in illuminated objects caused by altered illuminant color temperature, for example moving between areas lit by mercury and sodium vapor lamps.

The Automotive Imaging Environment

A possible methodology for estimating the dynamic range of the automotive vision environment is based on photometric and spectral measurements together with the statistical photospace model. In addition, knowledge of the spectral characteristics of colored light sources is important when designing VIS–NIR color night vision systems.

Scene Photometry

To determine dynamic range requirements, a quantitative model of the image capture environment is needed. First, a measure of the brightness of light sources and illuminated objects in automotive scenes is required. The intensity of light is measured in radiometric power units, which are then converted to photometric units that represent the perceived brightness. This is done by weighting the radiant power at each wavelength by a spectral sensitivity function that models human brightness sensitivity, for example the photopic luminous efficiency function $V(\lambda)$ for the bright-adapted eye, or the scotopic luminosity function $V'(\lambda)$ for the dark-adapted eye. The amount of visible light reflected by or emitted from a surface area is measured as luminance with units of candela per square meter [cd/m^2]. Luminance is a good indicator of how bright a light source or illuminated object will appear. It measures the luminous power perceived at the surface of a light source or an illuminated object. It is independent of viewing distance and not changed by optical systems, e.g., lenses. Luminance measurements of objects in automotive scenes require spot luminance meters.

In the case of color and multispectral imaging, radiance must be measured [W/cm^2/sr] at specific wavelengths to characterize the night vision environment. This is done by a spot spectroradiometer that can measure not only the visible but also the NIR range.

Scene analysis relies on measuring the luminance of individual scene elements rather than the scene average [9]. Scene photometry in combination with scene analysis has been used to build statistical distributions

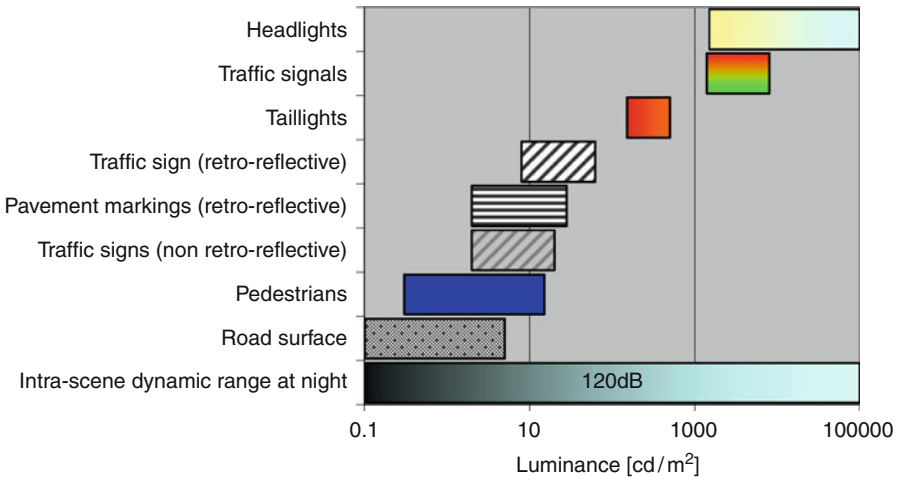

True Color Night Vision Video Systems in Intelligent Vehicles. Figure 3
Luminance ranges for light sources and reflective surfaces in typical night traffic scenes [8]

of light levels within a scene, ranging from the brightest lights to the darkest illuminated surfaces. Figure 3 shows an automotive vision example with luminance ranges for light sources and reflective surfaces typical of a night traffic scene.

Photospace in Automotive Vision

Photospace describes the environment as a statistical distribution that is populated by measuring average scene luminance levels for a great number of application-typical scenes [10]. By analyzing at least ten daytime and ten night traffic scenes, extended photospace distributions can be built based not on scene averages but rather on the probability that a scene element of a given luminance will occur (Fig. 4) [4, 11]. As more image data are added, such distributions will ever more closely represent application conditions. These extended photospace distributions for automotive vision by day and night show clusters representing light sources at high luminance levels (reflections of sun, vehicle lights, street lights, and traffic lights), and illuminated surfaces at lower luminance levels (road surface, traffic signs, and traffic participants). The luminance ratio within night scenes (10^6) is anticipated to be higher than that of daylight scenes (10^4–10^5) since poorly illuminated objects at night have much lower luminance. The highest luminance ratios in daylight scenes occur when the roadway enters or exits deep shade (bridges, tunnels). For the camera to detect image detail at night simultaneously in both the brightest (differentiation of headlights) and darkest scene areas (pedestrian detection), a dynamic range of 10^6:1 is required. However, a wide dynamic range is not the only requirement for an automotive camera to work in a night vision environment. The other necessity is that the camera is sensitive to the lowest luminance levels of the automotive photospace. The noise-limited sensitivity of the camera at the video frame rate should be such that its dynamic range covers the entire automotive photospace, including most of the mesopic range plus as much of the photopic range as possible (Fig. 5).

For a monochrome system, it is sufficient to render the brightest lights near the maximum signal level of the pixel in order to minimize halos and flare, thus maximizing differentiation between various lights, for example, headlights. However, in the case of color capture, this may be insufficient; a colored light captured near the maximum signal level will be too desaturated to be recognizable. As a rule of thumb, if a pixel's set of RGB signals is to be perceived as "green" (10% color saturation between the hue angles of 85° and 155°), each of the R and B signals has to be at least 10% lower on average than the G signal. However, if the green light increases in brightness, the G signal will reach then exceed

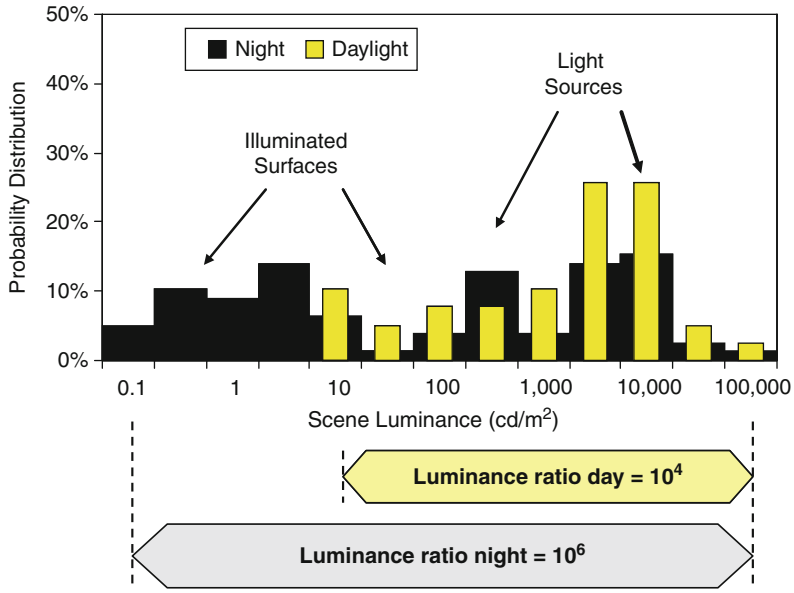

True Color Night Vision Video Systems in Intelligent Vehicles. Figure 4
Extended photospace distribution showing clusters for light sources and illuminated surfaces [5]

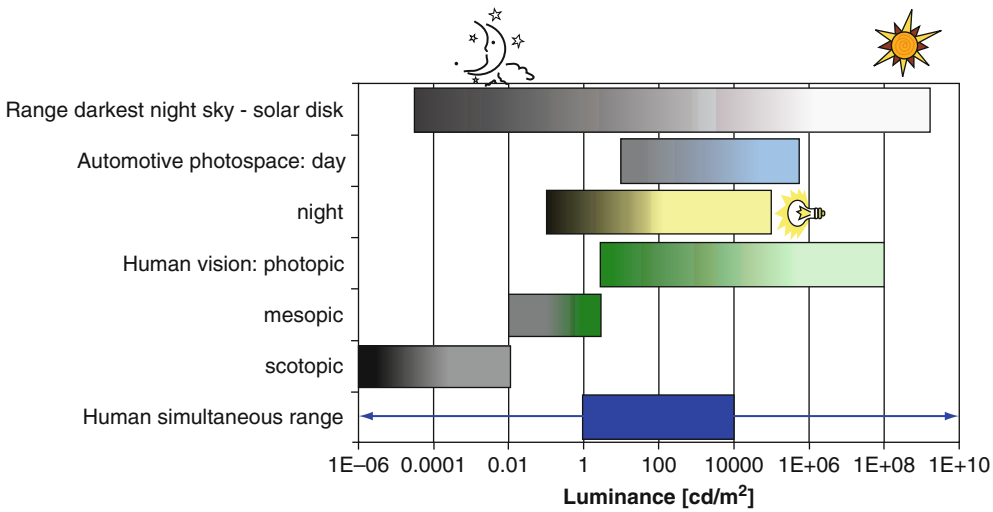

True Color Night Vision Video Systems in Intelligent Vehicles. Figure 5
Luminance levels and adaptation of the HVS [42]

saturation level before R and B, thus decreasing the G/R and G/B ratios so that the green color is barely distinguishable from "white" (see Fig. 6). Therefore, the dynamic range of a night vision color system must be wide enough to prevent any of the RGB color signals from being clipped.

Spectral Distribution of Light Sources

The diversity of spectral characteristics of colored light sources poses a challenge to automotive vision systems that combine NIR sensitivity with color differentiation. For example, a green traffic light might be an LED array

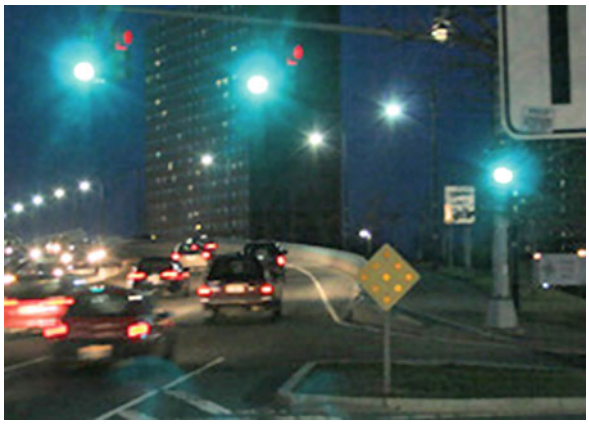

True Color Night Vision Video Systems in Intelligent Vehicles. Figure 6
Typical urban night traffic color scene where limited dynamic range results in clipped highlight colors appearing *white* (centers of *green* traffic lights, *red* tail lights) [35]

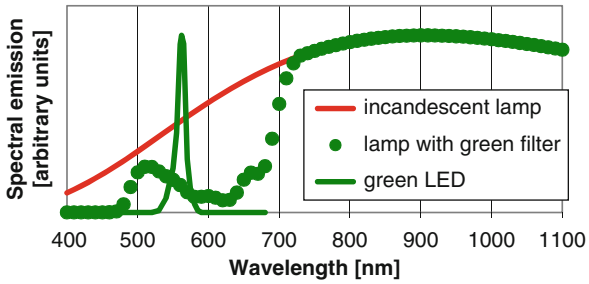

True Color Night Vision Video Systems in Intelligent Vehicles. Figure 7
Spectral VIS–NIR emission curves of an incandescent lamp (3,200 K), an incandescent lamp with a green glass filter, and a green LED [35]

or an incandescent lamp behind a colored filter. The former has a narrow spectral distribution peaking in the 500–600 nm range. The latter has a more complicated spectral distribution. Although in the VIS range, it has a peak in the green region of the visible spectrum, since most commonly used color filter materials are almost transparent in the NIR range and the spectral emission of incandescent lamps (color temperature 3,200 K) peaks in the NIR at about 800 nm, the strong NIR contribution might exceed that from the VIS range (400–700 nm), see Fig. 7. Spectral measurements of objects in automotive scenes require spot spectroradiometers.

This high NIR content of colored lights does not pose a problem for human vision and common RGB color cameras because the eye is insensitive to IR, and the latter has an IR-cut filter.

It follows that a VIS–NIR color night vision system has to combine high sensitivity in both spectral areas with good reproduction of those colors relevant to night traffic scenes. This requires the imager to have WDR to avoid signal saturation in colored lights, plus sufficient separation of NIR and color signals so that colors can be reproduced independently of the light source's IR content.

Conclusion: Automotive WDR Environment

Intra-scene dynamic range is determined by the range of intensities between bright lights (some of them carrying color information) and dark, dimly illuminated objects. The automotive vision environment can be measured by scene photometry to quantify the luminance ranges of traffic-relevant light sources and illuminated objects, and to populate statistical photospace distributions that show the probability that scene elements of a given brightness (luminance) will occur at night or day. Automotive scenes typically cover a WDR, highest at night due to lower background luminance levels. Challenges in daylight conditions are deep shadows (parked vehicle under bridge, tunnel entry) and blinding (solar glare, exit from tunnels or bridges). Night vision requires both high sensitivity (to distinguish shadow detail) and WDR (to distinguish highlight color detail). Preserving the color information of traffic-relevant lights requires an even wider dynamic range than for monochrome vision.

Extending the Dynamic Range

A possible methodology to extend the dynamic range of image sensors without compromising the transfer of scene information to image information can be developed from an information-theoretical model.

Definition of Dynamic Range

Dynamic range generally relates to an imager's ability to capture information about both bright and dark

objects in the same scene at the same exposure settings. There are several definitions of dynamic range. In its most general sense, dynamic range describes the ratio between the largest and smallest possible signal values of a changeable quantity such as light [4]. Dynamic range can be either input-referred (ratio of real-world light levels) or output-referred (ratio of the response signals delivered by a light detector). Since the output-referred definition can lead to dynamic range numbers built solely on technical specifications (such as the bit depth of an A/D converter) rather than on actual measurements, it has limited value in predicting dynamic range [13]. Therefore, dynamic range should refer strictly to input signals, for example luminance L in photopic units of cd/m^2. The relationship between input and output signals is established from the imager response curve.

In silver halide photography, the luminance ratio of the highlights to the shadows is called "object ratio" and the logarithm of this ratio "object range" [4]. The equivalent of "object range" in digital imaging is the input-referred dynamic range, which can be expressed in units of decibels [dB] by calculating 10 log of the luminance ratio. However, technical specifications of digital and video image sensors traditionally referred to ratios of output voltages or digitized light levels so that decibels represent 20 log of the ratio (even when the represented input luminance is directly proportional to the output voltage or level) not to its square [14]. In order to avoid disadvantaging input-referred data, the 20 log rule is also used to calculate the input-referred dynamic range from luminance ratios:

$$DR = 20 \cdot \log_{10}\left(\frac{L_{\max}}{L_{\min}}\right). \quad (1)$$

Reliability Criterion

Ascertaining dynamic range requires determining the maximum and minimum signal levels. Detection of the smallest possible signal is limited by the noise floor. To become detectable, a signal must exceed the noise floor; in other words, the signal-to-noise ratio (SNR) must be greater than 1. The largest possible detected signal is limited by saturation. Any input signal above the saturation level can only reproduce a saturation level output signal and thus remains indistinguishable from the saturation signal. This introduces the concept of signal variation as the carrier of information: object detail is carried by small variations in light level. Scene information can only be gathered reliably if the image capture system can detect and reproduce the small signal variations carrying that information. Thus, dynamic range needs a more precise specification to ensure detection reliability: it is the ratio between the maximum and minimum luminance signals where a camera can simultaneously capture detail carried by small signal variations.

A distinction has to be made concerning the spatial dimension of object details. Below a certain size, the details in an image are no longer formed independently; the signal at a given image point depends not only on the luminance at the corresponding object point but also on that of its surroundings [4]. This effect can be accounted for by the modulation transfer function (MTF). However, this estimation of dynamic range refers only to the reproduction of details large enough that the loss of detail due to MTF can be ignored. It is desirable to deduce dynamic range from objective measurements. This methodology is laid down in a progression of ISO/TC42 imaging performance standards [15–17].

Figure 8 shows the transfer of large-area detail (small luminance variation) by the response curve in

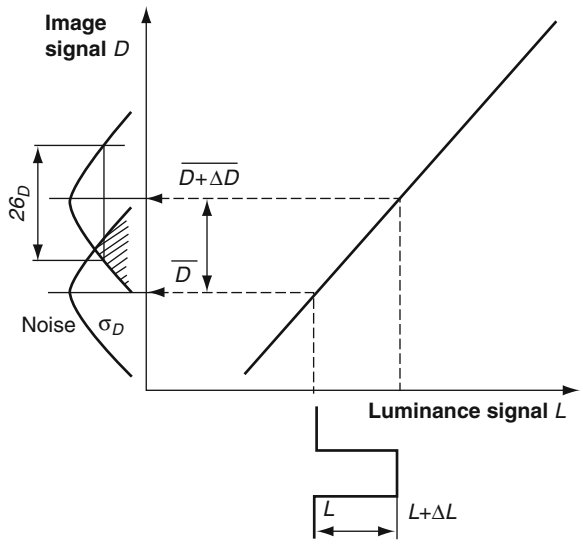

True Color Night Vision Video Systems in Intelligent Vehicles. Figure 8
Transfer of large-area detail (small luminance variation ΔL) by the response curve $D(L)$ in the presence of noise σ_D [5]

the presence of noise [18]. The response curve is the relationship $D(L)$ between input luminance signal L and output digital image signal D. ISO/TC42 refers to the response curve as opto-electronic conversion function (OECF). The slope of the OECF, the change dD in image signal due to a change dL in the luminance signal, is referred to as incremental gain $g(L)$:

$$g(L) = \frac{dD}{dL}. \tag{2}$$

Detection error is given by noise. Since dynamic range refers to the input luminance signal L, the noise σ_L has to be defined as the luminance-equivalent of the noise σ_D that can be observed and measured in the digital image [19]. At each luminance level L, the equivalent luminance variation σ_L can be calculated from the image noise σ_D via the incremental gain:

$$\sigma_L(L) = \frac{\sigma_D(L)}{g(L)}. \tag{3}$$

The criterion for detection reliability is the SNR, the ratio of the input luminance signal L and the luminance-equivalent noise σ_L. Detection reliability requires the SNR to stay above a threshold of one to fulfill the following condition:

$$\frac{L}{\sigma_L(L)} = \frac{g(L) \cdot L}{\sigma_D(L)} > 1. \tag{4}$$

The expression in (4) is referred to as "incremental SNR" (iSNR, also S/Nx and $\mathrm{SNR_{inc}}$); the incremental signal is defined as $iS(L) = g(L) \cdot L$. An equivalent concept for determining detection reliability in silver halide photography is known as noise-equivalent contrast (NEC) [20].

The threshold condition $iSNR > 1$ means that at any given luminance level L, detail carried by a small variation in luminance can only be reliably detected if the corresponding incremental image signal is high enough and the noise low enough. Fulfilling the iSNR criterion will be first explored for imagers with a linear response. At very low luminance levels, noise keeps iSNR below its threshold. The minimum reliable luminance level $L_{\min}$ is reached only when iSNR rises above the threshold. At very high luminance levels, the onset of saturation will clip further signal increases and thus cause the incremental gain to drop sharply. The maximum reliable luminance level $L_{\max}$ is reached when iSNR once more drops below the threshold. It follows that dynamic range for linear imagers is bounded by the two extreme luminance levels $L_{\min}$ and $L_{\max}$ at which the iSNR condition of (4) still holds.

The iSNR condition is now applied to imagers with extended dynamic range. This requires shifting saturation to higher input signal levels by a nonlinear response curve: at a so-called breakpoint, the response curve's slope (incremental gain) is suddenly lowered to delay saturation to higher luminance levels than for a linear imager (Fig. 9). However, lowering incremental gain will, in turn, decrease iSNR, pointing to a potential iSNR trade-off when increasing dynamic range. Rather than just using iSNR to determine the boundary luminance levels $L_{\min}$ and $L_{\max}$, the minimum iSNR criterion has to be maintained at every luminance level in between. Verifying this requires iSNR be measured as a function of luminance L. An equivalent strategy was used for silver halide photography where NEC curves were measured as function of exposure [20].

Therefore, nonlinear imagers require a more general definition beyond the recommendations of ISO/TC42; dynamic range is the input luminance range within which the threshold criterion for $iSNR(L)$ is met at all levels $L_{\min} \leq L \leq L_{\max}$. This suggests a strategy for maximizing the dynamic range of imagers with a nonlinear response curve: maintain the necessary minimum of $iSNR(L)$ over the largest possible range of luminances L. Thus, iSNR becomes a metric describing the reliability of detecting scene detail. The theoretical detection limit is 1, but the reliability requirements of applications may require

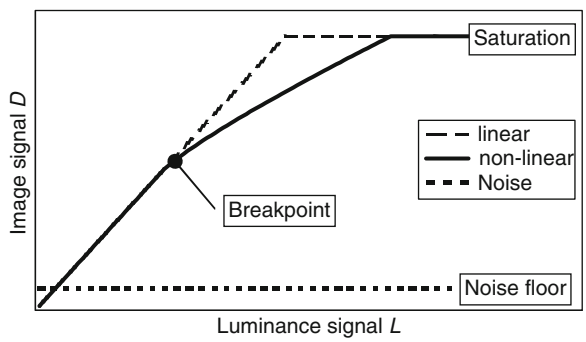

True Color Night Vision Video Systems in Intelligent Vehicles. Figure 9

Extending dynamic range with a nonlinear response curve [5]

higher thresholds. For example, a minimum of 10 is suggested for "acceptable" photographic image quality, and between 1.5 and 4 are estimated for machine-vision applications [18].

Technologies to Extend Dynamic Range

The following section reviews a selection of WDR technologies and explores the iSNR trade-offs of nonlinear dynamic range extension. A WDR video camera for automotive applications should combine good sensitivity with low noise at a given frame rate (10–60 fps) plus a WDR extension that can be adapted quickly to match typical automotive photospace conditions (80–120 dB). The first group of technologies for WDR extension are those that directly change the CMOS pixel response function (such as logarithmic response [21], linear-log combination [22], in-pixel light-to-frequency conversion [23], pixel-level A/D conversion [24], or pixels with overflow capacitors [25]), while a second group changes pixel response indirectly by altering the timing (multiple exposure, multiple partial reset [26]).

The first group, directly changing the response function, involves extensive pixel circuitry resulting in low fill-factor and thus poor low-light sensitivity. For example, in-pixel light-to-frequency conversion provides 115–130 dB WDR, but the required circuitry decreases the fill factor to 25%, and reduces low-light sensitivity. Similar sensitivity degradation currently limits the usefulness for automotive video of both pixel-level A/D conversion and pixels with overflow capacitors. Although pixels with direct logarithmic compression can provide WDR above 170 dB at low cost, the WDR extension is not adaptive, and at present, high fixed-pattern noise and dark current decrease low-light SNR. The combined linear-log CMOS pixel does avoid these drawbacks, but the required seven transistors per pixel limit the fill factor.

WDR can be covered with a linear image sensor by multiple exposure, but application to automotive video requires either fast readout (high frame rate with corresponding loss in low-light sensitivity), or local frame storage and processing.

Among WDR technologies that alter the timing, CMOS image sensors with multiple partial reset (multiple-slope) technology offer good imaging

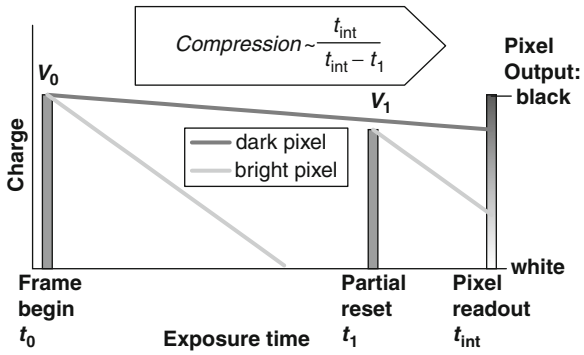

True Color Night Vision Video Systems in Intelligent Vehicles. Figure 10
Charge–time diagram for a CMOS WDR pixel with a single partial reset [5]

performance at low cost and are thus well suited to automotive video capture [4]. The example of a multiple-slope imager explains how to extend dynamic range while maintaining detection reliability.

At the heart of the CMOS pixel is a light-sensitive photodiode with a parasitic capacitance that is charged by applying a voltage pulse V_0 at frame begin t_0, then discharged as exposure generates photoelectron-hole pairs. Figure 10 shows the charge–time diagram of a CMOS pixel. The rate of discharge depends on the input luminance; a darker pixel is discharged at a lower rate, a brighter at a higher one. After integration time t_{int}, the remaining charge is read out and converted into the image signal D. This is proportional to the degree of discharge between t_0 and t_{int}; no discharge corresponds to $D = 0$, and full discharge to saturation level (Fig. 10). A darker pixel will only be partially discharged at t_{int}, proportional to the input luminance; its response will therefore resemble that of a linear pixel. A very bright pixel will be fully discharged before t_{int}, making it impossible to register any further increase in luminance; it has reached the saturation level of its response curve. However, this bright pixel could resume registering photons if a reset voltage pulse V_1 is applied at the time $t_1 < t_{int}$ to replenish the charge of each capacitor. The reset is only partial; the reset voltage V_1 is chosen to be lower than the initial V_0 so as to discriminate between darker pixels that would not be saturated at t_{int} and brighter ones that would. The partial reset does not affect those darker pixels that are still above the reset level V_1. It only recharges

the brighter pixels that are already discharged below V_1. For them, the reset overwrites any memory of previous exposure, and they resume registering photons in the shorter exposure time $t_{int} - t_1$. The corresponding pixel response curve will be piecewise linear, but with a lower incremental gain after the breakpoint that corresponds to the reset at t_1. The nearer t_1 is to t_{int}, the lower the incremental gain after reset, and the higher the saturation luminance L_{max} becomes. The reset allows a higher luminance range to be "compressed" into the same limited output image signal range; thus, the ratio of the total exposure time t_{int} to the remaining exposure time $t_{int} - t_1$ is referred to as "compression." To increase compression further, additional partial resets of successively decreasing voltage can be applied within the remaining time between t_1 and t_{int}, see Fig. 11a, thus creating a piecewise linear response curve where the incremental gain is further decreased after each of the breakpoints, see Fig. 11b. Theoretically, the number of additional resets is only limited by the smallest increments of timing and recharge voltage control, but in reality, it is limited by the requirement of detection reliability.

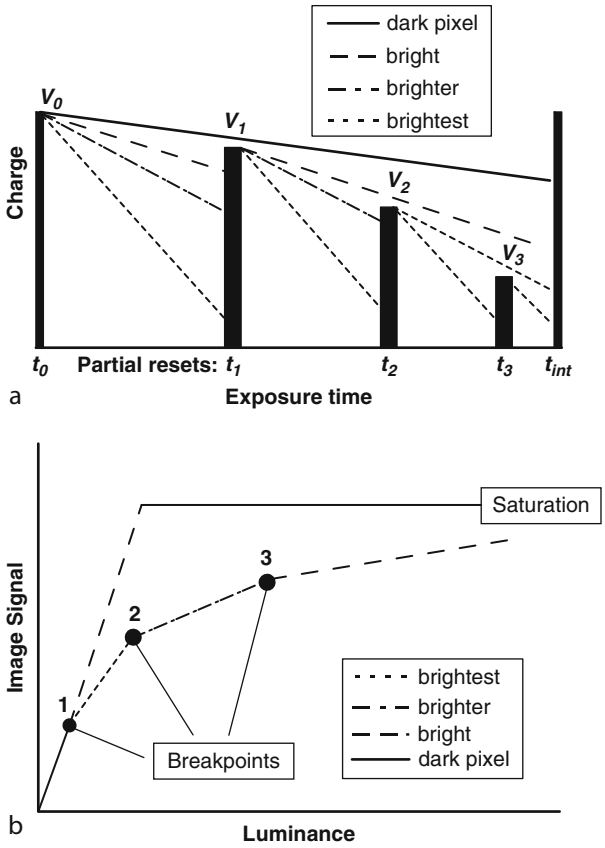

True Color Night Vision Video Systems in Intelligent Vehicles. Figure 11
(**a**) Charge–time diagram and (**b**) response curve for a CMOS WDR pixel with multiple partial resets [5]

Extending Dynamic Range Reliably

The partial resets of a multiple-slope WDR imager require precise control of the timing and recharge voltage so that it can adapt optimally to the changing dynamic range of a natural scene. Experimental observations and model calculations show how the iSNR criterion can be used to maximize dynamic range without compromising detection of scene detail. The methodology for measuring iSNR has been described in detail [5].

Experimental Observations One important goal of dynamic range extension is minimizing the number of saturated pixels and thus maximizing the capture of highlight detail. With the single-reset system shown in Fig. 10, high compression can be achieved by moving the reset time t_1 as close as possible to the frame end t_{int}. The highest compression is limited only by the increments of reset timing, given by one row time in common multiple-slope imagers and by one pixel time for the most advanced multiple-slope imagers. This can be explained in the example of a VGA imager with 480 rows of 640 pixels. The voltage reset can be placed as close as one row time before t_{int} (i.e., after 479 rows), achieving a maximum compression of $c = 480/(480–479) = 480$. This means that the ratio of exposure times in compressed and linear modes is 1:480 and that the pixel is 480× less sensitive in compressed mode. From exposure time ratios, dynamic range can be estimated to be extendable by 54 dB. In an advanced VGA imager where single pixel times are addressable, the dynamic range extension could be even more impressive. Each row contains 640 pixels. The shortest exposure time would be one pixel time before $t_{int} = 480 \times 640$ pixels so that a maximum compression of $c = (640 \times 480)/(640–639) = 307{,}200$ could be reached, extending the dynamic range by 110 dB.

Experiments like those shown in Fig. 12 and the corresponding imager response model of section

"Imager Response Model" show that although the practical implementation of high compression with just one partial reset can effectively prevent highlight saturation, it does come at the cost of usefulness, seen as severe loss of midtone image contrast. Figure 12a shows an image taken in linear mode where saturation prevents visibility of detail on the trunk of the car. Progressing from Fig. 12b to d, increased compression decreases the proportion of saturated pixels, making highlight detail more visible on the trunk but at the cost of lowered contrast of midtone detail (lane markings versus road surface). Figure 12d shows the limit of a single-reset system. There are still a fair number of saturated pixels, but the lane markings have become almost indistinguishable from the road surface, which has lost all texture detail. There is a trade-off; the higher the compression, the lower the midtone contrast. At levels of compression still far from theoretical limits, portions of midtone detail almost disappear, and the image becomes unnatural and less useful. The underlying mechanism of this is explained by the following imager response model.

Imager Response Model Response curve and noise models show that the loss of midtone detail as observed in Fig. 12 can be explained by a drop of iSNR that occurs at the reset point. Figure 13 shows modeled curves of OECF and iSNR as functions of log luminance. The model assumes a constant dark noise floor without considering photonic shot noise.

After the partial reset breakpoint, the slope of the response curve (and thus the incremental signal) is reduced so that saturation is delayed to a correspondingly higher luminance level. With increased compression, the drop in iSNR at the breakpoint becomes deeper until it drops below the reliability threshold as shown in Fig. 13c, thus creating an undesirable zone of extinguished local

True Color Night Vision Video Systems in Intelligent Vehicles. Figure 12
Natural scene captured with (**a**) linear camera and with a single-reset WDR camera at (**b**) low, (**c**) medium, and (**d**) high compression, demonstrating the trade-off between increased dynamic range and decreased midtone contrast [5]

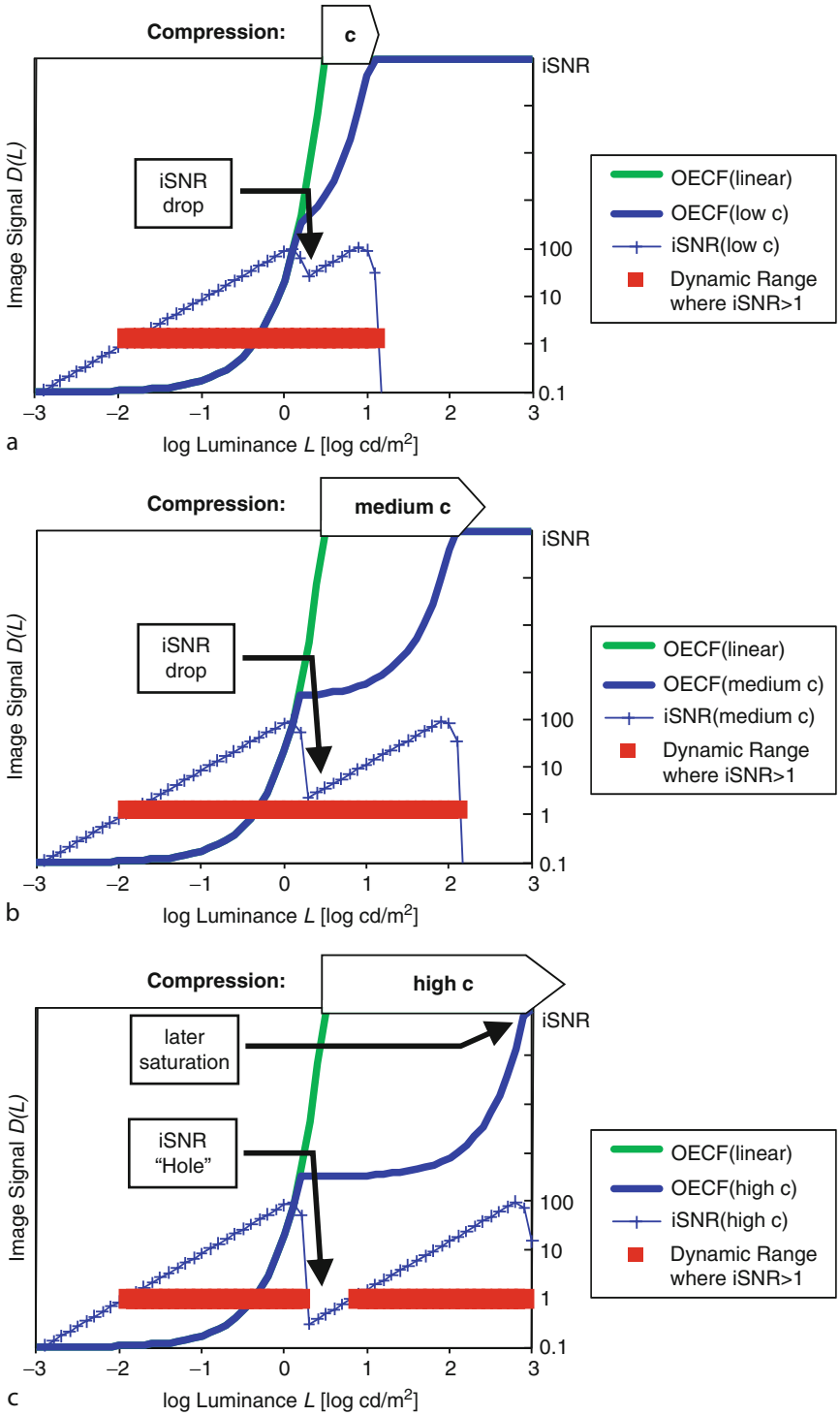

True Color Night Vision Video Systems in Intelligent Vehicles. Figure 13
Log-linear response curves (OECF) and incremental SNR of a single-reset model at (**a**) low compression, (**b**) medium, and (**c**) high compression [5]

contrast, a so-called iSNR hole. The luminance range within and near the "iSNR hole" corresponds to the luminance levels of those details such as road texture and lane markings that became almost indistinguishable in Fig. 12d.

Along with saturated pixels or those below the noise floor, "iSNR holes" make the detection of scene detail impossible. In linear imagers, the zones of iSNR failure occur only at very dark pixels (below noise floor) and very bright pixels (above saturation level). However, in multiple-slope WDR imagers, zones of iSNR failure can also occur at luminance levels corresponding to reset times. These levels cannot be predicted without exact knowledge of the response curve for a given set of reset times. If the resets are automatically adapted to the intra-scene dynamic range, then the luminance levels corresponding to the reset times would depend on scene content and thus be variable, making iSNR holes potentially interruptive to the visibility and automatic detection of scene detail. It follows that resets have to be controlled to prevent iSNR holes occurring in the first place. Dynamic range can only be extended as long as the incremental signal iS can be kept above the noise floor at every luminance level. Thus, iSNR is not just a criterion for determining the upper and lower dynamic range limits but becomes critical when controlling the reset times within the dynamic range. Adaptive WDR extension requires separate control loops for integration time and compression that both adapt the imager's response curve to include the darkest and brightest scene details. The control algorithms for timing the multiple partial resets in adaptive WDR extension must be designed specifically to avoid iSNR holes.

Reliably Extending Dynamic Range The example of a multiple-slope WDR camera demonstrates how the iSNR criterion can be used to extend dynamic range without sacrificing detection reliability.

If the number of resets is limited to one or two, then noise reduction is the most effective way of increasing dynamic range. Figure 14 compares two single-reset model imagers, one where altered pixel design (i.e., larger size, correlated double sampling, etc.) has cut noise in half (−6 dB). This leads to a twofold increase in dynamic range. Firstly, the 6 dB lower noise floor leads to a 6 dB lower noise-equivalent luminance signal L_{min}. In addition, the lower noise floor allows – without creating an iSNR hole – the compression to be increased by a factor of 2, halving the slope after reset and doubling the saturation luminance L_{max}, thus increasing the dynamic range by another 6 dB, a total of 12 dB. Assuming a minimum iSNR of 1, dynamic range is increased from 88 to 100 dB or twice that of a linear imager of 50 dB.

Where pixel-level noise reduction is not effective (small pixels, low fill factor, high operating temperatures, inexpensive pixel design), then increasing the number of partial resets is a better strategy. The drop in iSNR at a reset point depends on the ratio of

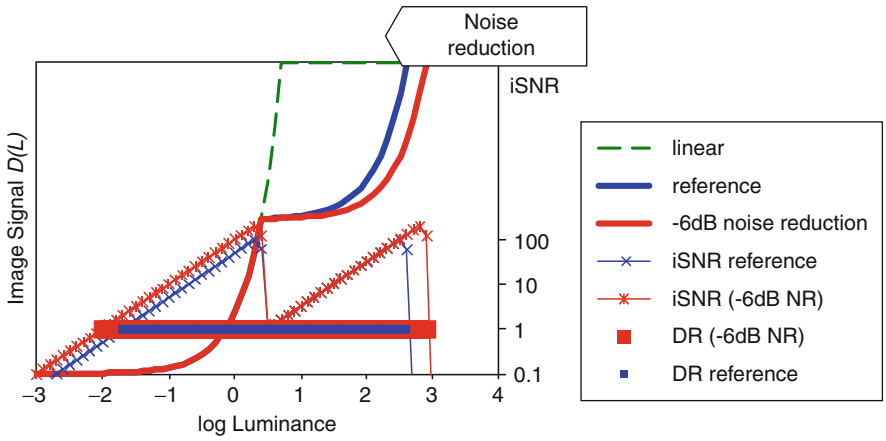

True Color Night Vision Video Systems in Intelligent Vehicles. Figure 14
Lower pixel-level noise increases dynamic range in a single-reset imager [5]

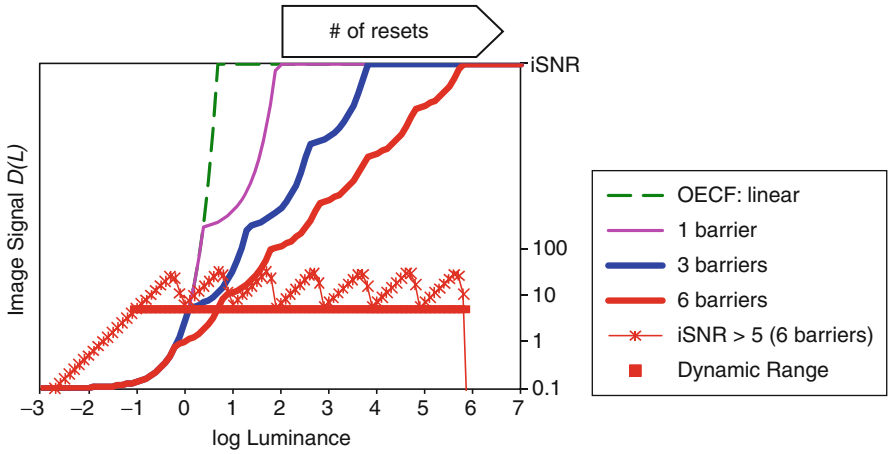

True Color Night Vision Video Systems in Intelligent Vehicles. Figure 15
More resets increase dynamic range while allowing a higher minimum iSNR threshold of 5 [5]

incremental gains after and before the reset, $k = g/g_0$. The more $g(L)$ is reduced by a reset, the deeper iSNR will drop. After each partial reset n, the sensitivity decreases geometrically by the factor $1/k^n$. When deploying multiple partial resets, their timing and charge (voltage) can be chosen so that the linear output signal range is equally distributed between the resets [5]. This ensures that iSNR at each reset point drops to the same minimum level (see Fig. 15). Having more resets has the added advantages: the decrease in incremental gain can be approached more gradually, and the iSNR threshold can be raised from one to a more practical level. Figure 15 shows a dynamic range model for an increasing number of resets. Assuming an increased iSNR threshold of 5, the linear imager will have a dynamic range of only 36 dB. Compression with a single reset will extend the dynamic range to 62 dB; two resets will reach 98 dB, and six resets 138 dB.

Conclusion

Although the concept of iSNR-based reliability has been modeled and tested only for multiple-slope CMOS imagers, it can be deduced that the concept applies to any other WDR extension technology that involves sudden changes in the incremental gain of the pixel response curve. In contrast, sensors with logarithmic response are in no danger of "iSNR holes" as their incremental gain decreases continuously during exposure time.

For the example of multiple-slope CMOS imagers, it has been shown that iSNR is a critical criterion governing the number, timing, and recharge voltage of partial resets. Dynamic range can be increased by reducing noise at the pixel level, by increasing the number of partial resets, and by distributing them equally to maintain a minimum iSNR necessary for reliable detail detection throughout the entire dynamic range. As technologies for extending the dynamic range evolve, new solutions will be added to the repertoire and tested for their suitability for intelligent vehicle technology. However, the methodology described here will provide a guideline for optimizing the pixel response for maximum dynamic range at the highest possible iSNR.

Extending Spectral Sensitivity into NIR

In order to capture dark scene detail illuminated by ambient light, the camera has to be very sensitive with high SNR. Exposure time is limited by the video frame rate and the need to limit motion blur. Sensitivity can be increased by either lowering noise (increasing SNR) and/or extending the range of spectral energy sensed.

IR Sensing

The spectral sensitivity of silicon-based image sensors extends beyond the long-wavelength edge of the visible spectrum (730 nm) into the infrared (IR). As longer

wavelengths penetrate further into silicon, CMOS imagers can be made more sensitive to IR by collecting photo charge carriers from greater depth and by increasing substrate thickness. The IR cut-off in CMOS imagers can thus be shifted as high as 1,100 nm. This spectral range coincides with the shorter wavelengths of the IR-A or near-infrared (NIR) range (700–1,400 nm). Imagers for longer wavelengths beyond the NIR rely on semiconductors with a narrower band gap, for example InGaAs (950–2,600 nm). Such far-infrared (FIR) cameras can sense the black body radiation that surfaces emit as a function of their temperature, and obtain a thermal image of the environment. They do not require any other source of radiation and can operate in complete darkness. Compared to NIR systems, FIR night vision systems are more costly, cannot be placed behind glass, and deliver unnatural images that are difficult to interpret [27, 28].

Passive and Active NIR Vision

The detection of objects by a NIR-sensitive camera requires them to be irradiated by a NIR source so that the camera can detect radiance image from reflected NIR. Passive sensing relies on ambient NIR. Ambient NIR at night comes mostly from artificial incandescent light sources such as vehicle headlights; vapor street lighting and natural light sources (moon, stars) emit comparatively little NIR. Daylight especially direct sunlight contains extremely high background NIR that is strongly reflected by vegetation; cameras may have to operate in WDR mode to avoid signal saturation. Active sensing requires sources that are mounted to the same vehicle as the NIR camera. Conventional metal halide (tungsten) headlamps emit more than 60% of their spectral energy in the NIR. Dedicated NIR-only headlamps, either tungsten lights with a VIS-cut filter or NIR LEDs at 850 nm, have the advantage that they are invisible to humans. As they cannot blind oncoming drivers, they can be operated on high-beam, thus extending the range of vision beyond that of dipped headlights [29]. One of the first active systems implemented was the Mercedes-Benz Night View Assist (2005).

Comparing the spectral sensitivity of a monochrome CMOS image sensor with the photopic and scotopic luminous sensitivity functions shows the range of spectral energy that the image sensor can utilize. For example, when the scene is illuminated by metal halide headlamps whose emission spectra peak in the NIR at about 900 nm, sensitivity stretches to the long-wavelength cut-off of the image sensor (Fig. 16).

The example in Fig. 17 shows an urban traffic scene taken without and with ambient NIR, showing the main

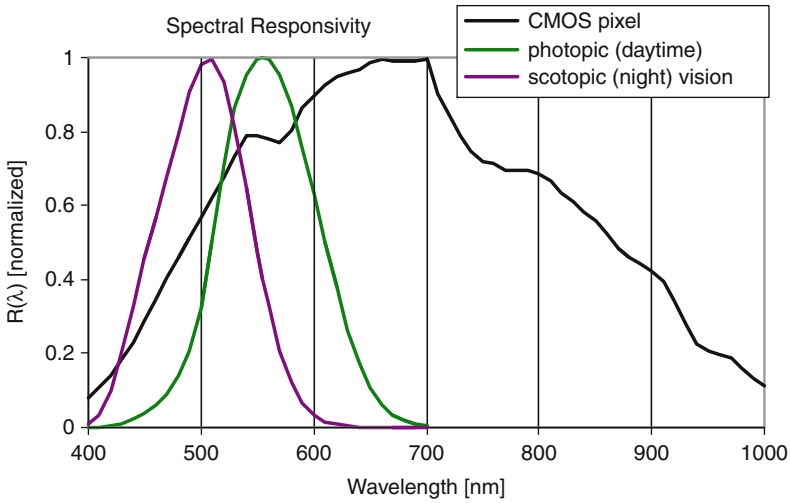

True Color Night Vision Video Systems in Intelligent Vehicles. Figure 16
Comparison of photopic and scotopic luminous sensitivity with the spectral sensitivity of a monochrome automotive CMOS image sensor [42]

True Color Night Vision Video Systems in Intelligent Vehicles. Figure 17
Monochrome image of urban traffic scene (**a**) without NIR and (**b**) with NIR

benefit of extended NIR sensitivity: better visibility of the roadway where it is illuminated by dipped headlights.

The range of visibility can be extended even further, without blinding oncoming drivers, if dedicated NIR-only high-beam headlights are used. These will, of course, "blind" any NIR-sensitive night vision cameras of other vehicles, unless they are capable of performing in a WDR environment.

Adding Color Differentiation to VIS + NIR-Sensitive Imager

Using NIR to increase the sensitivity of color imagers requires separation of the NIR and RGB color signals because the color filter materials used in standard CMOS and CCD technology are highly transparent to NIR so that each color pixel also detects NIR (Fig. 18).

Mixing color and NIR signals can result in extreme color de-saturation if the illumination contains high amounts of IR. This is the case when incandescent lamps are used with color temperatures typically about 3,200 K, where spectral power distribution peaks at about 800 nm (Fig. 7). Here, the signal contributions to RGB from the NIR are even higher than those from the actual colors so that all colors are rendered as off-gray, for example shades of pink (Fig. 19). The example demonstrates that the differentiation of color requires the NIR signal to be separated from the color signals.

Increasing the Spectral Sensitivity of Color Imagers

Color image sensors simply suppress the NIR information by an IR-cut filter. The sensitivity of such imagers can be improved by adding filterless "white" pixels to the RGB filter pattern [30, 31] (Fig. 20). Compared to the RGB color pixels, these "white" pixels have about three times higher spectral sensitivity.

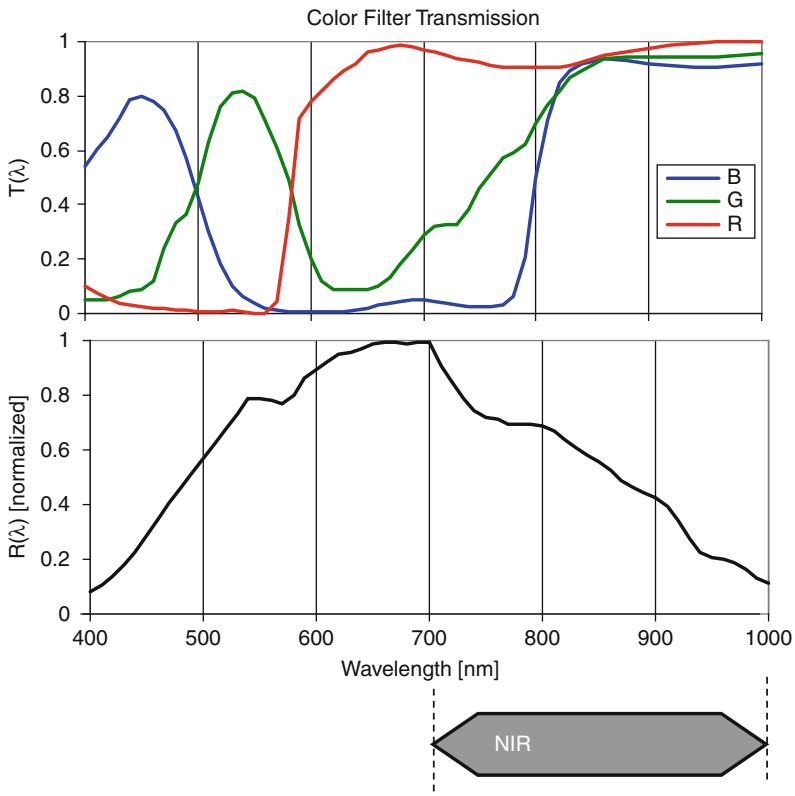

True Color Night Vision Video Systems in Intelligent Vehicles. Figure 18
VIS–NIR spectral transmission curves of typical RGB color filters used in CMOS imagers [35]

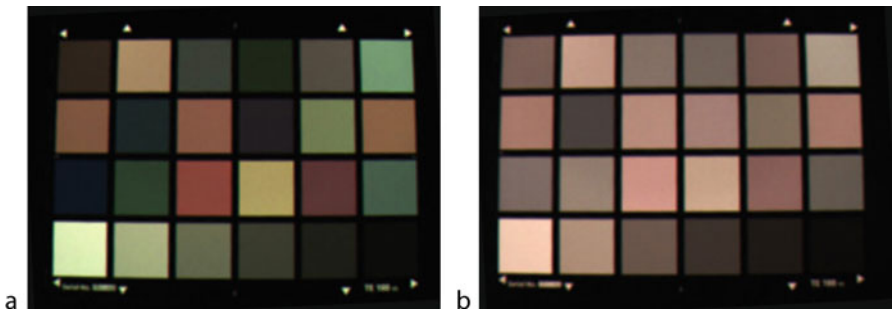

True Color Night Vision Video Systems in Intelligent Vehicles. Figure 19
Raw images of a Macbeth color checker chart illuminated by incandescent light (3,200 K) taken with a CMOS color camera (**a**) with IR-cut filter and (**b**) without IR-cut filter [35]

As scene illuminance decreases, information from color pixels is increasingly mixed with luminance information from the W-pixels by pixel binning. This requires high pixel counts plus special (nonstandard) filter patterns, and the NIR remains unutilized for night vision.

Extending the Spectral Sensitivity of Color Image Sensors into the NIR

Extending the light sensitivity of color imager sensors into the NIR requires a separation of the NIR and the color signals. This could be achieved by using a beam

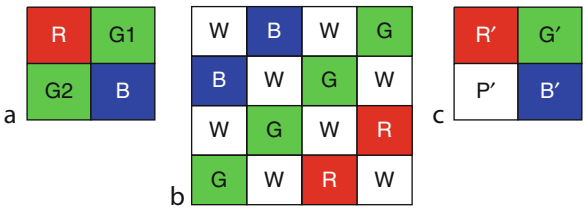

True Color Night Vision Video Systems in Intelligent Vehicles. Figure 20
CFA layouts: (**a**) standard Bayer, (**b**) RGBW, and (**c**) RGBP [35]

splitter and two image sensors, one monochrome for NIR, and one color for VIS. However, cost and form factor do not recommend this solution for automotive vision applications.

Single-imager solutions are based on the addition of a fourth pixel type to the RGB-pixels (Fig. 20c). This fourth pixel, which, for example, replaces the second G-pixel in the Bayer pattern, is either NIR-sensitive or "panchromatic," sensitive to both visible and NIR light. A variety of methods have been proposed to separate NIR signals from color signals:

- Patterned optical NIR-cut filters can be added to mosaic filter arrays, for example RGBW or CymG (cyan-yellow-magenta-green) [32], to protect all or a portion of color pixels from the effects of NIR radiation. The filters can be of the absorptive or interference type. Interference filters are preferred for their sharper absorption edge toward the NIR, but they do require patterned deposition of more than ten dielectric layers [36], which is both costly compared to dye-based filters and uses dielectric materials that are incompatible with standard Si processes. The effectiveness of such filters is limited by optical crosstalk of NIR into the color pixels after passing the NIR cut filter, especially at low incident angles.
- Nano-optical filters, currently still in the research stage, can be designed as short-pass edge filters or band-pass filters. They can either be integrated as metal layers into the pixel stack [37] or deposited on top of the imager [38]. Although nanostructured metal layers within the pixel stack have to follow the Si design rules for structure size (0.15, 0.13, 0.11, 0.09 μm) which limits the degrees of freedom for spectral tuning, they are practically free from optical crosstalk. Filters on top of the imager can be created by nanoimprint technologies which allow the creation of an array of plasmonic band-pass filters. However, the peak transmission of band-pass filters is relatively low (<0.4). Peak filter transmission decreases, and halfwidth increases with wavelength, making nano-optical filters less effective in the NIR (Fig. 21) [38].
- Virtual NIR filters separate NIR and color signals by image signal processing. One possible implementation adds filterless pixels to the RGB filter pattern, but in contrast to RGBW, no optical NIR-cut filter is used [33–35]. The filterless pixel has two functions: Firstly, it has a "panchromatic" spectral response that includes the NIR and is equivalent to that of a monochrome imager. The panchromatic P′-pixel is more than three times as sensitive as a color imager, capable of delivering a much brighter luminance image. Secondly, the P′-pixel delivers the reference signal necessary to estimate the NIR signal contribution to the R′G′B′ pixel signals. The raw color pixel responses are $R' = R + I$, $G' = G + I$, and $B' = B + I$ (Fig. 22). The panchromatic pixel response $P' = R + G + B + I$ provides the reference signal for estimating the NIR portion in the incident light, which is then used in the virtual NIR filter matrix to remove as much as possible of the NIR contributions to the R′G′B′ signals. The response of the P′-pixel can also be used to simply retrieve a panchromatic VIS–NIR luminance channel $L_{\mathrm{VIS-NIR}}$.

An example of raw spectral pixel responses ($R'(\lambda)$, $G'(\lambda)$, $B'(\lambda)$, $P'(\lambda)$) shows the high NIR signal contribution to the color signals as well as high amounts of crosstalk between the four pixel types. Since both deteriorate colors, they have to be minimized by determining the virtual NIR filter coefficients, for which two calibration methods are commonly used, global and spectral.

- The global method relies on a set of known reference colors, for example those of a Macbeth color checker chart, that have to be reproduced as faithfully as possible. The color match can be done in a standardized color space, for example CIE 1931 XYZ, and the matrix M_G optimized so that the

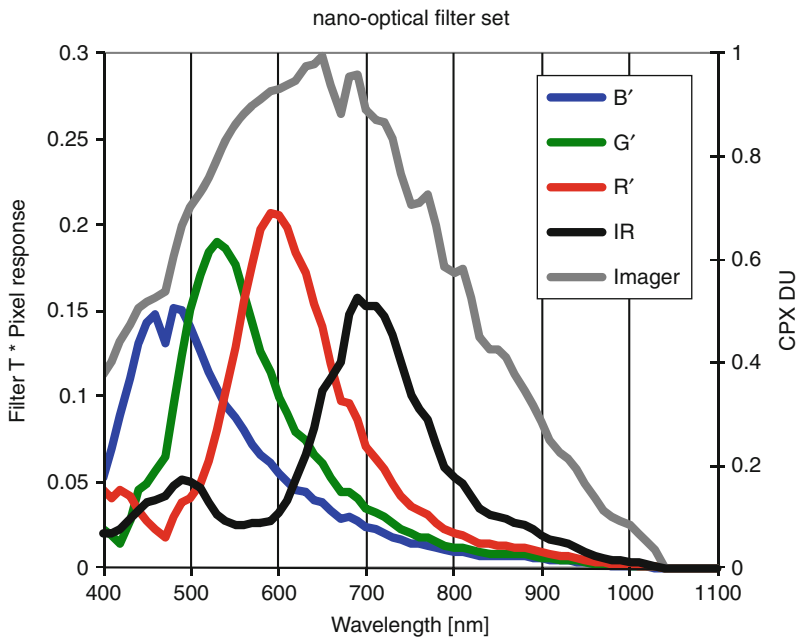

True Color Night Vision Video Systems in Intelligent Vehicles. Figure 21
Simulated response curves for CMOS imager with plasmonic nano-optical filters [38]

transformed colors match the reference colors $[XYZ]$ as closely as possible,

$$\begin{bmatrix} X \\ Y \\ Z \end{bmatrix} \approx M_G \cdot \begin{bmatrix} R' \\ G' \\ B' \\ P' \end{bmatrix}. \tag{5}$$

Global calibration works well for colors within and close to the reference set and under illumination conditions similar to those used in the calibration, but it is poorly suited for color night vision where the most relevant colors are not reflective but rather emissive colors whose brightness might lie far outside the set, and whose illuminant, and thus, relative NIR content varies widely.

- The spectral calibration method optimizes the matrix coefficients β_{mn} so that the filtered spectral response functions $(R(\lambda), G(\lambda), B(\lambda), I(\lambda))$ fulfill application-specific conditions.

$$\begin{bmatrix} R(\lambda) \\ G(\lambda) \\ B(\lambda) \\ I(\lambda) \end{bmatrix} = \begin{bmatrix} \beta_{11} & -\beta_{12} & -\beta_{13} & \beta_{14} \\ -\beta_{21} & \beta_{22} & -\beta_{23} & \beta_{24} \\ -\beta_{31} & -\beta_{32} & \beta_{33} & \beta_{34} \\ \beta_{41} & \beta_{42} & \beta_{43} & -\beta_{44} \end{bmatrix} \cdot \begin{bmatrix} R'(\lambda) \\ G'(\lambda) \\ B'(\lambda) \\ P'(\lambda) \end{bmatrix} \tag{6}$$

For example, in a machine-vision application, the coefficients are optimized to remove from the transformed spectral responses $(R(\lambda), G(\lambda), B(\lambda), I(\lambda))$ as much of the NIR and color crosstalk signals as possible. Instead of retrieving an IR channel, the P′- response can be mapped into a panchromatic luminance channel $L_{\text{VIS–NIR}}$. In human vision applications, a colorimetric calibration is better suited for achieving natural-looking colors. Colorimetric calibration as shown in Fig. 23c tries to optimize the matrix M_S so that the filtered spectral response curves of the imager approximate the spectral color matching functions $(b(\lambda), g(\lambda), r(\lambda))$ of the human visual system as specified in ISO 17321 [39]:

$$\begin{bmatrix} r(\lambda) \\ g(\lambda) \\ b(\lambda) \end{bmatrix} \approx M_S \cdot \begin{bmatrix} R'(\lambda) \\ G'(\lambda) \\ B'(\lambda) \\ P'(\lambda) \end{bmatrix}. \tag{7}$$

Spectral calibrations have the advantage of not relying on a particular set of reference colors, and also, they do not rely on a specific illuminant. The virtual NIR filter with colorimetric spectral calibration reduces the NIR crosstalk into color signals even under

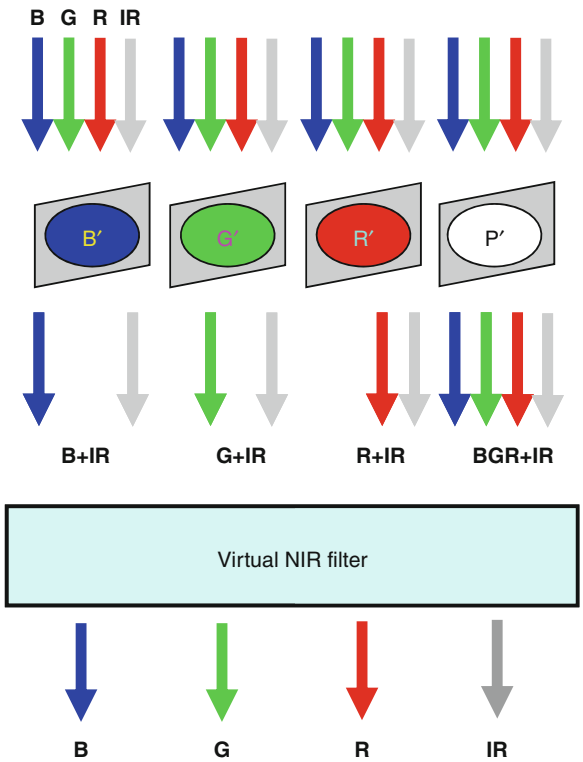

True Color Night Vision Video Systems in Intelligent Vehicles. Figure 22
Light, pixel responses of the R′G′B′P′ imager and image signals after virtual NIR filtering [35]

illumination conditions with high amounts of NIR, for example incandescent light at 3,200 K color temperature. The example in Fig. 24 shows images before (a), (b), and after virtual NIR filtering (c) with increasing amounts of NIR. Increasing NIR reduces color saturation of the raw R′G′B′ color channels, and increases brightness of the panchromatic P′-channel. The colors reconstructed by the virtual NIR filters become darker with increasing levels of NIR because of decreasing color-to-NIR signal ratios in the raw images.

However, residual spectral leakage limits the performance of the virtual NIR filter, especially in WDR mode where initial signal ratios are reduced. Careful management of NIR can further reduce the effects of NIR crosstalk and has to include pixel and microlens design to minimize optical and electrical crosstalk, high SNR to counter the noise-amplifying effect of high filter coefficients, and NIR-only headlights to minimize the proportion of NIR radiation with the highest leakage into the color signals.

Extending the Dynamic Range of Color Imagers with NIR Sensitivity

Signal saturation in color imagers leads to loss in color information; as the signals in the R, G, and B channels approach saturation levels, colorfulness decreases. In a RGB color imager, signal clipping in one or more color channels leads to a whitening of colors; clipping in a four-channel system such as R′G′B′P′ can also lead to false colors. WDR extension is therefore essential to capture color detail carried by bright lights. However, corrections have to be made for the effects of WDR extension on the color signals. In the example of multiple exposures with varying exposure time, each exposure maps a different range of input radiance signals into the same range of output image signals. Within the sequence of images to be combined into a single WDR image, the same output signal may be produced by different combinations of input signals so that the relationship between input and output signals is not unique. Therefore, the combination of exposures into the WDR image has to be preceded by linearization, which uses the camera response function in each color channel to create a unique map between the digital signal levels in the WDR image and the input radiance levels. The response function can be derived by techniques such as those proposed by Debevec and Malik [40], or Mitsunga and Nayar [41].

Direct WDR methods that extend the dynamic range in a single exposure have the great advantage of providing a unique map between input radiance and output image signal levels (Fig. 9). However, if the response function is nonlinear, for example piecewise linear as shown in Fig. 11, the signal ratios between the color channels will decrease with decreasing slope of the response curve. Increasing compression will thus decrease the input signal ratios between the raw R′G′B′P′ channels, thus decreasing chromaticity and iSNR of the output colors after virtual NIR filtering. To recover the color components and remove the NIR component from the highly compressed signals of bright colored lights, the raw R′G′B′P′ pixel signals have to be linearized with the inverse response curve of the imager so that the image signals can be referred

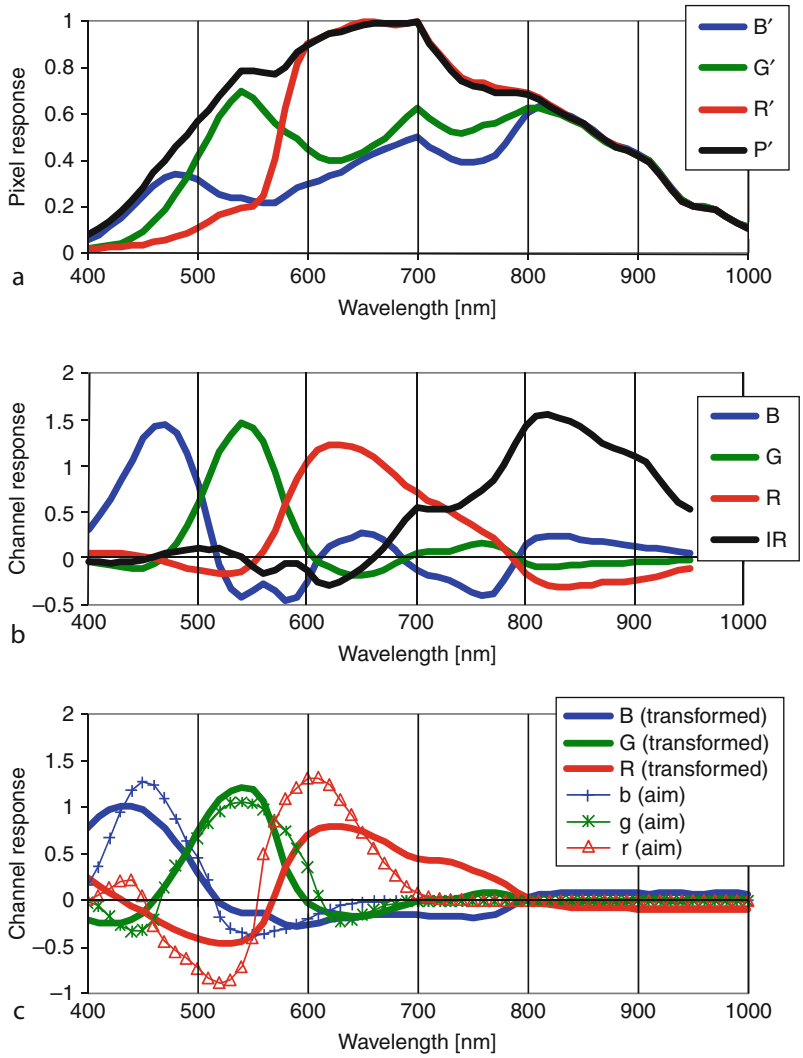

True Color Night Vision Video Systems in Intelligent Vehicles. Figure 23
Spectral pixel responses of (**a**) the R′, G′, B′, and P′ pixels and spectral channels after (**b**) separating NIR from the RGB color channels and (**c**) colorimetric calibration [42]

back to the corresponding scene radiances (inverse gamma correction). The effect of linearization is shown in Fig. 25 where it restores the colors in the highly compressed images of bright colored lights below the Macbeth color checker chart [42].

Visual Representation of the VIS + NIR Color Information

Section "Conclusion: Producing Natural Images Under Mesopic Conditions" outlined the requirements for rendering a natural-looking night vision image. In the example of a WDR imager with panchromatic and color pixels, NIR sensitivity increases the range of visibility, and the panchromatic image information can be displayed in the luminance channel. The virtual NIR-cut filter can recover traffic-relevant color information from backlit or retroreflective signage, traffic lights, and taillights. Virtual NIR filtering shows reasonably good performance in reconstructing colors even under illumination conditions with high amounts of NIR, for example incandescent light at a color temperature of

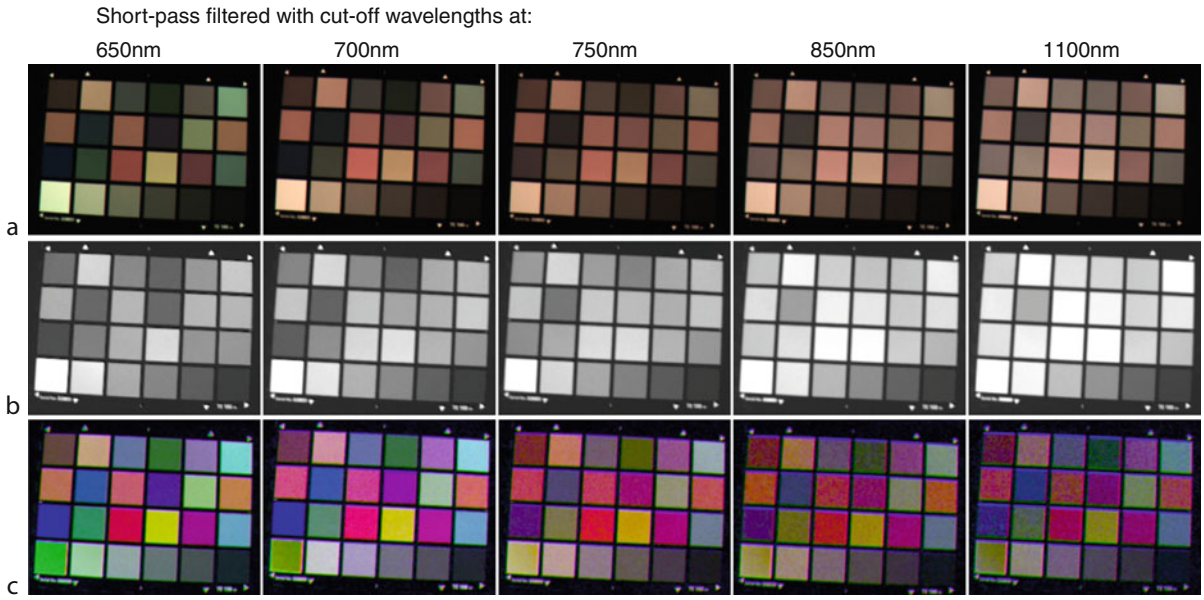

True Color Night Vision Video Systems in Intelligent Vehicles. Figure 24
Macbeth color checker chart illuminated by incandescent light (3,200 K) and imaged with short-pass filters allowing increasing amounts of NIR: (**a**) raw R′G′B′ image, (**b**) raw P′ image, and (**c**) RGB image after virtual NIR filtering [42]. The false colors in the brightest patch are caused by clipping of the P′-signal

3,200 K having 20% signal in the visual and 80% in the NIR range (Fig. 24). Since the filter array relies on standard RGB filter materials and fabrication processes, it can be produced at comparably low costs as conventional RGB imagers, without the extra cost of a patterned optical NIR-cut filter.

The VIS and NIR image information has to be represented in a way that the human observer viewing video on a dashboard screen can easily interpret. The VIS + NIR color camera with virtual NIR filter can provide multispectral image information, for example, in four channels, RGB and NIR. Multichannel image data could simply be mapped into a false-color representation, but this creates unnatural images that do not agree well with visual expectations and can even be confusing rather than useful. Natural image data representation that agrees with human expectations can be achieved by following certain design guidelines [43]: (1) orthogonal encoding to represent information with as little redundancy as possible; (2) anthropometric optimality to maximize usefulness to the human observer; (3) ecological invariance so ensure similarity of image interpretation over a variety of environmental parameters such as time of day, illuminants, and weather conditions; (4) computational simplicity to allow video implementation. For example, the achromatic channel of the HVS carries over 95% of the scene information and is much more sensitive to spatial information than the opponent color channels which process color information. Therefore, true-color image fusion is best suited for this application because it uses the extra information from the NIR to enhance the spatial and luminance information in the achromatic channel while mapping the color information from the visible range into the chrominance channels [32, 44, 45]. First, the RGB image obtained by virtual NIR filtering (6) must be transformed into a luminance–chrominance color space; then, its luminance component L_{VIS} is replaced by the luminance $L_{\mathrm{VIS+NIR}}$ estimated from the P′-pixels. Additional processing of $L_{\mathrm{VIS+NIR}}$ ensures that the fusion increases the brightness of the dark scene background but not so much that of colored lights, thus preventing the loss of color saturation in colored lights after fusion. For example, tone mapping using global, local, or Retinex algorithms significantly improves the visibility of grayscale and color detail in WDR images [46].

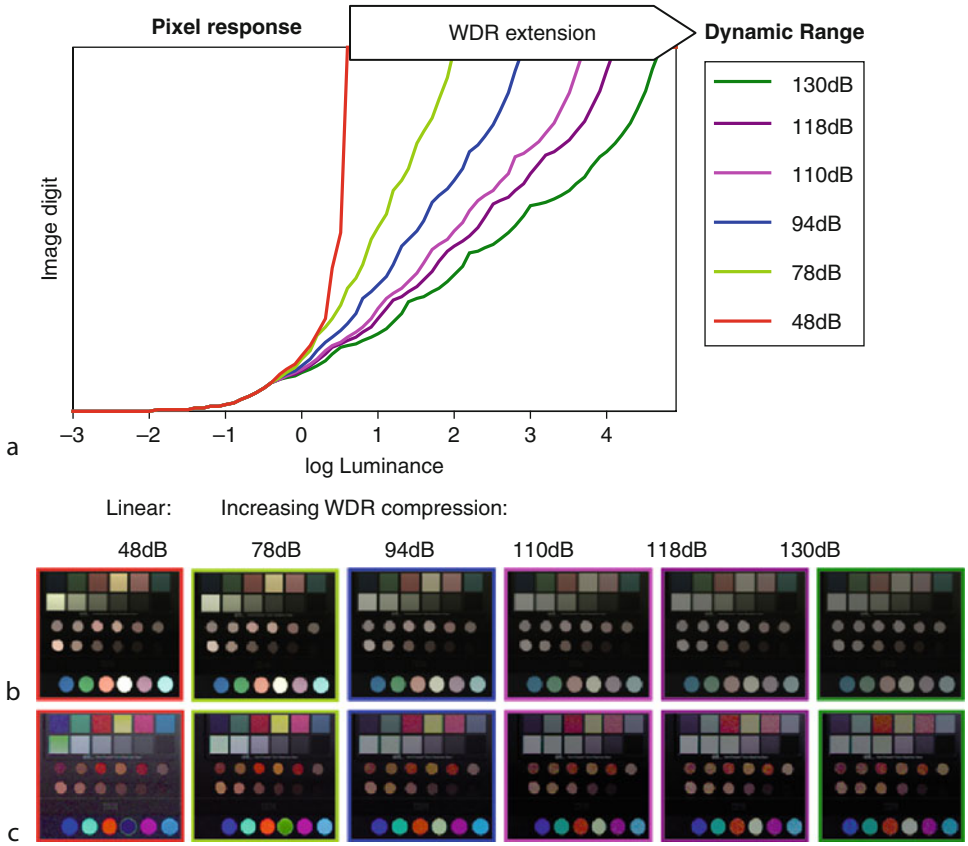

True Color Night Vision Video Systems in Intelligent Vehicles. Figure 25
WDR color scene consisting of dark reflective colors (*top*), bright transmissive colors with (*center*) and without NIR (*bottom*), taken with (**a**) imager response of increased compression and displayed (**b**) without and (**c**) with linearization [42]

The night scene in Fig. 26, illuminated only by the car's headlights, shows how image fusion effectively extends the field of vision, increases visibility of detail, and retains color in the retroreflective sign.

A previously described WDR scene simulator [5] composed of a digital display and a projector has been used for creating test scenes with controlled luminance levels, covering a wide dynamic range of 100 dB. Individual scene elements such as the road surface, lane markings, traffic signs, pedestrians, and headlights shown in Fig. 27 were calibrated so that their absolute luminance levels were within the ranges of typical traffic scenes as shown in Fig. 3. The example demonstrates that even if little or no IR is present in the scene, image fusion will still increase the brightness of dark scene detail because the filterless P′-pixels are more sensitive than any of the color pixels. Fusion utilizes the brighter luminance image from the P′-pixels, making the pedestrians in the dark background much apparent. The retroreflective sign and traffic lights are also brightened, but only to the extent that color saturation is not adversely affected.

In real-world night vision scenes, the panchromatic pixel can utilize the large NIR component of incandescent (tungsten) headlights that is invisible to the driver (Fig. 7). Furthermore, high-beam NIR-only headlights can be used to increase visibility beyond the distance range of headlights at low beam.

Example: Render Traffic-Relevant Color Information in Natural Images

Figure 28 demonstrates the image rendering of a VIS–NIR true-color WDR night vision camera for a typical urban night traffic scene.

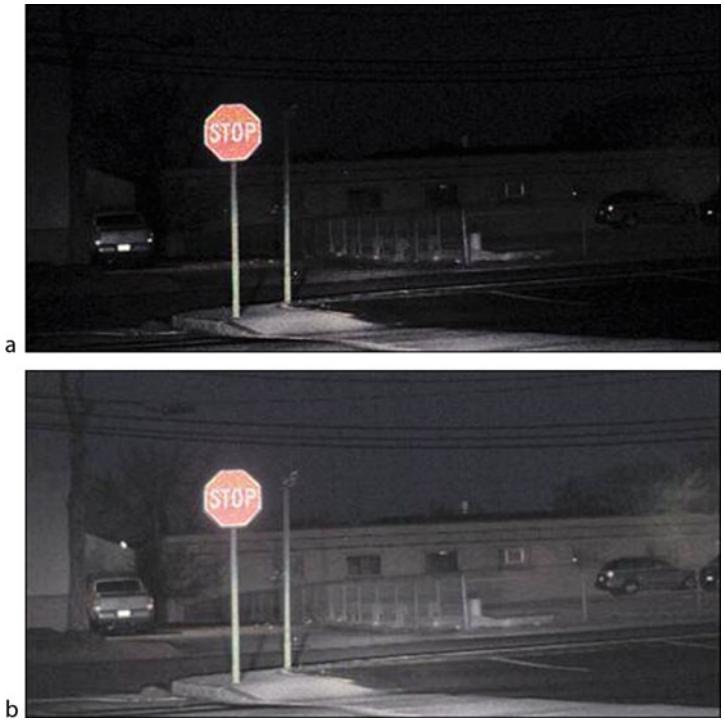

True Color Night Vision Video Systems in Intelligent Vehicles. Figure 26
Night scene with tungsten headlights as only light source, taken without image fusion (**a**) and with image fusion (**b**)

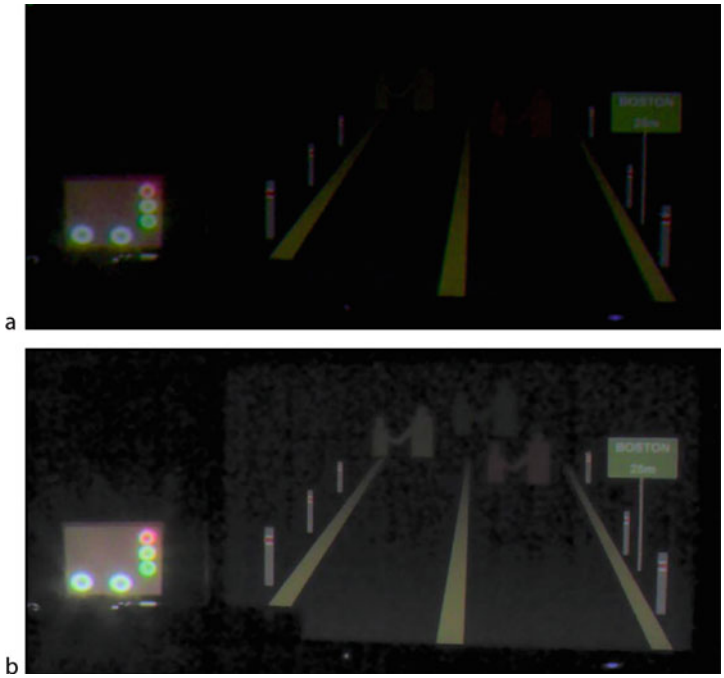

True Color Night Vision Video Systems in Intelligent Vehicles. Figure 27
Simulated 100 dB WDR traffic color scene (**a**) without and (**b**) with image fusion [35]

True Color Night Vision Video Systems in Intelligent Vehicles. Figure 28
Urban night traffic scene: (**a**) panchromatic P′ image, (**b**) RGB color image after virtual NIR filtering, and (**c**) final image after image fusion [8]

The monochrome image in Fig. 28a shows that the wide spectral sensitivity of the panchromatic P′-pixels delivers a sufficiently bright monochrome image even at a frame rate of 30 fps. The color image in Fig. 28b is comparatively dark, consisting mainly of the "unrelated colors" of traffic lights and vehicle taillights against an almost black background. The spectral energy in the visible band is small compared to the total energy within the imager's sensitivity range so that the luminance component of the filtered colors is much lower than the luminance from the P′-pixels. WDR compression and

subsequent linearization ensure that the bright highlight colors are preserved. The fused image in Fig. 28c then combines the bright monochrome background with the unrelated colors, leading to a more natural rendering of the scene that contains all traffic-relevant color information from traffic lights and car signal lights.

Conclusion

True-color night vision systems that utilize the NIR sensitivity and WDR capability of CMOS image sensors can aid the driver in dangerous situations where human vision is inadequate or challenged (Table 2). NIR sensitivity extends the range of vision when the safe braking distance exceeds the range of headlights. Cameras with adaptive WDR compression provide natural images of scenes where the intra-scene dynamic range exceeds that of the human eye, for instance when blinded by headlights of oncoming vehicles. Such cameras are able to adapt to sudden changes in scene brightness much faster than the HVS so that image information is available while the eye is still in the process of adapting, for example to the "black hole" after bright headlights of a passing car have left the field of vision.

True Color Night Vision Video Systems in Intelligent Vehicles. Table 2 Advantages of camera-based night vision systems

	Human visual system	True-color VIS–NIR camera with WDR	Advantages of camera
NIR sensitivity	No	Up to 1,100 nm	Extended range of vision
Adaptation to brightness and dynamic range	Transient 1–2 s	3–6 frames (0.2–0.1 s)	Image information available at WDR and during sudden changes in brightness
Color vision	Mesopic shift	Color constancy	Consistent color information

Future Directions

Vision-based DAS are one of a wide range of intelligent vehicle technologies that can be implemented either as stand-alone or cooperative systems. Some are already in use (antilock braking system, electronic stability control) while others are still in the research stage, under development, or in the process of being introduced into the market [47, 48].

Vision-based driver assistance systems aim to enhance the visual perception of the road ahead in situations where the human visual system is challenged or even fails to perceive dangerous situations. The scene information captured by the camera is processed into a natural-looking image and displayed in the driver's field of view. Since more than 90% of driving decisions and actions are based on vision, the fastest and most efficient human–machine interface is a visual display. Their combination of relative simplicity with high capacity and the speed of the visual information channel recommended display-based vision systems to early proponents of intelligent vehicle technology. Active NIR-sensitive night vision systems such as the Toyota Night View (2002) and Mercedes-Benz Night View Assist (2005) were pioneered in top-of-the-range cars. Despite the relative simplicity of camera-to-display night vision systems versus machine-vision-based automatic driver assistance systems (such as lane keeping, obstacle detection, etc.), the technical challenges and reliability requirements are so high that their penetration into the market is still low. The night vision system must deliver useful natural images under an extremely wide range of lighting conditions while experiencing changing proportions of color and NIR signals. Furthermore, they have to perform under adverse weather conditions that severely tax human vision, such as rain, drizzle, fog, snow, and salt spray. The performance and reliability of future night vision systems might be improved in many ways, perhaps including:

- Improved NIR management by integrating adaptive NIR-only headlights into the night vision system [49]
- Increased SNR of the image sensor to increase dark sensitivity and counter the increased visibility of color noise after virtual NIR filtering

- Reduced NIR crosstalk into the color signal through CFA and color pixel design, for example, nano-optical color filters [37, 38]
- Reduced NIR leakage in virtual NIR filtering by using algorithms that further reduce NIR leakage, for example, neural networks [50]
- Improved WDR color processing, for example, Retinex-based tone mapping [46]

In addition, head-up displays such as windscreen projection will be able to communicate visual information to the driver without shifting attention away from the road as necessitated by a head-down display outside the field of vision, for example, the dashboard displays of early night vision systems [28].

The main shortcoming of any display-based vision system is that it only improves traffic safety if the driver pays attention to the display at the critical moment. For example, it is of no use if the driver does not check the display as an obstacle beyond the field of vision is displayed by the NIR-sensitive system before the driver can see it through the windshield. Recent developments in intelligent vehicle technology work toward addressing this shortcoming and move beyond the early display-based vision systems. The two main strategies are intelligent stand-alone systems to enhance vehicle safety, and cooperative systems to improve road traffic safety [48].

- Stand-alone, in-vehicle systems use sensors to detect possible dangers and try to avoid or mitigate accidents by following a three tier strategy: (1) inform the driver as early as possible, (2) issue warnings if there is no driver reaction to the information, and (3) actively assist or ultimately intervene in the vehicle control [48]. In-vehicle systems will rely on multiple vision sensors and combine different sensor technologies such as radar and LIDAR (light detection and ranging) alongside vision sensors to improve overall detection reliability. Display-based vision systems can be expected to remain an important integral part of on-board safety systems because a visual display more immediately informs the driver of the nature of the danger than an acoustic warning would.
- Cooperative systems increase the capacity for gathering information by using communications from infrastructure or other sensor-equipped vehicles to make an individual vehicle less dependent on its own sensors and local environmental conditions. For example, if a car drives into a bank of fog, it can be guided by infrastructure and information from other vehicles outside the danger zone.

Forward-looking VIS–NIR cameras with color discrimination and WDR will continue to produce useful image information for both human and machine vision systems. Even if camera-based night vision systems with visual human–machine interfaces turn out to be only a transition stage toward future intelligent vehicle solutions, the technical experience gleaned by the implementation and application of pioneering vision systems may still prove indispensible for the future development of intelligent vehicle technology.

Bibliography

Primary Literature

1. Traffic Accident Causation in Europe (TRACE) (2007) Review of crash effectiveness of intelligent transport systems, Project No. 027763, Deliverable D4.1.1–D6.2, 55
2. Jones WD (2006) Safer driving in the dead of night – infrared vision systems are set to become standard in high-end cars. IEEE Spectrum Green Technology. http://spectrum.ieee.org/green-tech/advanced-cars/safer-driving-in-the-dead-of-night
3. Yendrikhovskij S (1999) Image quality: between science and fiction. In: Proceedings of the IS&T PICS, Savannah, pp 173–178
4. Hertel D, Betts A, Hicks R, ten Brinke M (2008) An adaptive multiple-reset CMOS wide dynamic range imager for automotive vision applications. In: Proceedings of the 2008 IEEE intelligent vehicles symposium, IEEE Press, Piscataway, pp 614–619
5. Hertel D (2010) Extended use of incremental signal-to-noise ratio as reliability criterion for multiple-slope wide-dynamic-range image capture. J Electron Imaging 19(1):011007
6. Marjukka E, Liisa H (2005) MOVE – performance based model for mesopic photometry. Helsinki University of Technology Report No. 35, ISBN 951-22-7566-X, Espoo, Finland
7. Fu C, Li C, Luo MR, Hunt RWG, Pointer MR (2007) Quantifying colour appearance for unrelated colour under photopic and mesopic vision. In: Proceedings of the IS&T 15th color imaging conference, Albuquerque, pp 319–324
8. Hertel D, De Locht C (2010) Utilizing near-infrared and colour information in an automotive wide-dynamic-range night vision system for driver assistance. In: Meyer G, Valldorf J (eds) Advanced microsystems for automotive applications 2010 – smart systems for green cars and safe mobility. Springer, Dordrecht/London/New York, pp 145–154
9. Carlson PJ, Urbanik T (2004) Validation of photometric modeling techniques for retroreflective traffic signs. Transp Res Rec 1862:109–118

10. Keelan BW (2002) Handbook of image quality. Dekker, New York, pp 329–399
11. Hertel D, Chang E (2007) OECF characterization of a non-linear HDR color camera for automotive applications. In: Proceedings of the IS&T 15th color imaging conference, Albuquerque, pp 244–248
12. Dierickx B (2008) Wide dynamic range: what should I care about? IEEE international solid-state circuits conference (ISSCC '08), imager design forum, wide dynamic range imaging, San Francisco
13. Williams D (2003) Debunking specsmanship: progress on ISO/TC42 standards for digital capture imaging performance. In: Proceedings of the IS&T PICS, Rochester, pp 77–81
14. Sangwine SJ, Horne REN (1998) The colour image processing handbook. Springer, New York, p 127
15. International Standard ISO 12232 (1997) Photography – electronic still picture cameras – determination of ISO speed
16. International Standard ISO 14524:1999(E) (1999) Photography – electronic still-picture cameras – methods for measuring opto-electronic conversion functions (OECFs)
17. International Standard ISO 15739:2003(E) (2003) Photography – electronic still-picture imaging – noise measurements
18. Görgens E (1987) Objective evaluation of image quality. J Inf Rec Mater 15:305–321
19. Kerr DA (2008) The ISO definition of the dynamic range of a digital still camera. http://dougkerr.net/Pumpkin/articles/ISO_Dynamic_range.pdf
20. Dainty JC, Shaw R (1974) Image science. Academic Press, London, pp 152–171
21. Chamberlain SG, Lee JPY (1984) A novel wide dynamic range silicon photodetector and linear imaging array. IEEE J Solid-State Circuits SC-19(2):41–48
22. Storm G, Henderson R, Hurwitz JED, Renshaw D, Findlater K, Purcell M (2006) Extended dynamic range from a combined linear-logarithmic CMOS image sensor. IEEE J Solid-State Circuits 41(9):2095–2106
23. Wang X, Wong W, Hornsey R (2006) A HDR CMOS image sensor with inpixel light-to-frequency conversion. IEEE Trans Electron Devices 53(12):2988–2992
24. Yang D, El Gamal A, Fowler B, Tian H (1999) A 640 × 512 CMOS image sensor with ultrawide dynamic range floating-point pixel-level ADC. IEEE J Solid-State Circuits SC-34(12):1821–1834
25. Kawahito S (2006) A sensitivity and linearity improvement on a 100 dB dynamic range image sensor using a lateral overflow integration capacitor. IEEE J Solid-State Circuits 41(4): 851–858
26. Decker S, McGrath RD, Brehmer K, Sodini CG (1998) A 256 × 256 CMOS imaging array with wide dynamic range pixels and column-parallel digital output. IEEE J Solid-State Circuits SC-33(12):2081–2091
27. Knoll PM (2002) A NIR based system for night vision improvement. SAE Convergence 2002, Detroit
28. Kallhammer J-E (2006) Night vision: requirements and possible roadmap for FIR and NIR systems. SPIE 6198, 61980 F
29. Hörter MH, Stiller C, Koelen C (2009) Hardware and software framework for automotive intelligent lighting. In: Proceedings of the 2009 IEEE intelligent vehicles symposium, Xi'an, China, p 299
30. Hamilton JF, Compton JT (2007) Processing color and panchromatic pixels. US Patent Application 20070024879
31. Honda H, Iida Y, Itoh G, Egawa Y, Seki H (2007) A novel Bayer-like WRGB color filter array for CMOS image sensors. In: Proceedings of the SPIE-IS&T electronic imaging, SPIE, vol 6492, pp 64921 J.1–64921 J.10
32. Kriesel M, Gat N (2008) True-color night vision cameras. In: Proceedings of the SPIE, vol 6540, pp 65400D.1–65400D.10
33. Frame WW (2006) One chip, low light level color camera. US 7,012,643 B2
34. Kidono K, Yoshiki N (2007) Visibility estimation under night-time conditions using a multiband camera. In: Proceedings of the 2007 IEEE intelligent vehicles conference, Istanbul, Turkey, pp 1013–1018
35. Hertel D, Marechal H, Tefera DA, Fan W, Hicks R (2009) A low-cost VIS-NIR true color night vision video system based on a wide dynamic range CMOS imager. In: Proceedings of the 2009 IEEE intelligent vehicles symposium, Xi'an, China, p 273
36. Koyama S et al (2009) A day and night MOS imager spectrally adjusted for a wide range of color temperatures. SPIE 7249, 72490 S
37. Catrysse PB, Wandell BA (2007) Integrated color pixel. U.S. Patent No. 7,248,297 (Filed 2001 – Issued 2007)
38. Choi B (2007) Nano-technology for color: plasmonic nano-optic filter technology for color capturing, expression, and management. In: Proceedings of the IS&T CIC15, Albuquerque
39. International Standard ISO 17321:1998 (1998) Graphic technology and photography – colour target and procedures for the colour characterization of digital still cameras (DSCs). ISO, Geneva, Switzerland
40. Debevec PE, Malik J (1997) Recovering high dynamic range radiance maps from photographs. In: Proceedings of the SIGGRAPH 97 annual conference, Los Angeles, pp 369–378
41. Mitsunga T, Nayar SK (1999) Radiometric self calibration. In: Proceeding of the IEEE computer vision and pattern recognition, Fort Collins
42. Hertel D (2010) Using spectral response measurements to optimise the colour processing of a wide dynamic range colour camera with near-infrared sensitivity. The royal photographic society, symposium on colour imaging 2010, http://www.rps-isg.org/SCI2010_programme.php
43. Scott Tyo J (2007) Displaying advanced optical imagery information for human observers. In: Proceedings of the IS&T CIC15, Albuquerque, pp 174–177
44. Ngo H, Tao L, Zhang M, Livingston A, Asari V (2005) A visibility improvement system for low vision drivers by nonlinear enhancement of fused visible and infrared video. IEEE computer society conference on computer vision and pattern recognition (CVPRW'05) – Workshops, p 25
45. Fredembach C, Süsstrunk S (2008) Colouring the near-infrared. In: Proceedings of the IS&T 16th color imaging conference, Portland, pp 176–182

46. Meylan L, Süsstrunk S (2006) High dynamic range image rendering using a retinex-based adaptive filter. IEEE Trans Image Process 15(9):2820–2830
47. Bertozzi M, Broggi A, Fascioli A (2000) Vision-based intelligent vehicles: state of the art and perspectives. Robot Auton Syst 32:1–16
48. European Commission, Information Society and Media: i2010 intelligent car initiative. http://ec.europa.eu/information_society/activities/intelligentcar/docs/icar/intelligent_car.pdf
49. Carley L (2009) News technologies for safer driving: adaptive lighting, night vision, backup cameras & blind spot detection. Import car, http://www.import-car.com/Article/60749/News_Techn.aspx
50. Kang HR, Anderson PG (1992) Neural network applications to the color scanner and printer calibrations. J Electron Imaging 1:125–134

Books and Reviews

Frieser H (1975) Photographische Informationsaufzeichnung. Focal Press, New York
Hunt RWG (2004) The reproduction of colour. Fountain Press, Tolworth, England
Proceedings of IEEE intelligent vehicles symposium 2007, Istanbul, Turkey, 13–15 June 2007, ISBN 1-4244-1068-1
Proceedings of IEEE intelligent vehicles symposium 2008, Eindhoven, The Netherlands, 4–6 June 2008
Proceedings of IEEE 2009 IEEE intelligent vehicles symposium, Xi'an, China, 3–5 June 2009, ISBN 978-1-4244-3502-9
Reinhard E, Ward G, Pattanaik S, Debevec P (2006) High dynamic range imaging – acquisition, display, and image-based lighting. Morgan Kaufmann Publishers, San Francisco
Sharma G (2003) Digital color imaging. CRC Press, Boca Raton
Wyszecki G, Stiles WS (2000) Color science. Wiley, New York

Tuberculosis, Epidemiology of

Giovanni Sotgiu[1], Matteo Zignol[2], Mario C. Raviglione[2]
[1]Epidemiology and Biostatistics Unit, Department of Biomedical Sciences, University of Sassari, Sassari, Italy
[2]STOP TB Department (STB), HIV/AIDS, TB & Malaria Cluster (HTM), World Health Organization, Geneva, Switzerland

Article Outline

Glossary
Definition of the Subject and Its Importance
Introduction
Basic and Descriptive Epidemiology of Tuberculosis
Etiologic Epidemiology of Tuberculosis
Tuberculosis/HIV Coinfection
Drug-Resistant Tuberculosis
Control of Tuberculosis
Global Epidemiological Situation
Future Directions
Bibliography

Glossary

Acquired immunodeficiency syndrome (AIDS) Clinical syndrome caused by the Human Immunodeficiency Virus (HIV). Its pathogenesis is related to a qualitative and quantitative impairment of the immune system, particularly a reduction of the CD4+cell count (surrogate marker of the disease). After an average of 10 years if untreated, HIV + individuals can develop opportunistic diseases (i.e., infections and neoplasias rarely detected in immunocompetent subjects). The natural history of the disease can be dramatically modified with administration of combination therapy composed of at least three antiretroviral (ARV) drugs.

Human immunodeficiency virus (HIV) Virus that causes Acquired Immunodeficiency Syndrome (AIDS). It belongs to *Retroviridae* family and was discovered in 1983 by Luc Montagnier and Robert Gallo. It is transmitted mainly through sexual intercourse, exchange of contaminated syringes among intravenous drug users, and contaminated blood transfusion. HIV-1 is the type most frequently detected worldwide.

Incidence Rate describing the number of new cases of disease occurring within a unit of time in a defined cohort at risk of disease (expressed in cases per 100,000 population per year).

Latent tuberculosis infection (LTBI) Infection caused by *Mycobacterium tuberculosis* transmitted mainly through the air. Clinical and/or radiological signs of latent tuberculosis infection cannot be detected in the majority of the cases. The infection can be presumptively diagnosed by a positive tuberculin skin testing and/or a positive interferon-γ release assay (IGRA), being able to identify a persistent adaptive immunological reactivity against mycobacterial antigens. In most individuals

mycobacteria can be eliminated through chemoprophylaxis. It is estimated that one third of the human population is infected by *Mycobacterium tuberculosis* worldwide.

Mortality Rate describing the number of deaths from a disease occurring within a unit of time in a defined cohort at risk of death (expressed in deaths per 100,000 population per year).

Mycobacterium tuberculosis Bacterium that causes tuberculosis, discovered by Robert Koch in 1882. It is genetically closely related to other mycobacteria with which it forms a complex (*Mycobacterium africanum*, frequently detected in Western Africa, and *Mycobacterium bovis*, frequently detected in the past in cows and transmitted to human beings through unpasteurized milk).

Prevalence Number of cases of disease in a defined population at a specific point in time; it is mainly presented as a relative frequency (i.e., proportion usually expressed per 100,000 population).

Tuberculosis Infectious disease caused by *Mycobacterium tuberculosis*. It usually involves the lungs (pulmonary tuberculosis) but can also affect other organs (i.e., kidneys, central nervous system, lymph nodes, bones, etc.: extrapulmonary tuberculosis). Pulmonary tuberculosis, which is the most frequent clinical form, can be classified as smear-positive or smear-negative according to the result of the sputum bacteriological examination. The former is a major public health problem being highly contagious. Only a few individuals develop tuberculosis after a mycobacterial infection, and most of them soon after infection: it is estimated that the lifetime risk is 5–10% in HIV-negatives and 5–15% yearly in HIV-positives.

Definition of the Subject and Its Importance

Tuberculosis is a disease caused by bacilli belonging to the *Mycobacterium tuberculosis* complex, which includes the species *Mycobacterium tuberculosis* (most frequently detected in human beings), *Mycobacterium africanum*, and *Mycobacterium bovis*. It is primarily an airborne disease. Mycobacteria enter into the human airways through the inhalation of droplet nuclei, i.e., particles containing mycobacteria aerosolized by coughing, sneezing, talking, or singing. Other rare, recognized ways of transmission are the ingestion of cow milk contaminated by *Mycobacterium bovis* (frequent route of transmission in the past), cutaneous inoculation in laboratory workers and pathologists, and sexual intercourse [1].

Tuberculosis is a major public health issue worldwide. Together with HIV/AIDS, it is one of the main infectious killers of individuals in their productive years in low-income countries [2]. However, tuberculosis is a highly curable disease if diagnosed and treated with combination chemotherapy. As a result of the global implementation of the World Health Organization's (WHO) STOP TB Strategy, during the period 1995–2009, 41 million tuberculosis patients were successfully treated and 6 million deaths averted compared to what would have happened if current standards were not implemented [3, 4].

Introduction

The epidemiology of tuberculosis studies the dynamics and interactions between *Mycobacterium tuberculosis* and human beings in a specific environment. Furthermore, it qualitatively and quantitatively evaluates all the covariates (for instance, the administration of antituberculosis drugs) that could interfere with the outcomes of the natural history of this interaction (i.e., exposure, infection, disease, and death) [5].

Basic and Descriptive Epidemiology of Tuberculosis

The global burden of tuberculosis is measured using epidemiological indicators (incidence, prevalence, mortality, and case fatality). Estimates of these indicators are computed yearly by the World Health Organization which collates information obtained from surveillance systems (notification system and mortality registries), special epidemiological studies (surveys of tuberculosis prevalence and in-depth analyses of surveillance data), and experts' opinion [6].

Epidemiological Indicators

Tuberculosis incidence: number of new cases of tuberculosis occurring within a specific time period (usually 1 year) in a defined cohort. It is usually presented as a rate per 100,000 inhabitants and describes the probability of developing tuberculosis in a specific time period [6, 7].

Tuberculosis prevalence: number of cases of tuberculosis in a defined population at a specific point in time. It is presented as an absolute or a relative (usually per 100,000 inhabitants) frequency and can be considered the product of the incidence of tuberculosis by the duration of the disease. This indicator assesses the global, national, regional, and local burden of tuberculosis.

Tuberculosis mortality: number of deaths from tuberculosis occurring within a specific time period (usually 1 year) in a cohort of individuals with tuberculosis disease. It is often presented as a rate per 100,000 people and describes the probability of dying from tuberculosis in a specific time period.

Tuberculosis case fatality: number of deaths from tuberculosis occurring within a specific time period (usually 1 year) in a defined cohort of individuals with tuberculosis. It is presented as a percentage.

Incidence of sputum smear-positive pulmonary tuberculosis cases: number of new sputum smear-positive cases of pulmonary tuberculosis occurring within a specific time period (usually 1 year) in a defined cohort. It is usually presented as a rate per 100,000 population. It identifies the most contagious tuberculosis cohort, that is, the most important source of infection.

Incidence of sputum culture-positive pulmonary tuberculosis cases: number of new sputum culture-positive cases of pulmonary tuberculosis occurring within a specific time period (usually 1 year) in a defined cohort. It is usually presented as a rate per 100,000 population.

Etiologic Epidemiology of Tuberculosis

Natural History

The dynamics of the probabilistic model of tuberculosis are complex and the associated covariates, as well as their quantitative effects, are not always known. The potential interaction between a human being and the strains of *Mycobacterium tuberculosis* could result in the following non-deterministic outcomes: subclinical infection, pulmonary and/or extrapulmonary disease, and death. The incidence of the above mentioned outcomes is regulated by the occurrence and the additive and/or the synergistic combination of multiple risk factors. Several environmental, bacterial, and human risk factors have been identified. Some of them could play an important role since the first crucial event, that is, the exposure to a source of mycobacteria [1, 5, 8].

Exposure

A critical exposure to transmission of mycobacteria from a contagious patient to a susceptible individual could be a close physical contact or permanence in a small room with limited ventilation [5].

The most important variable significantly increasing the likelihood of exposure to a source of *Mycobacterium tuberculosis* is the prevalence of contagious patients in a specific setting. This is estimated as the product of the incidence of infectious individuals by the duration of their infectiousness. The number of incident cases greatly varies between settings and depends on numerous factors.

Duration of infectiousness is strictly related to the capacity of the health system for early detection and adequate treatment of an index case [5, 8]. After a microbiological diagnosis, which should include drug-sensitivity testing, proper anti-tuberculosis treatment should be started without delay [3]. Correct drug combinations and dosages should be used to avoid sub-optimal anti-bacterial activity [5, 9, 10]. Strict clinical follow-up of patients in nosocomial or community settings should be undertaken to ensure adherence to anti-tuberculosis medications for the full duration of treatment. Compliance could be compromised by the long duration of therapy and/or the emergence of adverse events. The capacity of a patient to adhere to antituberculosis therapy depends on factors related to the health system, socioeconomic conditions of the individual, type of therapy, and the disease and patient's characteristics. The concept of early case detection and immediate treatment is supported by the evidence that on average 30–40% of the close contacts of a sputum smear-positive pulmonary case are estimated to be infected at the time of diagnosis. The public health consequences of a diagnostic and/or therapeutic delay are dramatic [5].

It is clear that quality and quantity of human relations modify the risk of critical exposures and, consequently, the risk of acquiring the infection [5]. In particular, population density is a critical element: the higher the population density, the greater the risk of

interactions. High population density can be experienced in urban areas or in household crowding associated with poor housing [5, 8]. Climatic condition is an additional environmental variable that plays a relevant role in the likelihood of exposure. In cold climates, people tend to spend more time in indoor activities, increasing the risk of exposure because of the higher chances of close contact. On the other side, in warm climates people tend to spend more time outdoors, diminishing frequency and duration of case–contact interactions per unit of space. At the same time natural indoor ventilation and the effect of the solar ultraviolet rays that kill mycobacteria contribute to control the spreading of infection [5].

Other relevant non-environmental modifiers of the risk of exposure are sex and age. In several low-income countries and social groups, males and females have different opportunities of social contact and therefore a different risk of exposure. For instance, in some countries females are excluded from public activities and spend most of their time indoors. The median age of tuberculosis cases, and consequently of contagious sources of infection, is considerably different between low- and high-income countries, with elderly people representing the majority of the autochthonous patients in industrialized areas and young adults counting for the largest proportion of patients in low-income countries [5, 11–13].

Infection

The risk of infection by *Mycobacterium tuberculosis* is directly associated to the probability of exposure to infectious particles produced by a tuberculosis patient through coughing, sneezing, talking, or singing [1, 5, 8, 14]. Such risk is related to the concentration of contagious droplet nuclei containing mycobacteria and to the time of exposure [1, 5].

Infectious particles must be suspended in the air in order to be inhaled by a contact of a tuberculosis patient. The speed of falling to the ground is directly correlated to the square of their diameter. However, the tendency of liquid particles to evaporate and, consequently, to reduce their diameter, increases the speed of their descent. The effect of evaporation on very large liquid particles is less important. Furthermore, humidity and temperature could influence the evaporation: high humidity hinders the evaporation of infectious particles and, indirectly, increases the speed of dropping to the ground. Overall, the effect of the diameter of the particle is more influential than that of humidity [5].

Droplet nuclei should be 1–5 μm large to be inhaled and retained in the pulmonary alveoli. It has been demonstrated that a diameter >5 μm increases the probability of being entrapped in the upper airways through the continuous movement of both the vibrissae and the muco-ciliary system. On the other hand, contagious droplets whose diameter is <1 μm can arrive to the alveolar spaces, but the probability of retention in the peripheral pulmonary alveoli is very low [1, 5].

A crucial variable that can dramatically change the air density of contagious droplet nuclei in a specific indoor environment (for instance, in a nosocomial setting) is the natural, mixed-mode, or mechanical ventilation [15]. Several authors described transmission of mycobacterial strains in health-care settings with flawed or missing ventilation systems both in low- and high-income countries. The typology of the ventilation system should be chosen taking into account several variables: the building structure, outdoor climatic conditions and air quality, purchase and maintenance costs, and national and local regulations. However, modifiers should not alter the main principle of a ventilation system that must promote an airflow direction from the infectious source to the air exhaust area [5, 15]. Ventilation rate can be evaluated measuring the volume of the space (i.e., air changes per hour – ACH) or the number of individuals in a space (i.e., liters/second/person): every individual should have a definite supply of fresh air to dilute the concentration of mycobacteria. The World Health Organization recommends more than 11 air changes per hour for an isolation room of 24 m^3 (i.e., at least 80 l/s/person). Natural ventilation may be improved by increasing the size of windows and positioning them on opposite walls. Well-designed fans can improve the airflow direction when natural ventilation rates are not adequate (mixed-mode ventilation). However, continuous maintenance of those fans is essential. In some circumstances it may be necessary to use upper room or shielded ultraviolet germicidal irradiation (UVGI) devices. In settings with frequent climatic changes or

high risk of transmission of multi-drug resistant mycobacterial strains, UVGI devices could be helpful in addition to a mechanical ventilation system.

Several measures should be implemented in household settings to reduce the risk of transmission: improvement of natural ventilation, education on cough etiquette, and respiratory hygiene. Furthermore, a tuberculosis patient should sleep isolated in a well-ventilated room or, if his/her clinical conditions are favorable, should spend as much time as possible outdoors.

Personal protective equipment may considerably reduce the possibility of infection, especially when the ventilation system is weak. In this regard only high-efficiency particulate air-filter respirators filtering out droplet nuclei sized 1–5 μm can be protective. Particulate respirators meeting or exceeding the N95 standards set by the United States Centers for Disease Control and Prevention/National Institute for Occupational Safety and Health (CDC/NIOSH) or the CE certified FFP2 standards are recommended for health-care workers (particularly during the management of multi-drug resistant tuberculosis cases and aerosol-generating procedures) and visitors. Health education on the importance of respirators in communities at risk should be carried out in order to avoid stigma, and continuous training of health-care providers on the correct use (fit testing) and on indications of respirators should be organized. Surgical masks can be worn by contacts of a patient but do not protect from exposure [15]. The probability of being infected can be decreased if the source of droplet nuclei is isolated or if both mouth and nose are covered.

The most efficient measure to stop transmission is to rapidly detect and adequately treat a tuberculosis case [3, 5, 8, 15]. Patients are normally not infectious after 2–3 weeks of effective treatment. However, not all tuberculosis patients are equally infectious and there is a correlation between the number of mycobacteria in a milliliter (ml) of sputum and the efficiency of transmission. At least 5,000 mycobacteria in 1 ml of sputum are necessary to classify a sputum smear examination as positive.

Several studies demonstrated that sputum smear-positive patients are significantly more contagious than those who are sputum smear-negative and culture-positive. Furthermore, the latter are not much more infectious than tuberculosis patients who have a negative smear and culture [5, 8].

Although sputum smear-positive patients are the most contagious population, those who are sputum smear-negative need equal attention, as 17% of mycobacterial transmissions, in some industrialized settings, are due to this group of patients [5].

According to estimates computed in the pre-antibiotic era and used to model the tuberculosis epidemic, an undiagnosed sputum smear-positive patient can infect 10–12 contacts annually. Since after 2 years, the probability of death or spontaneous conversion to sputum smear-negativity is high, the average number of contacts infected by a single smear-positive case was estimated to be 20–24 [5, 8, 16]. The delay of diagnosis and/or of treatment of just 2–3 months could result in infection of several contacts [5].

Numerous factors determine patient's delay to diagnosis: these include alcohol or substance abuse, low income, difficult access to health care facilities, disabilities, and beliefs about tuberculosis. On the other hand, other concomitant pulmonary diseases, sputum smear-negative or extra-pulmonary tuberculosis, inexperience of health care workers, weak health care infrastructure, and absence of respiratory symptoms are all factors associated with healthcare delay [17, 18].

The annual burden of the most relevant source of tuberculosis infections is assessed through an epidemiological indicator: the incidence of sputum smear-positive pulmonary tuberculosis cases. This describes the number of new sputum smear-positive cases of pulmonary tuberculosis occurring within 1 year in a defined population at risk of tuberculosis [5, 6, 8]. The average annual risk of latent tuberculosis infection is an important epidemiological indicator that assesses the probability of becoming infected with *Mycobacterium tuberculosis* in a period of 1 year [5, 8].

Clinical and/or radiological signs of latent tuberculosis infection cannot be detected in the majority of the cases. However, it can only be presumptively diagnosed through a tuberculin skin testing (TST) and/or an interferon-γ release assay (IGRA), which identifies a persistent adaptive immunological reactivity against mycobacterial antigens [14, 19–22]. The tuberculin skin test, performed with an intradermal injection of purified protein derivative (PPD) obtained from *Mycobacterium*

tuberculosis culture filtrate, has been considered as the gold standard diagnostic tool for identifying individuals latently infected with *Mycobacterium tuberculosis*. The main limitation of this technique is the low specificity, due to antigenic similarities between PPD, Bacille Calmette-Guerin (BCG) strains, and nontuberculous mycobacterial strains. Furthermore, its application and interpretation significantly depend on the health worker responsible for the test [14, 19, 22].

Interferon Gamma Release Assays (IGRA), available in two different commercial forms, that is, QuantiFERON-TB Gold In Tube (QFT-IT; Cellestis Ltd., Chadstone, Australia) and T-SPOT.TB (Oxford Immunotec, Abingdon, UK), are tools for the in vitro diagnosis of latent tuberculosis infection. They detect cellular immune reactivity toward *Mycobacterium tuberculosis*–specific antigens (ESAT-6, CFP-10, and TB7.7). As such, contrary to PPD, they can discriminate between people previously immunized with Bacille Calmette-Guerin vaccination or those infected by non-tuberculous mycobacteria from tuberculosis patients [14, 19–22].

The average annual risk of tuberculosis infection can be estimated with direct or indirect methods:

- The direct evaluation assesses the proportion of individuals who convert to tuberculin skin test in a defined period of time. The main limitations are related to the sample size, which should be large enough in order to obtain an adequate statistical power, and to the boosting phenomenon (an apparent conversion related to repeated tests).
- The indirect evaluation relies on the relationship between the prevalence of tuberculosis infection in a specific time-point and the average annual risks of infection.

The probability of being infected is estimated to be very low in high-income countries (from 0.1% to 0.01%) especially among the young. On the other hand, the prevalence of infection is high in most developing countries, due to ongoing transmission [5, 8]. Overall, one third of the global population is estimated to be infected by *Mycobacterium tuberculosis* [5, 6, 8].

Disease

Active tuberculosis is the outcome of infection with *Mycobacterium tuberculosis* [1, 5, 8, 23]. As for exposure and infection, the likelihood of clinical tuberculosis is strictly dependent on risk factors, the impact of which is not only related to their effect on the pathogenesis of the disease but also to their prevalence in the general population [5, 8].

After the establishment of tuberculosis infection the probability of developing a disease is higher in the first 12–24 months after the entry of *Mycobacterium tuberculosis* into the human body, and decreases as time elapses from the infection. It is generally estimated that the risk of disease is about 5% in the first 1–2 years after infection, and up to 5% in the subsequent years [1, 5, 8]. The age of primary infection is an important determinant of the cumulative risk, as this is the highest in young individuals (from 35% to 50% in children aged less than 15 years and those who are in close contact with a sputum smear-positive patient) [5, 8].

The key pathogenic factor favoring the development of tuberculosis is the quantitative and/or functional deficiency of the innate and/or adaptive immune system, which is responsible for the control of tuberculosis infection [2, 5, 8, 23]. The host cellular and molecular mechanisms triggered by mycobacterial infections are only partially known. After reaching the lower respiratory tract, the mycobacteria grow, partially controlled for the first few weeks by nonspecific immunity. CD4+ lymphocytes producing interferon-γ are recruited after 2 weeks but their number is not sufficient to activate the pool of alveolar macrophages. Their priming in the draining lymph nodes occurs only after the first 7–10 days because mycobacteria are initially phagocytosed by non-motile phagocytic cells. T-cell priming and accumulation could additionally be delayed through the activation of regulatory T lymphocytes. Continuous activation of T lymphocytes is vital to control mycobacteria in the granuloma; nevertheless, several experimental data demonstrated that once exposed to chronic mycobacterial stimulation, T lymphocytes can experience a functional collapse [1, 23]. Numerous medical conditions can modify one or more components of the immune response against *Mycobacterium tuberculosis*, compromising the control of the infection, and, then, increasing the probability of development of disease [1, 5, 8]. For these reasons and due to its global burden, HIV/AIDS is recognized as the most important risk

factor for the development of tuberculosis [1, 2, 5, 8, 24, 25]. Numerous studies demonstrated that the lower the CD4+ lymphocytes counts the higher the risk of developing pulmonary as well as extrapulmonary disease. The qualitative and quantitative role of CD4+ lymphocytes in the adaptive immune response against mycobacteria is crucial, particularly their interaction with macrophages, which need to be activated in order to be effective. The risk of development of tuberculosis disease is 5–15% per year if the mycobacterial infection precedes HIV transmission. On the contrary, such risk could be significantly higher if mycobacterial infection develops in a seriously immunocompromised host. Generally, the probability of developing tuberculosis is 20–37-fold higher in HIV-infected compared to HIV-negative individuals. The relative risk is 20.6 in countries with a generalized HIV epidemic, 26.7 in countries with concentrated epidemics, and 36.7 in low HIV-prevalence countries [1, 2, 5, 8, 26].

Another medical condition that could compromise the immune key players against mycobacterial strains is diabetes mellitus. The estimated prevalence of diabetes is 180 million individuals globally, a figure expected to increase to 360 million by 2030 [5, 27]. The probability of developing tuberculosis is 1.5–8 times higher among individuals with diabetes compared to healthy subjects. No significant differences in terms of risk of disease have been detected between low- and high-income countries [28–32]. Experimental studies showed that hyperglycemic mice have higher mycobacterial loads, impaired production of interferon-γ and interleukin-12 together with an impaired T helper 1 response. Leukocyte bactericidal activity is reduced in diabetic patients compared to healthy individuals. Diabetic patients have an altered chemotaxis and oxidative killing of neutrophils. Furthermore, impaired immunity is frequently associated with other relevant risk factors like chronic renal failure, malnutrition, and pulmonary microangiopathy [28, 33, 34]. Nevertheless, several epidemiological analytical studies assessing the relative risk or the odds ratio of diabetic patients are biased because routine data sources were used, which do not allow controlling for all confounders. The population-attributable risk for diabetes is similar to that of HIV/AIDS; although the relative risk related to HIV/AIDS is highest, ranging from 6.5 to 26 (i.e., 2–9 times higher than the relative risk of diabetes), it is less prevalent than diabetes [28–33, 35].

Chronic renal failure and the hemodialytic treatment increase the risk of developing tuberculosis from 6.9 to 52.5 times compared to the general population [5, 36]. Some epidemiological studies highlight a greater incidence of tuberculosis in the first year of dialysis due to the occurrence of a severe immune depression. It is difficult to understand the role of chronic renal failure because the majority of the studies enrolled principally hemodialytic patients. The crucial pathogenetic feature is the impaired immune response to mycobacterial isolates, in particular type 1 helper T-cell responses involving interleukin-12 and interferon-γ production and co-stimulatory function of antigen-presenting cells. In the final stages of a chronic renal failure, a high rate of anergy to mycobacterial antigens administered intracutaneously has been documented (i.e., from 32% to 40%). Other relevant elements are the continual inflammatory phase of monocytes/macrophages due to the uremia and to the dialysis, malnutrition (mainly related to vitamin D intake), and hyperparathyroidism [5, 36–38].

Silicosis increases the likelihood of pulmonary tuberculosis from 2.8 to 39 times if compared to healthy controls whereas the probability of developing extra-pulmonary tuberculosis is 3.7-fold greater (the pleural form is the most common form, 61% of cases) [1, 5, 24, 39–41]. The average time elapsing between the diagnosis of silicosis and the development of tuberculosis is 6.8 years. The incidence of tuberculosis seems to be proportional to the severity of silicosis and the intensity of exposure to crystalline silica dust. Occupational activities in the mines seem to modify considerably the risk of developing tuberculosis: in particular, drilling has been associated with a greater intensity of exposure. Some studies identified a higher relative risk (i.e., 1.1–4.0) of developing tuberculosis in miners exposed to silica but without silicosis. These epidemiological findings support the results of experimental studies demonstrating that silica modifies the pulmonary immune response, and impairs the metabolism and the function of pulmonary macrophages till their apoptosis after long exposure [5, 24, 39–41]. The incidence of silica-related tuberculosis has been increased by the increased prevalence of HIV infection in resource-limited countries. The incidence of

pulmonary tuberculosis in South African gold miners is 3,000 per 100,000 population. For this reason, several authors strongly recommend the treatment for latent tuberculosis infection in individuals with and without silicosis (especially for HIV-infected people) [5, 39–41].

Smoking is another relevant modifier, being associated to a relative risk of developing tuberculosis ranging from 2.3 to 2.7 [1, 5, 24, 42, 43]. Furthermore, it increases the risk of infection (relative risk of 1.7). The relative risk for latent tuberculosis infection and disease is not independent: the increase of the risk of infection directly increases the proportion of individuals at risk of disease. Therefore, the independent relative risk for tuberculosis in an infected population is obtained computing the ratio of the two relative risks (i.e., 1.4–1.6). Smoking reduces adaptive immune responses, decreasing CD4+ cell counts, altering macrophages, and mechanically disrupting the cilia in the upper respiratory airways. A dose–response effect has been documented: the likelihood of tuberculosis is directly linked to the number of cigarettes smoked daily.

Being treated with immunosuppressive drugs could increase the risk of tuberculosis, as recently demonstrated with the anti-TNFα therapies for the treatment of chronic inflammatory diseases (for instance, rheumatoid arthritis, psoriasis and psoriatic arthritis, ankylosing spondylitis, juvenile idiopathic arthritis, and inflammatory bowel disease) [44]. TNF is a protein crucial for granuloma initiation and stability in the lungs. It fosters the phagocytic and killing activities of the alveolar macrophages and favors the gathering of cells at the inflammatory site inducing adhesion molecules. Four monoclonal anti-TNF antibodies are currently available and are used for the treatment of chronic inflammatory diseases: adalimumab, certolizumab pegol, golimumab, and infliximab. The risk of developing tuberculosis is amplified by 1.6–25.1 times and varies depending on the clinical setting and type of anti-TNF therapy prescribed [44–46].

The role of a corticosteroid treatment in the pathogenesis of tuberculosis is debated [5]. Daily dose of 10 mg or higher of corticosteroids, prescribed for a few days, appears to not be associated with an increased risk of developing tuberculosis but experimental studies on rabbits documented their role in increasing the risk of disease.

Numerous studies evaluated the impact of several tumors as risk factors for tuberculosis, but only lymphomas, pulmonary neoplasia, and head/neck cancers seem associated to the development of the disease [5]. Other relevant diseases and medical events that could increase the risk of tuberculosis are malnutrition, substance abuse, gastrectomy, and jejunoileal by-pass [5, 24]. Intravenous drug and alcohol abuse could increase the risk of tuberculosis by compromising the immune system. Malnutrition, meat and fish deficiencies, or a vegetarian diet are epidemiologically associated to increased probability of tuberculosis [5, 24].

Mortality

The wide availability of anti-tuberculosis drugs has decreased mortality from tuberculosis and case fatality in developed countries. In the pre-antibiotic era, 30% and 66% of patients with tuberculosis died after 1 and 5 years from the notification of the disease, respectively [5, 8]. The most important prognostic variables are the site and type of tuberculosis, the early and adequate administration of anti-tuberculosis treatment, and adherence to treatment [3, 5, 8]. The majority of deaths caused by tuberculosis are attributable to sputum smear-positive tuberculosis [5, 8].

Patient's delay and/or health-care system's delay are associated to increased mortality. Patient's delay can be reduced with health education measures, decreasing tuberculosis stigma, and improving the health-care network. The delay of the health-care system could be related to several factors, particularly poor availability of diagnostic means and misdiagnosis; furthermore, negative prognostic health-care–associated factors are poor accessibility to antituberculosis drugs, incorrect prescription of anti-tuberculosis regimens in terms of dosages, time of exposure, and drug susceptibility of the infecting mycobacterial strains.

Tuberculosis/HIV Coinfection

HIV infection has dramatically changed the epidemiology of tuberculosis in high- and low-income countries, mostly in sub-Saharan Africa, Southeast Asia, and Eastern Europe. It was estimated that tuberculosis incidence in 2008, if compared with the rate computed in 1990, increased by 11% due to the HIV pandemic. In sub-Saharan Africa, tuberculosis mortality has tripled

in the last two decades and 29% of tuberculosis-related deaths are associated to HIV infection [1, 2, 5, 8, 47, 48]. The increase in tuberculosis notification rates mirrored the increase in the HIV prevalence with a delay of 4–7 years [2, 48–50].

By the end of 2008, 33.2 million individuals were estimated to be living with HIV. Incidence and mortality in 2007 were 2.7 million and 2.1 million, respectively [48, 49]. Tuberculosis is estimated to be the cause of 26% of the deaths in people living with HIV. The majority of TB/HIV patients is located in sub-Saharan Africa but in numerous high HIV prevalence areas only 20% HIV-infected individuals know their HIV status. The infection is principally transmitted through sexual relationships, exchange of contaminated syringes among intra-venous drug users, and transfusion of infected blood. The risk of developing tuberculosis ranges from 3% to 15% per year in HIV coinfected patients, while the cumulative lifelong risk in non-HIV-infected individuals is 10%. However, surveys carried out in high HIV prevalence areas estimated an annual probability of developing tuberculosis up to 30% in advanced immunocompromised patients [1, 2, 5, 8, 48–50].

The risk of developing tuberculosis is directly correlated to the degree of immunodeficiency, particularly with the quantitative impairment of CD4+ cell counts, which are considered a relevant surrogate marker of infection together with the HIV-viral load. For this reason tuberculosis is the main opportunistic disease and cause of death in HIV + individuals globally [1, 2, 5, 8, 48, 50].

It is crucial to detect HIV-positive individuals and to start antiretroviral therapy (ART) to decrease the probability of developing tuberculosis and, consequently, the probability of transmitting mycobacterial strains to susceptible individuals. The risk of developing tuberculosis is reduced by 70–90% in patients treated with ART if compared with untreated HIV-positive individuals. In 2008, more than four million individuals were treated with antiretroviral drugs [1, 2, 5, 8, 48–54].

The role of HIV infection on tuberculosis incidence is strictly related to the prevalence of latent tuberculosis infection in the population, particularly in those aged 15–54 years. In industrialized countries, where the prevalence of the mycobacterial infection is low in all age groups, incidence and prevalence of tuberculosis in HIV + individuals are also low. However, in some metropolitan areas an epidemiological scenario comparable to that described in some low-income countries, with high proportions of coinfected individuals has been documented [2, 5, 8, 47, 48].

It is estimated that 30% of HIV + individuals are infected by mycobacterial strains worldwide, with a wide variability from 14% in Europe to 46% in Southeast Asia.

A series of tuberculosis/HIV collaborative activities have been developed to address tuberculosis/HIV coinfection (Table 1) [2, 3, 48, 49, 51, 55, 56]:

- Establishment of a tuberculosis/HIV coordinating body to plan and carry out common activities, such as monitoring and evaluation of the epidemiological indicators and clinical outcomes.
- Surveillance of the prevalence of HIV infection in patients with tuberculosis.
- Intensified tuberculosis case finding aimed at identifying tuberculosis symptoms and clinical signs in HIV-positive individuals attending specialized

Tuberculosis, Epidemiology of. Table 1 Tuberculosis/HIV collaborative activities [3]

1.	*Establishment of the mechanisms for collaboration* • Set up a coordinating body for tuberculosis/HIV collaborative activities that could be effective at all levels • Carry out surveillance of HIV-prevalence among tuberculosis cases • Carry out joint tuberculosis/HIV planning • Conduct monitoring and evaluation
2.	*To decrease the burden of tuberculosis in people with HIV/AIDS* • Implement intensified tuberculosis case finding • Introduce isoniazid preventive therapy • Ensure the control of latent tuberculosis infection in health-care and congregate settings
3.	*To decrease the burden of HIV in patients with tuberculosis* • Provide HIV testing and counseling • Introduce HIV-prevention methods • Introduce cotrimoxazole preventive therapy • Ensure care and support for people with HIV/AIDS • Introduce antiretroviral therapy

health-care settings (HIV clinics, sexually transmitted diseases, clinics, etc.).
- Isoniazid preventive therapy (IPT) in HIV-positive individuals latently infected by mycobacterial strains. In these cases, it is strongly recommended to microbiologically exclude tuberculosis before the administration of the anti-tuberculosis drug.
- Infection control measures in health care and congregate settings to avoid the spread of mycobacterial strains.
- HIV counseling together with HIV rapid testing in tuberculosis patients.
- Introduction of HIV-prevention methods.
- Cotrimoxazole preventive therapy.
- Wide availability of antiretroviral (ARV) drugs.

Delivery of ART to HIV-positive patients with tuberculosis is deemed one of the most important measures for a successful DOTS strategy as it can prevent the shift from latent tuberculosis infection to active tuberculosis following the immunological recovery. However, several issues can hamper the efficacy of ART in tuberculosis patients: pharmacokinetic interactions between anti-HIV drugs and anti-tuberculosis drugs and immune-reconstitution syndrome (IRIS) could increase morbidity and mortality, for instance, decreasing the adherence and, then, the clinical efficacy of the specific treatment regimens [2, 48, 50–54].

The combination of three of the above mentioned tuberculosis/HIV activities, that is, Intensified Case Finding, Isoniazid Preventive Therapy and Infection Control measures, known as the "Three I's", can have a significant role in the prevention of mycobacterial infections and tuberculosis, and in the early identification of tuberculosis cases [2, 3, 55, 56].

Intensified Case Finding helps to rapidly identify tuberculosis suspects using questionnaires focused on symptoms and clinical signs of tuberculosis. Individuals with or at high risk of HIV infection or in congregate settings (such as mines, prisons, etc.) are regularly screened and counseled by HIV services and/or by community-based organizations supporting HIV-positive patients.

Isoniazid Preventive Therapy can be administered to HIV-positives without tuberculosis, reducing the risk of developing the disease by 33–67% for up to 4 years. The criteria for treatment include HIV-positive individuals living in areas with a proportion of latent tuberculosis infection above 30% or HIV-positives with documented latent tuberculosis infection or exposure to a contagious tuberculosis index case. The efficacy of its combination with the ART in preventing the development of tuberculosis has been proven.

Tuberculosis Infection Control measures can prevent the spread of mycobacterial strains to vulnerable patients, health-care workers, the community, and those living in congregate settings.

However, slow implementation of the "Three I's" has been documented because of the difficulty faced by some national programs to integrate these components in the framework of HIV care. Some national tuberculosis programs do not support the implementation of some activities (for instance, the use of isoniazid preventive therapy) and gaps in policy and operational guidance remain a major obstacle in some settings. Infection control still represents a serious challenge at national-, regional-, and facility-level for the absence of a coordinating body or for multiple coordinating bodies, lack of technical expertise, trained health care workers, and laboratory biosafety. Furthermore, inadequate diagnostic tools for latent tuberculosis infection and tuberculosis have hampered the implementation of intensified tuberculosis case finding and the delivery of isoniazid preventive therapy predominantly in resource-limited settings [2, 48, 55, 56]. Nevertheless, it was estimated that 1.4 million tuberculosis cases were tested globally for HIV infection in 2008, which is a 64-fold increase if compared with the estimates in 2002. The increase was significant in sub-Saharan Africa (from 4% to 45% in 2004 and 2008, respectively). A significant improvement has been documented in the number of HIV-infected people screened for tuberculosis: from 600,000 in 2007 to 1.4 million in 2008. Improvements were also recently recorded on the provision of preventive and therapeutic drugs, particularly trimethoprim-sulfamethoxazole preventive treatment (200,000 HIV-positives with tuberculosis in 2008), isoniazid preventive therapy (50,000 HIV-positives in 2008), and ART (100,000 HIV-positives with tuberculosis in 2008) [2, 48, 49].

All countries with a high HIV prevalence should be committed to rapidly implement and scale-up all tuberculosis/HIV collaborative activities.

Future investments in the translational research aimed at identifying new diagnostics and therapeutics as well as international and national political commitment could improve the epidemiology of tuberculosis/HIV coinfection [2, 5, 8, 48, 50, 53].

Drug-Resistant Tuberculosis

Development of resistance to anti-tuberculosis drugs has been documented since the early years of introduction of chemotherapy for the treatment of tuberculosis. The large majority of patients treated with streptomycin in the first Medical Research Council randomized clinical trial in the 1940s acquired resistance to that drug [57]. The spread of drug-resistant strains was soon recognized, and a survey of clinics in England in the 1950s found that over 5% of patients with tuberculosis without a history of previous treatment had strains resistant to at least one of the three major drugs in use at that time [58]. If even once the three effective drugs are used in combination, the development of drug resistance is theoretically impossible [59]. However, despite the introduction of combination regimens throughout the world many years ago, drug resistance has been progressively documented [60].

In the early 1990s, several reports were published on the emergence of multi-drug resistant TB (MDR-TB), but the populations surveyed were not comparable, and methods used to quantify the problem were not standardized thus making it difficult to estimate the global magnitude of drug-resistant TB [61–64].

In 1994, the Global Project on Anti-tuberculosis Drug Resistance Surveillance was established in order to estimate the global burden of drug-resistant TB worldwide using standardized methodologies so that data could be compared across and within regions [65]. The Project aimed to monitor trends in resistance, evaluate the performance of TB control programs, and advise on drug regimens. The Supranational TB Reference Laboratory Network (SRLN), a network now consisting of 29 laboratories globally, was developed in order to provide quality assurance to drug resistance surveys including panel testing before the start of a survey and rechecking of isolates during the survey [66]. Since 1994 drug resistance data have been systematically collected and analyzed from 119 countries worldwide (62% of all countries of the world). Out of them, 48 countries can rely on continuous surveillance systems based on routine diagnostic drug susceptibility testing of all patients. The remaining 71 countries have relied on special surveys of representative samples of patients.

The distributions of multidrug-resistant TB (MDR-TB), defined as TB caused by strains of *Mycobacterium tuberculosis* that are resistant to at least isoniazid and rifampicin, are given in Figs. 1 and 2, for new and

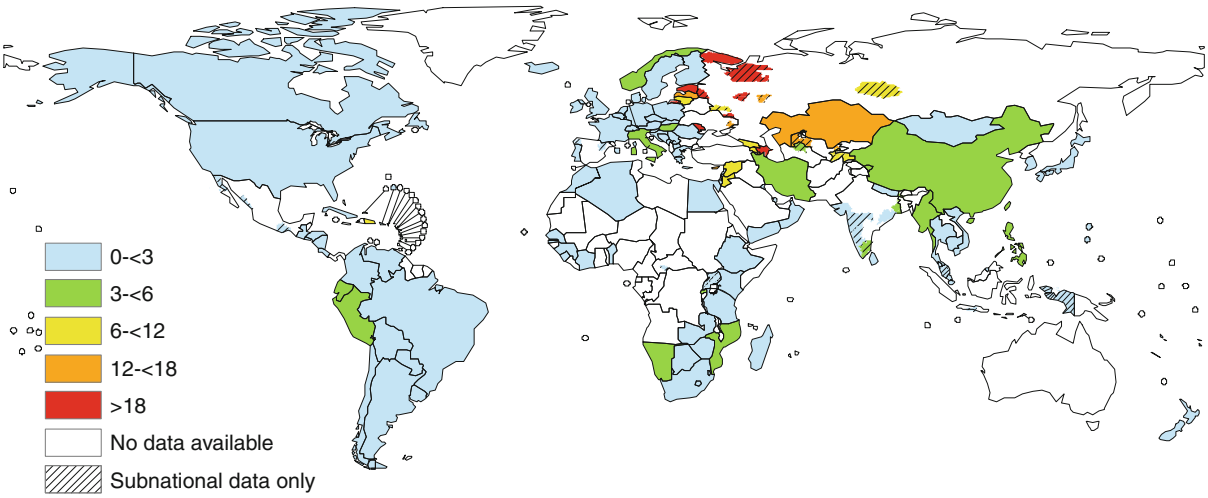

Tuberculosis, Epidemiology of. Figure 1
Distribution of MDR-TB among new TB cases, 1994–2010

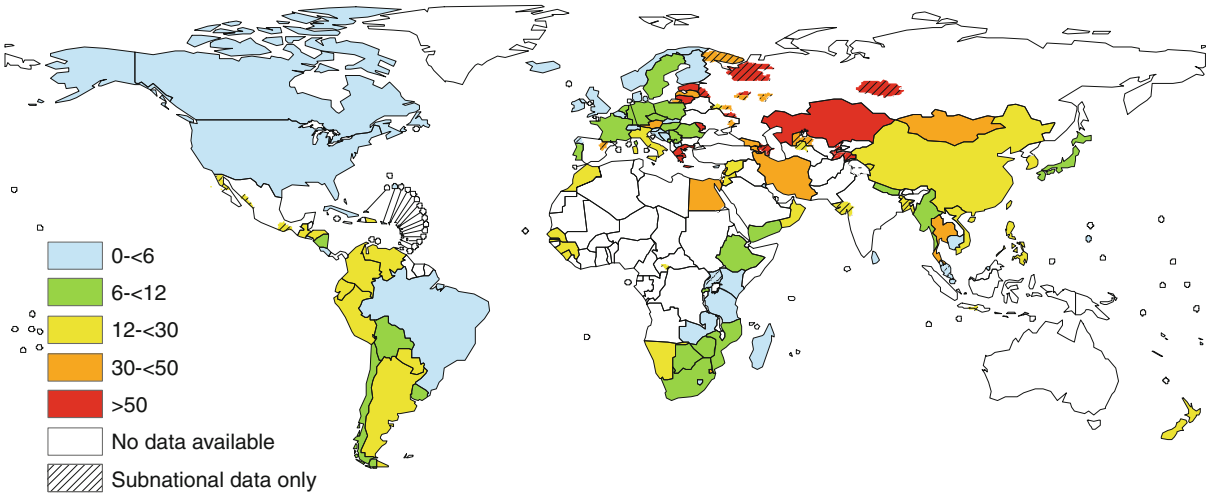

Tuberculosis, Epidemiology of. Figure 2
Distribution of MDR-TB among previously treated TB cases, 1994–2010

previously treated TB cases, respectively. Proportions of MDR-TB exceeding 18% among new TB cases (in countries reporting more than ten MDR-TB cases) have been documented in Estonia (22.0%), Russian Federation (Arkhangelsk Oblast, 25.7%, Belgorod Oblast, 19.8%, Ivanovo Oblast, 20.3%, Kaliningrad Oblast, 22.3%, Murmansk Oblast, 28.9%, Pskov Oblast, 24.3%, and Vladimir Oblast, 20.9%). Proportions of MDR-TB exceeding 50% among previously treated TB cases (for countries reporting more than ten MDR-TB cases) are found in Estonia (51.6%), Lithuania (51.5%), Russian Federation (Arkhangelsk Oblast, 58.8%, Belgorod Oblast, 51.6%, Ivanovo Oblast, 57.7%, and Tomsk Oblast, 53.8%), and Tajikistan (Dushanbe city and Rudaki district, 61.6%, 95% CI: 52.5–70.2) [67, 68].

Since 2006, WHO has also been collecting and analyzing data on resistance to second-line anti-TB drugs. Extensively drug-resistant TB (XDR-TB), defined as MDR-TB plus resistance to a fluoroquinolone and at least 1 second-line injectable agent – amikacin, kanamycin, and/or capreomycin-, has been documented in 69 countries globally [67].

Overall, there were an estimated 390,000–510,000 cases of MDR-TB (primary and acquired) arising in 2008, with the best estimate at 440,000 cases. Among all incident TB cases globally, 3.6% (95% CI: 3.0–4.4) are estimated to have MDR-TB.

The estimated global number of incident MDR-TB episodes among new and relapse TB cases in 2008 was between 310,000 and 430,000 episodes, with the best estimate at 360,000 episodes. The estimated global number of incident acquired MDR-TB episodes was between 83,000 and 110,000 episodes, with the best estimate at 94,000 episodes. Almost 50% of MDR-TB cases worldwide are estimated to occur in China and India. These estimates refer to cases of MDR-TB that arose in 2008 and do not reflect the number of prevalent cases of MDR-TB. The number of prevalent cases of MDR-TB in many parts of the world is estimated to be much higher than the number arising annually.

An estimated 150,000 deaths caused by MDR-TB occurred globally in 2008, including those with HIV infection (range: 53,000–270,000). The estimated number of MDR-TB deaths excluding those with HIV infection was 97,000 (range: 6,000–220,000) [69].

Although the association of HIV and MDR-TB has been widely documented in hospital outbreaks of drug-resistant TB among people living with HIV, based on the population-based data gathered till now, it is not possible to conclude whether an overall association between MDR-TB and HIV epidemics exists [70–72].

More work is needed to understand global trends of the MDR-TB epidemic but in a group of countries and settings, decreasing trends in absolute numbers of

MDR-TB are documented (Estonia, Latvia, China, Hong Kong, United States of America, and two Oblasts in the Russian Federation, Tomsk and Orel) [69].

Control of Tuberculosis

In the second half of the nineteenth century more than one third of deaths globally were due to infectious diseases and 15% were due to tuberculosis. In particular, more than 30% of men and women during their productive years died of tuberculosis.

In industrialized nations, before the availability of the first anti-mycobacterial antibiotics in the second half of 1900, the incidence of tuberculosis notification dramatically decreased because of the reduction or elimination of some risk factors favoring the spread of mycobacterial strains in the community (for instance, improvement of the social and economic conditions of many families) and the implementation of public health interventions, such as the identification and isolation of contagious tuberculosis patients [1, 5, 8, 16, 73].

The first sanatorium was built in Germany in 1857 in order to isolate contagious tuberculosis patients and to provide them with adequate food, rest, sunlight, and fresh air. The dispensary system was introduced in 1897 in Scotland, England, following the basic German principle of the separation of an infectious patient from the community. After the Italian, Forlanini proved the efficacy of artificial pneumothorax to increase the likelihood of cure in tuberculosis cases in 1907, sanatoria increased their surgical activities to create pulmonary collapse (for instance, plombage and thoracoplasty) [1, 5, 8, 16, 74, 75].

The wide distribution of antituberculosis drugs and the scale-up of therapeutic combination, together with the establishment of the first National Tuberculosis Programs (NTPs) and the further improvement of the socio-economic situation, have been significantly associated with a rapid decline of tuberculosis incidence and prevalence in the USA and in numerous European countries [1, 5, 8, 16]. However, in the mid-1980s the erroneous feeling of imminent elimination of tuberculosis, supported by the persistent decline of incidence and prevalence, has led to a reduction of tuberculosis control measures with numerous sanatoria closed or converted into non-tuberculosis specialized facilities. The escalation of the HIV/AIDS epidemic, the increasing number of migrants from high tuberculosis incidence countries, socioeconomic changes due to the collapse of the Soviet Union contributed to the rapid increase of tuberculosis incidence in low-incidence countries [1, 5, 8, 16, 76, 77]. Epidemiological trends in low-income countries are partially known but in the last decades the improvement of surveillance systems has increased the confidence on morbidity and mortality estimates [5, 8].

The World Health Organization has played a crucial role in the fight against tuberculosis worldwide. In 1993, tuberculosis was declared a global public health emergency and reiterated in 2000 by the United Nations Millennium Development Goals (MDGs). The Millennium Development Goal mainly focused on the tuberculosis issue aims at combating HIV, malaria, and other infectious diseases.

In the last 20 years, two public health strategies have changed the natural history of tuberculosis worldwide: DOTS strategy since 1996 and Stop TB Strategy since 2006. Both of them were launched after interactive and proactive debates and discussions between governmental and non-governmental organizations and national representatives of high tuberculosis incidence countries (tuberculosis control program managers and their staffs) [8, 78–82].

DOTS strategy is based on finding and treating contagious cases. It consists of five components: government commitment to tuberculosis control, bacteriological diagnosis through smear microscopy (mainly on individuals complaining of characteristic tuberculosis symptoms), short-course antituberculosis therapy that has to be standardized and supervised (i.e., directly observed, at least during the initial phase), uninterrupted high-quality drug supply, and individual outcome evaluation through a standardized recording and reporting system. Its targets were to detect 70% of sputum smear-positive tuberculosis cases and to successfully treat 85% of them by 2005. DOTS can reduce annual tuberculosis notifications from 6% to 8%, decreasing the incidence, the prevalence, and the mortality.

In 2005, the World Health Organization launched the new Stop TB Strategy (Table 2) [82]. The former strategy was revisited to pursue DOTS expansion, adding six other components to be implemented to

Tuberculosis, Epidemiology of. Table 2 WHO-recommended Stop TB Strategy [82]

1.	*Pursue high-quality DOTS expansion and enhancement* • Secure political commitment, with adequate and sustained financing • Ensure early case detection, and diagnosis through quality-assured bacteriology • Provide standardized treatment with supervision, and patient support • Ensure effective drug supply and management • Monitor and evaluate performance and impact
2.	*Address TB/HIV, MDR-TB, and the needs of poor and vulnerable populations* • Scale up collaborative TB/HIV activities • Scale up prevention and management of multidrug-resistant TB (MDR-TB) • Address the needs of TB contacts, and of poor and vulnerable populations, including women, children, prisoners, refugees, migrants, and ethnic minorities
3.	*Contribute to health system strengthening based on primary health care* • Help improve health policies, human resource development financing, supplies, service delivery, and information • Strengthen infection control in health services, other congregate settings, and households • Upgrade laboratory networks, and implement the Practical Approach to Lung Health (PAL) • Adapt successful approaches from other fields and sectors, and foster action on the social determinants of health
4.	*Engage all care providers* • Involve all public, voluntary, corporate, and private providers through Public–Private Mix (PPM) approaches • Promote use of the International Standards for TB Care (ISTC)
5.	*Empower people with TB, and communities through partnership* • Pursue advocacy, communication, and social mobilization • Foster community participation in TB care • Promote use of the Patients' Charter for TB care
6.	*Enable and promote research* • Conduct program-based operational research, and introduce new tools into practice • Advocate for and participate in research to develop new diagnostics, drugs, and vaccines

reach the 2015 Millennium Development Goal related to tuberculosis control, that is, to reduce prevalence of and mortality due to tuberculosis by 50% relative to those of 1990.

The new Stop TB Strategy can be summarized in the following elements [82]: (1) pursuing high-quality DOTS expansion and enhancement; (2) addressing tuberculosis/HIV coinfection, multi-drug resistant tuberculosis, and other challenges; (3) contributing to the strengthening of health-care systems; (4) engaging all care providers; (5) empowering people and communities with tuberculosis; and (6) enabling and promoting research.

This new Strategy addresses several issues that emerged during the implementation and scale-up of the DOTS strategy: spread of tuberculosis/HIV coinfection and increased rates of multi-drug resistant tuberculosis, weak health care systems, exclusion of the private sector from national tuberculosis control strategies (often managing poor and marginalized individuals), passive involvement of tuberculosis patients and communities, few resources in research and development of new diagnostics, drugs, and vaccines.

The first component, that is, "to pursue quality DOTS expansion and enhancement" is aimed at improving the previous strategy: political commitment should be strong in terms of financial resources available for tuberculosis control at national- and regional-level as well as for strengthening of health system. National laboratory networks should be improved with the introduction of culture methods and drug susceptibility testing as well as new effective evidence-based diagnostic technologies. In order to obtain high-treatment rates and to avoid the emergence and spread of drug-resistant strains treatment support should be provided through a patient-centered approach. A national body should manage the continuous supply of quality-assured anti-tuberculosis drugs. Continuous monitoring of the national TB program and evaluation of the tuberculosis control activities should be regularly implemented.

The second component of the strategy describes all the interventions that should be implemented to control and avoid further emergence of the rising issues: tuberculosis/HIV coinfection and multi-drug resistant tuberculosis. Tuberculosis and HIV national programs

should implement collaborative activities. Patients with drug-resistant tuberculosis should have access to diagnosis and proper treatment with second-line anti-TB drugs. More attention should be given to groups at highest risk of developing tuberculosis (such as prisoners, immigrants, etc.).

The third component is focused on strengthening of health system, highlighting all the elements necessary to improve a national health system: human and financial resources, information systems, and national policies.

The fourth component underlines the importance of the engagement of all health-care providers, including those outside national health system (public–private mix approach) and those working in prisons, general hospitals, and medical colleges.

The fifth component is aimed at describing the empowerment of people with tuberculosis and of communities, sharing some tuberculosis activities like treatment support. Furthermore, communities could have a role in reducing tuberculosis stigma.

The sixth component highlights the importance of the operational and biomedical research aimed at improving program performance and at developing new diagnostic, therapeutic, and preventive tools.

The Stop TB Strategy addresses all the risk factors associated to the development of mycobacterial infection and tuberculosis, including the reduction of the social and economic consequences of the disease. It supports the Global Plan to Stop TB (2011–2015), developed by the Stop TB Partnership [81]. The plan is aimed at identifying political and public health strategies to be implemented, and financial needs and existing gaps to address in order to scale up the Stop TB Strategy. Finally, International Standards of Tuberculosis Care (ISTC) have been issued to help both public and private health care providers to deliver quality DOTS services [83–85]. The aim is to describe an evidence-based standard of care for health-care workers managing confirmed or suspected tuberculosis individuals. The following principles of care are highlighted: early and accurate bacteriological diagnosis; administration of standardized and effective anti-tuberculosis drug regimens as well as appropriate treatment support and supervision; and monitoring of treatment outcomes.

Global Epidemiological Situation

Incidence

According to the last global estimates the number of new cases of tuberculosis in 2009 was 9.4 million, ranging from 8.9 million to 9.9 million (137 cases per 100,000 inhabitants). During the recent years the incidence trend has slowly decreased but the absolute frequency has increased due to population growth. The regions contributing the most to the global estimated incidence of tuberculosis are the South-east Asian region with 35% of cases (3,300,000), the Western Pacific region with 20% (1,900,000 cases), the African region with 30% (2,800,000 cases) followed by the Eastern Mediterranean region (7%), the European region (4%), and the Region of the Americas (3%) [4, 6].

The World Health Organization identified 22 so-called high burden countries (HBCs), accounting for more than 80% of the incident cases estimated globally. India accounts for 21% of all tuberculosis patients and China for 14%. The highest incidence rates in 2009 were estimated in India (range: 1.6–2.4 million), China (range: 1.1–1.5 million), South Africa (range: 0.40–0.59 million), Nigeria (range: 0.37–0.55 million), and Indonesia (range: 0.35–0.52 million). The incident tuberculosis/HIV coinfection was estimated in 1.1/9.4 million (12%; 1.0–1.2 million, 11–13%) individuals, with the vast majority of patients in the African region. Among the incident cases estimated in 2008, 440,000 (range: 390,000–510,000) patients were infected by multi-drug resistant mycobacterial strains, that is, with resistance in vitro to at least isoniazid and rifampicin (MDR-TB).

Prevalence

The estimated tuberculosis prevalence in 2009 was 200 cases per 100,000 inhabitants as a consequence of 14 million (range: 12–16 million) prevalent patients.

Mortality

In 2009 about 1.7 million individuals (i.e., 26 cases per 100,000 inhabitants) died of tuberculosis, with 400,000 (range: 320,000–450,000) and 1.3 million (range: 1.2–1.5 million) deaths among tuberculosis/HIV coinfected and HIV-negative patients, respectively.

Case Notifications

National tuberculosis programs registered 5.8 million tuberculosis patients in 2009: most of them were new cases (94.8%) and 0.3 million were relapses (i.e., previously treated cases whose most recent anti-tuberculosis treatment outcome was "cure" or "treatment completed" but who were afterward diagnosed with sputum smear and/or culture-positive tuberculosis); 57% of the pulmonary tuberculosis cases was considered highly infectious, that is, sputum smear-positive. Among the 5.5 million new cases notified in 2009, 47.3% (2.6 million) was sputum smear-positive, 36.4% (2.0 million) sputum smear-negative while 16.4% (900,000) was affected by extrapulmonary tuberculosis.

The causes behind the global under-reporting could be linked to the patients (limited knowledge of tuberculosis; economic and/or geographical barriers to access health care; etc.) and/or to the health systems (poor clinical and laboratory capacities; few trained health care workers; poor compliance to national laws on notification after tuberculosis diagnosis).

Treatment Outcomes

The global treatment success ("cured" plus "treatment completed") rates for new sputum smear-positive cases treated during the years 2007 and 2008 were higher than the target set in 1991, that is, 85%.

In 2008 three WHO regions contributed to this result: Eastern Mediterranean Region, the South-east Asian Region, and the Western Pacific Region; the worst treatment success rate was documented in the European Region (66%), followed by the Region of the Americas (77%) and the African Region (80%).

Future Directions

Elimination of tuberculosis, or reducing the incidence of new sputum smear-positive cases below one per one million inhabitants, is the goal for the next decades. The target endorsed by Stop TB Partnership is the elimination of tuberculosis as a public health problem by 2050 [6–88].

The objectives of the tuberculosis elimination strategy are:

- Reduction of the incidence of latent tuberculosis infection.
- Reduction of the prevalence of latent tuberculosis infection.

The aim is to decrease the burden of future new tuberculosis cases.

In low tuberculosis-incidence countries, the lowest prevalence and incidence of latent tuberculosis infection are detected in the autochthonous youngest groups. The epidemiological projections indicate that each generation will be substituted by a generation with a lower risk of infection and, then, characterized by a lower prevalence of latent tuberculosis infections [5, 8, 86, 88].

Early detection and adequate treatment of contagious tuberculosis patients are of paramount importance in order to achieve a positive epidemiological trend. Moreover, the progression to tuberculosis in individuals infected by mycobacterial strains should be prevented, particularly focusing on high-risk groups (migrants, HIV-positives, ethnic minorities, prisoners, elderly people, and close contacts of tuberculosis index cases) [5, 8, 86].

This combined approach is deemed essential to reach the elimination goal, and it should be supported by international and national policies, embracing the following components [2, 5, 8, 86, 87]:

- Political commitment toward control and elimination, particularly providing human resources, facilities, and funds
- Case detection through case-finding among symptomatic individuals presenting at health services and active case finding in special groups through quality-assured laboratories and trained health-care providers
- Access to tuberculosis diagnostic and treatment services, implementing collaborative activities with health bodies or organizations working with migrants, prisoners, homelessness, etc.
- Standard approach to treatment of tuberculosis and latent tuberculosis infection, following international evidence-based recommendations
- Surveillance and treatment outcome monitoring, following standard internationally accepted definitions

However, tuberculosis indicators could potentially worsen in the next decades due to the following public health challenges:

- Drug-resistant mycobacterial strains (mostly multi/extensively drug-resistant mycobacteria)
- HIV/AIDS
- Immunocompromised individuals
- Political unrests and wars, natural disasters, and starvation

Adequate funds, constant international and national political commitment, and an effective supply of anti-tuberculosis and anti-HIV drugs and diagnostics represent relevant components for a successful strategy. In particular, the research and development of new effective anti-tuberculosis drugs with an improved toxicity, tolerability, and efficacy profile and the evaluation of the activity of potential adjunctive treatments, such as vitamin D, as well as of new primary preventive measures (i.e., vaccines) are crucial priorities for the near future. Basic and applied research would need to be followed by operational research, as new diagnostic, therapeutic, and preventive approaches must be tested at the program-level (field trials) after clinical trials [89].

Bibliography

1. Fitzgerald D, Haas DW (2005) *Mycobacterium tuberculosis*. In: Mandell GL et al (eds) Principles and practice of infectious diseases, 6th edn. Churchill Livingstone, Philadelphia, pp 2852–2886
2. Nunn P, Williams B, Floyd K, Dye C, Elzinga G, Raviglione M (2005) Tuberculosis control in the era of HIV. Nat Rev Immunol 5(10):819–826
3. Raviglione MC (2006) The global plan to stop TB, 2006–2015. Int J Tuberc Lung Dis 10(3):238–239
4. World Health Organization (2010) Global tuberculosis control. A short update to the 2009 report. WHO, Geneva, 2010
5. Rieder H (1999) Epidemiologic basis of tuberculosis control. International Union Against Tuberculosis and Lung Disease, Paris
6. World Health Organization (2010) Global tuberculosis control 2010. World Health Organization Document 2010, Publication No. WHO/HTM/TB/2010.7
7. Everitt BS, Palmer C (2011) Encyclopedic companion to medical statistics, 2nd edn. Wiley, Chichester
8. Styblo K, Raviglione MC (1997) Tuberculosis, public health aspects. In: Encyclopedia of human biology, vol 8, 2nd edn. Academic, San Diego, pp 537–558
9. Stýblo K, Danková D, Drápela J, Galliová J, Jezek Z, Krivánek J, Kubík A, Langerová M, Radkovský J (1967) Epidemiological and clinical study of tuberculosis in the district of Kolin, Czechoslovakia. Report for the first 4 years of the study (1961–64). Bull World Health Organ 37(6):819–874
10. Krivinka R, Drápela J, Kubík A, Danková D, Krivánek J, Ruzha J, Miková Z, Hejdová E (1974) Epidemiological and clinical study of tuberculosis in the district of Kolín, Czechoslovakia. Second report (1965–1972). Bull World Health Organ 51(1):59–69
11. Borgdorff MW, Nagelkerke NJ, van Soolingen D, Broekmans JF (1999) Transmission of tuberculosis between people of different ages in The Netherlands: an analysis using DNA fingerprinting. Int J Tuberc Lung Dis 3(3):202–206
12. Rieder HL (1999) Socialization patterns are key to the transmission dynamics of tuberculosis. Int J Tuberc Lung Dis 3(3):177–178
13. Stead WW (1998) Tuberculosis among elderly persons, as observed among nursing home residents. Int J Tuberc Lung Dis 2(9 Suppl 1):S64–S70
14. Leung CC, Rieder HL, Lange C, Yew WW (2011) Treatment of latent infection with *Mycobacterium tuberculosis*: update 2010. Eur Respir J 37(3):690–711
15. WHO (2009) WHO policy on infection control in health-care facilities, congregate settings and households. World Health Organization, Geneva. WHO/HTM/TB/2009.419
16. Migliori GB, Sotgiu G, Lange C, Centis R (2010) Extensively drug-resistant tuberculosis: back to the future. Eur Respir J 36(3):475–477
17. Storla DG, Yimer S, Bjune GA (2008) A systematic review of delay in the diagnosis and treatment of tuberculosis. BMC Public Health 8:15
18. Ngadaya ES, Mfinanga GS, Wandwalo ER, Morkve O (2009) Delay in tuberculosis case detection in Pwani region, Tanzania. A cross sectional study. BMC Health Serv Res 9:196
19. European Centers of Disease Prevention and Control (2011) Use of interferon-γ release assays in support of TB diagnosis. ECDC, Stockholm, 2011
20. Cellestis (2006) QuantiFERON-TB Gold (In-Tube Method) Package Insert. Valencia, 2006
21. Oxford_Immunotec (2009) T-Spot. TB Package Insert. 2009
22. Diel R, Goletti D, Ferrara G, Bothamley G, Cirillo D, Kampmann B, Lange C, Losi M, Markova R, Migliori GB, Nienhaus A, Ruhwald M, Wagner D, Zellweger JP, Huitric E, Sandgren A, Manissero D (2011) Interferon-γ release assays for the diagnosis of latent *Mycobacterium tuberculosis* infection: a systematic review and meta-analysis. Eur Respir J 37(1):88–99
23. Torrado E, Robinson RT, Cooper AM (2011) Cellular response to mycobacteria: balancing protection and pathology. Trends Immunol 32(2):66–72
24. Creswell J, Raviglione M, Ottmani S, Migliori GB, Uplekar M, Blanc L, Sotgiu G, Lonnroth K (2010) Tuberculosis and noncommunicable diseases: neglected links, missed opportunities. Eur Respir J 37(5):1269–1282

25. Lönnroth K, Jaramillo E, Williams BG, Dye C, Raviglione M (2009) Drivers of tuberculosis epidemics: the role of risk factors and social determinants. Soc Sci Med 68(12):2240–2246
26. Schutz C, Meintjes G, Almajid F, Wilkinson RJ, Pozniak A (2010) Clinical management of tuberculosis and HIV-1 co-infection. Eur Respir J 36(6):1460–1481
27. World Health Organization (2006) Diabetes fact sheet No. 312
28. Jeon CY, Murray MB (2008) Diabetes mellitus increases the risk of active tuberculosis: a systematic review of 13 observational studies. PLoS Med 5(7):e152
29. Stevenson CR, Forouhi NG, Roglic G, Williams BG, Lauer JA, Dye C, Unwin N (2007) Diabetes and tuberculosis: the impact of the diabetes epidemic on tuberculosis incidence. BMC Public Health 7:234
30. Stevenson CR, Critchley JA, Forouhi NG, Roglic G, Williams BG, Dye C, Unwin NC (2007) Diabetes and the risk of tuberculosis: a neglected threat to public health? Chronic Illn 3(3):228–245
31. Harries AD, Billo N, Kapur A (2009) Links between diabetes mellitus and tuberculosis: should we integrate screening and care? Trans R Soc Trop Med Hyg 103(1):1–2
32. Dooley KE, Chaisson RE (2009) Tuberculosis and diabetes mellitus: convergence of two epidemics. Lancet Infect Dis 9(12):737–746
33. Martens GW, Arikan MC, Lee J, Ren F, Greiner D, Kornfeld H (2007) Tuberculosis susceptibility of diabetic mice. Am J Respir Cell Mol Biol 37(5):518–524
34. Stalenhoef JE, Alisjahbana B, Nelwan EJ, van der Ven-Jongekrijg J, Ottenhoff TH, van der Meer JW, Nelwan RH, Netea MG, van Crevel R (2008) The role of interferon-gamma in the increased tuberculosis risk in type 2 diabetes mellitus. Eur J Clin Microbiol Infect Dis 27(2):97–103
35. Lienhardt C, Rodrigues LC (1997) Estimation of the impact of the human immunodeficiency virus infection on tuberculosis: tuberculosis risks re-visited? Int J Tuberc Lung Dis 1(3): 196–204
36. Hussein MM, Mooij JM, Roujouleh H (2003) Tuberculosis and chronic renal disease. Semin Dial 16(1):38–44
37. Woeltje KF, Mathew A, Rothstein M, Seiler S, Fraser VJ (1998) Tuberculosis infection and anergy in hemodialysis patients. Am J Kidney Dis 31(5):848–852
38. Girndt M, Sester U, Sester M, Kaul H, Köhler H (1999) Impaired cellular immune function in patients with end-stage renal failure. Nephrol Dial Transplant 14(12):2807–2810
39. Rees D, Murray J (2007) Silica, silicosis and tuberculosis. Int J Tuberc Lung Dis 11(5):474–484
40. Barboza CE, Winter DH, Seiscento M, Santos Ude P, Terra Filho M (2008) Tuberculosis and silicosis: epidemiology, diagnosis and chemoprophylaxis. J Bras Pneumol 34(11):959–966
41. Hnizdo E, Murray J (1998) Risk of pulmonary tuberculosis relative to silicosis and exposure to silica dust in South African gold miners. Occup Environ Med 55(7):496–502
42. Bates MN, Khalakdina A, Pai M, Chang L, Lessa F, Smith KR (2007) Risk of tuberculosis from exposure to tobacco smoke: a systematic review and meta-analysis. Arch Intern Med 167(4):335–342
43. Arcavi L, Benowitz NL (2004) Cigarette smoking and infection. Arch Intern Med 164(20):2206–2216
44. Solovic I, Sester M, Gomez-Reino JJ, Rieder HL, Ehlers S, Milburn HJ, Kampmann B, Hellmich B, Groves R, Schreiber S, Wallis RS, Sotgiu G, Schölvinck EH, Goletti D, Zellweger JP, Diel R, Carmona L, Bartalesi F, Ravn P, Bossink A, Duarte R, Erkens C, Clark J, Migliori GB, Lange C (2010) The risk of tuberculosis related to tumour necrosis factor antagonist therapies: a TBNET consensus statement. Eur Respir J 36(5): 1185–1206
45. Ehlers S (2005) Tumor necrosis factor and its blockade in granulomatous infections: differential modes of action of infliximab and etanercept? Clin Infect Dis 41(Suppl 3):S199–S203
46. Bekker LG, Freeman S, Murray PJ, Ryffel B, Kaplan G (2001) TNF-alpha controls intracellular mycobacterial growth by both inducible nitric oxide synthase-dependent and inducible nitric oxide synthase-independent pathways. J Immunol 166(11): 6728–6734
47. Raviglione MC, Harries AD, Msiska R, Wilkinson D, Nunn P (1997) Tuberculosis and HIV: current status in Africa. AIDS 11(Suppl B):S115–S123
48. Getahun H, Gunneberg C, Granich R, Nunn P (2010) HIV infection-associated tuberculosis: the epidemiology and the response. Clin Infect Dis 50(Suppl 3):S201–S207
49. Joint United Nations Programme on HIV/AIDS (2008) Report on the global AIDS epidemic. Joint United Nations Programme on HIV/AIDS, Geneva, 2008
50. Corbett EL, Watt CJ, Walker N, Maher D, Williams BG, Raviglione MC, Dye C (2003) The growing burden of tuberculosis: global trends and interactions with the HIV epidemic. Arch Intern Med 163(9):1009–1021
51. Reid A, Scano F, Getahun H, Williams B, Dye C, Nunn P, De Cock KM, Hankins C, Miller B, Castro KG, Raviglione MC (2006) Towards universal access to HIV prevention, treatment, care, and support: the role of tuberculosis/HIV collaboration. Lancet Infect Dis 6(8):483–495
52. World Health Organisation (2006) Antiretroviral therapy for HIV infection in adults and adolescents in resource limited settings: towards universal access. World Health Organisation, Geneva
53. World Health Organization (2010) Treatment of tuberculosis guidelines, 4th edn. World Health Organization, Geneva, Document WHO/HTM/TB/2009.420
54. Abdool Karim S, Naidoo K, Grobler A, et al. Initiating ART during TB treatment significantly increases survival: results of a randomised controlled clinical trial in TB/HIV co-infected patients in South Africa. Presented at 16th conference on retroviruses and opportunistic infections. Montreal, 8–11 Feb 2009
55. WHO (2011) Guidelines for intensified tuberculosis case-finding and isoniazid preventive therapy for people living with HIV in resource constrained settings. WHO, Geneva, 2011
56. WHO Three I's Meeting. 2008

57. Medical Research Council (1948) Streptomycin treatment of pulmonary tuberculosis. A Medical Research Council investigation. BMJ 2:769–782
58. Fox W, Wiener A, Mitchison DA, Selkon JB, Sutherland I (1957) The prevalence of drug-resistant tubercle bacilli in untreated patients with pulmonary tuberculosis: a national survey, 1955–1956. Tubercle 38:71
59. Zhang Y, Yew WW (2009) Mechanisms of drug resistance in *Mycobacterium tuberculosis*. Int J Tuberc Lung Dis 13(11):1320–1330
60. Wright A, Zignol M, Van Deun A, Falzon D, Gerdes SR, Feldman K, Hoffner S, Drobniewski F, Barrera L, van Soolingen D, Boulabhal F, Paramasivan C, Kam KM, Mitarai S, Nunn P, Raviglione M (2009) For the Global Project on Anti-Tuberculosis Drug Resistance Surveillance. Epidemiology of antituberculosis drug resistance 2002–07: an updated analysis of the Global Project on Anti-Tuberculosis Drug Resistance Surveillance. Lancet 373(9678):1861–1873
61. Ellner JJ, Hinman AR, Dooley SW et al (1993) Tuberculosis symposium: emerging problems and promise. J Infect Dis 168:537–551
62. Frieden TR, Sterling T, Pablos-Mendez A et al (1993) The emergence of drug-resistant tuberculosis in New York City. N Engl J Med 328:521–526
63. Rastogi N (1993) Emergence of multiple-drug-resistant tuberculosis: fundamental and applied research aspects, global issues and current strategies. Res Microbiol 144:103
64. Sbarbaro JA (1993) TB control in the 21st century. Monaldi Arch Chest Dis 48:197–198, Editorial
65. Cohn DL, Bustreo F, Raviglione MC (1997) Drug-resistant tuberculosis: review of the worldwide situation and the WHO/IUATLD global surveillance project. Clin Infect Dis 24(Suppl 1):S121–S130
66. Van Deun A, Wright A, Zignol M, Weyer K, Rieder HL (2011) Drug susceptibility testing proficiency in the network of supranational tuberculosis reference laboratories. Int J Tuberc Lung Dis 15(1):116–124
67. World Health Organization (2011) Towards universal access to diagnosis and treatment of multidrug-resistant and extensively drug-resistant tuberculosis by 2015 (WHO/HTM/TB/2011.3). Geneva, 2011
68. Ministry of Health and Social Development of the Russian Federation (2010) Tuberculosis in the Russian Federation 2009. An analytical review of the TB statistical indicators used in the Russian Federation. The Russian Federation, Moscow, 2010
69. World Health Organization (2010) Multidrug and extensively drug-resistant TB (M/XDR-TB) - 2010 global report on surveillance and response (WHO/HTM/TB/2010.3). Geneva, 2010
70. Edlin BR, Tokars JI, Grieco MH, Crawford JT, Williams J, Sordillo EM, Ong KR, Kilburn JO, Dooley SW, Castro KG, Jarvis WR, Holmberg SD (1992) An outbreak of multidrug-resistant tuberculosis among hospitalized patients with the acquired immunodeficiency syndrome. N Engl J Med 326:1514–1521
71. Moro ML, Gori A, Errante I, Infuso A, Franzetti F, Sodano L, Iemoli E (1998) An outbreak of multidrug-resistant tuberculosis involving HIV-infected patients of two hospitals in Milan, Italy. Italian Multidrug-Resistant Tuberculosis Outbreak Study Group. AIDS 12:1095–1102
72. Wells CD, Cegielski JP, Nelson LJ, Laserson KF, Holtz TH, Finlay A, Castro KG, Weyer K (2007) HIV infection and multidrug-resistant tuberculosis: the perfect storm. J Infect Dis 196(Suppl 1):S86–S107
73. Raviglione M (2006) XDR-TB: entering the post-antibiotic era? Int J Tuberc Lung Dis 10(11):1185–1187
74. Dawson JJ, Devadatta S, Fox W, Radhakrishna S, Ramakrishnan CV, Somasundaram PR et al (1966) A 5-year study of patients with pulmonary tuberculosis in a concurrent comparison of home and sanatorium treatment for one year with isoniazid plus PAS. Bull World Health Organ 34(4):533–551
75. Styblo K, Meijer J, Sutherland I (1969) Tuberculosis surveillance research unit report no. 1: the transmission of tubercle bacilli; its trend in a human population. Bull Int Union Tuberc 42: 1–104
76. Dahle UR, Eldholm V, Winje BA, Mannsåker T, Heldal E (2007) Impact of immigration on the molecular epidemiology of *Mycobacterium tuberculosis* in a low-incidence country. Am J Respir Crit Care Med 176(9):930–935
77. McKenna MT, McCray E, Onorato I (1995) The epidemiology of tuberculosis among foreign-born persons in the United States, 1986 to 1993. N Engl J Med 332(16):1071–1076
78. World Health Organisation (2015) The global plan to stop TB 2006–2015
79. World Health Organization (2005) Fifty-eighth world health assembly: resolutions and decisions. WHA58/2005/REC/1. WHO, Geneva, 2005
80. WHO (2004) Report on the meeting of the second ad hoc Committee on the TB Epidemic (WHO/HTM/STB/2004.28). World Health Organization, Geneva, 2004
81. WHO (2006) Stop TB partnership and the World Health Organization. The global plan to stop tuberculosis, 2006–2015. WHO/HTM/STB/2006.35. WHO, Geneva, 2006
82. Raviglione MC, Uplekar MW (2006) WHO's new stop TB strategy. Lancet 367(9514):952–955
83. Migliori GB, Hopewell PC, Blasi F, Spanevello A, Raviglione MC (2006) Improving the TB case management: the international standards for tuberculosis care. Eur Respir J 28(4):687–690
84. Tuberculosis Coalition for Technical Assistance (2006) International standards for tuberculosis care (ISTC). Tuberculosis Coalition for Technical Assistance, The Hague, 2006
85. Tuberculosis Coalition for Technical Assistance (2009) International standards for tuberculosis care (ISTC), 2nd edn. Tuberculosis Coalition for Technical Assistance, The Hague, 2009
86. Clancy L, Rieder HL, Enarson DA, Spinaci S (1991) Tuberculosis elimination in the countries of Europe and other industrialized countries. Eur Respir J 4(10):1288–1295
87. Broekmans JF, Migliori GB, Rieder HL, Lees J, Ruutu P, Loddenkemper R, Raviglione MC (2002) World Health

Organization, International Union Against Tuberculosis and Lung Disease, and Royal Netherlands Tuberculosis Association Working Group. European framework for tuberculosis control and elimination in countries with a low incidence. Recommendations of the World Health Organization (WHO), International Union Against Tuberculosis and Lung Disease (IUATLD) and Royal Netherlands Tuberculosis Association (KNCV) Working Group. Eur Respir J 19(4):765–775

88. Migliori GB, Loddenkemper R, Blasi F, Raviglione MC (2007) 125 years after Robert Koch's discovery of the tubercle bacillus: the new XDR-TB threat. Is "science" enough to tackle the epidemic? Eur Respir J 29(3):423–427
89. Migliori GB, D'Arcy Richardson M, Sotgiu G, Lange C (2009) Multidrug-resistant and extensively drug-resistant tuberculosis in the West. Europe and United States: epidemiology, surveillance, and control. Clin Chest Med 30(4):637–665

U

Ultraviolet Radiation: Distribution and Variability

Julian Gröbner
European Ultraviolet Calibration Center,
Physikalisch-Meteorologisches Observatorium Davos,
World Radiation Center, Davos Dorf, Switzerland

Article Outline

Glossary
Definition of the Subject and Its Importance
Introduction
Factors Affecting Surface Ultraviolet Radiation
Future Directions
Bibliography

Glossary

Effective surface albedo The effective surface albedo represents the reflectivity of a homogeneous surface which produces the same downwelling UV irradiance as in the presence of an inhomogeneous surface.

Erythemal UV radiation UV radiation weighted with the nominal action spectrum for the spectral sensitivity of Human skin to sunburn (erythema).

Solar zenith angle Angle between the sun and the normal to the Earth's surface. An SZA of 0° corresponds to an overhead sun (solar elevation 90°), while a SZA of 90° corresponds to the sun at the horizon.

Spectroradiometer Instrument using a grating or prism to split the incoming radiation in its spectral components so as to measure the intensity of the solar spectrum at individual wavelengths.

Stratosphere Part of the atmosphere between approximately 10 and 40 km which is characterized by increasing atmospheric temperatures with height due to the photo dissociation of ozone molecules by solar UV radiation.

Irradiance Radiation flux through a unit surface area.

Radiation dose Amount of radiation reaching a subject during a defined time interval. A daily dose corresponds to the total radiation reaching the surface during one whole day.

UV Radiation Radiation in the wavelength range 100–400 nm. It is subdivided into three regions called UV-C (100–280 nm), UV-B (280–315 nm), and UV-A (315–400 nm).

Definition of the Subject and Its Importance

Solar UV radiation is the most energetic radiation that is able to penetrate the atmosphere and reach the Earth's surface. Due to the very low intensities of the radiation in this wavelength range, its investigation started comparably late with respect to the other spectral regions of the solar spectrum. Dorno was the first to investigate systematically the seasonal and spectral variability of solar UV radiation at Davos, Switzerland. Starting in 1907, his measurements allowed to determine the distinct differences of radiation in this wavelength range, which were later explained by the absorption of atmospheric ozone (mainly located in the stratosphere). Using a specially designed spectroradiometer, he discovered the relationship between the cut-on of the solar spectrum in the UV-B and the path through the atmosphere. In view of his achievements, UV radiation at the time was also called Dorno radiation. In the 1960s, Paul Bener, also from Davos, continued the investigations initiated by Dorno, by building specially designed spectroradiometers that were unique in his time. Systematic measurements under different atmospheric and environmental conditions provided for the first time a benchmark dataset to use as reference for validating radiative transfer models (RTMs), which were emerging at the time. Thus, the

Robert A. Meyers (ed.), *Encyclopedia of Sustainability Science and Technology*, DOI 10.1007/978-1-4419-0851-3,
© Springer Science+Business Media, LLC 2012

dependence of solar UV radiation on clouds, aerosols, surface reflectivity, and altitude were investigated systematically. Moreover, polarization measurements of the sky radiance were obtained at that time, and are still among the most precise measurements available. Recently, the interest for UV radiation has been linked to its biological effects on humans and on the biosphere in general. The discovery of decreasing ozone levels due to anthropogenic chemicals released in the atmosphere in the early 1980 s has led to intense research activity in the field of solar UV measurements to determine the effect of declining ozone levels on UV radiation and its implications for the environment.

In this entry, the spatial distribution of solar UV radiation at the surface will be discussed, as well as the most important parameters responsible for variations in intensity of the surface solar UV radiation.

Introduction

Solar ultraviolet radiation falling on the Earth's surface originates from the sun. On its passage through the atmosphere, the radiation is scattered and absorbed depending on a variety of factors. Even though the mechanisms are qualitatively similar to what occurs at longer wavelengths, several important differences exist: Ultraviolet radiation is strongly absorbed by atmospheric ozone, located high up in the atmosphere. Furthermore, ultraviolet radiation is strongly scattered by air molecules.

Ultraviolet radiation is classified into three wavelength regions: Radiation at wavelengths just shorter than visible light is called UV-A and extends from 315 to 400 nm. The radiation at shorter wavelengths is more energetic and is classified as UV-B radiation, from 280 nm to 315 nm. At even shorter wavelengths between 100 and 280 nm, the radiation is termed UV-C and is fully absorbed by atmospheric trace gases before reaching the Earth's surface [1]. Due to the spectral characteristics of the ozone absorption cross sections, UV radiation shows a dramatic decrease in intensity – over several orders of magnitude – between approximately 330 and 290 nm. This short wavelength cutoff at around 290 nm is therefore mainly influenced by ozone absorption.

Solar ultraviolet radiation contains only a small part of the total energy of the solar radiation reaching the Earth's surface. Nevertheless, radiation at these short wavelengths is energetic enough to affect biological tissue, such as breaking DNA bonds [2]. Ultraviolet radiation has detrimental effects on plants, human beings, and underwater life forms such as plankton, fish, larvae, and algae.

Information on the level of ultraviolet radiation reaching the Earth's surface can be obtained from ground-based measurements, radiative transfer modeling, and more recently can be inferred from measurements by satellite sensors.

The most precise and accurate method is to measure the incoming UV radiation from the surface using spectroradiometers [3]. These instruments measure the intensity of radiation in very narrow wavelength bands and can thereby reconstruct the solar spectrum with high fidelity. Since the UV spectrum shows such important intensity changes with wavelength, the knowledge of the solar spectrum gives the most complete knowledge on the surface UV radiation.

Narrowband multifilter radiometers measure the solar spectrum in several narrow UV wavelength bands with resolutions of the order of 2–10 nm. This type of instrument is more compact and robust than a spectroradiometer, but requires a spectroradiometer for its calibration [4].

The most common type of instrument measuring solar UV radiation is a broadband filter radiometer. This instrument uses filters to be sensitive to a broad wavelength interval, and returns a single value representing the solar UV spectrum weighted with the instrument spectral sensitivity. Various types of such broadband instruments exist, depending on what spectral range they are sensitive: UV-B, UV-A, or the total UV range. While these instruments are easy to operate and require very little maintenance, their calibration is complex and necessitates experienced and well-equipped laboratories [5]. Furthermore, due to the gradual deterioration of their filters, these instruments need frequent recalibrations if long-term measurements are required.

Radiative transfer models (RTMs) solve the radiation equation to retrieve the surface UV radiation from a prescribed atmospheric state [6, 7]. While current RTMs solve the radiation equation with sufficient precision, the results are practically limited by the knowledge of the model parameters that are input to the

model. These model parameters (essentially the composition of the atmosphere and the vertical distribution of their components) are usually not very well known and induce corresponding large uncertainties in the computed UV radiation [8].

Knowledge of the spatial distribution of UV radiation is readily obtained from remote-sensing instruments located on satellite platforms. These instruments determine UV radiation from the backscattered solar radiation that is reflected by the atmospheric layers and the Earth's surface [9]. The surface UV radiation is then obtained from elaborate model calculations. Due to the difficulty inherent in such an approach, the accuracy of the retrieved UV radiation, although determined over large areas with high spatial resolution, has much larger uncertainties than the corresponding surface point-like measurements. For example, a typical problem faced by satellite sensors is the distinction between snow and clouds, which both have a high reflectivity as seen from space. In the first case, surface UV radiation is enhanced, whereas in the second case it is strongly reduced, depending on cloud type and thickness [10]. Additionally, comparisons between surface UV measurements and different satellite sensors have shown that the radiation absorbed by tropospheric aerosols is not well taken into account by satellite sensors and retrieval algorithms. Thus, UV radiation in polluted areas can be overestimated by up to 30% [11, 12].

Factors Affecting Surface Ultraviolet Radiation

The map shown in Fig. 1 displays the daily erythemal UV dose reaching the Earth's surface, averaged over the whole year 2005. The map was obtained from measurements by the Ozone Monitoring Instrument (OMI) [13]. Each pixel has a size of $1 \times 1°$. As can be seen in the figure, the highest UV radiation is found close to the equator, where the solar elevation is the highest. In addition, the Andes and the Himalayas mountain ranges are clearly visible due to the much higher UV radiation with respect to the surrounding areas. Less obvious is the reduced UV radiation over large parts of the Amazonian rainforest, due to the predominant cloud cover over this area compared to the Atlantic and Pacific Ocean at the same latitude.

In what follows, the parameters affecting surface UV radiation will be described in detail.

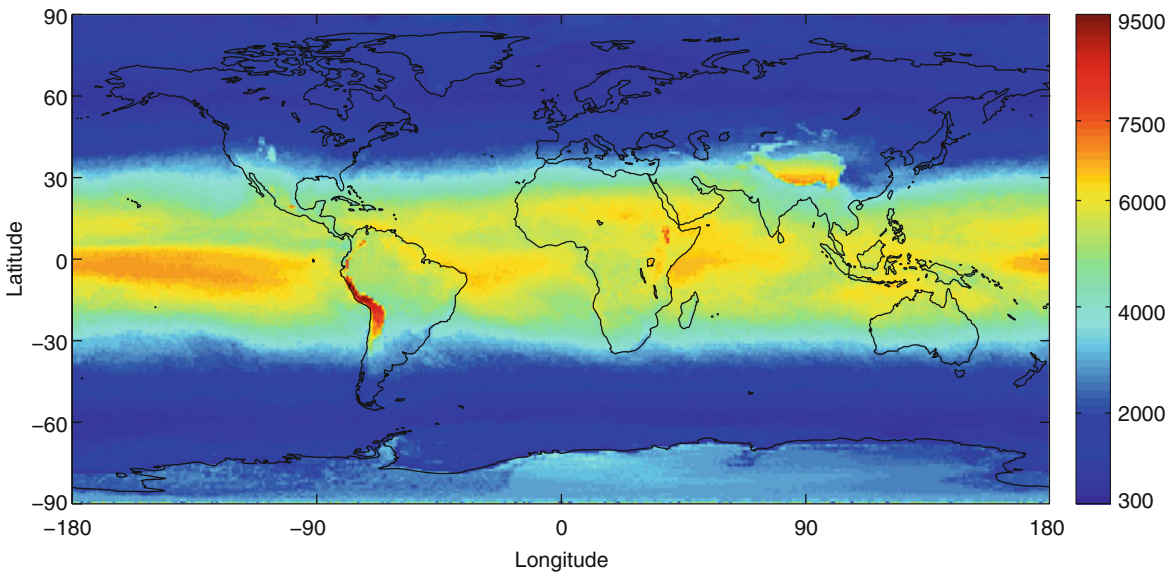

Ultraviolet Radiation: Distribution and Variability. Figure 1
Average daily dose of surface solar erythemal UV radiation in J/m^2 from the OMI Satellite for the year 2005

Earth to Sun Distance

Due to the point-like size of the sun as seen from Earth, the radiation intensity coming from it decreases as the inverse square of the distance between it and the Earth. This variability is of geometric nature and is therefore independent of wavelength, that is, radiation at all wavelengths is affected equally. Since the Earth path around the Sun follows an ellipse in which the sun is at one focus, slight changes in the distance during one annual rotation are evident. The Earth is closest to the sun in early January and farthest from it in early July. The relative difference between the minimum and maximum intensity is 6.8%. This radiation variability has consequences on the geographical distribution of UV radiation since the maximum occurs during the winter in the Northern hemisphere and correspondingly in (austral) summer in the Southern hemisphere and vice versa. Thus, purely from geometrical considerations, the radiation intensity is higher in summer in the Southern hemisphere than in the Northern hemisphere.

Solar Zenith Angle

The largest variation of surface UV radiation is due to the elevation of the sun above the horizon. The dependence of solar UV radiation on solar zenith angle (SZA) is responsible for the diurnal variation of cloud-free solar UV radiation, which normally has a maximum at local noon. The solar zenith angle is also responsible for the latitudinal dependence of surface UV radiation, as shown in Fig. 1. The overall latitudinal gradient dominates the UV variability on a global scale. This pronounced variability is much higher than at longer wavelengths and is due to the absorption of UV radiation by atmospheric ozone, as explained below.

When the solar zenith angle is low, that is, the sun is high in the sky, the path through the atmosphere is short, so that both the absorption and scattering processes are minimized with respect to high SZA when the path through the atmosphere is much larger. This dependence on SZA is mainly due to the atmospheric ozone contained in the atmosphere, since it strongly absorbs UV radiation on its passage through the atmosphere. As is shown in Fig. 2, the diurnal shape of UV-B radiation is much steeper compared with the variation at longer wavelengths, which are not affected by atmospheric ozone.

Clouds

After SZA, clouds represent the most important factor responsible for surface UV variability [14]. Due to their high temporal and spatial variability, clouds are the main reason why it is so difficult to accurately predict UV radiation. Surface UV radiation can be attenuated by up to 99% under certain specific thick cloud types, such as cumulonimbus clouds. In the presence of scattered cumulus clouds, UV radiation is frequently enhanced by the lensing effect from tall adjacent vertical cloud sides [15]. This enhancement can be up to 20% and occurs usually only during short periods of time for particular solar and cloud situations. Figure 3 displays the UV radiation measured at Ispra, Italy between 1992 and 2004. The red curve represents the radiation level possible on a cloud-free day, while the individual points are actual measurements. The large scatter is predominantly due to attenuation by clouds, while the overall yearly variability is due to seasonal changes in solar elevation.

Molecular Scattering

Air molecules in the atmosphere scatter incoming radiation according to its wavelength. As shown by Lord Rayleigh in 1871, the scattering efficiency scales with the inverse fourth power of wavelength ($1/\lambda^4$), thereby scattering short wavelengths much more than longer ones [16]. This relationship, for example, leads to the blue color of the sky in the visible radiation spectrum. For UV wavelengths, the effect is even stronger and is the reason why a large fraction of the incoming solar UV radiation is scattered and reaches the Earth as diffuse radiation. Indeed, even at low SZA, as much as half of the surface UV radiation flux is scattered solar radiation.

Ozone

The inverse correlation between UV Radiation and atmospheric ozone is well documented, and has been thoroughly discussed in the popular and scientific literature. As has been shown, a 1% decrease in total atmospheric ozone leads to an approximately 1% increase in UV-B radiation [17]. The relationship between UV radiation and ozone is strongly dependent on wavelength because the efficiency of ozone in

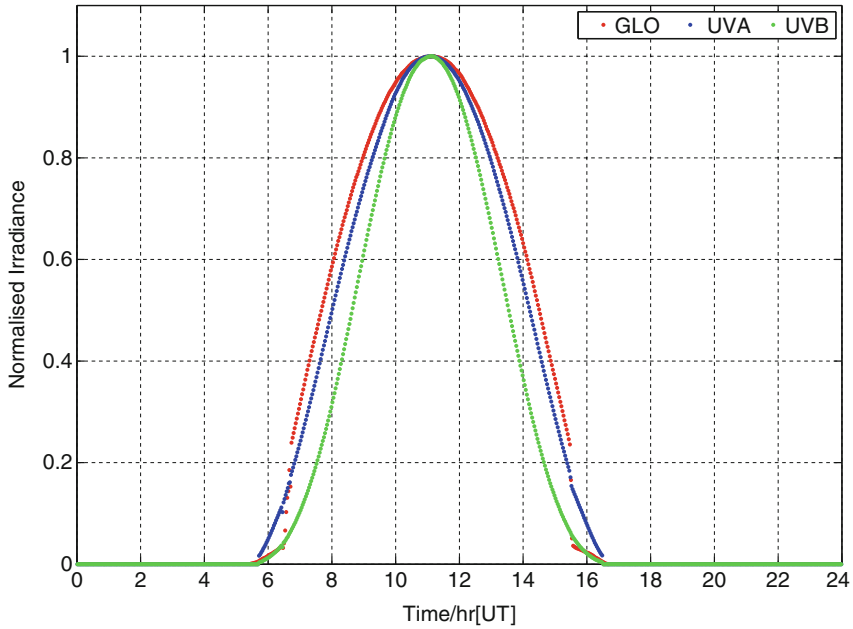

Ultraviolet Radiation: Distribution and Variability. Figure 2
Typical diurnal variation of global solar radiation (0.3–3 μm), red curve, UV-A radiation, blue curve, and UV-B radiation, green curve, during a clear day at Davos. The discontinuity in global radiation around both 7 and 16 UT is due to surrounding mountains blocking the path of the direct radiation from the sun

absorbing UV radiation increases exponentially with decreasing wavelength.

Due to this inverse relationship, a global decrease in total column ozone would raise UV levels to a level that would become deleterious to many life forms living on the Earth.

The inverse correlation between UV radiation and ozone is generally masked by the much larger variability due to SZA and clouds. In Fig. 4, the correlation between UV-B radiation and ozone is shown by normalizing the irradiance at 305 nm by that at 324 nm. The resulting ratio remains very sensitive to ozone, while becoming insensitive to parameters such as clouds or aerosols, which both affect radiation at 305 and 324 nm nearly equally.

Stratospheric Ozone Hole

A dramatic ozone decrease has been occurring in the spring period over the Antarctic continent since the early 1980s [18]. Man-made chemical species accumulate in the winter period over the Antarctic, due to atmospheric conditions specific to the Antarctic continent during winter. In the presence of sunlight, these chemical species react with ozone molecules in the stratosphere and destroy a large fraction of the atmospheric ozone. As much as two thirds of the total ozone contained in the atmosphere can thus be destroyed, which leads in turn to important enhancements in the UV radiation reaching the Earth's surface.

Due to the dynamical nature of the polar vortex, ozone-poor air occasionally reaches also Punta Arenas and Ushuaia at the southern extreme of the South American continent. For instance, during periods of significant ozone reductions, biologically effective UV radiation at Punta Arenas in Chile were more than a factor of 2 higher than during normal conditions [19].

Aerosols

Aerosols in the atmosphere both scatter and absorb radiation. The amount and nature of these processes depend directly on the microphysical properties of the aerosols. Due to the large spatial and temporal variability in aerosols created by anthropogenic or natural

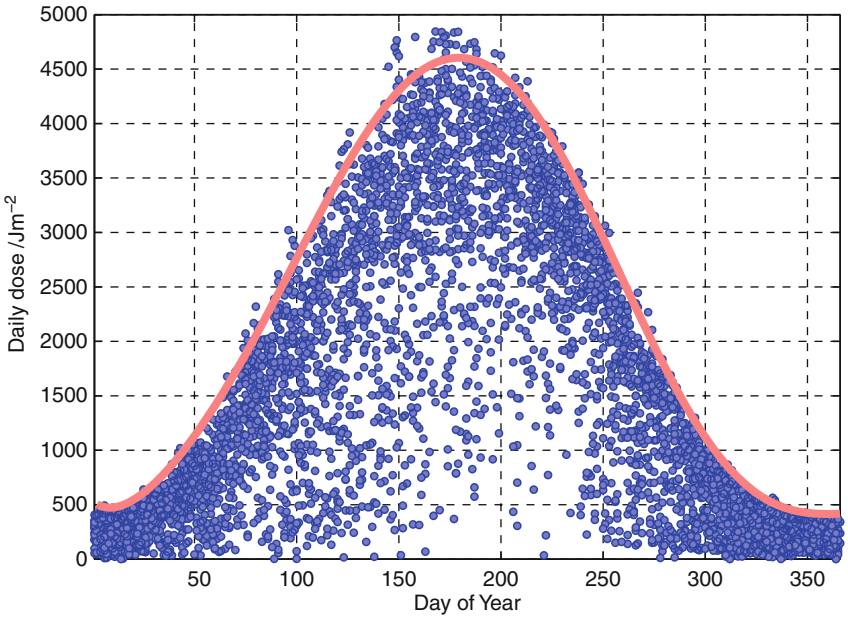

Ultraviolet Radiation: Distribution and Variability. Figure 3
Daily erythemally weighted UV radiation dose at Ispra, Italy for the years 1992–2004. Each point represents the radiation dose reaching the Earth's surface during a single day. The red curve represents the maximum radiation dose expected on a cloud-free day. The large scatter around this curve is due to the effect of clouds, which can reduce UV radiation by up to 99%. Instances of UV radiation higher than the theoretical cloud-free maximum are due to enhanced UV radiation caused by the lensing (or funnel) effect from the sides of cumulus clouds. This effect can locally and temporarily increase UV radiation by up to 20%

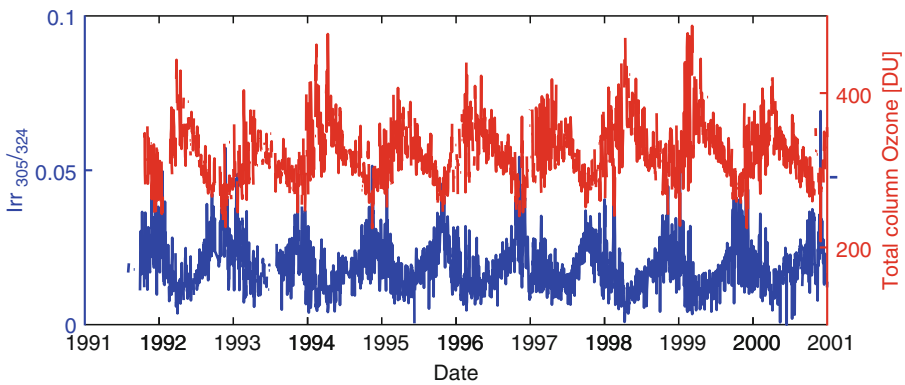

Ultraviolet Radiation: Distribution and Variability. Figure 4
Measurements of UV radiation and total column ozone at Ispra, Italy from 1991 to 2001. The UV radiation at 305 nm is strongly affected by ozone, whereas radiation at 324 nm is only weakly attenuated by ozone. The ratio between radiation at 305 nm and 324 nm (*blue curve*) is largely insensitive to clouds and other parameters that are only weakly depending on wavelength, thus highlighting the dependence on ozone. The total column ozone (*red curve*) measured at the same site shows a systematic yearly shape that is anti-correlated with the UV radiation at 305 nm

processes, the quantification of these processes remains very challenging.

Two main parameters are used to quantify the effect of aerosols on UV radiation. The amount of aerosols, termed the aerosol optical depth (AOD) is a measure of the total aerosol load of the atmosphere. Incoming direct solar UV radiation is attenuated due to scattering and absorbing processes, which are a direct function of AOD. The relative efficiency of aerosols in either scattering or absorbing radiation is described by a second parameter, called the single-scattering albedo (SSA). This parameter can be obtained from microphysical properties of the aerosols. In practice, SSA is very difficult to quantify for a particular atmospheric situation due to the large variability of the aerosol composition. UV radiation can be attenuated by 30% or more in presence of heavy aerosol loads [20].

Surface Reflectivity

Radiation reflected from the surface is backscattered by the atmosphere and thus increases diffuse radiation. This enhancement of diffuse radiation occurs from the scattering that occurs on the molecules and aerosols present in the lower atmospheric layers. Due to the large molecular scattering effect in the UV wavelength range, a significant fraction of the reflected radiation is scattered back to the Earth surface, thereby enhancing the downwelling solar UV radiation. As can be seen in Fig. 5, this enhancement increases toward shorter wavelengths as is expected from the increased molecular scattering efficiency.

The largest enhancement occurs in presence of snow, which has a reflectivity of up to 90% [21]. Studies have shown that in regions with a complete snow cover UV radiation can be enhanced by up to 50% comparatively to a snow-free situation [22]. Radiative transfer models are generally used to infer the effect of surface albedo on UV radiation. As is shown in Fig. 4, the enhancement due to surface albedo has a specific spectral signature, which is mainly due to the interplay between two parameters: At wavelengths above $\approx$ 330 nm, where ozone absorption is negligible, the enhancement is due to Rayleigh scattering. Around 320 nm, a distinct maximum is found followed by a gradual decrease toward shorter wavelengths, which is due to the increasing effectiveness of tropospheric

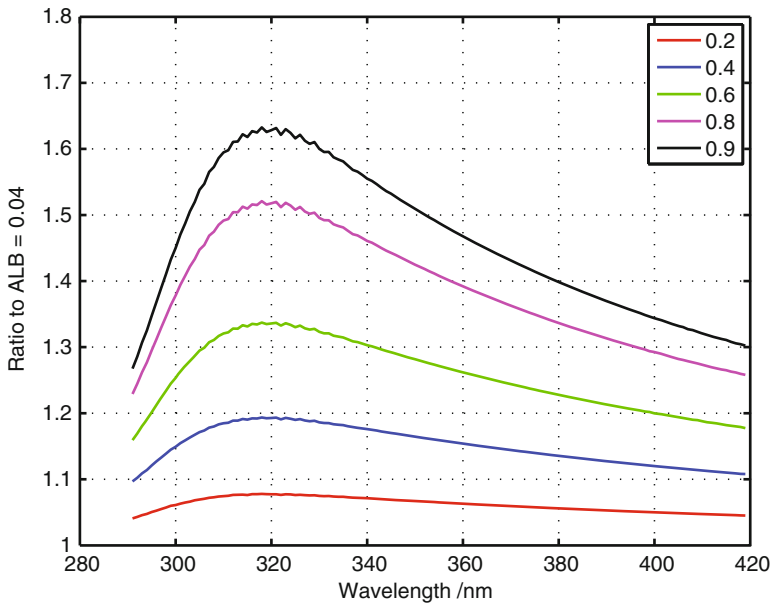

Ultraviolet Radiation: Distribution and Variability. Figure 5
Enhanced UV radiation for different surface albedo values with respect to the case with a UV albedo of 0.04. The gradual increase with decreasing wavelength is due to the increasing scattering efficiency of air molecules, while the decrease below about 320 nm is caused by tropospheric ozone absorption

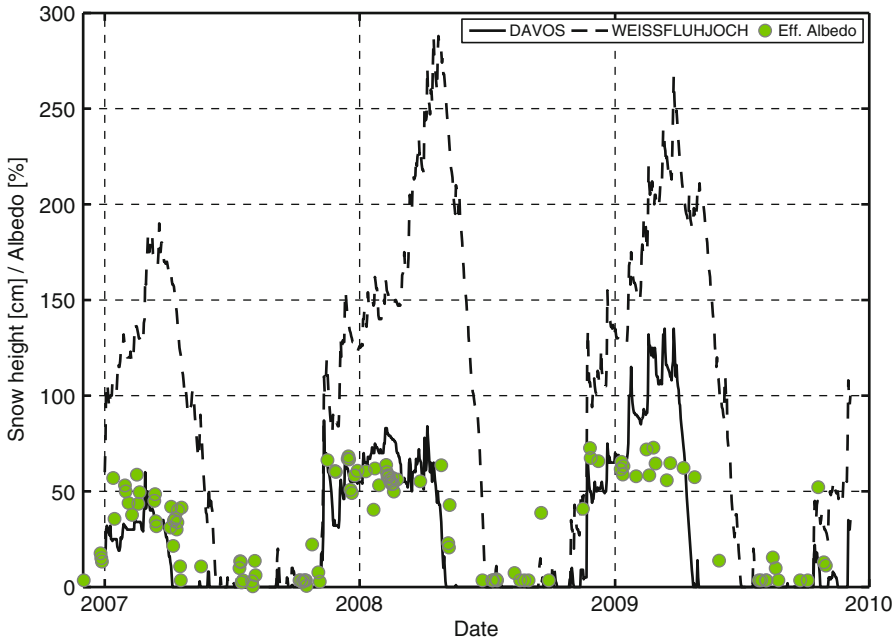

Ultraviolet Radiation: Distribution and Variability. Figure 6
Effective surface albedo in percent, as determined from UV measurements during cloud-free periods at Davos (elevation 1,590 m). The black and dotted lines represent the actual snow height measured in Davos and Weissfluhjoch (elevation 2,540 m, horizontal distance from Davos, 2 km), respectively. During winter, the effective albedo is as high as 70%, enhancing UV radiation by up to 30% with respect to snow-free conditions. During summer, the effective albedo drops to values close to 2–3%

ozone in absorbing UV radiation. Since the reflected radiation is scattered several times before reaching the surface, the likelihood of being absorbed by tropospheric ozone is enhanced.

The enhancement of surface UV radiation due to reflected radiation from the surface that is backscattered to the surface is influenced by the surrounding area around the measurement site. Indeed, model calculations demonstrate that radiation reflected as far away as 30 km can influence the locally incident radiation [23, 24]. State-of-the art three-dimensional radiative transfer models can calculate the actual radiation for an arbitrary surface environment composed of a complex patchwork of albedo conditions, and be only limited by the spatial resolution of the model. In contrast, most common radiative transfer models can only prescribe a single albedo value for the whole surface, which is then called an effective surface albedo [25]. This effective surface albedo represents the overall reflection characteristics of a usually inhomogeneous surface over a circular area with a radius of up to 30 km.

Figure 6 shows the effective albedo determined for Davos from 2007 to 2009 by combining measurements and radiative transfer calculations. As can be seen in the figure, during the winter period when Davos and the surrounding areas are fully covered by snow, the effective albedo has an average value of about 0.6, whereas during the summer months the surface albedo decreases to values around 0.03. The corresponding radiation increase with respect to the snow-free summer period is as large as 30%. It should be noted however that, due to the lower solar elevation in winter than summer, the daily radiation dose is much higher in summer than winter.

Future Directions

The intensity of solar UV radiation in the future will depend on possible changes in several factors, in

relation to global and regional changes in the climate system. These factors include ozone, aerosols, clouds, and surface reflectivity, which are all expected to change on both a regional and global scale due to climate change. Changes in stratospheric ozone can be modeled quite accurately using global chemistry models. Their results indicate that the total ozone levels will not only recover as a consequence of the measures taken under the Montreal protocol and its amendments, but that a "super-recovery" of ozone is likely to occur around 2050 [26]. This super-recovery will manifest itself with higher ozone levels than prior to the global ozone decrease, with correspondingly reduced UV levels, depending on the region considered [27].

Bibliography

Primary Literature

1. Coblentz WW (1932) The Copenhagen meeting of the second international congress on light. Science 76:412–417
2. Diffey BL (1991) Solar ultraviolet radiation effects on biological systems. Phys Med Biol 36(3):299–328
3. Gröbner J (2001) Characterisation of spectrophotometers used for spectral solar ultraviolet radiation measurements. Rad Prot Dosimetry 97:415–418
4. Dahlback A (1996) Measurements of biologically effective UV doses, total ozone abundances, and cloud effects with multichannel, moderate bandwidth filter instruments. Appl Opt 35:6514–6521
5. Hülsen G (2007) Characterization and calibration of ultraviolet broadband radiometers measuring erythemally weighted irradiance. Appl Opt 46:5877–5886
6. Chandrasekhar S (1960) Radiative transfer. Dover Press, New York. ISBN 0-486-60590-6
7. Stamnes K et al (1988) Numerically stable algorithm for discrete-ordinate-method radiative transfer in multiple scattering and emitting layered media. Appl Opt 27:2502–2509
8. Weihs P et al (1997) Accuracy of spectral UV model calculations 1. Consideration of uncertainties in input parameters. J Geophys Res 102(D1):1541–1550
9. Herman J et al (1999) Distribution of UV radiation at the Earth's surface from TOMS-measured UV-backscattered radiances. J Geophys Res 104(D10):12059–12076
10. Arola A et al (2003) A new approach to estimating the albedo for snow-covered surfaces in the satellite UV method. J Geophys Res 108:4531. doi:10.1029/2003JD003492
11. McKenzie R et al (2001) Satellite retrievals of erythemal UV dose compared with ground-based measurements at northern and southern midlatitudes. J Geophys Res 106:D20. doi:10.1029/2001JD000545
12. Arola A et al (2005) Assessment of TOMS UV bias due to absorbing aerosols. J Geophys Res 110:D23211. doi:10.1029/2005JD005913
13. Tanskanen A et al (2007) Validation of daily erythemal doses from Ozone Monitoring Instrument with ground-based UV measurement data. J Geophys Res 112:D24S44. doi:10.1029/2007JD008830
14. Bener P (1964) Investigation on the influence of clouds on the ultraviolet sky radiation. Contract AF 61(052)-618, Tech. Note 3, Davos-Platz, Switzerland
15. Mims FM III, Frederick JE (1994) Cumulus clouds and UV-B. Nature 371:291
16. Rayleigh (1871) On the scattering of light by small particles. Phil Mag 41, 107, 274
17. Madronich S et al (1998) Changes in biologically active ultraviolet radiation reaching the Earth's surface. J Photochem Photobiol B Biol 46(1–3):5–19
18. Farman JC et al (1985) Large losses of total ozone in Antartica reveal seasonal ClOx/NOx interaction. Nature 315:207–210
19. Kirchhoff V et al (1997) UV-B enhancements at Punta Arenas, Chile. J Photochem Photobiol B Biol 38:174–177
20. Kylling A et al (1998) Effect of aerosols on solar UV irradiances during the photochemical activity and solar ultraviolet radiation campaign. J Geophys Res 103:26051–26060
21. Blumthaler M et al (1988) Solar UVB albedo of various surfaces. Photochem Photobiol 48(1):85–88
22. Bernhard G et al (2007) Ultraviolet and visible radiation at Barrow, Alaska: climatology and influencing factors on the basis of version 2 National Science Foundation network data. J Geophys Res 112:D09101. doi:10.1029/2006JD007865
23. Degünther M et al (1998) Case study on the influence of inhomogeneous surface albedo on UV irradiance. Geophys Res Lett 25:3587–3590
24. Mayer B, Degünther M (2000) Comment on "Measurements of erythemal irradiance near Davis station, Antarctica: effect of inhomogeneous surface Albedo". Geophys Res Lett 27: 3480–3490
25. Kylling A et al (2000) Determination of an effective spectral surface albedo from ground-based global and direct UV irradiance measurements. J Geophys Res 105(D4):4949–4959
26. Austin J et al (2006) Ensemble simulation of the decline and recovery of stratospheric ozone. J Geophys Res 111:D16314. doi:10.1029/2005JD006907
27. WMO (2007) Scientific assessment of ozone depletion: 2006. Global ozone research and monitoring project report No. 50. World Meteorological Organization, Geneva

Books and Reviews

Seckmeyer et al (2001) Instruments to measure solar ultraviolet radiation, part 1: spectral instruments (WMO TD No. 1066), available at http://www.wmo.ch/pages/prog/arep/gaw/gaw-reports.html

Seckmeyer et al., Instruments to measure solar ultraviolet radiation – Part 2: Broadband instruments measuring erythemally

weighted solar irradiance (WMO TD No. 1289), 55 p, July 2008, available at http://www.wmo.ch/pages/prog/arep/gaw/gaw-reports.html

Webb et al (2003) Quality assurance in monitoring solar utraviolet radiation: The state of the art (WMO TD No. 1180), available at http://www.wmo.ch/pages/prog/arep/gaw/gaw-reports.html

Zerefos C (1997) Solar ultraviolet radiation: modelling, measurements and effects (NATO ASI Series/Global Environmental Change). ISBN 3-540-62711-1

Underground Cable Systems

Yamille Del Valle, Nigel Hampton, Josh Perkel, Caryn Riley
National Electric Energy Test Research and Application Centre (NEETRAC), Forest Park, GA, USA

Article Outline

Glossary
Definition of the Subject
Introduction
Cable System Structure
MV, HV, and EHV Cable Systems
Uses of Cables
AC and DC Transmission
Cable Types
Components of the Cable
Cable Manufacture
Failure Processes
Dry Aging Thermoelectric Aging
Future Directions
Understanding Life Expectancy of Cable Systems
Improving Cable Performance with Respect to Aging
Recyclable/Recoverable Cable Designs
Increased Use of Long Length Links
Bibliography

Glossary

Breakdown Permanent failure through insulation.

Cable system Cable with installed accessories.

CCV Catenary continuous vulcanization extrusion line for extruded dielectrics.

Cross-linked polyethylene (XLPE) A thermoset unfilled polymer used as electrical insulation in cables.

Diagnostic test A field test made during the operating life of a cable system. It is intended to determine the presence, likelihood of future failure and, for some tests, locate degraded regions that may cause future cable and accessory failure.

Dielectric loss An assessment of the electric energy lost per cycle. A poorly performing cable system tends to lose more energy per AC cycle. Measurements can be made for selected voltages or over a period of time at a fixed voltage. The stability of the loss, the variation with voltage and absolute loss are used to estimate the condition. Data can be derived from time-based (if sufficient time is taken) or frequency-based test methods.

Electrical trees Permanent dendritic growths, consisting of nonsolid or carbonized micro-channels, that can occur at stress enhancements such as protrusions, contaminants, voids, or water trees subjected to electrical stress. The insulation is damaged irreversibly at the site of an electrical tree.

Ethylene propylene rubber (EPR) A type of thermoset-filled polymer used as electrical insulation in cables and accessories. There are several different formulations of EPR and they have different characteristics. For purposes here, the term also encompasses ethylene propylene diene monomer rubber (EPDM).

Extra high voltage (EHV) Cable systems within the voltage range 161–500 kV, though more often between 220 kV and 345 kV. Also referred to as transmission class, though usually has higher design stress levels than HV.

Extruded dielectrics Insulation such as EPR, HMWPE, PE, WTRXLPE, XLPE, etc., applied using an extrusion process.

Filled insulation Extruded insulations where a filler (carbon black or clay) has been incorporated to modify the inherent properties of the base polymer. This class includes all types of EPR, Vulkene, etc.

High pressure fluid filled (pipe type or HPOF) paper insulated and installed in trefoil in steel pressure pipes and impregnated with high-pressure nondegradable fluid which is maintained at high

pressures by pumping plants – common in USA at HV & EHV.

High voltage (HV) Cable systems within the voltage range from 46–161 kV, though more often between 66 kV and 138 kV. Also referred to as transmission class, though usually has lower design stress levels than EHV.

Jacket An extruded outer polymeric covering for cables designed to protect the cable core and the metallic shielding (wires, tapes, or foils).

Joint A device to join two or more sections of power cable together. A joint includes a connector to secure the cable conductor and a stress controlling/insulating body to manage the electrical stress.

Laminated dielectrics Insulation formed in layers typically from tapes of either cellulose paper or polypropylene or a combination of the two. Examples are the PILC (paper-insulated lead-covered) and MIND (mass-impregnated non-draining) cable designs.

Mass impregnated non-draining Cable (MIND) A cable design using paper insulation impregnated with a thick compound such that the compound does not leak out when the lead is breached.

Maximum electrical stress The highest level of stress also corresponds to the highest probability of instantaneous failure or, equivalently, the highest rate of electrical aging.

MDCV Mitsubishi Dainichi continuous vulcanization, often called long land die, extrusion line for XLPE, typically for HV & EHV.

Mean or average electrical stress This is most important if the most serious defects are uniformly located throughout the bulk of the insulation.

Medium voltage (MV) Cable systems within the voltage range from 6 kV to 46 kV, though more frequently between 15 kV and 35 kV. Also referred to as distribution class.

Metallic shield A concentric neutral surrounding the cable core. The shield provides (to some degree) mechanical protection, a current return path, and, in some cases, a hermetic seal (essential for impregnated cables).

Minimum electrical stress This is most important if cable system reliability is determined by the performance of accessories or if the electrical design or installation method of accessories degrades cable performance.

Paper insulated lead covered (PILC) A cable design using paper insulation impregnated with a fluid and encased in lead to prevent the fluid from leaking out of the insulation.

Partial discharge A low voltage (mV or μV) signal resulting from the breakdown of gas enclosed in a dielectric cavity. The signals travel down the cable system and may be detected at the end, thereby enabling location.

PE-based Extruded insulations that do not have an incorporated filler (carbon black or clay). This class includes all types of HMWPE, PE, WTRXLPE, XLPE, etc.

Polyethylene (PE) A polymer used as electrical insulation in cables.

Power frequency A substantially sinusoidal waveform of constant amplitude with an alternating frequency in the range of 49–61 Hz.

Self-contained fluid filled (FF or LPOF or PILC) Paper or paper polypropylene laminated (PPL) insulated with individual metal sheaths and impregnated with a dielectric fluid. Where used these are common in land cable applications. This type of cable is one of the first to be installed in the 1890s.

Shielded cable A cable in which an insulated conductor is encapsulated in a conducting "cylinder" that is connected to ground.

Space charge Quasi-permanent injected charge that is trapped within the insulation of a cable system. This charge is sufficient to modify the applied AC and impulse voltage stresses.

Splice A joint.

Tan δ (TD) The tangent of the phase angle between the voltage waveform and the resulting current waveform.

Termination A device that manages the electric stress at the end of a cable circuit, while sealing the cable from the external environment and providing a means to access the cable conductor. Devices referred to as elbows or potheads are types of terminations.

VCV Vertical continuous vulcanization extrusion line for XLPE, typically for HV & EHV

Water tree retardant cross-linked polyethylene (WTRXLPE) A thermoset polymer used as electrical insulation in cables that is designed to retard water tree growth.

Water trees Dendritic pattern of electro-oxidation that can occur at stress enhancements such as protrusions, contaminants, or voids in polymeric materials subjected to electrical stress and moisture. Within the water tree the insulation is degraded due to chemical modification in the presence of moisture.

Definition of the Subject

Underground cables have been used from the earliest time as integral parts of the power distribution and transmission system. Compared to their overhead analogues, they have been long regarded as the most critical of components due in part to their high total installed cost, their unique ampacity requirements, and the complexity of their installation. Thus, even from the very first technical papers, the sustainability, through reliability and longevity, has been of paramount importance. This contribution addresses the focus on sustainability today while maintaining a linkage to the lessons that have been already learned.

Introduction

Almost all electric power utilities distribute a portion of the electric energy they sell via underground cable systems. Collectively, these systems form a vast, interlinked, and valuable infrastructure. Estimates for the USA indicate that underground cables represent 15–20% of installed distribution system capacity. This percentage is much closer to 50% in Europe. These cable systems consist of many thousands of miles of cable and hundreds of thousands of accessories installed under city streets, suburban developments, and the countryside. Utilities have a long history of using underground system with some of these cable systems installed as early as the 1890s. Very large quantities of cable circuits were installed in the 1950s–1980s. Today, the size of that infrastructure continues to increase rapidly as the majority of newly installed electric distribution lines are placed underground. There are a number of drivers and brakes that control this process and they are shown in Table 1.

Cable systems are designed to have a long life with high reliability. However, the useful life is not infinite. These systems age and ultimately reach the end of their reliable service lives. Estimates set the design life of underground cable systems to be in the range of 30–40 years. Today, a large portion of this cable system infrastructure is reaching the end of its design life, and there is evidence that some of this infrastructure is reaching the end of its reliable service life. This is a result of natural aging phenomena as well as the fact that the immature technology used in some early cable systems is decidedly inferior compared to technologies used today. Increasing failure rates of these older systems are now adversely impacting system reliability, and it is readily apparent that action is necessary to manage the consequences of this trend.

Underground Cable Systems. Table 1 Factors encouraging and discouraging the installation of underground cable systems

Encouraging installation of underground cable systems	Discouraging installation of underground cable systems
Public perception of risk	Capital cost – higher for cable systems
Reliability (frequency of outages) – frequency is lower for underground cable systems	Return to service after failure (repair time) – longer repair time
Total operating cost – lower electrical losses & lower repair and maintenance costs	Need for reactive compensation on long lengths AC systems
Public perception of visual impact – lower impact	

Cable System Structure

The name "cables" is given to long current-carrying devices that carry their own insulation and present an earthed outer surface [1]. In this context, overhead lines, for example, are not considered as cables. Power cables have a coaxial structure: Essentially, they comprise a central current-carrying conductor at line voltage, an insulation surrounding the conductor, and an outer conductor at earth potential. AC cables are generally installed as a 3-phase system, and hence, the outer conductor should only carry fault and loss currents. In practice, a more sophisticated construction is

adopted. The interfaces between the metal conductors and the insulation (laminated or polymeric) would tend to include contaminants, protrusions, and voids, features that would lead to electrical stress enhancement, accelerated aging, and premature failure [2, 3]. To overcome this, a "semicon" layer, a conductive paper or polymeric composite, is placed at both interfaces. The inner semicon, the insulation, and the outer semicon ensure the interfaces are smooth and contaminant-free. Surrounding this cable are layers to protect the cable during installation/operation and carry the loss/fault currents. These layers also serve to keep out water, which may lead to water treeing in polymer insulations or elevated losses in laminated insulations. A schematic diagram of a power cable is shown in Fig. 1.

MV, HV, and EHV Cable Systems

Cable systems that are used for distribution and transmission purposes are generally categorized according to the voltage rating:

- Medium voltage (MV): 6–36 kV
- High voltage (HV): 36–161 kV
- Extra high voltage (EHV): 161–500 kV (or more)

There is no international consistency on the distinction between "distribution" and "transmission." Which means that although clear in the bulk of the ranges, the edges/transitions get somewhat blurred. Table 2 shows the relationship between the voltages and voltage classes of cable systems for selected regions of the world.

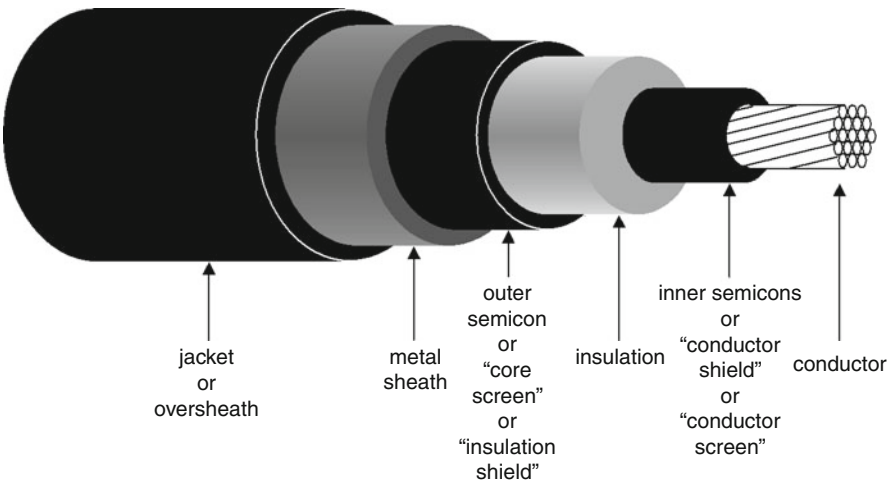

Underground Cable Systems. Figure 1
Cut-away section of a typical power cable

Underground Cable Systems. Table 2 Voltage classes for AC cable systems in selected regions

	MV	HV	EHV
Asia	6.6, 10, 15, 22, 33	66, 90, 110, 132, 154, 161	187, 220, 275, 345, 400, 500, 525
Europe	11, 20, 33	63, 66, 90, 110, 132, 145, 150	220, 275, 380, 400
North America	15, 25, 35, 46	69, 115, 138	220, 230, 345, 500
	Distribution	Transmission	
Nordic	20	90, 132, 145	220, 400

Electrical Stresses

The operation of a cable system is very dependent upon the electrical stresses (E) to which it is subjected, for example:

- Dielectric heating $\propto E^2$
- Probability of failure $\propto 1-\exp(E/\alpha)^{\beta}$
- Insulation aging $\propto E^n$

Thus, to understand the many issues associated with sustainability, it requires a firm understanding of the electric stresses in the whole system.

Alternating Current (AC) The electrical stress within a cable is given by [1].

$$E = \frac{V}{x \ln\left(\frac{R}{r}\right)} \tag{1}$$

where V is the applied voltage, r is the radius over the inner semiconductive screen, R is the diameter over the insulation, and x is the intermediate radius (between r and R) at which the electric stress is to be determined.

The probability of failure depends upon the electrical stress and increases with stress. The effect of an increased stress is most commonly estimated using the Weibull probability function [4]:

$$P_f = 1 - \exp\left\{-\left(\frac{E}{\alpha}\right)^{\beta}\right\} \tag{2}$$

where P_f is the cumulative probability of failure, i.e., the probability that the cable would have failed if the stress is increased to a value E. The two parameters, α and β, are known, respectively, as the characteristic stress and the shape parameter.

Inspection of Eq. 1 shows that the electric stress varies with the position within the cable. There are three potentially useful stresses that can be considered:

- Maximum stress at conductor screen
- Mean geometric average stress for the whole insulation
- Minimum stress at the core screen

The decision as to which of these to consider is an important one and is guided by the potential modes of failure:

- Maximum: The highest level of stress also corresponds to the highest probability of instantaneous failure or, equivalently, the highest rate of electrical aging. This is most important if the most serious cable defects are located on or near the conductor screen.
- Mean: This is most important if the most serious defects are uniformly located throughout the bulk of the insulation.
- Minimum: This is most important if cable system reliability is determined by the performance of accessories or if the electrical design or installation method of accessories degrades cable performance. It is also important if the most serious cable defects are located on or near the core screen.

The range of electrical stresses employed is shown in Table 3.

Direct Current (DC) The stress in AC cables is determined by the capacitance (permittivity) of the structure. However, in DC cable systems, the resistance (resistivity) determines the stress [1, 5].

Underground Cable Systems. Table 3 Average stress levels for selected insulations

Type	Stress (kV/mm)	EHV	HV	MV
Fluid filled	Average at core screen	10.0	8	8
	Average at conductor screen	17	14	10.0
EPR	Average at core screen	4	3	2
	Average at conductor screen	8	5	3
XLPE	Average at core screen	5.0	3	2
	Average at conductor screen	11	6	3

The permittivity of insulations is essentially stress and temperature independent (within the range of normal use), whereas the resistivity has significant voltage and temperature dependence.

Inspection (Fig. 2) shows that in the temperature range (20–60°C), the resistivity can change by 2–3 orders of magnitude. The dependence of the resistivity ρ on stress E and temperature T can be characterized equally well by using the formats of Eqs. 3 or 4.

$$\rho = \rho_0 \exp(-\alpha T - \beta \mathrm{E}) \tag{3}$$

$$\rho = \rho_0 \exp(-\alpha T)\mathrm{E}^{-\gamma} \tag{4}$$

where ρ_o is the resistivity at reference temperature, α is the temperature coefficient, and β and γ are the stress coefficients of the insulation.

The practical consequence is that the stresses in a DC cable system are primarily determined by the dimensions, voltage, and the temperature distribution. Thus, the design of DC systems is technologically much more challenging than AC. The most obvious manifestation is the difference (with respect to AC systems) of the location of the maximum stress: In AC systems, this is always located close to the conductor (termed Laplace field in Fig. 3); in DC systems, this can move from the conductor (no load case) to the outside (highly loaded case) – this is termed stress/temperature inversion.

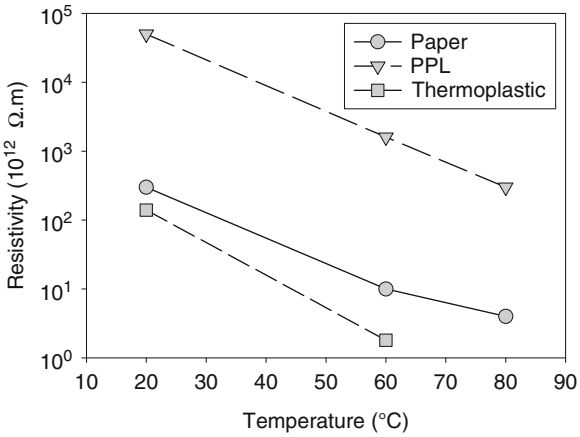

Underground Cable Systems. Figure 2
Resistivity of selected insulations at different temperatures

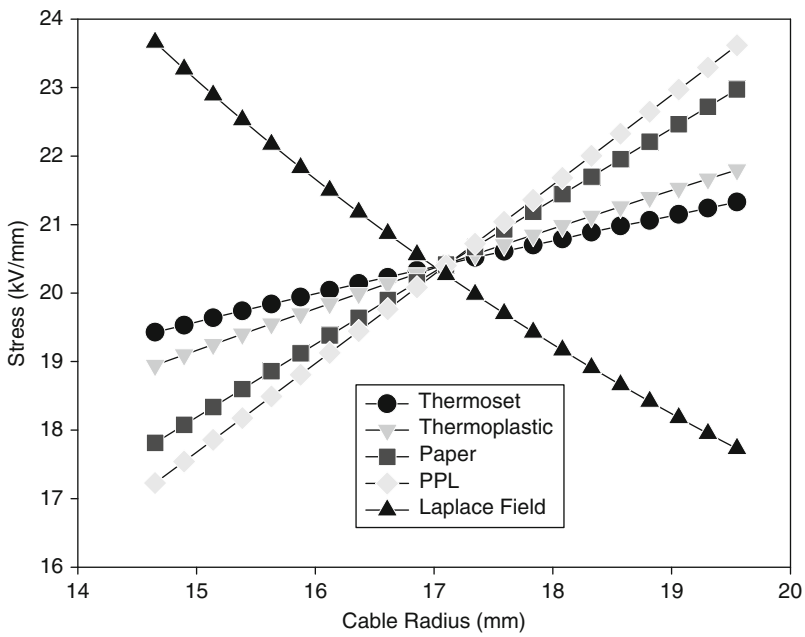

Underground Cable Systems. Figure 3
Electrical stress distribution, under load, for a 100 kV DC cable manufactured using different insulants. The power loss *W* is the same for all designs

One of the ways to calculate the electrical stress distribution E_r across the cable insulation at radius r can is shown below:

$$E_r = \frac{\delta V (r/r_2)^{\delta-1}}{r_2\left[1-(r_1/r_2)^{\delta}\right]} \tag{5}$$

$$\delta = \frac{\alpha W/2\pi\lambda + \beta V/(r_2 - r_1)}{\beta V/(r_2 - r_1) + 1} \tag{6}$$

where λ is the thermal conductivity, r_1 is the conductor screen radius, r_2 is the radius over insulation, $W = I^2R$ is the conductor loss, and V is the applied voltage. The α and β parameters are extracted from the resistivity data using Eq. 3.

Uses of Cables

Power cables are commonly used in underground or underwater (submarine) connections. Cables are placed at strategic points of the transmission grid to supplement overhead lines or, in some cases, they can form the whole "backbone." Interconnections between networks are particularly well suited to cable solutions [3] for security of supply reasons.

Cables may also be used in other applications rather than just underground or underwater. For example, overhead covered conductors allow smaller phase clearance between the conductors on medium-voltage overhead lines. Objects, particularly tree branches, may touch the lines without tripping or customer outage. This has led to substantial improvements in service reliability (e.g., [5]). In most cases, the aluminum alloy conductor is covered with black UV-resistant cross-linked polyethylene and filled with grease, to provide corrosion protection and longitudinal watertightness. Arcing guides are applied at insulator tops, to protect the line from arcing damage. Another application is the "Powerformer" [6] and the related "motorformer." These new generators are able to supply electricity directly to the high voltage grid without the need for a step-up transformer. It is suitable for power generation at output voltages of several 100 kV. One example of this is the Troll motorformer project on an natural gas rig in the North Sea. The new concept is based on circular conductors for the stator winding, and it is implemented by using proven high-voltage cable technology. Thus, the upper limit for the output voltage from the generator is only set by that of the cable.

AC and DC Transmission

Cable systems are used in both alternating current (AC) and direct current (DC) schemes. The cable designs used in each case are outwardly very similar and have many identical design elements. However, the detailed engineering and the materials used are very different. AC is the globally preferred means of transferring electric power. This form of transfer makes it straightforward to generate electricity and to transform voltages up and down. This means of transfer accounts for more than 98% of the global power infrastructure.

In long-distance transmission schemes, especially those that are of interest in the future such as windfarms or solar plants, there are very significant advantages in using DC over AC. System instabilities caused by connecting regions with slightly different AC phases and frequencies are obviated. Capacitive charging current implies that there is a maximum useful length of AC cables without the use of shunt reactors. DC cables are therefore particularly useful for long-distance submarine connections. Furthermore, the lack of electromagnetic effects under DC conditions eliminates the skin effect in which the conductor resistance can rise by up to 20% at 50 Hz. The drawbacks for a DC solution are that the terminal equipment for AC/DC conversion is seen as more costly and less efficient than AC transformers. (Reviews on AC/DC power transmission are contained in [7].) Thus, the system must be sufficiently long to be economically viable. In addition, the control of the electrical stress in a DC cable insulation is also much more difficult due to thermally induced stress inversions and stress modifications due to trapped space charge. The space charge issues are particularly onerous at interfaces, such as those that occur at accessories (joints and terminations).

Before 2000, cables using lapped/impregnated (oil or compound) insulations were almost exclusively used for DC transmission up to 500 kV and very long distance. Even today this technology is preferred for the highest voltages (EHVDC) and distances. However, the recent development in the HVDC and lower power

Underground Cable Systems. Table 4 HVDC projects using extruded cable systems

Project	Type of Project	Power MVA	Voltage rating KV	Cable length km	In service Year
Gotland/SE	S	60	80	140	1999
Directlink/AU	TL	180	84	390	2000
Tjœreborg/DK	WIND	8	10	8	2000
Cross Sound/US	S	330	150	82	2002
Troll/NO	OFF	80	60	70	2004
Estlink/FI	S	350	150	105	2006
Valhalla/NO	OFF	78	150	292	2009
NordEon/DE	WIND	400	150	390	2009
Transbay/US	S	400	200	95	2010

S Subsea Interconnection, *OFF* Offshore Power Supply, *WIND* Windpower Delivery to Shore, *TL* Trading Link

range has seen the symbiotic development of cable systems and converter technologies. The pace of this development has been quite rapid such that the current installed lengths (not at similar voltages) of paper and extruded cables are approximately equal at 22,500 km. A selection of HVDC projects using extruded cables is shown in Table 4.

Cable Types

There are, in general, four types of underground power cable technologies in use today:

- *Polymeric*: Cross-linked polyethylene (XLPE), water tree retardant cross-linked polyethylene (WTRXLPE), or ethylene propylene rubber (EPR).
- *Self-contained fluid filled (FF or LPOF or PILC)*: Paper or paper polypropylene laminated (PPL) insulated with individual metal sheaths and impregnated with a dielectric fluid. Where used these are common in land cable applications. This type of cable is one of the first to be installed in the 1890s.
- *Mass impregnated non-draining (MIND or solid)*: Paper insulated with individual metal sheaths and impregnated with an extremely high viscosity polybutene compound that does not flow at working temperatures – common at MV and submarine HVDC.
- *High pressure fluid filled (Pipe Type or HPOF)*: Paper insulated and installed in trefoil in steel pressure pipes and impregnated with high pressure nondegradable fluid which is maintained at high pressures by pumping plants – common in USA at HV & EHV.

The typical electrical stresses employed in cables are shown in Table 3.

Up until the mid-1980s, paper-insulated cables (PILC, MIND & LPOF) were the system of choice at medium and high voltages. However, improvements in polymeric cables and accessories plus environmental concerns with the impregnation (dielectric fluid and the associated lead sheaths) have led to a significant reduction in the use of paper cables for land applications. In particular, at MV, there has been a strong preference for XLPE & WTRXLPE cables over EPR (except in Italy and USA). XLPE/WTRXLPE and EPR have emerged as the favored polymeric insulations through the 90°C continuous operating temperature that can be achieved when they are used. This temperature matches that which can be attained when fluid-filled lapped insulations (paper and PPL) are used. In contrast, LDPE and HDPE are limited to operating temperatures of 70°C and 80°C, respectively. As a consequence, these insulations have fallen into disuse.

Tables 5 and 6 identify some of the main advantages of the respective technologies at distribution and transmission voltages.

The situation today is:

- Almost all new HV and EHV systems that are being installed are new build/expansion.

Underground Cable Systems. Table 5 Advantages (+) and disadvantages (−) of MV cable insulations

XLPE 11–46 kV	EPR 11–46 kV	WTRXLPE 11–46 kV	Paper 11 to 46 kV (PILC and MIND technologies)
+ No risk of oil leakage	+ No risk of oil leakage	+ No risk of oil leakage	– Oil leakage in PILC technology 0 Reduced compound leakage in MIND technology
+ Very low dielectric losses	0 Medium dielectric losses	+ Low dielectric losses	– High dielectric losses
+ Simple accessory designs which require competent workmanship	+ Simple accessory designs which require competent workmanship	+ Simple accessory designs which require competent workmanship	0 Simple/robust accessories which require high level of workmanship – installation skills disappearing with aging of the workforce
– Likely to suffer from water trees if no metal sheath	0 Less likely to suffer from water trees if no metal sheath	0 Less likely to suffer from water trees if no metal sheath	+ Metal sheath required to contain fluid, thus water is excluded
0 Standard Size	0 Standard Size Reduced size available in special designs	0 Standard Size	+ Small size – higher design stresses – important for installation in ducts

Underground Cable Systems. Table 6 Advantages (+) and disadvantages (−) of HV & EHV cable insulations

XLPE 66–500 kV	EPR 66–138 kV	Paper 66–500 kV (low-pressure and high-pressure technologies)
+ No risk of oil leakage	+ No risk of oil leakage	0 Oil leakage is a concern
+ Simple design	+ Simple design	– Complicated design – High maintenance burden
+ Very low dielectric losses	0 Medium dielectric losses	0 Medium dielectric losses
+ Acceptable fire performance	+ Acceptable fire performance	– Fire performance in tunnel and substation applications is a concern due to the copious supply of flammable oil
+ Simple accessory designs which require high level of workmanship	+ Simple accessory designs which require high level of workmanship	0 Simple accessories which require high level of workmanship – installation skills disappearing with aging of the workforce
0 Growing track record	– Limited track record	+ Extensive track record
– Likely to suffer from water trees if no metal sheath	– Likely to suffer from water trees if no metal sheath	+ Metal sheath required to contain fluid, thus water is excluded
– Large size	– Large size	+ Small size – higher design stresses

- The majority of HV cables, *already installed* within the existing system, are insulated with paper (83% paper and 17% polymeric).
- There is very little replacement of existing paper cables: Most of installed capacity is based on paper.
- Most HV transmission is by overhead lines (OHLs).
- HV cables are replacing OHLs in environmentally sensitive areas but there is limited impact (globally) on new OHLs.

- XLPE cables make up 80–90% of the HV cable capacity *presently being installed.*

The reasons that there has been little replacement of paper cables are:

- Paper cables continue to operate reliably.
- Operating temperatures have been considerably below the temperature limits
- The designs of XLPE cables are too large to fit existing rights of way or pipes that have been designed for paper cables. This is of special importance in the USA where there are many paper cables and small tight ducts. In this area, the key task is to develop polymeric cables designs that are flexible, small (i.e., working at high stresses), and easy to join as it is essential to use the existing pipes/ducts. Present designs address these issues, and now, cables exist that match the size and performance of paper cables [8, 9].

Components of the Cable

Conductor

Conductors in the USA tend to be based on the American wire gauge (AWG), but, in the rest of the world, are based on IEC228 and are therefore described using the metric convention. Stranded conductors have generally comprised concentric layers, but, in order to make them smoother and more compact, they are often specially shaped in rolling mills nowadays. When operating at high voltages and currents, the AC current is preferentially carried more in the outer than in the inner conductors (the skin effect). In addition, the electromagnetic fields induce eddy currents (proximity effect). These effects tend to increase the conductor resistance under AC above that which is seen under DC. The AC/DC ratio ($R_{AC/DC}$) can be as large as 1.15. This increased resistance serves to increase the Joule heating losses within the conductor and increases the temperature of the cable. Thus, special "Milliken" conductors may be used for large conductor designs to reduce the AC/DC ratio.

Conductors are virtually all made from either copper or aluminum. Copper has the advantage of being more conductive, and therefore, requires less material to carry a given current. Copper conductors, therefore, have the advantage of being small. However, the cost of aluminum, although variable, is lower than that of copper, and even though it has a lower conductivity, it is often used as the conductor. An additional advantage of aluminum over copper is that the conductors are lower in weight even though more volume of material is used. At MV, aluminum is preferred whereas, at HV and EHV, the smaller size of copper provides the greatest advantage.

Semicon

Semiconductive screening materials are based on carbon black, manufactured by the complete and controlled combustion of hydrocarbons. The carbon conducting medium is dispersed within a paper or polymer matrix depending upon the type of cable involved. In early designs of polymeric cable, paper tapes or painted carbon screens were used. These displayed extremely poor service performance as they were seen to dramatically accelerate the growth of water trees. In these cases, failures occurred many years short of the anticipated design life. Current designs of polymeric cables (XLPE, WTRXLPE, or EPR) use extruded polymeric materials to construct the semiconducting screen. Optimal performance is obtained when the screens are coextruded with the insulation in a closed "true triple" extrusion head.

The concentration of carbon black, in both paper and polymeric screens, needs to be sufficiently high to ensure an adequate and consistent conductivity. The incorporation must be optimized to provide a smooth interface between the conducting and insulating portions of the cable. The smooth surface is important as it decreases the occurrence of regions of high electrical stress [10]. To provide the correct balance of these properties, it is essential that both the carbon black and polymer matrix be well engineered.

The same care needs to be paid to the manufacture of the matrix materials (paper or polymer) for semicons as for the insulation. In the case of extruded screens, the chemical nature of the polymers is subtly different from those used for the insulations because of the need to incorporate the carbon black. The carbon black and other essential additives (excluding cross-linking package) are compounded into the matrix. The conveying and compounding machinery used are designed to maintain the structure of the carbon black within

a homogeneous mix. Before the addition of the cross-linking package, filtration may be applied to further assure the smoothness of the material, to a higher standard than that provided by the compounding process.

The smoothness of the extruded cable screens is assured by extruding a sample of the complete material in the form of the tape. The tape is optically examined for the presence of pips or protrusions. Once detected, the height and width of these features are estimated, thereby enabling width-segregated concentrations to be determined. When using such a system, care needs to be exercised when examining the present generation of extremely smooth (low feature concentration) screens, as the area of tape examined needs to match the likely number of detected features: Smooth screens require larger areas of examination.

Insulation

It seems clear that, globally, XLPE or its WTRXLPE variants are the most commonly used cable insulations currently being installed. Insulating XLPE compounds need to fulfill a number of requirements. They should act as thermoplastic materials within the extruder and crosshead. They should cross-link efficiently with the application of high temperatures and pressures within the vulcanization tube. They should be immune to thermal degradation throughout the cable manufacture process and operation at the maximum cable temperature for the life of the system. They must display an extremely low occurrence of the features that can enhance the applied electrical stress and thereby lead to premature failure. To deliver these requirements, it is essential that the greatest care is paid to the design and manufacture of the polymer and the engineering of the appropriate cross-linking and stabilizing packages.

The manufacturing technology employed for XLPE compounds to be used for power applications needs to ensure the highest level of cleanliness at all points of the production chain. The sequence comprises three main parts: base polymer manufacture, addition of a stabilizing package, and addition of the cross-linking package. The most common route for cross-linking in cables (XLPE, WTRXLPE, and EPR) is peroxide cure – thermal degradation of an organic peroxide after extrusion causes the formation of cross-links between the molten polymer chains.

Cleanliness The cleanliness of XLPE and WTRXLPE insulation materials may be assessed by converting a representative sample of the polymer into a transparent tape and then establishing the concentration of any inhomogeneities. This is not possible for monosil as the chemistry occurs immediately prior to the cable extrusion. The inhomogeneities are detected by identifying variations in the transmission of light through the tape. To gain the required level of consistency and sensitivity, the tape is inspected by an automated optical system.

Metal Sheath

For many years, lead or lead alloys were the main materials used for the metal sheath layer. This is principally because the low melting temperature allows the lead to be extruded at a temperature of approximately 200°C over the polymeric cable. The main disadvantages of lead are its high density (11,400 kgm^{-3}) leading to a heavy product; environmental concerns; and the tendency to creep, flow, or embrittle under cyclic temperature loadings. This latter effect has led to a number of cases where the sheath ruptured. There are also environmental concerns relating to the use of lead. Its use may become restricted by European Union (EU) directives. In 2000, the EU Commission officially adopted the waste electrical and electronic equipment (WEEE) and reduction of hazardous substances (ROHS) proposals. The ROHS proposals required substitution of lead and various other heavy metals from 2008. To address these problems a number of materials have been used.

- *Extruded aluminum*: This has excellent mechanical performance but requires a large bending radius and can be difficult to manufacture since it requires corrugations. It can be heavy.
- *Aluminum foil*: This is light and easy to manufacture but small thicknesses (0.2–0.5 mm) do not give mechanical protection; the strength comes from the polymer oversheath. It relies on adhesive to make a watertight seal, and it can suffer from corrosion.
- *Copper foil*: This is light, easy to manufacture but not as flexible as aluminum foil. It also relies on adhesive to make a watertight seal.
- *Welded copper*: This is strong, robust, and capable of carrying significant current but difficult to

manufacture since it requires corrugation and it is difficult to ensure perfect longitudinal welds in practical situations.

- *Welded stainless steel*: This is strong, robust, and capable of carrying significant current but has similar manufacturing difficulties to welded copper.

Oversheath (Jacket)

In addition to the meticulous attention that must be paid to the insulation system, care also needs to be taken with the oversheath layer. One of the earliest lessons that was learned from MIND and PILC cables (where a lead sheath is employed) is that installation damage and corrosion can compromise the metallic sheath [11, 12]. Once sheath integrity is lost, water may enter and impregnant leak out. In these cases failures in service occurred quite rapidly. These issues were soon resolved on neoprene tape or extruded oversheaths were used. When extruded cables were introduced in the mid-1960s, it was believed that there was no longer a need for an oversheath as the insulating polymers were themselves waterproof. However, the phenomena of water treeing soon showed that a good-quality cable jacket was extremely valuable even at the low electrical stresses prevalent at MV.

The vast majority of HV and EHV XLPE cables are of the "dry design" type, which means that a metal barrier is included. The purpose of the metal barrier is to protect the core within from mechanical damage, carry fault and loss currents, and to exclude water from the construction. (The electrical aging rate is significantly higher in the presence of moisture.) The metal barrier is a key part of the cable design and much care needs to be taken as this significantly affects how a cable system may be installed in practice. In a similar way to that at MV, the metal layer is itself protected by a polymeric oversheath. Due to the critical performance needed from the oversheath, there are a number of properties that are required: good abrasion resistance, good processing, good barrier properties, and good stress crack resistance. Experience has shown that the material with the best composite performance is an oversheath that is based on polyethylene.

Cable Manufacture

Stages of Cable Manufacture

The stages in cable manufacture may be summarized as:

1. *Conductor manufacture*: This involves
   - *Wire drawing* to reduce the diameter to that required
   - *Stranding* in which many wire strands and tapes are assembled
   - *Laying up*: the assembly of noncircular (Milliken) segments into a quasi-circular construction
2. *Core manufacture*: This involves
   Paper (LPOF, MIND, PILC) cables
   - *Lapping* in which the core of the cable is formed by wrapping semiconducting and insulation tapes around the conductor with prescribed tensions and paper tape overlaps
   - *Laying up (triplexing)* for three core cables
   - *Drying* which improves the dielectric properties of the cable core and is carried out at elevated temperatures and under vacuum

   Polymer (XLPE, WTRXLPE, and EPR) cables
   - *Triple extrusion* in which the core of the cable is formed comprising the inner semicon, insulation, and outer semicon.
   - *Cross-linking* which is carried out directly after extrusion (peroxide cure).
   - *Degassing* in which peroxide cross-linking by-products are removed by heating offline. The diffusion time depends upon temperature and insulation thickness.
3. *Cable manufacture*: This involves
   Paper (LPOF, MIND, PILC) cables
   - *Impregnation* where the dry paper tapes are impregnated at elevated temperatures with dry/degassed dielectric fluid
   - *Metal sheathing*: the application of a metal impregnant enclosure
   - *Oversheathing*: the application of high strength extruded polymeric oversheath (jacket)
   - *Armouring*: the application of high strength metal components (steel) to protect the cables; essential for submarine cables
   - *Routine testing*: voltage withstand and ionization factor tests

Polymer (XLPE, WTRXLPE, and EPR) cables

- *Core taping* during which cushioning, protection, and water exclusion layers inner semicon, insulation, and outer semicon are applied over the extruded core
- *Metal sheathing*: the application of a metal moisture and protection layer
- *Oversheathing*: the application of high strength extruded polymeric oversheath (jacket)
- *Armouring*: the application of high strength metal components (steel) to protect the cables; essential for submarine cables
- *Routine testing*: voltage withstand and partial discharge tests

Methods of Core Manufacture for Extruded Cables

All of the production processes will be common to all methods of manufacture, with the exception of the extrusion process where there are three types of peroxide cross-linking methods. (Cross-linking is often referred to as vulcanization or curing.)

- *VCV*: Vertical continuous vulcanization
- *CCV*: Catenary continuous vulcanization
- *MDCV*: Mitsubishi Dainichi continuous vulcanization, often called long land die

In all of these processes, the three layers of the cable core are extruded around the conductor. This un-cross-linked core then passes directly into the curing tube; this is where differences in the processes become apparent. In the moisture cure approach, which takes place offline after extrusion, the manufacturing process is considerably simplified as the length of the tube following extrusion only has to be long enough for the thermoplastic core to cool sufficiently to prevent distortion.

The general relationship between manufacturing method, the insulation technologies, and voltage classes is shown in Table 7.

Failure Processes

Power cable systems are designed to be high-reliability products. The failure of a major power cable is likely to have a considerable effect on the power transmission grid and may take several days/weeks to repair. If it is under the sea, it may take months/years to repair and cost well in excess of $3 million (€3 million). Cables have a good service history. The majority of cable failures are caused by external influences such as road diggers or ship anchors. Cable system failures may also occur at joints and terminations.

Underground Cable Systems. Table 7 General correlation of extrusion equipment with extruded insulation materials

	MV			HV			EHV		
	EPR	WTR XLPE	XLPE	EPR	WTR XLPE	XLPE	EPR	WTR XLPE	XLPE
Catenary vulcanization 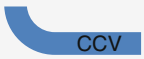	X	X	X	X	–	X	–	–	X
Vertical vulcanization	–	–	–	–	–	X	–	–	X
Horizontal vulcanization	–	–	–	–	–	X	–	–	X

Underground Cable Systems. Table 8 System performance for a 20kV XLPE ([13])

Class	Fault rate (#/year/100 cct km)
Total system	2.0
Third party damage	1.0
Accessories	0.9
Cable	0.1

A study of MV cable systems in France [13] has shown that the failure rate for paper cables is 3.5 failures per 100 cable km per year which compares with a rate of 2 failures per 100 cable km per year for XLPE cables. The failure rate for XLPE has been classified in Table 8. This analysis shows that the XLPE cables form the most reliable component of the cable system. Further inspection would suggest that the XLPE cable system is 2.5 times more reliable than the paper system when third party damage is excluded. (It is assumed that a paper cable is as likely to get dug up as an XLPE one!) This estimate may well overstate the case and illustrates one of the major problems of evaluating field failure statistics, namely, the differing ages of the populations. XLPE data are based on a population which is 15 years old whereas the paper data are based on a population that is 30–40 years old; thus, higher failure rates of the paper system are expected since it contains older devices; this would be quite independent of the intrinsic reliabilities of the systems.

The service performance of cable system accessories (joints and terminations) depends upon six essential elements:

- Connector design
- Joint/termination body design
- Installation methods
- Installation quality
- Operating conditions

A more recent study in the USA [11] estimated a median failure rate of 3.5 failures per 100 cct miles per year. Figure 4 shows an estimate of how these failures are disbursed by the sources of failure. At first sight, these figures seem to be quite different to the EDF study; however, it should be recognized that there will be considerable variation due to utility and geographical location. For example, the average percentage of failures ascribed to splices is 37%; however, this can range from 5% to 80% depending upon utility. Nevertheless, these studies both show that it is important to consider the cable system as a whole entity.

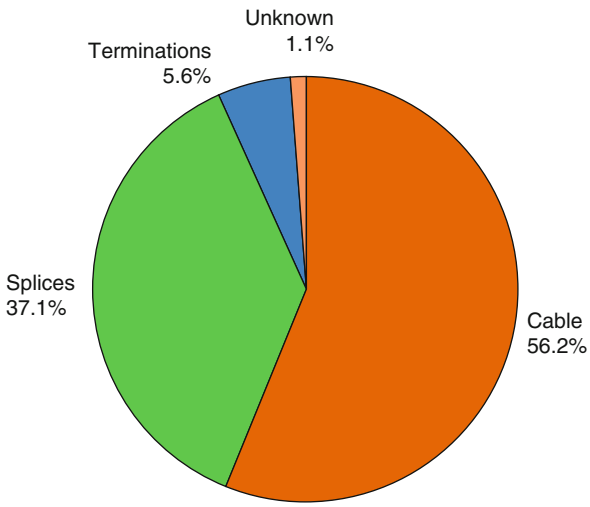

Underground Cable Systems. Figure 4 Estimated dispersion of North American MV cable system failures by equipment type

In general, the causes of insulation breakdown will include the causes listed below. Table 9 shows how the types of defects may be related to the failure modes for the different voltage classes of cables. Many of these defects are shown schematically in Fig. 5.

- Extrinsic defects (contaminants, protrusions, or voids) caused during manufacture or installation. These would normally lead to electrical treeing or direct breakdown soon after production of the void and cable energization.
- Water treeing ("wet aging") caused by water leakage through the sheath or inappropriate design or deployment of a cable without a water barrier. Water trees lead to a weakening of the insulation and electrical treeing or direct breakdown.
- Water ingress caused by failure of the metal water barriers. Water increases the dielectric loss and thereby leads to local overheating. Failure proceeds by thermal runaway in a region with compromised local breakdown strength.

Underground Cable Systems. Table 9 Role, in general terms, of defects in cable failure modes

Cause of failure	MV	HV	EHV
Extrinsic defects *Contaminants* *Delaminations* *Protrusions* *Shield interruptions* *Voids/cracks*	Accelerants for water treeing	Major source of failure Accelerants for electrical treeing	Major source of failure
Water treeing *Bowtie* *Vented – partial* *Vented bridging*	Major source of failure for extruded	Can be an issue if robust metallic water barriers are not used	Rarely an issue due to the use of robust metallic water barriers
Water ingress	Major source of failure for laminar	Major source of failure for laminar	Rarely an issue due to the use of robust metallic water barriers
Thermoelectric aging	Rarely an issue due to the low temperatures and stresses of operation	Major source of failure accelerated by extrinsic defects	Major source of failure accelerated by extrinsic defects

- Thermoelectric aging: The combination of the electric field, acting synergistically with a raised temperature, causes the insulation to weaken over time and for breakdown to occur eventually. This process may not always be significant within the lifetime of a well-designed cable.

Extrinsic Defects

The efforts made have already been described, from the earliest times, by cable manufacturers to exclude and detect contaminants, protrusions, and voids (CPVs) in their products. Contaminants within the bulk of the insulation and protrusions into the insulation from the semicon cause field intensifications that lead to premature failure of the polymer.

The degree of aging follows the empirical Inverse Power Law relationship with the electric stress ($\propto E^n$) [2, 3, 12, 14, 15].

Contaminants and Protrusions Many studies [2, 3, 5, 11, 12, 14–18] have shown the degradation caused by large metallic contaminants. Generally contaminants and protrusion type defects reduce the characteristic strengths of insulators; furthermore, the increasing size of contaminants changes the statistical nature of the failures, making them less scattered or more certain.

The effects may be explained by the fact that metallic contaminants increase the electric stress within their immediate locality such that the local electric stress is higher than the breakdown strength of the insulator. This effect is best described in terms of a stress enhancement factor that acts as a multiplier for the Laplacian stress (i.e., the geometrically calculated stress). It is interesting to note that it is possible to get large stress enhancements at sharp metallic contaminants but that the magnitude of the enhancement falls dramatically with distance from the tip; for a 5-μm radius, the field falls by 50% within 1.5 radii of the tip [10]. Thus, the calculated stress enhancements should be viewed as providing the upper limits of any assessment and it is quite challenging to relate them directly to the likelihood of failure.

The electrical stress enhancements are not only based on the size and concentration but they have a significant influence from the nature (conducting, insulating, high permittivity), the shape (sharp or blunt), and the way that they are incorporated into the matrix. The effect of the shape of contaminants has been assessed [18] using XLPE cups with a Rogowski profile. It was shown that contaminants with irregular surfaces reduced the AC ramp breakdown strength by a greater degree than those with smooth surfaces.

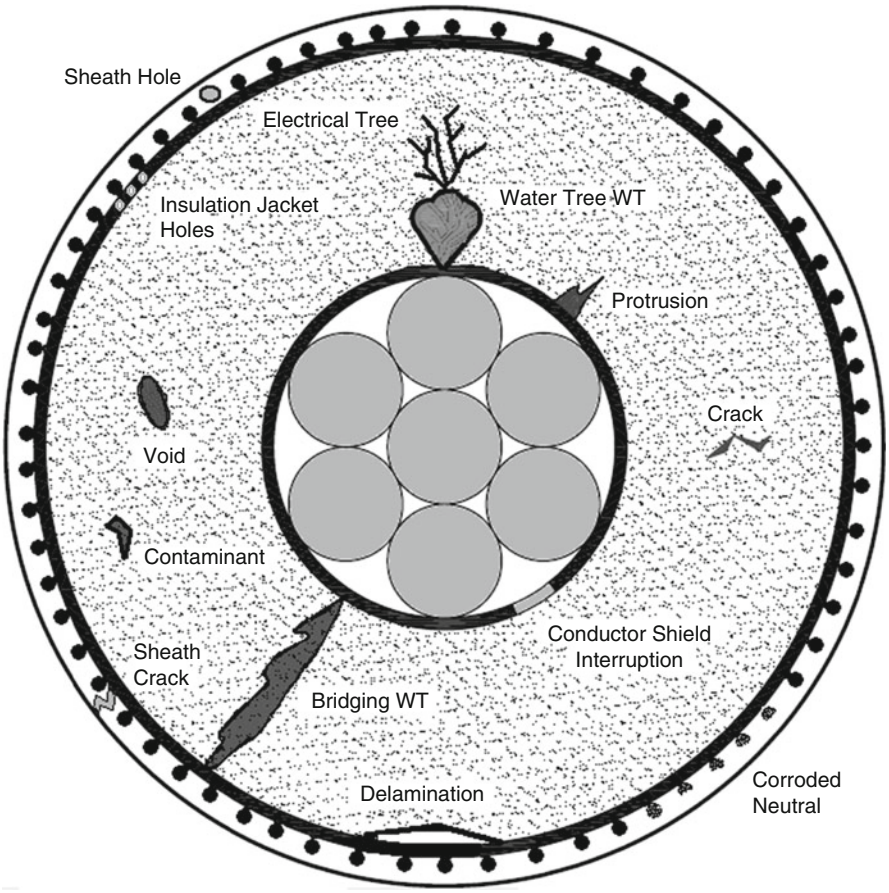

Underground Cable Systems. Figure 5
Typical power cable defects

The local stress enhancement experienced within an insulator will have contributions from the size of the contaminants, their concentration, and the nature (conducting or high permittivity) of the contaminants. This is shown in Eq. 7:

$$\eta = 1 - \frac{1}{\alpha}\left(0.5\ \ln\frac{\lambda+1}{\lambda-1} - \frac{\lambda}{\lambda^2-1}\right) \tag{7}$$

where:

$$\alpha = 0.5\ \ln\frac{\lambda+1}{\lambda-1} - \frac{1}{\lambda} + \frac{1}{(k-1)\lambda\left(\lambda^2-1\right)}$$

$$k = \frac{\varepsilon_2}{\varepsilon_1} \quad \lambda = \frac{1}{\sqrt{1-\frac{r}{a}}}$$

η = stress enhancement factor,
r = radius of the ellipse,
$2a$ = length of the ellipse,
ε_1 = permittivity of the matrix, and
ε_2 = permittivity of the defect.

Voids Voids are likely to lead to breakdown *if* discharges occur inside them. These discharges are known as "partial discharges" since they are not, in themselves, a complete breakdown or "full discharge." The least problematic (and perhaps the least likely) shaped void is the sphere. The field inside an air-filled, sphere-shaped void is higher than the field in the insulation by a factor equal to the relative permittivity of the solid. For other shaped voids, the field in the void will be higher than this. For example, a void inside XLPE (relative permittivity = 2.3) will have a field inside it of at least 2.3 times that of the field in the XLPE itself. The criterion for a discharge in a void is that the void

field must exceed the threshold described by the Paschen curve (see [12] for example); this is dependent on the size of the void and the gas pressure within it. The Paschen field has a minimum for air at atmospheric pressure for a void diameter of 7.6 μm. The breakdown voltage at this diameter is 327 V. This equates to a void field (ignoring the nonlinear effects) of 43 kV/mm or an applied field of 19 kV/mm within the XLPE. Below this void size, the Paschen field increases rapidly; for example, a 2-μm void would require an applied field of approximately 150 kV/mm to cause discharging. It is clear then that voids of diameter exceeding a few microns are likely to allow severe electrical damage to occur.

Partial Discharges and Electrical Treeing In an electrical discharge, electrons are accelerated by the electric field such that their kinetic energy may exceed several electron-volts. With such energies, collisions with gas molecules may cause further electrons to be released, thus strengthening the discharge or they may cause electroluminescence and the release of energetic photons. The surface of the void is therefore likely to be bombarded by particles (photons or electrons) with sufficient energy to break chemical bonds and weaken the material. In the case of sharp protrusions or contaminants, which give rise to high local electric fields, electrons may be emitted and very quickly acquire the kinetic energy required to cause permanent damage to the insulation. Electrons may accumulate – i.e., they may be trapped – around such defects and cause a further increase in local electric fields. Mechanical stress, which may already be increased due to the modulus and thermal expansion coefficient differences between the host materials and the CPVs, may be further enhanced by electromechanically induced stress. These effects, catalyzed by CPVs in an electric field may lead directly to a breakdown path, but are more likely to lead first to the formation of an electrical tree.

An electrical tree is shown in Fig. 6. For the sake of clarity, this has been grown in a translucent epoxy resin from a needle acting as a protrusion. A breakdown path can be seen to be growing back through the electrical tree from the plane counter-electrode. Electrical trees have a branched channel structure roughly oriented along the field lines. Typically, the diameters of the channels are 1–20 μm, and typically, each channel is 5–25 μm long before it branches. There is considerable evidence that the branching is determined by the local electric field, which is grossly distorted by trapped electrons emanating from the discharges within the tree. There is a considerable body of work on this subject (e.g., [12]). Trees tend to grow more directly across the insulation if they are spindly, so-called branch trees. The other type of tree, the "bush" tree, uses the energy to produce a lot more dense local treeing and, therefore, tends to take longer to bridge the insulation. Because branch trees occur at *lower* voltages, there is a non-monotonic region between branch and bush growth in which failure occurs more quickly at lower voltages. Trees grown from larger voids can be clearly distinguished from those due to protrusions; it is noticeable that the fields must cause the voids to discharge before the trees initiate. After an initial period in which the tree grows fast, the rate of growth decreases. Finally, as the tree approaches the counter-electrode, a rapid runaway process ensues.

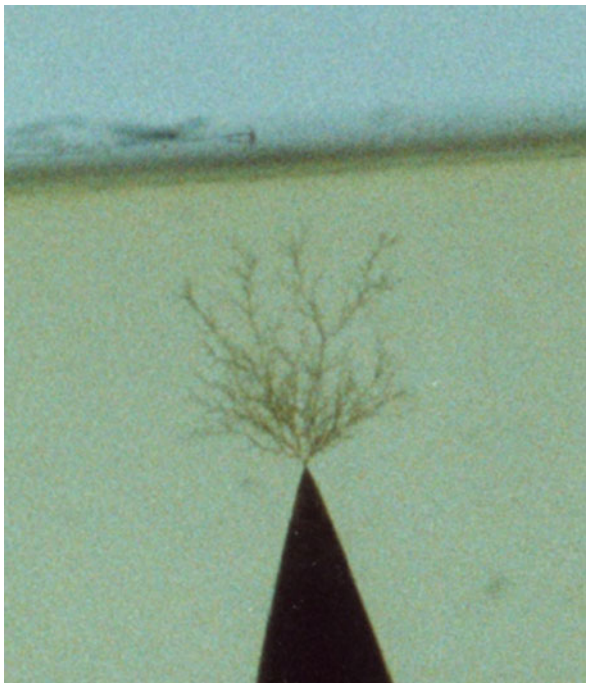

Underground Cable Systems. Figure 6
An electrical tree grown in epoxy resin

Although the electric tree processes are now quite well understood, apparently little can be done to

prevent electrical tree propagation in polymeric insulation once it has started. It is thought that electrical trees take relatively little time to grow and cause breakdown in cables, perhaps a few minutes to a few months. Once an electrical tree has been initiated, the cable can be considered to be "terminally ill." It is therefore vital to prevent the inclusion of CPVs during cable manufacture and installation. The triple extrusion continuous vulcanization techniques and appropriate cable protection and deployment techniques appear to have been successful in this regard, and cables rarely suffer from these problems. There are more likely to be problems at joints or terminations where high field stresses may inadvertently be introduced or if water trees, described in the following section, are allowed to grow.

Interaction Between Moisture and Temperature One of the effects of water entering an insulation is that it tends to increase the permittivity and loss of the insulation [1, 19, 20]. The energy lost per cycle within an insulation is proportional to both the permittivity and the loss. Thus, at a given electrical stress, the increasing energy loss due to the presence of water will lead to an elevated temperature. If this temperature becomes too high, other mechanisms come into play and there is a thermal runaway to failure.

Although this happens in principle in all insulations, and may be very important at the high stresses of HV & EHV systems, this is most commonly observed in paper-insulated MV cables. The sensitivity of these cables is due to the fact that the dielectric losses are initially much higher and the paper and oils have a higher propensity to absorb water. Some basic measurements were made by Blodgett [19] who showed that the loss in paper insulations increased with both temperature and moisture. These data can be used within cable system rating models to estimate the thermal equilibrium for selected temperatures and moisture contents. The results are shown in Fig. 7 which shows the increment above the base-case temperature in the form of a contour-plot for selected moisture contents and temperatures. Inspection shows that significant temperature rises can be expected for quite reasonable moisture contents. A separate study has shown that cables removed from service but not failed might be expected to have a median moisture content of 1%, but cables that failed had moistures in excess of 3%. Thus, the thermal runaway mechanism seems to be a reasonable explanation of the observed phenomena. Moreover, the calculations show the difficulty of setting wide-reaching criteria; a common empirically determined maximum permitted moisture level is 3%. However, the impact of this level of moisture is quite different for different cables and temperatures: 3°C, 7.5°C, 14°C for 15 kV/90°C, 35 kV/90°C, and 35 kV/105°C, respectively.

Wet Aging: Water Trees

In the early days of polymer-insulated cables, it was assumed that the polymers would be essentially immune to the deleterious effects of water that were well known in paper cables. Consequently, the first designs of cables were installed with little or no water precautions. Within a few years, a large number of cables started to fail in service. Upon examination, tree-like structures were seen to have grown through the insulation. It was assumed that they continued to grow and failure occurred when the whole insulation was breached. This is the phenomenon of water treeing [1–3, 21].

Many studies have been carried out into the phenomena and its solution. Looking back, it is clear that a number of improvements in cable design, manufacture, and materials have reduced the incidence of cable failures by water treeing. These improvements have included

- Water barriers (metal or polymeric) to exclude the water
- Triple extrusion (all polymer layers extruded at the same time)
- Semiconductive polymer screens to replace carbon paint or paper tapes
- Cleaner insulations
- Smoother semicons
- Internationally recognized approval methods
- Special long life insulations based either on additives or polymer structure

The laboratory studies have concluded that the growth of water trees is affected by:

- Test voltage
- Test frequency

- Mean temperature
- Temperature gradient
- Type of material
- Presence of water (external and within the conductor)

There are essentially two types of water trees: (a) vented trees that grow across the insulation and are potentially the most dangerous and (b) bow-tie trees that grow across the insulation and tend to grow to a limiting size without breaching the insulation. These trees do *not* comprise tubules containing water as might be surmised from the earlier description of electrical trees. The "branches" of a water tree actually appear to comprise a high density of water-filled voids of typical diameter 1–10 μm. Such branches are therefore similar to a "string of pearls," but in practice, even branches of water trees are not usually discernible. They are simply diffuse regions of water-filled voids. If dried up, re-immersion in water reopens the voids. Boiling stabilizes the structure but probably also produces extra small voids. There is limited evidence that a percolation network does interconnect the voids, but the size scale of the interconnecting features is at around 10 nm. Electrolyte material accompanies the water into the voids and the ability of cationic dyes, such as rhodamine B, to stain the trees permanently indicates that some oxidation must have taken place. Chemical modification has also been shown using IR and FTIR spectroscopy and by fluorescence techniques.

Water trees grow much more slowly than electrical trees. Typically, they may not be observed at all for several years, even if the prevailing conditions for their growth are in place. They will then grow fast initially and then very slowly. Indeed, in the case of bow-tie water trees, there is much evidence that they stop growing completely after a given length

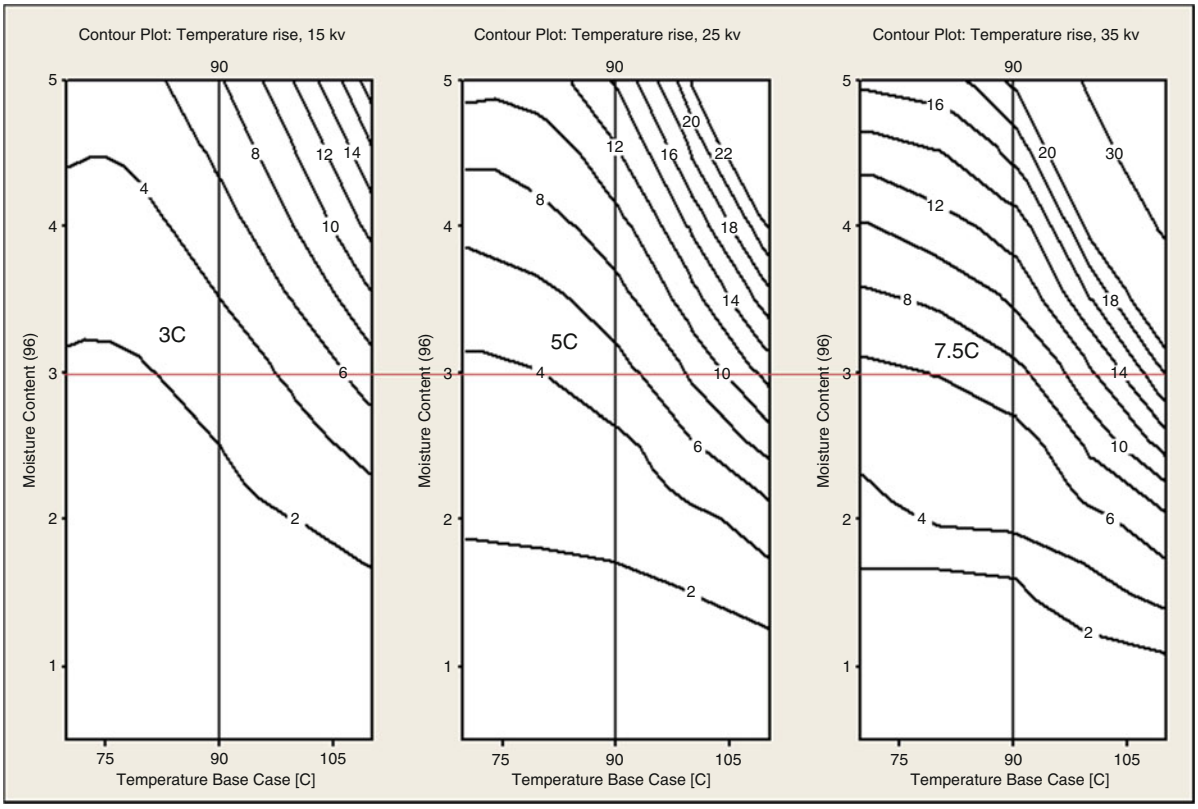

Underground Cable Systems. Figure 7
Contour plot of temperatures increment (°C) above base-case temperature for selected base temperatures and moisture content. The calculations have been made for three difference cable voltages

(dependent on prevailing conditions) and that they might not precipitate breakdown. Vented water trees may cross the insulation completely without breakdown occurring, but they do greatly weaken the insulation. Generally, an electrical tree or a breakdown path may grow back through an electrical tree.

It is important to recognize that water trees occur in all extruded insulations (EPR, WTRXLPE, XLPE) and have been found in failure locations retrieved from service. It is often suggested that the water tree–retarding insulations (EPR and WTRXLPE) do not grow water trees. Unfortunately, this is not correct, though it is more difficult to detect water trees in these insulations; however, this is due to the lower initiation and growth rates (EPR and WTRXLPE) and the opaque nature of the insulation (EPR). Nevertheless, longer endurances and lower failure rates are seen for EPR and WTRXLPE for comparable designs and ages, with respect to cable XLPE analogues.

There are many proposed mechanisms of water treeing and these have been critically reviewed in Reference [12]. Essentially, it is likely that solvated ions are injected at partially oxidized sites. These catalyze further oxidation by maintaining the ion concentration. A sequence of metal-ion-catalyzed reactions is proposed in which bonds break and cause microvoids to develop. Alternating electromechanical stresses open up pathways for solvated ions; these initiate new microvoids. Many tree-retardant polymers contain "ion catchers" to prevent the metal ion catalysis, and these have been found to successfully delay the onset and growth rate of water trees.

The tree inception time, i.e., the time between the conditions being right for water tree growth and the first observation of water trees, is highly dependent upon the electrical stress. Typically, the inception time is inversely proportional to a high power (≈4–10) of electric field. For this reason, low-voltage cables, which tend to run at lower electric fields, may not have a water barrier to prevent water ingress and hence electrical treeing. In such cases, with fields typically <4 kV/mm (see Table 3), the probability of failure through electrical treeing is low and a water barrier would make little difference. HV and EHV polymer–insulated cables generally use water barriers, and these become mandatory above 66 kV. Furthermore, the conductor is often water blocked (a water-swellable compound or an extruded mastic) to prevent the transport of water along the conductor. The water may enter the conductor either after a cable breakdown or during installation or through an incorrectly installed accessory.

Dry Aging: Thermoelectric Aging

The requirement for extra high voltage (EHV) underground power cables is increasing [1, 2, 12, 14, 22, 23]. There is commercial pressure to push the mean electric field in the insulation of such cables toward 16 kV/mm, and the most common insulation used is cross-linked polyethylene (XLPE). Long-term experience of XLPE, however, is limited to moderately stressed cables with mean fields of 5–7 kV/mm. Furthermore, the introduction of cross-linking processes has permitted the continuous operating temperature of polymeric cables (XLPE and EPR) to be increased to 90°C, equaling that of oil-filled (LPOF and HPOF) paper and polypropylene paper laminate (PPLP) cables. The use of XLPE as the insulation for transmission cables has grown steadily since the early 1990s. Many extruded power cables have been operating for 20 years and are approaching the end of their 30-year design life. If robust methodologies could be found for improving or/and evaluating the reliability of AC power cables, it may be possible to continue to use them without compromising the reliability of the system. Such methodologies require considerable improvements in the understanding of any aging or degradation mechanisms of cable insulation. They would enable XLPE cables to be more competitive at EHV levels.

Future Directions

When looking at the history of underground power cable systems, it is possible to discern a number of rather constant trends:

- Longer length systems get installed as service experience increases.
- Utilities are looking for technologies with easier and less expensive installation and maintenance.
- Manufacturing and material technologies permit higher operating stresses leading to reduced wall thicknesses.
- Reduced wall thicknesses:

  - Lower the total installed system costs
  - Improve the thermal capacity
  - Place greater strains on the accessory and cable installation practices
- End users are looking for longer lives, though the end of life criteria remain undefined.
- Higher reliabilities for systems.
- Public pressure on the location of transmission lines underground.
- Increasing use of underground distribution cables in urban and suburban areas.

It seems clear that all of these trends will continue in the foreseeable future.

Considering the growth of energy requirement (Fig. 8), the increasing environmental awareness and the ever-growing level of information transfer, it can be seen that there will be a need to widen our future considerations to include:

- Much lower levels of electrical losses within the transmission and distribution systems – required for increased efficiency
- Higher attention to electric and magnetic field issues – required for increased acceptance of cable systems
- Even higher levels of urban undergrounding to improve the visual environment – required for increased acceptance of electric energy [25, 26]
- Integration of data and energy transmission – required for increased control and optimal use of corridors
- Improved levels of power delivery reliability as there is increasing reliance on more electrically powered systems – required for increased customer satisfaction

There can be no doubt that the use and importance of cables will increase.

The areas where most activity will be seen are:

- Understanding life expectancy of cable systems
- Improving cable performance with respect to aging
- Recyclable/recoverable cable designs
- Increased use of long length links
- Diagnostic trends for cable systems
- Impact of smart grid initiatives
- High temperature superconductivity (HTS)
- Gas-insulated lines (GIL)

Understanding Life Expectancy of Cable Systems

Utilities the world over continue to strive to increase the useful life of their underground or subsea cable system assets. However, this activity is taking place in an environment where there is an absence of any actuarial life expectancy or a good understanding of the factors that determine the end of useful life of a cable

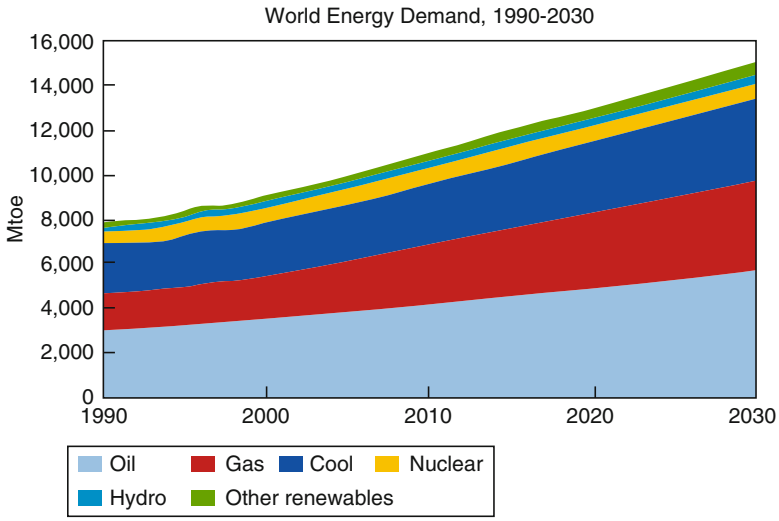

Underground Cable Systems. Figure 8
Estimated world energy demand including split of primary energy sources [24]

system. This does not mean that some of the causes of failure are not understood, in fact an extensive amount of work has been done on early failures in the 15–30 year range (e.g., water treeing, effects of contaminants). Thus, the life estimate for cable systems of 40 years is difficult to justify in any rigorous way.

A good example of the issues is the case of MV PILC cables installed in the USA [11]. These cables make up 15% of the total US installed capacity; however, in certain critical locales, this can rise to 80%. The median age of the oldest of these cables is 80 year with lower and upper quartiles at 70 and 90 years. Yet these cables are not failing at a rate that is discernibly higher than the average population of PILC cables: median age of 44 years. Thus, it is not possible to classify them as reaching the end of life because they are old or when they have not reached the right-hand portion of the "bathtub curve." It is equally unhelpful to assert that these cables have an infinite life as it is known that the paper and oil components will inexorably degrade.

These concerns become important when considering the economics/reliability and sustainability of any technology: The impact of a system that might last for 60 years is considerably less than today's arbitrary estimate of 30–40 years.

Improving Cable Performance with Respect to Aging

If one builds on the life expectancy concepts discussed previously, then it becomes possible to ascribe a value to technologies that might increase that longevity. Figure 9 shows the financial benefits of improved reliability within MV system. The experience over the recent past has shown that the most efficient way to measure and assure cable reliability is to require long-term wet aging tests (CENELEC – 2 years and ICEA – 1 year) with success levels that comfortably exceed the specified minimums.

The total cost perspective of two cable installations is shown in Fig. 9. The first shows the classic reference scenario, where the installed cost of cables is higher than the overhead analogue but the total lifetime cost is lower (92%). The second shows the scenario where a longer-lived cable has a longer life (30 years rather than

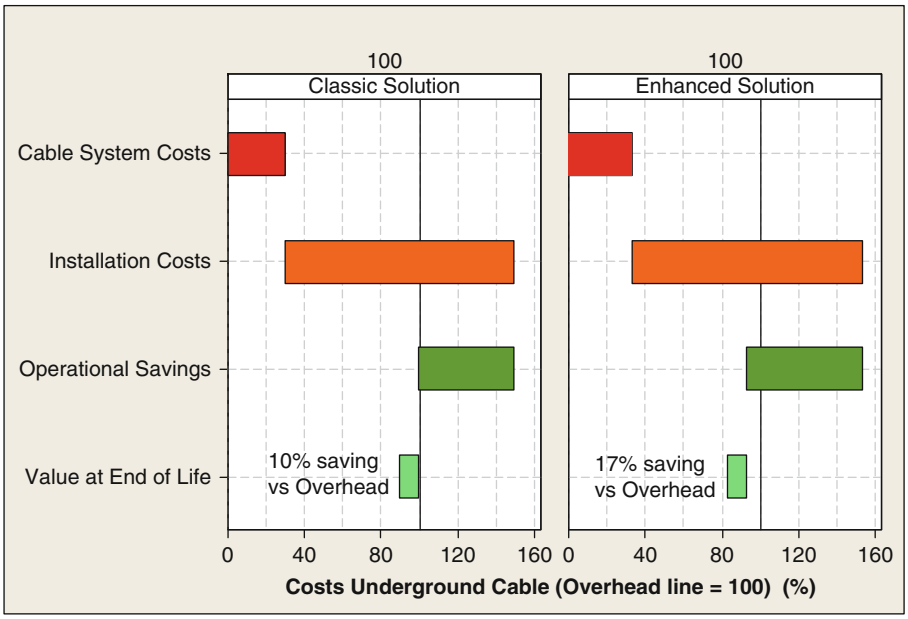

Underground Cable Systems. Figure 9
Total cost perspective of two cable installations when compared to an Overhead Line. Initial costs are significantly offset by operational (maintenance, losses, and unreliability – all of these are assumed to be constant over a 30-year period) costs. Two cases are shown: 25 year life is the base case; the other is where a 10% higher cable cost brings higher quality and a 20% increase in life length (30 years)

Underground Cable Systems. Table 10 110kV Cable versus overhead cost (excluding permitting cost and time). Studies from The Technical University of Graz [26]

Type	Loading conditions	Installed costs (Euros/km)	Operating costs (Euros/km)	Total lifetime costs (Euros/km)	Cost ratio cables to overhead lines
Overhead lines	Low Load	149,000	15,000	164,000	**1.18**
Underground cable		181,000	12,000	193,000	
Overhead lines	High Load	149,000	165,000	314,000	**0.76**
Underground cable		181,000	58,000	239,000	

25 years in the reference) and lower operational costs, due to the better reliability throughout the longer life. Clearly the total cost is lower (82%) for the longer-lived cable. This approach is even more favorable than shown here for the higher-quality, longer-lived, cable; this is because the reference scenario would require that the cable and installation costs be incurred again in years 25–30.

A similar story is seen at HV: In Austria, a very detailed study of total lifetime costs at 110 kV (Table 10) shows that cables have lower costs compared to overhead lines when the normal high loading of lines is considered. The ratios favor overhead lines at low loading but the gap is likely to narrow when the cost of obtaining wayleaves and negative customer/regulator pressure is included [26].

Recyclable/Recoverable Cable Designs

Today there is little activity associated with the recovery of abandoned cable systems as it is believed that there is little economic value associated with them. However, this may well change in the future as:

- There is likely to be public and environmental pressure to rehabilitate the land.
- The cables represent considerable natural resources.
- There will be a pressure to reuse the land previously used for cables and more importantly their associated substations/transformers/switches.

Evidence of these trends can be seen in the recovery of submarine fluid-filled cables (such as those that previously lay in Long Island Sound); here the regulation authorities required their removal as a prerequisite to the installation of new links. This reuses the structures can be seen with the replacement of gas compression cables in Germany and other places with extruded cables; but thie the reuse of the existing pipes/containment structures.

One of the limitations on recycling is the mixed nature of the nonmetallic components, i.e., the insulations and jackets [27]. This is because it is relatively simple to separate metals and metals from paper/plastic. However the plastic separation is not straightforward. Thus, to enable this separation in the future, the key element is the use of a whole polyolefin concept: XLPE and a HDPE jacket. With this approach the material mass is low and there is no expensive ($50/T at 2003 costs) separation step at the end of useful life. The metal within the cable may be reused, and the energy content of the polymer will be liberated and provide a value extremely close to the prevailing cost of oil, which is likely to be significant in 25–30 years' time [27].

Increased Use of Long Length Links

Submarine Cable Systems

Submarine power cables is the term given to cables that carry power underwater. They may be major transmission systems running under the sea, river crossings, or links to islands. Most submarine cable systems, of short to moderate length, are AC, whereas very long lengths employ DC (see later). The reason for the preference for AC is the simplicity of integration with existing infrastructures. The AC embodiments suffer from

reactive losses, due to the natural capacitance and inductive properties of wire; hence, there are limitations on length. However, considerable accommodations can be made with solid state control devices and reactive compensation. DC transmission does not suffer reactive losses; the losses in the DC transmission line are the resistive losses. However, the losses in the AC/DC converters need to be included. Furthermore, the converter stations are a considerable capital and maintenance cost. However, from a pure power delivery standpoint, a DC cable system will carry between 1.3 and 1.6 times the power of an equivalently sized AC analogue.

Submarine cables are considerably longer than their terrestrial analogues: hundreds of kilometers versus tens of kilometers. They are laid in very long lengths from a variety of barges or ships. Thus, the manufacture and reliability requirements are much more challenging than for land cables. The importance of these considerations is obvious when the actions for repair after a failure in service are considered. The parties involved need to mobilize considerable marine resources, locate suitable repair materiel, obtain necessary environmental permits, physically attend to the site, retrieve the cable from the ocean floor, effect a repair, and confirm the integrity of the repair. If these elements are not challenging enough, the user and manufacturer need to determine some means to reestablish their confidence in the future problem-free operation of the link. Thus the design, specification, testing, manufacture and installation phases of a submarine project are many orders of magnitude more onerous than a similar terrestrial solution.

Nevertheless, in the future, it is clear that power grids will install larger amounts of submarine cable systems; the drivers will be:

- Increased network interconnection and stability
- Power trading
- Elimination of costly and inefficient local generation (islands)
- Integration of hydro and wind energy
- Reduced public reaction with respect to terrestrial power links

Efficient DC Power Transmission

Direct current (DC) power transmission has been shown to be highly efficient for highly controlled long-distance delivery (experience in Nordpool). Long-distance AC transmission is possible (Horns Rev and Isle of Man); however, it requires complex system control and reactive compensation of the cable capacitance. Thus, today the only technology that is capable of delivering long-distance power utilizing underground cables is HVDC. Inspection of the Gotland, Cross Sound, Murraylink, Troll and Estlink projects shows us that voltage source converter (VSC) technology and cables manufactured with cross-linked polyethylene designed for the rigors of DC are already proven and in commercial use. It is interesting to note how many appliances used today operate with DC power supplies (PC, TVs, etc.) – perhaps Thomas Edison had it right all along!!

In the early days of DC, the increased cost of the converters limited its use to EHV grid interconnections (UK/France, Baltic Cable, etc.). However, recent innovations (VSC) in converter technology, cross-linked polyethylene cables, and the flexibility of system design have seen a very rapid growth of DC at high voltage (50–150 kV).

There have been interesting laboratory studies and qualifications of extruded cables using filled insulations at EHV; however, all of the world's commercial installations and the experience shown in Fig. 10 has been achieved with specially designed unfilled cross-linked materials. It is clear that unfilled cross-linked technology will be used when extruded cables are integrated into EHV DC systems.

The increased use of DC is being supported within the international committees. Specific recommendations have been prepared and published by CIGRE WG 21.01 within Technical Brochure 219. This document provides a very solid base for the extension to extruded HVDC cables. DC cable design presents the engineer with a coupled thermal and electrical problem with the stresses experienced by the cable depending upon the temperature and stress (polarity) inversions. There can be no doubt that HVDC cable design presents as many challenges as EHV ac systems. These include:

- Stress inversions
- Electrical stresses higher than those seen at EHV AC
- Ultralong lengths
- Testing and approvals
- Accessory technology
- System integration

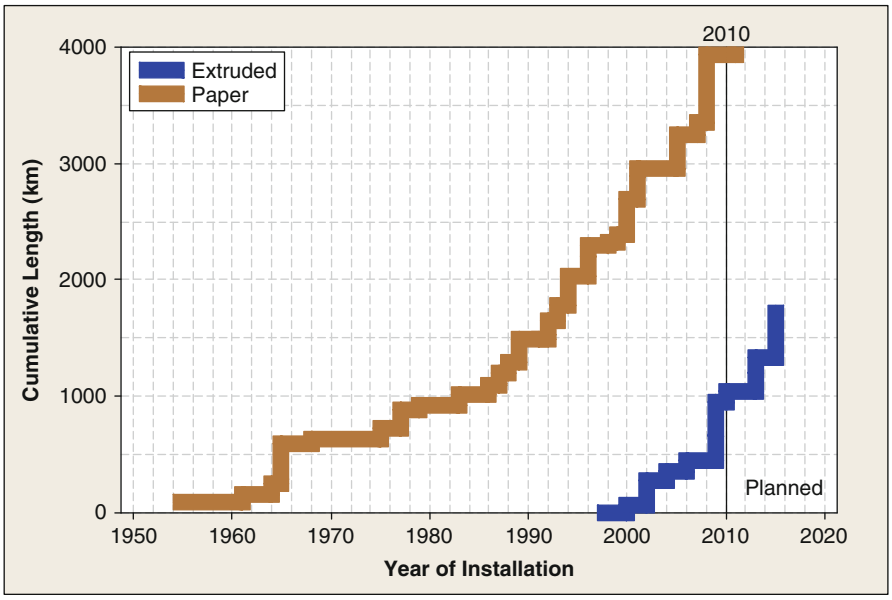

Underground Cable Systems. Figure 10
Global installed DC cable capacity segregated by type of cable insulation

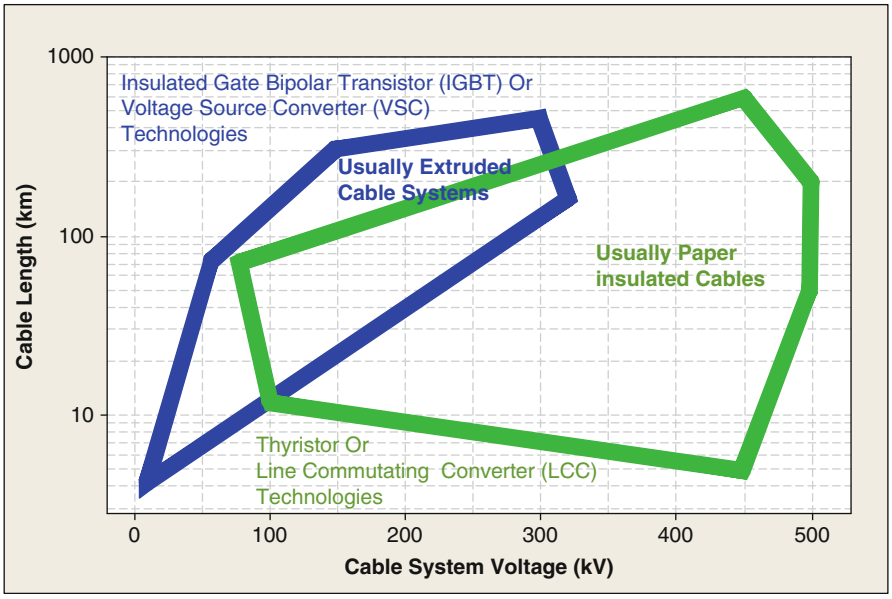

Underground Cable Systems. Figure 11
Global installed DC cable capacity segregated by converter technology

However, as with EHV AC, careful attention to the insulation system makes it possible to succeed with some very impressive projects (Murraylink, Troll, and Cross Sound).

A complimentary aspect is the increasing usage of extruded cables using cross-linked DC polyethylene and voltage source converters (VSC) (Figs. 10 and 11). These developments have significantly increased the

speed of implementation, lowered the total cost, and increased the types of projects for DC systems. It is interesting to reflect in Fig. 10 that paper systems required 30 years to achieve 1,000 km of cumulative installed capacity whereas extruded cables within 13 years. It is clear that the trend toward extruded cable systems with VSC technology will increase both in the submarine and terrestrial environments.

Diagnostic Trends for Cable Systems

The use of diagnostics on cable systems is growing and will clearly be an important part of network management for the future. New cables and accessories will probably have features integrated into them that will provide significant amounts of data. Older systems do not benefit from these developments, and thus, a diagnosis will need to be made without optimal sensors and a baseline condition. Nevertheless, considerable advances have been made. However, the challenge for cable and system engineers will come in transforming these data into useful information. Although the new installations will bring exciting opportunities, the major challenge will be associated with the "dumb" cable systems of today and yesterday.

The major areas of activity for diagnostics are:

- Real-time control of cable system rating – This is normally achieved through the use of fiber-optic temperature systems which are coupled to sophisticated thermal models of the cable system.
- Cable system commissioning/acceptance tests – Cable system components are separately tested in the factory; however, there is overwhelming consensus that most of the cable system issues are associated to incidents that occur during installation. Thus, there is a growing trend for cable system acceptance tests which permit these defects to be detected prior to acceptance for service, thereby enabling repair in a timely and cost-effective manner.
- Cable system diagnostic tests [11] – These are tests where the "health" of the cable system is determined, together with essentially a probabilistic assessment of future performance. These results enable a proactive level of asset optimization within the operator.

Real-time control of cable system and cable system commissioning tests are well established, and mature approaches and implementation is proceeding through international standardization bodies such as CIGRE and IEC. In many cases, the challenge is not technical but is the availability of the appropriate knowledge within the user community on the appropriate implementation.

Cable System Diagnostic Tests Almost all electric power utilities distribute a portion of the electric energy they sell via underground cable systems. Collectively, these systems form a vast and valuable infrastructure. Estimates indicate that underground cables represent 15–20% of installed distribution system capacity. Utilities have a long history of using underground system with some of these cable systems installed as early as the 1920s. Very large quantities of cable circuits were installed in the 1970s and 1980s due to the introduction of economical, polymer-based insulation compounds and the decreasing acceptance of overhead distribution lines. Today, the size of that infrastructure continues to increase rapidly as the majority of newly installed electric distribution lines are placed underground.

Cable systems are designed to have a long life with high reliability. However, the useful life is not infinite. These systems age and ultimately reach the end of their reliable service lives. Estimates set the design life of underground cable systems installed in the range of 30–40 years. Today, a large portion of this cable system infrastructure is reaching the end of its design life, and there is evidence that some of this infrastructure is reaching the end of its reliable service life. This is a result of natural aging phenomena as well as the fact that the immature technology used in some early cable systems is decidedly inferior compared to technologies used today. Increasing failure rates on these older systems are now adversely impacting system reliability, and it is readily apparent that action is necessary to manage the consequences of this trend.

Complete replacement of old or failing cable systems is not an option. Many billions of dollars and new manufacturing facilities would be required. Electric utilities and cable/cable accessory manufacturers are simply not in a position to make this kind of investment.

However, complete replacement of these systems may not be required because cable systems do not age uniformly. Cable researchers have determined that many cable system failures are caused by isolated cable lengths or isolated defects within a specific circuit segment. Thus, the key to managing this process is to find these "bad actors" and to proactively replace them before their repeated failures degrade overall system reliability. Various cable system diagnostic testing technologies were developed to detect cable system deterioration. The results of diagnostic tests are used to identify potential failures within cable systems and then again, after repair, to verify that the repair work performed did indeed resolve the problem(s) detected.

Appropriate maintenance and repair practices enable system aging to be controlled and help manage end-of-life replacements. Diagnostics to determine the health of the cable system are critical to this management program.

A number of cable diagnostic techniques are now offered by a variety of service providers and equipment vendors. However, no one service has definitively demonstrated an ability to reliably assess the condition of the wide variety of cable systems currently in service. Implementing cable system diagnostics in an effective way involves the management of a number of different issues. This includes the type of system (network, loop, or radial), the load characteristics (residential, commercial, high density, government, health care, etc.), the system dielectric (XLPE, EPR, paper, mixed), and system construction (direct buried or conduit). The basic cable diagnostic testing technologies used to assess cable circuit conditions are listed below.

- Time domain reflectometry (TDR)
- Partial discharge (PD) at operating, elevated 60 Hz, elevated Very Low Frequencies (VLF) or damped AC (DAC) Voltages [11, 28]
- Tan δ/dielectric spectroscopy at 60 Hz, VLF or variable frequencies [28–30]
- Recovery voltage
- DC leakage current
- Polarization and depolarization current
- Simple withstand tests at elevated VLF, 60 Hz AC, or DC Voltages [11, 31]
- Acoustic PD techniques
- Monitored withstand tests at elevated VLF, 60 Hz AC, or DC voltages with simultaneous monitoring of PD, tan δ, or Leakage Current [11, 31]
- Combined diagnostic tests at 60 Hz AC, very low frequencies (VLF), or damped AC (DAC) voltages using PD and tan δ

There is no doubt that cable system diagnostic testing can be used to improve system reliability. However, to be effective, the technology should be appropriate to the circuit to be tested. Setting accurate and reasonable expectations is also a critical part of the process.

In general, the work performed in the CDFI [11] led to the following observations:

- Diagnostic tests can work. They often show many useful things about the condition of a cable circuit, but not everything desired.
- Diagnostics do not work in all situations. There are times when the circuit is too complex for the diagnostic technology to accurately detect the true condition of the circuit.
- Diagnostics are generally unable to determine definitively the longevity of the circuit under test. Cable diagnostics are much like medical diagnostics. They can often tell when something is wrong (degraded), but it is virtually impossible to predict the degree to which a detected defect will impact the life of the system tested.
- Field data analysis indicates that most diagnostic technologies examined do a good job of accurately establishing that a cable circuit is "good." They are not as good at establishing which circuits are "bad." In most cases, there are far more good cable segments than bad segments. However, it is virtually impossible to know which "bad" circuits will actually fail. Therefore, utilities must act on all replacement and repair recommendations to achieve improved reliability.
- The performance of a diagnostic program depends on:
  - Where diagnosis is used?
  - When diagnosis is used?
  - Which diagnosis to use?
  - What is done afterward?
- A quantitative analysis of diagnostic field test data is very complex. The data comes in many

different formats and the level of detail is extremely variable. However, an in-depth analysis of the data clearly highlights the benefits of diagnostic testing.
- Diagnostic data require skilled interpretation to establish how to act. In almost all cases, the tests generate data requiring detailed study before a decision can be made on whether to repair or replace the tested cable circuit.
- No one diagnostic is likely to provide sufficient information to accurately establish the condition of a cable circuit.

Impact of Smart Grid Initiatives

Much has been written about Smart Grid Initiatives. Smart grid is defined rather differently in Europe and USA; however, one commonality is that the goal is to insert intelligent and interactive devices in the existing grid infrastructure to fulfill a number of goals, such as:

- Better facilitate the connection and operation of generators of all sizes and technologies
- Allow consumers to play a part in optimizing the operation of the system
- Significantly reduce the environmental impact of the whole electricity supply system
- Maintain or even improve the existing high levels of system reliability, quality, and security of supply
- Dynamic optimization of grid operations and resources, with full cyber-security
- Deployment and integration of distributed resources and generation, including renewable resources
- Development and incorporation of demand response, demand-side resources, and energy-efficiency resources
- Deployment of "smart" technologies (real-time, automated, interactive technologies that optimize the physical operation of appliances and consumer devices) for metering, communications concerning grid operations and status, and distribution automation
- Deployment and integration of advanced electricity storage and peak-shaving technologies, including plug-in electric and hybrid electric vehicles, and thermal-storage air conditioning

Thus, it is clear that the existing grid will be operated in a different manner to the one that it is accustomed and that the demands placed upon it will be increased. A natural consequence will be that a number of hitherto unseen failure or degradation modes will become prevalent. It is already possible to postulate what a number of them might be:

- Overheating of nonoptimally designed/installed components, which have not presented themselves due to the lower level of grid loading [32]
- Accelerated degradation due to transients/harmonics superposed on the grid by the smart devices themselves, the most obvious are third, and higher, harmonics
- A heightened sensitivity of consumers to power quality issues
- More aggressive load profiles due to changing demand and supply side protocols, as a consequence of reducing the traditional "low load recovery periods"

High-Temperature Superconductivity (HTS)

Equally there are technologies of today that will find some niche uses, but are unlikely to come into immediate and widespread use. The first is high-temperature superconductivity (HTS) that may well find application where people wish to transmit large amounts of power over relatively short distances. However, the issues associated with long-distance cryogenics, termination temperature differences, and complicated start-up procedures need to be addressed before this technology becomes attractive to utilities.

Gas-Insulated Lines (GIL)

Gas-insulated Lines offer the hope of large current ratings, low capacitances, and reduced dielectric losses for longer transmission distances. Yet, in most practical cases, the short lengths, and the associated difficulties of fabrication, plus the large environmental issues around large amounts of SF_6 gas, even in mixtures, will limit its use. By comparison, it would seem that GIL has much wider application than superconducting cables. A typical gas-insulated line design is shown in Fig. 12.

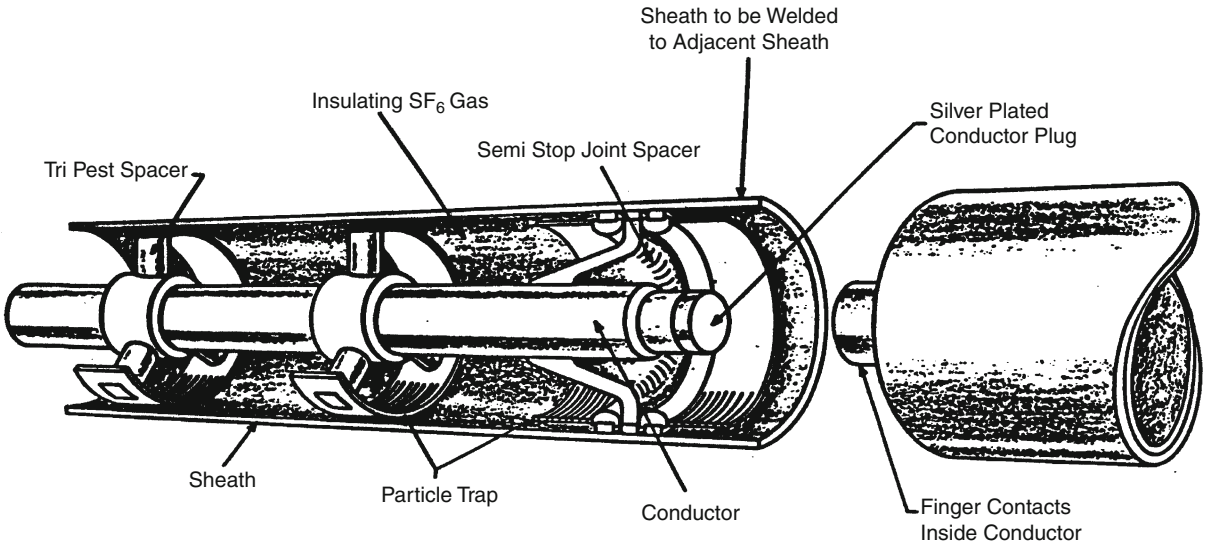

Underground Cable Systems. Figure 12
Typical design of a gas-insulated line (GIL)

Bibliography

1. Moore GF (1997) Electrical cables handbook. Blackwell Science, San Diego. ISBN 0 632 04075 0
2. Densley J (1995) Ageing and diagnostics in extruded insulations for power cables. In: IEEE 5th international conference on conduction and breakdown in solid dielectrics, IEEE publication 95CH3476-9, pp 1–15
3. Fothergill JC, Hampton RN (2004) Polymer insulated cable. In: Haddad A, Warne D (eds) Advances in high voltage engineering. IEE, London, pp 477–507, Chapter 10. ISBN 0 85296 158 8
4. Abernethy RB (1996) The new Weibull handbook, 2nd edn. Robert B. Abernethy, North Palm Beach. ISBN 0965306208
5. Hampton RN (2008) Some of the considerations for materials operating under High Voltage Direct Current Stresses. IEEE Electrical Insulation Magazine 24(1):5–13
6. Leijon M (1999) Novel concept in high voltage generation: Powerformer™. IEE Conference Publication, v5, n467, 1999. In: Proceedings of the 1999, 11th International symposium on "High Voltage Engineering", 23–27 Aug 1999, London, UK, p 5.379.S5-5.382.P5, IEE, ISSN: 0537–9989 IECPB4 ISBN: 0-85296-719-5
7. Jenkins N (2002) Power Engineering Journal 16(3):90–91
8. Karlstrand J, Sunnegardh P, Zenger W, Ghafurian R, Boggia R (2002) Water-cooled 345 kV solid-dielectric cable system, Cigré paper 21–111
9. Halvarsson P, Karlstrand J, Larsson D, Larsson M, Reinholdsdóttir K, Sigurösson E (2002) A novel approach to long buried AC transmission system, Cigré paper 21–201
10. Bartnikas R, Eichhorn RM (eds) (1983) Engineering dielectrics, vol IIA, Electrical properties of solid insulation, Philadelphia, ASTM-STP 783
11. Diagnostic Testing of Underground Cable Systems (Cable Diagnostic Focused Initiative) DOE Award No. DE-FC02-04CH11237, December 2010
12. Dissado LA, Fothergill JC (1992) Electrical degradation and breakdown in polymers. In: Peter Peregrinuns for the IEE, London
13. Brincourt T, Regaudie V (1999) Evaluation of different diagnostic methods for the French underground MV network. In: JICABLE'99, Versailles, p 451
14. Peschke E, Schroth R, Olshausen R (1995) Extension of XLPE cables to 500 kV based on progress in technology. In: JICABLE'95, Montreal, pp 6–10
15. Griffiths CL, Betteridge S, Hampton RN (1998) Thermoelectric ageing of cable grade XLPE in dry conditions. Conduction and breakdown in solid dielectrics ICSD '98. Proceedings of the 1998 IEEE 6th international conference, pp 279–282, doi:10.1109/ICSD.1998.709279
16. Coppard RW, Bowman J, Dissado LA, Roland SM, Rakowski RT (1990) The effect of aluminium inclusions on the dielectric breakdown strength of polyethylene. J Appl Phys 23:1554–1561
17. Antoniscki JR, Nilsson U, Gubanski SM (1997) The effect of metal inclusions on the breakdown strength of XLPE cables. In: CEIDP 1997, Minneapolis, pp 283–286
18. Hagen ST, Ildstad E (1993) Reduction of AC breakdown strength due to particle inclusions in XLPE cable insulation. In: Conference on power cables and accessories 10 kV–500 kV, London, pp 165–168

19. Blodgett RB (1962) Influence of absorbed water and temperature on tan delta and dielectric constant of oil-impregnated paper insulation. Trans AIEE 81:93–100
20. Hartlein RA, Hampton RN, Perkel J (2008) Some considerations on the selection of optimum location, timing, and technique, for diagnostic tests. In: IEEE Power Engineering Society (PES) general meeting panel session, Pittsburg
21. Steennis EF (1989) Water treeing: the behaviour of water trees in extruded cable insulation. ISBN 90-353-1022-5, Kema, pp 132–133
22. Gregory B, Griffiths CL, Hampton RN and Mainwaring SP (2000) A probabilistic design method for polymeric structures to operate at high electrical stress. In: 8th international conference on dielectric materials, measurements and application, IEE Conference Publication no 473, pp 419–424
23. Ogawa K, Kosugi T, Kato N, Kawawata Y (1990) The worlds first use of 500 kV XLPE insulated aluminium sheathed power cables at the Shimogo and Imaichi power stations. IEEE Trans Power Delivery 5(1):26–32
24. International Energy Agency. www.iea.org
25. Gorham and Partners (1995) Undergrounding – A success story already in Europe – Potentially worldwide. Report to ICF Congress 1995
26. Campbell A (2003) Undergrounding HV and EHV – window of opportunity opens. In: ICF Congress 2003, St Petersburg, pp 169–193
27. Hampton RN (2005) Electrical insulation systems for energy technology and clean environment. In: Nordic insulation symposium (NORDIS), Trondheim, June 2005
28. Hampton RN, Olearczyk M, Perkel J, Weisenfeld N (2010) Cable fleet management. IEEE Power and Engineering, Nov 2010
29. Perkel J, Hernández JC, Hampton RN, Drapeau JF, Densley (2011) Challenges associated with the interpretation of dielectric loss data from power cable system measurements. In: International conference on insulated power cables JICABLE11, Versailles France, June 2011, C.4.5
30. Drapeau J-F, Cantin B, Hampton N, Perkel J (2011) Dielectric loss characterization of hydro-quebec medium voltage (MV) submarine cables – phase 1. In: International conference on insulated power cables JICABLE11, Versailles France, June 2011, Paper A.7.6
31. Fletcher CL, Perkel J, Hampton RN, Hernandez JC, Hesse J, Pearman MG, Wall CT, Zenger W (2011) First practical utility implementation of monitored withstand diagnostics in the USA. In: International conference on insulated power cables JICABLE11, Versailles France, June 2011, Paper A.10.2
32. Parker T, Hampton RN (2011) Impact of filled-strand conductor on connector temperature for medium voltage joints. In: International conference on insulated power cables JICABLE11, Versailles France, June 2011, Paper C.1.5

Unscented Kalman Filter in Intelligent Vehicles

Moustapha Doumiati[1], Daniel Lechner[2]
[1]B2i Automotive Engineering Company, Massy, France
[2]Department of Accident Mechanism Analysis, IFSTTAR-MA Laboratory, Salon de Provence, France

Article Outline

Glossary
Definition of the Subject
Introduction
Estimation Process Description
Four-Wheel Vehicle Model
Tire-Road Interface
Observers Design
Experimental Results
Conclusion and Future Perspectives
Acknowledgments
Bibliography

Glossary

Lateral tire forces They are responsible to hold on the vehicle during a turn.

Longitudinal tire forces They are responsible to accelerate/brake the vehicle.

Observer or estimator It models a real system in order to provide an estimate of its internal state, given measurements of the input and output of the real system.

Sideslip angle It is the angle between the velocity heading and the true heading of the vehicle.

Tire forces The developed forces (longitudinal and lateral) are function of tire properties (material, tread pattern, tread depth, profile, etc.), the normal load on the tire, and the velocities experienced by the tire.

Vehicle control systems They provide commands and instructions to control the movements of the vehicle in order to maintain stability and enhance passengers security and comfort.

Vehicle dynamics It includes analytical and experimental technology used to study and understand

the dynamical responses of a vehicle in various in-motion situations.

Vertical (normal) tire forces They are responsible to support the weight of the vehicle.

Definition of the Subject

The principal concerns in driving safety with standard vehicles are understanding and preventing risky situations. A close examination of accident data reveals that losing the vehicle control is the main reason for most car accidents. To help the driver to prevent such accidents, vehicle control systems may be used. For their optimal operation, these control systems require certain input data concerning vehicle dynamic parameters and vehicle–road interaction. Unfortunately, some fundamental parameters like the tire-road forces and the sideslip angle are difficult to measure in a car, for both technical and economic reasons. To face this problem, this study presents a dynamic modeling and observation method to estimate these variables. The ability to accurately estimate lateral tire forces and sideslip angle is a critical determinant in the performances of many vehicle control systems. To address nonlinearities and unmodeled vehicle dynamics, an observer derived from unscented Kalman filtering technique is proposed. The estimation process method is based on the dynamic response of a vehicle instrumented with easily available and potentially integrable sensors. Performances are tested using an experimental car in real driving situations. Experimental results show the potential of the proposed estimation method.

Introduction

Vehicle dynamics and stability have been of considerable interest to automotive engineers, automobile manufacturers, government, public safety groups, and general public for a number of years. The obvious dilemma is that people naturally desire to drive faster and faster on the roads and highways, yet they expect their vehicles to be stable and safe during all normal and emergency maneuvers. For the most part, people pay little attention to the limited handling potential of their vehicles until some unusual behavior is observed that often results in fatality. According to statistics, worldwide, an estimated 1.2 million people are killed in road crashes each year and as many as 50 million are injured [1]. Preventing car accidents requires to know what determines vehicle dynamics during motion [2].

Today, automotive electronic technologies are developing for safe and comfortable traveling of drivers and passengers. Nowadays, there are a lot of vehicle control system such as the Anti-lock Braking System (ABS) that prevents wheel lock during braking [3], and the Electronic Stability Control (ESC) that enhances lateral vehicle stability [4, 5]. These control systems installation rate is increasing all around the world. Vehicle control algorithms have made great strides toward improving the handling and safety of vehicles. For example, experts estimate that ESC prevents 27% of loss-of-control accidents by intervening when emergency situations are detected [6]. While nowadays vehicle control algorithms are undoubtedly a lifesaving technology, they are limited by the available vehicle state information.

Vehicle control systems currently available on production cars rely on available inexpensive measurements such as longitudinal velocity, accelerations, and the vehicle yaw rate. Sideslip rate can be evaluated using the yaw rate, lateral acceleration, and vehicle velocity [7]. Calculating the sideslip angle is possible from the sideslip rate integration. However, it is prone to uncertainty and errors from sensor bias. Besides, these control systems use unsophisticated, inaccurate tire models to evaluate lateral tire dynamics. In fact, measuring tire forces and sideslip angles is very difficult for technical and economic reasons. Therefore, these important data must be observed or estimated. If control systems were in possession of the complete set of lateral tire characteristics, namely lateral forces, sideslip angle, and the tire-road friction coefficient, they could greatly enhance vehicle handling and increase passenger safety.

As the motion of a vehicle is governed by the forces generated between the tires and the road, knowledge of the tire forces is crucial when predicting vehicle motion. For example, a vehicle can turn because of the applied lateral tire forces. In fact, what happens is that when the front wheels of a vehicle are steered, a slip angle is created, which gives rise to a lateral force. This lateral force turns or yaws the vehicle. Under normal driving situations (low slip angle), a vehicle responds predictably to the driver's inputs. As the vehicle

approaches the handling limits, for example, during an evasive emergency maneuver, or when a vehicle undergoes high accelerations, high slip angle occurs, and the vehicle's dynamic becomes highly nonlinear and its response becomes less predictable and potentially very dangerous.

Accurate data about tire forces lead to a better evaluation of the vehicle possible trajectories, to a better vehicle control and rollover prevention. Moreover, it enables the development of a diagnostic tool for evaluating the potential risks of accidents related to poor adherence or dangerous maneuvers.

In the literature, many studies have looked at the vehicle dynamic states estimation. Several ones have been conducted regarding the estimation of tire/road forces [8–20]. For example, in [8], a study of a 14-degrees-of-freedom (DOF) vehicle model is proposed where the dynamics of the roll center are used to calculate vertical tire forces. In [9], the authors propose an estimation method in order to estimate vertical and lateral forces per axle. The authors in [10–13] estimate the vehicle vertical forces and other dynamic states for a four-wheel vehicle model (FWVM) comprising four DOF. Consequently, lateral tire forces at each tire are calculated based on the estimated states and using a quasi-static tire model. In [14], Ray estimates the vehicle dynamic states and lateral tire forces per axle for a nine-DOF vehicle model. The author uses measurements of the applied torques as inputs to his model. We note that the torque is difficult to get in practice; it requires expensive sensors. More recently, authors in [15, 16] propose observers to estimate lateral forces per axle without using torque measures. In [17], the authors propose an estimation process based on a three-DOF vehicle model, as a lateral tire force estimator. In [15–17], lateral forces are modeled with a derivative equal to random noise. The authors in [17] remark that such modeling leads to a noticeable inaccuracy when estimating individual lateral tire forces, but not in axle lateral forces. This phenomenon is due to the non-representation of the lateral load transfer when modeling. Studies in [21–24] focus on the tire–road friction estimation.

The main goal of this study is to present an estimation method that uses simple vehicle-road models and a certain number of valid measurements in order to estimate in real time and in accurate way the sideslip angle and the lateral force at each individual tire/road contact point. This study presents two significant particularities (Fig. 1):

1. First, the estimation process does not use the measurements of wheel torques which are very expensive.
2. Second, the estimation process uses accurate normal tire forces, in contrast to many existing approaches that assume constant vertical forces. This approach is more realistic since during cornering, accelerating, and braking, the load distribution varies significantly in a car, thus cornering stiffness and lateral forces evaluation are directly affected.

The developed estimation process is model-based and built using Kalman filter technique. The Kalman filter is known as the most commonly used real-time estimator for linear and nonlinear systems. In order to show the effectiveness of the estimation method, some real-time validation tests were carried out on an instrumented vehicle in realistic driving situations.

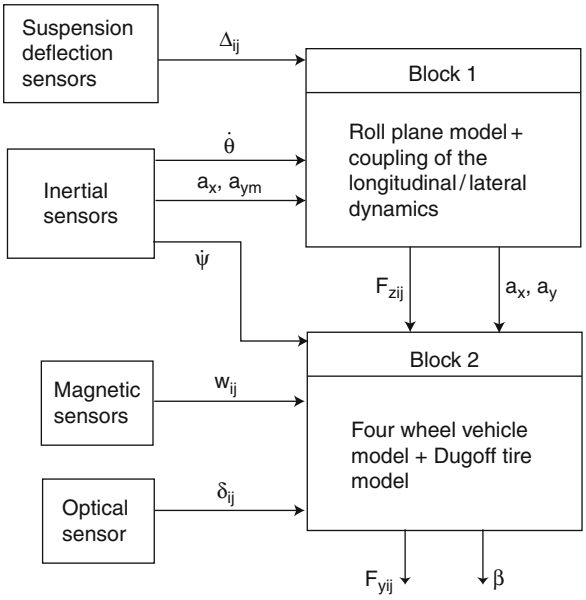

Unscented Kalman Filter in Intelligent Vehicles. Figure 1 Process estimation diagram

Estimation Process Description

The estimation process is shown in its entirety by the block diagram in Fig. 3, where a_x and a_{ym} are, respectively, the longitudinal and lateral accelerations; $\dot{\psi}$ is the yaw rate, $\dot{\theta}$ is the roll rate, Δ_{ij} (the index i represents the front *(1)* or the rear *(2)* and the index j represents the left *(1)* or the right *(2)*) is the suspension deflection; w_{ij} is the wheel velocity; F_{zij} and F_{yij} are, respectively, the normal and lateral tire-road forces; β is the sideslip angle at the center of gravity (cog). The whole estimation process consists of two blocks, and its role is to estimate sideslip angle at the cog, normal, and lateral forces at each tire/road contact point, and consequently evaluate the used lateral friction coefficient. The following measurements are needed:

- Yaw and roll rates measured by gyrometers
- Longitudinal and lateral accelerations measured by accelerometers
- Suspension deflections using suspension deflections sensors
- Steering angle measured by an optical sensor
- Rotational velocity for each wheel given by magnetic sensors

The first block aims to provide the vehicle's mass, lateral load transfer, normal tire forces, and the corrected lateral acceleration a_y (by canceling the gravitational acceleration component that distorts the accelerometer signal a_{ym}). It contains observers based on vehicle's roll dynamics and model that couples longitudinal and lateral accelerations. Authors have looked at the first block in some previous studies [10, 11]. This work focuses only on the second block, whose main role is to estimate individual lateral tire force and sideslip angle. The second block makes use of the estimations provided by the first block. In fact, as will be shown in the sections, the impact of including accurate normal forces in the calculation of lateral forces is fundamental.

One specificity of this estimation process is the use of blocks in series. By using cascaded observers, the observability problems entailed by an inappropriate use of the complete modeling equations are avoided, enabling the estimation process to be carried out in a simple and practical way. In the following, the model-based observer of the second block will be explained in details. Therefore, the vehicle-road model and the estimation method will be illustrated, respectively.

Four-Wheel Vehicle Model

The Four-Wheel Vehicle model (FWVM) is chosen for this study because it is simple and corresponds sufficiently to our objectives. The FWVM is widely used to describe transversal vehicle dynamic behavior [12–14, 17, 18].

Figure 2 shows a simple diagram of the FWVM model in the longitudinal and lateral planes.

In order to simplify the lateral and longitudinal dynamics, rolling resistance is neglected. Additionally, the front and rear track widths (E) are assumed to be equal. L_1 and L_2 represent the distance from the vehicle's center of gravity to the front and rear axles, respectively. The sideslip at the vehicle center of gravity (β) is the difference between the velocity heading (V_g) and the true heading of the vehicle (ψ). The yaw rate ($\dot{\psi}$) is the angular velocity of the vehicle about the center of gravity. The forward and lateral velocities are, respectively, V and U. The longitudinal and lateral forces ($F_{x,y,i,j}$) are shown for front and rear tires of the vehicle.

Longitudinal forces should be taken into account to enable accurate lateral forces estimation during vehicle

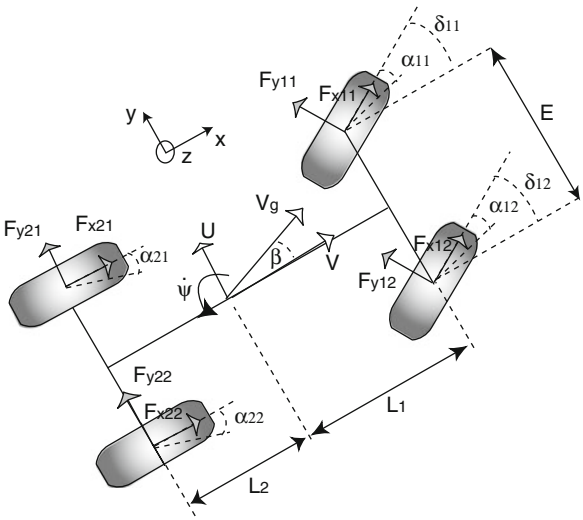

Unscented Kalman Filter in Intelligent Vehicles. Figure 2 Four-wheel vehicle model

braking or acceleration. While considering their effect is certainly important, its inclusion makes solving the lateral estimation problem considerably more complex. Thus, it may be desirable to solve the lateral estimation problem in the absence of longitudinal forces first and include them in later studies. This can be done by focusing on solving the estimation problem when the vehicle is driven at constant speeds [20].

This study extended the hypothesis of moving in a constant speed and addresses the case of a front-wheel drive, where rear longitudinal forces are neglected relative to the front longitudinal forces. Longitudinal front axle forces are considered by assuming that:

$$F_{x1} = F_{x11} + F_{x12} \tag{1}$$

The longitudinal force evolution is modeled with a random walk model, where its derivative is equal to random noise ($\dot{F}_{x1} = 0$). This is due to the lack of knowledge on the longitudinal slip and the effective radius of the tire [25].

The lateral dynamics of the vehicle can be obtained by summing the forces and moments about the vehicle's center of gravity. Consequently, the simplified FWVM is formulated as the following dynamic relationships [19]:

$$\begin{cases} \dot{V}_g = \dfrac{1}{m}\begin{bmatrix} F_{x1}\cos(\beta-\delta) + F_{y11}\sin(\beta-\delta) \\ + F_{y12}\sin(\beta-\delta) + (F_{y21}+F_{y22})\sin\beta \end{bmatrix} \\ \ddot{\psi} = \dfrac{1}{I_z}\begin{bmatrix} L_1\left[F_{y11}\cos\delta + F_{y12}\cos\delta + F_{x1}\sin\delta\right] \\ -L_2[F_{y21}+F_{y22}] \\ +\dfrac{E}{2}\left[F_{y11}\sin\delta - F_{y12}\sin\delta\right] \end{bmatrix} \\ \dot{\beta} = \dfrac{1}{mV_g}\begin{bmatrix} -F_{x1}\sin(\beta-\delta) + F_{y11}\cos(\beta-\delta) \\ + F_{y12}\cos(\beta-\delta) + (F_{y21}+F_{y22})\cos\beta \end{bmatrix} - \dot{\psi} \\ a_y = \dfrac{1}{m}\left[F_{y11}\cos\delta + F_{y12}\cos\delta + (F_{y21}+F_{y22}) + F_{x1}\sin\delta\right] \\ a_x = \dfrac{1}{m}\left[-F_{y11}\sin\delta - F_{y12}\sin\delta + F_{x1}\cos\delta\right] \end{cases} \tag{2}$$

where m is the vehicle mass, and I_z is the yaw moment of inertia.

The tire slip angle (α_{ij}), as shown in Fig. 2, is the difference between the tire's longitudinal axis and the tire's velocity vector. The tire velocity vector can be obtained from the vehicle's velocity (at the cog) and the yaw rate. Assuming that rear steering angles are approximately null, the direction or heading of the rear tires is the same as that of the vehicle. The heading of the front tires includes the steering angle (δ). The front steering angles are assumed to be equal ($\delta_{11} = \delta_{12} = \delta$). The forward velocity V, steering angle δ, yaw rate $\dot{\psi}$, and the vehicle body slip angle β are then used to calculate the tire slip angles α_{ij}, where:

$$\begin{cases} \alpha_{11} = \delta - \arctan\left[\dfrac{V\beta + L_1\dot{\psi}}{V - E\dot{\psi}/2}\right] \\ \alpha_{12} = \delta - \arctan\left[\dfrac{V\beta + L_1\dot{\psi}}{V + E\dot{\psi}/2}\right] \\ \alpha_{21} = -\arctan\left[\dfrac{V\beta - L_2\dot{\psi}}{V - E\dot{\psi}/2}\right] \\ \alpha_{22} = -\arctan\left[\dfrac{V\beta - L_2\dot{\psi}}{V + E\dot{\psi}/2}\right] \end{cases} \tag{3}$$

Tire–Road Interface

As the motion of a vehicle is governed by the forces generated between the tires and the road, knowledge of the tire forces is crucial in order to predict the vehicle's motion. This section presents the tire–road interaction phenomenon, especially the lateral tire forces. Since the quality of the observer largely depends on the accuracy of the tire model, the underlying model must be precise. Taking real-time calculation requirement, the tire model should also be simple.

Dugoff Tire Model

Many different tire models, based on the physical nature of the tire and/or on empirical formulations deriving from experimental data, can be found in the literature. These models include the Burckhardt, Dugoff, and Pacejka models [19, 26, 27]. One of the most commonly used model is the Pacejka's "Magic Formula." It is an effective method for predicting real tire behavior. However, it requires a large number of tire-specific parameters that are usually unknown. Another commonly used model is the Dugoff tire model. It synthesizes all the tire property parameters into two constants Cx and Cy, referred to as the longitudinal and cornering stiffness of the tire. Dugoff's model is the one used in this study. Neglecting

longitudinal forces, the simplified nonlinear lateral tire forces are given by:

$$\overline{F_{yij}} = -Cy_{ij} tan\alpha_{ij} f(\lambda) \tag{4}$$

where Cy_{ij} is the cornering stiffness, α_{ij} is the slip angle, and $f(\lambda)$ is given by:

$$f(\lambda) = \begin{cases} (2-\lambda)\lambda, & \text{if } \lambda < 1 \\ 1, & \text{if } \lambda \geq 1 \end{cases} \tag{5}$$

$$\lambda = \frac{\mu F_{zij}}{2Cy_{ij}|tan\alpha_{ij}|} \tag{6}$$

In the above formulation, μ is the friction coefficient and F_{zij} is the vertical load on the tire. This simplified tire model assumes pure slip conditions with negligible longitudinal slip, a uniform pressure distribution, a rigid tire carcass, and a constant friction coefficient for sliding rubber. The original Dugoff tire model has a constant stiffness in respect to weight transfer. It is worthy to note that, according to [28], load transfer affects the cornering stiffness Cy_{ij}. It can be represented by a second-order polynomial with respect to the normal force as shown in (7):

$$Cy_{ij}(F_z) = (aFz_{ij} - bFz_{ij}^2) \tag{7}$$

where a and b are, respectively, the first and second-order coefficient in the cornering stiffness polynomial. They are identified once using a set of experimental data treated offline, where the tires remain in their linear operation zone. Therefore, (7) is compared to the calculated cornering stiffness obtained from the ratio of the measured lateral force to the measured tire's slip angle. Hence, a and b are calculated, in such a way that the (7) fits the calculated cornering stiffness well.

This study proposes a modified Dugoff tire model, where the cornering stiffness varies with respect to load.

As shown in (4), vertical forces and the tire slip angles can be used to find the lateral force on each tire. Figure 3, based on the modified Dugoff's tire model, is a graph of the lateral force versus tire slip angle. It will be noted that as the load increases, the peak lateral force occurs at somehow higher slip angle.

It is clear that for small slip angles, the force profile can be defined by a linear region. When operating in this region, a vehicle responds predictably to the driver's inputs.

As the slip angle continues to grow, the tire begins to saturate and reaches a peak value; this area is commonly called the nonlinear region of the tire curve. It represents the tire limits, and it is rarely reached

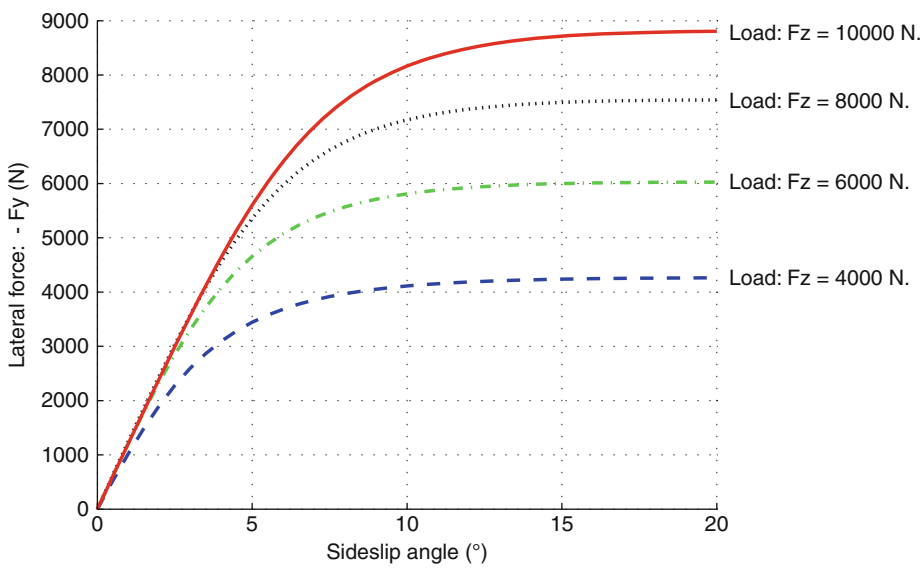

Unscented Kalman Filter in Intelligent Vehicles. Figure 3
Generic tire curve: lateral force versus slip angle

under normal driving conditions. If the front tires saturate first, the vehicle is said to display understeer and may plow out of a bend. If the rear tires saturate first, the vehicle limit oversteers and may spin out. Because most drivers are not accustomed to operate in the nonlinear handling regime, both of these responses are potentially very dangerous. Noting that oversteer situation is much more difficult to be controlled than the understeer [29].

Observers Design

This section presents a description of the observer devoted to lateral tire forces and sideslip angle. The state-space formulation, the observability analysis, and the estimation method will be presented.

Stochastic State-Space Representation

The nonlinear stochastic state-space representation of the system described in previous section is given as:

$$\begin{cases} \dot{X}(t) = f(X)(t), \;\; U(t)) + w(t) \\ Y(t) = h(X(t), \;\; U(t)) + u(t) \end{cases} \tag{8}$$

The input vector, U, comprises the steering angle and the normal forces considered estimated by the first block (see Fig. 3):

$$U = [\delta, F_{z11}, F_{z12}, F_{z21}, F_{z22}]^T = [u_1, u_2, u_3, u_4, u_5]^T \tag{9}$$

The measure vector, Y, comprises yaw rate, vehicle velocity (approximated by the mean of the rear-wheel velocities calculated from wheel-encoder data), longitudinal and lateral accelerations:

$$Y = [\dot{\psi}, V_g, a_x, a_y]^T = [y_1, y_2, y_3, y_4]^T \tag{10}$$

The state vector, X, comprises yaw rate, vehicle velocity, sideslip angle at the cog, lateral forces, and the sum of the front longitudinal tire forces:

$$\begin{aligned} X &= [\dot{\psi}, V_g, \beta, F_{y11}, F_{y12}, F_{y21}, F_{y22}, F_{x1}]^T \\ &= [x_1, x_2, x_3, x_4, x_5, x_6, x_7, x_8]^T \end{aligned} \tag{11}$$

Authors would like to emphasize that the consideration of the lateral forces as states allows:

1. A better evaluation of the tire forces. In fact, whatever the complexity of the tire models, there are several reasons why such models do not match the actual tire forces perfectly [30]. From these reasons, we can cite especially the changes in the tire's pressure and temperature and the changes in the road characteristics. Therefore, authors believe that according to the closed loop observer theory, the integration of the tire forces in the state vector may lead to better results than just using an open loop tire model.
2. A better understanding of the tire behaviors using the relaxation-length formulation, especially in transient maneuvers [31].
3. The forces reconstruction to be done robustly with respect to some parameter variations. In fact, it is well known that the Kalman filters have proven to be robust to parameter changes.

Taking these observations in mind, one can infer the contribution of this study with respect to others existing studies in the literature like [12, 13], which estimate dynamic variables of the vehicle, and then assess the tire forces using a properly adjusted tire model.

The process and measurements noise vectors, respectively, w and u, are assumed to be white, zero mean, and uncorrelated.

Consequently, the particular nonlinear function $f(.)$ of the state equations is given by:

$$\begin{cases} f_1 = \dfrac{1}{I_z} \begin{bmatrix} L_1 [x_4 \cos u_1 + x_5 \cos u_1 + x_8 \sin u_1 \\ - L_2 [x_6 + x_7] \\ + \dfrac{E}{2} [x_4 \sin u_1 - x_5 \sin u_1] \end{bmatrix} \\ f_2 = \dfrac{1}{m} \begin{bmatrix} x_8 \cos(x_3 - u_1) + x_4 \sin(x_3 - u_1) \\ + x_5 \sin(x_3 - u_1) + (x_6 + x_7) \sin(x_3) \end{bmatrix} \\ f_3 = \dfrac{1}{m x_2} \begin{bmatrix} - x_8 \sin(x_3 - u_1) + x_4 \cos(x_3 - u_1) \\ + x_5 \cos(x_3 - u_1) + (x_6 + x_7) \cos x_3 \end{bmatrix} - x_1 \\ f_4 = \dfrac{x_2}{\sigma_1} (-x_4 + \overline{F_{y11}} (\alpha_{11}, u_2)) \\ f_5 = \dfrac{x_2}{\sigma_1} (-x_5 + \overline{F_{y12}} (\alpha_{12}, u_3)) \\ f_6 = \dfrac{x_2}{\sigma_2} (-x_6 + \overline{F_{y21}} (\alpha_{21}, u_4)) \\ f_7 = \dfrac{x_2}{\sigma_2} (-x_7 + \overline{F_{y22}} (\alpha_{22}, u_5)) \\ f_8 = 0 \end{cases} \tag{12}$$

The observation function $h(.)$ is:

$$\begin{cases} h_1 = x_1 \\ h_2 = x_2 \\ h_3 = \dfrac{1}{m}[-x_4 \sin u_1 - x_5 \sin u_1 + x_8 \cos u_1] \\ h_4 = \dfrac{1}{m}[x_4 \cos u_1 + x_5 \cos u_1 + (x_6 + x_7) + x_6 \sin u_1] \end{cases} \tag{13}$$

The state vector $X(t)$ will be estimated by applying the unscented Kalman filter technique.

Observability

Observability is a measure of how well the internal states of a system can be inferred from knowledge of its inputs and external outputs. This property is often presented as a rank condition on the observability matrix. Using the nonlinear state-space formulation of the system presented in section "Stochastic State-Space Representation," the observability definition is local and uses the Lie derivative [32]. An observability analysis of this system was undertaken in [33]. It was shown that the system is observable except when:

- Steering angles are null.
- The vehicle is at rest ($V_g = 0$).

For these situations, we assume that lateral forces and sideslip angle are null, which approximately corresponds to the real cases.

Estimation Method: Kalman Filter Algorithms

The aim of an observer or a virtual sensor is to estimate a particular unmeasurable variable from available measurements and a system model in a closed loop observation scheme, as illustrated in Fig. 4. Because of the vehicle system-model mismatches (unmodeled dynamics, parameter variations, etc.) and the presence of unknown and unmeasurable disturbances, the calculation obtained from vehicle's model would deviate from the actual values over time. In order to reduce the estimation error, at least some of the measured outputs are compared to the same variables estimated by the observer. The difference is fed back into the observer after being multiplied by a gain matrix K, and so we have a closed loop observer (see Fig. 4). All developed observers are implemented in a first-order Euler approximation discrete form. At each iteration, the state vector is first calculated according to the evolution equation and then corrected online with the measurement errors (innovation) and filter gain K in a recursive prediction–correction mechanism. In this study, the gain is calculated using the Kalman filter method which is a set of mathematical equations and is widely represented in [34–36].

The EKF (Extended Kalman Filter) is probably the most commonly used estimator for nonlinear systems. However, in this study, the UKF (Unscented Kalman Filter) [38–40] is chosen for the following fundamental reasons:

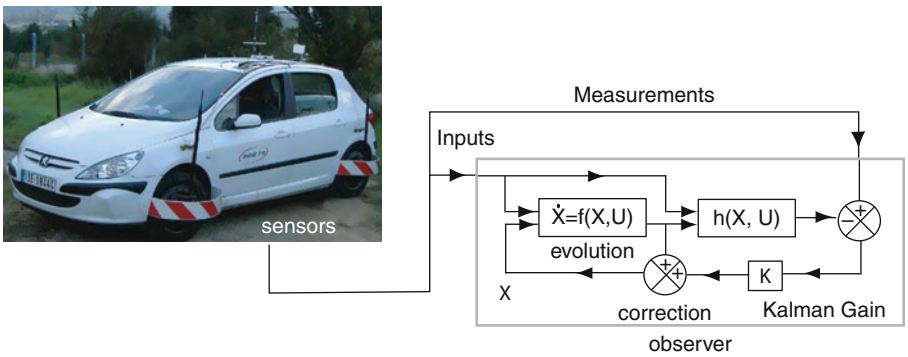

Unscented Kalman Filter in Intelligent Vehicles. Figure 4
Process estimation diagram

- The high nonlinearities of the vehicle-road model.
- The calculation complexity of the Jacobian matrices which causes implementation difficulties.

UKF Algorithm In this subsection, the principle of the UKF is summarized. Consider the general discrete nonlinear system:

$$\begin{cases} X_{k+1} = f(X_k, U_k) + w_k \\ Y_k = h(X_k) + v_k \end{cases} \tag{14}$$

where $X_k \in R^n$ is the state vector, $U_k \in R^r$ is the known input vector, $Y_k \in R^m$ is the output vector at time k, w_k, and v_k are, respectively, the disturbance and sensor-noise vector, which are assumed to be Gaussian white noise with zero mean and uncorrelated.

The UKF can be formulated as follows [37–40]:

Initialization

$$\begin{cases} \bar{X}_0 = E[X_0] \\ P_0 = E[(X_0 - \bar{X}_0)\ (X_0 - \bar{X}_0)^T] \end{cases} \tag{15}$$

where $\bar{X}_0$ and P_0 are, respectively, the initial state and the initial covariance.

Sigma points calculation and time update

$$\begin{cases} \chi_{k-1} = [\bar{X}_{k-1}, \bar{X}_{k-1} \pm \sqrt{(n+\lambda)P_{k-1}}] \\ \chi^*_{k|k-1} = f(\chi_{k-1}, U_{k-1}) \\ \bar{x}_{k|k-1} = \sum_{i=0}^{2n} w_i^m\ \chi^*_{i,k|k-1} \\ P_{k|k-1} = \sum_{i=0}^{2n} w_i^c\ (\chi^*_{i,k|k-1} - \bar{X}_{k|k-1}) \\ \qquad \times (\gamma^*_{i,k|k-1} - \bar{X}_{k|k-1})^T + Q \\ \chi_{k|k-1} = [\bar{X}_{k-1}, \bar{X}_{k-1} \pm \sqrt{(n+\lambda)P_{k|k-1}}] \\ \gamma_{k|k-1} = h(\chi_{k|k-1}) \\ \bar{Y}_{k|k-1} = \sum_{i=0}^{2n} w_i^m\ \gamma_{i,k|k-1} \end{cases} \tag{16}$$

where

$$\begin{cases} w_0^m = \dfrac{\lambda}{n+\lambda} \\ w_0^c = \dfrac{\lambda}{n+\lambda} + (n - \alpha^2 + \beta) \\ w_i^m = w_i^c = \frac{1}{2(n+\lambda)} \quad i = 1, \ldots, 2n \\ \lambda = n(\alpha^2 - 1) \end{cases} \tag{17}$$

Measurement update

$$\begin{cases} P_{\bar{Y}_k\bar{Y}_k} = \sum_{i=0}^{2n} w_i^c(\gamma_{i,k|k-1} - \bar{Y}_{k|k-1}) \\ \qquad \times (\gamma_{i,k|k-1} - \bar{Y}_{k|k-1})^T + R \\ P_{\bar{X}_k\bar{Y}_k} = \sum_{i=0}^{2n} w_i^c(\chi_{i,k|k-1} - \bar{X}_{k|k-1}) \\ \qquad \times (\gamma_{i,k|k-1} - \bar{Y}_{k|k-1})^T \\ K_k = P_{\bar{X}_k\bar{Y}_k}\ P^{-1}_{\bar{Y}_k\bar{Y}_k} \\ P_k = P_{k|k-1} - K_k\ P_{\bar{Y}_k\bar{Y}_k}\ K_k^T \\ \bar{X}_k = \bar{X}_{k|k-1} + K_k(Y_k - \bar{Y}_{k|k-1}) \end{cases} \tag{18}$$

where the variables are defined as follows: $\bar{X}_k$ and $\bar{Y}_{k|k-1}$ are the estimations, respectively, of the state and of the real measurement at each instant k, w_i is a set of scalar weights, and n is the state dimension; the parameter α determines the spread of the sigma points around $\bar{X}$ and is usually set to $1e-4 < \alpha < 1$. The constant β is used to incorporate part of the prior knowledge of the distribution of X, and for Gaussian distributions, $\beta = 2$ is optimal. Q and R are, respectively, the disturbance and sensor-noise covariance: R takes into account the uncertainty in the measured data and Q is tuned depending on the model quality. Remember that the computation of the Kalman gain is a subtle mix between process and observation noises. The less noise in the operation compared to the uncertainty in the model, the more the variables will be adapted to follow measurements. Since the lateral forces are modeled using a relaxation model based on reliable tire models, the uncertainty affected to them is not too high. However, the longitudinal force per front axle is not modeled at all; hence, it is represented by a high noise level. The other states (yaw rate, longitudinal and lateral vehicle velocity) are modeled using the vehicle's equations. Therefore, they are said to have an average noise. On the other hand, since the embedded sensors have good accuracy, the noises on the measurements are quite small. In order to reduce the complexity of the problem, both measurement covariance matrix, R, and the process covariance matrix, Q, are assumed to be constant and diagonal. The off-diagonal elements are set to 0. That means that both the measurement noises and the process noises are supposed uncorrelated.

Experimental Results

In this section, the experimental car used to evaluate the observer performances is presented. Moreover, the test conditions and the results of the previously developed observers are discussed and analyzed.

Experimental Car

The experimental vehicle shown in Fig. 4 is the INRETS-MA (Institut National de Recherche sur les Transports et leur Sécurité – Département Mécanismes d'Accidents) Laboratory's test vehicle [7]. It is a Peugeot 307 equipped with:

- Gyrometers and accelerometers that measure, respectively, the rotations (roll, pich, and yaw rates) and accelerations (longitudinal, lateral, and vertical) of the car body.
- Suspension sensors that measure the distances between the wheels and the car body.
- Three Correvit noncontact optical sensors:
  1. One is located in chassis rear overhanging position, and it measures longitudinal and lateral vehicle speeds.
  2. The other two are installed on the front right and rear right tires, and they measure front- and rear-tires longitudinal/lateral velocities and sideslip angles.
- Dynamometric wheels fitted on all four tires, which are able to measure tire forces and wheel torques in and around all three dimensions.
- Steering-rack displacement sensor that is used to determine the steering angle.
- Magnetic sensors that measure rotational velocity for each wheel.

It is important to note that the Correvit and the wheel-force transducers (see Fig. 5) are very expensive sensors. They are used in this study as a reference for

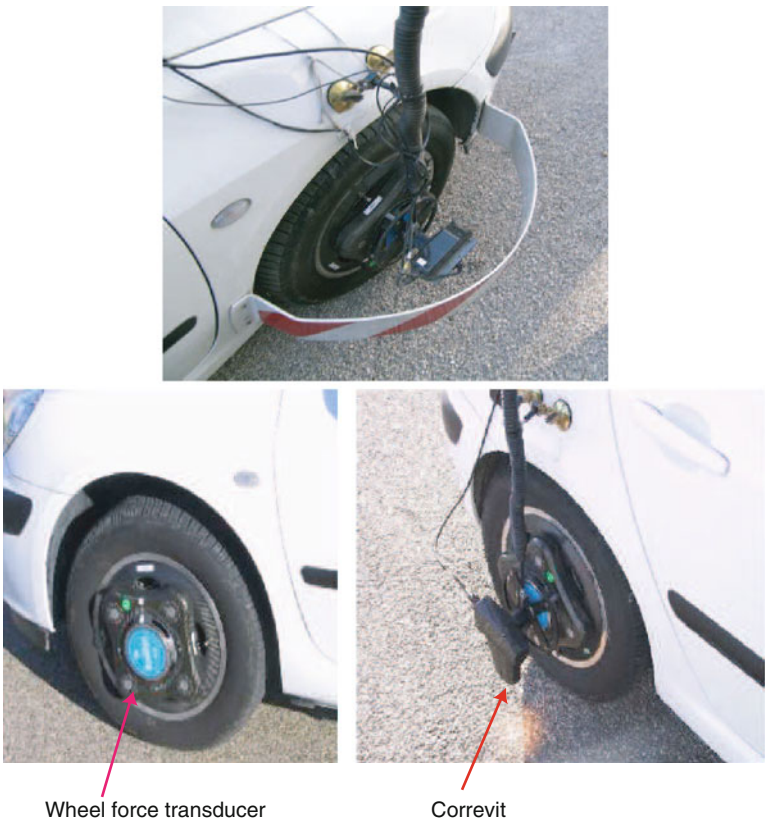

Unscented Kalman Filter in Intelligent Vehicles. Figure 5
Wheel-force transducer and sideslip sensor installed at the tire level

validating the estimation process. The sampling frequency of the different sensors is 100 Hz.

Test Conditions

Test data from nominal as well as adverse driving conditions were used to assess the performance of the observer presented in section "Observers Design," in realistic driving situations. We report a lane-change maneuver where the dynamic contributions play an important role. Figure 6 presents the Peugeot's trajectory (on a dry road), its speed, steering angle, and "g-g" acceleration diagram during the course of the test. The acceleration diagram, that determines the maneuvering area utilized by the driver/vehicle, shows that large lateral accelerations were obtained (absolute value up to 0.6 *g*). This means that the experimental vehicle was put in a critical driving situation.

The estimation process algorithm was written in C++ and has been integrated into the laboratory car as a DLL (Dynamic Link Library) that functions according to the software acquisition system.

Validation of Observers

The observer results are presented in two forms: as tables of normalized errors, and as figures comparing the measurements and the estimations. The normalized error for an estimation z is defined as:

$$\epsilon_z = 100 \times \frac{\| z_{obs} - z_{measured} \|}{max\,(\| z_{measured} \|)} \tag{19}$$

where z_{obs} is the variable calculated by the observer, $z_{measured}$ is the measured variable, and $max(\|z_{measured}\|)$ is the absolute maximum value of the measured variable during the test maneuver.

Figures 7 and 8 show lateral forces on the front and rear wheels. According to these plots, the observers are relatively good with respect to measurements. Some small differences during the trajectory are to be noted. These might be explained by neglected geometrical parameters, especially the camber angles, which also produce a lateral forces component [41]. It is also shown that the lateral forces on the right-hand tires exceed those on the left-hand tires. This result is

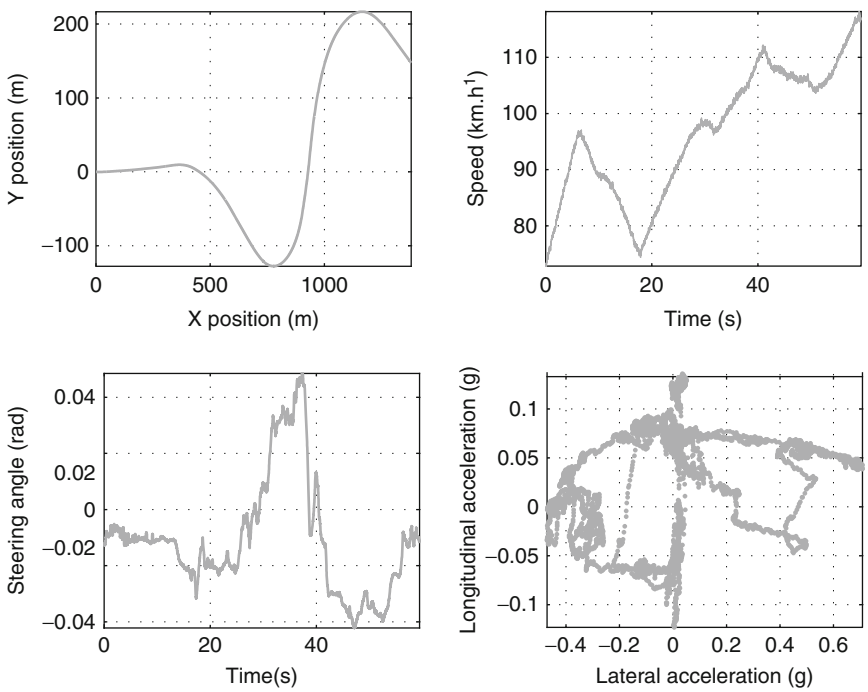

Unscented Kalman Filter in Intelligent Vehicles. Figure 6
Experimental test: vehicle trajectory, speed, steering angle, and acceleration diagrams for the lane-change test

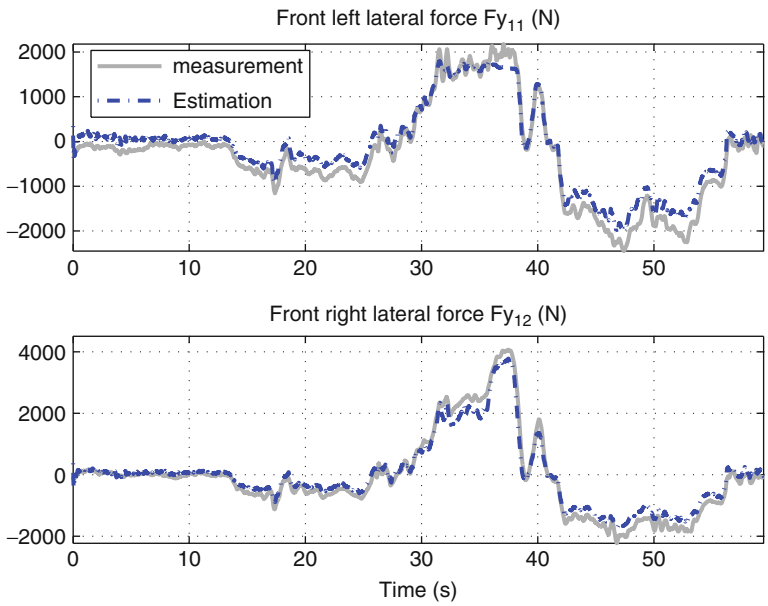

Unscented Kalman Filter in Intelligent Vehicles. Figure 7
Estimation of front lateral tire forces

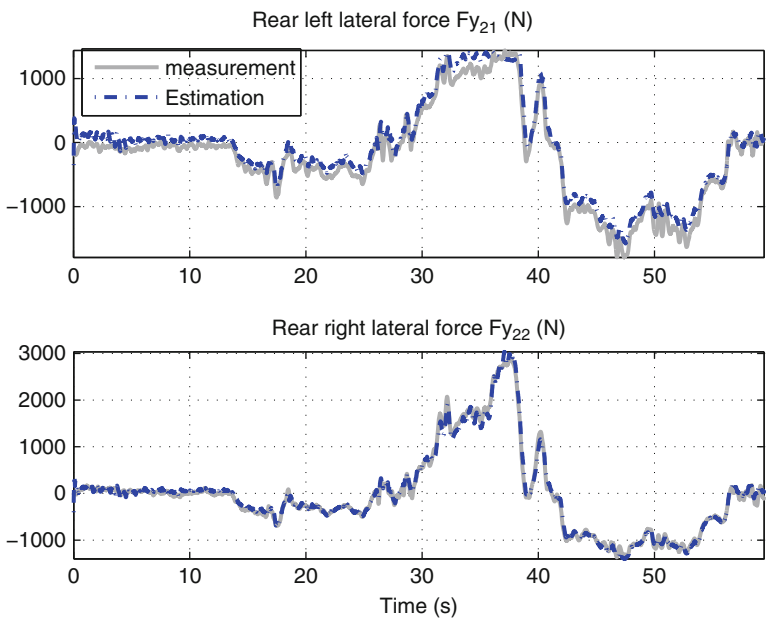

Unscented Kalman Filter in Intelligent Vehicles. Figure 8
Estimation of rear lateral tire forces

clearly a consequence of the load transfer produced during cornering from the left- to the right-hand side of the vehicle. In fact, lateral force increases as normal force increases. Figure 9 shows how sideslip angle changes during the test. Reported results are relatively good.

Table 1 presents maximum absolute values, normalized mean errors, and normalized std (standard

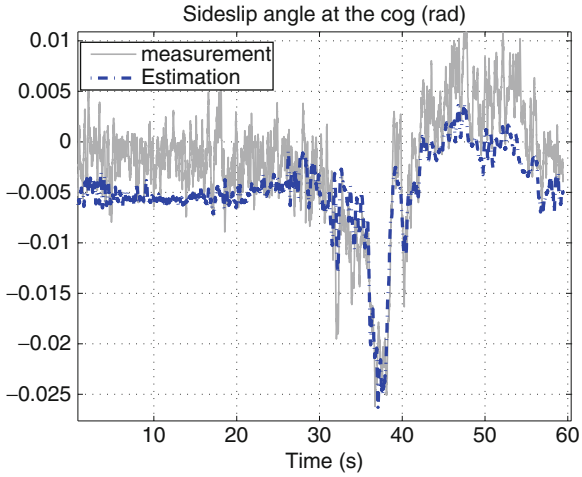

Unscented Kalman Filter in Intelligent Vehicles. Figure 9
Estimation of the sideslip angle at the cog

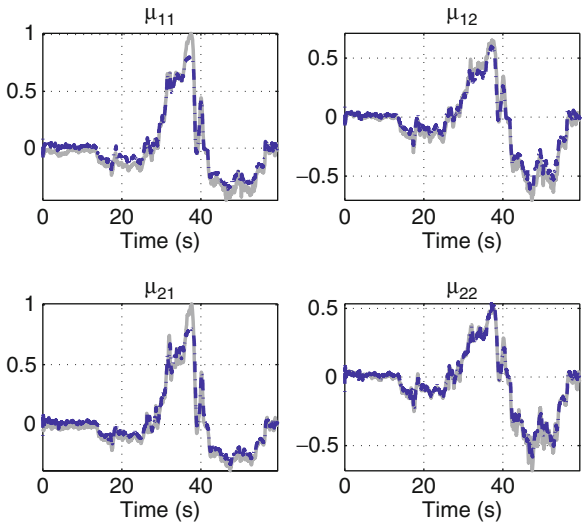

Unscented Kalman Filter in Intelligent Vehicles. Figure 10
Used lateral friction coefficients developed by the tires

Unscented Kalman Filter in Intelligent Vehicles. Table 1 Maximum absolute values, normalized mean errors, and normalized Std

	Max |||	Mean%	Std%
F_{y11}	2180 (*N*)	8.23	4.80
F_{y12}	4070 (*N*)	3.70	3.74
F_{y21}	1441 (*N*)	7.51	3.52
F_{y22}	2889 (*N*)	1.91	1.77
β	0.027 (*rad*)	8.32	6.41

deviations) for lateral tire forces and sideslip angles. Despite the simplicity of the model, we can deduce that for this test, the performance of the observer is satisfactory, with normalized error globally less than 8%.

Given the vertical and lateral tire forces at each tire-road contact level, the estimation process is able to evaluate the used lateral friction coefficient μ. This is defined as the ratio of friction force to normal force, and is given by [29, 41]:

$$\mu_{ij} = \frac{Fy_{ij}}{Fz_{ij}} \tag{20}$$

The lateral friction coefficients in Figure 10 show that the estimated μ_{ij} are close to the measured values. A closer investigation reveals that the used lateral friction coefficients μ_{12} and μ_{22} corresponding to the overloaded tires during cornering are lower than μ_{11} and μ_{21}. This phenomenon is due to the tire load sensitivity effect: the lateral friction coefficient is normally higher for the lighter loads, or conversely, falls off as the load increases [29, 41].

This test also demonstrates that μ_{11} and μ_{21} are high, especially for lateral accelerations up to 0.6, and that they attain the limit for the dry road friction coefficient. In fact, dry road surfaces show a high friction coefficient in the range 0.9–1.2 (implying that driving on these surfaces is safe), which means that for this test the limits of handling were reached.

Conclusion and Future Perspectives

This paper presents an interesting method for estimating lateral tire forces and sideslip angle, that is to say, two of the most important parameters affecting vehicle stability and the risk of leaving the road. Consequently, the developed observer could feed control systems with fundamental vehicle-dynamics data in order to enhance vehicle safety.

The proposed observer is derived from a simplified four-wheel vehicle model and is based on unscented Kalman filtering technique. Tire–road interaction is represented by the Dugoff model. A comparison with real experimental data demonstrates the potential of

the estimation process. It is shown that it may be possible to replace expensive correvit and dynamometric hub sensors by real-time software observers. This is one of the important results of this report. Another important result concerns the estimation of individual lateral forces acting on each tire. This can be seen as an advance with respect to the current vehicle-dynamics literature.

Future studies will improve the vehicle-road model in order to widen validity domains for the observer (take into account road irregularities and road bank angle), and make it adaptive with the road conditions (especially the road friction). Moreover, it will be of major importance to study the effect of coupling longitudinal/lateral dynamics on lateral tire behavior.

Acknowledgments

This work was done at Heudiasyc Laboratory UMR CNRS 6599, UTC University (Compiègne, France) in collaboration with Alessandro Victorino and Ali Charara.

Bibliography

Primary Literature

1. FARS (2007) Fatality analysis reporting system (FARS). Technical report, National Highway Traffic Safety Administration, National Center for Statistics and Analysis
2. Aparicio F, Paez P, Moreno F, Jimenez F, Lopez A (2005) Discussion of a new adaptive speed control system incorporating the geometric characteristics of the road. Int J Veh Auton Syst 3(1):47–64
3. Bosch R (2004) Bosch automotive handbook, 6th edn. SAE Society of Automotive Engineers, Bosch company, New York
4. ESC (2003) Electronic stability control fact sheet. Technical report, ESC Coalition and DEKRA Automotive research
5. Van Zanten A (2002) Evolution of electronic control systems for improving the vehicle dynamic behavior. In: Proceedings of the 6th international symposium on advanced vehicle control (AVEC), Hiroshima, pp 7–15
6. Hsu Y, Gerdes JC (2005) Stabilization of a steerby-wire vehicle at the limits of handling using feedback linearization. In: Procedings of IMECE2005, AMSE international mechanical engineering congress and exposition, Florida
7. Lechner D (2008) Embedded laboratory for vehicle dynamic measurements. In: International symposium on advanced vehicle control, Kobe
8. Shim T, Ghike G (2007) Understanding the limitations of different vehicle models for roll dynamics studies. Veh Syst Dyn 45:191–216
9. Doumiati M, Baffet G, Lechner D, Victorino A, Charara A (2008) Embedded estimation of the tire/road forces and validation in a laboratory vehicle. In: International symposium on Advanced Vehicle Control, Kobe
10. Doumiati M, Victorino A, Charara A, Lechner D, Baffet G (2008) An estimation process for vehicle wheelground contact normal forces. In: IFAC World Congress, Seoul Korea
11. Doumiati M, Victorino A, Charara A, Lechner D (2009) Lateral load transfer and normal forces estimation for vehicle safety experimental evaluation. Veh Syst Dyn 47(12):1511–1533
12. Wenzel TA, Burnham KJ, Blundell MV, Williams RA (2006) Estimation of the nonlinear suspension tyre cornering forces from experimental road test data. Veh Syst Dyn 44:153–171
13. Dakhlallah J, Glaser S, Mammar S, Sebsadji Y (2008) Tire-road forces estimation using extended Kalman filter and sideslip angle evaluation. In: American control conference, Seattle
14. Ray LR (1997) Nonlinear tire force estimation and road friction identification: simulation and experiments. Automatica 33(10):1819–1833
15. Baffet G, Charara A, Dherbomez G (2007) An observer of tire road forces and friction for active-security vehicle systems. IEEE/ASME Trans Mechatron 12:651–661
16. Baffet G, Charara A, Lechner D, Thomas D (2008) Experimental evaluation of observers for tire-road forces, sideslip angle and wheel cornering stiffness. Veh Syst Dyn 45:191–216
17. Wilkin MA, Manning WJ, Crolla DA, Levesley MC (2006) Use of an extended Kalman filter as a robust tyre force estimator. Veh Syst Dyn 44:50–59
18. Venhovens PT, Naab K (1999) Vehicle dynamics estimation using Kalman filters. Veh Syst Dyn 32:171–184
19. Kiencke U, Daiss A (1997) Observation of lateral vehicle dynamics. Control Eng Pract 5(8):1145–1150
20. Hsu YHJ (2009) Estimation and control of lateral tire forces using steering torque. PhD, Department of mechanical engineering, Stanford University
21. Haffner L, Kozek M, Shi J, Jorgel HP (2008) Estimation of the maximum friction coefficient for a passenger vehicle using the instantaneous cornering stiffness. In: American control conference, Seattle
22. Gustafsson F (1997) Slip-based tire-road friction estimation. Automatica 33(6):1087–1099
23. Hahn JO, Rajamani R, Alexander L (2002) GPS-Based real time identification of tire-road friction coefficient. IEEE Trans Control Syst Technol 10(3):331–343
24. Uchanski MR (2001) Road friction estimation for automobiles using digital signal processing methods. PhD thesis, University of California, Berkley
25. Koo SL, Tan HS (2007) Tire dynamic deflection and its impact on vehicle longitudinal dynamics and control. IEEE/ASME Trans Mechatron 12(6):623–631
26. Dugoff J, Fanches P, Segel L (1970) An analysis of tire properties and their influence on vehicle dynamic performance. Society of Automotive Engineers Paper 700377
27. Pacejka HB (2002) Tyre and vehicle dynamics. Elsevier, Amsterdam

28. Gillespie TD (1992) Fundamental of vehicle dynamics. Society of Automotive Engineers, Warrendale
29. Rajamani R (2005) Vehicle dynamics and control. Springer, New York
30. Lidner L (1993) Experience with the magic formula tyre model. In: Proceedings of the 1st international colloquium on tyre models for vehicle dynamic analysis, Amsterdam
31. Svendenius J (2007) Tire modeling and friction estimation. PhD thesis, Lund University, Sweden
32. Nijmeijer H, Van der Schaft AJ (1991) Nonlinear dynamical control systems. Springer, New York
33. Doumiati M, Victorino A, Charara A, Lechner D (2009) Unscented Kalman filter for real-time vehicle lateral tire forces and sideslip angle estimation. In: IEEE intelligent vehicles symposium, Xi'an, Shaanxi
34. Kalman RE (1960) A new approach to linear filtering and prediction problems. Trans ASME J Basic Eng 82(D):35–45
35. Welch G, Bishop G (2001) An introduction to the Kalman filter, Course 8. University of North Carolina, Departement of computer science
36. Durrant-Whyte H (2001) Multi sensor data fusion. Technical report, Australian center for field robotics, University of Sydney
37. Mohinder GS, Angus PA (1993) Kalman filtering theory and practice. Prentice Hall, Englewood Cliffs
38. Julier SJ, Uhlman JK (1997) A new extension of the Kalman filter to nonlinear systems. In: International symposium aerospace/defense sensing, simulation and controls, Orlando
39. Julier SJ, Uhlman JK, Durrant-Whyte HF (1995) A new extension approach for filtering nonlinear systems. In: American control conference, Seattle
40. Wan EA, Merwe RVD (2000) The unscented Kalman filter for nonlinear estimation. In: Proceedings of the adaptive systems for signal processing, communications, and control symposium, Atlanta, pp 153–158
41. Milliken W, Milliken DL (1995) Race car vehicle dynamics. Society of Automotive Engineers, Warrendale

Books and Reviews

Aga M, Okada A (2003) Analysis of vehicle stability control (VSC)'s effectiveness from accident data. In: Proceedings of the 18th international technical conference on the enhanced safety of vehicles, Nagoya

Aguirre LA, Letellier C (2005) Observability of multivariate differential embeddings. J Phys A Math Gen 38:6311–6326

Bakker E, PAcejka HB, Lidner L (1987) A new tire model with application in vehicle dynamic systems, SAE Paper 890087

Besanon G (2007) Nonlinear observers and applications. Springer, Berlin

Bevly DM, Gerdes JC, Wilson C, Zheng G (2000) The use of GPS based velocity measurements for improved vehicle state estimation: proceedings of the American Control Conference, Chicago. American Automatic Control Council, New York

Brown T, Hac A, Martens J (2004) Detection of vehicle rollover. SAE World Congress, Detroit

Doumiati M, Sename O, Martinez J, Poussot C, Dugard L (2010) Gain scheduled steering and braking control for improvement of vehicle handling and stability. In: IEEE conference on decision and control, Georgia

Doumiati M, Sename O, Martinez J, Dugard L, Gaspar P, Szabo Z, Bokor J (2011) Vehicle yaw control via coordinated use of steering/braking systems. IFAC World Congress, Milano

Heydinger G, Howe J (2000) Analysis of vehicle response data measured during severe maneuvers, SAE Paper 2000-01-1644

Jazar RN (2008) Vehicle dynamics, theory and application. Springer, New York

Smith ND (2004) Understanding parameters influencing tire modeling. Colorado State University, Formula SAE Platform

Uranium and Thorium Resources

J. Stephen Herring
Idaho National Laboratory, Idaho Falls, ID, USA

Article Outline

Glossary
Definition of the Subject
Introduction
Estimates of Uranium Reserves
Global Estimates of Overall Uranium and Thorium Resources
Mechanisms for the Concentration of Uranium
Unconventional Resources
New Technologies for Uranium Extraction
Impact of Uranium Scarcity and Higher Extraction Costs
Future Directions
Bibliography

U

Glossary

Cross section Probability of neutron interaction with a nucleus, expressed in terms of area, in units of barns (b). One barn equals 1.0×10^{-24} cm^2.

Enrichment The fraction of an isotope, usually fissile ^{235}U, in a mass of uranium. Enrichment is commonly quoted as the weight percent of the particular isotope. Natural uranium has an enrichment of

0.711 wt%, commercial reactor fuel is 3–5% enriched, and depleted uranium is 0.2–0.3% ^{235}U.

Enrichment tails (also depleted uranium) The uranium remaining after the enrichment of natural uranium into fuel, today about 0.3% ^{235}U, earlier 0.2–0.25% ^{235}U.

Fractionation Crystallization from a magma in which the initial crystals are prevented from equilibrating from the parent liquid, resulting in a series of residual liquids of more extreme composition than would have resulted from continuous reaction [1].

Highly enriched uranium (HEU) Uranium containing more that 20 wt% ^{235}U.

J_{th} Joule (i.e., Watt-second) thermal. One British thermal unit (BTU) equals 1,055 J_{th}.

Log-normal distribution Distribution of the form $f(x) = e^{-(\ln x)^2}$. In the present usage, the tonnage of an element available at concentration c, $T(c)$, is given by $T(c) = C_1\, e^{-(\ln c_o - \ln c)^2}$, where c_o is the average crustal abundance and C_1 is a constant.

Low-enriched uranium (LEU) Uranium containing less than 20 wt% ^{235}U.

Mafic Composed chiefly of dark ferromagnesian minerals.

MOX Mixed oxide fuel, usually consisting of a ceramic mixture of uranium dioxide and plutonium dioxide.

MSWU Mega-separative work unit, a million separative work units. A separative work unit is the separative work that must be done to one kilogram of a mixture of isotopes to change its separation potential by one unit. The separation potential, a dimensionless function, is defined by $\phi\ (x_k) = (2x_k - 1)\ln\frac{x_k}{1-x_k}$, where x_k is the atomic fraction of the isotope, k. See Benedict 1981, p. 667 for a more complete definition [2].

Pegmatite An exceptionally coarse-grained igneous rock, with interlocking crystals, often found at the margins of batholiths.

Placer A mineral deposit at the surface formed by sedimentary concentration of heavy mineral particles from weathered debris.

Quad Quadrillion (i.e., 10^{15}, also written 1E15) British thermal units. One quad = 1.055×10^{18} J_{th}.

t Metric ton, also used in *Mt*, million metric tons, and *Tt*, trillion metric tons (teratons).

Unconformity A break or gap in the geologic record, such as an interruption in the normal sequence of deposition of sedimentary rocks, or a break between eroded metamorphic rocks and younger sedimentary strata [1].

Yellowcake A concentrate of uranium ore, containing 80–90% U_3O_8. Yellowcake ranges from yellow to black, depending on impurities, processing temperature, and degree of hydration [3]. Although uranium prices are sometimes colloquially cited as "dollars per pound of yellowcake," the actual prices are $ per lb of U_3O_8, where all of the uranium is assumed to be present in the yellowcake as that oxide.

Definition of the Subject

Uranium is a widely distributed element which is essential, at least in the near term, to the use of nuclear fission as a source of energy. Uranium is ubiquitous in the earth because of the wide variety of minerals in which it can occur, and because of the variety of geophysical and geochemical processes that have transported it since the primordial formation of the earth from the debris of supernovae. Uranium is approximately as common in the earth's crust as tin or beryllium, and is a minor constituent in most rocks and in seawater. The average crustal abundance of uranium is 2.76 weight parts per million (wppm), higher than the average concentrations of such economically important elements as molybdenum (1.5 wppm), iodine (0.5 wppm), mercury (0.08 wppm), silver (0.07 wppm), and gold (0.004 wppm).

Introduction

Beginning with the discovery of nuclear fission, uranium has been seen as a valuable but scarce resource. Uranium-235 (^{235}U) is the only naturally occurring isotope that can be made to fission with thermal neutrons. Consequently, the resources of uranium have been believed to inherently limit the sustainability of nuclear energy. There have been two periods of extensive exploration for uranium, in the 1950s and in the 1970s, both followed by long periods of severe contraction in the market and in exploration activity. With the peak of uranium prices to about $350/kg in 2007, there

was an increased effort in exploration. However, that exploration quickly resulted in increased known reserves in several deposits and the return of prices to about $140/kg. Today, exploration activity is at a moderate level for several reasons: (1) deposits found during earlier exploration periods have proven to be larger than initially estimated, (2) nuclear energy is growing, but not as rapidly as earlier forecast, (3) improved nuclear fuel management techniques and materials are allowing higher burnup and longer operating cycles, and (4) the conversion ("downblending") of highly enriched uranium of military origin to civilian purposes has postponed the need for large amounts of newly mined natural uranium.

Concern that uranium would soon be exhausted was one of the driving forces in the development of fast breeder reactors, particularly in the 1960s and 70s. Fast breeder reactors convert the fertile isotope ^{238}U into the fissile isotope ^{239}Pu. These concerns also led to the development of thermal breeder reactors capable of converting thorium into the fissile, but not naturally occurring, isotope ^{233}U. Thorium, consisting almost entirely of the isotope ^{232}Th, is about four times more abundant than uranium and thus may represent a source of nuclear fuel in the distant future.

Estimates of Uranium Reserves

The importance of the overall uranium and thorium resource is demonstrated by the attention given to the estimates by such international agencies as the International Atomic Energy Agency (IAEA) and the Nuclear Energy Agency (NEA) of the Organisation for Economic Co-operation and Development (OECD). The estimates of these organizations are based on information provided by the member states and backed by research from others. The results are regularly compiled in the "Red Book" [4].

However, the estimates of uranium resources in the Red Book are based on the known and expected reserves that can be economically extracted using present or near-future technology. Because of the wide range of uranium concentrations in various minerals, the cost of extraction serves as the independent variable against which resources are estimated. Any reported amount of reserves/resources should be accompanied by the estimated cost of recovery of those reserves.

The Red Book [4] estimates the economically recoverable uranium reserves based on current and prospective mining projects ("Total Identified Resources Reasonably Assured and Inferred") as of January 2009 are 5.4 million metric tons (Mt) of uranium of the best-proven category recoverable worldwide at a marginal cost of <$130/kg of uranium metal. When the high-cost category (between $130/kg and $260/kg of U metal) is added, the total identified resources are estimated to be 6.3 Mt. Total undiscovered resources (prognosticated resources and speculative resources) as of January 2009 were estimated to be 10.4 Mt. The 2008 consumption of natural uranium by the 438 reactors worldwide was 59,065 t, and consequently, these total identified resources could be expected to last about 100 years at current rates and 250 years if speculative resources are included. These ratios of identified and speculative resources to consumption rate are longer than those for nearly all metals and fossil fuels, with the exception of coal.

Low market prices, the slow growth of nuclear power, and the downblending of highly enriched uranium (HEU) have in the past resulted in both very low levels of exploration and little effort in the development of advanced extraction technologies. Downblending agreements with the Russian Federation are due to expire in 2013. The discovery of additional total identified resources has shown a strong correlation with exploration expenditures, averaging 0.65 kg of additional resources per exploration dollar from 1987 to 2005 and 0.32 kg/exploration dollar from 2005 to 2009, following the uranium price increases after 2005 [5]. Those transient price increases led to an increase in the average annual expenditures for exploration from $127 million/year for 1987–2005 to $1.1 billion/year for 2005–2009.

It is important to note that uranium today is used overwhelmingly in the light water reactor fuel cycle, where only about 1.1–1.5% of the ultimate energy of the mined uranium is extracted via fissioning of ^{235}U and the small amounts of ^{239}Pu bred in situ. The rest of the uranium remains either in the used fuel or in the depleted uranium tails remaining after enrichment. Of the 1.8 Mt of uranium mined worldwide since 1945, the location of all but about 1,500 t is known. Only the location of that uranium dispersed either in nuclear explosions or as armor-piercing projectiles is not known. The inventory of used fuel and of depleted

uranium represents a very significant resource that could become fuel for fast breeder reactors.

While uranium is an essential input for the production of nuclear energy, the costs of natural uranium are a minor component of the overall cost. Today, at uranium prices of about \$140/kg U (\$53/lb of U_3O_8), the natural uranium required for the light water reactor (LWR) fuel cycle is responsible for only about 2.5–3% of generating costs. The fuel cost is 15–20% of the generating costs, but those costs include conversion of the uranium ore to UF_6, enrichment of the natural uranium, production of the ceramic UO_2 fuel pellets, and fabrication of the fuel assemblies. A tenfold increase in the cost of natural uranium would not be welcome, but would not fundamentally change the economics of nuclear power. A tenfold increase in uranium prices would, at first estimate, be expected to increase the cost of nuclear electricity by 25–30%. However, a more detailed calculation, optimizing the ^{235}U content of the depleted uranium tails and adjusting fuel management for a higher priced resource, would result in an increase in the cost of electricity significantly less than 20%.

This entry discusses uranium resources in a global sense, beyond the official estimates of the IAEA and the OECD. As an introduction to that discussion, the origins of the earth's present inventory of uranium, the geophysical and geochemical processes that serve to concentrate uranium into economically viable deposits, and the technologies now being used for the extraction and concentration of uranium ores are described. Finally, the potential impacts of technologies now under development and the overall impact of the cost of uranium on the cost of energy from nuclear fission will be reviewed.

Thorium as a Nuclear Fuel

For the foreseeable future, uranium will probably continue to be the only source of nuclear energy. Nevertheless, for completeness, thorium resources should also be considered because of thorium's unique characteristics as a nuclear fuel. There are basically four reasons for considering thorium resources within the overall discussion of nuclear fuel resources. First, thorium is about 3.9 times more abundant than uranium, on a mass basis, as indicated both by samples of the continental crust and by spectroscopy of supernova debris, from which planets are formed. Secondly, because similarities of the geochemistry and mineralogy of thorium and the lanthanides, thorium and the lanthanides (often called the "rare earth elements") are often found in the same ore bodies. Since the lanthanides are of increasing technical and strategic importance due to their widespread use in magnets and electronics, thorium is often treated as a waste since it has only a small market and since it is radioactive. Thus research on the efficient separation and purification of thorium could enhance both rare earth and thorium resources. Third, thorium can be directly substituted in the UO_2 crystal, making it a long-term supplement for uranium for in situ ^{233}U breeding. Thorium, as ThF_4, can also be used in the molten salt reactor in combination with UF_4, where the uranium would be a mixture of ^{233}U, ^{235}U, and ^{238}U. Finally, because thorium has only one oxide, ThO_2, which has high thermal stability, it can serve as a very robust matrix for actinide transmutation, after which the ThO_2 would serve as the waste form for the transmutation targets.

Thorium averages 12 parts per million in the earth's crust, and is the 39th most abundant of the 78 crustal elements. Soil commonly contains an average of 6 wppm of thorium. When thorium is used as a nuclear fuel, much less plutonium and other minor transuranics (i.e., neptunium, americium, curium, berkelium, ...) are produced than are produced in uranium fuel cycles. The reduced production of transuranics occurs for two reasons. First, the fissile product of neutron absorption by ^{232}Th is ^{233}U, which is further down the actinide series from plutonium and the minor actinides, and secondly, the fission to capture ratio of ^{233}U is approximately nine, while that of ^{239}Pu is about three, thus resulting in lower production of the transuranics.

The generation of thorium deposits occurs in a fundamentally different manner from deposits of uranium. Uranium has some nine oxides and is dissolved or precipitated depending on the oxygen content and pH of the groundwater. Thus deposits are often formed where there is a decrease in the oxygen content of groundwater. Thorium, on the other hand, has only one oxide, ThO_2, which is very refractory and insoluble. Thus thoria (along with many of the lanthanide oxides) is not dissolved in erosion by groundwater

and flowing rivers. The surviving grains, containing the thoria from the base rock, form into alluvial deposits of monazite sands.

Thorium occurs as the ores thoriatite (ThO_2), thorite ($ThSiO_4$) and mainly as monazite ((Ce, La, Nd, Th) PO_4). Thorium and its compounds have been produced primarily as a by-product of the recovery of titanium, zirconium, tin, and rare earths from monazite, which contains 6–8.5 wt% thorium oxide. Only a small portion of the thorium produced is consumed. Limited demand for thorium, relative to the demand for rare earths, has continued to create a worldwide oversupply of thorium compounds and mining residues. Most major rare-earth processors have switched feed materials to thorium-free intermediate compounds to avoid the handling of radioactive thorium. Excess thorium not designated for commercial use is either disposed of as a radioactive waste or stored for potential use as a nuclear fuel or other applications. Increased costs to comply with environmental regulations and potential legal liabilities and costs to purchase storage and waste disposal space were the principal deterrents to its commercial use. Health concerns associated with thorium's natural radioactivity have not been a significant factor in switching to alternative nonradioactive materials. US consumption of thorium, all for nonenergy uses, has decreased from 11.4 t (thorium content) to 0.7 t since 1997. The principal applications of thorium today make use of the very high melting point of ThO_2 (3,300°C, the highest of all binary oxides) and of the electron emitting capability of thorium when alloyed with tungsten for use in filaments for high-powered magnetrons for radar.

In the short term, thorium is available for the cost of extraction from rare-earth processing wastes. In the longer term, large resources of thorium are available in known monazite deposits in India, Brazil, China, Malaysia, and Sri Lanka. The world total thorium resources identified and prognosticated amounts to 3.6 million tons Th. Though reported values vary because of the difficulty in measuring such low concentrations, ^{232}Th is present in seawater at only about 0.050 wppb, due primarily to the insoluble nature of its only oxide, ThO_2. Thus the recovery of thorium from seawater is not a realistic option.

Because ^{232}Th is the only isotope of natural thorium, there are no enrichment plant tails from thorium nuclear fuel. Therefore, the cost of thorium in a mixed thorium-uranium LWR fuel or in a pure thorium-^{233}U fuel cycle is relatively small. However, the cost of chemically processing of ThO_2-based fuel and the separation of ^{233}U is significant.

Energy Content of Uranium and Thorium

Uranium has 18 known isotopes, none of which are stable and only two of which have half-lives longer than a million years, ^{235}U (704 Ma) and ^{238}U (4.47 billion years). Only ^{235}U, which is about 0.711 wt% (0.720 atom%) of natural uranium, is fissile, i.e., will fission using thermal (i.e., low velocity) neutrons. Uranium-238, which is by far the dominant isotope at 99.2745 wt%, will fission if struck by high-energy neutrons. However, ^{235}U is the only naturally occurring isotope of any element capable of sustaining a neutron chain reaction in a suitably designed reactor.

^{238}U is a fertile isotope and can be transformed into ^{239}Pu through the capture of a neutron and two subsequent beta decays, as shown in the following reaction:

$$^{238}\mathrm{U}(n,\gamma)^{239}\mathrm{U} \xrightarrow[\beta^- \, t_{1/2} = 23.5 \text{ min}]{}$$

$$^{239}\mathrm{Np} \xrightarrow[\beta^- \, t_{1/2} = 2.35 \text{ days}]{}$$

$$^{239}\mathrm{Pu} \xrightarrow[\sigma_{f\ \mathrm{thermal}} = 750b]{} \text{fission}$$

where β^- indicates a beta decay with electron emission and $\sigma_{f\ \mathrm{thermal}}$ is the fission cross section in barns at a neutron energy of 0.025 eV.

Thorium has 25 isotopes, of which only the nonfissile isotope ^{232}Th is long-lived, with a half-life of 14 billion years. However, in the reaction shown below, ^{232}Th can be transmuted into ^{233}U, a fissile isotope:

$$^{232}\mathrm{Th}(n,\gamma)^{233}\mathrm{Th} \xrightarrow[\beta^- \, t_{1/2} = 22.3 \text{ min}]{}$$

$$^{233}\mathrm{Pa} \xrightarrow[\beta^- \, t_{1/2} = 27.0 \text{ days}]{}$$

$$^{233}\mathrm{U} \xrightarrow[\sigma_{f\ \mathrm{thermal}} = 531\ b]{} \text{fission}$$

The fission energy of ^{233}U is 190 MeV and that of ^{239}Pu is 200 MeV. If 1 kg of thorium were bred into ^{233}U, the fission energy available would be 78.9×10^{12} $J_{thermal}$ (78.9 TJ_{th}). The fission energy in 1 kg of natural uranium, bred to ^{239}Pu, is 80.4 TJ_{th}. Thus thorium and uranium are quite similar in maximum energy content, but uranium is far more important in the near term because ^{235}U is a naturally occurring fissile isotope.

Global Estimates of Overall Uranium and Thorium Resources

Uranium and thorium have two unique characteristics when compared with other fuels. First, their energy is contained in the nucleus, rather than in the chemical bonds between the atoms, as is the case with fossil fuels. Thus, chemical reactions within the earth, due to pressure, high temperatures, or the presence of oxygen, have no effect on the nuclear energy available from uranium or thorium. In contrast, exposure of fossil fuels to the oxygen in the atmosphere or to volcanic activity releases the energy stored in their chemical bonds. The vast majority of the solar energy originally stored in fossil fuels through photosynthesis of the source biomass has been lost in chemical reactions with the atmosphere, groundwater, and lava.

A second, less obvious, characteristic of uranium and thorium is that they are constantly signaling their presence via the products of radioactive decay. Everyone is familiar with pictures of the prospector with a Geiger counter searching for uranium. Gamma rays and beta particles can be detected with a handheld instrument if the uranium ore is at the surface. However, even as little as a meter of overlying soil will shield the gammas and beta particles from the counter. Therefore, any ore deposits more than a meter below the surface will have to be detected through well logs or core samples or via their gravitational or magnetic signatures, rather than through their radiation.

Astrophysical Origins of Uranium

Uranium, thorium, and all other elements heavier than nickel result from the sudden collapse of massive stars as supernovae. The lifetime of stars and the results of these gravity-driven implosions are very dependent on the stars' initial mass. A star having the mass of our sun lasts for about ten billion years but can only produce elements up to iron. A star having ten solar masses lasts for only 10 Ma until it explodes as a supernova, producing all the elements in the periodic table.

The groundbreaking work by Burbidge, Burbidge, Fowler, and Hoyle [6] led to the realization that all of the elements heavier than nickel are the result of less than a minute of tremendous neutrino and neutron fluxes during the collapse and explosion of a supernova [7]. The nuclide distribution as a function of time in a supernova has been simulated [8] and indicates that isotopes with the maximum number of neutrons ("the neutron drip edge") form during few seconds of intense activity at the center of the imploding supernova. From this nuclear modeling of a supernova explosion, it can be inferred that uranium and thorium are about seven orders of magnitude below silicon in the composition of the supernova debris – the material from which planets are formed. This is in rough agreement with Bulk Silicate Earth model, shown in Fig 1.

Earlier studies are also in agreement. Urey cites estimates by Goldschmidt of the primordial abundance of 41 weight parts per billion (wppb) for uranium and 106 wppb for thorium. Alpher's theoretical curves and Harrison S. Brown's observed astrophysical data show uranium approximately 6.5 orders of magnitude less abundant than silicon, resulting in a primordial abundances of 57 wppb. Deffeyes, accounting for the decay of uranium since the expansion of the primordial neutron gas, estimates global uranium abundance at 10.5 wppb [9].

Recent work on the physics of supernova collapse offers some insight into the expected global inventories of uranium and thorium. These two elements, and all other elements heavier than nickel, are formed in a few seconds of extremely violent conditions during the collapse and explosion of massive stars. During the last few minutes of such a massive star's evolution, hydrogen, helium, and all of the elements lighter than nickel at the center of the star are depleted through fusion reactions. With no more energy available for continued fusion reactions, the center cannot withstand the outer shells of material, and the matter in the center is compressed to a degenerate state in which matter is broken into the constituent particles, primarily neutrons and neutrinos. The torrent of neutrons from the center of the supernova irradiates the infalling

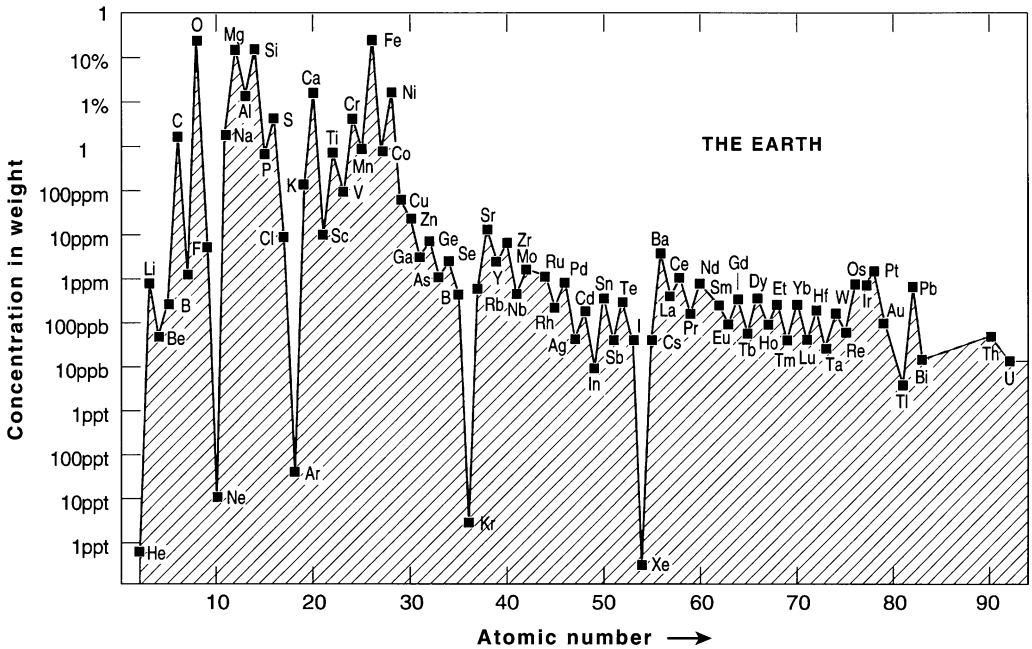

Uranium and Thorium Resources. Figure 1
Composition of the bulk silicate Earth

outer layers of stellar material, producing heavier isotopes at a rate faster than the radioactive decay of those isotopes. The result is the production of isotopes stretching from nickel through uranium and beyond, all saturated with neutrons.

This type of supernova explosion is estimated to occur, somewhere in the universe, at the rate of one per second. Obviously, most such explosions are too distant or masked by dust clouds and are not detected from the earth. Since the beginning of the universe, some interstellar material has gone through multiple cycles of collapse, explosion, dispersal, and accretion into new stars.

The hydrodynamic instabilities of the implosion result in a wide variation in the shapes of the resulting nebulae. Nevertheless, neutron transport and reaction codes have been developed to estimate the distribution of isotopes resulting from a supernova implosion. Wanajo and others [8] have modeled the first few seconds of isotope production and shown that the uranium mass should be about seven orders of magnitude less than that of silicon. Since the chemical and planetary accretion characteristics of silicon, uranium, and thorium are similar, and since the earth is about 10% silicon, one would expect that the overall concentration of uranium in the earth is about 10 wppb. The geoneutrino data from KamLAND and from newer detectors indicate that the global uranium inventory is, in fact, about 10 wppb.

Therefore, based on these astrophysical models, it is fairly clear that the earth taken as uniform body contains about 10 wppb uranium and about 40 wppb thorium. Stated in other terms, the present global inventory is thus 63 Tt (63×10^{12} t) of uranium and approximately 400 Tt of thorium. Although this inventory is a vast amount of both elements, if uranium and thorium had a uniform distribution throughout the earth, as assumed in the cold accretion model, concentrations of uranium and thorium would be far too small to be economically extracted.

Geoneutrino Estimates of Uranium and Thorium

In the last 20 years, however, another decay product of the 4.5 billion year half-life of ^{238}U and the 14.2 billion year half-life of ^{232}Th has been used to estimate the total global inventory of uranium and thorium. These particles, called neutrinos, are extremely difficult

to detect and most neutrinos pass completely through the earth without interacting. Thus neutrino detectors are usually a thousand tons in mass and must be located deep underground to avoid unwanted signals caused by cosmic rays.

Neutrinos occur in three types: electron, muon, and tau. Each of the three types has a corresponding antineutrino. Neutrinos originating within the earth, termed *geoneutrinos*, are actually electron antineutrinos primarily resulting from the decay of ^{40}K, ^{238}U, and ^{232}Th. Geoneutrinos provide a means for estimating the total uranium and thorium content of the earth and also may provide limited information on the location of those resources. These elementary particles have been measured over the past decade by massive detectors in Japan, Canada, and Europe in an effort to differentiate the radiogenic and gravitational components of the total geothermal energy flux through the earth's surface [10]. Neutrino and antineutrino fluxes have also been measured to understand neutrino oscillations, to investigate solar fusion processes, and as a first signal of supernova events. Neutrinos (and antineutrinos) travel close to the speed of light, have a small mass (<2 eV), and lack an electric charge. When an electron antineutrino collides with a proton, the result is a neutron and a positron (i.e., an antielectron). This reaction, known as the neutron inverse β decay, was used in the first detection of the neutrino in the Cowan–Reines experiment of 1956. Following the neutron inverse β decay, the positron reacts with a nearby electron to produce two 511 keV gamma rays. The neutron is absorbed by a hydrogen nucleus, releasing a characteristic 2.2 MeV gamma with a mean delay of ~200 μs. Circuitry in the detector registers a neutrino event through the delayed emission of a 2.2 MeV gamma following two 511 keV gammas.

The KamLAND (the Kamioka Large Antineutrino Detector), in central Japan, consists of a 18 m diameter spherical vessel which in turn contains a 13 m diameter nylon balloon. The balloon contains approximately 1,000 t of a liquid scintillator (mineral oil, benzene, and fluorescent compounds). The volume between the balloon and the spherical vessel contains highly purified oil which shields the balloon from external radiation and provides buoyancy to support the liquid scintillator. About 1,900 photomultiplier tubes are mounted on the inner surface of the spherical vessel. Surrounding the spherical vessel is a water Cherenkov detector which provides additional shielding and acts as a muon veto counter.

The decay chain of ^{238}U into ^{206}Pb results in six antineutrinos, one antineutrino for each beta decay. Similarly, the decay of ^{232}Th in ^{208}Pb results in four antineutrinos [11]. Because the neutron inverse β decay requires an electron antineutrino threshold energy of 1.80 MeV, KamLAND cannot detect ^{40}K antineutrinos, but antineutrinos from both ^{238}U and ^{232}Th are within the range of this instrument.

The overall results of the KamLAND geoneutrino study [12] show that the sum of the global U and Th inventory is approximately 30×10^{16} kg. Since the global Th/U mass ratio is 3.9, the global U inventory is about 6×10^{16} kg or ~10 ppb of the mass of the earth. The geoneutrino signal also indicates that the majority of the uranium is in the upper continental crust (UCC) and that relatively little of the inventory is in the oceanic crust, the mantle, or the core. The partitioning of the uranium among the upper, middle, and lower continental crust and the upper mantle occurs via geochemical processes [13].

Thermal models of the earth point to inevitable melting of the earth soon after its accretion due to gravitation energy and due to radioactive decay of uranium, thorium, and potassium. Because of its large ionic size and heating due to radioactive decay, uranium is transferred into low melting temperature fractions and out of the earth's core and mantle into the crust. These geochemical and geophysical models predict that two thirds of initial 63 Tt of uranium present in the earth are now concentrated in the crust, which constitutes only 0.4% of the earth's total mass. The low uranium and high iron concentrations predicted for the earth's mantle and core have been supported by concentrations in iron meteorites and in mantle issuing from oceanic spreading zones (0.1 ppm U), compared with U concentrations in magma and crust in subduction zones, (2 ppm U).

Preliminary results from the newer antineutrino detector Borexino at Gran Sasso in the Apennines [14] generally confirm the KamLAND results but indicate a geoneutrino flux 60% higher. Because of very low radioactive contamination in the materials of construction for Borexino, a signal-to-noise ratio of 50:1 was achieved. This greater sensitivity allowed the Borexino

Uranium and Thorium Resources. Table 1 The main properties of geoneutrinos

Decay	Q (MeV)	$\tau_{1/2}$ (10^9 year)	E_{max} (MeV)	ε_H (W/kg)	$\varepsilon_{\bar{\nu}_e}$ ($kg^{-1}\ s^{-1}$)
$^{238}U \rightarrow {}^{206}Pb + 8\ {}^4He + 6\ e + 6\ \bar{\nu}_e$	51.7	4.47	3.26	0.95×10^{-4}	7.41×10^7
$^{232}Th \rightarrow {}^{208}Pb + 6\ {}^4He + 4\ e + 4\ \bar{\nu}_e$	42.7	14.0	2.25	0.27×10^{-4}	1.63×10^7
$^{40}K \rightarrow {}^{40}Ca + e + \bar{\nu}_e$	1.32	1.28	1.31	0.36×10^{-8}	2.69×10^4

$\bar{\nu}_e$ denotes electron antineutrinos
where:
Q is the energy release for the overall decay chain
$\tau_{1/2}$ is the half-life of the parent isotope
E_{max} is the maximum antineutrino energy in the decay chain
ε_H is the heating rate, per kg of the parent isotope
$\varepsilon_{\bar{\nu}_e}$ is the electron antineutrino source rate, per kg of the parent isotope

researchers to place an upper bound on the power of any critical fissioning zones in the core at 3 TW, significantly below the indicated global radiogenic heat production of about 18 TW. Collection of geoneutrino data by Borexino is continuing.

Geoneutrino data collected to date indicates that the uranium content of the earth is several orders of magnitude greater than conventional resource estimates. Limited geoneutrino data and an understanding of geochemical processes suggest that most of that uranium content is in the upper continental crust. This data provides some confidence that, with further local exploration or advanced extraction technologies, sufficient uranium could be found for several centuries of expanded nuclear power (Tables 1 and 2).

The overall results of the KamLAND geoneutrino study [10, 12] show that the sum of the U and Th inventory is 3E17 kg and since the global Th/U mass ratio is 3.9, the global U inventory is 6E16 kg or 10 ppb of the mass of the earth, in agreement with the supernova production ratio with silicon. Further note that the geoneutrino signal indicates that the majority of the uranium is in the upper continental crust and that relatively little of the inventory is in the oceanic crust. The partitioning of the uranium into the UCC via geochemical process is discussed in the next section.

Mechanisms for the Concentration of Uranium

Unlike other energy resources such as coal or petroleum, the resources of uranium are not fundamentally changed by geological processes. Whereas petroleum

Uranium and Thorium Resources. Table 2 U, Th, and K global inventories, radiogenic heating, and neutrino luminosities according to the Bulk Silicate Earth (BSE) model

	m (10^{17} kg)	H_R (10^{12} W)	L_ν ($10^{24}\ s^{-1}$)
U	0.8	7.6	5.9
Th	3.1	8.5	5.0
^{40}K	0.8	3.3	21.6

might be lost through evaporation or combustion or a natural gas reservoir may vent into the atmosphere, uranium is lost only through radioactive decay or through the relatively rare formation of a natural reactor. Therefore the primordial inventory of uranium, reduced by radioactive decay, remains present somewhere in the earth. The crucial question is "where?"

The natural distribution of elements in the earth's crust is controlled by two major factors. The first is the set of ambient geological fractionating processes that leads to regions of depletion and concentration of the element. The second factor includes the overall geochemical characteristics of the element. Elements that are concentrated by a small number of fractionation processes can be expected to have a multimodal distribution, with a peak in the tonnage versus grade curve for each of the modes of geochemical concentration. For elements having a large number of applicable concentration processes, the peaks overlap and the resulting tonnage versus grade curve takes on

a log-normal characteristic. For example, the element chromium, whose distribution at high concentrations is solely governed by fractional crystallization in mafic magmas (i.e., high in magnesium and iron), one would expect a bimodal distribution of concentrations, with one peak at the average crustal abundance and the high concentration peak at the mafic fractionation concentration. On the other hand, most elements, uranium included, can undergo a wide variety of fractionating processes, and deposits would be expected over a wide range of concentrations. In this latter case, the tonnage versus grade distribution would be expected to be log-normal. Bear in mind that geological conditions change over time and therefore the distribution patterns have varied with time.

In considering uranium in particular, it is important to examine the tectonic and igneous processes that have redistributed the uranium within the crust. In the past four billion years, the most important processes are continental accretion and plate tectonics. In the accretion process, crust formed into masses of continental dimensions. In the second, continuing, process, the continental crust and the oceanic crust have taken on quite different characteristics in terms of uranium concentration.

Igneous Processes

Igneous processes begin with the melting of mantle rocks at depths of 60–200 km, followed by the migration of less dense liquids to the surface. The migration of these less dense minerals to the surface is a predominant process in the formation of the continental crust. The extruded liquid forms crust in two general locations, at mid-oceanic ridges, where the upwelling material forms new oceanic crust and in subduction zones, where the oceanic crust plunges back into the mantle, usually passing under the edge of a continent.

The behavior of uranium in igneous processes is dominated by two characteristics of the element. In the +4 oxidation state, the condition expected in the earth's mantle, the U^{+4} ion has an ionic radius of 97×10^{-12} m (picometers, pm) about the same as Na^{+1} ion (97 pm). Other ions common in the core and mantle are significantly smaller in radius: Fe^{+2}, 74 pm; Ni^{+2}, 69 pm, Mg^{+2}, 66 pm; and Al^{+3}, 51 pm. Thus, like sodium and the other large ions, uranium ions selectively enter partial melts within the mantle and are transported to the surface.

The second characteristic of uranium is its radioactivity, serving as a source of heat for melting the mantle and core. Like Th^{+4} (ionic radius 102 pm) and K^{+1}(133 pm), these heat-producing elements are readily fractionated out of the mantle and toward the surface. Deffeyes notes that the earth would be a radically different place if the heat-producing elements had small radii, since the geothermal energy source would then be located deep within the core and the convection currents driving plate tectonics would be much stronger [15].

The rocks forming the oceanic crust at mid-oceanic ridges are characterized by a uniform uranium concentration of about 0.1 wppm. Conversely, the crust formed above subduction zones is characterized by uranium concentrations of about 2 wppm. The wide difference in concentration is due to the differences in the source materials and to the different chemistry. The upwelling mantle at the oceanic ridge has a uranium concentration of about 0.005 wppm, while the subduction zones have as their source material oceanic crust and bits of continental crust, with an average uranium concentration of about 0.1 wppm. The continuous upwelling at the oceanic ridges serves as a mechanism for depleting the core and mantle of uranium and incorporating that uranium in the oceanic crust. The relatively low concentration of uranium in the oceanic crust is augmented with uranium from continental runoff, which subsequently precipitates in the ocean basins. At the subduction zones, the oceanic crust is again subjected to partial melting and the uranium is again fractionated in the melt and transported to the surface.

Average Vertical Distribution of Uranium and Thorium

As a result of the various igneous processes, the average concentration of uranium is highest at the surface of the continental crust and decreases approximately exponentially with depth.

The anticipated variation of uranium concentration with depth is given by the equation $U(z) = U(z = 0)\, e^{(-z/h_r)}$, where z is the depth in m, h_r is the depth parameter (discussed below), and $U(z)$ is

Uranium and Thorium Resources. Table 3 Sources of heat in the upper continental crust

Isotope	Thermal output
U-238	0.095 mW/kg
Th-232	0.027 mW/kg
K-40	3.6 nW/kg

the concentration at depth z, in wppm. $U(z = 0)$ is the average continental crustal abundance of uranium at the surface, 2.76 wppm.

This approximation is based on the presence of heat-producing elements, U-238, Th-232, and K-40, in the continental crust, measurements of the thermal conductivity of the crustal materials, and the linear temperature distribution with depth measured at many locations. The heat produced in the crust is divided about evenly between U-238 and Th-232, since the crustal abundance mass ratio between Th and U is 3.9. K-40 is about four orders of magnitudes lower, although potassium has a crustal abundance of 2.1%, since K-40 is only 117 ppm of natural potassium and the thermal energy output of K-40 is about four orders of magnitude below U-238 and Th-232, as shown by Lachenbruch, below [16] [17] (Table 3).

Obviously, this method assumes one-dimensional heat transport and a fairly uniform thermal conductivity, without a significant contribution from flowing fluids. A more recent review by Brady et al. [18] provides more details on the technique.

Several measured values of the depth parameter are listed in Table 4. [19].

If a depth parameter of 8,500 m is assumed, based on the above data, then 11% of the crustal uranium inventory would be expected to be within 1,000 m of the surface and 21% within 2,000 m.

Geochemical Beneficiation Processes

Uranium occurs in ores such as uraninite [UO_2, pitchblende], carnotite [$K_2(UO_2)_2V_2O_8{\cdot}3(H_2O)$], autunite [$Ca(UO_2)_2(PO_4){\cdot}11(H_2O)$], uranophane [$Ca(UO_2)_2(HSiO_4)_2{\cdot}5H_2O$), davidite [Ce0.75La0.25Y 0.75U0.25$Ti_{15}Fe_3$ + 5O38 and $La_{0.7}Ce_{0.2}Ca_{0.1}Y_{0.75}$ $U_{0.25}Ti_{15}Fe_3$ + 5O38], torbernite [$Cu(UO_2)_2(PO_4)_2{\cdot}$ $12H_2O$], and other minerals containing U_3O_8 (actually a stable complex oxide of $U_2O_5{\cdot}UO_3$).

Uranium and Thorium Resources. Table 4 Temperature distribution depth parameter

Location	h_r (m)
Sierra Nevada	10,000
Eastern USA	7,500
Norway and Sweden	7,200 ± 700
Eastern Canadian Shield	7,100 ± 1,700
Canadian Appalachians	10,000 ± 2,000
US Appalachians	8,100 ± 1,300

In the other references the depth parameter is denoted as D, rather than h_r

The governing characteristic in the geochemical transport of uranium is the fact that uranium is highly soluble in oxidizing environments and essentially insoluble in reducing environments. The change in the earth's atmosphere from a reducing to an oxidizing condition about 1.8 billion years ago is thus responsible for a fundamental change in the dominant processes in uranium transport. In the earlier age, igneous processes and fractionation of uranium in partial melts due to its large ionic size were dominant. In the last 1.8 billion years the transport of uranium by means of groundwater oxygenated at the surface has been dominant.

Thus, in the period more than 1.8 billion years ago, uranium was primarily concentrated in placer deposits as a chemically inert and physically dense phase. Because of the low solubility of uranium in reducing environments, rivers, lakes, groundwater, and thus the sea contained very low uranium concentrations. The placer deposits at Elliott Lake, Canada and at Witwatersrand, South Africa are typical of the deposits formed during this period.

With the dominance of photosynthesis in the last 1.8 billion years, the atmospheric and groundwater conditions have been oxidizing and uranium minerals have been highly soluble in the sedimentary weathering cycle. Placer deposits no longer formed and, in fact, began to dissolve. The uranium content of rivers, lakes, and groundwater increased and gradually, the uranium concentration in the oceans also increased. Nevertheless, the uranium concentration remained well below saturation.

In a few isolated locations, however, oxidation of organic-rich beds by groundwater led to locally

reducing conditions. In these locations, the uranium ions or their complexes would reach supersaturation and re-precipitate. An important example of this re-precipitation is in the Mesozoic sandstones of the Colorado Plateau. The uranium ores are found in organic-rich zones where the oxygen in groundwater was removed by carbon-rich debris. Precipitation of uranium has also occurred where restricted circulation in the oceans and organic-rich sediments led to anoxic conditions. Good examples are the black Chatanooga Shale and the phosphorite shale of the Phosphoria Formation [9].

Specific Deposit Types

Before the discovery of the McArthur River deposit, the highest grade uranium ores were obtained from igneous sedimentary deposits such as Great Bear Lake in Canada, Joachimsthal in the Czech Republic, and Katanga in the Congo. The deposits at Oklo in the Gabon Republic in Africa were of high enough concentration and the uranium, 1.7 billion years ago, contained 3% ^{235}U rather than the present 0.711% such that several critical natural reactors occurred in the deposit. The reactor zones released about 15,000 MW-years of fission energy over the course of about 250,000 years. These deposits were formed by the movement of hot water through fractures in blocks of rock heated by their own uranium and thorium content.

Precambrian sandstones overlie much older Precambrian granites and metamorphic rocks. At the interface, there is a discontinuity in the age of the rocks. This type of discontinuity is termed an unconformity. Unconformity deposits, such as those in Saskatchewan and northern Australia occur where uranium from the sandstone, has formed into veins in the open spaces of the interface, and has been heated to temperatures of several hundred degrees Celsius.

Roll-Front Deposits As mentioned earlier, uranium oxide precipitates when the solution enters a reducing environment. The uranium oxide can be redissolved in situ by oxygenated leach solutions. In sandstone deposits, the uranium minerals have been deposited in the interstices between the sand grains. The deposits are often moving very slowly through the sandstone because of the flow of groundwater, much like the movement of a front through a liquid chromatography column. Oxygenated water from the surface enters the sandstone where reducing agents, such as sulfides or organic matter, are located in the interstitial spaces. The organic carbon in one pore volume of sandstone can remove all the oxygen dissolved in 50,000 pore volumes of oxygenated groundwater.

Therefore, the front between the oxygenated groundwater and oxygen-free groundwater moves slowly through the sandstone. Uranium dissolved at the surface and uranium dissolved from the sandstone by the oxygenated groundwater is swept along and precipitated at the front. Upstream of the front the uranium is present in the groundwater as the soluble hexavalent uranyl carbonate complex. As the oxygen is removed from the groundwater at the front, the soluble hexavalent uranium is reduced to the insoluble quadrivalent state.

The quadrivalent uranium precipitates in the form of the mineral uraninite (UO_2). Thus the location of ore bodies is often associated with deposits of carbonaceous materials where the carbon, in much larger quantities compared with the uranium, has removed the oxygen from the groundwater.

Based on the various modes for the formation of uranium ore bodies, reviewing the large body of prior research, Deffeyes and MacGregor estimated the uranium content of the various crustal regimes in a report for the USDOE in 1978 [9].

The distribution of mass versus grade for the various types of uranium deposits is shown in Fig. 2 with additional data [9, 15]. The three gray bars on the left (grade >1,000 ppm U) indicate deposits of the type now mined for uranium alone. The expected log-normal distribution is shown and the mass and grade of two Canadian mines discovered since 1978 are also indicated: (1) the McArthur River deposit, 137,000 t U of proven reserves averaging 18 wt% U and (2) the Cigar Lake deposit, 90,000 t U at an average grade of 17 wt% U. Other known larger, but lower grade deposits, such as Olympic Dam in Australia, have not been shown.

Present mining activities are recovering uranium at market prices of \$150/kg from ores containing 0.027–20% U_3O_8. Given the log-normal distribution and the known quantities of the various uranium

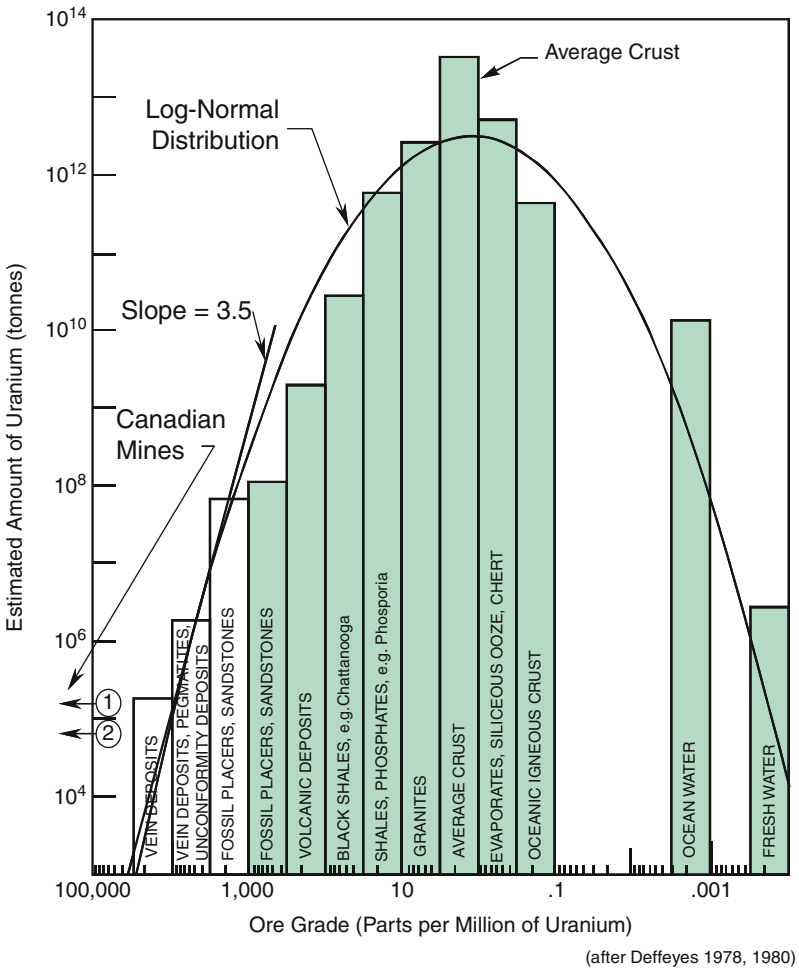

Uranium and Thorium Resources. Figure 2
Distribution of uranium in the Earth's crust

mineralizations, a tenfold increase in the price of uranium (and thus a tenfold decrease in economically viable ore grade) would result in a 300-fold increase in the amount of uranium available. Equivalently, the World Nuclear Association (formerly the Uranium Institute) estimates that a doubling of uranium prices would result in a tenfold increase in supply [5] (WNA 2010).

The slope of the log-normal curve at presently mined grades is also shown in Fig. 2. This slope, about +3.5, indicates that for a doubling of the cost of mining (i.e., mining ore at half the present concentration), the economically available resources of uranium would increase by more than an order of magnitude ($2^{3.5} \approx 11$). This estimate presumes a continuation of present mining techniques and does not consider the increased using of in situ leaching and recovery of uranium as a by-product in gold, copper, and phosphate mining.

Unconventional Resources

Existing Enrichment Tails

Another potential source of uranium is the re-enrichment of depleted uranium by using today's overcapacity of enrichment. Because of low price of natural uranium in recent years, many enrichment plants have been operating with tails assays of up to 0.3% ^{235}U. The 1.18 million tons of depleted uranium currently stored at enrichment plants could therefore supplant a few

hundred thousand tons of natural uranium if demand required. The inventory of depleted uranium is expected to increase by about 51,400 t U/year though at least 2010. The enrichment capacity in 2010 was reported to be 57 MWSU/year compared with an annual demand of 49 MWSU/year. The present spare capacity in enrichment plants in the world, around 8 MSWU/year, theoretically represents an equivalent of around 3,000 tons/year of natural uranium if this spare capacity was utilized for enrichment of depleted uranium with an assay of 0.3% and a new tails assay of 0.1%.

The economics of re-enrichment depend on the ^{235}U assay of the depleted uranium and the relationship between the price of uranium and the cost of enrichment services. A tails assay of above 0.3% is preferable if re-enrichment of depleted uranium is to be considered a possibility. Re-enrichment of depleted uranium for the production of low-enriched uranium (LEU) in the Russian Federation has taken place for several years in times of excess enrichment capacity. However, decreasing amounts of excess enrichment capacity makes re-enrichment a marginal source of light water reactor fuel. On the other hand, the eventual use of enrichment tails as breeding blankets for fast reactors, as will be discussed shortly, represents a large long-term source of fuel.

Gold and Phosphate Tailings

In addition to the discovery of new resources through increased exploration, improvements in mining technology are also lowering the cost of previously high-cost deposits. In particular, in situ leaching (ISL) is of growing significance and could be applied to existing gold and phosphates tailings piles. The resource base of 16.2 million tons U does not include uranium in gold and phosphate tailings. The phosphate deposits are estimated at 22 million t U.

Uranium from Seawater

The recovery of uranium from seawater places an upper limit on the cost of uranium. Uranium is dissolved in seawater at 3 mg/m^3 (3 wppb) and represents a well-known resource of 4.2 billion tons, 250 times the known land-based resource. The uranium content of the oceans is relatively constant and large-scale extraction can be done without local depletion of the resource. Since only about 3% of global population lives in landlocked countries, extraction of uranium from seawater is truly the bounding cost for uranium.

New Technologies for Uranium Extraction

The current prices for uranium provide little motivation for the development of new extraction technologies. However, regulations to minimize the impact of mining on the environment and radiation exposure to workers have led to the use of technologies where uranium is extracted in situ or where ores previously mined for another element are processed for uranium extraction. In addition, the technologies described above for the extraction of uranium from seawater could have a major impact in minimizing environmental impact and radiation exposure.

In Situ Leaching

During conventional mining, the rock of the ore body is removed from the ground, transported to a mill, and treated to remove the minerals of economic value. The opening of the mine, the transport of the ore, the milling and the disposal of remaining treated rock can create severe environmental impacts. In situ leaching (ISL), sometimes known as solution mining, involves the use of liquids to dissolve the desired elements from the ore body without removing it from the ground. The liquid is pumped through the ore body and returned to the surface, where the desired elements are removed from the solution by precipitation, by electrochemistry, or other means. The leaching liquid is then returned to the ore body and the process is repeated. ISL eliminates the need to remove large quantities of ore from ground and to transport it to the mill, thus minimizing surface disturbance. ISL also eliminates the need to dispose of the tailings or waste rock. However, for ISL to be effective, the ore body must be permeable to the flow of the leaching liquid. Furthermore, the ISL site must be located so as not to contaminate ground water away from the ore body.

Today, because of its reduced surface impact and lower cost, ISL is used for 85% of US uranium production. Most of the operations in Wyoming, Nebraska, and Texas are less than 10 years old. Worldwide, about 16% of world uranium production uses ISL, including all the production in Uzbekistan and Kazakhstan.

ISL can be used to extract uranium from deposits below the water table in permeable sand or sandstone, provided that the deposit is confined above and below by impermeable strata. Suitable candidates are often roll-front deposits as described earlier. The uranium mineral are usually uranium oxide or uranium silicate coatings on the individual sand grains. The ISL process replicates, in a few months, the conditions that led to the formation of the roll-front deposit in the sandstone initially.

There are two types of ISL, depending on the chemistry of the deposit and groundwater. When the ore body is limestone or gypsum, i.e., containing significant amounts of calcium, then an alkaline leaching agent such as sodium bicarbonate and CO_2 must be used. Otherwise an acid leaching agent, such as weak sulfuric acid plus oxygen at a pH of 2.5–2.8 (about the same as vinegar) is preferred. ISL in Australia is primarily acid, while ISL in the USA is primarily alkaline.

Generally the uranium is extracted by progressively drilling wells into the deposit on a rectangular grid with ~30-m spacing. The leaching fluid is pumped into four wells surrounding a central extraction well, into which a submersible pump has been lowered. The wells are cased to assure that the fluids do not enter strata above the deposit. In the USA the production life of an individual alkaline ISL well is typically 6–10 months. The most successful operations have extracted 80% of the uranium from the ore. Production life is often limited when the sandstone is plugged by mobilized clay and silt. Sometimes the blockages can be dislodged by reversing the flow through the field or by increasing the injection pressure.

The uranium is recovered from the extracted solution in an ion exchange or solvent extraction process. Solvent extraction is preferred if the groundwater is saline, while ion exchanges is most effective if the chloride content is below 3,000 ppm. With alkaline leaching, ion exchange is effective until the total dissolved solids reach 3,000 ppm. The uranium is then stripped from the resin or solution for further processing [20].

Before the process solution is reinjected, it is reoxygenated or recharged with sulfuric acid, for alkaline or acidic processes respectively. About 1% of the process solution is bled off to maintain a pressure gradient toward the wellfield. The pressure gradient ensures that groundwater from any surrounding aquifer flows into the wellfield and that ISL mining solutions does not enter the aquifer.

Recovery of Uranium from Seawater

The recovery of uranium from seawater is highly speculative and may never prove to be economic. One cubic meter of seawater contains 3 mg of natural uranium, which can deliver 244 MJ_{th} in a breeder or about 2.5 MJ_{th} in a present day LWR. Simple calculations show that the pumping energy needed in an extraction plant could easily consume all the energy available, particularly in the LWR case. Thus seawater extraction conceptual designs relying on ion exchange or adsorption have utilized ocean currents or wave action to move the seawater past the uranium-collecting surfaces.

However, the magnitude of the seawater resource places an upper limit on the cost of uranium for several reasons. First, seawater is available to nearly all countries of the world at virtually the same uranium concentration and without local depletion due to the extraction of uranium. Secondly, because no group of countries can form a cartel over the uranium supply if seawater extraction is practiced, the price of uranium is unlikely to be driven artificially high through market manipulation. Furthermore, the only present limitation on the extraction of uranium from seawater is knowledge of the technology and resins. Thus one would expect that, if conventional sources of uranium become limiting, a healthy competition in research and development would drive down the cost of extraction.

Uranium recovery from seawater has been studied in Japan for a very long term or to face a very strong development of fission energy. In a laboratory scale experiment performed by the Japan Atomic Energy Agency (JAEA) where uranium is trapped by an amidoxime adsorbent which has been prepared on nonwoven polyethylene material with the aid of radiation-induced cografting. This experiment, 7 km offshore from Sekine-Hama in Aomori Prefecture, Japan, produced more than 1 kg of U on 350 kg of nonwoven fabric during a total submersion time of 240 days [21]. However, at this stage of the study, it is difficult to predict the practical application of uranium recovery from seawater. An economic assessment has

been reported indicating a possible cost for this uranium process in a 1,000-t U/year commercial plant of approximately $600/kgU [22].

Impact of Uranium Scarcity and Higher Extraction Costs

Table 5 shows the approximate impact of increases in the price of natural uranium on the cost of electricity from a light water reactor. In this set of calculations, the cost of natural uranium is set at $140/kg U (approx. average price of domestic U to US utilities, 2011), $500/kg U, representing an optimistic cost of extraction from seawater and $1,000/kg U, representing a more pessimistic (or perhaps more realistic) cost for extraction from seawater. Two burnups are shown for each uranium price, 45 MW-day (thermal) per kg of initial uranium (MW-day/kg) and 60 MW-day/kg. The specific power of the fuel remains constant at 37.9 kWth/kg of initial uranium, as does the interest charged on the fuel during the fuel cycle. In the cases with higher cost uranium, the tails assay ("Tails U-235 content") to optimize the balance between raw materials and enrichment costs. As shown in the last two lines of the table, an increase in the cost of natural uranium from $140/kg U to $1,000/kg U results in an increase in the cost of electricity of about $0.018/kW-h. For comparison, an increase in the prices of natural gas of $2.80 per million BTU, as has occurred five times since 2005, also results in an increase in the cost of electricity of $0.018/kW-h.

Uranium Compared with Future Energy Needs

A simple calculation is needed to place the magnitude of current uranium mining in perspective. If it is assumed that the world population reaches a steady-state level of 10 billion and each of those people consumes energy at the average rate of a US resident in 2011, then the total annual world consumption of energy would be about 3.7×10^{21} J_{th}. While that high rate of consumption would probably not be sustainable for a variety of other reasons, the required natural uranium input to a system of fast reactors to produce 3.7×10^{21} J_{th} would be about 45,000 t U. Average worldwide uranium usage, from both mining and the downblending of HEU, is now about 59,000 t U/year [4].

The Need for Fast Reactors

The early development of fast breeder reactors and of thermal breeder reactors using thorium was driven in part by the apparent global scarcity of fissile isotopes to fuel a rapidly growing set of nuclear reactors. Slow growth in nuclear power and large discoveries of natural uranium in a few regions of the world have reduced the global urgency for breeding more fissile material. In those regions of the world lacking known uranium resources, particularly Europe and Japan, there has been continuing interest in the development of sodium-cooled fast breeder reactors. Such reactors reduce the need for natural uranium by a factor of ~50, compared with light water reactors and thus the cost and availability of natural uranium is a much smaller consideration.

However, beyond the breeding of fissile isotopes, the use of a fast neutron spectrum offers unique capabilities for the consumption of the long-lived actinides, particularly plutonium, neptunium, americium, and curium.

In the long term, the capability of a fast reactor to make use of both ^{238}U and ^{235}U will be critical in meeting future energy needs. However, in the next century, fast reactors will be crucial for the management of actinides and the reduction of the long-term radiotoxicity of the nuclear fuel cycle by at least two orders of magnitude.

Comparison of Fossil Fuel and Uranium Reserves

It is interesting to compare the cited uranium known reserves and the inventory of depleted uranium with the estimated reserves of coal, oil, and natural gas. In Table 6, the reserves of fossil fuels and uranium are compared on the basis of known, economically recoverable reserves.

Fossil fuel reserves are those of the World Energy Council, the *Oil & Gas Journal*, and *World Oil* [23]. In the use of Table 6, the caveat cited above applies. Resources of both fossil fuels and of uranium are undoubtedly much larger than the reserves cited. Nevertheless, it is noteworthy that the uranium resources are energetically equivalent to about 20% of natural gas or oil resources, even with the use of LWRs only. The 1.2 million tons of

Uranium and Thorium Resources. Table 5 Impact of uranium costs on the cost of electricity

Impact of uranium costs on the cost of electricity							
	Current uranium prices		Uranium from unconventional sources				Units
			Optimistic: $500/kg		Pessimistic: $1,000/kg		
	UO_2 fuel 45 MWd/kg	UO_2 fuel 60 MWd/kg	UO_2 fuel 45 MWd/kg	UO_2 fuel 60 MWd/kg	UO_2 fuel 45 MWd/kg	UO_2 fuel 60 MWd/kg	
Specific power	37.9	37.9	37.9	37.9	37.9	37.9	kWth/kg
Cycle parameters							
Total cycle length	3.6	4.8	3.6	4.8	3.6	4.8	years
Capacity factor	90%	90%	90%	90%	90%	90%	
Effective full power days	1183	1578	1183	1578	1183	1578	efpd
Burnup	45	60	45	60	45	60	MWd/kg ihm
Feed U-235 content	0.711%	0.711%	0.711%	0.711%	0.711%	0.711%	wt%
Product U-235 enrichment	4.00%	5.34%	4.00%	5.34%	4.00%	5.34%	wt%
Tails U-235 content	0.25%	0.25%	0.20%	0.20%	0.10%	0.10%	wt%
Separative work	5.874	8.692	6.546	9.636	8.953	13.020	kg-SWU/ kg fuel
Natural uranium	8.089	10.964	7.439	10.050	6.385	8.569	kg/kg fuel
	0.180	0.183	0.166	0.168	0.142	0.143	kg/MWd
Rates							
Interest rate	5.0%	5.0%	5.0%	5.0%	5.0%	5.0%	/year
Natural uranium	$140	$140	$500	$500	$1,000	$1,000	/kg U
Conversion U3O8 to UF6	$54	$54	$193	$193	$385	$385	/lb U3O8
	$11	$11	$11	$11	$11	$11	/kg natural U
Separative work	$150	$150	$150	$150	$150	$150	/kg-SWU
Costs							
Natural uranium	$1,132	$1,535	$3,719	$5,025	$6,385	$8,569	/kg fuel
Separative work	$881	$1,304	$982	$1,445	$1,343	$1,953	/kg fuel
Conversion	$89	$121	$82	$111	$70	$94	/kg fuel
Fabrication	$500	$500	$500	$500	$500	$500	/kg fuel
Total cost	$2,602	$3,459	$5,283	$7,081	$8,298	$11,116	/kg fuel
Interest during use	$234	$415	$475	$850	$747	$1,334	/kg fuel

Uranium and Thorium Resources. Table 5 (Continued)

Impact of uranium costs on the cost of electricity							
	Current uranium prices		Uranium from unconventional sources				Units
			Optimistic: $500/kg		Pessimistic: $1,000/kg		
	UO_2 fuel 45 MWd/kg	UO_2 fuel 60 MWd/kg	UO_2 fuel 45 MWd/kg	UO_2 fuel 60 MWd/kg	UO_2 fuel 45 MWd/kg	UO_2 fuel 60 MWd/kg	
Total fuel cost	$2,837	$3,874	$5,758	$7,931	$9,045	$12,450	/kg fuel
	$63.19	$64.73	$128.27	$132.50	$201.48	$208.00	/MWth-day
	$0.772	$0.790	$1.566	$1.618	$2.460	$2.540	/million BTU
	$7.81	$8.00	$15.86	$16.38	$24.91	$25.72	/MWe-h
COE increase due to high uranium prices			$8.05	$8.38	$16.91	$17.71	/MWe-h
			0.8	0.84	1.69	1.77	cents/kWe-h

Uranium and Thorium Resources. Table 6 Comparison with fossil reserves

Coal		909	Billion tons
	=	2.01E + 22	Jth
	=	19,089	Quadrillion BTU (quad)
Petroleum		1340	Billion barrels
	=	8.20E + 21	Jth
	=	7,772	Quad
Natural gas		6261	Trillion cubic feet
	=	6.84E + 21	Jth
		6,480	Quad
Total fossil reserves		3.52E + 22	Jth
	=	33,341	Quad
Uranium		5.404	Million t natural U
	+	1.2	Million t depleted U
	=	2.33E + 21	Jth in LWRs
	=	2211	Quad in LWRs
	=	5.36E + 23	Jth in fast reactors
	=	508,000	Quad in fast reactors

depleted uranium currently in storage itself represents an energy source larger than the fossil reserves if used in a fast reactor.

Future Directions

Uranium is ubiquitous in the continental crust and concentrated in economically recoverable deposits by several relatively well-understood processes. Today uranium is being mined from the richest and most convenient of the deposits though little exploration has taken place in the last 20 years. Uranium and thorium are often being extracted as by-products of mining for other elements. It is likely that other similarly rich deposits exist in relatively unexplored regions of Asia and Africa.

Prices in the present uranium market are dominated by large discoveries in the last 20 years and by the conversion of military HEU to civilian purposes. The continued use of nuclear energy and the end of downblending can be expected to raise uranium prices, encourage exploration, and return the uranium to a slightly higher-priced equilibrium.

However, because of the wide range of igneous and geochemical processes that are responsible for the

formation of uranium deposits, it can be expected that uranium will be found in significant quantities with renewed exploration.

Emerging technologies for the extraction of uranium, particular in situ leaching, will make resources in sandstone and shale economically recoverable and minimize the surface disruption due to open pit mining and the occupational radiation exposures of underground mining.

In more distant future, the extraction of uranium from seawater will make this fuel available to virtually every nation. While extraction from seawater is likely to be five to ten times more expensive than uranium is today, the overall increase in the cost of electricity or other energy products would be minimal.

Therefore, the need for fast reactors in the near term, with a global view in mind, is not driven by a scarcity of uranium but rather by a need to effectively manage the long-lived actinides in spent fuel. A fast neutron spectrum is uniquely capable of fissioning the higher actinides and reducing the long-term radiotoxicity and volume of the nuclear fuel cycle. Likewise, although thorium is more abundant than uranium, the primary use of thorium will probably not be for the breeding of ^{233}U, but rather as a host material for the transmutation of the higher actinides in fast neutron spectrum reactors.

There are many challenges in the development of safe, proliferation-resistant, and economical reactors and fuel cycles. Fortunately, the uranium and thorium resources do not appear to be a near-term limitation.

Bibliography

1. Bates RL, Jackson JA, American Geological Institute (eds) (1984) Dictionary of geological terms, 3rd edn. Anchor Books, New York
2. Benedict M, Pigford TH, Levi HW (1981) Nuclear chemical engineering. McGraw-Hill, New York
3. NRC Glossary (2011) Yellowcake. http://www.nrc.gov/reading-rm/basic-ref/glossary/yellowcake.html. Updated 27 May 2011
4. OECD Nuclear Energy Agency, International Atomic Energy Agency (2010) Uranium 2009: resources, production and demand: a joint report. OECD, Paris
5. World Nuclear Association (2010) Supply of uranium, Dec 2010. www.world-nuclear.org/info/inf75.html
6. Burbidge EM, Burbidge GR, Fowler WA, Hoyle F (1957) Synthesis of the elements in stars. Rev Mod Phys 29(4):547
7. Burrows A (2000) Supernova explosions in the Universe. Nature 403:727–733, 17 Feb 2000
8. Wanajo S et al (2003) The r-process in supernova explosions from the collapse of O-Ne-Mg cores. Astrophys J 593:968–979, 20 Aug 2003
9. Deffeyes KS, MacGregor ID (1978) Uranium distribution in mined deposits and in the Earth's crust: final report. GJBX–1(79). Dept of Geological and Geophysical Sciences, Princeton University, Princeton. Prepared for the USDOE, Grand Junction Office, Aug 1978
10. Araki T et al (2005) Experimental investigation of geologically produced antineutrinos with KamLAND. Nature 436:499–503, 28 Jul 2005
11. Fiorentini G, Lissia M, Mantovani F, Vannucci R (2004) Geo-Neutrinos: a short review. arXiv:hep-ph/0409152v1, 14 Sep 2004
12. Enomoto S, Ohtani E, Inoue K, Suzuki A (2005) Neutrino geophysics with KamLAND and future prospects. arxiv.org/ftp/hep-ph/papers/0508/0508049.pdf
13. Herring JS (2004) Uranium and thorium resources. In: Cleveland CJ (ed) The encyclopedia of energy. Academic, Amsterdam/Boston
14. Borexino Collaboration (2010) Observation of geo-neutrinos. Phys Lett B 687:299–304
15. Deffeyes KS, MacGregor ID (1980) World uranium resources. Sci Am 242(1):66–76
16. Lachenbruch AH (1968) Preliminary geothermal model of the Sierra Nevada. J Geophys Res 73(22):6977–6989, 15 Nov 1968
17. Lachenbruch AH (1970) Crustal temperature and heat production: implications of the linear heat-flow relation. J Geophys Res 75(17):3291–3300, 10 June 1970
18. Brady RJ, Ducea MN, Kidder SB, Saleeby JB (2006) The distribution of radiogenic heat production as a function of depth in the Sierra Nevada Batholith, California. Lithos 86:229–244
19. Schubert G, Turcotte DL, Olson P (2001) Mantle convection in the Earth and planets. Cambridge University Press, Cambridge/New York, p 146
20. World Nuclear Association (2010) In situ leach (ISL) mining of uranium. http://www.world-nuclear.org/info/inf27.html. Updated Mar 2010
21. Seko N et al (2003) Aquaculture of uranium in seawater by fabric-adsorbent submerged system. Nucl Technol 144: 274–278
22. Joint Nuclear Energy Action Plan, Fuel Cycle Technology Working Group (2010) Uranium extraction from seawater, 1st information exchange meeting. Lawrence Berkeley National Laboratory, Berkeley, Meeting record, 24–25 June 2010
23. EIA (2010) Annual energy review 2009, DOE/EIA-0384(2009). Energy Information Administration, US Department of Energy, Washington, DC, Aug 2010

Uranium in the Environment: Behavior and Toxicity

Glen A. Bird
EcoMetrix Incorporated, Mississauga, ON, Canada

Article Outline

Glossary
Definition of Subject
Introduction
Nuclear Fuel Cycle
Background U Concentrations
Uranium Speciation
Terrestrial Environment
Aquatic Ecosystems
Uranium Toxicity
Future Directions
Bibliography

Glossary

Acute toxicity test A toxicity test of short duration in relation to the life span of the test organism (e.g., ~ 4 days for fish).

Chronic toxicity test A toxicity test that spans a significant portion of the life span of the test organism (e.g., 10% or more) and examines effects on such parameters as metabolism, growth, reproduction, and survival.

Concentration ratio (CR) The ratio of the steady-state concentration of a substance in an organism to the concentration of the substance in filtered water and/or the ratio of the uptake-rate constant to the depuration-rate constant.

Critical toxicity value (CTV) The quantitative expression of low toxic effect (e.g., EC_{10}) to the measurement endpoint. CTVs are used in risk characterization for the calculation of an Estimated-No-Effect Value (ENEV).

Depleted uranium (DU) The by-product of uranium enrichment and has a ^{235}U content that is less than that of natural uranium (0.71 wt.%) usually 2 to 4 wt.%.

EC_x The concentration of a substance in water, soil, or sediment that is estimated to cause a specified toxic effect (e.g., immobilization, reduced growth) on x% (most often 50%) of the test organisms. The duration of the test must be specified. The EC_x describes quantal effects, lethal or sublethal, and is not applicable to quantitative effects (see IC_x).

Estimated-no-effect value (ENEV) The concentration of a contaminant that should not have an effect on a sensitive endpoint of ecological relevance such as survival, growth, or reproduction, and is derived by dividing the critical toxicity value by an appropriate application factor.

IC_x The inhibiting concentration for a substance for a specified x% impairment in a quantitative biological function such as the attained size over a growth period, reproductive performance, or respiration.

LD_{50} The dose that causes mortality in 50% of the organisms tested.

Lowest-observed-effect level (LOEL) The concentration at which actual ecotoxic effects become apparent, usually the fifth percentile of the screening-level concentration.

No-observed-effect level (NOEL) The highest dose in a toxicity test not causing a statistically significant effect compared with the controls.

Partition coefficient (K_d) A measure of the propensity of a particular radionuclide to associate with solid phases defined as the ratio of the concentration of the radionuclide on the particulate fraction to the concentration in water ($L \cdot kg^{-1}$ dry sediment).

Transfer coefficient (TC) A ratio of the concentration ratio (unit less) and the rate of intake of the organism ($kg \cdot day^{-1}$) to predict the fraction of the radionuclide in the diet that is accumulated in the body on a daily basis ($day \cdot kg^{-1}$).

Definition of Subject

Uranium (U) is a primordial radionuclide that is naturally present in the environment at low concentrations. Natural U is mainly a chemical hazard as opposed to a radiological hazard. The chemical speciation of U influences its bioavailability and toxicity. Under anoxic conditions, U is in the tetravalent state forming insoluble compounds and is immobile. Under oxic conditions, U is in the hexavalent state is mobile, bioavailable, and tends to have higher toxicity. Low absorption in the gut and a tendency to decrease in

concentration up the food chain makes U toxicity of little concern at typical background concentrations, but at elevated concentration U may be toxic.

Considerable work has investigated the toxicity of U to humans using animal models. This work is applicable to wildlife. In comparison to mammals, little effort has focused on the toxicity of U to terrestrial plants and soil invertebrates. For some aquatic species, U toxicity decreases with an increase in hardness and alkalinity. For some species U toxicity is not ameliorated with increasing hardness and alkalinity, and U can be toxic at low concentrations.

This entry provides an overview of the presence of U in the environment, its chemical speciation, behavior in the environment, and toxicity to organisms at low concentrations to assist the practitioner in establishing ecotoxicological benchmarks for protection of the environment.

Introduction

Uranium is a member of the actinide series of elements with an atomic number of 92 and atomic weight of 238.029. Uranium is a heavy, silvery-white, ductile, and slightly paramagnetic metal, which is pyrophoric when finely divided [1]. Uranium is not found in elemental form in nature, but is found in about 155 mineral forms [2]. All 16 isotopes of U are radioactive; ^{238}U (99.27% by weight), ^{235}U (0.72%), and ^{234}U (0.0055%) are the three most common isotopes. Natural materials have ^{238}U: ^{235}U ratios of 137.5 ± 0.5 [3]. Uranium decays primarily by emitting an alpha (α) particle (two neutrons and two protons) from its nucleus [4]. The penetration range of a typical 5 MeV alpha particle is about 4 cm in air and about 50 μm in soft tissue, not enough to penetrate the superficial keratin layer of the human skin [1]. The dominant isotope, ^{238}U, has a physical half-life of 4.5×10^9 years, giving it a very low specific activity (1.24×10^4 Bq·g^{-1} U). For these reasons, U is primarily a chemical toxicant rather than a radiological toxicant. Uranium-238, ^{235}U ($t_{1/2} = 7.0 \times 10^8$ years) and ^{232}Th ($t_{1/2} = 1 \times 10^{10}$ years) are the long-lived parents of the U, actinium, and thorium decay series.

Major sources of anthropogenic releases of U include U mining/milling and refining processes, combustion of fossil fuels, roasting of sedimentary rocks for cement production, and the use of phosphate fertilizers. Atmospheric emissions are mainly through the burning of wood, peat, coal, and petroleum, the roasting of rock minerals in the metal extraction, refining, and cement industries, and the incineration of solid wastes.

Uranium is mainly used in the production of electricity by the nuclear industry. Depleted U (18.97 g·cm^3) is denser than iron (7.87 g·cm^3), has a high melting point (1,132°C), is highly pyrophoric, with a high tensile strength comparable to most steels, is abundant and is relatively cheap. Therefore, depleted U is used for nonnuclear fuel purposes rather than natural U. Depleted U is used for internal guidance devices for missiles, radio emissions shielding, photographic emulsions, as a catalyst in analytical chemistry, photographic toners, pigments and glazes, protective armor on tanks and other vehicles, and for ammunition [1].

Depleted U is a by-product of U enrichment and has a ^{235}U content that is less than that of natural U, for example, about 70% of the ^{235}U is removed [3] so the ^{235}U content is about 0.2–0.4 wt.% ^{235}U isotope. Depleted U is about 42% less radioactive than natural uranium and is indistinguishable from natural uranium in terms of chemotoxicity. A separate discussion of depleted U and its health and environmental effects as a result of military use is beyond the scope of this entry.

Because of the author's greater familiarity with the Canadian situation, examples are largely from Canada. However, the examples should also be relevant to other parts of the world.

Occurrence

Uranium is relatively common in low concentrations in the earth's crust, averaging about 3 mg·kg^{-1} [5]. Concentrations are frequently elevated near U mining/milling operations [6, 7]. The relative abundance of U in the earth's crust is comparable to silver, gold, and the light rare earth elements and is more abundant than tin, mercury, and lead. The concentration of U in non-ore grade rocks is as follows: 1–5 mg·kg^{-1} igneous rocks; 3–4 mg·kg^{-1} shales; 0.5–1.5 mg·kg^{-1} sandstones; and 2–5 mg·kg^{-1} limestones. Phosphoratic rocks may have 120–300 mg·kg^{-1} of U. Shales and other fine-grained

sedimentary rocks have higher concentrations of U than coarser-grained rock, because of the presence of clays and organic material to which U adsorbs.

Uranium is commonly found in association with oxygen in minerals in the tetravalent (4^+) state as uranous hydroxide ($U(OH)_4$) or in the hexavalent (6^+) state as uranyl ion (UO_2^{2+}). The main uranium minerals are uraninite (pitchblende) and potassium uranyl vanadate (carnotite). U is also found in phosphatic rocks and monzanite sands in commercially extractable concentrations [8].

In air, U easily oxidizes and is mainly found in its oxidized form in nature. Weathering of rocks releases about 27,275–31,325 t of U annually. Natural leaching of U from the rock involves the oxidation and dissolution of the soluble uranyl ion by surface or groundwater. Oxygenation of ores by bacteria such as *Thiobacillus ferrooxidans* in the presence of moisture produces sulfuric acid. Acid conditions enhance the dissolution of U from rocks. Phosphate ion also increases the solubility of uraninite. In rock unaffected by weathering for a million years, ^{238}U, ^{235}U, and ^{230}Th are in secular equilibrium with their decay products (activity ratios are equal to 1). Weathering of the rock causes disequilibrium.

Uranium is mobile in the environment with most U deposits being derived from nearby geological rock formations, through dissolution, mobilization, and recrystalization/redeposition in receptor formations. For example, the U-rich deposits of the Athabasca Basin of northern Saskatchewan originated from dissolution of U from clastic minerals in the Athabasca Group by heated groundwater, followed by precipitation of the U at redox traps situated near peletic zones in the basement rock [9]. Uranium concentrations in the environment (water, sediment, and soil) reflect the concentrations in nearby rock formations and are generally low. The behavior of U in the environment has been extensively studied and the subject of several reviews [5, 10–14].

Nuclear Fuel Cycle

Mining and Milling

In 1990, about 90% of the world's total U production occurred in nine countries: Australia, Canada, Kazakhstan, Namibia, Niger, the Russian Federation, South Africa, the USA, and Uzbekistan. Underground mining of the ore accounted for about 40% of the world's production in 1996, open-pit mining for 39%, and in situ leaching about 13%. The remaining 8% was recovered as a by-product of other mineral processing [15]. The mining method depends on the location of the ore, local conditions, and the economics. Uranium ores mined commercially may contain as little as 0.04% U or may be highly concentrated, for example, the average U concentration in ore at McArthur River Mine in northern Saskatchewan is about 20%. Recovery of U from the ores in modern milling operations may exceed 97%.

In Canada, the first mining and milling operations for U commenced in 1942 at Port Radium and in the 1950s near Elliot Lake, Ontario, and Beaverlodge Lake, northern Saskatchewan. Depletion of the ore bodies and a decline in the demand for U resulted in these older mines and mills ceasing operation by the mid-1990s or earlier. Today there are three operating mines and three operating mills in the Athabasca basin of northern Saskatchewan. However, with higher prices for U ore, several new mines are scheduled to come on stream. There are also several decommissioned or abandoned mines in the basin.

In other parts of the world, U mining and milling has been going on much longer than in Canada, for example, in Germany U was discovered in 1789 in the Erzgebrige (Ore Mountain) area and abandoned mines and mills are a common legacy of early operations [3].

Uranium mills extract U_3O_8 from crushed, ground ores either by an acid or by an alkaline leaching process. After leaching, the resultant solution containing U goes through a solvent extraction process in which the U is purified and concentrated. Yellowcake, the end product of the milling process, is shipped to a U refinery. The residual material (tailings), which is crushed ore minus most of the U, is pumped as slurry to a tailings management facility. Uranium tailings contain up to 85% of the radioactivity initially present in the U ore, since most of the U decay products remain in the tailings [16]. Releases from early mines and mills were not treated. Effluent treatment in Canada only started in the 1970s with the introduction of federal regulations. For this reason, the more significant environmental effects of U mining and milling are mainly associated with older operations. At older operations, untreated

tailings were often discharged to a nearby lake which served as a tailings pond. Subsequently tailings were flushed downstream with discharge events contaminating downstream water bodies. An example is the deposition of tailings in Mudford Lake resulted in tailings moving downstream to Langley Bay, Lake Athabasca, covering the bay with a 2–4 m thick blanket of tailings [17].

Uranium mill tailings have been dewatered and deposited directly on land. These are relatively dry and prone to wind erosion. Dust particles contaminated with U and decay products can be dispersed over much larger areas. Dust particles from tailings and from mill vents constitute a potential exposure pathway for terrestrial biota through inhalation. Wet and dry deposition may increase U concentrations in surrounding soils and vegetation [18] and hence U enters the terrestrial food chain albeit in a localized area. For example, the impact due to aerial transport of aerosols and radon generated from mining in Brazil was restricted to an area less than 15 km^2 [15].

Tailings may also be a source of U released to groundwater [6]. Uranium enters surface waters as a result of releases of treated mill effluent and from mine dewatering activities. Generally, the effluent treatment plants also treat contaminated water collected from tailings management facilities.

Uranium operations not only release U to the environment but they release other contaminants including members of the U decay chain such as ^{226}Ra, ^{222}Rn, ^{232}Th, ^{210}Pb, and ^{210}Po; metals such as cadmium, copper, bismuth, arsenic, and molybdenum; organic contaminants such as kerosene, amine, and isodecanol which may be released when the mill's solvent extraction process is upset [19]; and salinity stressors [6].

Refining, Conversion, Enrichment, and Fabrication Facilities

The major processing steps involved in U refining and conversion are the purification of yellowcake from U mills to UO_3 in the UO_3 circuit, and conversion of UO_3 to either uranium hexafluoride (UF_6) or uranium dioxide (UO_2). Yellowcake is chemically complex, but contains 26–28% ammonium and magnesium diuranate, which are biologically available. Yellowcake is refined by nitric acid digestion to an intermediate product, uranyl nitrate, which is thermally decomposed into uranium trioxide (UO_3). This in turn is either converted to uranium dioxide (UO_2) as an end product, or reacted with hydrofluoric acid to form uranium tetrafluoride (UF_4), which is calcined and further fluorinated to produce uranium hexafluoride (UF_6). The UO_2 is pressed and sintered into high-density fuel pellets, and inserted into zircalloy tubes assembled in bundles to serve as fuel in heavy-water reactors that use natural uranium.

UF_6 is one of the few non-uranyl compounds of hexavalent uranium. UF_6 is volatile at temperatures above 60°C, is highly corrosive, and is stored as uranium metal. Enrichment plants take UF_6 from a conversion facility and enrich it usually to 3–5 wt.% ^{235}U depending on the specific reactor requirements. An end product of enrichment is tailings of depleted uranium (DU) ranging from 0.25 to 0.35 wt.% ^{235}U [20]. Re-enrichment is the further depletion or stripping of depleted uranium tailings to produce U with a ^{235}U content of natural U (0.71%). Thus the tailing is upgraded to natural ^{235}U grade, which may then be further enriched to reactor grade [21]. Enriched uranium hexafluoride (3–5% ^{235}U) is used as reactor fuel in power reactors or as weapon grade material (>90% ^{235}U). The enriched UF_6 is converted into uranium dioxide powder that is then processed into pellet form. The pellets are then fired in a high-temperature, sintering furnace to create hard, ceramic pellets of enriched uranium. Releases that occur at different stages of the U refining and conversion process are vented to the atmosphere or treated and released to surface waters.

Nuclear Power Plants

Nuclear power plants generally do not release significant quantities of U and, therefore, there is no U impact on the environment from these sources. Impacts on the environment from nuclear power plants are mainly confined to impingement, entrainment, and thermal effects on aquatic ecosystems. Releases of radionuclides to the environment are generally low and, although of great concern to the public, usually have no effect on the environment or to the public.

Waste Management (Nuclear Power Plants)

Waste management facilities for radioactive wastes were developed to handle a variety of wastes ranging from contaminated soils (historical contamination), liquid and solid wastes, contaminated filters and resins from pollution control systems of nuclear power plants and reactor spent fuel. Modern facilities are well-engineered structures with well-controlled releases, whereas older facilities (e.g., pre-1970s) are generally not as well designed and are more likely to have releases that have the potential to impact on the environment.

Background U Concentrations

Atmospheric U concentrations measured over the North Atlantic are about 4×10^{-6} μg·m^3 and are considered to represent background concentrations [8]. Typical atmospheric U concentrations range from 0.025 to 0.1×10^{-3} μg·m^3 [10]. Higher values are found in developed regions, for example, values from 0.10×10^{-3} to 1.47×10^{-3} μg·m^3 are reported over upper New York reflecting industrial emissions [8]. Background concentrations of U in southern Ontario are about 0.1×10^{-3} μg·m^3 [22].

In mineralized soil, U concentrations are generally about 1–4 mg·kg^{-1}. Fine-textured soils develop primarily from the weathering of sedimentary rocks and have U concentrations similar to the rock (~4 mg·kg^{-1}). Uranium concentrations up to 250 mg·kg^{-1} may be present in phosphate rock, which points to the importance of phosphorus fertilizers as a source of radiation in the environment (see Waller this section). Uranium concentrations in soil generally increase with increasing clay and organic content, because of the high affinity of U for clay and organic material. Coarser sandy soil has low U concentrations.

Background concentrations of U in surface water including seawater are generally quite low with values usually a few parts per billion or less. The total U concentration in the Atlantic and Pacific oceans is about 3.1 μg·L^{-1} [23, 24]. This natural background concentration in seawater is 9–11 times greater than those for freshwater. Average U concentrations in rivers are 0.2–0.6 μg·L^{-1} [3]. Concentrations in drinking water in the USA average about 3 μg·L^{-1} with a range of 0.1–973 μg·L^{-1} [8]. Higher values are probably associated with the use of groundwater as drinking water.

Background concentrations of U in lake water across Canada are generally low with a median concentration of < 0.05 μg·L^{-1} and a maximum concentration of 1,350 μg·L^{-1} [25]. The maximum value is associated with the U deposits of northern Saskatchewan. The median U concentration in streams is higher at 0.06 μg·L^{-1}, with a maximum of 255 μg·L^{-1} in a stream in the Yukon Territory. In northern Saskatchewan, an area known for its U mines, the median aqueous background U concentration is below the detection limit of 0.05 μg·L^{-1} with an upper 95th percentile of 0.35 μg·L^{-1}.

Uranium concentrations in sediments in lakes generally range from 0.5 to 5 μg·g^{-1} (dry weight sediment unless specified otherwise), with an average of 3 μg·g^{-1} [5]. Freshwater sediments from Canadian Rocky Mountain streams have U concentrations ranging from 0.1 to 430.0 μg·g^{-1} with a median value of 3.4 μg·g^{-1}, whereas U sediment concentrations in Canadian Shield lakes range from 0.1 to 733 μg·g^{-1} with a median value of 4.6 μg·g^{-1}. Sediment concentrations in northern Saskatchewan have a geometric mean of 3.7 mg·kg^{-1} sediment, with a 95% confidence level (CL) of 29.5 μg·g^{-1} dry weight (dw) sediment. A maximum sediment U concentration of 648 μg·g^{-1} dw and several other high values in northern Saskatchewan were associated with the ore deposits [6]. The few lakes with high U sediment concentrations have been drained and mined.

U concentrations are generally low but under natural conditions can be extremely high in certain areas. Groundwater U concentrations are generally in the range of 0.1–50 μg·L^{-1} and occasionally as high as 2,000 μg·L^{-1} [11]. Uranium concentrations in groundwater in the USA, Europe, and Australia range from 0.1 to 1,870 μg·L^{-1} with most values less than 2.2 μg·L^{-1} [8]. In the region of Helsinki, Finland, U concentrations in deep groundwater are up to 14,870 μg·L^{-1} [26].

Uranium Speciation

Freshwater

An understanding of U speciation is essential to understanding the bioavailability and toxicity of U. Uranium exists in four valence states: U^{3+}, U^{4+}, U^{5+}, and U^{6+}, but only tetra- and hexavalent states are commonly

found in the environment. Tetravalent U occurs in reducing environments such as anoxic sediments and water, and in mineral formations. The tetravalent form has a high affinity for organic materials and very low solubility (0.06 $\mu g \cdot L^{-1}$) [11]. Hexavalent U exists in oxidizing environments such as surface waters and weathered rock [14]. Most mobilization of U occurs during weathering processes in which uranous (U^{4+}) compounds, generally uraninite, are released from rock and oxidized to the uranyl ion by surface waters. The uranyl ion is the principal form of uranium found in aquatic environments. Uranyl ion is a very large divalent positively charged ionic species similar in size to potassium, calcium, and cesium [14]. In natural waters, U usually forms complexes, typically with chloride, fluoride, phosphate, sulfate and carbonate, hydroxide, and perhaps silicate ions and organic materials, with fluoride complexes predominating below pH 5 and phosphate complexes predominant between pH 4 and 7.5 [27]. The formation of U complexes generally greatly increases the solubility of U in oxidizing environments.

The chemical speciation of U, like that of other metals, is influenced by water quality variables such as alkalinity, hardness, pH, and natural organic matter (e.g., [28, 29]). The pH of a solution has a strong influence on the chemistry of U. U oxides and their hydrolysis products have the highest solubility at pH 4–6. Figure 1 shows the distribution of U species with pH based on thermodynamic simulations. Note that there is large uncertainty in the predictive power of the simulations [7, 30] and that predictions can only be validated for waters with low total dissolved solid concentrations [5]. Furthermore, the output of different geochemical speciation models can differ substantially [31].

Speciation modeling provides evidence that UO_2^{2+} is the most toxic form of U, although some studies suggest exceptions at different pH values [29, 32, 33]. Markich et al. [29] also attribute U toxicity to UO_2OH^+. UO_2SO_4 and UO_2CO_3 do not contribute to toxicity [34]. The free uranyl ion (UO_2^{2+}) is calculated to be the predominant species at pH $\leq$ 5, but is insignificant at pH > 6 (Fig. 1). UO_2OH^+ is also important at pH $\leq$ 5. At high pH, the uranyl ion forms soluble complexes with carbonate ions. Uranium carbonate complexes such as uranyl carbonate (UO_2CO_3) are very soluble especially at pH 6 and higher, and have an overall negative charge. Since CO_2 and carbonates are abundant and readily available in water, uranyl carbonates commonly contribute significantly to U concentrations in water. From pH 5.5 to 6, UO_2CO_3 is the predominant uranyl species. From pH 6 to 7.5, the mixed uranyl-hydroxide-carbonate species, $(UO_2)_2(OH)_3CO_3^-$, is the dominant uranyl species, whereas $UO_2(OH)_3^-$ dominates at pH > 7.5. At high U concentrations (30 $\mu g \cdot L^{-1}$), $(UO_2)_2(OH)_3CO_3^-$ dominates from pH 5 to 8.5 (Fig. 1b). Polymeric uranyl-hydroxide species are only important in natural waters when U concentrations are greater than 200 $\mu g \cdot L^{-1}$ [5]. Conditions that favor the formation of free ion UO_2^{2+} include low pH, low natural organic matter concentrations, and low alkalinity [29, 35].

The distribution of U species varies with the total U concentration as well as the concentration of ligands [29, 36]. When the concentration of ligands is much greater than that of the metal concentration, the relative distribution of the metal speciation tends to remain stable. However, when the metal concentration is higher than the ligand concentration, there is a significant shift in the metal distribution with U tending to form hydroxyl and carbonate complexes [32].

The organic carbon of surface water is usually in the range of 1–10 $mg \cdot L^{-1}$ [37]. In brown-water (organic-rich) lakes and streams of low hardness and alkalinity, U complexes predominantly with humic substances. Complexation of U increases up to about pH 6, because of increasing ionization of the carboxylate (COOH) functional groups of humic substances. Uranium is strongly absorbed by the carboxyl group, but is not reduced. The adsorption equilibrium of humic acids is described by the Langmuir iso-pH curves. Above pH 6, U complexation with humic substances decreases, because of the higher binding affinity with carbonate and hydroxide ($UO_2(OH)_3^-$, $UO_2(CO_3)_3^{4+}$, $UO_2(CO_3)_2^{2+}$, and/or $(UO_2)_2(OH)_3CO_3^-$) [5]. The binding of U to humics is often underestimated in studies, because humic substances are not accounted for in many speciation models, the chemistry of humic substances is poorly defined, their stability constants are poorly known, and most speciation modeling is done with simple, chemically defined experimental water rather than natural water [5]. In most instances, ligands decrease the bioavailability of U [32].

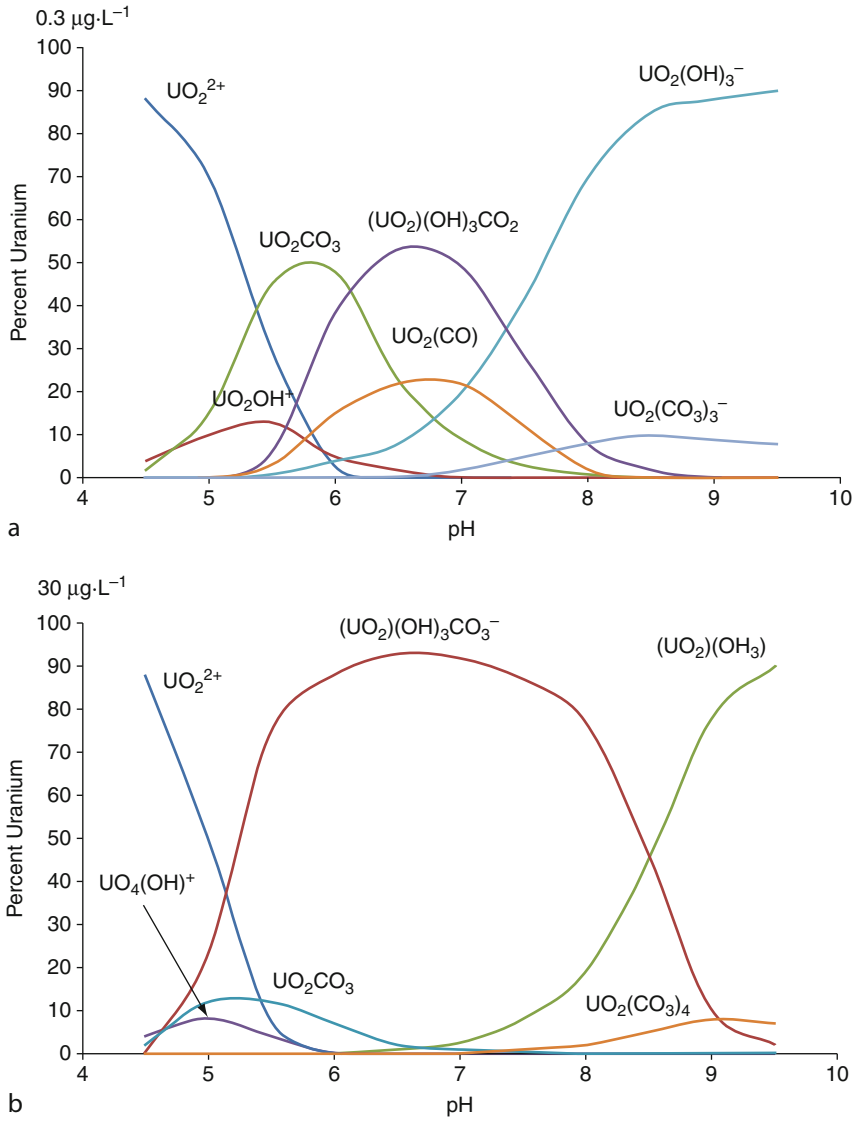

Uranium in the Environment: Behavior and Toxicity. Figure 1
Percent distribution of uranium speciation with pH (4.5–9.5) in freshwater at uranium concentrations of (**a**) 0.3 μg·L^{-1} and (**b**) 30 μg·L^{-1} (Modified from Markich [5])

Uranium uptake generally correlates with free uranyl ion concentration as predicted by the free ion activity model and biotic ligand model, although hydrophilic metal ligand complexes may increase the bioavailability of U above the predicted free ion concentration [5, 32]. Increased toxicity in the presence of ligands involves organic ligands that can be assimilated by the organism, for example, low molecular weight metobolites such as citrate and thiosulfate. The ligand is assimilated along with the metal. This is seen in the plant–soil system, where uptake of U by roots can be enhanced by the presence of organic chelators that increase the solubility of U, that is, citric acid addition decreases pH which increases U desorption from the soil and the binding of uranyl by the citrate anion further increases the solubility and mobility of U, increasing U availability for plant uptake [14].

Seawater

In oxic seawater, pH 8, U behaves conservatively and is predominately (80–90%) present as a stable, soluble uranyl tricarbonate complex $UO_2(CO_3)_3^{4+}$. Minor portions of U are bound to peroxide ligand, $UO_2(CO_3)_2(HO_2)^{3-}$ [5].

Effect of Mine and Mill Effluents on Speciation

Bernhard et al. [38] assessed uranium speciation in three different uranium mining areas in Germany by measuring speciation using time-resolved laser-induced fluorescence spectroscopy and laser-induced photoacoustic spectroscopy and by speciation modeling. The water samples were filtered through a 1-nm cellulose filter before analysis and did not appear to be treated to remove contaminants or neutralize pH. In mine water from Schlema, with neutral pH (pH 7.13, total organic carbon of 62 mg·L^{-1} and 1.9 g·L^{-1} SO_4^{2-}), the calcium uranyl carbonate complex dominated. In the Königstein mine, U was leached underground with dilute sulfuric acid. This resulted in a very acidic mine water with pH 2.6 and sulfate as the major anion (2.2 g·L^{-1}). In the Königstein mine water, uranyl sulfate complexes, mainly $UO_2SO_4/UO_2(SO_4)_2^{2-}$ and UO_2^{2+}, were the major species. In contrast, the Helmsdorf mill tailing water had high concentrations of sulfate, hydrogen carbonate/carbonate and chloride ions, pH 9.76, and elevated concentrations of phosphate, arsenate, and total organic carbon. In the Helmsdorf tailing water, uranyl carbonate complexes, mainly $UO_2(CO_3)_3^{4-}$ and $UO_2(CO_3)_2^{2-}$ were dominant. Therefore, water chemistry has a marked effect on U speciation.

At U mines/mills, the release of treated effluent complicates the interpretation of U toxicity to aquatic organisms, since treated effluent not only increases U and sulfate concentrations, but also increases calcium and magnesium concentrations in the receiving surface water. For example, as a result of mill effluent releases in Island Lake from the Cluff Lake Operations (now decommissioned) in northern Saskatchewan, mean baseline hardness increased from 36 mg·L^{-1} $CaCO_3$ to 1,113 mg·L^{-1} $CaCO_3$ between 1978 and 1988; calcium increased from 7.18 to 292 mg·L^{-1}; and magnesium increased from 4.4 to 96.5 mg·L^{-1}. In comparison, HCO_3 only increased from 36.3 to 55.0 mg·L^{-1}, and CO_3 from about 0.0 to 6.7 mg·L^{-1}, whereas SO_4 increased from 1.28 to 1,140 mg·L^{-1} [39].

To assess the potential compounding effects of effluent treatment on increased U concentrations, U chemical speciation modeling using the PHREEQC code and WATEQ4F database, was performed by Environment Canada and Health Canada (EC and HC) [6] for Beaverlodge Lake, a decommissioned site which used an alkaline leaching process, and for Key Lake Operations. For Beaverlodge Lake carbonate species of U were predicted to represent 98% or more of the total U, with less than 0.5% of U present in the form of the toxic species UO_2^{2+} and UO_2OH^+. For the Key Lake Operation the presence of elevated sulfate concentrations in the treated effluent resulted in a significant increase in the proportion of UO_2SO_4 (50–60%) and in the toxic U species UO_2^{2+} (17–29%) and UO_2OH^+ (4–17%) and in a decrease in the proportion of carbonate species of U to $\leq$15% as well as the absolute amount. Based on these studies, treated mill effluent from mining and milling operations may increase the concentration of U in the receiving environment including the concentration of toxic U species (UO_2^{2+}). However, it also increases the concentration of calcium and magnesium which may have ameliorating effects on U toxicity. It is obvious from these studies that site-specific studies are required to quantify impacts.

Terrestrial Environment

Atmospheric emissions may contaminate the surrounding terrestrial environment through atmospheric deposition of U. This may be in the form of both dry deposition, where particles and gases impinge directly onto surfaces such as foliage and soils, and wet deposition, or washout, where the particles and gases are extracted from the atmosphere by rain or snow and are deposited with the precipitation.

Dry deposition tends to dominate closer to the source because particles gradually settle out downwind of the plume. At greater distances, the particles remaining in the plume are smaller and tend to stay aloft until precipitation occurs. The extent of dry deposition depends more on features such as topography and surface roughness than does wet deposition. Elevated (hilltop) areas may receive relatively more dry deposition because the landscape effectively intersects

the airborne plume. Particles in the plume become impinged on the elevated surfaces. Surface roughness influences the extent of dry deposition, for example, trees intersect and entrain more airborne particles than low-lying vegetation such as grass.

Wet deposition is less dependent on the topography and surface roughness than is dry deposition. However, the underlying surfaces affect the fate of the contaminants washed out of the plume. Some contaminants may dissolve in the water droplets, whereas others will remain as particles. Dissolution will also happen as the precipitation interacts with contaminants previously deposited on surfaces by dry deposition processes. Dissolved contaminants may be absorbed directly into the foliage or will be washed off the foliage surface. Contaminants can be washed off the surface at the drip line of the vegetation (through fall) or along stems and trunks (stem flow). Through fall and stem flow can result in an uneven distribution of contaminants in the underlying soil with elevated soil concentrations at the drip line and immediately adjacent to the trunk. The wash off is a mass action process that generally follows first-order kinetics with a half-time in the order of 2 weeks regardless of particle size [40].

In the soil, dissolved contaminants will interact with the soil solids. Contaminants accumulate in soil litter, but ultimately the litter is decomposed and incorporated into the underlying soil. Contaminants that sorb to the litter reach the underlying soil in a relatively short time (months to years). Contaminated particles may be incorporated into the soil or be subjected to dissolution and leached from the soil.

Uranium moves in solution in soil both vertically and horizontally. Downward movement is in response to gravitational potential, whereas upward movement is by capillary rise or forces exerted by plant roots extracting water. Horizontal movement or through flow occurs in a sloping landscape coupled with gravitational potential. Redistribution of fine soil particles over time, also contributes to the movement of U in soil. The "A" horizon of the soil profile usually has the highest U concentration, whereas the "C" horizon has the next highest and the lowest is in the "B" horizon. This is because of the leaching and gravity settling of soluble and ultrafine particulate materials from the middle zone to the lower horizon, and because of retention of organically bound U in the surface humus [14].

Mobility of U in soil is a function of soil type and conditions. In the absence of carbonates and under oxidizing conditions, U in soil water is present as an uranyl ion or an uranyl hydrolysis product. Uranyl ion is common at pH 5.5 and below, and has a positive charge. Uranyl hydrolysis products exist above pH 5.5, with either positive or neutral charge. In the presence of carbonates at neutral pH, or above, negatively charged uranyl carbonates are common.

Soil particles and associated organic matter have negatively charged absorption sites to which positively charged metals and complexes can bind. Therefore, positively charged uranous ions, uranyl ion, and uranyl hydrolysis products are relatively immobile in soils, and negatively charged uranyl carbonates are highly mobile [8]. Alluvial soils, which tend to have high clay and organic matter content, bind U tightly, whereas in sandy soil, U is more mobile and are at lower concentrations. Anaerobic soils, such as wet marshy soils or sediments, have reducing conditions, which results in the adsorption of positively charged uranous ions. Under oxidizing conditions U is readily lost from the water to the peat by cation exchange, identical to the exchange of Ca^{2+} and K^{+} and other cations in soil. Therefore, adsorption of U is dependent on cation-exchange capacity, but does not always correlate with the cation-exchange capacity. In a soil with a high organic matter and clay content, mean extractable U was about 10% with a range of 4–24%. In comparison, mean extractable U in a sandy, acidic soil was 40% with a range of 7–65% [41]. Therefore, a relatively large portion of the U associated with soil may be bioavailable (extractable).

Storm events selectively erode finer clay and silt particles that have high contaminant concentrations such as U [42] transporting U downslope from contaminated floodplains to adjacent streams [43] or to topographically low areas such as wetlands and surface water bodies. These areas become secondary locations for exposure.

Direct exposure of terrestrial biota to atmospheric contaminants is from either inhalation or foliar uptake. However, more significant impacts usually occur as a result of accumulation of the contaminants in environmental media. Contaminants that are not very mobile in soil tend to accumulate where they are deposited, which exposes resident biota to elevated concentrations.

Terrestrial plants are exposed to contaminated soil by way of their roots. In the case of trees, their fine roots occupy the area just below the litter layer and tend to be more prevalent at the edge of the tree drip line in order to optimize extraction of nutrients and water. Tree roots will also penetrate unsaturated soil to intersect subsoil moisture, and this may predispose them to absorb contaminants in groundwater. Plant roots have the ability to change the chemical and physical makeup of the soil, to optimize growing conditions. The rhizosphere, which is the area occupied by the roots of plants, has an altered pH, an active microbial community, and may be enriched in organic ligands, some originating in the root, which solubilize elements that would otherwise be insoluble. These special features of the rhizosphere optimize the absorption of relatively insoluble nutrients such as phosphorus, iron, manganese, and zinc and can also influence the bioavailability of contaminants such as U.

Uranium is absorbed with water by the root with U penetrating the epidermis of the root. However, U is precipitated as a yellowish deposit in the meristem region with little U entering the root sap system. The storage of U as a yellow deposit in the cell nuclei of the meristem results in the destruction of chromatin and cessation of the cell nucleus activity, preventing U translocation [14]. However, others have reported that the action of U in plant tissues appears to be mainly at the cell surface. In the shrub, *Corprosma australis*, at least 50% of the U was bound to cell wall proteins in the form of U-protein complexes [8]. The binding of positively charged U complexes to cell walls and membranes and to carboxyl groups of proteins may restrict transport mechanisms responsible for movement and deposition of sugars and other metabolic products in plant cells.

Uranium concentrations are highest in the root, and generally follow the order: roots > fruits (seeds) > branches > bark > leaves (needles) > wood and tend to be higher in older branches [18].

Decomposers such as insects and earthworms recycle nutrients (U) in dead plants and animals. In contaminated areas, plant litter often accumulates on the soil surface because the decomposer community has been disrupted [44, 45]. This not only illustrates the importance of decomposers, but suggests that decomposers may be more sensitive to contaminants than primary producers.

Decomposers such as insects and earthworms are important in the comminution of the litter into smaller pieces, which accelerates decomposition by microbes. Microbes colonizing litter take up contaminants from the surrounding pore water, and transfer the contaminants to higher trophic levels through the detrital food web.

Soil invertebrates are also exposed to contaminants through contact with and ingestion of soil and soil pore water. Soil nematodes live in the pore water, so direct absorption of contaminants in pore water is a primary exposure pathway for nematodes. Larger invertebrates consume soil along with the litter, so their exposure may be directly with soil solids. Feces egested by invertebrates may also be re-ingested by other invertebrates to extract additional nutrients and associated contaminants.

Concentration Ratios, K_d, and Transfer Factors

The migration of contaminants in the environment is complex. However, simplified models have been widely adopted to predict contaminant transfer and the resultant concentration in media. Concentration ratios (CRs), solid/liquid partition coefficients (K_d), and transfer coefficients (TCs) assume that the transfer of contaminants is dependent on concentration. Their values are empirically derived so they can be robust and self-validating.

The CR may also include the assumption that contaminant uptake is for a specified soil depth, usually the depth of cultivation and that uptake is from the root, that is, absorption by foliage is lumped with root uptake. It is also assumed that CR data can be transferred from one setting to another. Databases are available to describe the distribution of CR, K_d, and TC [46–52]. However, it is best to undertake studies to establish site-specific parameter values when possible as generic values may not necessarily describe local conditions [53].

The U content of plants is derived mainly from soil water. Plant to soil concentration ratios generally range from 0.0001 to 0.1 which results in low U concentrations. However, some plant species may have a U concentration as high as 0.5% dw. The mosses, *Sorbus aucuparia*, and *Astralagus* sp., are indicator plants for U and have been used in prospecting for

U ore. *Sphagnum* spp. and *Ledum groenlandecum* reflect soil U concentrations in lowland areas, *Umbilicaria* spp. and *Cladonia* spp in rock outcrops, and *Picea mariana* and *Betula papyrifera* in upland locations [54].

Agricultural plants typically have higher U concentrations. Root crops and leafy crops contain more U than other crops. Starchy roots contain approximately 1 $\mu g \cdot kg^{-1}$, cereals 0.5 $\mu g \cdot kg^{-1}$, and fruit and vegetables 0.8 $\mu g \cdot kg^{-1}$ U [8]. Plants high in potassium and calcium have lower U concentration. Agricultural plants accumulate more U from irrigation waters than from the soil. Concentration ratios between agricultural plants and soils are generally 10^{-5} to 10^{-3} and between plants and irrigation water are 1–100 [14].

As the soil U concentration increases, the U concentration in plants generally increases. An exception is marshy soil where U concentrations may be high, but associated plant U concentrations are low because U is tightly bound under anaerobic conditions. Hence, it is both the amount of U in the soil and soil conditions that determine the plant U concentration. Uranium concentrations in plants in arid areas may exceed that in soil. At neutral to alkaline pH in aerobic soils in arid areas, soluble and mobile uranyl carbonates are available for uptake. There are also plant species-specific differences in uptake. Among different plant species growing in soil with a given U content, U concentration may vary by a factor of 10 [14].

Terrestrial Environmental Pathways/Food Chain

Uranium does not biomagnify and is transferred inefficiently through the food web. U has a high partition coefficient (K_d) in most soils and a relatively low mean plant/soil CR of 0.0045. Uranium concentrations tend to decrease with successive trophic level (Table 1). Therefore, the risk of U toxicity in the terrestrial environment is low.

Uranium is taken up through ingestion of drinking water and contaminated food, inhalation and absorption through the skin. The respiratory route is not usually important except for small mammals living in heavily contaminated areas [56].

Soil Ingestion

Soil ingestion may represent a major source of U for wildlife [57]. Soil ingestion is usually considered an important pathway in environmental risk assessments, but is generally not addressed in feeding studies. Linsalata et al. [58] estimated that over 90% of the daily U intake in cattle from natural sources is from soil. Animals may consume soil incidentally, while ingesting roots and vegetation or while grooming, or may intentionally ingest soil at salt licks that provide nutrients during the spring [59]. Sheppard [40] suggested a mean ingestion rate of 50 mg soil·kg^{-1} food in the diet of animals for modeling purposes. Wildlife preying on soil-dwelling invertebrates may ingest a higher proportion. High rates of soil ingestion up to 87% of the diet have been reported for some wild

Uranium in the Environment: Behavior and Toxicity. Table 1 Concentrations of uranium in a plant–rodent food chain and through a plant–deer food chain based on Mahon [55]

Plant–rodent food chain		Plant–deer food chain	
Taxa	ng U·g^{-1} dw	Taxa	ng U·g^{-1} dw
Deer mice (*Peromyscus maniculatus*)	<5	Mule deer (*Odocoileus hemionus*) flesh	24
Chipmunk (*Eutamius amoenus*)	10	Mule deer (*Odocoileus hemionus*) bone	9
Fireweed seed heads (*Epilobium angustifolia*)	22.1 ± 8.1	Mule deer (*Odocoileus hemionus*) liver	5
Grouseberry (*Vaccinium scoparium*)	16.2 ± 10.4	Grouseberry (*Vaccinium scoparium*)	16.2 ± 10.4
		Lichens (*Bryoria freemontia* and *Alectoria sarmentosa*)	17.5 ± 10.4
		Grass (*Calamagrostis rubescens*)	69.3 ± 71.9

species [57, 59]. Feces of whitetail deer average 29% inorganic matter. Soil ingestion is highly variable and may change seasonally [57].

The amount of U retained from ingested soil is a function of the total amount of U ingested and its bioavailability [40], which varies with soil type. At present, there is no reliable method to predict the bioavailability of U through this exposure route. A gut absorption rate of 5% is often used for adult mammals, with a higher value of 10% for juvenile and immature animals. A value of 30% may be expected for neonates, based on the work of Sullivan [60] for plutonium uptake by neonate swine. EC and HC [6] assumed soil to be 2–5% of the diet depending on the wildlife species, and made the assumption that soil U was assimilated at the same rate as U in food.

Aquatic Ecosystems

Since U in industrial effluent releases is mainly to surface waters, it is the aquatic system that is most affected by effluent releases. In the case of U mining/milling, releases of treated effluents are frequently to small headwater lakes or streams.

The fate of U and other radionuclides will depend on their chemical characteristics and the nature of the water body. The physical state of the contaminant, particulate or dissolved, the pH and chemical composition of the water, particularly dissolved organic matter (DOM) or ligand content will have a strong influence on the fate of the contaminant. In carbonate-rich water, U exists as the uranyl-hydroxy-carbonate and is poorly sorbed [37]. In soft-water lakes carbonate concentrations are low, and sorption of the uranyl ion occurs to particulates. Upon entering a water body, contaminants partition among the various compartments. A portion becomes associated with dissolved inorganic and organic ligands in solution. The remainder becomes associated with particulate matter as a result of adsorption, precipitation, coprecipitation, and uptake by plankton and eventually settles out of the water column.

Effluents from mines/mills usually enter the epilimnion of the receiving water body as opposed to deeper waters. Mixing in the epilimnion is rapid. Hesslein [61] found that complete mixing takes place within 24 h in a thermally stratified 16 ha lake. Particle-reactive radionuclides, such as ^{60}Co, ^{65}Zn, and ^{210}Pb (and U) are rapidly adsorbed to DOM, suspended solids, and epilimnetic bottom sediments or are taken up by algae. Dissolved radionuclides also diffuse into interstitial sediment pore waters.

Continuous input of U mine effluents to the surface (epilimnion) waters of a thermally stratified lake in summer will result in the rapid loss of U to littoral sediments. Sediments in deeper waters will gradually become contaminated through the process of sediment focusing. Despite losses from littoral sediments to deep waters, the U concentration of littoral sediment will not decrease because of the continuous input of U and other contaminants to the lake from the effluent. Therefore, sediment U concentrations in shallow water sediments can be high especially if the sediment is high in organic content.

In the water column, dissolved radionuclides are rapidly taken up by algae. The contaminated algae are fed upon by zooplankton, which in turn is a source of food for higher trophic levels. Particle-reactive radionuclides taken up by algae may be routed to the hypolimnion of the lake via the rapid sedimentation of zooplankton fecal pellets. This appears to be the case for U as algae, sediment-trap material, and deepwater organic particles were found to have similar U (and Ra) concentrations [62]. Uranium associates with organic particles (plants, algae, and microbes) in the water column, which eventually sink to the bottom to produce organic sediments. Sedimentation of algae and aggregates formed by the coagulation of colloidal particles will also result in the transfer of radionuclides to bottom sediments, but at a slower rate than that by fecal pellets. Uranium in sediment may be almost completely associated with algae, debris, and humic acids [63].

The transfer of contaminants such as U from water to sediment is an important process for their removal from the water column. The behavior of contaminants in lake water can be described as being nonreactive (conservative) or reactive (non-conservative), depending upon their sorption to suspended particles and retention within the lake [64, 65]. Nonreactive radionuclides tend to remain in the water column and are lost from the lake via the outflow. Thus, there is little retention of these radionuclides within the lake. In comparison, reactive radionuclides are rapidly transferred to sediment and are retained in the lake.

Bird et al. [65] defined probability distribution functions for the transfer rate of U and other elements from the water column to the sediments based on published data and mass balance equations. A high transfer rate indicates that the element has a high affinity for sorption to particles and is lost from the water column [66, 67]. In lakes, nonreactive radionuclides tend to have transfer rates <0.1, whereas more reactive radionuclides usually have transfer rates >1.0. In terms of residence time in a non-flushing system, a radionuclide with a transfer rate of 0.1 would have a half-time in the water column of 6.93 years, whereas a radionuclide with a value of 1.0 would have a half-time of only 0.69 years. The transfer rate of U from water to sediment was found to have a lognormal distribution with a geometric mean of 0.5 and a geometric standard deviation of 3.0. Therefore, the overall behavior of U in the range of conditions expected in lakes essentially falls midway between a particle-reactive element and a nonreactive element and can be considered a moderately reactive radionuclide. U tends to partition to sediments as evidenced by a relatively high K_d of 0.36–3.2 × 10^3 L·kg^{-1} [68]. K_d values vary among sites and are lower at contaminated sites than uncontaminated sites, that is, as contaminant concentrations increase, K_d values and CRs decrease. This is probably because at high levels of contamination, the number of available sorption sites in the sediments becomes limiting.

In a study of the effect of sediment type, temperature, and natural colloids (humic and fluvic acids) on the transfer of radionuclides from water to natural sediments, Bird and Evenden [69] found that the loss of U from water was generally in the order: organic sediment > clay > sand sediment and was slower for U than cobalt, zinc, and cesium. The transfer rate for U was 0.001–0.084·day^{-1} depending on the experimental conditions. The transfer rate for U to sediment increased significantly for each 10°C increase in temperature between 5°C and 25°C in the presence of organic sediment, presumably due to enhanced microbial activity. There was no difference with temperature in the presence of sand sediment, whereas a greater loss rate was observed at 5°C than 15°C for the clay sediment. An increase in temperature is reported to reduce the sorption rate of uranyl ions to clays [70].

Loss of radionuclides from water was slower in the presence of natural colloids [69]. The chemical behavior of metals and radionuclides becomes dominated by the physical behavior of the colloids following surface complexation [71]. Colloids are usually negatively charged and are known to increase the mobility of radionuclides [37, 72] and to alter their bioavailability and toxicity [73].

In lakes, size-selective sorting and ultimate transport of smaller particles from littoral areas to the deeper profundal waters, a process termed sediment focusing [74] will, over time, result in greater accumulation of sediment and sediment-associated contaminants in the deeper waters. In general, there is a linear relationship between sediment accumulation and lake depth, with flocculent sediments tending to accumulate at depths greater than 10 m in Canadian Shield lakes [75]. Thus, there will be a gradual transfer of the particle-bound radionuclides from littoral regions to the deeper profundal region via sediment focusing, the result of water mixing events over time. In shallow lakes, sediment focusing is not an important process as sediments are continuously redistributed throughout the basin. In these shallow, well-mixed lakes, little difference in sediment contaminant concentration is expected with water depth, but concentrations will vary with sediment type.

Considerable decomposition of organic particles may occur en route to the bottom sediment, particularly in the metalimnion, resulting in a substantial release of the radionuclides, including U into the deeper waters. In Chesapeake Bay, U is transferred from the water column to the sediments with the detritus that forms during periods of high productivity. Degradation of detritus results in the release of U to bottom waters and porewater and there is redox-dependent cycling of U between sediment and bottom water. During summer, anoxic conditions in the hypolimnion inhibit the exchange of U with overlying water due to the stability of reduced U(IV). However, with reoxygenation of the water with fall turnover, U is released back into the water column [76]. In a meromictic lake which has anoxic bottom waters, U in sediment was mainly associated with colloids (80%) with about 40% associated with fulvic and hydrophilic acids [77].

Once U is transferred to the sediment, decomposition may release U and other contaminants to porewater. Decomposition of algae and other detritus in sediment results in about 20% of the U being released to the porewater. Epiphilic algae or periphyton growing at the sediment–water interface are very efficient at taking up radionuclides released from the sediments and from the overlying water. Bioaccumulation of the radionuclides by periphyton may result in the transfer to higher trophic levels via the food chain [73].

As redox potential (E_h) decreases (usually with depth in the sediment), U(VI) may be reduced to U (IV). The reduction of U(VI) to U(IV) and the subsequent chemical reactions and transformation of U sulfide, carbonate, or other biogenic ore requires strongly reducing conditions, that is, U(VI) reduces to U(IV) at low E_H (<200 mV). In the sediment profile, redox conditions change with oxygen being reduced first, followed by denitrification, then by UO_2CO_3 reduction to uraninite and sulfate reduction to sulfide. Uranium reduction and removal from pore water is related to bacterially mediated sulfide reduction. When the sediment undergoes bioturbation or when sulfate reduction is halted, U is released back into the pore water. The release of U is associated with the reduction of U hydroxides of Fe and possibly Mn [7].

The uranyl ion adsorbs by base exchange onto clay and other crystal layer-lattice minerals in the sediment. Sorption to clay minerals occurs at or below pH 5 and sorption to Fe and Al (oxy)hydroxides, silica, and biotic surfaces occurs at higher pH. Both processes reduce the mobility of U in freshwater. The configuration of uranyl ion (UO_2^{2+}) with the oxygen atoms located collinearly allows for a strong structure when absorbed to minerals. This provides considerable resistance to mobility particularly when adsorbed between the layers of carbonaceous material. The enrichment or depletion of radionuclides, including U is influenced by oxides of iron and manganese. These oxides may reduce U from U^{6+} to U^{4+}. The partitioning of U in sediment can be very stable, for example, Edgington et al. [78] reported that U in sediments of Lake Baikal has not been significantly redistributed over at least the past 250,000 years.

In sediments, trace metals and radionuclides can bind to sediments through absorption at particle surfaces, incorporation into the lattices of primary or secondary minerals, or occlusion in amorphous material [70, 79, 80]. The binding of metals and radionuclides to sediment reduces their mobility and bioavailability. Jenne [81] proposed that hydrous oxides of manganese and iron are primarily responsible for the fixation of metals to sediment. The binding of metals to the oxides is affected by E_h, pH, concentration of the metal and competing metals, concentrations of other ions capable of forming inorganic complexes and organic chelates [81]. Sediment characteristics, such as particle size, organic content, cation-exchange capacity, and microbial dynamics also influence retention in sediment [70, 79]. Because of internal lake mixing, sediments in profundal areas tend to be finer and higher in organic content than shallow littoral sediments and in many respects similar to the upper most A_o horizon of soils [82]. U concentrations in sediment are dependent on sediment organic matter content [83]. Consequently, U in floodplain soils is largely associated with organic matter as a result of sediment deposition [84] and is associated with the acid-soluble fraction in sequential extractions [85].

Changes in environmental conditions may facilitate the release of radionuclides from sediment to the overlying water. For instance, changing environmental conditions such as E_h, pH, temperature, salinity, biological activity, and ligand types and concentrations may affect the speciation of radionuclides, their complexation, and consequently their mobility, bioavailability and toxicity. If the bottom waters of the hypolimnion are anoxic, U strongly sorbs to particles and the sediment, whereas other redox-sensitive radionuclides may be released back into the water where they persist, mainly in the colloidal form, until reaeration of the water column with lake turnover. Lake mixing will result in the redistribution of the radionuclides throughout the water column and the subsequent loss of particle-reactive radionuclides to bottom sediments [73, 86]. Resuspension of contaminated sediment particles may also result in release of radionuclides into the water column with the degradation of the suspended particles. For example, Simpson et al. [87] found that resuspension of sediments for several hours reduced acid volatile sulfide concentrations, which resulted in release of a significant fraction of the trace radionuclide sulfide phases in the marine environment.

Aquatic organisms may take up radionuclides directly from the water column via respiration, by

adsorption of radionuclides to their outer body surface and from ingestion of food. The latter includes ingestion of suspended particles by filter feeders such as zooplankton and clams, ingestion of bottom sediment by benthic organisms, and the indirect ingestion of sediment in the gut of prey organisms. Benthic organisms are also exposed to radionuclides in sediment pore waters. The major route of exposure may vary with the life stage of the organism and the radionuclide's concentration and bioavailability in a particular medium. For example, when aqueous concentrations are high, the major route for uptake may be from the water, whereas when aqueous concentrations are low, uptake may be mainly from sediments by way of the food chain [73].

Aquatic Food Chain

Uranium does not biomagnify through the food web and tends to decrease with successive trophic levels (Table 2). Therefore, U generally poses minimal risk to aquatic and semiaquatic wildlife. The exception is waterbodies where U concentrations are greatly elevated.

In contaminated Beaverlodge Lake, the food chain pathway was sediment → insects → forage fish → lake whitefish (*Coregonus clupeaformis*) and white sucker (*Catostomus commersoni*). The bottom-feeding fish, the whitefish, and sucker, had much higher U concentrations than pelagic fishes, for example, lake trout (*Salvelinus namaycush*) [68].

Since U mine/mill effluent releases are mainly to surface waters, it is the aquatic system that is most affected by effluent releases. In freshwater systems, the CR between aquatic plants and water may be high [47], which can lead to secondary toxicity via the accumulation of U in organisms feeding on aquatic plants. Bird and Schwartz [47] reported geometric mean U concentration ratios for shield lakes of 1,780 $L \cdot kg^{-1}$ (GSD = 1.6) for algae, 1,750 $L \cdot kg^{-1}$ (GSD of 2.2) for macrophytes, 950 $L \cdot kg^{-1}$ (GSD =16) for freshwater invertebrates, and 6.2 $L \cdot kg^{-1}$ (GSD = 6.2) for freshwater

Uranium in the Environment: Behavior and Toxicity. Table 2 Uranium concentrations in the aquatic food chain

Lake Michigan [88]		Lake in central interior of British Columbia [55]		Beaverlodge Lake Area, northern Saskatchewan [68, 89]	
Taxa	ng $U \cdot g^{-1}$	Taxa/media	μg $U \cdot g^{-1}$	Taxa/media	μg $U \cdot g^{-1}$ ww
Pisivorous fish	0.5–0.7	Water	0.34 ± 0.17 $\mu g \cdot L^{-1}$	White sucker (*Catastomus commersoni*)	0.06 ± 0.01
Planktivorous fish	0.3–0.6	Rainbow trout (*Oncorhynchus mykiss*)	<0.005	White fish (*Coregonus clupeaformis*)	0.08 ± 0.02
Benthic invertebrates	2–8	Finescale sucker (*Catastomus Catastomus*)	0.005	Lake trout (*Salvelinus namaycush*)	0.005
Zooplankton	16–44	Snail (*Pisidium* sp.)	0.4	Spottail shiner (*Notropis hudsonius*)	1.03
Benthic filamentous algae	51	Plankton	0.6 ± 0.2	Lake chub (*Couesius plumbeus*)	0.62 ± 0.11
Phytoplankton	88–156	Algae	13.4	Juvenile white sucker (*Catostomus commersoni*)	2.67
Macrophytes	62–615	Sediment	10.3 ± 6.2	Blackflies (*Simulium* spp.)	2.6 ± 0.5
				Chironomus spp.	15
				Caddisflies (*Nemotaulius* sp.)	25.6 ± 2.6
				Sediment	109 ± 22

fish. Concentration ratios tend to be higher at low contaminant concentrations, and lower at higher contaminant concentrations. For example, in lakes near Canadian U mines where U concentrations were elevated, EC and HC [6] calculated site-specific geometric mean concentration ratio of 89 (maximum of 158) was calculated for algae, 1.5 (maximum 38) for macrophytes, and 1.24 (maximum of 38) for fish. Wildlife that feed in and along the contaminated waterways have the potential to become contaminated through ingestion of high levels of U in plants, water, and sediment. EC and HC [6] concluded that at some mine sites consumption of macrophytes, fish, water, and sediment were important pathways for U uptake and risk quotients (RQs) indicated potential toxicity to terrestrial mammals. For example, EC and HC [6] reported a RQ of 0.17 for muskrat at background concentrations of U (0.35 $\mu g \cdot L^{-1}$) and RQs up to 21 for muskrat at a site where the U concentration was 1,061 $\mu g \cdot L^{-1}$. In the marine environment, water exposure was the main route of uptake of U by crab (*Pachygrapsus laevimanus*) and zebra winkle (*Austrocochlea constricta*) [90].

Sediment Ingestion

Sediment ingestion may represent a major source of U for wildlife [57] and is usually considered an important pathway in environmental risk assessments. The amount of U retained from dietary sediment is a function of the total amount of U ingested and its bioavailability (see soil ingestion). Sediment ingestion is highly variable and may change seasonally [57]. Wildlife preying on invertebrates in sediments may ingest much sediment. For example, the diet of mallard ducks on average contained 3.3% sediment but 10% of the 88 specimens examined consumed 26% sediment in their diet at certain times of the year [57]. Sandpipers consumed 7–30% sediment in their diet and two wood ducks contained >70% sediment in their gut. Information is not available on the portion of sediment in the diet of other animals such as the muskrat that often dig into the sediment to acquire their food and feed primarily on roots during winter [91], or the moose which has been observed to feed on the rhizomes of aquatic plants shortly after ice-out in spring, before new plant growth has developed (personal observation). It is assumed that these animals periodically ingest a high proportion of sediment in their diet. Higher accumulation of U occurs in the roots of cattails (*Typha* sp.) than other parts of the plants [92]. Muskrats and similar animals may also consume sediment indirectly while grooming themselves. Sequential extraction studies to determine the bioavailability of sediment-bound U at Beaverlodge Lake area showed that between 69% and 90% of the U in contaminated sediment may be bioavailable [93]. EC and HC [6] assumed sediment to be 2–5% of the diet depending on the wildlife species and made the assumption that sediment U was assimilated at the same rate as U ingested from food.

Uranium Toxicity

The remainder of this entry focuses on the toxicity of U, with emphasis on more sensitive organisms to assist the practitioner in establishing toxicity benchmarks.

The most commonly used compounds to assess the toxicity of U are uranyl nitrate ($UO_2(NO_3)_2 \cdot 6H_2O$) and uranyl sulfate ($UO_2SO_4 \cdot 3H_2O$). Uranyl acetate ($UO_2(C_2H_3O_2)_2 \cdot 2H_2O$) is occasionally used. These ionize in water to form hexavalent uranyl ions (UO_2^{2+}).

Toxicity Benchmark Values

Benchmark values are the measurement endpoint of the environmental assessment. The values are used to protect the species or communities of concern based on toxicological data. Benchmarks are the toxicological concentrations of a contaminant where low effects or no effects are expected to the species, population, or community based on ecologically relevant endpoints such as survival, growth, and reproduction. Application factors are often applied to the lowest observed effect concentration (LOEC) or critical toxicity value (CTV) to ensure protection of more sensitive species than the test species.

Toxicity to Terrestrial Plants

There have been surprisingly few studies on the toxicity of U to plants (Table 3), particularly in comparison to the work on U toxicity to mammals (below). In a literature review, Sheppard [97] reported U toxicity to plants at soil concentrations ranging from 0.5 to 2,600 $mg \cdot kg^{-1}$ dw. Work by Aery and Jain [94] showed that the

Uranium in the Environment: Behavior and Toxicity. Table 3 Uranium toxicity to terrestrial plants and soil organisms based on soil concentrations (mg U·kg^{-1} dry soil)

Taxa	Endpoint	Effect concentration	Reference
Plants			
Wheat (*Triticum aestivum*) L. var. WH-147	EC_{44} # seeds/spike	1	Aery and Jain [94]
	EC_{58} # seeds/spike	5	
Cotton and sugar beet	EC_{25} for yield	5	Shevchenko et al. (1987 cited in [94])
Wheat (*Triticum aestivum*), and *Lycopersicon esculentum*	EC_{25} for biomass yield	6	Gulati et al. [95]
Native range grasses purple threeawn (*Aristida purpurea*), buffalograss (*Buchloe dactyloides*) and little bluestem (*Schizachyrium scoparium*)	LOEC for biomass increase	50	Meyer et al. [96]
Crop plant	EC_{11} for yield	50	Zhukov and Zudilkin (1971 cited in [97])
Scots pine (*Pinus sylvestris*)	NOEC for growth	>100	Sheppard et al. [98]
Rice	EC_{25} for survival at harvest	250	Bufatin et al. (1985 cited in [99, 100])
Crop plants and pine (*Phaseolus vulgaris*, *Zea mays*, *Lactuca sativa*, *Lycopersicon esculentum*, *Brassica rapa*, and *Pinus strobes*)	EC_{25} for pod yield in beans	300	Sheppard et al. [99]
Grass (*Elymus lanceolatus*)	NOEC for emergence, length, and biomass	1,000	Sheppard et al. [100]
Soil fauna			
Collembola (*Onychiurus folsomi*)	EC_{20} for survival and reproduction in fine sand	92–190	Sheppard et al. [100]
Earthworm (*Lumbricus* sp.)	LOEC for survival	300	Sheppard and Evenden [100]
Collembola (*Folsomia candida*)	EC_{20} for survival in fine sand	350	Sheppard et al. [100]
Collembola (*Onychiurus folsomi*)	EC_{20} for survival and reproduction in loam soil	>390	Sheppard et al. [100]
Collembola (*Folsomia candida*)	EC_{20} for survival and reproduction in loam soil	>710	Sheppard et al. [100]
Earthworm (*Lumbricus* sp.)	NOEC for survival	1,000	Sheppard et al. [100]

addition of only 1 mg U·kg^{-1} dry soil affected the growth of wheat (*Triticum aestivum*). At 1 mg U·kg^{-1}, there was an 11% decrease in the number of spikes per plant, 44% decrease in the number of seeds per spike, and 8% decrease in seed weight. This is a toxic effect to a plant species at a U concentration representative of background conditions. A dose-dependent response was seen in each of these endpoints as soil U concentration increased. At 125 mg U·kg^{-1} soil, number of spikes and seeds per spike each declined by more than 70%. Thus, U may inhibit the growth of certain plants at natural concentrations. In contrast, Sheppard et al. [99] found that seed germination of corn, lettuce, tomato, rapeseed (*Brassica rapa*), and

pine was not affected by U at concentrations as high as 1,000 mg U·kg^{-1} dw in garden soil (high organic carbon content), presumably because of the lower bioavailability of U. In limed brunisol soil, seed germination was significantly reduced at 1,000 mg U·kg^{-1} dw. Pine seeds exposed to 1,000 mg U·kg^{-1} dw soil did not germinate, whereas seed germination was not affected by 300 mg U·kg^{-1} dw soil. However, germination apparently is not as sensitive to U toxicity as plant growth [101]. In plants grown in Hoagland's nutrient solution, Weinberger and Murthy [101] found that tomato seedlings are more sensitive to U than other plant species tested, showing a 24% reduction in growth at 4.24 mg U·L^{-1} and 44% at 42.4 mg U·L^{-1}. Greater sensitivity of tomatoes to U in their study [101] is probably due to increased bioavailability of the U in the absence of soil. Considerable differences can be expected in the toxicity of U between studies using natural soils and nutrient solutions; the latter have little relevance to natural systems.

Addition of uranyl nitrate solution to soil suppressed the growth of spring wheat by 50% at 50 mg·kg^{-1} soil and by 91% times at 100 mg·kg^{-1} soil, but had no effect at 10 mg·kg^{-1} soil. Addition of phosphorus fertilizers to soil reduces the effect of U on plant growth, probably because insoluble uranyl phosphate complexes are formed at high phosphorus (>75 μg·L^{-1}) concentrations rendering U unavailable for plant uptake [14]. In contrast, a positive response is seen in some studies when uranyl nitrate is used due to the plants responding to nitrate.

In a 22-day bioassay with northern wheatgrass (*Elymus lanceolatus*) a significant decrease in shoot and root length and in total plant biomass was observed at 3,000 mg U·kg^{-1} soil compared to controls in neutral pH loam and for root length at 3,000 mg U·kg^{-1} compared to controls in a fine sand with pH of 6.2 [99]. Sheppard et al. [100] reported an overall EC_{25} in the range of 300–500 mg U·kg^{-1} dry soil for terrestrial plants and derived a value of 250 mg U·kg^{-1} dry soil as the Estimated-No-Effect-Concentration (ENEC).

Soil Invertebrates

The toxicity of U to soil invertebrates also has been little investigated (Table 3). In garden soil, survival of earthworms (*Lumbricus terrestris*) to 75 days was not affected by U concentrations of 3–1,000 mg·kg^{-1} dw soil [99]. However, the study only investigated the effects of U on mature earthworms. In another study, Environment Canada's bioassay protocol was followed for three different soil organisms: an acute 14-day survival and a 56-day chronic reproduction bioassay with the worm *Eisenia andrei*; a 28-day reproduction test with the collembolan, *Folsomia candida*; and 35-day reproduction test with mature adults of the collembolan *Onychiurus folsomi* [100]. No effect was seen on earthworm survival at 1,000 mg U·kg^{-1} soil compared to controls for the three soils, and for reproduction in two of the three soils. An EC_{20} of 350 mg U·kg^{-1} soil for survival of *F. candida* was observed in limed fine-sand soil with pH 6.2. EC_{20}s of 710 to > 3,000 mg U·kg^{-1} were recorded in the other two soils. Results for *O. folsomi* were similar with EC_{20}s from 390 to >1,000 mg U·kg^{-1}. *O. folsomi* a root-eating springtail was much more sensitive to U in the limed fine-sand soil with survival and reproduction EC_{20}s as low as 92 mg U·kg^{-1}.

Sheppard et al. [100] proposed an ENEC of 100 mg U·kg^{-1} dry soil for the protection of soil invertebrates. This value is below the Province of Ontario [41] guideline of 300 mg U·kg^{-1} dw soil for soil and higher than the maximum background U soil concentration [41, 102]. CCME [10] derived a soil uranium quality guideline of 23 mg·kg^{-1} for residential, parkland, and agricultural land use for protection of both human and environmental health.

Uranium Accumulation and Toxicity in Mammals

The uptake and deposition of U in the body is dependent on the mode of entry, inhalation or ingestion, and the form of U. Early studies demonstrated that U compounds could be grouped into those that are slightly toxic (UO_2, U_3O_8, and UF_4), moderately toxic (UO_2, NaU_2O_2, $(NH_4)_2U_2O_7$, and high-grade ore), and highly toxic (UO_2F_2, UCl_2, UO_4). In toxicity studies, it is a common practice to inject the U intravenously to follow the fate of U once it has entered the bloodstream following ingestion and uptake by the gastrointestinal tract.

Inhalation to Lungs Inhalation is not generally considered a major pathway for uptake of U by wildlife.

However, resuspension of respirable particles in the upper few millimeters of soil may be important in the contamination of small mammals at highly contaminated sites [56]. For humans, inhalation of natural U is only important in industrial settings; however, inhalation of dust is considered the major pathway for depleted U exposure both in combat and noncombat situations [1].

Absorption of U through the lungs is related to U solubility in water and its ability to form stable bicarbonate complexes. Insoluble, UO_3, UO_4, UF_4, or ammonium or sodium diuranate are deposited primarily in the lungs with little absorption into the blood. In contrast, dusts of UF_6, UO_2F_2, $UO_2(NO_3)_2{\cdot}6H_2O$, and UCl_4 are absorbed from the lungs and circulate in the blood to bone and kidney [103]. Their effect is primarily on the kidney as described for ingestion below.

In a long-term study of up to 6.5 years duration in which dogs and monkeys were exposed for 1–5 years to natural UO_2 aerosol, Leach et al. [104] found that the lungs and the tracheobronchial lymph node were the principal sites of U retention and the only tissues that exhibited pathological effects. The kidney showed no evidence of U toxicity. At the end of 5 years of inhalation exposure, U concentrations in the lungs of dogs were in the 2,000 $\mu g{\cdot}g^{-1}$ range (~22 mSv/week) and those of the monkeys were 4,000 $\mu g{\cdot}g^{-1}$ range (~44 mSv/week); values well above the maximum permissible organ concentration of 25 $\mu g{\cdot}g^{-1}$ for natural uranium [105]. They observed dose-dependent pulmonary and tracheobronchial lymph node fibrosis in the lungs, consistent with radiation effects. Effects were more marked in the monkey than in dogs. Biological half-times for U in the dog and monkey lungs ranged from 420 to 660 days. For the rat, the biological half-time in the lung averaged about 300 days.

Uptake Through the Digestive Tract The amount of U that resides in an organ at steady state is proportional to the amount of ingested U absorbed from the gut, the fraction of absorbed U deposited in the organ, and the biological half-time of U in that organ [106]. For wildlife almost all the daily U intake is from food, water, and ingestion of soil/sediment. Inhalation and dermal exposure may also be important pathways in some instances [107]. For humans, the U content of most food is in the range of 0.01–0.1 $\mu g{\cdot}g^{-1}$, but because of poor absorption in the gastric tract, the average daily intake of U is only about 1.0 $\mu g{\cdot}day^{-1}$ [108]. On average, food contributes about 15% of ingested U and drinking water contributes about 85% [108].

Ingestion is probably the major exposure route to U for wildlife. A key consideration in determining the importance of ingestion is the assimilation rate from the gut. This value determines how much material is ultimately transported to the blood for deposition in critical organs and is the greatest source of uncertainty in dose estimates for the ingestion of long-lived alpha-emitting radionuclides [109]. Uptake of U following ingestion has been reviewed by Wrenn et al. [110, 111], Durbin and Wrenn [103], Yuile [107], the International Commission on Radiological Protection (ICRP) [112], and Leggett and Harrison [113] for the development of models to estimate allowable daily intakes in humans. These reviews provide data on laboratory studies with mammals and are applicable to wild species.

The uptake rate of U from the gut is generally low, ranging from <1% of the diet to 3–4% [110, 113] and can be quite low, for example, about 0.06% for both rats and rabbits with values ranging up to about 2.8% [60, 114–117]. Factors affecting this rate are the feeding status of the organism and the species [118]. The ICRP [112] assumed for adult humans, a conservative absorption rate of 5% of diet for soluble U and 0.2% for insoluble U. Slightly higher rates of uptake (up to 5%) are reported for water than food [113]. In chronic clinical studies with humans, Hursh et al. [119] reported that only about 0.5–5% of an orally administered acute dose of 11 mg U as uranium nitrate hexahydrate was absorbed. However, in another study based on daily intake rates and daily U excretion rates, absorption of 12–31% was calculated [120]. The value of 5% is considered conservative for humans. Therefore, the uptake of U by ingestion is low.

Elimination Through Feces Most of the U intake through ingestion remains in the digestive tract and is lost in the feces.

Elimination Through Kidney Absorbed U is eliminated from the body primarily by kidney excretion. More than 90% of the U absorbed into the blood is excreted into the urine and less than 1% is eliminated

by feces. Daily urinary excretion is about 0.15–0.38 μg for humans. There is a rapid initial phase of excretion in which 70–80% of the U is lost in the first 24 h following administration of the dose. The remaining 20–30% has a biological half-time of 6 months to 1 year.

The chemical toxicity of U to mammals has been reviewed by Durbin and Wrenn [103], Leggett [121], and Ribera et al. [2]. A selection of more sensitive uranium toxicity findings for mammals is presented in Table 4. The major site of U burden in mammals is the skeleton, followed by the kidney. In the skeleton, U replaces calcium in the surface of bone crystals. Effects observed in bone (i.e., osteosarcoma) are attributed to radiotoxicity and not chemical toxicity [2]. Although U accumulates in bone and kidney [103, 107, 121], chemical effects are primarily in the kidney. Literature values for the fraction of U deposited in the bone range from 20% to 32% with retention half-times of 40–180 days [114] and in the kidney range from 7.2% to 45% with retention times of 5–9 days [117]. The removal of U in the urine follows a power function $Y_u = 0.015\ t^{-1.5}$ where t is in hours. Uranium deposited in the peripheral part of the renal cortex and in bones is eliminated very slowly.

Kidney Toxicity The kidney is the critical organ in terms of U chemical toxicity. This is despite the fact that much of the U in the kidney is excreted rapidly. Renal damage occurs when U reacts chemically with the protein of columnar cells lining the tubular epithelium, leading to cellular injury and necrosis [131]. In the blood, uranyl ion circulates as a relatively inert bicarbonate-uranyl complex. When this is filtered in the kidney tubules, the uranyl ions dissociate from the carbonates in the acidic environment of the kidney. The uranyl ion is concentrated in the tubular lumen where the ions may cause damage to kidney structure. If the damage is severe enough, kidney failure may occur. Necrosis of kidney tubules results in albuminuria, elevated blood urea nitrogen, and a loss of weight. The proximal convoluted tubule of the nephron is the site most affected. Uranium toxicity occurs through the disruption of kidney function by binding to the membranes of renal tubular cells, restricting the reabsorption of glucose, sodium, amino acids, protein, water and other substances, and causing cell death by suppression of cell respiration [121]. Uranyl ion also competes with ATP for a binding site on the Ca^{+} and Mg^{2+} adenosine triphosphatase (ATPase) and this may be a factor in renal toxicity [114]. Damage to the kidney

Uranium in the Environment: Behavior and Toxicity. Table 4 Selected more sensitive U toxicity findings for mammals (mg U·kg^{-1} body weight·day^{-1})

Taxa	Endpoint	Effect concentration	Reference
Male rat	LOEC for effects on testes	0.03	Malenchenko et al. (1978 cited in [122])
New Zealand white rabbits	LOEC for change in kidney histopathology	0.05	Gilman et al. [123, 124]
Sprague-Dawley rats	LOEC for renal damage	0.06	Gilman et al. [125]
New Zealand white rabbits	LOEC for renal damage	1.36	Gilman et al. [124]
Swiss mice	LOEC for growth of pups from exposed mothers	2.8	Paternain et al. [126]
Mice	LOEC for maternal weight gain and developmental effects	< 5	Domingo et al. [127]
Rabbit	LOEC for weight loss and limited renal damage	3	Maynard and Hodge [128]
Swiss mice	LOEC for pregnancy rate (untreated mates?)	5.6	Llobet et al. [108]
Dog	Histological effects in kidneys	9	Maynard et al. [129]
Mice	LOEC for litter size	< 50	Domingo et al. [130]

becomes evident as the cells of the proximal tubules stop functioning and die. The tubular epithelium undergoes massive cellular necrosis resulting in cell rupture and discharge of cellular contents into the urine. Cellular necrosis appears to be brought about by alternations in the transport of organic compounds and ions across tubule cell membranes along with changes in intercellular protein binding. Severe impairment may result in death. Sublethal damage is usually repairable.

Commonly used serum parameters of renal function such as creatine and urea concentration only become abnormal when a significant impairment of organic function has been sustained. Injury to the glomerulus typically increases glomerulus permeability, permitting the passage of high molecular weight proteins the size of albumin (69,000 Da) or larger to pass into the urinary filtrate. Injury to the renal proximal tubules prevents the usual reabsorption of low molecular weight proteins from the filtrate, permitting these to appear in increased concentrations in the urine, a condition called tubular proteinuria. Low molecular weight proteins are largely taken up by pinocytosis in the proximal renal tubules and then degraded to the amino acid level in the lysosomes. The proximal reabsorption of small proteins is possibly selective and seems to be a vulnerable process [114].

Toxicity of U compounds is governed by their solubility. The soluble hexavalent U compounds have LD_{50} values after injection in the range of 0.1–1 mg U·kg^{-1} bw in different animal species, whereas after oral application the acute toxicities are a few hundred mg·kg^{-1} bw. Less soluble tetravalent U compounds are generally nontoxic at concentrations up to 20% of the diet.

For U, lethality is a common endpoint used for acute studies, while kidney function is the predominant endpoint for chronic studies. Acute exposures have demonstrated that U has low toxicity to most species, often requiring concentrations greater than 2% in the diet to elicit an acute response. Rabbits are a sensitive species, with LD_{50} values below 0.5% of the diet. An LD_{50} value of 23 mg U·kg^{-1} bw·d^{-1} has been reported for the rabbit in a 30-day feeding study with soluble U [103].

Animal studies performed at the Universities of Rochester and Chicago in the 1940 s and 1950 showed that the dog is more susceptible to U^{6+} effects than the rodent; UO_2F_2 is the most toxic uranyl compound in acute lethality studies in rats, two times more toxic than uranyl nitrate and in long-term feeding studies was four to six times more toxic than uranyl nitrate; and U-induced renal injury (catalauria in 2–4 days) occurs in the rabbit with a dose as low as 10 μg·kg^{-1} of U^{6+}. Uranyl fluoride metabolism agrees generally with that of uranyl nitrate, uranyl citrate, and uranium trioxide. Renal tubular dysfunction (glucosuria) occurred in response to a 10 μg·kg^{-1} absorbed (injected) dose. Retention half-times in the dog were 79.5 days for the kidney and 883 days for bone [132].

Environment Canada [8] in their review of U toxicity to mammals reported LD_{50}s for U toxicity administered orally of 12 mg·kg^{-1} for dogs and 238 mg·kg^{-1} for cats. The LD_{50} of uranyl nitrate to rats was 135–204 mg·kg^{-1} over 24 h and 1–2 mg·kg^{-1} over 1–21 days. Chronic intake of U in concentrations of 0.6–1 mg·L^{-1} causes essentially no accumulation of U in kidney or bone. The minimum oral dose given for 1 year that produced renal damage in the dog was 25 mg·kg^{-1}·day^{-1} for uranyl fluoride; a value considerably higher than the tolerable daily intake of U of 0.6 μg·kg^{-1} body weight from drinking water [133, 134].

Moss [114] reported that renal tissue U concentrations in the range of 1–3 mg U·kg^{-1} lead to renal tubular changes, which are rapidly followed by adaptive and regenerative changes. Histological changes occur in rats at renal burdens of 0.7–1.3 mg·kg^{-1}. The threshold for toxic damage is as low as 0.1 mg U·kg^{-1} bw [107, 135].

Since the kidney is the most sensitive organ to U toxicity, the threshold effect level for U in the kidney is an appropriate benchmark for the assessment of U toxicity. The ICRP [136] adopted a maximum permissible concentration of 3 mg·kg^{-1} ww in kidney for the protection of humans, but reduced the value to 1 mg·kg^{-1} as indicators of kidney function became more sensitive [26, 110]. SuLu and Fu-Yao Zhao [137] recommended that the kidney U burden should not be allowed to exceed 0.26 mg·kg^{-1} in kidney of humans based on a tenfold safety factor and mild impairment of kidney function at 2.6 mg·kg^{-1}. This is in agreement with Morrow et al. [132], who found a renal concentration of 0.3 mg·kg^{-1} kidney was close to a threshold concentration for renal injury. Damage

to kidney becomes evident in virtually all species at levels of about 0.5 mg·kg^{-1} ww [26, 118]. Although the kidney has substantial reserve capacity, and may function with the loss of a proportion of the nephrons, the loss of reserve capacity is considered an adverse effect.

Based on long-term feeding studies with dogs, a No-Observed-Effect Level (NOEL) for U of 1 mg·kg^{-1}·day^{-1} was estimated [26]. Gilman et al. [123–125] studied the effect of U on kidney damage in the rabbit and the rat. The Lowest-Observed-Effect Level (LOEL) in rabbits exposed to U as uranyl nitrate hexahydrate in their drinking water over a 91-day period was 0.05 mg U·kg^{-1} bw·day^{-1} (0.04 mg U·kg^{-1} ww kidney) in males and 0.49 mg U·kg^{-1} bw·day^{-1} (0.02 mg U·kg^{-1} ww kidney) in females [123]. A NOEL was not identified. In their study, four male rabbits developed *Pasteurella multocida* infection and were removed from the study. The highest doses administered, 28.7 mg U·kg^{-1}·day^{-1} (4.98 mg·kg^{-1} ww kidney) and 43.02 mg U·kg^{-1}·day^{-1} (1.03 mg U·kg^{-1} kidney) were toxic with significant effects on kidney physiology and pathology and in some cases may have been lethal [123]. Permanent kidney damage was likely in male rabbits. Female rabbits were less affected than males, although significant nuclear changes (anisokaryosis and vesiculation) were seen even at the lowest exposure (0.49 mg U·kg^{-1}·day^{-1}). Sensitivity of male rabbits was greater in this study than in a subsequent study with specified pathogen-free male rabbits [125]. This caused Gilman et al. [125] to speculate that subclinically expressed disease stress may have caused the male rabbits to be more susceptible to the effects of U in the initial study.

In a similar study using male and female Sprague-Dawley rats, a LOEL of 0.06 mg U·kg^{-1} bw·day^{-1} for males and 0.09 mg U·kg^{-1} bw·day^{-1} for females was reported [124]. At the lowest exposure level (0.09 mg U·kg^{-1} bw·day^{-1}), significant changes were seen in renal tubules of males, which may result in permanent injury to basement membranes with loss of nephrons and reduced renal function [124]. In females, the most important changes were sclerosis of glomerular capsules and reticulin sclerosis of tubular basement membranes and interstitial scarring, which are non-repairable and occurred at the lowest exposure level. The authors suggested that sustained exposure would likely have increased the number of damaged glomeruli and ultimately impaired renal function.

Effects on Offspring Domingo et al. [127] observed an increased incidence of external malformations, specifically exeacephaly, cleft palate, micrognathia, and short or curled tails in response to maternally toxic doses to mice. The incidence of hematomas, especially in facial or dorsal areas, also increased. No internal soft tissue malformations were observed. Undeveloped renal papillae (a developmental alteration) occurred in fetuses from the 5 and 25 mg·kg^{-1}·day^{-1} groups.

In another study, Paternain et al. [126] looked at the effects of uranyl acetate dehydrate on the reproduction, gestation, and postnatal survival of mice. They found that the number of dead offspring increased with oral dose. The total number of dead per total number of offspring produced per treatment over the 21-day study period expressed as a percentage was 8.2% at 0 mg·kg^{-1} bw·day^{-1}, 23% at 5 mg·kg^{-1} bw·day^{-1}, 26.5% at 10 mg·kg^{-1} bw·day^{-1}, and 42.3% at 25 mg·kg^{-1} bw·day^{-1}. The mortality of offspring between birth and day 21 (viability index) was significantly greater (Chi-squared test) in each of the U-treated groups than the controls [6]. Growth, measured as body weight over the 21-day period, was also significantly reduced in each of the U-treated groups compared with the control group. The number of dead young per litter was significantly greater than controls in the 10 and 25 mg U·kg^{-1} bw·day^{-1} groups at day 0.

On the basis of dead offspring per treatment over the 21-day period of lactation, mortality was three times greater at 5 mg·kg^{-1} bw·day^{-1} (2.8 mg U·kg^{-1} bw·day^{-1}) than that for controls. The value of 2.8 mg U·kg^{-1} bw·day^{-1} was considered a critical toxicity value (CTV) for effects on reproduction of the mouse by EC and HC [6], who used an application factor of three to derive the Estimated-No-Effect Value (ENEV) of 0.93 mg U·kg^{-1} bw·day^{-1} for effects on mortality of offspring in mice. The three-fourth power function for body weight [138] was used to derive species-specific ENEVs for the wildlife [6].

It can be concluded that U is a highly toxic element when soluble salts are administered peritoneally, but toxicity is lower when ingested due to low gastrointestinal absorption. Therefore, U is generally not a chemotoxic threat as an environmental contaminant

unless concentrations are elevated. Benchmark values of 0.5 mg·kg^{-1} ww kidney and about 1.0 mg U·kg^{-1} bw·day^{-1} should be protective of kidney function in most mammals.

Waterfowl

Reviews of U uptake indicate that birds may retain greater amounts of U than mammals at the same levels of exposure [139]. Sample et al. [138] reported a NOEL value of 16 mg U·kg^{-1} bw·day^{-1} for U toxicity to birds. This value was based on a toxicity study by Haseltine and Sileo [140] on the black duck using depleted U. However, the use of this study to derive a NOEL for birds is questionable, because depleted U is a metallic form of U which has very low bioavailability in the gut.

Growing chicks are relatively tolerant of U with a 7-day LD_{50} of 235 mg·kg^{-1} body weight, which is considerably higher than 24-h LD_{50} of 135–305 mg·kg^{-1} bw for rats [141]. Hepatotoxicity is a predominant feature of U toxicity in chickens.

Fish

Absorption of U by fish takes place in the gut, epidermis, and gills. Uptake of U via the diet is considered to be the primary route of U exposure for fish [68, 142–144], although others consider uptake to be primarily via the gill as is common for metals [145]. In laboratory studies, Simon and Garnier-Laplace [146] found that trophic transfer through the diet was minimal as is the case for many terrestrial species. Uranium accumulates in intestine, bone, scales, gonad, kidney, liver, and gill when U is taken up through the gut from the diet (Fig. 2).

The renal tubular excretion system in fish is similar to other vertebrates [8]; therefore, the toxicity of U to fish is expected to be similar to that of mammals. For example, lake whitefish (*Coregonus clupeaformis*) fed a commercial diet contaminated with U developed renal lesions in proximal tubules similar to those reported for mammals [143]. Focal hepatocyte necrosis of the liver and alterations of the bile ductile epithelium were also observed.

Acute and chronic toxicity data for aquatic biota are summarized in Table 5. In several studies, toxicity was greater in soft water than in hard water. For example, Tarzwell and Henderson [148] reported LC_{50}s for fathead minnow (*Pimephales promelas*) of 2.8 mg·L^{-1} in soft water (20 mg·L^{-1} hardness) and 135 mg·L^{-1} in hard water (400 mg·L^{-1} hardness) for uranyl sulfate. Parkhurst et al. [149] reported a sixfold increase in hardness from 35 to 208 mg·L^{-1} decreased the 96-h LC_{50} of U to brook trout (*Salvelinus fontinalis*) by a factor of four. In soft water, U LC_{50} values ranged from 0.73 to 3.46 mg·L^{-1} for six tropical species of fish [145], while the threshold toxicity for growth in a larval

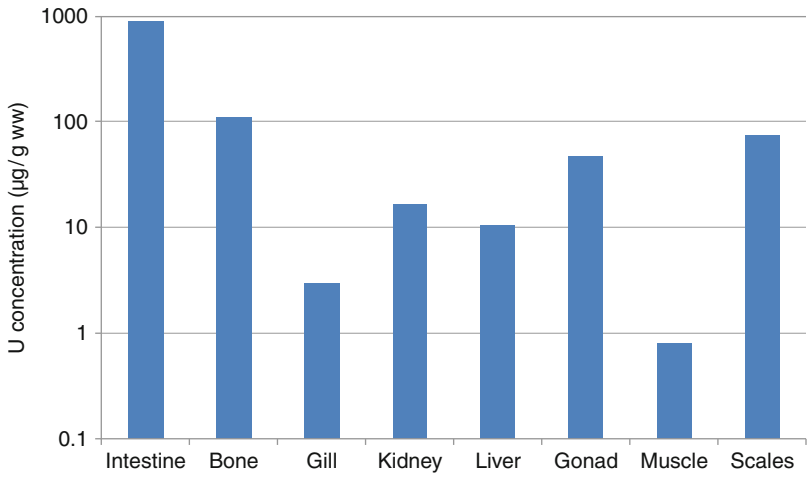

Uranium in the Environment: Behavior and Toxicity. Figure 2
Uranium concentration in tissues of white fish exposed to contaminated diet for 100 days (Based on Cooley and Klaverkamp [144])

Uranium in the Environment: Behavior and Toxicity. Table 5 Uranium toxicity ($\mu g \cdot L^{-1}$) to freshwater aquatic organisms with emphasis on hardness as a modifying parameter. *H* hardness as $mg \cdot L^{-1}$ $CaCO_3$, *A* alkalinity as $mg \cdot L^{-1}$ $CaCO_3$

Taxa	Endpoint	Aqueous parameters	Effect concentration ($\mu g \cdot L^{-1}$)	Reference and true hardness assessed yes or no[a]
Fish				
Fathead minnow (*Pimephales promelas*)	96-h LC_{50}	H23, A12, pH 6.3–7.0	2,000	Vizon SciTec Inc [147] Yes, no effect
	96-h LC_{50}	H72, A14, pH 6.5–6.8	2,000	
	96-h LC_{50}	H131, A10, pH 6.4–6.8	2,100	
	96-h LC_{50}	H244, A10, pH 6.4–6.8	1,800	
	7-day LC_{50}	H23, A12, pH 6.3–7.0	1,600	
	7-day LC_{50}	H72, A14, pH 6.5–6.8	2,100	
	7-day LC_{50}	H131, A10, pH 6.4–6.8	2,000	
	7-day LC_{50}	H244, A10, pH 6.4–6.8	1,500	
	7-day LOEC		1,300–2,000	
Fathead minnow (*Pimephales promelas*)	96-h LC_{50}	H20, A18, pH 7.4	1,572	Tarzwell and Henderson [148] No
	96-h LC_{50}	H400, A360, pH 8.2	75,778	
Brook trout (*Salvelinus fontinalis*)	48-h LC_{50}	H184, A146, pH 7.4	59,000	Parkhurst et al. [149] No
	96-h LC_{50}	H32, A12, pH 6.7	5,500	
	96-h LC_{50}	H210, A54, pH 7.5	23,000	
	60-day embryo larval NOEC	H201, A189, pH 8.0	$>$ 9,080	
Brook trout (*Salvelinus fontinalis*)	96-h LC_{50}	H31, A26, pH 6.8–7.0	8,000	Davies [150] No
Rainbow trout (*Oncorhynchus mykiss*)	96-h LC_{50}	H20, A20, pH 6.2–7.0	4,200	Vizon SciTec Inc [147] Yes, no effect
	96-h LC_{50}	H68, A12, pH 6.6–7.0	3,900	
	96-h LC_{50}	H126, A11, pH 6.5–6.9	4,000	
	96-h LC_{50}	H243, A12, pH 6.5–7	3,800	
Rainbow trout (*Oncorhynchus mykiss*)	30-day EC_{50}, NOEL/LOEL embryo/alevin	H6,A7, pH 6.3–7.2	460 $<$280 280	Vizon SciTec Inc [147] Yes, minor effect
	31-day EC_{50} embryo/alevin NOEL/LOEL	H61,A6, pH 6.3–7.2	640 310 610	

Uranium in the Environment: Behavior and Toxicity. Table 5 (Continued)

Taxa	Endpoint	Aqueous parameters	Effect concentration ($\mu g \cdot L^{-1}$)	Reference and true hardness assessed yes or no[a]
Rainbow trout (*Oncorhynchus mykiss*)	96-h LC_{50}	H31, A26, pH 6.8–7.0	6,200	Davies [150] No
Lake trout (*Salvelinus namaycush*)	141-day NOEC 141-day LOEC embryo/alevin/fry	H74–88, A69–77, pH 7.9–8.1	6,050	Liber et al. [151] No
			29,780	
Bluegill (*Lepomis machrochirus*)	96-h LC_{50}	H2.5–3.2, A $<$ 0.1–3.8, pH 5.1–5.6	1,670	Trapp [152] No
Zebra fish (*Brachydanio rerio*)	96-h LC_{50}	H178, pH 7.9	3,050	Labrot et al. [153] No
Colorado squawfish (*Ptychocheilus lucius*)	96-h LC_{50} Swim-up, fry, small, and larger juvenile	H196, A107, pH 7.8	46,000 all stages	Hamilton [154] No
Razorback sucker (*Xyrauchen texanus*)	96-h LC_{50} Swim-up, fry, small, and larger juvenile	H196, A107, pH 7.8	46,000	Hamilton [154] No
Bonytail (*Gila elegans*)	96-h LC_{50} Swim-up, fry, small, and larger juvenile	H196, A107, pH 7.8	46,000	Hamilton [154] No
Flannelmouth sucker (*Catostomus latipinnis*)	96-h LC_{50}	H144, A103, pH 7.9	43,500	Hamilton and Buhl [155] No
Chequered rainbowfish (*Melanotaenia splendida inornata*)	96-h LC_{50} 7-day old	H4.6, A3.3, pH 6.6	2,660	Bywater et al. [145] No
	96-h LC_{50} 14-day old	H4, A3.2, pH 6.6	1,390	
	96-h LC_{50} 90-day old	H4.6, A3.3, pH 6.6	3,460	
Chequered rainbowfish (*Melanotaenia splendida inornata*)	96-h LC_{50} 14-day old	H4.1, A1.8, pH 6.3	1,390	Holdway [156] No
	7-day LC_{50} 31-day old	H4.1, A1.8, pH 6.3	1,570	
Black-banded rainbowfish (*Melanotaenia nigrans*)	96-h LC_{50} 7-day old	H4.7, A3.3, pH 6.6	1,700	Bywater et al. [145] No
	96-h LC_{50} 90-day old	H4.7, A3.3, pH 6.6	1,900	
Northern purple-spotted gudgeon (*Mogurnda mogurnda*)	96-h LC_{50} 6-day old	H4, A3.2, pH 6.6	1,570	Bywater et al. [145] No
	96-h LC_{50} 7-day old	H4.6, A3.3, pH 6.6	1,110	
	96-h LC_{50} 40-day old	H4, A3.2, pH 6.6	329	
	96-h LC_{50} 70-day old	H4, A3.2, pH 6.6	329	
	96-h LC_{50} 90-day old	H4.6, A3.3, pH 6.6	1,460	

Northern purple-spotted gudgeon (*Mogurnda mogurnda*)	96-h LC_{50} 6-day old	H4, A3.2, pH 6.6	1,570	Holdway [156] No
	96-h LC_{50} 40-day old	H4, A3.2, pH 6.6	3,290	
	96-h LC_{50} 70-day old	H4, A3.2, pH 6.6	3,290	
	7-day LC_{50} 1-day old	H4, A1.8, pH 6.3	1,590	
	7-day LC_{50} 1-day old + 7-day postexposure	H4, A1.8, pH 6.3	890	
	7-day LC_{50} 40-day old	H4, A1.8, pH 6.3	2,690	
	7-day LC_{50} 40-day old + 7-day postexposure	H4, A1.8, pH 6.3	1,440	
	7-day LC_{50} 70-day old	H4, A1.8, pH 6.3	3,290	
	7-day LC_{50} 70-day old + 7-day postexposure	H4, A1.8, pH 6.3	2,700	
	14-day LC_{50}, 1-day old	H3.6, A3, pH 6.4	>1,790	
	14-day LC_{50} +15-day postexposure	H3.6, A3, pH 6.4	1,290	
	14-day LOEC,1-day old		1,790	
	14-day NOEC,1-day old		880	
Reticulated perchler (*Ambassis macleayi*)	96-h LC_{50} juvenile	H4.6, A3.3, pH 6.6	800	Bywater et al. [145] No
Delicate blue-eyes (*Pseudomugil tenellus*	96-h LC_{50} juvenile	H4.6, A3.3, pH 6.6	730	Bywater et al. [145] No
Mariana's Hardyhead	96-h LC_{50} juvenile	H4.6, A3.3, pH 6.6	1,220	Bywater et al. [145] No
Zooplankton				
Water flea (*Daphnia magna*)	48-h LC_{50}	H67-73, A54-60, pH 8	5,340–7,620	Poston et al. [157] No
	48-h LC_{50}	H126–140, A93, pH 8	30,440–44,570	
	48-h LC_{50} survival	H188–205, A124–133, pH 8	29,560–74,340	
	21-day LOEC reproduction	H200, pH 7.8–8	520	
Water flea (*Daphnia magna*)	48-h LC_{50}	H91, A62, pH 7.7	5,180–9,360	Barata et al. [36] No
		H179, A126, pH 8.1	15,300–25,400	

Uranium in the Environment: Behavior and Toxicity. Table 5 (Continued)

Taxa	Endpoint	Aqueous parameters	Effect concentration ($\mu g \cdot L^{-1}$)	Reference and true hardness assessed yes or no[a]
Water flea (*Daphnia magna*)	48-h LC_{50}	H250, A2.7, pH 7	390	Zeman et al. [158]
		H250, A34, pH 8	7,800	
	21-day LC_{10}	H250, A2.7, pH 7	100	
	21-day EC_{50} reproduction	H250, A2.7, pH 7	91	
	21-day EC_{10} reproduction	H250, A2.7, pH 7	14	
Water flea (*Daphnia pulex*)	48-h LC_{50}	H2.3–3.3, A < 0.1–0.6, pH 5.1–5.6	220	Trapp [152] No
Water flea (*Ceriodaphnia dubia*)	96-h LC_{50}	H176, A126, pH 8.4	10,500	Kuhne et al. [159] No
	7-day NOEC	H190, A148, pH 8.5	1,970	
	7-day LOEC	H190, A148, pH 8.5	3,910	
Water flea (*Ceriodaphnia dubia*)	IC_{50} LOEC NOEC reproduction	H60, A22, pH 7.7	44 35 10	Liber [160] No
	IC_{50} LOEC NOEC reproduction	H120, A69, pH 8.3	> 1,147 380 127	
	IC_{50} LOEC NOEC reproduction	H240, A141, pH 8.6	> 4,295 4,295	
Water flea (*Ceriodaphnia dubia*)	3-brood LC_{50} LC_{25}	H5, A5, pH 6.5–6.9	160 150	Vizon Scitec Inc [147] Yes, No effect
	3-brood LC_{50} LC_{25}	H17, A5, pH 6.6–7	140 120	
	3-brood LC_{50} LC_{25}	H124, A8, pH 6.6–7.3	100 58	
	3-brood LC_{50} LC_{25}	H252, A8, pH 6.7–7.1	110 54	
Water flea (*Ceriodaphnia dubia*)	48-h LC_{50} NOEC MATC	H6.1, A1.1, pH 6.9–7.7	60 and 89 two tests < 1.3, < 7, 2.5 2	Pickett et al. [161]
Diaphanosonia excisum	24-h LC_{50}	H4.6, A3.3, pH 6.6	1,000	Bywater et al. [145] No
Latonopsis fasciculate	24-h LC_{50}	H4.6, A3.3, pH 6.6	410	Bywater et al. [145] No
Dadaya macrops	24-h LC_{50}	H4.6, A3.3, pH 6.6	1,100	Bywater et al. [145] No
Water flea (*Moinodaphnia macleayi*)	48-h LC_{50}	H4.6, A3.3, pH 6.6	1,290	Bywater et al. [145] No

Water flea (*Moinodaphnia macleayi*)	48-h EC_{50}	pH 6.3–6.9	160–390	Semaan et al. [162] No
	48-h LOEC		100–370	
	48-h NOEC		100–270	
	5–6 day LOEC reproduction	pH 6.85	20– >46	
	5–6 day NOEC reproduction		8–46	
Phytoplankton				
Chlorella sp.	72-h EC_{50} LOEC NOEC	H8, A8, pH 7	56 1.6 0.7	Charles et al. [163] Yes
	72-h EC_{50} LOEC NOEC	H40, A8, pH 7	72 1.7 0.7	
	72-h EC_{50} LOEC NOEC	H100, A8, pH 7	150 4.4 2.3	
	72-h EC_{50} LOEC NOEC growth inhibition	H400, A8, pH 7	270 12 4.5	
Chlorella sp.	72-h EC_{50} LOEC NOEC	H4, pH 5.7	78 34 21	Franklin et al. [164]
	72-h EC_{50} LOEC NOEC growth inhibition	H4, pH 6.5	44 13 11	
Chlorella sp.	72-h IC_{50} NOEC LOEC growth synthetic water	H3.9, A4, pH 6.2	74 38 70	Hogan et al. [165] 4 reps
			177 150 179	
	72-h IC_{50} NOEC LOEC growth natural water		166 109 136	
			238 157 187	
			137 72 120	
Pseudokirch neriella subcapitata (previously *Selenastrum capricornutum*)	72-h IC_{50} IC_{25} NOEL LOEL	H5, A7, pH 6.8–7.8	160 27 14 29	Vizon SciTec Inc [147] Yes, no, or little effect
	72-h IC_{50} IC_{25} NOEL LOEL	H15, A7, pH 7.8–8.2	170 94 57 110	
	72-h IC_{50} IC_{25} NOEL LOEL	H64, A7, pH 7.2–7.3	100 60 56 110	
	72-h IC_{50} IC_{25} NOEL LOEL	H122, A8, pH 7.2–7.4	200 100 220 430	
	72-h IC_{50} IC_{25} NOEL LOEL	H228, A8, pH 7.2–7.3	200 150 110 210	
Macrophytes				
Duck weed (*Lemna minor*)	7-day IC_{50} IC_{25} dw	H35, A7, pH 5.8–7.4	13,100 6,400	Vizon SciTec Inc [147] Yes, effect
	7-day IC_{50} IC_{25} dw	H137, A9, pH 6.5–7.3	35,500 3,300	
	7-day IC_{50}, IC_{25} frond #	H35, A7, pH 5.8–7.4	7,400 4,700	
	7-day EC_{50} EC_{25} frond #	H137, A9, pH 6.5–7.3	16,400 12,300	

Uranium in the Environment: Behavior and Toxicity. Table 5 (Continued)

Taxa	Endpoint	Aqueous parameters	Effect concentration ($\mu g \cdot L^{-1}$)	Reference and true hardness assessed yes or no[a]
Duck weed (*Lemna aequinoctialis*)	IC_{50}		> 2,850	Van Dam et al. [166]
	IC_{10}		250	
Benthic invertebrates				
Freshwater snail (*Amerianna cumingi*)	IC_{50}		250	Van Dam et al. [166]
	IC_{10}		22	
Amphipod (*Hyalella azteca*)	14-day LC_{50} EC_{25} NOEC LOEC	H17, A8, pH 6.4–7.0	17 5.3 5.7 11	Vizon SciTec Inc [147] yes, effect
	14-day LC_{50} EC_{25} NOEC LOEC	H61, A8, pH 6.4–6.9	140 100 70 170	
	14-day LC_{50} EC_{25} NOEC LOEC	H123, A9, pH 6.5–7.1	200 130 63 130	
	14-day LC_{50} EC_{25} NOEC LOEC	H238, A10, pH 6.5–7.0	340 130 94 190	
Amphipod (*Hyalella azteca*)	14-day LC_{50} Depleted U – low biovailability	H157, A137, pH 7.9	1,520	Kuhne et al. [159] No
Amphipod (*Hyalella azteca*)	7-day LC_{50}	H18, A14, pH 7.4–8.3	21	Borgmann et al. [167] No
	7-day LC_{50}	H124, A84, pH 8.2–8.5	1,651 nominal value	
Amphipod (*Hyalella azteca*)	Adults		Adults	Alves et al. [168]
	28-day LC_{50}	H12, A8.4, pH 6.9	42	
	28-day LC_{50}	H12, A8.4, pH 7.2	15	
	28-day LC_{50}	H120, A8.4, pH 7.2	30	
	28-day LC_{50}	H60, A42, pH 7.6	48	
	28-day LC_{50}	H12, A84, pH 8.0	94	
	28-day LC_{50}	H120, A84, pH 7.9	1,042	
	28-day LC_{50}	H120, A84, pH 8	2,066	
	Juveniles		Juveniles	
	28-day LC_{50}	H12, A8.4, pH 6.9	14.5	
	28-day LC_{50}	H12, A8.4, pH 7.2	47	
	28-day LC_{50}	H120, A8.4, pH 7.2	44	

	28-day LC_{50}	H60, A42, pH 7.6	198	
	28-day LC_{50}	H12, A84, pH 8.0	132	
	28-day LC_{50}	H120, A84, pH 7.9	664	
	28-day LC_{50}	H120, A84, pH 8	714	
	Growth		Growth	
	28-day EC_{25}	H12, A8.4, pH 6.9	11	
	28-day EC_{25}	H12, A8.4, pH 7.2	21	
	28-day EC_{25}	H120, A8.4, pH 7.2	28	
	28-day EC_{25}	H60, A42, pH 7.6	59	
	28-day EC_{25}	H12, A84, pH 8.0	45	
	28-day EC_{25}	H120, A84, pH 7.9	595	
	28-day EC_{25}	H120, A84, pH 8	262	
Midge (*Chironomus tentans*)	10-day EC_{50}	H125, A84, pH 7.2	10,200	Burnett and Liber [169] No
	MATC		800	
Chironomid larvae (*Chironomus riparius*)	10-day $\sim LC_{72}$ 6.07 $\mu g\ U \cdot g^{-1}$ sediment dw	H48, pH 7.2	28	Dias et al. [170]
	10-day $\sim LC_{77}$ 11.4 $\mu g\ U \cdot g^{-1}$ sediment dw	H48, pH 7.2	51	
	10-day $\sim LC_{77}$ 11.4 $\mu g\ U \cdot g^{-1}$ sediment dw	H48, pH 7.2	85	
Bivalve (*Velesunio angasi*)	EC_{50}, NOEC, LOEC	H3.7, A2.7 pH 5	117 95 92	Markich et al. [29]
	EC_{50}, NOEC, LOEC	H3.7, A2.7 pH 5	144 118 113	
	EC_{50}, NOEC, LOEC	H3.7, A2.7 pH 5	247 208 197	
	EC_{50}, NOEC, LOEC	H3.7, A2.7 pH 5.3	141 114 108	
	EC_{50}, NOEC, LOEC	H5.5, A2.7 pH 5.5	163 132 125	
	EC_{50}, NOEC, LOEC	H5.5, A2.7 pH 5.5	242 228 192	
	EC_{50}, NOEC, LOEC	H5.5, A2.7 pH 5.5	497 417 399	
	EC_{50}, NOEC, LOEC	H5.8, A2.7 pH 5.5	290 224 214	

Uranium in the Environment: Behavior and Toxicity. Table 5 (Continued)

Taxa	Endpoint	Aqueous parameters	Effect concentration ($\mu g \cdot L^{-1}$)	Reference and true hardness assessed yes or no[a]
	EC_{50}, NOEC, LOEC	H6.0, A2.7 pH 5.5	634 440 416	
	EC_{50}, NOEC, LOEC	H6.0, A2.7 pH 5.5	824 598 558	
	EC_{50}, NOEC, LOEC valve movement	H6.0, A2.7 pH 5.5	1,228 958 913	
Bivalve (*Corbicula fluminea*)	EC_{50}, EC_{20}	H6, pH 5.5,10 min	40 19	Fournier et al. [33]
	EC_{50}, EC_{20}	H6, pH 5.5, 20 min	40 19	
	EC_{50}, EC_{20}	H6, pH 5.5, 30 min	40 19	
	EC_{50}, EC_{20}	H6, pH 5.5, 60 min	40 19	
	EC_{50}, EC_{20}	H6, pH 5.5, 120 min	28.6 <DL	
	EC_{50}, EC_{20}	H6, pH 5.5, 300 min	11.9 <DL	
	EC_{50}, EC_{20}	H5.9, pH 6.5, 10 min	150 90	
	EC_{50}, EC_{20}	H5.9, pH 6.5, 20 min	143 79	
	EC_{50}, EC_{20}	H5.9, pH 6.5, 30 min	138 52	
	EC_{50}, EC_{20}	H5.9, pH 6.5, 60 min	83 4.8	
	EC_{50}, EC_{20}	H5.9, pH 6.5, 120 min	38 <DL	
	EC_{50}, EC_{20}	H5.9, pH 6.5, 300 min	31 <DL	
Hydra (*Hydra viridissima*)	96-h EC_{50}, LOEC	H6.6, A4, pH 6	114 32	Rietmuller et al. [35]
	96-h EC_{50}, LOEC	H165, A4, pH 6	177 90	
	96-h EC_{50}, LOEC	H165, A102, pH 6	171 42	
	96-h EC_{50}, LOEC	H330, A4, pH 6	219 62	
Hydra (*Hydra viridissima* or *H. vuldaris*)	LOEC		400–550	Hyne et al. [171]

[a]True hardness – varying the hardness concentration without varying alkalinity, so alkalinity does not covary with hardness.

tropical fish was reported at 0.20 mg·L^{-1} [156]. In very soft water, bluegill (*Lepomis macrochirus*) is also sensitive with a 96-h LC_{50} of 1.7 mg·L^{-1} [152]. Hamilton [154] reported that the toxicity of U to the Colorado squawfish (*Ptychocheilus lucius*), razorback sucker (*Xtrauchen texanus*), and bonytail (*Gila elegans*) is low (LC_{50} of 46 mg·L^{-1}) in hard water (Table 5). Hamilton [154] found that the acute toxicity of the three fishes to U was the same for the three early life stages tested: swim-up fry, young juvenile, and older juvenile. This is in contrast to most studies where early life stages are usually more sensitive to toxicants than later life stages. Hamilton [154] also found that toxicity to fish was in the order vanadium = zinc > selinite > lithium = uranium > selenate > boron. Uranium was also more toxic than lead to the zebra fish *Brachydanio rerio* [153].

Rainbow trout (*O. mykiss*) appear to be moderately tolerant of U with 96-h LC_{50}s ranging from 3.8 to 6.2 mg·L^{-1} [147, 150] at various levels of hardness (Table 5). However, rainbow trout embryos and alvins were sensitive to U in moderately hard water with low alkalinity in longer-term exposures. Based on survival after 31 days, the LOEC and EC_{25} were 280 μg·L^{-1} and 340 μg·L^{-1} respectively [147]. In another study, lake trout (*S. namaycush*) embryos and fry had a LOEC of 29.78 mg U·L^{-1} for time to hatch, hatching success, and survival in moderately hard water (72 mg $CaCO_3$·L^{-1}) after 141 days of exposure but the exposure had no effect on growth [151]. These studies demonstrate that there is a marked difference in sensitivity to U for the two trout species in water that differed primarily in the level of alkalinity.

For fathead minnow (*P. promelas*) embryos in 7-day exposure tests, NOECs ranged from 810 to 1,200 μg·L^{-1} and LOECs from 1,300 to 2,000 μg·L^{-1} over a range of water hardness [147]. White sucker (*C. commersoni*) fry in moderately hard water (72 mg $CaCO_3$·L^{-1}) were relatively tolerant of U with a NOEC of 7.33 mg·L^{-1} and a LOEC of 27.86 mg·L^{-1} for growth [172]. In general, as the duration of the test increases, toxicity occurs at lower U concentrations for the same species and endpoints, although little difference was observed between 96-h and 7-day LC_{50} values for the fathead minnow [147].

It is sometimes suggested that in areas of elevated U concentrations, the local fauna will adapt to local conditions and become more tolerant to U. To test this conjecture, Keklak et al. [173] compared the toxicity of U to second-generation mosquitofish from parents chronically exposed to elevated aqueous concentrations of 4.2 μg U·L^{-1} and sediment concentrations of 6,165 μg U·g^{-1} dw with that of specimens from a reference site. After 7 days of exposure to 2.57 mg·L^{-1} of U as uranyl nitrate, 98% and 96% of the reference population had died in two replicate tanks compared to 25% and 57% of the offspring of fish that had been exposed for multiple generations. They concluded that the increased tolerance to U was genetically based since the test organisms were second-generation postexposure. However, this is not a substantial increase in tolerance and from data presented in their paper, it can be seen that the mortality of exposed fish was still increasing and had the experiment continued, all exposed fish likely would have died.

Zooplankton

Pickett et al. [161] found that *Ceriodaphnia dubia* was very sensitive to U with a threshold effect value of 3 μg·L^{-1} (GM of the NOEC and LOEC) for reproduction in soft water (~ 4 mg·L^{-1} $CaCO_3$) (Table 5). In another study, *C. dubia* had a 48-h threshold effect concentration for reproduction of 19 ± 2 μg U·L^{-1} in 7-day chronic toxicity tests with water from a stream near McClean Lake Operations in northern Saskatchewan, adjusted to a hardness of 60 mg·L^{-1} as $CaCO_3$ [160]. When the hardness was adjusted to 120 mg·L^{-1} $CaCO_3$ toxicity was considerably lower with a threshold effect concentration for reproduction of 218 μg U·L^{-1} [160]. Vizon SciTec [147] reported LC_{25}s of 54–150 μg·L^{-1} for *C. dubia* at hardness of 5–252 mg·L^{-1} as $CaCO_3$ and low alkalinity (5–8 mg·L^{-1} as $CaCO_3$). In contrast, Kuhne et al. [159] reported low toxicity in hard water (182 mg·L^{-1} as $CaCO_3$) for *C. dubia* with a 96-h LC_{50} of 10.5 mg·L^{-1} and a LOEC of ≥ 3.91 mg·L^{-1} for depleted U.

Poston et al. [157] reported that the 48-h LC_{50} for *D. magna* to U decreased sixfold as hardness increased from 70 to 195 mg·L^{-1}, whereas Barata et al. [36] reported a threefold decrease in toxicity as hardness increased from 90 to 180 mg·L^{-1}. The LOEL was 520 μg·L^{-1} for daphnid reproduction in water with hardness of 66–73 mg·L^{-1} [157], whereas the 48-h LC_{50} for *Daphnia pulex* in soft water was 220 μg·L^{-1} [152].

In a more detailed study on the effect of U on *D. magna*, Zeman et al. [158] reported a 48-h LC_{50} of 390 μg·L^{-1} at pH 7 and 7,800 μg·L^{-1} at pH 8. Much greater sensitivity was observed in 21-day exposures. The 21-day LC_{10} was 100 μg·L^{-1} and the EC_{10} for reproduction was 14 μg·L^{-1}. Decreased feeding activity and increased oxygen consumption at 25 μg·L^{-1} of U after 7 days exposure affected growth. Growth and reproduction decreased 50% and 65%, respectively, at 50 μg·L^{-1} of U after 7 days and at 25 μg·L^{-1} of U after 21 days. Therefore, *D. magna* is sensitive to low concentrations of U, but not as sensitive as *C. dubia*.

Bywater et al. [145] reported U LC_{50} values ranging from 0.14 to 0.9 mg·L^{-1} for four species of tropical cladocerans in water of low hardness and low alkalinity. LOECs ranged from 20 to 49 μg·L^{-1} and NOECs from 8 to 31 μg·L^{-1} for three different populations of the tropical cladoceran *Moinodaphnia macleayi* [162]. The population of *M. macleayi* obtained from a pond with elevated U concentrations was found to be no more tolerant than the populations from background conditions.

Phytoplankon

Cellular Uptake of U Uranium is believed to mimic calcium at the cell surface and is readily transported into the cell as if it were calcium. Once inside the algal cell, U is concentrated into vacuoles and may be precipitated as U(VI) phosphates [7]. Internal deposition of U may have ultimately killed the cells of *Pseudomonas fluorescens* [174]. Cellular toxicity may occur as a result of binding of U to enzymes disabling enzyme function [175]. Uranium may also exert toxicity at the cellular level by interfering with calcium homeostasis. Uptake and deposition of U in marine red algae is primarily by ion exchange or coprecipitation of the U ion with the calcium carbonate matrix and secondarily by complex formation with either protein nitrogen or other components of the organic fraction. Competition for sites on cell walls is strongly pH dependent as H^+ ions behave like other cations. At pH below 5, H^+ concentrations are high enough to compete with other metals in solution and strip metals from the ligands. Uranium(IV) also competes with other metals for binding sites based on molecular size and shape, and the configuration of the ligand.

Algae are very efficient at removing nutrients and metals, including U, from solution. Iron reduces the uptake of U by *Anacystis nidulans* (Cyanobacteria) [176], as do phosphate and carbonate for U uptake by *Chlorella regularis* (Chlorophyta) [177]. Adsorption of U and other metals (Cu, Ni, Mn, and Zn) reaches steady state rapidly, within a few minutes. Uranium is concentrated from water by a factor of 330 in 48 h by the alga *Ochromonas* sp. B and by a factor of 2,098 based on wet weight by the green alga *Spirogyra* sp. in a U enriched stream (12.5 μg·L^{-1}) [6]. Both living and nonliving *Chlorella regularis* accumulate U from water [178]. Figure 3 shows the uptake of U by algae after 30 min due to intracellular uptake and extracellular adsorption. Intracellular U content of cells was greatly reduced in the presence of ligands. About 75% of the intracellular U was associated with the insoluble fractions – (vacuoles, nuclei, flagella, and membranes), and 25% with the cytosol [32].

Algal cells take up U in the cation form UO_2^{2+} or UO_3OH^+ [177]. The optimum pH for U uptake by algae is usually acidic to neutral. At pH 5.9–6.8 uranyl ions exist as hydrolysis products, which are more strongly bound to cell absorption sites. Above pH 7, uranyl carbonate complexes exist. These negatively charged and extremely soluble ionic complexes experience charge conflicts at cell absorption sites, which inhibit uptake thereby decreasing U uptake. Optimum pH range for U uptake by algae is about pH 2.5–8.5 (Table 6) and between pH 4 and 5 for lichen. Uptake optima under acidic conditions correspond to the fact that carboxyl, amino, and phosphate ligands are probably the major complexing agent on or in the cell walls.

Toxicity to Phytoplankton Franklin et al. [164] found that a tropical alga (*Chlorella* sp.) was more sensitive to U in soft water (2–4 mg·L^{-1} as $CaCO_3$) at pH 6.5 than at pH 5.7 (Table 5). In their study, the LOEC was 34 μg·L^{-1} at pH 5.7 and 13 μg·L^{-1} at pH 6.5. At pH 5.7, U concentrations up to 34 μg·L^{-1} had no significant effect on growth rate, but at 60 μg·L^{-1} relatively small increases in U concentrations caused pronounced growth inhibition. At pH 6.5, *Chlorella* sp. was more sensitive to U with concentrations >8 μg·L^{-1} resulting in pronounced growth inhibition with small increases in U concentration. Increasing the U concentration from 40 to 250 μg·L^{-1} resulted in an

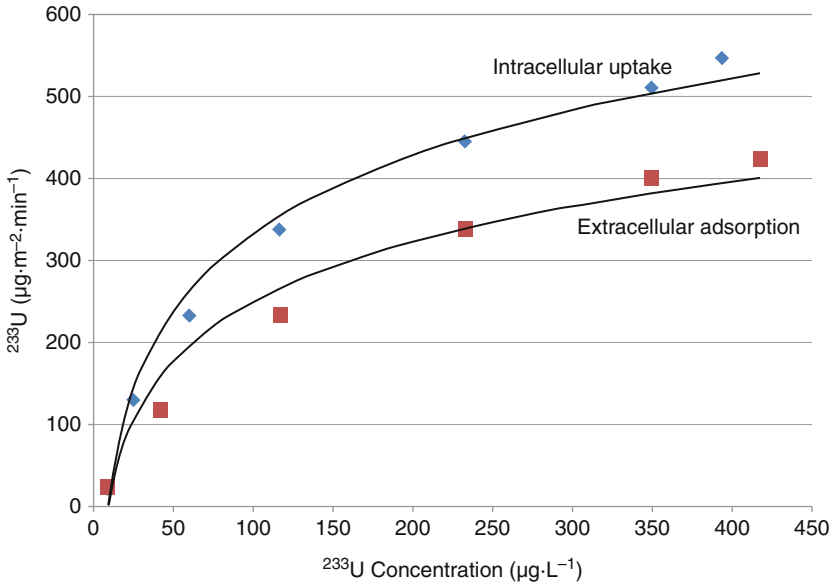

Uranium in the Environment: Behavior and Toxicity. Figure 3
Uranium uptake after 30 min by the unicellular green alga *Chlamydomonas reinhardtii* (Modified from Fortin et al. [32])

Uranium in the Environment: Behavior and Toxicity. Table 6 Optimum pH for uptake of uranium by several algal species (Kalin et al. [7])

Taxa	Optimum pH
Anacysti (Cyanobacterium)	3.0 and 5.0
Sargassum (Phaeophyta)	2.5 and 4.0
Scenedesmus (Chlorophyta)	5.0 and 8.5
Scenedesmus (Chlorophyta)	5.9 and 6.8
Chlorella regularis (Chlorophyta)	6.0 and 7.0

eightfold increase in both intracellular and extracellular U at both pH 5.7 and 6.5. Intracellular U concentrations were greater at pH 6.5 that at pH 5.7 with about two times the U located in the cell. Greater toxicity at pH 6.5 corresponded with greater uptake of U to the cell surface and uptake of U into the cell. Speciation modeling indicates that the decreasing toxicity of U to *Chlorella* sp. with decreasing pH may have been the result of H^+ inhibiting intracellular U uptake at the lower pH. At the pH range 5.7–6.5, $UO_2(OH)_3CO_3^-$ is expected to dominate (70–93%) and <4% would occur as UO_2^{2+} [5].

Charles et al. [163] assessed the effect of hardness at 8, 40, 100, and 400 mg·L^{-1} as $CaCO_3$ on the 72-h growth inhibition of *Chlorella* sp. A 50-fold increase in hardness resulted in a fivefold decrease in U toxicity, from 56 to 270 µg U·L^{-1}. Reduction in toxicity was attributed to competition with calcium and magnesium for binding sites. The effect of hardness on extracellular and intracellular U concentrations, and U toxicity is summarized in Table 5. Intracellular U concentrations decreased with increasing hardness, whereas the ratio of extracellular to intracellular U increased with increasing U concentration. Hardness also reduced the toxicity of U to *Chlorella* sp (Table 7). The toxicity of U to *Pseudokirchneriella subcapitata* (previously *Selenastrum capricornutum*) was in general agreement with the findings for *Chlorella*. The alga *P. subcapitata* had IC_{25}s for inhibition of growth of 27–150 µg·L^{-1} depending on hardness (Table 5) [147].

Macrophytes

Van Dam et al. [166] investigated the toxicity of U to the tropical duckweed *Lemna aequinoctialis*. An IC_{50} of > 2,850 µg·L^{-1} U for growth inhibition and an NOEC of 250 µg·L^{-1} were reported for *L. aequinoctialis*. These values indicate that duckweed is not very sensitive to U.

Uranium in the Environment: Behavior and Toxicity.
Table 7 Effect of hardness (mg·L^{-1} $CaCO_3$) on uranium uptake by *Chlorella* sp. (From Charles et al. [163])

Hardness	μg U·L^{-1}	Intracellular (× 10^{-6} ng μm^{-3})	Extracellular U (× 10^{-6} ng μm^{-2})
8	12	0.60	0.41
	53	0.82	0.80
	270	4.6	15
400	17	0.07	0.03
	62	0.10	0.22
	310	0.15	0.36
	520	1.1	5.0

This is in agreement with the findings for *Lemna minor*, which had a 7-day IC_{50} of 7,400 μg·L^{-1} and 7-day IC_{25} of 4,700 μg·L^{-1} for number of fronds and IC_{50} of 13,100 μg·L^{-1} and IC_{25} of 6,400 μg·L^{-1} for growth at low hardness [147].

Benthic Invertebrates

Sediments are a sink for particle-reactive contaminants released into aquatic ecosystems. Sediment-associated contaminants may have adverse effects on benthic macroinvertebrates and fish that feed on contaminated invertebrates. Borgmann et al. [167] reported a 7-day LC_{50} of 21 μg·L^{-1} (measured) for *H. azteca* in soft water (hardness 18 mg·L^{-1}) and a LC_{50} of 1,651 μg·L^{-1} (nominal) in hard water (hardness 124 mg·L^{-1}). This is in agreement with the 14-day LC_{50} of 17 μg·L^{-1} reported for *H. azteca* in soft water by Vizon SciTec [147] and the 14-day LC_{50} reported for *H. azteca* of 1.52 mg·L^{-1} in hard water by Kuhne et al. [159]. A pronounced hardness effect was seen in the Vizon SciTec [147] study.

When *H. azteca* was exposed to U spiked sediment, it was concluded that toxicity was mainly from the water rather than the sediment [168]. The pH of the water (pH 6.9–8.0) had a marked effect on the uptake of U by *H. azteca*, whereas calcium concentration (4, 30 or 40 mg) had little effect on U uptake but did influence U speciation in aqueous solution. The 28-day LC_{50}s for juvenile *H. azteca* ranged from 14.5 to > 714 μg·L^{-1} (4.6–14 mg·g^{-1} dry sediment) depending on pH and calcium concentration (Table 5), whereas 28-day LC_{50}s ranged from 15 to 2,060 μg·L^{-1} (5.5–13.1 mg U·g^{-1} dry sediment) for adult specimens (Table 5). BEAK International Inc. [177] reported juvenile *H. azteca* were much more sensitive to U than the adults with a LC_{20} of 15 mg U·kg^{-1} dw for juveniles compared to a LC_{20} of 116 mg U·kg^{-1} dw for adults in hard water (105–308 mg·L^{-1} as $CaCO_3$).

The midge *Chironomus tentans* was found to be quite tolerant to U with a 10-day LC_{50} of 6,400 μg·L^{-1} and a LOEC of 1,519 μg·L^{-1} [169]. Survival was a more sensitive endpoint than growth. In contrast, *Chironomus riparius* appears to be quite sensitive to U. First-instar larvae of *C. riparius* were exposed to sediment U concentrations up to 23.84 mg U·kg^{-1} dw in 10-day bioassays, and associated aqueous U concentrations up to 85.17 μg·L^{-1} as a result of desorption of U from the sediment [170]. Mortality of larvae was higher at sediment U concentrations of 6.07 mg U·kg^{-1} dw, than 2.97 mg U·kg^{-1} dw sediments and the control. Growth of fourth instar larvae was significantly lower at 2.97 mg U·kg^{-1} dw sediment than in control sediment. No larvae matured to the fourth instar stage over the 10-day study in the 23.84 μg U·kg^{-1} dw sediment. However, desorption of U from sediments resulted in aqueous U concentrations of 10, 28, 51, and 85 μg·L^{-1}, respectively (Table 5), and it can be speculated that the toxicity was mainly from the water pathway as reported by Alves et al. [168].

The freshwater snail *Amerianna cumingi* was found to be sensitive to U with an IC_{50} of 250 μg·L^{-1} and an IC_{10} of 22 μg·L^{-1} for inhibition of egg production [165]. The Asiatic clam (*Corbicula fluminea*) was more sensitive to U at pH 5.5 than at pH 6.5. The minimal sensitivity threshold that caused closure of the valve by 50% of the bivalves was 12 μg·L^{-1} at pH 5.5 after 5 h of exposure. Higher concentrations of UO_2^{2+} were required at pH 6.5 to illicit the same response. In both marine and freshwater mollusks and crustaceans, U accumulates in lysosomes [179].

In another investigation using the mayfly *Hexagenia limbata* nymphs exposed to contaminated sediment from historic uranium mining operations, Jaagumagi and Bedard [180] reported a 63% mortality rate in nymphs exposed to 491 mg U·kg^{-1} dw sediment

in 22-day sediment bioassays. No effect on mortality or growth was observed for mayfly nymphs at U sediment concentrations of 78, 83, and 100 mg·kg^{-1} dw.

From the above it can be concluded that U can be toxic at low concentrations to certain aquatic organisms under specific conditions such as low alkalinity.

Overview of Parameters Affecting U Toxicity

Hardness Hardness is reported to reduce the toxicity of uranium to freshwater organisms [148, 149, 157]. However, a quantitative relationship describing U toxicity as a function of hardness is lacking. This is because many experiments designed to investigate the effects of hardness on U toxicity have confounded the effects of true water hardness (calcium or magnesium concentrations) with alkalinity (carbonate concentrations) and pH (H^+ concentration) [35].

Hardness (calcium or magnesium concentrations) and alkalinity (carbonate concentration) influence toxicity through different mechanisms. In the case of hardness, calcium and/or magnesium competitively inhibit the uptake at the cell surface of trace metals thereby reducing their toxicity. About sevenfold more Mg is needed to exhibit the same ameliorative effect as Ca on toxicity [181, 182]. In the case of alkalinity, complexation of trace metals with carbonate modifies metal speciation and reduces the concentration of the toxic metal species, UO_2 and UO_2OH^+ [34].

In studies on the effect of hardness on U toxicity in which $CaSO_4$ was added to prevent alkalinity from covarying with hardness, hardness was found to decrease the toxicity of U to the alga *Chlorella* sp. [163] and the macrophyte *L. minor* [147]. A 50-fold (mg·L^{-1}) increase in hardness resulted in a 4.8-fold (mg·L^{-1}) decrease in U toxicity [163]. In contrast, U toxicity to the alga *P. subcapitata* [147] was not influenced by hardness. The invertebrate *H. azteca* responded markedly to hardness; a 16-fold increase in hardness decreased U toxicity by 12-fold in 14-day toxicity tests [147] (Table 5). Other studies that increased hardness with alkalinity also reported reduced toxicity, for example, to *D. magna* [36, 157] and the green hydra *Hydra viridissima* [35].

Equations have been developed to predict the effect of hardness on U toxicity to aquatic organisms [100, 157]. However, when EC [25] plotted hardness versus LC_{50} data similar to that described by Sheppard et al. [100], but included more recent data that did not covary with alkalinity [147], they found no significant relationship with which to predict U toxicity with hardness.

Not all organisms show a hardness effect in their response to U toxicity. For example, for rainbow trout and fathead minnow, U toxicity did not vary in short-term tests where alkalinity was held constant as hardness increased [147]. Similar results were found in long-term tests on *C. dubia* [147]. Therefore, in setting benchmarks to protect aquatic biota the hardness should not be a consideration if the goal is to protect most species.

Alkalinity Only two toxicity studies were found that altered alkalinity at constant hardness. Riethmuller et al. [35] varied alkalinity from 4.0 to 102 mg $CaCO_3$·L^{-1} to assess U toxicity to the freshwater hydrazoan *Hydra viridissima*. Increased alkalinity changed the speciation of U (percent $UO_2(CO_3)_2^{2-}$ from <1% to 20% and UO_2^{2+} from 6% to 1%) but had no effect on U toxicity. Markich et al. [34] reported toxicity was inversely proportional to alkalinity when pH and hardness were kept constant. U toxicity decreased 20% with a fivefold increase in alkalinity at pH 5 and hardness of 3.5 mg·L^{-1} as $CaCO_3$.

There is not enough information on the effect of alkalinity on U toxicity, and further studies are required with a variety of organisms to establish a relationship.

Natural Organic Matter Natural organic matter has the potential to bind the toxic free ion forms of a metal and hence reduce toxicity similar to alkalinity. Markich et al. [29] found that an increase in fulvic acid from 0 to 7.91 mg·L^{-1} decreased U toxicity to a freshwater bivalve by a factor of 2–3. In another study, Hogan et al. [164] found increasing dissolved organic matter decreased U toxicity in *Chlorella* sp. More work is required to assess the effect of organic matter on U toxicity.

Temperature Water temperature may affect U toxicity by changing U solubility, speciation or kinetics, and the metabolic rate of organisms, for example, uptake rate, depuration rate, and survival. Information could not be found on the effect of temperature on U speciation or

toxicity. However, temperature affects the metabolism of poikilotherms, which will affect toxicity, for example, a 10°C increase in temperature may increase metabolism by factor of 2 and toxicity by a factor of 2 or 3 [183]. Transfer of U to organic sediments is also more rapid at higher temperature [69].

Metal Mixtures Only one study examined the toxicity of mixtures of U and other metals. Hamilton and Buhl [169] exposed the flannelmouth sucker, *C. latipinnis*, to metal mixtures consisting of copper, zinc, selenium, boron, vanadium, uranium, and arsenic, based on concentrations found at their study site, the San Jan River, USA. Toxicity of metals was found to be additive. Further work needs to be done in this area, especially since mine and mill effluents contain elevated levels of various metals, including U.

Regulatory Guidelines Regulatory guidelines are available from a number of jurisdictions (Table 8). Until recently, the Canadian Water Quality Guidelines for Protection of Aquatic Life and Wildlife was 300 $\mu g \cdot L^{-1}$ [8]. Recently Environment Canada prepared a draft guideline which is undergoing review. The proposed guideline is considerably lower than their former guideline and is more in line with those derived independently by several Canadian provinces. However, it is considerably higher than the guideline of 0.5 $\mu g \cdot L^{-1}$ for Australia and New Zealand [184], which includes an application factor of 20 because of the limited amount of long-term data available for tropical species.

Uranium in the Environment: Behavior and Toxicity.
Table 8 Water Quality Guidelines for Protection of Aquatic life from U

Jurisdiction	U concentration ($\mu g \cdot L^{-1}$)	Hardness ($mg \cdot L^{-1}$ $CaCO_3$)
Quebec	14	20–100
	100	100–210
Saskatchewan	15	
Ontario	5	
China	50	
Australia	0.5	
New Zealand	0.5	
Canada	300 (being revised)	

Future Directions

Studies demonstrate that background concentrations of U found in the environment are unlikely to be toxic to biota, and if toxicity occurs, it is more likely to be chemotoxic than radiotoxic because of the low specific activity of ^{238}U. Uranium usually has low toxicity primarily because oral uptake rates are low and concentrations decrease up the food chain. However, U may be toxic to organisms in areas with elevated U concentrations above background levels.

The toxicity of U to human and terrestrial wildlife has been well documented based on human epidemiological studies and laboratory studies on mammals. Further worked is required on the toxicity of U to terrestrial plants and soil invertebrates, as few studies have focused on these organisms.

A substantial amount of work has been undertaken on the effects of U on the aquatic ecosystem. Nevertheless, there remain many unanswered questions because of the complex chemistry of U and the interactions between U and environmental parameters. For aquatic organisms, U toxicity for several species decreases with an increase in hardness and alkalinity. However, not all organisms show a hardness effect on toxicity, and U may be toxic at low concentrations as observed for fish (*M. mogurnda* and early life stages of rainbow trout), zooplankton (*C. dubia*, *D. pulex*, and *D. magna*), algal spp. (*Chlorella* sp. and *P. subcapitata*), and benthic invertebrates (*H. azteca*, *C. riparius*, *C. fluminea*, and *H.viridissima*) under the conditions given in Table 5. Other parameters, such as pH, alkalinity, and ligands affect U speciation and their effect on toxicity needs assessment at environmentally relevant concentrations and conditions. In the case of aqueous releases from mining/milling operations, the interactions of the ameliorating effects of elevated calcium and magnesium concentrations from effluent treatment, elevated U concentrations with potentially increased abundance of toxic U species (UO_2^{2+} and UO_2OH^+) along with increased concentrations of sulfate and other metals must be considered. Site-specific testing of the receiving surface waters is required to assess the potential toxicity of complex effluents from mining/milling U operations.

Bibliography

Primary Literature

1. Bleise A, Danesi PR, Burkart W (2003) Properties, use and health effects of depleted uranium (DU): a general overview. J Environ Radioact 64:93–112
2. Ribera D, Labrot F, Tisnerat G, Narbonne JF (1996) Uranium in the environment: occurrence, transfer, and biological effects. Rev Environ Contam Toxicol 146:53–89
3. Meinrath A, Schneider P, Meinrath G (2003) Uranium ores and depleted uranium in the environment, with a reference to uranium in the biosphere from the Erzgebirge/Sachsen, Germany. J Environ Radioact 64:175–193
4. Harley NH (1996) Toxic effects of radiation and radioactive materials. In: Klaassen CD (ed) Casarett and Doull's toxicilogy: the basic science of poisons. McGraw-Hill, New York, pp 773–800
5. Markich S (2002) Uranium speciation and bioavailability in aquatic systems: an overview. Sci World J 2:707–729
6. Environmental Canada, Health Canada (2003) Canadian Environmental Protection Act 1999. Priority substances list assessment report releases of radionuclides from nuclear facilities (Impact on non-human biota). Final Report May 2003
7. Kalin M, Wheeler WN, Meinrath G (2005) The removal of uranium from mining waste water using algal/microbial biomass. J Radiochem Radioact 78:151–177
8. Environment Canada (1983) Guideline for surface water quality volume 1: inorganic chemical substances URANIUM. Inland Waters Directorate, Water Quality Branch, Ottawa
9. Painter S, Cameron EM, Allan R, Rouse J (1994) Reconnaissance geochemistry and its environmental relevance. J Geochem Explor 51:213–246
10. CCME (Canadian Council of Ministers of the Environment) (2007) Canadian soil quality guidelies for uranium: environmental and human health scientific supporting document PN 1371 ISBN 978-1-896997-64-3 PDF
11. Gascoyne M (1992) Geochemistry of the actinides and their daughters. In: Ivanovich M, Harmon RS (eds) Uranium series disequilibrium: applications to earth, marine and environmental sciences, 2nd edn. Clarendon, Oxford, pp 34–61
12. Macdonald CR (1998) The chemical toxicity of uranium to wildlife. Report to the Commercial Chemical Division, Environment Canada. Contract Number K2221-7-0076. Pinawa, MB. 32 pp
13. Ragnarsdottir KV, Charlet L (2000) Uranium behavior in natural environments. In: Cotter-Howells JD, Campbell LS, Valsami-Jones E, Batchelder M (eds) Environmental mineralogy: microbial interactions, anthropogenic influences, contaminated land and waste management, vol 9, Mineralogical Society Series. Mineralogical Society, London, pp 245–289
14. Sheppard MI (1980) The environmental behaviour of uranium and thorium. Whiteshell Nuclear Research Establishment, Atomic Energy of Canada Limited, Pinawa, Manitoba, 44 pp. (Technical Report AECL-6795)
15. Fernandes HM, Filho FFLS, Perez V, Franklin MR, Gomiero LA (2006) Radioecological characterization of a uranium mining site located in a semi-arid region of Brazil. J Environ Radioact 88:140–157
16. Landa ER, Gray JR (1995) US Geological Survey research on the environmental fate of uranium mining and milling wastes. Environ Geol 26:19–31
17. Joshi SR, Waite DT, Platford RF (1989) Vertical distribution of uranium mill tailings contaminants in Langley Bay, Lake Athabasca sediments. Sci Tot Environ 87(88):85–104
18. Thomas PA (1997) The ecological distribution and bioavailability of uranium series radionuclides in terrestrial food chains: key Lake uranium operations, northern Saskatchewan. Prepared for Environmental Protection, Prairie and Northern Region, Environment Canada, Regina, Saskatchewan, by P.A. Thomas, University of Saskatchewan, Saskatoon, Saskatchewan
19. Robertson EL, Liber K (2007) Bioassays with caged *Hyalella azteca* to determine in situ toxicity downstream of two Saskatchewan, Canada, uranium operations. Environ Toxicol Chem 26:2345–2355
20. Shropshire DE, Williams KA, Boore WB, Smith JD, Dixon BW, Dunzik-Gougar M, Adams RD, Combert D, Schneider E (2008) Advanced fuel cycle cost basis. Report prepared for Idaho National laboratory, INL/EXT-07-12107 Rev. 1
21. Diehl P (1999) Depleted uranium: a by-product of the nuclear chain. http://www.antenna.nl/wise-database/uranium/dhap99f.html. Accessed 22 Nov 2009
22. Tracy BL, Prantl FA (1985) Radiological impact of coal-fired power generation. J Environ Radioact 2:145–160
23. Chen JH, Edwards RL, Wasserburg GJ (1986) ^{238}U, ^{234}U & ^{232}Th in seawater. Earth Planet Sci Lett 80:241–251
24. Choppin GR, Stout BE (1989) Actinide behaviour in natural waters. Sci Total Environ 83:203–216
25. Environment Canada (2008) Canadian water quality guidelines for uranium: Scientific supporting document (Draft) 10th March, 2004 original draft updated 5 Feb 2008
26. Bosshard E, Zimmerli B, Schlatter Ch (1992) Uranium in the diet: risk assessment of its nephro- and radiotoxicity. Chemosphere 24:309–321
27. Langmuir D (1978) Uranium solution-mineral equilibria at low temperatures with application to sedimentary ore deposits. Geochim Cosmochim Act 42:547–569
28. Hamelink JL, Landrum PF, Bergman HL, Benson WH (1994) Bioavailability: physical, chemical and biological interactions. Lewis, Boca Raton
29. Markich SJ, Brown PL, Jeffree RA, Lim RP (2000) Valve movement responses of *Velesunio angasi* (Bivalvia: Hyriidae) to manganese and uranium: an exception to the free ion activity model. Aquat Toxicol 1:155–175
30. Denison FH, Garnier-Laplace J (2005) The effects of database parameter uncertainty on uranium (VI) equilibrium calculations. Geochim Cosmochim Acta 69:2183–2191
31. Unsworth ER, Jones P (2002) The effect of thermodynamic data on computer model predictions of uranium speciation in natural water systems. J Environ Monit 4:528–532
32. Fortin C, Dutel L, Garnier-Laplace J (2004) Uranium complexation and uptake by green alga in relation to chemical

speciation: the importance of the free uranyl ion. Environ Toxicol Chem 23:974–981
33. Fournier ED, Tran F, Denison J, Massabuau C, Garnier-Laplace J (2004) Valve closure response to uranium exposure for a freshwater bivalve (*Corbicula fluminea*): qualification of the influence of pH. Environ Toxicol Chem 23:1108–1114
34. Markich SJ, Brown PL, Jeffree RA (1996) The use of geochemical speciation modelling to predict the impact of uranium to freshwater biota. Radiochemica Acta 74:321–326
35. Reithmuller N, Markich SJ, Van Dam RA, Parry D (2001) Effects of water hardness and alkalinity on the toxicity of uranium to a tropical freshwater hydra (*Hydra viridissima*). Biomarkers 6:45–51
36. Barata C, Baird DJ, Markich SJ (1998) Influence of genetic and environmental factors on the tolerance of *Daphnia magna* straus to essential and non-essential metals. Aquat Toxicol 42:115–137
37. Higgo JJW (1987) Clay as a barrier to radionuclide migration. Progr Nucl Energy 19:173–207
38. Bernhard G, Geipel G, Brendler V, Nitsche H (1998) Uranium speciation in waters of different uranium miningareas. J Alloy Comp 271–273:201–205
39. Melville GE (1995) Changes in the pelagic crustacean zooplankton of high-boreal Island Lake, Saskatchewan, associated with uranium mining. Environ Monit Assess 34:45–58
40. Sheppard SC (1995) Parameter values to model the soil ingestion pathway. Environ Monit Assess 34:27–44
41. Fleming S, Marsh M, Wagenaar A, McLaughlin D, Bloxam R (2000) Proposed ambient air quality standards for uranium. Rational Document: for discussion with Port Hope stakeholders. Ontario Ministry of the Environment
42. Sheppard SC, Evenden WG (1992) Bioavailability indices for uranium: effect of concentration in eleven soils. Arch Environ Contam Toxicol 23:117–124
43. Batson VL, Bertsch PM, Herbert BE (1996) Transport of anthropogenic uranium from sediments to surface waters during episodic storm events. J Environ Qual 25:1129–1137
44. Babich H, Stotzky G (1985) Heavy metal toxicity to microbe-mediated ecological processes: a review and potential application to regulatory policies. Environ Res 36:111–137
45. Coughtrey PJ, Jones CH, Martin MH, Shales SW (1979) Litter accumulation in woodlands contaminated by Pb, Zn, Cd and Cu. Oceologia 39:51–60
46. Bird GA, Stephenson M, Cornett RJ (1993) The surface water sub model for the assessment of Canada's Nuclear fuel waste management concept. AECL research report AECL-10290, COG-91-193. Pinawa, Manitoba
47. Bird GA, Schwartz W (1996) Nuclide concentration factors for freshwater biota. Atomic Energy of Canada limited, Pinawa, Manitoba (Technical Record TR-703, COG-95-397)
48. FASSET Frederica radiation effects database federica-online.org http://www.frederica-online.org/panel.asp. Accessed 22 Nov 2009
49. International Atomic Energy Agency (1985) Radionuclides in the marine environment. Technical Reports Series No. 247
50. International Atomic Energy Agency (1994) Handbook of parameter values for the prediction of radionuclide transfer in temperate environments. Tech Report Series No 364
51. International Atomic Energy Agency (2010) Modeling the environmental transfer of tritium and carbon-14 to biota and man. Final report, Tritium and Carbon-14 Working Group, IAEA EMRAS Program, International Atomic Energy Agency, Vienna Australia
52. Sheppard MI, Thibault DH (1990) Default soil solid/liquid partition coefficients, K_ds, for four major soil types: a compendium. Health Phys 59:471–482
53. Kumblad L, Kautsky U, Naeslund B (2006) Transport and fate or radionuclides in aquatic environments – the use of ecosystem modelling for exposure assessments of nuclear facilities. J Environ Radioact 87:107–129
54. Sheppard MI, Thibault DH (1984) Natural uranium concentrations of native plants over a low-grade ore body. Can J Bot 62:1069–1075
55. Mahon DC (1982) Uptake and translocation of naturally-occurring radionuclides of the uranium series. Bull Environ Contam Toxicol 29:697–703
56. Hanson WC, Miera FR Jr, (1976) Long-term ecological effects of exposure to uranium. Technical Report LA-6269 Los Alamos Scientific Lab, New Mexico, USA
57. Beyer WN, Connor EE, Gerould S (1994) Estimates of soil ingestion by wildlife. J Wildl Manage 58:375–382
58. Linsalata P, Morse R, Ford H, Eisenbud M, Franca EP, de Castro MB, Lobao N, Sachett I, Carlos M (1989) Transport pathways of Th, U, Ra and La from soil to cattle tissues. J Environ Radioact 10:115–140
59. Weeks HP, Kirkpatrick CM (1976) Adaptations of white-tailed deer to naturally occurring sodium deficiencies. J Wildl Manage 40:610–625
60. Sullivan MF (1980) Absorption of actinide elements from the gastrointestinal tract of neonatal animals. Health Phys 38:173–185
61. Hesslein RH (1987) Whole-lake metal radiotracer movement in fertilized lake basins. Can J Fish Aquat Sci 44(suppl 1): 74–82
62. Fisher NS, Teyssie JL, Krishnaswami S, Baskaran M (1987) Accumulation of Th, Pb, U, and Ra in marine phytoplankton and its geochemical significance. Limnol Oceanogr 32:131–142
63. Degens ET, von Bronsart G, Ho Kim W, Khoo F, Dickman MD (1979) Environmental parameters responsible for the fixation of uranium in recent sediments; test area Bow lake, Ontario, Canada, Part 1. Mitteilungen aus dem Geologisch-Palaeontologischen Institut der Universitaet Hamburg, no. 49, pp 27–60
64. Nyffeler UP, Santschi PH, Li YH (1986) The relevance of scavenging kinetics to modelling of sediment-water interactions in natural waters. Limnol Oceanogr 31:277–292
65. Bird GA, Stephenson M, Cornett RJ (1993) The surface water model for assessing Canada's nuclear fuel waste disposal concept. Waste Manag 13:153–170

66. Santschi PH, Nyffeler UP, Anderson RF, Schiff SL, O'Hara P, Hesslein RH (1986) Response of radioactive trace metals to acid-base titrations in controlled experimental ecosystems: evaluation of transport parameters for application to whole-lake radiotracer experiments. Can J Fish Aquat Sci 43:60–77
67. Carignan R, Nriagu JO (1985) Trace metal deposition and mobility in the sediments of two lakes near Sudbury, Ontario. Geochim Cosmochim Acta 49:1753–1764
68. Swanson SM (1985) Food-chain transfer of U-series radionuclides in a northern Saskatchewan aquatic system. Health Phys 49:747–770
69. Bird GA, Evenden WG (1994) Effect of sediment type, temperature and colloids on the transfer of radionuclides from water to sediment. J Environ Radioact 22:219–242
70. Ames LL, McGarrah JE, Walker BA (1983) Sorption of uranium and radium by biotote, muscovite, and phlogopite. Clays Clay Mater 31:343–351
71. Santsci PH, Honeyman BD (1989) Radionuclides in aquatic environments. Radiat Phys Chem 34:213–40
72. Livens FR (1991) Chemical reactions of metals with humic material. Environ Pollut 70:183–208
73. Bird GA, Schwartz WJ, Motycka M (1998) Fate of ^{60}Co and ^{134}Cs added to the hypolimnion of a Canadian Shield lake: accumulation in biota. Can J Fish Aquat Sci 55:987–998
74. Likens GE, Davis MB (1975) Post-glacial history of Mirror Lake and its watershed in New Hampshire, U.S.A. An initial report. Int Ver Theor Angew Limnol 19:982–993
75. Evans RD, Rigler FH (1983) A test of the lead-210 dating for the measurement of whole lake soft sediment accumulation. Can J Fish Aquat Sci 40:506–515
76. Shaw TJ, Sholkovitz ER, Kinkhammer G (1994) Redox dynamics in the Chesapeake Bay; The effect on sediment/water uranium exchange. Geochim Cosmochim Acta 58:2985–2995
77. Alberic P, Viollier EP, Jezequel D, Grosbois C, Michard G (2000) Interactions between trace elements and dissolved organic matter in the stagnant anoxic deep layer of a meromictic lake. Limnol Oceanogr 45:1088–1096
78. Edgington DN, Robbins JA, Colman SM, Orlandini KA, Gustin MP (1996) Uranium-series disequilibrium, sdimentation, diatom fustules, and paleoclimate change in Lake Baikal. Earth Plant Sci Lett 142:29–42
79. Hart BT (1982) Uptake of trace metals by sediments and suspended particulate: a review. Hydrobiologia 91:299–313
80. Alberts JJ, Wahlgren MA, Orlandini KA, Durbahn CA (1989) The distributions of ^{29,240}Pu, ^{238}Pu, ^{241}Am and ^{137}Cs among chemically-defined components of sediments, settling particulates and net plankton of lake Michigan. J Environ Radioact 9:89–103
81. Jenne EA (1968) Controls on Mn, Fe, Co, Ni, Cu, and Zn concentrations in soils and water: the significant role of hydrous Mn and Fe oxides. In: Gould RF (ed) Trace inorganics in water, vol 73. American Chemical Society, Washington DC, pp 337–387
82. Wetzel RG (1975) Limnology. WB Saunders, Philadelphia
83. Kovalsky VV, Vorotnitskaya IE (1965) Biogenic migration of uranium in Lake Issyk-Kul'. Geokhimiya 6:724–732
84. Otton JK, Zielinski RA, Been JM (1989) Uranium in Holocene valley-fill sediments, and uranium, radon and helium in waters, Lake Tahoe-Carson Range Area Nevada and California. U.S.A. Environ Geol Water Sci 13:15–28
85. Landa ER (1982) Leaching of radionuclides from uranium ore and mill tailings. Uranium 1:53–64
86. Bird GA, Schwartz WJ, Motycka M, Rosentreter J (1998) Behaviour of ^{60}Co and ^{134}Cs in a Canadian shield lake over five years. Sci Tot Environ 212:115–135
87. Simpson SL, Apte SC, Batley GE (1998) Effect of short-term resuspension events on trace metal speciation in polluted anoxic sediment. Environ Sci Technol 32:620–625
88. Walgren MA, Alberts JJ, Nelson DM, Orlandin KA (1976) Study of the behaviour of transuranics and possible chemical analogues in Lake Michigan water and biota. In: IAEA, Transuranium nuclides in the environment. Symposium Proceedings, San Francisco, pp 9–24. STI/PUB/410, International Atomic Energy Agency,Vienna
89. Swanson SM (1983) Levels of ^{226}Ra, ^{210}Pb, and ^{total}U in fish near a Saskatchewan uranium mine and mill. Health Phys 45:67–80
90. Ahsanullah M, Williams AR (1989) Kinetics of uranium uptake by the crab *Pachygrapsus laevimanus* and the zebra winkle *Austrocochlea constricta*. Mar Biol 101:323–327
91. Mirka MA, Clulow FV, Dave NK, Lim TP (1986) Radium-226 in cattails, *Typha latifolia* and bone of muskrat, *Ondatra zibethica* (L.) from a watershed with uranium tailings near the city of Elliot Lake, Canada. Environ Pollut 91:41–51
92. Waite DT, Joshi SR, Sommerstad H (1988) The effect of uranium mine tailings on radionuclide concentrations in Langley Bay, Saskatchewan, Canada. Arch Environ Contam Toxicol 17:373–380
93. Golder Associates Ltd. (2002) Final report on current period environmental monitoring program for the Beaverlodge Mine site in northern Saskatchewan. Submitted to Cameco Corporation, Saskatoon, Saskatchewan, by Golder Associates Ltd., Saskatoon, Saskachewan
94. Aery NC, Jain GS (1998) Influence of uranium on the growth of wheat. J Environ Biol 19:5–23
95. Gulati KL, Oswal MC, Nagpaul KK (1980) Assimilation of uranium by wheat and tomato plants. Plant Soil 55:55–59
96. Meyer MC, Paschke MW, McLendon T, Price D (1998) Decreases in soil microbial function and functional diversity in response to depleted uranium. J Environ Qual 27:1306–1311
97. Sheppard SC (1989) Toxicity levels of arsenic and uranium in soils. Atomic Energy of Canada Limited, Pinawa, Manitoba (AECL Technical Report TR-480)
98. Sheppard MI, Thibault DH, Shepppard SC (1985) Concentrations and concentration ratios of U, As and Co in Scots pine grown in waste-site soil and an experimentally contaminated soil. Water Air Soil Pollut 26:85–94
99. Sheppard SC, Evenden WG, Anderson AJ (1992) Multiple assays of uranium toxicity in soil. Environ Toxicol Wat Qual 7:275–294

100. Sheppard SC, Sheppard MI, Gallerand M-O, Sanipelli B (2005) Derivation of ecotoxicity threshold for uranium. J Environ Radioact 79:55–83
101. Weinberger P, Murthy TCSS (1985) Uranium uptake and its effects on the germination and early growth of some crop species. Report for Atomic Energy of Canada Limited, Whiteshell Nuclear Research Establishment, Pinawa, Manitoba Technical Record TR-329
102. Kabata-Pendias A, Pendias H (1992) Trace elements in soils and plants, 2nd edn. CRC Press, Boca Raton, 365 pp
103. Durbin PW, Wrenn ME (1975) Metabolism and effects of uranium in animals. Conference on occupational health experience with uranium. Arlington, Virginia, April 28–30, 1975. U.S. Energy Research & Development Administration; U.S. Government Printing Office, Washington, DC, pp 68–129 (ERDA 93)
104. Leach LJ, Yuile CL, Hodge HC, Sylvester GE, Wilson HB (1973) A five-year inhalation study with natural uranium dioxide (UO_2) dust –II. Postexposure retention and biological effects in the monkey, dog and rat. Health Phys 25:239–258
105. Leach LJ, Maynard EA, Hodge HC, Scott JK, Yuile CL, Sylvester GE, Wilson HB (1970) A five year inhalation study with natural uranium dioxide (UO_2) dust –1. Retention and biological effect in the monkey, dog and rat. Health Phys 18:599–612
106. Kocher DC (1989) Relationship between kidney burden and radiation dose from chronic ingestion of U: implications for radiation standards for the public. Health Phys 57:9–15
107. Yuile CL (1973) Animal experiments. In: Hodge HC, Stannard JN, Hursh JB (eds) Uranium, plutonium, transplutonic elements. Springer, NewYork, pp 165–196
108. Llobet JM, Sirvent JJ, Ortega A, Domingo JL (1991) Influence of chronic exposure to uranium on male reproduction in mice. Fund Appl Toxicol 16:821–829
109. Harrison JD (1991) The gastrointestinal absorption of the actinide elements. Sci Tot Environ 100:43–60
110. Wrenn ME, Durbin PW, Howard B, Lipsztein J, Rundo J, Still ET, Willis DL (1985) Metabolism of ingested U and Ra. Health Phys 48:601–633
111. Wrenn ME, Bertelli L, Durbin PW, Eckerman KF, Lipsztein JL, Singh NP (1995) A biokinetic and dosimetric model for the metabolism of uranium. Atomic Energy Control Board, Ottawa, Ontario 79 pp (INFO-0500)
112. International Commission on Radiological Protection (1979) Limits on intake of radionuclides by workers. ICRP Publication 30, Part 1. Pergamon, New York
113. Leggett RW, Harrison JD (1995) Fractional absorption of ingested uranium in humans. Health Phys 68:484–498
114. Moss MM (1989) Study of the effects of uranium on kidney function. Atomic Energy Control Board INFO-0306
115. Sullivan MF, Gorham LS (1982) Further studies on the absorption of actinide elements from the gastrointestinal tract of neonatal animals. Health Phys 43:509–519
116. LaTouche YD, Willis DL, Dawydiak OI (1987) Absorption and biokinetics of U in rats following oral administration of uranyl nitrate solution. Health Phys 53:147–162
117. Tracy BL, Quinn JM, Lahey J, Gilman AP, Mancuso K, Yagminas AP, Villenueve DC (1992) Absorption and retention of uranium from drinking water by rats and rabbits. Health Phys 62:65–73
118. Morris SC, Meinhold AF (1995) Probabilistic risk assessment of nephrotoxic effect of uranium in drinking water. Health Phys 69:897–908
119. Hursh JB, Neuman WF, Toribara T, Wilson H, Waterhouse C (1969) Oral ingestion of U by man. Health Phys 17:619–621
120. Berlin M, Rudale B (1979) Uranium. In: Friberg L, Norberg GF, Vouk VB (eds) Handbook on the toxicology of metals. Elsevier/North Holland Biomedical, Amsterdam, pp 647–658
121. Leggett RW (1989) The behavior and chemical toxicity of U in the kidney: a reassessment. Health Phys 57:365–383
122. Domingo JL (2001) Reproductive and developmental toxicity of natural and depleted uranium: a review. Reprod Toxicol 15:603–609
123. Gilman AP, Villeneuve DC, Secours VE, Yagminas AP, Tracy BL, Quinn JM, Valli VE, Moss MA (1998) Uranyl nitrate: 91-day toxicity studies in the New Zealand white rabbit. Toxicol Sci 41:129–137
124. Gilman AP, Villeneuve DC, Secours VE, Yagminas AP, Tracy BL, Quinn JM, Valli VE, Willes RJ, Moss MA (1998) Uranyl nitrate: 28-day and 91-day toxicity studies in the Sprague-Dawley rat. Toxicol Sci 41:117–128
125. Gilman AP, Moss MA, Villeneuve DC, Secours VE, Yagminas AP, Tracy BL, Quinn JM, Long G, Valli VE (1998) Uranyl nitrate: 91-day exposure and recovery studies in the male New Zealand White rabbit. Toxicol Sci 41:138–151
126. Paternain JL, Domingo JL, Ortega A, Llobet JM (1989) The effects of uranium on reproduction, gestation and postnatal survival in mice. Ecotoxicol Environ Saf 17:291–296
127. Domingo JL, Paternain JL, Llobet JM, Corbella J (1989) The developmental toxicity of uranium in mice. Toxicol 55: 143–152
128. Maynard EA, Hodge HC (1949) Studies of the toxicity of various uranium compounds when fed to experimental animals. In: Voegtlin C, Hodge HC (eds) 1953 Pharmacology and toxicology of uranium compounds chronic inhalation and other studies. McGraw-Hill, New York, pp 309–376
129. Maynard EA, Downs WL, Hodge HC (1949) Oral toxicity of uranium compounds. In: Voegtlin C, Hodge HC (eds) The Pharmacology and toxicology of uranium compounds. McGraw-Hill, New York, pp 1221–1369
130. Domingo JL, Ortega A, Paternain JL, Corbella J (1989) Evaluation of the perinatal and postnatal effects of uranium in mice upon oral administration. Arch Environ Health 44:395–398
131. Harvey RB, Kubera LF, Phillips TD, Heidelbaugh ND (1986) Validation of impaired renal function chick model with uranyl nitrate. Bull Environ Contam Toxicol 36:67–72
132. Morrow P, Gelein R, Beiter H, Scott J, Picano J, Yuile C (1982) Inhalation and intravenous studies of UF_6/UO_2F_2 in dogs. Health Phys 43:859–873
133. World Health Organization (2004) Uranium in Drinking-water: background document for development of WHO guidelines

for drinking-water quality. World Health Organization, Geneva, Switzerland, WHO/SDE/WSH/03.04/118
134. Health Canada (1999) Uranium guidelines for canadian drinking water quality: supporting documentation. http://www.hc-sc.gc.ca/ewh-semt/pubs/water-eau/uranium/guideline-recommandation-eng.php
135. Hursh JB, Spoor NL (1973) Data on man. In: Hodge HC, Stannard JN, Hursh JB (eds) Handbook of experimental pharmacology: uranium, plutonium, transplutonic elements, vol 36. Springer, Berlin, pp 197–239
136. International Commission on radiological protection (1959) Permissible dose for internal radiation. International Commission on radiological protection Publication 2. Pergamon, Oxford
137. SuLu Fu-Yao Zhao (1990) Nephrotoxic limit and annual limit on intake for natural U. Health Phys 58:619–623
138. Sample BE, Suter GW, II (1996) Estimating exposure of terrestrial wildlife to contaminants. Oak Ridge National Laboratory, U.S. Department of Energy, Oak Ridge, Tennessee, 59 pp. (ES/ER/TM-125)
139. Linsalata P (1994) Uranium and thorium decay series radionuclides in human and animal foodchains – a review. J Environ Qual 23:633–642
140. Haseltine SD, Sileo L (1983) Response of American black ducks to dietary uranium: a proposed substitute for lead shot. J Wildl Manage 47:1124–1129
141. Harvey RB, Kubera LF, Lovering SL, Mollenhauer HH, Phillips TD (1986) Acute toxicity of uranyl nitrate to growing chicks: a pathophysiologic study. Bull Environ Contam Toxicol 37:907–915
142. Kovalsky VV, Vorotnitskaya IE, Lekarev VS (1967) Biogeochemical food chains of uranium in aquatic and terrestrial organisms. In: Aberg B, Hungate FP (eds) Radioecological concentration processes. Pergamon, London, pp 329–332
143. Cooley HM, Evans RE, Klaverkamp JF (2000) Toxicology of dietary uranium in lake whitefish (*Coregonus clupeaformis*). Aquat Toxicol 48:495–515
144. Cooley HM, Klaverkamp JF (2000) Accumulation and distribution of dietary uranium in lake whitefish (*Coregonus clupeaformis*). Aquat Toxicol 48:477–494
145. Bywater JF, Banaczkowski R, Bailey M (1991) Sensitivity to uranium of six species of tropical freshwater fishes and four species of cladocerans from northern Australia. Environ Toxicol Chem 10:1449–1458
146. Simon O, Garnier-Laplace J (2005) Laboratory and field assessment of uranium trophic transfer efficiency in the crayfish *Orconectes limosus* fed the bivalve *C. fluminea*. Aquat Toxicol 74:372–383
147. Vizon SciTec (2004) Final Report on the toxicity investigation of uranium to aquatic organisms. Prepared for the Canadian Nuclear Safety Commission, Ottawa, Ontario by Vizon SciTec, Vancouver, British Columbia RSR-019-80
148. Tarzwell CM, Henderson C (1960) Toxicity of less common metals to fish. Ind Waste 5:52–67
149. Parkhurst BR, Elder RG, Meyer JS, Sanchez DA, Pennak RW, Waller WT (1984) An environmental hazard evaluation of uranium in a Rocky Mountain stream. Environ Toxicol Chem 3:113–124
150. Davies PH (1980) Acute toxicity of uranium to brook trout (*Salvelinus fontinalis*) and rainbow trout (*Salmo gairdneri*) in soft water. Fort Collins, Coloradao, Colorado Division of Wildlife F-33-R-15
151. Liber K, Stoughton S, Janz D (2003) Uranium toxicity testing using early life stage lake trout (*Salvelinus namaycush*). Draft report submitted to Saskatchewan Environment, Saskatoon, Saskatchewan by Toxicology Centre, University of Saskatchewan, Saskatoon, Saskatchewan
152. Trapp KE (1986) Acute toxicity of uranium to waterfleas (*Daphnia pulex*) and bluegill (*Lepomis macrochirus*). Environmental & Chemical Sciences, Inc., Aiken, South Carolina (Report ECS-SR-30)
153. Labrot F, Narbonne JF, Ville P, Saint Denis M, Ribera D (1999) Acute toxicity, toxicokinetics, and tissue target of lead and uranium in the clam *Corbicula fluminea* and the worm *Eisenia fetida:* comparison with the fish *Brachydanio rerio*. Arch Environ Contam Toxicol 36:167–178
154. Hamilton SJ (1995) Hazard assessment of inorganics to three endangered fish in the Green River, Utah. Ecotoxicol Environ Saf 30:134–142
155. Hamilton SJ, Buhl KJ (1997) Hazard evaluation of inorganics, singly and in mixtures, to flannelmouth sucker *Catostomus latipinnis* in the San Juan River, New Mexico. Ecotoxicol Environ Saf 38:296–308
156. Holdway DA (1992) Uranium toxicity to two species of Australian tropical fish. Sci Tot Environ 125:137–158
157. Poston TM, Hanf RW Jr, Simmons MA (1984) Toxicity of uranium to *Daphnia magna*. Water Air Soil Pollut 22: 289–298
158. Zeman FA, Gilbin R, Alonzo F, Lecomte-Pradines C, Garnier-Laplace J, Aliaume C (2008) Effects of waterbourne uranium on survival, growth, reproduction and physiological processes of the freshwater cladoceran *Daphnia magna*. Aquat Toxicol 86:370–378
159. Kuhne WW, Caldwell CA, Gould WR, Fresquez PR, Finger S (2002) Effects of depleted uranium on the health and survival of *Ceriodaphnia dubia* and *Hyalella azteca*. Environ Toxicol Chem 21:2198–2203
160. Liber K, George T (2000) Toxicity of uranium to *Ceriodaphnia dubia* at different water hardnesses representative of northern Saskatchewan conditions. Report for COGEMA Resources Inc., Saskatoon, Saskatchewan. Toxicity Centre, University of Saskatchewan, Saskatoon, Saskatchewan
161. Pickett JB, Specht WL, Keyes JL (1993) Acute and chronic toxicity of uranium compounds to *Ceriodaphnia dubia*. Westinghouse Savannah River Co., Aiken, South Carolina. Prepared for the Department of Energy under contract DE-AC09-89SR 18035, 57 pp (WSRC-RP-92-995)
162. Semaan M, Holdway DA, van Dam RA (2001) Comparative sensitivity of three populations of the cladoceran *Moinodaphnia macleayi* to acute and chronic uranium exposure. Environ Toxicol 16:365–376

163. Charles AL, Markich SJ, Stauber JL, De Filippis LF (2002) The effect of water hardness on the toxicity of uranium to a tropical freshwater alga (*Chlorella* sp.). Aquat Toxciol 60:61–73
164. Franklin NM, Stauber JL, Markich SJ, Lim RP (2000) pH-dependent toxicity of copper and uranium to a tropical freshwater alga (*Chlorella* sp.). Aquat Toxicol 48:275–289
165. Hogan A, van Dam R, Masrkich S, Camerilleri C (2005) Chronic toxicity of uranium to a tropical green alga (*Chlorella* sp.) in natural waters and the influence of dissolved organic carbon. Aquat Toxicol 75:343–353
166. van Dam R, Hogan A, Houston M, Noul S, Lee N (2006) Chronic toxicity of uranium to *Lemna aequinoctialis* and *Amerianna cuming*, In: Jones DR, Evans KG, Webb A (eds) Eriss research summary 2005–2006, Supervising Scientist Report 193, Supervising Scientist, Darwin NT
167. Borgmann U, Couillard Y, Doyle P, Dixon DG (2005) Toxicity of sixty-three metals and metalloids to *Hyalella Azteca* at two levels of water hardness. Environ Toxicol Chem 24:641–652
168. Alves LC, Borgmann U, Dixon DG (2008) Water-sediment interactions for *Hyalella azteca* exposed to uranium-spiked sediment. Aquat Toxic 87:187–199
169. Burnett C, Liber K (2006) Can *Chironomus tentans* develop tolerance to uranium exposures over several generations? Society of environmental Toxicology and Chemistry (SETAC) North America 27th Annual meeting, Montreal
170. Dias V, Ksas B, Camilleri V, Bonzom JM (2005) Sublethal effects of sediment-associated uranium on *Chironomus riparius* (Diptera: *Chironomidae*) larvae. Radioprotection Suppl 40:S191–S197
171. Hyne RV, Rippon GD, Ellender G (1992) pH-dependent uranium toxicity to freshwater hydra. Sci Tot Environ 125:159–173
172. Liber K, Stoughton S, Rosaasen A (2004) Chronic uranium toxicity to white sucker fry (*Catostomus commersoni*). Bull Environ Contam Toxicol 73:1065–1071
173. Keklak MM, Newman MC, Mulvey M (1994) Enhanced uranium tolerance of an exposed population of the eastern Mosquitofish (*Gambusia holbrooki* Girard 1859). Arch Environ Contam Toxicol 27:20–24
174. Krueger S, Olson GJ, Johnsonbaugh D, Beveridge TJ (1993) Characterization of binding of gallium, platinum, and uranium to *Pseudomonas fluorescences*by small-angle x-ray scattering and transmission electron microscopy. Appl Environ Microbiol 59:4056–4064
175. Khangarot BS (1991) Toxicity of metals to a freshwater tubificid worm, *Tubifex tubifex* (Muller). Bull Environ Contam Toxicol 46:906–912
176. Liu H-H, Wu JT (1993) Uptake and recovery of americium and uranium by *Anacystis* biomass. J Environ Sci Health part A Environ Sci Engin 28:491–504
177. Nakajima A, Horikoshi T, Sakaguchi T (1979) Ion effects on the uptake of uranium by *Chlorela regularis*. Agric Biol Chem 43:625–629
178. Horikoshi T, Nakajima A, Sakaguchi T (1979) Uptake of uranium by *Chlorella* cells grown under autorophic, heterotrophic and mixotrophic cultue conditions. Agric Biol Chem 45:781–783
179. Chassard-Bouchard C (1983) Cellular and subcellular localization of uranium in the crab *Carcinus maenas*: a microanalytical study. Mar Pollut Bull 14:133–136
180. Jaagumagi R, Bedard D (2001) Bancroft area mines (Madawaska, Bicroft and Dyno Mines): assessment of impacts on water, sediment and biota from historical uranium mining activities. Final Report Prepared for Peterborough District Eastern Region Ministry of the Environment
181. Carroll JJ, Ellis SJ, Oliver WS (1979) Influence s of total hardness constituents on the acute toxicity of cadmium to brook trout (*Salvelinus fontinalis*). Bull Environ Contam Toxicol 22:575–581
182. Welsh PG, Lipton J, Chapman GA, Podrarsky TL (2000) Relative importance of calcium and magnesium in hardness-based modification of copper toxicity. Environ Toxicol Chem 19:1624–1631
183. Holdway DA (1992) Uranium mining in relation to toxicological impacts on inland waters. Ecotoxicology 1:75–88
184. Australian and New Zealand guidelines for fresh and marine water quality: Vol 2 – Aquatic ecosystems – Rationale and background information, Section 8.3.7 (http://www.mincos.gov.au/_data/assets/pdf_file/0020/316136/gfmwq-guidelines-vol2-8-3b.pdf). Accessed 14 Jan 2010
185. BEAK International incorporated (1998) Toxicity of uranium and trace metal discharged to the aquatic environment. Prepared for Atomic Energy Control Board, Ottawa, Ontario, August 1998. Dorval, Quebec (Solicitation No. 87055-7-5010/1)

Books and Reviews

Voegtlin C, Hodge HC (eds) (1953) Pharmacology and toxicology of uranium compounds chronic inhalation and other studies. McGraw-Hill, New York

Urban Air Quality: Meteorological Processes

David Carruthers[1], Silvana Di Sabatino[2], Julian Hunt[3]
[1]Cambridge Environmental Research Consultants, Cambridge, UK
[2]Dipartimento di Scienza dei Materiali, Università del Salento, Lecce, Italy
[3]University College London, London, UK

Article Outline

Glossary
Definition of the Subject
Introduction
Characteristic Regions of the Flow and Drivers
Urban Data

Computational Models for Meteorology and Air Flow in Urban Areas
Examples of Output of Modelling Calculations
Future Directions
Notation and Abbreviations
Subscripts
Abbreviations
Bibliography

Glossary

Mesoscale Scale of weather systems smaller than synoptic scale but larger than microscale or urban scale; tens to hundreds of kilometers.

Neighborhood scale Scale typical of groups of buildings or streets; hundreds of meters to a few kilometers.

Building and street scales Scales of buildings or streets; tens to hundreds of meters.

Fully computational model (FCM) A model which explicitly represents flow and turbulence around buildings.

Fast approximate model (FAM) A model which uses approximations and parameterizations of the fine scale flow to speed up model run times and reduce complexity.

Porosity The volume fraction of air between buildings and therefore a measure of building density.

Urban air quality A general term representing concentrations of pollutants in an urban area. Good air quality corresponds to low concentrations of pollutants.

Urban meteorology Meteorology within an urban area; the urban environment significantly affects mean flow turbulence and temperature.

Definition of the Subject

Meteorological processes in urban areas that are relevant to urban air quality. Of most significance are the impacts of the urban morphology on the mean flow and turbulence, which determines the transport and dispersion of pollutants and therefore their concentration.

Introduction

Concentrations of pollutants within an urban area depend on a number of different factors. These include the emissions of pollutants within the urban area, pollutant concentrations transported into the area, and the meteorology within the urban area, in particular, the mean airflow and turbulence (which determines the movement and mixing of the emitted pollutants) and the temperature and solar insolation (which impacts on chemical transformation taking place). This entry discusses meteorology within the urban area with the focus being on the mean flow and turbulence, as these may be substantially different from the upstream flow. Discussed here are the current understanding, experimental and numerical simulation data, and the relative merits of different modelling approaches. For discussions of dispersion within urban areas, see, for example, [1].

Section "Characteristic Regions of the Flow and Drivers" presents the underlying concepts and prediction methods related to the airflow and meteorology of urban areas that are particularly relevant for understanding and modelling dispersion from the urban sources. It is noted how spatial and temporal patterns of flow and dispersion in urban areas greatly depend on their location (e.g., flat, hilly terrain, coastal, or desert), the types of surface, prevailing meteorological conditions (e.g., strong/weak geostrophic winds), and on the patterns and forms of urban building/street/open space (e.g., isolated buildings or canyons; high or low range of building heights, etc.). It will be convenient to describe the flow in terms of three characteristic ranges of length scale, namely, mesoscale, neighborhood scale, and building/street scales, each with their own general features and where different modelling approaches are necessary, depending on the requirements for accuracy and speed of computation. Section "Urban Data" presents some details of data, and sections "Computational Models for Meteorology and Air Flow in Urban Areas" and "Examples of Output of Modelling Calculations" provide details of modelling methods for flow in urban areas and examples of model calculations.

Characteristic Regions of the Flow and Drivers

Characteristic Regions of the Flow

In urban areas, there are usually considerable variations in the types, sizes, and layout of buildings and streets as illustrated in Fig. 1, and over larger urban areas there are often also significant variations in the natural

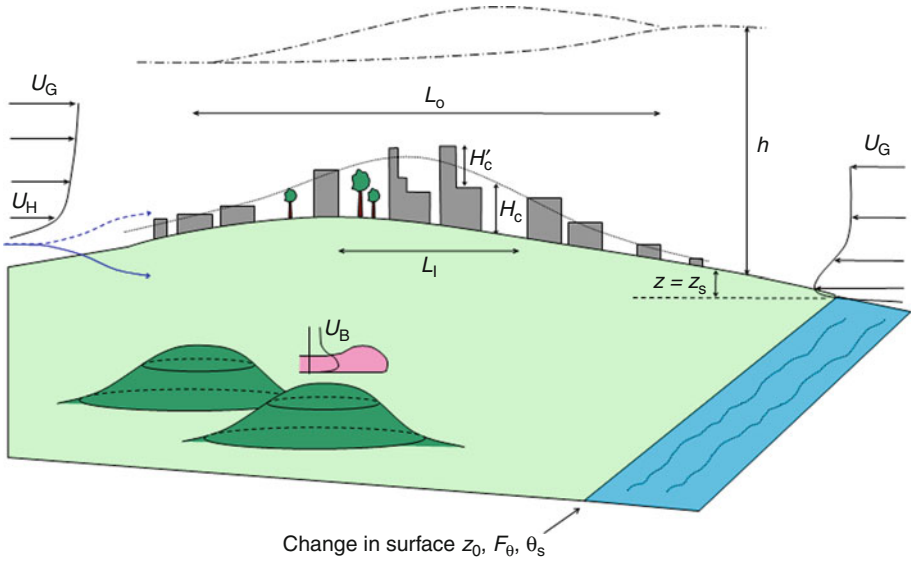

Urban Air Quality: Meteorological Processes. Figure 1
Characteristic features of the terrain, buildings, and meteorology on the meso- (regional) scale of significance for urban dispersion. L_o and L_I are the overall and inner city length scales, respectively. Note that U_G is the geostrophic wind, U_B is the typical wind speed associated with local buoyancy effects, for example, downslope winds from nearby mountains. H_c is the canopy height and H_c' is the standard deviation of canopy height

Urban Air Quality: Meteorological Processes. Table 1 Scale ranges of urban air flow and dispersion

	Range	Determining factor(s)	Relation to urban and meteorological scales
1.	Mesoscale L_M (~30 km)	Flow over buildings Significant orographic/Coriolis effects Surface influences and pollutants mixed through boundary layer	$L_M \sim L_O$ for large urban areas l_O (x ~ L_M) ~ h
2.	Neighborhood scale L_N (1–10 km)	Flow and dispersion above and between buildings Average geometrical features dominate mean flow/dispersion Growing internal layer above buildings	$L_N < L_O \lesssim L_M$ Typically $L_N \sim L_I$, inner city scale l(x ~ L_N) $\lesssim$ h
3.	Building/street scale L_{BS} (~3–1,000 m)	Flow and dispersion determined by features below building level (except for elevated releases) Mean geometrical and flow features on scale L_{BS} (not smaller) mainly determine dispersion Internal mixing layers below/above buildings are of order of building/street dimensions	$10\,H \gtrsim L_{BS} \gtrsim w, b, d$ $l \lesssim H$ (this defines upper scale of L_{BS})

topography. Both these urban scale features and the meteorology have general characteristics over different length scales. These need to be understood and related to each other when developing a picture of the urban airflow as illustrated in Tables 1 and 2.

Over level terrain, except in very light wind conditions, the direction and speed of the airflow only changes significantly over the mesoscale (of order 30 km) or greater scales. These changes are determined by Coriolis effects, by the effect of the urban area on

Urban Air Quality: Meteorological Processes. Table 2 Main types and features of urban mesoscale

	Increasing effects of orography/heat island, lighter geostrophic wind →			
←Increasing scale	$F = U_G/U_B$ / L_O/L_{RO}	>1 (typically windy environment over flat plain)	~1 (typically moderate wind over flat surface)	<1 (hilly terrain; near coast)
	$\lesssim 1$	(i) Roughness slow down; boundary layer depth varies.	(iii) Weak flow convergence, change in stability over urban area	(v) Slope flows in open valleys; sea breezes; slope flows and pooling in bounded valleys
	$\gtrsim 1$	(ii) in addition to effects of (i) above anticyclonic turning of wind; weak convergence /divergence on left/right.	(iv) Strong central convergence and cyclonic turning.	(vi) Interactions between orographic and urban heat island flows. Significant variations in orographic and heat island flow across the urban area.

Note: U_G is the geostrophic wind speed,
$U_B = (gh|\Delta\theta|/\theta)^{1/2}$ is the buoyancy-induced local wind speed
L_f is the Coriolis advection length (= U/f)
L_{Ro} is the Rossby length scale defined by stratification and Coriolis effects (= hN/f)

convergence/divergence and turning of the wind, and by temporal variations in the flow forced by diurnal and synoptic effects. Where there are sharp variations in topography the *surface* air flow may change locally (e.g., at the coast or edge of an urban area). However, the whole boundary layer flow does not adjust immediately to the change of surface conditions: this takes place over a mesoscale distance L_M which, in the atmosphere, is typically of order 30–50 km. This distance is usually determined by the Rossby length scale $L_{Ro}= hN/f$ where f is the Coriolis parameter and N is the buoyancy frequency of the stable layer at or above the boundary layer of height h. At midlatitudes $f \sim 10^{-4}\ s^{-1}$, and typically $N \sim 10^{-3}\ s^{-1}$, $h \sim 1{,}000$ m. In neutral conditions, L_M is determined dynamically by inertia and turbulence stresses, when $L_M \sim L_f = U/f$, usually a distance of greater than 30 km, while close to large mountains of height H_M, $L_{Ro}= H_M N/f$.

Figure 2 shows that in the zone where the boundary layer is adjusting to the changed surface conditions, there is an internal layer with depth $l(x, y)$ above the ground, separating the air flow and pollutants above and below it. The depth of this layer tends to increase slowly over the area where the surface conditions (temperature or surface roughness) have changed; see, for example, [2] and [3]. Over the mesoscale L_M, the internal layer reaches the top of the boundary layer, and then the vertical profiles of velocity and temperature over the whole boundary layer are changed.

Over shorter horizontal scales, the internal layer depth is much less than h. Here the perturbed flow has separate characteristics over the intermediate neighborhood scales L_N ($\lesssim 5$ km) and over the shorter building/street scales L_{BS} ($\lesssim 300$ m). The former scale L_N extends over groups of buildings/streets of similar size and type, and the internal layer depth l_N is greater than the height of the envelope or canopy of the buildings H_C. Note that there is significant mass, momentum and energy transfer between the flow in and above the canopy on this scale. Even though the neighborhood scale includes many buildings, the types of buildings and their patterns have significant effects on this exchange process and on the flow within the canopy.

Mesoscale

In the following section, the main features of the flow and meteorology in the three characteristic flow regions of urban areas are discussed, beginning with

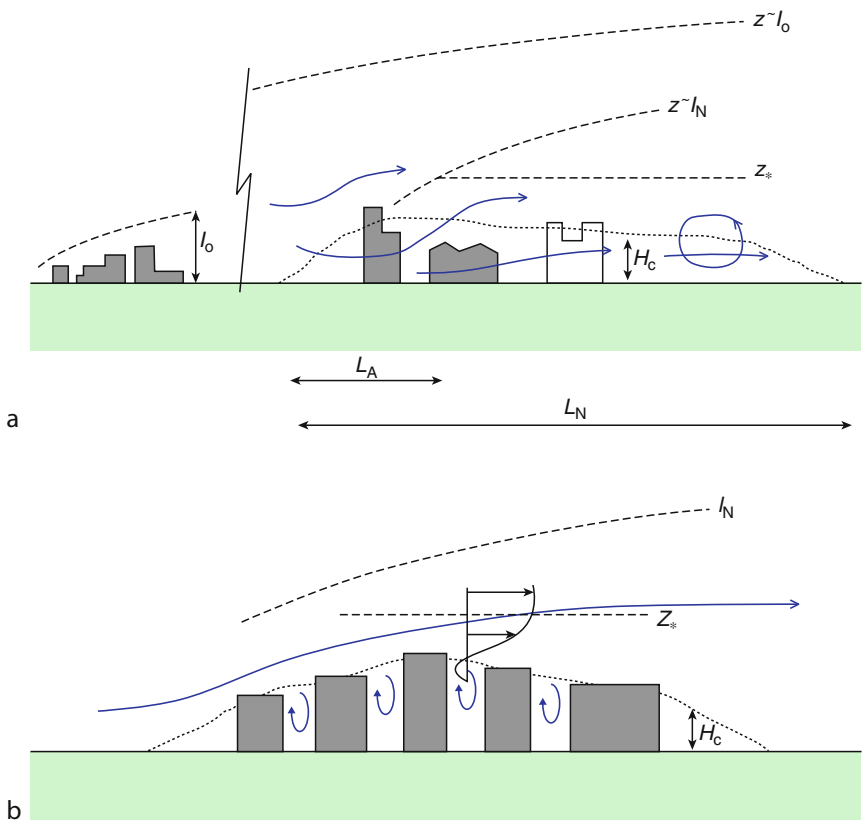

Urban Air Quality: Meteorological Processes. Figure 2
Characteristic features of building envelope and zones of air flow in neighborhod scale. (Note that the definition of this scale depends partly on the level of detail of the computation.) (**a**) "Porous" canopy – with isolated buildings. l_O and l_N are the heights of the perturbed layers above the buildings; z_* is the height of the top of the shear layer above the buildings. L_A is the adjustment distance. (**b**) Non-porous canopy, where the mean flow passes over the canopy

those on the mesoscale. These are broadly categorized in Table 2 according to the relative effects of buoyancy to inertial forces produced by orographic or heat island effects on the one hand and the effects of Coriolis forces acting over the overall scale L_O of the urban area on the other. The buoyancy and inertial forces are essentially indicated by the value of the Froude number, defined as the ratio of the geostrophic wind U_G to the average velocity U_B produced by the buoyancy forces acting over the urban area, i.e., $F = U_G/U_B$. U_B is driven by the horizontal temperature and hence density changes $\Delta\theta$, which may be natural or caused by the urban heat island, and is defined by $U_B = \sqrt{gl_0|\Delta\theta|/\theta}$, where l_0 is the internal layer thickness or the height of the nearby mountains if these dominate the flow and g is gravitational acceleration. Note that $\Delta\theta/\theta$ depends on a number of features of the urban area, the most important being the increased heat storage due to urban buildings, which increases temperature (urban heat island) and the impact of vegetation inside and outside the urban area, which may reduce temperature. Typically the heat island causes increases in temperature of a few degrees in a small town ([4, 5]) so that $|\Delta\theta|/\theta \sim 0.01$ and $U_B \sim 3$ m/s. Larger urban areas show a much higher urban heat island effect (up to 12 C for cities in arid or semiarid environments, [6]) leading to larger values of U_B. Coriolis effects are significant if L_o is comparable or greater than the mesoscale length scales.

Referring to Table 2, it is seen that for typical small to medium scale urban areas (case (i)), buoyancy and Coriolis effects are negligible, $F > 1$, and L_f, $L_{Ro} > L_O$,

the scale of the urban area. For case (ii), as L_O increases, and if there are no thermal effects, Coriolis effects begin to become significant with turning of the wind. Case (iii) corresponds to the case in which the urban heat island, and hence the buoyancy velocity, increases. This will change the stability and boundary layer depth over urban areas. But if the area is even larger so that L_f, $L_{Ro} < L_O$, as in case (iv), then the heat island and Coriolis effects are larger. In this case there is convergence with the flow toward the urban area turning cyclonically (i.e., anticlockwise in the northern hemisphere), as has been measured, especially at night [3].

Strong buoyancy forces occur in the presence of mountains and sloping terrain, so that $F < 1$, leading to marked diurnal variations in the wind speed and direction, over the urban area and outside it. Such areas are associated with sudden changes in the airflow, internal fronts, and pooling of the air in valleys, all of which greatly influence dispersion of air pollution.

Note that because of release of heat stored in buildings at night and increased mixing due to the high surface roughness, the static stability of the air stream usually changes as it moves into and out of the urban area, typically becoming less and more stable, respectively.

Where there are significant buoyancy forces or orographic effects, the boundary layer profiles over the urban area and downwind may not simply adjust toward the equilibrium states found in neutral, stable, and unstable boundary layers over flat terrain. In fact there are characteristic features of the air flow on these scales, especially near hills, coasts, and urban/rural boundaries, that can significantly affect dispersion, such as blocked flow, unsteady slope flows, gravity currents, and boundary layer jets ([7, 8]).

Neighborhood Scale

The characteristic features of the air flow on the neighborhood scale are dependent on the grouping of the buildings/streets (with average building height H, breadth b, width w, and distance between buildings d). In suburban areas or spaciously designed urban centers, the buildings are effectively isolated. However, in dense suburbs and inner city areas there may be "canyons" with long rows of buildings neighboring streets.

The suburban areas or spacious urban centers are essentially porous to the oncoming boundary layer; the airflow slows down as it passes between the buildings, as a result of both the bulk displacement of the flow over and around the "envelope" or canopy of the buildings and their drag. Downwind of a characteristic adjustment distance L_A (which is of the order of $H(d^2/wb)$ or H/β where 1-β is the volume occupied by the buildings and β is the volume of air between buildings and therefore a measure of porosity), or typically 10–30 building widths [9], the drag force dominates but is weakened by the sheltering effect of upwind buildings (see Table 3). Over this adjustment distance the air flow above the buildings first accelerates as a result of the vertical displacement by the buildings, and then decelerates as slow moving fluid is expelled from below the level of the building envelope or canopy. Downwind of the adjustment distance (Fig. 2a), if the neighborhood scale is large enough (i.e., $L_N > L_A \sim 30\ H$), the air flow (speed U_c) within the canopy is largely driven by turbulent shear stresses generated in the shear layer just above buildings $H_c < Z < Z_* < l_N(x)$ (rather than by the oncoming airflow). Above this shear layer, $Z_* > Z > l_N(x)$, the airflow is characteristic of a surface layer with displacement height z_d, so that

$$U(z) \cong \frac{u_*}{\kappa} \ln\left(\frac{z - z_d}{z_0}\right), \tag{1}$$

where z_0 is the aerodynamic roughness length, and κ is von Karman's constant as discussed by Grimmond and Oke [10], Britter and Hanna [11], and Belcher et al. [9]. Application of Eq. 1 requires knowledge of z_0, z_d, and u_*. The estimation of these parameters is not straightforward in urban areas. The determination of the friction velocity is also difficult because of the large variability of momentum fluxes inside the urban canopy [12].

The aerodynamic roughness length z_0 is a measure of the turbulence-generating capacity of the ground. The larger the roughness length, the more turbulent the air for a given wind speed. Generally, tall features such as buildings have a larger roughness length than short features. However a densely built area may have a smaller roughness length than a less dense one because the interaction between the air and the region

Urban Air Quality: Meteorological Processes. Table 3 Typical street/building configurations in urban areas

	Increasing separation, d →		
← Increasing width *w*	*b/s* / *b/w*	≳2	≲1
	≳10	(i) Canyon (*H/w* > 2) Residential street (*H/w* ≲ 1)	(iv) City squares*, parksides
	1–5	(ii) Long blocks (e.g. industrial estates)	(v) Enclosed spaces (e.g. courtyards)
	≲2	(iii) Closely-packed industrial sites; ancient settlements**	(vi) Square blocks (e.g. houses), *H/w* ≲ 1 Office blocks, *H/w* ≥ 1

* Long buildings with large space are rare except for city squares/courtyards.
** Wide buildings close together are rare except on certain industrial estates.
In the above *s* is the distance to the nearest building.
Note:
(a) Mixed cases occur, such as office blocks as part of streets (so H/w varies).
(b) Long and square blocks are usually aligned in streets (i.e. angle between two nearest cases Δθ is 180°).

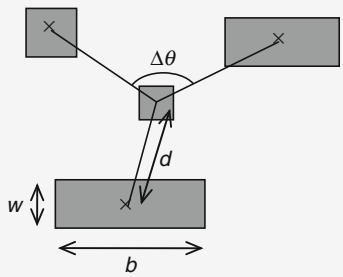

beneath is reduced. The wind speed close to a rough surface is reduced by friction and a velocity profile can be plotted from the surface to the free fluid. This reduction in wind speed as the surface is approached can be equated to a transfer of momentum from the bulk fluid to the surface, caused by the friction force. The momentum transfer (transport) is large if the roughness is large.

The displacement height z_d according to Jackson [13] can be interpreted as the level of mean momentum absorption. According to the Jackson's formulation this can be determined by the following relation:

$$(z_d - z_s)(\overline{u'w'_s}) \int_{z_s}^{z_d} \left(\overline{u'w'_s} - \overline{u'w'(z)}\right) dz, \qquad (2)$$

where z_s is the average elevation of the surface and $\overline{u'w'_s}$ is the peak of the shear stress profile. Accurate knowledge of the aerodynamic characteristics of cities is vital to describe, model, and forecast the behavior of urban winds, turbulence, and the dispersion of pollutants at all scales. The calculation of z_d (which is of order H) based on Eq. 2 is rarely feasible due to the lack of measurements. The classical way to estimate z_0 and z_s in open flat terrain is based on the measurements of wind speed profiles from a tall mast or, less accurately, on the inference from published aerodynamic roughness values for similar terrain elsewhere [14, 15]. Both methods, however, are very difficult to apply to urban areas. A promising alternative that has become available in recent years, due to increased computing resources and the availability of high-resolution 3-D building databases, is based on the calculation of z_0 and z_d from the analysis and measurement of the city geometry (urban morphometry). Morphometric methods express the cities' aerodynamic characteristics in

terms of average building height (H), planar area index (λ_p), frontal area index (λ_f), and other measurable parameters related to the urban morphology (e.g., [10, 16, 17]. While λ_p for a given neighborhood is independent of wind direction, λ_f represents the total area of buildings projected into the plane normal to the incoming wind direction and is a function of orientation. For a given wind direction, λ_f is smaller if the wind angle is oblique, rather than perpendicular, to the front face of the building.

Starting from the lambda parameters z_d and the aerodynamic roughness length, z_0 can be computed using the equations derived by Macdonald et al. [18]:

$$\frac{z_d}{\overline{H}} = 1 + (\lambda_p - 1)\alpha^{-\lambda_p}, \tag{3}$$

$$\frac{z_0}{\overline{H}} = \left[1 - \frac{z_d}{\overline{H}}\right] \exp\left\{-\left[\frac{0.5\beta C_D \lambda_F}{\kappa^2}\left(1 - \frac{z_d}{\overline{H}}\right)\right]^{-0.5}\right\}, \tag{4}$$

where $\alpha = 4.43$, $\beta = 1.0$, $\kappa = 0.4$, $C_D \sim 1$.

Even though Eqs. (3) and (4) provide good operational estimations for z_d, as far as z_0 is concerned, there is a warning due to the intrinsic difficulty linked to limited fetch, typical in urban areas, which prevents the flow from being in equilibrium with the changing surface as noted above. Equations (3) and (4) provide a first estimate of surface characteristics, but aerodynamic properties need to be evaluated on a case by case basis. Besides, while z_0 is an important parameter for the above canopy flow description as expressed by Eq. (1), within the urban canopy its use can be replaced by a combination of lambda parameters and their variation with height [19].

Going back to the discussion on the flow characteristics, it is worth mentioning that despite the unevenness and inhomogeneity of these boundary layer flows, the ratios of the r.m.s. values of the three components of turbulent velocity (σ_u,σ_v, σ_w) to the friction velocity u_* are quite comparable with their values over level terrain, i.e., $\sigma_u/u_* \cong 2.5$, $\sigma_v/u_* \cong 2.0$, $\sigma_w/u_* \cong 1.3$[20].

Downwind of the "neighborhood" or urban area where the buildings decrease in height, the mean air flow descends and accelerates. Typically in neutral conditions the mean velocity adjusts to within 10% of its ultimate (rural) value within about 30 lengths [21].

When the urban area is more densely packed with buildings and they are distributed in the "canyon" form, the urban area is effectively "non-porous" (Fig. 2b). An example of this case is the central area of Nantes [22]. The air does not flow continuously between the buildings but the mean streamlines and the cloud/plume pass above the buildings and air flow is largely above the canopy envelope (average height H_C); the ratio U_c/U_H is much less than σ_w/U_H.

Within the canopy the flow depends on the particular street and building configuration at that scale. There are mean flows along streets at an angle to the mean flows above the buildings, which results in extra lateral diffusion.

The flow above the canopy is essentially equivalent to airflow over a wide hill with length L_N and height H_C, but with a significant value of the roughness length z_0 that is of the order of the thickness of the shear layer over the buildings and the "canyons" between them [23]. The flows in the inner layer above the buildings and in the wake downwind of the neighborhood region are similar to those for the porous case.

Building and Street Scale

On the building/street scale there are also characteristic features of the flow corresponding to different categories of building street shape and configuration. Various planning criteria and concepts have been proposed for defining these categories, for example, rugosity (or mean canopy height H_C), relative rugosity (defined by building height variability or canopy height variability H'_C), sinuosity (of canyons), the Sky View Factor (SVF), which signifies the fraction of sky dome visible from a specific outdoor position and is important for estimating the amount of incoming solar radiation for energy calculation, and the "compactness index," which is defined as the ratio of building surface area (excluding the plan area) to the surface area of a cube that has the same volume as the building. For microscale phenomena the urban morphometry is the more important, but at the mesoscale both the geometry and surface thermal characteristics play an equal role [24]. These, and related concepts, have been used to guide the suggested categorization shown in Table 3 for

building/street configurations and the consequences for air flow features illustrated in Fig. 3.

Fluid mechanical studies have shown how flows around individual buildings become significantly distorted in the presence of other buildings depending on the ratio b/d of the breadth b to separation distance d from the nearest building, on the ratio b/w of breadth to the width w of the building, and on the relative height to width ratio H/w. When there are many buildings, as in urban areas, these flow interactions build up into characteristic flow patterns; this is now examined.

Separated Buildings b/w, w/b <2. The separation distances d are large enough that $b/d \leq 1/3$ ((vi) of Table 3 and Fig. 3a). The flow around each building

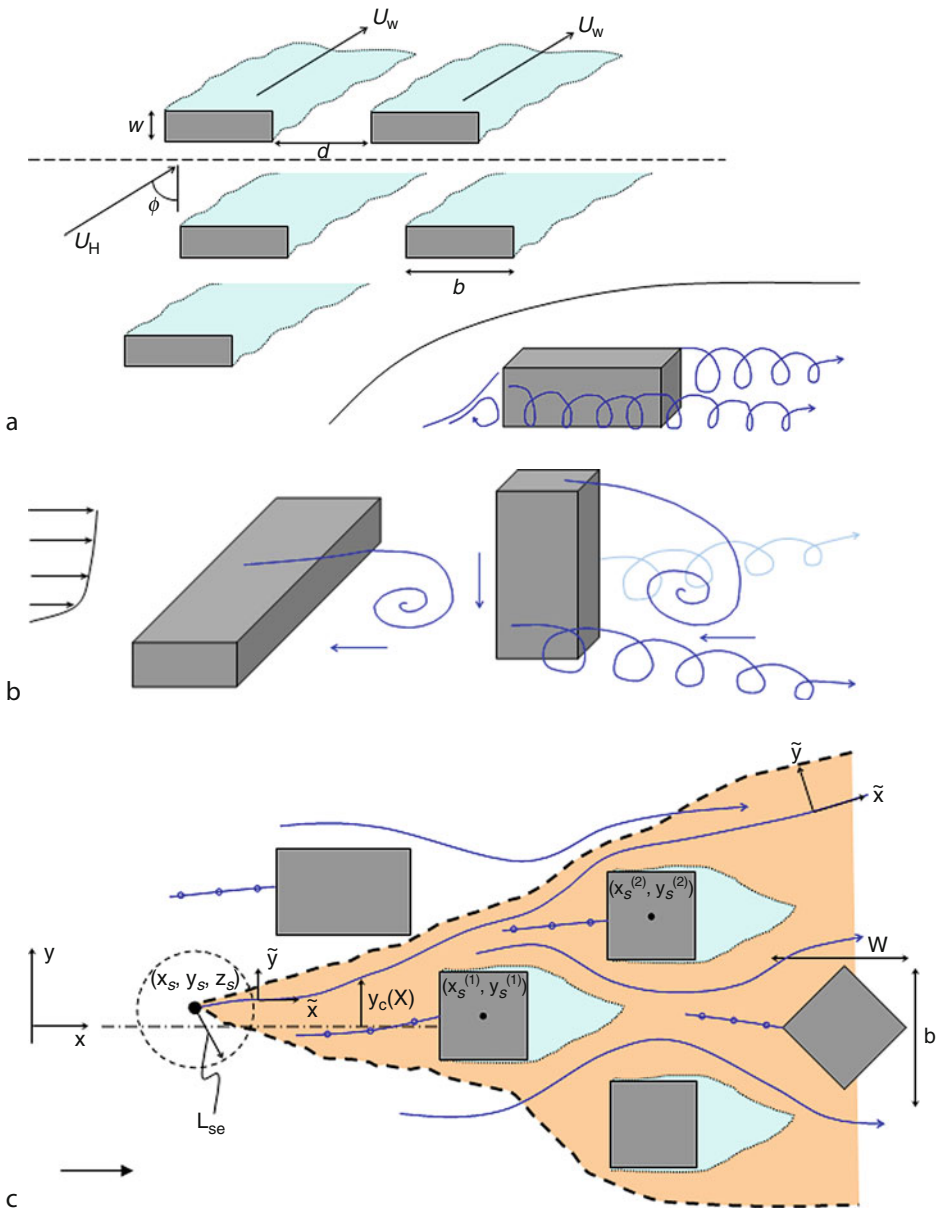

Urban Air Quality: Meteorological Processes. Figure 3 (Continued)

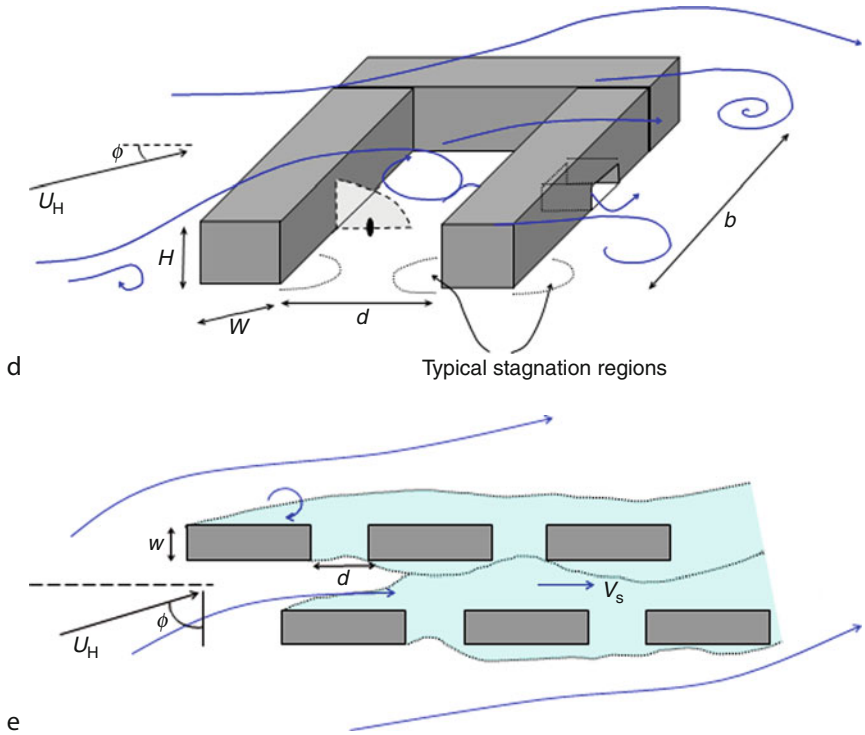

Urban Air Quality: Meteorological Processes. Figure 3
Typical building/street configuration. (**a**) Normal approach angle ϕ small enough (i.e., cosϕ > 2w/d) for independent wakes to be formed (approximately parallel to the approach wind). Note the complex forms of building wakes, in which swirl may persist. (**b**) Effects of uneven building heights. Note strong reverse and downdraft winds (e.g., [26, 27]). (**c**) Staggered tall buildings (comparable height), located at $\{x_B^{(i)}, y_B^{(i)}\}$, close to each other. Note how wakes can "disappear" through converging streamlines, while lateral diffusion is enhanced by diverging streamlines ("topological" diffusion). Streamlines are indicated by solid arrowed lines. The streamline through the source at (x_s, y_s, z_s) is $y_c(x)$; $\tilde{x}, \tilde{y}$ are coordinates parallel and perpendicular to this streamline. Streamlines marked with small circles are mean streamlines ψ_{stag} passing through stagnation points where plumes split. The cloud/plume resulting from the source is the shaded area enclosed by heavy dashed line. L_{Se} is the effective size of the source outside which atmospheric turbulence determines the dispersion. (**d**) Enclosed spaces – Typical instantaneous streamlines of the large-scale flow in a courtyard, where b/d ∼ 1, b/w ∼ 3, H/d ∼ 1/3, and H/w ∼ 1. The shaded area indicates the region of highest concentration of matter released in the courtyard. (**e**) Normal approach angle ϕ large enough (i.e., cosϕ ≲ 2w/d) for wakes to merge and "canyon" flow to develop in streets between the buildings

has approximately the same form as that of an isolated building, with recirculating flow regions, turbulent wakes, and horseshoe vortex structures around the base of the building. In slightly stable conditions the vortex structures can persist far downwind but in most urban cases where the flow is neutral and highly turbulent they are not significant. On the other hand the turbulent wakes from upwind buildings do impact on those downwind, enhancing the mixing. Isolated buildings, especially in slightly stable conditions can produce swirling wakes far downwind [25]. When there are marked variations in the height of adjacent buildings, the wake vorticity shed from upwind buildings can produce sharp down-flows and increased trailing vorticity in the flow direction as discussed by Lawson [26]. These effects contribute to mixing between the canopy and external flow.

For tall buildings that are not closely packed and where $H/b > 1$ (Fig. 3b), there is strong mixing in the horizontal plane and to a lesser extent in the vertical direction because of the high turbulence generated. Buildings placed sufficiently close to each other may result in wake interaction, which tends to cause downwash [27] and strong swirl around the sides of tall buildings. This enhances vertical mixing in the lower part of the downwind wakes and through lateral convergence reduces their downwind extent. When $b/d < 1/3$, corresponding to long buildings that are sufficiently separated from each other, the flow over an upwind building can descend into the space between the buildings. This flow is significantly sheltered and stagnation areas are larger than for isolated buildings.

Close Packed Buildings not Aligned. In some city centers and some types of industrial plant, the spacing between buildings are within about two or three widths (i.e., $b/d \gtrsim 1/3$), but the gaps between the building do not form continuous "canyons"((iii) of Table 3). The air flow passes around the buildings and the streamlines move irregularly between the buildings, converging and diverging as they do so, as sketched in Fig. 3c [28]. The wakes tend to be reduced in length because of cancellation of vorticity.

Where the separation distance is smaller, i.e., $b/d \geq 1$, the flow is further changed because there may be other complicating geometrical factors, such as the effect of a courtyard, which further slows up the flow, or open gateways, which can lead to sufficiently high local winds that affect the overall flow pattern (Fig. 3d). Here the interaction between the vorticity layer from the top of the buildings and impacting on surrounding buildings leads to even more complex recirculating flows than in street canyons. However, because of the finite extent of these flow regions, it can generally be assumed that (unlike elongated street canyons) there is only a small mean velocity component U_C below the building height, i.e., $U_C/U_H \lesssim 0.1$. However, the turbulence level is quite high in these recirculating flows, with $\sigma_u \sim \sigma_v \sim (0.5\text{–}1.0) \cdot \sigma_u(z_*) \sim 1.2\text{–}2.5\ u_*$, so that $\sigma_u \sim V_s$ [23].

Flow Aligned with Rows of Buildings ($b/w > 1$, $H/d \gtrsim 1/3$). In this case buildings are located in rows with separation gaps d that are comparable with their height H (i.e., streets). The case includes buildings that are loosely aligned in rows or continuous canyons ((ii), (iii), and (iv) of Table 3). Where the downwind buildings are nearly aligned with the wind (Fig. 3e, $\cos\phi \leq w/d$), they distort the wake's vorticity so that the wakes tend to be aligned with the building [29]. The recirculating flow in the wake of the upwind row tends to extend across the "street," and there is usually a significant mean velocity V_s along the street. The mean flow has a component along the street and, when the external flow is not aligned with the "canyon," a swirling motion in the perpendicular direction that tends to extend up to the top of the buildings. The peak mean and fluctuating velocities near the ground are comparable with those at the level of the top of the buildings. The key quantitative parameter for dispersion modelling is the ratio of the mean wind along the street V_s to the mean wind U_H above the buildings at the height H (in the approach flow). Computation and field observations [23] have suggested a large range of this ratio from 0.3 to 1.0. The analysis also suggests that the value of V_s can be quite sensitive to the value of V_s at the upwind end of the canyon. Thus a major crossroad can have a large effect on the canyon flows downwind.

In conclusion it has been shown that most of the usual types of building/street shape and configuration found in urban areas can be categorized in geometrical terms that also correspond to the characteristic air flow patterns found in these situations for typical wind conditions. In particular there is a major distinction between, on the one hand, flows determined by random interactions of wakes of well-separated buildings and, on the other hand, flows where the interaction of wakes is of less relevance, for example, highly organized "canyon" like flows that occur when the buildings form street canyons or, if they are separated, when they are positioned along streets and flows in enclosed areas (e.g., courtyards) or between very densely packed buildings.

Urban Data

Experiments and dedicated simulations have shown features of urban dispersion at the neighborhood and street buildings scale. This includes how the mean transport direction differs from the mean flow above the buildings, the rapid vertical and horizontal spreading of plumes in wakes and canyons, the more complete mixing by the interacting wakes (with lower relative

levels of fluctuation compared with rural terrain), the transition of dispersion below the buildings level to above them and the variation in concentration downwind of sources and within the buildings.

In the context of urban air quality, the full use of models based on an up-to-date understanding of the flow as described in the previous sections is somehow limited by the scarcity of available data. Urban flow and dispersion models require input information and source distribution data about the mean flow field, turbulence, and source distribution. Until very recently velocity field data in urban areas were quite sparse and typically derived from the experiments in the USA. Some progress has been made in recent years with some field experiments performed in some European cities even though one has to accept that datasets from field experiments are yet not fully complete given the inherent difficulty and the cost of urban flow and dispersion experiments. This aspect has motivated the increase of laboratory experiments of flow and dispersion over simplified groups of buildings (building arrays) as well as over scaled reproduction of real city quarters. In addition to field studies, laboratory experiments allow easier validation of physical or numerical models because of carefully controlled flow conditions and the possibility of making numerous measurements. The laboratory experiments can be either wind-tunnel experiments [30–32] or water-channel experiments [33]. Some field studies have focussed on real cities, releasing a tracer gas in selected neighborhoods, for example: Copenhagen [34]; Salt Lake City, "Urban 2000" [35]; Oklahoma City, "Urban Joint 2003" [36]; Basel (BUBBLE experiment) [37]; London (the Dispersion of Air Pollution and its Penetration into the Local Environment known as the "Dapple" experiments) [38, 39].

The advantage of such experiments is to simulate flow and pollution dispersion in real conditions, but an important drawback is that the complexity of the urban morphometry can obscure the "true" impact of buildings from other complex phenomena due to the specific configuration of the selected city or neighborhoods. In the case of the Mock Urban Setting Test (MUST, [40]) it was determined that the focus would be on a simplified representation of a city by modelling it as a regular array of shipping containers, while keeping meteorological conditions real. This study has helped to clarify and give scientific evidence of specific flow phenomena as outlined in the previous sections. One important aspect for dispersion application has been the quantification of the deflection of the mean plume axis relative to the incoming wind direction induced. This can be significant, being up to 23° for a wind direction of 27° relative to the axis of the array, as found in the MUST experiment. Extrapolations to the real conditions are not always straightforward. The full field experiments mentioned above confirmed that, depending on building density and morphology, transport and dispersion may lead to complications not observed in simpler building array distributions. Near street level, for example, the dispersing plume may travel several blocks in a direction opposing the prevailing wind and many blocks laterally. This topological dispersion can lead to secondary sources and significantly alter the rate of lateral dispersion. A ground-level source can rise several hundred meters in depth in less than a block when caught in the updraft just downwind of a tall building. Buildings also alter the timing of the transport and dispersion, generally resulting in much longer residence times as compared to open terrain. Even though it is difficult to generalize the time of residence of a pollutant cloud, the Birmingham experiments suggested a few hours for a single source. However, the Dapple experiments did not give a definite conclusion on this. A further observation important for air quality applications is that the experiments have shown the presence of stable stratification during the night when consequently street level flow is less well coupled to the upper level reference. This might be more frequent in US cities than in European cities. As observed by Barlow et al. [39], stable conditions occur in London only occasionally. The analysis by Allwine et al. [35] carried out using data from the Joint Urban campaign in July 2003, Oklahoma City, showed that a stable layer is often observed overnight, with a nocturnal jet. Thus, there is no common pattern regarding the frequency of stable conditions; such conditions are a strong function of thermal advection due to regional scale flow processes and also depend on the specific materials used in the different cities.

The above are only some examples and are far from being a complete discussion of specific results obtained from the urban experiments.

Computational Models for Meteorology and Air Flow in Urban Areas

This section discusses those computational models for both meteorology and air flow in urban areas that are used as input to models for calculating dispersion. The numerical and physical basis and operational attributes are summarized in Table 4 for the three ranges of length scale introduced in section "Characteristic Regions of the Flow and Drivers", and for the different types of model, ranging from off-line, fully computational models (FCM) to the fastest approximate models (FAM) that can be run on PCs. The choice of the model depends on their practical purpose (in relation to dispersion modelling), the required level of spatial/temporal detail and scientific understanding involved, and on the detail and accuracy of meteorological and topographical input data. For research and for off-line

Urban Air Quality: Meteorological Processes. Table 4 Types of computational models for urban meteorology and air flow

1. Mesoscale
(i) Full computational models (FCM) Based on grid box numerical methods; full physics (fluid dynamics and thermodynamics). Input: from synoptic (or regional) numerical weather prediction models and local surface conditions, for example, surface fluxes for heat, F_θ, water vapor, F_v, roughness length, $z_0(x, y)$, and surface elevation, $z_s(x, y)$. Output: mean flow, turbulence statistics from above building envelope up to tropopause as a function of space and time over the urban area. Typical number of grid boxes for 1/3–1 km resolution on 30–100 km grid is 10^6–10^7. Takes about 3 h per 1 simulation hour, faster for lower resolution model.
(ii) Fast approximate models (FAM) (a) Flow perturbation models (suitable where $U_G/U_B \gtrsim 1$) using fast/approximate numerical and analytical methods, simple physics (for turbulence, stratification profiles), input from observational data (reduced) or NWP models and from local surface conditions. (b) Local flow/thermal models (especially where $U_G/U_B \lesssim 1$) using formula/fast approximate models for special conditions/physics, for example, slope winds, sea breeze, and thermal convection; often adjusted for local conditions. (c) Mass consistent models to compute flow fields given data at several points in the flow domain and surface elevation z_s. (Only suitable if such data exist for all relevant cases.) (d) Typical resolutions can be on a horizontal scale of 100 m or less. (e) These models can be run over a few minutes on PCs for each case. Current simplified models do not account for unsteady conditions over large urban areas (where L_O/L_f, $L_O/L_{Ro} \gtrsim 1$).
2. Neighborhood scale
(i) FCM using CFD methods Grid point numerical models with approximate representation of buildings and open spaces (as porous medium; as distributed forces; or as approximate shapes); approximate turbulence and heat transfer models; input from mesoscale models or measured data. Output: mean and turbulence profiles within the building envelope and up to the boundary layer/inversion layer height. Typical horizontal resolution is greater than the spacing between buildings. For a "neighborhood" of 5 km (e.g., city center) with 10^6–10^7 points, the resolution would be 100 m for an "accurate" computation.
(ii) FAM (a) Flow perturbation models (applicable where ln z_0 or F_θ vary significantly) using fast/approximate numerical and analytical methods with buildings/open spaces described by average properties and their relative fluctuations (e.g., average building height H, spacing d, and also typical r.m.s fluctuations in H and d); simple turbulence and heat transfer models for canopy flows; input from mesoscale models or local data, and estimates of distributed effects of buildings. Output: mean flow within and above the canopy and turbulence above the canopy. (b) Local flow/thermal models (where ln z_0 or F_θ are approximately uniform). Formulae based on local dynamical and thermodynamic balance and estimates of distributed effects of buildings; input based on average wind, thermal flux, and estimates of distributed effects.

Urban Air Quality: Meteorological Processes. Table 4 (Continued)

3. Building/street scale
(i) FCM using CFD methods Grid box numerical models with accurate representation of buildings, approximate turbulence and heat transfer models; input from neighborhood models or assumed data. (Very fast versions using idealized (e.g., inviscid) equations with finite numerical diffusion and approximate boundary conditions for buildings.) Output: mean flow and turbulence profiles around buildings of different shapes and grouping within an urban area. Typical computational domain is greater than building length or spacing L, or d (100 m) and grid size of 1 m or less. Note: sensitivity to inflow conditions from other buildings and atmospheric turbulence. Models better for clusters of buildings than isolated buildings (where large-scale atmospheric turbulence has less influence). Simpler methods are accurate/fast enough for practical use in off-line diffusion calculations.
(ii) FAM (a) Turbulent wakes of individual buildings based on perturbation methods and typical flows near buildings. (b) Closed packed buildings modelled by ideal (potential) flow. (c) Idealized models for interactions when wakes of upwind building impinge on downwind structures. (d) Canyon models (semiempirical formulae – not yet well established). (e) Canyon/street intersection models (e.g., ideal potential flow).

validation studies, a variety of types of model tend to be used: some studies require great detail and accuracy about particular or commonly occurring situations; others require simpler models for rapidly calculating a wide range of meteorological and topographic boundary conditions. When models are analytically based, their predictions can be easily understood and may be expressed in useful formulae.

The reason why it is necessary to have different types of model for the different distances is because every type of model can only represent a finite range of length scales, limited by the capacity and speed of the computational systems and data input.

Mesoscale Models

On the mesoscale range, the inputs to the models are the representation/parameterization of the topography and the natural features of the surface necessary for computations down to the smallest scale L_M/R_M (which typically is of order 1/3–1 km). This is therefore the scale over which the surface conditions are averaged, including ground surface elevation $z_s(x, y)$, roughness length $z_0(x, y)$, surface heat flux $F_\theta(x, y, t)$, and surface temperature $\theta_s(x, y, t)$ (which is usually derived in operational mesoscale models by coupling the atmospheric model to a thermal model for ground temperature, allowing for radiation from/to the earth's surface). In fully computational models, FCMs, the boundary conditions at the edges of the domain (and, in some models, above the domain) have to be specified and are usually derived from larger scale regional or global numerical models. These are usually updated at regular intervals, for example, every 3–12 h, with observational data taken at all levels in the atmosphere. This process of "data assimilation" is also beginning to be applied directly to mesoscale models, for example, in urban areas with many measurement sites.

A critical feature of any FCM, especially in the boundary layer and when the flow is influenced by mountains, buildings, surface heating etc., is the representation of the effects on residual (or computed) scales greater than L_M or R_M of the turbulence at the smaller space and timescales. Some models, such as HOTMAC [41], contain quite complex sub-models of the turbulence statistics (with extra equations for the turbulent kinetic energy and turbulent dissipation rate (k-ε)), while others, for example, WRF [42], COAMPS [43], MM5 [44], MESONH [45], and UK Met. Office unified models [46], use eddy viscosity or even simpler parameterizations (e.g., assuming a known form of the velocity profile). The experience from field studies in the USA is that for urban areas located on sloping terrain where buoyancy forces are significant (i.e., $F \lesssim 1$), the models with the more complex turbulence models are more accurate in these conditions. But the greatest improvements in accuracy, especially in predicting the mean wind speeds and wind direction

in changing meteorological conditions, and in complex terrain, arise from using these models with finer resolution of the order of 1 km or less. However even with finer resolution and complex modelling, such models still cannot predict some significant features of surface layer turbulence, such as evening transition of upslope flows and formation of gravity currents, or calculate relevant statistics of the turbulence for dispersion models, unless they are used as large eddy simulations [47], which, because of computational requirements, is currently only possible in research mode.

As explained in Table 4, these models take many hours to compute a single meteorological situation. Nevertheless, they are sufficiently reliable indicators to be used operationally. Fast approximate models, FAMs, for air flow and meteorology over mesoscale distances are being developed, based on recent research. These models are useful as qualitative guides to the complex flow that might occur on the mesoscale, for quantitative predictions as input to dispersion computations.

As shown in Table 4, when local buoyancy effects are weak (i.e., $U_G/U_B \geq 1$), the air flow over an urban area is generally a perturbation of the oncoming flow. Then, from semi-analytic models using perturbation methods, faster computational schemes have been devised, and are being developed in a general way to allow for orography, roughness change, and some effects of surface heating [8], [48]. Although these are perturbation methods, the changes in wind speed and direction predicted (and verified) by these models can be quite large (~50% or more).

The perturbation modelling approach being adopted in this range of meteorological flows is similar to that used for sub-mesoscale/neighborhood scale orographic flows (for example, in the FLOWSTAR model [49] and RIMPUFF [50]), the main difference being that over the larger scale the internal layer l reaches the top of the boundary layer h, so that the inversion height is affected and Coriolis effects have to be included (which, for example, significantly influences flows along coasts and up and down large river valleys, [51]). Typically these models are run in the steady state. Once the time dependence over several hours is significant, a fully computational model is necessary.

When buoyancy forces are significant, $U_G/U_B < 1$, no FAM is yet available to cover all the most significant types of air flow and meteorological conditions that might be needed for dispersion calculations. However, models and physical estimates have been derived for some particular situations, especially when Coriolis forces play a small role, for example, in wide valleys with low slopes, large heat island effects, and sea/lake breezes [48, 52, 53]. Not only are the quasi-steady features of these flows now quite well described, but also their time/space dependence over the diurnal cycle. In the absence of strong geostrophic winds (or very stable local conditions) the local diurnally varying buoyancy forces may control the flow and therefore they are quite predictable (e.g., a valley wind, or sea/lake breeze on a still day). Since the single most important aspect of the air flow needed for dispersion calculations is the direction of the wind, such physically based models provide vital information for estimating the dispersion in complex terrain.

Neighborhood Scale Models

On the neighborhood scale (typically 5 km), fully computational models, even with the latest computing systems, cannot generally resolve the flow around every building. Typically, for computations with 10^6–10^7 grid boxes, the horizontal grid spacing is about 100 m or greater in the horizontal direction. To resolve the velocity field around a building in order to calculate its drag effect on the overall flow, the grid boxes would have to be of the order of 1 m or less. Therefore even FCMs can, at present, only calculate average features of the flow over these grid box scales by estimating the average effects of buildings and streets in the model. This is expected to change in the near future with further increases in computational power.

For most practical applications in urban areas, different modelling approximations are needed (even with an FCM) depending on whether the buildings in the neighborhood being considered form effectively porous or non-porous regions of resistance. In the case of effectively porous buildings (Fig. 3; category (i) of Table 3), the effect of the buildings is estimated by a drag coefficient averaged over the whole volume occupied by the buildings and the space between them (typically this is of the order of the porosity β).

The FCM input is the mesoscale flow field approaching the neighborhood region (or the flow

leaving the adjoining neighborhood), for example, suburbs adjoining a city center as in Fig. 1. FCM output will be the mean flow and basic turbulence statistics that depend on the particular closure model used, for example, mixing length, turbulent energy-dissipation (k-ε) closure, or Reynolds stress closure [54, 55]. All three of these models lead to estimates of turbulent kinetic energy, but only the latter also provides estimates of length scale, and the space/time dependent evolution of turbulence structure, which is significant where the areas of building density or height change sharply. The third method allows for the anisotropy of turbulence, which changes in these transition zones. Such models predict the mean velocity field everywhere (spatially averaged over the grid box) and the turbulence outside the canopy. Within the canopy, where large-scale inhomogeneous turbulence is generated by the shear layer over the top and by eddying motions around buildings, the spatially averaged models are deficient.

In the second case, an effectively non-porous neighborhood, the mean air flow passes over the building envelope as if over a hill with elevation $z_s(x, y)$. The roughness length z_0 also changes as a result of turbulence and recirculating flows in the courtyards, streets, etc. between the buildings. Estimating these parameters z_s, z_0 in terms of the building layout is only approximate, (e.g., $z_s \cong H_c$, $z_0 \sim$ H/30). As with porous built-up areas, the parameterizations for calculating average flow properties can be estimated approximately by detailed computation of typical local areas. These calculations can also provide estimates of the local turbulence, needed for dispersion computations [23]. FCMs using turbulence closure models have been extensively applied to the kinds of recirculating flows that occur between buildings in non-porous urban areas; most validation has been for wind tunnel tests and engineering flows, where the kind of very-large-scale eddies and downdrafts found in atmospheric flows are absent. Such motions can lead to more rapid exchange between the upper flow above and within the canopy layer, as discussed in the review by Mestayer and Anquetin [5].

As shown in Table 4, and reviewed by Britter and Hanna [11], most FAMs for the neighborhood scale tend to focus on equilibrium flows within and just above the canopy. In a "porous" canopy (Fig. 2a), the mean velocity within the canopy $U_c(z)$ is driven by the turbulent shear stresses generated in the intense shear layer just above the canopy. Here the ratio of $U_c/U(z_*)$, where $U(z_*)$ is the velocity at the top of, or above, the roughness layer (Fig. 2), depends on the porosity – a typical value being 0.3. In a non-porous canopy, typically in the inner city, where flows are determined by canyon and downdraft effects, this mean velocity ratio varies considerably over the range 0.1–0.3 [23].

The approximate average velocity profile (Eq. 2.1) is not applicable at the edges of "neighborhoods" where the density and heights of buildings vary, or in the interiors of such regions, such as near parks, squares, etc. At the edges of porous canopies, where the air flow in the canopy varies rapidly, an FAM approximate model has been developed based on the same approach as FCM by representing the canopy as a porous layer and (as for the FAM in the mesoscale range) solving perturbation equations semi-analytically to provide fast computation of the mean velocity and shear stress [9, 56]. These have been verified against field and wind tunnel studies.

Over non-porous canopies (typically categories (i)–(v) in Table 3), the determining parameters (H_c, $z_0(x, y)$) are the same as for FCM over these elevation/roughness changes. The linearized FAM approaches give very similar results to those using FCMs [57, 58].

Modelling the Building and Street Scale

The purpose of detailed flow modelling in and around individual buildings and the surrounding streets is firstly to understand how rapidly released matter disperses locally. Secondly, detailed studies of these local scale flows are necessary, as explained in the previous section, to develop models over neighborhood scales for flow and dispersion.

Fully computational methods, using a variety of turbulence modelling methods, have been extensively applied to computing flows around single buildings in turbulent boundary layers. Using turbulence closure methods, many models have predicted mean velocities near the buildings within one or two widths; but such models (e.g., k-ε models) have tended to over-predict small-scale turbulence around the structure [59] and under-predict the large-scale atmospheric eddies. This leads to an over/under-prediction of the mean velocity

defects in the wakes downwind of 3-D/2-D structures in the atmospheric boundary layer. Only the computationally intense method of Large Eddy Simulation (LES), or unsteady modelling of the fluctuating flows using turbulence closure models, can accurately represent the distortion of the large-scale eddy motion around the building and its effect on downwind wakes [60, 61].

Calculations using FCM with turbulence closure have also been performed on flow around small groups of buildings using resolutions down to about 0.1 *H*. The predictions of the turbulence in these flows are more reliable than those of isolated structures because most of the turbulence in this instance is generated locally between the buildings and is of smaller scale (similarly, wind tunnel models of dispersion around buildings are generally more reliable when the buildings are in groups than when isolated because wind tunnels cannot simulate the low frequency fluctuation in wind direction). This is because the primary interactions between the wake of one building and its impact on adjacent buildings are not sensitive to the structure of turbulence; however, the wakes of isolated or well-separated buildings are strongly affected by the form of the low frequency spectrum of turbulence. This is why in some institutions, for example, the US Naval Laboratory [62] and more recently at Los Alamos [63], work is being undertaken on dispersion in dense urban areas with fast FCMs in which approximate velocity fields are computed using classical grid box methods of finite size (say 1 m) but neglecting completely any modelling of turbulent stress. This reduces the number and the order of the equations to be solved and speeds up the computation by a factor of 10 or more. The finite size of the grid effectively introduces numerical diffusion that simulates many of the same mean flow features developed using the more complex turbulence closures.

Another simplification to speed up the computation of the mean velocity field is to represent the effects of the individual buildings as a distributed force acting on the flow (or source/sink distribution) and thereby only approximately representing the shape of the building [64]. In most FCM calculations, considerable computational resource and time is spent on exactly representing the building shape, while at the same time making considerable approximations in the flow.

There are at present no general FAMs that are capable of calculating the detailed flow around any isolated building or group of buildings, or even calculating those broad features of the flow needed for modelling dispersion close to the building. The main reason is that the unsteady separated shear layers that control the flow are of much smaller scale than the building. This means that the recirculating flow region, which greatly affects the magnitude and timescale of concentration fluctuation, is not only highly unsteady but also very sensitive to the effects of nearby buildings. Nevertheless, the main features of the mean flow patterns and typical magnitudes of the mean and fluctuating velocity have been classified and partially quantified for many types of buildings and groupings. Therefore, although no practical FAM for the mean flow is available at present, these features of the flow field are now well enough known to derive useful quantitative FAMs for the dispersion. For example, when buildings are far enough apart that their near-flow fields and their wakes are approximately independent, the wakes can be approximated as a perturbation to the approach flow, a theory by Counihan et al., 1974 [21] that is used in the "Buildings" module in ADMS [67]. The same model can be used approximately with linear superposition when buildings are separated by at least $3H$, where H is their height. As the ratio of breadth to height, b/H, increases from 1.0 to 10, this minimum separation distance $d_{\min}$ increases linearly to about 10 H (Fig. 3a(i)).

When d is less than $d_{\min}$ (Fig. 3a(ii)), it is found that the recirculating regions of the wakes of the upwind buildings are elongated and extend to the nearest downwind building [65]. For buildings designed in rows nearly parallel with the wind direction, the flow structure consists of turbulent recirculating regions in the spaces downwind of the buildings and relatively high-speed streams in the open streets between the buildings [28]. Describing the flow structure in this way provides the basis for FAM for dispersion calculations.

By contrast, when the buildings are placed in a staggered pattern relative to the wind direction, the wakes tend to disappear and the mean flow between the buildings consists largely of unidirectional bifurcating patterns of diverging and converging streamlines, with small regions of recirculating flow. Such flow can be

computed by fast potential flow methods [28], which are even faster if the shape of the layout of the buildings is approximated [64].

When the buildings are long enough and close enough (i.e., categories (i), (ii), and (iii) of Table 3) and the wind is at any angle, or if they are situated in rows and the wind is at a small glancing angle to the row (Fig. 3a(ii)), then the characteristic canyon flows are formed in the streets between the buildings. When the buildings either side of the street are of comparable height, a strong feature of the helical canyon flow is that it does not extend above the buildings. Therefore the appropriate FAM for these flows is to assume a canyon flow below the building level and a rough wall boundary layer flow above it [23].

The final consideration is of the air flow in typical courtyards and "squares" connected to adjoining streets (Fig. 3c). Simulations confirm that these are regions where fluid trajectories are well mixed. This provides a basis for constructing FAMs for dispersion in these regions using semi-analytical diffusivity models.

Examples of Output of Modelling Calculations

A series of examples of recent model calculations showing the impact of buildings on flow are now reported. The cases considered are a single building, a regular building array, and a complex urban junction. The examples mainly comprise simulations using an FCM (specifically a CFD model); one example using an FAM is also presented.

CFD models do not describe all meteorological phenomena as described earlier; however, they are useful tools for predicting flow characteristics in street canyons and within urban areas at the neighborhood, building, and street scale. They can also be used to interpret wind tunnel and field data and their outputs can therefore be used to improve operational models. Most available general purpose CFD models currently still need to be validated against wind tunnel or field data to obtain confidence before applying them to a particular case study [67]. Some FAM models used for calculating dispersion at the building and street scale are reviewed in [68].

Single Building

Table 5 summarizes cases investigated by means of both wind tunnel and CFD simulations by Wang and McNamara [69]. The Launder and Spalding's standard k-ε model [70] for turbulence and the advection-diffusion model for dispersion was used for the computation with a computational grid comprising 500,000 cells and smallest dimensions equal to 0.005 m. The cases comprised a cube (1), a tall building (4), a wide building (5), and intermediate cases (2 and 3).

Mean concentrations are expressed as dimensionless values K which are defined as:

$$K = \frac{CU_{ref}H^2}{Q},$$

where Q is the emission rate, C is the measured/calculated concentration, and U_{ref} is the reference velocity. Figure 4a shows the geometric setup and Figs. 4b–d show examples of model outputs for Cases 1 and 3 together with comparisons with measurements from controlled wind tunnel experiments. In detail, Fig. 4b shows the x-velocity component (along the wind direction) contour obtained from CFD simulations, where it

Urban Air Quality: Meteorological Processes. Table 5 Summary of the single building case. *H*, *W*, and *L* are the building height, width, and length, respectively. *H* = 0.3 m for case 4 and *H* = 0.1 m for all other cases

Case		Model details	Source details
1	Isolated rectangular building	Cube	The stack, 0.5 *H* high, is installed at an upwind distance of 2 *H* from the building
2		*W/H* = 2, *L/H* = 1	
3		*W/H* = 1, *L/H* = 2	
4		*W/H* = 1/3, *L/H* = 1/3	
5		*W/H* = 6, *L/H* = 1	

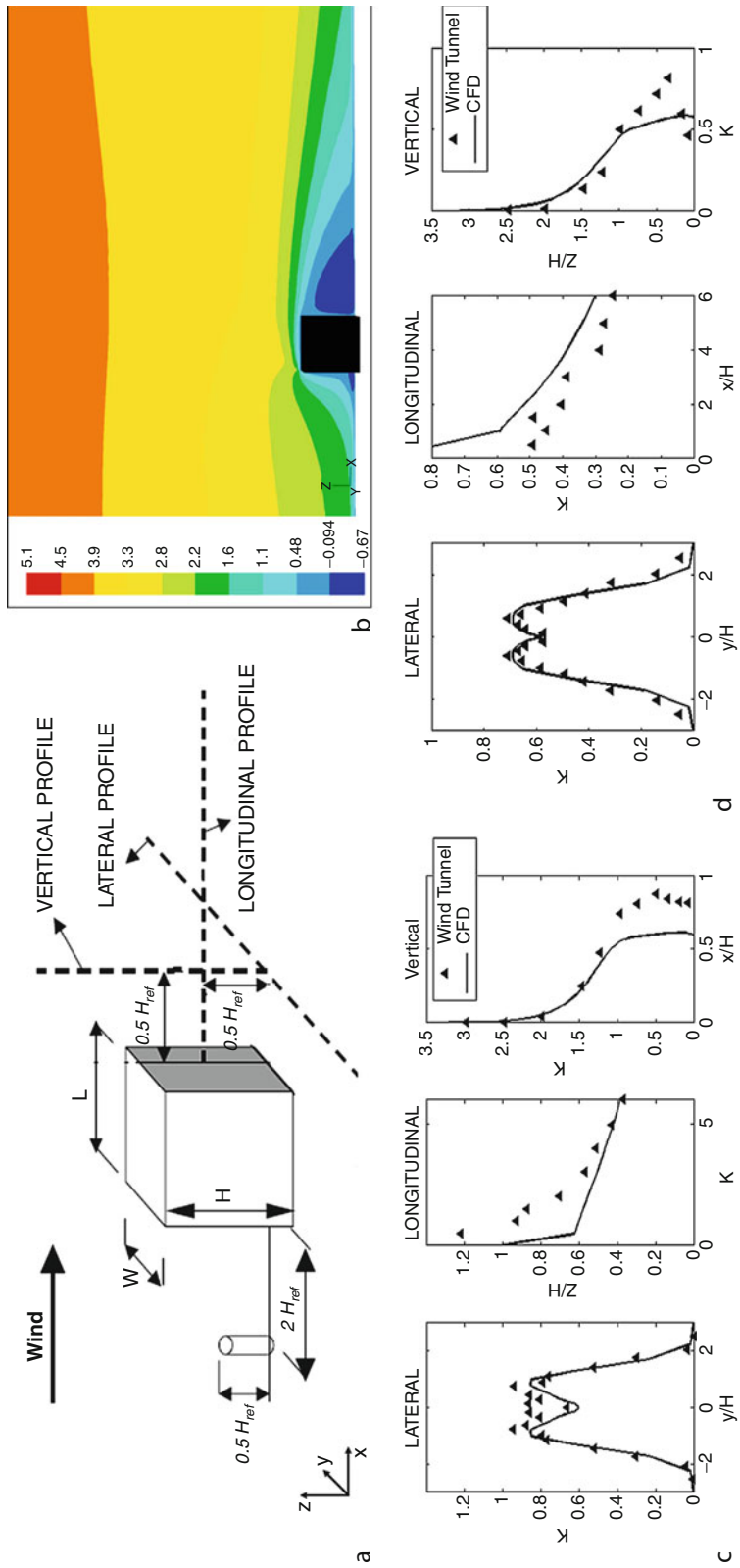

Urban Air Quality: Meteorological Processes. Figure 4
(**a**) Sketch of the single building with indication of the upstream source position and profiles where wind tunnel and CFD results are compared. (**b**) Contour of the x-velocity component in the middle of the building from CFD simulations. (**c**) Concentration profiles for Case 1. (**d**) Concentration profiles for Case 3

can be noted that the k-ε model was successful in predicting the typical vortex which develops in the wake zone behind the building. Figs. 4c and 4d also show the comparison between wind tunnel and CFD data for Case 1 and Case 3. In particular, it can be noted that in Case 1 the model under-predicts concentrations slightly. The hit rate q, a statistical quantitative score of the model performance [71], is equal to 75%. It is recalled that the Hit Rate validation test is performed using a fractional deviation $RD = 0.25$ and an absolute deviation $W = 0.06$ ($q > 66\%$ is typically requested for the comparison with wind tunnel data). Nowadays, statistical metrics are typically used to assess model performance during the model evaluation process. Usually k-ε models give a satisfactory performance for wind profiles according to the q tests. For this study, the Case 2 and Case 3 model predictions are in general agreement with observations from wind tunnel measurements, with hit rate test scores of $q = 82\%$ and $q = 77\%$, respectively. Finally, Case 4 and Case 5 model predictions are also in general agreement with observations from wind tunnel measurements with hit rate test scores of $q = 78\%$ and $q = 68\%$, respectively.

Isolated Street Canyons

Recent interest has risen in employing LES models ([72], [73]) to overcome the shortcomings of RANS in its inability to capture the unsteady and inherent fluctuations of the flow field within the street canyon on which the dispersion of pollutants depends. RANS, which is the most widely used approach in industry for the modelling of turbulent flows, assumes that non-convective transport in a turbulent flow is governed by stochastic three-dimensional turbulence possessing a broadband spectrum with no distinct frequencies and, therefore, models the entire range of the eddy length scales. This approach has obvious weaknesses and poses serious uncertainties in flows for which large-scale organized structures dominate, such as flows around buildings. In addition, RANS models assume gradient transport, which may not be the case for pollutant exchange at the roof level of a street canyon. LES, although computationally more expensive, has an advantage over RANS in that it explicitly resolves the majority of the energy carrying large-scale organized structures and the internally or externally induced periodicity involved, whereas only the universal small-scale eddies are modelled.

As an example, an illustration is provided of the flow structure and pollutant dispersion within an urban street canyon of width to height ratio $W/H = 1$ using the standard k-ε model, the Reynolds Stress Model (RSM), and LES, coupled with the advection-diffusion method for species transport [74] (Fig. 5). In the case shown, the computational domain was built by using about one million cells with smallest dimensions equal to 0.077 H. Numerical results, which include the statistical properties of pollutant dispersion, for example, the mean concentration distributions, three-dimensional spreads of the pollutant, etc., are then compared to wind-tunnel measurements from the online database [75]. Integrated into the model street, four tracer gas emitting line sources were used for simulating the release of traffic exhausts. Mean concentrations are normalized according to:

$$c^{+} = \frac{CU_{ref}H}{Q/l},$$

where C is the measured/calculated concentration, H the building height, U_{ref} the flow velocity at height H in the undisturbed approaching flow, and Q/l the tracer gas source strength per unit length. Figure 5 shows normalized concentration contours at wall A (leeward) and wall B (windward) of the street canyons.

It is observed that amongst the two RANS models, RSM performed better than standard k-ε, however, LES proved better than RANS in predicting the concentration distribution because it was able to capture the unsteady and intermittent fluctuations of the flow field, and hence, resolve the transient mixing process within the street canyon.

Regular Building Arrays

Wind tunnel experiments have demonstrated that street ventilation is reduced in the presence of upstream buildings. This seems to be because of the upward displacement of the flow and the consequent perturbed momentum exchange between the street canyon and the outer region of the flow. Also, numerical results have indicated that the surrounding building configuration affects pollutant dispersion in a street canyon, therefore it should be taken into account in numerical

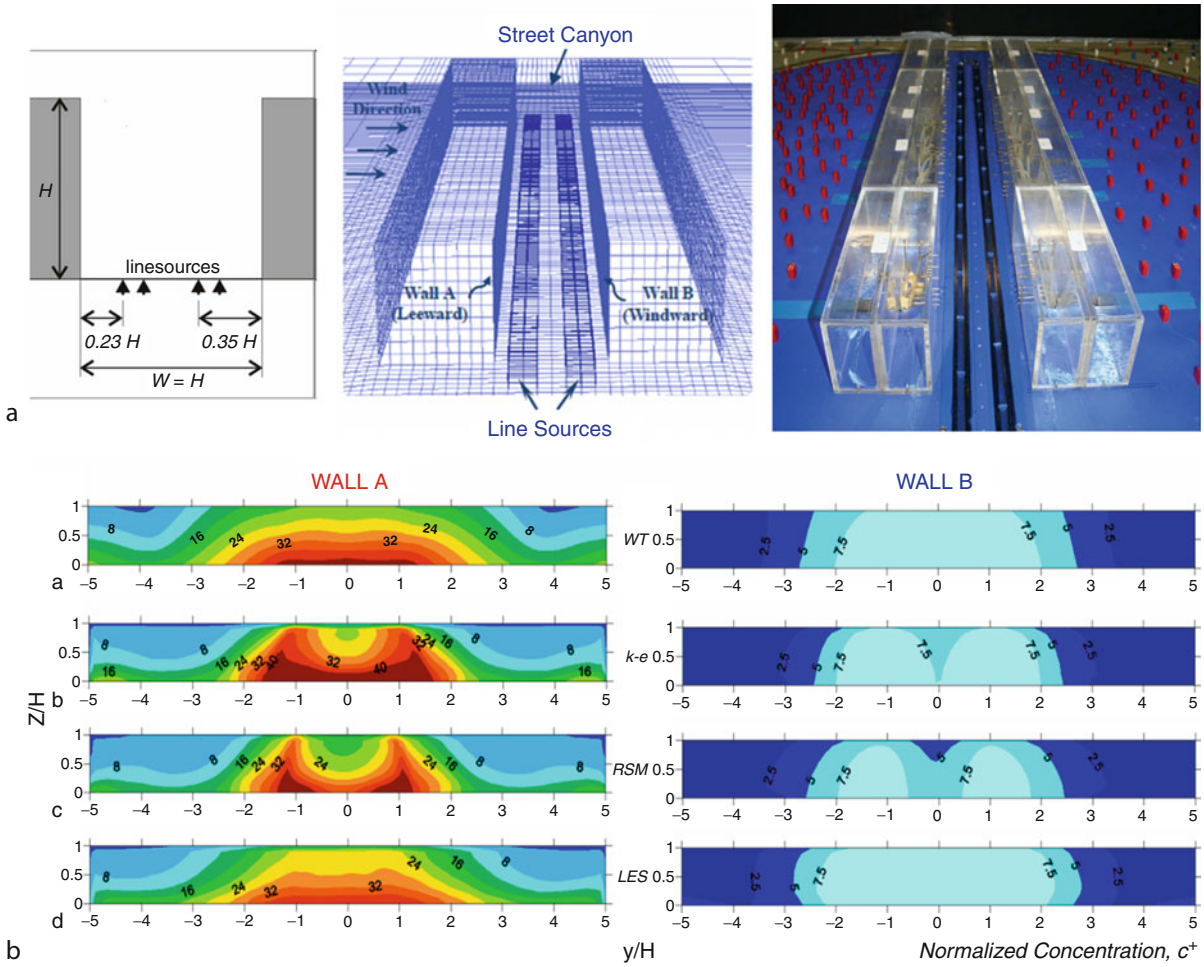

Urban Air Quality: Meteorological Processes. Figure 5

(**a**) Sketch of the street canyon with indication of the position of line source, grid, and wind tunnel model (from [74] CODASC, 2008). (**b**) Mean normalized concentrations at wall A (leeward) and wall B (windward) showing comparison between WT data (available from CODASC) and numerical results performed with k-ε, RSM, and LES simulation

dispersion modelling (see, for example, [76]). Two examples of flow and pollutant dispersion distributions for regular building geometries are shown in Fig. 6, investigated by means of wind tunnel experiments and numerical simulations as previously described.

The experiment is set up in a boundary layer wind tunnel to simulate the case of dispersion of pollutants from naturally ventilated underground parking garages [77]. A finite array of idealized building blocks with 0.1 m by 0.15 m base dimensions and 0.125 m height (three buildings crosswind and seven buildings along wind direction) are considered, as shown in Fig. 6a. The aspect ratio of the street canyons resulting from the building arrangement is $W/H = 0.8$. Four ground-level emission sources were mounted close to the building. RANS type simulations [78] were performed by employing the standard k-ε model and the advection-diffusion model. The computational grid was built by using 500,000 cells, with smallest dimensions equal to 0.005 m. Flow and dispersion were measured within the street canyon positioned downwind of the building equipped with the sources.

Wind tunnel experiments and CFD simulations show that a recirculation flow region forms within a street canyon exposed to a perpendicular flow. Both wind tunnel measurements and CFD predictions show

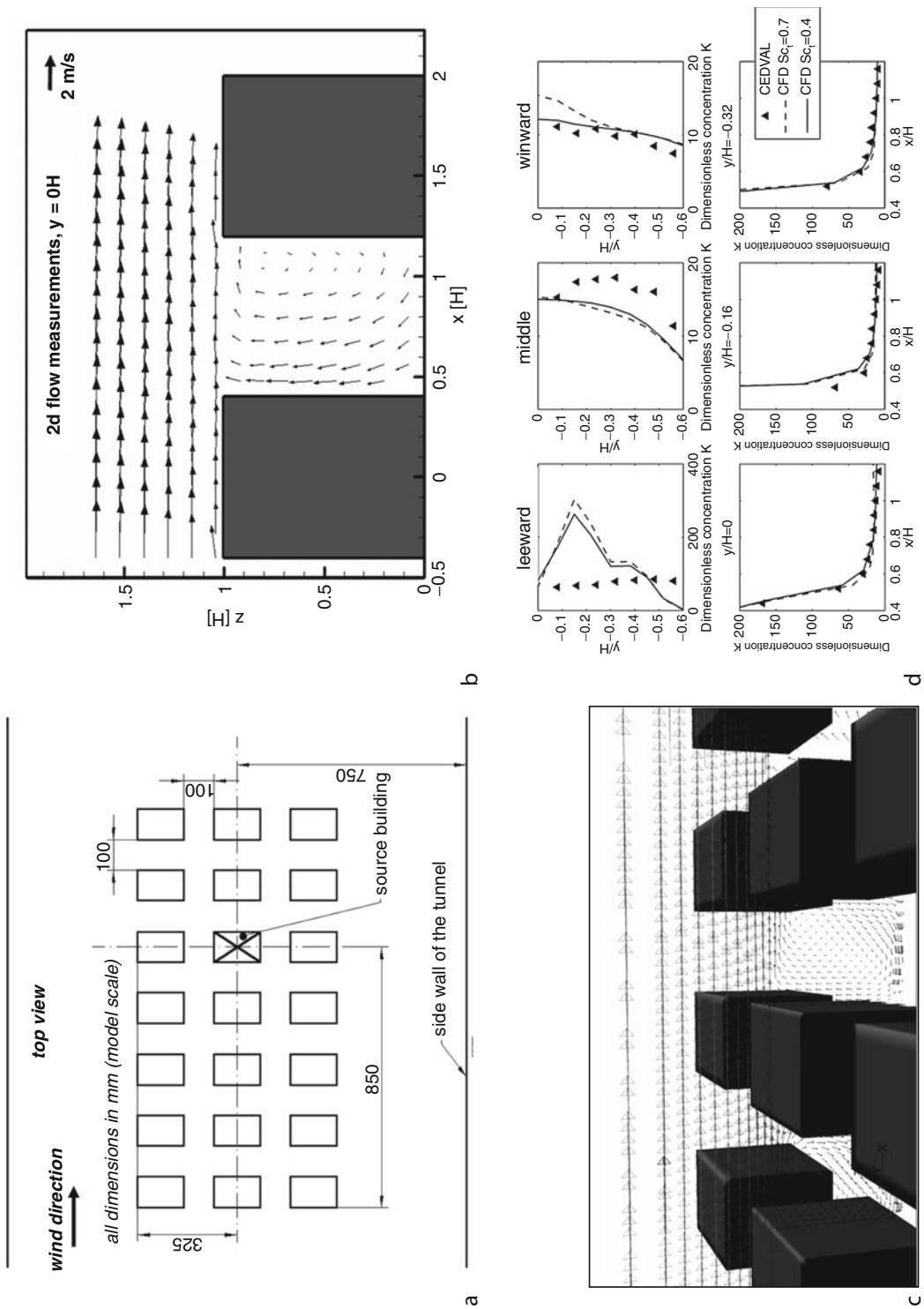

Urban Air Quality: Meteorological Processes. Figure 6
(**a**) Sketch of the regular building array with indication of the source building. (**b**) Velocity vectors obtained from wind tunnel experiments showing the vortex inside the canyon downwind of the source building. (**c**) Velocity vectors obtained from CFD simulations. (**d**) Concentration profiles at different positions within the same street canyon with a sensitivity to the Schmidt number value

that for aspect ratio $W/H = 0.8$ a single vortex forms inside the canyon. In particular, Fig. 6 shows velocity vectors on the vertical plane in the middle of the street canyon obtained from wind tunnel experiments (Fig. 6b) and CFD simulations (Fig. 6c). The figure shows that the shape and dimension of the vortex predicted by the CFD simulations is very similar to that observed by CEDVAL experiments [77] compiled at the University of Hamburg. The ability to capture the right dimension of the vortex is very important as the vortex drives the distribution of pollutants within the street canyon.

As outlined in [79] and [80], it should be noted that typical CFD codes predict dispersion spread that is smaller than that predicted by the well-validated integral model ADMS-Urban [81]. From a sensitivity test on the turbulent Schmidt number value (the standard value is 0.7), the value of 0.4 was found to be the most appropriate in order to artificially increase plume dispersion, even though such tuning should be avoided. Figure 6d (top) shows the dimensionless coordinate y/H versus the dimensionless concentration K near the floor ($z/H = 0.06$) within the street canyon downwind the source building and dimensionless concentration K versus dimensionless coordinate x/H on the same vertical plane (bottom). The horizontal velocity near the floor is negative because the vortex in the canyon is clockwise. Thus, pollutants are carried toward the leeward side and mixed in the street canyon. CFD results agree well with wind tunnel measurements.

It is known that FCM type of models still suffers from their high computational cost which prevents them from being largely employed in operational applications. This has pushed the development of FAM models yet incorporating new understanding of flow and dispersion processes within the urban canopy layer. Recently, di Sabatino et al. [82] have proposed a new modelling approach for the computation of the spatially-averaged flow field, where the average is defined at the neighborhood scale, i.e., from 0.2 km up to 10 km. The underlying idea is the description of the drag forces in terms of height-dependent morphological parameters based on detailed knowledge of building geometry such as the planar area index λ_p and λ_f (introduced in section "Characteristic Regions of the Flow and Drivers") and the reduction of the complete three-dimensional flow field to a one-dimensional quantity, given by the mean wind direction, and the three-dimensional spatial dependence to a much more simple dependence from the height z. As a consequence, only mean profiles are needed as input to the model. There are examples in the literature [83] showing the possibility of extending this modelling approach to an Eulerian dispersion model for the computation of the concentration field. Figure 7 shows the spatially-averaged profiles of wind velocity and diffusivity coefficient resulting from full CFD simulations.

This reduced description of the wind field and the diffusivity coefficient was used as input into the developed three-dimensional Eulerian dispersion model for

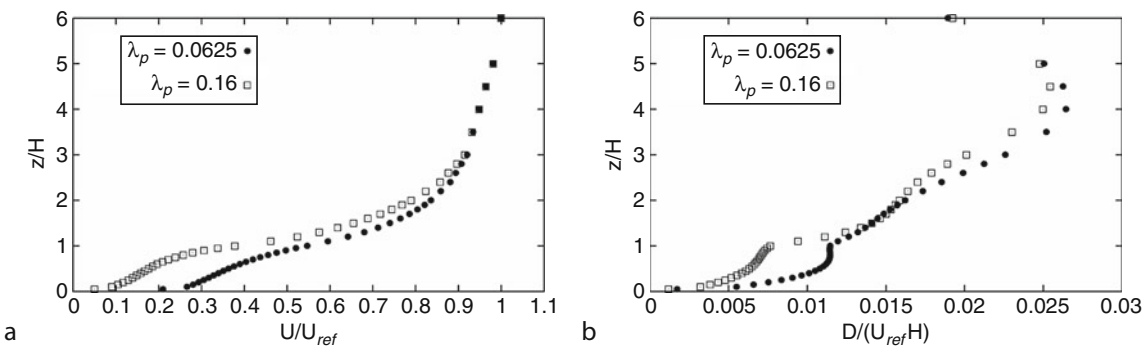

Urban Air Quality: Meteorological Processes. Figure 7
Spatially-averaged profiles of wind velocity (**a**) and diffusivity coefficient (**b**). H is the building (cube) height and U_{ref} the average velocity at the top

the dispersion simulation of a pollutant released from a point source. Results were then compared with CFD predictions.

Figure 8 shows concentration contours for the case $\lambda_p = \lambda_f = 0.16$. The pollutant source was placed along the x direction at a distance from the inlet of approximately 1/3–1/4 of the domain length and equidistant from both boundaries in the y direction. The domain height was 6 H, where H is the building height. The figure refers to a source height $Z_s = 0.5\ H$ and shows the comparison at three horizontal sections at $z = 0.05\ H$, $z = H$, and $z = 2\ H$.

Inside the canopy, CFD concentrations tend to show some periodicity, due to the presence of cubic buildings. This specific behavior cannot be reproduced by the simplified Eulerian model. However, by using spatially-averaged one-dimensional profiles, the model is able to reproduce the order of magnitude of fully computational CFD concentration predictions, even if contour shapes may differ qualitatively. The quality of the comparison is not homogeneous over the domain. As expected, the comparison is quite poor close to the source and improves downstream. Large differences are also found near the top boundary, but this is most probably an effect related to the boundary condition. Overall, the plume width predicted by the FAM type model is comparable to the CFD model. Similar results were obtained in the case of small packing density ($\lambda_p = \lambda_f = 0.0625$), not shown here.

Results highlight the potential of the approach based on the parameterization of one-dimensional wind and diffusivity profiles in terms of routinely available meteorological parameters and morphological parameters such as λ_p and λ_f, which synthesize the main geometric characteristics of the urban canopy.

Complex Urban Junction

The geometry of idealized building arrays is far less complicated than the morphology of real urban areas,

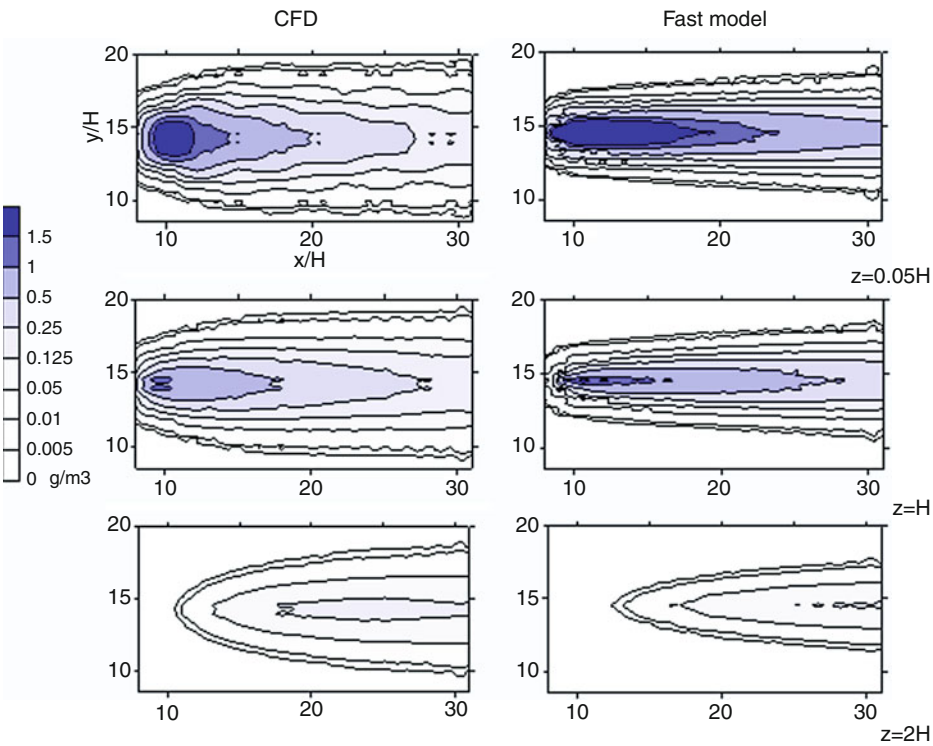

Urban Air Quality: Meteorological Processes. Figure 8
Intermediate canopy ($\lambda_p = \lambda_f = 0.16$), $Z_s = 0.5$ H: concentration (g/m^3) contours from the CFD model (*left*) and the fast model (*right*) at several horizontal planes

where urban neighborhoods are characterized by street intersections, asymmetric street canyons, and staggered arrays of buildings of irregular and/or highly variable shapes. These local features significantly alter the flow and dispersion patterns, as experimental and numerical studies have concluded (see for example [32], [84] and [85]). Reported here are some results of a modelling study performed with a CFD code by employing the RSM [86], and the advection-diffusion scheme in a neighborhood in the city of Bari in southern Italy. The real geometry comprises both step-up and step-down street canyons and consists of two asymmetric streets as shown in Fig. 9a. The wider street canyon is characterized by an average aspect ratio $W/H \sim 1.8$ and it is perpendicular to the wind direction. The other street canyon is characterized by an average aspect ratio $W/H \sim 0.5$ and is parallel to the wind direction. The tallest building is ~46 m. The two canyons intersect orthogonally forming four major blocks of buildings and a junction. For the sake of computational convenience the real geometry was slightly simplified, yet maintaining the main geometrical details of the street canyons. A fine mesh close to the ground (up to a height of 4 m) was used (Fig. 9b), with cell dimensions $\delta x_{\min} = \delta y_{\min} = 1$ m, $\delta z_{\min} = 0.3$ m. The number of computational cells was approximately three and a half million. Vectors of velocity magnitude (m/s) and turbulent kinetic energy (m^2/s^2) at $z = 2$ m are shown in Fig. 9c, d, respectively. Due to the interaction of the wind with buildings, the resulting flow is channelled along the wider street canyon (which is that perpendicular to the wind direction), predominately blowing along the negative y direction. Obviously, the distribution of the turbulent kinetic energy is highly asymmetric, showing large values in the windward region. This example shows that flow pattern and turbulent kinetic energy are strongly affected by the geometry.

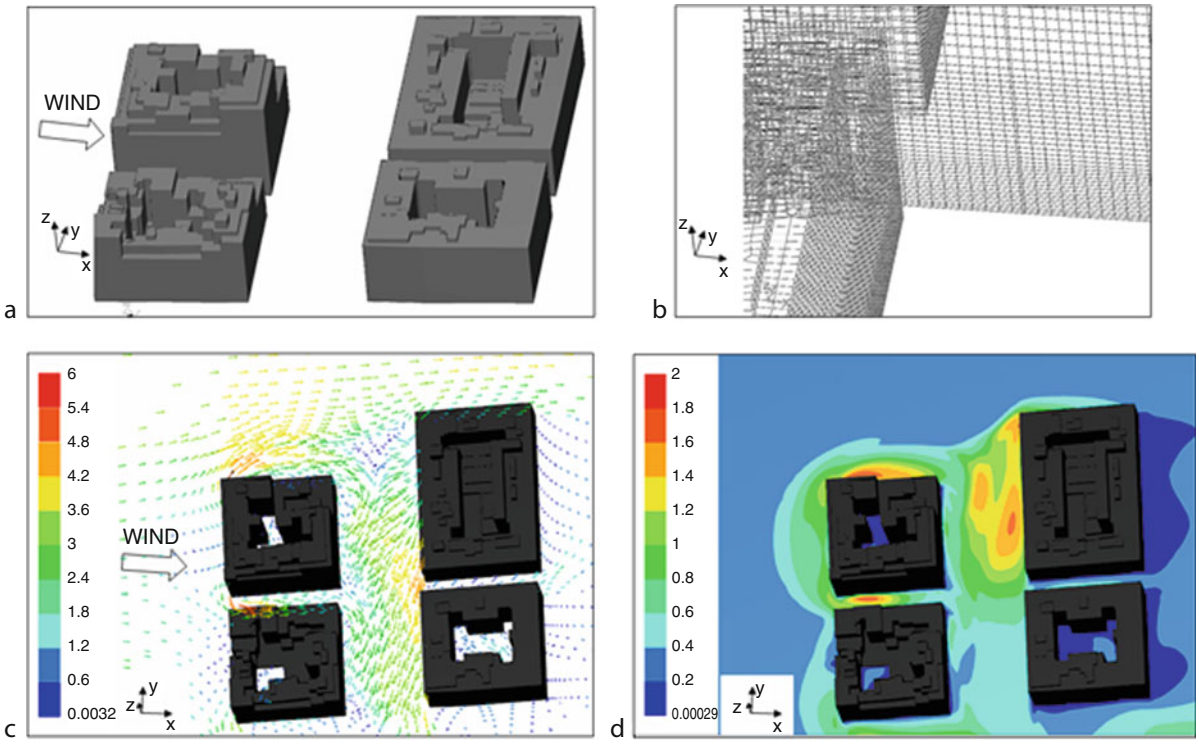

Urban Air Quality: Meteorological Processes. Figure 9
(**a**) Sketch of the urban junction. (**b**) Grid refinement close to the ground. (**c**) Flow pattern at $z = 2$ m developed within the urban junction. (**d**) Turbulent kinetic energy at $z = 2$ m

Future Directions

The entry has described the impacts of urban areas on urban meteorology at the mesoscale, neighborhood, and building street scale. While our general understanding of the processes is good and this enables us to construct approximate models, it is clear that at this time there is a paucity of detailed field data and the most detailed numerical models are still not able to resolve all the features of the flow in good time. With the availability of faster response and cheaper instrumentation, the continuing improvements in computer speeds, and the current strong interest in this topic, it is certain that more detailed data and more advanced models of urban meteorology will increasingly become available, resulting in huge data resources. Understanding of such data will continue to rely on the general concepts and categorizations described in this entry. Also of great relevance to future developments is both the impact of climate change on urban meteorology and the response of the urban environment to climate change. These issues are discussed in [87].

Notation and Abbreviations

b	Building breadth
C	Measured/calculated concentration
C_D	Drag coefficient
c^+	Normalized mean concentration for a line source
d	Gap or separation distance between buildings
f	Coriolis frequency
F	Froude number
F_v	Surface water vapor flux
F_θ	F_θ
g	Gravitational acceleration
h	Boundary layer height
H	Building height
H_c	Canopy height
H_c'	Standard deviation of canopy height, H_c
H_M	Mountain height
K	Normalized mean concentration for a point source
k-ε	Kinetic energy and energy-dissipation model of turbulence
l	Vertical length scale of internal layer
l_O, l_N	Vertical length scales of internal layers over the urban area, neighborhood scale
L_A	Adjustment length for mean flow to adjust as it enters the porous canopy
L	Building length
L_f	Coriolis advection length
L_I	Inner city length scale
L_M, L_N, L_{BS}	Length scales of the (sub-)regions M, N, BS
L_O	Overall city length scale
L_{Ro}	Rossby length scale
L_{Se}	Effective source size
N	Buoyancy frequency
q	Hit rate test score
Q	Emission rate
RD	Fractional deviation
R_M	Ratio of the length of the sub-region L_M to the smallest scales resolved in that region
s	Distance to the nearest building
u_*	Friction velocity of the turbulent velocity profile of the atmosphere
U	Mean velocity, with subscripts denoting location/physical process
U_B	Typical wind speed associated with local buoyancy effects
U_C	Wind speed within the canopy
U_G	Geostrophic wind
U_H	Mean wind above the buildings (at height H)
U_{ref}	Reference velocity
U_c	Mean wind along the street canyon
V_S	Mean wind along street
w	Building length or width
W	Absolute deviation, Building width
$x = (x, y, z)$	Coordinates of a point
$x_B^{(i)}$, $y_B^{(i)}$	Coordinates of staggered building i
x_s, y_s, z_s	Coordinates of source
$y_c(x)$	Streamline through source at x_s, y_s, z_s
$z_0(x, y)$	Roughness length for wind profile
z_d	Displacement height for logarithmic wind profile
$z_S(x, y)$	Surface elevation of the ground
Z_s	Source height

Z_*	Height of top of shear layer above buildings
β	"Porosity" of an urban canopy [$\beta \sim bw/d^2$]
θ	Mean temperature
θ_s	Surface temperature
κ	Von Karman's constant
λ_p	Planar area index
λ_f	Frontal area index
σ_u, σ_v, σ_w	R.m.s velocity components (of the order of u_*)
ϕ	Angle between wind direction and normal direction to a street (Figs. 3 and 6), i.e., $\phi = 90°$ if wind is along the street.

Subscripts

B	Buoyancy
BS	Building/Street scale
c	Canopy
C	Cloud concentration
f	Coriolis
G	Geostrophic
H	At top of buildings/canyon
M	Mesoscale
N	Neighborhood scale
O	Overall urban area
Ro	Rossby
s	Surface, street
S	Source
Se	Effective source
*	Turbulence-related level for log profile, or turbulent source

Abbreviations

BS	Building/street sub-region
CFD	Computational fluid dynamics
FAM	Fast approximate model
FCM	Fully computational model
LES	Large eddy simulation
M	Mesoscale region
N	Neighborhood sub-region
RANS	Reynolds averaged Navier–Stokes
RSM	Reynolds stress model
r.m.s	Root mean square
SVF	Sky view factor

Bibliography

1. Hunt JCR, Carruthers DJ, Britter RE, Daish NC (2004) ADMLC, http://www.admlc.org.uk/documents/ADMLC20023_000.pdf
2. Garratt JR (1993) The atmospheric boundary layer. Cambridge University Press, Cambridge, 334 p
3. Hunt JCR, Simpson JE (1982) Atmospheric boundary layers over non-homogeneous terrain. In: Plate E (ed) Engineering meteorology. Elsevier Science, Amsterdam, New York, pp 269–318
4. Oke TR (1978) Boundary layer climates. Methuen, London, 372 pp
5. Mestayer PG, Anquetin S (1995) Climatology of cities. In: Gyr A, Rys FS (eds) Diffusion and transport of pollutants in atmospheric mesoscale flow fields. Kluwer, Dordrecht, pp 165–189
6. Emmanuel R, Fernando HJS (2007) Effects of urban form and thermal properties in urban heat island mitigation in hot humid and hot arid climates: the cases of Colombo, Sri Lanka, and Phoenix, USA. Clim Res 34:241–251
7. Högström U, Smedman A (1984) The wind regime in coastal areas with special reference to results obtained from the Swedish wind energy program. Bound Lay Meteorol 33:351–373
8. Owinoh A, Orr A, Hunt JCR, Clark P (2003) Numerical modelling of boundary layer flow over a low hill with abrupt surface heat flux change (submitted)
9. Belcher SE, Jerram N, Hunt JCR (2003) Adjustment of a turbulent boundary layer to a canopy of roughness elements. J Fluid Mech 488:369–398
10. Grimmond CSB, Oke TR (1999) Aerodynamic properties of urban areas derived from analysis of surface form. J Appl Meteor 38:1262–1292
11. Britter RE, Hanna SR (2003) Flow and dispersion in urban areas. Ann Rev Fluid Mech 35:469–496
12. Kastner-Klein P, Rotach MW (2004) Mean flow and turbulence characteristics in an urban roughness sublayer. Bound Lay Meteorol 111:55–84
13. Jackson PS (1981) On the displacement height in the logarithmic velocity profile. J Fluid Mech 111:15–25
14. Davenport AG (1960) Rationale for determining design wind velocities. J Struct Div Amer Soc Civ Eng 86:39–68
15. Davenport AG, Grimmond CSB, Oke TR, Weiringa J (2000) Estimating the roughness of cities and scattered country. In: Proceedings of 12th AMS conference on applied climatology, 2000. Asheville, NC, USA
16. Cionco R, Ellefsen R (1998) High resolution urban morphology data for urban wind flow modeling. Atm Env 32:7–17
17. Ratti CS, Di Sabatino S, Britter RE (2006) Urban texture analysis with image processing techniques: winds and dispersion. Theor Appl Climatol 84:77–90
18. Macdonald RW, Griffiths RF, Hall DJ (1998) An improved method for estimation of surface roughness of obstacle arrays. Atmos Environ 32:1857–1864

19. Di Sabatino S, Leo LS, Cataldo R, Ratti C, Britter R (2010) On the construction of DEMs of a southern European city and a comparative morphological analysis with respect to northern European and North American cities. J Appl Meteor Climatol 49:1377–1396
20. Rotach MW (1995) Profiles of turbulence statistics in and above an urban street canyon. Atmos Environ 29:1473–1486
21. Counihan J, Hunt JCR, Jackson PS (1974) Wakes behind two-dimensional surface obstacles in turbulent boundary layers. J Fluid Mech 64:529–563
22. Mestayer PG, Vachon G, Rosant J-M (2002) The Nantes'99 data base for model validation of air quality in streets. In: Proceedings of 8th International Conference on harmonisation within atmospheric dispersion modelling for regulatory purposes, Sofia, Bulgaria, 14–17 October 2002, pp 297–300
23. Soulhac L (2000) Modélisation de la dispersion atmosphérique à l'intérieur de la canopée urbaine. Ph.D. thesis, École Centrale de Lyon
24. Todhunter PE (1990) Microclimatic variations attributable to urban-canyon asymmetry and prientation. Phy Geog 11(2):131–141
25. Kothari KM, Peterka JA, Meroney RN (1986) Perturbation analysis and measurements of building wakes in a stably-stratified turbulent boundary layer. J Wind Eng Ind Aerodyn 25:49–74
26. Lawson TV (1980) Wind effects on buildings, vol 1. Design, Applied Science
27. Britter RE, Hunt JCR (1979) Velocity measurements and order-of-magnitude estimates of the flow between two buildings in a simulated atmospheric boundary layer. J Ind Aero 4:165–182
28. Davidson MJ, Mylne KR, Jones CD, Phillips JC, Perkins RJ, Fung JCH, Hunt JCR (1995) Plume dispersion through large groups of obstacles – a field investigation. Atmos Environ 29: 3245–3256
29. Eames I, Hunt JCR, Belcher SE (2004) Lagrangian and Eulerian properties of steady flows through groups of obstacles. J Fluid Mech 515:371–389 [Summary version in ERCOFTAC Bulletin No. 56]
30. Kastner-Klein P, Plate EJ (1999) Wind-tunnel study of concentration fields in street canyons. Atmos Environ 33:3973–3979
31. Schatzmann M, Leitl B (2002) Validation and application of obstacle-resolving urban dispersion models. Atmos Environ 36:4811–4821
32. Kastner-Klein P, Berkowicz R, Britter R (2004) The influence of street architecture on flow and dispersion in street canyons. Meteorol Atmos Phys 87:121–131
33. Macdonald RW, Ejim CE (2002) Flow and dispersion data from a hydraulic simulation of the MUST array. Technical Report 2002–2003, Department of mechanical engineering, University of Waterloo, Canada
34. Gryning S-E, Lyck E (1984) Atmospheric dispersion from elevated sources in an urban area: comparison between tracer experiments and model calculations. J Clim Appl Meteorol 23:651–660
35. Allwine KJ, Shinn JH, Streit GE, Clawson KL, Brown M (2002) Overview of Urban 2000: a multiscale field study of dispersion through an urban environment. Bull Am Meteorol Soc 83:521–536
36. Allwine KJ, Leach MJ, Stockham LW, Shinn JS, Hosker RP, Bowers JF, Pace JC (2004) Overview of joint urban 2003 – an atmospheric dispersion study in Oklahoma City. Symposium on Planning, Nowcasting and Forecasting in the Urban Zone, American Meteorological Society, Seattle, Washington, January 11–15
37. Rotach MW, Gryning S-E, Batchvarova E, Christen A, Vogt R (2004) Pollutant dispersion close to an urban surface – the BUBBLE tracer experiment. Meteorol Atmos Phys 87:39–56
38. Wood CR, Arnold SJ, Balogun AA, Barlow JF, Belcher SE, Britter RE, Cheng H, Dobre A, Lingard JJN, Martin D, Neophytou MK, Petersson FK, Robins AG, Shallcross DE, Smalley RJ, Tate JE, Tomlin AS, White IR (2009) Dispersion experiments in Central London: The 2007 DAPPLE project. Bull Amer Meteor Soc 90:955–969
39. Barlow JF, Dobre A, Smalley RJ, Arnold SJ, Tomlin AS, Belcher SE (2009) Referencing of street-level flows: results from the DAPPLE 2004 campaign in London, UK. Atmos Environ 43:5536–5544
40. Yee E, Biltoft CA (2004) Concentration fluctuation measurements in a plume dispersing through a regular array of obstacles. Bound Lay Meteor 111:363–415
41. Brown MJ, Williams MD (1998) An Urban Canopy Parameterization for Mesoscale Meteorological Models. Los Alamos National Laboratory, Report LA-UR-98-3831
42. WRF – http://www.wrf-model.org/index.php (2010) The weather research and forecasting model
43. Hodur R (1997) The Naval Research Laboratory's Coupled Ocean/Atmosphere Mesoscale Prediction System (COAMPS). Mon Wea Rev 125:1414–1430
44. MM5-MM5 community model (2008) http://www.mmm.ucar.edu/mm5/overview.html
45. MESONH-Meso-NH, non-hydrostatic mesoscale atmospheric model (2011) http://mesonh.aero.obs-mip.fr/mesonh/
46. Cullen MJP (1993) The unified forecast/climate model. Meteorol Mag 122:81–94
47. Carlotti P (2002) Two point properties of atmospheric turbulence very close to the ground: comparison of a high resolution LES with theoretical models. Bound Lay Meteor 104:381–410
48. Hunt JCR, Orr A, Rottman JW, Capon R (2004) Coriolis effects in mesoscale flows with sharp changes in surface conditions. Quart J Roy Meteor Soc 130:2703–2731, Conference on shallow layer flows, Delft
49. Carruthers DJ, Hunt JCR, Weng WS (1988) A computational model of stratified turbulent airflow over hills – FLOWSTAR I. In: Zanetti P (ed) Computer techniques in environmental studies. Springer, Berlin, pp 481–492
50. Thykier-Nielsen S, Deme S, Mikkelsen T (1999) Description of the atmospheric dispersion module RIMPUFF. Report RODOS

(WG2)-TN(98)-02. Risø National Laboratory. See also http://www.rodos.fzk.de/RodosHomePage/RodosHomePage/ Documents/Public/Handbook/Volume3/4_2_6_RIMPUFF.pdf
51. Wippermann F (1984) Air flow over and in broad valleys: channeling and counter-current. Beitr Phys Atmos 57:92–105
52. Blumen W (ed) (1990) Atmospheric processes in complex terrain. American Meterological Society, Monograph vol. 23, Number 45, June 1990, 323 pp
53. Ohashi Y, Kida H (2002) Effects of mountains and urban areas on daytime local-circulations in the Osaka and Kyoto regions. J Meteorol Soc Jpn 80:539–560
54. Pope SB (2000) Turbulent flows. Cambridge University Press, Cambridge UK, 806 pp
55. Hunt JCR, Olafsson H, Bougeault P (2001) Coriolis effects on orographic and mesoscale flows. Quart J Roy Met Soc 127:601–633
56. Coceal O, Belcher SE (2004) A canopy model of mean winds through urban areas. Quart J Roy Meteor Soc 130:1349–1372
57. Belcher SE, Xu DP, Hunt JCR (1990) The response of a turbulent boundary layer to arbitrarily distributed roughness change. Quart J Roy Met Soc 116:611–635
58. Hunt JCR, Tampieri F, Weng W-S, Carruthers DJ (1991) Air flow and turbulence over complex terrain: a colloquium and a computational workshop. J Fluid Mech 227:667–688
59. Murakami S (1992) Computational wind engineering one: Proceedings of the 1st International symposium on computational wind engineering (Cwe92). Elsevier Science, Tokyo, 21–23 August 1992, pp 924
60. Rodi W (1997) Comparison of LES and RANS calculations of the flow around bluff bodies. J Wind Eng Ind Aerodyn 69–71:55–75
61. Kim S-E, Boysan F (1999) Application of CFD to environmental flows. J Wind Eng Ind Aerodyn 81:145–158
62. Boris JP, Grinstein FF, Oran ES, Kolbe RL (1992) New insights into large eddy simulation. Fluid Dyn Res 10:199–228
63. Singh B, Hansen BS, Brown MJ, Pardyjak ER (2008) Evaluation of the QUIC-URB fast response urban wind model with a cubical building array and wide building street canyon. Environ Fluid Mech 8:281–312
64. Moulinec C, Hunt JCR, Nieuwstadt F (2004) Disappearing wakes and scalar diffusion in tube bundles. J Flow Turb Comb 73:95–116 (See also ERCOFTAC Bulletin 56:5–9)
65. Robins AG, Apsley DD (2000) Modelling of building effects in ADMS. ADMS technical specification, Paper P16/01 N/00. See http://www.cerc.co.uk/software/pubs/ADMS3-1TechSpec/P16_01.pdf
66. Stoesser T, Mathey F, Froelich J, Rodi W (2003) LES of flow over multiple tubes. ERCOFTAC Bulletin 56:15–19
67. Britter R, Schatzmann M (eds) (2007) COST Action 732, Background and justification document to support the model evaluation guidance and protocol. COST Office, Brussels
68. Vardoulakis S, Fisher BEA, Pericleous K, Gonzalez-Flesca N (2003) Modelling air quality in street canyons: a review. Atmos Environ 37(2):155–182
69. Wang X, McNamara KF (2006) Evaluation of CFD simulation using RANS turbulence models for building effects on pollutant dispersion. Environ Fluid Mech 6:181–202
70. Launder BE, Spalding D (1974) The numerical computation of turbulent flows. Comput Meth Appl Mech Eng 3:269–289
71. Schlünzen KH, Bächlin W, Brünger H, Eichhorn J, Grawe D, Schenk R, Winkler C (2004) An evaluation guideline for the prognostic microscale wind field models. Proceedings of the 9th International conference on harmonisation within atmospheric dispersion modelling for regulatory purposes, Garmisch-Partenkirchen (Germany)
72. Cai XM, Barlow JF, Belcher SE (2008) Dispersion and transfer of passive scalars in and above street canyons–Large-eddy simulations. Atmos Environ 42:5885–5895
73. Letzel MO, Krane M, Raasch S (2008) High resolution urban large-eddy simulation studies from street canyon to neighbourhood scale. Atmos Environ 42:8770–8784
74. Salim SM, Buccolieri R, Chan A, Di Sabatino S (2011) Numerical simulation of atmospheric pollutant dispersion in an urban street canyon: comparison between RANS and LES. J Wind Eng Ind Aerod 99:103–113
75. CODASC (2008) Concentration data of street canyons. Laboratory of Building- and Environmental Aerodynamics, IfH, Karlsruhe Institute of Technology. www.codasc.de
76. Xie X, Huang Z, Wang J (2005) Impact of building configuration on air quality in street canyon. Atmos Environ 39:4519–4530
77. CEDVAL (2001) Compilation of experimental data for validation of mesoscale dispersion models, http://www.mi.uni-hamburg.de/Introduction.433.0.html
78. Di Sabatino S, Buccolieri R, Pulvirenti B, Britter R (2007) Application and validation of FLUENT flow and dispersion modelling within complex geometries. In: Borrego C, Renner E (eds) Air pollution modeling and its application XVIII, vol 6. Elsevier, Amsterdam, pp 3–11
79. Riddle A, Carruthers D, Sharpe A, McHugh C, Stocker J (2003) Comparisons between fluent and ADMS for atmospheric dispersion modelling
80. Di Sabatino S, Buccolieri R, Pulvirenti B, Britter R (2007) Simulations of pollutant dispersion within idealised urban-type geometries with CFD and integral models. Atmos Environ 41:8316–8329
81. Carruthers DJ, Edmunds HA, Lester AE, McHugh CA, Singles RJ (2000) Use and validation of ADMS-urban in contrasting urban and industrial locations. Int J Environ Pollut 14:1–6
82. Di Sabatino S, Solazzo E, Paradisi P, Britter RE (2008) A simple model for spatially-averaged wind profiles within and above an urban canopy. Bound Lay Meteor 127:131–151
83. Di Sabatino S, Buccolieri R, Paradisi P, Palatella L, Corrado R A fast model for pollutant dispersion at the neighbourhood scale. Int J Environ and Pollut. Manuscript accepted for publication
84. Wang J, Huang Z (2006) Numerical study on flow and dispersion in urban street canyons of asymmetrical configurations. J Hydrodynamics 18:146–150

85. Wood CR, Barlow JF, Belcher SE, Dobre A, Arnold SJ, Balogun AA, Lingard JJN, Smalley RJ, Tate JE, Tomlin AS, Britter RE, Cheng H, Martin D, Petersson FK, Shallcross DE, White IR, Neophytou MK, Robins AG (2009) Dispersion experiments in central London: the 2007 DAPPLE project. Bull Am Meteorol Soc 90:955–969
86. Launder BE, Reece GJ, Rodi W (1975) Progress in the development of a reynolds-stress turbulence closure. J Fluid Mech 68:537–566
87. Hunt JC, Bohnenstengel SI, Belcher SE, Timoshkina Y (2010) Implications of climate change for expanding cities worldwide. J Urban Design and Planning. Manuscript accepted for publication

Urban Air Quality: Sources and Concentrations

Michael Evan Goodsite, Ole Hertel
Department of Atmospheric Environment, National Environmental Research Institute, Aarhus University, Roskilde, Denmark

Article Outline

Glossary
Definition of the Subject and Its Importance
Introduction
Sources in Urban Airsheds
Impact of Physical Parameters: Geography, Topography, and Meteorology
Pollutant Dispersion in Urban Streets
Nitrogen Dioxide Pollution in Urban Areas
The Impact of Particle Pollution
Polycyclic Aromatic Hydrocarbons (PAHs) and Urban Air Quality
Trace Elements to Include Heavy Metals in Urban Areas
Conclusions
Future Directions
Bibliography

Glossary

Air pollutants Anything in the air around us man-made or natural that contaminates the natural steady state of and constituents in the air as required for life categorized as gaseous or particulate pollutants.

Air pollution The state of pollutants contaminating the air/atmosphere around us.

Air quality A subjective often locally or nationally determined state of the amount of pollutants in the air around us. The best air quality is when there are very low pollutant levels.

Air quality index A numerical index for air pollution, for example, in the United Kingdom it is from 1 to 10 and related to the air quality bands of "low," "moderate," "high," or "very high" (http://www.airquality.co.uk/glossary.php?glossary_id=5, accessed February 13, 2010).

Ambient air Air outside of structures at any given time. The "outdoor air" as opposed to the "indoor air."

Atmosphere The envelope of gases surrounding the Earth.

Coarse particles The coarse particle mass fraction is defined as the difference between measured PM_{10} and $PM_{2.5}$.

Diffuse sources of air pollutants Sources for which the release cannot easily be traced, for example, that are not geo coded like gases and particle emissions from smaller industry and domestic heating and ammonia from grassing cattle, etc.

Emissions The discharge of man-made or natural compounds into the environment.

Fine particles The $PM_{2.5}$ fraction of particles.

Particulates Fine and coarse liquid and solid particles of organic or inorganic substances present in the atmosphere/suspended (floating) in the air. Particulate matter (PM) consists of very small liquid and solid particles floating in the air.

Photochemical smog The resulting haze and reduced visibility from pollutants formed in reactions induced by sunlight and involving nitrogen oxides (NO_x) and hydrocarbons (HC). Photochemical smog including elevated ozone (O_3) levels occurs generally on warm sunny days that promote the photochemical reactions.

$PM_{2.5}$ The mass concentration of particles in the air less than 2.5 microns (μm) in diameter and thus capable of penetrating into the deepest parts of the lungs and therefore often those that can cause great health concern.

PM_{10} The mass concentration of particles <10 μm in aerodynamic diameter. PM_{10} is generally used as an

indicator for suspended particulate matter (e.g., regulated in EU directives) and routinely measured at many locations throughout the world.

Point (stationary) sources of air pollutants Source that emit pollutants from one location, for example, power plants.

Smog A word combining "smoke" and "fog" first used by Dr. HA Des Voeux in 1905 describing the poor visibility and often sharp, unpleasant, and soot pertaining haze occurring during periods when air pollutants are trapped at ground level. There are two processes producing smog: photochemical and physical processes respectively referred to as photochemical smog and urban smog.

Ultrafine particles Particles in the size fraction below 0.1 μm in diameter. These particles are also often termed nanoparticles.

Urban An area with a large population, that is, town or city, generally with a high density and large amount of population.

Urban smog Smog where air pollutants particularly smoke and sulfur dioxide are trapped at ground level usually occurring on cold, wind-still winter days. The Great London Smog episode of 1952 is a historical example still seen in developing countries in today. In western countries, photochemical smog consisting of nitrogenoxides, ozone, and PAN is more common nowadays.

Winter smog Winter smog episodes including elevated levels of nitrogen oxides (NO_x) occur on cold calm days when air pollutants are trapped in urban areas by an inversion layer, that is, a layer of warmer air above the wind-still cold air.

Definition of the Subject and Its Importance

Urban air quality refers to how "clean" the ambient air is inside of cities with a density, population, and level of activity that generally are recognized as "urban." Urban air quality generally differs from rural air quality since there are more concentrated sources and the ability for the pollutants in the air to be dispersed are limited by the physical constraints of the urban environment. Urban air quality varies significantly in urban cities in industrialized worlds, and nonindustrialized world generally because of the difference between control on pollution sources and use of open fires in the urban areas. Nevertheless, illness, deaths, and damage to the environment are still attributed across the world to air pollution.

Worldwide, the United Nations Environmental Programme (UNEP) (http://www.unep.org/urban_environment/issues/urban_air.asp, accessed February 13, 2010) reports that an estimated more than one billion people annually are exposed to outdoor air pollution. Further, up to one million premature deaths are linked to urban air pollution in the ambient environment and about 1.5 million are linked to indoor air pollution. Given primarily these deaths and other health costs and loss of productivity, urban air pollution is estimated to cost approximately 2% of GDP in developed countries and 5% in developing countries.

UNEP further reports that rapid urbanization has resulted in increasing urban air pollution in major cities, especially in developing countries with over 90% of air pollution in major cities in developing countries attributed to vehicle emissions brought about by high numbers of older vehicles coupled with poor vehicle maintenance, inadequate infrastructure, and poor fuel quality with high amounts of sulfur in the fuel.

Most developed countries have put in measures to reduce vehicle emissions, in terms of fuel quality, for example, by regulating the amount of sulfur, benzene, and additives like lead in vehicle fuel and vehicle emission reduction technologies such as catalytic converters, these measures are yet to be adopted in most cities in developing countries and there are recent cases where vehicle manufactures save costs by not utilizing such technologies, while at the same time, lowering overall vehicle prices, thus enhancing the number of vehicles on the road with all of the subsequent effects on air quality.

Air quality as a term, is subjectively defined, generally through laws regulating the maximum concentrations of pollutants in the atmosphere via the maximum allowable emissions from sources. The quality of the ambient (outside) air is monitored, in some urban environments continuously with advanced equipment and generally reported in some type of index by local or national authorities; a so-called air quality index.

Despite relatively unchanged levels of pollutants, the air quality can be improved or degraded based on

the weather and topography of the urban environment. It is therefore a very complicated issue to manage and predict. Many municipalities therefore have air quality management (AQM) offices and/or plans.

There are specific mathematical models developed to predict air quality and support the air quality policies that naturally must be aligned with policies affecting the other environmental compartments.

In cities in the industrialized world, air quality has generally improved after controls and policies on pollution and emittants were emplaced during the past decades. The policies have been the result of international treaties, as well as national and local legislation. The United Nations Environmental Programme (UNEP) maintains a Register of International Treaties and Other Agreements in the Field of the Environment for the interested reader (http://www.unep.org/law/PDF/register_Int_treaties_contents.pdf). Specifically, the 1979 Convention on the Long-range Transboundary Air Pollution and its eight associated protocols, generally named after the cities in which they were signed such as Aarhus, Denmark are relevant for air quality as with the signing of the convention it is recognized as a transboundary issue. There is likewise an international agreement regarding transboundary haze pollution.

Air quality issues are generally on a long-term scale, however in urban areas, municipal authorities need to be prepared for acute events such as those that may be arising from an industrial accident such as what occurred at a pesticide plant in Bhopal, India in December, 1984, or from elevated levels of air pollution such as experienced in London during the "Great London Smog" of 1952. It has been estimated that just in this single event about 12,000 deaths could be directly attributed to the incident [1].

As point sources such as those responsible for the acute incidents above are addressed by policies, other man-made sources, generally the "mobile sources" (i.e., vehicular traffic) are becoming the new primary contributor to degraded air quality in urban areas.

Natural sources are also an important contributor depending on the locality with dust, sea spray, and other types of particulate matter (PM) such as pollen as well as volatile organic compounds (VOCs) emitted from plants and trees being those that contribute often to degraded air quality.

Historically in urban areas across the world, high levels of smoke and sulfur dioxide from domestic burning of coal in people's homes and later combustion of fossil fuels in coal-fired power plants have been the major point source of air pollutants, and this has led to major episodes of air pollution with resultant degraded air quality and associated health effects, including deaths directly attributed to the poor air quality.

Air quality in urban environments, especially in developed countries is nearly always a function of vehicular traffic and the emissions arising from vehicles. Both petrol- (gasoline) and diesel-driven vehicles emit vast amounts of pollutants. These include carbon monoxide (CO), the oxides of nitrogen (NO_x), and volatile organic compounds (VOCs). Particulates (PM_{10}) and finer-sized particles ($PM_{2.5}$) are emitted not just from the combustion processes in the motor but also and more predominantly from physical processes, such as resuspension of road dust and wear of tires, brakes, and road material.

Introduction

Air pollution is estimated by WHO to cause about two million premature deaths (half of this is associated with outdoor and the other half with indoor air pollution) worldwide annually [2], and this is in addition to a variety of other adverse health effects like asthma and other airway diseases, cardiovascular disease, different types of cancer, as well as adverse pregnancy outcome. The most hazardous of the ambient pollutants are generally believed to be related to the particulate matter (PM), although the mechanisms behind these health effects are not yet fully understood. It is therefore still very uncertain what it is about the particles that cause these negative health effects. Despite the uncertainties related to the mechanism behind these effects, it has, for example, been estimated by WHO that reducing ambient air concentrations of PM_{10} from 70 to 20 $\mu g/m^3$ would lower the number of air quality related deaths by approximately 15% [2].

People are generally most at risk in the urban areas with respect to health effects related to air pollution. More than half of the world's population reside in cities, and it is here that the highest air pollution exposure [3] and thus also most of the associated

negative health impact takes place. The projections for the next 50 years furthermore indicate that the worldwide urban population will be increasing by two thirds [3]. As a result of rapid urbanization, the urban air pollution has been increasing in many major cities, especially those found in developing countries (such as in Brazil, Russia, India, Indonesia, and China). The cost to society of the associated health effects is very significant, and has been estimated to be approximately 2% of the gross domestic product (GDP) in developed countries, whereas it is even 5% of the GDP in developing countries (www.unep.org/urban_environment/issues/-urban_air.asp). There may also be significant associated losses in productivity [5].

Origins of Air Quality: Sources and Formation of Urban Air Pollution

Urban ambient air pollution concentrations arise from the continuous competition between the emission processes that increase pollutant concentrations, and the dispersion, advection, and deposition processes that reduce and remove them. Pollutant differences between different urban areas are naturally reflecting differences in emission densities and pattern, but also in the dispersion and removal processes. The local meteorological conditions are governing the impact on pollution levels of these dispersion and removal processes, and these meteorological conditions vary heavily with the physical location of the city. Air pollution concentrations in an urban environment are naturally the result of the contribution from local emissions, but also contributions arising from pollution from more remote sources may play a very important role (Fig. 1). The size of the city domain together with the density of pollutant emissions governs the local contribution to urban air pollution [6]. Naturally, the temporal pattern in urban air pollution levels is a function of the temporal pattern in the local releases. However, the extent of the urban area, and the spatial distribution in the local emission density, also play central roles for the local contribution to air pollution levels in the urban environments. The local contribution to pollution levels also varies heavily from one pollutant to another. In addition, the meteorological conditions greatly affect the actual pollution levels in a given situation as they govern the dispersion conditions and the pollutant transport in and out of the city area. In this context, the presence of the building obstacles plays a crucial role in causing generally high pollutant levels in the urban environment. This is especially true inside the street canyons with buildings on both sides of the street and where the canyon vortex flow governs the pollution distribution.

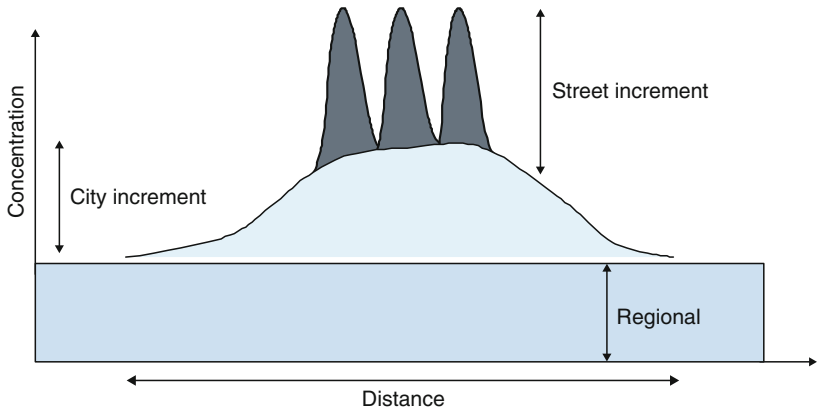

Urban Air Quality: Sources and Concentrations. Figure 1
City cross section. A schematic illustration of the air pollutant contribution from regional transport, the city area, and the street. The relative magnitude of the various contributions depends on the considered pollutant and the actual dispersion conditions (governed by the meteorology)

Air Quality and Health Effects

Air quality and health effects have been shown to be linked. Particulate matter (PM) is generally believed to be the most hazardous of ambient pollutants. More than half of the world's population reside in cities and the number is expected to grow [3]. Cities and especially their urban centers are where air quality is generally the poorest, and the highest air pollution exposure [4] and associated negative health impact therefore take place.

With projections for the next 50 years indicating that the worldwide urban population will increase by two thirds [3], urban air quality will continue to deteriorate as air pollution continues to increase in major cities, especially those in developing countries (such as in Brazil, Russia, India, Indonesia, and China).

Urban Air Pollution Concentrations in General

Urban air pollution arises from the competition between emission processes that increase pollutant concentrations, and dispersion, advection, and deposition processes that reduce and remove them. Differences in pollution levels reflect differences in emission densities and emission patterns. They also reflect processes of pollutant dispersion and removal. Pollution is dispersed by the flow of wind. It is removed generally via chemical conversion to other compounds and/or by being deposited either through wet or dry deposition processes.

The dispersion and removal processes are governed by the local meteorological conditions, which also vary heavily with the physical location of the city. Therefore, air pollution concentrations in an urban environment are naturally the result of local emissions as well as contributions from pollution transport from more remote sources (Fig. 1).

Also of importance to the local contribution to urban air pollution are demographic/geographic factors such as the size of the city domain and the density of pollutant emissions inside the domain [5].

The temporal pattern in urban air pollution levels varies as a function of the local releases. However, it is the variations in the meteorological parameters that govern the dispersion and also the pollutant transport into and out of the city from surrounding rural areas.

The temporal variations in emissions and meteorology are not the only contributors, the emission release height also plays an important role with respect to how quickly the air pollution is dispersed and deposited, with air quality generally improving with areas with very tall and technologically up-to-date smoke stacks. This is because air pollution emitted from a high release height will in many cases be transported out of the urban area before being dispersed down to ground level, although this is of course depending on the size of the urban domain. This is the principle that the "solution to pollution is dilution" when often, the pollution and subsequent air quality issues are just moved from one jurisdiction to another.

Urban industries, power plants, and other sources for which the releases come from tall chimneys therefore only rarely contribute to the local ground level air pollutant concentrations inside the urban area, and instead they are usually contributing primarily to the regional air pollution.

Pollutant emissions related to vehicular transport, local domestic heating, and smaller industries have low release heights [less than 10 m above ground level (a.g.l.)]. Consequently, the releases are not diluted as efficiently before reaching ground level as in the case for emissions from tall (more than 20 m a.g.l.) release heights. The contribution from "low" sources, both point and mobile, therefore often dominates the pollutant concentrations at ground levels inside the urban area.

A steady growth in vehicular transport and centralization of domestic heating have made road traffic the most important source of urban air pollution in many countries including most of the industrialized nations [7].

There are usually significant differences between developed and developing countries when comparing emissions from different industrial sectors. With respect to the local contribution from the various sectors, a comparison of two so-called megacities (Beijing and Paris) showed that aerosol particles and volatile organic compounds (VOCs) have a complex and multi-combustion source in Beijing, whereas a single traffic pollution source completely dominates the urban atmospheric environment in Paris [8]. Both municipalities recognize the above and are taking steps to improve air quality.

Urban Air Quality: Sources and Concentrations. Table 1 Ranges in annual average urban ambient air concentrations ($\mu g\ m^{-3}$) of PM_{10}, NO_2, SO_2, and 1 h average maximum concentrations of O_3 for different regions, based on a selection of urban data from WHO report [1] and previously presented by Hertel and Goodsite [66]

Region	Annual average concentrations			1 h max concentration
	PM_{10}	NO_2	SO_2	O_3
Africa	40–150	35–65	10–100	120–130
Asia	35–220	20–75	6–65	100–250
Australia/New Zealand	28–127	11–28	3–17	120–310
Canada/United States	20–60	35–70	9–35	150–380
Europe	20–70	18–57	8–36	150–350
Latin America	30–129	30–82	40–70	200–600

Source: Reproduced from Hertel and Goodsite [66]

Although ambient air quality is that which is often the subject of research and the type of pollution that is heard about (and also the subject of this entry), indoor air quality cannot be forgotten. Since many people spend most of their time indoors, indoor air quality is a major health concern and may be worsened by the location of the office or home in the urban environment.

The issue, as with case of ambient air quality, is generally worse in the developing countries. Emissions from household use of fossil fuels in the year 2000 were estimated to account for 1.6 million deaths, mainly among women and children in the poorest countries [9] that are being exposed to elevated pollutant levels in the indoor environment.

The actual ambient air pollutant load and therefore average air quality greatly varies from one city to another, but, generally, major urban areas throughout the world have poor air quality, and, among these, the cities in the developing countries face the greatest challenges.

WHO has compiled a survey on typical ranges in ambient air concentrations of four indicator pollutants, summarized in Table 1.

Urban Air Quality Concentrations and Indices

The greatest levels of pollutants like PM_{10} and SO_2 are presently found in urban air concentrations in Africa, Asia, and Latin America, whereas, the highest levels of secondary pollutants (i.e., produced via reaction in the atmosphere with primary pollutants) like O_3, PAN, and NO_2 are observed in Latin America and in some of the larger cities and urban areas in the developed countries.

The environmental and human health impacts are particularly severe in megacities, which are cities of about ten million or more inhabitants [10].

Urban air pollution has thus become one of the main environmental concerns in Asia, and especially in China where the pollution load in megacities like Beijing, Shanghai, Guangzhou, Shenzhen, and Hong Kong is substantial and air quality can be greatly affected (Photo 1).

In these cities, between 10% and 30% of days exceed the so-called Grade-II national air quality standards [11] by a factor of three to five times that of the WHO AQG (air quality grade). These cities experienced a 10% growth in traffic each year over the last 5–6 years. Therefore even with enhanced emission controls, NO_2 and CO concentrations have remained almost constant over the same period of time.

Air quality indices (AQIs) are commonly used as tools in air quality management. A description of widely used indices and how they are expressed mathematically is given in Gurjar et al. [12]. AQIs may be designed to handle single or a multitude of pollutants, and they may also be used for comparing the loads in different municipalities or describing the current load in relation to average loads or air quality standards and target values.

Urban Air Quality: Sources and Concentrations. Photo 1
Photo from a Beijing Hotel, October, 2008 showing reduced visibility due to the poor air quality (Photo by M. Goodsite)

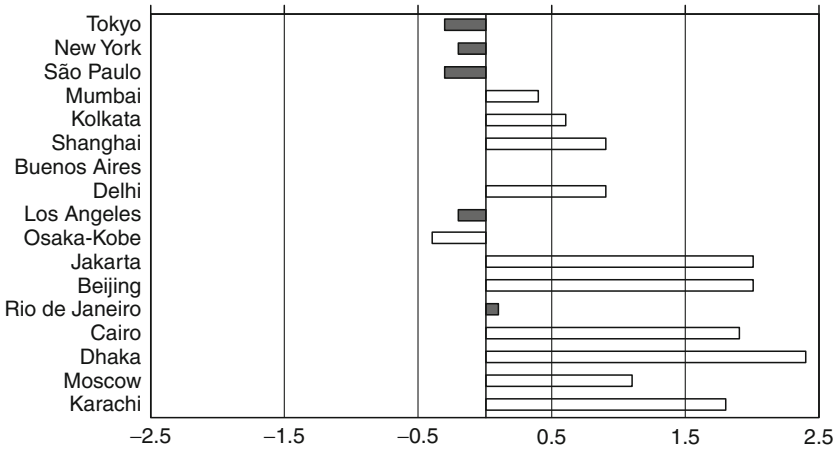

Urban Air Quality: Sources and Concentrations. Figure 2
Megacities pollution indices (MPI) based on measurements of the classical air pollutants and aggregated into an index for total pollution level (multipollutant). The plot is reproduced from Gurjar et al. [12], and 30% of the local NO_x contribution is related to aircraft, whereas the remaining 95–70% is from road traffic [15]

In an example of a multi component AQI (the authors applied the term MPI) a comparison over megacities throughout the world showed that the highest MPI values were found for Dhaka, Beijing, Cairo, and Karachi with values about double those of Delhi, Shanghai, and Moscow [12] (Fig. 2).

Sources in Urban Airsheds

Urban airsheds are the areas in and around the urban areas where air mass generally reaches a steady state given that they are facing stable, normal meteorological conditions.

Urban Air Quality: Sources and Concentrations. Photo 2
(**a**) and (**b**) Delhi in July 2010, immediately prior to rainfall at the Delhi airport and immediately after rainfall from the Delhi University Main Campus, showing the effectiveness of wet deposition in improving air quality (Photos by M. Goodsite)

There are many potential sources in urban areas that are generally located physically away from the urban center but still have to be considered as a part of the urban airshed. Airports are one of these.

Airports are usually located in the vicinity of larger cities and often mentioned as potential sources of high pollution loads in the urban areas (note: the haze in Photo 2a at the Delhi airport is probably not from the airport activities alone, but from the construction activities and traffic around the airport).

Several studies have thus been carried out to determine the potential impact of emissions from airport activities. These studies generally point at the main influence on air quality is coming from the road traffic going to and from the airport, whereas the impact of aircraft emissions has been found to be very limited. A study carried out in Frankfurt Airport, showed that aircraft-specific emissions generally could not be identified, whereas emissions from vehicle traffic on surrounding motorways had measurable impact on the air quality [13]. A study from Munich Airport had similar findings [14], as did a study inside Heathrow Airport [15].

Ship traffic has been estimated to be responsible for about 60,000 lung cancer and cardiopulmonary deaths annually [16], but this outcome is linked to the contribution from ship emissions to the background particulate matter load and not directly related to contribution from ship emissions to the urban air quality.

Harbors may nevertheless be a local source contributing to urban pollution as they are often part of the urban airshed in coastal areas, but studies indicate that as with airports, that local road traffic often dominates the contribution from harbors. For example, a study in the harbor of Aberdeen thus showed a gradient of increasing NO_2 and soot concentrations from the harbor toward the city center [17], indicating that the contribution from the harbor had very limited impact on the local air quality in comparison with the emissions taking place in the urban environment.

Wood combustion in households is a concern in areas with many wood stoves. These areas have relatively high local emissions of PM in comparison with other anthropogenic pollution sources generally in the airshed. Investigations of wood combustion and air quality in developed countries like New Zealand [18], Sweden [19], the United States [20, 21], and Denmark [22] have documented that residential wood combustion likely significantly elevates the local PM concentrations in outdoor air. Emission inventories for Denmark, where wood-burning stoves are generally secondary sources of domestic heating, point at wood combustion as the largest anthropogenic source of

primary particle emissions in the country, being responsible for about 60% of the countrywide primary particle emissions.

Impact of Physical Parameters: Geography, Topography, and Meteorology

Impact of Geography

The location of the city has a great impact on the dispersion conditions and thus air quality as it affects the local meteorological conditions. Los Angeles for example, is situated in a valley with stagnant conditions during temperature inversions. The stagnant conditions lead to very low wind speeds, and this results in little air exchange between the valley and the surrounding areas. The hot and sunny climate and high emissions from traffic, industry, and other sources make the valley act like a large pollutant reaction chamber, and this is ultimately leading to high concentrations of photochemical products like ozone, nitrogen dioxide, and peroxy acetyl nitrate (PAN) with the resultant degradation of air quality.

Wind speed through a city plays an important role. For example, nitrogen oxide (NOx) levels in the street Via Senato in Milan, Italy compared with the street Jagtvej in Copenhagen, Denmark show similar concentrations at the two sites despite the much higher traffic load in the street of Copenhagen [23]. This is directly the result of generally higher wind speeds in Copenhagen compared with Milan. High wind speeds and neutral conditions prevail in Copenhagen, whereas low wind speeds and stable or near stable conditions are frequent in Milan. Copenhagen has a cold coastal climate whereas Milan has a warm subtropical climate and the local wind conditions are furthermore affected by the location inside the Po Valley. Air quality planners must take their own geography into consideration.

Impact of Topography

Most cities have characteristic wind systems as a result of local topography. An example is the rising air over a warm mountainside during daytime often leading to local formation of clouds and the subsequent release of precipitation.

During the night, the system reverses and the cooling of the air in the mountain valley leads to stable conditions that may lead to local air pollution problems. The impact of Katabatic winds is another example affecting cities along the Norwegian coast. Katabatic winds are formed when cold air masses move downslope (Katabatic is Greek for moving downhill) and meeting the colder snow- and glacier-covered areas, which then cool the air mass further as it continues flowing downhill.

Katabatic winds may lead, for example, to high levels of local dust with resulting air quality issues, though their occurrence is highly location specific. The warm and dry Foehn wind formed on the backside of a mountain chain, for example, on the north side of the European Alps is another case in point. As the wind flows over the mountain, the air mass is cooled and releases moisture. The air is subsequently warmed as the air mass flows downhill. This system may then form an inversion with the effect of reducing the dispersion of local air pollutants.

Impact of Meteorology

Ambient temperature in the urban atmosphere of larger cities is usually a couple of degrees Celsius higher than that found in the surrounding rural areas due to the so-called urban heat island effect [24]. The phenomenon is due to the much smaller reflection or albedo of the city as compared with its surrounding area and therefore absorbs more energy to release it later in the form of heat.

There is in addition a high consumption of energy inside the city, as a result of domestic heating and intense road traffic, which further contributes to the higher releases of heat than rural surroundings. Buildings act as heat reservoirs so the city has a less pronounced diurnal temperature variation compared with the rural area. Lastly, buildings and other urban constructions form a physical barrier for the wind flow. This shielding leads to less cooling of the surfaces inside the city.

In calm weather, an urban circulation cell, so-called heat island circulation, may be formed by warm air rising from the city. As it moves away from the city, the heated air may sink and then in another circulation, be returned to the city at a low altitude. A similar phenomenon is known in coastal regions, where a sea breeze may be formed as a result of the temperature difference between the sea and land surfaces.

A study in London showed that due to the heat island circulation over the city, the wind speed is never below about 1 m s^{-1} [25]. Therefore, the heat island effect is very important during low wind speed conditions in urban areas where it may dominate the dispersion and thereby be the limiting factor for the highest local air pollution concentrations and therefore local air quality. The urban heat island effect may thus be the limiting factor for the highest pollution concentrations and thereby air quality parameters in the urban environment.

Pollutant Dispersion in Urban Streets

Pollution "hot spots" are areas where large concentrations of pollution are emitted or concentrate. In urban areas, trafficked streets are air pollution hot spots (Fig. 1). The concentration inside the urban street are generally the result of two contributions, one from emissions from the local traffic in the street itself and one from background pollution entering the street canyon from above roof level [26]:

$$C = c_b + c_s$$

where c is the concentration in the street, c_b the urban background contribution, and c_s the contribution from traffic inside the street itself. The background contribution arises from two contributions: (1) the contribution from nearby sources in the urban area (typically this will be the traffic in surrounding streets) and (2) the regional (sources within a distance of a few hundred kilometers) and long-range transported (sources placed up to thousands of kilometers away) of air pollution.

The pollutant levels in the urban streets are strongly affected by the emissions from traffic taking place on the street itself. The concentration level and the distribution of air pollution inside the street canyon (the street "boxed in" by buildings on each side) are largely governed by the surrounding physical conditions. These physical conditions heavily affect the wind speed and the wind direction inside the street, with residence time for an air packet in the vicinity of an urban street usually on the order of seconds to a few minutes depending on the street topography. This means that only very fast chemical conversions of pollutants have time to take place [26].

The airflow generated inside the streets and around building obstacles may result in very different concentration levels at different places in the street.

The street canyon vortex flow (Fig. 3) physically governs the pollutant distribution inside the street canyon. The street canyon is characterized by the presence of tall buildings on both sides of the street. Within the vortex, relatively clean air flows from rooftop height and down the windward face of the street, across the road at street level, in the reverse of the wind direction at roof top, thus transporting the pollutants from the road-level traffic to the leeward face of the canyon. The result is that pollution concentrations are up to ten times higher on the leeward side compared with the windward side of the street. This means that air quality depending on prevailing wind conditions may often be much poorer on one side of the street than another.

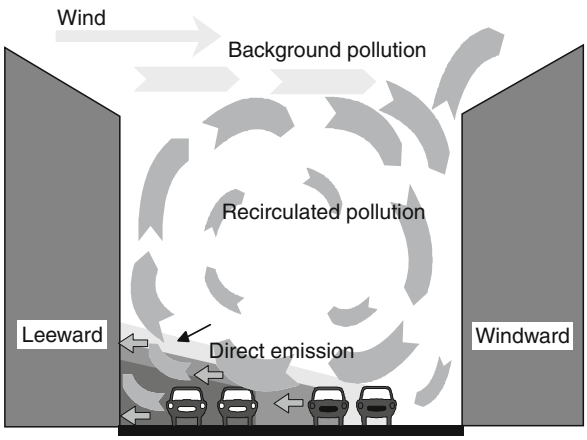

Urban Air Quality: Sources and Concentrations. Figure 3 Illustration of the flow and dispersion inside a street canyon. The wind above roof level blows perpendicular to the street in the above figure, thus creating a vortex inside the street canyon with the wind direction at street level opposite to the wind direction above roof level. The result of these flows is that there may be differences in air pollution concentrations of up to a factor of 10 between the two pavements inside the street canyon. Air quality on one side of the street might thus be poorer than on the opposite side of the street, if there are prevailing winds

Nitrogen Dioxide Pollution in Urban Areas

For example, the chemistry of nitrogen oxides [NO_x: the sum of nitrogen monoxide (NO) and nitrogen dioxide (NO_2)] in urban streets may be described by only two reactions: the reaction between ozone (O_3) and NO forming NO_2, and the photo dissociation of NO_2 [27]:

$$NO + O_3 \rightarrow NO_2 \quad (1)$$

$$NO_2 + h\nu \rightarrow NO + O(^3P) \quad (2)$$

$$O(^3P) + O_2 \rightarrow O_3 \quad (3)$$

where $O(^3P)$ is ground state atomic oxygen. Reaction (3) is very fast, and therefore for most practical applications it may be disregarded. The products of reaction (2) may thus be considered to be NO and O_3.

NO_x is therefore mainly emitted as NO and to a lesser extent, NO_2.

Long-term exposure to elevated NO_2 levels is a health hazard, and may decrease lung function and increase the risk of respiratory symptoms such as acute bronchitis, cough, and phlegm, particularly in children [28], whereas NO at current ambient air concentrations is considered to be harmless.

The fraction of NO_x directly emitted as NO_2 used to be only about 5–10% in countries with a small fraction of diesel engines. However, due to the use of catalytic converters and an increasing number of diesel engines with high fraction of NO_2 in the exhaust, this value may in some regions be now up to as much as 40% [29]. This extremely simple chemical mechanism of two reactions and a direct emission describes very well the concentrations of NO_2 inside urban streets [27], for many cities it may also be applied for describing NO_2 concentrations in urban background air (see [6] documenting this the case for many Northern European cities).

The use of catalytic converters in automobiles has in recent years led to a major reduction in NO_x concentrations in the urban streets of many industrialized countries. For several reasons, NO_2 levels have not followed the same trends (Fig. 4). Part of the explanation is the chemical conversion of NO to NO_2 in the reaction with O_3, but the other explanation is, as mentioned above, the increased fraction of NO_2 in the NO_x emission from vehicles with catalytic converters. Despite the overall reduction in NO_x emissions, this is contributing to elevated NO_2 concentrations.

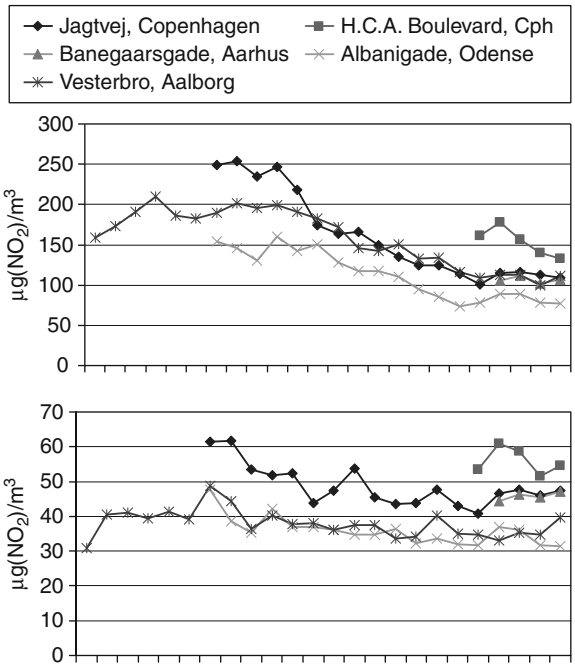

Urban Air Quality: Sources and Concentrations. Figure 4 The measured trend in annual mean concentrations of NO_x and NO_2 (both shown in µg $(NO_2)/m^3$) at the street stations in the largest Danish cities: Copenhagen, Aarhus, Odense, and Aalborg. The upper plot shows NO_x and lower plot NO_2. The plots include measurements from the time period 1982–2005, and illustrate a decrease in NO concentrations resulting from increasing number of vehicles with catalytic converters in Danish car fleet, but also illustrates that this decrease is not reflected in the NO_2 concentrations that have remained more or less constant during this time period [64]

The Impact of Particle Pollution

Ambient urban air contains a complex mixture of particles from natural and anthropogenic sources of varying sizes and chemical composition [30–34]. The particle size is crucial for the atmospheric fate [35] and the human health impact as both the particles' atmospheric behavior and their deposition in the human respiratory system is governed in part by its size [36].

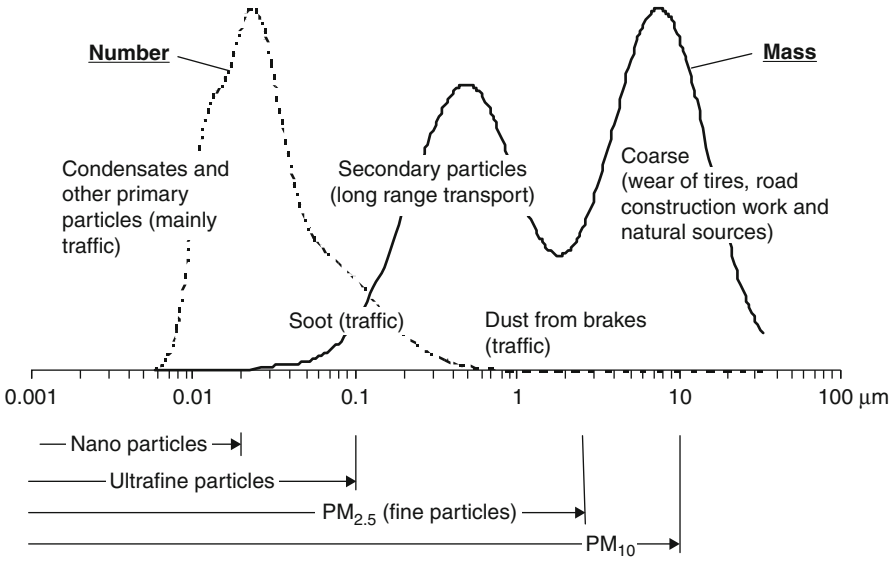

Urban Air Quality: Sources and Concentrations. Figure 5
Typical size distribution of particles in urban air: both as mass and number concentration. The horizontal axis is the particle diameter in micrometers. The black line is mass distribution, dominated by the coarse and secondary particles. The dashed line is the number distribution, dominated by ultrafine particles. Note that one particle with a diameter of 10 μm has the same weight as one billion particles with a diameter of 0.01 μm [65]

Particles in ambient air generally appear in two rather distinct size classes (referred to as "modes") usually termed fine particles (diameter: 0.1–2.5 μm) and coarse particles (diameter: >2.5 μm). In addition, it is common to talk about the ultrafine particles (diameter: 0.01–0.1 μm or 10–100 nm) that usually dominate the number concentrations (Fig. 5).

Particle Mass Concentrations

Mass concentration of particles <10 μm and <2.5 μm in aerodynamic diameter (PM_{10} and $PM_{2.5}$) are generally used as an indicator for suspended particulate matter (e.g., regulated in EU directives) and routinely measured at many locations throughout the world. Particle mass is dominated by particles >0.1 μm in diameter. Particles in traffic exhaust are mainly in the ultrafine fraction and include elemental carbon (EC) as well as organic carbon (OC) [37]. The ultrafine mode particles from traffic sources contribute considerably to the PM number concentrations but only little to the PM mass.

While some health studies have demonstrated a relationship between both acute and long-term health effects and the ultrafine particle mode (particle diameters <0.1 μm) [38], other studies are less conclusive concerning the health effects of the ultrafine mode particles. Even though ultrafine particles are a minor contribution to total particle mass concentration, they represent most of the particles in terms of the number concentration. Most studies to this point of the health effects air particles have been related to particle mass. Neither of the mechanisms are yet fully understood and the need for more studies has been called for [39].

With respect to streets with a high level of vehicular traffic, a significant fraction of the particle pollution originates from this traffic [40]. The direct emissions from car exhaust contain particles formed inside the engine as well as in the air just after leaving the exhaust pipe. The latter depend on the sulfur content in the fuel.

Studies have shown that reducing the sulfur content in diesel significantly reduces the particle number concentrations in urban streets and this parameter is therefore important for air quality planning and management.

Directly emitted particles are mainly found in the ultrafine particle fraction of the total particle

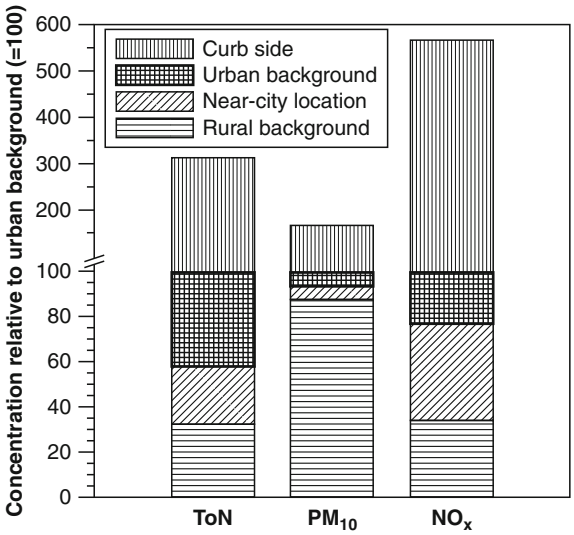

Urban Air Quality: Sources and Concentrations. Figure 6 Comparison of average concentrations of total particle number (ToN), particle mass (PM_{10}), and NO_x at rural, near-city, urban, and curb side measurement stations relative to urban background levels in the area of Copenhagen, Denmark. The concentration bars are stacked so only the additional contributions are marked with the pattern shown in the legend. Note that the scale of the vertical axis changes at 100 (Adapted from Ketzel et al. [40])

concentration. Traffic, however, also contributes to the mechanically formed particles in the fine and especially the coarse fraction, typically produced from wear of tires and brakes, wear from road surface material as well as resuspended dust.

For the particle mass (PM_{10}), long-range transport is usually the dominating source for regional background levels. Studies have shown that less than 10% of the urban PM_{10} originate from local urban sources [40]. For NO_x as well as particle numbers a larger difference between the urban, rural, and curb side levels have been observed, indicative of a large contribution from local traffic sources (Fig. 6).

Particle Number Concentrations

A high correlation (one study [40] found $R > 0.9$) between concentrations of NO_x and total particle number indicating that both components of air pollution originate from the same (traffic) source.

The correlation is seen as the components are emitted in a similar ratio (particle number : NO_x) from different traffic categories, in other words, high NO_x emitters such as diesel vehicles (especially heavy-duty vehicles) are also the high particle emitters (when these are expressed in particle number concentrations) [41].

The Danish Operational Street Pollution Model (OSPM) [42] is an example of a numerical model that through its calculations, have been shown to reproduce well the observed particle number, when treating particles as inert tracers (i.e., by disregarding transformation and loss processes) [43]. The particle emission factors depend on ambient temperature with higher emissions at lower temperatures, which is accounted for in the simulations reported in [44] and other refined numerical models.

Long-range transport however, is a significant contributor to fine fraction particles and leads to the main part of particulate sulfate and ammonium and a large part of particulate nitrate. These secondary particles are formed from anthropogenic sulfur dioxide (SO_2), ammonia (NH_3), and NO_x emissions [45] and often constitute more than 30% of the PM_{10}. A separate fraction of particulate nitrate appears in the coarse mode, which also contains contributions from sea spray and resuspended dust [46, 47] with relatively large mass and thus quickly deposits by gravitational settling, such as road dust. Due to the quick deposition, coarse particles, therefore, generally have a relatively short lifetime in the atmosphere when compared with fine particles.

Particles of low-temperature combustion processes from wood-burning stoves and other poorly controlled burning processes may be soot particles that often have high contents of polycyclic aromatic hydrocarbons (PAHs) and other carcinogens or just generally degrade the air quality in the urban environment, despite the "charm" or in developing countries, necessity, for burning with these methods.

Air Quality Measurement Locations

When comparing observed levels of particulate matter or air quality in different cities, aside from assuring that the indices are the same, the location of the monitoring stations must be taken into account, as they may be very different. An index that reports the "average"

might consist of a station in the urban center and one on the outskirts. There is a real risk of comparing sites in the vicinity of large pollution sources with sites at some distance from local sources. The location of measurement stations must be very carefully considered, and it is not generally good enough to just replicate what another town is doing. For all of the physical and anthropogenic factors previously discussed, locating stations is critical and must be done in conjunctions with city planners. Recently in the Danish press, scientists speculated if air quality levels improved as a result of newly laid road tar thus keeping down the dust at a roadway at the measurement station.

In addition to the ambient measurements, modern air quality management is starting to consider locating measurement stations where many people spend most of their time: indoors. Exposure to air pollution in the home is an important fraction of a person's overall exposure. A Danish study in an uninhabited apartment in central Copenhagen revealed that particle pollution inside the apartment was to some extent linked to the activity level of the neighboring apartments [48] indicating that sources in the neighboring environment must also be considered in the analysis of overall exposure. Measuring air quality is therefore not a simple matter of purchasing machines. They need to be carefully located and the measurements are best coupled with other data such as meteorology and with numerical models that help provide additional value with the measured numbers.

Natural Sources

A 2006 WHO study (Fig. 7) indicates that PM_{10} concentrations in Asia and Latin America are higher than are observed in Europe and North America [1]. The highest particle levels are observed in Asia and are attributed to forest fires, poor fuel quality, and aeolian (windblown) dust. Wind erosion originating especially in the deserts of Mongolia and China contributes to the general level of PM in the region.

Polycyclic Aromatic Hydrocarbons (PAHs) and Urban Air Quality

Sources and Emissions of PAHs

Polycyclic aromatic hydrocarbons are a group of chemicals that are formed during incomplete burning of coal, oil, gas, wood, garbage, or other organic substances, such as tobacco and charbroiled meat. There are more than 100 different PAHs. PAHs generally occur as complex mixtures normally as part of combustion products such as soot and not as single compounds.

PAHs can also be found in materials such as crude oil, coal, coal tar pitch, creosote, and roofing tar. There are numerous other sources [49, 50].

In the air, they are either attached to dust particles or as solids in airborne soil or sediment. This is of great concern due to the mutagenic [51] and carcinogenic [52] properties of PAHs; the United States Agency for Toxic Substances (ATSDR, 1995) has listed 17 PAHs as of priority concern with respect to their toxicological profile.

PAHs that have been studied in urban and other areas appear to represent only a fraction of a percent of the ambient particle mass [53]. However, there are compelling arguments that the previously commonly employed measurement techniques produced artifacts. Despite the toxicological profile of PAHs, no country has mandatory guidelines with respect to their ambient air quality standards [54].

Sampling Artifacts in Measuring PAHs

In order to reduce the risk of sampling artifacts [52], in the spring of 2003 the Mexico City Metropolitan Area (MCMA) air quality campaign employed three independent methods to measure particle-bound PAHs [57, 58]. Peak concentrations of PAHs on the order of 120 ng m^{-3} during the morning rush hour were observed in excellent agreement that 20% of the vehicles account for 50% of the PAH emissions [59]. Like other atmospheric gaseous and particulate constituents, PAHs are removed from the atmosphere by wet or dry deposition and may also be converted or degraded in heterogeneous processes. Despite the systematic approach, there may have been significant concentrations of very toxic and very reactive PAHs in the MCMA atmosphere that were missed due to filter reaction artifacts [58] thus attesting to how complicated measuring PAHs are as a part of air monitoring programmes and the need for further development.

Long-Range Transport of PAH

Together with the local emission, the long-range transport of PAHs is of concern. PAHs are designated as one

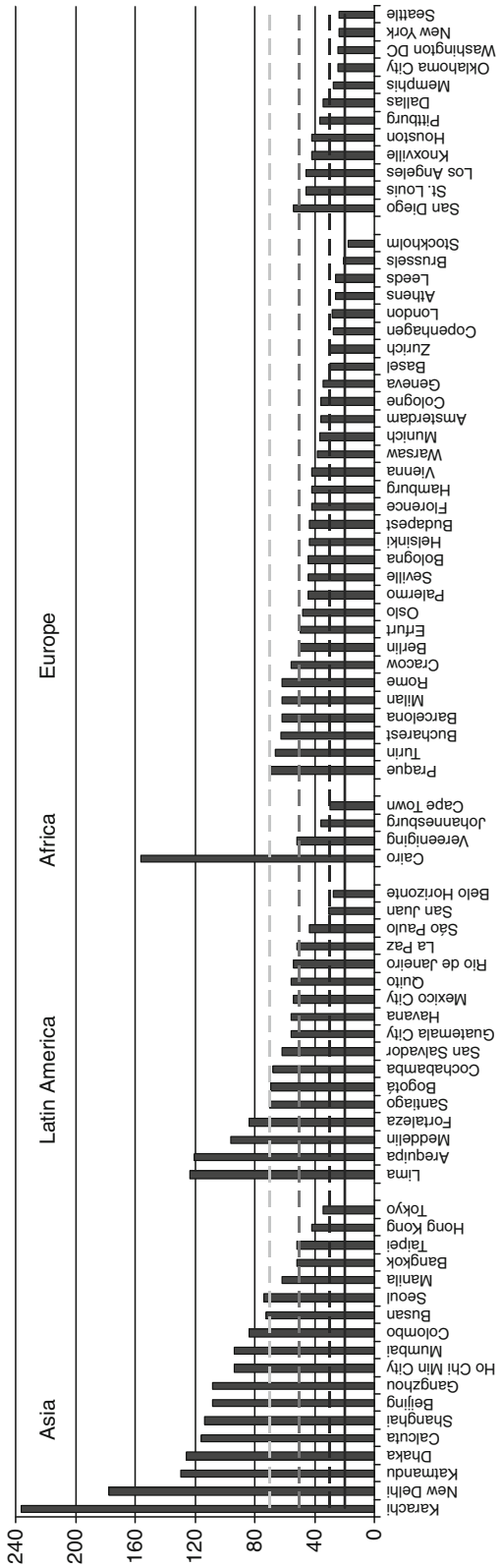

Urban Air Quality: Sources and Concentrations. Figure 7

PM_{10} concentrations ($\mu g\ m^{-3}$) in selected large cities throughout the world. The plot has been derived on basis of WHO (2006) [1]. The WHO Air Quality Guideline (AQG) (shown in the figure) is defined at the lowest level at which total, cardiopulmonary and lung cancer mortality has been shown to increase with more than 95% confidence in response to long-term exposure. Shown also are the WHO interim target values 1–3

of the persistent toxic substances in central and northeast Asia under the Stockholm Convention (UNEP, 2002). It has been demonstrated that transformation processes can lead to PAHs that are more toxic than their precursors [57].

The source apportionment of particulate PAHs at Seoul, Korea, during a measurement campaign between August 2002 and December 2003 were analyzed [60] by applying the US EPA (2004) chemical mass balance (CMB) model. Seoul is in the atmospheric footprint of major coal-burning industries and power plants of China and Japan, as well as contributing itself to the Northeast Asia particle footprint. In Seoul, similar to MCMA, gasoline and diesel vehicles accounted for 31% of the measured PAHs and thus were the major sources. Daily and seasonal variations were noted and attributed to differences in biomass burning and coal (heating) with a 19% difference in the total concentrations observed between fall (63%) and winter (82%). The sources showed an inverse profile when moving away from the city. The study authors used source analysis to attribute this to the long-range transport of atmospheric pollutant (LRTAP) of PAHs and their precursors from sources in China or North Korea thus demonstrating that for certain urban environments, in footprints of major industrial areas, PAHs from local and long-range transport must be taken into greater consideration as air quality management plans are updated.

Trace Elements to Include Heavy Metals in Urban Areas

Trace elements including heavy metals (HMs) are ubiquitous in the atmosphere of urban areas and many are classified by authorities as hazardous air pollutants (HAPs).

These represent serious environmental and health risks and are especially of concern in urban and industrial climates, with megacities in developing nations being the obvious sites of concern for populations at risk for trace element exposure.

Air quality can be affected and trends in urban areas have been noted. One study has provided trends and levels of trace metals in three Danish cities as well as at background sites [61]. The levels reported are less than literature values for megacities, as expected, but in many cases the trends are similar, though the numbers of studies are very limited.

Heavy Metals in the Urban Atmosphere

Heavy metals are still a problem for ambient and indoor air quality, especially in general in urban and industrial areas despite that many nations have tightened and continue to restrict emissions of such trace elements as mercury. Even with history of progressive regulation of trace metals, they still represent a real and pressing health and environmental hazard in the United States (US EPA, 2006) and most certainly in other western nations and other countries as well. Trace metals have been measured in nearly all aerosol size fractions so it is of paramount importance to characterize the particle size distribution and relate these to the potential adverse health effects in the urban population [62].

Humans are exposed to metals via ambient air inhalation, and consuming contaminated food or water, as well as, in the case of lead and children, chewing on lead-painted toys, and exposure from walls or furniture. Metals were of great concern in western cities prior to lead being banned as an anti-knock agent in gasoline in the mid-1970s, as well as other regulations regarding the use of lead in, for example, house paints.

The United States Environmental Protection Agency (US EPA) lists many trace metals as among the worst urban air toxics (www.epa.gov/ttn/atw/nata/34poll.html, November 28, 2008) and several metals aside from mercury and lead are classified by the United States Clean Air Act as HAPs: chromium, manganese, nickel, and cadmium. There is no reason that other countries should not also endorse this classification in their air quality plans.

Trace Elements in the Urban Atmosphere

Trace elements (and metals) and the observed high levels of them in the urban environment have led to extensive monitoring with consequential regulations and international agreements that have greatly reduced the concentrations.

The sources of emission into the urban atmosphere of commonly measured trace elements: Be, Co, Hg,

Mo, Ni, Sb, Se, Sn, and V, with smaller concentrations of As, Cr, Cu, Mn, and Zn, are primarily human activities, especially the combustion of fossil fuels and biomass, industrial processes, and waste incineration [62].

As with PAHs, there are seasonal variations of trace metals in PM_{10} and $PM_{2.5}$ observed in campaigns conducted seasonally. Higher winter values of nearly all trace elements are observed suggesting a significant source of particles from domestic heating in most temperate urban areas, and/or less efficient dispersion of emissions in winter.

Many trace elements are primarily observed from natural sources and have local, regional, and global effects. Sources include sea spray near coastlines, dust from aeolian processes and weathering (especially noted in Asia), and volcanoes.

The main source of trace elements in most urban environments are nevertheless, anthropogenic activities, and national regulations, especially with regard to limits in gasoline, and emissions from coal-fired power plants, as well as other industrial control are in most cases effective in mitigating their emissions. Thus, developing nations generally have higher levels in general than industrialized nations.

Conclusions

Urban air quality is subjectively determined based on levels mandated generally by law. It is a function of a complex and dynamic mixture of gaseous and particulate pollutants emitted from natural and human environments and their interaction with natural and built environment. The concentration of pollutants both produced in photochemical reactions and suspended in the air of the urban environment and therefore air quality is weather dependent and thus exhibits daily and seasonal variation due to both anthropogenic and biologic activity levels and weather conditions.

The actual pollution load in a given urban area is the result of both local conditions and emissions and transport from nearby and remote sources. The location of the city is very important for the local dispersion conditions, which are governed by meteorology but are also heavily affected by topographical conditions (e.g., effects of coastline, mountains, and valleys).

Studies of the impact of transportation hubs such as local harbors and airports on urban air quality have generally pointed at a limited influence, with the impact on the air quality mainly related to the road traffic that these facilities are generating.

The highest urban air pollutant concentrations of the pollutants PM_{10} and SO_2 are generally found in developing urban environments such as those in Africa, Asia, and Latin America.

The highest levels of photochemical pollutants such as O_3 and NO_2 are observed in Latin America and certain developed countries – topographical conditions and weather conditions are very important factors in this respect.

The negative health effects of urban air pollution are well documented and are found to be particularly severe in the megacities, where quality of life is lessened due to air pollution. The interaction of poor air quality with other lifestyle decisions such as smoking generally results in a synergistic effect. The negative health effects of poor ambient air quality are likely enhanced by exposure to tobacco smoke, indoor particulate and gaseous sources from cooking, candles, stoves, etc., but also by exposures to the non-airborne agents in textiles, food, etc. The possibility of reduced productivity from toxics and their associated costs should be investigated and valuation models should be further developed [5].

Even though the health effects of poor urban air quality have been documented in numerous studies, there are still many unknowns and through their investigation, there is a possibility for improving health, environment, and the climate. The reader is referred to Hertel and Goodsite, 2009 [66] – from which this entry was based; as well as the supplemental literature list where recent reviews across various aspects of the field of urban air quality are included.

Future Directions

The European programme Integaire (see www.integaire.org: Integaire was established in March 2002 under the key action "City of Tomorrow and Cultural Heritage" of the European Fifth Framework of Research Programme) made extensive recommendations (http://www.integaire.org/project/Integairere-searchrecommendations%5B2%5D.pdf) still valid

today as a way forward. These recommendations, along with those addressed with the article are required future directions on the development of Urban Air Quality science.

Integaire's recommendations have been summarized below, combining them into fewer points where convenient.

1. Quantify sources of particulate matter for example resuspension of dust may contribute significantly, but it cannot be quantified.
2. Investigate the health effects of particulate matter and methods to demonstrate how PM relates to citizens' health should be developed. Especially $PM_{2.5}$ should be monitored.
3. Assess the impact of local policies on climate change and vice versa. Some local air quality measures, in particular many emission reduction measures, are known to reduce the greenhouse effect too, but there are also local measures to reduce air pollution that have a negative effect on greenhouse gas emissions – these dynamics must be investigated.
4. Investigate the possibilities of cleaner vehicles and alternative fuel.
5. Quantify the emissions of traffic as a function of engine conditions and traffic behavior.
6. Study possibilities for controlling particulate matter and NO_2.
7. Improve the insight in the effect of buildings on hot spot concentrations.
8. Improve the possibilities of improving horizontal integration of air, water, soil, and waste policies. Strategies across these management areas must be harmonized.
9. Continue to improve insight into photochemical air pollution.
10. Develop more knowledge on the reliability of air pollution, air quality as well as air transport and deposition models, including validation procedures. Urban air quality models need to be developed and operationalized with the manager in mind, that is, results developed with the regulator in mind, integrating measurements and model results. Tools for valuation need to continue to be developed and integrated into the models.
11. Clarify and give more guidance on PM_{10} and $PM_{2.5}$ monitoring.
12. Develop methods for taking "soft" aspects (communication, attitudes, and participation as well as management governance structures) into account.

Given the number and complexity of the above challenges, it is also important that educational programmes and efforts to develop the air quality scientists and managers of tomorrow are increased.

There is an urgent need for field studies dedicated to a better characterization of urban particle pollution together with studies focusing at gaseous and particulate PAHs and trace elements such as heavy metals. Such studies are needed for the full assessment of the health impact on the urban population and for providing the necessary basis for future urban air pollution management. Of the pollutants dominating urban air pollution climates, particulate pollution in general together with gaseous and particulate polycyclic aromatic hydrocarbons (PAHs) and heavy metals are those where further field measurements, characterization, and laboratory studies are urgently needed in order to fully assess the health impact on the urban population and provide the right basis for future urban air pollution management.

PAHs in the urban atmosphere as well as their transformation, transport, and conversion are urgently needed to be studied. Although air quality of megacities and urban areas in most cases fall within the jurisdiction of local governments, the studies provide compelling evidence that effort at international levels to regulate LRTAP must specifically look at PAHs and their precursors. This will require an international, strategic joint collaboration among Asia, Europe, and North America to investigate these complicated mechanisms and analyze the data.

With respect to air quality models, the authors of a regional model for atmospheric photochemistry and particulate matter applied to predict the fate and transport of lead, manganese, total chromium, nickel, and cadmium, over the continental United States during January and July 2001 [63] recommend research to improve the model results on emission data for aerial suspension of particles and biomass burning. They further cite the need to better quantify anthropogenic emissions of chromium, nickel, and cadmium [in the

US National Emission Inventory (NEI)]. It is our opinion that their recommendations are valid for most NEI, which are necessary management tools for air quality policy development.

Bibliography

Primary Literature

1. Bell ML, Davis DL, Fletcher T (2003) Environ Health Perspect 112:6–8
2. WHO (2006) WHO Air quality guidelines for particulate matter, ozone, nitrogen dioxide and sulfur dioxide – summary of risk assessment. WHO, Geneva
3. UNFPA (2007) UNFPA State of World Population 2007 – unleasing the potential of urban growth. UNFPA, Geneva
4. Hertel O, de Leeuw FAAM, Raaschou-Nielsen O, Jensen SS, Gee D, Herbarth O, Pryor S, Palmgren F, Olsen E (2001) Pure Appl Chem 73:933–958
5. Hylander LD, Goodsite ME (2006) Sci Total Environ 368:352–370
6. Berkowicz R, Kunzli F, Kaiser R, Medina S, Studnika M, Chanel O, Filliger P, Herry M, Horak F, Puybonnieux-Texier V, Quenel P, Schneider J, Reethaler R, Vergnaud JC, Sommer H (2000) Environ Monit Assess 65:259–267
7. Kunzli N et al (2000) Public-health impact of outdoor and traffic-related air pollution: a European assessment. Lancet 356:795–801
8. Gros V, Sciare J, Yu T (2007) CR Geosci 339:764–774
9. Smith KK et al (2004) Indoor air pollution from household use of fossil fuels. WHO, Geneva
10. Gurjar BR, Lelieveld J (2005) Atmos Environ 39:391–393
11. Chan CK, Yao X (2008) Atmos Environ 42:1–42
12. Gurjar BR, Butler TM, Lawrence MG, Lelieveld J (2008) Atmos Environ 42:1593–1606
13. Crecelius HJ, Sommerfeld M (2005) Gefahrstoffe Reinhalt Luft 65:49–54
14. Suppan P, Graf J (2000) Int J Environ Poll 14:375–381
15. Farias F, ApSimon H (2006) Environ Model Softw 21:477–485
16. Corbett JJ et al (2007) Environ Sci Technol 41:8512–8518
17. Marr IL, Rosser DP, Meneses CA (2007) Atmos Environ 41:6379–6395
18. Wang HB, Shooter D (2002) Atmos Environ 36:3519–3529
19. Hedberg E, Johansson C (2006) J Air Waste Manag Assoc 56:1669–1678
20. Sexton K, Liu KS, Hayward SB, Spengler JD (1985) Atmos Environ 19:1225–1236
21. Maykut NN, Lewtas J, Kim E, Larson TV (2003) Environ Sci Technol 37:5135–5142
22. Glasius M, Ketzel M, Wåhlin P, Bossi R, Stubkjær J, Hertel O, Palmgren F (2008) Atmos Environ 42:8686–8697
23. Vignati E, Berkowicz R, Hertel O (1996) Sci Total Environ 190:467–473
24. Eliasson I, Holmer B (1990) Theo App Climatol 42:187–196
25. Rigby M, Toumi R (2008) Atmos Environ 42:4932–4947
26. Berkowicz R, Palmgren F, Hertel O, Vignati E (1996) Sci Total Environ 190:259–265
27. Palmgren F, Berkowicz R, Hertel O, Vignati E (1996) Sci Total Environ 190:409–415
28. Brauer M, Hoek G, van Vliet P, Meliefste K, Fischer PH, Wijga A, Koopman LP, Neijens HJ, Gerritsen J, Kerkhof M, Heinrich J, Bellander T, Krunekreef B (2002) Am J Respir Critic Care Med 166:1092–1098
29. Carslaw DC, Beevers SD (2005) Atmos Environ 39:167–177
30. Beddows DCS, Beddows MCS, Donovan RJ, Harrison RM, Kinnersley RP, King MD, Nicholson DH, Thompson KC (2004) J Environ Monit 6:124–133
31. Harrison RM, Jones AM, Lawrence RG (2004) Atmos Environ 38:4531–4538
32. Wåhlin P, Berkowicz R, Palmgren F (2006) Atmos Environ 40:2151–2159
33. Salcedo D, Onasch TB, Dzepina K, Canagaratna MR, Zhang Q, Huffman JA, DeCarlo PF, Jayne JT, Mortimer P, Worsnop DR, Kolb CE, Johnson KS, Zuberi B, Marr LC, Volkamer R, Molina LT, Molina MJ, Cardenas B, Bernabe RM, Marques C, Caffney JS, Marley NA, Laskin A, Shutthanandan V, Xie Y, Brune W, Lsher R, Shirley T, Jimenez JL (2006) Atmos Chem Phys 6:925–946
34. Viana M, Kuhlbusch TAJ, Querol X, Alastuey A, Harrison RM, Kopke PK, Winiwarter W, Vallius A, Szidat S, Prevot ASH, Heuglin C, Bloemen H, Wåhlin P, Vecchi R, Miranda AI, Kasper-Giebl A, Maenhaut W, Hitzenbergerq R (2008) J Aerosol Sci 39:827–849
35. Harrison RM, Shi JP, Xi SH, Khan A, Mark D, Kinnersley R, Yin JX (2000) Philos Trans R Soc Lond A Math Phys Eng Sci 358:2567–2579
36. Løndahl J, Pagels J, Swietlicki E, Zhou JC, Ketzel M, Massling A, Bohgard M (2006) J Aerosol Sci 37:1152–1163
37. Harrison RM, Yin JX (2008) Atmos Environ 42:1413–1423
38. Peters A, Wichmann HE (2001) Epidemiol 12:S97
39. Harrison RM, Yin JX (2000) Sci Total Environ 249:85–101
40. Ketzel M, Wåhlin P, Kristensson A, Swietlicki E, Berkowicz R, Nielsen OJ, Palmgren F (2004) Atmos Chem Phys 4:281–292
41. Harrison RM, Tilling R, Romero MSC, Harrad S, Jarvis K (2003) Atmos Environ 37:2391–2402
42. Berkowicz R (2000) Environ Monit Assess 65:323–331
43. Ketzel M, Berkowicz R (2004) Modelling the fate of ultrafine particles from exhaust pipe to rural background: an analysis of time scales for dilution, coagulation and deposition. Atmos Environ 38:2639–2652
44. Ketzel M, Omstedt G, Johansson C, During I, Pohjolar M, Oettl D, Gidhagen L, Wahlin P, Lohmeyer A, Haakana M, Berkowicz R (2007) Estimation and validation of PM2.5/PM10 exhaust and non-exhaust emission factors for practical street pollution modelling. Atmos Environ 41:9370–9385
45. Baek BH, Aneja VP (2004) J Air Waste Manag Assoc 54:623–633
46. Pakkanen TA, Kerminen VM, Hillamo RE, Makinen M, Makela T, Virkkula A (1996) J Atmos Chem 24:189–205
47. Pakkanen TA (1996) Atmos Environ 30:2475–2482

48. Schneider T, Jensen KA, Clausen PA, Afshari A, Gunnarsen L, Wåhlin P, Glasius M, Palmgren F, Nielsen OJ, Fogh CL (2004) Atmos Environ 38:6349–6359
49. International Agency for Research in Cancer (1983) IARC monographs on the evaluation of the carcinogenic risk of chemicals to humans. WHO, International Agency for Research in Cancer, Geneva
50. ATSDR (1995) Toxicological profile for polycyclic aromatic hydrocarbons (PAHs). Department of Health and Human Services, Public Health Service, Atlanta
51. Hanigan IC, Johnston FH, Morgan GG (2008) Environ Health 7:42
52. Denissenko MF, Pao A, Tang MS, Pfeifer GP (1996) Science 274:430–432
53. Molina LT, Kolb CE, de Foy B, Lamb BK, Brune WH, Jimenez JL, Ramos-Villegas R, Sarmiento J, Paramo-Figueroa VH, Cardenas B, Gutierrez-Avedoy V, Molina MJ (2007) Atmos Chem Phys 7:2447–2473
54. Ravindra K, Sokhi R, Van Grieken R (2008) Atmos Environ 42:2895–2921
55. Perwak J, Byrne M, Coons S, Goyer M, Harris J, Cruse P, Derosier R, Moss K, Wendt S (1982) Exposure and risk assessment for Benzo(a)pyrene and other polycyclic aromatic hydrocarbons, vol 4. US Environmental Protection Agency Office of Water Regulations and Standards, Washington, DC
56. Hazardous Substances Data Bank (HSDB) (1994) National Library of Medicine, National Toxicology Program (via TOXNET) http://www.nlm.nih.gov/pubs/factsheets/hsdbfs.html, specifically as linked in the previous to http://toxnet.nlm.nih.gov/. Accessed 3 February 2011
57. Marr LC, Dzepina K, Jimenez JL, Reisen F, Bethel HL, Arey J, Gaffney JS, Marley NA, Molina LT, Molina MJ (2006) Atmos Chem Phys 6:1733–1745
58. Dzepina K, Arey J, Marr LC, Worsnop DR, Salcedo D, Zhang Q, Onasch TB, Molina LT, Molina MJ, Jimenez JL (2007) Int J Mass Spectrom 263:152–170
59. Jang C, Lee J (2005) Proc Inst Mech Eng D J Automobile Eng 219:825–831
60. Lee JY, Kim YP (2007) Atmos Chem Phys 7:3587–3596
61. Kemp K (2002) Nucl Instrum Meth Phys Res Sec B Beam Interact Mater Atoms 189:227–232
62. Rajsic S, Mijic Z, Tasic M, Radenkovic M, Joksic J (2008) Environ Chem Lett 6:95–100
63. Hutzell WT, Luecken DJ (2008) Sci Total Environ 396:164–179
64. Hertel O, Ellermann T, Palmgren F, Berkowicz R, Løfstrøm P, Frohn LM, Geels C, Skjøth CA, Brandt J, Christensen J, Kemp K, Ketzel M (2007) Environ Chem 4:65–74
65. Hertel O, Jensen SS, Hvidberg M, Ketzel M, Berkowicz R, Palmgren F, Wåhlin P, Glasius M, Loft S, Vinzents P, Raaschou-Nielsen O, Sørensen M, Bak H (2007) Assessing the impact of traffic air pollution on human exposures and linking exposures to health effects. In: Jensen-Butler C, Sloth B, Larsen MM, Madsen B, Nielsen OA (eds). Road Pricing, the Economy and the Environment, Series: Advances in Spatial Science, Springer, Berlin, p 425
66. Hertel O, Goodsite ME (2009) Urban air pollution climates throughout the world. In: Hester RE, Harrison RM (eds) Air quality in urban environments, vol 28. RSC, Cambridge, UK, pp 1–22

Books and Reviews

Anderson LG (2009) Ethanol fuel use in Brazil: air quality impacts. Energy Environ Sci 2(10):1015–1037

Chan CK, Yao X (2008) Air pollution in mega cities in China. Atmos Environ 42(1):1–42

Cimino-Reale G et al (2008) Toxicogenomic study of indoor and outdoor air chemical mixtures. Fresenius Environ Bull 17.9B:1485–1491

Colbeck I, Nasir ZA, Ali Z (2010) The state of ambient air quality in Pakistan-a review. Environ Sci Pollut Res 17(1):49–63

Deguen S, Zmirou-Navier D (2010) Social inequalities resulting from health risks related to ambient air quality-A European review. Eur J Public Health 20(1):27–35

Ebi KL, McGregor G (2008) Climate change, tropospheric ozone and particulate matter, and health impacts. Environ Health Perspect 116(11):1449–1455

El-Fadel M, bi-Esber L (2009) In-vehicle exposure to carbon monoxide emissions from vehicular exhaust: a critical review. Critic Rev Environ Sci Technol 39(8):585–621

Farmaki EG, Thomaidis NS (2008) Current status of the metal pollution of the environment of Greece – a review. Glob Nest J 10(3):366–375

Goyal SK et al (2006) Understanding urban vehicular pollution problem vis-a-vis ambient air quality – case study of a megacity (Delhi, India). Environ Monit Assess 119(1–3):557–569

Gros V, Sciare J, Yu T (2007) Air-quality measurements in megacities: focus on gaseous organic and particulate pollutants and comparison between two contrasted cities, Paris and Beijing. CR Geosci 339(11–12):764–774

Hidalgo J et al (2008) Advances in urban climate modeling. Trends Dir Climate Res 1146:354–374

Holmes NS, Morawska L (2006) A review of dispersion modelling and its application to the dispersion of particles: an overview of different dispersion models available. Atmos Environ 40(30):5902–5928

Jacob DJ, Winner DA (2009) Effect of climate change on air quality. Atmos Environ 43(1):51–63

Just J et al (2007) Air pollution and asthma in children. Rev Fr D Allergol D Immunol Clin 47(3):207–213

Kanda M (2007) Progress in urban meteorology: a review. J Meteorol Soc Jpn 85B:363–383

Kindzierski WB et al (2009) Automotive wastes. Water Environ Res 81(10):1545–1568

Krewski D, Rainham D (2007) Ambient air pollution and population health: overview. J Toxicol Environ Health A 70(3–4):275–283

Kuykendall JR et al (2009) Chemicals present in automobile traffic tunnels and the possible community health hazards: a review of the literature. Inhal Toxicol 21(8–11):747–792
Liu Y et al (2009) Review of the applications of multiangle imaging spectroradiometer to air quality research. Sci China, Ser D Earth Sci 52(1):132–144
Mejia JF, Morawska L (2009) An investigation of nucleation events in a coastal urban environment in the Southern Hemisphere. Atmos Chem Phys 9(20):7877–7888
Morawska L et al (2008) Ambient nano and ultrafine particles from motor vehicle emissions: characteristics, ambient processing and implications on human exposure. Atmos Environ 42(35):8113–8138
Nuvolone D, Barchielli A, Forastiere F (2009) Assessing the effectiveness of local transport policies for improvements in urban air quality and public health: a review of scientific literature. Epidemiol Prev 33(3):79–87
Ooi GL (2007) Urbanization in Southeast Asia – assessing policy process and progress toward sustainability. J Ind Ecol 11(2):31–42
Paoletti E (2009) Ozone and urban forests in Italy. Environ Pollut 157(5):1506–1512
Ravindra K, Sokhi R, Van Grieken R (2008) Atmospheric polycyclic aromatic hydrocarbons: source attribution, emission factors and regulation. Atmos Environ 42(13):2895–2921
Rodriguez S et al (2007) Atmospheric particulate matter and air quality in the Mediterranean: a review. Environ Chem Lett 5(1):1–7
Sarnat JA, Holguin F (2007) Asthma and air quality. Curr Opin Pulm Med 13(1):63–66
Sidiropoulos C, Tsilingiridis G (2009) Improved sectoral allocation of NMVOC emissions from solvent use in Greece. Sci Total Environ 407(13):4075–4083
Sitaras LE, Siskos PA (2008) The role of primary and secondary air pollutants in atmospheric pollution: Athens urban area as a case study. Environ Chem Lett 6(2):59–69
van den Elshout S, Leger K, Nussio F (2008) Comparing urban air quality in Europe in real time – a review of existing air quality indices and the proposal of a common alternative. Environ Int 34(5):720–726
Vardoulakis S et al (2007) Operational air pollution modelling in the UK – street canyon applications and challenges. Atmos Environ 41(22):4622–4637
Vautard R et al (2007) Air quality in Europe during the summer of 2003 as a prototype of air quality in a warmer climate. CR Geosci 339(11–12):747–763
Whitehead PG et al (2009) A review of the potential impacts of climate change on surface water quality. Hydrol Sci J J Sci Hydrol 54(1):101–123
Yearley S (2006) Bridging the science – policy divide in urban air-quality management: evaluating ways to make models more robust through public engagement. Environ Plann C Gov Policy 24(5):701–714
Zhang JJ, Smith KR (2007) Household air pollution from coal and biomass fuels in China: measurements, health impacts, and interventions. Environ Health Perspect 115(6):848–855

Urban Atmospheric Composition Processes

William Bloss
School of Geography, Earth & Environmental Sciences, University of Birmingham, Birmingham, UK

Article Outline

Glossary
Definition of the Subject
Introduction
Historical Perspective
Meteorology, Dynamics and Mixing
Basic Composition and Key Pollutants
Key Emission Characteristics
Urban Atmospheric Composition Processes
Trends in Urban Atmospheric Composition
Future Directions
Bibliography

Glossary

Boundary layer The lowermost layer of the atmosphere, in contact with the surface and well mixed. Extending from 100 to 200 m at night, up to 1–2 km during the day.

Mixing ratio The fraction of the air which a given species comprises, typically parts per million (10^6), billion (10^9) or trillion (10^{12}), by volume.

NO_x The sum of nitric oxide (NO) and nitrogen dioxide (NO_2).

NO_x limited The ozone production regime in which VOCs are (relatively) plentiful, and ozone production is limited by the availability of NO_x.

Photostationary steady state The rapid chemical/photochemical balance between a number of reactants, usually applied to NO, NO_2 and O_3.

PM_{10} Suspended airborne particulate matter, with an aerodynamic diameter of 10 μm or less.

Primary pollutants Those emitted directly to the atmosphere, typically from mechanical or combustion processes.

Secondary pollutants Those formed within the atmosphere by chemical reactions.

Street canyon The semi-isolated atmospheric compartment formed by adjacent rows of multi-story buildings.

Temperature inversion An increase in temperature with increasing altitude, which usually isolates ground-level air from the overlying atmosphere, resulting in increased (primary) pollutant concentrations.

Transboundary pollution The transport of long-lived chemical species, such as O_3 and CO, across national boundaries.

VOC Volatile Organic Compound, one commonly found overwhelmingly in the gas phase.

VOC limited The ozone production regime where NO_x is plentiful, and ozone production is limited by the availability of hydrocarbons.

Definition of the Subject

The majority of the population now live in cities (the 50% point was passed during 2007 [1]) and are exposed to the urban atmosphere every day of their lives. As global population has also doubled over the past 50 years, urban air quality is a major factor in pollutant exposure for billions of individuals. The urban atmospheric environment is unique, with the city landscape defining particular meteorological characteristics, and a wide range and high density of emission (or pollution) sources, which combine to determine local air quality. Air pollutants, ranging from gases such as carbon monoxide, ozone and nitrogen dioxide, to suspended particles of varying size and composition, have been shown to be linked to respiratory and cardiovascular health issues. Urban atmospheric composition processes affect the abundance of primary pollutants, and are wholly responsible for the formation of secondary species such as ozone. In this article, the principle urban atmospheric components and their sources are introduced, followed by an account of the predominant atmospheric composition (chemistry) processes which affect urban air quality. The article concludes with a brief consideration of the potential impacts of future changes in emissions, physical and political climates upon urban atmospheric composition.

Introduction

Increasing population density implies an increasing human exposure to urban atmospheric pollutants. Countering this basic trend, growing scientific understanding of atmospheric composition processes, coupled with technological developments in emissions control and policy measures to limit pollution, have led to improved urban air quality over the past several decades in many cities, although this conclusion is dependent upon the species measured and metric chosen. The predominant air quality conditions are therefore a strong function of the level of development of a city (Fig. 1), and have changed substantially over the past few decades, with (in many cases) the removal of heavy industry from urban regions, while traffic has

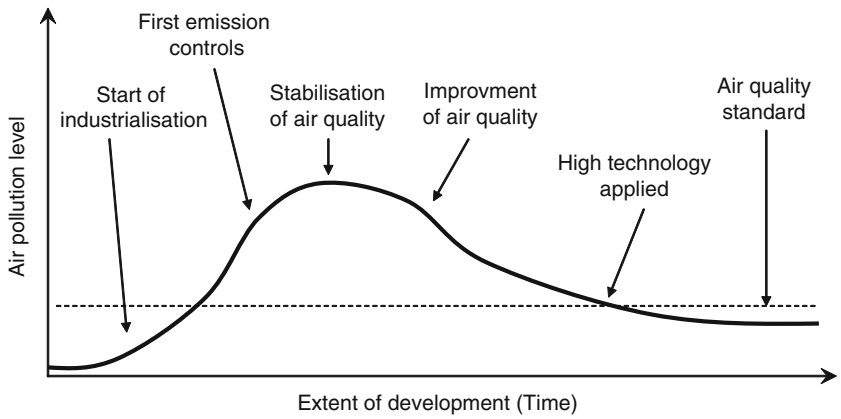

Urban Atmospheric Composition Processes. Figure 1
Schematic representation of the evolution of air pollution vs. development. Adapted from Fenger [2]/Mage et al. [3]

become the dominant emission source; the concept of urban atmospheric pollution thus varies in time, and between different cities across the world.

Historical Perspective

The history of urban atmospheric composition and air pollution reflects developments in fuel usage for domestic heating, cooking, emerging industrial activities and power generation, and the spread of the internal combustion engine. The earliest reports of atmospheric pollution issues, associated with the combustion of coal for domestic heating and cooking, and for industrial operations such as lime production, are noted in historical documents dating to at least the thirteenth century, when a Commission was established to address the problems associated with coal smoke in London. By the sixteenth or seventeenth century, some of the earliest proposals for "emission control legislation" such as John Evelyn's *Fumifugium* of 1661 were drafted for (unsuccessful) presentation to Parliament [4]. Increasing domestic and industrial coal combustion led to the London smogs of the nineteenth and twentieth centuries, in which the major pollutants were highly acidic particulates and fog droplets arising from use of high-sulfur fuels. Another prominent atmospheric pollution event of the time was the Donora Valley episode of 1948, in which local industrial emissions of sulfur dioxide, carbon monoxide and heavy metal particles were trapped in a week-long temperature inversion leading to tens of deaths and thousands suffering from respiratory illness. These events primarily concerned primary pollutants, those emitted directly to the atmosphere (although strictly speaking sulfuric acid is formed within the atmosphere following the release of sulfur dioxide). Subsequent legislation, mandating the use of tall chimneys to aid dispersion, use of low-sulfur and smokeless fuels in populated areas, the migration of heavy industry away from cities and the introduction of emissions control technologies and policies (including emissions trading schemes on the case of SO_2), have greatly reduced these pollution phenomena in many nations. Over the past 50 years, motor vehicle emissions have come to dominate urban atmospheric composition in most developed nations, as the global vehicle fleet has increased by an order of magnitude over this timeframe. In developing nations, combustion of biofuels (primarily wood) and coal for domestic cooking and heating remain major urban pollutant sources. Alongside the reduction in some of the traditional primary pollutants (sulfur dioxide, carbon monoxide), levels of secondary components formed in the atmosphere, such as ozone and (much of) nitrogen dioxide and particulate matter, have in many cases been rising, and have become the focus of concern.

Meteorology, Dynamics, and Mixing

The urban atmosphere may be defined horizontally by the extent of the particular city in question (see comments below regarding export of urban atmospheric pollutants), and vertically as encompassing the boundary layer, the first few 100 m to kilometer or so of the atmosphere, which is regarded as well mixed. The urban boundary layer height determines the size of the atmospheric compartment into which emissions are mixed – a lower boundary layer height (as commonly found at night) results in higher concentrations for an equivalent emission strength, all other things being equal. The urban boundary layer may be further divided into vertical regions determined by the interaction between the city topography and airflow: At the street scale, urban canyons, formed between rows of buildings, represent semi-isolated environments into which traffic-related emissions are initially discharged. The urban canopy layer encompasses multiple street canyons at rooftop level. Above the canopy layer, the overlying boundary layer is sometimes divided into the roughness sub-layer, where building wake-induced turbulence effects predominate and atmospheric composition (as far as it relates to urban emissions) is highly variable, and the higher inertial sub-layer which exhibits a more homogeneous composition [5].

Local wind speed and direction critically affect local pollutant levels – on a street canyon scale, winds perpendicular to the canyon may lead to the establishment of within-canyon vortices, leading to the upwind side of the canyon, at ground level, experiencing higher levels of primary pollutants (those from local traffic at least) – Fig. 2. Conversely, along-canyon wind effectively ventilates the ground-level emissions into the overlying boundary layer. While most pollutant levels fall with increasing windspeed as a consequence of

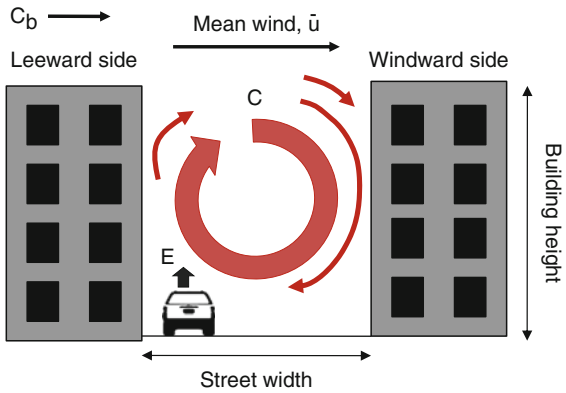

Urban Atmospheric Composition Processes. Figure 2 Typical within-canyon vortex circulation, driven by overlying perpendicular airflow, increases primary pollutant levels on the upwind (leeward) side of the street at ground level

increased dilution, re-suspension of coarse particulate matter (dust, sand, tyre, and brake debris) is found to increase atmospheric PM (particulate matter) levels at elevated windspeeds [6].

The ventilation of the urban airshed as a whole affects the pollutant levels experienced for a given emission source. Certain cities (notable examples include Mexico City, Santiago, Los Angeles) are partially to almost entirely surrounded by mountain ranges, leading to build-up of emissions within the (urban) boundary layer (e.g., Molina and Molina [7]). In other locations, regional weather patterns lead to persistent patterns of pollutant exposure, for example, the daily sea breeze circulation affecting Hong Kong and the Pearl River Delta [8]. Local circulation patterns and topography can therefore exacerbate, or ameliorate, the atmospheric composition resulting from a given emissions situation [9]; and the combined effects of local and regional scale dynamics, mixing and chemical transformations must be considered in the development of urban air quality management policies.

Basic Composition and Key Pollutants

The bulk atmospheric composition is essentially constant throughout the troposphere, comprising gases such as nitrogen, oxygen, argon, helium, carbon dioxide and a variable amount of water vapor. Most concern over urban atmospheric composition and air pollution arises from the trace components – gaseous constituents such as ozone, nitrogen oxides and volatile organic compounds, and suspended particulate material (PM) commonly referred to as aerosol (although strictly the term denotes both the condensed phase material and the gas it is suspended within).

Urban air pollution issues primarily relate to local emissions and the chemical processing of pollutants and natural atmospheric species which occurs on timescales of a few hours to a few days. This can be distinguished from the wider, regional impacts of air pollution (such as increasing background ozone levels, and the abundance of sulfate aerosol), although these also impact on the urban environment and are considered here. Global air pollution issues related to long-lived species such as CFC, HCFC and halon compounds contributing to stratospheric ozone depletion, and the climate-related issues associated with the global abundance of longer-lived greenhouse gases such as carbon dioxide and methane, are not discussed further here – although some urban air pollutants are also important greenhouse gases, for example, ozone. Table 1 gives typical abundances for key urban air components which would be found in the remote boundary layer, away from anthropogenic emission sources, and compares these with those observed in selected urban atmospheres. It should be noted that point measurements such as these may be representative of a local microenvironment only, rather than the wider city-scale environment – if cities do not have representative networks for air quality monitoring, this concern persists into reported pollution levels.

As understanding of the impact of air pollutants upon health has developed, various national and international air quality standards and targets have been established, by national governments, the European Union (EU), and the World Health Organization (WHO). Selected current standards for key urban pollutants are summarized in Table 2. These species – the gases nitrogen dioxide NO_2, ozone (O_3), carbon monoxide (CO), sulfur dioxide (SO_2), benzene (C_6H_6), 1,3-butadiene (C_4H_6), and polycyclic aromatic hydrocarbons (PAH), plus the integrated particulate matter (PM) measures PM_{10} and $PM_{2.5}$ (see below for definitions) are the focus of this chapter. An issue in comparing pollution levels is the differing units commonly used – measurements of trace gases for scientific

Urban Atmospheric Composition Processes. Table 1 Comparison of typical unpolluted boundary layer abundance of selected pollutants, and their equivalent levels in various urban centers. All concentrations expressed in μg m^{-3}

Species	Remote MBL	London: MR	London: NK	Beijing	Lagos
NO_2	0.04	98	37	66	95
O_3	58	18	34	109[b]	64
SO_2	0.2	7.7	1.9	53	186
CO	140	650	280	2,100	6,700
Benzene	0.01	1.3	–	13.4[a]	–
1.3-butadiene	<0.01	0.57	–	–	–
PM_{10}	–	27	17	161	228
$PM_{2.5}$	–	18	11	130[b]	–

Notes: Remote MBL (Marine Boundary Layer) data taken from the Cape Verde Atmospheric Observatory in the tropical Atlantic Ocean [10, 11] except SO_2, benzene, 1-3-butadiene from Mace Head. London NK (North Kensington) is an urban background site while London MR (Marylebone Road) is a roadside monitoring station on a congested major road. London data are annual averages (for 2010) taken from the UK Air Quality Archive (www.airquality.co.uk). PM data are TEOM FDMS measurements. Beijing data are averages across the city for 2006, as given by [12] except (a): [13] and (b) [14]. Lagos data are averages of several sites taken from [15] except O_3 from [16]

Urban Atmospheric Composition Processes. Table 2 (Selected) EU air quality limit values and WHO air quality guidelines. Values in μg m^{-3}

Species	EU	WHO
NO_2	40 (annual mean)	40 (annual mean)
O_3	120 (target, <25 times/year)	100 (8 h mean)
SO_2	124 (24 h mean, <3 times/year)	20 (24 h mean)
CO	10,000 (running 8 h mean)	10,000 (8 h mean)
Benzene	5 (annual mean)	–
1.3-butadiene	2.25 (UK, annual mean)	–
PM_{10}	40 (annual mean)	20 (annual mean)
$PM_{2.5}$	25 (2020 target)	10 (annual mean)

EU limits are those in force as of 2010; *target* values not legally binding. Additional limit values/future reductions also apply for some pollutants. WHO guidelines from 2005 update [17] except CO (1997 update)

purposes are frequently presented in terms of (volume) mixing ratio (vmr), in parts-per-million, billion or trillion (10^6, 10^9, and 10^{12}, respectively) while for PM, and for legislative purposes, concentration values (usually expressed as μg m^{-3}) are used. Conversion between these is straightforward but is also dependent upon the local temperature and pressure; care is needed as different standard conditions for the conversion are mandated by, for example, the EU (20°C) and the WHO (25°C). While mixing ratio units are commonly preferred for atmospheric chemistry research where gaseous species are concerned, as they are invariant to changes in temperature and pressure (i.e., air parcel transport), and preserve the stoichiometry of the

chemical reactions (i.e., the relationship between reactants and products), here mass concentration units are used for consistency and ease of comparison with air quality standards.

Key Emission Characteristics

Ambient urban air pollutant emissions in most developed regions are primarily associated with vehicle traffic – direct exhaust emissions from petrol (spark) and diesel (compression) powered vehicles, and mechanical sources such as brake and tyre erosion and road surface material and dust re-suspension from all vehicles. Fugitive emissions of fuel vapor from filling station operations are a further significant vehicle-related source of gaseous organic (hydrocarbon) air pollutants. Other significant sources include emissions from local point sources such as domestic and office heating, cooking, and industrial processes, in particular the use of solvents, paints and lubricants which may have a significant vapor pressure, and combustion processes. Large-scale industrial emissions associated with heavy industry (power generation, steel making, etc.) are not major contributors to general *urban* air quality issues in most developed nations, as the plants responsible have largely been removed from the city centers, and as readily identifiable point sources in most cases have their direct emissions scrubbed at source, for example, in the case of sulfur dioxide from coal-fired power stations. In urban regions within developing nations, which incorporate many of the fastest-growing megacities on the planet, a different picture of emission sources is observed; again vehicle emissions are a major contributor, although the fleet composition differs with typically older vehicles (i.e., conforming to less stringent, if any, emission regulations), reduced diesel prevalence and a greater contribution from small two-stroke (oil burning) powered two wheelers. Domestic heating and cooking, where this is primarily through wood burning, is a major contributor to urban atmospheric composition (and indeed to overall pollutant exposure, through indoor effects within the home).

Characteristics of Motor Vehicle and Domestic Fuel Emissions

Within internal combustion engine vehicles, emissions of a range of pollutants reflect the composition of the fuel and oil burnt, and the high-temperature decomposition of atmospheric oxygen and nitrogen leading to the production of nitrogen oxides. NO_x ($NO+NO_2$) at the tailpipe is conventionally assumed be partitioned (on average) into 95% NO and 5% NO_2, although there is some evidence that the direct fraction of NO_2 may be greater than this, and increasing across the fleet on average – in particular, for diesel-engined HGVs (heavy goods vehicles) [18]. Incomplete combustion leads to the production of carbon monoxide (CO), a vast range of hydrocarbons which may be gases (if they are sufficiently small and volatile) or may condense to form the organic component of exhaust particulates, as the exhaust gases cool. The introduction of catalytic converters has greatly reduced emissions of NO, CO and hydrocarbons (which are converted to N_2, CO_2 and H_2O) for petrol-engined vehicles, while diesel oxidation catalysts have reduced CO and hydrocarbon emissions from diesel engines. Increasingly stringent emissions regulations, such as the EURO-1 to EURO-5 EU series of emissions standards for various vehicle classes, have substantially reduced emissions per unit activity (at least within the parameters of the defined driving cycles), and (disregarding CO_2) the principal emission concerns from modern vehicles are NO_x and particulate matter, for which in both cases diesel engine emissions tend to be higher emitters. Exhaust PM in particular is known to incorporate toxic and carcinogenic components such as PAH and heavy metals, and (as new particles are formed through condensation/nucleation) to contribute substantially to the population of the smallest particles particularly associated with adverse health effects [19]. The introduction of biofuels (ethanol) in some markets (notably, South America) has been associated with increased emissions of aldehydes such as formaldehyde and acetaldehyde [20] which are toxic, and also potent radical precursors leading to photochemical smog formation (see below). Biofuel (wood and charcoal) combustion for domestic heating and cooking is a substantial source of pollutants within many homes in developing nations, leading to indoor air pollutant exposure, and forming a major emission source within urban regions. The relatively low temperatures commonly found lead to substantial emissions of carbon monoxide, black carbon (soot) and a range of trace compounds VOCs, oxygenated compounds and acids, including toxic

substances such as polycyclic aromatic hydrocarbons (PAHs), particularly within the organic component of the emitted particulate matter [21].

Urban Atmospheric Composition Processes

Gas-Phase Composition Processes

Gas-phase processes in urban environments are dominated by the oxides of nitrogen, (primarily) NO and NO_2, emitted directly from the exhausts of high-temperature (i.e., internal combustion engine) vehicles. Following emission, a number of gas-phase processes follow. In close proximity (within a few meters) to the tailpipe, NO levels may be sufficiently high before mixing and dilution that the NO-self-reaction, converting NO into NO_2, may occur:

$$NO + NO + O_2 \rightarrow 2NO_2 \quad (1)$$

However the dominant chemistry of NO_x in the urban environment is the interaction between NO, NO_2, and ozone. In daylight, these three species are very closely coupled by the $NO+O_3$ reaction, and the solar decomposition (photolysis) of NO_2:

$$NO + O_3 \rightarrow NO_2 + O_2 \quad (2)$$

$$NO_2 + h\nu \rightarrow NO + O \quad (3)$$

The O atoms formed through NO_2 photolysis rapidly and near-exclusively recombine with molecular oxygen (O_2) to form ozone (reaction 4), where M denotes the involvement of a third body, nitrogen or oxygen, which removes some of the excess energy from the nascent ozone molecule.

$$O + O_2 + M \rightarrow O_3 + M \quad (4)$$

As these reactions dominate the $NO/NO_2/O_3$ interconversion, it is possible to define two further quantities, NO_x ($=NO+NO_2$), and total oxidant O_x ($=NO_2+O_3$), which, in the absence of further processes, are conserved. NO_x and O_x provide useful metrics for assessing variations in the sum of NO and NO_2, and of NO_2 and O_3, without need to consider the partitioning between these species. The reaction of fresh, vehicle-emitted NO with O_3 reduces ozone levels in many urban areas compared with the surrounding regions, leading to an *urban decrement* in ozone (compare O_3 concentrations for the MR and NK sites in Table 1) – discussed further below.

The timescales of reactions 2 and 3 in the boundary layer under sunlit conditions is of the order of 1–2 min, while reaction 4 proceeds in milliseconds; consequently away from direct emission sources NO, NO_2 and O_3 are found in equilibrium defined by the Leighton Relationship [22]:

$$\frac{[NO_2]}{[NO]} = \frac{k_2[O_3]}{j_3}$$

where k_2 is the rate constant for the $NO+O_3$ reaction, and j_3 is the (solar radiation intensity-dependent) rate of photolysis of NO_2. It follows that for a given abundance of NO_x and O_3, in the absence of other processes, NO_x will exist primarily as NO_2 when light levels are lower (i.e., at dawn and dusk), while the NO fraction will maximize at midday. In practice the values of k_2 and j_3 are such that the NO_2:NO ratio is typically in the range 2–5 during the day – see Fig. 3.

NO_x is removed from the atmospheric system through chemical conversion to more stable species, which in turn are removed by deposition and by their uptake or incorporation into aerosol particles. During the day, NO_2 reacts with the OH radical, the gaseous oxidant which dominates the removal of many pollutants on a global scale, forming nitric acid, HNO_3. Nitric acid is then lost through dry deposition (i.e., contact with surfaces), wet deposition/rainout, and through uptake into aerosol particles (see below).

$$OH + NO_2 + M \rightarrow HNO_3 + M \quad (5)$$

The OH radical is formed primarily through sunlight-driven photolysis processes, so has a very low abundance at night; in the absence of sunlight, the NO_2 photolysis reaction also ceases, and a separate chain of reactions dominate NO_x:

$$NO + O_3 \rightarrow NO_2 + O_2 \quad (2)$$

$$NO_2 + O_3 \rightarrow NO_3 + O_2 \quad (6)$$

$$NO_2 + NO_3 + M \Leftrightarrow N_2O_5 + M \quad (7)$$

The nitrate radical, NO_3, is rapidly photolysed during the day, effectively suppressing reactions 6 and 7. At night however NO and NO_2 may be converted into N_2O_5 on a timescale of hours; N_2O_5 is then removed from the urban atmosphere through wet and dry deposition, and uptake into aerosol particles (it is also photolysed slowly during the day). In both cases,

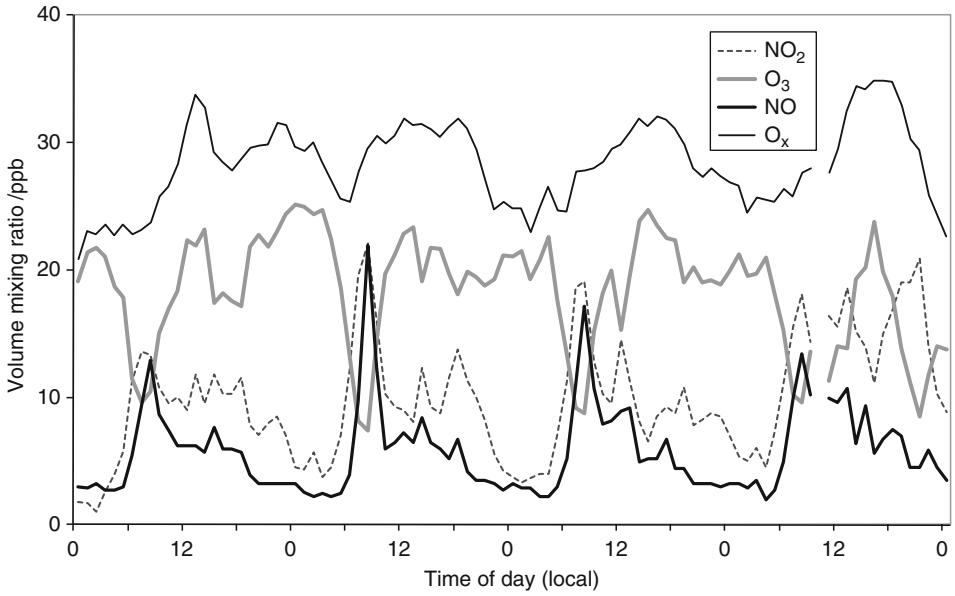

Urban Atmospheric Composition Processes. Figure 3
Diurnal variation in NO, NO_2, O_3, and O_x over a 4-day period for Birmingham City Centre; from Bloss [23]

following removal from the gas phase HNO_3 and N_2O_5 contribute to the nitrate (NO_3^-) content of aerosol particles (see below), and to the acidity of precipitation. The combination of reactions 5 and 7 determine a chemical lifetime for NO_x (strictly, time for concentrations to fall to 1/e of their initial value) of the order of 12–24 h in urban environments.

A further major air pollution consequence of the interaction of NO_x and VOCs in sunlight is the photochemical production of ozone, a major secondary pollutant. Figure 4, below, summarizes the major reaction processes responsible (after Wayne, [24]). The process is initiated by the production of an oxidant radical, OH, shown in Fig. 4 from the photolysis of ozone in the presence of water vapor (although other indirect sources also occur, e.g., aldehyde photolysis). OH radicals react with organic compounds (VOCs and CO) which leads to the formation of organic and hydro peroxy radicals, RO_2 and HO_2. In the absence of NO_2, these undergo self-reaction to form peroxides (not shown); however in the urban environment substantial levels of NO are usually present, and the peroxy radicals react with NO, converting it to NO_2, and

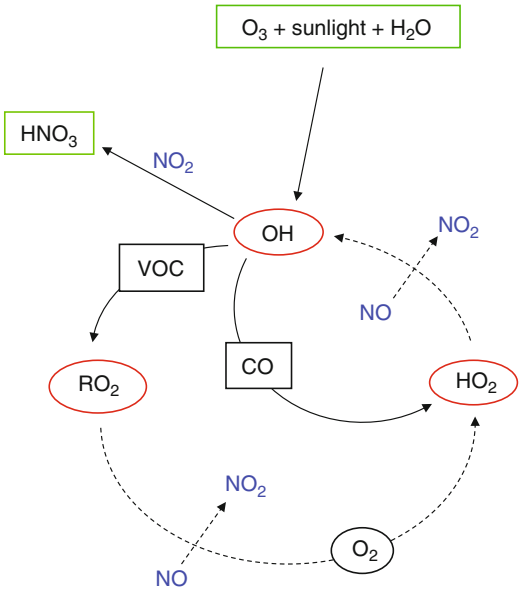

Urban Atmospheric Composition Processes. Figure 4
Some important steps in the gas-phase oxidation of volatile organic compounds (VOCs) in the presence of NO_x. The photolysis of NO_2 regenerates NO and leads to net ozone production

regenerating the radical species HO_2 and subsequently OH. The peroxy radical–NO reaction therefore leads to the conversion of NO to NO_2 without the consumption of O_3 (cf. reaction 2), and the subsequent photolysis of NO_2 and reaction of the O atom formed with molecular oxygen (reactions 3 and 4) results in ozone formation. While initiation of the process consumes ozone, the cyclical nature of the reactions leads to net ozone production overall.

The timescale of ozone production ranges from hours to days, but is complex to determine directly. In the boundary layer, ozone removal is dominated by deposition, however as the atmospheric lifetime of ozone is several days to weeks, advection (of ozone-rich or ozone-poor air from upwind locations) and atmospheric mixing also have a substantial influence upon measured ozone levels. Observed ozone pollution episodes vary in extent from hours in highly polluted conditions to a few days, and are closely associated with the prevailing weather conditions. In the case of Western Europe, ozone pollution events commonly correspond to summertime anticyclonic periods in which air masses have looped over Europe accumulating pollutants. Ozone is chemically formed along the airmass trajectory at rates of the order of 20–30 ppb per day (daytime chemical production, part of which is offset by night-time chemistry and deposition [25]). If a typical episode is characterized by ozone levels of the order of 90 ppb compared with the rural background of around 30–40 ppb, several days are clearly required to achieve this level. In more extreme conditions, ozone production proceeds more rapidly: during the 2003 Western Europe heatwave event, a photochemical model constrained by in situ observations of long-lived species from suburban North-East London determined the peak ozone production to be 17 ppb h^{-1}, with an average production rate during midsummer at midday of 7.2 ppb h^{-1} [26]. Observations in Mexico City have led to calculated ozone production rates of up to 50 ppb h^{-1} [27] during stagnant meteorological conditions.

Exposure to ozone has substantial human health consequences, being associated with irritation to eyes and nose, inflammatory reactions and reduced lung function. Ozone is also harmful to vegetation and ecosystems, and certain materials (erosion of polymers through reaction with component double bonds), and is an important greenhouse gas in its own right; consequently reduction in ozone levels is a major goal of air quality policy. The long lifetime of ozone limits the impact that local/national air quality legislation can have upon boundary layer ozone levels, and dictates that ozone is treated as a *transboundary* pollutant.

The secondary nature of ozone further complicates attempts to reduce its abundance: The precursor species, NO_x and VOCs, must be controlled; however the response of the chemical ozone production rate to the level of, for example, NO_x and CO is not straightforward: As can be seen from inspection of Fig. 3, at high NO_x levels, the reaction of OH with NO_2, forming HNO_3, can compete with the reaction of OH with VOCs. In this instance, reducing NO_x levels (e.g., through emission controls) would have the effect of increasing the abundance of OH, and the rate of the OH+VOC reactions, and hence would lead to an increase in ozone production. At lower NO_x levels, where NO_2 is not competing effectively with VOCs for OH, reduction in NO_x leads to a reduction in the ozone production rate, by reducing the rate of the peroxy radical–NO reaction (or strictly, by allowing other competing processes, not shown on Fig. 3, to occur – [24]). Two overall regimes for ozone production can be identified: VOC-limited, where NO_x levels are high, and ozone production rates will rise or fall with increase/decreases in VOC levels respectively, and NO_x-limited, where VOCs are relatively more abundant, NO_x levels low, and ozone levels rise and fall with increases/decreases in NO_x. Reduction of NO_x in a VOC-limited regime may lead to increased ozone production. Many urban environments correspond to VOC-limited conditions (i.e., higher NO_x levels); as air is advected from the urban centre to surrounding rural regions, with reduced emission sources, NO_x levels fall and the ozone production regime undergoes a transition to a NO_x-limited state. The complex dependence of the ozone production rate upon the abundance of primary pollutants between urban and rural areas, which is compounded by the reduction in ozone levels on the street canyon scale within

urban areas by the titration of O_3 to NO_2 by fresh vehicle NO emissions, presents a major challenge to the development of effective policy for mitigation of ozone pollution – see below.

Different organic compounds have differing potentials for ozone production (reflecting their chemical identity/size, and the rates of their reactions with oxidants such as OH), and of course are emitted in varying quantities. Metrics to rank species in terms of their contribution to ozone levels (such as Photochemical Ozone Creation Potentials, POCP values) have been developed to account for the integrated effect of these factors; in the case of the UK, the highest POCP values are assigned to tri-methylbenzene, however considering the mass-weighted emissions, the largest contributors to the ozone levels experienced are toluene and n-butane [28]. These values are specific to the UK case, that is, to the emissions, and in particular NO_x levels, typically experienced by an air parcel advected from continental Europe to southern Britain.

Peroxy acetyl nitrate (PAN, $CH_3C(O)OONO_2$) is the simplest example of a range of acetyl nitrate compounds, secondary pollutants which are the principal lachrymator (tear inducing) component of photochemical smog. PAN is formed from the reaction between peroxy acetyl radicals, $CH_3C(O)OO$, and NO_2, and in terms of the chemical cycling acts as a temporary reservoir for the HO_x and NO_x radicals involved in ozone production. A key feature of the equilibrium between PAN and its precursor species is the strong temperature dependence, with lower temperatures favoring PAN stability. A scenario which arises then is that PAN is formed in a polluted urban area, transported aloft (where temperatures are lower and PAN is stable) over long distances, before airmass descent and warming leads to PAN decomposition and release of the component NO_x in otherwise unpolluted regions.

Sulfur dioxide (SO_2) is possibly the classic air pollutant formed from the combustion of sulfur-containing fuels. SO_2 emissions have been successfully reduced in many regions, through a combination of the use of low sulfur fuels, and application of flue gas desulphurization technologies on major plants (e.g., power stations). Within the atmosphere, SO_2 is processed to H_2SO_4 on a timescale of days, both in the gas phase, initiated by reaction with the OH radical, and in the condensed phase, within water droplets, where the oxidation reactions are driven predominantly by hydrogen peroxide, H_2O_2. Gas phase sulfuric acid has a very low vapor pressure, and is readily incorporated into aerosol and condensation, raising PM acidity. More widely, co-condensation of H_2SO_4 with water vapor and/or ammonia leads to the production of new particles in the atmosphere.

Condensed Phase Composition Processes

Particulate matter is an important component of urban atmospheric composition, in particular where health effects are concerned. Sources of particulate matter include the local primary emissions from vehicles and combustion described above, including mechanical sources related to vehicle brake pad/disc, tyre and road surface wear, wider atmospheric inputs such as wind-blown dust and crustal material, and secondary contributions arising from the condensation of low-volatility gases to form new or (predominantly) contribute to the growth of existing particles.

Levels of particulate matter or aerosol are usually expressed as a mass concentration below a certain size; the size ranges commonly selected relating loosely to the extent to which particles penetrate the human respiratory system. PM_{10} and $PM_{2.5}$ define the fractions of suspended particulate matter with (aerodynamic) diameters below 10 and 2.5 μm respectively (the aerodynamic diameter is a concept used to allow for the varying morphology or shape of particles; a particle with an aerodynamic diameter of 1 μm will exhibit the same inertial properties as a sphere with a diameter of 1 μm and a density of 1 g cm^{-3} – irrespective of the actual size, shape or density of the particle). PM_{10} and $PM_{2.5}$ correspond approximately to size ranges which may be inhaled into the thoracic cavity (lungs) and into the alveolar regions respectively. The size distribution of urban particles typically exhibits several modes, reflecting the varying dominance of different processes responsible for particle formation and growth: The nucleation mode, below approximately 0.1 μm in diameter, where secondary particles are formed from the condensation of low-volatility gases (or, more commonly, condenses onto pre-existing particles); the accumulation mode (0.1–2.5 μm), where particles grow by condensation

and coagulation (collisions), but within which the mass is too small for gravitational setting to be a major sink (hence the size range where particles accumulate, until removal primarily by precipitation) and the coarse mode, which incorporates most mechanically generated particles, and within which gravitation settling begins to be a significant loss process. As simple geometric considerations show, the largest number of particles is found in the nucleation mode, while the mass is dominated by the coarse and accumulation modes. It is perhaps unfortunate then that most current air quality metrics focus upon particle mass concentration (PM_{10} or $PM_{2.5}$), while scientific evidence suggests that many human health impacts are related to exposure to the fine-mode particles which can penetrate most deeply into the alveolar structure.

Measurements of the composition of urban particulate matter are less common than total mass concentration, but a number of composition measurements are now performed routinely at a small number of sites in various countries. Within the sphere of such semi-routine monitoring, the (mass) contributions from sulfate, nitrate, ammonium, chloride and other elemental components may be determined, alongside the elemental and organic carbon fractions. Figure 5, below, shows the composition of $PM_{2.5}$ and PM_{10} in Birmingham city centre. Components which are apparent include iron and calcium components from crustal erosion, salt (sea-salt derived, possibly with some contribution from winter road salting), elemental carbon (essentially soot, from incomplete combustion; in these measurements, likely to arise almost entirely from diesel vehicles), organic compounds, ammonium bisulphate, ammonium nitrate and sodium nitrate. Of these, the ammonium, sulfate and nitrate components are likely to be largely secondary, arising from agricultural emissions, combustion of sulfur-containing fuels and the atmospheric processing of NO_x respectively (see above), while within the organic (carbon) fraction comprises elemental carbon (soot, likely primarily from diesel vehicles) and a substantial contribution from organic compounds.

Research-focused field measurements can disaggregate the organic fraction in more detail, and typically find that this is primarily secondary in origin (up to 64% in urban regions [30]), arising (in urban environments) largely from aromatic VOCs (e.g., benzene, toluene), which in turn are sourced primarily from vehicle emissions. As in the case of ozone, the substantial secondary component of urban particulate matter complicates air quality management and control. A component of particulate matter worth of further consideration is polycyclic aromatic hydrocarbons (PAH). Formed from two or more aromatic rings fused together, and produced from the incomplete combustion of coil, oil, petrol and wood, in particular

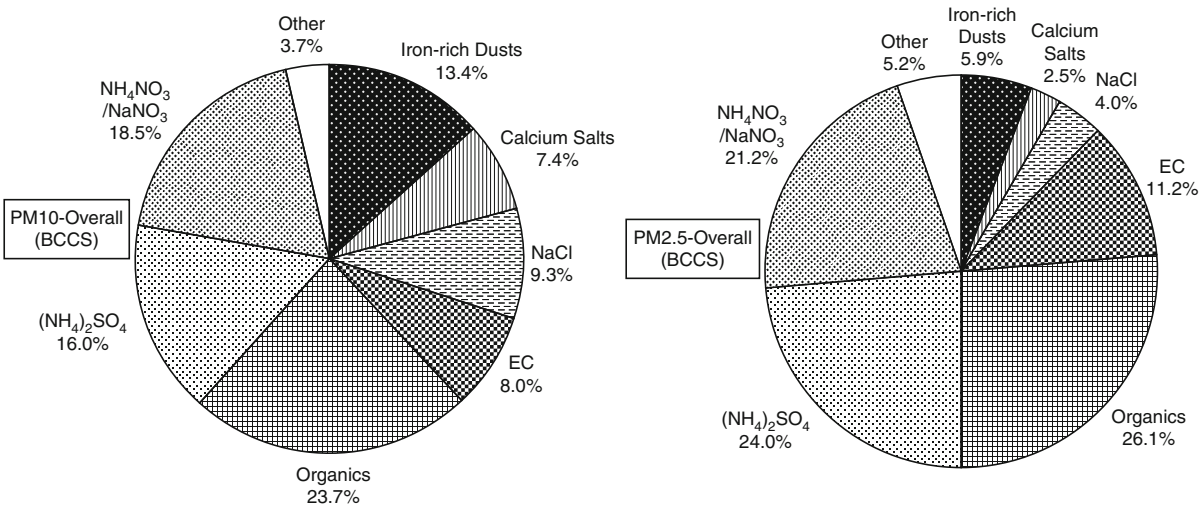

Urban Atmospheric Composition Processes. Figure 5
Chemical composition of particulate matter (PM_{10} and $PM_{2.5}$) from Birmingham City Centre. Data from Yin & Harrison [29]

domestic fuel usage, PAH are persistent bioaccumulative organic compounds; human exposure leads to a range of toxic and carcinogenic effects. One specific PAH, benzo-a-pyrene, is commonly used as a marker for the abundance of this family of compounds; the EU has established a target concentration of 1 ng m^{-3} for B[a]P by end of 2010, which may be compared with current (UK) levels of 0.16 ng m^{-3} (mean across all sites for 2006).

Trends in Urban Atmospheric Composition

This section concerns trends in the key urban atmospheric components over the forthcoming few decades. The trends observed reflect the integration of a number of independent effects: background levels of atmospheric components on a regional and global basis; changes in emissions of primary pollutants per unit activity (i.e., from improvements in vehicle technology and penetration of exhaust treatments such as catalytic converters through the vehicle fleet); and changes in the overall activity level, that is, increasing economic prosperity and population levels, particularly in many megacities in developing nations. A further external driver which may affect future urban composition is the interaction between atmospheric composition processes and global climate.

For the gaseous pollutants, the species of particular concern on an ongoing basis are nitrogen oxides (specifically NO_2 as this is the NO_x component against which legislation is commonly framed) and ozone. Of the other regulated pollutants (Table 2), sulfur dioxide levels are falling as the intensive sources (power and heavy industry) have emissions controlled at source and carbon monoxide levels have greatly reduced with the advent of catalytic converters.

Urban NO_x levels show a downward trend in most developed cities when viewed on a 2–3 decade timescale, driven by improved emission control technologies in the vehicle fleet; for example, across a range of UK urban sites, annual mean NO_x levels have fallen by 40% over the period 1993–2005, from 135 to 80 μg m^{-3} [18]. Within this overall trend, there are some significant local variations, for example, data from London suggests that the fraction of NO_x emitted as NO_2 has risen in recent years, possibly due to the introduction of diesel particulate filters, while traffic control measures such as the London Congestion Zone have altered the average fleet composition in central London to favor diesel vehicles with increased NO_x emissions, thought to be responsible for the 7% increase in NO_2 observed in central London over the period 2003–2008. More widely however, NO_x levels in most developed cities have fallen dramatically over the past 2–3 decades [18].

Globally, background ozone levels have risen over the past century – the earliest instrumental data thought to be reliable, the Montsouris measurements recorded on the outskirts of Paris from 1876, indicate average background ozone levels of 22 μg m^{-3} over the period 1876–1910 [31]. The equivalent values for the past decade from background locations are much higher – for example, ca. 80 μg m^{-3} for background air at Mace Head, Ireland (value for 2006 from Derwent et al. [32]); background levels have increased over the past 2–3 decades at up to 10 μg m^{-3} per decade (5 ppb per decade) [33]. On top of this hemispheric trend, urban ozone levels respond to regional pollution events, and to the extent of local titration of O_3 to NO_2 through NO_x (strictly, NO) emissions. Emissions controls have reduced the prevalence and extent of ozone episodes over the past 1–2 decades, reducing this contributor to urban ozone; however reductions in NO_x emissions have offset some of this change, reducing the ozone urban decrement. These effects are clearly seen in the UK over the period 1990–2006 (e.g., AQEG [34]), where the maximum hourly mean values (associated with regional ozone pollution episodes) have decreased substantially due to European controls on emissions of VOCs and NO_x, while at intermediate percentiles, urban sites show a positive trend in ozone with time due to the reduced urban decrement. The lowest hourly mean ozone levels show no change as these essentially correspond to total titration of O_3 to NO, consequently ozone levels are zero across the time period considered.

Primary sources (vehicle exhaust) of PM have been substantially reduced in may developed nations, and PM levels (measured as PM_{10}) have fallen substantially over the past few decades. Recently however, the downward trend appears to have been arrested, at least for PM_{10} in Europe, and the sulfate and nitrate

components of this PM_{10} [35]. It is unclear if this is a temporary departure from the general trend or reflects an ongoing leveling off, possibly reflecting non-exhaust sources, changing meteorology, and the interaction between sulfate and nitrate via ammonia availability to form ammonium nitrate.

Future Directions

In many developing megacities, the outcome of the opposing effects of increasing population density and economic activity, and adoption of improved (i.e., lower emission) technologies for transport, industry and domestic heating/cooking will determine local atmospheric composition over the coming decade. Dramatic improvements have been shown to be possible in cities when suitably stringent emission controls are implemented, for example, during the Beijing Olympics in 2008 [14, 36]. A key issue for future urban atmospheric composition processes is the potentially changing climate within which the air chemistry takes place, and the global perspective of cities as sources of a range of pollutants into the wider atmosphere. A number of the processes outlined above are strongly temperature-dependent, in particular the stability of PAN and other organic nitrates which sequester NO_x, and the equilibria between the condensed and vapor phases for many of the secondary components of PM, in particular nitrate. Changed temperatures will also affect emission sources, including evaporative losses of fuels, and emissions of biogenic VOCs, many of which are strongly (and non-linearly) temperature-dependent, and has been suggested to affect the prevalence of the meteorological patterns which favor ozone pollution episodes, such as the western European heatwave of 2003 [37]. These latter effects may particularly influence the background atmospheric composition (ozone levels) upon which localized urban influences build. Urban heat island effects already drive some of these changes on a local scale. A potentially larger climate-related impact may however arise from the widespread adoption of non-fossil-fuel-based transportation systems, driven by carbon emission considerations. Should this occur, our currently low understanding of the non-exhaust contributions to urban air pollution will assume much greater importance.

Bibliography

Primary Literature

1. United Nations Department of Economic and Social Affairs/Population Division (2008) World urbanization prospects: the 2007 revision. United Nations, New York
2. Fenger J (1999) Urban air quality. Atmos Environ 33:4877–4900
3. Mage D, Ozolins G, Peterson P, Webster A, Orthofer R, Vandeweerd V, Gwynne M (1996) Urban air pollution in megacities of the world. Atmos Environ 30:681–686
4. Brimblecombe P (1987) The big smoke. Methuen, London
5. Salmond JA, McKendry IG (2009) Influences of meteorology on air pollution concentrations and processes in urban areas. In: Hester RE, Harrison RM (eds) Air quality in urban environments, vol 28, Issues in environmental science and technology. Royal Society of Chemistry, London, pp 23–41
6. Thorpe AJ, Harrison RM, Boulter PG, McRae IS (2007) Estimation of particle resuspension source strength on a major London road. Atmos Environ 41:8007–8020
7. Molina LT, Molina MJ (2004) Improving air quality in megacities Mexico city case study. Ann NY Acad Sci 1023:142–158
8. Ding A, Wang T, Zhao M, Wang T, Li Z (2004) Simulation of sea-land breezes and a discussion of their implications on the transport of air pollution during a multi-day ozone episode in the Pearl river delta of China. Atmos Environ 39:6737–6750
9. Vardoulakis S, Fisher BEA, Pericleous K, Gonzalez-Flesca N (2003) Modelling air quality in street canyons: a review. Atmos Environ 37:155–182
10. Lee JD, Moller SJ, Read KA, Lewis AC, Mendes L, Carpenter LJ (2009) Year-round measurements of nitrogen oxides and ozone in the tropical north Atlantic marine boundary layer. J Geophys Res 114:D21302. doi:10.1029/2009JD011878
11. Read KA, Lee JD, Lewis AC, Moller SJ, Mendes L, Carpenter LJ (2009) Intra-annual cycles of NMVOC in the tropical marine boundary layer and their use for interpreting seasonal variability in CO. J Geophys Res 114:D21303. doi:10.1029/2009JD011879
12. United Nations Environment Programme (2007) Beijing 2008 Olympic games – an environmental review. Report of the United Nations Environment Programme. United Nations Environment Programme, Nairobi
13. Gros V, Sciare J, Yu T (2007) Air-quality measurements in megacities: focus on gaseous organic and particulate pollutants and comparison between two contrasted cities, Paris and Beijing. C R Geoscience 339:764–774
14. Wang T et al (2010) Air quality during the 2008 Beijing Olympics: secondary pollutants and regional impact. Atmos Chem Phys 10:7603–7615
15. Abam FI, Unachukwu GO (2009) Vehicular emissions and air quality standards in Nigeria. Eur J Sci Res 34:550–560
16. Raheem AMOA, Adekola FA, Obioh IO (2009) The seasonal variation of the concentrations of ozone, sulfur dioxide, and nitrogen oxides in two Nigerian cities. Environ Model Assess 14:497–509

17. World Health Organisation (2006) Air quality guidelines. Global update 2005. Particulate matter, ozone, nitrogen dioxide and sulfur dioxide. World Health Organisation, Copenhagen
18. Air Quality Expert Group (2007) Trends in primary nitrogen dioxide in the UK, Fourth report of the Air Quality Expert Group. DEFRA, London
19. Maynard RL (2009) Health effects of urban pollution. In: Hester RE, Harrison RM (eds) Air quality in urban environments, vol 28, Issues in environmental science and technology. Royal Society of Chemistry, London, pp 108–128
20. Jacobson MZ (2007) Effects of ethanol (E85) versus gasoline vehicles on cancer and mortality in the United States. Environ Sci Technol 41:4150–4157
21. Andrae MO, Merlet P (2001) Emission of trace gases and aerosols from biomass burning. Glob Biogeochem Cycles 15:955–966
22. Leighton PA (1961) Photochemistry of air pollution. Academic, New York
23. Bloss WJ (2009) Atmospheric chemical processes of importance in cities. In: Hester RE, Harrison RM (eds) Air quality in urban environments, vol 28, Issues in environmental science and technology. Royal Society of Chemistry, London, pp 42–64
24. Wayne RP (2001) Chemistry of atmospheres. Oxford University Press, Oxford
25. Jenkin ME, Davies TJ, Stedman JR (2002) The origin and day-of-week dependence of photochemical ozone episodes in the UK. Atmos Environ 36:999–1012
26. Emmerson KM, Carslaw N, Carslaw DC, Lee JD, McFiggans G, Bloss WJ, Gravestock T, Heard DE, Hopkins J, Ingham T, Pilling MJ, Smith SC, Jacob M, Monks PS (2007) Free radical modelling studies during the UK TORCH campaign in summer 2003. Atmos Chem Phys 7:167–181
27. Wood EC, Herndon SC, Onasch TB, Kroll JH, Canagaratna MR, Kolb CE, Worsnop DR, Neuman JA, Seila R, Zavala M, Knighton WB (2009) A case study of ozone production, nitrogen oxides, and the radical budget in Mexico city. Atmos Chem Phys 9:2499–2517
28. Derwent RG, Jenkin ME, Saunders SM (1996) Photochemical ozone creation potentials for a large number of reactive hydrocarbons under European conditions. Atmos Environ 30:181–199
29. Yin J, Harrison RM (2007) Pragmatic mass closure study for $PM_{1.0}$, $PM_{2.5}$ and PM_{10} at roadside, urban background and rural sites. Atmos Environ 42:980–988
30. Zhang Q et al (2007) Ubiquity and dominance of oxygenated species in organic aerosols in anthropogenically-influenced northern hemisphere midlatitudes. Geophys Res Lett 34: L13801. doi:10.1029/2007GL029979
31. Volz A, Kley D (1988) Evaluation of the montsouris series of ozone measurements made in the nineteenth century. Nature 332:240–242
32. Derwent RG, Simmonds PG, Manning AJ, Spain TG (2007) Trends over a twenty year period from 1987–2006 in surface ozone at the atmospheric research station at Mace Head, Ireland. Atmos Environ 41:9091–9098
33. Raes F, Hjorth J (2006) Answers to the Urbino questions. ACCENT Secretariat, Universita di Urbino, Italy. ISBN 92-79-02413-2
34. Air Quality Expert Group (2009) Ozone in the United Kingdom. Fifth report of the Air Quality Expert Group, DEFRA, London
35. Harrison RM, Stedman J, Derwent D (2008) New directions: why are PM_{10} concentrations in Europe not falling? Atmos Environ 42:603–606
36. Fang M, Chan CK, Yao X (2009) Managing air quality in a rapidly developing nation: China. Atmos Environ 43:79–86
37. Lee JD et al (2006) Ozone photochemistry and elevated isoprene during the UK heatwave of August 2003. Atmos Environ 40:7598–7613

Books and Reviews

Ayres J, Maynard RM, Richards R (eds) (2006) Air pollution and health, London: Imperial College Press reports of the air quality expert group. DEFRA, UK

Brimblecombe P (1987) The big smoke. Methuen, London

Brimblecome P, Maynard RL (2001) The urban atmosphere and its effects, vol 1, Air pollution reviews. Imperial College Press, London

Fenger J (1999) Urban air quality. Atmos Environ 33:4877–4900

Harrison RM, Hester RE (eds) (2009) Air quality in urban environments, vol 28, Issues in environmental science and technology. Royal Society of Chemistry, Cambridge

Holloway AM, Wayne RP (2010) Atmospheric chemistry. RSC, Cambridge

Singh HB, Brimblecome P, Veenstra F (2009) Atmospheric environment special issue fifty years of endeavour and papers therein. Atmos Environ 43:1

Tiwary A, Colls J (2010) Air pollution: measurement, modelling and mitigation, vol 3. Routledge, London

WHO/UNEP (1992) Urban air pollution in megacities of the World. Blackwell, Oxford

WHO (2006) Air quality guidelines. Global update 2005. Particulate matter, ozone, nitrogen dioxide and sulfur dioxide. World Health Organisation, Copenhagen

Urban Ecology

S. T. A. Pickett[1], M. L. Cadenasso[2]
[1]Cary Institute of Ecosystem Studies, Millbrook, NY, USA
[2]Department of Plant Sciences, University of California, Davis, CA, USA

Article Outline

Glossary
Definition of the Subject

Introduction
Urban Ecology Principles
Future Directions
Bibliography

Glossary

City A dense, demographically and economically heterogeneous settlement containing businesses, residences, intensive transportation infrastructure, multistory buildings, and warehousing or manufacturing. Economies of cities focus on services, processing commodities, manufacturing, or finance rather than on agricultural or resource management. Cities are often characterized by a population representing diverse social groups and economic classes in relatively close spatial proximity. As a caution, it should be noted that the term "city" is sometimes used to refer to an entire urban (definition 1) area, and sometimes used in a narrow sense to contrast with suburb (definition 2).

CSE City-suburban-exurban system. A comprehensive term referring to all components of a complex urban system, metropolitan area, or other cluster of urban areas.

Ecology The science of the relationship of organisms to each other and the physical environment, and the transformation of resources mediated by those interactions. Human ecology includes the social and institutional structures established by people as components of the system studied.

Ecosystem A system comprising the organisms, the physical environment, and the interactions among them within a specified volume of the Earth. Ecosystems may be of any size, depending on the research questions of interest, and are open to material and energetic flows with adjacent systems. Although this definition encompasses human ecosystems, for completeness it is considered that human ecosystems include biological components, the physical environment of air, water, soil, energy, the social and human institutions, and the built environment.

Suburb This term has two meanings, depending on whether an Old World or a New World context is intended. In the New World, a suburb is a component of a broadly recognized urban area, a primarily residential land cover in which single or multiple household dwellings are interspersed with the open spaces of lawns and generous street landscaping. New World suburbs are often a locus of wealth and power. Modest commercial nodes, mostly as service rather than manufacturing or warehousing, may be included in such suburbs. In contrast, Old World suburbs may be less green and more densely built than New World suburbs, and in many cases may host concentrations of lower income, less empowered persons. In the expanding cities of the global south, shanty towns and informal settlements may constitute much of the suburban realm.

Urban Definition 1 refers to all components of densely settled and built up areas, and contrasts with rural, agricultural, or wild lands. An alternative terminology for this inclusive definition is city-suburban-exurban (CSE) system. Definition 2 refers to dense commercial, industrial, and residential lands in contrast to suburbs and exurbs.

Definition of the Subject

Within the science of ecology, urban ecology is defined as the study of structure, dynamics, and processes in urban ecological systems. Urban ecology is the study of the relationships of human and nonhuman organisms in urban areas, the interactions of these organisms with the native and built physical environment, and the effects of these relationships on the fluxes of energy, materials, and information within individual urban systems and between urban and nonurban systems. Urban ecology applies the methods and concepts of the biological science of ecology to urban areas, but requires and integrates with the concerns, concepts, and approaches of social sciences to produce a hybrid discipline. Urban ecological systems include individual organisms, populations, communities, and landscapes, as well as buildings and infrastructure. Urban ecology further recognizes specific urban ecosystems as a part of the global biogeochemical, economic, and human demographic system.

Importance of Urban Ecology

Urban ecology is important because it brings the insights and knowledge from contemporary biological ecology to bear on urban areas [1]. It replaces the

earlier and superseded versions of ecological science that had been used by social scientists, geographers, and urban planners in justifying and predicting urban dynamics in the second half of the twentieth century. Urban ecology as a branch of contemporary ecological science now emphasizes spatial heterogeneity, feedbacks between natural and human system components, probabilistic system change, and the integration between human perceptions and environmental processes.

Urban ecology is also important because urban habitats are increasing worldwide. The United Nations estimates that more than 50% of the global population now resides in urban areas, as defined by the various member nations. In addition, the next three billion people to be added to the world population are expected to live in urban areas. Hence, urban systems are becoming the predominant habitat of humanity, and are an increasingly widespread land cover type worldwide. In the USA, constructed surfaces now cover an area equivalent to that of the state of Ohio [2].

If the disciplines and practices of urban planning and design, ecological restoration, and ecosystem management are to draw more effectively upon ecological knowledge and data, then the science of urban ecology will become an increasingly key resource for these pursuits.

Brief History

Urban ecology has emerged as a subdiscipline of biological ecology only in the last 30 years [3]. It began as an ecological science in the study of the species and biotic communities of conspicuously green patches in cities and metropolises. Parks, vacant lots, disturbed, and derelict lands were the first focal areas of the discipline [4]. More recently, ecologists began to examine areas actively inhabited and managed by people, including lawns and streetscapes [5]. Another contrasting tradition in urban ecology focuses on the coarser scale, to quantify energy and material budgets of cities. This focus, sometimes called urban metabolism, deals with the energy, matter, and information that flow through and are transformed by cities. In all cases, how the biological components and fluxes affect the well-being of people in the city is a concern. However, the contemporary approach to urban ecology differs from the past traditions. First, all areas in the city are now subject to ecological analysis, not just the conspicuous green areas. Second, even in the budgetary approach, the internal spatial configuration of different components of the urban area is recognized as potentially influencing the fluxes and transformations within the larger metropolis. Finally, the fully hybrid nature of the systems is acknowledged, so that cities are seen as neither fully human nor fully natural entities. Rather, they are inextricably both human constructions and biophysical features [6, 7]. Urban ecology was once a study of green spaces in the city. Now it is the study of the ecology of the entire urban area, including biological, built, social, and physical components.

Other scholarly disciplines beyond biology have used the term "urban ecology." Principal among these has been sociology. This use originated in the 1920s at the University of Chicago under the leadership of Robert Park and Ernest Burgess, who brought concepts of community, competition, and succession that were then current in biological ecology into their new discipline of sociology. Human ecology, which has roots in geography, anthropology, and other social sciences, is closely related to urban ecology when the study subject is urban populations and their interactions. However, other disciplines tend to neglect the physical and biological components of the environment when they address urban ecology.

Introduction

Urban ecology has been used by several disciplines which have different foci and concerns. These contrast or complement the conceptions of urban ecology as a biological science, which is the approach emphasized here.

History

Urban ecology has a long history. The first flowering of urban ecology was a sociological phase established by Park and Burgess at the University of Chicago in the 1920s. Although this was a sociological pursuit, it was centrally informed by analogies from the biological science of ecology, for which the University of Chicago was one of the founding schools. Park, Burgess, and their students explained the unprecedented growth and social change in Chicago in terms of invasion of new human communities, competition among

communities, and spatial isolation between different communities and functions in the city. These scholars were disturbed by the doubling of the population of Chicago at the time, and the role of new migrants from the American South or from eastern and southern Europe. The racial, ethnic, and class novelty in the city begged explanation and incited the Chicagoans to seek explanatory and predictive models to serve in the face of such unprecedented changes. This approach to urban ecology was informed by a tacit antiurbanism, as the Chicago sociologists held village and agricultural communities as the paragons of human societies. One of the central tenets of the Chicago school was that cities had a life cycle, analogous to the expected, but incorrect, prediction that ecological communities had predictable life cycles starting from invasion, extending through competition and sorting, and ending in a mature state. This phase of urban ecology ended when social science critics prompted a move toward more individual behavioral explanations of urban change, as opposed to community-based models. A similar, but independent shift occurred in mainstream ecology at about the same time. Even though the academic community moved beyond the deterministic, life-cycle approach to cities, urban policy in the USA continued to assume life-cycle patterns through the 1960s, basing urban conservation and urban renewal policies on this flawed assumption.

Oddly, during the early twentieth century, while their major ideas were informing the birth of sociology and being widely applied in urban systems, most biological ecologists heartily ignored cities and urban systems. European and Japanese ecologists began to explore ecology in urban contexts after World War II. The manifest destruction in the cities in which they lived invited their interest as biologists. What would be the patterns and mechanisms of plant establishment in derelict sites? How would the newly established biotic communities change over time? What benefit might they provide the cities in which they occurred? The questions of the immediate postwar researchers in Europe and Japan were standard ecological questions, but asked in a novel location. This tradition became linked with urban planning in Europe and has remained active in that form [8].

The second wave of urban ecology rose in the 1970s in the USA. Associated with the birth of environmentalism and its concern with the Earth's exponential human population growth, the urban ecology of this era tended to assume that humans were a negative influence on ecosystems, and urban areas provided an extreme case of the human impact that was beginning to worry scientists and the public. A key document from this era is the volume by Stearns and Montag [9]. In it, the problems of urban areas are outlined, and the nature of potential ecologically informed solutions is suggested. However, the ecology of the time was rather coarse-scaled, and assumed equilibrium tendencies of systems, rather than recognizing fine-scale heterogeneity as a causal feature of systems [10]. Furthermore, although failure of the old ecological ideas that had informed the Chicago School was evident, no clear replacement had emerged. Urban ecology in this era concentrated on investigations of conspicuously green patches in the city. Hence, this approach can be characterized as ecology in the city [3]. Parks, cemeteries, gardens, and abandoned lots exemplify this literature.

Another feature of this second wave of urban ecology was a budgetary, systems approach. Epitomized by work in Hong Kong [11], this approach to urban ecology addressed energy and material budgets of cities, and detailed the human costs of pollution and crowding. This approach is characterized as a budgetary feature of ecology of the city. It shares with the early Chicago School an assumption of the importance of urban "pathologies" in the human population. Industrial ecology and urban metabolism are branches from this tradition. Both of these schools of thought analyze the material and energetic inputs, efficiencies, and outputs of urban systems and their components. Life-cycle analysis of materials is a strategy that aims to reduce the use of resources and the generation of wastes associated with contemporary material use. This era of urban ecology did not persist in the USA as a comprehensive field.

A new wave of urban ecology is currently on the rise. It is characterized by several features that differentiate it from prior instances of urban ecology, and make it more comprehensive than earlier approaches. First, it attempts to unify social and biological knowledge, concerns, and approaches [12]. Second, it acknowledges and exploits spatial heterogeneity and fine-scale dynamics as a feature and cause of urban change.

Third, it seeks to understand the controls of biogeochemical processes throughout urban systems, including retention, fluxes, and leakage of limiting nutrients and pollutants. Contemporary urban ecology brings the three previously separate goals together for the first time.

Will this current interest in urban ecology wane, as did the previous ones in the USA? One difference between the current manifestation of urban ecology and the previous ones is institutional support. The pioneers of urban ecology in Europe, Japan, and the USA did not have long-lasting research support. As a result, their pioneering efforts were sometimes short-lived. Now there are two urban Long-Term Ecological Research (LTER) sites in the USA, and International Long-Term Ecological Research programs and Zones Ateliers are including urban areas among their rosters. Already the US LTER urban sites are 13 years old. Such longevity promotes interdisciplinary collaboration, continued use of research areas, developing ongoing relationships with communities and decision-makers, and accumulation of lengthy data runs which can expose causal links and the role of pulse events [13]. Acknowledging that urban areas both contribute to and are vulnerable to global changes [13] will tend to keep them in focus in ecological science.

Examples

Urban ecology is such a diverse science that examples are required to give a sense of its breadth.

Patterns of diversity and abundance associated with urbanization are complex and competing explanations exist. Tests of island biogeography theory in urban areas find that species–area relationships are preserved in urban patches [14]. However, in some studies, patch size influenced species composition rather than species richness as a result of organisms at higher trophic levels being preferentially lost from smaller patches [15]. Attempts to directly quantify the extinction and colonization processes that island biogeography relies on have shown that immigration and extinction characterize different kinds of patches [16, 17]. The species composition in a patch is the result of species colonizing the novel habitats formed by urbanization along with those remaining after local extinctions due to isolation or habitat alteration. One prediction of the view of complex causes of urban biodiversity is that urban habitats are not always less diverse than rural patches. Rather, diversity depends on the sum of extinction and colonization rates, which differ regionally and taxonomically. At moderate levels of urbanization, species richness may actually be higher than in nearby wild lands.

A second example is the disconnection between riparian zones of urban streams and the water table [18]. This disconnection limits the capacity of urban riparian zones to convert nitrate, a pollutant in groundwater derived from fertilizer and sewage, to gaseous forms that do not pollute streams. Research in agricultural landscapes has suggested that riparian restoration, inserting woody and grass vegetation between crops and stream banks, is an effective strategy to mitigate nitrate pollution in streams. When the capacity of urban riparian zones to accomplish such mitigation was examined in Baltimore, MD, USA, it was discovered that riparian zones had become disconnected from the groundwater sources that control their ability to convert nitrate to nitrogen gas. With reduced infiltration of stormwater into the ground due to impervious surfaces, and with high incision leaving stranded droughty floodplains in cities, urban riparian zones no longer support the anaerobic conditions and high organic matter required to fuel denitrifying bacteria. Hence, the expected denitrification in urban riparian zones may not always occur [19]. This example demonstrates that knowledge obtained in nonurban environments may not apply to urban situations.

Guide to the Article

It is now clear that urban areas express different combinations of ecological processes than do nonurban areas and that urban areas are an increasingly important component of the global biosphere. It is now possible to examine key principles that are emerging from the new ecological focus on urban research. Future directions for research and management are addressed at the conclusion of the article.

Urban Ecology Principles

Thirteen principles characterize the contemporary science of urban ecology. Of course, such principles are

likely to be improved or replaced with advances in this rapidly growing scientific field. The principles can be divided into four groups: (1) the human ecosystem, (2) urban form, (3) urban function, and (4) methodology.

Principles Concerning Human Ecosystems

Much of the history of urban research has proceeded as though city and ecology were different and mutually exclusive. At the same time that the social scientists of the Chicago School were applying bioecological concepts of the day to their work in the cities, another member of the University of Chicago faculty was establishing the concept of plant succession. A member of the Botany Department, Henry Chandler Cowles, was working on the seemingly pristine plant communities of the Indiana Dunes, distant from Chicago's immigrant-driven hurley burley. There was conspicuously no empirical or theoretical collaboration between the pioneering ecologists and social scientists at the University of Chicago in the early twentieth century [20].

The tradition of treating city and nature as opposites was challenged by adventuresome scholars and practitioners in the closing decades of the twentieth century [21]. This has led to a new conception of cities or urban areas as hybrid socio-bioecological systems. In other words, urban places may be considered to be human ecosystems. As such, they incorporate not only the traditionally recognized biotic and physical components of ecosystems, but also the social structures and built components so conspicuous in cities and towns [7].

The new conception of human ecosystems prompts researchers, planners, and managers in urban systems to study and exploit the reciprocal feedbacks between the social components in all their demographic, institutional, behavioral, and economic complexity, and bioecological processes, whether conspicuous or not. For example, the mitigation of urban heat extremes by trees is well known [22]. Put simply, there is an ecosystem feedback between vegetation and human comfort or risk of heat stress. However, because of the multifaceted nature of the human ecosystem, the embedding of human values and culture, and the linkage of vegetation cover with water demand, the causal link between the desire to mitigate heat stress and the willingness to plant trees is complex. Included are citizen concerns over private property access, commitments to tree maintenance and litter removal on their property, fear of crime associated with vegetated hiding places, risk of treefall, root fouling of infrastructure, and aesthetic judgments [23]. Other examples of such processes are associated with later principles.

Two principles emerge from these considerations about human-natural system coupling in urban contexts:

Principle 1: Cities and urban areas are human ecosystems in which socioeconomic and bioecological processes feed back to one another.

Principle 2: Human values and perceptions are a key link mediating the feedbacks between social and bioecological components of human ecosystems.

Principles Concerning Urban Form

One of the most remarkable features of urban areas is their spatial form. Architects and urban planners have traditionally used figure-ground representations of urban areas, which emphasize the built component of the human ecosystem. Pioneering efforts by landscape architects have shown the need and power of going beyond such classic representations to include both the hidden and the conspicuous bioecological features of urban areas.

Urban form has changed dramatically through time. Early walled cities were physically and socially distinct from the surroundings and often were centered on a cosmologically significant, ceremonial core. The industrial city spread beyond the location of former city walls and established porosity for the purposes of exchange of goods and the accumulation of immigrants needed as labor. After World War II, the industrial city was further disaggregated into a mixture of new suburbs, dispersed commercial districts, and older core cities that were reduced in density. This is the city as part of a network in a dispersed megalopolis [24].

This simple, linear typology does not necessarily reflect the temporal trends in all parts of the world. Indeed in some cities of the global south, no industrial period existed before they began the sprawling growth driven by migration of persons from the provinces seeking opportunity and a better life in the modern city of consumption. Shanty towns outpacing the urban infrastructure are one feature of such cities.

Hence, urban form is evolving, which leads to the following principle of urban form:

Principle 3: Urban form is a dynamic phenomenon and exhibits contrasts through time and across regions that express different cultural and economic contexts of urbanization.

Why is urban form important ecologically? The establishment of street grids and major road patterns alters surface drainage [25] and presents barriers and corridors for the movement of native and introduced plants and animals [26]. The adding of new vegetation and the obliteration of the forest, savanna, desert, wetland, or grassland that had previously occupied the urban site follows the dictates and needs of the new urban form. In addition, the infrastructures for supplying clean water and for dealing with fouled water are large alterations to watershed structure and regional water balances. The placement of main sanitary sewers and main storm drains in stream valleys and the shortcutting of ground and surface water flows are components of the universal urban alteration of hydrology. Furthermore, the shapes of heterogeneity introduced by urban form are often rectilinear and of different scale than the former regional and local patterns of environmental gradients and patches. In addition to spatial heterogeneity of the biophysical components of urban systems, the social features of cities, towns, and suburbs are notably patchy [27]. Urbanists have long acknowledged the fine-scale change – often from block to block – in economic activity, wealth, social group, architecture, and land use that characterize cities. Although traditional postwar suburban development typically occupies rather large tracts which they homogenize, the abrupt shifts in urban structure persist. This patchiness is reinforced by the near universal employment of zoning in large urban areas of wealthy countries. All of these heterogeneous structural alterations can have significant effects on urban and adjacent natural ecosystem function, as will be detailed in a later section "Principles Concerning Urban Function". These insights about the nature of urban form at scales as small as residential parcels or a stroll to the corner of the block can be summarized in a principle:

Principle 4: Urban form is heterogeneous on many scales, and fine-scale heterogeneity is especially notable in cities and older suburbs.

The heterogeneous form of contemporary urban systems extends into the surroundings [28]. The suburban fringe in rapidly growing cities may abut farms, desert, forest, or whatever landscape constitutes the predominant rural or wild land cover. Indeed, the adjacencies are often convoluted and complex, leading to interdigitation of urban elements with the wilder or more rural landscape. In some wealthy urban regions, individual homes are embedded in what is otherwise a wild matrix [29]. An example is the building of suburban houses in chaparral shrublands in Mediterranean climates, such as Southern California. A similar case is the construction of houses in the forest fringe of the Pacific Northwest metropolises, or in forested foothills of the exurban lands of the Southern Appalachians in the USA. The insertion of households whose financial equity, lifestyle identity, social connections, and environmental attitudes have been defined by urban life rather than a life of logging, farming, fishing, or other natural resource management is perhaps a more significant interdigitation than the mere presence of their homes. Similar juxtapositions exist for resorts that serve as remote summer or winter destinations for urban dwellers. The interdigitation of urban with wild or less-intensively managed lands results not only from the invasion of wild land by new housing, commercial, or transportation corridors, but also by the afforestation of foothill developments in arid or semiarid climates in which the lower slopes would have been savanna or grassland. The well-to-do suburbs of Oakland, CA, are an example, which now merge to some extent with the ridgetop forests of the Coast Ranges, and where fire is now a real risk. The fact that urban land cover is growing more rapidly than urban population in oil-subsidized economies [24] suggests that such interdigitation will be the source of increasing conflicts and changing exposure to natural disturbance regimes [29]. Recognizing the ongoing interaction of urban and wild lands suggests this principle:

Principle 5: Urban land covers and uses extend into and interdigitate with rural or wild land covers and uses.

Urban form and hence its interaction with less-urbanized landscapes is the result of a complex of causes. One cause of urban form is conformity to regional plans. This cause is rare in many countries, such as the USA, but more common in Europe.

Successful constraint on urban sprawl is exemplified in the USA by the metropolitan green line in Portland, OR, or the Urban-Rural Demarcation Line of Baltimore County, MD [30]. In Baltimore County, more than 90% of residents live within the URDL. The line has been in force since the 1970s and is controlled through zoning, the restriction of sewer infrastructure, and the focusing on urban growth in the county to specific corridors. However, the rarity of such regional controls is compensated for by the commonness of the role of developer self-interest in determining urban form. Indeed, urban planners often lament the predominance of the real estate market as a driver of urban form. On the social roster of causes of urban form are those that are described as "push and pull" factors. Persons and households choose to live at specific places in the metropolis based on such pull factors as attraction to open space, commodious housing, affordability, good schools, and access to desirable commercial establishments. Push factors include high taxes, small and old housing, lack of personally controlled open space, perceived risk of crime, underperforming schools, and the like. Firms also experience push and pull factors. In the case of businesses, a customer base, access to efficient delivery routes, free parking, access to a trained work force, and similar concerns are pull factors. The push factors for businesses mirror those experienced by households.

Many of the factors that control urban form are accidental or unintentional. Pollution, traffic congestion, and the concentration of heat in built areas are examples of unintentional disamenities. Urban flooding is an unintended result of successfully draining stormwater from upstream. Drawing down of groundwater is a similar result of successful stormwater drainage. In neighborhoods built on filled wetlands in Boston, such drying of the soil is threatening the wooden piles supporting the foundations of some buildings. These examples suggest attending to both the intended and unintended consequences of urban development and environmental modification. The principle that emerges is the following:

Principle 6: Urban form reflects planning, incidental, and indirect effects of social and environmental decisions.

Because ecology as a science has been absent from cities for so long the need for data is great. However, ecologists cannot rely on the tried and true experimental approach which they employ with such enthusiasm and success in more wild and rural lands. In urban areas, multiple ownerships, the involvement of individuals and communities in land-use decisions even on private land, and the ethical constraints about manipulations that affect people's well-being or pleasure all limit the applicability of controlled, replicated experiments.

However, while ethics and property regimes close one door to experimentation, the processes of urban design, development, and neighborhood revitalization open others [31]. Urban design projects, whether they be landscape architecture projects in the public realm, private development of a subdivision, or installation of environmental retrofits in older residential or commercial areas, can themselves be treated as experiments. Two examples show the power of this approach. One, the classic case of Jordan Cove, CT, compared an alternative suburban development to a traditional layout of homes. The goal was to test the potential to mitigate stormwater quality and amount with minimal effect on real estate development. A second example is the proposed subdivision of a forested tract in the Hudson Highlands region of New York State. The goal in this case was to reduce the impact on a salamander population that is of conservation concern in the State. The landscape architect employed ecological principles to suggest altering the traditional suburban design to reorient roads, preserve small vernal ponds upon which the salamanders depend for breeding, and install rain gardens as a component of the yard of each house to maintain the hydrologic regime of the complex network of ponds and overland drainage. The development is planned to contain drift fences and pitfall traps as infrastructure to continually monitor the salamander population. Hence the development itself can act as an experiment. To work with designs as experiments, partnerships with urban designers and developers will be required. These examples suggest a principle to test in further application:

Principle 7: Urban designs and development projects at various scales can be treated as experiments to expose the ecological effects of different design and management strategies.

Principles Concerning Urban Function

The tradition in both the social and biophysical sciences to see urban areas as distinct and opposed to

nature has resulted in a bias against finding natural processes in City-Suburban-Exurban systems. Both the pioneering research in landscape architecture and urban ecology [5] as well as the more recently established projects [13] have, however, confirmed and extended the understanding of ecological processes as parts of cities and their more extensive urban mosaics. Several examples show the power of bioecological phenomena in urban contexts.

In Philadelphia and Boston, buried floodplains, thought to have been engineered in a reliable stormwater management structure or filled to provide substrate for building, continued to manifest higher levels of soil water and were associated with property damage and abandonment [32]. In Philadelphia, the collapse of the sewer that had replaced Mill Creek was a catastrophic outcome of ignoring the function of the urban landscape. Landscape designs envisioned with the participation of neighborhood residents account for hazard and vulnerability, and provide an opportunity to convert a disturbance prone site to an open space amenity. Such sites can contribute constructively to regional stormwater management, recreation, and education.

A second example shows the capacity of open space to perform biogeochemical ecosystem functions in the urban matrix. Nitrate pollution in streams can be used as an index of environmental quality to assess ecosystem function. Researchers who started the Baltimore Ecosystem Study expected suburban lands to be detrimental to the environmental quality of the urban mosaic. This hypothesis was suggested by the large amounts of nitrogen fertilizer and water applied to many American lawns. When small watersheds that drain areas having different amounts of green space in their landscapes were studied however, it was discovered that the suburban subwatersheds exhibited relatively high nitrate retention [18, 33].

A third example of the role of ecological processes is shown in the net carbon flux between surface and atmosphere. In a location near the boundary between Baltimore City and County, an atmospheric flux tower assesses the upward versus downward movement of moisture, temperature, and carbon dioxide, among other factors. Although the urban area is a net generator of carbon dioxide to the atmosphere due to the use of fossil fuels for heating and transportation, there is lower net flux on weekends and when the wind blows across areas of higher vegetation cover compared to winds from areas or greater built cover.

Examples such as these suggest a principle:

Principle 8: Urban areas contain remnant or newly emerging vegetated and stream patches that exhibit bioecological functions.

One of the fluxes that exercises the interest of urban planners and managers worldwide is water. This concern extends well beyond those cities that are located in arid or semiarid environments. Indeed, some cities, such as Phoenix, AZ, and Los Angeles, CA, are so well connected to distant water supplies via diversions from the Colorado River that they may seem impervious to drought. Ironically, although arid-land cities do show concern for water, many cities from moist climates are coming to acknowledge the sensitivity of their reservoir systems to periodic drought [34]. New York City, with its system of impoundments more than 200 km to the north, or Boston with its reservoir in rural central Massachusetts must now plan for the impacts of periodic drought and of the drying that may come with climate change. Even now, development in some counties in eastern Maryland faces limits due to shortages of groundwater, which are the sources for these suburban-style developments.

Such concerns with water supply are not limited to the USA. Urbanization on the Indian subcontinent is sensitive to projected reduced snowpack in the Himalaya Mountains, in which its rivers originate. Water withdrawal for agriculture and forestry in highlands of South Africa stands to alter water availability for which lowland settlement and wildlife compete. Similar diversions along the tributaries of the Nile are of concern for international relationships in East Africa.

Water supply is not the only aspect of water flux that is of concern. All cities, no matter whether they are in moist or dry climates, must deal with periods of high rainfall. Even desert cities are subject to occasional local thunderstorms, or to floods from the foothills and mountains upstream. Hence, stormwater management in spates is as of as much concern in Mediterranean Santiago, Chile, as it is in temperate Seattle, Washington. The traditional mode of stormwater management is to collect it and pass it off downstream as rapidly as possible. While this solves

local problems, it creates problems downstream. Stream bed erosion, scouring out the habitats of aquatic organisms and the spawning grounds of anadromous fish, and increasing the temperature of downstream reaches affected by runoff from hot paved surfaces are some of the consequences to the engineering approach to stormwater management. Many urban management plans now reference water supply and stormwater management as key concerns.

A principle emerges from these sorts of events and situations:

Principle 9: The flux of water, including both clean water supply and stormwater management, is of concern to urbanizing areas worldwide, and connects them explicitly to larger regions.

Ecologists and other biologists have recognized the presence of wildlife and plants in cities for a long time. This tradition is especially strong in Europe, but also has early roots in Japan and the USA. Interest has focused both on organisms that represent the native biota and those that represent threats to either native biota or to human health.

Native biological diversity, or biodiversity, is usually reduced in urban areas, with native species declining in richness compared to species introduced from elsewhere [35]. An example of altered species distribution that may have an impact on the future composition of urban forests is the greater number of vine species, especially introduced species, in the treefall gaps found in urban compared to rural forests. Such vines can impede the regeneration of trees in canopy gaps. Still, the total number of species, including both native and exotic species, can be larger in urban areas than in nearby rural areas in the temperate zones. However, in some central German cities, the richness of even native species is greater in urban areas than in the adjacent countryside. Urban wildlife is subsidized by purposeful feeding, by the incidental increase in resources found in garbage, or for fruit-feeding birds, by the large abundance of fleshy-fruited horticultural species planted in settlements [36].

Urban fauna and flora can respond to the novel conditions of urban ecosystems. For example, bird populations in San Diego exhibit genetically different plumage from rural counterparts [37]. Although that difference is not necessarily adaptive, other changes are functional. Urban bird populations have been demonstrated to raise pitch and volume of their songs, presumably selected by the higher noise levels in cities than in the countryside [38]. Plants are well known to genetically adapt to the heavy metals found in brownfields or associated with urban construction.

An important question is the contribution of exotic and native species to ecosystem services in urban areas. Biophilia, the affinity that humans express for natural settings and living things or the salubrious effects of plants and wild animals in the surroundings, are benefits of wildlife and plants in cities. Other services are performed by the biota of cities, including moderation of climate through shading and transpiration, stabilization of soil surfaces and stream banks, and absorption of pollution. These services can be performed by both introduced and native species. Indeed, some introduced species, such as the exotic Norway maple, were imported due to their tolerance of urban stresses. Ironically, this species is one that has escaped into the wild, and due to the deep and seasonally long-lasting shade it casts, poses a threat to the herbaceous species of the forest understory and to regeneration of other canopy tree species [39].

Because of the damage that exotic species can do to native biotic communities and the functional changes they can cause in ecosystems, they are often targeted for removal. Although the introduction, either purposeful or accidental, of new exotic species should be avoided, in urban areas the removal of exotics as a blanket policy may be problematic. The contribution of the species to ecosystem services in urban areas, the ability of native species capable of performing that function to tolerate urban conditions, or the potential to breed native species for these capacities are all issues that must be considered in planning the management of exotic species. Some exotics can contribute to ecological functions in city-suburban-exurban habitats.

A principle that emerges from knowledge about urban biota is this:

Principle 10: Urban biodiversity has multiple components, and the contributions of each kind of species to ecosystem services in cities must be evaluated.

One important aspect of urban function is how equitably the ecological benefits and risks in urban systems are distributed across the human population. This concern, labeled environmental justice, first emerged in communities of color or economically

disadvantaged communities that were adjacent to contaminated sites, or sites that produce hazardous pollution. The frequent locations of such communities in topographic positions subject to flooding or landslides are other cases of environmental injustice. An example is the disproportionate damage suffered by low-lying neighborhoods such as the lower 9th Ward of New Orleans during 2005 in the wake of Hurricane Katrina, or the location of informal settlements with their flimsy construction in some South American cities on erodible slopes. Poor and disempowered populations may be actively excluded from desirable sites, as was the case with segregation practices historically in some US cities, or they may be indirectly priced out of locating to sites on higher ground, more distant from polluting businesses, or from facilities that process waste. The patterns and mechanisms of environmental injustice suggest a principle:

Principle 11: Bioecological processes are differentially distributed across the metropolis and the limitation of services and excess of hazards is often associated with the location of populations that are poor, discriminated against, or otherwise disempowered.

Methodological Principles

Two methodological principles of urban ecology complete the survey of guiding concepts for contemporary urban ecological science. These principles draw on conceptual and empirical principles outlined above and can help shape future urban research.

The first methodological principle deals with setting the boundary and scope of the study system. This step is key to quantification and comparison within and across urban systems. However, there is no a priori, universally correct scientific specification of an urban system [40]. Using legally set municipal or town borders may be convenient for policy purposes, but they may not be appropriate limits for scientific research [28]. This is because a large urban system may be made up of many such legally distinct jurisdictions. In addition, materials, energy, and information that are important in structuring an urban system are likely to move across political boundaries. For example, while it is possible and useful to measure species richness in a city, the collection of species so identified may depend on and interact with the larger, regional species pool [14]. A second example compares boundaries chosen for watershed-based studies with those chosen for a policy analysis. The 17,150 ha Gwynns Falls Watershed, which extends from its headwaters in Baltimore County to its confluence with Baltimore Harbor near downtown in the City of Baltimore, provides a sampling transect. Measurements of stream water quality and flow integrate across the two jurisdictions [18]. In contrast, measurements intended to help managers in Baltimore City define tree planting goals and identify priority areas for planting were conducted solely within the city limits. It is the responsibility of the investigators to state what the boundaries of their study units are and what the criteria for inclusion in the urban system are [40]. Such considerations suggest a methodological principle for urban ecology:

Principle 12: Definition of the boundaries and content of an urban study system is set by the researchers based on their research questions or the spatial scope of its intended application.

The second methodological concern is how to frame comparisons within urban systems. Because urban systems are hybrid human–natural complexes and because they are heterogeneous, there are many possible axes of comparison within them [27]. Comparisons may be based on criteria as divergent as the proportion of impervious surface, the amount of woody vegetation, the density of the human population, the surface area of buildings, the accumulated wealth of residents, the lifestyle characteristics of neighborhoods, or the power relationships of local institutions. Many other criteria are possible. However, different criteria are appropriate bases for different comparisons. For example, hydrology and flood risk may be compared on the basis of impervious surface [25]. The amount of woody vegetation may be used in comparisons of the exchange of heat or carbon dioxide between the surface and the atmosphere. The density of human population may be used as a predictor of water quality. Lifestyle contrasts may form the basis for comparisons of environmental decisions made by households in different parts of a metropolis, or in different metropolitan areas [41].

The fact that these many criteria are often patchily arranged suggests that comparisons will rarely be accomplished by running linear transects across metropolitan maps. Although raw distance is

sometimes useful in making coarse-scale urban comparisons, as it was along the urban-rural transect in metropolitan New York [42], in many cases the spatial heterogeneity as it exists on the ground may better be presented as a rearranged, abstract gradient [43]. An example of a gradient abstracted from an array of plots is the gradient of wealth along which bird biodiversity was distributed in Phoenix. Thus, while linear transects may be appropriate bases for initial comparison, ordinated gradients are in fact the general case which should be used to frame comparisons over different scales. The principle is as follows:

Principle 13: Urban comparisons can be framed as linear transects or as abstract gradients, and the abstract comparisons acknowledge the spatial complexity of urban heterogeneity.

The baker's dozen of principles present above frame the current state of urban ecology. As a biological discipline closely related to social and economic sciences and the theory and practice of urban design and planning, it is a relatively new and outward-looking field [13]. Hence, these principles are not the final roster that the field may exhibit. Nor are they in what is likely to be their final form. However, these broad ideas should continue to be useful over the next decade as this field consolidates by accumulating more data on specific urban places through time and by comparing amongst urban areas across the globe. These working principles identify assumptions and suggest hypotheses that can be used to guide future research on urban socio-ecological systems.

Future Directions

Although, as shown above, urban ecology has deep roots as a biological science as well as important parallels in social sciences and the design professions, it remains a young discipline. It is poised for significant growth and increased practical importance. There are three realms in which future directions cluster.

Interdisciplinary Integration for Understanding

Urban areas have been studied by many different disciplines, ranging from sociology, physical and human geography, economics, anthropology, and the more recent offshoots of these classic fields, such as political ecology, political economy, and human ecology. There is a large opportunity for integration across these perspectives. Accomplishing that integration is beyond the scope of this article, but ecological science has an important role to play in promoting integration among the diverse perspectives these disciplines represent. Ecology can play this role because it is preeminently an integrative discipline. It incorporates several contrasting perspectives that together define a goal for a more complete understanding of systems that contain biophysical components and biologically driven processes among their complex structures and functions. Ecology as a science focuses on (1) the interactions of organisms and environment through feedbacks, (2) the interactions of organisms with each other, (3) and the transformations that organisms generate within the environment. It is thus a science of interaction, feedback, and change. These three features are among the most important characteristics of urban systems.

Ecology can be a further stimulus to integration within urban systems because of its growing appreciation and study of the role of humans in ecosystems ranging from remote wilderness to suburbs and downtown districts [12]. This biological science has begun to link effectively with economics, with social sciences, with hydrology, and with atmospheric sciences, for example, in order to contribute to more comprehensive models of inhabited and built landscapes [44]. Yet there is still more work to be done on these various frontiers of integration, and the range of urban systems and ecosystem patches within complex city-suburban-exurban systems is an important arena in which to test hypotheses and models combining the perspectives of the different disciplines. Furthermore, data that integrate different disciplinary perspectives and the attempt to generalize cautiously from these data are important empirical activities.

A useful guide to these integrative approaches is the human ecosystem framework. Introduced originally by the social scientist William R. Burch, Jr., and his colleagues [21], this framework has been modified to reflect more bioecological content and thus to better support the integrative program of urban ecology [44]. The framework is not itself a model, but rather an organized roster of potential causes, mechanisms, and interactions upon which specific models can draw. The human ecosystem framework does take a human-centered perspective on inhabited and

managed systems and thus breaks the concept of human ecosystem down into the social system as the primary focus and into the biophysical foundations and sociocultural foundations of that social system (Fig. 1). This framework is an excellent abstract picture of any urban ecosystem. The components contained in this causal framework will have specific instances and representations in any urban area.

The biophysical foundations start metaphorically with the earth, air, fire (or energy), and water perspectives that must comprise any environment [45]. However, to prevent neglecting important environmental features that ecologists have come to appreciate in all systems they study, it goes on to include nutrients, which at some concentration often become pollutants, toxic materials and contaminants, soil structure and

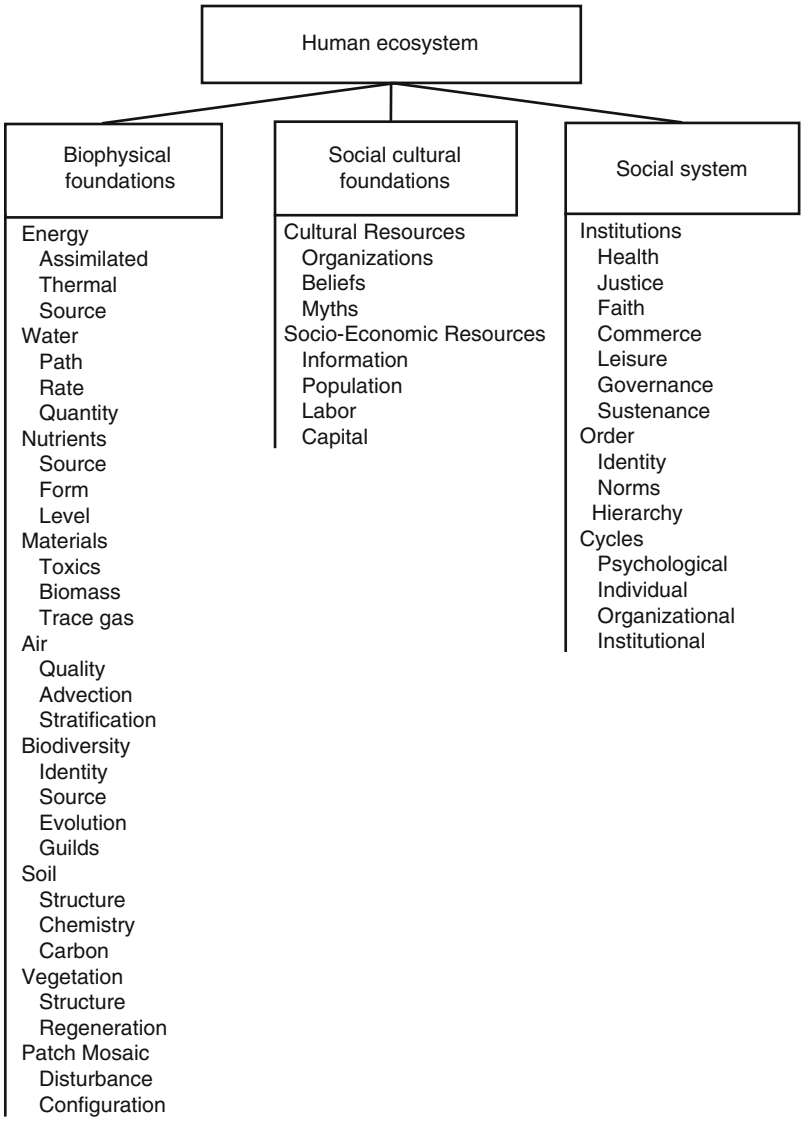

Urban Ecology. Figure 1
The human ecosystem framework as a hierarchy of potential causes and interactions within human ecosystems (Modified after Machlis et al. [21])

chemistry, vegetation composition and dynamics through time, and the spatial mosaic that the biophysical and built components jointly define in urban systems. Each of these categories has at least as much component complexity, if not more, than appears in Fig. 1. The sociocultural foundations include the resources provided by culture in its material, mental, and spiritual forms. Socioeconomic resources among the sociocultural foundation include information, population, labor, and capital. Capital of course refers not only to financial resources but also to the talents and skills of individual persons and the social capital embodied in networks of human interaction. The social system is the structure that enables and constrains the social interactions that all humans depend upon for their immediate well-being. The social system is characterized by the intuitions, in the broad sense, that humans construct to accomplish the tasks of survival, interaction, health, and control. The social system also establishes order among persons and does so in the form of social identity, formal and informal norms of behavior, and the establishment of social rank hierarchies along several dimensions (Fig. 1). The framework identifies cycles as a way of recalling that the components of the social system are not fixed in time or space, but can change with the collective changes in individual and household life cycles, individual and group psychological changes, organizational age as expressed in capacity and flexibility, and the degree of persistence of the various institutional structures in a society. The current intensification of globalization suggests that in many cases local or regional dynamics will be affected by biophysical, economic, and social changes that originate at a distance. For example, the massive migrations from countryside to cities, or from countries in which unemployment is high to different countries where people know or perceive there to be greater opportunities, or the displacements by war and disaster, all suggest looking beyond immediate boundaries for causes of change in city-suburban-exurban systems.

Urban Comparisons

Some generalizations have emerged in discussing the principles. For example, biotic homogenization is a common feature of urban systems [46], although not all taxa or functional groups express homogenization. Likewise, there is an urban stream syndrome, in which downcutting of stream beds is associated with stranding of flood plains and reduction of riparian and in-stream ecological function, and with simplification of the heterogeneity and biotic diversity in stream channels [47]. On a more hypothetical level are generalizations about the increasing similarity of carbon budgets of cities based on planting and maintenance of mesic vegetation in all types of climates [48]. Although these generalizations seem robust so far, they must be challenged, refined, or rejected based on further comparisons with additional cities. Of course, to conduct appropriate comparisons, cities may have to be more explicitly classified according to some globally relevant schema than they are now [27]. City-suburban-exurban systems differ based on location relative to rivers, streams, or coastal waters; regional climate and form of original vegetation; kind of geological substrate; and exposure to natural hazards. In the broad social realm, cities experience different forms of governance; different histories with respect to development, industry, shipping, and ground transportation; access to commodities and sources of wealth; cultural context and diversity; and porosity of social groups. Not all of these may be major axes of comparison, but they point to some of the many dimensions that may affect differences among cities in their bioecological structure and function.

An important aspect of the comparison of cities is their ability to represent global change processes. Cities may well stand in as a laboratory for global change, as temperate cities are now often drier than their mesic surroundings, and due to the urban heat island effect, are generally hotter. Portions of some highly irrigated desert cities may be an exception and in fact be cooler during some hours than the surrounding arid lands due to the evaporation of massive quantities of surface irrigation water or introduced mesic plants [22]. Another feature of global change that some cities may mimic is a great exposure to flood risk due to the building of floodwalls and levees upstream.

Comparisons within cities can benefit from new land cover classifications. The usual "Anderson Level II" classification uses such categories as commercial, industrial, transportation, and residential in low,

medium, and high intensities of occupancy. These categories may be too coarse for some desirable ecological comparisons [49]. Likewise, the census geography of block groups based on clusters of approximately 400 households may be rather coarse relative to some levels of ecological function [19]. Both the land use/land cover and the census geographies fail, for example, to adequately match the fine-scale watershed behaviors in urban areas. Social perceptions of edges, enclaves, corridors, and so on may also match other scales of observation than the classical tools of differentiation within urban areas. One example of a classification scheme devised to expose aspects of joint biophysical and social differentiation is the High Ecological Resolution Classification for Urban Landscapes and Environmental Systems (HERCULES) [49]. Rather than assuming land use as the determining criterion, it focuses on land cover in order to provide a structural base to test against bioecological functioning. HERCULES classifies patches in urban systems based on (1) surface characteristics, whether bare or paved, (2) presence and amount of either tall or short vegetation, and (3) cover and kinds of buildings. The classes may be extracted from continuous variation along these three axes, or may be defined to represent percentiles of the different categories. This and other classifications are a frontier tool for urban ecology to promote within and cross-system comparisons.

Integration for Practice

Urban ecological science can be integrated with a number of professional practices. This section illustrates its potential for linkage with urban design and planning, environmental justice, and adaptive processes supporting sustainability. Further integration can emerge from dialog with the concerns of urban policy makers and managers.

Integrating with Urban Design and Planning

Urban design incorporates the activities of architects and landscape architects and often focuses on individual sites, on neighborhoods, or spatially extensive development or redevelopment projects. Urban planning, in contrast, brings aspects of that same knowledge set together with knowledge about policy, governance, and regulation and generates coarse-scale designs for large areas or regions. Master planning is a synonym for this coarser-scale pursuit. Both have traditions that express concern with ecology as a relevant knowledge base or approach. One tradition takes analogies with evolution or ecological processes as a touchstone. This tradition began with Geddes in Scotland, who is one of the founders of modern landscape architecture [50]. Ecological analogies have been common among those who wish to bring an ecological perspective to the urban design and planning professions. This is in part because there has been until recently so little empirical ecological research in urban systems. In this knowledge gap, idealized successional trends from simple to spatially complex systems, ending in a stable "climax," have been brought to bear. Other analogies adopted in the design professions have been the classical ecological expectation of equilibrium in systems. A still larger and deeply flawed analogy has been the adoption of an organism-like life cycle for cities and towns. The life cycle analogy was used to justify policies of physical intervention to circumvent undesired changes in cities. Of course, the assumption that physical change was sufficient to address social problems is another questionable assumption, often tacit, that was used along with life cycle analysis to justify such interventions as slum clearance. Unfortunately, these analogies are not supported by the contemporary knowledge base in ecological science itself. Succession is a probabilistic process that does not lead inexorably toward some ideal state. Equilibrium composition is rarely obtained in ecological systems, even though material balances and thermodynamic processes can be used to understand the structure and function of ecosystems.

In contrast to the use of ecological analogies, which is necessarily limited by the superficiality of the visualizations transferred to design, ecological substance has informed a growing number of designers. In Europe, analyses of "ecotopes," patches that hosted biodiversity or complex bioecological structure, were incorporated into plans to meet aesthetic or functional needs the patches were perceived to satisfy. In the realm of greenfield development, McHarg [51] famously introduced a multilayered strategy to analyze ecological, physical, historical, and cultural features of an area to be developed. The site design was spatially arranged to optimize the joint benefits and reduce the hazards associated with the layers representing different features of the

landscape. Spirn [32] applied a careful analytic approach to established urban areas in her work in Boston and west Philadelphia. She used an understanding of watershed dynamics to explain where disempowered communities faced risks due to design in their neighborhood that had been insensitive to ecological processes. This information then informed appropriate neighborhood redevelopment and plans for renewed green space in these old city neighborhoods. This evolving tradition is notable for taking account of both bioecological processes and social concerns. Other designers and planners are promoting the integration of ecological substance with their professional theory and practice [52]. Shared work between designers and ecologists has several advantages. One advantage to working with designers is the entry they provide into the intricacies of development and construction in urban environments, thus making new sites available to their ecological research partners [31]. A second advantage of the increasing interaction between ecologists and designers is to treat constructed design projects as experimental venues [30]. Indeed, because designs provide alternative arrangements of various kinds of surfaces, vegetation, and slopes, for example, they may yield important and novel information on the relationship between urban form and its ecological function [53]. Scaling these relationships from individual small sites to large developments provides another dimension of experimental comparison. Measurements taken in contrasting built projects and landscapes provide an essentially untapped resource for increasing the ecological understanding of urban systems [54].

Environmental Justice Environmental justice refers to the concern about equal access of all persons to environmental goods and services, and equal avoidance of or capacity to respond to environmental hazards. As a social movement, it emerged from communities of color and from communities with poor access to resources and power, in which people noted an unusual association with toxic sites or other serious environmental disamenities. As a result of this origin, environmental justice has an activist dimension and a scholarly dimension. Ecology can contribute to the scholarship of environmental justice by enhancing the understanding of environmental benefits and environmental hazards. Traditionally, environmental justice has focused on environmental negatives or disamenities. In cities, ecologists and related scientists are increasing the stock of knowledge about not only the disamenities, but increasingly about the benefits that emerge from the biotic components of human ecosystems. This focus on benefits is part of the study of ecosystem services [55]. Examples of urban ecosystem services include the mediation of local climate by trees, the tempering of human behavior by green views, the reduction of stormwater flows, provision of recreation, conversion of some pollutants to neutral forms, and the sequestration of carbon dioxide in biomass, soils, and organic litter [56]. Cultural benefits also accrue to the biotic components of urban ecosystems. These include a sense of place provided by ecological structures such as particular patches of vegetation or streams. Environmental justice can be enhanced by a broader understanding of the spatial distribution of hazards such as fire and exposure to winds, and to the potential for mitigation and other positive services provided by the biotic components of urban ecosystems.

Sustainability and Adaptive Processes An emerging frontier in urban systems is the nature and processes of sustainability. Sustainability is defined in two main ways. One definition suggests that sustainability is the capacity to meet present needs without compromising the ability of future generations to meet their own needs. A second definition focuses on the reconciliation of demands within economic, social, and environmental spheres that permit the entire integrated system to persist and continue to adapt to change. This second definition is important for giving equal weight to the three facets of the global hybrid system as well as accommodating social justice as a key aspect of the social dimension. Indeed, some scholars define sustainability in terms of economy, environment, and equity, following the assumption that a social system that does not provide for equity is less likely to persist.

Sustainability, as the ability to adjust to changing conditions originating within and beyond the system of interest, is closely related to the concept of resilience. Resilience is the capacity of systems to experience disturbance and shocks and still remain within a given structural or functional domain. Such resilience requires adaptive processes (Fig. 2). Adaptive processes

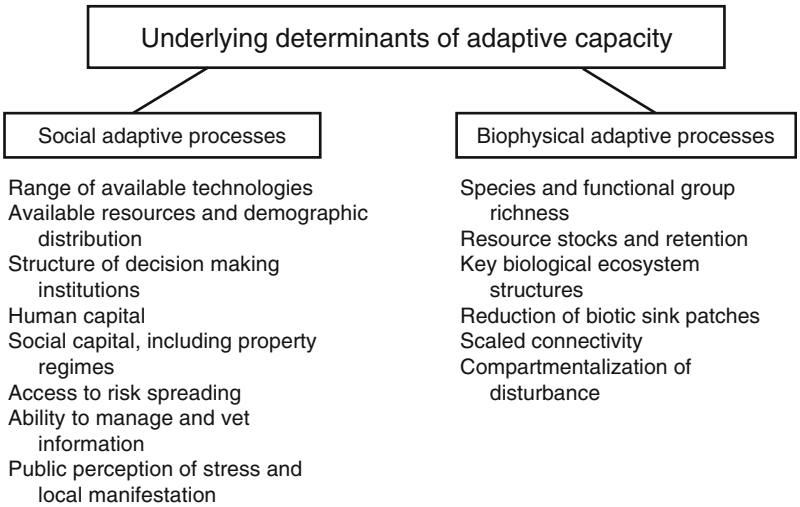

Urban Ecology. Figure 2
Underlying determinants of adaptive capacity in socio-ecological systems. Social components derived from Yohe and Tol [57] and biophysical components derived from Gunderson and Pritchard [58] and Walker et al. [59]

are both social [57] and bioecological [58, 59], in keeping with the understanding of most contemporary ecosystems as human ecosystems (Fig. 2). Adaptive processes bring the components of human ecosystems into the dynamic realm of sustainability and resilience.

Sustainability has become a goal of many urban jurisdictions. This development is the latest stage in an ongoing evolution of cities in industrial countries. The industrial city was the epitome of overcrowding, contaminated water, and industrially generated pollution, for example. Reformers followed two paths to correct the flaws of the industrial city. One was to abandon it altogether. This strategy motivated the establishment of suburbs, or of garden cities in green sites well outside the shadow of the dark Dickensian industrial city. The second strategy was to alter the industrial city itself. Providing clean water, removing waste, alleviating overcrowding, and reducing the local impact of pollution were hallmarks of this second strategy, which can be labeled, following historian Martin Melosi [60], the "sanitary city." The sanitary city installed infrastructure to carry sewage away from the populated areas. Ultimately, treatment was added, so that downstream systems did not have to bear the burden of the displaced sewage. Smokestacks were built taller so that local pollution was alleviated. Ultimately, newer fuels or scrubbing technologies for coal-fired installations also contributed to reduced pollution. Sanitary landfills were established, and odoriferous wetlands were drained or filled. Many of the solutions employed in the sanitary city were engineered tactics to deal with specific problems. The departmental structure of cities followed this issue-by-issue approach, so that water supply, waste water, solid waste, streets, housing, parks, and so on were dealt with by separate agencies of municipal government.

The emerging sustainable city contrasts with the key characteristics of the older sanitary city. Cities will always be heterotrophic systems, garnering food and other resources from beyond their boundaries. Furthermore, they will generate waste that must be dealt with, requiring commitments of land and other resources – an urban footprint – that extends well beyond their geopolitical boundaries [61]. However, as an ideal, sustainable cities aim to reduce their ecological footprint. A sustainable city is one that reduces its demand and its impact on the environment by reducing resource use and waste generation. Sustainable cities manage potable water, gray water, and stormwater in ways that reduce flood risks, contamination of water, and waste of potable water. They reduce energy use via building standards, landscape design, and reducing per capita use of fuel in transportation. Limiting sprawl while maintaining space for ecological processes and

capacities in the urban matrix is an important feature of the sustainable city. Hence, other dimensions of sustainability must be supported. In the environmental realm, reducing vulnerability to natural and human-generated hazards is a sustainability goal, as are supporting native biodiversity and achieving the ecosystem services that eminate from green spaces in the urban matrix. Reduced contribution to global warming can be achieved through enhanced carbon sequestration.

Sustainability by definition also must deal with social processes. Too often in the past, urban interventions have focused on the physical form of the city, assuming that social benefits will follow. Contemporary focus on sustainability recognizes that social capital, community cohesion, and social equity are issues that must be addressed in and of themselves for generating and maintaining liveable cities. Equity is a major component of the social realm, as discussed above, and is reflected in exposure to environmental hazards, access to environmental benefits, and inclusion in the process of making environmentally relevant decisions.

The economic aspect of sustainability is well known, and because of the traditional predominance of attention in urban studies to issues of jobs, finance, the real estate industry, and the relationships of business and political processes, it is not necessesary to review it further in this article. Clearly, however, economic resources and sustainability of economic capacity contribute to well-being in urban systems.

One of the potentially most powerful aspects of the sustainable city ideal is how management and policy are conducted in this new kind of city. As mentioned before, the sanitary city is managed by discrete departments or authorities, often having little cross-communication. For example, the concern with street cleaning are isolated in the transportation department, whereas street sweeping in fact affects stormwater quality. Another cross-cutting issue is how the presence of vegetation can influence aggression, which joins the concerns of a parks department with those of public safety. These simple examples suggest that sustainability can be enhanced by integrated management in urban systems. Indeed, cross-cutting management and policy are hallmarks of the emerging sustainable city. This suggests that sustainability can be usefully considered a central function of city administration and not an isolated pursuit to be marginalized in a special office isolated from the traditional activities of municipal government. Indeed, there are growing numbers of examples of cross-sectoral management as part of sustainability strategies. For example, in the city of Baltimore, neighborhood tree planting and gardening, removal of unneeded pavement in school yards, altered street cleaning schedules, community environmental activities, and installation of fine-scale best management practices such as rain gardens specifically designed to be both attractive and to allow infiltration of stormwater into the soil, engage multiple city departments in specific neighborhoods to achieve social, environmental, and economic revitalization. Ecological research can help inform and evaluate sustainability plans, which are often mostly metaphorical or assessed only by indices of human outcomes.

Communication between researchers and decision-makers is a key ingredient in the success of the sustainable city. Growing experience shows that communication is enhanced when approached as a two-way dialog, rather than a one-way flow of information from science to policy. Indeed, such a dialog can help shape scientific research and identify practical management projects that provide data about the structure and function of urban ecosystems. Mutual respect for the knowledge, constriants, and rewards of each group involved in the dialog is a firm foundation for effectively shaping the science and the practice of urban sustainability. Establishing effective and lasting forums for such communication is a practical part of the frontier of urban ecological science. Such dialog is one tool for the sustainable city, which remains a goal rather than a reality. Combining the knowledge, concerns, and networks represented by problem solving and knowledge generation is perhaps the most urgent frontier for further research and action.

Bibliography

Primary Literature

1. Collins JP et al (2000) New urban ecology. Am Sci 88:416–425
2. Elvidge CD et al (2004) US constructed area approaches the size of Ohio. Euro Opt Soc 85:233–240
3. Grimm NB et al (2000) Integrated approaches to long-term studies of urban ecological systems. BioScience 50:571–584
4. Numata M (1977) The impact of urbanization on vegetation in Japan. In: Miyawaki A, Tuxen R (eds) Vegetation science and environmental protection. Maruzen, Tokyo

5. Loucks OL (1994) Sustainability in urban ecosystems: beyond an object of study. In: Platt RH, Rowntree RA, Muick PC (eds) The ecological city: preserving and restoring urban biodiversity. University of Massachusetts Press, Amherst, pp 48–65
6. Alberti M et al (2003) Integrating humans into ecology: opportunities and challenges for studying urban ecosystems. BioScience 53:1169–1179
7. Pickett STA, Grove JM (2009) Urban ecosystems: what would Tansley do? Urban Ecosyst 12:1–8
8. Sukopp H (1990) Urban ecology and its application in Europe. In: Sukopp H, Hejny S, Kowarik I (eds) Urban ecology: plants and plant communities in urban environments. SPB Academic, The Hague, pp 1–22
9. Stearns F, Montag T (eds) (1974) The urban ecosystem: a holistic approach. Dowden, Hutchinson and Ross, Stroudsburg, p 217
10. Wu J, Loucks OL (1995) From balance of nature to hierarchical patch dynamics: a paradigm shift in ecology. Q Rev Biol 70:439–466
11. Boyden S et al (1981) The ecology of a city and its people: the case of Hong Kong. Australian National University Press, Canberra, pp 21–473
12. Redman C, Grove JM, Kuby L (2004) Integrating social science into the long-term ecological research (LTER) network: social dimensions of ecological change and ecological dimensions of social change. Ecosystems 7:161–171
13. Grimm NB et al (2008) Global change and the ecology of cities. Science 319:756–760
14. Fernández-Juricic E, Jokimäki J (2001) A habitat island approach to conserving birds in urban landscapes: case studies from southern and northern Europe. Biodivers Conserv 10:2023–2043
15. Gibb H, Hochuli DF (2002) Habitat fragmentation in an urban environment: large and small fragments support different arthropod assemblages. Biol Conserv 106:91–100
16. Crooks KR et al (2001) Extinction and colonization of birds on habitat islands. Conserv Biol 15:159–172
17. Leston LFV, Rodewald AD (2006) Are urban forests ecological traps for understory birds? An examination using northern cardinals. Biol Conserv 131:566–574
18. Groffman PM et al (2003) Down by the riverside: urban riparian ecology. Front Ecol Environ 1:315–321
19. Cadenasso ML et al (2008) Exchanges across land-water-scape boundaries in urban systems: strategies for reducing nitrate pollution. Ann NY Acad Sci 1134:213–232
20. Light JS (2009) The nature of cities: ecological visions and the American urban professions 1920–1960. Johns Hopkins University Press, Baltimore
21. Machlis GE, Force JE, Burch WR (1997) The human ecosystem. 1. The human ecosystem as an organizing concept in ecosystem management. Soc Nat Resour 10(4):347–367
22. Baker LA et al (2002) Urbanization and warming of Phoenix (Arizona, USA): impacts, feedbacks and mitigation. Urban Ecosyst 6:183–203
23. Troy AR et al (2007) Predicting opportunities for greening and patterns of vegetation on private urban lands. Environ Manage 40:394–412
24. Alig RJ, Kline JD, Lichtenstein M (2004) Urbanization on the US landscape: looking ahead in the 21st century. Landscape Urban Plann 69:219–234
25. Gurnell A, Lee M, Souch C (2007) Urban rivers: hydrology, geomorphology, ecology and opportunities for change. Geogr Compass 1(5):1118–1137
26. Snep RPH et al (2006) How peri-urban areas can strengthen animal populations within cities: a modeling approach. Biol Conserv 127:345–355
27. Dow K (2000) Social dimensions of gradients in urban ecosystems. Urban Ecosyst 4:255–275
28. Theobald DM (2004) Placing exurban land-use change in a human modification framework. Front Ecol Environ 2:139–144
29. Radeloff VC et al (2005) The wildland urban interface in the United States. Ecol Appl 15:799–805
30. Outen DC (2007) Pioneer on the frontier of smart growth: the Baltimore County, MD experience, in Smart growth @ 10: a critical analysis of Maryland's landmark landuse program. The National Center for Smart Growth Research and Education, Annapolis and College Park, Maryland, p 49
31. Felson AJ, Pickett STA (2005) Designed experiments: new approaches to studying urban ecosystems. Front Ecol Environ 3:549–556
32. Spirn AW (2005) Restoring Mill Creek: landscape literacy, environmental justice and city planning and design. Landscape Res 30:395–413
33. Groffman PM et al (2002) Soil nitrogen cycling processes in urban riparian zones. Environ Sci Technol 36:4547–4552
34. Kennedy C, Cuddihy J, Engel-Yan J (2007) The changing metabolism of cities. J Ind Ecol 11:43–59
35. McKinney ML (2002) Urbanization, biodiversity, and conservation. BioScience 52:883–891
36. Beissinger SR, Osborne DR (1982) Effects of urbanization on avian community organization. Condor 84:75–83
37. Yeh PJ (2004) Rapid evolution of a sexually selected trait following population establishment in a novel habitat. Evolution 58:166–174
38. Slabbekoorn H, Peet M (2003) Birds sing at a higher pitch in urban noise. Nature 424:267
39. Wyckoff PH, Webb SL (1996) Understory influence of the invasive Norway maple (*Acer platanoides*). Bull Torrey Bot Club 123:197–205
40. McIntyre NE, Knowles-Yanez K, Hope D (2000) Urban ecology as an interdisciplinary field: differences in the use of "urban" between the social and natural sciences. Urban Ecosyst 4:5–24
41. Zhou W et al (2008) Can money buy green: demographic and socioeconomic predictors of lawncare expenditures and lawn greenness in urban residential areas. Soc Nat Resour 22:744–760
42. Pouyat RV, Turechek WW (2001) Short- and long-term effects of site factors on net N-mineralization and nitrification rates along an urban-rural gradient. Urban Ecosyst 5:159–178
43. McDonnell MJ et al (1997) Ecosystem processes along an urban-to-rural gradient. Urban Ecosyst 1:21–36

44. Pickett STA et al (2011) Urban ecological systems: scientific foundations and a decade of progress. J Environ Manag 92:331–362
45. Spirn AW (1984) The granite garden: urban nature and human design. Basic Books, New York, pp 1–334
46. Clergeau P et al (2006) Avifauna homogenisation by urbanisation: analysis at different European latitudes. Biol Conserv 127:336–344
47. Walsh CJ et al (2005) The urban stream syndrome: current knowledge and the search for a cure. J N Am Benthol Soc 24:706–723
48. Carreiro MM et al (2009) Carbon and nitrogen cycling in soils of remnant forests along urban-rural gradients: case studies in the New York metropolitan area and Louisville, Kentucky. In: McDonnell MJ, Hahs A, Breuste J (eds) Ecology of cities and towns: a comparative approach. Cambridge University Press, New York, pp 308–328
49. Cadenasso ML, Pickett STA, Schwarz K (2007) Spatial heterogeneity in urban ecosystems: reconceptualizing land cover and a framework for classification. Front Ecol Environ 5:80–88
50. Welter VM (2002) Biopolis: Patrick Geddes and the city of life. MIT Press, Cambridge, p 355
51. McHarg I (1969) Design with nature. Doubleday/Natural History Press, Garden City, p 197
52. Musacchio LR (2009) Pattern:process metaphors for metropolitan landscapes. In: McDonnell MJ, Hahs A, Breuste J (eds) Ecology of cities and towns: a comparative approach. Cambridge University Press, New York, pp 484–502
53. Pickett STA, Cadenasso ML (2008) Linking ecological and built components of urban mosaics: an open cycle of ecological design. J Ecol 96:8–12
54. Cook WM et al (2004) Learning to roll with the punches: adaptive experimentation in human dominated systems. Front Ecol Environ 2:467–474
55. Boone CG et al (2009) Parks and people: an environmental justice inquiry in Baltimore, Maryland. Ann Assoc Am Geogr 99:767–787
56. Bolund P, Hunhammar S (1999) Ecosystem services in urban areas. Ecol Econ 29:293–301
57. Yohe G, Tol RSJ (2002) Indicators for social and economic coping capacity – moving toward a working definition of adaptive capacity. Glob Environ Change 12:25–40
58. Gunderson LH, Pritchard L Jr (eds) (2002) Resilience and the behavior of large-scale systems. Island Press, Washington, DC, p 287
59. Walker B et al (2004) Resilience, adaptability and transformability in social-ecological systems. Ecol Soc 9(2): Article 5
60. Melosi MV (2000) The sanitary city: urban infrastructure in America from colonial times to the present. Johns Hopkins University Press, Baltimore, 600 pp
61. Rees WE (1992) Ecological footprints and appropriated carrying capacity: what urban economics leaves out. Environ Urbanization 4:121–129

Books and Reviews

Alberti M (2008) Advances in urban ecology: integrating humans and ecological processes in urban ecosystems. Springer, New York

Beatley T (2000) Green urbanism: learning from European cities. Island, Washington, DC

Bullard RD (ed) (2005) The quest for environmental justice: human rights and the politics of pollution. Sierra Club Books, San Francisco

Burch WR Jr (1988) Human ecology and environmental management. In: Agee JK, Johnson DR (eds) Ecosystem management for parks and wilderness. University of Washington Press, Seattle, pp 145–159

Burger J (1999) Animals in towns and cities. Kendall/Hunt Publishing Company, Dubuque

Cadenasso ML, Pickett STA (2008) Urban principles for ecological landscape design and management: scientific fundamentals. Cities Environ 1(2):1–16

Catterall CP (2009) Responses of faunal assemblages to urbanisation: global research paradigms and an avian case study. In: McDonnell MJ, Hahs A, Breuste J (eds) Ecology of cities and towns: a comparative approach. Cambridge University Press, New York, pp 129–155

Curwell S, Deakin M, Symes M (eds) (2005) Sustainable urban development, volume 1: the framework and protocols for environmental assessment. Routledge, New York

Forman RTT (2008) Urban regions: ecology and planning beyond the city. Cambridge University Press, New York

Frumkin H, Frank L, Jackson RB (2004) Urban sprawl and public health: designing, planning and building for healthy communities. Island, Washington, DC

Gleick PH (2009) The world's water: 2008–2009. Island, Washington, DC

Grove JM (2009) Cities: managing densely settled social-ecological systems. In: Chapin FS III, Kofinas GP, Folke C (eds) Principles of ecosystem stewardship: resilience-based natural resource management in a changing world. Springer, New York, pp 281–294

Gunderson LH (2000) Ecological resilience – in theory and application. Annu Rev Ecol Syst 31:425–439

Marzluff JM, Schulenberger E, Endlicher W, Alberti M, Bradley G, Ryan C, Simon U, ZumBrunne C (eds) (2008) Urban ecology: an international perspective on the interaction between humans and nature. Springer, New York

McDonnell MJ, Breuste J, Hahs A (2009) Introduction: scope of the book and need for developing a comparative approach to the ecology of cities and towns. In: McDonnell MJ, Hahs A, Breuste J (eds) Ecology of cities and towns: a comparative approach. Cambridge University Press, New York, pp 1–5

McGrath BP, Marshall V, Cadenasso ML, Grove JM, Pickett STA, Plunz R, Towers J (eds) (2007) Designing patch dynamics. Columbia University Graduate School of Architecture, Preservation and Planning, New York

Sukopp H, Numata M, Huber A (1995) Urban ecology as the basis of urban planning. SPB Academic, The Hague

United Nations Population Fund (2007) State of world population 2007: unleashing the potential of urban growth. United Nations Population Fund, New York

Urban Forest Function, Design and Management

Kjell Nilsson[1], Cecil C. Konijnendijk[1], Anders Busse Nielsen[2]
[1]Danish Centre for Forest, Landscape and Planning, University of Copenhagen, Frederiksberg C, Denmark
[2]Department of Landscape Management, Design and Construction, Swedish University of Agricultural Sciences, Alnarp, Sweden

Article Outline

Glossary
Definition of the Subject with Brief Historical Background
Introduction: Urban Forest Resources in a Global Context
The Benefits of Urban Greening
Urban Forest Policies
Design and Management of the Urban Forest
Future Directions
Bibliography

Glossary

Green infrastructure Green infrastructure is a planned network of multifunctional green spaces and interconnecting links which is designed, developed and managed to meet the environmental, social, and economic needs of communities.

Urban forest The sum of all woodland and other tree-based vegetation in and immediately surrounding an urban area.

Urban forestry The art, science, and technology of managing trees and forest resources in and around urban communities for the environmental, social, economic, and esthetic benefits trees provide to people.

Urban green space All vegetated lands in urban areas, including parks, woodland, gardens, cemeteries, orchards, etc. Often urban green space is used in terms of publicly owned green space.

Urban greening The planning and management of all urban vegetation to create or add values to the local community in an urban area.

Urban woodland Forested land located in or close to urban agglomerations, with a multiple forest functions approach. Typically, social and environmental forest services are the focus of urban woodland management.

Definition of the Subject with Brief Historical Background

Land use planners have increasingly been focusing on urban green infrastructure rather than individual green elements. Moreover, politicians, researchers, and practitioners have had to deal with the contributions of this urban green infrastructure to the quality of urban life and environment. They have started to realize that more integrated green area planning and management are required to meet current societal demands when operating in high-pressure environments. This has led to the emergence of new concepts and approaches of a more integrative kind. Urban greening, for example, has developed as the planning and management of all urban vegetation to create or add values to the local community in an urban area [40, 66]. Another more integrative concept resulting from the above-mentioned developments is that of urban forestry.

Urban forestry has become defined as the art, science, and technology of managing trees and forest resources in and around urban communities for the environmental, social, economic, and esthetic benefits trees provide to people (developed from [27, 50]). In its broadest sense, urban forestry embraces a multi-managerial system that includes municipal watersheds, wildlife habitats, outdoor recreation opportunities, landscape design, recycling of municipal wastes, tree care in general, and the production of wood fiber as a raw material. Urban forestry includes activities carried out in the city center, suburban areas, and the peri-urban or interface area with rural lands.

Growing awareness about the need for more integrated approaches to urban green planning and management, and specific threats to urban tree populations caused by pests and diseases (such as Dutch Elm Disease) led to the emergence of urban forestry in North America during the 1960s. Europe and other parts of the world followed with, for example, international research networking intensifying during the late 1990s (e.g., [35, 39, 50]). In spite of this, urban forestry is an

emerging and still developing field. Differences can be noted in the definition and implementation of the urban forestry concept in different parts of the world, with, for example, a traditional focus on urban woodland in Europe (e.g., [40]). However, the concept of urban forestry as encompassing the planning, design, establishment, and management of trees and forest stands with amenity values situated in or near urban areas, has become more widely accepted.

In Europe, the definition of urban forestry has been adapted into the Urban Forestry Matrix see (Fig. 1).

The matrix shows the integrative scope of urban forestry, incorporating urban and peri-urban tree resources, including single trees and groups of trees along streets, in public and private parks and gardens, cemeteries, and so forth. The distinction between the three types of locations included in the matrix arises from three different levels of planning and management hierarchy, stress, establishment techniques, average life times, and costs in relation to establishment and management [55]. Street trees, for example, are usually single trees with a low average lifetime due to a high stress level. Moreover, street trees generally involve the highest management costs. Park trees are also to be found individually or in small groups, with a medium or high average lifetime, medium stress level, and medium costs for establishment and management. Urban woodland trees are usually established in stands by means of seeding or planting of small trees, with a high average lifetime, low establishment cost, and, relatively, low management costs.

The matrix also shows the different relationships and interactions between human society and urban forest resources. At the more strategic level, form and function of urban forests provide a basis for policy-making, planning, and design. The selection of plants for the urban environment, and tree establishment involve technical activities. Management, finally, is aimed at bringing strategies and technical operations together in order to maintain and develop sustainable and multifunctional urban forest resources.

As visualized in the matrix, urban forestry is an integrative approach, combining street and garden trees with urban woodland, and extending from

	Street trees	Trees in parks, private yards, cemeteries	Urban woodlands
Form, functions, design, policies and planning			
Selection, establishment and other technical approaches			
Management			

Urban Forest Function, Design and Management. Figure 1
The Urban Forestry Matrix (Based on [37], photos by Kjell Nilsson)

policy-making to establishment, maintenance, and management activities. Integration has been described as one of the key characteristics (and strengths) of urban forestry [35]. Other characteristics include its strategic scope, its social inclusiveness (emphasizing stakeholder involvement), its focus on multifunctionality of the urban forest resource, and its embracing of the urban settings and dynamics in which urban forests are situated.

Introduction: Urban Forest Resources in a Global Context

In 2008, for the first time in human history, the number of people living in urban areas exceeded the rural population. Urban areas in developing countries will account for nearly 90% of the projected world population increase of 2,700 million people between 1995 and 2030.

Urbanization is a worldwide phenomenon; the World Resources Institute [87] estimated that in 2025, more than 50% of the African and Asian populations would be living in urban areas. In Central and South America these figures will be between 75% and 85% (Fig. 2).

Managing urban population change will be one of the most important challenges during the next decades, along with moderating the impacts of climate change. In developed countries, the urban future will involve dealing with complex changes in the composition of urban populations and containing urban sprawl beyond the suburbs to retain the critical ecosystem services that will sustain population growth. In developing countries, where 80% of the world's population resides, central issues will be how to cope with an unprecedented increase in the number of people living in urban areas and with the growing concentration of these urbanites in large cities with millions of residents and declining availability of natural resources.

Throughout Europe, the proportion of urban green areas varies considerably, from less than 5% in cities like Tirana and Bratislava to nearly 70% of the area of Oslo and Gothenburg [11] (Fig. 3). In comparison, the figure for Mexico City is only 2.2%; in relation to the number of inhabitants, this only provides 1.94 m^2 per inhabitant, which is far below the 9 m^2 recommended by the World Health Organization [6]. However, these figures should be taken cautiously since definitions of green space and city boundaries differ a lot between cities. A suggested measure of urban environmental quality is the location of green areas within a walking distance of 15 min or less from all housing areas. This criterion is met for the citizens in, for example, Brussels, Copenhagen, Glasgow, Madrid, Milan, and Paris and, in general, for more than 50% of the population in most European cities [78].

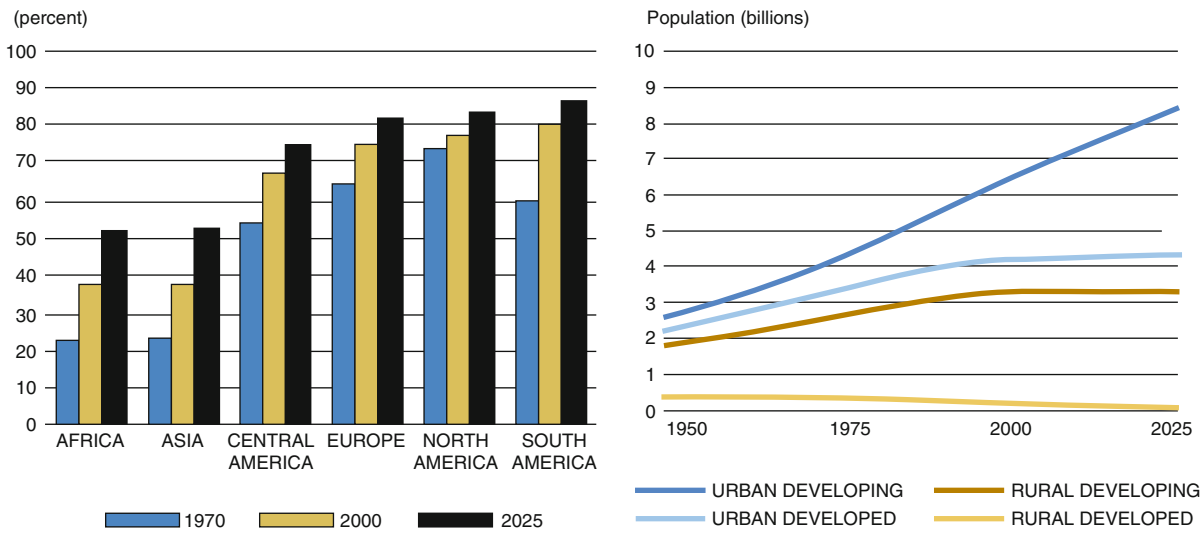

Urban Forest Function, Design and Management. Figure 2
Estimated urban population by region (From [87])

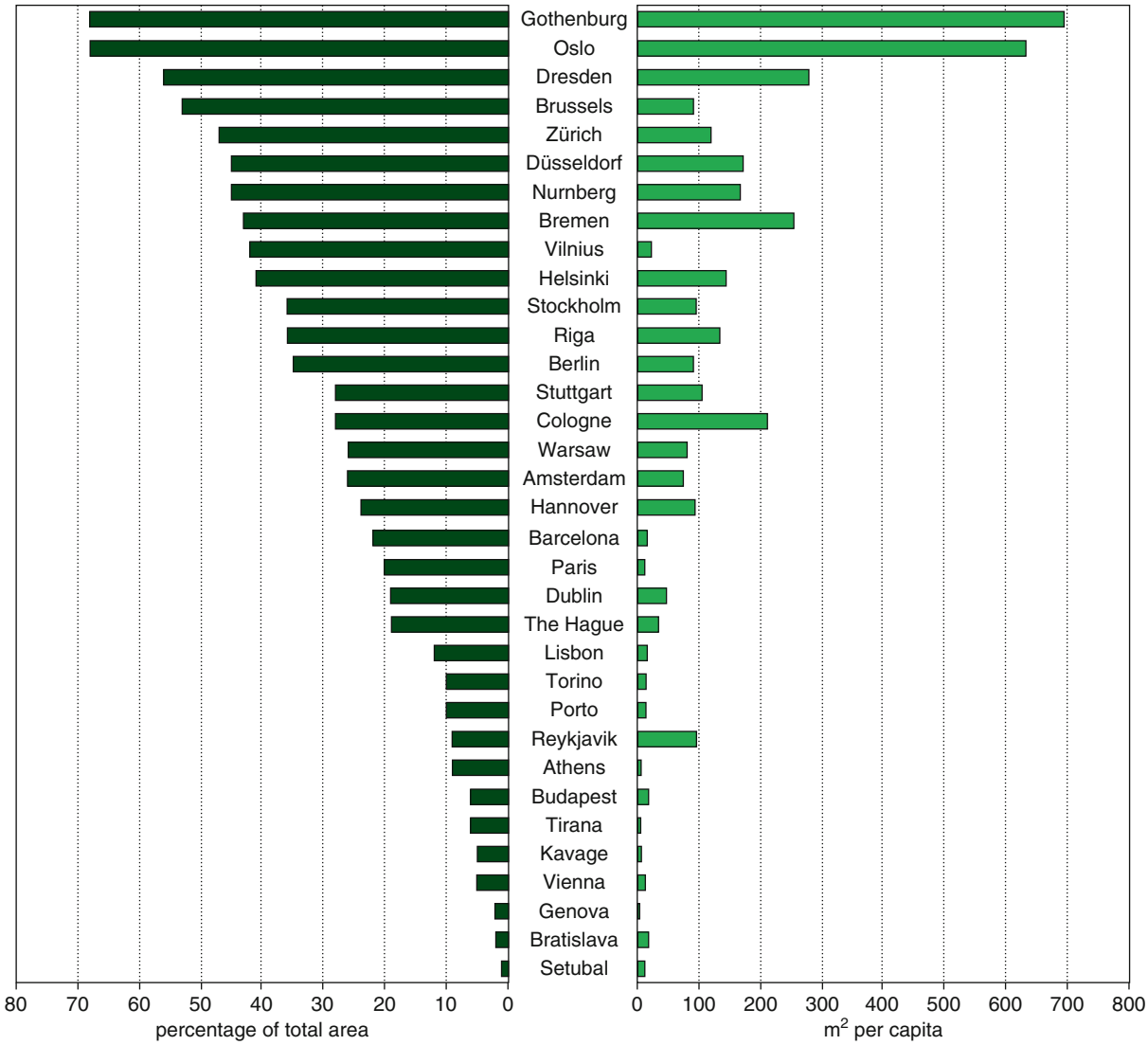

Urban Forest Function, Design and Management. Figure 3
Green areas in selected European cities [11]

The Benefits of Urban Greening

The green infrastructure of cities provides urban society with an essential range of goods and services, representing the three dimensions of sustainable development: Environmental, economic, and social sustainability.

Environmental and Ecological Functions

Reduce Air Pollution Trees intercept particulate matter and absorb such gaseous pollutants as ozone, sulfur dioxide, and nitrogen dioxide, thus removing them from the atmosphere. Several studies conducted in the USA as well as in Germany and China have shown that urban tree cover has the potential for improving air quality [7, 57, 88]. Protective plantations along heavily trafficked roads and around industrial areas are, therefore, an effective means of reducing air pollution. In Santiago de Chile, urban forests were found to be a cost-effective air quality improvement policy [15]. But this should obviously not be taken as an excuse for neglecting to combat pollution at its source.

Even though plants absorb carbon dioxide and produce oxygen, it is still important not to assign plants excessive significance to the urban environment. Harris [26] reminds that plants really have only a minor effect on the carbon dioxide and oxygen content of urban air. Photosynthesis in the oceans accounts for between 70% and 90% of the world's total oxygen production, for which reason it is absolutely vital that they be protected against pollution. Even a minor reduction in the oxygen content of the air will cause a large percentage increase in its carbon dioxide content, which would reinforce the greenhouse effect, thus leading to a rise in the global temperature. Harris [26] also stresses that urban vegetation has an especially beneficial effect on air pollution through its ability to cool urban heat lands and reduce the quantity of airborne particles.

Protect Water Resources and Reduce Stormwater Runoff Before modern urban areas made their appearance, rainwater was handled locally. It ran in stone fascines in the ground or out onto fields and pastures. The towns also had streams and wetlands that functioned as recipients. The great change came after the Second World War, when serious attempts were made to drain the water away from residential areas, streets, and squares in underground sewer pipes. Thus, the traditional water cycle of the towns lost its main source. Instead, costly drinking water is now used for watering greens and plantations.

When it falls on roofs and paved areas, rain has become an environmental problem, instead of being a resource that appeals to the senses and benefits plants and animals. Run-off from roads, streets, parking areas, and even some roofs is polluted. Thus, draining rainwater into sewers means that these pollutants end in watercourses, lakes, and the sea. On the other hand, rainwater that has filtered through the soil is considerably cleaner than the water from purification plants [30].

Protection of riparian woodland can be of particular importance for surface water quality. The hydrological function of urban woodland and trees is increasingly stressed as protection of drinking water resources. For example, in Denmark, new woodland areas established close to cities consider this function as a primary one next to recreational benefits [29].

Reduce Harmful Influence of Sun, Wind, and Temperature By transpiring water and shading surfaces, trees lower local air temperatures. Because trees lower air temperatures, shade buildings in the summer, and block winter winds, they can reduce the consumption of building energy and consequently reduce the emission of pollutants from power-generating facilities [48].

Temperatures will change in the future and the so-called urban heat island effect will strengthen the effects of climate change. Results from the ASCCUE (Adaptation Strategies to Climate Change in the Urban Environment) project show that green areas can play an important role for smoothing the effects of rising temperatures. The results show that for the city of Manchester increasing green cover by 10% in urban areas could keep extreme surface temperatures at current levels up until the end of the century, despite climate change [21].

Biodiversity Older gardens and parks often contain noticeably rich biodiversity [59]. These are the main habitats of urban plants and animals. Older, well-established installations attract, for instance, birds and mammals, the natural habitat of which is the forest. Since an increasing part of the population lives in urban areas and receives its daily perception of nature therein, nature in urban areas is important to environmental awareness and an understanding of nature.

Urban landscapes create new habitats for species establishment and germination and colonization sites [86, 89]. These new habitats can affect biodiversity and change community structure. Although an urban landscape may not have a full complement of natural species, the existing natural and seminatural ecosystems can provided a suite of benefits compared to the urban built infrastructure and other technologies.

Economic Functions

The aim of sustainable development is to meet the needs of both present and future generations by promoting development that does not degrade the environment and is technically appropriate, economically viable, and socially acceptable.

Food from trees in private gardens, fruit orchards, or allocated plots in public gardens can contribute

significantly to food security in developing countries [41]. Low-care wild edible plants are often excellent candidates for multipurpose use as ornamental roadside plantings. Older fruits varieties in aging orchards are an important genetic repository.

Woodfuel provides between 25% and 90% of urban household energy supplies; it is particularly important as a source of energy in smaller urban centers in developing countries, especially in dry zones [41]. Poor urban households spend a significant proportion of their cash income in obtaining wood energy. If the urban poor population continues to grow, an increase in the consumption of traded woodfuel is likely to be a consequence. Under favorable circumstances, fuelwood from non-rural forests and agroforestry systems can contribute significantly to fuelwood supply.

In rich countries, urban green spaces can contribute to the local economy, by enhancing real estate prices and by attracting economic activity and improving the local tax base. Several Scandinavian studies show that the prices of apartments are significantly raised in the presence of nearby woodlands or other types of green space (e.g., [81]). Trees and greenspace also help to conserve global energy reserves in developed nations where they are consumed at the greatest rates.

Social Functions

Health Aspects City life is stressful, but research shows that urban green areas have a beneficial influence on the health and well-being of the urban population. Several studies conducted in Europe and the USA indicate that visits to green areas can counteract stress, renew vital energy, and speed healing processes [56].

Kaplan and Kaplan [32] formulated a theory on the interaction between man's attention and his surroundings. This means that urban living, with fast vehicles, flashing neon signs, and strong colors, causes constant stress. The research indicates that vegetation and nature reinforce one's spontaneous attention, allow one's sensory apparatus to relax, and infuse one with fresh energy. Visits to green areas bring relaxation and sharpen one's concentration, since one only needs to use one's spontaneous attention. At the same time, one gets fresh air and sunlight, which have significance for one's diurnal and annual rhythms.

Furthermore, Ulrich [83] showed that hospitalized patients recovered faster when they had a view through a window, allowing them to see trees. In 1991, he conducted a new study showing a gory film on industrial accidents to 120 people [84]. Half of the people were then shown a nature film, whereas the other half were shown a film on the city, with sequences of buildings and traffic. The subjects' heartbeat, muscular tension, and blood pressure were monitored throughout. All subjects exhibited strong signs of stress during the first film, on industrial accidents. The stress levels of the half of the subjects that then watched the nature film had returned to a normal level after 4–6 min, whereas the half that watched the film on buildings and traffic continued to exhibit high stress levels.

Another important health function is recreation provided by parks in areas that are used for recreational activities such as walking, biking, and spaces for children to play. Finally, when several metric tons of air pollutants are removed by urban forests in Mexico City, this also can lead to substantial health benefits [14].

Educational Functions Closely related with the ecological and social values of urban green spaces is their educational function. Since a rapidly increasing part of the world's population lives in urban areas and receives its daily perception of nature therein, nature in urban areas is important to increase environmental awareness and an understanding of nature.

Richard [45] coined the term *nature deficit disorder*, to refer to the trend that children are spending less time outdoors resulting in a wide range of behavioral problems. He claims that causes for the phenomenon include parental fears for their children in urban areas, restricted access to natural areas around cities, and the lure of the computer and television screen. Result of nature deficit disorder can include childhood obesity, attention disorders, and depression. Providing youth time in nature during the school day can help reduce anxiety and have a positive effect on the attention span, stress reduction, creativity, cognitive development, and children's sense of wonder and connection to the earth.

Urban Forest Policies

Urban Forest Policies Defined

A policy is a generally agreed-to and purposeful course of action that has important consequences for a large number of people and for a significant number and magnitude of resources [12]. Policies can be informal as well as formalized in written documents. Usually policies are selected from a number of alternative courses of action – by government agencies, as well as by institutions, groups, and even individuals.

Drawing on the political sciences, Ottitsch and Krott [58] mention three central concepts for strategic decision-making about urban forests. "Polity" comprises the institutional dimension at formal levels relating to, for example, constitutions, laws, taxes, parliament, as well as at informal (e.g., traditions) levels. "Politics" then refers to the procedural dimension, looking at the dynamics of political processes, as, for example, concerning will formulation, interest mediation, bargaining, and communication processes. "Policy," finally, refers to the substantial or normative dimension, which includes issues and objectives as well as outcomes of the political process. A policy document can be a typical outcome of the political process.

While politics and policy-making relate to the choice of and releasing of certain political decisions, planning encompasses a search for implementation options [34]. Planning has also been described as coordinating management in order to meet the objectives the community would like to see met [58].

In an urban forestry context, policy-making and policies define the strategic choices regarding urban forests, typically for a period of at least 10 years. These typically relate to which urban forest functions should be in focus, depending on societal demands. But urban forest policy-making is also about how to conserve and develop urban forests in highly dynamic, high-pressure urban settings. Conflicts are an integral part of urban forestry, and, not surprisingly, urban forest policy-making has thus been defined as a social bargaining process between stakeholders for the regulation of conflicts related to different interests concerning urban forest utilization and protection [58].

As urban forests comprise a form of urban land use, planning helps to relate urban forest to other types of land use, as well as helps guides choices within urban forest areas. Planning can be seen as the intermediate level between decision-making (policy) and actual implementation of decisions. In urban forestry, the latter comprises, for example, the design and management activities described elsewhere in this chapter.

Urban forest policies and planning deal with a highly complex field, with a large variety of actors in play. Complexity also relates to the complexity of the urban forest itself. As is seen, it constitutes an overall green network that includes tree elements ranging from street trees to large woodland areas.

Urban Forest Policies and Plans Today

Research has shown that across the globe, urban forest policies are scarce when regarded in terms of formalized policies that specifically focus on a city's "urban forest," incorporating all tree-dominated vegetation [34, 60]. A growing number of cities in especially the industrial world have developed policies and strategies for (part of) their green spaces, as, for example, reflected by green structure plans. Green belt policies inspired by the London Green Belt have been in place in many parts of the world [2]. But a strategic perspective on what should happen with a city's woodlands and trees is seldom present. Exceptions are North American and British cities with specific urban forest plans. The most typical level of plans, however, has been that of (park and forest) management plans which pay less attention to strategic, longer-term decisions, and focus more on short-term, operational maintenance tasks. There are exceptions, however, such as the strategic management guidelines developed for forests in and near major German cities.

As urban forest policies are largely absent at the local level, it is not surprising that they are even more scarce at the national level. Still, some national urban forest policy-making has occurred, with countries such as the USA and China as important examples. In the USA, a nationwide urban forestry program has helped raise political awareness about urban forestry, as well as aided implementation of urban forestry at state and local level (e.g., [13]). Moreover, the national program has been supported by substantial research funding. In China, urban forestry and urban greening policies have been developed by the national government. As part of the national programs, cities with ambitious and

successful greening programs being awarded awards and privileges [43]. Elsewhere, countries such as Malaysia and Singapore have developed ambitious national "greening" programs (e.g., [60, 77]) in which tree planting plays a major role.

In Europe, the UK has probably been the country with the most ambitious urban forestry policies. Urban and community forests were described as a priority and powerful tool in the England Forestry Strategy issued in 1998 [18]. In a national program called the Community Forest Program, woodland establishment and management near large agglomerations has been used to tackle significant social, economic, and environmental challenges [36]. The Community Forests were set up as partnerships between national and local public bodies, as well as a range of private actors. When focusing on the woodland element of urban forests, the last 2 decades have shown a boom in new policies that have incorporated the importance of urban forests and/or urban forest elements. Countries such as Belgium (Flanders), Denmark, Ireland, Netherlands, and Great Britain issued afforestation policies in which urban agglomerations have the highest priority. Woodland grant schemes thus favor urban settings. Social and environmental services such as providing opportunities for outdoor recreation and protection of drinking water for primarily urban populations have become prioritized in national forest policies.

At the international level, the Food and Agriculture Organization (FAO) of the United Nations started to actively engage with "urban and peri-urban forestry" during the late 1980s. From the late 1990s, efforts intensified (e.g., [38]). FAO, for example, assigned a series of urban forestry case studies in the developing world, demonstrating that urban forestry was not only a promising approach for western countries, but could help developing-country cities in dealing with environmental and economic challenges. FAO also assessed the status of urban forestry legislation and released a series of guidelines for good practice in, for example, urban forest policy-making. Urban forestry became integrated in the so-called Regional Outlook Studies for forestry, starting with the Forest Outlook Study for West and Central Asia [17].

Policy objectives for urban forestry have changed over time, in line with changing societal demands and focus on different urban forest benefits. During a large part of history, for example, especially urban woodland was conserved and managed as provider of local timber, fuelwood, and animal fodder [36]. City forests such as the Sihlwald near Zurich, Switzerland, for example, were gradually "annexed" by the neighboring city eager to guarantee a steady supply of timber for construction. Urban woodland areas were also protected by kings and other rules as hunting domains. Throughout history hunting was not only a favorite pastime of those in power but also a means of obtaining status and prestige. Prestige was also an important reason for developing the first city parks and boulevards, inspired by the work of Haussmann in Paris.

Over time, urban forestry became targeted toward a wider range of users, with the benefits of green space, for example, for public health and worker well-being becoming recognized in the industrialized world. Recreation and other social benefits came in focus – where they still are today, as described elsewhere in this chapter. This can be illustrated by various studies of urban forest policies in Europe (e.g., [34, 58]). The social benefits of urban forests are prioritized in most cities, with environmental services such as protection of drinking water, improving the urban climate and nature protection ranking second. Economic benefits in terms of, for example, timber production is only of secondary importance in most western cities, although several cities in, for example, Central Europe do manage their forests for timber. Moreover, new focus on bioenergy as alternative to fossil fuels also makes wood harvesting more attractive once again [36]. In developing countries, urban forests often make important contributions to local livelihoods.

Although there seems to be agreement that urban forests primarily have amenity values, this does not mean that conflicts over the green spaces and their use do not occur. In fact, urban forestry policy-making is very much about managing conflicts, for example, between a range of different recreational uses. Relatively small areas of urban forest near to cater for the wishes of thousands and sometimes millions of people.

Conflicts are also mentioned as an important element of urban forestry policies and planning by Ottitsch and Krott [58] in their study of urban forestry policies and planning in 14 European cities. They describe a number of common elements apart from a joint focus on social and environmental benefits.

The authors stress the importance of municipal land property and regulative policy instruments – and the fact that current urban forest policy mostly deals with publicly owned land, even though a considerable part of a city's urban forest is in private ownership (e.g., private garden trees). In the case of private ownership, public authorities use legislation such as tree protection orders and financial instruments such as subsidies for private land owners offering recreational access to their lands.

Actors and Stakeholders

From a "polity" perspective, municipal authorities are the main decision-makers for urban forests. The strong role of municipal actors is partly due to what Ottitsch and Krott [58] call the traditional "property strategy" according to which city governments attempted to transfer green space within their boundaries or within their otherwise described spheres of interest to municipal property.

In spite of the dominant role of municipal governance, however, decision-making about urban forests is seldom a comprehensive process with one central actor. Typically, different components of the urban forest are the responsibility of different municipal departments. Comprehensive policies are difficult to develop, as city trees, parks, and woodland areas are often placed in units or divisions each with their own culture and way of doing things. As Liu [43] has shown for the Chinese city of Weihai, city park and forestry units have had difficulties in cooperating or at least followed their own agendas. A trend in many European countries has been, however, to integrate the different green space elements (e.g., parks, nature areas, and forests) in one division or department, something which could be expected to lead to more comprehensive urban forest policies and planning.

Other public actors also play a role in urban forestry decision-making, especially through state forest agencies that manage forest areas surrounding cities and towns. In some cases, state forests are even part of the city proper. Often these state forests are former royal hunting domains [34].

Private land owners do play a role in urban forestry, for example, through privately owned wooded estates. Moreover, a large part of a city's tree population is typically located in private gardens.

In addition, urban forestry policy-making and planning involve a wide range of other stakeholders. Obviously residents and users play an important role, as primary beneficiaries of urban forestry. Participation and communication regarding urban forest issues has steadily increased during recent decades. As Moll [52] states, "Where we find healthy city forests, we usually find strong citizen support. In the end, the support of city managers and government agencies comes back to citizens. They are the conscience of the community and the clients all political leaders work for. No other group feels the sense of place trees offer of organizes a force to change conditions more effectively than citizens. City forests decline when city foresters consider citizens a group to avoid, and the forest improve when lines of communication are opened." Although public participation has been increasingly called for in urban forestry, it is not always a well-developed component of decision-making processes [58, 85]. Another important group of policy actors are nongovernment groups such as nature conservation and outdoor recreation associations.

Policy Integration and Governance

Urban forest policy-making and planning are changing in response to a series of challenges to urban forests and local authorities. Ottitsch and Krott [58] speak of a number of "tension lines" in urban forest policies. In many cases, as described, there are no comprehensive policies for urban forests, but rather a patchwork of segmented policies, different spheres of interests, and competition between different municipal bodies. The role of urban forestry as a public service is also under debate. Urban forests are seen as a public service and public good, which has led to focus on expensive property strategies. In a time of public budget cuts, alternative funding mechanisms and policy instruments need to be developed. Conflicts over urban forests (and their use) have intensified and urban demands are rapidly changing.

However, urban forestry also involves a range of promising opportunities. The role of trees and other vegetation in tackling major political issues such as climate change mitigation and adaptation, promoting human health and well-being, and enhancing city competitiveness in a globalized society is increasingly

recognized. Forests and trees can play a role in large, market-driven development projects, for instance for new sustainable urban development schemes. Through the strong associations people have with forests and trees, these can play an important role in symbolic communication. One example is representing a physical sign of how the local environment is improving [42]. This symbolic role has been intensively used in programs such as the English Community Forests, but also in the "rebranding" and greening programs of a city like Chicago. In a time of, on the one hand, individualization, and on the other hand migration, urban forests are among the final truly public areas where all of society's segments and groups can meet each other. Thus urban forests can help strengthen social cohesion (e.g., [62]).

Developing the potential of urban forestry requires closer collaboration between stakeholders. Municipal authorities alone can no longer manage the task alone, hampered by government reform, lack of finances, and calls for greater involvement. New modes of governance are needed – with governance being defined as the process of making decisions that define expectations, grant authority, and verify performance [33]. In urban forestry, the traditional approach of "governance by government" needs to be (and is increasingly) replaced by modes of "governance with government," as, for example, reflected in public–private partnership and public involvement processes.

New forms of governance for urban forests are being explored. In Finland and Sweden, for example, National Urban Parks have been established. The Stockholm National City Park, which includes the Norra Djurgården city forest, was the first of its kind. The park, established by parliamentary decision in 1994, is the result of new environmental and land use legislation and the national level. National urban parks are developed as a partnership between state and municipal authorities, as well as other stakeholders. The overall aim for the NCP is to act as a model for sustainable development, with focus on nature and ecology, recreation and culture. Swedish legislation stipulates that national urban parks should contain natural areas important for the preservation of urban biodiversity, cultural milieus – including buildings – important for an understanding of national history or that of the city itself, and parks and green areas of architectural or esthetic significance [71]. Multi-stakeholder schemes for urban forests of national as well as local importance also include the Biosphere Reserves developed near cities from Vienna to Sao Paolo [36].

Urban forestry can "feed in" to emerging, integrative planning approaches such as "green infrastructure planning." The term "green infrastructure" has become frequently used in countries such as the UK and the USA in reference to urban renaissance and green space regeneration. It can be defined as creating networks of multifunctional green spaces that are carefully planned to meet the environmental, social, and economic needs of a community [44]. All green spaces, both public and private, are considered. By using the term "infrastructure," focus is on functionality and green spaces enter the urban planning discourse at an essential public service.

Design and Management of the Urban Forest

As reflected in the overall concept of urban forestry as described above, design and management of urban forests is an interdisciplinary and participatory field at the interface of, among others, landscape architecture, landscape planning, horticulture, arboriculture, forestry, ecology, and the social sciences. Whether urban forest elements are of natural, seminatural, or man-made origin, and whether new elements need to be added to the urban green structure or existing components require changes due to evolving demands, proper design and management are needed to ensure that woodlands, parks, and trees in streets and other urban spaces can provide the environmental, economic, and social functions society attributes to and demands from the urban forest resource. The disciplines, professions, and stakeholders involved vary depending on the location, setting, and social and cultural context, and not at least on the type of urban forest element concerned.

Across the world, urban forest design and management relate to very different circumstances. The climate, the ecosystem, the character of the people, the cultural history, city development, and the political settings over time varies between cities, between regions, between countries, and between the continents. Design and management aim to maintain and

incorporate the rich variety of climate, ecology, tradition, and cultural heritage contained in the existing resources, whilst at the same time meeting current demands and incorporate flexibility for changes in future requirements (population pressure and social values) and climate (climate change) [5].

Many of the most appreciated urban woodlands, parks, street tree plantations, and private gardens are characterized by old and graceful trees recognized for their cultural–historical and natural values. An inventory of the Belvoir Park Forest at the fringe of Belfast, Northern Ireland, for example, found 270 single stem trees with a diameter at breast height of 3 m or more [75]. Such trees act as landmarks and offer important habitats for biodiversity [31] and management often aim to maintain them for as long as they do not pose a security risk [28]. Design and management of urban forest therefore have to consider the full life cycle that trees have in nature, including developing stages of establishment, growth, early maturity, and degrading stages of late maturity and degradation, and today continuous design and redesign over time is perceived as a crucial part of sound, sustainable urban forest management [5, 25].

Whereas the urban forest traditionally has been designed and managed with the mature stage in mind only [24], the pace of urbanization and social changes leading to cities being transformed and renewed faster than trees can grow, has resulted in a changed professional mindset. Design is increasingly perceived as a continuing process rather than a one-off action. It is seen as a crucial part of sound, sustainable management [5, 25]. This has led to an upsurge in integrative and adaptive approaches in urban forest design and management that focus on developing qualities through all stages of development, from establishment and growth through maturity and to degradation (e.g., [10, 53]), while in streets, squares and other "gray spaces" the demand for "instant" values have implied that planting of large trees of 20–30 cm circumference or more, is becoming increasingly common practice [79].

Design of urban forests operates on different levels [5]. At the integrative and strategic level, design operates on the regional scale where urban green areas are linked to the landscape structure of the wider region, such as the "Finger Plan" of the greater Copenhagen area in Denmark. At the city level, urban green structures are designed to give strength and depth to the urban forest by linking individual components and their form and functions. Frederik Law Olmsted's design of the "Emerald Necklace" in Boston, Massachusetts, from the 1870s is one of the first and most known examples of design constituting a green infrastructure. At the site level, the form, structure, and content of individual green spaces are designed with linkages to local aspirations and use patterns, including the detailed layout and use of different vegetation elements, such as the number of plants involved, what types they are (trees, shrubs, herbaceous plants), the mix of species, how the plants are assembled in space, and their age or maturity.

The concept of urban forest management relates to management as operations and management in terms of organizations carrying out the management [25]. Municipal authorities are the main managers of urban forests but following the introduction of New Public Management doctrines a growing number of cities in especially the industrial world have outsourced management to private enterprises (e.g., [65]). Trees in private or commercial spaces such as gardens or business premises often represent a significant proportion of the tree population of a town or city. Although it is difficult to control how trees on private property are used and managed, urban foresters are increasingly becoming aware of the need of including them in the complete urban forest resource. During the last decades many cities throughout the world have developed and implemented orders and legislations that protect and prohibit removal or damage of trees in public and/or private areas by use of, for example, felling licenses, replacement planting regulations and enforcement systems such as penalties [64, 73].

Management operations address different levels. Gustavsson et al. [25] write "At the level of strategic management, the overall visions for management are developed. In line with policies and planning, objectives and targets are formulated, means are allocated and a time frame is set. Specific, well-defined tasks are defined and carried out in line with this at the level of operation management. While strategic management typically addresses a period of 10 years or more, operational management focuses on annual or biannual activities. As an intermediate level, tactical management brings the two together."

Design and management of urban forests are directed by objectives and targets, economic and other frames, and not at least the type of green area concerned. The variety of urban situations that trees relate to has been grouped into three types [66]. The first type of location is trees in street, square, and other "gray spaces" with sealed surfaces. The second include parks and other green spaces such as yards, gardens, and commercial areas. The third is stands of trees which are referred to as "woodlands" or "woods" to distinguish between the wider urban forest resource and its components that have traditionally been defined as "forest." The main design and management issues, concepts, and principles vary between the three types of locations.

Trees in Streets and Other Paved Areas

Row plantings of uniformly spaced trees are one of the earliest and simplest expressions of intentional and functional design. Over the ages, trees have been an integral part of the urban infrastructure and a mirror of the prosperity and achievements of society, such as the *Platanus* alley in the Agora of Athens, 500 BC. In Europe, the use of actual street trees became more widespread following Haussmann's renewal of Paris during the 1850s and beyond. Here trees became substantial street fixtures perceived as providing important esthetic and climatic benefits [49], and today systematic tree planting in streets and boulevard is a powerful characteristic of the city.

Trees in streets and paved areas are an important component of the urban forest, as well as an important architectural element in the cityscape where they ameliorate esthetic, social, and microclimatic conditions [3]. The natural, graceful shapes of trees provide a transition between human size and the scale of buildings and streets, as well as an element of continuity and uniformity in heterogeneous districts of mixed uses, building styles and variable scales [5]. Trees can be designed to relate to built form in different ways by use of different architectural principles of scale, massing, enclosure, and perspective, by use of different design concepts (e.g., boulevard, avenue, alley, single line, block, grid, or groups design) as well as different functional characteristics related to tree from size, texture, color, and different degrees of light and shade [3, 20]. In many cities, the "web" of trees along streets, squares, etc., weaves through the city and supports the overall sense of a citywide forest by creating ecological corridors and visual links between woodland, parks, and other open spaces. In the historical or commercial core of larger cities, streets and not in the least parking areas are often the only location available for trees. In countries with a warm climate, the shade provided by trees encourages life to take place in the street.

Streets and other paved urban areas with surface sealing are generally characterized by limited space for planting pits, alkaline and compaction soils resulting from construction work, utility trenching, and in the many parts of the world use of deicing salt. The complex stressed environment challenge tree growth [74] and integration of adequate spaces and growth substrates in the overall street design is increasingly called for [61, 76], as is the use of stress-tolerant tree species (e.g., [4, 79, 80]). In the Central European region, an important contribution is the Climate-Species-Matrix developed by Roloff and colleagues [67] to support choice of tree species for urban habitats considering climate change. The matrix contains 250 woody species used in Central European green spaces. Based on drought tolerance and winter robustness, each species is assessed and classified with regards to usability after predicted climate changes of increased average temperatures and more frequent heat waves and periods of drought.

Research has shown that a limited number of tree species dominate the tree stock in streets, but drawing on the severe consequences of Dutch elm disease a growing number of experts emphasize the use of a diversity of species as key component of design strategies aimed at increasing the resilience of the tree stock to pests and diseases [4, 51]. The most comprehensive recommendation of the latter concept is provided by Santamour [70], who suggests that no species should represent more than 10%, a genus not more than 20%, and a family not more than 30% of the population.

Besides selection of suitable tree species and proper design and planting, aftercare is essential to maintain healthy, esthetic, and safe trees in the harsh conditions of streets and other urban paved sites. Urban tree management techniques and activities are grouped under the field of arboriculture, that is, the cultivation and management of individual or small groups of

woody plants, primarily in urban areas. Arboriculture includes watering, fertilization, mulching, protection with (stakes, supports), and formative pruning of young plantings, as well as training, vitality, and safety inspections of mature trees to reduce hazard [9]. It is based on a detailed understanding of tree biology and responds to cultural practices of pruning and to wounds and environmental conditions. Arboriculture also plays an important role in management of trees in parks, gardens, and other urban green spaces, but here, management of other types of vegetation also comes in.

Parks and Other Green Spaces

Parks, gardens, and other urban spaces dominated by vegetation often contain a considerable number of trees, but actual forest stands are often limited or absent. Instead elements such as lawns, pastures, garden elements such amenities as seating and different types of infrastructure and/or buildings dominate [5]. Design and management aim to integrate elements into attractive areas that are enticing for people of all ages, genders, and backgrounds, and stimulate use on regular basis during all parts of the day, week, and year, where trees are used to provide ornamental values as well as mass and structure and define the character and scale of space.

Park design has evolved through a number of phases where different styles have reflected the social, cultural, and artistic movement of the times when they were created. Beautification has traditionally been one of the main arguments for greening cities with parks, gardens, and other types of green spaces [36, 82]. The park first became an integral part of city planning and development in England during the 1830s, and then subsequently spread throughout Europe, North America, and eventually the world. In the polluted and densely populated cities that followed the industrial revolution, parks were seen as a solution to both social and hygienic problems. Peoples could gather and socialize in the fresh air, which promoted public health [8]. Playgrounds, sports fields, and other facilities stimulation activity evolved as one of the most important features of public parks, and remain so today. Yet, as evidence has mounted about the multiple functions urban green spaces provide, their design and management has gradually shifted to also encompassing environmental, conservation, and economic benefits with the aim to develop functioning ecosystems as well as settings for cultural and social activity [5, 25, 47].

Recognizing the interconnection of natural resources and human resources and design and management of parks and other green spaces have become essential for the concept of sustainable urban ecosystems. The political movements of sustainability and protection of biodiversity have caused a more restricted use of the richness of exotic species, which for centuries have been a predominant element in park design due to their ornamental values. The focus of decision makers, professionals, as well as residents on protecting local nature and cultural history have implied that the design and management of urban parks and woodlands increasingly are carried out as part of varying restoration programs which either concentrate on ecosystems functions or cultural history, or both (e.g., [22]). One example is the "Isar Plan," where the strongly regulated Isar river course in the inner-city of Munich, Germany, has been redesigned as part of a program that combines flood protection with the restoration of a near-natural river landscape and the improvement of nature-oriented leisure and recreational use of the urban population in the river bank zone [16].

Trees in private or commercial spaces such as gardens or business premises often represent a significant proportion of the tree population of a town or city, and give people the chance to express themselves and to develop their own, personal relationships with trees and plants. Although it is difficult to control how trees on private property are used, urban foresters are increasingly becoming aware of the need of including them in the design and management of the complete pattern of urban woods, parks, street trees, and trees in private spaces [5]. In recognition of this, an increasing number of cities have developed tree protection orders that also include private trees [64, 73], as also described elsewhere in this chapter.

Woodlands

Urban woodlands are designed and managed for a variety of purposes. Originally, provision of timber and fuelwood was the main reason for cities and towns to own and manage forests, but this function is

presently only of secondary importance [36]. Recreation and nature protection typically are the main functionalities of urban woodlands today [5, 82]. Woodlands tend to be more multipurpose than parks and other urban forest elements, and their design and management need to accommodate more uses, some of which might conflict. Aspiration of woodland character differs greatly between users, for example, according to age, sex, profession, and cultural background, and it is important to consider the social status and recreational use of the individual woodland as well as the ecological status and potential for nature conservation, and to rank the use priorities when deciding on their design and management [28, 46].

Bell et al. [5] define woodland design as "...accomplished through the manipulation of the spatial pattern of different stands of trees, their species composition and vertical structure(...) These elements are manipulated through woodland management and the adoption of different silvicultural systems." However, the importance of urban woodlands has from a silvicultural perspective been widely overlooked and approaches that are suited to the capacities of woodlands and the realities in urban contexts are still under development. Much urban woodland has developed over time from commercial production plantations and mainly consists of even-aged monoculture types with interiors resembling the "pillared hall." However, canopy trees, undergrowth, and the main characteristics of the ground flora are all of importance for biodiversity and for the human experience of character, size, and atmosphere of forest interiors [25]. Municipal authorities throughout Europe and North America are increasingly applying a variety of management techniques to achieve different structures of vegetation and atmospheres within individual woodlands as well as across woodland lots. Form- and species-rich forest stand types associated with selection cutting methods are considered among the most valuable types to integrate high esthetic and biological qualities [25, 90], especially in smaller-scale woodland lots. Historical/cultural forest management regimes, such as coppice forests, forest pastures, and unmanaged forests are also increasingly applied to assist diversifying woodland interior rooms and habitats within and across urban woodlands for the benefit of people, plants, and wildlife [25, 54, 69]. Natural colonization has also been identified as a management tool that can give strength to urban woodland design and that is readily transferable, although regional differences have to be taken into account [68].

Compared to "commercial" forests with a management regime aimed at wood production, and where the stand is the functional unit, the higher functional level – that is, the woodland landscape – is of equal importance when it comes to developing recreational and ecological functionalities in urban woodlands [25]. Hence, design and management of urban woodlands should not only give attention to stands, but also to the wooded landscape. Variation between wooded areas and open habitats and recreational areas is a common characteristic for many of the most appreciated and well-known urban woodland landscapes in Europe, such as Amsterdamse Bos, the Netherlands, Helsinki's Central Park, Finland, and Jægersborg Deer garden north of Copenhagen, Denmark. The mosaic of interiors under closed canopies, intimate glades, and canopy openings, semi-open savannah-like areas with scattered trees, open spaces of varying sizes and types and a diversity of edges along the boundary of forested and open parts are mutually supportive for multipurpose uses [5], while they also create habitat diversity, something which is of the utmost importance for biodiversity conservation.

Urban growth has in many cases led to woodland fragmentation, cutting woodland areas into more or less isolated patches of varying sizes, ranging from small copses and woodland remnants to large wooded landscapes. This fragmentation should be considered when designing and managing urban woodlands. While larger woodland landscapes are often the most used for recreational purposes, small wooded lots account for a large share of the woodland resource in many cities. In the case of Ljubljana, Slovenia, for example, Pirnat [63] idenfitied as much as 606 woodland lots of a size of 0.5–10 ha. While woodlands in general are able to absorb many uses, small woods limit recreational as well as ecological opportunities whilst larger woods can absorb many uses and provide a wider range of ecosystem services [1, 5]. Zoning different functions and applying different silvicultural systems in order to separate and provide attractive and safe environments for various forms of recreation and

ecosystem functions within woodland lots and across the diversity of urban woodlands are frequently applied [19, 23, 69].

Urban Forest Information and Inventory

To support sound urban forestry programs, policies, planning design, and management, high quality information is needed. Schipperijn et al. [72] divide the wide range of information requirements into basic green space information, environmental and ecological information, and sociocultural information. The need for reliable information has led to the development of different methods, tools, and systems, such as remote sensing, tree inventory systems, biotope mapping, sociotope mapping, GIS systems, and decision support systems to help collect, compile, and use available information, many of which are described in Schipperijn et al. [72]. Following the introduction of New Public Management doctrines, an increasing number of cities in especially the industrial world have outsourced urban green space management or implemented internal division of purchasers and providers in order to reduce management costs and to gain more insight into the daily management routine tasks and costs (e.g., [65]). In this process, detailed inventories and monitoring have been carried out to establish "basic green space information" about the location of green areas, green elements, and street trees, characteristics and quantity of different elements (species, age, size, height, and so forth), as well as information on type and quantity of the different management activities in use. In comparison, inventory and monitoring providing "information about the environmental and ecological" conditions that influence green spaces, as well as the environmental benefits of green spaces are still under development and implementation, as are methods for collect and compile "sociocultural information" dealing with user preferences, cultural values, economic benefits, and information on health and other social services.

Future Directions

The world's urban population will only increase in the coming years, which means that the focus on cities as sustainable human habitats must increase as well. There will be a growing need for research and policy support in the field of sustainable urban development. What should cities of the future look like? What constitutes a "good city"? How much green space is necessary to sustain a healthy population? Each city has its own specific problems, mainly related to economic status and geographic location.

At present, research results indicate that the urban population in general would benefit from a well-developed green infrastructure, especially when the urban green space is well integrated in the overall city planning. It is important to realize that planting more trees or creating more green in urban areas is not enough. Studies indicate the importance of well-funded, long-term management and proper maintenance of the green infrastructure. It is also clear that public participation ensures the success of government investment and is an important tool in providing sustainable green space and in creating sustainable cities.

The increased interest in urban ecology and environmental problems will drive investment in parks and green areas over the coming decades. Most of these should be laid out in the larger and rapidly expanding cities of Asia, Africa, and Latin America to ensure an equitable distribution of green space and healthy, sustainable population growth. Similar expansion of protected green infrastructure was carried out in North America and Europe during the years after the Second World War and up to the 1970s. Planning has not kept up with growth in many cases, and the need exists to look at a mega-regional scale to identify remnant urban and peri-urban open space and critical lands for protection that will be sufficient to supply a steady source of ecosystem services to sustain long-term population growth. Over the coming years, the main challenge will be to ensure that the expansion of green infrastructure in the world's urban areas is implemented within the framework of sustainable development, optimizing the ecosystem services provided by these natural resources with the use of appropriate technology, community participation, and without a heavy dependence on chemicals and irrigation. This will ensure that the rapidly expanding urban landscapes remain resilient and healthy habitat for a growing society.

Today's focus on climate change will raise the demands for more compact cities. But a compact city with a lot of sealed surface and lack of green space is

very vulnerable for the effects of climate change. Therefore, the issue of urban density is a good example of a potential conflict between mitigation and adaptation concerns. If increasing density, in order to reduce energy by lowering travel demand and heating requirements, leads to the consumption of green space resources, its consequence will be the loss of a vital adaptation resource. The concept of the city of tomorrow is such an oxymoron. The challenge is how to combine the need for a compact city with people's need for green space close to where they live – The Green Compact City. *Inter alia* Scandinavian planning and building tradition contains several examples which could inspire. Better coordination between transport, land use, and open space planning; urban containment and preservation of the green infrastructure; the creation of new urban landscapes; and promotion of the urban–rural interface are basic principles for this. Urban forestry is one of the promising approaches to support this process.

Bibliography

1. Alvey AA (2006) Promoting and preserving biodiversity in the urban forest. Urban Forest Urban Greening 5:195–201
2. Amati M (ed) (2008) Urban green belts in the twenty-first century. Ashgate, Aldershot
3. Arnold HF (1993) Trees in urban design, 2nd edn. Van Nostrand Reinhold, New York
4. Bassuk N, Curtis DF, Marranca BZ, Neal B (2009) Recommended urban trees: site assessment and tree selection for stress tolerance. Urban Horticulture Institute, Cornell University, Ithaca, New York
5. Bell S, Blom D, Rautamäki M, Castel-Branco C, Simson A, Olsen IA (2005) Design of urban forests. In: Konijnendijk CC, Nilsson K, Randrup TB, Schipperijn J (eds) Urban forests and trees. Springer, Berlin, pp 149–186
6. Benavides Meza HM (1992) Current situation of the urban forests in Mexico City. J Arboric 18:33–36
7. Bernatzky A (1994) Baumkunde und Baumpflege. Thalacker Verlag, Braunschweig
8. Bucht E (2002) Traditions in urban park planning and management in Sweden and other European countries. In: Randrup TB, Konijnendijk CC, Christophersen T, Nilsson K (eds) Urban forests and trees, Proceedings No.1. COST Action E12. Office for Official Publications of the European Communities, Luxembourg, pp 215–226
9. Dujesiefken D, Dreno C, Oven P, Stobbe H (2005) Arboricultural practices. In: Konijnendijk CC, Nilsson K, Randrup TB, Schipperijn J (eds) Urban forests and trees. Springer, Berlin, pp 419–441
10. Dunnet N, Hitchmough J (eds) (2004) The dynamic landscape. Spon Press, London
11. EEA (European Environment Agency) (1998) Europe's environment: the second assessment. Office for Official Publications of the European Communities, Luxembourg
12. Ellefson PV (1992) Forest resources policy: process, participants, and programs. McGraw-Hill, New York etc
13. Elmendorf WF, Cotrone VJ, Mullen JT (2003) Trends in urban forestry practices, programs, and sustainability: contrasting a Pennsylvania, US, study. J Arboric 29(4):237–246
14. Escobedo F, Chacalo A (2008) Estimación preliminar de la descontaminación atmosférica por parte del arbolado urbano de la Ciudad de México (A preliminary estimate of air pollution removal by Mexico City's urban forest). Interciencia 33:29–33
15. Escobedo FJ, Wagner J, Nowak DJ, de la Maza CL, Rodríguez M, Crane DE (2008) Analyzing the cost-effectiveness of Santiago Chile's policy of using urban forests to improve air quality. J Environ Manage 86:148–157
16. European Urban Knowledge Network (2010) European Urban Knowledge Network Web site, http://www.eukn.org. Retrieved 3 March 2010
17. FAO (2006) Urban and peri-urban forestry and greening in West and Central Asia: experiences, constraints and prospects. Compiled by Åkerlund U, Knuth L, Randrup TB, Schipperijn J. FAO, Rome
18. Forestry Commission (1998) England forestry strategy. A new focus for England's woodlands – strategic priorities and programmes. Forestry Commission, Cambridge
19. Forestry Commission (1992) Forest recreation guidelines. HMSO, London
20. Forrest M (2006) Landscape trees and shrubs, use and management. CABI, Wallingfrod
21. Gill S, Handley J, Ennos R, Pauleit S (2007) Adapting cities for climate change: The role of the green infrastructure. Built Environ 33(1):115–133
22. Gobster PH (2007) Models for urban forest restoration: human and environmental values. In: Proceedings of the IUFRO conference on forest landscape restoration, Seoul, Korea, May 14–19, pp 10–13
23. Gundersen VS, Frivold LH (2008) Public preferences for forest structures: A review of quantitative surveys from Finland, Norway and Sweden. Urban Forest Urban Greening 7:247–258
24. Gustavsson R (2004) Exploring woodland design: designing with complexity and dynamics – woodland types, their dynamic architecture and establishment. In: Dunnet N, Hitchmough J (eds) The dynamic landscape. Spon Press, London, pp 246–293
25. Gustavsson R, Hermy M, Konijnendijk CC, Steidle-Schwahn A (2005) Management of Urban Woodland and Parks – Searching for Creative and Sustainable Concepts. In: Konijnendijk CC, Nilsson K, Randrup TB, Schipperijn J (eds) Urban forests and trees. Springer, Berlin, pp 369–397
26. Harris RW (1992) Arboriculture: integrated management of landscape trees, shrubs and vines, 2nd edn. Prentice Hall, Upper Saddle River
27. Helms J (ed) (1998) Dictionary of forestry. Society of American Foresters, Bethesda

28. Hodge SJ (1995) Creating and managing woodlands around towns, vol 11, Forestry Commission Handbook. HMSO Publications Centre, London
29. Jensen FS (1995) Forest recreation. In: Hytönen M (ed) Multiple-use forestry in the Nordic countries. The Finnish Forest Research Institute, Helsinki, pp 245–278
30. Jensen MB, Persson B, Guldager S, Reeh U, Nilsson K (2000) Green structure and sustainability – developing a tool for local planning. Landscape Urban Plann 52:117–133
31. Jonsell M (2004) Old park trees: a highly desirable resource for both history and beetle diversity. J Arboric 30:238–244
32. Kaplan R, Kaplan S (1989) The experience of nature. Cambridge University Press, Cambridge
33. Kleinschmit D, Böcher M, Giesen L (2009) Discourse and expertise in forest and environmental governance – an overview. For Policy Econ 11(5–6):309–312
34. Konijnendijk CC (1999) Urban forestry in Europe: a comparative study of concepts, policies and planning for forest conservation, management and development in and around major European cities. Doctoral dissertation, Research Notes No. 90, Faculty of Forestry, University of Joensuu, Joensuu
35. Konijnendijk CC (2003) A decade of urban forestry in Europe. For Policy Econ 5(3):173–186
36. Konijnendijk CC (2008) The Forest and the City: the cultural landscape of urban woodland. Springer, Berlin
37. Konijnendijk CC, Randrup TB (2004) Urban forestry. In: Burley J, Evans J, Younquist JA (eds) Encyclopedia of forest sciences. Elsevier Science, London, pp 471–478
38. Konijnendijk CC, Sadio S, Randrup TB, Schipperijn J (2004) Urban and peri-urban forestry in a development context – Strategy and implementation. J Arboric 30(5):269–276
39. Konijnendijk CC, Nilsson K, Randrup TB, Schipperijn J (2005) Urban forests and trees. Springer, Berlin, Heidelberg, New York
40. Konijnendijk CC, Ricard RM, Kenney A, Randrup TB (2006) Defining urban forestry – A comparative perspective of North America and Europe. Urban Forest Urban Greening 4(3–4):93–103
41. Kuchelmeister G (1999) Urbanization in developing countries – time for action for national forest programs and international development cooperation for the urban millennium. Forest policy research forum: the role of national forest programs to ensure sustainable forest management, 14–17 June 1999, Joensuu, Finland
42. Lawrence HW (2006) City trees: a historical geography from the Renaissance through the nineteenth century. University of Virginia Press, Charlottesville & London
43. Liu L (2009) Status and prospects for urban green structure planning in China – Weihai city as a case study. Forest and landscape research 41/2008. Danish Centre for Forest, Landscape and Planning, University of Copenhagen, Frederiksberg
44. Longhurst J (2007) Chain reaction. Green Places 2007(36):20–22
45. Louv R (2008) Last child in the woods. Algonquin, Chapel Hills
46. Lucas OWR (1991) Design of forest landscapes. Oxford University Press, New York
47. McPherson EG (2000) Urban forestry issues in North America and their global linkages. Presentation for the 20th Session of the North American Forestry Commission Food and Agriculture Organization of the United Nations, St. Andrews, New Brunswick, Canada. 12–16 June 2000
48. McPherson EG, Rowntree RA (1993) Energy conservation potential of urban tree planting. J Arboric 19(6):321–331
49. Meyer FH (1978) Baüme in der Stadt. Verlag Eugen Ulmer, Stuttgart
50. Miller RW (1997) Urban forestry: planning and managing urban greenspaces, 2nd edn. Prentice Hall, Englewood Cliffs
51. Miller RH, Miller RW (1991) Planting survival of selected street tree taxa. J Arboric 17:185–191
52. Moll G (1989) In search of an ecological urban landscape. In: Moll G, Ebenreck S (eds) Shading our cities, a resource guide for urban and community forests. American Forestry Organisation, Island Press, Washington
53. Nielsen AB, Jensen RB (2007) Some visual aspects of planting design and silviculture across contemporary forest management paradigms – perspectives for urban afforestation. Urban Forest Urban Greening 6:143–158
54. Nielsen AB, Møller FG (2008) Is coppice a potential for urban forestry? - The social perspective. Urban Forest Urban Greening 7:129–138
55. Nilsson K, Randrup TB, Wandall B, (2001) Trees in the urban environment. In: Evans J (ed) The forest handbook, vols. 1 and 2. Blackwell Science, Oxford, pp 347–361 and 260–271
56. Nilsson K, Baines C, Konijnendijk CC (2007) Health and the natural outdoors, COST Strategic Workshop in Larnaca, Cyprus, Final report. COST, Brussels
57. Nowak DJ, Crane DE, Stevens JC, Ibarra M (2002) Brooklyn's urban forest. United States Department of Agriculture, Forest Service, General Technical Report NE-290, Radnor
58. Ottitsch A, Krott M (2005) Urban forest policy and planning. In: Konijnendijk CC, Nilsson K, Randrup TB, Schipperijn J (eds) Urban forests and trees. Springer, Berlin, pp 117–148
59. Owen J (1992) The ecology of a garden. Cambridge University Press, Cambridge
60. Palijon A (2004) Urban forestry in Asia: state of the art. In: Konijnendijk CC, Schipperijn J, Hoyer KK (eds) Forestry serving urbanised societies. Selected papers from the conference held in Copenhagen, Denmark, 27 to 30 August 2002, vol 14, IUFRO World Series. IUFRO, Vienna, pp 25–40
61. Pauleit S (2003) Urban street tree plantings: Identifying the key requirements. Proc Inst Civ Eng Munic Eng 156:43–50
62. Peters K, Elands B, Buijs A (2010) Social interactions in parks: Stimulating social cohesion? Urban Forest Urban Greening 9(2):93–100
63. Pirnat J (2005) Multi-functionality in urban forestry – a dream or a task? In: Konijnendijk CC, Schipperijn J, Nilsson K (eds) Urban forests and trees, Proceedings No. 2. COST Action E12. Office for Official Publications of the European Communities, Luxembourg, pp 101–118

64. Profous GV, Loeb RE (1990) The legal protection of urban trees: a comparative world survey. J Environ Law 2:179–193
65. Randrup TB, Persson B (2008) Public green spaces in the Nordic countries: Development of a new strategic management regime. Urban Forest Urban Greening 8:31–40
66. Randrup TB, Konijnendijk C, Kaennel Dobbertin M, Prüller R (2005) The concept of urban forestry in Europe. In: Konijnendijk CC, Nilsson K, Randrup TB, Schipperijn J (eds) Urban forests and trees. Springer, Berlin, pp 9–20
67. Roloff A, Korn S, Gillner S (2009) The Climate-Species-Matrix to select tree species for urban habitats considering climate change. Urban Forest Urban Greening 8:295–308
68. Ryan J, Simson AJ (2002) Identifying good practice in the design of urban woodlands. Arboricultural J 26:309–331
69. Rydberg J, Falck J (2000) Urban forestry in Sweden from a silvicultural perspective: a review. Landscape Urban Plann 47:1–18
70. Santamour FS Jr (1990) Trees for urban planting: Diversity, uniformity and common sense. In: Proceedings of the 7th conference of the metropolitan tree improvement alliance, Lisle, pp 57–65
71. Schantz P (2006) The formation of National Urban Parks: a Nordic contribution to sustainable development? In: Clark P (ed) The European city and green space: London, Stockholm, Helsinki and St Petersburg, 1850–2000, Historical Urban Studies. Ashgate, Hants, pp 159–174
72. Schipperijn J, Pillmann W, Tyrväinen L, Mäkinen K, O'Sullivan R (2005) Information for urban forest planning and management. In: Konijnendijk CC, Nilsson K, Randrup TB, Schipperijn J (eds) Urban forests and trees. Springer, Berlin etc, pp 399–417
73. Schmied A, Pillmann W (2003) Tree protection legislation in European cities. Urban Forest Urban Greening 2:115–124
74. Sieghardt M, Mursch-Radlgruber E, Paoletti E, Couenberg E, Dimitrakopolus A, Rego F, Hatzistathis A, Randrup TB (2005) The abiotic urban environment: impact of urban growing conditions on urban vegetation. In: Konijnendijk CC, Nilsson K, Randrup TB, Schipperijn J (eds) Urban forests and trees. Springer, Berlin etc, pp 281–323
75. Simon B (2005) The history of Belvoir Park. In: Simon B (ed) A treasured landscape – the heritage of Belvoir Park. The Forest of Belfast, Belfast, pp 16–42
76. Simons K, Johnson GK (2008) The road to a thoughtful street tree master plan – a practical guide to systematic planning and design. http://www.forestry.umn.edu/extension/urban_com/street%20Tree%20manual.REVISED_2008.pdf
77. Sreetheran M, Philip E, Adnan M, Siti Zakiah M (2006) A historical perspective of urban tree planting in Malaysia. Unasylva 57(223):28–33
78. Stanners D, Bourdeau P (eds) (1995) Europe's environment. The Dobris assessment. Europe's Environment Agency, Copenhagen
79. Sæbø A, Borzan Z, Ducatillion C, Hatzistathis A, Lagerström T, Supuka J, Garcia-Valdecantos JL, Rego F, Slycken JV (2005) Selection of plant materials for street trees, park trees and urban woodland. In: Konijnendijk CC, Nilsson K, Randrup TB, Schipperijn J (eds) Urban forests and trees. Springer, Berlin, pp 257–280
80. Tello ML, Tomalak M, Siwecki R, Motta E, Mateo-Sagasta E (2005) Biotic urban growing conditions – threats, pests and diseases. In: Konijnendijk CC, Nilsson K, Randrup TB, Schipperijn J (eds) Urban forests and trees. Springer, Berlin, pp 325–365
81. Tyrvainen L (1999) Monetary valuation of urban forest amenities in Finland. Doctoral dissertation. Research Paper No. 739. Finnish Forest Research Institute, Vantaa, Finland
82. Tyrväinen L, Pauleit S, Seeland K, de Vries S (2005) Benefits and uses of urban forests and trees. In: Konijnendijk CC, Nilsson K, Randrup TB, Schipperijn J (eds) Urban forests and trees. Springer, Berlin, pp 81–114
83. Ulrich RS (1984) View through a window may influence recovery from surgery. Science 224:420–421
84. Ulrich RS, Simons RF, Losito BD, Fiorito E, Miles MA, Zelson M (1991) Stress recovery during exposure to natural and urban environments. J Environ Psychol 11:201–230
85. Van Herzele A, Collins K, Tyrväinen L (2005) Involving people in urban forestry – a discussion of participatory practices throughout Europe. In: Konijnendijk CC, Nilsson K, Randrup TB, Schipperijn J (eds) Urban forests and trees – a reference book. Springer, Berlin, pp 207–228
86. Williams NSG, Schwartz MW, Vesk PA, Mccarthy MA, Hahs AK, Clemants SE, Corlett RT, Duncan RP, Norton BA, Thompson K, Mcdonnell MJ (2008) A conceptual framework for predicting the effects of urban environments on floras. J Ecol 97:4–9
87. World Resources Institute (2001) Earthtrends: the environmental information portal. World Resources Institute, Washington DC
88. Yang J, McBride J, Zhou JX, Sun ZY (2005) The urban forest in Beijing and its role in air pollution reduction. Urban Forest Urban Greening 3:65–78
89. Zipperer WC, Wu J, Pouyat RV, Pickett S (2000) The application of ecological principles to urban and urbanizing landscapes. Ecol Appl 10:685–688
90. Larsen JB (2000) From plantation management to nature-based silviculture – a Danish perspective, Third International Congress on Sustainability in Time and Space. Pro Silva Europe 187

Urban Redevelopment and Quality of Open Spaces

Juliane Mathey[1], Dieter Rink[2]
[1]Leibniz Institute of Ecological and Regional Development (IOER), Dresden, Germany
[2]Helmholtz Centre for Environmental Research (UFZ), Leipzig, Germany

Article Outline

Glossary
Definition of the Subject

U

Introduction
Dimensions of Shrinkage and Vacant Land in East Germany
The Joint Program of the German Federal and State Governments: "Urban Redevelopment East"
The Demands Made of the New Open Spaces
Strategies and Tools for Open Space Development
Conclusion: New Open Space Qualities Through Urban Redevelopment?
Bibliography

Glossary

Brownfield Brownfield is an usused urban site of derelict or underused land, which require intervention to bring it back to beneficial use and which may have real or perceived contamination problems (see also: http://www.cabernet.org.uk).

Perforated city The concept is used in the sense of a city whose physical fabric contains a scattering of vacant sites and which is undergoing progressive redistribution.

Renaturation The concept is employed here not in the narrower nature conservation sense but as used by the Federal Ministry for Building, Transport and Housing, and the Federal Office for Building and Spatial Planning to refer to urban redevelopment projects that are basically concerned with the temporary or permanent downzoning of building land into green and open spaces [36].

Shrinking city Shrinking City can be defined as an urban area that has faced a population loss in large parts of it for more than 2 years and is undergoing economic transformations with some symptoms of a structural crisis.

Urban Redevelopment Program "Stadtumbau Ost" ("Urban Redevelopment East") Federal funding scheme in Germany which has the aim to demolish a certain number of flats in order to regulate the housing market.

Definition of the Subject

Urban shrinkage has become a new normality for a growing number of European cities and urban regions. It is a result of different but strongly interconnected processes: uneven economic development, demographic change, shifts in land use and urban form, as well as housing preferences and lifestyles. Shrinking urban regions develop their own patterns of development, and form distinctive dynamics that differ from those of their growing counterparts. Shrinkage, however, produces brownfield sites or open spaces of various sizes practically everywhere in the urban fabric. Many local authorities engage in scattered downsizing within existing settlements. But this type of urban redevelopment reaches its limits when "holes" steadily multiply and the physical urban fabric disintegrates. Redevelopment and downsizing raise the question of how the design of open and green space can provide a new quality of urban development. The major issue for the future is how public funding can best be deployed in handling vast areas of previously developed land within increasingly perforated cities. This paper looks systematically at the solutions already available and what contribution they can make to improving the ecological quality and the quality of life in cities.

Introduction

The current discussion on shrinking cities stresses the long-term nature and irreversibility of shrinkage, necessitating the abandonment of long-established planning principles. Furthermore, note is repeatedly taken of the fragmentation and perforation of urban areas, caused not least by parallel shrinkage and growth. However, the discussion has focused primarily on housing and to some extent on infrastructural problems. Abandoned industrial land and new brownfield sites in residential areas, in contrast, tend to be given only cursory attention – they are literally a "marginal problem."

Shrinking cities are not a new phenomenon, but in the past they have been regarded only as isolated or regionally limited exceptions [1]. During the last decades shrinking cities have become a distinct urban process in particular in Europe [2]. While a considerable share of "urban Europe" has been growing during the last decades and continues to do so, other urban regions have been suffering from deindustrialization, population loss and decay for decades. Nearly one third of all of Europe's cities with more than 200,000 inhabitants have at least undergone one decade of population decline [3] in the last 45 years. Whereas some of these

cities have been losing population ever since the 1960s, the majority of cases started declining only in the 1980s and 1990s. While population losses and economic decline can also be found in numerous Western and Southern European cities, they are especially pronounced in Central Eastern and Eastern Europe [4]. Here, declining urban population numbers are rather the normal case than the exception [3]. It is a result of different but strongly interconnected processes, that is, uneven economic development, demographic change, as well as shifts [5] in land and resource use, urban form, housing preferences, and lifestyles. As these drivers of shrinkage will increasingly impact on urban and regional development in the future, shrinkage clearly represents a key regional development challenge in Europe. Recent statistics show that processes of shrinkage will even gain more importance over the next decades: According to estimations by the UN, the population of western, northern, and – most of all – southern Europe will decrease. Current calculations of the UN predict a decline in Europe's population from 729 million in the year 2000 to 628 million people in the year 2050.

Shrinkage has thus not only become a new normality for a growing number of European cities but a serious challenge for urban planning. In many cases, shrinkage is caused by the sudden vacating of waste sites or a systematic retreat from extensive development in the course of redevelopment. The question of the quality and use capability of the (new) open spaces therefore takes on new dimensions: How can or should previously developed land be integrated into the urban fabric? What contribution can it make to local residential amenity? What interim and after-uses can be envisaged?

This paper looks at the dimensions of shrinkage and vacancies in East Germany, where this process is in particular pronounced due to the interaction of outmigration, demographic change, and suburbanization. As a reaction to the shrinkage processes in East Germany, the federal government established the "Urban Redevelopment East" program, which seeks to create solutions to this development. It also investigates how open spaces in shrinking cities are treated, what solutions have hitherto been adopted, and what approaches are desirable from an ecological, social, and/or economic point of view. Examples are presented from various cities in East Germany. The idea of the paper is that these solutions are applicable as well in other European cities or worldwide.

Dimensions of Shrinkage and Vacant Land in East Germany

In East Germany, 90% of all towns and cities with over 20,000 inhabitants have suffered a population decline ([6]; [7], p. 62). Shrinkage in such dimensions and at such speed is a new phenomenon in Europe [8].

It follows on from a process that began in GDR times. Between 1949 and 1989, the German Democratic Republic lost about two million inhabitants. Local authorities also lost population owing to government-planned concentration processes, so that there were old gaps in the fabric of many towns and cities, often in a derelict state. At present, three main processes are causing shrinkage in East Germany: (1) the deindustrialization that set in with regime change, (2) the suburbanization or disurbanization of the 1990s, and (3) demographic decline.

1. Deindustrialisation set in immediately after the change in regime, affecting practically all sectors of the industry and with dire consequences for the economic basis of East German towns and cities. Seventy percent of all job losses were due to the collapse of the industry ([9], p. 4). Thus many industrial and commercial sites fell vacant, especially in the late nineteenth-century urban extensions. An estimated 3–4% or more of land in urban areas, and up to 5% in industrial cities lies vacant (own estimates on the basis of data on Leipzig), and will probably remain unused in the future. Completely new dimensions in brownfield land in cities are being dealt with here – a process that will continue with the advance of urban redevelopment.
2. From the early 1990s to the mid-decade, the rapid expansion of the housing supply topped the list of local government priorities. In view of the housing shortage in East Germany and positive population forecasts, both the rehabilitation of old city centers and the construction of new housing were pushed. Housing was built everywhere with the aid of tax relief, write-offs, and government subsidies. Between 1991 and 1999 alone, 773,368 new dwellings were built [10], almost exclusively newly

constructed on greenfield sites. This led to parallel shrinkage and growth, stepped up land take, and, finally, a government subsidized housing surplus that now – again with government aid – has to be reduced.

3. Demographic decline in East Germany has been caused by outmigration and natural population development. Between 1989 and 2005, some 1.4 million people moved from East Germany to West Germany; if about 500,000 foreigners had not arrived, the migration loss would have been even greater [11]. In addition, there was a natural decline in the population of some 600,000 owing to the massive fall in the birth rate from 1990 ([11], p. 12). Over this period, the total population of East Germany fell by 11.7%. Further decline can be expected owing to demographic change. If the trend in East Germany persists, the population will have halved by 2050. More and more towns and cities, not only in East Germany but also in the western states, are expected to experience stagnation or shrinkage [12].

Owing to demographic developments and outmigration, as well as developments on the property and housing markets, some one million dwellings had fallen vacant by the end of the 1990s. But these vacancies were only one element in the shrinkage problem, which must be understood as a many-facetted upheaval involving economic, social, and cultural factors ([7], p. 58ff.). The many dimensions of this upheaval are beginning to emerge in outline. East Germany has embarked on a specific path in the development of settlement structures which finds little to compare with in West Germany. Some authors have described it as a "disurbanization process" (intra-regional deconcentration of the population in an overall context of demographic decline) [13]. Since shrinkage can be expected to continue in the long term, "reasonable strategies for a retreat from extensive development" are called for [14]. Cities already have to cope with the loss of functions.

The Joint Program of the German Federal and State Governments: "Urban Redevelopment East"

In response to housing vacancies, the federal and state governments set up an expert commission in the late 1990s on "Housing Structural Change in the New States," on whose recommendation the federal government launched the "Urban Redevelopment East" program in 2002 [15]. The scheme was endowed with some €2.7 billion. By 2010, about 350,000 of the circa one million surplus dwellings were to be demolished. The demolition program is currently being implemented almost throughout East Germany. About 350 larger local authorities are now integrated in the program covering about 650 development areas, approximately three quarters of all East German towns and cities with populations of over 10,000 [6]. Most communities receiving support have a vacancy rate of about 10–15%, some even 20%. So far about 220,000 dwellings have been demolished (status end of 2009), reducing the vacancy rate to some 13%. Meanwhile, the demolition program is no longer limited to cautious downsizing: in many cities entire neighborhoods are being razed ([6], p. 11). Redevelopment has so far focused on large housing estates on the urban fringe. Some 40% of development areas are characterized by prefabricated high-rise housing from GDR times. Only one quarter have older housing stock dating from before 1948.

"Urban Redevelopment East" is clearly conceived as a consolidation program for the local housing market, but also pursues ambitious urban development objectives. Support is mainly provided for the demolition of housing, but the remaining stock, infrastructure, and the residential environs are to be upgraded, which includes the provision of new, attractive green structures. The aim is an integrated procedure, linking housing industry problems with urban development aspects. With an eye to ensuring the sustainability of the city as a whole, planned demolitions are to be embedded in urban structures and the neighborhoods involved are to be upgraded at the same time [16]. To ensure that downsizing, redevelopment, and upgrading works are coordinated and that demolition is adapted to the given urban structure, funding is made contingent on the elaboration of integrated urban development plans. Their purpose is "to coordinate the individual measures of urban redevelopment and combine them into a sustainable, meaningful whole" [17] and hence to improve urban amenity. The "Urban Redevelopment East" program thus sets high standards – also for the creation and design of

open spaces – which, however, both funding policy and local sectoral authorities have since substantially lowered. The thrust is now clearly toward rapid consolidation of the housing market. Funding for the after-use or conversion of cleared demolition sites are now scarcely available ([16], p. 758); in only one third of cases are upgrading measures undertaken, mostly planting. It is increasingly apparent that downsizing on the "onion-ring principle" from the periphery inward, as preferred by most local authorities, faces considerable difficulties in implementation. Urban redevelopment measures are now almost impossible to embed in an urban development concept, and in many cases they lead to the perforation of the urban structure. As a result, many isolated open spaces and vacant sites of varying sizes are created in the urban fabric. Perhaps for this reason every second local authority regards coping with previously developed land in central and significant locations as a serious problem [18].

In sum, the strategy of controlled shrinkage adopted by many cities has already come up against its limits, since it takes no account of these new needs but continues to be pursued for lack of feasible alternatives. Coping with existing and new brownfield land cleared in the course of urban redevelopment is proving to be a growing problem for which, as it has been seen, the program no longer provides anything like adequate funding.

The Demands Made of the New Open Spaces

The permanent rezoning of residential and industrial land, as well as infrastructure land in such dimensions, is a new urban development task. Initially, traditional demands are made of the new open spaces; they are to serve recreational purposes, for instance, in the form of small parks, green spaces, or playgrounds, and generally contribute to improving residential amenity. Ecological demands are formulated, for example, that habitat networks or green corridors should be created, thus contributing to nature conservation in the city.

Furthermore, new demands are advanced, notably that the new open spaces should help enhance the image of the locality and contribute to the positive presentation of the shrinkage process and its consequences. What is accordingly envisioned is not isolated, planted plots: notions of a "new urban landscape" predominate in which the new open space elements are interlinked ([19], pp 645ff.). The hope is that this will not only improve residential amenity but encourage demand and investment, thus upgrading entire neighborhoods. The new open spaces are hence expected to help stabilize residential areas and counteract vacancies, thus maintaining urban and socio-spatial structures. Open space systems are to provide a solid framework for the maintenance of urban structural contexts ([20], p. 737ff.), help integrate peripheral settlements into the surrounding landscape, and to improve and create recreational and locational amenities in inner cities ([6], p. 23; [21]). One particular goal is to establish green corridors that serve both recreational and nature conservation purposes.

The urban redevelopment program treats the creation of green spaces primarily as an element in design upgrading; seldom are ecological or nature conservation goals in focus. Apart from municipal demands for improved residential amenity and better quality of life for local residents, the call for active participation by the public plays a steadily growing role. Top-down urban development is longer judged sufficient: the committed involvement of residents and private actors is also needed. This development also means that more is expected from the open spaces cleared during redevelopment.

In the course of urban redevelopment, neighborhoods, cities, and entire regions set their hopes in the new open spaces as "identity-forming elements" for "when buildings are demolished and entire neighbourhoods downsized, the only remaining key factor in urban development is open space" [22]. What is more, the uses to which open spaces are put change with population decline, aging, diversification, and individualization. The focus shifts increasingly to specific user groups: the elderly, youth, singles, families, women and men, Germans, and immigrants ([22], p. 7). The question is whether the new, differentiated demands can really be met by traditional amenities. They are replaced by uses not typical of the city, with open spaces being understood as creative spaces. They include experience, art, and nature areas such as wild gardens, farmland, event venues, etc. The new open spaces are particularly suitable for social intercourse, offering opportunities for a highly varied urban stage

set by the population. Security in such areas plays a major role, and problems can be caused by informal use, for example, as rubbish tips, dog runs, drug trafficking locales, or camp sites for the homeless.

Strategies and Tools for Open Space Development

The current after-uses for previously developed sites range from (complete) clearance or clearance with simple planting or afforestation without precisely defined use requirements, to the layout of permanent green areas (parks, green belts, sport grounds, playgrounds, and other amenities). The *renaturation* (see our definition of the term within the glossary) of such areas is increasingly envisaged for the urban fringe. For some years now, new strategies have been tested, especially in East German cities, experimenting with interim uses in the form of temporary greening (recreation, events, nature conservation), but also with unconventional solutions for permanent green spaces, such as the layout of compensatory areas, downzoning to farmland and urban forest, and urban wilderness. Support is given for the renaturation of land no longer used for building purposes by both the Federal Spatial Planning Act [23] and the Federal Nature Conservation Act [24]. Section 2 (2) (8) of the Federal Spatial Planning Act, listing the principles of spatial planning, lays down that "if land is no longer used on a permanent basis, the productivity of the soil shall be maintained or restored." Section 2 (1) (11) of the Federal Nature Conservation Act prescribes that "Sealed surfaces which are no longer required shall be renatured or, where desealing is not possible or excessively expensive, they shall be left to natural development." In addition, the "National Strategy on Biological Diversity" adopted by the federal government on November 7, 2007, explicitly calls for more greenery in cities [25].

The examples of current and new subsequent uses of urban brownfield sites and their urban development, aesthetic, and ecological value are discussed below.

(Complete) Clearance of Redundant Sites

The consequences of the abandonment of large industrial areas, especially from the early to mid-1990s, have still not always been satisfactorily overcome. In many cases it was sought to revitalize areas through the massively subsidized demolition of buildings and complete clearance of sites, which preparatory land-use plans continued to register as industrial land. Where land could not be successfully marketed or only partially put to new use, unplanned reintegration of the area into the surrounding countryside was often the result, especially on the urban fringe. An undisturbed succession of vegetation thus took over large areas. Although interesting from an ecological point of view, this development met with a very mixed reception among nature conservationists owing the preponderance of ubiquitous species. Aesthetic aspects also gave cause for criticism, and acceptance among the local urban population was often lacking. Such derelict areas provoked anxiety, recalling the decline of entire industries and the associated loss of jobs ([26], p. 79) (Fig. 1).

Simple Clearance

Many downsizing projects funded by the "Urban Redevelopment East" program have already proved problematic, since they leave behind them nothing but simple, often dreary and derelict open spaces for whose maintenance no one accepts responsibility. Many local authorities have demolished or downsized single buildings within existing settlements (prefabricated housing estates, *Gründerzeit* neighborhoods), where, although the buildings have been removed, the technical infrastructure is left in place and sealed and streets retained. Vacant land is usually planted with lawn, and sometimes with a few shrubs or trees. As a rule, these areas are still zoned in the preparatory land-use plan as residential. In some redeveloped areas, especially prefabricated housing estates, vast land-use gaps have now opened up in the once closed structure of the city. Attempts to create extensive green corridors are often in vain; clearance sites tend to be scattered throughout the community. Their ecological value is thus low and their recreation value limited (Figs. 2 and 3).

Development of Permanent Green Spaces

A number of brownfield sites have, however, also been permanently converted into green spaces. Larger brownfield or clearance sites are linked up to form green corridors in the hope of improving social and ecological qualities, and, particularly on the urban

Urban Redevelopment and Quality of Open Spaces. Figure 1
Abandoned land with undisturbed succession on a former industrial zone along the River Elbe in Heidenau (Germany) (Photo: M. Arendt)

Urban Redevelopment and Quality of Open Spaces. Figure 2
Demolition of a prefabricated housing estate in Dresden-Prohlis (Germany) (Photo: R. Bendner)

outskirts, establishing a transition to the landscape. It is hoped that improving the quality of life and enhancing the image of the locality will help prevent urban sprawl [27]. One successful example of this strategy is the Leipzig-Grünau green corridor (planning and implementation 1993–1996), where the abandoned route of a planned road bordering on rural areas offered favorable conditions for creating a green belt. After

Urban Redevelopment and Quality of Open Spaces. Figure 3
Simply green former housing area with lawn, few shrubs, and trees in Dresden-Prohlis (Germany) (Photo: R. Bendner)

demolition of the prefabricated housing, new recreational amenities and green spaces with native trees and shrubs were created in the area, which had been short on greenery and open spaces. Local residents and institutions were involved in planning and design [28]. Such green spaces are generally of great value for recreational uses and, if well designed, can contribute to the ecological upgrading of the neighborhood or of the entire urban territory. Sustained conservation and maintenance can prove problematic, and more and more reliance is put on participation by local residents (Figs. 4 and 5).

Interim Use as Temporary Green Space

Ownership structures can make it difficult for municipal programs to reactivate smaller gap sites scattered throughout the city. Private property owners are wary of the legal repercussions of "official," even temporary, use of their plots and fear for the value of their building land. In order to induce landowners to tackle their vacancy problems, the "authorization agreement" has been developed [29, 30], a tool that provides for the meaningful, temporary public use of private brownfield sites without affecting existing building rights. A contract is concluded between the municipality and the property owner under which the owner makes unused sites available for concrete public uses (simple green areas, playgrounds, neighborhood gardens). In compensation, the municipality offers to pay for design and layout and limited maintenance and provides relief from property tax. Owners have accordingly been more willing to make land temporarily available for a wide range of uses, providing more opportunities for individually designed life spaces [29, 30]. Leipzig has pioneered the temporary use of open spaces under authorization agreements. The municipality has pursued a central objective: "more greenery, less density." The "Guidelines for Urban Renewal" [31] calls for more and better green areas and open spaces. Under authorization agreements, Leipzig has so far managed to develop some 140,000 m^2 of new green areas and open spaces ([29], p. 46), covering a wide range of interim uses. Most temporary green space uses focus on recreation. Depending on how these areas are designed and used, they can also be of incidental and targeted value in attaining urban-ecological goals and offer opportunities for nature conservation in the city (Fig. 6).

Use as Compensatory Areas

The use of inner-city brownfield sites for ecological compensation purposes gives local authorities a valuable opportunity to assert the interests of nature conservation in urban life spaces. For they provide debt-strapped municipalities with a possibility to use the duty imposed by Section 1a (3) of the Federal Building Code to mitigate the impact of development on nature specifically for urban-ecological measures, hence improving quality of life for residents [32]. However, difficult ownership structures and often high preliminary financing costs mean that hardly any suitable sites are available. Ecological upgrading mostly involves de-sealing and planting works. However, the extent to which nature conservation areas can be used

Urban Redevelopment and Quality of Open Spaces. Figure 4
New designed green spaces in Leipzig-Grünau (Photo: Municipality of Leipzig)

Urban Redevelopment and Quality of Open Spaces. Figure 5
Public allotments in the Lehne-Voigt-Park in Leipzig (Photo: J. Mathey)

by the urban population is problematic. In order to steer impact mitigation compensatory measures into the inner cities, a number of municipalities have formed land pools that include previously developed land. In Leipzig, for example, the city council decided that 50% of compensatory measures under the environmental impact mitigation rules were to involve inner-city brownfield sites (information from the

Urban Redevelopment and Quality of Open Spaces. Figure 6
Temporary use of former brownfield as green spaces in the east of Leipzig (Photo: J. Mathey)

Leipzig Office of the Environment). There is now an intermunicipal compensatory land pool which included most of the land that comes into question. However, as in other cities, it is difficult to find areas for permanent planting in Leipzig.

Permanent Downzoning to Farmland or Forest

Urban and peri-urban agriculture has a long tradition [33]. Regardless of the type and intensity of farming, agricultural areas also provide city dwellers with a wide range of recreational and other amenities [34]. The discussion on the greater use of renewable energies and the growing demand for biomass production can be an economically attractive after-use option for clearance sites in the city. An ongoing Experimental Housing and Urban Development study is examining the use of urban open spaces for renewable energy [35]. Examples of agricultural uses are the short rotation plantations in Halle-Neustadt and the Green Bow in Leipzig-Paunsdorf, the layout of which took account of nature conservation aspects and recreational needs. The types of farming feasible on previously developed urban land will depend on the size of the areas, their location in the urban structure, and on locational prerequisites (e.g., soil quality), but not least on what actors can be found to manage them.

A frequently envisaged category of after-use in renaturation projects is forest or woodland. Forest does not necessarily require the reallocation of holdings, and ensures secure, long-term management, generally by the forest authorities [36]. In contrast to use as conventional green spaces, managing land under the terms of the Forests Act involves much lower investment and maintenance costs, less stringent traffic safety obligations than for the more usual urban open spaces (problem of liability), much lower land values, but also new use options, since public access is maintained. In keeping with the principle of downsizing from the periphery inward, conversion into forest is envisaged primarily on the urban outskirts, with the aim of establishing interconnectivity with the surrounding countryside [37, 38]. In Schwedt "Am Waldrand," for example, the afforestation of clearance sites is planned; in Weißwasser-Süd forest-like mixed plantations have been established, which after 4 years of development care are to be transferred to the forestry authorities. The "Waldstadt" in Halle-Silberhöhe is being laid out on the periphery of the large housing estate, bordering on an extensive young-stand, near-natural deciduous

Urban Redevelopment and Quality of Open Spaces. Figure 7
Farmland combined with nature conservation on a former military area in Leipzig-Paunsdorf (Photo: Municipality of Leipzig)

forest [36]. Woodland is used in the inner-city to cover gap sites, maintaining the illusion of density and compactness (e.g., "Dunkler Wald" in Leipzig). Such forested areas attain spatial significance only after a relatively long period, and only then do they correspond to the accustomed image, which can initially lead to problems of public acceptance (Figs. 7 and 8).

Experiment "Wilderness in the City"

In many cases, however, the development of brownfield sites proceeds unsystematically. Depending on how long a vacant plot remains undisturbed or on the way in which it is used, different stages of vegetation development with the associated animal species will predominate. This often results in ecologically valuable habitat mosaics [39–41], which can be precious recreation areas and offer opportunities to experience nature [42]. The question of wilderness in the city is much discussed in the debate on urban redevelopment. This is, however, to be understood not so much as a "free succession" of vegetation with land being completely left to its own devices but as a "regulated succession," a mix of planned, partly cultivated, and "wild" areas [43]. The overgrowth of vacant sites is

Urban Redevelopment and Quality of Open Spaces. Figure 8
"Dark Forest" on a former brownfield in Leipzig (Photo: I. Hartmann)

accepted only if it remains in the prescribed limits and fits into the pattern of new open spaces [44]. "Orderly succession" constitutes a many-facetted habitat mosaic that also exhibits a certain order. This new aesthetic is more acceptable than impenetrable

Urban Redevelopment and Quality of Open Spaces. Figure 9
"Orderly Succession" on a former military area in Dresden-Nickern (Photo: R. Bendner)

wilderness. Moreover, in comparison with conventional green spaces, considerable savings can be made on layout and maintenance. In contrast to the substantial attention that this subject attracts among the public and experts, it has so far played hardly any role at all in urban redevelopment, and there are very few examples of projects. On a former military site in Dresden-Nickern, a sort of "ruderal park" has been developed, retaining existing spontaneous vegetation, which includes wilderness and natural succession. This ruderal park is accepted and well used by the residents, however, often the development value and amenity quality of such areas is criticized and public acceptance is low ([26], p. 73f.; [45]) (Fig. 9).

Conclusion: New Open Space Qualities Through Urban Redevelopment?

Urban redevelopment has opened up a new field of experimentation and opportunity in the design and use of inner-city open spaces. The new possibilities and opportunities face a complex of obstacles, primarily financial but also legal in nature. They cannot be overcome by traditional strategies: new forms of cooperation are needed. This is also true of coping with the changing demands made on the use of open spaces. Overall, a change of awareness is required, a shift from growth toward a novel combination of growth and shrinkage. Approaches directed toward a subdivided or fragmented urban structure would appear to be more suitable in handling the new open spaces [46].

The advantages offered by "new greenery" such as improved open space amenity, the concomitant ecological upgrading, or the attention paid to the interests of nature conservation are counterbalanced by a number of disadvantages. One is the fragmentation of the physical urban fabric, the perforation of the city, and, not seldom, the limited use capability of the new open spaces. What is more, these new open spaces are often still encumbered by the remains of urban infrastructure. Sometimes they have a derelict aspect, which contributes to stigmatization. Although urban redevelopment produces many new open and green spaces, it leads to a loss of design quality and amenity when measured against existing standards and the associated demands made of urban open space. The importance of open space planning in shrinking cities is therefore increasing; it is becoming one of the "most important tools of urban development" ([19], p. 648).

In the course of urban redevelopment, new open spaces are also expected to perform urban development

tasks and functions. It is questionable whether they are suitable, for the new open space qualities envisioned by integrated urban development concepts do not emerge at once. To begin with, much takes the appearance of isolated pieces of a puzzle or tiles in a mosaic without recognizable outline, or is provisional and transitory in nature. For example, it is not yet clear what is to become of the experiments with vegetation succession. Many experimental projects – including forms of extensive maintenance, wilderness, and succession – are experienced as impoverishment [47]. In the short and medium term, many cities will have to live with open spaces that attain their aesthetic qualities only gradually ([26], p. 74). Since planning practice largely stands by the accustomed types of open space [46, 48], the permanent conversion of redundant building land into urban green spaces of conventional design and function (e.g., parks, playgrounds and recreation facilities, and allotment gardens) is, despite financial restrictions, likely to remain the most frequent after-use for clearance sites in the inner-city and residential areas. However, as budgets shrink, urban parks departments are already scarcely able to maintain their green areas, let alone take on additional cleared sites. In the future, new types of open spaces are therefore likely to be established alongside the accustomed ones, especially areas that allow stronger forms of succession. Thus a growing number of cities undertaking urban redevelopment can be expected to embark on the adventure of succession ([49], p. 12), but they will by no means be overgrown as a result. One outcome of urban redevelopment in the cities concerned will be a more self-stabilizing nature. In view of the far-reaching transformations that redevelopment cause in the cityscape, however, these changes can be regarded as secondary. In sum, urban redevelopment and more greenery will not directly enhance quality in the conventional sense. The population will have to get used to a new quality of the city and its new open spaces. And the decisive innovation will perhaps be a shift in perspective that allows open spaces to be seen with new eyes.

Outlook: Future Directions

As pointed out (in the conclusions) above, the reintegration of brownfields into the urban fabric by developing green and open spaces (renaturation) is a big challenge, which in future times will become of more and more importance. There is a chance to reconstruct the urban structure (urban fabric) and give cities new faces, but new overall strategies are necessary and a lot of obstacles have to be overcome. In the planning, practice cities have to face a lot of implementation problems such as (1) availability of brownfields (sites not in the ownership of the community), (2) financing of measurements and maintenance, (3) missing cooperation of different city departments, (4) meeting the needs of residents (public relation, participation), (5) considering legal and strategic requirements, and (6) necessitating the profit gain out of the sites. Finding solutions demands for interdisciplinary (research) approaches, where ecological, social, economical, and planning aspects are taken into consideration to develop overall strategies (and concepts) that lead to a "new urban landscape" with valuable, usable, and accepted green and open spaces in a sustainable urban structure.

Bibliography

Primary Literature

1. Lampen A, Owzar A (2008) Schrumpfende Städte. Ein Phänomen zwischen Antike und Moderne. Böhlau, Köln
2. Oswalt P, Reiniets T (2006) Atlas of shrinking cities. Ostfildern-Ruit, Hatje Cantz
3. Turok I, Mykhnenko V (2007) The trajectories of European cities, 1960–2005. Cities: Int J Urban Policy Plan 24:165–182
4. Demuth B, Moorfeld M, Heiland S (2010) Demografischer Wandel und Naturschutz. In: Bundesamt für Naturschutz (BfN) (ed) Naturschutz und Biologische Vielfalt Heft 88. Bonn-Bad Godesberg
5. Haase D, Schetke S (2010) Potential of biodiversity and recreation in shrinking cities: contextualization and operationalization. In: Müller N, Werner P, Kelcey JG (eds) Urban biodiversity and design, Conservation science and practice series. Wiley-Blackwell, Oxford, pp 518–538
6. BMVBS (Bundesministerium für Verkehr, Bau- und Stadtentwicklung) & Bundestransferstelle Stadtumbau Ost (2008) Evaluierung des Bund-Länder-Programms Stadtumbau Ost. Berlin
7. Rink D (2010) Schrumpfen als Transformationsproblem. Ursachen und Verlaufsformen von Schrumpfung in Ostdeutschland. In: Bernt M, Haus M, Robischon T (eds) Stadtumbau und lokale Politik. Darmstadt, Schader Stiftung pp 58–77
8. Gatzweiler H-P, Meyer K, Milbert A (2003) Schrumpfende Städte in Deutschland? Fakten und Trends. In: Informationen zur Raumentwicklung, H.10/11, pp 557–574

9. Hannemann C (2003) Schrumpfende Städte in Ostdeutschland – Ursachen und Folgen einer Stadtentwicklung ohne Wirtschaftswachstum. In: Aus Politik und Zeitgeschichte, Beilage zur Zeitschrift DAS PARLAMENT, B 28, S. 3–8
10. Expertenkommission (2001) Wohnungswirtschaftlicher Strukturwandel in den neuen Bundesländern, Bericht, Berlin, p 4
11. Ragnitz J (2006) Demographische Entwicklung in Ostdeutschland. Halle
12. Müller B, Siedentop S (2004) Wachstum und Schrumpfung in Deutschland – Trends, Perspektiven und Herausforderungen für die räumliche Planung und Entwicklung. In: Deutsche Zeitschrift für Kommunalwissenschaften. Jg. 43, H. 1, pp 14–32
13. Siedentop S, Kausch S (2003) Die siedelungsstrukturelle Dimension der Schrumpfung – Räumliche Trends der Bevölkerungsentwicklung in Ostdeutschland nach der Wende. In: Müller B, Siedentop S (eds) Schrumpfung – Neue Herausforderung für die Regionalentwicklung in Sachsen. Sachsen-Anhalt und Thüringen, Hannover, pp 11–24
14. Herfert G (2004) Die ostdeutsche Schrumpfungslandschaft. In: Geographische Rundschau, Issue 2, pp 57–62
15. Häussermann H, Glock B (2004) New trends in urban development and public policy in Eastern Germany: dealing with the vacant housing problem at the local level. Int J Urban Reg Res 28(4):919–929
16. Bernt M (2009) Partnerships for demolition: the governance of urban renewal in East Germany's shrinking cities. Int J Urban Reg Res 33(3):754–769
17. BMVBW (Bundesministerium für Verkehr, Bau- und Wohnungswesen) (2001) Wettbewerb Stadtumbau Ost. Für lebenswerte Städte und attraktives Wohnen, Berlin
18. BMVBS & BBR (Bundesministerium für Verkehr, Bau- und Stadtentwicklung & Bundesamt für Bauwesen und Raumordnung) (2007) 5 Jahre Stadtumbau Ost – Eine Zwischenbilanz. Zweiter Statusbericht der Bundestransferstelle, Bonn
19. Kunz W (2004) Stadträumliche Qualität durch Freiräume. Beispiele für innovative Planungsideen und –methoden aus dem Stadtumbauprozess in Leipzig. In: Informationen zur Raumentwicklung, H. 11–12, pp 645–658
20. Schwartz C (2004) Extensive Freiraumgestaltung als Strategie im Stadtumbau. In: Informationen zur Raumentwicklung, H. 11–12, pp 735–747
21. Roch I, Banse J (2007) Entwicklungsperspektiven für die Lebensqualitäten Wohnen und Freiraumnutzung in den Städten Bonn und Dresden. In: Schrenk M, Popovich VV, Benedikt J (eds) REAL CORP 2007, proceedings, Vienna, 20–23 May 2007, pp 563–578
22. Böhme C (2007) Die "grüne" Stadt – urbane Qualitäten durch Freiraumentwicklung. In: Deutsche Zeitschrift für Kommunalwissenschaften, J. 46, H. 1, pp 5–9
23. Raumordnungsgesetz (ROG) vom 18. August 1997 (BGBl. I S. 2081, 2102), zuletzt geändert durch Artikel 10 des Gesetzes vom 9. Dezember 2006 (BGBl. I S. 2833)
24. Bundesnaturschutzgesetz (BNatSchG) vom 25. März 2002 (BGBl. I S. 1193), zuletzt geändert durch Artikel 3 des Gesetzes vom 10. Mai 2007 (BGBl. I S. 666)
25. BMU (Bundesministerium für Umwelt, Naturschutz und Reaktorsicherheit (ed.) (2007): Nationale Strategie zur biologischen Vielfalt self-published
26. Rink D (2005) Surrogate nature or wilderness? Social perceptions and notions of nature in an urban context. In: Kowarik I, Körner S (eds) Wild urban woodlands. Berlin/Heidelberg, Springer pp 67–80
27. GreenKeys Team (2008) GreenKeys @ Your City – a guide for urban green quality. Leibniz Institute of Ecological and Regional Development (IOER), Dresden
28. URGE-Team (2004) Making Greener Cities – a practical guide. UFZ-Bericht Nr. 8/2004 (Stadtökologische Forschungen Nr. 37), UFZ Leipzig-Halle
29. Heck A (2005) "STADTHALTEN" – Leipzig. Temporäre Nutzungen in urbanen Räumen. In: Planerin, 01/05, pp 45–47
30. Heck A (2006) Gestattungsvereinbarungen als Handlungsinstrument der Stadtentwicklung. In: DRL (Deutscher Rat für Landespflege) (ed) Freiraumqualitäten in der zukünftigen Stadtentwicklung. Schriftenreihe des DRL Heft 78, pp 111–114
31. Stadt Leipzig (2005) Das Neue Leipzig. Sterneuerung. Neue Freiräume im Leipziger Osten. Leipzig
32. Mathey J, Kochan B, Stutzriemer S (2003) Biodiversität auf städtischen Brachflächen? Planerische Aspekte naturverträglicher Folgenutzungen. In: Bayrisches Landesamt für Umweltschutz (ed) StadtNatur – Bedeutung der Stadt für die Natur und der Natur für die Stadt, pp 47–57
33. Lohrberg F (2000) Urbane Landwirtschaft als Erlebnisraum. In: Garten + Landschaft, Heft 3, pp 9–12
34. Lauinger H (2005) Urbane Landwirtschaft. In: Oswalt P (Hrsg.) Schrumpfende Städte. Band 2: Handlungskonzepte. Ostfildern-Ruit, Hatje Cantz pp 156–164
35. BBR (2007) ExWoSt Programm. Forschungsprojekt "Nutzung städtischer Freiflächen für erneuerbare Energien." Bonn
36. BMVBW & BBR (Bundesministerium für Verkehr, Bau- und Wohnungswesen & Bundesamt für Bauwesen und Raumordnung) (2004) Zwischennutzungen und neue Freiflächen. Städtische Lebensräume der Zukunft, Berlin
37. Kowarik I, Körner S (eds) (2005) Wild urban woodlands. Berlin/Heidelberg, Springer
38. Burckhardt I et al (2008) Urbane Wälder – Ökologische Stadterneuerung durch Anlage urbaner Waldflächen auf innerstädtischen Flächen im Nutzungswandel – ein Beitrag zur Stadtentwicklung. Bonn
39. Wittig R, Zucchi H (eds) (1993) Städtische Brachflächen und ihre Bedeutung aus der Sicht von Ökologie, Umwelterziehung und Planung, Geobotanische Kolloquien, 9. Frankfurt, Verlag Natur & Wissenschaft Harro Hieronimus & Jürgen Schmidt, Solingen
40. Rebele F, Dettmar J (1996) Industriebrachen. Ökologie und Management, Stuttgart
41. Kowarik I (2004) Neue Wildnis, Naturschutz und Gestaltung. In: Garten + Landschaft 2/2004, pp 12–15
42. Rebele F (2003) Was können Brachflächen zur Innenentwicklung beitragen? In: Arlt G, Kowarik I, Mathey J, Rebele F (eds) Urbane Innentwicklung in Ökologie und Planung. IÖR-Schriften, Bd. 39, Dresden, pp 63–74

43. Rink D (2009) Wilderness: the nature of urban shrinkage? The debate on urban restructuring and renaturation in eastern Germany. Nat Cult 4(3):275–292
44. Dettmar J (2002) Alternative Wildnis. In: Garten + Landschaft, Heft 5, pp 15–17
45. Heydenreich S (2006) Baulücke? – Zwischennutzungen! Bürgerschaftliche Zwischennutzungen in schrumpfenden Stadtteilen – das Beispiel Solidago e. V., Leipzig Schönefeld. In: Friedrich-Ebert-Stiftung (Hrsg.) Luxus der Leere – Chancen für den Stadtumbau, pp 15–21
46. Rößler S (2010) Freiräume in schrumpfenden Städten. Chancen und Grenzen der Freiraumplanung im Stadtumbau, Dresden
47. Mathey J, Rink D (2010) Urban wastelands – a chance for biodiversity in cities? Ecological aspects, social perceptions and acceptance of wilderness by residents. In: Müller N, Werner P, Kelcey JG (eds) Urban biodiversity and design, Conservation science and practice series. Wiley-Blackwell, Oxford, pp 406–424
48. Rößler S (2008) Green space development in shrinking cities – opportunities and constraints. In: GreenKeys Team (ed) Urban green spaces – a key for sustainable cities. Conference reader for the international conference in Sofia, Bulgaria, 17–18 Apr 2008. Leibniz Institute of Ecological and Regional Development (IOER), Dresden, pp 71–74
49. Kil W (2005) Die neue Leere – eine Chance für's Grün? In: Stadt + Grün, H. 9/2005, S. 9–14

Books and Reviews

BMVBS (Bundesministerium für Verkehr, Bau- und Stadtentwicklung) (2009) Renaturierung als Strategie nachhaltiger Stadtentwicklung. Berlin

BMVBS & BBR (Bundesministerium für Verkehr, Bau- und Stadtentwicklung & Bundesamt für Bauwesen und Raumordnung) (2006) Stadtumbau Ost – Stand und Perspektiven. Erster Statusbericht der Bundestransferstelle, Bonn

Broggi MF (1999) Ist Wildnis schön und "nützlich"? In: Konold W, Böcker R, Hampicke U (Hrsg.) Handbuch Naturschutz und Landschaftspflege. Landsberg, Ecomed pp 1–7

UV Effects on Living Organisms

Philipp Weihs[1], Alois W. Schmalwieser[2]
Günther Schauberger[2]
[1]University of Natural Resources and Applied Life Sciences, Vienna, Austria
[2]WG Environmental Health, University of Veterinary Medicine, Vienna, Austria

Article Outline

Glossary
Definition of the Subject
Introduction
Biological Effectiveness of UV Radiation
Transmission to the Effective Skin Dose
Biological Effects on Microorganisms
Effects of UV Radiation on Plants
Animals
Future Directions
Bibliography

Glossary

Abiotic An abiotic factor is a feature or process that is not derived from, or caused by, living organisms but that might affect living organisms in their environment.

Biologically effective UV radiation The biologically effective UV radiation is obtained by integrating the biologically effective spectral irradiance over the whole wavelength range.

Biotic A biotic factor is a feature or process derived from, or caused by, living organisms, which might affect other living organisms in their environment.

Chloroplast Chloroplast is the site of photosynthesis. It is distinguished by its green color, caused by the presence of chlorophyll.

Chromophore A chemical group capable of selective light absorption resulting in the coloration of certain organic compounds. In biological molecules that serve to capture or detect light energy, the chromophore is the moiety that causes a conformational change of the molecule when hit by light.

Ecotherm An organism that regulates its body temperature largely by exchanging heat with its surroundings (e.g., fish, reptile, . . .).

Eye damage This includes the keratoconjunctivitis (an inflammation of the cornea and conjunctiva, snow blindness), an acute effect, and chronic damage of the eye lens, caused by absorbing UVA radiation.

Flavonoids An umbrella term that designates a wide spectrum of pigments (including anthocyanins, among others).

Genetic damage DNA absorbs UVB radiation and the absorbed energy can break bonds in the DNA. Most of the DNA breakages are repaired by proteins present in the cell nucleus, but unrepaired genetic damage of the DNA can lead to skin cancers.

Health effects In humans and animals, prolonged exposure to solar UV radiation may result in acute and chronic health effects on the skin, eye, and immune system. UVB exposure induces the production of vitamin D in the skin. The majority of positive health effects are related to this vitamin.

Minimal erythemal dose (MED) The amount of UV radiation exposure required to cause a just perceptible reddening of the skin.

Mitochondria "Powerhouse" of the cell, which acts as the site for the production of high-energy compounds. These high-energy compounds are the vital energy source for several cellular processes.

Monomer A molecule that can combine with others to form a polymer.

Morphogenesis Biological process of growth, structure, form, or shape.

Phototaxis A response to a directional light stimulus that involves movement of a whole organism. This is advantageous for phototrophic organisms as they can orient themselves most efficiently to receive light for photosynthesis. Phototaxis is called positive if the movement is in the direction of increasing light intensity and negative if the direction is opposite.

Plant growth The rate of increase in weight and size of plant organs, such as leaf, stem, or root.

Skin damage Beside the sunburn (erythema), a well-known acute effect, chronic skin damage is also observed. This includes elastoses (damage of collagen fibers) and, thereby, aging of the skin and skin cancer. (The three most common skin cancers are basal cell cancer, squamous cell cancer, and melanoma, each of which is named after the type of skin cell from which it arises. Melanoma is one of the less common types of skin cancer but causes the majority (75%) of skin cancer–related deaths.)

Spectral weighting function Wavelength dependency of biologic efficiency of UV radiation. The multiplication of spectral irradiance and a spectral weighting function delivers the biologically effective spectral irradiance. The spectral weighting function is unique for each photobiological process.

UV (ultraviolet) radiation Electromagnetic energy in the wavelength range between 200 and 400 nm. In the solar spectrum on Earth's surface the wavelength range is limited to 280 and 400 nm. The spectral range is divided in UVC (200–280 nm), UVB (280–315 nm), and UVA (315–400 nm).

Yield Economic product harvested from plants, for example, seed from pods of soybean, roots from carrots (*Daucus carota*), grain from wheat (*Triticum aestivum*), or seed and lint from cotton (*Gossypium hursutum*).

Definition of the Subject

Since the energy of an electromagnetic photon increases with decreasing wavelength, the biological effectiveness – defined as the capacity of radiation to produce a specific biological effect – also increases with decreasing wavelength. The largest biological effects are therefore generated in the shortest wavelength range (280–400 nm) of the incident solar radiation spectrum, which is referred to as ultraviolet (UV) radiation. Living organisms (i.e., living systems such as animals, plants, and microorganisms) are influenced by solar radiation and especially also by UV radiation. Three important aspects have to be taken into account in an investigation regarding the UV impact on living organisms: First, the damage potential of UV has to be studied; second, the faculty of living organisms to protect themselves and to adapt has to be examined; and third, the environment and its impact on the UV radiation field has to be taken into account.

Introduction

The decrease in the ozone layer, which was discovered in the early 1980s, has raised big concerns among the scientific community and among the decision makers. The ozone layer shields the Earth from the very harmful UV radiation that belongs to the part of the solar spectrum with the largest photon energy. Before the ozone hole discovery, it was well known that UV radiation may lead to sunburn on humans and animals, and it was also known that UV may have a negative impact on the eyes. It was, however, not clear what impact UV would have on the biosphere if the ozone layer was to diminish more. Would the biosphere be able to adapt? Or, conversely, would the expected increase in UV eradicate all life on Earth? A lot of money was therefore invested in research on the impacts of UV on the biosphere: the UV effects on humans, as well as on microorganisms, plants and

animals, were investigated. In this article, the focus is on microorganisms, plants and animals. An overview of the research results obtained in these topics during the last 30 years is given, in the form of a detailed review of the findings on the damage potential of UV, and on the adaptation potential and the UV defense mechanisms of microorganisms, plants and animals.

Biological Effectiveness of UV Radiation

The main concept that is used throughout this article is that of the "dose," which describes the biologically effective UV radiation reaching the skin, considered as a relevant receiving surface, and taking into account the Grotthus–Draper law (named after the chemists Christian J.D.T. von Grotthus and John W. Draper). This law states that a tissue effect can only occur if radiation is absorbed. However, absorbed radiation does not necessarily cause a biochemical reaction. Absorbed radiation may simply be converted into heat, or it may be re-emitted as light at a different wavelength. The latter phenomenon is called fluorescence.

The spectral sensitivity of these biochemical effects is taken into account by a spectral weighting function, whose convolution with the incident solar spectrum results in biologically effective radiation (it would be good to introduce the MED here or in next section).

Biologically Effective Irradiance and Dose

The biologically effective irradiance E_{biol} is calculated by a dimensionless biological weighting function σ_λ and the incident spectral irradiance E_λ from:

$$E_{biol} = \int_{280\ \text{nm}}^{400\ \text{nm}} E_\lambda\, \sigma_\lambda\, \mathrm{d}\lambda. \tag{1}$$

The corresponding biologically effective dose (irradiation) is obtained as the product of the biologically effective irradiance E_{biol} and the time of exposure t:

$$D_{biol} = E_{biol}\ t \tag{2}$$

if it can be assumed that E_{biol} is constant over the period. Otherwise, a summation over time would be necessary.

According to the rule of Bunsen and Roscoe [1] see (Fig. 1), also called reciprocity law, a photochemical reaction is directly proportional to the dose D_{biol}, irrespective of the time t over which this dose is

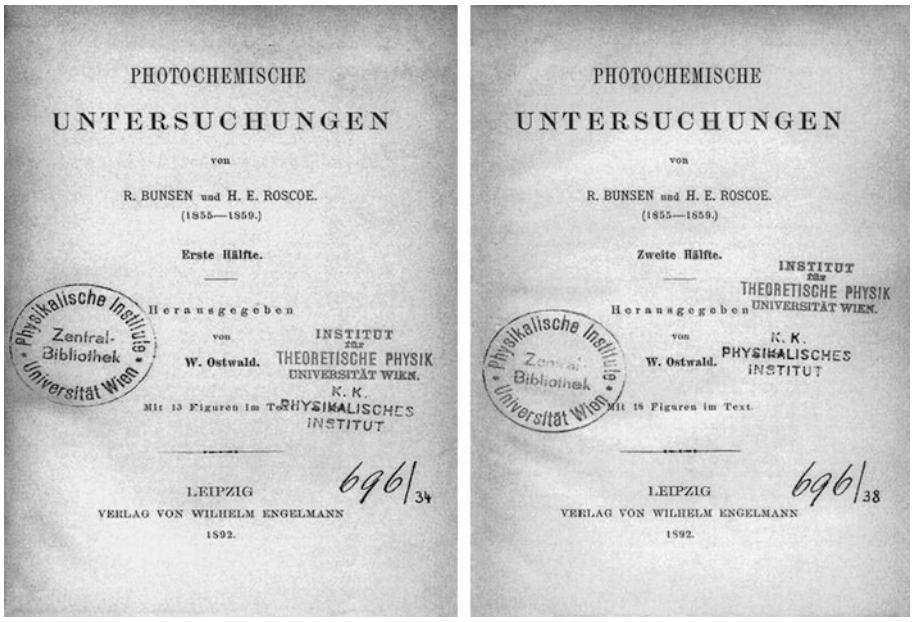
PHOTOCHEMISCHE
UNTERSUCHUNGEN
von
R. BUNSEN und H. E. ROSCOE.
(1855—1859.)
Erste Hälfte.
Herausgegeben
von
W. Ostwald.
LEIPZIG
VERLAG VON WILHELM ENGELMANN
1892.

PHOTOCHEMISCHE
UNTERSUCHUNGEN
von
R. BUNSEN und H. E. ROSCOE.
(1855—1859.)
Zweite Hälfte.
Herausgegeben
von
W. Ostwald.
Mit 18 Figuren im Text.
LEIPZIG
VERLAG VON WILHELM ENGELMANN
1892.

UV Effects on Living Organisms. Figure 1
Cover page of a re-print of the paper by Bunsen and Roscoe [1], published by Wilhelm Engelmann in the series "Ostwalds Klassiker der modernen Wissenschaft," Leipzig 1892 [2]

delivered. This often implicit assumption is a simple working hypothesis even though it has been shown that at a constant total dose, the irradiance (intensity) is a major factor that determines both the quality and quantity of the response [2, 3], in the case of UV-induced cell death, photocarcinogenesis, psoralen photochemistry, and effects of low-level laser radiation.

Reciprocity law failures were commonly observed in experiments conducted at either very low or very high radiant fluxes. To account for these failures, Schwarzschild, an astronomer, proposed a modification of the reciprocity law that resulted in a better fit to his low intensity, stellar data. This empirical model later became known as Schwarzschild's law [4] and is given by either [5]

$$D_{biol} = E^{p}{}_{biol}\ t \tag{3}$$

or

$$D_{biol} = E_{biol}\ t^{p} \tag{4}$$

where p is the Schwarzschild coefficient. When $p = 1$, then the Schwarzschild and the reciprocity law are identical. Martin et al. [5] found in a review that, in 11 experiments with erythema, only one deviated from the reciprocity law by $p = 1.2$. For many other biological effects the Schwarzschild coefficient was found to be $p = 1$ for the majority of experiments.

Dose–Response Relationship

A dose-response function (DRF) describes the influence of a biologically effective UV dose, D, on an observed biological effect.

Erythema The erythema is caused by ultraviolet radiation. It can be observed on animals in the same way as on humans. In particular, the dose-response functions and the time course of the reddening of the skin of pigs were investigated in detail.

The dose-response function of skin reddening can be described by a logit function,

$$\Delta EI = \frac{\Delta EI_{\max}}{1 + e^{\frac{\log D - \log D_{0.5}}{-k}}} \tag{5}$$

The erythema index ΔEI is defined via the international color system, L*a*b*. The ΔEI value is the difference of the red color value a* before and after UV exposure, the UV Dose D (J/m^2), the plateau of the dose-response function (maximum value of the erythema index) $\Delta EI_{\max}$, the dose of the midpoint of the function $D_{0,5}$ and the slope of the logit function at the midpoint k (Fig. 2). The measurements of the redness of the skin can be done by a color meter (e.g., Minolta Chroma Meter CR 300) that uses the international color system L*a*b*.

Most photobiological effects do not appear immediately after or during exposure but after a certain latent period. For certain effects, the latent period may be in the order of decades (e.g., skin cancer in human), while for other effects, the period is rather short (e.g., erythema).

The visibility of an effect may depend also on time. In a first phase the visibility of an effect increases until reaching a maximum. Afterward the visibility decreases. If an effect is reversible, the visibility of the effect goes back to zero; if the effect is irreversible, it stays visible. Repair mechanisms (photorepair) of the organisms are crucial to make the effect disappear. Sustained irradiation can be additive and enhances the remaining effect (cumulative effect).

The temporal course of an effect may depend on dose and wavelength.

The dose-response function, as well as the time course of the erythema in pigs, were investigated by

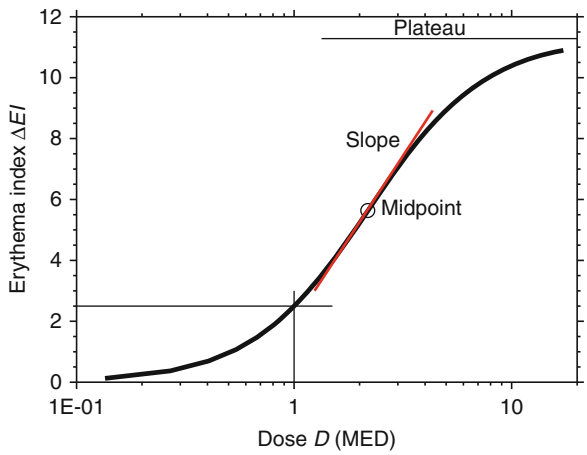

UV Effects on Living Organisms. Figure 2
UVB-caused dose-response curve, 24 h after exposure, for a pig with a minimal erythema dose of MED = 148 J/m^2. In this specific case, the plateau $\Delta EI_{\max}$ equals 11.28, the midpoint $D_{0.5}$ is 2.75 MED, and the slope k is 0.269

Reischl et al. [6] (Fig. 3). In Fig. 4, the normalized dose-response function of ten pigs (crossbreeding of "Edelschwein" and "Landrasse") show similar behavior. The differences of the plateau and the slope of the function can be explained by individual sensitivity, similar to the four skin types of humans. The median of the MED was calculated as 165 J/m^2, the lower quartile 143 J/m^2, and the upper quartile 184 J/m^2. In Table 1 the minimal erythema dose (MED) is summarized for cattle, horse and pig.

To describe the time course of the erythema index ΔEI, the doses were divided into three groups: low doses if below 1 MED (sub-erythemal doses), medium doses between 1 and 7 MED, and high doses above 7 MED. The time course of the artificial UVB and UVC exposure is depicted in Fig. 5.

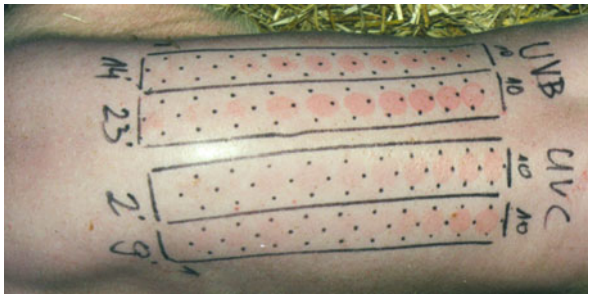

UV Effects on Living Organisms. Figure 3
Erythema (on pig skin?) caused by UVB and UVC radiation [6]

The time course of erythema was bimodal after UVB and UVC exposure. Both spectral ranges show a peak for low doses within about 12 h. Higher doses showed a greater intensity of redness and later fading by UVB than by UVC. Two effects could be distinguished. The first effect caused an early maximum of erythema by low doses, whereas the second effect caused a later, higher maximum by higher doses. These two effects can also be observed in studies on humans [7]. For both spectral ranges, the time course of erythema was primarily related to the UV dose and not to the spectral range.

Action Spectra

If one would like to estimate the effectiveness of UV radiation in causing a certain effect, the action spectrum (or biological weighting function) has to be known to weigh the incident spectral irradiance. An action spectrum (AS) describes the spectral efficiency of light in initiating a photochemical or photobiological process.

Conventionally, an AS is determined by exposing a sample to $n(\lambda)$ photons at wavelength λ to produce the effect. Then the wavelength and photon number are varied in such a way that the same effect is produced at all wavelengths. The AS s is then

$$s(\lambda) = C/n(\lambda) \tag{6}$$

where C is a constant.

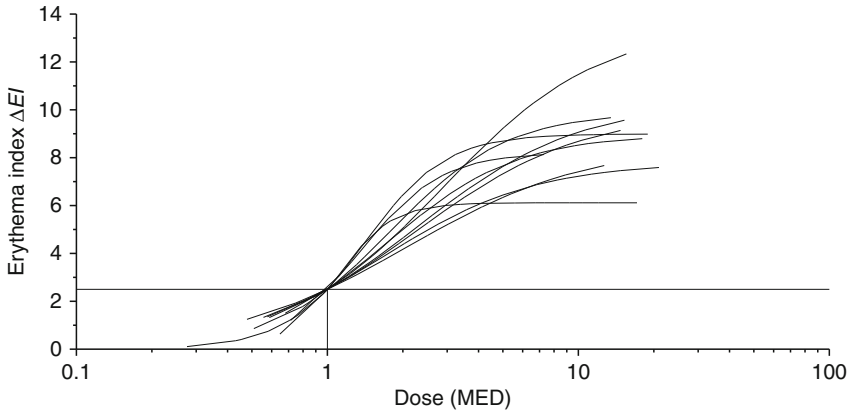

UV Effects on Living Organisms. Figure 4
Dose-response function for pigs, normalized by the individual minimal erythema dose (MED). The MED was determined by an erythema index $\Delta EI = 2.5$, which is the limit of the visual detection 24 h after a UVB exposure [6]

UV Effects on Living Organisms. Table 1 Minimal erythema dose (MED) for several species

Specie	Minimal erythema dose (MED) (J/m^2)	Author
Cattle	100	Mehlhorn and Steiger [8][a]
Horse	450	Kasper [9][b]
Pig	165	Reischl et al. [6][b]

[a]Spectral weighting function not clearly defined
[b]Reference erythema weighting function by MacKinley and Diffey [10]

The number of photons is called radiant exposure or dose. It is the product of irradiance and the duration of irradiation.

If only one chromophore is present and if this chromophore is in an unbound and monomeric state, the action spectrum will have a shape identical to that of the absorption spectrum of the chromophore. In samples with many absorbing molecules, action spectroscopy is a powerful tool used to identify the specific chromophore for the process under scrutiny.

If free monomeric chromophore molecules are present together with bound or aggregated molecules, the

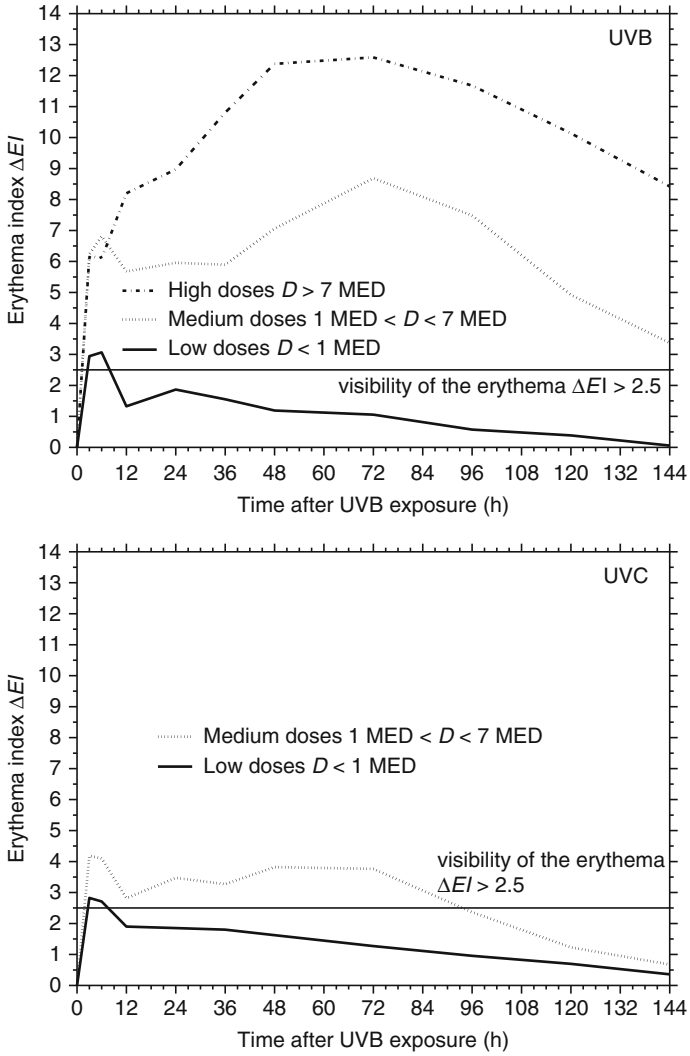

UV Effects on Living Organisms. Figure 5
Time course of the erythema intensity caused by UVB and UVC radiation, measured by the erythema index ΔEI for three dose levels [6]

situation is more complicated. Aggregated or bound molecules usually have distorted or shifted spectra as compared with monomeric molecules, but are usually less efficient in initiating photochemical processes.

If different chromophores are involved, the AS is a superposition of several absorption spectra.

Action spectra are specific to each process. They may obviously differ, as in the cases of DNA damage, Erythema, and Pigmentation see (Figs. 6–8), depending on the absorbing molecules.

Comparisons between experimentally determined action spectra and absorption spectra of appropriate molecules can sometimes give insight into which molecule is primarily responsible for the effect. Using the bactericidal AS derived by Gates [11] see (Fig. 6), it becomes possible to identify DNA as the genetic material [11, 12]. This observation was confirmed with other unicellular organisms and led to the realization that nucleic acids have a fundamental role in ultraviolet photobiology.

Although it is still possible to glean more information about the photoresponses of organisms that do not meet the criteria above, it may be impossible to identify either the molecule(s) or the mechanism(s) involved in the process being studied. It may not be possible to circumvent these limitations if a complex process, such as plant "growth," is to be analyzed. An action spectrum for this latter process may be nothing more than a determination of effects as a function of wavelength, but the exact mechanism causing the effect might remain unknown. Even in this case, such action spectra can be useful in estimating the response to ambient of changing light exposures.

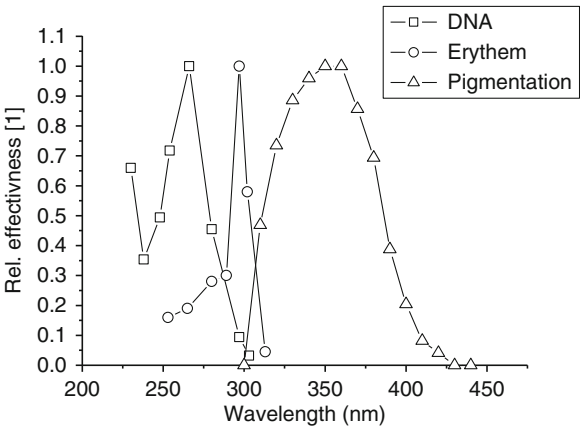

UV Effects on Living Organisms. Figure 6
Early known action spectra such as DNA damage [11], erythema in humans [19], and pigmentation [28]

After the discovery of infrared [13, 14] and ultraviolet radiation [15], the crude action spectroscopy was done by dividing whether a certain photobiological effect is caused by UV, or rather visible or infrared radiation. During the nineteenth century action spectroscopy was refined by using colored glass filters to select wavelength ranges. This technique has already allowed identifying chlorophyll as the chromophore most responsible for the growth of plants [16–18].

The first spectral resolved AS (Fig. 6) was reported by Hausser and Vahle [19] after constructing a high-quality quartz-prism monochromator. They first reported the erythema action spectrum, which showed a major peak of activity at 297 nm. The general form of this curve was confirmed by other investigators in the following 10 years [20–22]. Then, in 1934, Coblentz and Stair proposed a "standard erythema curve," which was subsequently adopted by the Commission Internationale de l'Eclairage [23] in 1935. This was the first standardized AS, which maintained its status until 1987 [24].

In the 1930s, a variety of other important ASs were derived, like for the killing of bacteria [25] and bacteriophage [26], vitamin D synthesis (healing rickets) [27], pigmentation of human skin [28] (Fig. 6), or cell division [29].

Most of the ASs were derived in the 1980s after the ozone depletion issue became known, to the effect that biologically effective radiation became a topic of interest.

Transmission to the Effective Skin Dose

The estimation of the effective skin or surface dose needs knowledge of the orientation of the receiver in respect to the sun, of the nearby UV environment (reflection, scattering, sky obstruction, . . .) and of the protection of the hair coat and behavior (Fig. 7).

Orientation and UV Environment

Measured or calculated solar UV data incident on horizontal surfaces are commonly used to assess

UV Effects on Living Organisms. Figure 7
3D model of an animal and its environment

the risk to a biological system from the local UV environment. Usually, standard solar radiation measurements are performed for horizontal surfaces and include the incoming irradiance from the whole sky. This incident global irradiance on a horizontal surface is the sum of direct beam and scattered diffuse radiation.

In reality, few biological surfaces are horizontal or flat. However, the surface of an organism can be decomposed into many small inclined planes or "facets."

Figure 8 depicts such a surface mesh for a cow, along with the corresponding frequency distribution of the tilt of these surface patches. This is convenient for an immobile subject. Obviously, the task of assessing the radiant exposure becomes much more complex when the subject is moving.

The incident irradiance on inclined planes (e.g., body parts of an animal) includes the sum of three radiation components see (Fig. 9):

- Direct beam irradiance: The intensity of the incident direct beam on an inclined plane depends not only on the intensity of the direct beam irradiance but also on the incidence angle between the sun and the normal to the plane.
- Diffuse sky irradiance: The inclined plane does not "see" the whole hemisphere, and the diffuse irradiance is therefore reduced compared to a horizontal receiver.
- Ground-reflected radiation toward the receiver: This reflected radiation depends on the illumination of the reflecting facet (incident irradiance on ground), on the solid angle of the facet, on the reflectance (albedo) (Table 2) of the facet, and of course on the inclination of the receiving plane.

Direct Beam Radiation The direct beam, I, on a given plane depends on the initial intensity of the direct solar beam irradiance incident on a normal plane (I0), which can be measured or calculated, and on the angle of incidence, β, which is the angle between the solar beam and the surface normal (also called illumination angle)

$$I = \mathrm{I0} \cos \beta \tag{7}$$

β is calculated using the following equation:

$$\cos \beta_{\mathrm{i}} = \cos \theta_{\mathrm{s}} \cos \theta_{\mathrm{n,i}} + \sin \theta_{\mathrm{s}} \sin \theta_{\mathrm{n,i}} \cos(\varphi_{\mathrm{s}} - \varphi_{\mathrm{n,i}}) \tag{8}$$

where θ_s is the solar zenith angle, $\theta_{n,i}$ the slope inclination (or tilt angle), $\varphi_{n,i}$ the azimuth (orientation) of the slope, and φ_s the solar azimuth.

Diffuse Irradiance The diffuse irradiance D incident on a horizontal plane is the integral of the sky radiance I over the whole sky hemisphere (please replace I here by something else to avoid confusion since it is already used in Eq. 7).

$$D = \int_0^{\pi/2} \int_0^{2\pi} I \sin\theta \cos\theta \, \mathrm{d}\theta \mathrm{d}\gamma \tag{9}$$

where θ is the zenith angle and γ the azimuth angle of a sky element.

For the calculation of the incident radiation on an inclined plane, the sky radiance has to be integrated only over the portion of sky seen from the plane. The diffuse irradiance on a given plane may be approximated, assuming an isotropic hemispherical sky radiance distribution, using the following equation [31, 32]:

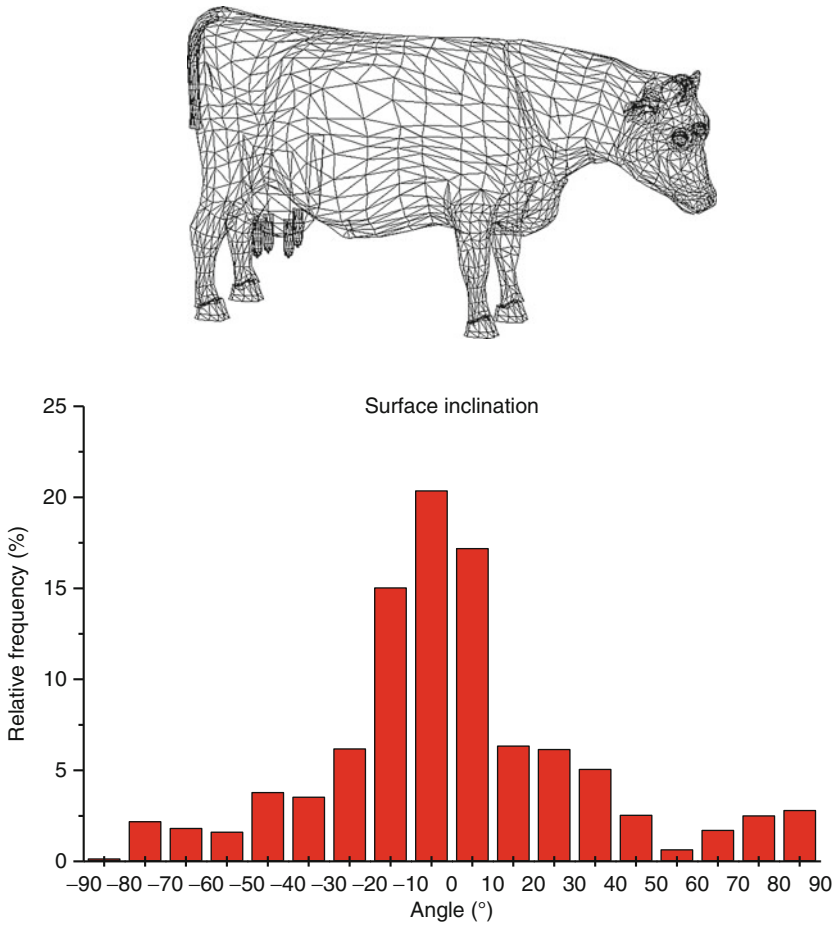

UV Effects on Living Organisms. Figure 8
3D model of a cow and frequency distribution of surface tilt (0° denoted vertically, +90° horizontally face up and −90° face down)

$$\mathrm{Dt} = \left(1 + \cos\left(\theta_{\mathrm{n,i}}\right)\right)\mathrm{D}/2 \tag{10}$$

where $\theta_{n,i}$ is the tilt angle of the plane, and D is the diffuse horizontal irradiance (Eq. 9). Equation 10 does, however, not take into account the reflected irradiance emanating from the ground, which should be added to the quantity Dt.

Measurements showed that the ratio of the irradiance on a horizontal plane to the irradiance on the vertical plane has a strong seasonal course, resulting in higher irradiance on the horizontal plane in summer and higher irradiance on the vertical plane in winter at mid- to high-latitudes. The irradiance on vertical planes in winter may be up to 2.5 times higher than in summer [33]. In summer, the ratio of irradiance incident on vertical to irradiance incident on horizontal planes may be as low as 0.2 for solar zenith angles around 45°. Over snow surfaces the incident irradiance can be much higher [34–36]. Figure 10 shows the influence of the UV albedo on theUV irradiance incident on an inclined plane.

Obstruction of the Sky The obstruction of the horizon shields a sensor/subject from a part of the diffuse irradiance. The surroundings, however, also reflect some radiation toward the sensor or subject.

The obstruction of the horizon may be calculated by integrating the shadow line over all azimuth angles [32]:

$$\mathrm{Obstr} = \int \mathrm{d}\alpha\, \mathrm{d}\varphi \tag{11}$$

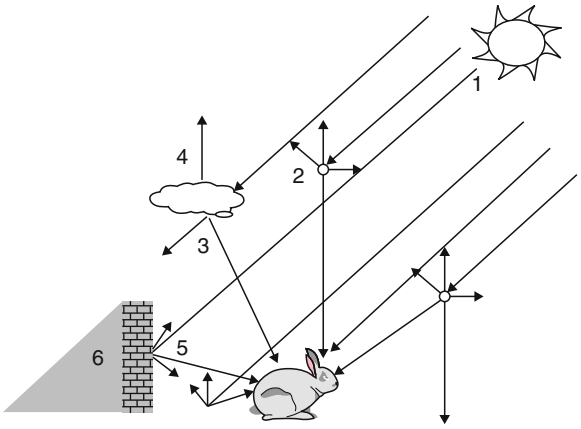

UV Effects on Living Organisms. Figure 9
Overview of the various radiation components and phenomena that have an impact on the radiation exposure of an animal. *1* direct beam irradiance, *2* radiation scattered by molecules and aerosols, *3* radiation scattered by clouds. (*2* and *3* make up the diffuse radiation component), *4* radiation reflected by clouds, *5* reflection by the surroundings, *6* shading (here, by a wall)

UV Effects on Living Organisms. Table 2 Albedo of various surfaces in the UV and visible range

Surface	UV	Visible
Woodland	0.07	0.2
Grass	0.05	0.18
Bare soil	0.1	0.3
New, deep snow	0.9	0.8

Source: Blumthaler and Ambach [30]

where α is the elevation of the object over the horizon and φ its azimuth.

Obstr is the angular obstruction of the horizon (due to the surrounding obstacles, such as mountains) in addition to the obstruction already occurring due to the inclination of the sensor.

By taking this obstruction of the horizon into account, the effective diffuse irradiance Dt on a given plane may be calculated under the assumption of isotropic sky radiance distribution and no reflected irradiance, by using the following equation [31, 32], which is a modification of Eq. 10:

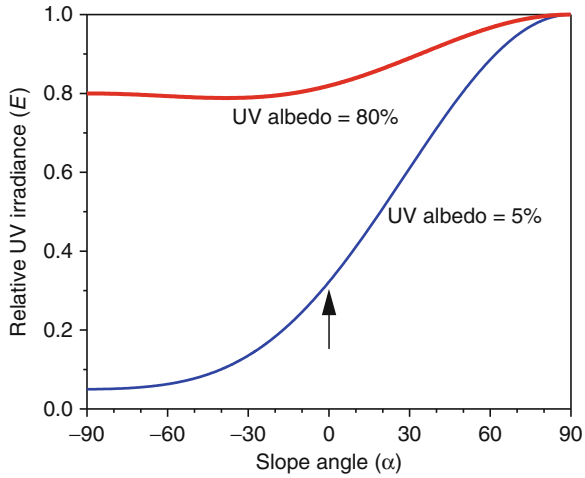

UV Effects on Living Organisms. Figure 10
Relative irradiance on a sloped receiving surface in dependence of slope angle and UV albedo

$$\mathrm{Dt} = \left(1 + \cos\left(\theta_{\mathrm{n,i}}\right)\right)\mathrm{D}(1 - \mathrm{Obstr})/2 \tag{12}$$

where Obstr is obtained from Eq. 11.

Models Using Eqs. 7 and 8, the calculation of the incident beam UV radiation on inclined planes is straightforward. Equations 10 and 12, for the determination of the diffuse irradiance on incident planes, bear some uncertainty, because the sky radiance is not perfectly isotropic. Several geometrical models [37–41] for the calculation of the broadband (rather than UV) diffuse irradiance which account also for the non-isotropic component of the sky radiance are available [42]. (Note that [37, 39–41] deal with broadband irradiance, not UV; in the UV, the sky radiance is more isotropic than at longer wavelengths, so that these models should not be used in the present situation ....) Models reproduce adequately the incident UV radiation on planes facing the equator with a mean bias deviation lower than 4.5%. For planes with other orientations, a larger bias may be found, for example, 10% or more. In recent years, radiative transfer models were adapted to calculate the incident UV on inclined planes [43], taking also into account the obstruction of the horizon [44].

Vegetation In addition to direct shading, vegetation can also be used by animals as protection against UV

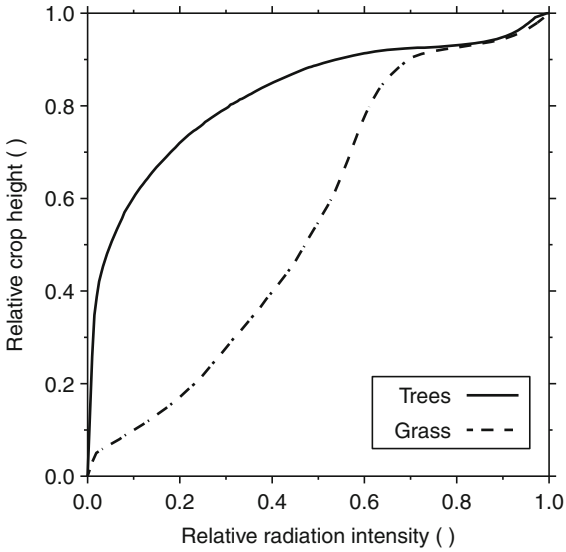

UV Effects on Living Organisms. Figure 11
Effect of the relative crop height of trees and grass on the relative radiation intensity normalized to unity by the intensity above the crop, according to Dirmhirn [45]

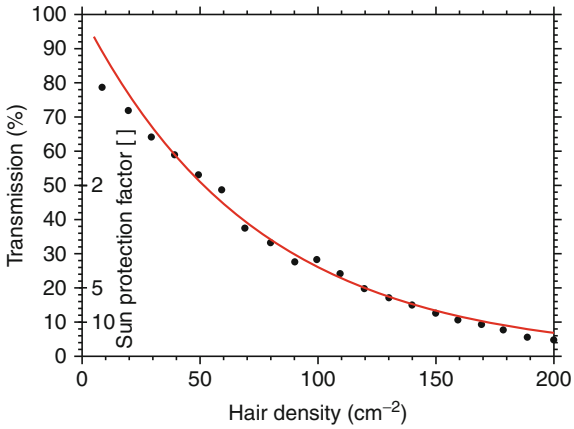

UV Effects on Living Organisms. Figure 12
UV Transmission and the resulting UV sun protection factor SPF due to the hair coat of cattle, according to Bianca and Wegmann [54]

radiation. The attenuation of radiation results from shadowing by leaves, branches, or stems. Therefore, the geometrical structure of vegetation affects its UV attenuation and protection capacity (Fig. 11). Moreover, the protection is dependent on the seasonal changes like height of vegetation, density, and leaf area [45, 46]. Figure 11 depicts the influence of the relative crop height of trees and grass on the relative radiation intensity normalized to unity by the intensity above the crop, as modeled by Dirmhirn [45].

Behavior

The biggest problem for estimating the effective skin dose is the consideration of the behavior, because it affects the duration of stay within the vegetation. Many herbivores forage in the open field and afterward go back into higher vegetation for cooling, resting, and cowering. For this no investigations are available. The biggest problem for estimating the effective skin dose is the consideration of the behavior, because it affects the duration of exposition. For this only a few investigations are available especially for ecotherms. [please condense these 2 paragraphs]

In 1997, Manning and Grigg [47] found that, for the freshwater turtle, basking (moving and positioning the body to maximize sun exposure) lasts longer than its thermoregulation would require. Ferguson et al. [48, 49] have shown that Panther chameleons can behaviorally regulate UV exposure or regulate absorption by changing skin color, to an absorption level at which the body already responds with vitamin D production at low UV levels. Karsten et al. [50] have shown that in dependence of their dietary Vitamin D_3 intake, Panther chameleons behaviorally regulate their exposure to solar UV to ensure an optimal Vitamin D_3 status. For some species of lizards, it was previously known that they possess a vitamin D_3 receptor in the brain [51]. Their retina is sensitive to the UV [52, 53] and may therefore be helpful for sun seeking and predator avoidance.

Hair Coat

One important barrier that keeps the ambient dose below the effective skin dose is the hair cover of animals. In addition to its important role as the primary thermal protection of the body, the hair cover is an effective UV protection.

Investigations on the hair coat of horses [9, 55, 56] found a biologically effective UV radiation transmission factor to the skin below 2%. This transmission corresponds to a sun protection factor (SPF) of approximately 50. In to the case of cattle, similar results were obtained [8, 54]. Figure 12 depicts the relation

UV Effects on Living Organisms. Figure 13
Erythema of a newborn pig due to outdoor UV exposure

between transmission and hair density. This leads to the conclusion that, whenever the biological effects of UV radiation are analyzed, the natural protection of the hair coat has to be considered.

The lack of UV protection was described by Chapman et al. [57] for newborn furless sheep and for pigs [58]. In Fig. 13, a pig is shown with a whole-body erythema due to outdoor UV exposure.

Transmission Through Water, Snow, and Ice

Water For aquatic life, the optical properties of the immediate habitat – both atmosphere and water – are of great relevance. At the boundary, the optical properties of the interface between air and water, as well as the spectral reflection properties of the benthic division, are crucial [59]. At the water–air boundary, the index of refraction changes and must be taken into account. Reflection is in the order of 5–7% in the UVB and 6–9% in the UVA (e.g., [60]), where the higher values are measured at lower solar elevations.

The penetration of UV radiation into water depends on the optical properties of water as well as on wavelength. Transmittance in water is much lower than in the atmosphere.

Solutes and salinity decrease transmittance due to increased absorption, but most important is the amount of absorbing and scattering suspended particles in the water. Particulate matter is either of terrigenous (erosion and pulverization) or biological origin (dissolved organic carbon, pigments such as chlorophyll or pheophytin, etc.). Especially in eutrophic fresh water systems and coastal regions, the transparency is affected strongly by these.

Dissolved organic carbon (DOC) is organic material from plants and animals broken down into such a small size that it is "dissolved" into water. DOC is an umbrella term for thousands of different dissolved compounds. The humic or tannin types of DOC are yellow to black in color and can have a great influence on the water's visible color.

DOC attenuates UVB effectively [61, 62]. Moderate levels of DOC may decrease the UVB within 5 cm down to only 2% compared to the level at the surface [63].

DOC is photochemically degraded by UV [64] into dissolved inorganic carbon (CO, CO_2, H_2CO_3, ...) [65]. Through this process, UV indirectly affects its own transmission.

Other important absorbers are photosynthetic pigments like chlorophyll, pheophytin, and others.

UV is also absorbed and scattered by organisms living in water, such as plankton, algae, and sea grasses, which may build large canopies.

In general, transparency is highest in the clear ocean water [61] and high-latitude (dry valleys) [66, 67] or high alpine lakes [68], and lowest in brown (humic) waters (e.g., [69, 70]). Altogether, the depth for a 10% UV transmission can vary from about dozens of meters in the clearest waters to a few centimeters in brown humic waters.

A multicomponent model developed by Smith and Baker [71, 72] describes the total attenuation as the sum of numerous partial attenuation coefficients from water, DOC, pigments, particulate matter, and undefined residuals:

$$K_{Total}(\lambda) = K_{Water}(\lambda) + K_{DOC}(\lambda) + K_{Pigm}(\lambda) + K_{PM}(\lambda) + K_{Residual}(\lambda) \quad (13)$$

All individual attenuation coefficients on the right-hand side of Eq. 13 depend on wavelength (λ). As a result, UVB is attenuated stronger than UVA and the visible radiation (e.g., [70, 73–75]). In most cases, the main contributor to $K_{Total}(\lambda)$ is either K_{DOC} (e.g., lowland lakes) or K_{Pigm} (e.g., high alpine lakes) (e.g., [76]).

Once K_{Total} is evaluated, the spectral irradiance $E_\lambda{}^z$ at a certain depth z can be approximated [77, 78] by:

$$E_\lambda^z = -E_\lambda^0 \cdot w_\lambda \cdot \left(e^{-K_{Total}(\lambda)\cdot z} - 1\right) \cdot \frac{1}{K_{Total}(\lambda)} \quad (14)$$

where w_λ is a weighting function for a certain photobiological effect, and E_λ^0 is the spectral irradiance at the surface.

As can be seen from Fig. 14, shorter-wavelength UV radiation is absorbed more effectively than longer-wavelength UV [59, 79].

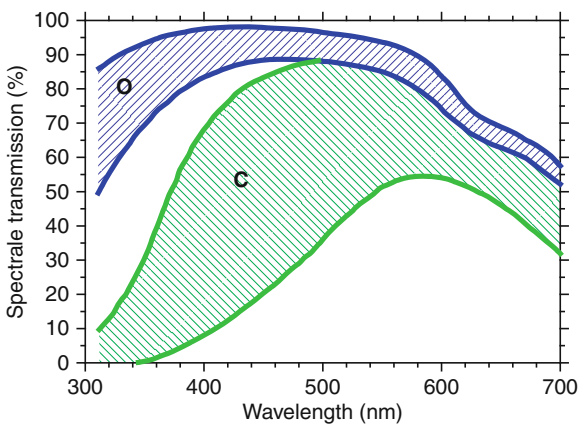

UV Effects on Living Organisms. Figure 14
Spectral transmission through 1 m of ocean (o) and coastal waters (c)

The transparency of water is not constant over time, but shows a temporal (seasonal) variability, which goes hand in hand with the changing amount of solved and dissolved matter in the water (e.g., [64, 69, 80]). As can be seen from Fig. 15, even the transparency of groundwater and well water (drinking water quality) is not constant during the year.

Meteorological factors may also cause variability – snow melting and flood water may transport large amounts of unsolved substances.

In aquatic regions where water becomes occasionally scarce due, for example, to low water flow or, of course, to the tide cycle, UV radiation on sessile aquatic livings may become extreme, weather permitting.

Smith and Baker [78] have weighted the transmitted UV irradiance with the action spectrum for DNA damage [81]. In Fig. 16, the spectral biological effective radiation for waters with a small amount of soluble organic material and a small content of chlorophyll (clear oceanic water), as well as offshore water with high biological activity, is depicted. The spectral maximum of the 10-m depth line is attenuated by less than an order of magnitude, whereas it is four orders of magnitude for offshore waters.

It can also be seen that the ozone-affected UVB range provides the largest amount of irradiance for DNA damage, although the UVB from the sun, after transmittance through water, has a lower magnitude than UVA.

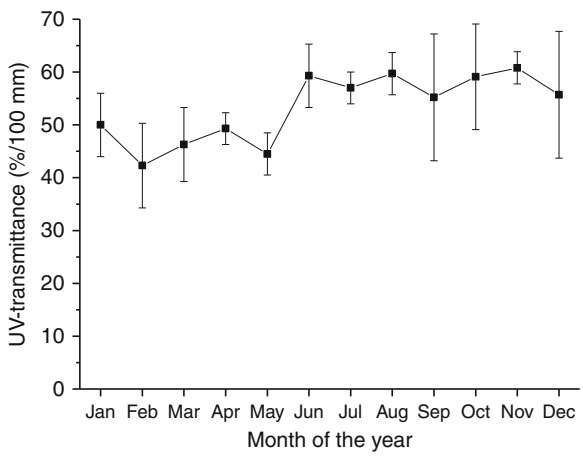

UV Effects on Living Organisms. Figure 15
Annual course of transmittance (100 mm) of groundwater (drinking water)

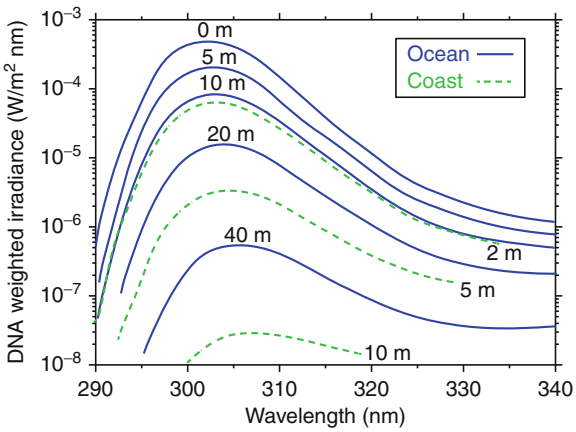

UV Effects on Living Organisms. Figure 16
DNA-weighted spectral irradiance in ocean and coastal waters at various depths

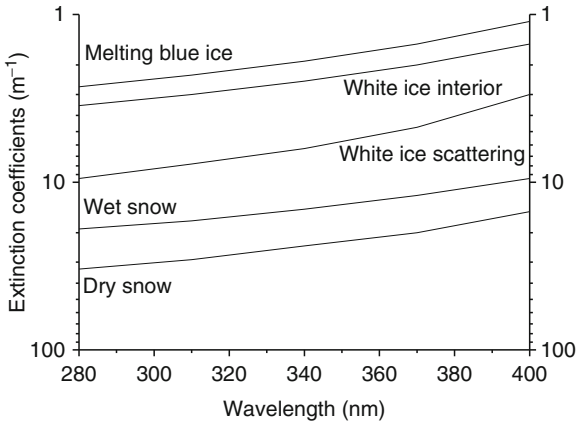

UV Effects on Living Organisms. Figure 17
UV extinction coefficients of ice and snow (After data from [89, 92])

Ice and Snow Ice and snow reflect a significant part of the incoming UV radiation. New dry snow may reflect over 90% of the incident UVB. New wet snow reflects over 80%. The amounts reflected by old dry snow and old wet snow are 82% and 74%, respectively [82, 83]. The albedo of snow may change within a day by around ±0.05 with lower values shortly after noon, which may be caused by a change in the optical properties of snow [84], and by an increase in specularity effects at low sun angles.

Organisms living above the snow cover are therefore at serious risk of UV overexposure because they receive high amount of additional UV. Moreover, the intense reflected UV emanates from below, which represents a completely different direction than usual. This upwelling UV irradiance may hit body parts that are seldom exposed to UV, and are therefore less protected by pigmentation or fur, or less shielded by other body parts. A well-known effect is snow blindness, which humans also experience.

In spite of this high reflectance, a certain amount of UV penetrates into the snow cover (Fig. 17). Nevertheless, snow cover usually provides high UV protection for the organisms living beneath it (see, e.g., [85]). For instance, a snow layer of 5 cm can reduce the UV radiation down to 15–20%, and a layer of 15 cm can reduce it by nearly two orders of magnitudes [85, 86].

The reflectance of ice is somewhat lower than that of snow. It varies from about 30–80%, as a function of surface structure and temperature [87–89]. The transparency of ice to UV depends on age and clearness of the ice and on wavelength (Fig. 17). UVB is attenuated stronger than UVA or visible radiation. In ice, a layer of 2.5 m can reduce UVA and UVB by up to 2 and 2.5 orders of magnitudes, respectively [90].

One meter of fresh, thin sea ice transmits roughly 20% of the incident UV radiation, whereas cold first-year ice transmits less than 2%. Different layers within the ice, from very white interior ice to almost clear surface ice have different UV extinction coefficients [89, 91, 92].

It was shown by Vincent et al. [67] that the transmitted UV below 3.5 m of very clear ice is still intense enough to inhibit algal growth.

Ice on lakes and rivers is more transparent than that on seawater, because during freeze-up DOC is removed from the ice [93].

Ice is often covered with snow. This combination, of course, affects both albedo and transmittance [87]. A snow cover of ≈5 cm (1–9 cm) on top of ≈0.9 m (0.5–1.3 m) of ice reduces UVB by 2–13% and UVA by 5–19% [94].

Small changes in snow and ice depth can have an extreme influence on UV radiation. This effect is much stronger than that caused by usual changes in atmospheric parameters like cloudiness or total ozone column [95].

Nowadays, special consideration on the transmittance of ice and snow is needed in the context of

climate change. During shorter periods of snow and ice cover, the "underlying" aquatic or terrestrial organisms can become exposed, even though they are normally shielded from UV radiation. In addition to changing temperatures, a change in water flow can be responsible. An ecologically very important effect is the thinning of ice cover of the Arctic and Antarctic Seas, which leads to an enhanced exposure of a very large aquatic ecosystem.

Ice and snow also provide habitat for microbial assemblages (microalgae, bacteria, protozoa, ...). They can be found in melt ponds on the ice surface, in brine channels within the ice, in slush layers between ice and snow, or between black and white ice, attached to the bottom of the ice or in the sub-ice platelet layer (e.g., [96, 97]). In hypersaline melt ponds above the surface of ice, microbial life can be found at temperatures around −10°C.

On the top of ice and snow, the so-called snow algae (cold-tolerant algae and cyanobacteria) can be found during alpine and polar summers. Algal bloom colors ice and snow with red hues, resulting in what is called red snow or watermelon snow.

Biological Effects on Microorganisms

What are called microorganisms or microbes consist of various types of very small life forms. Microorganisms can be found in the air, in waters, in the ground, on surfaces, and inside other organisms. They can also be found in the harshest environments. For instance, bacteria have been found around hydrothermal vents (hot springs, fumaroles, geysers, or "black smoke" at the sea ground), where water effuses at temperatures up to 350°C. These thermophiles grow best at temperatures above 80°C and accept temperature up to 113°C. At the other extreme, microorganisms can grow in hypersaline lakes at temperatures as low as −10°C. Regarding their tolerance to pressure, both extremes can be accommodated: there are barophilic deep-sea bacteria, and there are also microorganisms in the mesosphere.

Microorganisms (such as viruses, bacteria, fungi, and protozoa) are as manifold and different as one can imagine. Their size may be smaller than the wavelength of light (e.g., 40 nm for viruses). Virus and bacteriophage are the most simple microorganisms. They consist only of RNA or DNA surrounded by a protein. Both need a host cell for reproduction. Bacteriophages are viruses that infect bacteria. The cells become lysed, which gave bacteriophages their name: "bacteria eaters."

For humans and animals, a variety of microbes are necessary to stay healthy (e.g., in the gastrointestinal tract, skin, mucous membranes, ...), while other microbes can cause severe diseases (pathogens). The human body consists of approximately 10^{13} cells, but also hosts ten times more microorganisms [98, 99].

Finally, microorganisms play an important role in the biosphere as they build up to 90% of the DNA biomass in marine ecosystems, and play a vital role in the geochemical and global carbon cycle.

UV Environment of Microorganisms

The life span of microorganisms outside a host is defined by temperature, humidity, and solar (UV) radiation. Free moving microorganisms receive UV radiation from all directions. Therefore, the optical properties of the surrounding medium, including its reflectance, are of importance.

On the one hand, solid or organic particulate matter in water or air reduces transmittance of UV, and on the other hand, microorganisms have the ability to adhere on surfaces, so they can make use of particulate matter as radiation protection and vehicles. Clumping of microorganisms is also a strategy of radiation protection in an open environment.

Airborne Microorganisms Microorganisms can be found at all heights in the atmosphere. In the late 1800s and early 1900s, microorganisms were already collected during balloon flights [100, 101]. In 1936, Rogers and Meier [102] collected microorganisms at a height of 20 km. Imshenetsky et al. [103] could even collect reproductive forms of microorganisms (spores of Cicirnella, Pencicillium, Aspergillus, and Papulaspora, as well as Micrococcus and Mycobacterium) from the mesosphere between 48 and 77 km (−60°C) using meteorological rockets. Five of the six microorganisms had synthesized pigmentation. At such an altitude, UV radiation is several times higher than on the ground. Moreover, the spectral range is broader, extending to the UVC range, since most of

ozone is below that level, in the stratosphere at about 20–22 km.

Altitude-dependent UV radiation defines the species composition [104]. Bacteria species in the stratosphere are more resistant than in the troposphere or at the ground [105]. Beside pigmentation, clumping and forming aggregates enhances the chances of survival of microorganisms in the stratosphere [105]. In the boundary layer of the atmosphere (i.e., below about 2 km), only around 65% of microorganisms are pigmented [106]. Predominant species are Staphylococcus, Listeria, and Micrococcus.

Small sizes and low density allow microorganisms to remain airborne for long periods before they sediment to the ground. Long-distance transport of fungal spores was observed already in the 1930s [107]. Desert dust enables intercontinental exchanges by offering a UV-shielding vehicle for microorganisms [108–110]. Biomass fires cause strong convection, which is more effective in bringing up microorganisms that are not burned to heights of 3 km than surface stormy winds. Smoke clouds shield them from UV and act as a vehicle over long distances [111]. This explains why, for example, plant fungi can cause allergic reactions or trigger asthma at locations thousands kilometers away from their origin [112].

Airborne microorganisms are influenced strongly by UV. This can be seen by the fact that nonpigmented microorganisms decline strongly with increasing solar UV radiation during the day and during a year. Pigmented microorganisms exhibit a similar pattern but with lower amplitude [113].

Microorganisms released from humans or animals (coughing, sneezing, and talking) into the air have a rather short range (around 12 m) [114] before adhering on surfaces. From these surfaces, they can be reaerosoled. Survival may last up to 48–72 h. It is assumed that the survival of some microorganisms like influenza virus in air depends less on humidity and temperature than on UV radiation [115, 116].

Waterborne Microorganisms In aquatic environments, bacterioplankton may contribute up to 90% of the total cellular DNA [117–121], and up to 40% of the total planktonic carbon biomass [122]. In addition, bacteria may process up to 50% of algal primary productivity in marine systems [123].

The size of most bacterioplankton cells precludes effective cellular shading or protective pigmentation [124]. Their metabolism is affected by solar UVB down to a depth of 5 m, and by UVA down to 15 m in clear ocean waters [125]. It has been shown that bacterial abundance [126] depends on light cycle as well as on metabolism [127], DNA, protein synthesis, and degradative enzyme activities [128]. Various studies have investigated the effect of UV on different aquatic systems, especially in marine environments [129–132]. Studies on the impact of UV radiation on bacterioplankton have also been carried out in other aquatic systems, such as (alpine) lakes [69, 76, 128, 130, 132–134].

Other authors have done research on biodiversity at extreme UV locations, such as the Himalayas [135–138] and the Andes [139–141]. Moreover, viruses were found in ice-covered Antarctic lakes [142]. The effects of UV in rivers are still poorly investigated.

The most resistant waterborne microorganisms are *Bacillus* sp., *Acinetobacter* sp., *Pseudomonas* sp., *Sphyngomonas* sp., *Staphylococcus* sp., and *Stenotrphomonas* sp. These were found in lakes [139, 141] and wetlands [140] up to an altitude of 4,600 m, where UV radiation is approximately 170% that at sea level.

Ecologically and economically important are cyanobacteria (blue-green algae), which are found on wet farmland (rice) all over the world. Cyanobacteria are quite sensitive to UV. Cyanobacteria fix atmospheric nitrogen and are important primary producers in the ocean, but are also found in habitats as diverse as freshwater or hypersaline inland lakes, or arid areas where they are a major component of biological soil crusts.

Effects of UV Radiation on Microorganisms

Damage Microorganisms can be easily damaged by UV radiation. In 1877, Downes and Blunt [143] established that a beneficial effect of sunlight is bactericidal. The experiments that followed revealed that blue/violet is the most effective color to kill bacteria. Hertel [144, 145] could then definitively show that it is the UV part of the spectrum that is responsible. In parallel, it was also found that the bactericidal effect increases with altitude. A detailed review of the early

years of research on the damaging effect by UV is given by Hockberger [146].

Damage can be manifold, and includes growth reduction, decrease of reproduction rate, of metabolism rate, of infectivity, of mobility, or other effects. The main targets for UV damage are RNA, DNA, and proteins.

The wavelength range where UV is most effective in inactivation is quite similar to that where DNA has the highest absorptance (UVC and UVB range) with maximum effectiveness – of course outside the natural UV – i.e., around 265 nm. The range of highest efficiency is also called germicidal range.

Our knowledge of UV-induced damage results mainly from studies in the UVC and UVB, where efficiency is much lower than in the UVA [147]. However, solar UVA is magnitudes higher than solar UVB. It can thus be assumed that solar UVA contributes also to damage, although only a few action spectra have been proposed for the UVA (Fig. 18).

Disinfection Whereas sterilization results in a total absence of microorganisms, disinfection denotes a substantial reduction of the number of microorganism, by at least four orders of magnitude. Hygiene applications like disinfection make use of UV inactivation [149–152]; inactivation means that the existing microorganisms lose their ability to reproduce. UV inactivation results from the direct absorption of UV radiation by the microorganism. This absorption triggers an intracellular photochemical reaction that changes the biochemical structure of nucleic acids. These changes may lead to the inhibition of transcription and replication of nucleic acids, thus making the organism sterile and incapable of spreading infection when entering a host.

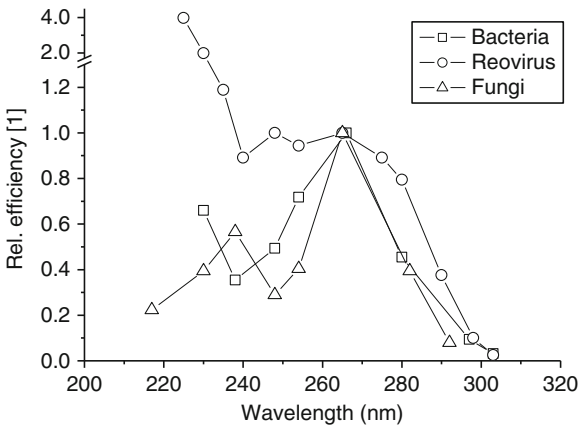

UV Effects on Living Organisms. Figure 18
Action spectra for inactivation of Bacteria *Escherichia coli* [11], Reovirus-3 [148], and fungi *Trichophyton mentagrophytes* [12]

At the beginning of the twentieth century, Henry et al. [153] found that UVC's disinfection potential was much stronger than UVB or UVA. After developing a mercury vapor quartz lamp and a quartz tube for protecting the lamp against water, the first application of UV irradiation in disinfection of drinking water was realized in Marseilles, France.

Nowadays, disinfection of air, water, and surfaces is generally done by the application of low- or medium-pressure mercury lamps, which emit up to 90% of their light around 254 nm. However, disinfection of drinking water is also possible with solar UV radiation (e.g., Wegelin et al. [154]). The methods can be as simple as using UV-transmitting PET bottles (e.g., McGuigan et al. [155]) or batch reactors (e.g., Navntoft et al. [156]). Serious pathogens like *Salmonella*, *Shigella dysenteriae*, *Escherichia coli*, *Vibrio cholera*, *Pseudomonas aeuriginosa*, oocysts of *Cryptosporidium parvum*, cysts of *Giardia muris*, *Candida albicans* (yeast), fungus like *Fusarium solani*, or the Poliovirus can be inactivated effectively by solar radiation. With the current booming interest in solar energy applications, various methods of detoxification and disinfection of water by means of concentrated solar radiation are being successfully experimented, both for small-scale (rural) and industrial-scale operations (e.g., [157–159]).

Protection and Repair The simplest microorganisms have no intrinsic mechanism for UV protection, since their small size does not allow pigmentation or cellular shading. Microorganisms that possess pigments in their outer layer are more resistant. Highly resistant to UV radiation are spores and (oo)cysts. However, UV sensitivity varies a lot, even within a single group, by a factor of up to 10 [160].

Spores and (oo)cysts are reproductive structures that can adapt to dispersal and can survive under unfavorable conditions for extended periods of time.

In such a stage, microorganisms have suspended "life," but are able to start again as soon as the environment becomes more favorable.

Mechanical strategies for radiation protection are clumping of microorganisms, forming aggregates, and building films. Dead microorganisms can act as a shield. Additionally, the biological effectiveness of UV is decreased by orders of magnitude if the targeted (pathogenic/parasitic) microorganism has entered a host.

A strategy for UV protection that microorganisms have elaborated is to postpone UV-sensitive processes until the end of the day or nighttime [161]. Microorganisms exhibit a 24-h cell division cycles, whereas DNA replication and cell division occurs during the night, since all division processes are sensitive to solar UV radiation.

Microorganisms – like all other life forms – know how to defend themselves against damage from UV radiation. There are repair mechanisms that may reduce damage to a certain degree. Nucleic acids, for example, can be repaired in a process termed "photoreactivation" in the presence of light, or "dark repair" in the absence of light. Viruses and phages can take advantage of the reactivity capacity of their host.

The action spectra for photorepair exhibit maxima at three different wavelengths: 345, 400, and 430 nm. Figure 19 depicts the action spectra for damage and photorepair. It can be seen that UVA and blue light are responsible for photorepair.

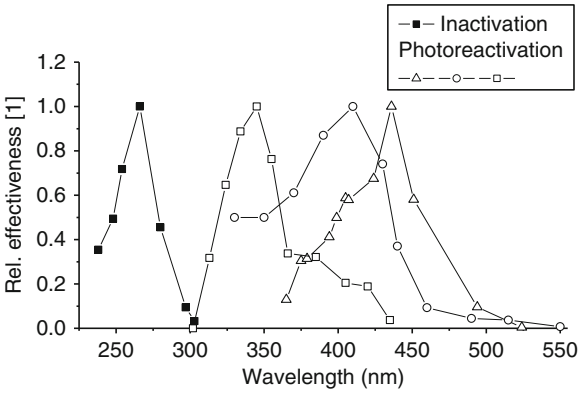

UV Effects on Living Organisms. Figure 19
Action spectra for DNA damage and photorepair

Since damage is caused by UVB and reactivation by UVA, their ratio is important. This ratio changes during the day, with season, latitude, altitude, total ozone column, and to a certain extent with cloudiness. Low solar radiation, low altitude, high total ozone amount, and high cloudiness tend to favor UVA.

Recent studies have reported an increased UV resistance of environmental bacteria and bacterial spores, compared to lab-grown strains [162]. This means that they could have the ability to adapt to their UV environment.

Vital Effects Damage is not the only effect of UV radiation on microorganisms. In many species of fungi, for instance, UV may also act by igniting new stages in development, like sporulation. Moreover, a variety of morphogenetics depends on UV radiation. Microorganisms can make use of UV for environmental information too. Metabolism, as well as the circadian clock, can also be triggered by UV.

UV modulates activity of bacteria that are responsible for geochemical transformative reactions in the nitrogen and phosphor cycles [163–165].

Changing UV Environment

As any other organism, microorganisms are well adapted to their environment. However, they have the important advantage to adapt very rapidly to any environmental change, and mutate if necessary.

In general, an increase in UV radiation is detrimental to them, resulting in reduced life span, decreased ability to reproduce, shorter mobility range, reduced habitat, or reduced population.

Still, there are many ways by which microorganisms may profit from environmental or climatic changes. Decreased UV radiation, for example, by enhanced cloudiness, aerosol load or dust, results in decreased damage, which in turn may allow a longer pathway to find a potential host (e.g., [116]). In the case of pathogens, a higher transmission rate and therefore outbreaks of diseases in humans may occur more frequently. For instance, the seasonal outbreak pattern of influenza in many parts of the world is currently believed to result from annual changes in solar UV [166]. Differences in the spring and autumn outbreaks could be explained by different total ozone amounts

and cloudiness, which in turn change the relationship between damage and photoreactivation.

If other environmental parameters change (like temperature or the availability of vectors), microorganisms can settle in a new environment where damage through solar radiation is maybe lower and potential hosts are not prepared for the blight. It has been observed that during the past few years, pathogens have already started to migrate toward higher latitudes.

An important factor controlling infections is the immune response of the host which can be suppressed by solar UV [167]. A lowered immune suppression within a human population enables higher infection rates and more frequent outbreaks. How the UV-initiated vitamin D level in humans could influence the outbreak of infection diseases is currently being discussed [168] (Fig. 20).

Effects of UV Radiation on Plants

One factor that increases the risk of UVB damage on plants is the fact that they are sessile organisms that are fixed on the ground. UVB damaging effects on plants include the destruction of the cell membranes and all organelles within the cell, including mitochondria, chloroplasts, and deoxyribose nucleic acid (DNA) within the nucleus [169]. These damages to the cell organelles in turn influence the metabolic processes of

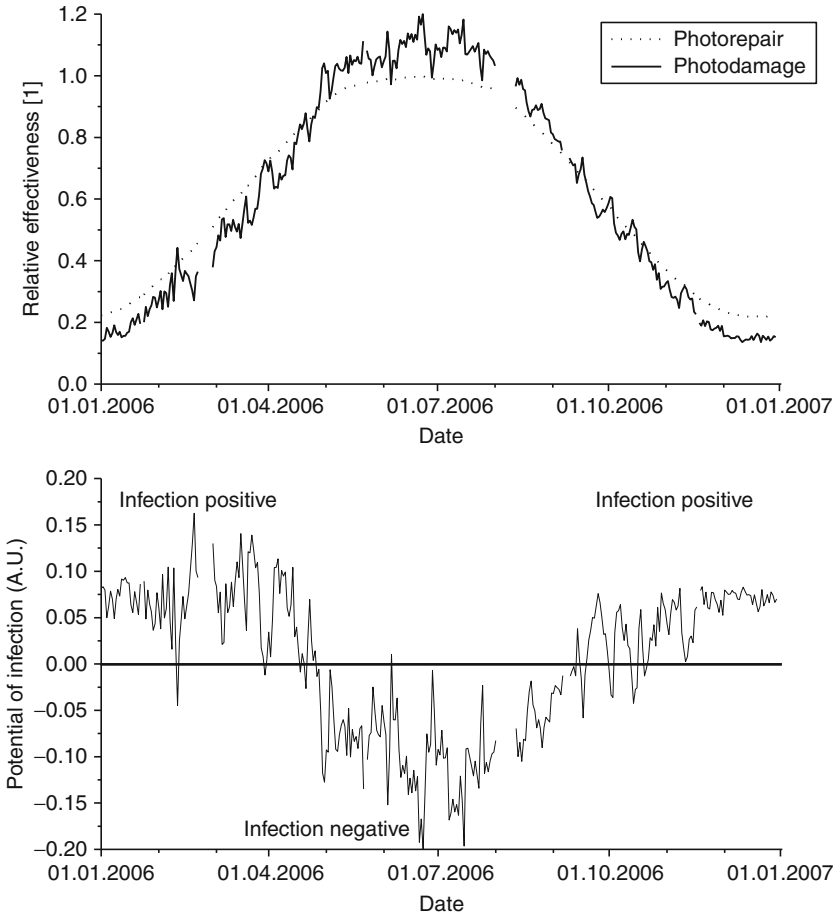

UV Effects on Living Organisms. Figure 20
Relative annual course of damaging and reactivating efficiency of solar UV over Vienna, Austria. Calculations are done for clear skies to point out the influence of total ozone

UV Effects on Living Organisms. Table 3 Effects of UVB exposure on various physiological processes in plants

Trait	Decreases	Increases	No effect
DNA damage		X	
Protein destruction		X	
Fatty acid destruction		X	
Photosynthesis	X		
Photosystem I	X		
Photosystem II	X		
Rubisco	X		
Stomata closure		X	
Chlorophylls	X		
Flavonoids		X	
Waxes		X	
Epidermal hairs		X	
Cuticle thickness		X	
Reproduction			
Pollen viability	X		
Pollen tube growth	X		
Fertilization	X		
Cell division	X		
Cell size			X

Source: Prasad et al. [170]

UV Effects on Living Organisms. Table 4 Effects of exposure to UVB radiation on various growth and yield parameters in plants

Trait	Decreases	Increases	No effect
Photosynthesis	Y		
Stomatal conductance	Y		
Phenology			Y
Senescence		Y	
Plant height	Y		
Branching		Y	
Leaf area	Y		
Leaf growth and expansion	Y		
Leaf thickness		Y	
Specific leaf weight		Y	
Dry matter production	Y		
Flowering	Y	Y	
Fruit (grain) number	Y		
Fruit (grain) weight	Y		
Yield	Y		
Quality	Y		
Disease incidence			
Powdery mildew	Y		
Rust		Y	
Insect	Y	Y	

Source: Prasad et al. [170]

the plant such as respiration, photosynthesis, growth, and reproduction. These UVB damages eventually impact crop yield and quality. The qualitative effects of UVB radiation exposure on the physiological processes, growth, and yield of plants are shown in Tables 3 and 4 [170]. Many factors may influence the extent of the UV impact on plants. The intensity and length of exposure, as well as the type of species and cultivar directly influences the sensitivity of plants to UV.

UVB Radiation Damages

Genetic Damage (DNA Damage) The nucleus of each cell contains deoxyribonucleic acid (DNA), nucleic acid, which contains the genetic instructions used in the development and functioning of plants. DNA is very sensitive to UV radiation [81, 171], which is primarily absorbed in the UVB region by the cell. If DNA is exposed to UVB radiation, effects include (1) breakage of bonds in the DNA and DNA-protein crosslinks, (2) chromosomal aberrations, (3) chromosomal breakage, and (4) exchange and production of toxic and mutagenic photoproducts.

Ultrastructural Cell Damage Ultrastructural changes may occur due to exposure to UV. Among other things, these ultrastructural changes include damage and dilation of the nuclear membrane, rupture of the chloroplast wall, swelling of chloroplasts,

dilation of thylakoids, swollen cisternae in the endoplasmic reticulum, and damage to mitochondria [170].

Inhibition of Photosynthesis Photosynthesis is the process by which plants convert carbon dioxide and water into organic compounds, especially sugars. The photosynthesis apparatus is one important target site of UVB destruction.

Among the direct effects of UVB that affect photosynthesis are [170]: (1) damage to the ultrastructure of chloroplasts, which are principal sites for photosynthesis; (2) impairment of light energy transfer of photosystem II and to a lower extent photosystem I; (3) reduction of activity of Rubisco (rubilos 1,5-bisphosphate carboxylase-oxygenase); (4) reduction of carbon dioxide fixation and oxygen evolution; and (5) diminution of the starch and chlorophyll content. For field crops [172], a decrease in photosynthesis was observed and was explained both by direct effects (on the photosystem) and indirect effects (decrease in leaf pigments and leaf area).

Plant Morphology and Architecture UVB leads to strong morphological changes in plants [170]. Leaves that are exposed to enhanced UVB radiation first develop irregular chlorotic patches. With a continuation of exposure to UVB, the chlorotic patches (Fig. 21) turn to brown necrotic spots before they later die.

Other effects of UVB are: reduction of the plant height, decrease in individual leaf size (Fig. 22), decrease of tiller number, and reduction of branch length [172]. These morphological changes also lead to a reduction of the density of the canopy, which in turn intercepts less UVB radiation than a plant grown under favorable conditions.

Phenology and Reproductive Processes Neither early bud, flower development, nor the time of first flower is influenced by UVB radiation. Shedding of early-formed floral buds is usually the reason for any time delay of first flower observed in crop species. However, in many plant species, UVB radiation affects the size of flowers, anther number, pollen production, pollen germination, and pollen tube growth [170].

In general, the reproductive organs of most plants are highly protected. Sepals, petals, and ovary walls "screen" the reproductive organs from UVB. Pollen is therefore "at risk" when it falls on the stigma. Then pollen germination and rate of pollen tube growth are also affected by UVB radiation. A decrease in pollen tube growth by 10–25% may result. The fertilization process of sensitive plants is affected too, resulting in fewer seeds in these plants. However, the walls of the style and ovary may provide some protection once the pollen tube has penetrated the stigma.

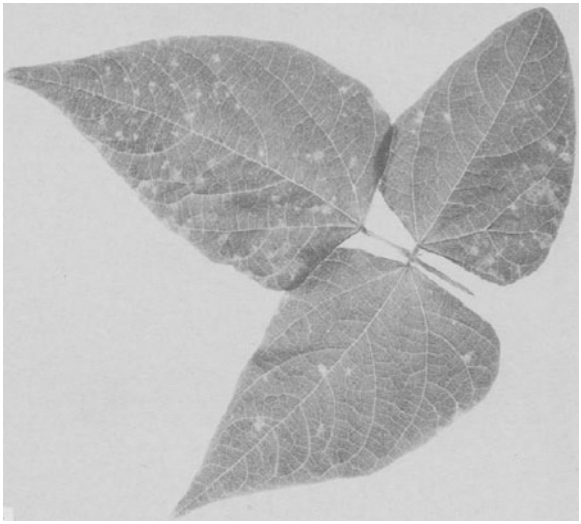

UV Effects on Living Organisms. Figure 21
Example of foliar symptoms (chlorotic patches) on bean leaves strongly enhanced by UV radiation exposure (Taken from [173])

UV Effects on Living Organisms. Figure 22
Comparison between leaves (from Patagonian *Jaborosa magellanica* Brisben) from nonirradiated plants (*left*) and leaves from irradiated plants (*right*) (Taken from [174])

Growth and Dry Matter Production Increases in length of organs (e.g., roots, leaf, or stem) or in weight are usual indicators of plant growth. For any given plant, several "quantities," such as dry matter increase, increase in cell number, or increase in volume, are generally used to monitor growth [175]. For many plant species, studies in the field [176–179] or in controlled environment [180–182] have shown a decrease in growth of leaves and of stems caused by enhanced UVB radiation (Fig. 22). The observed growth reduction is explained by a reduction of the cell division rather than by a reduction in cell dimension. Reduction in plant height in connection with enhanced UVB radiation is explained by decreased growth hormone levels. On one hand, smaller and more compact canopies will better protect the plant by transmitting less solar radiation and UVB. On the other hand, the potential, or total, photosynthetical area, which is essential for growth, will be reduced [170]. Altogether, these factors will lead to a reduction in total dry matter and in biomass production. According to [170] 60% of crop species show a reduction in dry matter production after exposure to UVB radiation, 24% show no change, whereas only 8% show an increase in dry matter production.

Strategies for Protection Against UVB Radiation

During the process of evolution, plants developed repair and defense mechanisms by which UVB damages to the cell are limited and tolerance to solar UV-radiation is increased. Several UV-driven repair and defense mechanisms exist, which modify the optical characteristics of the leaves or other parts of the plant, or which work at the biochemical-molecular level [169, 170].

Repair Mechanisms

Cellular life forms usually possess repair enzymes that can recognize chemically modified bases, including those formed by UV radiation [170, 183]. In addition, a variety of biochemical mechanisms exist to restore the integrity of the genetic material after DNA damage, and thus to maintain its stability. These DNA repair mechanisms include photoreactivation, excision, and postreplication repair. During the process of photoreactivation, an enzyme (photolyase) responsible for the splitting of pyrimidine cyclobutane dimers is involved. Excision repair consists in eliminating the damaged part of DNA by removing the bases in the damaged strand and then by synthesizing the gap. During the process of postreplication repair, the DNA damage is bypassed during DNA replication, and the resulting gaps are later filled in by using the sister duplex information. These kinds or repair mechanisms are observed in chloroplast and nuclear DNA [170, 183]. The ability to repair DNA varies a lot among the different plant species.

Defense Mechanisms

The first kind of defense mechanism is based on a better adaptation of the surface structure, physiology, and composition of the epidermal layer to attenuate the transmission of UVB through the epidermal layers, and eventually to better shield cells from UVB radiation [183]. The protective structures have the capacity to attenuate radiation damage by reflecting, absorbing, and scattering the incident flux. Among other mechanisms, hairs and wax coating have a prominent role [184]. UVB radiation leads to oxidative stress in plant systems, similarly to what is observed for abiotic and biotic stress. As a result, plants increase production of some chemicals such as flavonoids and antioxidant enzymes, which provide defense against UVB radiation [185–187]. Flavonoids, which are produced and mostly deposited in leaf hairs and in epidermal and mesophyll layers, are very efficient in mitigating the effects of UVB radiation. In this way, flavonoids may reduce damage to sensitive cell organs (e.g., DNA, chloroplasts, and mitochondria). Other compounds that could have the potential to protect against UV radiation effects are anthocyanins and carotenoids. They can protect the pollen grains, especially in flowers. They do not directly influence photosynthesis and other physiological processes, since they attenuate incoming radiation only in the UVB spectral range and not in the range of photosynthetic active radiation [170].

Selection or Genetic Improvement Plant species adapt and protect themselves from UVB in more or less adapted ways. The variable stimulation of protective and repair mechanisms may explain the difference among the various plant species. These variations

provide an opportunity for genetic improvement – either through traditional plant breeding techniques (crossing or selection) or through modern molecular biology techniques, such as plant transformation including some genetic modification. As a possible method, it may prove useful to identify tolerant species or cultivars by screening wide germplasm from various locations, and investigate the origin of UV tolerance [170].

Effect of UVB on Aquatic Plants and Macroalgae

In general, UVB radiation constitutes a significant stressor for macroalgae, aquatic mosses, liverworts, and aquatic flowering plants [130].

UVB affects macroalgae on the cellular, molecular, individual, and community levels [188]. UVA and UVB both affect photosynthesis and growth rate, and lead to accumulation of DNA damage. In addition, some studies report about the "impairment" of phototaxis used, e.g., by motile gametes of brown algae to accumulate at the water surface in order to increase the chance of finding a mating (do you mean: mating?) partner [189].

UVB sensitivity varies a lot among species. This results in vertical and in geographical "distributions" of the various species according to their sensitivity to UV. UV-tolerant species populate the tidal zone and are in general closer to the water surface. More sensitive species are found in deeper waters [190, 191]. Seasonal changes in UV and visible radiation also result in a succession of species over the year [192]. Macroalgae show an "ability" to adapt to UV. For instance, young specimens are more sensitive to UV than older specimens, and species collected shortly after the winter are found to be more sensitive than those harvested later in the year [193]. Most macroalgae have efficient repair mechanisms. In many macroalgae, efficient ROS (reactive oxygen species) (has ROS been defined earlier?) scavenging enzymes are found in addition to the DNA repair mechanisms.

Aquatic mosses and liverworts show a UVB-related inhibition of photosynthesis, growth, and pigmentation [194, 195].

For aquatic flowering plants, studies [130] show that the photosynthetic quantum yield dramatically decreases under unfiltered solar radiation, and that removal of UVB or total UV leads to an increase in photosynthetic activity [196]. Experiments show also an efficient adaptation of sea grasses to solar UV [197].

UVB and Agricultural and Natural Terrestrial Plants

A meta-analysis comparing the overall reaction of woody and herbaceous plants under high supplemental UVB levels showed that the changes in "physiological" variables due to UVB observed in woody plants were significantly smaller than those observed in herbaceous plants [198].

Methodologies Used for the UV Experiments To investigate the effects of UV on plants, two different methodologies are followed:

1. Experiments in climate rooms and glasshouses
2. Experiments in the field

The experiments in climate rooms and glasshouses have the considerable advantage of a controlled environment. The drawbacks of this methodology are the unfavorable PAR to UVB ratio and differences between the PAR and UV spectra of the lamps and that of solar radiation. Results from indoor studies cannot therefore be easily extrapolated to outdoor conditions. Conversely, results from outdoor experiments are more realistic than those from indoor studies [199, 200]. Outdoor studies consist of experiments using some UV lamps to increase, or filters to decrease, the UV levels. In general, the increase or decrease in UV should be comparable to expected realistic changes in UV that may be simulated using a radiative transfer model.

UVB and Woody Plants Studies showed contradictory results regarding the effect of UVB on growth and photosynthesis in woody plants. Some investigations [201] demonstrated a sensitivity of woody plants to UVB irradiance, and also showed that these kinds of effects may be cumulative [202]. Other studies, however, found that even large increases in UVB radiation would not lead to any harmful effects on growth and photosynthesis in some woody plants [203, 204].

Radiative transfer in tree canopies is very complex: radiation incident on leaves depends on the orientation and inclination of the leaf and on the position of the leaf in the canopy. Whereas the upper foliage may be

fully exposed to UVB, the lower foliage is benefits from the shading by branches, leaves and twigs. This results in a very variable radiation environment with sunflecks and gaps. In various forests with closed canopies, as little as 1–2% of the incident UVB may be transmitted to the lower levels [205].

At the individual leaf level, surface reflectance and absorption by pigments are major determining factors for the plant's UVB sensitivity. In general the UVB surface reflectance of leaves is lower than 10% [205]. The UVB surface reflectance depends on leaf surface waxes and hairiness. Leaf hairs are one major protector against UVB radiation [206–208].

In general, the amount of UVB radiation reaching the photosynthetic mesophyll is relatively low in evergreen species and higher in deciduous species [209], due to a higher concentration of absorbing compounds in the epidermis of evergreen plants.

UVB and Herbaceous Plants Studies showed that herbaceous plants would suffer a negative effect in biomass production under elevated UVB radiation levels. Reductions of 7–14.6% have been found, compared to values under normal ambient UV levels. Elevated UVB leads to decrease in plant height and specific leaf area, as well as increases in herbaceous UVB absorbing compounds [198].

UVB and Field Crops Indoor or glasshouse experiments conducted with additional UVB lamps to increase UVB, or with filters to reduce UVB, usually show dramatic effects of UVB radiation. Due to the supplemental UVB sources, however, the tested UV levels are usually much higher than what would ever occur under natural outdoor conditions. Several studies also showed that it is much more complex to simulate and investigate the effects of changing UVB that would occur under natural conditions [172].

Many of the studies showed that enhanced UVB radiation levels could lead to visual symptoms consisting of chlorotic or necrotic patches on leaves exposed to UVB. UVB radiation alters the vegetative and reproductive morphology. Changes in leaf anatomy consisting of changes in thickness of epidermal, palisade, and mesophyll layers occur. After enhanced exposure to UVB, a decrease in chlorophyll content (10–70%), and an increase in UVB-absorbing compounds (10–300%) are observed in many crops [172]. A decrease in photosynthesis (3–90%) is particularly observed at higher UV doses.

Yield and Yield Components The decrease in chlorophyll pigments and photosynthesis usually results in lower biomass and yield of crop plants. Some genotypes of crop species show a thicker leaf wax layer, a loss of chlorophyll, and an increase in phenolics (that allow a better UVB protection), ultimately resulting in changes in biomass and yield [172]. The effects of UVB on yield vary very much with crop species, however. In any case, most of the studies show that UVB increases lead to yield loss (Table 5).

Some species such as cowpea (*Vigna unguiculata*) [210, 211], millet (*Setaria italica*), and tobacco (*Nicotiana tabacum*) [212] show almost no yield reduction. Other species (e.g., pea [179], barley (*Hordeum vulgare*) [176, 179], mustard (*Brassica nigra*) [213], Black gram, Mung bean [214], and wheat [215]) show a strong reduction (Table 6). This yield loss consists of a reduced fruit grain number due to failure in fertilization, destruction of fruiting structures, and reduced fruit size due to decreased supply of assimilates to the growing sink (fruits). UVB also affects the yield quality. For instance, protein content and seed oil are reduced in soybeans that are exposed to enhanced UVB radiation.

Animals

Animals are divided here depending on the utilization of the species in the following four groups: pets (animals kept for companionship and enjoyment, or a household animal), farm animals (including horses for sport reasons), zoo animals, and finally fish and fishery-related animals.

A general finding is that animals show similar UV-induced changes of eye and skin as humans do. For the skin, two distinctive forms can be distinguished: malign melanoma and non-malign skin cancer, predominantly squamous cell carcinoma (SCC), and basal cell carcinoma (BCC).

Pets

UV Hazards The UV exposure of pets depends strongly on how these animals are kept. Cats and dogs

UV Effects on Living Organisms. Table 5 Selected results quantifying the influence of increased UV radiation on crop yield

Crop	Simulation of O_3 depletion (%)	Experimental condition	Observed change in yield (%)	Reference
Barley	–	F	−17 to −31	Mazza et al. [176]
Black gram	−15	F	−63	Singh [214]
Corn	−20	F	−22 to −33	(Correia et al. [177]
Mung bean	−15	F	−76	Singh [214]
Soybean	−16	F, GH	−41	Teramura and Murali [216]
Wheat	−12, −20, −25	F	−43	Li et al. [215]
	15	F	15	Al-Oudat et al. [217]

F outdoor experiments, *GH* Greenhouse experiment
Source: Kakani et al. [172]

UV Effects on Living Organisms. Table 6 Sensitivity of selected crops to enhanced levels of UVB radiation. Results of experiments performed in controlled environments

Sensitive	Moderately sensitive	Relatively tolerant
Barley (*Hordeum vulgare*)	Common bean (*Phaseolus* spp.)	Corn (*Zea mays*)
Carrot (*Daucus carota*)	Lettuce (*Lactuca sativa*)	Cotton (*Gossyptum hirsutum*)
Cucumber (*Cucurnis sativus*)	Peanut (*Arachis hypogaea*)	Cowpea (*Vigna unguiculata*)
Mustard (*Brassica* spp.)	Pepper (*Piper nigrum*)	Clover (*Trifolium* spp.)
Oats (*Avena sativa*)	Petunia (*Petunia* spp.)	Millet (*Setaria italica*)
Pea (*Pisum sativum*)	Potato (*Solanum tuberosum*)	Radish (*Raphanus sativus*)
Soybean (*Glycine max*)	Rice (*Oryza sativa*)	Sunflower (*Helianthus annuus*)
Sweet corn (*Zea mays* var. *saccharata*)	Rye (*Secale cereale*)	Tobacco (*Nicotiana tabacum*)
Tomato (*Lycopersicon* spp.)	Sorghum (*Sorghum vulgare*)	Wheat (*Triticum aestivum*)

Source: Prasad et al. [170]

can stay outdoors for longer periods, whereas several other species that are kept as pets live predominantly indoor. For humans, it is well known that the incidence of melanoma and non-melanoma skin cancer depends on the UV exposure, which can be assessed by the geographic latitude, elevation, and/or annual global radiation (itself related to sunshine hours). For dogs, this correlation between environmental factors and the incidence of skin neoplasms could not be found in experiments conducted in Australia (Melbourne and Queensland), USA, and UK [27, 218–227]. Two arguments could explain this discrepancy between humans and dogs: first, the fact that dogs stay predominantly indoors, so that the influence of environmental factors is reduced, and second, the different distribution of breeds in these regions. For farm animals, it is well known that some breeds are not adapted to areas with high UV exposure due to lack of pigmentation (e.g., Herford cattle).

Teifke and Lohr [228] analyzed 106 SSC immunohistochemically for overexpression of p53,

which is an indicator of a UV-related incidence. In 9 of 11 (82%) feline SCCs of the ear and in 7 of 14 (50%) feline SCCs of other locations, p53 immunoreactivity was detected. For dogs, 7 of 25 (30%) cutaneous SCCs gave a positive reaction. This is a good indicator that UV exposure is an important external factor for SCC.

The clinical picture of eye cancer, such as cutaneous SCCs in the close vicinity of the eye, could be observed in guinea pigs, hamsters, rats, and mice, which are used as pets as well. Pigmented rats and mice showed a significant reduction in the incidence of development of such cancerous eyes compared with nonpigmented animals [229].

Dogs A study on humans estimated that 0.25–1% of actinic keratosis (AK), which is mainly caused by UV exposure, progress toward SCC. Similar data do not exist for cats or dogs. Nevertheless, it can be observed that AK is common in the vicinity of SCC. In dogs, they are found primarily on the central abdomen; ventral flanks; and medial thighs of short-coated, white-haired, or piebald breeds. Dalmatians, Pit Bull Terriers, Beagles, Basset Hounds, and other dogs with similar coat characteristics have an increased incidence of AK, as well as other solar-induced neoplasms [230]. The occurrence of AK on the nose is often called "collie nose" (nasal solar dermatitis), even though it is not restricted to this breed [231]. As possible therapy, the application of sun screens with a high sun protection factor, or the tattooing of the nonpigmented areas of the nose, is recommended.

A genetically homogeneous group of 991 Beagles was housed in gravel-based, outdoor pens with dog-houses in a high-altitude, high-sunshine environment, in Colorado (40.5°N, USA). Solar dermatosis was restricted to the sparsely haired, nonpigmented abdominal skin. Solar dermatosis was diagnosed in 363 of the 991 dogs, representing an incidence of 36.6%. There were 175 cases of hemangiomas, hemangiosarcomas, or SCC of the skin among the 991 dogs. Of these, 129 tumors occurred in dogs with, and only 46 in dogs without, solar dermatosis [232].

Nielsen and Cole [233] found that there is no preferred location for SCC, contrarily to humans, whose preferred sites are the most UV-exposed areas of the body.

The influence of age is mentioned by Nesbitt [234], who observed the occurrence of SCC mainly for dogs older than 5 years. The cumulative incidence for such lesions for Beagles was observed with 47% at the age of 12 years [235]. For a genetically homogeneous group of 991 Beagles, Nikula et al. [232] investigated the role of age on the cumulative incidence of hemangiomas, hemangiosarcomas, and SCC. For SCC, the slope gets steeper for an age of 7 years (Fig. 23).

A breed disposition for the incidence of SCC was observed for dogs with insufficient pigmentation on the lips and nose, as well as on toes and ventral abdomen. Worse affected are: White German Shepherd, White Australian Shepherd, and Welsh Corgi [234].

Cats In the case of cats from sunny places, SCC could be found on the head. Risk factors are UV radiation, nonpigmented skin, and thin hair [236]. Actinic keratoses occur most often on the pinnae, nose, and eyelids of white-faced cats [230]. The influence of pigmentation was shown by Dorn et al. [237] for white-faced, blue-eyed cats. The prevalence of SCC in white cats is 11-fold higher than in nonwhite cats (Fig. 24).

In cats, melanomas could be hardly observed. After Jörger [236], no race-specific or sex-specific predispositions are known.

Vitamin D in Pets

Cats and Dogs Vitamin D is synthesized by UV in the skin of omnivores (rats, pigs, humans) and herbivores (horses, sheep, cattle). On the contrary, carnivores are solely dependent on oral intake to meet their vitamin D requirement [220–222].

How et al. [223] have shown that there is no photosynthesis of vitamin D_3 in cat skin. Although not strictly carnivores, dogs lack in the ability to photosynthesize vitamin D_3 [223]. It could be shown that hypovitaminosis D occurs in dogs irradiated with UV but with no vitamin D in their food [220].

Both natural food and commercially available complete dog food contain sufficient vitamin D_3 to fulfill a dog's requirement. Therefore, in domesticated dogs and cats, rickets is only seen under extreme circumstances, such as a strict vegetarian diet, biliary atresia, and inborn errors of vitamin D_3 metabolism [226]. Hypervitaminosis D and coupled hypercalcemia are rarely reported [225].

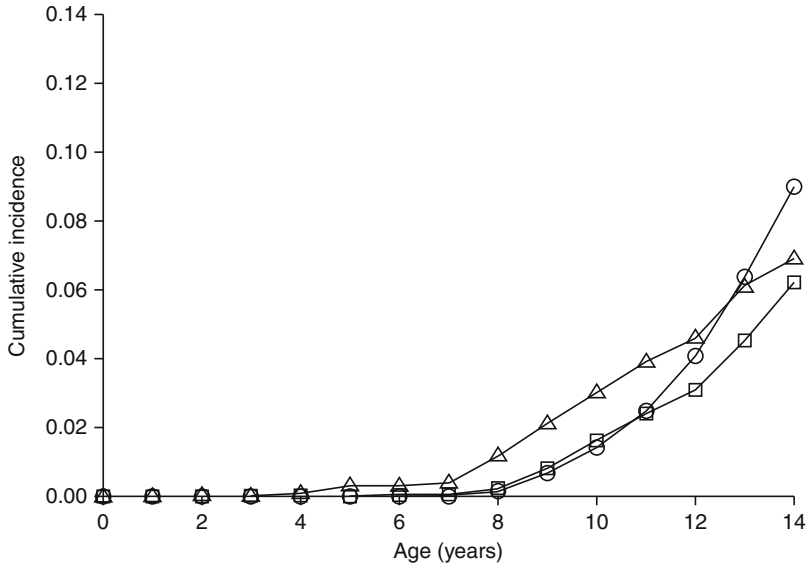

UV Effects on Living Organisms. Figure 23
Cumulative incidence of hemangiomas (○), hemangiosarcomas (□), and SCC (Δ) for Beagle dogs (Source: Nikula et al. [232])

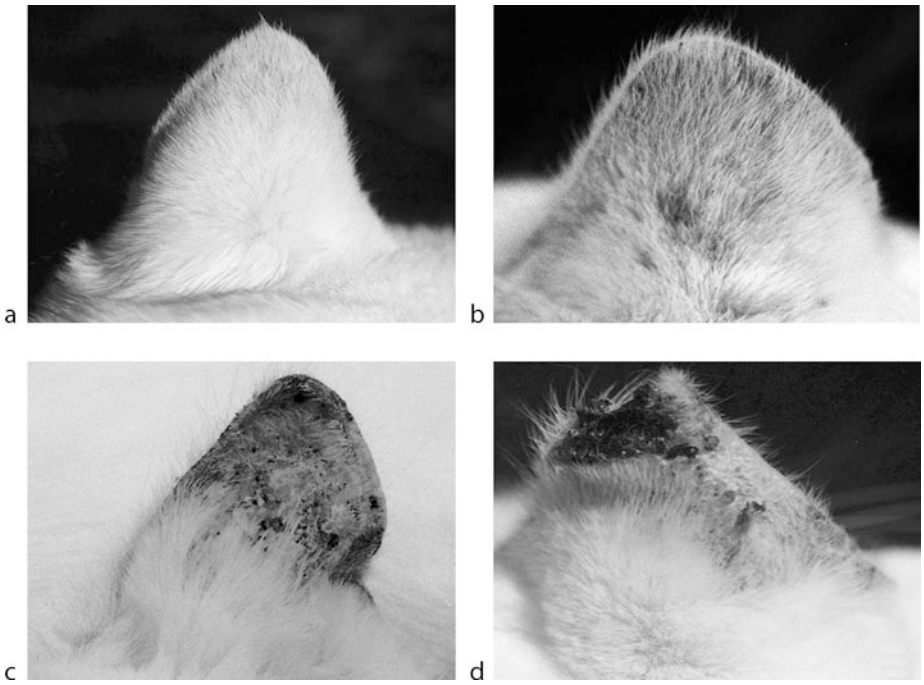

UV Effects on Living Organisms. Figure 24
Demonstration of progressive stage of photo damage shown on the ear of cats. (**a**) Normal, (**b**) initial photo damage, with erythema and scaling, (**c**) advanced photo damage, with erythema, scaling, erosion, ulceration, and plaques, and (**d**) advanced photo damage and SCC (Source: Almeida et al. [238])

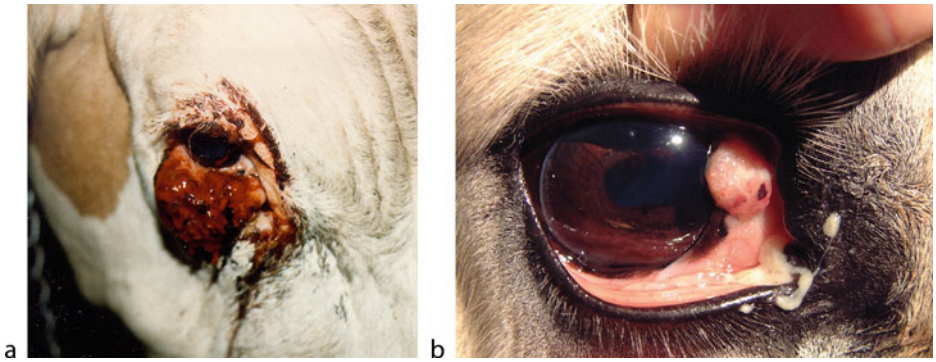

UV Effects on Living Organisms. Figure 25
Cancer eye (ocular squamous cell carcinoma) around a sparsely pigmented skin area (**a**) cattle (Source: [9]) and (**b**) horse (Source: [241])

Rabbits In rabbits, there is a clear difference in vitamin D concentration between animals housed in hatches and animals kept in free range. A strong seasonal variation in plasma vitamin D_3 concentration has been reported in rabbits [219]. For animals that had the opportunity to bask in the sun, the highest concentration was found between May and September. It takes about 5 months for the vitamin D reserve to become depleted after exposure has stopped, in conjunction with a vitamin D deficient diet [224]. Vitamin D content of forage and vegetables being negligible, only high-quality hay could contribute to the vitamin D level in rabbits.

Rats The fact that UV radiation cures rickets in rats was reported by Sonne and Rekling [27]. Beside a dose–response relationship, they were also able to derive an action spectrum. This action spectrum is quite similar to that for humans, with high efficiency in the UVB. How et al. [222] showed directly that after UV exposure an increase in vitamin D_3 in rats could be observed.

Farm Animals

UV Hazards Beside the known short-term effects like erythema, several long-term effects can be detected, such as elastosis and skin cancer. Farm animals of several species – cattle [9, 239], goats, sheep [240], and horses [241] – can develop skin cancer, mainly squamous cell carcinoma (SCC), in sparsely haired and sparsely pigmented areas of the skin.

Several farm animal species can also develop the so-called cancer eye, which is a squamous epithelial carcinoma near the eye. This disease typically occurs because the eyelid is hairless, and is dependent on both pigmentation and UV exposure. This cancer eye (Fig. 25) can be observed predominantly in Herford and Simmentaler cattle, Ayreshire, Shorthorn, black-pied cattle, Indian water buffalo, and their cross breedings [9, 239], but also in horses [241].

Teifke and Lohr [228] analyzed 106 SCC immunohistochemically for overexpression of p53, which is an indicator of a UV-related incidence. All of six (100%) equine ocular SCCs and seven of nine (78%) SCCs of the equine penis or vulva gave positive reactions. Therefore, UV radiation can be assumed as a major etiological factor for SCC.

Cattle Heeney and Valli [242] reviewed several epidemiological studies about bovine ocular SCC (cancer eye). Etiological factors were UV radiation, circumocular apigmentation, and viruses. Concerning pigmentation, Hereford cattle are commonly affected. The incidence of ocular lesions was found between 8.1–45.7% [243], 35–58% [244], 21% [245], and 25–35% [242]. For Holstein cattle, a much lower incidence was observed, $<1\%$ [242], as a result of a denser circumocular pigmentation.

In a study of Gharagozlou et al. [246], 32 cases of ocular neoplasms were diagnosed. The affected animals were female (100%), adult and more than 50% of them aged more than 5 years. In most cases (70%), the lesions were located in the nictitating membrane and palpebral conjunctiva. Intraocular invasion was noted in seven cases (22%). Microscopically, in 12 cases out of

32 (38%) the tumors were noninvasive SCC or carcinoma in situ; 18 cases (56%) were invasive SCC; a single case (3%) was lymphosarcoma, while a further single case (3%) was malignant hemangioendothelioma.

Morris [247] investigated the heritability of predictors that are closely related to skin cancer. The heritability of the eyelid pigmentation was estimated at 0.64–0.83. The Hereford cattle also appear to be highly sensitive to eye cancer. Estimates indicated a moderate heritability: 0.17–0.29 for eye cancer, 0.10 ± 0.08 for the incidence, and 0.30 ± 0.09 for the number of tumors.

The influence of UV exposure on the incidence of cancer eye can be related to geographic latitude, duration of sunshine, and altitude. Anderson and Skinner [248] classified 5,000 Hereford cattle into groups, describing the UV exposure based on latitude, sunshine duration, and altitude (Table 7). The stratification of the data showed that for all three parameters, the incidence of skin cancer stays proportional to the UV exposure.

Anderson and Badzioch [245] performed epidemiological investigations on 34 Hereford herds in North America (Table 8). For some parameters that are correlated with UV intensity (sunshine duration, elevation, cloudiness index, and global radiation) a relationship with ocular SCC was found. The odds ratios for these parameters, as a measure for the risk to develop a SCC, are summarized in Table 8. Because of the similar geographical latitudes of the statistical investigated territory, these results can be applied to midlatitude countries and southern Europe as well.

In Zimbabwe, ocular SCC was frequently observed in Simmental cattle, and exposure to intense solar radiation has been proposed as the cause, especially when cattle are kept at high altitude (1,500 masl) in a sunny and warm climate [249]. No cases were observed for fully pigmented cattle breeds.

The influence of the age t (in years) of Hereford cattle on the incidence I (in %) is depicted in Fig. 26, showing an exponential growth according to $I = 0.519\exp(0.193\ t)$ (with an adjusted coefficient of determination $r^2 = 0.541$), based on the data from Woodward and Knapp [250] and Russel et al. [244]. The half value period gives 3.6, which means that the incidence I doubles every 3.6 years. The first data set was collected in Montana at a latitude of about 46°N, and the second one in Colorado at a latitude of about 37°N. Anderson and Badzioch [245] found a 2% increase of risk per month of age, compared to 1.6% per month for the exponential model in Fig. 26. For New Mexico, Blackwell et al. [251] found an incidence for ocular SSC which was 2.5 times larger than in the two previous data sets. This could be caused by different climatic conditions, combined with a lower geographic latitude of about 35°N. Therefore, these data

UV Effects on Living Organisms. Table 7 Relationship between solar UV exposure and the incidence of cancer eye in Hereford cattle

Criterion	UV exposure	# animals	Incidence	Arithmetic mean within each level		
				Latitude (°)	Sunshine (h)	Altitude (masl)
Latitude (°)	Low	3,445	3.6 ± 0.3	46.4	2,593	809
	Medium	361	7.8 ± 1.4	43.4	2,840	1,143
	High	1,154	9.2 ± 0.8	33.6	3,150	776
Sunshine duration (h)	Low	3,445	3.6 ± 0.3	46.4	2,593	809
	Medium	823	5.6 ± 0.8	38.1	2,800	691
	High	692	11.7 ± 1.2	33.4	3,400	1,068
Altitude (masl)	Low	670	4.8 ± 0.8	36.1	2,880	357
	Medium	3,909	5.1 ± 0.1	44.4	2,718	846
	High	381	9.7 ± 1.5	43.9	2,704	1,433

Source: Anderson and Skinner [248]

UV Effects on Living Organisms. Table 8 Relationship between solar UV exposure and the incidence of cancer eye in Hereford cattle in North America (After Anderson and Badzioch [245]) (Global radiation is expressed in ly (1 ly = 4.184 J/cm^2), and cloudiness index as the global horizontal irradiation normalized with its extraterrestrial equivalent)

UV exposure described by	No of animals	Affected (%)	Odds ratio
Sunshine duration (h)			
1,800–2,299	273	13.6	1.0
2,300–2,599	335	16.1	1.1
2,600–2,899	1,158	21.2	1.8
2,900–3,499	1,009	25.7	2.5
Global radiation (ly)			
200–299	283	17.3	1.0
300–399	1,455	19.1	2.1
400–499	1,037	25.8	3.1
Cloudiness index (–)			
0.400–0.499	1,067	13.6	1.0
0.500–0.599	690	27.2	3.4
0.600–0.699	1,018	25.7	2.9
Altitude (ft)			
0–1,999	1,308	13.7	1.0
2,000–2,999	564	30.3	2.8
3,000–3,999	381	33.6	4.6
4,000–9,200	522	22.4	3.2

were not included into the regression model for the incidence (Fig. 26).

For cattle, SCC could be observed also on the vulva [232]. Wettmuny [252] found that pigmentation is a main criterion for the incidence of vulva carcinoma in Ayreshire cattle in Ceylon (8°N; 1,800 masl). The same relationship was obtained by Hünermund [253] for Kenya (1°S, 2,200 masl). The incidence of SCC on nonpigmented areas of the vulva reached between 1% in Israel (30°N) [254] and about 10% in Ceylon [255].

Like the skin, the eye is also sensitive to UV exposure. In an epidemiological survey about infectious keratoconjunctivits in Australian cattle, Slatter et al. [239] derived a relationship between season and

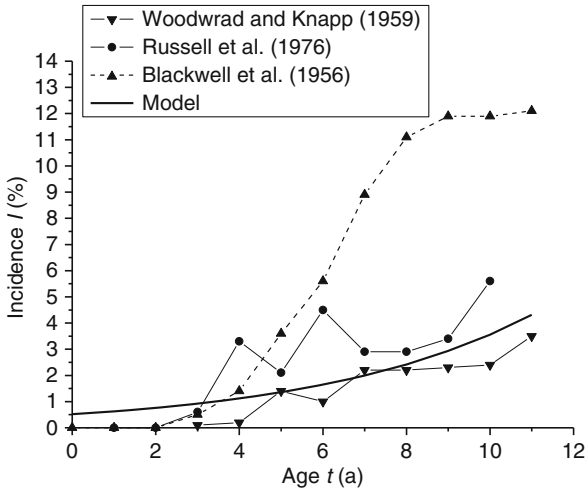

UV Effects on Living Organisms. Figure 26 Influence of age (years) of Hereford cattle on the incidence of cancer eye $I = 0.519\ \exp(0.193\ t)$ (%) (Data for the regression model from [244, 250])

frequency of disease. Similarly, Kopecky et al. [256] established that solar radiation was an amplifying factor for this disease.

Small Ungulates (Sheep and Goat) For sheep and goat, SCC could be observed on the vulva, eyelid, ear, and other parts poorly covered by wool [232].

The clinical and pathological characteristics of the outbreak of SCC observed in that study suggest that the breed of sheep, its lack of skin pigmentation, the farm's southern latitude (where UV is comparatively stronger than at the same latitude in the northern hemisphere), and factors related to the type of farming played a decisive role in the development of SCC in these sheep [240]. For Marino sheep, Forrest and Fleet [257] could show the lack of tanning capability as well as a distinct erythemal response to UV radiation. Due to a long-term UV exposure of over 28 days, the thickening of the epidermis from 23 to 120 μm was observed.

Horse For horses, a histological examination of 21 suspected neoplasms confirmed the presence of SSC (76% of cases). The remaining cases were diagnosed as lymphoid hyperplasia (14%), mast cell tumor (5%), and sebaceous gland adenocarcinoma (5%) [241]. Beside SCC, melanoma is also a common equine tumor [258]. Approximately 80% of gray horses over

15 years of age show melanotic growths. The neoplasms are generally found at the perineum, vulva, and undersurface of the root of the tail, but also on the male genitalia, neck, and ears. Melanomas remain benign for 10–20 years on the skin; however, the disease is rapidly fatal once vital organs are involved.

Genetic disposition of horses for ocular SCC were found by Dugan et al. [259], who analyzed the databases of 14 veterinarians in the USA. It was found that breed and hair color had a significant effect on the prevalence of ocular SSC. The increasing prevalence with increasing age can be calculated by the odds ratio (OR). The influence of UV radiation on the prevalence of ocular SSC was found as a function of longitude (do you mean: latitude?), altitude, and annual solar exposure [259], win good agreement with epidemiological studies for other species (e.g., cattle [245]).

The adjusted OR results summarized in Table 9 provide the relative prevalence $P_{\mathrm{rel}}(x, y)$ describing the change of prevalence of an older horse (age x, in years) in relation to a young horse (age y, in years) according to $P_{\mathrm{rel}}(x, y) = OR^{x-y}$. The age effect on OR is 1.1 ($p < 0.001$). This means, for instance, that a 12-year-old horse has a 2.6-fold higher risk to develop ocular SSC than a 2-year-old horse (of the same breed and hair color) based on $P_{\mathrm{rel}} = OR^{12-2} = 1.1^{10}$.

UV Effects on Living Organisms. Table 9 Adjusted odds ratio (OR) of variables that are correlated with the occurrence of ocular SSC in horses (After Dugan et al. [259]). Variables with a nonsignificant OR ($p < 0.05$) are not shown here

Variable		OR	*p*-value
Breed	Mixed breed	3.1	<0.001
	Paint, pinto	4.5	<0.001
	Apaloosa	7.6	<0.001
	Draft breed (Belgium, Clydesdale, Shire)	21.6	<0.001
Hair color	Chestnut, sorrel	3.8	<0.001
	Buckskin	4.4	<0.01
	Red/white or strawberry/white	4.7	<0.001
	Gray	6.7	<0.001
	Creamello, polomino	13.7	<0.001
	White	26.7	<0.001

Photosensitivity Photosensitivity defines an abnormal reaction of the skin to visible light and UV radiation. Basically, two forms of sensitivity can be distinguished: Phototoxic reactions and photo-allergenic reactions. The former occur after absorption of radiation by molecules, and the membrane and DNA damages that follow. The reaction of the skin is restricted to exposed areas. Photo-allergenic reactions are a more seldom phenomenon, where the agent evokes immunologic reactions. An observed photo-allergenic reaction can persist many years, even when the causing noxa has already been eliminated.

Photosensitive substances can be found in either drugs or feed. For instance, buckwheat (*Fagopyrum esculentum*) is known to cause photosensitivity.

This disease can be observed mainly in sheep and swine, rarely in cattle and goat, and hardly in horse. Saint-John's-wort (*Hypericum perforatum*) causes a disease in sheep, which manifests as a depigmentation by hypericin. Other sensitizers exist, such as furanocoumarin, which can be found in apiaceae or umbelliferae (like hogweed [*Heracleum mantegazzianum*], chervil [*Anthriscus cerefolium*], angelica [*Angelica archangelica*]) and yarrow (*Achillea millefolium*).

The application of veterinary medicines and medicated feed may expose agricultural workers to antimicrobial drugs, tranquilizers, and other chemicals with phototoxic and photoallergic side effects, like phenothiazin, acriflaviniumchlorid, tetrazyklin, mansonil, or sulphonamide. Olaquindox, a growth promoter for swine, is known to cause photosensitization in farmers, probably due to a photoallergic mechanism. Moreover, olaquindox was found to be phototoxic in animal experiments [260–263].

Vitamin D Vitamin D_3 is synthesized by UV radiation in the skin of omnivores (pigs, humans) and herbivores (horses, cows, sheep, goats). This synthesis works in fur-bearing animals even in the presence of hair.

For animals, both types of vitamin D – namely, cholecalciferol (vitamin D_3) and ergocalciferol (vitamin D_2) – are of importance. Whereas vitamin D_3 is produced in the skin, vitamin D_2 is ingested with feed.

Vitamin D is negligibly low in forage and silage, as well as in corns, roots, seeds, and grains. The only exception is silage made of maturity corn. Contrarily, hey contains a significant amount of vitamin D.

For animals in agricultural use, the antirachitic properties of vitamin D are brought by vitamin D_2 supplementation to food [8]. From animal welfare reasons outdoor areas for farm animals are also quite common. In such a case, supplementation is not necessary [264]. The free-range practice can also be a problem, because most swine have a very low minimal erythema dose (in MED) due to a lack of photoprotection by hair coat or low pigmentation. Exceptions are found in older races, like Mangaliza pigs, which are well adapted to solar UV radiation.

In calves, exposition to UV was shown to enhance weight gain [265] compared to nonexposed calves.

Cattle can receive vitamin D from two sources: either UV radiation or plants exposed to the sun. Vitamin D_2 is produced by UV radiation by ergosterol in forage. However, common forage (grass, grass silage) is often poor in vitamin D [266]. This explains why, in cattle, vitamin D_3 is the major form in cattle blood plasma, whereas vitamin D_2 is minor [267]. When cattle are brought in the sun or specially exposed to UV, vitamin D_3 concentrations increase within the first 5 weeks of exposure up to a plateau level [268]. In pasture animals, the annual cycle of vitamin D_3 is correlated with the annual course of solar UV exposure [269, 270]. A plateau is held from June to August. In animals that have no longer access to UV radiation, the plasma concentration in vitamin D_3 decreases rapidly, whereas the concentrations of calcium and magnesium remain much longer, and even increase for a certain period after UV exposure has stopped [268, 269]. The rather rapid decrease in vitamin D concentration may be caused by tits release into the milk [269]. Milk contains only low vitamin D concentrations – even in summer when cows are at the pasture [269]. The vitamin D content of milk can be enhanced by a factor of 100 just by irradiating it with UV.

In sheep, vitamin D is gained from both dietary sources and photosynthesis in the skin exposed to UV. In the grazing sheep, D_3 plays a dominant role in the vitamin D status [270]. When sheep are kept indoors, they need a diet that delivers vitamin D; otherwise, vitamin D supplementation has to be given. In sheep, D_2 is the dominant form of vitamin D in the blood plasma [264]. However, the presence of vitamin D_3 increases with UV exposure [271, 272], although there seems to be no linear relationship between vitamin D_3 and UV exposure. Experiments have shown that sheep easily reach their optimum vitamin D_3 level through UV exposure. Plasma D_3 and 25-OH D_3 are still detectable 7 days after the UV exposure has stopped (whereas it lasts 14 days in the case of D_2 from diet) increasing for the next 7 weeks up to a plateau. The UV caused vitamin D concentration plateau was two times higher than the plateau caused by vitamin D supplemented diets. After treatment (UV or diet), the vitamin D level stays stable twice as long as that from diet. It is concluded that UV is faster and more effective than diet to improve the vitamin D level.

Sheep kept outdoors show strong seasonal variations in plasma 25-OH D_3 concentration [273]. In winter, its level depends strongly on geographical latitude.

Wool has an important influence on the vitamin D level. As shown by Zintzen and Boyazoglou [274], the concentration of vitamin D in shorn sheep was two to three times greater than in unshorn animals. With increasing Fleece length, the vitamin D level decreases.

For goats and pigs, studies on vitamin D with respect to UV radiation are very rare.

Horses exposed to 4–6 h of solar radiation (including cloudy days) can synthesize sufficient quantities of vitamin D [275]. Solaria for horses (Fig. 27) have been recommended for animals that were held predominantly in stables, to compensate for the lack of solar UV exposure. Such radiation devices use lamps for visible and infrared radiation, as well as UV lamps, to simulate the entire spectrum of the Sun. From this exposure to simulated solar radiation, several positive physiological effects are expected. The spatial distribution of UV radiation over the entire horse body, as received either from the sun or from solaria, has been investigated by Keck et al. [55], Fig. 28.

This study showed that the UV skin dose from outdoor exposure had a totally different spatial distribution than that resulting from exposure beneath a solarium, as depicted in Fig. 28. The UV dose distribution was measured by 17 polysulphon dosimeters that were fixed with mastic on the hair coat of the horses. The dose distribution beneath the solarium

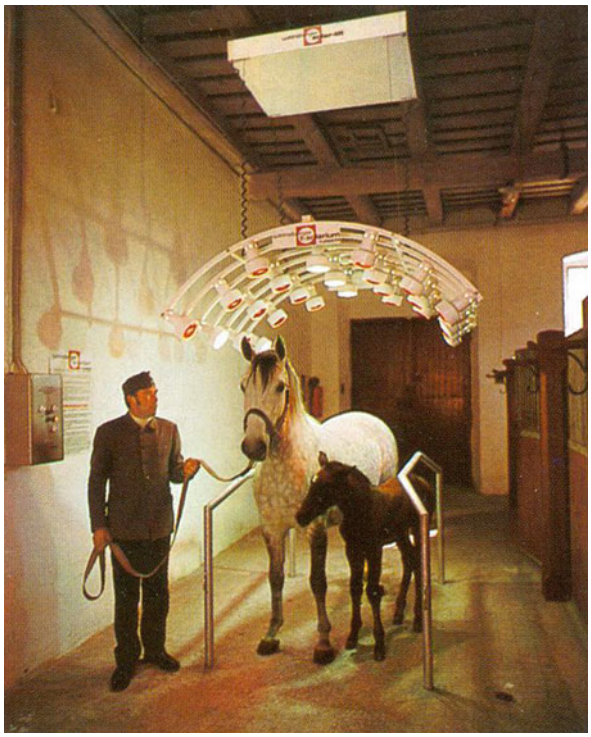

UV Effects on Living Organisms. Figure 27
Application of a solarium for horses in the Spanish Riding School of Vienna (Source: Weinsberger SW GmbH, Germany)

depends on the geometry of the UV lamps (Fig. 27), whereas the solar radiation field is much more homogeneous due to the presence of hemispherical diffuse radiation from the sky. Consequently, in outdoor conditions, hairless or little haired regions of the horse's skin receive a considerable portion (up to 60%) of radiation compared to a horizontal receiving surface. This means that UV effects can be assumed especially in these body regions.

The local maximum of the UV dose was ≈3,500 J/m^2 for outdoor exposure and ≈400 J/m^2 for solarium exposure. Considering a UV transmission of the hair coat of horses of less than 2% [55] the effective skin dose is about 70 J/m^2 for outdoor exposure and less than 9 J/m^2 for the solarium. Based on the Grotthus-Draper law, there is only little evidence that the (low) skin dose of horses beneath a solarium can contribute to positive UV effects like vitamin D synthesis. Longer exposure times, or more powerful UV lamps, would have to be used.

Horses exhibit a strong diurnal variation (50%) in vitamin D_3 serum level [276, 277]. This phenomenon seems to be restricted to horses.

Chicken can gain vitamin D from feed and UV exposure. Early studies [278–281] on poultry indicated that 10–30 min of daily sun exposure could prevent all

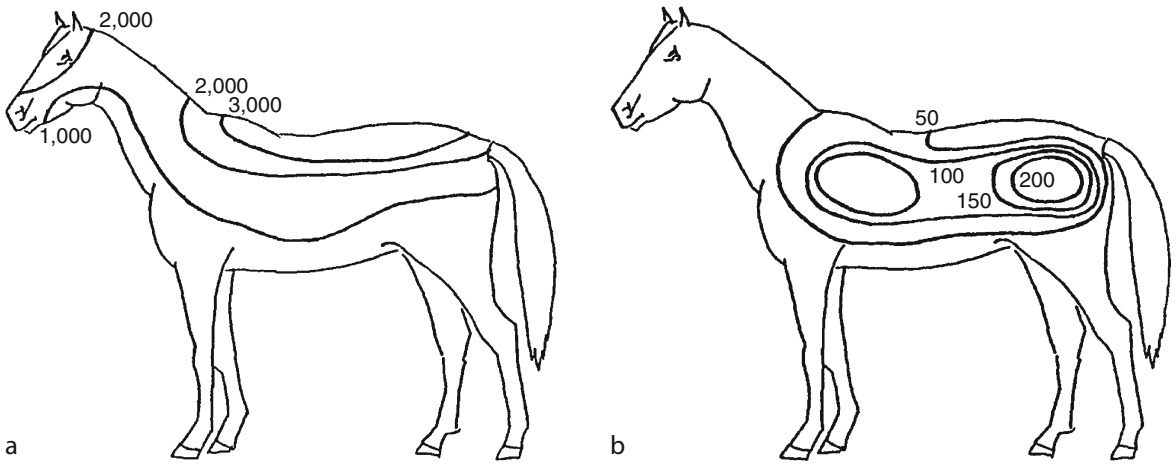

UV Effects on Living Organisms. Figure 28
Spatial distribution of the biologically effective UV dose outside of the hair cover of horses (J/m^2) (**a**) typical 1-day outdoor exposure, (**b**) solarium with a recommended exposure time of 22 min (Source: Keck et al. [55])

signs of vitamin D deficiency in growing chicken. It has also been known for a long time that a 15-min exposure to a quartz mercury vapor arc lamp produced similar effects [281].

Because of the dense plumage covering the chicken body, photosynthesis occurs in the featherless skin of legs and feet. The chicken's skin of the legs and feet contains eight times as much 7-dehydrocholesterol as their body skin [282]. Bernard et al. [283] pointed out that UV exposure (from lamps) and vitamin supplementation of food had similar efficiency. Higher hardness of egg shells can also be observed in chicken with sufficient vitamin D supply [8].

A known problem with chicken is that viable eggs produced by apparently healthy adults may incubate full term but then fail to hatch. The fully developed, dead embryos appear normal but have poorly mineralized skeletons. This problem can be successfully corrected by providing UV to the adult female prior to oviposition [284–287].

Fish and Fisheries

UV Hazards Fish and fisheries are part of the aquatic ecosystem, which produces more than 50% of the total biomass of our planet. The primary producers (phytoplankton) in freshwater and marine ecosystems constitute the basis of the food webs, providing energy for the primary (e.g., zooplankton) and secondary (e.g., fish) consumers and are thus important contributors to the production of staple diet. Humans use about 8% of the productivity of the entire oceans, but this amounts to 35% of the productivity of temperate continental shelf systems [130].

Phytoplankton and bacterioplankton are primary producers, since they use solar energy for photosynthetic conversion of CO_2 and nutrients into carbohydrates (in the so-called photic or euphotic zone). They account for about 95% of the primary productivity of oceans, and about half of all primary productivity on earth. Phytoplankton occurs predominantly in cooler, midlatitude zones with sufficient nutrients, especially nitrogen. The two major primary producers are the diatoms, which are located in temperate and polar oceans. They contribute about 60% of the primary productivity of oceans, with a typical size of about 30 μm. In contrast, the coccolithophores, with a typical size of 5–10 μm, dominate in regions of moderate turbulence at midlatitudes in late spring, as well as in subpolar and equatorial regions. They contribute about 15% to the primary productivity of oceans.

Zooplankton is the primary consumer of phytoplankton. They range in size from single-celled organisms to larger multicelled organisms. Small zooplankton is eaten by larger zooplankton. Zooplankton include ciliates (single-celled animals), copepods, shrimp, and larval forms of barnacles, mollusks, fish, and jellyfish.

The UV sensitivity of primary producers (phytoplankton) and consumers (zooplankton) in the food chain is an important predictor of biomass production. The UV protection capability of plankton is inversely related to its size. Bacteria and nano- or pico-plankton are too small to effectively protect themselves against UV radiation by absorption. There is an upper limit for the concentration of absorbing substances due to osmotic restrictions [288]. DNA damage correlates strongly with the penetration of UVB radiation into the water column. As long as the repair mechanisms keep up with the UV-caused damage, the plankton population is not threatened. However, when cyclobutane pyrimidine dimers accumulate under high-UV exposure, the population decreases.

The UV sensitivity of aquatic plankton (bacterioplankton, phytoplankton, and zooplankton) can be expressed by the radiation amplification factor, RAF, which is defined as the relative increase of UV-caused damage for a relative change in total ozone (Table 10).

By using a model that describes the UV-induced DNA damage in oceanic bacterioplankton, the sensitivity on varying ozone thickness (which conditions the UV exposure at the sea surface), dissolved organic matter concentration, chlorophyll concentration, wind speed, and mixed layer depth was investigated. From the model, the total amplification factor (TAF; a relative measure of the increase in UV damage associated with a decrease in ozone thickness) for net DNA damage in the euphotic zone is 1.7, as compared to 2.1–2.2 for UV radiation weighted for damage to DNA at the surface [291]. The link between producers and consumers in the food web has been successfully shown by Kouwenberg and Lantoine [293] for trophic plankton interactions. Diatom (*Skeletonema costatum*) was exposed to UV radiation in doses of 10% higher

UV Effects on Living Organisms. Table 10 Radiation amplification factor (RAF) for aquatic species

Species	RAF
Phytoplankton motility (*Evglena gracilis*)	1.5–1.9
Phytoplankton photosynthesis (*Phaeodactylum* sp.)	0.2–0.3
Phytoplankton photosynthesis (*Prorocentrvm micans*)	0.3–0.4
Phytoplankton photosynthesis, in Antarctic community	0.8
Phytoplankton photosynthesis (*Nodularia spumtgena* cyanobacteria)	0.2
Bacterioplankton DNA damage (euphotic zone)	1.7
Bacterioplankton DNA damage (surface water)	2.1–2.2
Green alga *Prasiola stipitata*	0.7
Dinoflagellate *Gyrodinium dorsum*	0.4
Cyanobacterium *Anabaena* sp	1.0
Corals photosynthesis	0.21

Source: References [289–292]

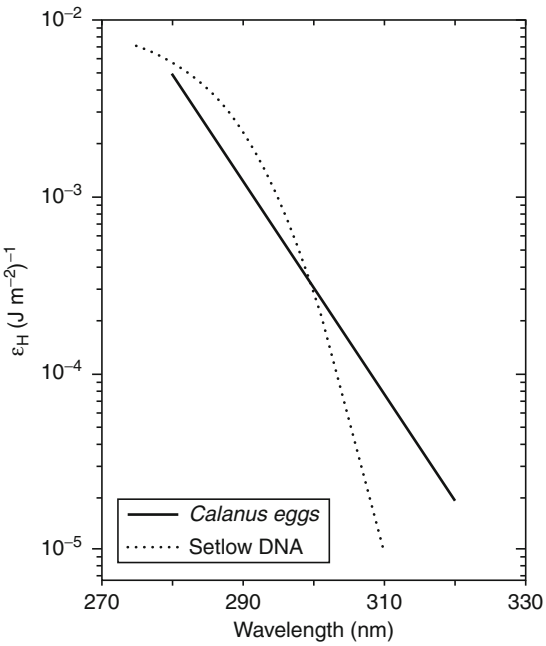

UV Effects on Living Organisms. Figure 29 Action spectra of the copepod egg mortality and of the DNA damage [81] (Source: Kouwenberg et al. [294])

than the natural UV exposure. UVB-exposed algae showed modifications in cell structure, volume increases, and delay in cell division. These UVB-stressed *S. costatum* cultures were used as food for wild copepods (*Calanus helgolandicus*), which showed an indirect UVB effect on their reproductive output.

The sensitivity of copepoda *Calanus finmarchicus* to UV is an important factor conditioning the planktonic food chain of the St. Lawrence Gulf, Canada [294]. The biological weighting function of the mortality of copepods eggs is similar to that of DNA damage (Fig. 29).

Based on the spectral UV sensitivity of copepods eggs, their mortality corresponding to solar UV irradiance at noon was calculated by an exponential law

$$N = N_0 \exp(-E_{biol}\ t) \tag{15}$$

where the egg number of live eggs is N_0, and N is the egg number after exposure of the eggs to a biologically effective irradiance E_{biol} during a time t. The weighting of the irradiance was done by a weighting function that was derived from Fig. 29. For an egg mortality of 50% at the sea surface, a 2.5 h exposure time was assumed. At a depth of 50 cm the exposure time was rather 4.6 h, due to the UV absorption of the water column [294].

To investigate the natural protection of Antarctic marine organisms against solar UV exposure, 57 species (1 fish, 48 invertebrates, and 8 algae) were collected during austral spring (Anvers Island, Antarctic Peninsula), and were analyzed for the presence of mycosporine-like amino acids – compounds that absorb UV radiation and may provide shielding from UV radiation. Nearly 90% of the 57 examined species contained mycosporine-like amino acids [311].

To assess the ecological UV sensitivity of plankton and aquatic animals, the vertical distribution of the species (e.g., Uitz et al. [312], Kesler et al. [313]) and the spectral absorption of the water column have to be taken into account [85, 314, 315].

For fish, several experiments were done to investigate their sensitivity to solar UV radiation. In addition to the mortality of eggs, skin lesions and eye damages were observed and summarized (Table 11). Rodgers [305] referred to the UV damage of the skin as the "summer syndrome." Photobiologic responses in fish are also referred to as "sunburn" [308].

UV Effects on Living Organisms. Table 11 Biological UV effects in fish

Biological effects	Fish species	Author
Skin lesions, damage on eggs and larvae; damage of the brain, eyes, disorders in growth and development	Anchovies (*Engraulis mordax*)	Hunter et al. [295]
	Pacific mackerels (*Scomber japonicus*)	
Dose-response functions for mortality of eggs	Sockeye salmon (*Oncorhynchus nerka*)	Bell and Hoar [296]
Dose-response functions for mortality	Galaxiids (*Galaxus maculatus*)	cit. by Zagarese et al. [297]
	Odonthestes hatcheri	
Dose-response functions for mortality of eggs	Atlantic cod (*Gadus morhua*)	Kouwenberg et al. [298]
Skin lesions, sunburn	Chinook salmon	Brocklebank and Armstrong [299]
	Arctic char	
Skin lesions, sunburn	Hammerhead shark (*Sphyrna lewini*)	Lowe and Goodman-Lowe [300]
Skin lesions, sunburn	Juvenile rainbow trout (*Salmo gairdneri*)	Dunbar [301], Bullock and Couts [302]
Skin lesions, sunburn	Juvenile paddles fish (*Polyodon spathula*)	cit. by Zagarese et al. [297]
Skin lesions, sunburn	Juvenile plaice (*Pleuronectes platessa*)	cit. by Zagarese et al. [297]
Skin lesions, sunburn	Atlantic salmon (*Salmo salar*)	McArdle and Bullock [303], Kaweewat and Hofer [304], and Rodger [305]
Skin lesions, sunburn	Koi carp (*Cyprinus carpio*)	Bullock et al. [306]
Skin lesions	Rainbow trout (*Oncorhynchus mykiss*)	Markkula et al. [307]
Immune system	Carp (*Cyprinus carpio*)	Markkula et al. [307]
Cataract	Rainbow trout (*Oncorhynchus mykiss*)	Markkula et al. [307]
Cataract	Lake trout (*Salvelinus namayush*)	Roberts [308], Allison [309]
Cataract	Atlantic salmon (*Salmo salar*)	Wall [310]

The biological weighting function derived for UVB-induced mortality in cod eggs is similar to that reported for DNA [81], which suggests that mortality is a direct result of DNA damage. No evidence was found that UVA had any influence on the UV sensitivity. Calculations based on this biological weighting function indicate that, under current noon surface UV irradiance, 50% of cod eggs located at, or very near below (within 10 cm), the ocean surface would be dead after 42 h of exposure [298]. To counterbalance this high sensitivity to UV exposure (found in the laboratory), many effects actually reduce the solar irradiance on fish eggs: surface water mixing, UV absorption in the water column, cloud cover, etc.

Browman et al. [316] investigated the UV effects on the early life stages of a planktonic Calanoid copepod (*calanus finmarchicus gunnerus*) and of Atlantic cod (*Gadus morhua*). Both are key species for the North Atlantic food webs. The wavelength-specific DNA damage (cyclobutane pyrimidine dimer [CPD] formation per megabase of DNA) is similar to the action spectrum for damage to T7 bacteriophage DNA.

Cases of skin lesions in fish have been reported long ago, as early as 1930. Skin lesions were described as white-to-gray necrotic areas and erosions [297]. As explained by Roberts [308], the sensitivity of fish skin to UV radiation results from the absence of a keratin layer, the poor melanin content, and the presence of dividing cells in all layers of the skin. Therefore, the skin of fish is more sensitive to UV than that of humans [297]. Lesions are typically found on the head, dorso and tail, because these regions are exposed most. Bullock [317] wrote a detailed review about skin alterations in fish. Such lesions could be found in Koi carps [306], rainbow trouts [301, 302, 318, 319], brown trout [309], Atlantic salmon [303, 305], and plaice [320]. Exposure of Atlantic salmon to enhanced UVB radiation retarded growth, and decreased the hematocrit value and plasma protein concentration. Furthermore, enhanced UVB radiation affected the plasma immunoglobulin concentration. These results also demonstrated that juvenile Atlantic salmons are not able to fully adapt to increased ambient UVB levels over long-term exposures. The interference with the immune system function suggests a negative effect of UVB on disease resistance [321]. Markkula et al. [322] studied the effect of UVB exposure on common carp (*Cyprinus carpio*), based on the immunomodulation in the blood and head kidney. Their results emphasize the potentially harmful impact of increased solar UVB radiation on the fish immune functions, and show that the effects of short- and long-term exposure differ from each other.

Armstrong et al. [323] investigated larvae of Japanese medaka (*Oryzias latipes*) to determine whether pigmentation modifies the UVB-inducible damage. One-day post-hatch medaka were exposed to UVB radiation, with or without photoreactivating light, 7 h per day for 5 days. At the higher UVB dose tested, wild-type melanophore-containing medaka formed significantly more dimers than at least one of the other strains tested. Wild-type medaka also showed significantly less photorepair capability than the white melanophore-lacking medaka. The presence of melanophores in the wild-type medaka may have contributed to an increased level of tissue damage in this strain when compared to the other strains.

Juvenile rainbow trout were also exposed to UVB using a UV-transparent respirometer chamber. A direct relationship between UVB exposure and the oxygen consumption was observed. Increased swimming activity and restless behavior were also noted [324].

Keeping fish in fish farms with high stocking rates results in a much higher UV exposure [325]. A relationship for UV-induced abnormalities was found for fish farms at high elevation in Bolivia [302] and for different seasons [305, 309].

Sunburn is in many cases the first stage before an outbreak of infectious diseases can be observed [326]. For example, fungal infections commonly occur in fish exposed to excessive sunlight. Outbreaks of *flexibacteriosis maritimus* in cultured Atlantic salmon in Tasmania (Fig. 30) occurred due to high UV exposure during cloud-free days with water temperatures above 21°C [327]. Markkula et al. [307] studied the effect of UVB on the resistance of rainbow trout (*Oncorhynchus mykiss*) against a bacterium (*Yersinia ruckeri*), the causative agent of enteric red mouth disease, and a trematode parasite (*Diplostomum spathaceum*), which causes cataracts in fish. As a result of increased UVB exposure, a significantly higher number of parasites was detected in the eyes of the irradiated fish, indicating reduced resistance against the pathogen. Furthermore, UVB exposure altered the

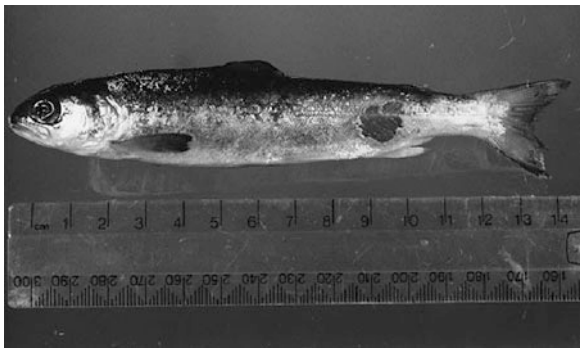

UV Effects on Living Organisms. Figure 30
Skin lesions of salmonid cutaneous erosion disease caused by *Flexibacter maritimus* in experimentally infected Atlantic salmon (From Handlinger et al. [327])

immunological and hematological parameters of fish, which also verified the immunomodulatory potential of UVB.

In a retrospective study conducted at 13 salmon farms in Western Ireland, Rodgers [305] showed that economic losses resulting from UV-induced skin damages (sunburn) could be reduced by the use of broadband antibiotics. Six out of 13 farms using antibiotics suffered from such losses, mounting to 10–23% of the post-smolt stocks over the sampling period. In 4 out of the 13 farms, where the cages were shaded, no sunburn cells in the histology of the skin could be observed.

In addition to skin lesions, eye damages can be observed in fish. Cullen et al. [328] exposed rainbow trouts (*Onchorynchus mykiss*) to broadband UV exposure over a period of 205 days. The results support the hypothesis that chronic exposure to ambient levels of UV radiation is cataractogenic. For the Atlantic salmon (*Salmo salar*), Wall [310] could show that the incidence of cataracts was very variable between sites (Ireland, Scotland, and Norway). Whereas in some farms 95% of the salmons had cataract, this fraction was less than 5% in other farms. Blind fish could often be seen near the surface. The pattern of these outbreaks suggested that the diet could be involved, beside other factors like UV exposure. For juvenile scalloped hammerhead sharks (*Sphyrny lewini*), the absorption in their corneal tissues, particularly at wavelengths below 310 nm, increases proportionally to UV exposure [329].

Cataract could also be observed in fish [308]. Allison [309] reported on trout kept in open but covered basins. In these sun-protected basins, 6% of the brown trouts developed cataract, whereas it was as much as 22% in uncovered basins.

To study repair mechanisms and the effects of UV radiation in animals, the Zebra fish is becoming an important model system. Their embryos are easily treated with UV radiation. The DNA damage repair pathways appear to be conserved in Zebra fish and mammals [330].

Due to UV exposure, aquatic organisms also developed protection measures and avoidance strategies. For them, a variety of physiological and biochemical mechanisms are available for reducing the damage by UV exposure. Screening mechanisms include both physical and chemical protection measures. Physical methods are UV absorption of mucus, sporopollenin, and multiple cell walls. Chemical screening methods include UV absorption by mycosporines, mycosporine-like amino acids, scytonemin, 3-Hydroxykynurenin, melanin, and fluorescent pigments. When screening does not eliminate penetration of UVR into the cell, there is a variety of quenching and repair processes available to overcome damage to sensitive cellular components (antioxidants, carotenoids, and the xanthophyll cycle). Damaged proteins are usually replaced by de novo synthesis (turnover), whereas damaged DNA is generally repaired. Several different mechanisms exist for repairing DNA, including photoreactivation, nucleotide excision repair, dimer bypass, and recombinational repair [331].

Coral reef fish were recently discovered to have ultraviolet (UV) radiation screening compounds, most commonly known as mycosporine-like amino acids (MAAs), in their external body mucus. However, little is known about the identity and quantity of MAAs in the mucus of reef fish, or what factors affect their abundance and distribution. In seven species of reef fish (*Labroides dimidiatus* and *Thalassoma lunare* [*Labridae*]; *Chlorurus sordidus, Scarus flavipectoralis, S. niger, S. rivulatus, and S. schlegelii* [*Scaridae*]) from Queensland, Australia, the UV absorptance of mucus was measured. The mucus of all fish investigated contained MAAs. Depending on species, different combinations and quantities of the MAAs asterina-330, palythene, and mycosporine-N-methylamine

serine were present [332]. Zamzow [333] could show that the UV protective agent in the mucus depends on the level of UV exposure. For shallow-water Caribbean fish (*Scarus iseri* and *Halichoeres bivittatus*), different ways of coping with UV radiation were discovered: *H. bivittatus* shifted the spectral quality of its mucus to increase absorptance of shorter, more damaging wavelengths, whereas *S. iseri* increased the overall UV absorbance of its mucus, with minimal spectral shifting. The influence of the diet and gender on the UV protection by the mucus could be shown for tropical wrasse, *Thalassoma duperrey* [334]. Females had higher rates of skin damage than males. Females sequester UV absorbing compounds in their pelagic eggs as well as their epithelial mucus, whereas males do not sequester these compounds in the testes.

Behavioral avoidance strategies (Table 12) are not only protection measures, but also a way to reduce UV exposure. Both laboratory and field experiments have demonstrated that many species are negatively phototactic to UV. In addition, UV photoreceptors were found in a variety of fish and invertebrates, suggesting that UV vision may be prominent in aquatic organisms [335–337]. These UV photoreceptors are thought to be used for navigation, communication, enhanced foraging, and possibly UV radiation avoidance. Given the presence of negative phototactic behaviors as well as UV vision, UV radiation may be an important factor

UV Effects on Living Organisms. Table 12 Behavioral avoidance of aquatic organism caused by UV radiation in laboratory (L) and field (F) experiments

Organism	Behavioral activity in the presence of UV radiation	Laboratory/field study
Marine cyanobacteria *Microcoleus chthonoplastes*	Migrate to greater depths	L
Ciliate *Btepharisma japonicum*	Backward swimming	L
Cladocerans	Negatively phototactic	L
Daphnia magna	Negatively phototactic	L
Cyclopoid *Cyclops serrulatus*	Avoid UV exposure	L
Marine echinoid larva *Dendraster excentricus*	Avoid UV exposure	L
Oplophorid shrimp *Systellaspis debilis*	Pitching, changing swimming speed, moving the feeding appendages	L
Zebra mussel *Dreissena polymorpha*	Ceased all swimming and crawling motions	L
D. pulicaria	Rapidly descended from the surface waters	F
D. catawba	Negatively phototactic	F
D. catawba	Negatively phototactic	F
Copepod *Diaptomus nevadensis*	Negatively phototactic	F
Marine copepod *Acartia tonsa*	Negatively phototactic	F
Cladoceran *Daphnia magna*	Negatively phototactic	F
Hydromedusan *Polyorchis penicillatus*	Negatively phototactic	F
Juvenile rainbow trout (*Oncorhynchus mykiss*)	Increased swimming activity	F
Juvenile coho salmon (*Oncorhynchus kisutch*)	Negatively phototactic	L/F

Sources: Leech and Johnsen [338], Alemanni et al. [324], Holtby and Bothwell [340]

influencing migration and abundance patterns, as well as predator-prey and intraspecific interactions [338].

UV vision has been documented in a variety of terrestrial organisms including insects, birds, amphibians, reptiles, and mammals. It is therefore not surprising that many aquatic organisms also perceive light in the UV range. Most UV photoreceptors in aquatic organisms have been described in fish species; however, UV photoreceptors have also been reported in bacteria and algae as well as in some species of protozoan, annelids, cnidarians, and crustaceans. Many UV photoreceptors have a maximum absorptance peak in the UVA range, although UVB photoreceptors have also been documented in some species. One explanation for the rarity of UVB vision is that UVB radiation is potentially more damaging to the eye [338, 339].

Vitamin D Fish store large quantities of vitamin D in their liver and fat tissues, including the fat associated with muscles, and this makes fish an important dietary source of vitamin D for their predators or for humans. Plankton, the chief food source of fish, was assessed [341] as the possible dietary origin of vitamin D in fish. High amounts of provitamins D and vitamins D (D_2 and D_3) were found in freshwater plankton [342] during summer months. Thus, plankton may be an important contributor to vitamin D in fish.

For some species of fish (rainbow trout and Mozambique tilapia) photosynthesis of vitamin D_3 from 7-DHC was reported [343]. However, it is unlikely that the photosynthesis of vitamin D_3 plays a significant role under natural conditions, where fish are less exposed to UV light.

The role of vitamin D in fish physiology is still enigmatic [344]. Until the 1970s, the consensus was that fish accumulated but not metabolized vitamin D. Now, 4 decades later, there is substantial evidence that fish have a vitamin D endocrine system with similar functions as in mammals.

Zoo Animals

The geographical origins of many exotic animals are areas with high-UV intensity. When brought into zoological gardens, they might suffer under a deficiency of UV exposure, especially at mid- and high-latitudes. On the other hand, increased UV exposure may cause photodamage of the skin and the eyes. To provide these animals with an appropriate environment, their solar UV exposure has to be taken into account.

Lack of UV radiation strongly reduces the availability of vitamin D_3. Therefore, animals can suffer from rachitis (rickets) and osteodystrophy, which causes irreversible bone degeneration of the locomotion system and substantial deformation of the jaw. This handicaps both their movement and food intake. Vitamin D can also be supplied by feed. However, excessive dietary vitamin D can result in toxic effects and death. Conversely, high-UV exposure does not result in excessive vitamin D levels [345].

For some species, the vitamin D supply can be substituted by vitamin D_2 supplementation in the feed. However, Göltenboth [346] illustrated that rachitis in primates could not be healed by such vitamin D_2 supplementation. The symptoms could only be eradicated by exposure to lamps with a high UV output (Ultravitalux-lamps, Osram). Several species of New World primates have an absolute requirement for vitamin D_3, either from the diet or through exposure to UV radiation. They seem to metabolize vitamin D_2 too quickly to maintain adequate serum levels of 1,25-dihydroxyergocalciferol [347]. Hofmann-Parisot [348] described typical differences in diverse primate species concerning the vitamin D metabolism.

Tonge [349] has shown that the application of supplemental UV radiation can prevent the deformation of the tail of lizards. Bosch and Frank [350] pointed out that in terrariums, 11% of turtles and 7% of iguanas display a vitamin D deficiency syndrome.

McCrystal and Behler [351] and Townsend and Cole [352] indicated that for the breeding success in lizards, a sufficient supply in UV is necessary. This can be attributed to interactions with the calcium metabolism, because calcium is responsible for the mechanical stability of their eggs (Fig. 31).

Another fundamental problem for lizards raised in captivity may be that their viable eggs incubate full term but then fail to hatch, even when produced by apparently healthy adults. The fully developed, dead embryos appear normal but have poorly mineralized skeletons. This problem is similar to that of chicken, and can also be corrected by supplementing UV to the adult female prior to oviposition [284, 285].

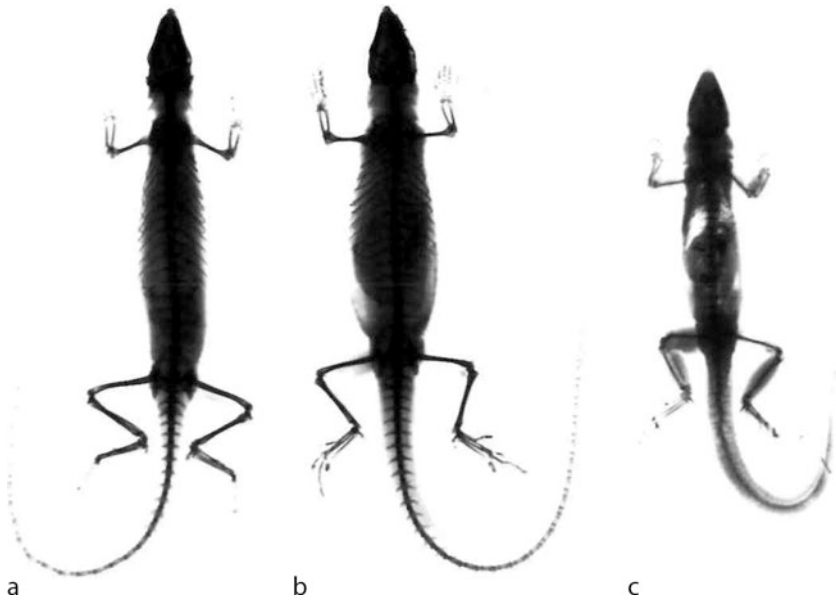

UV Effects on Living Organisms. Figure 31
X-ray image of whiptail lizards (*Cnemidophorus exsanguis*). (**a**) Healthy, wild-caught adult. (**b**) Healthy laboratory-reared adult. (**c**) Laboratory-reared young adult with metabolic bone disease (Source: Townsend and Cole [352])

Turtles receive vitamin D either from dietary or from UV exposure. It was shown by Acierno et al. [353] that UV is much more effective than diet. In 1997, Manning and Grigg [47] found that basking in a freshwater turtle is longer than thermoregulation would require, which indicates that turtles regulate their vitamin D status by basking.

For snakes and turtles, Acierno et al. [354] investigated the vitamin D supply following 28 days of additional UV exposure. As a result of such an additional UV exposure, the plasma concentration of 25-hydroxyvitamin D_3 was about 3.4 times higher than the control group in snakes, and 2.3 times higher in turtles.

For various lizards, snakes, and chameleons [50, 345], it could be shown that the exposure behavior to natural sunlight depends on the vitamin D status. Animals with low dietary vitamin D_3 intake significantly increased their spontaneous exposure to solar radiation, compared to those with a high dietary vitamin D_3 intake. These results demonstrate the importance of basking for nonthermoregulatory purposes and, more specifically, that basking constitutes an integral mechanism for the regulation of a vital hormone, vitamin D_3. Ferguson et al. [49] found some evidence that the vitamin D photosynthesis in the skin may reflect a correlated response associated with the need of vitamin D. However, the possibility that specific adaptations for the photosynthesis of vitamin D and for the protection from skin damage could involve independent mechanisms still needs more investigation.

Ferguson et al. [48, 49] have shown that Panther chameleons (*Furcifer pardalis*) can regulate UV exposure behaviorally or by a change in skin color, so that their vitamin D production is enhanced at low UV levels. As Karsten et al. [50] have shown, Panther chameleons and possibly reptiles, in general, bask also for reasons other than thermoregulation. In dependence of their dietary vitamin D_3 intake, Panther chameleons behaviorally regulate their exposure to solar UV to ensure an optimal vitamin D_3 status with high precision. Their UVA-sensitive retina is helpful in this respect. Vitamin D supplementation in lizards is not easy. It may become toxic, and possibly lethal [284].

Hofmann-Parisot [348] investigated the use of artificial UV sources that were used in keeping zoo animals healthy. It was found that ≈60% of the zoo gardens surveyed apply artificial UV radiation to animals.

Of that number, 48% use UV only for treating reptiles, and 52% do this also for mammals and avian. Interestingly, this survey also provided a very fuzzy picture of the UV supplementation practice: UV intensity and exposition times, types of lamps, and radiation geometry were highly variable, illustrating that no sufficient information is available concerning the UV needs of specific animal species. As illustrated by the case of chameleons, animal behavior has to be taken into account.

Gehrmann [355] realized the importance of using UV sources in animal husbandries and investigated different types of lamps, as well as the reflection and transmission properties of some materials that are used in zoos [356]. (Note that, in this kind of study, the spectral distribution of these UV sources and the specific animal requirements would have to be considered as well.)

Even though it is well known that most of the observed diseases related to vitamin D deficits are caused by a lack of UV exposure, no systematic investigations have been performed to optimize the UV irradiance or the exposure time for various animals. Most of the applications of artificial UV sources resulted from "educated guess." For snakes and lizards, however, Ferguson et al. [345] estimated the natural UV irradiance by using the UV index of their natural environment. The conversion rate of vitamin D due to UV exposure was investigated by Ferguson et al. [285] for panther chameleons (*Furcifer pardalis*).

Although insufficient natural UV radiation is typical in zoo animals, overexposure to artificial UV can also appear, if inappropriate UV sources are in use. For a ball python (*Python regius*) and a blue tongue skink (*Tiliqua nigrolutea*), the application of an otherwise appropriate UV lamp, but with an extremely high UVB output, showed epidermal erosion and ulceration, with severe epidermal basal cell degeneration and necrosis, and superficial dermatitis as well as bilateral ulcerative keratoconjunctivitis with bacterial colonization [357]. Veterinarians who are consulted for reptiles with ocular and/or cutaneous disease of unapparent cause should fully evaluate the specifics of the vivarium light sources. In general, overexposure to UV radiation can cause eye and skin damage, skin cancer, and poor reproduction in reptiles and amphibians [345].

Future Directions

The so-called ozone hole was detected in ozone measurements of the late 1970s [358]. The reduction of the total ozone content in the stratosphere and the resulting decrease of absorbing capacity for UV radiation [359] cause a hype in research on the biological effects of UV radiation. Up to this moment the solar radiation and therefore also the spectral range of UV radiation was assumed to be constant without remarkable variability. In the following 2 decades, a steep increasing number of investigations were published which were concentrated primarily to the monocausal effects of UV radiation on plants, animals, and humans.

These research activities of biologically effective UV radiation due to ozone depletion were replaced by the climate change discussion starting in the late 1990s. By more sophisticated general circulation models (GCM) also parameters like solar radiation were predicted for the next century. This leads to the opportunity to predict the biologically effective UV radiation as well. These climate change scenarios for a century were the basis for a more holistic approach to describe the interaction between UV radiation and flora as well as fauna. The coupling of the biosphere with GCM can be used to assess effects of the climate change on the biosphere and vice versa (e.g., reduced cloud cover leads to a higher UV exposure of plankton which reduces the plankton reproduction, which causes a reduction of carbon storage and finally an increase of CO_2 release, influencing the radiative forcing as an important input parameter of GCM). For humans the resulting migration scenarios and the adaptation of the behavior to the changing climate can be used to calculate the modification of the UV skin exposure and the health implications.

Beside UV effects, which cause a damage (e.g., eye, skin), also beneficial effects are under discussion, which are correlated with the vitamin D synthesis due to UV radiation. A sufficient supply with vitamin D is necessary for skeletal health. Further it is assumed as protective measure against several kinds of cancer in humans. For these investigations an appropriate animal model would be a great help.

For several UV effects different working hypothesis are in use, which are verified very rarely. First of all the assumption of reciprocity is a simple prerequisite

which says that the effect is depending on the UV dose, which is calculated by the intensity of the radiation times the exposure time. Secondly we assume that a polychromatic UV exposure is caused by an unweighted sum of all spectral UV doses. This means that the weighting of the UV radiation and the resulting biologically effective UV radiation can be described as photoadditive, without photoprotection or photoaugmentation due to certain wavelength ranges [360].

Bibliography

Primary Literature

1. Bunsen RW, Roscoe HE (1857) Photochemische Untersuchungen. Poggendorfs Ann 100:51
2. Schindl A, Rosado-Schlosser B, Trautinger F (2001) Die Reziprozitätsregel in der Photobiologie. Eine Übersicht Der Hautarzt 52:779–785
3. Diffey BL, Kochevar IE (2007) Basic principles of photobiology. In: Lim HW, Hönigsmann H, Hawk JL (eds) Photodermatology. Informa Healthcare USA, New York, pp 15–27
4. Schwarzschild K (1900) On the law of reciprocity for bromide of silver gelatin. Astrophys J 11:89
5. Martin JW, Chin JW, Nguyen T (2003) Reciprocity law experiments in polymeric photodegradation: a critical review. Prog Org Coat 47:292–311
6. Reischl S, Henrich J, Schauberger G (2000) Time course and dose-response-relationship of erythema of the pigs induced by UVB- and UVC-radiation. In: 13th international congress on photobiology, San Francisco, 1–6 July 2000, p 136
7. Farr PM, Besag JE, Diffey BL (1988) The time course of UVB and UVC erythema. J Investig Dermatol 91:454–457
8. Mehlhorn G, Steiger A (1974) Künstliche UV-Strahlung in der Tierproduktion. Gustav Fischer Verlag, Jena
9. Kasper I (1986) Abschätzung biologischer UV-Wirkungen durch Bestrahlung von Großtieren mit künstlichen UV-Quellen. Dissertation Veterinärmedizinische Universität Wien, Wien
10. MacKinley AF, Diffey BL (1987) A reference action spectrum for ultraviolet induced erythema in human skin. CIE J 6:17–22
11. Gates FL (1930) A study of the bactericidal action of ultra violet light. III. The absorption of ultra violet light by bacteria. J Gen Physiol 14:31–42
12. Hollaender A, Emmons CW (1941) Wavelength dependence of mutation production in the ultraviolet with special emphasis on fungi. Cold Spring Harb Symp Quant Biol 9:179–185
13. Herschel W (1800) Investigation of the powers of the prismatic colours to heat and illuminate objects; with remarks, that prove the different refrangibility of radiant heat. To which is added, an inquiry into the method of viewing the sun advantageously, with telescopes of large apertures and high magnifying powers. Philos Trans R Soc Lond 90:255–283
14. Herschel W (1800) Experiments on the refrangibility of the invisible rays of the sun. Philos Trans R Soc Lond 90:284–292
15. Ritter JW (1801) Ann Phys 7:527
16. Daubeny C (1836) On the action of light upon plants and plants upon the atmosphere. Philos Trans R Soc Lond 126:149–176
17. Draper JW (1884) Note on decomposition of carbonic acid by the leaves of plants under the influence of yellow light. Philos Mag 25:159–173
18. Engelmann TW (1882) Über Sauerstoffausscheidung von Pflanzenzellen im Microspectrum. Bot Zeit 40:419–426
19. Hausser KW, Vahle W (1921) Die Abhängigkeit des Lichterythems und der Pigmentbildung von der Schwingungszahl (Wellenlänge) der erregenden Strahlung. Strahlentherapie 13:41–71
20. Coblentz WW, Stair R (1934) Data on the spectral erythemic reaction of the untanned human skin to ultraviolet radiation. Bur Stand J Res 12:13–14
21. Luckiesh M, Holladay LL, Taylor AH (1930) Reaction of untannted human skin to ultraviolet radiation. J Opt Soc Am 20:423–426
22. Hausser KW, Vahle W (1927) Sonnenbrand und Sonnenbräunung. Wiss Veröfftl Siemens Konzern 6:101–120
23. CIE (1937) Neuvieme Session Berlin und Karlsruhe Juillet 1935. Cambridge University Press, Cambridge, UK
24. McKinley AF, Diffey BL (1987) A reference action spectrum for ultraviolet induced erythema in human skin. CIE J 6:17–22
25. Duggar BM, Hollaender A (1934) Irradiation of plant viruses and of microorganisms with monochromatic light: I. The virus of typical tobacco mosaic and serratia marcescens as influenced by ultraviolet and visible light. J Bacteriol 27: 219–239
26. Gates FL (1934) Results of irradiating staphylococcus aureus bacteriophage with monochromatic ultraviolet light. J Exp Med 60:179–188
27. Sonne C, Rekling E (1927) Behandlung experimenteller Rattenrachitis mit monochromatischem ultravioletten Licht. Strahlentherapie 35:552–558
28. Henschke U, Schulze R (1939) Über Pigmentierung durch langwelliges Ultraviolett. Strahlentherapie 65:14–42
29. Reiter T, Gabor D (1928) Ultraviolette Strahlen und Zellteilung. Strahlentherapie 28:125–132
30. Blumthaler M, Ambach W (1988) Solar UV-B albedo of various surfaces. Photochem Photobiol 54:429–432
31. Monteith JL (1973) Principles of environmental physics. Arnold, London
32. Quaschning V, Hanitsch R (1998) Irradiance calculation on shaded surfaces. Sol Energy 62:369–375
33. Blumthaler M, Ambach W, Ellinger R (1996) UV-Bestrahlung von horizontalen und vertikalen Flächen im Hochgebirge. Wetter Leben 1:25–31
34. Schauberger G (1990) Model for the global irradiance of the solar biologically-effective ultraviolet radiation on inclined surfaces. Photochem Photobiol 52:1029–1032

35. Grant RH (1998) Ultraviolet irradiance of inclined planes at the top of the plant canopies. Agric For Meteorol 89:281–293
36. Webb AR, Weihs P, Blumthaler M (1999) Spectral UV irradiance on vertical surfaces: a case study. Photochem Photobiol 69:464–470
37. Hay JE (1979) Calculation of monthly mean solar radiation for horizontal and inclined surfaces. Sol Energy 23:301–307
38. Schauberger G (1992) Anisotropic model for the diffuse biologically effective irradiance of solar UV radiation on inclined surfaces. Theor Appl Climatol 46:45–51
39. Klucher TM (1979) Evaluation of models to predict insolation on tilted surfaces. Sol Energy 26:179–184
40. Hay JE, McKay DC (1985) Estimating solar irradiance on inclined surfaces: a review and assessment of methodologies. Int J Sol Energy 3:203–240
41. Reindl DT, Beckmann WA, Duffie JA (1990) Diffuse fraction correlations. Sol Energy 45:1–7
42. Utrillas MP, Marin MJ, Esteve AR, Estelles V, Tena F, Canada J et al (2009) Diffuse ultraviolet erythemal irradiance on inclined planes: a comparison of experimental and modeled data. Photochem Photobiol 85:1245–1253
43. Mech M, Koepke P (2004) Model for UV irradiance on arbitrarily oriented surfaces. Theor Appl Climatol 77:151–158
44. Hess M, Koepke P (2008) Modelling UV irradiances on arbitrarily oriented surfaces: effects of sky obstructions. Atmos Chem Phys 8:3583–3591
45. Dirmhirn I (1964) Das Strahlungsfeld im Lebensraum. Akademische Verlagsgesellschaft, Frankfurt
46. Geiger R (1961) Das Klima der bodennahen Luftschicht, 4. Aufl. ed. Viehweg, Braunschweig
47. Manning B, Grigg GC (1997) Basking is not of thermoregulatory significance in the "basking" freshwater turtle Emydura signata. Copeia 1997:579–584
48. Ferguson GW, Gehrmann WH, Karsten KB, Hammack SH, McRae M, Chen TC et al (2003) Do panther chameleons bask to regulate endogenous vitamin D_3 production? Physiol Biochem Zool 76:52–59
49. Ferguson GW, Gehrmann WH, Karsten KB, Landwer AJ, Carman EN, Chen TC et al (2005) Ultraviolet exposure and vitamin D synthesis in a sun-dwelling and a shade-dwelling species of Anolis: are there adaptations for lower ultraviolet B and dietary vitamin D_3 availability in the shade? Physiol Biochem Zool 78:193–200
50. Karsten KB, Ferguson GW, Chen T, Holick MF (2009) Panther chameleons, furcifer pardalis, behaviorally regulate optimal exposure to UV depending on dietary vitamin D status. Physiol Biochem Zool 82:218–225
51. Bidmon HJ, Stumpf WE (1996) Vitamin D target systems in the brain of the green lizard Anolis carolinensis. Anat Embryol 193:145–160
52. Bowmaker JK, Loew ER, Ott M (2005) The cone photoreceptors and visual pigments of chameleons. J Comp Physiol A Neuroethol Sens Neural Behav Physiol 191:925–932
53. Tovee MJ (1995) Ultra-violet photoreceptors in the animal kingdom: their distribution and function. Trends Ecol Evol 10:455–460
54. Bianca W, Wegmann H (1974) Die Durchlässigkeit von Rinderhaaren für ultraviolette Strahlung. Schweiz Arch Tierheilk 116:114–146
55. Keck G, Kasper I, Schauberger G, Cabaj A (1987) Biological effects of UV-irradiation on horses with artificial UV-sources. In: Passchier WF, Bosnjakovic BFM (eds) Human exposure to ultraviolet radiation – risk and regulations. Elsevier, Amsterdam
56. Keck G, Kasper I, Schauberger G, Cabaj A (1988) UV-Wirkungen in Pferdesolarien? Berl Münchner Tierärztl Wochenschr 101:49–52
57. Chapman RS, Cooper KD, De Fabo EC, Frederick JE, Gelatt KN, Hammond SP et al (1995) Solar ultraviolet radiation and the risk of infectious disease: summary of a workshop. Photochem Photobiol 61:223–247
58. Schauberger G (1997) Biological relevance of solar radiation to animals. Wien Tierärztl Mschr 84:2–13
59. Wolfe WL, Zissig GJ (1978) The infrared handbook. Office of Naval Research, Department of the Navy, Washington
60. Chadysiene R, Girgzdys A (2008) Ultraviolet radiation albedo of natural surfaces. J Environ Eng Landscape Manage 16:83–88
61. Morris DP, Zagarese H, Williamson CE, Balseiro EG, Hargreaves BR, Modenutti B et al (1995) The attenuation of solar UV radiation in lakes and the role of dissolved organic carbon. Limnol Oceanogr 40:1381–1391
62. Reitner B, Herndl GJ, Herzig A (1997) Role of ultraviolet-B radiation on photochemical and microbial oxygen consumption in a humic-rich shallow lake. Limnol Oceanogr 42:950–960
63. Booth CR, Morrow JH (1997) The penetration of UV into natural waters. Photochem Photobiol 65:254–257
64. Morris DP, Hargreaves BR (1997) The role of photochemical degradation of dissolved organic carbon in regulating the UV transparency of three lakes on the Pocono Plateau. Limnol Oceanogr 42:239–249
65. Graneli W, Lindell M, Tranvik L (1996) Photo-oxidative production of dissolved inorganic carbon in lakes of different humic content. Limnol Oceanogr 41:698–706
66. Markager S, Vincent WF (2000) Spectral light attenuation and the absorption of UV and blue light in natural waters. Limnol Oceanogr 45:642–650
67. Vincent WF, Rae R, Laurion I, Howard-Williams C, Priscu JC (1998) Transparency of Antarctic ice-covered lakes to solar UV radiation. Limnol Oceanogr 43:618–624
68. Sommaruga R, Psenner R (1997) Ultraviolet radiation in a high mountain lake of the Austrian Alps: air and underwater measurements. Photochem Photobiol 65:957–963
69. Sommaruga R, Augustin G (2006) Seasonality in UV transparency of an alpine lake is associated to changes in phytoplankton biomass. Aquat Sci 68:129–141
70. Huovinen PS, Penttilä H, Soimasuo MR (2003) Spectral attenuation of solar ultraviolet radiation in humic lakes in Central Finland. Chemosphere 51:205–214

71. Smith RC, Baker KS (1981) Optical properties of the clearest natural waters (200–800 nm). Appl Opt 20:177–184
72. Baker KS, Smith RC (1982) Bio-optical classification and model of natural waters. Limnol Oceanogr 27:500–509
73. De Lange HJ (2000) The attenuation of ultraviolet and visible radiation in Dutch inland waters. Aquat Ecol 34:215–226
74. Bukaveckas PA, Robbins-Forbes M (2000) Role of dissolved organic carbon in the attenuation of photosynthetically active and ultraviolet radiation in Adirondack lakes. Freshw Biol 43:339–354
75. Squires MM, Lesack LFW (2003) Spatial and temporal patterns of light attenuation among lakes of the Mackenzie Delta. Freshw Biol 48:1–20
76. Sommaruga R (2001) The role of solar UV radiation in the ecology of alpine lakes. J Photochem Photobiol B 62:35–42
77. Smith RC, Baker KS (1978) Optical classification of natural waters. Limnol Oceanogr 23:260–267
78. Smith RC, Baker KS (1979) Penetration of UV-B and biologically effective close-rates in natural waters. Photochcm Photobiol 29:311–323
79. Jerlov NG (1968) Optical oceanography. Elsevier, Amsterdam
80. Williamson CE, Stemberger RS, Morris DP, Frost TM, Paulsen SG (1996) Ultraviolet radiation in North American lakes: attenuation estimates from DOC measurements and implications for plankton communities. Limnol Oceanogr 41:1024–1034
81. Setlow RB (1974) The wavelengths in sunlight effective in producing skin cancer: a theoretical analysis. Proc Natl Acad Sci USA 71:3363–3366
82. Grenfell TC, Warren SG, Mullen PC (1994) Reflection of solar radiation by the Antarctic snow surface at ultraviolet, visible, and near-infrared wavelengths. J Geophys Res 99: 18669–18684
83. Blumthaler M, Ambach W (1988) Solar UVB-albedo of various surfaces. Photochem Photobiol 48:85–88
84. Meinander O, Kontu A, Lakkala K, Heikkilä A, Ylianttila L, Toikka M (2008) Diurnal variations in the UV albedo of arctic snow. Atmos Chem Phys 8:6551–6563
85. Perovich DK (1993) A theoretical model of ultraviolet light transmission through Antarctic sea ice. J Geophys Res 98:22579–22588
86. Cockell CS, Rettberg P, Horneck G, Wynn-Williams DD, Scherer K, Gugg-Helminger A (2002) Influence of ice and snow covers on the UV exposure of terrestrial microbial communities: dosimetric studies. J Photochem Photobiol B 68:23–32
87. Warren SG, Brandt RE, Grenfell TC (2006) Visible and near-ultraviolet absorption spectrum of ice from transmission of solar radiation into snow. Appl Opt 45:5320–5334
88. King MD, France JL, Fisher FN, Beine HJ (2005) Measurement and modelling of UV radiation penetration and photolysis rates of nitrate and hydrogen peroxide in Antarctic sea ice: an estimate of the production rate of hydroxyl radicals in first-year sea ice. J Photochem Photobiol A 176:39–49
89. Perovich DK (2001) UV radiation and the optical properties of sea ice and snow. In: Hessen D (ed) UV radiation and Arctic ecosystems, pp 73–89
90. Lesser MP, Lamare MD, Barker MF (2004) Transmission of ultraviolet radiation through the Antarctic annual sea ice and its biological effects on sea urchin embryos. Limnol Oceanogr 49:1957–1963
91. Fritsen CH, Priscu JC (1999) Seasonal change in the optical properties of the permanent ice cover on Lake Bonney, Antarctica: consequences for lake productivity and phytoplankton dynamics. Limnol Oceanogr 44:447–454
92. Grenfell TC, Maykutt GA (1977) The optical properties of ice and snow in the Arctic basin. J Glaciol 18:445–463
93. Belzile C, Gibson JAE, Vincent WF (2002) Colored dissolved organic matter and dissolved organic carbon exclusion from lake ice: implications for irradiance transmission and carbon cycling. Limnol Oceanogr 47:1283–1293
94. Belzile C, Johannessen SC, Gosselin M, Demers S, Miller WL (2000) Ultraviolet attenuation by dissolved and particulate constituents of first-year ice during late spring in an Arctic polynya. Limnol Oceanogr 45:1265–1273
95. Kepner JRL, Wharton RA Jr, Collier RD, Cockell CS, Jeffrey WH (2000) UV radiation and potential biological effects beneath the perennial ice cover of an antarctic lake. Hydrobiologia 427:155–165
96. Felip M, Camarero L, Catalan J (1999) Temporal changes of microbial assemblages in the ice and snow cover of a high mountain lake. Limnol Oceanogr 44:973–987
97. Felip M, Wille A, Sattler B, Psenner R (2002) Microbial communities in the winter cover and the water column of an alpine lake: system connectivity and uncoupling. Aquat Microb Ecol 29:123–134
98. Savage DC (1977) Microbial ecology of the gastrointestinal tract. Annu Rev Microbiol 31:107–133
99. Berg RD (1996) The indigenous gastrointestinal microflora. Trends Microbiol 4:430–435
100. Cristiani H (1893) Analyse bacteriologique de l'air des hauteurs, puise un voyage en ballon. l'Inst Pasteur 7:665–671
101. Harz CO (1904) Bakteriologische Untersuchungen der freien Atmosphäre mittels Luftballons nebst Bemerkungen über den atmosphärischen Staub. Fb dtsch Luftsch Verb 1904:293–302
102. Rogers LA, Meier FC (1936) U.S. Army Air Corps stratosphere flight of 1935 in the balloon "Explorer II." Technical papers, The National Geographic Society, Washington, DC, pp 146–151
103. Imshenetsky AA, Lysenko SV, Kazakov GA (1978) Upper boundary of the biosphere. Appl Environ Microbiol 35:1–5
104. Fulton JD (1966) Microorganisms of the upper atmosphere. 3. Relationship between altitude and micropopulation. Appl Microbiol 14:237–240
105. Yang Y, Itahashi S, Yokobori S, Yamagishi A (2008) UV-resistant bacteria isolated from upper troposphere and lower stratosphere. Biol Sci Space 22:18–25
106. Tong Y, Che F, Xu X, Chen M, Ye B (1993) Population study of atmospheric bacteria at the Fengtai district of Beijing on two representative days. Aerobiologia 9:69–74
107. Meier FC, Lindbergh CA (1935) Collecting micro-organisms from the Arctic atmosphere. Sci Mon 40:5–20

108. Griffin DW, Garrison VH, Herman JR, Shinn EA (2001) African desert dust in the Caribbean atmosphere: microbiology and public health. Aerobiologia 17:203–213
109. Griffin DW, Kubilay N, Koçak M, Gray MA, Borden TC, Shinn EA (2007) Airborne desert dust and aeromicrobiology over the Turkish Mediterranean coastline. Atmos Environ 41: 4050–4062
110. Griffin DW, Westphal DL, Gray MA (2006) Airborne microorganisms in the African desert dust corridor over the mid-Atlantic ridge, Ocean Drilling Program, Leg 209. Aerobiologia 22:211–226
111. Mims SA, Mims FM III (2004) Fungal spores are transported long distances in smoke from biomass fires. Atmos Environ 38:651–655
112. Brown JKM, Hovmoll MS (2002) Aerial dispersal of pathogens on the global and continental scales and its impact on plant disease. Science 297:537–541
113. Tong Y, Lighthart B (1997) Solar radiation is shown to select for pigmented bacteria in the ambient outdoor atmosphere. Photochem Photobiol 65:103–106
114. Reiling F (2000) Dissemination of bacteria from the mouth during speaking, coughing, and otherwise. JAMA 284:156
115. Giese AC (1976) Living with our suns's ultraviolet rays. Plenum, New York
116. Mims FM III (2005) Avian influenza and UV-B blocked by biomass smoke. Environ Health Perspect 113(12):A806–A807
117. Coffin RB, Velinsky DJ, Devereux R, Price WA, Cifuentes LA (1990) Stable carbon isotope analysis of nucleic acids to trace sources of dissolved substrates used by estuarine bacteria. Appl Environ Microbiol 56:2012–2020
118. Paul JH, Jeffrey WH, DeFlaun M (1985) Particulate DNA in subtropical oceanic and estuarine planktonic environments. Mar Biol 90:95–101
119. Paul JH, Carlson DJ (1984) Genetic material in the marine environment: implication for bacterial DNA. Limnol Oceanogr 29:1091–1097
120. Fuhrman JA, Sleeter TD, Carlson CA, Proctor LM (1989) Dominance of bacterial biomass in the Sargasso Sea and its ecological implications. Mar Ecol Prog Ser 57:207–217
121. Boehme J, Frischer ME, Jiang SC, Kellogg CA, Pichard S, Rose JB et al (1993) Viruses, bacterioplankton, and phytoplankton in the southeastern Gulf of Mexico: distribution and contribution to oceanic DNA pools. Mar Ecol Prog Ser 97:1–10
122. Cho BC, Azam F (1990) Biogeochemical significance of bacterial biomass in the ocean's euphotic zone. Mar Ecol Prog Ser 63:253–259
123. Azam F, Fenchel T, Field JG, Gray JS, Meyer-Reil LA, Thlngstad F (1983) The ecological role of water-column nilcrobes In the sea. Mar Ecol Prog Ser 10:257–263
124. Garcia-Pichel F (1994) A model for internal self-shading in planktonic organisms and its implications for the usefulness of ultraviolet sunscreens. Limnol Oceanogr 39:1704–1717
125. Aas P, Lyons MM, Pledger R, Mitchell DL, Jeffrey WH (1996) Inhibition of bacterial activities by solar radiation in nearshore waters and the Gulf of Mexico. Aquat Microb Ecol 11:229–238
126. Sieracki ME, Sieburth JM (1986) Sunlight-induced growth delay of planktonic marine bacteria in filtered seawater. Mar Ecol Prog Ser 33:19–27
127. Bailey CA, Neihof RA, Tabor PS (1983) Inhibitory effect of solar radiation on amino acid uptake in Chesapeake Bay bacteria. Appl Environ Microbiol 46:44–49
128. Herndl GJ, Muller-Niklas G, Frick J (1993) Major role of ultraviolet-B in controlling bacterioplankton growth in the surface layer of the ocean. Nature 361:717–719
129. Alonso-Sáez L, Gasol JM (2007) Seasonal variations in the contributions of different bacterial groups to the uptake of low-molecular-weight compounds in Northwestern Mediterranean coastal waters. Appl Environ Microbiol 73:3528–3535
130. Häder DP, Kumar HD, Smith RC, Worrest RC (2007) Effects of solar UV radiation on aquatic ecosystems and interactions with climate change. Photochem Photobiol Sci 6:267–285
131. Joux F, Jeffrey WH, Lebaron P, Mitchell DL (1999) Marine bacterial isolates display diverse responses to UV-B radiation. Appl Environ Microbiol 65:3820–3827
132. Sommaruga R, Obernosterer I, Herndl GJ, Psenner R (1997) Inhibitory effect of solar radiation on thymidine and leucine incorporation by freshwater and marine bacterioplankton. Appl Environ Microbiol 63:4178–4184
133. Halac S, Felip M, Camarero L, Sommaruga-Wögrath S, Psenner R, Catalan J et al (1997) An in situ enclosure experiment to test the solar UVB impact on plankton in a high-altitude mountain lake. I. Lack of effect on phytoplankton species composition and growth. J Plankton Res 19:1671–1686
134. Winter C, Moeseneder MM, Herndl GJ (2001) Impact of UV radiation on bacterioplankton community composition. Appl Environ Microbiol 67:665–672
135. Jiang H, Dong H, Yu B, Liu X, Li Y, Ji S et al (2007) Microbial response to salinity change in Lake Chaka, a hypersaline lake on Tibetan plateau. Environ Microbiol 9:2603–2621
136. Liu Y, Yao T, Jiao N, Kang S, Zeng Y, Huang S (2006) Microbial community structure in moraine lakes and glacial meltwaters, Mount Everest. FEMS Microbiol Lett 265:98–105
137. Zhang G, Niu F, Ma X, Liu W, Dong M, Feng H et al (2007) Phylogenetic diversity of bacteria isolates from the Qinghai-Tibet Plateau permafrost region. Can J Microbiol 53:1000–1010
138. Zhang G, Ma X, Niu F, Dong M, Feng H, An L et al (2007) Diversity and distribution of alkaliphilic psychrotolerant bacteria in the Qinghai-Tibet Plateau permafrost region. Extremophiles 11:415–424
139. Dib J, Motok J, Zenoff VF, Ordonez O, Farias ME (2008) Occurrence of resistance to antibiotics, UV-B, and arsenic in bacteria isolated from extreme environments in high-altitude (above 4400 m) Andean wetlands. Curr Microbiol 56:510–517
140. Fernandez-Zenoff V, Sineriz F, Farias ME (2006) Diverse responses to UV-B radiation and repair mechanisms of bacteria isolated from high-altitude aquatic environments. Appl Environ Microbiol 72:7857–7863

141. Ordonez OF, Flores MR, Dib JR, Paz A, Farias ME (2009) Extremophile culture collection from Andean lakes: extreme pristine environments that host a wide diversity of microorganisms with tolerance to UV radiation. Microb Ecol 58:461–473
142. Kepner RL Jr, Wharton RA Jr, Suttle CA (1998) Viruses in Antarctic lakes. Limnol Oceanogr 43:1754–1761
143. Downes A, Blunt TP (1877) Researches on the effect of light upon bacteria and other organisms. Proc R Soc Med 26: 488–500
144. Hertel E (1904) Ueber Beeinflussung des Organismus durch Licht, speziell durch die chemisch wirksamen Strahlen. Z Allg Physiologie 4:1–43
145. Hertel E (1905) Ueber physiologische Wirkung von Strahlen verschiedener Wellenlänge. Z Allg Physiologie 5:95–122
146. Hockberger PE (2002) A history of ultraviolet photobiology for humans, animals and microorganisms. Photochem Photobiol 76:561–579
147. Cabaj A, Sommer R, Pribil W, Haider T (2002) The spectral UV sensitivity of microorganisms used in biodosimetry. Water Sci Technol Water Supply 2(3):175–181
148. Rauth AM (1965) The physical state of viral nucleic acid and the sensitivity of viruses to ultraviolet light. Biophys J 5:257–273
149. EPA (1999) Alternative disinfectants and oxidants guidance manual. EPA 815-R-99-014, United States Environmental Protection Agency, Cincinnati
150. Solsona F, Méndez JP (2003) Water disinfection. PAHO/CEPIS/PUB/03.89
151. WHO (2006) Guidelines for safe recreational water environments, vol 2, Swimming pools and similar environments. WHO, Geneva
152. WHO (2003) Guidelines for safe recreational water environments, vol 1, Coastal and fresh waters. WHO, Geneva
153. Henry V, Helbronner A, Recklinghausen M (1910) Nouvelles recherches sur la sterilization de grandes quantited d'eau par les rayons ultraviolets. Comp Rend Acad Sci 151:677–680
154. Wegelin M, Canonica S, Mechsner K, Fleischmann T, Pesaro F, Metzler A (1994) Solar water disinfection: scope of the process and analysis of radiation experiments. Aqua J Water Supply Res Technol 43:154–169
155. McGuigan KG, Joyce TM, Conroy RM, Gillespie JB, Elmore-Meegan M (1998) Solar disinfection of drinking water contained in transparent plastic bottles: characterizing the bacterial inactivation process. J Appl Microbiol 84:1138–1148
156. Navntoft C, Ubomba-Jaswa E, McGuigan KG, Fernández-Ibáñez P (2008) Effectiveness of solar disinfection using batch reactors with non-imaging aluminium reflectors under real conditions: natural well-water and solar light. J Photochem Photobiol B 93:155–161
157. Sommer B, Mariño A, Solarte Y, Salas ML, Dierolf C, Valiente C et al (1997) SODIS – An emerging water treatment process. J Water Supply Res Technol AQUA 46:127–137
158. Spiewak I, Benmair R, Messalem R, Radchenko O (1998) Water detoxification and disinfection using high solar concentration and homogeneous photocatalysts. J Chem Sci 110:229–238
159. Ubomba-Jaswa E, Fernández-Ibáñez P, Navntoft C, Polo-López MI, McGuigan KG (2010) Investigating the microbial inactivation efficiency of a 25 L batch solar disinfection (SODIS) reactor enhanced with a compound parabolic collector (CPC) for household use. J Chem Technol Biotechnol 85:1028–1037
160. Hijnen WAM, Beerendonk EF, Medema GJ (2006) Inactivation credit of UV radiation for viruses, bacteria and protozoan (oo) cysts in water: a review. Water Res 40:3–22
161. Nikaido SS, Johnson CH (2000) Daily and circadian variation in survival from ultraviolet radiation in Chlamydomonas reinhardtii. Photochem Photobiol 71:758–765
162. Nicholson WL, Munakata N, Horneck G, Melosh HJ, Setlow P (2000) Resistance of Bacillus endospores to extreme terrestrial and extraterrestrial environments. Microbiol Mol Biol Rev 64:548–572
163. Zepp RG, Erickson DJ III, Paul ND, Sulzberger B (2007) Interactive effects of solar UV radiation and climate change on biogeochemical cycling. Photochem Photobiol Sci 6:286–300
164. Zepp RG, Callaghan TV, Erickson DJ (1998) Effects of enhanced solar ultraviolet radiation on biogeochemical cycles. J Photochem Photobiol B 46:69–82
165. Zepp RG, Callaghan TV, Erickson DJ (1995) Effects of increased solar ultraviolet radiation on biogeochemical cycles. Ambio 24:181–187
166. Sagripanti JL, Lytle CD (2007) Inactivation of influenza virus by solar radiation. Photochem Photobiol 83:1278–1282
167. Kripke ML (1984) Immunologic unresponsiveness induced by UV radiation. Immunol Rev 80:87–102
168. Lipsitch M, Viboud C (2009) Influenza seasonality: lifting the fog. Proc Natl Acad Sci USA 106:3645–3646
169. Hollosy F (2002) Effects of ultraviolet radiation on plant cells. Micron 33:179–197
170. Prasad PVV, Kakani VG, Reddy KR (2003) Plants and the environment: ozone depletion. In: Encyclopedia of applied plant sciences. Elsevier Academic, Oxford, pp 749–756
171. Jagger J (1967) Introduction to research in photobiology. Prentice Hall, Englewood Cliffs
172. Kakani VG, Reddy KR, Zhao D, Sailaja K (2003) Field crop responses to ultraviolet-B radiation: a review. Agric For Meteorol 120:191–218
173. Roosien J, van Klaveren P, Van Vloten-Doting L (1983) Competition between the RNA 3 molecules of wildtype alfalfa mosaic virus and the temperature-sensitive mutant Tb ts 7(UV). Plant Mol Biol 2:113–118
174. Cuadra P, Herrera RI, Fajardo V (2004) Effects of UV-B radiation on the Patagonian Jaborosa magellanica Brisben. J Photochem Photobiol B 76:61–68
175. Mohr H, Schopfer P (1992) Pflanzenphysiologie, 4th edn. Springer, Berlin/Heidelberg
176. Mazza CA, Battista D, Zima AM, Szwarcberg BM, Giordano CV, Acevedo A et al (1999) The effects of solar ultraviolet-B radiation on the growth and yield of barley are accompanied by increased DNA damage and antioxidant responses. Plant Cell Environ 22:61–70

177. Correia CM, Coutinho JF, Bjorn LO, Torres PJMG (2000) Ultraviolet-B radiation and nitrogen effects on growth and yield of maize under Mediterranean field conditions. Eur J Agron 12:117–125
178. Pal M, Sengupta UK, Srivastava AC, Jain V, Meena RC (1999) Changes in growth and photosynthesis of mungbean induced by UV-B radiation. Indian J Plant Physiol 4:79–84
179. Mepsted R, Paul N, Stephen J, Nogues S, Corlett JE, Baker NR et al (1996) Effects of enhanced UV-B radiation on pea (Pisum sativum L.) grown under field conditions. Glob Change Biol 2:325–334
180. Tevini M, Mark U, Saile-Mark M (1991) Effects of enhanced solar UV-B radiation on growth and function of crop plant seedlings. Curr Top Plant Biochem Physiol 10:13–31
181. Gonzalez R, Mepsted R, Wellburn AR, Paul ND (1998) Non-photosynthetic mechanisms of growth reduction in pea (Pisum sativum L.) exposed to UV-B radiation. Plant Cell Environ 21:23–32
182. Kumagai T, Hidema J, Kang HS, Sato T (2001) Effects of supplemental UV-B radiation on the growth and yield of two cultivars of Japanese lowland rice (Oryza sativa L.) under the field in a cool rice-growing region of Japan. Agric Ecosyst Environ 83:201–208
183. Taylor RM, Tobin AK, Bray CM (1997) DNA damage and repair in plants. In: Lumsden PJ (ed) Plants and UVB responses to environmental changes. Cambridge University Press, Cambridge
184. Robberecht R, Caldwell MM (1978) Leaf transmittance of ultraviolet radiation and its implications for plant sensitivity to ultraviolet-radiation induced injury. Oceologia 32:277–287
185. Caldwell MM, Robberecht R, Flint SD (1983) Internal filters: prospects for UV-accumulation in higher plants. Physiol Plant 58:445–450
186. Tevini M, Iwanzik W, Teramura AH (1983) Effects of UV-B radiation on plants during mild water stress. II Effects on growth, protein, and flavonoid content. Z Pflanzenphysiol 110:459–467
187. Beggs CJ, Schneider-Ziebert U, Wellmann E (1986) UV-B radiation and Adaptive Mechanisms in Plants. In: Worrest RC, Caldwell MM (eds) Stratospheric ozone reduction, solar ultraviolet radiation and plant life. Springer, Berlin, pp 235–250
188. Bischof K, Wiencke C (2006) Auswirkung der Zunahme der UV-Strahlung. In: Lozan J, Graál H, Hubberten HW, Hupfer P, Piepenburg D (eds) Warnsignale aus den Polarregionen. Druckerei in St. Pauli, Hamburg, pp 259–263
189. Wiencke C, Roleda MY, Gruber A, Clayton MN, Bischof K (2006) Susceptibility of zoospores to UV radiation determines upper depth distribution limit of Arctic kelps: evidence through field experiments. J Ecol 94:455–463
190. Johansson G, Snoeijs P (2002) Macroalgal photosynthetic responses to light in relation to thallus morphology and depth zonation. Mar Ecol Prog Ser 244:63–72
191. Roleda MY, Wiencke C, Hanelt D, van de Poll WH, Gruber A (2005) Sensitivity of Laminariales zoospores from Helgoland (North Sea) to ultraviolet and photosynthetically active radiation: implications for depth distribution and seasonal reproduction. Plant Cell Environ 28:466–479
192. Lotze HK, Worm B, Molis M, Wahl M (2002) Effects of UV radiation and consumers on recruitment and succession of a marine macrobenthic community. Mar Ecol Prog Ser 243:57–66
193. Bischof K, Hanelt D, Aguilera J, Karsten U, Vögele B, Sawall T et al (2002) Seasonal variation in ecophysiological patterns in macroalgae from an artic fjord. I. Sensitivity of photosynthesis to ultraviolet radiation. Mar Biol 140:1097–1106
194. de Bakker NVJ, van Bodegom PM, van de Poll WH, Boelen E, Nat E, Rozema J et al (2005) Is UV-B radiation affecting charophycean algae in shallow freshwater systems? New Phytol 166:957–966
195. Martinez-Abaigar J, Nunez-Olivera E, Beaucourt N, Garcia-Alvaro MA, Tomas R, Arroniz M (2003) Different physiological responses of two aquatic bryophytes to enhanced ultraviolet-B radiation. J Bryol 25:17–30
196. Figueroa FL, Jimenez C, Vinegla B, Perez-Rodriguez E, Aguilera J, Flores-Moya A et al (2002) Effects of solar UV radiation on photosynthesis of the marine angiosperm Posidonia oceanica from southern Spain. Mar Ecol Prog Ser 230:59–70
197. Brandt LA, Koch EW (2003) Periphyton as a UV-B filter on seagrass leaves: a result of different transmittance in the UV-B and PAR ranges. Aquat Bot 76:317–327
198. Li FR, Peng SL, Chen BM, Hou YP (2010) A meta-analysis of the responses of woody and herbaceaous plants to elevated ultraviolet-B radiation. Acta Oecologica 36:1–9
199. Rozema J, Van de Staaij JWM, Tosserams M (1997) Effects of UV-B radiation on plants from agro- and natural ecosystems. In: Lumsden PJ (ed) Plants and UV-B responses to environmental change. Cambridge University Press, Cambridge
200. Caldwell MM, Flint SD (1994) Solar ultraviolet radiation and ozone layer change: implications for crop plants. In: ASo A (ed) Physiology and determination of crop yield. American Society of Agronomy, Madison
201. Sullivan JH, Teramura AH (1992) The effects of UV-B radiation on loblolly pine. 2. Growth of field-grown seedlings. Tree Struct Funct 6:115–120
202. Naidu SL, Sullivan JH, Teramura AH, DeLucia EH (1993) The effects of ultraviolet-B radiation on photosynthesis of different aged needles in field-grown loblolly-pine. Tree Physiol 12:151–162
203. Bassman JH, Edwards GE, Robberecht R (2002) Long-term exposure to enhanced UV-B radiation is not detrimental to growth and photosynthesis in Douglas-fir. New Phytol 154:107–120
204. Trost-Sedej T, Gaberscik A (2008) The effects of enhanced UV-B radiation on physiological activity and growth of Norway spruce planted outdoors over 5 years. Trees 22:423–435
205. McLeod AR, Newsham KK (1997) Impacts of elevated UV-B on forest ecosystems. In: Lumsden PJ (ed) Plants and UV-B responses to environmental change, 64th edn. Cambridge University Press, Cambridge

206. Karabourniotis G, Papadopoulos K, Papamarkou M, Manetas Y (1992) Ultraviolet-B radiation absorbing capacity of leaf hairs. Physiol Plant 86:414–418
207. Karabourniotis G, Kyparissis A, Manetas Y (1993) Leaf hairs of Olea europaea protect underlying tissues agains ultraviolet-B radiation damage. Environ Exp Bot 33:341–345
208. Grammatikopoulos G, Karabourniotis G, Kyparissis A, Petropoulou Y, Manetas Y (1994) Leaf hairs of olive (Olea europaea) prevent stomatal closure by ultraviolet-B radiation. Aust J Plant Physiol 21:293–301
209. Day TA, Howells BW, Rice WJ (1994) Ultraviolet absorption and epidermal-transmittance spectra in foliage. Physiol Plant 92:207–218
210. Nedunchezhian N, Kulandaivelu GL (1991) Effects of UV-B enhanced radiation on ribulose 1, 5-bisphophate carboxylase in leaves of Vigna sinensis. Photosynthetica 25:431–435
211. Premkumar A, Kulandaivelu G (1996) Influence of ultraviolet-B enhanced solar radiation on growth and photosynthesis of potassium deficient cowpea seedlings. Photosynthetica 32:521–528
212. Basiouny FM (1986) Sensitivity of corn, oats, peanuts, rice, rye, sorghum, soybean and tobacco to UV-B radiation under growth chamber conditions. J Agron Crop Sci 157:31–35
213. Pal M, Jain V, Sengupta UK (1998) Influence of enhanced UV-B radiation on mustard: cultivar response. Indian J Plant Physiol 3:188–193
214. Singh A (1995) Influence of enhanced UV-B radiation on tropical legumes. Trop Ecol 36:249–252
215. Li Y, Yue M, Wang XL (1998) Effects of enhanced ultraviolet-B radiation on crop structure, growth and yield components of spring wheat under field conditions. Field Crops Res 57:253–263
216. Teramura AH, Murali NS (1986) Intraspecific differences in growth and yield of soybean exposed to ultraviolet-B radiation under greenhouse and field conditions. Environ Exp Bot 26:89–95
217. Al-Oudat M, Baydoun SA, Mohammad A (1989) Effects of enhanced UV-B on growth and yield of two Syrian crops wheat (Triticum durum var. Horani) and broad beans (Vicia faba) under field conditions. Environ Exp Bot 40(1):11–16
218. Finnie JW, Bostock DE (1979) Skin neoplasia in dogs. Aust Vet J 55:602–604
219. Fairham J, Harcourt-Brown FM (1999) Preliminary investigation of the vitamin D status of pet rabbits. Vet Rec 145: 452–454
220. Hazewinkel HAW, Tryfonidou MA (2002) Vitamin D_3 metabolism in dogs. Mol Cell Endocrinol 197:23–33
221. Morris JG (1999) Ineffective vitamin D synthesis in cats is reversed by an inhibitor of 7-dehydrocholestrol-Δ^7-reductase. J Nutr 129:903–908
222. How KL, Hazewinkel HAW, Mol JA (1994) Dietary vitamin D dependence of cat and dog due to inadequate cutaneous synthesis of vitamin D. Gen Comp Endocrinol 96:12–18
223. How KL, Hazewinkel HA, Mol JA (1995) Photosynthesis of vitamin D in the skin of dogs cats and rats. Vet Q 17(Suppl 1):S29
224. Brommage R, Miller SC, Langman CB, Bouillon R, Smith R, Bourdeau JE (1988) The effects of chronic vitamin D deficiency on the skeleton in the adult rabbit. Bone 9:131–139
225. Mellanby RJ, Mee AP, Berry JL, Herrtage ME (2005) Hypercalcaemia in two dogs caused by excessive dietary supplementation of vitamin D. J Small Anim Pract 46: 334–338
226. Schulze C, Rothuizen J, Van Sluijs FJ, Hazewinkel HAW, Van Den Ingh TSGAM (2000) Extrahepatic biliary atresia in a border collie. J Small Anim Pract 41:27–30
227. Ladds PW, Kraft H, Sokale A, Trueman KF (1983) Neoplasms of the skin of dogs in tropical Queensland. Aust Vet J 60:87–88
228. Teifke JP, Lohr CV (1996) Immunohistochemical detection of P53 overexpression in paraffin wax-embedded squamous cell carcinomas of cattle, horses, cats and dogs. J Comp Pathol 114:205–210
229. UNEP (1991) Environmental effects of ozone depletion: 1991 update. United Nations Environment Programme (UNEP), Nairobi
230. Gross TL, Ihrke PJ, Walder EJ, Affolter VK (2005) Skin diseases of the dog and cat: clinical and histopathologic diagnosis. Blackwell, Oxford
231. Moss LC, Severin GA (1963) Tattooing as therapy for chronic solar dermatitis (Collie nose) in the dog. J Am Vet Med Assoc 142:609–610
232. Nikula KJ, Benjamin SA, Angleton GM, Saunders WJ, Lee AC (1992) Ultraviolet radiation, solar dermatosis, and cutaneous neoplasia in beagle dogs. Radiat Res 129:11–18
233. Nielsen SW, Cole CR (1960) Cutaneous epithelial neoplasms of the dog-a report of 153 cases. Am J Vet Res 21:931
234. Nesbitt GH (1983) Canine and feline dermatology: a systematic approach. Lea & Febiger, Philadelphia
235. Hargis AM, Thomassen RW, Phemister RD (1977) Chronic dermatosis and cutaneous squamous cell carcinoma in the beagle dog. Vet Pathol 14:218–228
236. Jörger K (1988) Skin tumors in cats. Occurrence and frequency in the research material (biopsies from 1984 to 1987) of the Institute for Veterinary Pathology, Zurich. Schweiz Arch Tierheilk 130:559–569
237. Dorn CR, Taylor DO, Schneider R (1971) Sunlight exposure and risk of developing cutaneous and oral squamous cell carcinomas in white cats. J Natl Cancer Inst 46:1073–1078
238. Almeida EMP, Caraca RA, Adam RL, Souza EM, Metze K, Cintra ML (2008) Photodamage in feline skin: clinical and histomorphometric analysis. Vet Pathol 45:327–335
239. Slatter DH, Edwards ME, Hawkins CD, Wilcox GE (1982) A national survey of the occurrence of infectious bovine keratoconjunctivitis. Aust Vet J 59:65–68
240. Méndez A, Pérez J, Ruiz-Villamor E, García R, Martín MP, Mozos E (1997) Clinicopathological study of an outbreak of squamous cell carcinoma in sheep. Vet Rec 141:597–600

241. Payne RJ, Lean MS, Greet TRC (2009) Third eyelid resection as a treatment for suspected squamous cell carcinoma in 24 horses. Vet Rec 165:740–743
242. Heeney JL, Valli VEO (1985) Bovine ocular squamous cell carcinoma: an epidemiological perspective. Can J Comp Med 49:21–26
243. Sloss V, Smith TJ, De Yi G (1986) Controlling ocular squamous cell carcinoma in Hereford cattle. Aust Vet J 63:248–251
244. Russell WC, Brinks JS, Kainer RA (1976) Incidence and heritability of ocular squamous cell tumors in Hereford cattle. J Anim Sci 43:1156–1162
245. Anderson DE, Badzioch M (1991) Association between solar radiation and ocular squamous cell carcinoma in cattle. Am J Vet Res 52:784–788
246. Gharagozlou MJ, Hekmati P, Ashrafihelan J (2007) A clinical and histopathological study of ocular neoplasms in dairy cattle. Veterinarski Arh 77:409–426
247. Morris CA (2007) A review of genetic resistance to disease in Bos Taurus cattle. Vet J 174:481–491
248. Anderson DE, Skinner PE (1961) Studies on bovine ocular squamous carcinoma ("Cancer Eye") XI. Effects of sunlight. J Anim Sci 20:474–477
249. Radostits OM, Arundel JH, Gay CC, Blood DC, Hinchcliff KW (2000) Veterinary medicine: a textbook of the diseases of cattle, sheep, pigs, goats and horses. W.B. Saunders, London
250. Woodward RR, Knapp B Jr (1950) The hereditary aspect of eye cancer in hereford cattle. J Anim Sci 9:578–581
251. Blackwell RL, Anderson DE, Knox JH (1956) Age incidence and heritability of cancer eye in hereford cattle. J Anim Sci 15:943–951
252. SGdS W (1974) Das Vulvacarcinom beim Rind auf Ceylon. Zbl Vet Med A21:834–843
253. Hühnermund G (1973) Disposition der Ayreshirerasse zu karzinomatösen Veränderungen an Vulva und Membrana nicitans bei extremen Sonneneinwirkungen in den Tropen. Berl Münchn Tierärztl Wsch 21:414–415
254. Yeruham I, Perl S, Orgad U, Yakobson B (1999) Tumours of the vulva and vagina in cattle – a 10-year survey. Vet J 158: 237–239
255. Wettimuny SG (1974) Bovine vulval carcinoma in Ceylon. Zentralbl Veterinärmed A 21:834
256. Kopecky KE, Pugh GW Jr, Hughes DE (1980) Wavelength of ultraviolet radiation that enhances onset of clinical infectious bovine keratoconjunctivitis. Am J Vet Res 41:1412–1415
257. Forrest JW, Fleet MR (1985) Lack of tanning in white Merino sheep following exposure to ultraviolet light. Aust Vet J 62:244–246
258. Turner AS, Mansmann RA, McAllister ES, Pratt PW (1982) Equine medicine and surgery, 3rd edn. American Veterinary, Santa Barbara
259. Dugan SJ, Curtis CR, Roberts SM, Severin GA (1991) Epidemiologic study of ocular/adnexal squamous cell carcinoma in horses. J Am Vet Med Assoc 198:251–256
260. Eberlein B, Bergner T, Przybilla B (1992) Demonstration of olaquindox phototoxicity in vitro. Photodermatol Photoimmunol Photomed 9:63–66
261. Bovenschen HJ, Peters B, Koetsier MI, Van Der Valk PG (2009) Occupational contact dermatitis due to multiple sensitizations in a pig farmer. Contact Dermat 61:127–128
262. Schauder S, Schröder W, Geier J (1996) Olaquindox-induced airborne photoallergic contact dermatitis followed by transient or persistent light reactions in 15 pig breeders. Contact Dermat 35:344–354
263. Belhadjali H, Marguery MC, Journé F, Giordano-Labadie F, Lefebvre H, Bazex J (2002) Allergic and photoallergic contact dermatitis to Olaquindox in a pig breeder with prolonged photosensitivity. Photodermatol Photoimmunol Photomed 18:52–53
264. Bartussek H (1988) Haltung. In: Haiger A, Storhas R, Bartussek H (eds) Artgemäße Nutztierhaltung. Ulmer, Stuttgart
265. Sozonov JI, Inesin VA (1975) Ergebnisse der UV-Bestrahlung von Kälbern. Landwirtschaftliches Zentralbl 4:460
266. Hidiroglou M, Proulx JG, Roubos D (1979) 25-hydroxyvitamin D in plasma of cattle. J Dairy Sci 62:1076–1080
267. Horst RL, Littledike ET, Riley JL, Napoli JL (1981) Quantitation of vitamin D and its metabolites and their plasma concentrations in five species of animals. Anal Biochem 116:189–203
268. Hidiroglou M, Williams CJ, Proulx JG (1985) Plasma vitamin D3 response in cattle and sheep exposed to ultraviolet radiation. Int J Vitam Nutr Res 55:41–46
269. Flachowsky E, Graf H, Matthey M, Ochrimenko WI, Beyersdorfer S, Dorn W et al (1993) Einfluß von Jahreszeit, Haltungsform und einer Vit.D3 Zulage auf den Vit.A, D und E Gehalt von Kuhmilch sowie die 25-OH Vit-D3-Konzentration im Blutplasma von Milchkühen. Mh Vetmed 48:197–202
270. Richter GH, Flachowsky G, Matthey M, Ochrimenko K, Wolfram D, Schade T (1990) Einfluß der Stall- bzw. Auslaufhaltung auf die 25-OH-Vitamin-D3-Blutplasmakonzentration bei Mastbullen. Mh Vet Med 45:227
271. Hidiroglou M (1987) Kinetics of intravenously administered 25-hydroxyvitamin D3 in sheep and the effect of exposure to ultraviolet radiation. J Anim Sci 65:808–814
272. Hidiroglou M, Karpinski K (1989) Providing vitamin D to confined sheep by oral supplementation vs ultraviolet irradiation. J Anim Sci 67:794–802
273. Smith BS, Wright H (1984) Relative contributions of diet and sunshine to the overall vitamin D status of the grazing ewe. Vet Rec 115:537–538
274. Zintzen H, Boyazoglu PA (1973) Vitamin D and its relation to calcium phosphorus metabolism in ruminants. J S Afr Vet Med Assoc 44:25–36
275. El Shorafa WM, Feaster JP, Ott EA, Asquith RL (1979) Effect of vitamin D and sunlight on growth and bone development of young ponies. J Anim Sci 48:882–886
276. Piccione G, Assenza A, Fazio F, Bergero D, Caola G (2008) Daily rhythms of serum vitamin D-metabolites, calcium and phosphorus in horses. Acta Vet Brno 77:151–157

277. Piccione G, Assenza A, Grasso F, Caola G (2004) Daily rhythm of circulating fat soluble vitamin concentration (A, D, E and K) in the horse. J Circadian Rhythms 2(1):3
278. Hart EB, Steenbock H, Lepkovsky S, Halpin JG (1923) The nutritional requirements of baby chicks: III. The relation of light to the growth of the chicken. J Biol Chem 58:33–42
279. Bethke RM, Kennard DC, Kik MC (1925) Nutritional studies of the growing chick: I. The relation of sunlight and green clover to leg weakness in chicks. J Biol Chem 63:377–390
280. Mussehl FE, Bancroft PM (1925) Nutrient requirements of growing chicks. Poult Sci 4:118–122
281. Heuser GF, Norris LC (1929) Rickets in chicks: III. The effectiveness of mid-summer sunshine and irradiation from quartz mercury vapour arc in preventing rickets. Poult Sci 8:89–98
282. Scott ML, Nesheim MC, Young RJ (1982) Nutrition of the chicken. M. L. Scott and Associates, Ithaca
283. Bernard JB, Watkins BE, Ullrey DE (1989) Manifestations of vitamin D deficiency in chicks reared under different artificial lighting regimes. Zoo Biol 8:313–395
284. Ferguson GW, Jones JR, Gehrmann WH, Hammack SH, Talent LG, Hudson RD et al (1996) Indoor husbandry of the panther chameleon Chamaeleo [Furcifer] pardalis: effects of dietary vitamins A and D and ultraviolet irradiation on pathology and life-history traits. Zoo Biol 15:279–299
285. Ferguson GW, Gehrmann WH, Chen TC, Dierenfeld ES, Holick MF (2002) Effects of artificial ultraviolet light exposure on reproductive success of the female panther chameleon (Furcifer pardalis) in captivity. Zoo Biol 21:525–537
286. Narbaitz R, Tsang CPW (1989) Vitamin D deficiency in the chick embryo: effects on prehatching motility and on the growth and differentiation of bones, muscles, and parathyroid glands. Calcif Tissue Int 44:348–355
287. Packard MJ, Clark NB (1996) Aspects of calcium regulation in embryonic lepidosaurians and chelonians and a review of calcium regulation in embryonic archosaurians. Physiol Zool 69:435–466
288. Häder DP, Sinha RP (2005) Solar ultraviolet radiation-induced DNA damage in aquatic organisms: Potential environmental impact. Mutat Res Fundam Mol Mech Mutagen 571:221–233
289. Madronich S, Flocke S (1995) Theoretical estimation of biologically effective UV radiation at the Earth's surface. In: Zerefos CS, Bais AF (eds) Solar ultraviolet radiation: modelling, measurements, and effects, pp 23–48
290. Rozema J, Björn LO, Bornman JF, Gaberscik A, Häder DP, Trost T et al (2002) The role of UV-B radiation in aquatic and terrestrial ecosystems-An experimental and functional analysis of the evolution of UV-absorbing compounds. J Photochem Photobiol B 66:2–12
291. Huot Y, Jeffrey WH, Davis RF, Cullen JJ (2000) Damage to DNA in bacterioplankton: a model of damage by ultraviolet radiation and its repair as influenced by vertical mixing. Photochem Photobiol 72:62–74
292. Zepp RG (2003) UV exposure of coral assemblages in the Florida Keys. Environmental Protection Agency Report No. 600/R-03/095. U.S. Environmental Protection Agency, Washington, DC
293. Kouwenberg JHM, Lantoine F (2007) Effects of ultraviolet-B stressed diatom food on the reproductive output in Mediterranean Calanus helgolandicus (Crustacea; Copepoda). J Exp Mar Biol Ecol 341:239–253
294. Kouwenberg JHM, Browman HI, Runge JA, Cullen JJ, Davis RF, St-Pierre JF (1999) Biological weighting of ultraviolet (280–400 nm) induced mortality in marine zooplankton and fish. II. Calanus finmarchicus (Copepoda) eggs. Mar Biol 134:285–293
295. Hunter JR, Taylor JH, Moser HG (1979) Effect of ultraviolet irradiation on eggs and larvae on the northern anchovy, Engraulis mordax, and the Pacific mackerel, Scomber japonicus, during the embryonic stage. Photochem Photobiol 29:325–338
296. Bell G, Hoar W (1950) Some effects of ultraviolet radiation on sockeye salmon eggs and alevins. Can J Res 28:35–43
297. Zagarese HE, Williamson CE (2001) The implications of solar UV radiation exposure for fish and fisheries. Fish Fish 2: 250–260
298. Kouwenberg JHM, Browman HI, St-Pierre JF, Runge JA, Cullen JJ, Davis RF (1999) Biological weighting of ultraviolet (280–400 nm) induced mortality in marine zooplankton and fish. I. Atlantic cod (Gadus morhua) eggs. Mar Biol 134:269–284
299. Brocklebank JR, Armstrong RD (1994) Solar dermatitis in hatchery-reared salmonids in British Columbia. Can Vet J 35:651–652
300. Lowe C, Goodman-Lowe G (1996) Suntanning in hammerhead sharks. Nature 383:677
301. Dunbar C (1959) Sunburn in fingerling rainbow trout. Prog Fish Cult 21:74
302. Bullock AM, Coutts RR (1985) The impact of solar ultraviolet radiation upon the skin of rainbow trout, Salmo gairdneri Richardson, farmed at high altitude in Bolivia. J Fish Dis 8:263–272
303. McArdle J, Bullock AM (1987) Solar ultraviolet radiation as a causal factor of "summer syndrome" in cage-reared Atlantic salmon, *Salmo solar* L.: a clinical and histopathological study. J Fish Dis 10:255–264
304. Kaweewat K, Hofer R (1997) Effect of UV-B radiation on goblet cells in the skin of different fish species. J Photochem Photobiol B 41:222–226
305. Rodger HD (1991) Summer lesion syndrome in salmon: a retrospective study. Vet Rec 129:237–239
306. Bullock AM, Roberts RJ, Waddington P, Bookless WD (1983) Sunburn lesions in koi carp. Vet Rec 112:551
307. Markkula SE, Karvonen A, Salo H, Valtonen ET, Jokinen EI (2007) Ultraviolet B irradiation affects resistance of rainbow trout (Oncorhynchus mykiss) against bacterium Yersinia ruckeri and trematode Diplostomum spathaceum. Photochem Photobiol 83:1263–1269
308. Roberts R (2001) Fish pathology. Churchill Livingstone, Edinburgh

309. Allison L (1960) "Sunburning" fingerling lake trout with ultraviolet light and the effect off a niacin-fortified diet. Prog Fish Cult 22:114–116
310. Wall AE (1998) Cataracts in farmed Atlantic salmon (Salmo salar) in Ireland, Norway and Scotland from 1995 to 1997. Vet Rec 142:626–630
311. Karentz D, McEuen FS, Land MC, Dunlap WC (1991) Survey of mycosporine-like amino acid compounds in Antarctic marine organisms: Potential protection from ultraviolet exposure. Mar Biol 108:157–166
312. Uitz J, Claustre H, Morel A, Hooker SB (2006) Vertical distribution of phytoplankton communities in open ocean: an assessment based on surface chlorophyll. J Geophys Res 111: C08005
313. Kessler K, Lockwood RS, Williamson CE, Saros JE (2008) Vertical distribution of zooplankton in subalpine and alpine lakes: Ultraviolet radiation, fish predation, and the transparency-gradient hypothesis. Limnol Oceanogr 53:2374–2382
314. Yamashita Y, Tanoue E (2009) Basin scale distribution of chromophoric dissolved organic matter in the Pacific Ocean. Limnol Oceanogr 54:598–609
315. Loiselle SA, Bracchini L, Dattilo AM, Ricci M, Tognazzi A, Cózar A et al (2009) Optical characterization of chromophoric dissolved organic matter using wavelength distribution of absorption spectral slopes. Limnol Oceanogr 54:590–597
316. Browman HI, Vetter RD, Rodriguez CA, Cullen JJ, Davis RF, Lynn E et al (2003) Ultraviolet (280–400 nm)-induced DNA damage in the eggs and larvae of Calanus finmarchicus G. (Copepoda) and Atlantic cod (Gadus morhua). Photochem Photobiol 77:397–404
317. Bullock AM (1982) The pathological effects of ultraviolet radiation on the epidermis of teleost fish with reference to the solar radiation effect in higher animals. Proc R Soc Edinb 81B:199–210
318. Bullock AM, Roberts RJ (1979) Skin photosensitisation by phenothiazine in cultured rainbow trout (Salmo gairdneri Richardson). Vet Rec 104:55
319. Bullock AM, Roberts RJ (1981) Sunburn lesions in salmonid fry: a clinical and histological report. J Fish Dis 4:271–275
320. Bullock AM (1985) The effect of ultraviolet-B radiation upon the skin of the plaice, Pleuronectes platessa L., infected with the bodonid ectoparasite Ichthyobodo necator (Henneguy, 1883). J Fish Dis 8:547–550
321. Jokinen IE, Markkula ES, Salo HM, Kuhn P, Nikoskelainen S, Arts MT et al (2008) Exposure to increased ambient ultraviolet B radiation has negative effects on growth, condition and immune function of juvenile Atlantic salmon (Salmo salar). Photochem Photobiol 84:1265–1271
322. Markkula SE, Salo HM, Immonen AK, Jokinen EI (2005) Effects of short- and long-term ultraviolet B irradiation on the immune system of the common carp (Cyprinus carpio). Photochem Photobiol 81:595–602
323. Armstrong TN, Reimschuessel R, Bradley BP (2002) DNA damage, histologial changes and DNA repair in larval Japanese medaka (Oryzias latipes) exposed to ultraviolet-B radiation. Aquat Toxicol 58:1–14
324. Alemanni ME, Lozada M, Zagarese HE (2003) Assessing sublethal effects of ultraviolet radiation in juvenile rainbow trout (Oncorhynchus mykiss). Photochem Photobiol Sci 2:867–870
325. Bullock AM (1982) The pathological effects of ultraviolet radiation on the epidermis of teleost fish with reference to the solar radiation effect in higher animals. Proc R Soc Edinb B Biol Sci 81:199–210
326. Nowak BF (1999) Significance of environmental factors in aetiology of skin diseases of teleost fish. Bull Eur Assoc Fish Pathol 19:290–292
327. Handlinger J, Soltani M, Percival S (1997) The pathology of Flexibacter maritimus in aquaculture species in Tasmania, Australia. J Fish Dis 20:159–168
328. Cullen AP, Monteith-McMaster CA, Sivak JG (1994) Lenticular changes in rainbow trout following chronic exposure to UV radiation. Curr Eye Res 13:731–737
329. Nelson PA, Kajiura SM, Losey GS (2003) Exposure to solar radiation may increase ocular UV-filtering in the juvenile scalloped hammerhead shark, Sphyrna lewini. Mar Biol 142:53–56
330. Zeng Z, Richardson J, Verduzco D, Mitchell DL, Patton EE (2009) Zebrafish have a competent p53-dependent nucleotide excision repair pathway to resolve ultraviolet B-induced DNA damage in the skin. Zebrafish 6:405–415
331. Banaszak AT (2003) Photoprotective physiological and biochemical responses of aquatic organisms. In: Helbling EW, Zagarese HE, Zagarese H (eds) UV effects in aquatic organisms and ecosystems. Royal Society of Chemistry, Cambridge, UK, pp 329–356
332. Eckes MJ, Siebeck UE, Dove S, Grutter AS (2008) Ultraviolet sunscreens in reef fish mucus. Mar Ecol Prog Ser 353:203–211
333. Zamzow JP (2007) Ultraviolet-absorbing compounds in the mucus of shallow-dwelling tropical reef fishes correlate with environmental water clarity. Mar Ecol Prog Ser 343:263–271
334. Zamzow JP (2004) Effects of diet, ultraviolet exposure, and gender on the ultraviolet absorbance of fish mucus and ocular structures. Mar Biol 144:1057–1064
335. Rick IP, Bakker TCM (2008) Color signaling in conspicuous red sticklebacks: do ultraviolet signals surpass others? BMC Evol Biol 8:189
336. Gacic Z, Damjanovic I, Mickovic B, Hegedis A, Nikcevic M (2007) Spectral sensitivity of the dogfish shark (Scyliorhinus canicula). Fish Physiol Biochem 33:21–27
337. Matsumoto T, Ihara H, Ishida Y, Yamamoto S, Murata O, Ishibashi Y (2010) Spectral sensitivity of juvenile chub mackerel (Scomber japonicus) in visible and ultraviolet light. Fish Physiol Biochem 36(1):63–70
338. Leech DM, Johnsen S (2003) Behavioral response – UVR avoidance and vison. In: Helbling EW, Zagarese HE, Zagarese H (eds) UV effects in aquatic organisms and ecosystems. Royal Society of Chemistry, London, pp 329–356

339. Leech DM, Johnsen S (2009) Light, biological receptors. In: Likens GE (ed) Encyclopedia of inland waters. Elsevier, Oxford, pp 671–681
340. Holtby LB, Bothwell ML (2008) Effects of solar ultraviolet radiation on the behaviour of juvenile coho salmon (Oncorhynchus kisutch): avoidance, feeding, and agonistic interactions. Can J Fish Aquat Sci 65:701–711
341. Rao DS, Raghuramulu N (1996) Food chain as origin of vitamin D in fish. Comp Biochem Physiol A Physiol 114:15–19
342. Copping AM (1934) Origin of vitamin D in cod-liver oil: vitamin D content of zooplankton. Biochem J 28:1516–1520
343. Rao DS, Raghuramulu N (1997) Vitamin D_3 in Tilapia mossambica: relevance of photochemical synthesis. J Nutr Sci Vitaminol 43:425–433
344. Lock EJ, Waagbo R, Wendelaar Bonga S, Flik G (2010) The significance of vitamin D for fish: a review. Aquac Nutr 16:100–116
345. Ferguson GW, Brinker AM, Gehrmann WH, Bucklin SE, Baines FM, Mackin SJ (2010) Voluntary exposure of some western-hemisphere snake and lizard species to ultraviolet-B radiation in the field: how much ultraviolet-B should a lizard or snake receive in captivity? Zoo Biol 29(3):317–334
346. Gölthenboth R (1982) Höhensonne für Zootiere im Zoo Berlin. Berliner Münchner Tierärztliche Wochenschrift 95(11):220
347. Morrisey JK, Reichard T, Lloyd M, Bernard J (1995) Vitamin-D-deficiency rickets in three colobus monkeys (Colobus guereza kikuyuensis) at the Toledo Zoo. J Zoo Wildl Med 26(4):564–568
348. Hofmann-Parisot M (1995) Result of a European-wide inquiry about the use of artificial UV radiation sources in zoo animal husbandry with special regard to the mammals (Primates/Simiae/monkeys). Berl Münch Tierärztl Wschr 108:185–191
349. Tonge S (1985) The management of juvenile telfair's skinks leiolopisma telefairii with particular reference to the role of ultra violet light. In: Reptiles: breeding, behaviour and veterinary aspects. British Herpetological Society, London, pp 61–72
350. Bosch H, Frank W (1983) Häufige Erkrankungen bei im Terrarium gehaltenen Amphibien und Reptilien. Salamandra 19:29–54
351. McCrystal HG, Behler JL (1982) Husbandry and reproduction of captive Giant ameiva lizards. Int Zoo Yearb 22:159–163
352. Townsend CR, Cole CJ (1985) Additional notes on requirements of Captive whiptail lizards (cnemidophorus) with emphasis on ultraviolet radiation. Zoo Biol 4:49–55
353. Acierno MJ, Mitchell MA, Roundtree MK, Zachariah TT (2006) Effects of ultraviolet radiation on 25-hydroxyvitamin D_3 synthesis in red-eared slider turtles (Trachemys scripta elegans). Am J Vet Res 67:2046–2049
354. Acierno MJ, Mitchell MA, Zachariah TT, Roundtree MK, Kirchgessner MS, Guzman DSM (2008) Effects of ultraviolet radiation on plasma 25-hydroxyvitamin D_3 concentrations in corn snakes (Elaphe guttata). Am J Vet Res 69:294–297
355. Gehrmann WH (1987) Ultraviolet irradiances of various lamps used in animal husbandry. Zoo Biol 6:117–127
356. Burger RM, Gehrmann WH, Ferguson GW (2007) Evaluation of UVB reduction by materials commonly used in reptile husbandry. Zoo Biol 26:417–423
357. Gardiner DW, Baines FM, Pandher K (2009) Photodermatitis and photokeratoconjunctivitis in a ball python (Python regius) and a blue-tongue skink (Tiliqua spp.). J Zoo Wildl Med 40:757–766
358. Farman JC, Gardiner BG, Shanklin JD (1985) Large losses of total ozone in Antarctica reveal seasonal ClO_x/NO_x interaction. Nature 315:207–210
359. Blumthaler M, Ambach W (1990) Indication of increasing solar ultraviolet-B radiation flux in alpine regions. Science 248:206–208
360. Rünger TM (2007) How different wavelengths of the ultraviolet spectrum contribute to skin carcinogenesis: The role of cellular damage responses. J Investig Dermatol 127: 2103–2105

Books and Reviews

Björn LO (2008) Photobiology. The science of life and light. Springer, New York

Cockell C, Blaustein AR (2001) Ecosystems, evolution, and ultraviolet radiation. Springer, New York

Gao W, Schmoldt DL, Slusser JR (2010) UV radiation in global climate change. Measurements, modeling and effects on ecosystems. Springer, Heidelberg

Ghetti F, Checcucci G, Bornman JF (2006) Environmental UV radiation: impact on ecosystems and human health, NATO science series, IV earth and environment sciences. Springer, Dordrecht

Helbling EW, Zagarese HE, Zagarese H (2003) UV effects in aquatic organisms and ecosystems, Comprehensive series in photochemical and photobiological sciences. Royal Society of Chemistry, Cambridge

Lumsden PJ (1997) Plants and UV-B: responses to environmental change, Society for experimental biology seminar series. Cambridge Univeristy Press, Cambridge

Mora SJD, Demers S, Vernet M (2000) The effects of UV radiation in the marine environment, Cambridge environment chemistry series. Camridge University Press, Cambridge

Reichrath J (2008) Sunlight, vitamin D and skin cancer, Advances in experimental medicine and biology. Springer, New York

V

Vehicle Biofuels

Mark Holtzapple
Department of Chemical Engineering, Texas A&M University, College Station, TX, USA

Article Outline

Glossary
Definition of the Subject
Introduction
Vehicle Fuels
Biomass
Biomass Processing
Conversion Processes
Future Directions
Bibliography

Glossary

Biodiesel Methyl or ethyl ester of fatty acids.

Biomass Biological material from living or recently living organisms.

Bio-oil The liquid resulting from biomass pyrolysis.

Equivalence ratio The actual oxygen fed to the reactor divided by the stoichiometric oxygen needed for complete combustion.

Gasohol A mixture of gasoline and ethanol, typically 90% gasoline and 10% ethanol.

Lignocellulose Biomass composed of lignin, cellulose, and hemicellulose.

Oleaginous microorganisms Microorganisms that accumulate triacylglycerol (TAG) within their cells.

Saccharification Hydrolysis of polysaccharides to produce sugar.

Synthesis gas Mixture of carbon monoxide and hydrogen.

Triacylglycerol (TAG) A natural product containing three fatty acids linked to glycerol via ester bonds.

Definition of the Subject

Vehicle biofuels are solid, liquid, and gaseous fuels derived from biomass (e.g., corn, sugarcane, grasses, and wood) used for transportation (e.g., automobiles, trucks, planes, and trains). Among biofuels, liquids are the most valuable because they are easily stored, have a high energy density, and are readily metered into engines. Biofuels are infinitely renewable provided appropriate agricultural practices are followed.

Introduction

Historically, biological feedstocks have been used to power transportation. For example, early steam-powered trains were fueled by wood, Rudolph Diesel designed his engine to run on peanut oil, and Henry Ford designed the Model T to run on ethanol.

From 1880 to 1973, the price of crude oil was $15–30/bbl (current dollars), so it was very difficult for biofuels to compete. As a consequence, during this time period, very few vehicles were powered by biofuels. However, during crisis situations, biofuels were employed. For example, during World War II, Europeans had difficulty obtaining gasoline, so millions of vehicles were adapted to run on gasified wood. The Arab Oil Embargo (1973) and Iranian Hostage Crisis (1979) caused the price of crude oil to rise to about $90/bbl (current dollars), which precipitated interest in biofuels. In 1978, the US Energy Tax Act provided tax credits for ethanol ($0.54/gal ethanol), which promoted the conversion of corn into biofuel. This act was designed to reduce dependence on foreign oil (36% imports in 1978) and to create a new market for corn, which had depressed prices at the time. In 2005, the US government provided a tax subsidy for biodiesel ($1.00/gal). In 2008, the Farm Bill included a subsidy for cellulosic ethanol ($1.01/gal).

Through these subsidies, the US government is promoting the use of biofuels for the following reasons:

Robert A. Meyers (ed.), *Encyclopedia of Sustainability Science and Technology*, DOI 10.1007/978-1-4419-0851-3,
© Springer Science+Business Media, LLC 2012

- Energy security – In 2009, the United States imported 59% of its net crude oil consumption, which makes its economy vulnerable to supply disruptions.
- Balance of trade – When crude oil sells for about $90/bbl, the United States spends about $1 billion per day on imports. If retained within the United States, this money would help develop domestic jobs.
- Rural economic development – The sale of biofuels will bring additional revenue to rural economies.
- Environment – The production of biofuels from polluting biomass feedstocks (e.g., manure, municipal solid waste) removes these hazards from the environment.
- Global warming – The combustion of biofuels does not contribute net carbon dioxide to the atmosphere; any CO_2 released from the combustion of biofuels is fixed via photosynthesis which recycles it as plant matter.

Vehicle Fuels

For transportation, liquid fuels are preferred because of their high energy density, ease of transport, and controllability; therefore, they command a premium price as described below:

- Liquid (e.g., gasoline, jet fuel, diesel) – $15 to $25/GJ.
- Gaseous (e.g., methane) – $2 to $5/GJ.
- Solid (e.g., coal) – $1 to $3/GJ.

Conventional Fuels

Gasoline is used primarily in spark-ignited piston engines (Otto cycle). It is composed of hydrocarbons containing 4–12 carbon atoms (average about 7–8). Gasoline grades are determined by the *octane number*, which characterizes the tendency of the fuel to *knock*, i.e., prematurely detonate. Gasoline-powered engines have a compression ratio (maximum: minimum gas volume) of about 7:1–12:1. During the compression of the air–fuel mixture, the temperature increases. Fragile molecules (e.g., large linear hydrocarbons) readily detonate whereas stable molecules (e.g., branched hydrocarbons, aromatics, oxygenates) resist detonation. High-compression engines are more efficient and powerful, and require high-octane fuels to prevent knocking. Because knocking pressurizes the gas at the wrong point in the engine cycle, it can rob efficiency and potentially cause damage. (Note: A fuel with an octane number of 100 has knocking characteristics identical to an idealized fuel containing 100% iso-octane and 0% *n*-heptane. Similarly, a fuel with an octane number of 0 has knocking characteristics identical to an idealized fuel containing 0% iso-octane and 100% *n*-heptane. Other fuel octane numbers correspond to other idealized mixtures.)

Jet fuel is used primarily in jet engines (Brayton cycle). It is composed of hydrocarbons containing 8–16 carbon atoms (average of about 12), which is similar to kerosene. Jet fuel formulations are adjusted to ensure the fuel does not freeze at high altitudes, where the temperature is cold. Also, the composition is adjusted to reduce smoke formation.

Diesel fuel is used primarily in diesel engines. It is composed of hydrocarbons containing 10–22 carbon atoms (average of about 16). Diesel engines have a high compression ratio (typically 14:1–24:1), which greatly increases the air temperature during the compression stroke. To ignite the fuel, they do not employ a spark; rather, they rely on the high temperature of the compressed air. When atomized diesel fuel is injected into the hot compressed air, it decomposes and ignites. The burn characteristics of diesel fuel are determined by the *cetane number*, which quantifies how quickly the fuel starts to auto-ignite in a diesel engine. Analogous to octane rating, the cetane rating assigns a value of 100 to a fuel that behaves like cetane (*n*-hexadecane) whereas a value of 0 is assigned to a fuel that behaves like 1-methyl napthalene.

Biofuels

Biofuels come in many forms, as described in Table 1. Table 2 provides properties of both biofuels and conventional fuels.

In the United States, ethanol is the dominant biofuel. Figure 1 shows the US ethanol capacity from 1980 to 2010. In 2010, the US ethanol capacity was 13.2 billion gallons per year and US gasoline consumption was 138.5 gal per year (Fig. 2); thus, about 8.7% of the gasoline–ethanol pool was ethanol. In 2010, approximately 40% of the US corn crop was converted to fuel ethanol. Table 3 shows global ethanol production in 2009.

Vehicle Biofuels. Table 1 Examples of biofuels

Fuel type	Generic	Examples	
Primary alcohols	R–OH	$H_3C–OH$	methanol
		$H_3CH_2C–OH$	ethanol
Secondary alcohols	OH | R–C–R'	OH | $H_3C–C–CH_3$	isopropanol
Ethers	R–O–R'	$H_3C–O–CH_3$	dimethyl ether
		$H_3CH_2C–O–CH_2CH_3$	diethyl ether
Ketones	O || R–C–R'	O || $H_3C–C–CH_3$	Acetone
Esters	O || R–CO–R'	O || $H_{34}C_{18}–CO–CH_3$	Biodiesel

In 2009, the US biodiesel capacity was 2.0 billion gallons per year [4] and US diesel consumption was 55.7 billion gallons per year [5]; thus, about 3.5% of the diesel pool was biodiesel.

Biofuel Blends

Biofuels are often blended with other components. Common designations are described below.

E10 *E10* is a blend of 10% ethanol and 90% gasoline, and is commonly described as *gasohol*. It is widely used in the United States; nearly the entire gasoline pool contains ethanol. Modern gasoline engines are designed to be compatible with E10 without the need for modifications.

Addition of ethanol to gasoline has some benefits, such as (1) reducing gasoline imports, (2) improving the fuel octane rating, and (3) improving combustion. Regarding the latter point, the 1990 US Clean Air Act required the addition of oxygenates to *reformulated gasoline* in cities that could not attain carbon monoxide or ozone standards. In those cities, fuels were required to contain 2.7% oxygen, which could be met by adding oxygenates such as methyl tertiary butyl ether (MTBE) or ethanol. When MTBE was found to contaminate groundwater, its use was banned so the demand for ethanol increased dramatically.

Addition of ethanol to gasoline also has some detriments, such as (1) reducing fuel economy because of its lower energy content (~3%); (2) raising the fuel vapor pressure, which reduces the amount of low-cost, high-octane butanes that can be added to fuel; (3) increasing production of formaldehyde and acetaldehyde in tail-pipe emissions; and (4) absorbing water into the fuel. Regarding the latter point, ethanol is very polar compared to gasoline and attracts water, which is also polar. Common-carrier pipelines that transport hydrocarbon fuels often contain water. If ethanol-containing fuel were transported through these pipelines, it would absorb water, which adversely affects fuel quality. To avoid this problem, anhydrous ethanol is transported via rail or trucks and is "splash blended" at the fuel terminal.

E15 *E15* is a blend of 15% ethanol and 85% gasoline. As ethanol is increasingly added to the gasoline pool, the United States will soon reach a "blend wall" for E10. The US Environmental Protection Agency has authorized the use of E15 in certain vehicles (e.g., automobiles, SUVs, light-duty trucks) after model year 2001, which potentially would allow the percentage of ethanol to increase by 50%. The ruling has spurred controversy regarding potential damage to engines, emission systems, and air quality. Further, E15

Vehicle Biofuels. Table 2 Properties of fuels[a]

Fuel	Heat of combustion[b] (MJ/kg)	Density (kg/L)	Heat of combustion[b] (MJ/L)	Octane rating[c]
Hydrocarbons				
Diesel	44.8	0.83	37.2	15–25
Jet	46.6	0.81	37.7	
Gasoline	47.3	0.74	35.0	91–99
Esters				
Biodiesel	39.9	0.88	35.1	
Alcohols				
Methanol	19.9	0.79	15.7	106
Ethanol	28.9	0.79	22.8	108
n-Propanol	30.7	0.80	24.6	
Isopropanol	30.5	0.80	24.4	
n-Butanol	33.1	0.81	26.8	96
Isobutanol	33.0	0.80	26.4	
Tertbutanol	32.6	0.78	25.4	103
n-Pentanol	34.7	0.81	28.1	
Ethers				
Dimethyl ether	28.7	0.67	19.2	
Diethyl ether	33.9	0.71	24.1	
Dipropyl ether	36.4	0.74	26.9	
Dibutyl ether	37.8	0.77	29.1	
Ketones				
Acetone	28.6	0.78	22.3	
Methyl ethyl ketone	31.5	0.80	25.2	
Diethyl ketone	35.7	0.82	29.3	

[a]Data derived from Wikipedia
[b]Higher heating value (i.e., water product is a liquid)
[c]Research Octane Number (RON)

would need to be sold in a manner to prevent it from being used in unauthorized vehicles (e.g., motorcycles, heavy-duty vehicles, off-road vehicles, and vehicles older than model year 2000).

E85 *E85* is a blend of 85% ethanol and 15% gasoline. Because ethanol has lower energy content than gasoline, the fuel mileage of E85 decreases by 25–30%. Compared to gasoline, ethanol has a higher latent heat of vaporization and lower vapor pressure; thus, it is potentially difficult to start the engine during cold weather. To overcome this problem, gasoline is a component of E85. During very cold weather, fuel retailers will increase the percentage of gasoline to 30%. Conventional spark-ignited engines are not designed to combust E85; however, flexible-fuel vehicles (FFVs) can accept any ratio of E0 to E85. In FFVs, the metals, polymers, and elastomers in the fuel system and

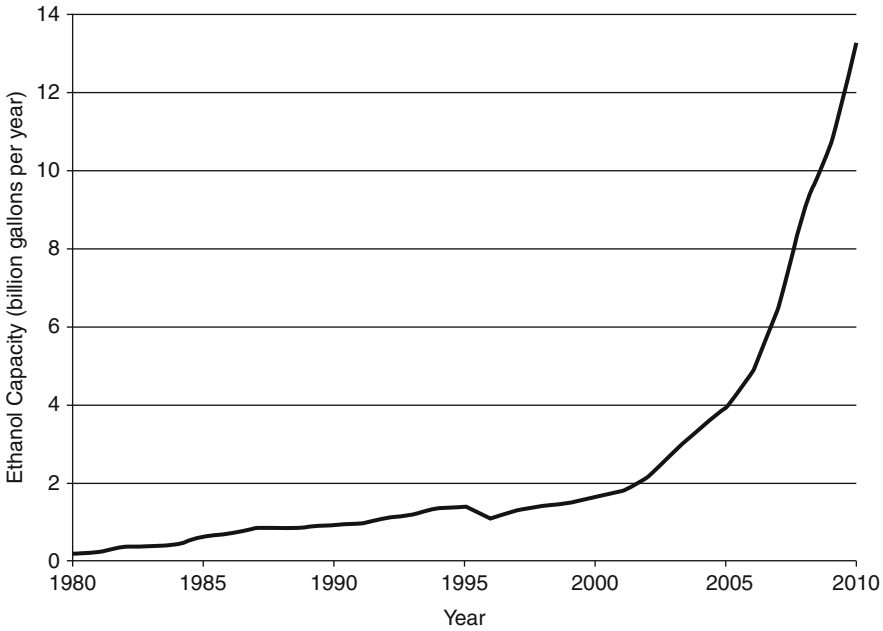

Vehicle Biofuels. Figure 1
US ethanol capacity [1]

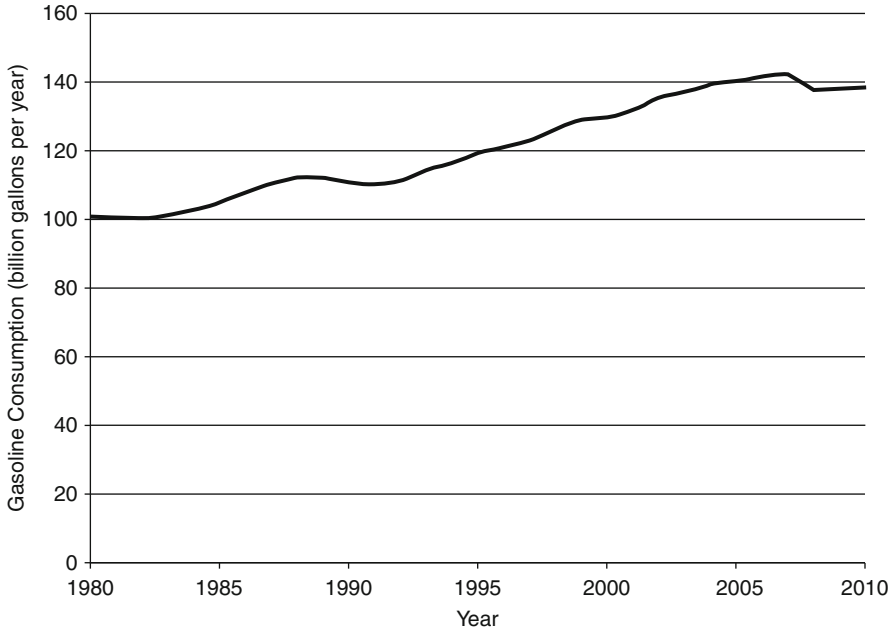

Vehicle Biofuels. Figure 2
US gasoline consumption [2]

Vehicle Biofuels. Table 3 Global fuel ethanol production in 2009 [3]

Country	Annual Production (million gallons)
United States	10,600.00
Brazil	6,577.89
European Union	1,039.52
China	541.55
Thailand	435.20
Canada	290.59
India	91.67
Colombia	83.21
Australia	56.80
Other	247.27
Total	19,963.70

engine components must be compatible with the range of fuels. Further, engine sensors detect the fuel composition and automatically adjust the fuel injector and spark timing. For the automobile manufacturer, the marginal cost of producing an FFV is about $150 per vehicle.

E100 *E100* is 100% ethanol and 0% gasoline. The previously discussed fuels (E10, E15, E85) contain ethanol blended with gasoline. In these fuels, only anhydrous ethanol can be used; otherwise, water will phase out when the gasoline is added. However, E100 is a *neat fuel* (i.e., it contains no additives), so it can contain water. In the production of ethanol, it must be distilled from water. The top of the distillation column reaches the *azeotrope*, where the composition of the liquid and vapor are identical (95.63% ethanol and 4.37% water, by weight). To break the azeotrope requires additional technology (e.g., the use of molecular sieves to remove water from the solution), which adds cost. In Brazil, many vehicles operate on azeotropic ethanol; therefore, the cost of the final dehydration step is eliminated. To overcome potential cold-start problems, it is common practice to start the engine on gasoline and then switch to E100 once the engine is warmed. Direct injection of ethanol into the engine shows an effective octane rating of 130. With appropriate engine controls, it is possible to burn neat ethanol in engines with a compression ratio up to 19.5:1, which has a thermal efficiency similar to diesel engines. The higher efficiency of the high-compression engine compensates for the lower energy content of ethanol, so the fuel mileage is similar to gasoline.

Biodiesel *Biodiesel* is produced from vegetable oil or animal fats. It has a carbon number similar to petroleum-derived diesel fuel, so it can be combusted in conventional diesel engines. Common blends include B2, B5, B10, and B100, which contain 2%, 5%, 10%, and 100% biodiesel, respectively. Disadvantages of biodiesel include the following: (1) potential cold-start problems (not unlike conventional diesel), which can be overcome using additives that prevent clogging of filters; (2) deposits and clogging from low-quality or oxidized fuel; (3) slightly higher NO_x emissions; and (4) lower energy content. Regarding the latter point, because biodiesel contains oxygen, B100 has 3–5% less energy content than petroleum-derived diesel. Advantages of biodiesel include the following: (1) better lubricity (short-term studies with biodiesel show that it has less wear than conventional diesel) and (2) lower emissions. Regarding the latter point, because of its oxygen content, biodiesel burns more completely. Further, it has no sulfur or aromatic emissions.

Although biodiesel is more commonly used in diesel engines, it can be used in aircraft engines as well. Usually, it is blended with conventional jet fuel; however, there are some reports of aircraft operating with B100.

E-Diesel Because of its hydroxyl group, ethanol has hydrophilic properties and is completely soluble in water in any ratio. Because of its ethyl group, ethanol has oleophilic properties and is completely soluble in diesel fuel in any ratio. However, if a small amount of water (0.2%) is present in the fuel, two phases form: one ethanol-rich and the other diesel-rich [6]. To prevent phase separation, additives (e.g., surfactants, emulsifiers, and co-solvents) can be included in the fuel. The addition of biodiesel to petroleum-derived diesel allows significant quantities (5–15%) of ethanol to be added to the fuel [7]. Rather than adding ethanol

directly to diesel fuel, ethanol can be stored in a separate tank and introduced as a fog or vapor into the air intake of the engine.

Biomass

Biomass is biological material from living or recently living organisms. In the context of biofuels, usually biomass is used to describe plant matter such as wood, grass, agricultural residues, energy crops, and algae. The dominant components of biomass are described below.

Free Sugars

Free sugars are found in fruits and plant juices. Figure 3 shows examples including glucose, fructose, and sucrose (a disaccharide of glucose and fructose).

Starch

As shown in Fig. 4, starch is a polymer of glucose joined by α bonds. It occurs in two forms: amylose (unbranched) and amylopectin (branched). In plants, starch is used primarily as an energy-storage compound.

Cellulose

As shown in Fig. 5, cellulose is an unbranched polymer of glucose joined by β bonds. Because of extensive internal hydrogen bonds (Fig. 6), cellulose is crystalline and rigid; therefore, it is used as a structural component of roots, stems, and leaves. Because these components are so common in plants, cellulose is the most abundant biological material produced on earth.

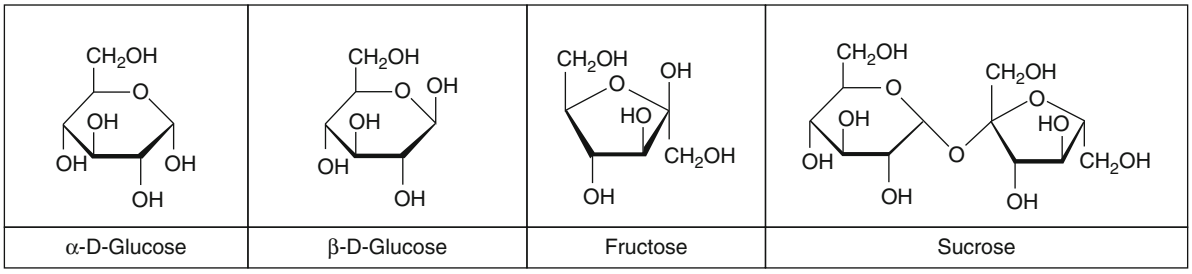

Vehicle Biofuels. Figure 3
Free sugars. (Note: For simplicity, the hydrogens bonded to carbon are not shown)

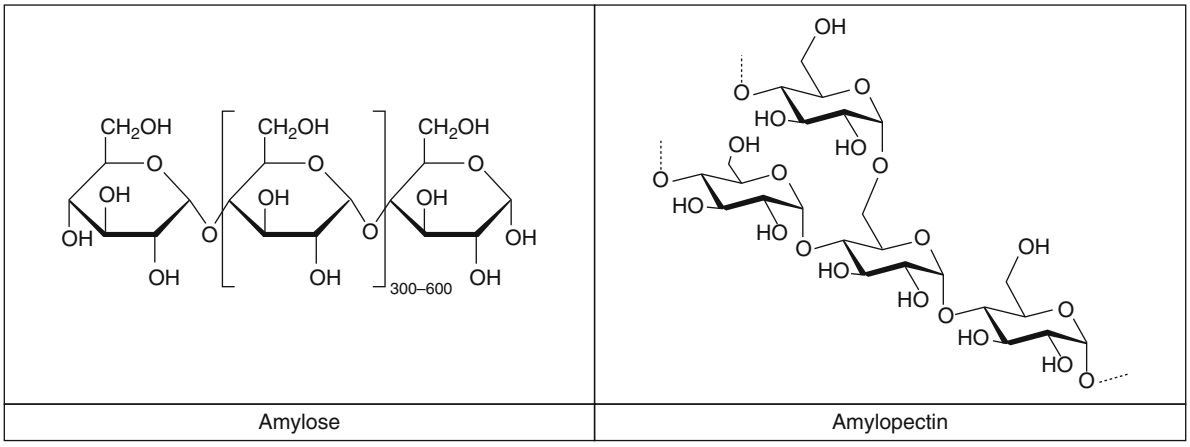

Vehicle Biofuels. Figure 4
Two forms of starch. (Note: For simplicity, the hydrogens bonded to carbon are not shown)

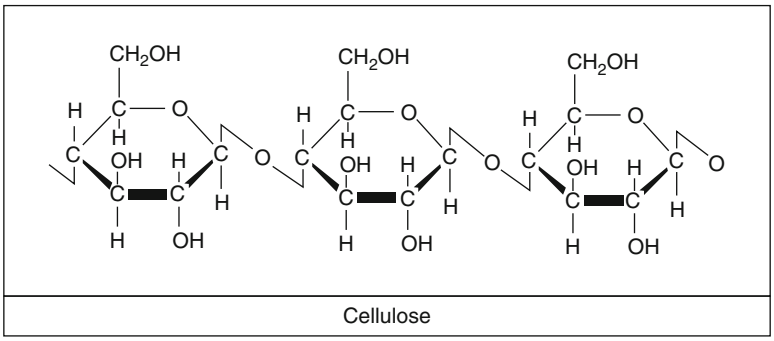

Vehicle Biofuels. Figure 5
Cellulose structure

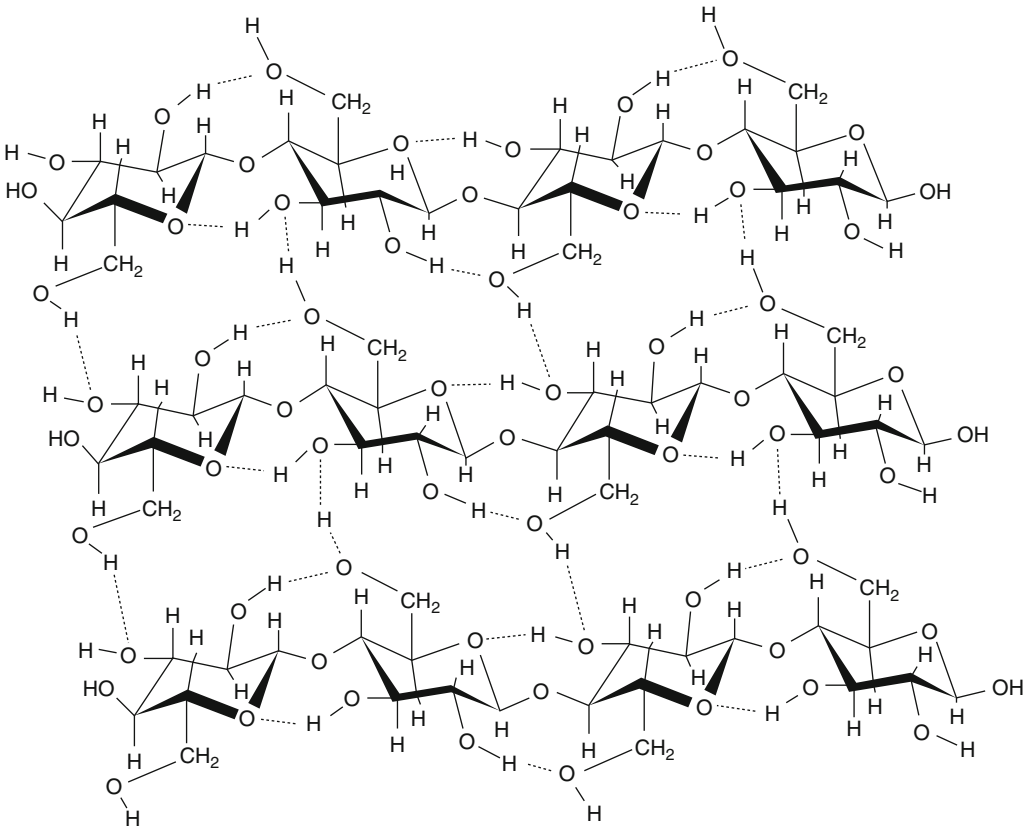

Vehicle Biofuels. Figure 6
Cellulose has extensive hydrogen bonds, shown as *dotted lines*

Hemicellulose

As shown in Fig. 7, hemicellulose is a polymer with a backbone of xylose (a five-carbon sugar) joined by β bonds. In addition to xylose, hemicellulose contains glucose, mannose, galactose, rhamnose, arabinose, mannuronic acid, and galacturonic acid. Hemicellulose is randomly acetylated, which helps it resist degradation by sterically hindering hemicellulose enzymes.

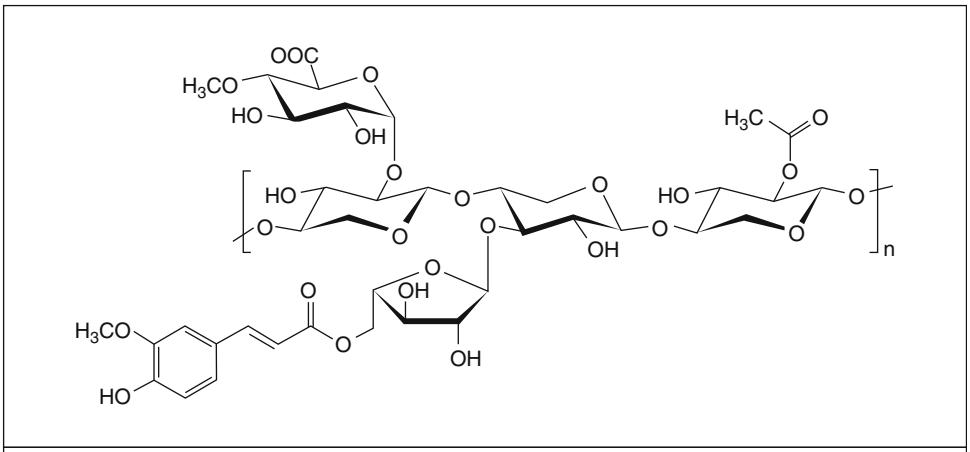

Vehicle Biofuels. Figure 7
Hemicellulose structure

Lignin

Lignin is a complex polymer composed of three monomers (Fig. 8), which are highly cross-linked (Fig. 9). Lignin is the "glue" that holds biomass together. By analogy to fiberglass composites, lignin functions like epoxy resin whereas cellulose functions like glass fibers. Lignin is hydrophobic and reduces evaporation of water from plant vessels. Further, lignin resists biological attack by insects and microorganisms.

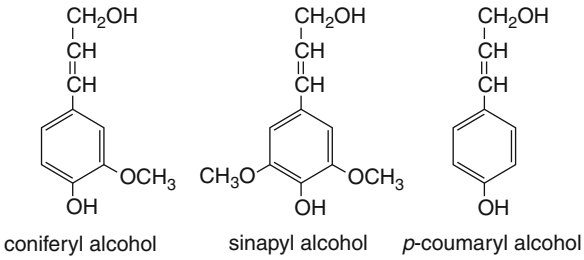

Vehicle Biofuels. Figure 8
Lignin monomers

Triacylglycerol

Triacylglycerol (TAG) is the main component of vegetable oil and animal fats and is composed of fatty acids bonded to glycerol via ether linkages (Fig. 10). In Fig. 10, the value of *n* typically ranges from 14 (palmitic acid) to 16 (oleic and stearic acids). Although Fig. 10 shows the hydrocarbon chain is fully saturated with hydrogen, naturally occurring fatty acids often have some unsaturated bonds as well.

Proteins

Figure 11 shows the chemical structure of an amino acid, which contains an amine group ($-NH_2$) and a carboxylic acid ($-COOH$). In naturally occurring amino acids, there are 20 standard R groups, which are coded by DNA. By eliminating water, the amine and carboxylic acid groups form a peptide bond, thus creating a protein polymer. In nature, proteins have many functions, including catalyzing reactions (enzymes) and providing mechanical structure.

Biomass Processing

Figure 12 shows an overview of processes that convert biomass into fuels, which is described in more detail below.

Raw Materials

Lignocellulose includes wood, grass, agricultural residues, and aquatic plants. Lignocellulose is the structural component of biomass and is composed of cellulose (30–50%), hemicellulose (20–40%), and

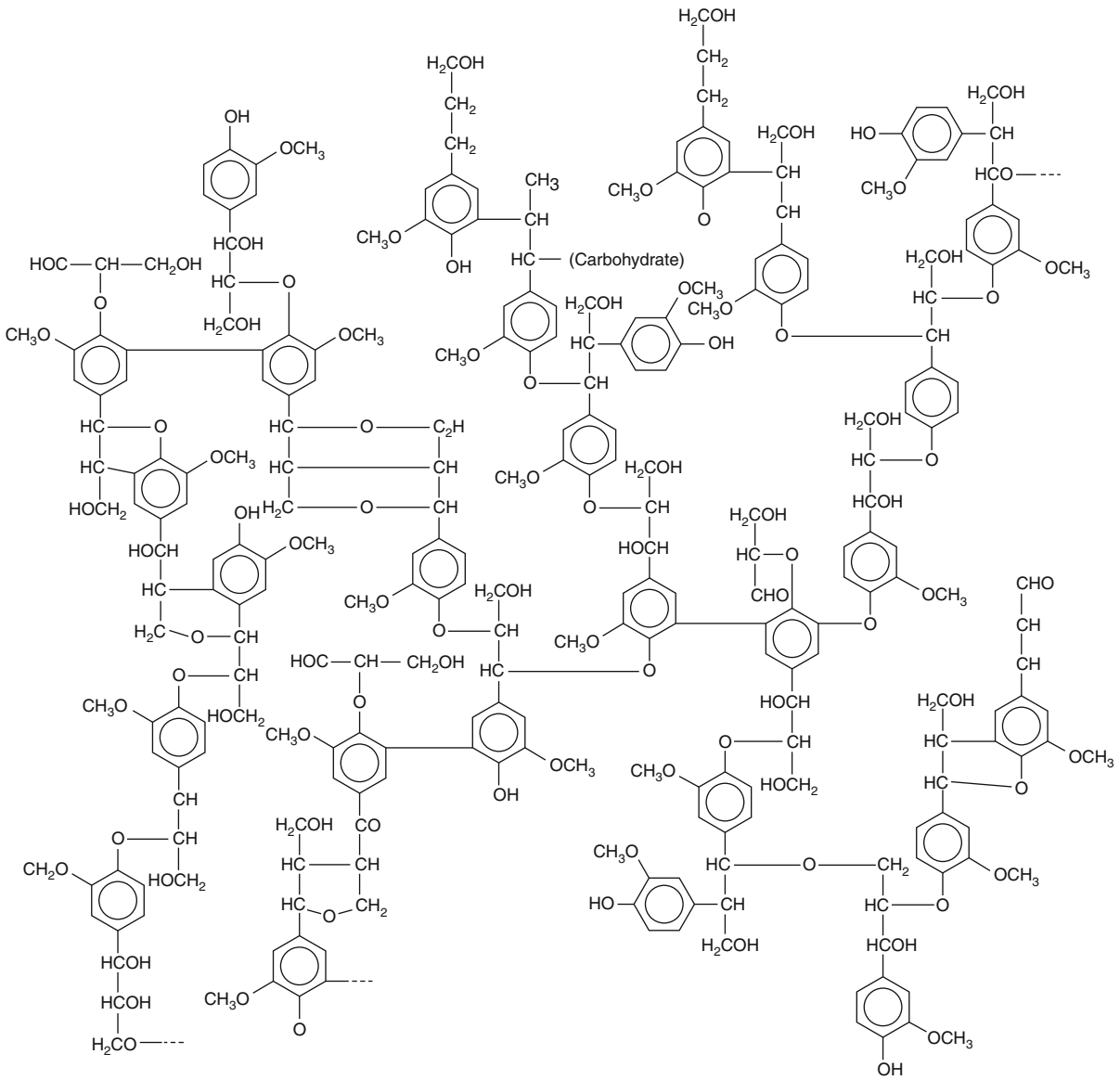

Vehicle Biofuels. Figure 9
Lignin structure

lignin (20–30%). By far, lignocellulose is the dominant form of biomass produced on earth. Table 4 catalogs the land available in the United States. Table 5 summarizes the potential lignocellulose resources in the United States. Tables 6 and 7 focus on waste biomass whereas Table 8 describes the productivity of energy crops.

Sugar crops include sugarcane, sweet sorghum, and sugar beets. The dominant sugar is sucrose with minor amounts of glucose and fructose. Table 9 shows the productivity of sugar crops.

Starch crops include grains (e.g., corn, grain sorghum) and tubers (e.g., potatoes, cassava). Table 10 shows the productivity and abundance of US grain crops. Figure 13 shows the historical increase in US corn productivity.

Oil crops include palm, soybeans, rape, and Chinese tallow. Also, animal fats and waste frying oil can be

used as raw material. Table 11 shows the productivity of oil crops.

Algae include primarily microalgae (e.g., cyanobacteria, diatoms) but also macroalgae (e.g., kelp, seaweed). Table 12 shows the range of lipid contents and biomass productivities of microalgae grown under laboratory conditions. Table 13 shows lipid contents, biomass productivities, and lipid productivities for microalgae grown in outdoor ponds.

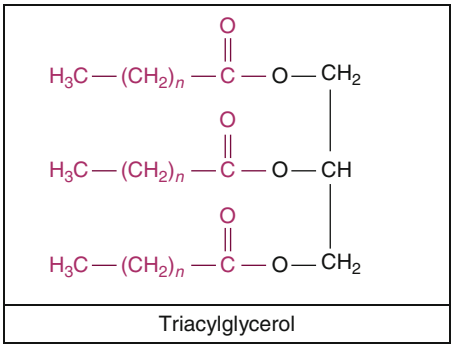

Vehicle Biofuels. Figure 10
Structure of triacylglycerol

Intermediates

Figure 12 describes the following intermediates:

Bio-oil is the liquid resulting from biomass pyrolysis. Visually, it looks like crude oil; however, the composition is very different. Unlike crude oil, bio-oil contains a substantial amount of oxygen and is water soluble. A typical composition includes saccharides (2.4–3.3%), anhydrosugars (6.5–6.8%), aldehydes (10.1–14.0%), furans (0.35%), ketones (1.24–1.4%), alcohols (1.2–2.0%), carboxylic acids (8.5–11.0%), and pyrolytic lignin (16.2–20.6%). Because of the acids, the pH is low (1.5–3.8) [27].

Synthesis gas is the common name for a mixture of carbon monoxide and hydrogen, so named because it can be catalytically converted to a wide variety of products.

Acid degradation products result when biomass is heated with strong mineral acids. Components include acetaldehyde, formic acid, 2-furfural, glucose, 5-hydroxymethyl-furfural, 5-methyl-2-furfural, levulinic acid, saccharinic acid, and 2-furoic acid [28, 29].

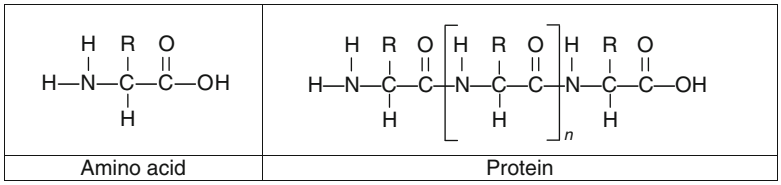

Vehicle Biofuels. Figure 11
Structure of amino acids and proteins

Raw Material	Intermediate	Fuel
(1) Lignocellulose	(a) Bio-oil	(A) Hydrocarbon
(2) Sugar crops	(b) Synthesis gas	(B) Alcohol
(3) Starch crops	(c) Acid degradation products	(C) Ether
(4) Oil crops	(d) Sugar	(D) Ester
(5) Algae	(e) Carboxylate	(E) Ketone

Vehicle Biofuels. Figure 12
Overview of processes that convert biomass to fuels

Vehicle Biofuels. Table 4 US land categories [8]

Land categories	Percentage (%)	Land (million acre)	Land (million hectare)
Forest	33	747	302
Grassland pasture and range	26	588	238
Crop	20	453	183
Special use (e.g., public facilities)	8	181	73
Misc. (e.g., urban, swamp, desert)	13	294	119
Total	100	2,263	916

Vehicle Biofuels. Table 5 Summary of potential lignocellulose feedstocks [8]

Biomass resource	Availability (million dry ton/year)	Potential gasoline[a] (billion gal/year)
Woody		
Logging and other residues	64	4.5
Fuel treatments	60	4.2
Urban wood residues	47	3.3
Fuelwood	52	3.6
Sub-total	223	15.6
Herbaceous		
Perennial crops	377	26.4
Crop residues	446	31.2
Process residues	87	6.1
Sub-total	910	63.7
Grand total	1,133	79.3

[a]Assumed yield = 70 gal/t

Sugar intermediates include glucose, xylose, arabinose, galactose, mannose, rhamnose, and fructose, which are derived from sucrose, starch, cellulose, and hemicellulose.

Vehicle Biofuels. Table 6 Residues that are sustainably recovered under moderate crop yield increases without land use changes [8]

Biomass resource	Yield (dry ton/(acre·year))	Availability (million dry ton/year)	Potential gasoline[a] (billion gal/year)
Crop residues			
Corn	4.1	169.7	11.88
Sorghum, grain	1.7	1.3	0.09
Barley	2.2	2.8	0.20
Oats	1.9	0.7	0.05
Wheat, winter	2.3	27.4	1.92
Wheat, spring	1.4	7.4	0.52
Soybeans	1.8	0.0	0.00
Rice	5.1	10.3	0.72
Cotton lint	1.1	5.5	0.39
Other crops	1.2	20.8	1.46
Wastes			
Manure	–	43.5	3.05
Fats and grease	–	2.0	0.14
Municipal solid waste	–	29.4	2.06

[a]Assumed yield = 70 gal/t

Carboxylates are salts of carboxylic acids and include salts of volatile fatty acids (e.g., acetate, propionate, butyrate, valerate, caproate, heptanoate) and fatty acids (e.g., palmitate, stearate, oleate).

Products

Figure 12 describes the following products: hydrocarbons, alcohols, ethers, esters, and ketones. All of these products have been described previously.

Conversion Processes

Biomass is converted to fuels using either thermochemical or biological processes [30].

Vehicle Biofuels. Table 7 Maximum potential of municipal solid waste (2009) [9]

	Percentage (%)	Wet weight (mill ton/year)	Assumed moisture (%)	Dry weight (mill ton/year)	Gasoline potential (bill gal/year)
Organic					
Wood	6.5	15.8	7	14.7	1.03
Yard trimmings	13.7	33.3	70	10.0	0.70
Food scraps	14.1	34.3	80	6.9	0.48
Paper & paperboard	28.2	68.5	6	63.7	4.46
Inorganics					
Glass	4.8	11.7	0	11.7	0
Metal	8.6	20.9	0	20.9	0
Plastic	12.3	29.9	0	29.9	0
Rubber/leather/textiles	8.3	20.2	0	20.2	0
Other	3.5	8.5	0	8.5	0
Total	100.0	243.0		186.5	6.67

Vehicle Biofuels. Table 8 High-yield lignocellulosic crops

Crop	Yield (dry ton/(acre·year))	Potential gasoline[a] (gal/(acre·year))	Potential gasoline[a] (L/(ha·year))
Mixed prairie grass [10]	1.64–2.67	115–187	1,070–1,740
Switchgrass [11]	2.3–4.9	161–343	1,500–3,200
Poplar [12]	4.5–6.7	315–469	2,940–4,380
Willow [12]	4.5–6.7	315–469	2,940–4,380
Miscanthus [12]	5.3–13.4	371–938	3,460–8,760
Photoperiod-sensitive sorghum [13]	8–17	560–1,190	5,230–11,100
Conventional sugarcane [14]	17	1,190	11,100
Giant cane (*Arundo donax*) [15]	25	1,720	16,300
Energy cane [16]	30	2,100	19,600
Elephant grass (*Pennisetum purpurcum*) [17]	37–47	2,590–3,290	24,200–30,700
Water hyacinth [18]	111	7,770	72,500
Water hyacinth with enriched CO_2 [18]	146	10,220	95,400

[a]Assumed yield = 70 gal/t

Thermochemical

At elevated temperatures, thermochemical conversion processes react biomass with air or oxygen to form solid (char), liquid, and gaseous products. Except for minor amounts of nitrogen and sulfur, the elemental composition of biomass is dominated by carbon, hydrogen, and oxygen (Table 14). Free of ash, nitrogen, or sulfur, a typical formula for woody biomass is $CH_{1.4}O_{0.59}$ [31].

Vehicle Biofuels. Table 9 US sugar crops (2010)

Crop	Land harvested (acre)	Yield (wet ton/(acre·year))	Sugar content (ton sugar/t wet biomass)	Yield (ton sugar/(acre·year))	Potential ethanol yield (gal/(acre·year))
Sugarcane [8]	1,766,400	31.8	0.12	3.8	536
Energy cane [16]	Negligible	100	0.09	9	1,270
Sugar beets [8, 19]	1,155,700	27.6	0.15	4.1	578
Sorghum, sweet [20, 21]	negligible	13–20	0.06	0.78–1.2	110–169

Ton = 2,000 lb
Assumed yield = 141 gal per ton of sucrose

Vehicle Biofuels. Table 10 US grain crops (2010) [22]

Crop	Land harvested (acre)	Yield	Bushel weight (lb)	Water (%)	Yield (ton/(acre·year)	Yield (tonne/(ha·year)
Corn	81,446,000	152.8 bu/acre	56	15.5	3.62	8.11
Wheat	47,637,000	46.4 bu/acre	60	13.5	1.20	2.69
Sorghum, grain	4,808,000	71.8 bu/acre	56	13.0	1.75	3.92
Rice	3,615,000	6,725 lb/acre	NA	14.0	2.89	6.47
Oats	1,263,000	64.3 bu/acre	32	12.0	0.91	2.04

Tonne = 1,000 kg
Ton = 2,000 lb

The *equivalence ratio* ϕ is defined as the actual oxygen fed to the reactor divided by the stoichiometric oxygen needed for complete combustion. Using a typical formula for woody biomass, the stoichiometric amount of oxygen is calculated as follows:

$$CH_{1.4}O_{0.59} + 1.055O_2 \rightarrow CO_2 + 0.7H_2O.$$

As a function of equivalence ratio, Fig. 14 shows the equilibrium energy content of the char and gases exiting an air-fired thermochemical reactor [31]. Under *pyrolysis* conditions ($\phi < 0.1$), char is about 40–55% of the energy content of the raw biomass with the remaining energy in the form of gases. Under *gasification* conditions ($0.2 < \phi < 0.4$), char is less than 15% of the energy content of the raw biomass; most of the energy is in the form of gases. Figure 15 shows the equilibrium composition of the gases exiting an air-fired thermochemical reactor. Other than char, the only equilibrium products are CH_4, CO, H_2, CO_2, and N_2. Real thermochemical reactors also produce complex tars and bio-oils; however, these are non-equilibrium products.

Combustion A biomass combustor can be as simple as a bonfire or a sophisticated as a fluidized bed. The objective of the combustion process is to produce heat (Table 14), which typically is used to generate steam. To ensure that there is negligible carbon monoxide in the combustion gas, a biomass combustor is typically operated at an equivalence ratio of 1.05–1.10. In an air-fired combustor, the combustion temperature is about 2,050°C and in an oxygen-fired combustor, combustion temperature is about 2,800°C [31].

As a solid fuel, biomass competes with coal. Because of its lower oxygen content, coal has higher energy

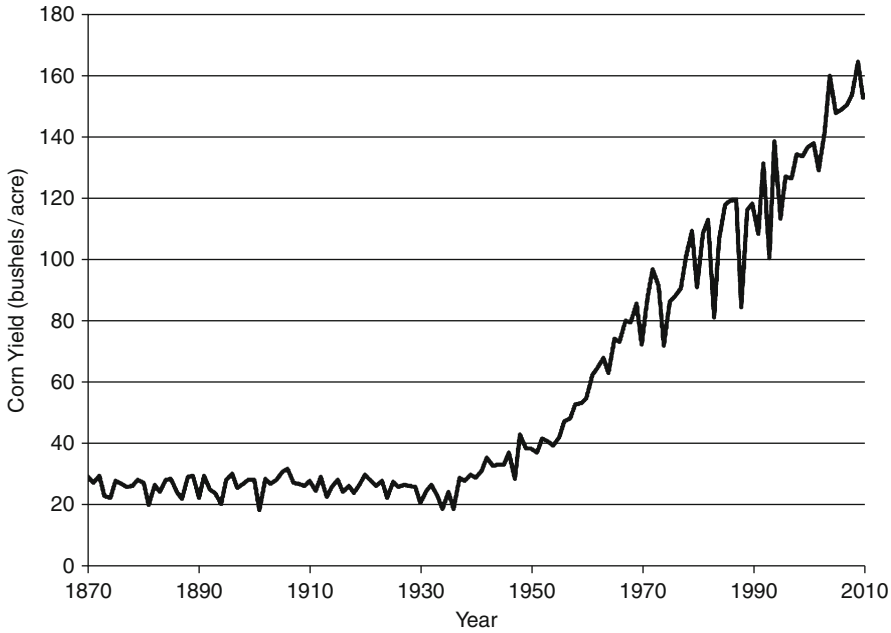

Vehicle Biofuels. Figure 13
Historical corn productivity [22]

content than biomass. Heating biomass in an oxygen-free environment drives off volatiles to produce charcoal, which has lower oxygen content than biomass and hence its heating value is similar to coal. Compared to coal, biomass has fewer impurities (N, S), so less treatment of stack gases is required, which lowers the capital cost of the combustor.

Gasification Commonly, gasifiers are operated at an equivalence ratio of about 0.25 (1.6 g air/g biomass). Gasification typically occurs at temperatures of 700–1,100°C with air and about 100°C higher with oxygen [31]. Table 15 shows the energy content of the gases exiting a gasifier fired with air or oxygen. In Europe during World War II, the low-energy gas from air-fired gasifiers was fed to millions of vehicles.

The mechanical design of gasifiers follows [31]:

Updraft gasifiers employ a bed of biomass in which fresh biomass is introduced at the top. Air (or oxygen) is introduced at the bottom of the bed and is blown upward. The bottom zone is richest in oxygen, which is where combustion reactions occur thereby releasing heat and increasing the temperature. As the hot gases flow upward through the upper zone of fresh biomass, gases and liquids are generated. Ideally, to prevent liquid condensation, the hot products are burned directly.

Downdraft gasifiers also employ a bed of biomass in which fresh biomass is introduced at the top. Air (or oxygen) is introduced at an intermediate zone in the bed. The gas flows downward with the biomass and passes through the hot combustion zone. Because the gas exits at very high temperatures, less tar and bio-oil is produced. The hot product gas can be used to preheat the incoming biomass feed.

Fluidized-bed gasifiers mix high-velocity air and steam with the biomass to create an ebullating bed. Unlike fixed-bed gasifiers, fluidized-bed gasifiers can employ a wider range of particle sizes and have a higher throughput because of the uniformly high temperature. To maintain high velocities, the hot product gas is often recycled into the fluidized-bed gasifier. These gasifiers often employ a solid heat transfer agent, such as sand or catalyst.

Vehicle Biofuels. Table 11 Productivity of oil-producing crops

Crop	Latin Name	Productivity (gal/(acre·year))	Productivity (L/(ha·year)
Corn [23]	*Zea mays*	18	168
Soybean [23]	*Glycine max*	46	429
Peanut [23]	*Ariachis hypogaea*	109	1,020
Rape seed [23]	*Brassica napus*	122	1,140
Castor bean [23]	*Ricinus communis*	145	1,350
Jojoba [23]	*Simmondsia chinensis*	186	1,740
Jatropha [23]	*Jatropha curcas*	194	1,810
Coconut [23]	*Cocos nucifera*	276	2,580
Macauba palm [23]	*Acrocomia aculeata*	461	4,300
Oil palm [23]	*Elaeis guineensis*	610	5,700
Chinese tallow [24]	*Triadica sebifera*	645	6,020

Vehicle Biofuels. Table 12 Productivity of microalgae [25]

Algae species	Lipid content (%)	Biomass productivity (tonne/(ha·year))
Ankistrodesmus sp.	24–31	42–63
Botryoccus braunii	25–75	11
Chlorella emersonii	25–63	3.3–3.5
Chlorella vulgaris	5–58	2.1–3.5
Chlorella sp.	10–48	5.9–91
Chlorella pyrenoidosa	2	264–474
Chlorella	18–57	13–51
Dunaliella salina	6–25	5.8–131
Dunaliella primolecta	23	51
Haematococcus pluvialis	25	37–133
Monallanthus salina	20–22	43
Nannochloropsis sp.	12–53	7–19
Nitzchia sp.	16–47	32–79
Oocystis pusilla	11	148–167
Phaeodactylum tricornutum	18–57	8.8–77
Porphyridium cruentum	9–61	91
Scenedesmus sp.	20–21	8.9–49
Spirulina platensis	4–17	1.5–186
Spirulina maxima	4–9	91
Tetraselmis suecica	8–23	69

The primary product from gasifiers is a mixture of carbon monoxide and hydrogen, often called *synthesis gas*. The hydrogen content of the synthesis gas can be enriched using the *shift reaction*

$$CO + H_2O \rightarrow CO_2 + H_2.$$

Commonly, the process employs two stages: high-temperature shift (350°C, iron oxide catalyst) and low-temperature shift (190–210°C, copper catalyst).

Synthesis gas can be converted to a variety of products, as described below.

Methanol (1 → b → B) (*Note:* Codes are described in Fig. 12) Using ZnO catalyst operating at 240–400°C and 50–300 atm, methanol can be produced from synthesis gas according to the following reaction [31]:

$$CO + 2H_2 \rightarrow CH_3OH.$$

Mixed Alcohols (1 → b → B) Using Mo_2C catalyst operating at 300°C and 80 atm, mixed alcohols (e.g., C2 to C7) can be produced from synthesis gas [32]. A representative reaction is the formation of ethanol [32]

$$CO + 4H_2 \rightarrow C_2H_5OH + H_2O.$$

Hydrocarbons (1 → b → A) Fischer–Tropsch catalysts (e.g., cobalt, iron) typically operate at 150–300°C and produce hydrocarbons according to the following reaction:

$$(2n + 1)H_2 + nCO \rightarrow C_nH_{(2n+2)} + nH_2O.$$

Vehicle Biofuels. Table 13 Productivity of microalgae grown in outdoor ponds [26]

Algae species	Lipid content (%)	Biomass productivity (tonne/(ha·year)	Lipid productivity (L/(ha·year))	Lipid productivity (gal/(acre·year))
Amphora	40	142	64,500	6,910
Chaetoceros muelleri	26	95	28,100	3,010
Cyclotella cryptica	24	99	27,000	2,890
Isochrysis galbana	22	102	25,500	2,730
Nannochloropsis	21	55	13,100	1,410
Nannochloropsis salina	16	91	16,500	1,770
Tetraselmis suecica	22	69	17,200	1,850

The product distribution tends to be very wide and includes heavy waxes. Although waxes are valuable products, the market is small, so they often must be refined into lighter fuels (e.g., gasoline, jet fuel, diesel). During World War II, Fischer–Tropsch chemistry was used by the Germans to produce liquid fuels from coal. Currently, South African SASOL uses Fischer–Tropsch chemistry to produce hydrocarbons from coal. A number of commercial plants (Malaysia, Qatar) use Fischer–Tropsch chemistry to produce hydrocarbons from natural gas.

Hydrocarbons (1 → b → B → A) Through an alternative route, methanol (or higher alcohols) can be converted to hydrocarbons using zeolite catalysts, such as ZSM-5 [31].

$$n\mathrm{CH_3OH} \rightarrow \mathrm{C}_n\mathrm{H}_{2n} + n\mathrm{H_2O}$$

Ethers (1 → b → B → C) Methanol can also be converted to dimethyl ether (DME) using a zeolite catalyst, such as ZSM-5 [33].

$$2\mathrm{CH_3OH} \rightarrow \mathrm{H_3COCH_3} + \mathrm{H_2O}$$

DME can be used in diesel engines as a clean-burning fuel [34].

Pyrolysis (1 → a → A) As stated previously, liquids are not thermodynamically stable products from thermochemical reactors; however, they are produced as reaction intermediates. *Fast pyrolysis* involves rapidly heating biomass (less than 1–5 s) to 450–600°C and then rapidly cooling the products to "freeze" the reaction [35]. On a weight basis, a typical product spectrum consists of the following:

- Char = 10–25%
- Gas = 8–30%
- Bio-oil = 45–65%
- Water = 8–15%

Although the bio-oil physically looks like crude petroleum, its properties are very different [36]. It has high water content (15–30%) that is difficult to remove via distillation. Further, it has high oxygen content (35–40%) and low pH (∼2.5). Crude bio-oil can be used directly in boilers and engines (e.g., diesel, gas turbines); however, there are issues with fuel stability and corrosiveness. Using processes similar to those used to refine crude oil (e.g., hydrotreating and catalytic vapor cracking), the bio-oil can be upgraded to products similar to those obtained from petroleum [36]. At the moment, upgrading bio-oil is expensive and energy yields are low.

Acid Degradation (1 → c → C) To produce fuels using acid degradation, lignocellulose is thermochemically treated in a multi-step process [37]:

- *Step 1* – The biomass is hydrolyzed at 210–230°C for 13–25 s using 1–5% mineral acid. This produces primarily hydroxymethylfurfural, which is removed continuously.
- *Step 2* – The hydroxymethylfurfural is hydrolyzed further at 195–215°C for 15–30 min to produce primarily levulinic acid, which is continuously removed.

Vehicle Biofuels. Table 14 Elemental composition and energy content of solid fuels [31]

Feedstock	Elemental composition (wt%)						Higher heating value[a]	
	C	H	N	S	O	ash	(Btu/lb)	(MJ/kg)
Coal								
Pittsburg seam coal	75.5	5.0	1.2	3.1	4.9	10.3	13,650	31.754
West Kentucky No. 11 coal	74.4	5.1	1.5	3.8	7.9	7.3	13,460	31.312
Utah coal	77.9	6.0	1.5	0.6	9.9	4.1	14,170	32.963
Wyoming Elkol coal	71.5	5.3	1.2	0.9	16.9	4.2	12,710	29.567
Lignite	64.0	4.2	0.9	1.3	19.2	10.4	10,712	24.919
Charcoal	80.3	3.1	0.2	0.0	11.3	3.4	13,370	31.102
Biomass								
Douglas fir	52.3	6.3	0.1	0.0	40.5	0.8	9,050	21.053
Douglas fir bark	56.2	5.9	0.0	0.0	36.7	1.2	9,500	22.010
Pine bark	52.3	5.8	0.2	0.0	38.8	2.9	8,780	20.425
Western hemlock	50.4	5.8	0.1	0.1	41.4	2.2	8,620	20.052
Redwood	53.5	5.9	0.1	0.0	40.3	0.2	9,040	21.030
Beech	51.6	6.3	0.0	0.0	41.5	0.6	8,760	20.378
Hickory	49.7	6.5	0.0	0.0	43.1	0.7	8,670	20.169
Maple	50.6	6.0	0.3	0.0	41.7	1.4	8,580	19.959
Poplar	51.6	6.3	0.0	0.0	41.5	0.6	8,920	20.750
Rice hulls	38.5	5.7	0.5	0.0	39.8	15.5	6,610	15.377
Rice straw	39.2	5.1	0.6	0.1	35.8	19.2	6,540	15.214
Sawdust pellets	47.2	6.5	0.0	0.0	45.4	1.0	8,814	20.504
Paper	43.4	5.8	0.3	0.2	44.3	6.0	7,572	17.615
Redwood wood waste	53.4	6.0	0.1	0.1	39.9	0.6	9,163	21.316
Alabama oak waste wood	49.5	5.7	0.2	0.0	41.3	3.3	8,266	19.229
Animal waste	42.7	5.5	2.4	0.3	31.3	17.8	7,380	17.168
Municipal solid waste	47.6	6.0	1.2	0.3	32.9	12.0	8,546	19.880

[a]Water product is assumed to be liquid

- *Step 3* – Through a series of dehydration and reduction reactions, levulinic acid is converted to methyltetrahydrofuran, an oxygenate that can be added to conventional gasoline.

Biodiesel (4 → e → D or 5 → e → D) A component of oil seeds and algae, triacylglycerol (TAG) can be extracted using a solvent (e.g., hexane). TAG can be used directly in diesel engines; however, its high viscosity causes operational problems in the fuel injectors. To overcome this problem, the diesel engine can be modified to include fuel-line heaters that lower the TAG viscosity. Rather than modify the engine, the fuel itself can be modified to lower its viscosity. Typically, this is accomplished by converting TAG to esters ("biodiesel") by a base-catalyzed reaction with an

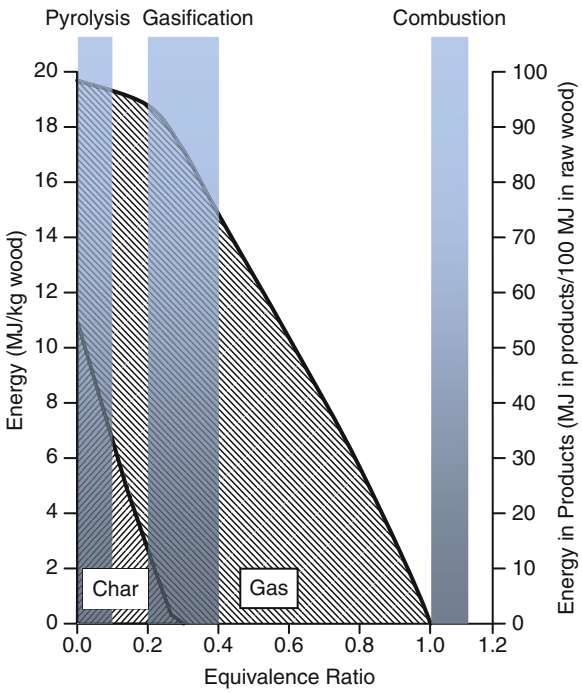

Vehicle Biofuels. Figure 14
Equilibrium energy content of gas and char exiting a thermochemical reactor using air as the oxidant. The equivalence ratio is the actual air employed compared to the stoichiometric amount needed for complete combustion [31]

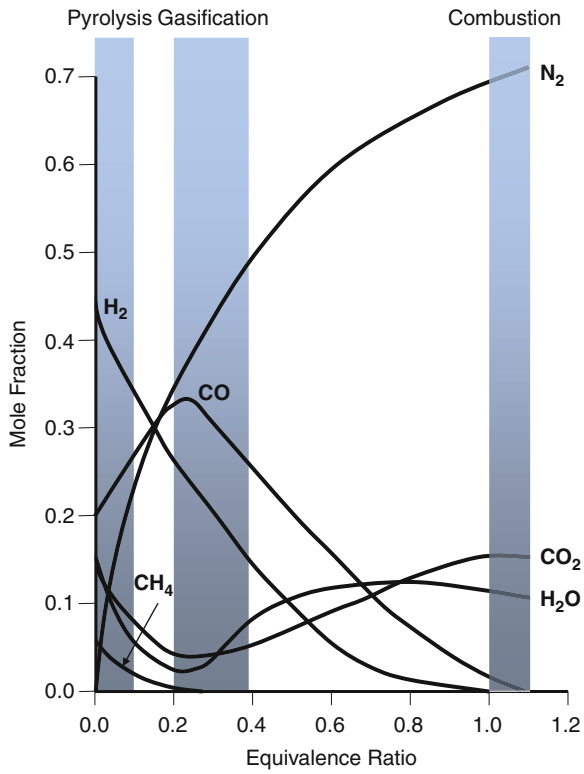

Vehicle Biofuels. Figure 15
Equilibrium gas composition exiting a thermochemical reactor using air as the oxidant. The equivalence ratio is the actual air employed compared to the stoichiometric amount needed for complete combustion [31]

alcohol [38, 39]. Because of its low cost, methanol is the preferred alcohol; however, other alcohols (e.g., ethanol) can be used as well. A by-product of biodiesel production is glycerol.

Biological Processes

Biological processing of biomass involves the use of fermentation to convert biomass to fuels.

Sugar Platform The sugar platform employs processes that convert sugar to fuel (typically alcohol) via fermentation (Fig. 16).

Sugar Crop (2 → d → B) In Brazil, the dominant sugar crop is sugarcane (*Saccharum officinarum*). Traditionally, prior to harvest, the sugarcane field is set afire to burn off leaves, which contain negligible amounts of sugar. (*Note:* Because of the pollution that results from burning sugarcane fields, many governments are banning this practice.) After the fire, the stalks are brought to the sugar mill for processing. On a wet basis, the harvested plant contains 68–72%

Vehicle Biofuels. Table 15 Energy content of gaseous fuels [31]

Name	Source	Energy content (Btu/scf)[a]
Low-energy gas	Air gasifier	150–200
Medium-energy gas	Oxygen gasifier Pyrolyzer	300–500
Biogas	Anaerobic digestor	600–700
High-energy gas	Natural gas	1,000

[a]*scf* standard cubic foot (ft^3) where $T = 60°F$ and $P = 1$ atm

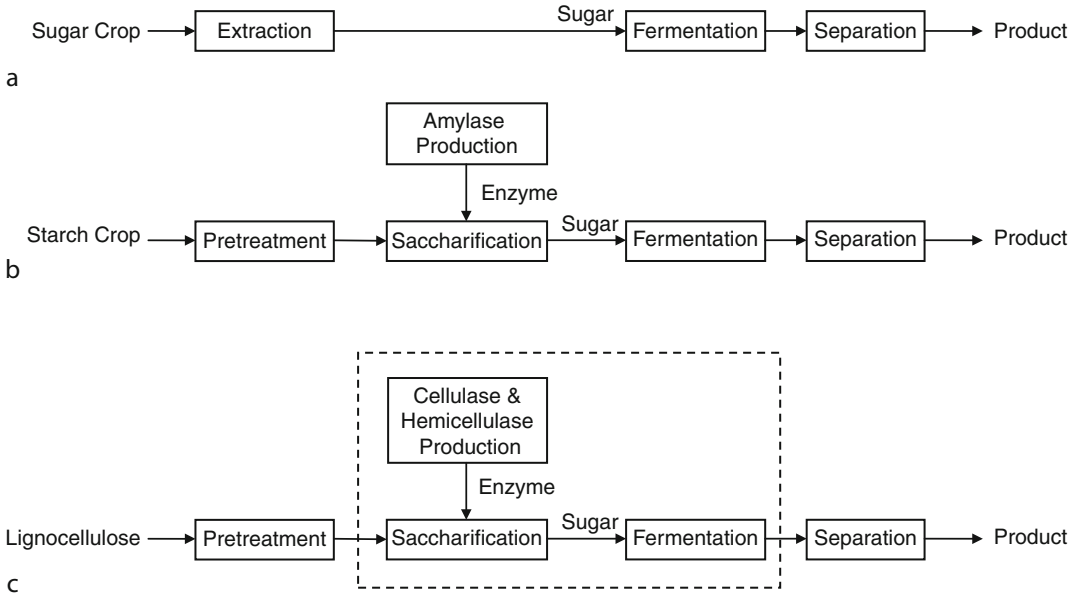

Vehicle Biofuels. Figure 16
Sugar platform. (**a**) sugar crop; (**b**) starch crop; (**c**) lignocellulose

moisture and 12–17% total sugars that are 90% sucrose and 10% glucose or fructose [40].

To extract the sugar, the sugarcane stalks are chopped using a hammer mill and washed countercurrently with water in a multi-stage operation. The most common extraction method uses roller mills that intensely squeeze the fiber to recover the maximum juice per stage. Typically three to four stages are employed. Another common extraction method employs diffusers in which the fiber is placed on a conveyor belt and is repeatedly washed in a countercurrent manner with water that has ever-lower sugar concentrations. Typically, 10–18 washing stages are employed [40]. The extraction process usually recovers >95% of the sugar in fiber. The washed fiber is called *bagasse*, and is used to fuel boilers that power the sugar mill.

Commercial sugarcane varieties are bred to have high sugar concentrations, which reduces the amount of fiber that must be processed by the sugar mill. In contrast, energy cane varieties are bred to have high per-acre yields of both fiber and sugar, at the expense of lower sugar concentrations. To economically recover sugar from energy cane, a novel screw-press conveyor extraction system can be employed that uses a "gentle squeeze" between extraction stages [41]. Typically eight extraction stages would be employed.

In Brazil, both continuous and batch fermentations are employed [42]. Continuous fermentations are more productive; however, they are more prone to contamination, thus batch fermentations are preferred. In both processes, centrifuges recover yeast (*Saccharomyces cerevisiae*) from the fermentation broth and recycle it to subsequent fermentations. Yeast grow at acid pH whereas bacteria prefer neutral pH; therefore, to reduce bacterial contamination, the recycled yeast is contacted with dilute sulfuric acid. Typical fermentations employ the following conditions: cell density 8–17% v/v, temperature 33–35°C, ethanol concentration 8–11% v/v, ethanol yield 90–92% of theoretical, and fermentation time 6–10 h. Contaminants are unable to take over the fermentation because of the short residence time, high ethanol concentrations, and addition of antibiotics.

The ethanol product is distilled to the azeotrope (95.5% v/v) and then can be dehydrated using molecular sieves [42]. In Brazil, azeotropic ethanol is sold as a neat fuel; however, it cannot be blended into gasoline or diesel fuel because the water will form a separate phase.

Starch Crop (3 → d → B) The most common starch crop is corn, which has a typical composition shown in Table 16. Corn is processed by wet mills and dry mills (Fig. 17). Wet mills fractionate corn into oil, fiber, gluten (i.e., protein), and starch; the later which may be fermented into ethanol. Purpose-built ethanol plants use dry milling, which is less capital intensive and produces the majority of corn ethanol in the United States.

Vehicle Biofuels. Table 16 Typical corn composition [43]

Component	Wet basis (g/100 g wet corn)	Dry basis (g/100 g dry corn)
Starch	59.5	70.0
Fiber	7.0	8.2
Ash and other	6.7	7.9
Protein	8.4	9.9
Oil	3.4	4.0
Water	15.0	0.0
Total	100.0	100.0

In dry mills [43], the corn is hammer-milled and then is mixed with water, lime, and ammonia at 88–110°C for 75 min. During this cooking process, the starch hydrates and swells. To reduce the viscosity, thermo-stable α-amylase is added which begins the *saccharification* (i.e., sugar-production) process. After cooking, the temperature is lowered to 61°C and glucoamylase is added, which completes the saccharification of starch to glucose in about 5 h. After saccharification, the temperature is lowered to 32°C to begin the fermentation using yeast (*Saccharomyces cerevisiae*). Typically, batch fermentations are used with a residence time of about 68 h. The final ethanol concentration in the beer is about 10.8% ethanol (w/w). To recover the ethanol, the beer is distilled. The bottoms of the first distillation column contain solids (e.g., yeast, gluten, fiber, and germ), which are recovered by centrifugation and evaporation and sold as distiller's dried grains with solubles (DDGS). The DDGS has high protein content (about 28%) and is

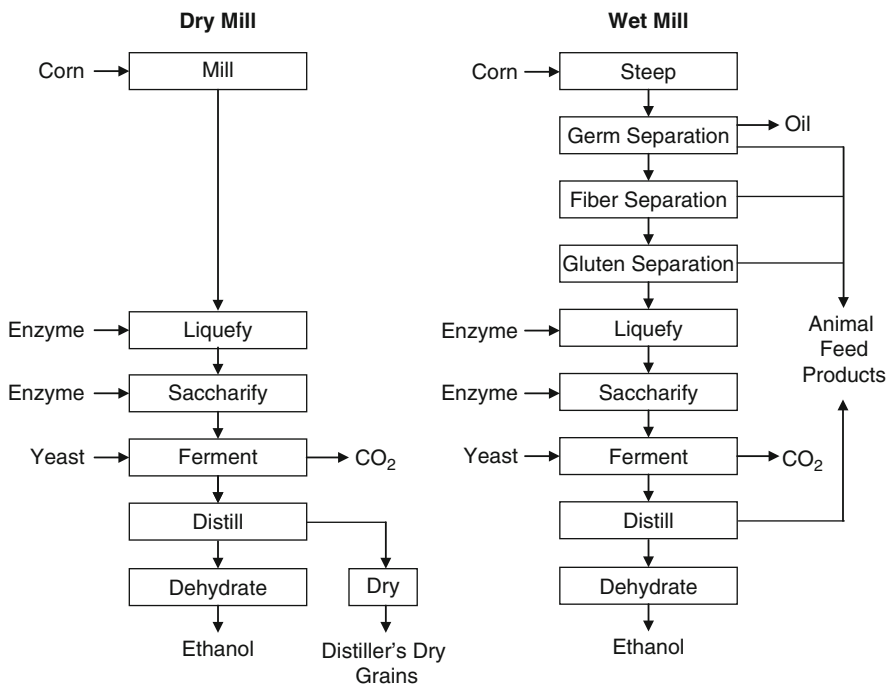

Vehicle Biofuels. Figure 17
Corn-to-ethanol processes

sold as animal feed. The tops from the first distillation column contain ethanol and water, which is further distilled and finally dehydrated using molecular sieves.

In wet mills [44], first the corn is *steeped*, i.e., soaked in water containing 0.06–0.2% sulfur dioxide at about 51°C for about 36 h. The steeping softens the kernels and breaks the protein matrix allowing the corn to be separated into its various components (germ, fiber, gluten, starch). From the germ, corn oil is extracted leaving germ meal. The germ meal, corn fiber, and gluten are formulated into various animal feed products (e.g., gluten meal, gluten feed). The corn starch has numerous uses (e.g., production of high-fructose syrup) and can be used to produce ethanol in a process similar to that used in dry mills.

Although ethanol is the dominant alcohol produced from starch, butanol is also being produced [45].

Lignocellulose (1 → d → B) In lignocellulose, the dominant polysaccharide is cellulose, which is composed of β-linked glucose monomers. Because of its similarity to starch (α-linked glucose), many lignocellulose-conversion processes are modeled after starch-conversion processes (Fig. 16). In starch-conversion processes, the pretreatment step involves soaking in water, which swells the starch rendering it more susceptible to enzymatic hydrolysis. In lignocellulose-conversion processes, a more aggressive pretreatment is required.

The enzymatic digestibility of lignocellulose is affected by the following factors: lignin content, acetyl content of hemicellulose, cellulose crystallinity, degree of polymerization, pore volume, and accessible surface area. To increase its enzymatic digestibility, lignocellulose may be treated with steam, alkali (e.g., ammonia, lime, sodium hydroxide), dilute acids (e.g., sulfuric), liquid hot water, solvents (e.g., ethanol, acetone, butanol, ionic liquids), oxidants (e.g., hydrogen peroxide, oxygen, ozone), and machines (e.g., ball mill, two-roll mill) [46].

After pretreatment, the lignocellulose is saccharified using cellulase and hemicellulase enzymes, which produce primarily glucose and xylose [47]. Traditional yeast (*Saccharomyces cerevisiae*) can ferment only the glucose, so xylose-fermenting microorganisms (e.g., *Pichia stipitis*) are required to utilize all sugars. Using genetic engineering, microorganisms have been developed that ferment both glucose and xylose to ethanol [48]. Economies can be realized via *consolidated bioprocessing* in which enzyme production, saccharification, and fermentation occur in the same vessel using a single microorganism, as shown in the dotted box of Fig. 16 [49]. Although genetic engineering is being used to develop consolidated bioprocessing microorganisms, naturally occurring microorganisms have been identified as well [50].

The conversion of lignocellulose to ethanol has not been commercialized, so typical industrial fermentation conditions have not yet been established. Compared to starch, lignocellulose is much less reactive; therefore, lignocellulose fermentations are likely to take much longer and produce lower ethanol concentrations.

Lignocellulosic ethanol will be recovered via distillation, much like ethanol from conventional starch or sugar processes.

The main impediments to lignocellulosic ethanol are the high cost of pretreatment and enzymes. Some processes overcome this barrier by using dilute acids to saccharify lignocellulose [51]. In the early and mid twentieth century, this process was used commercially in Germany and the former Soviet Union, and was piloted in the United States during World War II. The main obstacle to widespread commercialization is sugar degradation, which reduces yields and inhibits the fermentation. Another process option is the use of concentrated acid to saccharify lignocellulose [52]. Compared to dilute-acid hydrolysis, sugar degradation is much less; however, acid recovery is a challenge. One promising approach is industrial-scale chromatography.

Carboxylate Platform (1 → e → B) The carboxylate platform is a type of consolidated bioprocessing in which lignocellulose is biologically converted to carboxylate salts (e.g., calcium acetate) that are subsequently chemically converted to fuels and chemicals [53, 54]. Generally, a mixed culture of microorganisms is used, which has a great operational advantage: sterile operating conditions are not required. Nonetheless, because they have greater control over the products and yields, some processes use a monoculture and do require sterile operating conditions [55].

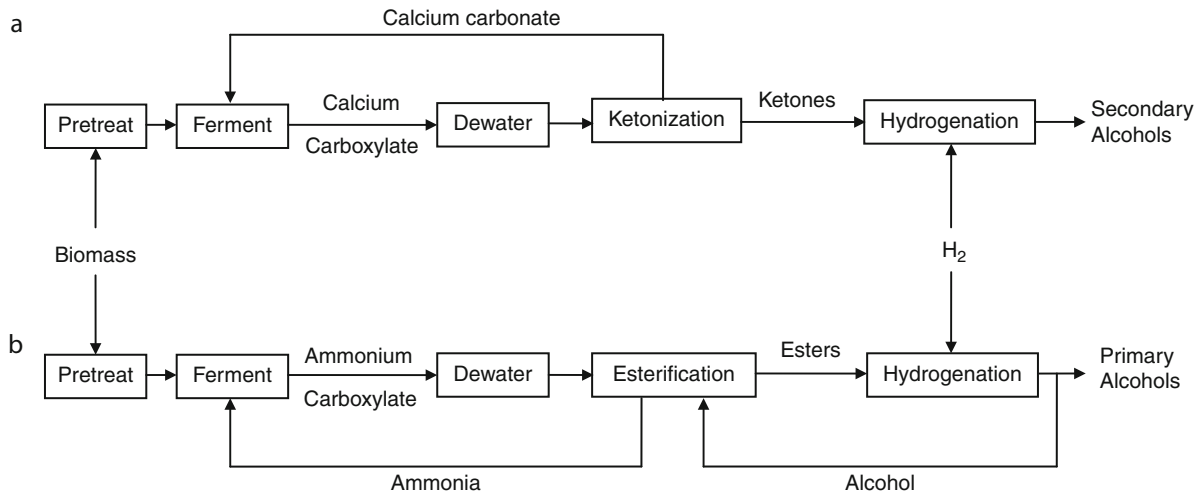

Vehicle Biofuels. Figure 18
Carboxylate platform. (**a**) secondary alcohol route; (**b**) primary alcohol route

Figure 18 shows a schematic of the carboxylate platform, which has routes to secondary and primary alcohols.

In the secondary alcohol route [56], the biomass is pretreated to enhance its digestibility. In principle, any pretreatment can be used; however, alkaline pretreatments (e.g., lime) are favored because the cations help neutralize the carboxylic acids produced in the fermentation. The biomass is then fed to a mixed culture of microorganisms that ferments biomass components (e.g., cellulose, hemicellulose, starch, free sugars, pectin, protein, fats) into carboxylic acids (e.g., acetic, propionic, butyric acids) and hydrogen. To maintain a near-neutral pH, a buffer is added (e.g., calcium carbonate). The mixed culture of microorganisms can originate from a variety of sources, such as cattle rumen or marine swamps. An inhibitor (e.g., iodoform) is added to suppress the generation of methane, an unwanted by-product. Via vapor-compression evaporation, the carboxylate salts in the fermentation broth are dewatered. The concentrated carboxylate salts (e.g., calcium acetate) are thermally converted to ketones (e.g., acetone). The ketones are hydrogenated using a hydrogenation catalyst (e.g., Raney nickel) to produce secondary alcohols (e.g., isopropanol). Potential sources of hydrogen include the fermentor gas, gasified undigested residues, reformed methane, and water electrolysis.

In the primary alcohol route [57], the early steps (pretreatment, fermentation, and dewatering) are nearly identical to the secondary alcohol route. After dewatering, the concentrated carboxylate salts (e.g., ammonium acetate) react with a recycled high-molecular-weight alcohol (e.g., hexanol) to form esters (e.g., hexyl acetate), which is subsequently hydrogenated to form two alcohols (e.g., ethanol and hexanol). The high-molecular-weight alcohol is recycled and the low-molecular-weight alcohol is harvested as product.

Syngas Platform (1 → b → B) As described previously, syngas ($CO + H_2$) is produced by gasifying biomass. The syngas can be fermented to acetate, butyrate, ethanol, and butanol [58–60].

Biomass to Hydrocarbons Because of their high energy density, hydrocarbons are the preferred source of transportation fuels. Various routes to hydrocarbons are described below.

Biogas (1 → e → A) As described previously, the carboxylate platform uses a mixed culture of microorganisms to produce carboxylate salts and hydrogen. If no methanogen inhibitor is included, these products are converted to biogas ($CH_4 + CO_2$), which simply bubbles out of the fermentation broth [61].

Because of its simplicity, this process is used all over the world, including developing countries, to convert waste biomass into fuel. Normally, this fuel is used for stationary applications (e.g., cooking, electricity production); however, it could be purified by removing carbon dioxide using acid-gas absorbents (e.g., triethanol amine). The resulting pure methane could be cryogenically liquefied and used for transportation purposes.

Hydrocarbons from Alcohols (B → A) Fermentation-derived alcohols can be converted to hydrocarbons using zeolite catalysts, such as H-ZSM-5 [62].

$$nC_2H_5OH \rightarrow C_{2n}H_{4n} + nH_2O$$

The reaction proceeds by dehydrating the alcohol to form an alkene (olefin), which then oligomerizes to form higher molecular weight hydrocarbons (e.g., olefins, aromatics). If desired, the final product can be hydrogenated to saturate the bonds. Compared to low-molecular-weight alcohols, high-molecular-weight alcohols retain a greater percentage of their combustion energy within the hydrocarbon product [63].

Oleaginous Microorganisms *Oleaginous microorganisms* accumulate triacylglycerol (TAG) within their cells, typically as a result of environmental stress such as nutrient limitations (e.g., nitrogen, phosphorous). As with algae and oil crops, the TAG can be extracted from the cell and converted to methyl esters (biodiesel) or hydrotreated to hydrocarbons [64]. In some cases, the TAG floats to the top of the fermentor and can be removed by skimming.

Hydrocarbons from Sugar (d → A) Under appropriate fermentation conditions, naturally occurring microorganisms accumulate TAG. For example, the yeast *Rhodosporidium toruloides* ferments sugar and accumulates 67% of its cellular dry weight as lipids and can produce TAG concentrations over 70 g/L in the fermentor [64]. To enhance TAG production, researchers are applying genetic engineering techniques to *Saccharomyces cerevisiae* and *Escherichia coli* [65].

Hydrocarbons from Lignocellulose (1 → A) Some microorganisms that grow directly on lignocellulose accumulate TAG within their cells [66].

Hydrocarbons from Carboxylates (e → A) Some microorganisms (e.g., *Alcanivorax borkumensis* SK2) accumulate and secrete TAG when growing on acetate [67].

Future Directions

For biofuels to make a significant impact on transportation, it is necessary to minimize land area requirements, which is accomplished by (1) growing the most productive crops and (2) utilizing the whole plant.

Crop Productivity

Among oil-producing land crops, Chinese tallow is one of the most productive and it can grow on marginally productive lands. Despite these advantages, it is not a significant source of biodiesel. In the United States, soybean oil dominates, yet it is among the least productive oil-seed crops. Chinese tallow is not widely grown because it is an invasive species and governments restrict its growth; however, the very properties that make it invasive (rapid growth, robust) make it an ideal biomass source. Perhaps plant breeders can create varieties that maintain the desirable traits, yet eliminate its invasive properties. For example, it might be possible to create varieties in which the seeds are sterile.

Among aquatic plants, water hyacinth has the highest productivity and rivals algae, which are the most productive photosynthetic organisms. Water hyacinth is also an invasive species; therefore, production systems must be developed to prevent its release into local rivers and lakes.

Among land crops, lignocellulose is the most productive. Further, numerous lignocellulosic wastes (municipal solid waste, manure, agricultural residues) are inexpensive and many are already collected.

Whole Plant Utilization

In recent years, much attention has been paid to algae because they do not compete with agricultural land, and they produce high concentrations of TAG, which is readily converted to biodiesel or hydrocarbons. Nonetheless, only a portion of the algae is TAG. Rather than focusing only on TAG, greater yields will be realized by converting the entire organism to fuel.

Given the diverse composition and high water content of algae, the best process candidate is the carboxylate platform.

Lignocellulose conversion processes use the whole plant, not just the seed or the root. Although many lignocellulose conversion processes are being developed, the technology is still immature so no processes have been fully commercialized.

Closing Thoughts

Although biofuels currently contribute to the global supply of transportation fuels, the industry is in its infancy. Once lignocellulose conversion technology is perfected, the full potential of biofuels will be realized.

Bibliography

Primary Literature

1. Renewable Fuels Association. http://www.ethanolrfa.org/pages/statistics#A
2. Energy Information Administration. http://www.eia.gov/dnav/pet/hist/LeafHandler.ashx?n=PET&s=MGFUPUS2&f=A
3. Renewable Fuels Association (2010) Ethanol industry outlook: climate of opportunity. http://www.ethanolrfa.org/page/-/objects/pdf/outlook/RFAoutlook2010_fin.pdf?nocdn=1
4. Energy Information Administration. http://www.eia.doe.gov/cneaf/solar.renewables/page/biodiesel/biodiesel.html
5. Energy Information Administration. http://www.eia.gov/dnav/pet/pet_cons_psup_dc_nus_mbblpd_a.htm
6. Zhang RD, He H, Shi XY, Zhang CB, He BQ, Wang JX (2004) Preparation and emission characteristics of ethanol-diesel fuel blends. J Environ Sci (China) 16:793–796
7. Subbaiah GV, Gopal KR, Hussain SA, Prasad BD, Reddy KT (2010) Rice bran oil biodiesel as an additive in diesel-ethanol blend for diesel engines. Int J Res Rev Appl Sci 3:334–342
8. Perlack RD, Wright LL, Turhollow AF, Graham RL, Stokes BJ, Erbach DC (2005) Biomass as feedstock for a bioenergy and bioproducts industry: the technical feasibility of a billion-ton annual supply. Oak Ridge National Laboratory, Oak Ridge. DOE/GO-102995–2135, ORNL/TM-2005/66
9. US Environmental Protection Agency (2010) Municipal solid waste generation, recycling, and disposal in the United States: facts and figures for 2009. Franklin Associates, EPA530-R-10–012. http://www.epa.gov/epawaste/nonhaz/municipal/pubs/msw2009-fs.pdf
10. Tilman D, Hill J, Lehman C (2006) Carbon-negative biofuels from low-input high-diversity grassland biomass. Science 314:1598–1600
11. Schmer MR, Vogel KP, Mitchell RB, Perrin RK (2008) Net energy of cellulosic ethanol from switchgrass. Proc Nat Acad Sci USA 105:464–469
12. McKendry P (2002) Energy production from biomass (part 1): overview of biomass. Bioresour Technol 83:37–46
13. McCollum III T, McCuistion K, Brent B (2005) Brown mid-rib and photoperiod-sensitive forage sorghums. AREC 05–20. Agricultural Program, Texas A&M University, Amarillo
14. Waclawovsky AJ, Sato PM, Lembke CG, Moore PH, Souza GM (2010) Sugarcane for bioenergy production: an assessment of yield and regulation of sucrose content. Plant Biotechnol J 8:263–276
15. Westlake DF (1963) Comparisons of plant productivity. Biol Rev 38:385–425
16. Alexander AG (1985) The energy cane alternative, vol 6, Sugar series. Elsevier, Amsterdam
17. Klass DL (1998) Biomass for renewable energy, fuels, and chemicals. Academic, San Diego, 70
18. Spencer W, Bowes G (1986) Photosynthesis and growth of water hyacinth under CO_2 enrichment. Plant Physiol 82:528–533
19. http://waterquality.montana.edu/docs/irrigation/sugarbeet101.shtml
20. Freeman KC, Broadhead DM, Zummo N, Westbrook FE (1986) Sweet sorghum culture and syrup production. U.S. Department of Agriculture, Washington, DC, Handbook No. 611, 55 pp
21. Reddy BVS, Ramesh S, Reddy PS, Ramaiah B, Salimath PM, Kachapur R (2005) Sweet sorghum – a potential alternate raw material for bio-ethanol and bioenergy. SAT eJournal 1(1). www.ejournal.icrisat.org
22. US Department of Agriculture, National Agricultural Statistics Service. http://www.nass.usda.gov/
23. Tickell J (2000) From the fryer to the fuel tank: the complete guide to using vegetable oil as an alternative fuel, 3rd edn. Tickell Energy Consulting, Tallahassee, 162
24. Breitenbeck GA (2008) Chinese tallow trees a potential bioenergy crop for Louisiana. Louisiana Agr 51:10–12
25. Mata TM, Martins AA, Caetano NS (2010) Microalgae for biodiesel production and other applications: a review. Renew Sust Energy Rev 14:217–232
26. Griffiths MJ, Harrison STL (2009) Lipid productivity as a key characteristic for choosing algal species for biodiesel production. J Appl Phycol 21:493–507
27. Piskorz J, Scott DS, Radlein D (1988) Composition of oils obtained by fast pyrolysis of different woods. In: Soltes EJ, Milne TA (eds) Pyrolysis oils from biomass, vol 376, ACS symposium series. American Chemical Society, Washington, DC, pp 167–178
28. Emsley AM, Stevens GC (1994) Kinetics and mechanisms of the low-temperature degradation of cellulose. Cellulose 1:26–56
29. Klinke HB, Thomsen AB, Ahring BK (2004) Inhibition of ethanol-producing yeast and bacteria by degradation products produced during pre-treatment of biomass. Appl Microbiol Biotechnol 66:10–26

30. Wu X, McLaren J, Madl R, Wang D (2010) Biofuels from lignocellulosic biomass. In: Singh OV, Harvey SP (eds) Sustainable biotechnology: sources of renewable energy. Springer, New York, pp 19–41
31. Reed TB (1981) Biomass gasification: principles and technology. Noyes Data Corporation, Park Ridge
32. Woo HC, Park KY, Kim YG, Nam I-S, Chung JS, Lee JS (1991) Mixed alcohol synthesis from carbon monoxide and dihydrogen over potassium-promoted molybdenum carbide catalysts. Appl Catal 75:267–280
33. Xu M, Lunsford JH, Goodman DW, Bhattacharyya A (1997) Synthesis of dimethyl ether (DME) from methanol over solid-acid catalysts. Appl Catal A Gen 149:289–301
34. Semelsberger TA, Borup RL, Greene HL (2006) Dimethyl ether (DME) as an alternative fuel. J Power Source 156:497–511
35. Bridgwater AV, Meier D, Radlein D (1999) An overview of fast pyrolysis of biomass. Org Geochem 30:1479–1493
36. Czernik S, Bridgwater AV (2004) Overview of applications of biomass fast pyrolysis oil. Energy Fuels 18:590–598
37. Bozell JJ, Moens L, Elliott DC, Wang Y, Neuenscwander GG, Fitzpatrick SW, Bilski RJ, Jarnefeld JL (2000) Production of levulinic acid and use as a platform chemical for derived products. Resour Conserv Recycl 28:227–239
38. Balat M, Balat H (2010) Progress in biodiesel processing. Appl Energy 87:1815–1835
39. Chisti Y (2007) Biodiesel from microalgae. Biotechnol Adv 25:294–306
40. Rein PW (1995) A comparison of cane diffusion and milling. In: Proceedings of the South African sugar technologists' association, pp 196–200
41. Granda CB, Holtzapple MT (2006) Low-pressure sugar extraction with screw-press conveyors. Int Sugar J 108:555–568
42. Wheals AE, Basso LC, Alves DMG, Amorim HV (1999) Fuel ethanol after 25 years. Trends Biotechnol 17:482–487
43. Kwiatkowski JR, McAloon AJ, Taylor F, Johnston DB (2006) Modeling the process and costs of fuel ethanol production by the corn dry-grind process. Ind Crop Prod 23:288–296
44. Ramirez EC, Johnston DB, McAloon AJ, Yee W, Singh V (2008) Engineering process and cost model for a conventional corn wet milling facility. Ind Crops Prod 27:91–97
45. Manzer LE (2010) Recent developments in the conversion of biomass to renewable fuels and chemicals. Topics Catal 53:1193–1196
46. Sierra R, Smith A, Granda C, Holtzapple MT (2008) Producing fuels and chemicals from lignocellulosic biomass. Chem Eng Prog 104:S10–S18
47. Sun Y, Cheng J (2002) Hydrolysis of lignocellulosic materials for ethanol production: a review. Bioresour Technol 83:1–11
48. Zaldivar J, Nielsen J, Olsson L (2001) Fuel ethanol production from lignocellulose: a challenge for metabolic engineering and process integration. Appl Microbiol Biotechnol 56:17–34
49. Lynd LR, van Zyl WH, McBride JE, Laser M (2005) Consolidated bioprocessing of cellulosic biomass: an update. Curr Opin Biotechnol 16:577–583
50. Warnick TA, Methe BA, Leschine SB (2002) *Clostridium phytofermentans* sp. nov., a cellulolytic mesophile from forest soil. Int J Syst Evol Microbiol 52:1155–1160
51. Lee YY, Iyer P, Torget RW (1999) Dilute-acid hydrolysis of lignocellulosic biomass. Adv Biochem Eng Biotechnol 65:93–114
52. Lindsey TC (2010) Conversion of existing dry – mill ethanol operations to biorefineries. In: Blaschek HP, Ezeji TC, Scheffran J (eds) Biofuels from agricultural wastes and byproducts. Wiley-Blackwell, Oxford
53. Agler MT, Wrenn BA, Zinder SH, Angenent LT (2011) Waste to bioproduct conversion with undefined mixed cultures: the carboxylate platform. Trends Biotechnol 29:70–78
54. Chang HN, Kim N-J, Kang J, Jeong CM (2010) Biomass-derived volatile fatty acid platform for fuels and chemicals. Biotechnol Bioprocess Eng 15:1–10
55. Verser D, Eggeman T (2003) Process for producing ethanol. US Patent 6,509,180 B1
56. Pham V, Holtzapple M, El-Halwagi M (2010) Techno-economic analysis of biomass to fuel conversion via the MixAlco process. J Ind Microbiol Biotechnol 37:1157–1168
57. Granda CB, Holtzapple MT, Luce G, Searcy K, Mamrosh DL (2009) Carboxylate platform: the MixAlco process. Part 2: process economics. Appl Biochem Biotechnol 156:537–554
58. Datar RP, Shenkman RM, Cateni BG, Huhnke RL, Lewis RS (2004) Fermentation of biomass-generated producer gas to ethanol. Biotechnol Bioeng 86:587–594
59. Younesi H, Najafpour G, Mohamed AR (2005) Ethanol and acetate production from synthesis gas via fermentation processes using anaerobic bacterium, *Clostridium ljungdahlii*. Biochem Eng J 27:110–119
60. Vega JL, Prieto S, Elmore BB, Clausen EC, Gaddy JL (1989) The biological production of ethanol from synthesis gas. Appl Biochem Biotechnol 20(21):781–797
61. Santosh Y, Sreekrishnan TR, Kohli S, Rana V (2004) Enhancement of biogas production from solid substrates using different techniques – a review. Bioresour Technol 95:1–10
62. Oudejans JC, Van den Oosterkamp PF, Van Bekkum H (1982) Conversion of ethanol over zeolite H-ZSM-5 in the presence of water. Appl Catal 3:109–115
63. Holtzapple MT, Granda CB (2009) Carboxylate platform: the MixAlco process. Part 1: comparison of three biomass conversion platforms. Appl Biochem Biotechnol 156:525–536
64. Li Q, Du W, Liu D (2008) Perspectives of microbial oils for biodiesel production. Appl Microbiol Biotechnol 80:749–756
65. Rude MA, Schirmer A (2009) New microbial fuels: a biotech perspective. Curr Opin Microbiol 12:274–281
66. Hui L, Wan C, Hai-tao D, Xue-jiao C, Qi-fa Z, Zhao Yu-hua (2010) Direct microbial conversion of wheat straw into lipid by a cellulolytic fungus of *Aspergillus oryzae* A-4 in solid-state fermentation. Bioresour Technol 101:7556–7562
67. Manilla-Pérez E, Lange AB, Hetzler S, Steinbüchel A (2010) Occurrence, production, and export of lipophilic compounds by hydrocarbonoclastic marine bacteria and their potential use to produce bulk chemicals from hydrocarbons. Appl Microbiol Biotechnol 86:1693–1706

Books and Reviews

Bungay HR (1981) Energy, the biomass options. Wiley-Interscience, New York

Cheremisinoff NP, Cheremisinoff PN, Ellerbusch F (1980) Biomass: applications, technology, and production, vol 5, Energy, power, and environment. Marcel Dekker, New York

Klass DL (1981) Biomass as a nonfossil fuel source, vol 144, ACS symposium series. American Chemical Society, Washington, DC

Klass DL (1998) Biomass for renewable energy, fuels, and chemicals. Academic, San Diego

Moo-Young M, Blanch HW, Drew S, Wang DIC (1985) Comprehensive biotechnology, vol 3, The practice of biotechnology: current commodity products. Pergamon, New York

Saha BC, Woodward J (1997) Fuels and chemicals from biomass, vol 666, ACS symposium series. American Chemical Society, Washington, DC

Sarkanen KV, Tillman DA (1979) Progress in biomass conversion, vol 1. Academic, New York

Smil V (1983) Biomass energies: resources, links, constraints. Plenum, New York

Stafford DA, Hawkes DL, Horton R (1980) Methane production from waste organic matter. CRC Press, Boca Raton

Waldron K (2010) Bioalcohol production: biochemical conversion of lignocellulosic biomass, vol 3, Woodhead publishing series in energy. CRC Press, Boca Raton

Zaborsky OR, McClure TA, Lipinsky ES (1981) Handbook of biosolar resources, vol II, Resource materials. CRC Press, Boca Raton

Vehicle Detection, Tightly Coupled LIDAR and Computer Vision Integration for

Lili Huang, Matthew Barth
Department of Electrical Engineering, University of California, Riverside, CA, USA

Article Outline

Glossary
Definition of the Subject
Introduction and Background
A Novel Multi-planar LIDAR and Computer Vision Calibration Procedure Using 2D Patterns
Tightly Coupled LIDAR and Computer Vision Integrated System for Vehicle Detection
Conclusions and Future Work
Future Directions
Disclaimer
Bibliography

Glossary

Calibration Comparison and alignment between two or more measurements or coordinates; coordinate systems are defined for different devices and the relationships between systems are established through calibration.

Computer vision Technology using computers to extract information from an image, a series of images, or video sequences to aid sensing applications.

Intelligent transportation system (ITS) System of technologies including information processing, control, communications, and system management applied to vehicles and infrastructure to improve transportation. ITS aims to improve safety, transportation efficiency, and reduce environmental impacts.

Laser range finder (LIDAR) A device that uses laser beams to determine the distance to an object. The most common technique used for distance measurement works on the time-of-flight principle.

Vehicle detection Detect, count, and classify vehicles using video camera, loop sensors, or wireless sensors. Vehicle detection systems are typically "nonintrusive" to traffic.

Vehicle tracking A combination of techniques to track a vehicle's location, record position data, and deliver data to an owner or a third party. Devices used in vehicle tracking include GPS, and possibly a video camera and other electronic devices.

Definition of the Subject

The demand on today's transportation systems is growing quite rapidly, with an estimated 30% travel demand increase predicted over the next decade [1]. Transportation infrastructure growth is not keeping pace with this traffic demand, therefore researchers and practitioners have turned to intelligent transportation systems (ITS) to improve overall traffic efficiency, thereby maximizing the current infrastructure's capacity.

ITS uses sensors, communication, and traffic control technologies to better handle the increased

demands in traffic, to enhance public safety, and to reduce environmental impacts of transportation [2]. One key ITS function that is important for many applications is the ability to gather traffic information using vehicle detection and surveillance techniques. Vehicle detection technology is widely used to provide information for vehicle counting, classification, and traffic characterization. Further, when it is implemented on a moving vehicle, it can even be utilized for vehicle navigation purposes [3]. The generalized vehicle detection problem from a moving vehicle is challenging, which aims to determine the surrounding vehicle's (relative) position, speed, and trajectory. A driver is able to determine a short-term and long-term trajectory based on the vehicle's current position and information about the surrounding vehicles.

In the case where vehicle detection is carried out on a moving vehicle, the surrounding vehicles' information is commonly collected by various sensing systems. These sensing systems typically consist a suite of sensors that can provide real-time measurements, and play an important role in the development of driver assistant systems (DAS).

One of the most common sensing techniques used is computer vision. Computer vision sensors provide a large amount of information on the surrounding environment. However, the computer vision sensors often suffer from intensity variations, narrow fields of view, and low-accuracy depth information [4]. In contrast, a laser ranging method (i.e., LIDAR) measures distance and relative angle from the sensor to the target by calculating time of flight of the laser. Its measurements depend on the size and reflectivity of the target, so the probability of detection decreases with distance [5]. Since their characteristics of computer vision and LIDAR complement each other, it is useful to integrate both computer vision and LIDAR for detecting different objects around the vehicle's environment.

A tightly coupled LIDAR and computer vision system is proposed in this entry to solve the vehicle detection problem. This sensing system is mounted on a test vehicle, as is shown in Fig. 1. A pair of LIDAR sensors is mounted on the front bumper of the vehicle, and a camera is mounted behind the front windshield.

Since sensor fusion systems are commonly used to integrate sensory data from disparate sources, the output will be more accurate and complete in comparison to the output of a single sensor. In order to effectively extract and integrate 3D information from both computer vision and LIDAR systems, the relative position and orientation between these two sensor modalities should be obtained. A sensor calibration process is used to identify the parameters that describe the relative geometric transformation between sensors [6, 7], which is a key step in the sensor fusion process. However, current calibration methods work only for visible beam LIDAR, 3D LIDAR, and 2D LIDAR [8–12]. To date, there does not exist any convenient calibration methods for multi-planar "invisible-beam" LIDAR and computer vision systems.

Vehicle Detection, Tightly Coupled LIDAR and Computer Vision Integration for. Figure 1
The mobile sensing platform. This probe vehicle carries one camera and two IBEO ALASCA XT LIDAR sensors

A novel calibration approach of a camera with a multi-planar LIDAR system is proposed in this entry, where the laser beams are invisible to the camera. The camera and LIDAR are required to observe a planar pattern at different positions and orientations. Geometric constraints of the "views" from the LIDAR and camera images are resolved as the coordinate transformation coefficients. The proposed approach consists of two stages: solving a closed-form equation, followed by applying a nonlinear algorithm based on a maximum likelihood criterion. Compared with the classical methods which use "beam-visible" cameras or 3D LIDAR systems, this approach is easy to implement at low cost.

The combination of LIDAR and camera is employed in vehicle detection since the geometric transformation between two sensors is known from calibration. In the sensor fusion system, LIDAR sensor estimates possible vehicle positions. This information is transformed into the image coordinates. Different regions of interest (ROIs) in the imagery are defined based on the LIDAR object hypotheses. An Adaboost object classifier is then utilized to classify the vehicle in ROIs. A classifier error correction approach chooses an optimal position of the detected vehicle. Finally, the vehicle's position and dimensions are derived from both the LIDAR and image data. This sensor fusion system can be used in ITS applications such as traffic surveillance and roadway navigation tasks.

This entry is organized as follows: section "Introduction and Background" reviews background and related work, including the calibration methods for LIDAR and camera, and sensor fusion–based vehicle detection algorithms. Section "A Novel Multi-Planar LIDAR and Computer Vision Calibration Procedure Using 2D Patterns" focuses on the calibration of LIDAR and camera system. The coordinate systems of the LIDAR and camera sensors are introduced, followed by the mathematical derivation of geometric relations between the two sensors. The equations are then solved in two stages: a closed-form solution, followed by applying a nonlinear algorithm based on a maximum likelihood criterion. Section "Tightly Coupled LIDAR and Computer Vision Integrated System for Vehicle Detection" describes the sensor fusion–based vehicle detection system. Both hardware and data processing software of the sensor fusion system are introduced in this section. Finally, future work is discussed in section "Conclusions and Future Work".

Introduction and Background

During the past decade, a variety of research has been carried out in the traffic surveillance area, where numerous techniques have been developed to obtain parameters such as vehicle counts, location, speed, trajectories and classification data, for both in-vehicle navigation and freeway traffic surveillance applications [13].

As one of the most popular traffic surveillance techniques, computer vision-based approaches are one of the most widely used and promising techniques. LIDAR is another attractive technology due to its high accuracy in ranging, wide-area field of view, and low data processing requirements [5]. The other sensors used in vehicle detection include radar and embedded loop sensors. A brief comparison of the sensor technologies and their advantages as well as disadvantages is given in Table 1.

Sensor fusion systems in the vehicle detection application aim to gather information from the far-field as well as near-field sensors, and combine them in a meaningful way [15]. The output of the sensor fusion system should be the states of objects around the test vehicle.

In this section, a few of the most popular LIDAR sensors that are available commercially today are introduced. This is followed by a discussion of current LIDAR and computer vision calibration methods. The calibration methods include the visible LIDAR beam–based calibration, 3D LIDAR and the 2D single planar LIDAR calibration. Sensor fusion techniques for vehicle detection and tracking systems are also discussed here.

Laser Range Finder (LIDAR)

The vehicle detection solution aims to estimate the states of surrounding vehicles. Vehicle state includes position, orientation, speed, and acceleration. State estimation addresses the problems of estimating quantities from sensors that are not directly observable [16].

LIDAR sensors are commonly utilized in vehicle navigation for detecting surrounding vehicles, infrastructure, and pedestrians. It can also be used in vehicle

Vehicle Detection, Tightly Coupled LIDAR and Computer Vision Integration for. Table 1 Performance comparison of existing sensor technologies used in ITS [14]

Sensor technology	Advantage	Disadvantage
LIDAR	Detect distance and angle with high accuracy	High cost
	Low data processing requirement	Limited detection range
	Operational in fog and rain	Difficult to classify the object
Radar	Direct measurement of speed or distance	Relatively low precision
	Compact size	Limited field of view
	Low data processing requirement	May have identification problem in multilane applications
		Medium cost
Video camera	Provide real-time image of traffic	High requirement for data processing and storage
	Low cost	
	Multiple lanes observed	Different algorithms required for day- and nighttime
	No traffic interruption for installation and repair	
	Large field of view	Susceptible to atmospheric obscurants and weather change
Infrared camera	Day and night operation	High requirement for data processing
	Operational in fog	Susceptible to weather change
Inductive loop detector	Low cost per unit	Installation and maintenance require traffic disruption
	Large experience base	Easily damaged

localization, either as the only sensor or in some combination with GPS and INS.

One of the most popular LIDAR sensors is the SICK LMS 2xx series [17]. A SICK LIDAR operates at distance up to 80 m with an angular resolution of 0.5° and a measurement accuracy of typically 5 cm. The distance between the sensor and an object is calculated by measuring the time interval between an emitted laser pulse and a reception of the reflected pulse. Amplitude of the received signal is used to determine reflectivity of the object surface. The SICK LIDAR is able to detect dark objects at long ranges. Moreover, compared to the CCD cameras and RADAR systems, the view angle of SICK LIDAR is larger, e.g., 180°. Figure 2a illustrates the SICK LMS200 LIDAR.

The HOKUYO UXM-30LN LIDAR is another single planar range sensor for intelligent robots and vehicles [18]. Its detection range is up to 60 m, and the horizontal field of view is 190°. The distance accuracy is 30 mm when the range is less than 10 m, and 50 mm when the range is between 10 and 30 m. The angular resolution is 0.25°. The device is shown in Fig. 2b.

As another example, the ALASCA XT laser scanner made by IBEO is a multi-planar LIDAR, which splits the laser beam into four vertical layers. The aperture angle is 3.2°. The distance range is up to 200 m, and the horizontal field of view is 240° [19]. Figure 2c shows the IBEO sensor.

The Velodyne HDL-64E LIDAR is a 3D sensor which is specifically designed for autonomous vehicle navigation [20]. With 360° horizontal by 25° vertical field of view, 0.09° angular resolution, and 10 Hz refresh rate, Velodyne provides surrounding 3D traffic information with high accuracy (<5 cm resolution)

Vehicle Detection, Tightly Coupled LIDAR and Computer Vision Integration for. Figure 2
A variety of LIDAR sensors: (**a**) SICK LMS LIDAR, (**b**) HOKUYO UXM-30LN LIDAR, (**c**) IBEO ALASCA XT LIDAR, and (**d**) Velodyne HDL-64E LIDAR

and efficiency. The detection range is 100 m for cars, and the latency is less than 0.05 ms. Figure 2d illustrates the Velodyne sensor.

LIDAR sensors were initially used by automatic guided vehicles in indoor environments. More recently, the performance of these ranging sensors has been improved, so that they now can be used in outdoor environments on vehicles. A primary application example is the DARPA Urban Challenge in 2007, in which autonomous vehicles were capable of driving in traffic and performing complex maneuvers such as acceleration and deceleration, lane change, and parking [13]. IBEO and SICK LIDARs were used in many of the finalists for object detection and localization. The Velodyne sensor was used by the five out of six of the finishing teams.

LIDAR and Computer Vision Calibration

Sensor fusion systems are commonly used to combine the sensory data from disparate sources, so that the result will be more accurate and complete in comparison to the output of one sensor. As an example, the winner of the 2007 DARPA Urban Grand Challenge performed sensor fusion between a GPS receiver, long- and short-range LIDAR sensors, and stereo cameras [21].

In order to effectively extract and integrate 3D information from both computer vision and LIDAR systems, the relative position and orientation between these two sensor modalities can be obtained. The relative geometric transformation can be solved through a calibration process [6, 7]. Several approaches have been defined and utilized for LIDAR and computer vision calibration. These techniques can be roughly classified into three categories.

Visible Beam Calibration Visible beam calibration is performed by using cameras to observe the LIDAR beams or reflection points. The calibration system usually consists of an active LIDAR and some infrared or near-infrared cameras. The LIDAR system typically projects stripes with a known frequency, while these stripes are visible to the camera [8–10]. For example, the LIDAR beams used in [9] are captured by a 955fps high-speed camera. However, the image of the high-speed camera is not suitable for monitoring. Color image of the LIDAR beams is generated by letting the vision output go through a beam splitter.

This approach requires a high-cost infrared camera, which should be sensitive to the spectral emission band of the LIDAR. Therefore, this method is not suitable for the low-cost sensor fusion systems.

Three-Dimensional (3D) LIDAR-Based Calibration The 3D LIDAR-based calibration method calibrates the computer vision system with a 3D LIDAR system. Various features are captured by both the camera and the LIDAR. These features are usually in the form of planes, corner, or edges of specific calibration object. An elaborate setup is required. Moreover, dense LIDAR beams in both the vertical and horizontal directions are necessary for the calibration.

The 3D calibration algorithm presented in [11] uses checkerboard in calibration, which is commonly used

for camera calibration. Coefficients of the checkerboard plane are first calculated by LIDAR, and then the coefficients are computed by camera in computer vision coordinates. A two-stage optimization procedure is implemented to minimize the distance between the calculated results and the measurement output.

When the features are edges or corners, accuracy of the calibration method depends on the accuracy by which features are localized [22]. When the features are planes, the LIDAR beams must be sufficiently dense [11]. Therefore, these methods cannot easily be applied to single planar or sparse multi-planar LIDAR systems.

Two-Dimensional (2D) Planar-Based Calibration This approach works for the calibration of camera and 2D LIDAR integration system. The calibration system proposed in [23] consists of a monochrome CCD camera and a LIDAR. The camera and the LIDAR have been pre-calibrated so that their coordinates are parallel to each other. A "V"-shaped pattern is designed to obtain the translation between these two sensors. The calibration procedure is implemented in two steps: the LIDAR detects the "V" shape and finds the vertex, and camera detects the intersection line which cuts the pattern into two parts.

Another calibration approach is proposed in [12] using a checkerboard for calibration. This method is based on observing a plane of an object and solving distance constraints from the camera and LIDAR systems. This approach works for a single planar LIDAR only, e.g., the SICK LMS 2xx series LIDAR.

To date, there does not exist any convenient calibration methods for multi-planar "invisible-beam" LIDAR and computer vision systems. Section "A Novel Multi-Planar LIDAR and Computer Vision Calibration Procedure Using 2D Patterns" proposes a method to handle this case, which is the first calibration method for this system as to the author's best knowledge.

Sensor Fusion–Based Vehicle Detection and Tracking

Computer vision is generally used on mobile platform–based object detection and tracking systems, either separately or along with LIDAR sensors [24]. Most of the computer vision techniques utilize a simple segmentation method such as background subtraction or temporal difference to detect objects [25]. However, these approaches suffer with the fast background changes due to camera motion. A trainable object detection method is proposed in [26] based on a wavelet template, which defines the shape of an object in terms of a subset of the wavelet coefficients of the image. However, the application of vision sensors in vehicle navigation is far from sufficient: clustering, illumination, occlusion, among many other factors, affect the overall performance. Fusion of camera and active sensors such as LIDAR or RADAR, is being investigated in the context of on-board vehicle detection and classification.

A LIDAR and a monocular camera–based detection and classification system is proposed in [27]. Detection and tracking are implemented in the LIDAR space, and the object classification work both in LIDAR space (Gaussian Mixture Model classifier) and in computer vision system (Adaboost classifier). A Bayesian decision rule is proposed to combine the results from both classifiers, and thus a more reliable classification is achieved.

Another integration structure is proposed in [28], in which a LIDAR is integrated with a far-infrared camera and an ego motion sensor. LIDAR-based shape extraction is employed to select region of interests (ROIs). This system combines a straightforward methodology with a backward loop one. Kalman filtering is used as the data fusion algorithm.

A similar technique is presented in [29], which makes use of RADAR, velocity, and steering sensors to generate position hypotheses. Examination of the hypotheses is implemented by a computer vision sensor. Classification is performed using a shape model for either the monocular camera vision or the infrared spectrum images.

A Novel Multi-planar LIDAR and Computer Vision Calibration Procedure Using 2D Patterns

In this section, a novel calibration approach is proposed for a LIDAR and computer vision sensor fusion system. This system consists of a camera with a multi-planar LIDAR, where the laser beams are invisible to the camera. This calibration method also works for computer vision and 3D LIDAR systems.

Although several calibration methods have been developed to obtain the geometric relationship

between two sensors, only a few of them have provided a complete sensitivity analysis of the calibration procedure (see section "LIDAR and Computer Vision Calibration"). As part of the calibration method proposed in this section, the effects of LIDAR noise level as well as total number of poses on calibration accuracy are also discussed.

This section is organized as follows: section "Sensor Alignment" gives the setup using planar planes and defines the calibration constraint. Section "Calibration Solutions" describes in detail how to solve this constraint in two steps. Both a closed-form solution and a nonlinear minimization solution based on maximum likelihood criterion are introduced. Experimental results with different poses are provided in section "Experimental Results". Finally, a brief summary is given in section "Summary".

Sensor Alignment

The setup for a multi-planar LIDAR and camera calibration is described here.

Sensor Configuration In the calibration system, an instrumented vehicle is equipped with two IBEO ALASCA XT LIDAR sensors which are mounted on the front bumper. The LIDAR sensor scans with four separate planes. The distance range is up to 200 m, the horizontal field of view angle of a single LIDAR is 240°, and the total vertical field of view for the four planes is 3.2°. A camera is mounted on the vehicle behind the front windshield, as is shown in Fig. 1.

In order to use the measurements from different kinds of sensors at various positions on the vehicle, the measurements should be transformed from their own coordinate into some common coordinate system. This section focuses on obtaining the spatial relationship between video and LIDAR sensors. The geometric sensor model is shown in Fig. 3.

Vision, LIDAR, and World Coordinate Systems There are several coordinate systems in the overall system to be considered: the camera coordinates, the LIDAR coordinates, and the world coordinate systems.

A camera can be represented by the standard pinhole model. One 3D point in the camera coordinate denoted by $\mathbf{P}_c = [\mathbf{X}_c \quad \mathbf{Y}_c \quad \mathbf{Z}_c]^T$ is projected to a pixel $\mathbf{p} = [u \quad v]^T$ in the image coordinate. The pinhole model is given as [30]:

$$s\mathbf{p} \sim \mathbf{A}[\mathbf{R} \quad \mathbf{t}]\mathbf{P}_c \quad \text{with} \quad \mathbf{A} = \begin{bmatrix} \alpha & \gamma & u_0 \\ 0 & \beta & v_0 \\ 0 & 0 & 1 \end{bmatrix} \tag{1}$$

where s is an arbitrary scale factor. $\mathbf{A}$ is the camera intrinsic matrix defined by coordinates of the principal point $(u_0 \quad v_0)$, scale factors α and β in image u and v

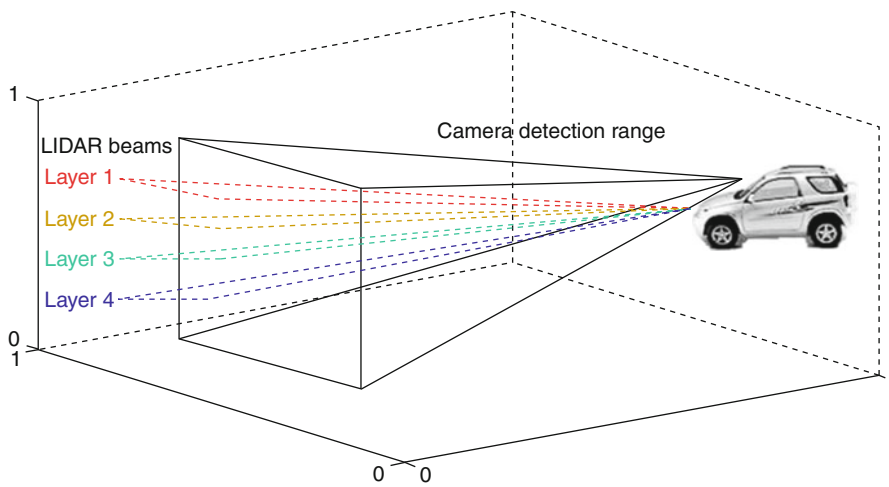

Vehicle Detection, Tightly Coupled LIDAR and Computer Vision Integration for. Figure 3
Geometric model with the camera and the LIDAR

axes, and skewness of the two image axes γ. $(\mathbf{R}, \quad \mathbf{t})$ are called extrinsic parameters. The 3×3 orthonormal rotation matrix $\mathbf{R}$ represents the orientation of world coordinates to the camera coordinate system. The translation matrix $\mathbf{t}$ is a three-vector representing origin of world coordinates in the camera's frame of reference. In the real world, lens of the camera may also have image distortion coefficients, which include radial and tangential distortions and are usually stored in a five-vector [31]. In this entry, the lens is assumed to have no significant distortion, or the distortion has already been eliminated.

The LIDAR sensor provides distance and direction of each scan point in LIDAR coordinates. Distances and directions can be converted into a 3D point denoted by $\mathbf{P}_l = [X_l \quad Y_l \quad Z_l]^T$ [19]. The origin of LIDAR coordinates is the equipment itself. X, Y, and Z axes are defined as forward, leftward, and upward from the equipment, respectively. The camera and LIDAR reference systems are shown in Fig. 4.

In addition to the camera and LIDAR reference systems, another coordinate system is used in the calibration procedure: the world frame of reference. In the calibration process, a checkerboard is placed in front of the sensors. The first grid on the upper-left corner of this board is defined to be the origin of the world coordinates [31].

Suppose a fixed point $\mathbf{P}$ is denoted as $\mathbf{P}_c = [X_c \quad Y_c \quad Z_c]^T$ in the camera coordinates, and $\mathbf{P}_l = [X_l \quad Y_l \quad Z_l]^T$ in the LIDAR coordinates. The transformation from LIDAR coordinate to camera coordinate is given as:

$$\mathbf{P}_c = \mathbf{R}_l^c \mathbf{P}_l + \mathbf{t}_l^c \tag{2}$$

where $\left(\mathbf{R}_l^c, \quad \mathbf{t}_l^c\right)$ are the rotation and translation parameters which relate LIDAR coordinate system to the camera coordinate system.

The purpose of this calibration method is to solve Eq. 2 and obtain coefficients $\left(\mathbf{R}_l^c, \quad \mathbf{t}_l^c\right)$, so that any given point in the LIDAR reference system can be transformed to the camera coordinates.

Basic Geometric Interpretation A checkerboard visible to both sensors is used for calibration. In the following sections, the planar surface defined by the checkerboard is called the *checkerboard plane*. Without loss of generality, the checkerboard plane is assumed to be on $Z = 0$ in the world coordinates. Let $\mathbf{r}_3$ denotes the i-th column of the rotation matrix $\mathbf{R}$. $\mathbf{r}_3$ is also the surface normal vector of the calibration plane in camera coordinate systems [31].

Note the origin of world coordinate is the upper-left corner of the checkerboard, and the origin of camera coordinate is the camera itself. The translation vector $\mathbf{t}$ represents relative position of the checkerboard's upper-left corner in the camera's reference system. Since both $\mathbf{t}$ and $\mathbf{P}_c$ are points on the checkerboard plane denoted in camera coordinates, a vector $\vec{v}$ is defined as $\vec{v} = \mathbf{P}_c - \mathbf{t}$. Note that $\vec{v}$ is a vector on the checkerboard plane, and $\mathbf{r}_3$ is orthogonal to this plane, so:

$$\mathbf{r}_3 \cdot \vec{v} = 0 \tag{3}$$

where $\cdot$ denotes the inner product. The geometric interpretation for Eq. 3 is illustrated in Fig. 5.

By substituting Eq. 2 into Eq. 3, Eq. 3 becomes:

$$\mathbf{r}_3^T \left(\mathbf{R}_l^c \mathbf{P}_l + \mathbf{t}_l^c - \mathbf{t}\right) = 0 \tag{4}$$

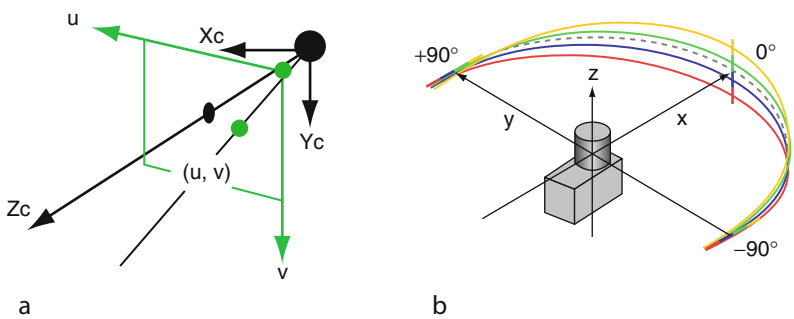

Vehicle Detection, Tightly Coupled LIDAR and Computer Vision Integration for. Figure 4
Two coordinate systems. (**a**) The camera coordinates and screen coordinate systems, and (**b**) the LIDAR coordinate system

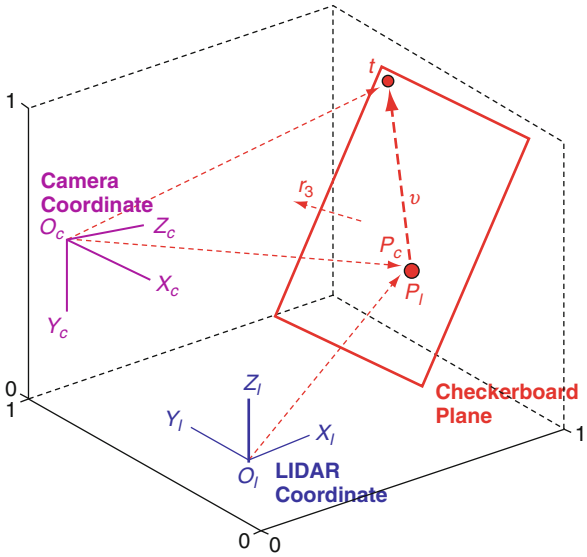

Vehicle Detection, Tightly Coupled LIDAR and Computer Vision Integration for. Figure 5
Geometric interpretation of the camera coordinates, the LIDAR coordinates, and checkerboard

Since point $\mathbf{P}_l$ in LIDAR coordinates is $[X_l \quad Y_l \quad Z_l]^T$, from Eq. 4:

$$\mathbf{r}_3^T \left[\mathbf{R}_l^c \quad \mathbf{t}_l^c - \mathbf{t}\right] \begin{bmatrix} X_l \\ Y_l \\ Z_l \\ 1 \end{bmatrix} = 0 \tag{5}$$

For each LIDAR point on the checkerboard plane, Eq. 5 explains the geometric relationships and constraints on $\left(\mathbf{R}_l^c, \quad \mathbf{t}_l^c\right)$. This is the basic constraints for the calibration from the LIDAR to the vision coordinate system.

Calibration Solutions

This subsection provides the method to efficiently obtain calibration coefficients $\left(\mathbf{R}_l^c, \quad \mathbf{t}_l^c\right)$. An analytical solution is proposed, followed by a nonlinear optimization technique based on the maximum likelihood criterion.

Closed-Form Solution Initially, the camera's intrinsic parameters are calibrated using a standard Camera Calibration Toolbox [31]. For each pose of the checkerboard, there is one set of camera extrinsic parameters $(\mathbf{R}, \quad \mathbf{t})$. Each $(\mathbf{R}, \quad \mathbf{t})$ is determined also using the toolbox, after which $\mathbf{r}_3$ and $\mathbf{t}$ in Eq. 5 are obtained.

For simplicity, it is defined that $\mathbf{r}_3 = [r_{31} \quad r_{32} \quad r_{33}]^T$, $\Delta_i = \mathbf{t}_l^c - \mathbf{t} = [\Delta_x \quad \Delta_y \quad \Delta_z]^T$, and m_{ij} is the element on the i-th row, j-th column in matrix $\mathbf{R}_l^c$. Suppose for one pose of the checkerboard, there are p LIDAR points on the checkerboard plane, denoted as $\mathbf{P}_{l,1} = [X_{l,1} \quad Y_{l,1} \quad Z_{l,1}]^T$, $\mathbf{P}_{l,2} = [X_{l,2} \quad Y_{l,2} \quad Z_{l,2}]^T, \ldots, \mathbf{P}_{l,p} = [X_{l,p} \quad Y_{l,p} \quad Z_{l,p}]^T$. The geometric interpretation becomes a $\mathbf{Ax} = \mathbf{0}$ problem, where $\mathbf{A}$ is a $N \times 12$ matrix, and $\mathbf{x}$ is a 12-vector to be solved. $\mathbf{A}$ and $\mathbf{x}$ are given in Eq. 6.

$$\begin{aligned} \mathbf{A} &= [r_{31}\mathbf{P}_{l,p} \; r_{31}\mathbf{E} \; r_{32}\mathbf{P}_{l,p} \; r_{32}\mathbf{E} \; r_{33}\mathbf{E}_{l,p} \; r_{33}\mathbf{E}] \\ \mathbf{x} &= [\mathbf{m}_1 \, \Delta_x \, \mathbf{m}_2 \Delta_y \, \mathbf{m}_3 \, \Delta_z]^T \end{aligned} \tag{6}$$

where $\mathbf{P}_{l,p} = \left[\mathbf{P}_{l,1} \;\; \mathbf{P}_{l,2} \;\; \ldots \;\; \mathbf{P}_{l,p}\right]^T$, $[\mathbf{E} = [1 \;\; 1 \;\; \cdots \;\; 1]^T$ is a $(p \times 1)$ vector, and $\mathbf{m}_i = [m_{i1} \;\; m_{i2} \;\; m_{i3}]$, $i = 1, 2, 3$.

By getting the LIDAR points $\mathbf{P}_{l,1}, \mathbf{P}_{l,2}, \ldots, \mathbf{P}_{l,p}$, $\mathbf{x}$ is estimated using the least square method. In order to avoid the solution $\mathbf{x} = \mathbf{0}$, normalization constraints are proposed. Faugeras and Toscani suggested the constraint $m_{31}^2 + m_{32}^2 + m_{33}^2 = 1$, which is singularity free [32]. This restriction is proposed from the coincidence that $[m_{31} \quad m_{32} \quad m_{33}]$ is the third row of the rotation matrix $\mathbf{R}_l^c$. Thus solving the equation $\mathbf{Ax} = \mathbf{0}$ is transformed into minimizing the norm of $\mathbf{Ax}$, i.e., minimizing $|\mathbf{Ax}|$ with the restriction $m_{31}^2 + m_{32}^2 + m_{33}^2 = 1$.

$|\mathbf{Ax}|$ can be minimized using a Lagrange method [33]. Let $\mathbf{m}_3 = [m_{31} \; m_{32} \; m_{33}]$ and $\mathbf{m}_9$ be a vector containing the remaining nine elements in $\mathbf{x}$. The Lagrange equation is written as:

$$L = \mathbf{A}_9 \cdot \mathbf{m}_9 + \mathbf{A}_3 \cdot \mathbf{m}_3 + \lambda\left(\mathbf{m}_3^T \mathbf{m}_3 - 1\right) \tag{7}$$

where $\mathbf{A}_3$ contains the 9th to 11th columns of $\mathbf{A}$, and $\mathbf{A}_9$ contains the remaining nine columns corresponding to $\mathbf{m}_9$.

The closed-form linear solution is:

$$\begin{aligned} \lambda\mathbf{m}_3 &= \left(\mathbf{A}_3^T\mathbf{A}_3 - \mathbf{A}_3^T\mathbf{A}_9\left(\mathbf{A}_9^T\mathbf{A}_9\right)^{-1}\mathbf{A}_9^T\mathbf{A}_3\right)\mathbf{m}_3 \\ \mathbf{m}_9 &= -\left(\mathbf{A}_9^T\mathbf{A}_9\right)^{-1}\mathbf{A}_9^T\mathbf{A}_3\mathbf{m}_3 \end{aligned} \tag{8}$$

It is well known that $\mathbf{m}_3$ is the eigenvector of the symmetric positive definite matrix $\mathbf{A}_3^T\mathbf{A}_3 - \mathbf{A}_3^T\mathbf{A}_9\left(\mathbf{A}_9^T\mathbf{A}_9\right)^{-1}\mathbf{A}_9^T\mathbf{A}_3$ associated with the smallest eigenvalue. $\mathbf{m}_9$ is obtained after $\mathbf{m}_3$. Once $\mathbf{m}_3$

and $\mathbf{m}_9$ are known, the rotation and translation matrix $\left(\mathbf{R}_l^c, \mathbf{t}_l^c\right)$ is available.

Because of data noise, the rotation matrix $\mathbf{R}_l^c$ may not in general satisfy $\left(\mathbf{R}_l^c\right)^T \mathbf{R}_l^c = \mathbf{I}$. One solution is to obtain $\hat{\mathbf{R}}_l^c$, which is the best approximation of given $\mathbf{R}_l^c$. This $\hat{\mathbf{R}}_l^c$ has the smallest Frobenius norm of the difference $\hat{\mathbf{R}}_l^c - \mathbf{R}_l^c$, subject to $(\widehat{R}_l^c)^T \hat{\mathbf{R}}_l^c = \mathbf{I}$ [30].

Maximum Likelihood Estimation The closed-form solution is obtained by minimizing an algebraic distance $|\mathbf{Ax}|$, which is not physically meaningful. In this subsection, the problem is refined through maximum likelihood function using multi-pose checkerboard planes, which is more meaningful.

In the proposed camera calibration approach, differences of image points and the corresponding projection of the ground truth point in an image are minimized [30]. This method is also valid for visible-beam LIDAR calibration [12]. In the test, the Euclidean distances from camera to the checkerboard are checked. Note that Eq. 4 can be written as:

$$\mathbf{r}_3^T\left(\mathbf{R}_l^c \mathbf{P}_l + \mathbf{t}_l^c\right) = \mathbf{r}_3^T \mathbf{t} \tag{9}$$

where both $\mathbf{R}_l^c \mathbf{P}_l + \mathbf{t}_l^c$ and $\mathbf{t}$ are points on the calibration plane surface, and $\mathbf{r}_3$ is the normal vector to this surface. Therefore, both the left and right sides of Eq. 9 are the distance between the checkerboard plane and the origin of the camera reference system.

Suppose there are totally n poses of the calibration plane. For the i-th pose, there is a set of $(\mathbf{r}_3, \mathbf{t})$ denoted as $\left(\mathbf{r}_3^i, \mathbf{t}^i\right)$. LIDAR points are assumed to be corrupted by Gaussian distributed noise. The maximum likelihood function is defined by minimizing sum of the difference between $\mathbf{r}_3^T\left(\mathbf{R}_l^c \mathbf{P}_l + \mathbf{t}_l^c\right)$ and $\mathbf{r}_3^T \mathbf{t}$ for all the LIDAR points. Suppose for the i-th plane, there are p_i LIDAR points. The solution satisfies:

$$\arg\min_{\mathbf{R}_l^c, \mathbf{t}_l^c} \sum_{i=1}^{n} \frac{1}{p_i} \sum_{j=1}^{p_i} \left(\left(\mathbf{r}_3^i\right)^T \left(\mathbf{R}_l^c \mathbf{P}_{l,j}^i + \mathbf{t}_l^c\right) - \left(\mathbf{r}_3^i\right)^T \mathbf{t}^i \right)^2 \tag{10}$$

where $\mathbf{R}_l^{c,i} \mathbf{P}_{l,j}^i + \mathbf{t}_l^{c,i}$ is the coordinate of $\mathbf{P}_{l,j}^i$ in the camera reference system, according to Eq. 2.

By using Rodriguez formula [32], the rotation matrix $\mathbf{R}_l^c$ is transformed into a vector, which is parallel to the rotation axis and whose magnitude is equal to the rotation angle. Thus $\left(\mathbf{R}_l^c, \mathbf{t}_l^c\right)$ forms a vector. Equation 10 is solved using the Levenberg–Marquardt algorithm (LMA) [34, 35], which provides numerical solutions to the problem of minimizing nonlinear functions. LMA requires an initial guess for the parameters to be estimated. In this algorithm, $\left(\mathbf{R}_l^c, \mathbf{t}_l^c\right)$ in the closed form is used as this initial state. For each pose, a set of $\left(\mathbf{R}_l^c, \mathbf{t}_l^c\right)$ is obtained. The weighted average is used as an initial guess, where the scalar weight is normalized as a relative contribution of each checkerboard pose. Then LMA gives a robust solution even if the initial state starts far off the final solution.

Summary of Calibration Procedure The calibration procedure proposed in this approach can be summarized as:

1. Place the checkerboard in view of the camera and LIDAR systems. Make sure that the plane is within the detection zone of both sensors. The different poses of checkerboard cannot be parallel to each other, otherwise the parallel poses do not provide enough constraints on $\mathbf{R}_l^c$.
2. Take a few measurements (images) of the checkerboard under different orientations. For each orientation, read the LIDAR points on this plane from the output.
3. Estimate the coefficients using the closed-form solution given in section "Closed-Form Solution".
4. Refine all the coefficients using the maximum likelihood estimation in section "Maximum Likelihood Estimation".

Experimental Results

The proposed vision-LIDAR calibration algorithm has been tested on both a computer simulation platform and with real-world data.

Computer Simulations The camera is assumed to have been calibrated. It is simulated to have the following properties: $\alpha = 1,200$, $\beta = 1,000$, and the skewness coefficient $\gamma = 0$. The principal point is $(320, 240)$, and the image resolution is 640×480. The calibration checkerboard consists of 10×10 grids. The size of each square grid is 5cm $\times$ 5cm. The position and orientation of the LIDAR relative to the camera have also been defined. The LIDAR's position in camera coordinates is $\mathbf{t}_l^c = [10 \quad 150 \quad 100]^T$ centimeters, and the rotation

matrix $\mathbf{R}_l^c$ is parameterized by a three-vector rotation vector $[-85^o \quad 10^o \quad -80^o]^T$.

The LIDAR points are calculated based on the location of the camera, and relative position as well as orientation of the checkerboard. Gaussian noise is added to the points.

Performance with respect to Gaussian Noise Level A checkerboard plane is placed in front of the camera and the LIDAR. Three poses are used here. All of them have $\mathbf{t} = [-20 \quad -20 \quad -550]^T$. Three rotation matrices are defined by the rotation vectors as $\mathbf{r}_1 = [170^o \quad -5^o \quad 85^o]^T$, $\mathbf{r}_2 = [170^o \quad 15^o \quad 85^o]^T$, $\mathbf{r}_3 = [170^o \quad -25^o \quad 85^o]^T$, respectively. Gaussian noise with zero mean and standard deviation (from 1 to 10 cm) is added to the LIDAR points. The estimation results are then compared with ground truth. For each noise level, 100 independent random trials are delivered. The averaged calibration error is shown in Fig. 6, where the calculation results are denoted as $\hat{\mathbf{R}}_l^c$ and $\hat{\mathbf{t}}_l^c$, respectively. This figure illustrates that the calibration error increases with noise level, as expected. For $\sigma < 7$cm (which is larger than the normal standard deviation for most LIDAR sensors), the error of norm of $\mathbf{R}_l^c$ is less than 0.01. With three checkerboard poses, the relative translation error is less than 5% when $\sigma < 5$cm.

Performance with respect to the Number of Checkerboard Positions The checkerboard was originally setup as parallel to the image plane. Then it is rotated by, where the rotation axis is randomly selected in a uniform sphere. The number of checkerboards used for calibration varies from 4 to 20. Gaussian noise with zero mean and standard deviation $\sigma = 4$cm is added to the LIDAR points. For each position, 100 trials of independent rotation axes are implemented. The averaged result is illustrated in Fig. 7. This figure shows that when the number of checkerboard positions increases, the calibration error decreases.

Performance with respect to the Orientation of Checkerboard The checkerboard plane is initially set as parallel to the image plane. It is then rotated around a randomly chosen axis with angle θ. The rotation axis is randomly selected from a uniform sphere. The rotation angle θ varies from 10° to 80°, and 10 checkerboards are used for each θ. Gaussian noise with zero mean and standard deviation $\sigma = 4$cm is added to the LIDAR points. For each rotation angle, 100 trials are repeated and the average error is calculated. The simulation result is shown in Fig. 8. The calibration error decreases when the rotation angle increases. When the rotation angle is too small, the calibration planes are almost parallel to each other,

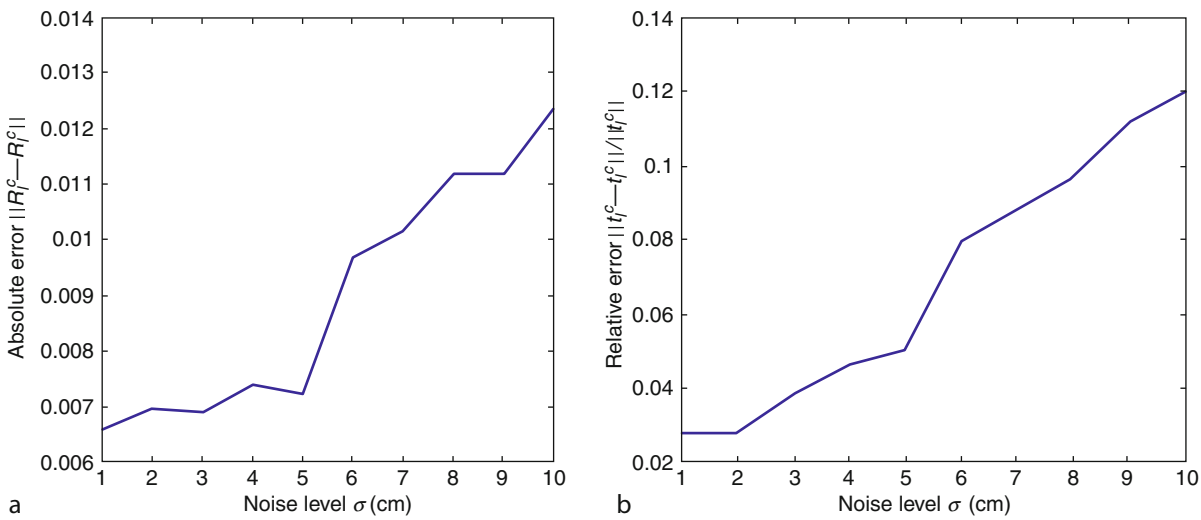

Vehicle Detection, Tightly Coupled LIDAR and Computer Vision Integration for. Figure 6
Rotation and translation error with respect to the noise level. (**a**) Rotation error with respect to noise level. (**b**) Translation error with respect to noise level

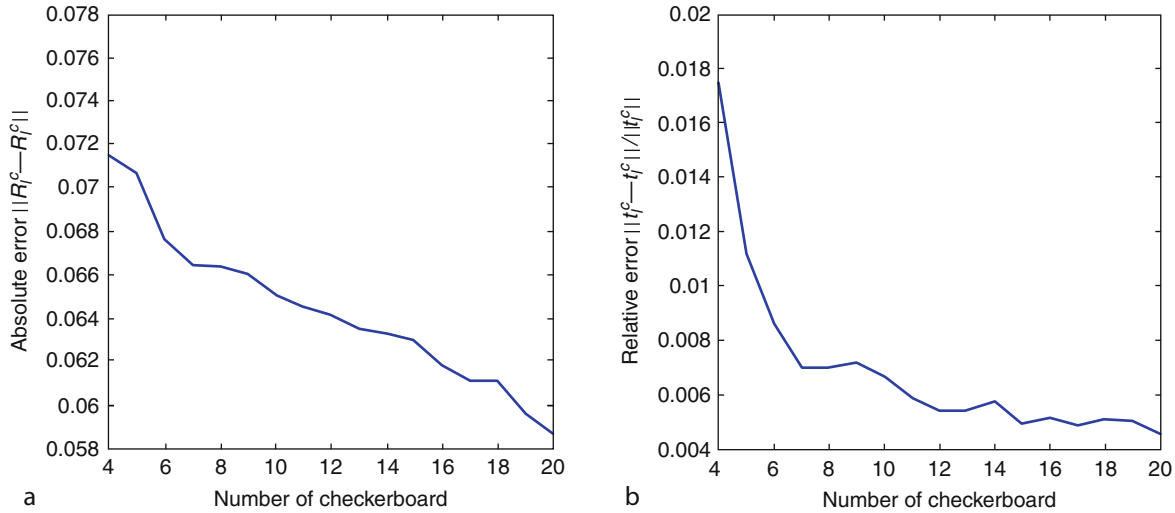

Vehicle Detection, Tightly Coupled LIDAR and Computer Vision Integration for. Figure 7
Rotation and translation error with respect to number of checkerboard positions. (**a**) Rotation error with respect to number of checkerboard. (**b**) Translation error with respect to number of checkerboard

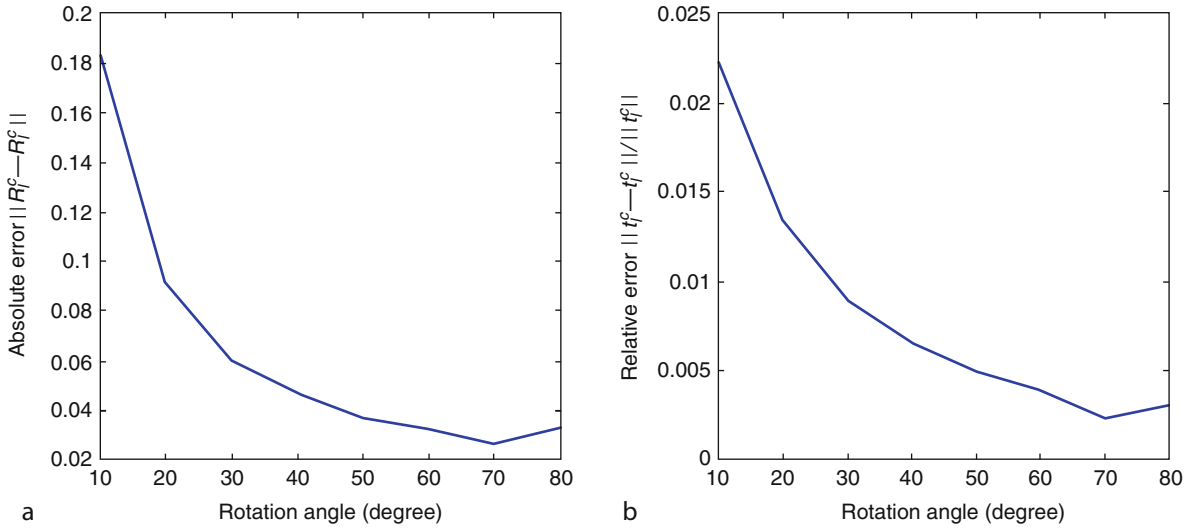

Vehicle Detection, Tightly Coupled LIDAR and Computer Vision Integration for. Figure 8
Rotation and translation error with respect to the orientation of the checkerboard plane. (**a**) Rotation error with respect to orientation of the checkerboard plane. (**b**) Translation error with respect to orientation of the checkerboard plane

which cause error. When the rotation angle is too large, the calibration plane is almost perpendicular to the image plane, which makes the LIDAR measurement less precise.

Real Data Calibration The calibration method has been tested using an IBEO ALASCA XT LIDAR system and a Sony CCD digital camera with a 6 mm lens. The image resolution is 640 × 480. The checkerboard plane

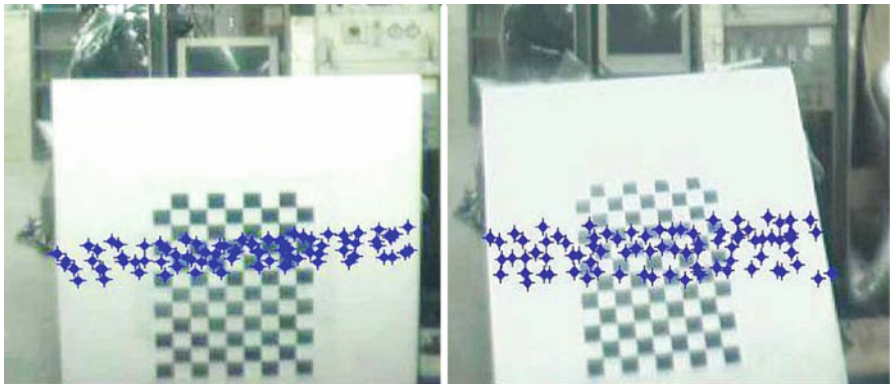

Vehicle Detection, Tightly Coupled LIDAR and Computer Vision Integration for. Figure 9
Two checkerboard positions. The LIDAR points are indicated by *blue dots*. The calibration method proposed in this entry is used to estimate $\mathbf{R}_l^c$ and $\mathbf{t}_l^c$

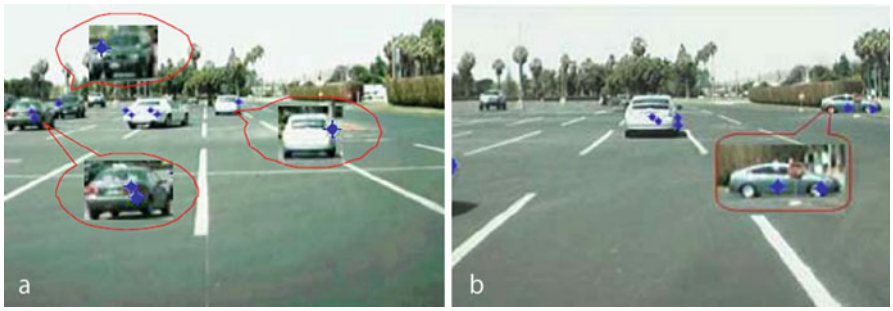

Vehicle Detection, Tightly Coupled LIDAR and Computer Vision Integration for. Figure 10
Two sensor fusion image frames. The *red rectangle* is an enlarged image of the detected area

consists of a pattern of 16×16 squares, so there are totally 256 grids on the plane. The size of each grid is 2.54cm $\times$ 2.54cm (1 $\times$ 1 in.).

Twenty images of the plane were taken with different orientations, and the LIDAR points are recorded simultaneously. Two examples of the calibration results are shown in Fig. 9, where the LIDAR points are mapped to image reference system using estimated $\mathbf{R}_l^c$ and $\mathbf{t}_l^c$. Although the ground truth of $\mathbf{R}_l^c$ and $\mathbf{t}_l^c$ are not known, Fig. 9 shows that the estimation results are pretty reasonable.

Application in Vehicle Detection The calibration method has been integrated into a mobile sensing system. This mobile sensing system is designed to detect and track surrounding vehicles, which is the first and fundamental step for any of the automatic traffic surveillance systems. However, object detection is a big challenge for the moving platform. Both the foreground and the background are rapidly changing, which makes it difficult to extract the foreground regions from the background. The sensor fusion technique is used to compensate for the spatial motion of the moving platform. Figure 10 gives two images from the vehicle detection video.

In Fig. 10a, there are totally four vehicles detected by the LIDAR, where the farthest vehicle is 55 m away from the mobile sensing system. It is hard to obtain the vehicle's distance and orientation from an image alone. The LIDAR points provide a reliable estimation of this vehicle's position. In Fig. 10b, one car parallel to the probe vehicle is detected by the LIDAR. Meanwhile, it is

partially visible in the image, together with its shadow on the ground. Although this vehicle is hardly recognizable in the image, with a wide angle of view, LIDAR data provide enough information to reconstruct the location of this vehicle.

The experiment results illustrate that the calibration algorithm provides good results. The sensor fusion system combining LIDAR and computer vision information sources presents distance and orientation information. This system is helpful for vehicle detection and tracking applications.

Summary

In this section, a novel calibration algorithm was developed to obtain the geometry transformation between a multi-plane LIDAR system and a camera vision system. This calibration method requires LIDAR and camera to observe a checkerboard simultaneously. A few checkerboard poses are observed and recorded. The calibration approach has two stages: closed-form solution followed by a maximum likelihood criterion–based optimization. Both simulation and real-world experiments have been carried out. The experiment results show that the calibration approach is reliable. This approach will be used in the vehicle detection and tracking system.

Tightly Coupled LIDAR and Computer Vision Integrated System for Vehicle Detection

Computer vision sensors are generally used in current mobile platform–based object detection and tracking systems. However, the application of vision sensors is far from sufficient: clustering, illumination, occlusion, among many other factors, affect the overall performance. In contract, a LIDAR sensor provides range and azimuth measurements from the sensor to the targets. However, the accuracy of its measurements depends on the reflectivity of the targets and the weather. The fusion of camera and active sensors such as LIDAR is being investigated in the context of on-board vehicle detection and tracking.

In this section, a tightly coupled LIDAR/CV system is proposed, in which the LIDAR scanning points are used for hypothesizing regions of interest and for providing error correction to the classifier, while the vision image provides object classification information. LIDAR object points are first transformed into image space. ROIs are generated using the LIDAR feature detection method. An Adaboost classifier based on computer vision systems [36] is then used to detect vehicles in the image space. Dimensions and distance information of the detected vehicles are calculated in body-frame coordinates. This approach provides a more complete and accurate map of surrounding vehicles in comparison to the single sensors used separately. One of the key features of this technique is that it uses LIDAR data to correct the Adaboost classification pattern. Moreover, the Adaboost algorithm is utilized both for vehicle detection and for vehicle distance and dimension extraction. Then the classification results provide compensatory information to the LIDAR measurements.

This section is organized as follows: in section "Overview of the Vehicle Detection System" a brief introduction of the vehicle detection system is given. Section "Vision-Based System" describes the vision-based system. The vehicle detection algorithm is introduced in section "Moving Vehicle Detection System". A vehicle tracking approach using particle filter is proposed in section "Vehicle Tracking System". Experimental results of vehicle detection are provided in section "Experiment Results", followed by conclusions and future work in section "Summary and Discussion".

Overview of the Vehicle Detection System

Vehicle detection is the first and fundamental step for any driver assistant system (DAS). With sensors mounted on a moving platform, the detected data change rapidly, making it difficult to extract objects of interest. In the proposed approach, spatial motion of the moving platform has been compensated by using the sensor fusion approach.

Multi-module Architecture The input of vehicle detection system consists of two LIDAR sensors and a single camera, as is shown in Fig. 1. The detection area is covered by two LIDAR sensors overlapping with each other. The camera is placed behind the rearview mirror. The field of view of this camera is fully covered by the LIDAR ranging space.

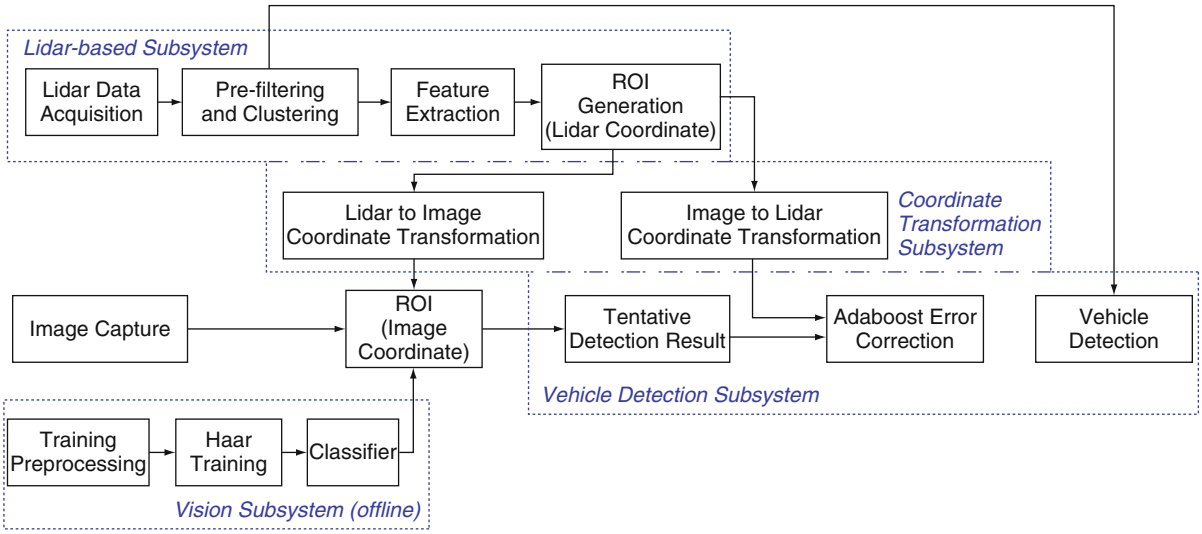

Vehicle Detection, Tightly Coupled LIDAR and Computer Vision Integration for. Figure 11
Flowchart of the mobile sensing system

Figure 11 presents the flowchart of this vehicle detection system. It consists of four subsystems: a LIDAR-based subsystem, a coordinate transformation subsystem, a vision-based subsystem, and a vehicle detection subsystem.

LIDAR-Based Subsystem *The LIDAR Data Acquisition Module* uses IBEO External Control Unit (ECU) to communicate, collect, and combine data from a pair of LIDAR sensors.

The Prefiltering and Clustering Module aims to transform scan data from distances and azimuths to positions, and cluster the incoming data into segments using a Point-Distance-Based Methodology (PDBM) [12]. If there exists any segment consisting of less than three points, and the distance of this segment is greater than the given threshold, these points are considered as noise. The segment will be disregarded.

The Feature Extraction Module extracts primary features in the cluster. The main feature information in one segment is its geometrical representation, such as lines and circles. One of the advantages of geometrical features is that they occupy far less space than storing all the scanned points.

A vehicle may have any possible orientation. The contour of a vehicle is constructed by four sides: front, back, left side, and right side. The LIDAR sensor can capture one side, or two neighboring sides, as is shown in Fig. 12.

When the object is close to the probe vehicle, the extracted feature provides enough information for object classification. However, if the target is far away, it may be represented by only one or two scanning points. For those objects with only a few LIDAR points, it is difficult to get reliable size, location, and orientation information from the scan data alone. Note that the computer vision image also contains size and orientation information, which can be extracted by the object classification technique. By employing the sensor fusion technology, LIDAR scan data and Adaboost output are complementary to each other.

The ROI Generation Module calculates positions of ROI bounding boxes in LIDAR coordinates. It is worth mentioning that the ROI is not defined by LIDAR points alone, since the scan points of one target may not be able to represent its full dimension. In this algorithm, the width and length of ROI are defined by both LIDAR data points and the maximum dimension of a potential vehicle.

Each ROI is defined as a rectangular area in the image. The bottom of the rectangle is the ground. The top of the rectangle is set to be the maximum height of

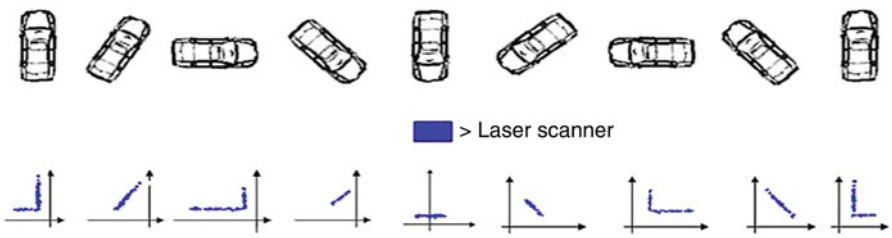

Vehicle Detection, Tightly Coupled LIDAR and Computer Vision Integration for. Figure 12
Orientation of the vehicle significantly changes its appearance in the scan data frame. The rectangles show position of the LIDAR

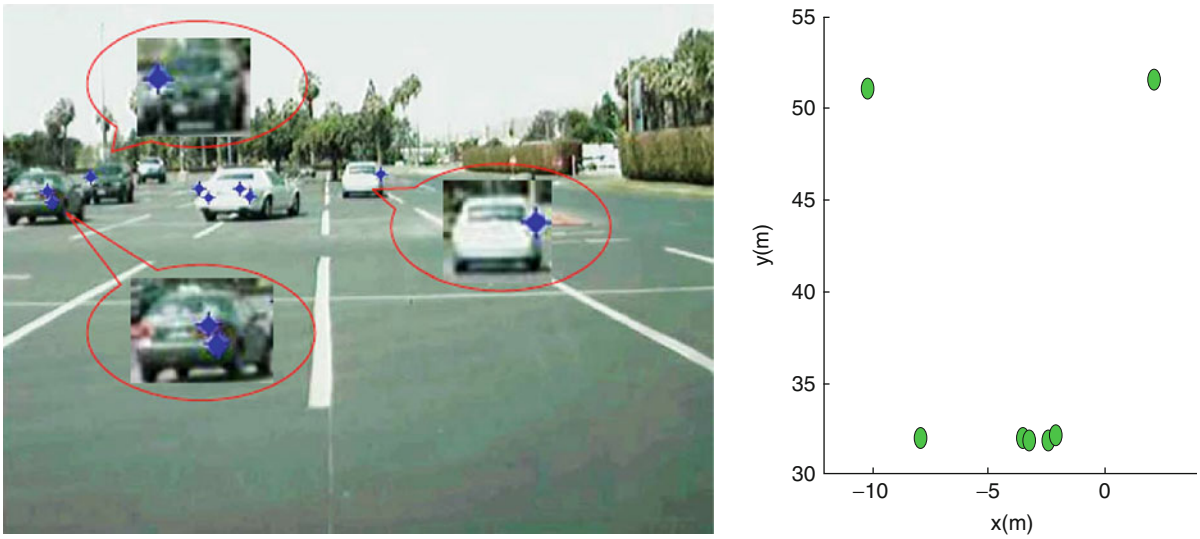

Vehicle Detection, Tightly Coupled LIDAR and Computer Vision Integration for. Figure 13
The LIDAR scan points. (**a**) Points in the LIDAR coordinate system. Each green dot is one scan point. (**b**) These points are transformed to the image frame. Each blue star in the image is one LIDAR point. Vehicles in the red circles are the enlarged image of the detected area

a car. The left and right edges are obtained from the furthest left and right scanning points in a cluster, as well as the typical width of a car.

The LIDAR to Image Coordinate Transformation Module transforms all the LIDAR points into the image frame. The relative position and orientation between LIDAR and camera sensors should be obtained for the transformation. A unique multi-planar LIDAR and computer vision calibration algorithm is described in section "A Novel Multi-Planar LIDAR and Computer Vision Calibration Procedure Using 2D Patterns", which calculates the geometry transformation matrix between "multiple invisible beams" of LIDAR sensors and the camera. The calibration results are used in the sensor fusion system.

During the road test, each LIDAR scan point $\mathbf{P}_l$ is transformed into camera coordinate as $\mathbf{P}_c$. $\mathbf{P}_c$ is then transformed into point $\mathbf{p}_c$ in the image plane. Figure 13 illustrates LIDAR scan points and the transformation results in the image reference system.

After the LIDAR to image transformation coefficients are calculated, ROIs generated in the

LIDAR-based subsystem is converted into image frame. A larger ROI is generated due to inaccuracy of the transformation from LIDAR data to image data.

The Image to LIDAR Coordinate Transformation Module is called to correct Adaboost classification result. More details are given in the following sections.

Vision-Based System

Object classification from the hypothesized ROIs is required for vehicle detection purpose. Feature representations are used for object classifiers by an Adaboost algorithm [36]. Viola et al. proposed that the object is detected based on a boosted cascade of feature classifiers, which performs feature extraction and combines features such as simple weak classifiers to a strong one.

The Adaboost classifier requires off-line training using target as well as nontarget images. In the vehicle detection applications, the target images, i.e., the rearview of vehicles, are called positive samples; while the non-vehicles are named as negative samples. Figure 14 illustrates some of the positive as well as negative samples in the training dataset. Training samples are taken from both Caltech vehicle image dataset [37] and video collected by the test vehicle. The positive samples include passenger cars, vans, trucks, and trailers. The negative sample sets include roads, traffic signs, buildings, plants, and pedestrians.

Image Training Preprocessing Both the positive and negative samples are used by computer vision system for data training. All the samples are originally colored images. In order to remove the effects of various illumination conditions and camera differences, gray-level transformation is required as a preprocessing step. The gray-level normalization method is applied to the whole image dataset, which transforms gray level of the image to be in [0, 1] domain. The color image is transformed by [38]:

$$I^*(x, y) = \frac{I(x, y) - I_{\min}}{I_{\max} - I_{\min}} \tag{11}$$

where $I(x, y)$ is the intensity of pixel (x, y), $I_{\min}$ and $I_{\max}$ are the minimum and maximum values in this image, respectively. $I^*(x, y)$ is the normalized gray-level value.

The next step is to normalize the sizes of all the positive samples. It is implemented before training

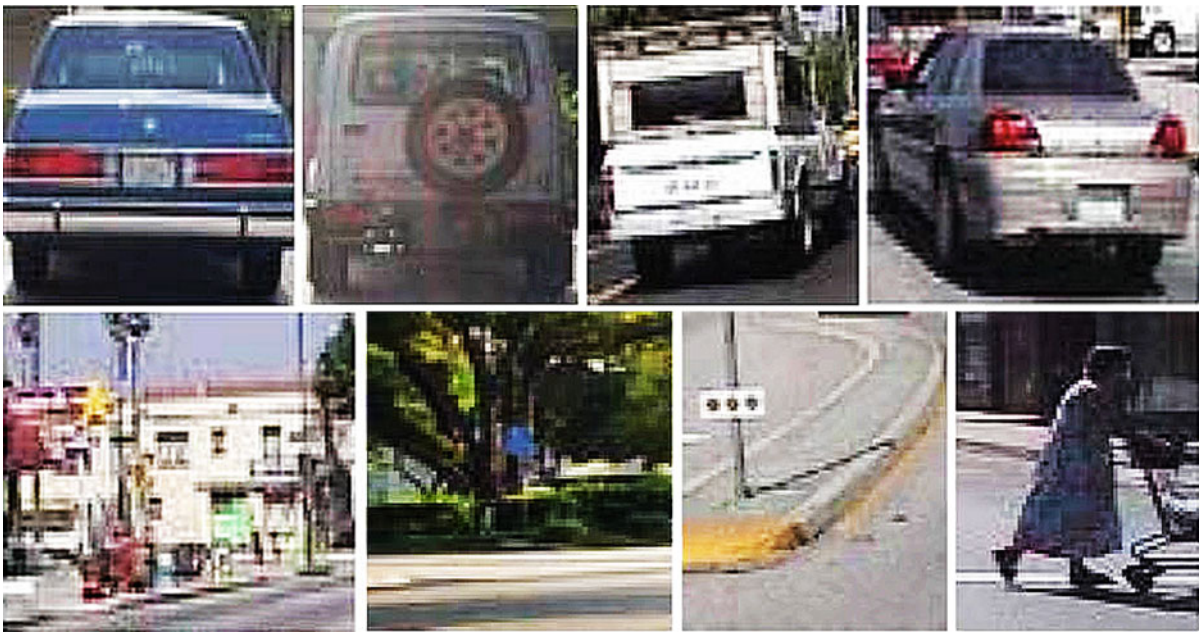

Vehicle Detection, Tightly Coupled LIDAR and Computer Vision Integration for. Figure 14
Positive and negative samples used in Adaboost training

since different resolutions may cause different number of features to be counted. The sizes of the normalized positive samples determine the minimum size of objects that can be detected [39]. In this test, the normalized image size is set as 25 × 25 pixels.

Haar Training In the vision-based system, Haar-like features are used to classify objects [36]. This approach combines more complex classifiers in a "cascade" which quickly discard the background regions while spending more computation on the Haar-like area [36].

More specifically, 14 feature prototypes are utilized for the Haar training [40]. These features represent characteristic properties like edge, line, and symmetry. The features prototypes can be grouped into three categories:

- Edge features: The difference between sums of the pixels within two rectangular regions

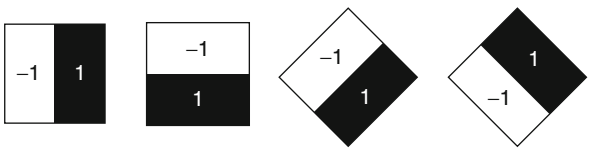

- Line features: The sum within two outside rectangular regions subtracted from the sum in the center rectangular

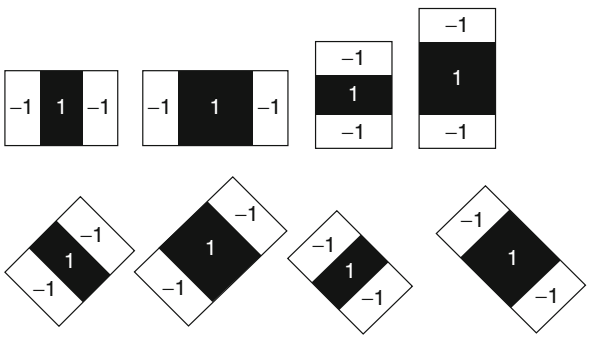

- Center-surround features: The difference between the sums of the center rectangular and the outside area

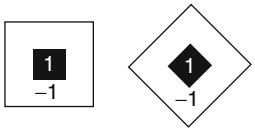

Here black areas with "−1" have negative weights, and white areas with "1" have positive weights.

After the weak classifier has been trained at each stage, the classifier is able to detect almost all the targets of interest while rejecting certain nontarget objects. A cascade of classifiers is generated to form a decision tree. The training process consists of totally 15 stages. Each stage is trained to eliminate 60% of the non-vehicle patterns, and the hit rate (HR) in each stage is set to be 0.998. Therefore, the total false alarm rate (FAR) for this cascade classifier is supposed to be $0.4^{15} \approx 1.07e-06$, and the hit rate should be around $0.998^{15} \approx 0.97$.

Moving Vehicle Detection System

The Adaboost algorithm designs a strong classifier that can detect multiple objects in the given image. However, there is no guarantee that this strong classifier is optimal for the object detection. In contrast to the classic Adaboost algorithm, in this test there is only one vehicle in each ROI defined by the LIDAR clustering algorithm. Therefore, it is not necessary for the Adaboost algorithm to detect several possible targets in one ROI. A classification correction technique is proposed to utilize the LIDAR scanning data to reduce redundancy in the Adaboost detection results.

There are two kinds of redundancy errors in the classification results. Figure 15 gives some examples of these two cases. Both have detected more than one object, while the ground truth is that there is only one vehicle. One kind of error is that the Adaboost detects two possible targets, while the area of the smaller one is almost covered by the larger one, as is shown in Fig. 15a. Another error shown in Figure 15b is that all the detected areas belong to the same object, while none of them cover the full body of the target.

Suppose in the i-th ROI, there exists a LIDAR point cluster $\Re_i$, which has the following features in LIDAR coordinate system: c_i^{LIDAR} as the center of the cluster, w_i^{LIDAR} as the width of the object, and l_i^{LIDAR} as the possible length of the vehicle. On the image side, there are detected target candidates denoted as d_1, d_2,. . ., d_n. Initially, d_1, d_2,. . ., d_n are transformed from image coordinate to camera coordinate, then to LIDAR coordinates.

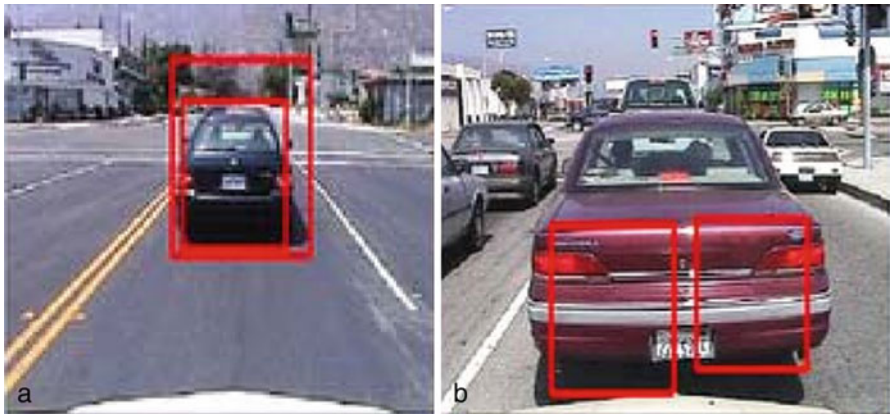

Vehicle Detection, Tightly Coupled LIDAR and Computer Vision Integration for. Figure 15
Two kinds of redundancy errors in Adaboost detection. (**a**) Two bounding boxes overlap on the same target. (**b**) Two bounding boxes detected with no overlap on the same target

The scan points in LIDAR coordinates are denoted as D_1, D_2,..., D_n. The j-th candidate D_j has center $c_{i,j}^{DETECT}$, width $w_{i,j}^{DETECT}$, and height $h_{i,j}^{DETECT}$. In LIDAR coordinate frame, two vectors are defined as $\mathbf{m}_i^{LIDAR} = \left(c_i^{LIDAR}, w_i^{LIDAR}\right)$ and $\mathbf{m}_i^{DETECT} = \left(c_{i,1}^{DETECT}, w_{i,1}^{DETECT}, \cdots, c_{i,n}^{DETECT}, w_{i,n}^{DETECT}\right)$. Here $\mathbf{m}_i^{LIDAR}$ is the size information obtained by LIDAR, and $\mathbf{m}_i^{DETECT}$ consists of measurements in LIDAR coordinate systems which are transformed from the image reference system. The coefficient $\mathbf{w}_i$ for mapping multiple target areas to the LIDAR information satisfies:

$$\mathbf{w}_i = \arg\min \left\| \mathbf{m}_i^{LIDAR} - \sum\nolimits_{j=1:n} \mathbf{w}_{i,j} \mathbf{m}_{i,j}^{DETECT} \right\| \tag{12}$$

where $\|.\|$ is the Euclidean norm. $\mathbf{w}_i$ is used as a weight to recalculate the detected area, which is a combination of all the detected objects in one ROI.

LIDAR scanning points and Adaboost classification results are then combined to generate a complete map of vehicles. A summary of the vehicle detection process is given here:

Algorithm 1: Vehicle Detection. Given LIDAR points cluster $\Re_i$ with features $\left(c_i^{LIDAR}, w_i^{LIDAR}, l_i^{LIDAR}\right)$, detected target candidate $d_1, \ldots, d_n$ in the image;

if no object detected in the ROI
  enlarge ROI and search again
else
  define $\mathbf{m}_i^{LIDAR} = \left(c_i^{LIDAR}, w_i^{LIDAR}\right)$
  transform $d_1, \ldots, d_n$ in the image coordinate frame to LIDAR reference frame
  define $\mathbf{m}_i^{DETECT} = \left(c_{i,1}^{DETECT}, w_{i,1}^{DETECT}, \cdots, c_{i,n}^{DETECT}, w_{i,n}^{DETECT}\right)$
  calculate the weight vector which minimize $\left\| \mathbf{m}_i^{LIDAR} - \sum \mathbf{w}_{i,j} \mathbf{m}_{i,j}^{DETECT} \right\|$
end if
The detected vehicle is located at $\sum_{j=1:n} \mathbf{w}_{i,j} c_{i,j}^{DETECT}$.

The vehicle detection system proposed in this section can be summarized as:

- The Adaboost classifier training is implemented off-line with both positive and negative samples.
- ROI is defined by the LIDAR scan data. No more than one vehicle is assumed to exist in each ROI.
- Use the Adaboost classifier to make a preliminary vehicle detection.
- LIDAR data is used to correct the Adaboost redundancy error, and to merge detected areas in one ROI.
- Combine the Adaboost detected area (in LIDAR coordinate) and the LIDAR output to generate a complete vehicle distance and dimension map.

Vehicle Tracking System

LIDAR and computer vision sensors are integrated in a probabilistic manner for vehicle tracking. A sampling

importance resampling (SIR) particle filter is used as the tracker, which is a sophisticated model estimation technique [41]. Unlike the commonly used Kalman filter and extended Kalman filter (EKF), this particle filter does not assume that the linear dynamic system is perturbed by Gaussian noise. The key idea of particle filter is to represent the estimation by a set of random samples (they are called *particles*) with associated weights.

Particle Filter Let $\mathbf{x}_t^{(i)}$ be the i-th sample of the position and velocity of the target at time t, $i = 1, 2, \cdots, N_s$, where N_s is the total number of samples or particles in the particle filter. $w_t^{(i)}$ is the i-th weight at time $_t$ associated with $\mathbf{x}_t^{(i)}$. The procedure of SIR particle filter is defined as follows:

1. Initial Particle Generation
   Generate N_s particles $\left\{\mathbf{x}_0^{(i)},\ w_0^{(i)}\right\}$, $i = 1, 2, \cdots, N_s$. Here $\mathbf{x}_0^{(i)}$ is obtained from vehicle detection results and $w_0^{(i)} = 1/N_s$.
2. Particle Updating
   For each particle $\mathbf{x}_{t-1}^{(i)}$ at time $t-1$, generate a particle $\mathbf{x}_t^{(i)}$ at time t. This step corresponds to the prediction step in Kalman filter and EKF. However, in Kalman filter and EKF, at time t the state is updated only once. Here in the particle filter, each of the particles should be updated, so totally N_s particle updating calculations are implemented. In this system, $\mathbf{x}_t^{(i)} = \begin{bmatrix}\mathbf{p}_t^{(i)} & \mathbf{v}_t^{(i)}\end{bmatrix}$ is the sample of the position and velocity, so a linear model is used to update the particles:
   $$\mathbf{p}_t^{(i)} = \mathbf{p}_{t-1}^{(i)} + \mathbf{v}_{t-1}^{(i)} T + n \tag{13}$$
   where T is the time interval and n is the noise.
3. Particle Weighting
   Each particle $\mathbf{x}_0^{(i)}$ at time t is associated with the weight $w_t^{(i)}$, which is also called the *importance factor*. The weight at time t is a function of the weight at time $t-1$, and the probability function of measurements and states at time t. The importance factor is commonly calculated as [41]:
   $$w_t^{(i)} = w_{t-1}^{(i)} p\left(\mathbf{z}_t \middle| \mathbf{x}_t^{(i)}\right) \tag{14}$$
   where $\mathbf{z}_t$ is the measurement at time t. In the proposed sensor fusion system, both LIDAR and computer vision sensors are utilized for vehicle tracking. Therefore, the measurement is $\mathbf{z}_t = \left\{{}^l\mathbf{z}_t;\ {}^c\mathbf{z}_t\right\}$, where ${}^l\mathbf{z}_t$ is the output of LIDAR and ${}^c\mathbf{z}_t$ is the measurement of the camera. This step corresponds to the update step in Kalman filter and EKF. The probability $p\left(\mathbf{z}_t \middle| \mathbf{x}_t^{(i)}\right)$ will be discussed in the following subsection.
4. Resampling
   A common problem with the particle filter is the degeneracy, which is the phenomenon that after a few iterations only one particle has non-negligible weight [41]. $\widehat{N_{eff}}$ has been defined to measure the degeneracy, which is calculated as [41]:
   $$\widehat{N_{eff}} = \frac{1}{\sum_{i=1}^{N_s}\left(w_t^{(i)'}\right)^2} \tag{15}$$
   where $w_t^{(i)'}$ is the normalized weight of the i-th particle at time t with $w_t^{(i)'} = \frac{w_t^{(i)}}{\sum_{i=1}^{N_s} w_t^{(i)}}$. If $\widehat{N_{eff}}$ is less than a given threshold N_T, the degeneracy is detected.

   Resampling is performed at each iteration. It is designed to eliminate particles that have small weights and replicate particles that have large weights. Particles that have large weights are considered to be the "good" particles while the particles with small weights are "bad" particles. The resampled weights are set as $w_t^{(i)} = 1/N_s$.

   After obtaining $w_t^{(i)}$, the posterior filtered density can be approximated as [41]:
   $$p(\mathbf{x}_t|\mathbf{z}_{1:t}) \approx \sum_{i=1}^{N_s} w_k^i \delta\left(\mathbf{x}_t - \mathbf{x}_t^{(i)}\right) \tag{16}$$

The Sensor Model The sensor model describes the process by which sensor measurements are made in the physical world. It relates sensor output to the state of the vehicle. In the vehicle detection application it is defined as the conditional probability $p\left({}^l\mathbf{z}_t;\ {}^c\mathbf{z}_t \middle| \mathbf{x}_t^{(i)}\right)$, which is the probability of LIDAR and computer vision sensor measurements given the state of the vehicle.

A LIDAR sensor model is described in [42], which represents the probability as a mixture of four distributions corresponding to four types of measurement errors: the small measurement noise, errors due to unexpected objects or obstacles, errors due to failure to detect objects, and random unexplained noise.

Let $z_t^{(k)*}$ denote the true distance to an obstacle, $z_t^{(k)}$ denote the recorded measurement, and $z_{\max}$ denote the maximum possible reading. The small measurement error is defined as a Gaussian distribution p_{hit} over the range $[0, \quad z_{\max}]$ with mean $z_t^{(k)*}$ and standard deviation σ_{hit}.

The LIDAR detection zone is often blocked by the moving vehicles, which leads to the measurement whose length is shorter than the true length. This particular type of measurement error is modeled by a truncated exponential distribution p_{short} with the coefficient λ_{short}.

LIDAR sometimes fails to detect obstacles due to low reflectivity of the target. The errors due to failure to detect objects is defined as a pseudo point-mass distribution $p_{\max}$ centered at $z_{\max}$.

Finally, unexplainable measurements may be returned by the LIDAR sensor, which is caused by interference. This type of error is modeled by a uniform distribution p_{rand} over the entire measurement range.

$p\left({}^l\mathbf{z}_t \middle| \mathbf{x}_t^{(i)}\right)$ is calculated as a combination of the four types of errors as [42]:

$$\begin{aligned} p\left({}^l\mathbf{z}_t \middle| \mathbf{x}_t^{(i)}\right) = {} & \alpha_{\text{hit}} p_{\text{hit}}\left({}^l\mathbf{z}_t \middle| \mathbf{x}_t^{(i)}\right) \\ & + \alpha_{\text{short}} p_{\text{short}}\left({}^l\mathbf{z}_t \middle| \mathbf{x}_t^{(i)}\right) \\ & + \alpha_{\max} p_{\max}\left({}^l\mathbf{z}_t \middle| \mathbf{x}_t^{(i)}\right) \\ & + \alpha_{\text{rand}} p_{\text{rand}}\left({}^l\mathbf{z}_t \middle| \mathbf{x}_t^{(i)}\right) \end{aligned} \tag{17}$$

where α_{hit}, α_{short}, $\alpha_{\max}$, and α_{rand} are the weights for p_{hit}, p_{short}, $p_{\max}$, and p_{rand}, respectively. $\alpha_{\text{hit}} + \alpha_{\text{short}} + \alpha_{\max} + \alpha_{\text{rand}} = 1$. The parameters in Eq. 17 are commonly used as the a priori information, which are obtained by data training.

A camera weight model is proposed in [43] as:

$$p\left({}^c\mathbf{z}_t \middle| \mathbf{x}_t^{(i)}\right) = \begin{cases} S & \text{the object is in the camera detection zone.} \\ 1-S & \text{the object is out of the camera detection zone.} \end{cases} \tag{18}$$

where S is a constant, $0 \le S \le 1$. This model is based on the assumption that the camera is able to detect all the objects in the detection zone.

The sensor fusion probability model is calculated based on the LIDAR probability model as well as the camera probability model. It is proposed in [43] that ${}^l\mathbf{z}_t$ and ${}^c\mathbf{z}_t$ are independent measurements. So

$$p\left({}^l\mathbf{z}_t; {}^c\mathbf{z}_t \middle| \mathbf{x}_t^{(i)}\right) = p\left({}^l\mathbf{z}_t \middle| \mathbf{x}_t^{(i)}\right) p\left({}^c\mathbf{z}_t \middle| \mathbf{x}_t^{(i)}\right) \tag{19}$$

However, in the proposed sensor fusion system, LIDAR and the camera are not two independent sensors. They have been calibrated to observe the same target, and the geometric relationships are given as a priori information. Moreover, the classification result of the camera is corrected by the LIDAR output.

In this section, a novel sensor fusion probability model is proposed. As defined in [42], LIDAR tracking process is modeled as a mixture of four types of errors: the small measurement noise, unexpected objects detection error, detection failure error, and random unexplained noise. In the field test, small measurement noise error is found to be the exclusive error source of the LIDAR sensor. The other types of errors are removed by integration of LIDAR and camera. The LIDAR tracking model is [42]:

$$p\left({}^l\mathbf{z}_t \middle| \mathbf{x}_t^{(i)}\right) = \begin{cases} \frac{1}{\sqrt{2\pi}\delta} \exp\left(-\frac{\left({}^l\mathbf{z}_t - {}^l\mathbf{z}_t^*\right)^2}{2\delta^2}\right) & 0 \le {}^l\mathbf{z}_t \le z_{\max} \\ 0 & \text{otherwise} \end{cases} \tag{20}$$

The computer vision-based vehicle tracking is implemented by KLT tracking [36, 47]. A function $s\left(x_{t(i)}^m\right)$ is used to determine if a predicted corner $x_{t(i)}^m$ is close to an observed corner $z_{t(i)}$. $s\left(x_{t(i)}^m\right)$ is defined as $s\left(x_{t(i)}^m\right) = -\sum_{j=1}^{M} \exp\left(d_{t(i,j)}^m\right)^2$, where M is the total number of corners, $\left(d_{t(i,j)}^m\right)^2 = \left\| z_{t(j)} - x_{t(i)}^m \right\|^2$ is the Euclidean distance between i-th detected corner of the m-th particle $x_{t(i)}^m$ and j-th extracted corner $z_{t(j)}$ [47]. The camera model is defined as [47]:

$$p\left({}^c\mathbf{z}_t \middle| \mathbf{x}_t^{(i)}\right) = \exp\left(-\sum\left(s\left(x_{t(i)}^m\right) - 1\right)^2\right) \tag{21}$$

Finally, the sensor fusion tracing system has totally three measurement situations: (1) the vehicle is tracked by both the LIDAR and the camera. In this case, the single sensor tracking error is eliminated by sensor integration technique proposed in section "Moving

Vehicle Detection System"; (2) the vehicle is out of camera detection zone, so it is tracked by the LIDAR alone; and (3) the vehicle is tracked by the camera but not detected by the LIDAR sensor due to factors such as distance or weak reflection. The sensor fusion model is given as:

$$p\left({}^{l}\mathbf{z}_t;{}^{c}\mathbf{z}_t \middle| \mathbf{x}_t^{(i)}\right) = \begin{cases} \alpha p\left({}^{l}\mathbf{z}_t \middle| \mathbf{x}_t^{(i)}\right) + \beta p\left({}^{c}\mathbf{z}_t \middle| \mathbf{x}_t^{(i)}\right) \\ \text{target is tracked by both LIDAR and camara} \\ p\left({}^{l}\mathbf{z}_t \middle| \mathbf{x}_t^{(i)}\right) \\ \text{target is tracked by LIDAR alone} \\ p\left({}^{l}\mathbf{z}_t \middle| \mathbf{x}_t^{(i)}\right) \\ \text{target is tracked by camara alone} \end{cases} \tag{22}$$

where the weight $0 \le \alpha \le 1$ and $0 \le \beta \le 1$ are two coefficients obtained by data training, $\alpha + \beta = 1$, which allows to balance the LIDAR and computer vision information.

The weight $w_t^{(i)}$ can be calculated using Eq. 14. The particle filter is summarized in Algorithm 2. Unlike the Kalman filter or EKF, particle filter can track vehicle state with multi-model or arbitrary distributions.

Algorithm 2: Particle Filter for Sensor Fusion Systems. Input: $\left\{x_{t-1}^{(i)}, w_{t-1}^{(i)}\right\}$, $i = 1, 2, \cdots, N_s$: set of weighted particles at time $t-1$
$\mathbf{z}_t = \left({}^{l}\mathbf{z}_t; {}^{c}\mathbf{z}_t\right)$: LIDAR and computer vision measurement at time t
Output: $\left\{x_t^{(i)}, w_t^{(i)}\right\}$, $i = 1, 2, \cdots, N_s$: set of weighted particles at time t
Process:
for $i = 1$ to N_s do
Predict $\mathbf{x}_t^{(i)}$ as $\mathbf{p}_t^{(i)} = \mathbf{p}_{t-1}^{(i)} + \mathbf{v}_{t-1}^{(i)} T + n$
$w_t^{(i)} = w_{t-1}^{(i)} p\left(\mathbf{z}_t \middle| \mathbf{x}_t^{(i)}\right)$
end for
calculate $\widehat{N_{eff}}$
if $\widehat{N_{eff}} < N_T$
for $i = 1$ to N_s do
computer $w_t^{(i)}$ using Eq. 14, in which $p\left({}^{l}\mathbf{z}_t; {}^{c}\mathbf{z}_t \middle| \mathbf{x}_t^{(i)}\right)$ is given in Eq. 20
update the particle with $\left\{x_t^{(i)}, 1/N_s\right\}$
end for
else
$Z = \sum_{i=1}^{N_s} w_t^{(i)}$
for $i = 1$ to N_s do
update the particle with $\left\{x_t^{(i)}, Z^{-1} w_t^{(i)}\right\}$
end for
end if

Experiment Results

The experiment results of vehicle detection are discussed in this section. To evaluate the performance of this system, a dataset of 377 images was used for training and testing. These images are taken from both the Caltech vehicle image dataset [37] and the video samples collected by probe vehicles. Another test dataset consists of 526 images with synchronized scanning data that are used for performance evaluation. The test dataset was recorded in a local parking lot on different days during different seasons.

Hit rate (HR), false alarm rate (FAR), and region detection rate (RDR) are used to evaluate the performance of this system. Here HR is the number of detected vehicles over total number of vehicles. RDA denotes the percentage of "real" vehicle detection rate. A "real" vehicle detection is that majority area of the vehicle is covered by a rectangle, and there is only one rectangle that covers this object. Therefore, a target that is hit may not be a region "really" detected; and a region detected object is always a hit. The higher the RDR is, the more accurate the detection result will be. Figure 16 illustrates several cases for hit, false alarm, and region detection. In this figure, TR represents the target region in the image, and DR is the detected region by the classifier.

Table 2 gives the detection performance of Adaboost classifier (detection with camera only), the classic LIDAR–camera sensor fusion system, and the proposed LIDAR and computer vision-based detection and error correction approach. Here in both the classic sensor fusion technique and the proposed approach, LIDAR data are utilized for ROI generation. The difference lies in the fact that in the proposed approach LIDAR data help correct the classification result. Table 2 shows that this approach both improves the hit rate and reduces the false alarm rate in comparison with Adaboost classifier. Compared with the classic LIDAR–camera fusion system, this approach improves the

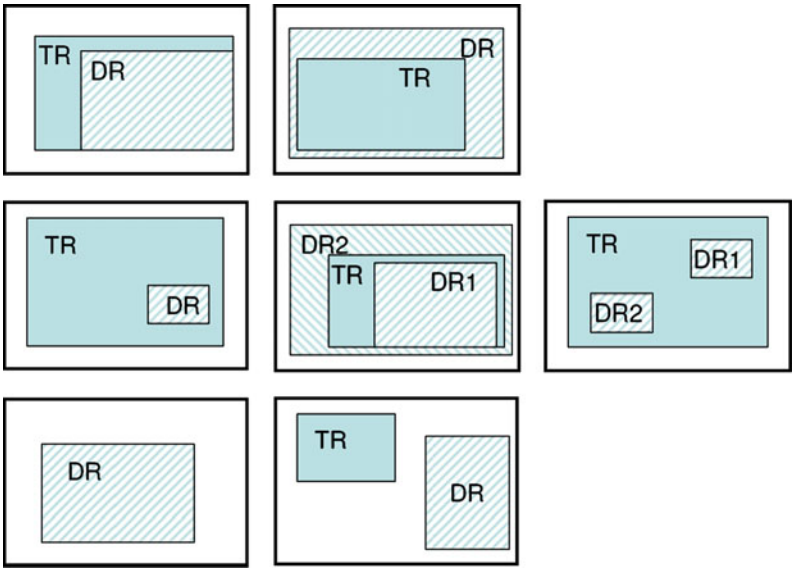

Vehicle Detection, Tightly Coupled LIDAR and Computer Vision Integration for. Figure 16
Three target detection cases. The first row is region detected, the second row is hit but not region detected, and the third row is false alarm

Vehicle Detection, Tightly Coupled LIDAR and Computer Vision Integration for. Table 2 Detection result

Type	HR (%)	FAR (%)	RDR (%)
Adaboost	84.17	3.27	78.00
Classic LIDAR–camera fusion	91.33	1.78	84.85
Proposed approach	91.33	1.78	89.32

region detect rate from 84.85% to 89.32%, since for each hit but not accurately covered object the LIDAR scanning data helps to recomputed position of the target. Most of the overlapping or partial target detection areas are merged during the LIDAR correction process.

Figure 17 illustrates some of the vehicle detection results. The left column presents LIDAR scan points, and the right column illustrates camera images with information from the sensor fusion system. In Figure 7a, all the vehicles are detected and are marked with a rectangle. Figure 7b shows that the classifier found two vehicles only, which are bounded in a red rectangle. The other two ROIs (shown in blue rectangles) are classified to have non-vehicle objects. In fact, one of them is a trash can. The other is a vehicle at a distance of 92.78 m. This vehicle is too far away and too small in the image for the classifier to recognize.

During the test, the hit rate decreases when the distance between the probe vehicle and the target vehicles increases. The targets are detected frame by frame. Therefore, the target vehicles may not be recognized by the classifier in certain frames even if it was recognized in the last frame. Vehicle tracking technique helps solve this problem. By running a particle filter–based tracking algorithm, the target is initially detected in the initial frame or in several initial frames, after which it is tracked in the following frames. This approach both improves the detection accuracy and reduces the required amount of calculation. HR and RDR will be further improved by vehicle tracking.

Summary and Discussion

A novel vehicle detection system has been proposed based on tightly integrating LIDAR and computer vision sensors. Distances to the objects are first defined by the LIDAR sensors, and then the object is classified based on computer vision images. In addition, data from these two complementary sensors are combined for classifier correction and vehicle detection.

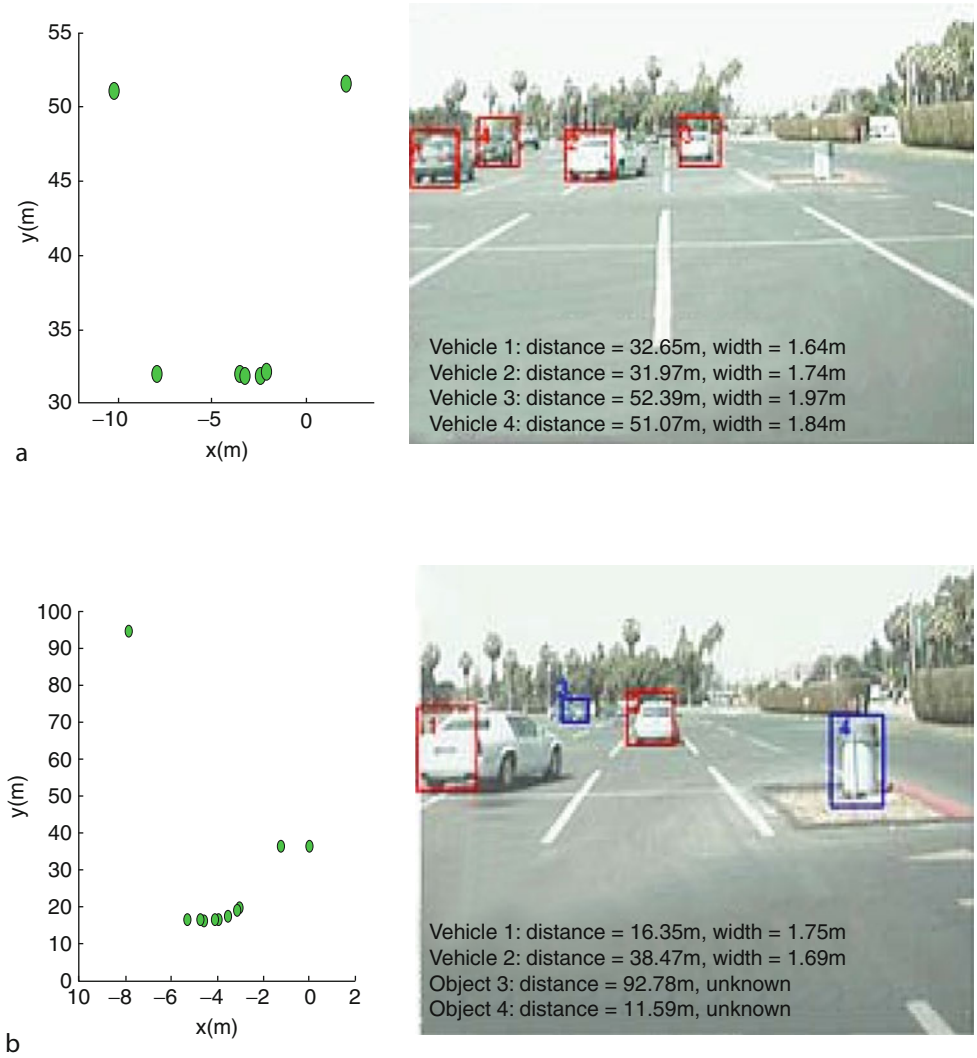

Vehicle Detection, Tightly Coupled LIDAR and Computer Vision Integration for. Figure 17
LIDAR scan points and the final vehicle detection results

The experimental results have indicated that, when compared with image-based and classic sensor fusion–based vehicle detection systems, this approach has a higher hit rate and a lower false alarm rate. It is quite useful for modeling and prediction of the traffic conditions over a variety of roadways. This system may be used in future autonomous navigation systems.

Conclusions and Future Work

This entry presents a multi-sensor equipped vehicle detection system that was developed to specifically obtain the state of surrounding vehicles. It involves the development of a tightly coupled LIDAR and computer vision system, calibration of a pair of multi-planar LIDAR sensors and the camera system, and the methodology of sensor fusion-based vehicle detection technique.

This section provides a brief summary of this entry, as well as the possible future work.

Summary

Automatic vehicle detection techniques are becoming an essential part of our daily lives. They open up many potential opportunities but they also come with

challenges in terms of sensing capability and accuracy. In this entry, the problem of vehicle detection is addressed, and some novel approaches have been demonstrated to solve the problem in a traffic environment.

The goal of this research is to provide a solution to measure the state of surrounding vehicles. State of the vehicle includes position, orientation, speed, and acceleration. Sensor fusion techniques are utilized to provide a direct measurement of the state. A variety of sensors have been used in this entry, including LIDAR and computer vision. The goal is to quantitatively show that the integration of sensors provides a more accurate and effective estimation of the vehicle state. The proposed system has successfully met this goal.

The developed multi-planar LIDAR and computer vision sensor calibration approach, as to the author's best knowledge, is the first calibration method for an "invisible-beam" multi-planar LIDAR and a camera. In comparison to the commonly used calibration methods that require a infrared camera to "see" the LIDAR beams or a special designed calibration shape, this approach is easy to implement with low cost. It has been theoretically and experimentally proven to be able to estimate the geometric relationships between the two sensors.

Based on this unique calibration method, a sensor fusion-based vehicle detection system is designed and implemented. It consists of three major components: (1) ROIs are generated by the LIDAR sensor; (2) vehicle classification using a computer vision-based Adaboost algorithm, and (3) vehicle position is verified using the output of the LIDAR sensor. A vehicle tracking model is also presented in this entry, which uses a joint probability model-based particle filter to predict state of the vehicle. The experiment result shows that the designed sensor fusion system achieves higher detection rate and lower positive as well as negative error rates, when compared with a single sensor-based detection method. The positions of detected vehicles have been represented in vehicle coordinates to generate a local traffic map.

Taken together, the tests in this entry demonstrate that a good vehicle detection performance can be achieved using a LIDAR and computer vision sensor-based moving platform. Such results are especially important for vehicle navigation systems, as well as traffic surveillance systems that are equipped with multiple sensors.

Future Directions

Although a sensor fusion system is developed in this entry for the on-board vehicle detection application, it is believed that the introduction of sensor fusion-based system in the automobile industry is still couple of years away. In the future driver assistance systems, sensor fusion techniques can be employed to support, even replace the driver. Moreover, falling costs of sensors, such as RADAR, GPS, inertial sensors (INS), and LIDAR, combined with increasing image processing capability provides a bright future for on-board intelligent transportation applications.

Disclaimer

Much of the material for this entry comes from the 2010 dissertation of Lili Huang, at the University of California-Riverside (see [44]). Portions of this entry have also appeared in [45] and [46].

Bibliography

1. Proper AT, Cheslow MD (1997) ITS benefits: continuing successes and operational test results. FHWA-JPO-98-002, Oct 1997
2. Mimbela L, Klein LA (2000) Summary of vehicle detection and surveillance technologies used in intelligent transportation systems. Report to Federal Highway Administrations (FHWA) Intelligent Transportation Systems Joint Program Office
3. Apogee/Hagler Bailly (1998) Intelligent transportation systems: real world benefits. FHWA-JPO-98-018, Jan 1998
4. Kim MY, Cho H, Lee H (2004) An active trinocular vision system for sensing mobile robot navigation environments. In: Proceedings of the IEEE intelligent robots and systems, Sendai, pp 1698–1703
5. Jung YK, Ho Y-S (1999) Traffic parameter extraction using video-based vehicle tracking. In: IEEE/IEEJ/JSAI international conference on intelligent transportation systems, Tokyo, pp 764–769
6. Baltzakis H, Argyros A, Trahanias P (2003) Fusion of laser and visual data for robot motion planning and collision avoidance. Mach Vision Appl 12:431–441
7. Liu Y, Emery R (2001) Using EM to learn 3D environment models with mobile robots. In: Proceedings of the 18th international conference on machine learning, Williamston, 2001
8. Jokinen O (1999) Self-calibration of a light striping system by matching multiple 3-D profile maps. In: Proceedings of the second international conference on 3-D digital imaging and modeling, Ottawa, pp 180–190
9. Hayashibe M, Nakamura Y (2001) Laser-pointing endoscope system for Intra-operative 3D geometric registration. In: Proceedings of the international conference on robotics and automation, Seoul, pp 1543–1548

10. Mahlisch M, Schweiger R, Ritter W, Dietmayer K (2006) Sensorfusion using spatio-temporal aligned video and lidar for improved vehicle detection. In: Proceedings of intelligent vehicles symposium, Meguro-Kupp, pp 424–429
11. Unnikrishnan R, Hebert M (2005) Fast extrinsic calibration of a laser rangefinder to a camera. Technical report CMU-RI-TR-05-09, Robotics Institute, Carnegie Mellon University, July 2005
12. Zhang Q, Pless R (2004) Extrinsic calibration of a camera and laser range finder (Improves camera calibration). In: IEEE proceedings of international conference on intelligent robots and systems, Sendai, pp 2301–2306
13. DARPA urban challenge http://www.darpa.mil/grandchallenge/index.asp
14. Mahmassani HS, Haas C, Zhou S, Peterman J (1998) Evaluation of incident detection methodologies. Technical Report FHWA/TX-00/1795-1, Center of Transportation Research, The University of Texas at Austin, Oct 1998
15. University of Central Florida (2007) I2Lab, TeamUCF – DARPA urban challenge. Technical Report, June 2007
16. Thrun S (2003) Learning occupancy grid maps with forward sensor models. Autonomous Robots 15(2):111–127
17. SICK USA, see http://www.sick.com/us/en-us/home/Pages/Homepage1.aspx
18. HOKUYO UXM-30LN LIDAR, see http://www.hokuyo-aut.jp/02sensor/07scanner/uxm_30ln.html
19. The laser scanner product overview, see http://www.ibeoas.com/english/products.asp
20. Velodyne HDL-64E LIDAR, http://www.hizook.com/blog/2009/01/04/velodyne-hdl-64e-laser-rangefinder-lidar-pseudo-disassembled
21. Whittaker WR (2005) Red team DARPA grand challenge 2005 technical paper. Carnegie Mellon University, CSC Technical Report, Aug 2005
22. Cobzas D, Zhang H, Jagersand M (2002) A comparative analysis of geometric and image-based volumetric and intensity data registration algorithms. In: IEEE international conference on robotics and automation (ICRA), Washington, DC, 2002
23. Wasielewski S, Strauss O (1995) Calibration of a multi-sensor system laser rangefinder/camera. In: Proceedings of intelligent vehicles symposium, Detroit, pp 472–477
24. Neira J, Tard JD, Horn J, Schmidt G (1999) Fusing range and intensity images for mobile robot localization. IEEE Trans Robot Autom 15(1):76–84
25. Toyh D, Aach T (2003) Detection and recognition of moving objects using statistical motion detection and Fourier descriptors. In: 12th international conference on image analysis and processing, Mantova, pp 430–435
26. Oren M, Papageorgiou C, Sinha P (1997) Pedestrian detection using wavelet templates. In: IEEE proceedings on computer vision and pattern recognition, San Juan, 1997
27. Premebida C, Monteiro G, Nunes U, Peixoto P (2007) A lidar and vision-based approach for pedestrian and vehicle detection and tracking. In: IEEE intelligent transportation systems conference, Seattle, pp 1044–1049
28. Fardi B, Schuenert U, Wanielik G (2005) Shape and motion-based Pedestrian detection in infrared images: a multi sensor approach. In: Proceedings of the IEEE intelligent vehicles symposium Las Vegas, pp 18–23
29. Milch S, Behrens M (2001) Pedestrian detection with radar and computer vision. In: Proceedings of the conference on progress in automobile lighting, Darmstadt, 2001
30. Zhang Z (2000) A flexible new technique for camera calibration. IEEE Trans Patt Anal Mach Intell 22:1330–1334
31. Bouguet J-Y (2003) Camera calibration toolbox for matlab, 2003
32. Faugeras OD, Toscani G (1987) Camera calibration for 3D computer vision. In: Proceedings of the international workshop on industrial applications of machine vision and machine intelligence, Silken, Japan, pp 240–247
33. Ricolfe Viala C, Sanchez Salmeron AJ (2004) Performance evaluation of linear camera calibration techniques. In: IEEE Proceedings on world automation congress, Spain, vol 18, pp 49–54
34. Levenberg K (1944) A method for the solution of certain problems in least squares. Quart Appl Math 2:164–168
35. More J (1977) The Levenberg-Marquardt algorithm, implementation and theory. In: Numerical analysis. Lecture notes in mathematics, vol 630. Springer, Berlin
36. Viola P, Jones MJ (2001) Rapid object detection using a boosted cascade of simple features. In: Proceedings of the IEEE computer vision and pattern recognition, Hawaii, pp 511–518
37. Caltech vehicle image dataset, see http://www.vision.caltech.edu/htmlfiles
38. Haselhoff A, Kummert A, Schneider G (2007) Radar-vision fusion with an application to car-following using an improved adaboost detection algorithm. In: IEEE intelligent transportation systems conference, Seattle, pp 854–858
39. Tutorial OpenCV Haartraining, see http://sourceforge.net/projects/opencvlibrary
40. Lienhart R, Kuranov A, Pisarevsky V (2003) Empirical analysis of detection cascades of boosted classifiers for rapid object detection. In: 25th pattern recognition symposium, Madgeburg, Sep 2003, pp 297–304
41. Arulampalam MS, Maskell S, Gordon N, Clapp T (2002) A tutorial on particle filters for online nonlinear/non-Gaussian Bayesian tracking. IEEE Trans Signal Process 50(2):174–188
42. Thrun S, Burgard W, Fox D (2005) Probabilistic robotics. The MIT Press, Cambridge, MA
43. Kurazume R, Yamada H, Murakami K, Iwashita Y, Hasegawa T (2008) Target tracking using SIR and MCMC particle filters by multiple cameras and laser range finders. In: IEEE/RSJ international conference on intelligent robots and systems, Nice, pp 3838–3844
44. Huang L (2010) LIDAR, Camera and inertial sensors based navigation techniques for advanced intelligent transportation systems, PhD dissertation, University of California Riverside
45. Huang L, Barth M (2009) A novel multi-planar LIDAR AND computer vision calibration procedure using 2D patterns for automated navigation. In: IEEE intelligent vehicles symposium, Xi'an, pp 117–122

46. Huang L, Barth M (2009) Tightly-coupled LIDAR and computer vision integration for vehicle detection. In: IEEE intelligent vehicles symposium, Xi'an, pp 604–609
47. Dore A, Beoldo A, Regazzoni CS (2009) Multitarget tracking with a corner-based particle filter. In: IEEE 12th international conference on computer vision workshops, Kyoto, pp 1251–1258

Vehicle Dynamics and Performance

Yimin Gao
Department of Electrical and Computer Engineering, Texas A&M University, College Station, TX, USA

Article Outline

Glossary
Definition of the Subject
Introduction
Vehicle Performance
Fuel Economy and Energy Consumption
Vehicle Braking Performance
Future Directions
Bibliography

Glossary

Braking forces The forces acting on the contact area of the running wheels and ground, generated by the brake system.

Braking performance The vehicle behavior underlying braking, braking distance, and direction stability.

Braking system A vehicle subsystem that is used to slow the vehicle quickly.

Fuel consumption Fuel consumed in unit traveling distance.

Power plants The machines that supplies power for propelling vehicle.

Tractive effort The thrust force acting on the contact area of running wheels and ground that push the vehicle forward.

Transmissions Mechanical devices that transmit the powers of the power plants to vehicle wheels.

Vehicle performance The capability of a vehicle, in terms of speed, acceleration, and gradeability.

Vehicle resistance The forces that is against the vehicle motion.

Definition of the Subject

Vehicle system is a complex system that includes many mechanical and electric components and operates in very different traffic environments. There are many requirements, including traffic conditions, mission requirements, energy supplies, environmental protection, cost, etc. Vehicle dynamic and performance analysis supplies the basic methodologies for vehicle performance evaluation, design principle, and quantitative computation methods for system and component design.

Introduction

Vehicle dynamics and performance are broad topics that deal with vehicle's drivability, fuel economy, braking performance, handling characteristics, noise, vibration and harshness (NVH), etc. The research for improving vehicle dynamics and performance never ceased in 100 years since vehicles have been invented. The research in this area has been developed for the purposes of basic understanding of the system operation behaviors, system and components design, and development of more advanced control technologies, such as engine control, transmission control, traction control, braking control, vehicle stability control, etc. In recent years, more efficient and clean vehicle technologies have been developed quickly, especially, electric propulsion, fuel cell, and hybrid technologies. These require the research on vehicle dynamics and performance being extended beyond the scope of conventional vehicles that has focused on gasoline and diesel power vehicles. However, although there are many differences between conventional and electric-based vehicles, they share some similarities of drivability and braking performance. The fundamentals of vehicle dynamics and performance established for conventional vehicles are still, to a great degree, valid. This section reviews the fundamentals of vehicle's dynamics and performance for providing reference for electric, hybrid electric, and fuel cell vehicle design. The following sections focus on the traction and braking performance. Other performance, such as handling characteristics, noise, vibration and harshness (NVH), etc., will not be discussed in this entry.

Vehicle Performance

Vehicle performance discussed in this article will be restricted to propelling and braking performance in terms of vehicle speed, acceleration, gradeability, braking deceleration, and braking force distribution on front and rear wheels.

Overview of Vehicle Power Train Structure

Vehicle propelling performance is dictated by the power train structure, tractive power rating, and power plant operation characteristics and transmission design. Generally, vehicle power train consists of energy source (fuel, batteries), power plant (engine, electric motor), transmission, and drive wheels. The power train may be configured into front wheel drive, rear wheel drive, and all wheel drive, as shown in Fig. 1. The engine power is transmitted to drive wheels through clutch or torque converter, transmission, shaft, final drive, and transaxles. The torque on the drive wheels reacts with road surface to develop tractive effort to push the vehicle forward, as shown in Fig. 2.

The tractive effort developed on the drive wheel, together with the vehicle resistances, determines the vehicle performance (speed, acceleration, and gradeability).

Tractive Effort and Vehicle Speed

Tractive effort is produced on drive wheels by the reaction between the tractive torque and road surface as shown in Fig. 2. The tractive effort is proportional to the tractive torque, T_w, by

$$F_t = \frac{T_w}{r} \tag{1}$$

where T_w is the tractive torque on the drive wheels and r is the wheel radius.

The tractive torque acting on the drive wheels is produced by the engine or motor, transmitted through transmission gear box and final drive. It can be expressed as

$$T_w = T_e\, i_0\, i_g\, \eta_t \tag{2}$$

where T_e is the engine torque, i_0 is the gear ratio of the final drive, i_g is the gear ratio of the transmission, and η_t is the efficiency from the engine to the drive wheels. Combining (1) and (2), the tractive effort can be further expressed as

$$F_t = \frac{T_w\, i_0\, i_g \eta_t}{r} \tag{3}$$

The gear ratios of final drive and transmission are defined as the ratio of the input speed to the output speed. The transmission efficiency should include all the losses in the driveline components, such as, torque converter, transmission, torque distributor, final drive, etc. The typical efficiency values for individual components may be evaluated by [1, 2]

Clutch	99%
Each pair of meshed gears	95–97%
Bearing and joint	98–99%

It should be mentioned here that efficiency of torque converter is closely related to its operating point, that is, the speed ratio of the torque converter [1, 2].

Vehicle speed is related to the rotating speed of the drive wheels as

$$V = \omega_w\, r \quad (\mathrm{m/s}) \tag{4}$$

where ω_w is the rotating speed of the drive wheels in rad/s. In terms of revolution per second (rpm) N_w, the vehicle speed can be further expressed as

$$V = \frac{\pi N_w\, r}{30} \quad (\mathrm{m/s}). \tag{5}$$

The wheel rotating speed is related to the engine rotating speed by

$$N_w = \frac{N_e}{i_0\, i_g}, \tag{6}$$

where N_e is engine rpm.

It should be noted that gear ratio of torque converter should be included into the gear box gear ratio, i_g. Gear ratio of torque converter is the reciprocal of the speed ratio of the torque converter [1, 2].

Combining (5) and (6), the vehicle speed can be further expressed as

$$V = \frac{\pi N_e\, r}{30\, i_0\, i_g} \quad (\mathrm{m/s}) \tag{7}$$

Equation 3 is only valid while the vehicle is running on well-prepared road, where no obvious slip

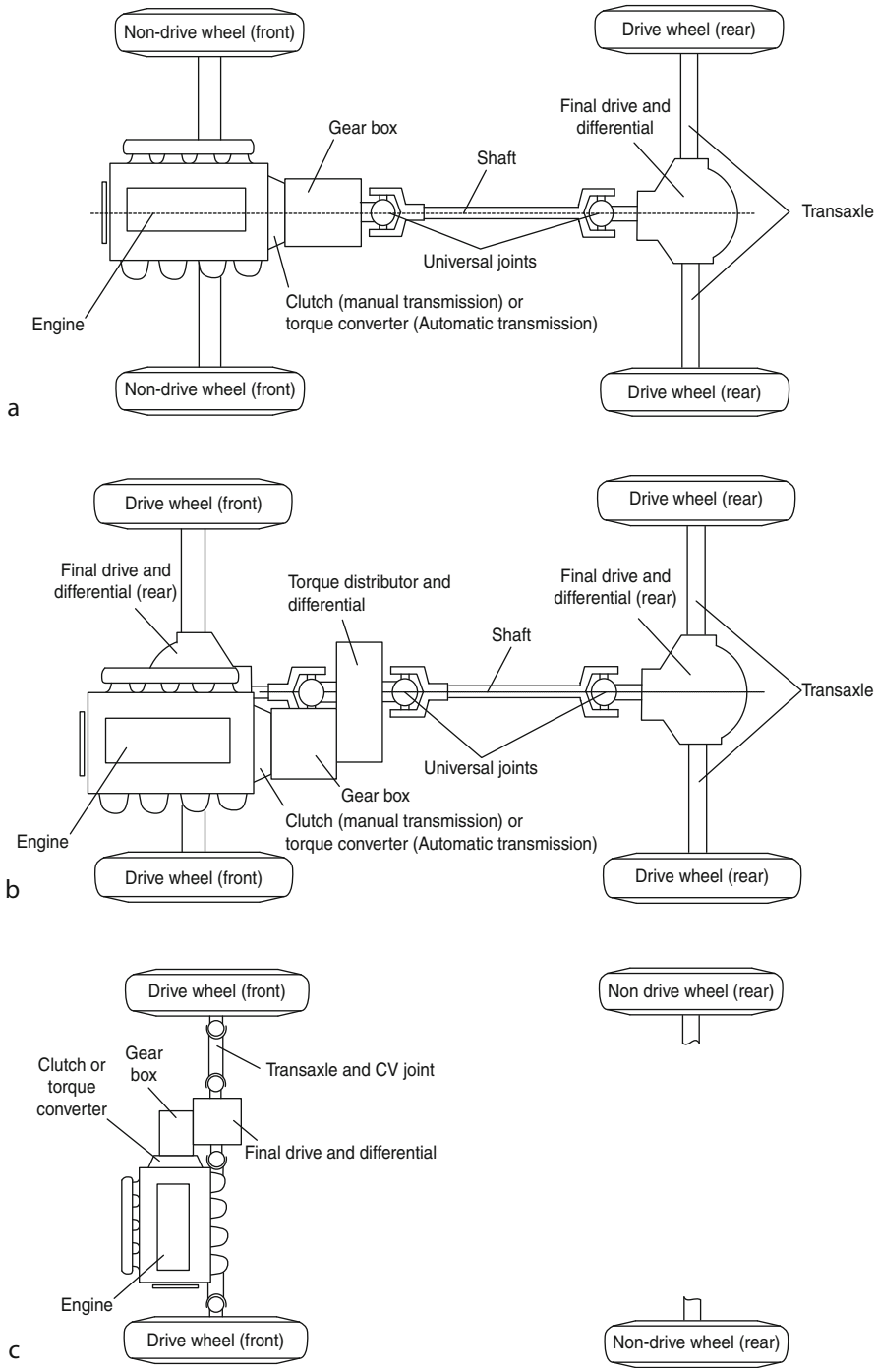

Vehicle Dynamics and Performance. Figure 1

Typical vehicle power trains: (**a**) rear wheel drive, (**b**) front wheel drive, and (**c**) all wheel drive

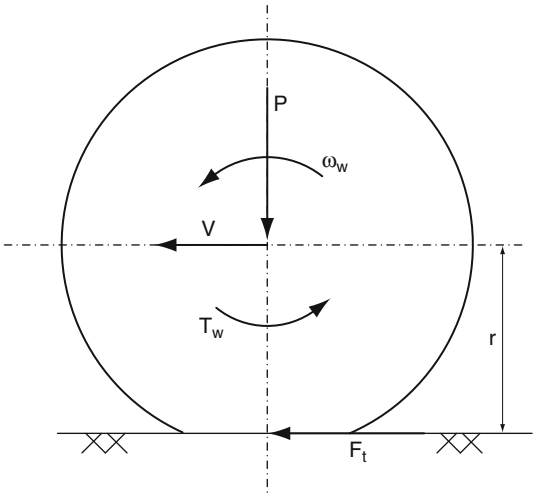

Vehicle Dynamics and Performance. Figure 2
Tractive effort, F_t, produced by wheel torque T_w

between tire and road surface occurs. For off-road operation, refer [1].

Torque (Power)-Speed Characteristics

For maximizing vehicle performance at a given power plant power capacity, the ideal power plant is one that can produce a constant power in its full speed range. In this case, the power plant can apply its maximum power for propelling the vehicle in its whole speed range, yielding the highest vehicle performance. However, in practice, the maximum torque acting on drive wheels is limited by road adhesive capability. Beyond this limitation, obvious tire slip will occurs. Therefore, at low speed, high torque is usually cut off with a constant torque as shown in Fig. 3.

For evaluating vehicle performance, such as maximum speed, acceleration, and gradeability, the maximum tractive torques in its whole speed range are used, that is, the torque produced by a fully opened throttle engine. Figure 4 shows a typical gasoline engine operation characteristics with full open throttle [2]. Figure 5 shows the operation characteristics of a typical gasoline engine with partial open throttle.

The torque-speed profile of the engine is quit flat and is very different from the ideal profile shown in Fig. 3. Consequently, a multi-gear or continuous varying transmission (CVT) is required to modify this profile as shown in Fig. 6, in which, the envelope curve is a constant power curve as required.

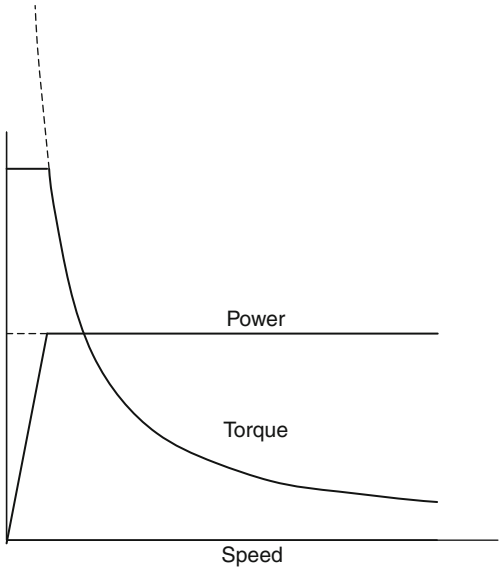

Vehicle Dynamics and Performance. Figure 3
Ideal torque (power)-speed performance of a vehicle power plant

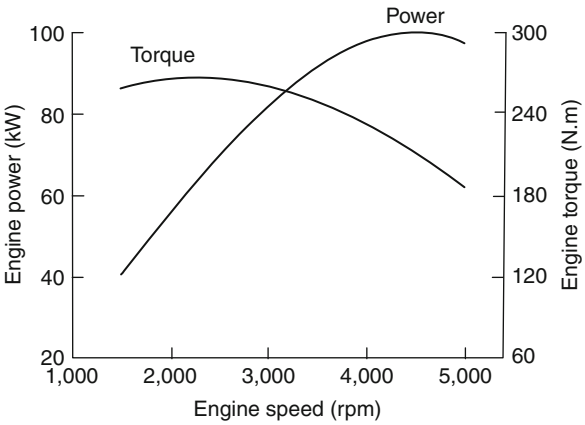

Vehicle Dynamics and Performance. Figure 4
Typical performance characteristics of gasoline engine with full open throttle [1]

Compared with the toque-speed profile of internal combustion engine, well-controlled electric motors possess the torque-speed profile much closer to the ideal as shown in Fig. 7. At low speeds, the motor develops constant torque, and at high speeds, constant power. The corner speed is called as base speed. A traction motor is usually controlled in such ways

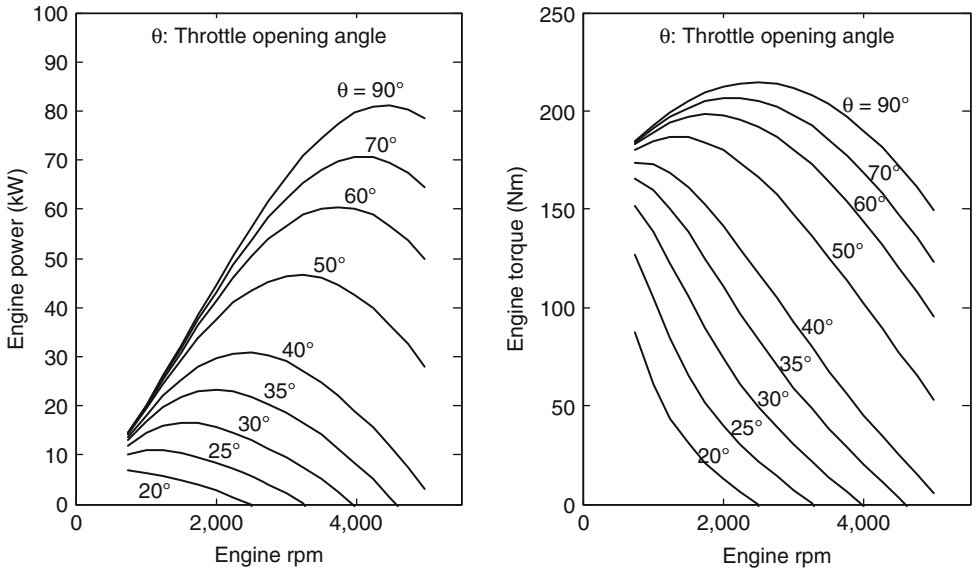

Vehicle Dynamics and Performance. Figure 5
Typical performance characteristics of gasoline engine with partial open throttle

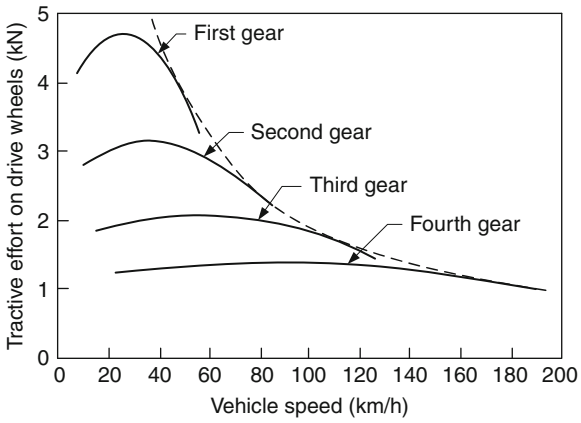

Vehicle Dynamics and Performance. Figure 6
Gasoline engine–powered tractive effort with a multi-gear transmission

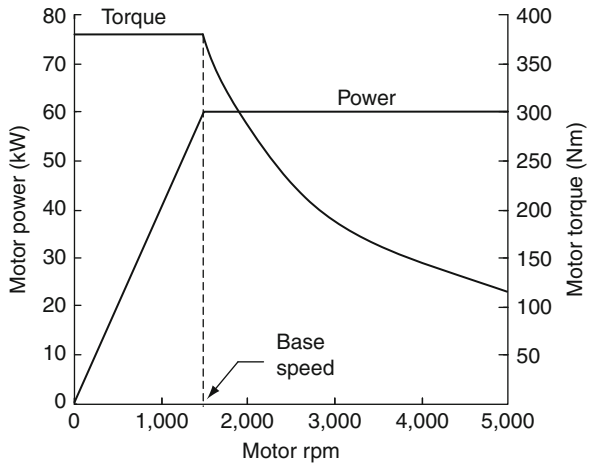

Vehicle Dynamics and Performance. Figure 7
Typical torque-speed profile of a well-controlled electric motor

that terminal voltage is linearly increased from zero speed to its base speed; meanwhile, the magnetic field is kept constant. Beyond the base speed, the terminal voltage is kept constant and magnetic field is linearly weakened. Since its torque-speed profile is naturally closer to the required, an electric motor–driven vehicle usually needs fewer gears than that of an engine-driven vehicle. A single- or double-gear transmission may meet the performance requirement.

Transmission Characteristics

As discussed above, torque-speed characteristic of internal combustion engine is far away from the ideal one and the engine cannot be directly connected to wheels. A multi-gear transmission or continuous varying transmission (CVT) is installed between the engine and drive wheels for modifying the torque-speed

characteristic of the engine output. A transmission is a gear box, in which there are several gear ratios for use. The gears are selected by driver based on real-time operation, such as vehicle speed and tractive effort requirement. This kind of transmission is referred to as manual transmission. The gear selection action may be performed automatically by a transmission control actuator, which is referred as automation or automatic transmission.

Transmission gear ratio design plays an importance role in vehicle performance. It should ensure the engine operating in its best speed range for torque producing and low fuel consumption.

Generally, there are several gears in a gear box. Each gear has a fixed gear ratio. Gear number depends upon vehicle performance requirements and specific power of the vehicle, which is defined as the power capacity per unit vehicle weight. More gear number results in a torque-speed profile closer to the ideal one, thus better vehicle performance can be obtained. However, more gears leads to complex transmission structure, and increased manufacturing difficulty, volume, weight, and cost. Therefore, the gear number design is usually a trade-off. In general, fewer gears are used in the vehicles that have large specific power. For passenger cars, four or five gears are common. For heavy-duty vehicles, over ten gears are common and two gear boxes are usually used.

Gear ratio design should ensure the engine operating in the best speed range. The design rule is interpreted as following.

As indicated by (7), for each gear, vehicle speed is proportional to engine speed. Gear changing procedure in acceleration driving is interpreted by Fig. 8 with a four-gear transmission.

1. Vehicle starts with first gear from zero speed to a speed, V_1 (point a), at which the engine speed reaches N_{e2}.
2. At point a, gear is changed from first to second (from point a to point b), in which vehicle speed does not change due to the very short gear change duration.
3. Start from point b, second gear is engaged, and continuous acceleration to point c.
4. At point c, gear is changed to third (from point c to point d).

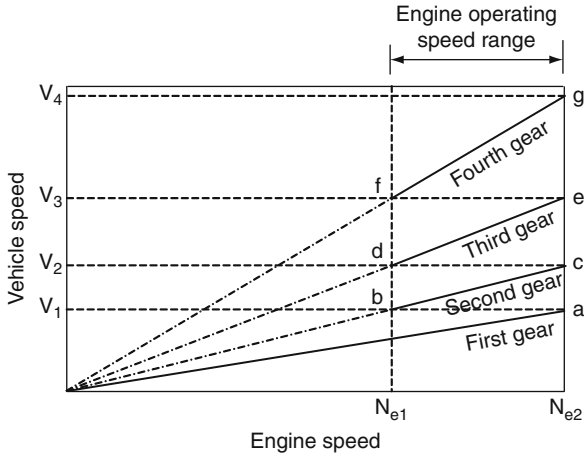

Vehicle Dynamics and Performance. Figure 8
Engine speed versus vehicle speed at each gear

Using the speed relations, for example, the speed at point a equals to the speed at point b, the speed at point c equals to the speed at point d, and so on, and using (7), one obtains

$$V_1 = \frac{\pi N_{e2}\, r}{30\, i_0\, i_{g1}} = \frac{\pi N_{e1}\, r}{30\, i_0\, i_{g2}}$$
$$V_2 = \frac{\pi N_{e2}\, r}{30\, i_0\, i_{g2}} = \frac{\pi N_{e1}\, r}{30\, i_0\, i_{g3}} \tag{8}$$
$$V_3 = \frac{\pi N_{e2}\, r}{30\, i_0\, i_{g3}} = \frac{\pi N_{e1}\, r}{30\, i_0\, i_{g4}}$$

Equation 8 gives

$$\frac{N_{e2}}{N_{e1}} = \frac{i_{g1}}{i_{g2}} = \frac{i_{g2}}{i_{g3}} = \ldots.. = \frac{i_{g,n-1}}{i_{g,n}} = k \tag{9}$$

Equation 9 indicates that the ratios of two adjacent gears, k, is a constant, which determines the engine speed range, N_{e1}–N_{e2}. Small k allows engine operating in a narrow speed range, but more gears are needed.

When gear number and ratio, k, are determined, the gear ratio of each gear can be obtained using (9).

In transmission design, gear ratio of the highest speed gear is usually designed by selecting an engine speed, at which the vehicle has its top speed, that is,

$$i_{gh} = \frac{\pi\, N_{ed}\, r}{30\, i_0\, V_{\max}} \tag{10}$$

where i_{gh} is the gear ratio of highest speed gear, $V_{\max}$ is the top speed of the vehicle with the highest speed gear,

N_{ed} is the desired engine speed with highest speed gear at maximum vehicle speed, and r is tire radius. After determination of the gear ratio of the highest speed gear, gear ratios of other gears can be determined by (9). It should be pointed out that the gear ratio of the lowest speed gear (first gear) should ensure the vehicle has its maximum tractive effort at low speed for meeting gradeability requirement.

In practice, gear ratio design may not exactly follow the rule of (9). For passenger cars, high-speed gears are used more often than low-speed gears in normal driving, thus gear ratios are usually designed more "dense" than low-speed gears, that is,

$$\frac{i_{g1}}{i_{g2}} > \frac{i_{g2}}{i_{g3}} > \ldots\ldots > \frac{i_{g,n-1}}{i_{g,n}}. \tag{11}$$

Vehicle Resistance

In operation, the tractive effort needs to overcome vehicle resistances and inertias. In steady-state operation, vehicle resistance consists of rolling resistance, aerodynamic drag, and gravity component along the vehicle moving direction during climbing a grade. In acceleration, the tractive effort also needs to overcome the vehicle inertias for picking up its speed.

Rolling Resistance Rolling resistance stems from the energy loss inside tire due to hysteresis effect of rubber materials and deformation of road surface [1, 2]. When vehicle is running on well-prepared hard road, the rolling resistance is mainly caused by tire hysteresis effect. However, when vehicle is running off-road, the ground deformation becomes the major factor.

The rolling resistance is usually interpreted by a rolling coefficient, f_r defined as the horizontal force acting on the wheel rotating center, which maintains the wheel rotating on a road while unit load acting on the wheel center perpendicular to the road surface as shown in Fig. 9.

The rolling resistance of a vehicle is mathematically expressed as

$$F_r = M\,g\,f_r \cos\alpha, \tag{12}$$

where M is vehicle mass, g is gravity acceleration, 9.81 m/s^2, f_r is the rolling resistance coefficient, and α is the road grade angle as shown in Fig. 12.

The rolling coefficient is close to the tire and road conditions, such as tire material, tire structure, temperature, inflation pressure, tread geometry, road roughness, and presence of liquid on the road. In vehicle performance evaluation, at not very high speeds, rolling resistance can be taken as constant. Typical values on various roads are listed in Table 1 [1].

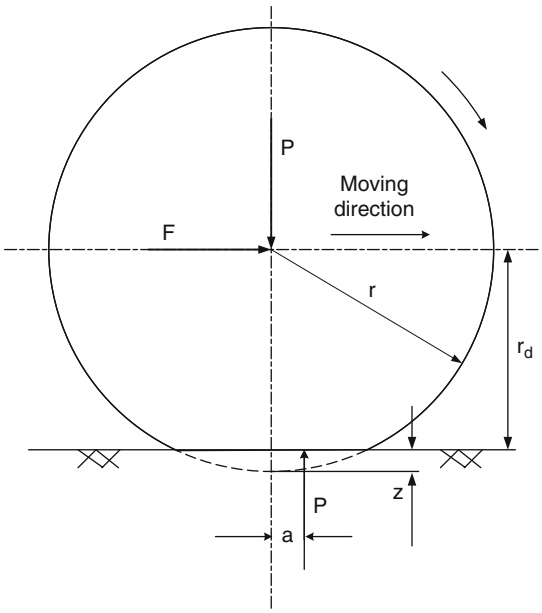

Vehicle Dynamics and Performance. Figure 9 Rolling resistance due to hysteresis effect inside tire material [2]

Vehicle Dynamics and Performance. Table 1 Rolling resistance coefficient [1]

Conditions	Rolling resistance coefficient
Car tire on a concrete or asphalt road	0.013
Car tire on a rolled gravel road	0.02
Tar macadam road	0.025
Unpaved road	0.05
Field	0.1–0.35
Truck tire on concrete or asphalt road	0.006–0.01
Wheel on iron rail	0.001–0.001

Vehicle speed should be taken in account for more accuracy at high speeds. Many experiments have been performed for determination of the effect of vehicle speed to the rolling resistance. Many empirical formulas have been proposed for calculation of rolling resistance coefficient on hard road. For example, the rolling resistance coefficient for a passenger car running on concrete road may be calculated by [1]

$$f_r = f_0 + f_s\left(\frac{V}{100}\right)^{2.5}, \tag{13}$$

where V is vehicle speed in km/h, and f_0 and f_s depend on inflation pressure of the tire [1]. For most common range of tire pressure, the rolling resistance coefficient of passenger cars on hard concrete road may be estimated by [1]

$$f_r = 0.01\left(1 + \frac{V}{160}\right). \tag{14}$$

This equation is effective to predict acceptable accuracy for speeds up to 128 km/h [1].

Aerodynamic Drag A moving vehicle in air subjects a force that resists the vehicle's motion. This force is referred to as aerodynamic drag. The aerodynamic drag is mainly resulted from the pressure difference between front and back of the vehicle as shown in Fig. 10. When the vehicle is moving, high-pressure areas are formed ahead of the vehicle. On the other hand, low-pressure areas are also formed behind the vehicle. The pressure difference between the high pressure in front of the vehicle and low pressure behind the vehicle results in a resultant force that tries to stop the vehicle. One effective approach to reduce the aerodynamic drag is to design the vehicle body shape for minimizing the areas of both high pressure and low pressure.

Aerodynamic drag of a vehicle in Newton is calculated by

$$F_w = \frac{1}{2} C_D \rho_a A_f (V - V_w)^2, \tag{15}$$

where C_D is the aerodynamic drag coefficient that is determined by the vehicle body shape, ρ_a is the air density, 1.205 kg/m^3 for close earth surface, A_f is the front area of the vehicle body, V is the vehicle speed in m/s, and V_w is the wind velocity component in the vehicle moving direction, which has a positive value when this component in the same direction of the vehicle speed and negative when it is opposite to the vehicle speed. Typical values of aerodynamic drag for various types of vehicles are shown in Fig. 11 [3].

Grading Resistance The weight of a vehicle running on a grade produces a component that always directs toward downhill as shown in Fig. 12. This gravity weight component is a resistance for uphill and a drive force for downhill. For vehicle performance evaluation, only uphill operation is considered.

From Fig. 12, the grading resistance can be expressed as

$$F_i = M g \sin\alpha. \tag{16}$$

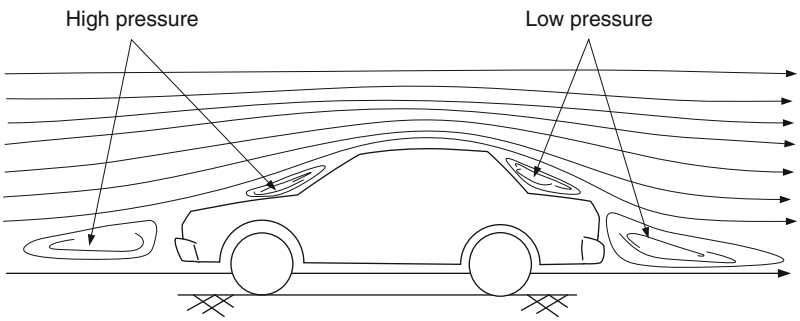

Vehicle Dynamics and Performance. Figure 10
Formation of aerodynamic drag

Vehicle type	Coefficient of aerodymanic drag
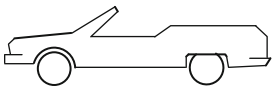 Open convertible	0.5–0.7
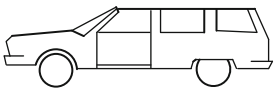 Van body	0.5–0.7
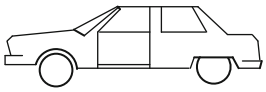 Ponton body	0.4–0.55
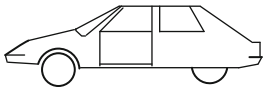 Wedged-shaped body; headlamps and bumper are integrated into the body, covered underbody, optimized cooling	0.3–0.4
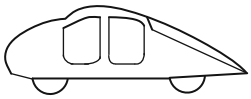 Headlamp and all wheels in body, covered underbody	0.2–0.25
K-shaped (small reaksway section)	~ 0.23
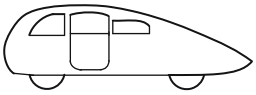 Optimum streamlined design	0.15...0.20
Trucks, road trains	0.8–1.5
Buses	0.6–0.7
Streamlined buses	0.3–0.4
Motorcycles	0.6–0.7

Vehicle Dynamics and Performance. Figure 11
Aerodynamic drag coefficients of various body shapes [3]

For simplifying calculation, $\sin\alpha$ is usually replaced by a grade value, i, with a small road angle. The road grade is defined as

$$i = \frac{H}{S} = \tan\alpha \approx \sin\alpha. \tag{17}$$

Further, the grading resistance can be expressed as

$$F_i = M\,g\,i. \tag{18}$$

Inertia Force When a vehicle is in acceleration, its translational and rotational inertias induce reaction force and reaction torque that are against the driving force and driving torque. For translational vehicle mass, the corresponding inertial force can be simply written as

$$F_{a-l} = M\,\frac{dV}{dt}. \tag{19}$$

where dV/dt is the acceleration rate of the vehicle in m/s^2.

Along vehicle power line, there are many rotating components whose angular acceleration is related to the vehicle liner acceleration through gear ratios and wheel radius. For simplifying calculation, the rotational inertias are equivalently converted into translational inertia, which uses equal kinetic energy approach.

Suppose that a rotating component, i, in the drive line has the moment of inertia of J_i, and gear ratio of i_i to the drive wheel, using the equal kinetic energy principle, one obtains

$$\frac{1}{2}M_{i-e}V^2 = \frac{1}{2}J_i\omega_i^2. \tag{20}$$

where M_{i-e} is the equivalent linear mass inertia of rotating component i, V is the vehicle speed, and ω_i is

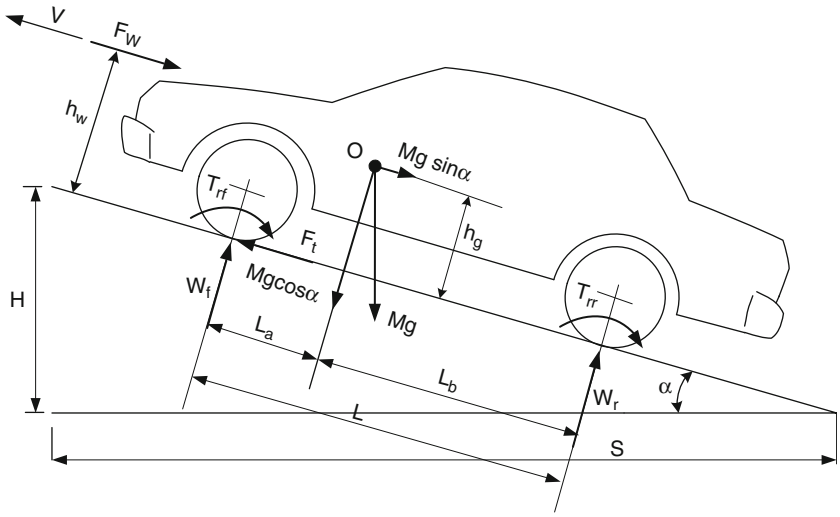

Vehicle Dynamics and Performance. Figure 12
Forces acting on uphill vehicle

the angular speed of the rotating component i. Thus, M_{i-e} can be expressed as

$$M_{i-e} = J_i \frac{\omega_i^2}{V^2}. \tag{21}$$

since ω_i and V have the relationship as

$$V = \frac{\omega_i\, r}{i_i} \tag{22}$$

Thus, (21) can be further expressed as

$$M_{i-e} = J_i \frac{i_i^2}{r^2} \tag{23}$$

where r is the radius of the drive wheel.

In vehicle acceleration performance analysis, only relative large rotating inertias are considered, typically the engine shaft components, such as flywheel, and running wheels. The equivalent translational mass inertia can be expressed as

$$M_{eq} = \frac{J_e\, i_0^2\, i_g^2}{r^2} + \frac{J_w}{r^2} \tag{24}$$

where J_e is the moment of inertia of the rotating components that are attached on the engine shaft, i_0 and i_g are the final drive and transmission gear ratios, respectively, and J_w is the total moment of inertia of all wheels.

The total inertial force can be expressed as

$$F_a = (M + M_{eq})\frac{dV}{dt} = M(1 + \frac{M_{eq}}{M})\frac{dV}{dt} = M\delta\frac{dV}{dt} \tag{25}$$

where $\delta = (1 + M_{eq}/M)$ is defined as the equivalent mass factor.

Calculating equivalent mass factor, δ, needs to know the moments of inertia of all the rotating components. In the case of not knowing these values, δ of passenger cars would be estimated by empirical equation as

$$\delta = 1 + \delta_1 + \delta_2 i_0^2\, i_g^2 \tag{26}$$

where δ_1 represents the term that is related to the moment of inertia of running wheels with a estimated value of 0.04 and δ_2 represents the term that is related to the moments of inertia of the engine-attached components with an estimated value of 0.0025 [2].

Vehicle Performance

Vehicle performance represented by maximum speed, gradeability, and acceleration is completely determined by the vehicle tractive effort developed by the engine or electric motor and the resistance in the vehicle motion direction. Figure 12 illustrates the forces acting on a vehicle, which is running uphill.

The forces acting on the vehicle in the vehicle moving direction are tractive effort, F_t, and resistances including rolling resistance, aerodynamic drag, grading resistance, and inertial force induced by acceleration. All these forces are always in a balanced state, which can be described by

$$F_t = F_r + F_w + F_i + F_a, \tag{27}$$

or more detail

$$\frac{T_e\, i_0\, i_g \eta_t}{r} = M\, g\, f_r \cos\alpha + \frac{1}{2} C_D \rho_a A_f V^2 + M\, g\, \sin\alpha + M\, \delta \frac{dV}{dt}. \tag{28}$$

When grade angle α is small, $\cos\alpha \approx 1$ and $\sin\alpha \approx \tan\alpha = i$. Equation 28 can further be written as

$$\frac{T_e\, i_0\, i_g \eta_t}{r} = M\, g\, f_r + \frac{1}{2} C_D \rho_a A_f V^2 + M\, g\, i + M\, \delta \frac{dV}{dt} \tag{29}$$

Equation 28 or 29 interprets the general operation behavior of a vehicle and is used to analyze vehicle performance. Depicting (29) using a tractive effort versus rolling resistance and aerodynamic drag on grade road is very helpful for vehicle performance analysis as shown in Figs. 13 and 14.

1. Maximum vehicle speed

   The maximum speed of a vehicle is defined as the speed that can be reached when the power plant operates with its maximum capability (full open throttle for an IC engine and maximum current for an electric motor) on a flat road. Running on its maximum speed, no grading resistance and inertia force exists. Thus, (29) becomes

$$\frac{T_e\, i_0\, i_g \eta_t}{r} = M\, g\, f_r + \frac{1}{2} C_D \rho_a A_f V^2. \tag{30}$$

   On the diagrams of Figs. 13 and 14, maximum speed of vehicle can be obtained as the intersection of the tractive effort curve and the resistance curve at zero grade road.

2. Gradeability

   Gradeability of a vehicle is defined as the road grade or grade angle that the vehicle can overcome at a specified speed, for example, 100 km/h, or the

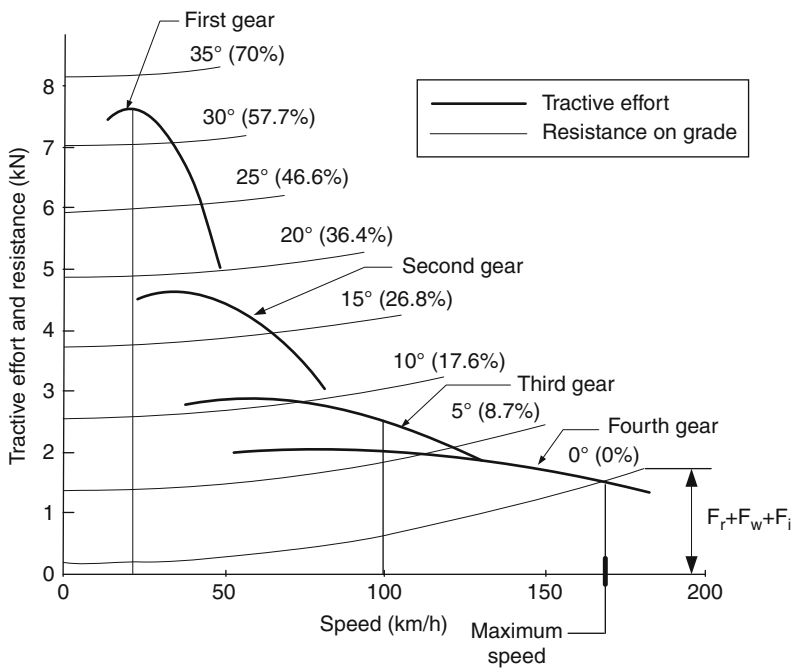

Vehicle Dynamics and Performance. Figure 13
Tractive effort versus vehicle resistance for a gasoline engine–powered vehicle [2]

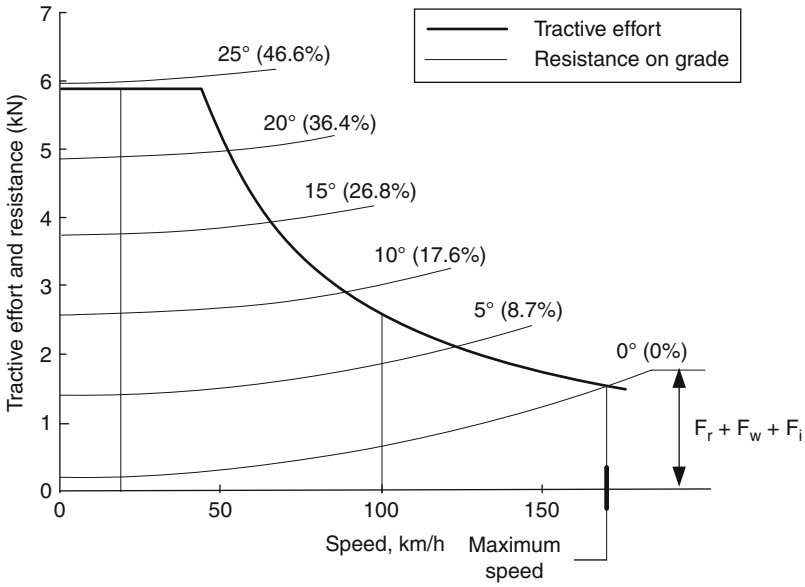

Vehicle Dynamics and Performance. Figure 14
Tractive effort versus vehicle resistance for an electric motor–powered vehicle [2]

maximum grade at low speed. While running on an uphill grade with constant speed, 28 and 29 become

$$\frac{T_e i_0 i_g \eta_t}{r} = M g f_r \cos\alpha + \frac{1}{2} C_D \rho_a A_f V^2 + M g \sin\alpha \tag{31}$$

and

$$\frac{T_e i_0 i_g \eta_t}{r} = M g f_r + \frac{1}{2} C_D \rho_a A_f V^2 + M g i \tag{32}$$

The gradeability can be directly obtained by reading Figs. 13 and 14. For instance, for the gasoline engine–powered vehicle, running at 100 km/h, gradeabilities of 5.5° (9.6%) for fourth gear, 7.5° (13%) for third gear, and 32.5° (63.7%) at speed of about 20 km/h are obtained. Similarly, for the electric motor–powered vehicle, around 8° (14%) at the speed of 100 km/h and 24° (44.5%) at speeds lower than 50 km/h are obtained.

3. Acceleration performance

Acceleration performance of a vehicle is interpreted by the time used for accelerating the vehicle from a low speed (general zero speed) to a specified high speed (e.g., 100 km/h) on a level road. The acceleration time can be calculated by

$$t = \int_0^{V_f} \frac{1}{a} dV. \tag{33}$$

where V_f is the specified final speed and a is the acceleration rate in m/s^2, which can be obtained from (29) as

$$a = \frac{dV}{dt} = \frac{\frac{T_e i_0 i_g \eta_t}{r} - M g f_r + \frac{1}{2} C_D \rho_a A_f V^2}{M \delta} \tag{34}$$

The distance covered during acceleration can be calculated by

$$d = \int_0^{t_a} V dt \tag{35}$$

A digital integration method may be used to solve (33)–(35). Figures 15 and 16 show the acceleration time and distance for a gasoline engine–powered and electric motor–powered vehicle.

Fuel Economy and Energy Consumption

Fuel economy is one of the most important performances of a vehicle, which is evaluated by the fuel consumed in number of liters per 100 km. In the United States it is usually evaluated by the mileages per gallon fuel. In electric energy–driven vehicle, it is

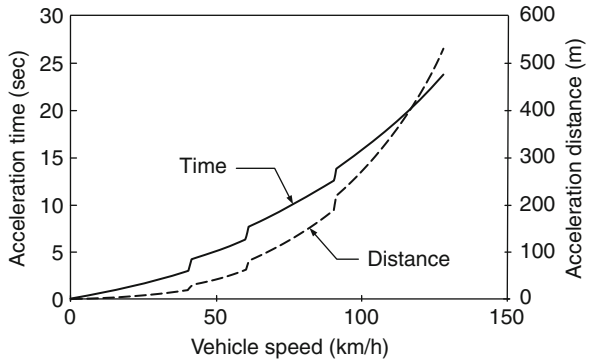

Vehicle Dynamics and Performance. Figure 15
Acceleration time and distance of a gasoline engine–powered vehicle with a four-gear transmission

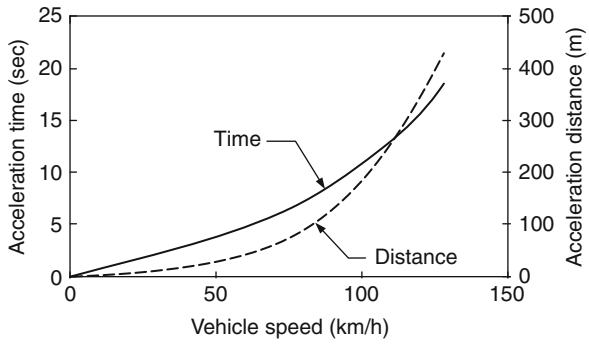

Vehicle Dynamics and Performance. Figure 16
Acceleration time and distance of an electric motor–powered vehicle with single-gear transmission

usually evaluated by kilowatt-hour (kWh) number of electric energy per unit traveling distance (km or mile). In plug-in hybrid vehicle, both fuel consumption and electric energy consumption are used at the same time.

Obviously, fuel and electric energy consumptions are associated with driving environments, typically, on highway and in urban. Highway driving is characterized by almost constant speeds. However, frequent stop-and-go is the common driving pattern in urban. These two very different driving patterns result in different fuel and energy consumptions. A vehicle specification usually lists the values for both highway and city driving.

Fuel and energy consumptions are determined by the energy consumed to overcome the vehicle resistances and the efficiency of the power train.

For engine-powered vehicle, the engine is the most inefficient component and its efficiency depends very much upon its operating points in terms of speed and torque or power. In practice, fuel usage efficiency of an engine is evaluated by fuel grams consumed per kWh energy output from its shaft, which is referred to as specific energy consumption (g/kWh). The typical fuel consumption characteristic of a gasoline engine is shown in Fig. 17 [2].

Fuel consumption varies with the operating points of the engine. The most efficient operating points are close to its full open throttle operation. At a given output power, the engine running at lower speed (point *a* in Fig. 17) results in lower fuel consumption than at higher speed (point *b* in Fig. 17). That is the reason that running in high-speed gear is more efficient than in low-speed gear. The transmission with more gears increases the chance for the engine operating close to its optimum operation line. Ideally, a continuous variable transmission (CVT) is capable of choosing a gear ratio that, at any driving condition, can operate the engine at its optimum line.

Based on the specific fuel consumption of engine, the fuel consumption rate (fuel amount consumed in unit time) of the engine can be determined by

$$Q_t = \frac{P_e\, g_e}{1000\gamma_f} \quad (\text{liter/h}), \tag{36}$$

where P_e is the engine power in kW, g_e is the specific fuel consumption (g/kWh) of the engine, which depends on its operating point (speed vs. power), and γ_f is the mass density of the fuel in kg/L. The engine power can be calculated by

$$P_e = \frac{V}{\eta_t}(F_a + F_w + F_i + F_a). \tag{37}$$

Specific fuel consumption of the engine, g_e, can be obtained on the fuel consumption characteristic map (Fig. 17) with respect to the engine speeds, which can be determined by the vehicle speed and gear ratio as

$$N_e = \frac{30\, i_0\, i_g}{\pi\, r} V. \tag{38}$$

With constant speed, fuel consumption of a vehicle in a driving distance, S, is obtained by

$$Q_t = \frac{P_e\, g_e}{1000\gamma_f} \frac{S}{V}. \tag{39}$$

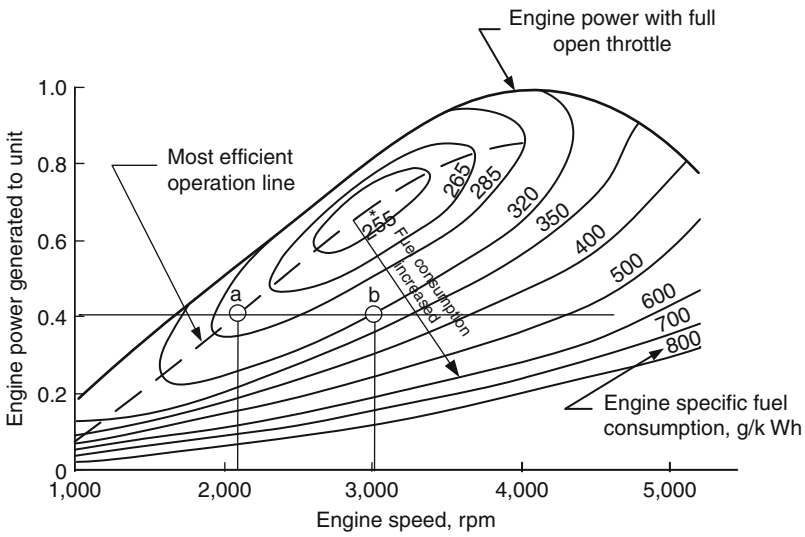

Vehicle Dynamics and Performance. Figure 17
Fuel consumption characteristics of a gasoline engine [2]

Since the complexity of vehicle operation in real world, fuel consumption at constant speeds cannot reflect the real fuel consumption scenario. Various driving cycles have been developed to emulate the real operation of a vehicle in specific driving environments. Figure 18 shows some typical driving cycles.

Driving cycles are interpreted by vehicle speed profiles versus driving time. For calculation of vehicle fuel consumption in a cycle, numerical computing method is usually used. The whole cycle is divided into many time intervals, usually 1 s, then, the fuel consumption in each time interval is calculated. The fuel consumption in the whole cycle can be obtained by summation of the fuel used in all the time intervals.

Figures 19 and 20 show the fuel consumption of a vehicle and engine operating points overlapping the engine fuel consumption map in FTP 75 urban and highway driving cycles [2]. It can be seen from these two diagrams that the engine operating points are far away from its most efficient area. This is one of the major reasons why conventional vehicle is inefficient, which hybrid technologies intend to cure.

Vehicle Braking Performance

Braking performance of a vehicle is one of the most important requirements. The basic requirements of a vehicle brake system includes (1) fast reducing vehicle speed to complete stop, (2) braking effectiveness sustainability, and (3) maintaining vehicle stability during braking. Meanwhile, when a vehicle operates with stop-and-go pattern in urban areas, significant amount of energy is consumed, which is one of the major factors that result in low fuel efficiency. With more and more involvement of electric tractions, such as electric vehicle, hybrid electric vehicle, and fuel cell electric vehicle, braking energy recovery are becoming practice, in which, the kinetic energy of the vehicle body can be converted into electric energy by an electric machine. The recovered energy is charged into on-board energy storage, mostly chemical batteries, and can be reused in later traction. This is called regenerative braking. In vehicle brake system design, a new requirement is added, that is, recovering braking energy as much as possible. Nevertheless, braking safety is still the primary consideration.

Vehicle behavior during braking is determined by the reaction between the braking force and road. The basic requirements are to supply sufficient braking force to quickly stop the vehicle and at the same time, maintain the vehicle running direction stable and controllable.

Braking Force

Braking force of a vehicle determines the deceleration rate. Effective braking force is determined by two

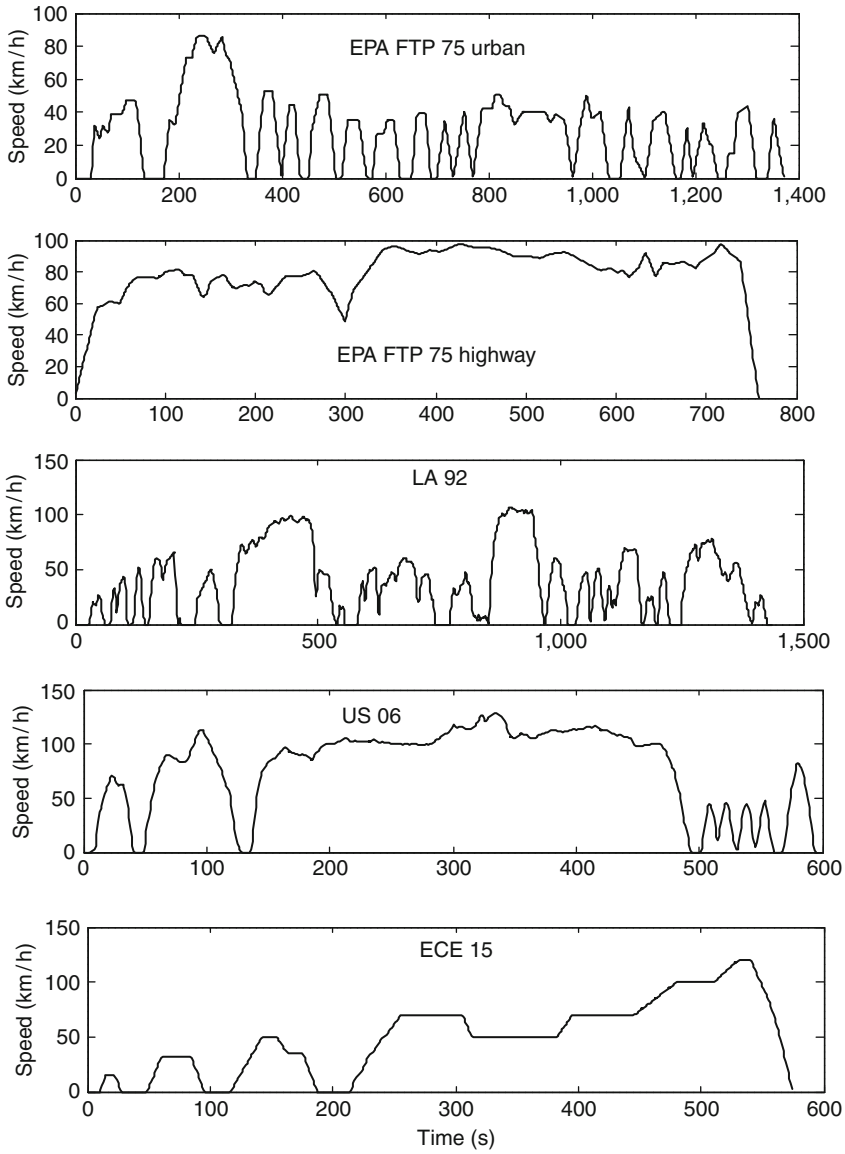

Vehicle Dynamics and Performance. Figure 18
Some typical driving cycles

factors. One is the braking torque developed by the brake system and the other is the road adhesive condition. When braking force is not large enough to lock the vehicle wheels, the braking force is determined by the braking torque generated by the braking system. However, when the wheels are locked, the braking force depends solely on the road adhesive condition.

Figure 21 shows a braked wheel. The brake pad is pushed against the brake plate, generating a braking torque around the wheel's rotating center. This braking torque induces a braking force in the tire-ground contact area. In the case of unlocked wheel, the braking force is proportional to the braking torque as

$$F_b = \frac{T_b}{r}. \tag{40}$$

However, when the braking force goes up until locking the wheel, the braking force is completely

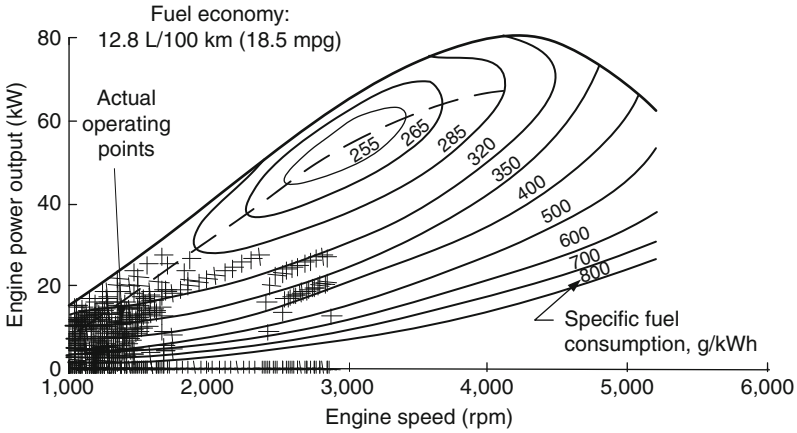

Vehicle Dynamics and Performance. Figure 19
Fuel consumption and engine operating points in EPA FTP 75 urban driving cycle [2]

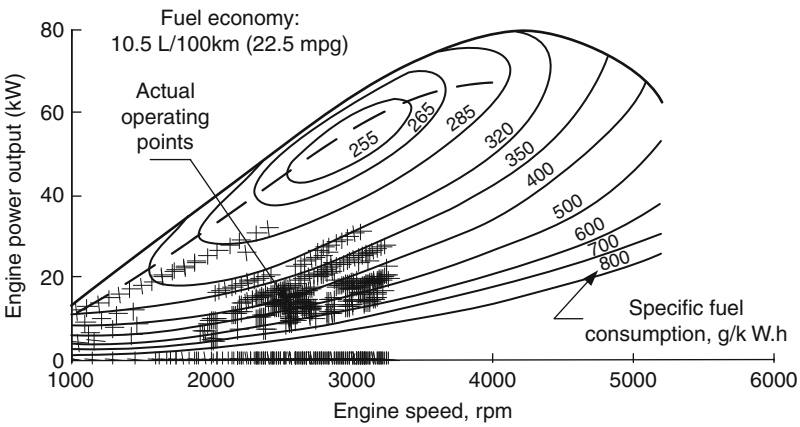

Vehicle Dynamics and Performance. Figure 20
Fuel consumption and engine operating points in EPA FTP 75 highway driving cycle [2]

determined by the road adhesive capability, as shown in Fig. 22, which is expressed as

$$F_{b\max} = \mu W, \tag{41}$$

where W is the vertical load between the wheel and ground and μ is the adhesive coefficient of the wheel to ground. A well-prepared road has high adhesive coefficient. Contrary, a slippery road has low adhesive coefficient. Generally, adhesive coefficient is a function of wheel slip, s, as shown in Fig. 23. The wheel slip is defined as

$$s = \left(1 - \frac{r\,\omega}{V}\right) \times 100\%, \tag{42}$$

where V is vehicle speed (the translator speed of the wheel center), ω is angular speed of the wheel, and r is the wheel radius. With a free rotating wheel, $r\omega = V$ and $s = 0$. On the other hand, with a locked wheel, $\omega = 0$ and $s = 100\%$.

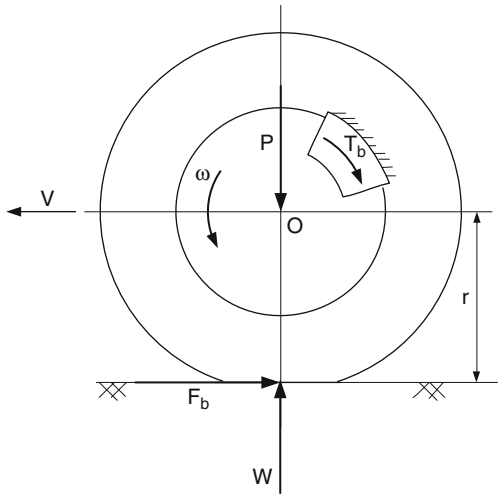

Vehicle Dynamics and Performance. Figure 21
Braking torque and braking force on a braked wheel

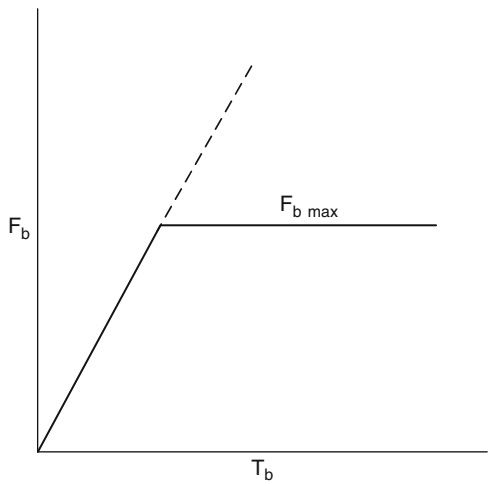

Vehicle Dynamics and Performance. Figure 22
Braking force versus braking torque

Figure 23 indicates that with a small slip (between 0 and A), the adhesive coefficient is almost linearly proportional to the slip value. In this case, no obvious slip occurs in the wheel-ground area. The small slip is caused by the elastic property of the tire. Further increase in the braking force will cause actual slip at some points in the contact area. With increase in the braking force, more and more points go into slipping. In this case, the relationship between the slip and

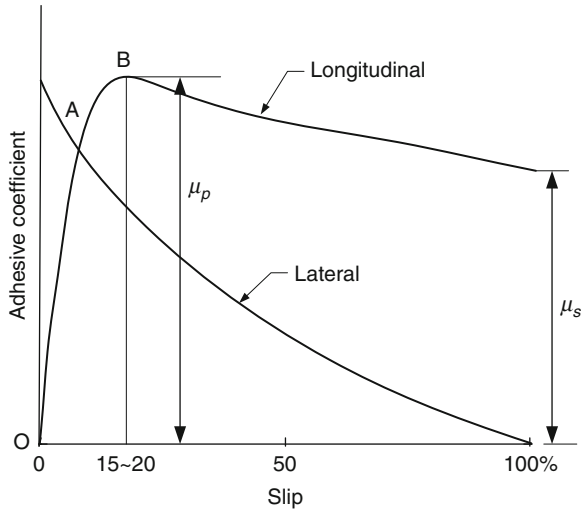

Vehicle Dynamics and Performance. Figure 23
Adhesive coefficient varying with wheel slip

adhesive coefficient is nonlinear with a small increase rate. The adhesive coefficient reaches its maximum at a slip of about 15–20%. Beyond this peak point, the wheel will become unstable and is quickly locked up, even no further increase in the braking force. The adhesive coefficient at complete slipping is generally named as slipping value, which is smaller than the peak value.

It should be noted that the adhesive coefficient in lateral direction drops monotonously with the increase of wheel slip. At complete locked wheel, it becomes close to zero. Lateral adhesive coefficient represents the capability of resisting lateral disturbance. A completely locked wheel loses this capability, consequently, leading to unstable vehicle behavior during braking. Anti-lock brake systems (ABS) have been developed in order to prevent wheels from being completely locked, therefore improving vehicle braking stability.

Table 2 shows the average values of adhesive coefficients on various roads [1, 2].

Braking Strength and Braking Force Distribution on Front and Rear Wheels

Braking strength is defined as the deceleration rate, m/s^2 or g ($g = 9.81\ m/s^2$), which is completely determined by the total forces acting on the vehicle in the opposite direction of the vehicle travel. Rolling

resistance and aerodynamic drag also functions as braking forces. However, they are quit small, compared to road braking force, and ignored in braking performance analysis.

Figure 24 shows all the forces acting on a vehicle during braking on a flat road, where j is the braking strength in m/s^2, and F_{bf} and F_{br} are the braking forces acting on the front and rear wheels, respectively. The braking strength, j can be expressed as

$$j = \frac{F_{bf} + F_{br}}{M}, \tag{43}$$

where M is the vehicle mass.

Vehicle Dynamics and Performance. Table 2 Average values of adhesive coefficient on various roads [1, 2]

Surface	Peaking values, μ_p	Slipping values, μ_s
Asphalt and concrete (dry)	0.8–0.9	0.75
Concrete (wet)	0.8	0.7
Asphalt (wet)	0.5–0.7	0.45–0.6
Grave	0.6	0.55
Earth road (dry)	0.68	0.65
Earth road (wet)	0.55	0.4–0.5
Snow (hard packed)	0.2	0.15
Ice	0.1	0.07

It is considered to be ideal design for distribution of the total braking force on front and rear wheels in such a way that the slips on the front and rear wheels are always equal. This strategy can ensure front and rear wheels reach their maximum road adhesion at the same time, consequently, achieving the shortest braking distance. This approach is interpreted as that the braking forces are proportional to their vertical loads, which is expressed as

$$\frac{F_{bf}}{W_f} = \frac{F_{br}}{W_r} \tag{44}$$

Referring to Fig. 24, the vertical loads on front and rear wheels can be obtained as

$$W_f = \frac{M\,g}{L}\left(L_b + h_g\frac{j}{g}\right), \tag{45}$$

and,

$$W_r = \frac{M\,g}{L}\left(L_b - h_g\frac{j}{g}\right). \tag{46}$$

Then, (44) can be further expressed as

$$\frac{F_{bf}}{F_{br}} = \frac{L_b + h_g j/g}{L_a - h_g j/g}. \tag{47}$$

Equations 43 and 47 dictate the ideal braking force distribution on front and rear wheels, which can further be written as

$$F_{br} = \frac{M\,g}{2h_g}\sqrt{L_b^2 + \frac{4h_g L}{M\,g}F_{bf}} - \left(F_{bf} + \frac{M\,g\,L_b}{2h_g}\right) \tag{48}$$

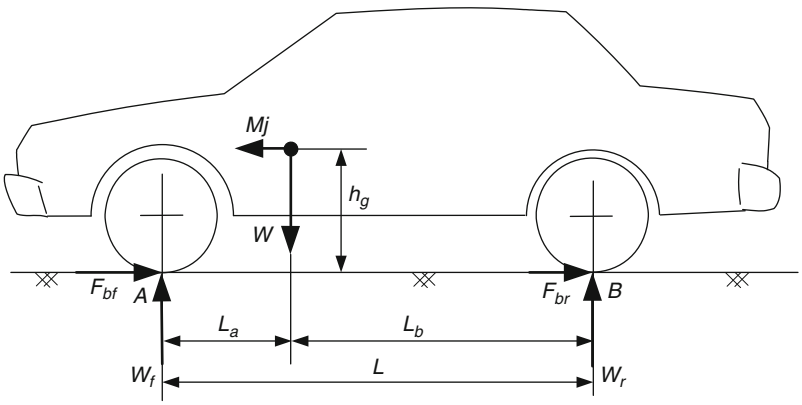

Vehicle Dynamics and Performance. Figure 24 Forces acting on a vehicle during braking

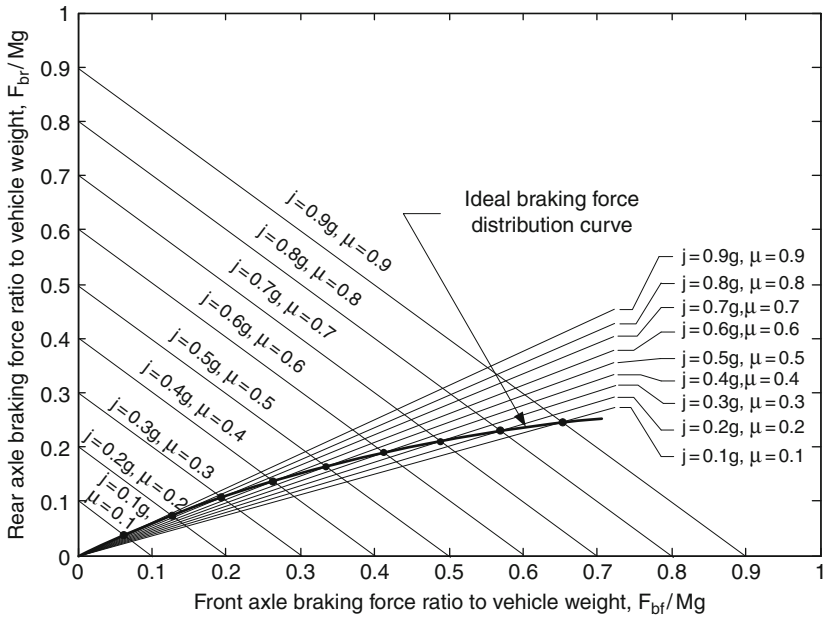

Vehicle Dynamics and Performance. Figure 25
Ideal braking force distribution on front and rear wheels [2]

Figure 25 shows the ideal distribution curve (simply *I* curve), which has a parabolic shape. This figure also shows two sets of lines that represent (43) and (47) with respect to various braking strengths. When the braking forces reach their maximum values determined by the wheel-road adhesion, the maximum braking strength is achieved as

$$j_{\max} = \frac{F_{bf\,\max} + F_{br\,\max}}{M} = \frac{(W_f + W_r)\mu}{M} = g\mu. \tag{49}$$

Due to the nonlinear property of the ideal braking force distribution curve, design of a brake system to follow the ideal distribution curve becomes complicated. However, implementation of advanced electronic control may make this happen.

In practice, braking forces on front and rear wheels are usually designed to have a linear relationship. The proportion is represented by a ratio of the braking force on front wheel to the total braking force of the vehicle, that is,

$$\beta = \frac{F_{bf}}{F_b} = \frac{F_{bf}}{F_{bf} + F_{br}}. \tag{50}$$

β is determined by the brake system design, such as the diameters of front and rear wheel cylinders. For a given β, the applied braking forces on the front and rear wheels can be expressed as

$$F_{bf} = \beta F_b, \tag{51}$$

and

$$F_{br} = (1 - \beta) F_b, \tag{52}$$

and then

$$\frac{F_{bf}}{F_{br}} = \frac{\beta}{1 - \beta} \tag{53}$$

The braking force distribution represented by (53) is different from that described by (48) as shown in Fig. 26. One intersection point of these two lines exists, at which both front and rear wheels have the same slips, or both wheels are locked at the same time. This point specifies a specific adhesive coefficient, μ_0. Referring to (47), in which j/g is replaced by μ_0, one obtains

$$\frac{\beta}{1 - \beta} = \frac{L_b + h_g \mu_0}{L_a - h_g \mu_0}. \tag{54}$$

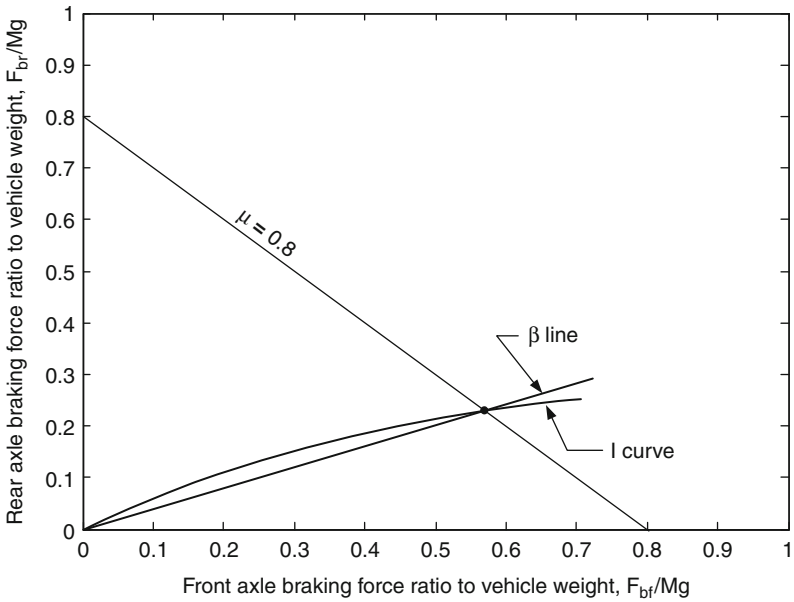

Vehicle Dynamics and Performance. Figure 26
Ideal and actual braking force distribution curve [2]

From (54), one obtains

$$\mu_0 = \frac{L\beta - L_b}{h_g} \tag{55}$$

As shown in Fig. 26, μ_0 divides the whole range into two sections. While braking on the road with an adhesive coefficient less than μ_0, front wheels are locked prior to rear wheels. Otherwise, rear wheels are locked prior to front wheels.

Braking Stability

As discussed in a previous section, completely locked wheels will lose their capacity of resisting lateral disturbance. Consequently, any disturbance, such as wind, uneven road surface, and running along a curve road, would cause significant lateral movement and instability. Much more serious instability would occur with rear wheels locked than with front wheel locked. This can be interpreted in Fig. 27.

As shown in Fig. 27a, while a lateral slip on front wheels occurring, due to the lateral disturbance force F_d, the vehicle speed changes its motion from straightforward direction V to a curved running speed, V_r, which causes the whole vehicle body rotating around the point O. At the same time, the curved running of the vehicle body induces a centrifugal force, F_j, which acts on the gravity center, C, of the vehicle body. It can be seen from Fig. 27a that this centrifugal force has the effect of resisting against the lateral movement of the front wheel. When the disturbance force disappeared, the centrifugal force quickly brings the vehicle back to its straight motion.

While lateral slip occurs on rear wheels due to lateral disturbance, the induced centrifugal force augments the lateral slip, causing the vehicle very instable. Even after the lateral disturbance disappears, the lateral movement may continuous. Experiments have shown that when rear wheels are locked up over 0.5 s prior to the front wheels lockup, serious directional deviation would occur. In extreme case, vehicle body would swing 180° [1].

Front wheel lockup causes losing of steering capability. However, it can be detected more readily by the driver and correction can be made by the driver to release or partial release of the brake pedal. This is a less dangerous than rear wheel lockup swing.

Anti-lock brake system (ABS) can effectively present the wheels from lockup. This system monitors the wheel operation status. When it finds a wheel tending

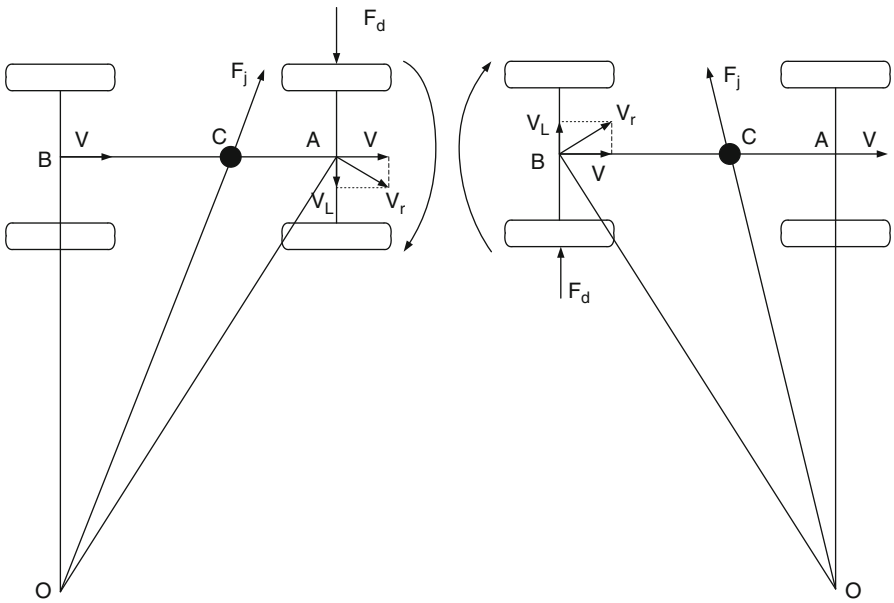

Vehicle Dynamics and Performance. Figure 27
Vehicle behaviors with (**a**) lateral slip on front wheels and (**b**) lateral slip in rear wheels

to be locked, a control system reduces the braking force for this wheel and therefore brings the wheels back to its rotation.

Brake Design Regulation

For maintaining braking stability, rear wheel lockup is required not prior to the front wheel lockup. This requirement results in the braking force distribution always below ideal braking force distribution curve (I curve) as shown in Fig. 26. This can be realized by increasing the front wheel braking force and decreasing the rear wheel braking force. However, when most of the braking forces are applied to the front wheels and very small to rear wheels, it would cause a problem of reduced utilization of road adhesive capability. That is, when front wheels are locked and rear wheels are not locked, the maximum braking force of rear wheels is never used. Consequently, the stop distance will be longer. For avoiding this situation, some brake design regulations have been developed. A typical one is the ECE R13 regulation.

The ECE R13 regulation for passenger cars is represented by

$$\frac{F_{bf}}{W_f} \geq \frac{F_{br}}{W_r}, \tag{56}$$

and,

$$\frac{j}{g} \geq 0.1 + 0.85(\mu - 0.2). \tag{57}$$

Equation 56 dictates rear wheels being never locked prior to the front wheels, that is, β line is always below the I curve. Equation 57 dictates that, with locked front wheel, the braking force on rear wheels must be large enough to ensure to generate a braking strength j/g that is equal to or greater than a value dictated by (57).

Equations 56 and 57 are interpreted in a diagram as shown in Fig. 28. Obviously, the real braking force distribution design must fall into the area between the I curve and ECE regulation curve.

Future Directions

Vehicle system is a very complex system. With rapid development of computing technologies, the analysis methods of vehicle dynamics and performance are becoming more and more accurate and reliable by employing computer-based modeling and simulation. The advanced computing technologies allow solving much more complicated mathematical problems in

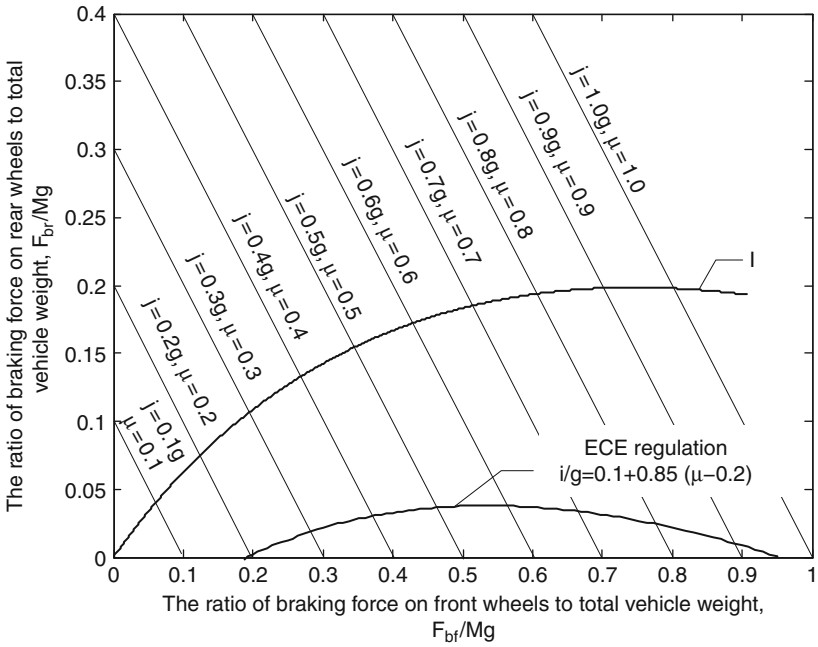

Vehicle Dynamics and Performance. Figure 28
The upper and low boundaries of braking force distribution dictated by ECE regulation

real time, which was impossible before computer age. Advanced data accessing, acquisition, processing, and control technologies provide great opportunity for vehicle dynamic control to improve vehicle performances.

Advanced electrical propulsion and electric energy storage create a way for high efficiency and clean vehicles that include electric vehicles, hybrid vehicles, and fuel cell vehicles.

Bibliography

Primary Literature

1. Wong JY (1978) Theory of ground vehicles. Wiley, New York
2. Ehsani M, Gao Y, Emadi A (2010) Modern electric, hybrid electric and fuel cell vehicles—fundamentals, theory and design, 2nd edn. CRC press, Boca Raton
3. Bosch R (2000) Automotive handbook. Tobert Bosch GmbH, Karsruhe

Books and Reviews

Gillespie TD (1992) Fundamentals of vehicle dynamics. SAE international, Warrendale
Mizutani S (1992) Car electronics. Sankaido Co., Tokyo

Vehicle Energy Storage: Batteries

Y. S. Wong[1], C. C. Chan[2]
[1]State Grid Energy Research Institute, State Grid Corporation of China, China
[2]Department of Electrical and Electronic Engineering, University of Hong Kong, Hong Kong, China

Article Outline

Glossary
Definition of the Subject
Introduction
Electrical Powertrain
Power and Energy Demands of EVs and HEVs
Batteries for Vehicle Applications
Future Directions
Bibliography

Glossary

Battery A string of rechargeable electrochemical cells.

Battery electric vehicle An electric vehicle in which the electrical energy to drive the motor(s) is stored in an onboard battery.

Capacity The electrical charge that can be drawn from the battery before a specified cut-off voltage is reached.

Depth of discharge The ratio of discharged electrical charge to the rated capacity of a battery.

Electric vehicle A vehicle in which propulsion torque is delivered exclusively by one or more electric motors.

Energy capacity The electrical energy that can be drawn from the battery before a specified cut-off voltage is reached.

Fuel cell electric vehicle An electric vehicle in which the propulsion energy is delivered from an onboard fuel cell and battery hybrid system.

Hybrid electric vehicle A vehicle in which propulsion energy is provided from two or more kinds or types of energy stores, sources, or converters, and at least one of them delivers electrical energy.

Open circuit voltage The difference of electrical potential between two terminals of a battery when no external load is connected.

Vehicle energy source The onboard energy storage device of a vehicle.

Definition of the Subject

With ever-increasing concerns on energy efficiency, energy diversification, and environmental protection, electric vehicles (EVs), hybrid electric vehicles (HEVs), and low-emission vehicles are on the verge of commercialization. EVs not only offer higher energy efficiency than that of internal combustion engine (ICE) vehicles, but also mitigate one country's dependence on oil by diversifying the energy sources to renewable energies.

Vehicle energy source is bottleneck of EV and HEV commercialization. At present and in the foreseeable future, the viable energy sources for EVs and HEVs are batteries, fuel cells, and ultracapacitors (supercapacitors). The battery is the most mature energy source and it has been the most important component of an EV since commercialization of the first EV. This entry gives an overview of batteries for vehicle applications and discusses the research and development roadmap of next-generation batteries for vehicle applications.

Introduction

The EV has higher energy efficiency than that of the ICE vehicle and it also mitigates the one country's dependence on oil by diversifying the energy sources to renewable energies such as hydro, wind, and solar energies. The EV also facilitates load leveling of power systems and achieves zero local and minimal global vehicular emissions. At present, there is no economically viable energy source for commercialization of EVs.

The battery has been the most important component of an EV since commercialization of the first EV. In 1801, Richard Trevithick built a steam-powered carriage, opening the era of horseless transportation. The first battery-powered electric bicycle was built by Thomas Davenport in 1834. It was powered by a nonrechargeable battery and used on a short track. In 1838, Robert Davidson built a nonrechargeable battery-powered electric locomotive.

After the invention of lead-acid (Pb-Acid) battery in 1859, Sir David Salomons built a rechargeable battery-powered EV in 1874. The first petrol-powered ICE vehicle was built in 1885 and the first HEV was presented by J. Lohner and F. Porsche in 1901. The ICE vehicle outperformed the EV and HEV in the automotive century because there was no high performance battery for EVs and HEVs to overcome four major barriers to commercialization of EVs and HEVs, namely, short driving range, long charge time, long recharge time, and high life-cycle cost [1].

The battery for EVs has evolved from flooded lead acid (Pb-Acid) battery in 1859 to lithium ion (Li-Ion) polymer in 1999. Table 1 lists some historic events of vehicle batteries. The EV has also evolved a lot but it still holds its position in niche areas, like postal services [2].

The HEV has been introduced as an interim solution before the full implementation of the EV when there is a breakthrough in vehicle energy sources. The HEV extends greatly the driving range of the EV by three to four times and offers rapid fuel refueling. There are several types of EVs and HEVs in the market [3–5].

Technical requirements of batteries for vehicle applications are discussed by analyzing vehicle topologies and energy management systems in EVs' and HEVs' electrical powertrain. Viable batteries for EV and HEV applications are reviewed and the research and development roadmaps are discussed at the end of this entry.

Vehicle Energy Storage: Batteries. Table 1 Vehicle battery history

Year	Inventor	Battery
1859	Raymond Gaston Planté	Planté lead-acid cell
1881	Camille Alphonse Faure	Improved lead-acid cell
1899	Waldmer Junger	Nickel-cadmium cell
1899	Waldmer Junger	Nickel-iron cell
1946	Union Carbide Company	Alkaline manganese secondary cell
1970	Exxon laboratory	Lithium-titanium cell
1980	Moli Energy	Lithium-molybdenum disulfide
1990	Samsung	Nickel-metal hydride
1991	Sony	Lithium ion
1999	Sony	Lithium ion polymer

Electrical Powertrain

Motor drive and battery are two major components of an electrical powertrain in EVs and HEVs. Energy efficiency of motor drives is, intrinsically, higher than that of an ICE. In addition, the electrical powertrain can absorb kinetic energy during braking and assist engine in acceleration in HEVs. Thus, the efficiency improvement of an EV or an HEV over an ICE vehicle depends on power ratings and functionality of the electric motor drive and the onboard batteries [6, 7]. Key motor drive features and battery characteristics are discussed in the following sections.

Motor Drive Features

Regenerative Braking Regenerative braking is a unique feature of an electrical powertrain. The motor drive converts vehicle's kinetic energy back to electrical energy during braking, deceleration, and downhill running. The converted electrical energy is stored in the receptive energy sources such as batteries or ultracapacitors to extend the driving range. If the receptive sources are fully charged up, regenerative braking can no longer be applied and the vehicle is braked by the conventional hydraulic braking system.

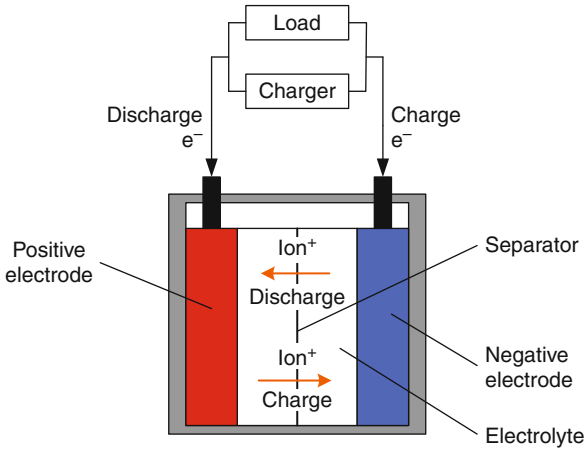

Vehicle Energy Storage: Batteries. Figure 1 Basic components of an electrochemical cell

Power Boost The HEV allows both the engine and the electric motor to deliver power simultaneously to drive the vehicle. Generally, the engine and electric motor are coupled to the drive shaft of the wheel via two clutches, such that, the propulsion power may be supplied by the engine alone or by both of them. The motor cranks the engine and assists vehicle acceleration for maximization of engine fuel economy.

Battery Characteristics

Electrochemical Batteries The battery refers to the rechargeable electrochemical battery. Electrochemical cell is the basic element of each battery. A connection of a number of cells in series forms a battery. Figure 1 shows the basic components of an electrochemical cell in which both the positive and negative electrodes are immersed in the electrolyte. The electrolyte is an ion-conducting material, which can be in the form of aqueous, molten, or solid solution. The separator is a membrane that physically prevents direct contact between the two electrodes and allows ions, but not electrons, to pass through.

During discharge, the negative electrode performs oxidation reaction, which drives electrons to the external circuit, while the positive electrode carries out reduction reaction, which accepts electrons from the external circuit. During charge, the process is reversed so that electrons are injected into the negative electrode to perform reduction while the positive electrode releases electrons to carry out oxidation.

Battery Capacity Energy capacity (EC) of a battery refers to the electrical energy that can be drawn from the battery before a specified cut-off voltage is reached. EC is commonly presented in watt-hour (Wh). Coulometric capacity (C) refers to the total amount of electrical charge that can be drawn from the battery before the specified cut-off voltage is reached. C is typically measured in ampere-hour (Ah). C is widely employed to describe battery capacity, but EC is more common than C in addressing battery capacity in vehicle applications. Both EC and C, intrinsically, depend on the battery design, discharge current, temperature, and cyclic history.

Depth of Discharge and State of Charge Depth of discharge (DoD) and state of charge (SoC) are key parameters in battery energy management systems. DoD refers to the ratio of discharged electrical charge to the rated capacity. SoC refers to the ratio of usable charge to the rated battery capacity. SoC is an indicator of available electrical charge, while DoD is an indicator of discharged charge of a battery. Thus, sum of SoC and DoD of a battery is 100%. The SoC of a fully charged battery is 100% and the DoD is zero. When 20% of the stored charge is dissipated, SoC of this battery reduces to 80% and the DoD rises to 20% correspondingly.

Electrical Efficiency Energy efficiency of a battery refers the ratio of output electrical energy during discharging to the input electrical energy during charging. The energy efficiency is different from the charge efficiency, which is defined as the ratio of discharged charge to the charged charge. For vehicle applications, the energy efficiency is more informative than the charge efficiency. Typical energy efficiency of a battery is 55–75%.

Energy Density and Specific Energy Energy densities of an energy source refer to the usable energy capacity per unit mass or volume. The gravimetric energy density is usually named as the specific energy in watt-hour per kilogram (Wh/kg). The volumetric one is loosely named as energy density in watt-hour per litre (Wh/L). Specific energy is more instructive than the energy density for vehicle batteries because the battery weight is highly correlated with the vehicle fuel economy while the volume only affects the usable space. The specific energy is a key parameter to assess the pure electric driving range. The usable energy capacity greatly varies with discharge rate. The larger the discharge rate, the smaller the usable energy. Generally, specific energy and energy density are quoted with a discharge rate.

Power Density and Specific Power Power densities of a battery denote the deliverable rate of energy per unit mass or volume. The gravimetric power density is named specific power and measured in watt per kilogram (W/kg) and the volumetric power density is named power density and measured in watt per litre (W/L). The specific power changes with DoD. Thus, specific power and power density are quoted with DoD.

Cycle Life Cycle life is a key parameter to describe the service life of a battery based on the storage capacity of the battery. It is defined as the number of charge and discharge cycles it can undergo before its capability falls to 80% of the rated capacity. Cycle life is greatly affected by DoD of each discharge cycle, thus, it is usually quoted with DoD. For example, a battery can be claimed to offer 500 cycles at 80% DoD and 1,000 cycles at 50% DoD [1].

Calendar Life Calendar life refers to life period of a battery until failure in years. The battery calendar life depends on charge rate, discharge rate, DoD, temperature, and chemistries of the battery.

Power and Energy Demands of EVs and HEVs

EVs and HEVs can be further divided into six types of vehicles according to the demands of energy and power on vehicle batteries. Instead of grouping HEVs by vehicle architecture, it is more informative to group them by functionality of the electrical powertrain, which affects the fuel economy significantly.

HEVs are classified into four specific hybrids: micro hybrid vehicle (MHV), mild hybrid electric vehicle (MHV), full hybrid electric vehicle (FHEV), and plug-in hybrid electric vehicle (PHEV). On the other hand, EVs are classified into battery EV (BEV) and fuel cell EV (FCEV). A BEV is an EV where the electrical energy to drive the motor(s) is stored in onboard rechargeable batteries while an FCEV is an EV making

use of fuel cell and battery hybrid system as onboard energy sources [4, 8].

The battery is still the most important component of these vehicles but the requirements on power, energy, cycle life, and system voltage are different. Functionality of the electrical powertrain and the favorable battery voltages in these vehicles are shown in Fig. 2.

Hybrid Electric Vehicles

Energy management strategies of HEVs aim to satisfy four key goals: maximum fuel economy, minimum emissions, minimum system costs, and high acceleration rate. The major challenges of HEV design are management of multiple energy sources, battery sizing, and battery management. HEVs take the advantages of electric drive to compensate the inherent weakness of engine. HEVs can avoid engine idling and increase the engine efficiency during starting, low-speed, and high-speed operations. HEVs can also absorb energy during regenerative braking [3, 9].

Hybrid Electric Vehicle Configuration The three basic hybrid architectures of HEVs are series, parallel, and series-parallel hybrids. Figure 3 shows the energy paths in these hybrids. The series hybrid couples the engine and the battery by a generator. Both the engine and the battery power the electric motor to propel the vehicle. The parallel hybrid couples the mechanical power from the engine and from the electric motor to propel the vehicle. The series-parallel hybrid is a direct combination of the series and parallel hybrids.

Micro Hybrid Vehicles The MHV has an electric motor with peak power of about 2.5 kW. The electrical powertrain is driven by a battery system at 12–42 V. The motor is small and simple in structure. It can be an integration of starter and alternator in an ICE vehicle. The electrical and mechanical powertrains in an MHV are governed by an automatic stop-start mechanism, in which, the engine shuts down under vehicle braking and rest. The MHV is favorable for city driving, where

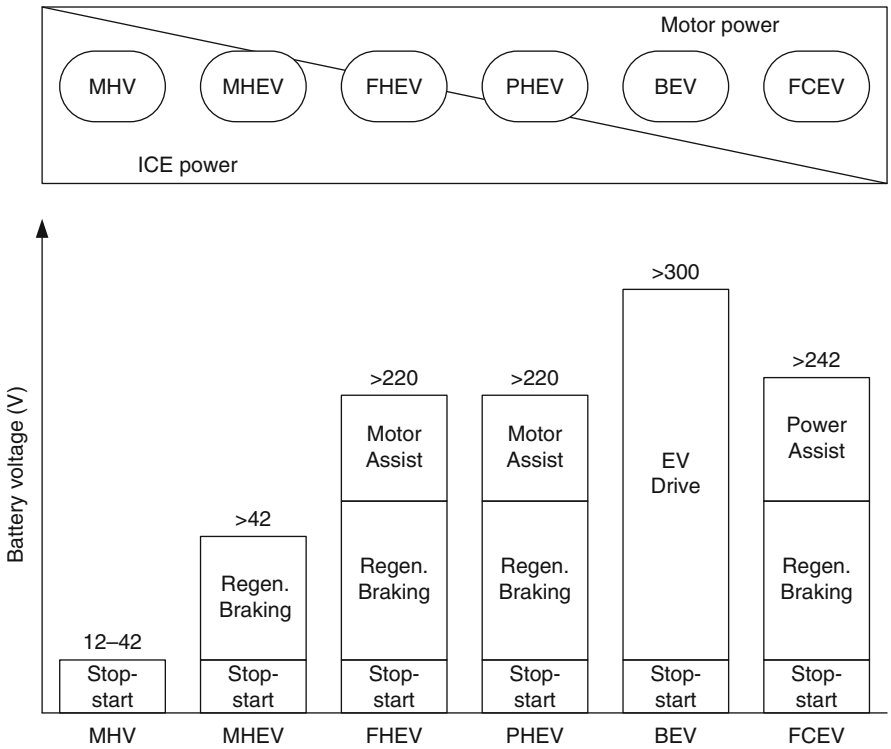

Vehicle Energy Storage: Batteries. Figure 2
Battery operating voltages in EVs and HEVs

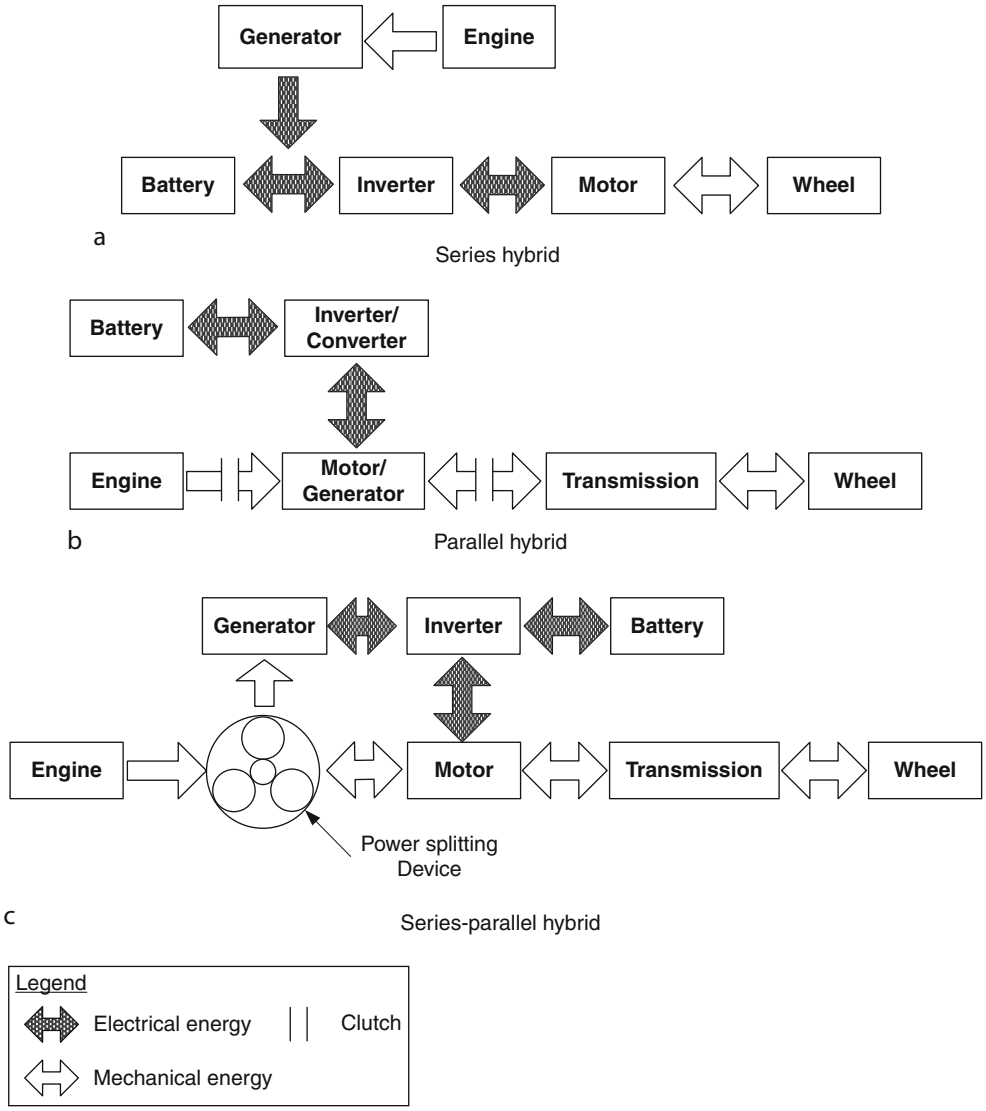

Vehicle Energy Storage: Batteries. Figure 3
Energy flow in series, parallel, and series-parallel HEVs

there are frequent stops and starts. An MHV's fuel economy can be 5–10% higher than that of an ICE vehicle in city driving. The Citroen C3 is an MHV using the Valeo motor system.

The battery discharges frequently in cranking the engine in MHVs. Thus, there is a demand for high cycle life for batteries in MHVs. Table 2 lists some key technical data of batteries for MHVs.

Mild Hybrid Electric Vehicles The MHEV has a more powerful electrical powertrain than an MHV's. The typical electric motor power of a sedan MHEV is about 10–20 kW at 100–200 V. The motor is directly coupled with the engine. The motor has a large inertia such that it can replace the original flywheel of the engine. The motor and the engine are generally coupled in parallel hybrid configuration. Table 3 shows some technical data of batteries for MHEVs. The electrical powertrain is designed to crank the engine and perform regenerative braking during braking. There are demands of high specific power and long service life for batteries in MHEVs. Battery's charge and

Vehicle Energy Storage: Batteries. Table 2 Technical data of batteries for MHVs

Parameters	Unit	MHV
Voltage	V	12–42
Discharge power	kW	4.2–6
Low temperature (−28°C) discharge power	kW	>3
Energy capacity	kWh	0.2–1
Operating temperature	°C	−30 to +52
Calendar life	Year	>3

Vehicle Energy Storage: Batteries. Table 3 Technical data of batteries for MHEVs

Parameters	Unit	MHEV
Voltage	V	42–200
Discharge power	kW	>15
Low temperature (−28°C) discharge power	kW	>4
Recharge power	kW	>15
SoC window	%	40–70
Recharge pulse power	kW	>20
Energy capacity	kWh	0.8–1
Operating temperature	°C	−30 to +52
Calendar life	Year	>10

discharge power depend on its SoC. The battery's discharge power decreases with its SoC. The minimum operating SoC is around 40–50% to uphold sufficient power for launch and acceleration support. On the other hand, the battery's recharging power drops when the SoC is high, thus, the maximum operating SoC is regulated at around 70–80% to maintain sufficient recharge power for regenerative braking. Typically, the batteries operate in an SoC window between 40% and 70%.

Comparing with an ICE vehicle, the MHEV can boost the fuel economy by 20–30% in city driving. MHEVs in the market include Honda Insight Hybrid, Honda Civic Hybrid, and Ford Escape Hybrid.

Vehicle Energy Storage: Batteries. Table 4 Technical data of batteries for FHEVs

Parameters	Unit	FHEV
Voltage	V	220–350
Discharge power	kW	>35
Low temperature (−28°C) discharge power	kW	>4
Recharge power	kW	>30
SoC window	%	40–80
Recharge pulse power	kW	>40
Energy capacity	kWh	1–2
Operating temperature	°C	−30 to +52
Calendar life	Year	>10

Full Hybrid Electric Vehicles The FHEV has a high power electrical powertrain to drive the vehicle purely by electricity in a short driving range. The typical electric motor power for sedan FHEV is about 50 kW at 200–350 V. Generally, the motor, generator, and engine are coupled in series-parallel configuration. With the aid of power split devices, which are mainly built by planetary gear sets and clutches, the energy management system of the engine, motor, and generator is designed to maximize energy efficiency and minimize emissions.

The FHEV can be driven in pure EV mode and hybrid mode. The electrical powertrain assists the engine, not only at the starting, but also during acceleration in the hybrid model, which is also called charge-sustaining mode. In this mode, the discharged energy of the battery is recharged not only during braking but also by the engine to maintain the SoC in high and narrow window. Table 4 shows the technical data of batteries for FHEVs.

The FHEV can achieve higher fuel economy than that of the ICE vehicle by 30–50% in city driving. FHEVs in the market include Toyota Prius, Highlander, and Lexus RX 400 h.

Plug-in Hybrid Electric Vehicles The electrical powertrain of a PHEV is similar to that of an FHEV. The key differences are the additional battery pack and the functionality of grid recharging. In addition to the charge-sustaining mode, the PHEV can also operate in

the charge depletion mode, in which the PHEV operates in pure EV mode. Thus, the battery SoC drops in the charge depletion mode.

The electrical drivetrain of a PHEV works in a high voltage at 220–350 V. The battery energy capacity in PHEVs is the largest among all HEVs and it is determined by the targeted pure electric driving range. The PHEV operates in the charge depletion mode first and then the charge-sustaining mode. In the charge depletion mode, the batteries decline from 100% to a threshold SoC, which triggers the operation mode change. In the charge-sustaining mode, the battery SoC is regulated between the bottom of the SoC window and the threshold SoC. The battery is recharged from the grid at the end of the trip. Similar to the EV, the PHEV suffers from complexity and costliness. However, the PHEV delivers longer driving range than the EV's. Table 5 shows technical data of batteries for PHEVs.

The BYD F3DM is the world's first mass production PHEV, which went on sale to the government agencies and corporations in China in December 2008. Toyota also works on a plug-in version of the Prius. The plug-in Prius is converted from the Prius by adding additional 1.3 kWh battery pack into the car and a charging unit. The plug-in Prius and F3DM adopt the series-parallel hybrid powertrain.

A PHEV can also be implemented in a series hybrid topology. The GM Chevrolet Volt is a series PHEV, which is also called extended-range electric vehicle (EREV). The EREV is driven by one sole electrical powertrain, powered by the battery and a small engine.

Hybrid Electric Buses The battery in hybrid electric buses (HEBs) functions for engine start, power boost, and regenerative braking, which are very similar to the application in FHEVs. The HEB is heavier than a sedan HEV, such that the batteries needed for HEBs are a scale up of that in a sedan FHEV. The battery operates at a significantly higher voltage of 400–700 V. Table 6 shows the technical data of batteries for HEBs.

Electric Vehicles

Battery Electric Vehicles Battery is the sole energy source for the electrical powertrain and accessory systems in a BEV. The typical electric motor power for sedan BEV is about 50–80 kW and the battery operates in a high voltage, over 300 V. Figure 4 shows the bidirectional energy flow in the BEV powertrain and Table 7 lists some key data of batteries for BEVs. In city driving, the EV's fuel economy can be double that of an ICE vehicle [10, 11]. The Mitsubishi i-MiEV and Nissan Leaf are typical BEVs in the market.

Fuel Cell Electric Vehicles An FCEV is driven by a fuel cell and battery hybrid system. A fuel cell system

Vehicle Energy Storage: Batteries. Table 5 Technical data of batteries for PHEVs

Parameters	Unit	PHEV
Voltage	V	220–350
Discharge power	kW	>50
Low temperature (−28°C) discharge power	kW	>6
Recharge power	kW	>30
SoC window	%	20–100
Recharge pulse power	kW	>20
Energy capacity	kWh	5–20
Charge time	Hour	<5
Operating temperature	°C	−30 to +52
Calendar life	Year	>10

Vehicle Energy Storage: Batteries. Table 6 Technical data of batteries for HEBs

Parameters	Unit	HEB
Voltage	V	400–700
Discharge power	kW	100–200
Low temperature (−28°C) discharge power	kW	>20
Recharge power	kW	50–100
SoC window	%	40–70
Energy capacity	kWh	>10
Operating temperature	°C	−30 to +52
Calendar life	Year	>5

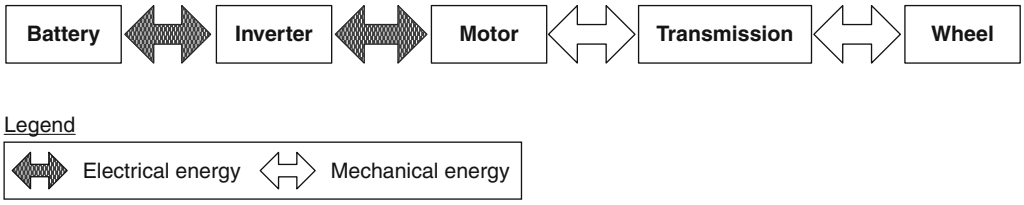

Vehicle Energy Storage: Batteries. Figure 4
Energy flow in a BEV

Vehicle Energy Storage: Batteries. Table 7 Technical data of batteries for BEVs

Parameters	Units	BEV
Voltage	V	>300
Discharge power	kW	>50
Low temperature (−28°C) discharge power	kW	>40
Recharge power	kW	>30
SoC window	%	20–100
Energy capaciy	kWh	50–90
Charge time	Hour	<8
Operating temperature	°C	−30 to +52
Calendar life	Year	>10

consists of a fuel cell stack with plant components for air supply, fuel control, temperature control, and humidification control. Most FCEVs combine the fuel cell stack with a high-voltage battery in a hybrid system for regenerative braking and acceleration boost. The batteries operate in an SoC window between 40% and 70%. Figure 5 shows the energy flow in an FCEV and Table 8 shows technical data of batteries for FCEVs [5].

Batteries for Vehicle Applications

The battery has to be intrinsically tolerant to abuse conditions such as overcharge, short circuit, crush, fire exposure, and mechanical shock and vibration. Battery cells are connected in series and parallel in a vehicle battery system, thus, cells' SoCs have to be balanced to prevent undercharge and overcharge. The operating temperature range of the battery is wide such that active thermal management systems are needed [1, 12].

Key requirements for vehicle batteries are high specific energy and specific power, long cycle life, high efficiency, wide operating temperature, and low cost for commercialization. Figure 6 shows the power and energy requirements of battery for various EVs and HEVs.

The United States Council for Automotive Research LLC (USCAR) and the United States Advanced Battery Consortium (USABC) have set technical targets for vehicle batteries. The MHVs need batteries with long cycle life. The MHEVs, FCEVs, FHEVs, and HEBs need batteries with high specific power for power boost and regenerative braking. Table 9 shows some USABC's key goals for batteries in HEV applications [12–15].

The EV needs batteries with high specific power for quick charge and with high specific energy for long driving range. Table 10 shows some USABC's key goals for batteries in EV applications. The EV commercialization goals were developed to provide lower and possibly reachable goals for car manufacturers to enter the EV market in the near future.

The PHEV needs batteries with high specific power but the requirements on specific energy vary with the targeted pure electric driving range. Table 11 shows some USABC's key goals for batteries in PHEV applications. The high power to energy ratio battery is required for PHEVs with 10-mile pure electric driving range, while the high energy to power ratio battery is required for a pure electric driving range of 40 miles.

The viable batteries for vehicle applications consist of the valve-regulated lead-acid (VRLA), nickel-cadmium (Ni-Cd), nickel-zinc (Ni-Zn), nickel-metal hydride (Ni-MH), zinc/air (Zn/Air), aluminium/air (Al/Air), sodium/sulfur (Na/S), sodium/nickel chloride ($Na/NiCl_2$), lithium metal-polymer (LiM-Polymer), and lithium-ion (Li-Ion) batteries. The specific energy and specific power of these batteries are shown in Fig. 7. These batteries are classified into lead-acid,

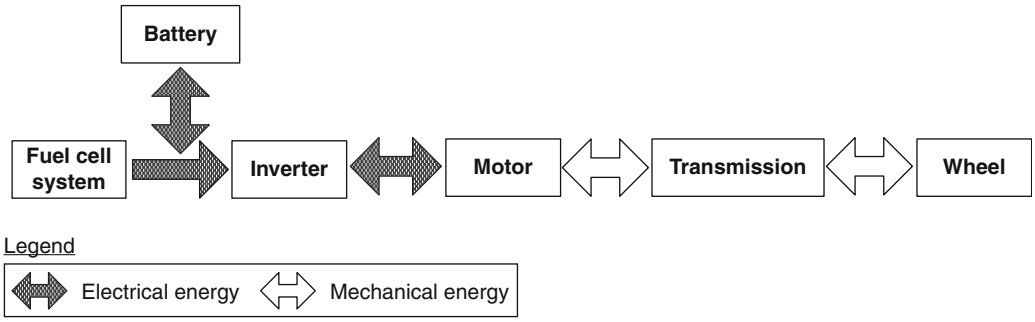

Vehicle Energy Storage: Batteries. Figure 5
Energy flow in an FCEV

Vehicle Energy Storage: Batteries. Table 8 Typical specification of batteries for FCEVs

Parameters	Unit	FCEV
Voltage	V	200–440
Discharge power	kW	>15
Low temperature (−28°C) discharge power	kW	>4
Recharge power	kW	>15
SoC window	%	40–70
Recharge pulse power	kW	>20
Energy capacity	kWh	0.6–1.5
Operating temperature	°C	−30 to +52
Calendar life	Year	>10

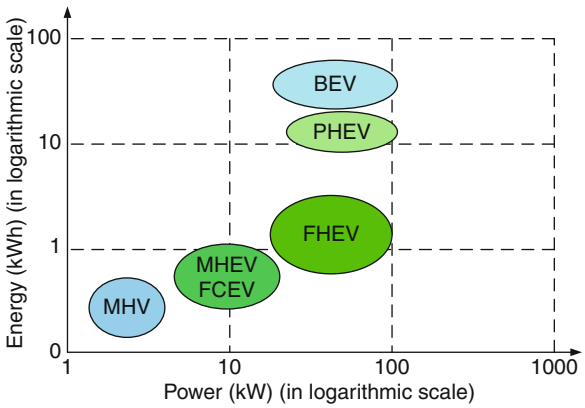

Vehicle Energy Storage: Batteries. Figure 6
Power and energy requirements of batteries for various EVs and HEVs

nickel-based, zinc/halogen, metal/air, sodium-beta, and ambient-temperature lithium batteries, as shown in Fig. 8 [9–11].

Lead-Acid Batteries

The lead-acid (Pb-Acid) battery was invented in 1859. It has been a successful commercial product for over a century. The Pb-Acid battery is mature and has low cost. It has a nominal cell voltage of 2 V, specific energy of 35 Wh/kg, energy density of 90 Wh/L, and specific density of 200 W/kg. It uses metallic lead as the negative electrode and lead dioxide as the positive electrode. The electrolyte is a sulfuric acid solution [16].

On discharge, both lead and lead dioxide are converted into lead sulfate. On charge, the reactions are reversed. The overall electrochemical reactions are described in (1). The electrolyte, sulfuric acid, participates in the electrochemical reactions, and its concentration changes with SoC. Open-circuit voltage of the Pb-Acid battery cell depends only on the acid concentration and is independent of the amount of lead, lead dioxide, or lead sulfate in the cell as long as these components are available. On discharge, the cut-off voltage at moderate rates is 1.75 V and can be as low as 1.0 V at extremely high rates at low temperature. On charge, the charge voltage is regulated below the gassing voltage, about 2.45 V, to avoid evolutions of hydrogen and oxygen gases with the loss of water.

$$\mathrm{Pb} + \mathrm{PbO_2} + 2\mathrm{H_2O} \underset{\text{charge}}{\overset{\text{discharge}}{\rightleftharpoons}} 2\mathrm{PbSO_2} + 2\mathrm{H_2O} \tag{1}$$

Vehicle Energy Storage: Batteries. Table 9 Typical USABC goals for batteries in HEV applications

Parameters	Unit	MHV	MHEV	FHEV	FCEV
Discharge pulse power	kW	6	13–25	40	20
Regenerative pulse power	kW	N.A.	8–20	35	25
Energy capacity	kWh	0.25	0.30	0.50	0.25
Calendar life	Year	15	15	15	15
Cycle life	Cycle	150,000	300,000	300,000	N.A.
Maximum operating voltage	V	48	400	400	440
Operating temperature	°C	−30 to +52	−30 to +52	−30 to +52	−30 to +52

N.A.: not applicable

Vehicle Energy Storage: Batteries. Table 10 Typical USABC goals for batteries in EV applications

Parameters	Unit	EV Commercialization goals	EV Long-term goals
Discharge specific power at 80% DoD for 30 s	W/kg	300	400
Regenerative specific power at 20% DoD for 10 s	W/kg	150	200
Power density	W/L	460	600
Onboard energy capacity	kWh	40	40
Specific energy at C/3 discharge rate	Wh/kg	150	200
Energy density at C/3 discharge rate	Wh/L	230	300
Calendar life	Year	10	10
Cycle life to 80% DoD	Cycle	N.A.	1,000
Operating temperature	°C	−40 to +50	−40 to +85
Selling price	USD/kWh	<150	<100
Normal recharge time	Hour	6	3 to 6
High recharge rate	Hour	0.5 (20–70% SoC)	0.25 (40–80% SoC)

N.A.: not applicable

Valve-Regulated Lead-Acid Battery In the sealed Pb-Acid battery, a special porous separator is employed in the cell such that the evolved oxygen is transferred from the negative electrode to the positive electrode and then combines with hydrogen to form water. Thus, it provides a definite advantage of maintenance-free operation. Moreover, the immobilization of the gelled (Gel) electrolyte or absorbed electrolyte with absorptive glass mat (AGM) separators allows the battery to operate in different orientations without spillage. The sealed Pb-Acid battery is so-called valve-regulated lead-acid (VRLA) battery [16].

Absorptive Glass Mat The AGM separator in the VRLA batteries serves not only as a permeable electronic insulating diaphragm, resistant to strong acid and oxidation, but also as an acid reservoir for the electrochemical reactions. The separator also plays an active role and has a critical influence on the battery performance and service life. The AGM VRLA battery

Vehicle Energy Storage: Batteries. Table 11 Typical USABC goals for batteries in PHEV applications

Parameters	Unit	High power to energy ratio battery	High energy to power ratio battery
Reference equivalent electric range	Mile	10	40
Peak pulse discharge power for 2 s	kW	50	46
Peak regenerative power for 10 s	kW	30	25
Available energy for charge-depleting mode at 10 kW discharge rate	kWh	3.40	11.60
Available energy for charge-sustaining mode	kWh	0.50	0.30
Cold cranking power at −30°C	kW	7	7
Calendar life at 35°C	Year	15	15
Maximum system weight	kg	60	120
Maximum system volume	l	40	80
Maximum operating voltage	V	400	400
Operating temperature	°C	−30 to +52	−30 to +52

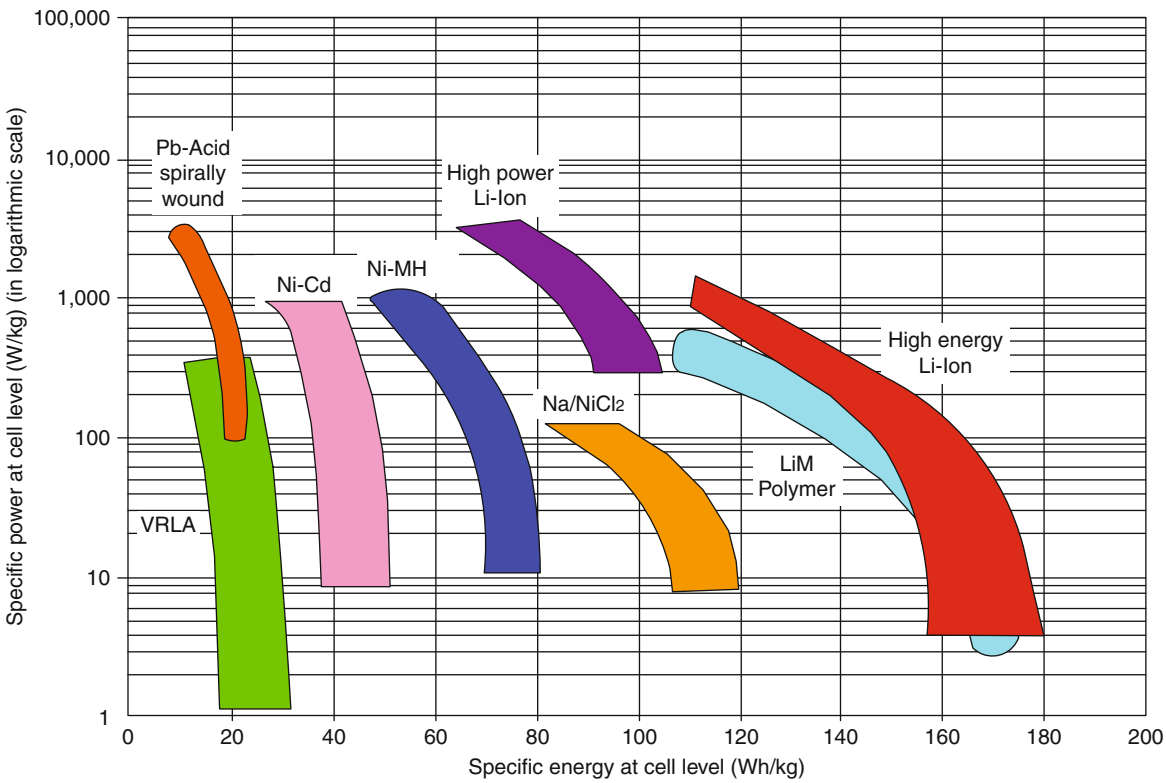

Vehicle Energy Storage: Batteries. Figure 7
Specific energy and specific power of vehicle batteries

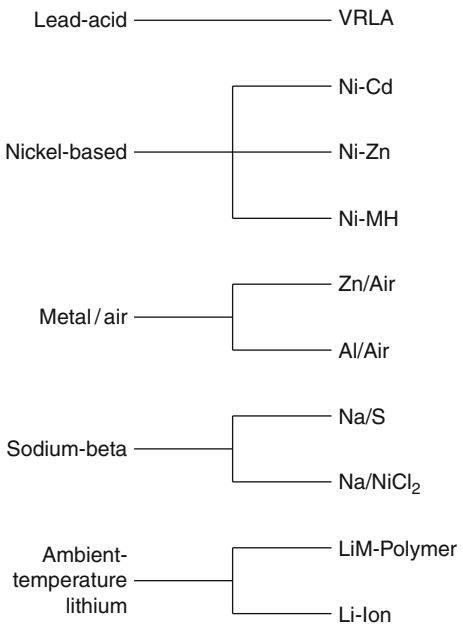

Vehicle Energy Storage: Batteries. Figure 8
Classification of vehicle batteries

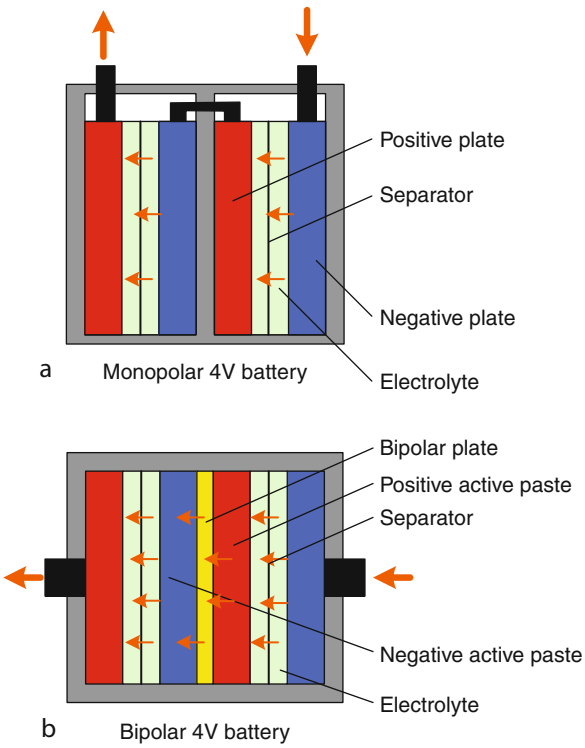

Vehicle Energy Storage: Batteries. Figure 9
Conduction paths inside a monopolar battery and inside a bipolar Pb-Acid battery

has penetrated the market of 12 V starting-lighting-ignition (SLI) batteries in premium cars and MHVs. They are attractive for HEBs and low-cost MHVs [17].

Gel Electrolyte In Gel VRLA batteries, the electrolyte is absorbed in a silica gel rather than an AGM. Ionic conductivity of the gelled electrolyte is low such that power density of the Gel VRLA battery is lower than that of the AGM or flooded Pb-Acid batteries. The Gel VRLA battery is not appropriate for starter batteries or power-optimized HEV batteries. Cycling capability of Gel VRLA battery is good but the discharge rate at low temperature is low. Therefore, Gel VRLA batteries are widely used in electric bicycles, BEVs, and in-house transportation systems, where cold cranking is not required but cyclic stress is extreme [18].

Bipolar Cell Stacks Conventional monopolar cell operates at approximately 2 V in its own plastic compartment and the system battery voltage is achieved by connecting a sufficient number of cells in series. In bipolar Pb-Acid batteries, the positive active material of a battery cell is pasted on one side of a conductive plate, so-called bipolar plate, and the negative active material is pasted on the other side. The positive material on one side of a bipolar plate faces the negative material of the neighboring plate with a separator between them. The battery capacity is determined by surface area of the bipolar plate and the paste material utilization [19]. Figure 9 shows the structure and conduction paths in a monopolar battery and in a bipolar Pb-Acid battery.

Bipolar Pb-Acid cells are favorable for high-voltage applications. In the bipolar Pb-Acid battery system, the system voltage increases by 2 V per unit of additional electrode. The bipolar construction shortens the current path between the positive and negative terminals of adjacent cells of the battery. This reduces the battery's internal resistance and creates uniform current distribution such that the paste materials are utilized efficiently and the power intensity is improved.

UltraBattery™ The UltraBattery™ is a hybrid energy storage battery that integrates an asymmetric supercapacitor and a Pb-Acid battery in a single unit

without extra electronic control. The Pb-Acid component comprises one positive plate, lead dioxide (PbO_2), and one negative plate, lead (Pb). The asymmetric supercapacitor consists of one lead dioxide positive electrode and one carbon-based negative electrode. Lead dioxide is the common material of the Pb-Acid cell and the asymmetric supercapacitor such that negative electrodes of the Pb-Acid cell and the asymmetric supercapacitor are connected in parallel and share the same positive electrode in the UltraBattery™ as shown in Fig. 10 [20].

The charge and discharge currents at the negative electrode consists of two components: capacitor current ($i_{Capacitor}$) and Pb-Acid negative electrode current ($i_{Pb\text{-}Acid}$). The capacitor electrode acts as buffer of the Pb-Acid electrode to mitigate peak charge and discharge currents in HEV applications.

The results from tests at the CSIRO laboratory demonstrated that the UltraBattery™ has greater charge and discharge power and significantly long cycle life than that of a traditional VRLA battery. The UltraBattery™ is at the preproduction stage and prototype batteries have been produced at the Furukawa Battery Co., Ltd, Japan for field testing in HEVs.

Vehicle Applications The VRLA battery has maintained its prime position for more than a century. There are a number of advantages contributing to this outstanding position: proven technology and mature manufacturing, low cost, high cell voltage, good high-rate performance that is suitable for vehicle applications, good low-temperature and high-temperature performances, high energy efficiency (75–80%), and availability in a variety of sizes and designs.

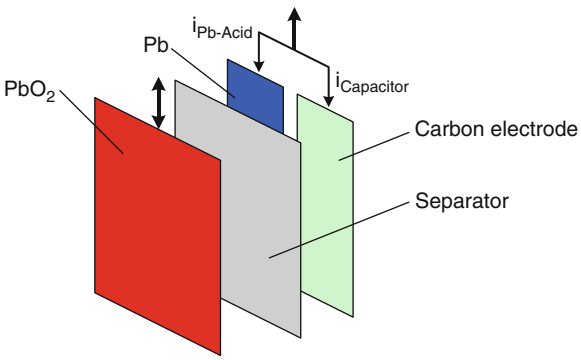

Vehicle Energy Storage: Batteries. Figure 10 Configuration of an UltraBattery™

The VRLA battery still suffers from some disadvantages and needs continual development. Its specific energy and energy density are relatively low, typically, 35 Wh/kg and 70 Wh/L. Its self-discharge rate is relatively high at about 1% per day at 25°C.

Advanced Pb-Acid batteries with improved performance are being developed for vehicle applications. Improvements of the VRLA battery in specific energy over 40 Wh/kg and energy density over 80 Wh/L with the possibility of rapid recharge have been attained. The bipolar VRLA battery and UltraBattery™ are promising Pb-Acid batteries for vehicle applications.

Nickel-Based Batteries

There are many kinds of electrochemical batteries using nickel oxyhydroxide as the active material for the positive electrode, including the Ni-Cd, Ni-Zn, and Ni-MH. Among them, the Ni-MH battery has been well accepted for EV and HEV applications because of its proven technology and good performance. The Ni-Zn battery is still under development.

Ni-Cd Battery For more than 90 years, the Ni-Cd battery has been successfully utilized in heavy-duty industrial applications. Due to the resurgence of interest in EVs in the late 1970s and early 1980s, it led to further development of the Ni-Cd battery for EV applications. The Ni-Cd battery possesses the nominal parameters of 1.3 V, 56 Wh/kg, 110 Wh/L, and 225 W/kg. Its active materials are metallic cadmium for the negative electrode and nickel oxyhydroxide for the positive electrode. The alkaline electrolyte is an aqueous potassium hydroxide solution [21].

The electrochemical reactions of discharge and charge are described in (2). On discharge, metallic cadmium is oxidized to form cadmium hydroxide and nickel oxyhydroxide is reduced to nickel hydroxide with consumption of water. On charge, the reverse reactions occur. In contrast to the sulfuric acid electrolyte used in the Pb-Acid battery, the potassium hydroxide electrolyte in the Ni-Cd battery is not significantly changed in density or composition during discharge and charge.

$$2NiOOH + Cd + 2H_2O \underset{\text{charge}}{\overset{\text{discharge}}{\rightleftharpoons}} 2Ni(OH)_2 + Cd(OH)_2 \quad (2)$$

The Ni-Cd battery has gained enormous technical importance because of the advantages of high specific power (over 220 W/kg), long cycle life (up to 2,000 cycles), highly tolerant of electrical and mechanical abuse, flat voltage profile over a wide range of discharge currents, rapid recharge capability (about 40–80% in 18 min), wide operating temperature range (from −40°C to 85°C), low self-discharge rate (less than 0.5% per day), excellent long-term storage due to negligible corrosion, and available in a variety of sizes and designs. The Ni-Cd battery has some disadvantages which offset its wide acceptance for vehicle applications, namely, low cell voltage, memory effect, and the carcinogenicity and environmental hazard of cadmium.

The Ni-Cd battery can be divided into vented and sealed types. The vented sintered-plate type has higher specific energy but is more expensive. It is characterized by its flat discharge profile and superior high-rate and low-temperature performance. Similar to the sealed Pb-Acid battery, the sealed Ni-Cd battery incorporates a specific cell design feature to prevent build-up of pressure in the cell caused by gassing during overcharge. As a result, the battery can be sealed and requires no maintenance other than recharging.

Major manufacturers of the Ni-Cd battery for vehicle applications are SAFT and VARTA. EVs powered by the Ni-Cd battery included the Chrysler TE Van, Citroën AX, Mazda Roadster, Mitsubishi EV, Peugeot 106, Renault Clio, and HKU U2001.

Ni-Zn Battery Starting from the 1930s, the Ni-Zn battery has been studied for vehicle applications. The Ni-Zn battery has high specific energy and low material cost; however, it has not achieved any commercial importance because of the short life in the zinc electrode [22].

The Ni-Zn battery nominally operates at 1.6 V and has energy and power densities of 60 Wh/kg, 120 Wh/L, and 300 W/kg. It uses zinc as the negative electrode and nickel oxyhydroxide as the positive electrode. The electrolyte is an alkaline potassium hydroxide solution. The discharge and charge reactions are described in (3).

$$Zn + 2NiOOH + 2H_2O \underset{\text{charge}}{\overset{\text{discharge}}{\rightleftharpoons}} Zn(OH)_2 + 2Ni(OH)_2 \quad (3)$$

On discharge, metallic zinc in the negative electrode is oxidized to form zinc hydroxide and nickel oxyhydroxide in the positive electrode is reduced to nickel hydroxide. On charge, the reactions are reversed.

Among the nickel-based batteries, the Ni-Zn battery has the advantages of higher specific energy and specific power than the Ni-Cd battery's, high cell voltage (the highest of the nickel-based family), nontoxicity (more environmental friendliness than the Ni-Cd), tolerance of overcharge and overdischarge, capability of high discharge and recharge rates, and wide operating temperature (from −20°C to 60°C). However, the major and serious drawback of the Ni-Zn battery is its short cycle life (about 300 cycles). It is mainly due to the partial solubility of zinc species in the electrolyte.

Ni-MH Battery The Ni-MH battery has been on the market since 1992. Its characteristics are similar to the Ni-Cd battery. The principal difference between them is the use of hydrogen, absorbed in a metal hydride, for the active negative electrode material in the Ni-MH battery [23].

Active materials of Ni-MH batteries are hydrogen in the form of metal hydride for the negative electrode and nickel oxyhydroxide for the positive electrode. The metal hydride undergoes reversible hydrogen desorbing-absorbing reactions when the battery is discharged and recharged. An aqueous solution of potassium hydroxide is the major component of the electrolyte. The overall electrochemical reactions are described in (4). When the battery is discharging, metal hydride in the negative electrode is oxidized to form metal alloy and nickel oxyhydroxide in the positive electrode is reduced to nickel hydroxide. During charge, the reverse reactions occur.

$$\mathrm{MH} + \mathrm{NiOH} \underset{\text{charge}}{\overset{\text{discharge}}{\rightleftharpoons}} \mathrm{M} + \mathrm{Ni(OH)_2} \tag{4}$$

The hydrogen storage metal alloy is a key component of the Ni-MH battery. It is well formulated to maintain stable over a large number of cycles. The rare-earth alloys based around lanthanum nickel, known as the AB5, and the alloys consisting of titanium and zirconium, known as the AB2, are the two major metal alloys used in Ni-MH batteries. Although the AB2 alloys typically have higher capacity than that of the AB5 alloys, the AB5 alloy is widely used because of its superiority in charge retention and stability.

The Ni-MH battery has a nominal voltage of 1.32 V and attains specific energy of 65–110 Wh/kg for EV applications and 45–60 Wh/kg for HEV applications. It operates in a temperature from −20°C to +45°C. A number of battery manufacturers, such as GM Ovonic, GP, GS, Panasonic, SAFT, VARTA, and YUASA, have actively engaged in the development of this battery for HEVs.

Metal/Air Batteries

The rechargeable metal/air batteries include the electrically or mechanically rechargeable zinc/air (Zn/Air) battery and the mechanically rechargeable aluminum/air (Al/Air) battery. These metal/air batteries have very high specific energy and energy density (as high as 600 Wh/kg and 400 Wh/L for Al/Air), low cost, and are environment friendly. In addition, those mechanically rechargeable batteries have two distinct advantages which are very essential for EV applications, namely, fast and convenient refueling (comparable to petrol refueling in a few minutes) and centralized recharging and recycling (most efficient and environmentally sound use of electricity). The disadvantages associated with rechargeable metal/air batteries are low specific power (at most 105 W/kg for Zn/Air), narrow operating temperature window, carbonation of alkaline electrolyte due to carbon dioxide in air, and evolution of hydrogen gas from corrosion in electrolyte.

Zn/Air Battery The Zn/Air battery has been developed as an electrically and mechanically rechargeable battery. Although both of them have been applied to EV applications, the mechanically rechargeable battery is more favorable [24].

The electrically rechargeable Zn/Air battery nominally operates at 1.2 V and has the specific energy of 180 Wh/kg, energy density of 160 Wh/L, and specific power of 95 W/kg. The negative electrode consists of zinc particles and the positive electrode is a bifunctional air electrode. The electrolyte is potassium hydroxide. The simplified electrochemical reactions are described in (5).

$$2\mathrm{Zn} + \mathrm{O_2} \underset{\text{charge}}{\overset{\text{discharge}}{\rightleftharpoons}} 2\mathrm{ZnO} \tag{5}$$

On discharge, zinc is first oxidized to potassium zincate dissolved in the electrolyte and then to a precipitation of zinc oxide. On charge, the reactions are reversed. However, the zinc electrode generally suffers from the problem of shape change during cycling.

The mechanically rechargeable Zn/Air battery avoids the use of bidirectional air electrode and the shape change problem. Hence, it can offer a higher specific energy of 230 Wh/kg and a higher specific power of 105 W/kg. The depleted zinc negative electrode cassettes can be replaced robotically by a mechanically refueling system at a fleet servicing point or at a public service station. The discharged fuel is then electrochemically recharged at central facilities. There are four steps in a recharging process. Firstly, the discharged cassettes are mechanically taken apart and the zinc oxide discharge product is removed. Secondly, zinc oxide is dissolved in a potassium hydroxide solution to form a zincate solution. Thirdly, the zincate solution is electrolyzed in an electrowinning bath. Finally, the electrowon zinc is compacted onto the negative electrode cassettes.

A mechanically rechargeable Zn/Air battery was developed for field test. A 160-kWh Zn/Air battery was installed and tested in a Mercedes-Benz 180E van in 1994. The driving range at a constant speed of 64 km/h was 689 km.

Al/Air Battery The Al/Air battery has a nominal voltage of 1.4 V. The negative electrode is aluminum metal and the positive electrode is only a simple

unifunctional air electrode for discharge. The electrolyte can be either saline solution or alkaline potassium hydroxide solution. The discharge reaction of this mechanically rechargeable battery is described in (6).

$$4Al + 3O_2 + 6H_2O \xrightarrow{\text{discharge}} 4Al(OH)_3 \qquad (6)$$

The Al/Air battery with a saline electrolyte is attractive only for low-power applications. On the other hand, the alkaline Al/Air battery offers high specific energy and energy density of 250 Wh/kg and 200 Wh/L and is suitable for high power applications. Nevertheless, the corresponding specific power is as low as 7 W/kg. Because of its exceptionally low specific power, the Al/Air battery is seldom used as the sole energy source for EVs and it is commonly used in conjunction with other batteries in a battery hybrid system.

Sodium-Beta Batteries

The sodium-beta battery refers to the Na/S and $Na/NiCl_2$ batteries, which have liquid sodium as one reactant and beta-alumina ceramic as the electrolyte.

Na/S Battery The Na/S battery operates at 300–350°C with a nominal cell voltage of 2 V, specific energy of 170 Wh/kg, energy density of 250 Wh/L, and specific power of 390 W/kg. The active materials are molten sodium for the negative electrode and molten sulfur/sodium polysulfides for the positive electrode. The beta-alumina ceramic electrolyte functions as a sodium ion-conducting solid medium and works as a separator for the molten electrodes to prevent any direct self-discharge [25]. The electrochemical reactions of the Na/S battery are described in (7).

$$2Na + xS \underset{\text{charge}}{\overset{\text{discharge}}{\rightleftharpoons}} Na_2S_x, \quad x = 2.7 - 5 \qquad (7)$$

On discharge, sodium is oxidized to form sodium ions, which migrate through the electrolyte and combine with the sulfur that is being reduced in the positive electrode to form sodium pentasulfide. Then, the sodium pentasulfide is progressively converted into polysulfides with higher sulfur compositions (Na_2S_x) where x is from 2.7 to 5. On charge, these reactions are reversed.

Barriers to commercialization of the Na/S battery are safety issues (high reactivity and corrosiveness of molten active materials), inadequate freeze-thaw durability (weak ceramic electrolyte subjected to mechanical stress), and need of thermal management (additional energy and thermal insulation).

$Na/NiCl_2$ Battery In $Na/NiCl_2$ battery, the active materials are molten sodium for the negative electrode and solid nickel chloride for the positive electrode. In addition to the beta-alumina ceramic electrolyte as used in the Na/S, there is a secondary electrolyte, namely, sodium-aluminum chloride, in the positive electrode chamber. The secondary electrolyte conducts sodium ions from the primary beta-alumina electrolyte to the solid nickel chloride positive electrode [26]. The corresponding electrochemical reactions are described in (8)

$$2Na + NiCl_2 \underset{\text{charge}}{\overset{\text{discharge}}{\rightleftharpoons}} Ni + 2NaCl \qquad (8)$$

On discharge, the solid nickel chloride is converted into nickel metal and sodium chloride crystal. On charge, these reactions are reversed. The $Na/NiCl_2$ battery operates at 155–350°C with a nominal cell voltage of 2.58 V. In a battery system, the system specific energy and specific power can be 86–120 Wh/kg and 150–300 W/kg. Comparing with the Na/S battery, the $Na/NiCl_2$ battery has higher open circuit cell voltage, wider operating temperature, safer products of reaction (less corrosive than molten Na_2S_x), and better freeze-thaw durability (smaller temperature difference).

The AEG ZEBRA (Zero Emission Battery Research Activity) has been the major developer of the $Na/NiCl_2$ battery. The ZEBRA battery, namely, Z12, offered a specific energy of 103 Wh/kg and a specific power of 180 W/kg.

Ambient Temperature Lithium Batteries

There are a number of approaches being taken in the design of rechargeable ambient-temperature lithium

batteries. One approach is to use metallic lithium for the negative electrode and a solid inorganic intercalation material for the positive electrode. The electrolyte can be a solid polymer, leading to name as the lithium metal polymer (LiM-Polymer) battery. Another approach is the use of a lithiated carbon material as the negative electrode such that lithium ions move forth and back between the positive and negative electrodes during cycling. The "rocking-chair" movements of Li-Ions lead to the name lithium-ion (Li-Ion) battery [1, 27].

Lithium Metal Polymer Batteries The LiM-Polymer battery uses lithium metal and a transition metal intercalation oxide (M_yO_z) for the negative and positive electrodes, respectively. A thin solid polymer electrolyte (SPE) is used, which offers the merits of improved safety and flexibility in design [28]. The general electrochemical reactions are described in (9).

$$x\mathrm{Li} + \mathrm{M}_y\mathrm{O}_z \underset{\text{charge}}{\overset{\text{discharge}}{\rightleftharpoons}} \mathrm{Li}_x\mathrm{M}_y\mathrm{O}_z \tag{9}$$

On discharge, lithium ions formed at the negative electrode migrate through the SPE and are inserted into the crystal structure at the positive electrode. On charge, the process is reversed. By using a lithium foil negative electrode and vanadium oxide (V_6O_{13}) positive electrode, the Li/SPE/V_6O_{13} cell is a typical LiM-Polymer battery. It operates at a nominal voltage of 3 V and has the specific energy of 155 Wh/kg, energy density of 220 Wh/L, and specific power of 315 W/kg. The advantages are high cell voltage (3 V), very high specific energy and energy density (155 Wh/kg and 220 Wh/L), very low self-discharge rate (about 0.5% per month), and capability of fabrication in a variety of shapes and sizes. However, its low-temperature performance is weak [1].

Lithium Ion Batteries Since the commercialization of the Li-Ion battery by Sony Energytec in 1990, the Li-Ion battery has been considered to be the most promising rechargeable battery of the future. The Li-Ion battery has already gained acceptance for HEV applications. The specific energy of Li-Ion battery was 98 Wh/kg in 1990 and increased to 195 Wh/kg in 2008 [27].

The Li-Ion battery consists of two electrodes, a porous separator impregnated with electrolyte, and two current collectors. Lithium cobalt oxide ($LiCoO_2$) typically serves as an active electrode material for the positive electrode. The negative electrode is usually made of lithiated carbon or graphite (LiC_6). Electrodes are electrically isolated by the separator, where the space between them is filled by electrolyte. Copper foil is used for the negative current collector and aluminum for the positive current collector.

The Li-Ion battery employs insertion reactions for both positive and negative electrodes. The Li-Ions are inserted into the negative electrode when the battery is fully charged and they move between positive and negative electrodes during cycling. Thus, the Li-Ion battery is also called "rocking-chair battery" or "shuttle-cock battery." The main reactions at the positive electrode are described in (10).

$$\mathrm{Li}_{1-x}\mathrm{CoO}_2 + x\mathrm{Li}^+ + xe^- \underset{\text{charge}}{\overset{\text{discharge}}{\rightleftharpoons}} \mathrm{LiCoO}_2 \quad 0 \le x \le 0.5 \tag{10}$$

The Li-Ion is extracted from the positive electrode during charging and inserted into the electrode during discharging, where x represents the mol fraction of Li^+ ions inside the positive electrode. For a proper reversible functioning of a Li-Ion battery, not all Li^+ ions can be extracted from the electrode. The corresponding reactions at the negative electrode are described in (11).

$$\mathrm{Li}_z\mathrm{C}_6 \underset{\text{charge}}{\overset{\text{discharge}}{\rightleftharpoons}} \mathrm{C}_6 + z\mathrm{Li}^+ + ze^- \quad 0 \le z \le 1 \tag{11}$$

Where z describes the mol fraction of Li^+ ions inside the negative electrode.

The electrolyte is based on a dissociated lithium-containing salt, such as lithium hexafluorophosphate ($LiPF_6$) or lithium perchlorate ($LiClO_4$). Mixtures of ethylene carbonate (EC), diethyl carbonate (DEC), and dimethyl carbonate (DMC) are used as nonaqueous solvents. The ions in the electrolyte are transported by both diffusion and migration, which is induced by the

electric field between the electrodes. The overall reactions are described in (12)

$$Li_{1-x}CoO_2 + Li_{z+x}C_6 \underset{\text{charge}}{\overset{\text{discharge}}{\rightleftharpoons}} LiCoO_2 + Li_zC_6 \tag{12}$$

Development of Positive Active Materials The $LiCoO_2$ has been used as positive active material since 1990. Extensive works have been done for new materials with higher energy density and lower cost. Electrode with nickel compounds shows larger capacity than that of $LiCoO_2$. The lithium nickel oxide ($LiNiO_2$) is a potential material for the positive electrode of the Li-Ion battery. The $LiNiO_2$ is a layered oxide with lithium, oxygen, and nickel layers, and it has the same crystalline structure of $LiCoO_2$. The $LiNiO_2$ is not commercialized because the $LiNiO_2$ electrode showed a rapid capacity decay with cycling, due to the movement of nickel to the lithium layer during cycling. In addition, the thermal stability of $LiNiO_2$ at charged state is low such that it goes to thermal runaway easily. Partial substitutions of nickel with Co, Al, and Mn have been studied to enhance thermal stability.

The manganese-based compounds, namely, $LiMnO_2$ and $LiMn_2O_4$ are potential materials for the positive electrode. The three-dimensional structure and spinel $LiMn_2O_4$ is more stable than the $LiCoO_2$ at fully charged state and the cost is lower. The Li-Ion battery with spinel $LiMn_2O_4$ was commercialized in 1996. However, the battery capacity of $LiMn_2O_4$ is lower than that of $LiCoO_2$ and the capacity decays rapidly. Partial substitutions of $LiMn_2O_4$ with Co, Mg, Cr, Ni, Fe, Ti, and Zn improve cycle life of spinel $LiMn_2O_4$.

The positive electrode with polyanions (SO_4^{2-} and PO_4^{2-}) are promising in reducing cost and enhancing thermal stability. The lithium iron phosphate ($LiFePO_4$) is electrochemically active and shows a flat discharge voltage at about 3.5 V. The $LiFePO_4$ electrode is thermally stable, because it does not release oxygen at fully charged state at an elevated temperature. The electric conductivity is enhanced by coating nanosized $LiFePO_4$ particles with ultrathin carbon layer. Moreover, lithium manganese phosphate ($LiMnPO_4$) and lithium cobalt phosphate ($LiCoPO_4$) are under development for enhancements of battery voltage and capacity [29–34].

Development of Negative Active Materials The capacity of negative electrode has increased by replacing coke (non-graphitic carbon) with graphite, which has larger capacity and flat discharge profile. The capacity of graphic carbon used in Li-Ion batteries is close to the theoretical limit. Commercially available graphic carbons are natural graphite, synthetic graphite, and mesocarbon microbead (MCMB). Intermetallic components and lithium titanium oxide are potential materials for negative electrodes of Li-Ion batteries [35].

Lithium alloys have been developed for negative electrode since 1970s. Cycle life of lithium alloy was short due to alloy pulverization caused by large volume change during cycling. Intermetallic components, such as Cu – Sn, Cu – Sb, and In – Sb, have been investigated aiming at suppressing volume change in lithium alloys during cycling. In 2005, Sony demonstrated a lithium alloy, composed of Sn, Co, and C, that showed 50% increase in volumetric capacity, comparing with a conventional graphite electrode.

The lithium titanate spinel has been investigated as a negative electrode material since the commercialization of the Li-Ion battery, which uses $LiCoO_2$ cathode and carbon anode. The lithium titanate materials, particularly the $Li_4Ti_5O_{12}$, have demonstrated significant improvements in charge and discharge rates in laboratory and in commercial batteries [36].

Vehicle Applications The Li-Ion battery can be made from different advanced positive electrode and negative electrode materials. The mature positive electrode materials are $LiCoO_2$, $LiMn_2O_4$, $LiFePO_4$, lithium nickel manganese cobalt (NMC) oxide ($LiNiMnCoO_2$), and lithium nickel cobalt aluminum (NCA) oxide ($LiNiCoAlO_2$). The mature negative electrode materials are graphite and titanate. Table 12 shows the potential Li-Ion batteries for vehicle applications. Each Li-Ion battery in Table 12 can only overcome one of the barriers to EV commercialization. However, these high-power and thermally stable Li-Ion batteries are promising for HEV applications.

Future Directions

The battery is the most significant factor of commercialization of EVs and HEVs. Developments of batteries for EV and HEV applications are continued and

Vehicle Energy Storage: Batteries. Table 12 Advanced Li-Ion batteries

Positive electrode	Negative electrode	Manufacturers	Key feature
$LiCoO_2$	Graphite	Sony	Mature
$LiMn_2O_4$	Graphite	NEC, GS, Yuasa, LG	High power
NCA/NMC	Graphite	SAFT, Samsung, Sanyo, Evonik	High energy
$LiFePO_4$	Graphite	A123, Valence Tech, BYD	Highly stable
$LiMn_2O_4$	Titanate	Toshiba, Enerdel	High discharge rate

Vehicle Energy Storage: Batteries. Table 13 Key features of promising batteries

Type	Pb-Acid	Nickel-based		Lithium	
Feature	VRLA	Ni-Cd	Ni-MH	Li-Ion	Li-Titanate
Specific energy (Wh/kg)	30–40	40–60	60–70	160	70–90
Cycle life at 100% DoD (cycle)	50–80	300–600	300–500	500–750	25,000
Safety	Fire hazard	Moderate	Fire hazard	Fire hazard	Safest
Charge time (0–90% SoC) (h)	8	2	2	2	0.1
Operating temperature (°C)	−10 to 60	0–50	0–40	0–40	−40 to 70
Environmental impact	Toxic	Toxic	Low	Minimal	Minimal
Memory effect	Very low	High	Moderate	None	None
Power delivery	Good	Moderate	Moderate	Moderate	High
Manufacturability	Easy	Adequate	Adequate	Easy	Easy
Maintenance	Moderate	Moderate	Moderate	Moderate	Moderate
Market position	High volume	Sliding	Modest	Good	Rising
Cost	Low	Tied to Ni	Tied to Ni	Moderate	Moderate

accelerated. The key requirements for vehicular applications are safety, high specific energy, high specific power, short recharge time, long life cycle, and low cost.

The mature and promising batteries for EVs and HEVs are VRLA, Ni-Cd, Ni-MH, and Li-Ion batteries. The specific power and specific energy of the batteries are plotted in Fig. 3 and their features are compared in Table 13. The VRLA battery is popular for MHVs and low-cost EVs due to its maturity and cost-effectiveness. Features of the Ni-MH battery are superior to those of the Ni-Cd battery, so the Ni-Cd battery is being superseded by the Ni-MH battery in the market for MHEVs, FHEVs, and PHEVs.

The Li-Ion batteries are the promising batteries in the future. The advanced Li-Ions batteries have demonstrated the potentials of improvements in specific power, specific energy, charge rate, and safety.

Bibliography

Primary Literature

1. Chan CC, Chau KT (2001) Modern electric vehicle technology. Oxford University Press, Oxford
2. Kurzweil P (2009) Secondary batteries. In: Encyclopedia of electrochemical power sources. Elsevier, Amsterdam, pp 565–578
3. Chau KT, Wong YS (2002) Overview of power management in hybrid electric vehicles. J Energy Conver Manage 43:953–1968
4. Chan CC, Wong YS, Bouscayrol A, Chen K (2009) Powering sustainable mobility: roadmaps of electric, hybrid, and fuel cell vehicles. Proc IEEE 97:603–607

5. Chan CC (2007) The state of the art of electric, hybrid, and fuel cell vehicles. Proc IEEE 95:704–718
6. Chan CC, Wong YS (2004) The state of the art of electric vehicles technology. IPEMC 2004 1:46–57
7. Chau KT, Chan CC (2007) Emerging energy-efficient technologies for hybrid electric vehicles. Proc IEEE 95:821–835
8. Chan CC, Bouscayrol A, Chen K (2010) Electric, hybrid, and fuel-cell vehicles: architectures and modeling. IEEE Trans Veh Technol 59:589–598
9. Köhler U (2009) Hybrid electric vehicles: batteries. In: Encyclopedia of electrochemical power sources. Elsevier, Amsterdam, pp 269–285
10. Chau KT, Wong YS (2001) Hybridization of energy sources in electric vehicles. J Energy Conver Manage 42:1059–1069
11. Gutmann G (2009) Electric vehicle: batteries. In: Encyclopedia of electrochemical power sources. Elsevier, Amsterdam, pp 219–235
12. USCAR (2006) Energy storage system goals: USABC goals for advanced batteries for EVs. USCAR. http://www.uscar.org
13. USCAR (2006) Energy storage system goals: power assist HEV battery goals. USCAR. http://www.uscar.org
14. USCAR (2006) Energy storage system goals: 42 V battery goals. USCAR. http://www.uscar.org
15. USCAR (2008) USABC requirements of end of life energy storage systems for PHEVs. USCAR. http://www.uscar.org
16. Rand DAJ, Moseley PT (2009) Lead-acid system overview. In: Encyclopedia of electrochemical power sources. Elsevier, Amsterdam, pp 550–575
17. Weighall MJ (2009) Valve-regulated batteries: absorptive glass mat. In: Encyclopedia of electrochemical power sources. Elsevier, Amsterdam, pp 715–726
18. Kramm F, Niepraschk H (2009) Valve-regulated batteries: gel. In: Encyclopedia of electrochemical power sources. Elsevier, Amsterdam, pp 727–734
19. Loyns AC (2009) Bipolar batteries. In: Encyclopedia of electrochemical power sources. Elsevier, Amsterdam, pp 750–754
20. Lam LT, Furukawa J (2009) Supercap hybrid (UltraBattery™). In: Encyclopedia of electrochemical power sources. Elsevier, Amsterdam, pp 755–763
21. Shukla AK, Venugopalan S, Hariprakash B (2009) Nickel–cadmium: overview. In: Encyclopedia of electrochemical power sources. Elsevier, Amsterdam, pp 452–458
22. Cairns EJ (2009) Nickel–Zinc. In: Encyclopedia of electrochemical power sources. Elsevier, Amsterdam, pp 528–533
23. Hariprakash B, Shukla AK, Venugoplan S (2009) Nickel–metal hydride: overview. In: Encyclopedia of electrochemical power sources. Elsevier, Amsterdam, pp 494–501
24. Haas O, Van Wesemael J (2009) Zinc–air: electrical recharge. In: Encyclopedia of electrochemical power sources. Elsevier, Amsterdam, pp 384–392
25. Holze R (2009) Sodium–sulfur. In: Encyclopedia of electrochemical power sources. Elsevier, Amsterdam, pp 302–311
26. Sudworth JL, Galloway RC (2009) Sodium–nickel chloride. In: Encyclopedia of electrochemical power sources. Elsevier, Amsterdam, pp 312–323
27. Yamaki J (2009) Lithium rechargeable systems – lithium-ion overview. In: Encyclopedia of electrochemical power sources. Elsevier, Amsterdam, pp 183–191
28. Kobayashi Y, Seki S, Terada N (2009) Lithium-ion polymer batteries. In: Encyclopedia of electrochemical power sources. Elsevier, Amsterdam, pp 375–382
29. Goodenough JB (2009) Positive electrode: layered metal oxides. In: Encyclopedia of electrochemical power sources. Elsevier, Amsterdam, pp 243–248
30. Arai H, Hayashi M (2009) Positive electrode: lithium cobalt oxide. In: Encyclopedia of electrochemical power sources. Elsevier, Amsterdam, pp 258–263
31. Zaghib K, Mauger A, Gendron F, Julien CM, Goodenough JB (2009) Positive electrode: lithium iron phosphate. In: Encyclopedia of electrochemical power sources. Elsevier, Amsterdam, pp 264–296
32. Kanno R (2009) Positive electrode: lithium nickel oxide. In: Encyclopedia of electrochemical power sources. Elsevier, Amsterdam, pp 297–306
33. Wohlfahrt-Mehrens M (2009) Positive electrode: manganese spinel oxides. In: Encyclopedia of electrochemical power sources. Elsevier, Amsterdam, pp 318–327
34. Liu DW, Cao GZ, Wang Y (2009) Positive electrode: nanostructured transition metal oxides. In: Encyclopedia of electrochemical power sources. Elsevier, Amsterdam, pp 337–355
35. Inaba M (2009) Negative electrodes: graphite. In: Encyclopedia of electrochemical power sources. Elsevier, Amsterdam, pp 198–208
36. Ariyoshi K, Ohzuku T (2009) Negative electrode: spinel-type titanium oxides. In: Encyclopedia of electrochemical power sources. Elsevier, Amsterdam, pp 209–213

Books and Reviews

Encyclopedia of electrochemical power sources. Elsevier

Vehicle Traction Motors

C. C. Chan[1], Ming Cheng[2]

[1]Department of Electrical and Electronic Engineering, University of Hong Kong, Hong Kong, China

[2]School of Electrical Engineering, Southeast University, Nanjing, China

Article Outline

Glossary
Definition of the Subject
Introduction
Classification

Design Consideration
Control Consideration
Future Directions
Bibliography

Glossary

AC motor An electric motor driven by an alternating current. There are two types of AC motors, depending on the type of rotor used. The first is the synchronous motor, which rotates exactly at the supply frequency or a submultiple of the supply frequency. The magnetic field on the rotor is either generated by current delivered through slip rings or by a permanent magnet. The second is the induction motor, which runs slightly slower than the supply frequency. The magnetic field on the rotor of this motor is created by an induced current.

Armature winding The conducting coils that are wound around the armature in which voltage is induced, causing it to rotate within a magnetic field.

Brushless DC motor Also called electronically commutated motors. Synchronous motors powered by direct current supply and having electronic commutation system, rather than mechanical commutators and brushes. The current-to-torque and voltage-to-speed relationships are linear.

CVT Continuous variable transmission is a transmission which can change steplessly through an infinite number of effective gear ratios between maximum and minimum values. This contrasts with other mechanical transmissions that only allow a few different distinct gear ratios to be selected. The flexibility of a CVT allows the driving shaft to maintain a constant angular velocity over a range of output velocities.

DC motor An electric motor that runs on direct current (DC) supply.

DTC Direct torque control is a method used in variable frequency drives to control the torque of three-phase AC motors based on stator flux control in the stator fixed frame using direct control of the inverter switching. It involves estimating the motor's magnetic flux and torque based on the measured voltage and current of the motor.

emf Electromotive force is the force that pushes electrons through a conductor.

Field winding The electric circuit is usually a number of coils wound on individual poles and connected in series, which produces the magnetic field in a motor or generator.

FOC Field-oriented control, also called vector control, is a method used in variable frequency drives to control the torque (and thus finally the speed) of three-phase AC motors by controlling two orthogonal current vectors.

Generator A machine that converts mechanical energy into electrical energy by magnetic induction.

ISG Integrated starter/generator, an advanced electric machine controlled by electronics and is designed for integration with internal combustion engines. It replaces the conventional starter motor and alternator, which are the two indispensable electric units for almost every engine.

mmf Magnetomotive force, also known as magnetic potential, is the property of certain substances or phenomena that give rise to magnetic fields. Magnetomotive force is analogous to electromotive force or voltage in electric field.

Motor A machine that converts one form of energy, such as electricity, into mechanical energy or motion.

Definition of the Subject

The traction motor of EVs is responsible for converting electrical energy to mechanical energy in such a way that the vehicle is propelled to overcome aerodynamic drag, rolling resistance drag, and kinetic resistance.

Some engineers and even researchers may consider traction motors kindred or similar to industrial motors. However, traction motors usually require frequent start/stop, high rate of acceleration/deceleration, high-torque low-speed hill climbing, low-torque high-speed cruising, and very wide speed range of operation, whereas industrial motors are generally optimized at rated conditions. Thus, traction motors are so unique that they are deserved to form an individual class. Hence, the general requirements of traction motor are significantly different from those of industrial motors. Their major differences in load

requirement, performance specification, and operating environment are as follows:

- Traction motors need to offer the maximum torque that is four to five times of the rated torque for temporary acceleration and hill climbing, while industrial motors generally offer the maximum torque that is twice of the rated torque for overload operation.
- Traction motors need to achieve four to five times the base speed for highway cruising, while industrial motors generally achieve up to twice the base speed for constant-power operation.
- Traction motors should be designed according to the vehicle driving profiles and drivers' habits, while industrial motors are usually based on a typical working mode.
- Traction motors demand both high power density and good efficiency map (high efficiency over wide speed and torque ranges) for the reduction of total vehicle weight and the extension of driving range, while industrial motors generally need a compromise among power density, efficiency, and cost with the efficiency optimized at a rated operating point.
- Traction motors desire high controllability, high steady-state accuracy, and good dynamic performance for multiple-motor coordination, while only special-purpose industrial motors desire such performance.
- Traction motors need to be installed in mobile vehicles with harsh operating conditions such as high temperature, bad weather, and frequent vibration, while industrial motors are generally located in fixed places.

Introduction

An electric motor drive is the heart of electric vehicles (EVs). Its job is to interface energy source (such as batteries) with vehicle wheels, transferring energy in either direction as required, with high efficiency, under control of the driver at all times. Hence, the electric motor drives are the core technology for electric, hybrid, and fuel cell vehicles. The major requirements of the traction motor drive are the following: [1–3]:

1. High torque density and power density
2. Very wide speed range, including constant-torque and constant-power regions
3. High efficiency over wide torque and speed ranges
4. High torque for low-speed starting and climbing, and high power for high-speed cruising
5. Fast torque response
6. High intermittent overload capability for overtaking
7. High reliability and robustness for vehicular environment
8. Low acoustic noise
9. Reasonable cost

Typical torque/power-speed characteristics required for traction motor drives are illustrated in Fig. 1.

To satisfy these special requirements, the power rating and torque-speed requirements of the motor drive should be determined on the basis of driving cycles and system-level consideration. New motor design technologies and control strategies are being pursued to extend the speed range, to optimize the system efficiency, and to enlarge the high-efficiency region. Newly developed electronic products are also adopted to improve the system performance and to reduce the total cost.

From the functional point of view, a traction motor drive system can be divided into two parts – electrical and mechanical. The electrical part consists of the subsystems of motor, power converter, and electronic controller, whereas the mechanical part includes the subsystems of mechanical transmission (optional) and vehicle wheels. The boundary between the

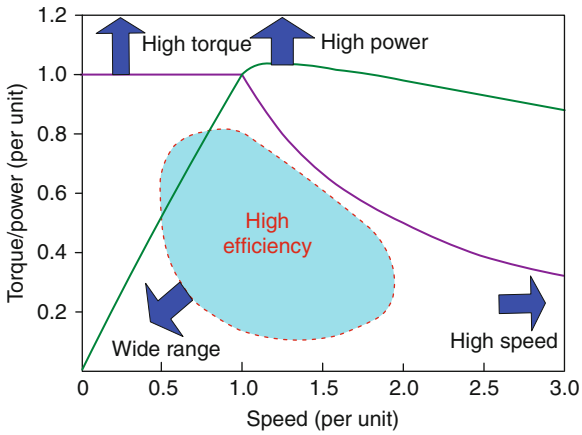

Vehicle Traction Motors. Figure 1
Torque/power requirements for traction motors

electrical and mechanical parts is the air-gap of the motor, where electromechanical energy conversion is taken place. The electronic controller can be further divided into three functional units – sensor, interface circuitry, and processor. The sensor is used to translate the measurable quantities, such as current, voltage, temperature, speed, torque, and flux, into electronic signals. Through the interface circuitry, these signals are conditioned to the appropriate level before being fed into the processor. The processor output signals are usually amplified via the interface circuitry to drive power semiconductor devices of the power converter. The converter acts as a power conditioner that regulates the power flow between the energy source and the electric motor for motoring and regeneration. Finally, the motor interfaces with the vehicle wheels via the mechanical transmission. This transmission is optional because the electric motor can directly drive the wheel as in the case of in-wheel drives. The functional block diagram of a motor drive for EVs is shown in Fig. 2.

Based on the technological growth of electric motors, power electronics, microelectronics, and control strategies, more and more kinds of motor drives become available for EVs. DC motor drives have been traditionally used for EV propulsion because of their ability to achieve high torque at low speeds and easy control. However, the DC motor needs careful maintenance due to its commutator and brushes. Recent technological developments have enabled a number of advanced motor drives to offer definite advantages over those DC motor drives, namely, high efficiency, high power density, efficient regenerative braking, robust, reliable, and maintenance free. Among them, the vector controlled induction motor drive is most popular and mature, though it may suffer from low efficiency at light-load ranges. On the other hand, permanent magnet (PM) brushless motors possess the highest efficiency and power density over the others, but may suffer from a difficulty in flux weakening control for the constant-power high-speed region. The PM hybrid motor is a special type of PM brushless motors. In this motor, an auxiliary DC field winding is so incorporated that the air-gap flux is a resultant of the PM flux and field-winding flux.

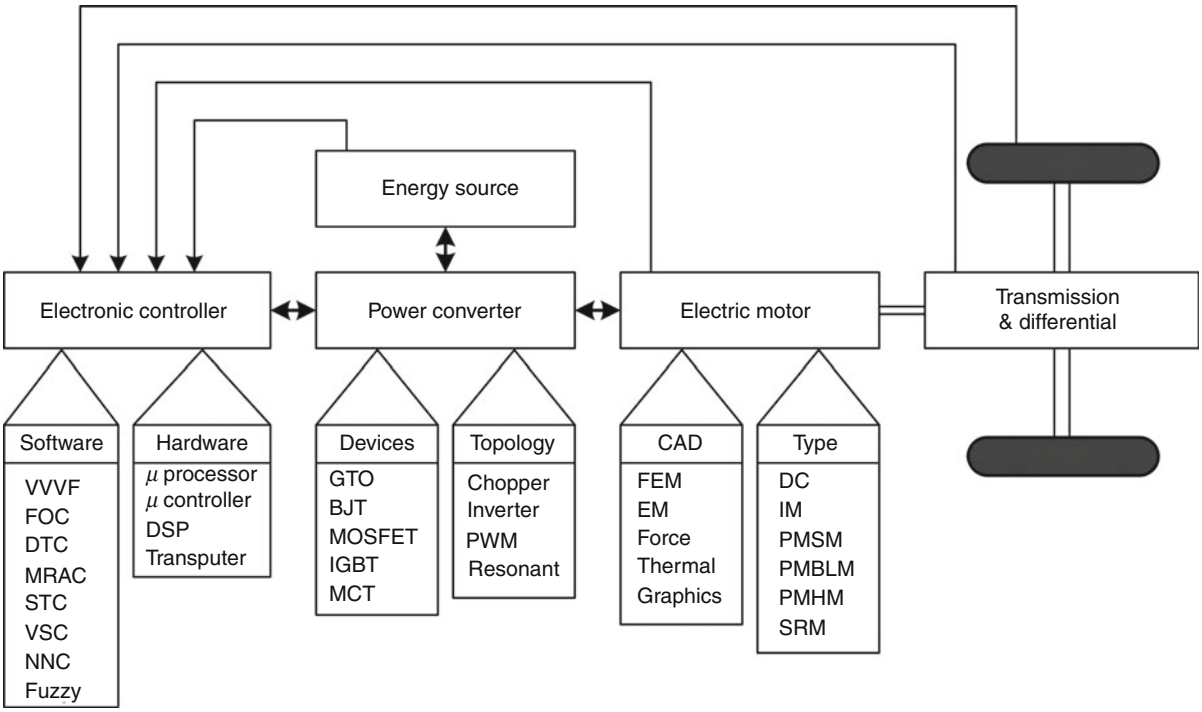

Vehicle Traction Motors. Figure 2
Functional block diagram of an EV drive system

By adjusting the field-winding excitation current, the air-gap flux can be varied flexibly, hence offering optimal efficiency over a wide speed range. Switched reluctance (SR) motors offer promising features for EV applications due to their simplicity and reliability in both motor construction and power converter configuration, wide speed range, favorable thermal distribution, and efficient regenerative braking. However, they may suffer from torque ripples and acoustic noise problems.

The choice of traction motor drive for EVs mainly depends on three factors – driver expectation, vehicle constraint, and energy source. The driver expectation is defined by a driving profile which includes the acceleration, maximum speed, climbing capability, braking, and range. The vehicle constraint depends on the vehicle type, vehicle weight, and payload. The energy source relates with batteries, fuel cells, capacitors, flywheels, and various hybrid sources. Thus, the process of identifying the preferred features and packaging options for electric motor drive has to be carried out at the system level. The interactions between subsystems and those likely impacts of system trade-offs must be examined.

Classification

Electric motors have been available for over a century. The evolution of motors, unlike that of electronics and computer science, has been long and relatively slow. Nevertheless, the development of motors is continually fuelled by new materials, sophisticated topologies, powerful computer-aided designs (CAD), as well as modern power electronics and microelectronics. Based on the technological growth of electric motors, power electronics, microelectronics, and control strategies, more and more kinds of motor drives become available for EVs. As illustrated in Fig. 3, those traction motors applicable to EVs can be classified as two main groups, namely, the brushed motors and brushless motors. The former simply denote that they generally consist of the commutator and brushes, mainly traditional DC motors, while the latter have no brushes.

DC Motor

Traditionally, DC brushed motors have been loosely named as DC motors. There are typically four types of wound-field DC motors, depending on the mutual interconnection between the field and armature windings, namely, separately excited, shunt excited, series excited, and compound excited. By replacing the field winding of DC motors with PMs, PMDC motors permit a considerable reduction in stator diameter due to the efficient use of radial space. Owing to the low permeability of PMs, armature reaction is usually reduced and commutation is improved. The control principle of DC motor is simple because of the orthogonal disposition of field and armature mmfs. Figure 4 illustrates the cross section of a wound-field DC motor.

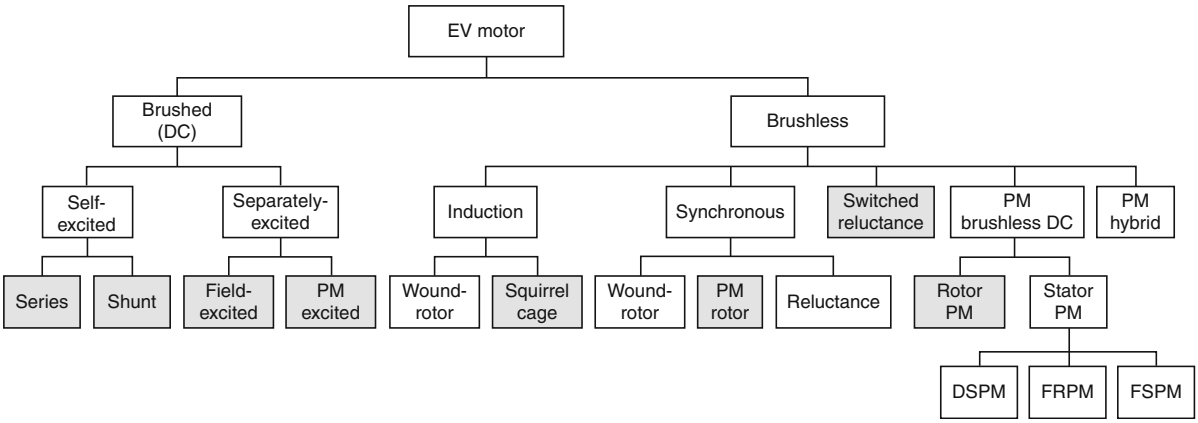

Vehicle Traction Motors. Figure 3
Classification of traction motors for EVs

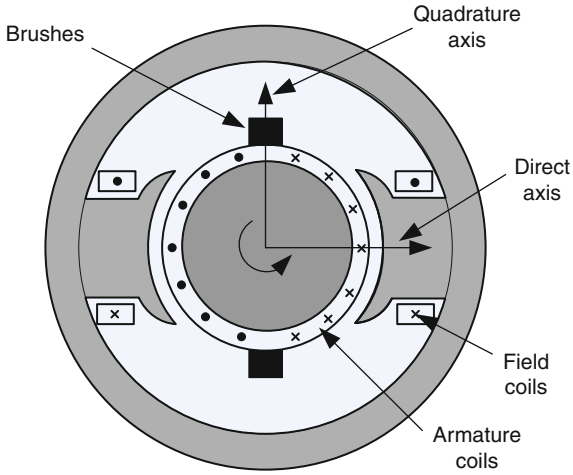

Vehicle Traction Motors. Figure 4
Schematic of DC motor

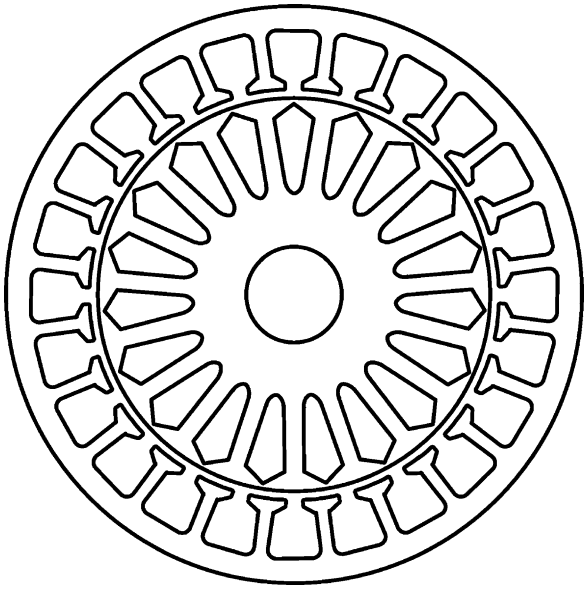

Vehicle Traction Motors. Figure 5
Induction motor with squirrel cage

However, the principal problem of DC motors, due to their commutators and brushes, makes them less reliable and unsuitable for maintenance-free operation. Nevertheless, because of mature technology and simple control, DC motors have ever been prominent in electric propulsion. Actually, various types of DC motors, including series, shunt, separately excited, and PM excited, have ever been adopted by recent EVs.

Recently, technological developments have pushed brushless motors to a new era, leading to take the advantages of higher efficiency, higher power density, lower operating cost, more reliable, and maintenance free over DC brushed motors. As high reliability and maintenance-free operation are prime considerations for electric propulsion in EVs, brushless motors are becoming attractive.

Induction Motor

Induction motors (IM) are a widely accepted brushless motor type for EV traction because of their low cost, high reliability, and free from maintenance. There are two types of induction motors, namely, wound rotor and squirrel cage motors. The wound-rotor IMs are less attractive than their squirrel-cage counterparts due to their higher cost, more maintenance, and lack of sturdiness. The most common types of induction motor rotors are the squirrel cage in which aluminum bars are cast into slots in the outer periphery of the rotor, as shown in Fig. 5 [4, 5].

The main advantages of IM include: (1) Robust structure and relatively low cost; (2) Light weight, small volume, and high efficiency. The disadvantages include: (1) The limited constant-power range (only two to three times the base speed); (2) Relatively difficult control schemes due to the variable equivalent parameters.

Conventional control of induction motors such as variable-voltage variable frequency (VVVF) cannot provide the desired performance. One major reason is due to the nonlinearity of their dynamic model. With the advent of microcomputer era, the principle of field-oriented control (FOC) of induction motors has been accepted to overcome their control complexity due to the nonlinearity. Notice that FOC is also known as vector control or decoupling control. Nevertheless, these EV induction motors employing FOC still suffer from low efficiency at light loads and limited constant-power operating region. On the one hand, an online efficiency-optimizing control scheme has been developed for these EV induction motors [6], which can reduce the consumed energy by about 10% and increase the regenerative energy by about 4%, leading to extend the driving range of EVs by more than 14%. On the other hand, an electrically pole changing scheme has been

developed for EV induction motors [7, 8], which can significantly extend the constant-power operating region to over four times the base speed.

Permanent Magnet Brushless Motors

Permanent magnet brushless motors (PMBM) include sinusoidal and trapezoidal back-EMF machines. From the control schemes, they are divided into brushless DC (BLDC) and brushless AC (BLAC) motors. Generally, a trapezoidal back-EMF waveform in BLDC or a sinusoidal back-EMF waveform in BLAC is needed so as to achieve high-torque density and low-torque pulsation. The PM brushless AC motor with sinusoidal back-EMF is also called as the PM synchronous motor. The most obvious advantage of these motors is the removal of brushes, leading to eliminate many problems associated with brushes.

The PM BLAC motor can run from a sinusoidal or PWM supply without electronic commutation. When PMs are mounted on the rotor surface, they behave as non-salient synchronous motors because the permeability of PMs is similar to that of air. By burying those PMs inside the magnetic circuit of the rotor, the saliency causes an additional reluctance torque which leads to facilitate a wider speed range at constant-power operation. Similar to induction motors, those PM synchronous motors usually employ FOC or DTC for high-performance applications. Because of their inherent high power density and high efficiency, they have been accepted to have great potential to compete with induction motors for EV applications. To achieve optimal efficiency throughout the operating region, a self-tuning control has been developed for PM synchronous motors [9].

The PM BLDC motor has surface-mounted magnets on the rotor, and a concentrated fractional stator winding, which results in a low copper loss. Different from PM synchronous motors, these PM BLDC motors generally operate with shaft position sensors. Recently, a phase-decoupling PM BLDC motor has been developed for EVs, which offers the merits of outstanding power density, no cogging torque, and excellent dynamic performance [10]. Also, it can adopt advanced conduction angle control to greatly extend the constant-power operating range [11].

The main advantages of PM brushless motors are: (1) Light weight, small volume, and high power density as the magnetic field is excited by high-energy PMs; (2) High efficiency, high reliability, and good heat dissipation.

The main disadvantages include: (1) A comparatively narrow range of constant-power operation due to the difficultly in weakening the air-gap flux. By using some new schemes, the speed range can reach three times the base speed. However, the PM may suffer from demagnetization and possible fault. (2) Relatively high cost due to PM materials, especially in high power application [5].

Figure 6 illustrates the typical topologies of the PM brushless motors.

It should be emphasized that all the PM machines mentioned above have the magnets located in the rotor, and are referred as "rotor-PM machines," which are predominated in EV applications due to their outstanding advantages. However, the magnets usually need to be protected from the centrifugal force by employing a retaining sleeve, which is made of either stainless steel or non-metallic fiber. The rotor temperature rise may be a problem due to poor thermal dissipation, which may cause irreversible demagnetization of magnets and ultimately limit the power density of the machine. Recently, in contrast, a new type of PM machines having magnets in stator, nominated as "stator-PM machines," have reemerged and developed, which can overcome the problems suffered by rotor-PM counterparts [12]. Conceptually, the stator-PM machines employ the polarized reluctance principle, in which torque and emfs are resultant from the flux-switching action of rotor saliencies on a unipolar flux produced by PMs in the stator. Since the rotor has neither PMs nor windings, these stator-PM machines are mechanically simple and robust, hence very suitable for high-speed operation. Compared with conventional rotor-PM brushless machine topologies, generally, it is easier to limit the temperature rise of the magnets as heat is dissipated more effectively from the stator. According to the location of the PMs in stator, they can be classified as the doubly salient PM (DSPM) machine [13, 14], flux-reversal PM (FRPM) machine [15, 16], and flux-switching PM (FSPM) machine [17–19].

(a) Doubly Salient PM Machine: In this DSPM machine, the PMs are placed in stator back-iron.

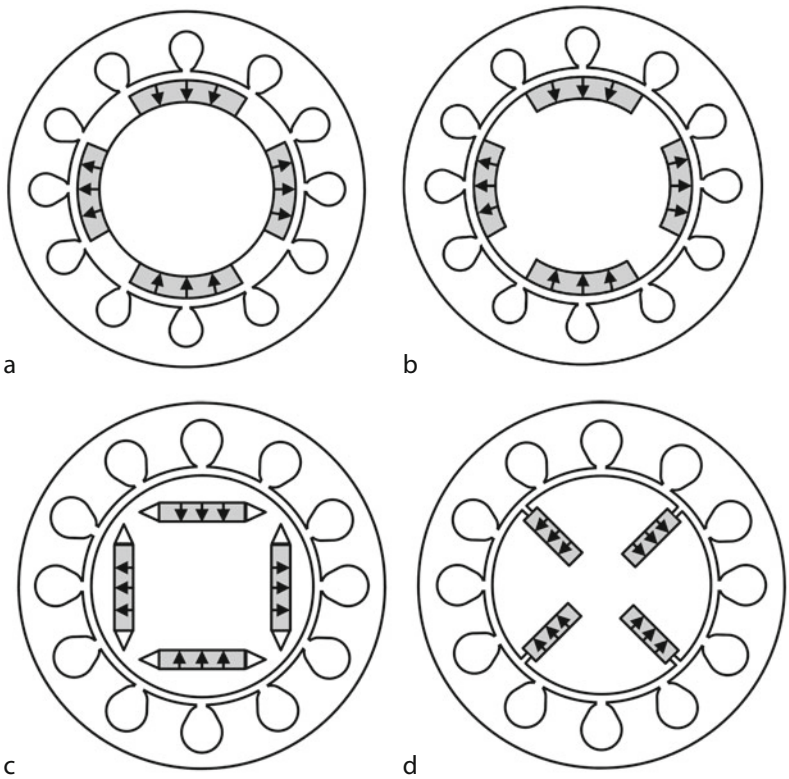

Vehicle Traction Motors. Figure 6
Typical topologies of PM brushless motors. (**a**) Surface mounted; (**b**) surface inset; (**c**) interior radial; (**d**) interior circumferential

Figure 7 shows a 12/8-pole DSPM machine topology (with 12 stator poles and 8 rotor poles). For a three-phase machine a magnet is required in the stator back-iron for every three teeth, while for a four-phase machine a magnet is required for every four teeth. The variation of the flux-linkage with each coil as the rotor rotates is unipolar, while the back-EMF waveform tends to be trapezoidal [12]. Thus, this topology is more suitable for BLDC operation. However, a major disadvantage of the DSPM motor is relatively poor torque density as compared to that of other PM brushless machines [20] due to the unipolar flux-linkage, although, as reported in [14], it can still be higher than that of an induction machine.

(b) Flux-Reversal PM Machine: The FRPM machine has the magnets located on the surface of stator teeth and concentrated windings. Figure 8 illustrates a 12/10-pole FRPM machine topology. Each stator tooth has a pair of magnets of different polarity mounted at its surface. When a coil is excited, the field under one magnet is reduced while that under the other is increased, and the salient rotor pole rotates toward the stronger magnetic field. The flux-linkage with each coil reverses polarity as the rotor rotates. Thus, the phase flux-linkage variation is bipolar, while the phase back-EMF waveform is, again, essentially trapezoidal. Thus, it is suitable for BLDC operation mode. Additionally, it is found that the FRPM machine exhibits fault-tolerance capability due to its natural isolation between the phases, and the variation of inductances versus rotor position is small. Such a machine topology exhibits a low winding inductance, while the magnets are more vulnerable to partial irreversible demagnetization. In addition, significant eddy-current loss may be

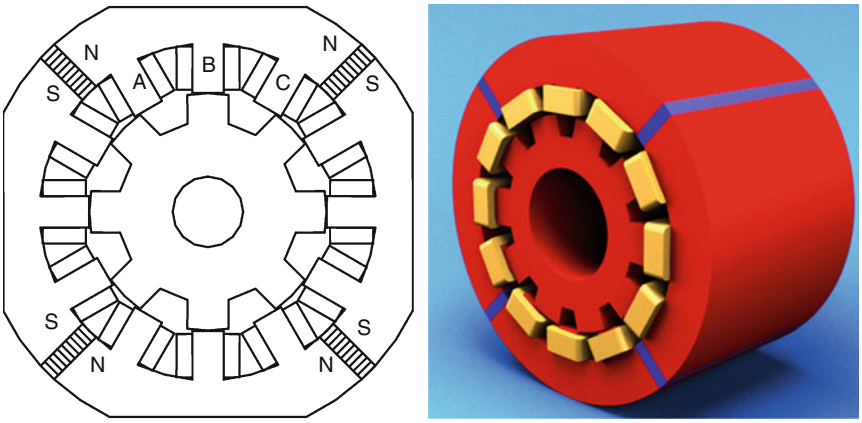

Vehicle Traction Motors. Figure 7
A 12/8-pole DSPM machine

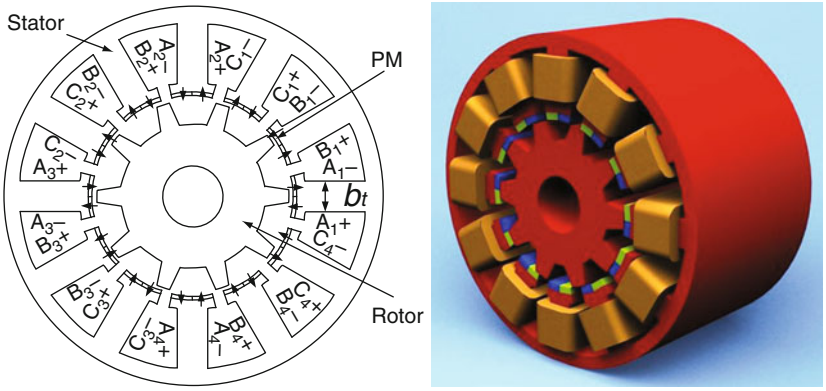

Vehicle Traction Motors. Figure 8
FRPM machine

induced in the magnets, which also experience a significant radial magnetic force. Further, since the air-gap flux density is limited by the magnet remanence, the torque density may be compromised [2].

(c) Flux-Switching PM Machine: In this FSPM machine, the stator consists of U-shaped laminated segments between which circumferentially magnetized PMs are sandwiched, while the direction of magnetization is being reversed from one magnet to the next. Figure 9 shows a 12/10-pole FSPM machine topology. Each stator tooth comprises two adjacent laminated segments and a PM. Thus, flux-concentration can be readily incorporated, so that low-cost ferrite magnets can be employed [2]. In addition, in contrast to conventional PM brushless machines, the influence of the armature reaction field on the working point of the magnets is minimal. As a consequence, the electric loading of FSPM machines can be very high. Therefore, since the phase flux-linkage waveform is bipolar, the torque capability is significantly higher than that of a DSPM machine [20]. Due to the magnetic reluctance difference between the two pairs of coils composing a phase, the resultant phase emf waveforms are essentially sinusoidal without any additional measures [18], which makes them more appropriate for BLAC

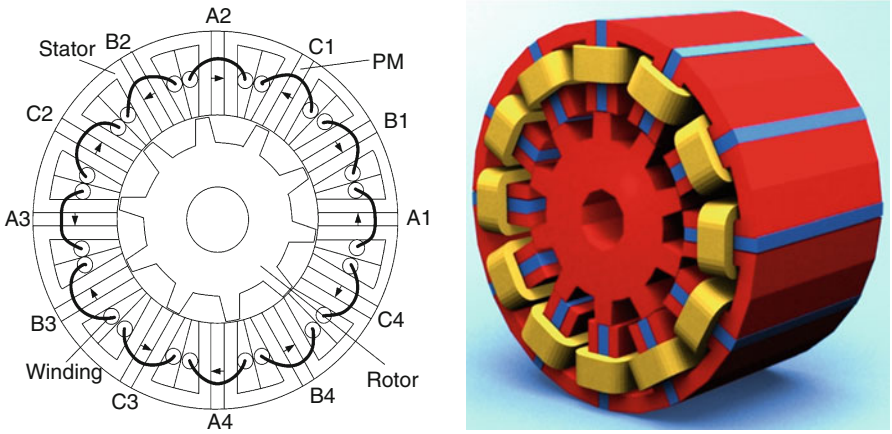

Vehicle Traction Motors. Figure 9
FSPM machine

operation. In addition, since a high per unit winding inductance can readily be achieved, such machines are eminently suitable for constant-power operation over a wide speed range.

PM Hybrid Motor

Although the PM brushless motors possess the highest efficiency and power density over the others, they suffer from a difficulty in flux control. Hence, the current phase angle has to be progressively advanced as the speed is increased above the base-speed so that a demagnetizing d-axis current component is produced which reduces the flux-linkage. Ultimately, however, this may cause partial irreversible demagnetization of the magnets. At the same time, due to the inverter voltage and current limits, the torque-producing q-axis current component has to be reduced correspondingly. Consequently, the torque and power capabilities are limited [2]. Thus, a compromise has to be made between the low-speed torque capability and high-speed power capability. Hybrid PM and field current excitation have been shown to be beneficial in improving the power capability in the extended speed range, enhancing the low-speed torque capability, and improving the overall operational efficiency. Figures 10 and 11 show PM hybrid motors with rotary and stationary PMs, respectively [10, 21]. The PM hybrid motor is a special type of PM brushless motors. In this motor, an auxiliary DC field winding is so incorporated that the air-gap flux is a resultant of the PM flux and field-winding flux. These PM hybrid motors offer many attractive features due to the presence of the hybrid PM field [3]:

1. By varying the polarity and magnitude of the DC field current, the air-gap flux density becomes easily controllable.
2. By realizing flux strengthening, the machine can offer the exceptionally high-torque feature, which is very essential for cold cranking HEVs or providing temporary power for vehicular overtaking and hill climbing.
3. By realizing flux weakening, the machine can offer the exceptionally wide speed constant-power feature, which is very essential for EV cruising.
4. By online tuning the air-gap flux density, the machine can maintain a constant voltage output under generation or regeneration over a very wide speed range, which is very essential for battery charging of various EVs.
5. By online tuning the air-gap flux density, the machine can also offer efficiency-optimizing-control (EOC), which is highly desirable for EVs.

Switched Reluctance Motor

SR motors have been recognized to have considerable potential for EV applications. Figure 12 shows the schematic of an 8/6-pole SR motor. SR motors have the definite advantages of simple construction, low manufacturing cost, inherent fault tolerance, and outstanding torque-speed characteristics for EV

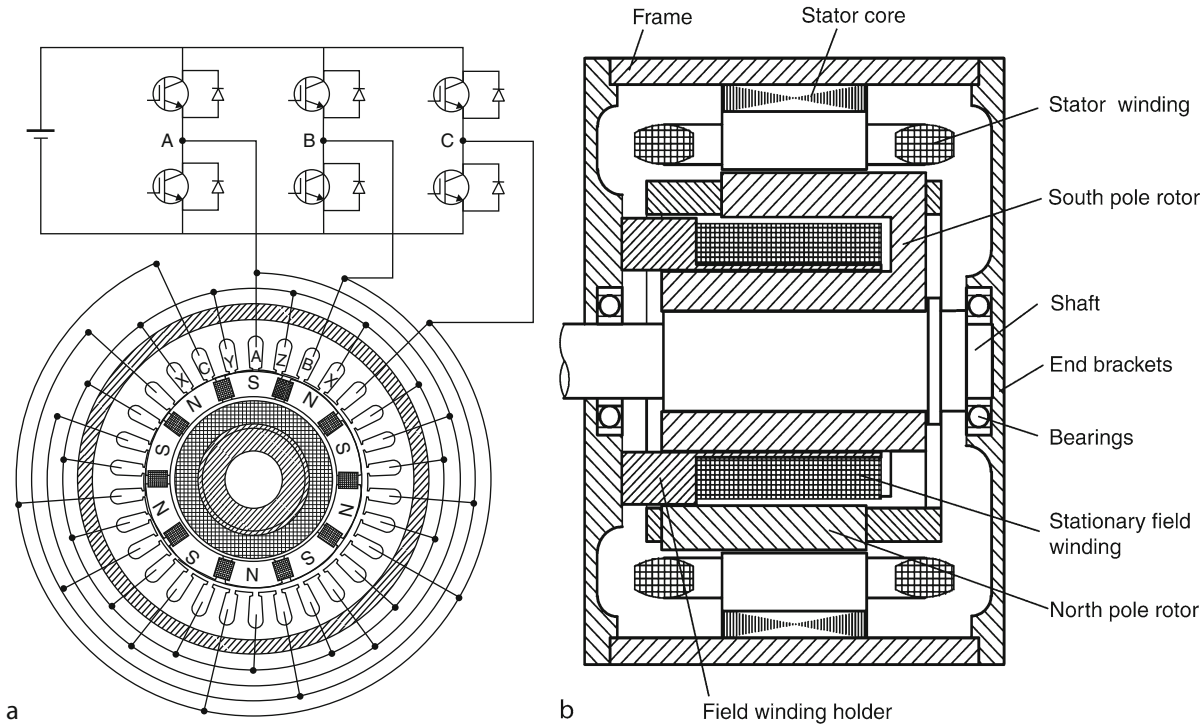

Vehicle Traction Motors. Figure 10
Hybrid PM machine with rotary PMs

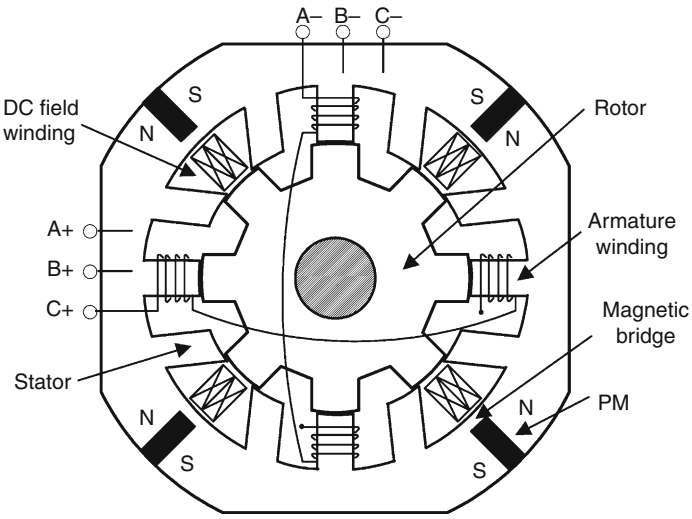

Vehicle Traction Motors. Figure 11
Hybrid PM machine with stationary PMs

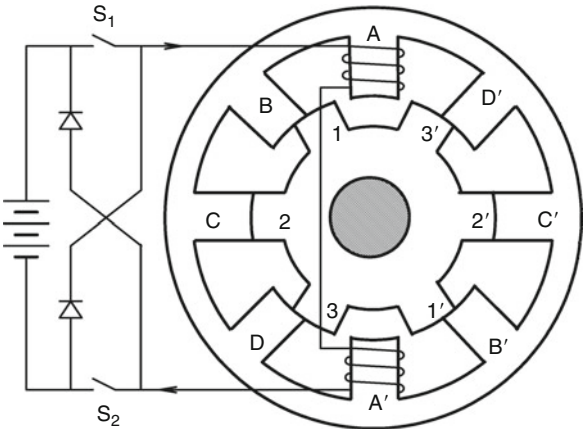

Vehicle Traction Motors. Figure 12
Basic structure of switched reluctance motor drive (only one phase winding shown)

Vehicle Traction Motors. Table 1 Applications of EV motors

EV models	EV motors
Fiat Panda Elettra	Series DC motor
Mazda Bongo	Shunt DC motor
Conceptor G-Van	Separately excited DC motor
Suzuki senior tricycle	PMDC motor
Fiat Seicento Elettra	Induction motor
Ford Th!nk City	Induction motor
GM EV1	Induction motor
Honda EV Plus	PM synchronous motor
Nissan Altra	PM synchronous motor
Toyota RAV4	PM synchronous motor
Chloride Lucas	Switched reluctance motor
Toyota Prius (2005)	PM BLDC motor
Honda Civic	PM BLDC motor

propulsion. Although they possess the simplicity in construction, it does not imply any simplicity of their design and control. Because of the heavy saturation of pole tips and the fringe effect of poles and slots, their design and control are difficult and subtle. Also, they usually exhibit relatively high acoustic noise, vibration, and torque ripple problems. Recently, an optimum design approach to SR motors has been developed [22], which employs finite-element analysis to minimize the total motor losses while taking into account the constraints of pole arc, height, and maximum flux density. Also, fuzzy sliding mode control has been developed for those EV SR motors so as to handle the motor nonlinearities and minimize the control chattering [23, 24].

The motor types that have ever been adopted by recent EVs are indicated by shaded blocks in Fig. 3. Table 1 also illustrates their recent applications to flagship EVs.

In order to evaluate the aforementioned EV motor types, a point grading system is adopted. The grading system consists of six major characteristics and each of them is graded from one to five points. As listed in Table 2, this evaluation indicates that induction motors and PM brushless motors are relatively most acceptable. When the cost of PM material has significant improvements, the PM brushless (including AC or DC) motors will be most attractive. Conventional DC motors seem to be losing their competitive edges, whereas both SR and PM hybrid motors have increasing potentials for EV propulsion.

Design Consideration

Basic Consideration

The basic consideration of motor design includes magnetic loading – the peak of fundamental component of radial flux density in the air-gap of the motor, electric loading – the total rms current per unit length of periphery of the motor or ampere-turns per unit periphery, power per unit volume and weight, torque per unit volume and weight, flux density at each part of the magnetic circuit, speed, torque and power, losses and efficiency, and thermal design and cooling.

The corresponding key issues are better utilization of steel, magnet, and copper; better electromagnetic coupling; better geometry and topology; better thermal design and cooling; understanding the limits on the motor performance; and understanding the relationship among geometry, dimensions, parameters, and performance, thus to achieve higher power per unit weight, higher torque per unit weight, and better performance.

Vehicle Traction Motors. Table 2 Evaluation of EV motors

	DC motor	Induction motor	PM brushless motor	SR motor	PM hybrid motor
Power density	2.5	3.5	5	3.5	4
Efficiency	2.5	3.5	5	3.5	5
Controllability	5	4	4	4	4.5
Reliability	3	5	4	5	4
Maturity	5	5	5	4	3
Cost	4	5	3	4	3
Total	22	26	26	24	23.5

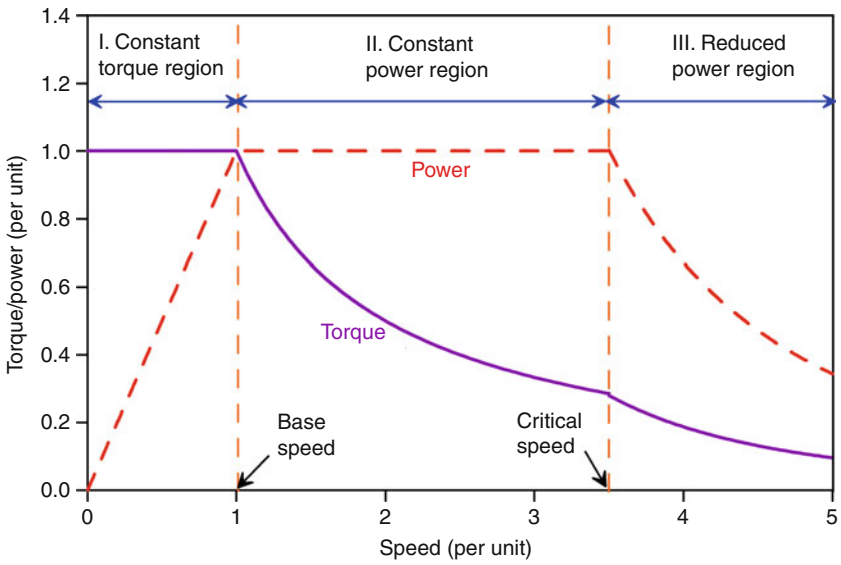

Vehicle Traction Motors. Figure 13
Ideal torque/power-speed characteristics

Traction motor drives for EVs should be designed, as close as possible, to the ideal torque/power-speed characteristics as shown in Fig. 13. In the constant-torque region I, the maximum torque capability is determined by the current rating of the inverter, while in the constant-power region II, flux weakening or commutation phase advance has to be employed due to the inverter voltage and current limits. In region III, the torque and power are reduced due to the increasing influence of the back-emf. However, the power capability and the maximum speed can be enhanced without sacrificing the low-speed torque capability by employing a DC–DC voltage booster [2], a technique which is employed in the Toyota hybrid system, or by employing series/parallel winding connections, i.e., series connection at low speed and parallel connection at high speed, as demonstrated in [25] and [26].

Electrical machine design cannot be undertaken in isolation, but must account for the control strategy and the application requirements, both static and dynamic. Hence, a system-level design approach is essential.

System Consideration

Vehicle operation consists of three main segments. They are: (1) the initial acceleration; (2) cruising at

vehicle rated speed; and (3) cruising at the maximum speed. These three operations provide the basic design constraints for the EV and HEV drive train.

Apart from satisfying the aforementioned special requirements, the design of traction motors also depends on the system technology of EVs. From the technological point of view, the following key issues should be considered:

1. Single- or multiple-motor configurations. One adopts a single motor to propel the driving wheels, while another uses multiple motors permanently coupled to individual driving wheels. The single-motor configuration has the merit of using only one motor which can minimize the corresponding size, weight, and cost. On the other hand, the multiple-motor configuration takes the advantages to reduce the current/power ratings of individual motors and evenly distribute the total motor size and weight. Also, the multiple-motor one needs additional precaution to allow for fault tolerance during the electronic differential action. The functional block diagrams of single- and dual-motor configurations are shown in Fig. 14, while their comparison is listed in Table 3. Since these two configurations have their individual merits, both of them have been employed by modern EVs. For example, the single-motor configuration has been adopted in the GM EV1 while the dual-motor configuration has been adopted in the NIES Luciole. Nevertheless, as reliability is of utmost importance for EVs, the use of single-motor configuration is rekindling, especially for commercialization.
2. Fixed- or variable-gearing transmissions. It is also classified as single-speed and multiple-speed transmissions. The former adopts single-speed fixed-gearing, while the latter uses multiple-speed variable gearing together with the gearbox and clutch. Based on fixed-gearing transmission, the motor should be so designed that it can provide both high instantaneous torque (three to five times the

Vehicle Traction Motors. Table 3 Comparison of single- and dual-motor configurations

	Single motor	Dual motor
Cost	Lower	Higher
Size	Lumped	Distributed
Weight	Lumped	Distributed
Efficiency	Lower	Higher
Differential	Mechanical	Electronic
Reliability	Higher	Lower
Failure modes	Better	Worse

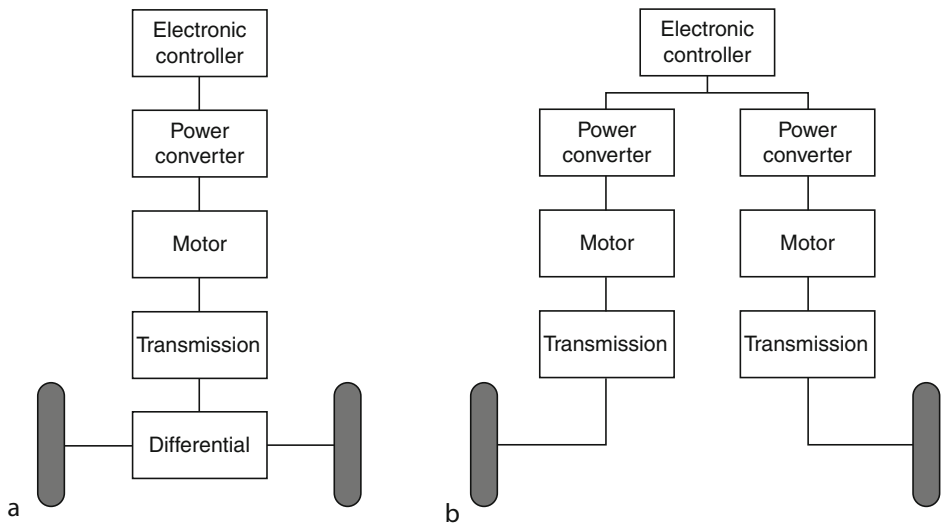

Vehicle Traction Motors. Figure 14
(**a**) Single-motor and (**b**) dual-motor configurations

rated value) in the constant-torque region and high operating speed (three to five times the base speed) in the constant-power region. On the other hand, the variable-gearing transmission provides the advantage of using conventional motors to achieve high starting torque at low gear and high cruising speed at high gear. However, there are many drawbacks on the use of variable gearing such as the heavy weight, bulky size, high cost, less reliable, and more complex. Table 4 gives a comparison of fixed-gearing and variable-gearing transmissions. Actually, almost all the modern EVs adopt fixed-gearing transmission.

3. Geared or gearless. The use of fixed-speed gearing with a high gear ratio allows EV motors to be designed for high-speed operation, resulting high power density. The maximum speed is limited by the friction and windage losses as well as transaxle tolerance. On the other hand, EV motors can directly drive the transmission axles or adopt the in-wheel drive without using any gearing (gearless operation). However, it results the use of low-speed outer-rotor motors which generally suffer from relatively low-power density. The breakeven point is whether this increase in motor size and weight can be outweighed by the reduction of gearing. Otherwise, the additional size and weight will cause suspension problems in EVs. The functional block diagrams of geared and gearless in-wheel motor configurations are shown in Fig. 15. Both of them have been employed by modern EVs. For examples, the high-speed geared inner-rotor in-wheel motor has been adopted in the NIES Luciole while the low-speed gearless outer-rotor in-wheel motor was adopted in the TEPCO IZA. Nevertheless, with the advent of compact planetary gearing, the use of high-speed planetary-geared in-wheel motors is becoming more attractive than the use of low-speed gearless in-wheel motors.
4. System voltage. The design of traction motors is greatly influenced by the voltage level of the EV system. Reasonable high-voltage motor design can be adopted to reduce the cost and size of inverters. If the desired voltage is too high, a large number of

Vehicle Traction Motors. Table 4 Comparison of fixed- and variable-gearing transmissions

	Fixed gearing	Variable gearing
Motor rating	Higher	Lower
Inverter rating	Higher	Lower
Cost	Lower	Higher
Size	Smaller	Larger
Weight	Lower	Higher
Efficiency	Higher	Lower
Reliability	Higher	Lower

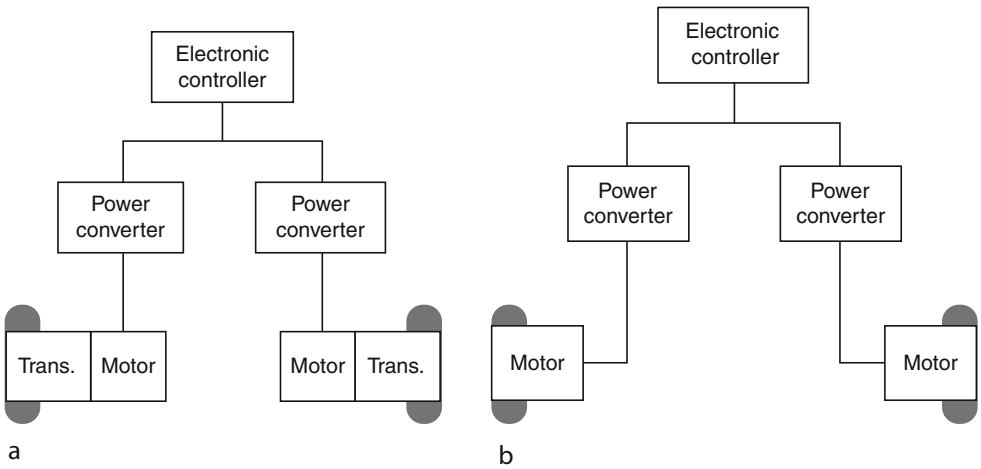

Vehicle Traction Motors. Figure 15
In-wheel motor configurations. (**a**) Geared motor; (**b**) Gearless motor

batteries will be connected in series, leading to the reduction of interior and luggage spaces, the increase in vehicle weight and cost, as well as the degradation of vehicle performances. Since different EV types adopt different system voltage levels, the design of EV motors needs to cater for different EVs. Roughly, the system voltage is governed by the battery weight which is about 30% of the total vehicle weight. In practice, higher power motors adopt higher voltage levels. For examples, the GM EV1 adopts the 312-V voltage level for its 102-kW motor, whereas the Reva EV adopts the 48-V voltage level for its 13-kW motor.

5. Integration. The integration of the motor with the converter, controller, transmission and energy source is prime important consideration. The EV motor designer should fully understand the characters of these components, thus to design the motor under these given environments. It is quite different with the normal standard motors under standard power source for normal industrial drives.

Efficiency

The efficiency may be classified into two types, namely, energy efficiency and power efficiency. The energy efficiency η_e is the ratio of energy output to energy input, while the power efficiency η_p is the ratio of power output to power input. So, they can simply be expressed as:

$$\eta_e = \frac{E_{out}}{E_{in}}$$

$$\eta_p = \frac{P_{out}}{P_{in}}$$

For industrial operation, these two efficiencies may not be necessarily distinguishable. On the contrary, for vehicular operation, there is a significant difference because the power efficiency varies continually during the operation of most vehicles. Thus, it is necessary to delineate the power efficiency associated with the speed and torque conditions. Instead of using a particular operating point (such as rated power at rated torque and rated speed) to describe the power efficiency of a vehicle subsystem or component, an efficiency map is generally adopted. Figure 16 shows typical efficiency maps of a three-phase induction motor and a PM BLDC motor for propelling an EV. Hence, the energy efficiency can be derived by summing powers over a given time period.

Regenerative braking is a definite advantage of EVs over internal combustion engine vehicles (ICEVs). During braking, the motor operates in the regenerative mode which converts the reduction of kinetic energy during braking into electrical energy, hence recharging the batteries. On average, the amount of convertible energy is only about 30–50% as there is significant dissipation in road load. Assuming that the in/out efficiency of the drivetrain and energy source is about 70%, the amount of energy actually stored in the batteries is about 21–35%. This is known as the regenerative braking efficiency. Similar to the previous case, in order to depict the value at different loads, a regenerative braking efficiency map should be adopted.

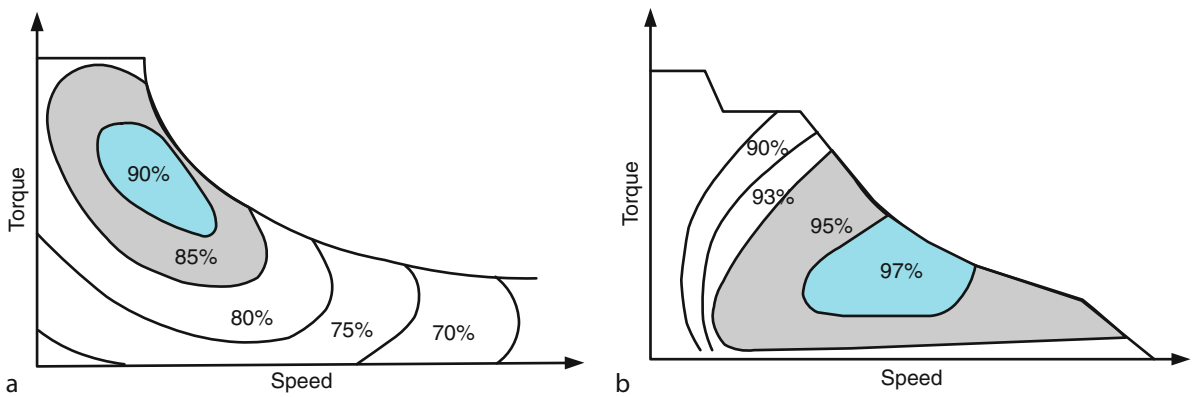

Vehicle Traction Motors. Figure 16
Typical power efficiency maps of EV traction motors. (**a**) Induction motor; (**b**) PM BLDC motor

Design Methodology

To keep up with the stringent requirement and fast changing motor topologies, the design of motors has turned to CAD. Basically, there are two major design approaches – circuit and field. In essence, the circuit approach is based on equivalent circuit analysis while the field approach depends on electromagnetic field analysis. The field approach takes the advantages of more accurate results, greater knowledge of the critical areas, as well as capabilities of handling complicated machine geometry and nonlinear materials. Recently, the finite-element method (FEM) has been regarded as one of the most powerful tools for electromagnetic field analysis of EV motors. The FEM outranks other numerical methods because of its flexibility and applicability in stress and thermal field analyzes.

The performance of a motor drive depends on not only the motor, but also the control circuits. And there are strong coupling between the magnetic circuit and electric circuit of a motor drive. Traditionally, magnetic circuit and electric circuit of electric machines, however, are separately dealt with in dynamic simulations. To evaluate accurately the performance of a motor drive in design procedure, the co-simulation method for the motor drive may be required. In co-simulation, the magnetic circuit and the electric circuit are coupled in time-domain, providing the possibility of system-level simulation. Finite-element time-domain modeling coupled with the equations of circuit and motion is an accurate and detailed approach of simulating drive system performance. Figure 17 illustrates the field-circuit-motion coupled method. The modeling tools for the co-simulation consist of two separate packages, namely, the magnetic solver, Maxwell 2D® and the circuit solver, Simplorer®. The magnetic solver calculates two-dimensional transient magnetic problem of motor drive, while electric circuit and controller are supplied by the circuit solver. Incorporating electric circuit equations into equations of the finite-element system, the magnetic solver uses a loop form of the magnetic equations. At the same time, the circuit solver uses a nodal form of the circuit equations. In each time step, the circuit solver forms a Norton equivalent source of the drive circuit at the coupling pins between the motor and the rest of the drive system.

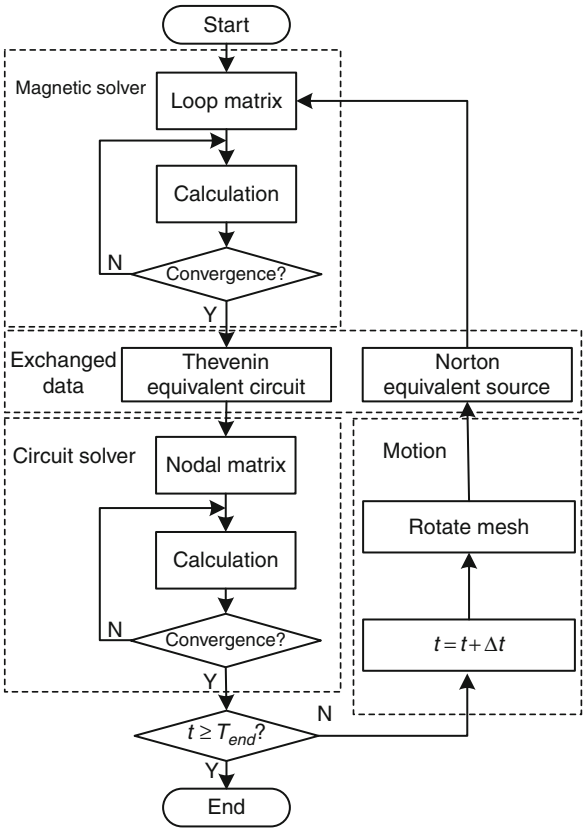

Vehicle Traction Motors. Figure 17
Flowchart of a co-simulation method

The magnetic solver converts it to a loop matrix and solves the finite-element equations. Finally, the magnetic solver outputs a Thevenin equivalent circuit for the next time step of the circuit solver. This parameter-based coupling enhances the solution accuracy and stability. When the simulation runs in the circuit solver, the magnetic solver will start automatically in a co-simulation mode. At each co-simulation time step, both the simulators exchange the calculated data, and results achieved by one solver will be exported to the other solver in the next step. The co-simulation model allows an easy access to all available components such as linear or nonlinear resistances, capacitances, inductances, various diodes, controlled switches, independent sources, voltages, and current probes [27, 28].

Control Consideration

Power Electronics

EV Power Devices In the past decades, power semiconductor device technology has made tremendous progress. These power devices have grown in power rating and performance by an evolutionary process. Among existing power devices, the power diode behaves as an uncontrolled switch, whereas the others, including the thyristor, gate turnoff thyristor (GTO), power bipolar-junction transistor (BJT), power metal-oxide field-effect transistor (MOSFET), insulated-gate bipolar transistor (IGBT), static-induction transistor (SIT), static-induction thyristor (SITH), and MOS-controlled thyristor (MCT), are externally controllable. Active research is still being pursued on the development of high performance power devices.

Before selecting the preferred power devices for electric propulsion, the following requirements have to be considered:

- Ratings. The voltage rating is based on the battery nominal voltage, maximum voltage during charging, and maximum voltage during regenerative braking. On the other hand, the current rating depends on the motor peak power rating and number of power devices connected in parallel. When paralleling these devices, on-state and switching characteristics have to be matched.
- Switching frequency. Switching at higher frequencies can bring down the filter size and help to meet the electromagnetic interference (EMI) limitation requirements. Over the switching frequency of 20 kHz, there is no acoustic noise problem.
- Power losses. The on-state conduction drop or loss should be the minimum while the switching loss should be as low as possible. Since higher switching frequencies increase the switching loss, switching the device at about 10 kHz seems to be an optimum for efficiency, power density, acoustic noise, and EMI considerations. The leakage current should also be less than 1 mA to minimize the off-state loss.
- Base/gate driveability. The device should allow for simple and secure base/gate driving. The corresponding driving signal may be either triggering voltage/current or linear voltage/current. The voltage-mode driving involves very little energy and is generally preferable.
- Dynamic characteristics. The dynamic characteristics of the device should be good enough to allow for high dv/dt capability, high di/dt capability, and easy paralleling. The internal antiparallel diode should have similar dynamic characteristics as the main device.
- Ruggedness. The device should be rugged to withstand a specific amount of avalanche energy during overvoltage and be protected by fast semiconductor fuses during over-current. It should operate with no or minimal use of snubber circuits. Since EVs are frequently accelerated and decelerated, the device is subjected to thermal cycling at frequent intervals. It should reliably work under these conditions of thermal stress.
- Maturity and cost. Since the cost of power devices is one of the major parts in the total cost of electric propulsion systems, these devices should be economical. Some recent power devices such as the high power MCT are not yet mature for EV applications.

Taking into account the above requirements, the GTO, power BJT, power MOSFET, IGBT, and MCT are considered for electric propulsion. The thyristor is not considered because it requires additional commutating components to turn off and its switching frequency is limited to 400 Hz. The SIT and SITH are also excluded because of their normally turn-on property and limited availability. In order to evaluate their suitability, a point grading system is adopted, which consists of eight major characteristics and each of them is graded from one to five points. From Table 5, the power MOSFET, IGBT, and MCT score high points which indicate that they are particularly suitable for EV propulsion. Due to its highest score, the IGBT is almost exclusively used for modern EVs. Nevertheless, the power MOSFET has also been accepted for those relatively low-power electric tricycles and bikes.

EV Power Converters The evolution of power converter topologies normally follows that of power devices, aiming to achieve high power density, high efficiency, high controllability, and high reliability [29].

Vehicle Traction Motors. Table 5 Evaluation of EV power devices

	GTO	BJT	MOSFET	IGBT	MCT
Ratings	5	4	2	5	3
Switching frequency	1	2	4	4	4
Power losses	2	3	4	4	4
Base/gate driveability	2	3	5	5	5
Dynamic characteristics	2	3	5	5	5
Ruggedness	3	3	5	5	5
Maturity	5	5	4	4	2
Cost	4	4	4	4	2
Total	24	27	33	36	30

Power converters may be AC–DC, AC–AC at the same frequency, AC–AC at different frequencies, DC–DC or DC–AC. Loosely, DC–DC converters are known as DC choppers while DC–AC converters are known as inverters, which are respectively used for DC and AC motors for electric propulsion.

Initially, DC choppers were introduced in the early 1960s using force-commutated thyristors that were constrained to operate at low switching frequency. Due to the advent of fast-switching power devices, they can now be operated at tens or hundreds of kilohertz. In electric propulsion applications, two-quadrant DC choppers are desirable because they convert battery DC voltage to variable DC voltage during the motoring mode and revert the power flow during regenerative braking. Furthermore, four-quadrant DC choppers are employed for reversible and regenerative speed control of DC motors. A four-quadrant DC chopper is shown in Fig. 18.

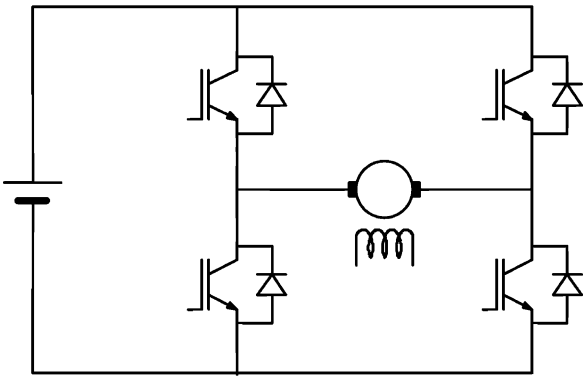

Vehicle Traction Motors. Figure 18
Four-quadrant DC chopper

Inverters are generally classified into voltage-fed and current-fed types. Because of the need of a large series inductance to emulate a current source, current-fed inverters are seldom used for electric propulsion. In fact, voltage-fed inverters are almost exclusively used because they are very simple and can have power flow in either direction. A typical three-phase full-bridge voltage-fed inverter is shown in Fig. 19. Its output waveform may be rectangular, six-step or PWM, depending on the switching strategy for different applications. For example, a rectangular output

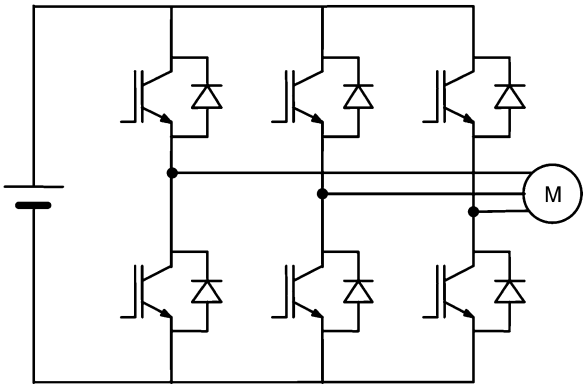

Vehicle Traction Motors. Figure 19
Three-phase full-bridge voltage-fed inverter

waveform is produced for a PM BLDC motor, while a six-step or PWM output waveform is for an induction motor. It should be noted that the six-step output is becoming obsolete because its amplitude cannot be directly controlled, and its harmonics are rich. On the other hand, the PWM waveform is harmonically optimal and its fundamental magnitude and frequency can be smoothly varied for speed control.

Starting from the last decade, numerous PWM switching schemes have been developed for voltage-fed inverters, focusing on the harmonic suppression, better utilization of DC voltage, tolerance of DC voltage fluctuation, as well as suitability for real-time and microcontroller-based implementation [29]. These schemes can be classified as voltage-controlled and current-controlled PWM. The state-of-the-art voltage-controlled PWM schemes are natural or sinusoidal PWM, regular or uniform PWM, harmonic elimination or optimal PWM, delta PWM, carrierless or random PWM, and equal-area PWM. On the other hand, the use of current control for voltage-fed inverters is particularly attractive for high-performance motor drives because the motor torque and flux are directly related to the controlled current. The state-of-the-art current-controlled PWM schemes are hysteresis-band or band–band PWM, instantaneous current control with voltage PWM, and space vector PWM.

Soft-Switching EV Converters Instead of using hard or stressed switching, power converters can adopt soft or relaxed switching. The key of soft switching is to employ a resonant circuit to shape the current or voltage waveform such that the power device switches at zero-current or zero-voltage condition. In general, the use of soft-switching converters possesses the following advantages:

- Due to zero-current or zero-voltage switching condition, the device switching loss is practically zero, thus giving high efficiency.
- Because of low heat sinking requirement and snubberless operation, the converter size and weight are reduced, thus giving high power density.
- The device reliability is improved because of minimum switching stress during soft switching.
- The EMI problem is less severe and the machine insulation is less stressed because of lower *dv/dt* resonant voltage pulses.
- The acoustic noise is very small because of high frequency operation.

On the other hand, their key drawbacks are the additional cost of the resonant circuit and the increased complexity. Although soft-switching DC–DC converters have been widely accepted by switched-mode power supplies, the corresponding development for EV propulsion is much slower. As the pursuit of power converters having high efficiency and high power density for EV propulsion is highly desirable, the development of EV soft-switching power converters is in progress [30–32]. Table 6 gives a comparison between hard-switching and soft-switching converters for EV propulsion.

Although there have been many soft-switching DC–DC converters developed for switched-mode power supplies, these converters cannot be directly applied to DC motors for EV propulsion. Apart from suffering excessive voltage and current stresses, they cannot handle backward power flow during regenerative braking. It should be noted that the capability of regenerative braking is very essential for EVs as it can

Vehicle Traction Motors. Table 6 Comparison of hard switching and soft switching for EV converters

	Hard switching	Soft switching
Switching loss	Severe	Almost zero
Overall efficiency	Norm	Possibly higher
Heat-sinking requirement	Norm	Possibly lower
Hardware count	Norm	More
Overall power density	Norm	Possibly higher
EMI problem	Severe	Low
Dv/dt problem	Severe	Low
Modulation scheme	Versatile	Limited
Maturity	Mature	Developing
Cost	Norm	Higher

extend the vehicle driving range by up to 25%. Recently, a new soft-switching DC–DC converter, having the capability of bidirectional power flow for motoring and regenerative braking as well as the minimum hardware count, has been developed for EV DC motors [33].

The development of soft-switching inverters for AC motors (including induction motors, PM brushless motors, and PM hybrid motors) has become a research direction in power electronics. Figure 20 shows a milestone of soft-switching inverters, namely, the three-phase voltage-fed resonant DC link inverter developed in 1986 [34]. Consequently, many improved soft-switching topologies have been proposed, such as the quasi-resonant DC link, series resonant DC link, parallel resonant DC link, synchronized resonant DC link, resonant transition, auxiliary resonant commutated pole, and auxiliary resonant snubber inverters. A number of development goals of soft-switching inverters for EV propulsion have been identified, namely, efficiency over 95%, power density over 3.5 W/cm^3, switching frequency over 10–20 kHz, *dv/dt* below 1,000 V/μs, zero EMI, zero failure before the end of the vehicle life, and redundant with "limp-home" mode. Recently, the delta-configured auxiliary resonant snubber version has satisfied most of these goals, and has been demonstrated to achieve an output power of 100 kW.

Compared with the development of soft-switching inverters for AC motors, the development for SR motors has been very little [35]. Recently, a new soft-switching converter, so-called the zero-voltage-transition version, has been particularly developed for SR motors [36]. This new converter possesses the advantages that all main switches and diodes can operate at zero-voltage condition, unity device voltage and current stresses, as well as wide operating range. Moreover, it offers simple circuit topology, minimum hardware count, and low cost, leading to achieve high switching frequency, high power density, and high efficiency.

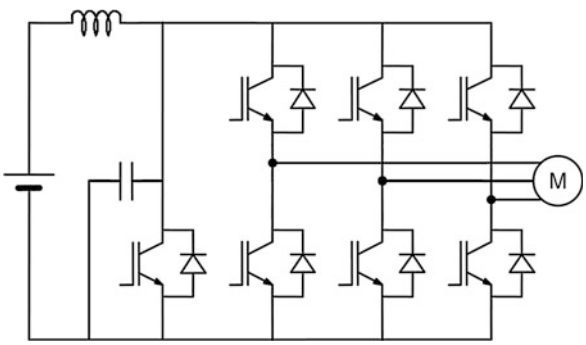

Vehicle Traction Motors. Figure 20
Three-phase voltage-fed resonant DC link inverter

Microelectronics

Since the introduction of microcomputers in 1970, the microelectronics technology has gone through an intense evolution in last 5 decades. Modern microelectronic devices can generally be classified as microprocessors, microcontrollers, and digital signal processors (DSPs).

Microprocessor technology has been used to recognize the milestone of the development of microelectronics, such as the 8086, 80186, 80286, 80386, 80486, Pentium, Pentium II, Pentium III, Pentium IV, Pentium M, and so on. Microprocessors are the CPU of microcomputer systems, which decode instructions, control activities, as well as perform all arithmetic and logical computations. Unlike microprocessors, microcontrollers, such as the 8096, 80196, and 80960, include all resources (CPU, ROM or EPROM, RAM, DMA, timers, interrupt sources, A/D and D/A converters, and I/O ports) to serve as stand-alone single-chip controllers. Thus, microcontroller-based electric propulsion systems possess definite advantages of minimum hardware and compact software. Digital signal processors (DSPs), such as the TMS320C24x/LC24x, TMS320C28x, etc., include several microcontroller peripherals such as Memory, Pulse Width Modulation (PWM) generator, Analog to Digital Converters (ADC), and Event Manager module, and have the capability of high- speed computation to implement sophisticated control algorithm for high performance motor drives for electric propulsion.

By integrating microelectronic devices and power devices on the same chip (like the integration of brain and muscle), power ICs (PICs), loosely named as "smart power," aim to further reduce the cost, minimize the size, and improve the reliability. The PIC may include the power module, control, protection, communication, and cooling. The main problems in PIC synthesis are the isolation between high-voltage and

low-voltage devices as well as cooling. Nevertheless, this technology has promising applications to electric propulsion in near future. The key is the integrating and packaging.

Control Strategies

Conventional linear control such as PID can no longer satisfy the stringent requirement placed on high-performance motor drives. In recent years, many modern control strategies have been proposed. The state-of-the-art control strategies that have been proposed for motor drives are direct torque control (DTC), efficiency optimizing control (EOC), artificial intelligent control, position-sensorless control (PSC), and so on [3].

Direct Torque Control DTC is becoming attractive for EVs, particularly for those equipped with dual-motor propulsion which desires fast torque response. It does not rely on current control and depends less on parameters. For the PM BLAC drives, the DTC controls both the torque and the flux-linkage independently [37, 38]. The controller outputs provide proper voltage vectors via the inverter in such a way that these two variables are forced to predefined trajectories.

Efficiency-Optimizing Control (EOC) EOC of motor drives is highly desirable for EVs since their on-board energy storage is very limited. Different types of motor drives may employ different ways for efficiency optimization. For the rotor-PM BLAC drives, the EOC can be achieved by online tuning the input voltage or the d-axis armature current I_{2d} to minimize the total losses P_{loss} [9], [39]

$$P_{loss}(I_{2d}, T, \omega) = P_{cu}(I_{2d}, T, \omega) + P_{Fe}(I_{2d}, T, \omega)$$

where P_{Cu} is the copper loss, and P_{Fe} is the iron loss for the given torque T and speed ω. It can be found that there is a unique optimal operating point. In particular, the minimum total losses occur at a lower d-axis armature current than that of the minimum copper loss, hence illustrating that the maximum torque per ampere control cannot maximize the efficiency of the PM BLAC drives. For the hybrid PM BLAC drive incorporated with an additional DC field winding [40], the EOC can be easily achieved by tuning the polarity and magnitude of the DC field current.

Artificial Intelligent Control All artificial intelligence-based control strategies, such as fuzzy logic control, neural network control, neuro-fuzzy control, and genetic control, are classified as artificial intelligent control (AIC). Among them, the fuzzy logic control [41] and the neural network control [42] are most mature and attractive since they can effectively handle the system's nonlinearities and sensitivities to parameter variations.

Position-Sensorless Control In order to achieve high performance for EV drives, position feedback is almost mandatory. In order to get rid of the costly and bulky position encoder, position-sensorless control (PSC) is becoming attractive [43–45]. There are various PSC techniques which can be classified as motional EMF, inductance variation, and flux-linkage variation. Basically, the position information is derived by online analysis of the voltages and currents in the machine windings.

It should be noted that the PSC can be readily incorporated into other control strategies such as the EOC, the DTC, and the AIC.

Comparison of Control Strategies As shown in Table 7, the aforementioned control strategies are compared in terms of their major advantages, major disadvantages, and typical techniques [3]. Since there are many possible strategies for the AIC, the self-tuning fuzzy PI control [41] is used for exemplification. The corresponding control block diagrams are shown in Fig. 21. Finally, some sample results of these control strategies have illustrated that the EOC can achieve the minimum total losses [39], the DTC can provide direct bang–bang control of torque [38], the AIC can achieve fast and accurate response [41], and the PSC can offer accurate estimation of rotor position [44].

Future Directions

Thanks to persistent hard work of both academic and industrial communities in the past years, the performance of traction motors for EVs has been improved greatly. With quick development of industry technology, motor drives in EVs would meet with new renovations.

Vehicle Traction Motors. Table 7 Comparison of control strategies

	Advantage	Disadvantage	Techniques
DTC	Fast torque response; no need for current control; less parameter dependence	Cause errors due to drift flux-linkage estimation and variation of stator resistance	Generate the voltage vectors using independent torque and flux computations
EOC	Minimize the overall losses; no need for accurate loss model; work for wide speed and torque range	Originate system oscillation or convergence problem	Control the input voltage or d-axis armature current; control DC field current
AIC	Flexible control algorithms; adapt nonlinearities and parameter variations	Require expert knowledge or intensive computation and sophisticated hardware	Incorporate fuzzy logic, neural network, and other AI into traditional controls
PSC	Eliminate position sensor, hence reduce system size and cost; readily merge into other controls	Require intensive computation and sophisticated hardware	Estimate the position based on motional EMF, inductance variation, or flux- linkage variation

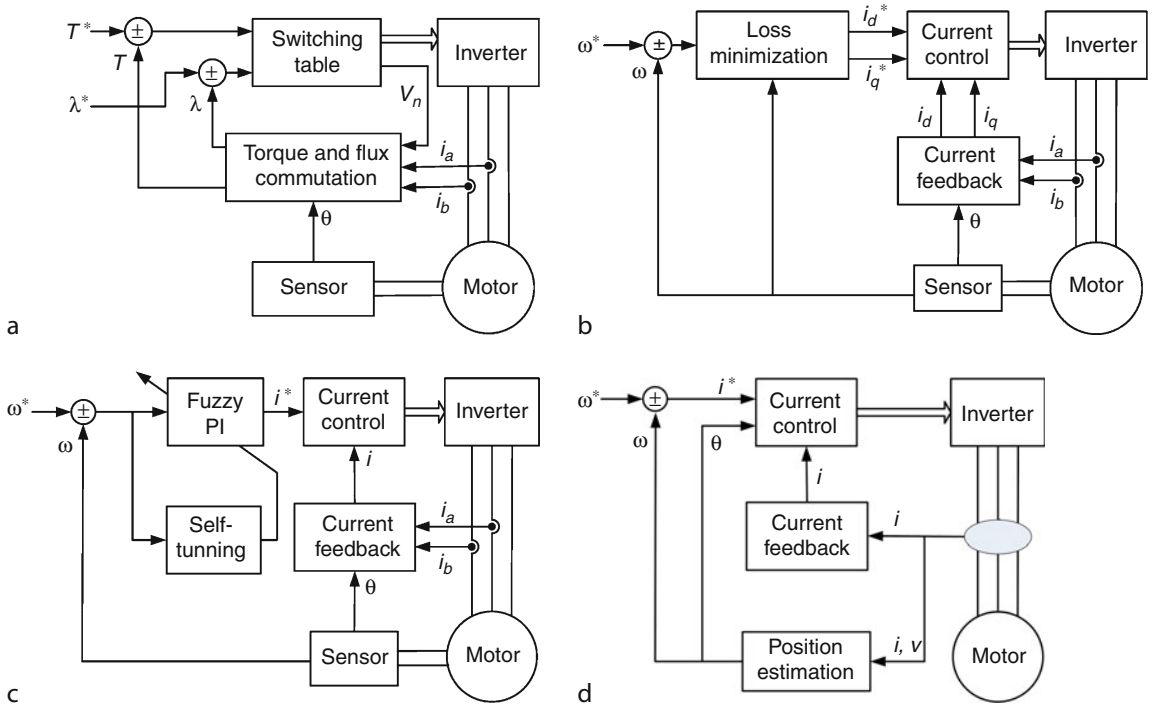

Vehicle Traction Motors. Figure 21
Control block diagrams. (**a**) DTC; (**b**) EOC; (**c**) AIC; (**d**) PSC

The development of traction motor drives is no longer limited to the design and operation of a single motor or drive. The research trends of the traction motor drive in EVs may be concluded as follows.

1. High-speed motors. By increasing speed, the size of electric motors may be reduced greatly, namely, higher power from smaller machines and redesigning for increased material utilization [3, 46]. Some

companies have started to focus on high speed of 16,000 r/min PM motors that can achieve field weakening within the structure of the motor and eliminate the need for a DC–DC boost converter [47].

2. System integration. It is necessary for the designers to take electrical machine, power electronics, such as converter, and energy source into consideration altogether. Furthermore, control methods will be analyzed during the machine design so as to extend the constant-power speed range, increase the starting torque, and etc.
3. Redundant and fault-tolerant motor structure. Continued operation of motor drive is an essential requirement in EV application. Therefore, the need for high degree of reliability in motor drive system has inspired much research in the area. To achieve high reliability, redundant or conservative design techniques have been employed in many motor drives. Figure 22 illustrates a 6-phase 8-pole rotor-PM motor [48] and a flux-switching motor.
4. Novel manufacture techniques. To achieve high power density, high efficiency, and low-cost motors for EVs, the manufacture technique of motors is being improved. The segmented stator and concentrated winding are examples [49]. In addition, using flat wire to replace round wire in motor windings can increase slot filling factor, enabling both a higher torque constant and a lower copper loss.
5. Novel machine topologies with composite structures and new materials. For traditional machines, each has its own merits and demerits. The composition of different machines may significantly improve the performance. Hence, the traction machines consist of different structures may be noticed in the next step.

EVT Systems

In 1997, Toyota developed the first EVT system for its flagship HEV, Prius, which is a full hybrid. The schematic configuration of this EVT is shown in Fig. 23, which is mainly composed of a planetary gear, a motor, and a generator. The internal combustion engine (ICE) is attached to the planet carrier, the motor is coupled with the driveline shaft so that both are attached to the ring gear, and the generator is mounted to the sun gear [50]. By controlling the power taken by the generator and then feeding back into the motor, the ICE speed can be maintained constant when the driveline-shaft speed is varying. Thus, a continuously variable ratio between the ICE speed and the wheel speed can be achieved. Hence, this EVT system takes the following advantages.

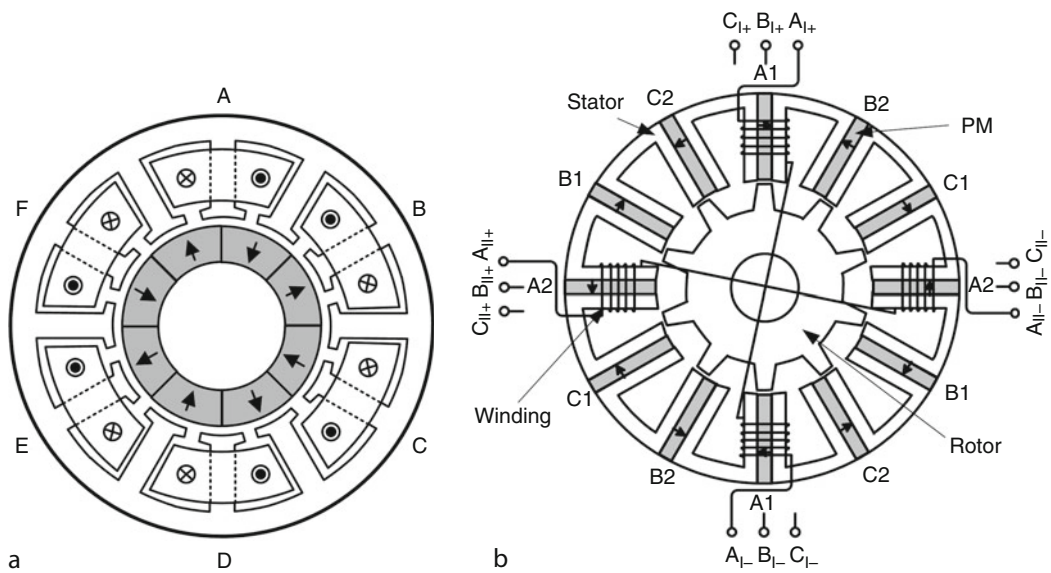

Vehicle Traction Motors. Figure 22
Fault-tolerant motor topologies. (**a**) 6-phase 8-pole rotor-PM motor; (**b**) Flux-switching PM motor

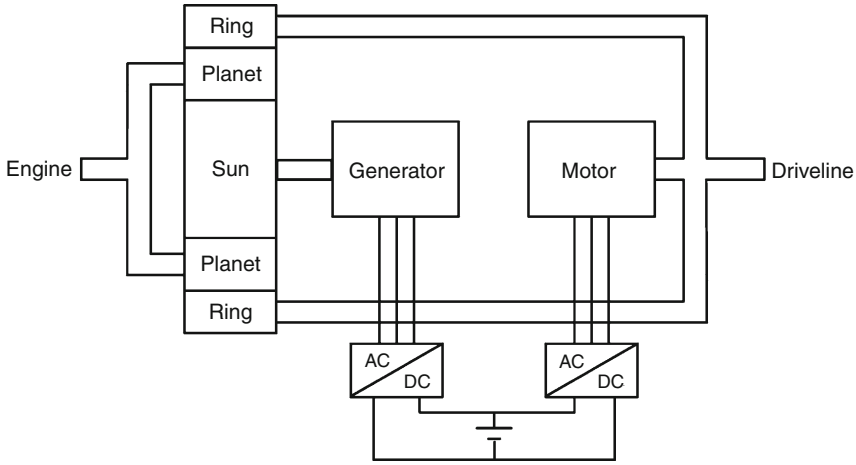

Vehicle Traction Motors. Figure 23
Planetary-geared EVT system

1. Because of the absence of clutches or shifting gears, it can significantly improve the transmission efficiency and reduce the overall size, hence increasing both the energy efficiency and the power density.
2. In the presence of continuously variable ratio between the ICE speed and the wheel speed, the ICE can always operate at its most energy-efficient operating point, hence resulting in a considerable reduction of fuel consumption.
3. The system can fully enable the idle stop, electric launch, regenerative braking, and full-throttle acceleration features, which are particularly essential for the full hybrids.

However, this planetary-geared EVT system inherits the fundamental drawbacks of planetary gearing, namely, transmission loss, gear noise, and need of regular lubrication.

In recent years, active research works have been conducted to eliminate this mechanical planetary gear while retaining the EVT propulsion. One viable approach is the use of the dual mechanical port (DMP) machine to realize power splitting for the full hybrids [51]. Figure 24 shows the EVT system integrated with the DMP machine. When installing this EVT system in a full hybrid, it offers four modes of operation, namely, cranking, charging, launching, and continuous variable transmission (CVT) [52].

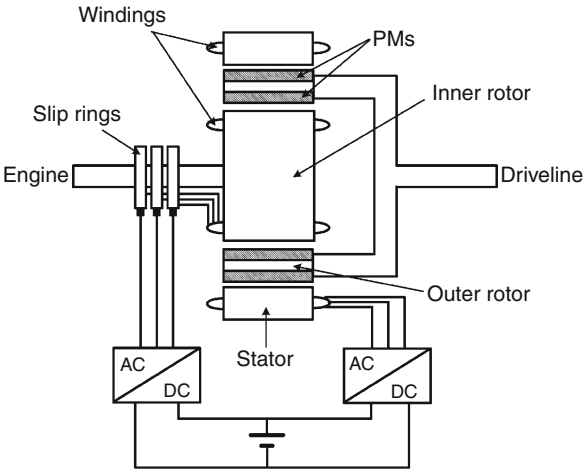

Vehicle Traction Motors. Figure 24
EVT system using integrated DMP machine for HEVs

1. In the cranking mode, the battery delivers the power to crank the ICE via the primary machine until the ICE reaches the speed for ignition.
2. In the charging mode, the battery is either charged by the ICE via the inner-rotor winding when the vehicle stops motion or by the stator winding during regenerative braking.
3. In the launching mode, the battery delivers the power to launch the vehicle via the stator winding without using the ICE.

4. In the CVT mode, the input and output shafts are controlled to change the speed and the torque, respectively, so that the optimal operating line of the ICE can be achieved.

Magnetic-Geared PM Brushless Drives

For EVs, in-wheel motor drives are very attractive since they play the role of electronic differential [1]. As the wheel speed is only about 600 r/min, the in-wheel motor drive is either a low-speed gearless outer-rotor one or a high-speed planetary-geared inner-rotor one.

Although the former one takes the advantage of gearless operation, its low-speed operation causes bulky size and heavy weight. On the other hand, although the latter one takes the merits of reduced overall size and weight, the planetary gear inevitably involves transmission loss, acoustic noise, and regular lubrication. Magnetic gearing is becoming attractive since it offers the advantages of high efficiency, reduced acoustic noise, and maintenance free [53]. By artfully integrating the magnetic gear into a motor drive, the low-speed requirement for direct driving and the high-speed requirement for machine design can be achieved simultaneously [54]. Figure 25 shows the detailed configuration of a magnetic-geared in-wheel PM BLDC motor. The artfulness is the share of a common PM rotor, namely, the outer rotor of a PM BLDC motor and the inner-rotor of a concentrically arranged magnetic gear. The operating principle of this magnetic-geared PM BLDC drive is similar to that of a high-speed planetary-geared inner-rotor drive, but with the difference that this one is an outer-rotor drive. That is to say, the motoring operation is the same as the PM BLDC drives. First, the stator is fed by three-phase voltages, which are rated at 220 Hz, to achieve the rated speed of 4,400 r/min. Then, the magnetic gear steps down the rated speed to 600 r/min, which in turn boosts up the torque for direct driving. The torque transmission is based on the modulation of the air-gap flux density distributions along the radial and circumferential directions. The space harmonic is modulated by the 25 stationary steel pole pieces from three pole pairs in the inner air-gap to 22 pole pairs in the outer air-gap. Hence, the torque in the outer rotor can be significantly amplified to about seven times that of the inner-rotor.

ISG Systems

In conventional automobiles, the starter motor and generator are separately coupled with the ICE, hence providing high starting torque for cold cranking and

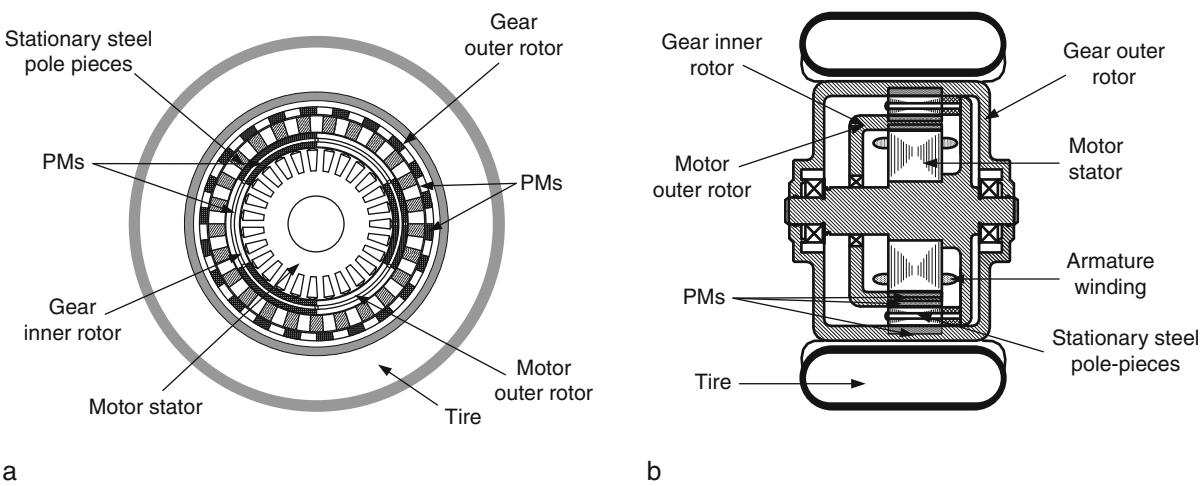

Vehicle Traction Motors. Figure 25
Magnetic-geared in-wheel motor drive. (**a**) Elevation view; (**b**) Side view

generating electricity for battery charging, respectively. This arrangement takes the advantage of simplicity but suffers from the poor utilization of both machines, hence resulting in heavy weight and bulky size. In order to incorporate both functions in a single unit, the development of integrated starter-generator (ISG) systems is accelerating.

By incorporating the inherent merits of PM brushless machines into the ISG, the resulting PM brushless ISG system is attractive for the latest micro- and mild HEVs. The stator doubly fed DSPM brushless machine [55] is a particular type of the aforementioned PM hybrid brushless machine topologies, which is promising for application to the ISG system. Its configuration is shown in Fig. 26, in which there are two magnetic field excitations, namely, the PMs and the DC field windings, air bridges in shunt with the PMs in the inner stator, AC armature windings in the salient-pole outer stator, and the salient-pole outer rotor with no PMs or windings.

This stator doubly fed DSPM brushless ISG system offers several distinct advantages:

1. The DC field current can be bidirectionally controlled to strengthen and weaken the air-gap flux density, hence offering high starting torque for cold cranking and constant output voltage over a wide speed range for battery charging. Meanwhile, the air bridge amplifies the effect of flux weakening.
2. The outer-rotor topology can fully utilize the space of the inner stator to accommodate the PMs and the DC field windings, hence reducing the overall size of the machine.
3. Since the outer rotor does not involve any windings or PMs, it can provide high mechanical integrity which is essential to handle the high starting torque during cold cranking.
4. Since the stator adopts fractional-slot concentrated windings, it can effectively reduce the cogging torque which usually occurs in the PM BLDC machines. In addition, it can shorten the length of end windings, hence saving the copper material and improving the power density.

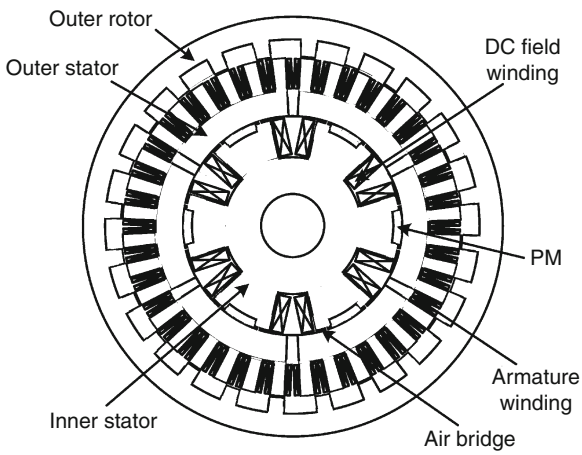

Vehicle Traction Motors. Figure 26
ISG system based on a stator doubly fed DSPM machine

Memory Brushless Machine Topologies

Although the DC field winding in PM hybrid motors enables the air-gap flux controllable, the use of DC field current inevitably causes additional power loss and degrades the efficiency. Hence, a new class of flux controllable PM machines, namely, the memory brushless machine was advent, which has the distinct ability to change the intensity of magnetization and also memorize the flux-density level in the PMs [56]. Figure 28 shows the topologies of memory brushless machines. In Fig. 27(a), it consists of aluminum nickel cobalt (AlNiCo) PMs sandwiched by soft iron, which are then mechanically fixed to a nonmagnetic shaft. The online magnetization is achieved by properly applying a short DC current pulse flowing through the stator armature winding to change the magnetization level of the AlNiCo PMs in the rotor. Figure 27(b) is a memory DSPM motor that adopts two-layer inner stator and outer rotor. In the stator, the armature windings are located in the outer layer, while both the PMs and magnetizing windings are placed in the inner layer, hence achieving a compact structure. Since the outer rotor is simply composed of salient poles without PMs or windings, it is very robust. The PM material used in the motor is an AlNiCo alloy [57]. Due to its direct magnetization of PMs by a temporary current pulse in the magnetizing windings, the flux control is highly effective and highly efficienct.

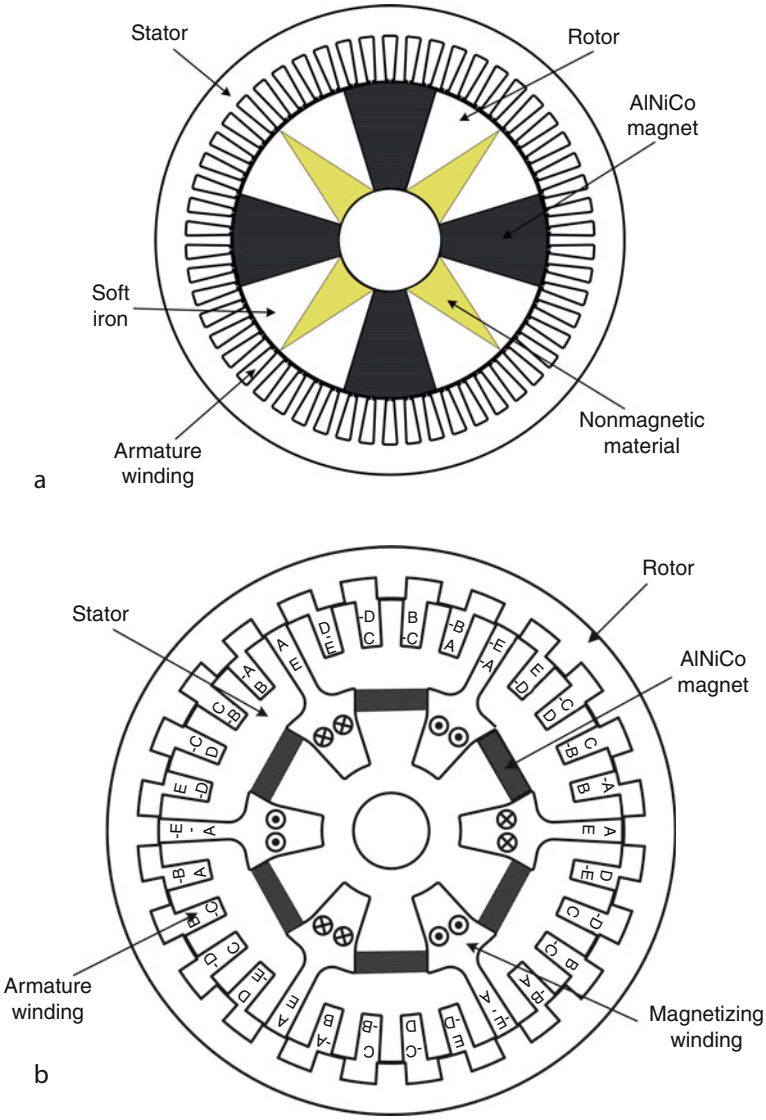

Vehicle Traction Motors. Figure 27
Memory brushless machines. (**a**) Rotor-PM; (**b**) Stator-PM

Transverse Flux Machine

PM transverse flux machine (TFM) [58, 59] is claimed to exhibit a higher torque density compared to the induction motor, SR motor, PM BLDC motor, and normal PM synchronous motor. In the TFM, the flux enters segments of stator core in transverse, i.e., perpendicular to the direction of rotor movement in the cross section plane, therefore, it is called transverse flux machine. The TFM stator iron core has two basic structures: (1) U-shape poles which have both teeth in the same axial plane and (2) claw-poles. Figure 28 shows the schematic configurations of the TFM. For each phase, a toroidal winding is placed inside the stator teeth or poles. Generally, TFMs have a relatively large number of poles, all of which interact with the total ampere-conductors of each phase. This enables very high electric loadings and, hence, high-torque densities to be achieved. Hence, it is especially suited

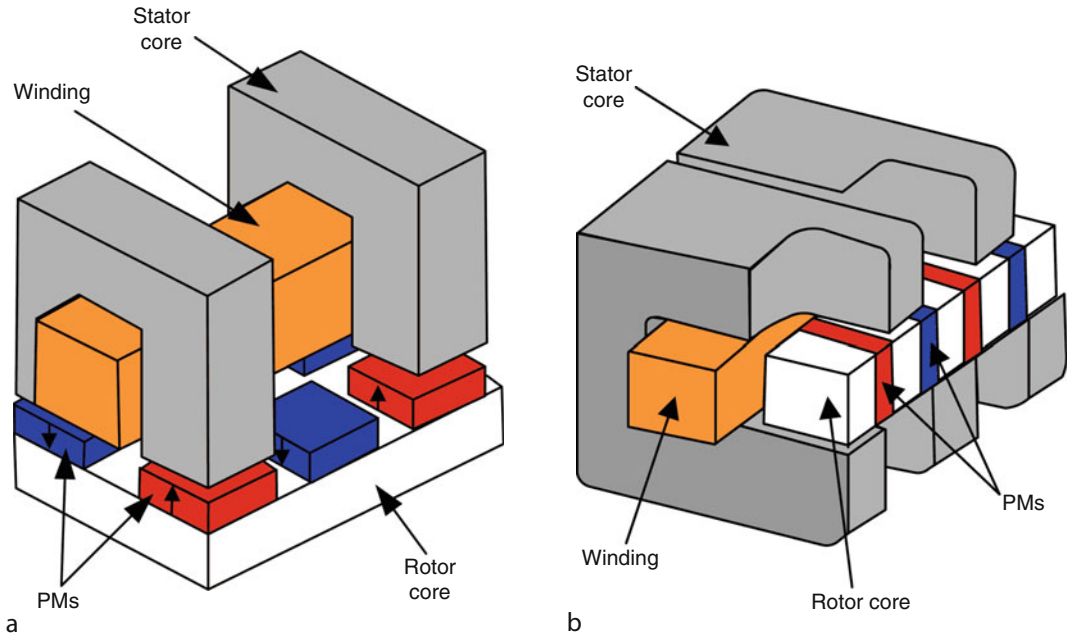

Vehicle Traction Motors. Figure 28
PM transverse flux motor. (**a**) Surface PMs; (**b**) Flux concentrated PMs

for in-wheel direct drive. However, they have a significant leakage flux and a relatively high winding inductance, as well as a poor power factor. This impacts significantly on the associated VA rating of the power electronics converter.

Bibliography

Primary Literature

1. Chan CC, Chau KT (2001) Modern electric vehicle technology. Oxford University Press, Oxford, UK
2. Zhu ZQ, Howe D (2007) Electrical machines and drives for electric, hybrid, and fuel cell vehicles. Proc IEEE 95:746–765
3. Chau KT, Chan CC, Liu C (2008) Overview of permanent-magnet brushless drives for electric and hybrid electric vehicles. IEEE Trans Ind Electron 55:2246–2257
4. Fuhs A (2008) Hybrid vehicles and the future of personal transportation. CRC, Boca Raton
5. Xu W, Zhu J, Guo Y et al (2009) Survey on electrical machines in electrical vehicles. In: IEEE international conference on applied superconductivity and electromagnetic devices, Chengdu, 25–27 Sept 2009, pp 167–170
6. Yamada K, Watanabe K, Kodama T et al (1996) An efficiency maximizing induction motor drive system for transmission less electric vehicle. In: Proceeding the 13th international electric vehicle symposium, Osaka, vol II, pp 529–536
7. Jiang SZ, Chau KT, Chan CC (2002) Performance analysis of a new dual-inverter pole-changing induction motor drive for electric vehicles. Electr Power Compon Syst 30:11–29
8. Jiang SZ, Chau KT, Chan CC (2003) Spectral analysis of a new six-phase pole-changing induction motor drive for electric vehicles. IEEE Trans Ind Electron 50(1):123–131
9. Chan CC, Chau KT (1996) An advanced permanent magnet motor drive system for battery-powered electric vehicles. IEEE Trans Veh Technol 45:180–188
10. Chan CC, Chau KT, Jiang JZ et al (1996) Novel permanent magnet motor drives for electric vehicles. IEEE Trans Ind Electron 43:331–339
11. Chan CC, Jiang JZ, Xia W, Chau KT (1995) Novel wide range speed control of permanent magnet brushless motor drives. IEEE Trans Power Electron 10:539–546
12. Cheng M, Hua W, Zhang J, Zhao W (2011) Overview of stator-permanent magnet brushless machines. IEEE Trans Ind Electron. doi:10.1109/TIE.2011.2123853
13. Liao Y, Liang F, Lipo TA (1995) A novel permanent magnet machine with doubly salient structure. IEEE Trans Ind Appl 3(5):1069–1078
14. Cheng M, Chau KT, Chan CC (2001) Static characteristics of a new doubly salient permanent magnet motor. IEEE Trans Energy Convers 16(1):20–25
15. Deodhar RP, Andersson S, Boldea I, Miller TJE (1996) The flux-reversal machine: a new blushless doubly-salient permanent-magnet machine. In: Proceedings of the IEEE IAS Annual Conference. San Diego, 6–10 Oct 1996, pp 786–793

16. Kim TH, Jang KB, Chun YD et al (2005) Comparison of the characteristics of a flux reversal machine under the different driving methods. IEEE Trans Magn 41(5):1916–1919
17. Hoang E, Ben-Ahmed AH, Lucidarme J (1997) Switching flux permanent magnet polyphased machines. In: Proc. Eur. Conf. Power Electron. Appl., Trondheim, pp 903–908
18. Hua W, Cheng M, Zhu ZQ et al (2008) Analysis and optimization of back EMF waveform of a flux-switching permanent magnet motor. IEEE Trans Energy Convers 23(3):727–733
19. Zhu ZQ, Chen JT (2010) Advanced flux-switching permanent magnet brushless machines. IEEE Trans Magn 46(6): 1447–1453
20. Hua W, Zhu ZQ, Cheng M et al (2005) Comparison of flux-switching and doubly-salient permanent magnet brushless machines. In: Proc. Int. Conf. electrical machines and systems, Nanjing, pp 165–170
21. Zhu X, Cheng M (2010) Design, analysis and control of hybrid excited doubly salient stator-permanent-magnet motor. Sci China Tech Sci 53(1):188–199
22. Chan CC, Jiang Q, Zhou E (1995) A new method of dimension optimization of switched reluctance motors. In: Proceedings of Chinese international conference on electrical machines, Hangzhou, pp 1004–1009
23. Chan CC, Jiang Q, Zhan YJ, Chau KT (1996) A high-performance switched reluctance drive for P-star EV project. In: Proceedings of 13th international electric vehicle symposium, Osaka, vol II, pp 78–83
24. Zhan YJ, Chan CC, Chau KT (1999) A novel sliding-mode observer for indirect position sensing of switched reluctance motor drives. IEEE Trans Ind Electron 46:390–397
25. Krishnan R (1996) Review of flux-weakening in high performance vector controlled induction motor drives. In: Proc. IEEE Int. Symp. Industrial Electronics, Warsaw, pp 917–922
26. Miller JM, Gale AR, McCleer PJ et al (1998) Starter/alternator for hybrid electric vehicle: comparison of induction and variable reluctance machines and drives. In: Proceedings of the industry applications Society Annual Meeting, Oct 1998, St Louis, pp 513–523
27. Zhu X, Cheng M, Zhao W et al (2007) A transient co-simulation approach to performance analysis of hybrid excited doubly salient machine considering indirect field-circuit coupling. IEEE Trans Magn 43(6):2558–2560
28. Zhao W, Cheng M, Zhu X et al (2008) Analysis of fault tolerant performance of a doubly salient permanent magnet motor drive using transient co-simulation method. IEEE Trans Ind Electron 55(4):1739–1748
29. Bose BK (1992) Modern power electronics: evolution, technology, and applications. IEEE, New York
30. Chan CC, Chau KT, Chan DTW, Yao JM (1997) Soft switching inverters in electric vehicle. In: Proceedings of the 14th international electric vehicle symposium, CD-ROM, Orlando
31. Lai JS (1997) Resonant snubber-based soft-switching inverters for electric propulsion drives. IEEE Trans Ind Electron 44:71–80
32. Murai Y, Cheng J, Yoshida MA (1997) Soft-switched reluctance motor drives circuit with improved performances. In: Proc of IEEE power electronics specialists conference, 22–27 June 1997, St Louis, pp 881–886
33. Chau KT, Ching TW, Chan CC, Chan DTW (1997) A novel two-quadrant zero-voltage transition converter for DC motor drives. In: Proceedings of IEEE international conference on industrial electronics, New Orleans, pp 517–522
34. Divan DM (1986) The resonant DC link converter – a new concept in static power conversion. In: Proceedings of IEEE industry application society annual meeting, Denver, pp 648–656
35. Cho JG, Kim WH, Rim GH, Cho KY (1997) Novel zero transition PWM converter for switched reluctance motor drives. In: Proceedings of IEEE power electronics specialists conference, St Louis, pp 887–891
36. Ching TW, Chau KT, Chan CC (1998) A new zero-voltage-transition converter for switched reluctance motor drives. In: Proceedings of IEEE power electronics specialists conference, Fukuoka, pp 1295–1301
37. Rahman MF, Haque ME, Tang L, Zhong L (2004) Problems associated with the direct torque control of an interior permanent-magnet synchronous motor drive and their remedies. IEEE Trans Ind Electron 51(4):799–809
38. Pascas M, Weber J (2005) Predictive direct torque control for the PMsynchronous machine. IEEE Trans Ind Electron 52(5):1350–1356
39. Cavallaro C, Tommaso AOD, Miceli R et al (2005) Efficiency enhancement of permanent-magnet synchronous motor drives by online loss minimization approaches. IEEE Trans Ind Electron 52(4):1153–1160
40. Shu Y, Cheng M, Kong X (2008) Online efficiency optimization of stator-doubly-fed doubly salient motor based on a loss model. In: Proceedings of 11th international conference on electrical machines and systems, Wuhan, pp 1174–1178
41. Cheng M, Sun Q, Zhou E (2006) New self-tuning fuzzy PI control of a novel doubly salient permanent-magnet motor drive. IEEE Trans Ind Electron 53(3):814–821
42. Pajchrowski T, Zawirski K (2007) Application of artificial neural network to robust speed control of servo drive. IEEE Trans Ind Electron 54(1):200–207
43. Acarnley PP, Watson JF (2006) Review of position-sensorless operation of brushless permanent-magnet machines. IEEE Trans Ind Electron 53(2):352–362
44. Silva C, Asher GM, Sumner M (2006) Hybrid rotor position observer for wide speed-range sensorless PM motor drives including zero speed. IEEE Trans Ind Electron 53(2): 373–378
45. Angelo CD, Bossio G, Solsona J et al (2006) Mechanical sensorless speed control of permanent-magnet AC motors driving an unknown load. IEEE Trans Ind Electron 53(2):406–414
46. Emadi A, Young Joo L, Rajashekara K (2008) Power electronics and motor drives in electric, hybrid electric, and plug-in hybrid electric vehicles. IEEE Trans Ind Electron 55(6):2237–2245
47. U.S. Department of Energy (2007) Plug-in hybrid electric vehicle R&D plan. http://www1.eere.energy.gov/vehiclesandfuels/pdfs/program/phev_rd_plan_june_2007.pdf

48. Mecrow BC, Jack AG, Haylock JA, Coles J (1996) Fault-tolerant permanent magnet machine drives. IEEE Proc Electric Power Appl 143(6):437–442
49. Akita H, Nakahara Y, Miyake N, Oikawa T (2003) New core structure and manufacturing method for high efficiency of permanent magnet motors. In: Conference record of IEEE IAS annual meeting, Amagasaki, 12–16 Oct 2003, pp 367–372
50. Miller JM (2006) Hybrid electric vehicle propulsion system architectures of the e-CVT type. IEEE Trans Power Electron 21(3):756–767
51. Xu L, Zhang Y, Wen X (2007) Multi-operational modes and control strategies of dual mechanical port machine for hybrid electrical vehicles. In: Proceedings of the IEEE IAS Annual meeting, New Orleans, pp 1710–1717
52. Cheng Y, Cui S, Song L, Chan CC (2007) The study of the operation modes and control strategies of an advanced electromechanical converter for automobiles. IEEE Trans Magn 43(1):430–433
53. Atallah K, Howe D (2001) A novel high performance magnetic gear. IEEE Trans Magn 37(4):2844–2846
54. Chau KT, Zhang D, Jiang JZ, Liu C, Zhang Y (2007) Design of a magnetic-geared outer-rotor permanent-magnet brushless motor for electric vehicles. IEEE Trans Magn 43(6):2504–2506
55. Chau KT, Li YB, Jiang JZ, Liu C (2006) Design and analysis of a stator doubly fed doubly salient permanent magnet machine for automotive engines. IEEE Trans Magn 42(10):3470–3472
56. Ostovic V (2003) Memory motor. IEEE Ind Appl Mag 9(1):52–61
57. Yu C, Chau KT, Liu X et al (2008) A flux-mnemonic permanent magnet brushless motor for electric vehicles. J Appl Phys 103(07103):1–3
58. Henneberger G, Bork M (1997) Development of a new transverse flux motor. In: IEE Colloq. new topologies for permanent magnet machines, London, pp 1/1–1/6
59. Baserrah S, Orlik B (2009) Comparison study of permanent magnet transverse flux motors (PMTFMs) for in-wheel applications. In: Proceedings of the international conference on power electronics and drive systems, Taipei, pp 96–101

Books and Reviews

Chan CC (2002) The state of the art of electric and hybrid vehicles. Proc IEEE 90:247–275

Chan CC, Chau KT (1997) An overview of power electronics in electric vehicles. IEEE Trans Ind Electron 44:3–13

Chau KT, Ming C (2010) New drive technology for electric vehicles. China Machine, Beijing (In Chinese)

Ehsani M, Rahman KM, Toliyat HA (1997) Propulsion system design of electric and hybrid vehicles. IEEE Trans Ind Electron 44:19–27

Ehsani M, Gao Y, Gay SE, Emadi A (2005) Modern electric, hybrid electric, and fuel cell vehicles: fundamentals, theory, and design. CRC, Boca Raton

Husain I (2003) Electric and hybrid vehicles-deign fundamentals. CRC, Boca Raton

Rashid MH (2005) Modern electric, hybrid electric, and fuel cell vehicles: fundamentals, theory, and design. CRC, Boca Raton

Vehicular Ad Hoc Networks, Enhanced GPSR and Beacon-Assist Geographic Forwarding in

Ping Wang, Fuqiang Liu, Wenjie Shu, Wenqiang Xu
Department of Information and Communication Engineering, Tongji University, Shanghai, China

Article Outline

Glossary
Definition of the Subject
Introduction
Describing Enhanced GPSR Using Neighbor-Awareness Position Update and Beacon-Assist Geographic Forwarding
Survey of Different Strategies to Enhance GPSR
Future Directions
Bibliography

Glossary

BGF Beacon-Assist Geographic Forwarding, one of the approaches for enhanced GPSR in packet-forwarding strategy to enable nodes to forward packets by considering their neighbors' beacon interval in neighbor list.

Geographical routing A kind of routing protocol in VANET that uses geographic information to help complete packets delivery. This kind generally contains two parts: location server and packets forwarding.

GPSR The famous geographical routing protocol, named greedy perimeter stateless routing, uses greedy forwarding strategy to select a next hop and perimeter forwarding strategy to cope with routing failure caused by local minimum.

ITR Inaccuracy-Tolerant Range represents the inaccurate degree of location information.

Local minimum No neighbor exists which is closer to the destination than the intermediate node itself.

NUR Neighbor-Awareness position Update, one of the approaches for enhanced GPSR in beaconing to set the position update interval dynamically.

SDR The Successful Date Rate defines as the ratio of packets successfully delivered to the destination node to those generated by the sender.

VANET The VehiculAr NETwork is a special communication network comprising of radio-enabled vehicles and roadside units, including vehicle-to-vehicle communication and vehicle-to-roadside unit communication.

Definition of the Subject

In vehicular network (VANET), moving vehicles always have a high speed and a frequent change of their moving direction. These make the network topology highly dynamic. Because of the highly dynamic nature of the mobile nodes, finding and maintaining routes is very challenging in VANET.

GPSR is considered as a promising geographical routing protocol applicable for VANET. In order to cope with the problem of highly dynamic topology, it makes routing decisions at the intermediate nodes instead of building a constant route. Under this strategy, routing failure caused by nodes disconnection in constant routing approach can be efficiently mitigated. However, there are still some problems in GPSR. As in greedy forwarding strategy, the intermediate node always selects the next hop node that lies close to the relaying nodes' transmission range border; the selected one has high possibility to leave the transmission range because of the high speed node movement. GPSR does not take this into consideration. Another problem comes from the constant beacon interval strategy. Such principle may lead to high routing overhead and poor performance in various nodes density environment.

Introduction

Researches on routing protocol in VANET come from the bases of earlier researches on routing protocol in Mobile Ad hoc network (MANET). They share the characteristics of self-organization, self-management, low-bandwidth, and short radio transmission range. However, VANET differs from MANET by its highly dynamic topology. The traditional topology-based routing strategies in MANET, such as AODV (Ad hoc On-demand Distance Vector) and DSR (Dynamic Source Routing), are not approving enough to be used in VANET. These routing protocols are under the principle of building a constant route table and maintaining the pre-build route table. Due to the highly dynamic mobility, routing protocols under such principle are unable to quickly find, maintain, and update long routes in VANET. The route will become invalid if some intermediate nodes disconnected. Thus, frequent route recovery will make the whole performance inefficient. Take AODV for example. It has been tested in real-world experiments. Results show that packets are excessively lost due to route failures.

Vehicles are not only simply mobile nodes, but also they have characteristics of high speed, limited movement along roads, and capability to equip with GPS system. As GPS systems are widely used in vehicles now, the mobile nodes can easily get their position information. This trend brings a new type of routing protocol, geographical routing, or position-based routing, which uses the position information to help deliver packets. Position-based routings mainly content two parts: location server and forwarding strategy. Location server is responsible for providing location information of the destination nodes to the source nodes. After getting location information of the destination nodes, different kinds of forwarding strategies will be used at the intermediate nodes to make the forwarding decisions in order to select an appropriate next hop. As introduced above, one of the main characteristics of position-based routings is that they do not try to build a constant route table. In this way, it makes position-based routings more applicable to VANET with highly dynamic mobility. Researchers see position-based routing as a more promising approach and do researches on them.

GPSR is one of the most typical position-based routing protocols. It uses the positions of routers and a packet's destination to make packet forwarding decisions. It contains two modes of forwarding strategy: greedy forwarding mode and perimeter forwarding mode. GPSR makes greedy forwarding decisions using only information about a router's immediate neighbors in the network topology. When a packet reaches a region where greedy forwarding is impossible, the algorithm recovers by routing around the perimeter of the region. By keeping state only about the local topology, GPSR scales better in per-router state than shortest-path and topology-based routing protocols as the number of

network destinations increases. Under mobility's frequent topology changes, GPSR can use local topology information to find correct new routes quickly.

Although GPSR shows a much higher performance than the traditional topology-based routing protocols in VANET, it still has some drawbacks within its routing strategy. GPSR uses a fixed period beaconing mechanism to send HELLO messages. Such mechanisms may lead to several problems such as wasted bandwidth, delaying of data packet, and increased network congestion. As GPSR adopts greedy forwarding algorithm, in which the intermediate node always selects the next hop node that lies close to the relaying nodes' transmission range border. The selected route may be not stable enough for the chosen next hop nodes have a high possibility to move away from the relaying nodes. One more drawback comes from the perimeter forwarding strategy. GPSR lacks considering the usage of road topology that restricts nodes' movements. Under such perimeter approach, the select route path may be not the most efficient and shortest one.

Describing Enhanced GPSR Using Neighbor-Awareness Position Update and Beacon-Assist Geographic Forwarding

The enhanced GPSR is modified by the algorithm called GPSR-N&B. It includes two parts: Neighbor-Awareness position Update (NAU) and Beacon-Assist Geographic Forwarding (BGF). GPSR-N&B uses NAU to set the position update interval dynamically, according to the neighbors' number and position of the relaying nodes. And BGF strategy enables nodes to forward packets by considering their neighbors' beacon interval in neighbor list. This algorithm aims to reduce beacon overhead and medium access control (MAC) layer collisions in different densities and velocities of VANET, while ensuring the Successful Date Rate (SDR) performances well.

Neighbor-Awareness Position Update (NAU)

GPSR-N&B is based on the following assumptions (a) all links are bidirectional and (b) all nodes can easily get their current location information and velocity.

In VANET, a vehicle's movement has effect on its neighbors' movement. NAU adapts the beacon update intervals according to the number, position, and velocity of the nodes in the neighborhood. The Neighbor-Awareness position Update (T_i) is shown as follows:

$$T_i = \frac{1}{2} T_i' + \frac{1}{2} T_i''. \quad (1)$$

T_i' is affected by the neighbors' position, while T_i'' is affected by the number of neighbors.

1. T_i'

   In GPSR-N&G, an aspect of inaccuracy-tolerant range (ITR) is supposed to represent the inaccurate degree of location information that can be accepted. Intuitively, within maximum transmission range, the larger the distance between two nodes is and the more the probability the link may break, the shorter the beacon interval should be.

   Figure 1 demonstrates the inaccuracy-tolerant range around node A. For example, node E which is located between the maximum transmission range (250 m) and ITR threshold (240 m) will not forward packets from node A, because of the changeable environment and distance between them, which may often lead to link breakdown.

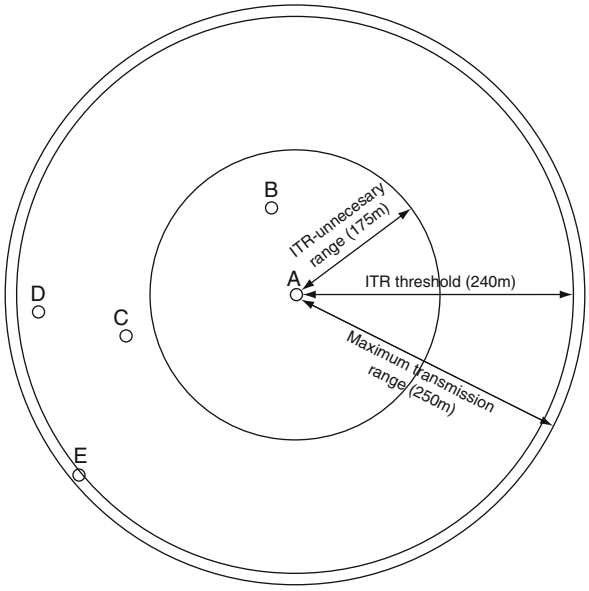

Vehicular Ad Hoc Networks, Enhanced GPSR and Beacon-Assist Geographic Forwarding in. Figure 1 Inaccuracy-tolerant range

As node D is within the range of 200–240 m, ITR equals to 240-d, where d is the distance between nodes A and D: $d = \sqrt{(x_A - x_D)^2 + (y_A - y_D)^2}$. The relative beacon interval time T_{AD} will be set to be $\text{Max}\left[\frac{(240-d)T_{\text{MINbeacon}}}{240-175}, T_{\text{MINbeacon}}\right]$.

As node B is within the range of 175 m, the default beacon interval $T_{\text{MINbeacon}}$ is then used as T_{AB}, instead of calculating the effect of ITR.

In Fig. 2, node A and B are neighbors. After considering A and B, a relative beacon interval T_{AB} will be got as well as T_{AC} and T_{AD} in a similar way. Then T'_A can be set as:

$$T'_A = \frac{T_{AB} + T_{AC} + T_{AD}}{3}. \tag{2}$$

Then, $T'_i = \frac{\sum_{j=2}^{k} T_{ij}}{K}$, where K is the number of node i's neighbors.

2. T''_i

T''_i is set as $T''_i = wK$, in which w is computed in simulation test. Finally, node i's new beacon interval is shown in Eq. 3:

$$T_i = \frac{1}{2}\frac{\sum_{j=2}^{k} T_{ij}}{K} + \frac{1}{2}wK \tag{3}$$

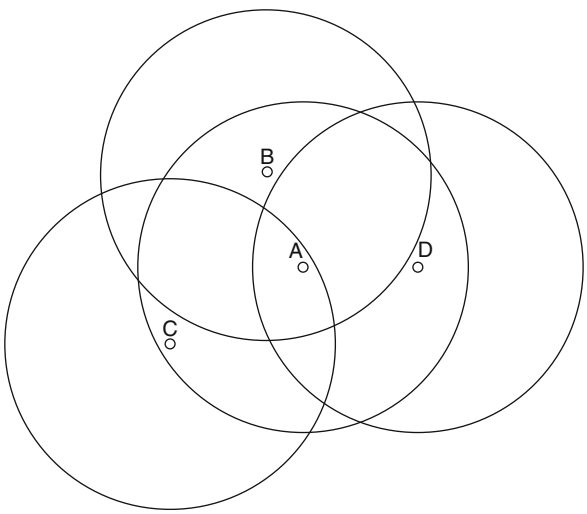

Vehicular Ad Hoc Networks, Enhanced GPSR and Beacon-Assist Geographic Forwarding in. Figure 2 Neighbor-awareness position update

Upon initialization, each node broadcasts a beacon informing its neighbors about its current location (x_i, y_i) and velocity (v_{xi}, v_{yi}) using default beacon interval $T_{\text{DEFbeacon}}$, which is set to $\frac{175}{V_{\text{MAX}}}$ in the following simulation. Here, V_{MAX} is the maximum node velocity.

After initialization, each node replaces its own beacon interval by T_i.

Beacon-Assist Geographic Forwarding (BGF)

In NAU, the way to set position update time is based on the change of relative distance, instead of change of position. The neighbor list is changed by using relative distance in x and y directions, instead of the position as Table 1 shows.

In Table 1, X-Distance and Y-Distance are the distance between current node and its neighbor in x direction and y direction. V_x and V_y are the relative velocity of current node and its neighbor in x direction and y direction. T_{beacon} is the neighbor's beacon interval time.

As in NAU, each neighbor's T_{beacon} includes the topology information in its vicinity. So the neighbors' T_{beacon} can be used as the topology information of the next hop in choosing the efficient forwarding node. In BGF, a routing metric is defined which depends on (a) relative distance and (b) T_{beacon} as follows:

$$M_j(l_j, T_{j\text{beacon}}) = \alpha g(l_j) + \beta h(T_{j\text{beacon}}) \tag{4}$$

$$g(l_j) = \exp(-(l_j - l_i)) \tag{5}$$

$$h(T_{j\text{beacon}}) = \exp\left(-(T_{j\text{beacon}} - T_{\text{DEFbeacon}})\right) \tag{6}$$

Here α and β are the weights to distance and T_{beacon}. l_i is the distance between the destination and node i. l_j is

Vehicular Ad Hoc Networks, Enhanced GPSR and Beacon-Assist Geographic Forwarding in. Table 1 Node A's neighbor list

	X-distance	Y-distance	V_x	V_y	*Tbeacon*
B	−50	210	10	15	2
C	−202	−45	−20	5	3
–	–	–	–	–	–

the distance between the destination and node j in node i's neighborhood, and $T_{j\text{beacon}}$ is node j's beacon interval.

Simulation Results

Performance of GPSR-N&B is evaluated by simulation varying the beacon interval, the maximum speed of mobile nodes and the network density for freeway models. NS-2 is used to estimate the effect of inaccurate location information with different beacon intervals, speeds, and densities on GPSR, which has been proven to perform efficiently with accurate location information.

1. Set w in T_i''
   In the simulation, w of 1/5,2/5,3/5,4/5,5/5 is tested in different number of nodes (20,40,60). In Fig. 3, w equaling to 3/5 outperforms the others in terms of the SDR. As a result, in following simulation, w is set to 3/5.
2. Results and Analysis
   The results represented here are averaged over ten runs, each using a different random seed. Nodes are randomly placed over a 1,000*50 m^2 freeway created by sumo and move.

Performance of various beacon intervals (0.5, 1, 2, 4, 8) is compared as well as GPSR-N&B by varying maximum moving speed (10, 20, 30 m/s) and different number of nodes (20, 40, 60). Each simulation lasts 100 simulation seconds. The size of data packets is 32 bytes. Five random source–destination pairs, using CBR as the traffic flows and lasting about 20 s, are selected. Different aspects of the performance of the routing protocol are evaluated using the following metrics:

Successful date rate (SDR): The ratio of packets successfully delivered to the destination node to those generated by the sender.

Routing overhead: The total number of beacon packets transmitted.

Number of MAC layer collisions: The number of collisions in MAC layer due to the beacon packets.

Figure 4a, b, and c illustrates that GPSR-N&B outperforms from GPSR with fixed beacon interval with various numbers of nodes and maximum node speed. GPSR with fixed beacon interval results in low SDR, and cannot cope with the topology change with high mobility.

Firstly PSR-N&B controls the routing overhead and decreases the MAC layer collisions to leave more channel resource for the CBR packets which will be discussed later. Secondly, GPSR-N&B using BGF makes use of the beacon intervals of neighbors for estimating the next hop topology, which makes the greedy forwarding more stable and efficient. The greedy forwarding is extended to two-hop area.

Figure 5a, b, and c shows that the routing overhead of GPSR-N&B is very low in all the simulations. The most important thing is that routing overhead of GPSR-N&B does not increase a lot with the increasing density of nodes, so GPSR-N&B fits the large number of nodes. In NAU, the node beacon interval is set according to the number of neighbors.

GPSR-N&B makes lower MAC layer collisions as shown in Fig. 6a, b, and c, due to the different beacon intervals of nodes in the network compared with GPSR using fixed beacon intervals. The overhead packets in high-density neighbor area are less than in low-density neighbor area due to the addition of T″ in NAU.

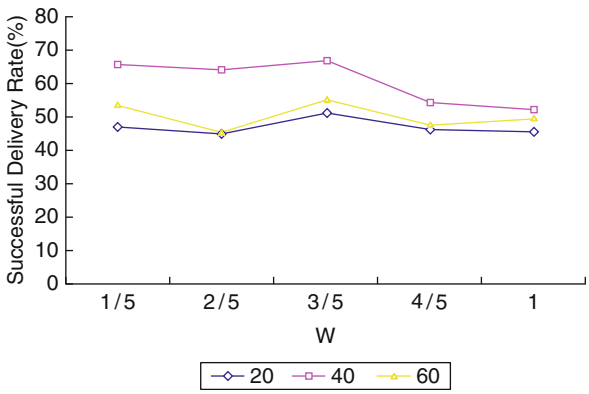

Vehicular Ad Hoc Networks, Enhanced GPSR and Beacon-Assist Geographic Forwarding in. Figure 3
SDR of different w

Survey of Different Strategies to Enhance GPSR

GPSR does not take cars' mobility characteristics into consideration which limits the performance in VANET. The movement of nodes is assumed to be arbitrary in MANET while bound to a street in VANET. It makes sense that many researchers are going to exploit the different characteristics to increase packet-forwarding

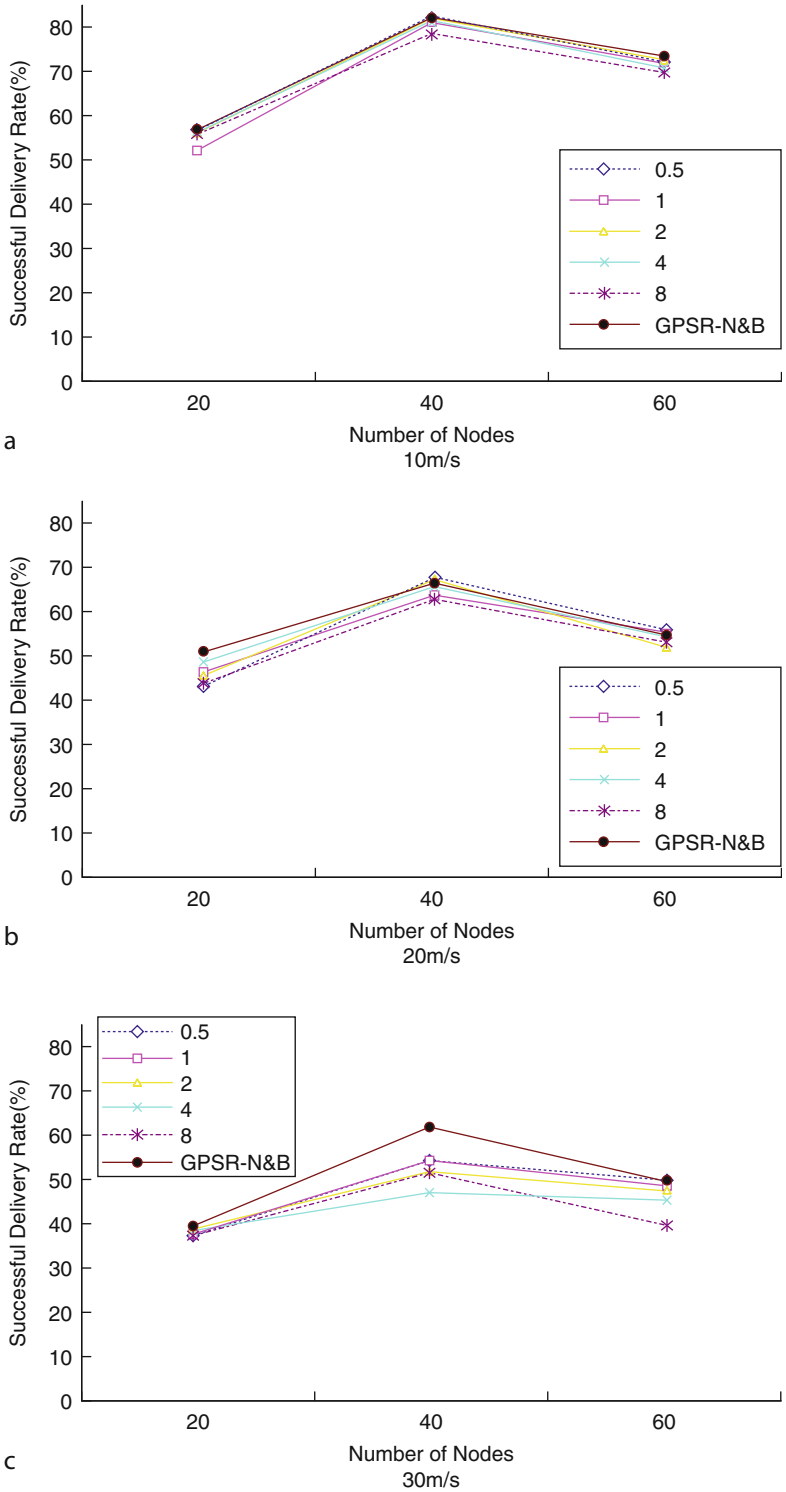

Vehicular Ad Hoc Networks, Enhanced GPSR and Beacon-Assist Geographic Forwarding in. Figure 4
SDR varying maximum node speed

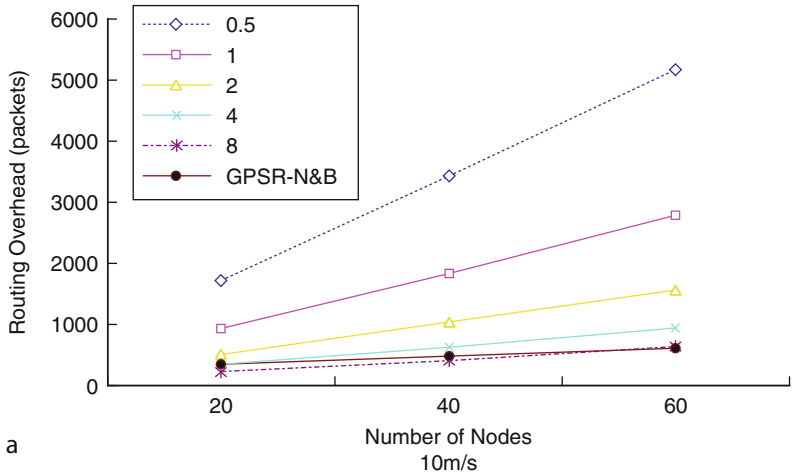

a

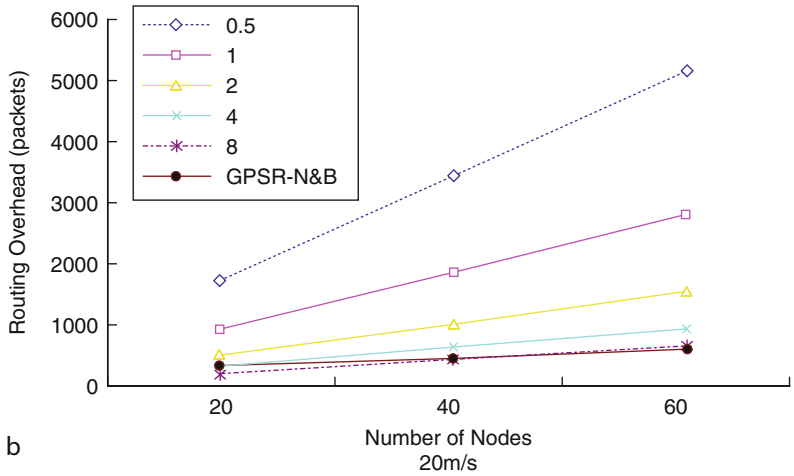

b

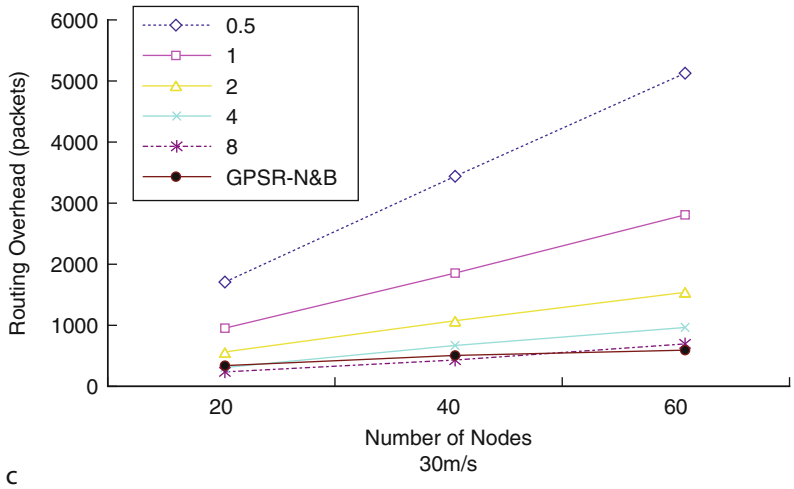

c

Vehicular Ad Hoc Networks, Enhanced GPSR and Beacon-Assist Geographic Forwarding in. Figure 5
Routing overhead varying maximum node speed

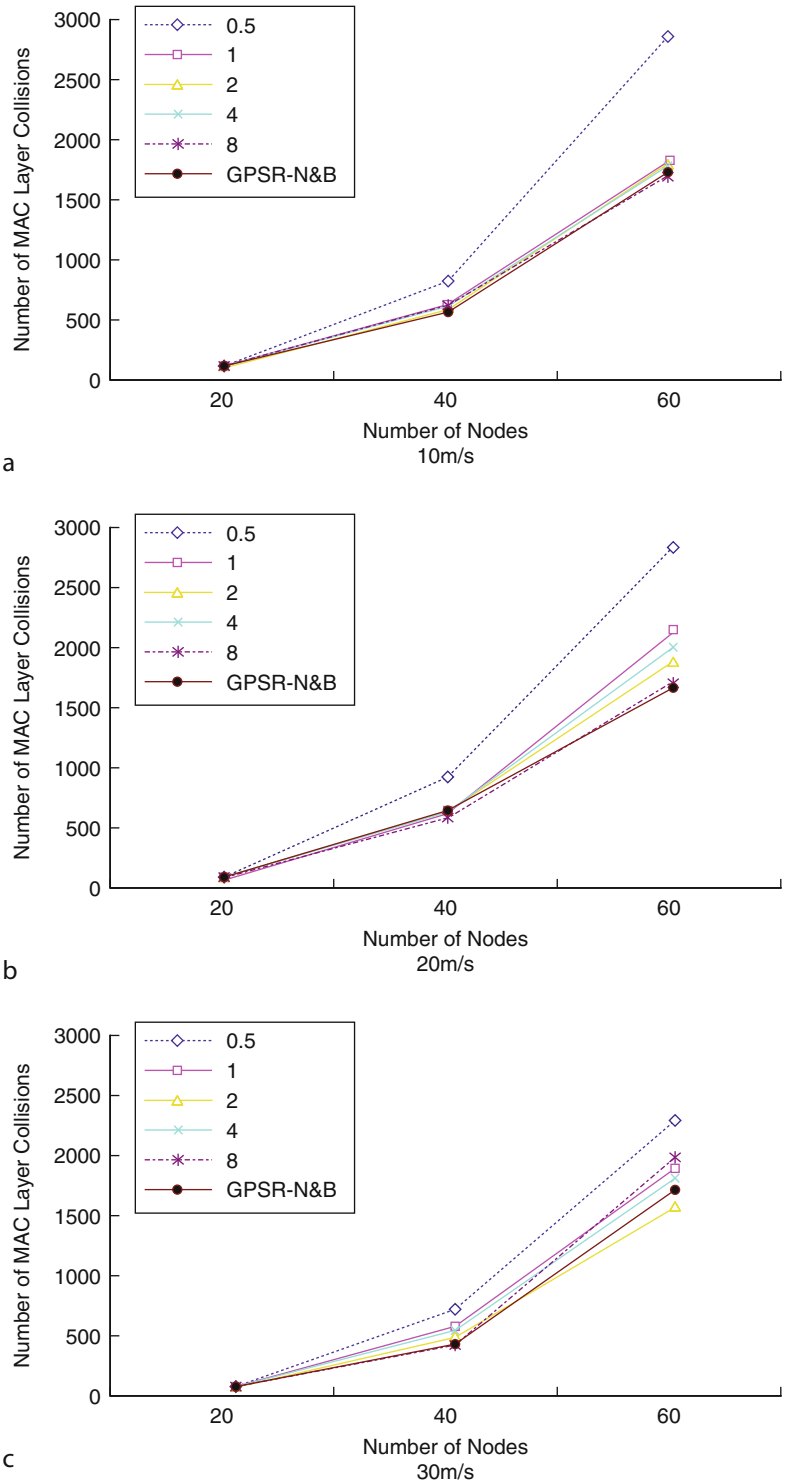

Vehicular Ad Hoc Networks, Enhanced GPSR and Beacon-Assist Geographic Forwarding in. Figure 6
Number of MAC layer collisions varying maximum node speed

performance. Going from simple to complex, scenarios of cars movement can be classified as highway and city scenario.

Considering these characteristics in highway and city scenario, which will be discussed in following sections, researchers have developed other approaches to improve the routing performance in VANET compared with GPSR.

Strategies of Enhancement in Highway Scenario

Definition of the Subject In highway scenario, cars may move in different directions or in different lanes, but the main extent of movement is along the road, not across, which makes the movement one dimensional. This makes packet forwarding fairly easy but much sensitive to speed because cars may move in highway very fast.

Advanced Greedy Forwarding (AGF)

V. Naumov, R. Baumann, and T. Gross in [1] proposed the Advanced Greedy Forwarding (AGF) algorithm to significantly improve GPSR performance in VANETs.

Both the source and the destination nodes inform each other with the help of the location discovery service (e.g., reactive location service [2]) about their moving directions and speeds – velocity vectors. Velocity vector information is also added into HELLO beacons of all nodes. Velocity vector requires two additional bytes to store the information about nodes' speed and direction. The first byte encodes the direction in the range of 0–127. The second byte stores the speed in km/h (enough for representing the allowed maximum speed in most countries).

Also the information about the packet travel time is added in a data packet header. Every node forwarding a data packet adds its own processing time into packet header. A next hop node is chosen based on the velocity vectors information stored in the neighbor tables.

A node receiving a data packet checks if the destination is listed in its neighbor table and the entry is still valid, taking into account the packet travel time and the node's and the destination's velocity vectors. If this is the case, the node sends the packet directly to the destination. If the destination is in the neighbor table, but the new position estimation tells that the destination is most likely already out of the range, then the node closest to the new position of the destination is chosen as a next hop.

If no destination is found in the neighbor table, the node consults the packet travel time and estimates whether it may potentially reach the position of the destination recorded in the packet header within one hop, taking into account a distance potentially traveled by the destination node within the packet travel time. If yes, the non-propagating broadcast is sent around, with the search for the destination. If no answer is received (either from the destination or the node that has the destination in its table and is closer to the destination than the current node), then the next closest to the destination node is chosen, and the process repeats.

Movement Prediction–Based Routing

This routing concept, based on vehicles movement prediction, estimates the stability of each communication link in the network in terms of communication lifetime, and then selects the most stable route composed by the most stable intermediate links from the source till the destination. This concept can be applied to position-based routing protocols and has been implemented with GPSR under the network simulator NS2. By this way, GPSR's performance is improved.

Movement Prediction-Based Routing (MOPR) [3] determines the most stable path from a source to a destination in terms of communication lifetime by selecting the most stable intermediate links, then, the best intermediate vehicles. For example, assuming there is a network protocol which is capable to provide several unicast paths to a destination, one of those paths can result to be more stable with respect to the others. A stable path can increase the probability that link failures will be avoided during the whole communication. MOPR, based on vehicles' movement information, guarantees the selection of the best next hop for data forwarding. Using MOPR, each vehicle estimates the Link Stability (LS) for each neighboring vehicle before selecting the next hop for the data forwarding/sending. The LS is a relation between the link communication lifetime and a constant value (σ) which represents in general cases the routing route validity time, and it depends on the used routing protocol. Figure 7 shows how link lifetimes are estimated based on neighbors' movement information.

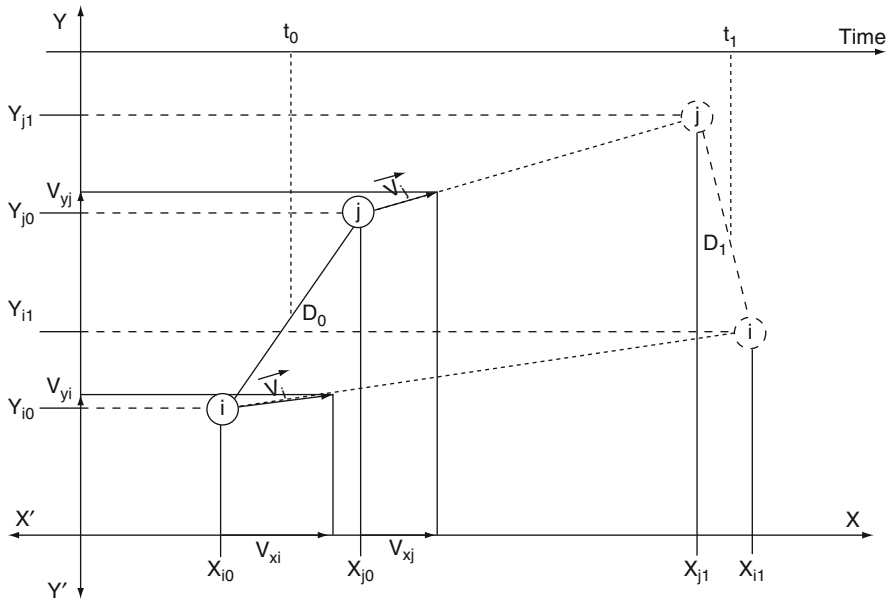

Vehicular Ad Hoc Networks, Enhanced GPSR and Beacon-Assist Geographic Forwarding in. Figure 7 Link lifetime estimation

The lifetime of the link (i, j) (LifeTime$[i,j]$) corresponds to the estimated time $\Delta t = t_1 - t_0$ with t_1 is the time when D_1 becomes equal or bigger than the communication range R (i.e., the time when j goes out of the communication rage of i). D_1 and Δt are estimated using the initial positions of i and j ((X_{j0}, Y_{j0}), and their initial speeds $\bar{V}_j$ and $\bar{V}_j$, respectively):

$$D_1^2 = ((X_{i0} + Vx_i\Delta t) - (X_{j0} + Vx_j\Delta t))^2 + ((Y_{i0} + Vy_i\Delta t) - (Y_{j0} + Vy_j\Delta t))^2$$

$$D_1^2 = A\Delta t^2 + B\Delta t + C$$

$$\text{with}\begin{cases} A = (Vx_i - Vx_j)^2 + (Vy_i - Vy_j)^2 \\ B = 2[(X_{i0} - Y_{j0})(Vx_i - Vx_i) \\ \qquad + (X_{i0} - Y_{j0})(Vy_i - Vy_i)] \\ C = (X_{i0} - X_{j0})^2 + (Y_{i0} - Y_{j0})^2 \end{cases}$$

By solving the equation $A\Delta t^2 + B\Delta t + C - R^2 = 0$ it is easy to get Δt which corresponds to the LifeTime$[i,j]$. LS is calculated as follows:

$$LS[i,j] = \frac{\text{Life Time}[i,j]}{\sigma}, \text{ with } LS[i,j] = 1 \text{ when Life Time } [i,j] \geq \sigma$$

Once LS is calculated for each neighboring vehicle, MOPR selects as a next hop for data forwarding/sending the one corresponding to the highest LS (corresponding to the most stable neighboring link).

This approach should help as well in minimizing the risk of broken links and in reducing data loss and link-layer and transport retransmissions.

F. Granelli et al. have proposed a Movement-Based Routing Algorithm (MORA) [4] for vehicular ad hoc networks. It is applied to GPSR. MORA takes into account the physical location of neighboring vehicles and their movement direction when selecting the next hop for sending/forwarding packets. MOPR believes that considering only the position and the movement direction is not enough for a best next hop selection in VANETs. The vehicle's driving speed is important and should be taken into account as well. A vehicle which is almost out of communication range should not be selected as a next hop, which cannot be guaranteed without taking into account the speed. Thus, with MOPR, a vehicle which is estimated to go out of communication range in a short duration will not be selected as a next hop for data routing if a better candidate is available.

To show the performance improvements of MOPR over position-based routing protocols, it is applied over GPSR. It is not suitable to apply MOPR to GPSR as it is done to unicast routing [3, 5], where MOPR tries to select the path with the longest lifetime. When applying MOPR to GPSR as it is, the selected paths should be same or longer in terms of number of hops when compared to basic GPSR. And the calculation of neighboring links' LS before sending/forwarding each packet takes a considerable time. All this decreases the routing performances. To face this problem, MOPR is applied in a different way. When a vehicle wants to send or forward data, it first estimates the future geographic location after a duration time T in seconds for each neighbor. T is counted in seconds, and it is fixed to 1 s in the simulations. Then, it selects as next hop the closest neighbor to the destination which does not have a future location out of its communication rage after the time T.

By doing this, MOPR-GPSR avoids the case when a next hop goes out of communication range during a data packet transmission, thus, decreasing data loss and link-layer and transport retransmissions, which increases the routing performances.

To evaluate the performances of MOPR over position-based routing protocols, it is implemented on top of GPSR, named MOPR-GPSR. A Hierarchical Location Service (HLS) is used to provide the exact position information of the neighboring and the destination vehicles. More information on HLS is given in [6].

The simulations use a 5,000 m length highway scenario, with 200 vehicles moving on it as shown in Fig. 8. In each direction, there are three lanes with different speed ranges starting from a minimum speed value of 70 km/h and a maximum speed value which is increased from 120 to 220 km/h. In each direction there is a density of five vehicles every 150 m. The classical 802.11 Medium Access Control (MAC) functionalities are used. Traffic type was CBR with 1,024 Bytes of packet size and a 512 bps of maximum CBR rate. A transmitting source and a destination vehicle are selected randomly along the middle lane (normal vehicles' lane) in each direction.

Figure 9 shows the Packet Delivery Ratio (PDR) obtained for each routing protocol as function of vehicles' maximum speed. It is clearly shown that both MOPR and MORA guarantee a better PDR when compared to basic GPSR. As shown, higher the vehicles' maximum speed, higher the PDR of MOPR when compared to MORA. This means that MOPR guarantees the best PDR when speed is higher.

Figure 10 shows the delay for each routing protocol as a function of vehicles' maximum speed. MOPR improves the delay by at least two times when compared to both basic GPSR and MORA.

Figure 11 shows the routing overhead as a function of vehicles' maximum speed. MOPR decreases the routing overhead when compared to basic GPSR, but MORA decreases the routing overhead more. That means that MORA is the best in terms of routing overhead. But, in Fig. 12 the Hierarchical Location Service (HLS) overhead caused in the network which should be taken into account to evaluate the real performance of this routing protocol in terms of routing overhead. And it is clearly shown that MOPR is the best in terms of HLS overhead when compared to both basic GPSR and MORA.

To evaluate the performance of any routing protocol in terms of routing overhead, it is important to

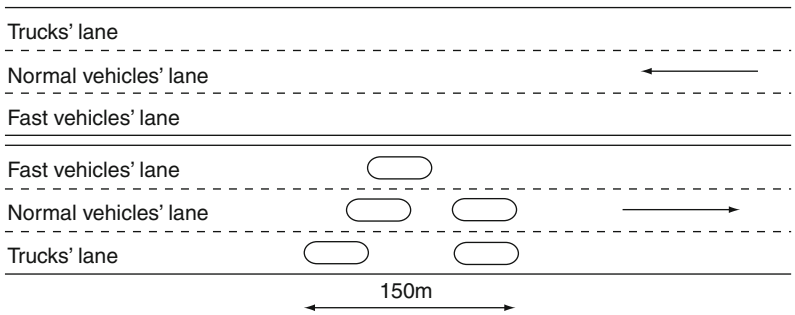

Vehicular Ad Hoc Networks, Enhanced GPSR and Beacon-Assist Geographic Forwarding in. Figure 8
The highway scenario in simulations

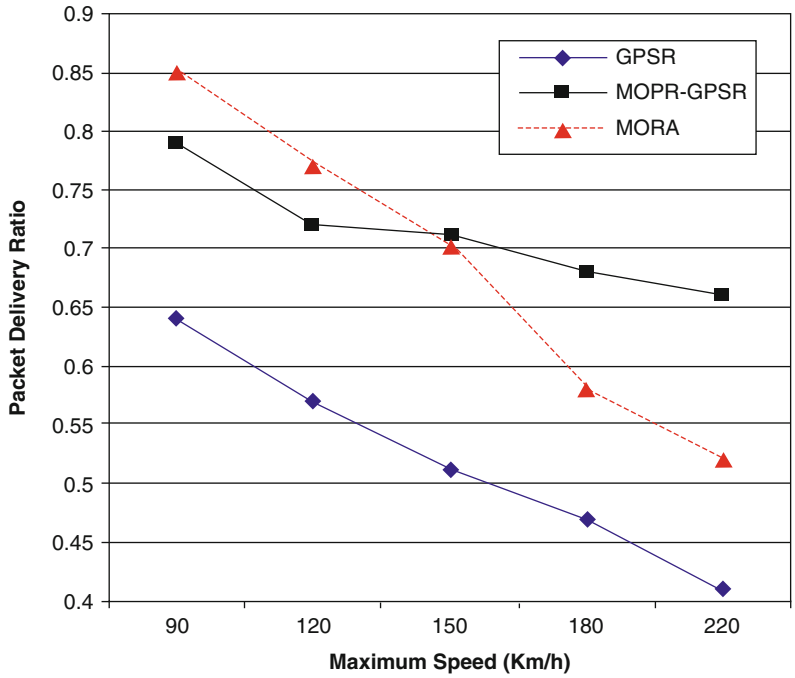

Vehicular Ad Hoc Networks, Enhanced GPSR and Beacon-Assist Geographic Forwarding in. Figure 9
Packet delivery ratio comparison between GPSR, MOPR, and MORA

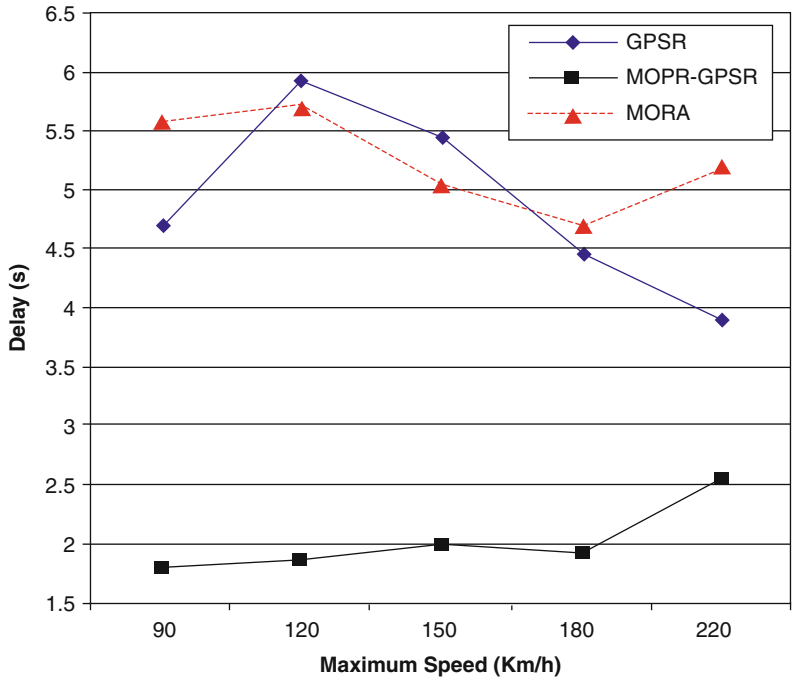

Vehicular Ad Hoc Networks, Enhanced GPSR and Beacon-Assist Geographic Forwarding in. Figure 10
Delay comparison between GPSR, MOPR, and MORA

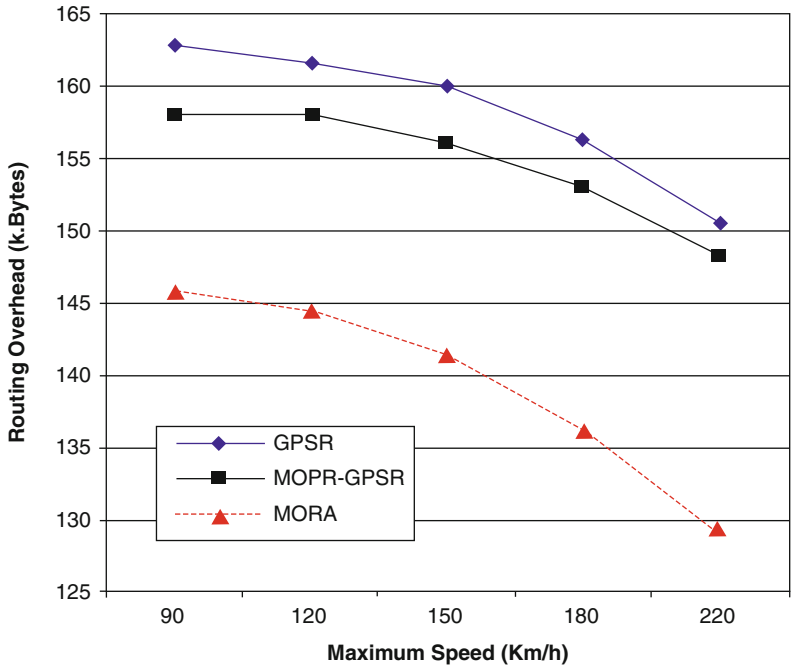

Vehicular Ad Hoc Networks, Enhanced GPSR and Beacon-Assist Geographic Forwarding in. Figure 11
Routing overhead comparison between GPSR, MOPR, and MORA

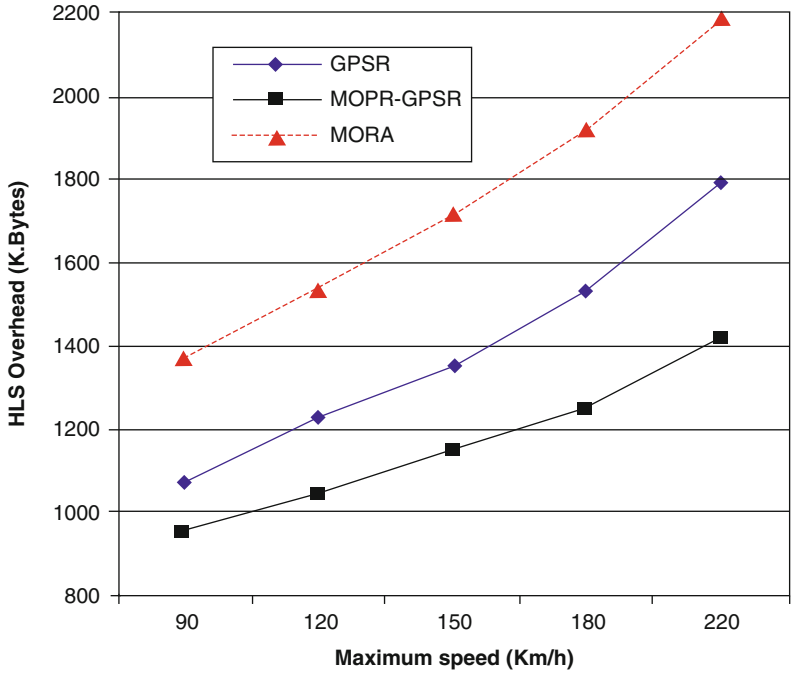

Vehicular Ad Hoc Networks, Enhanced GPSR and Beacon-Assist Geographic Forwarding in. Figure 12
HLS overhead comparison between GPSR, MOPR, and MORA

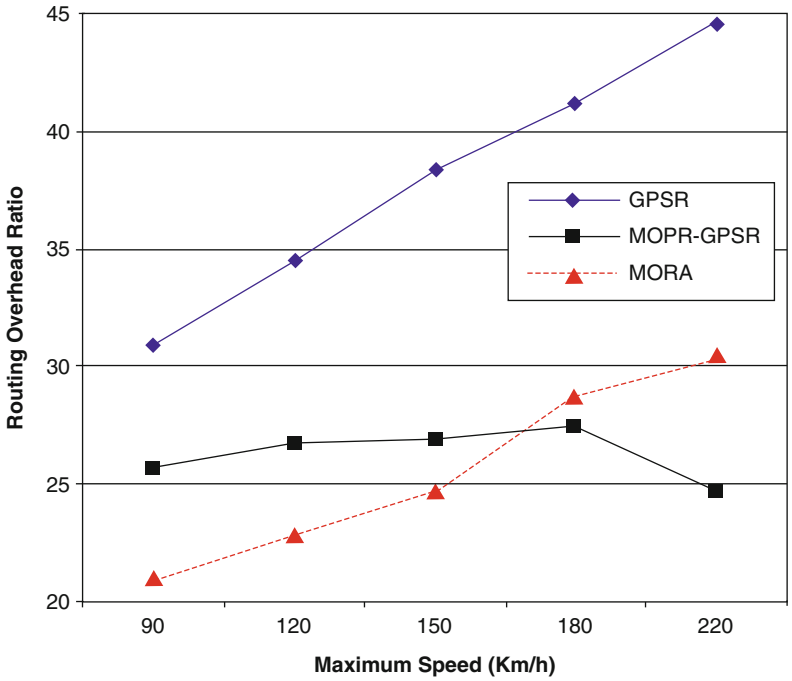

Vehicular Ad Hoc Networks, Enhanced GPSR and Beacon-Assist Geographic Forwarding in. Figure 13
Routing overhead ratio comparison between GPSR, MOPR, and MORA

calculate the Routing Overhead Ratio (ROR). Figure 13 shows the ROR caused in the simulation network while taking into account only the routing overhead (i.e., without counting the HLS overhead). It is clearly shown that both MOPR and MORA improve the ROR when compared to basic GPSR. And MOPR shows an almost stable ROR compared to MORA which increases when the maximum speed increases.

The ROR is important, but in such kind of routing protocol, the global ROR overhead, while taking into account the HLS overhead as well, is more important. Figure 14 shows clearly how MOPR improves the network performance in terms of global ROR by about two times when compared to both basic GPSR and MORA.

All simulation results presented in this section show that MOPR improves the routing performances from all sides. Consequently, MOPR shows a big potential for position-based routing in VANETs.

Strategies of Enhancement in City Scenario

Definition of the Subject A city scenario is much more complicated. Communication between cars driving in a city environment creates different challenges, largely due to the more complex geometry of the scenario. The challenges can be summarized as follows:

Geometric two-dimensionality: Cars change their movement direction all the time and can move at any relative angle to each other allowed by the street geometry. This weakens the correlation of the destination position to a suitable next hop.

Obstacles: A city is usually characterized by the presence of radio obstacles, which creates problems with position-based next hop selection because the nodes are not able to communicate whenever the line of sight between two nodes goes through an obstacle. And multipath propagation and complex obstacle surfaces create a much more complicated situation in reality.

Node density: the node density can be expected to be rather high with respect to the radio range, especially at "density hot spots" like junctions. Node density creates better ad hoc connectivity while it also poses a challenge to flooding mechanisms that need to be very efficient.

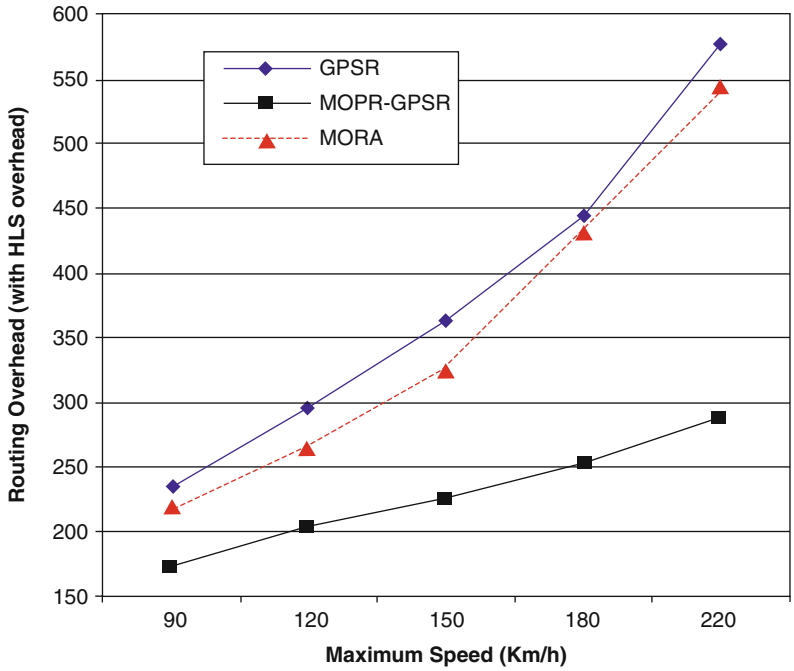

Vehicular Ad Hoc Networks, Enhanced GPSR and Beacon-Assist Geographic Forwarding in. Figure 14
Global routing overhead (routing + HLS) ratio comparison between GPSR, MOPR, and MORA

Low mobility: Compared to highway scenarios, nodes move at lower speeds, influenced by node density and are constrained by speed limits.

Greedy Perimeter Coordinator Routing

Greedy perimeter coordinator routing (GPCR) [7] does not use map information or densities in the streets, nor does it use the idea of a list of junctions that a packet must pass until it reaches the destination. It aims to avoid overhead. GPCR proposes a position-based algorithm. The main idea is to take into account the fact that the streets and junctions form a natural planar graph and, hence, it is possible to apply geographic routing directly. GPCR consists of two parts: restricted greedy routing and repair strategy.

Restricted greedy routing. Data packets should be routed along streets because they cannot get through buildings. The junctions are the only places where actual routing decisions are taken. Therefore, packets should always be forwarded to a node on a junction rather than being forwarded across a junction. This is illustrated in Fig. 15, where node *b* would forward the packet beyond the junction to node *c* if greedy forwarding is used. But by forwarding the packet to any of the nodes in the corner it finds an alternative path to the destination without getting stuck in a local optimum. A local optimum is produced when a forwarding node does not find a neighbor closer to the destination than itself. A node on a junction usually has more available options to route a message. Nodes that are located close to a junction are called coordinators. A coordinator broadcasts its role into its beacon packets. Thus, its neighbors will know its role when they have to forward these beacons. As a node must know whether it is a coordinator or not, two methods have been proposed to learn that.

The first one consists of including neighbors' locations and identifiers in beacons, so that each node can have information about the two-hop distance. Then, a node is considered to be in a junction when it has two neighbors that are within transmission range to each other but do not list each other as neighbors. Figure 16 shows *v* and *w* are neighbors of node *u* but they do not list each other as neighbors. This method might have problems. In Fig. 17 the requirement is correct but

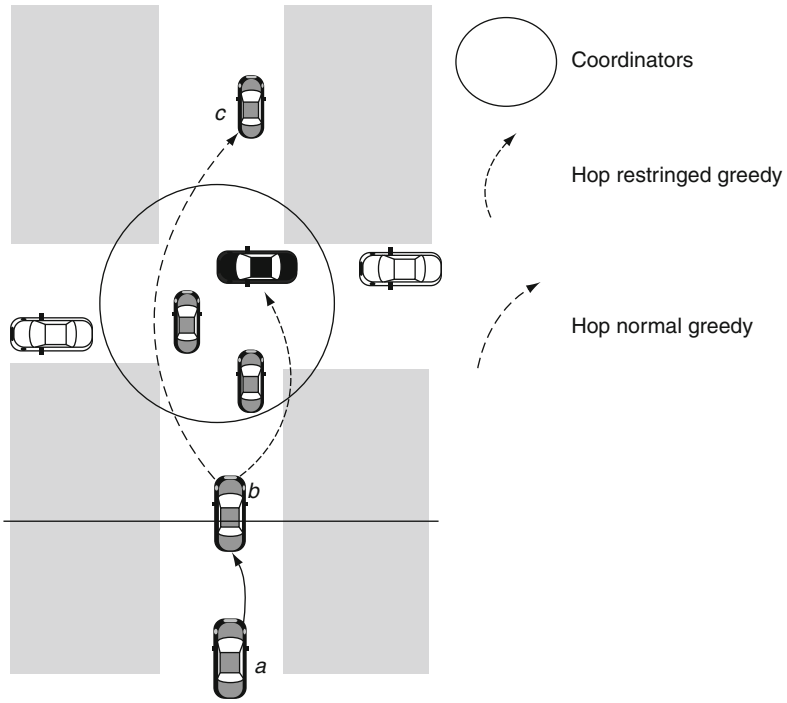

Vehicular Ad Hoc Networks, Enhanced GPSR and Beacon-Assist Geographic Forwarding in. Figure 15
Preference coordinator nodes in GPCR

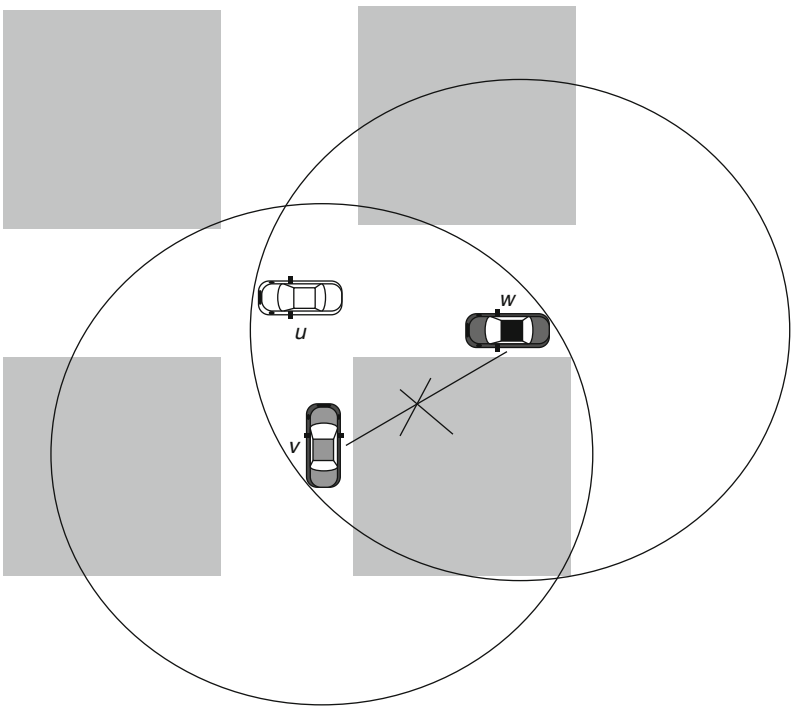

Vehicular Ad Hoc Networks, Enhanced GPSR and Beacon-Assist Geographic Forwarding in. Figure 16
Discovery method of coordinators in GPCR

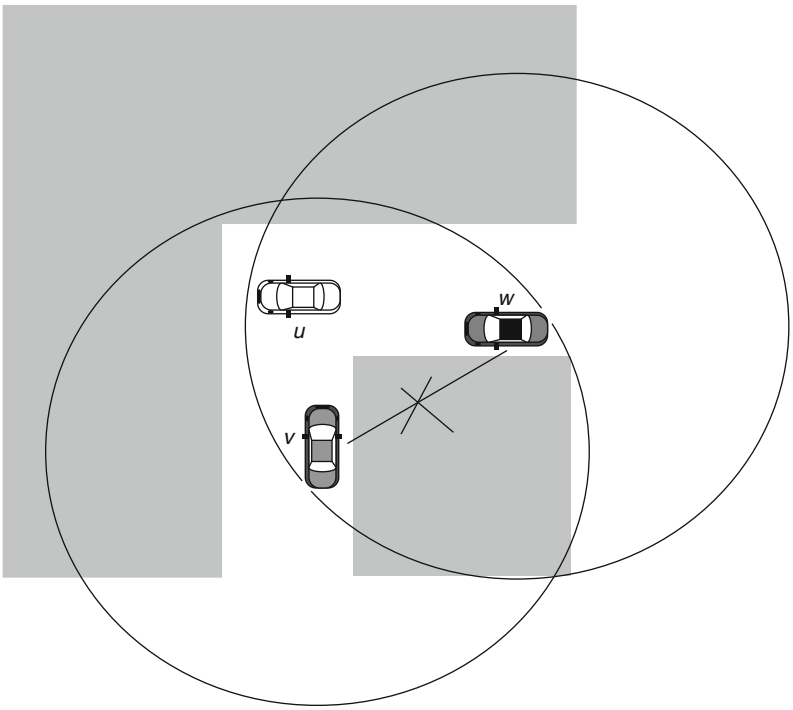

Vehicular Ad Hoc Networks, Enhanced GPSR and Beacon-Assist Geographic Forwarding in. Figure 17
Failed discovery coordinator in GPCR

node u is not really a coordinator because it is located in a curve.

The second one consists of calculating the correlation coefficient (CC) with respect to the position of the neighbors. In this method, it is not necessary to include additional information into beacon messages. Let x_i and y_i be the (x, y) coordinates of a node i. Also let $\bar{x}$ and $\bar{y}$ be the mean of x-coordinates and y-coordinates, respectively. σ_{xy} indicates covariance of x and y. σ_x and σ_y indicates the standard deviation of x and y, respectively. Finally, the correlation coefficient is defined in Eq. 7:

$$\rho_{xy} = \left|\frac{\sigma_{xy}}{\sigma_x \sigma_y}\right| = \left|\frac{\sum_{i=1}^{n}(x_i - \bar{x})(y_i - \bar{y})}{\sqrt{\left(\sum_{i=1}^{n}(x_i - \bar{x})^2\right)\left(\sum_{i=1}^{n}(y_i - \bar{y})^2\right)}}\right| \tag{7}$$

with $\rho_{xy} \in [0,1]$. If the value is close to 1 it indicates a linear coherence that is normally found when a vehicle is located in the middle of a street (Fig. 18). On the other hand, a value close to 0 might indicate a linear coherence and, hence, a vehicle can be determined to be located in a junction. By adjusting a threshold $\in$, a node can evaluate the correlation coefficient and assume with $\rho_{xy} \geq \in$ that it is located on a street and then the node is a coordinator. But if $\rho_{xy} \leq \in$, it can be concluded that the node is close to a junction. 0.9 is considered to be a good value for 2, but it may be arbitrary.

If the forwarding node is located on a street and not on a junction, the packet is forwarded along the street toward the next junction. To achieve this, the forwarding node draws a line between the forwarding node's predecessor and the forwarding node itself. The neighbors that approximate the extension of the line will be candidates. The farthest candidate node is selected. In Fig. 18, node w is selected based on the line between u and v. In the event that some candidate node is a coordinator it will be selected before any non-coordinator node. If there were more coordinators, one of them is randomly selected (Fig. 15). This prevents a packet from crossing a junction. Once a packet reaches a coordinator, a decision has to be made

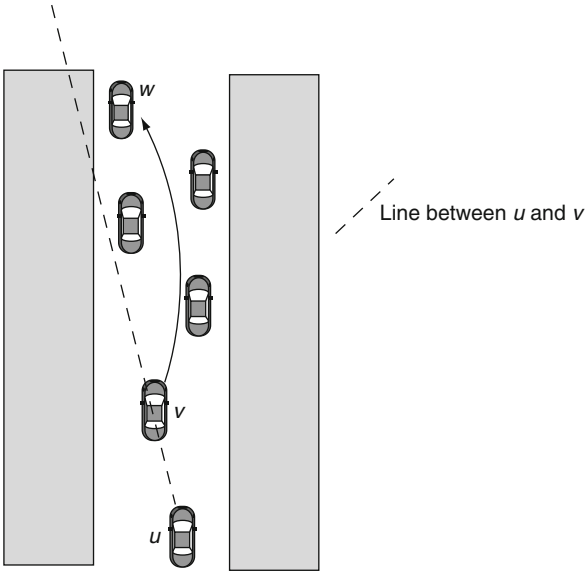

Vehicular Ad Hoc Networks, Enhanced GPSR and Beacon-Assist Geographic Forwarding in. Figure 18
Restricted greedy in a street

about the street that the packet should follow. This is done in a greedy mode: the neighbor with the largest progress toward the destination is chosen. This implies a decision on the street that the packet should follow (Fig. 19).

Repair strategy. Despite the new greedy routing model, there exists the risk that a packet gets stuck in a local optimum. Hence a repair strategy is required. The vehicle tries to infer the topology of the roads by applying the recovery strategy over the set of neighbors. If the forwarding node is a coordinator and the packet is in repair mode, then the node needs to determine which street the packet should follow next. To this end the right-hand rule [8] is applied (Fig. 20). Using the right-hand rule it chooses the street that is the next one counterclockwise from the street the packet has arrived on. But if the forwarding node with a packet in repair mode is not a coordinator, then the node applies restricted greedy routing.

In GPCR, there exists a risk that a packet could be forwarded back over the same street from which the packet has arrived. When a packet is being forwarded in repair mode and reaches a coordinator node, it applies

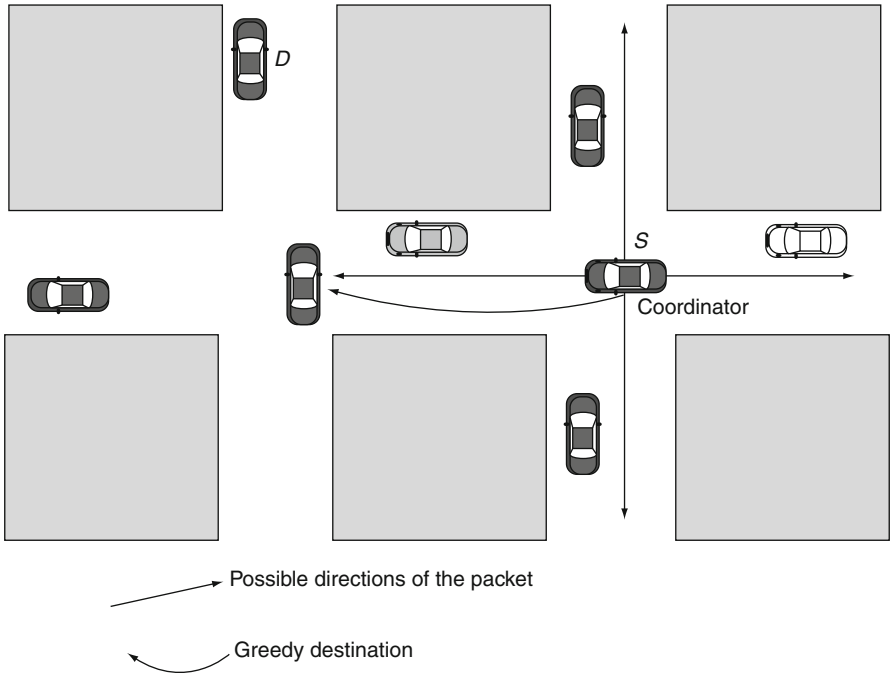

Vehicular Ad Hoc Networks, Enhanced GPSR and Beacon-Assist Geographic Forwarding in. Figure 19
Restricted greedy in a street

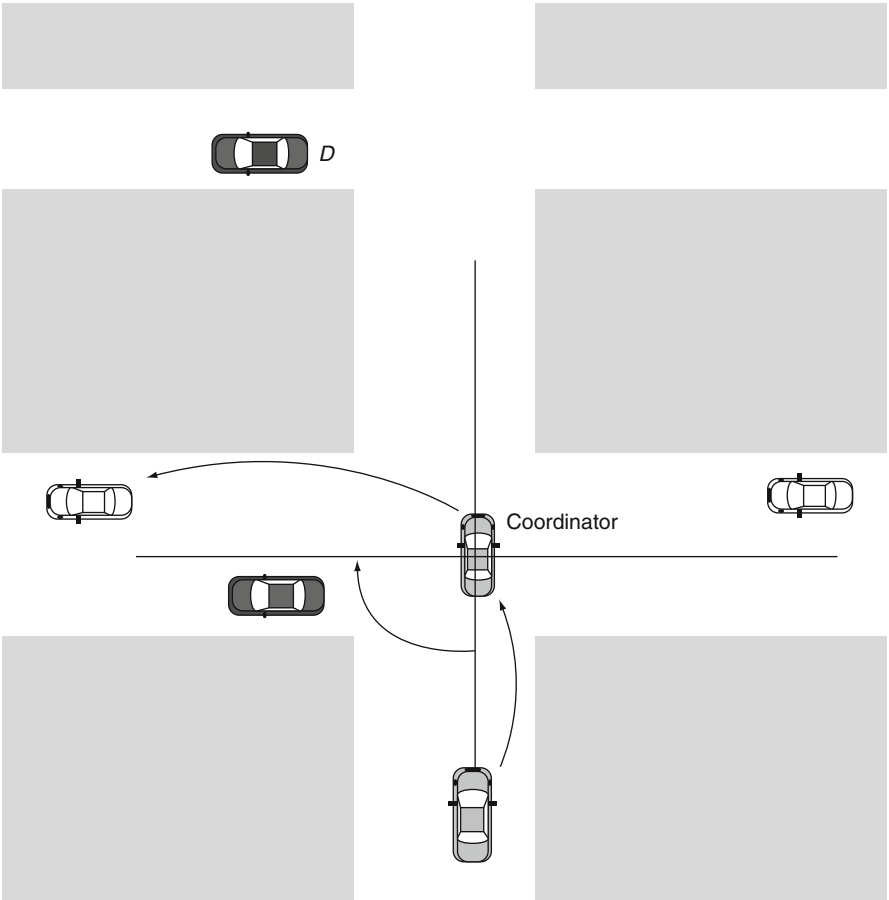

Vehicular Ad Hoc Networks, Enhanced GPSR and Beacon-Assist Geographic Forwarding in. Figure 20 Coordinator applying perimeter in GPCR

perimeter routing. In Fig. 21, it shows how if the node u applies the right-hand rule (in this case left-hand rule) from the line formed between nodes u and v, the coordinator chooses the node w as the next hop, instead of the node x which is located along the next street. Therefore, the packet does not turn the junction, but it remains on the same street.

Simulation of GPCR is implemented with the ns-2 simulator version ns-2.1b9a. In the simulation, a real city topology is used, which is a part of Berlin, Germany. The scenario consists of 955 cars (nodes) on 33 streets in an area of 6.25 × 3.45 km. The movement of the nodes was generated with a dedicated vehicular traffic simulator and represents a real-world movement pattern for this given scenario [9]. IEEE802.11 was used as MAC with a transmission rate of 2 Mbps. The transmission range was set to 500 m. Real-world tests with cars have shown this to be a reasonable value when using external antennas. For each simulation run ten sender–receiver pairs are randomly selected. Each pair exchanges 20 packets over 5 s. Figure 21 shows the achieved packet delivery rate versus the distance between the two communication partners and Fig. 22 shows the number of hops. The communication distance between two nodes is calculated as the minimal distance based on the street topology at the beginning of the communication.

Figure 21 also depicts how the delivery rate is influenced by the algorithms used for junction detection. It shows that calculating the correlation coefficient (CC) is slightly better than relying on the comparison of the neighbor tables (NT).

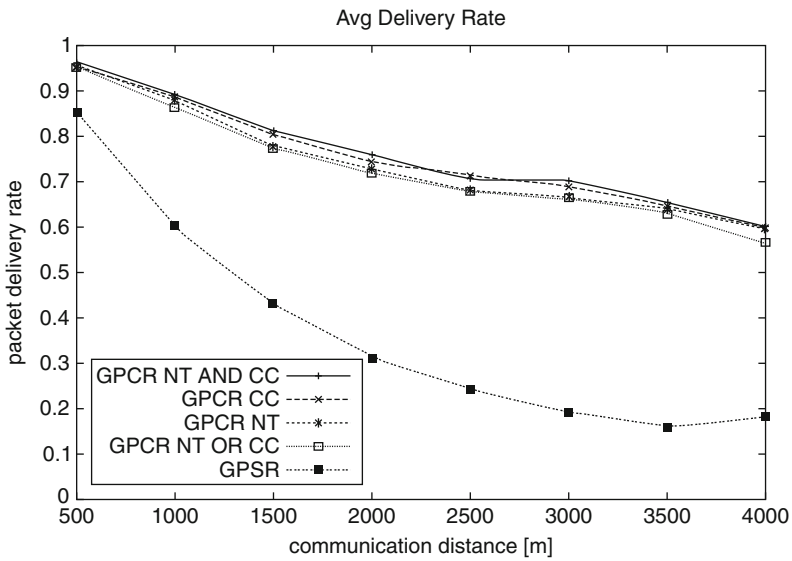

Vehicular Ad Hoc Networks, Enhanced GPSR and Beacon-Assist Geographic Forwarding in. Figure 21
GPCR versus GPSR – delivery rate

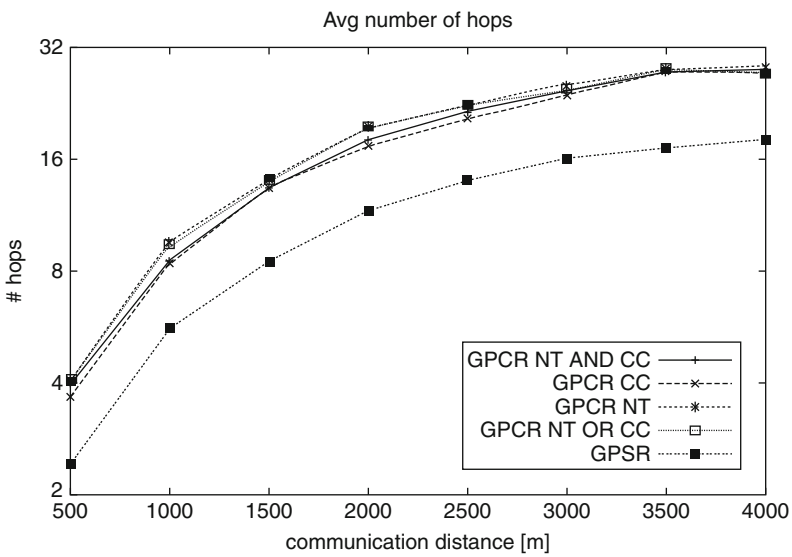

Vehicular Ad Hoc Networks, Enhanced GPSR and Beacon-Assist Geographic Forwarding in. Figure 22
GPCR versus GPSR – average number of hops

A compound decision consisting of the neighbor table comparison and correlation coefficient is also analyzed, concatenated by logical OR as well as by logical AND. The latter one outperforms the other approaches slightly but it does not come for free: the size of the beacon packets increases for each of the two approaches. Therefore, GPCR simply uses the correlation coefficient. In general, the study on achievable

packet delivery rate (Fig. 21) shows good results for the approach compared to GPSR. This improvement in performance comes at the expense of a higher average number of hops and a slight increase in latency. This increase in hop counts and latency is mainly caused by those packets that could not be delivered at all by GPSR and thus did not impact the hop-count and latency for GPSR.

Connectivity-Aware Routing

Connectivity-aware routing (CAR) [10] is a position-based routing scheme. The protocol is aimed at solving the problem of determining connected paths between source and destination nodes. VANETs' nodes present a high degree of mobility, and nodes cannot know the position of the rest of the vehicles due to several well-known scalability problems. This lack of information makes it impossible to determine a priori which streets have enough vehicles to allow messages to be routed through them.

CAR's algorithm is designed to deal with these problems, and to do that it is divided into three stages: (1) finding the location of the destination as well as a connected path to reach it from the source node, (2) using that path to relay messages, and (3) maintaining the connectivity of the path in spite of the changes in the topology due to the mobility of vehicles.

In the first stage, the source node broadcasts a route request message. The idea behind this initial broadcast is the following: The reception of, at least, one of these route request messages at the destination means that at least one connected path exists. The destination node answers the route request message with a response message including its current location so that the first problem is solved. But the source node also needs to know the path to reach the destination.

In CAR, it is proposed to include in the header of every route request message the list of junctions (called anchor points) traversed by that message in its way toward the destination. Thus, adding that list to the response message issued by the destination solves the second problem. Besides, nodes periodically transmit short messages including the issuer's identifier, location, and current velocity vector. These short messages (called beacons) keep the neighbor's tables updated. Moreover, the determination of junctions is made by means of comparing the direction of the vehicles. That is, a node determines if it is currently located at a junction when the angle between its velocity vector and one of the neighbors is not parallel. Two velocity vectors are parallel if the smallest angle between the vectors is less than α (equal to 18°). Otherwise the velocity vectors are nonparallel. Nodes that have neighbors with nonparallel velocity vectors identify themselves as being near a crossing or road curve and can serve as relays.

Additionally, to select not only a connected path between the source and the destination but also a short one, the destination does not respond immediately. Instead, it waits a predefined amount of time and then the path selected is the shortest one among those included in the different route request messages received. CAR uses the preferred group broadcast (PGB) [2] protocol to reduce as much as possible the overhead of flooding.

Once the source node has determined a path to reach the destination, data messages are routed geographically from an anchor node to the next one until the destination is reached. To do that, the source node uses a source routing approach. The full list of anchor nodes is included as a header in every data message transmitted. CAR uses the advance greedy forwarding (AGF) [2] algorithm to deliver messages between each pair of anchor nodes. In AGF, relay nodes select as next hop the neighbor located closest to the destination. In this case, it is the vehicle located closest to the next anchor point.

CAR defines the concept of "guards" (see Fig. 23) to help nodes determine if a message has reached a certain anchor point. A guard is a set of information tied to a geographical area. That area is defined by the location of the anchor point and a radius. Thus, guards contain both the location and the radius. Nodes create guards when they identify a new anchor point. A node creating a guard is the first one including it on its beacon messages. Nodes store the guards received during beaconing periods, but only nodes located inside the area defined in the guard retransmit it on their beacons.

A node receiving a message being routed toward the anchor point a can determine that the message has reached a by checking if it has already received a guard for a. Moreover, the mobility of vehicles causes

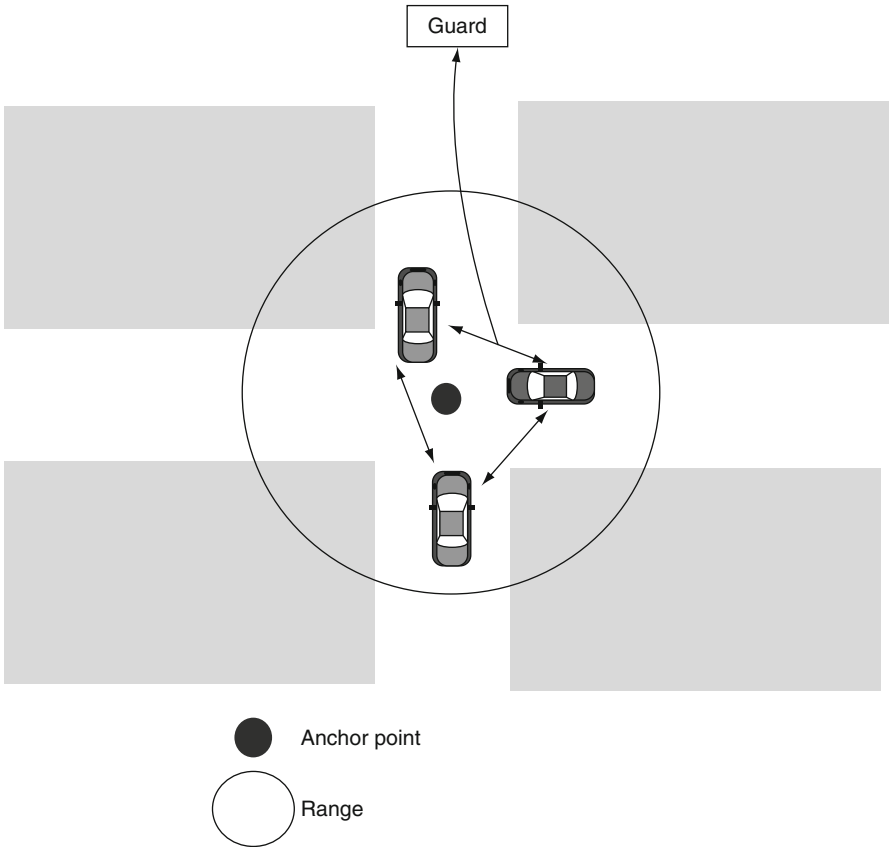

Vehicular Ad Hoc Networks, Enhanced GPSR and Beacon-Assist Geographic Forwarding in. Figure 23
Three vehicles interchanging a guard about an anchor point.

constant topology changes. Thus, the connected path found at the beginning of a data transmission can become disconnected over time. To overcome this issue, CAR uses the guards to help maintain the connectivity of the path, or at least to dynamically auto-adjust it on the fly without resorting to a new route discovery process.

Concretely, it is assumed that there cannot be disconnection problems between anchor points, so that only the movement of the destination node represents an issue. Therefore, when a destination node changes its direction, then a new guard is generated including also the new velocity vector of the destination node. When a data message arrives to the old destination node's location, the guarding nodes (those interchanging that guard) can retransmit the packet toward the new estimated location of the destination. Of course, this assumption may not hold in general, which means that the protocol may fail to maintain the path connected.

Finally, as CAR makes extensive use of beacons, an adaptive beaconing mechanism is proposed to reduce control overhead while keeping neighbor tables as accurate as possible, especially when the number of neighbors or their mobility makes them very unstable. The idea is to adapt the beaconing rate to the nodes density, so that the fewer the number of neighbors, the higher is the beaconing frequency. By this way, several drawbacks, such as wasted bandwidth, delaying of data packet, increased network congestion, coming from fixed period beacon strategy, can be mitigated.

In CAR, there are two possibilities for routing error to occur. First, the AGF algorithm may fail to forward a packet between two anchor points due to

(a) a temporary gap between vehicles (or raised interference level), such gaps may appear and disappear with time at any place on a road; or (b) long-term disconnections due to a suddenly closed road or an unusually big gap in the vehicular traffic. Second, a packet may reach the estimated destination position after passing the last anchor point but fails to find the destination there. The reason for that event could be that the destination changed direction but could not activate a guard due to lack of neighbors within communication range, or the guard was activated but later could not be retransmitted due to the same problem. CAR uses two approaches to handle these routing errors: (1) *Timeout algorithm with active waiting cycle* – One approach to tackle temporary gaps (or a raised interference level) is the use of timeout with packet buffering and an active waiting cycle. The forwarding node suspends the packet and periodically checks if the next hop neighbor has appeared. A long-term disconnection recovery algorithm should be invoked when a simple timeout approach failed. (2) *Walk-around error recovery* – If the AGF algorithm fails to find the destination at its estimated position (case 1), or the timeout algorithm could not find the next hop host (case 2), the node that detected the problem informs the source about the error and starts a local destination location discovery process. In case (1) the scope of this discovery is limited to half the number of anchor points in the old source–destination path. The broadcast is allowed to travel no more than one half of the old path length. In case (2) the scope is limited to the number of anchor points in the old path to the destination (from the current node) plus 50%. The same applies to the path length.

Simulations are made under version 2.28 of the ns-2 simulator with the probabilistic Shadowing model. The performances of CAR protocol without and with enabled walk-around error recovery (CAR + WA) are compared with GPSR and GPSR + AGF. Three different densities of nodes (low – less than 15 vehicles/km of road, medium – 30–40 vehicles/km, and high – more than 50 vehicles/km) are used in the following movement scenarios: highway (averaged over three different highway areas, ten sub-scenarios each for every density of vehicles) and city (averaged over three different city areas, ten sub-scenarios each for every density of vehicles) [2]. 20 CBR traffic sources with a sending rate of 4 packets/s are considered. Sources stop generating data packets 50 s before the simulation ends. Source/sink nodes stay inside the simulated area (do not leave the area and do not park) for the duration of the simulations (300 s).

Figure 24 shows packet delivery ratio for city and highway scenarios with different densities of vehicles. For all traffic densities, GPSR performs very poorly in the city scenario, with 5–7% of data packets delivered. Also, the advanced greedy forwarding algorithm (GPSR + AGF) shows moderate performance (up to

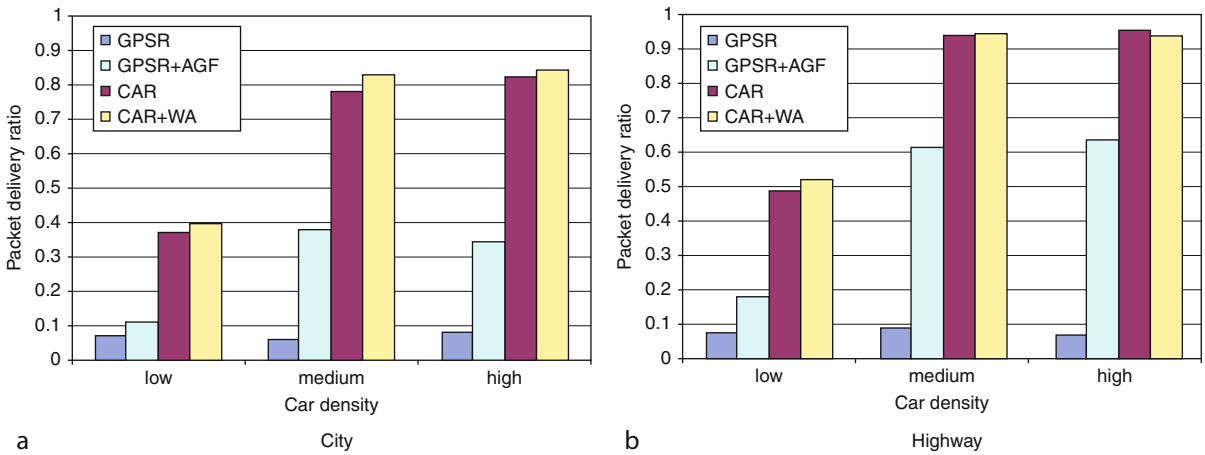

Vehicular Ad Hoc Networks, Enhanced GPSR and Beacon-Assist Geographic Forwarding in. Figure 24
Packet delivery ratio

only 38% of data packets delivered), although performance is noticeably higher than for standard GPSR. Note that GPSR and GPSR + AGF use an idealized location service in the simulation: source nodes obtain the true location of destinations each time a data packet is originated. Despite the additional overhead to discover the real paths and to obtain destination coordinates, CAR and CAR + WA demonstrate much better results than GPSR + AGF. The highway scenarios are geographically less sophisticated than the city scenarios, thus all studied protocols show better PDR in highway areas. Again, CAR and CAR + WA outperform GPSR and GPSR + AGF, despite the need to obtain and maintain paths between source–destination pairs.

In terms of the average data packet delays (Fig. 25), the original GPSR and the GPSR + AGF are always worse than CAR and CAR + WA. For CAR, the route discovery process precedes every first data transmission to an unknown destination, this step adds to the delay of the first data packets. However, the average delay of the data packet for CAR and CAR + WA is much lower than for GPSR and GPSR + AGF. This result is a consequence of CAR's use of real connected paths between source and destination pairs, whereas GPSR and GPSR + AGF often fail due to local maximum resolution encountered by the perimeter mode. CAR easily tolerates short-term disconnections due to gaps or a temporary high interference level (e.g., frequent MAC collisions).

Figure 26 shows the total routing protocol overhead, measured in total number of routing packets sent network-wide during the entire simulation. For the CAR protocol, the overhead is presented as accumulative contribution of (1) beaconing, (2) path discoveries, and (3) path maintenance with the help of guards. The use of adaptive beaconing allows CAR to keep the average beaconing overhead from 1.5 to 3 times lower than the beaconing overhead of GPSR, without harming the performance.

GpsrJ+

GpsrJ+ is a position-based routing protocol which consists of two modes, yet using a special form of greedy forwarding. As obstacles (e.g., buildings) block radio signals, packets may only be greedily forwarded along road segments as close to the destination as possible. Accordingly, the major directional decisions are made at junctions. When packets reach a local maximum, a point at which there is no node closer to the destination, the node switches to GpsrJ+'s recovery mode.

In recovery mode, packets are greedily backtracked along the perimeter of the roads. GpsrJ+ removes the unnecessary stop at a junction while keeping the efficient planarity of topological maps. It is not necessary to back forward in small steps through planarized links, for reasons that the general direction of the right-hand

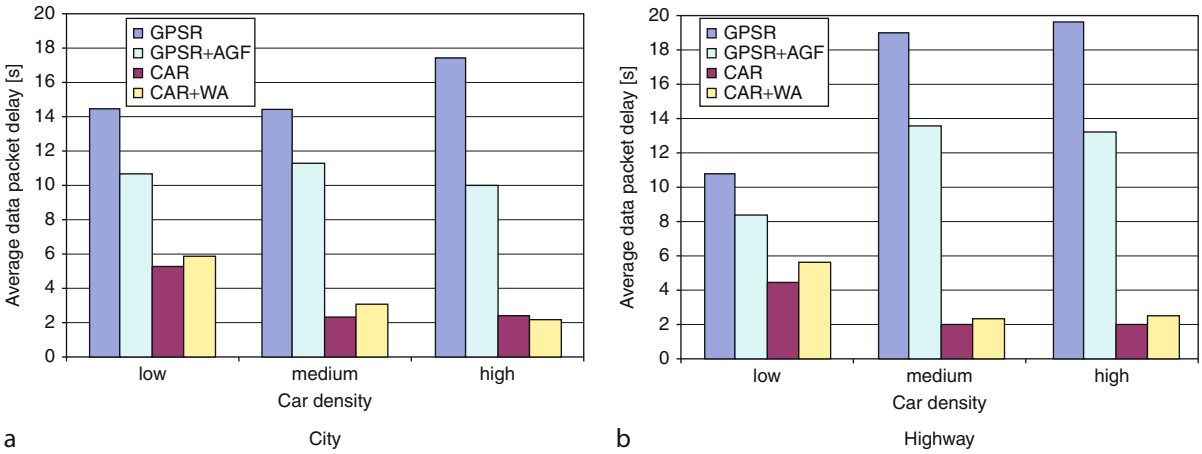

Vehicular Ad Hoc Networks, Enhanced GPSR and Beacon-Assist Geographic Forwarding in. Figure 25
Average delay of a data packet

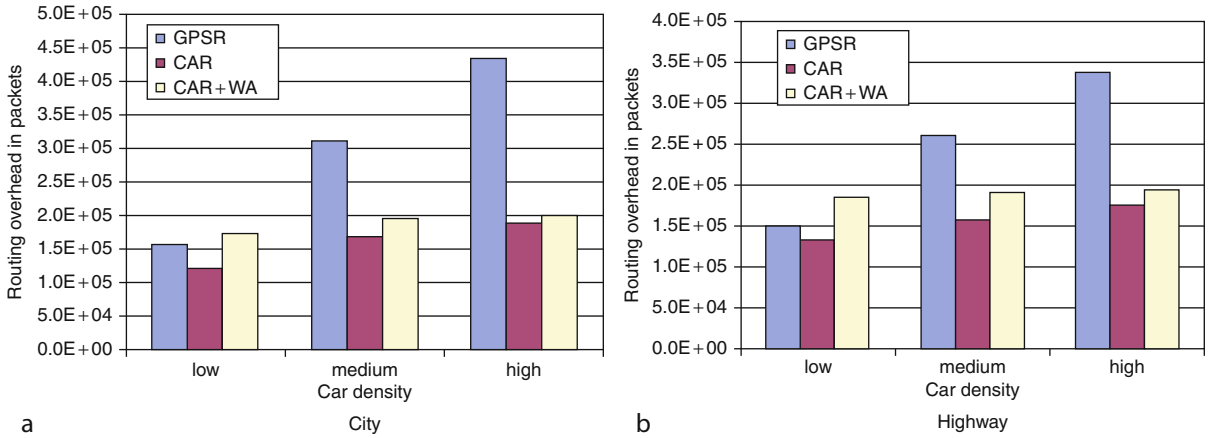

Vehicular Ad Hoc Networks, Enhanced GPSR and Beacon-Assist Geographic Forwarding in. Figure 26
Routing overhead in packets

rule always results in the opposite direction of where packets were going before recovery, and the objective is to come back as fast as possible to a junction. Unlike GPCR, where packets must be sent to a junction node since junction nodes coordinate the next forwarding direction, GpsrJ+ lets nodes that have junction nodes as their neighbors predict on which road segment its junction nodes would forward packets onto, and thus may safely overpass them if not needed. GpsrJ+ uses the right-hand rule to determine the best direction (as opposed to final destination direction) and thereby the best forwarding node. That is, if the furthest node is in the same direction as the best direction, the best forwarding node is the furthest node; otherwise, the best forwarding node is a junction node. Figure 27 illustrates the advantage of prediction. The figure shows that GpsrJ+ can bypass the junction area and forward the packet to node *E* directly, yet GPCR forwards it to the junction node *B*, thus causing more transmissions.

Moreover, GpsrJ+ uses a two-hop neighbor enhanced beaconing. In addition to the node's position in the beacon, each node also broadcasts the road segments that its neighbors are on. In the neighbor list, each node has its neighbor's location and the associated road segments on which its neighbor's neighbors are.

GpsrJ+ is analyzed by comparing it with GPSR and GPCR under Qualnet 2.95 simulator software, with 75 nodes up to 175 nodes, with a 25-node increment. Generally, GpsrJ+ improved recovery strategy brings significant results compared to GPSR and GPCR. In the simulation, an urban topology is employed, which is a user-defined Manhattan-grid of 1,500 × 1,500 m.

Figure 28 shows the packet delivery ratio (PDR) between GPSR, GPCR, and GpsrJ+. Clearly, taking aggressive hops in the recovery mode along the perimeter improves the PDR. This is further verified by the fewer hops GpsrJ+ needs compared to GPSR as shown in Fig. 29a. A higher number of hops imply an increased probability of channel contention; therefore, there is a higher probability that a packet gets dropped along the way. Although GPCR and GpsrJ+ stop at each junction node in greedy mode, this is not sufficient to increase the hop count dramatically. The total hop count of GPCR and GpsrJ+ is still lower than that of GPSR. Figure 29b shows the number of hops a packet experiences before being dropped. GPSR's failed hop is twice as much as GPCR and GpsrJ+. This is consistent with that planarization of nodes produces too many hops. The undeliverable packets, as a result of disconnections between the source and destination, engage in perimeter forwarding most of the time and explore all possible perimeters in a limited way caused by planarization. Since more nodes are involved in forwarding, there is a lot of resource wastage. The situation worsens for undeliverable packets as they create a loop and the same route formed by the same

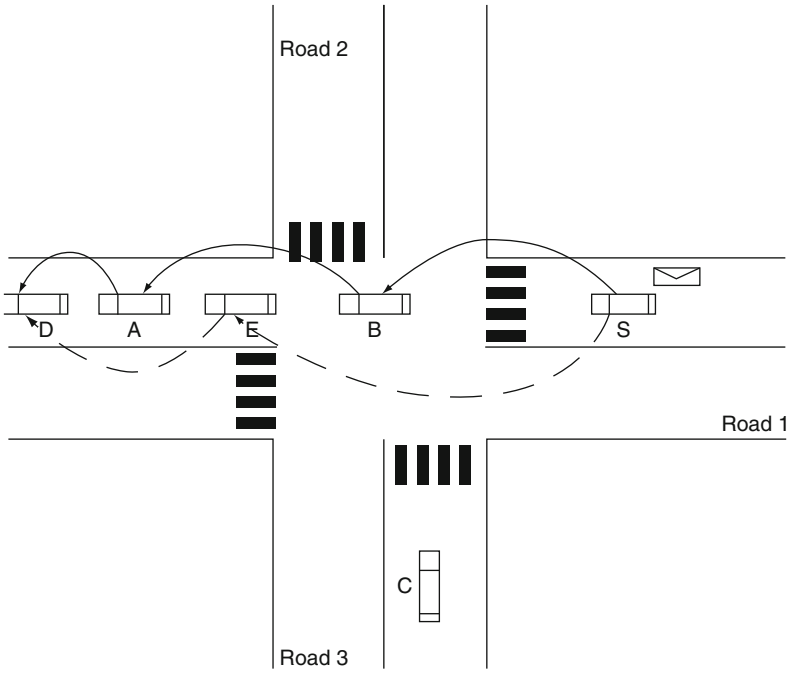

Vehicular Ad Hoc Networks, Enhanced GPSR and Beacon-Assist Geographic Forwarding in. Figure 27
Dashed arrows are GpsrJ+ and *solid arrows* are GPCR

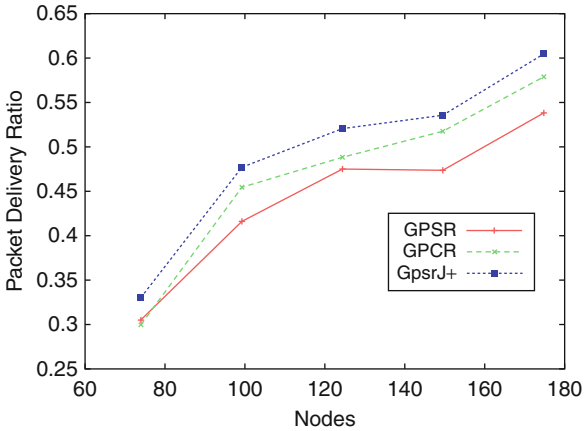

Vehicular Ad Hoc Networks, Enhanced GPSR and Beacon-Assist Geographic Forwarding in. Figure 28
PDR among GPSR, GPCR, and GpsrJ+

nodes in the same hops is visited again. In summary, the inefficiency of node planarization strategies in urban vehicular scenarios to forward packets in perimeter mode not only affects the delivery ratio but also impacts the hop count and network resources as packets stay longer in the network before being dropped.

Figure 28 also shows that GpsrJ+ possesses a higher PDR than GPCR thanks to prediction. The slight increase in hop count and latency in Fig. 29a and c, respectively, is the result of packets that do not get delivered to the destination and thus do not contribute to GPCR's hop count and latency. The reason is that the smoother decrease in hop count in GpsrJ+ compared to GPCR is due to the fact that nodes do not necessarily have to go through junction nodes, which might be heavily used for forwarding in GPCR. Consequently, the interference and collision of multiple packet transmission cause packets either to be dropped or to be forwarded on a longer route. The slight increase in failed hops in GpsrJ+ compared to GPCR in Fig. 29b illustrates a longer expectancy of packets as GpsrJ+ makes a better effort to deliver them. Once again, the ability not to rely on junction nodes that get flooded with traffic prolongs the life expectancy of a packet before it gets dropped. The improved PDR in GpsrJ+ also brings in the advantage of the fraction of times a packet travels in greedy mode.

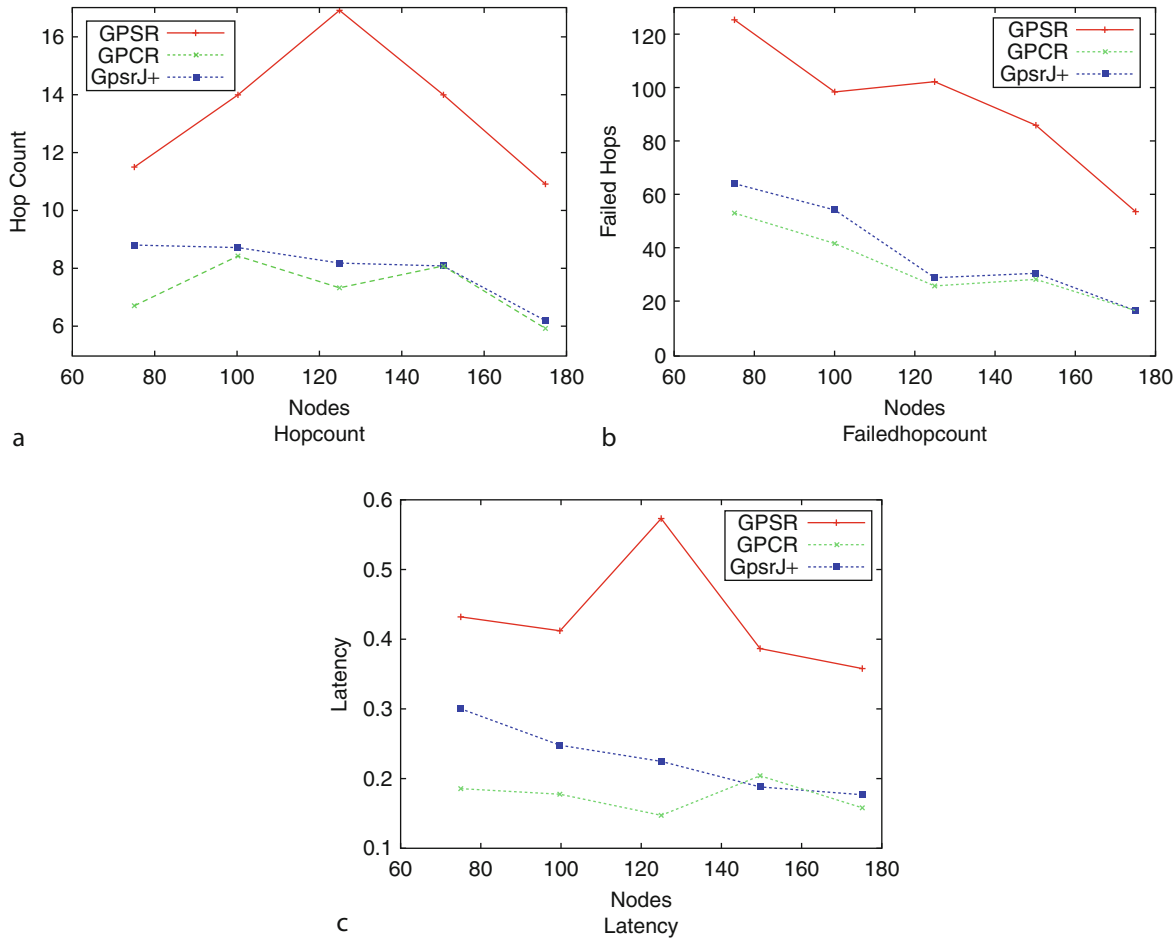

Vehicular Ad Hoc Networks, Enhanced GPSR and Beacon-Assist Geographic Forwarding in. Figure 29
Hop count and latency among GPSR, GPCR, and GpsrJ+

Figure 30 indicates that GpsrJ+ is in greedy mode a higher fraction of time than GPCR, and implies that GpsrJ+ minimizes the number of times a packet gets into a local maximum and maximizes the number of times a packet gets out of a local maximum.

Vehicle-Assisted Data Delivery

Zhao and Cao [11] proposed several vehicle-assisted data delivery (VADD) protocols. All of them share the idea of storing and forwarding data packets. That is, nodes can decide to keep the message until a more promising neighbor appears on their coverage range, but trying always to forward them as soon as possible. Additionally, decisions about which streets must be followed by the packet are made using vehicle and road information such as current speed, distance to the next junction, and maximum speed allowed. These routing decisions are dynamically taken at junctions because the authors state that precomputed optimal paths used by other protocols might rapidly lose their optimality due to the unpredictable nature of VANETs.

In VADD, the main goal is to select the path with the smallest packet delivery delay. The behavior of the protocol depends on the location of the node holding the message. Two cases are considered: when nodes routing the message are located in the middle of a road and when they are located in a junction. The first case (also called routing in straight way) presents less alternatives: forwarding the packet toward the next junction or to

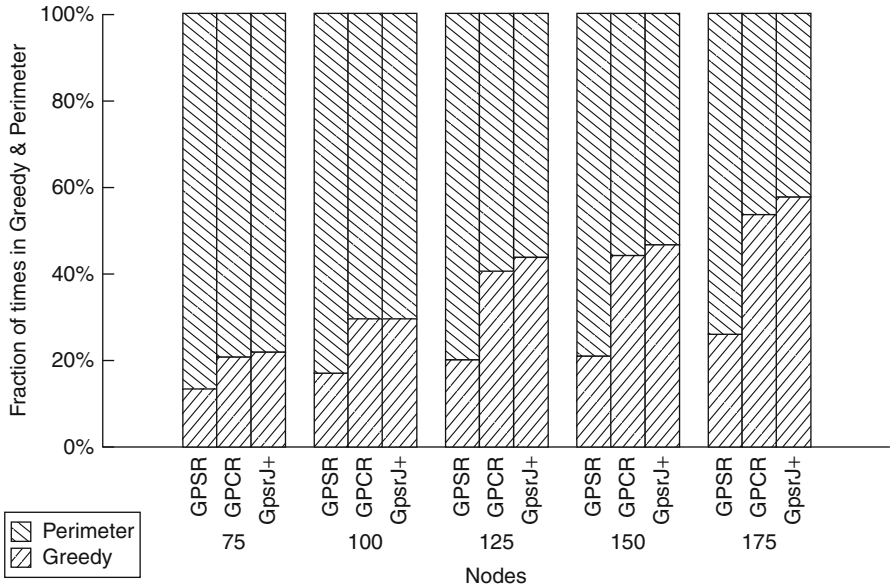

Vehicular Ad Hoc Networks, Enhanced GPSR and Beacon-Assist Geographic Forwarding in. Figure 30
Fraction of times in greedy and perimeter

the previous one. However, the second case (also called routing in intersections) is much more complicated because at junctions, the routing decision must consider the different roads, so that the number of options is higher.

Both cases use the same approach, determining the next road the message must follow, and then selecting the next relay among the current neighbors. In VADD, a common way of determining the next road is proposed, while the determination of the next hop remains different. Concretely, the outgoing road with the lowest estimated delay would be selected. In the "straightway" case, there are two possible outgoing roads, the two segments of the roads in which the node divides the current road. In the "intersection" case, each road starting in that junction represents a different option.

The authors call roads to the street segments delimited by two consecutive junctions. The estimation of the delay of routing a message through a certain road takes into account the road's length, its maximum speed, the mean traffic density, and other traffic-specific parameters. But, to estimate the delay to the destination, the authors also incorporate the estimated delay of the next possible roads along with the probability of choosing them. Figure 31 depicts the delay model used in VADD. A car located near intersection I_m computes the delay for the road between I_m and I_n (D_{mn}) accounting also the estimated delay of choosing the road between I_n and I_a, the one between I_n and I_b, or the one between I_n and I_c.

To estimate message delays for the different roads, the authors propose to solve an $n \times n$ linear equation system using the Gaussian elimination algorithm $[\Theta(n^3)]$, n being the number of junctions. To limit the complexity of this computation, a boundary area around the current location is defined, so that only the junctions inside that area are considered in the equation system.

Once the next road has been selected, it is time to determine which neighbor must be the next relay. In the "straightway" the decision is simple, the one located closest to the next junction according to the next road selected. In this case, the next junction can be the next one in the direction of the current vehicle or the one the vehicle has just passed by. In both cases, the packet is stored only if no neighbors are available at the moment.

The "intersection" case is more complex. Obviously, if no neighbor is available, or every outgoing road has a longer estimated delay than the current one, the decision taken consists of storing the message waiting for the next forwarding opportunity.

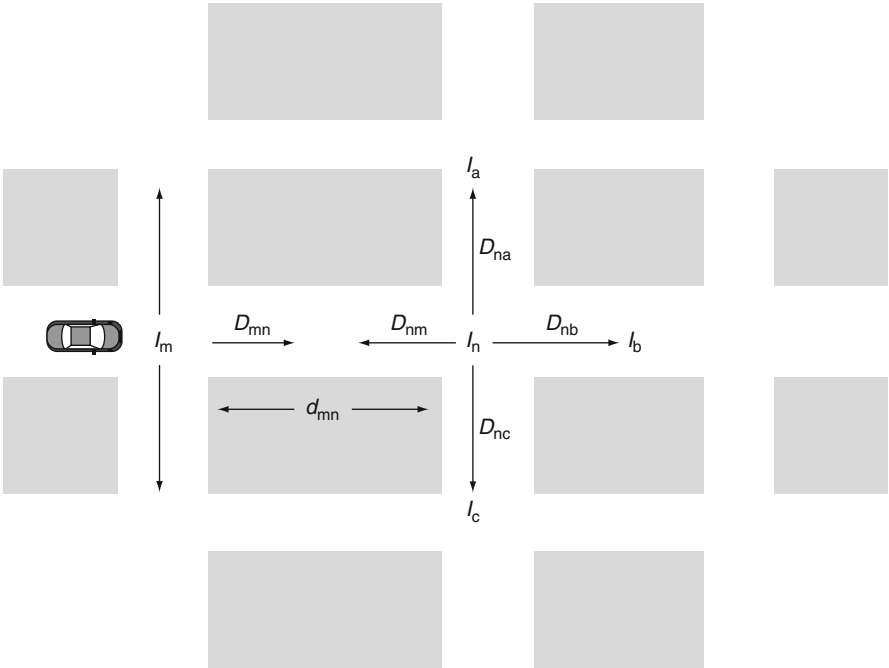

Vehicular Ad Hoc Networks, Enhanced GPSR and Beacon-Assist Geographic Forwarding in. Figure 31
Example of VADD model

Additionally, the authors propose three alternative ways to select the next forwarder when more than one candidate neighbor is available:

Location first: The node located closest to the next selected junction in the most promising road is chosen. This scheme presents routing loops.

Direction first: The node located closest to the next selected junction in the most promising road among the ones moving in the right direction.

Hybrid: Location first is applied unless a cycle is detected, in that case direction first scheme is used. This scheme seems a little bit unrealistic due to the difficulty of detecting routing loops.

VADD's main drawbacks are its complexity and difficulty of parameterization. The size of the bounding area is by far the most important parameter and, at the same time, it is responsible for the complexity of the computation needed at every node. Determining a value for this parameter to achieve a good trade-off between computational complexity and accuracy can be a hard task. Additionally, the authors claim that their hybrid scheme achieves the best performance; however, it is not clear how to implement this scheme due to the difficulty of detecting cycles.

Future Directions

The ways of strategies to enhance or extend performance of GPSR routing protocol have been introduced. The density of vehicles in each possible route as well as the travel direction and movement of the vehicles have been taken into account to improve the forwarding algorithm performance, and thus increasing the packets delivery ratio. Beaconing strategy has also been modified by these facts, and finally decreasing the route overhead.

Although data dissemination and routing have been extensively addressed, many unique characteristics of VANET together with the diversity in promising applications offer newer research challenges. Authors in [12, 13] have focused on the problems of radio obstacle during data transmission in city scenario.

They use an intersection-based approach to forward packets along successions of road from the source to destination in order to find robust and optimal routes. And the digital map information is used in these routing strategies to get information of intersections.

A VANET may exhibit a bipolar behavior, i.e., the network can either be fully connected or sparsely connected depending on the time of day or on the market penetration rate of the wireless communication devices. Authors in [14] have mentioned the issue when routing is within sparse vehicular ad hoc wireless networks. Simulation results show that the network re-healing time can vary from a few seconds to several minutes. This suggests a new ad hoc routing protocol will be needed as current routing protocol may not work with such long re-healing times for most of them are designed under an assumption that the networks are full and well connected.

Bibliography

Primary Literature

1. Naumov V, Baumann R, Gross T (2006) An evaluation of inter-vehicle ad hoc networks based on realistic vehicular traces. In: Proceedings of ACM MOBIHOC'06, Florence, pp 108–119
2. Lochert C et al. (2003) A routing strategy for vehicular ad hoc networks in city environments. In: IVS'03, pp 156–161
3. Menouar H, Lenardi M, Filali F (2005) A movement prediction-based routing protocol for vehicle-to-vehicle communications. In: First international vehicle-to-vehicle communications workshop, co-located with MobiQuitous 2005, V2VCOM 2005, San Diego
4. Granelli F, Boato G, Kliazovich D (2006) MORA: a movement-based routing algorithm for vehicle ad hoc networks. In: IEEE workshop on automotive networking and applications (AutoNet 2006), San Francisco
5. Menouar H, Lenardi M, Filali F (2006) An intelligent movement-based routing for VANETs. In: ITS world congress 2006, London
6. Kieß W, Füßler H, Widmer J, Mauve M (2004) Hierarchical location service for mobile ad-hoc networks. Proc ACM SIGMOBILE Mobile Comput Commun Rev 8:47–58
7. Christian L, Martin M (2005) Geographic routing in city scenarios. ACM SIGMOBILE Mobile Comput Commun Rev Arch 9(1):69–72
8. Frey H, Stojmenovic I (2006) On delivery guarantees of face and combined greedy face routing in ad hoc and sensor networks. In: Proceedings of the ACM annual international conference on mobile computing and networking (Mobicom), Los Angeles
9. Lochert C, Hartenstein H, Tian J, Füßler H, Hermann D, Mauve M (2003) A routing strategy for vehicular ad-hoc networks in city environments. In: Proceedings of IEEE IV'03, Columbus, pp 156–161
10. Naumov V, Gross TR (2007) Connectivity-aware routing (CAR) in vehicular ad-hoc networks. In: Proceedings of 26th IEEE international conference on computer communications (INFOCOM'07), Anchorage, pp 1919–1927
11. Zhao J, Cao G (2006) VADD: vehicle-assisted data delivery in vehicular ad hoc networks. In: Proceedings of 25th IEEE international conference on computer communications (INFOCOM'06), Barcelona
12. Nzouonta J, Rajgure N, Wang G, Borcea C (2009) VANET routing on city roads using real-time vehicular traffic information. IEEE Trans Veh Technol 58(7):3609–3626
13. Jerbi M, Senouci S-M, Rasheed T, Ghamri-Doudane Y (2009) Towards efficient geographic routing in urban vehicular networks. IEEE Trans Veh Technol 58(9):1–1
14. Wisitpongphan N, Bai F, Mudalige P, Sadekar V, Tonguz O (2007) Routing in sparse vehicular ad hoc wireless networks. IEEE J Sel Area Commun 25(8):1538–1556

Books and Reviews

Lee KC, Haerri J, Uichin L, Gerla M (2007) Enhanced perimeter routing for geographic forwarding protocols in urban vehicular scenarios. In: 2007 IEEE Globecom workshops, 26–30 Nov 2007, pp 1–10

Vitrification of Waste and Reuse of Waste-Derived Glass

Enrico Bernardo, Giovanni Scarinci, Paolo Colombo
Department of Mechanical Engineering – Materials Division, University of Padova, Padova, Italy

Article Outline

Glossary
Definition
Introduction
Advantages and Prospects of Vitrification
Treatment of High-Level Radioactive Waste
Vitrification Processes and Plants
Waste Sources
Valorization of Waste-Derived Glasses
Future Directions
Bibliography

Glossary

Crystallization Crystallization is the formation of crystals (i.e., a solid phase possessing short-, middle-, and long-range order) from a liquid or a solid. It occurs via a process consisting of two steps: nucleation and crystal growth. During nucleation, the structural units (atoms, ions, or molecules) spontaneously arrange themselves according to a regular geometry, which is specific for the crystal phase being formed. If this cluster, typically of the order of a few nanometers, has reached a critical size, which depends on the operating conditions (temperature, supersaturation, etc.), it becomes thermodynamically stable. The crystal growth is the subsequent growth of the nuclei that succeed in achieving the critical cluster size. In a crystal, the constituents are arranged in a defined and periodic manner (unit cell) that defines the crystal structure.

Durability Durability is the ability of a substance (or a structure) to withstand the interaction with the surrounding environment without detrimental effects for its properties. Highly durable materials can be subjected to a variety of chemical attacks without significant release of constituents (leaching) or decrease in their physical-mechanical characteristics.

Glass A glass is an inorganic solid material whose structure does not possess any middle- or long-range order. This condition is referred to as an amorphous (in comparison to crystalline) phase, featuring the distinctive phenomenon of glass transition. The most common glasses are based on oxides, and their composition may vary in a very wide range of values. A formal definition of glass is that it is an inorganic product of fusion, which has been cooled through its glass transition to the solid state without crystallizing.

Glass-ceramic A glass-ceramic contains both an amorphous phase and one or more crystalline phases. They are produced by a so-called, deliberate "controlled crystallization" process, which involves keeping the material for a certain time at temperatures at which the crystals first nucleate and then grow within the amorphous (glassy) matrix. In comparison to glasses, glass-ceramics possess a wider ranging set of thermo-mechanical properties.

Hazardous waste Waste are unwanted or unusable materials, which derive from natural or human (civil and industrial) processes. Hazardous waste are waste that pose substantial or potential threats to public health or the environment, and they can be flammable, radioactive, corrosive, toxic or have a genetic, carcinogenic, mutagenic, and teratogenic potential.

Vitrification Vitrification is the transformation of a substance into a glass, typically accomplished via a process involving the formation a liquid phase at high temperature, in the presence of an adequate content of vitrifying oxides (i.e., the so-called "network forming oxides," normally SiO_2, B_2O_3, P_2O_5). This subsequently cools to a solid without the formation of any crystalline phases. In this context, the substance of interest is hazardous waste, with the addition or not of additional glass-forming raw materials.

Definition

In the context of various technologies for the disposal of waste material, vitrification has proved to be the safest technology for the treatment and remediation of noncombustible hazardous waste. Vitrification is a process comprising the thermal destruction of waste. It is performed by melting the waste at high temperature, if necessary with the addition of glass-forming oxides (notably silica), and then cooling the melt quickly enough to prevent crystallization. In this process, the organic fraction is decomposed and burned off, whereas the inorganic fraction is stabilized by embedding its constituents at the atomic level within the glass network. The ability of glass to incorporate nearly all the elements of the periodic table into its structure is of fundamental importance: if formulated with an adequate composition, the resulting glass features a high chemical inertness, so that it can be landfilled without any particular concerns but it can also be recycled as secondary raw material for the manufacturing of new products.

In the early 1960s, it was first recognized that the immobilization of high-level radioactive waste (HLW) in glass was the most appropriate treatment to obtain an extremely durable and long-term stable waste form. After the establishment of the first vitrification plant of

Marcoule (France), more advanced vitrification systems have been developed and used in the USA, the UK, France, Germany, Belgium, Japan, and Russia. At present, vitrification is internationally still accepted as the best demonstrated available technology for the treatment of HLW [1, 2]. Given the excellent results achieved by HLW vitrification, in the 1980s and 1990s the technology of vitrification was gradually extended to other types of hazardous waste, and various types of melters – such as Joule-heated melters, electric arc furnaces, and plasma torch melters – were tested and commercialized. In Japan, because of the high cost and scarcity of available landfill sites, vitrification of municipal solid waste (MSW) incinerator residues (bottom ash and fly ash, containing hazardous substances such as heavy metals and dioxins) was developed in the 1980s, and has been in operation in a great number of MSW incineration facilities [3]. By this process, dioxins and furans in the residues are decomposed in the furnace at a temperature of approximately 1,400°C, and metallic compounds are stabilized in the structure of the product. In the USA, vitrification technologies were successfully commercialized [4–6] in the same period for the inertization of high-volume waste, including municipal sludge, paper sludge, soils, and dredged sediments. In this way, the need for disposal was eliminated and a glass aggregate was produced, marketable for many construction uses. During the 1980s, in situ vitrification earth-melting technology was developed by Battelle Memorial Institute [7] for DOE (US Department of Energy) and commercialized in the USA as GeoMelt^{TM} technology [8]. This method can be utilized for treatment of soils contaminated with high concentrations of both organic and inorganic polluting substances, and is the preferred methodology when there is need to avoid the risk connected with the excavation of the waste. Many applications of the in situ vitrification technology were carried out in the USA and Australia for the decontamination of polluted sites and soils. In the last years, plants based on the plasma torch melting technology have been realized in France for asbestos and fly ash vitrification [9].

Despite the soundness of vitrification technology, confirmed by numerous scientific studies and experimental tests, it has found difficulties in establishing itself. In fact, a cost analysis for vitrification [10], in comparison to other inertization options such as chemical processes or solidification/stabilization treatments, has shown that limited opportunity exists for a viable application of this process. An extensive use of vitrification can be carried out only when the absolute necessity of environmental safety has priority over cost, as is the case for radioactive waste. However, if the glassy material obtained by waste vitrification instead of being landfilled or used as inert aggregate for road foundations or other low value applications will be transformed into value added and competitive products, it will be possible not only to offset its production costs but also to make a profit. In the past years, a lot of experimental research has demonstrated the feasibility of such a transformation, with the realization of glass-ceramics, cellular glass, glass fibers, and other products from a variety of inorganic hazardous waste. Furthermore, recent studies have highlighted the possibility of utilizing the glass obtained from waste as a secondary raw material in manufacturing processes of ceramic articles of large consumption, such as bricks or paving tiles.

Introduction

Waste can be, in a first approximation, divided in two main categories: organic and inorganic waste, and each category includes both hazardous and nonhazardous waste. Organic waste are combustible, and today incineration of organic waste of all kinds (hazardous and not-hazardous) is the most common destruction treatment throughout the world, as it is easy to set up and operate and the heat generated can be utilized. A large variety of hazardous organic waste, including pesticides, polychlorinated biphenyls (PCBs), and persistent organic pollutants (POPs), is at present destroyed with very high efficiency by dedicated incinerators [11]. Inorganic hazardous waste derive mostly from many types of industrial processes, particularly in the metallurgical, steel, and chemicals production areas, but can come also from the demolition of buildings and civil infrastructures (realized, e.g., with cementitious materials containing asbestos), or form as a residue in many combustion processes, as the bottom and fly ashes produced by municipal solid waste (MSW) incineration plants. They require to be rendered inert before their landfill disposal or recovery, and their inertization can be achieved through chemical and physical processes such as: (1) stabilization using chemical agents, (2) extraction using acid or other solvents, (3) calcination at high temperature, (4) stabilization-solidification,

and (5) vitrification. The last two processes immobilize pollutants in a suitable matrix that indefinitely prevents their release into the environment upon disposal or reutilization. The goal is therefore that of reducing the polluting potential and the hazardousness of the waste, making them suitable for subsequent treatments (landfill disposal or recovery).

Stabilization-solidification processes include two stages: the first (stabilization) decreases the waste hazardousness by converting the chemical contaminants in a less soluble, less mobile and less toxic form; the second (solidification) only affects the physical state of the waste, turning them into a solid material with high structural and chemical integrity, thereby decreasing the mobility of pollutants. These processes can be carried out using thermoplastic or thermosetting polymers (which are however not frequently used because of their cost), or inorganic reagents such as cement, lime, or clay. However, in the latter case they increase the volume of waste, do not thermally decompose hazardous organics and do not give sufficient long-term guarantees in terms of the release of pollutants in the leachate [12].

Vitrification consists of the immobilization of hazardous waste, predominantly inorganic or with a low content of organics, in an inert amorphous matrix in the form of oxides, which, soluble in the molten glass at high temperatures, are then homogeneously incorporated into the vitreous structure following the cooling of the melt. It is therefore possible to successfully exploit one of the main characteristics of glass, which is to be a material characterized by high chemical stability that can contain a huge variety of pollutants in the form of oxides [12]. Hazardous waste can be vitrified by melting them and then cooling the melt at a rate sufficient to avoid crystallization. The waste, however, do not necessarily have to be intrinsically vitrifiable: if its composition does not contain enough glass-forming oxides (notably silica), it can be appropriately corrected through the use – to keep cost down – of vitrifying substances which are themselves waste, such as glass cullet or residues from the processing of feldspars. Glass cullet is particularly useful also as a low-cost flux to reduce the glass working temperature when this is too high, thereby helping to limit the cost of the process. Given the large quantity of thermal or electrical energy needed to melt the waste, the vitrification process is more expensive than others. Nevertheless, it is becoming increasingly important considering the rising cost of landfill, the exhaustion of available landfill sites and the hostility of the people toward the opening of new ones. Furthermore, the tightening of controls and sanctions against illegal disposal procedures and the enactment of increasingly stringent legal standards – which require preventive inertization of hazardous wastes – have given a significant boost to the technology of vitrification in all the most advanced countries.

Advantages and Prospects of Vitrification

The main advantages of vitrification can be summarized as follows:

1. Flexibility of the process, which allows to treat many types of waste, such as sludge, contaminated soil, ash, slag from hazardous processing, wet and dry solids (including asbestos, whose microfibers are destroyed only by heat), in large and variable proportions, often without the need for preliminary treatment
2. Destruction of all organics (including the most toxic substances such as dioxins and furans) with an efficiency exceeding 99.99%
3. Complete immobilization of the hazardous inorganic substances (such as heavy metals, radioactive elements, etc.) within the glassy network in ionic form
4. Substantial reduction in volume of the treated waste (from 20% to 97%, depending on the type of waste)
5. Good mechanical and thermal properties of the vitreous product
6. Excellent chemical stability and durability of the product, that is, resistance against attack from water or other chemical agents. Consequently, low environmental impact and possibility of landfill disposal without any problem, because any inorganic contaminant is retained permanently (any leakage of contaminants is so slow that no detectable adverse environmental effects are produced)
7. Well-established technology

The certainty that vitrification is the best available technology to ensure that the inertized waste do not

release toxic substances stems from the fact that it is the only process that has been adopted, since more than 40 years, for the long-term inertization of high-level radioactive waste in all countries that produce nuclear energy. Nevertheless, vitrification has been slow to become established in the field of hazardous waste inertization because it is expensive (for the high consumption of energy required to produce the oxide melt). Therefore, cheaper and easier solutions have been preferred, such as the immobilization in cementitious matrices (albeit less safe in the long term), the disposal in special landfills, or even illegal disposal methods (used for unspecified, but certainly very significant quantities of waste). However, if the glass obtained by vitrification, instead of simply being disposed of as an inert material or used for low value applications (e.g., road foundations, reinforcing filler for asphalt, drainage aggregates, the containment or consolidation of buildings and constructions, etc.), is transformed into value-added and competitive products, its intrinsic processing cost will be remunerated and may be even possible to make a profit. It should be noted that vitrification is the only method that allows such a transformation of the inert materials produced.

In terms of experimental research (especially in Italy, Britain, and Spain), over the past few years cellular glass for thermal and acoustic insulation, glass-ceramic materials for building applications (such as paving tiles), insulating or reinforcing vitreous fibers, glass, or glass-ceramic matrix composites were obtained, while just a few plants for the production of insulating fibers have been so far realized at an industrial level.

Treatment of High-Level Radioactive Waste

In the 1960s, it was recognized that the immobilization of high-level radioactive waste (HLW) in glass was the most appropriate treatment to obtain an extremely durable and long-term stable waste form. Significant advantages of the glass waste form include, in fact, its tolerance in terms of variability in chemical composition and its processability. At present, vitrification is internationally still accepted as the best demonstrated available technology [1, 2]. Since the combination of high temperatures and high-level radioactivity in the course of the vitrification process requires particularly sophisticated technologies to meet all safety requirements, a large number of experiences and tests was carried out in the past. The vitrification plant of Marcoule (France) was the first one starting worldwide to operate with HLW originating from spent fuel reprocessing plants (1978) [13]. The process was carried out in two stages: in the first one, successive steps of evaporation, drying, and calcination of the waste and the addition of borosilicate glass frit slurry were performed in a rotary tube; in the second one, the calcined product was melted – in a discontinuous process – inside a metallic pot heated by a multi-zone induction furnace. The melt, after homogenizing, was drained into a stainless steel canister, where it solidified transforming into an inert and stable glass form. The canister was then sealed and decontamined to be isolated in a deep geological formation. Emissions generated in the melter from the vitrification process were treated by an off-gas system to remove radioactive contamination and destroy nitrogen oxides (NOx). This technology was adopted by the vitrification plants in La Hague (France) and, with a few modifications, in Sellafield (UK), in the 1980s.

Because of the limited throughput and short melter life – the latter due to high temperatures glass corrosion – a more advanced vitrification system was then developed, starting from the second half of the 1970s [14] based on a Joule-heated ceramic melter (JHCM). In the JHCM, thermal energy is generated by passing an electric current through the molten glass across multiple pairs of electrodes. Since glass in the molten state is an ionic conductor of electricity, it can increase its temperature due to Joule effect. This technology was developed mainly in the USA [15] and, afterward, in Germany [16]. Operational plants were built in Belgium (Mol), the USA (Savannah River, West Valley), and Japan (Tokai Mura). At present, JHCM technology is the standard vitrification method for high-activity waste worldwide. Advantages of the JHCM over metallic pot induction heated melters are: capability for direct liquid feeding, higher throughput, enhanced life of the melter (whose walls are made of high corrosion resistant alumina-zirconia-silica refractory), and better operational flexibility, due to an unrestrained heat transfer area and the possibility of adopting a continuous mode of operation. Limitations of the process are: shortened life of the electrodes (if they

are utilized at temperatures in excess of 1,200°C), possibility of electrical short-circuiting (causing failures in the melter) due to redox conditions and presence of free metal, and difficulties in the decommissioning of the ceramic melter at the end of its life.

In the last few years, a new attractive technology has been emerging, that is, cold crucible induction melting (CCIM) [17]. This process is a modification of induction heating in which cooling is applied to form a protective layer of solidified glass on the internal walls of the crucible. This technology looks very promising for the future, and could be applied to many other types of hazardous waste, in addition to radioactive waste.

Vitrification Processes and Plants

The various vitrification processes can be distinguished according to the heating method employed in the furnace, into which the waste to be vitrified are continuously fed. High temperatures are generally used, and often the heterogeneous nature of the waste may give rise, in addition to the vitrified material itself, to other products that must be removed safely. For example, molten metal can be deposited at the bottom of the furnace, while at the surface a thin layer of liquid salts can form, especially if the batch contains a significant amount of chlorides, sulfates, or other species of limited solubility in molten glass. The output stream of gas and vapors is comprised (besides of the combustion products) of organic substances, often found in the batch, or their pyrolysis products, the most volatile heavy metals (such as mercury and cesium), particularly if reduced by carbon or other reducing substances contained in the feed, heavy metals, chlorides, particulate (dust), etc. These substances must be properly separated and collected, or chemically treated, to be recycled in the process or disposed of separately in a landfill. Thus, it can be inferred that the choice of a vitrification process cannot be limited to a simple choice of the melter, but should also consider systems and installations for the treatment of secondary effluent.

The main types of melters used for the vitrification of waste are:

Furnaces based on conventional combustion [18–22]. The thermal energy necessary for waste melting is provided by the combustion of natural gas, fuel oil, or coke. These melters can be of various types:

- *Tank melters*, such as those used in the production of flat or container glass, but with some modifications. The waste feed is introduced onto the glass pool, which is contained in a refractory-lined tank. Burners are directed at the waste feed to provide the required energy. These melters are characterized by high reliability, long life, ability to vitrify waste of very different composition.
- *Cyclone melters*, in which the particulate waste feed is incorporated in the flowing combustion gases which are forced to spiral around the inside of the melter. In this way, the particles are melted and the melt runs down the walls of the cyclone toward an orifice in the bottom. Although the high processing rate is advantageous, the control of composition and other processing parameters may be difficult. These melters, similarly to rotary furnaces, are often preferred in the presence of a high content of organic matter, but can give an inhomogeneous melt, requiring an additional conditioning unit.
- *Surface melting furnaces*, in which the waste are pushed onto the refractory-lined furnace floor, whose inclined surface receives radiation heat from burners located on the roof.
- *Small-scale blast furnaces*, which use coke for burning, but the highly reducing processing conditions increase the loss of heavy metals, chlorides, and sulfur in the form of gaseous effluents.

Ultimately, the disadvantages of all these melters consist especially in the volatilization of heavy metals, in particulate-rich exhaust gases and in the large volume of off-gases, which must be purified in high cost facilities. The use of oxygen instead of air as oxidizer increases the direct operating cost, but decreases by over 70% the volume of effluent gases, greatly reducing the capital and operating costs of the purification systems.

Fluidized bed gasifying melting systems [23]. A new technology for the incineration of waste has been developed in Japan [24]. The waste, milled and dried if necessary, are treated (at temperatures between 500°C and 650°C) in a fluidized bed gasifying plant, with the generation of a gas stream and a solid residue. Both of these products are then completely oxidized (at temperatures between 1,250°C and 1,450°C) in a two-stage vortex combustion plant, in which dioxins are completely destroyed and the ashes are melted to

obtain a vitreous slag. The gas enthalpy is recovered in a particular heat exchanger with circulation of alumina grains, which enables preheating of the combustion air without problems of fouling or corrosion. The gaseous effluents are then cooled, de-pulverized by bag filter, and treated by a NOx destruction system.

Electric furnaces heated by Joule effect [5, 18, 19, 21, 22]. In this type of melter, an electric current is passed by ionic transport through the molten charge from one electrode to another between which a potential difference is applied. The electrodes (one or two couples) are positioned in the hearth or in the side walls of the melter and are immersed in the melt. The electric energy of the current is dissipated as heat by Joule effect, with a very high conversion efficiency. Since the electrical conductivity of the initial solid charge is negligible and starts to have an appreciable value only above ~800°C (when the heated material gradually melts and becomes an electrolytic conductor), the charge must first be melted by a secondary heating system (e.g., by resistors or by special burners). Once the initial charge is completely melted, further batch is fed continuously from the top of the melter and, falling into the melt, is in turn heated and fused at expense of the available energy, while in parallel a certain amount of molten glass is discharged from the melter. The molten material is more or less conductive depending on its chemical composition, and this should be taken into account for setting the temperature of the process, since electric conductivity increases with temperature. The lack of combustion gases entails a drastic reduction of the gaseous effluents; their volume may in fact be even two orders of magnitude smaller than for combustion-based melters, so off-gas treatment plants (needed in the presence of hazardous organic materials) are of minimal size and rather simple. This type of melter is particularly suited to process homogeneous inorganic materials that are finely divided, such as sludge, soils, and crushed concrete. To increase the efficiency of the process, the feedstock must be accurately controlled; if it is not finely divided, it is slow to dissolve and, besides, inappropriate materials can slow down the melting or even corrode the electrodes. The molten material, once extracted from the melter and cooled, solidifies in a glassy form. To achieve the waste vitrification, that is, its complete transformation into a homogeneous and chemically durable glass, vitrifying additives (to be chosen among other waste, e.g., cullet) may be added and intimately mixed to the charge before it is fed to the melter.

Joule-heated melters have a refractory-lined cylindrical chamber made of stainless steel and cooled by a water jacket. An opening on the bottom allows for the discharge of molten material through a channel. The crown, that is also refractory-lined, has an opening for the introduction of the feedstock and one for the off-gas release (see Fig. 1). To prevent the volatilization of heavy metals, cold top Joule-heated melters are used, that is, with the melt surface kept at low temperature, because it is covered by a layer of feedstock continuously supplied and not yet melted. In this case, the volatile substances released at the bottom of the furnace, which is warmer, ascend and condense upon contact with the cold top, and are then mixed again with the residual melt by convection currents. Even salts (as chlorides or sulfates) condense, forming a liquid layer at the interface between feedstock and melt, and can be removed with special drainage techniques. The cold blanket acts as a thermal insulation shielding the crown from thermal radiation; the crown thus remain at low temperature and the off-gas is cooled (to about 150°C). Additional heating elements at the top of the melter (hot top Joule-heated melters) can be inserted to obtain the complete destruction of hard to treat hazardous organics, but in this case there is an increase of particulate and volatile species in the

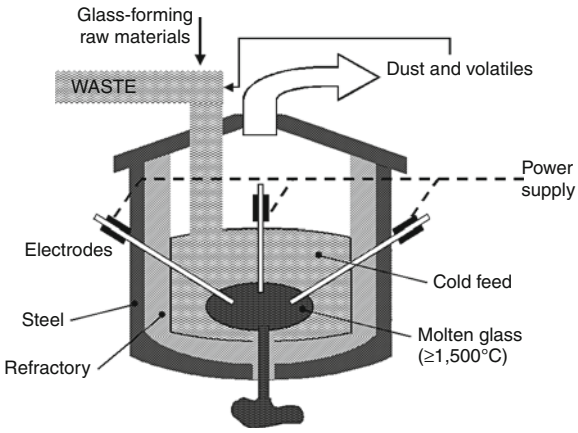

Vitrification of Waste and Reuse of Waste-Derived Glass. Figure 1
Sketch of an electric furnace heated by Joule effect

off-gas. Intensive stirring inside small volume Joule-heated melters results in high throughput. The electrodes, usually made of molybdenum or graphite, are corroded by free metals if they are contained in significant amounts in the waste, so that very small quantities of unoxidized metals can be tolerated. In some cases, more expensive electrodes (made of tin oxide or chromium oxide) can be utilized. The type of electrode used may strongly influence the maximum operating temperature. Moreover, the free metals can alter the electric current distribution within the melt and cause a significant decrease in the efficiency of the process. Both water and organic substances in the feedstock should never exceed 5 wt%, as they require large amounts of energy for heating, evaporation, gasification and molecular dissociation, as well as an increase in the cost of the plant because of the need of an off-gas treatment equipment. In any case, to ensure process reliability parameters, a careful formulation of the batch composition is required.

Terra-Vit melter [25, 26]. The Terra-Vit melter was designed to increase the life of the melter and reduce capital and operating costs. It is a Joule-heated melter and consists basically in a pit of semi-spherical form, that is excavated in the ground and covered by a refractory brick roof. Electrodes are introduced into the molten pool through holes in the roof; their position must be such as to limit corrosion and erosion of side walls and floor, which are lined with refractory clays and can be water-cooled to further limit corrosion. Waste is continuously fed through the roof onto the molten pool and melts progressively. The molten material is discharged through an opening in the wall, located at the same level of the melt surface. If the waste contains organic or combustible fractions, oxidation air is blown onto the molten pool surface. It is also possible to add some coal to the waste to burn these components and therefore lower the energy costs. If the waste feed contains steel or other metals, they melt and accumulate on the bottom of the melter, and must be oxidized with injected air.

Electric arc furnaces [18–22]. This technology has been adopted from steelmaking, and is most applicable to mainly inorganic, dry waste. The melting of the feedstock is caused by the heat produced by means of the arc generated by an electrical three-phase current passing through three graphite electrodes, which penetrate into the furnace (see Fig. 1). The previously dried solid charge is fed from the top of the furnace and falls, spreading out, on the already melted material. The furnace operates at high temperature (>1,400°C), and therefore any ferrous materials contained in the charge can be melted evenly within a short time. The slag exceeding a given level is continuously released from the melting tank through a refractory channel, in which an additional electrode can be inserted. The melted slag is then quenched with water and carried out by conveyor. Any organic components in the charge are burnt completely in this type of furnace, and are then removed by the exhaust gas. The atmosphere within the furnace is maintained oxidizing and there are no water-cooled parts; therefore, risks of explosion are minimized. These furnaces are characterized by structural simplicity, low thermal losses, and high throughput.

Plasma torch furnaces [27–30]. The process is similar to that which occurs in electric arc furnaces, except for the use of a thermal plasma to convey the arc energy. The electric arc is generated by a potential difference applied between two electrodes, and may be either of a non-transferred (both the metallic electrodes are confined within the torch) or a transferred type (from one electrode inside the torch to another of graphite inside the hearth). The electric arc overheats a processing gas (air in case of waste) flowing inside the torch, causing its ionization. The thermal plasma thus obtained may reach very high temperature (even higher than 15,000°C), and heat transfer occurs mostly by radiation. The plasma jet hits with high energy density a limited area of the waste, whose temperature is raised to 3,000–4,000°C. The organic substances contained in the waste undergo sublimation, molecular scission, reforming reactions, and carbon oxidation by steam injected in the kiln in a controlled amount (e.g., $C + H_2O \rightarrow CO + H_2$), with complete gasification and production of a synthetic gas named "syngas." Syngas is a fuel gas which is composed primarily of H_2 and CO, with varying percentages of N_2, CO_2, water vapor, CH_4, and other light hydrocarbons (depending on the chemical composition of the feedstock). It undergoes various cleaning treatments aimed at (a) removing particulate matter (which is then collected and batch-fed back into the plasma vessel), (b) hindering the formation of dioxins and furans by quenching from

high temperatures, (c) performing selective catalytic reduction of NOx, and (d) dissolving any acid gas and other inorganic ions (chloride, fluoride, sulfate, phosphate, sodium, and calcium) into the liquid of a packed column scrubber. After purification, syngas can be used as fuel for electricity generation, or for the production of precursors (e.g., methanol, ethanol) for the chemical industry or for the separation of pure hydrogen through ultrafiltration. The hydrogen from syngas can find use in the petrochemical (hydrogenation of petrol) or food (hydrogenation of fats) industry, and in hydrogen fuel cells which can power transportation (cars, trucks, buses, and ships).

The inorganic fraction of waste treated by plasma is melted and transformed, after being extracted from furnace and cooled, into a vitrified material similar to a glassy volcanic rock such as obsidian, in whose matrix the heavy metals (together with any contaminant from the syngas purification sections) are incorporated and completely inertized. The obtained material, because of its very low leachability, can be utilized without environmental risks as secondary raw material for road embankments, concrete mix, filling, etc. The plasma vessel is a cylindrical stainless steel container, lined with refractory materials, that is maintained at a slight negative pressure to ensure that no gases can escape to atmosphere. The plasma torch is inserted in the crown (see Fig. 2a); there are openings for the introduction of solid, liquid, and gaseous feedstock, by themselves or in any proportion or combination, and an exit port in the bottom part to remove excess molten material (followed by cooled rollers – see Fig. 2b – or not, with the direct casting in metal containers – see Fig. 2c).

The advantages of this technology are:

- Very wide flexibility (it is possible to treat every kind of waste materials – even those containing large amounts of metals – in any physical state and with large variations in composition and ratio between organic and inorganic components).
- The power input can be quickly adjusted to match process requirements.
- The process can be stopped and restarted easily, eliminating the need for large waste storage.
- High efficiency – because of very high temperatures – of destruction of organic compounds (including hazardous organic micropollutants such as dioxins, furans, and polycyclic aromatic hydrocarbons).
- Lack of waste products (particulate and sewage sludge from the cleaning treatments of the syngas are sent back to the reactor to be vitrified).
- Compact plant (and consequent possibility of realization of mobile units).

The drawbacks of this technology are: limited yield of the plant, very expensive technology because of the high energy consumption (much higher than for other types of furnaces) and frequent maintenance operations (duration of the torches is very limited, because of the consumption of electrodes). Moreover, the maximum water content in the waste to be treated must be less than 10 wt% and the net heat value of the waste must be at least 12–15 MJ/kg, otherwise the whole process becomes uneconomical.

Because of these reasons, plasma technology is particularly suited for the treatment of hazardous waste which require very high temperatures to be totally destroyed (e.g., concentrated organic waste types, including PCBs, pesticides, and persistent organic pollutants) and therefore cannot be eliminated by using technologies such as incineration, gasification, or pyrolysis, or need operating conditions that can minimize the risk to human health and the environment (e.g., asbestos containing waste, fly ash from incineration of MSW, hospital waste, etc.).

Cold-crucible induction melters [17, 31, 32]. This technology has been so far mainly applied to the vitrification of highly radioactive waste. The metallic crucible of an induction heated melter is cooled in order to cause the formation, on its inner walls, of a solidified glass layer, which protects the crucible against glass corrosion. The inductive coupling of a water-cooled high frequency electrical coil with the glass causes eddy currents with the production of heat and effective stirring of the melt. Since the molten glass is contained inside a frozen layer of the same composition, and because of the lack of electrodes, no contamination can occur and melts with high purity are attainable. As there are no limitations arising from the corrosion of refractories or failure of the electrodes, high process temperature (up to 3,000°C) can be achieved for the treatment of waste otherwise difficult to process.

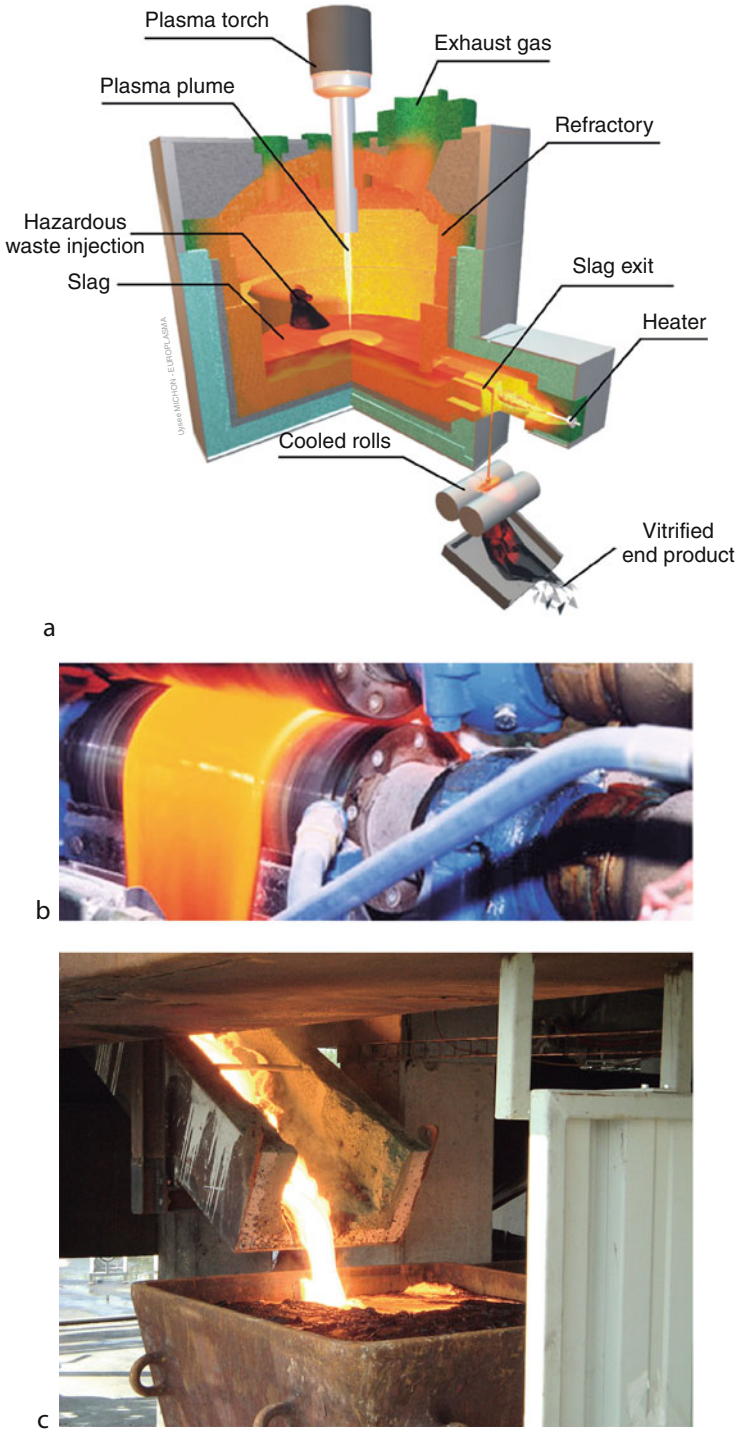

Vitrification of Waste and Reuse of Waste-Derived Glass. Figure 2

(**a**) Example of a plasma torch furnace; (**b**) vitrified MSW incinerator fly ash cooled between rollers; (**c**) pouring of vitrified asbestos-containing waste (Courtesy of Dr. Erika Edme, Europlasma, Bruges, France – http://www.europlasma.com)

Moreover, the reaching of high temperatures increases the processing rate and allows for greater throughput.

In addition to employing variously heated melters, two other vitrification technologies are currently in use, namely direct in situ vitrification and self-sustaining vitrification.

In situ vitrification [7, 8]. In situ vitrification (ISV) is a waste treatment technology that uses electrical power to melt in place contaminated earthen media such as soil, sediments, and mine tailings. It has been marketed by GeoMelt^{TM} (Richland, WA-USA) from the early 1990s and has been applied the first time at a Superfund site in Grand Ledge, Michigan (1993–1994) to treat soils and sediments contaminated with pesticides, metals, and dioxins. Afterward, several contaminated soils and debris have been successfully remediated in the USA, Japan, and Australia. This type of vitrification technology consists of four electrodes (placed symmetrically and fed by a two-phase alternating current), which are immersed into a portion of the contaminated soil circumscribed by the electrodes and melt it completely, causing its vitrification into a monolithic block. The solid ground, poorly and only occasionally conductive, is initially heated to melting by inserting between the electrodes (to which a potential difference is applied) a conductive medium, formed, for example, by a strand of glass fibers, in itself highly insulating, impregnated by electrically conductive graphite. When power is supplied to the electrodes, this medium conducts the current through the soil, heating the surrounding area and forming a pool of molten soil at the surface of a treatment zone between and directly adjacent to the four electrodes. The electrically conductive molten pool serves then as the heating element for the process, wherein electrical energy is transformed into heat by Joule effect. As the soil becomes molten, the electrodes are lowered further into the soil, continuing the melting process to the desired depth of treatment. In this way, the molten mass grows outward and downward (up to a maximum area of ~12 m in diameter and to a depth of 6–7 m), thereby creating individual batch melts at an average rate of approximately 3–4 tons per h. Melt temperatures are in the range of 1,500–2,000°C, and energy consumption varies from 500 to 800 kWh/ton in most applications, so that the process is very efficient. When the desired volume has been melted, power is shut off and the molten mass cools to form a hard, monolithic product of glass and crystalline material that incorporates and immobilizes the inorganic compounds and metals. This material is stable and chemically inert, with very low leaching characteristics, and is effectively and permanently isolated from the surrounding environment. The high temperature of the melt promotes pyrolysis and/or vaporization of all the organic substances in the hot soil surrounding the melt. Consequently, organic contaminants and any other volatile constituent escape and migrate to the surface. In the GeoMelt^{TM} system, a dome-shaped hood completely covers the treatment area, supports the electrodes and collects the gaseous emissions, which are then conveyed to the wet and dry off-gas treatment system. Combined with the destructive action of the melt, the off-gas treatment system contributes with very high efficiency to the further destruction and/or removal of trace quantities of contaminants present in the off-gas. The ISV equipment is mobile and can be repositioned in another area of the contaminated soil after any treatment. It is also possible to collect, melt, and vitrify waste of different types, or coming from different locations, that are enclosed in one or more reusable cells. Cost is affected by the depth of the contamination, the degree of homogeneity of soil, the presence of debris, and excess moisture. Moreover, in several countries the price of electricity can be an important factor. The generally high cost of the process makes it especially suited for hard to treat hazardous wastes, such as mixtures of metals and organics. The process is highly effective for remediating soils contaminated with heavy metals (including Cr, Pb, Cd, and As) and virtually all chlorinated organic compounds (including solvents, pesticides, herbicides, dioxins, furans, and poly-chlorinated biphenyls). Even sites contaminated by radioactive materials have been successfully remediated using the GeoMelt^{TM} process.

Self-sustaining vitrification [10, 33]. Self-sustaining vitrification uses the energy released during exothermic chemical reactions (similar to the well-known thermite reactions) that occur in a mixture of waste and powder metal fuel (PMF) to form a melt, which cools down to produce a glass-like material. The process is controlled by the composition of the initial mixture of dried and crushed waste and PMF; it does not require either an external power supply or large and expensive

equipment, and it is economically viable particularly for small volume hazardous waste. PMF is a specially designed blend of heat generating components; generally, it consists of combustible powder metals (as Al, Mg), oxygen-containing components, and some additives such as stabilizers and surface active substances. A suitable PMF composition must: (1) release an amount of heat sufficient to sustain waste melting without external heating, (2) produce a glass-like end product binding contaminants in its structure, and (3) minimize carryover of toxic chemicals, heavy metal vapors, oxides, and radionuclides. After initial ignition, a combustion wave propagates within the mixture at a velocity of ~1 mm/s; PMF must therefore be tailored in order to maintain the reaction parameters within a controlled and stable range, providing a good quality product. Self-sustaining vitrification has been demonstrated to be a feasible immobilization technology for many types of waste, including radioactive waste, [33] contaminated soils [34] and ashes [34].

The vitrification technologies most suited to the treatment of waste are reported in Table 1, along with their main characteristics.

To summarize, several technologies are currently available for the vitrification of waste, and the choice of which one to adopt depends on several parameters, among which are: the composition, form, amount and geographical location of the waste to be treated, the cost of the plant itself (including treatment of off-gases), the cost of energy, the cost of labor, the flexibility in terms of waste composition accepted (a single plant could serve several industries, but then the cost of waste transport should be added), the issuing of economical incentives from local government agencies, the existence of local laws regulating the handling/recycling of special waste, etc. Therefore, the choice of the most suitable technology, even for the same typology of waste, will vary with the location of the plant and the local political and labor circumstances.

Waste Sources

A definition of hazardous substance or hazardous waste is neither easy nor simple. A legal definition of a hazardous waste by EPA (the US Environmental Protection Agency) is: (1) any waste or combination of waste of a solid, liquid, contained gaseous, or semisolid form which cause or significantly contribute to an increase in mortality or an increase in serious irreversible or incapacitating reversible illness, or (2) pose a substantial present or potential hazard to human health or the environment when improperly treated, stored, transported or disposed of, or otherwise managed [35]. EPA compiled a detailed list of hazardous materials that includes tens of thousands of chemicals, and pointed out six tests that enable to classify a substance as hazardous. These tests measure specific properties of the material, such as: (1) level of radioactivity, (2) bioconcentration, (3) flammability, (4) reactivity, (5) toxicity, (6) genetic, carcinogenic, mutagenic, and teratogenic potential. According to EPA, if a substance does not fail any of the six tests, it is not hazardous, and it is possible to dispose of it in ordinary landfills.

In the European Union, the List of Waste (formerly the European Waste Catalogue), is a catalogue of all waste types generated in the EU. It was established by Commission Decision 2000/532/EC of May 3, 2000 [36] and has been amended by Commission Decision 2001/118/EU, 2001/119/EU, and 2001/573EU. The List of Waste classifies all waste, whether intended to disposal or recovery, in 20 chapters (see Table 2), according to the activity that originated them. Each of the 20 chapters is grouped into subchapters and includes a detailed list of specific waste. Every waste is fully defined by a six-digit code, with two digits each for chapter, subchapter, and waste type. Hazardous wastes are those marked with an asterisk next to their appropriate identification code.

The European List of Waste is a harmonized list of waste and is subject to regular revisions and/or amendments, to take into account scientific and technical progress. Waste classified as hazardous are considered to display one or more of the properties listed in Annex III to Directive 91\689\EEC (Table 3) and, in reference to labels H3–H8, H10, and H11 of the said Annex, one or more characteristics related to their flash point or to the concentration limits of some specific pollutant contained in the waste (Article 2 of the Commission Decision 2000/532/EC, as amended).

There are test methods which serve the purpose to give specific meaning to the definitions reported in Annex III. The methods to be used are those described in Annex V to Directive 67/548/EEC, in the version as

Vitrification of Waste and Reuse of Waste-Derived Glass. Table 1 Main technologies used to vitrify waste

Vitrification technology	Heat source	Advantages (A), disadvantages (D), and limitations (L)
Combustion based melters (tank melters, cyclone melters, surface melting furnaces and small-scale blast furnaces)	Combustion (natural gas, fuel oil, or coke)	(A) High reliability, long life, ability to vitrify waste of very different composition (tank melters). High processing rate (cyclone melters) (D) High capital cost. Inhomogeneous melt, volatilization of heavy metals, particulate in the off-gas, large volume of the off-gas (to be treated in large and expensive depuration plants). Pure oxygen as combustion agent decreases the off-gas volume by over 70% (but extra-cost has to be considered)
Fluidized bed gasifying melting systems	Combustion (natural gas, fuel oil, or coke)	(A) Optimum thermal efficiency. Complete destruction of toxic contaminants as dioxins. Melting of ashes into a vitreous slag
Joule-heated melters (JHMs): cold top JHMs, hot top JHMs, intensively stirred small volume-high throughput JHMs	Electrical power (Joule heating, due to ionic conduction inside the melt)	(A) Drastic reduction of the off-gas volume and thus of the purification plant size. By employing cold top JHMs it is possible to hinder volatilization of heavy metals and to obtain salts condensation. With hot top JHMs complete destruction of hazardous organics is obtained (D) Free metals attack graphite or Mo electrodes and decrease the process efficiency (L) System particularly suitable to vitrifying properly divided homogeneous inorganic materials (mud, soils, and finely ground concrete). Careful formulation of the charge is required: water and organics must not exceed 5 wt%
Terra-Vit melter (JHM)	Electrical power	(A) Reduced capital and operating costs. Increased melter life
Electric arc furnaces	Electrical power (electric arc generated by three electrodes on the furnace top)	(A) Systems characterized by simplicity of construction, low thermal losses, high output. High process temperature (>1,400°C). Fast ferrous materials melting. Risks of explosion minimized (L) Technology most applicable to essentially inorganic, dry waste
Plasma torch melters	Electrical power (ionization of a process gas by the electric arc generated, and formation of a very high temperature plasma)	(A) Compact plant (mobile units can be used). Very high temperatures attainable. High efficiency of toxic organic compounds destruction. Very wide flexibility, that is, possibility of direct treatment of highly different types of waste, even containing large quantities of metals. Absence of waste products (D) Limited yield of the plant. Plasma torch melters consume more energy, need frequent maintenance and are less durable than combustion-based or electric furnaces (L) Technology most suited to waste requiring high destruction temperature or operating conditions that minimize risks to human health and the environment
Cold-crucible induction melters	Electrical power (induction heating of a water-cooled crucible)	(A) Crucible protected against corrosion. Effective stirring of the melt. High purity melts attainable. Very high processing temperatures achievable, if required
In situ vitrification	Electrical power (Joule heating of contaminated soils)	(A) Mobile equipment. High melting temperatures attainable. Highly effective process for remediating soils contaminated by heavy metals, chlorinated organic compounds and radioactive materials (L) High cost of the process makes it sustainable only for hard to treat hazardous waste

Vitrification of Waste and Reuse of Waste-Derived Glass. Table 1 (Continued)

Vitrification technology	Heat source	Advantages (A), disadvantages (D), and limitations (L)
Self-sustaining vitrification	Exothermic chemical reactions between powder metal fuel and the waste	(A) No need of external power supply. Large and expensive equipment not required (L) Technology most suited for small volume hazardous waste

amended by Commission Directive 84/449/EEC13, or by subsequent Commission Directives adapting Directive 67/548/EEC to technical progress. These methods are themselves based on the work and recommendations of the competent international bodies. Selected examples of important and representative categories of hazardous waste are reported in Table 4.

Vitrification has been investigated and successfully achieved for many of the waste listed in Table 4, and reports on the operation of vitrification plants can be found in the literature [37].

It should be stressed that the chief aim of vitrification is to produce a homogeneous glass possessing a high chemical durability, and detailed and complete tests have to be performed in order to be able to predict the long-term behavior of the material under the complex conditions prevailing in a repository environment or in an actual reuse of the glass. Because of the importance of this aspect, some studies tried to understand and predict the correlation between leaching behavior and composition of the waste or of the glasses [38, 39]. Furthermore, thermochemical modeling of oxide glasses or the determination of solubility limits of some pollutants in oxide glasses allows to predict crystal formation or phase separation, both greatly affecting leaching behavior [40, 41]. Some authors assessed the risk posed by leachates coming from waste-derived glasses (obtained from fly ash), proving indeed that they pose a minimum ecotoxicological risk, thus opening the possibility of reusing such glass for the development of commercial products [42].

The most frequently treated waste typologies will be briefly discussed below [43].

Slags from ferrous and nonferrous metallurgical industries are the first industrial waste that were vitrified with the aim of inertization and recovery producing, after crystallization, tiles possessing properties suitable for the building sector. The first example dates back to the early 1960s [44] followed by other examples, employing blast-furnace slag, which were reported in the early literature [45–47]. They are produced in large volume and are characterized by a high content in glass-forming and network-modifying oxides (SiO_2, Al_2O_3, CaO). In most cases, vitrification is followed by crystallization, either during cooling or via a controlled secondary heat treatment, and the process is facilitated by the presence of large amounts of elements prone to the formation of crystalline phases (such as iron oxides) or by the addition of suitable nucleating agents (such as TiO_2, Cr_2O_3, P_2O_5, sulfides, and fluorides) [44]. While blast-furnace (BF) slag is widely used in the cement industry, the vitrification route is at present the only treatment suitable for the recovery of basic oxygen furnace (BOF) slag (up to 60%, added to sand and Na_2O), because of its higher iron and lower silica content [48]. Compositional adjustment have been required in some cases to form a stable glass upon cooling. For instance, blast-furnace (BF) slag was added to ash from a coal-fired electric power station and a waste product from the copper producing industry, producing a homogeneous glass, which was subsequently crystallized [49]. Steelwork slag has also been successfully vitrified, [50] with the addition of residues of bauxite extraction, limestone, sand, and TiO_2 as nucleating agent (added as ilmenite), forming then an iron rich glass-ceramic. Slag deriving from the hydrometallurgy of zinc ores, containing a large amount of Fe (~50 wt%), of Zn (~6 wt%) and of Pb (~4 wt%), has been also vitrified and ceramized (with the addition of 30–60% of cullet), producing materials with a Fe content higher than 20 wt% [51, 52]. The durability depends on the

Vitrification of Waste and Reuse of Waste-Derived Glass. Table 2 Chapters of the List of Waste (EU)

01.	Waste resulting from exploration, mining, dressing and further treatment of minerals and quarry
02.	Waste from agricultural, horticultural, hunting, fishing, and aquacultural primary production, food preparation and processing
03.	Waste from wood processing and the production of paper, cardboard, pulp, panels, and furniture
04.	Waste from the leather, fur, and textile industries
05.	Waste from petroleum refining, natural gas purification, and pyrolytic treatment of coal
06.	Waste from inorganic chemical processes
07.	Waste from organic chemical processes
08.	Waste from the manufacture; formulation; supply; and use (MFSU) of coatings (paints, varnishes, and vitreous enamels), adhesives, sealants, and printing inks
09.	Waste from the photographic industry
10.	Inorganic waste from thermal processes
11.	Inorganic metal-containing waste from metal treatment and the coating of metals and nonferrous hydrometallurgy
12.	Waste from shaping and surface treatment of metals and plastics
13.	Oil waste (except edible oils, 05 and 12)
14.	Waste from organic substances used as solvents (except 07 and 08)
15.	Waste packaging; absorbents, wiping cloths, filter materials, and protective clothing not otherwise specified
16.	Waste not otherwise specified in the list
17.	Construction and demolition waste (including road construction)
18.	Waste from human or animal health care and/or related research (except kitchen and restaurant waste not arising from immediate health care)
19.	Waste from waste treatment facilities, off-site waste water treatment plants and the water industry
20.	Municipal waste and similar commercial, industrial, and institutional waste including separately collected fractions

Vitrification of Waste and Reuse of Waste-Derived Glass. Table 3 Properties that render waste hazardous (EU)

H1"Explosive": substances and preparations which may explode under the effect of flame or which are more sensitive to shocks or friction than dinitrobenzene
H2 "Oxidizing": substances and preparations, which exhibit highly exothermic reactions when in contact with other substances, particularly flammable substances
H3-A "Highly flammable": - liquid substances and preparations having a flash point below 21°C (including extremely flammable liquids), or - substances and preparations which may become hot and finally catch fire in contact with air at ambient temperature without any application of energy, or - solid substances and preparations which may readily catch fire after brief contact with a source of ignition and which continue to burn or to be consumed after removal of the source of ignition, or - gaseous substances and preparations which are flammable in air at normal pressure, or - substances and preparations which, in contact with water or damp air, evolve highly flammable gases in dangerous quantities
H3-B "Flammable": liquid substances and preparations having a flash point equal to or greater than 21°C and less than or equal to 55°C
H4 "Irritant": noncorrosive substances and preparations which, through immediate, prolonged or repeated contact with the skin or mucous membrane, can cause inflammation
H5 "Harmful": substances and preparations which, if they are inhaled or ingested or if they penetrate the skin, may involve limited health risks
H6 "Toxic": substances and preparations (including very toxic substances and preparations) which, if they are inhaled or ingested or if they penetrate the skin, may involve serious, acute or chronic health risks and even death
H7 "Carcinogenic": substances and preparations which, if they are inhaled or ingested or if they penetrate the skin, may induce cancer or increase its incidence
H8 "Corrosive": substances and preparations which may destroy living tissue on contacts

Vitrification of Waste and Reuse of Waste-Derived Glass. Table 3 (Continued)

H9 "Infectious": substances containing viable microorganisms or their toxins which are known or reliably believed to cause disease in man or other living organisms
H10 "Teratogenic"9: substances and preparations which, if they are inhaled or ingested or if they penetrate the skin, may induce nonhereditary congenital malformations or increase their incidence
H11 "Mutagenic": substances and preparations which, if they are inhaled or ingested or if they penetrate the skin, may induce hereditary genetic defects or increase their incidence
H12 Substances and preparations which release toxic or very toxic gases in contact with water, air, or an acid
H13 Substances and preparations capable by any means, after disposal, of yielding another substance, for example, a leachate, which possesses any of the characteristics listed above
H14 "Ecotoxic": substances and preparations which present or may present immediate or delayed risks for one or more sectors of the environment

crystalline phase assemblage, and can be higher than that of the parent glass [53]. Finally, waste coming from a geothermic plant and containing a large amount SiO_2 were used as silica source for the production of glass-ceramics or optical glass [54, 55].

Fly ash, which derives from various industrial processes, is also one of the most important examples of waste that have been successfully vitrified by several researchers [56]. In particular, fly ash deriving from municipal solid waste (MSW) incineration is one of the most extensively investigated residues. In fact, early studies demonstrated that vitrification of MSW fly ash enables the immobilization of hazardous metals and destroys the organic pollutants, [57, 58] with the advantage, at the same time, of achieving a significant reduction in the volume of waste (as high as 80–90%). Such waste consists of the finer fraction of ash separated from the effluent gas by the filters, and represents a serious environmental problem because it contains a significant amount of hazardous organic and inorganic constituents, such as dioxin, furans, and heavy metals (mainly Cd, Cr, Cu, Pb). Typically, the content of glass formers (mainly silica) in this type of waste is rather low (<35 wt%), and therefore the addition of other raw materials (e.g., cullet or silica) to correct the composition of the batch is needed. However, several examples of direct vitrification of MSW fly ash without

Vitrification of Waste and Reuse of Waste-Derived Glass. Table 4 Selected examples (EU) of hazardous waste (HW)

HW from the manufacture, formulation, supply, and use (MFSU) of acids; from the MFSU of halogens; from the MFSU of basic organic chemicals; from the MFSU of plastics, synthetic rubber and man-made fibers; from the MFSU of organic solvents
Bottom and fly ashes (e.g., from incineration of MSW) containing dangerous substances
Waste from the iron and steel industry containing dangerous substances
HW from Al, Pb, Cu, Zn, and other nonferrous thermal metallurgy
HW from casting of ferrous and nonferrous pieces
HW from petroleum refining
HW from the MFSU of pharmaceuticals; from the MFSU of fats, grease, detergents, soaps, disinfectants, and cosmetics; from the MFSU of fine chemicals
HW from the MFSU and removal of paint and varnish; from the MFSU of adhesives and sealants
HW from the photographic industry
HW from electrical and electronic equipments
Insulation materials containing asbestos
Lead batteries, Ni-Cd batteries, mercury-containing batteries
Waste organic solvents, refrigerants, and propellants
Oil waste and waste of liquid fuels
HW from galvanic processes, zinc coating processes, pickling processes, etching, phosphating, alkaline degreasing, anodizing
Waste explosives
MSW hazardous components (fluorescent tubes; batteries and accumulators; adhesive, paint, inks; discarded electrical and electronic equipments; detergents and solvents)
Hospital and medical waste
Soil, stones, and dredging spoil containing dangerous substances

any cullet addition exist, [59–61] and some reports show the successful formation of a (highly crystallizable) glass starting from fly ash containing <12 wt% of silica [62, 63]. Due to the low content of network formers, the durability of the glasses resulting from the vitrification of fly ashes needs to be carefully evaluated, to verify the lack of heavy metal leaching [64] and the degree of inertness of the material. In some cases, the presence of salt (added to food) and plastic packaging in the ash residues constitutes a problem, as it is a source of chlorine, which is difficult to dissolve into the glass and can lead to the formation of dioxins during cooling by reaction with hydrocarbons [65]; this difficulty may however be overcome by the vitrification of fly ash after washing in water [66]. Often, the addition of alkali-containing chemicals (such as Na_2CO_3 or waste from the production of feldspar) is performed to improve the viscosity and working characteristics of the melt [67, 68]. Electric arc furnace baghouse dust (EAFD) from steelmaking processes typically contains a high amount of heavy metals (Cr, Pb, Zn, Cu, Cd, Ni), in addition to a large amount of Fe and again a low silica content, which requires the addition of glass cullet to the batch in an amount depending on the composition of the waste [69]. On the contrary, the composition of coal fly ash, which is produced in large amounts by the burning of coal in thermal power plants, is particularly rich in silica (>45 wt%) and alumina, so it can be directly vitrified, if precursors for alkaline and alkaline earth oxides are added to the batch to tailor the rheological characteristics of the melt [70]. Another type of fly ash is one rich in lead, produced by the incineration of sludge recovered from tetraethyl lead and leaded gasoline storage tanks. As they are constituted mainly of inorganic Pb compounds and iron oxide, with a silica content of ~2 wt %, a maximum amount of 60 wt% can be incorporated in a glass formed by the addition of other raw materials [67, 71].

Differently from the majority of other waste, fly ash are often not vitrified by themselves, with just the addition of minor amounts of cullet or other glass-forming raw materials. Several types of fly ash are, in fact, typically either mixed together [72–74, 76] or added as a minor constituent to a glass-forming mixture [73–76], which can itself contain other types of waste [77, 78], in order to obtain a more suitable composition of the batch. The mixing of fly ash with bottom ash may represent a further solution for the above mentioned problem of limited chloride solubility in waste glasses [65]. In all cases discussed above, the amount of fly ash that can be present in a batch depends on the general composition of the waste and the operating conditions of the vitrification process. The glasses obtained from fly ash (in limited or large amount) generally belong to the system $CaO–Al_2O_3–SiO_2$ or $CaO–MgO–Al_2O_3–SiO_2$ and, due to the frequent presence of significant amounts of components that could promote some phase separation and therefore heterogeneous nucleation (e.g., Fe_2O_3 (~10 wt%), P_2O_5 (~2 wt%), and TiO_2 (>1 wt%)), they are easily converted into glass-ceramics through a subsequent controlled heat treatment [59, 61, 67, 79–83].

Air pollution control (APC) residues, produced from the flue gas cleaning processes, represent a secondary important type of waste from incineration operations. Amutha Rani et al. [84] reported that this waste is classified as hazardous mainly due to its high alkalinity, although heavy metals, organics (primarily dioxins and furanes), and chlorides are present in significant amounts. These authors successfully applied plasma vitrification to APC residues mixed with alumina and silica.

Mud or sediments constitute another typology of waste that has been successfully vitrified. They derive either from contaminated environments (e.g., Venice lagoon dredging spoils) [85, 86] or from industrial processes (sludge from wastewater treatment, [87–89] Cr-containing mud from the tanning process, sludge from traditional ceramics cutting or polishing procedures, [78] red muds from the alumina Bayer process of bauxite or from beryllium extraction from its ore) [78, 90]. They are characterized by a large variation in their composition (especially if coming from dredging operations), the presence of a large amount of water and organic matter (frequently requiring extensive pretreatment before introduction in the melter) and often by the predominance of a specific component in their composition (thus requiring extensive compositional corrections using glass-forming materials). For a successful vitrification of this waste, a highly flexible process should be used, and a control of the average composition of the waste material before each melting campaign should be performed, to ensure the

production of a glass with chemical durability within the regulation limits. Volume reduction of the waste can be as high as 40–60%.

Among other types of waste that have also been successfully vitrified, asbestos-containing residues are of particular relevance because of the health concerns they raise. They do not contain heavy metals in significant amounts, differently from all the waste described previously; however, vitrification enables the complete destruction of the fibrous structure, which constitutes the main hazard. Because they are comprised of silicates, large quantities of such residues can be added to a glass-forming mixture, and after the thermal treatment leading to the formation of the melt, a glass of conventional composition and good chemical inertness is produced, which can be disposed of safely or reused [91, 92].

Glass cullet should also be considered in the context of vitrification of waste. Despite not being classifiable as an hazardous waste in itself, except in the case of glasses from dismantled cathode ray tubes (CRTs), featuring a remarkable content of heavy metal oxides (i.e., BaO, SrO [from the front part, known as the panel] and PbO [from the internal part, known as the funnel or cone]), [93] cullet is collected in large quantities by community glass recycling programs. Although recommended for limiting the consumption of energy and natural raw materials, the use of cullet in manufacturing traditional products (especially container glass) is possible only after an expensive sorting step, aimed at the removal of impurities (of metallic or ceramic nature). This separation leads to a fraction of almost pure glass, suitable for the industry, and a fraction enriched in contaminants, which remains practically unused, and is mostly disposed of in landfills [94, 95]. However, as mentioned before, cullet can be used to modify the composition of other waste, therefore playing the fundamental role of supplying the needed glass-forming oxides lacking from the waste to be treated. Albeit most experimental work has been carried out with soda-lime-silica glass, the Ba-Sr glass deriving from the front part of CRTs has also been used [96, 97]. Alternatively, it can be used to fabricate less conventional, glass-based products (such as glass foams), [93] or it can be added to conventional batches for the fabrication of traditional ceramic products (tiles, bricks) [98–102].

In Table 5, the various typologies of hazardous waste, for which both successful vitrification and suitable durability of the produced glass or glass-ceramic have been proven, have been grouped according to their source. It has to be noted, in fact, that the chemical-physical characteristics of waste often overlap, making it difficult to classify them according to the choice of the most valid vitrification process, from a technological and economical point of view. It is indeed because of the great flexibility of glass to accommodate large variations of composition without detrimental effects on its chemical durability, that all these experiments were successful.

In Table 6, the typical compositional range of various waste is reported, as a reference. Naturally, other waste and residues specific to particular processes and geographical locations might have widely different compositions from the ones listed below.

Despite the several successful experiences reported in the scientific literature, a fundamental difficulty in moving vitrification toward large-scale implementation consists in the fact that, typically, the incoming waste stream is largely inconsistent in composition. Naturally, this would affect greatly the day-to-day plant operations, but also make extremely difficult the reuse of the produced glass as either a vitrified product or as raw material for other industrial processes. Improvements could be achieved with more extensive and selection separation of waste, which however would require the cooperation of the waste producers as well as, in most cases, of the public.

Valorization of Waste-Derived Glasses

The vitrification process is capital and energy intensive. The process is consequently hardly sustainable, if the economic advantage is related only to the avoided disposal costs. These costs are particularly significant for highly hazardous waste, such as asbestos-containing materials, which are vitrified even by employing the most expensive technologies, such as plasma heating [105]. Even if it is rather straightforward that waste landfilling will become more and more complicated in the future, so that disposal costs are expected to rise, vitrification should be economically encouraged by favoring some sources of extra revenue, such as the use of the produced glass to fabricate

Vitrification of Waste and Reuse of Waste-Derived Glass. Table 5 Typologies of hazardous waste that have been vitrified

Waste	Comments
BF, BOF, and other steelwork slag	Direct vitrification of BF [47]
	60 wt% BOF, additions of sand (glass formation) and Na_2O (workability) [48]
	Additions of bauxite residues, limestone, sand [50]
Zn hydrometallurgy slag	30–60 wt% of glass cullet or granite scraps and mud; high Fe content (>20 wt%) in the final glass [51, 52]
MSW fly ash	Addition of SiO_2 (10 wt%) to promote glass formation, MgO (5 wt%) to promote diopside formation upon conversion to glass-ceramic [61]
	Addition of 40 wt% SiO_2 and Na_2CO_3 powders, high Fe content leading to a nonhomogeneous glass [67]
	Addition of (30 wt%) waste from feldspar production [68]
	Ash rich in Pb; maximum ash content 60 wt%; addition of 40 wt% SiO_2 (glass former oxides in the ash <4 wt%) and Na_2CO_3 [67, 75]
Coal fly ash	Additions of Na_2CO_3 (to improve workability) and $CaCO_3$ (to improve chemical durability) [70]
Steel plant fly ash (+ MSW fly ash)	MSW fly ash gives chemical constituents of glass; addition of cullet (workability); and steel plant fly ash (crystallization) [73, 74, 76]
EAFD from stainless and carbon steel plants	55 wt% of glass cullet and sand; evaporation of Zn from the batch to increase the stability of the produced glass [69]
APC residues	Addition of silica (22 wt%) and alumina (8 wt%); soluble salt evaporated upon plasma melting [84]
Sewage sludge ash	Addition of limestone to obtain glass compositions prone to the formation of calcium alumino-silicates [87]
Mud from Bayer process (bauxite extraction)	Vitrification of a mixture of mud, coal fly ash, residues from the polishing of porcelain stoneware tiles and $CaCO_3$ [78]
Mud from Be extraction process	Additions of Na_2CO_3, Na_2SiF_6, and Na_3FeF_6 [90]
Dredging spoils	Addition of glass cullet (20 wt%) to promote glass formation [85, 86]
Asbestos-containing residues	Addition of K_2CO_3, $MgCO_3$, Ca-phosphate [91, 92]
Cullet	Composition corrections of batches comprising other types of inorganic waste (vast literature on the use of soda-lime-silica glass; limited experiences with Ba-Sr glass from the front part of CRTs) [96, 97]

high-value products, that is, by the introduction of a "valorization" step in the overall process. This opportunity depends on the fact that glass is a very versatile material and allows for the manufacturing of a wide range of products suitable for various applications. The use of waste-derived glass in a mass market application is highly attractive since it would enable a safe disposal of a large quantity of waste, even when the waste glass contributes only to a limited extent to the final composition of the material, with the additional benefit of reducing the use of natural raw materials. A major drawback of the approach is represented by the fact that glasses obtained from waste have often widely varying composition (and thus rheological behavior). Therefore, the process parameters of the selected production generally need to be reassessed for each starting

Vitrification of Waste and Reuse of Waste-Derived Glass. Table 6 Typical composition of different waste (wt% to one decimal place)

Waste	SiO_2	Al_2O_3	Fe_xO_y	MgO	CaO	Na_2O	K_2O	ZnO	PbO	Other[a]	C+LOI
BF, BOF, and other steelwork slag [47, 50]	7.6–35.5	0.9–11.5	0.3–36	6.2–11.6	39–43.5	–	–	–	–	1.3–5	–
Zn hydrometallurgy slag [51]	3.7	0.3	49.3	0.2	0.1	–	–	5.6	3.6	–	37.2
MSW fly ash [10]	2.5–52.1	0.5–18	0.3–25.6	0.6–4.6	5.8–44.5	1.2–33	0.3–17.3	0.2–1.7	0–0.5	0.9–41	1.2–17.1
Coal fly ash [103]	15.2–66.2	11.4–29.6	3.8–43.5	0.6–9	2.6–23.7	0.2–5.1	0.3–2.1	<1.4	<0.1	<6.5	<41
EAFD from stainless and carbon steel plants [69]	4.4–5.9	0.7–1.5	24.2–52.8	5.2–9.6	7.5–20.7	0.9–6.6	1–1.7	7.6–13.8	<0.5	6.7–23.1	–
Sewage sludge ash [10]	14.4–57.7	4.6–26	2.7–24.6	0.9–4.2	4.1–38	0.1–1.2	0.1–2.7	0–0.5	–	0.6–26.7	0.3–15.1
Mud from Bayer process (bauxite extraction) [78]	7.8	17.1	44.1	0.6	11.7	3.2	0.1	–	–	5.6	9.8
Mud from Be extraction process [90]	75–80	16.9–19	0.3–9	0.1–0.2	0.1–0.2	0.3–2.6	–	–	–	1–1.7	–
Dredging spoils (calcined) [85]	42.4	12.9	5.2	8.2	25.8	1.5	2.3	–	–	0.9	–
Asbestos-containing residues [92]	30	3.9	2.5	8	33	0.3	0.3	–	–	0.3	21.5
CRT panel glass [93, 104]	58.9–60.7	3–1.7	0–0.1	0–0.9	0.1–1.7	7.5–8.1	6–6.9	0–0.1	0–3.4	18.4–18.5	–
CRT funnel glass [93, 104]	54.1–55.5	1.8–4.1	0–0.2	0–1.3	2.7–3.5	6.1–6.2	6.1–8.2	0–0.1	12–22	1.5–5.5	–

[a] B_2O_3, P_2O_5, MnO, BaO, SrO, ZrO_2, TiO_2, SO_3, Cl, F, etc.

material. Moreover, glasses from waste can be used only in applications where a high transparency is not required, because of the large amount of transition metal ions they contain, leading to dark-colored products.

Glass-Ceramics by Nucleation and Growth

Glass-ceramics represent a vast range of materials obtained by controlled crystallization of a glass of selected composition; the overall process leads to materials often possessing outstanding properties, such as high hardness and mechanical strength, a thermal expansion coefficient adjustable in a wide range of values (from negative to more than 12×10^{-6} °C^{-1}), high refractoriness, high chemical durability, and excellent dielectric properties [44]. The most valuable glass-ceramics, also known as "technical glass-ceramics," can be produced only from base glasses with a carefully controlled chemical composition, obtainable from particularly refined raw materials. However, the glass-ceramic technology has been applied to glasses obtained from waste since the early 1960s, that is, quite soon after the discovery of glass-ceramics occurred [44]. The significant variability in composition of the inorganic residues may be accommodated by using mixtures of different waste materials (changes in the waste ratio could compensate variations in the composition of a single waste) and by considering not particularly sophisticated applications, such as the manufacturing of tiles for the building industry [103].

Classical glass-ceramic technology relies on a double step treatment of a previously formed glass object (shaped into the desired form), corresponding to the nucleation of a crystal species within the base glass, favored by the separation of some glass components (such as Ag or Au colloids, or oxides like TiO_2 and ZrO_2), and to the crystal growth. These components are generally added to the formulation of the base glass, and are referred to as "nucleating agents." The base glass is heated first to the temperature of maximum nucleation and then to the temperature of maximum crystal growth (slightly higher than the previous one), with a holding time at each temperature, before cooling. These temperatures are different for each glass composition, and need to be determined precisely using, for instance, Differential Thermal Analysis (DTA).

The nucleation and growth heat treatment, often termed "ceramization," is the basis of a well-established production of glass-ceramics from waste glasses, known as "Slagsitalls," [44] and "Slagceram" [45]. Sheeted and pressed Slagsitalls have been produced for the last 40 years in more than 20 billion square meters and used in construction, chemical, mining, and other branches of industry. The base glasses for both Slagsitalls and Slagceram products belong to the systems $CaO–Al_2O_3–SiO_2$ and $CaO–MgO–Al_2O_3–SiO_2$, and are obtained from slags of ferrous and non-ferrous metallurgy, ashes and waste of mining and chemical industries, with minor compositional adjustments via addition of network-forming oxides (mainly SiO_2 and Al_2O_3) to form a stable glass upon cooling. Tiles are obtained mainly by a rolling process of a melt containing more than 50% of waste material, followed by crystallization. The addition of nucleating agents helps to achieve a uniform crystal growth under specific heat treatment conditions. The products obtained have very good mechanical strength and excellent abrasion resistance, due to the high percentage of crystals distributed uniformly in the whole volume and whose sizes range from 0.1 to 1 μm. Calcium silicate (wollastonite, $CaO \cdot SiO_2$) and calcium feldspar (anorthite, $CaO \cdot Al_2O_3 \cdot 2SiO_2$) are generally the main crystal phases, with other silicates and alumino-silicates (pyroxenes, i.e., rather complex chain silicates, expressed by the general formula $XY(Si,Al)_2O_6$, where $X = Na^+, Ca^{2+}, Fe^{2+}, Mg^{2+}$, etc., and $Y = Mg^{2+}, Fe^{2+}, Fe^{3+}, Al^{3+}, Cr^{3+}, Ti^{4+}$, etc., [106] or gehlenite $2CaO \cdot Al_2O_3 \cdot SiO_2$ and its solid solutions) present as secondary phases. However, depending on the composition, the secondary phases may in some cases replace the main ones and vice versa [44].

Microcrystalline products obtained from extensive nucleation (i.e., containing a very large number of nuclei) possess of very remarkable mechanical properties, even when produced from waste. Boccaccini et al. [58] showed an almost threefold increase of bending strength (from 90 to 240 MPa) and fracture toughness (from 0.6 to 1.7 MPa m$^{0.5}$) for a glass-ceramic with respect to the parent glass, produced from vitrification of MSW ash. Oveçoglu [75] produced slag-based glass-ceramics with a high bending strength (>300 MPa) and an excellent fracture toughness (5.2 MPa m$^{0.5}$). Peng et al. [107] demonstrated the feasibility of glass-ceramics with nano-sized

crystals (<200 nm), from the controlled crystallization of a glass from high alumina coal fly ash.

It must be observed that waste-derived glasses usually have an inherent strong tendency to devitrification, attributable to the presence of specific components in the formulation of waste, and therefore there is no need to add nucleating agents to the batch. The separation of magnetite (Fe_3O_4) crystals is particularly significant in iron-rich waste glasses. Karamanov and Pelino observed the dependence of crystallization on the ratio Fe^{3+}/Fe^{2+} [108, 109]. They showed that the crystallization of iron-rich glasses begins with the separation of small magnetite crystals, but the surface oxidation of Fe^{2+} to Fe^{3+} causes a change of the chemical composition, with the formation of hematite (Fe_2O_3), thus decreasing the total amount of crystal phase and changing the reaction order of the crystallization process. Bloomer et al. [110] also showed that oxidized glass from dc arc melting of highly iron containing waste were highly durable, since oxidative conditions promote the dissolution of heavy metals, but poorly prone to devitrification. Iron-rich waste glasses are known also for the opportunity of obtaining glass-ceramics with interesting functional properties: Romero-Perez et al. [63] showed that with Fe_2O_3 contents in the base glass superior to 26%, the precipitated magnetite particles were large enough to exhibit full magnetic order, so that glass-ceramics showed ferromagnetic behavior. Compositions with low waste introduction, up to 18% Fe_2O_3 concentration, behaved in paramagnetic way, due to iron dissolution in the glass matrix; intermediate compositions showed super-paramagnetic behavior due to fine precipitated magnetic clusters. Fe_2O_3 is also interesting for its interaction with sulfur: Susuki et al. [87] showed that, due to the presence of Fe_2O_3, sulfur and carbon, iron sulfide, FeS, could be formed and act as crystal nucleating agents for the precipitation of anorthite. Sulfides are also known to control the color of Slagsitalls: the addition of ZnO turns the color of glass-ceramics from grayish black, given by FeS or MnS, to white, due to the formation of ZnS (together with FeO or MnO) [44].

Glass-Ceramics by Sinter-Crystallization

The above described nucleation/crystal growth step may be difficult to control and economically expensive. A major drawback concerns the presence of defects in the glass articles, like pores, which remain in the glass-ceramic, causing a decrease in the mechanical properties. The evolution of gas bubbles from the glass melt requires high temperatures and long holding times, that is, a carefully controlled refining step. This refining is particularly complicated with waste glasses, which are usually dark and feature a low thermal conductivity by radiation, due to the amount of heavy metals. A further detrimental issue for glass-ceramics obtained by the traditional route is their visual appearance, which is generally rather inferior to that of natural stones and traditional ceramics. With a sintering approach, the problems of defects and visual appearance are generally avoided. In fact, when applying the sintering route, there is no need to refine the melt before casting into a frit, thus reducing cost and gaseous emissions. The ground glass powder is subsequently heated to a certain temperature, at which viscous flow sintering of glass powders occurs together with crystallization. The densification operated by the viscous flow greatly reduces the presence of pores; the crystallization, generally starting at the contact points between adjacent glass granules, [44] gives a pleasant marble-like visual appearance to the products (see Fig. 3a).

The simultaneous sintering and crystallization treatment is known as sinter-crystallization, [111] and it has been exploited commercially since the 1970s, for the manufacturing of the well-known Japanese, wollastonite-based, "Neoparies" tiles for the building industry [44]. The approach has been greatly reevaluated in the last 20 years for the conversion of waste glasses into useful products, again in the form of tiles, mainly due to the work of Gutzow and Karamanov [49]. In fact, remarkable advantages in both the vitrification and ceramization steps are achievable. As mentioned above, refining is not needed, so that the vitrification may be conducted in small plants and in particularly short times, favoring the immobilization of components, which could vaporize with longer heat treatments. Furthermore, a relatively high degree of crystallization may be achieved in very short times; the surface of glass is in fact a preferred site for crystallization, [112–115] and thus ground glass is easier to devitrify than bulk glass with the same composition, and nucleating agents are not needed. In some cases, the holding time at the sintering temperature may not exceed 30 min, being also accompanied by very fast heating rates (even "direct heating" is possible, that is

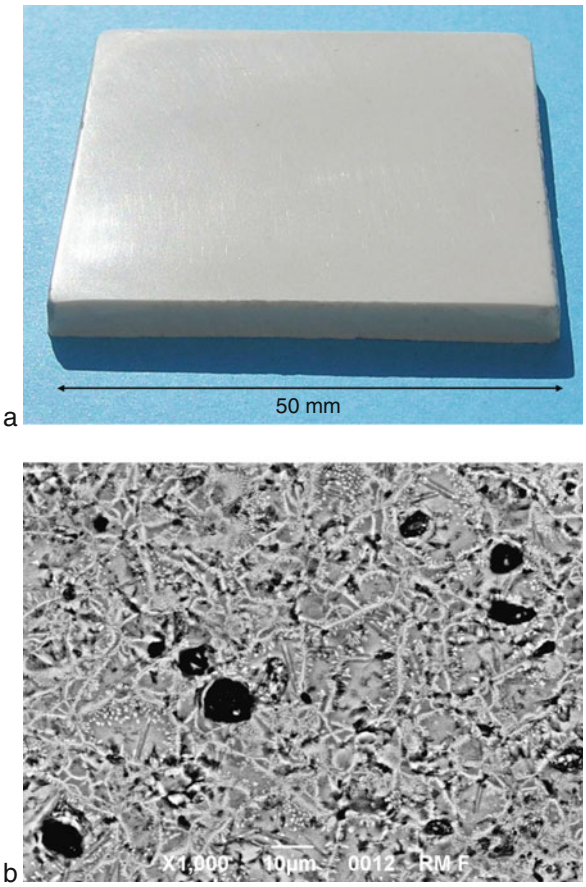

Vitrification of Waste and Reuse of Waste-Derived Glass. Figure 3
(**a**) Visual appearance of a sintered sanidine-based glass-ceramic tile; (**b**) typical microstructure of a sintered glass-ceramic from vitrified waste, containing red mud from the Bayer process (the lighter crystals correspond to pyroxenes)

the direct insertion of glass powder compacts in the furnace directly at the sintering temperature), thus configuring a "fast sinter-crystallization" process [61, 116]. The base glasses for the manufacturing of sintered glass-ceramics have similar chemical compositions, except for lack of nucleating agents, to those of glass-ceramics from waste glasses obtained by conventional nucleation and growth. Pyroxenes, wollastonite, and anorthite (with solid solutions) are very common crystal phases (see Fig. 3b). However, the remarkable nucleation activity of fine glass powders (<40 μm) has been found to enable the very unusual precipitation of alkali feldspars and feldspathoids, such as sanidine and nepheline, as main crystal phases [96, 97].

The sinter-crystallization process relies on a quite complicated balance between viscous flow sintering, surface crystallization, and even bulk crystallization, that is, crystallization operated by the separation of components acting as nucleating agents. This balance is sensible to many conditions, for example, the oxidation state and the heating rate. Starting from an iron-rich waste glass, Karamanov et al. [117] observed that the addition of C (1.5–2%) to the glass batch increased the magnetite phase and enhanced the crystallization rate. Bernardo et al. [78] starting from a base waste glass with a low Fe^{2+}/Fe^{3+} ratio, observed that magnetite was promoted by oxidation, more sensible for fine glass powders (<40 μm) than for coarse ones (<80 μm). Karamanov et al. [118, 119] reported that the balance between surface crystallization and bulk crystallization is strongly affected by the heating rate: low heating rates favor bulk crystallization, and sintering may be inhibited by the crystal phase, causing incomplete densification. High heating rates favor sintering so that low porosity remains in the material; however, the amount of crystal phase formation is lower, because crystallization occurs only at the surface. It has been shown in many papers [78, 86, 96, 97, 116] that, in the presence of fine glass powders (<40 μm), the crystallization may be achieved right at the temperature of the crystallization exothermic peak in the DTA plot of the same powders. More recent investigations, [61] however, highlighted that optimum crystallization is achievable only if the crystallization peak is located at a temperature suitably higher than that corresponding to the dilatometric softening point, that is, the temperature at which viscous flow becomes appreciable [120]. If the temperature difference is limited, the obtained glass-ceramics are remarkably porous and improvements in the densification are achievable only by increasing the sintering temperature and the heating rate (direct heating, as described above, enables sintering of the powders before the crystallization can "freeze" the viscous flow, due to the very large increase in viscosity associated to crystal precipitation).

Glass-Ceramics by the Petrurgic Method

Glass-ceramics from waste may be produced by a third method, known as the "petrurgic method" [121], named in this way because of the similarity with the process of crystallization of natural rocks. This method has actually been applied since the 1970s, with the development of "Silceram" ceramics from metallurgical slags [103]. In this process, crystals nucleate and grow directly upon cooling of glass from the melting temperature, with an intermediate temperature holding stage, [66] which can sometimes be avoided. Francis et al. [83] reported the feasibility of crystallization upon controlled cooling (from 1°C to 10°C/min) of glasses obtained from mixtures of coal ash and soda lime glass melted at 1,500°C, without any intermediate step. The cooling rate is a dominant factor in controlling the formation and morphology of the crystal phase, particularly in relation to iron containing raw materials. Faster cooling rates allow for the formation of magnetite, with samples exhibiting magnetic properties, while slow cooling rates cause the formation of plagioclase and augite.

"Glass-Ceramics" by Direct Sintering of Silicate Waste

The above mentioned techniques for the manufacturing of glass-ceramic all involve the previous formation of a glass. However, some interesting sintered materials may be produced by mixing glass cullet, of various origins, with silicate waste, leading to components which cannot, strictly speaking, be termed glass-ceramics, since they are not produced by the (controlled) crystallization of any parent glass. Francis et al. [122] as an example, produced glass-ceramics from high iron containing coal ash, adding Pyrex glass powder. The presence of iron led to soft magnetic materials, due to ferrite phases formation depending on the ash/glass ratio. A similar approach was followed by Fidancevska et al. [123]. In these cases, the crystallization is associated to the interaction between recycled glass and the silicate waste.

Fibers

Whereas glass-ceramics have constituted so far the main application for waste-derived glasses, glass fibers for composites and thermal insulation represent also a valid opportunity (see Fig. 4). Scarinci et al. [124] obtained glass fibers from glasses derived by the vitrification of MSW ashes and sludge excavated from the lagoon of Venice, with glass cullet added as melting aid. The glass fibers displayed a good tensile strength (maximum value of 1.6 GPa) and an elastic modulus up to 75 GPa. Glass fibers for reinforcement of plastics or bituminous materials, possessing physical and chemical properties comparable to those of commercially available materials, were also produced from a variety of waste [125]. The production of glass fibers is also a promising application for panel glass from cathode ray tubes (CRT), as shown by Hreglich et al. [126]. The addition of about 15 wt% of panel glass to the typical batch composition for type A glass fibers does not significantly modify the working range temperature, enabling the production of fibers of comparable quality to commercially available ones. These fibers could find application in textiles for radiation protection. Marabini et al. obtained glass wool by melting talc and cromite mine tailings (with basalt rock employed as an additive) at 1,350°C and running the fluid onto a rapid rotating heated plate; the obtained glass fibers were subsequently crystallized [127].

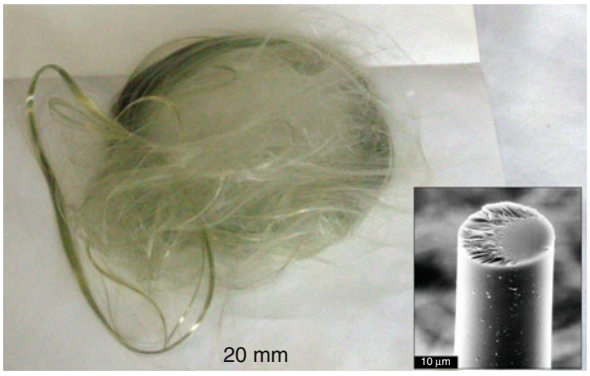

Vitrification of Waste and Reuse of Waste-Derived Glass. Figure 4
Glass fiber tow derived from waste (Courtesy of Dr. Roberto Falcone, Stazione Sperimentale del Vetro, Venice, Italy – http://www.spevetro.it). Inset: a typical SEM micrograph of a single fiber

Cellular Glasses and Glass-Ceramics

Glass foams represent a particularly interesting type of components for thermal and acoustic applications [128].

They are produced in limited quantities due to high processing costs, but their characteristic of un-flammability, thermal and chemical stability will lead to an increased use in substitution for organic foams. Moreover, the closed cell structure makes the material watertight and an efficient barrier against soil humidity. The production of glass foams may follow two distinct processes: [128] the first, dating back to the 1930s, consists of the direct introduction of gases ("blowing") into molten glass; the second one, much less expensive, is based on the viscous flow sintering of fine glass powders, which creates a pyroplastic mass, which is foamed by the action of specific powder additives (foaming agents), owing to decomposition or oxidation reactions. The decomposition reactions involve carbonates and sulfates, while oxidation reactions are due to the interaction of carbon-containing species (C, SiC) with oxygen, coming mainly from the atmosphere of the sintering furnace. The adoption of a sintering approach paved the way for the use of glass not specifically designed for foam production; significantly, the sintering approach led to the extensive use of cullet for this application. Soda-lime glass is the common raw material; however, a number of recent investigations showed that it is possible to fabricate foams using other glasses, such as CRT glass [93]. The low characteristic temperature of these glasses enables foaming at particularly low temperature (even below 750°C), through the decomposition of added calcium carbonate. Furthermore, this foaming procedure has the significant advantage of producing chemically stable foams, avoiding any risk of reduction of heavy metal oxides into metal colloids, which is often experienced when using reducing compounds (SiC or TiN) [129].

Glass foams represent an interesting way to directly use industrial residues, without converting them into a glass, with the addition of recycled soda-lime glass. Brusatin et al. [130] used fuel oil-derived fly ashes (with SiC as foaming agent), processing at temperatures between 800°C and 900°C, producing foams with a crushing strength of about 3.5 MPa and a density of ~0.35 g/cm^3. Bernardo et al. [94] used a SiC-containing waste, deriving from the polishing operations of artistic glass articles, as the only foaming agent (although the oxidation of SiC was favored by the addition of MnO_2), obtaining very high porosities (up to 92%); the heavy metal oxides present in the waste (mainly lead and cadmium deriving from artistic glass) were found to be immobilized in the glass matrix. Fernandes et al. also employed waste as raw materials containing a foaming agent, using ash produced after the burning out of SiC-based abrasive paper [131].

The foaming of waste-derived glasses is quite complicated, due the above discussed tendency of these glasses to crystallize upon heating. Significantly, a porous structure is associated to a high specific surface, which enhances surface nucleation. If extensive crystallization occurs during foaming, problems in the homogeneity and reproducibility of the overall foam morphology arise. This issue may be overcome by using a combined approach, that is, by the foaming of mixtures of soda-lime glass and a glass undergoing crystallization, [132] or again of soda-lime glass and selected waste (like in the case of "glass-ceramics" from direct sintering of silicate waste) [133]. In this case the crystallization may actually be useful, since it enhances the mechanical properties. A similar situation is found when using mixtures of soda-lime glasses with cullet of other origin, more difficultly recycled but quite prone to crystallization (e.g., glass residue from the manufacturing of glass fibers, having a $CaO–Al_2O_3–SiO_2$ composition similar to that of many waste glasses used for the preparation of glass-ceramics), as observed by Bernardo et al. [95] (see Fig. 5a).

The remarkable crystallization of waste glasses may be even advantageous when other types of cellular materials are desired. Common glass foams are mostly closed cell foams, thus maximizing the thermal insulation; on the other hand, this makes them unsuitable to filtering applications. Open-celled glass-ceramics may be obtained by the mixing of glass powders with polymeric microspheres or by the deposition of slurries onto polyurethane sponges, [134] followed by the burn-out of the sacrificial polymers and sinter-crystallization (see Fig. 5b). The crystallization, enhanced by the high amount of free glass surface, "freezes" the structure modeled by the polymeric templates, greatly limiting the viscous collapse. A similar concept was reported by Fidancevska et al., who used slurries composed of mixtures of coal fly ash and recycled glasses to coat a polyurethane foam or to envelop sacrificial carbon fibers [123].

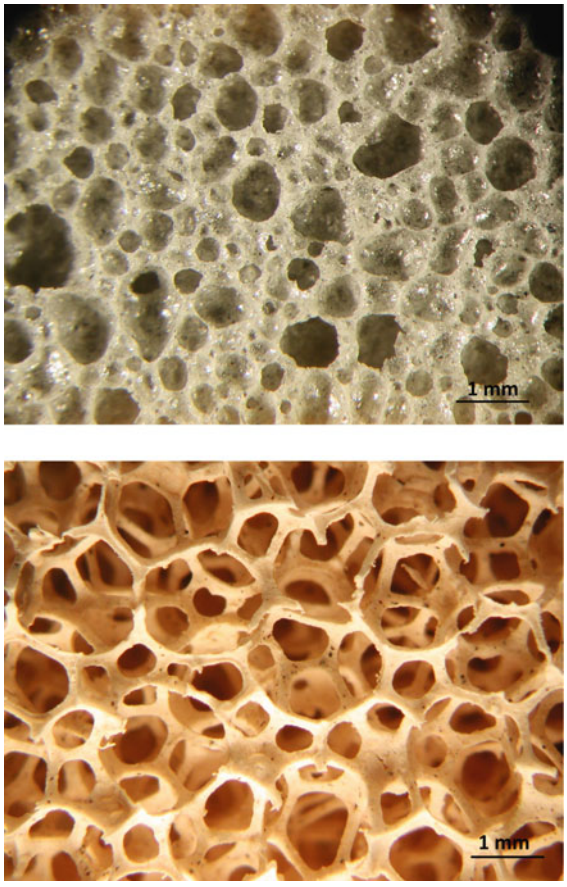

Vitrification of Waste and Reuse of Waste-Derived Glass. Figure 5
(**a**) Glass foam obtained from a mixture of recycled glasses; (**b**) cellular glass-ceramic produced by sinter-crystallization of fine glass powders deposited on a polyurethane sponge

Glass and Glass-Ceramic Matrix Composites

The development of glass matrix composites from waste was pioneered by Boccaccini et al. [135] who reported the introduction of up to 20 vol% low-cost alumina platelets in a glass matrix developed by sintering borosilicate glass cullet mixed with fly ash, leading to an increase in Young's modulus, modulus of rupture, hardness, and fracture toughness with platelet volume fraction. The reinforcement is mainly intended to improve the fracture toughness of the matrix, the most important limit for extensive structural use applications of glass-based products. Ferraris et al. [136] following the same approach, reported the introduction of solid waste from aluminum foundry.

Glass-ceramic composites can also be easily obtained using the sinter-crystallization approach, by adding the reinforcement directly to glass powders, subsequently heated. Bernardo et al. [96] prepared composites with a bending strength of 163 ± 14 MPa and a fracture toughness of 1.9 ± 0.1 MPa·m$^{0.5}$, by the addition of up to 15 vol% alumina platelets to a waste glass capable of sinter-crystallization and leading to a nepheline-based glass-ceramic matrix. Appendino et al. [137] and Aloisi et al. [138] found similar results with a glass from MSW incinerator fly ash mixed with alumina waste. However, the addition of alumina platelets is more significant because it gives origin to an alternative material to glass-ceramics, rather than being used for the reinforcement of glass-ceramics. Pressureless sintered alumina-reinforced glass matrix composites have in fact been prepared from CRT glasses [139] and from waste glass not prone to sinter-crystallization [140]. In both cases, the overall mechanical properties (e.g., a bending strength of about 100 MPa) are very close to those exhibited by Slagsitalls, although processed at much lower temperature (e.g., only 650°C for the composites based on CRT glasses). The alumina reinforcement may also be exploited even for "glass ceramics" from direct sintering of silicate waste; Rozenstrauha et al. [141] reported in fact a significant enhancement in fracture strength (from 57 to 97 MPa) with a 20 wt% addition of platelets.

Further Applications

A number of secondary applications for waste-derived glass, in addition to those previously presented, is available. Minor applications include products such as tableware, optical glass, insulators, and solid fertilizers. Hreglich et al. [126] successfully produced colored tableware glass using panel glass from cathode ray tubes, with a limited addition of sodium nitrate as a fining material. Diaz et al. [55] prepared transparent optical glass from the vitrification of geothermic waste, added with Pb_3O_4 and K_2CO_3, acting as modifiers and stabilizers. Saccani et al. [142] showed that a glass derived from the melting of MSW incinerator ashes and cullet possesses an electrical resistivity comparable

to that of E glass, so that it could be employed for high voltage insulators. Barba et al. [143] produced low cost phosphorous and potassium containing glass-ceramic frits by melting phosphates and feldspar with bones and glass cullet and pouring the melt into water. The leaching behavior of such frits suggests their application as solid fertilizers. A very similar approach was recently followed by Dall'Igna et al. [92] using vitrified asbestos-containing waste as a low cost raw material.

Glazes, tiles, road pavement, and concrete represent an important opportunity for using waste-derived glasses, because of the very large volume of production of such articles. Waste-derived glass may be used as inert aggregate in concrete, [144] asphalt concrete for road pavements, [145, 146] filler in plastics and paints etc. Finally, some studies illustrated the possibility of producing high-performance abrasive powders (Vickers' hardness >9 GPa) from the crystallization of vitrified electric arc furnace dust and foundry sand [147].

The use of waste-derived glass in the ceramic industry needs a more detailed discussion. Most of the applications of waste glasses presented in the previous paragraphs are related to products made almost completely of glass from waste, but they are of interest only to a limited market. The ceramic products discussed below, on the contrary, do not feature glass as their main constituent, but have a mass market. The manufacturing of ceramic tiles is particularly interesting due to their higher added value. Waste-derived glasses may be used in both coatings and body formulation, acting as a sintering aid. Glazes were developed from panel glass cullet [126], metallurgical slags [148], or granite waste [149]; vitrified MSW ash were employed as a sintering aid in the fabrication of porcelain stoneware or other traditional ceramics [86, 150] in analogy to glass cullet, for which a vast literature is already available [98–102]. It was observed that vitrified MSW ash in the fabrication of porcelain stoneware may cause an undesirable darker coloration with respect to the base body, with a slight coarsening in the tiles planarity, and this limited the maximum amount of waste-derived glass that can be used. Recent investigations [151] showed that this conclusion is probably premature. Firstly, the unpleasant coloration may be modified by the use of pigments; secondly, waste-derived glasses may represent an opportunity for the development of a new type of porcelain stoneware, fired at much lower temperatures than the traditional ones and with a much reduced use of natural raw materials. For instance, feldspar sands were completely replaced by a $CaO–Al_2O_3–SiO_2$ waste-derived glass, [151] obtaining a ceramic (fired at 1,000°C) with the same mechanical properties than that produced from traditional raw materials (fired above 1,150°C). The key advantages in the replacement of feldspars are the fact that the waste glass may provide a liquid phase by softening at much lower temperature than that required by the melting of feldspars, and the fact that some crystallization occurs, leading to an increase of viscosity that stabilizes the shrinkage. The complete replacement of feldspar with recycled soda-lime glass and CRT glasses has been recently proposed [104]. The stabilization of shrinkage could be caused by a viscosity increase, operated by the addition of calcium hydroxide (for soda-lime glass) promoting the formation of wollastonite, or by the addition of alumina platelets (for CRT glasses). In both cases, the firing temperatures were particularly low (880–920°C and 750–775°C, respectively).

In Table 7 are reported the main typologies of products that have been so far fabricated using glass produced from waste. The references quoted refer to the selected representative papers, for example, those reporting values for some engineering properties of the material (mechanical strength, hardness, etc.) or significant advances in the processing.

Future Directions

The vitrification of waste is a technology that is successful and suitable for the inertization of a large variety of waste, differing in composition and form; however, it still has to be proven economically viable on any substantial scale due to the substantial energy cost required to produce the high temperature necessary for obtaining a workable and homogeneous melt. If the primary economic driver toward vitrification is only the avoidance of landfill cost, then this additional energy-intensive process is not justifiable per se. However, when in some instances the hazardous nature of the waste is such that immobilization is absolutely required to meet regulation requirements or, as in the case of contaminated land remediation where the cost of vitrification can be sometimes comparable to alternative cleanup costs, sufficient incentives to pursue

Vitrification of Waste and Reuse of Waste-Derived Glass. Table 7 Main products fabricated from waste-derived glasses

Product fabricated	Main typologies of waste used	Comments	Selected references
Glass-ceramic tiles (by nucleation and growth)	MSW incinerator ashes; metallurgical slag; coal fly ash; cullet	Nucleation triggered by additives to the glass batch (e.g., TiO_2 or P_2O_5) or by separation of iron oxide already present in the waste. Most treatments require a two-step (nucleation and growth) heat treatment for crystal phase development	[58, 63, 75, 87, 107]
Glass-ceramic tiles (by sinter-crystallization)	MSW incinerator ashes; dredging spoils; mixtures of various waste	No need for second heat treatment; influence of oxidation state and heating rate; possibility of "fast sinter-crystallization"	[49, 61, 68, 116–119]
Glass-ceramic tiles (by petrurgic method)	Coal fly ash; cullet	Crystalline material forms upon cooling, with or without intermediate temperature holding stage	[83]
Fibers	MSW incinerator ashes; dredging spoils; cullet	Suitable for reuse of CRT cullet	[124, 125, 127]
Porous glasses and glass-ceramics	Cullet	Viscosity of glass affects choice of foaming agents; crystallization to be limited (in closed cell foams) or exploited (in open-celled foams)	[93, 94, 131, 134]
Glass and glass-ceramic matrix composites (tiles)	MSW incinerator ashes; Al foundry waste; coal fly ash; cullet	Alumina platelets as main reinforcement. Suitable for reuse of CRT cullet	[96, 137–139]
Frits (for glazes)	Metallurgical slags; granite waste	Difficulties in controlling color. Suitable for crystalline coatings	[148, 149]
Porcelain stoneware tiles	MSW incinerator ashes; cullet; mixtures of various waste	Possible complete replacement of feldspars and reduction of firing temperature; controlled shrinkage (by crystallization)	[104, 150, 151]
Solid fertilizers	Bones; cullet; asbestos waste	Very specific compositions need to be achieved	[92, 143]
Aggregate in concrete (cementitious or bituminous)	Cullet	Low cost and low bulk density; decorative; problems with debonding of glass particles	[144–146]

this route exist. Moreover, the reuse of the glass or glass ceramic produced from the vitrification of waste, either as new products or as raw materials for other processes, would contribute to further offset the overall cost of the technology.

The forecasted future developments concern a rationalization and specialization of the melting technologies, based from one hand on a more exact knowledge of the initial batch (composition, physical state, particle size, toxicity, etc.), and the other hand on precise selection rules (based on economic or plant criterions) of the off-gas purification systems. Alternatively, the development of a multipurpose melter (such as the cold-crucible induction melter, recently devised for the treatment of nuclear waste) could meet the growing demand of successfully vitrifying waste with vastly different chemical-physical characteristics, however increasing the cost and requirements relative to the gas depuration system. Changes in legislatory regulations would also prove crucial toward aiding to establish vitrification as not only the safest, but also the most viable hazardous waste management process.

The present trend, which will be more and more continued in the future due to economic reasons, is toward the fabrication of marketable products using glass obtained from waste, such as glass-ceramics, tiles

for flooring or lining, foam glass, insulating or reinforcing fibers, glass or glass-ceramic composites. The scientific and technological challenge will be to produce components possessing the chemical, mechanical, and esthetic characteristics required by the specific application.

Bibliography

Primary Literature

1. Roth G, Weisenburger S (2000) Vitrification of high level liquid waste: glass chemistry, process chemistry and process technology. Nucl Eng Des 202:197–207
2. Park J-K, Song M-J (1998) Feasibility study on vitrification of low-and intermediate-level radioactive waste from pressurized water reactors. Waste Manag 18:157–167
3. Sakai S, Hiraoka M (2000) Municipal solid waste incinerator residue recycling by thermal processes. Waste Manag 20:249–258
4. US Environmental Protection Agency (1994) 1994 EPA contaminated sediment management strategy, EPA 823-R-94-001. Office of Water, US Environmental Protection Agency, Washington
5. SITE (Superfund Innovative Technology Evaluation) Emerging Technology Bulletin (1995) Ferro Corporation waste vitrification through electric melting, U.S. EPA/540/F-95/503. US Environmental Protection Agency, Cincinnati
6. Nechvatal TM, Jansen TJ (1996) Converting paper mill sludge or the like. US Patent 5,549,059. Assignee: Minergy
7. Buelt JL, Oma KH, Eschbach EA (1994) Apparatus for in situ heating and vitrification. US Patent 5,316,411, 31 May 1994
8. U.S. Environmental Protection Agency (1995) Geosafe Corporation in situ vitrification. innovative technology evaluation report. Risk reduction engineering laboratory, Office of Research and Development. Report EPA/540/R-94/520
9. Poiroux R, Rollin M (1996) High temperature treatment of waste: from laboratories to the industrial stage. Pure Appl Chem 68:1035–1040
10. Bingham PA, Hand RJ (2006) Vitrification of toxic waste: a brief review. Adv Appl Ceram 105:21–31
11. http://www.epa.gov/epawaste/hazard/tsd/td/combustion.htm. Accessed 10 Feb 2009
12. Marra JC, Jantzen CM (2004) Glass: an environmental protector. Am Ceram Soc Bull 83(11):12–16
13. Baehr W (1989) Industrial vitrification processes for high-level liquid waste solutions. IAEA Bulletin 31(4):47–51
14. Buelt JL, Chapman C (1978) Liquid fed ceramic melter. Doc. N° PNL-2735, UC 70, U.S. Department of Energy
15. Jantzen C, Bickford DF, Brown KG, Cozzi AD et al (2000) Savannah river site waste vitrification projects initiated throughout the United States: disposal and recycle options. US Department of Energy, Office of Scientific and Technical Information, Oak Ridge
16. Roth G (1995) Atomwirtschaft 40(Jg3):174–177
17. Jouan A (2001) La vitrification des déchets, une contribution au respect de notre terre. Verre 7:20–27
18. US Environmental Protection Agency (1992) Handbook on vitrification technologies for treatment of hazardous and radioactive waste, report EPA/625/R-92/002. Office of Research and Development, Washington
19. Buelt JL (1997) Molten glass processes. In: Freeman HM (ed) Standard handbook of hazardous waste treatment and disposal, 2nd edn. McGraw-Hill, New York, pp 45–77
20. Wakamura Y, Nakazato K (1994) Recent trend of ash management from MSW incineration facilities in Japan. In: National Waste Processing Conference Proceedings ASME 91–96
21. Richards RS, Plodinec MJ (1998) Overview of current and emerging waste vitrification technologies. In: Proceedings of the XVIII international congress on glass, San Francisco, 5–8 July 1998. Paper No. A7-I (CD ROM). The American Ceramic Society, Westerville
22. Hollander H (1995) Vitrification of combustion ash residue for beneficial use. Solid Waste Technol 9:31–40
23. Terasawa Y, Yasuda S, Horizoe H, Sato J, Gotou Y (2001) Commercialization of MSW incineration system with direct ash melting by thermal cracking for high efficient generation of electricity, Mitsubishi Heavy Industries, Ltd. Tech Rev 38(2):82–86
24. Miyata H, Sadatsuka T (2005) Technology applicable to "Heat recovery facilities", Sanki Engineering. J Solid Liq Waste 35(9):43–44, in Japanese
25. Chapman C (1995) Earth melter. US Patent 5,443,618. Assignee Battelle Memorial Institute, Richland
26. Chapman C (1993) State-of-the-art of waste glass melters. In: Varshneya AK, Bickford DF, Bihuniak PP (eds) Ceramic Transactions v.29. American Ceramic Society, Westerville, pp 485–493
27. Park JK, Moon YP, Park BC, Song MJ, Ko KS, Cho JM (2001) Noncombustible waste vitrification with plasma torch melter. J Environ Sci Health A Tox/Hazard Subst Environ Eng 36:861–871
28. Tendler M, Retberg P, Van Oost G (2005) Plasma based waste treatment and energy production. Plasma Phys Controlled Fusion 47:A219–A230
29. Moustakas K, Fatta D, Malamis S, Haralambous K, Lozidou M (2005) Demonstration plasma gasification/vitrification system for effective hazardous waste treatment. J Hazard Mater 123:120–126
30. Park HS, Kim SJ (2005) Analysis of a plasma melting system for incinerated ash. J Ind Eng Chem 11:657–665
31. Kushnikov VV et al. (1995) Using an induction melter with a cold crucible for the immobilization of Plutonium. In: Plutonium Stabilization and Immobilization Workshop Proceedings, Washington, pp 319–326
32. Jouan A, Boen R, Merlin S, Pujadas V (1997) New development for medium and low level waste vitrification. In: Nuthos-5, Beijing, 14–18, April 1997
33. Ojovan MI, Lee WE (2003) Self sustaining vitrification for immobilisation of radioactive and toxic waste. Glass Technol 44:218–224
34. Karlina OK, Varlakova GA, Ojovan MI, Tivanski VM, Klimov VL, Pavlova GY, Dmitriev SA (2001) Ash and soil conditioning using exothermic metallic compositions. Mater Res Soc Symp Proc 663:65–70

35. Blackman WC (1993) Basic hazardous waste management. Lewis, Boca Raton
36. European Council (2000) European Waste Catalogue, Council Decision 2000/532/EC, Official Journal of the European Communities L226:3–24
37. Räbiger K, Keldenich K, Scheffer J (1995) Experience in operation of a pilot plant melting residual substances. Glastech Ber Glass Sci Technol 68:84–90
38. Frugifer P, Godon N, Vernaz E, Larché F (2002) Influence of composition variations on the initial alteration rate of vitrified domestic waste incineration fly-ash. Waste Manag 22:137–142
39. Piepel G, Redgate T (1997) Mixture techniques for reducing the number of components applied for modeling waste glass sodium release. J Am Ceram Soc 80:3038–3044
40. Besmann TM, Spear KE (2002) Thermochemical modeling of oxide glasses. J Am Ceram Soc 85:2887–2894
41. Kim C-W, Choi K, Park J-K, Shin S-W, Song M-J (2001) Enthalpies of chromium oxide solution in soda lime borosilicate glass systems. J Am Ceram Soc 84:2987–2990
42. Lapa N, Santos Oliveira JF, Camacho SL, Circeo LJ (2002) An ecotoxic risk assessment of residue materials produced by the plasma pyrolysis/vitrification (PP/V) process. Waste Manag 22:335–342
43. Colombo P, Brusatin G, Bernardo E, Scarinci G (2003) Inertization and reuse of waste materials by vitrification and fabrication of glass-based products. Curr Opin Solid State Mater Sci 7:225–239
44. Höland W, Beall G (2002) Glass-ceramic technology. American Ceramic Society, Westerville
45. Davies MW, Kerrison B, Gross WE, Robson MJ, Witchall DF (1973) Slag ceramics: a glass ceramic from blast-furnace slag. J Iron Steel Inst 208:348–370
46. Nakamura S (1976) Crystallized glass article having a surface pattern. US patent 3,955,989. 11 May 1976
47. Fredericci C, Zanotto ED, Ziemath EC (2000) Crystallization mechanism and properties of a blast furnace slag glass. J Noncryst Solids 273:64–75
48. Ferreira EB, Zanotto ED, Scudeller LAM (2002) Glass and glass-ceramic from basic oxygen furnace (BOF) slag. Glass Sci Technol 75:75–86
49. Karamanov A, Gutzow I, Chomakov I, Christov J, Kostov L (1994) Synthesis of wall-covering glass-ceramics from waste raw materials. Glastech Ber Glass Sci Technol 67:227–230
50. Gomes V, De Borba CDG, Riella HG (2002) Production and characterization of glass ceramics from steelwork slag. J Mater Sci 37:2581–2585
51. Pelino M (2000) Recycling of zinc-hydrometallurgy waste in glass and glass ceramic materials. Waste Manag 20: 561–568
52. Karamanov A, Taglieri G, Pelino M (1999) Iron-rich sintered glass-ceramics from industrial waste. J Am Ceram Soc 82(11):3012–3016
53. Pisciella P, Crisucci S, Karamanov A, Pelino M (2001) Chemical durability of glasses obtained by vitrification of industrial waste. Waste Manag 21:1–9
54. Diaz C, Valle-Fuentes FJ, Zayas ME, Avalos-Borja M (1999) Cordierite glass-ceramic from geothermic waste. Am Ceram Soc Bull 78:62–64
55. Diaz C, Gracia H, MaE Z, Espinoza FJ, Valle-Fuentes FJ (2000) Producing optical glass with geothermal waste. Am Ceram Soc Bull 79:57–59
56. Ferreira C, Ribeiro A, Ottosen L (2003) Possible applications for municipal solid waste fly ash. J Hazard Mater B96:201–216
57. Romero M, Rawlings RD, Rincón JM (1999) Development of a new glass-ceramic by means of controlled vitrification and crystallization of inorganic waste from urban incineration. J Eur Ceram Soc 19:2049–2058
58. Boccaccini AR, Kopf M, Stumpfe W (1995) Glass-ceramics from filter dusts from waste incinerators. Ceram Int 21:231–235
59. Cheng TW, Chen YS (2003) On formation of CaO-Al_2O_3-SiO_2 glass-ceramics by vitrification of incinerator fly ash. Chemosphere 51:817–824
60. Park YJ, Heo J (2002) Conversion to glass-ceramics from glasses made by MSW incinerator fly ash for recycling. Ceram Int 28:689–694
61. Bernardo E, Scarinci G, Edme E, Michon U, Planty N (2009) Fast-sintered gehlenite glass–ceramics from plasma-vitrified municipal solid waste incinerator fly ashes. J Am Ceram Soc 92:528–530
62. Romero M, Rawlings RD, Rincón JM (2000) Crystal nucleation and growth in glasses from inorganic waste from urban incineration. J Noncryst Solids 271:108–118
63. Romero M, Rincon JMa, Rawlings RD, Boccaccini AR (2001) Use of vitrified urban incinerator waste as raw material for production of sintered glass-ceramics. Mater Res Bull 36:383–395
64. Park YJ, Heo J (2002) Vitrification of fly ash from municipal solid waste incinerator. J Hazard Mater B91:83–93
65. Siwadamrongpong S, Koide M, Matusita K (2004) Prediction of chloride solubility in CaO–Al_2O_3–SiO_2 glass systems. J Noncryst Solids 347:114–120
66. Kim JM, Kim HS (2004) Glass-ceramic produced from a municipal waste incinerator fly ash with high Cl content. J Eur Ceram Soc 24:2373–2382
67. Kavouras P, Komninou Ph, Chrissafis K, Kaimakamis G, Kokkou S (2003) Microstructural changes of processed vitrified solid waste products. J Eur Ceram Soc 23:1305–1311
68. Karamanov A, Pelino M, Hreglich S (2003) Sintered glass-ceramics from municipal solid waste-incinerator fly ashes-part I: the influence of the heating rate on the sinter-crystallization. J Eur Ceram Soc 23:827–832
69. Pelino M, Karamanov A, Pisciella P, Crisucci S, Zonetti D (2002) Vitrification of electric arc fornace dusts. Waste Manag 22:945–949
70. Leroy C, Ferro MC, Monteiro RCC, Fernandes MHV (2001) Production of glass-ceramics from coal ashes. J Eur Ceram Soc 21:195–202
71. Kavouras P, Kaimakamis G, Ioannidis ThA, Kehagias Th, Komninou Ph, Kokkou S, Pavlidou E, Antonopoulos I, Sofoniou M, Zouboulis A, Hadjiantoniou CP, Nouet G, Prakouras A, Karakostas Th (2003) Vitrification of lead-rich solid ashes

from incineration of hazardous industrial waste. Waste Manag 23:361–371
72. Cheng TW (2003) Combined glassification of EAF dust and incinerator fly ash. Chemosphere 50:47–51
73. Barbieri L, Ferrari AM, Lancellotti I, Leonelli C (2000) Crystallization of (Na_2O-MgO)-CaO-Al_2O_3-SiO_2 glassy systems formulated from waste products. J Am Ceram Soc 83:2515–2520
74. Barbieri L, Corradi A, Lancellotti I (2000) Alkaline and alcaline-earth silicate glasses and glass-ceramics from municipal and industrial waste. J Eur Ceram Soc 20:2477–2483
75. Öveçoğlu ML (1998) Microstructural characterization and physical properties of a slag-based glass-ceramic crystallized at 950 and 1100°C. J Eur Ceram Soc 18:161–168
76. Barbieri L, Corradi A, Lancellotti I (2002) Thermal and chemical behavior of different glasses containing steel fly ash and their transformation into glass-ceramics. J Eur Ceram Soc 22:1759–1765
77. Barbieri L, Lancellotti I, Manfredini T, Queralt I, Rincon JM, Romero M (1999) Design, obtainment and properties of glasses and glass-ceramics from coal fly ash. Fuel 78:271–276
78. Bernardo E, Esposito L, Rambaldi E, Tucci A, Pontikes Y, Angelopoulos GN (2009) Sintered esseneite–wollastonite–plagioclase glass–ceramics from vitrified waste. J Eur Ceram Soc 29:2921–2927
79. Boccaccini A, Rawlings R (2002) Waste not – Producing glass-ceramics from waste materials. Mater World 10:16–18
80. Rincon JM, Romero M, Boccaccini AR (1999) Microstructural characterisation of a glass and a glass-ceramic obtained from municipal incinerator fly ash. J Mater Sci 34:4413–4423
81. Boccaccini AR, Petitmermet M, Wintermantel E (1997) Glass-ceramics from municipal incinerator fly ash. Am Ceram Soc Bull 76:75–78
82. Erol M, Demirler U, Küçükbayrak S, Ersoy-Meriçboyu A, Öveçoğlu ML (2003) Characterization investigations of glass-ceramics developed from Seyitömer thermal power plant fly ash. J Eur Ceram Soc 23:757–763
83. Francis AA, Rawlings RD, Boccaccini AR (2002) Glass-ceramics from mixtures of coal ash and soda lime glass by the petrurgic method. J Mater Sci Lett 21:975–980
84. Amutha Rani D, Gomez E, Boccaccini AR, Hao L, Deegan D, Cheeseman CR (2008) Plasma treatment of air pollution control residues. Waste Manag 28:1254–1262
85. Bernstein AG, Bonsembiante E, Brusatin G, Calzolari G, Colombo P, Dall'Igna R, Hreglich S, Scarinci G (2002) Inertization of hazardous dredging spoils. Waste Manag 22:865–869
86. Brusatin G, Bernardo E, Andreola F, Barbieri L, Lancellotti I, Hreglich S (2005) Reutilization of waste inert glass from the disposal of polluted dredging spoils by the obtainment of ceramic products for tiles applications. J Mater Sci 40:5259–5264
87. Suzuki S, Tanaka M, Kaneko T (1997) Glass-ceramic from sewage sludge ash. J Mater Sci 32:1775–1779
88. Park YJ, Moon So, Heo J (2003) Crystalline phase control of glass ceramics obtained from sewage sludge fly ash. Ceram Int 29:223–227
89. Toya T, Nakamura A, Kameshima Y, Nakajima A, Okada K (2007) Glass-ceramics prepared from sludge generated by a water purification plant. Ceram Int 33:573–577
90. Bhat PN, Ghosh DK, Desai MVM (2002) Immobilisation of beryllium in solid waste (red-mud) by fixation and vitrification. Waste Manag 22:549–556
91. Roberts D, Stuart JH (1989) Vitrification of asbestos waste. US Patent 4,820,328, 11 April 1989
92. Dall'Igna R, Falcone R, Hreglich S, Profilo B, Vallotto M, Cadore A, Grattieri W (2002) Production of mineral fertilizer glass from inertized asbestos containing waste. Riv Staz Sper Vetro 6:13–15
93. Bernardo E, Scarinci G, Hreglich S (2005) Foam glass as a way of recycling glasses from cathode ray tubes. Glass Sci Technol 78:7–11
94. Bernardo E, Cedro R, Florean M, Hreglich S (2007) Reutilization and stabilization of wastes by the production of glass foams. Ceram Int 33:963–968
95. Bernardo E, Scarinci G, Bertuzzi P, Ercole P, Ramon L (2009) Recycling of waste glasses into glass and glass-ceramic foams. J Porous Mater 17(3):359–365
96. Bernardo E, Andreola F, Barbieri L, Lancellotti I (2005) Sintered glass-ceramics and glass-ceramic matrix composites from CRT panel glass. J Am Ceram Soc 88:1886–1891
97. Bernardo E, Castellan R, Hreglich S, Lancellotti I (2006) Sintered sanidine glass-ceramics from industrial wastes. J Eur Ceram Soc 26:3335–3341
98. Tucci A, Esposito L, Rastelli E, Palmonari C, Rambaldi E (2004) Use of soda-lime scrap-glass as a fluxing agent in a porcelain stoneware tile mix. J Eur Ceram Soc 24:83–92
99. Pontikes Y, Christogerou A, Angelopoulos G, Rambaldi E, Esposito L, Tucci A (2005) Use of soda-lime-silica scrap glass in the traditional ceramic industry. Glass Technol 46:200–207
100. Tarvornpanich T, Souza GP, Lee WE (2005) Microstructural evolution on firing soda-lime-silica glass fluxed whitewares. J Am Ceram Soc 88:1302–1308
101. Tucci A, Rambaldi E, Esposito L (2006) Use of scrap glass as raw materials for porcelain stoneware tiles. Adv Appl Ceram 105:40–45
102. Raimondo M, Zanelli C, Matteucci F, Guarini G, Dondi M, Labrincha JA (2007) Effect of waste glass (TV/PC cathodic tube and screen) on technological properties and sintering behaviour of porcelain stoneware tiles. Ceram Int 33:615–623
103. Rawlings RD, Wu JP, Boccaccini AR (2006) Glass-ceramics: their production from wastes – a review. J Mater Sci 41:733–761
104. Bernardo E, Esposito L, Rambaldi E, Tucci A (2009) Glass-based stoneware as a promising route for the recycling of waste glasses. Adv Appl Ceram 108:2–8
105. http://www.europlasma.com/
106. Morimoto N et al (1988) Nomenclature of pyroxenes. Am Mineralog 73:1123–1133
107. Peng F, Liang K, Hu A (2005) Nano-crystal glass–ceramics obtained from high alumina coal fly ash. Fuel 84:341–346
108. Karamanov A, Cantalini C, Pelino M, Hreglich S (1999) Kinetics of phase formation in jarosite glass-ceramic. J Eur Ceram Soc 19:527–533

109. Karamanov A, Pelino M (2001) Crystallization phenomena in iron-rich glasses. J Noncryst Solids 281:139–151
110. Bloomer PE, Feng X, Chantaraprachoom N, Gong M, McCready DE (1999) Effect of crystallization, redox, and waste loading on the properties of several glassy waste forms. J Am Ceram Soc 11:2999–3011
111. Gutzow I, Pascova R, Karamanov A, Schmelzer J (1998) The kinetics of surface induced sinter-crystallization and the formation of glass-ceramic materials. J Mater Sci 33:5265–5273
112. Müller R, Zanotto ED, Fokin VM (2000) Surface crystallization of silicate glasses: nucleation sites and kinetics. J Noncryst Solids 274:208–231
113. Prado MO, Zanotto ED (2002) Glass sintering with concurrent crystallization. C R Chimie 5:773–786
114. Francis AA, Rawlings RD, Sweeney R, Boccaccini AR (2004) Crystallization kinetic of glass particles prepared from a mixture of coal ash and soda-lime cullet glass. J Noncryst Solids 333:187–193
115. Hernandez-Crespo MaS, Romero M, Rincon JMa (2006) Nucleation and crystal growth of glasses produced by a generic plasma arc-process. J Eur Ceram Soc 26:1679–1685
116. Bernardo E (2008) Fast Sinter-crystallization of a glass from waste materials. J Noncryst Solids 354:3486–3490
117. Karamanov A, Pisciella P, Cantalini C, Pelino M (2000) Influence of Fe^{3+}/Fe^{2+} ratio on the crystallization of iron-rich glasses made with industrial waste. J Am Ceram Soc 83:3153–3157
118. Karamanov A, Pelino M, Hreglich S (2003) Sintered glass-ceramics from municipal solid waste-incinerator fly ashes-part I: the influence of the heating rate on the sinter-crystallization. J Eur Ceram Soc 23:827–832
119. Karamanov A, Aloisi M, Pelino M (2005) Sintering behaviour of a glass obtained from MSWI ash. J Eur Ceram Soc 25:1531–1540
120. Ray A, Tiwari AN (2001) Compaction and sintering behaviour of glass-alumina composites. Mater Chem Phys 67:220–225
121. Romero M, Rincon JMa (1999) Surface and bulk crystallization of glass-ceramic in the Na_2O-CaO-ZnO-PbO-Fe_2O_3-Al_2O_3-SiO_2 system derived from a goethite waste. J Am Ceram Soc 82:1313–1317
122. Francis AA, Rawlings RD, Sweeney R, Boccaccini AR (2002) Processing of coal ash into glass ceramic products by powder technology and sintering. Glass Technol 43:58–62
123. Fidancevska E, Mangutova B, Milosevski D, Milosevski M, Bossert J (2003) Sci Sinter 35:85–91
124. Scarinci G, Brusatin G, Barbieri L, Corradi A, Lancellotti I, Colombo P, Hreglich S, Dall'Igna R (2000) Vitrification of industrial and natural waste with production of glass fibres. J Eur Ceram Soc 20:2485–2490
125. Hreglich S, Cioffi F (2009) Continuous glass fibres from waste and their application in reinforced materials. Adv Appl Ceram 108:22–26
126. Hreglich S, Falcone R, Vallotto M (2001) The recycling of end of life panel glass from TV sets in glass fibres and ceramic productions. In: Dhir RK, Limbachiya MC, Dyer TD (eds) Recycling and reuse of glass cullet. Thomas Telford, London, pp 123–134
127. Marabini AM, Plescia P, Maccari D, Burragato F, Pelino M (1998) New materials from industrial and mining waste: glass-ceramics and glass- and rock-wool fibre. Int J Miner Process 53:121–134
128. Scarinci G, Brusatin G, Bernardo E (2005) Production technology of glass foams. In: Scheffler M, Colombo P (eds) Cellular ceramics. structure, manufacturing, properties and applications. Wiley-VCH, Weinheim
129. Méar F, Yot P, Viennois R, Ribes M (2007) Mechanical behaviour and thermal and electrical properties of foam glass. Ceram Int 33:543–550
130. Brusatin G, Scarinci G, Zampieri L, Colombo P (2002) Foam glass from cullet. Glass Mach Plant Accessory 1:108–110
131. Fernandes HR, Tulyaganov DU, Ferreira JMF (2009) Production and characterisation of glass ceramic foams from recycled raw materials. Adv Appl Ceram 108:9–13
132. Tulyaganov DU, Fernandes HR, Agathopoulos S, Ferreira JMF (2006) Preparation and characterization of high compressive strength foams from sheet glass. J Porous Mater 13:133–139
133. Wu JP, Boccaccini AR, Lee PD, Kershaw MJ, Rawlings RD (2006) Glass ceramic foams from coal ash and waste glass: Production and characterisation. Adv Appl Ceram 105:32–39
134. Bernardo E (2007) Micro- and macro-cellular sintered glass-ceramics from wastes. J Eur Ceram Soc 27:2415–2422
135. Boccaccini AR, Bücker M, Bossert J, Marszalek K (1997) Glass matrix composites from coal fly ash and waste glass. Waste Manag 17:39–45
136. Ferraris M, Salvo M, Smeacetto F, Augier L, Barbieri L, Corradi A, Lancellotti I (2001) Glass matrix composites from solid waste materials. J Eur Ceram Soc 21:453–460
137. Appendino P, Ferraris M, Matekovits I, Salvo M (2004) Production of glass-ceramic bodies from the bottom ashes of municipal solid waste incinerators. J Eur Ceram Soc 24:803–810
138. Aloisi M, Karamanov A, Taglieri G, Ferrante F, Pelino M (2006) Sintered glass ceramic composites from vitrified municipal solid waste bottom ashes. J Hazard Mater 137:138–143
139. Bernardo E, Scarinci G, Hreglich S (2005) Development and mechanical characterization of Al_2O_3 platelet-reinforced glass matrix composites obtained from glasses coming from dismantled cathode ray tubes. J Eur Ceram Soc 255:1541–1550
140. Bernardo E, Castellan R, Hreglich S (2007) Al_2O_3-platelet reinforced glass matrix composites from a mixture of wastes. J Mater Sci 42:2706–2711
141. Rozenstrauha I, Cimdins R, Berzina L, Bajare D, Bossert J, Boccaccini AR (2002) Sintered glass-ceramic matrix composites made from Latvian silicate wastes. Glass Sci Technol 75:132–139
142. Saccani A, Sandrolini F, Barbieri L, Corradi A, Lancellotti I (2001) Structural studies and electrical properties of recycled glasses from glass and incinerator waste. J Mater Sci 36: 2173–2177
143. Barba MF, Callejas P, Arabe JO, Ajò D (1998) Characterization of two frit ceramics materials in low cost fertilizers. J Eur Ceram Soc 18:1313–1317
144. Jin W, Meyer C, Baxter S (2000) Glascrete-concrete with glass aggregate. ACI Mater J 97:208–213

145. Schroeder RL (1994) The use of recycled materials in highway construction. Public Roads 58:32–41
146. Su N, Chen JS (2002) Engineering properties of asphalt concrete made with recycled glass. Resour Conserv Recycl 35:259–274
147. Gao Z, Drummond CH (1999) Thermal analysis of nucleation and growth of crystalline phases in vitrified industrial waste. J Am Ceram Soc 82:561–565
148. Romero M, Rincon JMa, Acosta A (2002) Effect of iron oxide content on the crystallisation of a diopside glass-ceramic glaze. J Eur Ceram Soc 22:883–890
149. Zubekhin AP, Zhabrev VA, Kondyurin AM (1993) Glass formation and crystallization in the SiO_2–CaO–MgO–Fe_2O_3–MnO_2–K_2O–Na_2O for synthesizing heat resistant coatings. Steklo i Keramica 5:26–28
150. Barbieri L, Corradi A, Lancellotti I, Manfredini T (2002) Use of municipal incinerator bottom ash as sintering promoter. Waste Manag 22:859–863
151. Bernardo E, Esposito L, Rambaldi E, Tucci A, Hreglich S (2008) Recycle of waste glass into "Glass-ceramic Stoneware". J Am Ceram Soc 91:2156–2162

Books and Reviews

Gomez E, Rani DA, Cheeseman CR, Deegan D, Wise M, Boccaccini AR (2008) Thermal plasma technology for the treatment of wastes: a critical review. J Hazard Mater 161:614–626
Oh CO (2001) Hazardous and radioactive waste treatment technology. CRC Press, Boca Raton
Scholze H (1991) Glass: nature, structure and properties. Springer, New York
Strnad Z (1986) Glass-ceramic materials. Elsevier, Amsterdam
Vesilind PA, Worrell W, Reinhart D (2002) Solid waste engineering. Rooks/Cole, Pacific Grove

Volcanoes of Mexico

Nick Varley
Centre of Exchange and Research in Volcanology, Universidad de Colima, Col. Villas San Sebastián, Colima, Mexico

Article Outline

Glossary
Definition of the Subject
Introduction
The Basics of Volcanism
The Importance of Mexico's Volcanoes
Tectonics
Baja California and Sonora
Pacific Islands
Tepic-Zacoalco Rift
Volcán de Colima
Central Stratovolcanoes
Volcanic Fields
Volcanoes of Chiapas
Future Directions
Bibliography

Glossary

Andesite Magma of intermediate composition of silica, a common product of eruptions from stratovolcanoes.

Basalt Magma of a low silica composition, has a low viscosity and usually is emplaced in lava flows or as scoria.

Dacite Magma of a composition higher in silica, between andesite and rhyolite.

Debris avalanche Large collapse event which produces an extensive deposit, often characterized by hummock-shaped hillocks. Occur from most likely all stratovolcanoes, due to their inherent instability.

Holocene The time period since the end of the last glaciation (11,700 years ago to present).

Lahar Mudflow with the remobilization of active volcanic pyroclastic deposits. Can be hot if occurring during or soon after the eruption.

Maar Explosive craters surrounded by a ring-shaped deposit of pyroclasts. Form due to phreatomagmatic interactions, often in basins with extensive aquifers.

Monogenetic field Region featuring the growth of cinder cones or maars, with each eruptive centre typically exhibiting only one eruption.

Phreatomagmatic Explosive eruption resulting from the interaction between magma and water. Results in the expulsion of juvenile material. *Phreatic* implies no juvenile component.

Pleistocene The epoch between 2.58 million and 11,700 years ago, which included the major period of glaciation.

Pyroclastic flow or pyroclastic density current A gravity-driven mobile flow of hot gases mixed with ash and rocks, which descend volcano flanks

at fast speeds posing a great threat to anything in their path.

Rhyolite Evolved magma with a high silica contents, often associated with large explosive eruptions.

Strombolian Explosive eruption of low magnitude, occur usually with low-viscosity basaltic magma. Activity that produces scoria cones: accumulation of vesiculated magma around the vent.

Surtseyan type Eruption occurring through shallow water with the formation of an island from the deposition of pyroclastic material resulting from the highly explosive interaction between magma and seawater.

Vulcanian Explosive eruption of medium magnitude: result from the failure of an impermeable layer above the magma column, which restricts the process of magma degassing. Produce a lot of ballistics.

Xenolith Material of external origin and different composition incorporated within magma. They are often pieces of upper mantle or lower crustal rocks.

Definition of the Subject

Volcanoes represent one of nature's most formidable yet beautiful spectacles. They represent an omnipresent threat in many parts of the world, but also attract an increasing number of visitors, who have the urge to scale their flanks and peer into the depths of their craters. This entry includes a brief introduction to volcanoes: the reason they form, where they are located, and the hazard presented by the products of different types of eruption. Mexico is one of the world's most volcanic regions and a summary of the volcanoes of this country is presented. Included is a list of the active volcanoes of Mexico, defined for the first time using systematic criteria.

Introduction

In a small village somewhere in Mexico, a farmer awoke one morning and headed off to tend his crops, not expecting that anything out of the ordinary was going to happen that day. But his farm included a field that was not any ordinary cornfield, but a cornfield which all Mexican children now learn about in primary school. It was a cornfield which on that particular day was to become host to the birth a volcano. That farmer was to become one of the few people to witness a birth of one of nature's most spectacular creations.

The eruption of Paricutín took place between 1943 and 1952. It is the youngest of at least 1,040 volcanoes that are located in the Michoacán-Guanajuato volcanic field. Perhaps there is no better country than Mexico to study this type of volcanism. The country hosts at least 13 major monogenetic fields, each with countless scoria cones and other features. Many new fields are only now being defined.

The Basics of Volcanism

Volcanoes are located within certain regions on the Earth's surface related either to plate tectonics or to so-called hot spots, which represent locations below which convection-driven mantle plumes carry hotter material toward the surface. Plate boundaries can be divergent, such as mid-ocean ridges, which host the largest numbers of volcanoes on the planet, or rift zones, such as in East Africa. Other boundaries are convergent, which results in subduction, if one or both plates are thinner oceanic plates. In this process, one plate descends below the other carrying ample quantities of water within the rocks' structure. The water is a key ingredient to the formation of volcanoes since it lowers the melting point of the mantle, which becomes buoyant and rises toward the surface. A variable amount of the subducted plate is carried with it. Rather than erupt at the surface, the majority of magma accumulates within the crust after it loses its buoyancy, then cools with crystals slowly forming to create intrusive igneous rock. Some magma however will make it to the surface producing an eruption.

Volcanic eruptions can be divided into two broad categories: explosive or effusive. Various factors combine to determine how the magma emerges, the key ingredient again is water. Magma contains typically a few percent of water by weight, which is adequate to cause violent explosive eruptions if the magma rises to the surface sufficiently quickly. During ascent, decompression means that the dissolved water (and other gases) starts to form bubbles, which grow, and in the case of explosive eruptions, the volume of gas becomes much larger than the residual liquid magma. This gas can expand at alarming rate, which can produce the largest eruptions known as Plinian. Plinian eruptions

produce columns of gas and ash which can rise to 20 km or more above the surface. The larger eruptions produce enormous clouds of ash which enter the stratosphere, are dispersed widely by winds, and promote significant reductions in atmospheric temperatures. If the volume of magma emerging is large and its ascent rapid, the evacuation of the magma chamber below can promote collapse and the formation of a caldera. Some historical caldera-forming eruptions have had a considerable impact on the world's climate (e.g., the volcano Tambora, Indonesia, in 1815).

Less explosive types of explosive eruption, such as Strombolian, result from the ascent of less viscous magma (such as basalt). Bubbles of volcanic gas are able to flow through the magma, which prevents the buildup of extremely high pressures. This type of activity can result in the construction of a scoria cone, a common feature of the Mexican landscape. Larger stratovolcanoes are constructed over thousands of years with the erupted magma accumulating to form the volcanic edifice. The interaction of the rising magma with the ocean, a lake, or groundwater can escalate the explosivity, through the formation of rapidly expanding steam, and produce phreatic or phreatomagmatic eruptions. On land, the result can be a maar.

Effusive eruptions on the other hand produce lava domes and flows. In this case, the most important characteristics of the ascending magma: its temperature, viscosity, volatile contents, amount of crystals, combine to produce this less hazardous type of eruption. Lava flows can displace human settlements and destroy cultivated land, such as what happened at Paricutín, but they seldom endanger lives.

The products of explosive eruptions consist of ballistic rocks, ash, and pyroclastic density currents. The secondary remobilization of the pyroclastic deposits by water can produce immense mudflows or lahars. With the exception of ballistics, which do not reach very far from the volcano, each of these hazards can present a major risk to the population living close-by. Volcanologists need to investigate the deposits of previous eruptions to understand what might happen in the future. Hazard maps can be created to indicate where the eruptive products might accumulate. Several of Mexico's volcanoes have hazard maps and for several others, maps are in progress.

The Importance of Mexico's Volcanoes

Figure 1 shows the location of the major volcanoes of Mexico. The majority are located in the Trans-Mexican Volcanic Belt (TMVB), which extends across the country and has been described as the world's largest intracontinental volcanic arc. Over 40% of the population lives in this zone, which includes the large cities of Mexico City, Guadalajara, and Puebla. This makes volcanic risk an important issue. Enormous stratovolcanoes lie here within, like Nevado de Toluca, Popocatépetl, and the tallest volcano in North America: Citlaltépetl (or Pico de Orizaba, the name given by the Spanish colonialists). Construction of these edifices took place from the late Pleistocene onward. Figure 2 illustrates the magnitude of the most important eruptions of Mexico's active volcanoes.

Apart from the eruption of magma, stratovolcanoes can drastically influence their surroundings in another form: debris avalanches. These are huge collapses of a large proportion of the volcanic edifice and are common within the lifetime of a large volcano, given its unstable nature. Mexico has many examples with extensive deposits [1], which represent an important contribution to the shaping of the landscape.

The TMVB also includes nine identified large calderas with their associated ignimbrite deposits, such as Los Humeros or La Primavera, with 182 other circular features identified on satellite images [2]. Most likely many of these are also collapse caldera structures. It is easy to observe other expressions of volcanism such as maars, shield volcanoes, fissure eruptions, domes, volcanic islands, etc. Some of these calderas play an important role in the energy supply in Mexico. Currently some 958 MW of geothermal power are produced, which puts the country in fourth place in the world's rankings [3]. Production is dominated by Cerro Prieto in Baja California, with Los Azufres and Los Humeros contributing in the TMVB.

Volcanoes make their appearance throughout the different chapters of Mexican history. Eruptions of Popocatépetl drove the population out of prehispanic cities such as Cuicuilco, on the outskirts of Mexico City. The Aztecs reported various eruptions of Popocatépetl, which means "the smoking mountain" in the Náhuatl language. Other sacred centres, such as La

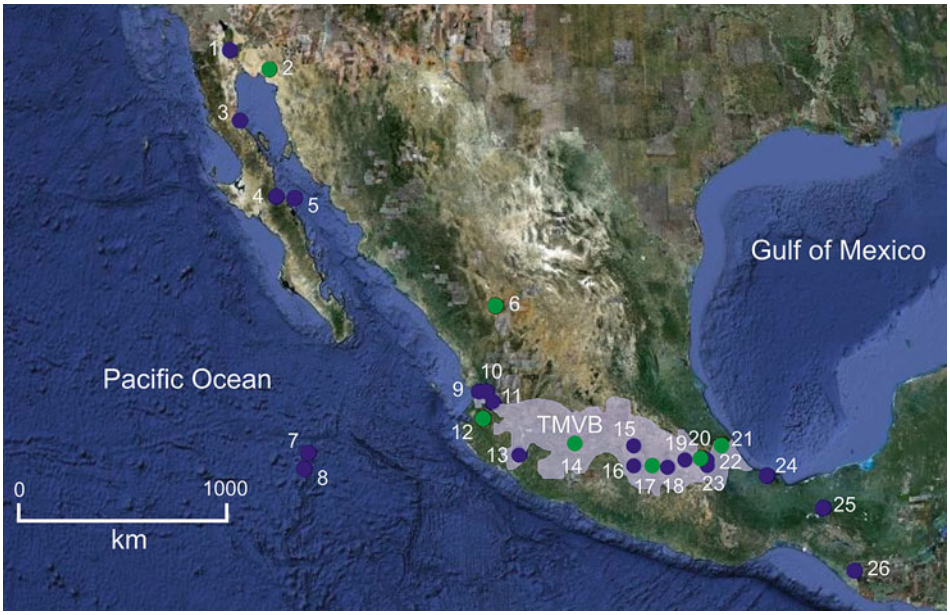

Volcanoes of Mexico. Figure 1

Map of Mexico showing the locations of the active volcanoes or volcanic fields. TMVB: Trans-Mexican Volcanic Belt. *1* – Cerro Prieto; *2* – Pinacate; *3* – Isla Tortuga; *4* – Tres Virgenes; *5* – Isla San Luis; *6* – Durango Volcano Field; *7* – Bárcena; *8* – Isla Socorro; *9* – San Juan; *10* – Sangangüey; *11* – Ceboruco; *12* – Mascota Volcanic Field; *13* – Volcán de Colima; *14* – Michoacán-Guanajuato Volcanic Field; *15* – Jocotitlán; *16* – Nevado de Toluca; *17* – Chichinautzin Volcanic Field; *18* – Popocatépetl; *19* – La Malinche; *20* – Serdán-Oriental volcanic field; *21* – Naolinco volcanic field; *22* – Las Cumbres; *23* – Citlaltépetl; *24* – San Martín; *25* – El Chichón; *26* – Tacaná

Campana in Colima, show evidence that the construction of certain pyramids tried to mimic distant volcanic peaks. Vast valleys are filled with soils that owe their fertility to the outpourings of countless eruptions, and other value has been reaped, such as the hugely important volcanic product that is obsidian. This volcanic glass, usually shiny black in colour, can be fashioned without much skill into knifes and weapons. It was clearly important in the development of the early Mexican people. Cortes during his conquest of Mexico had run out of gunpowder. Unfortunately for countless indigenous people, he was able to get the sulphur to replenish his stocks by sending his men into the crater at Popocatépetl. The Paso de Cortes, situated high up between Popocatépetl and its older neighbour Iztaccíhuatl, is host to the only statue to Cortes in the whole of Mexico.

During the nineteenth century various pioneers of exploration and scientific observation made important discoveries, and their documents along with the paintings of various travellers are important documentation of the early eruptive record of many volcanoes.

Volcanology in Mexico is a young science, having only taken off following the 1982 eruption of El Chichón. An enormous amount of work remains to be done: identification of deposits; geochemical analyses to determine details of magma ascent and emplacement; geophysical work to establish the location of magma chambers, hydrothermal systems, etc.; risk assessments and the creation of hazard maps. There are countless young lava flows, some possibly matched by accounts of activity from prehispanic stories or texts from European missionaries or explorers. But many question marks remain regarding the date of the most recent activity for many centres.

The number of volcanoes described as being "active" varies depending upon the text being consulted. Here, the list in Table 1 includes 26 volcanoes or volcanic fields ascribed as being active, and represents the first systematic attempt to create

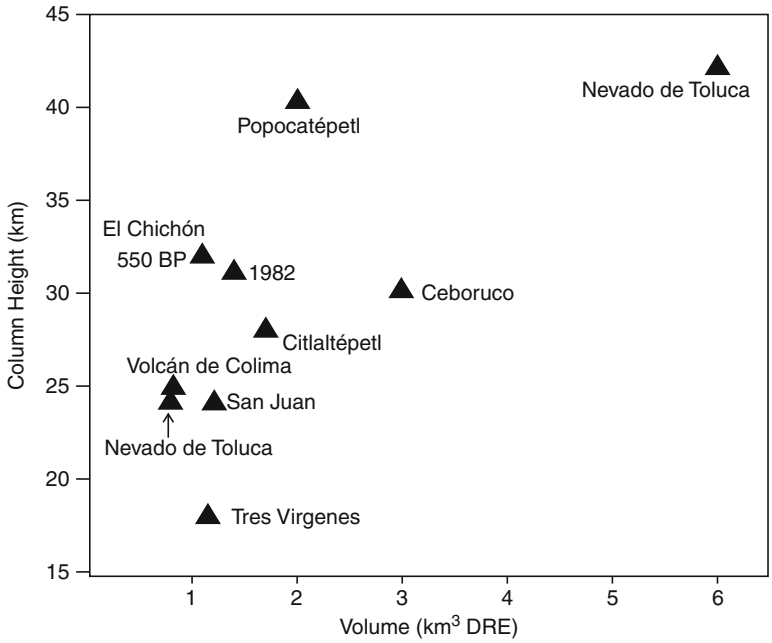

Volcanoes of Mexico. Figure 2
Eruption column height v. erupted volume of magma for Mexico's most recent large (Plinian) eruptions. DRE = Dense rock equivalent, thereby taking into account any vesicles or pores within the deposits. Eruption ages: El Chichón 1982 and 550 year BP; Volcán de Colima 1913; Ceboruco 1,060 ± 55 year BP; Popocatépetl 4,965 ± 65 year BP; Tres Vírgenes 6,500 year BP; Citlaltépetl 8,500–9,000 year BP; Nevado de Toluca 10,500 year BP and 21,700 year BP; San Juan 14,770 ± 480 year BP (Figure modified from Arana-Salinas et al. 2010)

a definitive list. An active volcano is one that could erupt again, which means the presence of a magma body present at depth. This should give certain telltale signs, such as seismicity, heat dissipated through the interaction with ground water, resulting in hot springs, or direct degassing in the form of fumaroles. A seismic network may not be present to detect these movements and the thermal manifestations will not always be present. Medina et al. [4] in their early work considered the existence of fumarolic activity as a criterion for considering a volcano active. The other consideration is the repose interval since the last eruption. Mexico has many volcanoes with long repose intervals, often of several thousand years, hence a somewhat arbitrary limit can be taken as 10,000 years (following the definition of the Smithsonian Institute, Washington, D.C.). Since volcanic fields feature monogenetic volcanoes (those that erupt just once), these are taken as a single active entity. Several other volcanic fields, or scoria cone complexes not considered here, could also be active, in that they feature lava emissions that may have occurred within the Holocene. However, they have not been included in the list since no strong evidence exists to date. Examples are La Gloria field in Veracruz and Isla Isabel in Nayarit, where, as is the case at many locations, further studies are needed to clarify the situation. Three Pleistocene calderas in the TMVB still have fumarolic activity with extensive geothermal fields: La Primavera, Los Azufres, and Los Humeros. These have not been included as active since the probability of future eruptive activity is regarded as negligible, given the long periods that have passed since their last eruptions. Prehistoric calderas sometimes feature persistent hydrothermal activity, which unlike the case of stratovolcanoes or domes, is not necessarily regarded as evidence for the likelihood of a future eruption.

Monitoring has been expanded greatly in the last 20 years with sophisticated networks feeling the pulse of Popocatépetl and Volcán de Colima. Seismic and geochemical monitoring (water samples) is being carried out at El Chichón and Tacaná with some seismic

Volcanoes of Mexico. Table 1 Active volcanoes of Mexico, in order starting with the most recently active

Volcano/field	Date of last eruption	Details	References
Volcán de Colima	Currently erupting[a]	Cyclic effusive and Vulcanian explosions	[38]
Popocatépetl	Currently erupting[a]	Cyclic effusive and Vulcanian explosions	[42]
Isla Socorro	1993	Submarine flank eruption	[21]
Tacaná	1986	Phreatic explosion	[67]
El Chichón	1982	Plinian eruption	[59]
Bárcena	1953	Explosive eruption	[20]
Michoacán-Guanajuato volcanic field	1943–1952	Formation of cinder cone – Paricutín	[50]
Ceboruco	1870–1875	Dacitic lava flow	[26]
Citlaltépetl	1846	Explosive	[47]
St. Martin Tuxtla	1793	Summit cinder cones	[58]
Tres Virgenes	1746	Explosive though unconfirmed	[15]
Sangangüey	1742	Unconfirmed eruption of flank cone	[27]
Jocotitlán	1270	Explosive	[41]
Chichinautzin volcanic field	340 AD	Xitle cinder cone and flow	[55]
La Malinche	1170 BC	Ash fall and pyroclastic flow	[45]
Naolinco volcanic field	1200 BC	Cinder cone and lava flow	[57]
Isla San Luis	Recent but undefined age	Rhyolitic obsidian domes	[16]
Nevado de Toluca	3,300 BP	Pyroclastic flow and surge	[40]
Mascota Volcanic Field	Maybe 5,600 BP	Lava flow and scoria	[53]
Las Cumbres	5,900 BP	Rhyolitic lava dome	[49]
Durango Volcanic field	Few thousand years	Maar formation, scoria cones and lava flows	[52]
Pinacate volcanic field	Holocene	Unknown	[10]
Cerro Prieto	Holocene	Unknown	[3]
Isla Tortuga	Holocene	Unknown	[17]
Serdán-Oriental volcanic field	Holocene or late Pleistocene	Las Derrumbadas – fumaroles	[56]
San Juan	Holocene or late Pleistocene	Plinian eruption 14,770 BP	[28]

[a]Effusive eruption still ongoing at the time of writing: June 2011

monitoring of Citlaltépetl and Ceboruco. Much effort is being directed at increasing the quality and diversity of the information being generated, as well as the definition of models of the eruption mechanisms, thus advancing what can be interpreted from the data.

Tectonics

Volcanism in the north of Mexico can be clearly divided into various regions, each with its characteristic tectonic situation. Volcanism can be associated with

extension; this gives rise to various volcanic centres in Baja California and Sonora. Further south the oceanic Rivera and Cocos plates collide with the continental North America plate; the resulting subduction gives rise to the majority of volcanoes which are located in the TMVB. Further to the south the Central American Volcanic Belt (CAVB) starts with the potentially dangerous volcano Tacaná, shared between Mexico and Guatemala. Whereas this belt, which extends through Central America, is parallel to the subduction trench, the TMVB clearly extends obliquely across the country, making an angle of about 15° with respect to the Middle American Trench. This intriguing characteristic has been explained using geophysical and geochemical observations that suggest a decreasing angle of subduction as one moves down the coast from the NW to SE [5, 6]. This results in an increasing distance between the trench, the point where the descent of the oceanic plate commences, and the zone of melting, which typically occurs at pressures corresponding to a 100 km depth.

One fascinating feature within the belt is the existence of several small chains of volcanoes, which demonstrate a decreasing age from north to south: Cántaro – Nevado de Colima – Volcán de Colima; Tlaloc – Itzaccihuatl – Popocatépetl; and Cofre de Perote – Las Cumbres – Citlaltépetl –Sierra Negra. Evidence of an overall southern migration of the magma chamber has been identified [7].

At each end of the TMVB things get tectonically more complicated. Firstly to the east, between the TMVB and CAVB the very active volcano El Chichón is found along with other extinct peaks forming the Pliocene to Recent age Chiapanecan Volcanic Arc (CVA). This rather esoteric arc stretches some 150 km in a NW to SE direction. The subducting Cocos plate changes from being a virtually flat slab in Central Mexico to a ~45° dip angle beneath the CVA, with the slab being located an unusually deep ~200 km below the arc [8]. At the north-western extreme of the TMVB evidence of rifting, or the separation of two plates, is present. Here magmas with a higher alkaline content have been erupted, which combined with geomorphological evidence, such as the alignment of scoria cones or fault scarps, suggests that the so-called Jalisco Block might one day separate from mainland Mexico [9, 10].

The following summary of Mexico's different volcanic centres starts in the NW of the country, continues with the TMVB, going from W to E, continues with monogenetic fields and finishes with the volcanoes of Chiapas. The account concentrates on active volcanic centres, though some important extinct volcanoes are included.

Baja California and Sonora

Sierra Pinacate Volcanic Field

This region includes more than 400 cinder cones and lava flows, and eight large maar craters of late-Pleistocene to Holocene age [11]. As with many cases of volcanic fields in Mexico, the cones follow alignments determined by the regional tectonics. Maars are the result of phreatomagmatic activity and this field has excellent examples. Crater Elegante is the largest with a diameter of 1.6 km and depth of 240 m. Eruptions here generally commenced with Stombolian eruptions and the construction of cinder cones. Unusually, the phreatomagmatism occurred later, probably a reflection of the aridity of the region. Despite a lack of any firm dates of Pinacate rocks placing the most recent activity from the field in the Holocene, the low level of erosion suggests activity within this period and hence its inclusion in the list of active Mexican volcanic fields [3].

Cerro Prieto

This is the location of the most productive geothermal field in Mexico. The dacitic lava dome is located within an active continental rift, which marks the transition from the famous San Andreas transform fault system to the north to the spreading ridge of the East Pacific Rise in the Gulf of California to the south. Geophysical evidence gave 10,000 years as an approximate youngest date [12] and the presence of geothermal manifestations at the surface also suggests its inclusion in the active list. In addition, legends of the local Cucupas people describe hot rocks being thrown by a monster and fires coming from the soil, suggesting it may have been active much more recently [4].

San Quintín, Jaraguay, and San Borja Volcanic Fields

These three fields are not being included as active, although some early authors thought they are of Holocene age [4, 13], there is no clear evidence. Recent

dating suggests the San Quíntin field is no younger than 20,000 years [14]; however, the Jaraguay and San Borja fields have less vegetation on their flows, suggesting younger ages [15]. The three fields consist of cinder cones and lava flows, San Quintín with ten distinct complexes [13].

Tres Virgenes

The only large stratovolcano in the Baja California region is the Tres Virgenes complex. It consists of three cones, with a progression to younger ages to the SW, La Virgen being the youngest. There may have been an eruption in 1746, according to a record of observations, but there is no hard evidence [16]. The last major Plinian eruption occurred about 6,500 years ago. Volcanism here is associated with dominantly extensional faulting.

Isla San Luis and Isla Tortuga

These two islands represent the youngest volcanism in the Sea of Cortés. The oldest deposits of Isla San Luis show that it was born like the island of Surtsey, in Iceland, with corresponding highly explosive eruptions producing pyroclastic surges [17]. This activity was followed by dacitic flows and the formation of tuff rings, then finally two rhyolitic domes were emplaced. The activity can be thus characterized by a successive eruption of progressively more differentiated lavas. Suggestions have been made that the two rhyolitic domes are less than 100 years old [4]. While this might be wishful thinking, they certainly are relatively young, warranting the inclusion of this island in the active volcanoes list.

Isla Tortuga is a shield volcano with young lava flows located further south. The latest stage of activity culminated in caldera collapse, extrusion of the surficial flows, and the formation of a lava lake. Medina et al. [4] defined it as being Holocene, though no evidence was given. The spatter cones within the caldera appear to be recent as do many of the flows that cover its flanks [18].

Isla Isabel

This small island off the state of Nayarit represents an emergent Surtseyan-type volcanic complex. Various craters on this island show evidence that there was a general migration of volcanic activity from northwest to southeast [19]. It is one locality where it is possible to find abundant mantle xenoliths. It has been suggested that the most recent eruptions were less than 10,000 years ago, though due to the lack of hard evidence, the island is not included in the list of active Mexican volcanoes.

Pacific Islands

The Revillagigedo archipelago is volcanic with two active centres. It is located on the Mathematician Ridge, which was the location of an active spreading centre prior to its migration 3.15 Ma BP [20]. The volcano Bárcena on the small 4.5 km long unpopulated island of San Benedicto formed in an eruption in 1952–1953 [21]. Since, it has remained quiet and unstudied.

Famous for its marine life and endemic species of fauna and flora, Isla Socorro represents the other active volcano of the archipelago. The only human occupancy is a naval base in the SE corner of the island. In Fig. 3 you can see a view from off the southern coast, showing domes and old lava flows, one with beautiful levees (ridges at the edge of the flow parallel to its flow direction). The last eruption occurred in 1993: a relatively small submarine event which sent blocks of gas-filled pumice hurtling to the surface [22]. The summit area has not seen an eruption since at least 15,000 years ago [20], but has an extensive hydrothermal field, emitting gases which contain unusually high concentrations of methane and hydrogen [23]. The island is covered with extensive lava flows and domes, unusually of peralkaline composition, and more recent cinder cones in the SE part of the island. Here the ^{14}C method was used to date some lacustrine deposits, which are clearly older than nearby cones [24]. An age of about 5,000 years was obtained.

Tepic-Zacoalco Rift

This zone stretches from beyond Tepic southeast to Guadalajara. It includes a mesmerizing density of volcanic features, including five andesitic stratovolcanoes, plus maars, domes, and countless scoria cones. Many groups of cinder cones are aligned in a NW-SE direction, the same as the rift. To the NE of

Volcanoes of Mexico. Figure 3
View from the south side of Isla Socorro. Various domes and lava flows can be distinguished on the slopes of the volcano

the zone the mountains represent the huge deposits of the Sierra Madre Occidental volcanic province, while to the SW the micro-plate known as the Jalisco Block is located [25]. The zone is dominated by several large stratovolcanoes, but also includes many fascinating features such as the maar Santa Maria del Oro, which contains a picturesque lake.

Ceboruco

The most recent activity in this region was a lava flow which emanated from Ceboruco in 1870 and descended down the south-west flank. Recent activity at this volcano has been in the form of various lava flows of either a dacitic or andesitic composition, some originating from near the summit, others from lower on the flanks. Two roads extend along the rift zone, one to the north, the other to the south of Ceboruco. Both provide stunning views of the many lava flows which have covered the flanks of this volcano. The last major explosive eruption occurred only 1,000 years ago [26] and produced an extensive pyroclastic flow and pumice fall deposit. A caldera was formed with a 4 km diameter. The eruptive episode was terminated by the emplacement of two small domes and a lava flow within the crater. Following, there was a period of about 500 years with the formation of six different andesitic or dacitic lava flows on the flanks [27]. Since then the volcano has been quieter, with just the one recent 7 km long lava flow.

Sangangüey and San Juan

Further to the NW, Sangangüey is an impressive mass with a spectacular lava spine at its summit and large collapse scars on its flanks. The spine can be seen in Fig. 4, which was taken from the summit of Ceboruco. Many cinder cones exist along the rift, all aligned in the NW-SE direction in five different linear groups. There are no records of historic activity from the peak, although historical accounts coupled with low levels of erosion suggest that some of the flank cinder cones have erupted less than 1,000 years ago [28]. For this reason the volcano is included in the list of active volcanoes of Mexico.

At the Tepic end of the rift, in fact adjacent to the city of Tepic, there lies San Juan, a volcano which is not termed active using the 10,000 year rule. However, it has been pointed out that its explosive past, with the last Plinian event occurring about 14,770 years ago, suggests that a reawakening should not be totally ruled out [29].

Volcanoes of Mexico. Figure 4
Sangangüey shown in the distance, looking from Ceboruco. Many scoria cones can be seen following the NW-SE trending faults

Volcán Tequila

Tequila, apart from being a notorious Mexican export, gives its name to a large stratovolcano, located further to the SE along the rift. The youngest associated volcanic feature (~60 ka) is a small andesitic vent called Cerro Tomasillo [30]. The region features various cones, domes, and flows with a large variety of compositions from basalt to rhyolite. Volcán Tequila itself also has a summit spine; in this case it is a 300 m high pinnacle, which dominates any view to the volcano from an east or north direction.

La Primavera

Very close to Mexico's second largest city, Guadalajara, there is a picturesque zone of obsidian and hot springs, otherwise known as La Primavera. A large 11 km diameter caldera was formed about 95,000 years ago, with the Tala Tuff being emplaced which has a volume of about 20 km^3 [31]. The caldera was then filled by a lake. Subsequent activity included the formation of many domes, which along with uplift ended the life of the lake. Its legacy can be seen in the form of a notorious deposit of so-called giant pumices, some of which are more than 1 m across [32]. The exploitation of the remnant heat for geothermal energy was commenced but never made it to production due to objections due to the environmental impact.

Volcán de Colima

Being the most active volcano in North America, Volcán de Colima deserves special attention. It currently is undergoing its most active period since the last major eruption, which occurred in 1913. The Colima Volcanic Complex shows a southern migration of activity, the oldest edifice being Cántaro which was active between 1.6 and 1 million years before present. Volcanism then moved 15 km south to Nevado de Colima, and more recently to the current location, a further 6 km to the south [33]. The existence of a group of undated domes, called Los Hijos about 3 km further south, possibly corresponds to the first signs of further migration. Some major debris avalanches have occurred from the edifice, including a large one 18,500 years ago, which formed a dam across the Naranjo river [34]. The breaking of this dam produced an enormous debris flow which reached the Pacific Ocean, 120 km away. More recently,

3,600 years ago, a smaller collapse went toward the SW, this time damming the Armería river [35]. The relatively large frequency of such events is demonstrated by evidence of a more recent event still, which has been dated at 2,500 years ago. Emergency response plans cannot consider events of such large magnitude. The probability of occurrence remains low; however, sooner or later a debris avalanche will occur, if not at Colima, at one of Mexico's other sizable stratovolcanoes.

Since the most recent collapse, pyroclastic deposits and lava flows have been accumulating and building the current edifice. It has grown to a height of about 3,860 m, though the current altitude is not really known due to the frequent construction and destruction of summit domes. The 1913 Plinian eruption produced a 23 km altitude column and pyroclastic flows that reached 15 km from the volcano [36]. The historical records show that Volcán de Colima has a large Plinian (or at least sub-Plinian) eruption every 100 years, more or less [37]. Previous to 1913 there were eruptions in 1818, 1690, and 1606. This is very frequent for a volcano.

Volcán de Colima has produced a large number of andesitic domes and flows during recent years. The most recent episode of activity commenced in 1998 [38] and has since produced four different phases of dome growth (1998–1999, 2001–2003, 2004, 2007–2011 [effusive eruption still ongoing at the time of writing: June 2011]). The effusive activity has been interspersed with explosive eruptions (Fig. 5). This peaked in 2005, when at least 30 Vulcanian eruptions occurred, each producing a pyroclastic flow resulting from column collapse. The longest flow reached 5.4 km along a ravine to the SE of the volcano. An even longer flow occurred in October 2004 when a relatively large dome collapse produced a pyroclastic flow which headed down a ravine on the SW flank to a point 6.1 km from the volcano. Since 2003, the volcano has produced several Vulcanian explosions each day (like the example in Fig. 6).

The population occupying the flanks of this volcano is much larger today than it was at the time of the last large eruption. Monitoring efforts include a variety of techniques applied in the quest to identify precursors of any large-scale acceleration of activity.

Volcanoes of Mexico. Figure 5
Volcán de Colima in January 2002. In the photo the older part of the complex, Nevado de Colima can be seen behind to the north. The volcano itself is covered with lava flows of different ages, the longest recent flows to the south having formed in 1998–1999. The black-looking lava dome had been growing since May 2001 and reached the crater rim and began forming rockfalls the following month. The Los Hijos domes can be seen in the bottom right-hand corner of the photo

Volcanoes of Mexico. Figure 6
Small typical Vulcanian explosion at Volcán de Colima, February 2009

The seismic network had its first seismometers installed in the 1980s. Useful precursors have been identified like swarms of long-period events prior to Vulcanian explosions or effusion (2004 and 2005; [39]) and volcanotectonic events signaling the ascent of magma in 1997–1998. The recent introduction of monitoring methods such as the thermal monitoring of fumaroles [40], the dome and explosions have expanded the possibilities of forming models to explain the transition between different regimes of activity, which form various cycles of activity: from the daily explosive cycle, the several year cycle of effusive episodes, to the 100 year cycle of large explosions. The integration of monitoring data will be vital to try and determine whether a cataclysmic eruption is imminent.

Central Stratovolcanoes

The Eastern-central zone of the TMVB features five large stratovolcanoes, four of which are considered active, along with a number of smaller edifices like Jocotitlán, also considered active. Here the descriptions start to the west and head east.

Nevado de Toluca

Nevado de Toluca reaches 4,680 m above sea level and features a pair of lakes within its caldera. Fig. 7 shows the smaller Laguna de la Luna (moon) within the summit caldera. The lakes have proved to be interesting to archaeologists, whose finds suggest they were used for prehispanic rituals. Its final episode of effusive activity 9,100 years ago produced a small dacitic lava dome. This followed the most recent major Plinian eruption, which produced the Upper Toluca Pumice deposit 10,500 years ago [41]. This major eruption produced a column that is thought to have reached 42 km in altitude and deposited about 14 km^3 of material. This was the largest eruption in Mexico in the last 15,000 years. An extensive record of large explosive activity and major collapses of the edifice can be observed in the surrounding region. The most recent deposits date about 3,300 years before present and consist of a pyroclastic flow and surge emplaced on the NE flank.

Jocotitlán

Nearby the smaller Jocotitlán is a fine example of an edifice that has collapsed to produce a debris avalanche deposit. In contrast to the larger stratovolcanoes, it rises only 1,300 m above the surrounding plains. Large conical hummocks have been identified with the collapse event that occurred 9,690 years ago [42].

Volcanoes of Mexico. Figure 7
Laguna de la Luna, within the crater of Nevado de Toluca

The 2.8 km^3 deposit reached a distance of 12 km. The most recent eruption of Jocotitlán was only 680 years ago; the material deposited from pyroclastic density currents on the upper flanks of the edifice makes it obligatory to include this peak in the list of active volcano of Mexico.

Popocatépetl

The potentially biggest volcanic threat in Mexico is Popocatépetl, which at 5,472 m towers above the surroundings, and is only 65 km from Mexico City and 45 km from Puebla (Fig. 8). The population within a radius of 40 km is in excess of one million. Popocatépetl reawoke in December of 1994. Since then activity has been characterized by the growth of lava domes within the crater, periodic Vulcanian explosions and the release of large volumes of gas. This eruption has been the first since El Chichón in 1982 to produce fatalities. Unfortunately five intrepid individuals decided to ignore official warnings and they climbed to the crater rim in April 1996. As well as ending their lives, an explosion sent cm-sized fragments of the destroyed lava dome to the nearest villages.

During the last 10,000 years there have been at least three large Plinian eruptions [43]. 4,965 years ago an eruption sent clasts with a diameter of up to 2.5 cm to a distance of 19 km from the volcano [44]. This implies that the height of the eruption column was 37–41 km. The eruption deposited 4.9 km^3 of material and was the second largest in Mexico within the Late Pleistocene–Holocene period. A similar eruption today would have an enormous impact on some 15 million people living in the surrounding region. More recently, two further large eruptions occurred 2,150 and 1,100 years ago. These two would have affected the local population centres at this time.

During the current activity there have been two reasonably sized lahar events in 1997 and 2001 [45]. The first had more water with a partial melting of the glacier making a contribution. Both events reached the most vulnerable village on the flanks: Santiago Xalitzintla, some 15 km from the crater, though nobody was hurt.

La Malinche

The indigenous wife of Cortés certainly would not have guessed that her name, or the Mexican nickname for her, would one day be given to a large stratovolcano. Like many volcanoes in this country, activity is punctuated by large periods of rest [46]. La Malinche is one

Volcanoes of Mexico. Figure 8
Popocatépetl, which gets a frequent covering of snow during the rainy season. Its permanent glacier has greatly diminished in size over recent years

volcano that has not appeared on lists of active Mexican volcanoes, explained by its lack of a clear crater or fumaroles. However, the local land is covered by pyroclastic deposits with poor soil development on top, and one layer has been dated at 3,100 years old. Given that over two million people live on its lower slopes, it needs to be considered carefully, with eruption scenarios determined [46].

Citlaltépetl

Citlaltépetl has the honor of being the highest active volcano of North America. Its prehispanic name is perhaps less used than the name which resulted from the Spanish invasion: Pico de Orizaba. At 5,675 m it is no mean feat to cross the glaciers and reach the rim of the crater. In recent years it has not shown much activity; however, over 750,000 people live within a radius of 40 km. The last major eruption, which occurred 4,100 years ago, produced a series of block and ash flows and lahars whose deposits have been found up to 28 km from the crater [47]. The most recent event was a smaller eruption that left deposits of tephra, having been dated at 690 years ago [48].

Like many of Mexico's volcanoes, widespread devastation is one possible future scenario in the event of a debris avalanche. There is evidence that Citlaltépetl has suffered many such events possibly without any eruptive activity [49], with some reaching the Gulf of Mexico, 120 km away. The edifice of this volcano has often been weakened by intense hydrothermal alteration, which combined with a large elevation difference of 4,400 m dropping down to the Gulf Coastal Plain have produced favourable conditions for these large-scale edifice collapses. This lack of precursory eruptive activity means that an event could occur one day without any warning.

Las Cumbres

Las Cumbres, located only about 10 km north of Citlaltépetl volcano, is an eroded stratovolcano which was once possibly as large as its neighbour [50]. It is the middle member of the enormous N-S chain of volcanoes which starts with Cofre de Perote in the north and ends with Citlaltépetl to the south. Its last big eruption was 20,000 years ago and produced the widespread Quetzalapa pumice deposit. More recently various scoria cones were formed as well as the Yolotepec dome,

Volcanoes of Mexico. Figure 9
The church of San Juan Parangaricutiro which was buried by the lava flows from Paricutín. The cone can be seen in the background

which has been dated at less than 6,000 years [50]. Large debris avalanches have also resulted from major collapses within this complex [49].

Volcanic Fields

Michoacán-Guanajuato Volcanic Field

Driving through this large expanse of territory, one cannot escape the awe-inspiring impact of the extent of this volcanic field. In places the cinder cones are so close they are touching one another. The recent addition of Paricutín is the most famous, but previously the birth of Jorullo was also witnessed in 1759. The field covers a vast area measuring 250 × 200 km in the two states which give the field its name. It contains at least 1,040 volcanic vents. The majority are cinder cones, but there are also small shield volcanoes, lava domes and maars. In general, the cones are randomly distributed, although there are local areas where alignments can be identified [51]. The region with the largest density of cones is that of Paricutín, where the median spacing between each one is 1.15 km. The cones are not so large, the median height being 90 m with a basal diameter of 800 m. A visit to Paricutín today awards the visitor with views of the famous church which was partly spared by the advancing lava flows. Figure 9 shows the church partially submerged.

One northern region of the field is Valle de Santiago, which features the stunning beauty of its seven major maars. There are a total of 20 within a zone with dimensions of 7 × 50 km [52]. The youngest, La Alberca, has been dated at 73,000 years old. Unfortunately, overexploitation of the groundwater has meant that the maars have almost all lost their lakes over recent years.

Durango Volcanic Field

This large field covers some 2,100 km^2 and contains about 100 cinder cones [53]. The La Brefia-El Jagüey Maar Complex is one of the youngest centres in the field and the only section studied in detail. Being maars, they were formed by the interaction between magma and groundwater (phreatomagmatic eruption), which produced large explosions. The final phase of the activity was the formation of several scoria cones within the crater and related lava flows. The age of this complex has been estimated at a few thousand years [53].

Mascota Volcanic Field

Several volcanic fields are located within the Jalisco Block, the youngest being close to the city of Mascota. This field is notorious for the geochemistry of its lavas, which are dominated by minettes, an unusual type of lava which, instead of the more common feldspar crystals dominating, contains large mica crystals [54]. The youngest flow of this field stands out through the lack of vegetation or soil on its surface. This led the authors to believe its age to be a few thousand years old. Further evidence of its age could be a correlation with scoria found in nearby lake deposits that was dated at less than 5,600 years old.

Chichinauzin Volcanic Field

The extensive Chichinauzin field lies to the south of Mexico City and covers some 2,500 km^2. It contains more than 200 monogenetic scoria cones and associated lava flows [55]. The last eruption was 1,670 years ago [56] and given that its historic <1,250 years reoccurrence time has been greatly exceeded, it represents one of the more likely regions for the birth of the next Mexican volcano. During the past 10,000 years, at least six monogenetic eruptions have occurred (Pelado, Cuauhtzin, Tláloc, Guespalapa, Chichinautzin, and Xitle). The cone of Xitle is a clear landmark within the southern limits of the city boundary, reminding us of its eruption 1,670 years ago. Obviously when the day arrives for the next eruption, the effect will be catastrophic and resulting lava flows and ash fall will paralyze the capital city.

Serdán-Oriental Volcanic Field

No evidence has been found for activity within the last 10,000 years; however, it has been included in Table 1 for two main reasons. Firstly, Las Derrumbadas are a pair of volcanic domes within this field. They still have active fumaroles outputting measurable quantities of sulphur dioxide. This volcanic field also hosts several maars, some with lakes, some without, other rhyolitic domes and scoria cones. An interesting dome named Cerro Pizarro shows evidence that it has produced multiple eruptions, unusual for this type of volcano, which normally is monogenetic [57]. Furthermore, the repose periods could be greater than 65,000 years, which is another reason for not declaring this field as no longer capable of producing an eruption.

Cofre de Perote Vent Cluster and Naolinco Volcanic Field

These recently identified mafic fields are located on the flank of the largely Pleistocene Cofre de Perote shield volcano, in the case of the Cofre de Perote Vent Cluster (CPVC) and to the north of Jalapa, Veracruz, the Naolinco Volcanic Field (NVF) [58]. The CPVC consists of an extensive lava field that covers >100 km^2. The most recent eruption was from the El Volcancillo scoria cone and it produced an impressively large flow which traveled 50 km only about 870 years ago. The Rincón de Chapultepec scoria cone in the NVF produced a lava flow ~2,980 BP. Interestingly these flows are some of the largest in the whole TMVB, but remained almost totally ignored until within the last 10 years.

San Martín Tuxtla

The basaltic volcano San Martín Tuxtla is located near the coast of the Gulf of Mexico, in southern Veracruz. It actually represents the active centre within another volcanic field containing monogenetic volcanic cones, maars, and three other large volcanoes which have not shown evidence of activity in the Holcene [59]. It is so far unclear whether this volcano is the eastward end-member of the TMVB or related to extensional tectonics. Its most recent eruption in 1793 was a succession from phreatomagmatic explosions, to Strombolian explosions and then an effusive episode, which produced a 3 km lava flow. At least nine other eruptions took place within the last 6,000 years of scoria cones and maars in this field.

Volcanoes of Chiapas

El Chichón

The largest historic eruption to occur in Mexico was the 1982 eruption of El Chichón, which resulted in the death of around 2,000 people and impacted the world's climate through a measurable reduction in temperature. Prior to the eruption it was almost totally unknown, with nobody aware of its potential for

devastation. El Chichón is not a towering stratovolcano like those of the TMVB, but an unassuming hill, which is difficult to see until one has almost arrived at its lower flanks. Ironically, several months before the eruption, El Chichón was the subject of a geothermal prospecting trip. In a report it was stated that the volcano needed to be studied and might reactivate in the future.

Three large explosions occurred within a week from 28 March to 4 April, 1982. The authorities were taken by surprise [60]. The volcano had been asleep for 550 years previous to this Plinian eruption. Lack of experience largely affected the handling of the emergency, with a proportion of the deaths occurring due to the early return of evacuees. The eruption attracted a lot of international interest, one reason being that the magma had an unusually high sulphur content. This increased the impact on the world's climate from the eruption cloud, with aerosols in the stratosphere producing a decrease of 0.2–0.5°C in temperature in the Northern Hemisphere [61].

The eruption at El Chichón formed a 1 km diameter and 180 m deep crater (Fig. 10). Geochemical and geophysical studies have attempted to define the hydrothermal system which includes the shallow crater lake, bubbling springs, and geysers [62, 63]. The lake can be observed to vary considerably in size, seemingly following a cycle that is independent of the local rainfall. Another interesting observation is that some hot springs found outside of the crater appear to be part of a system that was undisturbed by the Plinian eruption.

Research has now shown that the volcano has had a large eruption approximately every 800 years [64]. Studies looking at the stratigraphy of local deposits have deduced that during the past 8,000 years it has produced at least 11 eruptions [65], with many being similar to that of 1982. Larger magnitude events occurred in the year 750 and 1450 AD. The former of the two coincided with the collapse of the Mayan civilization in that region. Perhaps it played a role. A future large eruption would impact more than 70,000 people living in a radius of 35 km from the volcano.

Tacaná

This volcano sits right on the Mexico–Guatemala border and presents a largely unacknowledged hazard. The most recent eruption was in 1986: the phreatic explosion resulted in the formation of a new fumarole field

Volcanoes of Mexico. Figure 10
The crater of El Chichón taken on 5 May 2004

below the summit. Although it was a small event, it indicates the proximity of a magma body to the surface. The study of the geochemical characteristics of a number of springs at different elevations has provided an interesting insight into the often little-understood interaction between magmatic gases and the aquifers within the volcanic edifice [66].

The new fumaroles are located in a scar that was left by a collapse that occurred about 10,610 years ago after the growth of a summit dome [67]. More recently during the Holocene Tacaná had a series of eruptions, both explosive and effusive, the most recent being about 1,950 years ago [68]. Following the eruption, a series of lahars devastated the surrounding countryside. There is evidence that the construction of a nearby prehispanic settlement called Izapa was interrupted by these events. New activity of a similar magnitude could impact the approximately 300,000 people who live within 35 km of the volcano, an order of magnitude higher than its more famous neighbour in Chiapas.

Future Directions

Hopefully this entry has provided a useful introduction to the many volcanoes of Mexico. The cultural and geographical richness of the country is exemplified in its volcanoes. For their study, Mexico offers a huge variety of landforms and endless geophysical and geochemical case studies. There is a considerable potential for future eruptions with a significant impact. The most dangerous volcanoes in Mexico for their potential for large eruptions are probably Popocatépetl, Volcán de Colima, Tacaná, Citlaltépetl, and Ceboruco. But monogenetic fields such as Chichinautzin could also wreak havoc with the birth of a new cinder cone. The reactivation of one of its other sleeping giants always remains a distinct possibility.

Studies are only just being initiated of many of the active or potentially active volcanic centres of Mexico. There are many areas of research to be explored, with many more waiting to be defined. In certain cases the origin of extensive deposits emplaced during historic or prehistoric eruptions is unknown. With others the eruption mechanism has yet to be fully understood, which creates a dilemma when attempting to define a monitoring strategy, whilst faced with the possibility of an impending cataclysmic event. This lack of understanding makes it difficult to set threshold levels for monitored parameters, such as gas flux or seismicity, which should trigger a change in the alert system or an action within the emergency risk mitigation plan.

Hazard maps have been published of Popocatépetl, Volcán de Colima, Citlaltépetl, El Chichón, and Nevado de Toluca. These represent vital tools for the mitigation of volcanic risk by improving land-use planning and for defining procedures during emergencies. These need to be regarded as dynamic, with constant updating as new information becomes available. Work is underway to construct risk maps for certain hazards, which not only consider the geographical extent, but also the probability of occurrence and the vulnerability of the local population. Similar maps are required for some of the other active volcanoes of Mexico.

After the large loss of life at the hands of El Chichón, much progress has been made to reduce the risk at many of Mexico's volcanoes. More needs to be done in areas such as education to prepare for future potentially devastating eruptions.

Bibliography

Primary Literature

1. Capra L, Macías JL, Scott KM, Abrams M, Garduño-Monroy VH (2002) Debris avalanches and debris flows transformed from collapses in the Trans-Mexican Volcanic Belt, Mexico – behavior, and implications for hazard assessment. J Volcanol Geotherm Res 113:81–110
2. Anguita F et al (2001) Circular features in the Trans-Mexican Volcanic Belt. J Volcanol Geotherm Res 107(4):265–274
3. Asociación Geotérmica Mexicana. http://www.geotermia.org.mx. Accessed June 2011
4. Medina F, Suarez F, Espindola JM (1989) Historic and holocene volcanic centers in NW Mexico. Bull Volcanol 51:91–93
5. Pardo M, Suárez G (1995) Shape of the subducted Rivera and Cocos plates in southern Mexico: seismic and tectonic implications. J Geophys Res 100(B7):12357–12373
6. Ferrari L (2004) Slab detachment control on mafic volcanic pulse and mantle heterogeneity in central Mexico. Geology 32(1):77–80
7. Márquez A, Oyarzun R, de Ignacio C, Doblas M (2001) Southward migration of volcanic activity in the central Mexican Volcanic Belt: asymmetric extension within a two-layer crustal stretching model. J Volcanol Geotherm Res 112(1–4):175–187
8. Manea M, Manea VC (2008) On the origin of El Chichón volcano and subduction of Tehuantepec Ridge: a geodynamical perspective. J Volcanol Geotherm Res 175(4):459–471

9. Luhr JF, Nelson SA, Allan JF, Carmichael ISE (1985) Active rifting in Southwestern Mexico: manifestations of an incipient eastward spreading-ridge jump. Geology 13:54–57
10. Frey HM, Lange RA, Hall CM, Delgado-Granados H, Carmichael ISE (2007) A Pliocene ignimbrite flare-up along the Tepic-Zacoalco rift: evidence for the initial stages of rifting between the Jalisco Block (Mexico) and North America. GSA Bull 119(1/2):49–64
11. Gutmann JT (2002) Strombolian and effusive activity as precursors to phreatomagmatism: eruptive sequence at maars of the Pinacate volcanic field, Sonora, Mexico. J Volcanol Geotherm Res 113(1–2):345–356
12. de Boer J (1980) Paleomagnetism of the Quaternary Cerro Prieto, Crater Elegante, and Salton Buttes volcanic domes in the northern part of the Gulf of California rhombochasm, 2. symposium on the Cerro Prieto Geothermal Field. Baja California, Mexico, p 10
13. Luhr JF (1995) San Quintin volcanic field, Baja California Norte, Mexico: geology, petrology, and geochemistry. J Geophys Res 100(B7):10353–10380
14. Ortega-Rivera A, Bohnel H, Lee J (2004) The San Quintin volcanic field – $^{40}Ar/^{39}Ar$ geochronology and paleomagnetism. Geological Society of America Penrose Conference, Metepec, Puebla, p 59
15. Rogers G, Saunders AD, Terrell DJ, Verma SP, Marriner GF (1985) Geochemistry of Holocene volcanic rocks associated with ridge subduction in Baja California, Mexico. Nature 315:389–392
16. Capra L, Macías JL, Espíndola JM, Siebe C (1998) Holocene plinian eruption of La Virgen volcano, Baja California, Mexico. J Volcanol Geotherm Res 80:239–266
17. Paz Moreno FA, Demant A (1999) The recent Isla San Luis volcanic centre: petrology of a rift-related volcanic suite in the northern Gulf of California, Mexico. J Volcanol Geotherm Res 93(1–2):31–52
18. Batiza R (1978) Geology, petrology, and geochemistry of Isla Tortuga, a recently formed tholeiitic island in the Gulf of California. Geol Soc Amer Bull 89:1309–1324
19. Housh TB, Aranda-Gómez JJ, Luhr JF (2010) Isla Isabel (Nayarit, México): quaternary alkalic basalts with mantle xenoliths erupted in the mouth of the Gulf of California. J Volcanol Geotherm Res 197(1–4):85–107
20. Bohrson WA et al (1996) Prolonged history of silicic peralkaline volcanism in the eastern Pacific Ocean. J Geophys Res 101(B5):11457–11474
21. Richards AF (1959) Geology of the Islas Revillagigedo, Mexico 1. Birth and development of Volcan Barcena, Isla San Benedicto. Bull Volcanol 22:73–124
22. Siebe C et al (1995) Submarine eruption near Socorro Island, Mexico: geochemistry and scanning electron microscopy studies of floating scoria and reticulite. J Volcanol Geotherm Res 68:239–271
23. Taran YA, Varley NR, Inguaggiato S, Cienfuegos E (2010) Geochemistry of H_2- and CH_4-enriched hydrothermal fluids of Socorro Island, Revillagigedo Archipelago, Mexico. Evidence for serpentinization and abiogenic methane. Geofluids 10:542–555
24. Farmer JD, Farmer MC, Berger R (1993) Radiocarbon ages of lacustrine deposits in volcanic sequences of the Lomas Coloradas area, Socorro Island, Mexico. Radiocarbon 35(2):253–262
25. Ferrari L, Pasquarè G, Venegas-Salgado S, Romero-Rios F (1999) Geology of the western Mexican volcanic belt and adjacent Sierra Madre Occidental and Jalisco Block. Cenozoic tectonics and volcanism of Mexico. Geological Society of America, Special paper 334, pp 65–83
26. Gardner JE, Tait S (2000) The caldera-forming eruption of Volcán Ceboruco, Mexico. Bull Volcanol 62:20–33
27. Sieron K, Siebe C (2008) Revised stratigraphy and eruption rates of Ceboruco stratovolcano and surrounding monogenetic vents (Nayarit, Mexico) from historical documents and new radiocarbon dates. J Volcanol Geotherm Res 176(2): 241–264
28. Nelson SA, Carmichael ISE (1984) Pleistocene to recent alkalic volcanism in the region of Sanganguey volcano, Nayarit, Mexico. Contrib Mineral Petrol 85(4):321–335
29. Luhr JF (2000) The geology and petrology of Volcán San Juan (Nayarit, México) and the compositionally zoned Tepic Pumice. J Volcanol Geoth Res 95(1–4):109–156
30. Lewis-Kenedi CB, Lange RA, Hall CM, Delgado-Granados H (2005) The eruptive history of the Tequila volcanic field, western Mexico: ages, volumes, and relative proportions of lava types. Bull Volcanol 67(5):391–414
31. Mahood GA (1981) A summary of the geology and petrology of the Sierra La Primavera, Jalisco, Mexico. J Geophys Res 86(B11):10137–10152
32. Walker GPL, Wright JV, Clough BJ, Booth B (1981) Pyroclastic geology of the rhyolitic volcano of La Primavera, Mexico. Geol Rundschau 70:1100–1118
33. Luhr JF, Carmichael ISE (1980) The Colima volcanic complex, Mexico. 1. Post-caldera andesites from Volcan Colima. Contrib Minerol Petrol 71:343–372
34. Capra L, Macías JL (2002) The cohesive Naranjo debris-flow deposit (10 km^3): a dam breakout flow derived from the Pleistocene debris-avalanche deposit of Nevado de Colima Volcano (Mexico). J Volcanol Geotherm Res 117(1–2):213–235
35. Cortés A, Macías JL, Capra L, Garduño-Monroy VH (2010) Sector collapse of the SW flank of Volcán de Colima, México: the 3600 yr BP La Lumbre-Los Ganchos debris avalanche and associated debris flows. J Volcanol Geotherm Res 197(1–4): 52–66
36. Saucedo R et al (2010) Eyewitness, stratigraphy, chemistry, and eruptive dynamics of the 1913 Plinian eruption of Volcán de Colima, México. J Volcanol Geotherm Res 191(3–4):149–166
37. Luhr JF (2002) Petrology and geochemistry of the 1991 and 1998–1999 lava flows from Volcán de Colima, Mexico: implications for the end of the current eruptive cycle. J Volcanol Geotherm Res 117(1–2):169–194

38. Zobin VM et al (2002) Overview of the 1997–2000 activity of Volcán de Colima, Mexico. J Volcanol Geotherm Res 117(1–2): 1–19
39. Varley N, Arámbula-Mendoza R, Reyes-Dávila G, Stevenson J, Harwood R (2010) Long-period seismicity during magma movement at Volcán de Colima. Bull Volcanol 72(9): 1093–1107
40. Stevenson JA, Varley N (2008) Fumarole monitoring with a handheld infrared camera: Volcán de Colima, Mexico, 2006–2007. J Volcanol Geotherm Res 177(4):911–924
41. Arce JL, Macías JL, Vázquez-Selem L (2003) The 10.5 ka Plinian eruption of Nevado de Toluca volcano, Mexico: stratigraphy and hazard implications. GSA Bulletin 115(2):230–248
42. Siebe C, Komorowski J-C, Sheridan MF (1992) Morphology and emplacement of an unusual debris avalanche deposit at Jocotitlán volcano, central Mexico. Bull Volcanol 54:573–589
43. Siebe C, Abrams M, Macías JL, Obenholzner J (1996) Repeated volcanic disasters in Prehispanic time at Popocatépetl, central Mexico: past key to the future? Geology 24:399–402
44. Arana-Salinas L, Siebe C, Macías JL (2010) Dynamics of the ca. 4965 yr ^{14}C BP "Ochre Pumice" Plinian eruption of Popocatépetl volcano, México. J Volcanol Geotherm Res 192(3–4): 212–231
45. Capra L, Poblete MA, Alvarado R (2004) The 1997 and 2001 lahars of Popocatépetl volcano (Central Mexico): textural and sedimentological constraints on their origin and hazards. J Volcanol Geotherm Res 131(3–4):351–369
46. Castro-Govea R, Siebe C (2007) Late Pleistocene-Holocene stratigraphy and radiocarbon dating of La Malinche volcano, Central Mexico. J Volcanol Geotherm Res 162(1–2):20–42
47. Carrasco-Núñez G (1999) Holocene block-and-ash flows from summit dome activity of Citlaltepetl volcano, Eastern Mexico. J Volcanol Geotherm Res 88(1–2):47–66
48. De la Cruz-Reyna S, Carrasco-Núñez G (2002) Probabilistic hazard analysis of Citlaltépetl (Pico de Orizaba) Volcano, eastern Mexican Volcanic Belt. J Volcanol Geotherm Res 113(1–2):307–318
49. Carrasco-Núñez G et al (2006) Multiple edifice-collapse events in the Eastern Mexican Volcanic Belt: the role of sloping substrate and implications for hazard assessment. J Volcanol Geotherm Res 158:151–176
50. Rodriguez SR (2005) Geology of Las Cumbres Volcanic Complex, Puebla and Veracruz states, Mexico. Rev Mex Cienc Geol 22(2):181–199
51. Hasenaka T, Carmichael ISE (1985) The cinder cones of Michoacán-Guanajuato, Central Mexico: their age, volume and distribution, and magma discharge rate. J Volcanol Geotherm Res 25:105–124
52. Uribe-Cifuentes RM, Urrutia-Fucugauchi J (1999) Paleomagnetic study of the Valle de Santiago volcanics, Michoacán-Guanajuato volcanic field, Mexico. Geofís Intern 38(4):217–230
53. Aranda-Gómez JJ, Luhr JF, Pier G (1992) The La Breña – El Jaguey Maar Complex, Durango, México: I. Geological evolution. Bull Volcanol 54(5):393–404
54. Carmichael ISE, Lange RA, Luhr JF (1996) Quaternary minettes and associated volcanic rocks of Mascota, western Mexico: a consequence of plate extension above a subduction modified mantle wedge. Contrib Mineral Petrol 124(3):302–333
55. Siebe C, Rodríguez-Lara V, Schaaf P, Abrams M (2004) Radiocarbon ages of Holocene Pelado, Guespalapa, and Chichinautzin scoria cones, south of Mexico city: implications for archaeology and future hazards. Bull Volcanol 66:203–225
56. Siebe C, Arana-Salinas L, Abrams M (2005) Geology and radiocarbon ages of Tlaloc, Tlacotenco, Cuauhtzin, Hijo del Cuauhtzin, Teuhtli, and Ocusacayo monogenetic volcanoes in the central part of the Sierra Chichinautzin, Mexico. J Volcanol Geotherm Res 141(3–4):225–243
57. Carrasco-Núñez G, Riggs NR (2008) Polygenetic nature of a rhyolitic dome and implications for hazard assessment: Cerro Pizarro volcano, Mexico. J Volcanol Geotherm Res 171(3–4):307–315
58. Siebert L, Carrasco-Núñez G (2002) Late-Pleistocene to precolumbian behind-the-arc mafic volcanism in the eastern Mexican volcanic belt; implications for future hazards. J Volcanol Geotherm Res 115(1–2):179–205
59. Espíndola JM, Zamora-Camacho A, Godinez ML, Schaaf P, Rodríguez SR (2010) The 1793 eruption of San Martín Tuxtla volcano, Veracruz, Mexico. J Volcanol Geotherm Res 197(1–4): 188–208
60. Tilling RI (2009) El Chichón's "surprise" eruption in 1982: lessons for reducing volcano risk. Geofís Intern 48(1):3–19
61. Luhr JF, Carmichael ISE, Varekamp JC (1984) The 1982 eruptions of El Chichón Volcano, Chiapas, Mexico: mineralogy and petrology of the anhydritebearing pumices. J Volcanol Geotherm Res 23(1–2):69–108
62. Rouwet D, Taran Y, Inguaggiato S, Varley N, Santiago Santiago JA (2008) Hydrochemical dynamics of the "lake-spring" system in the crater of El Chichón volcano (Chiapas, Mexico). J Volcanol Geotherm Res 178(2):237–248
63. Jutzeler M, Varley N, Roach M (2011) Geophysical characterization of hydrothermal systems and intrusive bodies, El Chichón volcano (Mexico). J Geophys Res 116(B4):B04104
64. Macías JL et al (2008) Hazard map of El Chichón volcano, Chiapas, México: constraints posed by eruptive history and computer simulations. J Volcanol Geotherm Res 175(4):444–458
65. Espíndola JM, Macías JL, Tilling RI, Sheridan MF (2000) Volcanic history of El Chichón volcano (Chiapas, Mexico) during the Holocene, and its impact on human activity. Bull Volcanol 62(2):90–104
66. Rouwet D, Inguaggiato S, Taran Y, Varley N, Santiago SJ (2009) Chemical and isotopic compositions of thermal springs, fumaroles and bubbling gases at Tacaná volcano (Mexico-Guatemala): implications for volcanic surveillance. Bull Volcanol 71(3):319–335
67. Macías J et al (2010) Late-Pleistocene flank collapse triggered by dome growth at Tacaná volcano, México-Guatemala, and its relationship to the regional stress regime. Bull Volcanol 72(1):33–53
68. Macías JL et al (2000) Late Holocene Peléan style eruption at Tacaná volcano, Mexico-Guatemala: past, present, and future hazards. Geol Soc Am Bull 112:1234–1249

Books and Reviews

Delgado-Granados H, Aguirre-Díaz G, Stock JM (eds) (1999) Cenozoic tectonics and volcanism of Mexico. GSA special paper 334
Francis P, Oppenheimer C (2003) Volcanoes. Oxford University Press, Oxford, p 536
Houghton B, Rymer H, Stix J, McNutt S, Sigurdsson H (1999) Encyclopedia of volcanoes. Academic, San Diego, p 1417
Luhr JF, Varekamp JC (eds) (1984) El Chichón volcano, Chiapas, Mexico: special issue. J Volcanol Geotherm Res 23(1/2):1–191
Macías JL (2007) Geology and eruptive history of some active volcanoes of Mexico. Geol Soc Am Bull 422:183–232
Nelson SA (1990) Volcanic hazards in Mexico – a summary. Univ Nacional Autón México Inst Geol Rev 9(1):71–81
Parfitt L, Wilson L (2008) Fundamentals of physical volcanology. Wiley-Blackwell, Malden, p 256
Schminke H-U (2005) Volcanism. Springer, Berlin/Heidelberg, p 334

Volcanoes, Observations and Impact

Clifford Thurber[1], Stephanie Prejean[2]
[1]Department of Geoscience, University of Wisconsin-Madison, Madison, WI, USA
[2]Seismology, USGS Volcano Science Center, Alaska Volcano Observatory, Anchorage, AK, USA

Article Outline

Glossary
Definition of the Subject
Introduction
Observations
Impacts
Volcanoes and Sustainability
Future Directions
Bibliography

Glossary

Caldera Large crater formed by collapse of an overlying structure when an eruption empties a magma reservoir.

Effusive Eruption of fluid molten material that later solidifies.

Fumarole A volcanic vent that emits hot gas.

Infrasound Sound waves at frequencies below the range of human hearing (<20 Hz).

Interferogram A pattern of satellite radar wave "fringes" formed by interference, analogous to the colorful pattern from light reflected by a thin film of oil or gas, that can indicate ground deformation.

Lahar Heavy flow of mud, water, and debris triggered by interactions of hot material with ice of water or when heavy rain falls on recently erupted unconsolidated material.

Phreatic Explosion caused by heating and expansion of ground water.

Pyroclastic Composed of rock fragments ejected explosively from an erupting volcano.

Tremor Continuous vibration of the ground related to magma movement.

Volatiles Dissolved gases contained in magma.

Definition of the Subject

Volcanoes are critical geologic hazards that challenge our ability to make long-term forecasts of their eruptive behaviors. They also have direct and indirect impacts on human lives and society. As is the case with many geologic phenomena, the time scales over which volcanoes evolve greatly exceed that of a human lifetime. On the other hand, the time scale over which a volcano can move from inactivity to eruption can be rather short: months, weeks, days, and even hours. Thus, scientific study and monitoring of volcanoes is essential to mitigate risk. There are thousands of volcanoes on Earth, and it is impractical to study and implement ground-based monitoring at them all. Fortunately, there are other effective means for volcano monitoring, including increasing capabilities for satellite-based technologies.

In recent history, the destructive power of earthquakes and earthquake-induced tsunamis has been quite salient. Over the centuries and millennia, however, volcanic eruptions and eruption-induced tsunamis have had impacts that rival those of earthquakes, and in some cases have had a global reach. A prime example is the 1815 eruption of Tambora in Indonesia. That eruption is blamed for the catastrophic "Year without a Summer," when global cooling due to reflection of the Sun's energy by aerosols and ash injected into the atmosphere during the eruption led to massive crop failures and many deaths from starvation around the world [1, 2]. The Earth has also not witnessed a massive caldera-forming

eruption, such as those that gave rise to Yellowstone and Long Valley calderas, since the formation of Toba caldera (also in Indonesia) about 75,000 years ago [3].

There is also a contrast between earthquakes and volcanoes in terms of predictability. Although reliable and effective earthquake prediction remains an elusive goal [4] and warning systems are operational in very few places (e.g., Japan), there are numerous examples of successful eruption forecasts and warnings. An example is the impressive success of the US Geological Survey's Volcano Disaster Assistance Program (VDAP), which reports dozens of successful eruption forecasts and warnings in the 25 years of the program's history [5]. Somewhat ironically, it is the monitoring of seismic activity that has been the key to VDAP's success.

Introduction

Although most of the world's magmatic activity occurs underneath the oceans, primarily along mid-ocean ridges, the discussion is restricted to volcanism on continents and islands. Within this subaerial class of volcanism, there are three main categories in terms of tectonic setting: subduction zones, hotspots, and continental rifts, with examples provided by Indonesia, Hawaii, and East Africa, respectively. Iceland is a special example of an above sea level section of mid-ocean ridge. The first-order classification of erupted products is based on silica content, with further distinctions based on alkali content (sodium and potassium) [6] and the size of crystallized mineral grains. More silica-rich (felsic) lavas are predominant at subduction zones and more silica-poor (mafic) lavas are predominant at hotspots and continental rifts. In general, mafic lavas erupt more effusively whereas felsic lavas are more prone to explosiveness. For a thorough introduction to types of volcanoes and lavas and their potential for explosivity, the interested reader is referred to Lockwood and Hazlett [7].

The magnitude and violence of volcanic eruptions can be quantified in several ways. A common measure that is used in this entry is the Volcanic Explosivity Index (VEI) [8]. Volume of erupted material, ash cloud height, eruption duration, and qualitative observations describing eruption intensity are used in the calculation of VEI. Worldwide eruptions to date have been classified as VEI 0-8, with each increasing integer corresponding to an order of magnitude increase in eruption severity. The 1980 and 2004–2008 eruptions of Mount St. Helens, for example, are classified as VEI 4 (large eruption) and VEI 2 (moderate eruption), respectively. The largest eruptions of the twentieth century were of VEI 6, including the 1912 eruption of Novarupta on the Alaska Peninsula and the 1991 eruption of Mt. Pinatubo, Philippines. A second commonly used measure of eruption size is the dense-rock equivalent (DRE) of erupted material. This parameter specifies the actual amount of magma erupted and is dependent on careful field studies of erupted deposits. The Smithsonian Museum of Natural History keeps an updated database of these two eruption size parameters for recent and historical eruptions (http://www.volcano.si.edu/world/). Pyle [9] summarizes these and other measures of eruption sizes.

In this entry, the focus is mainly on geophysical observations of volcanoes and calderas as they pertain to eruption forecasting and prediction. Some key aspects of the impacts that eruptions have on humans and selected aspects related to sustainability have also been characterized.

Observations

The Role of Geologic Mapping

Our focus is primarily on geophysical volcano monitoring, but the importance of geologic mapping and associated studies cannot be overstated in providing the background information necessary to interpret these data correctly. In the case of erupting volcanoes, the past is generally the key to the present. Volcanoes often erupt similar magmas in similar volumes; thus, geological mapping to determine eruption histories provides a framework in which to interpret renewed unrest at a previously quiet volcano. In the case when a volcano's behavior diverges from its historical activity, knowledge of eruptive history allows us to understand how the magma system is evolving with time. Geologic mapping also characterizes the spatial distribution of hazards from previous eruptions including tephra fall, lahars and pyroclastic and lava flows. These maps can have an important role in land use planning. In addition, careful petrologic, petrographic, and isotopic analyses of erupted material can provide valuable evidence regarding magma storage and transport

history. These analyses complement the geophysical measurements described below to characterize the magmatic system at depth. For further details, the interested reader is referred to Decker [10], Simkin and Siebert [11], and Lockwood and Hazlett [7].

Seismology

Earthquake monitoring is certainly one of the most basic and widely used techniques for observing volcanic activity [12, 13]. In fact, seismic monitoring of volcanoes has generally been the most fruitful approach for short-term eruption prediction. The successes of the US Geological Survey's Volcano Disaster Assistance Program (VDAP) [5] in using simple measures of earthquake activity to predict eruptions is a remarkable testament to the value of real-time seismic monitoring for taking the pulse of a volcano in a state of unrest. VDAP has assisted with or directly provided more than 50 successful eruption forecasts and/or predictions for more than 30 volcanoes worldwide in the first 25 years of its history (1986–2011), using simple instrumentation and basic observations of seismicity and ground shaking [5].

Earthquakes associated with volcanoes are commonly grouped into four classes: volcano-tectonic (VT, predominant frequencies of 1–20 Hz), long-period (LP, predominant frequencies of 1–5 Hz), hybrid (VT event transitioning into an LP event), and very-long-period (VLP) [14, 15]. The former are generally believed to be normal brittle-failure earthquakes, although they commonly occur in swarms of similar-sized small events rather than a main shock-aftershock sequence style. This can be quantified by the log frequency versus magnitude (i.e., Gutenberg-Richter) relation (i.e., b-value), which is characterized by a linear trend with a slope around 1 for earthquakes on crustal faults but frequently has a higher slope, up to roughly two, for volcanic swarms.

The mechanism of LP's remains a subject of debate, centered mainly on the effect of fluids on the earthquake source versus the effects of wave propagation (path effects), and the connection between LP's and the phenomenon known as volcanic tremor is also controversial. Volcanic tremor is a more or less continuous signal lasting minutes to hours to days, with a comparable frequency content to LP's. Some researchers believe volcanic tremor is simply the superposition of repeated LP events or, in the case of harmonic tremor, VT events with the observed frequency content controlled by the earthquake repetition rate [16]. A somewhat more common hypothesis is that the tremor is due to resonant oscillations in a magma conduit or a nonlinear response to fluid flow through cracks [17, 18]. The initiation of volcanic tremor is clearly associated with the movement of magma and the potential for an eruption, and thus tremor is one of the important precursors for eruption prediction [13]. In addition, deep LP's (typically 20–50 km depth) have been observed prior to a number of eruptions, presumably reflecting magma movement at depth [19–21], so additional focus has been placed on identifying these events. The nature of hybrid events is also debated, again centered on source versus path effects [22].

With the increasing use of broadband seismometers (instruments with a wide frequency range) in volcano monitoring, VLP earthquakes have been identified in many places [15, 23–38]. Similar to LP events, the source of VLP's is generally attributed to fluid-rock interaction, specifically transport of magma through the shallow crust. Waite et al. [38] for example, found that at Mount St. Helens, the VLP source is best modeled as a combination of volumetric and single-force components, the former due to compression and expansion of a shallow, magma-filled sill, and a smaller component of expansion and compression of a dike, and the latter due to mass transport in the magma conduit. A cartoon suggesting possible interrelationships among VLP, LP, and VT earthquakes based on the Hill fracture mesh concept [39] is shown in Fig. 1.

Some seismic path measurements have unveiled time dependencies that have been associated with eruptions, but for the most part these techniques have been applied retroactively. One of the earliest such studies was by Foulger et al. [40], who found changes in the ratio of the velocity of P waves (primary, or compressional) to S waves (secondary, or shear) (i.e., Vp/Vs, equivalently Poisson's ratio) at Mammoth Mountain, California, that correlated spatially and temporally with increased tree kill due to CO_2 emission. They hypothesized that an increased presence of gas in fractures led to a reduction in Vp/Vs, which was imaged using seismic tomography. Such changes in Vp/Vs have

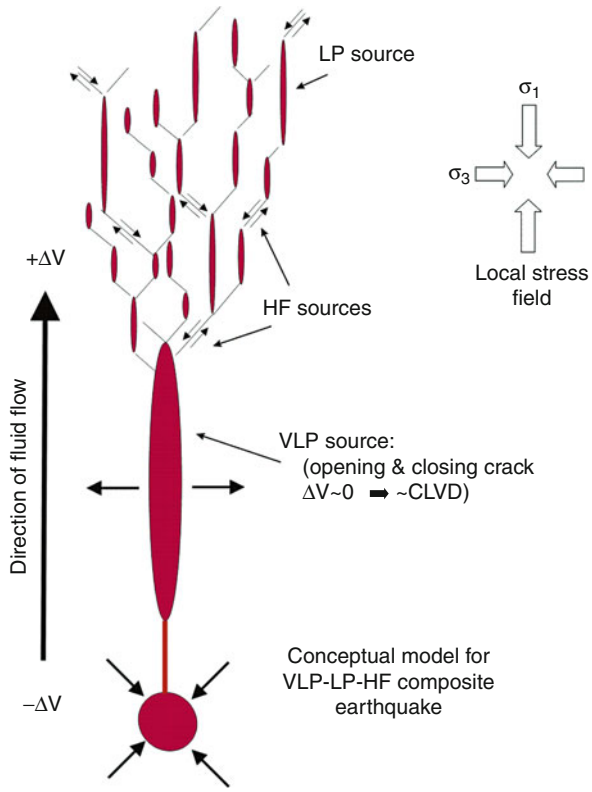

Volcanoes, Observations and Impact. Figure 1 Cartoon of the hypothetical relationship among VLP, LP, and HF (i.e., VT) earthquakes. In this model, the VLP source is upward flow of magma with volume change ΔV. Volatiles from the magma permeate the crust above the VLP event, triggering high frequency (HF) and LP earthquakes in a stress field with most and least compressive stress directions, σ_1 and σ_3 respectively, as shown (Modified from [39])

also been identified at Mt. Etna, Italy [41]. Recently, temporal changes in seismic wave attenuation, in this case associated with magmatic activity, have been found at Mt. Ruapehu, New Zealand [42] as well as Mt. Etna [43].

Two other types of seismic path observations that have been reported to show temporal change associated with magmatic activity are shear wave splitting, which is caused by birefringence in the Earth, and ambient noise correlations, which yield an estimate of the wave propagation behavior (the Green's function) between two seismic stations. Miller and Savage [44] identified a change in the polarization direction of the fast shear wave at Mt. Ruapehu, which they associated with an eruption. Subsequent studies have also reported such changes elsewhere related to magmatic activity [45–49], but extreme care must be taken to separate spatial versus temporal variations. Brenguier et al. [50] compared a reference Green's function (created from 18 months of background or "ambient" noise data) to Green's functions from sequential 10-day periods of data at Piton de la Fournaise Volcano on La Reunion island and found shifts in apparent travel times corresponding to a small reduction in seismic velocity within the volcano. Their interpretation was that decreases in seismic velocity a few weeks before eruptions were related to preeruptive inflation of the volcanic edifice, presumably due to increased magma pressure.

Deformation

Uplift and subsidence associated with magmatic and eruptive activity have been recognized for centuries, with the Temple of Serapis in the town of Pozzuoli in Campi Flegrei caldera, Italy, being one of the most famous examples [51]. Geodetic surveying techniques, such as leveling and tilt measurements, began to be applied to volcanoes in the early twentieth century [52]. In the modern era, Global Positioning System (GPS) and interferometric synthetic aperture radar (InSAR), along with tilt, are the primary types of geodetic observations applied to the study and monitoring of volcanoes. The sensitivity of these different techniques is compared in Fig. 2. Continuous GPS (cGPS) and InSAR are quite complementary, with the former providing fine temporal resolution at particular points on the Earth's surface and the latter providing exceptional spatial resolution of position changes over a wide area for pairs of observation times. Deformation modeling is commonly done to estimate pressure changes in and the geometry of magma source zones.

GPS Since the 1990s, GPS has become a central technique for volcano monitoring. Initial applications required repeated visits to benchmarks, known as campaign GPS. Continuous GPS (cGPS) has become relatively commonplace, allowing near-real-time tracking of site positions and, when multiple cGPS sites are available, a time history of volcano deformation.

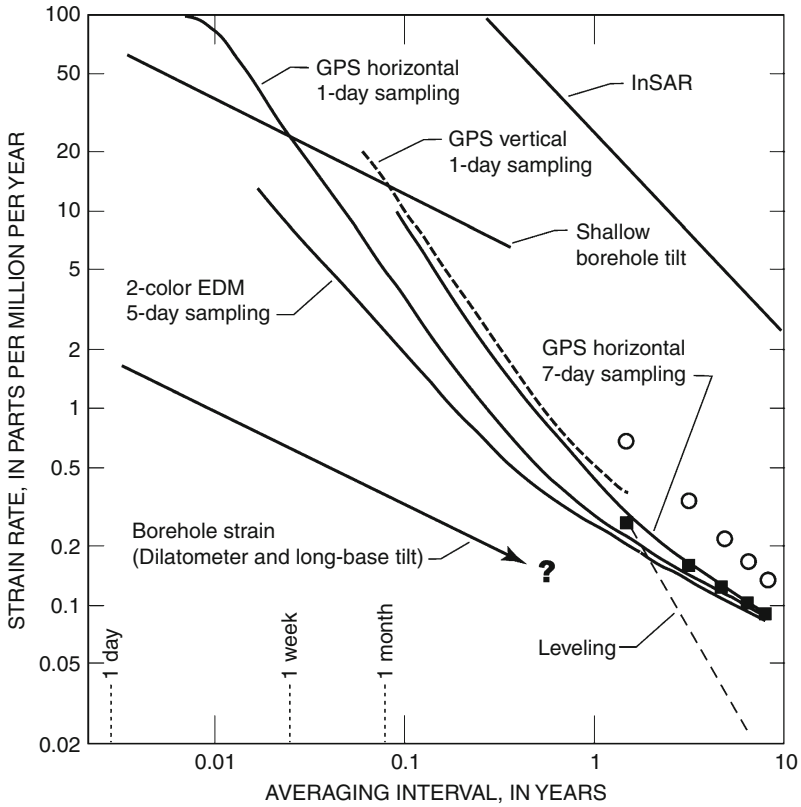

Volcanoes, Observations and Impact. Figure 2

Comparison of rate sensitivity for GPS, InSAR, borehole strainmeters at 200 m depth, and borehole tiltmeters (which measure the gradient in vertical deformation) at 2 m depth. The x-axis indicates the time period that may be spanned by the different data types. For example, daily GPS measurements may span 1 day or longer. The y-axis indicates the strain rate that can be resolved as a function of the period. Strain is the change in length (area or volume) per a unit length (area or volume), and thus is unitless and can be expressed as parts per million (ppm). As can be seen from the plot, the borehole tiltmeters and strainmeters are more sensitive than GPS at shorter periods, but at periods longer than a few days and a few months, respectively, GPS measurements provide better resolution of strain rates (Figure modified from [52])

For example, with two cGPS sites on opposite sides of a volcano's summit or straddling a rift zone, relative changes in separation of the sites would reflect volcano inflation/deflation or rift zone extension/contraction. With enough sites, detailed modeling of deformation sources is possible, providing constraints on the locations, depths, and pressure/volume changes of buried magma reservoirs and conduits. An example of the use of cGPS in monitoring an impending eruption at Augustine Volcano, Alaska [53] is described in some detail later.

GPS works by having a receiver on the surface of the Earth receive signals simultaneously from four or more satellites. These signals carry information about the signal origin time and the position of the satellite, so that determining the receiver position is done by trilateration, essentially analogous to locating an earthquake. The interested reader is referred to [52] for a lucid and comprehensive discussion of the details of this process.

GPS is not without its complications and limitations. GPS is a point measurement of position, so good spatial coverage requires multiple GPS sites. Data reduction requires knowledge of the GPS satellite orbits, which are known only approximately at any instant. Final orbital information is distributed by

International GNSS Services (where GNSS stands for Global Navigation Satellite System) with about a 2-week delay [54]. The use of differential and kinematic GPS techniques effectively overcomes orbital (and some other) error effects, if only relative positions are desired. Atmospheric effects, due to ionosphere and troposphere delays, also impart positioning errors. Finally, elevation uncertainty is significantly greater than that for latitude and longitude.

InSAR InSAR burst onto the geophysics scene in 1993 with the publication of the famous Landers, CA, earthquake interferogram on the cover of Nature [55]. Applications to volcanoes and calderas around the world followed soon thereafter, including Mt. Etna, Italy [56], Long Valley caldera, CA [57], Yellowstone caldera, WY [58], Piton de la Fournaise Volcano, La Reunion [59], a number of volcanoes in Alaska [60–65], the Galapagos Islands [66], Afar [67], Chile [68], and many more.

InSAR works by having a satellite (or constellation of satellites) acquire a pair of radar images of the same area on Earth from about the same point in space at different times, which are then combined, or interfered, to produce a map of the difference in phase of the two returned radar signals, represented by colored "fringes." The phase difference is related to the line-of-sight (LOS; i.e., in the direction of the satellite) displacement of the ground in the time between the two image acquisitions. Converting the phase differences into a map of LOS surface displacement is a process known as "unwrapping" [69, 70]. As in the case of GPS, source models can be derived to fit the observed displacements.

The spatial extent and resolution of InSAR coverage is extraordinary (scenes typically 10s to 100 km on a side with 1–30 m pixel size and <cm resolution of surface displacements). There are many more subtleties and complexities with InSAR data and their interpretation than for GPS, however. Repeated image acquisitions are limited by the configuration and orbits of the satellites. An accurate digital elevation model (DEM) is critical for removing the effects of topography from the images. Noise in the data can lead to an incorrect assessment of LOS ground movement. Signal decorrelation, for example, due to vegetation variations, the presence of water, snow and ice, or steep topography, can yield areas with no usable signal. Atmospheric delay anomalies, due mainly to variations in tropospheric water content, can also cause artifacts in InSAR images. With the need for repeated imaging and the inherently limited temporal coverage for forming interferometric pairs, there is no guarantee that a good image can be created for a particular time interval of interest.

Tilt and Strain Although far less ubiquitous in volcano monitoring settings than seismic and GPS instrumentation, tiltmeters and strainmeters are valuable observational tools that can provide complementary information about deformation. Both have remarkable sensitivity, with standard (bubble) tiltmeters able to measure the equivalent of 0.1 mm of uplift over a range of a kilometer (0.1 μrad, or 10^{-7} strain). Strainmeters can measure strain on the order of 10^{-11} to 10^{-12} (10 to 1 parts per billion). Tiltmeters have a number of advantages over strainmeters, including much lower cost, simpler installation, and, for biaxial sensors, the ability to provide information on the direction to the source of deformation. These advantages have been responsible for the much greater use of tiltmeters than strainmeters by volcano observatories. Due to their excellent sensitivity to vertical deformation, in contrast to GPS with its more precise determination of horizontal position, and real-time capability, tiltmeters can be of great value in volcanic crisis situations [52]. Strainmeters have also proven their value in long-term observatory settings, though, such as the successful prediction of an eruption of Hekla Volcano, Iceland, in 2000 [71].

Gravity Gravity measurements can be used to infer vertical surface displacements with an accuracy comparable to GPS and some leveling techniques, but its real power comes from the ability to infer subsurface mass or density changes when surface deformation is constrained independently [52]. When uplift or subsidence occurs, the change in gravity can be compared to that predicted from the free-air gravity gradient. Deviations from the expected change in gravity reflect either an increase or decrease in mass in the subsurface [72], and the degree and sign of the difference constrains the

density change. At Long Valley caldera, CA, for example, the combination of gravity and deformation observations allowed the inference of an intrusion of volatile-rich magma as the source of inflation in the period 1982–1999 [73].

For monitoring purposes, standard campaign-style gravity observations are of limited use, although such repeated measurements are vital for the types of research noted above. There is significant monitoring potential with continuous networks of gravimeters [74]. An example is the continuous gravity network at Mt. Etna, Italy. Continuous gravity observations at the start of the 2002–2003 eruption, showing a reduced gravity decrease followed by recovery over a few hours, have been interpreted as indicating the initial opening of dry fractures that were subsequently filled by magma [75]. Although seismicity commenced several hours before the beginning of the gravity change, the detection of the opening of fractures would certainly be a key part of identifying the likely onset of an eruption.

Volcanic Gas

Detection of volcanic gas is an early indicator of magma ascent that can provide clues to speed of ascent, magma chemistry and explosivity, volume of intruding magma, and the state of the hydrothermal system at a volcano. As magma ascends in the Earth's crust, the decrease in confining pressure leads to exsolution of volatiles from the melt. Additional volatiles can also be released from the existing hydrothermal system as newly emplaced magma heats the surrounding rock. The resulting gases and fluids work their way toward the surface through fractures and can be observed through soil monitoring and space-, air-, and ground-based monitoring of fumaroles and gaseous plumes.

Interpreting the emission rates and compositions of volcanic gases to evaluate magmatic unrest is a challenging task. The compositions of volatiles released from magma vary with tectonic setting, melt composition, and pressure, but the most common gases include, in order of decreasing abundance, water, carbon dioxide (CO_2), sulfur dioxide (SO_2), and halogens. Arc volcanoes often host hydrothermal systems, crater lakes, or can be covered in snow and ice. For these reasons, volcanic gases emitted from arc volcanoes often have chemical reactions with water and other compounds on their way to the surface, which change their chemical form. For example, hydrolysis reactions can change SO_2 into H_2S and native sulfur [76]. This characteristic makes interpreting SO_2 emissions difficult at volcanoes with active hydrothermal systems (e.g., [77]). In contrast, because CO_2 exsolves from magma before other chemical species and because its chemical form is relatively stable as it ascends, its detection at the surface can be an early indicator that magma is ascending and accumulating beneath a volcano [78, 79]. The later appearance of increased SO_2 may then indicate continued magma ascent or drying out of the hydrothermal system. Given these complexities, it is necessary to consider the ratios of CO_2, SO_2, and H_2S to interpret the presence of these gases correctly. An additional complication in the interpretation of gas emissions is that most active volcanoes emit low levels of gas passively; therefore, background monitoring of quiescent time periods must be established before gas emissions associated with unrest can be interpreted correctly. Several strategies must be employed to measure the complete suite of emitted volcanic gases, including both continuous and episodic ground and/or aircraft-based gas monitoring of fumaroles, satellite monitoring, and measurement of CO_2 flux through soils (see [80–82] for reviews of monitoring techniques).

Visual and Thermal Remote Sensing

Recent advances in satellite monitoring and ground-based and airborne remote sensing capabilities have revolutionized volcano monitoring and ash cloud tracking and provided a new perspective for understanding eruption dynamics. In the case of remote volcanoes that lack local seismic and GPS monitoring, satellite data often provide the only data stream documenting unrest and eruption. Data from satellites operated by the various international space agencies are primarily used for weather and climate research and forecasting, but are also used for volcano monitoring tasks including detecting and measuring anomalous thermal emissions, tracking ash clouds, and making visual observations. Rather than describe a complete

list of satellite-based tools used in volcano studies, here the applicability of several satellite systems commonly used at US volcano observatories are highlighted, and readers are referred to more detailed reviews in the literature [82–84]. Some land- and aircraft-based imaging techniques are also briefly described.

When magma intrudes into a volcano, heat flow increases at the Earth's surface, resulting in hot fumaroles and fractures and melting of snow and ice. Thus, thermal remote sensing measurements can provide an early indicator of volcanic unrest in addition to defining the existence and spatial extent of lava flows, domes, and pyroclastic flows. The Moderate Resolution Imaging Spectroradiometer (MODIS) sensors on NASA research satellites and Geostationary Operational Environmental Satellite (GOES) and Advanced Very High Resolution Radiometer (AVHRR) sensors on NOAA satellites provide frequent, low resolution (~1 km pixel) data. Mid-infrared data (3.5–4 μm wavelength) from these sensors are used to study the extent and temporal development of lava and pyroclastic flows and to estimate effusion rates and thermal flux associated with an eruption.

Thermal infrared data from satellites (8–14 μm wavelength) are used to detect and track volcanic ash and gas clouds in the atmosphere, complementing ground- and satellite-based radar measurements of ash clouds. By comparing the brightness temperature difference in two different frequency bands, 11 and 12 μm, clouds containing ash can be discriminated from those containing only water using the Brightness Temperature Difference Method [85]. This method was used for tracking ash clouds from many eruptions (e.g., [86]) and has improved our understanding of the global atmospheric effects of large eruptions. The use of this technique to detect and measure volcanic ash clouds is limited by temporal coverage, atmospheric and cloud water content, tephra particle size, and thermal contrast between the cloud and the surface beneath it. Timing and intervals between images are dependent on satellite position and global location. For northern Pacific volcanoes, for example, GOES data are available every 15 min, while AVHRR data are available 1–12 times per day depending on specific location [87]. Landsat TM and ETM+, Advanced Spaceborne Thermal Emission Reflection Radiometer (ASTER), and other high-resolution sensors provide a complementary dataset to these sensors. Although these data cannot be obtained in real time and images are less frequent, they provide high spatial resolution (15–90 m or better) for detailed visual and thermal observations. A recent compilation of capabilities to detect and measure volcanic clouds can be found in a European Space Agency report [88].

Thermal monitoring is not limited to satellite sensors. As an example of a sensor that can be hand held or mounted on an aircraft or tripod, the Forward Looking Infrared Radiometer (FLIR) camera is highlighted. FLIR surveys and installations often record simultaneous visual and infrared images or movies, providing maps of temperature distributions in ash clouds and on land surfaces. These images can be used to detect fumaroles, map pyroclastic flow deposits, and define spatial extent and structure of lava flows and domes. Frequently, gas emissions visually obscure volcanic activity, but FLIR thermal images can "see" through some gas, as demonstrated at volcanoes such as Mount St. Helens and Augustine [89, 90]. FLIR data have also been used successfully to characterize individual explosion characteristics at Stromboli Volcano [91].

Satellite remote sensing data are used for more than thermal imaging. Ultraviolet spectrometers, such as Total Ozone Mapping Spectrometers (TOMS) and the newer Ozone Monitoring Instrument (OMI) sensor operated by NOAA, can be used to map paths and concentrations of SO_2 clouds emitted from volcanoes by UV absorption of SO_2 in the atmosphere [92, 93]. Thanks to improved capabilities from the OMI sensor, scientists are better able to detect precursory SO_2 emissions in the atmosphere, to quantify eruptive SO_2 more accurately, and to track the SO_2 for longer periods of time. Thus, OMI data provide early indicators of magmatic unrest in addition to improving our understanding of eruption dynamics and hazard to aviation.

The remote sensing capabilities described here will undoubtedly evolve rapidly in the coming decade as technologies continue to advance and new satellites are launched. New remote monitoring tools will continue to emerge as well. For example, recent technical advances permit the measurement of volcanic lightning, both from ground and satellite sensors, to detect and study large ash clouds [94]. Improved resolution in digital cameras has permitted scientists to construct spectacular three-dimensional models of lava dome growth using aerophotogrammetric techniques [95].

Infrasound

Infrasound is the subaudible (<20 Hz) range of sound waves. Infrasound observations are made with either commercial or custom-built low-frequency microphones. These can be deployed individually or, more commonly, as arrays. Array data can be stacked to diminish noise, which can be significant in these data, and can be used to determine the direction to the source. Infrasound disturbances can regularly be detected up to a few hundred kilometers from a volcano during eruptions. The use of infrasound for volcano monitoring was sufficiently rare at the beginning of the twenty-first century for the technique to be absent from some past reviews of volcano monitoring techniques (e.g., [12]), but now such observations are being made at dozens of volcanoes.

Infrasound observations are of great value for monitoring and quantifying eruptions, and are potentially useful for eruption prediction, especially in open-vent systems [96]. Unlike seismic observations, where variations in materials and structure in the Earth's crust along the seismic ray path have a strong influence on the recorded wavefield, the atmosphere alters infrasonic airwaves relatively little at high frequencies [97]. This advantage makes infrasound quite useful for studying eruption dynamics and for quantitative comparisons of eruptions among different volcanoes [98]. Another advantage is that it is very difficult to distinguish between earthquakes at very shallow depths versus earthquakes directly associated with surface explosions using seismic data alone, but in many cases the absence or presence of an infrasound signal can serve to distinguish between the two possibilities and thus provide direct evidence that magmatically driven activity has reached the surface.

Infrasound data provide a new and unique perspective on the dynamics of volcanic eruption columns. Comparing ratios of seismic and acoustic energy between discrete explosions can offer compelling evidence for gas distributions in the magma column and eruption violence. Matoza et al. [99] have used infrasound data to investigate the spectra of volcanic jets and showed that they are similar to noise from aircraft jet engines. Infrasound has also been used to estimate the velocity of material ejected from volcanic vents during eruptions [100]. Observations of this sort could potentially be helpful in estimating ash output at erupting volcanoes when they cannot be observed directly.

Impacts

The literature on the impacts of volcanic eruptions is vast, so only brief and rather general information about selected topics is presented in this entry. The focus is on key primary and secondary volcanic hazards, and in particular those that have relatively immediate and direct impact. As a result, topics such as climatic effects are not covered here.

Lava Flows, Pyroclastics, and Tephra

Primary volcanic hazards that are direct eruption products can be categorized somewhat generally into lava flows, pyroclastic ejecta, and tephra. Lava is molten rock, and surface lava flows can travel many kilometers, or tens of kilometers in the case of basaltic tube-fed flows [101]. Their impact, though, will generally be spatially limited for any single eruption, although cases such as the decades-long rift eruption of Kīlauea Volcano are exceptions. Basaltic lava flows cause direct damage to the natural environment and human infrastructure, as well as igniting fires and/or touching off explosions that result in further damage. Fatalities due to basaltic lava flows are typically minimal, however, due to their modest flow rates, at least on terrain that is not particularly steep. Andesitic-dacitic stratovolcanoes, such as Mount St. Helens, grow blocky and viscous lava domes. Although generally limited in spatial extent to only the volcanic crater and its drainages, these domes can become unstable and fail, producing ash fall and hot block and ash flows down slope.

In contrast to lava flows, pyroclastic flows and surges (dense and dilute solid-gas mixtures, respectively, with a range of possible temperatures) travel at great speed, 10s of meters per second (m/s) to about 150 m/s (over 500 km/h), and large flows can travel 50 km or more from their source vents. The potential for destruction and death is summarily greater. For example, in the 1990s, deaths due to pyroclastic flows comprised the vast majority of directly caused mortality by volcanic eruptions [102].

Tephra is a general term encompassing various types of pyroclastic ejecta that are typically classified

according to size, including blocks and bombs, lapilli, ash, and dust [7]. The larger fragments follow ballistic trajectories, whereas smaller particles can remain suspended in the atmosphere for some time (minutes to weeks) before falling to the surface. Tephra accumulations can amount to tens of centimeters to a few meters at distances of tens to hundreds of kilometers for very large eruptions [103]. Lockwood and Hazlett [7] point out that ballistic fragments are produced in greater abundance by smaller explosive eruptions. Annen and Wagner [102] report a similar number of deaths due to collapse of ash-covered roofs as due to pyroclastic flows and surges in the 1990s.

Lahars

Although a less familiar term to many, these mudflows or debris flows originating from volcanoes can have an enormous impact and cause many fatalities. Lahars can be generated directly and immediately by pyroclastic flows, or in a delayed manner upon collapse of volcanic deposits (for example, due to very heavy rainfall) or due to a lake breakout [104]. Flow rates are generally slower compared to pyroclastic flows, less than 10 m per second except on steep slopes.

A prime example of a lahar is from the eruption of Nevado del Ruiz, Colombia, in 1985. When the volcano erupted violently on the night of November 13, a massive lahar was initiated when pyroclastic flows caused massive melting of snow and glacial ice on the volcano. The lahar swept through and buried the town of Armero nearly 75 km away, resulting in more than 20,000 fatalities [105]. Sadly, the potential for a lahar from Nevado del Ruiz striking Armero had been well documented beforehand – mudflows from Nevado del Ruiz eruptions in 1595 and 1845 buried the same area [106]. Destructive lahars were also produced by the 1980 eruption of Mount St. Helens and the massive 1991 eruption of Mt. Pinatubo, Philippines.

Landslides, Lateral Blasts, and Tsunamis

Weaknesses in the interiors of volcanoes (fracturing and poorly consolidated material, hydrothermal alteration, etc.) leaves them prone to major landslides, which here is meant to encompass also avalanches and sector collapses. Avalanches are common on composite volcanoes, aka stratovolcanoes [7]. Some avalanches are triggered by the shaking from an earthquake. A landslide that grows and becomes more chaotic as it descends is termed a debris avalanche. At a larger scale, a sector collapse is the breaking away of a wedge-shaped flank of a volcano. When combined with an eruption, it can produce a lateral blast. Sector collapses are surprisingly common, at least on a geologic time scale. A number of Hawaii's volcanoes have experienced sector collapses, for example. The 1980 Mount St. Helens eruption began with a sector collapse producing a large debris avalanche, followed by a lateral blast and the initiation of a vertical eruption column. Lateral blasts are somewhat rare, but others have occurred at Arenal Volcano, Costa Rica [107] and Bezymianny Volcano, Russia [108]. For island volcanoes, there is the potential for landslides or especially sector collapses to produce a tsunami. The famous 1883 eruption of Krakatoa was accompanied by repeated tsunamis reportedly as high as 30–40 m around the Sunda Strait, killing tens of thousands of people [11]. Similarly, partial collapse of a volcano neighboring Unzen in 1792 generated a giant tsunami reaching heights of 60 m that caused on the order of 15,000 fatalities [7].

Volcanic Gases

As described above, volcanic gases are important indicators of magma transport, but they also represent a critical hazard. For example, although CO_2 is a significant component of the air we breathe regularly, this odorless, colorless gas is lethal at high concentrations. A tragedy involving CO_2 occurred in 1986 at Lake Nyos, Cameroon, a crater lake formed ~400 years ago. Dissolved CO_2 accumulated in the lake and was released in a discrete event, killing all living things within a 25 km radius, including 1,700 people [109]. In the United States, CO_2 emissions at Mammoth Mountain, CA, led to the deaths of four people between 1998 and 2006. CO_2 is far from the only harmful volcanic gas, however. For example, vog, a form of air pollution resulting from emissions of SO_2 and other volcanic gases, plagues the Island of Hawaii, as the actively erupting Kīlauea Volcano is a prolific producer of several gas species [110].

Eruption Forecasting: Strategies and Challenges

Earthquakes have been recognized to herald volcanic eruptions throughout history. For example, prior to

the well-known eruption of Mount Usu, Japan in 1663, earthquake ground shaking caused local residents to evacuate. Eruption forecasting became a science with the advent of real-time seismic monitoring capabilities. Although earthquake observations still form the backbone of eruption forecasting, they are now complemented by more sophisticated analyses of seismic data and data from many other disciplines. Geodesy, gas chemistry analysis, satellite remote sensing, visual observations and high-resolution photography, petrography, and geochemistry all provide critically important indicators of the state of a magmatic system. Detectable manifestations of magma ascent vary widely between volcanoes based on several factors including the magma chemistry and crystallinity, the physical state of the volcano's conduit system and surrounding crust, the tectonic setting of the volcano, and time since last eruption. Thus, no one-size-fits-all forecasting approach exists. Modern volcano observatories are dynamic organizations that integrate a variety of data streams with knowledge of volcanic history to evaluate the state of unrest and potential future activity at a volcano.

In the United States volcano observatories use a color code alert level system to describe the state of volcano unrest [111]. One of the biggest challenges in forecasting volcanic eruptions and applying this alert system is assessing the time scale over which an eruption might occur. Here, the terms "forecast" and "prediction" as defined by [112] are used. Long-term forecasts, which address hazards on time scales of decades and centuries, are based on geological mapping of volcanoes and their deposits. Correct forecasts that describe likely hazards on time scales of hours to months based on geophysical and gas monitoring are common. However, reliable short-term predictions which specify the time and size of eruptions are difficult and fraught with complexities, not only in correctly interpreting the physical processes responsible for observations but in the delicacies of communicating with the emergency managers who coordinate societal response.

Almost all volcanic eruptions have earthquakes as precursors, but seismological response to magma ascent can vary significantly in character and in magnitude between volcanic systems. Although many eruptions of VEI 3 or smaller at frequently active volcanoes have only small earthquakes (magnitude (M) less than ~2.5) that may not be noticed without local seismic monitoring (e.g., [113]), large eruptions at volcanoes that erupt infrequently can have large earthquakes. For example, the 1980 eruption of Mount St. Helens, the 1991 eruption of Pinatubo Volcano, and the 2008 eruption of Kasatochi Volcano all had associated earthquakes of M5.1 or greater [114]. The cataclysmic rhyolitic eruption of Novarupta in 1912, the largest eruption of the twentieth century, was associated with a staggering nine M6.0 and larger earthquakes [115].

Earthquakes at volcanoes often have unique characteristics that are not observed in purely tectonic systems, like the San Andreas Fault in California. The most obvious difference is that earthquakes at volcanoes tend to occur in swarms of many small earthquakes of similar size, as noted above. Unlike on tectonic faults, these earthquakes tend to increase in magnitude and frequency of occurrence with time before an eruption as magmatically driven pressure increases in the Earth's crust. The time history of seismicity is therefore critical in eruption forecasting. Earthquakes at volcanoes can also have distinctive frequency characteristics. LP and VLP earthquakes and volcanic tremor, for example, reflect fluid movement in the Earth's crust (see the "Seismology" section). Kasatochi Volcano, in the central Aleutian Islands, displayed the classic seismological eruption precursor sequence in 2008 [114]. In the 48 h prior to eruption, the rate and magnitude of earthquakes gradually increased, reflecting pressurization in the Earth's crust. In the 2 h prior to eruption and shortly after a M5.8 earthquake, strong volcanic tremor was observed, indicating that the earthquake likely increased permeability in the crust sufficiently for volatiles and magma to ascend rapidly.

Advanced analyses of seismic data, including some techniques described in the "Seismology" section, are actively being explored for eruption forecasting applications. For example, in some situations, real-time high-precision earthquake locations may be useful. In the 2000 eruption of Miyakejima, earthquakes were observed to migrate laterally as a dike was emplaced [116]. In other situations, however, such as the Long Valley caldera of California, earthquake locations can be misleading, as they reflect geothermally active areas

and the fluid pathways rather than the location of magma itself.

The value of geodesy as an eruption forecasting tool was emphasized to the volcanological community during the 1980 eruption of Mount St. Helens. Prior to eruption, scientists at the Cascades Volcano Observatory documented a growing bulge on the north flank of the mountain. The eruption began as the bulge failed in an earthquake-induced landslide. The surprising and deadly horizontal blast of pyroclastic material that resulted highlighted the importance of deformation data in determining not only volume of magma intruded into volcanic edifices, but also eruption style and potential edifice collapse. Development of continuous GPS technologies in the late twentieth century made near-real-time deformation monitoring a reality. Later development of InSAR methods further improved the role of geodesy in volcano monitoring by providing spatially complete snapshots of volcano deformation. GPS is now a common component of volcano monitoring networks, although it is still significantly less common than seismic monitoring [117]. Dzurisin [118] describes monitoring strategies in which deformation data may be useful in making longer-term forecasts than are typically possible with seismic data alone.

Although seismic and geodetic monitoring are the most common data streams used in eruption forecasting, many other disciplines provide highly valuable information that can be critically important. For example, explosive eruptions of Bezymianny Volcano (Kamchatka), which generally begin with growth of a new lava dome that subsequently becomes unstable and fails, have been forecasted successfully based solely on thermal satellite data by KVERT (the Kamchatkan Volcanic Eruption Response Team). During the preeruptive stage of the 2009 eruption of Redoubt Volcano, Alaska, CO_2 levels provided one of the most conclusive early indicators that the unrest would advance to full eruption, rather than resulting in a stalled intrusion. Geochemical and physical tephra analyses often provide the first indicator that a juvenile magma is involved in an eruption, a critical indicator to understanding the size and potential explosivity of eruptions.

The challenge in interpreting geologic and geophysical indicators of eruption lies in determining the time scale and type of eruption, or even whether the magmatic activity will result in eruption at all. Earthquake swarms, for example, are common in volcanic and geothermal environments, and at least 2/3 and possibly as many as 9/10 of these do not result in eruption [119]. As magmas ascend, volatile exsolution and crystallization reduce overpressure and buoyancy in the magma body. Thus, most ascending magma bodies stall long before reaching the Earth's surface. Rejuvenation of a stalled magma body often involves an external trigger. Magma can be remobilized by many processes including accumulation of volatiles within the body, interaction of magma with water, a decrease in regional confining stress, or infusions of additional gas-rich magma from depth.

Eruption Forecasting: Case Studies

To demonstrate the variability in eruption precursors, two contrasting eruption case studies managed by the Alaska Volcano Observatory (AVO) are described: the 2006 eruption of Augustine Volcano and the 2008 eruption of Okmok Volcano. Both volcanoes were seismically and geodetically monitored, geologically mapped, and had documented historical eruptions. While the Augustine eruption exemplifies a successful eruption response, the Okmok eruption demonstrates how even thorough volcano monitoring does not guarantee that an eruption can be forecast.

The unrest preceding the 2006 eruption of Augustine Volcano, an andesitic stratovolcano located in the lower Cook Inlet of Alaska, proceeded in a "textbook" manner (see Power et al. [120] for a detailed review of the eruption). Scientists had observed this volcano erupt twice previously in 1976 and 1986, providing a template for interpreting unrest. Conveniently for the volcano observatory staff, the volcano closely followed the 1986 template. An increase in earthquake rate was first noted in late April 2005 (Fig. 3; [121]). Subsequently in fall 2005, airborne gas monitoring revealed that SO_2 output increased [122] and GPS monitoring showed that the volcano began to inflate [53]. These data together strongly suggested that magma was ascending beneath and accumulating within the volcanic conduit. Thus, AVO raised the color code for level of concern from Green to Yellow in late November 2005 (see Neal et al. [123] for

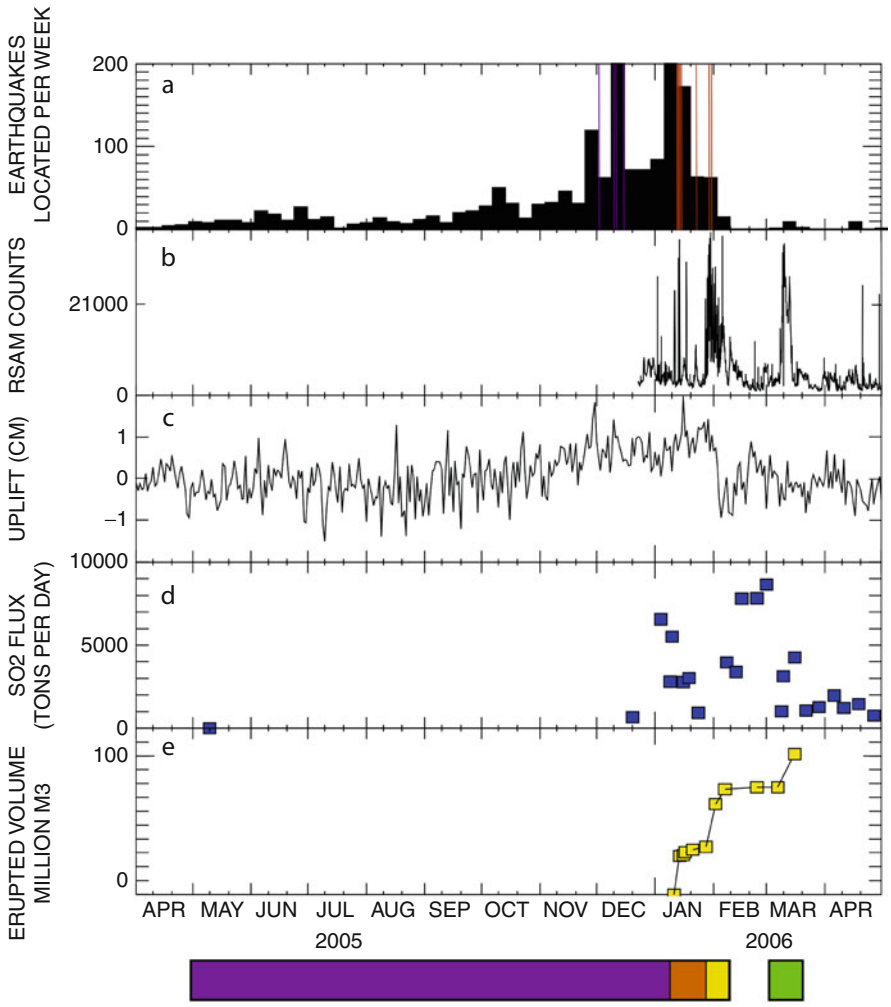

Volcanoes, Observations and Impact. Figure 3

Time history of the 2006 eruption of Augustine volcano, Alaska (From [121] and references therein). (**a**) Number of earthquakes located per week. *Purple* and *red lines* indicate phreatic and magmatic explosions, respectively; (**b**) hourly RSAM (reduced seismic amplitude measurement) from station AU13, indicating overall level of seismicity and tremor; (**c**) Uplift relative to GPS stations A59 and AV02; (**d**) SO_2 flux; and (**e**) erupted volume

a detailed chronology of color codes). On December 2, 2005, the first small phreatic (steam) explosion occurred, presumably as ascending magma interacted with water in the conduit. In response to this event, the color code was raised to Orange. Explosions of this type are often interpreted as "vent clearing" events, as they open the pathway for new magma to ascend. In the following month, anomalous activity waxed and waned, but continued to increase gradually in severity, until January 11, 2006, when the volcano had its first significant ash-rich explosion of magma, and the color code was raised to Red. This phase of the eruption continued with intermittent explosions for 2 weeks. Subsequently, the volcano effused small amounts of ash nearly continuously for two additional weeks, through early February 2006. The eruption gradually transitioned to effusive lava dome growth as magma was degassed sufficiently to permit more passive eruption of andesitic magma. A lava dome grew at the volcano's summit through mid-March 2006 and the volcano subsequently returned to a quiet state. This series of increased unrest, phreatic explosions,

magmatic explosions, and effusion is relatively common in andesitic stratovolcanoes and relatively easy to forecast correctly.

Okmok Volcano, a large caldera located in the eastern Aleutian Islands, had a history of small explosions and basaltic and basaltic-andesite lava flows prior to the 2008 eruption, with the most recent of these in 1997. In the decade between eruptions, earthquakes were rare and volcanic tremor was common enough to be considered background activity for the volcano. GPS and InSAR data revealed that Okmok experienced periods of both inflation and deflation since at least 2000 and was inflating continuously for 6 months prior to eruption [124, 125]. On the morning of July 12, 2008, the volcano was quiet and deformation data revealed no unusual increase in the rate of inflation. However by 11:30 AM AKDT of that day, seismicity ramped up dramatically from quiescence to near constant small earthquakes of $M < 3$ (Fig. 4) over a 60 min interval. Phreato-magmatic eruptive activity followed the first earthquake in the series by less than 2 h. In response, AVO raised the color code from Green directly to Red. Unlike previous effusive lava flow eruptions at Okmok Volcano, the 2008 eruption propelled ash into the atmosphere, affecting north Pacific air traffic for several months. Geologic studies of the eruption deposits reveal that the interaction of magma with a large quantity of groundwater likely drove the eruption to be more explosive and ash-rich than previous eruptions at the volcano [126]. Johnson et al. [127] speculate that prior to the eruption, the shallow open magmatic system was able to degas easily, preventing build up of overpressure and earthquakes. Either a subtle addition of melt or sudden contact with water may have triggered the eruption. This scenario is a worst-case example in terms of forecasting. It is arguably the only eruption at a monitored United States volcano with a well-established seismic network that was not forecast since 1989.

Volcano-Earthquake Interactions

Volcanism and large earthquakes near plate margins are two different manifestations of plate tectonics; thus, over time scales of millennia the processes are closely linked. How earthquakes and volcanoes affect one another over shorter timescales, such as days to months, remains an open and intriguing problem. One frequently asked question in times of crisis is, "can a large earthquake trigger eruption of a nearby volcano?" There are a few compelling examples of eruptions following large earthquakes that suggest a causal relationship between the two, such as the brief eruption of Kīlauea Volcano following the M 7.2 Kalapana Hawaii earthquake in 1975 and the eruption of Puyehue-Cordon Caulle Volcano immediately following the M 9.5 Chile earthquake in 1960. However, it is also true that large earthquakes occur commonly without related eruptions. For example, although the 1964 M9.2 Alaska earthquake occurred in a region with dozens of active volcanoes, the only report of volcanic activity in the subsequent months was a suggestion of increased steaming at Wrangell Volcano, Alaska. Establishing a causal, statistically significant relationship between a large earthquake and a subsequent volcanic eruption is difficult, as it requires an accurate understanding of the probabilities of each event occurring independently. This in turn requires a robust long-term record of eruption and earthquake occurrence, which is rarely available. Studies to date [128–130] suggest that evidence exists for earthquake-triggered eruptions, but it is not a common phenomenon. In the rare occasion where this does occur, there are several possible mechanisms that may explain eruption triggering [131]. Static stress changes in the Earth's crust related to the earthquake may change the confining pressure on a magma reservoir, destabilizing it. Alternatively, high frequency dynamic seismic waves may destabilize the magma by causing bubble nucleation or increasing convection within the reservoir. Finally, violent shaking may cause fractures, landslides, or other changes to the crustal volume surrounding a shallow magma reservoir, leading to eruption.

Large earthquakes commonly affect volcanoes in subtle ways, however. Following the 1992 M 7.3 Landers, California earthquake, volcanic and geothermal areas across the western United States showed an increase in earthquake activity [132]. Since that time, small earthquakes triggered at great distances by surprisingly small amplitude oscillatory seismic waves from large earthquakes ($\leq$0.01 MPa dynamic stress change) have been documented at many areas around the world (see Prejean and Hill [133] for review). Although dynamic triggering of small earthquakes

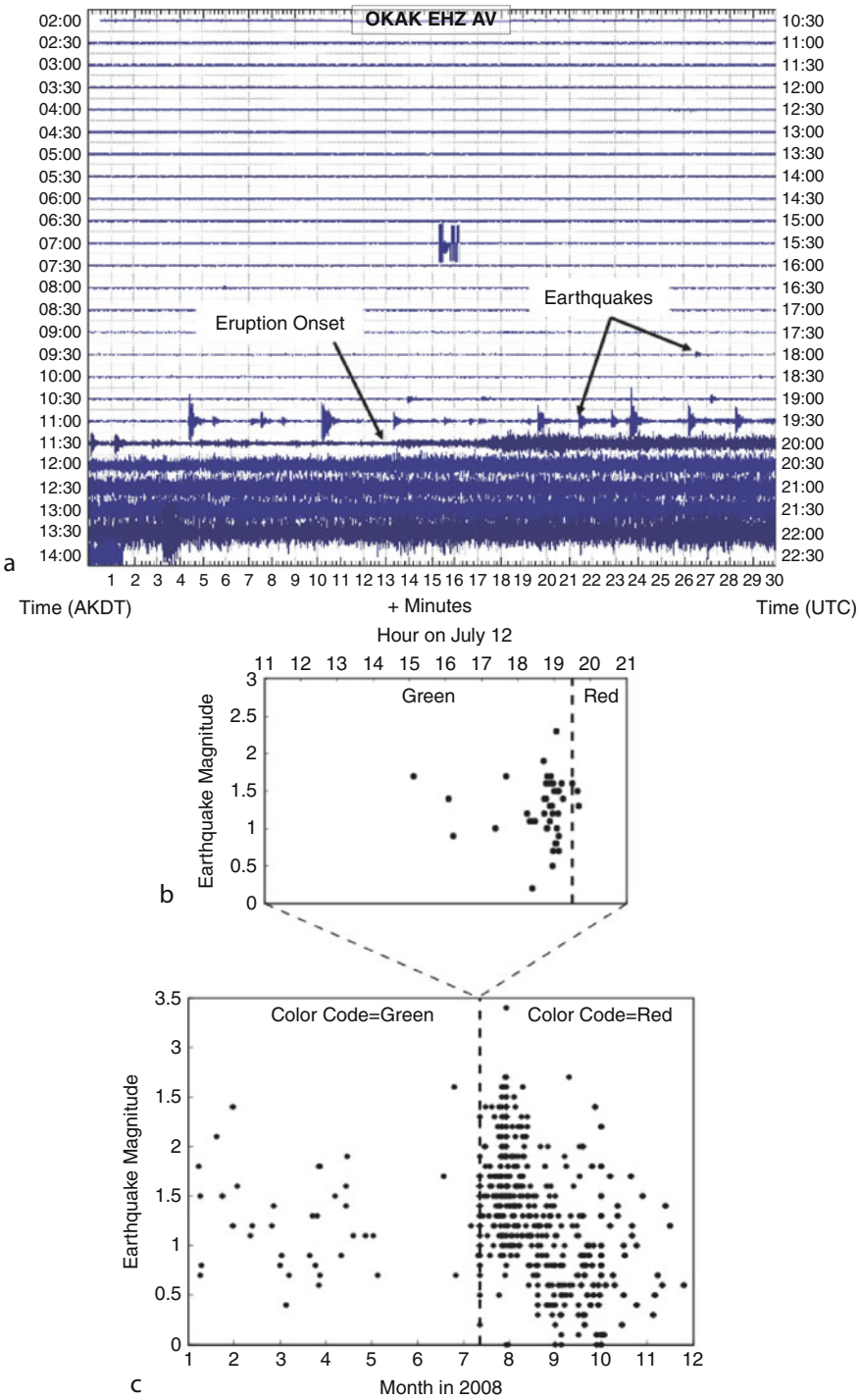

Volcanoes, Observations and Impact. Figure 4

Seismicity related to the 2008 eruption at Okmok caldera, Alaska, from [125]. (**a**) Twelve hours helicorder plot of seismic data from station OKAK, showing quiescence in the hours prior to eruption. (**b**) Located earthquakes over 10 h near the time of eruption onset. (**c**) Located earthquakes at Okmok by the Alaska Volcano Observatory in 2008. *Colors* indicate color code alert level assigned by the Alaska Volcano Observatory

happens in many environments, volcanoes appear to be particularly susceptible to dynamic earthquake triggering [133]. A range of physical models have been proposed to explain how small amplitude dynamic waves trigger earthquakes, including changing fluid pathways in delicate hydrothermal systems, changing the crustal stress field by disrupting magma chambers, and directly exceeding the frictional strength of faults [134]. Most models require very high pore-fluid pressures in the volume where the triggered earthquakes occur.

Volcanoes and Sustainability

The focus of this section is on three direct and immediate connections between volcanoes and sustainability. One is the societal hazard factor – as with other geologic hazards, population growth puts more and more people at risk for possible volcanic impacts. A second, related impact is eruption effects on aviation, which received global attention in 2010 due to the eruption of Eyjafjallajökull Volcano in Iceland. The third is magmatic activity as a source of geothermal energy. Areas being tapped for commercial-scale geothermal energy are in regions of magmatic activity if not actually on the flanks of a volcano (e.g., the Puna Geothermal Venture on Kilauea). Longer-term connections between volcanoes and sustainability, including climatic effects and connections to ore deposits, are not covered here but are discussed in numerous sources (e.g., [135, 136]).

Volcanoes and Human Population

About 10% of the world's population lives on or near active volcanoes [137], and this percentage is steadily increasing with time. Lockwood and Hazlett [7] estimate that more than 100 million people live in areas near calderas that have been subjected to pyroclastic flows. There have been a number of large eruptions in the past several centuries, but nothing rivaling the very large explosive volcanic eruptions ("super volcanoes") that are present in the geologic record [138], so in historic times, humans have not experienced the full impact that volcanic eruptions can produce. However, the number of eruptions causing fatalities has steadily increased each century since the 1500s, which Simkin et al. [139] attribute to increased global population, as opposed to an increase in the frequency of eruptions.

Quantifying the hazard from volcanic eruptions is certainly a challenge, especially considering the shortness of the historic record in comparison to the frequency of occurrence of large to very large eruptions (centuries to many millennia). Interestingly, eruption size on the VEI scale [8] follows a roughly linear size-log frequency distribution, similar to the Gutenberg-Richter relation for earthquakes. Simkin and Siebert [11] found that VEI 6 eruptions occur about once or twice a century, VEI 5 about once per decade, VEI 4 once or twice a year, etc. Ewert and Harpel [140] combined the global distributions of population and volcanoes to derive a Volcano Population Index (VPI), and applied it to Central America. VPI quantifies the population within 5 (VPI5) or 10 (VPI10) km of a volcanic system, corresponding to eruptions of VEI 2–4. They found that roughly 2.5 million people were at risk as measured by VPI10, and also suggested that only Indonesia might have a larger exposed population than Central America. As in the case of earthquake and tsunami hazards, population centers in harm's way of a possible future eruption are certainly not going to relocate. Mitigation, warning strategies and systems, and education efforts are therefore essential.

Volcanoes and Aircraft

The prolonged eruption of Eyjafjallajökull in Iceland in 2010 is a prime example of the impact volcanic eruptions can have on air travel. That disruption cost airlines billions of dollars [141], and certainly caused additional losses to businesses and people impacted by the shut down in air travel. The most critical hazard is the intake of ash into jet engines, which can severely damage engine parts and potentially cause engine failure. For example, KLM Flight 867, with 245 passengers and crew on board, encountered the ash cloud from the eruption of Alaska's Redoubt Volcano on December 15, 1989, causing all four engines to shutdown. The airplane plunged nearly 15,000 ft before the pilots were able to restart the engines and ultimately land safely, albeit with tens of millions of dollars of damage to the airplane. In the 1980s through the mid 1990s, about one airplane per year experienced damage from volcanic ash on North Pacific air routes [142]. The USGS, along with

Alaskan state agencies, established the Alaska Volcano Observatory in 1988 in large part to address the volcanic ash-aircraft problem in that region.

Assessing and monitoring the ash hazard to aircraft requires the application of essentially all the tools available. This includes forecasting, monitoring, and prediction efforts prior to an eruption and 24/7 geophysical monitoring and remote sensing to track eruptive activity and the spread of ash clouds during an eruption. Because volcanic ash from large eruptions can remain in the atmosphere at flight altitudes for weeks or longer, circling the globe multiple times, addressing the hazard requires international cooperation of air traffic controllers, scientists, and weather agencies. As air passenger and cargo air traffic continues to increase globally, the risk will escalate.

Volcanoes and Geothermal Energy

Volcanoes can provide part of the solution to global energy needs, as heat generated inside the Earth can be harnessed for geothermal energy. Although volcanic activity is not required for geothermal energy production in enhanced geothermal systems (EGS), such as that at Soultz-sous-Forets, France, volcanic activity brings heat nearer the Earth's surface, potentially lowering the cost of energy production. The United States is currently the largest producer of geothermal energy [143], although many other countries are developing their own resources. Successful geothermal energy plants located on active volcanoes or above magma chambers are currently in operation in the United States at Kīlauea Volcano in Hawaii, the Long Valley caldera, California, and many other sites in California, Nevada, and Idaho, although in total geothermal sources provided less than a half a percent of the electricity in the US in 2009 [144]. The potential to produce geothermal energy at additional volcanoes in Alaska and the Pacific Northwest is being explored aggressively. Most current geothermal energy operations involve tapping hot ground water. In contrast, the Geysers, California – the largest geothermal field in the United States – is a dry steam field that taps superheated steam.

A potential risk associated with geothermal power is triggering earthquakes. Generally, earthquakes associated with geothermal production are small ($M < 2$), but occasional larger earthquakes have disrupted communities, most notably in Basel, Switzerland. A second less common but significant risk to geothermal energy production at active volcanoes in Hawaii and Alaska involves eruptions disrupting the energy supplies and potentially destroying infrastructure.

Future Directions

Technological developments to improve and expand observational capabilities are likely to have the greatest impact on the development of volcano studies in the future [145]. An example is the use of autonomous sensor networks [146, 147]. The combination of ease of deployment and networked communication makes such systems extremely appealing for volcano monitoring. Deployment of a constellation of radar satellites with wavelengths that are tuned to "see" through vegetative cover could cut InSAR repeat observation cycles to intervals of days, allowing for high spatial resolution observations of deformation on a time scale of use for eruption forecasting. One can imagine a day when radar satellites detect significant deformation of a volcano anywhere in the world (on land), an autonomous sensor network is deployed rapidly (e.g., [148]), and a team of volcanologists forecasts the activity as the episode of unrest unfolds, comparable to severe storm forecasting.

In closing, the concern that population growth and expanding commercialism (especially air travel) will inexorably lead to increasing impact of volcanic activity on humans, either directly or indirectly, is reiterated. Although volcanoes certainly cannot be controlled, monitoring technologies and strategies for forecasting and predicting their behavior can be effective. It therefore seems clear that increased efforts in volcano monitoring are required to mitigate future risks.

Bibliography

1. Oppenheimer C (2003) Climatic, environmental and human consequences of the largest known historic eruption: Tambora volcano (Indonesia) 1815. Prog Phys Geogr 27:230–259
2. Stothers RB (1984) The great Tambora eruption in 1815 and its aftermath. Science 224:1191–1198
3. Rose WI, Chesner CA (1987) Dispersal of ash in the great Toba eruption, 75 ka. Geology 15:13–917
4. Hough S (2009) Predicting the unpredictable: the tumultuous science of earthquake prediction. Princeton University Press, Princeton

5. White RA, McCausland WA, Lockhart AB (2011) Volcano monitoring: keep it simple – less can be more during volcano crises; 25 years of VDAP experience. Seism Res Lett 82:330
6. Le Bas MJ, Le Maitre RW, Streckeisen A, Zanettin B (1986) A chemical classification of volcanic rocks based on the total alkali-silica diagram. J Petrol 27:745–750
7. Lockwood JP, Hazlett W (2010) Volcanoes – global perspectives. Wiley-Blackwell, Hoboken
8. Newhall CG, Self S (1982) The volcanic explosivity index (VEI): an estimate of explosive magnitude for historical volcanism. J Geophys Res 87:1231–1238
9. Pyle DM (2000) Sizes of volcanic eruptions. In: Sigurdsson H, Houghton BF, McNutt SR, Rymer H (eds) Encyclopedia of volcanoes. Academic Press, San Diego
10. Decker RW (1986) Forecasting volcanic eruptions. Ann Rev Earth Planet Sci 14:267–291
11. Simkin T, Siebert L (1994) Volcanoes of the world. Geoscience, Tucson
12. McNutt SR (1996) Seismic monitoring of volcanoes: a review of the state-of-the-art and recent trends. In: Scarpa R, Tilling R (eds) Monitoring and mitigation of volcano hazards. Springer, Berlin
13. McNutt SR (2000) Seismic monitoring. In: Sigurdsson H, Houghton BF, McNutt SR, Rymer H (eds) Encyclopedia of volcanoes. Academic Press, San Diego
14. Lahr JC, Chouet BA, Stephens CD, Power JA, Page RA (1994) Earthquake classification, location, and error analysis in a volcanic environment: implications for the magmatic system of the 1989–1990 eruptions at Redoubt volcano, Alaska. J Volcanol Geotherm Res 62:137–151
15. Hill DP, Dawson P, Johnston MJS, Pitt AM, Biasi G, Smith K (2002) Very-long-period volcanic earthquakes beneath Mammoth Mountain, California. Geophys Res Lett 29:1370. doi:10.1029/2002GL014833
16. Hotovec AJ, Prejean SG, Vidale JE, Gomberg J (in press) Strongly gliding harmonic tremor during the 2009 eruption of Redoubt volcano. J Volcanol Geotherm Res
17. Chouet B (1985) Excitation of a buried magmatic pipe: a seismic source model for volcanic tremor. J Geophys Res 90:1881–1893
18. Julian B (1994) Volcanic tremor: nonlinear excitation by fluid flow. J Geophys Res 99:11859–11877
19. White RA (1996) Precursory deep long-period earthquakes at Mount Pinatubo: spatial-temporal link to a basaltic trigger. In: Newhall CG, Punongbayan RS (eds) Fire and mud: eruptions and lahars of Mount Pinatubo, Philippines. University of Washington Press, Seattle
20. Power JA, Stihler SD, White RA, Moran SC (2004) Observations of deep long-period (DLP) seismic events beneath Aleutian arc volcanoes; 1989–2002. J Volcanol Geotherm Res 138: 243–26
21. Mavonga T, Zana N, Durrheim RJ (2010) Studies of crustal structure, seismic precursors to volcanic eruptions and earthquake hazard in the eastern provinces of the Democratic Republic of Congo. J Afr Earth Sci 58:623–633. doi:10.1016/j.jafrearsci.2010.08.008, ISSN 1464-343X
22. Harrington RM, Brodsky EE (2007) Volcanic hybrid earthquakes that are brittle-failure events. Geophys Res Lett 34:L06308. doi:10.1029/2006GL028714
23. Kawakatsu H, Ohminato T, Ito H, Kuwahara Y (1992) Broadband seismic observation at the Sakurajima volcano, Japan. Geophys Res Lett 19:1959–1962
24. Kawakatsu H, Ohminato T, Ito H (1994) 10s-period volcanic tremors observed over a wide area in southwestern Japan. Geophys Res Lett 21:1963–1966. doi:10.1029/94GL01683
25. Neuberg J, Luckett R, Ripepe M, Braun T (1994) Highlights from a seismic broadband array on Stromboli volcano. Geophys Res Lett 21:749–752. doi:10.1029/94GL00377
26. Kaneshima S, Kawakatsu H, Matsubayashi H, Sudo Y, Tsutsui T, Ohminato T, Ito H, Uhira K, Yamasato H, Oikawa J, Takeo M, Iidaka T (1996) Mechanism of phreatic eruptions at Aso volcano inferred from near-field broadband seismic observations. Science 273:642–645
27. Ohminato T, Chouet BA, Dawson P, Kedar S (1998) Waveform inversion of very long period impulsive signals associated with magmatic injection beneath Kilauea volcano. J Geophys Res 103:23839–23862. doi:10.1029/98JB01122
28. Arciniega-Ceballos A, Chouet BA, Dawson P (1999) Very long period signals associated with vulcanian explosions at Popocate´petl volcano, Mexico. Geophys Res Lett 26:3013–3016. doi:10.1029/1999GL005390
29. Legrand D, Kaneshima S, Kawakatsu H (2000) Moment tensor analysis of near-field broadband waveforms observed at Aso volcano, Japan. J Volcanol Geotherm Res 101:155–169. doi:10.1016/S0377-0273(00)00167-0
30. Nishimura T, Kobayashi T, Ohtake M, Sato H, Nakamichi H, Tanaka S, Sato M, Ueki S, Hamaguchi H (2000) Source process of very long period seismic events associated with the 1998 activity of Iwate volcano, northeastern Japan. J Geophys Res 105:19135–19147. doi:10.1029/2000JB900155
31. Rowe CA, Aster RC, Kyle PR, Dibble RR, Schlue JW (2000) Seismic and acoustic observations at Mount Erebus volcano, Ross Island, Antarctica, 1994–1998. J Volcanol Geotherm Res 101:105–128. doi:10.1016/S0377-0273(00)00170-0
32. Kumagai H, Ohminato T, Nakano M, Ooi M, Kubo A, Inoue H, Oikawa J (2001) Very-long-period seismic signals and caldera formation at Miyake Island, Japan. Science 293:687–690. doi:10.1126/science.1062136
33. Almendros J, Chouet B, Dawson PB, Bond T (2002) Identifying elements of the plumbing system beneath Kilauea volcano, Hawaii, from the source locations of very-long-period signals. Geophys J Int 148:303–312
34. Hidayat D, Voight B, Chouet B, Dawson P, Ratdomopurbo A (2002) Source mechanism of very-long-period signals accompanying dome growth activity at Merapi volcano, Indonesia. Geophys Res Lett 29. doi:10.1029/2002GL015013
35. Aster R, Mah S, Kyle P, McIntosh W, Dunbar N, Johnson J, Ruiz M, McNamara S (2003) Very long period oscillations of Mount Erebus volcano. J Geophys Res 108:2522. doi:10.1029/2002JB002101

36. Chouet B, Dawson P, Ohminato T, Martini M, Saccorotti G, Giudicepietro F, Luca GD, Milana G, Scarpa R (2003) Source mechanisms of explosions at Stromboli volcano, Italy, determined from moment-tensor inversions of very-long-period data. J Geophys Res 108:2019. doi:10.1029/2002JB001919
37. Chouet B, Dawson P, Arciniega-Ceballos A (2005) Source mechanism of Vulcanian degassing at Popocate´petl volcano, Mexico, determined from waveform inversions of very long period signals. J Geophys Res 110:B07301. doi:10.1029/2004JB003524
38. Waite GP, Chouet BA, Dawson PB (2008) Eruption dynamics at Mount St. Helens imaged from broadband seismic waveforms: interaction of the shallow magmatic and hydrothermal systems. J Geophys Res 113:B02305. doi:10.1029/2007JB005259
39. Hill DP (1977) A model for earthquake swarms. J Geophys Res 82:1347–1352. doi:10.1029/JB082i008p01347
40. Foulger GR, Julian BR, Pitt AM, Hill DP, Malin P, Shalev E (2003) Three-dimensional crustal structure of Long Valley Caldera, California, and evidence for the migration of CO_2 under Mammoth Mountain. J Geophys Res 108:B3. doi:10.1029/2000JB000041
41. Patanè D, Barberi G, Cocina O, De Gori P, Chiarabba C (2006) Time resolved seismic tomography detects magma intrusions at Mount Etna. Science 313:821–823
42. Titzschkau T, Savage M, Hurst T (2010) Changes in attenuation related to eruptions of Mt. Ruapehu volcano, New Zealand. J Volcanol Geotherm Res 190:168–178
43. De Gori P, Chiarabba C, Giampiccolo E, Martinez-Arevalo C, Patane D (2011) Body wave attenuation heralds incoming eruptions at Mount Etna. Geology 39:503–506
44. Miller V, Savage M (2001) Changes in seismic anisotropy after volcanic eruptions: evidence from Mount Ruapehu. Science 293:2231–2233
45. Patanè D, De Gori P, Chiarabba C, Bonaccorso A (2003) Magma ascent and the pressurization of Mount Etna's volcanic system. Science 299:2061–2063
46. Volti T, Crampin S (2003) A four-year study of shear-wave splitting in Iceland: 2. Temporal changes before earthquakes and volcanic eruptions. In: Nieuwland DA (ed) New insights into structural interpretation and modeling, Geological Society of London, Special Publication 212. Geological Society, London, pp 135–149
47. Musumeci C, Cocina O, De Gori P, Patanè D (2004) Seismological evidence of stress induced by dike injection during the 2001 Mt Etna eruption. Geophys Res Lett 31:L07617. doi:10.1029/2003GL019367
48. Bianco F, Scarfı L, Del Pezzo E, Patanè D (2006) Shear wave splitting changes associated with the 2001 volcanic eruption on Mt. Etna. Geophys J Int 167:959–967
49. Roman DC, Savage MK, Arnold R, Latchman JL, De Angelis S (2011) Analysis and forward modeling of seismic anisotropy during the ongoing eruption of the Soufrière Hills volcano, Montserrat, 1996–2007. J Geophys Res 116:B03201. doi:10.1029/2010JB007667
50. Brenguier F, Shapiro N, Campillo M, Ferrazzini V, Duputel Z, Coutant O, Nercessian A (2008) Towards forecasting volcanic eruptions using seismic noise. Nat Geosci 1:126–130
51. Poland M, Hamburger M, Newman A (2006) The changing shapes of active volcanoes: history, evolution, and future challenges for Volcano Geodesy. J Volcanol Geotherm Res 150:1–13
52. Dzurisin D (2007) Volcano deformation: geodetic monitoring techniques. Springer, Berlin
53. Cervelli PF, Fournier TJ, Freymueller JT, Power JA, Lisowski M, Pauk BA (2010) Geodetic constraints on magma movement and withdrawal during the 2006 eruption of Augustine volcano. In: Power JA, Coombs ML, Freymueller JT (eds) The 2006 eruption of Augustine volcano, Alaska, U.S. Geological Survey Professional Paper 1769. U.S. Geological Survey, Reston, pp 427–452
54. Dow JM, Neilan RE, Rizos C (2009) The International GNSS service in a changing landscape of Global Navigation Satellite Systems. J Geodesy 83:191–198. doi:10.1007/s00190-008-0300-3
55. Massonnet D, Rossi M, Carmona C, Adragna F, Peltzer G, Feigl K, Rabaute T (1993) The displacement field of the Landers earthquake mapped by radar interferometry. Nature 364:138–142
56. Massonnet D, Briole P, Arnaud A (1995) Deflation of Mount Etna monitored by spaceborne radar interferometry. Nature 375:567–570
57. Thatcher W, Massonnet D (1997) Crustal deformation at Long Valley Caldera, eastern California, 1992–1996 inferred from satellite radarinterferometry. Geophys Res Lett 24:2519–2522
58. Wicks C Jr, Thatcher W, Dzurisin D (1998) Migration of fluids Beneath Yellowstone Caldera inferred from satellite radar interferometry. Science 282:458–462
59. Sigmundsson F, Durand P, Massonnet D (1999) Opening of an eruptive fissure and seaward displacement at Piton de la Fournaise volcano measured by RADARSAT satellite radar interferometry. Geophys Res Lett 26:533–536
60. Lu Z, Fatland R, Wyss M, Li S, Eichelberer J, Dean K, Freymueller J (1997) Deformation of New Trident volcano measured by ERS-1 SAR interferometry, Katmai National Park, Alaska. Geophys Res Lett 24:695–698
61. Lu Z, Mann D, Freymueller JT, Meyer DJ (2000) Synthetic aperture radar interferometry of Okmok volcano, Alaska: radar observations. J Geophys Res Solid Earth 105:10791–10806
62. Lu Z, Wicks C, Dzurisin D, Thatcher W, Freymueller JT, McNutt SR, Mann D (2000) Aseismic inflation of Westdahl volcano Alaska, revealed by satellite radar interferometry. Geophys Res Lett 27:1567–1570
63. Lu Z, Wicks C, Power JA, Dzurisin D (2000) Ground deformation associated with the March 1996 earthquake swarm at Akutan volcano Alaska, revealed by satellite radar interferometry. J Geophys Res 105:21483–21495
64. Lu Z, Power JA, McConnell VS, Wicks C, Dzurisin D (2002) Preeruptive inflation and surface interferometric coherence characteristics revealed by satellite radar interferometry at Makushin volcano, Alaska: 1993–2000. J Geophys Res 107:B11

65. Lu Z, Masterlark T, Power J, Dzurisin D, Wicks C (2002) Subsidence at Kiska volcano, Western Aleutians, detected by satellite radar interferometry. Geophys Res Lett 29:18
66. Jonsson S, Zebker K, Cervelli P, Segall P, Garbeil H, Mouginis-Mark P, Rowland S (1999) A shallow-dipping dike fed the 1995 flank eruption at Fernandina volcano, Galapagos, observed by satellite radar interferometry. Geophys Res Lett 26:1077–1080
67. Amelung F, Oppenheimer C, Segall P, Zebker H (2000) Ground deformation near Gada 'Ale volcano, Afar, observed by radar interferometry. Geophys Res Lett 27:3093–3096
68. Pritchard ME, Simons M (2002) A satellite geodetic survey of large-scale deformation of volcanic centres in the central Andes. Nature 418:167–171
69. Goldstein RM, Zebker HA, Werner CL (1988) Satellite radar interferometry – two-dimensional phase unwrapping. Radio Sci 23:713–720
70. Gens R (2003) Two-dimensional phase unwrapping for radar interferometry: developments and new challenges. Int J Remote Sens 24:703–710
71. Sturkell E, Einarsson P, Sigmundsson F, Geirsson H, Olafsson H, Pedersen R, de Zeeuw-van Dalfsen E, Linde AT, Sacks SI, Stefansson R (2006) Volcano geodesy and magma dynamics in Iceland. J Volcanol Geotherm Res 150:14–34
72. Rymer H (1996) Microgravity monitoring. In: Scarpa R, Tilling R (eds) Monitoring and mitigation of volcano hazards. Springer, Berlin
73. Battaglia M, Hill D (2009) Analytical modeling of gravity changes and crustal deformation at volcanoes: the Long Valley Caldera (CA) case study. Tectonophysics 471:45–57
74. Williams-Jones G, Rymer H, Mauri G, Gottsmann J, Poland M, Carbone D (2008) Toward continuous 4D microgravity monitoring of volcanoes. Geophysics 73:WA19–WA28
75. Carbone D, Budettaa G, Greco F, Rymer H (2003) Combined discrete and continuous gravity observations at Mount Etna. J Volcanol Geotherm Res 123:123–135
76. Symonds RB, Gerlach TM, Reed MH (2001) Magmatic gas scrubbing: implications for volcano monitoring. J Volcanol Geotherm Res 108:303–341
77. Doukas MP, Gerlach TM (1995) Sulfur dioxide scrubbing during the 1992 eruption of Crater Peak, Mount Spurr, Alaska. In: Keith T (ed) The 1992 eruptions of Crater Peak Vent, Mount Spurr Volcano, Alaska, U.S. Geological Survey Bulletin B-2139. U.S. G.P.O.: U.S. Dept. of the Interior, US Geological Survey, Washington, DC, pp 47–57
78. Aiuppa A, Moretti R, Federico C, Giudice G, Gurrieri S, Liuzzo M, Papale P, Shinohara H, Valenza M (2007) Forecasting Etna eruptions by real-time observation of volcanic gas composition. Geology 35:1115–1118
79. Werner C, Kelly PJ, Doukas M, Lopez T, Pfeffer M, McGimsey RG, Neal CA (in press) Degassing associated with the 2009 eruption of Redoubt volcano, Alaska. J Volcanol Geotherm Res (Special Issue on the 2009 Redoubt Eruption)
80. Francis P, Horrocks L, Oppenheimer C (2000) Monitoring gases from andesite volcanoes. Philos Trans Math Phys Eng Sci 358:1567–1584
81. Edmonds M (2008) New geochemical insights into volcanic degassing. Philos Trans Math Phys Eng Sci 366:4559–4579
82. Moran SC, Freymueller JT, LaHusen RG, McGee KA, Poland MP, Power JA, Schmidt DA, Schneider DJ, Stephens G, Werner CA, White RA (2008) Instrumentation recommendations for volcano monitoring at US volcanoes under the National Volcano Early Warning System. USGS Scientific Investigations Report 2008–5114
83. Dean KG, Dehn J, Engle K, Izbekov P, Papp K (2002) Operational satellite monitoring of volcanoes at the Alaska Volcano Observatory. In: Harris AJH, Wooster M, Rothery DA (eds) Monitoring volcanic hotspots using thermal remote sensing. Adv Environ Monit Model 1:70–97
84. Mouginis-Mark PJ, Crisp JA, Fink JH (eds) (2000) Remote sensing of active volcanism, AGU Geophysical Monograph 116. American Geophysical Union, Washington, DC
85. Prata J (1989) Observations of volcanic ash clouds in the 10–12 μm window using AVHRR/2 data. Int J Remote Sens 10:751–761
86. Corradini S, Merucci L, Prata AJ, Piscini A (2010) Volcanic ash and SO_2 in the 2008 Kasatochi eruption: retrievals comparison from different IR satellite sensors. J Geophs Res 115:D00L21. doi:10.1029/2009JD013634
87. Schneider DJ, Dean KG, Dehn J, Miller TP, Kirianov VY (2000) Monitoring and analysis of volcanic activity using remote sensing data at the Alaska Volcano Observatory: case study for Kamchatka, Russia, December 1997. In: Mouginis-Mark PJ, Crisp JA, Fink JH (eds) Remote sensing of active volcanism, AGU Geophysical Monograph 116. American Geophysical Union, Washington, DC
88. Zehner E (2010) Monitoring volcanic ash from space. European Space Agency, Noordwijk, p 110
89. Schneider DJ, Vallance JW, Wessels RL, Logan M, Ramsey MS (2008) Use of thermal infrared imaging for monitoring renewed dome growth at Mount St. Helens, 2004. In: Sherrod DR, Scott WE, Stauffer PH (eds) A volcano rekindled; the renewed eruption of Mount St. Helens, 2004–2006, U.S. Geological Survey Professional Paper 1750. U.S. Dept. of the Interior, U.S. Geological Survey, Reston, p 856 and DVD-ROM [http://pubs.usgs.gov/pp/1750/]
90. Wessels RL, Coombs ML, Schneider DJ, Dehn J, Ramsey MS (2010) High-resolution satellite and airborne thermal infrared imaging of the 2006 eruption of Augustine volcano. In: Power JA, Coombs ML, Freymueller JT (eds) The 2006 eruption of Augustine volcano, Alaska, U.S. Geological Survey Professional Paper 1769. U.S. Geological Survey, Reston, pp 527–552
91. Patrick MR, Harris AJL, Ripepe M, Dehn J, Rothery DA, Calvari S (2007) Strombolian explosive styles and source conditions: insights from thermal (FLIR) video. Bull Volcanol 69:769–784
92. Krueger AJ, Schaefer SJ, Krotkov N, Bluth G, Barker S (2000) Ultraviolet remote sensing of volcanic emissions. In: Mouginis-Mark PJ, Crisp JA, Fink JH (eds) Remote sensing of active volcanism, AGU Geophysical Monograph 116. American Geophysical Union, Washington, DC

93. Carn SA, Krueger AJ, Krotkov NA, Yang K, Evans K (2009) Tracking volcanic sulfur dioxide clouds for aviation hazard mitigation. Nat Hazard 51:325–343
94. McNutt SR, Williams ER (2010) Volcanic lightening: global observations and constraints on source mechanisms. Bull Volcanol 72:1153–1167
95. Schilling SP, Thompson RA, Messerich JA, Iwatsubo EY (2008) Use of digital aerophotogrammerty to determine rates of lava dome growth, Mount St. Helens, Washington, 2004–2005. In: Sherrod DR, Scott WE, Stauffer PH (eds) A volcano rekindled; the renewed eruption of Mount St. Helens, 2004–2006, U.S. Geological Survey Professional Paper 1750. U.S. Dept. of the Interior, U.S. Geological Survey, Reston, p 856 and DVD-ROM [http://pubs.usgs.gov/pp/1750/]
96. Garces MA, Iguchi M, Ishihara K, Morrissey M, Sudo Y, Tsutsui T (1999) Infrasonic precursors to a Vulcanian eruption at Sakurajima volcano, Japan. Geophys Res Lett 26:2537–2540
97. Johnson JB (2003) Generation and propagation of infrasonic airwaves from volcanic explosions. J Volcanol Geotherm Res 121:1–14
98. Johnson JB, Aster RC, Ruiz MC, Malone SD, McChesney PJ, Lees JM, Kyle PR (2003) Interpretation and utility of infrasonic records from erupting volcanoes. J Volcanol Geotherm Res 121:15–63
99. Matoza RS, Fee D, Garces MA, Seiner JM, Ramon PA, Hedlin MAH (2009) Infrasonic jet noise from volcanic eruptions. Geophys Res Lett 36. doi:1029/2008GL036486
100. Caplan-Auerbach J, Bellesiles A, Fernandes JK (2010) Estimates of eruption velocity and plume height from infrasonic recordings of the 2006 eruption of Augustine volcano, Alaska. J Volcanol Geotherm Res 189:12–18
101. Blong R (1996) Volcanic hazards risk assessment. In: Scarpa R, Tilling R (eds) Monitoring and mitigation of volcano hazards. Springer, Berlin
102. Annen C, Wagner J-J (2003) The impact of volcanic eruptions during the 1990s. Nat Hazard Rev 4:169–175
103. Hoblitt RP, Miller CD, Scott WE (1987) Volcanic hazards with regard to siting nuclear-power plants in the Pacific Northwest. U.S. Geological Survey Open-File Report 87-297
104. Siebert L (1996) Hazards of large debris avalanches. In: Scarpa R, Tilling R (eds) Monitoring and mitigation of volcano hazards. Springer, Berlin
105. Ewert JW, Murray T, Lockhart A, Miller C (1993) Preventing volcanic catastrophe: the U. S. International Volcano Disaster Assistance Program. Earthq Volcanoes 24:270–291
106. Wright TL, Pierson TC (1992) Living with volcanoes: The U. S. Geological Survey's Volcano Hazards Program, USGS Circular 1973. United States Government Printing Office, Washington, DC
107. Alvarado GE, Soto GJ, Schmincke H-U, Blge LL, Sumita M (2006) The 1968 andesitic lateral blast eruption at Arenal volcano, Costa Rica. J Volcanol Geotherm Res 157:9–33
108. Fisher RV, Heiken G, Hulen J (1998) Volcanoes: crucibles of change. Princeton University Press, Princeton
109. Holloway M (2000) The killing lakes. Sci Am 283:92–99
110. Sutton AJ, Elias T (1993) Volcanic gases create air pollution on the Island of Hawai'i: U.S. Geological Survey. Earthq Volcanoes 24:178–196
111. Gardner CA, Guffanti MC (2006) U.S. Geological Survey's alert notification system for volcanic activity. U.S. Geological Survey Fact Sheet 2006-3139p
112. Swanson DA, Casadevall TJ, Dzurisin D, Holcomb RT, Newhall CG, Malone SD, Weaver CS (1985) Forecasts and predictions of eruptive activity at Mount St. Helens, USA: 1974–1984. Science 3:397–423
113. Power JA, Jolly A, Nye C, Harbin M (2002) A conceptual model of the Mount Spurr magmatic system from seismic and geochemical observations of the 1992 Crater Peak eruption sequence. Bull Volcanol 64:206–218
114. Ruppert NA, Prejean S, Hansen RA (2011) Seismic swarm associated with the 2008 eruption of Kasatochi volcano, Alaska: earthquake locations and source parameters. J Geophys Res 116:B00B07. doi:10.1029/2010JB007435
115. Abe K (1992) Seismicity of the caldera-making eruption of Mount Katmai, Alaska in 1912. Bull Seismol Soc Am 82:175–191
116. Japan Meteorological Agency (JMA) (2000) Recent seismic activity in the Miyakejima and Niijima-Kozushima region, Japan – the largest earthquake swarm ever recorded. Earth Planets Space 52:i–iv
117. Guffanti M, Diefenbach AK, Ewert JW, Ramsey DW, Cervelli PF, Schilling SP (2008) Volcano-monitoring instrumentation in the United States, 2008. USGS Open-File Report 2009-1165
118. Dzurisin D (2003) A comprehensive approach to monitoring volcano deformation as a window on the eruption cycle. Rev Geophys 41:1–29
119. Benoit JP, McNutt SR (1996) Global volcanic earthquake swarm database and preliminary analysis of volcanic earthquake swarm duration. Annali de Geofisca 39:221–229
120. Power JA, Coombs ML, Freymueller JT (eds) (2010) The 2006 eruption of Augustine volcano, Alaska, U.S. Geological Survey Professional Paper 1769. U.S. Geological Survey, Reston
121. Power JA, Lalla DJ (2010) Seismic observations of Augustine volcano, 1970–2007. In: Power JA, Coombs ML, Freymueller JT (eds) The 2006 eruption of Augustine volcano, Alaska, U.S. Geological Survey Professional Paper 1769. U.S. Geological Survey, Reston, pp 527–552
122. McGee KA, Doukas MP, McGimsey RG, Neal CA, Wessels RL (2010) Emission of SO_2, CO_2, and H_2S from Augustine volcano, 2002–2008. In: Power JA, Coombs ML, Freymueller JT (eds) The 2006 eruption of Augustine volcano, Alaska, U.S. Geological Survey Professional Paper 1769. U.S. Geological Survey, Reston, pp 609–630
123. Neal CA, Murray TL, Power JA, Adleman JN, Whitmore PM, Osiensky JM (2010) Hazard information management, interagency coordination, and impacts of the 2005–2006 eruption of Augustine volcano. In: Power JA, Coombs ML, Freymueller JT (eds) The 2006 eruption of Augustine volcano, Alaska, U.S. Geological Survey Professional Paper 1769. U.S. Geological Survey, Reston, pp 645–667

124. Freymueller JT, Kaufman AM (2010) Changes in the magma system during the 2008 eruption of Okmok volcano, Alaska, based on GPS measurements. J Geophys Res 115:B12415, 14 pp. doi:10.1029/2010JB007716
125. Lu Z, Dzurisin D, Biggs Wicks JC Jr, McNutt S (2010) Ground surface deformation patterns, magma supply, and magma storage at Okmok volcano, Alaska, from InSAR analysis: 1. Intereruption deformation, 1997–2008. J Geophys Res 115: B00B02. doi:10.1029/2009JB006969
126. Larsen J, Neal C, Webley P, Freymueller J, Haney M, McNutt S, Schneider D, Prejean S, Schaefer J, Wessels R (2009) Eruption of Alaska volcano breaks historic pattern. Eos Trans Am Geophys Union 90:173–174
127. Johnson JH, Prejean S, Savage MK, Townend J (2010) Anisotropy, repeating earthquakes, and seismicity associated with the 2008 eruption of Omok volcano, Alaska. J Geophs Res 115. doi:10;1029/2009JB006991
128. Linde AT, Sacks IS (1998) Triggering of volcanic eruptions. Nature 395:888–890
129. Manga M, Brodsky EE (2006) Seismic triggering of eruptions in the far field: volcanoes and geysers. Annu Rev Earth Planet Sci 34:263–291
130. Walter TR, Amelung F (2007) Volcanic eruptions following M > = 9 megathrust earthquakes: implications of the Sumatra-Andaman volcanoes. Geology 35:539–542
131. Hill DP, Pollitz F, Newhall C (2002) Earthquake-volcano interactions. Phys Today 55:41–47
132. Hill DP, Reasenberg PA, Michael AJ, Arabasz WJ, Beroza GC (1993) Seismicity remotely triggered by the magnitude 7.3 Landers, California earthquake. Science 260:1617–1623
133. Prejean SG, Hill DP (2009) Earthquakes, dynamic triggering of. In: Encyclopedia of complexity and system science, editor in-cheif Meyers RA. Complexity in earthquakes, tsunamis, and volcanoes, and forecast, Lee WHK (ed). Springer, Berlin
134. Spudich P, Steck LK, Hellweg M, Fletcher JB, Baker LM (1992) Transient stresses at Parkfield, California, produced by the M 7.4 Landers earthquake of June 28, 1992: observations from the UPSAR dense seismograph array. J Geophys Res 100:675–690. doi:10.1029/94JB02477
135. McGee KA, Doukas MP, Kessler R, Gerlach TM (1997) Impacts of volcanic gases on climate, the environment, and people. U.S. Geological Survey Open-File 97-262
136. Robb LJ (2005) Introduction to ore-forming processes. Blackwell Science, Carlton
137. Peterson DW (1996) Mitigation measures and preparedness plans for volcanic emergencies. In: Scarpa R, Tilling R (eds) Monitoring and mitigation of volcano hazards. Springer, Berlin
138. Self S (2006) The effects and consequences of very large explosive volcanic eruptions. Philos Trans R Soc A 364:2073–2097
139. Simkin T, Siebert L, Blong R (2001) Volcano fatalities: lessons from the historical record. Science 291:255
140. Ewert JW, Harpel CJ (2004) In harm's way: population and volcanic risk. Geotimes 49:14–17
141. International Air Travel Association (2010) Volcano crisis cost airlines $1.7 billion in revenue – IATA urges measures to mitigate impact, IATA press release
142. USGS (1997) Volcanic ash – danger to aircraft in the North Pacific. U.S. Geological Survey Fact Sheet 030-97
143. Geothermal Energy Association (2010) Geothermal energy: international market update, 7 pp
144. U.S. Energy Information Administration (2009) Annual Energy Review
145. Ewert JW, Guffanti M, Murray TL (2005) An assessment of volcanic threat and monitoring capabilities in the United States: framework for a National Volcano Early Warning System. USGS Open-File Report 2005-1164
146. Song W-Z, Shirazi B, Huang BR, Xu M, Peterson N, LaHusen R, Pallister J, Dzurisin D, Moran S, Lisowski M, Kedar S, Chien S, Webb F, Kiely A, Doubleday J, Davies A, Pieri D (2010) Optimized autonomous space in-situ sensor web for volcano monitoring. IEEE J Sel Topics Appl Earth Observ Remote Sens 3:541–546
147. Fleming K, Picozzi M, Milkereit C, Kuehnlenz F, Lichtblau B, Fischer J, Zulfikar C, Oezel O, Zschau J, Veit I, Jaeckel KH, Hoenig M, Nachtigall J, Woith H, Redlich JP, Ahrens K, Eveslage I, Heglmeier S, Erdik M, Kafadar N (2009) The self-organizing seismic early warning information network (SOSEWIN). Seismol Res Lett 80:755–771
148. Huang R, Song W-Z, Xu M, Picone N, Shirazi B, LaHusen R (2011) Real-world sensor network for long-term volcano monitoring: design and findings. IEEE Trans Parallel Distrib Syst 99, doi:10.1109/TPDS.2011.170

W

Waste Collection and Transport

Jess W. Everett
Civil and Environmental Engineering,
Rowan University, Glassboro, NJ, USA

Article Outline

Glossary
Definition of the Subject and Its Importance
Introduction
Source Activities
Collection
Transfer and Transport
Case Studies
Future Directions
Bibliography

Glossary

Source activities Actions that take place at the waste generation point that result in the proper presentation of the waste to the waste collection system.

Generation The act of creating a waste.

Separation Placing different waste materials in different containers.

Storage Keeping waste materials at the generation point until they can be collected.

Processing Changing the properties of a waste material, e.g., compacting cans.

Presentation Placing waste materials in the proper location for collection by the municipal waste collection program.

Participation rate The fraction of households that regularly present materials properly.

Residual waste Materials remaining as waste after reuse, recycling, or processing.

Set-out rate The fraction of households that present materials on collection day.

Curbside collection Collecting materials from each household, at the front curb or back alley.

Drop-off center A centrally located facility, with large containers for each type of material, from which material is collected.

Collection Obtaining materials from the curbside or drop-off centers and bringing that material to an unloading point.

Collection vehicle Vehicle designed to collect waste.

Transfer Moving wastes from a collection vehicle to a transport vehicle.

Transfer station Facility at which transfer is performed.

Material recovery facility Special type of transfer station, where recyclables are processed before transport.

Transport Moving wastes long distances for treatment, disposal, or recycling.

Transport vehicle Vehicle designed to move waste long distances.

Definition of the Subject and Its Importance

Concise definition of the subject and its importance with brief historical background.

Solid wastes must be collected from generation points and moved to a transfer station, or treatment, disposal, or recycling facility. Source activities are carried out at generation points. They include generation, processing, storage, and presentation to the collection system. Collection involves moving the waste from the presentation point to an unloading point, i.e., a transfer station, etc. Wastes are taken to a transfer station when the ultimate destination is far away. Environmental impact from collection and transport arise primarily from the operation of collection and transport vehicles.

Introduction

The functional elements of an integrated solid waste management system include generation, source activities,

Robert A. Meyers (ed.), *Encyclopedia of Sustainability Science and Technology*, DOI 10.1007/978-1-4419-0851-3,
© Springer Science+Business Media, LLC 2012

collection, processing, transfer and transport, treatment, and disposal [1]. Generation is the creation of waste, when an item becomes unwanted. Source activities are things that must be done to the waste at the generation point to deliver it to the collection system, e.g., storage in a recycling or waste container that is placed at the curb on collection day. Collection involves obtaining the waste from the presentation point and bringing it to the unloading point of the collection vehicle. Processing is anything that must be done before transfer, transport, or disposal. Transfer moves the waste from the collection vehicle to a transport vehicle, perhaps via a processing facility. Transport involves moving waste significant distances from a transfer location to processing, treatment, or disposal facilities. Treatment facilities reduce the volume, mass, or toxic nature of a waste. Treatment facilities include composting facilities and incinerators with energy recovery. Disposal facilities store wastes, e.g., landfills. All landfills combine aspects of treatment and disposal, with bioreactor landfills tending more toward treatment than traditional landfills.

The purpose of this entry is to describe the collection and transport of waste, with emphasis on associated environmental impacts. The functional elements most related are source activities, collection, transfer, and transport.

Source Activities

Source activities take place at the point of waste generation, i.e., residences, commercial, industrial and institutional establishments, and outdoors (picnics, camping, travel, etc.). Source activities must be carried out properly if waste is to be properly delivered to the solid waste collection system. Source activities include separation, storage, processing, and presentation. For the collection of recyclables and compostables, the participation rate is also very important.

The environmental impacts of source activities are relatively small and have not yet been subjected to analysis or estimation. The discussion here is focused on their description.

Separation

Separation requirements can vary depending on the solid waste management system. If no recycling or composting is included in the system, no separation is required; all wastes can be placed in a single container. A single container can also be used if a centralized facility is used to separate recyclable or compostable materials from residual waste.

Waste Collection and Transport. Table 1 Common residential separation schemes

Scheme	Description
Wet/Dry/Residual	The wet stream is composted while the dry stream is incinerated. Residual wastes are landfilled. Recyclables are often separated from the residual wastes via a drop-off center program.
Single-stream recycling	All recyclables (paper, bottles, cans) are separated into a single stream, which is further separated at a central processing facility. Residual wastes are also separated. Compostable wastes may be separated from residuals.
Two-stream recycling	Paper and cardboard are separated into one stream, while bottles and cans are separated into another. The bottle and can stream typically consisted of plastic, glass, aluminum, and steel. Residual wastes are also separated. Compostable wastes may be separated from residuals.

In many solid waste management systems, waste must be separated into two or more fractions. Common residential separation schemes are described in Table 1.

The separations employed at industrial and institutional establishments will depend on the waste characteristics of a particular facility. Very specific separations may be justified, depending on the predominance of a particular type of waste, e.g., grocery stores may separate corrugated boxes, offices may separate white paper, and cafeterias may separate food waste.

Storage

A two-step storage process is often followed in residences. Small containers are kept in the kitchen (under the sink or in a cabinet) or in a laundry or utility room. When these small containers become full, they are emptied into larger containers kept

outside the living area. At single-family dwellings, the containers are often kept next to the house, along an alley if present, or next to or in a garage or outbuilding. In the case of compostables, materials may be stored for a brief time in the home and then moved to an outside storage container or a home composting unit.

At multistory apartment complexes garbage chutes may be available in the hallways. In some cases, these chutes can accept multiple fractions. A switch is used to identify the fraction about to be placed in the chute and a carousel rotates the proper container under the chute. Alternatively, convenience areas may be located outside the apartment building. Convenience areas may contain one container (for the entire waste stream) or multiple containers for recyclables, compostables, and residual waste. An apartment complex convenience center in Börlange, Sweden contains separate containers for batteries, compostables (wet), combustibles (dry), residual waste, colored glass, and clear glass.

Storage at industrial or institutional establishments may also be two-stage. For example, at an office facility, small containers may be located in offices and/or public areas. These containers will be periodically emptied into larger containers in utility areas or outside.

A relatively small number of municipal solid waste (MSW) systems are pneumatic. In this case, containers may be located inside or near buildings. These containers are periodically emptied by suction and the materials moved through pneumatic tubes to larger containers for longer-term storage.

Processing

Home composting is a relatively common process employed at residences. Composting is controlled aerobic or anaerobic biodegradation in which microbes consume the more biodegradable portions of a waste, though worms can also be used. Backyard composters can range from a simple enclosure of wire fence to a container that is rotated to mix and aerate. Worm composters consisting of a tower of trays can be located inside the home. Fresh waste is deposited in a top tray, causing worms to move out of composted material in a lower tray, leaving it worm free and ready to be removed. Yard and food waste are the most common materials composted at home. Maximum savings to communities are realized from home composting, as a portion of the waste stream is treated at zero cost to the municipality. Even more convenient is the "let it lie" process, in which leaves or cut grass are allowed to remain in the yard and degrade naturally.

Most processing at the source is carried out to make it easier to store waste. Some items must be cleaned before placement in a recycling container, such as a mayonnaise jar. Other items may be crushed by hand to increase density and store more items before a container must be emptied. In some houses an appliance is used to compact residual waste, to minimize the frequency with which it must be taken to the outside storage container.

Processing may be required at industrial or institutional establishments, e.g., at a grocery store, corrugated boxes may be compacted to optimize storage.

Presentation

The last source activity is "presenting" the waste to the collection system. If curbside collection is employed, a collection vehicle passes each single-family residence. In some cases, the collection crew may walk onto the property to retrieve container(s). The crew may even return the container to its storage location. In this case, the resident does not need to do anything other than fill the container. More commonly, residents move their containers to the curb or alley on collection day and/or return them to the storage location after collection.

Where a large centralized container is located near an apartment complex or industrial or institutional establishment, no special presentation is required. Simply storing the waste puts it in the proper place for presentation to the municipal solid waste system.

In communities that employ drop-off centers, large centralized containers are located at a relatively small number of centrally located public areas, e.g., along streets or at grocery stores, government buildings, transfer stations, or landfills. Residents are responsible for bringing materials to these drop-off centers, where they are stored temporarily before collection. For the residents of the Börlange apartment complex mentioned above, additional materials were presented to the MSW system at a nearby grocery store. Containers included in-store storage for deposit/refund beverage containers (glass, plastic, and aluminum), and storage containers in the parking lot for packaging (paper,

plastic, and metal). While drop-off centers are less expensive to operate for the municipality, locations should be picked so that users can walk or, if driving is required, use combined trips. Otherwise, the economic and environmental costs incurred by the generators may exceed any municipal savings.

According to Belton et al. [2], drop-off centers should be within 500 m if an individual is walking or 0.5 to 2.5 km if the person is driving.

Valeo et al. [3] used geographical information systems (GIS) to locate drop-off centers for recyclables in a community of 22,000 in Southern Ontario, Canada. Location–allocation modeling was used. Shopping centers, municipal parking lots, and roadside sites were considered. Five-hundred potential sites were identified. If people were assumed to walk to drop-off centers, 35 centers were needed to adequately serve 99% of the population.

Bacha et al. [4] developed a model predicting the collected amount of waste paper based on 649 Austrian municipalities using drop-off centers. Municipalities with a higher number of overnight hotel stays per person and year had higher quantities of collected waste paper, attributed to the increased waste potential of municipalities in tourist regions. The index of purchasing power per capita (the sum of net income per year) showed a strong effect on the amount of waste paper collected. Municipalities with a higher percentage of households in which one member works in the home for no pay showed a significantly lower amount of waste paper per person. Higher amounts of waste paper were collected in municipalities with a higher percentage of employees in businesses and industry as well as in the service sector. A higher number of agricultural firms were associated with a smaller amount of collected paper. The density of collection sites positively influenced the amount of collected waste paper, probably due to increased convenience.

Surveys can be used to improve the operation of drop-off centers. Williams and Taylor [5] administered two surveys in order to better understand how to maximize the use of 26 drop-off centers in Lancashire, UK. A telephone survey was carried out among the drop-off center attendants to identify the effects of recent site improvements and obtain their opinions regarding overall customer satisfaction. An on-site questionnaire survey was conducted among customers at five drop-off centers, over three seasons, on weekends and weekdays. Customers were asked their opinion of the drop-off centers and were asked to identify methods that would maximize recycling. Site attendants stated that they actively encouraged customers to segregate waste more efficiently, and that a bonus scheme had provided incentive regarding this effort. Site attendants had a key role in effective use of the drop-off centers. Lancashire drop-off center customers were mostly male, used private cars, and showed high levels of customer satisfaction. Practical changes to encourage more recycling at drop-off centers included longer opening hours and the provision of boxes to enable pre-separation of waste.

Participation

In residential areas, the participation rate in collection programs is the fraction of residences that present all or most or their waste materials (residual, recyclable, or compostable) to the collection system. Typically, 100% of residences present residual waste, because municipal collection is the most convenient way to get rid of a material that otherwise will cause odors and attract flies. Smaller fractions of residences participate in municipal recyclables or compostables collection programs, because it is more convenient to leave them in the residual fraction.

The set-out rate is the fraction of homes that set out materials on a given collection day. Set-out rates are lower than participation rates because some participating households do not set out materials on every collection day. Set-out rates for residual waste programs are also close to 100%, while set-out rates for recycling programs vary greatly. According to Canadian researchers, set-out rates for recycling programs have been reported to range from less than 20% to more than 70% [6].

Given that it is typically more convenient to leave recyclables and compostables with residual waste, it is useful to investigate reasons why significant numbers of people participate in recyclables and compostables collection programs. Recycling and composting programs have been described as individual-level environmental collective actions (IECAs). According to Everett [7], IECAs involve the widespread adoption of particular individual behaviors to produce environmental collective

goods. Collective goods are defined as any good "such that, if any person X_i in a group $X_1, X_2, \ldots, X_i, \ldots, X_n$ consumes it, it cannot be feasibly withheld from others in the group" [8]. Some collective goods have what is called "jointness of supply." For collective goods with jointness of supply, the consumption of the collective good by one member of the group in no way reduces the ability of other members to enjoy it. The classic example is the lighthouse. Once one is built, any ship passing near it benefits (a collection good), and the benefit of one ship does not reduce the benefit for other ships (jointness of supply).

Collection programs are IECAs because they require individuals to adopt behaviors concerning municipal solid waste management in order to produce environmental collective goods such as cleaner air, water, and soil. Of course, not all of the goods provided by collection programs are collective in nature, e.g., lower MSW management bills.

Figure 1 can be used to understand the factors leading to participation in IECAs in general and recycling and composting programs in particular [7]. The Figure provides a flowchart that describes the various scenarios under which various assessment rationales and incentives are effective. In the discussion that follows, the Figure is interpreted for recycling programs; however, the discussion can easily be applied to composting programs.

The first condition is knowledge of the recycling program. People who do not know that a recycling collection program exists will not participate. Furthermore, while it is unlikely that a curbside collection program can remain unknown for a long time, residents that do not learn what or how to recycle may not participate. With regard to drop-off programs, residents may remain ignorant of the existence of a program, especially when drop-off centers are located in places rarely visited for purposes other than recycling.

Once a resident has knowledge of the recycling program, participation requires sufficient incentive. Incentives can be described by two dimensions,

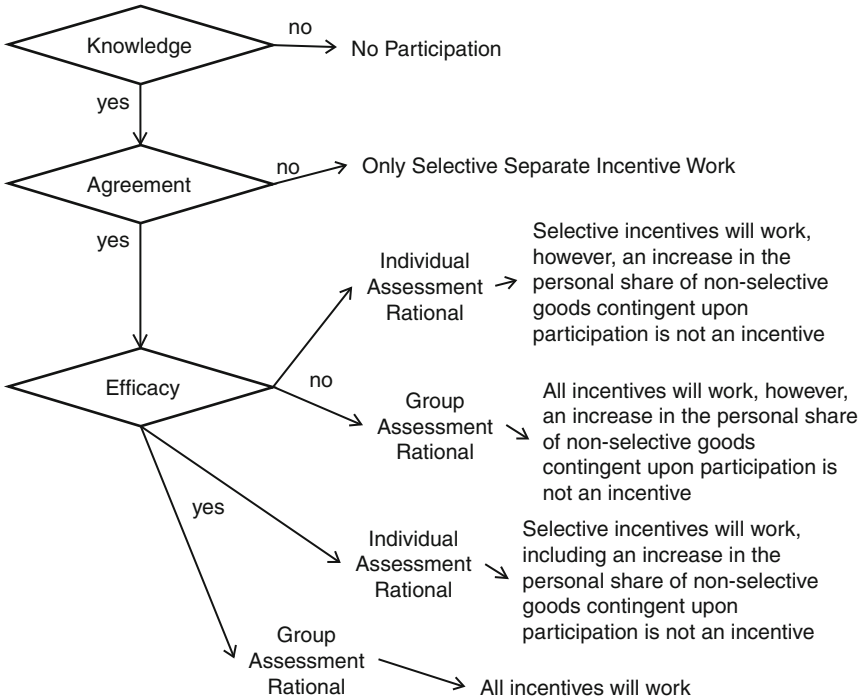

Waste Collection and Transport. Figure 1
Conditions to participate in recycling programs [7]

separation and selectivity. Separate incentives do not depend on ideological agreement with the goals of the recycling program, e.g., monetary incentives. Not-separate incentives are related to the goals of the recycling program, e.g., saving natural resources or reducing waste management costs. Selective incentives are contingent on participation, e.g., awards or avoiding punishment. Nonselective incentives are the collective goods provided by the IECA. Anyone in the group receives them, whether or not they participate.

There are four combinations of these two dimensions: selective-separate (e.g., monetary rewards); selective-not-separate (e.g., awards); nonselective-not-separate (collective goods directly related to the goals); and nonselective-separate (collective goods supplied by the recycling program, but not related to the goals). The last combination is rarely encountered.

The effectiveness of each type of incentive depends on ideological agreement, assessment rationale, and belief in efficacy. Individuals in ideological agreement with a recycling program believe that its goals are valid. Only selective-separate incentives work for individuals not in ideological agreement.

For those that agree with the goals of an IECA, their perception of individual efficacy and their assessment rationale jointly determine what incentives will have influence. With many collective actions "...no single individual's contribution makes a perceptible difference to the group as a whole, or the burden or benefit of any single member of the group," i.e., individual efficacy is negligible [8]. For IECAs, even though an individual's contribution to the overall collective good may be small, it exists and its production is directly linked to participation. As each individual's ability to produce the collective good, though small, is approximately the same, each individual has about the same effectiveness. Some individuals focus on the direct relationship between their participation and production of the collective good and end up believing in their own efficacy. Others focus on the small amount of collective good their participation produces, and believe that they are not efficacious.

Two assessment rationales can be employed, individual and group. An individual assessment rationale is based only on personal gain from participation. Collective goods, the receipt of which does not depend on participation, enter into individual assessments only if the *increase* in an individual's share of a collective good consequent to participation is greater than the cost of participation. Such an individual, by Olson's terminology [8], is "privileged." It is difficult to imagine such a person with respect to collection programs. If greater profit – personal benefit minus personal cost – is gained from not participating, nonparticipation will be the choice of action of individuals operating under an individual assessment rationale. This is the logic behind "free riders."

Individuals following a group assessment rational consider group benefits. Some employing the group assessment rationale will participate any time the group benefits outweigh their personal cost. Since the small improvement in environmental quality from recycling a single item is shared by all living beings on the planet, it is very likely that the group benefit will outweigh the individual cost. Others employing the group assessment rationale may not be so altruistic; they will participate as long as their benefits outweigh their personal costs. They differ from people employing the individual assessment rationale because they may participate when nonparticipation would increase their personal net benefit. Figure 1 identifies the types of incentives that influence people falling into the four combinations of efficacy and assessment rationale.

At least five major factors are related to participation in collection programs: market incentives, coercive incentive, convenience strategies, promotional efforts, and demographic and attitudinal variables [7]. Market incentives are selective and separate. They consist of direct payments, deposit programs, and pay-as-you-throw (PAYT) schemes. In communities using PAYT, residents pay different rates for different volumes or mass of waste collection. Pay-as-you-throw programs are an effective method for encouraging source reduction and recycling. The US EPA [9] estimated that each person participating in a PAYT program reduced their annual greenhouse gas (GHG) emissions by an average of 0.085 MTCE. An MTCE (metric ton carbon equivalent) is an amount of greenhouse gases (e.g., CO_2, Methane, water vapor, or ozone) with the greenhouse potential of an amount of CO_2 containing 1 metric ton of carbon.

Coercive incentives use the force of law to produce desired behaviors. A nationwide study in the USA found that mandatory programs collecting newspaper,

glass, and aluminum collected almost 60% more materials than voluntary programs collecting the same materials [10]. Though numerous programs have rules requiring participation, and even punishments specified in ordinances and codes, enforcement is rare.

Though separating wastes into additional fractions for recycling or composting can never be more convenient that placing everything in one container, convenience strategies can be employed to reduce that additional cost as much as possible. Convenience strategies can employ delivery methods, separation requirements, container provision, collection frequency, and program reliability [10, 11].

Promotion efforts give people knowledge of a program, describing where, when, what, and how to recycle. They can also affect ideological agreement and efficacy, e.g., by advertising recycling benefits and describing the positive outcomes of an individual's recycling behavior. Promotions can also change people's perceptions of all types of incentives, e.g., lowering personal cost perceptions by describing the convenience of a particular program. Promotions should be tailored for each program, highlighting its particular benefits and conveniences, and minimizing its costs.

The explanatory power of demographic and attitudinal variables can be related to recycling activity [7]. Demographic variables such as higher education, higher income, neighborhood stability and networks, type of building, and age group have all been associated with recycling behavior. So have attitudinal variables such as a sense of being in control of one's life, a sense of personal responsibility for environmental problems, and frugality.

Collection

Collection is needed to move wastes from widely distributed generation points to a transfer station or treatment/disposal facility. In the case of residual wastes, collection frequency has an upper limit based on the breeding cycle of pests, such as maggots and flies. For example, it takes 9 to 11 days for flies to multiply in residual waste at typical temperatures [1], hence residual wastes are generally collected at least once a week. While recyclables can typically be stored for at least 2 weeks, the once per week collection frequency is often used, as it is easier to remember to collect every Wednesday, e.g., rather than every other Wednesday.

Collection programs can be privately or publicly operated. García-Sánchez [12] examined street cleaning and waste collection services in Spanish municipalities to identify factors influencing service efficiency. Information from 38 of 113 towns with populations over 50,000 was obtained. Measures of success included tonnage collected, number of collection points, collection point density, and length of streets washed. They found no significant difference in the efficiency of street cleaning and waste collection services between towns with private versus public programs.

Collection containers can be divided into two major types, hauled and stationary. Full hauled containers are carried by the collection vehicle to the unloading point. Once emptied, they are returned to their next collection point. A common use for hauled containers is at construction and demolition sites. Stationary containers are permanently located at a particular site. When full, or at regular intervals, the stationary container is emptied into the collection vehicle and immediately returned to its location.

Stationary containers range from relatively small containers used in curbside collection programs to specialty containers and dumpsters. In curbside collection programs, vehicles drive by each setting out household or business and collect materials. Curbside programs most commonly collect from neighborhoods of one- and two-family residences or districts of small businesses. Typical curbside containers in the USA range from 32 to 96 gallons (121–363 L). Figure 2 is used to demonstrate the typical activities of a collection vehicle collecting two routes per workday. The vehicle is stored in a parking facility. At the start of the workday, the truck is driven to the first route and collection begins. When the route is finished, the truck drives to the unloading facility, unloads, and travels to the second collection route. Once the second route is finished, the truck again travels to the unloading facility, unloads and returns to the parking facility. Unloading facilities can be processing centers, transfer stations, landfills, or incinerators.

Dumpsters and specialty containers are located at large generation sites (e.g., apartment complexes and businesses) or at drop-off centers. In communities that rely on drop-off centers, householders must take

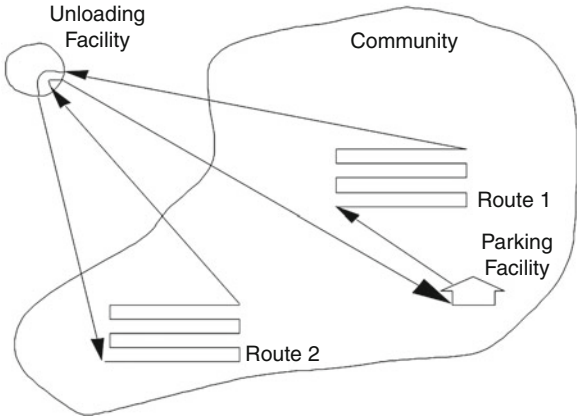

Waste Collection and Transport. Figure 2
Collection truck activities (Residual waste, recyclables, or compostables)

recyclables or compostables, and, in some cases, residual wastes to containers located at public access points, e.g., along streets in urban areas, shopping center parking lots, municipal facilities, transfer stations, or landfills. Specialty containers are often used at drop-off centers, e.g., containers with openings designed to accommodate different recyclable items. Collection vehicles periodically empty the containers.

The collection of residual or compostable waste is most often done in compaction vehicles. By compacting waste during the collection process, more waste can be collected before the vehicle must be unloaded. Compaction can be used with recyclables, but care must be exercised to avoid breaking glass.

Vehicle loading can be manual, semiautomatic, or automatic. Manual loading requires the collection crew to push or pull containers to the collection vehicle and lift them to empty. Semiautomatic still requires a crew member to push or pull the container to the collection vehicle, but a pneumatic lifting system is used to empty the container into the truck. In automatic collection, the driver of the truck maneuvers close to a container, "grabs" it with a crane or "forklift" type device, and automatically empties it. Automatic systems use the crane with curbside collection and the "forklift" type device with dumpsters. Single compartment trucks are the norm for residual waste collection. The collection of recyclables can be done in single- or multi-compartment trucks.

Manual and semiautomatic collection can result in health issues for crew members. Rogers et al. [13] administered a survey to municipal solid waste (MSW) collectors and their supervisors/safety officers in both public and private companies to evaluate occupational risks to Florida MSW workers. Data were obtained for 251 workers. Results of the survey indicated high rates of lacerations, contusions, strain/sprains, and illness. Seventy-five percent of the collectors reported having been injured in the previous 12 months.

According to Medina [14], many cities in developing countries spend 20–50% of municipal revenues on MSW while collecting only a fraction of MSW generated, in many cases less than 50%. In Mexico, informal private collectors often provide collection in low-income areas, where no official collection is provided. While informal refuse collection is illegal in Mexico, response varies from city to city, including repression, neglect, collusion, and even encouragement. Medina argues that informal refuse collection can be a valid part of solid waste management where a regulatory and policy framework is in place that encourages self-help, private investment, and entrepreneurship. Many cities in developing countries are simply unable to provide complete collection coverage, especially in low-income areas. Informal refuse collection can fill the gap, providing an important service and improving the quality of life.

Factors Influencing Collection Efficiency

WRAP [15], a nonprofit based in the UK, completed an analysis of three types of curbside collection systems for recyclables: curbside sort; single stream comingled; and two stream partially comingled. In curbside sort systems, materials are sorted by type at the curbside and collected in different compartments of a multi-compartment vehicle. In single stream comingled systems, materials are placed at the curb in one bin and collected in a single compartment vehicle, with the sorting of the materials occurring at a Materials Recovery Facility (MRF). In two stream partially comingled systems residents separate materials into two categories, usually fibers (paper and cardboard) and containers (glass, cans, and plastic bottles), which are collected in a two compartment vehicle. Each comingled stream is handled separately at the MRF.

The following general observations were made after investigating programs in the UK:

- Curbside sort schemes had lower costs than single stream comingled schemes, when the income from material sales was considered.
- The net costs of curbside sort schemes are strongly affected by income from the sale of materials.
- The net costs of comingled schemes are strongly affected by MRF fees.
- Two stream comingled collections schemes keeping paper separate from containers have similar net costs to curbside sort schemes.
- There is little variation in material yields between the three main curbside schemes.
- Programs that collect glass and/or have alternate weekly collection of refuse exhibit the greatest diversion rates.
- Recycling collections are maximized when more or larger containers are provided and/or recyclable materials are collected weekly.
- The best scheme does not appear to be impacted by the "urban" or "rural" nature of the area served.

Wilson and Batz [6] developed a derived probability model to estimate vehicle and labor requirements for municipal solid waste collection systems. The set-out distribution was modeled using the binomial distribution, leading to the application of the geometric distribution to stop-to-stop distance. The total loading time and delay time were modeled using the normal distribution. The number of households a truck passes before filling was modeled using the negative binomial distribution. The model was used to explore three scenarios: route size when the collection vehicle is constrained by time; route time when the vehicle is constrained by capacity; and the effect of vehicle capacity on costs [16]. Parameters included route size (the number of houses served before the truck became full or runs out of time), set-out rate (the fraction of houses setting out materials on a given day), average loading time (time to load materials on the vehicle at a given stop), and average stop spacing (the distance between setting out houses).

In routes constrained by time, route size is sensitive to set-out rate, e.g., the same vehicle on a route with a 20% set-out rate could serve more than twice as many households as on a route with a set-out rate of 80% [16]. Route size was also sensitive to average loading time, e.g., a change in loading time from 10 to 20 s/stop required a reduction in route size of almost 40%. Route size was somewhat less dependent on average stop spacing, with an increase in average stop spacing from 10 to 25 m resulting in an approximately 20% reduction in route size.

Constraining routes by vehicle capacity results in relatively little variance in route time, because the number of stops will be constant [16]. This suggests that trucks of similar capacity, starting routes at similar times, will finish those routes at about the same time, resulting in long lines at unloading locations. When comparing trucks of 15, 20, and 25 yd^3 capacity (11.5, 15.3, and 19.1 m^3), the medium-sized truck was rarely the lowest-cost option. Large vehicles run up against a time constraint before filling to capacity whereas small vehicles fill well before the end of the collection day. In most cases, either situation was preferred to that of a medium-sized vehicle that meets both constraints at approximately the same point.

Dahlén et al. [17] investigated the effect of different collection systems on recycling in six municipalities in Sweden. PAYT schemes based on weight-reduced residual household waste collection by 50%; however, preliminary results indicated a relatively high rate of impurities (12% in 2004), i.e., wrongly sorted materials, in the biowaste fraction. Curbside collection programs recycled more metal, plastic, and paper packaging then drop-off programs. When separate collection of biodegradables was included in the curbside system, the overall sorting of dry recyclables increased. It appeared that the handling of biodegradables facilitated sorting dry recyclables.

In Sweden, a producer responsibility ordinance mandates that producers, i.e., plastic manufacturers, collect and recycle packaging materials. Hage and Soderholm [18] investigated the relationship between collection rates of household plastic packaging waste and various factors for 252 Swedish municipalities. The results of a regression analysis indicate that local policies, geographic/demographic variables, socioeconomic factors, and environmental preferences provide some explanation of inter-municipality collection rates. The collection rate was positively affected by increases in the unemployment rate, the fraction of private houses, and the presence of immigrants (unless newly arrived) in

the municipality. Distance to recycling industry, urbanization rate, and population density were not significantly related to collection rate. Municipalities with weight-based waste management fees typically experienced higher collection rates than those municipalities in which flat and/or volume-based fees were used.

Gomes et al. [19] simulated the costs of compostables collection using a fixed container system and a transfer station, for a municipality with a population of 28,000 inhabitants. The main goal was to compare three scenarios: traditional, unsorted collection; separate collection of compostables; and separate collection of compostables from urban communities with home composting elsewhere. Input data from 2001 were used, including waste quantities, travel times, work crew composition, crew time shifts, vehicles, and containers. Separate collection of compostables resulted in comparable collection costs to traditional, unsorted collection. When only urban compostables were collected and nonurban compostables were home composted, the costs were lower than traditional, unsorted method. This emphasizes the importance of home composting.

McLeod and Cherrett [20] assessed the effects of three domestic waste collection methods using data from three Hampshire, UK authorities: cooperation between neighboring waste collection authorities and vehicles based at waste disposal sites. Cooperation could reduce vehicle mileage by 5.9% if vehicles were optimally reallocated to depots. Vehicle mileage was reduced by 13.5% when vehicles were based at the two waste disposal sites rather than existing depots. This work identified some basic methods for optimizing waste collection.

Optimization

Numerous optimization studies have been applied to MSW Collection, often identifying significant saving opportunities. According to Tavares et al. [21], the collection of MSW can be more than 70% of the total waste management budget. Fuel costs can be a major portion of the collection cost. Optimization of the routing network used for waste collection and transportation can be used to minimize fuel costs. GIS optimization models can take into account the effects of road inclination and vehicle weight on fuel consumption. Tavares et al. [21] optimized routes two different ways, minimizing the travel distance or fuel consumption. For the Praia city region (Cape Verde), optimizing for fuel consumption used 8% less fuel than optimizing for route distance. When the model was applied to a waste transport problem, a 12% fuel reduction was obtained. The results indicated the importance of designing routes to minimize uphill climbs to reduce fuel consumption. Reducing fuel consumption will also reduce greenhouse gas (GHG) emissions.

Chang et al. [22] used compromise programming within a GIS framework to optimize waste collection in Kaohsuing city, the second largest city in southern Taiwan. Compromise programming was used to optimize multiple objectives: shortest collection distance, lowest collection cost, and shortest collection time. Optimization was performed on the current management districts and new proposed districts. The model was able to significantly reduce the number of collection points and collection distance and time. The number of collection points was reduced from 1,788 to 617, collection distance was reduced from 80,528 to 51,176 m, and collection time from 1,629 to 1,521 min. Furthermore, the average distances residents had to walk to collection points was also reduced, as was the average service frequency of the collection vehicles.

Kardimas et al. [23] used the ant colony system (ACS) algorithm, within a GIS environmental to monitor, simulate, and optimize solid waste collection in a portion of Athens that produced an amount of waste equivalent to the vehicle capacity. The program was able to reduce travel time by approximately 25%, resulting in an overall reduction in collection time (travel plus loading) of approximately 9%. Filipiak et al. [24] used the Chinese postman problem algorithm to optimize MSW collection costs in the Township of Millburn, NJ. They were able to develop a set of optimal collection routes that reduced the distance traveled by approximately 10%. Nuortioa et al. [25] optimized vehicle routes and schedules for collecting municipal solid waste in Eastern Finland using a guided variable neighborhood thresholding metaheuristic. The method was able to optimize three routes by an average of 46%.

Kima et al. [26] presented algorithms for collection vehicle routing problems that consider multiple unloading trips per day and driver's lunch breaks. This scenario is most appropriate for commercial waste collection, in which each vehicle can make many unloading trips per day. The algorithms were successfully implemented and used by Waste Management, Inc. In one case study, a collection scenario requiring ten 9-h routes with productivity of 57.06 yd^3/h (43.63 m^3/h) was improved to nine 9-h routes and 63.40 yd^3/h (48.47 m^3/h). This reduced the annual number of routes by 984, resulting in a savings of $18 million.

Green House Gas Emissions and Other Environmental Impacts

The collection of municipal solid waste generates pollution, e.g., vehicle emissions. For isolated communities, the pollution generated by long transport distances required to bring recyclables to processing or manufacturing centers may outweigh the benefits of avoided extraction and processing of virgin materials. A number of researchers have studied the environmental impacts of collection.

Batool and Chuadhry [27] estimated greenhouse gas (GHG) emissions from solid waste management for Data Ganj Bukhsh Town (DGBT) in Lahore, Pakistan using the life cycle assessment (LCA) methodology. There were 1,624,169 people living in 232,024 dwellings in DGBT, with an average per capita MSW generation rate of 0.84 kg/day. Solid waste management options considered included the collection and transportation of waste, composting, biogasification, collection of recyclables with single and mixed material bank container systems, and landfilling. CO_2 equivalents, emitted and avoided, were based on electricity consumption and production, fuel consumption, and emissions.

The baseline scenario was the current MSW system, collection of waste for landfilling without energy recovery [27]. In Scenario 1, 70% of biowaste was collected at the curb for composting. In scenario 2, the biowaste was collected for biogasification. Scenarios 3 and 4 involved drop-off systems for recyclables. Scenario 5 was a combination of scenarios 1 and 3. Scenario 6 combined scenario 5 with energy recovery at the landfill.

LCA results showed that the baseline scenario produced 838,116 tons of CO_2 equivalents annually. Scenarios 1, 2, and 5 resulted in reductions ranging from 58% to 75%. The recycling only options, scenarios 3 and 4, resulted in little savings, primarily because of the low percentage of materials available for recycling (26%). The sixth scenario was a carbon sink, with 33,773 tons stored each year. The authors' calculations indicate that GHG emissions associated with collection are less than reductions associated with recycling.

Solano et al. [28] developed an integrated solid waste management optimization and life cycle assessment (LCA) model that considers cost, energy, and environmental releases. They applied the model to a number of scenarios using a hypothetical, but realistic case study representing an urban region of medium size [29]. Both cost and GHG emission minimization could be determined by the model.

A minimum-cost MSW management system was identified in which residential and multifamily sectors were served by a recyclable materials drop-off center [29]. Approximately 5% of the waste of these two sectors was recovered. The remaining 95% was collected as mixed MSW and disposed of in a landfill. Approximately 26% of commercial sector waste was collected as presorted recyclable material, while the rest was collected as mixed MSW and disposed of in a landfill. Collection and landfill costs constituted 83% of the net cost. The drop-off option for recyclables was incorporated into the minimum-cost MSW system because it costs very little and was easily offset by the revenue generated from the recyclable materials.

According to Solano et al. [29] the majority of MSW management environmental impacts are associated with collection and landfill activities. Collection uses significant amounts of energy, while landfills emit significant amounts of GHG. This assumes that landfill gases are not captured or are flared.

In the minimum GHG emission scenario, the model selected recycling for some combustible and noncombustible items [29]. Recycling of combustible items was favored when recycling was more beneficial than combustion with energy recovery. This was the case for paper and plastic. Recycling of noncombustible items was favored when emissions savings at the remanufacturing facility were greater than the emissions associated with recyclables recovery activities.

This was the case for metal and glass. A costly mixed waste MRF was selected to recover those recyclables not separated by the residents, emphasizing the GHG emissions benefit of recyclable recovery. Almost the entire commercial waste stream was combusted.

Though not adequately described in the paper, it appeared that the only traditional landfilling option considered was one without energy recovery [29]. Other authors have concluded that landfilling with highly efficient gas capture and energy recovery is an optimal solution for minimizing GHG emissions. This points to the importance of base assumptions in LCA analyses.

Iriarte et al. [30] estimated the environmental impacts of three collection systems using an LCA model. Estimates were made for a scenario in which 1,500 tons a month of MSW were generated in a European urban locality with a density of 5,000 inhabitants/km^2. In the multi-container system, citizens placed materials in permanent containers located in two areas of the street. The organic and residual fractions were placed in containers at the curb at a maximum distance of 50 m from each household. Containers for glass, paper, and packaging were located at a maximum distance of 300 m.

In the door-to-door system, citizens left each fraction outside their house, according to a preestablished collection schedule. The organic fraction was placed at the curb in a community bin. Paper, packaging, and residual waste was left in plastic bags. Glass was collected in permanent containers situated at a maximum distance of 300 m from the citizens.

The mobile pneumatic system used a network of pipes and pneumatic suction trucks. Citizens dropped each fraction of waste through doors located in the street into underground tanks. The tanks were emptied into suction truck via a network of underground pipes connected to suction points situated in the street. Organic, paper, packaging, and residual fractions were collected pneumatically at preset times. Glass was stored in the underground containers, but was collected by top loader trucks.

Three stages of the collection system were explored separately: storage; urban transport; and intercity transport [30]. Storage included containers and, for the pneumatic system, the tanks and underground pipes. Urban transport included loading and transport from collection points to the locality border. The storage and urban transport stages were together called the urban stages. Intercity transport included transporting the materials from the locality borders to the recycling, processing, or disposal facilities and unloading. Collection vehicles were used for urban and intercity transport.

For the urban stages, the multi-container system had the least environmental impact of all systems [30]. The mobile pneumatic system had greatest environmental impact for global warming, fresh water aquatic ecotoxicity, terrestrial ecotoxicity, acidification, and eutrophication. The door-to-door system had the greatest environmental impact for abiotic depletion, ozone layer depletion, and human toxicity. The intercity transport stage was very important. For intercity distance of 11 km and upward, this stage contributed the most global warming impact and energy demand, for all the systems. This points to the importance of using transfer stations to transfer materials to more efficient transport vehicles.

Di Nino and Baetz [31] examined the link between air emissions from vehicles involved in the collection and transport of recyclable and residual materials and the urban form, i.e., population density, land-use mix, land-use pattern, and scale of development. Two hypothetical cities were evaluated, representing extremes of urban form. The "spread" city was comprised of large single-family homes and homogeneous land-use development with 6.3 units/ha. The "Nodal" city contained compact developments at higher densities and intermixed land use, with 18.01 units/ha. As expected, the "spread" city resulted in significantly more air emissions associated with recyclables and residuals collection. This was true for all of the air pollutants evaluated, including hydrocarbons, carbon monoxide, carbon dioxide, oxides of nitrogen, and particulates. For many of the pollutants, the "Spread" City resulted in more than twice the emissions of the "Nodal" city.

Special Collection Programs

Collection programs for household hazardous waste are common. Though some programs employ curbside collection, drop-off centers are much more common. In some cases, the drop-off centers are not active all the time. Some drop-off centers only collect materials once

Waste Collection and Transport. Figure 3
Battery collection box, Sweden

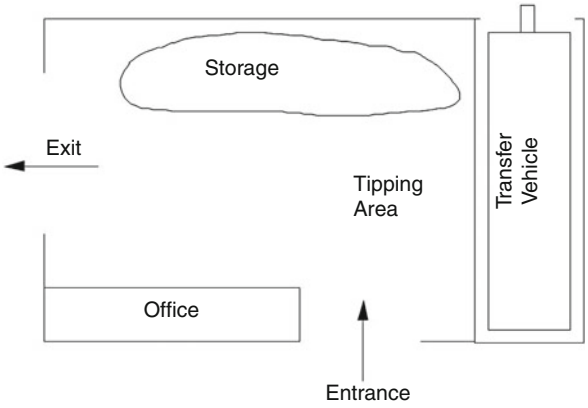

Waste Collection and Transport. Figure 4
Simple transfer station schematic

a month or four times a year. Common materials collected are paints, pesticides, cleansers, oil, electronics, and batteries.

Some communities have separate collection programs for batteries [32]. In some jurisdictions, only household batteries are considered a non-hazardous waste. In such cases, non-household batteries are often excluded to avoid hazardous waste regulations. Collected batteries can be disposed of at hazardous waste facilities or recycled. Collection programs range from drop off to curbside collection programs. Some drop-off programs have used widely distributed battery collection boxes (Fig. 3). Curbside collection can be with non-hazardous recyclables or hazardous waste. Program costs can be high, especially for curbside collection programs. In Spokane, WA, curbside collection with recycling cost $2,260 per ton, while curbside collection with landfill disposal cost $1,822 per ton [32].

Transfer and Transport

Transfer stations are an important part of municipal solid waste management systems. The location of transfer stations has traditionally been driven by a desire to minimize transport costs. Transfer stations are used to combine many small loads from collection vehicles into a few large loads in transport vehicles. Transfer stations are typically located close to population centers because it is cheaper to transport large amounts of waste over long distances in large loads than in small ones. Material recovery facilities are a special type of transfer station, used to process recyclables or compostables before transferring them to long-haul vehicles.

A simple transfer station is shown in Fig. 4. Not shown in the figure is a scale, commonly used to determine the amount of material brought by each vehicle. Collection vehicles empty in the tipping area. This can be onto the tipping floor, into a pit, or directly onto a transfer mechanism. Transfer mechanisms include front-end loader, conveyor, and crane. The transport vehicle is often located at a lower level then the tipping floor, allowing transfer by pushing material horizontally.

Wilson and Vincent [33] used on-board global positioning system (GPS) recorders to collect field data on the movement of solid waste collection vehicles at transfer stations. Five vehicles using four transfer stations were compared for 1 year. Spatial data were analyzed using geofences, determining the time each truck spent on four activities: queuing at the scale, weighing, queuing at the tipping floor, and unloading waste. The authors were able to identify and measure queuing delays. The average total time was 16.4 min per visit, with a standard deviation of 14.3 min. Time per visit ranged from 2 to 111 min per visit. The distribution was positively skewed. Multi-compartment vehicles

(co-collection and recycling trucks) spent more time at the unloading facilities than single compartment vehicles. At one facility, the longest delays were encountered queuing at the scale, at two facilities trucks experienced delays queuing at the tipping floor, while at the fourth facility no significant delays developed.

Collection vehicles are designed for collection, while transport vehicles are designed for long-distance hauling. If the final destination for the collected materials is far away, costs and environmental impacts can be reduced by transferring materials to more efficient transport vehicles, which include tractor trailers, trains, and ships.

Optimization

Numerous authors have developed algorithms for optimizing transfer and transport. Komilis [34] presented two conceptual mixed integer linear optimization models to optimize the transfer and transport of municipal solid waste (MSW) prior to landfilling. One model was based on minimizing time. The other was based on minimizing total cost. Both models identified an optimum route to haul MSW from generation points to landfills via transfer stations. The models assumed the locations of generation, transfer, and landfills were fixed. The basic input data were distances, average vehicle speeds, haul costs, equipment and facilities' operating and investment cost, labor cost, and tipping fees.

A case study at the Municipality of Athens was used to illustrate the models [34]. The time-based optimization model is simpler, as it is primarily based on the distances among generation points, transfer stations, and landfills; however, it is best used when no transfer stations are included in the system, as it is difficult to interpret the effect of the average speeds of the collection and transport vehicles. The cost optimization model is more appropriate for systems with transfer stations. For the baseline scenario – 100 tons/day MSW, transfer station location 15 km from generation point, and queue times of 0.5 h – the use of the transfer station was warranted when the distance to the landfill was at least 65 km. This is referred to as the threshold distance. Increasing the tons/day to 500 reduced the threshold distance to 56 km. The minimum threshold distance, for any amount of waste, was 54 km. Increasing the queuing time at the landfill to 1 h decreased the threshold distance to 56 km for the baseline scenario. Similarly, moving the transfer station location to 5 km reduced the threshold distance to 48 km.

Green House Gas Emissions and Other Environmental Impacts

Transfer stations can negatively impact the environment. Bovea et al. [35] compared the environmental impact of taking municipal wastes directly to the nearest waste treatment facility with waste management systems that include a transfer station. They applied a life cycle methodology to the Plana region of Castellón, Spain. They found that reductions in environmental impact from incorporating a transfer station ranged from 14.0 to 20.7%, depending upon the LCA method used.

Eshet et al. [36] estimated the economic value of externalities related to Israeli waste transfer stations. Most externalities were associated with impacts on residents living near transfer stations, such as noise, odor, litter, vermin, visual intrusion, and perceived discomfort. After mapping active transfer stations in Israel, problem sites near residential areas were identified and four were selected for further study. The Hedonic Price Method was used to examine the impact on property values. The maximum spatial impact occurred within 2.8 km of a transfer station. There was an increase of approximately $5,000 in housing price for each additional kilometer away from the site. There also was a 0.06% rise in the price of the average house for each 1% increase in average distance from the local transfer station. Transfer stations create externalities that should be taken into account during the siting process and when considering compensation for nearby residents.

Eisted et al. [37] reviewed electricity and fuel consumption associated with the collection, transfer, and transport of waste and quantified the associated greenhouse gas (GHG) emissions. Emission factors were assigned a global warming potential and aggregated into global warming factors (GWFs) that can be used to estimate the contribution to global warming from collecting, transporting, and transferring 1 metric ton of wet waste. Not considered were GHG emissions

Waste Collection and Transport. Table 2 Global warming factors (GWFs) for six scenarios

Scenario	Collection	Transfer	Transport	Total
Residual waste with 20 km of transport by truck, urban apartment blocks with pneumatic system	43–46	–	4–11	47–57
Residual waste with 20 km of transport by truck, urban apartment blocks with dumpsters	5.0–5.5	–	4–11	9–17
Residual waste with 150 km of transport by truck, single-family homes, transfer station	10–11	0.05–4.5	14–28	24–44
Recyclable paper with 2,000 km of transport by truck, drop-off centers, transfer station	6–11	0.05–4.5	182–380	189–396
Recyclable paper with 3,000 km of transport by diesel train, drop-off centers, transfer station	6–11	0.05–4.5	6–174	13–190
Recyclable materials with 10,000 km of transport by ship, private car brings materials to transfer station, 100 km to port	100–300	0.10–8.9	29–59	129–368

related to production, maintenance, and disposal of vehicles, equipment, infrastructure, and buildings. The estimated GWFs varied from 9.4 to 368 kg CO_2-equivalent (kg CO2-eq.) per metric ton of waste, depending on method of collection, capacity, and choice of transport equipment, and travel distances. Six scenarios are described in Table 2. GHG emissions can be reduced by avoiding the use of private cars and by optimizing long-distance transport, i.e., using trains and ships. As also found by Iriarte et al. [30], the environmental impact of pneumatic collection was very high.

Chunping et al. [38] measured environmental quality at five MSW Transfer Stations in Beijing from 2001 to 2006. Wastewater, air, and noise were monitored during wet and dry seasons. Levels of total suspended particles, odor, noise, ammonium nitrogen, chemical oxygen demand, biochemical oxygen demand, suspended solid, and fecal coliform were all above the criteria limit in China on numerous occasions. Poor environmental quality was measured at each transfer station in at least 5 of the 7 years evaluated.

Modern waste management in Western Europe has resulted in a remarkable increase in waste transportation. Salhofer et al. [39] investigated the ecological significance of increased waste transport for recycling refrigerators, paper, polyethylene films, and expanded polystyrene. Specifically, they examined the point at which increasing transportation distance drove the overall environmental impacts associated with recycling over that of disposal. Only in the case of expanded polystyrene were disposal impacts lower than recycling within the upper range of practical transportation distances. For other materials, disposal impacts were higher for all practical distances, indicating that efforts should focus on increasing recovery, e.g., through curbside recycling.

Case Studies

Two case studies further point to the importance of collection, transfer, and transport. The first, Beijing, China, describes a modern waste management system with little recycling. The second, Toronto, Canada, has significant recycling.

Current situation: Beijing, China

Beijing had an urban population of approximately 13.33 million in 2006 [40]. The average generation

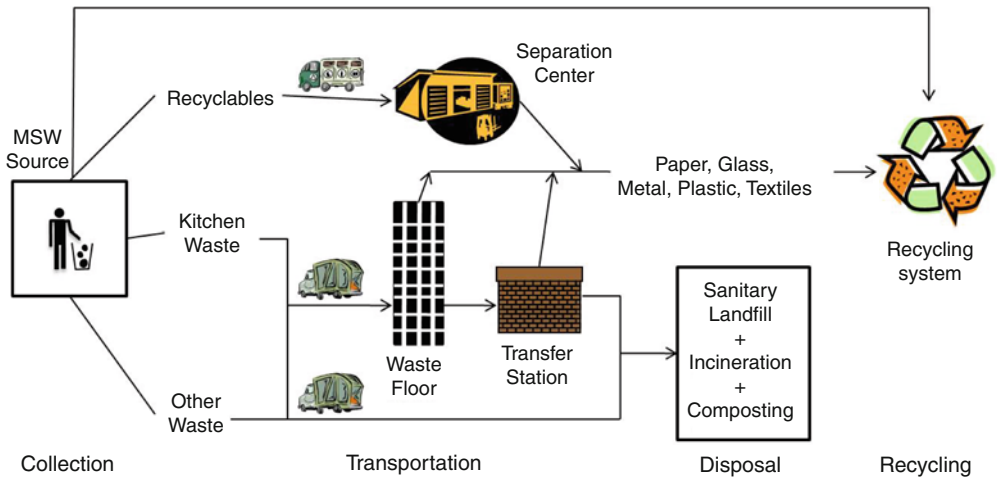

Waste Collection and Transport. Figure 5
Beijing MSW system. Adapted from Zhen-Shan [40]

rate of MSW in 2006 was 0.85 kg/capita/day. MSW generation in Beijing City increased from 1.04 million tons in 1978 to 4.134 million tons in 2006. Waste was predominately food waste (63.39%), followed by paper (11.07%), plastics (12.7%), and dust (5.78%), with all other wastes (tiles, textiles, glass, metals, and wood) accounting for less than 3%. In 2009, 90% of MSW generated in Beijing was landfilled, 8% incinerated, and 2% composted. Figure 5 is a schematic of the waste management system. Separate collection was available as a demonstration project to approximately 4.7 million people until 2007. Important MSW characteristics included moisture (61%), combustible waste (92%), recyclable waste (25%), compostable waste (77%), and low calorific value (4,600 kJ/kg). Though the fraction of the combustible waste is high, the low calorific value and high moisture content indicate that incineration would be ineffective without fuel addition or diversion of wet materials.

In 2006, Beijing City expended approximately $243 million on MSW management. Staffing accounted for $108 million, followed by waste collection-transportation ($47 million), treatment ($33 million), street sweeping ($32 million), equipment maintenance and repair ($18 million), and other costs ($6 million). There were six transfer stations in Beijing, where waste was compressed and transferred to more efficient vehicles for transport to landfills or incineration/composting facilities. At two transfer stations, waste was separated for recycling. There were 13 landfill sites and four incineration/composting plants, with a total designed capacity of 10,350 tons/day. At the end of 2005, there were 1,242 formal recycling sites in Beijing City, including 704 community-based sites and 538 floating sites. Approximately 1.6 million tons of materials were recycled in 2006, 7.3% higher than in 2005, including 0.36 million tons of paper, 0.87 million tons of metal, 0.17 million tons of plastic, and 0.08 million tons of glass. There were approximately 300,000 people living off the proceeds of waste recycling. Materials recycled by waste pickers were worth $0.44 million. The waste management system is shown in Fig. 5.

Aeration was the most popular method for odor control in separation workshops. Sprinklers are used to control dust. Approximately 50 tons of wastewater (including leachate and sewage) were generated each day at the transfer station with recyclables recovery. Leachate was mainly from waste compression and dust control water. An anaerobic–anoxic–aerobic reactor followed by a membrane filtration was used to treat the leachate.

Asuwei was the oldest and biggest landfill site, with a design capacity of 2,000 tons/day. Approximately 5,000 m^3 of landfill gas was generated every day in 2006. Before 2001, landfill gas was discharged. As of 2009, it is used to generate electricity.

Future Simulations: Toronto, Canada

Diaz and Warith [41] applied the Waste Analysis Software Tool for Environmental Decisions (WASTED) model – which provides a comprehensive view of the environmental impacts of MSW management systems – to Toronto, Canada. The model includes waste collection, material recovery, composting, energy recovery, and landfilling. WASTED uses compensatory systems to account for avoided environmental impacts. Upstream compensation incorporates the effects of processes that precede the waste management system (e.g., raw material extraction), while downstream compensation incorporates environmental effects of processes that

Waste Collection and Transport. Table 3 Waste Analysis Software Tool for Environmental Decisions (WASTED) results for Toronto, 2001 to 2021 [41]

	Collection/transport	Recycle	Compost	Landfill	Total
MSW Tonnes managed	$1.956E10^{7}$	$5.585E10^{6}$	$1.905E10^{6}$	$1.207E10^{7}$	$1.956E10^{7}$
Energy consumed (GJ)	$7.104E10^{9}$	$3.641E10^{8}$	$2.875E10^{6}$	$4.700E10^{8}$	$7.941E10^{9}$
Air pollutants					
Total CO_2 (ton)	$6.024E10^{5}$	$-2.010E10^{7}$	$2.096E10^{6}$	$2.446E10^{6}$	$-1.495E10^{7}$
Non-biogenic CO_2 (ton)	$6.024E10^{5}$	$-2.010E10^{7}$	$-3.483E10^{5}$	$-1.135E10^{6}$	$-2.098E10^{7}$
CH_4 (ton)	$7.246E10^{2}$	$-5.481E10^{3}$	$2.932E10^{-1}$	$3.250E10^{5}$	$3.202E10^{5}$
CO_2 equivalent (ton)	$6.177E10^{5}$	$-2.021E10^{7}$	$2.096E10^{6}$	$9.270E10^{6}$	$-8.227E10^{6}$
Non-biogenic CO_2 equivalent (ton)	$6.177E10^{5}$	$-2.021E10^{7}$	$-3.483E10^{5}$	$5.689E10^{6}$	$-1.425E10^{7}$
NO_x (ton)	$4.233E10^{3}$	$-2.983E10^{4}$	1.713	$-1.781E10^{3}$	$-2.738E10^{4}$
VOC_s (ton)	$1.861E10^{3}$	$3.039E10^{4}$	$3.238E10^{3}$	$2.732E10^{3}$	$3.822E10^{4}$
SO_x (ton)	$1.147E10^{3}$	$-2.362E10^{4}$	$4.643E10^{-1}$	$-4.423E10^{3}$	$-2.690E10^{4}$
PM (ton)	$3.360E10^{2}$	$-8.417E10^{3}$	$1.360E10^{-1}$	$-4.485E10^{2}$	$-8.529E10^{3}$
HCl (ton)	$1.113E10^{-2}$	$3.200E10^{4}$	0.000	$-2.626E10^{2}$	$3.174E10^{4}$
Pb (ton)	$2.631E10^{-2}$	21.428	$1.035E10^{-5}$	−17.277	41.77
Cd (ton)	$2.083E10^{-3}$	4.074	0.000	−49.136	−45.060
Hg (ton)	$8.468E10^{-4}$	$2.574E10^{-3}$	$3.421E10^{-7}$	−3.623E10-2	−3.280E10-2
NH_3 (ton)	0.000	0.000	$7.237E10^{2}$	0.000	$7.237E10^{2}$
Dioxins (kg)	$2.676E10^{-12}$	$3.718E10^{-9}$	$3.162E10^{-16}$	$-4.468E10^{-8}$	$-4.096E10^{-8}$
H^2S (ton)	0.000	0.000	0.000	42.731	42.731
Water pollutants					
BOD (kg)	$7.956E10^{-1}$	$1.248E10^{3}$	$3.220E10^{-4}$	$2.321E10^{6}$	$2.323E10^{6}$
COD (kg)	$7.956E10^{-1}$	$1.248E10^{3}$	$3.220E10^{-4}$	$3.316E10^{6}$	$3.318E10^{6}$
Pb (kg)	$9.472E10^{-2}$	0.425	$3.824E10^{-5}$	8.414	8.934
Cd (kg)	$1.023E10^{-2}$	$-1.748E10^{2}$	$4.139E10^{-6}$	11.055	$-1.637E10^{2}$
Hg (kg)	$9.738E10^{-5}$	$1.054E10^{-4}$	$3.938E10^{-8}$	0.131	0.131
NH_3 (ton)	0.000	0.000	0.000	2.211E105	$2.211E10^{5}$
Dioxin equivalent (ton)	0.000	$-6.271E10^{-5}$	0.000	0.000	$-6.271E10^{-5}$

take place after the waste management (e.g., avoided fossil fuel consumption from energy recovery from waste).

Diaz and Warith [41] applied the WASTED model to the city of Toronto, Canada from 2001 to 2021 (Table 3). From the table, one can see that collection was responsible for a majority of the energy consumption and significant portions of GHG emissions and other gas emissions and water pollutants. The authors also compared the results to the outcomes from two previous models, the Integrated Waste Management Model for Municipalities (IWM), and the Waste Reduction Model (WARM). While the models were in general agreement, fairly large differences were reported, indicating the importance of the underlying assumptions in the LCA models.

Future Directions

Waste collection and transport need to be made more efficient to conserve more natural resources and emit fewer pollutants, including green house gases. One way this can be done is to use the many optimization algorithms already developed, in conjunction with geographical information and global positioning systems, to design more efficient routes. Improvements can also be made to collection and transport vehicles, reducing fuel consumptions and pollution emissions. Greater use of trains and ships for transport, where appropriate, should also be pursued. Waste collection improvements will include the spread of recycling to more communities in more countries, through curbside and drop-off collection programs. This will require more material recovery facilities. As landfills become larger and, on average, more distant from waste generation points the use of efficient transport vehicles becomes more important.

Bibliography

Primary Literature

1. Tchobanoglous G, T Hilary, Vigil S (1993) Integrated solid waste management: engineering principles and management issues. Irwin/Mc-Graw-Hill, New York
2. Belton V, Crowe D, Matthews R, Scott S (1994) A survey of public attitudes to recycling in glassgo (UK). Waste Manage Res 12:351–367
3. Valeo C, Baetz B, Tsanis I (1998) Location of recycling depots with GIS. J Urban Plann Dev 124(2):93–99
4. Bacha H, Mild A, Natter M, Weber A (2004) Combining socio-demographic and logistic factors to explain the generation and collection of waste paper. Resour Conserv Recycl 41:65–73
5. Williams I, Taylor C (2004) Maximising household waste recycling at civic amenity sites in Lancashire, England. Waste Manage 24:861–874
6. Wilson B, Baetz B (2001) Modeling municipal solid waste collection systems using derived probability distributions. I: model development. J Environ Eng 127(11):1031–1038
7. Everett J (1994) Environmental collective action: residential recycling programs. J Prof Issues Eng Educ Pract 120(2):158–176
8. Olson M (1965) The logic of collective action. Harvard University Press, Cambridge, MA
9. USEPA (2003) Pay-as-you-throw: a cooling effect on climate change. US Environmental Protection Agency, EPA 530-F-03-008
10. Everett J, Peirce J (1991) National analysis of recycling material recovery rates. J Resour Manage Technol 19(4):148–152
11. Everett J, Peirce J (1993) Curbside recycling in the USA: convenience and mandatory participation. Waste Manage Res 11:49–61
12. García-Sánchez I (2008) The performance of Spanish solid waste collection. Waste Manage Res 26:327–336
13. Rogers J, Englehardt J, An H, Fleming L (2002) Solid waste collection health and safety risks – survey of municipal solid waste collectors. J Solid Waste Technol Manage 28(3):154–160
14. Medina M (2005) Serving the unserved: informal refuse collection in Mexico. Waste Manage Res 23:390–397
15. WRAP (2008) Kerbside recycling: indicative costs and performance. WRAP, Banbury, Oxon, UK
16. Wilson B, Baetz B (2001) Modeling municipal solid waste collection systems using dervice probability distributions. II: extensions and applications. J Environ Eng 127(11): 1039–1047
17. Dahlén L, Vukicevic S, Meijer J-E, Lagerkvist A (2007) Comparison of different collection systems for sorted household waste in Sweden. Waste Manage 27:1298–1305
18. Hage O, Soderholm P (2008) An econometric analysis of regional differences in household waste collection: the case of plastic packaging waste in Sweden. Waste Manage 28:1720–1731
19. Gomes A, Matos M, Carvalho I (2008) Separate collection of the biodegradable fraction of MSW: an economic assessment. Waste Manage 28:1711–1719
20. McLeod F, Cherrett T (2008) Quantifying the transport impacts of domestic waste collection strategies. Waste Manage 28:2271–2278
21. Tavares G, Zsigraiova Z, Semiao V, Carvalho M (2009) Optimisation of MSW collection routes for minimum fuel consumption using 3D GIS modeling. Waste Manage 29:1176–1185
22. Chang Ni-Bin, Lu H, Wei Y (1997) GIS technology for vehicle routing and scheduling in solid waste collection systems. J Environ Eng 123(9):901–910

23. Karadimas N, Papatzelou K, Loumos V (2007) Optimal solid waste collection routes identified by the ant colony system algorithm. Waste Manage Res 25: 139–147
24. Filipiak K, Abdel-Malek L, Hsieh H-N, Meegoda J (2009) Optimization of municipal solid waste collection system: case study. Practice Periodical of Hazardous, Toxic, and Radioactive Waste Management 13(3):210–216
25. Nuortioa T, Kytöjokib J, Niskaa H, Bröysyb O (2006) Improved route planning and scheduling of waste collection and transport. Expert Syst Appl 30:223–232
26. Kima B-I, Kimb S, Sahoob S (2006) Waste collection vehicle routing problem with time windows. Comput Oper Res 33:3624–3642
27. Batool S, Chuadhry M (2009) The impact of municipal solid waste treatment methods on greenhouse gas emissions in Lahore, Pakistan. Waste Manage 29:63–69
28. Solano E, Ranjitan R, Barlaz M, Brill D (2002) Life-cycle-based solid waste management I: model development. J Environ Eng 128(10):981–992
29. Solano E, Dumas R, Harrison K, Ranjitan R, Barlaz M, Brill D (2002) Life-cycle-based solid waste management II: illustrative applications. J Environ Eng 128(10):981–992
30. Iriarte A, Gabarrell X, Rieradevall J (2009) LCA of selective waste collection systems in dense urban areas. Waste Manage 29:903–914
31. Nino D, Tony BB (1996) Environmental linkages between urban form and municipal solid waste management infrastructure. J Urban Plann Dev 122(3):83–99
32. Shapek R (1995) Local government household battery collection programs: costs and benefits. Resour Conserv Recycl 15:1–19
33. Wilson B, Vincent J (2008) Estimating waste transfer station delays using GPS. Waste Manage 28:1742–1750
34. Komilis D (2008) Conceptual modeling to optimize the haul and transfer of municipal solid waste. Waste Manage 28:2355–2365
35. Bovea M, Powell J, Gallardo A, Capuz-Rizo S (2007) The role played by environmental factors in the integration of a transfer station in a municipal solid waste management system. Waste Manage 27:545–553
36. Eshet T, Baron M, Shechter M, Ayalon O (2007) Measuring externalities of waste transfer stations in Israel using hedonic pricing. Waste Manage 27:614–625
37. Eisted R, Larsen A, Christensen T (2009) Collection, transfer and transport of waste: accounting of greenhouse gases and global warming contribution. Waste Manage Res 27: 738–745
38. Chunping L, Guoxue L, Yiming L, Yanfu L, Jian H (2008) Environmental monitoring and fuzzy synthetic evaluation of municipal solid waste transfer stations in Beijing in 2001–2006. J Environ Sci 20:998–1005
39. Salhofer S, Schneider F, Obersteiner G (2007) The ecological relevance of transport in waste disposal systems in Western Europe. Waste Manage 27:S47–S57
40. Zhen-Shan L, Lei Y, Xiao-Yan Q, Yu-mei S (2009) Municipal solid waste management in Beijing City. Waste Manage 29:2596–2599
41. Diaz R, Warith M (2006) Life-cycle assessment of municipal solid wastes: development of the WASTED model. Waste Manage 26:886–901

Waste Diversion

Shirley Thompson, Mary Rezai, Jeff Valdivia
Natural Resources Institute, University of Manitoba, Winnipeg, MB, Canada

Article Outline

Glossary
Definition of the Subject and Its Importance
Introduction
Hierarchy of Waste Diversion
Source Reduction
Recycling
Biological Treatment: Composting and Anaerobic Digestion
Organic Waste
Future Directions
Bibliography

Glossary

Waste diversion Directs garbage away from landfills or incinerators through reuse, recycling, composting, or gas production through anaerobic digestion. Waste diversion is a key component of effective and sustainable waste management.

Waste management The process of collecting, processing, and disposing of waste.

Extended producer responsibility (EPR) Entails making manufacturers responsible for the entire life cycle of the products and packaging they produce based on the "polluter pays principle."

Waste prevention (aka Source reduction) Refers to changes in the design, manufacturing process, purchase, or use of materials or products that reduces their contribution to the waste stream.

Definition of the Subject and Its Importance

Waste diversion or landfill diversion is the process of diverting waste from landfill. Diverting waste from the landfill is done through recycling, composting, burning, compacting, etc., to reduce its threat to human health and the environment, make it more disposable, or capture some of its value [1]. There is a hierarchy of waste diversion that lists diversion methods in order of importance, namely, waste prevention (aka source reduction), preparing waste for reuse, recycling/composting, other recovery methods such as energy recovery from waste and biological transformation of waste.

Introduction

Without doubt, diverting waste provides a resource with a value [1], substituting for virgin resources, while conserving the products' embedded energy, and reducing the waste management problems of declining landfill space, leachate, and landfill gas. Unfortunately, the true value of waste is typically underestimated, since placing a value on improved human health or environmental quality is difficult [1]. Whether the value of waste can be captured will often depend on local circumstances, like the cost of labor, equipment, energy, and land [1]. Effective and timely waste diversion policies are needed to ensure the value is seen and help correct the various problems associated with the waste management sector. Waste diversion helps to resolve many of the problems facing waste management including declining landfill space, leachate, landfill gas, and toxins and gases emitted as a result of incineration.

Hierarchy of Waste Diversion

There is a hierarchy of waste diversion, which lists broad waste management measures in order of their importance [2]. The measures from greatest to least importance are waste prevention (aka source reduction), preparing waste for reuse, recycling/composting, other recovery (such as energy recovery from waste) and biological transformation of waste [2, 3]. The EU Directive on Waste stipulates that the following of the hierarchy should avoid human health hazards and environmental damage [2].

Source Reduction

Source reduction refers to changes in the design, manufacturing process, purchase, or use of materials or products that reduces their contribution to the waste stream [3]. It has been observed that source reduction is the best way of decreasing greenhouse gas emissions from the waste sector and decreasing overall waste generation [3, 4]. Reusing materials or products is considered a kind of source reduction as it frees space in landfills for other waste and prevents the creation of new materials or products to be used in their place [3–5].

Extended producer responsibility (EPR) programs, which are programs designed so that producers bear the financial burden of the disposal of their products, is another type of source reduction technique [3, 6]. This tactic attempts to relieve local governments of the costs of managing certain priority products by forcing manufacturers to internalize the cost of recycling within the product price. EPR promotes that producers (usually brand owners) have the greatest control over product design and marketing and therefore have the greatest ability and responsibility to reduce toxicity and waste. In this way, EPR shifts responsibility for waste from government to private industry, obliging producers, importers, and/or sellers to internalize waste management costs in their product prices and ensuring the sustainable and safe handling of the remains of their products [7].

Recycling

Recycling refers to taking used materials and creating new products in order to prevent the disposal of these products in landfills. Recycling material can include glass, paper, metal, plastic, textiles, and electronics. Because recycled materials can act as substitutes for raw materials in many manufacturing processes, recycling helps to reduce the amount of raw materials extracted and processed [3, 6], which results in several favorable outcomes. First, for instance, since recycling aluminum requires far less energy than extracting and processing virgin aluminum, making aluminum cans from recycled aluminum rather than virgin aluminum reduces emissions by 94% and energy use by 93% [3]. Second, since recycled materials are not sent to

landfills, recycling opens up space in landfills for other waste [3, 5].

Ferrara and Missios [8], for instance, investigated the relationship between recycling policy options and recycling behaviors and came to many of the following important findings [9]:

1. User fees for waste disposal increases recycling intensity; however, user fees may lead to illegal dumping.
2. Weekly recycling has a positive effect on the recycling of glass, aluminum, and toxic chemicals, but has a negligible effect on the recycling of newspaper, plastic bottles, tin cans, and cardboard. This result is consistent with the idea that recycling intensity increases when it occurs concurrently with waste collection, that is, when recycling is more convenient.
3. Offering free units under a use fee program for waste disposal negatively impacts recycling.
4. Limiting the number of bags at the curb has a negligible impact on recycling.
5. Promoting curbside recycling increases the rate of non-curbside recycling (i.e., the recycling of toxic materials).
6. For most materials, education level does not significantly affect recycling intensity, except for university undergraduate and/or postgraduate degrees, which increases the intensity of newspaper, aluminum, tin can, and toxic chemical recycling. Education has a positive impact on the recycling of glass above a high school degree.
7. Recycling generally decreases as income increases for newspaper, plastic, and toxic chemicals. This may occur because as income increases, time is more valuable to the recycler.
8. Home ownership is strongly, and positively, correlated to recycling. This suggests that homeowners are more attached to their community and/or are more concerned about their neighbors' perception of them, causing them to recycle more.

Although these behavioral traits are associated with recyclables rather than organics, these findings should apply to how people would react to the implementation of specific organic waste disposal programs.

Biological Treatment: Composting and Anaerobic Digestion

In addition to reusing materials waste products can go through biological treatment, which is the breaking down of material through the action of microorganisms. There are two types of biological treatments: anaerobic digestion and composting. Materials are broken down to carbon dioxide, water, and biomass. Some materials easily break down, others do not. The environment in which the material is placed determines the speed of breakdown.

Organic Waste

Organic waste is comprised of food/kitchen waste, yard waste, and paper [9, 10]. Organic waste amounts to almost 40% in high- and middle-income countries and roughly 30% in low-income countries by weight of municipal solid waste [10]. This portion of municipal solid waste is largely responsible for leachate and landfill gas problems [11]. In landfills, organic wastes, including food waste and yard waste, undergo anaerobic decomposition to produce various gases, including methane [3, 11, 12]. Landfill gas capture for energy recovery is used in many places, since methane is an excellent source of energy when combusted [3, 13]. Methane capture for energy recovery is useful because, although carbon dioxide is produced by the combustion of methane, carbon dioxide is a much less potent greenhouse gas than methane [3, 6, 11, 12].

Therefore, preventing or limiting organic waste from entering landfills would help to solve these problems [10]. There are several benefits to composting the organic portion of the waste stream. According to Gautam et al. [10], these benefits include the following:

1. Backyard and midsize composting at the source reduces the amount of waste to be collected and transported to landfills.
2. Composting reduces the production of leachate and landfill gas, which are both harmful to the environment.
3. Composting increases the life of landfills.
4. Composting and recycling result in a relatively inert waste stream going into landfills so that landfills require less daily cover, less equipment and labor

during operation, and reduced monitoring after closure.
5. Composting produces a useful soil conditioner with some fertilizer value that can often be sold.
6. Composting is one of the least expensive methods of dealing with organic waste.
7. Composting can significantly help municipalities achieve waste diversion targets.

It is probably impossible to draw general conclusions regarding the economics of waste management options [14]. Chynoweth et al. (1992) propose that, for the organic fraction of MSW, anaerobic digestion is better than aerobic composting because aerobic composting requires aeration or mixing, and anaerobic digestion produces a valuable fuel gas, in addition to compost [15]. Braber (1995) found that the anaerobic digestion of the organic fraction of MSW is slightly more expensive than aerobic composting [14]. In Indonesia, Aye and Widjaya (2006) estimate that composting in a centralized facility (CPC) is more cost-effective and environmentally friendly than composting in small, labor-intensive local facilities (CPL), producing biogas and compost simultaneously (BGP), engineering landfills for landfill gas capture to produce electricity (LFE), and business as usual (open dumping). Aye and Widjaya (2006) found that the benefit–cost ratios for CPC, CPL, BGP, and LFE were 2.2, 1.4, 1.3, and 1.03, respectively [16]. In contrast, Renkow and Rubin (1998) found from a survey of MSW composting facilities that their operating costs are generally around $50 US per ton and that the majority of facilities receive no revenue from their compost [17].

Future Directions

The more widely waste diversion options are available (to residents in single-family households and multifamily buildings and to the institutional, commercial, and industrial sectors) the easier it is to reach a high diversion rate. For this, policy and legislation are essential that support waste diversion efforts. Municipal bylaws limiting waste disposal, charging for garbage collection, or banning divertible materials from landfills can help enforce waste diversion practices. Broader policies, such as formal state, provincial, or municipal waste diversion targets, can also motivate change.

A number of trends in waste diversion are emerging including zero waste commitments, economic instruments, and green procurement. Zero waste is a long-term commitment to reduce waste through measures such as extended producer responsibility programs, economic instruments to encourage waste reduction, green procurement, and product design that includes end-of-life management. Economic instruments include Pay-As-You-Throw (PAYT) programs that require residents to pay on a volume basis for the disposal of their waste. The program may employ a tag or bag system or a cart system. Other economic instruments include tipping fee surcharges and fines on contaminated loads (waste that has not been source separated). Green procurement and consumer education policies encourage businesses and residents to reuse more and purchase goods with less packaging. For example, some communities or states have introduced bans on organic waste and different products at the landfill and levies on packaging and bottles. This approach requires strong education and enforcement to ensure a level playing field for businesses and change consumer behavior.

Bibliography

Primary Literature

1. Beede DN, Bloom DE (1995) The economics of municipal solid waste. World Bank Res Obs 10(2):113–150
2. Europa (2009a) Directive on waste. <http://europa.eu/legislation_summaries/environment/waste_management/ev0010_en.htm#KEY>. Accessed 26 Mar 2010
3. Mohareb AK, Warith M, Narbaitz RM (2004) Strategies for the municipal solid waste sector to assist Canada in meeting its Kyoto Protocol commitments. Environ Rev 12:71–95
4. Min H, Galle WP (1997) Green purchasing strategies: trends and implication. J Supply Chain Manage 33(3): 10–17
5. Huhtala A (1997) A post-consumer waste management model for determining optimal levels of recycling and landfilling. Environ Resour Econ 10:301–314
6. Statistics Canada (2005a) Human activity and the environment: solid waste in Canada. Government of Canada. Catalogue no. 16-201-XIE. <http://www.statcan.gc.ca/pub/16-201-x/16-201-x2005000-eng.pdf>. Accessed 15 Mar 2010
7. Nicol S, Thompson S (2007) Policy options to reduce consumer waste to zero: comparing product stewardship and extended

producer responsibility for refrigerator waste. Waste Manage Res 25(3):227–233
8. Ferrara I, Missios P (2005) Recycling and waste diversion effectiveness: evidence from Canada. Environ Resour Econ 30:221–238
9. Thompson S, Sawyer J, Bonam R, Valdivia JE (2009) Building a better waste generation model: validating models with recovery rates at 35 Canadian landfills. Waste Manage 29:2085–2091
10. Gautam S, Bundela PS, Pandey AK, Awasthi MK, Sarsaiya S (2010) Composting of municial solid waste of Jabalpur City. Glob J Environ Res 4(1):43–46
11. Ackerman F (2000) Waste management and climate change. Local Environ 5(2):223–229
12. Spokas K, Bogner J, Chanton JP, Morcet M, Aran C, Graff C, Moreau-Le Goluan Y, Hebe I (2006) Methane mass balance at three landfill sites: what is the efficiency of capture by gas collection systems? Waste Manage 26(5):516–525
13. Environment Canada (2007) Landfill gas – overview. Government of Canada. http://www.ec.gc.ca/wmd-dgd/default.asp?lang=En&n=10E36DBA-1. Accessed 11 Feb 2009
14. Braber K (1995) Anaerobic digestion of municipal solid waste: a modern waste disposal option on the verge of breakthrough. Biomass Bioenergy 9:365–376
15. Chynoweth DP, Owens J, O'Keefe D, Earle JFK, Bosch G, Legrand R (1992) Sequential batch anaerobic composting of the organic fraction of municipal solid waste. Water Sci Technol 25:327–339
16. Aye L, Widjaya ER (2006) Environmental and economic analyses of waste disposal options for traditional markets in Indonesia. Waste Manage 26:1180–1191
17. Renkow M, Rubin AR (1998) Does municipal solid waste composting make economic sense? J Environ Manage 53:339–347

Books and Reviews

Abbasi PA, Al-Dahmani J, Sahin F, Hoitink HAJ, Miller SA (2002) Effect of compost amendments on disease severity and yield of tomato in conventional and organic production systems. Plant Dis 86:156–161

Anand S, Sen A (2000) Human development and economic sustainability. World Dev 28(12):2029–2049

Barlaz MA, Green G, Chanton JP, Goldsmith CD, Hater GR (2004) Evaluation of a biologically active cover for mitigation of landfill gas emissions. Environ Sci Technol 38:4891–4899

Barrieu P, Sinclair-Desgagné B (2006) On precautionary policies. Manage Sci 52(8):1145–1154

Bishop RC (1993) Economic efficiency, sustainability, and biodiversity. Ambio 22(2/3):69–73

Bogner J, Matthews E (2003) Global methane emissions from landfills: new methodology and annual estimates 1980–1996. Glob Biogeochem Cycles 17(2):34-1–34-18

Borjesson G, Samuelsson B, Galle J, Svensson BH (2000) Methane emissions from landfills: options for measurement and control. Warwickshire, Stratford-upon-Avon

Canadian Council of Ministers of the Environment (CCME) (2009) Canada-wide action plan for extended producer responsibility. Government of Canada. Retrieved 29 June 2010 from <http://www.ccme.ca/assets/pdf/epr_cap.pdf>

Christensen TH, Kjeldsen P, Bjerg PL, Jensen BD, Christensen JB, Baun A, Albrechtsen HJ, Heron G (2001) Biogeochemistry of landfill leachate plumes. Appl Geochem 16:659–718

City of Vancouver (2009) Vancouver landfill & vancouver south transfer station rates. Engineering services. Retrieved 20 February 2009 from http://vancouver.ca/engsvcs/solidwaste/landfill/rates.htm

City of Winnipeg (2008a) Water and waste. Retrieved 20 June 2008 from http://www.winnipeg.ca/waterandwaste/recycle/recyclingReport.stm

City of Winnipeg (2008b) Water and waste. Retrieved 20 June 2008 from http://www.winnipeg.ca/waterandwaste/garbage/residentialReport.stm

City of Winnipeg (2009) Brady road landfill. Retrieved 20 February 2009 from http://www.winnipeg.ca/WaterandWaste/garbage/bradyroad.stm

Curmally A (2004) Exploring economic incentives for effective solid waste management in Rhode Island. Retrieved 19 January 2009 from http://envstudies.brown.edu/oldsite/env/theses/master0304/Curmally_Atiyah/Atiyah%20Curmally.pdf

Czepiel P, Shorter J, Harriss R, Kolb C, Lamb B (2002) The influence of atmospheric pressure on whole-landfill methane emissions observed during a multi-season study. Scientific poster. Retrieved 7 July 2008 from http://lst.sb.luth.se/iclrs/web/post2002/ppt/poster/Czepiel.pdf

Danish Environmental Protection Agency (1999a) Waste 21: waste management plan 1998–2004. Government of Denmark. Retrieved 13 May 2010 from http://www2.mst.dk/Udgiv/publications/1999/87-7909-571-2/pdf/87-7909-570-4.pdf

Danish Government (2007) Greenhouse gas emissions trends and projections in Europe 2007: Denmark – country profile 2007. European Environment Agency. Retrieved 10 June 2010 from http://www.eea.europa.eu/publications/eea_report_2007_5/Denmark.pdf

David A (2007) Overview of municipal solid waste (MSW) management in Canada. Environment Canada. Government of Canada. In: Proceedings "Municipal waste management workshop: different approaches and solutions." Retrieved 16 January 2009 from http://www.awma-ovc.ca/AWMA_OVC_WMWorkshop_Alain_David.pdf

Denman KL, Brasseur G, Chidthaisong A, Ciais P, Cox PM, Dickinson RE, Hauglustaine D, Heinze C, Holland E, Jacob D, Lohmann U, Ramachandran S, da Silva Dias PL, Wofsy SC, Zhang X (2007) Couplings between changes in the climate system and biogeochemistry. In: Solomon S, Qin D, Manning M, Chen Z, Marquis M, Averyt KB, Tignor M, Miller HL (eds) Climate change 2007: the physical science basis. Contribution of working group I to the fourth assessment report of the intergovernmental panel on climate change. Cambridge University Press, Cambridge/New York

Department of Environment, Climate Change, and Water (DECCW) (2007) NSW waste avoidance and resource recovery strategy 2007. NSW Government. Retrieved 25 February 2010 from http://www.environment.nsw.gov.au/resources/warr/07226_WARRreport07.pdf

Department of Environment, Climate Change, and Water (DECCW) (2008) NSW resource recovery industries survey 2006–07: organics reprocessing. NSW Government. Retrieved 1 March 2010 from http://www.environment.nsw.gov.au/resources/sustainbus/08584organicsRecovery.pdf

Department of Environment, Climate Change, and Water (DECCW) (2009a) About POEO legislation. NSW Government. Retrieved 25 February 2010 from http://www.environment.nsw.gov.au/legislation/aboutpoeo.htm#major

Department of Environment, Climate Change, and Water (DECCW) (2009b) DECCW act summaries. NSW Government. Retrieved 25 February 2010 from http://www.environment.nsw.gov.au/legislation/DECCActsummaries.htm#waarra

Department of Environment, Climate Change, and Water (DECCW) (2009c) NSW waste avoidance and resource recovery progress report 2008. NSW Government. Retrieved 26 February 2010 from http://www.environment.nsw.gov.au/resources/warr/09155WARRreport08.pdf

Department of Environment, Climate Change, and Water (DECCW) (2010) The waste and environment levy. NSW Government. Retrieved 3 March 2010 from http://www.environment.nsw.gov.au/wr/index.htm

Department of Justice (2010) Constitution acts, 1867 to 1982. Government of Canada. Retrieved 5 March 2010 from http://laws-lois.justice.gc.ca/eng/Const/Const_index.html

Department of Local Government (2009) Comparative information on NSW local government councils 2007/08. Retrieved 2 March 2010 from http://www.dlg.nsw.gov.au/dlg/dlghome/documents/Comparatives/Comparatives_2007_08.pdf

Department of the Environment, Water, Heritage, and the Arts (DEWHA) (2007a) National strategy for ecologically sustainable development. Australian Government. Retrieved 24 February 2010 from http://www.environment.gov.au/esd/national/nsesd/index.html

Department of the Environment, Water, Heritage, and the Arts (DEWHA) (2007b) National strategy for ecologically sustainable development. Australian Government. Retrieved 24 February 2010 from http://www.environment.gov.au/esd/national/nsesd/strategy/intro.html#GoalsEtc

Department of the Environment, Water, Heritage, and the Arts (DEWHA) (2007c) National strategy for ecologically sustainable development. Australian Government. Retrieved 24 February 2010 from http://www.environment.gov.au/esd/national/nsesd/strategy/wastes.html

Department of the Environment, Water, Heritage, and the Arts (DEWHA) (2009a) About the EPBA Act. NSW Government. Retrieved 24 February 2010 from http://www.environment.gov.au/epbc/about/index.html

Department of the Environment, Water, Heritage, and the Arts (DEWHA) (2009b) National environmental protection council. NSW Government. Retrieved 9 June 2010 from http://www.environment.gov.au/about/councils/nepc/index.html

Department of the Environment, Water, Heritage, and the Arts (DEWHA) (2009c) What is protected under the EPBA Act? Australian Government. Retrieved 24 February 2010 from http://www.environment.gov.au/epbc/protect/index.html

Division for Sustainable Development (n.d.) U.N. department of economic and social affairs. Retrieved 18 February 2009 from http://www.un.org/esa/dsd/dsd/dsd_index.shtml

El-Fadel M, Findikakis AN, Leckie JO (1997) Environmental impacts of solid waste landfilling. J Environ Manage 50:1–25

Elliott A (2008) Is composting organic waste spreading? Statistics Canada. Government of Canada. Retrieved 19 January 2009 from http://www.statcan.gc.ca/pub/16-002-x/2008001/10540-eng.htm#4

Environment Canada (2005b) A guide to understanding the Canadian environmental protection act, 1999: section 2: environmental management in Canada. Government of Canada. Retrieved 5 March 2010 from http://www.ec.gc.ca/CEPARegistry/the_act/guide04/s2.cfm

Environment Canada (2005c) A guide to understanding the Canadian environmental protection act, 1999: section 3: CEPA 1999 guiding principles. Government of Canada. Retrieved 5 March 2010 from http://www.ec.gc.ca/CEPARegistry/the_act/guide04/s3.cfm

Environment Canada (2006) Greenhouse gases. Government of Canada. Retrieved 16 January 2009 from http://www.ec.gc.ca/pdb/ghg/about/gases_e.cfm

Environment Canada (2009a) Canada's 2006 greenhouse gas inventory. Government of Canada. Retrieved 11 February 2009 from http://www.ec.gc.ca/pdb/ghg/inventory_report/2006/tab_eng.cfm

Environment Canada (2009b) Municipal solid waste (MSW). Government of Canada. Retrieved 9 March 2010 from http://www.ec.gc.ca/drgd-wrmd/default.asp?lang=En&n=7623F633-1

Environment Canada Weather Office Environment Canada (2006) Canadian climate normals or averages 1971–2000. Retrieved July 2007. http://www.climate.weatheroffice.ec.gc.ca/climate_normals/index_e.html

Environment Protection and Heritage Council (2009) National waste overview 2009. Australian Government. Retrieved 2 March 2010 from http://www.ephc.gov.au/sites/default/files/WasteMgt_Nat_Waste_Overview_PRINT_ver_200911.pdf

Europa (2006) Strategy on the prevention and recycling of waste. Retrieved 29 March 2010 from http://europa.eu/legislation_summaries/environment/waste_management/l28168_en.htm

Europa (2008a) Integrated pollution prevention and control: IPPC directive. Retrieved 30 March 2010 from http://europa.eu/legislation_summaries/environment/waste_management/l28045_en.htm

Europa (2008b) Waste incineration. Retrieved 29 Mar 2010 from http://europa.eu/legislation_summaries/environment/waste_management/l28072_en.htm

Europa (2009b) Waste disposal (until the end of 2010). Retrieved Mar 30 from http://europa.eu/legislation_summaries/environment/waste_management/l21197_en.htm

Europa (n.d.) The 27 member countries of the European Union. Retrieved 22 Mar 2010 from http://europa.eu/about-eu/27-member-countries/index_en.htm

European Commission (2009a) What are EU decisions? Retrieved 26 March 2010 from http://ec.europa.eu/community_law/introduction/what_decision_en.htm

European Commission (2009b) What are EU directives? Retrieved 26 March 2010 from http://ec.europa.eu/community_law/introduction/what_directive_en.htm

European Commission (2009c) What are EU regulations? Retrieved 26 March 2010 from http://ec.europa.eu/community_law/introduction/what_regulation_en.htm

European Commission (2009d) What is EU law? Retrieved 26 March 2010 from http://ec.europa.eu/community_law/introduction/treaty_en.htm

European Compost Network (n.d.) Biological waste treatment in Europe – technical and market developments. Retrieved 19 January 2009 from http://www.compostnetwork.info/index.php?id=10

Federation of Canadian Municipalities (FCM) (2004) Solid waste as a resource: guide for sustainable communities. Retrieved 9 March 2010 from http://www.sustainablecommunities.ca/files/Capacity_Building_-_Waste/SW_Guide_Overview.pdf

Folke C, Carpenter S, Elmqvist T, Gunderson L, Holling CS, Walker B (2002) Resilience and sustainable development: building adaptive capacity in a world of transformations. Ambio 31(5):437–440

Forcing In: Solomon S, Qin D, Manning M, Chen Z, Marquis M, Averyt KB, Tignor M, Miller HL (eds) Climate change 2007: the physical science basis. Contribution of working group I to the fourth assessment report of the intergovernmental panel on climate change. Cambridge University Press, Cambridge/New York

Forster P, Ramaswamy V, Artaxo P, Berntsen T, Betts R, Fahey DW, Haywood J, Lean J, Lowe DC, Myhre G, Nganga J, Prinn R, Raga G, Schulz M, Van Dorland R (2007) Changes in atmospheric constituents and in radiative forcing. In: Solomon S, Qin D, Manning M, Chen Z, Marquis M, Averyt KB, Tignor M, Miller HL (eds) Climate change 2007: the physical science basis. Contribution of working group I to the fourth assessment report of the intergovernmental panel on climate change. Cambridge University Press, Cambridge/New York

Friesen B (2000) Landfill ban stimulates composting programs in Nova Scotia. BioCycle Mag 41(3):53

Gollier C, Jullien B, Treich N (2000) Scientific progress and irreversibility: an economic interpretation of the precautionary principle. J Public Econ 75:229–253

Google Maps (2010a) Retrieved 24 February 2010 from http://maps.google.com.au/

Google Maps (2010b) Retrieved 4 March 2010 from http://maps.google.ca/

Government of Canada (2010) Provinces and territories. Government of Canada. Retrieved 4 March 2010 from http://www.canada.gc.ca/othergov-autregouv/prov-eng.html

Government of Nova Scotia (2008) Nova Scotia population by county. Government of Nova Scotia. Retrieved 16 March 2010 from http://www.gov.ns.ca/finance/statistics/agency/common/default.asp?p=1&s=1c

Green Manitoba (2009) Waste reduction and recycling support (WRARS) program guide. Government of Manitoba. Retrieved 29 June 2010 from http://www.greenmanitoba.ca/cim/dbf/wrars_guide_december_09_(v1.1).pdf?im_id=392&si_id=1001

Green Manitoba (2010) HHW events calendar for 2010. Government of Manitoba. Retrieved 29 June 2010 from http://www.greenmanitoba.ca/cim/dbf/2010_hhw_events.pdf?im_id=411&si_id=1001

Green Manitoba (n.d.) E-waste roundup. Government of Manitoba. Retrieved 29 June 2010 from http://www.greenmanitoba.ca/cim/1001.dhtm

Green Manitoba (n.d.) History of waste minimization in Manitoba. Government of Manitoba. Retrieved 23 June 2010 from http://www.greenmanitoba.ca/cim/dbf/history.pdf?im_id=150&si_id=1001

Hyder Consulting (2008) Waste and recycling in Australia: final report. Retrieved 25 February 2010 from http://www.environment.gov.au/settlements/waste/publications/pubs/waste-recycling2008.pdf

IPCC (2007) Summary for policymakers. In: Solomon S, Qin D, Manning M, Chen Z, Marquis M, Averyt KB, Tignor M, Miller HL (eds) Climate change 2007: the physical science basis. Contribution of working group I to the fourth assessment report of the intergovernmental panel on climate change. Cambridge University Press, Cambridge/New York

Kjeldsen P, Barlaz MA, Rooker AP, Baun A, Ledin A, Christensen TH (2002) Present and long-term composition of MSW landfill leachate: a review. Crit Rev Environ Sci Technol 32(4):297–336

Lay J, Li Y, Noike T (1996) Effect of moisture content and chemical nature on methane fermentation characteristics of municipal solid wastes. In: Proceedings: Japan society of civil engineers. J Environ Syst Eng Div 1:101–108

Manitoba Association for Resource Recovery Corporation (MARRC) (2010) On drop of used oil makes a difference. Retrieved 29 June 2010 from http://www.usedoilrecycling.com/en/mb

Manitoba Conservation (2010) News release. Government of Manitoba. Retrieved 29 June 2010 from http://news.gov.mb.ca/news/index.html?archive=&item=8282

Manitoba Conservation (N.d.b.) Waste reduction and pollution prevention (WRAPP) fund. Government of Manitoba. Retrieved 29 June 2010 from http://www.gov.mb.ca/conservation/pollutionprevention/wrapp/wrappfund.html

Manitoba Conservation (N.d.b.) Waste reduction and prevention. Government of Manitoba. Retrieved 29 June 2010 from http://www.gov.mb.ca/conservation/pollutionprevention/waste/index.html

Manitoba Local Government (n.d.) Municipalities. Government of Manitoba. Retrieved 17 May 2010 from http://web5.gov.mb.ca/public/municipalities.aspx

McCabe DJ (1976) Progress report of efforts completed during the second year of baled and unbaled solid waste studies. System Technology Corp, Xenia

National Capital Commission (2008) About Canada's capital. Government of Canada. Retrieved 5 March 2010 from http://www.capcan.ca/bins/ncc_web_content_page.asp?cid=16297-24515& lang=1&bhcp=1

Nevens F, Reheul D (2003) The application of vegetable, fruit and garden waste (VFG) compost in addition to cattle slurry in a silage maize monoculture: nitrogen availability and use. Eur J Agron 19:189–203

Nova Scotia Environment (2008) Final report on Nova Scotia's 1995 solid waste resource management strategy: not going to waste. Government of Nova Scotia. Retrieved 10 March 1995 from http://www.gov.ns.ca/nse/waste/docs/SolidWasteStrategyFinalReport1995.pdf

Nova Scotia Environment (2009a) Environmental goals and sustainable prosperity act: progress report 2009. Government of Nova Scotia. Retrieved 11 March 2010 from http://www.gov.ns.ca/nse/egspa/docs/EGSPA.2009.Annual.Report.pdf

Nova Scotia Environment (2009b) Renewal of Nova Scotia's solid waste resource management strategy: consultation summary report 2009. Government of Nova Scotia. Retrieved 10 March 2010 from http://www.gov.ns.ca/nse/waste/docs/SolidWasteStrategy.2009.Renewal.pdf

Nova Scotia Environment (2009c) Solid waste-resource management strategy. Government of Nova Scotia. Retrieved 10 March 2009 from http://www.gov.ns.ca/nse/waste/swrmstrategy.asp

Nova Scotia Environment and Labour (2004) Status report 2004 of solid waste-resource management in Nova Scotia. Government of Nova Scotia. Retrieved 11 March 2010 from http://www.gov.ns.ca/nse/waste/docs/WasteResourceStatus2004.pdf

NSW Legislation (2010) Protection of the environment operations act 1997 no. 156. New South Wales Government

Office of the Auditor General (2007) Audit of the province's management of contaminated sites and landfills. Government of Manitoba

Okeke C, Armour A (2000) Post-landfill siting perceptions of nearby residents: a case study of Halton landfill. Appl Geogr 20:137–154

Organic Waste Recycling Unit (2002) Soil carbon sequestration utilising recycled organics: a review of the scientific literature. NSW Agriculture. Retrieved 2 March 2010 from http://www.environment.nsw.gov.au/resources/warr/SPD_ORG_0208SoilCarbonSeq.pdf

Parliament of Australia (2003) Commonwealth of Australia constitution act. Australian Government. Retrieved 24 February 2010 from http://www.aph.gov.au/SEnate/general/constitution/par5cha1.htm

Parliamentary Education Office (PEO) (2009) A multi-tiered system: governing Australia. Australian Government. Retrieved 24 February 2010 from http://www.peo.gov.au/students/cl/multi.html

Pinamonti F (1998) Compost mulch effects on soil fertility, nutritional status and performance of grapevine. Nutr Cycl Agroecosyst 51:239–248

Press, Cambridge/New York

Read AD (1999) Making waste work: making UK national solid waste strategy work at the local scale. Resour Conserv Recy 26:259–285

RRFB Nova Scotia (2003) An assessment of the state of provincial compost processing facilities. Government of Nova Scotia. Retrieved 16 March 2010 from http://www.rrfb.com/pdfs/An%20Assessment%20of%20the%20State%20of%20Provincial%20Compost%20Processing%20Facilities.pdf

RRFB Nova Scotia (2008) Annual report 2008. Government of Nova Scotia. Retrieved 16 March 2010 from http://www.rrfb.com/pdfs/RRFB_AR_2008.pdf

Sathaye J, Najam A, Cocklin C, Heller T, Lecocq F, Llanes-Regueiro J, Pan J, Petschel-Held G, Rayner S, Robinson J, Schaeffer R, Sokona Y, Swart R, Winkler H (2007) Sustainable development and mitigation. In: Metz B, Davidson OR, Bosch PR, Dave R, Meyer LA (eds) Climate change 2007: mitigation. Contribution of working group III to the fourth assessment report of the intergovernmental panel on climate change, Cambridge University Statistics Canada (2010a) 2006 community profiles. Government of Canada. Retrieved 25 June 2010 from http://www12.statcan.ca/census-recensement/2006/dp-pd/prof/92-591/index.cfm?Lang=E

Statistics Canada (2005b) Land and freshwater area, by province and territory. Government of Canada. Retrieved 4 March 2010 from http://www40.statcan.ca/l01/cst01/phys01-eng.htm

Statistics Canada (2008a) Farm population and total population by rural and urban populations, by province (2001 and 2006 census of agriculture and census of population). Government of Canada. Retrieved 4 March 2010 from http://www40.statcan.ca/l01/cst01/agrc42a-eng.htm

Statistics Canada (2008b) Population and dwelling counts, for Canada, provinces and territories, and census subdivisions (municipalities), 2006 and 2001 censuses – 100% data. Government of Canada. Retrieved 25 June 2010 from http://www12.statcan.ca/english/census06/data/popdwell/Table.cfm?T=302&SR=1&S=3&O=D&RPP=25&PR=46&CMA=0

Statistics Canada (2008a) Disposal and diversion of waste, by province and territory, 2004 and 2006 (diverted materials per capita). Government of Canada. Retrieved 4 May 2010 from http://www40.statcan.ca/l01/cst01/envir32d-eng.htm

Statistics Canada (2008b) Waste management industry survey: business and government sectors. Government of Canada. Catalogue no. 16F0023X

Statistics Canada (2008c) Waste management industry survey: business and government sectors. Government of Canada. Catalogue no. 16F0023X. Retrieved 12 March 2010 from http://www.statcan.gc.ca/pub/16f0023x/16f0023x2006001-eng.pdf

Statistics Canada (2009) Population by year, by province and territory. Government of Canada. Retrieved 4 March 2010 from http://www40.statcan.ca/l01/cst01/demo02a-eng.htm

Statistics Canada (2010b) Waste disposal, by source, by province. Government of Canada. Retrieved 12 March 2010 from http://www40.statcan.gc.ca/l01/cst01/envir25a-eng.htm

Statistics Denmark (2009) Statistical yearbook 2009. Government of Denmark. Retrieved 22 March 2010 from http://www.dst.dk/pubpdf/14468/sy2009

Statistics Denmark (2010a) Population projections by municipality, age and sex. Government of Denmark. Retrieved 22 March 2010 from http://www.statbank.dk/statbank5a/default.asp?w=1680

Statistics Denmark (2010b) Quarterly population (ultimo). Government of Denmark. Retrieved 22 March 2010 from http://www.dst.dk/HomeUK/Statistics/Key_indicators/Population/pop_quarterly.aspx

Tanapat S (2004) A feasibility study of municipal waste-to-energy management: measurement of landfill gas quality at Brady Road Landfill in Canada. Unpublished master's thesis, University of Manitoba, Winnipeg

The City of Sydney (2010) Estimated resident population (ERP). Retrieved 24 February 2010 from http://profile.id.com.au/Default.aspx?id=148&pg=210

The Natural Step (n.d.) The four system conditions. Retrieved 6 March 2009 from http://www.thenaturalstep.org/en/canada/the-system-conditions

Thompson S, Bonam R Best practices for expanding the life of landfills: results of a 2005 Canadian landfill survey. Unpublished manuscript

Thompson S, Sawyer J, Bonam R, Smith S (2006) Recommendations for improving the Canadian methane generation model for landfills. University of Manitoba prepared for environment Canada, Mar 2006

Thompson S, Sawyer J, Valdivia JE (2009) Building a better methane generation model: validating models with methane recovery rates from 35 Canadian landfills. Waste Manage 29(7):2085–2091

Tiehm A, Nickel K, Neis U (1997) The use of ultrasound to accelerate the anaerobic digestion of sewage sludge. Water Sci Technol 36(11):121–128

Tire Stewardship Manitoba (2009) 2009 annual report. Retrieved 29 June 2010 from http://www.tirestewardshipmb.ca/cim/dbf/tsm-2009annualreport_web_s.pdf?im_id=54&si_id=1005

Tuomela M, Vikman M, Hatakka A, Itävaara M (2000) Biodegradation of lignin in a compost environment: a review. Bioresour Technol 72:169–183

US EPA (2009) Municipal solid waste generation, recycling, and disposal in the United States: facts and figures for 2008. EPA 530-F-009-021. US Government. Retrieved 10 May 2010 from http://www.epa.gov/osw/nonhaz/municipal/pubs/msw2008rpt.pdf

US EPA (2010a) Inventory of U.S. greenhouse gas emissions and sinks: 1990–2008. US Government. EPA 430-R-10-006. Retrieved 10 May 2010 from http://www.epa.gov/climatechange/emissions/downloads10/US-GHG-Inventory-2010_ExecutiveSummary.pdf

US EPA (2010b) Methane. US Government. Retrieved 10 May 2010 from http://www.epa.gov/methane/sources.html

van der Werf P, Cant M (2007) State of composting in Canada, part 2. Solid waste magazine Dec/Jan:43–46

Visit Denmark (2009) Geography. Government of Denmark. Retrieved 22 March 2010 from http://www.visitdenmark.com/usa/en-us/menu/turist/turistinformation/fakta-az/geography.htm

Vital Statistics (2006) Annual report. Nova Scotia Government. Retrieved 4 March 2010 from http://www.gov.ns.ca/snsmr/pdf/ans-vstat-2006-annual-report.pdf

Wagner T, Arnold P (2008) A new model for solid waste management: an analysis of the Nova Scotia MSW strategy. J Cleaner Prod 16:410–421

WCED (1987) Our common future: world commission on environment and development. Oxford University Press, Oxford

Westerman PW, Bicudo JR (2005) Management considerations for organic waste use in agriculture. Bioresour Technol 96:215–221

Wilson EJ, McDougall FR, Willmore J (2001) Euro-trash: searching Europe for a more sustainable approach to waste management. Resour Conserv Recy 31:327–346

Waste Management for Sustainable Society

Brian Bahor, Michael Van Brunt
Covanta Energy Corporation, Morristown, NJ, USA

Article Outline

Glossary
Definition of the Subject
Introduction
Greenhouse Gas Emissions
Emissions
Land Management
Summary
Bibliography

Glossary

Energy from waste (EfW) Synonym of WTE used by some companies.

Greenhouse gases (GHG) Carbon dioxide, methane, and other gases contributing to the greenhouse effect.

Integrated waste management Using a combination of all possible means of waste management so as to minimize adverse environmental impacts and optimize resource conservation.

Waste-to-energy (WTE) Recovery of the chemical energy contained in used materials by means of thermal treatment.

Definition of the Subject

The goal of this entry is to establish how an integrated waste management system can be part of the solution to the emerging crises of climate change and inadequate supply of renewable energy for future generations.

Developed and emerging countries societies are consuming natural resources at an increasing rate due to consumer habits and growing population. There is international agreement that a long-term solution to the energy and climate change issues must be a low, or neutral, carbon energy supply. There is no agreement on a solution; however, most discussion focuses on solar or wind energy and even these options are opposed sometimes at a local level. Waste is a resource that, when managed correctly with commercially proven technologies, can also be a sustainable source of renewable energy and contribute to greenhouse gas mitigation.

The waste hierarchy adopted by the European Union [1] and the US Environmental Protection Agency (USEPA) [2] provides a practical guideline for understanding general waste management priorities. Information provided in this entry quantifies the value of an integrated waste management system comprised of technology solutions including recycling, recovery, and disposal.

Introduction

The term "integrated waste management system" refers to a system that includes a combination of management options that provide a stable long-term solution based on a life-cycle assessment. The general principle is to manage the quantity of waste in accordance with the waste hierarchy as illustrated by Fig. 1.

The general concept of the hierarchy is that the "most sustainable" option is at the top because it conserves natural resources, saves or recovers energy, and reduces the emission of greenhouse gases. Options lower in the table are considered to be less desirable because, generally, they are not as effective.

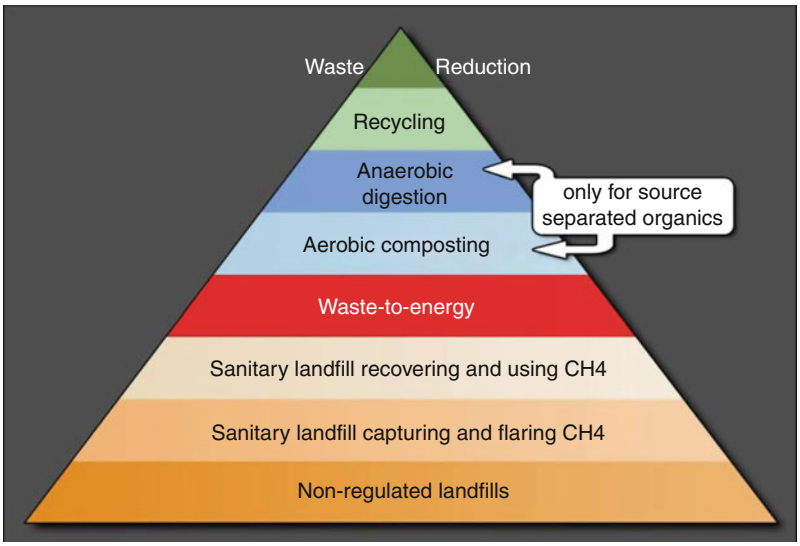

Waste Management for Sustainable Society. Figure 1
The hierarchy of waste management [3]

Waste reduction and reuse are correctly identified as the most preferable solution. However, implementation of these options requires a policy initiative whereas the last three options (recycling, energy recovery, and disposal in landfill) are technology options for the waste remaining after waste reduction and reuse efforts have been implemented. This sustainability evaluation therefore focuses on the technology options.

In regards to sustainability, the standard reference [4] is from the Brundtland commission where sustainable development is defined as development that meets the needs of the present without compromising the ability of future generations to meet their own needs. While that definition is a simple and effective metric, it does not capture the larger concept used by leading sustainability organizations that address a broad range of sustainability challenges, such as global climate change, dwindling resources, water scarcity, and the lack of available low carbon power options that are acceptable to society.

Principles Versus Practice

National and international organizations have determined that waste is a resource that when managed properly can provide a wide range of benefits to society, including preservation of natural resources, clean energy, reduction of greenhouse gas emissions, and stable long-term jobs that provide a community with a stable economy. The best example of a regulatory framework that considers waste as a resource is European Union Directive 2008/98 that establishes the waste hierarchy as a function of their Sixth Environmental Programme [5]. USEPA's 2009 report also determined that proper materials management can provide greenhouse gas mitigation while also yielding multiple environmental, human health, and economic benefits for communities and the nation; however this position has not been implemented as a matter of policy, legislation, or regulation.

Despite the abundant and growing analysis that supports management of MSW as a resource, and the progress made by the European Union (EU), the practices of many countries lag behind. Table 1 presents the amount of MSW managed by recycling, energy recovery, and landfills in three major areas of the world; North America, the European Union, and East Asia which is primarily China. These areas were selected due to readily available information on each and because each area is unique relative to waste management strategies.

Europe is the only area moving toward an integrated waste management system with Germany leading the effort with over 30 years of legislative efforts to change their waste management system. North American values are largely driven by the USA where there has not been a policy or regulatory driver to change the strong dependence on landfills. East Asia is interesting for several reasons. China is one of the world's largest economies and has adopted a policy to divert MSW from landfills by providing waste-to-energy capacity. China also influences the demand for recycled commodities, with both North America and Europe sending a majority of separated materials to China for transformation to recycled products.

The potential to diversify waste management on a national basis is demonstrated by several European Union (EU) Member States. Information from Eurostat [7] has been used to construct 10-year trends that illustrate how different paths toward advanced waste management have been followed. Note that the

Waste Management for Sustainable Society. Table 1 Allocation of MSW for existing practices

Reference information		Tons of MSW[a]			Percent of total		
Region	2004[a]	Landfill	EfW	Recycle	Landfill	EfW	Recycle
European Union	379	220	46	99	58	12	26
North America	371	252	22	96	68	6	26
East Asia	442	345	53	44	78	12	10

[a]MSW values (as million tons) and allocation as % of total is from [6]

Eurostat data is available for several years; however subsequent analysis presented herein is largely based on 2004 information which includes recycling data for conventional commodities (glass, paper, metals, plastic) and compost. It should be noted that waste management in the EU is, to some extent, driven by landfill diversion targets set out in the Landfill Directive. Also, the recent revision to the Waste Framework Directive requires a minimum of 50% overall recycling by 2020.

Figure 2 presents the average results for the 27 Member States and the general trend where MSW is being diverted from landfills to recycling and to a lesser extent to WTE. Figures 3 and 4 present results for Germany and the Netherlands respectively, two countries that have a long-term history of leading Europe in waste management and environmental concerns in general. Figures 5, 6, and 7 demonstrate trends in Spain, Italy, and Greece. Each has a relatively constant % of MSW being managed by WTE with Spain and Italy showing a growth in recycling due to diversion of MSW from landfills. Greece shows limited growth in recycling with no MSW being managed at a WTE facility.

Table 2 presents waste management data for the USA from two different sources. One set is from the USEPA's annual solid waste report [8] with the second set being reported by Biocycle [9, 10]. USEPA results are based on a survey of manufacturing information with waste generation rates being estimated from consumption rates of resources whereas Biocycle data is based on surveys completed by solid waste departments from all 50 states using data reported by waste management operations. The significant difference in results is largely attributable to the large difference in MSW landfilled in the USA, with USEPA estimating 135 million tons in 2008 and Biocycle estimating 265 million tons. Biocycle data is considered to be more useful and accurate and is in fact used by the USEPA in its greenhouse gas inventory report [11]. An independent analysis of USEPA reported values [12] concluded that the actual recycle rate is 27.8% when adjusting values to exclude commercial and industrial materials.

There is insufficient data to track long-term performance of the three waste management options in China.

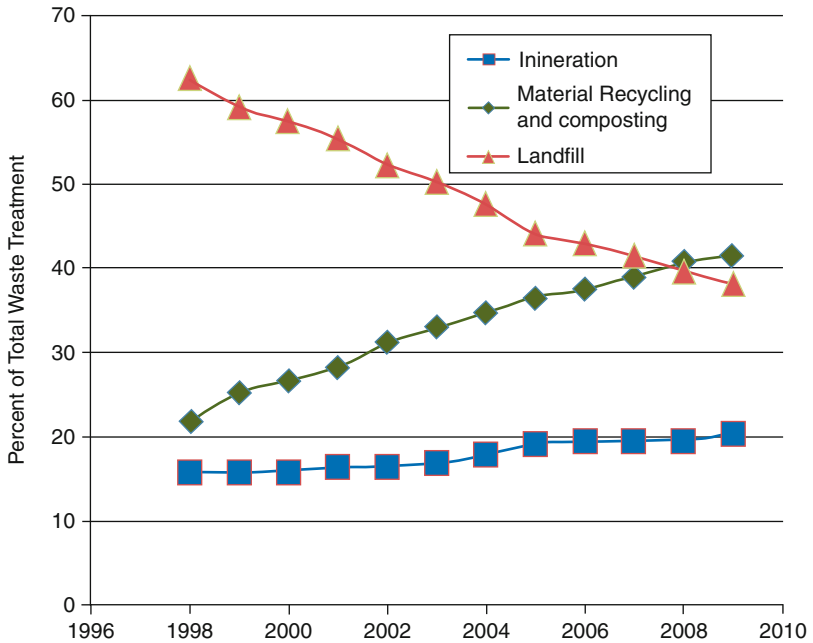

Waste Management for Sustainable Society. Figure 2
Waste management activities: EU 27

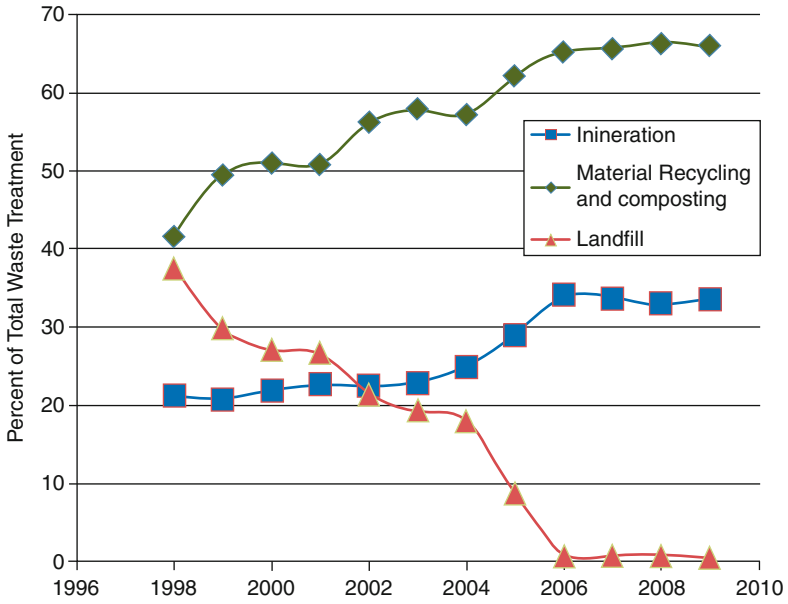

Waste Management for Sustainable Society. Figure 3
Waste management activities: Germany

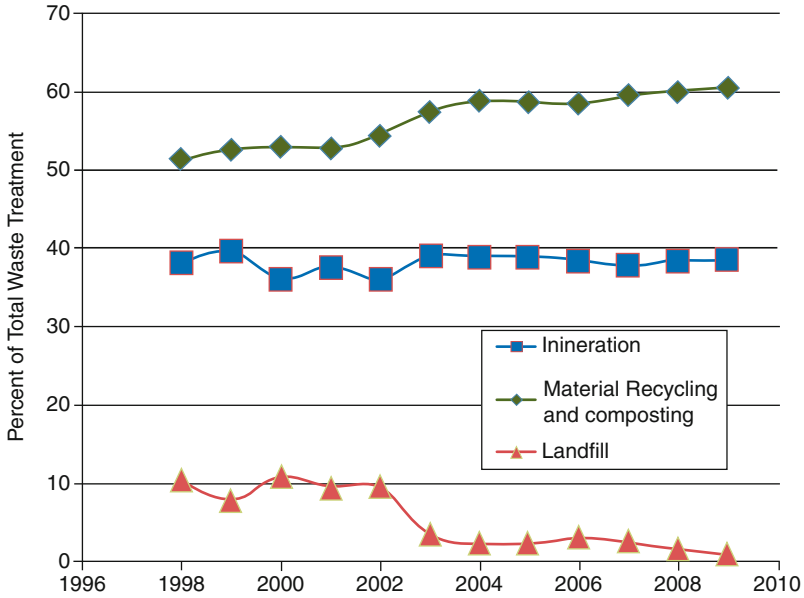

Waste Management for Sustainable Society. Figure 4
Waste management activities: Netherlands

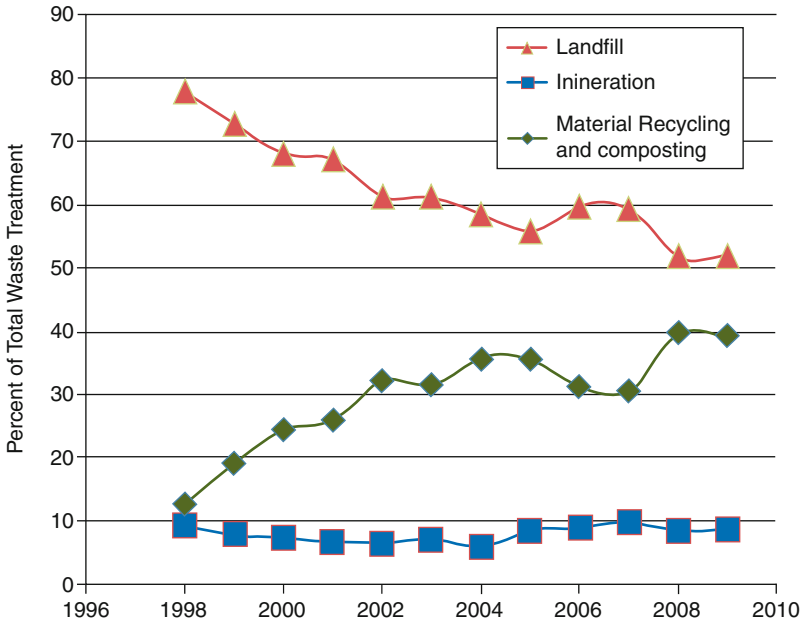

Waste Management for Sustainable Society. Figure 5
Waste management activities: Spain

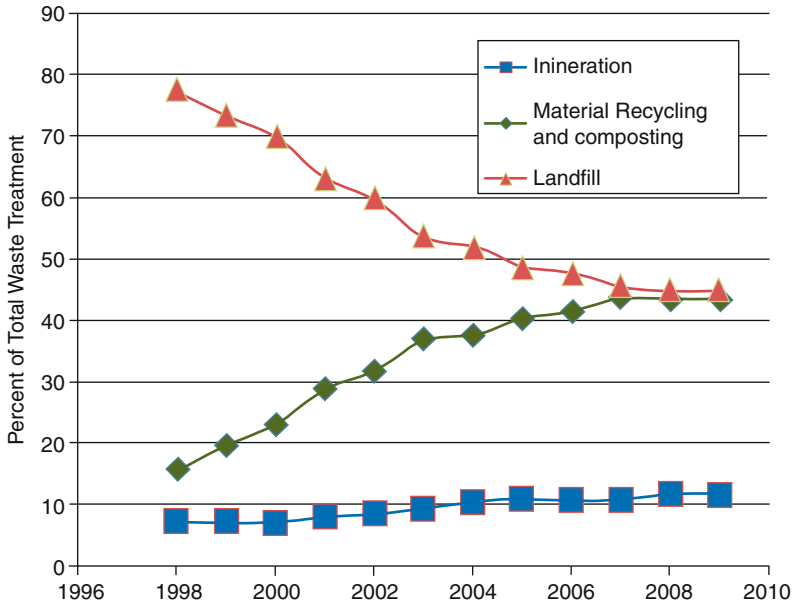

Waste Management for Sustainable Society. Figure 6
Waste management activities: Itlay

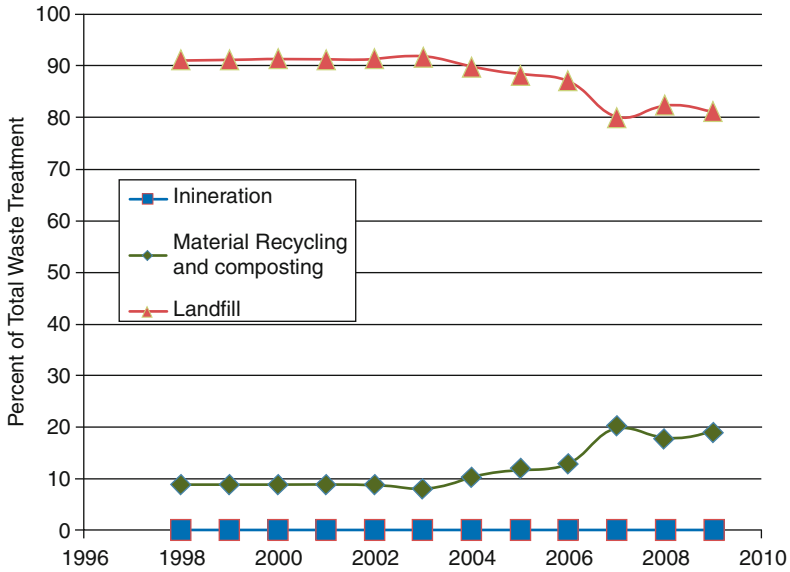

Waste Management for Sustainable Society. Figure 7
Waste management activities: Greece

Waste Management for Sustainable Society. Table 2 Waste management in the USA: 2000–2007

Reference		Year[a]		
Source	Option	2000	2005	2007
EPA	Recycling and composting	28.6	31.6	33.3
	WTE	13.9	12.5	12.5
	Landfill	57.5	55.9	54.2
Biocycle	Recycling and composting	32	28.5	28.6
	WTE	7	7.4	6.9
	Landfill	61	64.1	64.5

[a]Biocycle data from 2004 are used in 2005 and from 2006 in 2007 to enable a comparison

Observations from long-term Eurostat and USEPA data are:

- The most recent average recycle rate for the EU's 27 member States (41.5%) is significantly greater than the average USEPA adjusted factor (27.8%) and *Biocycle*'s (24%) factor.
- The USA continues to landfill the majority of its MSW although it is generally recognized to be the least sustainable alternative according to waste hierarchies.
- A national program, such as the EU's landfill directive and the Waste Framework Directive, can be the catalyst that forces a change in behavior to direct MSW from the low cost disposal alternative.
- Even in the presence of a binding Directive, certain countries have ignored compliance.
- The recycle rate is not impeded by the presence of WTE whether it is a low or moderate value, further supporting the position that recycle rates are dependent on a national policy and not the presence of a WTE industry.

Waste Management for Sustainable Society. Table 3 Comparison of primary input and outputs of WARM and MSW-DST

Parameter	Units	MSW-DST	WARM
Input options			
Energy recovery	kWh/MMBtu input	Variable	Constant
Efficiency of landfill gas collection	%	Variable	Constant
Oxidation of methane by soil	%	Variable	Constant
Carbon grit intensity	kg CO_2/kWh	Variable	Constant
Carbon storage	kg C/kg MSW	Variable	Constant
Output values			
Energy saved/consumed	MMBtu	Yes	Yes
Greenhouse gas emissions	Tons	Yes	Yes
SO_2, NOx, particulate	Tons	Yes	No
Solid waste	Tons	Yes	No
Water discharges	Tons	Yes	No

Life-Cycle Assessment (LCA) Methodology

The European Union formulates environmental directives according to a thematic strategy that is a multidisciplinary plan to assure that directives consider the big picture and interrelationship between different media including air, water, waste, toxics, etc. Their Integrated Pollution Prevention and Control [13] is an example of the multidisciplinary approach to decision making and introduces the concept of a life-cycle assessment (LCA) into the decision making process. A LCA is a long-term multidisciplinary evaluation methodology to assure that long-term implications are considered when selecting an option.

LCA methodology for waste management is endorsed by a variety of groups (USEPA, IPCC, Ceres) with there being a wide variety of LCA computational programs available in the market. The USEPA has two LCA's available for public use, the Waste Reduction Model (WARM) [14] and the Municipal Solid Waste Decision Support Tool (MSW-DST) [15]. EPA is currently reviewing each of these with a goal of creating consistency between the two. Table 3 provides a general comparison of the two and where they are different.

Evaluation of an Integrated Waste Management System

The following sections address several of the major parameters that warrant consideration when evaluating and/or designing an integrated waste management system.

- Energy – does the proposed system provide energy recovery, energy savings, or is it a sink?
- Greenhouse gases – does the proposed system provide mitigation (reduction) of greenhouse gases (GHGs) or is it a source?
- Land Management – can the proposed system be located in close proximity to the point of waste generation and what are the long-term impacts?
- Air emissions – does the system and its components provide for mitigation of air emissions including air toxics?

Energy is addressed first because it is a key parameter in determining the GHG and air emission characteristics.

Energy

A two-step approach is used to present and evaluate the energy parameter. Step 1 identifies the energy

savings/sink for specific components managed by various waste management options. Step 2 applies these component-based factors to national inventories as a means to present the energy recovery/savings for an integrated waste management system. A similar sequence is also followed with greenhouse gas (GHG) emissions in order to understand the relationship between energy and GHG emissions.

Derivation of Energy Factors

Primary energy represents all of the energy consumed, including the energy required to produce, generate, distribute, and transmit the electricity, petroleum, and natural gas used. This metric is used by the International Energy Association (IEA) and the US Energy Information Administration (EIA) and is well suited to compare different waste management options which generate electricity (WTE & LFGTE) and save electricity and fuels (recycling).

The primary energy savings or consumption for the three options was determined by USEPA for various waste components and composites through a life-cycle assessment (LCA). Table 4 presents USEPA's LCA energy factors [16] for various components managed by recycling, EfW, and landfills, with landfills being characterized by three types: vents (no gas collection and no energy recovery), flare (gas collection but no energy recovery), and energy (gas collection and energy recovery).

These energy factors are approximately 15–20 years old at this time and represent assumptions and operating conditions that may not necessarily represent existing conditions [16]. Several of the key parameters that should be considered when applied to a current situation are identified below according to the waste management option.

Recycling

1. There is one energy factor for a certain commodity regardless of its actual physical condition. As an example, there may be little variability in the energy savings when recycling aluminum cans, however, there may be significant differences when considering the variable quality of separated cardboard and paper, whether by contamination or being mixed with other materials. As a result – there is only one energy factor whether a country is separating 20% or 65% of a commodity.
2. Processes used to transform a separated commodity are likely to have changed in the last 20 years, however, any usullout danger the net energy difference between deriving a product from used and recovered items versus raw natural resources are not considered.
3. A large fraction of materials separated for "recycling" in North America and Europe are actually being "recycled" in China. The impact of energy savings in China versus other manufacturing locations is not considered by the USEPA factors.

Waste Management for Sustainable Society. Table 4 Energy factors for discrete components and mixed recyclables (mmbtu/t)[a]

Component	Recycling	WTE	LF-vent	LF-Flare	LF-Energy
Aluminum cans	−206.42	0.65	0.53	0.53	0.53
Steel cans	−19.97	−17.09	0.53	0.53	0.53
HDPE	−50.90	−19.61	0.53	0.53	0.53
Cardboard	−15.05	−7.21	0.53	0.53	−0.56
Office paper	−10.08	−6.95	0.53	0.53	−1.31
Mixed recyclables	−16.57	−7.22	0.53	0.53	−0.27
Compost	0.58	−2.32	0.53	0.53	−0.01
Recyclables and compost	−11.92	−5.89	0.53	0.53	−0.20

[a]Source WARM 10 using default values [14]

Waste-to-Energy (WTE; or Energy from Waste, EfW) USEPA's factors are based on operating characteristics of WTE facilities 20 years ago when the evaluation was completed. As a result, the estimated energy generation from WTE in WARM is low for several reasons:

1. Net energy distributed to the grid is based on a nominal thermal energy efficiency of 18% which is quite low in comparison to new units in Europe and North America that operate at up to 30% thermal efficiency (electricity generation only) and 90% when they also provide steam for local district heating.
2. Nearly all existing WTE facilities and *all* new WTE facilities recover both ferrous and nonferrous metals. This increases the energy savings because these materials are used in downstream recycling operations.

Landfills USEPA has a separate factor for three different landfill designs: landfill gas collection with vents, collection and flaring, and collection with combustion in a reciprocating engine. There are no expected changes to energy savings for landfills with vents or flares, however, a landfill that recovers more gas should yield more energy per ton of MSW buried. The absence of verifiable and proven long-term collection efficiencies and power generation make any improvements in energy generation speculative.

The results in Table 4 follow a logical pattern when evaluating component specific factors. As an example, it is common knowledge that recycling aluminum saves large amounts of energy but aluminum is a small weight percent of MSW and does not have much of an influence on a standard basket of mixed recyclables where the results are driven by large amounts of paper, plastic, and cardboard. A different and independent analysis by the Earth and Environmental Engineering Department of Columbia University [17] yielded similar results using a Resource Conservation Efficiency (RCE) metric that also placed energy savings of recycling ahead of WTE with landfills being in last place.

The energy factor associated with recycling represents the energy impact of collecting, processing, and remanufacturing the component. The "mixed recyclables" factor is based on USEPA's weight distribution which is limited to conventional materials including paper, glass, metals, and plastic. Compostable materials are treated as a separate line item and then combined with mixed recyclables.

Several major observations regarding Table 4 are:

- According to this data base, the ratio of energy saved by recycling to EfW is 2.2 for a mixed basket of recyclables (−16.57/−7.22) and 2.0 for one including both recyclables and compostable materials (11.92/5.89). This ratio is based on the assumptions identified above.
- The amount of energy saved by recycling is about 60 times greater than that recovered by a landfill with energy recovery whether the waste basket is recyclables (16.57/0.27) or recyclables and compost (11.92/0.2). Landfill with vents and flares are energy sinks (consume energy). This makes sense when considering the energy required for transportation and landfill management over the nominal 100 year anaerobic decomposition period for MSW.
- The amount of energy recovered/saved by EfW is 27–30 times more than landfills with energy recovery when considering recyclables or recyclables and compost.

The lifecycle assessment factors in Table 4 from USEPA's WARM model the different time requirements for each option. Both recycling and EfW are relatively short-term processes with EfW being a nominal 1-h process after MSW is charged to the grate. Recycling is also a short-term process when considering the time to transfer separated components to a transformation process where those components are converted to a recycled commodity. Landfills are very long-term processes due to the nominal 100 year anaerobic decomposition process. Landfills with gas collection and energy recovery generate electricity for export for a certain period when gas collection is of certain quantity and quality (25–35 years), however, there are energy demands for the entire life of the landfill. Independent analysis estimate that an average existing EfW facility generates 10 times the electricity delivered to the grid than a landfill gas to energy system with new EfW facilities using combined heat and power being significantly greater. As noted above, USEPA's LCA energy analysis demonstrates that a typical EfW is 27–30 times more effective than a landfill gas to energy option.

Application of Energy Factors

The approach used herein to assess the primary energy savings from an integrated waste management system is to compare results from two scenarios: Business as Usual (BAU) which is the situation today in each geographic area and a Sustainability Scenario (SUS) where an integrated waste management system is used with waste allocated according to the hierarchy. This approach allows a direct estimation of the energy benefits today if society simply changed the way it manages MSW. Table 5 presents the total amount of MSW (as millions of tons) and the percentage managed by each option. The BAU values are derived from a variety of sources whereas the distribution of MSW in the SUS scenario is based largely on the current situation in Germany where they have managed to achieve a nominal 65% recycle rate. The recycle rate in Germany (which is based on separating conventional materials (paper, plastic, metals, glass, cardboard, and composting) is the best in the EU.

The three examples (EU, USA, and East Asia (China)) were selected for several reasons:

- The EU provides the longest regulatory effort to advance recycling on a large scale. However despite several countries leading the way, the average value demonstrates that there is still room for improvement albeit less that the other two areas.
- The population and total waste of North America and the EU is about the same but the management of MSW is very different with the USA having a relatively stagnant waste management system compared to the European Union where diversion of MSW from landfills is considered to be a sustainable solution.
- China is the world's largest generator of MSW and has already demonstrated that its market, or absence thereof, for separated components can influence reported recycle rates. China, like the European Union, has also determined that landfills are the least sustainable option and is moving toward a sustainable integrated waste management system, however, they have not established a goal similar to Germany's operating condition, therefore there continues to be significant room for improvement.

Table 6 presents a comparison of the energy *savings* of the BAU and SUS Scenario using MSW rates listed in Table 5.

In order to provide some perspective on the magnitude of Quads, the Department of Energy [18] estimated the USA's 2008 energy use as 99.2 Quads with Table 7 providing a breakdown of that usage and the amount allocated to generating electricity.

Several observations regarding Tables 5, 6, and 7:

- Despite landfills being an energy sink – the majority of MSW in the EU, USA, and China is landfilled.
- Diversion of MSW from landfills to recycling and EfW provides a significant energy savings through the use of existing technology.
- The total energy savings of 2.2 Quads in the USA from the SUS Scenario is approximately 2.2% of the total energy use in the USA and 5.6% of that allocated to generating electricity. Approximately 2.2 Quads is the amount from hydro facilities and could offset a large fraction of electricity from coal and natural gas generation.

The amount of potential energy that can be saved/recovered from a sustainable allocation of MSW is

Waste Management for Sustainable Society. Table 5 Allocation of MSW for business-as-usual (BAU) and sustainability scenario (SUS)

Reference information		BAU scenario			SUS scenario		
Region	2004[a]	Landfill	EfW	Recycle	Landfill	EfW	Recycle
Europe	379	58	12	26	12	23	65
North America	371	68	6	26	12	23	65
East Asia	442	78	12	10	20	40	40

[a]MSW values (as million tons) and allocation as % of total is from [6]

Waste Management for Sustainable Society. Table 6 Primary energy savings (as Quads) for the business-as-usual (BAU) and sustainable scenario (SUS)[a]

MSW option	EU			USA			China		
	BAU	SUS	Delta	BAU	SUS	Delta	BAU	SUS	Delta
Landfill	0.0	0.0	0	−0.1	0	0.1	−0.1	0.0	0.1
Recycle	1.2	2.8	1.5	1.1	3.0	1.8	0.5	3.6	3.0
WTE	0.3	0.5	0.3	0.1	0.6	0.5	0.2	0.3	0.2
Total	1.5	3.3	1.8	1.1	3.5	2.4	0.7	3.9	3.3

[a]1 Quad = 10^{15} Btu

Waste Management for Sustainable Society. Table 7 Estimated US energy use in 2008 (as Quads)

Source	Total	Electricity generation
Solar	0.09	0.01
Nuclear	8.45	8.45
Hydro	2.45	2.43
Wind	0.51	0.51
Geothermal	0.35	0.31
Natural gas	23.84	6.82
Coal	22.42	20.54
Biomass	3.88	0
Petroleum	37.13	0
Total	99.12	39.07

significant on an absolute and relative basis. For the USA alone, the energy savings is equivalent to over 10% of our 2008 total oil imports or equivalent to the coal consumption of 63,500 MW coal plants. For the USA, Europe, and China together, the energy savings is equivalent to the coal consumption of nearly 200 large 500 MW coal plants.

An independent analysis by Columbia University Scientists evaluated the energy savings with their own metric called the Resource Conservation Efficiency (RCE) [22]. The RCE metric was applied to two leading cities in the USA, San Francisco and Honolulu, to evaluate their sustainable use of MSW as a resource according to their RCE metric. San Francisco has a higher recycle rate (34.4%) than Honolulu (27.2%) however 65.6% of MSW was landfilled yielding an RCE of 60.4. Honolulu minimized landfill (4.9%) with WTE managing 67.9% for a total RCE of 73.1. While Columbia's RCE metric is a different energy-based approach to evaluate sustainable use of MSW as a resource – its conclusions are consistent on a component basis and when applied to a larger source.

Subsequent sections consider the environmental impacts when diverting MSW from landfills to recycling and EfW.

Greenhouse Gas Emissions

Overview

Climate change has been correlated to an increase in the concentration of greenhouse gases (GHGs) driven predominately by anthropogenic emission sources. The most comprehensive report on the topic is the Fourth Assessment Report by the Intergovernmental Panel on Climate Change (IPCC) that included several key findings applicable to the topic of sustainable waste management:

- Increases in atmospheric CH_4 concentrations since preindustrial times have contributed a radiative forcing of $+0.48 \pm 0.05\ W\ m^{-2}$. Among greenhouse gases, this forcing remains second only to that of CO_2 in magnitude.
- Emissions of CO_2 from fossil fuel use and from the effects of land use change on plant and soil carbon are the primary sources of increased atmospheric CO_2.
- Current understanding of anthropogenic warming and cooling influences on climate has led to a very high confidence (at least 9 out of 10 chance) that the effect of human activities since 1750 has been a net positive radiative forcing of +1.6 (+0.6 to +2.4) $W\ m^{-2}$.

- It is very likely that anthropogenic greenhouse gas increases caused most of the observed increase in global average temperatures since the mid-twentieth century.

It is readily apparent from these IPCC findings that processes that reduce GHG emissions, including emissions of CO_2 and CH_4, should be preferred relative to attempts to capture and sequester GHG emissions after they have been generated. In other words, prevention of GHG emissions at the source is more effective than capturing and controlling GHG emissions.

Atmospheric measurements have demonstrated that the concentration of atmospheric CO_2 has increased from a preindustrial value of about 280 to 379 ppm in 2005 with future concentrations being dependent on a variety of complicated factors, one key factor being human behavior and the source of electrical energy to meet growing demand. In 2004, the journal *Science* published a pivotal paper by Pacala and Socolow that simplified the situation by considering two situations over a 50 year period, one where emissions are flat and one where emission increase according to the existing rate. This yields a right triangle or "stabilization wedge" with a growth of 7 billion tons of carbon over a 50 year period. The right triangle could then be broken down into more manageable "wedges," each of which could achieve a reduction in GHG emissions of at least 1 gigaton of carbon per year (GtC/year) by 2054 [19]). Seven 1 t wedges would stabilize carbon emissions. Fifteen stabilization wedges were presented in six categories: energy efficiency (vehicles, buildings, power plants), fuel shift (switching from coal power to nuclear, wind or natural gas), CO_2 capture and storage, nuclear fission, renewable energy (wind, photovoltaic, biogas), and forest and agricultural soils (reduced forestation and tillage).

Individual waste management options and an integrated system were not considered by this initial effort. However, application of an integrated solid waste management policy based on the waste hierarchy was subsequently identified as a stabilization wedge [6].

GHG Emission Characteristics of Waste Management Options

Each of the three waste management options considered in the energy section has GHG emission characteristics that must be considered in any discussion on sustainability. Table 8 presents an overview of the general GHG characteristics of each relative to CO_2 and CH_4 emissions.

Table 9, which presents GHG emission characteristics for specific waste components, is organized to be consistent with Table 4 which presents the energy factors for each component.

The GHG emission characteristics in Table 9 are absolute values for each option using a lifecycle

Waste Management for Sustainable Society. Table 8 Overview of GHG emission characteristics

Option	GHG	Characteristic	Mechanism
Recycling and composting	CO_2	Mitigation	Energy savings = avoided fossil CO_2[b]
	CH_4	Mitigation	Avoided landfill CH_4
Energy from waste	CO_2	Source	Combustion of plastics cutler anthropogenic also
	CO_2	Mitigation	Recovery of metals for recycling saver energy
	CO_2	Mitigation	Power generation = avoided fossil CO_2[a,b]
	CH_4	Mitigation	Avoided landfill CH_4
Landfill (disposal)	CO_2	Mitigation or source	Mitigation for landfills with energy recovery – avoided fossil CO_2
	CH_4	Source	All landfills emit CH_4 with the amount dependent on the effectiveness of the landfill gas collection system

[a]Does not include energy savings from recovery of metals
[b]Does not include upstream emissions from fuel production

Waste Management for Sustainable Society. Table 9 GHG emissions as Mg CO_2e/Mg MSW

Material	Recycling			EfW[a]	Landfill[b]
	Energy	Carbon storage	Total		
Aluminum cans	−0.37	0.0	−3.7	+0.02	+0.01
Steel cans	−0.49	0.0	−0.49	−0.42	+0.01
HDPE	−0.38	0.0	−0.38	+0.28	+0.01
Cardboard	−0.02	−0.83	−0.85	−0.17	+0.11
Office paper	0.05	−0.83	−0.78	−0.16	+0.53
Mixed recyclables	−0.13	−0.66	−0.79	−0.15	+0.05
Mixed MSW	Not applicable			−0.04	+0.41

[a]Factor assumes EfW does not include nonferrous recovery
[b]WARM version 10 using default values national averages, CH_4 emissions based on 75% collection and C sequestration

assessment (EPA WARM). Any one megagram (metric ton) of MSW or a discrete component can only be managed by one option, therefore difference between LCA results for two options is the net advantage or disadvantage relative to climate change. Observations from Table 9 on discrete components and different options are:

- Recovery of both ferrous and nonferrous metals is an effective GHG mitigation strategy.
- Management of paper and cardboard by recycling and EfW are GHG mitigation strategies, however, the recycling factors represent the high-end of separated commodities. The energy savings may not be the same for lower-end or contaminated materials.
- Landfills are a net source of GHG emissions even when assigning a favorable lifetime landfill gas collection efficiency of 75%.

The two GHG components of recycling, energy and carbon sequestration, are presented to highlight the value of each mechanism. Recycling is generally recognized as a demonstrated GHG mitigation technology because it can reduce GHG emissions at the manufacturing stage (saves energy), increase forest carbon sequestration, and avoid landfill CH_4 emissions, however close inspection shows that, depending on the material recycled, the majority of GHG mitigation can be from forest carbon sequestration.

While it is clear that recycling is a preferred management option for both energy savings and GHG mitigation – what is the best option for MSW that is not, or cannot be, recycled? Information in Tables 4, 5, and 6 demonstrated that WTE is the superior alternative when considering energy. Table 10 presents GHG emission factors on a lifecycle assessment basis when using USEPA's MSW-DST to compare the impact of managing one Mg of MSW by either EfW or the nationwide blend of landfills in the USA. The MSW-DST was used in this analysis because it allows the user to vary key parameters (methane generation rate, landfill gas collection efficiency, etc.) whereas WARM does not.

Observations from Tables 9 and 10 are:

- Recycling is a demonstrated GHG mitigation technology based on three different processes (save energy, forest carbon sequestration, and avoid landfill methane) with the exact values depending on local conditions.
- EfW is a demonstrated GHG mitigation technology based on energy recovery and avoided landfill methane with the exact values also depending on local conditions.
- Landfills are a source of GHG emissions with the exact amount being highly variable and dependent on sustained long-term performance at the landfill.
- A comparison of EfW and various landfill options demonstrates that EfW reduces GHG emissions with the amount being dependent on local conditions.

Waste Management for Sustainable Society. Table 10 Nationwide life cycle greenhouse gas emission factors for MWC versus landfill blend scenarios[a]

Integrated (lifetime) landfill gas collection efficiency	GHG emissions (Mg CO_2e/Mg MSW)			
	Landfill allocation (50/25/25)[a]		Landfill allocation (40/30/30)[b]	
	Lo = 100	Lo = 170	Lo = 100	Lo = 170
25	1.44	2.20	1.4	2.14
35	1.37	2.08	1.32	2.00
45	1.30	1.96	1.23	1.85
55	1.23	1.84	1.15	1.71
65	1.16	1.72	1.06	1.56
75	1.08	1.66	0.98	1.42

[a]50% vent, 25% flare, 25% with energy recovery
[b]40% vent, 30% flare, 30% with energy recovery

Application of GHG Emission Factors

Application of an integrated solid waste management policy based on the waste hierarchy has been identified as a stabilization wedge [6]. The analysis demonstrated that if MSW is allocated to recycling, waste-to-energy, and landfilling in descending order in lieu of existing "business-as-usual" practices with each option using modern technology and best practices, the system would reduce greenhouse gas emissions by more than 1 GtC/year. This integrated waste management system reduces CO_2 by displacing fossil electrical generation and avoiding manufacturing energy consumption and methane emissions from landfills.

As mentioned above, the concept of a stabilization wedge is to examine the GHG mitigation over a 50 year period on the premise that it takes that much time to implement change. Table 11 presents the GHG mitigation associated with immediate implementation of an integrated waste management system using MSW data in Table 4. These GHG mitigation results represent energy savings described in Table 6.

GHG mitigation is accomplished by two factors: (1) diverting MSW from landfills to recycling and EfW and (2) use of technology consistent with existing best practices. Diversion of MSW from landfills avoids methane emissions and by allocating MSW to recycling and EfW, there are significant energy savings and therefore avoidance of fossil CO_2 emissions.

Waste Management for Sustainable Society. Table 11 GHG mitigation attributable to an integrated waste management system

Land area	GHG mitigation	
	Million metric tons of C	Million metric tons as CO_2e
Europe[a]	40	148
North America[a]	60	220
East Asia[a]	94	337
Global[b]	1,009	

[a]Based on 2004 MSW tonnage and management
[b]Based on 2054 MSW tonnage and management

The original wedge analysis was a global assessment that considered a baseline condition and several sensitivity calculations. Table 12 provides an overview of the results.

The GHG mitigation for Europe, North America, and East Asia in the Waste Wedge was 0.41 GtC or about 41% if the total mitigation when considering growth of waste quantities by 2054. An immediate reduction of existing MSW in the three geographic areas, based on 2004 data, indicates an immediate

Waste Management for Sustainable Society. Table 12 Overview of integrated waste management as a stabilization wedge

Item	Reference	Results as GtC
Waste wedge	Baseline using 100-year GWP of 21	1.009
A	After maximizing recycling, maximize EfW	1.094
B	After maximizing recycling, minimize EfW	0.763
C	Maximize thermal efficiency of EfW in Waste Wedge	1.022
D25	Apply 100-year GWP of 25for methane instead of 21	1.153
D72	Apply 20-year GWP of 72 for methane instead of 21	2.842
E	Include carbon storage factor in recycling	2.132
F	Add source reduction in waste wedge analysis	1.251

Waste Management for Sustainable Society. Table 13 Overview of monitoring and testing requirements of WTE

Pollutant	European Union WID	USEPA CAAA
CEM		
Sulfur dioxide	Yes	Yes
Nitrogen oxides	Yes	Yes
Carbon monoxide	Yes	Yes
Particulate	Yes	Yes
Hydrogen chloride	Yes	[a]
Hydrogen fluoride	Yes	[a]
Hydrocarbons	Yes	[a]
Manual testing		
Metals	Yes	Yes
Dioxins and furans	Yes	Yes

[a]Not a national federal requirement however facility specific permits may include this requirement

reduction of about 0.2 GtC. This is a conservative and significant factor. It is conservative because:

- It is using a 100-year Global Warming Potential of 21 whereas the IPCC has raised the 100-year GWP to 25 and others recommend a 100-year GWP of 34 [20].
- The 20-year GWP of 72 is more appropriate when considering near term actions which can have an immediate impact on radiative forcing.

It is significant when considering the equivalencies. According to USEPA's equivalency calculator, 0.4 GtC is equivalent to the annual GHG emissions:

- Of approximately 350 large coal fired power plants,
- Of over 285 million automobiles, or
- From the energy consumption of every home in the USA.

Emissions

A direct comparison of emission from the three options is difficult for a variety of reasons. First, recycling of various separated commodities occurs at different operations (pulp and papermills, aluminum smelers, arc furnaces, etc.), each of which has a different set of standards in the USA, and with much material being exported to China, emissions are especially difficult to estimate. For MSW that is not recycled – regulations in the EU, USA, and elsewhere have led to a robust data set useful for characterizing WTE emissions. In contrast, landfills have not been subject to a comprehensive set of standards that requires testing and reporting of characteristic emissions.

WTE has been subject to extensive regulation in the EU through the Waste Incineration Directive (WID) [21] and through the Clean Air Act Amendments of 1990 (CAAA) in the USA [22]. While each set of regulatory standards has undergone a distinct history, the results are similar in that each set of regulations has identified the same proximate set of pollutants as being appropriate for effective management if emissions after 100% of flue gas have been managed by modern air pollution control technology. Both the WID and CAAA require continuous emissions monitoring (CEM) and periodic stack testing of other pollutants where CEM is not technically feasible with Table 13 presenting an overview of these requirements.

A directly comparable national standard for WTE was not available for China and Canada, however, WTE

Waste Management for Sustainable Society. Table 14 Landfill testing requirements in the European Union and the USA

Parameter	European Union landfill directive [23]	USEPA [22]
Gas collection	All landfills that accept biodegradable waste	Only those with NMOC emission above 50 mg per year
Gas collection period	Implies forever	Shutdown allowed 15 years after initial startup of system
Testing – bulk emissions (CH_4, CO_2, O_2, N_2, H_2S)	Operating landfill – monthly	None
	Closed landfill – Semiannual	
Testing – trace emissions		
Air toxics	No	No
Known carcinogens	No	No
Probable carcinogens	No	No
CEM required	No	No

projects in China are being permitted in accordance with the EU WID and recent projects in Canada have also been permitted in accordance with the EU WID or more stringent standards.

Continuous or intermittent measurement of emission from landfills is relatively complicated due to there being two basic sources: (1) an area source of landfill gas that is not collected by the landfill gas collection system and (2) emissions from the flare and/or engine where collected gas is combusted. Neither EU nor USEPA regulations require periodic testing of fugitive emission from landfills. Only minimal testing or monitoring (largely flue gas temperature) of combustion gas from the flare or engine is required. EU regulations are more rigorous, apparently due to the overall objective being to reduce negative impacts to the local environment (surface water, groundwater, soil and air) and global environment including the greenhouse effect and any resulting risk to human health during the whole life-cycle of the landfill. However, the EU standards do not require routine stack testing or monitoring in a manner similar to WTE.

Table 14 provides an overview of landfill test requirements in EU and USEPA.

USEPA's draft update of emission factors for landfills [24] listed 170 air pollutants of which 45 are Title III air toxics including several known carcinogens and many more reasonably anticipated carcinogens. A comparison of landfill emissions with either recycling or WTE operations is difficult because landfills are not required to test, resulting in a minimal data base.

A third source of emissions from landfills that warrants mention is surface and underground landfill fires. According to USEPA [25] and the Federal Emergency Management Agency (FEMA), [26] both types of landfill fires are known to be the source of emissions including dioxins. FEMA has estimated 8,400 landfills fires per year based on data from the National Fire Incident Reporting System (NFIRS) with USEPA estimating a possible dioxin emission of 1,100 g of toxic equivalence per year. At this estimated level, landfills would be the largest anthropogenic source of dioxin emission in the USA when compared to a recent USEPA dioxin inventory [27].

Land Management

Each of the three MSW management options has a land impact, however in a manner similar to emission, there is little data available to quantify the difference between each.

USEPA's life-cycle assessment of MSW management options recognized that when any material is separated for recycling, some portion of that material is unsuitable for use and is discarded. The loss rates [14] for different separated commodities were reported with

a range of 0.34 (textbooks) and 0.01 (copper wire). The typical mixed basket of recyclables, excluding compost, yields a loss factor of about 0.15, meaning that for every ton of recycled products there is 0.15 ton of material that must be managed by either WTE or landfill.

The automatically controlled combustion process at a modern WTE facility converts a ton of MSW into 0.25 ton of total inert residue in a nominal 1-hour period. This reduction in mass is proportional to a 90% reduction in volume. This essentially extends the lifetime of a landfill by a factor of 10 if both a WTE and landfill were to accept the same amount of material for any given period of time.

Summary

There is extensive information that documents that an integrated waste management system that manages municipal solid waste as a resource would be a sustainable solution for both generation of renewable energy and reduction of greenhouse gas emissions. Commercially available technology is available, however there are not sufficient existing policies and regulations to change dependence on landfills, the low cost option that has the least sustainable attributes.

Diversion of MSW from landfills to recycling and WTE systems would provide significant energy savings and a significant reduction in the emissions of GHG's. The European Union's establishment of directives is an example of how this can be accomplished.

Bibliography

1. European Parliament; Council of the European Union (2008) Directive 2008/98/EC of the European Parliament and of the Council of 19 November 2008 on waste and repealing certain Directives. J Eur Union L 312/3
2. U.S. EPA (2009) Opportunities to reduce greenhouse gas emissions through materials and land management practices. U.S. Environmental Protection Agency, Office of Solid Waste and Emergency Response
3. Kaufman SM, Themelis NJ (2009) Using a direct method to characterize and measure flows of municipal solid waste in the United States. J Air Waste Manag Assoc 59:1386–1390
4. United Nations World Commission on Environment and Development (WCED), 1987, Our Common Future, United Nations, New York. http://www.ceres.org/about-us/our-history
5. European Union (EU) (2002) Decision No 1600/2002/EC of the European Parliament and of the Council of 22 July 2002 laying down the Sixth Community Environment Action Programme. Off J Eur Communities L242:1–15
6. Bahor B, Van Brunt M, Blue K, Stovall J (2009) Integrated waste management as a climate stabilization wedge. Waste Manag Res 27:839–849
7. European Union (EU) Eurostat, Municipal waste generated and treated. http://epp.eurostat.ec.europa.eu/portal/page/portal/waste/data/sectors/municipal_waste. Accessed 25 Sept 2011
8. USEPA (2010) Municipal solid waste in the United States: 2009 facts and figures. EPA530-R-10-012. United States Environmental Protection Agency Office of Solid Waste (5306P), Washington, DC
9. Arsova L, Van Haaren R, Goldstein N, Kaufman S, Themelis N (2008) 16th Nationwide Survey of MSW Management in the US: The State of Garbage in America. BioCycle
10. Van Haaren R, Themelis N, Goldstein N (2010) 17th Nationwide Survey of MSW Management in the US: The State of Garbage in America. BioCycle
11. USEPA (2011) Inventory of U.S. GHG Emissions and Sinks: 1990–2009. USEPA
12. Berenyi E (2009) Recycling and waste to energy: are they compatable? 2009 update
13. European Commission (2006) Integrated pollution prevention and control – reference document on the best available technologies for waste incineration
14. US EPA (US Environmental Protection Agency) (2006) Waste Reduction Model (WARM). Version 10, November 2009. http://epa.gov/climatechange/wycd/waste/calculators/downloads/WARM_v10.zip. Accessed 17 June 2011
15. US EPA (US Environmental Protection Agency) (2002) Fact sheet: cutting edge software to cut emissions. http://www.epa.gov/osw/nonhaz/municipal/pubs/ghg/f02024.pdf. Accessed 25 Sept 2011
16. US EPA (2006) Solid waste management and greenhouse gases – a lifecycle assessment of emissions and sinks, 3rd edn. U.S Environmental Protection Agency, Washington, DC
17. Kaufman SM, Krishman N, Themelis N (2010) A screening lifecycle metric to benchmark the sustainability of waste management systems. Environ Sci Technol 44:5949–5955
18. Lawrence Livermore National Laboratory (2008) U.S. Energy flowchart 2008. https://www.llnl.gov/news/newsreleases/2009/images/energy-use.pdf. Accessed 25 Sept 2011
19. Pacala S, Socolow R (2004) Stabilization wedges: solving the climate problem for the next 50 years with current technologies. Science 305:968–972
20. Shindell DT, Faluvegi G, Koch DM, Schmidt GA, Unger M, Bauer SE (2009) Improved attribution of climate forcing to emissions. Science 326:716–718
21. European Union (EU) (2000) Directive 2000/76/EC of the European Parliament and of the Council of 4 December 2000 on the incineration of waste. Off J Eur Communities L332: 91–111
22. US EPA (Environmental Protection Agency) (1996) Standards of performance for Municipal Solid Waste Landfills. Fed Regist 49(61):9905–9944

23. Council Dircetive 1999/31/EC of 26 April 1999 on the landfill of waste. Official Journal of the European Committee, 16 Jul 1999
24. U.S. EPA (Environmental Protection Agency) (2008) Draft update, compilation of air pollutant emission factors, Section 2.4, Municipal Solid Waste Landfills, Oct 2008
25. U.S. EPA (Environmental Protection Agency) (2006) An inventory of sources and environmental releases of dioxin-like compounds in the United States for the years 1987, 1995, and 2000. National Center for Environmental Assessment, Washington, DC, EPA/600/P-03/002 F. National Technical Information Service, Springfield. http://epa.gov/ncea
26. FEMA (Federal Emergency Management Agency) (2002) Landfill fires: their magnitude, characteristics and mitigation. Federal Emergency Management Agency United States Fire Administration National Fire Data Center, May 2002/FA-225
27. US EPA (2006) An inventory of sources and environmental releases of dioxin-like compounds in the United States for the years 1987, 1995, and 2000. US EPA, Washington, DC

Waste Materials in Construction, Utilization of

Magdy Abdelrahman, Arash Saboori
Department of Civil Engineering (CIE 201F), North Dakota State University, North – Fargo, ND, USA

Article Outline

Glossary
Definition of the Subject
Introduction
Recycling
Recycling As a Rehabilitation Alternative
Types of Recycled Materials and Related Statistics
Applications of Waste Materials in Building Contruction
Applicability of Current Specifications to Recycled Materials
Future Directions
Acknowledgments
Bibliography

Glossary

By-product A secondary or incidental product deriving from a manufacturing process, a chemical reaction, or a biochemical pathway, and is not the primary product or service being produced.

Construction and Demolition Debris A large and varied waste stream that includes concrete, asphalt, wood, gypsum, and asphalt shingles generated from the construction, renovation, and demolition of buildings, roads, bridges, and dams.

Industrial Materials By-products of industrial processes.

Recycling Processing used materials into new products to prevent waste of potentially useful materials, reduce the consumption of fresh raw materials, reduce energy usage, reduce air pollution and water pollution by reducing the need for "conventional" waste disposal, and lower greenhouse gas emissions as compared to virgin production.

Rehabilitation Measures to improve, strengthen, or salvage existing deficient pavements to continue service with only routine maintenance. Deficient pavements exhibit distress in excess of what can be handled through routine maintenance.

Sustainability The capacity to endure. For humans, it is the potential for long-term maintenance of well-being, which in turn depends on the well-being of the natural world and the responsible use of natural resources.

Sustainable development A pattern of resource use that aims to meet human needs while preserving the environment so that these needs can be met not only in the present, but also for future generations.

Definition of the Subject

Recycling has always been a matter of obtaining an economic benefit or of helping the environment. Until the Industrial Revolution when materials became more available than labor, reuse and recycling was commonplace. Nearly 4,000 years ago, there was a recovery and reuse system of bronze scrap in operation in Europe and there is evidence that composting was carried out in China. Since the industrial revolution, the waste production rate has grown greatly. The idea of landfills came about in the 1940s and 1950s. When these huge depositories became available, they were extremely popular because of the ease of tossing unused products away. No one anticipated that soon these landfills would multiply to the extent that they have.

Considering the enormous volume of construction work done annually and the huge amount of waste materials produced each year, the issue of reusing the waste materials in construction is gaining increased attention, which can be observed by the extensive research being done on the subject. These wasted materials are either debris and demolition materials from construction industry or waste produced by other industries. The rapid growth of industries results in the need for more raw materials and the production of more waste materials, which makes the use of waste materials more feasible from two aspects, environmental and economical.

Introduction

Recycling has been a common practice throughout human history. In preindustrial times, scrap made of bronze and other precious metals was collected in Europe and melted down for perpetual reuse, and in Britain, dust and ash from wood and coal fires was downcycled as a base material in brick making. The main driver for these types of recycling was the economic advantage of obtaining recycled feedstock instead of acquiring virgin material.

Resource shortages caused by the world wars, and other such world-changing occurrences greatly encouraged recycling. Massive government promotion campaigns were carried out in World War II in every country involved in the war, urging citizens to donate metals and conserve fiber, as a matter of significant patriotic importance.

In the USA, the next big investment in recycling occurred in the 1970s, due to rising energy costs [1]. A main concern to deal with is the increasing volume of landfills due to large quantity of waste which are not recycled. Landfill usage peaked in the 1980s, when Americans sent almost 136 million metric tons (150 million US tons) of garbage to landfills each year. Today, Americans still dump more than 91 million metric tons (100 million US tons) of trash into landfills annually. However, recycling efforts in the United States divert 32% of waste away from landfills [2].

Among all the waste materials, two categories are of main concern in this entry, Industrial Waste and Construction and Demolition Materials (C&D) [3].

Construction and Demolition (C&D) waste accounts for a large part of the waste stream in the United States. While most of this waste accumulates in landfills, experts estimate that 90% of this waste stream is potentially reusable or recyclable. Recycling this waste can help to prolong our supply of natural resources and save money in the process [4]. Total US C&D waste was estimated to be 295 million metric tons (325 million US tons) in 2003 not including garbage.

Reducing and recycling C&D materials conserves landfill space, reduces the environmental impact of producing new materials, creates jobs, and can reduce overall building project expenses through avoided purchase/disposal costs [3]. Recycled Materials can be used in different categories of construction industry; their application in building and pavement as alternatives to virgin materials is discussed here.

Recycling

Literature defines recycling as processing used materials into new products to prevent waste of potentially useful materials, reduce the consumption of fresh raw materials, reduce energy usage, reduce air pollution (from incineration) and water pollution (from land filling) by reducing the need for "conventional" waste disposal, and lower greenhouse gas emissions as compared to virgin production [5].

Recycling or reuse of pavement materials is a powerful concept. Because of the reuse of existing material, pavement geometrics and thickness can also be maintained during construction. In some cases, traffic disruption is less than that for other rehabilitation techniques. Literature lists the specific benefits of recycling as:

1. Reduced costs of construction
2. Conservation of aggregate and binders
3. Preservation of the existing pavement geometrics
4. Preservation of the environment
5. Conservation of energy
6. Less user delay

Recycling as a Rehabilitation Alternative

Several studies have shown that it costs highway agencies less if the pavements are kept at a certain acceptable level of serviceability. According to World

Bank Sources, each $1.00 spent during the first 40% drop in quality will cost $4.00–$5.00 if delayed until the pavement loses 80% of its original quality. Rehabilitation is needed to maintain the pavement at a certain condition. Rehabilitation of pavement is also needed due to the following reasons:

1. Inadequate ride quality
2. Excessive pavement distress
3. Reduced surface friction
4. Excessive maintenance requirement
5. Unacceptable user costs
6. Inadequate structural capacity for planned use or projected traffic

Recycling is only one of the several rehabilitation alternatives available for asphalt pavements. Some of the other common methods are thick or thin hot mix asphalt (HMA) overlay. The choice of rehabilitation alternative depends on observed pavement distress, laboratory and field evaluation of existing material, and design parameters. Also, maintenance of geometrics and original thickness of pavements, especially in underpasses, influence the choice of rehabilitation method. However, recycling has some unique advantages which are not available with other types of rehabilitation techniques. For example, recycling can result in savings, help in conservation of natural resources, and can maintain pavement geometrics as well as thickness. Different recycling methods are now available to address specific pavement distress and structural needs.

Recycling presents environmental opportunities and challenges, which, when appropriately addressed, can maximize the benefits of reuse. The use of most recycled materials poses no threat or danger to the air, soil, or water. Furthermore, careful design, engineering, and application of recycled materials can reduce or eliminate the need to search for and extract new, virgin materials from the land. The engineering feasibility of using recycled materials has been demonstrated in research, field studies, experimental projects, and long-term performance testing and analysis. Significant advances in technology over the past decade have increased the types of recycled materials in use and the range of their applications. When appropriately used, recycled materials can effectively and safely reduce cost, save time, offer equal or, in some cases, significant improvement to performance qualities, and provide long-term environmental benefits [6].

The Federal Highway Administration (FHWA) policy toward recycling is [7]:

1. Recycling and reuse can offer engineering, economic, and environmental benefits.
2. Recycled materials should get first consideration in materials selection.
3. Determination of the use of recycled materials should include an initial review of engineering and environmental suitability.
4. An assessment of economic benefits should follow in the selection process.
5. Restrictions that prohibit the use of recycled materials without technical basis should be removed from specifications.

Types of Recycled Materials and Related Statistics

The different recycled and by-product materials which have application in construction industry are discussed and an estimation of annual production of each is presented [8–10].

Baghouse Fines

Hot mix asphalt baghouse fines are dust particles that are captured from the exhaust gases of asphalt-mixing plants. Secondary collection equipment called baghouses is commonly used to capture these very fine-sized materials. There are approximately 3,600 hot mix asphalt plants in the United States, accounting for a total annual production of 400–450 million metric tons (450–600 million US tons) of asphalt paving material. About 2,300 of these hot mix plants are batch plants, with the remaining 1,300 being drum mix plants. Roughly 40–50% of all hot mix asphalt plants are equipped with baghouse collections systems. It is estimated that approximately 5.4–7.2 million metric tons (6–8 million US tons) of baghouse fines are generated annually by the US asphalt production industry.

Blast Furnace Slag

In the production of iron, iron ore, iron scrap, and fluxes (limestone and/or dolomite) are charged into

a blast furnace along with coke for fuel. The coke is combusted to produce carbon monoxide, which reduces the iron ore to a molten iron product. This molten iron product can be cast into iron products, but is most often used as a feedstock for steel production. Blast furnace slag is a nonmetallic coproduct produced in the process. It consists primarily of silicates, aluminosilicates, and calcium-alumina-silicates. The molten slag, which absorbs much of the sulfur from the charge, comprises about 20% by mass of iron production. It is estimated that approximately 14 million metric tons (15.5 million US tons) of blast furnace slag is produced annually in the United States.

Coal Bottom Ash/Boiler Slag

Coal bottom ash and boiler slag are coarse, granular, incombustible materials that are collected from the bottom of furnaces that burn coal. The majority of coal bottom ash and boiler slag are produced at coal-fired electric utility generation stations, although bottom ash and boiler slag are produced by industrial and institutional coal-fired boilers and also from independent coal-burning electric generation facilities. The type of bottom ash or boiler slag produced depends on the type of furnace. The American Coal Ash Association (ACAA) estimates that during 2006, the utility industry in the United States generated 1.8 million metric tons (2.0 million US tons) of boiler slag.

Coal Fly Ash

The fly ash (fly ash) produced from burning pulverized coal in a coal-fired boiler is a fine-grained, powdery particulate material that is carried off in the flue gas and usually collected by means of electrostatic precipitators, baghouses, or mechanical collection devices such as cyclones. In 2006, the American Coal Ash Association (ACAA) reported that 65.7 million metric tons (72.4 million US tons) of coal fly ash were produced.

Flue Gas Desulfurization (FGD) Scrubber Material

The burning of coal produces sulfur dioxide (SO_2) gas. The 1990 Clean Air Act and subsequent amendments regulate SO_2 emissions from burning coal. Coal-fired power plants installed flue gas desulfurization (FGD) technology for reducing SO_2 emissions. The two most common scrubber technologies used today are wet or dry systems. Wet FGD systems introduce a spray of alkaline sorbent consisting of lime or limestone (primarily limestone) into the exhaust gas. The alkali reacts with the SO_2 gas to form calcium sulfite ($CaSO_3$) or calcium sulfate ($CaSO_4$) that is collected in a liquid slurry form. The calcium sulfite or sulfate is allowed to settle out, and the majority of the water is recycled. The settled material called FGD scrubber material or scrubber sludge is an off-white slurry with a solid content in the range of 5–10%. In 2006, FGD scrubber systems at coal-fired power plants generated approximately 27.4 million metric tons (30.2 million US tons) of material, or 24.2% of all coal combustion products.[7] Due to an expected increase in scrubbing applications, the amount of FGD produced is expected to grow during the next few decades.

Foundry Sand

Foundry sand is a high-quality silica sand that is used to form molds for ferrous (iron and steel) and nonferrous (copper, aluminum, brass, etc.) metal castings. The raw sand is normally of higher quality than typical bank run or natural sands used in construction. Of the 5.5–9 million metric tons (6–10 million US tons) of spent foundry sand generated annually, less than 15% is recycled.

Kiln Dust

Kiln dusts (CKD) are fine by-products of Portland cement and lime high-temperature rotary kiln production operations that are captured in the air pollution control dust collection system (e.g., cyclones, electrostatic precipitators, and baghouses). Approximately 12.9 million metric tons (14.2 million US tons) of CKD are produced annually.

Mineral Processing Waste

Mineral processing wastes are referred to in the Resource Conservation and Recovery Act (RCRA) as wastes that are generated during the extraction and beneficiation of ores and minerals. These wastes

can be subdivided into a number of categories: waste rock, mill tailings, coal refuse, wash slimes, and spent oil shale. The mining and processing of mineral ores results in the production of large quantities of residual wastes that are, for the most part, earth- or rock-like in nature. It is estimated that the mining and processing of mineral ores generate approximately 1.6 billion metric tons (1.8 billion US tons) of mineral processing waste each year in the United States.

Municipal Solid Waste (MSW) Combustor Ash

Municipal solid waste (MSW) combustor ash is the by-product that is produced during the combustion of municipal solid waste in solid waste combustor facilities. Approximately 29.5 million metric tons (32.5 million US tons) of solid waste is combusted annually at approximately 160 municipal waste combustor plants in the United States, existing and under construction.

Nonferrous Slag

Nonferrous slags are produced during the recovery and processing of nonferrous metal from natural ores. The slags are molten by-products of high-temperature processes that are primarily used to separate the metal and nonmetal constituents contained in the bulk ore. When cooled, the molten slag converts to a rock-like or granular material. The following nonferrous slags are included in these guidelines: copper, nickel, phosphorus, lead, lead-zinc, and zinc. Approximately 3.6 million metric tons (4 million US tons) each of copper and phosphorus slag are produced each year in the United States, while the annual production of nickel, lead, and zinc slags is estimated to be in the range of 0.45–0.9 million metric tons (0.5–1.0 million US tons).

Quarry By-Products

Processing of crushed stone for use as construction aggregate consists of blasting, primary and secondary crushing, washing, screening, and stockpiling operations. Quarry by-products are produced during crushing and washing operations. There are three types of quarry by-products resulting from these operations: screenings, pond fines, and baghouse fines. It is estimated that at least 159 million metric tons (175 million US tons) of quarry by-products are being generated each year, mostly from crushed stone production operations. As much as 3.6 billion metric tons (4 billion US tons) of quarry by-products have probably accumulated.

Reclaimed (or Recycled) Asphalt Pavement (RAP)

Reclaimed (recycled) asphalt pavement (RAP) is the term given to removed and/or reprocessed pavement materials containing asphalt and aggregates. These materials are generated when asphalt pavements are removed for reconstruction, resurfacing, or to obtain access to buried utilities. When properly crushed and screened, RAP consists of high-quality, well-graded aggregates coated by asphalt cement. It is estimated that as much as 80 million metric tons (88 million US tons) of RAP may be produced each year in the United States. A sample of RAP is shown in Fig. 1.

Reclaimed Concrete Material

Over two billion metric tons (2.2 billion US tons) of aggregate are produced every year in the USA. Production of aggregate is expected to reach 2.5 billion metric tons (2.8 US tons) by 2020, which raises concerns about

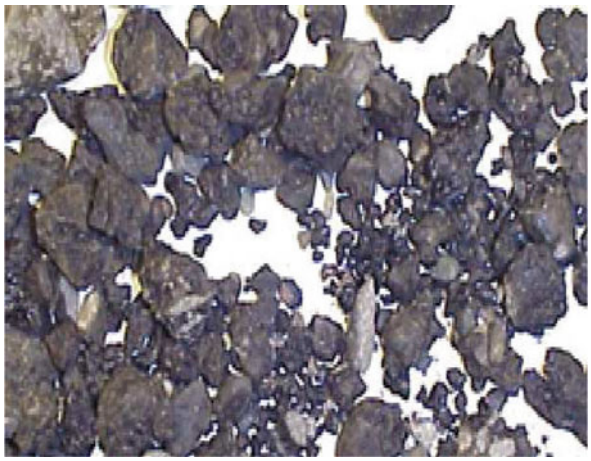

Waste Materials in Construction, Utilization of. Figure 1 RAP as aggregate replacement

where the new aggregate will come from. One alternative to using virgin aggregate is recycled concrete aggregate. Recycled concrete aggregate (RCA) consists of high-quality, well-graded aggregates (usually mineral aggregates), bonded by a hardened cement paste. The aggregates comprise approximately 60–75% of the total volume of concrete.

Roofing Shingle Scrap

There are two types of roofing shingle scraps. They are referred to as tear-off roofing shingles, and roofing shingle tabs, also called prompt roofing shingle scrap. Tear-off roofing shingles are generated during the demolition or replacement of existing roofs. Roofing shingle tabs are generated when new asphalt shingles are trimmed during production to the required physical dimensions or from "out-of-spec" shingles. Roofing shingle tab materials that result from shingle manufacture are estimated to range between 5% and 10% of the total production. Current estimates indicate that the percentage of roofing scrap generated by activity is as follows: 87.5% is manufacturing scrap and 12.5% is tear-off roofing scrap. Approximately 10 million metric tons (11 million US tons) of asphalt roofing shingle scrap is generated each year in the United States.

Scrap Tires

Approximately 400 million tires are discarded each year by American motorists, approximately one tire for every person in the United States. Around 30 million of these tires are retreaded or reused, leaving roughly 250 million scrap tires to be managed annually. About 85% of these scrap tires are automobile tires, the remainder being truck tires. Besides the need to manage the scrap tires, it has been estimated that there may be as many as 3–4 billion tires that have accumulated over the years and are contained in numerous stockpiles. Scrap tires can be managed as a whole tire, a slit tire, a shredded or chipped tire, as ground rubber, or as a crumb rubber product. Tire rubber is also known as crumb-rubber-modifier (CRM) as it is used for modifying asphalt properties. A sample of ground tire rubber is shown in Fig. 2.

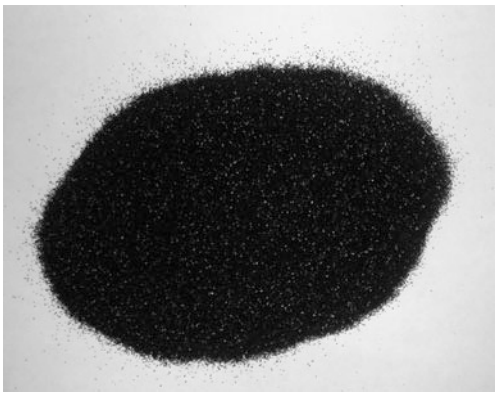

Waste Materials in Construction, Utilization of. Figure 2 Ground tire rubber

Sewage Sludge Ash

Sewage sludge ash is the by-product produced during the combustion of dewatered sewage sludge in an incinerator. Sewage sludge ash is primarily a silty material with some sand-sized particles. There are approximately 170 municipal sewage treatment plant incinerators in the United States, processing approximately 20% of the nation's sludge, and producing between 0.45 million and 0.9 million metric tons (0.5 and 1.0 million US tons) of sludge ash on an annual basis.

Steel Slag

Steel slag, a by-product of steel making, is produced during the separation of the molten steel from impurities in steel-making furnaces. The slag occurs as a molten liquid melt and is a complex solution of silicates and oxides that solidifies upon cooling.

Sulfate Waste

Fluorogypsum and phosphogypsum are sulfate-rich by-products generated during the production of hydrofluoric and phosphoric acid, respectively. Approximately 90,000 metric tons (100,000 US tons) of fluorogypsum are generated annually in the United States, mostly in Delaware, New Jersey, Louisiana, and Texas. Approximately 32 million metric tons (35 million US tons) of phosphogypsum are produced annually, mostly in central Florida, but also in Louisiana and southeastern Texas.

Applications of Waste Materials in Building Construction

Uses of waste materials is not limited to pavement applications. Huge amounts of recycled materials such as coal combustion products (CCPs), construction and demolition (C&D) materials, spent foundry sand, used tires, and slags are potentially usable in building construction applications. Reusing and recycling C&D materials onsite can reduce material hauling and disposal costs. In some cases, these materials have performance benefits over virgin materials. For example, fly ash and slag cement are used in concrete applications and can be used as partial replacements for cement, which helps in producing stronger, longer-lasting concrete. Recycled portland cement concrete has a very wide range of applications in construction. Concrete aggregate can include components from bottom ash, foundry sand, crushed concrete, and blast furnace slag. Coal bottom ash is used as bedding material for green roofs and is lighter than the alternatives. Tire shreds provide more effective drainage around building foundations in comparison with gravel and also put less pressure on the foundation walls.

Structural fills are engineered fills constructed in layers and compacted using coal fly ash, bottom ash, slag, and spent foundry. Spent foundry can be used in place of natural soil as base material for the building sites and because it does not freeze as readily as most soils, this can extend construction season. In backfills which surround the building's foundation to support it and provide drainage, waste materials can be used such as scrap tires which provide superior drainage, insulation, and wall pressure relief. Masonry blocks used in building are made from slag and aggregate, for which slag cement, fly ash, silica fume can substitute partially for cement and bottom ash; blast furnace slag and recycled concrete aggregate can be used instead of virgin aggregate.

Recycled materials are used to make sidewalks. Used tires are recycled to create rubberized sidewalks, and industrials by-products are used for concrete sidewalks. Recycled asphalt shingles and recycled asphalt pavement are used to make asphalt sidewalks. Flooring applications can also benefit from waste and recycled materials such as used tires and fly ash in carpet backing. Salvaged lumber or recycled wood is used for wood flooring and blast furnace slag or fly ash in flooring tile. For insulation, air-cooled blast furnace slag can be used to produce mineral or rock wool insulation. There are numerous applications of waste or recycled materials in construction and new applications are emerging every day out of ongoing research on this topic.

Applicability of Current Specification to Recycled Materials

In general, current specifications on construction materials do not reflect the current level of knowledge concerning desirable properties for construction applications. It is also reasonable to state that current testing does not provide all necessary property characterization to ensure field performance. Current testing may or may not be the best testing to characterize recycled material properties. The discussions with state engineers on the applicability of current specifications on recycled materials were focused on the following points:

- Are current requirements reflecting the needs of state agencies in material quality?
- Can an agency always use current specifications to specify the best quality recycled material?
- If new specification requirements are to be introduced, would the new requirements satisfy the performance-related properties of the applications?
- The need for additional testing must be justified by relating proposed testing to performance. For example, agencies express concerns that current relations between recycled aggregate testing and pavement performance are not sufficient and further correlations are needed before making changes to current specifications.
- The ease and affordability of testing to frequently ensure consistency of aggregate quality.
- Complicated and time-consuming testing is likely to be conducted less frequently and will not be sufficient to characterize recycled materials for their variability.

Can recycled materials fully replace virgin materials with respect to current specifications? For example, is RAP aggregate?

Future Directions

There is a need to evaluate compliance and consistency of recycled material properties with respect to current specification requirements and to assess property-based requirements of recycled materials. Officials are receptive to pursuing changes in the way they specify recycled materials. It is agreeable that current specifications are still outdated for virgin materials and do not reflect the current level of knowledge concerning desirable properties for pavement applications and do not provide all necessary property characterization to ensure field performance. Current procedures may or may not be the best testing to characterize the properties of recycled materials. There have been discussions regarding added testing procedures (to measure additional properties) in the current specifications to ensure the applicability of specifications on recycled materials. An example is asphalt-CRM binder stability. The concern regarding the relation between the suggested testing and performance has two aspects: If those relations are valid, then there is a need for a change in current specifications. If those relations do not exist, then marginal materials, including local sources that are poor in those properties, should be used successfully in most civil/construction applications.

Specific significant testing procedures that are well correlated to performance are difficult to implement on recycled materials. An example is aggregate compressive strength, ASTM C-170 Standard Test Method for Compressive Strength of Dimension Stone. The test cannot be considered for recycled aggregate sources because it requires a cubic-cut sample of the aggregate source of more than 5.0 cm each dimension. However, an alternative test, the point load test (ASTM D5731), uses much smaller sample and can provide reasonable accuracy for measuring the same property.

The comparison between the qualities of local materials vs. that of recycled materials is a sustainability issue. Aggregate is an example. There is a potential that local aggregate sources that are rejected for high-class pavement mixes can be used for local and low volume road applications. Aggregate quality is tied to the design process. The use of recycled materials, recycled asphalt pavement (RAP) for example, has been successful in same applications. Cost is a major factor in selecting aggregate sources. Life-Cycle-Cost analysis is a useful tool in determining the use of local aggregate vs. recycled materials applications. Having better quality aggregate would allow designing pavement for longer life, an aspect of sustainability.

Acknowledgments

This material is based upon work supported by the National Science Foundation under Grant No. 0846861. Any opinions, findings, and conclusions or recommendations expressed in this material are those of the author(s) and do not necessarily reflect the views of the National Science Foundation.

Bibliography

Primary Literature

1. Recycling Centers website. http://www.recyclingcenters.org
2. http://www.dosomething.org/whatsyourthing/Environment
3. Environmental Protection Agency website. http://www.epa.gov
4. The Construction Industry Compliance Assistance Center. http://www.cicacenter.org/
5. Recycling, Wikipedia. http://en.wikipedia.org/wiki/Recycling
6. Kandhal PS, Mallick RB (1997) Pavement recycling guidelines for state and local governments participant's reference book. Publication No. FHWA-SA-98-042, Federal Highway Administration, Washington, DC
7. Wright FG Jr (2002) Formal policy on the use of recycled materials. Federal Highway Association, Washington, DC
8. Recycled Materials Resource Center, User guidelines for byproducts and secondary use materials in pavement construction. http://www.rmrc.unh.edu/
9. Environmental Protection Agency, Using recycled industrial materials in building
10. Eighmy TT, Chesner WH (2000) Framework for evaluating use of recycled materials in the highway environment. Publication No. FHWA-RD-00-140, Federal Highway Administration, Washington, DC

Books and Reviews

Ahmed I (1993) Use of waste materials in highway construction. Noyes Data Corporation, Park Ridge

Boden F, Azaroual M, Piantone P (2000) Forecasting the behaviour of long-term municipal solid waste incineration bottom ash: rapid tests combined. In: Woolley GR, Goumans JJJM, Wainwright PJ (eds) Waste materials in construction. Proceedings of the international conference on the science and engineering of recycling for environmental protection, 1–2 June 2000. Elsevier, Amsterdam

Bossinik BAG, Brouwers HJH (1996) Construction waste: quantification and source evaluation. J Constr Eng Manag ASCE 122(1):55–60

Calkins M (2009) Materials for sustainable sites: a complete guide to the evaluation, selection and use of sustainable construction materials. Wiley, Hoboken

Carpenter AC, Gardner KH (2007) Recycled material highway construction environmental assessment: life cycle based risk assessment of recycled materials in roadway construction. RMRC Project No. 43 final report, Recycled Materials Resource Center

Carter A, Gardiner MS (2007) Indirect tension relaxation test to evaluate the effect of the addition of RAP to HMA mixes. J Mater Civ Eng ASCE 19(3):219–226

Chandra S (1997) Waste materials used in concrete manufacturing. Noyes Data Corporation, Westwood

Chen D-H, Hugo F (2001) Comparison of two pavement rehabilitation strategies. J Transp Eng ASCE 127(1):47–58

Cross SA (2002) Determination of N_{Design} for CIR mixtures using the superpave gyratory compactor. RMRC Research Project No. 15 final report, Recycled Material Resource Center

Federal Highway Administration (1993) A study of the use of recycled paving material – report to congress. Publication No. FHWA-RD-93-147, Federal Highway Administration, Washington, DC

Federal Highway Administration (2004) Transportation applications of recycled concrete aggregate. FHWA State of the Practice National Review. Federal Highway Administration, Washington, DC

Gidley JS, Sack WA (1984) Environmental aspects of waste utilization in construction. J Environ Eng ASCE 110(6): 1117–1133

Goumans JJJM, van der Sloot HA, Aalbers ThG (eds) (1994) Environmental aspects of construction with waste materials. Proceeding of the international conference on environmental implications of construction materials and technology developments, Maastricht, 1–3 June 1994. Elsevier, Amsterdam

Haselbach L (2008) The engineering guide to LEED–new construction: sustainable construction for engineers. McGraw-Hill, New York

Horvath A (2004) A life-cycle model and decision-support tool for selecting recycled versus virgin material for highway applications. RMRC Project No. 23 final report, Recycled Material Resource Center

Inyang HI (2003) Framework for recycling of wastes in construction. J Environ Eng ASCE 129(10):887–898

Kelly T (1998) Crushed cement concrete substitution for construction aggregates – a material flow analysis, U.S. Geological Survey Circular 1177. http://greenwood.cr.usgs.gov/pub/circulars/c1177/index.html

Kim JJ, Lee HD, Jahren CT, Heitzman M (2010) Long-term field performance of cold-in-place recycled road s in Iowa. J Perform Constr Facil ASCE 24(3):265–274

Kim Y, Lee HD, Heitzman M (2007) Validation of new mix design procedure for cold-in-place recycling with foamed asphat. J Mater Civ Eng ASCE 19(11):1000–1010

Lee KW, Brayton TE, Huston M (2002) Development of performance based mix design for cold-in-place recycling (CIR) of bituminous pavements based in fundamental properties. Publication No. FHWA-CIR-02-01, Federal Highway Administration, Washington, DC

Mallick RB, Mathisen PP, FitzPatrick MS (2002) Opening the window of sustainable development to future civil engineers. J Prof Issue Eng Educ Pract ASCE 128(4): 212–216

McDaniel RS, Soleymani H, Shah A (2002) Use of reclaimed asphalt (RAP) under superpave specifications. Publication No. FHWA / IN/JRTP-2002/6

Melton JS, Morgan T, Evaluation of tests for recycled material aggregates for use in unbound applications. RMRC Project 6 final report, Recycled Materials Resource Center

Naik TR (2008) Sustainability of concrete construction. Practice periodical on structural design and construction. Am Soc Civ Eng 13(2):98–103

Nassar K, Nassar W (2006) Reclaimed asphalt pavement detection and quality determination practice periodical on structural design and construction. Am Soc Civ Eng 11 (3):171–176

Polley C, Cramer SM, de la Cruz RV (1998) Potential for using waste glass in portland cement concrete. J Mater Civ Eng ASCE 10(4):210–219

Pratt E (1993) Current uses and evaluation of recycled materials in highway construction: overview of northeastern states. Northeastern Recycling Council

Rajendran S, Gambatese JA (2007) Solid waste generation in asphalt and reinforced concrete roadway life cycles. J Infrastruct Syst ASCE 13(2):88–96

Rubber Manufacturers Association (2009) Scrap tire markets in the United States, 9th biennial report. Rubber Manufacturers Association, Washington, DC

Saeed A (2008) Performance-related tests of recycled aggregates for use in unbound pavement layers. NCHRP Report 598, National Cooperative of Highway Research Program

Schimmoller VE et al (2000) Recycled materials in European highway environments: uses, technologies and policies. Publication No. FHWA-PL-00-025, Federal Highway Administration, Washington, DC

Shen D-H, Du J-C (2005) Application of gray relational analysis to evaluate HMA with reclaimed building materials. J Mater Civ Eng ASCE 17(4):400–406

Shen J, Amirkhanian S, Miller JA (2007) Effects of rejuvenating agents on superpave mixtures containing reclaimed asphalt pavements. J Mater Civ Eng ASCE 19(5):376–384

Sobhan K, Mashnad M (2000) Fatigue durability of stabilized recycled aggregate base course containing fly ash and waste-plastic strip reinforcement. Recycled Material Resource Center

Sorvari J (2003) By-products in earth construction: environmental assessments. J Environ Eng ASCE 129(10):899–899

Taha B, Nouno G (2009) Utilizing waste recycled glass as sand/cement replacement in concrete. J Mater Civ Eng ASCE 21(12):709–721

Tao M, Zhang Z, Wu Z (2008) Simple procedure to assess performance and cost benefits of using recycled materials in pavement construction. J Mater Civ Eng ASCE 20(11): 718–725

Tay J, Hong S, Show K (2000) Reuse of industrial sludge as pelletized aggregate for concrete. J Environ Eng ASCE 126(3):279–287

Venner M (2004) Environmental stewardship practices, procedures, and policies for highway construction and maintenance. NCHRP Project 25-25(4), National Cooperative Highway Research Program

Wang Y (2009) Sustainability in education. J Prof Issues Eng Pract ASCE 135(1):21–30

Wilburn DR, Goonan TG (1998) Aggregates from natural and recycled sources, economic assessment for construction applications – a material flow analysis, U.S. Geological Survey Circular 1176. http://greenwood.cr.usgs.gov/pub/circulars/c1176/c1176.html

Young HM, Sellasie K, Zeroka D, Sabnis G (2003) Physical and chemical properties of recycled tire shreds for use in construction. J Environ Eng ASCE 129(10):921–929

Zapata P, Gambatese JA (2005) Energy consumption of asphalt reinforced concrete pavement materials and construction. J Infrastruct Syst ASCE 11(1):9–20

Zhang W, Ingham JM (2010) Using recycled concrete aggregates in New Zealand ready-mix concrete production. J Mater Civ Eng ASCE 22(5):443–450

Related Websites

Aggregate Research Institute. http://www.aggregateresearch.com/

Asphalt Recycling and Reclaiming Association. http://www.arra.org/

Benefits of Recycling. http://www.benefits-of-recycling.com/recyclingstatistics.html

Center for Environmental Excellence by AASHTO website. http://environment.transportation.org/

Environmental Protection Agency, Waste-resource conservation. http://www.epa.gov/epawaste/conserve/index.htm

Federal Highway Administration recycling webpage. http://www.fhwa.dot.gov/pavement/recycling/index.cfm

National Demolition Association. http://www.demolitionassociation.com/

Pavement Recycling Systems. http://www.pavementrecycling.com/

Recycled Materials Resource Center. http://www.rmrc.unh.edu/

Recycling Centers. http://www.recyclingcenters.org

Recycling Today, The Industry's News and Resource Center. http://www.recyclingtoday.com/

Sustainable Sources, Construction waste recycling. http://constructionwaste.sustainablesources.com/

The Construction Industry Compliance Center. http://www.cicacenter.org/cdrecycling.html

Waste-to-Energy: Decreasing the Entropy of Solid Wastes and Increasing Metal Recovery

Helmut Rechberger
Institute of Water Quality, Resource and Waste Management, Vienna University of Technology, Vienna, Austria

Article Outline

Glossary
Definition of the Subject and Its Importance
Introduction: Material Balances and Entropy Evaluation
Description of Waste-to-Energy (WTE)
Statistical Entropy Analysis (SEA)
Application of SEA to Waste-to-Energy
Relationship Between SEA and Environmental Impact
Future Directions
Bibliography

Glossary

Statistical entropy Developed by C.E. Shannon as part of his information theory and used as a measure for distributions in statistics, formally similar to the thermodynamic entropy of mixing.

Waste-to-energy (WTE) Combustion of municipal solid waste (MSW) with energy recovery.

Material flow analysis (MFA) Systematic assessment of the flows and stocks of materials within a system, defined in space and time.

Statistical entropy analysis (SEA) Entropy-based method, based on material flow analysis, for quantifying the concentrating effect of a process or system.

Definition of the Subject and Its Importance

The turnover of materials used in a national economy has been described as the consumption of resources (low-entropy materials) that are used and transformed into wastes (high entropy materials); therefore, the economy is viewed as an entropy-producing process [1]. In a recycling economy, entropy generation must

be kept low and waste management should transform high-entropy wastes into low-entropy recycled products that can reduce the use of primary resources. Entropy reduction is achieved by the concentrating of materials. Evaluation of the materials balances, by means of statistical entropy analysis, within state-of-the-art incinerators shows that waste-to-energy is a major contributor to a sustainable materials management. It is shown that waste incineration results in significant concentrating of several substances.

Introduction: Material Balances and Entropy Evaluation

Stumm and Davis [2] described the life cycle of copper qualitatively by using the metric of entropy. They showed that entropy is reduced when consumer products are made from raw materials and entropy increases after the products are used and become waste (Fig. 1). Later, Rechberger and Graedel [3] applied the concept of statistical entropy to the global copper cycle and quantified the entropy trend (Fig. 2).

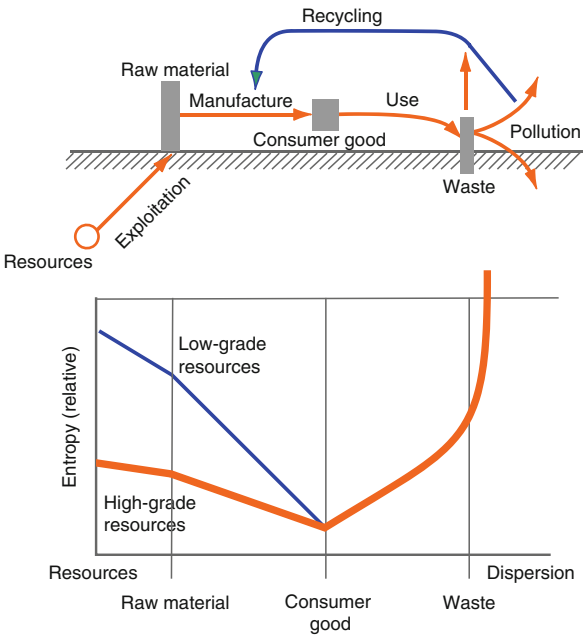

Waste-to-Energy: Decreasing the Entropy of Solid Wastes and Increasing Metal Recovery. Figure 1
The life cycle of copper and the change in its entropy [2]

The shape of the Relative Statistical Entropy (RSE) curve of Fig. 2 can be explained as follows: One tracks the life cycle of a batch of copper (e.g., 1 kg) and quantifies the state of this amount of copper by applying statistical entropy. There are two extreme states for the copper batch: either it appears as a 100% pure item, e.g., as a copper bar of 1 kg, which translates into a RSE of zero, or it is completely dissipated and contributes to the mean concentration in the earth's crust (ca. 70 mg/kg), which is defined as the maximum entropy state (RSE of 1). Any other state has to lie between these two extremes. The life cycle starts with copper ore (Fig. 2, point 1), which has a mean concentration of 0.5%. The "copper production" process comprises several concentrating and beneficiation steps resulting in high-grade cathode copper having a purity of 99.9% or higher (step 1 → 2 in Fig. 2). However, point 2 lies above the x-axis (RSE = 0) because extracting copper from its ore is not 100% efficient; there are some waste by-products (tailings, slag) and these account for the distance between point 2 and the zero-line in Fig. 2.

The process "production of goods" requires that copper metal be mixed or combined with other materials to form consumer products having copper concentrations between 0.01% and 100%; this results in an entropy increase (step 2 → 3 in Fig. 2). These products are then used and eventually become waste (step 3 → 4) with a typical copper concentration of <1% (MSW, waste electrical and electronic equipment, end-of-life vehicles, construction and demolition waste, etc.).

The process of "waste management" separates copper scrap and this results in an entropy decrease (step 4 → 5 in Fig. 2). The decrease is rather moderate because much of the copper becomes embedded in the stock of the process "consumption and use" that represents a future potential for recycling (and entropy decrease); because of this, the global recycling rate is rather low (about 50%).

The global total entropy trend for copper is rather balanced since point 1 (ore) and point 5 (wastes to landfill) have similar values. However, in a fully developed recycling economy where waste becomes a high-grade resource again, the life cycle of copper would end at point 5′ in Fig. 2. This means that waste management needs to realize a substantial reduction in entropy, posing a similar challenge as the

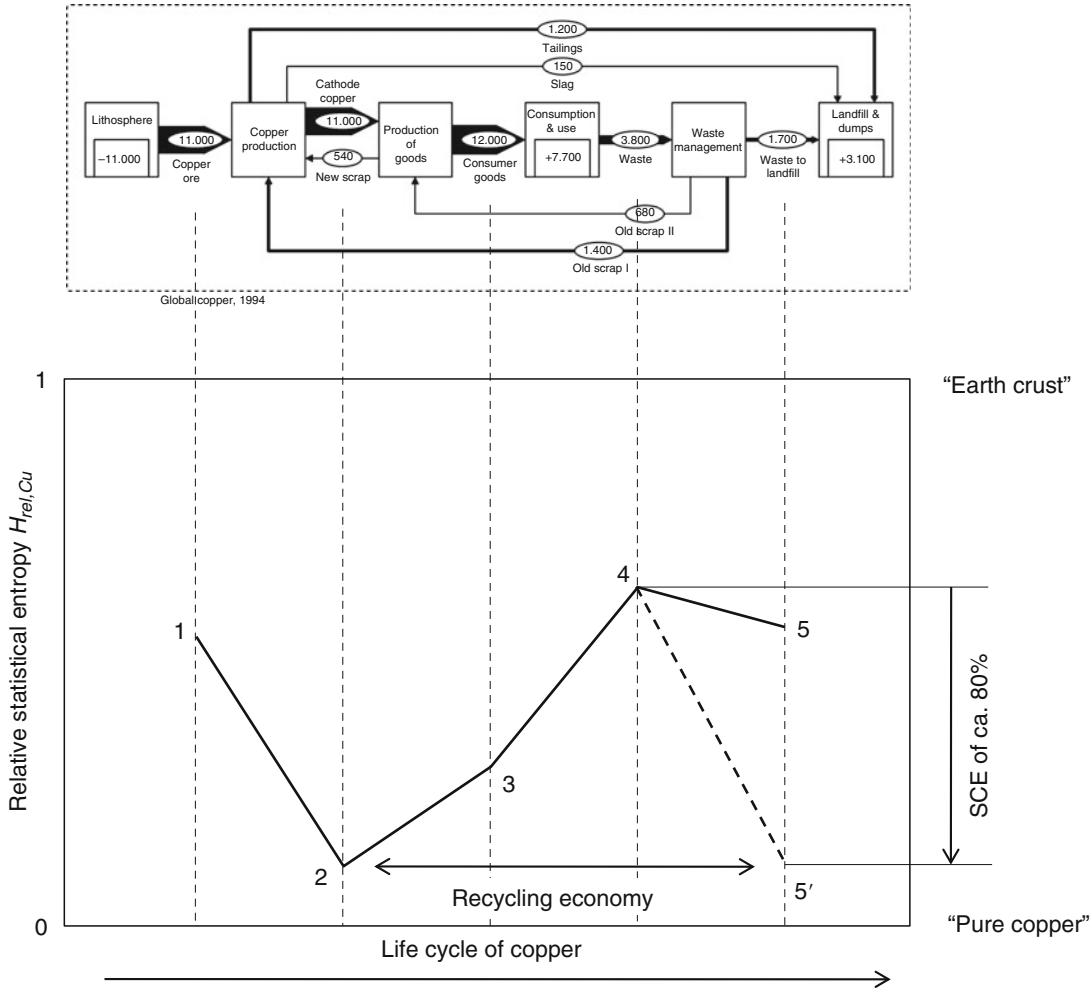

Waste-to-Energy: Decreasing the Entropy of Solid Wastes and Increasing Metal Recovery. Figure 2
Global production and use of copper (*upper diagram*) and corresponding change in its relative statistical entropy [3]

process from step 1 → 2 (Fig. 2), i.e., the production of pure cathode copper from copper ore. The latter is achieved by a series of processes, such as grinding, flotation, roasting, smelting, extraction, and refining. Therefore, it is straight forward to postulate that the path from 4 → 5′ (Fig. 2) will require a similar technological effort as the production path from 1 → 2. In other words, the realization of a substantial recycling economy will require high-tech waste management. At present, these high-tech technologies have not yet been introduced to waste management. Notable exceptions are state-of-the-art incinerators and a trend to sophisticated recycling technologies such as near-infrared spectroscopy detection and sorting equipment.

Description of Waste-to-Energy (WTE)

A waste-to-energy facility can be divided into the actual combustion process, the boiler and power generation turbine, and the air and water pollution control system. The choice for the combustion technology is mainly determined by the physical (particle size distribution, density, aggregate state, water content, etc.) and

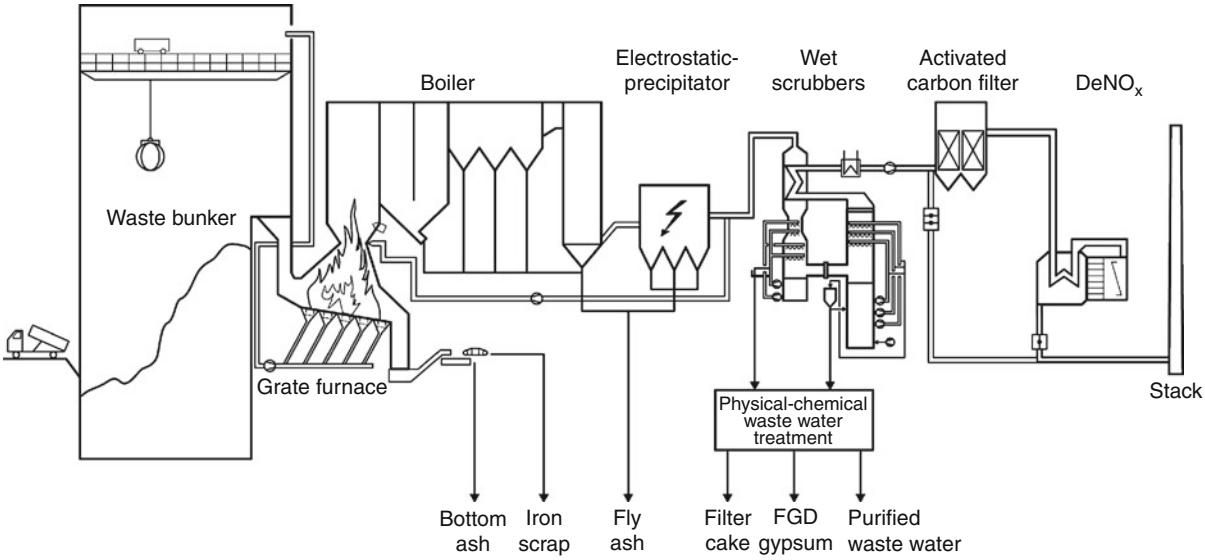

Waste-to-Energy: Decreasing the Entropy of Solid Wastes and Increasing Metal Recovery. Figure 3
Modern WTE facility with state-of-the-art air pollution control (APC) system

chemical (elemental composition, calorific value, ash content, etc.) characteristics of the waste. A widely used method for the incineration of municipal solid waste (MSW) is the so-called mass-burn grate combustion (Fig. 3).

In a typical mass-burn facility [4], waste is stored in a fully contained waste bunker for periods up to 1 week. Combustion air is taken from the bunker thus preventing odor outside the facility. An operator-controlled or automated crane mixes incoming wastes to provide some homogeneity with regard to calorific value and loads the waste into a hopper feeding a water-cooled gravity chute that serves as an air seal between bunker and furnace. A horizontal ram feeder at the bottom of the chute pushes the waste onto the furnace grate where it is combusted. The grate consists of moving and fixed elements (rows) that guarantee controlled transportation, mixing of the waste, and equal distribution across the grate. At the end of the grate, the bottom ash is discharged into a water basin, where it is cooled and then conveyed to the bottom ash bunker.

The flue gas leaving the combustion chamber contains high amounts of particulates (3–5 g/m^3), acids such as SO_2 (sulfur dioxide), HCl (hydrochloric acid), HF (hydrofluoric acid), and NO_x (nitrogen oxides) that require extensive flue gas treatment. Particulates are removed in electrostatic precipitators (ESP) or more commonly in bag house filters (also referred to as fabric filters). ESPs use electric forces to charge and move particulate matter in a flowing gas stream to a collecting surface. They are more robust toward temperature changes, have lower pressure drops, and are easy to maintain. Bag house filters (particulate removal by filtration on fiber surfaces) achieve high removal efficiencies for fine particles (<5 μm, >99.9%).

Various reagents are used in the APC system of WTEs, such as lime (CaO) or lime hydrate ($Ca(OH)_2$), to remove sulfur dioxide and hydrogen chloride, and activated carbon, to remove mercury and dioxins. Acids can be very efficiently and separately removed by a two-stage wet scrubber system. HCl and HF are physically absorbed in the first acid scrubber stage at pH1. The low pH prevents absorption of SO_2. The scrubber liquid is water, and no neutralization agent has to be used. Also mercury chlorides are removed from the flue gas at this stage. During the second stage SO_2 is chemically absorbed using either $CaCO_3$, $Ca(OH)_2$, or NaOH (sodium hydroxide) for neutralization at pH7. The final product of the sulfur removal is gypsum, which is dewatered and either

recycled in the gypsum industry or landfilled. Part of the scrubber water is continuously purified by an on-site physical-chemical wastewater treatment process. Neutralization sludge is precipitated and dewatered in a filter press. Chloride is discharged with the treated wastewater.

Hydrogen chloride (HCl) can be purified and concentrated to over 30% for recycling. Alternatively, the acid can be neutralized with NaOH, and sodium chloride brine can be recycled. NO_x is reduced to N_2 and H_2O by injecting NH_3 (ammonia). The reaction requires high temperatures (900–1,000°C). A ceramic catalyst (based on TiO_2 and V_2O_5) reduces the temperature need to 200–300°C and enhances the efficiency of the reaction from 70% to 80% up to 90%. With proper design, the catalyst can also be utilized to oxidize PCDD/F. Sometimes activated carbon filters are employed as a final stage to adsorb organic compounds (e.g., PCDD/F), metallic mercury (Hg°), and other trace pollutants passing the previous air pollution control (APC) stages. State-of-the-art combustion and APC systems destroy organic and remove inorganic pollutants with high efficiency. Various full-scale plants demonstrate the reliability of these technologies; they operate at emissions way below the stringent emission limits enacted, e.g., by the European Union [5].

An ongoing field of research and development with regard to WTE is how to produce bottom ash and filter residues that have improved landfill properties with regard to composition and emissions; and residues that can be utilized as secondary resources. This can be achieved either by after-treatment of bottom and/or fly ashes in thermal and/or chemical processes or by designing new technologies that are not necessarily based on the grate furnace technology.

Bottom ashes can also be further treated by mechanical processes (sieving, screening) and magnetic separation of iron scrap. Adequate thermal after-treatment of bottom ash results in three products: (1) a silicate product that can be utilized for construction purposes; (2) metals consisting mainly iron, copper, and other lithophilic metals (metals of low vapor pressure); and (3) a concentrate of atmophilic metals (metals of high vapor pressure). The last two fractions can be recycled in the metal industry.

Immobilization of leachable substances can also be achieved by solidification/stabilization using additives such as cement that physically and/or chemically immobilize hazardous substances in ashes. Some new incineration concepts combine pyrolysis and high-temperature processes with conventional APC as described in other entries of this encyclopedia. The goals of these technologies are to produce residues with better qualities with respect to disposal and recycling than mass burn systems. None of these new technologies have experienced a breakthrough. Up to now, they could not prove yet that they are able to reach the same or higher goals than traditional MSW incineration at lower costs and at the same reliability. Today, WTE combined with advanced APC represents a reliable, robust, and compared to other available options environmentally sound technology to dispose of combustible and hazardous wastes. Further development should be focused on producing more residues that can be recovered in an environmentally sound manner, and to use thermal processes to turn waste management into an integrated part of a sustainable materials management.

Table 1 provides the mass balance of a WTE facility consisting of mass-burn combustion, ESP, two-stage wet scrubber system, de-NO_x reactor, activated carbon filter, and chemical-physical wastewater treatment. Table 2 shows the respective transfer coefficients for selected metals. Both were determined by an intensive measurement campaign at a full-scale facility over 1 week [6].

Statistical Entropy Analysis (SEA)

The methodological framework of SEA is described in [7] and [8]. SEA employs statistical entropy to quantify the distribution of substances or elements in a process. In statistics, the entropy is used as a metric to describe distributions of any kind. Rechberger showed that the input as well as the output of a process (e.g., a WTE facility) can be described by distributions of substances as a result of a material flow analysis (MFA). Figure 4 and Table 3 show an example, the cadmium balance of a WTE facility.

The distribution of the input is rather simple since over 99% of the Cd enters the process via the material flow "MSW" that contains a concentration of

Waste-to-Energy: Decreasing the Entropy of Solid Wastes and Increasing Metal Recovery. Table 1 Normalized mass balance of a state-of-the-art WTE facility [6]

Input	t/t MSW	Output	t/t MSW
MSW	1.0	Bottom ash	0.26
Adsorbent	0.0011	FGD-gypsum	0.0040
Liquid ammonia solution	0.0030	Filter cake	0.0026
Air	4.1	Fly ash	0.029
Water	0.56	Iron-scrap	0.035
		Off-gas	4.9
		Purified waste water	0.39
Total	5.7		5.7

Waste-to-Energy: Decreasing the Entropy of Solid Wastes and Increasing Metal Recovery. Table 2 Transfer coefficients (%) of a WTE plant [6]

	Bottom ash %	Fly ash %	Iron-scrap %	FGD-gypsum %	Filter cake %	Pur. WW %	Off-gas %
Ag	83	16	0.001	0.0062	0.48	0.06	0.001
As	70	28	0.17	0.23	0.68	0.09	0.6
Cd	20	43	31	0.0052	5.9	0.01	0.04
Co	70	9	20	0.054	0.09	0.02	0.005
Cr	83	4	13	0.0006	0.032	0.0007	0.0006
Cu	96	0.9	3	0.0005	0.03	0.00005	0.00002
Fe	40	1.2	58	0.00026	0.08	0.00031	0.001
Hg	5	4.6	0.001	3.27	83	0.3	3.9
Mn	84	12	3.8	0.00032	0.16	0.034	0.0002
Ni	83	2	15	0.0022	0.027	0.001	0.0003
Pb	74	25	0.0049	0.0078	0.8	0.0006	0.0007
Sb	41	55	2.3	0.01	1.6	0.004	0.003
Sn	76	23	0.001	0.014	0.57	0.009	0.01
V	81	11	7.6	0.0026	0.39	0.02	0.005
Zn	72	26	0.6	0.011	1.27	0.006	0.0006

15 mg/kg MSW. The output distribution is more complex. Cadmium is partitioned among the outputs as follows: Bottom ash, 20% (11 mg/kg); iron scrap, 31% (130 mg/kg); fly ash, 43% (220 mg/kg); filter cake, 5.9% (340 mg/kg); FGD gypsum, 0.0052% (0.2 mg/kg); purified waste water, 0.01% (0.0038 mg/kg); and off-gas, 0.04% (0.0012 mg/kg). In other words, cadmium is transferred mostly to some output flows (fly ash, iron scrap) and at different concentrations in the various outputs. By applying the

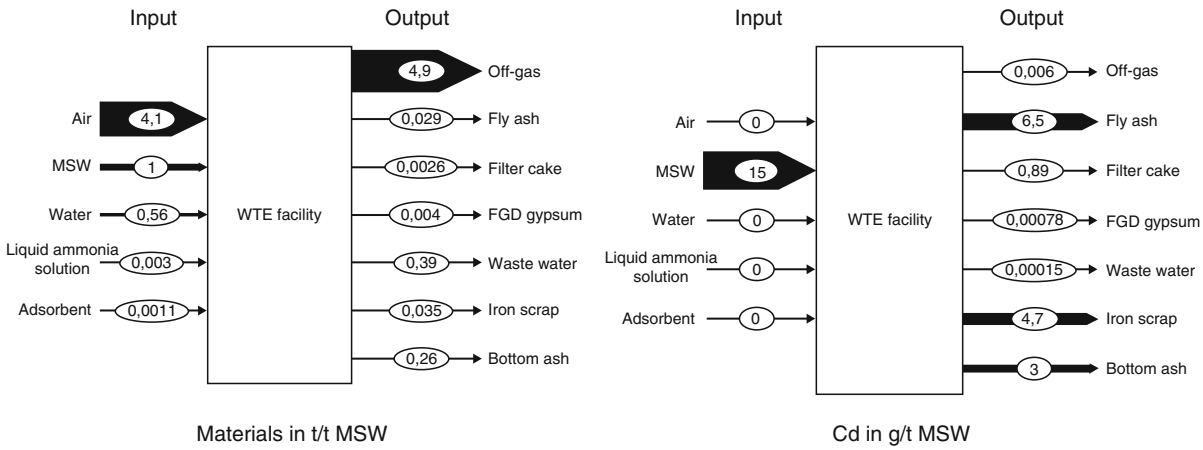

Waste-to-Energy: Decreasing the Entropy of Solid Wastes and Increasing Metal Recovery. Figure 4 Materials and Cd balance for a WTE facility. The WTE facility can be conceived as a transformer of distributions (input → output)

Waste-to-Energy: Decreasing the Entropy of Solid Wastes and Increasing Metal Recovery. Table 3 Result of an MFA for the flow of cadmium (Cd) through a WTE facility (material flows (M_i), concentrations (c), and resulting substance flows (X_i))

Input	M_i t material/ t MSW	c_i kg Cd/kg material	X_i kg Cd/t MSW	%	Output	M_i t material/ t MSW	c_i kg Cd/kg material	X_i kg Cd/t MSW	%
MSW	1.0	0.000015	0.015	99.9	Bottom ash	0.26	0.000011	0.003	20
Adsorbent	0.0011	0	0	0	FGD-gypsum	0.004	0.0000002	0.00000078	0.0052
Liquid ammonia solution	0.003	0	0	0	Filter cake	0.0026	0.00034	0.00089	5.9
Air	4.1	0	0	0	Fly ash	0.029	0.00022	0.0065	43
Water	0.56	0	0	0	Iron-scrap	0.035	0.00013	0.0047	31
					Off-gas	4.9	0.0000000012	0.000006	0.04
					Purified waste water	0.39	0.0000000038	0.0000015	0.01
Total	5.7		0.015	100		5.7		0.015	100

following equations, it is possible to quantify whether Cd is rather concentrated or diluted during the WTE operation.

X_{ij} . . . flow of substance j in material i
M_i . . . flow of material i
c_{ij} . . . concentration of substance j in material i

$$X_{ij} = M_i \cdot c_{ij} \tag{1}$$

with $i = 1 \ldots . n_I$ for input and $i = 1 \ldots . n_O$ for output
m_i. . . . normalized mass flows

$$m_i = \frac{M_i}{\sum_{i=1}^{n_I} X_{ij}} = \frac{M_i}{\sum_{i=1}^{n_O} X_{ij}} \tag{2}$$

The statistical entropy function for the input and output distribution is expressed as follows:

$$H_j(c_{ij}, m_i) = -\sum_{i=1}^{k} \bar{m}_i \cdot \bar{c}_{ij} \cdot ld(\bar{c}_{ij}) \quad (3)$$

where ld is the logarithm to the base 2 and $ld(0) = 0$.

The dilution of gaseous (g) and aqueous (a) emissions in the environment (only for the output) is considered by introducing the geogenic background concentration ($c_{j,geog.}$) of a substance in air and water. The assumption is that the emission via a stack or wastewater pipe into a river is diluted to 1% (therefore the factor of 100 in Eqs. 4 and 5) above the respective geogenic background concentration. Equations 4 and 5 are approximations and only valid if $c_{ij} >> c_{j,geog.}$. If this is not the case, a more complex formula has to be applied; for details see [7].

$$\bar{m}_i = \begin{cases} \dfrac{c_{ij} \cdot m_i}{c_{j,geog.,g}} \cdot 100 \\ \dfrac{c_{ij} \cdot m_i}{c_{j,geog.,a}} \cdot 100 \\ m_i \end{cases} \quad (4)$$

$$\bar{c}_{ij} = \begin{cases} c_{j,geog.,g}/100 \\ c_{j,geog.,a}/100 \\ c_{ij} \end{cases} \quad (5)$$

The maximum statistical entropy is expressed by

$$H_{max,j} = ld\left(\frac{1}{c_{j,geog,}} \cdot 100\right) \quad (6)$$

$$\text{with } c_{j,geog.} = c_{j,geog.,g} \quad \text{when} \quad c_{j,geog.,g} < c_{j,geog.,a}$$
$$\text{and } c_{j,geog.} = c_{j,geog.,a} \quad \text{when} \quad c_{j,geog.,g} > c_{j,geog.,a}$$

H_{max} is determined by assuming that the total substance flow ΣX_{ij} is diluted into the environmental compartment with the lowest background concentration (in the case of heavy metals, this is usually the atmosphere).

The relative statistical entropy is a normalized metric in the range [0, 1].

$$H_{rel,j} = H_j / H_{max,j} \quad (7)$$

The power of a process (e.g., WTE facility) to concentrate a substance j is then expressed by

$$\Delta H_{rel,j} = H_{rel,j,Output} - H_{rel,j,Input} \quad (8)$$

Alternatively, the "substance concentrating efficiency" (SCE) can be defined as a specific metric, in percentage:

$$SCE_j = \frac{-\Delta H_{rel,j}}{H_{rel,j,Input}} \cdot 100 \quad (9)$$

The SCE is positive for concentrating processes with a maximum of 100% (the "pure" substance) and negative for diluting processes (e.g., for Hg when refuse derived fuel is used for co-combustion in a cement kiln). As an example, Table 4 provides the calculation of ΔH_{rel} for cadmium in a WTE plant.

Application of SEA to Waste-to-Energy

By applying Eqs. 1–9 to the metals shown in Table 2, the resulting SCE-values for a specific WTE facility are shown in Fig. 5.

Generally, it can be said that the SCE of state-of-the-art WTE for most metals is in the range between 10% and 20%. For volatile (atmophilic) elements, it tends to be higher since these elements are rather transferred to and concentrated in the APC residues. The highest SCE is achieved for iron. Ferrous metals are easily separated and collected in a WTE facility, by means of magnetic separation.

Following the above discussion, it is clear that SCE-values of 10–20% are not sufficient to realize a noteworthy recycling economy (see Fig. 2). In the case of global copper management SEA shows that waste management should achieve a SCE of at least 80%.

On the other hand, it should be noted that a selective separation step does not have to be restricted to iron. Intensive characterization of bottom ash [6, 9] has shown that some metals appear to a large extent in metallic form in the ash and not as oxides or other compounds. For example, Fig. 6 shows that about 50% of the copper contained in the bottom ash would be recoverable by a mechanical process; particles larger than 4 mm are considered to be detectable and removable by a combination of near-infrared spectroscopy detection and pneumatic separators. This measure would increase the SCE for Cu from 21% to 51%. A melting process, described by Zeltner and Lichtensteiger [10] and shown in Fig. 7, would increase the SCE up to 80%. This last example shows that high recovery rates, i.e., high SCE values, can be achieved. However, they require the

Waste-to-Energy: Decreasing the Entropy of Solid Wastes and Increasing Metal Recovery. Table 4 Example: Calculation of ΔH_{rel} and the SCE of Cd in a WTE facility

	j = Cd	M_i	c_i	X_i	m_i	$c_i \times m_i$	$ld\ (c_i)$	$c_i \times m_i \times ld\ (c_i)$
n_I	Input	t material/ t MSW	kg Cd/kg of material	kg Cd/t MSW	kg of material/ kg Cd	–	–	–
1	MSW	1.0	0.000015	0.015	66,664	1.0	−16.0	−16.0
2	Adsorbent	0.0011	0	0	74	0.0	0.0	0.0
3	Liquid ammonia solution	0.003	0	0	200	0.0	0.0	0.0
4	Air	4.1	0	0	273,322	0.0	0.0	0.0
5	Water	0.56	0	0	37,332	0.0	0.0	0.0
	Total	5.7		0.015	377,593	1.0		−16.0
		M_i	$\bar{c}_i$	X_i	$\bar{m}_i$	$\bar{c}_i \times \bar{m}_i$	$ld(\bar{c}_i)$	$\bar{c}_i \times \bar{m}_i \times ld(\bar{c}_i)$
n_O	Output	t material/ t MSW	kg Cd/kg material	kg Cd/t MSW	kg material/kg Cd	–	–	–
1	Bottom ash	0.26	0.000011	0.003	17,400	0.2	−16.41	−3.3
2	FGD-gypsum	0.004	0.0000002	0.00000079	265	0.000052	−22.28	−0.00116
3	Filter cake	0.0026	0.00034	0.00089	173	0.59	−11.52	−0.68
4	Fly ash	0.029	0.00022	0.0065	1,934	0.43	−12.13	−5.22
5	Iron-scrap	0.035	0.00013	0.0047	2,347	0.31	−12.89	−4
6	Off-gas (g)	4.9	1.0E-14	0.000006	4E + 10	0.0004	−46.51	−0.0186
7	Purified waste water (a)	0.39	1.0E-12	0.00000015	1E + 08	0.0001	−39.86	−0.004
	Total	5.7		0.015	4.0E + 10	1.0		−13.2
	Geogenic concentration of Cd in				H_{max}	47		
	Air ($c_{geog.,g}$)	1.0E-12	kg Cd/kg air		$H_{rel,Input}$	0.34		
	Water ($c_{geog.,a}$)	1.0E-10	kg Cd/kg water		$H_{rel,Output}$	0.28	ΔH_{rel}	−0.06
					SCE (%)	18		

implementation of sophisticated and costly technology. Although it has not been established quantitatively as yet, it is safe to assume that SCE rates in the range of 70–90% are achievable for certain substances.

Relationship Between SEA and Environmental Impact

There is no scientific evidence that entropy is a direct measure of environmental impact. However, considering the stack emissions of a WTE facility, Fig. 8 shows that the actual emissions of Cd (0.0012 mg/m^3) are in a range where they do not contribute to $H_{rel,Output}$. A tenfold increase to 0.01 mg/m^3 would result in an entropy increase by 1%. The emission standard for Cd (0.025 mg/m^3) is in the range of 1–5% which is the area the cadmium emission in stack gas would become entropy relevant.

Therefore, from the point of view of statistical entropy analysis, the emission limit of Cd has been

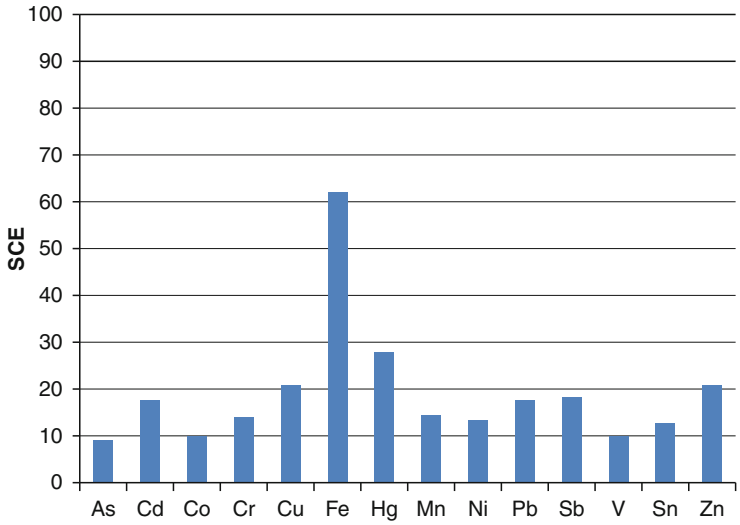

Waste-to-Energy: Decreasing the Entropy of Solid Wastes and Increasing Metal Recovery. Figure 5
Substance concentrating efficiency (SCE in %) of a WTE facility for selected metals

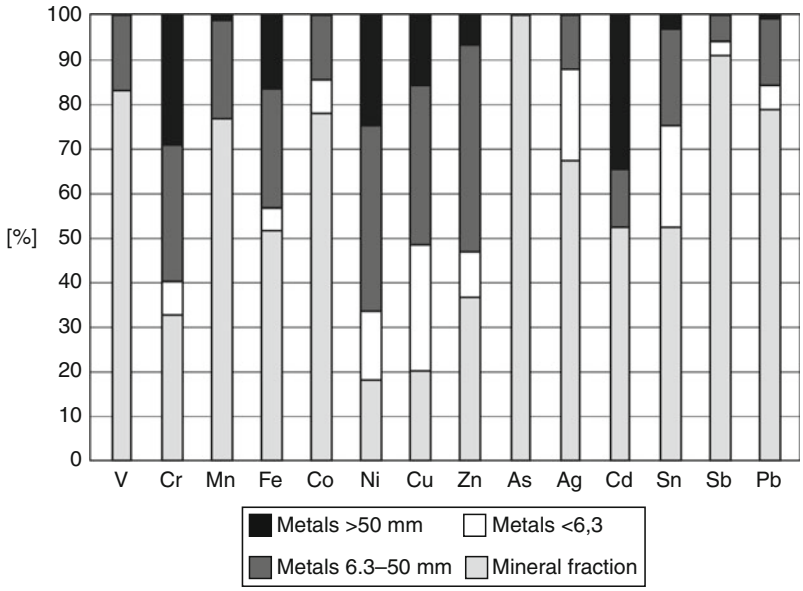

Waste-to-Energy: Decreasing the Entropy of Solid Wastes and Increasing Metal Recovery. Figure 6
Occurrence of metals (%) in the bottom ash of a WTE facility (mass burn) after magnetic separation of iron [6]

determined correctly. The European Directive on Waste Incineration [5] provides the following emission limits: Cd + Tl = 0.05 mg/m^3, Hg = 0.05 mg/m^3, and Sb + As + Pb + Cr + Co + Cu + Mn + Ni + V = 0.5 mg/m^3. For the sum of elements from Sb to V, Table 5 reveals that an emission of 1.1 mg/m^3 would result in an entropy increase ($H_{rel,j,Output}$) of 1%. For entropy increases by 5% and 10%, the emissions would have to be 6.3 and 11 mg/m^3, respectively. This calculation shows that, from an entropy point of view, the emission

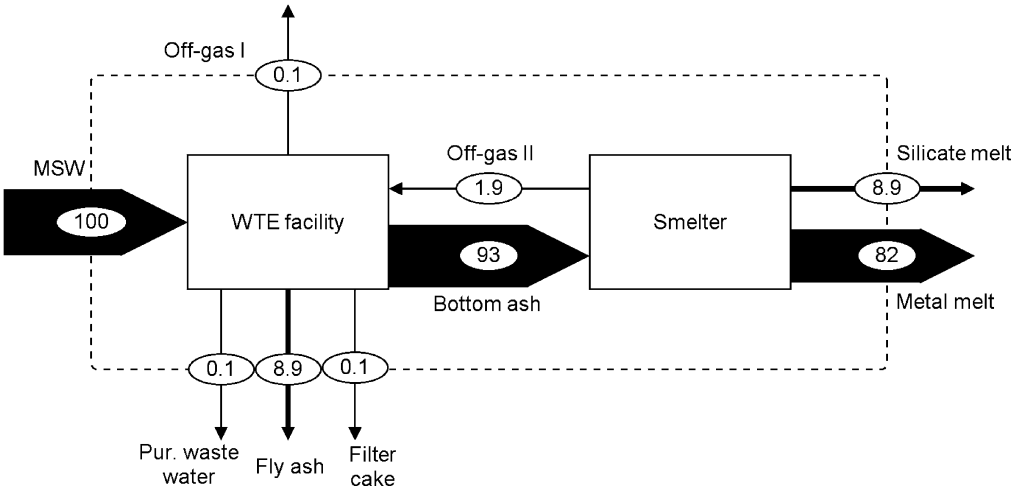

Waste-to-Energy: Decreasing the Entropy of Solid Wastes and Increasing Metal Recovery. Figure 7
Melting of bottom ash; copper flows. Some 80% of the copper in MSW could be recovered [9]

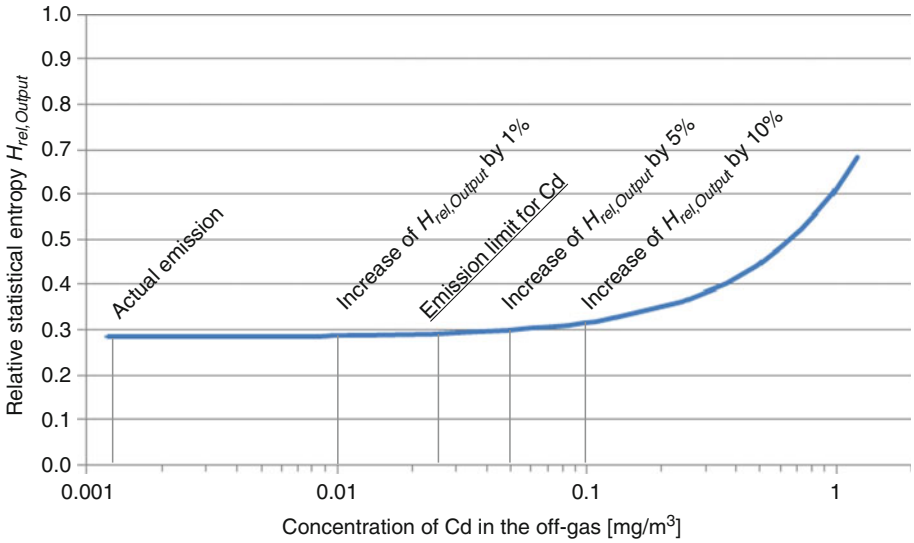

Waste-to-Energy: Decreasing the Entropy of Solid Wastes and Increasing Metal Recovery. Figure 8
Illustration of the influence of the stack gas emission of a WTE facility on the relative statistical entropy ($H_{rel,Output}$). The emission limit for Cd is in the transition area between 1 and 5% increase in entropy

standard for this group of metals is rather stringent. In the case of mercury (Hg), the entropy approach would suggest an emission limit of 0.01 mg/m^3. In this case, the actual emission standard of 0.05 mg/m^3 seems rather high.

However, it should be noted that the transfer coefficients for metals in the stack gas have high uncertainties because they are the result of a single point measurement; also the geogenic background concentrations of metals vary by one to two orders

Waste-to-Energy: Decreasing the Entropy of Solid Wastes and Increasing Metal Recovery. Table 5 Calculated emission values (mg/m^3) as a result of entropy increase

	Increase of $H_{rel,j,Output}$		
	1%	5%	10%
As	0.004	0.01	0.02
Co	0.005	0.03	0.05
Cr	0.1	0.7	1
Cu	0.5	3.5	5
Mn	0.2	0.7	1.3
Ni	0.08	0.4	0.7
Pb	0.23	0.8	2.4
Sb	0.02	0.1	0.2
V	0.008	0.04	0.07
Total (As + Co + Cr + Cu + Mn + Ni + Pb + Sb + V)	1.1	6.3	10.7
Emission limit for As + Co + Cr + Cu + Mn + Ni + Pb + Sb + V [5]			0.5

of magnitude. In summary, it can be stated with high certainty that the actual emissions of metals are not entropy relevant and with some certainty that the present emission standards are in the transition area where emissions to the air would become relevant. Therefore it seems that there is a weak relationship between entropy generation and environmental impact. This means that the entropy approach cannot replace human and eco-toxicological research to fix emission limits but can be used as a first approximation tool where limits are missing or need to be assessed.

Future Directions

At present, research is carried out to extend the concept of SEA from chemical elements to compounds. For example, instead of examining the nitrogen balance of a wastewater treatment plant, one would consider the different compounds of nitrogen in the inflow and effluent of the plant, such as nitrite, ammonium, nitrous oxide, etc. The consideration of the chemical speciation of an element is important for substances like carbon and nitrogen. Since the speciation of an element is crucial for its eco-toxicity, it will be interesting to find out whether there is a relationship between entropy and eco-toxicity. Another research topic is the testing of the applicability and usefulness of SEA in benchmarking studies for waste and wastewater treatment technologies and the employment of statistical entropy for the evaluation of resource consumption.

Bibliography

Primary Literature

1. Georgescu-Roegen N (1971) The entropy law and economic process. Harvard University Press, Cambridge, MA
2. Stumm W, Davis J (1974) Kann recycling die umweltbeeinträchtigung vermindern? In: Gottlieb Duttweiler-Institut für wirtschaftliche und soziale studien, Recycling: Lösung der Umweltkrise? Ex Libris, Zurich, pp 29–41
3. Rechberger H, Graedel TE (2002) The European copper cycle: statistical entropy analysis. Ecol Econ 42(1–2):59–72
4. Brunner PH, Morf LS, Rechberger H (2004) Thermal waste treatment – a necessary element for sustainable waste management. In: Twardowska I, Allen HE, Kettrup AAF, Lacy WJ (eds) Solid waste: assessment, monitoring and remediation. Elsevier, Kidlington, Oxford, pp 783–806
5. Directive 2000/76/EC of the European Parliament and of the Council of 4 December 2000 on the incineration of waste
6. Skutan S, Rechberger H (2007) Bestimmung von stoffbilanzen und transferkoeffizienten für die linie II der MVA Wels. Final Report, Institute for Water Quality, Resource and Waste Management, Vienna University of Technology, unpublished

7. Rechberger H (1999) Entwicklung einer methode zur bewertung von stoffbilanzen in der abfallwirtschaft. PhD-Thesis, Wiener Mitteilungen Band 158, Institute for Water Quality, Resource and Waste Management, Vienna University of Technology
8. Rechberger H, Brunner PH (2002) A new, entropy based method to support waste and resource management decisions. Environ Sci Technol 34(4):809–816
9. Mitterbauer G, Skutan S, Rechberger H (2009) Charakterisierung der rostasche der MVA Dürnrohr im hinblick auf die rückgewinnung von metallen. Institute for Water Quality, Resource and Waste Management, Vienna University of Technology, unpublished
10. Zeltner C, Lichtensteiger T (2002) Thermal waste treatment and resource management – a petrologic approach to control the genesis of materials in smelting processes. Environ Eng Policy 3:75–86

Books and Reviews

Brunner PH, Rechberger H (2004) Practical handbook of material flow analysis. Lewis Publishers, New York

Kaufman S, Krishnan N, Known E, Castaldi M, Themelis N, Rechberger H (2008) Examination of the fate of carbon in waste management systems through statistical entropy and life cycle analysis. Environ Sci Technol 42(22):8558–8563

Rechberger H (2001) An entropy based method to evaluate hazardous inorganic substance balances of waste treatment systems. Waste Manage Res 19:186–192

Rechberger H (2001) The use of the statistical entropy to evaluate the utilisation of incinerator ashes for the production of cement. Waste Manage Res 19:262–268

Waste-to-Energy Ash Management in Europe

Juergen Vehlow
Karlsruhe Institute for Technology, Institute for Technical Chemistry, Karlsruhe, Germany

Article Outline

Glossary
Definition of Subject
Introduction
Bottom Ashes
Boiler and Filter Ashes
Residues from Gas Cleaning
Conclusions
Future Directions
Bibliography

Glossary

Boiler ash Coarse fly ash separated from the flue gas inside the boiler and directly discharged or discharged after boiler cleaning by soot blowing or rapping.

Bottom ash Solid residue discharged from the grate of a waste incinerator.

Dioxins (PCDD/F) A group of 75 congeners of polychlorinated dibenzo-p-dioxins (PCDD) and 135 congeners of polychlorinated dibenzofurans (PCDF); concentrations are given in toxic equivalent accounting for the different toxicity of the single congeners.

Filter ash Fine dust separated from the flue gas by filters, mainly by electrostatic precipitators.

Incineration Combustion of waste, in Europe preferentially in grate furnaces.

Leaching Elution of inorganic (especially heavy metal) or organic species out of solid materials into liquids; leaching standards are typically regulating the access to disposal or the utilization of a material; leaching is measured by standardized tests.

Scrubbing Chemical gas cleaning step using wet or dry neutralizing agents; wet systems are typically designed in two stages.

Definition of Subject

In Europe, the environmentally compatible management of solid residues from waste incineration became a major topic of concern in the first decade of the new millennium. Tightened access criteria to landfills promoted in a number of countries, especially in the European Union, aim for beneficial use of the bottom ash. Furthermore, several attempts are seen to stabilize respectively inertize fly ash and gas cleaning residues so they need not be disposed of in hazardous landfills. Organic content and leaching stability are the most important environment-related quality parameters to be addressed.

Introduction

Some time ago, the debate about thermal processes was mainly driven by potential risks of air emissions, especially those related to dioxins. Meanwhile, the gas

cleaning devices implemented in municipal solid waste incineration (MSWI) or, as they are called in some areas, waste-to-energy (WTE) plants are among the most effective ones found in any technical process, and the interest is nowadays more focused on the quality of the solid residues from those processes. The actual objectives are to produce as much as possible inert bottom ashes and to enable their utilization as secondary building materials. This is especially promoted in the Netherlands, Denmark, and Germany, recently also in France. A further focus is the inertization and safe disposal – or even utilization – of the filter and boiler ashes as well as of the residues collected in the Air Pollution Control (APC) systems of WTE plants.

Already in early times attempts are seen to utilize bottom ashes from waste incineration plants. In the Frederiksberg incinerator, built in 1903, bricks were produced from bottom ash for utilization in the building sector [1]. However, the calorific value of the waste at that time and the resulting combustion temperature were most likely to generate a bottom ash quality which was far beyond the standards required and achieved today. The described procedure was only maintained for few years, supposably due to market constraints based on insufficient quality.

After World War 1 a tendency was seen not to burn but to melt the waste, again to produce secondary building materials. This practice, too, was finally not successful on the market because of problems with the refractory liners of the furnaces, varying product quality, and especially the high costs of the processes [2].

Starting the last decade of the twentieth century all kinds of secondary treatment processes have been developed to tailor the residue quality according to special needs. Secondary measures, however, are expensive and hence the better approach is an optimized control of the combustion process to

- Guarantee an excellent burnout of carbon compounds
- Promote the volatilization of heavy metals like Hg and Cd out of the fuel bed
- Fixate lithophilic elements in the silicatic and oxidic matrix of the bottom ash, thus reducing their leachability

The following discussion of the quality of residues from modern waste incineration plants will follow these objectives. Finally, this entry will investigate which rational options exist to inertize and eventually utilize bottom, boiler, and filter ashes, and flue gas cleaning residues. All considerations are based mainly on the results of an international perspective on the characterization and management of waste incineration residues, published by the International Ash Working Group in 1997 [3].

Mass Streams in a WTE Plant

The basis of all discussions about waste incineration residues is the knowledge of the different mass streams in a municipal solid waste incinerator. Figure 1 shows average ranges for these streams as found in modern mass burning systems. The air consumption is approx. 4,500 m^3/Mg of waste.

State-of-the-art plants in most industrialized countries produce typically between 150 and 250 kg of bottom ash per 1 Mg of burnt waste. The respective numbers in Japan are in the order of 100–120 kg due to different waste collection and eventual pre-treatment strategies.

Most published numbers include the grate siftings which are in many countries kept separate from the bottom ash. The mass flow of siftings depends on the type of grate and its time of operation. It accounts typically for less than 5 kg/Mg of waste. The siftings may increase the amount of unburnt matter in the bottom ash. In view of utilization, however, the inventory of metallic Al eventually dripping through the grate voids is of much higher concern. Metallic Al tends to form hydroxides in contact with water and this reaction is accompanied by a swelling of the material.

The production of boiler ash depends on the type of boiler and on the amount of dust released from the grate and carried over in the flue gas. Boiler ashes should be treated together with the filter ashes due to their similar level of toxic heavy metals and organic compounds. In some countries, this has already been enforced by legislative regulations. The data presented for filter ashes reflect the situation in modern plants that try to establish so-called gentle combustion with dust loads down to less than 2 g/m^3 [4].

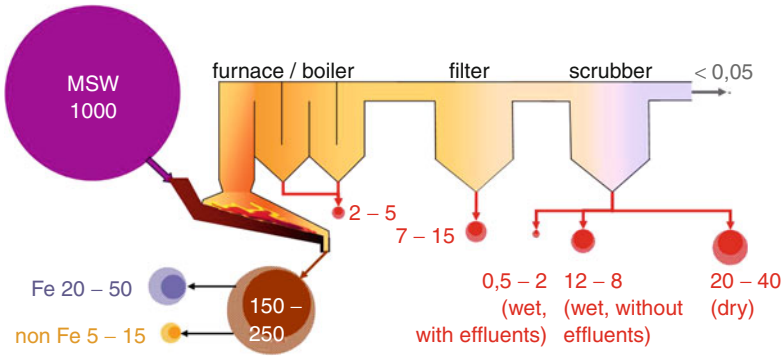

Waste-to-Energy Ash Management in Europe. Figure 1
Mass balance of a municipal solid waste incineration plant (in kg/Mg waste)

The mass flow of APC residues shows actually the highest variation of all residues. Wet scrubbing systems with liquid effluents discharge produce 0.5–2 kg of dry neutral sludge per Mg of burnt waste. In wet systems with internal or external evaporation of the scrubbing solutions additional 11–16 kg of neutralization products increase the total solid residues to approx. 12–18 kg/Mg. Whereas wet scrubbing operates close to stoichiometry and hence at minimum residues, in case of semi-dry or dry systems the necessary surplus of unreacted neutralizing reagents increases the total amount of scrubbing residues to 20–40 kg/Mg of waste.

Bottom Ashes

Disposal and Utilization Regulations

Waste incineration is performed to produce an inert residue, the bottom ash, which meets the respective disposal standards. Many countries aim for utilization of this residue stream in order to save space on landfill sites.

The disposal of residues is in the EU regulated by the EU landfill directive 1999/31/EC [5] and the Council Decision 2003/33/EC [6] which contains the landfill access criteria. For utilization of residues, however, no common regulations exist and the various countries have their own protocols.

Table 1 compiles selected standards laid down in the German Waste Storage Ordinance [7] for disposal on landfill class 1 – which are identical with those in the Council Decision – and for utilization of bottom ash in road construction which are laid down in a memorandum of the LAGA, a German working group of representatives of the ministers of environment of the federal states [8]. The leaching standards have to be measured according to the EU leaching protocol [9] which is in the table indicated by the respective national test DIN EN 12457-4. The table shows only small differences between the requirements for disposal and utilization. The challenge is to reach the utilization quality without further post-combustion treatment.

Waste-to-Energy Ash Management in Europe. Table 1
Selected German standards for disposal and utilization of WTE bottom ash

	Unit	German landfill class 1	Road construction (LAGA)
LOI	wt%	3	
TOC	wt%	1	1
DIN EN 12457-4			
Cl	mg/L	1,500	250
Cu	mg/L	1	0.3
Zn	mg/L	2	0.3
Cd	mg/L	0.05	0.005
Hg	mg/L	0.005	0.001
Pb	mg/L	0.2	0.05

In the case of utilization as secondary building material, additional standards are set for mechanical properties like density, mechanical strength, grain size distribution, or freeze-thaw-stability. This aspect will not be discussed here.

Characterization

Burnout and Organic Ingredients The "burnout" is the key parameter for disposal as well as for utilization of bottom ashes. The German Waste Storage Ordinance sets a total organic carbon (TOC) limit of 1 wt.-% for disposal on a class I landfill and the same number is found in the LAGA memorandum for utilization in road construction.

In modern well-operated WTE plants, the TOC in bottom ashes is typically well below 1 wt.% [10, 11]. Special combustion trials in the TAMARA test incinerator in Karlsruhe (Germany) demonstrated that an increasing heating value of the feed, and the resulting higher bed temperatures, improve the burnout of bottom ash (see Fig. 2) [12].

The TOC of bottom ashes consists mostly of elementary carbon; some organic compounds are also found that cover the spectrum from short-chain compounds [13] up to low volatile species such as PAH or PCDD/F. Typical concentrations of organic compounds in the various solid residues are compiled in Table 2.

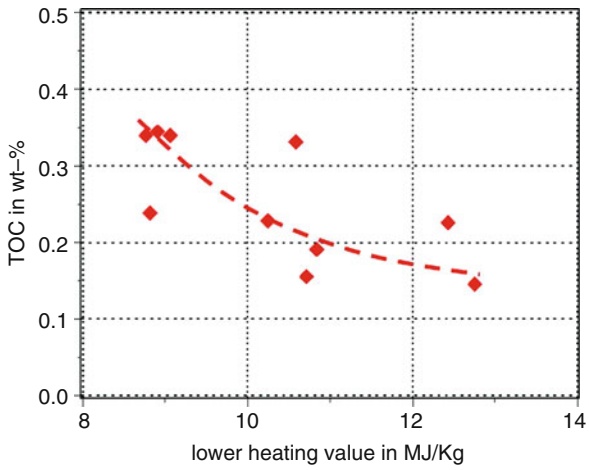

Waste-to-Energy Ash Management in Europe. Figure 2 Residual carbon in TAMARA bottom ashes versus heating value of the feed

The data are taken from modern facilities [12–15]. The PCDD/F numbers are given in terms of international toxic equivalence data (I-TE). It is evident that the organic pollution is higher in the boiler and fly ashes than it is in the bottom ash.

It should be noted that the I-TE levels detected in the bottom ashes of modern incineration plants were in the same order of magnitude as found in uncontaminated soils in Central Europe [16].

Chemical and Mineralogical Characterization

The mass and volume reduction occurring during combustion of solid wastes causes an enrichment of a number of heavy metals in the bottom ashes compared to their concentration in the earth's crust. This is demonstrated by the concentration ranges of selected species depicted in Fig. 3. The data are compiled from numerous publications and from the Handbook of Chemistry and Physics.

Some heavy metals, for example, As, Cd, Hg, and Pb are to a great extent volatilized out of the fuel bed, however, also these metals show in most cases higher concentrations in the bottom ashes than in the lithosphere.

In addition to the chemical analysis, a geochemical and mineralogical characterization provides useful information in view of the long-term behavior of a material. Bottom ashes can be characterized as a mixture of silicate and oxide phases. Some typical

Waste-to-Energy Ash Management in Europe. Table 2 Concentration ranges of organic compounds in bottom, boiler, and filter ashes (PCDD/F in I-TE)

	Bottom ash (ng/g)	Boiler ash (ng/g)	Filter ash (ng/g)
PCDD/F	<0.001–0.03	0.02–1	0.1–10
PCB	<5–50	4–50	10–250
PCBz	< 2–20	200–1,000	100–4,000
PCPh	<2–50	20–500	50–10,000
PAH	<5–10	10–300	50–2,000

mineral phases found in these residues are shown in the micrographs in Fig. 4 [17].

Some of these phases can provide information about the temperature the material has been exposed to on the grate. This important parameter controls mainly the fate of elements in the combustion chamber, but is not well known in full scale plants. The knowledge of formation temperatures of single phases and the specific search for high-temperature phases are promising ways to obtain better information in this area [18].

Post-combustion Treatment

As mentioned earlier, a number of countries have or are planning to set standards for the utilization of bottom ash. The major application area is road construction where ash is used in the support layers, mainly under water-tight capping. Among the few countries which have more or less country-wide common regulations is Germany which will be discussed more in detail below. Similar practice is followed in the Netherlands, Belgium, and Denmark. Countries like Sweden decide on utilization case by case.

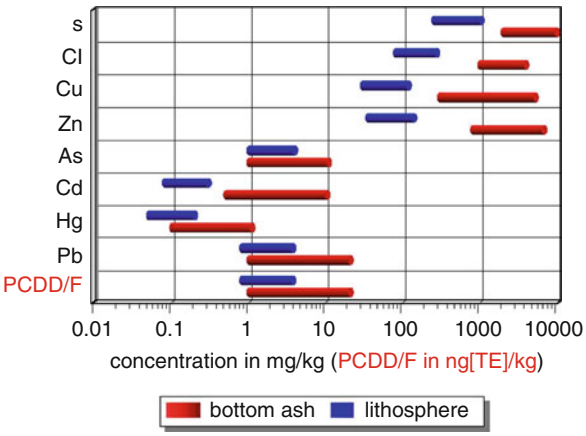

Waste-to-Energy Ash Management in Europe. Figure 3
Concentration ranges of selected elements and PCDD/F in bottom ash and in the earth's crust

The German guideline regulating use of ash in road construction is the LAGA memorandum mentioned earlier [8]. It requires mechanical pre-treatment, scrap removal, and aging of the ashes for 12 weeks.

The mass flow scheme in Fig. 1 indicated already that raw bottom ashes contain significant amounts of ferrous and non-ferrous metal scrap. It is common practice that at least the ferrous, but nowadays in most plants also the non-ferrous, metals are recovered if the final destination of the bottom ash is a landfill. Whereas revenue from ferrous scrap may often only cover the recovery costs, non-ferrous metals, mainly Al and Cu, have a high market value which cares for good economy.

Hence, scrap removal is the only pre-treatment if bottom ashes are landfilled. If utilization is envisaged, the obligatory post-combustion treatment is much more extended. A typical flow sheet of advanced ash treatment as performed at the Hamburg waste incinerator MVR is shown in Fig. 5.

The procedure starts typically already in the quench tank of the incinerator where a surplus of water reduces the salt content [10, 20]. After discharge, the ashes are stored for few days for de-watering before they undergo further treatment which consists of a sieving to remove bulky fractions and magnetic separation of ferrous

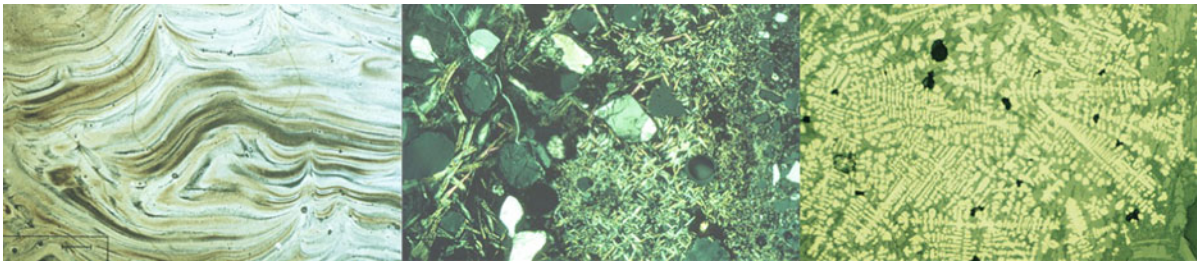

Waste-to-Energy Ash Management in Europe. Figure 4
Micrographs of minerals in bottom ashes: glass formed during combustion (*left*), gehlenite $Ca_2AlAlSiO_7$ in glassy matrix (*center*), magnetite, Fe_3O_4 (*right*)

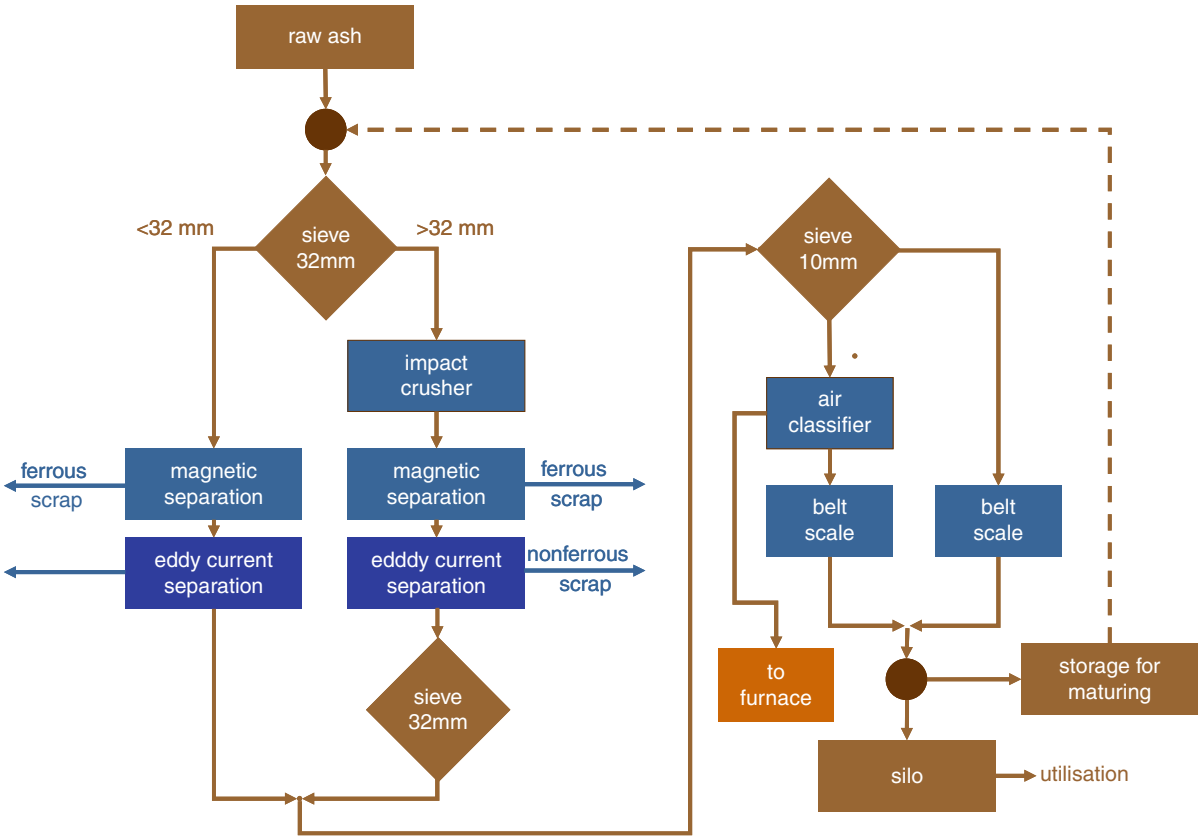

Waste-to-Energy Ash Management in Europe. Figure 5
Grate ash pre-treatment at the Hamburg waste incineration plant MVR (Adopted from [19])

scrap which is followed by an eddy-current separation of non-ferrous metals.

The metal fractions are sold to recycling companies. Considering the total amount of bottom ashes of 4–5 million Mg in Germany and a recovery efficiency of 60–70% more than 300,000 Mg of iron scrap and with a recovery efficiency of 30–40% up to 50,000 Mg of non-ferrous metals can be recovered. Especially, the latter fraction accounts for a not unwanted revenue for the operator.

The ashes are than stored for aging or maturing for 12 weeks and after the respective compliance tests, the ashes can be utilized as secondary building materials.

Leaching Properties

Leaching Fundamentals The chemical composition of a product may not allow determining its environmental impact. This is far more depending on the leaching stability of the material in question. Even if the matrix and the speciation of single elements are known, a reliable theoretical prediction of the short- and long-term behavior is almost impossible. The most important parameters influencing the leaching stability of a material are listed below:

- Its chemical composition
- Its chemical/geochemical/mineralogical speciation
- The fraction of a species available for leaching
- The particle morphology
- The properties of the leachant, especially its pH or the presence of complexing constituents
- The liquid-solid ratio (LS) in the leaching system

It seems evident, that no single or simple test procedure will deliver results that allow a sound evaluation of impacts on the environment. In fact a great number of different tests have been developed to get detailed

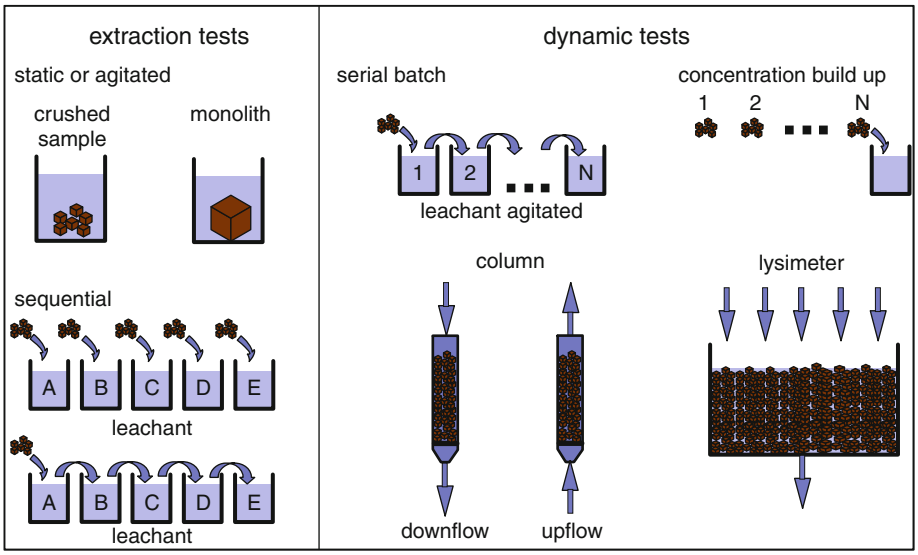

Waste-to-Energy Ash Management in Europe. Figure 6
Principles of leaching tests

information about the leaching properties of residues from waste incineration.

There are two principal categories of test procedures: extraction tests and dynamic tests. Indicator tests are in most cases extraction tests. The most common principles of these test categories are comprised in Fig. 6.

Extraction tests allow the determination of leaching equilibria. If the leachate is analyzed in time increments before equilibrium is reached, information on the kinetics of the system can be obtained. An example of such tests is the Dutch tank leaching test [21] for stabilized materials. This test also gives indication of the major parameters controlling the leaching process, for example, diffusion or solubility. Sequential tests in different leachants of increasing chemical strength are often used to investigate the chemical bond of specific elements in the matrix.

Dynamic tests are applied to reveal the leaching kinetics of granular material. One of these is the Dutch column leaching test [22]. This test is typically performed up to an accumulated liquid/solid ratio of 10 and enables the modeling of contaminant release over a period of 50–100 years.

In practice, a material in question is subject to a number of different tests that are selected to model as close as possible the envisaged disposal or utilization scenario. After the fundamental properties have been acquired, an indicator or compliance test – in most cases a standardized test procedure – is chosen to assess the quality of an actual sample in short time and with limited effort [23]. Since the early 2000s, the European Standardization Committee CEN has released unified test methods which will in future be applied in all EU countries [9].

The most important parameter influencing the results of a leaching test is the pH of the leachate [3, 24]. Figure 7 shows a schematic overview of the influence of the pH of the leaching solution on the solubility of metal cations and anions in aqueous solutions. It is well known that most heavy metals show rather low solubility in the weak alkaline range. Their solubility increases with decreasing pH. In the alkaline region, different metals behave differently: some (e.g., Cd) stay insoluble with increasing pH. Others, the amphoteric ones, are more or less solubilized if the pH is elevated. The amphoteric metal of highest interest in waste incineration is Pb.

Metals which tend to form anions in aquatic solutions like V, Cr, or Mo, have their highest solubility close to the neutral point.

The graph in Fig. 7 indicates the ranges of pH used in selected leaching tests of bottom ashes. In the DIN EN 12457-4 test with a LS ratio of 10, a duration of

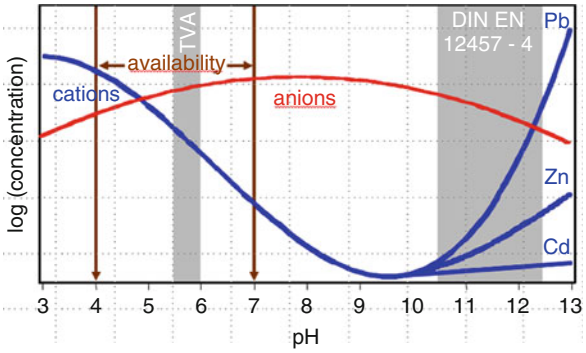

Waste-to-Energy Ash Management in Europe. Figure 7 Influence of the pH and the solubility of metal cations and anions

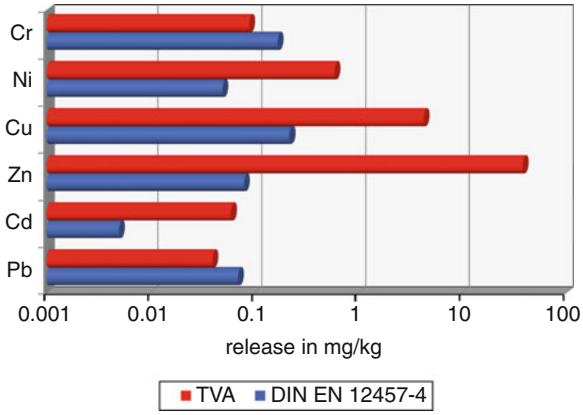

Waste-to-Energy Ash Management in Europe. Figure 8 Leaching results of the Swiss TVA and the German DIN EN 12457-4 test on one bottom ash sample (Adopted from [26])

24 h, and no pH control, the final pH values can vary between 10.5 and 12.5. These varying conditions have severe impacts especially on the test results for Pb as can be deduced from Fig. 7.

The Swiss TVA test [25], a compliance test with two steps, 24 h each, LS = 10, is characterized by a rather constant pH of 5.5–6 due to gaseous CO_2 injected permanently into the test solution.

Constant pH values are used for the Dutch availability test [22] which provides information about the leaching potential under assumed "worst" environmental conditions. The cation solubility is tested at a pH of 4 and that of anions at a pH of 7. The sample has to be finely ground in order to exclude any inhibition of the leaching by diffusion and the liquid-solid ratio is kept at 100 to avoid saturation effects in the solution.

Due to the different test conditions various leaching tests will produce different results when run on one and the same material. An example is shown in Fig. 8, where one bottom ash sample was tested using the Swiss and the German test procedure [26].

The bar plot indicates that Ni, Cu, and especially Zn show a significantly higher elution in the TVA then in the DIN EN test due to the formation of hydrogen-carbonates.

Effect of Aging and Utilization Potential In order to optimize the total burnout, the combustion temperature, and thus, the fuel bed temperature have been elevated in WTE plants compared to the operation mode during the 1980s. As an effect of such operation changes, a higher formation of CaO can be seen. The pH value of fresh bottom ashes is often exceeding 12. According to the German LAGA memorandum [8] bottom ashes have to be stored for 12 weeks prior to utilization in road construction for aging or maturing. During this time the uptake of CO_2 from the air converts the earth-alkali oxides into carbonates and neutralizes part of the alkalinity. Hence, aged bottom ashes establish a pH of about 10–11 in the DEV S4 test.

Data from a test program in a German full scale waste incineration plant illustrate the effect that aging has on the pH of bottom ash and on the leaching of metals [11]. The bar plot in the left part of Fig. 9 documents that the pH of fresh bottom ash in the DIN EN 12457-4 test exceeds in almost all test trials 12 and drops down by about two units during the aging process. As shown in the right graph of Fig. 9, this pH change has no effect on the leaching properties of Mo which is present mainly as molybdate. The leaching stability of Cu and Zn is moderately improved in the aged material whereas the leaching of Pb is reduced by almost two orders of magnitude.

This strong interdependency is responsible for the strange situation that due to German regulations fresh bottom ashes from some plants do not comply with the landfill standards while after aging they are excellent secondary building materials.

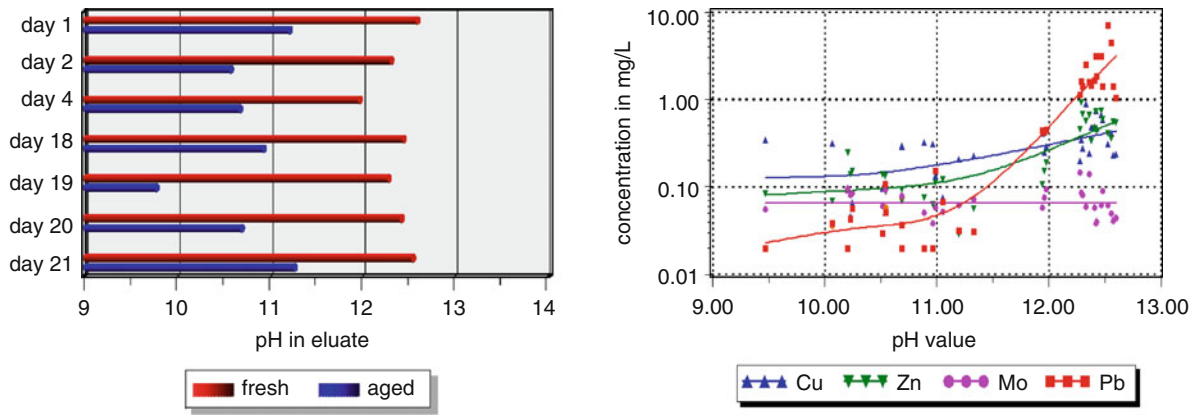

Waste-to-Energy Ash Management in Europe. Figure 9
pH value of fresh and aged bottom ash samples (left) and DIN EN 12457-4 test results on these samples for four metals (Adopted from [11])

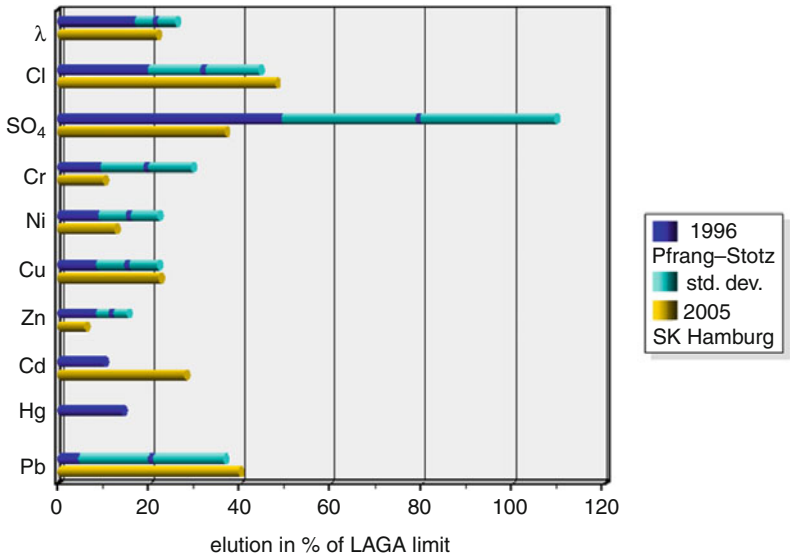

Waste-to-Energy Ash Management in Europe. Figure 10
Bottom ash leaching test results obtained by the German compliance test in 1996 (Adopted from [27]) and in 2005 (Adopted from [19]) (λ: electric conductivity)

Figure 10 shows the results for 26 samples taken routinely in 1994 over 1 year from an industrial ash treatment site [27]. The test at that time was almost identical with the DIN EN 12457-4 procedure. The results for the environmentally interesting heavy metals were always well below the respective standards. The only component exceeding the limit in a few cases was sulfate. This limit has been set to protect concrete structures from corrosion attack.

In 2005, equivalent data were published for bottom ashes of the Hamburg, Germany, waste incineration plants [19]. Except for the much better sulfate values the results are almost the same (Fig. 10).

Meeting standards is a prerequisite to get approval for utilization, more detailed information about the potential environmental impact may be achieved by running the same tests on bottom ashes and other building materials. This has been done using aged

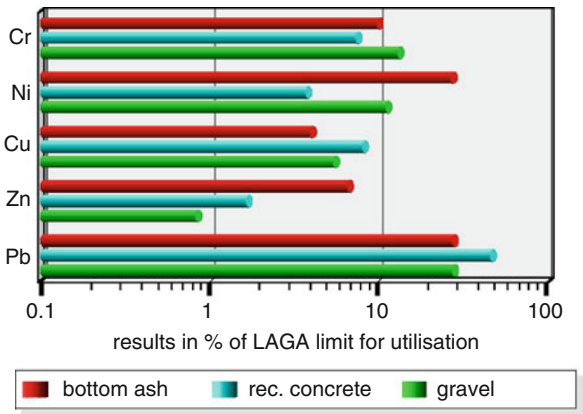

Waste-to-Energy Ash Management in Europe. Figure 11 Leaching test results obtained by the German compliance test on bottom ashes, recycled concrete, and gravel (Adopted from [28])

bottom ashes from a German waste incinerator, secondary building material recycled from a demolished highway bridge, and gravel from the river Rhine. The results are shown in Fig. 11 [28]. The bar plot documents that the difference in leaching stability of the three materials is surprisingly small, although there is no doubt, that the inventory of the selected metals in bottom ash is much higher than in concrete and especially in gravel.

Utilization of Bottom Ashes in Europe

According to the above discussed bottom ash quality, it can be stated that bottom ashes from modern and well-operated WTE plants meet the LAGA limits for utilization easily and do not behave significantly differently from conventional building materials. Hence, there is no reason not to utilize – after careful testing – such materials for e.g., road construction [29].

This use is common practice in countries with geological conditions hampering the siting of landfills like the Netherlands, Belgium, or Denmark. These countries utilize 90% and more of the bottom ashes. The respective number for Germany is approx. 85%. Some other countries like France are nowadays also encouraging bottom ash utilization.

A different strategy is followed by the Swiss authorities. According to their regulations, bottom ashes are categorized as reactive residues. Only stone-like materials are accepted as building materials and stone-like refers to the concentration and not to the mobility of a single constituent. Since the bottom ashes contain higher amounts of heavy metals than the lithosphere (see Fig. 3), almost no utilization is practiced. Bottom ashes have to be disposed of or they must be converted into stone-like materials by adequate measures.

The practiced management strategies for bottom ashes from European WTE plants are shown in Fig. 12. The data are taken from Eurostat, the statistical office of the EU [30], and from CEWEP, the Confederation of European Waste-to-Energy Plants [31].

As can be seen, most countries with a high share of waste incineration and hence high bottom ash figures utilize a significant fraction of that material, mainly in road construction.

Quality Improvement by Sintering

The above presented high leaching stability of bottom ash needs to be achieved permanently. This leads to the question, how to guarantee such high quality. A self-evident approach is the establishment of high temperatures in the fuel bed to volatilize mobile metals and halogens out of the bed material and to immobilize lithophilic species by sintering. Since sintering is a solid phase respeciation with stabilization of many heavy metals in the silicate-rich lattice of the bottom ash, a higher residence time of the ash at higher temperature in the furnace promotes the formation of inert species.

This strategy has been investigated in laboratory scale by sinter experiments using fresh bottom ashes from two German incineration plants [10]. The ashes were treated thermally under atmospheric air at temperatures of 850°C, 1,000°C, and 1,300°C for 30 min each. At the latter temperature, the material was melted. The resulting DEV S4 leaching data of the products of these tests are presented in Fig. 13.

The graph indicates a significant improvement of the leaching stability of four selected metals by the treatment. At 850°C and 1,000°C, comparable effects were observed. The fusion, however, did not improve the elution stability significantly. This finding is supported by the comparison of test results from bottom ashes with those published for molten residues

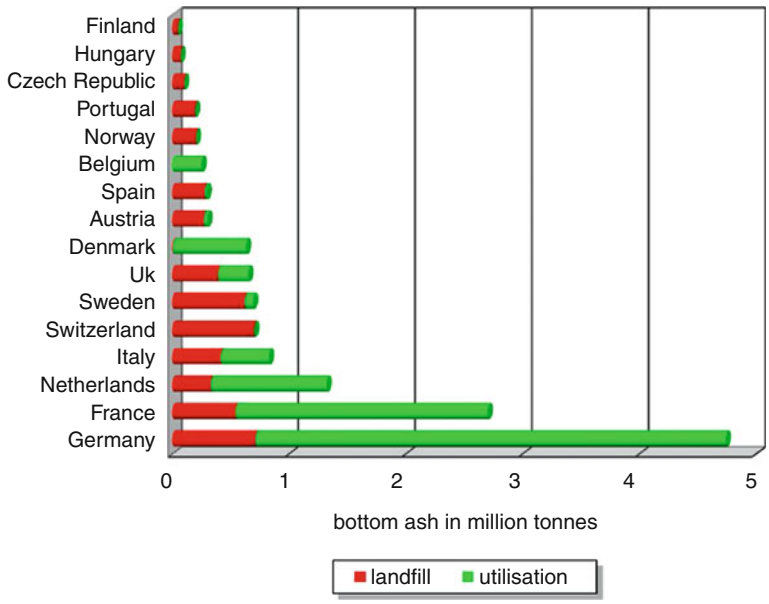

Waste-to-Energy Ash Management in Europe. Figure 12
Production, disposal on landfills, and utilization of bottom ashes in all European countries which operate WTE plants in 2008

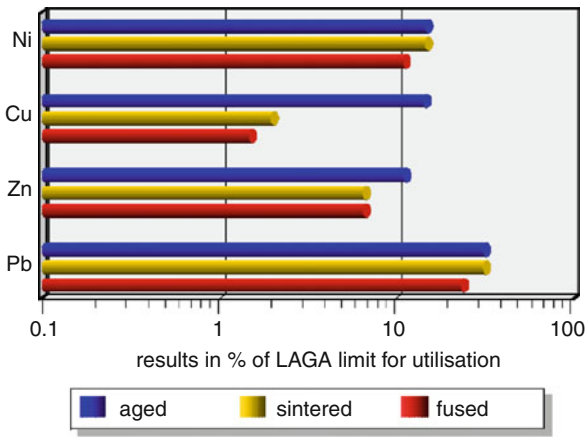

Waste-to-Energy Ash Management in Europe. Figure 13
Leaching test results of thermally treated bottom ashes and concrete

from high-temperature processes like Thermoselect or the Siemens Thermal Waste Recycling Process [32].

The stabilization by sintering was also validated in semi-technical experiments with fresh bottom ashes from a full scale incineration plant [33].

Based on these results, it can be concluded that sintering at temperatures of 850°C has a stabilizing effect upon heavy metals. The energy consuming – and thus more costly – fusion, however, does not pay since no significant further fixation could be observed. Hence, a simple in-plant measure to produce bottom ashes of high leaching stability can be recommended: The bed material should be kept at high temperature for as long as possible at the back end of the grate.

This is common practice in Europe today, attempts to implement melting or fusion processes into conventional waste incineration plants or to establish a market for combined processes with molten slag like Thermoselect [35], the Siemens Thermal Waste Recycling Process [36], or the Von Roll RCP Process [37] failed in Europe – in spite of strong efforts during the 1990s. Main reasons were energy consumption and complexity of the processes which caused high process costs as well as technical problems.

Other stabilization processes like stabilization by the addition of phosphates (WES-PHIX process) are also not common since the quality of bottom ashes from

well-operated incineration plants meets all requirements for safe long-term disposal or even utilization – as has been laid out above.

Boiler and Filter Ashes

Characterization

Boiler ashes are deposited at temperatures between approx. 800°C and 200°C, filter ashes typically at temperatures slightly below 200°C. That is why heavy metals and other species which are volatilized inside the combustion chamber are to some extent precipitated on the dust surfaces. The concentration of volatile elements like Zn, As, Cd, or Pb can exceed that in grate ashes significantly as is shown in Fig. 14. The inventory of halogenated organic micro-pollutants like PCDD/F or PCB which are mainly synthesized inside the boiler or of PAH which are an indicator for incomplete combustion is also increased compared to that in bottom ashes (compare Table 2).

Since filter ashes are precipitated at lower temperatures than boiler ashes and since they have a much finer particle size distribution and offer higher surfaces for condensation their concentrations of heavy metals, of halogenides, and of organic micro-pollutants are typically higher.

Disposal Practice

Due to their elevated pollutant inventory boiler and filter ashes have to be characterized as hazardous waste and must not be combined with the bottom ashes. They have to be typically disposed of on special – and expensive – disposal sites, preferentially in the underground. A compilation of filter ash production as well as disposal strategy in European countries is found in Table 3. The data have been compiled from CEWEP member's questionnaires [31].

The table documents that the by far prevailing management strategy is the disposal on hazardous landfill sites.

In Germany boiler and filter ashes can be used in old salt mines for backfilling of caverns. This practice is according to national regulations acknowledged as utilization. The same strategy is followed in Norway where filter ashes can be "utilized" for backfilling an old granite quarry on the small island Langøya. Norwegian

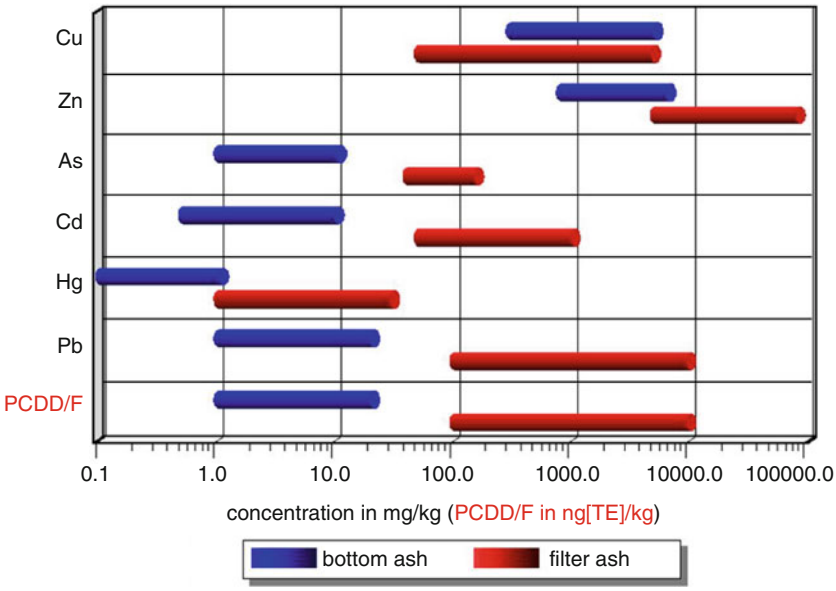

Waste-to-Energy Ash Management in Europe. Figure 14
Concentration ranges of selected elements and PCDD/F in bottom and filter ash

Waste-to-Energy Ash Management in Europe. Table 3 Filter ash production and management in selected countries [CEWEP 2006] ([1]estimated)

Country	Year	Production (Mg)	Management strategy
Austria	2004	40,000	Mainly salt mine backfilling, hazardous landfill
Belgium	2004	50,000	Solidification and hazardous landfill
Czech Republic	2004	6,000	5,000 hazardous landfill, 1,000 underground mine
Denmark	2004	86,834	100% recycled (salt mine after special treatment)
France		400,000	
Germany	2005	650,000	Utilization in salt mine, minor amount hazardous landfill
Hungary	2005	13,585	Hazardous landfill
Italy	2004	71,814	
Netherlands	2003	82,200	50% utilized in mines and construction (e.g., asphalt filler)
Portugal	2005	40,000	Inertization before hazardous landfill
Spain	2005	94,420	Hazardous landfill
Sweden	2004	138,000	Landfilling + utilization in Norway (Langøya)
United Kingdom[1]	2000	78,125	Hazardous landfill

data were not available but some filter ashes from Sweden are going to that place as well.

A different utilization of filter ashes is practiced in the Netherlands. Out of the noted 50% utilized ashes a certain amount is used as filler in asphaltic layers on roads, others are shipped to German salt mines for backfilling.

Stabilization Processes

The high expenses for a sustainable final disposal of boiler and filter ashes were reason for numerous attempts to detoxify these materials in order to get access to less expensive disposal routes or even to utilization scenarios. A broad spectrum of different processes has been proposed and tested in different scales. Table 4 tries to categorize the various treatment options.

It is evident that solidification or stabilization processes do not alter the toxic inventory of a material. The inertization by chemical reactions or the formation of a diffusion barrier does only last for a limited time. Two processes have been in full scale application for many years: the "Bamberg Model," where filter ashes are stabilized on a landfill by mixing with the neutralization sludge of the wet scrubber effluents [39], and in Switzerland the stabilization of filter ashes by cement after washing [40].

Waste-to-Energy Ash Management in Europe. Table 4 Procedures for treatment of boiler and filter ashes

Principle	Process
Solidification/ stabilization	Without additives (Bamberg Model) Cement based systems (e.g., Portland cement, alinite) Waste pozzolanic systems (e.g., coal fly ash) Chemical stabilization (e.g., sulphides, TMT 15™) Organic additives or matrix (e.g., bitumen)
Thermal treatment	PCDD/F destruction (Hagenmaier drum) Sintering (mineral respeciation) Fusion (melting without additives) Vitrification (melting with additives)
Combined processes	Acid extraction + sintering (3R process) Stabilisation with FeSO4, oxidation, sintering (Ferrox process)

Thermal treatment can be performed at moderate temperatures in the so-called Hagenmaier Drum at 400°C to destroy dioxins [41]. This process is actually used in Japan; in Germany only few plants operated it in the 1990s as pilot plants.

Another option is vitrification at high temperatures (>1,300°C) to produce glassy products. Vitrification is mainly favored in Japan as is the case for the bottom ashes. The molten products are distinguished by excellent leaching stability. Care has to be taken to avoid air pollution by evaporation of metal compounds. The energy consumption of all of these processes, however, is very high and is by far not compensated by the potential to recover metals. That is why such processes – although developed as described for the bottom ashes – did not conquer the market in Europe.

A third strategy – more in line with the demand for simple and in-plant measures – is followed by the 3R process which combines an acid extraction of soluble heavy metal compounds (by use of the acid flue gas cleaning solution) with a thermal treatment of the compacted extraction residues in the combustion chamber [42]. A plant equipped with this process has no filter and boiler ash stream and with that no need for a separate disposal of these critical residues. A scheme of the process is shown in Fig. 15. The technical demonstration revealed that the grate ashes from a 3R process which contain the leached filter ashes show excellent and not negatively altered leaching properties of heavy metals and that the PCDD/F are almost totally destroyed [43].

A similar process called FLUWA is practiced in a number of Swiss waste incineration plants. A main target in the further development of this process is the recovery of heavy metals out of the extraction solution [44].

The Ferrox process for treatment of filter ashes and APC residues involves washing of the residues in a ferrous sulfate solution and contemporary oxidation of the iron to form insoluble iron hydroxides and oxide hydrates [45]. The products have the quality to be landfilled or they can for quality improvement be fed back into the combustion chamber for further thermal treatment. Tests in a pilot plant documented the almost total destruction of PCDD/F and an excellent leaching stability of heavy metals after such sintering [46, 47].

Residues from Gas Cleaning

The residues from wet gas cleaning without water discharge and those from dry or semi-dry APC systems carry high levels of soluble salts, especially of alkali and earth-alkali chlorides or sulfates. Due to the high solubility, a safe disposal can only be guaranteed on special and expensive disposal sites. Attempts have been made to utilize parts of the ingredients of these residues in order to minimize the disposal problem. The challenge

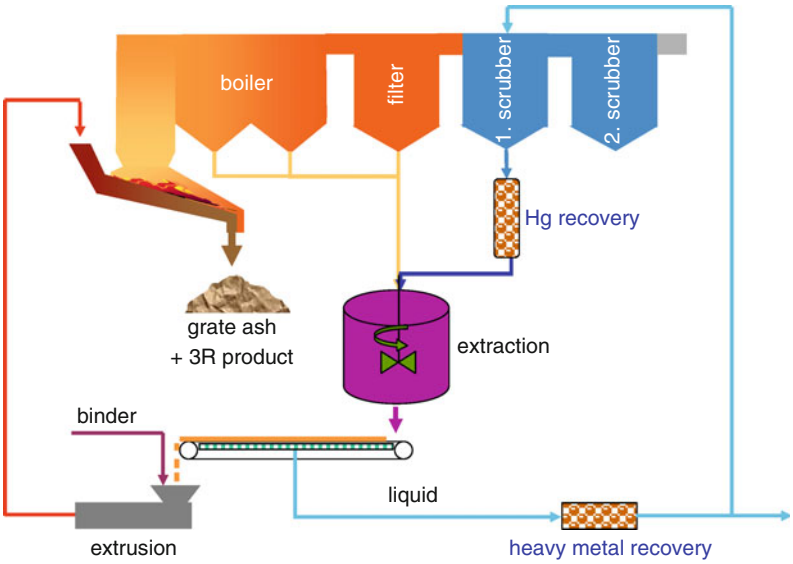

Waste-to-Energy Ash Management in Europe. Figure 15
Scheme of the 3R process

is the closing of the chlorine cycle. Different processes to recover NaCl [48], HCl [49], Cl_2 [50], or gypsum [49] have been tested. All such processes can only be successful if they end up with high quality products and if there is a long-term market for the products. Today, for example, in Germany only few MSWI plants produce HCl [51]. All other processes did not make it to the market due to unfavorable economy.

As mentioned above already, in Germany the disposal of gas cleaning residues and filter ashes for backfilling of caverns in old salt mines is acknowledged as utilization. This practice is widely used, to some extent also by neighboring countries.

Conclusions

European waste incineration plants aim since the early 1990s for the production of high quality bottom ashes for their safe disposal or even utilization as secondary building material. In line with this development also the sustainable management of boiler and filter ashes as well as of gas cleaning residues became of central concern.

Recommendations in that direction have been elaborated in the 1980s and 1990s; respective processes and operation protocols have been developed and have meanwhile been widely adopted by modern plants all over Europe. The major principles for achieving good management of WTE residues are compiled below.

- Adequate combustion control and careful sintering of the bed material at the back end of the grate guarantee an excellent burnout and cause a good fixation of heavy metals.
- Simple washing of the bottom ashes, preferentially in-plant in a modified quench tank, reduces the leaching of chlorides to very low levels.
- The resulting products have a high potential for utilization, for example, according to German regulations in road construction.
- Post-combustion treatment of bottom ashes increases the incineration cost without improving the elution stability significantly.

Most problems in the field of residue management are well understood today and in most cases appropriate technologies exist already. However, further development, especially in view of optimized energy recovery, is expected. It is obvious that primary and in-plant measures have to be preferred rather than secondary post-combustion techniques.

Future Directions

The process of unification of waste management in the EU member states will continue, and it is most likely that in future all countries will enact a landfill ban for reactive waste. It can also be envisaged that in all member states recycling will catch up with the actually leading countries. This development in line with the expected convergence of economy and lifestyle will promote WTE in the EU. The quality of residual waste will not change dramatically in view of its calorific value, but their inventory of some ingredients, especially of metallic species, will hopefully decrease by advanced recycling strategies.

With the increased application of WTE the generation of solid residues from this process will increase as well. The technological progress should care for a higher quality of bottom ashes. However, whether this will go along with an increased utilization has to be waited for. The niche market as secondary building material is limited, but the required quality will allow a safe and easy aftercare-free disposal of these materials.

The efforts for metal recovery from filter ashes – seen today in Switzerland – will find an echo in other countries and will pave the way for a tendency to inertize these actually problematic residues and to achieve their easier final disposal.

The today and also in future problematic residues from WTE processes are the scrubbing residues. For the time being there is no convincing solution for the management of these highly water soluble substances other than their disposal in old salt mines – may it be acknowledged as utilization or not. This option is for most countries not accessible. Hence further research is necessary, but from a chemical perspective most of the water soluble species, for example, alkali halogenides, cannot easily be stabilized against leaching. Hence, eventually other practicable approaches have to be considered.

Either recovery of chlorine and extended utilization of sulfur compounds are improved, or these species are discharged into their natural sink – the ocean. Of course, such strategy would need a significant change

in our present gas cleaning "philosophy." Which technology will be preferred in future is open; however, there is great hope that a sustainable solution will be found.

Bibliography

Primary Literature

1. de Fodor E (1911) Elektrizität aus Kehrricht. K.U.K Hofbuchhandlung von Julius Benkö, Budapest
2. Ude O (1934) Zur Frage der Müllschmelzung. Die Städtereinigung, *26*, No. 17 & 18
3. International Ash Working Group (IAWG): AJ Chandler, TT Eighmy, J Hartlén, O Hjelmar, DS Kosson, SE Sawell, HA van der Sloot J(1997) Vehlow (1997), Municipal solid waste incinerator residues. Elsevier, Amsterdam/Lausanne/NewYork/OxfordShannon/Tokyo
4. Vogg H, Hunsinger H, Merz A, Stieglitz L, Vehlow J (1991) Head-end-Techniken zur Dioxinminderung VDI Berichte 895:193
5. European Council (1999) Council directive 1999/31/EC of 26. April 1999 on landfill of waste. Official Journal of the European Communities, 16.7.1999, L182
6. European Council (2003) Council decision 2003/33/EC of 19 December 2002 establishing criteria and procedures for the acceptance of waste at landfills pursuant to Article 16 of and Annex II to Directive1999/31/EC. Official Journal of the European Communities, 16.1.2003, L11/27
7. Bundesministerium für Umwelt, Naturschutz und Reaktorsicherheit (2009) Verordnung zur Vereinfachung des Deponierechts. Bundesgesetzblatt I 2009, 900
8. LAGA (1994) Merkblatt Entsorgung von Abfällen aus Verbrennungsanlagen für Siedlungsabfälle, verabschiedet durch die Länderarbeitsgemeinschaft Abfall (LAGA) am 1. März 1994
9. CEN (2002) European Committee for Standardisation: CEN/T – Published Standards. http://www.cen.eu/CEN/Sectors/TechnicalCommitteesWorkshops/CENTechnicalCommittees/Pages/Standards.aspx?param=6273&title=CEN%2FT. Accessed March 2011
10. Schneider J, Vehlow J, Vogg H (1994) Improving the MSWI bottom ash quality by simple in-plant measures. In: Goumans JJJM, van der Sloot HA, Aalbers ThG (eds) Environmental aspects of construction with waste materials. Elsevier, Amsterdam/London/NewYork/Tokyo, p 605
11. Bergfeldt B, Däuber E, Seifert H, Vehlow J, Dresch H, Mark FE (2000) Rostaschenqualität nach Mitverbrennung der Shredderleichtfraktion in Abfallverbrennungsanlagen. Müll und Abfall 32:138
12. Vehlow J, Rittmeyer C, Vogg H, Mark F, Kayen H (1994), Einfluß von Kunststoffen auf die Qualität der Restmüllverbrennung, GVC-Symposium Abfallwirtschaft, Würzburg, 17.-19.10.1994, Preprints, 203
13. Köster R, Vehlow J (1998) Organische und anorganische Kontaminanten in Müllverbrennungsschlacken. FZK-Nachrichten 30:139
14. Vehlow J, Bergfeldt B, Hunsinger H (2006) PCDD/F and related compounds in solid residues from municipal solid waste incineration – a literature review. Waste Manag Res 24:404
15. Johnke B (1995) Schlackeverwertung und -entsorgung unter Beachtung der Vorgaben gesetzlicher und technischer Regelungen, VDI Bildungswerk, Seminar 43-76-03
16. Fiedler H (1996) Sources of PCDD/PCDF and impact on the environment. Chemosphere 32:55
17. Pfrang-Stotz G (1992), Mineralogische und geochemische Untersuchungen an Müllverbrennungsschlacken, Intern. Kongress für Umwelttechnologie und -forschung im Rahmen der Europäischen Messe für Umwelttechnik, Basel, CH, 5.-7. 10. 1992, Proc. Block 3, 33
18. Pfrang-Stotz G (1993) Gutbett-Temperatur-Bestimmungen an Müllverbrennungsschlacken unter besonderer Berücksichtigung mineralogischer Untersuchungsmethoden. Beihefte zum Eur J Mineral 5
19. Zwahr H. (2006) Eigenschaften mineralischer Abfälle, Stand der Aufbereitungstechnik und Untersuchungsverfahren von MVA-Schlacken. BMU- Workshop zu den Anforderungen an die ordnungsgemäße und schadlose Verwertung mineralischer Abfälle. 13. und 14. February 2006, Bundesumweltministerium, Bonn. http://www.bmu.de/files/abfallwirtschaft/downloads/application/pdf/abfw_workshop_zwahr.pdf. Accessed March 2011
20. Lahl U (1992) Verwertung von MV-Schlacken – durch Optimierung konventioneller Aufbereitung. Müll und Abfall 24:619
21. NEN 7345 (1993) Determination of the release of inorganic constituents from construction materials and stabilised waste products. Netherlands standardisation Institute (NNI), Delft
22. NEN 7341 (1993) Determination of leaching characteristics of inorganic components from granular (waste) materials. Netherlands standardisation Institute (NNI), Delft
23. Sloot HA van der (2005) Horizontal standardization and harmonization of leaching test methods for waste, secondary raw materials, construction materials and (contaminated) soil. http://www.ecn.nl/docs/library/report/2001/rx01009.pdf. Accessed March 2011
24. Dijkstra JJ, van der Sloot HA, Comans RNJ (2006) The leaching of major and trace elements from MSWI bottom ash as a function of pH and time. Appl Geochem 21:335
25. Schweizerischer Bundesrat (1990) Technische Verordnung über Abfälle (TVA) vom 10. Dezember 1990 (Stand am 1. Jan 1993)
26. Bergfeldt B, Däuber E, Vehlow J (1998) Norm und Wirklichkeit - zur Aussagekraft standardisierter Elutionstests. Terra Nostra, Schriften der Alfred-Wegener-Stiftung, Nr. 3

27. Pfrang-Stotz G, Reichelt J (1996) Müllverbrennungsschlacken. Mineralogie, Elutionsverhalten und technische Eigenschaften. Baustoff Recycling und Deponietechnik 12:4
28. Sauter J (2000) Vergleichende Bewertung der Umweltverträglichkeit von natürlichen Mineralstoffen, Bauschutt-Recyclingmaterial und industriellen Nebenprodukten. Diplomarbeit am Institut für Straßen- und Eisenbahnwesen der Universität Karlsruhe (TH)
29. Krass K, Mesters K (1993) Verwertung von Müllverbrennungsasche im Straßenbau. VGB Kraftwerkstechnik 73:841
30. Eurostat (2011) Waste statistics. http://epp.eurostat.ec.europa.eu/portal/page/portal/environment/data/database. Accessed March 2011
31. CEWEP (2011) Country reports. http://www.cewep.eu/information/data/subdir/index.html. Accessed March 2011
32. Vehlow J. (1995) Reststoffbehandlung – Schadstoffsenke "Thermische Abfallbehandlung". In: Die Thermische Abfallverwertung der Zukunft – Mit 100 Jahren Erfahrung ins nächste Jahrhundert. FDBR-Konferenz, Düsseldorf, 28 Sept 1995, Tagungsband, 56
33. Bergfeldt B, Schmidt V, Selinger A, Seifert H, Vehlow J (1997) Investigation of sintering processes in bottom ash to promote the reuse in civil construction (part 2) – long term behavior, WASCON'97, 4.-6.6.97, Houthem St. Gerlach, NL
34. Faulstich M. (1996) Behandlungsverfahren für feste Rückstände aus der Abfallverbrennung. In: Müllhandbuch, ESV Erich Schmidt Verlag, Berlin, A7125. http://www.muellhandbuchdigital.de/doi/MuA_a7125/dokument.html. Accessed Aug 2011
35. Stahlberg R, Feuerriegel U (1995) Das THERMOSELECT-Verfahren zur Energie- und Rohstoffgewinnung -Konzept. Verfahren, Kosten -, VDI Berichte 1192:319
36. Berwein H-J, Erlecke J (1990) Einsatzmöglichkeiten der Verschwelung als Homogenisierungsstufe in der thermischen Abfallverwertung. In: Thomé-Kozmiensky KJ (ed) Müllverbrennung und Umwelt 4. EF-Verlag, Berlin, p 225
37. Engweiler J (1997) Von Roll RCP: technological breakthrough in waste recycling. In: Barrage A, Edelmann X (eds) R'97 Recovery, recycling, re-integration congress proceedings, vol V. EMPA, St. Gallen, CH, 74
38. Striegel K-H (1997) Die untertägige Verwertung von Reststoffen in der Bundesrepublik Deutschland. In: Müllhandbuch. EVS Erich Schmidt Verlag, Berlin, A8196. http://www.muellhandbuchdigital.de/doi/MuA_a8196/dokument.html. Accessed Aug 2011
39. Reimann DO (1990) Reststoffe aus thermischen Abfallverwertungsanlagen. Beihefte zu Müll und Abfall 29:12
40. Tobler HP (1989) Konzepte zur Reststoffentsorgung in der Schweiz. VDI Berichte 753:9
41. Hagenmaier H, Kraft M, Brunner H, Haag R (1987) Catalytic effects of fly ash from waste incineration facilities on the formation and decomposition of polychlorinated dibenzo-p-dioxins and polychlorinated dibenzofuranes. Environ Sci Technol 21:1080
42. Vogg H (1984) Verhalten von (Schwer-)Metallen bei der Verbrennung kommunaler Abfälle. Chemie-Ingenieur-Technik 56:740
43. Vehlow J, Braun H, Horch K, Merz A, Schneider J, Stieglitz L, Vogg H (1990) Semi-technical demonstration of the 3R process. Waste Manag Res 8:461
44. Schlumberger S (2010) Neue Technologien und Möglichkeiten der Behandlung von Rauchgasreinigungs rückständen im Sinne eines nachhaltigen Ressourcenmanagements. In: Schenk K (ed) KVA-Rückstände in der Schweiz – Der Rohstoff mit Mehrwert Bundesamt für Umwelt BAFU, Bern. http://www.bafu.admin.ch/publikationen/publikation/01538/index.html?lang=de&lang=de. Accessed March 2011
45. Lundtorp KL, Jensen DL, Sørensen MA, Mogensen EPB, Christensen TH (2002) Treatment of waste incinerator air-pollution-control residues with FeSO4: concept and product characterization. Waste Manag Res 20:69
46. Bergfeldt B, Jay K, Seifert H, Vehlow J, Christensen TH, Baun DL, Mogensen EPB (2004) Thermal treatment of stabilized air pollution control residues in a waste incinerator pilot plant. Part 1: fate of elements and dioxins. Waste Manag Res 22:49
47. Baun DL, Christensen TH, Bergfeldt B, Vehlow J, Mogensen EPB (2004) Thermal treatment of stabilized air pollution control residues in a waste incinerator pilot plant. Part 2: leaching characteristics of bottom ashes. Waste Manag Res 22:58
48. Karger R (1990) Verfahren zur Rauchgasreinigung bei der Abfallverbrennung. AbfallwirtschaftsJournal 2:365
49. Kürzinger K, Stephan R (1989) Hydrochloric acid and gypsum (sulphuric acid) as utilisable end products obtained from the KRC process for cleaning flue gases from incinerators. In: Thomé-Kozmiensky KJ (ed) Recycling international. EF-Verlag, Berlin, p 1224
50. Volkman Y, Vehlow J, Vogg H (1991) Improvement of flue gas cleaning concepts in MSWI and utilisation of by-products. In: Goumans JJJ, van der Sloot HA, Albers ThG (eds) Waste materials in construction. Elsevier, Amsterdam, p 145
51. Menke D, Baars BA, Fiedler H (1999) Salzsäure aus Müllverbrennungsanlagen: Produkt oder Abfall? Müll und Abfall 31:490

Books and Reviews

Christensen TH (ed) (2011) Solid waste technology & management. Wiley, Chichester

Kranert M, Cord-Landwehr K (eds) (2010) Einführung in die Abfallwirtschaft. Vieweg + Teubner Verlag/Springer Fachmedien Wiesbaden GmbH, Wiesbaden

European Commission (2005) Integrated pollution prevention and control (IPPC) reference document on the best available techniques of waste incineration. Institute for Prospective Technological Studies, European IPPC Bureau, Seville, Spain, July 2005. http://www.ipcc.ch

Waste-to-Energy Ash Management in the United States

Floyd Hasselriis
Hasselriis Associates, Forest Hills, NY, USA

Article Outline

Glossary
Definition of the Subject
Introduction
Ash Residues from Waste Combustion Systems
Composition of Municipal Waste
Handling of Ash Residues
Landfill Disposal
Early Research on Ash Management
Regulatory Aspects of Ash Management
Treatment of Ash Residues
Environmental Impact of Use of WTE Ash
Ash Management Around the World
Future Directions
Bibliography

Glossary

Analysis Laboratory testing to determine composition and properties.

Ash residue Noncombustible solid matter remaining after combustion of municipal or other waste.

Beneficial use Application of ash residues to useful purposes as distinguished from disposal in landfills.

Bottom ash Noncombustible residues collected from the bottom of a combustion process such as a stoker.

Contaminants Minor and unwanted chemicals and salts that may be harmful to health and the environment.

Fly ash Fine solid particles derived from combustion and carried by gaseous products of combustion.

Heavy metals Metallic chemical element within the upper range of atomic weights, such as the lead and cadmium contained in ash residues.

Landfilling Placing municipal or other wastes upon the land.

Leaching Process of extraction of water-soluble metals and compounds by water passing through a solid waste.

Testing Laboratory analysis of ash residues to determine composition and properties.

Treatment Processing of ash residues to change characteristics or remove harmful components to reduce or eliminate contamination of the environment.

Definition of the Subject

Municipal solid waste (MSW) contains organics that can be converted to heat and power and should not be wasted by dumping in landfills. However, waste-to-energy (WTE) ash residues contain substances that have the potential to contaminate the environment. Management of ash residues therefore requires procedures that assure placement in landfills wherein leachate is collected, or treated to minimize the toxicity of the residues, possibly for beneficial use.

Regulations for management of ash residues have developed differently in various countries, in accordance with the physical and political situation and also the costs of the alternatives. Procedures used by WTE facilities in the USA require testing of the combined residues from the stoker, boiler, and emission control system to ensure meeting established federal and state regulations. Most of the "combined" ash produced in the USA is disposed in sanitary landfills as Alternative Daily Cover and for other landfill maintenance needs. In contrast, in many European countries bottom ash is used beneficially, for example, for road construction.

Procedures for managing WTE ash in the USA are described below. A following chapter in this Encyclopedia, by Dr. Jurgen Vehlow, discusses the management of WTE ash in Europe and Japan.

Introduction

In the past and even today in many parts of the world, waste materials have been simply dumped, out of sight and out of mind, without regard for their impact on the environment. Rain falling on these deposits leaches toxic metals, and other hazardous materials that can contaminate the soil, air, and waters. Recycling of usable materials is common practice but cannot recover more than one-half of the waste generated by our society, at the most. Landfilling can be reduced to

a minimum by means of combustion with energy recovery, also called waste to energy (WTE).

Municipal solid waste (MSW) is combusted to produce energy throughout the world, especially in developed countries where landfilling is very costly or prohibited. The energy stored in the hydrocarbons contained in MSW is recovered efficiently by means of combustion with heat recovery. The environmental impact of the combustion gases is minimized by the air pollution control (APC) system of the WTE plant. However, the noncombustible fraction remains as a residue, requiring processing, transportation, and disposal or, preferably, beneficial use. The cost of disposing of WTE residues represents a considerable part of the operating cost of the facility. Therefore, management and disposal of ash residues is an unavoidable and critical component of recovering energy from waste.

Ash residues from the combustion of MSW include the bottom ash, siftings, boiler ash, fly ash, and any other residues of the APC system. In particular, the APC residues contain the volatile metals contained in the raw waste in concentrated form and have the potential to contaminate the environment. Regulations controlling the management of ash residues vary from country to country, reflecting different political and physical situations and the cost of alternatives. In the USA, where over 60% of the MSW is still landfilled in sanitary landfills, all ash residues are usually mixed together ("combined ash"), tested for toxicity, and then disposed of in MSW landfills as daily cover of the working area and other maintenance needs, or in dedicated landfills called "monofills." All these landfills are lined so that the leachate can be collected and treated before being discharged. Bottom ash has also been used beneficially in the USA but to a very limited extent.

In northern Europe, where landfills have been phased out and are more costly and even prohibited, WTE bottom ash has been used beneficially, for example, as a substitute for aggregate materials, for use as road base, and for filling trenches carrying pipes for district heating. In Japan, ash residues must be vitrified or otherwise treated so as to permit beneficial use and/or to eliminate the risk of contamination of the environment.

The ash residues from combustion of municipal solid waste represent from 20% to 30% of the weight of incoming waste and 10% of its volume. Since they are generally in a wet condition when disposed, moisture represents 25 or more of their weight. Additives, such as calcium oxide, that are used to capture acid gases and other contaminants in the flue gas add to the weight to be disposed.

The disposal of ash residues must take into account the impact on the environment since soluble toxic metals can be leached out when subjected to rainfall or contact surface or groundwater. Also, reagents used to capture the acid gases may be soluble and influence the solubility of metals. Recognition of these hazards has led to strict environmental controls and requirements for testing of the residues and the leachate. Procedures have been developed to protect the environment and to encourage and permit beneficial uses of the ash, in preference to landfilling.

After passage of the Clean Air Act, the United States Environmental Protection Agency (U.S. EPA) was established. The Resource Conservation and Recovery Act of 1976 (RCRA) empowered the EPA to regulate residues from solid waste incinerators. The U.S. EPA then had to generate research needed to develop and promulgate regulation of waste disposal, particularly management of landfills. Regulations were also developed to assure environmentally acceptable combustion of wastes.

Ash Residues from Waste Combustion Systems

Ash residues are discharged at various locations from the combustion and emission control equipment:

- *Bottom ash* issuing from the discharge of the stoker grate consists of glassy residues, glass, and metallic objects, containing 1–3% carbon. It is usually quenched with water, although it can also be collected in a dry state.
- Stoker grate *siftings* fall though clearances in the grates and are collected with the bottom ash. These may include partially or totally unburned organic matter.
- *Boiler ash*, carried from the grate by the combustion gases, consists of flying particles and condensed metal vapor that may attach to refractory and

water-cooled walls and be caught on boiler surfaces, and has to be removed periodically. It may fall onto the stoker in the bottom ash, or it may be collected in hoppers and be discharged into the *bottom ash*.

- *Fly ash* is carried by the combustion gases through the furnace, boiler and emission controls. It may be collected in hoppers, by a wet scrubber or by an electrostatic or fabric filter. It may be removed separately or combined with the bottom ash.
- *Scrubber reaction products*, collected at the bottom of a spray-dry or dry lime-injection acid gas scrubber, include fly ash and reacted or partially reacted alkaline reagents such as lime, and activated carbon.
- *Mixed ash* may contain siftings, bottom ash, boiler deposits, fly ash, and scrubber residues.

Figure 1 is a schematic diagram of the Wheelabrator WTE facility built in Saugus, Massachusetts in 1975. Municipal solid waste (MSW) is fed by crane from the storage pit to the stoker, where it is burned. *Bottom ash* residues fall from the end of the stoker into a quench tank, and are conveyed to a trommel screen which removes bulk metal. The ash drops onto a conveyor, passes under a magnet to remove fine ferrous material, and drops into the aggregate hopper and a transport truck. *Fly ash* from the combustion chamber passes through the boiler, dropping some *boiler ash* into boiler and precipitator hoppers, then through the precipitator which collects the *fly ash* in storage hoppers before being sent out as cement supplement.

Composition of Municipal Waste

Municipal solid waste (MSW) typically contains about 50% combustible matter, 25% moisture, and 25% noncombustible inert materials (Fig. 2). A portion of

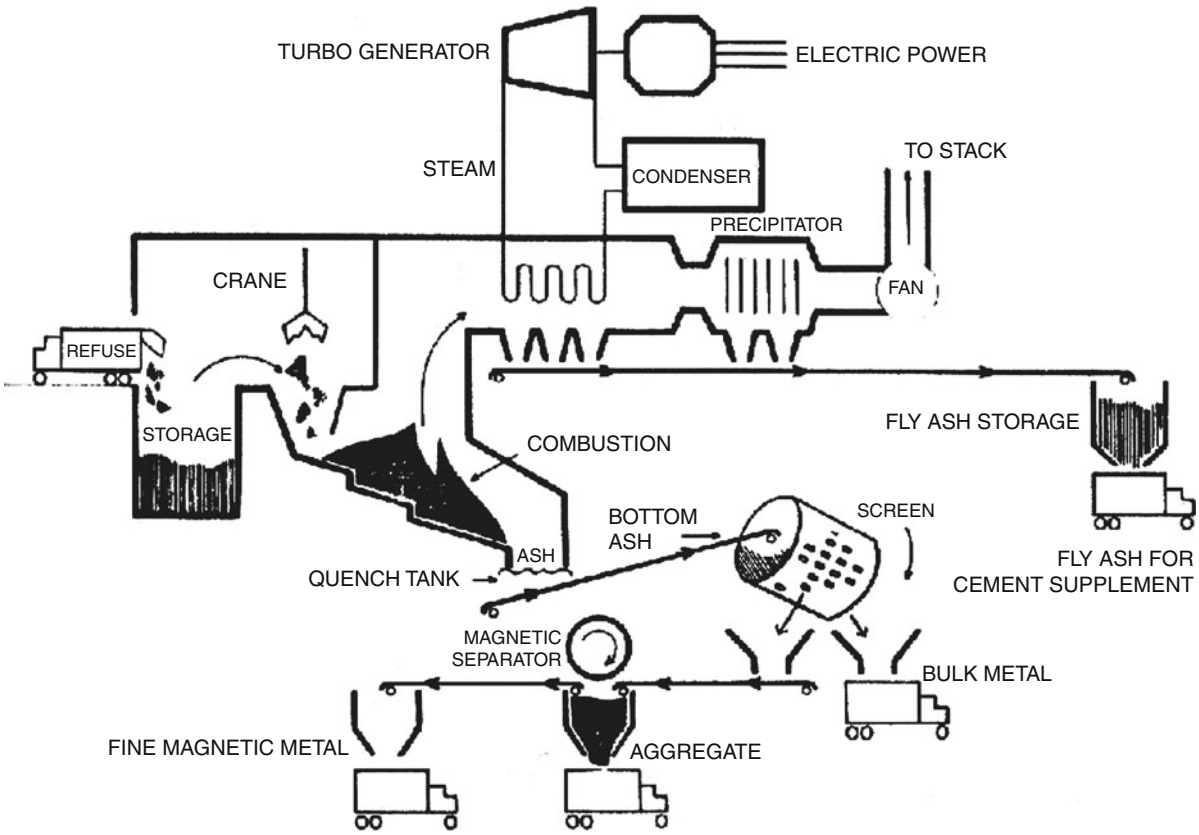

Waste-to-Energy Ash Management in the United States. Figure 1
Schematic of Wheelabrator waste management facility, Saugus, MA [33]

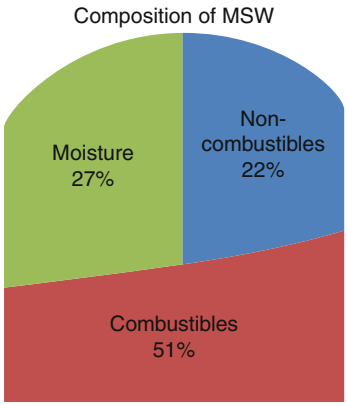

Waste-to-Energy Ash Management in the United States. Figure 2
Typical composition of municipal solid waste (MSW) [27]

the metals and glass can be reduced by recycling. *The chemical composition* of MSW is determined by laboratory analysis, after the large inert materials (metals, glass, and ceramics) are removed and accounted for, as performed by ASTM procedures [3]. Table 1 shows a typical ultimate analysis of the combustibles, containing 6.86% inherent ash. The noncombustible major metals constitute 99% of this, mainly aluminum, calcium, sodium potassium, and silicon, as shown in Fig. 3 [27]. Trace metals, totaling about 1% of the noncombustibles are mainly zinc, tin, lead, and chromium.

Table 2 shows the range of quantities of residues generated from combustion of MSW and associated emission controls in 1989. The dry bottom ash and fly ash may constitute 27–39% of the weight of MSW. Residues from various types of acid gas emission controls may add 1–5% [47].

Waste-to-Energy Ash Management in the United States. Table 1 Composition of municipal solid waste (MSW) [27]

Ultimate analysis of combustibles	Percent		Metals in ash	Percent
Carbon	35.02			
Oxygen	30.16			
Hydrogen	11.67			
Sulfur	1.88			
Chlorine	0.25			
Moisture	19.16			
Ash	6.86	→	Aluminum	33.21
Total	100.00		Calcium	30.20
			Sodium	17.50
			Potassium	13.12
			Silicon	5.00
			Major metals	99.04
			Zinc	0.400
			Lead	0.310
			Tin	0.150
			Chromium	0.047
			Nickel	0.020
			Cadmium	0.009
			Copper	0.007
			Minor metals	0.960
			(Total)	100.000

Metals Found in Bottom Ash and Fly Ash

The metals found in combined bottom ash and fly ash, in fly ash and in combined fly ash, and scrubber residues are shown in Table 3 [24]. Lead, cadmium, and zinc exist in high concentrations in the fly ash since they are volatilized at combustion temperatures. Potentially toxic metals in the fly ash, such as lead, cadmium, chromium, and nickel, are mainly derived from pigments, fillers, and inks used in or on paper and plastic products.

Chemical Composition of Ash Residues

The chemical composition of bottom ash and fly ash consists of the minerals found in earth. Fly ash contains greater amounts of the earth metals, the trace metals, lead, cadmium, and zinc, and the highly soluble chloride and sulfate salts. The fly ash/scrubber residues (Table 4) consist mainly of calcium, silica, alumina, and iron oxides. Table 4 compares the concentration of lime (calcium oxide) and other minerals found in air pollution control (APC) residue to that in Portland

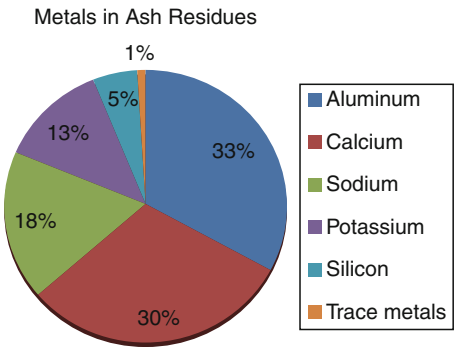

Waste-to-Energy Ash Management in the United States. Figure 3
Metals in ash residues from municipal waste [27]

Waste-to-Energy Ash Management in the United States. Table 2 Quantities of combustion and emission control residues

	Quantity of waste, lb/100 lb waste	% of total
Combustion residue		
Bottom ash (slag)	25.0–35.0	90
Filter dust (fly ash)	2.0–4.0	10
Total	27.0–39.0	100
Additional residues		
Wet scrubber residue	0.8–1.5	3–4
Spray-dry scrubber residue	1.6–3.5	6–9
Dry injection residue	2.5–4.5	9–12

Source: Thome-Kozmiensky [47]

cement and flue gas desulfurization (FGD) ash from a coal-fired power plant [28]. Vitrified slag from MSW consists primarily of silica, iron, calcium, sodium, and aluminum [1].

Density of Ash Residues

Combined ash produced by the combustion of MSW has densities ranging from 1,040 to 1,200 kg/m^3 at moisture content of 15–25%. In a monofill, combined ash is about 2,200 kg/m^3, at about 20% moisture [29].

Waste-to-Energy Ash Management in the United States. Table 3 Metals in combined ash, fly ash, and fly ash/scrubber residues

(Parts per million parts of ash by weight)			
Metal	Combined ash	Fly ash	Fly ash/scrubber residue
Aluminum	17,857	27,500	12,714
Calcium	33,642	64,857	176,428
Sodium	3,828	26,028	1,292
Potassium	3,071	36,928	8,450
Iron	20,428	10,857	3,314
Chloride	928	65,428	164,285
Sulfate	7	33	8
Lead	3,142	22,143	3,257
Cadmium	35	642	160
Zinc	4,107	53,500	9,143
Manganese	534	649	365
Mercury	ND	3	73

Source: Forrester [24]

Waste-to-Energy Ash Management in the United States. Table 4 Comparison of MSW APC waste with Portland cement

Component	MSW/APC[a] residue	Portland cement	Utility[b] FGD ash	MSW[c] slag
CaO	62–67	24	37	14
SiO	18–24	28	24	61
Al_2O_3	4–8	14	6	5
Fe_2O_3	1.5–4.5	5	3	

[a]MSW/APC residue: fly ash plus spray-dry acid gas control
[b]Utility scrubber residue (From Goodwin [28])
[c]Slag obtained by fusing MSW ash residues [1]

Densities of fine and coarse fly ash from a WTE using a dry lime-injection scrubber and baghouse range from 1,900 to 2,600 kg/m^3.

Moisture Content

Moisture content of ash residues can range widely, from 15% to 57%, depending on whether a semidry

ash discharger or a water quench tank is used. Excessive moisture content increases disposal costs. Maintaining minimum but sufficient moisture essentially eliminates dust liberation and fugitive dust problems. Controlling moisture can optimize landfill density. Dry fly ash needs to be conditioned with water to eliminate dusting.

Particle (Grain) Size Distribution

Typical size distributions of bottom ash and fly ash, an important factor in disposal and beneficial use of ash residues, are shown in Fig. 4. Typically, these distributions plot as straight lines on log-log paper. The "knee" in the fly ash curve indicates the presence of agglomerated fly ash. The size distribution of bottom ash corresponds well with specifications for aggregate materials [7].

Solubility of Metals in Water

Water containing high concentrations of dissolved metal compounds has the potential to contaminate the environment and drinking water supplies. The solubility of the trace toxic metals depends upon their chemical form and on the acidity or alkalinity (pH) of the water with which they are in contact. The acidity or alkalinity of ash residues in the presence of water, as measured by pH, generally ranges from neutral (pH = 7) to alkaline (pH = 9). When large amounts of unreacted lime are present, higher alkalinities, up to pH = 11, may be encountered.

Table 4 compares the amount of lime (calcium oxide) found in air pollution control (APC) residues with that found in Portland cement. Hydroxides, sulfates, and chlorides are more soluble and more readily available for leaching than oxides, silicates, and carbonates. The sulfate and chloride forms of lead and cadmium, found mainly in fly ash as the result of reaction with the sulfur and chlorine in MSW, are highly soluble.

Most metals are only slightly soluble in water at a pH range from 6 to 9. However, under acidic conditions, such as pH of 5 or less, solubility increases rapidly. While most metals are not soluble under alkaline conditions, lead becomes highly soluble at a pH greater than 10. Since lime has a pH of 12, large quantities of unreacted lime in the fly ash from acid gas control devices can increase the concentration of lead in the solution. See Fig. 5.

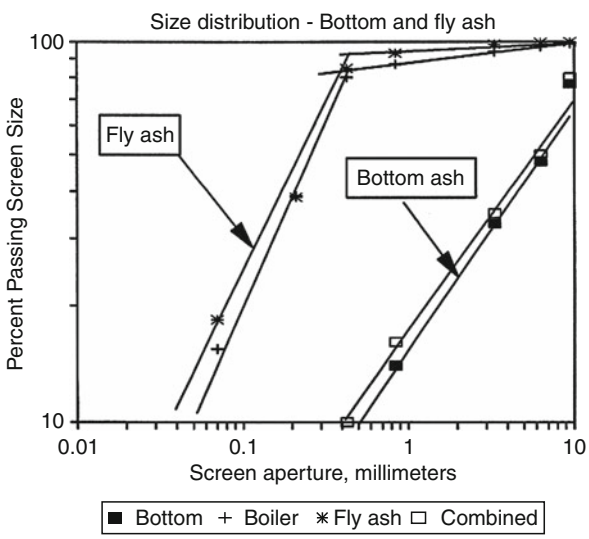

Waste-to-Energy Ash Management in the United States. Figure 4
Size distribution of particles in bottom and fly ash [7]

Soluble Salts in Fly Ash

In general, fly ash contains a large fraction of soluble salts, due to the sulfur and chlorine in the waste. Alkaline reagents such as caustic soda and lime, used as scrubbing agents for acid gas control, react with the acid gases to form soluble salts such as sodium and calcium chloride and various sulfates. Table 5 shows the analysis of the fly ash and scrubber residues from a spray-dry scrubber and the soluble fraction which totals 56% of the fly ash, primarily chlorides and sulfates [40].

Permeability of Ash Residues

Permeability is the property of a material that measures the velocity at which water will pass through the material, usually reported as centimeters per second (cm/s). The permeability of compacted ash has been measured to be from 1×10^{-6} to 1×10^{-9} cm/s. For comparison, landfill liners are typically required to have a permeability of 1×10^{-7} cm/s. It is possible to prepare ash for use as a landfill liner, thus meeting this specification by proper compaction, and by adding Portland cement and/or lime [24].

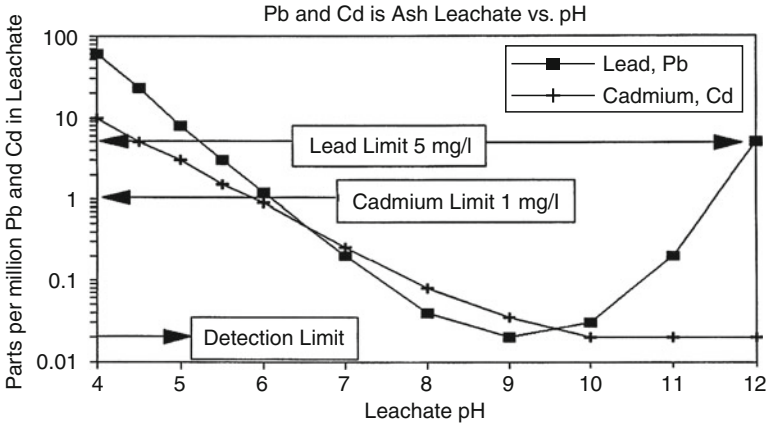

Waste-to-Energy Ash Management in the United States. Figure 5
Solubility of lead and cadmium as a function of pH of the solution. The limits set by the U.S. EPA are indicated: 5 mg/L for lead and 1 mg/L for cadmium. The detection limit is 0.02 mg/L (From Donnelly et al. [12])

Waste-to-Energy Ash Management in the United States. Table 5 Solubility of fly ash residues of dry scrubber [40]

Residue	Weight percent	Soluble percent
Fly ash	40	
$CaCl_2$	27	27
$CaS0_3$. 0.5 H_2O	20	20
$CaSO_4$-2 H_2O	5	5
CaF_2	2	2
Lime inerts	2	
$CaCO_3$	2	
$MnCl_2$	1	1
Heavy metals	$\frac{1-2}{100}$	$\frac{1}{56}$

Handling of Ash Residues

Wet quench systems cool the residues and permit them to be removed from the quench tank by means of *drag conveyors*. Ash residues commonly have a moisture content of about 50%.

Drag conveyors extract ash residues from water-filled quench tanks. They consist of flytes attached to moving chains carried over sprockets, configured to carry the ash residues up a slope so that they can be conveniently discharged.

Semi-wet systems quench the residues with water, but employ *mechanical dischargers* to push the residues out with a minimum amount of moisture. The heat remaining in the residues serves to drive off moisture so that the discharged residues may have moisture content close to 25%.

Dry removal of the ash residues makes it possible to remove the fine ash component by screening, leaving a useful granular aggregate and a relatively clean ferrous product.

Screw conveyors move powder-like dry ash from fly ash hoppers to other locations where they are dropped into water tanks, conditioning (wetting) devices for damp discharge, or into dry collecting containers.

Vibrating conveyors convey damp ash residues from ash dischargers to processing devices or receiving containers.

Vibrating screens separate ash residues into various size fractions, to remove rejects and produce useful fractions.

Grizzley screens remove oversize objects such as wood, bulky appliances, wheels, and miscellaneous metal objects from the ash residue. Vibrating rails separate out the oversize objects.

Trommels are rotary screens that remove oversize objects and clean ash residues to obtain more uniform products.

Magnetic separators used to recover ferrous metal are usually placed after grizzley screens to reduce interference by oversize objects.

Pneumatic conveyors transfer fly ash from ash hoppers to remotely located containers. Blower air and fabric filters are used to separate the fly ash from the transport air.

Handling and Storage

Handling and disposal of ash residues must not allow contamination of the environment by fugitive dust or by leaching into the environment or water supplies. Dusting is minimized by keeping the residues in a moist condition [30].

Stored ash residues must be properly managed to prevent unacceptable discharge of dust or leachate. Runoff and leachate must be collected, supervised, and properly disposed of so that soluble metal compounds and salts do not contaminate the environment.

Storing of ash allows chemical reactions that bind the metals to take place, reducing leaching potential. Rainwater percolating through the pile cleans the ash while slowly leaching out the available (soluble) metals.

Ash containers must be drainable to recover leachate, and watertight to prevent leachate from running off into the environment.

Transportation of ash residues must be in covered containers to prevent dust from escaping into the environment. Containers, vehicles, and roads must be washed if contaminated with ash. The wastewater must be disposed of properly or recycled back to the ash quench tank.

Processing

Ash residues can be processed at the waste-to-energy facility in order to reduce the rate of release of contaminants into the environment, facilitate disposal, improve the quality of the residues, remove valuable useful or harmful materials, and to prepare portions of the ash for beneficial use. The residues can be treated by washing, chemical treatment, or the use of additives and specific chemicals in order to retain, remove, or immobilize potentially toxic compounds.

Screening processes remove unwanted oversize and undersize components and separate the ash into usable products, including aggregate for use in construction.

Washing processes can provide clean aggregate materials and ferrous metals for beneficial use, and remove cementitious fly ash. Wash water can be processed and recirculated. The blowdown stream must be treated or evaporated to remove/recover and render harmless the dissolved metals and salts [20, 35].

Metal Separation

Metals are recovered not only for their commercial value, but also to minimize problems in beneficial use of the ash residues. As much as 15% of the bottom ash from mass-burn facilities is ferrous material that can be extracted magnetically. Conventional systems recover 60–70% of the ferrous metals and roughly 30% of aluminum, copper, and stainless steel, the nonmagnetic metals.

Tumbling of the ferrous product in a trommel can separate contaminants to improve quality.

Ferrous metals can be recovered and removed from bottom ash by magnetic separation systems, using either over-band or drum systems (Fig. 6). Nonferrous metals are recovered by eddy current separators (Fig. 7) [50].

After ferrous separation and screening, bottom ash residues have been used for fill and road base.

Treatment

Various methods of treatment of the bottom ash may be used to reduce the amount of leachable metal and salt concentrations, and thus render the ash more environmentally acceptable, as well as improve the chemical and physical stability and durability of the product so that it can be used for a variety of purposes. Treatment methods include ferrous separation and compaction, and various methods that modify release rates of the metals by chemical and physical changes, including solidification, stabilization, and encapsulation; addition of Portland cement, phosphates, waste pozzolans, and bituminous materials; washing and chemical treatment, thermal treatment, and vitrification.

Encapsulation in asphalt for use in bituminous paving mixtures and in cement serves to minimize the leaching of metals and salts from the product. Cement blocks and special forms can be made using aggregate processed from ash residues.

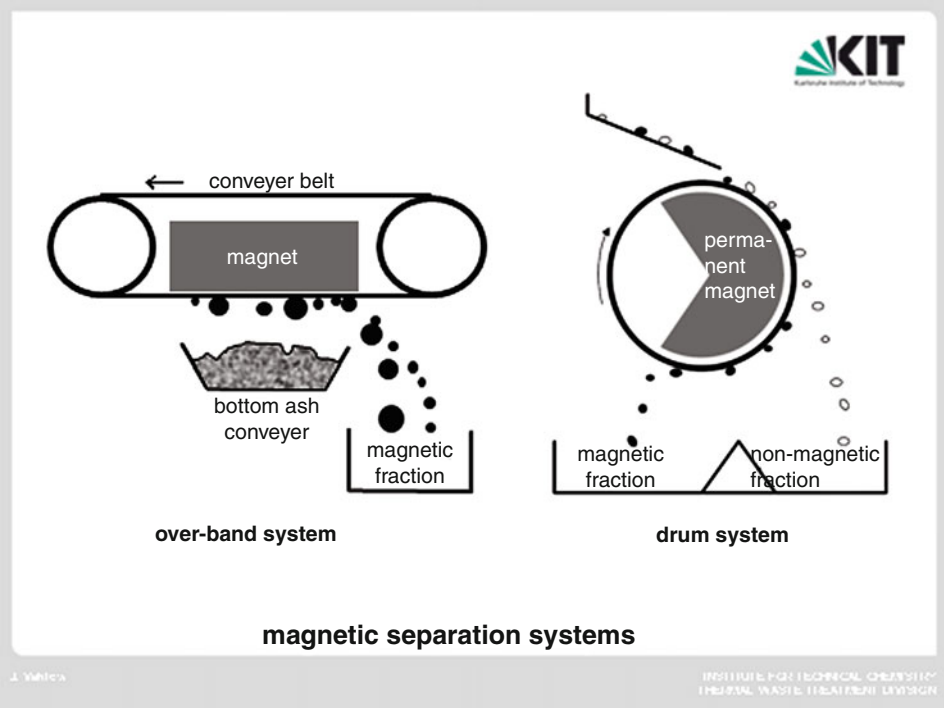

Waste-to-Energy Ash Management in the United States. Figure 6
Magnetic separation systems for ferrous metals [50]

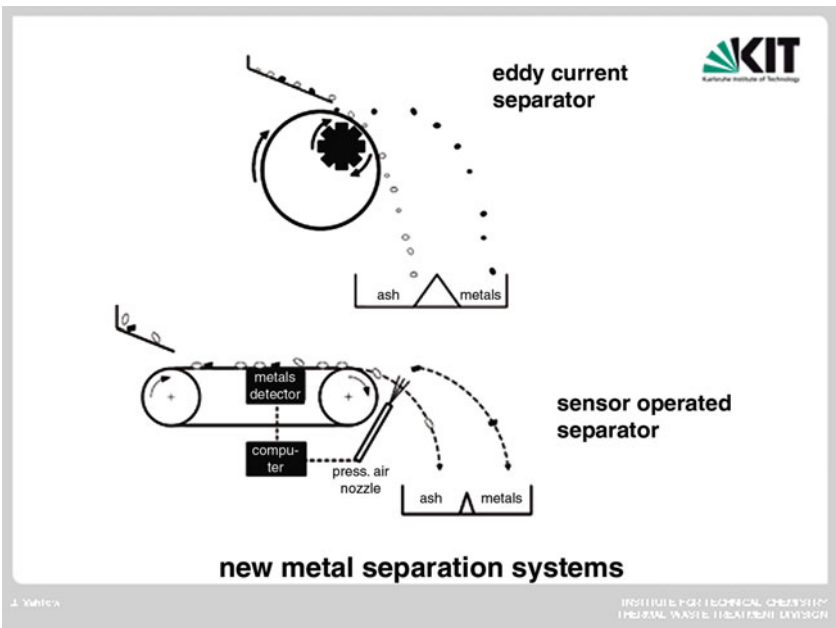

Waste-to-Energy Ash Management in the United States. Figure 7
Metal separation systems for nonferrous metals [50]

Lime and/or Portland cement can be mixed with fly ash to encapsulate the toxic metals and/or render them insoluble [38].

Phosphate treatment converts soluble lead compounds to insoluble phosphates, thus immobilizing the lead and reducing leaching to acceptable levels [14].

Carbonic acid absorbed from stack gases can convert soluble lead compounds into relatively insoluble lead carbonates [46, 51]. Heavy metals can be removed from fly ash by using carbonic acid recovered from flue gases, producing insoluble carbonates.

Chemical processing systems can process the ash residues while treating the flue gases and minimizing or eliminating water discharges. Calcium hydroxide specifically removes hydrogen chloride (HCl) and mercury; sodium hydroxide removes sulfur dioxide (SO_2); and ammonia (NH_3) can remove nitrogen oxides (NO_x). Hydrochloric acid is used in a primary gas scrubber to remove most of the cadmium and a major portion of the lead content of combined ash. Washing may especially be justified for treatment of fly ash, which can contain as much as 50% soluble salts in facilities employing acid gas controls.

Vitrification of bottom ash, mixed ash, or fly ash can be employed to obtain a high-quality glassy frit from which the trace toxic metals such as lead and cadmium do not leach out [10, 11]. Thermal treatment can produce glassy materials, or sintered and ceramic material [51].

Washing of Bottom Ash and Fly Ash

The bottom ash washing system shown in Fig. 8 accepts the bottom ash falling off the grate into a water-filled tank which separates out the slag and drops the residue into a sedimentation tank from which it goes to a bunker. The sediment goes to a treatment tank where HCl is added to force sedimentation of the soluble metals. Recirculated water is supplied to carry off the sedimented metals through the filters which recover the metals.

Figure 9 shows a system which can treat boiler ash and fly ash. The ash from the boiler hoppers is washed

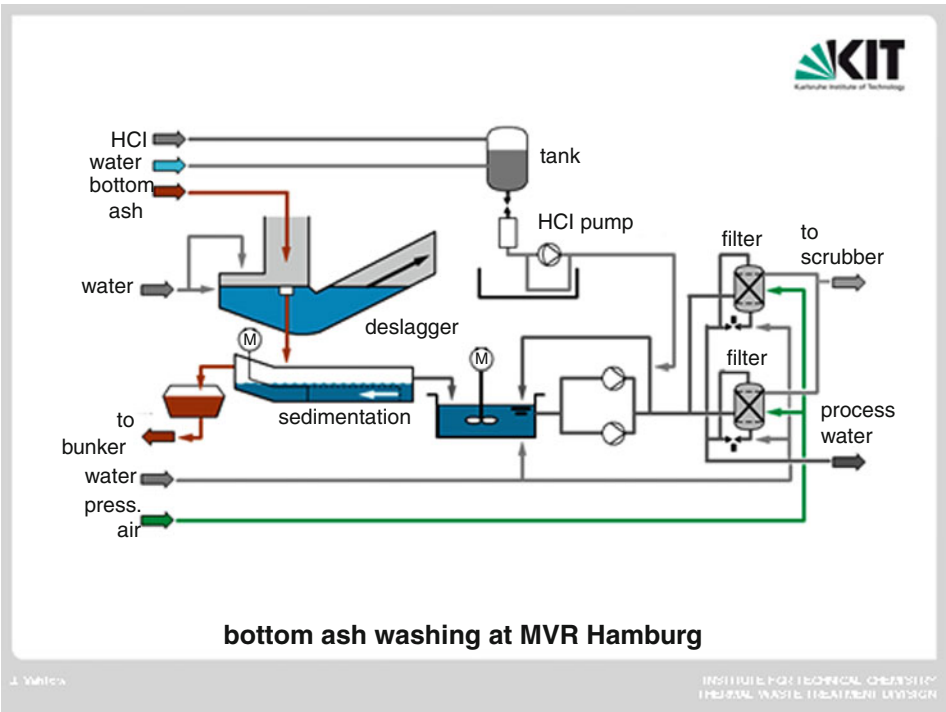

Waste-to-Energy Ash Management in the United States. Figure 8
Bottom ash washing system with treatment of the water at Hamburg [49]

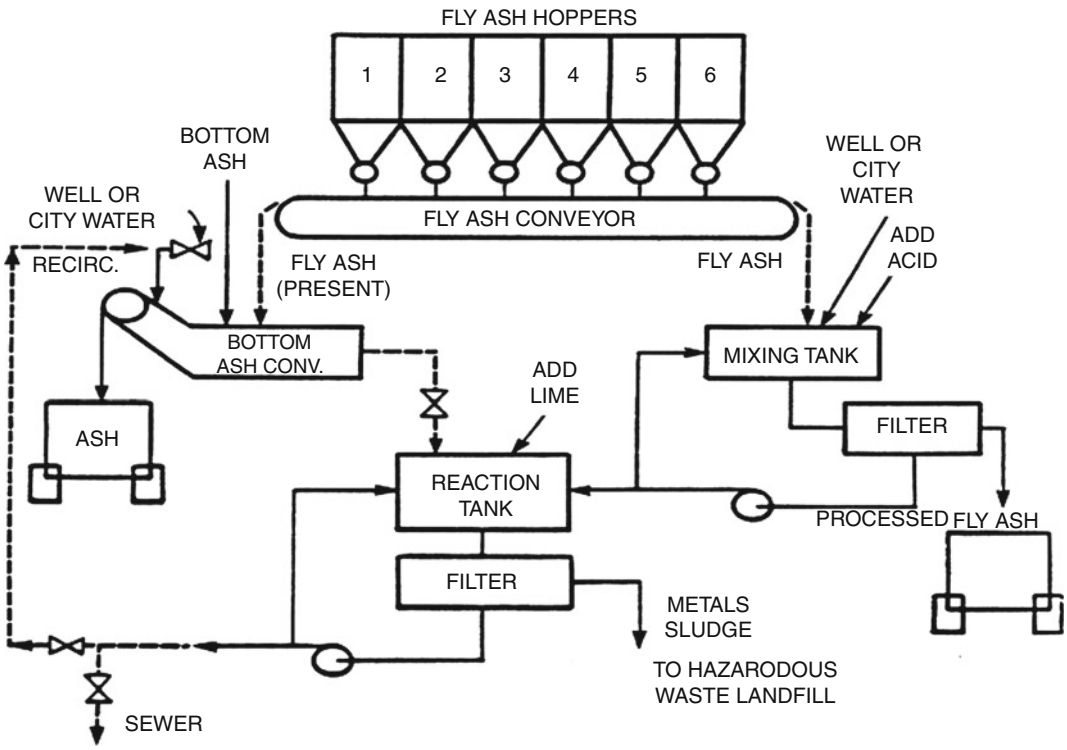

Waste-to-Energy Ash Management in the United States. Figure 9
Treatment system proposed for removing metal sludge and recovering processed fly ash at Saugus [32]

in the boiler ash tank from which it is dragged out to an ash container, for beneficial use. The wash water with this fine ash is passed to a reaction tank where lime is added to control the pH. The fines in the recirculated water are collected by a filter; the metals are discharged as metal sludge and sent to a hazardous waste landfill. A separate treatment system is provided for the precipitator hopper fly ash, where acid is added to precipitate metals. The fly ash can be collected separately, and sent to a mixing tank where acid is added to maintain pH. The fly ash then is filtered and collected for disposal or beneficial use.

Landfill Disposal

Landfilling of untreated ash is the simplest means of disposal. Ash residues are commonly codisposed of with municipal solid waste (MSW). They have been used to cover MSW as daily cover or as final cover. For various reasons it may be preferable to place ash residues in separate or dedicated cells, called ashfills or monofills.

Monofills or Ashfills

Monofills, or ashfills, are used for disposal of ash residues in cells separate from MSW. Placing ash residues in ashfills has the advantage that a solid, relatively impervious mass is created, over which trucks can drive as soon as it is placed. Ash residues have a high density and low permeability, which minimizes the need for leachate collection and treatment [29].

Compacting ash residues can increase the density to as high as 3,400 kg/m^3, as compared with about 1,900 kg/m^3 of uncompacted ash. Another benefit of compaction is the potential for reducing the permeability to as low as 1×10^{-6} to 1×10^{-9} cm/s. Ashfills are so impervious to water that only a small fraction of rain falling on the top surface is able to penetrate the fill; 90% or more will run off, without leaching much of the soluble material in the ash. It is important to provide effective runoff collection systems since the water may be significantly contaminated, especially when the ashfill is in the process of being filled, prior to capping [29].

Codisposal with MSW in Landfills

When ash residues are landfilled together with raw MSW, the acids generated by decomposing MSW could increase concentrations of soluble toxic metals in the collected leachate, requiring more stringent containment, leachate treatment, and groundwater monitoring [25]. On the other hand, the alkalinity of the ash has the ability to neutralize (buffer) the acids, thus reducing acid leaching.

Liners and Containment

Liners are provided in landfills and ashfills to contain the ash residues and to minimize or eliminate leachate penetration into the surroundings, as well as to provide means for collection of leachate and monitoring for indications of leakage. Only a small fraction of the rain falling on an ashfill can percolate through to the leachate collection system. The remainder is runoff that must be collected and properly managed [24].

Ash residues containing mixed bottom ash, fly ash, and acid gas scrubber residues have cementitious and compaction properties that make them relatively impervious to the penetration of leachate, especially if moisture and lime content are optimized. Completed cells can be covered with plastic liners, ash residues, or other relatively impervious materials to essentially eliminate the generation of leachate after the ashfill cell is closed [29].

Ash residues have been used as lining materials for landfills, in lieu of costly clay liners. To prepare the ash for use as a landfill liner, Portland cement can be added at the landfill at 6–10% plus lime at 6–7% by weight. If the fly ash component of the ash residues contains excess lime from the acid gas scrubber, less lime will be needed.

Leachate Disposal and Treatment

Rainfall on the landfill creates runoff and moisture, as it passes through the landfill, and generates leachate which contains various contaminants.

The leachate may be discharged or trucked to wastewater disposal plants if found to be acceptable, or it may require treatment before such disposal. The leachate from fly ash and from mixed bottom ash and fly ash contains substantial amounts (roughly 50%) of soluble salts resulting from the removal of acid gases by the emission controls that are required. It has been described as being similar to salt water [36]. The salt content may be more likely to require attention than the low concentrations of soluble metals.

Waste-to-Energy Ash Management in the United States. Table 6 Ranges of leachate concentrations of inorganic constituents from monofills [45]

Constituent	Concentration (CORRE study), mg/L	EP toxicity maximum allowable limit, mg/L	Primary drinking water standard, mg/L
pH	5.2–7.4		
Arsenic	nd–0.400	5.0	0.05
Barium	nd–9.22	100	1.00
Cadmium	nd–0.004	1.0	0.01
Chromium	nd–0.032	5.0	0.05
Copper		1.00	
Iron		0.30	
Lead	nd–0.054	5.0	0.05
Manganese	0.50		
Mercury	nd	0.2	0.002
Selenium	nd–0.340	1.0	0.01
Silver	nd	5.0	0.05
Zinc			5.00
Chloride			250

Table 6 shows actual leachate concentrations measured at various ashfill sites. The concentrations of the toxic metals were far below the EPA toxic limits. In most cases, the concentrations of the regulated toxic metals were close to the U.S. EPA drinking water limit [8, 45, 48].

Salinity of Leachate from Ash Residues

The effect of highly salty leachate on the environment has been studied. The salinity of leachate is measured by electrical conductivity. Soils producing leachates that have an electrical conductivity greater than 16 mhos/cm are classified as saline, causing interference

in the uptake of water by plants. Column simulations have shown that after 20 years of leaching, ash residues having an initial leachate conductivity of 21 mhos/cm were reduced by simulated annual acid rainfall to 8 mhos/cm, a level having relatively little impact on most plants [9].

Neutralizing Capacity: Ash/Acid Rain Mass Balance

The soluble toxic metals are only slowly released due to the presence of alkaline materials that provide powerful buffering against MSW-produced acids and the low quantity of weak acids in acid rain. It has been estimated that the effect of acid rain would be resisted for over 1,000 years. Long before this time, the leachable materials would presumably have been removed [31].

Early Research on Ash Management

Wheelabrator built a waste-to-energy plant in Saugus, Massachusetts in 1975, with the concept of total management of the ash residues (Fig. 1). Wheelabrator sponsored research programs at the Agriculture Center of the University of Massachusetts, at Amherst. [21, 32, 34]. In testing use of the ash as a soil conditioner it was found that the ash could enrich the soil, producing faster growth. Tests were run on the leaching of metals from the landfill, which was exclusively combined ash.

A comprehensive testing program was developed to understand the fate of lead and cadmium deposited in the course of flue gas passage through the boiler and the electrostatic precipitator, using samples taken from the dust hoppers of the boiler and the precipitator, and samples from the ash residue as it emerged from the plant [34].

The volatile metals, lead and especially cadmium, were found to collect on the boiler and precipitator surfaces. The suspended boiler tubes were shaken to clean the boiler sections once during each 8-h watch, dropping the metals-containing fly ash into the hoppers. Samples collected hourly revealed a "spike" in the metals content of the fly ash due to tube cleaning, which was reflected in the combined ash residues discharged from the plant. To obtain a true average of the lead content of the residues, a sufficient number of samples must be taken at regular intervals and these samples must be thoroughly mixed.

The leaching behavior of the ash residues was studied. It was discovered that the addition of phosphates to the residues would convert the lead to phosphates that are insoluble, inhibiting the leaching of lead and resulting in passing the Threshold Characteristic Leaching Procedure (TCLP) required by the U.S. EPA [19].

Extensive testing of leaching from landfills proceeded elsewhere: testing MSW landfills, monofills of ash only and codisposal landfills. California regulators concluded that the leaching procedure for ash residues should be performed with deionized water, simulating normal rainwater, not the strongly acidified solution of the "Threshold Characteristic Leaching Procedure" (TCLP) of EPA.

Leachates from ash residues at waste combustion plants throughout the country were tested, including testing of leachate from dedicated ashfills as distinguished from mixed landfills. Tests in Oregon found that the leachate from ash monofills was actually close to neutral, that is, pH = 7.0. Leaching of lead and cadmium is minimized at this pH level.

Since fly ash contains high concentrations of the volatile metals, the practice in Europe has been to keep Threshold it separate from bottom ash and dispose of it as a hazardous waste. Then the bottom ash can be used beneficially. In the USA, however, it has been considered to be more practical to mix the fly ash, and any scrubber residues, with the bottom ash, monitor its leaching properties, and apply additives as needed to pass the EPA leaching test.

Actual Leaching of WTE Ash

Several points are clear from a review of the data of field studies that characterized the leachates from ash monofills, TCLP testing of ash from several waste-to-energy facilities, and leaching of beneficially used products containing ash.

- Laboratory leach tests routinely overestimate the potential for constituents of concern to leach from an ash and ash product when compared to actual leaching from ash monofills and ash use in field applications.
- The combined ash of modern WTE facilities routinely passes the requirements of the TCLP test of EPA.

- Metal concentrations in leachates from ash monofills evaluated over time have routinely met ground water standards and often meet drinking water standards.
- Although leachates from combined ashes in monofills have low concentrations of heavy metals, the total dissolved salts concentration may be several orders of magnitude above drinking water standards.
- Levels of dioxins/furans in ash and ash leachates have been extremely low and considered not to be a concern when evaluating the environmental and health consequences of using ash.

Regulatory Aspects of Ash Management

The management, disposal, and beneficial use of ash residues and their products is subject to federal and state regulations which require sampling and analysis of the leaching characteristics of residues from combustion of municipal and other types of wastes.

Federal Regulations

Federal regulations broadly classify wastes into hazardous and nonhazardous categories. The Resource Conservation and Recovery Act of 1976 (RCRA) empowered the U.S. EPA to regulate residues from solid waste incinerators. In 1992, the U.S. EPA Administrator sent a memorandum to EPA Regional Administrators stating that the Resource Conservation and Recovery Act completely excludes ash from municipal waste combustors from regulation as a hazardous waste under Subtitle C as long as it is not characterized as toxic, since ash can be managed safely in solid waste landfills under Subtitle D, Section 3001(i) of RCRA. Prior to this statement, states developed various regulations, many requiring that MWC ash be disposed of in monofills, for ash only (ashfills), employing single liners, as compared with the double liners required for MSW landfills. Leachate collection and treatment are required in both cases. Landfills for hazardous wastes require much more stringent design and operation due to the greater potential hazards and uncertainty of their leachates.

The U.S. EPA has developed test procedures designed to screen wastes to determine their classification. Various states have developed different regulations as to whether or not ash must be sampled and analyzed prior to disposal. In any case, it is generally the responsibility of the producer of the ash to determine whether it exhibits the characteristic of toxicity in accordance with U.S. EPA procedures [18].

Ash Residue Extraction Leaching Procedures

The following leaching procedures have been applied to determine the characteristics of ash residues under a wide range of conditions to which they might be exposed, and also to discover which procedures might more closely simulate actual conditions of disposal or beneficial use:

- Extraction Procedure Toxicity (EP Tox) Test
- Acid No. 1. Acetic acid extraction fluid at pH of 4.87 to 5.2
- Threshold Characteristic Leaching Procedure (TCLP)
- Column Tests using simulated acid rain
- TCLP Fluid No. I (Acid No. 2). Similar to EP Tox
- TCLP Fluid No.2 (Acid No. 3). Similar to EP Tox
- California Waste Extraction Tests (WET), Uses citric acid
- Deionized Water (Method SW-924), also known as the Monofill Waste Extraction Procedure (MWEP)
- CO_2 saturated deionized water
- Simulated acid rain (SAR)
- ASTM Shake Extraction Procedure using distilled water leaching

The original Extraction Procedure (EP) toxicity test was replaced by the Threshold Characteristic Leaching Procedure (TCLP). These procedures use an acid leaching medium intended to simulate leaching of ash codisposed in a landfill in a proportion of 15% ash and 85% MSW. In the TCLP test, a unit sample of ash residue is immersed in 20 units of a specified acetic acid solution. The acidity of the solution is maintained at a pH value between 4.87 and 5.2 and stirred continuously for a 24-h period. The extract (leachate) is analyzed, and results are compared with the EPA-established limits. The sample would be characterized as hazardous if any of these limits were exceeded [18, 26]. These limits assume that a 100-time dilution would occur before the leachates could reach drinking water standards, hence they are established at 100 times the drinking water standard.

Actual leachate from MSW landfills as well as codisposal and ash residue landfills (ashfills) does not generally have pH values as low as 5.0. Extensive testing of leachate from these various types of landfills shows that they did not contain significant amounts of the toxic metals lead and cadmium, contrary to the results of laboratory tests employing the TCLP method. In other words, the TCLP test does not simulate actual disposal conditions [45].

A comparison of the effects of various laboratory leaching procedures on the cadmium and lead concentrations is shown in Table 7 [26]. Actual leachate concentrations from tests sponsored by CORRE/EPA are compared with the EPA toxic limits. The carbonic acid test was in closest agreement, while the EP toxicity procedure overestimated leaching by two orders of magnitude [45].

In general, leaching column tests more closely simulate actual leachates from landfills, as do tests *using simulated acid rain or carbon-dioxide-saturated water and/or deionized water*. More aggressive leaching tests such as the California WET test and EP or TCLP test, which represent conditions not likely to occur in the environment, serve as the basis for classifying the wastes as being *potentially* able to produce toxic levels of metals in the leachate.

Leaching column tests show that the soluble metals and salts are gradually removed from the ash as the leachate absorbs and removes them. The larger the quantity of acid in the water, the faster is the rate of removal. In some cases, two to four quantitative washes will have removed essentially all of the lead and cadmium that was soluble at the final pH level. Test borings of one ash pile showed that after several years of natural acid rainfall the leachable metals remaining in the ash pile had been reduced to the non-detectable level.

State Regulations

State regulations must be at least as stringent as federal regulations, but may be more detailed and suited to specific state environments. They require the collection and analysis of ash residue samples on a periodic basis, and require that these samples, on average, pass the prescribed toxicity tests.

Testing of ash residues is required to obtain confidence that there will be no harmful effects on the

Waste-to-Energy Ash Management in the United States. Table 7 Metal concentrations in extracts of MSW ash residues, in mg/L (parts per million) [16, 45]

Facility	Chicago	Sumner	Hampton	Auburn
Cadmium				
WET test	1.6	0.81	1.52	0.18
EP toxicity	0.71	0.24	0.50	0.02
Acetate	0.19	0.52	0.33	0.03
Carbonic acid	0.016	0.012	0.07	0.005
Water	<0.0005	<0.005	<0.005	<0.005
Lead				
WET test	29.0	35.0	46.0	29.0
EP toxicity	5.8	6.4	10.3	3.15
Acetate	0.5	0.28	1.62	4.20
Carbonic acid	0.025	0.004	0.095	0.012
Water	<0.002	<0.002	<0.002	<0.002

Source: Francis and Maskarinec [26]

environment after the residues are disposed of or used beneficially.

Samples of ash residues must represent the stream of ash residues from which they are taken. Mixing the fly ash properly with bottom ash avoids unrepresentative "hot spots." Aging samples with normal moisture allows the chemical reactions to take place that would occur under the conditions of disposal, such as converting soluble lead chlorides to insoluble lead carbonates.

Frequency of testing is generally regulated, including extensive testing after start-up of the plant, followed by one or more tests per year in order to assure consistent operation [22]. If some of the analytical results are found to be critically close to acceptable limits, more samples may be taken to obtain confidence in the average values.

Regularly time-spaced samples will represent the true average characteristic of the ash residues for the period of time over which they are produced, landfilled, or otherwise used.

Daily average samples are collected at uniform time intervals over the entire day. Daily samples are well mixed and coned and quartered to reduce the sample size and provide several identical samples. Weekly samples should include the entire week; monthly samples each week, and annual averages all months. As analyses are accumulated over long periods, confidence is established as to the true mean, and fewer analyses are required to assure representation of the residue stream.

Analysis of fly ash samples may show that untreated fly ash contains enough soluble lead and cadmium to exceed the toxic limit according to the EP or TCLP test.

Treatment of Ash Residues

If the ash residues should fail the TCLP test, they would have to be sent to a special and more costly landfill. To avoid these costs, and to assure that all products will pass the test, various chemical treatments have been used.

Processes have been developed to recover useful by-products from waste incinerators, and render the remaining residue nonhazardous, thereby eliminating the long-term environmental liability associated with disposing of these materials.

The fundamental mechanisms of phosphate stabilization of divalent metals in MSW combustion scrubber residues have been studied intensively [16].

The most prominent of these is the WES-PHix^{TM} process, in which the ash residue is sprayed with a phosphate solution while being tumbled in a drum. It has been demonstrated that this treatment reduces the solubility of lead which otherwise increases at the highly alkaline conditions such as 11 or 12 pH which result when excess lime is used for acid gas control. With this treatment, the ash residues may be disposed of in dedicated ashfills, and used for beneficial purposes [42]. Other treatments include control or addition of alkaline agents including Portland cement.

Residues from Air Pollution Control Systems

There are two predominant types of air pollution control (APC) systems: (1) wet scrubbers and (2) dry or semidry lime or other alkaline reagent injection systems. Wet scrubbers generally use sodium-based agents, such as $Na(OH)_2$, producing the highly soluble NaCl salt. In dry/semidry lime-injection APC systems, the calcium hydroxide ($Ca[OH]_2$) reacts with the acid gases to form significant concentrations of calcium chloride ($CaC1_2$) and calcium sulfate ($CaSO_4$) that comprise the bulk of the APC residue waste stream. The resulting $CaCl_2$ and the excess lime present in the APC residues are quickly solubilized upon contact with water. Furthermore, since the stoichiometric ratio of lime addition is greater than 1, the APC residues are highly alkaline, and the potential to solubilize amphoteric metal compounds (such as some Pb compounds) is greatly increased. Consequently, leachates from these residues may contain high concentrations of salts and trace metals, such as Al, Cr, Pb, and Zn.

Environmental Impact of Use of WTE Ash

Risk Assessments

Risk assessments to estimate environmental impact have been carried out for various uses of ash residues: combined ash as landfill daily cover; combined ash as final cover (bottom layer); use of treated ash aggregate (TAA) as a roadway base, as a structural fill, as daily and final landfill covers, as an aggregate substitute in

asphalt concrete paving, and reuse and final disposal of paving material containing TAA.

Boiler Aggregate™ from SEMASS, Massachusetts, has been demonstrated for use in producing an asphalt product, as an unregulated fill, and for milling and excavation for reuse. Stockpiling, handling, and transporting operations have also been evaluated, as well as in combined ash as a 30% substitution in bituminous pavement [17].

These assessments have covered specific situations, and generally evaluated the noncarcinogenic and carcinogenic effects on receptors from exposure to As, Ba, Cd. Direct and indirect exposure pathways evaluated included inhalation of fugitive dust on-and off-site, incidental ingestion and dermal contact with ash and ash products, residential exposure to soils potentially contaminated with particulates and/or leachates from ash and ash products, and similar pathways. In the case of landfill final cover, exposure pathways also included incidental ingestion and dermal contact with surface water and sediment while swimming in a nearby harbor, and consumption of fish from the harbor. Exposure from ingestion of food grown in soil potentially contaminated with TAA was evaluated. Also included was ingestion of drinking water containing leachate from Boiler Aggregate stockpiles, a road base, and recycled asphalt product pile.

In tests performed in the USA, on a 600-m section of U.S. Route 3 in Laconia, New Hampshire, with MWC bottom ash as 50% of the required aggregate in the binder course pavement, roadway runoff, surface water, and groundwater were monitored. Monolith leaching tests have indicated that release rates of chemical constituents are low and occur at levels similar to those for natural aggregates [16, 43, 44].

Use of Ash Residues for Construction

Ash residues from combustion of MSW have been used as roadway fill and subbase for parking lots, stabilized road base, bituminous paving mixtures, concrete masonry block, and Portland cement concrete. Concern about leaching of metals into the environment has led to extensive research into the characteristics and environmental impact of these practices. Table 8 describes the physical and chemical tests that may be used to evaluate the waste material for reuse [23].

Use of Ash Residues in Asphaltic Mixtures

Asphalt has been found to encapsulate ash residues effectively, reducing leaching potential to acceptable levels, so that the asphalt can be safely used for road construction [41]. The use of ash residue as an aggregate in bituminous-base course construction has been

Waste-to-Energy Ash Management in the United States. Table 8 Tests recommended for use of granular and asphaltic materials

Chemical tests	Physical tests
Elemental composition mineralogy Acid neutralizing capacity Distilled water leach test Bioavailability leach test Threshold characteristic leaching procedure (TCLP) Lysimeter leach test	Moisture content (ASTM d2216) Percent rejected (>% in) Organic content (loss on ignition) Ferrous content Particle size distribution (ASTM C136) Absorption and specific gravity (ASTM C127 and C128). Unit weight and voids (ASTM C29) Moisture density test (ASTM D1557) CBR (ASTM D 1863) Sodium sulfate soundness of aggregates (ASTM C-88). Los Angeles abrasion test (ASTM C131) Unconfined compressive strength (ASTM D2166). Marshall stability of asphaltic material (ASTM D1559)

Source: Lucido [41]

studied since the 1970s. Test sections have been continuously evaluated over periods from 1 to 5 years. The surface pavement and binder courses using combined bottom ash and fly ash from the Saugus facility in Lynn, Massachusetts, constructed in 1975, used 50% ash, 2% lime, 50% natural aggregate, and 13.5% asphalt, and were assessed in 1991 to be still performing well [15]. A section built in Washington, D.C., contained 68.5% residue, 1.5% hydrated lime, 15% sand, 15% limestone, and 9% asphalt. Surface asphalt road sections at the SEMASS facility in Rochester, Massachusetts, and in New Jersey, and ash use in road base and subbase structures at SEMASS and in New Hampshire were evaluated for soil contamination, runoff, and leachate [5, 52].

Portland Cement Treatment

A patented Portland cement-based ash aggregate, McKayanite, using combined ash or bottom ash, has been tested in Florida as landfill cover and as aggregate in road projects, and was found to meet physical standards for road construction materials, showing no adverse effects on groundwater, soil, or ambient air quality. The State of Tennessee Highway Department developed a standard for acceptable use of ash residues as aggregate in road base construction. Progress toward acceptance of ash residues for beneficial use was expected in other states [52].

At the Commerce WTE facility in Los Angeles, California, fly ash from the spray-dry scrubber/baghouse was mixed with Portland cement, and then blended with bottom ash in a cement mixer truck. The treated ash-concrete was poured into roll-off containers and stored for 24 h before transport to the landfill, where it was crushed for use as a subbase for roads at the landfill [13].

Building Blocks and Other Uses

Use of ash residue to produce aggregate material for use in concrete encapsulates the heavy metals and converts them to chemical forms that are essentially insoluble. Leaching tests of concrete blocks made from bottom ash only and mixed bottom ash/fly ash have shown that the rate of leaching of metals is insignificant in both underwater marine environments and in aboveground applications [52].

Cement blocks made from MSW combustion in Montgomery County, Ohio, have been used to construct buildings on the county landfill, after testing according to structural testing protocols, including ASTM tests for strength, Underwriter Laboratories (UL) tests for fire resistance, and TCLP tests. The blocks exhibited somewhat higher-than-normal shrinkage indices. The blocks made from coarser bottom ash released more easily from the molds than did blocks containing fly ash as a component [52].

Processing Ash for 100% Recovery and Use

A processing plant was built to use ash residues from the Nashville Thermal WTE facility, to achieve 100% recovery of products, that is, zero discharge to the landfill. The process involves sorting of the ash as it is received; bulk reduction; ferrous separation in three stages: ferrous processing; aggregate wet treatment; air classification to remove unburned product; and nonferrous separation, processing, and sorting. The unburned material was returned to the WTE plant. The product was treated by the WES-PHix process, expecting to sell it for uses in construction. The product was finally conditioned by storage in piles. In spite of successful operation for a long period of time, the facility was ultimately closed due to concern about groundwater contamination from the storage piles which resulted from failure to sell the product. The WTE facility (one of the earliest in the USA) was shut down to allow more profitable use of the downtown site [2].

Vitrification

Vitrification of residues from thermal processes produces a dense, grainless, amorphic, glass-like material which contains no organic material and from which inorganic mineral matter does not leach significantly, and which has many beneficial uses. The American Society of Mechanical Engineers (ASME) and the U.S. Bureau of Mines [10, 11] carried out an extensive investigation of vitrification. Tests were performed on combined furnace bottom ash and fly ash from three mass-burn WTE plants, fly ash from an RDF-fired WTE plant with acid gas scrubber, and combined ash from a multiple-hearth wastewater treatment sludge incinerator. The tests were performed in a sealed

submerged-arc electric furnace having a capacity of 1 t/h. Fumes from the furnace were cooled and the deposits analyzed. A fabric filter was used to collect particulate for analysis, and an afterburner was provided to burn off any possible organic matter. The stack gases were analyzed for trace organics and metals.

Approximately 83% of the feed weight was converted to vitrified product, and 5% metal was withdrawn, consisting mostly of about 75% Fe, and 8% copper, 6% phosphorous, and 7% silica. The matter, which collects on the top of the charge, contained about 48% copper, 15% iron, and about 27% sulfur. The principal components of the fume solids were NaCl, ZnS, and KCI. They contained 70% of the zinc and 37% of the lead in the furnace feed, and from 7% to 26% silica, varying with the carryover, which depended on the nature of the ash residues. Most of the chlorine in the feed material left the system in gaseous form, since essentially none was found in the solid products.

The vitrified product was tested in accordance with TCLP procedures that showed that the vitrified residues were environmentally benign. The levels of leaching from the samples were in all cases 10–50 times less than the EPA maximum limit.

The cost of vitrification was estimated to range from $200/t of dry ash residue for a 50 t/day facility to $115/t for a 300 t/day facility, based on electric power costing $0.051/kW-h. The components of the cost of vitrification can be roughly estimated to be 5% for drying, 45% for electric power, water, and gas, 30% for labor and maintenance, and about 20% for the cost of capital.

Ash Management Around the World

Worldwide, ash residues represent approximately 20% of the combusted MSW. Therefore, beneficial uses of ash can offer a substantial saving in landfill space and cost [6, 29]. Ash is a resource to be recycled, rather than

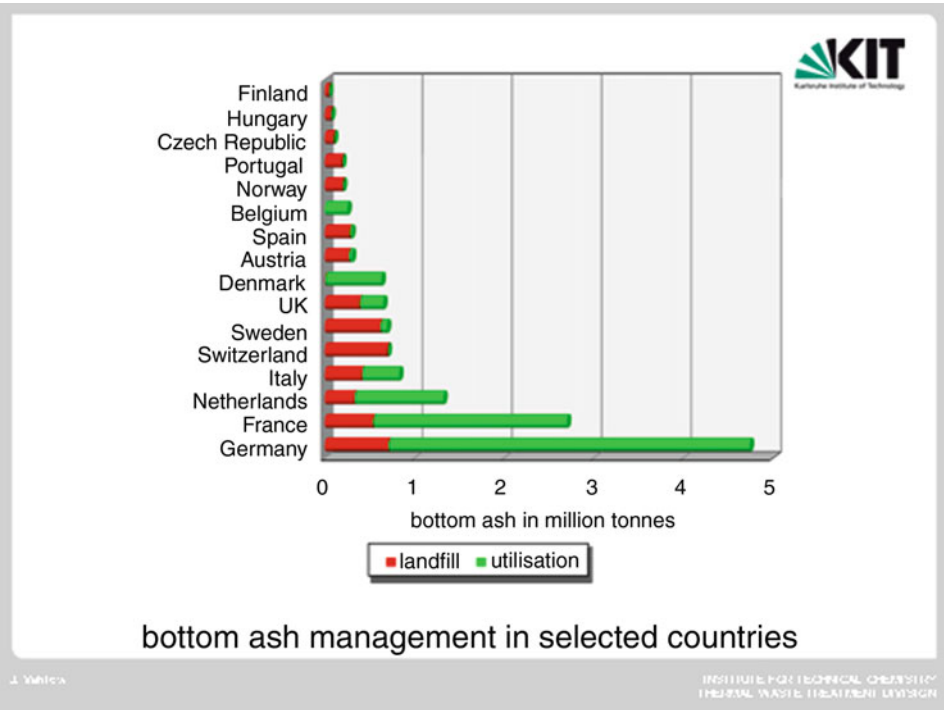

Waste-to-Energy Ash Management in the United States. Figure 10
Bottom ash management in selected countries in Europe [49] (KIT – University of the State of Baden-Wuerttemberg and National Laboratory of the Helmholtz Association)

bottom ash management in selected countries

	year	production (Mg/a)	utilisation (%)	specifics
Austria	2008	358,000	10	'slag concrete for landfill'
Belgium	2008	490,000	100	secondary building material
Czech Republic	2008	100,000	0	landfilling
Denmark	2008	631,000	99	80% road construction
Finland	2008	45,000	0	landfilled
France	2008	2,700,000	80	civil engineering
Germany	2009	4,740,000	85	mainly road construction
Hungary	2008	105,000	0	landfilling
Italy	2008	827,310	50	landfilling
Netherlands	2009	1,500,000	100	building material
Norway	2008	200,000	0	landfilling
Portugal	2008	193,000	0	landfilling
Spain	2005	293,693	5	road construction
Sweden	2008	690,000	10	rewcases of road construction
Switzerland	2008	700,000	0	landfilling
United Kingdom	2008	650,000	40	building material

Waste-to-Energy Ash Management in the United States. Figure 11
Bottom ash applications in Europe [49]

a waste to be disposed of into a landfill, provided that utilization is protective of the environment. Many countries have established criteria and procedures for determining acceptable use and disposal options, and continue to support research and development efforts for improved treatment and use technologies [52].

MWC ash is widely used in Europe in road construction as compacted road base; structural fill in wind barriers, sound barriers, and highway ramps; and in asphalt applications [4, 39]. For instance, approximately one-half of the MWC bottom ash generated in Germany is used in road construction. Figure 10 shows the bottom ash utilized in selected countries in Europe versus landfill. Figure 11 shows the quantities and percentages utilized and the specific applications.

Ash management practices in Bermuda, Japan, The Netherlands, Denmark, Germany, France, Sweden, and the UK were reviewed by the U.S. Department of Energy [26]. In Denmark, laws and regulations define how ash residues may be used, and in what quantities, so that environmental impact will be insignificant [37]. In general, in order to produce an environmentally benign bottom ash material by minimizing the quantity of soluble salts, fly ash is not mixed with bottom ash. The Netherlands, with many years of experience with MWC fly ash, has confirmed its suitability as a substitute for natural aggregate in asphalt road construction. No differences have been found in the leaching of metals between asphalt sections containing MWC fly ash compared to natural aggregates [52].

Future Directions

The many years of research and demonstration have produced a wealth of information which can be used to further sustainability and conservation of materials. The growing number of WTE facilities throughout North America, Europe, Asia, and the world will continue to manage ash residues in accordance with local, state, and federal regulations. The economic and social incentives to make use of these materials and derived products will continue to encourage processing and the marketing essential to favor beneficial use as distinguished from landfilling. Recovery of ferrous metals is

the most rewarding, but next of importance are the nonferrous metals. Ultimately, ash residues should be used for beneficial use in construction as a minimum, but more and more in fabricated products.

Bibliography

Primary Literature

1. Abe S (1984) Melting treatment of municipal waste. Recycling International, p 173 ff
2. Arcani GB (2000) Ash recycling in Nashville, Tennessee. Pub. No. GR-WTE-0108, SWANA, 8th annual North American waste-to-energy conference, Nashville
3. ASTM (1989) Standard guide for general planning of waste sampling (D4687). American Society for Testing and Materials, West Conshohocken
4. Chandler AJ et al (1997) Municipal solid waste incinerator residue. Studies in environmental science 67, The International Ash Working Group (IAWG). Elsevier, Amsterdam, The Netherlands
5. Chesner WA (1989) Aggregate-related characteristics of MSW combustion residue, Resource recovery report. In: Proceedings of the 2nd international conference on MSW combustor ash utilization, Washington, DC
6. Chesner WA (1993) Working toward beneficial use of waste combustor ash. Solid Waste Power 7(5):12
7. Chesner WH, Collins RJ, Fung T (1988) Assessment of the potential suitability of Southwest Brooklyn incinerator residue in asphaltic concrete mixes. NYSERDA report 90-15, State of New York, Albany, NY
8. Clark RA (1992) Summary of the field leachate generated from Northern States Power Company's Red Wing RDF ash disposal facility, Paper no. 92-47.02. In: 85th annual meeting of the air and waste management association, Kansas City
9. Cundari KL, Lauria JM (1986) The laboratory evaluation of expected leachate quality from a resource recovery ashfill. In: 1986 triangle conference for environmental technology, Chapel Hill, NC
10. DeCesare R, Plumley A (1992) Results from the ASME/US bureau of mines investigation – vitrification of residue from municipal waste combustion. In: 1991 ASME national waste processing conference, Detroit, MI
11. DeCesare R, Plumley A (1992) Results from the ASME/US Bureau of Mines Investigation – vitrification of residue from municipal waste combustion, Paper 92-47.03. In: 85th annual meeting of the air and waste management association, Kansas City
12. Donnelly JE, Jons E, Mahoney P (1987) By-product disposal from MSW flue gas cleaning systems, Paper #87-94A.3., 1987 APCA annual meeting, New York, NY
13. Eaton M (1992) The Commerce refuse-to-energy facility ash handling and treatment system. Chesner Engineering, 5th international conference on MSW combustor ash utilization
14. Eighmy TT et al (1989) Theoretical and applied methods of lead and cadmium stabilization in combined ash and scrubber residues, Resource Recovery Report. In: Proceedings of the 2nd international conference on MSW combustor ash utilization, Washington, DC
15. Eighmy T et al (1991/1993) The Laconia, NH, bottom ash paving project. Environmental Research Group, University of New Hampshire, Durham
16. Eighmy T et al (1997) Fundamental mechanisms of phosphate stabilization of divalent metals in MSW combustion scrubber residues. Pub. No. GRANITE 0105, SWANA. In: 5th annual North American waste-to-energy conference, Research Triangle Park, NC
17. Energy Answers, Energyanswers@Energyanswers.com
18. EPA US (1980) Hazardous waste management system: identification and listing of hazardous waste, toxicity test extraction procedure (EP). Fed Reg 45(98):33063–33285
19. EPA US (1995) Guidance for the sampling and analysis of municipal waste combustion ash for the toxicity characteristic. U.S Environmental Protection Agency, Washington, DC
20. Exner R et al (1989) Thermal effluent treatment for flue gas treatment systems in refuse incineration plants from the point of view of residue minimization by recycling. Recycling International, pp 1372–1392
21. Feder WA, Mika JS (1982) Summary update of research projects with incinerator bottom ash residue. Executive Office of Environmental Affairs, Commonwealth of Massachusetts, Boston
22. Fiesinger T (1989) Sampling of incinerator ash. Resource recovery report, p 51. In: Proceedings of the 2nd international conference on MSW combustor ash utilization, Washington, DC
23. Fiesinger T (1992) Incinerator ash management: knowledge and information gaps to 1987. Recovery Report 92-6, NYSERDA, Albany, NY
24. Forrester K (1989) State-of-the-art in refuse-to-energy facility ash residue characteristics, handling, reuse, landfill design and management – a summary, Resource Recovery Report, pp 167 ff. In: Proceedings of the 2nd international conference on MSW combustion ash utilization, Washington, DC
25. Francis CW (1984) Leaching characteristics of resource recovery ash in municipal waste landfills. DOE ERD-83-289, No. 2456, Oak Ridge National Laboratory, Oak Ridge
26. Francis CW, Maskarinec MP (1987) Leaching of metals from alkaline wastes by municipal waste leachate. ORNL/T-10050, Pub. No. 2846, Oak Ridge National Laboratory, Oak Ridge
27. GBB (1990) Studies of waste composition. Gershman, Brickner and Bratton, Inc., Falls Church
28. Goodwin RW (1982) Chemical treatment of utility and industrial waste. ASCE National Conference on Environmental Engineering, Minneapolis
29. Goodwin RW, Forrester KE (1990) MSW ash field study: achieving optimal disposal characteristics, Paper no. 25094. In: American Society of Civil Engineers, J Environ Eng Div 116(5):880–889

30. Hahn J et al (1990) Fugitive particulate emissions associated with MSW ash handling – results of full scale field program, 83 rd annual A&WMA, Pittsburg, PA
31. Harden J, Elander P (1986) Residues from waste incineration – chemical and physical properties, SGI Varia 172. Swedish Geotechnical Institute, Linkoping
32. Hasselriis F (1992) Alternative methods of disposal of residues from municipal incinerators. Wheelabrator Technologies.com.
33. Hasselriis F (1993) A comprehensive study of ash residue characteristics and statistical analysis of data. Air and Waste Management Association, Paper No. P-30
34. Hasselriis F (1994) Analysis of data obtained from an historic ash residue leaching investigation. In: ASME national waste processing conference, New York, NY
35. Hasselriis F, Drum D et al (1991) The removal of metals by washing of incinerator ash. In: 84th annual meeting of the air and waste management association, Vancouver, BC
36. Hjelmar O (1982) Leachate from incinerator ash disposal sites. In: International workshop on municipal waste incineration, Montreal, Canada
37. Hjelmar O (1990) Regulatory and environmental aspects of MSW ash utilization in Denmark, Resource Recovery Report. In: 3 rd international conference on ash utilization and stabilization (ASH III), Washington, DC
38. Holland P et al (1989) Evaluation of leachate properties and assessment of heavy metal immobilization from cement and lime amended incinerator residues, vol 1. In: Proceedings of the international conference on municipal waste combustion, Hollywood, FL
39. International Ash Working Group (IAWG) (1997) Municipal solid waste incinerator residues. Elsevier, Amsterdam
40. Lebedur H et al (1989) Emission reduction in the second domestic waste incinerator plant in the RZR Herten. Recycling International, p 1220
41. Lucido SP (2000) The use of municipal waste combustor ash as a partial replacement of aggregate in bituminous paving material. Pub. No GR-WTE-0108, SWANA, 8th annual North American waste-to-energy conference, Nashville
42. Lyons MR (1996) The WES-PHix ash stabilization process, pp 165ff, 17th Biennial ASME SWPD
43. Magee BH, Hahn J et al (1999) Environmental testing of municipal solid waste ash-amended asphalt, pp 103 ff. In: North American waste-to-energy conference, 1999
44. Musselman CN et al (1994) The New Hampshire bottom ash paving demonstration, Laconia, New Hampshire. In: ASME national waste processing conference, New York, NY
45. Roffman HK (1991) Major findings of the US. EPA/CORRE MWC-Ash Study. A&WMA VIP-19, Municipal Waste Combustion
46. Shinn CE (1987) Toxicity characteristic leaching procedure (TCLP), extraction procedure toxicity (EPtox) and deionized water leaching characteristics of lead from municipal waste incinerator ash. Department of Environmental Quality, Portland
47. Thorne-Kozmiensky K (1989) Measures to reduce incinerator emissions. Recycling International, p 1009
48. U.S. EPA (1988) National secondary drinking water regulations, 40-CFR 143. U.S. Environmental Protection Agency, Washington, DC
49. Vehlow J (2002) Bottom ash and APC residue management in Europe. In: Expert meeting on power production from waste and biomass, Espoo, Finland, 8–10 April 2002
50. Vehlow J (2010) Trends in utilizing WTE residues in Europe. WTERT 2010 bi-annual meeting, Columbia University, New York
51. Wakamura Y, Nakazato K (1992) Technical approach for flyash stabilization in Japan, Paper no. 92-20.08. In: 85th annual meeting of the air and waste management association, Kansas City, MO
52. Wiles C (1999) Beneficial use and recycling of municipal waste combustion residues – a comprehensive resource document. NREL/BK-570-25841, NREL, Boulder, CO

Books and Reviews

Hasselriis F (1984) Processing refuse-derived fuel. Ann Arbor Science, Boston (Available from author). ISBN 0-250-40315-3

Hasselriis F (2002) Waste-to-energy combustion, part 12B ash management and disposal. In: Tchobanoglous G, Kreith F (eds) Handbook of solid waste management, 2nd edn. McGraw-Hill, ISBN 0-07-135623-1

U.S. EPA (1993) Test methods for evaluating solid waste physical/chemical methods, 3rd edn. SW-846, sampling and testing methods for solid waste. U.S. Environmental Protection Agency, Washington, DC

Waste-to-Energy Facilities as Power Plants

M. A. J. (Marcel) van Berlo
Free University of Amsterdam and AEB-Amsterdam, Amsterdam, The Netherlands

Article Outline

Glossary
Definition of the Subject
Introduction
Waste to Energy History
Improving Energy Efficiency from Waste
Assessing the Energy from Waste
Future Directions
Bibliography

Glossary

CBA Cost benefit analysis.

CHP Combined heat and power: production of electricity combined with delivery of heat, e.g., for district heating.

EfW Energy from waste, synonym of WtE.

LCA Life cycle analysis.

MSW Municipal solid waste: residential, commercial, and other urban waste. It is the residual part, which is the non-source separated stream.

R1/D10 EU legislative distinction between Reuse and Disposal of waste.

RDF Refuse derived fuel: pretreated waste, mainly by shredding and recovery of some recyclable materials and removal of inert and wet fractions. It consists mainly of packaging paper and plastics.

WTE Waste to energy: Thermal treatment of wastes with energy recovery.

Definition of the Subject

This entry describes the history of WTE and technological developments with regard to increasing the energy efficiency of this process, and ways to assess energy efficiency.

In the history, four distinct stages are described involving improvements on the combustion system, flue gas cleaning, and energy efficiency.

An overview of options to improve energy efficiency is given, with the technical limitations to raise steam parameters, resulting efficiencies, and ways to evaluate the energy performance of WTE installations.

Introduction

Over the last century, Waste to Energy was developed in a few distinct stages. Originally, the objective was to manage urban wastes in order to avoid the spread of diseases. In the second stage, reduction of smoke issuing from the stack became the point of attention. Later, discovery of the effects of invisible pollutants, such as volatile metals and dioxins, in the stack gases led to important advancements of the air pollution control systems of WTE plants. Currently, sustainability and energy and materials conservation have shifted the focus of WTE research and development on obtaining higher energy efficiency and recovery of metals. This entry describes briefly the history of WTE and presents technological developments with regard to increasing energy efficiency.

Waste to Energy History

Pre–Nineteenth Century

Managing of waste became an urban issue when cities reached a certain size. Nuisance factors, both visual and unpleasant odor effects, led to the adoption of some rules for dealing with waste. In the nineteenth century, landfills were created to deal with the mounting amount of waste and collection was organized either by public or by private companies. The cholera epidemic that started in 1892 in Hamburg, swept over Europe, and even reached America, was a general political trigger for public responsibility for sanitation.

1900–1960: Hygiene

As a response to this political pressure, waste collection, sewer systems, and drinking water distribution were quickly developed in many European cities. Landfills were moved out of the cities and waste incinerators were built in many places. The focus of these incinerations was to dispose of the waste hygienically and reduce the amount of materials that had to be transported to landfills. In order to increase landfill space, in many cases the landfilled waste was often burned in the open. When the waste was burned in dedicated incineration facilities, the focus was on hygiene, and there were good examples of integrated systems of waste collection, transportation, and transfer into the bunker of the incineration plant. These systems were designed to minimize manual contact with the waste and keep it in closed containers to avoid rats, mice, birds, and flies.

However, in this focus on sanitation, there was not much attention paid to atmospheric pollution. A stack plume of black smoke was common and was considered to be a sign of economic activity and prosperity rather than a problem. Also, the bottom ash, and fly ash collected in a simple cyclone, of incinerators was landfilled or spread on roads to harden the surface. The incinerators were generally run as batch operations.

With regard to energy, most of these installations did not provide for energy recovery, but some were heating water for district heating. The very simple combustion systems were inadequately controlled, resulting in large amounts of air used, incomplete combustion causing massive amounts of black smoke and carbon monoxide, and very wide temperature fluctuations. This also led to corrosion problems so that only very simple and small heat exchangers were used to extract some of the combustion heat. As a result, the heat recovery was very small and most of the combustion heat was lost in the flue gasses leaving the stack.

Some incinerators in the first part of the twentieth century were equipped with a boiler for steam production that was used for either industrial use or electricity production. Electrical efficiency was very low, at about 5% in the best cases.

1960–1990: Dust Removal

Over time, the black deposits of the smoke and fly ash of waste incinerators became noticeable and gradually unacceptable. Therefore, standards emerged limiting smoke and dust for the next generation of incinerators. Technology improved in boiler designs, control of the fire, and fly ash separation by means of electrostatic precipitators that resulted in stacks without black smoke. This also enabled the recovery of more heat from the combustion gases and continuous operation of the incinerator and boiler for a period of a month or more. During this period, some cities were provided with a district heating network using hot water. This was done with a simple and inexpensive hot water boiler but did not take advantage of the potential work that can be done with the energy of cogenerating electricity and heat. For Combined Heat and Power (CHP), a steam boiler is needed plus a turbine for electricity production. In this period, CHP installations were mainly small backpressure turbines that were used to produce the heat and electricity.

Steam pressure from the boiler was initially in the range of 10–20 bar, but as designs improved, it was gradually raised for newer installations, reaching a common acceptance of about 40 bar as state of the art at the end of the 1980s. This 40-bar boiler pressure, and 400°C superheater temperature, resulted in an acceptable compromise between excessive corrosion of the boiler wall and superheater tubes and thermal efficiency achieved.

Also, energy loss in the flue gases was lowered by decreasing the boiler outlet temperature to 250–300°C. The resulting energy efficiencies were gradually improved to about 80% for hot water boilers and from 10% to 18% for electricity producing plants

In this period, some plants in Germany were built with higher steam parameters (e.g., Mannheim: 120 bar/525°C; Düsseldorf: 90 bar/495°C: Frankfurt 60 bar/500°C; Stuttgart 74 bar/525°C). However, these were based on coal-fired boiler concepts. In the case of burning Municipal Solid Waste, the high chlorine-to-sulfur ratio results in high corrosion rates and, also, the fly ash tends to be very stick at the higher temperatures of flue gas and boiler wall. The resulting large downtime periods for repairs and plant availabilities in the range of 70–80% lead to adaptations in the design of boilers that use municipal solid waste (MSW) as their fuel. But changing the steam parameters of a WTE plant is generally not possible without major rebuilding of boiler parts and turbine. Therefore, existing plants could not be retrofitted economically and had to continue operating at low plant availability.

The general consensus developed that 40 bar/400°C was the optimal compromise for the steam parameters, balancing corrosion and associated shutdowns and maintenance with the returns for the electricity produced. The overall efficiency with these parameters was commonly up to about 14–18%, but most operators paid little attention to improving electrical efficiency as the revenues from power production and sale were generally less than a quarter of total revenues.

1990–2005: Chemical Cleaning

At the end of the 1970s, it was discovered that although there was no visible smoke, dioxins and some volatile metals were present in alarming quantities in the flue gas of WTE plants. This raised great concerns and, within a period of about 10 years, political measures were taken to drastically limit the allowable quantities of emissions of dioxins and other critical pollutants such as mercury, other heavy metals, chlorine, sulfur dioxide, carbon monoxide, and particulate matter. The concerns were such that the new limits for dioxins were set at the detection limit, i.e., at about a factor 1,000

lower than average dioxin emissions of the time. In some EU countries standards emerged which were EU-wide implemented following the year 1991. These have by now been taken over by nearly all other countries with WtE installations.

The new standards have led to closure of many of the 1980s WTE plants and the addition of state-of-the-art air pollution control systems in all operating plants. As a result, in a period of ten to fifteen years, the WTE industry, worldwide, has been transformed from a major emitter of pollutants to being one of the cleanest power generators, having stricter limits than almost any other industry. For example, for dioxins, the emissions have been reduced by a factor 1,000 till a maximum limit of 0.1 ng/normalized cubic meter. As a result, by 2005 the issue of emissions from WTE was resolved. Although there remain some local debates at different countries, these are more a remnant of the past image rather than because of actual impacts of WTE plants.

With the focus on cleaning the WTE stack gases, there has been little attention to improvements with regard to energy efficiency. In many cases, there was an actual lowering of energy production, because of the increased use of energy within the plant for gas cleaning.

Some of the existing WTE plants have experimented with adding energy-saving improvements, such as additional heat exchangers in the flue gas (e.g., a second economizer or a condensing heat exchanger) so as to improve the recovery of heat for district heating or to replace internal heat consumption and to increase the plant's electrical efficiency.

Plants that were designed and built in this period generally followed the consensus of the 40 bar/400°C steam parameters. However, on the average, energy efficiency increased somewhat during this period, by reducing boiler outlet temperature (from about 250°C to 180°C), reducing the use of excess air from 1.8 to 1.6 (lowering oxygen content in the stack gas from 12% to about 8%), and simplifying the gas cleaning designs. Few plants that deliver only heat were built, as CHP was commonly employed to produce electricity and heat. When the plant is small compared to the heat demand, backpressure turbines were used. For bigger WTE plants, a vacuum turbine with a steam bleed was used. This allows maximum electricity production while the heat extraction can be controlled according to demand.

Some exceptional WTE plants were built in this period with high thermal efficiencies, such as:

- Falls (Bucks county, PA, USA, 1994): 90 bar/500°C and a boiler outlet temperature of about 180°C resulted in about 28% net electrical efficiency.
- Moerdijk (The Netherlands, 1996): 100 bar/400°C is directly coupled with a Combined Cycle Gas-fired power plant that further superheats the steam and includes it in its cycle. The total efficiency is in the order of 45%, but as natural gas can normally yield 58% efficiency, the net efficiency corresponding to the chemical energy from the waste is about 30%.
- Brescia (Italy, 1998): 61 bar/450°C two lines (plus a third line in 2004 operating at : 73 bar/480°C) and a boiler outlet temperature of 135°C results in about 25.8% net electrical efficiency plus 58% of heat for district heating.
- The Bilbao (Spain), 265,000 t/year WTE plant combusting presorted waste was started in 2004. The WTE steam parameters are 100 bar/330°C, but this steam is then superheated to 540°C in a Combined Cycle Gas Turbine and reheated halfway the turbine. The efficiency is similar to the Moerdijk WTE mentioned above.

Alternative thermal treatment technologies for treating solid wastes (e.g., fluidized bed, pyrolysis, and gasification) have not proven in practice to have as high energy efficiencies as the classical WTE installations that use the common grate technology. This is mainly due to the difficult physical and chemical properties of Municipal Solid Waste (MSW) or Refuse Derived Fuel (RDF) and associated operational problems, as compared to coal or biomass (e.g., wood chips).

2005 to Present: Sustainability

Since the mid-1990s, nickel–chromium alloys have been used to repair and protect corrosion-affected parts in WTE boilers. Especially, the alloy Inconel 625 has proven to be extremely successful in surviving the corrosive conditions encountered in MSW boilers. The gain in plant availability has paid for the high additional investment costs and by the year 2000, nearly all WTE plants were testing or using this alloy. Its high cost however prohibited its use by contractors for new installations. However, by 2005, this alloy was proven to be so effective

that in some new construction projects its use was prescribed for cladding the 1st-pass of the boiler already at construction of the plant. Steam parameters were still mostly around the conventional 40 bar/400°C.

At the same time, sustainability and the greenhouse gas effect came very much in focus, partly due to Al Gore's film, the "Inconvenient Truth." In two legal proceedings in the EU about cross-border transport of waste, it was ruled that the efficiency of the installation receiving the waste was the key criterion for deciding whether this should be allowed. This resulted in an efficiency formula in the EU "Best Available Technology" descriptions. In the new EU Waste Framework Directive, this resulted to the legal distinction between reuse/recovery (R1) and disposal (D10) status. This also meant that energy efficiency determines whether waste can be traded cross border and whether it may be used in the statistics for recovery.

The combination of more attention for energy efficiency and the availability of Inconel 625 as a good performing corrosion resistant material led to the use of higher steam parameters in new plant. Some examples are:

- In Amsterdam (The Netherlands), alongside the existing plant (1993, 800,000 t/year, 42 bar/430°C), the 530,000 t/year Waste Fired Power Plant was completed in 2007. The superior properties of Inconel 625 allowed in 2001 the choice for increasing the boiler steam parameters to 125 bar/440°C [1]. This high pressure with moderate superheater temperature was made possible by a steam-to-steam reheater, using drum steam to reheat the steam halfway the turbine. Energy efficiency was increased further by reducing boiler outlet temperature, reducing the combustion excess air ratio till 1.4 (equivalent to lowering oxygen content in the stack gas from 8% to about 6%), heat recovery from the gas cleaning system, reducing of internal heat and electricity consumption, and improved design of turbine and condenser. The net electrical efficiency of this unit is 30.4% and 34.5% gross.
- In Rüdersdorf near Berlin (Germany, 2009), a 250,000 t/year RDF plant was started with steam parameters of 90 bar/420°C. Also, reheating halfway the turbine is used, albeit with the reheating accomplished by a heat exchanger tube bundle in the flue gas. The net electrical efficiency of this plant is 29.1% and 31.8% gross.
- In Hameln (Germany), a 200,000 t/year plant was started in 2010 with steam parameters of 41 bar/400°C and external superheating of the steam to 520°C. The excess air ratio is only 1.39. The net electrical efficiency from the energy in the waste is 26.6% and 29.7% gross.
- Biomass combusting plants with reheaters were erected in Bischofferode (Thüringen, Germany, 128 bar/532°C), Leipzig (Germany, 20 MW fluidized bed boiler, fresh wood from forestry, 128 bar/532°C), Eberswalde (Germany, 80 bar/480°C), and Simmering (Vienna, Austria, 120 bar/520°C, 23.4 MWel, gross efficiency of 36.4%). The temperatures and hence efficiencies in these plants can be higher because the biomass combusted contains less chlorine than MSW, which results in less aggressive conditions in the boiler.

The above developments indicate that the focus on sustainable waste management along with favorable legislation and the availability of new corrosion-resistant materials have shifted the frontier of what WTE efficiencies can be commercially achieved. Especially, the general acceptance of using the high-cost Inconel 625 as a cladding on the boiler membrane walls has been a breakthrough in maintaining high availabilities with increasing steam parameters.

Historical Overview

Table 1 shows schematically the different generations of WTE power plants.

Improving Energy Efficiency from Waste

Waste to Energy plants all use a boiler to produce steam and a steam turbine to convert this steam to electricity in a Rankine cycle. The efficiency of this Rankine cycle depends directly on the ratio between maximum and minimum temperature, i.e., the superheated steam and the steam condenser at turbine outlet. The strongly corrosive properties of the combustion gases are limiting the maximum steam temperature that can practically be handled. This explains why WTE power plants cannot achieve the high energy efficiencies of a clean fuel like natural gas.

Waste-to-Energy Facilities as Power Plants. Table 1 Changing paradigms for WtE-plants

Generation	Period	Paradigm	Boiler	Heat efficiency	Electrical efficiency
0	Pre–1900	***Landfill***	–	–	–
1st	1900–1960	***Sanitation***, Incineration	Hot water or low steam parameters	~50%	Some cases
2nd	1960–1990	***Nuisance***, Dust separation	Medium steam parameters	<70%	~5–14%
3rd	1990–2005	***Pollution***, Chemical Flue gas cleaning	40 bar/400°C	CHP	~15–22%
4th	2005–	***Sustainability***, Energy efficiency & Material recovery	Higher steam parameters	CHP	~25–31%

In designing WTE boilers, great care has to be paid to the layout of superheaters with regard to their position in the boiler and the flue gas temperatures. The introduction of high-temperature corrosion-resistant alloys for the cladding of the membrane walling the first pass of the boiler has allowed to operate at higher boiler wall temperatures. This also allows for increasing steam pressure and the introduction of reheating of the steam halfway the turbine. The reheating increases efficiency even with moderate superheater temperatures. The following graph relates the steam parameters to the estimated corrosion resistance of normal boiler steel (e.g., 15 Mo3) and cladding of the steel with Inconel 625 (Fig. 1).

As shown in the above figure, a classical WTE boiler is operated at superheater temperatures of 40–60°C below the temperatures where corrosion starts to become important. However, it should be noted that the surface of the steel tube is between 20°C and 50°C above the temperature of the steam in the tube. The superheater temperatures for the new concepts can be increased till it is close to the transition area when the boiler design is optimized for this. Key parameters for this are especially low flue gas speeds in empty passes and in the superheater bundle. A long residence time of the flue gas allows for gradual cooling and a chemical equilibrium when reaching the superheater. Experiences with the use of Inconel in superheater bundles are mixed and are not generally cost-efficient. The good properties at high flue gas temperatures can best be exploited by cladding the membrane walls in combination with drum pressures of 80–150 bar, thus raising drum temperature by 50–80°C. These high pressures require the use of reheating halfway through the turbine in order to prevent too high levels of steam wetness in the turbine. For this there are three rivaling concepts.

Reheating can be done by a bundle in the boiler (Rüdersdorf plant) which allows reaching high reheating temperatures (~450°C) but requires an additional bundle near the superheaters. As a consequence, the flue gas at inlet of the bundles has to be hotter, leading to more molten fly ash deposits and corrosion. This makes this a maintenance-intensive solution.

In the alternative solution, the steam is reheated halfway the turbine by a steam–steam heat exchanger that uses steam from the drum. The temperature of the reheating is limited by drum steam temperature (~330°C) but the advantage is that it is a low maintenance solution because in this case the heat transfer is shifted from bundles to membrane wall, which is much lower in maintenance due to the Inconel.

The third alternative is to use external superheating (Moerdijk, Hameln, Bilbao) to circumvent the corrosion by using heat from another fuel to superheat or reheat the steam. This is thermodynamically a very good solution combining the low-temperature heat from waste (because the corrosion limits) with the high temperature from a good fuel like Natural gas. However, the total thermal efficiency of a plant using auxiliary fuel must be divided into the efficiency expected by the fossil fuel and that achieved only

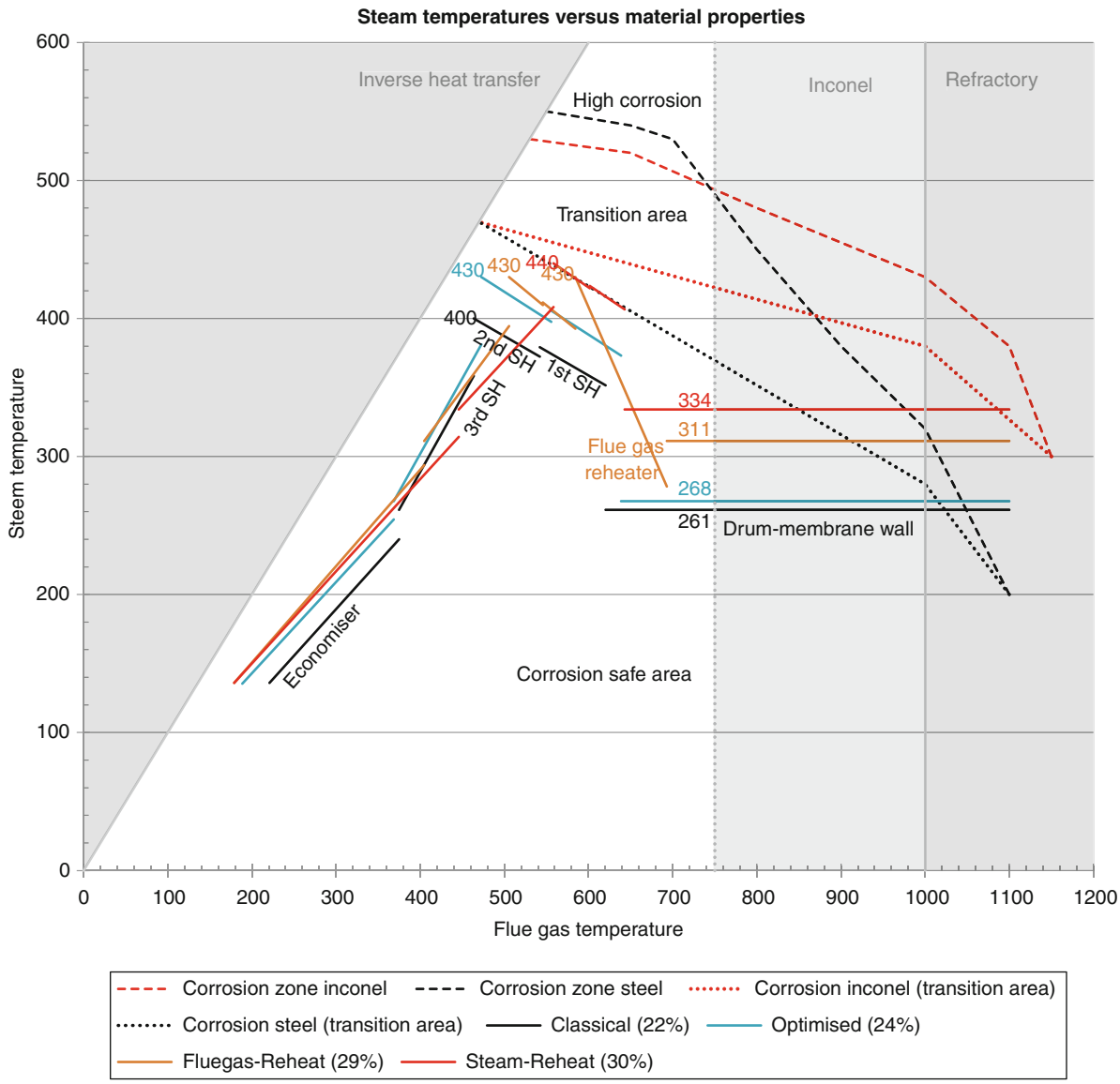

* corrosion performance of materials are estimates for real life fluegas and flyash conditions.
** Steam temperatures modeled in efficiency calculation model. ©AEB-MvB

Waste-to-Energy Facilities as Power Plants. Figure 1
Corrosion: Material properties and temperatures of steam and flue gas

from the energy in the waste. Therefore, the reference efficiency for gas (Combined Cycle Gas Turbine ca. 58%) must be deducted from the total output. The resulting efficiencies from the energy in the waste have been shown to be in the same range as the steam reheating concepts and they depend on the pressure at which the steam is delivered. Also, matching the scale of WTE boiler and the gas turbine can lead to practical problems since gas turbines are chosen preferably to be of high capacity (>200 MWel) in order to be more

efficient. Also, an economic disadvantage is that a WTE plant must be run in base load which means that the gas plant cannot be switched off during periods of low demand for electricity. This requires burning natural gas at times when electricity prices are low and makes maintenance planning critical.

Also, new WTE plants with classical steam parameters tend to have higher efficiencies due to energy optimization at other points:

- Lowering deaerator temperature from the common 135°C to 115°C
- Lowering boiler outlet temperature of 180°C further till 150°C
- After dust separation, a second economizer (for condensate preheating or for district heating) cooling the flue gasses till 90–100° (below the acid condensation point)
- A third economizer at the end of the flue gas cleaning (before induced draft fan) to extract the condensation heat of the flue gases (for condensate preheating)
- Large condenser design to improve turbine vacuum
- Flue gas recirculation as high-quantity secondary air/gas, with tertiary air above it
- Low stoichiometric combustion at 1.4 resulting in oxygen surplus of only 6%
- High efficient motor drives and the use of frequency converters to control them in order to avoid throttling by control valves
- Recovery of heat from blow-down water and steam bleeds (like deaerator off gas)
- Optimized steam bleeds from the turbine for staged heating of condensate, two-stage heating of water for district heating and primary air heating

Assessing the Energy from Waste

Efficiency Formulae

The simplest indicator of energetic efficiency of WTE power plants can be expressed as follows:

$$\text{Energy efficiency} = \frac{\text{Heat} + \text{Electricity}}{\text{Input from waste}} \tag{1}$$

In this formula, the total energy content in the waste (Lower Heating Value) is the input to the system, and the total output is the sum of the produced heat and electricity. Many different variations have been proposed for energy efficiency. In a Dutch study alone, there are listed 11 methods that are used in different legislation ([2], p. 14). This is mainly due to different definitions, deviations from the laws of physics, and using specific parameters and assumptions.

The definitions of the energy streams can be different; e.g., the *place* where the electricity is measured can be chosen at the generator (gross electricity production) or at the point of delivery to the grid (net electricity delivery). The difference is the in-plant consumption of electricity that can amount to 2–4 percentage points in efficiency. The *time* frame can be chosen as a specific measurement, e.g., over a short time of good operation (e.g., a day), or a year, including all variations in waste, operational disturbances, shutdowns, and start-ups. The difference between short term and long term average efficiency is typically 1–2 percentage points in efficiency. Also, corrections are needed to account for fossil fuels that may be used occasionally.

The R1/D10 formula in the EU Waste Framework directive is an energy efficiency formula developed specifically for WTE:

$$\text{R1/D10 efficiency factor} = \frac{\text{Ep} - (\text{Ef} + \text{Ei})}{0.97 \times (\text{Ew} + \text{Ef})} \tag{2}$$

where

E_p, annual primary energy substituted by the produced heat and electricity

E_f, annual energy input to the system from fuels contributing to the production of steam

E_w, annual energy contained in the treated waste calculated using the lower net calorific value

E_i, annual energy imported excluding E_w and E_f (GJ/year)

0.97, factor chosen for accounting for energy losses due to bottom ash and radiation

This formula is now the basis of a new EU ruling that determines the distinction between considering a WTE plant as reuse (R1-status) or disposal (D10-status) plant. The threshold is R1 = 0.6 for plants built before 2008 and R1 = 0.65 for new WTE plants. The figure is not to be compared with the

energy-output-efficiency as in formula (1) shown earlier. This formula expresses how much primary fuel is replaced by the energy recovered from the waste.

$$E_p = 1.1 * \text{Heat} + 2.6 * \text{Electr} \quad (3)$$

The equivalence factors 1.1 and 2.6 are expressing that the heat produced is substituting another boiler with an efficiency of 90% and the produced electricity is substituting a power plant with an average efficiency of 38% (1/90% = 1.0989 and 1/38% = 2.6316).

The EU R1/D10 formula for energy approach has some fundamental advantages:

- The equivalence factors account for the difference in thermodynamic quality of electricity and heat, which is a definite improvement over formula (1).
- Electrical efficiency for a plant can be measured by an established definition (ISO 1940).

This approach has some disadvantages:

- For both heat and electricity, the gross production is to be used, so internal consumption also contributes to a higher value.
- The Energy Efficiency definition is a new political definition, setting WTE power plants apart from electrical power production industry.
- Material/metal recovery is not taken into account.
- The offset from the biogenic content in the waste is not taken into account.
- The equivalence factors 1.1, 2.6, and 0.97 have no real physical background [3]. Heat is overvalued which makes it easy to fulfill the criterion in colder countries where district heating is common.
- The equivalence factor for heat does not take the temperature (and thereby enthalpy) of the heat delivery into account. This rewards (and stimulates) low-temperature district heating, but underestimates the even better effect of high-temperature steam delivery to industry. The use of *exergy* instead of energy is a possibility to physically correctly relate heat and electricity.

Many existing plants will meet the 0.6 criterion, only small plants delivering electricity only will be below. For new plants to be built, the 0.65 is not challenging for full optimization. Values up to the range of 0.9 till 1.1 have been reported.

Alternative Efficiency Evaluations

In order to address the performance of a WTE power plant in a specific context, several more integrated methods are available:

- Instead of efficiency (which is a ratio), the direct output can be expressed. Classical plants deliver about 500–650 kWh/t of waste when this has the average calorific value of 10 MJ/kg (standard waste, Lower Heating Value LHV). For the high-efficiency plants, this can be raised to as much as 850 kWh/t of waste. For presorted high calorific wastes with a calorific value of 12–14 MJ/kg, the recovery can reach 900–1,100 kWh/t of waste.Additionally, 1,500–2,500 kWh-heat/t of standard waste can be delivered with only a small de-rating of the capacity to produce electricity. De-rating depends on the temperature at which the heat is delivered and the configuration of the turbine, and can be 13–20% of the amount of heat extracted from the turbine, i.e., delivery of 1 kWh of heat reduces electrical output with 0.13–0.20 kWh.
- The use of *exergy* instead of energy is a possibility to physically and thermodynamically correctly relate heat and electricity, see [4, 5]. Exergy is the equivalent amount of work that can be performed by a stream of heat. A small formula uses the temperature to convert heat energy in it to equivalent exergy. This solves the use of arbitrary equivalence factors as used in the R1/D10 formula and expresses the output of a CHP plant in an equivalent amount of electricity that that plant could produce if no heat was extracted from the turbine.
- CO_2-evaluation is calculating the overall impact of the greenhouse gas effects. This constitutes the direct emission of CO_2 which originates partly from fossil origin (~450 kg/t of waste). The other half of the carbon in the waste is of biogenic origin content of the waste which is CO_2-neutral. The direct emissions are offset by the external effect of substitution of other fossil energy power production by the energy produced from waste. Also, the substitution of mining and materials processing by the recovery of metals can be calculated. For normal WTE installations, the combination of biogenic content and substitution results in a net greenhouse

effect of +100 to about zero kg CO_2/t of waste. For high-efficiency WTE installations, the higher substitution leads to a net avoidance (∼negative emission) of up to −200 kg CO_2/t of waste [6].

- Life Cycle Analyses (LCA) is doing the same as a CO_2-evaluation but it also adds a list of other impacts on the environment and health, like: human toxicity, ecotoxicity, acidification, eutrophication, injuries, mineral extraction, land use, nonrenewable energy, and ozone layer depletion. In the LCAs for different methods to manage wastes, it is generally shown that energy efficiency has a major effect in reducing the impact of waste management options. The process to conduct these studies is much more complicated but allows detailed analyses of the impacts [7].
- Cost Benefit Analyses (CBA) is doing the same as an LCA but monetizing all the effects. So comparisons of alternatives in a specific situation can be done using a single economic value. The economic value of different impacts has however high uncertainties which make the use of CBA often complicated and strongly depending on the boundary definitions of the system to be considered.

Future Directions

In the EU, there are strong legal drivers (e.g., formula for R1/D10 distinction and Best Available Technology Reference (BAT-BREF) documents) and in many nation members economic incentives (sustainable energy premiums) that encourage striving for higher efficiency of WTE. This promotes the use of more of the available energy efficiency optimization options. Even with classical steam parameters, new plants tend to be more energy efficient. WTE plants that produce only heat are becoming rare (with the exception of steam delivery to industry) and even in the case of Combined Heat and Power (CHP), electrical output is optimized. In the U.S.A., there is renewed interest in WTE which could also result in new high-efficiency plants. In Asia, a first wave of conventional installations is being built in China while in Japan there is up to now more focus on ash treatment than on energy efficiency.

It is to be expected that Europe will keep its technological leading position in getting more energy out of waste. After new advances in technology have been proven in the E.U., it is expected that they will also be implemented elsewhere.

As LCA studies have shown, consistently, that energy efficiency is a key parameter for reducing the overall cost as well as the environmental impact of waste management, it is expected that minimum standards for energy efficiency will be raised over time. Economical modeling shows that the additional energy produced by WTE power plants is among the least-cost sources of sustainable, and also renewable, energy.

Bibliography

1. Berlo MAJ, van en Wandschneider Jörn (2003) High efficiency waste-to-energy concept [Sectie van boek]//Municipal solid waste management, strategies and technologies for sustainable solutions/boekaut. Christian Ludwich, Hellweg Stefanie en Stucki Samuel. Springer, Berlin, Heidelberg. ISBN 3-540-44100-X
2. Erbrink H et al. (2001) Analysis of energy efficiency definitions for policy making (in Dutch) [Boek]. NOVEM/KEMA, Utrecht, publicatiecentrum@novem.nl. - Reportnr: 2EWAB01.03
3. Tebert C (2006) The energy efficiency formula of annex ii of the waste framework directive: a critical review. [Rapport] = R1/D10 formula Review/Ökopol gmbh, Institute for environmental strategies – [sl] : Ökopol. http://www.eeb.org/activities/waste/20060630-Okopol-Brief-on-MSWI-efficiency-formula-v5-final.pdf
4. Murer MJ et al. (2009) Comparison of energy efficiency indicators for energy-from-waste plants [Conferentie]/Internatonal waste management and landfill symposium, Sardinia: [sn], vol 12
5. Murer MJ et al. (2010) Exergetic analysis of heat transfer and efficiency in Efw plants [Conferentie]/Third international symposium on energy from biomass and waste. CISA, Environmental Sanitary Engineering Centre, Venice, Italy, vol 2010
6. Berlo MAJ, van en Waart Harry de (2008) Unleashing the power in waste, Comparison of greenhouse gas and other performance indicators for waste-to-energy concepts and landfilling [Conferentie] = Unleashing the power in waste// North American waste-to-energy conference. Philadelphia, Pennsylvania, USA: NAWTEC, 2008. vol 16, p 16, NAWTEC16-1937
7. EU – JRC (2007) Environmental assessment of municipal waste management scenarios: Part II – Detailed life cycle assessments [Rapport] = JRC 41241/EUR 23021 EN/2/Institute for environment and sustainability. European Commission, Joint Research Centre, Ispra, Italy. p 182 - http://www.jrc.ec.europa.eu. ISBN 978-92-79-07450-9

Waste-to-Energy for District Heating

Lasse Tobiasen, Bettina Kamuk
Ramboll Energy – Waste-to-Energy, København S, Denmark

Article Outline

Glossary
Definition of the Subject
Introduction
Waste Boilers
Grate-Fired Boilers
Different Types of Boiler Arrangements
Steam Turbines for Electricity Production
Process Concepts for a Complete Electricity-Only Energy for Waste Facility
WTE Facilities Delivering "Small-To-Medium" Amounts of Heat
Larger District Heating Networks and District Heat-Producing WTE Facilities
Advanced Solutions: Heat Pumps and District Cooling
Optimizing Energy for Waste Facilities for CHP Operation
Conclusions and Future Directions
Bibliography

Glossary

District heating (DH) A network of pipes, typically underground, that distributes hot water (or steam) used for space heating of residential homes and industrial spaces. This network allows for centralized production of heat to be distributed to many consumers.

Waste-to-energy (WTE) A thermal process where the chemical energy contained in solid wastes is converted to electricity and or heat.

Definition of the Subject

In Denmark, waste incineration has been used to provide district heating since 1903, when the Frederiksberg Municipality in Copenhagen realized that landfilling of municipal waste could not continue within the municipality boundaries [1]. The incineration plant of the municipality provided steam, hot water, and some electricity to a nearby hospital, while reducing the waste volume and mass at the same time.

The first waste-to-energy (WTE) plants in Denmark were producing heat only, while from the late 1980s, they started to produce combined heat and power (CHP). However, recovery of district heat for useful purposes requires large investments in energy infrastructure (district heating pipes distribution and transmission network), and the lack of such infrastructure makes combined heat and power difficult in many countries. Most countries at this time produce only electricity (and not heat) from their waste incineration plants.

Nevertheless energy recovery in district heating waste-to-energy plants is three- to fivefold higher than from electricity-only plants. Additionally, the revenues for a waste plant from selling district heat may substantially reduce the waste gate fee. For example, in 2007, 70% of the costs of the 29 Danish WTE plants were recovered by revenues from selling district heat. In Denmark today, about 20% of the total district heat production and approximately 4.5% of the electricity used are due to energy recovery from waste incineration [2].

This entry reviews waste-to-energy and district heating technologies, drawing on the considerable experience accumulated in Denmark.

Introduction

This entry deals with energy recovery in waste-fired boilers, using the Rankine steam cycle for electricity production; and also examines methods of producing district heat or process steam that allow combined heat and power production. The Rankine thermal cycle is used to produce approximately 90% of the world's electricity.

Figure 1 illustrates this process in its simplest form: Water is pressured in a pump, superheated in a boiler, and expanded in a steam turbine. It can be shown thermodynamically that the electricity yield at the turbine, $\dot{W}_{turbine}$, is much higher than the power consumed by the pump, $\dot{W}_{pump}$. It can be shown that the cycle efficiency – from fuel to turbine output – increases with higher steam temperatures and pressures (point 3); similarly, a higher efficiency is reached by lowering the steam condensing temperature (point 4). The

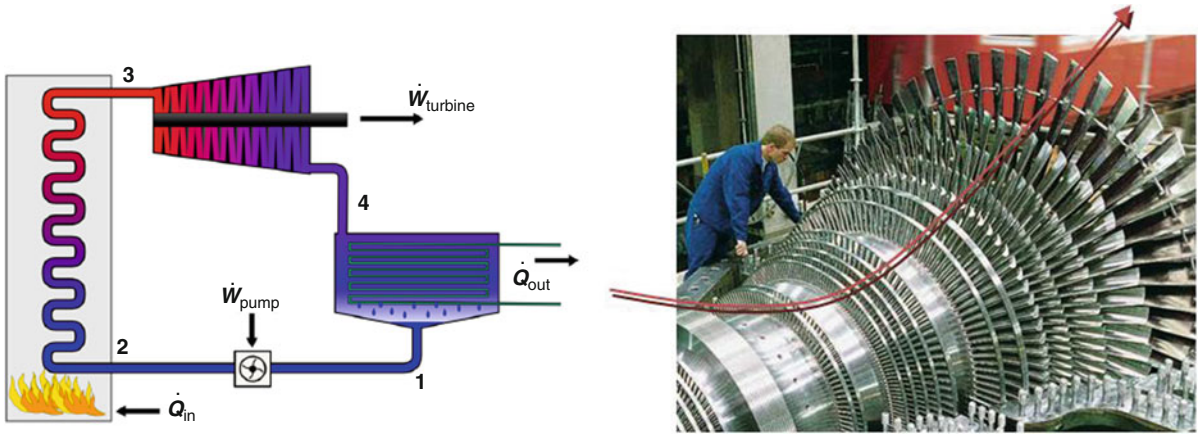

Waste-to-Energy for District Heating. Figure 1
Illustration of the Rankine water-steam cycle for electricity generation, as well as picture of a steam turbine rotor (Figure to the left from wikipedia.org. Picture of steam turbine rotor by Courtesy of MAN Diesel Turbo SE, see also http://www.mandieselturbo.com)

condensing temperature ultimately depends on the cooling temperature level available to the condenser; the condenser can be either water cooled (seawater or river/lake water) or air cooled. This is why power stations located in cold regions (access to cold seawater, for instance) have a higher electrical efficiency than power stations without such access.

Waste-to-energy facilities in Europe are often equipped with air-cooled condensers, which can be either wet (water consuming) or dry, and configured with either forced airflow or natural draught ("cooling tower"). Air-cooled condensers are the most common choice of WTE facilities.

Figure 2 shows the principle of such an air-cooled condenser system. In the top illustration in Fig. 2, low-pressure high-volume steam from a steam turbine exhaust is routed to a four-row air-cooled condenser unit, where the steam is condensed in finned tube bundles; large fans (often 10 m in diameter) force airflow across the condenser heat surface areas, thus removing the heat. Air-cooled condenser installations are necessary where there are no other means of cooling.

Therefore, WTE facilities with no access to a heat user must reject large amounts of heat through condensers, such as shown in Fig. 2. Typically, the net electrical efficiency of WTE facilities is in the region of 25%. Hence, for a 100 MW plant (corresponding to 32 t/h of waste with a calorific value of about 11 MJ/kg), roughly 25 MW of electricity can be sold to the grid. Of the 100 MW energy input, about 55 MW is rejected in water- or air-cooled condenser. Therefore, a very large amount of energy is lost.

However, if there is a demand for heat, such as space heating, in the vicinity of the WTE facility, it may very well be feasible to provide heat from the waste facility – thereby utilizing part of the heat rejected to condensers. Other options for using the WTE heat include the supply of process steam to a nearby factory or industry that would otherwise be produced by oil or gas.

Fuel input (waste):	100%
Electricity from waste:	~25%
Heat reject in Air-cooled condenser:	~55%
Other losses:	~20%
Useful heat potential (hot water or steam):	~**55–65%** (Flue gas condensation, a method of extracting additionally 10–15% of the fuel input as useful heat, but this is not included in this table)

There are various methods of producing heat from a WTE plant, as discussed in the following sections.

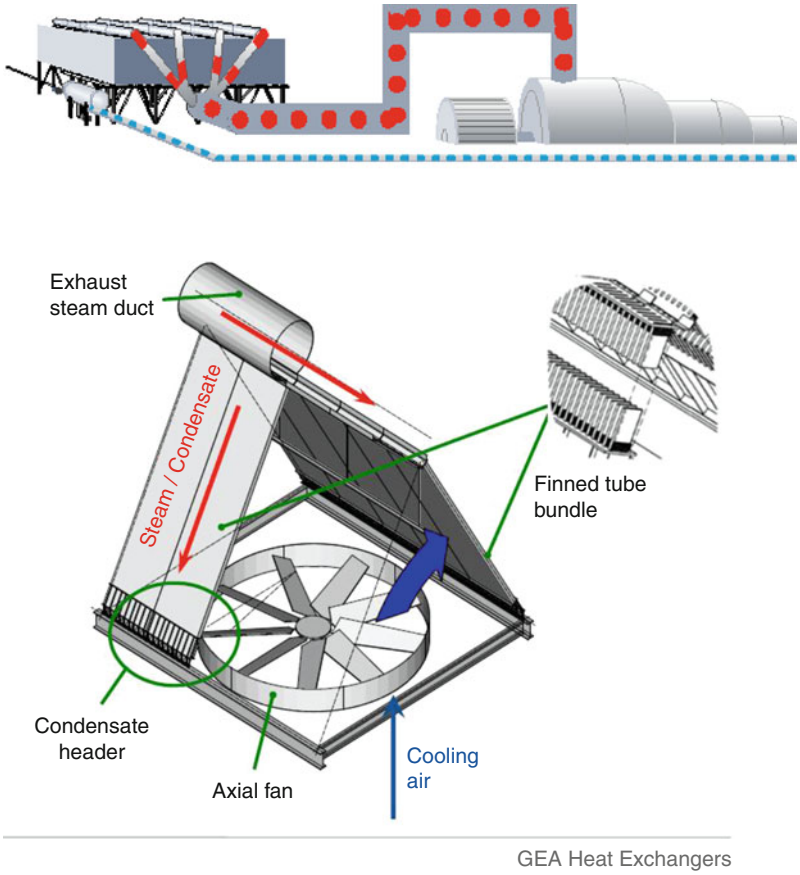

Waste-to-Energy for District Heating. Figure 2
Air-cooled condensers (Figures from http://www.gea-energietechnik.com, Courtesy GEA Energietechnik)

Waste Boilers

Waste incineration plants are designed to treat waste with great variation in the composition of the incoming waste (This chapter is mainly based on the following source: solid waste technology management, vol 1, chapter 8.1, as well as generally based on Ramboll knowledge and experience). This is the primary difference between waste incineration and other combustion systems, and it has large implications on the design of the incineration plant. Waste is not an ideal fuel and it is important to link the fuel characteristics to the combustion process. The main technologies described in this section are combustion of as-received municipal solid wastes (MSW) by means of a moving grate.

Common to waste boilers is the concept of the "capacity diagram," which determines limits of thermal capacity (energy input) for a particular boiler, given the variation of heating value in the waste. In the example shown in Fig. 3, the boiler can accept waste with a (lower) heating value from 9 to 15 MJ/kg, and a throughput from 7 to 14.4 t/h of waste.

Typical heating values for some waste fractions are as shown below [3]. Note the very large variations, and hence the need for a waste boiler to handle fuel input with a variety of lower heating values.

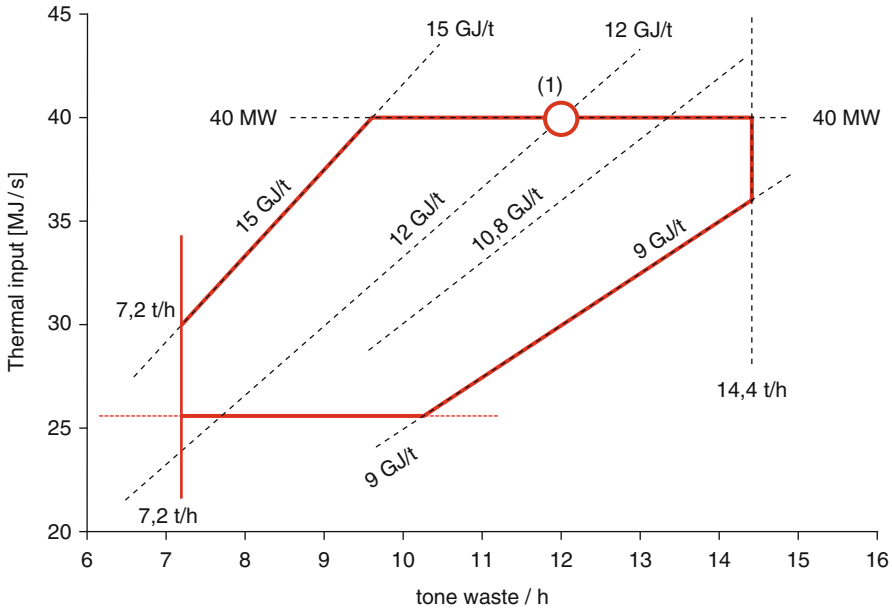

Waste-to-Energy for District Heating. Figure 3
Typical waste boiler capacity diagram. The nominal load point in this example is indicated by point (1), where the waste has a heating value of 12 MJ/kg

Fresh wood (50% moisture)	10 MJ/kg
Oven dried wood	17–19 MJ/kg
Paper/cardboard	14–15 MJ/kg
Plastic	28–35 MJ/kg
Metal, glass, concrete	0 MJ/kg
Organic waste	4 MJ/kg
Municipal waste (Copenhagen)	10–11 MJ/kg
Municipal waste (Bangkok)	2.5–12 MJ/kg

The minimum thermal load of a modern grate combustion waste boiler is 65–70%, limited by the ability to ensure proper burnout and upholding legislative requirements with regard to emission limits (like CO, Dioxins, etc.,) and flue gas temperature limits (flue gas at least 850°C for a minimum of 2 s, for instance).

Grate-Fired Boilers

A combustion grate is a transport device that moves the burning fuel from the inlet through the furnace to the bottom ash outlet. During transportation, the fuel is mixed and combustion air is added. Volatile material is released to the combustion chamber above the grate and fixed carbon is burned on the grate. The grate is an integrated part of the furnace, where the fuel is converted into energy. The grate ensures drying, ignition, combustion and energy release, and complete burnout before the bottom ash outlet [4].

Flue gases leaving the grate enter the actual "boiler," where the main steam generation takes place. A modern European waste boiler often consists of three empty flue gas passes, in which the flue gas is cooled to approximately 600–750°C while providing heat to evaporate the boiler water to generate (saturated) steam. The dominant means of heat transfer in this part of the boiler is radiation, due to the high temperature of the flue gases; thus, the first three passes are often called "radiation passes."

Boilers for waste facilities are "drum-type" boilers, characterized by a "drum" maintained below the critical steam pressure of 221 bar. The large cylindrical drum contains water at high pressure and is located at

the top of the boiler. Water circulates by natural convection by means of "down-comer" tubes and up through the evaporator tubes, since evaporated water (steam) has a lower density than the water in the down comers. Typically, the circulation ratio is 15–20, i.e., the circulating mass flow in the evaporator section is 15–20 times the dry steam flow exiting the drum.

A very simple analogy to the circulation principle in a drum-type boiler is a household electric drip brewing coffeemaker, where hot water is also moved upward without need of a pump, by the thermosyphon method.

When the flue gases enter the fourth pass of the boiler, the primary method of heat transfer changes to convection: Superheater tube bundles are located in the path of the flue gas flow, thus providing a large surface area to facilitate the transfer of heat from flue gas to steam. The superheater tube bundles heat the saturated steam from the drum to the desired final steam temperature.

The economizer is the last set of tube bundles in the boiler, seen from the flue gas point of view. Here the inlet water is heated to somewhere below the boiling point at the particular water pressure (e.g., heated to 200°C) while the flue gas is cooled to the desired set point temperature, e.g., 180°C.

Typically the pressure in the drum is 50–70 bar, and the final steam temperature 380–440°C.

The mechanisms described below are illustrated in Fig. 4.

Different Types of Boiler Arrangements

Depending on the needs and requirements of the purchaser of a WTE facility, the boiler heat transfer surfaces can be arranged in various ways, thus influencing up-front cost, operating and maintenance costs, availability, and efficiency.

The most common boiler configurations are described below (Table 3):

Steam Turbines for Electricity Production

The steam turbine is the equipment that transforms the energy in the steam (temperature and pressure) to mechanical energy, via a rotating generator that produces electricity. The thermodynamic process is

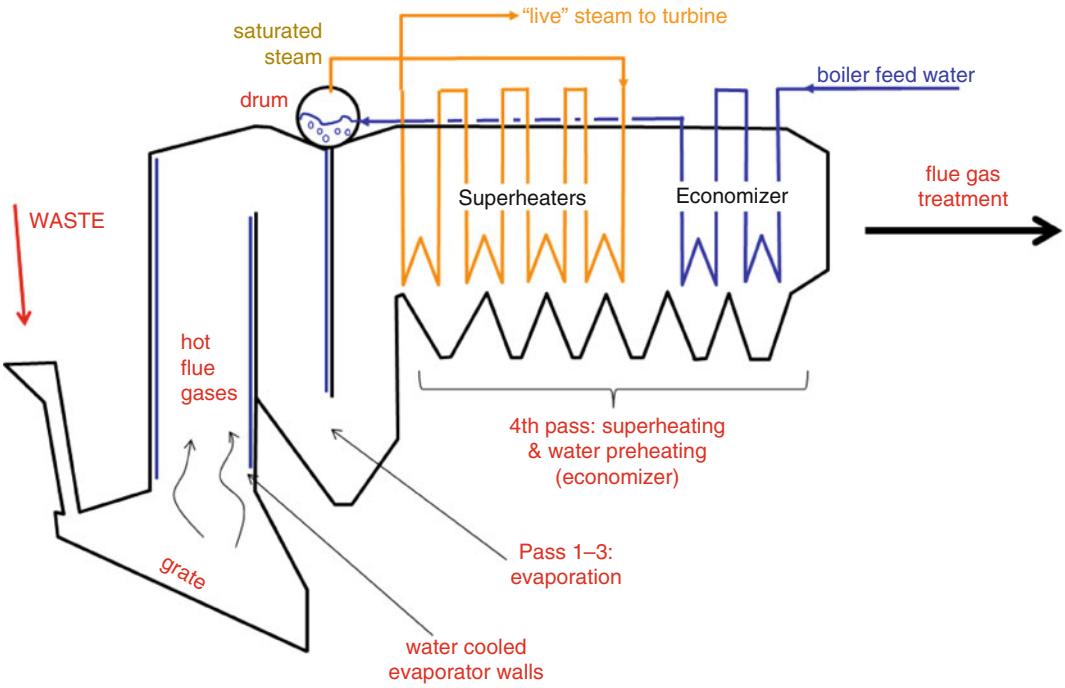

Waste-to-Energy for District Heating. Figure 4
Schematic of a modern European 4-pass waste boiler

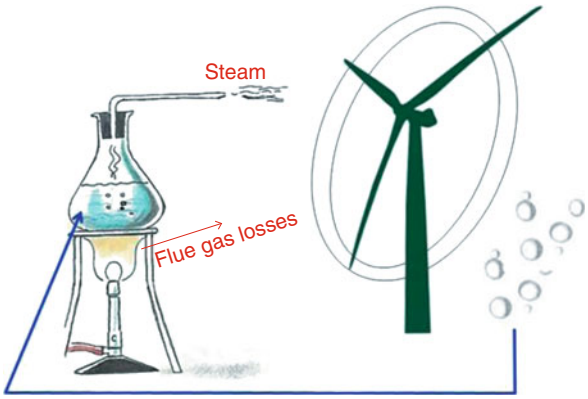

Waste-to-Energy for District Heating. Figure 5
Simple illustration of the steam cycle, with a wind-turbine analogy

expansion of the high-pressure steam that produces kinetic energy (high velocity) that is transferred to the blades of the steam and forces it to turn through an electromagnetic field.

This process, in very simple terms, can be compared to a wind turbine with the airflow past the wings (or "blades" as it is called in a steam turbine) being replaced by hot steam under pressure (Fig. 5).

It is often useful to plot a steam turbine expansion in a so-called mollier or hs diagram. "h" is the steam enthalpy and "s" is the entropy, both of which are thermodynamic variables of state, and can be thought of, as variables that can be looked up in tables provided that temperature and pressure are known (in the wet steam region this is not enough – here also steam dryness must be known).

In such a diagram, the enthalpy change during the steam expansion is shown "visually," which has particular interest due to the first law of thermodynamics stating the relationship between mechanical work, heat loss, and enthalpy drop (see equation below; its validity is subject to various assumptions for steam turbines, such as steady-state operation and negligible heat loss).

$$W[\text{Work}] = m \times (h_{in} - h_{out})$$
$$[\text{kW}] = [\text{kg/s}] \times [\text{kJ/kg}]$$

Since the heat loss from a steam turbine is negligible, and considering that approximately 97–99% of the mechanical shaft work can be translated into electrical power, the above equation shows that the steam turbine power output is mainly dependent on:

1. Mass flow of steam (given by the size of the boiler)
2. Inlet and outlet enthalpy (given by steam parameters, and available cooling, which sets the final expansion pressure)

A steam expansion from 40 bar to 1 bar is shown in Fig. 6 below, by means of the red line between the two yellow dots. The enthalpy drop on the y-axis can be read to be (3.24−2.56 MJ/kg) 0.68 MJ/kg. Therefore, for every kg/s of steam subjected to such an expansion, roughly 0.68 MW of electricity can be produced.

The "internal" efficiency of a steam turbine can be determined by the steepness of the red expansion line, where a completely vertical line represents 100% efficiency (limited by the second law of thermodynamics). This would correspond to an expansion to the green dot.

Figure 6 also clearly shows that each kg/s of steam would produce additional electricity if the inlet pressure and temperature were higher (see for instance the "200 bar" line) and if the outlet pressure were lower (see the "0.1 bar" line).

As noted earlier, thermal cycles are more efficient at higher steam temperatures and pressures. However, due to high-temperature corrosion of boiler tubes arising from chloride and other substances in the waste, waste boilers are for practical purposes limited to approximately 440–450°C and 60–90 bar, depending on the levels of maintenance a plant owner will accept.

Other examples of expansion lines can be seen in Fig. 7, using 8 kg/s as an example. This figure shows that, at 90% steam turbine efficiency, the potential power output is 4.1 MW, for an inlet state of 400°C and 40 bar and a fixed back pressure of 2 bar. This drops to 3.2 MW for an efficiency of 70%, and drops further to 2.6 MW when the steam temperature and pressure are decreased to 380°C and 22 bar.

Process Concepts for a Complete Electricity-Only Energy for Waste Facility

When the waste boiler and steam turbine technologies are combined, along with appropriate flue gas treatment, a waste-fired power plant concept is formed. Such a concept is illustrated in Fig. 8, comprising a horizontal-type boiler with a vertical economizer, a 400°C/40 bar steam turbine connected to an air-cooled condenser, and a dry flue gas cleaning system. The thermal cycle also

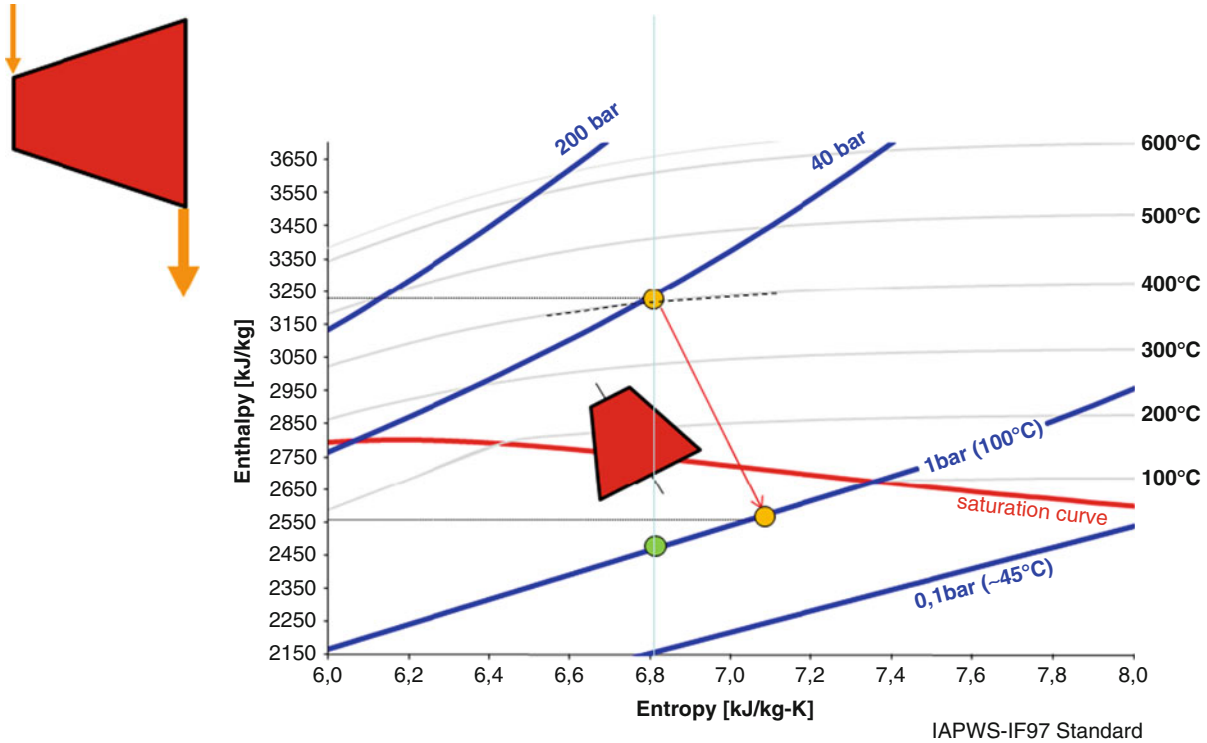

Waste-to-Energy for District Heating. Figure 6
hs-diagram for a hypothetical steam turbine expansion (Source: Ramboll)

shows other necessary components like a deaerator, which removes non-condensable gases from the boiler water/condensate. The process flow path of the water-steam flow and the flue gas, respectively, is shown in Fig. 9.

Experience with waste boilers has shown that the risk of high-temperature corrosion of the superheater tubes is greatly dependant on the flue gas temperature at the entrance to the fourth pass. It is therefore often a boiler design criterion that the flue gas does not exceed roughly 625–650°C, when passing across the hottest superheater tubes. Selection of correct/appropriate material (steel alloy) for the tubes is also important, although developments in anti-corrosive steel do not appear to have solved the corrosion problems in waste boilers.

Superheater tubes producing 400°C steam on a municipal waste facility are estimated by Ramboll to have a lifetime of up to 10–15 years, under the best conditions and with a modern boiler design. Even moderate increases to this temperature, say up to 450°C, may cause severe corrosion and reduce the lifetime of superheater tubes to perhaps 3–5 years. Ramboll estimates that further increases, say to 500°C, may entail boiler tubes maintenance several times a year due to severe high-temperature corrosion.

Waste boiler manufactures generally do not recommend higher steam temperatures than 440–450°C, unless special circumstances dictate otherwise. Methods of reducing corrosion include choosing high alloy steels, or specially resistant coatings.

WTE Facilities Delivering "Small-To-Medium" Amounts of Heat

An "electricity-only" waste-to-energy plant can easily be designed to produce small-to-medium amounts of heat; for example, when heat or process steam can be sold a number of months of the year (winter) while the remaining months, the plant can operate to produce electricity only.

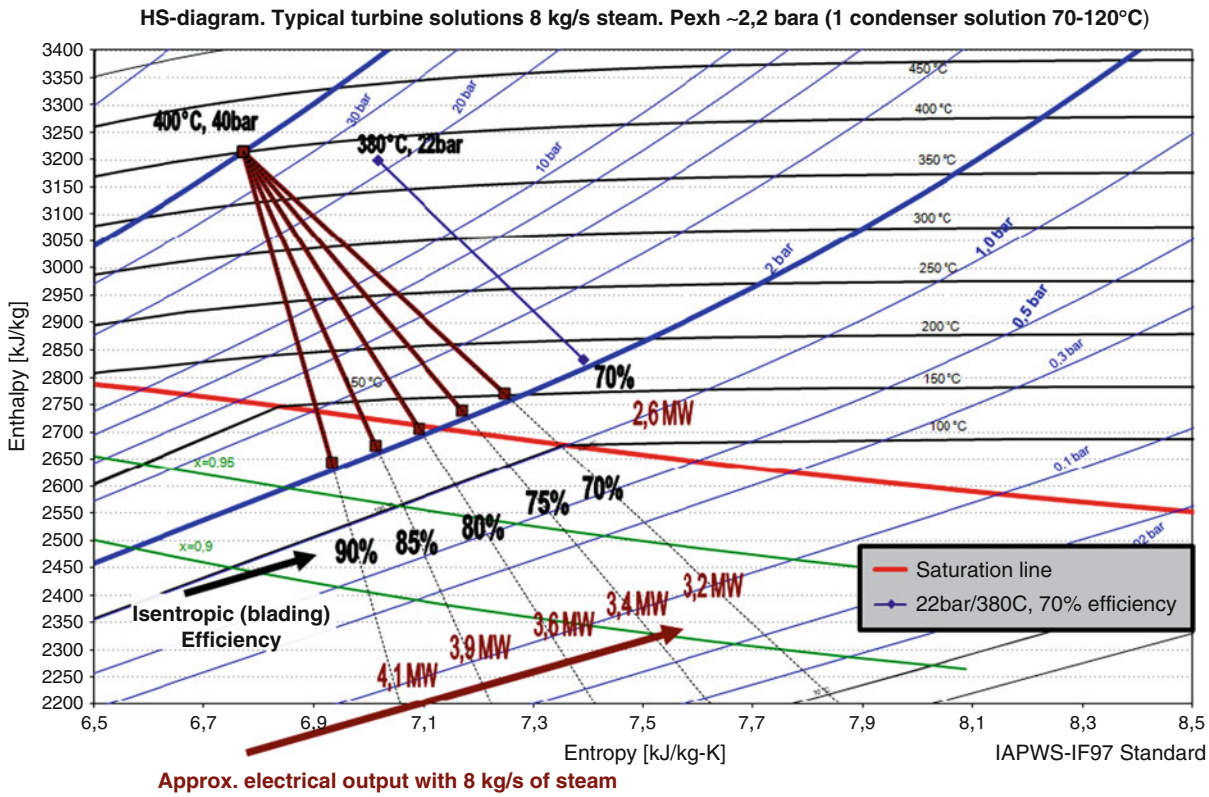

Waste-to-Energy for District Heating. Figure 7
Various expansion lines for 8 kg/s steam. The 2 bar back pressure equates to the necessary pressure level to produce hot water at 120°C (Diagram by Ramboll)

A technical solution to this is to have an "extraction" turbine, with a crossover valve placed somewhere along the turbine expansion line. When actuated toward the close position, the valve forces out steam to a hot water condenser which (Fig. 10) produces 80–110°C water. The crossover valve can thus divert steam to where it is mostly needed: either to produce heat, or to produce electricity, as required. As such, this type of turbine enables both "heat and power" operation as well as "electricity-only" operation.

Turbines such as the one shown in Fig. 10 could be the choice when the plant is connected to a small district heating network, or for the plant to be "CHP ready," for future district heating operation.

Figure 11 shows a cross-sectional view of an "extraction" steam turbine with the ability to operate freely between "electricity-only" and "combined heat and power" modes.

Figure 12 is an elaboration of Fig. 10, now showing also the major control principles relevant for an extraction turbine connected to a small district heating network.

The waterside district heating pumps (shown as a set of three pumps, for redundancy reasons) control to achieve a desired pressure drop in the district heating network, dP, for instance 2 bar. This allows enough pressure to operate the heating installations connected to the network.

If the heating consumers in the network turn on their radiators (call for more heat), the pressure in the network will drop, and the district heat pumps of the plant will respond by increasing the flow to again uphold the desired dP.

The steam turbine crossover valve, as well as the steam valve in the line to the DH condenser, is regulated to keep a constant district heating supply temperature. Thus, if the consumer calls for more

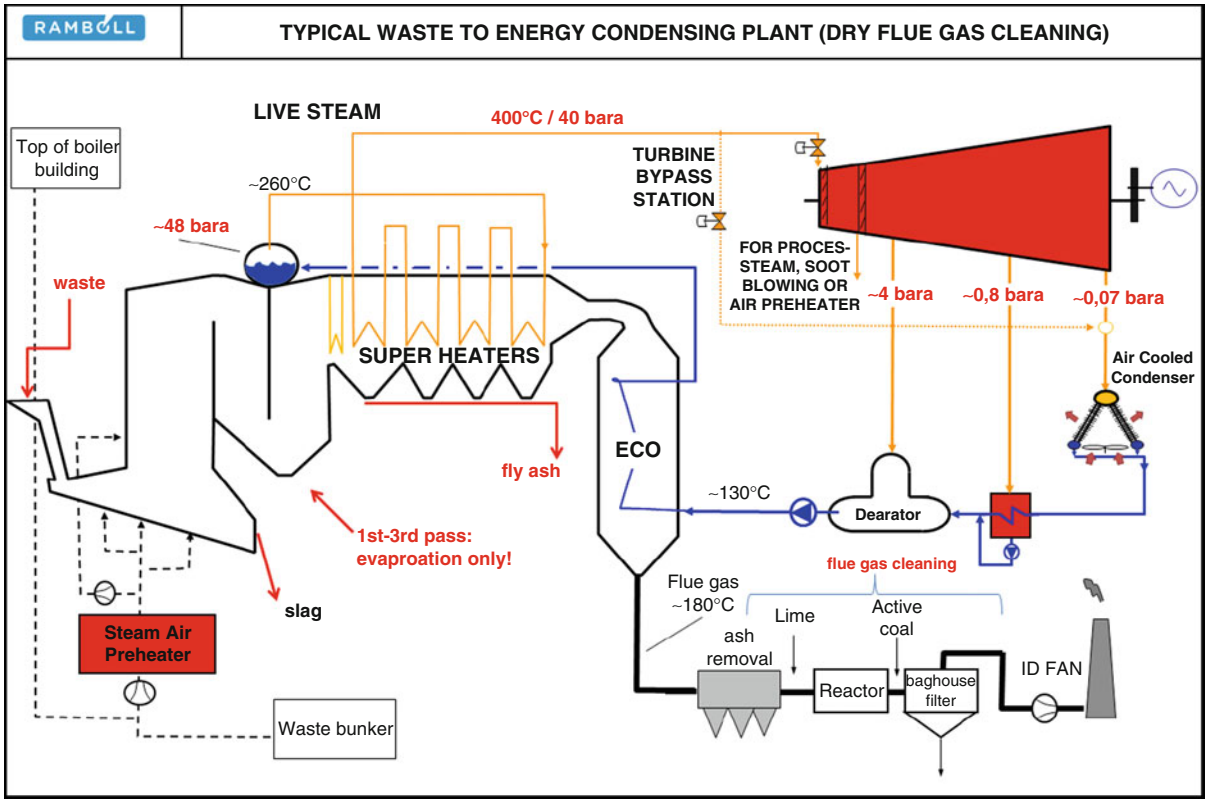

Waste-to-Energy for District Heating. Figure 8
Complete water-steam cycle for a typical European waste-to-energy facility, with no heat production (Source: Ramboll)

heat, the district heating pumps will increase the flow and the initial consequence will be a lower DH temperature. This is picked up by the turbine controls, which respond by providing more steam to the condenser until the set-point district heat temperature is obtained.

These controls in combination will thus match the consumer demand for heat (in MJ/s) and desired supply temperature, which is a set point determined by the heating network operators. For large transmission heat networks, the supply temperature is 100–120°C or more, whereas smaller heat networks may have supply temperatures as low as 75–85°C.

Generally, the supply temperature is a function of the ambient temperature, since a higher supply temperature will allow the transfer of more heat in the district heating pipework, which is also bound by hydraulic limits.

Table 1 below shows an example of set points for district heat network supply temperatures, as a function of ambient temperature.

Larger District Heating Networks and District Heat-Producing WTE Facilities

When a WTE facility has access to a large district heating network, such as in countries with a cold climate like Denmark, Sweden, and Finland, it is common to establish so-called back pressure turbines, where all the steam exiting the turbine is used to produce district heat (Fig. 13).

This configuration is illustrated in Fig. 14 (next page) where the very large air-cooled condenser has been replaced by two, and much smaller, surface steam condensers, where the condensing heat is transferred to the district heating water. To exemplify other options, a 14-bar process

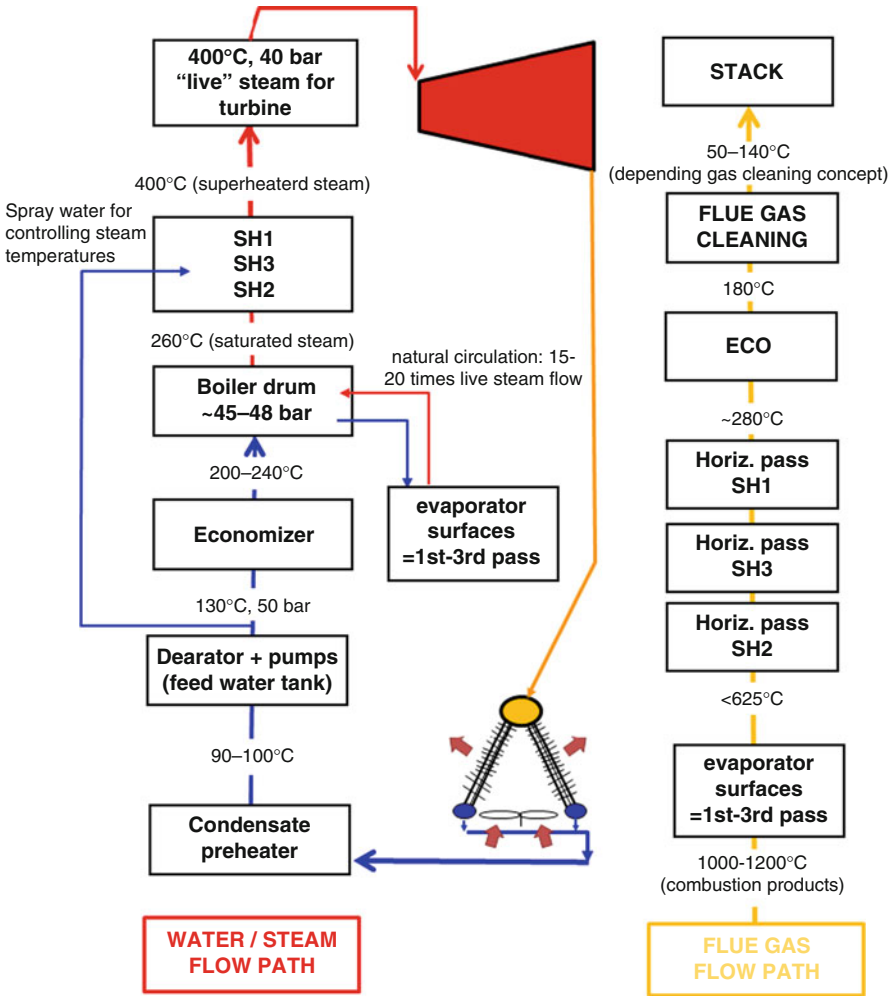

Waste-to-Energy for District Heating. Figure 9
Process flow path for water-steam (*left*) and flue gas (*right*) in a WTE facility (Source: Ramboll)

steam extraction to a hypothetical nearby factory is also shown.

Table 2 compares the electrical and total efficiencies of an "electrical-only" and combined heat and power "district heating" plant, configured as discussed in this chapter. Since the district heating water induces a higher back pressure (~1 bar) than an air-cooled condenser (~0.1 bar), the electrical efficiency of the "electrical-only" plant is higher.

As a result, the electrical-only plant will have an electrical efficiency approximately 3–6% points higher than the corresponding district heating plant (based on various assumptions).

Table 2 below shows typical figures based on a 100 MW thermal plant as an example. It is clear that the district heating plant produces 3.5 MW less electricity.

However, a total of 63 MJ/s of heat is produced instead – *hence 1 MW of electricity is converted to 18 MJ/s of heat* (63/3.5 = 18). This is *18 times more efficient* than electric space heating, and also even more efficient than highly efficient heat pump installations, which can produce up to approximately 4–6 MJ/s of heat for every MW of electricity.

The conclusion is that a waste-to-energy district heating turbine is an extremely efficient means of producing heat. Obviously, the "value" of the produced

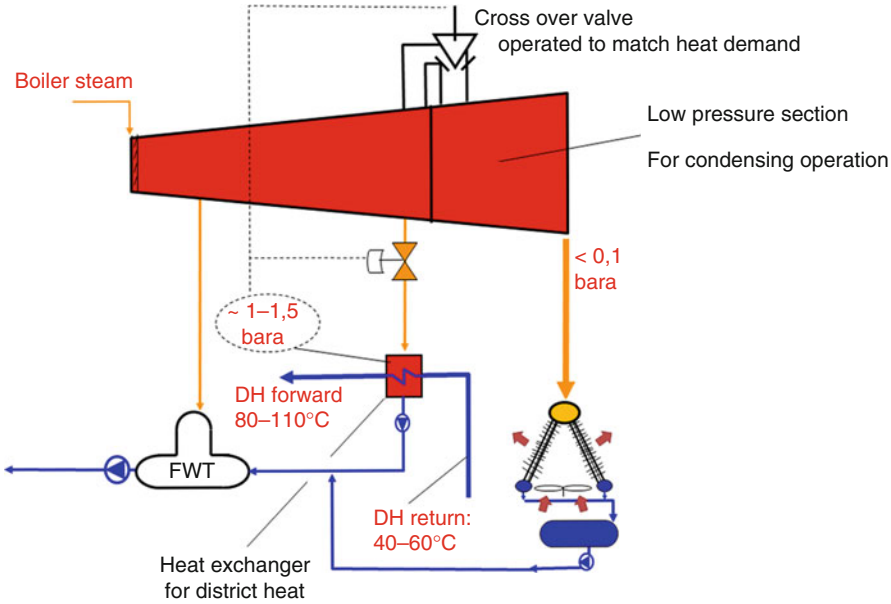

Waste-to-Energy for District Heating. Figure 10
Extraction turbine with the ability to provide variable quantities of hot water, depending on the heat requirement. The depicted solution is applicable for a plant to be operated both in "electricity-only" mode, as well as in "combined heat and power" mode (Figure by Ramboll)

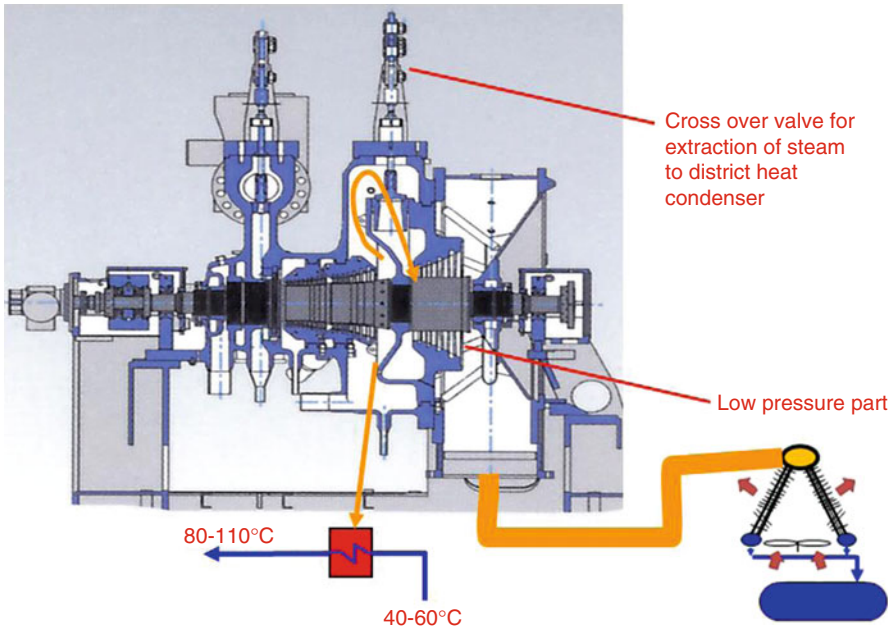

Waste-to-Energy for District Heating. Figure 11
Extraction steam turbine cross section. Crossover valve seen used to drive steam to the district heating condensers as per required heat demand (Courtesy of MAN Diesel & Turbo SE, see also http://mandieselturbo.com/0001157/PrimeServ/Turbomachinery/Steam-Turbines.html) (Figure by courtesy of MAN Diesel and Turbo SE, annotated by Ramboll)

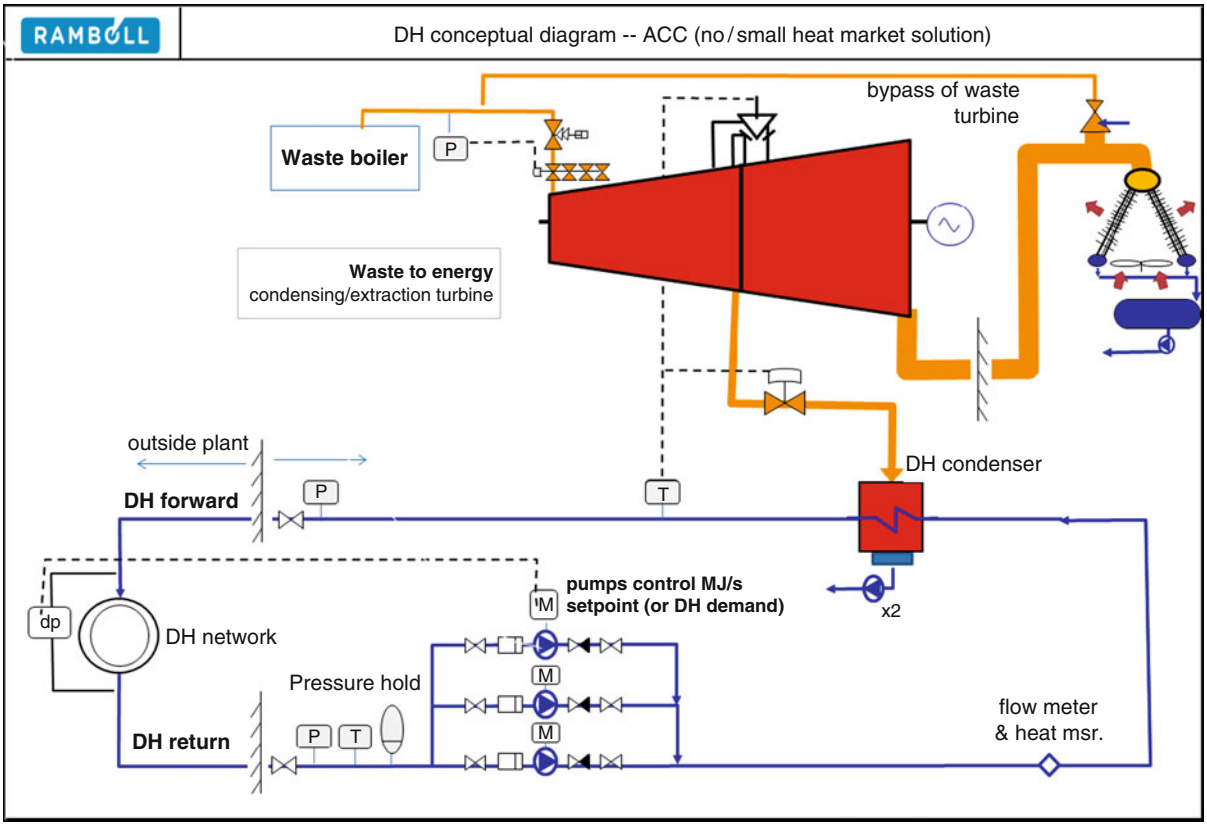

Waste-to-Energy for District Heating. Figure 12
Typical districting heating components and principle control mechanisms

Waste-to-Energy for District Heating. Table 1 Example of DH supply temperature versus ambient temperature for large Swedish DH network

	T ambient (°C)	T supply (°C)	T return (°C)
Very cold winter	<−15	115	52
Cold winter	−10 to −15	105	50
Winter	0 to −10	95	45
Spring/autumn	+10 to 0	85	42
Summer	> +10	75	45

heat depends on the local heat market and the size of the district heating network. Figure 15 shows the district heating network in the Copenhagen region that stretches over a distance of about 40 km from east to west.

The high total efficiencies of waste-to-energy plants connected to (medium-large) district heating networks result in low incinerator gate fees, since there is generally a higher energy-sales income than electricity-only plants.

The configuration of pumps and main control strategies for a district heating WTE facility can be seen in Fig. 16. The mechanisms are slightly different than the "electricity-only" concept shown in Fig. 12, since now the district heating pumps are controlled to sustain a given district heating supply temperature. The result is that the district heating pumps ensure that variations in the steam flow are taken up by the district heating water flow.

If, for instance, the thermal load on the waste boiler was to decrease (say due to a lower heating value of the waste), the steam flow to the turbine would be lower. The immediate consequence would be a lower district heat supply temperature.

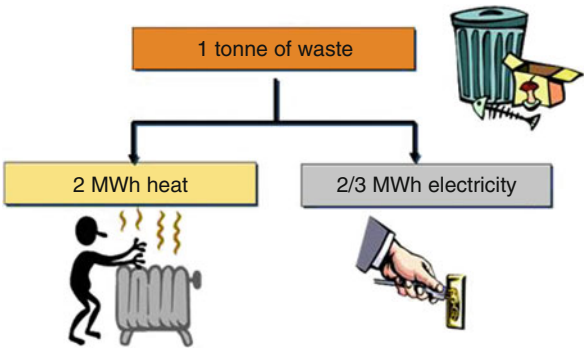

Waste-to-Energy for District Heating. Figure 13
1-2-3 rule of thumb for "district heat" configured waste-to-energy facilities. 1 t of waste yields approx. 2 MWh of heat, and 2/3 MWh of electricity

The district heat pumps would respond by decreasing the flow, to again obtain the desired district heat supply temperature. In such a system, the heat network is relying on other production units to balance the heat demand and heat production at any given point in time.

It is common, during summer, that a waste back pressure turbine produces more heat than the heat network demands. Since the MSW must be processed in the WTE plant, it is not always possible to reduce the thermal boiler load. Instead, plants often install water-to-air "summer coolers" to cool away the excess district heat.

Ultimately, the size of the district heating network, as compared to the size of the waste-to-energy facility,

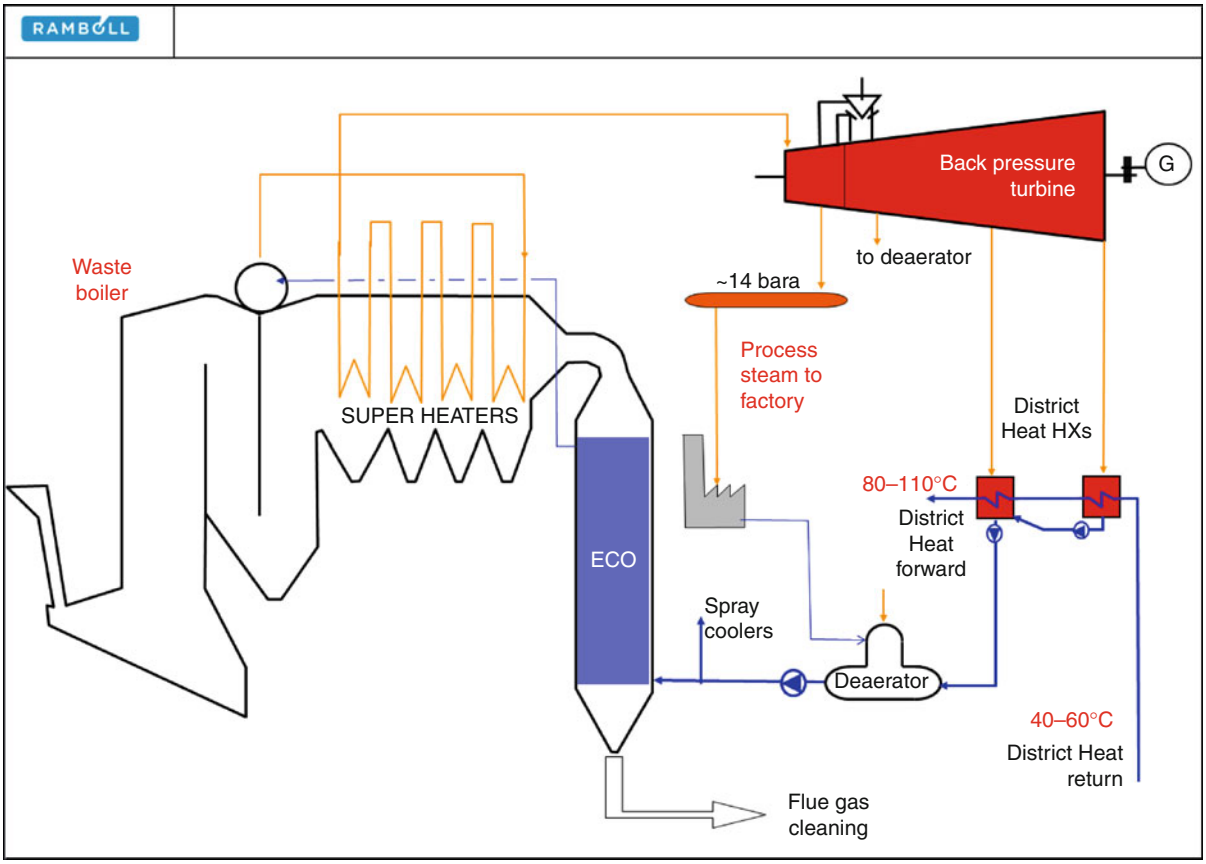

Waste-to-Energy for District Heating. Figure 14
Back pressure turbine for district heat production. Such a setup does not require a (large requiring) air-cooled condenser, since all the heat is transferred to the district heating network

Waste-to-Energy for District Heating. Table 2 Estimates of electrical and total efficiencies for "district heating" versus "electricity-only" Energy for waste facilities. Assumptions: electricity only back pressure = 100 mbar. District heating network temperatures = 50–90°C. Live steam parameters: 425°C/52 bar

Size: 100 MW thermal 36 t/h of waste (~300,000 t/year) CV = 10 MJ/kg	Net electrical efficiency (example)	Heat efficiency (example)	Total efficiency (example)
Back pressure (district heat) plant (without air-cooled condenser)	22.5% (22.5 MW sold)	63% (63 MJ/s heat sold)	85.5%
Electricity-only plant (with air-cooled condenser)	26% (26 MW sold)	0%	26%

will determine whether it is more cost-effective to install an extraction turbine with an air-cooled condenser, or a district heating back pressure turbine with a water-to-air hot water cooler.

Advanced Solutions: Heat Pumps and District Cooling

Waste-to-energy plants (and other thermal installations) can be equipped to supply both district or industrial heating and cooling. This could be a preferred solution for a geographic location with cold winters but hot summers. For this application, an electrically or steam-driven chiller could be used. The electricity or driving steam could be supplied by the waste-to-energy steam turbine, thus allowing for the complete installation to supply power, district heat, and district cooling, depending on the current demands.

A schematic diagram of such "tri-generation" is shown in Fig. 17, where the "generator package" is driven by a waste-fired steam turbine. District cooling is less common than district heating, and in most cases only makes sense in hot countries, or for supply of industrial cooling to large office buildings, airports, etc. District cooling on household level is not common.

Optimizing Energy for Waste Facilities for CHP Operation

A WTE facility typically has efficiencies in the following order of magnitude (MWt: thermal input) (Ramboll calculations and experience from Ramboll projects. Some plants may deviate from these values):

"Electricity-only" WTE facility up to 100 MWt	23–26% net electrical efficiency
"Electricity-only" WTE facility >100 MWt	Up to 30% net electrical efficiency
Heat and power WTE facility up to 100 MWt	17–23% net electrical efficiency
Heat and power WTE facility >100 MWt	Up to 25% net electrical efficiency

The lower efficiency of combined heat and power facilities is due to a higher turbine back pressure, as discussed earlier (Fig. 6). However, combined heat and power facilities have total efficiencies ranging from 82% to 86%; hence, a large amount of the energy in the waste is recovered for useful purposes.

WTE facilities can also be equipped with so-called flue gas condensation equipment, where the boiler flue gas is cooled to 30–50°C to produce additional district heat. This flue gas temperature is below the flue gas dew point of normally 52–60°C, and hence, moisture in the flue gas is condensed, causing a significant energy release (The flue gas dew point depends on excess air ratio and absolute pressure, as well as the moisture content in the flue gas. The latter is closely related to waste lower heating value (LHV), since a lower heating value usually arises from a wetter fuel. A dew point of 51°C corresponds roughly to an LHV of 12 GJ/t, and a dew point 60°C corresponds roughly to an LHV of 8 GJ/t).

Facilities using flue gas condensation may reach total energy recovery efficiencies of >100% (measured on lower heating value basis), and are thus extremely efficient.

In relation to optimizing electricity output for a combined heat and power plant, the temperature of

Waste-to-Energy for District Heating. Table 3 Typical boiler Configurations

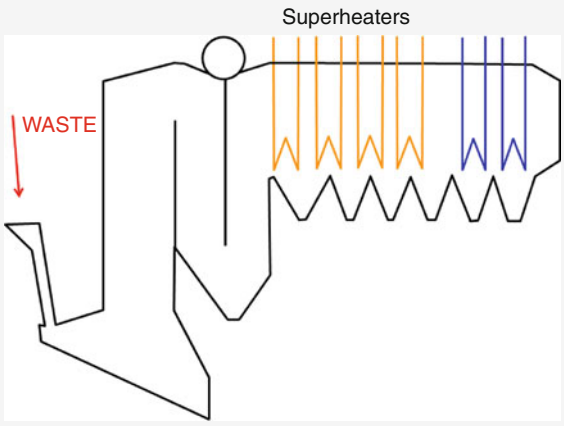	"Horizontal" *waste boiler* Often used in Europe for larger WTE facilities Advantages: – High efficiency, high availability – Good access to cleaning tubes in fourth pass, hence lower maintenance costs Disadvantages: – Higher initial investment
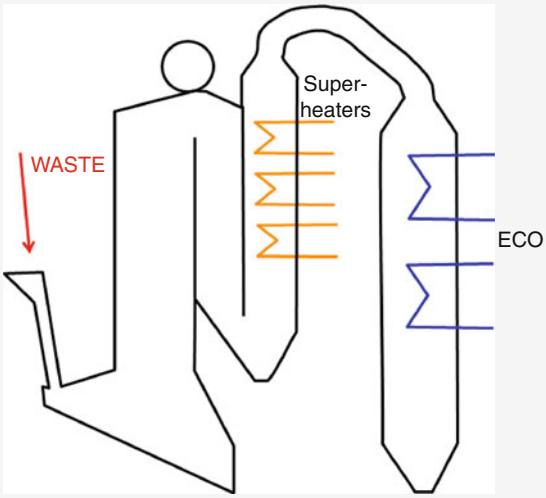	"Vertical" *waste boiler* Often used in smaller WTE facilities Advantages: – Low initial investment (smaller boiler) – Smaller plant footprint Disadvantages: – Replacement of superheaters, and in general maintenance, more difficult due to poorer access conditions – Economizer tubes cleaning by soot blower (= > lower efficiency)
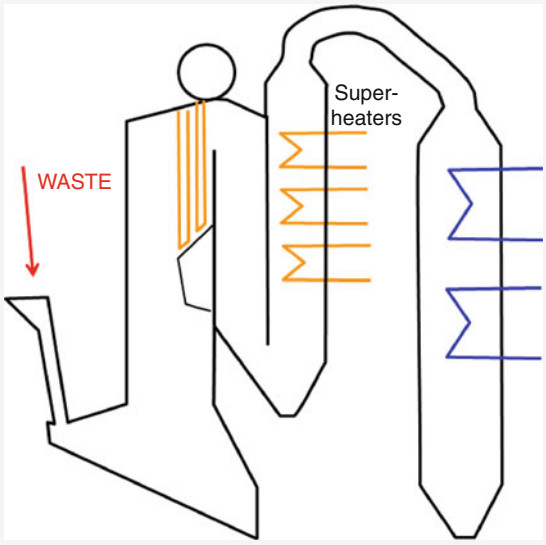	"Vertical" *waste boiler with superheater tubes in the radiation pass* This boiler configuration is often seen in USA Advantages: – As the "vertical" boiler, although even more compact Disadvantages: – The superheater tubes in the radiation pass may incur additional risk of corrosion and hence maintenance costs

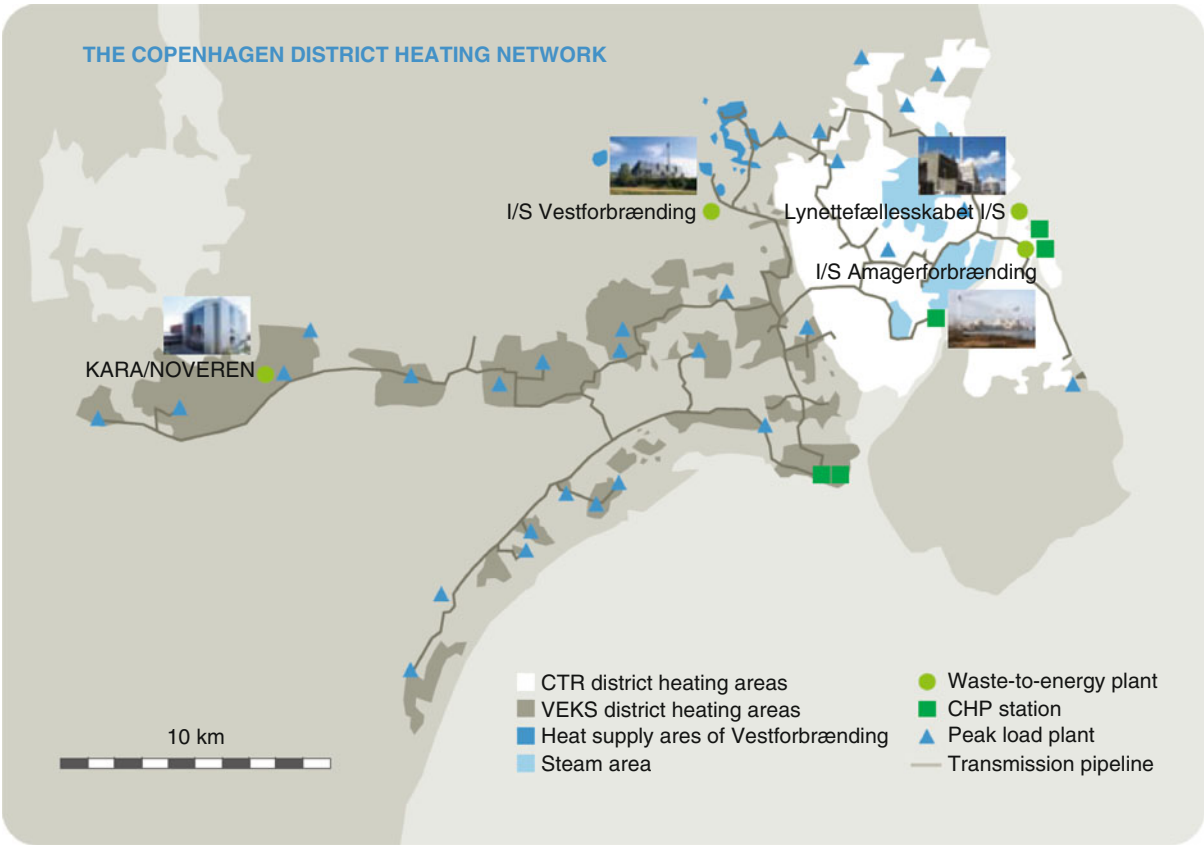

Waste-to-Energy for District Heating. Figure 15
Copenhagen district heating network spanning about 40 km from east to west (Figure courtesy of Ramboll Waste-to-Energy)

the district heating water (especially the supply temperature) has a big influence on efficiency, as can be seen in Fig. 18. The figure shows that the electrical efficiency is reduced by approximately 1%-point for every 10°C increase in hot water supply temperature, which compared to other measures is a strong impact. A lower district heating supply temperature also results in a lower heat loss in the network, so there are many benefits to be gained by striving toward the lowest possible supply temperature. On the other hand, as discussed earlier, a higher supply temperature will allow transfer of more heat (or a reduced water flowrate) in the district heating pipework, which is also bound by hydraulic limits. It is recommended by Ramboll that for new district heating networks, the design temperatures should be a focus point, among others, when optimizing the overall system. For existing districting networks, it is difficult to change supply and return temperatures, due to the coupling to exiting pipe sizes, hydraulics, and final user installation.

Even for relatively big changes in district heating temperatures, which would result in large/expensive impacts on the mechanical design, the effect on electrical efficiency is only within 1–5% points. Other optimization measures toward higher power output, such as higher steam parameters, higher boiler efficiency, etc., influence electrical efficiency also in the range of 1–5% points, at the most.

These relatively slight changes in electrical efficiency are in stark contrast to the benefits of combined heat and power, where the plant total efficiency can be increased by up to 60% points (from 25% to 85%) by using the "waste" heat for useful purposes, if possible.

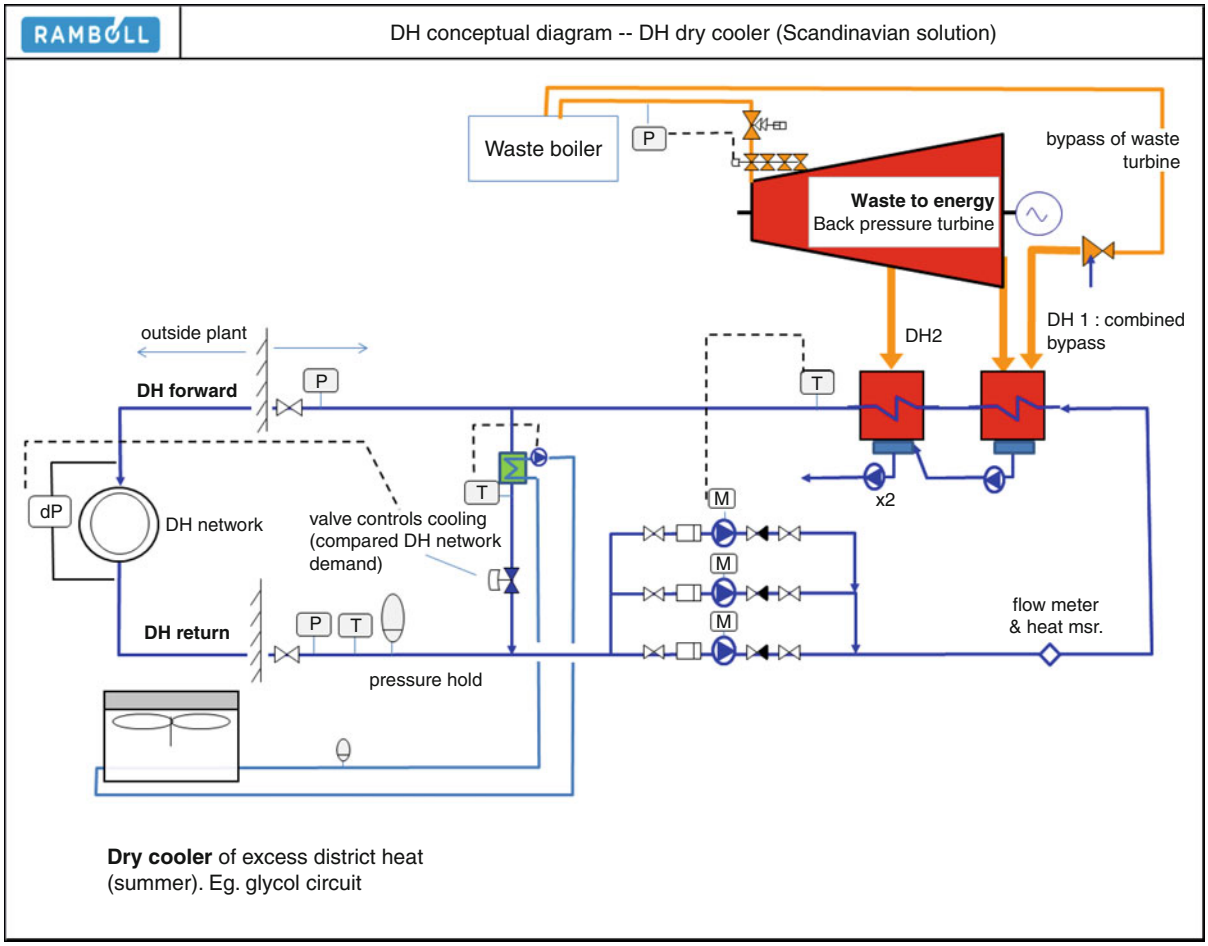

Waste-to-Energy for District Heating. Figure 16
Example of a district heat conceptual diagram for a "heat-only" back pressure plant

Obviously, heat and power requires a heat sales opportunity, which in practice means an energy infrastructure of district heating pipework and pump installations. The district heat network is not cost-effective on the short term, and certainly not for the individual producers of heat. However, municipalities, large energy companies, or governments interested in the long-term benefits of highly efficient energy facilities (for all fuels) can drive forward such infrastructure investments to the benefit of the whole community.

When using flue gas condensation in combination with a standard heat and power-configured plant, the total increase in efficiency can be up to 80–85%-points, resulting in total energy recovery rates above 100% (based on lower heating value).

Figure 19 illustrates the potential for flue gas condensation: up to approximately 20 MJ/s additional heat output for a 90MWt plant. As can be seen, the output is very sensitive toward the district heating return water, since the water is used as the media to cool the flue gas below the dew point of 52–60°C.

It is possible, and relatively common in Scandinavia, to incorporate absorption chillers to thus boost output of the flue gas condensation installation, if the district heat return temperature is high.

Conclusions and Future Directions

If a heat market exists or can be made available, waste-to-energy facilities can be a cheap source of

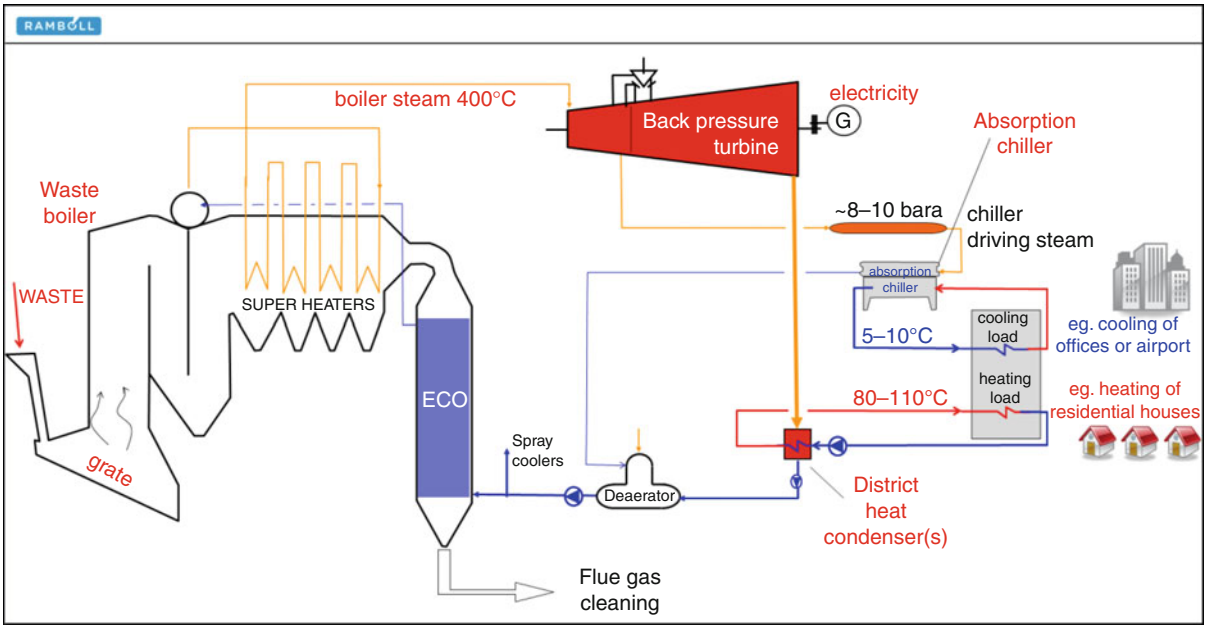

Waste-to-Energy for District Heating. Figure 17
Generation of power, heat, and cooling: "tri-generation". Cooling provided by an absorption chiller

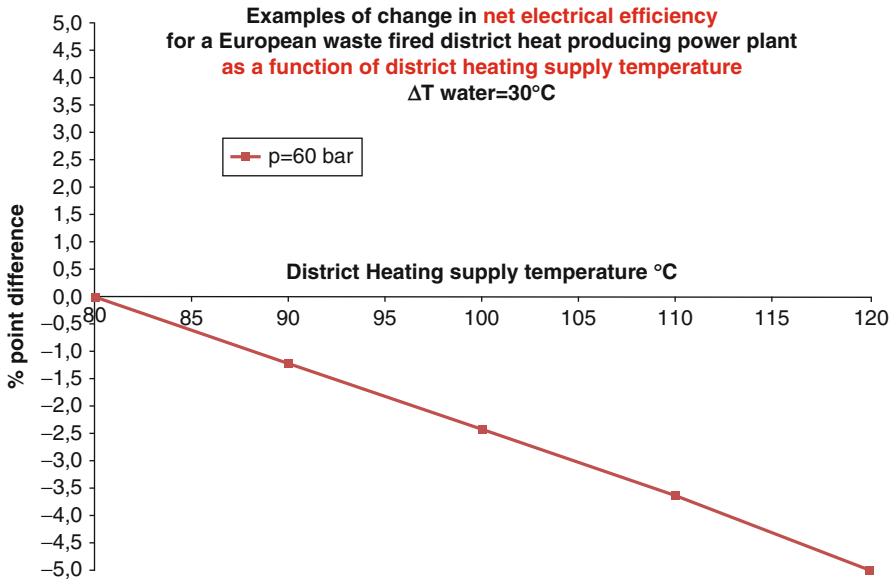

Waste-to-Energy for District Heating. Figure 18
Change in net electrical efficiency for a 100 MW WTE facility as a function of the supply temperature in the district heating network (Source: Ramboll calculations)

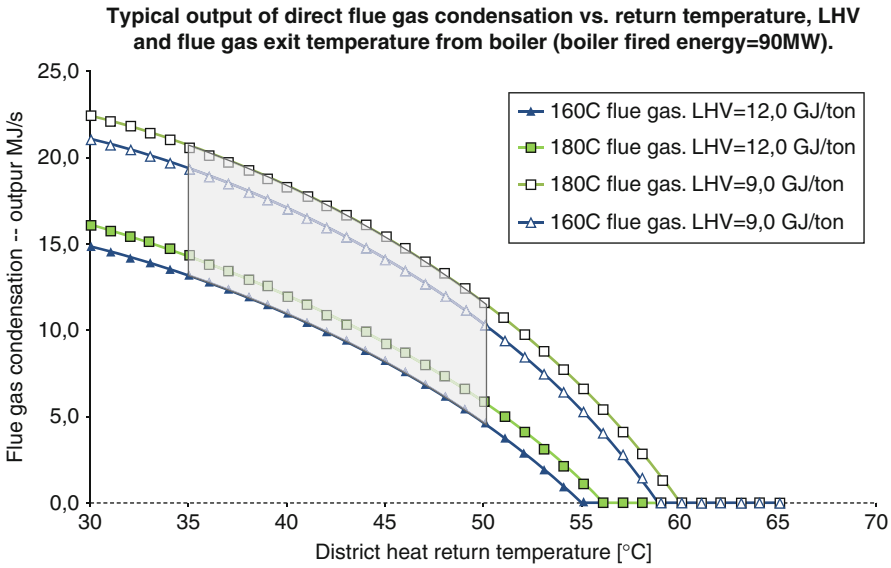

Waste-to-Energy for District Heating. Figure 19
Additional heat output from flue gas condensation for a 90 MJ/s plant. The additional increase in total efficiency is in the range of 0–20% (Source: Ramboll calculations)

heat – for example, the total energy recovery for "electricity-only" facilities of about 25% can be increased to 85–105% for combined heat and power installations. The loss in electrical efficiency by doing so is moderate: The electrical efficiency is reduced by only 3–6%-points.

Furthermore, configuring a steam turbine for "heat and power" instead of "heat-only" generates heat with high efficiency: an "electricity-to-heat" ratio of up to almost 20!

Even for smaller amounts of heat extraction from a waste plant, it is not uncommon to achieve an "electricity-to-heat" ratio of up to 10. Using such heat is particularly interesting given the fact that waste incineration continuously takes place mainly to reduce the mass and volume of (nonrecyclable) waste, and, hence, the alternative is to reject large amounts of heat in cooling installations with no real benefit.

Bibliography

Primary Literature

1. Kleis H, Dalager S (2004) 100 years of waste incineration in Denmark. Babcock and Wilcox, Vølund and Ramboll, Copenhagen
2. http://www.ens.dk/Documents/Faktaark/affald%20150709.pdf
3. Phyllis database www.ecn.nl/phyllis and "Accomplishments from IEA Bioenergy Task 23: Energy from Thermal Conversion of MSW and RDF" 2001 and "21′ Century Advanced Concept for Waste-Fired Power Plants." Babcock Wilcox Volund
4. 21′ Century advanced concept for waste-fired power plants. Babcock Wilcox Volund, p 20

Books and Reviews

Afval Energi Bedrijf, City of Amsterdam – Waste and Energy Company (2006) Value from waste, waste fired power plant. The new standard for recovery of sustainable energy, metals and building materials from urban waste

IEA Bioenergy (2000) Accomplishments from IEA Bioenergy Task 32: energy from thermal conversion of MSW and RDF

Danish Board of District Heating (2006) News from DBDH, Energy Environment. Journal number 4/2006. Theme issue: waste and district heating

Hesseling WFM, Rademakers PLF (2003) TNO environment, energy and process innovation, March 2003 (R2003/127): efficiency increase of waste-to-energy plants, evaluation of experience with boiler corrosion and corrosion reduction

Rand T, Haukohl J, Marxen U (2000) Municipal solid waste incineration – a decision maker's guide. World Bank, Washington, DC

Renosam and Ramboll (2006) The most efficient waste management system in Europe * Waste-to-energy in Denmark

Waste-to-Energy using Refuse-Derived Fuel

Floyd Hasselriis[1], Patrick F. Mahoney[2]
[1]Hasselriis Associates, Forest Hills, NY, USA
[2]Energy Answers International, Inc., Albany, NY, USA

Article Outline

Glossary
Definition of Subject
Introduction
Mass-Burn Incineration: Predominant Method for Waste Combustion
Early Efforts to Recover Materials and Energy from Processed Refuse
Advanced Resource Recovery Facilities
Processing Equipment
Air Quality Control Equipment
Properties of Municipal Waste and Processed Refuse Fuel
Power Production from Refuse Fuel
Future Directions
Bibliography

Glossary

Mass-burn incineration Mass-burn incineration is a waste treatment process used in many locations throughout the world that involves the combustion of unsorted, unprocessed mixed waste on a moving grate, generally with recovery of the heat generated.

Municipal solid waste (MSW) MSW is all the garbage, including organics like grass and leaves, generated by households, commercial sites (restaurants, stores, offices, etc.), and institutions (schools, museums, public parks, etc.). Materials such as packaging and office paper from small- to mid-size factories, called "light industrial sites," are also part of this mix.

Processed refuse fuel (PRF) PRF is a fuel created by the resource recovery system developed by Energy Answers International with minimum processing.

Refuse-derived fuel (RDF) RDF is produced from MSW through a number of processes to meet requirements for particle size, moisture content and noncombustible content dictated by the thermal unit that will receive the RDF. At its simplest, MSW is shredded to a maximum particle size to produce RDF. More often, additional steps are taken to remove noncombustible materials and control the particle size.

Renewable energy Renewable energy is energy generated from fuel sources that can be replenished. Unlike fossil fuels, which are exhaustible, renewable energy sources regenerate and can be sustained indefinitely. The five renewable sources used most often are: Biomass – including wood and wood waste, municipal solid waste, landfill gas, and biogas, ethanol, and biodiesel; water (hydropower); geothermal; wind and solar.

Sustainable energy Sustainable energy is energy that meets the needs of the present without compromising the ability of future generations to meet their needs. Sustainable energy sources are most often regarded as including all renewable sources.

Definition of Subject

Combustion of municipal refuse to produce energy and recover recyclable materials is consistent with goals to diversify energy generation sources and implement sustainable and renewable options. Using waste as a fuel can decrease dependency on non-sustainable fossil fuels, such as coal, oil, and gas, and provide a consistent and reliable source of recyclable materials, as well as get rid of the waste and minimize landfilling.

Processing the refuse to generate energy and recover materials before and after burning is an approach that has been provided as an alternative to mass-burn incineration. This alternative has been practiced as a parallel choice since the early 1970s, and, in many situations, has provided advantages in the form of increased energy production, lower landfill disposal requirements, higher quality combustion residues with low unburned carbon content, complete combustion, cleaner gases going to the air quality control system, higher materials recovery rates, lower capital costs, and lower operating costs.

With growing concerns related to greenhouse gas production, environmental impacts of landfills, and

dependency on foreign oil, as well as a shift toward renewable and diversified energy sources, processed refuse fuel technologies should see an increase in demand.

Introduction

Starting in the mid-1800s incinerators were used for the primary purpose of reducing waste volume. These incinerators, which burned the waste "as is" with no preprocessing, were widely used and were successful at reducing waste transport and disposal costs for densely populated urban areas. Numerous grate systems were designed and installed to burn the waste and move the ash residue out of the incinerator for disposal.

Early efforts to utilize the heat produced as motive force to operate in-plant equipment and to generate low-pressure steam for district heating or industry was the next step which began in many European locations. Urban areas in the USA, where land was becoming more valuable, followed suit as documented in the August 28, 1897 issue of the Scientific America Magazine featuring a heat recovery incinerator in operation in New York City producing electric power used for lighting the Williamsburg Bridge. However, despite waste volume reduction of up to 80%, energy recovery was an insignificant and inefficient part of the incineration solution and, because incinerators were operated with virtually no air pollution control systems, they were a major contributor of poor air quality.

Mass-burn incineration technology advanced in the mid-1900s with the addition of more efficient heat recovery units and, in some cases, equipment to recover a portion of the metals in the waste.

An important milestone in waste management strategy for the USA was the passage of the Resource Conservation and Recovery Act (RCRA) in 1976. As stated in Section 1003, "The objectives of the Act are to promote the protection of health and the environment and to conserve valuable material and energy resources. . ." The National Policy is presented in Section 4001 as ". . . developing and encouraging methods for the disposal of solid waste which are environmentally sound and which maximize the utilization of valuable resources including energy and materials which are recoverable from solid waste and to encourage resource conservation."

Another important milestone was the development of the Energy Policy and Conservation Act of 1975. This Act called for actions to encourage the expansion of domestic energy sources. Conversion of municipal solid waste (MSW) to energy is a noted alternative.

These government policies prompted regulatory agencies to demand closure of most of the old incinerators operating in the USA and required the addition of air pollution control systems on newer units. These policies also provided a strong foundation for advancing the technologies to process refuse for improved recovery of materials and energy.

With the world experiencing its first "energy crisis" in 1973, marked by the tripling of petroleum prices, a new opportunity for waste management engineers emerged. Waste, refuse, garbage, trash, etc., with a 75% combustible fraction, represented a potential source of energy which engineers could look to recover and reduce the cost of disposal. This historical event began the change in the design objectives of waste management engineers from waste reduction with some energy recovery to maximum resource recovery and efficient energy generation. Waste was now starting to be viewed as a "resource" and alternative fuel source.

Mass-Burn Incineration: Predominant Method for Waste Combustion

Mass-Burn incineration systems are the predominant method for combusting waste to produce energy. Combustion systems designed to process waste into a fuel in order to maximize energy generation and materials recovery have a distinctively different design philosophy and use different equipment. A brief description of mass-burn incineration and some of the disadvantages of the technology provides a foundation and rationale for the processing of refuse to recover materials and energy from refuse.

At a mass-burn incinerator, Municipal Solid Waste (MSW) is discharged from transfer vehicles or waste collection vehicles into a deep pit. There is no processing of the waste. Waste is removed from the pit by overhead crane and fed into hoppers which feed the furnace. Most of the time, the crane is used to mix the waste to try to obtain uniformity

of heating value, although this is somewhat difficult to do due to the distance from the crane cab to the waste itself.

In order to ensure continuous operation, it is necessary to have two cranes, while only one at a time is used. Crane cable replacement is a continuing and significant source of maintenance cost (Fig. 1).

The raw waste falls onto a traveling grate which is designed not only to move the waste from front to back (usually a distance of some 60 ft, divided into three 20-foot-long grates with drops from one to the next), but also to tumble the material in order to provide oxygen necessary for combustion. The grate size is determined by the amount of heat release anticipated, commonly about 200,000 BTU per square foot of grate per hour.

In order to facilitate movement of MSW through the furnace, the grate slopes downward from front to back such that the overall height of the grate is about 20 ft. This adds 20 ft to the overall height of the boiler house.

Because there is no presorting of material being fed to the furnace, there is always the problem of pieces of metal, cables, water tanks, propane tanks, etc., being fed into the furnace. This creates a potential erosion problem and therefore the waterwalls of the furnace are covered with refractory linings to protect the tubes. This refractory lining is carried to a point very high in the furnace to avoid corrosion at the point where the refractory stops and bare tubes are exposed. The use of refractory causes slower and reduced heat transfer into the tubes while slag from melting glass and low melting point metals tends to build up on the refractory linings low in the furnace. Thus, on a regular basis, the boiler must be shut down and refractory either cleaned or replaced.

As all the waste is burned on the grate, temperatures on the grate are above the melting point of glass such that clinkers are formed. On discharge from the furnace, the ash falls into a trough full of water where the clinkers shatter into small particles. These particles are amalgams of the noncombustibles originally fed into the furnace along with unburned material (carbon particles). Appearing often in the ash from mass-burning units may be unburned items such as large telephone directories, layered floor polisher pads, watermelon and grapefruit rinds, and other dense organics and similar materials which do not burn well because the necessary combustion air cannot reach in between the layers of paper or cloth. Because large metal objects are in the ash, plugging of the ash discharge systems can occur. Although the removal of some ferrous metal from the ash is often easily accomplished with magnets, mechanical removal and recycling of other metals and valuable products is virtually impossible. The use of water quenching for the ash produces an alkaline solution which generally must then be treated and neutralized.

Early Efforts to Recover Materials and Energy from Processed Refuse

Although mass-burn incinerators are viable methods for generating energy from waste, they are inherently inefficient for recovery of recyclable material. In the early 1970s technology emerged for processing waste to increase the recovery rates for energy and materials. Many of the early designs were flawed and were shut down but provide an understanding of the history and evolution of the technology which is currently implemented at the highly successful projects in operation or in development in 2010.

National Center for Resource Recovery (NCRR)

In the early 1970s, one of the concepts promoted by the newly formed "environmental" movement in the United States was that beverage containers made from metals and glass should all be reusable, thus reducing the amounts of new glass and metal which would have to be produced to meet the needs of future consumers. Container manufacturers, however, had only recently discontinued the use of "refillables" and were concerned that the costs of collecting, separating, returning, sterilizing, and reusing of containers would be very high compared to the cost of new containers. The National Center for Resource Recovery (NCRR) was formed and financed by several container manufacturers, aiming to demonstrate that recyclable material could be recovered from MSW at a central processing station and that this material could then be used to manufacture new containers and would negate the need for returnable containers.

Complications arose due to the fact that MSW contains not only containers but a wide variety of other waste materials including, but not necessarily

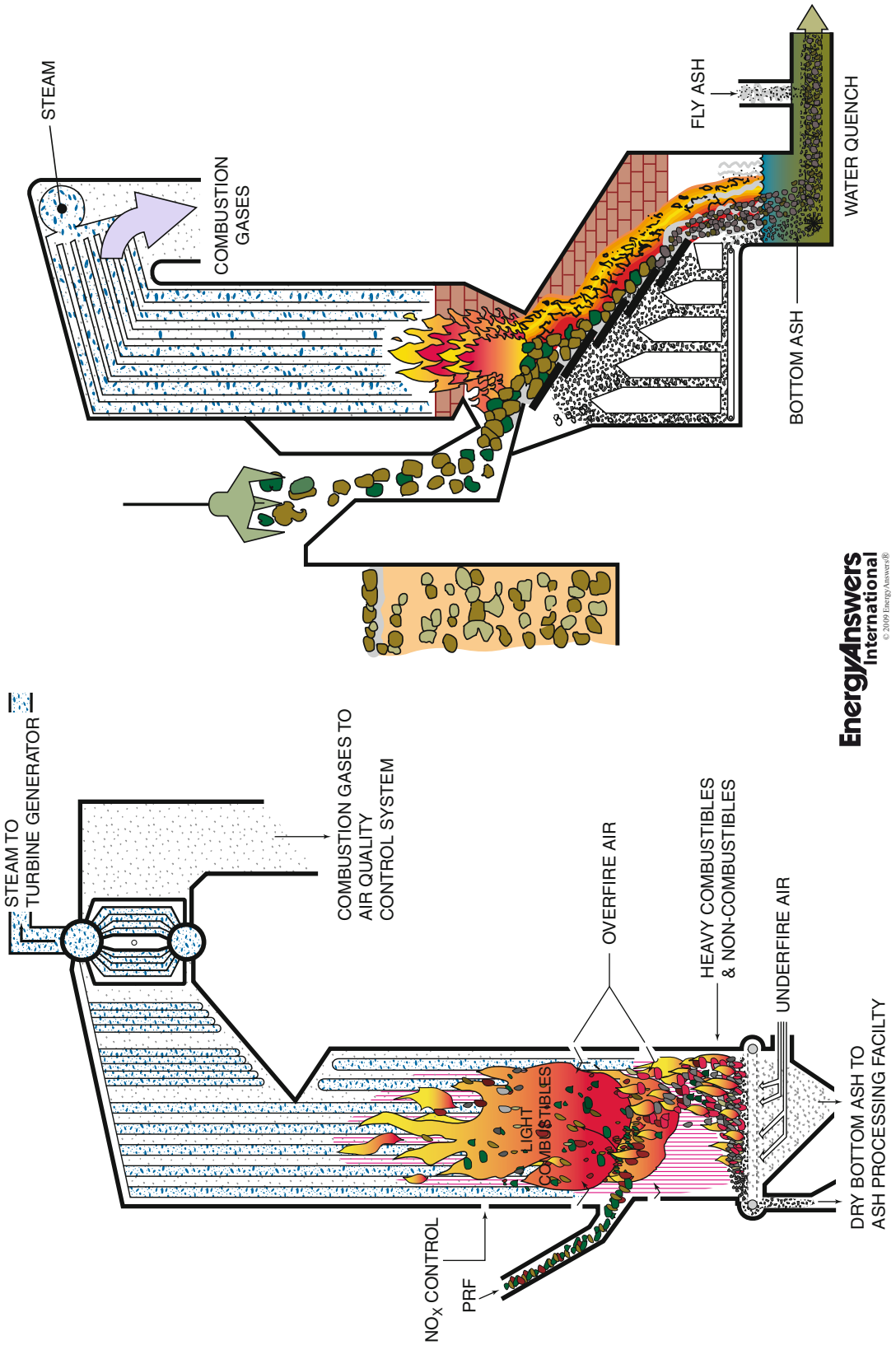

Waste-to-Energy using Refuse-Derived Fuel. Figure 1
Processed Refuse Fuel Combustion compared with Mass Burn Combustion. [Energy Answers International]

limited to, food waste, paper and cardboard, magazines, household chemicals, old clothes and rags, various plastic products (including containers), garden vegetation, trees and brush, flammable materials, sand and dirt, etc. What developed at NCRR was a series of systems and equipment aimed at separating not only containers, but also any other products which might be useful, including materials which might be used as fuel in place of coal or other fossil fuels, noncombustible materials (sand, grit, etc.), organic matter to create a soil conditioner; and valuable materials (metals, coins, jewelry, and the like).

One of the products which the NCRR tried to create was a "Refuse-Derived Fuel" (RDF) which could be used in existing furnaces and boilers as a substitute for, or in combination with, coal, oil, or gas [1]. The first stage was to separate the light combustible material (paper and light plastics) from the noncombustible materials by chopping all of the material into smaller pieces in a shredder and then separating the light fraction from the heavier material by means of air currents. Unfortunately, less than half the material became "air-classified" light combustible material while the balance, over 50% of the incoming waste, was destined to be disposed of in landfill. A further problem that existed in the preparation of this "fluff" RDF was the inability of equipment to handle the rags and streamers that occurred in shredded MSW. Various systems for the separation of these materials were tried with little long-term success.

Air-classified RDF did not prove to be a satisfactory fuel for use in facilities designed for fossil fuels. It was difficult to feed into the furnace, could cause fouling of flue gas paths, and, because of the high ground-glass content, significant slagging occurred on the grates and on the furnace walls. And because of the low density of the material, it was difficult and expensive to store and transport it.

The idea of creating very dense "pellets" made from MSW was born to solve the problems inherent in fluff RDF. MSW was ground into extremely small particles and a binder was added to enable the material to be extruded into pellets. Although this solved the high costs of storage and transport, the cost of manufacturing the pellets could not compete with the cost of normal fossil fuels. A further disadvantage was that the material remaining after production of pellets, at least 40% of the original incoming waste, was sent to a landfill.

Virtually all the systems developed at NCRR ultimately proved to be either technically impractical or economically unfeasible due to lack of markets capable of buying the recovered materials at a price necessary to cover NCRR's costs. Despite the unsatisfactory economics of the processes developed at NCRR, the facility operated for several years until finally the backers of NCRR withdrew financing and the facility has been closed since the 1980s.

Solid Waste Reduction Unit (SWARU)

In 1968, the City of Hamilton, Ontario, Canada, retained Gordon L. Sutin and Associates Limited, Consulting Engineers, and Consoer Townsend Engineers to design an incinerator which would burn 600 t/day of MSW, including a portion of combustible demolition waste [2].

SWARU was designed with a radically different philosophy in comparison to the combustion facilities in operation. Instead of designing a facility for burning waste, it was determined that the facility would become a manufacturing plant in which the raw material, municipal solid waste and demolition material, would be processed to create a finished product, ash. It was recognized that there would be by-products in the form of heat and air emission and possibly contaminated water. When this hypothesis was considered, it became clear that the problem was not really a "combustion" problem but rather a problem of receiving a "difficult-to-handle" raw material, feeding into a process for recovery of the heat generated in the combustion process, conversion to ash, removal of the finished product from the process, and control of air and water contamination.

An obvious result was the recognition of the need to handle the raw material and the finished product by the most simple and well-proven method known – conveyors. However, because of the nature of the raw material, movement on a conveyor reliably and without excessive belt damage could not be accomplished unless the waste could be converted to a more homogeneous mixture.

A literature search at the time indicated that only one large-scale, modern MSW combustion plant had

been built in Canada or the United States. The facility at the Norfolk Navy Base burned waste to generate steam but did not have any other recovery enhancement. However, many modern facilities had been built in Western Europe during the late 1950s and the 1960s that not only burned waste but also generated useful energy in the form of steam and/or electricity.

An evaluation of installations and equipment in Western Europe confirmed that none of the facilities processed MSW before burning. All technologies in Europe at that time were based on "Mass-Burn" techniques where, apart from the removal of large objects, all the waste was burned as received. There were significant components of the design which caused high cost and operational inefficiencies:

1. The use of the crane as a method of delivering waste to the furnace was expensive and inefficient with backup operators and crane equipment on standby to ensure continuous operation 24 h/day, 7 days/week.
2. The crane was also used, ineffectively, to reposition waste in the pit and to mix wet and dry waste in order to maintain a uniform heating value.
3. Despite the advantages of allowing for a large amount of waste to be stored in a small area with simplified odor control, the pit, which was in continuous use, could rarely be cleaned.
4. Different crane loads of waste had very different heating value and moisture content. Thus portions of the waste would burn more quickly than others and the result would be that where the waste had burned quickly, air flow through the grate to improve combustion and to cool the grate would be concentrated on those areas with the least resistance (where the waste had burned off quickly) while in other areas, there would not be enough air to support combustion. In these starved air areas, the waste would "cook" instead of burning, resulting in large clinkers and large percentages of unburned combustible materials.
5. Dense objects such as telephone directories and layered floor polisher pads could not be completely burned because char on the outside would act as an insulator and would block the flow of air necessary to burn all the materials. Thus, the job of burning all combustible material was not completely achieved, resulting in high combustible content in the ashes.
6. The temperature of the refractory linings would ultimately reach the melting point of glass, and glass in the waste would melt onto the linings, drip to the cooler bottom of the furnace, and harden on the refractory to form slag that needed to be removed on a regular basis using jackhammers and other heavy equipment.
7. Owing to the nature of the waste, a common occurrence was the breaking of a grate bar due to jamming of small metal pieces between adjacent bars. Such a failure would result in burning material falling into the air hoppers beneath the grate and causing damage.
8. Because many large metal objects (hot water tanks, bicycles, etc.) would often be fed to the furnaces by the crane, it was not uncommon for these objects to get caught at the discharge end of the grate just above the ash hopper. Thus, the ash would be restricted from entering the hopper and major plug-ups could occur, requiring the unit to be shut down while the plug-up was cleared.
9. The presence of large quantities of metals and other non-friable materials inevitably caused high wear on the drag chains used to remove the ash from the water-filled ash trough. Stretching and ultimate breaking of chain links caused jams of the equipment, necessitating repairs on an emergency basis. Further, it was noted that the wet ash systems used large quantities of water, and maintenance of workable conditions for employees in the ash receiving room was very difficult due to high moisture conditions.

As a result of the observations made of European equipment, it was determined that the design of the SWARU would not be based on the mass-burn technology but rather would be a design which would eliminate, if possible, all the problems common to the mass-burn facilities. Thus, the aim was to avoid the following systems and methods:

1. The use of cranes for moving waste from storage into the combustion system
2. The use of highly complex mechanical grate systems

3. The use of refractory linings on the walls of the furnace
4. Water quenching of the ash

SWARU was the first successful waste combustion system that recovered materials and energy from processed refuse. The operation was purposely designed to be simple and avoid the problems associated with more complex RDF systems.

- Instead of receiving and storing the incoming waste in a pit, the material was dumped on the floor of an enclosed building, examined so that undesirable objects could be removed before processing, and fed onto conveyors leading to the shredders.
- The actual processing of the waste into fuel consisted only of manual removal of objects from the waste which might jam a shredder or conveyors, and then shredding the waste, creating a relatively uniform, homogenous "Processed Refuse Fuel."
- The PRF is fed by conveyor into chutes that open into the lower part of a Babcock and Wilcox spreader-stoker boiler, just above the grate [3]. At the bottom of the chutes are deflectors that divert the material upward and additional throw is provided by a blast of air. The light materials, paper, plastic, textile, etc., catch fire in midair while the heavier material, glass, metal and chunks of wood and other combustibles are thrown to the back of the furnace where they land on the grate. The grate moves forward very slowly while air is blown through the grate to maintain temperatures below the melting point of glass. It takes about 1 h for the grate to move from back to front and on the last third of the grate, little burning is taking place but the ash is being cooled by the under-grate air.
- As a result of the simple fuel preparation and the "suspension-fired" combustion system, the ash was shown to be almost completely free of unburned combustible material, less than 1½% compared to up to 8% found in the mass-burn ash of the time. Buildup of slag was eliminated on the furnace walls; no water was used for removal of ash; and the grate material did not have to be manufactured from special metal alloys because the "hot spots" on the grate commonly experienced in mass-burn systems were not created.

SWARU went online in 1972 and, after a period of operation, underwent substantial modification, then continued to operate for 30 years, when it was shut down due to changes in permissible emission limits and the costs associated with the required retrofits. This was the first "dedicated" RDF-firing plant, as distinguished from "co-firing" with coal [4, 5].

US Bureau of Mines

In the 1970s, the United States Bureau of Mines concentrated research on the recovery of materials in municipal waste – paper, cardboard, ferrous, aluminum, and glass. The pilot research plant at College Park, Maryland, included a shredder (flail mill), trommel screen, air classifier, and metals recovery equipment that recovered materials from samples of municipal waste obtained from various parts of the country (Fig. 2).

The next concept that arose was the use of RDF for co-firing in utility boilers. In 1974, St. Louis Electric took up this concept at their Merrimac Plant in Missouri [6, 7]. With funding from the US Environmental Protection Agency, a shredding plant was erected, with a system capable of feeding the RDF to the existing boilers. The EPA-sponsored research program analyzed the waste in detail, over the course of a year. The research program included sampling and analysis of the stack emissions while burning this fuel, co-fired with coal (Table 5). The RDF was able to supply 10–15% of the total energy input. After the trial runs, it was decided to install magnets after the shredding operation to recover ferrous material, which would cause problems in feeding of the fuel to the boilers. It was also decided to add a second stage of shredding to make the RDF more suitable for feeding to the boilers.

Burning this low-sulfur RDF with coal significantly reduced the sulfur dioxide emissions, as expected. However, emissions from co-combustion included higher levels of heavy metals, such as lead and cadmium, than with firing only coal. The existing boilers were permitted for the emissions with coal firing: new compliance tests would be required for co-combustion. This would abrogate the "grandfathered" existing permits, which the utility was reluctant to do. Plans to build a processing facility taking waste from

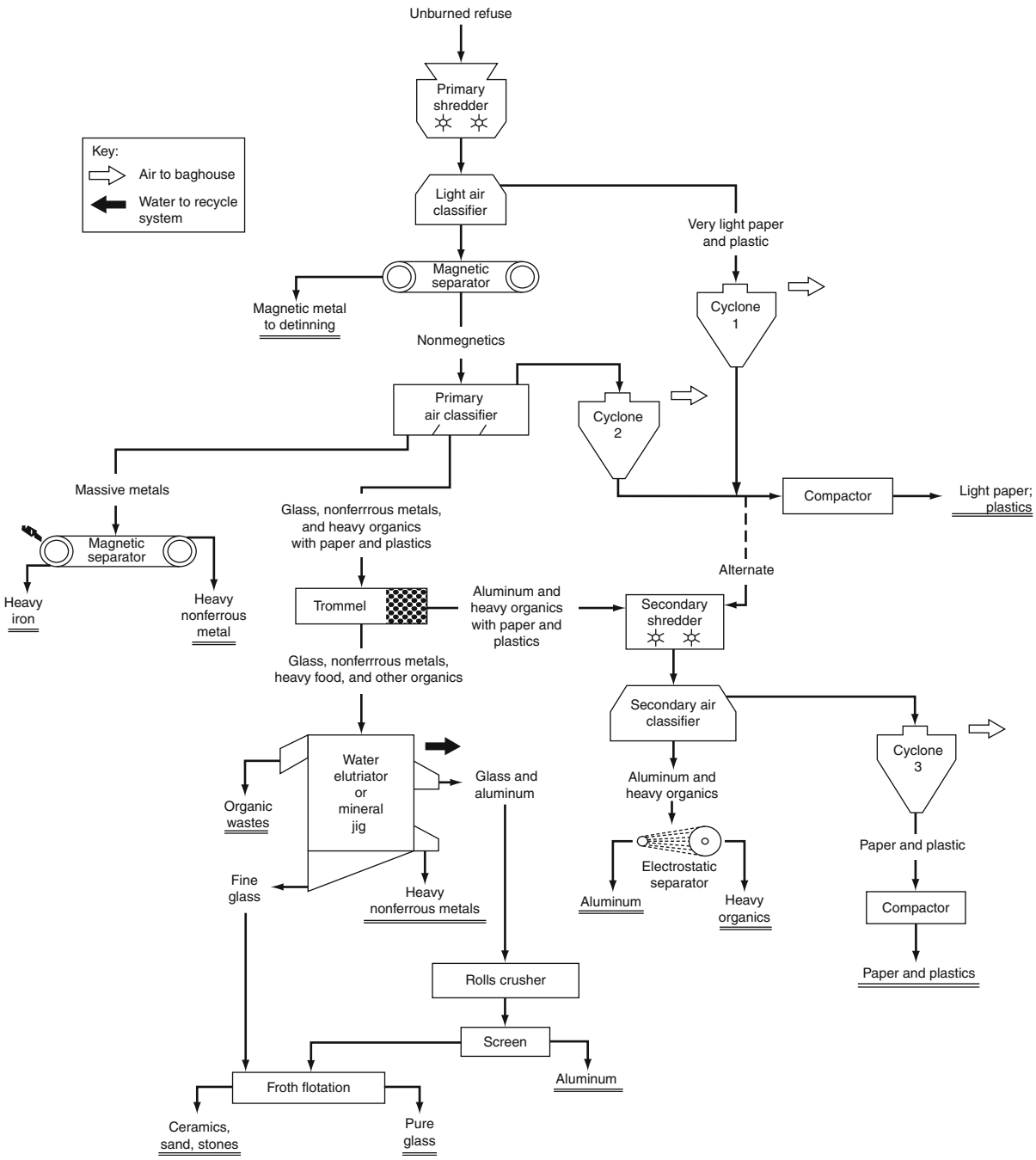

Waste-to-Energy using Refuse-Derived Fuel. Figure 2
US Bureau of Mines System (From [1])

the surrounding community were made and presented to the public. The public uproar convinced the utility that this would damage its public image.

In succeeding years, the US EPA sponsored extensive research on shredding, screening and air classification of RDF. Much of this work has been summarized in

Processing Refuse-Derived Fuel by Floyd Hasselriis, 1983 [1].

Co-Firing Operations

The City of Ames, Iowa, started up the second plant to process and burn its refuse in 1975 [8]. This plant employed two stages of shredding and an air classifier, and included a "silo" to store the RDF and feed it to the boiler, co-firing with coal. After a year of operation, it was decided to replace the air classifier with rotary screens made by Rader.

Combustion Engineering proposed burning RDF in their "corner-fired" boilers in Madison, Wisconsin, and in Chicago, Illinois [8]. Americology designed the process with two-stage shredding and air classification: it was started up in 1974. A shredder explosion damaged the plant, resulting in isolating the primary shredder in a concrete "cage." The plant was shut down in 1979. The City of Chicago designed a similar processing plant, which was started up in 1977. In this case, the RDF had to be conveyed the long distance from the plant to the boilers by pneumatically blowing it through 20-in. diameter pipes to the boilers. It was found that the blowers did not have sufficient capacity to convey the RDF without accumulating glassy sediment in the pipes.

A series of plants were designed for co-firing of RDF with coal, in Akron, Ohio; Columbus, Ohio; Madison, Wisconsin; Monroe County, New York; and Lakeland, Florida, but were shut down for various economic, political, and technical reasons. The City of Columbus built a processing plant in 1982, to produce RDF to be burned in their municipal power plant. Co-firing the RDF with coal was not successful and high emission levels caused a shutdown of this facility.

Northern States Power built a waste processing plant in Red Wing, Minnesota, in 1987 that employed two stages of shredding and a Rader disk screen. The RDF production facilities in Wilmarth, Minnesota, and Lacrosse, Wisconsin, are operating today.

The difficulties of co-firing with coal contributed to the decision to build only "dedicated" boiler installations [9]. Combustion Engineering promoted plants in Hartford, Connecticut; Detroit, Michigan; and Honolulu, Hawaii, in 1988, all based on two-stage shredding, magnetic separation and trommeling (Fig. 3).

Albany NY Energy Recovery System (ANSWERS)

The Albany NY Energy Recovery System (ANSWERS), which went online in 1981, was modeled after the Processed Refuse Fuel system at the SWARU in

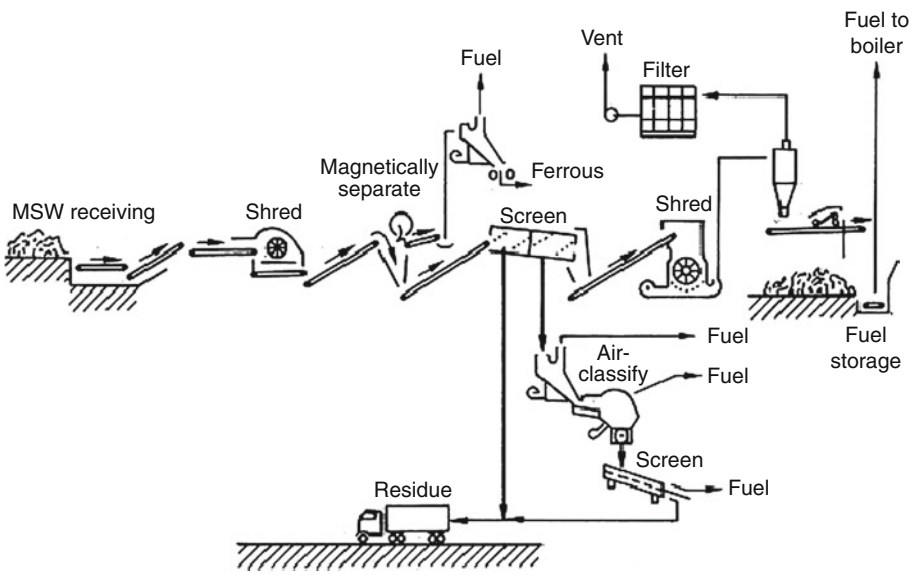

Waste-to-Energy using Refuse-Derived Fuel. Figure 3
Combustion engineering systems (From [8])

Hamilton, Ontario [2]. The ANSWERS process was divided into two sites. The City of Albany-owned site hosted a facility where waste was received and processed into Processed Refuse Fuel (PRF). At a second site, some 9 miles away, the PRF was burned to produce steam for the heating and cooling of State government office buildings in downtown Albany. The combustion facility was designed, owned, and operated by the State of New York Office of General Services, while the overall conceptual design of the entire system and the design and construction of the Processing Facility were by Smith and Mahoney, Engineers, of Albany, New York with Gordon Sutin acting as Technical Advisor and consultant to Smith and Mahoney. The steam plant burned PRF for 15 years until it was closed in order to avoid capital expenditures needed to meet new, more stringent air pollution control regulations.

As shown in Fig. 4, the municipal waste carters dumped their loads on the tipping floor. Front loaders moved the waste to the metal pan feed conveyors, where the waste was inspected and objectionable materials removed. The raw waste was then conveyed to the top of the shredders. Processing was done with two 1,000 HP diesel engine-driven shredders, in a single stage. After passing under magnets to remove ferrous material, the PRF was loaded into transfer trailers and shipped to the power plant where it was deposited into a pit for storage and feeding by crane to the boilers.

ANSWERS demonstrated the versatility of processed refuse fuel systems when waste can be processed into fuel at one location (or several locations if necessary) and transported by truck (or rail) to a power plant in a different location.

Bridgeport, Connecticut Eco-Fuel

In 1986, Combustion Equipment Associates built a plant to process MSW into a powder, called EcoFuel, to be transported and stored in silos, for co-firing with coal or oil in cyclone-furnace utility boilers at United Illuminating. The trash was shredded and ground in ball mills to a storable and retrievable powder. The process was demonstrated to be successful but could not compete with the low cost of landfills in the region. The project was shut down, as it was unable to contract with communities for the project's 2,300-t/day capacity [10].

The Southeastern Public Service Authority (SPSA)

The Southeastern Public Service Authority in Portsmouth, VA, built a facility in 1988 to produce RDF to be burned in the Naval Shipyard. This plant uses two-stage shredding, magnetic separation, and two stages of trommel screening to produce a fuel suitable for burning in the Navy boilers. Belt conveyors carry the fuel from the processing plant to the boilers where fuel feeders supply the fuel to the existing boilers (Table 1).

Advanced Resource Recovery Facilities

SEMASS Resource Recovery Facility

The SEMASS (Southeastern Massachusetts) Resource Recovery Facility in Rochester, MA, was developed by Energy Answers [2]. Construction began in 1986 and the facility went online in 1989, accepting 2,000 t/day of solid waste from communities on Cape Cod and in the southeastern section of Massachusetts. In 1996, SEMASS was expanded to 3,000 t/day with the addition of a third boiler, second turbine, and associated waste receiving, processing, and air quality control equipment.

An aerial photo of the SEMASS Resource Recovery Facility plant is shown in Fig. 5.

The first step takes place at the municipal level where residents participate in programs to reduce the amount of waste by recycling and composting. Whatever waste cannot be diverted through those programs is delivered to SEMASS by packer trucks, transfer trailers, and rail cars (Figs. 6 and 7).

After crossing the scales, waste is received on a tipping floor, where an attendant watches for unacceptable materials and either refuses them or sets them aside. Unacceptable items are such things as large rolls of carpet or wire fencing, tires, tree trunks, and similar items that should not be processed in the shredders. The waste is scanned for radioactive content or combustible potential (fireworks, propane tanks). It is then delivered by loaders to conveyors feeding shredders that reduce the material to pieces of nominal maximum size of 15–20 cm. Most of the particles in the shredded waste are below 5 cm and friable materials such as glass are still smaller. A magnet removes ferrous material, which goes to metal scrap dealers. Although the Processed Refuse Fuel (PRF) is in fact

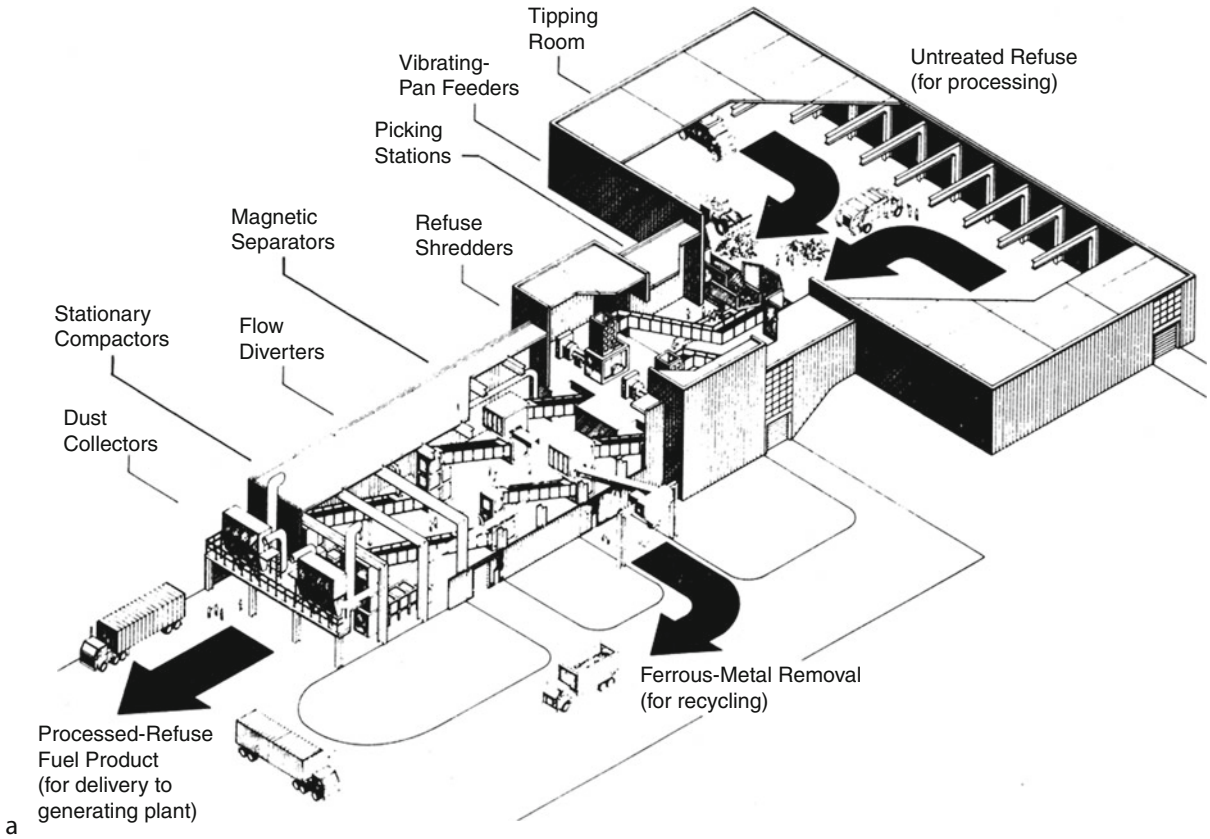

a

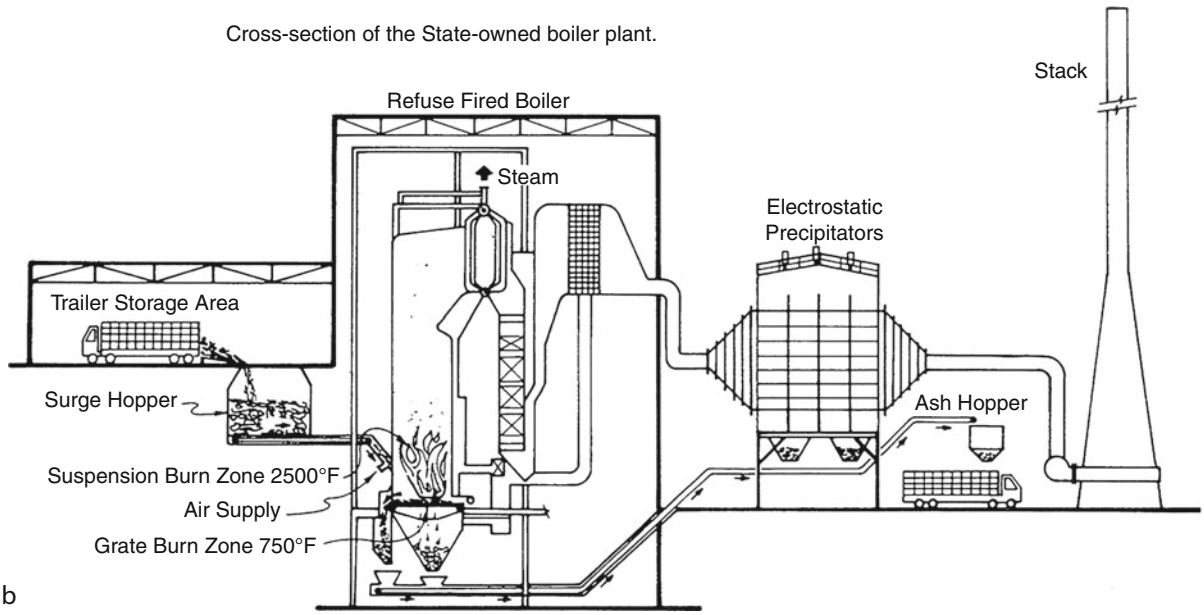

b

Waste-to-Energy using Refuse-Derived Fuel. Figure 4
(**a**) Refuse fuel processing facility, Albany New York; (**b**) Processed refuse-fuel combustion and power production facility, Albany, New York

Waste-to-Energy using Refuse-Derived Fuel. Table 1 Refuse processing power plants operating in the USA in 2007 [11, 12]

Plant name and location	Start date	Capacity (t/day)	Net power
Ames Municipal Electric Utility, Ames, IA	1975	1 line at 175 = 175 tpd	10 MW
Mid-Connecticut Resource Recovery Facility, Hartford CT	1987	3 lines at 666 = 2,000 tpd	68 MW
Miami-Dade County RRF, Miami FL	1979	4 lines at 750 = 3,000 tpd	77 MW
Maine Energy Recovery Company, Biddeford, ME	1987	2 lines at 300 = 600 tpd	22 MW
Penobscot Energy Recovery Company, Penobscott, ME	1988	2 lines at 750 = 1,500 tpd	25 MW
SEMASS RRF, Rochester, MA	1989	3 lines at 900 = 2,700 tpd	78 MW
Great River Energy – Elk River, MN	1989	2 lines at 250 tpd	35 MW
		1 at 500 = 1,000 tpd	
Xcel Energy – Red Wing Steam Plant, Red Wing, MN	1987	2 lines at 360 = 720 tpd	21 MW
Xcel Energy – Wilmarth Plant, Mankato, MN	1987	2 lines at 360 = 720 tpd	22 MW
Southeastern Public Service Authority, Portsmouth, VA	1988	4 lines at 500 = 2,000 tpd	50 MW
Xcel Energy French Island, LaCrosse, WI	1987	2 lines at 200 = 400 tpd	32 MW
North County Resource Recovery Facility – West Palm Beach, FL	1989	2 lines at 900 = 1,800 tpd	62 MW
Honolulu H-Power, Honolulu, HI	1990	2 lines at 925.5 = 1,851 tpd	57 MW
Greater Detroit Resource Recovery Facility, Detroit, IL	1991	3 lines at 944 tpd = 2,832	68 MW
Totals:		21,298 tpd	627 MW

Waste-to-Energy using Refuse-Derived Fuel. Figure 5
Aerial view of Southeast Massachusetts resource recovery facility (SEMASS) (© 2010 Energy Answers International, Inc)

Waste-to-Energy using Refuse-Derived Fuel. Figure 6
Processed refuse fuel in SEMASS storage building; front loader moving load to conveyor ((© 2010 Energy Answers International, Inc)

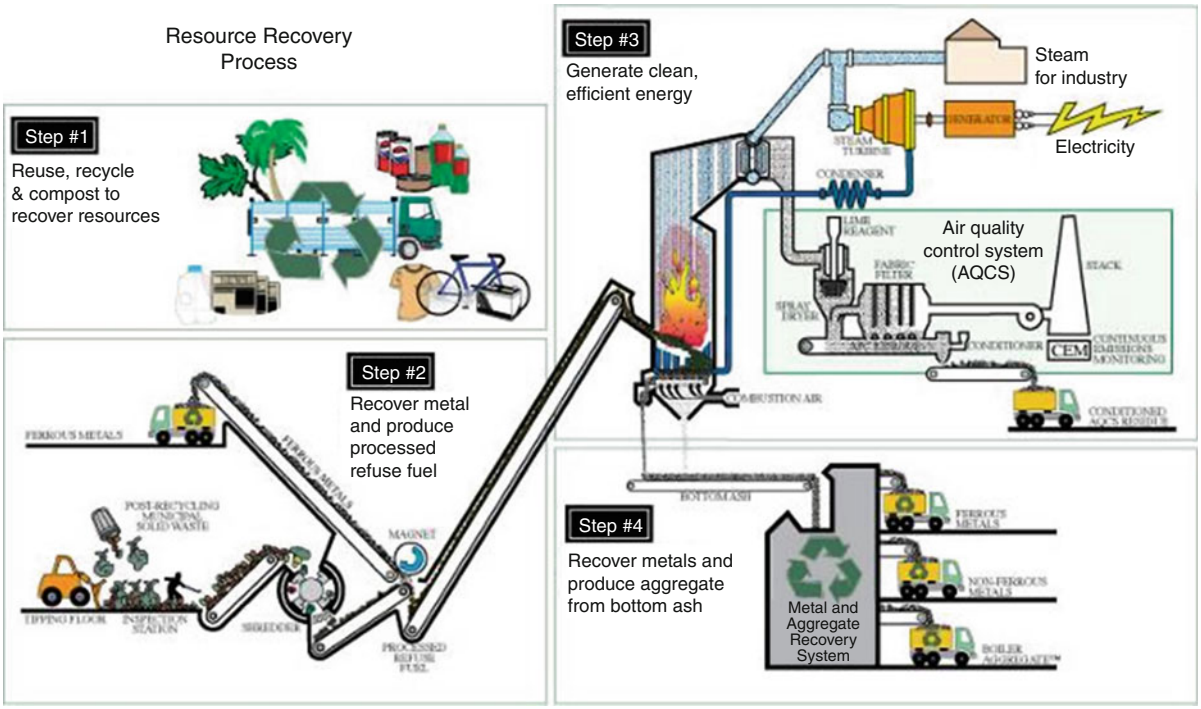

Waste-to-Energy using Refuse-Derived Fuel. Figure 7
SEMASS schematic process diagram (© 2010 Energy Answers International, Inc)

a "Refuse-Derived Fuel," the name PRF has been adopted to distinguish it from other Refuse-Derived Fuels such as "fluff" and "pellets," which require extensive processing of the waste compared to the two-step processing developed by Energy Answers.

The PRF leaves the shredders and is conveyed to the boiler building. Here the boilers each draw off the quantities needed to maintain steady steam generation. The PRF is fed into automatically controlled feed systems that blow the PRF into the furnace section of waterwall boilers. The steam produced drives the electric generators in the conventional power plant. Excess PRF is conveyed back to the storage floor, from which the loaders retrieve fuel as needed when the processing

floor is not operating, such as at night and on weekends.

Heavy materials drop onto a simple horizontal moving grate at the bottom of the furnace. The material on the grate consists of noncombustibles such as metal, glass, ceramic, and sand combined with small pieces of heavier combustible materials such as wood. The grate moves from back to front of the furnace over a 1-h period with a 20–30 cm deep bed on top. For the first 2/3 of the 6-m long grate, the heavy combustible materials burn on the grate. The grate temperatures are kept below the melting point of glass to avoid slag formation. Because of the long period allowed for the combustibles on the grate to burn, this "bottom ash" contains less than ½% carbon.

The lighter materials in the PRF go upward in the furnace and catch fire in midair forming a high-temperature "fireball" a few meters above the grate [3]. In this location, because of the ease with which the fuel can intermix with air, the amount of excess air which must be injected to complete combustion is a reduced and thus temperatures up to 1,250°C are reached. The reduced amount of excess air results in maximum thermal efficiency and therefore more electricity is generated per ton of waste than would normally be the case in a mass-burn system.

Bottom ash and fly ash are handled separately, so the fly ash can be treated to minimize the potential for leaching of heavy metals such as cadmium and lead. The bottom ash, which is generally granular in form, is discharged from the boiler without quenching in water, and is transported to the on-site Bottom Ash Processing Building. In this building, three products are recovered: the ferrous metals not removed prior to combustion, the nonferrous metals, and the Boiler Aggregate™, a granular material which can be substituted for natural aggregates used for landfill daily cover and as an ingredient in asphalt and concrete. The nonferrous metals are sold to a dealer who separates the contents of the mix, and the ferrous metals are sold to scrap dealers.

Because the heavy metals concentrate in the fly ash, the flyash needs to be conditioned with water as it is discharged from the silo into trucks for delivery to the landfill. Within 24 h the conditioned flyash hardens into a concrete-like material which, although not high-strength, does not absorb water. Testing of the conditioned flyash using state-mandated procedures indicates that the heavy metals are permanently bound and will not leach.

The SEMASS facility is provided with state-of-the-art acid-gas scrubbers [24]. The first two boiler units have electrostatic precipitators (ESPs) of a size greatly increased compared with previous units. The third boiler was installed using fabric filter emission controls. This facility has emissions well below US EPA standards, and even below standards of the European Union (see Table 3).

Palm Beach Florida Resource Recovery Facility

Babcock and Wilcox designed the boilers used for dedicated combustion of RDF produced in Biddeford, Maine, and Oronton, Maine, in 1987 and 1988, and later in Palm Beach, Florida, in 1989. The Palm Beach facility is another example of large-scale successful operation of an RDF combustion facility.

A model of the complete facility in Palm Beach is shown in Fig. 8. Municipal solid waste trucks enter the tipping floor and dump their loads on the floor. Front-loaders move the waste either directly to a metal pan feed conveyor, or to storage on the floor for later feeding. The loader operators inspect the waste as it is received, diverting over-size objects to a separate area, for recycling or disposal to landfill. The loaders feed the waste materials continuously, one bucket-load at a time, and deposit it onto feed conveyors. The front-loader operators in effect feed the conveyor as empty conveyor space appears, so that the feed is essentially steady. Shredders operate most efficiently and effectively at a full loading of the drive motor. Typically shredders are provided with 1,000 hp motors. The operators in the control room control the speed of these conveyors, so that the rate of feed is adjusted to the capacity of the shredders. Storage capacity is provided on the tipping floor as needed to handle the waste received at peak rates during the day while it is removed for processing at a steady rate.

The Palm Beach Facility has three shredders serving two basic processing lines. The feed conveyors are located in open space, rising to the shredder feed opening, and taking material out of the bottom of the shredder, again rising to feed the trommels, and again rising to feed the trommel screens. The RDF is then

Waste-to-Energy using Refuse-Derived Fuel. Figure 8
Palm Beach resource recovery facility [13]

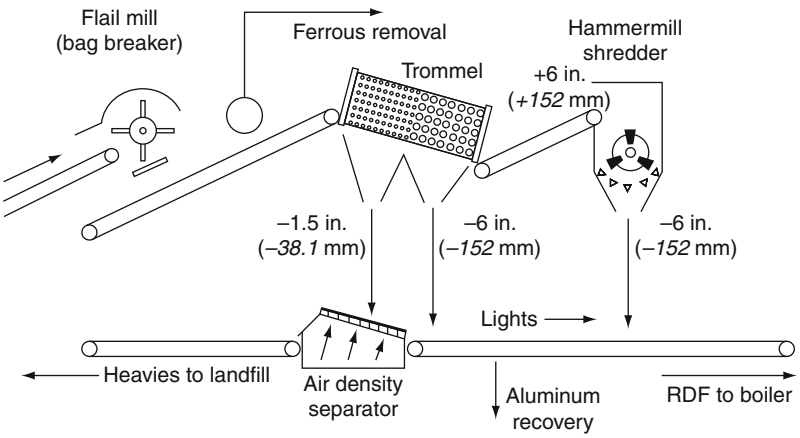

Waste-to-Energy using Refuse-Derived Fuel. Figure 9
Processing with flail mill before screening and shredding, Palm Beach [13]

carried by conveyors directly to the boilers or bypassed to a storage floor for future feeding to the boilers. Storage capacity is needed so that the boilers can operate 24 h/day, weekdays and weekends, and also to allow for shutdown of boilers, preferably one at a time.

RDF is produced using two-stage shredding and trommel screens, as shown in Fig. 9.

A flail mill is used to break the bags of refuse, avoiding excessive grinding of glass. A magnetic separator placed above a conveyor removes ferrous material,

especially cans, which are baled for shipment to metals recovery plants. The coarsely shredded waste is then screened by a trommel in two stages; the minus-1-1/2 fraction which contains broken glass, dirt, and miscellaneous fines, drops to an air density separator which blows light materials such as paper off the surface while the heavies pass through the screen and are removed as heavies to the landfill. Minus-6-in. holes pass aluminum and remaining steel cans, which are baled for shipment to recovery plants. The plus-6-in. material is then fed to a hammer mill shredder, which grinds the paper, cardboard, plastics and wood. The last operation is the disk screen that passes minus-6 in. material joining the screened lights to become the "prepared fuel" or RDF product that is conveyed to the storage room for feeding to the boilers.

Three shredding lines serve the plant, two having a capacity of 100 t/h. The raw MSW enters the flail mill, and passes under a belt magnet. The collected ferrous metal is then shredded, passing a second magnet that returns the entrained matter to the conveyor, while the ferrous material is air scrubbed to produce 5 t/h of clean ferrous material.

The two-stage trommel drops the minus1.5-in. material to an air density separator to produce 10 t/h of residue that goes to landfill. In this screening operation about 1.3 t/h of moisture is lost to the atmosphere. The RDF from the air density separator, air classifier, and disk screen is collected to produce an output of 83 t/h that is fed either directly to the boilers or stored on the tipping room floor. Typically, 0.7 t/h of aluminum is recovered. A shear shredder is shown, reducing tires to a size that can be burned in the boilers along with the RDF. The trommel removes the plus-2 in. material that is recycled to the shear shredder (Fig. 10).

The RDF is stored in a separate building, as shown in Fig. 11, from which it is loaded by front-loaders to the conveyors feeding the boilers. Shown are the RDF feeders that deliver to each of the boilers at speeds controlled by the operators in the control room. Figure 11 shows the boiler, the dry scrubbers and fabric filters followed by the induced-draft fans which discharge the combustion gases to the stacks.

The RDF feed system in front of the boiler is shown in Fig. 11. The feed conveyor delivers the RDF to the feed bin. A ram feeder pushes the feed onto the feed conveyor, which in turn carries the feed up and over to the drop chute after which it feeds the air-swept spout which injects it into the boiler (Fig. 12).

The air-swept spout is shown in Fig. 13. The RDF is directed over the traveling grate stoker upon which some of it is burned directly, and above which much of it is burned in suspension.

The ash residues are carried back to the ash hopper. Under-grate air supplies a portion of the combustion air. Secondary air (not shown) is supplied above the stoker.

Figure 13 shows the design of the Babcock and Wilcox combustion chamber above the firing grate. Overfire air is supplied at high pressure and passes through nozzles that direct the air so that turbulence is created in the combustion space, achieving effective mixing of fuel and air. The furnace walls are composed of alloy-faced or composite tubing that resists the intense heat and radiation and delivers the heat to the boiling water, to be released as steam. Figure 14 shows tubing which is used by Babcock and Wilcox, wherein the carbon steel core tubes are coated with stainless alloy in their manufacturing process. Some boiler manufacturers use solid alloy tubes, or apply the heat-resistant alloy coating after manufacture of the panels of tubes, and replace or restore the coatings periodically during annual shutdowns.

Ravenna, Italy Fluidized Bed System

The City of Ravenna, Italy, a seaport on the Adriatic, in 1998 commissioned a fluidized bed boiler/waste-to-energy system to combust approximately 50,000 t/year of RDF and generate electric power. The chosen site for a plant to convert this waste to energy is close to a landfill, whereas the RDF production plant is 26 km away. It was decided to pelletize the RDF to facilitate transportation by truck. In order to employ a pelletizer, it is necessary to process the MSW by shredding and screening the product. The processing of waste includes material sizing by shredding to size, followed by magnetic separation. The final waste stream is compressed through roller mill/punched grate to create a relatively "densified" fuel stream. The fluidized bed boiler system was designed to deliver about 70,000 lb/h of steam to generate approximately 7 MW of electricity [13].

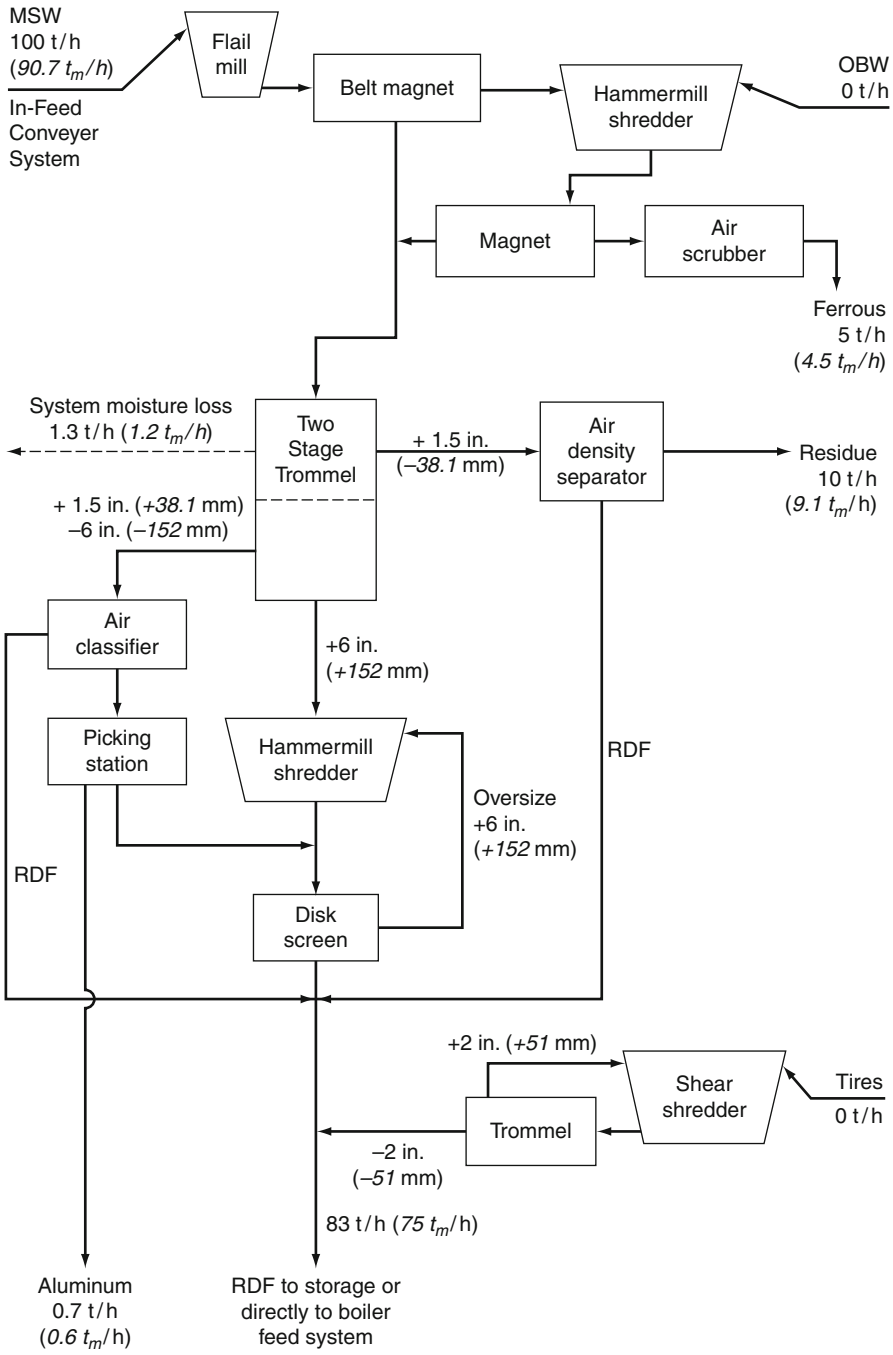

Waste-to-Energy using Refuse-Derived Fuel. Figure 10
Mass balance of waste in complete RDF processing system, Palm Beach [13]

Equipment Description The combustor/boiler flue gas train is shown in Fig. 15. Processed fuel is delivered to a dual screw-metering bin located adjacent to and elevated above the fluidized bed chamber. The metered fuel flows by gravity to the inlet of an air-swept spreader stoker centered on the narrow walls of the fluidized bed. Pulsating sweep air from the forced-draft fan disperses the fuel across the 20-ft span of the combustor.

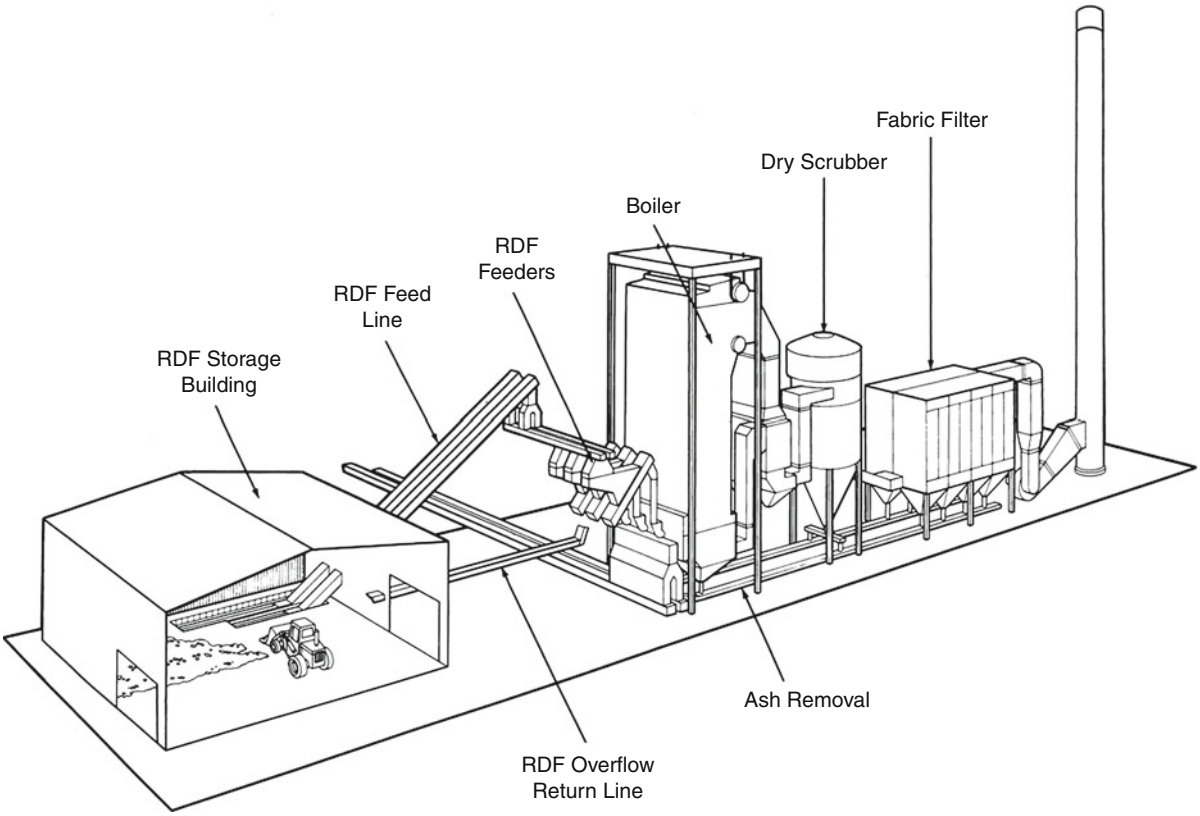

Waste-to-Energy using Refuse-Derived Fuel. Figure 11
Perspective drawing of complete RDF system with dry scrubber and fabric filter

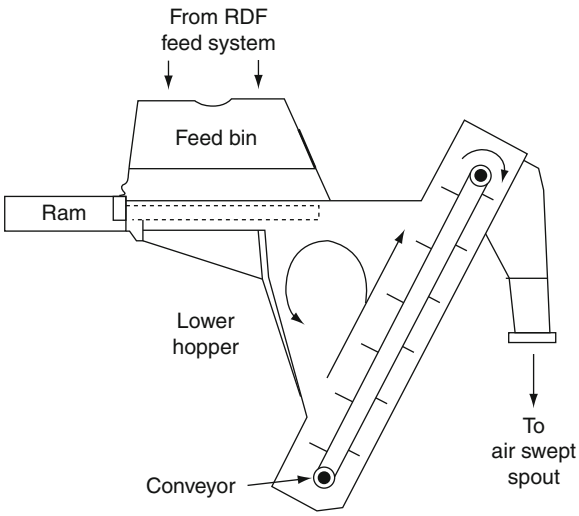

Waste-to-Energy using Refuse-Derived Fuel. Figure 12
RDF feeding system [13]

The fluid bed combustor is comprised of an internally insulated and refractor lined chamber having internal dimensions of approximately 10′ × 20′ and a height of approximately 42 ft. The bottom of the combustor is equipped with a pair of draw-down cones that comprise the patented and proprietary bed cleaning system that is the trademark of EA Technology. Fluidizing air from the FD fan is distributed throughout the combustor by a series of manifolds and nozzles that distribute the air uniformly. In addition to the underfire air, a pair of overfire air manifolds supplies and distributes the balance of the combustion air into the lower region of the vapor space. The 52 ft elevation above the fluidizing nozzle provide 4 s of residence time within the chamber with approximately 2.5 s of that after the second level of overfire air injections.

The furnace is designed to operate at about 50% excess air, sufficient to control combustor temperature

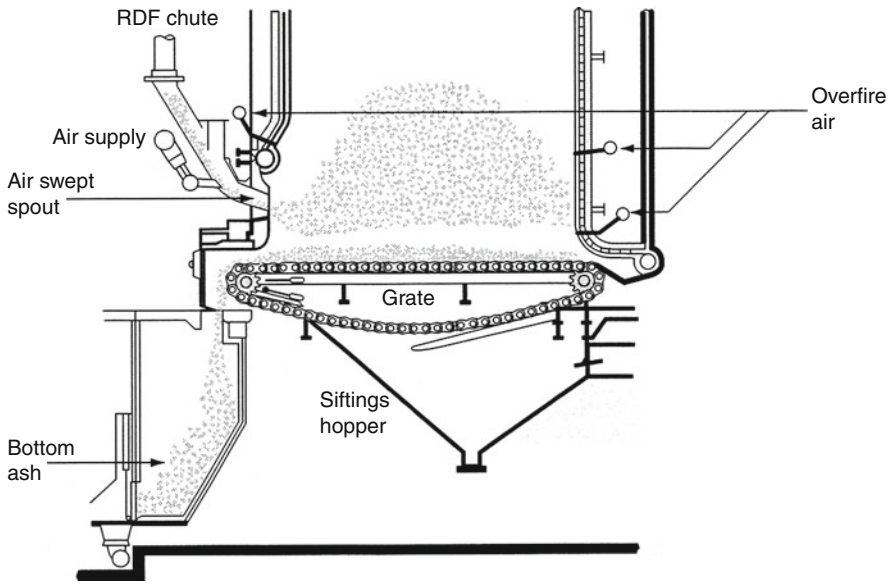

Waste-to-Energy using Refuse-Derived Fuel. Figure 13
Elevation of lower section of boiler [13]

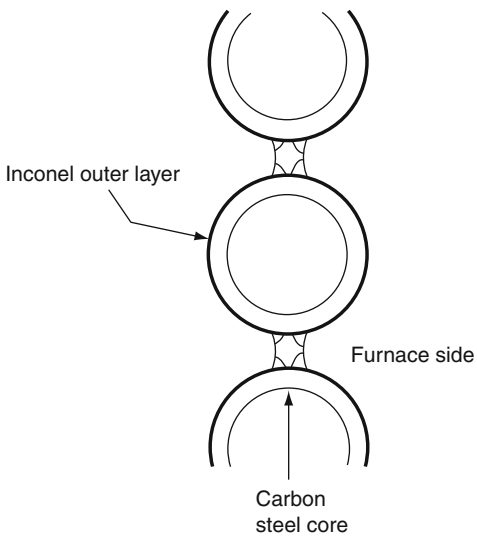

Waste-to-Energy using Refuse-Derived Fuel. Figure 14
Cross section of Babcock and Wilcox boiler tubes in waterwalls [13]

suppression: heat removal tubes provide the additional cooling effect for the gases to exit the furnace at about 1,700°F before entering the convective screen section where they are reduced to nearly 1,300°F before entering the superheater. Further steam production occurs in the final evaporator section designed to reduce the flue gas temperature out the boiler to 650°F (342°C).

Exiting the boiler the flue gases are cleaned of some particulate by a set of multicyclones. After the economizer the gases are reduced to about 325°F (162°C) while heating feedwater to around 390°F (199°C). The boiler is designed to generate 75,000 lb/h of steam at 595 psia and 716°F (41 bars, 380°C).

Emission Control Downstream of the boiler, particulate levels are controlled by a venturi reactor and bag house. The venturi reactor is a dry scrubber that incorporates a solid recirculation system, which optimizes the reactant equalization ratio. Hydrated lime and activated carbon are added as needed to reduce the acid gases and minimize dioxin/furan emissions. The flue gases at 300°F then enter a wet scrubber where they are quenched to 130°F. A solution of NaOH is sprayed into the flue gas prior to a series of demisters for final removal of any remaining acid gases and other soluble components of the gases. Prior to exiting the system through the induced-draft fan, the exhaust gases are reheated to 239°F (115°C). This comprehensive

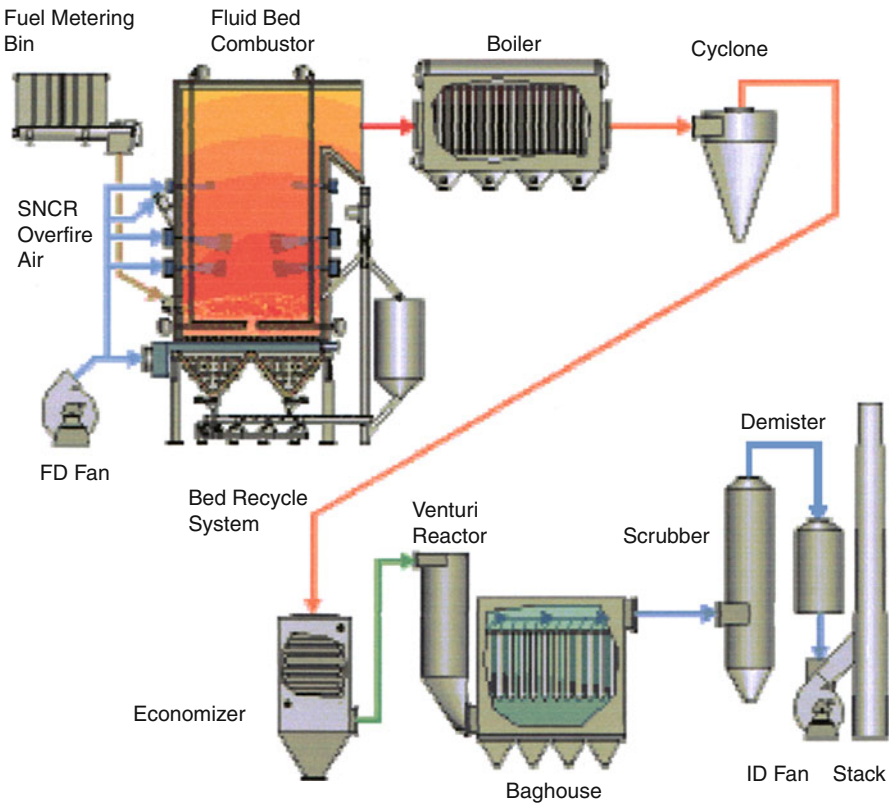

Waste-to-Energy using Refuse-Derived Fuel. Figure 15
Process flow schematic of Ravenna fluidized bed system firing refuse-derived fuel [15]

emission control system reduces emission levels well below the already stringent requirements of the Italian government [15].

Alliance, Ohio RDF Facility

A "greenfield" RDF facility in Alliance, Ohio, will process 2,400 t/day (TPD) of MSW and Construction and Demolition Debris (C&D). Two equipment trains to thermally process the material will consist of Riley Power's Advanced Stoker boiler, Turbosorb dry scrubber and the Regenerative Selective Catalytic Reduction (RSCR) nitrogen oxides (NO_x) control system. The boiler/emission control system is shown in Fig. 16 [16].

The Riley Advanced Stoker boiler has unique design features to ensure high efficiency, corrosion resistance, and fuel flexibility. The use of the Turbosorb will result in lower emissions of lead and other volatile heavy metals and mercury than a typical spray dryer/baghouse (Spray Dryer Absorber) system can achieve. Acid gas removal is also superior to an SDA system while utilizing less lime reagent and power. A Riley Selective Catalyst Remover (RSCR) follows the Turbosorb and baghouse as a "low-dust" Selective Catalytic Remover, having an auxiliary energy consumption about 85% lower than a typical low-dust, tail-end SCR. The RSCR reduces nitrogen oxides (NO_x) and carbon monoxide (CO) emissions to lower values compared with previous facilities producing energy from waste. This versatile system is capable of controlling emissions from combustion of commercial and demolition wastes (C&D) as well as refuse-derived fuel (RDF) from municipal waste.

The RDF and C&D conveyed to two Riley boilers and associated steam turbines will produce a total of 66 MW gross, which results in approximately 58 MW net electric power. At maximum continuous rating (MCR), 83,333 lb/h of RDF and C&D will be sent to each boiler.

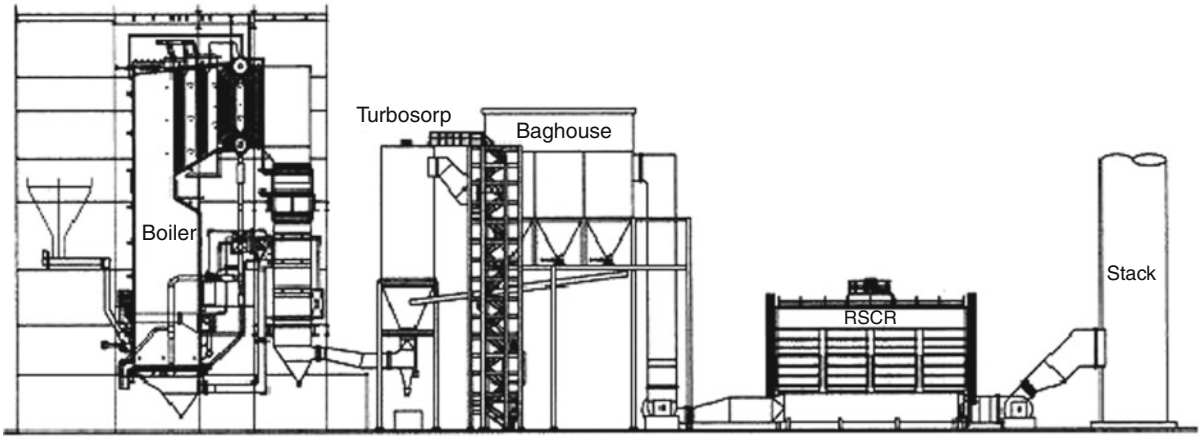

Waste-to-Energy using Refuse-Derived Fuel. Figure 16
Alliance Ohio boiler and AQC equipment [16]

The design higher heating value of the fuels is 4,500 BTU/lb for the RDF and 5,681 BTU/lb for the C&D, combined at 50%.

Figure 17 shows the Riley Advanced Stoker Boiler with a modular boiler bank, which replaces the conventional boiler bank. This design allows the evaporators to be shop assembled, resulting in fewer field execution hours.

A Turbosorp Dry Circulating Fluidized-Bed Scrubber (Fig. 18) removes acid gases from the boiler flue gas using lime injection. It is followed by a fabric filter (baghouse), which controls particulate emissions. Activated carbon injection is used to remove heavy metals, including mercury, as well as dioxins/furans. The flue gases enter a central pipe, rise to the top and then fall down through the annular outer pipe. This arrangement is very compact compared with the spray-dry scrubbers commonly in use.

The benefits of the Turbosorb technology over the spray dryer absorber (SDA) used heretofore include:

- Lower lime stoichiometry for the same removal efficiency and approach temperature.
- Higher removal efficiencies for acid gases, i.e., 95% or greater plus removal of sulfur trioxide (SO_3) sulfuric acid (H_2SO_4), hydrochloric acid (HCl) and hydrofluoric acid (HF), mercury, particulates, and dioxin/furans.
- Reduced power consumption since slurry atomization is not used.
- Simpler system with less maintenance since it uses dry lime, without the need for slurry handling.

The Turbosorp dry scrubbing technology employs high levels of solid circulation, with addition of finely atomized water, hydrated lime, and flue gas within the circulating bed reactor. The lime and finely atomized water are injected independently into the Turboreactor to lower flue gas temperature and enhance absorption capacity. The fluidized bed material is comprised of solids, including calcium hydroxide, recirculated flyash from the combustion process, and solid reaction products for the fabric filter.

Turbulent flow within the reactor permits intimate contact between the gas and the reagents promoting the chemical reaction between the gas and the active portions of the reagent. A portion of the solids is drawn out of the system and recirculated to maintain mass equilibrium. Provision to inject activated carbon into the gas stream will be made, but may not be required to achieve the emissions limits.

The Regenerative Selective Catalytic Reduction (RSCR) system shown in Fig. 19 is an advanced high-efficiency NO_x reduction system. Since the flue gas temperature is too low for the SCR catalyst to function efficiently, the RSCR temporarily elevates the flue gas temperature to the optimum level while using minimal auxiliary fuel, allowing NO_x reduction efficiencies greater than 70% to be achieved.

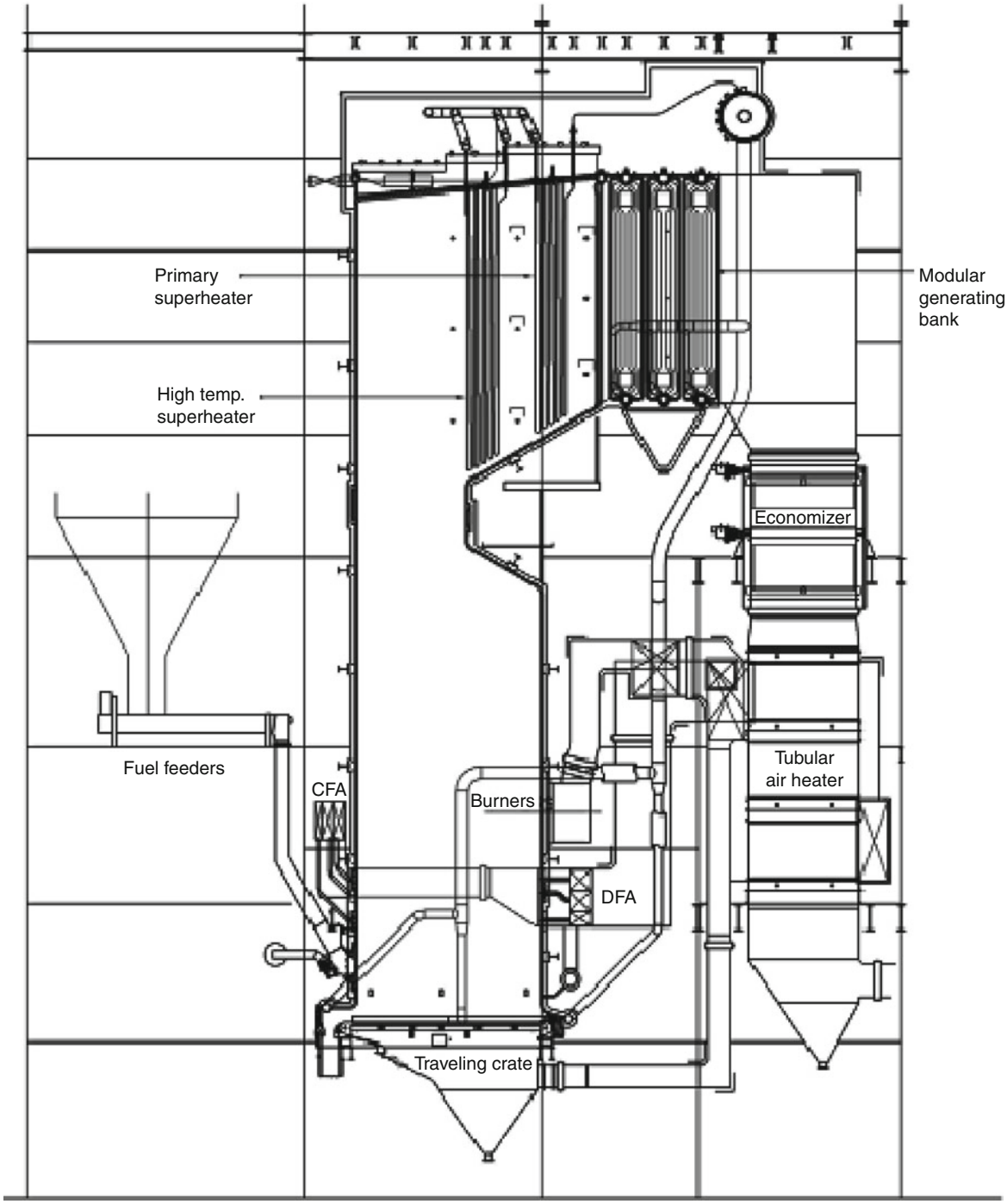

Waste-to-Energy using Refuse-Derived Fuel. Figure 17
Riley Power Inc. advanced stoker boiler [17]

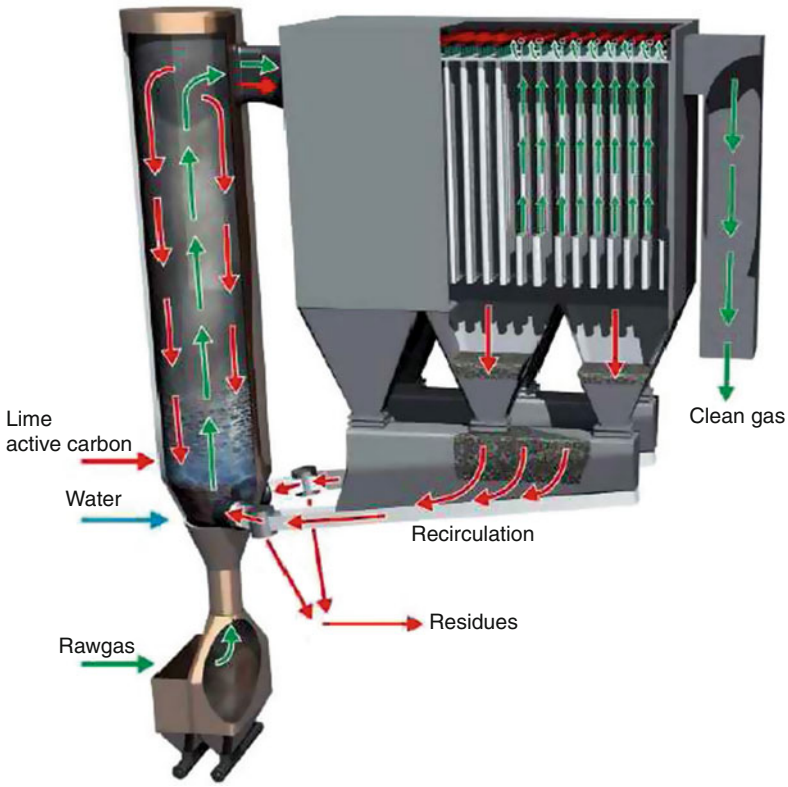

Waste-to-Energy using Refuse-Derived Fuel. Figure 18
Turbosorp and fabric filter filtration gas scrubbing system [17]

The RSCR device is a multi-chamber vessel, each chamber containing catalyst and ceramic beds [17]. Each chamber is arranged for vertical flow of gas in both the upward and downward direction. Dampers in the gas ductwork control the direction of gas flow. The catalyst mounted directly above the ceramic beds promotes the reduction of NO_x to nitrogen and water, while the ceramic bed is used to recover heat from the processed flue gas. The active reagent used for this process is 19% aqueous ammonia.

Flue gas enters an inlet header that connects to the four reaction canisters. At any time, one inlet duct and one outlet duct on each pair of canisters is open, and one of each is closed. Flue gas enters one canister and rises through a heat recovery medium, picking up heat to attain the proper temperature for NO_x removal (about 600°F). It then enters the catalyst, causing NO_x to be converted to nitrogen and water. After passing through the first catalyst, a small quantity of natural gas is combusted to raise the temperature of the flue gas by about 10°F. The gas then turns and goes down through the second canister, first passing through the catalyst, causing additional NO_x to be removed, then through the heat recovery medium, where the heat in the flue gas is transferred back to the medium. The gas then exits through the outlet header to the stack.

About every 3 min, the inlet and outlet dampers switch positions, reversing the flow. The flue gas picks up heat from the now heated side and gives up the heat to the cooler side. This process cools the gas to approximately 280°F before exiting to the stack.

Fairfield Renewable Energy Power Plant

Energy Answers International is developing a renewable energy power plant on an industrial-zoned site on Fairfield Peninsula in Baltimore, Maryland. The 140 MW combined heat and power plant is designed to provide wholesale energy to help meet regional demands, as well as reduced-price retail energy as an attraction for energy

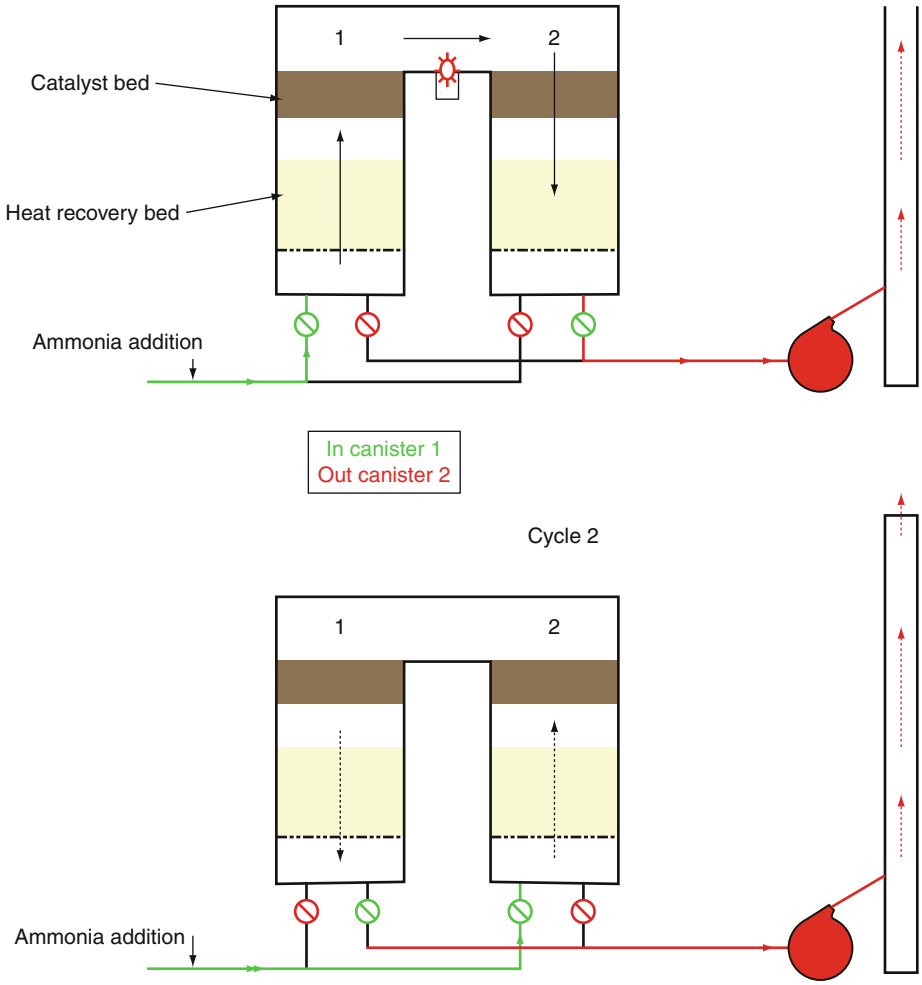

Waste-to-Energy using Refuse-Derived Fuel. Figure 19
Regenerative selective catalytic reduction (RSCR) nitrogen oxides (NO_X) system [18]

intensive industries to co-locate at an Eco-Industrial Park to be developed on the 90-acre "brownfield" site. The waste-derived fuel will be processed at various other sites and transported to the plant.

Processing Equipment

Typical equipment, common to RDF production, is described below.

Shredders for Size Reduction

Figures 20–22 show the typical shredders employed in RDF processing: shear shredders, flail mills, and hammer mills [1].

The flail mill has simple swinging hammers that reduce the size of bulky boxes, cardboard, and other materials, breaking bottles into large shards as the material is smashed onto the heavy steel table.

The shear shredder consists of counter-rotating wheels having knives or cutters that shear the materials as they are caught in the gap between the wheels. Hydraulic drives are used, so that when jams occur, the rotor can be stopped and started again to complete the grinding process. These machines are especially suited to processing tires, but also to screening RDF. The spacing of the wheels and the gap between the drums determines the size of the product.

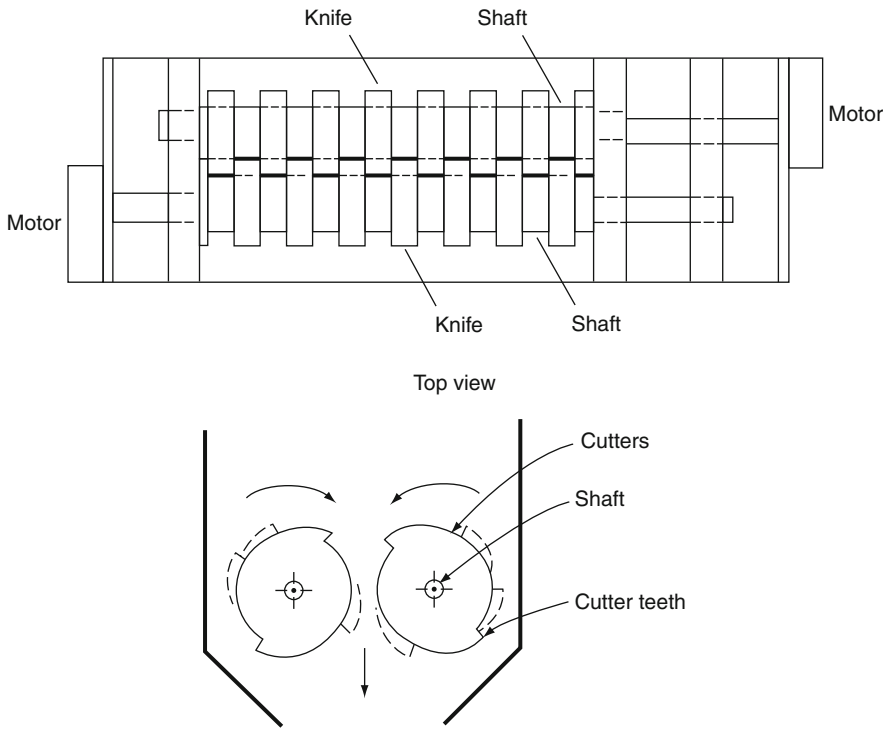

Waste-to-Energy using Refuse-Derived Fuel. Figure 20
Shear shredder

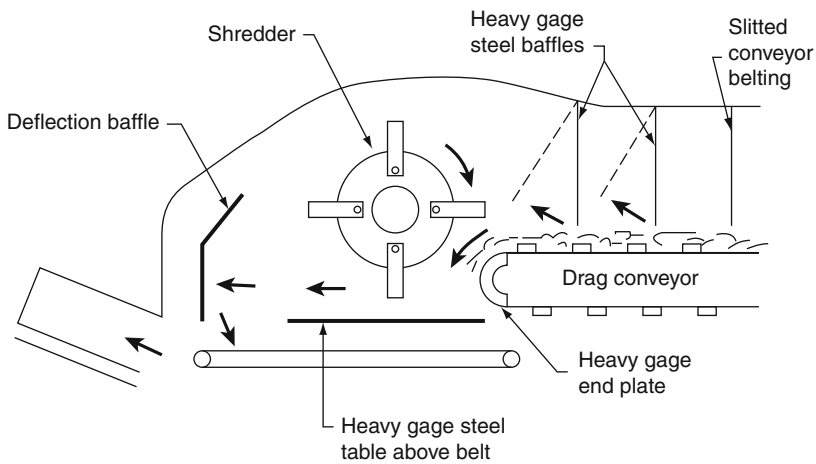

Waste-to-Energy using Refuse-Derived Fuel. Figure 21
Flail mill

A typical hammer mill has hammers mounted on the shaft, free to swing as they pass over grates on a quadrant of the circular shell. The hammers break the material by impact, and then force it through the grates as it is reduced in size. Material that is not shredded on the first pass circulates around until it can pass the grates. The spacing of the grates determines the size of the product. The rate of wear on the hammers is such that they have to be reversed or replaced periodically, typically on weekend downtime.

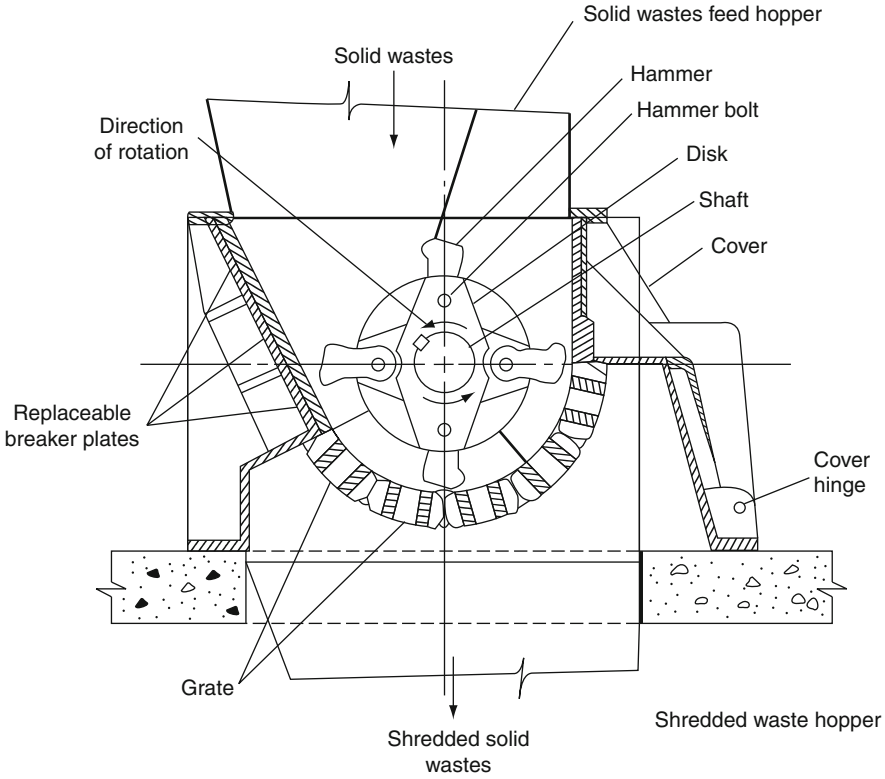

Waste-to-Energy using Refuse-Derived Fuel. Figure 22
Hammer mill

Magnets for Ferrous Recovery

Magnets are universally employed to separate ferrous metals from a stream of shredded refuse.

Figure 23 shows a typical Eriez magnet suspended above a belt conveyor. The magnet has a transverse belt that carries the collected metal away from the conveyor belt to a collection bin. An air density separator is employed to clean off entrained light material and return it to the RDF conveyor.

Screens Used in Resource Recovery

A variety of screens are used in RDF processing as shown in Fig. 24 – (a) vibrating flat, (b) vibrating double flat, (c) inclined flat, (d) disk, (e and f) rotary or trommel. Screens typically separate materials of smaller size from the mass passing over the screen, the size determined by the diameter of the hole, or the area of the passage. Rotary screens, called trommels, are especially suited to the operation, since the material is tumbled over the screen, exposing new material on every revolution.

Flat screens generally provide a vibratory or shaking motion, to assist the material in falling through the apertures in the screen. A flat screen, which incorporates an upward air flow, is shown in Fig. 25. This provides effective separation of light material from the heavy residue.

The Jeffrey Rader screen shown in Fig. 26 has rotating wheels provided with cutters: the spacing of the cutter drums and the gap between the opposing drums determines the size of the material that can pass through the screen.

Conveyors for Movement of Materials

Belt conveyors are the most common devices used for carrying RDF from one operation to another. The belts are carried on idler rolls, and are driven by a head pulley. Drop-off of material from one conveyor to

Waste-to-Energy using Refuse-Derived Fuel. Figure 23
Horizontal magnet used for ferrous recovery (Eriez)

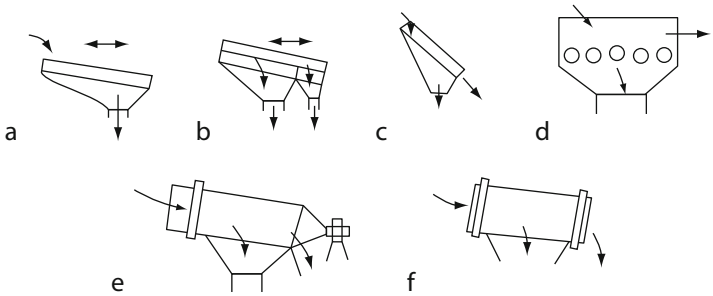

Waste-to-Energy using Refuse-Derived Fuel. Figure 24
Screens

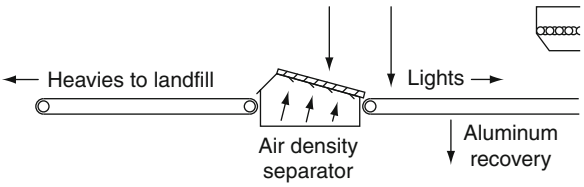

Waste-to-Energy using Refuse-Derived Fuel. Figure 25
Flat screen with upward air flow

another is a source of dusting and linting within the processing areas. Suitable covers must be used, and often a dust-collecting system is provided, which returns the dust to the processing line.

Belt conveyors are generally troughed to minimize fall-off of material. The slope of belt conveyors is limited to about 30°, so that material will not fall back (Fig. 27).

Vibrating-pan conveyors are employed with heavy or dense residual materials, including broken glass and combustion ash residues. Figure 28 shows the principles of operation. The movement "B" causes a rise and fall of the pan. The particles are suspended and fall back in a different place on the pan, progressing the material along. The oscillating drive forces movement over isolation springs, which are tuned to the natural frequency of the pans.

Steel Pan Conveyors

Pan conveyors as seen in Fig. 29 are used to handle raw municipal waste and other solid materials. The pans are hinged, and connected to steel rollers carried on tracks.

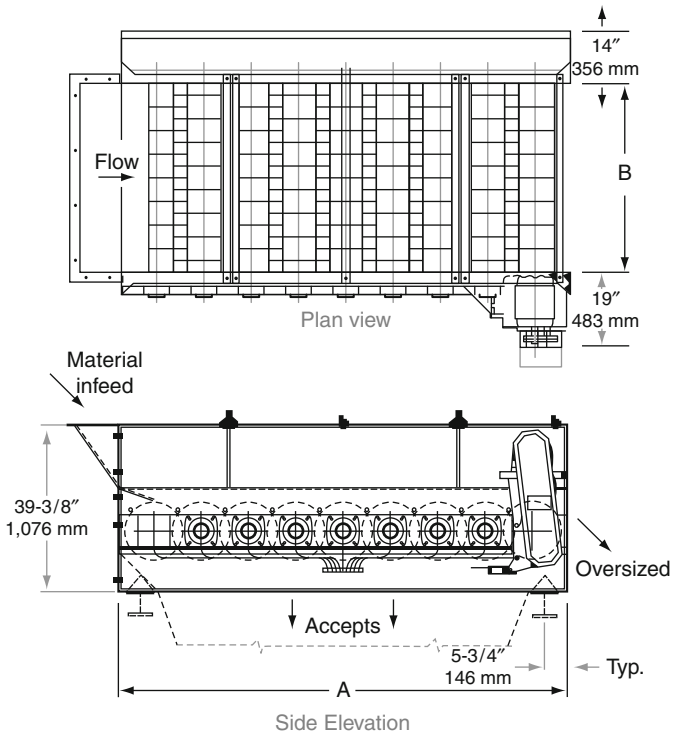

Waste-to-Energy using Refuse-Derived Fuel. Figure 26
Rotating disk screen for separating materials by size (Jeffrey Rader)

Waste-to-Energy using Refuse-Derived Fuel. Figure 27
Belt conveyor for moving light materials (typical)

Air Quality Control Equipment

Early Systems with Electrostatic Precipitators

The complete boiler and emission control system typical of early installations is shown in Fig. 30. A feed cyclone is shown, which drops the RDF into the air-swept spout onto the stoker. The boiler furnace has the rectangular shape commonly used in coal and wood stokers at the time. A "nose" deflects the gases into the top of the chamber where they enter the economizer. Next the gases pass through the convector section of the boiler where most of the steam is generated before passing through the superheater. An economizer is shown, cooling the gases before entering the electrostatic precipitator (ESP). The economizer heats the boiler feedwater before it enters the convection section

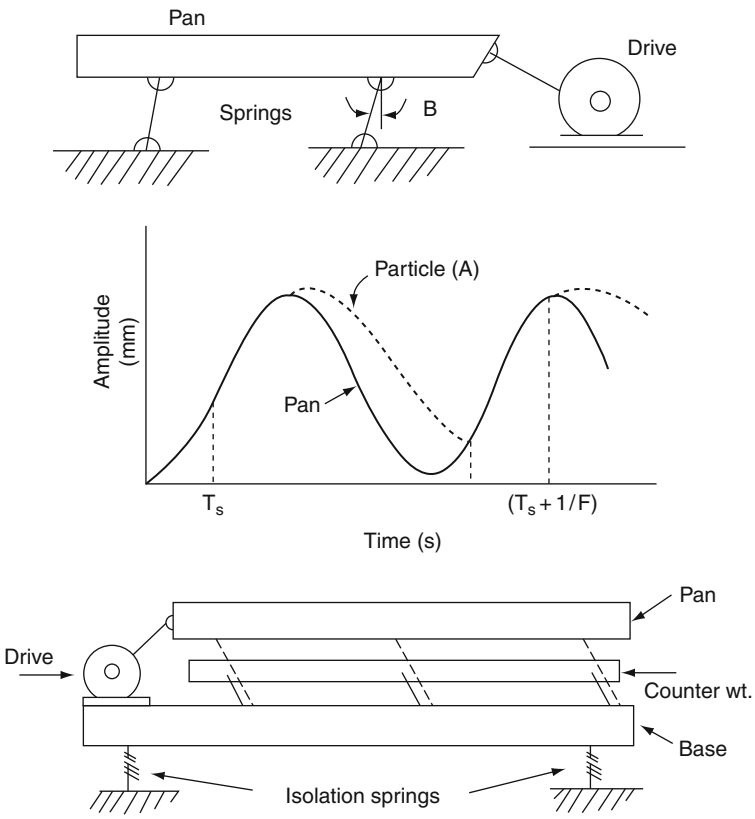

Waste-to-Energy using Refuse-Derived Fuel. Figure 28
Vibrating conveyors used to move heavy materials such as ash residues [1]

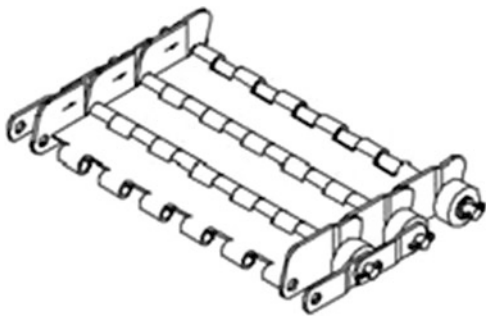

Waste-to-Energy using Refuse-Derived Fuel. Figure 29
Steel pan conveyor used for handling raw MSW

of the boiler. An air heater is shown, below the ESP. This preheats the combustion air, as needed to assist in driving off moisture in the RDF as it is fed to the stoker.

Contemporary Systems with Scrubber and Baghouse

Scrubbers and fabric filters, "baghouses," have replaced electrostatic precipitators in contemporary waste-to-energy plants. Dry scrubbers are commonly used to capture sulfuric acid and hydrochloric acid from emissions from waste-burning systems. Figure 31 shows flue

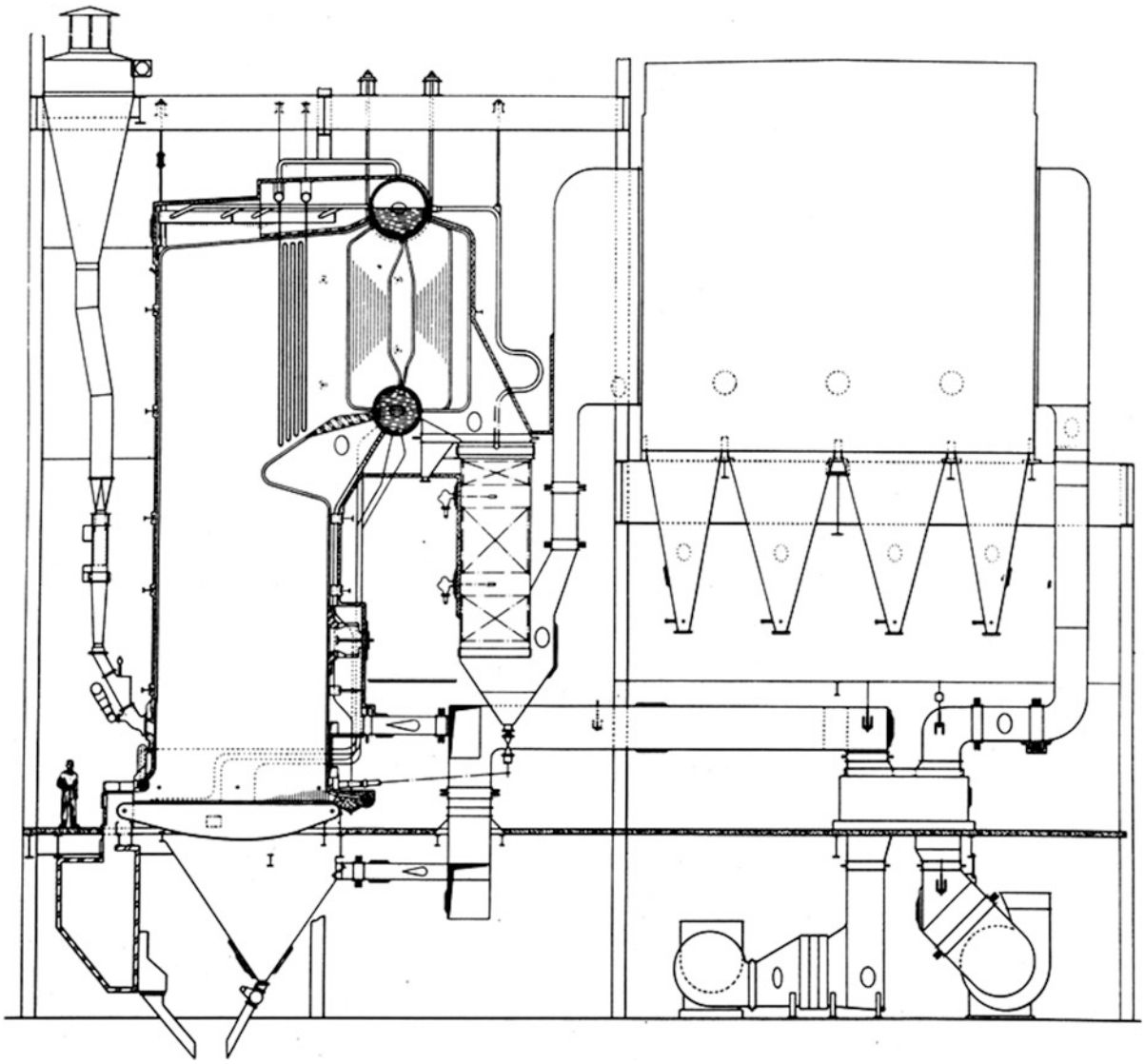

Waste-to-Energy using Refuse-Derived Fuel. Figure 30
Early Babcock and Wilcox RDF-fired stoker boiler with electrostatic precipitator

gases entering a spray-dryer tower within which a solution of caustic solution of lime, prepared by dissolving calcium oxide (CaO) in water, is atomized and sprayed into the gas stream passing through the tower. The scrubber functions by using the temperature potential of the entering gases (typically above 400°F) to evaporate the water in the droplets of lime, resulting in drying of the droplets while absorbing the acids, leaving the spray dryer at a temperature of about 350°F. The lime has reacted with the acids, producing calcium sulfate and calcium chloride as dry products that are collected by the fabric filter. Particulate matter (flyash or dust) entering with the combustion gases is also collected. Compressed air is used to loosen the dust from the surface of the fabric so the dry particulate and lime reactants will drop to the bottom of the filter housing, where they are released through a rotary sealing valve. This product must be "conditioned" by adding water in order to make "dust free" handling possible. The presence of free lime in the collected dust

helps to reduce or eliminate the toxicity of this product by forming compounds insoluble in water, reducing their environmental hazard.

Figure 32 shows the present technology of Babcock and Wilcox – a RDF-fired stoker boiler with dry scrubber and fabric filter. The economizer and air heater are in a downward pass, and the gases enter the acid gas scrubber tangentially, leaving at the bottom as they enter the baghouse before the induced draft (I.D.) fan discharging to the stack.

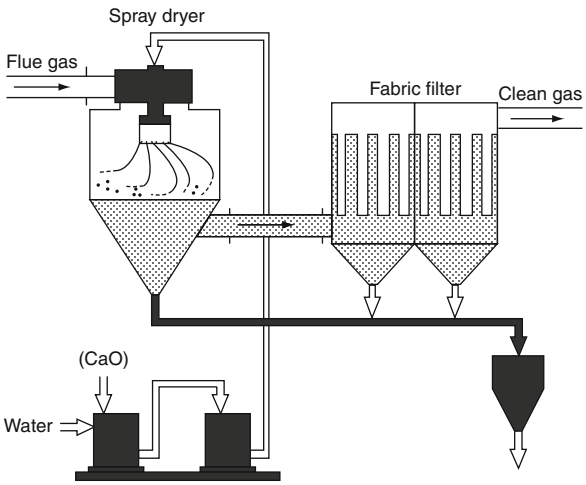

Waste-to-Energy using Refuse-Derived Fuel. Figure 31
Spray-dry acid gas absorber tower

Comparing Emissions of RDF Systems with those of Mass-Burn Facilities

The final emissions that exit the stack are a direct result of the operational efficiencies of the project and the air quality control equipment in place. All waste combustion facilities can operate in compliance with permit limits by employing advanced control technology and operating efficiently.

A major difference related to air quality control equipment in a processed-fuel facility and a mass-burn incineration system is the amount of air and gases that are generated and therefore need to be cleaned.

A Mass-Burn incinerator requires significantly more air to combust the waste in the boiler. This air then must pass through the air quality control equipment. It has a larger air volume hence requires larger

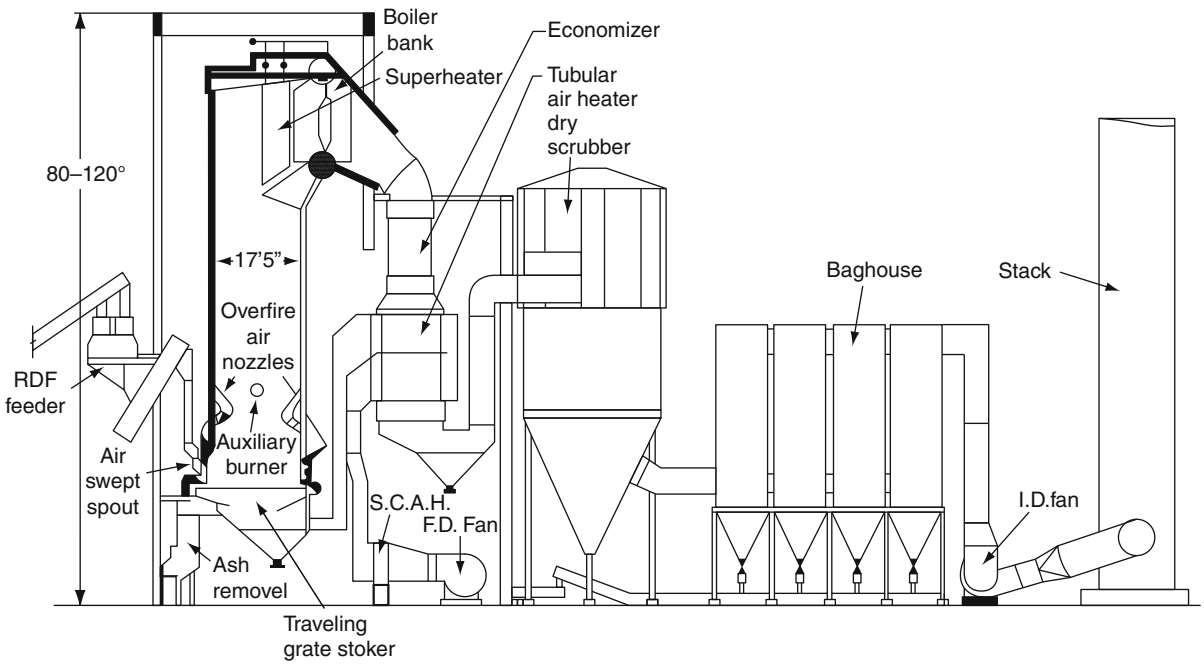

Waste-to-Energy using Refuse-Derived Fuel. Figure 32
Babcock and Wilcox RDF-fired stoker boiler with dry scrubber and fabric filter [13]

equipment with greater cost. Considering that the air quality control equipment is one of the largest expenses related to either technology, this can be a significant consideration in the technology choice.

Table 2 compares air emissions data from RDF and Mass-Burn combustion facilities. The RDF facilities show generally lower emissions of nitrogen oxides (NO_x) than do the typical mass-burn facilities, probably the result of more effective control of secondary air resulting in lower peak combustion temperatures. Carbon monoxide readings of the RDF facilities are higher, but this does not mean that trace organic emissions are high, as indicated by the extremely low PCDD/PCDF (dioxin) emissions measured. These were well below the European Union standard for dioxins. The mass-burn facilities as well as the RDF facilities today routinely employ activated carbon injection before the fabric filter to remove mercury, resulting in removing the dioxins before the gases leave the stack.

Table 3 shows the air quality test results for Boiler #3 at the SEMASS Resource Recovery Facility which has a scrubber and baghouse. The SEMASS current permit limits and MACT standards are provided for comparison.

In all tests, actual emissions were far below SEMASS permit limits, and the current MACT standards. . Note that these are the standards set forth in 40 CFR Part 60, Subpart Eb for new RDF-fired Municipal Waste Combustors. All emission standards and test results are corrected to 7% O_2, dry basis, and standard conditions (68°F and 1 atm).

Properties of Municipal Waste and Processed Refuse Fuel

The organic content of these fuels is "renewable" in the sense that most of it is produced from organic sources, trees, food, gas, and oil. Placing wastes in a landfill is not "renewable" but rather represents a waste of resources that could replace oil, coal, and gas in the production of energy for heating and for power production.

Energy from the sun is renewable, and sustainable. Likewise, organic material grown under the sun is renewable. Once this material is grown, it is wasteful not to use it, as distinguished from use of non-sustainable renewable fuels such as coal, oil, and gas recovered from the ground.

Waste-to-Energy using Refuse-Derived Fuel. Table 2 Comparison of air emissions from RDF and mass-burn facilities [13]

		RDF		Mass		
		MERC[a]	Mid-	Bridgeport[c]	Bristol[d]	Stanislaus[d]
	Facility	Biddeford ME	Conn[b] Hartford CT	Bridgeport CT	Bristol CT	Stanislaus Country CA
Pollutant	Units @ 12% CO_2					
NO_x	$ppmd_v$	202	190	225	280	300[e]
CO	$ppmd_v$	83	192	23	19	43
VOC	$ppmd_v$	<1	<1	<2	<2	4
SO_2	$ppmd_v$	5	4	9	13	3
HCL	$ppmd_v$	10	2	6	8	2
Particulate	gr/DSCF	0.008	0.006	0.001	0.005	0.004
PCDD/PCDF	ng/NM^3 (USEPA Toxic Eq.)	0.04	<0.03	0.015	0.09	0.06

[a][19]
[b][20]
[c][21]
[d][22]
[e]Stanislaus Country NO_x emission without thermal $DeNO_x$ system in operation

Waste-to-Energy using Refuse-Derived Fuel. Table 3 Air emission test results of SEMASS Boiler No. 3 (1994 through 2008) (©2010 Energy Answers International, Inc)

Regulated substance	SEMASS boiler no. 3 permit limits	Current MACT standards (a)	SEMASS boiler No. 3 test results				
			1994	1995	1996	1997	1998
Particulate (mg/Ncm)	21.0	15.3	3.50	1.40	0.350	0.875	3.50
Sulfur dioxide (ng/Ncm or % removal)	59 or 80%	61 or 80%	29.9	48.2	19.0	31.7	34.6
			87.4%	87.0%	Not available	89.4%	89%
Hydrogen chloride (mg/Ncm or% removal)	29 or 95%	29 or 95%	3.25	5.11	4.20	3.23	5.11
			96.2%	96.9%	99.5%	99.3	99%
Nitrogen oxides (mg/Ncm)	263	220	197	230	176	212	216
Carbon monoxide (mg/Ncm [24-h] or [97% of 10-min values])	134	134	55.5	5.0	56.6	46.1	41.9
Cadmium (μg/Ncm)	30.6	15.3	0.99	3.1	<0.084	0.29	0.326
Lead (μg/Ncm)	336	107	<18.6	<60.0	4.87	22.2	9.10
Mercury (μg/Ncm or% removal)	21.4	38.2	4.7	<6.7	2.81	2.64	2.62
	85%	85%	93.9%	Test not required	Test not required	Test not required	98.8%
Dioxins/furans (ng/Ncm [NATOTEQ] ng/Ncm [tetra-octa])	No standard	No standard	0.011	<0.015	0.00498	0.0122	0.0169
	22.9	9.9	0.586	<0.887	0.319	0.663	0.826

Regulated substance	SEMASS boiler no. 3 permit limits	Current MACT standards (a)	SEMASS boiler No. 3 test results				
			1999	2000	Jan 2001	Apr 2001	Apr 2004
Particulate (mg/Ncm)	21.0	15.3	3.15	9.27	1.15	1.19	5.9
Sulfur dioxide (ng/Ncm or% removal)	59 or 80%	61 or 80%	44.8	42.7	52.3	49.9	68
			80%	88%	78%	84.6%	85.6%
Hydrogen chloride (mg/Ncm or% removal)	29 or 95%	29 or 95%	6.96	5.22	11.5	9.85	5.69
			99%	99.3%	98.4%	98.7%	99%
Nitrogen oxides (mg/Ncm)	263	220	227	227	220	184	195

Waste-to-Energy using Refuse-Derived Fuel. Table 3 (Continued)

Regulated substance	SEMASS boiler no. 3 permit limits	Current MACT standards (a)	SEMASS boiler No. 3 test results				
			1999	2000	Jan 2001	Apr 2001	Apr 2004
Carbon monoxide (mg/Ncm [24-h] or [97% of 10-min values])	134	134	65.4	36.5	65.4	54.9	88
Cadmium (μg/Ncm)	30.6	15.3	0.634	0.520	0.34	0.28	0.72
Lead (μg/Ncm)	336	107	18.0	18.6	4.97	4.47	26.0
Mercury (μg/Ncm or% removal)	21.4	38.2	4.89	1.05	1.99	18.2	4.6
	85%	85%	94%	99%	99.0%	91.6%	96.8
Dioxins/furans (ng/Ncm [NATOTEQ] ng/Ncm [tetra-octa])	No standard	No standard	0.0864	0.013	0.0329	0.0138	0.0207
	22.9	9.9	5.27	0.910	2.53	1.00	1.29

Regulated substance	SEMASS boiler no. 3 permit limits	Current MACT standards (a)	SEMASS boiler No. 3 test results				
			Jan 2005	Nov 2005	July 2006	July 2007	Apr 2008
Particulate (mg/Ncm)	21.0	15.3	1.94	0.99	1.83	4.2	7.04
Sulfur dioxide (ng/Ncm or% removal)	59 or 80%	61 or 80%	57	52	77	16.0	29.1
			84.4%	81%	80.1%	80.1%	88.8%
Hydrogen chloride (mg/Ncm or% removal)	29 or 95%	29 or 95%	18	32	9	5.85	5.9
			97.7%	96.0%	99%	99.2%	99.1%
Nitrogen oxides (mg/Ncm)	263	220	188	235	219	135.8	161.8
Carbon monoxide (mg/Ncm [24-h] or [97% of 10-min values])	134	134	127.1	21.4	40.5	81.5	40.1
Cadmium (μg/Ncm)	30.6	15.3	0.34	0.34	0.11	0.92	1.07
Lead (μg/Ncm)	336	107	7.1	<1.91	13.6	31.1	26.8
Mercury (μg/Ncm or% removal)	21.4	38.2	1.99	4.59	0.99	1.8	3.68
	85%	85%	98.4%	97.0%	98.7%	97.8%	97.8%
Dioxins/furans (ng/Ncm [NATOTEQ] ng/Ncm [tetra-octa])	No standard	No standard	0.115	0.062	0.026	Not recorded	0.0465 EPA TEF
	22.9	9.9	7.57	5.89	2.75	3.9	2.52

The combustible content of raw MSW is about 70%. Typical noncombustibles are moisture, which may be 10% or more and ash, typically 20%. The moisture and ash-free heating value is about 9,000 Btu/lb, which can be compared with coal at about 12,000 Btu/lb, and oil having about 19,000 Btu/lb.

Table 4 shows typical constituents of MSW and their individual contributions to heating value. Multiplied by the mass percentage, the contribution of each constituent to the total heating value of the waste is obtained. The total is found to be 5,019 Btu/lb, which is fairly typical of contemporary waste, before recycling. The moisture-and-ash-free heating value is found to be 9,069 Btu/lb, which may be compared with coal, as received, at 9,000–12,000 Btu/lb. Recycling removes glass and metals, which do not contribute energy. Removing paper and plastics by recycling, to the extent practical, may actually result in a product with relatively higher heating value as fed to the boiler.

Analysis

The properties of MSW vary significantly, unlike those of fossil fuels. The properties of RDF are less variable due to processing and the inherent reduction in moisture. Table 5 shows the degree of variation of average daily values of RDF measured as it was sent from the storage bin to the boilers at the RDF plant owned by the City of Ames. Volatiles and fixed carbon amount to about 50%, with 23% moisture and 17.4% ash. The ultimate analysis was 30.9% carbon, 4.8% hydrogen, and 22.9% oxygen. The coefficient of variation, the percentage of the standard deviation to the mean, gives the best indication of property variation. Ash fusion temperatures, expressed in degrees Fahrenheit, give a useful indication of the temperatures at which the ash fuses, hence tends to form slag on the surfaces of the boilers. The Ames data indicates that fusion takes place at temperatures higher than about 1,100–1,200°F. Present-day furnaces are generally designed to cool the combustion gases to 1,000–1,400°F before the gases pass through the superheater tube passages where slagging is most likely to be a problem.

Table 6 gives a comparison of typical "reference" values of the composition and the characteristics of MSW and RDF, based on data obtained from operation of the Palm Beach RDF facility. Processing increases the heating value from 4,720 Btu/lb for MSW to 5,500 Btu/lb for RDF. Also important is the "yield" or fuel energy recovery, which is shown to be 83% for the RDF and 96% for the MSW.

Determining the Heating Value of MSW or RDF

The heating value of the MSW or RDF to be used to generate heat or power is essential to the calculation of the design and performance of the plant [1]. The heating value (HV) may be determined by (Table 7):

- Boiler as calorimeter: The boiler must be fully instrumented so that the heat liberated by the combustion, measured by steam generation, and the weights of feed and ash residues can be measured accurately, taking into account moisture added and lost. The ASME Boiler Code may be used for this determination.
- Laboratory calorimeter: The standard laboratory oxygen-bomb calorimeter can accept 1 g of milled refuse. Larger bomb calorimeters accept 2.5 g. The National Bureau of Standards (NBS) has developed a large flow calorimeter that can take 2.5 kg samples, permit heating value determinations of coarsely shredded MSW or RDF (see ASTM E-38 on Resource Recovery).
- Calculate heating value from ultimate chemical analysis. The weight component of each chemical component is multiplied by its heat of reaction and summed to obtain the total heating value.

The *higher heating value* (HHV) is the amount of heat that *would* be recovered by a boiler if the boiler condensed the water vapor in the combustion products. However, this is not generally the case, in reality, so the HHV is fictitious, although it is commonly used in the USA. Thus:

HHV = 14,447 (carbon) + 60,958 (Hydrogen–oxygen/8) + 33,980 (sulfur) + 1,040 (nitrogen), Btu/lb

The oxygen content is divided by 8 and subtracted from the hydrogen in order to take into account the portion of the hydrogen that has already reacted with oxygen and hence does not contribute heating value. It is convenient to rewrite this equation as follows:

HHV (Btu/lb) = 144.5 (%C) + 609.6 (%H) − 76.2 (%O) + 40 (%S) + 10 (%N)

Waste-to-Energy using Refuse-Derived Fuel. Table 4 Conversion of constituents to heating value by data [1, 23]

Conversion of constituents to heating value by data analysis[a]												
	As-received analysis					Products		Ultimate analysis				
Constituent	Wt%	% MC	% ASH	Btu/lb	Wt × Btu	Wt × MC	Wt × Ash	C	H	O	N	S
Newspaper	10.33	6.0	1.4	7,974	824	0.62	14.8	49.1	6.1	43.0	0.05	0.16
Brown paper	6.12	5.8	1.0	7,256	444	0.35	6.2	44.9	6.1	47.8	0	0.11
Magazine	7.48	4.1	22.5	5,254	393	0.31	168.0	32.9	5.0	38.6	0.07	0.09
Corrugated	25.68	5.2	5.1	7,043	1,809	1.34	130.0	43.7	5.7	44.9	0.09	0.21
Plastic coated	0.84	4.7	2.6	7,341	62	0.04	2.2	45.3	6.2	45.5	0.18	0.08
Waxed milk cartons	0.74	3.5	1.2	11,327	95	0.03	1.0	59.2	9.3	30.1	0.12	0.10
Paper cartons	2.27	6.1	6.5	7,258	165	0.14	41.8	44.7	6.1	41.9	0.15	0.16
Junk mail	3.03	4.6	13.1	6,088	184	0.14	40.0	37.9	5.4	42.7	0.17	0.09
Tissue paper	2.18	7.0	0.9	7,000	153	0.15	19.6	43.6	6.1	49.0	0.16	0.14
Food wastes	2.52	78.3	1.1	1,795	45	1.97	2.7	49.0	6.6	37.6	1.7	0.20
Citrus rinds	1.68	78.7	0.7	1,707	29	1.32	1.2	48.0	5.7	41.7	1.1	0.12
Cooked meats	2.52	38.7	3.1	7,623	192	0.97	7.8	59.6	9.5	24.7	1.0	0.19
Fried fats	2.52			16,466	415			73.1	12.0	14.3	0.4	0.07
Leather	0.42	7.5	21.2	7,243	30	0.03	8.9	42.0	5.3	22.8	6.0	1.0
Rubber	0.42	1.2	29.7	10,900	46	0.01	12.5	53.2	7.1	7.8	0.5	1.3
Plastics	0.84			15,910	134			78.0	9.0	13.0		
% Combustible 69.60				HHV = 5019		↓	↓	41.7	5.8	27.6	2.8	0.25
% Moisture in combustibles:						7.42		↓	↓	↓	↓	↓
% Ash in combustibles:							13.2					
HHV by ultimate analysis:			Ultimate analysis		= 79.4% =			41.7	5.8	27.6	2.8	0.25
			HHV of elements		=			145	609	−76	40	10
			HHV ×Wt.%		= 7,595.5 =			6,046	3,532	2,097	112	2.5
			HHV3(MAF)		= 7,596/(1−0.132)		= 8,751 Btu/lb					
HHV by components:			HHV1 (as received)		= 5,019/(0.696)		= 7,201 Btu/lb					
			HHV2 (dry)		= 7,201/(1−0.074)		= 7,776 Btu/lb					
			HHV3 (MAF)		= 7,201/(1−0.074−0.132)		= 9,069 Btu/lb					

Waste-to-Energy using Refuse-Derived Fuel. Table 5 Variability of daily values of characteristics of RDF - Ames Iowa [8]

Characteristic (%)	$\bar{X}$	Variability (about mean at 95% confidence coefficient) (±)	S_x standard deviation	Coefficient of variation (%)
Heating value (kv/kg)	13.050	590	1021.6	7.8
Bulk density (kg/m^3)	157	10.5	18.1	14.1
Proximate analysis (%)				
Moisture	23.0	2.4	4.2	18.3
Ash	17.4	1.8	3.2	18.3
Volatile	54.6	2.1	3.7	6.8
Fixed carbon	4.95	1.4	2.4	48.6
Ultimate analysis (%)				
Carbon	30.9	1.3	2.2	7.2
Hydrogen	4.8	0.2	0.3	6.8
Oxygen	22.9	2.3	3.9	17.1
Sulfur	0.43	0.1	0.2	44.8
Chlorine	0.24	0.06	0.11	45.1
Nitrogen	0.42	0.06	0.11	25.4
Ash analysis (%)				
SiO_2	48.19	2.3	4.1	8.4
Al_2O_3	11.75	1.3	2.3	19.5
Fe_2O_3	4.3	7.7	1.3	31.0
TiO_2	1.45	0.15	0.26	17.74
P_2O_5	0.79	0.16	0.28	34.9
CaO	12.71	0.93	1.7	12.7
MgO	2.38	0.18	0.31	13.1
Na_2O	4.37	0.35	0.60	13.7
K_2O	1.8	0.14	0.24	13.6
Ash fusion (°C)				
Reducing atomosphere				
Initial deform	1,106	72	42	3.8
Softening	1,143	31	18	1.6
Hemispherical	1,158	41	24	2.0
Fluidization	1,177	65	37	3.2
Oxidizing atmosphere				
Initial deform	1,149	41	23	2.0
Softening	1,165	50	29	2.5
Hemispherical	1,181	64	37	3.1
Fluidization	1,197	79	46	3.8

Waste-to-Energy using Refuse-Derived Fuel. Table 5 (Continued)

Characteristic (%)	$\bar{X}$	Variability (about mean at 95% confidence coefficient) (±)	S_x standard deviation	Coefficient of variation (%)
Particle size				
Geometric mean (mm)	12	1.2	1.4	13.0

Waste-to-Energy using Refuse-Derived Fuel. Table 6
Typical Reference values of Refuse [13]

	Reference	
	MSW (% by wt)	RDF (% by wt)
Component analysis		
Corrugated board	5.53	–
Newspaper	17.39	–
Magazines	3.49	–
Other paper	19.72	–
Plastics	7.34	–
Rubber, leather	1.97	–
Wood	0.84	–
Textiles	3.11	–
Yard waste	1.12	–
Food waste	3.76	–
Mixed combustibles	17.75	–
Ferrous	5.50	–
Aluminum	0.50	–
Other nonferrous	0.32	–
Glass	*11.66*	–
Total	100.00	
Ultimate analysis		
Carbon	26.65	31.00
Hydrogen	3.61	4.17
Sulfur	0.17 (Max. 0.30)	0.19 (Max. 0.36)
Nitrogen	0.46	0.49
Oxygen	19.61	22.72
Chlorine	0.55 (Max. 1.00)	0.66 (Max. 1.20)
Water	25.30	27.14

Waste-to-Energy using Refuse-Derived Fuel. Table 6 (Continued)

	Reference	
	MSW (% by wt)	RDF (% by wt)
Ash	*23.65*	*13.63*
Total	100.00	100.00
Heating value	4,720 Btu/lb (10,979 kJ/kg)	5,500 Btu/lb (12,793 kJ/kg)
Fuel value recovery (% MSW)	96	
Mass yield (% RDF/MSW)	83	

HHV (MJ/kg) = 0.336 C + 1.418 H – 0.148 O + 0.094 S + 0.059 N

As-Received, Dry and Moisture and Ash-Free Heating Values

- As-received heating value:
  HHV1 = HHV3 × (1 − (ash fraction) – (moisture fraction))
- Dry heating value: HHV2 = HHV3 × (1 − (ash fraction))
- Moisture and ash-free heating value:
  HHV3 = (HHV1/(1 − AF-MF) = HHV2/(1 −AF)

Air Required for Combustion

The air required for complete combustion of the combustible components of MSW or RDF can be calculated from the chemical equations, heat release and atomic weights of the components, expressed in pounds of air per million Btu of heat released by dividing by the HHV, as follows:

Theoretical air (TA) = {138.17 (C/12 + H/4 − 0.32 + S/32 + N/28) × $10E^6$}/HHV, lb/million Btu

Waste-to-Energy using Refuse-Derived Fuel. Table 7 Calculation of air required for combustion of RDF [1]

Component	% Wt	×	Heat release	=	HHV	% Wt	×	Factor	AIR
Carbon	26	×	144.47	=	3,756.22	26	×	11.51	299.26
Hydrogen	3.8	×	609.58	=	2,316.40	3.8	×	34.5	131.1
Oxygen	21.21	×	−76.2	=	–	21.21	×	−4.31	−91.63
Sulfur	0.18	×	39.82	=	7.17	0.18	×	4.32	9.78
Nitrogen	0.53	×	10.5	=	5.57				
Chlorine	0.18								
Nitrogen	0.4								
Moisture	26.54								
Ash	21.7								
Totals:	100	HHV = 4,469.15 Btu/lb							348.51

This form may be more convenient to use:

Theoretical air (TA) = {[11.51 (%C) + 34.5 (%H) − 4.32 (%O) + 4.3 (%S)] × 10^6}/HHV

It is convenient to use a tabular form to make these calculations, as follows, using typical values for weight percentages.

The value of theoretical air per unit of heat released by combustion, determined in this manner from chemical analysis of samples of MSW and RDF, appears to be independent of the nature of the waste, hence may be used with confidence in estimates of combustion air requirements.

Theoretical air (TA) = {348.5 × 10^4}/4,469.15 = 760 lb air per million Btu

Lower Heating Value. While the HHV is commonly used in the US, in other countries the lower heating value (LHV) is used. It can be calculated from the higher heating value (HHV) by subtracting the latent heat of evaporation of the water in the products of combustion. This water includes the water content of the fuel and the water produced by the combustion of hydrogen:

LHV = 144.5 (%C) + 609 (%H) – 76 (%O) + 40 (%S) + 10 (%N) − 10.5 (%H_2O)

The water produced by the combustion of hydrogen is nine times the weight of hydrogen in the fuel [(16 + 2)/2 = 9]. The hydrogen in the fuel is known from the ultimate analysis. For refuse fuels, the hydrogen is about 7.5% of the combustible matter. The latent heat at atmospheric pressure is 1,040 Btu/lb.

Loss of heating value due to not condensing water vapor = 7.5 × 9 × 10.50 = 712 Btu/lb combustible.

Power Production from Refuse Fuel

The energy yield of the Processed Refuse Fuel (PRF) process employed at the SEMASS Resource Recovery Facility would be expected to be higher, closer to the mass-burn yield. The simpler SEMASS process, with minimal processing, has only one stage of shredding and therefore uses less electric power and is simpler to operate and maintain. The SEMASS process has a higher overall plant efficiency than one burning more highly processed refuse, since some combustible material is lost due to the additional processing. RDF plants may be expected to have a higher thermal efficiency since the moisture content of the fuel is greatly reduced below that as received from the refuse trucks. The power used for shredding directly reduces the moisture content, hence is not wasted.

Other factors, such as the amount of excess air required and the steam pressures and temperatures at which the boiler generates the steam, make it difficult to compare the two approaches to processing municipal waste. The kilowatt-hours produced per ton of waste taken into the plant is the most telling ratio

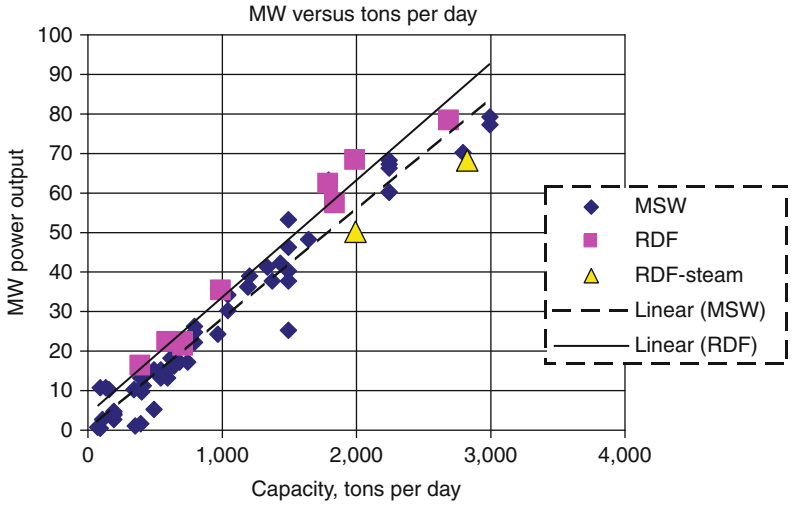

Waste-to-Energy using Refuse-Derived Fuel. Figure 33
Power produced per ton of waste (MW/TPD)

used in evaluating overall performance. This ratio varies throughout the year, since it depends on the heating value of the waste. A comparison between RDF and MSW facilities has been made using the design rating, nominal tons per day, at standard reference values of heating value, listed in Table 6. This is shown graphically in Fig. 33.

Future Directions

The technology for processing MSW and commercial waste to recover materials and generate energy has evolved since the 1970s and, 40 years later, is positioned to help achieve national and international goals of greenhouse-gas reduction and renewable energy generation. Concerns related to off-shore drilling, coal mining, foreign oil sources, nuclear waste disposal, and environmental contamination from landfills have forced a rethinking of waste as a viable fuel source.

One ton of fuel created from waste can produce the same amount of energy as 1 t of coal or a barrel of oil. "Replacing just 10% of the coal used to generate electricity in the United States in 2007 with RDF would create a potential demand for 225 million tons of RDF – significantly more than might be available if all the waste currently destined for landfills were diverted for RDF processing" [23].

Bibliography

Primary Literature

1. Hasselriis F (1984) Refuse-derived fuel processing. Butterworth Publishers, Boston (available from author)
2. Sutin GL (2004) The evolution of processed refuse fuel technology. Energy Answers Corporation, Albany, New York
3. Sutin GL (1998) Suspension firing – the heart of an integrated waste-to-energy system. Energy Answers Corporation, Albany
4. Rochford RS, Witkowski WJ (1978) Considerations in the design of shredded municipal refuse burning and heat recovery system. In: Proceedings of the 8th National Waste Processing Conference, Chicago, ASME, New York
5. France HA (1986) Hamilton SWARU retrofit. In: 1986 National Waste Processing Conference, ASME, Denver
6. Fiscus DE et al (1977) St. Louis demonstration final report. EPA-600/2-77-155a, MERL/ORD/U.S. EPA, Cincinnati
7. Gorman PG et al (1977) St. Louis Demonstration final report: power plant equipment, facilities, and environmental evaluations. U.S. Environmental Protection Agency Report EPA-600/2-77-1556
8. Hasselriis F (1983) Thermal systems for conversion of municipal waste, Vol. 4, Burning refuse-derived fuel in boilers. A Technology Status Report. ANL/CNSV-TM-120, Argonne National Laboratory
9. Fiscus DE et al (1983) Study of existing RDF-cofiring experience. Appendixes to Phase I Final Report, ANL/CNSV-TM-134, vol 2, Argonne National Laboratory

10. Hasselriis F (1980) The greater Bridgeport, Connecticut waste-to-power system. In: Proceedings of the 1980 National Waste Processing Conference, Paper Number WSS/CI 81-6
11. Energy Recovery Council. http://www.energyrecoverycouncil.org
12. Michaels T (2007) The 2007 IWSA directory of waste-to-energy plants: Integrated Waste Services Association, 31 p. http://www.wte.org/docs/IWSA_2007_Directory.pdf
13. Di Maria F, Pavesi G (2006) RDF to energy plant. . .energetic and economical analysis. Appl Therm Eng 26:1291–1300
14. Murphy ML (1999) Design and performance requirements for a fluidized bed boiler firing municipal refuse derived fuel in Ravenna, Italy. In: Proceedings of the 15th International Fluidized Bed Combustion Conference, Savannah, 16–19 May 1999, Paper FBC99-0128, epi2@energyproducts.com
15. Pope K (1998) Difficult fuels and stringent emissions requirements influence combustion technology preference in Europe, Energy Products of Idaho, epi2@energyproducts.com
16. Abrams RF et al (2010) 2,400 tons per day refuse-derived fuel facility with advanced boiler and air pollution control systems. In: Proceedings of the 18th Annual North American Waste-to-Energy Conference, Orlando, Florida
17. Abrams RF, Faia R (2009) RSCR system to reduce NO_x emissions from boilers. In: Proceedings of the 17th North American Waste-to-Energy Conference, Chantilly, Virginia
18. Ferraro FA et al (1988) Results of emissions and ash testing at the maine energy recovery WTE plant. WTI Energy, Inc., Biddeford, Maine
19. Bresowar GE et al (1988) Operating experience with a spray dry scrubbing system on a RDF-Fired boiler. Combustion Engineering, Inc.
20. Entropy Environmentalists Inc. (1988) Bridgeport Resco, Co., LP resource recovery facility compliance test report. Wheelabrator Environmental Systems, Inc.
21. J. L. Hahn, H. P. Von Dem Fange, D. Sofaer, Ogden Projects, Inc., "Recent Air Emissions Data from Ogden Martin Systems, Inc. Resource Recovery Facilities, Which Became Operational During 1988," June 1989, covantaenergy.com
22. Kaiser E (1966) Chemical analysis of refuse components. In: Proceedings of the 1966 National Incinerator Conference, American Society of Mechanical Engineers, New York
23. Gershman HW (2010) Fuel for the fire: a renewable energy push could spark demand for refuse-derived-fuel. Waste Age, March 2010
24. Mahoney PF, Zakaria J (1993) Basic design and operation information of the semass resource recovery facility. In: RDF Technology Seminar, Williamsburg, 29 Mar 1993

Books and Reviews

Beyond Sustainable: The Efficient Extraction of Energy & Marketable Products from Waste Materials. Keynote address – Waste Management & Recycling Congress, Berlin, Germany, October 2008

Bobman M, Culbertson J (2010) Waste composition in the Northeast U.S. – implications for resource recovery. In: Proceedings of the 18th Annual North American Waste-to-Energy Conference, NAWTEC, Orlando

Consonni S, Giuliano M, Grosso M (2005) Alternate strategies for energy recovery from municipal solid waste. In: WTERT 2005, Columbia University

Eco-Industrial Parks as a Vehicle for Converting Liability to Productive Redevelopment. 18th AHC Group Corporate Affiliates Workshop, Saratoga Springs, NY, June 2008

Efficient Recovery of Materials and Energy from Residual Waste. R'07 World Congress, Davos, Switzerland, September 2007

Energy Answers International (2010) Fairfield renewable energy plant and resource recovery project. Energy Answers International, EnergyAnswersInternational.com

Gershman HW (2010) Fuel for the fire: a renewable energy push could spark demand for refuse-derived-fuel. Waste Age, March 2010

Hasselriis F (1999) Practical design of waste incineration (Chapter 2.3) and Calculations for permitting and compliance (Chapter 2.4). In: Lee CC (ed) McGraw-Hill handbook of environmental calculations, ISBN 0-07-038183-6

Hollander H, Kieffer JK, Eller V, Stephenson JW (1980) A comprehensive municipal waste characterization program. In: Proceedings of the 1980 National Waste Processing Conference, ASME, New York

Lisiecki HG (1978) RDF storage and retrieval problems, cause-effect options. In: Proceedings of the National Waste Processing Conference, Chicago, ASME, New York

Mahoney PF (1980) ANSWERS: a comprehensive solution to the economic, technical and institutional problems of solid waste reuse. In: 8th Annual Industrial Pollution Conference, Houston

Mahoney PF, Mullen J (1988) Approaching total recovery in municipal solid waste to energy systems. In: 23rd Inter-Society Energy Conversion Engineering Conference, Denver

Murphy ML (2002) Advancing waste to energy technology design and performance of EPI fluidized bed RDF-fired power plants worldwide. In: 10th North American Waste to Energy Conference, ASME, Philadelphia, NAWTEC10-1011, epi2@energyproducts.com.

Nollet AR, Greeley RH (1982) New concepts for explosion alleviation in shred-first solid waste plants. In: Proceedings of the National Waste Processing Conference, ASME, New York

Providing Market Competitive Sustainable Solutions Drive the Bottom Line. AHC Corporate Affiliates Benchmarking Workshop, Phoenix, AZ, February 2007

Resource Recovery vs. Waste to Energy. Confederation of European Waste-to-Energy Plants Congress, Vienna, Austria, May 2006

Solid Waste as an Economic Generator for Sustainable Development. AHC Group 9th Annual Affiliate Program, Saratoga Springs, NY, June 2001

Tchobanoglous G, Kreith F (eds) (2002) Handbook of solid waste management. McGraw-Hill, New York

Waste-to-Energy, Introduction

Nickolas J. Themelis
Earth Engineering Center, Columbia University, New York, NY, USA

Article Outline

Municipal Solid Wastes (MSW)
Composition and Heating Value of MSW
Chlorine Concentration in MSW
Waste Reduction
Collection and Processing or Disposal of MSW
Recycling
Composting
Dealing with Mixed MSW and Post-recycling Residues
Energy Recovery from Wastes (Waste-to-Energy or WTE)
Landfilling
The Hierarchy of Waste Management
Greenhouse Gas Effects of Waste Management
Thermal Treatment Technologies
Grate Combustion of "As-Received" MSW
Combustion of Refuse-Derived Fuel (RDF)
Emerging WTE Technologies
Beneficial Use of WTE Ash
Need for Government Support
Bibliography

When I was asked by the Editor of the Encyclopedia of Sustainability Science and Technology, to put together a section on the role of waste-to-energy, I agreed to do it because the subject of resource recovery from the discards of society is an essential part of what the United Nations has defined as "sustainable development." Prior to the second half of the twentieth century, the consumption of materials and energy by humanity was a small fraction of what it is today. An example of the rapid growth in consumption is the use of copper, a metal that has been known since the beginning of history: A 1995 study by the author showed that more copper was consumed between 1945 and 1995 than in the preceding six millennia (Fig. 1).

Technology has made possible this rapid economic development and, also, the accompanying degradation of the global environment and the loss of innumerable species. However, in many cases technology has also helped immeasurably in mitigating or slowing down the adverse effects of economic development. On the basis of my studies and those of my graduate students in the past 15 years, I am convinced that waste-to-energy technology is definitely one of those bright spots where technology and ecology are not adversaries.

As noted in the excellent essay by William Ophuls "Plato's Revenge" (MIT Press 2011), there are similarities between the present age and that of the conquistadores: Scientists and engineers invent ways for producing the goods and arms that merchants and soldiers use to dominate markets and nations.

A very clear case of what can be called ecological imperialism is the massive transformation of greenfields to landfills. In the past, landfills were located in, or near, urban centers so there was a good reason for cities to manage their wastes and try to conserve land. In recent times, some cities, such as New York, have run out of landfill space and transport their wastes hundreds of kilometers away to mega-landfills. This is made possible by waste transfer stations, diesel trucks, and other technological equipment and, also, by the fact that cities are generally more affluent than the communities where the mega-landfills are created.

Fortunately, in the last 50 years, engineers have developed an alternative to landfills: waste-to-energy power plants that can be built within or near cities and transform the non-recycled residues of society to electricity, heat, and metals. Closing the materials loop in this way is a good example of industrial ecology using technology that mimics the age-long ecological cycle.

In developing the waste-to-energy (WTE) section of this Encyclopedia, the editor invited specified contributions from some of the most knowledgeable and prominent scientists and engineers in the area of integrated waste management.

– The essay by Johannes Martin and Ralf Koralewska of Martin GmbH (Germany) (► Martin Waste-to-Energy Technology) describes one of the oldest and constantly developing WTE technologies that is used in hundreds of plants in Europe, Asia, and North America.

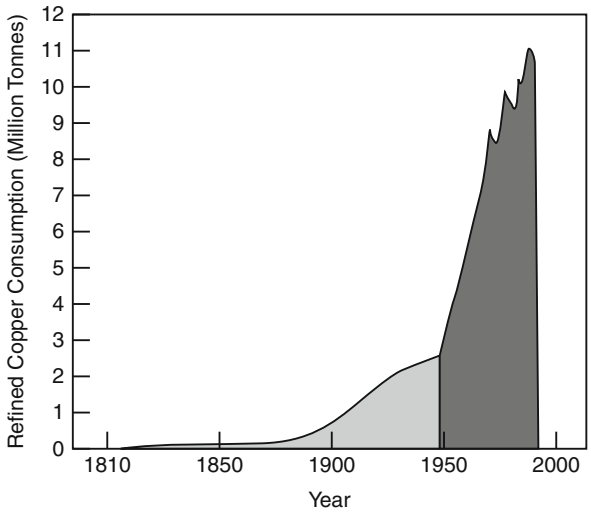

Waste-to-Energy, Introduction. Figure 1
Copper consumption in the twentieth century

- Craig Kedrowski and Peter Chromec of AE&E Inc. (USA) discuss the VonRoll grate combustion technology that is also used extensively throughout the world (▶ Hitachi Zosen Inova Technology). Both of the above technologies are based on the combustion of as-received municipal solid wastes (MSW) on a moving grate.
- Pat Mahoney of International EnergyAnswers Corp. (USA) and Floyd Hasselriis of Hasselriis Associates (USA) describe technologies that process the MSW mechanically before it is fed to the combustion chamber (▶ Waste-to-Energy using Refuse-Derived Fuel). Such technologies are called refuse-derived fuel (RDF) processes.
- The third largest waste-to-energy technology is fluidized bed combustion, discussed by Franz P. Neubacher (▶ Waste-to-Energy: Fluidized Bed Technology), author of the book Waste-to-Energy in Austria.
- Processes developed in Japan for converting MSW to gaseous or liquid fuels are the subject of the essay by Kunio Yoshikawa of the Tokyo Institute of Technology (▶ Gasification and Liquefaction Alternatives to Incineration in Japan).
- The description of various WTE technologies is completed by the essay of Nickolas Themelis of Columbia University and Armelle Vardelle of the University of Limoges that discusses thermal plasma-assisted WTE processes (▶ Plasma-Assisted Waste-to-Energy Processes).
- The transport and reaction phenomena in the combustion chamber are dealt with by J. Swithenbank and V.N. Sharifi of Shefield University (UK), the most prominent experimental group on WTE (▶ Incinerator Grate Combustion Phenomena).
- The very important role of WTE facilities as power generators is treated by M.A.J. (Marcel) van Berlo of the Free University of Amsterdam and co-developer of the highly efficient WTE plant of AEB Amsterdam (NL) (▶ Waste-to-Energy Facilities as Power Plants).
- Increasing the thermal efficiency of WTE facilities by using the "waste" stream for district heating (▶ Waste-to-Energy for District Heating), as practiced extensively in Denmark and some other nations in northern Europe, is discussed by Lasse Tobiasen and Bettina Kamuk of Ramboll Energy (Denmark).
- Dieter O. Reimann of the Confederation of European WTE plants reviews the material and energy balances in WTE facilities and the energy-production performance of European waste-to-energy plants (▶ Waste-to-Energy: Energy Resource in Solid Wastes).
- The beneficial use of WTE ash in Europe (WTE Ash Management in Europe) is discussed by Jurgen Vehlow of Karlsruhe Research Center (Germany) and in North America (WTE Ash Management in United States) by Floyd Hasselriis of Hasselriis Associates.
- Bernd Bilitewski and Christoph Wünsch of the Technical University of Dresden (Germany) describe the essential role of WTE in reducing greenhouse gas emissions (GHG) (▶ Greenhouse Gas Emission Reduction by Waste-to-Energy).
- The essay of Brian Bahor and Michael Van Brunt of Covanta Energy (USA) examines how integrated waste management can be part of the solution to the emerging crises of climate change and inadequate supply of renewable energy for future generations (▶ Waste Management for Sustainable Society).
- An LCA comparison of the environmental impacts of WTE to sanitary landfilling (LFGTE)

is presented in the essay by P. Ozge Kaplan, Joseph F. DeCarolis, and Morton A. Barlaz of North Carolina State University (USA), the foremost US research group on sanitary landfilling (► Life Cycle Comparison of Waste-to-Energy to Sanitary Landfill).

– Helmut Rechberger of Vienna University of Technology (Austria) shows how WTE decreases the entropy of solid wastes and increases metals recycling (► Waste-to-Energy: Decreasing the Entropy of Solid Wastes and Increasing Metal Recovery). Paul H. Brunner, also of Vienna University of Technology and winner of Columbia's 2006 WTERT Award, completes this extraordinary collection of essays, by explaining why thermal treatment of solid wastes is a key element of sustainable waste management (► Thermal Treatment of Waste: Key Element for Sustainable Waste Management).

I am grateful to all the authors for their contributions to this section. In the rest of this introductory entry, I will take the opportunity to summarize my own understanding of "sustainable waste management" and waste-to-energy, as derived from several dozens of studies and graduate theses sponsored by the Earth Engineering Center of Columbia University (EEC; www.eecny.org) and the Waste to Energy Research and Technology Council (WTERT; www.wtert.org), both headquartered at Columbia University.

Winner of Columbia/WTERT 2006 Industry Award: ASM Brescia, Italy

Municipal Solid Wastes (MSW)

Most of the solid wastes can be classified into municipal (residential and commercial), industrial, construction and demolition, and agricultural wastes. Municipal solid wastes (MSW) are the most heterogeneous since they consist of the residues of everything used by humanity: food and plant wastes, used furniture, papers, plastics, fabrics, leather, metals, glass, and other materials.

Composition and Heating Value of MSW

The composition of MSW varies somewhat from urban to rural settings and also from country to country. Table 1 shows a typical composition of MSW in a US city. The largest constituent is paper; other low-moisture organic materials are plastics, textiles, rubber, leather, and wood. These materials can be called "dry combustibles," in distinction to the "wet combustibles" of food, plants, and other wastes that may contain up to 70% water. The "noncombustible" wastes are metal, glass, and other inorganic compounds. Large items such as appliances and furniture can be broken down to recyclable metal or combustible wood and plastics. Hazardous wastes, such as paints, oils, and chemicals constitute only 0.4% of the total waste stream and are handled separately.

On the basis of the chemical composition of each material in Table 1 and the atomic weights of their chemical elements, Themelis et al. (2002) [1] showed that the chemical formula $C_6H_{10}O_4$ most closely approximated the mix of organic compounds in MSW. This formula corresponds to that of about ten organic compounds, such as adipic acid and ethylene glycol diacetate, whose heat of formation is about −960 kJ/mol (Roinen 1999). Using this value, the combustion of the $C_6H_{10}O_4$ "compound" can be represented by the chemical equation

$$C_6H_{10}O_4 + 6.5O_2 = 6CO_2 + 5H_2O$$

The above reaction is highly exothermic and at the reaction temperature of 1,000°C generates about 2.7 MJ/mol. Since the gram mol weight of $C_6H_{10}O_4$ is 0.146 kg, the "theoretical" heat of oxidation of the combustible components of MSW, that is, excluding moisture and inorganic materials, is calculated to be 18.5 MJ/kg. In the actual case where moisture and inorganic compounds are present, the average heat content of MSW in E.U. is about 10 MJ/kg. In terms

Waste-to-Energy, Introduction. Table 1 Composition of New York City MSW

Waste component	% weight
Paper (31.3%)	
Corrugated cardboard	4.7
Newspapers	9.2
All other paper	17.4
Plastics (8.8%)	
HDPE (clear and colour)	1.1
Films and bags	4.8
PET	0.5
Polypropylene, polystyrene	0.9
PVC	0.1
All other plastics	1.4
Wood	2.2
Textiles	4.7
Rubber and leather	0.2
Fines	2.3
Other combustibles	2.3
Food waste	12.7
Grass/leaves	3.4
Brush/prunings/stumps	0.7
Disposable diapers	3.4
Miscellaneous organics	7.8
Glass	5.0
Clear glass containers	2.9
All other glass	2.1
Aluminium	0.9
Ferrous metal	3.9
Hazardous waste	0.4
Bulk Items (appliances, furniture, etc)	5.0

of power generation potential, this value corresponds to 2.86 MWh of chemical energy per ton of typical MSW.

The effect of various waste materials and moisture on the heating value of MSW is illustrated in Fig. 2.

Chlorine Concentration in MSW

A troublesome element in MSW is chlorine because of its corrosive effect on boiler tubes. Table 2 shows that MSW contains much more chlorine than coal. This obliges WTE power plants to operate at lower steam temperatures and thus thermal efficiencies than coal fired plants.

The contribution of the various components of a typical US MSW to its chlorine concentration is shown in Table 3.

Waste Reduction

Economic development and prosperity are accompanied by the generation of more solid wastes per capita. The generation of wastes can be reduced to some extent by improved design of products and packaging materials, for example, by increasing intensity of service per unit mass of material used. However, the major factor is culture and lifestyle, as indicated by the fact that US citizens generate twice as much solid waste per capita, as northern Europeans and Japanese who live just as well. However, even in material-thrifty countries, there remains a large amount of solid wastes to be taken care of.

Collection and Processing or Disposal of MSW

Sustainable management of municipal solid wastes (MSW) requires that every possible effort be made to separate recyclable or compostable materials from the MSW stream. Experience has shown that it is best for these materials to be separated at the source, that is, at households, businesses, and institutions. The cost of source separation is then shared by the citizens (in terms of time and effort to sort out the recyclables) and the municipality (in terms of separate collection vehicles and processing systems).

Recycling

A 2009 study by Columbia University for Recycle America (USA) showed that it is environmentally and economically better to have a "single stream" rather than "multiple stream" collection of paper, metals, and designated plastic and glass materials. The single stream of recyclables is then collected by the municipality or a private company and brought to a Materials

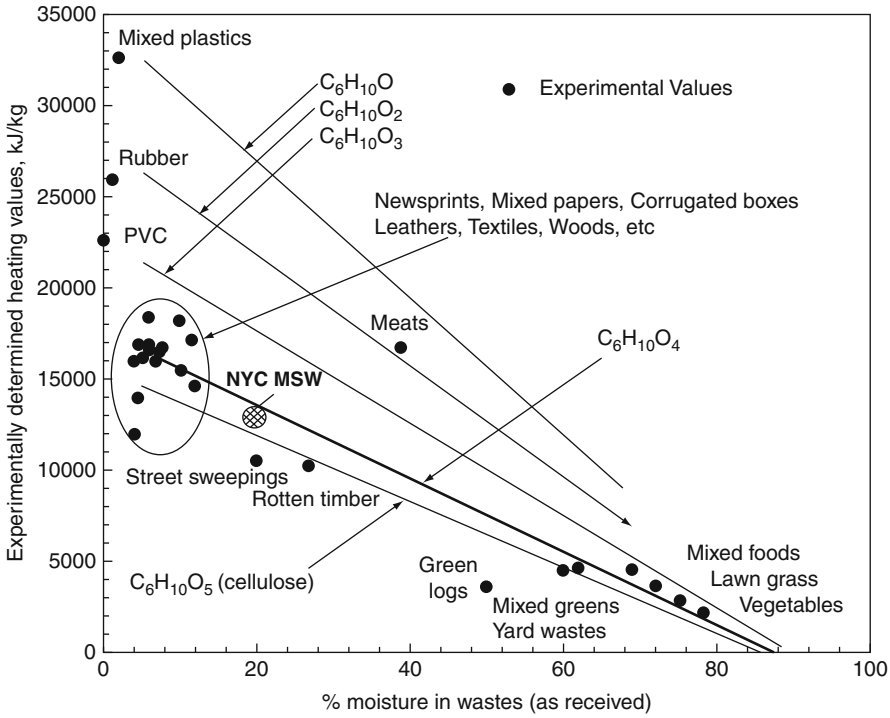

Waste-to-Energy, Introduction. Figure 2
Effect of constituents and moisture on calorific value of MSW [1]

Waste-to-Energy, Introduction. Table 2 Chlorine concentration in MSW and in coal

	New York City MSW	US typical MSW	UK typical MSW	US coals, range
Total Cl, g/kg	4.71	7.26	4.53	0.4–1
%	0.471	0.726	0.453	0.04–0.1

Recovery Facility (MRF) where it is separated to marketable streams, by means of electromechanical and manual methods.

It should be kept in mind that, unless the source-separated materials are usable, they will end up in landfills. An example of the lack of markets for certain materials is the fact that less than 10% of the plastic wastes generated in the USA are actually recycled; the corresponding figure in Germany is 20%.

The most easily recyclable materials are ferrous and nonferrous metals. The highest environmental and also economic benefit, per kilogram of material recycled, is derived from the recovery of aluminum because of the large amount of energy required to produce aluminum from bauxite ore. The largest component in MSW is mixed paper that can be re-pulped to produce wrapping paper and cardboard.

Composting

A second "stream" collected by many municipalities consists of yard or "green" wastes such as leaves, grass, tree branches, etc. Usually, these materials are brought by citizens to a collection center and are composted aerobically (i.e., in the presence of atmospheric oxygen) to carbon dioxide and a compost product that can be used as soil conditioner. Yard wastes can also be shredded and used as Alternative Daily Cover (ADC) in

Waste-to-Energy, Introduction. Table 3 Contribution of MSW components to its chlorine content

Material in MSW	Contribution to chlorine content (%)
Paper	10.1
Plastics	44.7
Organics	17.9
Textiles	9.4
Wood	5.8
Miscellaneous combustible	10.7
Glass	0.4
Metals	0.5
Miscellaneous noncombustible	0.5
Total	100.0

sanitary landfills, in place of soil. For example, nearly two million tons of yard wastes are used as ADC in California and the state considers this use to be equivalent to recycling. On the average, MSW contains 10% of yard wastes and the same or higher percentage of food wastes.

Food wastes generate undesirable odors in open windrow composting but can be composted *anaerobically* (i.e., in the absence of atmospheric air) in digesters to produce a biogas that contains about 50% of methane and, after a curing period, a compost product. However, composting of food wastes has not been successful on a large scale for two main reasons: First, it is not easy for households to collect odorous food wastes that decompose fairly rapidly in storage. Second, food wastes composted aerobically in windrows emit odors; therefore, they must be composted in closed composting systems or digested anaerobically (AD), both of which are costly to build and operate. As a result, in the USA about 50% of the yard wastes are collected and composted, while less than 5% of the generated food wastes are processed.

It should be noted that composting – both aerobic and anaerobic – is practical only for source separated organics. Otherwise, most of the compost product is not marketable as a soil conditioner and in many cases ends up in landfills.

Dealing with Mixed MSW and Post-recycling Residues

International experience has shown that there are only two ways to manage mixed MSW and the unavoidable residues from recycling and composting: (a) thermal processing, where the chemical energy of the wastes is recovered in the form of steam or syngas fuel, and (b) modern (sanitary) landfilling where some of the chemical energy in the MSW may be recovered in the form of landfill gas (LFG; 50% methane), thus reducing landfill methane emissions by 50–75%.

Energy Recovery from Wastes (Waste-to-Energy or WTE)

As stated earlier, energy is stored in chemical form in all waste materials that contain organic compounds containing carbon and hydrogen. These compounds are either of biogenic origin (e.g., paper, wood, food and plants, cotton, leather) or are anthropogenic materials created from fossil fuels, such as plastics and other petrochemicals. A carbon isotope analysis of stack gas from several WTE plants by Covanta Energy has shown that about two thirds of the carbon in the US MSW is biogenic and one third anthropogenic. The chemical energy content of metals, glass, and other inorganic materials is negligible.

The principal way of recovering the energy stored in wastes is by controlled combustion on a moving grate. The heat contained in the combustion gases is transferred to water and steam in a boiler and the superheated steam is used in a turbine generator of electricity and/or for district heating.

The chemical energy contained in MSW can also be recovered from wastes by means of partial combustion and gasification. The product of gasification is synthetic gas ("syngas"), consisting of carbon monoxide and hydrogen. It can be used as fuel in a gas engine or turbine generator of electricity or can be converted chemically to a liquid fuel (e.g., by means of the Fischer-Tropsch reaction).

Sorted plastic wastes, which have a high calorific value, can be converted into a liquid fuel by using an external source of heat, such as microwave energy. This process is called pyrolysis.

Landfilling

Landfilling is the ancient way of dealing with solid wastes and is still the principal means of waste management in most nations (Fig. 3). MSW that is not subjected to recycling, composting, or WTE, plus the residues from these processes (e.g., ash from combustion that is not used as construction material), must be disposed in properly designed and operated landfills.

Waste-to-Energy, Introduction. Figure 3
Landfill serving the island of Mauritius

A Columbia University study has shown that the urban MSW landfilled globally amounts to about one billion tons annually. Of this amount, only 200 million tons of MSW are deposited in modern landfills that try to collect some of the biogas generated.

A 2007 study by Columbia University showed that the current growth of WTE capacity, at about four million tons per year, will not be enough to curb landfill methane emissions by the year 2030 because population growth and economic development will result in a much greater rate of MSW generation and landfilling. The only way to reduce landfill greenhouse gases (GHG) between now and 2030 is by achieving a 7.5% growth in thermal treatment capacity on a global scale, or by increasing the amount of methane captured at landfills.

The Hierarchy of Waste Management

The "hierarchy of waste management" is a pyramid that illustrates the priorities that have been established in developed nations with regard to different methods for managing solid wastes. Waste reduction is placed at the top, followed by recycling and composting, waste-to-energy, and landfilling. In 2008, the Earth Engineering Center of Columbia University proposed the expanded hierarchy shown in Fig. 4 that divided

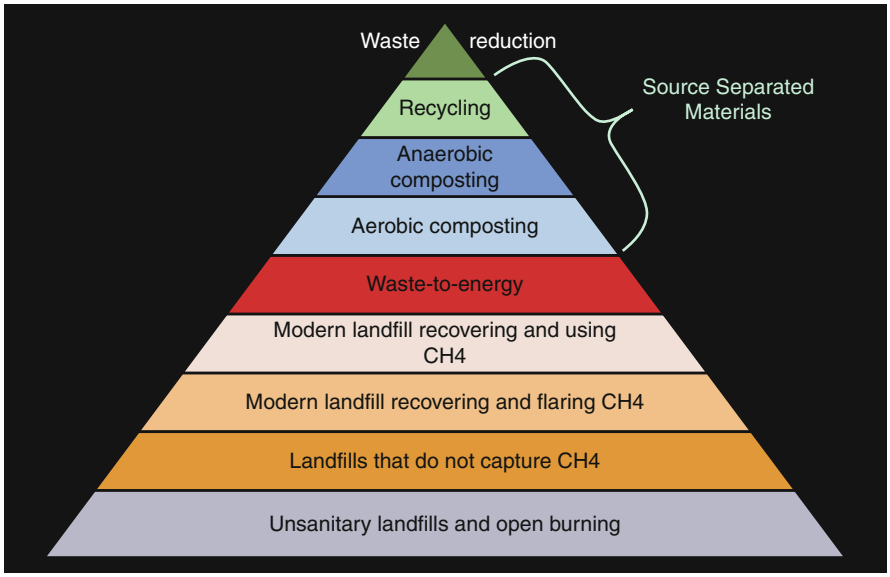

Waste-to-Energy, Introduction. Figure 4
The hierarchy of waste management

composting into anaerobic and aerobic, and landfilling into three categories: Modern landfills, also called "sanitary landfills," collect and treat their liquid effluents and also capture and use the generated biogas (about 50% methane). The next class of landfills burn their biogas in special flares to avoid the emission of methane to the atmosphere. At the very bottom of the waste management hierarchy are the age-old landfills that make no effort to collect their liquid and gas emissions and, regrettably, dot the surface of the Earth.

It should be kept in mind that, as in the case of every rule, there can be notable exceptions to the hierarchy of waste management. For example, as mentioned earlier, some yard wastes are used in California as Alternative Daily Cover (ADC) in sanitary landfills; in fact an LCA study by Columbia University (Rob van Haaren thesis) showed that the ADC use of yard wastes had a lower carbon footprint than composting, because of the avoidance of digging up and using soil as daily cover.

Greenhouse Gas Effects of Waste Management

Landfilling is presently a major anthropogenic source of methane, a gas that is considered to be the second most important of the greenhouse gases that are affecting climate change. The only two options for decreasing the emissions of methane in landfill gas (LFG), estimated presently to be 850 million tons of carbon dioxide, are accelerated growth of WTE capacity and increased LFG capture in the interim period. The global waste-to-energy capacity is about 190 million tons and at the current rate of growth of the WTE industry, about 2% annually, it cannot catch up with the projected growth of MSW generation. Therefore, it is necessary for governments to encourage WTE growth and also ensure that new and remaining landfills are constructed and operated so as to avoid contamination of ground and surface waters and maximize the capture and utilization of methane in landfill gas.

USA is the world's largest landfiller with about 225 million metric tons, followed by China with an estimated 200 million metric tons. However, the US landfilling industry and the USEPA Landfill Methane Outreach Project have made a determined effort to collect much of the landfill gas (LFG). Table 4 and Fig. 5 show the generation and capture of LFG

Waste-to-Energy, Introduction. Table 4 US and global generation and capture of LFG (in million metric tons)

	LFG methane generation	LFG methane utilization	LFG methane flaring	LFG fugitive methane	CO_2 equivalent
USA landfills	11.8	3.11	2.85	5.84	123
Global landfills	50	5	4.6	40.4	848
USA as % of global	23.6	62.2	62.0	14.5	14.5

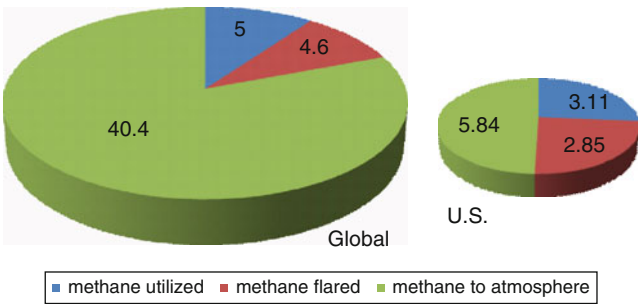

Waste-to-Energy, Introduction. Figure 5
Global and US. generation and capture of landfill methane (all numbers are in million tons per year)

(50% methane) in the USA and worldwide, as estimated by the author in a 2008 publication (GWMS).

Thermal Treatment Technologies

As stated earlier, the only proven alternative to landfilling mixed or post-recycling MSW is combustion or gasification to recover electricity, heat, syngas, and metals. Worldwide, there are over 800 thermal treatment plants, most of them in EU, Japan, and the USA.

Grate Combustion of "As-Received" MSW

In a mass burn WTE, the MSW bags and wastes are discharged from the collection vehicles into the waste bunker in a fully enclosed building. An overhead claw crane loads the solids in the charging hopper and a ram feeder at the bottom of the hopper pushes the solids on the moving grate (Fig. 6), which usually is inclined; the force of gravity and the periodic motion of the grate propel slowly the bed of wastes through the combustion chamber. The grate is 3–6 m wide, depending on the furnace capacity, and about 8–10 m long; the average residence time of solids on the grate is about 1 h.

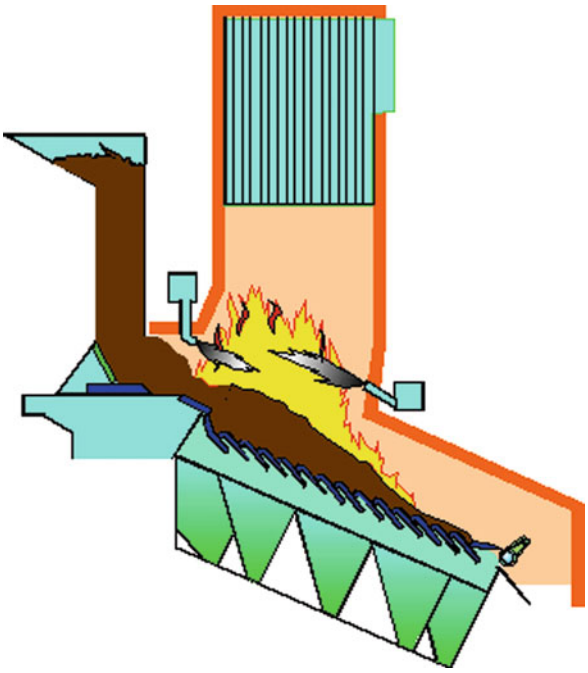

Waste-to-Energy, Introduction. Figure 6
WTE combustion chamber with inclined moving grate

As will be described in detail in other entries in the WTE section, the heat contained in the combustion gases is transferred, through the furnace water wall and superheater tubes, to the high-pressure steam that drives the turbine generator. The low-pressure steam from the generator exhaust is condensed or, preferably, used for district or industrial heating. The most efficient waste-to-energy (WTE) facilities are co-generators of electricity (>600 kWh) and district heating (>500 kWh) per ton of MSW processed. As an example, over 30% of the district heating needs of Denmark are provided by 28 WTE plants that serve this nation of five million people.

The mass burn WTE technology has the advantage of the cumulated experience of several decades and this has resulted in very high plant availability, over 8,000 h of operation per year. It is also the simplest way to thermally treat MSW because it requires little contact with the MSW and very few people to operate and maintain. A plant processing one million tons of MSW can be operated by fewer than 60 people. However, they are very costly to build.

Most WTE plants built in the last decade are of the grate combustion. A 2006 EEC survey of three dominant technologies (Martin, Von Roll, Keppel-Seghers) showed consistent growth of about three million tons of mass burn capacity per year. Other technologies, such as direct smelting (JFE, Nippon Steel), fluid bed (Ebara), and circulating fluid bed (Zhejiang University, China) have accounted for an additional estimated growth of another million tons per year.

Combustion of Refuse-Derived Fuel (RDF)

The MSW feedstock of WTE processes has a typical heating value of 10 MJ/kg. Whatever is done to decrease the MSW particle size (e.g., shredding), increase its calorific value (e.g., drying and sorting of inorganic constituents), or add auxiliary energy in the combustion chamber (e.g., oxygen enrichment or use of thermal plasmas) requires the use of electrical energy that must be justified by increased energy production per ton of MSW, or higher productivity per unit

volume of furnace and boiler that results in lower capital investment costs.

The Refuse-Derived Fuel (RDF) technology represents the simplest possible advance over grate combustion. The original RDF concept was to allow separation of marketable materials from the MSW feed before it enters the combustion chamber. Basically, this process consists of single-shredding of the MSW, sorting out some of recyclable materials, and then combusting the resulting RDF. This process is used mostly in the USA where there are 12 WTE facilities, ranging in capacity from 360 to 2,700 t per day and in total process about six million metric tons of MSW annually. A variation of the RDF process is the Mechanical Biological Treatment (MBT) process used in Europe that converts MSW to a solid recovered fuel (SRF) that can be co-combusted with coal in cement and also power plants, provided that their air pollution control systems can handle the resulting process gas.

Obviously, from a reaction engineering perspective, shredding of the highly heterogeneous MSW to a more uniform particle size and composition should be beneficial: Heat and mass transfer rates increase with smaller particle size; also, a certain degree of homogenization should facilitate combustion control in the furnace. Since the drying, volatilization, and combustion rates would be higher, the specific productivity (e.g., tons per unit volume of combustion chamber) of shredded WTE should also be higher than for a mass burn WTE. However, for wider adoption of the RDF technology, these advantages must translate into lower capital and operating costs than the grate combustion technology.

Emerging WTE Technologies

It should be stressed that while the novel WTE processes are called "gasification," they are in fact a combination of partial oxidation and gasification, followed either by combustion of the volatiles and steam generation, similarly to grate combustion, or using the syngas in an engine or turbine generator, or converting to a synthetic fuel.

As in the case of the RDF and MBT processes, gasification technologies need to demonstrate what are, or will be, the specific advantages of more complex systems over the constantly evolving grate combustion technology. It cannot be better control of emissions because, since the 1990s, all WTE plants have reduced their emissions to practically insignificant levels. It may be higher energy recovery because a gas turbine has higher thermal efficiency than the steam turbine used in grate combustion plants. There is a definite advantage of most gasification processes in vitrifying the ash residue. Also, a lower capital investment per ton of capacity than for grate combustion plants would be a definite advantage, especially for small city applications.

Beneficial Use of WTE Ash

The residues of waste-to-energy facilities are bottom ash, about 20–25% of the MSW by weight, and "fly" ash collected in the Air Pollution Control (APC) system, about 2–3% of the MSW. As the APC systems of WTE facilities have improved greatly, the captured heavy metals, dioxins, and other undesirable contaminants end up in the fly ash. At the present time, most of the US WTE facilities mix bottom and fly ash to form a "combined" ash that is chemically inert and is used for landfill maintenance and daily cover, in place of the 15-cm soil cover required by USEPA. Since the USA is the world's largest landfiller, there is a great need for use of WTE ash in landfills. However, since there are no alternative beneficial uses of WTE ash outside landfills, the WTE companies do not get much benefit from supplying it to landfills. In fact, its disposal for landfill maintenance represents a substantial operating cost.

Bottom ash does not contain dioxins and volatile metals and its chlorine and sulfur concentrations are very low. It can be used beneficially in road construction, remediation of extinct mines, and other uses, as is done in several other nations. Numerous demonstration programs, in the USA and abroad, have proven scientifically that bottom ash can be processed to generate an engineered and environmentally safe aggregate for diverse construction applications. In fact, the WTE facility of AEB Amsterdam (1.5 million tons of MSW annually) processes its ash in a novel way so that only 1% by weight of the MSW combusted has to be landfilled.

Need for Government Support

Government support for new WTEs in the USA, China, and other landfilling nations will increase the

rate of growth of WTE but, for several decades, humanity will continue to depend on landfilling. Eventually, only inorganic, non-recyclable materials will be landfilled, as is already done in several nations. However, until there is sufficient WTE capacity, there is much to be done with existing and new landfills. In particular, it is necessary for developing nations like China and India to follow the example of USA in constructing sanitary landfills that prevent liquid effluents from contaminating ground and surface waters and reduce methane and other gaseous emissions to the atmosphere.

Management of solid wastes has become as important in our times as the supply of water and the treatment of wastewater. All three are part of the Commons that is usually neglected by individuals but must be taken care by the community and the nation.

Bibliography

1. Themelis NJ, Kim YH, Brady MH (2002) Energy recovery from New York City municipal solid wastes, Waste Management & Research 20(3):223–233
2. EPA report (2011) GHG emissions of solid wastes. (http://www.epa.gov/climatechange/emissions/downloads/08_Waste.pdf)
3. Themelis NJ, Ulloa PA (2007) Methane generation in landfills. J Renew Energy 32(7):1243–1257
4. Themelis NJ, Ulloa PA (2005) Capture and utilization of landfill gas. In: Renewable energy 2005, pp 77–81. www.sovereign-publications.com/renewable-energy2005-art.htm
5. Matthews E, Themelis NJ (2007) Potential for reducing global methane emissions from landfills. In: Proceedings Sardinia 2007, 11th international waste management and landfill symposium, Cagliari, 1–5 Oct 2007, pp 2000–2030
6. USEPA, Inventory of U.S. greenhouse gas emissions and sinks: 1990–2006. (2006) www.epa.gov/climatechange/emissions/downloads/08_Waste.pdf
7. USEPA-LMOP (2010) Energy projects and candidate landfills. www.epa.gov/lmop/proj/index.htm
8. Themelis NJ (2007) Global growth of traditional and novel thermal treatment technologies. Waste Management World, Review Issue 2007–2008, pp 37–47, July–Aug 2007
9. HSC Chemistry (2011) Chemical reaction and equilibrium software. Outotec, Finland. http://www.hsc-chemistry.net/
10. Lee S-H, Castaldi M (2009) Effects of hydrogen chloride gas concentrations on corrosion rates of tube alloys under WTE environments. In: 16th annual North American waste-to-energy conference, NAWTEC 16. www.wtert.org/sofos
11. Kaufman SM, Themelis NJ (2009) Direct method to characterize and measure flows of municipal solid waste in the United States. J Air Waste Manage Assoc 59: 1386–1390

Waste-to-Energy: Energy Resource in Solid Wastes

Dieter O. Reimann
Confederation of European Waste-to-Energy Plants (CEWEP), Bamberg, Germany

Article Outline

Glossary
Definition of the Subject and Its Importance
Introduction
Recovery of Usable Energy from Waste
Potential for Increasing Energy Recovery of WTE Plants
Future Directions
Bibliography

Glossary

APC residues Residues collected in Air Pollution Control system of a plant.

Best available technology (BAT) The most effective methods for achieving a high level of protection for the environment; developed on a scale that allows implementation under technically and economically viable conditions (in the USA, called Maximum Achievable Control Technology: MACT).

BREF Reference Document on the Best Available Techniques (e.g., BREF Waste Incineration (WI) and BREF Energy Efficiency (ENE)).

Energy equivalence factors As per definition of the R1 formula, electricity produced must be multiplied by a factor of 2.6; heat produced must be multiplied by a factor of 1.1.

MSW incineration (MSWI also called waste-to-energy or WTE) a facility that includes waste storage bunker, waste feeding equipment to the furnace, boiler, flue gas cleaning system, and energy recovery system (steam turbine, etc.).

Municipal solid waste (MSW) Waste from households as well as commercial, industrial, and institutional waste that, by its nature and composition, is similar to waste from households. This includes, e.g., bulky waste, residual waste after recycling operations, RDF-refuse derived fuels mainly from

municipal waste. The categories of waste that may be treated in a WTE plant are listed in the permit by the competent authority.

Produced energy Total energy generated as electricity and heat for sale and use within the plant.

R1 energy efficiency factor Determines whether or not a WTE plant can be classified as a recovery operation, under EU legislation.

R1 formula Used to calculate the R1 factor under EU legislation.

Sankey diagram Flow diagram in which the width of the arrows is proportional to the flow quantity.

Waste incineration Thermal treatment of MSW in an environmentally sound way and recover its energy content as electricity, heat, or combined heat and power.

Definition of the Subject and Its Importance

In waste legislation and policy, the waste management hierarchy is a list of waste management methods, according to what constitutes the best overall environmental option. It consists of: prevention, reuse, recycling, composting, energy recovery, and disposal [1]. Waste incineration plants are classified either as "recovery," or as "disposal" operations. This depends on the fraction of energy recovered from that contained in the waste. It is important to note that "recovery" is defined as any operation through which wastes replace other materials that would be needed to fulfill a particular function in the plant or in the wider economy [1].

An appropriate method to assess whether or not a waste incineration plant is a recovery operation is to evaluate the energy produced and used from the waste. The European Commission has quantified this distinction by means of the R1 energy efficiency formula. A plant can only be classified as a recovery operation when its R1 factor is at least 0.60 for existing, and 0.65 for new plants. In the R1 formula this is determined using equivalence factors; a similar method is also used in Switzerland, but without using equivalence factors.

The R1 factor provides a major incentive for WTE plants to improve their energy efficiency. High R1 factors increase the contribution WTE plants make to the national energy supply, saving primary fossil fuel resources, e.g., in power or heating plants, and reducing the emission of greenhouse gases. The R1 factor also serves as a driving agent in the competition among operators of WTE plants to reach a higher ranking than other facilities.

Introduction

The three main purposes of MSWI or WTE are to reduce the volume of waste by means of thermal treatment; control effectively the emissions of this operation; and recover as much as possible of the energy content of the wastes.

Material Flow

The aim of the incineration process is to reduce the quantity of waste and produce as many recoverable materials from the residues as possible, so that only a very small part need to be deposited in a landfill. The technologies used to achieve the material flow are shown in Fig. 1 [5, 10]. They primarily depend on the type of grate or other combustion device, the composition and calorific value of the waste to be incinerated, the operating conditions in the furnace (e.g., % excess air), and the combustion temperature.

Pollutants and Emissions

One of the aims of the incineration process is to destroy organic pollutants and to separate heavy metals and inorganic pollutants that are contained in the incoming waste. By employing highly efficient flue gas cleaning technology, WTE plants can ensure that emissions into the ambient air are negligible. The data in Fig. 2 for the input and fate of pollutants in a WTE plant are from a life cycle assessment (LCA) study [2]. The destruction of organic pollutants takes place in the combustion chamber and in the first pass of the boiler, maintained at a temperature above 850°C; this is followed by adsorption of the remaining organic pollutants followed in the APC system, by means of the injection of activated carbon, or other method.

The heavy metals and other inorganic pollutants in the MSW are depending on their volatility volatilized during combustion. The higher the bed temperature, which should not exceed the melting point of bottom ash, the fewer pollutants will remain in the bottom ash. This is an important quality criterion for beneficial use of the bottom ash. The volatilized metals and inorganic

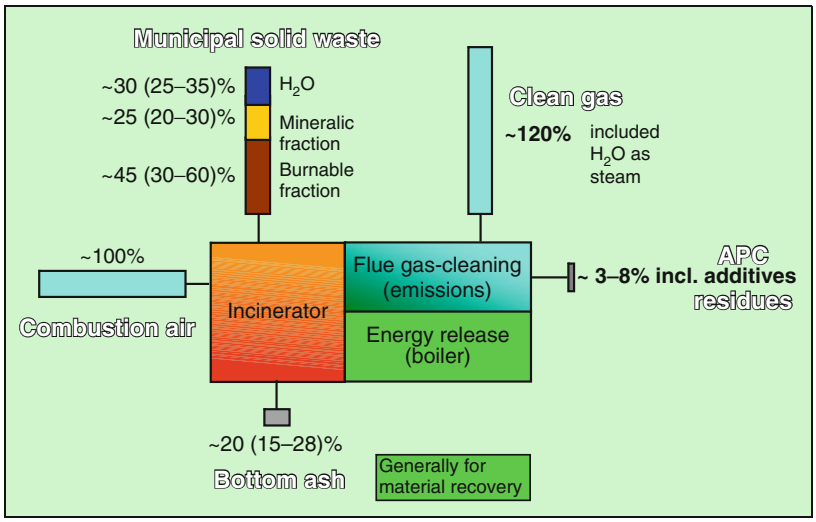

Waste-to-Energy: Energy Resource in Solid Wastes. Figure 1

MSWI: Material flow diagram showing range of MSW composition and distribution of MSW weight as flue gas, bottom ash, and APC residues

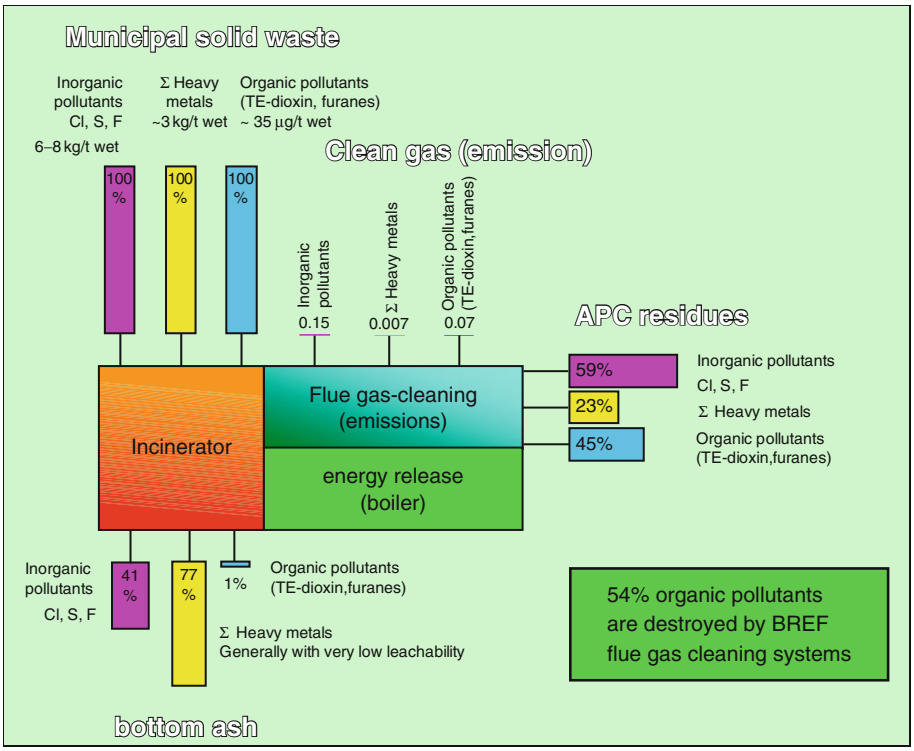

Waste-to-Energy: Energy Resource in Solid Wastes. Figure 2

MSWI: Path and percent distribution of pollutants contained in MSW processed in a WTE plant in Europe [2]

pollutants are then captured in the Air Pollution Control system, as described in detail in other chapters of this Encyclopedia. As a result, WTE plants designed and operated according to the Waste Incineration BREF [3], can meet the very stringent EU emission standards for waste incineration plants [4].

Energy from Waste

A waste incineration plant should aim to recover as much as possible of the energy available in the MSW feed. Figure 3 shows how the chemical energy stored in the waste is distributed in a WTE plant. The MSW feed into a WTE plant is a mixture of several fractions with very different calorific values, ranging from 1.6 to 4.3 MWh/t and an average value for Europe of 2.8 MWh (about 10 GJ) per ton of "as received" MSW (Fig. 3). An appropriate calculation method, based on the main data of a plant, is described in Section Net Calorific Value of MSW (NCV; Also Called Low Heating Value or LHV).

In the waste bunker, the different components of the MSW are mixed by the overhead crane, to ensure optimal combustion within the furnace and avoid the need to use auxiliary fuel, except during start-up or shutdown of a unit. The importance of the combustion control system within the furnace is discussed in detail in Waste to Energy (WTE): The AE&E Technology and The Martin WTE Technology entries of this Encyclopedia.

Projected Energy Losses of the Incineration Facility The heat loss in the bottom ash, the convection and radiation losses of furnace and boiler, and the loss associated with incomplete burnout of carbon in the ash correspond to about 3% of the energy input in the MSW feed. In the R1 formula, they are taken into account by the fixed correction factor of 0.97. This is the reason why only 97% of the heating value of MSW (plus any auxiliary heat used in the plants) is entered into the denominator of BREF WI [3].

Boiler Efficiency and Flue Gas Temperature After Boiler The temperature in the flue gas leaving the boiler affects the energy recovery by the boiler. It is independent of the heating value of the MSW and in state-of-the-art systems is in the range of 180–230°C. This range is associated with steam parameters of 40 bar/400°C and results in a mean boiler efficiency of 82% [8]; in other words, 18% of the input energy in the MSW is lost in the flue gas.

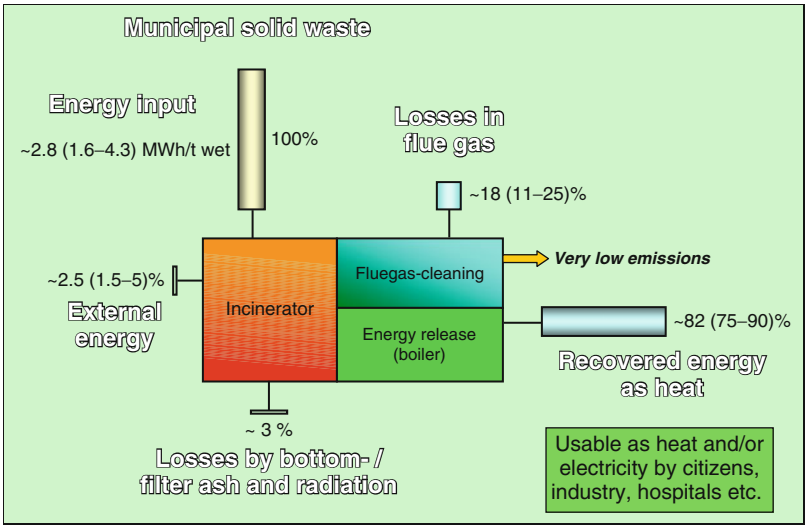

Waste-to-Energy: Energy Resource in Solid Wastes. Figure 3
MSWI: Flow diagram and distribution of energy contained in MSW processed in a WTE plant

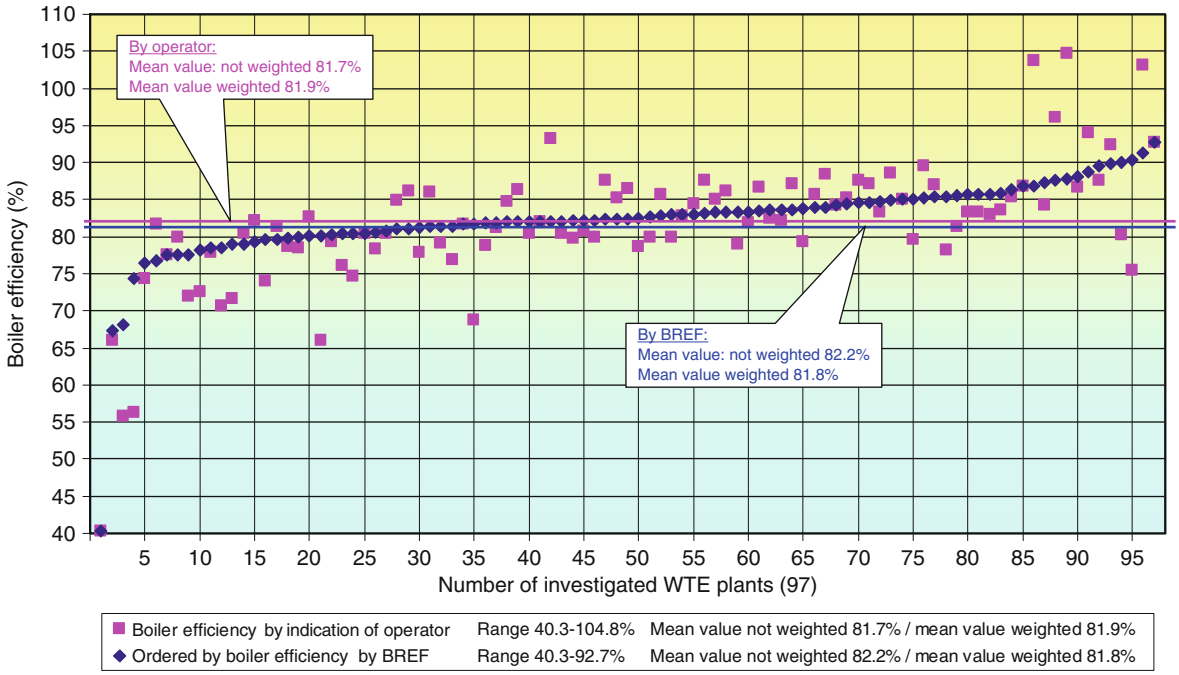

Waste-to-Energy: Energy Resource in Solid Wastes. Figure 4
Boiler efficiencies of 97 European WTE facilities (CEWEP 2006)

Figure 4 shows the calculated boiler efficiencies of 97 European WTE plants, investigated by the Confederation of European WTE Plants [8], using the formula:

% boiler efficiency = Energy contained in steam generated/0.97 (Energy contained in MSW feed + energy in any auxiliary fuel used in steam generation). The red squares show the actual data provided by the plant operators (2001–2004 data) and the blue triangles the calculated data according to the BREF WI formula.

It can be seen that many of the boiler efficiencies reported by the operators differ considerably from the BREF formula. This can be due to several factors, such as low or high estimated of heating values of MSW, inaccurate measurements of steam rates, etc.

When the steam energy is to be transformed to electricity, high steam parameters are required. In this case, relatively higher temperatures (up to 450°C) and pressures (up to 100 bar) of the steam are technically possible, but the surfaces of the boiler membrane walls, at least in the first and second pass and the superheater tubes must be protected against corrosion and abrasion, by cladding or other means.

Modern incineration plants reach boiler efficiencies over 85%. Even higher efficiencies are achievable with wastes containing low chlorine than MSW, which contains 0.4–0.6% per tonne of wet MSW.

Net Calorific Value of MSW (NCV; Also Called Low Heating Value or LHV) Many NCV (or LHV) data reported by the operators show a large deviation from the correct values of NCV. Because of this, a NCV formula has been defined by the BREF WI that in effect uses the furnace and boiler as a giant calorimeter. It is based on a simple energy balance between the energy inputs and the output of a WTE plant:

Formula 1: Formula for calculation of the net calorific value (NCV; or LHV in the USA) of MSW feed, according to BREF Waste Incineration (WI) using measured or calculated data:

$NCV = (1.133 \times (m_{st\,w}/m) \times c_{st\,x} + 0.008^{*}T_b)/1.085$, in GJ/t wet MSW
where
NCV = net (or lower) calorific value (NCV) of MSW, in GJ/t (wet)
$m_{st\,w} = m_{st\,x} - (m_f \times (c_f/c_{st\,x}) \times \eta_b)$, in t steam/t wet MSW
and
$m_{st\,w}$ = mass flow of steam produced from waste combustion, in t/year, or t/day
m_f = mass flow of steam from auxiliary fuel combustion, in t/year, or t/day
$m_{st\,x}$ = total amount of the steam produced, in t/year, or t/day
m = mass of waste combusted, in t/year, or t/day
$c_{st\,x}$ = net enthalpy of steam (i.e., minus enthalpy of boiler water), in GJ/t wet
c_f = net heating value (LHV) of auxiliary fuel used for steam production, in GJ/t
T_b = temperature of flue gas after boiler (at 4–12% O_2) − T_{input} of air, in °C
0.008 = specific sensible heat capacity of flue gas, GJ/t wet/°C
1.133 and 1.085 = constants derived from regression equations
η_b = efficiency of gas-to-steam heat transfer in the boiler (approx. 0.80)

Because the greatest part of the energy output goes to the steam exiting the boiler ($m_{st\,x}{}^{*}\ c_{st\,x}$), accurate measurement of the steam rate is very important in using the above formula to calculate the NCV (or LHV) of the waste. An example of "double counting" errors in the steam rate is steam used to preheat the combustion air. On the other hand, steam quantities that should be included in the steam rate of the plant are steam extracted ahead of the steam measuring device for heating the flue gases (e.g., before SCR, after wet scrubbers, before fabric filters) or injection of water for continuous boiler cleaning, or in the form of NH_4OH for NO_x reduction; the energy needed to evaporate these sources of water is not counted by the steam measuring device.

An example of NCV (or LHV) calculation, based on the NCV formula of BREF WI, is shown in Table 1 for a WTE plant with the annual energy flows shown in Table 1 [11, 12].

The calculations made in Table 1 show that by taking into account all relevant energy flows in this WTE plant, the calculated NCV (LHV) of the waste was 10.0 GJ/t of MSW at a boiler efficiency of 85.3%. In comparison, for a simplified NCV calculation, using only the energy of measured steam minus imported energy, the NCV would increase to 10.3 GJ/t and the boiler efficiency would decrease to 83.4%.

To get accurate and comparable NCVs of the waste combusted at WTE plants of different configurations, it is necessary to collect the complete energy flows from each plant. Figure 5 shows the results of an investigation that compared the net calorific values (NCV or LHV) of 97 European WTE plants, as calculated by the BREF WI formula (blue triangles) and reported by the plant operators (red squares; data for 2001–2004). A similar variation between these two values is observed as in Fig. 4 that compared calculated and reported boiler efficiencies.

The observed differences in calorific value among different European WTE plants may be due to several factors, including the prevailing rate of recycling, the degree of industrialization, and the economic development of the community served by a WTE. Figure 6 classifies NCV data from 231 European WTE plants into three regions: Northern, middle, and southern Europe [9].

The reason for the relatively wide range of calorific values of MSW combusted at different WTE within a region is most likely due to different fractions of high heating value wastes treated at different plants (e.g., industrial and commercial waste, nonrecyclable wrapping, and waste wood). For example, in northern Europe which is the coldest climate zone, high calorific waste is used to complement the available MSW and provide the demand for district heating and reduce the consumption of fossil fuels.

The low heating values in southern Europe are most likely due to the incineration of relatively larger quantities of food and green wastes and smaller quantities of plastics and paper.

Recovery of Usable Energy from Waste

The potential for energy recovery from WTE depends not only on the combustion technology used, but also

Waste-to-Energy: Energy Resource in Solid Wastes. Table 1 Example of calculation of NCV (or LHV) using the BREF WI formula

A	*Boiler efficiency* (1,738,100 + 15,992)/(0.97 * (210,000 * 10.038 + 12,100)) * 100 = 85.3%	η_b	85.3	%
B.1	Municipal waste incinerated	m_w	210,000	t/year
B.2	Measured steam quantity after boiler with the main measuring device	$m_{st\ x}$	630,000	t/year
B.3	Net enthalpy of steam 40 bar/400°C/130°C boiler water	c_{st} (3,214 + 544)	2,670.000	kJ/kg
B.4	Delivered steam to a third party with a second measuring device	m_w	20,000	t/year
B.5	Net enthalpy of steam 45 bar/257°C with no backflow of condensate	$c_{st} \times$ (2,800)	2,800	kJ/kg
B	*Total energy output based on measured steam quantities*	$m_{st\ x} \times c_{st\ x}$	1,738,100	GJ/year
C.1	Light fuel oil for start-ups and shutdowns	m_f steam producing	120	t/year
C.2	Light fuel oil for keeping combustion temperature >850°C	m_f steam producing	215	t/year
C.3	Sum of used light fuel oil	m_f steam producing	335	t/year
C.4	Energy input by fuel	$m_f \times c_f$ (42,73 GJ/t)	12,100	GJ/year
C	*Included in total energy output from measured stream*	$\eta_b \times m_f \times c_f$	10,321	GJ/year
D.1-1	Steam for soot blowing and for NH_4OH injection SNCR (both extracted after total steam measuring device)	$m_{st\ x}$	12,500	t/year
D.1-2	Net enthalpy of steam 40 bar/400°C/0.2 bar/220°C steam in flue gas	$C_{st} \times$ (3,214 − 2,918)	296	KJ/kg
D.1	*Energy by double measured steam quantity for soot blowing and NH_4OH injection of SNCR*	$m_{st\ x} \times C_{st\ x}$	3,700	GJ/year
D.2-1	Steam for heating up primary combustion air from 20°C to 130°C (extracted after steam measuring device)	$m_{st\ x}$	37,600	t/year
D.2-2	Net enthalpy of steam 3 bar/144°C/100°C in condensate	$C_{st\ x}$ (2,748 − 419)	2,329	kJ/kg
D.2-3	Energy input by steam	$m_{st\ x} \times C_{st}$	87,570	GJ/year
D.2	*Energy by double measured steam quantity for heating up primary combustion air from 20°C to 130°C*	$\eta_b \times m_{st\ x} \times C_{st\ x}$	74,698	GJ/year
D.3-1	Liquid quantity as water and NH_4OH injected before the total steam measuring device	m_{liquid}	4,600	t/year
D.3-2	Net enthalpy as steam 0.2 bar/220°C in flue gas	$C_{st} \times$ (2,918)	2,918	KJ/kg
D.3	*Not measured energy by injected liquids into the combustion chamber before steam measuring device*	$m_{liquid} \times C_{st\ flue\ gas}$	13,423	GJ/year

Waste-to-Energy: Energy Resource in Solid Wastes. Table 1 (Continued)

D.4-1	Steam extracted before the steam measuring device for heating up flue gas from 110°C to 120°C	$m_{st\ x}$	6,600	t/year
D.4-2	Net enthalpy of steam 45 bar/257°C/90°C condensate	$C_{st} \times (2{,}800 - 377)$	2,423	KJ/kg
D.4	*Not measured energy for heating up flue gas from 110°C to 120°C with steam out of the boiler drum*	$m_{st\ x} \times C_{st}$	15,992	GJ/year
D.5-1	Energy extracted by grate cooling before the steam measuring device for heating up the backflow of district heat		3,800	MWh/year
D.5-2	Transferred from MWh into GJ		3.6	GJ/MWh
D.5	Not measured energy from grate cooling for heating up the backflow of district heat		13,680	GJ/year
D	*Sum of double or not measured energies included in total energy output from measured steam*	$\eta_b \times m_f \times C_f$	−35,303	GJ/year
Σ (B − C + D): NCV relevant energy flows of this example			1,692,476	GJ/year
NCV determination by BREF WI formula based on the investigated, NCV relevant energy flows (η_b = 85.3%)			10.038	GJ/t MSW
NCV determination by BREF WI formula based only on the energy from the measured steam in B (η_b = 83.4%)			10.265	GJ/MSW

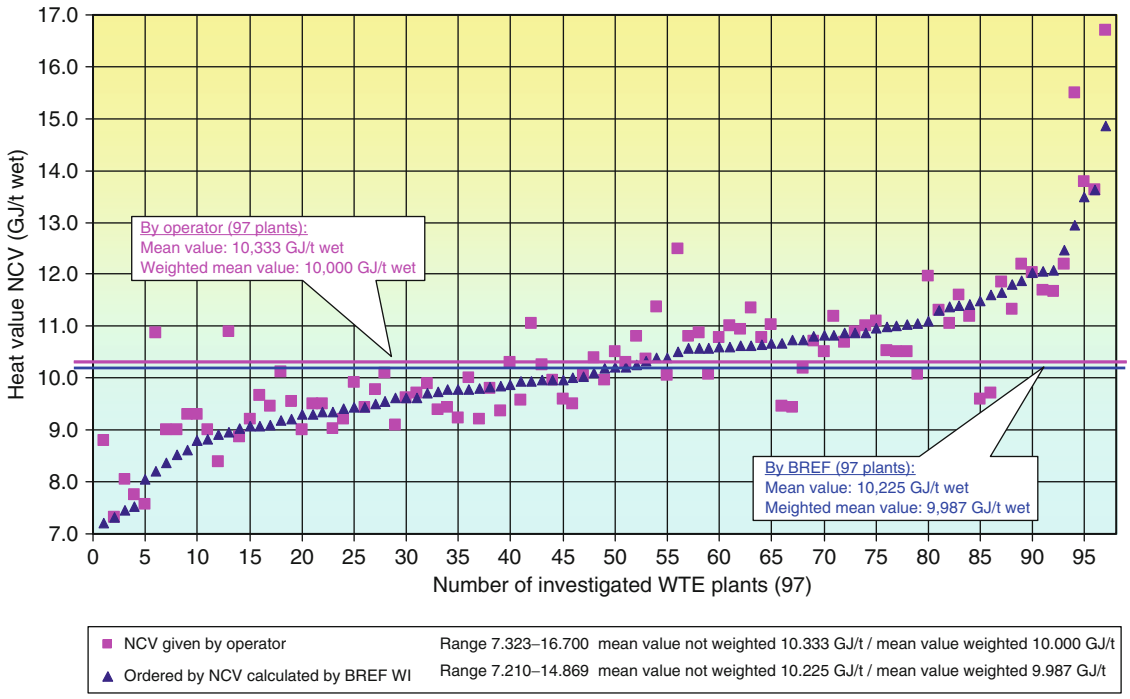

Waste-to-Energy: Energy Resource in Solid Wastes. Figure 5
Net calorific values (or LHV) of 97 European WTE plants (CEWEP 2006, 2009)

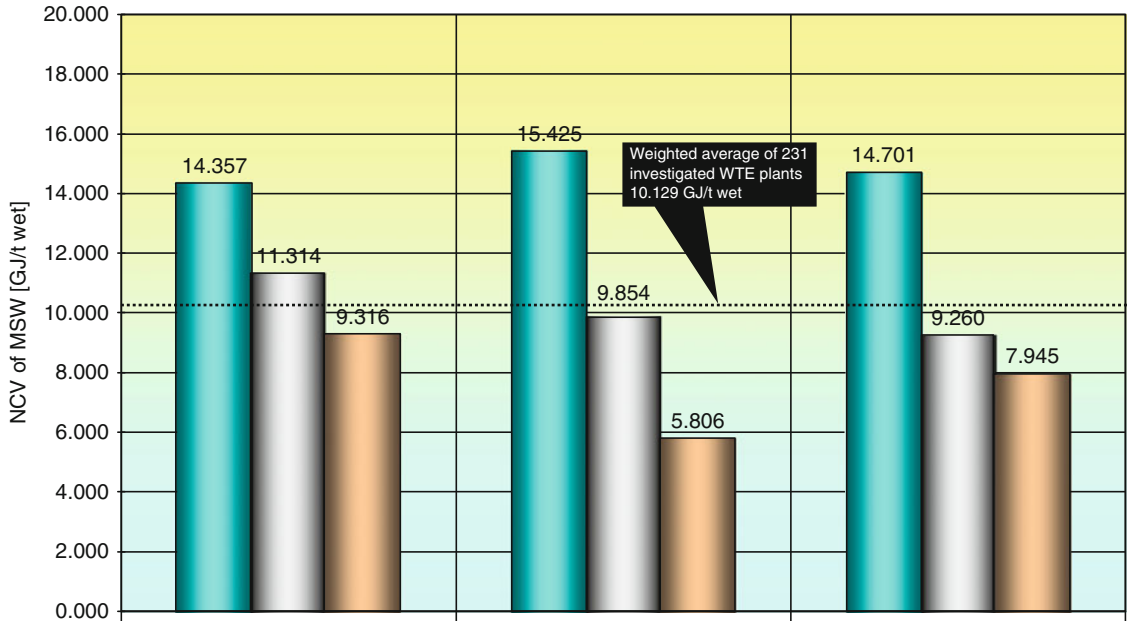

	Northern Europe (DK, FI, SE)	Middle Europe (AT, BE, CZ, FR, DE, HU, NL, GB, LU, CH)	Southern Europe (IT, PT, ES)
Max	14.357	15.425	14.701
Average weighted	11.314	9.854	9.260
Min	9.316	5.806	7.945

Waste-to-Energy: Energy Resource in Solid Wastes. Figure 6
Analysis of calorific values of MSW combusted in 231 WTE plants in Europe

on location and size of the plant, whether only electricity or heat are generated, and the incentives provided by government for the recovery of renewable energy and reduction of greenhouse emissions.

Status of Energy Recovery from Waste in Europe

Table 2 presents an overview of energy forms and average recovery rates of 231 European WTE plants, in 2004–2007. Forty-one plants produce only heat, 75 only electricity, and 115 plants both heat and power (CHP). The "specific" values denote energy recovered per ton of MSW; the percent values indicate the energy output (MWh of heat and/or electricity recovered) per MWh energy input in the MSW feed.

For WTE plants producing only heat, the energy recovery is over 70%, with a maximum of 96.8% for the most efficient plant (only hot water producing). Plants producing electricity exhibit a thermal efficiency of over 20%, with a maximum of 32.4% for the best plant. However, it should be kept in mind that electricity is a more valuable source of energy than heat; The EU BREF multiplies MWh of electricity by the factor of about 2.6; therefore, the 20% mentioned above corresponds to 52% actual thermal efficiency.

In the case of WTE plants that supply both heat and power (CHP), the thermal efficiency is over 35% for heat plus over 14% for electricity generation; the maximum value reported was 89.6% for a WTE plant recovering heat combined with 1.2% for electricity generation.

Classifying European WTE Plants as Recovery or Disposal Operations

As noted earlier, European WTE plants can be classified as recovery or disposal operations, depending

Waste-to-Energy: Energy Resource in Solid Wastes. Table 2 Generation of electricity and/or heat by 231 WTE plants in Europe (2001–2004)

Kind of energy recovery		All investigated WTE plants not classified	%	WTE plants only heat producing	%	WTE plants only electricity producing	%	WTE plants CHP producing	1.%
Number of WTE plants	[–]	231	100	41	17.7	75	32.5	115	49.8
Total throughput of MSW	t wet/ year	45,518,189	100	4,568,219	10.0	12,722,342	28.0	28,227,628	62.0
Specific energy input by MSW (without import) (NCV)	MWh abs./t wet	2.814	–	2.953	–	2.618	–	2.867	–
Total specific energy input (included import)	MWh abs./t wet	2.876	–	3.099	–	2.654	–	2.924	–
Total energy input (incl. import)	MWh abs./t wet	130,910,312	100	14,156,911	10.8	33,765,096	25.8	82,537,584	63.0
Specific electricity produced (Ep)	MWh abs./t wet	0.413	14.4	0	0.0	0.551	20.8	0.417	14.3
Specific electricity exported (Ep)	MWh abs./t wet	0.318	11.1	0	0.0	0.457	17.2	.306	10.5
Specific heat produced and used (Ep)[a]	MWh abs./t wet	0.905	32.2	2.210	71.3	0.092	3.5	1.067	36.5
Specific heat produced and used (Ep)[b]	*MWh abs./t wet*	1.202	41.8	2.486	80.2	0.399	15.0	1.356	46.4
Specific heat exported (Ep)	MWh abs./t wet	0.790	27.5	2.111	68.1	0.000	0	0.932	31.9
Specific total energy demand ((part of Ep) + Ef + Ei (th + el))[a]	MWh abs./t wet	0.272	9.5	0.245	7.9	0.222	8.4	0.303	10.4
Specific total energy demand ((part of Ep)+ Ef + Ei (th + el))[b]	*MWh abs./t wet*	0.569	19.8	0.521	16.8	0.529	19.9	0.592	20.2
Including in total specific demand as Ef	MWh abs./t wet	0.015	0.5	0.018	0.6	0.010	0.4	0.009	0.3
Including in total specfic demand as Ei(el)	MWh abs./t wet	0.019	0.7	0.101	3.3	0.004	0.2	0.017	0.6

Waste-to-Energy: Energy Resource in Solid Wastes. Table 2 (Continued)

Kind of energy recovery		All investigated WTE plants not classified	%	WTE plants only heat producing	%	WTE plants only electricity producing	%	WTE plants CHP producing	1.%
Including in total specific demand as Ei(th)	MWh abs./t wet	0.028	1.0	0.027	0.9	0.022	0.8	0.031	1.1
Including in total specific electricity produced as Ep (self-used electricity)	MWh abs./t wet	0.095	3.3	0.000	0.0	0.094	3.5	0.111	3.8
Including in total specific heat produced as Ep (self-used heat)[a]	MWh abs./t wet	0.115	4.0	0.099	3.2	0.092	3.5	0.135	4.6
Including in total specific heat produced as Ep (self-used heat)[b]	*MWh abs./t wet*	0.412	14.3	0.375	12.1	0.399	15.0	0.424	14.5

[a]In the real heat self used (demand) are, related to Sankey energy flow, beside the imported energy with 100% i.a. 18% energy self used for heating up of combustion air and all other processes with heat self demand, i.e., the steam to soot blowers, evaporation of APC residues, flue gas reheating, pipe heating, and building heating taken into account.
[b]In the heat self used (demand) related to the draft of the EU-Guidance for R1 formula, are additional to the load of "a" the total heat demand for boiler water heating up from an average temperature basis of 70°C to the individual boiler water temperature and 100% (instead of 18%) energy self used for heating up of combustion air included.

on their thermal efficiency [1]. The energy produced is calculated as the sum of energy exported plus energy used to operate the facility in a proper way, i.e., meeting at least all requirements specified by the permit of the plant.

Boundary Limits for Energy Balance

In order to calculate the energy efficiency of a plant, it is important to define the boundary limits of the plant, as illustrated in Fig. 7.

R1 Energy Efficiency Factor for the Member States of the European Union

The R1 energy efficiency factor is a nondimensional figure based on the first law of thermodynamics. Its purpose is to increase energy efficiency of WTE plants and minimize the demand of primary energy in the European Union [1]. This factor is calculated according to the following formula [6].

R1 = Energy efficiency factor = (Ep − (Ef + Ei))/(0.97 × (Ew + Ef))
where
Ep = energy produced per year as electricity or heat; electrical energy is multiplied by 2.6; heat produced for commercial use is multiplied by 1.1
Ef = energy input per year to the plant from fossil fuels
Ei = other external used per year in the plant
Ew = energy input per year to the plant from waste, on basis of its net calorific value (or LHV)
The factor 0.97 accounts for heat losses due to bottom ash and external radiation/convection

In the absence of external fossil fuels and electricity, formatting the R1 formula reduces to:

$$R1 = \text{Energy efficiency factor} = Ep/(0.97 \times Ew)$$

The equivalence factors for energy are based on savings of primary fuels in dedicated power and/or

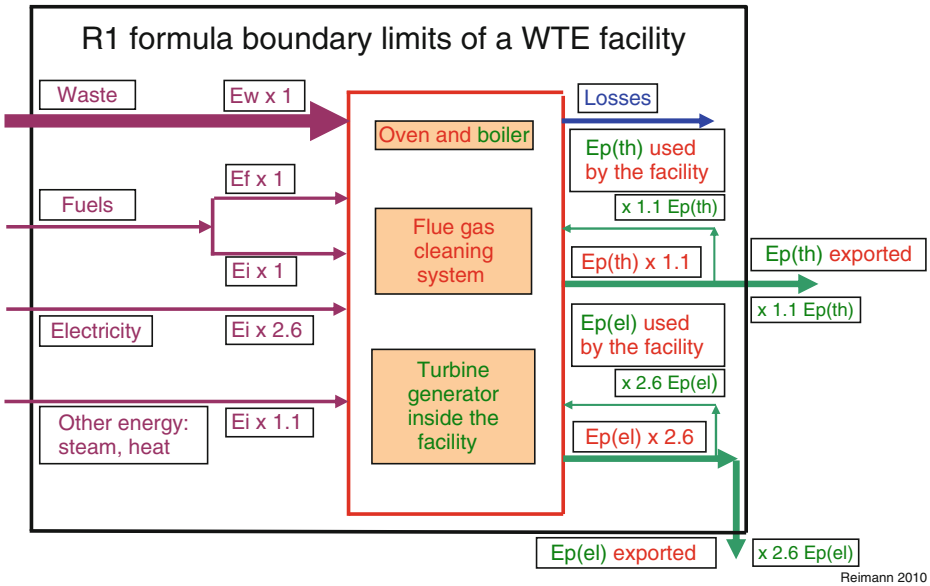

Waste-to-Energy: Energy Resource in Solid Wastes. Figure 7
Boundary limits for the determination of the energy efficiency of a plant

heat plants. In the R1 formula, electrical energy is multiplied by the equivalence factor 2.6 and heat by the factor 1.1. To reach the "recovery" status (R1), the computed R1 factor, according to the above formula, must be equal to or higher than

- 0.60 for plants in operation and permitted, in accordance with applicable EU legislation, before January 1, 2009
- 0.65 for plants permitted after December 31, 2008

Figure 8 is based on the data presented in Table 2 for 231 WTE plants in Europe. It divides these plants into three classes: Plants producing only heat, producing only electricity, and producing both heat and electricity (2003–2007 data). For each class, the maximum, average and minimum R1 factors are shown. The averages values of energy efficiency are calculated in two ways: On basis of the R1 formula and from the Sankey energy balance, as discussed earlier.

The highest R1 average based on CEWEP (0.88) was recorded for a CHP plant, producing both electricity and heat. The second highest average R1 factor was attained by a heat-generating WTE. The average R1 factor of WTE facilities generating only electricity was 0.71.

Potential for Increasing Energy Recovery of WTE Plants

Reimann [12] has suggested several ways to increase the energy efficiency of existing or new WTE facilities. For example, operators can aim to reduce excess air by optimal use of secondary air and recirculation of part of the flue gas stream. Other low cost measures are avoidance of fouling in boiler, ensuring a low flue gas temperature after boiler, reducing use of fossil fuel during start-up and shutdown, preheating the combustion air, and heating the flue gas for Selective Catalytic Reduction (SCR) by self produced steam instead of fossil fuels.

More costly measures recommended are frequent cleaning of heat exchanger tubes, providing for cooling of condenser by water sprinkling during high temperature excursions, increasing the boiler water temperature, use of a multistage turbine with reheating and dewatering of extracted steam in between the stages, and using boilers with higher steam parameters.

By far, the most effective means to increase the WTE thermal efficiency is by using the low-pressure steam for district heating or for providing heat to

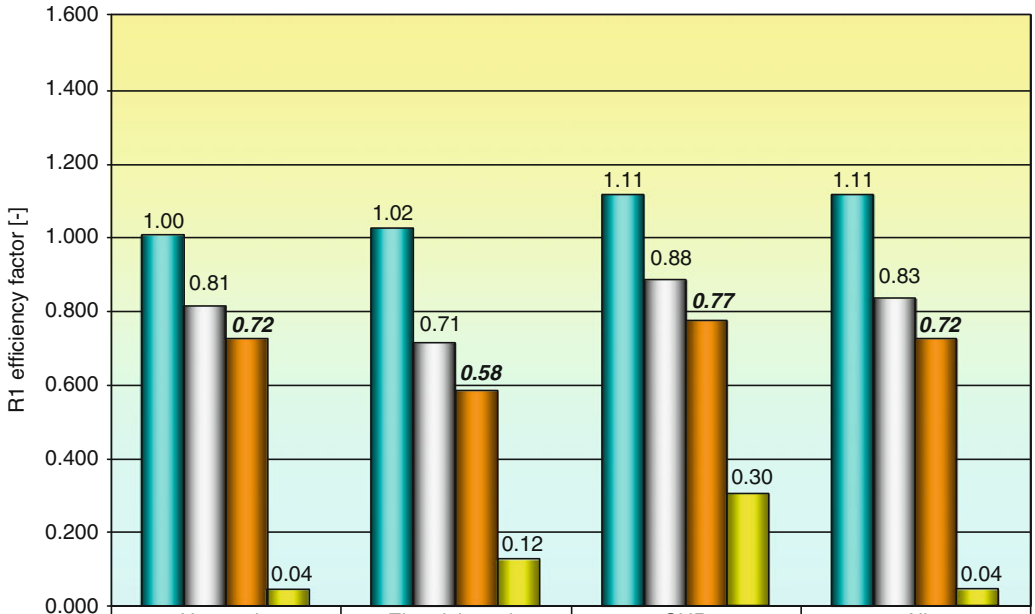

	Heat only	Electricity only	CHP	All
R1 max.	1.00	1.02	1.11	1.11
R1 average (CEWEP)	0.81	0.71	0.88	0.83
R1 average (EU guidance)	0.72	0.58	0.77	0.72
R1 min.	0.04	0.12	0.30	0.04

[1)]R1 calculation in accordance to Directive 2008/98/EC (WFD) 20/10/2008, ANNEX II, with equivalence factors: for electricity self produced and imported 1 MWh el=2.6 MWh el equ; for heat commercial used 1 MWh th=1.1 MWh th equ and according to BREF WI for imported fuel 1 MWh fuel=1.0 MWh fuel equ. Self used heat in Ep as described under [2)] in Table 2.

Waste-to-Energy: Energy Resource in Solid Wastes. Figure 8
Analysis of R1 energy efficiency factors of 231 WTE plants in Europe [9]

nearby industrial plants as base load, e.g., a paper recycling plant that requires a lot of heat. Of course, such measures are more applicable to new WTE plants and depend on the presence of customers for heat and the length of the heating or cooling period at a certain location.

Future Directions

Every WTE plant should strive not only to reach the R1 standard required for classification as a recovery plant but to exceed it. Higher recovery rates have several environmental and economic benefits, including the conservation of nonrenewable fuels and the reduction of greenhouse gas emissions with their climate change implications.

Bibliography

Primary Literature

1. European Parliament and Council (2008) Waste framework directive 2008/98/EC. Annex I and II. Off J L312:3–30, 22.11.2008. http://eur-lex.europa.eu/LexUriServ/LexUriServ.do?uri=CELEX:32008L0098:EN:NOT
2. PE International and CEWEP (2008) Life cycle assessment of WTE plants in Europe: Study, Table 2.2. http://www.cewep.eu/studies/climate-protection/art230,223.html (available on request from CEWEP)
3. European Commission (2006) BREF waste incineration (WI) for Integrated pollution prevention and control (IPPC) EIPPC Bureau Sevilla. http://eippcb.jrc.es/pages/FActivities.htm
4. European Parliament and Council (2000) EU waste incineration directive 2000/76/EC. Off J L332:0091–0111, 28.12.2000. http://eur-lex.europa.eu/LexUriServ/site/en/oj/2000/l_332/l_33220001228en00910111.pdf

5. Reimann DO, Hämmerli H (1995) Verbrennungstechnik für Abfälle in Theorie und Praxis (Waste incineration in theory and practice). Schriftenreihe Umweltschutz, Bamberg p 80ff (out of print)
6. Reimann DO (2003) Ermittlung und Bedeutung von Kennzahlen zur Energie und Anlagennutzung sowie zu Wirkungsgraden für die Abfallverbrennung (Determination and meaning of identification numbers for energy and plants as well as efficiencies of waste incineration) Müll und Abfall, Heft 10:512–520
7. European Commission (2010) Draft of the EU-Guidance for R1 formula, Version April 2011
8. CEWEP (2006) CEWEP energy report (Status 2001–2004) by Reimann DO, p 5ff. http://www.cewep.eu/studies/climate-protection/art230,223.html
9. CEWEP (2009) CEWEP energy report II (Status 2004–2007) by Reimann DO, p 4ff. http://www.cewep.eu/studies/climate-protection/art230,223.html
10. Reimann DO (1991) Rostfeuerungen zur Abfallverbrennung (Grate fired combustion of waste). EF Verlag, Berlin. ISBN 3-924511-55-1
11. Reimann DO (2004) Energetische Bilanzierung von Müllverbrennungsanlagen (Balancing of energy from waste incineration plants). Erich Schmitt, Berlin, ISBN 3 503 08324 3
12. Reimann DO (2010) R1 as efficiency indicator: status quo and optimization potential. In: Second conference on biomass and waste combustion, Oslo. www.sintef.no

Books and Reviews

Euroheat & Power (2005) District heating and cooling – Country by country/2005 Survey. Euroheat & Power, Belgium

IPCC-Ditective (2000) Good practice guidance and uncertainty management in National Greenhouse Gas Inventories – IPCC/OECD/IEA Programme. WMO Intergovernmental Panel on Climate Change UNEP, Bern, p 55ff

Waste-to-Energy: Fluidized Bed Technology

Franz P. Neubacher
UV&P Environmental Engineering
M.S. Chemical Engineering (T.U. Graz)
M.S. Technology & Policy (M.I.T), Vienna, Austria

Article Outline

Glossary
Definition of the Subject and Its Importance
Introduction
Technical Features and Limitations for Waste Treatment in FBC
Selected Concepts and Reference Projects for FBC
Emissions and Environmental Impact Assessment
Future Perspectives
Bibliography

Glossary

Combustion refers to the overall process of initial "drying" (evaporation of water), "degasification" (pyrolysis), "gasification" (of the solid carbon), and "oxidation" of the combustible gases.

Fluidized bed refers to fluid dynamics in an intensively mixed system of solid particles and gas flow which keeps the particles in dynamic movement somehow comparable to "bubbling" or "circulating," thus the mixture behaves much like a fluid. Fluidized bed is essentially a two phase flow phenomenon comprising a bulk of solids (e.g., quartz sand) which is kept in a fluidized state by an upward flow of gas (e.g., air) with velocities exceeding the minimum fluidization velocity. Thus the fluidized bed regime is characterized by intense movement of the solid particles resulting in high rates of heat and mass transfer. "Bubbling" and "circulating" fluidized bed systems can be distinguished depending on the gas velocity within the reaction chamber. In an "externally circulating" system the solids inventory is transported out of the reactor by gas flow at transport velocity.

Waste in the context of *waste-to-energy* typically refers to materials technically suitable for thermal treatment with ultimate oxidation of combustible matter. Treatment of waste may be necessary because of legal requirements for environmental protection (e.g., in order to destroy hazardous and other biologically or chemically reactive organic materials) or because of an economic advantage for recovery of energy by combustion of waste materials with a relevant calorific value (e.g., plastic wastes with high calorific value comparable to crude oil or bark and sawdust as a waste from processing wood). In advanced waste management regulations, the disposal of wastes exceeding 5% total organic carbon

(with some specific but limited exemptions) is legally prohibited in several European countries (e.g., in Austria, Germany, Switzerland).

Definition of the Subject and Its Importance

Waste is a complex issue. Disposal of waste in terms of "out of sight – out of mind" by burial on land or discharging into surface waters or by simple dumping onsite or in proximity of the origin of waste production has become a dramatic global problem and a cause for various forms of environmental degradation and severe damage to human health and the natural environment including fauna and flora. Increasing population and material wealth based on industrial production has led to tremendous waste problems. It has also led to greater understanding and the acknowledgment of resource limitations for an increasing human population on this planet. Therefore, the practice of dumping or disposal of waste must be viewed as wasteful, neglectful, and irresponsible to the needs of others and to those of future generations. It can also be viewed as a direct contradiction to "cultivating the earth" (the original concept for the human population on earth as described in the book of Genesis). Natural resources are often simply differentiated in "renewable" (based on the ongoing radiation of the sun onto the orbiting and rotating planet earth) and "nonrenewable" resources (particularly fossil resources such as mineral oil, natural gas, and coal). In any case, for both renewable and nonrenewable resources, whether material or energy, the issue of efficiency and recovery is vital for sustainability and the future quality of life on earth. The scientific basis for calculating resource efficiency, including recycling and recovery, is the first and second Law of Thermodynamics. Waste-to-energy is complementary to material recovery (including recycling). One unit of "ROE" (Raw Oil Equivalent) equals 40 MJ/kg or 40 GJ/t of calorific energy, which can be recovered by combustion and utilized in technical systems. Currently, about 90% of all presently consumed (nonrenewable) mineral oil in the form of various fuels goes directly into combustion. The use of mineral oil for production of materials such as plastic polymers allows for some recycling (recovery of materials for reuse in a recycling product) and also for ultimate recovery of the calorific value by waste-to-energy, rather than its disposal in a landfill (or dumping elsewhere).

According to state-of-the-art, there are various technical systems for waste-to-energy. The type of system used depends on the specific type and mixtures of waste to be treated and the specific demand for various forms of energy onsite (e.g., heat at a given level of temperature for specific industrial production processes or for heating or cooling by operating an absorption process, demand for electricity). A continuous demand for cogeneration of power and heat is economically favorable for locating a waste-to-energy facility on such a site.

Fluidized bed is the most appropriate technology for a large variety of specific wastes (as well as for some type of biomass and low-grade coal). The basic principles of waste-to-energy and fluidized bed technologies, their applications, and limitations for waste treatment, some selected reference projects, technical aspects on emissions and environmental impact assessment, and future perspectives for further development in recovery of materials and energy from waste by fluidized bed technologies will be presented and discussed.

Introduction

The basic principle of waste-to-energy refers to the overall process of energy recovery based on energy conversion by incineration of waste materials. The overall process of heat production by incineration of waste (or any other solid fuel, such as wood or lignite coal) comprises the individual processes of initial "drying" (evaporation of water by heat input), "degasification" (pyrolysis – cracking of large organic molecules with subsequent release of volatile fractions), "gasification" (of the solid carbon by gaseous molecules such as oxygen, water, and carbon dioxide), and "oxidation" of the combustible gases (ultimately the oxidation of carbon monoxide and hydrogen). The terms "incineration," "combustion" (like fuel in combustion engines), "thermal oxidation," "thermal treatment," and "gasification for generation of synthetic gas" (which will, of course, eventually be subject to some form of incineration) are often used interchangeably in waste-to-energy.

Figure 1 illustrates mass and heat transfer in the overall process of incineration with the four technically

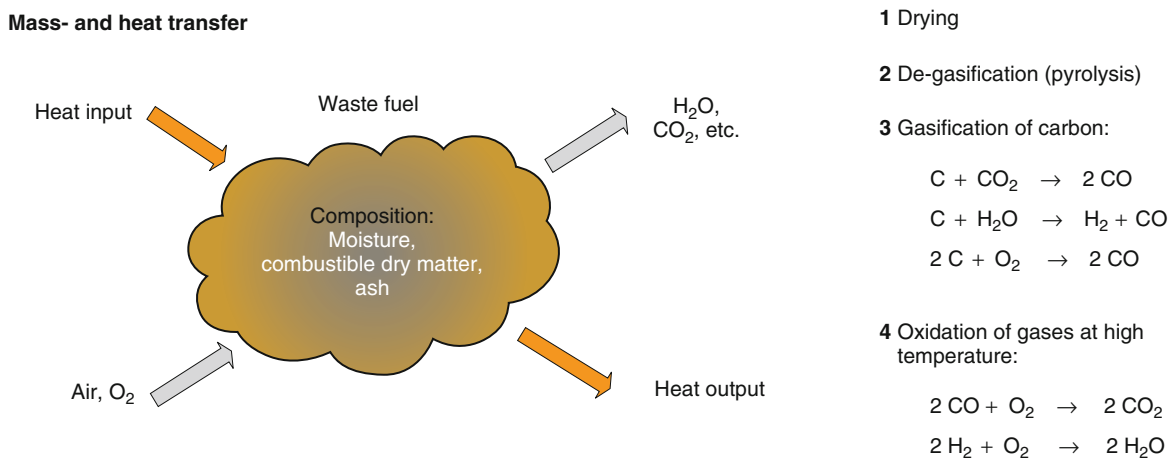

Waste-to-Energy: Fluidized Bed Technology. Figure 1
The four phases of the incineration process

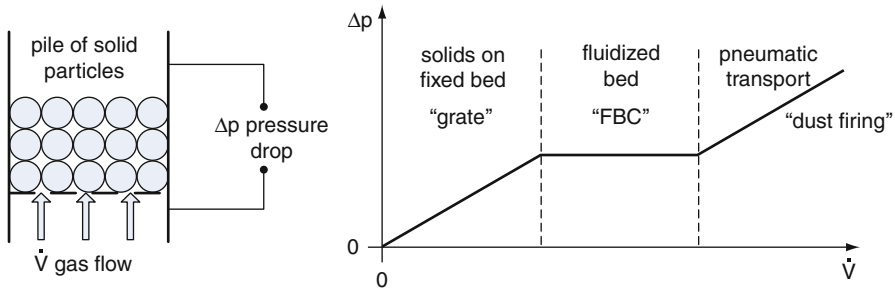

Waste-to-Energy: Fluidized Bed Technology. Figure 2
Pressure drop in gas flow through static and fluidized beds and pneumatic transport

distinct phases of drying, degasification, gasification, and combustion. The overall process of incineration can be illustrated by frying/burning a steak: At first the meat will shrink due to loss of water (drying), secondly it will start to release odorous molecules and visible organic fumes due to continued frying until the remains of the steak gradually turn into black charcoal (completion of degasification), until finally only gray ash remains. After gasification of black carbon, only a small quantity of ash (containing phosphates, calcium, etc.) will remain from the original large piece of a juicy steak.

The process of combustion is based on heat and mass transfer which includes a supply of oxygen necessary for the oxidation as well as the removal of carbon dioxide as a major reaction product (which would otherwise have the effect of a fire extinguisher). The necessary conditions for complete combustion are determined by the so-called 3T criteria, that is, "Temperature" (e.g., 850°C), "Time" (e.g., 2 s for the flue gas at the required minimum reaction temperature after the final supply of necessary oxygen) and "Turbulence" (rapid heat and mass transfer including thorough mixing of the combustible gases with the necessary oxygen in excess of the stoichiometric minimum need). The combustion process can effectively be monitored by the important parameters temperature, oxygen, and carbon monoxide.

The basic principles of fluidized bed reactors can be explained by the experiment (see Fig. 2) of a large number of particles (e.g., granular materials of defined particle size distribution) filled into a vertical cylinder

supported by a gas distributor at the bottom and a fluid (e.g., combustion air) passing upward through the bulk of solid particles. Initially, the particles remain at their original static position more or less densely packed. This state is like pieces of coal or wood lying on the grate of a furnace with air passing from underneath through the bed of solid fuel. This fluid regime is called "fixed bed." With further increase of gas flow, the pressure drop increases up to the point when the bed with the particles starts "bubbling" and some particles will be lifted due to aerodynamic forces and start floating like a "fluid." The fluidized bed behaves much like a liquid: It can be stirred; the bed surface remains horizontal when the vessel is tilted; the fluidized bed flows out like a liquid through a lateral opening; objects of greater specific gravity sink whereas those of lower specific gravity float; etc. [1].

With even greater gas flow, the particle bed becomes more "fluidized" and various forms of "internal circulation" will occur. Eventually, further increase of gas flow will carry away the particles, like fine coal being pneumatically conveyed and fired in a gas flow.

The term "fluidized bed" obviously refers to fluid dynamics in an intensively mixed system of solid particles and gas flow which keeps the particles in dynamic movement. Different systems can be described according to observation of the technical behavior as "bubbling," "turbulent," or "circulating" fluidized bed. Thus, various manufacturers refer to their system as a "bubbling bed," a "turbo," or a "circulating" fluidized bed. A fluidized bed system can be designed to induce specific forced circulation, for example, "internal circulation" (by specific geometry of the vessel – see example in Fig. 5) or "external circulation" (adjacent to the main combustion chamber is a large cyclone for separation of larger solid particles to be returned back into the fluidized bed and the hot flue gas leaving the cyclone through the afterburning zone). Technical examples are given in Figs. 4 and 10.

The complexity of large waste-to-energy projects is illustrated in Fig. 3. The incineration process (e.g., in the fluidized bed) may require some pretreatment of specific waste materials.

Figure 4 illustrates a waste-to-energy project with an "externally circulating fluidized bed combustion system." The overall process design is also based on Best Available Technique (BAT) according to Austrian and EU requirements. Specific waste materials are delivered and stored

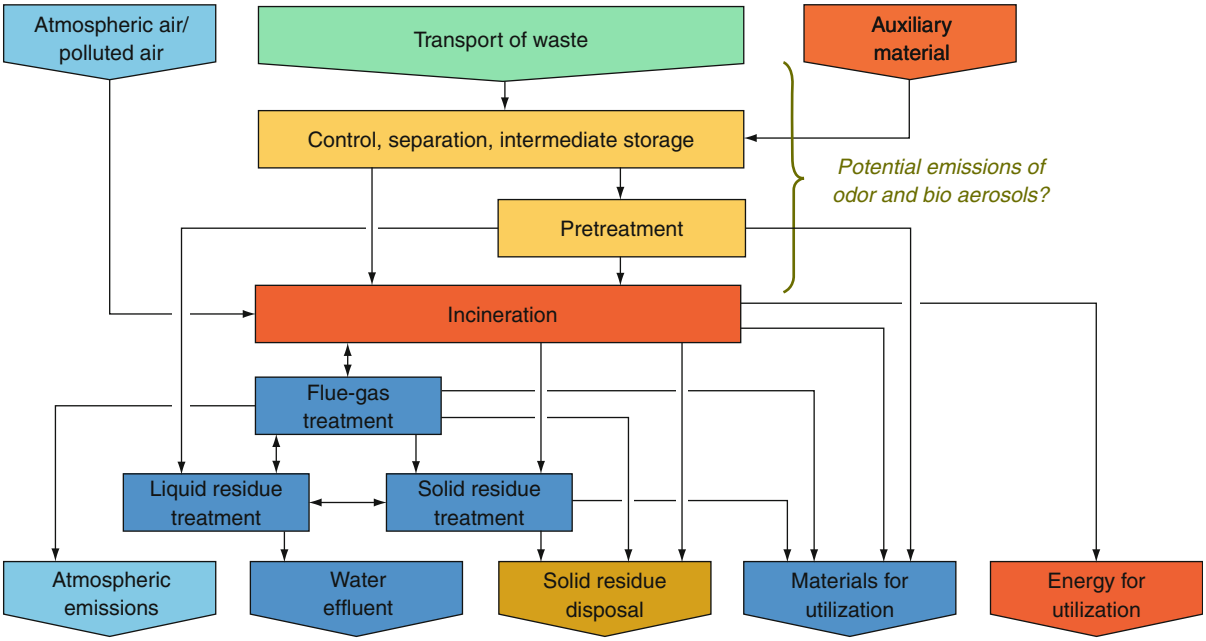

Waste-to-Energy: Fluidized Bed Technology. Figure 3
Overall scheme for the complexity of a waste-to-energy facility [2]

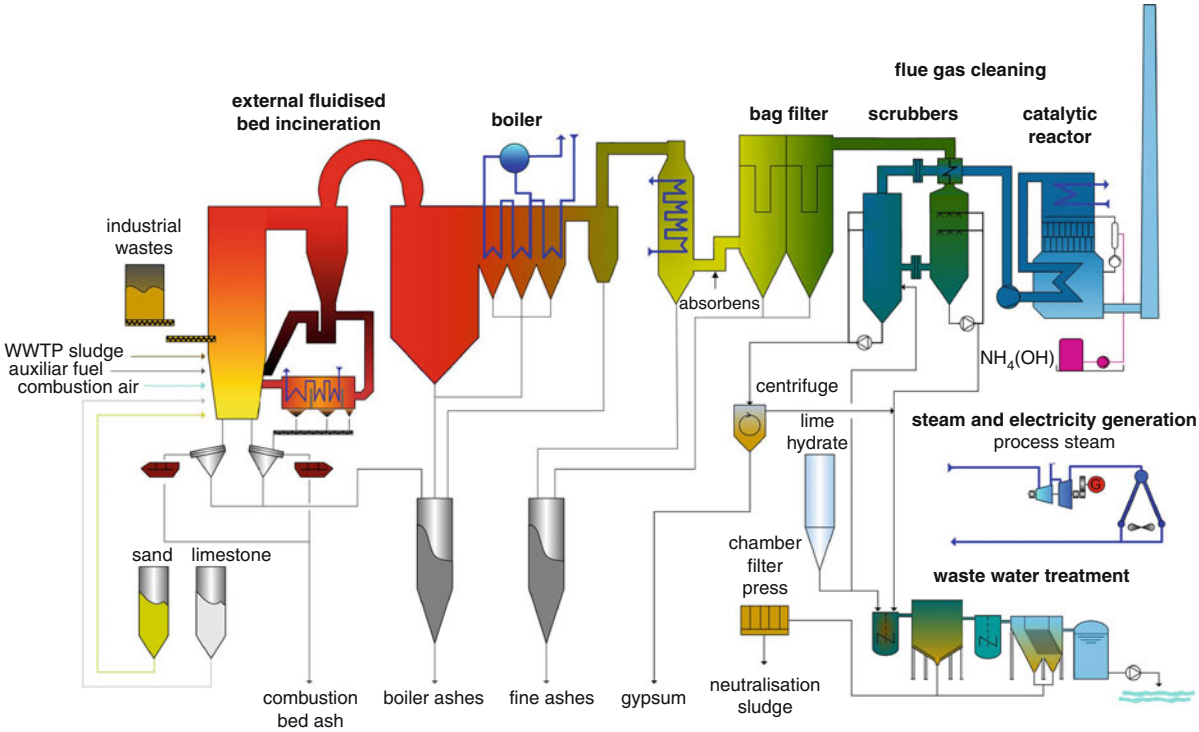

Waste-to-Energy: Fluidized Bed Technology. Figure 4
Example of waste-to-energy in an externally circulating fluidized bed system

in closed systems separately prior to incineration in the fluidized bed boiler. In this example the multistage flue-gas treatment process is effluent free because there is no ecologically acceptable discharge of chlorides into the river at the given location.

Technical Features and Limitations for Waste Treatment in FBC

Fluidized bed systems allow for intensive mass and heat transfer between the solid particles to be incinerated and the flow of gas, thus enabling highest efficiency and complete chemical reactions. The three key parameters turbulence, temperature, and time can be technically controlled in fluidized bed systems within narrow ranges. Because of precise control of mass flow (air flows as well as fuel supply) the maximum temperature can be kept within a very narrow range of around 900°C, just above the minimum temperature necessary for complete gasification and combustion. Therefore, combustion in the fluidized bed systems allows for very low formation of NO_x (nitrogen oxide) due to the absence of thermal formation by oxidation of nitrogen gas supplied with air for combustion. Such undesirable reactions do not occur at temperatures below 1,000°C.

The combustion process in a fluidized bed and the "freeboard" above it are complete. Thus, there are very low concentrations of unburned organic substances in the solid residues and in the flue gas.

Due to the precise process control, the excess air ratio (i.e., the excess oxygen content in the flue gas) after complete combustion can be kept very low including the option for controlled recirculation of cleaned flue gas extracted after the filter system (necessary removal of pollutants) back into the fluidized bed system. Reduced quantity of excess air minimizes the overall heat losses and atmospheric emissions of the system.

The following schemes in Figs. 5 and 6 illustrate the technical concept for precise control of gas flow in a waste-to-energy plant with an internally circulating fluidized bed as installed in Vienna: A small share of the

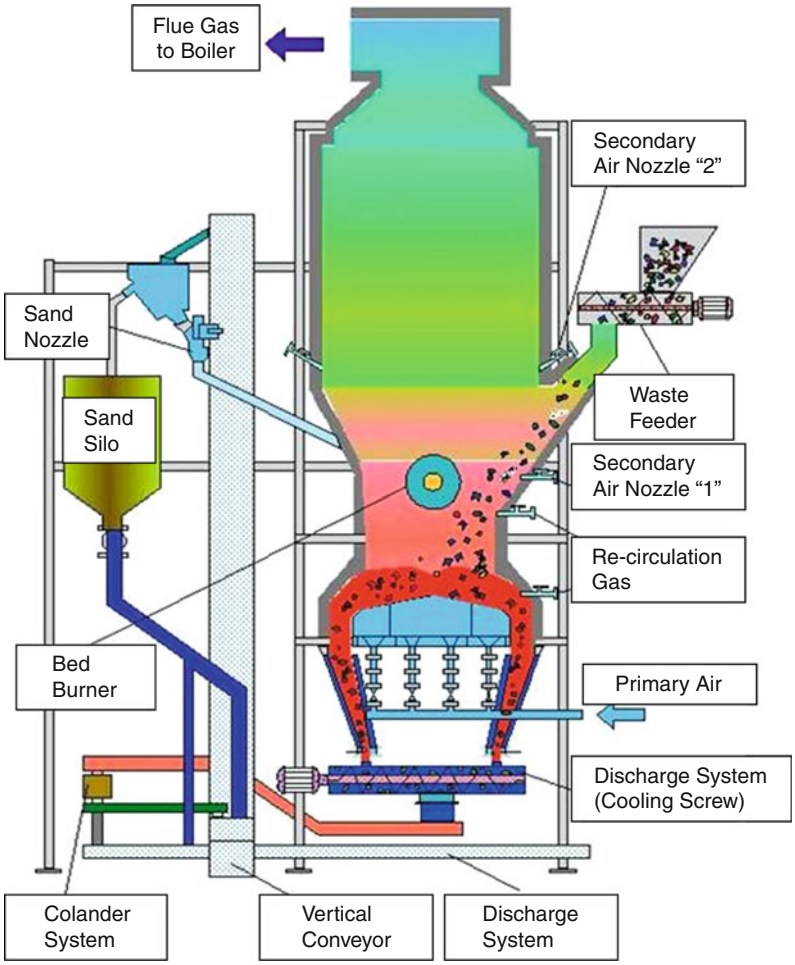

Waste-to-Energy: Fluidized Bed Technology. Figure 5
Example of an internally circulating fluidized bed system [9]

combustion air is the "primary air" necessary for fluidizing the bed material. It must be preheated in a heat exchanger in order to avoid condensation after mixing with high-pressure recirculation gas. The input of "secondary air" (for complete combustion of gas resulting from degasification and gasification of waste in the fluidized bed) can be varied by controlled utilization of recirculation gas and separately supplied ambient air. There is an additional supply of primary air (without need for preheating) by a separate ventilator for fostering internal circulation ("rotation") of the fluidized bed.

The intensive turbulence also allows for extensive sorption processes at the given conditions in the fluidized bed system, especially of sulfur oxide being chemically bound to calcium and magnesium oxides. These sorption agents are already present in waste material or fed into the fluidized bed, for example, in the form of calcium carbonate (limestone) or calcium hydroxide of defined fine particle size. This feature is also effectively used in the combustion of low-grade coal in fluidized bed systems with integrated reduction of sulfur dioxide emissions by about 90% (without secondary measures for sulfur oxide removal).

The precise control of fluidized bed systems also allows for a broad range of fuel properties with respect to calorific value. Fluidized bed systems can be designed and operated for average fuel mixtures ranging from about 5 to 8 MJ/kg up to values exceeding 40 MJ/kg (e.g., mixed plastic wastes). In extreme cases,

the average calorific value of waste to be incinerated can be below 3 MJ/kg (e.g., mechanically dewatered sewage sludge), with preheated combustion air (internal recovery of heat) and some waste flow being partly dried in a system utilizing low-pressure steam supplied from the own steam turbine.

The operating range also allows for reduced thermal load, e.g., as low as 50% of the maximum design capacity. The controllability of fluidized systems also allows for a very short shutdown time in case of an emergency because there is almost no unburned fuel within the fluidized bed system. In case of a temperature drop toward the minimum temperature requirement, auxiliary fuel supply or start-up burners can instantly be started. The emergency shutdown requires only a few minutes (stopping of waste supply, reduction and shut-off of air supply).

One of the limitations of fluidized bed systems is the maximum allowable particle size suitable for controlled and safe mechanical feeding into the combustion system, for example, screening at 80 mm for limiting maximum size of pieces to be fed into the fluidized bed.

The maximum particle size of waste to be expected is usually the maximum size technically possible due to the collection system. Thus, in the case of some large containers in collection of municipal wastes rather large particle size must be expected (e.g., a large tire together with the wheel rim, mattresses with steel wires and springs, large containers with unknown

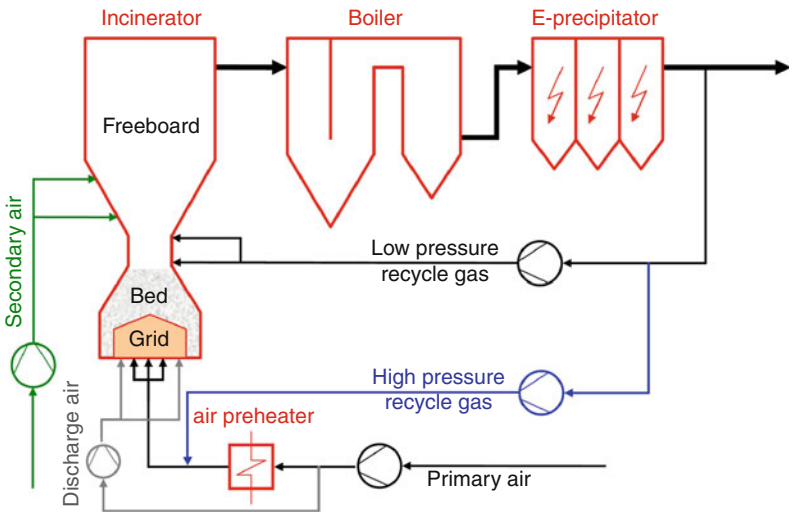

Waste-to-Energy: Fluidized Bed Technology. Figure 6
Example for air and gas flow in an internally circulating fluidized bed system [3]

Waste-to-Energy: Fluidized Bed Technology. Table 1 Comparison of technologies for waste-to-energy

Parameter	Incineration technology		
	Grate	Fluidized bed	Rotary kiln
Maximum fuel capacity per line	Approx. 90 MW	Approx. 160 MW	Approx. 40 MW
Excess air (oxygen) ratio (specific quantity of flue gas)	Medium	Low	High
Range of calorific value for waste and waste-derived fuel	Low	High	Medium
Fuel processing requirements	Low	High	Medium
Controllability of incineration and shutdown operation	Medium	High	Low

Waste-to-Energy: Fluidized Bed Technology. Table 2 Allocation of selected wastes to specific incineration technologies

Type of waste	Incineration technology		
	Grate	Fluidized bed	Rotary kiln
Mixed municipal solid waste (Residual mixed waste)	Well-suited	Pretreatment required	Suitable
Sewage sludge	Limited in terms of quantity	Well-suited	Suitable
Screening material from sewage treatment	Suitable	Pretreatment required	Limited suitability
Shredded plastic wastes	Limited in terms of quantity	Well-suited	Limited suitability
Scrap tires (from vehicles)	Limited suitability	Unsuitable	Limited suitability
Shredder waste (from metal scrap recycling)	Limited in terms of quantity	Well-suited	Limited suitability
Shredded waste wood (e.g., from processing bulky wastes)	Well-suited	Well-suited	Suitable
Lacquer and paint sludge,oil sludges	Unsuitable	Suitable	Suitable
Wastes in closed containers (e.g., medical and laboratory waste)	Limited suitability	Unsuitable	Suitable

Waste-to-Energy: Fluidized Bed Technology. Figure 7
Waste-to-energy facilities at Simmering, Vienna: 4 fluidized bed and 2 rotary kilns

content, etc.). Therefore, this type of waste with broad ranges of size and properties might require presorting or mechanical shredding prior to combustion in a specific fluidized bed system. The specific limitations on the maximum size and shape of waste for the technical feeding system as well as for the removal of coarse inert parts after incineration (which is removal of bed material and ashes) must be considered. In comparison

to fluidized bed systems, the typical grate systems for waste incineration are more suitable for typical large parts in unsorted municipal solid waste.

Some waste materials are neither suitable for fluidized bed nor for grate systems due to a broad range of (often unknown) potentially hazardous properties. Therefore, large rotary kilns with an integrated afterburning chamber are typically used for various mixes of hazardous wastes or closed containers with partly unknown content (e.g., infectious and other medical wastes, laboratory wastes). Tables 1 and 2 provide a general comparison of fluidized bed systems with other important systems for thermal waste treatment and waste-to-energy such as grate systems and rotary kiln (including an afterburning chamber).

Fluidized bed systems operate with high turbulence in the combustion process. This allows for the recovery of larger size of clean (like sandblasted) solid particles from the coarse bed material, but will also yield large quantities of very fine ash (although with a low content of unburned residues). This is of advantage with respect to maximum recovery of specific materials, but it may be a general disadvantage for disposal of untreated solid residues at lower costs. The quantity of (naturally fine) fly ash in a grate system firing typical municipal waste may be only about 10% of the total ash content, whereas in case of a fluidized bed, fly ash may be about 60–80% of the total ash quantity. Therefore, some fluidized bed systems use additional cyclones for particulate removal from flue gas in the boiler system at about 400°C in order to recover most of the (coarse) fly ash in a nonhazardous quality (no condensed pollutants such as metal chlorides at such temperature and no water-soluble chemical reaction products before

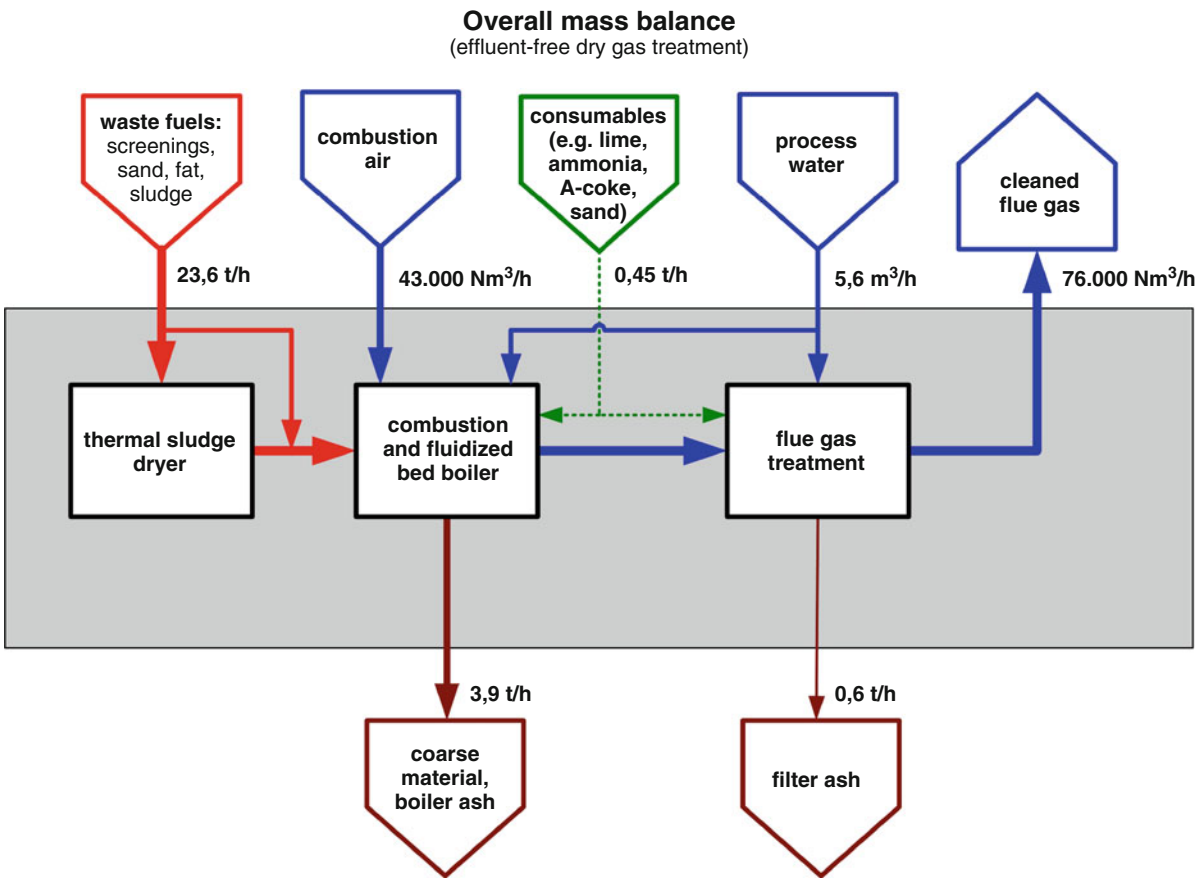

Waste-to-Energy: Fluidized Bed Technology. Figure 8
Overall mass balance for a fluidized bed system for residues from sewage treatment

injection of sorption agents into the flue gas). Slag from municipal waste combustion on grate systems is generally qualified as a nonhazardous material with the option of disposal at low cost in landfills.

Specific attention must be given to the potentially high content of metallic aluminum in waste combustion for two reasons: economic opportunity for recovery and recycling of aluminum and the potential risk of operational problems and hazardous properties of fine ash. Aluminum content in municipal waste has significantly risen throughout the last years (packaging, laminated materials, various aluminum products). Aluminum alloys have a melting point around or somewhat below 700°C; thus, metallic aluminum will be completely "dissolved" at such temperatures in the turbulence of fluidized bed systems. The very fine aluminum droplets (with a very stable surface of a thin layer of protective aluminum oxide) will be carried by the flue gas and will eventually either adhere in layers on surfaces with lower temperatures (also causing risk for sudden exothermic reactions) or become part of the removed fine ashes. These ashes have naturally high alkalinity and thus the fine aluminum will react in case of contact with water with the release of hydrogen gas (up to 1.3 l of H_2 per g of Al). Therefore, systems with temperatures below 650°C in the fluidized bed allow for recovery of aluminum parts in removal from coarse bed material. Systems operating at higher temperatures must strictly limit the maximum allowable content of metallic aluminum in ashes by operating with appropriate waste fuel mixes (including automated removal of nonferrous metallic parts before entering a combustion process).

The types and installed capacities of specific waste-to-energy technologies may vary significantly between various regions. According to many years of experience in Austria and some other European countries, the different technologies for thermal waste treatment and waste-to-energy are needed and applied.

The example of the city of Vienna and the more industrialized state of Upper Austria illustrate the successful operation of various technologies for

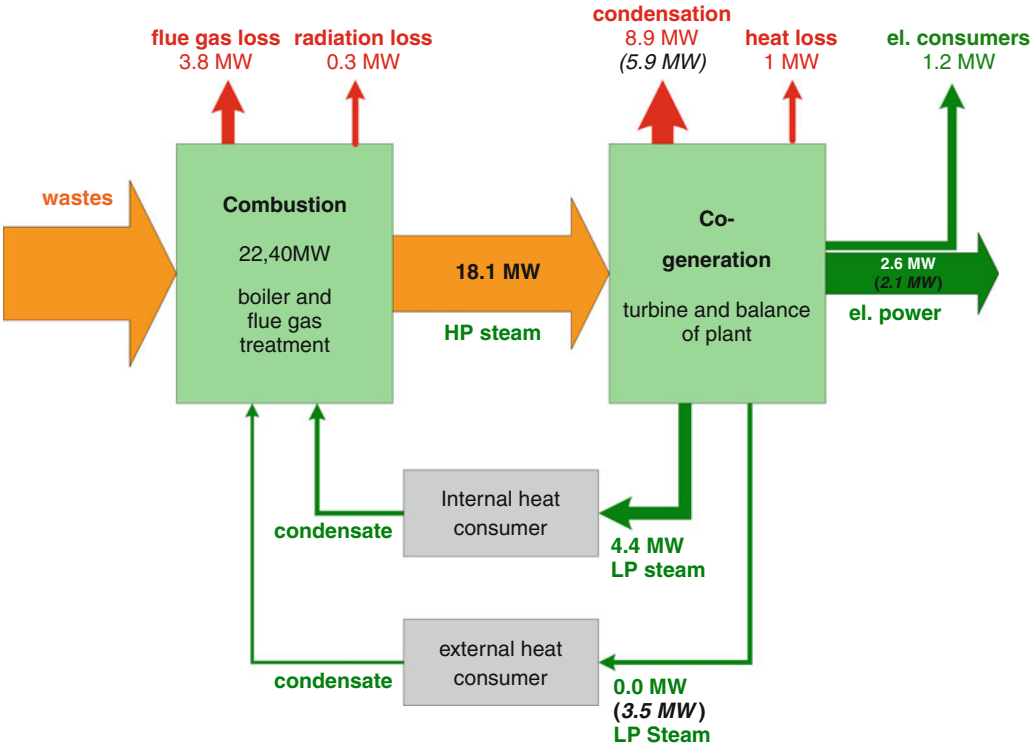

Waste-to-Energy: Fluidized Bed Technology. Figure 9
Energy balance for a fluidized bed system for residues from sewage treatment

waste-to-energy. Vienna operates four fluidized bed systems for sewage sludge and waste-derived fuel including mechanically pretreated municipal waste, seven grate systems for mixed residual municipal wastes, and two rotary kilns for hazardous wastes, the latter two serving all of Austria and some imports from other European countries.

In Upper Austria there is a larger capacity of fluidized bed systems operating with residual municipal waste than grate systems, plus additional fluidized bed systems for energy recovery from biomass wastes (e.g., mixed waste wood from processing of bulky wastes, bark and sawdust from wood processing, reject materials from paper recycling, residues from industrial and municipal wastewater treatment, etc.).

Selected Concepts and Reference Projects for FBC

Fluidized bed systems have been used for gasification and combustion for many decades throughout Europe and other industrialized countries [1]. Since the late 1960s and 1970s, treatment of waste water and sewage has become a high priority for municipalities and large industry. Subsequently, the need for sewage sludge treatment became obvious. Thus, an increasing number of fluidized bed systems were installed throughout the Western countries in order to treat those residues by thermal conversion (incineration). The first significant price increase for fossil fuels encouraged industry to utilize their burnable wastes (e.g., bark from processing wood in the pulp and paper industry) together with residues from mandatory wastewater treatment in appropriate boilers. Of course, these waste-to-energy plants also needed to be suitable for burning various types of coal for heat and power supply to the industrial production.

In 1980, two fluidized bed incinerators, based on the principle of "bubbling bed" (stationary fluidized bed), were installed in Vienna for treatment of mechanically dewatered sewage sludge with auxiliary fuel of waste oil or heating oil as needed. These

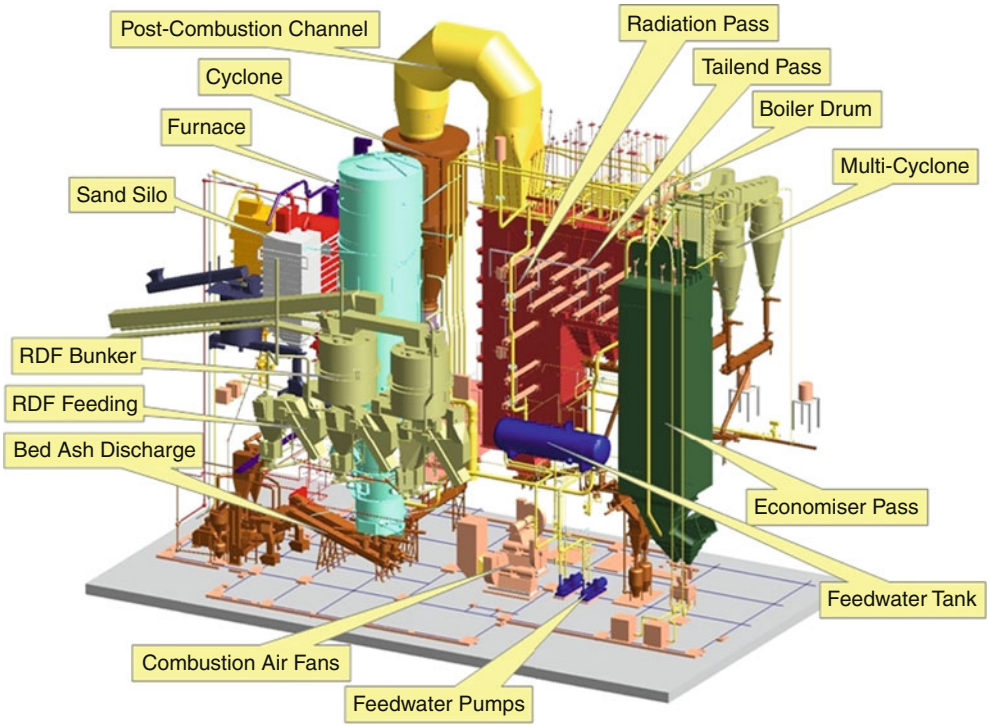

Waste-to-Energy: Fluidized Bed Technology. Figure 10
Layout of a waste-to-energy "circulating fluidized bed system" based on the successful project in Lenzing [10]

waste-to-energy plants are still in successful operation today, together with an additional similar fluidized bed system installed in 1992 [4]. For the purpose of standby and guaranteed treatment of all sludge generated at all times and for the purpose of waste-to-energy from pretreated municipal wastes an additional fluidized bed incinerator was installed at the same site in 2003. This incinerator is also a stationary system, but with a "rotating bed," also referred to as an "internally circulating fluidized bed" system (see Figs. 5 and 6). The overall performance of the four fluidized bed incinerators together with the two rotary kilns for hazardous wastes (plus a small rotary system for pretreatment of consumer batteries) at the site of Simmering is presented in Fig. 7. It should be noted that these facilities are situated next to the sewage treatment plant in the central area for vegetable production in Vienna – with full public acceptance of local residents.

The overall mass and energy balance for thermal treatment of residues from a large municipal wastewater treatment in a fluidized bed system is presented as example in Figs. 8 and 9. In order to operate the plant solely on residues from municipal sewage treatment (without auxiliary fuel), part of the mechanically dewatered sludge is dried in a machine operated with low-pressure steam from the waste-to-energy cogeneration facility.

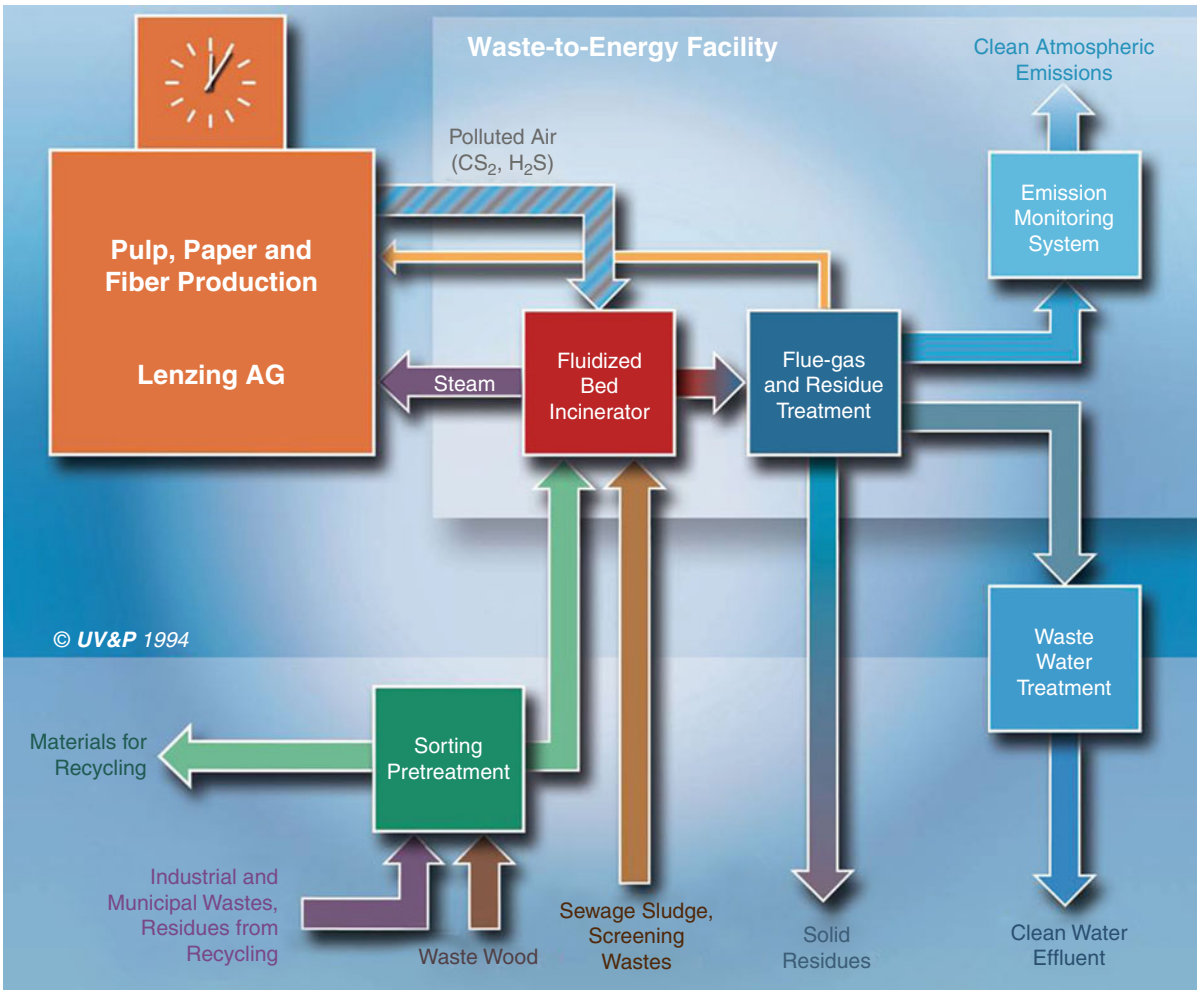

Waste-to-Energy: Fluidized Bed Technology. Figure 11
Scheme for integrated waste-to-energy in the industrial production at Lenzing

Waste-to-Energy: Fluidized Bed Technology. Figure 12 View of the industrial site Lenzing within a region of tourism and organic farming [2]

Fluidized bed systems for waste treatment and recovery are successfully in operation with small fuel (i.e., thermal generation) capacities below 5–10 MW in Europe. Examples include energy recovery with ORC (Organic Rankine Cycle) and simultaneous recovery of the mineral sand fraction from bituminous waste products at an industrial production site as well as a small plant for incineration of various solid, pasteous, and liquid hazardous wastes.

Large waste-to-energy facilities (up to 160 MW fuel capacity per line) for cogeneration of process heat and electricity at industrial sites are typically based on "externally circulating fluidized bed systems," as illustrated by the example of Lenzing in Upper Austria (see Figs. 11 and 12). This project was developed and planned in 1993 with subsequent heated

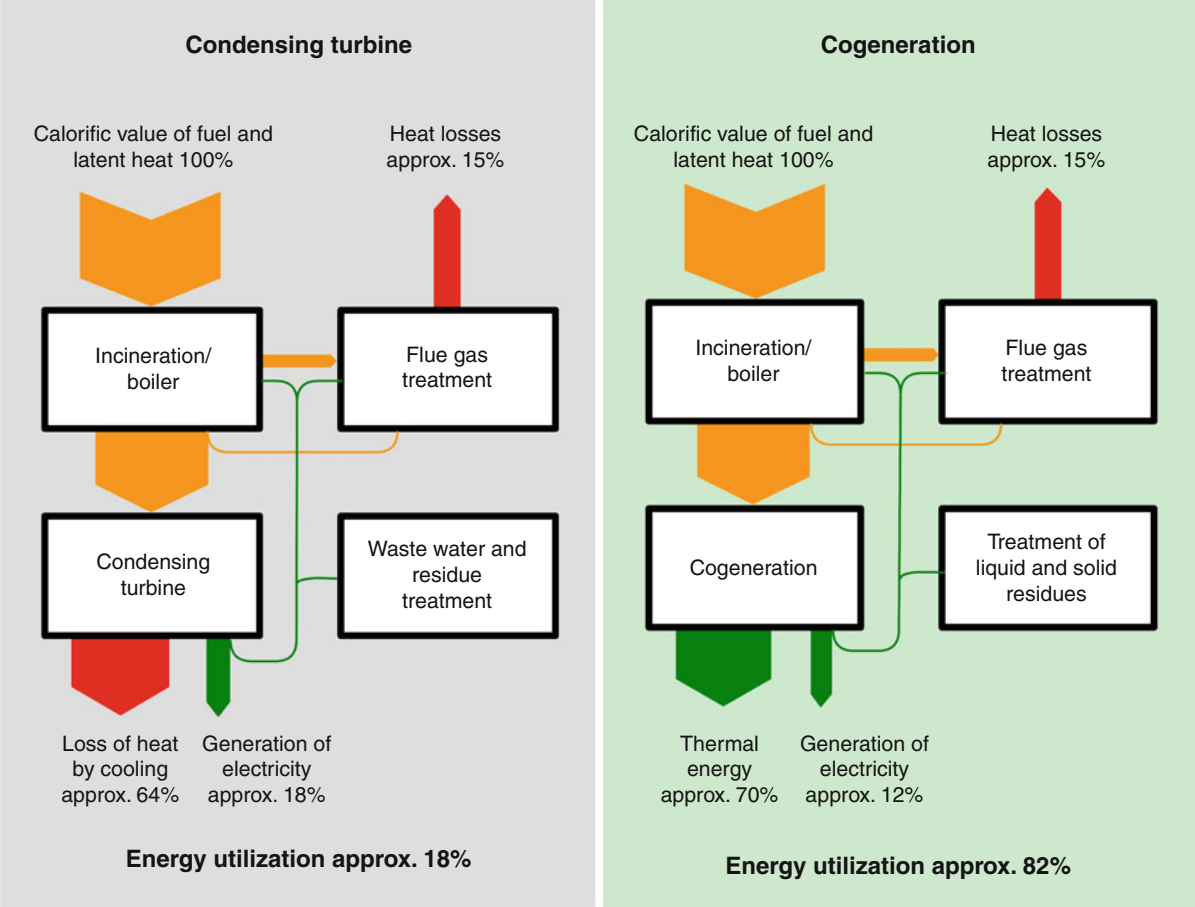

Waste-to-Energy: Fluidized Bed Technology. Figure 13
Energy utilization with a condensing turbine compared to cogeneration presented by the example of waste-to-energy at the more appropriate industrial site Lenzing

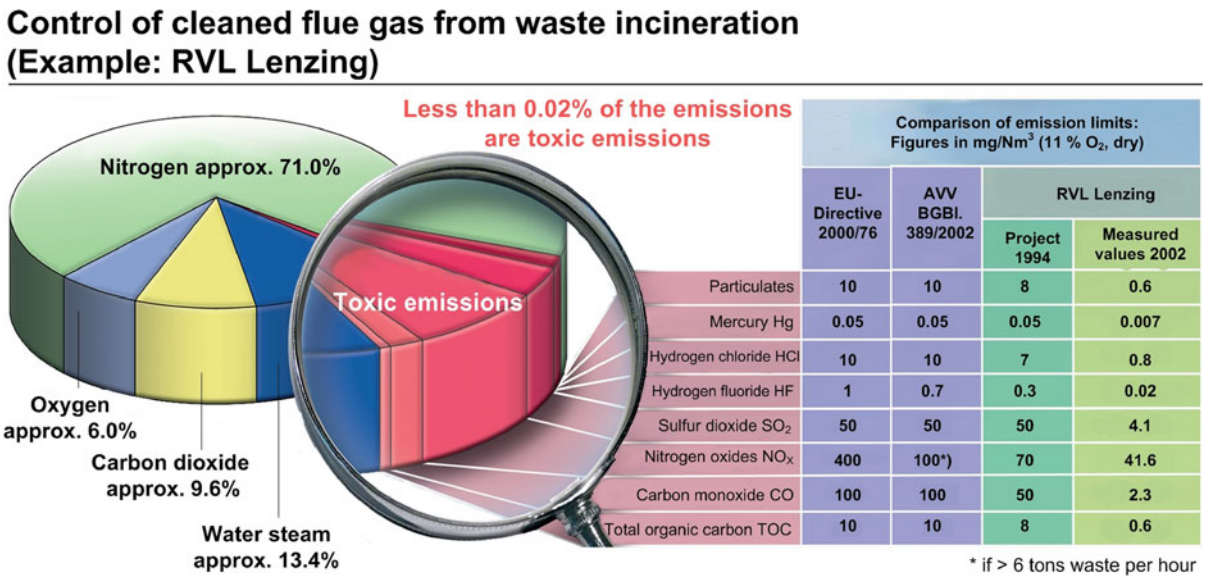

	Comparison of emission limits: Figures in mg/Nm³ (11 % O_2, dry)			
	EU-Directive 2000/76	AVV BGBl. 389/2002	RVL Lenzing	
			Project 1994	Measured values 2002
Particulates	10	10	8	0.6
Mercury Hg	0.05	0.05	0.05	0.007
Hydrogen chloride HCl	10	10	7	0.8
Hydrogen fluoride HF	1	0.7	0.3	0.02
Sulfur dioxide SO_2	50	50	50	4.1
Nitrogen oxides NO_x	400	100*)	70	41.6
Carbon monoxide CO	100	100	50	2.3
Total organic carbon TOC	10	10	8	0.6

Waste-to-Energy: Fluidized Bed Technology. Figure 14
Composition of atmospheric emissions and standards for the waste-to-energy project in 1994 in comparison to actual performance in 2002 and strictest legal emission standards

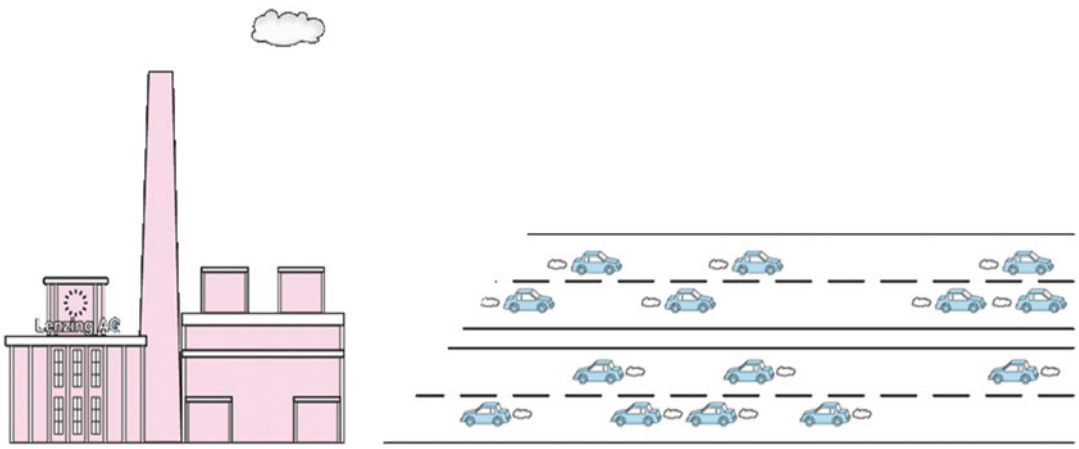

Calculation:
Car exhaust contains approx. 20 g C-org / kg fuel
Flue gas of the incineration plant contains less than 1,980 g C-org / h

Waste-to-Energy: Fluidized Bed Technology. Figure 15
Illustration for organic pollutants from the waste-to-energy plant compared with passenger cars (example [2])

discussions in the media and public hearings, nevertheless resulting in a successful start-up of operation in 1998. Based on the experience and know-how derived during optimization of this first plant of its kind, several more such large waste-to-energy plants have been built or are currently under construction by the supplier, ANDRITZ Energy & Environment (see Fig. 10).

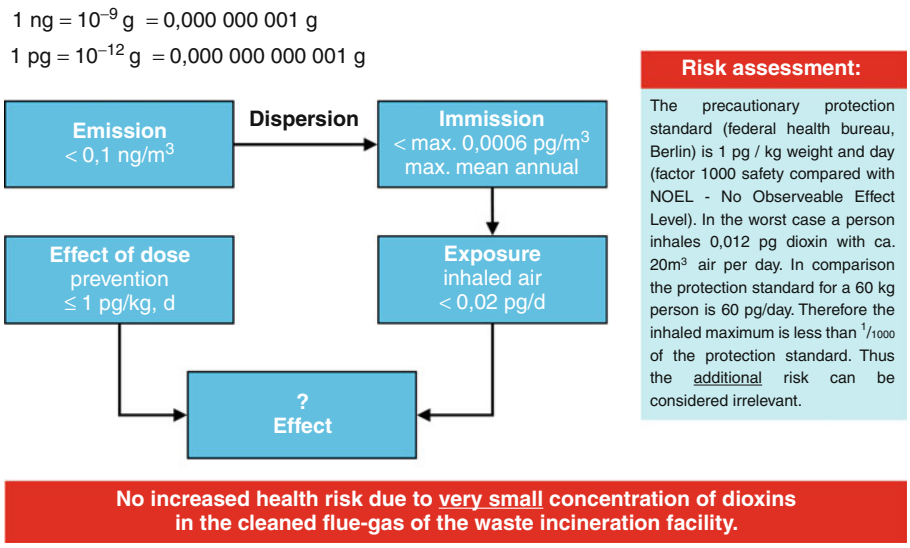

Waste-to-Energy: Fluidized Bed Technology. Figure 16
Risk assessment for atmospheric emissions of "dioxins" (example [2])

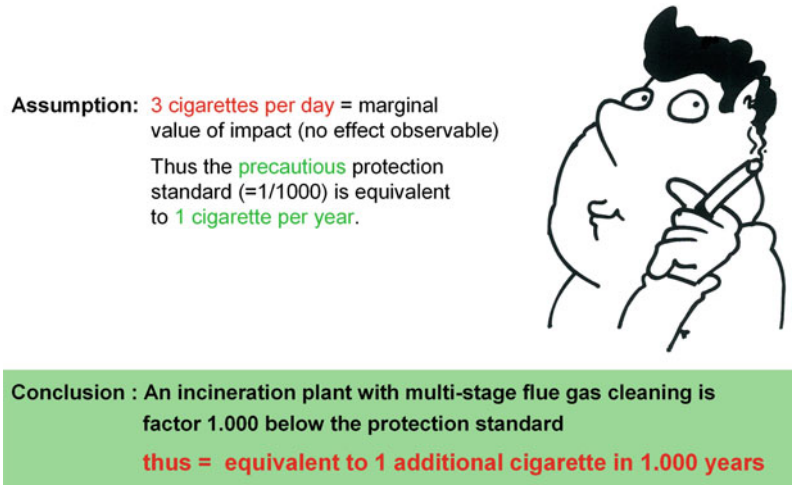

Waste-to-Energy: Fluidized Bed Technology. Figure 17
Illustration for risk assessment in comparison with cigarettes

Waste-to-Energy: Fluidized Bed Technology. Table 3 Development of emissions from waste incineration according to state-of-the-art in Austria and Switzerland [2] (figures in mg/m_N^3, PCDD/F in (TEQ) ng/m_n^3)

Year	Dust	Cd	HCl	SO_2	NO_x	Hg	PCDD/F
1970	100	0.2	1,000	500	300	0.5	50
1980	50	1.1	100	100	300	0.2	20
1990	1	0.005	5	20	100	0.01	0.05
2000	1	0.001	1	5	40	0.005	0.05

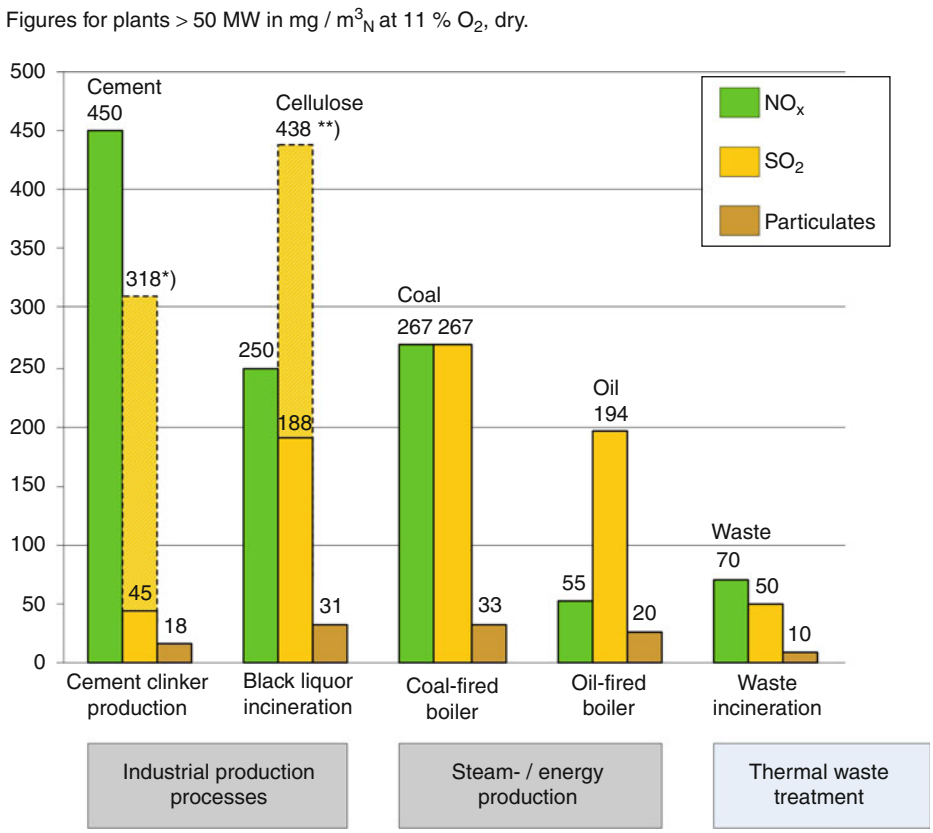

Waste-to-Energy: Fluidized Bed Technology. Figure 18
New source performance standards for flue gas from different industrial incineration processes in Austria

Emissions and Environmental Impact Assessment

Emissions and the assessment of environmental impact from a large waste-to-energy plant with fluidized bed technology can be presented based on the extensive public discussions in 1993/94 in Austria around the project in Lenzing. There were fundamental objections to such projects because of the fear of pollution from waste incineration by the local population and also due to strong opposition from the competing waste disposal industry outside of the planned project. Furthermore, the legal ban on disposal of wastes exceeding 5% TOC (total organic carbon) in landfills had not yet been established and was open for controversial public discussion.

Figure 11 summarizes the basic concept and technical features of the waste-to-energy project based on a fluidized bed system in Lenzing for comprehensive public information.

In extensive public discussions, justification for the considerable size of the project (thermal power of approx. 110 MW which allowed for the incineration of up to 1,000 t of waste per day) and the choice of the location (surrounded by organic farms and by the tourist region of Lake Attersee as depicted in Fig. 12) was successfully presented using the following three arguments:

1. Steam requirement for the industrial production of Lenzing (elimination of two old boilers from 1938/1939 at the site of the new plant, substitution of imported natural gas by waste-to-energy)

2. Improvement of local air quality by utilization of the malodorous air emitted from viscose fiber production for the necessary combustion air in the waste-to-energy boiler
3. Avoiding future disposal of reactive organic wastes in landfills (so-called reactor dumps), thus avoiding uncontrollable emissions from landfills and contaminated sites for future generations

The argument in favor of the proposed capacity at the highest level of energy efficiency in a fluidized bed boiler with high steam parameters (80 bar, 500°C) for cogeneration (based on continuous demand for process steam throughout the year) was illustrated by the comparison to a municipal waste incineration plant (with maximum production of electricity in a condensing turbine) as indicated in Fig. 13.

The fear of uncontrolled atmospheric emissions and possible adverse health impacts was of highest concern to local citizens in public discussions. Therefore, providing continuous measurements and monitoring of all relevant parameters was a priority. The development

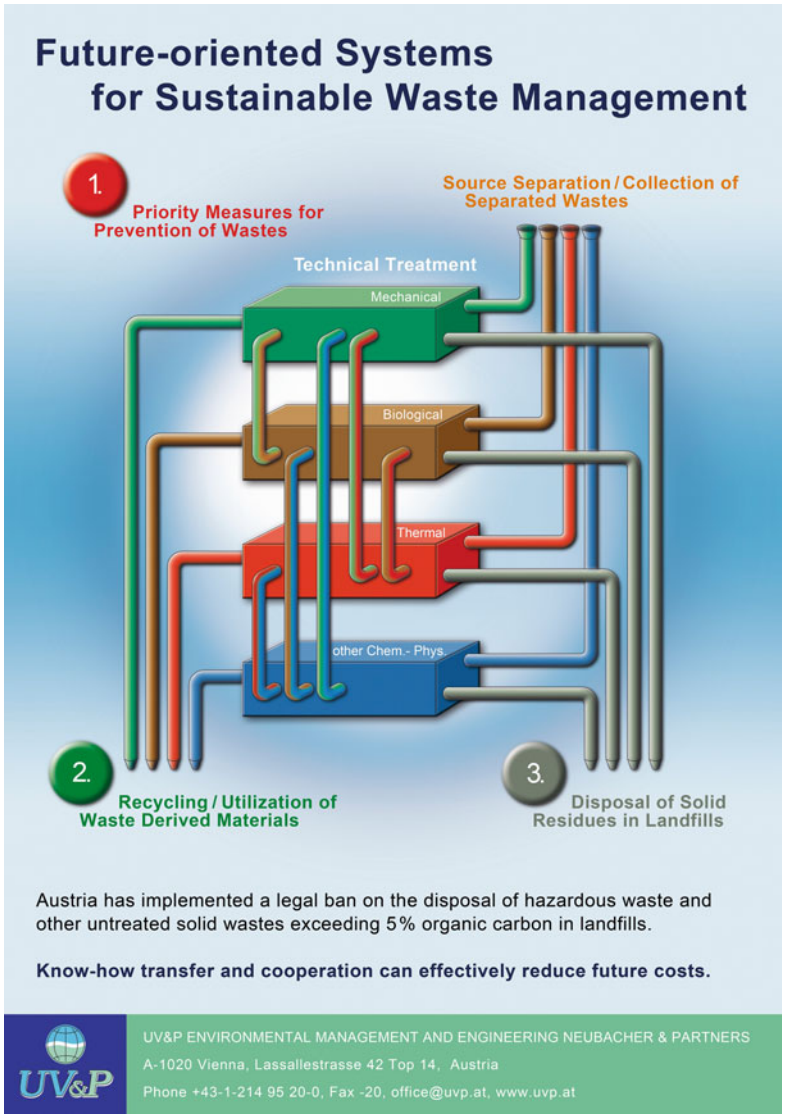

Waste-to-Energy: Fluidized Bed Technology. Figure 19
Integrated system for sustainable waste management

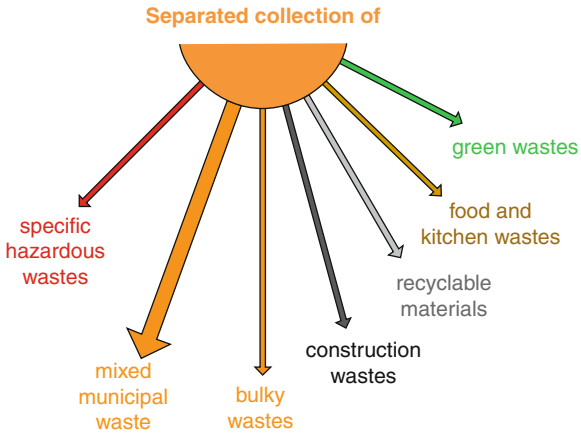

Waste-to-Energy: Fluidized Bed Technology. Figure 20
Separate collection of municipal wastes for recovery of materials and energy

Waste-to-Energy: Fluidized Bed Technology. Figure 21
Projected aerial view of waste-to-energy plant in Austria (design by architect H. Ganguly)

and planning of the waste-to-energy project was based on the most stringent emission standards worldwide (!). The public was also informed about the composition of the cleaned flue gas leaving the (already existing 152 m high) smokestack (see also Fig. 14). Subsequently, public concerns were expressed regarding the unknown organic pollutants as indicated by the summary parameter TOC (total organic carbon). However, the comparative calculation shows that the maximum allowable emission through the smokestack is equivalent to the organic carbon emissions of 14 passenger cars driving somewhere in the region (e.g., on the nearby highway A1, see Fig. 15).

The public discussion also showed great concern of some citizens for the need to analyze each delivery of incoming waste in order to be informed of the materials to be incinerated. However, the public has also been informed regarding the mass and emission balances for all of the six critical elements for thermal waste treatment processes. These include chlorine (predominant pollutant in various waste), fluorine, sulfur (predominant pollutant in some wastes, high load in the off-gas used for combustion air in the case of Lenzing), mercury (extremely volatile and toxic), cadmium (medium volatile and very toxic), and chromium (not volatile, but toxic in the water-soluble form of Chromium$^{(VI)}$). Thus, further chemical analyses are to be carried out only in the case of unknown production wastes and if there is suspicion of potentially high pollution load. The planned waste-to-energy plant will be equipped and operated to comply with the emission standards under all circumstances, also with the understanding that waste incineration in a fluidized bed can be halted within minutes in case of an emergency.

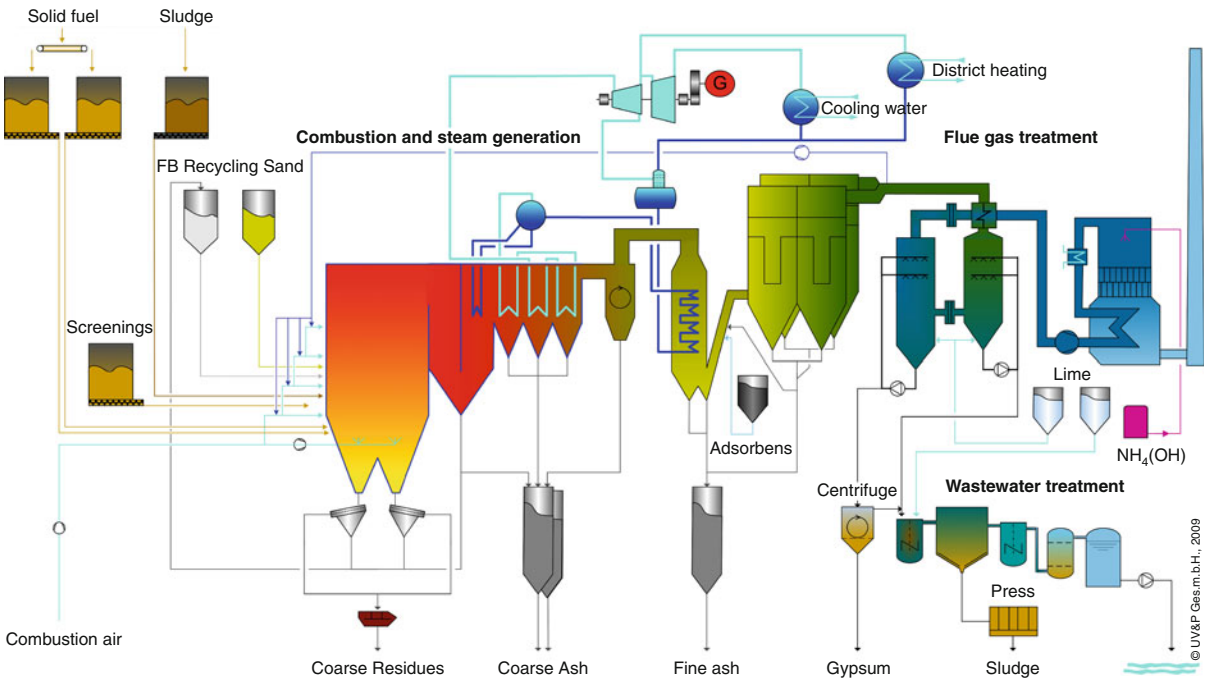

Waste-to-Energy: Fluidized Bed Technology. Figure 22
Waste-to-energy plant for processing municipal solid waste and residues from recycling and treatment of sewage in the region of Linz

Finally, some citizens (including lobbyists opposed to the waste-to-energy project) articulated concerns about the most dangerous emissions in the form of "dioxins." The answer was already prepared by a risk assessment based on a maximum allowable emission of 0.1 ng TE/m^3 (TE = toxicity equivalent of poly-chlorinated di-benzo-dioxins and -furanes expressed in 2,3,7,8 TCDD) and on the results of a dispersion model with meteorological data for an entire year measured onsite. The overall response presented by independent medical experts indicated a hypothetical, but extremely small additional risk (see Fig. 16). This risk was illustrated to the public by comparing the numbers with smoking a cigarette. Comparatively speaking, the amount of dioxin emitted from the waste-to-energy plant equals smoking one additional cigarette in 1,000 years, if the precautionary value for protection of health is supposed to be the maximum of one cigarette per year (see Fig. 17).

The discharge of dissolved chlorides within the small quantity of treated wastewater effluent (after removal of all heavy metals in multistage wastewater treatment) has been of no public concern due to the relatively small quantity in comparison to chlorides used for ion-exchange in the softening of hard water and salt applications on roads against ice in winter.

The negative public opinion regarding emissions from waste incineration is generally due to several factors: ignorance of the facts and figures and past achievements in making waste-to-energy an environmentally friendly option (as indicated by the development of atmospheric emissions according to state-of-the-art in Austria and Switzerland – see Table 3). The comparison of strict emission standards for various new sources of industrial production and heat and power generation indicates the outstanding environmental standard of waste-to-energy (Fig. 18).

Future Perspectives

Sustainable waste management will require an integrated approach for recycling and recovery based on material separation. Various specific technologies for

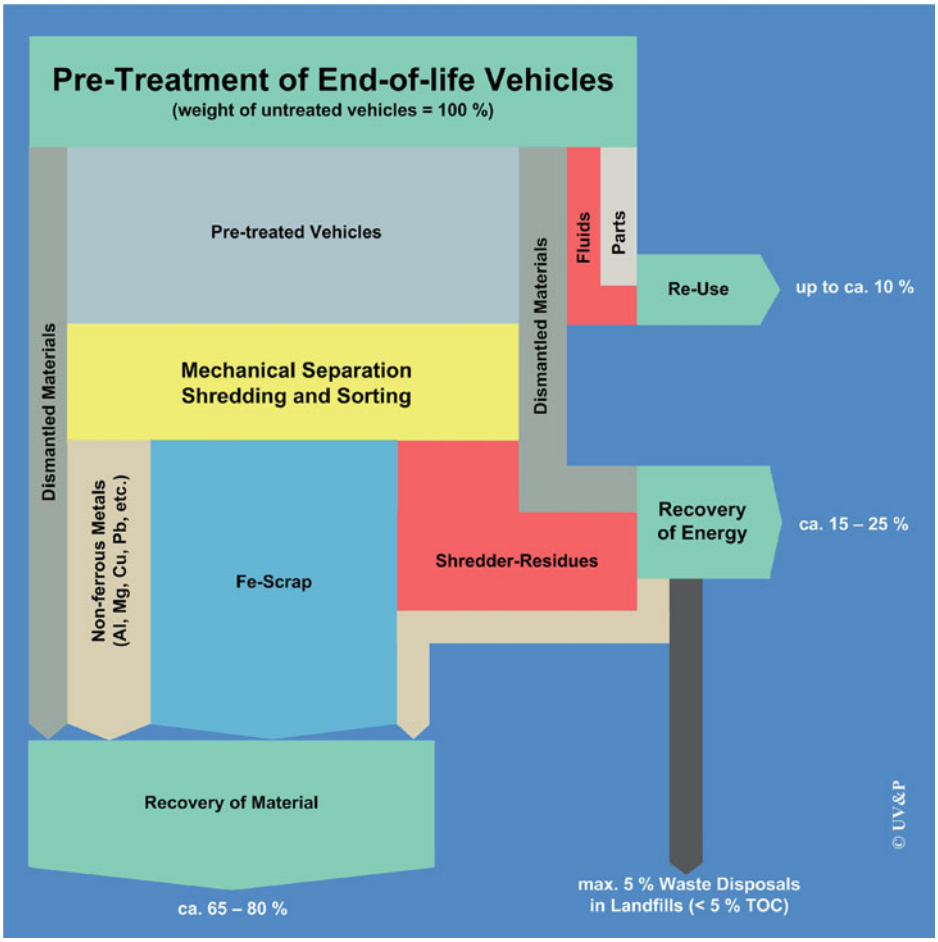

Waste-to-Energy: Fluidized Bed Technology. Figure 23
Processing of end-of-life vehicles in Austria and EU that includes material and energy recovery from automobile shredder residues

treatment of separated wastes are needed including thermal processes in context with recovery of materials and energy as illustrated in Fig. 19.

In the case of municipal waste management, waste-to-energy is needed for residues from recycling and material recovery as well as for mixed municipal wastes (Fig. 20). For practical purposes, fluidized bed systems for waste-to-energy at appropriate locations (with continuous demand for heat throughout the year, industrial infrastructure, and competence in operation and maintenance) should be considered as an option for integrated sustainable waste management in the future. The latest project in Central Europe for industrial waste-to-energy has been planned for integration into an existing cardboard recycling and production facility with a continuous demand of steam and electricity throughout the year. The planned project will substitute for imported natural gas and will use reject materials and other residues from paper and cardboard recycling for waste-to-energy in a fluidized bed boiler. The planned thermal capacity is 160 MW suitable for up to 450,000 t of waste fuel per year. The architectural design of the planned facility illustrates the option for aesthetic harmony with the surrounding environment (see Fig. 21).

The following example of waste-to-energy for district heating and power generation illustrates integrated waste management for the region of Linz in Upper Austria (see Fig. 22). This plant will start operations in 2011 [5]. It is designed for a fuel capacity of 72.6 MW and allows for the utilization of 200,000 t of various residues from

recycling and sewage treatment as well as for mechanically pretreated mixed municipal solid waste. The fluidized bed system comprises a sophisticated air control and distribution system that allows for highest efficiency in combustion and also for very low emissions [6]. This plant is located in the central area of the city of Linz and has been permitted based on a positive Environmental Impact Assessment without any objection from neighbors and citizens.

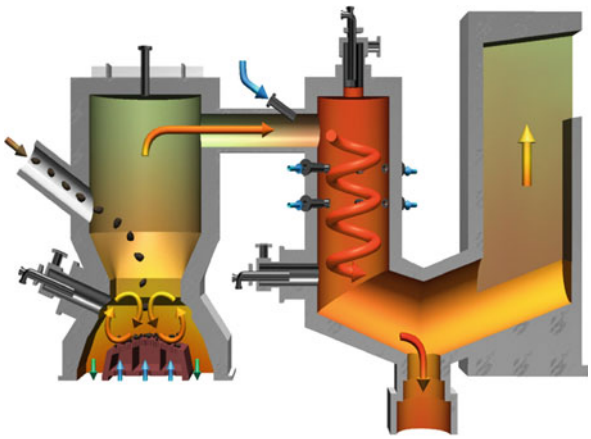

Waste-to-Energy: Fluidized Bed Technology. Figure 24
TwinRec core components gasifier and ash melting furnace [5] (© Ebara Environmental Plant Co., Ltd.)

The future challenges for waste-to-energy in fluidized bed systems include recovery of valuable materials prior, during, or after the thermal treatment process. This will be especially relevant for the treatment of shredder residues from end-of-life vehicles and other wastes containing metals and rare elements. The increase of recovery mandated in the European Directive 2000/53/EC on end-of-life vehicles to 95% (including 85% of reuse and material recovery) by 2015 will be a significant challenge for adaptation and further development of fluidized bed technologies (see Fig. 23). Such a solution may be provided by the Ebara internally circulating fluidized bed system (operating at around 600°C) followed by high-temperature combustion at around 1,400°C in an ash melting furnace that has been developed and is operating in Japan [7] (Figs. 24 and 25).

Waste-to-energy plants require a continuous fuel supply. However, waste-to-energy plants need planned shutdown times of typically 3 weeks or longer for maintenance, plus some for unexpected necessary repairs. Therefore, it is necessary to provide for intermediate storage of the feedstock to the plant.

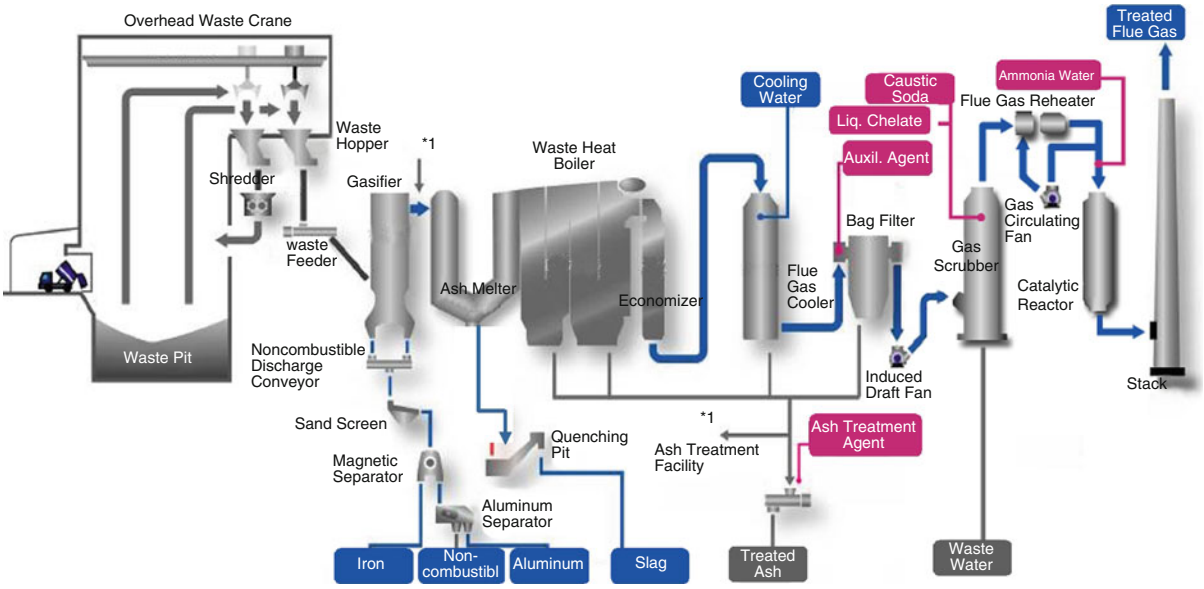

Waste-to-Energy: Fluidized Bed Technology. Figure 25
Combined energy and material recovery at the Aomori plant [5] (© Ebara Environmental Plant Co., Ltd.)

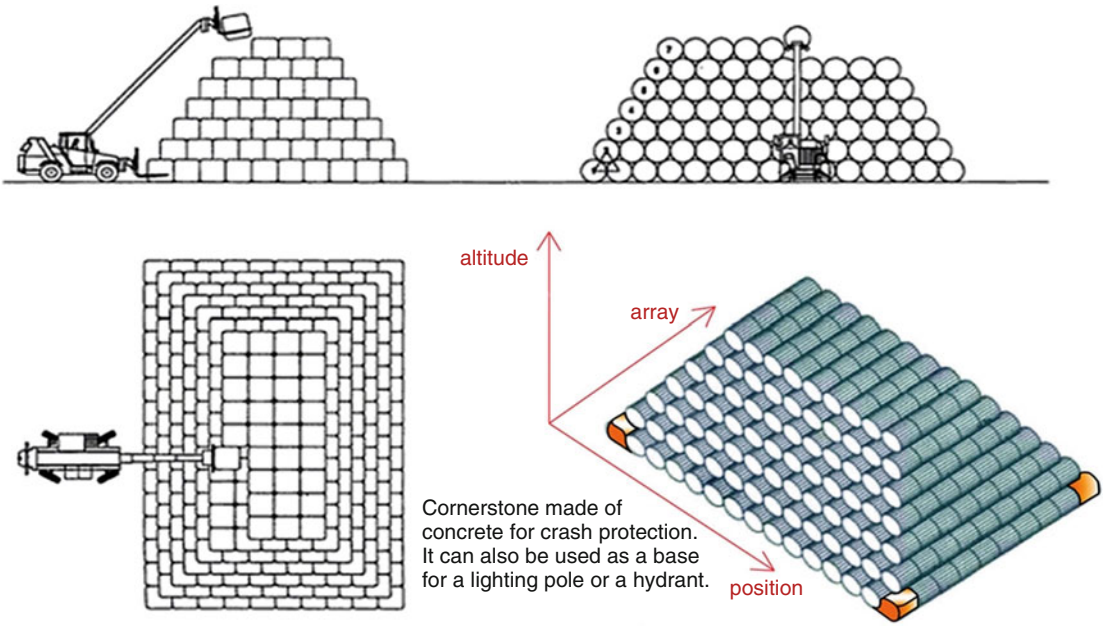

Waste-to-Energy: Fluidized Bed Technology. Figure 26
Logistic and intermediate storage in view of environmental protection and fire safety (Patent applications A 1037/2008, PCT/EP 2009/050238)

Technical guidelines have been developed for environmentally safe storage of different high-calorific and organic wastes [8]. As discussed in other entries in the waste-to-energy section of this encyclopedia, the bunker of a waste-to-energy plant can be designed to store up to 2 weeks of incoming wastes; when longer periods of storage are required, the wastes can be baled as illustrated in Fig. 26, based on proven know-how and experience in Europe. Cylindrical bales of approximately 1.2 m diameter and height can allow for a storage capacity of up to 60,000 t of solid wastes per hectare. Specific features for prevention of fire hazards and adverse environmental impacts of this method of storage and transport of wastes have been developed in Austria [8].

Bibliography

Primary Literature

1. Werther J (1992) Fluidized bed reactors. In: Ullmann's encyclopedia of industrial chemistry, vol B4. VCH, Weinheim
2. White Book Waste-to-Energy in Austria: Figures, Data, Facts (2010) Austrian Federal Ministry of Agriculture, Forestry, Environment and Water Management, Vienna
3. Strauss T et al. (2005) Start-up and operation optimization of a 39 MW_{th} bubbling fluidized bed incinerator for domestic waste and sewage sludge. Fernwaerme Wien, Vienna
4. Stubenvoll J et al. (2002) Stand der Technik bei Abfallverbrennungsanlagen, Austrian Federal Ministry of Agriculture, Forestry, Environment and Water Management, Vienna
5. Zschetzsche A (2011) RHKW Linz: engineering, contract specifications, supervision of erection and commissioning, AZ^2 Technisches Büro, Linz in cooperation with UV&P, Vienna
6. Seemann B (2010) BioCOM® – fluidized bed combustion technology for thermal utilisation of biomass and waste. HS energieanlagen, Freising
7. Seliger A, Steiner C (2004) Waste gasification in practice: TwinRec fluidized bed gasification and ash melting – review of four years of plant operation. In: IT3'04 conference, Phoenix, 10–14 May 2004
8. Huber KH et al. (2007) Anforderungen an die Zwischenlagerung von heizwertreichen Abfaellen, Austrian Federal Ministry of Agriculture, Forestry, Environment and Water Management, Vienna
9. Integral (2004) The fluidized bed incinerator #4 for the treatment of municipal waste and sewage sludge. INTEGRAL, Achau
10. Hashemian M (2011) ECOFLUID RC and POWER FLUID® RC fluidized bed technology for "Energy from Waste" ANDRITZ Energy and Environment, Raaba/Graz

Books and Reviews

Gleis M et al. (2011) German experiences with thermal treatment processes. In: Seventh international congress & exhibition for energy efficiency & renewable for south east Europe, Sofia, 13–15 April 2011

Grabda M et al. (2011) Waste to energy – practices and technologies in Japan. In: Seventh international congress & exhibition for energy efficiency & renewable for south east Europe, Sofia, 13–15 April 2011

Thomé-Kozmiensky K (1993) Reaktoren zur thermischen Abfallbehandlung, EF – Verlag für Energie und Umwelttechnik GmbH, Berlin

Thomé-Kozmiensky K (1994) Thermische Abfallbehandlung, EF – Verlag für Energie und Umwelttechnik GmbH, Berlin

Wlilén C et al. (2004) Finnish expert report on best available techniques in energy production from solid recovered fuels, Finnish Environment Institute, Helsinki

Wastewater Reclamation

In S. Kim[1], Byung Soo Oh[1], Seokmin Yoon[2], Hokyong Shon[3], Sangho Lee[4], Seungkwan Hong[5]

[1]Center for Seawater Desalination Plant, Gwangju Institute of Science and Technology (GIST), Buk-gu, Gwangju, Republic of Korea

[2]Environment Research Division, Research Institute of Industrial Science and Technology (RIST), Pohang, Republic of Korea

[3]School of Civil and Environmental Engineering, University of Technology, Sydney (UTS), Broadway, NSW, Australia

[4]Department of Water Resources and Environmental Research, Korea Institute of Construction Technology, Goyang-Si, Gyeonggi-Do, Republic of Korea

[5]Department of Civil, Environmental & Architectural Engineering, Korea University, Sungbuk-gu, Seoul, Republic of Korea

Article Outline

Glossary
Definition of the Subject
Introduction
Describing Wastewater Reclamation
Technologies for Wastewater Reclamation
Future Directions
Bibliography

Glossary

Agricultural water Water used for crop production and livestock uses.

Concentrate (also called retentate) The portion of the feed stream that contains salts rejected from the membrane system. The term can also refer to the rejected mixed liquor suspended solids (MLSS) in a membrane bioreactor (MBR) process, which is recycled or wasted to maintain a given biomass concentration in the biological treatment process.

Conventional treatment Technologies such as activated sludge and trickling filters that remove BOD and suspended solids from wastewater. Conventional treatment technologies are often coupled with anoxic and anaerobic processes for nutrient removal.

Direct potable reuse Introduction of reclaimed water directly into a drinking water distribution system, without intervening storage or additional treatment.

Indirect potable reuse Augmentation of a raw water supply with reclaimed water followed by an environmental buffer. The mixture of raw and reclaimed water typically receives additional treatment before distribution as drinking water.

Membrane bioreactor (MBR) A process that combines a suspended growth activated sludge reactor with a membrane separation system. Membrane separation is accomplished by either microfiltration or ultrafiltration and used in place of conventional gravity sedimentation.

Pathogens Disease-causing organisms capable of inflicting damage on a host it infects.

Potable water Water deemed safe for human consumption, food preparation, and bathing.

Reclaimed water Municipal wastewater that has gone through various treatment processes to meet specific water quality criteria with the intent of being used in a beneficial manner.

Renewable water resources The water entering a country's surface and groundwater systems. Not all of this water can be used because some falls in a place or time that precludes tapping it even if all economically and technically feasible storage and diversion structures were built.

Secondary treatment Activated sludge treatment, commonly with nitrification, used for the removal of soluble organic matter and particulate constituents.

Trace organics Organic compounds detected at very low (minute) levels by the use of sophisticated instrumentation capable of measuring concentrations in the range of 10^{-12} to 10^{-3} mg/L.

Wastewater reclamation Treatment or processing of wastewater to make it reusable with definable treatment reliability and meeting appropriate water quality criteria.

Wastewater reuse The use of treated wastewater for a beneficial use, such as agricultural irrigation and industrial cooling.

Wastewater Used water discharged from homes, business, cities, industry, and agriculture. Various synonymous uses such as municipal wastewater (sewage), industrial wastewater, and stormwater.

Definition of the Subject

Wastewater can be defined as used and contaminated water, mainly through human activities, which is adversely affected in quality by anthropogenic influence. The meaning of reclamation is the process of artificially converting an unusable entity to one that is usable. Accordingly, the definition of wastewater reclamation is the process of reclaiming wastewater into a reusable form by artificial treatments. Through the treatment processes, the reclaimed water is able to meet appropriate water quality criteria so it can be returned to the environment to augment the natural systems from which it came, or reused for numerous purposes related to human activities. The reuse of reclaimed wastewater makes two important contributions. The first is to produce sustainable water resources, and the second is to reduce adverse environmental effects. Furthermore, if wastewater could be completely reclaimed, it would be possible to have zero discharges in the water recycle between humans and the natural environment.

Introduction

The total amount of water on the earth rarely changes due to external impacts, but the world now suffers from a scarcity of usable water, which is due to the dislocation of the earth's water cycle, with the main reason being climate change. It is true that rapid industrialization and population growth have been accelerating climate change and contributing to the increasing scarcity of water around the world. Many countries are making great endeavor to overcome the water shortage problem by acquiring sustainable water resources via three main technologies; seawater desalination, rainwater harvesting, and wastewater reclamation. The properties of each of these technologies will be introduced in section "Sustainable Water Resource." All human activities use water, and this used water is discharged as wastewater (including sewage water and other discharged waters). The wastewater discharged from everywhere (e.g., homes, business, cities, industry, agriculture, and stormwater runoff) is treated in wastewater treatment plants to produce treated wastewater, called wastewater effluent, which will mix with natural water (e.g., river and lake). Target sources for wastewater reclamation include wastewater, wastewater effluent, and further treated wastewater effluent, but reuse of wastewater itself is significantly limited due to the water quality required for safe reuse. Technologies for wastewater reclamation are manifold according to the required purpose and water quality criteria. The applications of reclaimed water are categorized as follows: agricultural irrigation, landscape irrigation, industrial recycling and reuse, groundwater recharge, non-potable urban uses, and potable uses (see section "Applications and Water Qualities for Using Reclaimed Water"). The wastewater reclamation technologies can be divided into two types, conventional (processes installed in municipal wastewater treatment plants) and advanced (processes mainly related to membranes, such as membrane bioreactor, microfiltration, ultrafiltration, nanofiltration, and reverse osmosis for shifting wastewater to high-quality reclaimed water). For the most part, these methods are derived from physical, chemical, and biological treatment processes operated at municipal wastewater and drinking water treatment plants. The technical review of both conventional and advanced technology for wastewater reclamation will be discussed in sections "Conventional Treatment Practice" and "Advanced Technologies for Producing High-Quality Reclaimed Water." The keyword, "energy," is a critical issue around the world along with "water." Even though wastewater can be reclaimed as drinking water, it should be noted that the energy consumption of the applied technology is acceptable for its beneficial use. In the case of seawater desalination, a recent technical shift from thermal type to

reverse osmosis has been brisk because an energy-efficient plant is necessary for entering world markets. In section "Energy Consumption: Comparison of Wastewater Reclamation with Desalination," a comparative survey is presented for the energy consumption level between wastewater reclamation and seawater desalination. According to the applications for which the reclaimed water will be used, treatment goals are various.

Describing Wastewater Reclamation

Sustainable Water Resource

At global level, water source on Earth is abundant in nature, but the water source that is allowed to be accessed by humans is not enough. Over 97% of water on Earth is salt water; the remaining 5% is freshwater, including glaciers, groundwater, and surface water. Also, only 0.3% of the freshwater is surface water that can be easily used by humans. The global water cycle describes the continuous movement of water on Earth. Rivers flow into the oceans and seas, and the sun heats this water, which is the driving force of the water cycle. The heated water moves from oceans to land through a process of evaporation → condensation → precipitation, by which water becomes sustainable on land, supplying humans with sufficient water. However, the water cycle has changed due to global warming. Climate change has caused more frequent, severe rainfall and snowfall in some regions, and intensive drought in other regions, resulting in a significant reduction in the availability of renewable water resources for humans. In addition, the centralization of population into cities and industrial areas has made the use of various water sources difficult. About one third of the world's population (= about 6.8 billion in 2010) currently faces moderate to severe water shortages. An estimated 25% of the world population lacks access to clean drinking water and protection from waterborne diseases (US Census Bureau – World POPClock Projection). Recently, great efforts have been made to solve this water scarcity problem by finding alternative and sustainable water resources, which are classified into three main categories; rainwater harvesting, seawater desalination, and wastewater reclamation. First, a water storage device, such as a dam or reservoir, needs to be constructed that can store water when it rains. Rainwater harvesting used to be the best way to conserve water from flowing into seas and oceans, but there are many constraints on this method. First of all, building a dam causes deterioration of the water quality. Furthermore, it is unsuitable for securing sustainable water because precipitation and the time for rain cannot be controlled. Second, desalination could be a solution for changing unusable (seawater) into available water (freshwater). In this case, seawater can be classified as an unlimited water resource. However, there are space restrains because this water resource only exists on the sea shore. Third, wastewater reclamation is the most popular way to produce usable water from wasted water. Wastewater reclamation could surpass the limitations of the other reclamation methods, because wastewater is produced everywhere human activities take place.

Applications and Water Qualities for Using Reclaimed Water

A summary of categories for the application of reclaimed water is given in Table 1. The largest use of reclaimed water is for agriculture irrigation in most areas of the world. In 2002, about 46% of the total reclaimed water produced in California was used for agricultural irrigation (State of California 2003, 2004). Australia utilized 82% of their reclaimed water supply for agricultural irrigation in 2000 (Australian Bureau of Statistics 2004). In Israel, one of the most arid countries, it is estimated that 230 wastewater reclamation systems are in operation, recycling 72% of the municipal wastewater produced, primarily agricultural irrigation. The water supply from reclaimed water comprises about 15% of Israel's water recourses. In general, landscape irrigation is a major portion of the urban use of reclaimed water. For example, the Irvine Ranch Water District in southern California estimates that more than 70% of their total water use is for landscape irrigation. According to the data, the States of California and Florida are two largest users of reclaimed water in the United States, with golf course irrigation being major use of reclaimed water, comprising 50% and 36% of the total landscape irrigation use in each States, respectively. This indicates that landscape irrigation is a viable option for reducing the

Wastewater Reclamation. Table 1 Applications of reclaimed water [14]

Main category	Subcategory	Examples
Agricultural irrigation	Food crops	Crop grown for human consumption and consumed uncooked
	Nonfood crops and others	Fodder, fiber, seed corps, pastures, commercial plant nurseries, sod farms, and commercial aquaculture
Urban uses	Non-potable use	Landscape irrigation (parks, playgrounds, school yards, golf courses, cemeteries, greenbelts, and residential), fire protection, construction, ornamental fountains, road care/maintenance, car washing and in-building uses (toilets and air-conditioning)
	Potable use	Direct pipe to pipe water supply, blending with municipal water supply (reservoirs and groundwater)
Industrial uses	–	Cooling water, boiler feed, process water, construction activities, and washdown water
Environmental uses	Recreational use	Lakes and ponds used for swimming and snowmaking, fishing, and boating
	Environmental enhancement	Artificial wetlands, enhanced natural wetlands, sustained stream flows, and marsh enhancement
	Groundwater recharge	Groundwater replenishment, salt water intrusion control, and subsidence control

demand on potable water and decrease wastewater discharges to the environment. Industries commonly tend to use water at a relatively constant rate throughout the year compared to the seasonal and geographic variations associated with water use for agricultural and landscape irrigation. Therefore, a major benefit of using reclaimed water for industrial applications is that the water use requirements are consistent year-round. Other important considerations are the economic feasibility regarding system components and the related cost elements, such as reclaimed water supply, distribution system, onsite re-piping, engineering analysis of water quality and supplemental treatment alternatives, pretreatment capital and operating and maintenance costs, internal treatment needs, management of process residuals, including sludges and brines, as well as institutional, legal, and administrative activities. The contribution of reclaimed water for environmental enhancement has recently increased to satisfy the requirements of maintaining minimum water flows in rivers, streams, and wetlands, which is a major challenge in water resources management. The augmentation of various water resources using reclaimed water also increases the recreational opportunities.

When applying reclaimed water to its desired purposes, the water quality takes priority over everything else. A review of the required water quality for the application of reclaimed water is discussed below.

Concerns on pathogen when using reclaimed water: Encouraging wastewater reclamation and ensuring public health from wastewater reuse have been serious issues since the 1930s. Improperly treated wastewater may increase the risk to public health by exposing humans to microbial pathogens, chemicals, and heavy metals. Therefore, the safe use of wastewater has long been discussed with respect to the quality of water for various types of reuse; urban, agricultural, industrial, recreational and environmental reuse, groundwater recharge, and indirect potable reuse. Of the risks associated with water reuse, microbial pathogens have been considered the most significant, because sewage from urban and agricultural areas are major sources, which contain many pathogens, including viruses, bacteria, protozoan parasites, and helminthes. G. Kamizoulis [10] investigated the number of pathogens in raw sewage, as summarized in Table 2. Accordingly, thermotolerent coliforms (fecal colifoms) and enteric viruses were found to be the most abundant in raw sewage. It is clear that these pathogens cause various diseases to humans when they are exposed, either directly or indirectly, to the untreated sewage.

Wastewater Reclamation. Table 2 Typical numbers of excreted organisms in raw sewage [10]

Organisms	Numbers in wastewater (per L)
Bacteria	
Thermotolerant coliforms	10^8–10^{10}
Campylobacter jejuni	10–10^4
Salmonella spp.	1–10^5
Shigella spp.	10–10^4
Vibrio cholerae	10^2–10^5
Intestinal helminths	
Ascaris lumbricoides	1–10^3
Ancylostoma/Necator 03	1–10^3
Trichuris trichiura	1–10^2
Protozoa	
Cryptosporidium parvum	1–10^4
Entamoeba histolytica	1–10^2
Giardia intestinalis	10^2–10^5
Viruses	
Enteric viruses	10^5–10^6
Rotavirus	10^2–10^5

Wastewater Reclamation. Table 3 Survival times of pathogen at 20–30°C [6] (unit: days)

Pathogen	Freshwater and sewage	Crops	Soil
Viruses	<120 (<50)	<60 (<15)	<100 (<20)
Bacteria	<60 (<30)	<30 (<15)	<70 (<20)
Protozoa	<30 (<15)	<10 (<2)	<70 (<20)
Helminth	Many months	<60 (<30)	Many months

Figures in brackets show the normal survival time

Although many microbial pathogens exist in the raw sewage, the survival times outside of their hosts are limited, even without any disinfection process. Bradley (1983) investigated the survival time of pathogens at 20–30°C when exposed to environmental media, including freshwater and sewage, crops and soil (Table 3). According to the results, the survival time was shortest when the pathogens are in crops. Meanwhile, helminthes have been shown to survive for several months in water and soil.

Traditionally, coliforms and fecal coliforms are commonly used as pathogen indicators due to their large numbers in the feces of humans and warm-blooded animals, easy and rapid detection, and lack of growth in natural habitats outside of their hosts [7]. For the safe use of wastewater, the first guideline was enacted for irrigation in California, USA, in 1918 (California Table 22), which adopted a strict guideline for coliforms and fecal coliforms because California had advanced water treatment technology, but little available epidemiological evidences. The USEPA later developed federal guidelines on the basis of the treatment process, and finally published "Guidelines for water reuse" in 1992. The USEPA guidelines contain reclaimed water quality guidelines, with recommended monitoring and setback distances. The USA developed a water treatment process to meet the strict water quality, such as coagulation/flocculation, filtration, and disinfection, and these standards were also used for the safe quality of imported crops. In 1973, WHO announced the first wastewater reuse guidelines, with an epidemiological approach, which contained values for tolerable coliforms and fecal coliforms for the practical use of reclaimed wastewater in developing countries where sewage has been historically used for irrigation of crop without an appropriate treatment. The first guidelines have been revised with more epidemiological evidences, treatment processes, and irrigation systems, and WHO finally published the current guidelines in 1989, titled "Health Guidelines for the Use of Wastewater in Agriculture and Aquaculture." For the development of standards in the USA, California Table 22 influenced the regulation program of each state, but each state has different standards with different approaches according to the treatment process or water quality. A range of standards is now in use, as shown in Table 4. The USA standard consists of treatment technology, BOD5, TSS, Turbidity, and coliforms (total and fecal), with ten types of water use; urban reuse (restricted and unrestricted), agricultural (food crops and nonfood crops), recreational (restricted and unrestricted), environmental (wetland), industrial, groundwater recharge (non-potable aquifer), and

Wastewater Reclamation. Table 4 Examples of microbial quality standards used by various States in the USA [3]

Exposure route	Total coliforms per 100 mL		Fecal coliforms per 100 mL		Enteric viruses per 40 L	
	n[a]	Range of values	*N*	Range of values	*N*	Range of values
Spray irrigation[b]	4	2.0–100	3	2.2–200	1	1
Surface irrigation[b]	2	100	9	10–1,000	0	–
Parks and playgrounds[c]	8	2.2–100	3	10–100	1	128
Golf courses and open space[d]	6	2.2–1,000	5	0–100	0	–

[a]Number of states involved out of the 13 selected
[b]Includes food crop irrigation
[c]Includes playgrounds
[d]Includes cemeteries
[e]Arizona is the only state that has a virus standard

Wastewater Reclamation. Table 5 Recommended microbiological quality guidelines for wastewater use in agriculture[a]

Reuse conditions	Exposed group	Intestinal nematodes (/L[a,e])	Fecal coliforms (/100 mL[b,e])	Wastewater treatment expected to achieve required quality
Irrigation of crops likely to be eaten uncooked, sports fields, public parks[c]	Workers, consumers, public	<1	<1,000	A series of stabilization ponds designed to achieve the microbiological quality indicated, or equivalent treatment
Irrigation of cereal crops, industrial crops, fodder crops, pasture, and trees[d]	Workers	<1	None set	Retention in stabilization ponds for 8–10 days or equivalent helminth removal
Localized irrigation of crops if category B exposure of workers and the public does not occur[e]	None	n/a	n/a	Pretreatment as required by the irrigation technology, but not less than primary sedimentation

[a]Arithmetic mean
[b]Geometric mean
[c]In specific cases, local epidemiological, sociocultural, and environmental factors should be taken into account, and the guidelines modified accordingly
[d]*Ascaris* and *Trichuris* species and hookworms
[e]During the irrigation period
[f]A more stringent guideline (200 fecal coliforms/100 mL) is appropriate for public lawns with which the public may come into direct contact
[g]In the case of fruit trees, irrigation should cease 2 weeks before the fruit is picked and none should be picked off the ground

indirect potable reuse. The USA guidelines and standards influenced those of Australia, South Korea, and so on (Mehlika 1996; Ursula 2000; [9]), and the WHO guidelines affected European and Mediterranean nations in establishing their regulations. Particularly, a European level guideline has not been established, but is now being developed through the AQUAREC project [1].

Water quality of wastewater reuse for agriculture: Agricultural irrigation accounts for the largest part of water demand, approximately 80% of the worldwide; therefore, it also will also become the major water reuse application [21]. As describe before, the first standards are for microbiological parameters that show the presence of pathogens in wastewater. Water quality for irrigation in agriculture has been subdivided into three groups by the WHO (1989), as shown in Table 5; Group A (Irrigation of crops to be eaten uncooked, sports fields, and public parks), Group B (Irrigation of

cereal crops, industrial crops, fodder crops, pasture, and trees) Group C (exposure of workers and the public does not occur), in which the exposed group, helminthes, and fecal coliforms are described separately. The fecal coliforms in reclaimed water for uncooked crops are below 1,000 cfu/100 mL. The USEPA [20] guidelines for treated wastewater in agriculture are shown in Table 6, with type of use subdivided into three groups; similar to WHO (1989); Food crops not commercially processed, Food crops commercially processed, for nonfood crops. Contrary to the WHO guideline, zero fecal coliforms in 100 mL are required for irrigation water quality of uncooked crops, in addition to BOD_5, pH, SS, and residual chlorine. It is also recommended for reclaimed water monitoring and setback distances for each type of use. In the USA, each state has different microbiological standard, with different approach according to the treatment process or water quality, and a range of standards is in use. For unrestricted irrigation of food crops, the range is 2.2–20 fecal coliforms bacteria/100 mL, and for restricted irrigation is 23–200 fecal coliforms bacteria/100 mL.

Water quality of wastewater reuse for other type of applications: The USEPA standard for water quality (1992) describes the standards for each state for ten types of water use. As with water quality for agriculture, the regulatory items include treatment method, BOD5, TSS, Turbidity, and coliforms (total and/or fecal coliforms). In 1998, WHO published "Guidelines for Safe Recreational Water Environments." These guidelines deal with fecal coliforms' contamination of recreational water, with dose–response results used to develop criteria linking the microbial concentration in recreational waters to gastroenteritis. Table 7 shows the water quality for reclaimed wastewater and the qualitative requirements of eight types of water use.

Other water quality parameters: Besides microbial pathogens, other water quality parameters related with wastewater reuse are toxic metal accumulation and the salinity of wastewater. The availability and accumulation of heavy metals in crops depends on soil factors, such as pH, cation exchange capacity (CEC) and moisture content, and plant factors, such as species variety, plant parts used for consumption, and temperature. The salinity of wastewater is a problem in some Mediterranean countries, as it exerts an osmotic effect on plant growth. The USEPA updated the draft regulations in July 2003, requiring monitoring of emerging pollutants of concerns (EPOCs). The draft regulations require annual monitoring for pharmaceuticals, endocrine disrupting chemicals, and other chemical indicators in municipal wastewater [21].

Technologies for Wastewater Reclamation

Conventional Treatment Practice

Conventional wastewater treatment, which is also applied for water reuse, consists of a combination of physical, chemical, and biological processes, with operations to remove solids, organic matter and, sometimes, nutrients. Different degrees of treatment are used to achieve the desired levels of contaminant removal for water reuse, including preliminary, primary, secondary, tertiary, and disinfection, as well as advanced treatment.

1. *Preliminary treatment*: Preliminary treatment removes large solid materials from the raw wastewater before they are able to damage or clog the pumps and skimmers of the primary treatment clarifiers. Screening and grit removal are typical examples of preliminary treatment.
2. *Primary treatment*: Primary treatment aims to remove settable organic and inorganic materials by sedimentation and/or skimming. It is effective at removing large fractions of the total suspended solids, oils, and greases. Some organic nitrogen, organic phosphorous, and heavy metals associated with those solids are also removed, but colloidal and dissolved constituents are not removed. For nonfood crop irrigation, primary treatment may be a sufficient treatment. However, secondary treatment may be required to prevent potential adverse effects. Sedimentation tanks or clarifiers are generally used as a primary treatment. The sludge is processed by methods such as aerobic digestion, storage in sludge lagoons, land application, and others.
3. *Secondary treatment*: Secondary treatment is additional to the primary treatment of effluent to remove the residual organics (as indicated by BOD) and suspended solids. In most cases, secondary treatment involves aerobic biological treatment

Wastewater Reclamation. Table 6 US-EPA/USAID guidelines for agricultural reuse of wastewater [20]

Type of reuse		Treatment	Reclaimed water quality	Reclaimed water monitoring	Setback distance
Urban reuse					
Landscape irrigation, vehicle washing, toilet flushing, fire protection, commercial air conditioners, and other uses with similar access or exposure to the water		Secondary[a]	pH = 6–9	pH: weekly	50 ft (15 m) to potable water supply wells
		Filtration[b]	BOD < 10 mg/L	BOD: weekly	
		Disinfection[c]	Turbidity < 2NTU[d]	Turbidity: continuous	
			FC = zero coliform/100 mL[e]	Coliform: daily	
			Cl_2 residual = 1 mg/L min	Cl_2 residual: Continuous	
Agricultural reuse	*Food crops not commercially processed*				
	Surface or spray irrigation of any food crop, including crops eaten raw	Secondary	pH = 6–9	pH: weekly	50 ft from potable water supply wells
		Filtration	BOD ≤ 30 mg/L	BOD: weekly	
		Disinfection	Turbidity < 1NTU[d]	Turbidity: daily	
			FC = zero /100 mL[e]		
			Cl_2 residual = 1 mg/L min	Coliforms: daily	
				Cl_2 residual: continuous	
	Food crops not commercially processed				
	Surface irrigation of Orchards and Vineyards	Secondary	pH = 6–9	pH: weekly	100 ft from areas accessible to public
		Disinfection	BOD ≤ 30 mg/L	BOD: weekly	
			SS = 30 mg/L	SS: daily	
			FC ≤ 200/100 mL	FC: daily	
			Cl_2 residual = 1 mg/l min	Cl_2 residual: continuous	
	For nonfood crops				
	Pasture for milking animals; fodder, fiber and seed crops	Secondary	pH = 6–9	pH: weekly	300 ft (90 m) to potable water supply wells
		Disinfection	BOD ≤ 30 mg/L	BOD: weekly	
			SS < 30 mg/L	TSS: daily	
			FC < 200/100 mL[d]	Coliforms: daily	
			1 mg/L Cl_2 residual (min)	Cl_2 residual: continuous	

Wastewater Reclamation. Table 6 (Continued)

Type of reuse	Treatment	Reclaimed water quality	Reclaimed water monitoring	Setback distance
Indirect potable reuse				
Groundwater recharge by spreading into potable aquifiers	Site specific	Site specific	pH: daily	100 ft (30 m) to areas accessible to the public (if spray irrigation) site specific
	Secondary and disinfection (min)	Meet drinking waterstandards after percolation through vadose zone	Turbidity: continuous	
	May also need filtration and/or advanced wastewater treatment		Coliforms: daily	
			Cl_2 residual: continuous	
			Drinking water standards: quarterly	
			Other: depends on constituent	

Source: U.S. Environmental Protection Agency [20].
[a]Secondary treatment processes include activated sludge processes, trickling filters, rotating biological contactors, and many stabilization pond systems. Secondary treatment should produce effluent in which both the BOD and TSS do not exceed 30 mg/L
[b]Filtration means passing the effluent through natural undisturbed soil or filter media such as sand and/or anthracite
[c]Disinfection means the destruction, inactivation, or removal of pathogenic microorganisms. It may be accomplished by chlorination, or other chemical disinfectants, UV radiation, or other processes
[d]The number of fecal coliforms organisms should not exceed 800/100 mL in any sample
[e]The number of fecal coliforms organisms should not exceed 14/100 mL in any sample

processes. High-rate biological processes, such as activated sludge processes, trickling filters or biofilters, oxidation ditches, and lagoons, as well as rotating biological contactors (RBC), are commonly used. A combination of two of these processes in series can be used to treat municipal wastewater containing a high concentration of organic material from industrial sources.

High-rate biological processes are characterized by relatively small reactor volumes and high concentrations of microorganisms compared with low-rate processes. The microorganisms must be separated from the treated wastewater by sedimentation to produce clarified secondary effluent. High-rate biological treatment processes are effective at removing BOD and suspended solids, as well as some of the heavy metals. However, they remove very little of the phosphorous, nitrogen, nonbiodegradable organics, or dissolved minerals.

4. *Tertiary treatment*: Tertiary treatment is employed when specific undesirable wastewater constituents cannot be removed by secondary treatment. These constituents include nitrogen, phosphorous, additional suspended solids, refractory organics, and heavy metals and dissolved solids.
5. *Disinfection*: Disinfection is intended to reduce the number of pathogenic microorganisms in the water. Chlorine is normally used, but ozone and ultraviolet irradiation can also be used to meet advanced wastewater treatment requirements.

Wastewater Reclamation. Table 7 Consumptive user of reclaimed wastewater and qualitative water quality requirements [13]

Consumptive use	Removal of pathogens	Chlorine residual or other disinfection	Removal of susp. solids & turbidity	Presence of dissolved oxygen	Removal of BOD & COD	Removal of nutrients	Removal of taste, odor and color	Removal of trace organics & metals	Removal of excess salinity
Landscape	*	–	*	*	*	–	*	*	0
Nonfood crops	**	*	*	*	**	–	*	*	0
Food crops	***	***	***	**	***	–	**	**	*
Groundwater recharge	***	**	***	**	***	***	***	****	–
Industrial uses	**	**	***	***	***	***	***	**	**
Urban non-potable uses	****	****	****	****	****	***	****	****	**
Potable uses	*****	*****	*****	****	*****	****	*****	*****	***

(–) no need, (0) usually not essential, (*) slight need, (**) moderate need, (***) strong need, (****) stringent requirements, (*****) very stringent

6. *Advanced treatment*: Advanced treatment includes membrane technology (including ultra/nanofiltration or reverse osmosis) as well as water remineralization. The advanced technologies have gained interest for unrestricted uses of water because they are now much cheaper than in the past. This will be described in the next section (Fig. 1).
7. *Sludge treatment and disposal*: The sludge accumulated in a water reuse process must be treated and disposed of in a safe and effective manner. The most common treatment options are anaerobic digestion, aerobic digestion, and composting. Incineration is less common due to air emissions concerns. Anaerobic digestion is widely used for the treatment of domestic sewage. One major feature of anaerobic digestion is the production of biogas (with the most useful component being methane), which can be used for electricity production and/or heating purposes.

Advanced Technologies for Producing High-Quality Reclaimed Water

The increased need to secure a high-quality water supply from reclaimed water has resulted in the emergence of advanced technologies, including membrane bioreactors (MBR), nanofiltration (NF), reverse osmosis (RO), ion exchange (IEX), distillation, chemical oxidation, and carbon adsorption.

1. *Membrane bioreactor* (*MBR*): Membrane bioreactors combine activated sludge treatment with a membrane separation process. The reactor is operated in a similar way to conventional activated sludge, but a low pressure membrane (microfiltration or ultrafiltration) is used to perform the sludge separation. This allows the production of high-quality water in only a one unit operation.

   The MBR process has been shown to provide high-quality effluent, with high BOD removal and

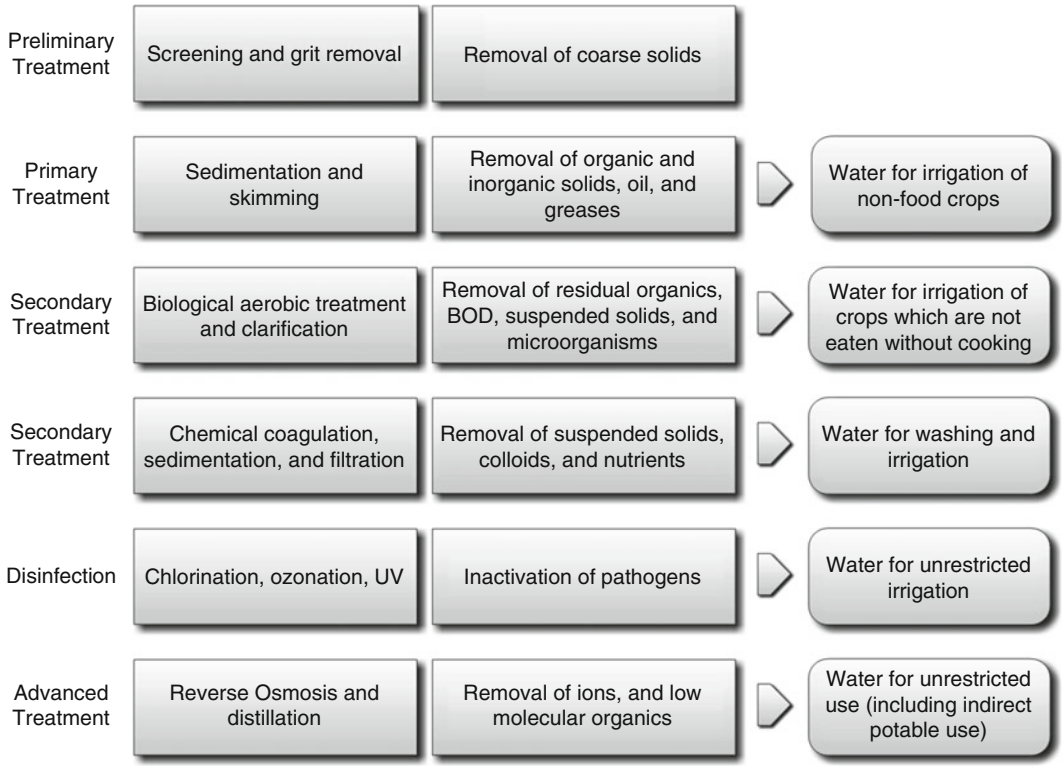

Wastewater Reclamation. Figure 1
Treatment technologies for water reuse

complete TSS reduction. Depending on the design, configuration, and need for nutrient removal, the activated sludge portion of the process can provide significant denitrification and phosphorus reduction. The MBR effluent has the added advantage of having low turbidity, making it possible for use as feed water to reverse osmosis (RO) in industrial or indirect potable reuse systems. Moreover, the overall footprint of an MBR system is much smaller than a conventional activated sludge facility.

Membrane configurations can be classified as: (1) sidestream and (2) submerged MBR. A sidestream MBR pumps sludge from an activated sludge reactor to a pressure-driven membrane for solid–liquid separation. A submerged MBR has membrane modules submerged in the bioreactor and operates under vacuum pressure. The submerged MBR configurations are preferred to the sidestream ones, especially for reuse of domestic wastewater. The energy demand of the submerged MBR can be up to two orders of magnitude lower than that of the sidestream systems.

MBR systems can be sited close to the points of potential reuse. Thus, local needs for reclaimed water are met more economically because of the reduced requirements for pipelines, pumping, and storage. Moreover, the product water quality is suitable for a variety of reclaimed water applications and, after disinfection, can be used for a number of non-potable, unrestricted uses.

During the operation of an MBR, the rejected constituents in the retentate tend to accumulate at the membrane surface, producing various phenomena, which lead to a reduction in the flow of water through the membrane (i.e., the flux) at a given transmembrane pressure (TMP) or, conversely, an increase in the TMP for a given flux (reducing the permeability, which is the ratio of flux to TMP). These phenomena are collectively referred to as fouling. Since membrane fouling represents the main limitation to membrane process operation, MBR systems are designed to mitigate fouling problems.

MBR systems using low pressure membranes cannot retain organic species and ions. To overcome these limitations, high retention membrane bioreactors (HRMBRs) have recently been investigated. HRMBRs use high rejection membranes, such as nanofiltration (NF), forward osmosis (FO), and membrane distillation (MD), in place of MF/UF. This allows a combination of the conventional MBR and high rejection membrane separation in a single step. However, this technology is still in its early stage of development, and many challenges, such as low recovery and accumulation of ions in the bioreactors, still have to be resolved.

2. *Nanofiltration/reverse osmosis*: With the increased use of reclaimed water for applications where quality and reliability are critical, such as indirect potable reuse and some industrial uses, the increased removal of dissolved solids and trace constituents may be required. In addition, dissolved solids may cause scaling or corrosion of equipment and piping systems, especially in cooling tower systems. Membrane technologies, such as nanofiltration (NF) and reverse osmosis (RO), can be applied to remove these constituents.

NF and RO are capable of separating dissolved ions from the feed stream, and require hydrostatic pressure to overcome the osmotic pressure of the feed stream. The key difference between NF and RO is the degree of removal of monovalent ions, such as sodium and chloride ions. Reverse osmosis removes monovalent ions in the 98–99% range, while removals with NF membranes vary between 50% and 90%, depending on the material and manufacture of the membrane. With the development of new low-pressure membranes, RO is finding increased use in water reuse applications.

NF is often used for removing salts to meet TDS requirements for groundwater recharge and for water softening applications. NF is also used in conjunction with RO to remove divalent and trivalent ions, which enable a higher recovery rate with RO. However, NF may not replace RO in reuse applications of municipal wastewater because of its low rejection of monovalent ions.

RO is effective at reducing TDS for unrestricted water reuse, including indirect portable use and power plant cooling water, and is also used to remove trace organics, such as endocrine disrupting chemicals and pharmaceuticals. However, RO is relatively ineffective at retaining non-charged small organic molecules (i.e., urea). Moreover, RO

requires high pressure to produce water, leading to a high energy cost.

Like all membrane processes, NF and RO membranes can be fouled by various constituents in the feed stream. Thus, pretreatment prior to the NF/RO process requires the removal of suspended particulates, such as colloidal material. This type of removal will normally require the use of a coagulant/filtration process, acid addition, and/or filtration, such as microfiltration (MF) or ultrafiltration (UF).

Another drawback for the implementation of NF/RO processes is the need for additional treatment of the concentrate. Membrane concentrate is primarily concentrated feed raw water materials, plus any added chemicals used for pretreatment purposes. Because of the high levels of dissolved solids, together with other toxic compounds in the raw water, the discharge of untreated membrane concentrate poses a significant risk to the environment. Various options exist for the disposal of concentrate from NF/RO plants, including discharge to surface water, discharge to wastewater treatment plants, deep wells, land application, evaporation ponds, and wastewater evaporators. Management of NF/RO residuals requires evaluation of the available management alternatives, regulations, costs and site-specific conditions.

3. *Electrodialysis*: Electrodialysis (ED) is an electrically driven process that separates mineral salts and other species using direct electrical potential as the driving force. When a direct current is passed through a solution, the positive and negative ions migrate to the negative and positive electrodes, or the cathode and anode, respectively. Accordingly, ED is not as effective at removing microorganisms and many anthropogenic organic compounds. Electrodialysis and electrodialysis reversal (a modification of the electrodialysis process) are used principally for desalting brackish water, and have also been used for demineralizing reclaimed water.
4. *Ion exchange*: Ion exchange is a process used for the removal of dissolved ionic constituents, where ions of a given species are displaced from a solid phase material by ions of a different species from the solution. This is applied for demineralization of water, removal of specific constituents (i.e., nitrate), and softening.

   Residual organic matter found in biological treatment effluents can cause blinding of the ion exchange beds, resulting in high pressure loss and inefficient operation, for example, where ion exchange is used following filtration. Therefore, some form of chemical treatment and clarification is required before ion exchange treatment. Moreover, ion exchange resins should be regenerated after a certain period of time, resulting in the challenge of brine management. The disposal of high TDS regeneration brine remains the primary obstacle to the wider use of ion exchange technology.
5. *Distillation*: Distillation is a unit operation, where the components of a liquid solution are separated by vaporization and condensation, which involves multiple effect distillation (MED), multistage flash evaporation (MSF), and vapor compression distillation (VCD). The principal issues with the application of distillation processes for water reclamation are the high energy input required to evaporate the feedwater, carryover of volatile constituents found in treated reclaimed water, and the degree of subsequent cooling and treatment that may be required to renovate the distilled water. In addition, all distillation processes reject part of the influent feedwater and produce a concentrated waste stream that must be managed. Scaling and corrosion are also problematic.
6. *Chemical oxidation*: Chemical oxidation is applied for the destruction of anthropogenic or synthetic toxic organics in water reuse systems. Oxidants used in water reclamation are chlorine, ozone, chlorine dioxide, permanganate, hydrogen peroxide, and hydroxyl radicals. The principal applications of conventional chemical oxidation in water reclamation are for odor control, hydrogen sulfide control, color removal, iron and manganese removal, disinfection, control of biofilm growth, and biofouling in treatment process and distribution system components, as well as the oxidation of selected trace organic constituents.

   The major concern with any chemical oxidation process is the potential for the formation of toxic byproducts due to incomplete oxidation. Oxidation processes using ozone can produce brominated

byproducts, as well as bromates, in water containing bromide ions. High concentrations of carbonate and bicarbonate in some reclaimed water can react with hydroxyl radicals and reduce the efficiency of oxidation processes. Metals ions and residual organics may also affect the performance of oxidation processes.

7. *Adsorption*: In water reclamation, adsorption is used for the removal of substances in solution by their accumulation on a solid phase. Adsorption treatment of reclaimed water is usually thought of as a polishing process for water that has already received normal biological treatment. Adsorption has been used for the removal of refractory organic constituents, residual inorganic constituents, such as nitrogen, sulfides and heavy metals, and for odorous compounds.

   The adsorption process in water reuse applications is limited by several factors; the relatively high capital cost due to the area requirements for the carbon contactors, and waste adsorbent due to the difficulty in its regeneration, which may require disposal as a hazardous waste due to the presence of toxic constituents (Fig. 2).

Energy Consumption: Comparison of Wastewater Reclamation with Desalination

Due to the high costs of power and an increasing concern over greenhouse gas emissions, the issue of energy reduction in wastewater treatment and reuse is becoming increasingly important. For instance, in California USA, an energy-efficiency program with the California Energy Commission is helping the state to achieve its goals of reducing per person water use by 20%, increasing renewable energy generation by 33%, and decreasing greenhouse gas emissions by 30% by 2020 [8], which could reduce the energy consumption in water/wastewater treatment plants by up to 30%.

The cost factors associated with wastewater treatment are pretreatment, chemical addition, cleaning, maintenance, and capital. In addition, water treatment and delivery require energy, which is another essential parameter in deciding on a wastewater treatment technology because it is a large fraction of the cost of water provision. Dreizin [5] reported that the energy cost was 25% and 65% of the total and operational costs, respectively, meaning that energy is the decision-making

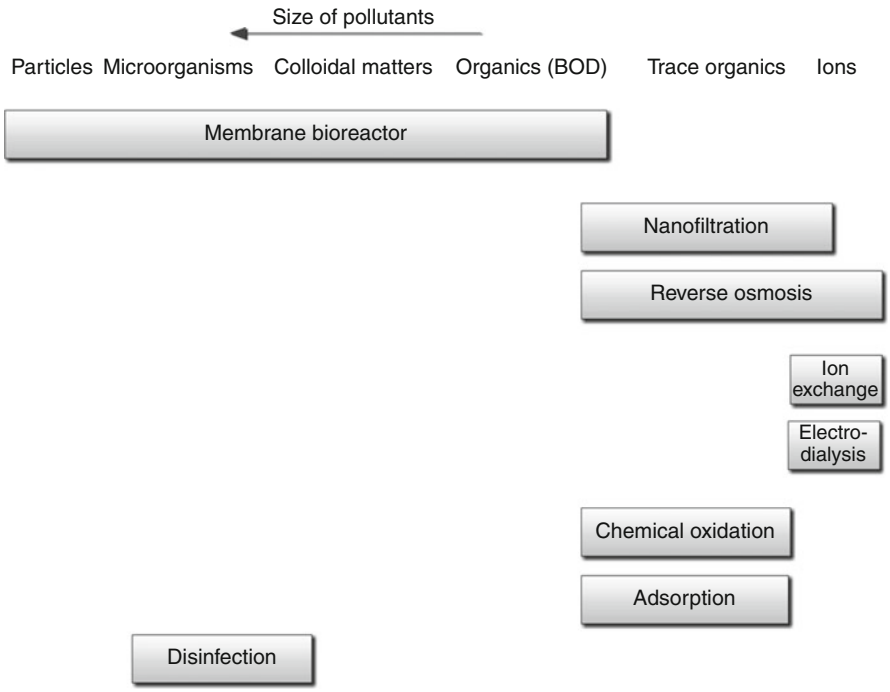

Wastewater Reclamation. Figure 2
Advanced treatment for constituents in wastewater

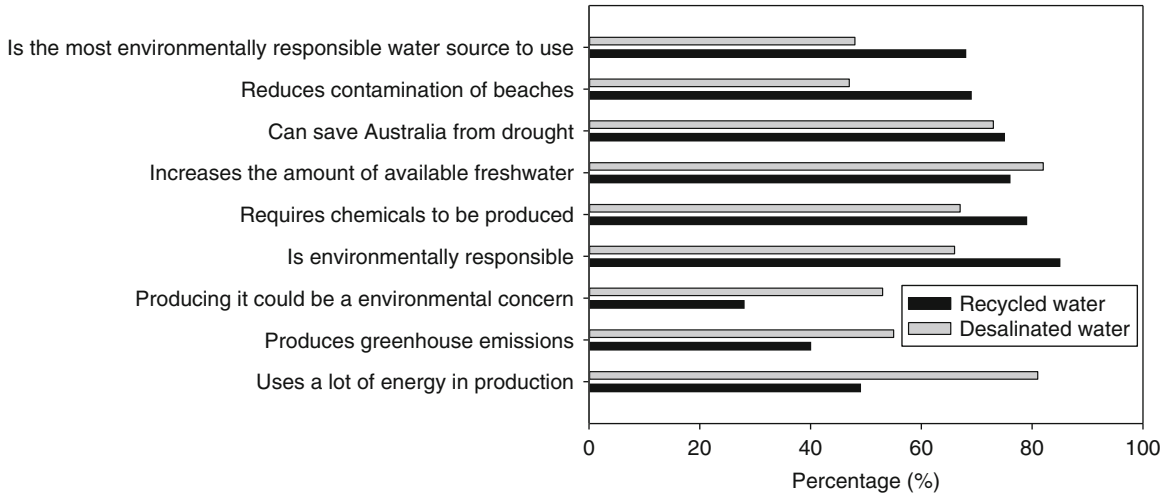

Wastewater Reclamation. Figure 3
Comparative perceptions/knowledge about environmental issues of recycled and desalinated water in Australia [4]

parameter with regards of the economics of different source waters. In general, the specific energy consumption for surface, brackish, or wastewater is 0.4–1.0 kWh/m^3; whereas, that for seawater is 3–3.4 kWh/m^3. As treatment systems advanced, the energy requirements will become higher. Especially, membrane technology is recognized as a cost-intensive process in water/wastewater treatment. These membrane processes, i.e., RO, can be applied to wastewater reuse and seawater desalination, which are the most suitable alternative water resources; therefore, these two processes are often compared in terms of energy consumption. In this section, the energy consumption of membrane-based solutions for wastewater reuse and desalination are compared.

Public perception of energy consumption for recycled versus desalinated water: Figure 3 shows a survey of the comparative perception/knowledge about environmental issues of recycled and desalinated waters [4], which was carried out by 1,000 respondents to a 30 min online questionnaire conducted in Australia. Health, environmental, and cost concerns were found to be the major issues. As expected, wastewater reuse is primarily perceived as a health issue, while the concerns about desalinated water are the environmental and cost issues. Many people recognize that desalinated water uses more energy and produces greenhouse emissions.

Wastewater Reclamation. Table 8 Comparison of energy and O&M costs for recycled water [11, 18]

	Pretreatment		Pretreatment-RO	
	CAS	MF	CAS-RO	MF-RO
Utilities (kWh/m^3)				
Power	0.2	0.2	1.3	0.5
O&M costs (US cents/m^3)				
Power	2	1.8	13.2	5.3
Other	14	3.2	12.7	10.6
Total	13	5	25.9	15.9

Thus, it is essential to evaluate the detailed comparative energy costs between recycled and desalinated waters.

Energy cost of recycled water: The relative contributions of surface water, groundwater, desalinated water, and recycled water to the total water abstracted for all uses for humans are 63.2%, 36.3%, 0.29%, and 0.19%, respectively [12]. Recycled water has the lowest percentage, possibly due to the strict public acceptance of health concerns. However, the quality of recycled water is as good as that of desalinated water, as both technologies utilize RO-based membranes.

Wastewater Reclamation. Table 9 Energy consumption for recycled and desalinated water [15]

Water	Total dissolved solid (mg/L)	CAS (kWh/m^3)	Pretreatment (kWh/m^3)	RO system (kWh/m^3)	Total treatment (kWh/m^3)
Surface water	50–300				0.15–0.3
Wastewater	300–800	0.3–0.6	0.1–0.2	0.4–0.5	0.8–1.0 (1.3)
Wastewater MBR	300–800		0.8–1.0	0.4–0.5	1.2–1.5
Brackish water	900–2,200		0.1–0.3	0.6–0.9	0.8–1.0
Seawater	38,000		0.3–1.0	2.0–3.0	2.3–4.0

Wastewater Reclamation. Table 10 Cost comparison for producing water from CAS and seawater (Cote et al. 2005)

Component	Units	CAS	Seawater	Ratio (seawater/CAS)
Capital costs				
Infrastructure and pretreatment	US$/m^3/day	161	320	1.9
RO	US$/m^3/day	321	624	1.9
Total	US$/m^3/day	482	944	2.0
Total life cycle costs				
Capital	US$/m^3	0.07	0.25	3.4
O&M	US$/m^3	0.21	0.37	1.8
Total	US$/m^3	0.28	0.62	2.2

Treatment of recycled water based on RO is divided into two processes: (1) conventional activated sludge (CAS) followed by MF/UF-RO, and (2) MBR-RO ([15]; Cote et al. 2005). The CAS in wastewater treatment is known as a biological process followed by clarification, but the CAS effluent is not appropriate as the feed water for RO due to severe membrane fouling. This leads to a combination of MF/UF and then on to RO. Prior to the MF/UF, lime clarification and sand filtration are used, which result in high chemical costs. Thus, the integrated MBR-RO systems for recycled water have been favorably used in many wastewater reuse plants. Integrated systems consist of screening, MBR, and RO, and do not require complex pretreatment steps, as required for CAS-MF/UF-RO. Reardon et al. [18] reported that the energy costs of the CAS versus MF pretreatment were similar, while the O&M costs of the CAS pretreatment were approximately three times higher than those of MF. On the other hand, when incorporated with RO, the energy consumption of the CAS-RO system was 2.6 times higher than that of the MF-RO. This suggests that the MBR-RO has various advantages and significant potential for wastewater reuse (Table 8).

Energy comparison of recycled versus desalinated water: The major issue of recycled versus desalinated water is energy, which plays an important role in deciding on alternative water resources from the areas suffering from water shortage. Desalination has been regarded as a cost-intensive process due to the high energy requirement. Assuming the cost of electricity as $0.10/kWh, for RO units using power generators, the cost of power would be $0.30/kWh based on 3 kWh/L (assumed diesel cost of $0.90/L). Compared to desalination, recycled water costs less due to: (1) no need for coagulant addition, (2) single pass RO, but 2-pass RO for desalination, (3) higher RO recovery, (4) higher RO flux, and (5) lower RO feed pressure (Cote et al. 2005).

Pearce [15] summarized the energy usages for various water and wastewater resources (Table 9).

Cote et al. (2005) reported a cost comparison for producing water from CAS and sweater (Table 10). Both surveys showed that desalinated water was 2–3 times more expensive than recycled water in terms of energy usage and water production costs. The key parameters of cost and energy usage differ between recycled and desalinated water due to the salinity of the latter. When the salinity increases, (1) the addition of chemical coagulant is needed, (2) smaller recovery (50%) from seawater (75% for wastewater), which leads to a larger pretreatment system, and (3) higher pressure due to high osmotic pressure with high salinity. This indicates that the difference (2–3 times) in the energy consumption and water production costs for recycled and desalinated water is unlikely to change as the difference in costs is generated due to the nature of saline water.

Future Directions

In recent years, the MBR process has become a viable alternative technology for wastewater treatment. Research on the MBR process has increased exponentially over the last decade, and is expected to keep increasing in the future. Despite rigorous and active research activities, membrane fouling still remains as a major obstacle for the practical and wide application of MBR technology. Furthermore, the great demand for wastewater reclamation and reuse due to the shortage of pristine water resources all over the world has pushed this technology to evolve into a more efficient process for controlling various micro-contaminants, in addition to the well-known biological nutrients, N and P. In this section, based on the current status of the knowledge obtained from the recent literature, the future directions of research and development on MBR technology are briefly discussed.

Various factors affecting fouling of the MBR process have been investigated and documented in numerous publications. However, many operational MBR plants have suffered from deterioration in the membrane productivity, mainly due to fouling. Thus, a fundamental understanding of membrane fouling mechanisms will continue to be the main focus of future research, with even more emphasis on enhancing the economic feasibility of this technology. More specifically, sophisticated analytical techniques will be developed to identify and characterize various chemical and biological components of membrane foulants. For example, the interactions between foulants and membrane surfaces or pores could be directly measured using various tools, including AFM, to determine the fouling potential of these components. Current lab-scale analytical technologies need to be further developed, refined, and simplified to be able to monitor fouling phenomena in real applications. In situ monitoring techniques will become more significant for the effective operation of full-scale MBR plants in the future.

In addition to fundamental assessment and practical monitoring of membrane fouling, more scientifically designed fouling control methods are expected to be developed in the future, which will be made possible by the elucidation of fouling mechanisms. A novel method utilizing a biological mechanism control, known as Quorum Sensing, is one example. Biological and chemical methods developed on the basis of fouling mechanisms should be easier and cheaper to apply to large-scale plants. Lastly, new, improved membrane modules for the control of fouling during MBR processes will continue to develop and reduce the capital costs, and enhance the hydrodynamic conditions.

The MBR technology was initially developed based on MF/UF membranes capable of achieving solid–liquid separation for SS and coliforms. However, environmental concern regarding the protection of natural water resources put more pressure on the development of MBR processes that were more suitable and effective for the control of biological nutrients, such as nitrogen and phosphorus. High nitrification can be easily accomplished under typical MBR processes operating conditions, characterized by high MLSS and high SRT, where slow-growing microorganisms, such as nitrifying bacteria, are enriched. Thus, the MBR process, combined with anoxic denitrification, is able to achieve high nitrogen removal. However, the operation of the MBR with such higher SRT is not detrimental to biological phosphate removal, which is achieved by the discharge of phosphate containing biomass, and results in an excessive amount of phosphate in the cell from wastewater systems. A variety of MBR processes have been configured with biological nutrients removal (BNR) systems, with their performance demonstrated for different applications, but have only shown limited success. Therefore, it is common to see additional

chemical methods incorporated into the MBR process to satisfy regulatory requirements. The development of the MBR process coupled with more efficient BNR systems will be the primary topic over the next decade.

As mentioned above, conventional MBR processes utilizing particle separating MF/UF membranes are not able to meet the effluent quality for wastewater reclamation and reuse, and often require tertiary treatment, including tighter membrane technologies, such as RO. In the future, however, water supply and wastewater management systems will be more decentralized for the optimum use of energy and resources, and thus, complicated MBR systems with tertiary treatment should be further simplified and compact. Such technological demands have resulted in the development of a high rejection MBR process, where tighter membranes reject not only particles, but also dissolved micropollutants also. The NF-MBR is the first alternative MBR process, where an NF membrane is submerged in the bioreactor and produces much better effluent water qualities than those by conventional MF-MBR. NF membranes, with chemical stability as well as reasonable water productivity, need to be developed for improving their applicability in the future.

In addition to traditional pressure-driven tighter membranes, two different types of membrane have been utilized in high retention MBR processes; membrane distillation and forward osmosis membranes. The membrane distillation bioreactor (MDBR) integrates a conventional bioreactor with a thermally driven membrane distillation process, which uses microporous hydrophobic membranes for distillation. With warm wastewater, a modestly elevated temperature (30–80°C) can easily be obtained, and water vapor can be transported through the membrane and condense into water, but nonvolatile components, such as contaminants, are not able to pass through the membrane and thus, will be rejected by the membrane. The energy demand for such systems is known to be low compared to conventional MBR coupled with RO, although the economics of scale-up systems will need to be examined further. Biological environments specific to this process should be further understood for the better design and operation of the process in the future. Forward osmosis bioreactors (FO-MBR) are another recent development. The FO membrane process utilizing a concentration gradient as the driving force is combined with a conventional bioreactor. Compared to RO processes, the FO process is characterized by low energy use and high recovery. A non-pressurized FO system is also known to enable increased fouling reversibility, thus making this process more suitable for wastewater applications where the fouling potential is very high. Although the benefits of such systems have been demonstrated in the literature, only limited performance data are available for small-scale applications. Therefore, newly developed high retention MBRs have a long way to go before they become a reality, but they are expected to attract many investigations and continue to grow as a promising technology to meet the demand for compact and reliable wastewater reuse systems.

Bibliography

Primary Literature

1. Bixio D, Thoeye C, Koning J, Joksimovic D, Savicc D, Wintgensd T, Melind T (2006) Wastewater reuse in Europe. Desalination 187:89–101
2. Bixio D, Thoeye C, Wintgens T, Ravazzini A, Miska V, Muston M, Chikurel H, Aharoni A, Joksimovic D, Melin T (2008) Water reclamation and reuse: implementation and management issues. Desalination 218:13–23
3. Cooper RC, Olivieri AW (1998) Infectious disease concerns in wastewater reuse. In: Asano T (ed) Wastewater reclamation and reuse. Technomic Publishing, Lancaster, pp 489–520
4. Dolnicar S, Schafer AI (2007) Desalination and recycling: Australians raise health, environment and cost concerns. Desalination Water Reuse 16:10–15
5. Dreizin Y (2006) Ashkelon seawater desalination project – off-taker's self costs, supplied water costs, total costs and benefits. Desalination 190:104–116
6. Feachem RG, Bradley DJ, Garelick H, Mara D (1983) World sanitation and disease: health aspects of excreta and wastewater management by Bank Studies, vol 3, Water supply sanitation. Wiley, Chichester
7. Fewtrell L, Bartram J (2001) WHO guidelines, standards and health. IWA Publishing, London
8. Force J (2010) Encouraging energy efficiency in US wastewater treatment. Water21, Magazine of the IWA, June 2009: 32–34
9. Hespanhol I, Prost AME (1994) WHO guidelines and national standards for reuse and water quality. Water Res 28(1): 119–124
10. Kamizoulis G (2008) Setting health based target for water reuse. Desalination 218:154–163
11. Kayaalp NM (1996) Regulatory framework in South Australia and reclaimed water reuse options and possibilities. Desalination 106(3):17–322

12. Kolodziejski J, Gasson C (2005) Water reuse markets 2005–2015: a global assessment and forecast. Media Analytics, Oxford (Global Water Intelligence)
13. Kretschmer N, Ribbe L, Gaese H (2003) Wastewater reuse for agriculture. Technol Resour Manage Dev 2:37–64
14. Levine AD, Asano T (2004) Recovering sustainable water from wastewater. Environ Sci Technol 38:201A–208A
15. Pearce GK (2008) UF/MF pre-treatment to RO in seawater and wastewater reuse applications: a comparison of energy costs. Desalination 222:66–73
16. Salgot M, Huertas E, Weber S, Dott W, Hollender J (2006) Wastewater reuse and risk: definition of key objectives. Desalination 187:29–40
17. Salgot M (2008) Water reclamation, recycling and reuse: implementation issues. Desalination 218:190–197
18. Reardon RD, Paranjape SV, Foussereau XJ, DiGiano FA, Aitken MD, Kim JH, Chong S-Y, Cramer R (2005) Water for reuse: membrane treatment of 2ry effluent for subsequent use. WERF Final Report, North Carolina University
19. Toze S (2006) Water reuse and health risks – real vs. perceived. Desalination 187:41–51
20. USEPA (1992) Process design manual: guidelines for water reuse. Report No. EPA-625/R-92-004, Cincinnati
21. USEPA (2004) Guidelines for water reuse. Report No. EPA/625/R-04/108

Books and Reviews

Asano T, Burton FL, Leverenz HL, Tsuchihashi R, Tchobanoglous G (2006) Water reuse: issues, technologies, and applications. Metcalf & Eddy/AECOM Press, McGraw-Hill, New York

Asano T, Jimenez B (2008) Water reuse: an international survey of current practice issues and needs. IWA Publishing, London

WHO (2006) A compendium of standards for wastewater reuse in the Eastern Mediterranean Region, WHO-EM/CEH/142/E

Wastewater Treatment and Control Through Wetlands

Jan Vymazal
Department of Landscape Ecology, Czech University of Life Sciences Prague, Kostelec nad Černými lesy, Prague, Czech Republic
ENKI, o.p.s., Třeboň, Czech Republic

Article Outline

Glossary
Definition of the Subject and Its Importance
Introduction
Types of Constructed Wetlands for Wastewater Treatment
The Use of Constructed Wetlands for Various Types of Wastewater
Future Directions
Bibliography

Glossary

Constructed wetland (CW) Constructed wetlands are engineered systems that have been designed and constructed to utilize the natural processes involving wetland vegetation, soils, and their associated microbial assemblages to assist in treating wastewater. Constructed wetlands offer several additional advantages compared to natural wetlands including site selection, flexibility in sizing, and most importantly, control over the hydraulic pathways and retention time.

CW with horizontal subsurface flow Constructed wetland where wastewater is fed in at the inlet and flows slowly through the porous medium under the surface of the bed in a more or less horizontal path until it reaches the outlet zone where it is collected before leaving via level control arrangement at the outlet. During this passage, the wastewater will come into contact with a network of aerobic, anoxic, and anaerobic zones.

CW with vertical flow Constructed wetlands where water is fed intermittently on the surface of the filtration bed and water percolates by gravity to the bottom where it is collected.

CW with free water surface Consists of basins or channels, with soil or another suitable medium to support rooted vegetation (if present) and water at a relatively shallow depth flowing through the unit.

Macrophytes Plants that are adapted to the life under anoxic and/or anaerobic soil conditions in wetlands.

Wetland Land that is saturated with water long enough to promote wetland or aquatic processes as indicated by poorly drained soils, hydrophytic vegetation, and various kinds of biological activity that are adapted to a wet environment.

Definition of the Subject and Its Importance

Wetlands are found on every continent except Antarctica and in every climate from the tropics to the frozen tundra. Any estimate of wetland extent in the world is difficult and depends on an accurate definition [1]. As the definitions vary, the estimated area of wetlands varies between 5.3 and 11.65 million square kilometers and between 3.5% and 7.7% [1–6]. As wetlands were considered as neither "true" terrestrial ecosystem nor "true" aquatic ecosystems, not many researchers were interested in wetland ecosystems. However, there has been an explosive growth of knowledge about, and a radical change of attitude toward wetlands since the 1950s [7]. Wetlands have been recognized as providing many ecosystem services such as hydrologic, biologic, biogeochemical, and cultural [8–12].

Natural wetlands have been used for wastewater treatment for centuries [13]. In many cases, however, the reasoning behind this use was disposal, rather than treatment and the wetland simply served as a convenient recipient that was closer than the nearest river or other waterway. Wetlands have been considered for a long time as "wastelands," were scientifically neglected and, therefore, the impact of wastewaters on different wetlands was not properly assessed. Uncontrolled discharge of wastewater led in many cases to an irreversible degradation of many wetland areas [14]. Although significant improvement in the quality of the wastewater is generally observed as a result of flow through natural wetlands, the extent of their treatment capability is largely unknown [15]. Natural wetlands are still used for wastewater treatment under controlled conditions [16, 17], but the use of constructed wetlands has become more popular and effective around the world since the 1980s.

Constructed wetland treatment systems are engineered systems that have been designed and constructed to utilize the natural processes involving wetland vegetation, soils, and their associated microbial assemblages to assist in treating wastewater. They are designed to take an advantage of many of the same processes that occur in natural wetlands, but do so within a more controlled environment. Constructed wetlands are essentially wastewater treatment systems and are designed and operated as such, though many systems do support other functional values [18]. Constructed wetlands can be built with a much greater degree of control than natural systems, thus allowing the establishment of experimental treatment facilities with well-defined composition of substrate, type of vegetation, and flow pattern. In addition, constructed wetlands offer several additional advantages compared to natural wetlands including site selection, flexibility in sizing, and most importantly, control over the hydraulic pathways and retention time [15].

Introduction

In 1953, Dr. Käthe Seidel for the first time presented methods for improvement of inland waterways, which suffered from overfertilizaton, pollution from sewage, and siltation by means of appropriate plant species [19]. Between 1952 and 1956, Seidel carried out numerous experiments on the use of wetland plants for treatment of various types of wastewater, including phenol, dairy, or livestock wastewater [20–22]. In the early 1960s, Seidel intensified her trials to grow macrophytes in wastewater and sludge of different origin and she tried to improve the performance of rural and decentralized wastewater treatment, which was either septic tanks or pond systems with inefficient treatment. To overcome the anaerobic septic tank systems, she integrated a stage of primary sludge filtration in vertically percolated sandy soils planted with *Phragmites australis*. So the system consisted of an infiltration bed through which the sewage flowed vertically and an elimination bed with a horizontal flow [23]. This system was the basis for hybrid systems, which were revived at the end of the twentieth century. However, Seidel´s concept to apply macrophytes to sewage treatment was difficult to understand for sewage engineers who had eradicated any visible plants on a treatment site for more than 50 years [24] and therefore, it was no surprise that the first full-scale constructed wetlands were built outside Germany.

In spite of many prejudices among civil engineers about odor nuisance, attraction of flies, and poor performance in cold periods, the IJssel Lake Polder Authority in Flevoland in the Netherlands constructed its first free water surface constructed wetland (FWS CW) in 1967 [25]. Contrary to the North America and Australia, FWS CWs did not spread throughout Europe significantly while CWs with subsurface horizontal

(HF CWs) and vertical (VF CWs) flow drew much more attention at the end of the twentieth century [26]. However, FWS CWs are in operation in many European countries, for example, Sweden, Denmark, Poland, Estonia, or Belgium [27].

Types of Constructed Wetlands for Wastewater Treatment

Constructed wetlands could be classified according to the various design parameters but two most important criteria are water flow regime (surface and subsurface) and the type of macrophytic growth (Fig. 1). Different types of constructed wetlands may be combined with each other (so-called hybrid or combined systems) in order to exploit the specific advantages of the different systems. The quality of the final effluent from the systems improves with the complexity of the facility.

Constructed Wetlands with Free Water Surface

Constructed wetlands (CWs) with surface flow are commonly referred to as "free water surface" (FWS CWs). They mimic the hydrologic regime of natural wetlands. In FWS CWs, treated wastewater enters one end of the basin, flows through an area with macrophytes, and is collected and discharged at the opposite end of the basin. The water is often shallow and moves through the wetland at a relatively slow velocity [28].

Systems with Free-Floating Macrophytes Constructed wetlands with free-floating macrophytes (Fig. 2) consist of one or more shallow ponds in which plants float on the surface. The shallower depth and the presence of aquatic macrophytes in place of algae are the major differences between constructed wetlands with free-floating macrophytes and stabilization ponds [29]. Free-floating macrophytes are highly productive and belong to the fastest growing plants on the Earth. The most commonly used species in constructed wetlands are Water hyacinth (*Eichhornia crassipes*) and species of the family Lemnaceae (Duckweed) such as *Lemna minor*, *L. trisulca*, or *Spirodela polyrhiza*.

A single Water hyacinth plant can produce approximately 65,000 offspring during a single season [30]

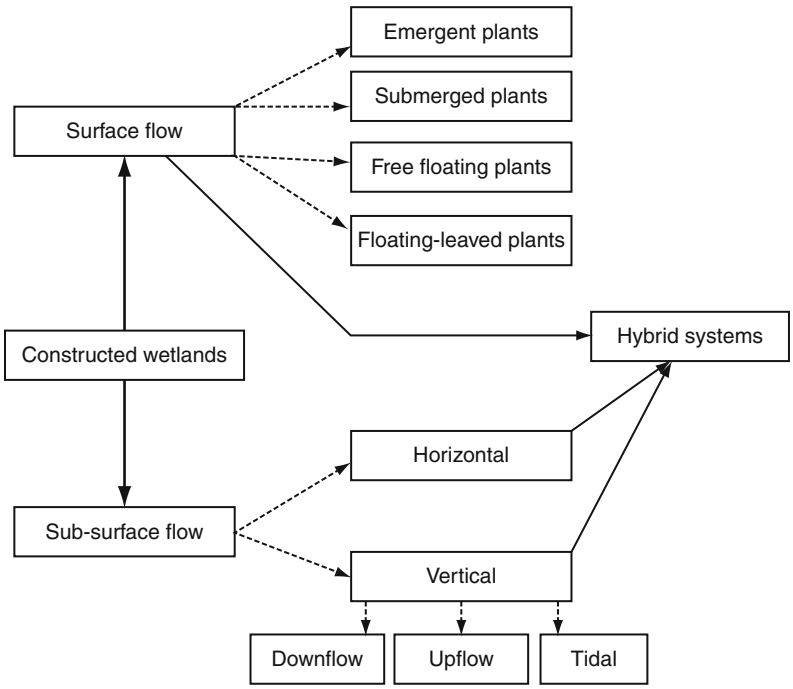

Wastewater Treatment and Control Through Wetlands. Figure 1
Types of constructed wetlands for wastewater treatment

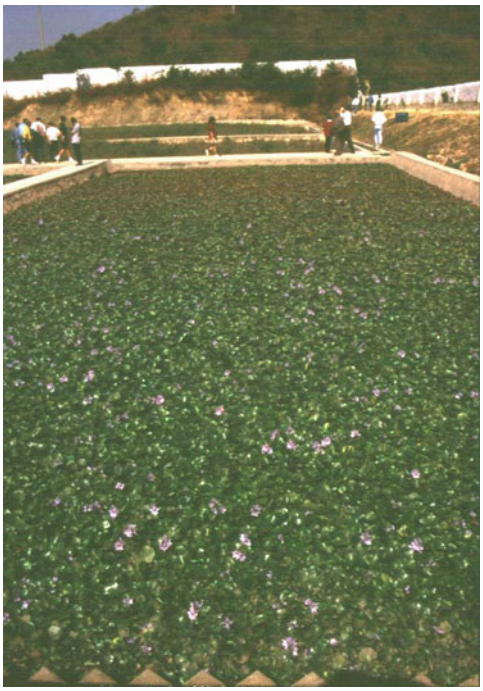

Wastewater Treatment and Control Through Wetlands. Figure 2
Constructed wetland with Water hyacinth (*Eichhornia crassipes*) in Yantian, South China as a part of hybrid constructed wetland for treatment of industrial wastewater (Photo: Jan Vymazal)

and ten plants can completely cover 0.4 ha of a water surface [31]. However, Water hyacinth does not survive the winter in temperate and cold climates, its growth rate is greatly reduced at temperatures below 10°C and, therefore, its use is restricted to subtropical and tropical regions. Moreover, the optimum water temperature is >25°C [32]. Duckweeds, compared to Water hyacinth, have a much wider geographic range as they are able to grow at temperatures as low as 1–3°C [15]. They even survive light freezes and continue to grow during the winter months but their growth optimum is at temperatures between 20°C and 30°C [33].

In CWs with free-floating macrophytes, organic substances are primarily removed by microbial degradation in water column by free-living bacteria or within a dense network of plant roots by attached bacteria. The degradation proceeds under both aerobic and anoxic/anaerobic conditions but aerobic processes are usually restricted only to the close vicinity of the roots or to the initial stages of plant development. As the plant density increases, oxygen diffusion into the water is restricted and also the plants cover completely the water surface and prevent oxygen-producing algae from growing in the water column [34]. Suspended solids are removed mainly through gravity sedimentation in the zone under the surface layer of floating plants but in Water hyacinth-based systems, substantial amount of suspended solids is retained in the root zone. The sedimentation rate is usually high as the plant layer on the surface eliminates the water movement and turbulence caused by wind. Phosphorus removal is mostly the result of the plant uptake and therefore it is desirable to keep plants in the exponential growth phase. This is realized by frequent harvesting of the plant biomass [35–37]. The harvesting has another beneficial effect because it opens the water surface for light penetration into the water and surface re-aeration. Nitrogen is removed via several processes including plant uptake (and subsequent harvesting), ammonia volatilization, and microbial nitrification/denitrification [38]. Ammonia volatilization is limited to early stages of wetland development when algae grow in water column and as a consequence of photosynthesis the pH values could be high enough for NH_3 volatilization. Nitrification occurs within the aerobic root zone and denitrification occurs in the much larger reduced zones in the water column. However, the nitrification/denitrification complex is usually not very effective for nitrogen removal because of limited nitrification in the system [38].

The CWs with Water hyacinth are very effective in pollutant removal. Vymazal [39] summarized the treatment efficiency of 14 systems in the USA and Japan and the average BOD_5, suspended solids, TN, and TP removal efficiencies amounted to 76%, 64%, 60%, and 47%, respectively. The mean outflow concentrations of respective parameters were 14.1, 9.3, 6.6, and 2.2 mg L^{-1}.

During the 1970s and early 1980s, constructed wetlands with free-floating macrophytes were intensively studied but the operational needs associated with large-scale applications have never been developed [29, 40]. Probably, the major obstacles to wider application of CWs with free-floating macrophytes are very high maintenance and operation costs and high amount of the biomass with no other use [41].

Systems with Submerged Macrophytes Submerged aquatic macrophytes have their photosynthetic tissue entirely submerged. Various experiments have proven that minerals can be taken up directly by shoot tissues of submerged plants; however, there is also no question regarding the uptake capability of nutrients by the roots of these plants. Most studies confirmed that although shoot uptake occurs, the major source for nutrients are sediments [42, 43]. Submerged plants, however, only grow well in oxygenated water and therefore cannot be used in wastewater with a high content of readily biodegradable organic matter because the microbial decomposition of the organic matter will create anoxic conditions [15]. In addition, the turbidity of the water must not be too high to prevent light transmission to the plants to support their photosynthetic activity [38]. Because of limiting conditions mentioned above (low light, high turbidity), the prime potential use of submerged macrophyte-based wastewater treatment systems (Fig. 3) is therefore for "polishing" secondary treated wastewaters [15].

There are many submerged species but the most promising are probably *Egeria densa* (Brazilian elodea), *Elodea canadensis* (Canadian waterweed), *Elodea nuttallii* (Western waterweed), *Ceratophyllum demersum* (Coontail), *Hydrilla verticillata* (Hydrilla), *Cabomba caroliniana* (Fanwort), *Myriophyllum* spp. (Watermilfoil), and *Najas guadalupensis* (Southern naiad). Submerged macrophytes are very often covered with periphyton, an attached community usually dominated by algae. The periphyton has a beneficial effect on nutrient removal but it also absorbs photosynthetically active radiation before it reaches the leaf surface of vascular plants thus making submerged plants light-limited [44]. The design criteria for CWs with submerged macrophytes still have not been fully developed, but there have been some good examples reported in the literature [45–47].

Constructed Wetlands with Floating-Leaved Macrophytes Floating-leaved macrophytes include plant species that are rooted in the substrate and their leaves on long peduncles float on the water surface. Typical examples are Water lilies (*Nymphaea* spp.), Spatterdock (*Nuphar lutea*), or Indian lotus (*Nelumbo nucifera*). In fact, this type combines the features of constructed wetlands with other types of macrophytes. The plants have huge underground rhizomes, leaf peduncles grow through the water column, and leaves float on the water surface. However, peduncle density is much lower as compared to submerged or emergent species and leaves rarely cover the entire surface of the

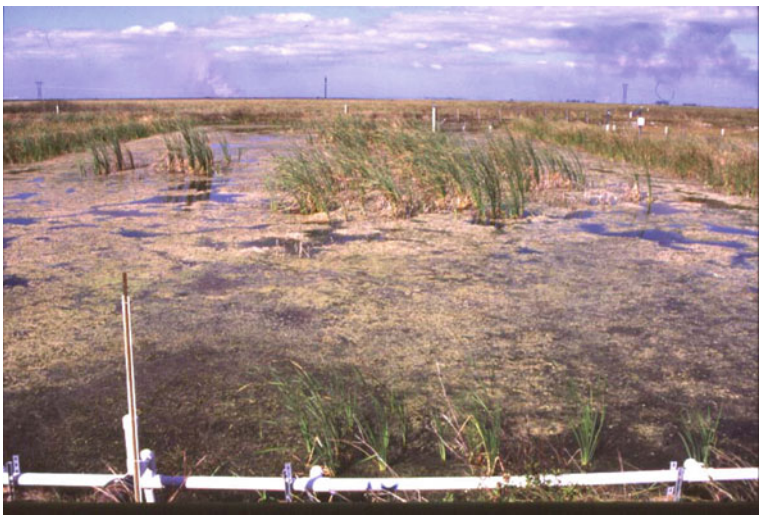

Wastewater Treatment and Control Through Wetlands. Figure 3
Constructed wetland with submerged vegetation (*Najas guadalupensis*) in the Florida Everglades Nutrient Removal Area (Photo: Jan Vymazal)

pond. So far, only a few constructed wetlands have used these plants [48] and therefore any sound conclusions on their efficiency and operation could be made.

Constructed Wetlands with Emergent Macrophytes
A typical free water surface constructed wetland (FWS CW) with emergent macrophytes is a shallow sealed basin or sequence of basins, containing 20–30 cm of rooting soil, with a water depth of 20–60 cm. Dense emergent vegetation covers significant fraction of the surface, usually more than 50% (Fig. 4). Besides planted macrophytes, naturally occurring species may be present [49]. Areas of open water may be incorporated in design to improve hydraulics and enhance wildlife habitat [28]. One of the primary design purposes is to provide wastewater with reactive biological surfaces. For FWS CWs, many plant species are used but the most common species are *Phragmites australis* (Common reed), *Typha* spp. (Cattails), and *Scirpus* (*Schoenoplectus*) spp. (Bulrush).

Suspended solids are mostly removed by gravitational settling. The largest and heaviest particles will predominantly settle out in the inlet open water zone, while slightly smaller and lighter particles may only settle out after flowing into wetland vegetation. Wetland vegetation promotes this enhanced sedimentation by reducing water column mixing and resuspension of particles from the sediment surface. The smallest of particles such as clay colloids may be removed by adhesion onto surfaces within the water column. The main surfaces within the water column are the emergent macrophytes and the biofilms growing on the surface of these plants [50].

Settleable organics are rapidly removed in FWS systems with emergent vegetation under quiescent conditions by deposition and filtration. Attached and suspended microbial growth is responsible for the removal of soluble organic compounds, which are degraded aerobically in the water column as well as anaerobically near the bottom within the litter layer. Oxygen is supplied to the wetland water column by diffusion through the air–water interface and via the photosynthesis of plants in the water column, namely algae [29, 50].

Nitrogen is most effectively removed by volatilization and nitrification/denitrification. Volatilization is very likely under higher pH values caused by photosynthesis of both planktonic and attached algae. Nitrification proceeds in aerobic zones, while nitrate is converted to free nitrogen or nitrous oxide in the

Wastewater Treatment and Control Through Wetlands. Figure 4
FWS CW Mc Grath Hill, Hawkesbury near Sydney, Australia planted with a mixture of *Phragmites australis* (Common reed) and *Bolboschoenus fluviatils* (River bulrush) (Photo: Jan Vymazal)

anoxic/anaerobic zones by denitrifying bacteria. Aerobic zones are usually in the water column and especially close to the water surface, while anerobic zones are mostly found in the litter layer on the bottom. FWS CWs with emergent vegetation provide sustainable removal of phosphorus, but at relatively slow rates. Phosphorus removal occurs from adsorption, absorption, complexation, and precipitation. However, the major retention process – precipitation with Al, Fe, and Ca ions – is limited by little contact between the wastewater and the soil [29, 51]. Substantial amounts of nitrogen and phosphorus may be stored in the peat/litter compartment. Algal and microbial uptake may be high but this retention is a short-term process and nutrients are washed out from the detritus back to the water [52].

Removal of nutrients via plant uptake is usually low as compared to inflow load. In addition, if the biomass is not harvested nutrients are released back into water during the biomass decay. Some of these nutrients could be subject to long-term accumulation in the soil, hence contributing to the wastewater-treatment capacity of the system [53].

Wetlands provide a suitable combination of physical, chemical, and biological factors for the removal of pathogenic organisms. Physical factors include mechanical filtration, exposure to ultraviolet radiation, and sedimentation. Chemical factors include oxidation, exposure to biocides excreted by some wetland plants, and absorption by organic matter. Biological removal mechanisms include antibiosis, predation by nematodes and protists, attack by lytic bacteria and viruses, and natural die-off [54].

In Europe, this technology started during the late 1960s. One of the first examples of full-scale FWS CWs with emergent vegetation are those built in 1967 in Lelystad, the Netherlands [25] and near Keszthely, Hungary [55]. This type of constructed wetlands have not spread too much throughout Europe as compared to subsurface constructed wetlands but recently many wetlands have been created in several countries, especially in Sweden and Denmark. More than 2,350 ha of wetlands have been created in Sweden in the agricultural landscape between 1996 and 2002 with different kinds of subsidies and in Denmark about 3,200 ha have been created until 2004 with the primary aim to reduce nitrogen input into Baltic Sea [27].

In North America, the FWS technology started with the ecological engineering of natural wetlands for wastewater treatment in the early 1970s in Florida [56] and Michigan [57]. Industrial stormwaters and process waters were applied to FWS CWs in North Dakota in 1975 [58] and in the early 1980s the use of FWS constructed wetlands for urban stormwater treatment was pioneered in California [59] and for mine wastewater throughout the USA [60]. At present, there are hundreds, and probably thousands of FWS constructed wetlands with emergent macrophytes treating municipal and industrial wastewaters, agricultural wastes and runoff, mine drainage waters, and stormwaters in North America [61]. Free water surface CWs are also commonly used in Australia and New Zealand, especially for treatment of municipal wastewater, stormwater, and pasture runoff [62, 63].

Constructed wetlands with free water surface and emergent vegetation are very effective in removing suspended solids, organics, and microbial pollution. Removal of nitrogen and phosphorus is moderate.

Constructed Wetlands with Floating Mats of Emergent Macrophytes Some emergent macrophytes are capable of forming floating mats, even though their individual plants are not capable of such existence (Fig. 5). Under field conditions, the floating islands of emergent macrophytes may occur naturally as a consequence of bottom disturbance. *Typha* spp. (cattails), *Glyceria maxima* (Mannagrass), *Phragmites australis* (Common reed), *Cyperus papyrus* (Papyrus), *Hydrocotyle umbellata* (Pennywort), or *Alternanthera philoxeroides* (Alligator weed) are examples of plants that are capable of growing in mats.

The floating mats need the support structures, which keep plants in upright position. This is realized either by various netlike structures or by floating, usually styrofoam islands. This technology spread gradually around the world [64, 65] but any design guidelines have not been developed yet.

Constructed Wetlands with Subsurface Flow

Constructed wetlands with subsurface flow may be classified according to the direction of flow into horizontal (HF or HSF) and vertical (VF). Vertical-flow treatment wetlands could be further categorized into

Wastewater Treatment and Control Through Wetlands. Figure 5
FWS CW with floating mats of emergent macropyhtes for treatment of stormwater runoff (Bornem, Belgium). Plants are kept in position with coconut strings (Photo: Jan Vymazal)

downflow and upflow whether the wastewater is fed onto the surface or to the bottom of the wetland (Fig. 1). In these systems, there is no free water surface and processes, which are responsible for pollution removal occur in the layer of filtration material.

Systems with Horizontal Subsurface Flow (HF CWs)
In HF CWs, mechanically pretreated wastewater flows slowly under the surface of the filtration bed, which is filled with porous material planted with emergent macrophytes (Fig. 6). During this passage, the wastewater will come into contact with a network of aerobic, anoxic, and anaerobic zones. The aerobic zones occur around roots and rhizomes that leak oxygen into the substrate [66, 67]. The filtration bed is sealed from the surrounding by an impermeable layer, in most cases plastic liner (PVC, DHPE, LDPE) to prevent leakage to the groundwater (Fig. 6). In order to protect the liner from damage, a geotextile is commonly used (Fig. 6).

The technology of wastewater treatment by means of constructed wetlands with horizontal subsurface flow was started in Germany based on research by K. Seidel commencing in the 1960s [20, 22, 23] and by R. Kickuth in the 1970s [68, 69]. The first full-scale HF Kickuth's type CW for treatment of municipal sewage was put in operation in 1974 in the community Liebenburg-Othfresen [69]. In 1981, the first HF constructed wetland was built in Weinitzen near Graz, Austria [70] and in 1983, the HF CW technology was introduced in Denmark where about 80 HF CWs were built by 1987. Despite problems with surface flow, soil-based systems exhibited high treatment effect for organics and suspended solids if vegetated bed area 3–5 m^2 PE^{-1} was used (PE = population equivalent, 60 g BOD_5 day^{-1}) [66].

In 1985, first two HF CWs were built in the UK (here called Reed Bed Treatment Systems) and by the end of 1986 more than 20 HF CWs were designed [71]. The major change in the design was the use of very coarse filtration material (5–10 mm fraction),which ensured subsurface flow similarly to former design by Seidel [23]. Also, specific area of 5 m^2 PE^{-1} was used in the UK. During the 1990s, HF CWs were built in many European countries and HF CWs became the most widely used concept in Europe in the 1990s [26, 72].

In the USA, between 1972 and 1976, F. Spangler and colleagues started the research aimed at the use of constructed wetlands with horizontal subsurface flow in Seymour, Wisconsin to treat municipal wastewater [73, 74]. This study was followed by other experiments

Wastewater Treatment and Control Through Wetlands. Figure 6
Constructed wetland with horizontal subsurface flow. *Top* – plastic liner (*right*) covered with a geotextile (*left*). *Bottom* – filtration bed filled with crushed rock (4–8 mm) with inflow and outflow zones filled with stones (32–64 mm) (*right*) planted with Reed canarygrass (*Phalaris arundinacea*) (*left*) (Photos: Jan Vymazal)

in New York [75] and Mississippi [76] and during the early 1980s in California [77] and Kentucky [78]. North America was slower to adopt subsurface technology as compared to Europe. However, in recent years, the use of these systems has drawn more attention and it is estimated that there are about 8,000 subsurface constructed wetlands at present [61]. HF CWs in Australia were also adopted in the late 1970s and early 1980s [79, 80] but at present mostly small on-site systems in rural areas are used treatment of domestic sewage [81].

Since the mid-1980s, the concept of HF CWs constructed wetlands has been used in South Africa [82]. At the end of the twentieth century, constructed wetland became more popular in tropical parts of Africa and there are now many fine examples of all types of constructed wetlands including HF systems treating municipal sewage as well as industrial wastewaters and mine drainage waters in [83, 84]. In Asia, the first information about the use of HF CWs appeared in the literature only in the early 1990s from India and China [85, 86] but at present, HF CWs are in

operation in many other Asian countries such as Korea, Taiwan, Japan, Nepal, Malaysia, or Thailand (e.g., [87, 88]). In South and Central America, the use of HF CWS is not widely distributed but this technology has recently got more attention (e.g., [89, 90]).

The early HF CWs were filled with local soil in order to provide high filtration effect. However, this filtration material did not provide sufficient hydraulic conductivity to keep the flow under the surface of filtration beds. After a short period of operation, the surface flow occurred. According to Kickuth's theory, the root formation would increase the hydraulic conductivity of the soil matrix by about two orders of magnitude within 2–4 years of operation [91], but this phenomenon has never been proved (e.g., [70]) and based on recent studies, the presence of plant roots and rhizomes in the HF beds will have a negative effect on hydraulic conductivity (e.g., [92]). However, most of the hydraulic conductivity decline is apparently associated with sediments trapped within the filtration bed from the wastewater. Therefore, more coarse filtration material were required and it turned out that gravel or crushed rock provide required hydraulic conductivity and do not clog rapidly when the wastewater is properly mechanically pretreated [71]. Since the mid-1980s, washed gravel or crushed rock with the grain size between 5 and 20 mm is most commonly used. In order to keep the water below the filtration bed surface, it is also important to have a good mechanical pretreatment and reliable outflow structure. The small secondary systems usually use septic tanks, larger secondary systems most commonly use a combination of screens, grit chamber, and Imhoff tank. However, many other combinations are possible.

For good hydraulics of HF CWs also distribution and collection of water is important. In HF constructed wetlands, the aim is to get even distribution across the full-sectional area of the inlet end of the bed. The early systems used long channels with castellated or vee-notch weirs, but this distribution system had problems with screenable material collected at edges and causing maldistribution and therefore they were replaced with single pipes with adjustable tees or orifices spread along their length and later with perforated pipes either buried or laid on the surface of the distribution zone. At the outlet end, most systems usually have a perforated agricultural drain pipe buried on the bottom of the outflow zone filled with stones. The pipe is connected with a sump where the water level is controlled by socketed pipes, swiveling elbows, or flexible hose(s) (Fig. 7), which can be held in position by a chain or rope.

The macrophytes growing in constructed wetlands have several properties in relation to the treatment

Wastewater Treatment and Control Through Wetlands. Figure 7
Swiveling elbow hanging on a chain in HF CW Sklené, Czech Republic (Photo: Jan Vymazal)

process that make them an essential component of the design. In HF CWs plants, macrophytes (1) insulate the surface during the periods of cold weather, (2) provide substrate for attached bacteria and oxygenation (even very limited) of areas adjacent to roots and rhizomes, (3) release root exudates that may have antimicrobial properties, and (4) sequester nutrients from the wastewater in the (aboveground) biomass that could be removed via harvesting [93]. The most commonly used plant around the world is *Phragmites australis* (Common reed) but many other species such as *Phalaris arundinacea* (Reed canarygrass), *Scirpus* (*Schoenoplectus*) spp. (Bulrush), *Iris pseudacorus* (Yellow flag) are used including the local species.

HF CWs provide high removal of suspended solids, organics, and microbial pollution; removal of nitrogen is moderate and removal of phosphorus is low unless special filtration media with high sorption capacity are used. Organic compounds are degraded by aerobic as well as anaerobic microorganisms attached to the plant's underground organs (i.e., roots and rhizomes) and media surface. The aerobic processes are usually restricted only to the close vicinity of roots where oxygen leaks to the rhizosphere as diffusion of oxygen from the atmosphere to a saturated filtration bed is very slow [94] and therefore anoxic and anaerobic decomposition play an important role in HF constructed wetlands.

The major removal mechanism for nitrogen in HF CWs is microbial nitrification/denitrification. However, the field measurements have shown that the oxygenation of the rhizosphere of HF constructed wetlands is insufficient and, therefore, the incomplete nitrification is the major cause of limited nitrogen removal. Volatilization, adsorption, and plant uptake play much less important role in nitrogen removal in HF constructed wetlands. Volatilization is limited by the fact that HF CWs do not have free water surface and algal activity is negligible in these systems. Nitrogen removal via plant uptake and subsequent harvesting is usually low as compared to inflow loads [95].

Phosphorus is removed primarily by ligand exchange reactions, where phosphate displaces water or hydroxyls from the surface of Fe and Al hydrous oxides. However, media used for HF wetlands (e.g., pea gravel, crushed stones) usually do not contain great quantities of Fe, Al, or Ca and therefore, removal of phosphorus is generally low [95]. Recently, several filtration materials such as LECA (lightweight clay aggregates) have been tested in constructed wetlands [96]. The removal of phosphorus is very high but it is important to realize that sorption and precipitation are saturable and the sorption decreases over the time. It has been found that removal of phosphorus through plant harvesting is negligible and forms only a tiny fraction of the amount removed. However, this mechanism may play more significant role in nutrient removal in tropical and partially subtropical regions where the growth seasonality and nutrient translocations between above- and below-ground parts are minimal [95].

Microbial pollution removal is mainly achieved through a combination of physical, chemical, and biological factors [97]. Physical factors include mainly filtration and adsorption. Chemical and biological factors may include oxidation, exposure to biocides excreted by a number of wetland plants, antimicrobial activity of root exudates, predation by nematodes and protists, activity of lytic bacteria or viruses, retention in biofilms and natural die-off [21, 93, 98].

Constructed wetlands with horizontal subsurface flow are primarily used to remove organics and suspended solids from the various types of wastewater. They are not effective in ammonia removal due to lack of oxygen in filtration bed but they provide suitable conditions for denitrification. Also, phosphorus removal is effective only when special filtration materials are used.

Systems with Vertical Subsurface Flow (VF CWs)

The earliest form of vertical-flow (VF) system is that of Seidel in Germany [23], which was used to oxygenate anaerobic septic effluents. Similar systems in the Netherlands were called "infiltration fields" [99]. Interest in the particular process seemed to wane but it was revived in the last decade because of the need to provide low ammonia concentrations in the discharged water.

Vertical-flow (VF) constructed wetlands comprise a sandy filtration bed planted with macrophytes. The wastewater is fed intermittently on the wetland surface (Fig. 8) and the next batch of wastewater is flushed only after the previous batch percolated through the filter. Wastewater is collected by a drainage network at the base. This feeding mode drains the bed completely free and it allows air to refill the bed. As a result,

Wastewater Treatment and Control Through Wetlands. Figure 8
Wastewater distribution in an experimental VF CW Carrion de Cespedes, Seville, Spain (picture taken before planting) (Photo: Jan Vymazal)

vertical-flow CWs provide good oxygen transfer and hence the ability to nitrify. The major purpose of macrophyte presence in VF CWs is to help maintain the hydraulic conductivity of the bed. By far, the most frequently used species is *Phragmites australis*. The early vertical-flow systems were usually staged systems with parallel and series beds. Such VF systems are now called first-generation VF systems [100]. Recently, VF systems with only one bed have been used. These systems are called second-generation VF CWs or compact vertical-flow beds [101].

The removal mechanisms in VF CWs are the same as in HF CWs. However, the major difference is the extent of processes responsible for nitrogen transformation and removal. VF CWs provide much higher degree of nitrification but removal of total nitrogen is comparable (Table 1) because the redox conditions in VF CWs are not suitable for denitrification and nitrogen is discharged as nitrate [95].

Vertical-flow constructed wetlands are very often used for on-site treatment [100, 101] but some countries such as France, the VF CWs are used to treat municipal sewage [102]. VF systems are getting more popular especially for their ability to remove ammonia. The most commonly used format is that a series of first stage beds dosed in rotation acts as combination of a sludge drying reed bed and pretreatment and the second stage is a "conventional" VF bed [102].

Besides vertical-flow CWs fed on the surface, there are VF wetlands that are fed on the bottom of the filter bed (so-called "upflow" systems). The water percolates upward and then it is collected either near the surface or on the surface of the wetland bed. These systems have commonly been used in Brazil since the 1980s [103], but they are used now in limited numbers in other countries as well.

Tidal flow systems are a new form of VF system [100]. These systems were developed to try to overcome some of the problems that were seen in the early forms of VF systems related to clogging of the surface. Upflow systems have been used for about 20 years but they suffer from the problem that distribution is below the surface and hence hidden from the observers. In tidal flow systems at the start of the treatment cycle the wastewater is fed to the bottom of the bed into the aeration pipes. It then percolates upward until the surface is flooded. When the surface is completely flooded the pump is then shut off, the wastewater is then held in the bed in contact with the microorganisms growing on the media. A set time later the wastewater is drained downward and

Wastewater Treatment and Control Through Wetlands. Table 1 Treatment performance of downflow, vertical-flow, and horizontal-flow constructed wetlands: worldwide experience

	Vertical flow				Horizontal flow			
	In	Out	Eff. (%)	*n*	In	Out	Eff. (%)	*n*
BOD_5	309	21	87.9	97	170	42	73.4	438
COD	547	70	78.6	115	427	143	62.7	292
TSS	188	18	77.1	74	141	35	68.6	367
TP	10.6	4.6	48.3	94	9.6	4.8	42.8	272
TN	70	37.6	44.0	64	63.1	36	39.7	208
NH_4-N	56.4	10.6	78.9	94	36.1	22.1	22.6	305
NO_3-N	0.62	25.3		70	8.0	5.9	26.0	210
FC*	5.95	3.0	97.6	20	8.22	5.17	92.4	95

In = inflow, Out = outflow, Eff. = efficiency, *n* = number of systems. *FC = fecal coliforms (log CFU 100 ml^{-1}) (Data from Vymazal and Kröpfelová 2008)

after the water has drained from the bed the treatment cycle is complete and air diffuses into the voids in the bed [100].

Hybrid Constructed Wetlands

Various types of constructed wetlands may be combined in order to achieve higher treatment effect, especially for nitrogen. Many of these systems are derived from original hybrid systems developed by Seidel at the Max Planck Institute in Krefeld, Germany. The process is known as the Seidel system, the Krefeld system, or the Max Planck Institute Process (MPIP) [23]. The design consisted of two stages of several parallel VF beds followed by two or three HF beds in series. This configuration provides nitrification in the first (VF) wetland and denitrification in the second (HF) wetland. Such systems were built, among others, in France [104], the UK [105], Norway [106], or Belgium [107].

In the mid-1990s, Johansen and Brix [108] introduced a HF-VF hybrid system with a large HF bed placed first and a small VF bed as the second stage. In this system, nitrification takes place in the vertical-flow stage at the end of the process sequence. If nitrate removal is needed it is then necessary to recirculate the effluent back to the front end of the system where denitrification can take place. It is possible to recycle the wastewater to the pretreatment unit (e.g., septic tank) or to the HF CW where conditions are favorable for denitrification (anoxic/anaerobic conditions and sufficient concentration of organics necessary for denitrification) [109].

Recently, hybrid constructed wetlands have combined even more types of CWs including FWS systems in order to achieve better treatment performance of the system. The FWS CWs help to oxygenate the water but very often contribute to the increase of suspended solids due to the presence of planktonic algae in the outflow. For example, Masi et al. [110], Mander et al. [111], and Brix et al. [112] reported the use of VF-HF-FWS-pond hybrid system to treat winery wastewaters in Ornellaia (Italy), sewage in Kõo (Estonia), and sewage in tsunami-destroyed area at the island of Phi Phi Don (Thailand).

The Use of Constructed Wetlands for Various Types of Wastewater

Constructed wetlands have mostly been used to treat municipal or domestic sewage. However, over the period of 4 decades, the constructed wetlands have also been used to treat nearly all types of wastewaters including industrial and agricultural, landfill leachate, mine drainage waters, and runoff waters (Table 2).

When municipal sewage treatment is concerned besides the common pollutants such as organics, suspended solids and nutrients also specific compounds,

such as linear alkylbenzene sulfonates, the most widely used synthetic surfactants [115], or PPCP (Pharmaceuticals and Personal Care Products) [116] are monitored. For both groups of compounds, constructed wetlands proved to be a suitable treatment technology.

Constructed wetlands are used to treat a wide variety of industrial wastewaters (Table 2). Industrial wastewaters vary widely in composition and also strength and some of these wastewaters such as those from food processing, distillery, winery or abattoir belong to the most concentrated wastewaters especially because of high concentrations of organics. However, it has been shown that constructed wetlands (Fig. 9) can handle these wastewaters successfully [117]. Also wastewaters from agroindustry operations are very strong and very often contain very high concentrations of suspended solids, organics, and ammonia. Therefore, it is necessary to include several steps of pretreatment and constructed wetlands are usually used as final treatment step.

Constructed wetlands are commonly used for treatment of various kinds of runoff. They improve water quality, modify the flow rates by storing water temporarily, attenuate flow, and reduce downstream scouring and erosion. Target pollutants differ among types of runoff. In highway, road and urban (Fig. 10) runoff, the targets are suspended solids, organics, oil and grease, and heavy metals [118]. In nursery, greenhouse, agricultural, pasture, and golfcourse (Fig. 11) runoff, the major targets are nitrates, phosphorus, and herbicides [119]. In airport runoff, the major targets are de-icing and anti-icing compounds applied to the aircraft and taxiways [120].

Wastewater Treatment and Control Through Wetlands. Table 2 The use of constructed wetlands for various types of wastewater [28, 29, 114, 115]

Industrial	Petrochemical, pulp and paper, electric utility, abattoir, tool industry, power station, sugar industry, olive mill, potato processing, soft drinks, explosives, chemicals, cheese, herbicides, textile, tannery, distillery, winery, laundry, fish farm, aquaculture (fish, shrimp)
Agriculture	Swine, livestock, poultry, dairy
Runoff	Dairy pasture, tile drainage, agriculture (row crops), residential areas, roads, highways, airport, golf-courses, greenhouse, nursery
Mine waters	Acid coal acid lignite, alkaline coal, coal slurry, metals (Cu, Zn, Pb, U), spoil heaps
Leachate	Landfill, compost, mushroom farm, wood

Wastewater Treatment and Control Through Wetlands. Figure 9
HF CW planted with *Typha domingensis* for treatment of abattoir wastewater in San Jacinto, Uruguay (Photo: Jan Vymazal)

Wastewater Treatment and Control Through Wetlands. Figure 10
FWS CW for urban stormwater runoff treatment in Woodcroft Estate near Sydney, Australia (Photo: Jan Vymazal)

Wastewater Treatment and Control Through Wetlands. Figure 11
FWS CW for treatment of golfcourse runoff (Rivertowne Country Club, Charleston, South Carolina, USA) (Photo: Jan Vymazal)

A very large application area for constructed wetlands is the treatment of mine drainage waters from coal (Fig. 12) and metal ores mining activities (Table 2). The target parameters are sulfates, iron, manganese, aluminum, acidity and alkalinity in coal mining drainage, and heavy metals in metal ores drainage waters.

Constructed wetlands are also used to treat various leachates. The most systems have been built to treat

Wastewater Treatment and Control Through Wetlands. Figure 12
Constructed wetland with free water surface and emergent vegetation (*Typha latifolia*) in Monastery Run, Pennsylvania, USA for treatment of mine drainage waters (Photo: Jan Vymazal)

landfill leachates [121, 122]. This application is getting more attention nowadays and examples of constructed wetlands could be found in Canada, the USA, Slovenia, Norway, Poland, the UK, among others [114].

Future Directions

Constructed wetlands have evolved over the period of nearly 4 decades into a widely accepted alternative for wastewater treatment of all types of wastewaters, despite the mistrust of many civil engineers and water authorities. These systems are very effective in removing pollution from wastewater and at the same time their operation and maintenance costs are much lower as compared to conventional treatment systems. Various types of constructed wetlands provide specific advantages and therefore their combination may enhance the treatment effect.

Indeed, constructed wetlands do have their "weak points" such as phosphorus removal. So far, constructed wetlands have not been recommended as an appropriate technology for phosphorus removal unless specific filtration materials are used. However, the artificially prepared materials are usually expensive and therefore intensive efforts are made to test various waste materials such as blast and electric arc furnace steel slags or fly ash (inorganic waste product from coal or oil shale combustion) to enhance phosphorus removal [123, 124].

It is desirable to pay more attention to secondary benefits of constructed wetlands designed primarily for wastewater treatment. For examples, the ecosystem services on the landscape are often neglected and seldom studied. Also the use of plant biomass from constructed wetlands is only scarce [125].

Bibliography

Primary Literature

1. Mitsch WJ, Mitsch RH, Turner RE (1994) Wetlands of the old and new worlds: ecology and management. In: Mitsch WJ (ed) Global wetlands: old world and new. Elsevier Science, Amsterdam, pp 3–56
2. Maltby E, Turner GE (1983) Wetlands of the world. Geogr Mag 55:12–17
3. Matthews E, Fung I (1987) Methane emission from natural wetlands: global distribution, area, and environmental characteristics of sources. Glob Biogeochem Cycles 1:61–86
4. Aselman I, Crutzen PJ (1989) Global distribution of natural freshwater wetlands and rice paddies, their net primary productivity, seasonality and possible methane emissions. J Atmos Chem 8:307–358

5. Aselman I, Crutzen PJ (1990) A global inventory of wetland distribution and seasonality, net primary productivity, and estimated methane emissions. In: Bouwman AF (ed) Soils and the greenhouse effect. Wiley, New York, pp 441–449
6. Patten BC (1990) Introduction and overview. In: Patten BC (ed) Wetlands and shallow continental water bodies, vol 1. SPB Academic, The Hague, pp 3–8
7. Williams M (1990) Understanding wetlands. In: Williams M (ed) Wetlands: a threatened landscape. Basil Blackwell, Oxford, pp 1–41
8. Chen ZM, Chen GQ, Chen B, Zhou JB, Yang ZF, Zhou Y (2009) Net ecosystem services value of wetlands: environmental economic account. Commun Nonlinear Sci Numer Simul 14:2837–2843
9. Geber U, Björklund J (2002) The relationship between ecosystem services and purchased input in Swedish wastewater treatment systems – a case study. Ecol Eng 19:97–117
10. Moreno D, Pedrocchi C, Comín FA, García M, Cabezas A (2007) Creating wetlands for the improvement of water quality and landscape restoration in semi-arid zones degraded by intensive agricultural use. Ecol Eng 30:103–111
11. Löffler H (1990) Human uses. In: Patten BC (ed) Wetlands and shallow continental water bodies, vol 1. SPB Academic, The Hague, pp 17–27
12. Sather JH, Smith RD, Larson JS (1990) Natural values of wetlands. In: Patten BC (ed) Wetlands and shallow continental water bodies, vol 1. SPB Academic, The Hague, pp 373–387
13. Stainbridge HH (1976) History of sewage treatment in Britain, part 5. Land treatment. Institute of Water Pollution Control, Maidstone
14. Wentz WA (1987) Ecological/environmental perspectives on the use of wetlands in water treatment. In: Reddy KR, Smith WH (eds) Aquatic plants for water treatment and resource recovery. Magnolia, Orlando, pp 17–25
15. Brix H (1993) Wastewater treatment in constructed wetlands: system design, removal processes, and treatment performance. In: Moshiri AG (ed) Constructed wetlands for water quality improvement. CRC Press, Boca Raton, pp 9–22
16. Kadlec RH (2009) The Houghton Lake wetland treatment project. Ecol Eng 35:1285–1286
17. Mander Ü, Jenssen P (eds) (2002) Natural wetlands for wastewater treatment in cold climates. WIT Press, Southampton
18. Hammer DA, Bastian RK (1989) Wetland ecosystems: natural water purifiers? In: Hammer DA (ed) Constructed wetlands for wastewater treatment. Lewis, Chelsea, pp 5–19
19. Seidel K (1953) Pflanzungen zwischen Gewässern und Land. J Max Planck Inst 17–20
20. Seidel K (1965) Phenol-Abbau in Wasser durch *Scirpus lacustris* L. wehrend einer versuchsdauer von 31 Monaten. Naturwissenschaften 52:398–406
21. Seidel K (1976) Macrophytes and water purification. In: Tourbier J, Pierson RW (eds) Biological control of water pollution. Pennsylvania University Press, Philadelphia, pp 109–122
22. Seidel K (1961) Zur Problematik der Keim- und Pflanzengewasser. Verh Internat Verein Limnol 14:1035–1039
23. Seidel K (1965) Neue Wege zur Grundwasseranreicherung in Krefeld, Vol. II. Hydrobotanische Reinigungsmethode. GWF Wasser/Abwasser 30:831–833
24. Börner T, von Felde K, Gschlössl T, Gschlössl E, Kunst S, Wissing FW (1998) Germany. In: Vymazal J, brix H, Cooper PF, Green MB, Haberl R (eds) Constructed wetlands for wastewater treatment in Europe. Backhuys, Leiden, pp 169–190
25. De Jong J (1976) The purification of wastewater with the aid of rush or reed ponds. In: Tourbier J, Pierson RW (eds) Biological control of water pollution. Pennsylvania University Press, Philadelphia, pp 133–139
26. Vymazal J (2005) Constructed wetlands with horizontal subsurface flow and hybrid systems for wastewater treatment. Ecol Eng 25:478–490
27. Vymazal J, Greenway M, Tonderski K, Brix H, Mander Ü (2006) Constructed wetlands for wastewater treatment. In: Verhoeven JTA, Beltman B, Bobbink R, Whigham DF (eds) Wetlands and natural resource management, vol 190, Ecological Studies. Springer, Berlin/Heidelberg, pp 69–94
28. Wallace SD, Knight RL (2006) Small scale constructed wetland treatment systems. Feasibility, design criteria, and O&M requirements. Water Environment Research Foundation, Alexandria
29. Kadlec RH, Knight RL, Vymazal J, Brix H, Cooper PF, Haberl R (2000) Constructed wetlands for water pollution control: processes, performance, design and operation. International Water Association Scientific and Technical report no. 8, London
30. Rogers HH, Davis DE (1972) Nutrient removal by waqter hyacinth. Weed Sci 20:423–427
31. Penfound WT, Earle TT (1948) The biology of the water hyacinth. Ecol Monogr 18:447–472
32. Crites R, Tchobanoglous G (1998) Small and decentralized wastewater management systems. McGraw-Hill, Boston
33. Culley DD Jr, Epps EA (1973) Use of duckweed for waste treatment and animal feed. J Water Pollut Control Fed 45:337–347
34. Rai DN, Munshi JD (1979) The influence of thick floating vegetation (waterhyacinth-*Eichhornia crassipes*) on the physicochemical environment of a freshwater wetland. Hydrobiologia 62:65–69
35. Wolverton BC (1979) Engineering design data for small vascular aquatic plant wastewater treatment systems. In: Bastian RK, Reed SC (eds) Aquaculture systems for wastewater treatment: seminar proceedings and engineering assessment. EPA 430/9-80-006. U.S. EPA, Washington, pp 179–192
36. Reddy KR, DeBusk WF (1984) Growth characteristics of aquatic macrophytes cultured in nutrient-enriched water. I. Water hyacinth, water lettuce and pennywort. Econ Bot 38:229–239
37. Rejmánková E, Rejmánek M, Květ J (1990) Minimizing duckweed (Lemnaceae) production by suitable harvest strategy. In: Whigham DF, Good RE, Květ J (eds) Wetland ecology and management: case studies. Kluwer, Dordrecht, pp 39–43
38. Reed SC, Middlebrooks EJ, Crites RW (1995) Natural systems for waste management and treatment, 2nd edn. McGraw-Hill, New York

39. Vymazal J (2008) Constructed wetlands, surface flow. In: Jørgensen SE (ed) Encyclopedia of ecology, vol 1. Elsevier B.V, Amsterdam, pp 765–777
40. Stewart EA III, Haselow DL, Wyse NM (1987) Review of operations and performance data of five water hyacinth based treatment systems in Florida. In: Reddy KR, Smith WH (eds) Aquatic plants for water treatment and resource recovery. Magnolia, Orlando, pp 279–288
41. Ozimek T, Czyprzňski P (2003) Ten years´ experience of constructed wetlands in Poland. Publ Inst Geogr Univ Tartuensis 94:163–167
42. Denny P (1980) Solute movement in submerged angiosperms. Biol Rev 55:65–92
43. Carignan R, Kalff J (1980) Phosphorus sources for aquatic weeds: water or sediments? Science 207:987–989
44. Twilley RR, Kemp WM, Staver KW, Stevenson JC, Boynton WR (1985) Nutrient enrichment of estuarine submersed vascular plant communities. 1. Algal growth and effects on production of plants and associated communities. Mar Ecol Prog Ser 23:179–191
45. Gu B, DeBusk TA, Dierberg FE, Chimney MJ, Pietro KC, Aziz T (2001) Phosphorus removal from Everglades agricultural runoff by submerged aquatic vegetation/limerock treatment technology: an overview of research. Water Sci Technol 44(11/12):101–108
46. Bishop PL, Eighmy TT (1989) Aquatic wastewater treatment using *Elodea nuttalii*. J Water Pollut Control Fed 61: 641–648
47. Toet S, Van Logtestijn RSP, Schreier M, Kampf R, Verhoeven JTA (2005) The functioning of a wetland system used for polishing effluent from a sewage treatment plant. Ecol Eng 25:101–124
48. Yang Y, Zhencheng X, Kangping H, Junsan W, Guizhi W (1994) Removal efficiency of the constructed wetland wastewater treatment system at Bainikeng, Shenzhen. In: Proceedings of the 4th international conference wetland systems for water pollution control. ICWS'94 Secretariat, Guangzhou, P.R. China, pp 94–103
49. Kadlec RH (1994) Overview: surface flow constructed wetlands. In: Proceedings of the 4th international conference wetland systems for water pollution control. ICWS Secretariat, Guangzhou, P.R.China, pp 1–12
50. Queensland Department of Natural Resources (QDNR) (2000) Guidelines for using freewater surface constructed wetlands to treat Municipal Sewage. QDNR, Brisbane
51. Vymazal J, Brix H, Cooper PF, Haberl R, Perfler R, Laber J (1998) Removal mechanisms and types of constructed wetlands. In: Vymazal J, Brix H, Cooper PF, Haberl R, Perfler R (eds) Constructed wetlands for wastewater treatment in Europe. Backhuys, Leiden, pp 17–66
52. Richardson CJ (1985) Mechanisms controlling phosphorus retention capacity in freshwater wetlands. Science 228:1424–1427
53. Sundblad K, Wittgren H-B (1989) *Glyceria maxima* for wastewater nutrient removal and forage production. Biol Waste 27:29–42
54. Gersberg RM, Gearhart RA, Ives M (1989) Pathogen removal in constructed wetlands. In: Hammer DA (ed) Constructed wetlands for wastewater treatment. Lewis, Chelsea, pp 431–446
55. Lakatos G (1998) Hungary. In: Vymazal J, Brix H, Cooper PF, Green MB, Haberl R (eds) Constructed wetlands for wastewater treatment in Europe. Backhuys, Leiden, pp 191–206
56. Ewel KC, Odum HT (eds) (1984) Cypress swamps. University of Florida Press, Gainesville
57. Kadlec RH, Tilton DL (1979) The use of freshwater wetlands as a tertiary wastewater treatment alternative. CRC Crit Rev Environ Control 9:185–212
58. Litchfield DK, Schatz DD (1989) Constructed wetlands for wastewater treatment at Amoco Oil Company's Mandan, North Dakota refinery. In: Hammer DA (ed) Constructed wetlands for wastewater treatment. Lewis, Chelsea, pp 233–237
59. Chan E, Bursztynsky TA, Hantzsche N, Litwin YJ (1982) The use of wetlands for water pollution control. U.S. EPA Report EPA-600/2-82-086, Municipal Environmental Research Lab, Cincinnati
60. Wieder RK (1989) A survey of constructed wetlands for acid coal mine drainage treatment in the eastern United States. Wetlands 9:299–315
61. Kadlec RH (2003) Status of treatment wetlands in North America. In: Dias V, Vymazal J (eds) Proc. Conf. The use of aquatic macrophytes for wastewater treatment in constructed wetlands. ICN and INAG, Lisbon, pp 363–401
62. Greenway M, Woolley A (1999) Constructed wetlands in Queensland: performance efficiency and nutrient bioaccumulation. Ecol Eng 12:39–55
63. Tanner CC, Nguyen ML, Sukias JPS (2005) Nutrient removal by a constructed wetland treating subsurface drainage from a grazed dairy pasture. Agric Ecosyst Environ 105:145–162
64. Kyambadde J, Kansiime F, Dalhammar G (2005) Nitrogen and phosphorus removal in substrate-free pilot constructed wetlands with horizontal surface flow in Uganda. Water Air Soil Pollut 165:37–59
65. Van Oostrom AJ (1995) Nitrogen removal in constructed wetlands treating nitrified meat processing effluent. Water Sci Technol 32(3):137–148
66. Brix H (1987) Treatment of wastewater in the rhizosphere of wetland plants – the root zone method. Water Sci Technol 19:107–118
67. Vymazal J (2001) Types of constructed wetlands for wastewater treatment: their potential for nutrient removal. In: Vymazal J (ed) Transformations of nutrients in natural and constructed wetlands. Backhuys, Leiden, pp 1–93
68. Kickuth R (1982) A low-cost process for purification of municipal and industrial waste water. Der Tropenlandwirt 83: 141–154
69. Kickuth R (1984) Das Wurzelraumverfahren in der praxis. Landschaft und Stadt 16:145–153
70. Haberl R, Perfler R (1990) Seven years of research work and experience with wastewater treatment by a reed bed system. In: Cooper PF, Findlater BC (eds) Constructed wetlands in water pollution control. Pergamon Press, Oxford, pp 205–214

71. Cooper PF, Green MB (1995) Reed bed treatment systems for sewage treatment – the first 10 years experience. Water Sci Technol 32:317–327
72. Vymazal J, Brix H, Cooper PF, Green MB, Haberl R (eds) (1998) Constructed wetlands for wastewater treatment in Europe. Backhuys, Leiden
73. Fetter CW, Sloey WE, Spangler FL (1976) Potential replacement of septic tank drain fields by artificial marsh wastewater treatment systems. Ground Water 14:1–7
74. Spangler FL, Sloey WE, Fetter CW Jr (1976) Artificial and natural marshes as wastewater treatment systems in Wisconsin. In: Tilton DL, Kadlec RH, Richardson CJ (eds) Freshwater wetlands and sewage effluent disposal. University of Michigan, Ann Arbor, pp 215–240
75. Small M, Wurm C (1977) Data report. Meadow/Marsh/Pond System. Brookhaven National Laboratory, BNL 50675
76. Wolverton BC (1987) Artificial marshes for wastewater treatment. In: Reddy KR, Smith WH (eds) Aquatic plants for water treatment and resource recovery. Magnolia, Orlando, pp 141–152
77. Gersberg RM, Elkins BV, Goldman CR (1983) Nitrogen removal in artificial wetlands. Water Res 17:1009–1014
78. Steiner GR, Watson JT, Hammer DA, Harker DF Jr (1987) Municipal wastewater treatment with artificial wetlands: a TVA/Kentucky demonstration. In: Reddy KR, Smith WH (eds) Aquatic plants for water treatment and resource recovery. Magnolia, Orlando, pp 923–932
79. Finlayson CM, Chick AJ (1983) Testing the potential of aquatic plants to treat abattoir effluent. Water Res 17:415–422
80. Bavor HJ, Roser DJ, McKersie S (1987) Nutrient removal using shallow lagoon-solid matrix macrophyte systems. In: Reddy KR, Smith WH (eds) Aquatic plants for water treatment and resource recovery. Magnolia, Orlando, pp 227–235
81. Davison L, Pont D, Bolton K, Headley T (2006) Dealing with nitrogen in subtropical Australia: seven case studies in the diffusion of ecotechnological innovation. Ecol Eng 28:213–223
82. Wood A (1990) The application of artificial wetlands in South Africa. In: Cooper PF, Findlater BC (eds) Constructed wetlands in water pollution control. Pergamon Press, Oxford, pp 235–244
83. Byekwaso E, Kansiime F, Logstrum J, Andersen S (2002) The optimisation of a reed bed filter for effluent treatment at Kasese Cobalt Company Limited – Uganda. In: Proceedings of the 8th international conference wetland systems for water pollution control. University of Dar es Salaam, Tanzania, pp 660–668
84. Kaseva ME (2004) Performance of a sub-surface flow constructed wetland in polishing pre-treated wastewater – a tropical case study. Water Res 38:681–687
85. Wang J, Cai X, Chen Y, Yang Y, Liang M, Zhang Y, Wang Z, Li Q, Liao X (1994) Analysis of the configuration and the treatment effect of constructed wetland wastewater treatment system for different wastewaters in South China. In: Proceedings of the 4th international conference wetland systems for water pollution control. ICWS'94 Secretariat, Guangzhou, P.R. China, pp 114–120
86. Juwarkar AS, Verma M, Meshram J, Bal AS, Juwarkar A (1992). Wastewater treatment in constructed wetlands. In: Proceedings of the 3rd international conference wetland systems for water pollution control. IWA and University of Western Sydney, pp 35.1–35.4
87. Lee CY, Lee CC, Lee FY, Tseng SK, Liao CJ (2004) Performance of subsurface flow constructed wetland taking pretreated swine effluent under heavy loads. Bioresour Technol 92:173–179
88. Lin YF, Jing SR, Lee DY, Chang YF, Chen YM, Shih KC (2005) Performance of a constructed wetland treating intensive shrimp aquaculture wastewater under high hydraulic loading rate. Environ Pollut 134:411–421
89. Dallas S, Ho G (2005) Subsurface flow reedbeds using alternative media for the treatment of domestic greywater in Monteverde, Costa Rica, Central America. Water Sci Technol 51(10):119–128
90. Platzer M, Cáceresy V, Fong N, Haberl R (2002) Investigations and experiences with subsurface flow constructed wetlands in Nicaragua, Central America. In: Proceedings of the 8th international conference on wetland systems for water pollution control. University of Dar es Salaam and IWA, Arusha, Tanzania, pp 350–365
91. Cooper PF, Boon AG (1987) The use of *Phragmites* for wastewater treatment by the Root Zone Method: the UK approach. In: Reddy KR, Smith WH (eds) Aquatic plants for water treatment and resource recovery. Magnolia, Orlando, pp 153–174
92. Young TC, Collins AG, Theis TL (2000) Subsurface flow wetland for wastewater treatment at Minoa. Report to NYSERDA and U.S. EPA, Clarkson University, New York
93. Brix H (1997) Do macrophytes play a role in constructed treatment wetlands? Water Sci Technol 35(5):11–17
94. Drew MC (1979) Plant responses to anaerobic conditions in soil and solution culture. Curr Adv Plant Sci 11: 36.1–36.14
95. Vymazal J (2007) Removal of nutrients in various types of constructed wetlands. Sci Total Environ 380:48–65
96. Vohla C, Põldvere E, Noorvee A, Kuusemets V, Mander Ü (2005) Alternative filter media for phosphorus removal in a horizontal subsurface flow constructed wetland. J Environ Sci Health 40:1251–1264
97. Vymazal J (2005) Removal of enteric bacteria in constructed treatment wetlands with emergent macrophytes: a review. J Environ Sci Health 40A:1355–1367
98. Decamp O, Warren A (2000) Investigation of *Escherichia coli* removal in various designs of subsurface flow wetlands used for wastewater treatment. Ecol Eng 14:293–299
99. Greiner RW, de Jong J (1984) The use of Marsh Plants for the treatment of waste water in areas designated for recreation and tourism. RIJP report no. 225, Lelystad, The Netherlands
100. Cooper PF (2005) The performance of vertical flow constructed wetland systems with special reference to the significance of oxygen transfer and hydraulic loading rates. Water Sci Technol 51(9):81–90

101. Weedon CN (2003) Compact vertical flow reed bed system – first two years performance. Water Sci Technol 48(5):15–23
102. Molle P, Liénard A, Boutin C, Merlin G, Iwema A (2005) How to treat raw with constructed wetlands: an overview of French systems. Water Sci Technol 51(9):11–21
103. Salati E Jr, Salati E, Salati E (1999) Wetland projects developed in Brazil. Water Sci Technol 40(3):19–25
104. Boutin C (1987) Domestic wastewater treatment in tanks planted with rooted macrophytes: case study, description of the system, design criteria, and efficiency. Water Sci Technol 19(10):29–40
105. Burka U, Lawrence P (1990) A new community approach to wastewater treatment with higher water plants. In: Cooper PF, Findlater BC (eds) Constructed wetlands in water pollution control. Pergamon Press, Oxford, pp 359–371
106. Mæhlum T, Stålnacke P (1999) Removal efficiency of three cold-climate constructed wetlands treating domestic wastewater: effects of temperature, seasons, loading rates and input concentrations. Water Sci Technol 40(3):273–281
107. Rousseau DPL, Vanrolleghem PA, De Pauw N (2004) Constructed wetlands in Flanders: a performance analysis. Ecol Eng 23:151–163
108. Brix H, Johansen NH (1999) Treatment of domestic sewage in a two-stage constructed wetland - design principles. In: Vymazal J (ed) Nutrient cycling and retention in natural and constructed wetlands. Backhuys, Leiden, pp 155–163
109. Brix H, Arias CA, Johansen NH (2003) Experiments in a two-stage constructed wetland system: nitrification capacity and effects of recycling on nitrogen removal. In: Vymazal J (ed) Wetlands-nutrients, metals and mass cycling. Backhuys, Leiden, pp 237–258
110. Masi F, Conte G, Martinuzzi N, Pucci B (2002) Winery high organic content wastewaters treated by constructed wetlands in Mediterranean climate. In: Proceedings of the 8th international conference wetland systems for water pollution control. University of Dar-es-Salaam, Tanzania and IWA, pp 274–282
111. Mander Ü, Teiter S, Lõhmus K, Mauring T, Nurk K, Augustin J (2003) Emission rates of N_2O and CH_4 in riparian alder forest and subsurface flow constructed wetland. In: Vymazal J (ed) Wetlands: nutrients, metals and mass cycling. Backhuys, Leiden, pp 259–279
112. Brix H, Koottatep T, Laugesen CH (2006) Re-establishment of wastewater treatment in tsunami affected areas of Thailand by the use of constructed wetlands. In: Dias V, Vymazal J (eds) Proceedings of the 10th international conference wetland systems for water pollution control, MAOTDR 2006, Lisbon, Portugal, pp 59–67
113. Vymazal J (2009) The use constructed wetlands with horizontal sub-surface flow for various types of wastewater. Ecol Eng 35:1–17
114. Vymazal J, Kröpfelová L (2008) Wastewater treatment in constructed wetlands with horizontal sub-surface flow. Springer, Dordrecht
115. Huang Y, Latorre A, Barcelo D, Garcia J, Aqguirre P, Mujeriego R, Bayona JM (2004) Factors affecting linear alkylbenzene sulfonates removal in subsurface flow constructed wetlands. Environ Sci Technol 38:2657–2663
116. Matamoros V, Arias C, Brix H, Bayona JM (2009) Preliminary screening of small-scale domestic wastewater treatment systems for removal of pharmaceutical and personal care products. Water Res 43:55–62
117. Vymazal J, Kröpfelová L (2009) Removal of organics in constructed wetlands with horizontal sub-surface flow: a review of the field experience. Sci Total Environ 407:3911–3922
118. Shutes RBE, Revitt DM, Scholes LNL, Forshaw M, Winter B (2001) An experimental constructed wetland system for the treatment of highway runoff in the UK. Water Sci Technol 44(11–12):571–578
119. Headley TR, Huett DO, Davison L (2001) The removal of nutrients from plant nursery irrigation runoff in subsurface horizontal-flow wetlands. Water Sci Technol 44(11–12):77–84
120. Worrall P, Revitt DM, Prickett G, Brewer D (2002) Constructed wetlands for airport runoff – the London Heathrow experience. In: Nehring KW, Brauning SE (eds) Wetlands and remediation II. Battelle Press, Columbus, pp 177–186
121. Urbanc-Berčič O (1997) Constructed wetlands for the treatment of landfill leachates: the Slovenian Experience. Wetlands Ecol Manage 4:189–197
122. Mæhlum T, Warner WS, Stålnacke P, Jenssen PD (1999) Leachate treatment in extended aeration lagoons and constructed wetlands in Norway. In: Mulamoottil G, McBean EA, Revers F (eds) Constructed wetlands for the treatment of landfill leachates. Lewis/CRC Press, Boca Raton, pp 151–163
123. Korkusuz EA, Beglioğlu M, Demirer GN (2005) Comparison of the treatment performances of blast furnace slag-based and gravel-based vertical flow wetlands operated identically for domestic wastewater treatment in turkey. Ecol Eng 24:187–200
124. Vohla C, Põldvere E, Noorvee A, Kuusemets V, Mander Ü (2005) Alternative filter media for phosphorous removal in a horizontal subsurface flow constructed wetland. J Environ Sci Health A 40:1251–1264
125. Maddison M, Soosaar K, Mauring T, Mander Ü (2009) The biomass and nutrient and heavy metal content of cattails and reeds in wastewater treatment wetlands for the production of construction material in Estonia. Desalination 246:120–128
126. Zurita F, De Anda J, Belmont M (2009) Treatment of domestic wastewater and production of commercial flowers in vertical and horizontal subsurface-flow constructed wetlands. Ecol Eng 35:861–869

Books and Reviews

Cooper PF (ed) (1990) European design and operation guidelines for reed bed treatment systems. Prepared for the European Community/European Water Pollution Control Association Emergent Hydrophyte Treatment System Expert Contact Group. WRc report UI 17

Cooper PF, Findlater BC (eds) (1990) Constructed wetlands in water pollution control. Pergamon Press, Oxford

Cooper PF, Job GD, Green MB, Shutes RBE (1996) Reed beds and constructed wetlands for wastewater treatment. Water Research Center, Swindon

Hammer DA (ed) (1989) Constructed wetlands for wastewater treatment. Lewis, Chelsea

Kadlec RH, Knight RL (1996) Treatment wetlands. CRC Press, Boca Raton

Kadlec RH, Wallace SD (2008) Treatment wetlands, 2nd edn. CRC Press, Boca Raton

Mander Ü, Jenssen P (eds) (2003) Constructed wetlands for wastewater treatment in cold climates. WIT Press, Southampton

Mitsch WJ, Gossselink JG (2007) Wetlands, 4th edn. Wiley, Hoboken

Mitsch WJ, Gosselink JG, Anderson CJ, Zhang L (2009) Wetland ecosystems. Wiley, Hoboken

Moshiri GA (ed) (1993) Constructed wetlands for water quality improvement. CRC Press/Lewis, Boca Raton

Mulamoottil G, McBean AE, Revers F (eds) (1999) Constructed wetlands for the treatment of landfill leachates. Lewis/CRC Press, Boca Raton

Price T, Probert D (1997) Role of constructed wetlands in environmentally-sustainable developments. Appl Energy 57:129–174

Reddy KR, Smith WH (eds) (1987) Aquatic plants for wastewater treatment and resource recovery, Magnolia Publishing. Orlando, Florida

Scholz M (2006) Wetland systems to control urban runoff. Elsevier, Amsterdam

Tinner RW (1999) Wetland indicators. A guide to wetland identification, delineation, classification, and mapping. Lewis, Boca Raton

Tourbier J, Pierson RW (eds) (1976) Biological control of water pollution. University of Pennsylvania Press, Philadelphia

Vymazal J (ed) (1999) Nutrient cycling and retention in natural and constructed wetlands. Backhuys, Leiden

Vymazal J (ed) (2001) Transformations of nutrients in natural and constructed wetlands. Backhuys, Leiden

Vymazal J (ed) (2003) Wetlands – nutrients, metals and mass cycling. Backhuys, Leiden

Vymazal J (ed) (2005) Natural and constructed wetlands: nutrients, metals and management. Backhuys, Leiden

Vymazal J (2008) Wastewater treatment, plant dynamics and management in constructed and natural wetlands. Springer, Dordrecht

Vymazal J, Kröpfelová L (2008) Wastewater treatment in constructed wetlands with horizontal sub-surface flow. Springer, Dordrecht

Wastewater Treatment Plant: Anthropogenic Micropollutant Indicators for Sustainable River Management

Eunkyung Lee[1], Sungyun Lee[1], Yunah Kim[1], Yu-Jeong Huh[2], Kap-Soon Kim[2], Jaeweon Cho[3]

[1]Department of Environmental Science and Engineering, Gwangju Institute of Science and Technology (GIST), Buk-gu, Gwangju, South Korea

[2]Yeongsan River Environment Research Center, Buk-gu, Gwangju, South Korea

[3]Gwangju Institute Science and Technology (GIST), Department of Environmental Science and Engineering, Natural Organic Matter Lab, Gwangju, Korea

Article Outline

Glossary
Definition of the Subject
Introduction
Materials and Methods
Results and Discussion
Conclusion
Future Directions
Acknowledgments
Bibliography

Glossary

Micropollutant Pollutant that exists in very small traces in aquatic environment including pharmaceutical drugs and endocrine-disturbing compounds.

Pharmaceuticals Chemical substances used in the medical diagnosis, cure, treatment, or prevention of disease.

Metabolites Intermediates and products formed by the metabolic transformations of a drug.

Personal care products Products used by individuals for personal cosmetic reasons, including fragrances and cosmetics.

Anthropogenic indicator Molecular markers of sewage-derived contaminants which is useful for

The two authors (Eunkyung Lee, Sungyun Lee) are equally contributing first authors.

identifying the sources of pollutants and tracing their transport pathways in aquatic environment.

Wastewater effluent Wastewater discharge from the wastewater treatment systems based upon physical, chemical, and biological processes.

Octanol-water partitioning coefficient Distribution equilibrium of a compound between water and *n*-octanol (K_{ow}) which is helpful to predict adsorption tendency of a compound.

Acidity constant Dissociation equilibrium constant for acid–base reactions, that is, acid dissociation constant.

Definition of the Subject

Micropollutants including pharmaceuticals, personal care products (PPCPs) have been an emerging issue in aquatic environment for several decades. Based on the improvement of the technology to detect and quantify these chemicals, the occurrence, fate, and removal mechanism of various micropollutants has extensively been investigated through different physical, chemical, and biological water treatments in different water sources. Rivers, lakes, estuarine waters, groundwaters, and even drinking waters are subject to the contaminations resulting from the release of anthropogenic micropollutants from wastewater treatment plants. The ubiquitous distribution of PPCPs and their metabolites is mainly caused by the discharge of partially eliminated wastewater contaminants into rivers, with growing concerns of potential ecotoxicological effects of pharmaceuticals on environment. With this point, the micropollutants have to be monitored for sustainable water management. Besides the existence, micropollutants with varying chemical characteristics, in terms of acidity constant (pK_a), octanol-water partitioning coefficient ($logK_{ow}$), may exhibit different transport behaviors in aquatic environment, with those being divided into conservative versus labile markers. There is a great need to suggest anthropogenic micropollutant indicators to predict the levels and behaviors of other micropollutants even with different physicochemical properties, for the sustainable management of the river, as measurements of all the micropollutants require complicated procedures and extensive time and expense.

Introduction

Micropollutants including pharmaceuticals and personal care products (PPCPs) have been extensively examined by a large number of research groups [1–6]. The worldwide occurrence of PPCPs has not been limited to wastewater plant effluents [2, 7], but have also been observed in river water [5, 8–10], groundwater [7], estuarine water [4, 12], and even drinking water [2, 13]. In an attempt to reduce the anthropogenic burden of these pollutants on the environment, recent studies have focused on the removal of micropollutants, including pharmaceuticals, by means of activated sludge treatment, bank filtration, oxidation, and wetland treatment [14, 15]. Some previous studies have also suggested that the existence of certain micropollutants could be used as anthropogenic molecular markers to trace wastewater-derived contaminants [4, 7, 16, 17].

According to Nakada et al. [4], in riverine catchments in Japan, there were relatively high correlations between the levels of crotamiton and carbamazepine and human population compared to biodegradable (ibuprofen), photodegradable (naproxen), volatile, and hydrophobic (triclosan) compounds. Some studies have attempted to use pharmaceuticals, especially those being used solely by humans, such as carbamazepine, diphenhydramine, and caffeine, as chemical indicators of human fecal contamination in water samples upstream and downstream of wastewater treatment plants and the corresponding wastewater effluent [7]. Clara et al. [18] also suggested that carbamazepine would be a good anthropogenic marker since it was highly persistent in 11 full-scale wastewater treatment plants in Austria, regardless of the wastewater treatment processes, including activated sludge, trickling filter, nitrification, denitrification, and phosphorus removal systems. The levels of caffeine, nitrate, and ammonia were also investigated in many different groundwater wells that were connected to either wastewater plants or septic tanks to test the potential of using caffeine as a wastewater discharge indicator. The results of this study demonstrated both the possibility and limitation of using caffeine as the indicator since the amount of discharged caffeine was very high and caffeine was not susceptible to biodegradation [19].

Several recent studies have been conducted to examine the potential fate and transport mechanisms of pharmaceuticals and to correlate these factors to wastewater contaminants [10, 20]. Correlation analysis with the representative parameters of wastewater

contaminants has provided statistically approved indicators. Yoon et al. [10] reported that the COD_{cr} was strongly correlated with EDC/PPCP concentrations ($r = 0.78$), and Santos et al. [20] reported that pharmaceuticals were positively correlated to wastewater characterization parameters such as TSS, BOD, and COD.

The hydrophobicity parameter, $logK_{ow}$, is believed to be an important indicator for specific compounds in predicting their bio-resistance and adsorption tendency, and consequently this parameter can be utilized to evaluate pharmaceuticals as potential markers of contamination in riverine and estuarine ecosystems. In a previous study conducted by Glassmeyer et al. [7], the $logK_{ow}$ parameters of selected pharmaceuticals, including carbamazepine, diphenhydramine, and caffeine, were not examined, but it is believed that information on the $logK_{ow}$ of the tested compounds can help explain their behaviors in aquatic ecosystems. The $logK_{ow}$ value (−0.07) of caffeine is relatively low, thus it is highly biodegradable; meanwhile, the values of carbamazepine and diphenhydramine are relatively high (2.45 and 3.20) and the $logK_{ow}$ value of diphenhydramine is dependent on pH. These factors suggest that carbamazepine holds great promise as an effective human fecal indicator, which is similar to the results reported in other studies. Functional groups, such as the carboxylic moiety, may substantially change the $logK_{ow}$ to normally lower values at neutral pH (e.g., 3.79–0.80 at pH 7.4 for ibuprofen with carboxylic group). The biodegradation potential of pharmaceuticals in constructed-engineered wetlands fed with wastewater effluent has been shown to be tightly related to the pH when considered in conjunction with $logK_{ow}$ (i.e., logD) [21]. The logD parameter has rarely been applied in micropollutant research, but is believed to provide important information in predicting the fate of micropollutants in an aquatic environment.

The objectives of this study were: First, to investigate the occurrence of selected micropollutants including pharmaceuticals and their metabolites in Yeongsan River water; second, to evaluate potential anthropogenic molecular markers in the river water by correlating their levels to wastewater quality parameters; and lastly, to elucidate the behaviors of pharmaceuticals with regard to the chemical characteristics, logD and pK_a.

Materials and Methods

Investigated Area and Sampling Sites

The Yeongsan River located in southwestern Korea was selected to investigate the possibility of using certain pharmaceuticals and personal care products (PPCPs) as anthropogenic indicators. The Yeongsan River system covers a basin area of 3,371 km^2 and has a total length of 115.5 km. The Yeongsan River starts from Damyang County, runs through three big cities, Gwangju, Naju, and Mokpo cities, and comes to the Yellow Sea through the estuarine barrier. Gwangju discharges a significant amount of wastewater to the Yeongsan River area, and has a population of approximately 1.4 million inhabitants. This city also contains several wastewater treatment plants that utilized the activated sludge process and discharges between 120,000 and 600,000 m^3/day. The Gwangju city is most likely the most important source of anthropogenic micropollutants, due to its dense population relative to adjacent cities around the Yeongsan River. As shown in Fig. 1, a total of 13 sampling sites upstream and downstream of the Yeongsan River were selected for micropollutants analysis. Sample collection was conducted four times from March to October in 2009. The precipitation in Gwangju area was mainly concentrated from June to September implying the dilution of contaminants (World Weather Information Service http://worldweather.wmo.int/095/c00335.htm). The weather conditions (water level, precipitation, temperature, and sun irradiation) in Gwangju are shown in Fig. 2. Sampling sites were changed between March and July from a project guideline switching, and maintained for later investigations.

Sample Collection and Water Quality Analysis

1 L river-water samples were collected from the Yeongsan River in amber glass bottles which had been previously cleaned with methanol and deionized pure water. One milliliter of 2 N sodium azide was spiked onsite into the sample bottles to prevent microbial activity. Samples were transported to the laboratory on ice and stored at 4°C until extraction. In situ measurements were conducted in terms of temperature, pH, conductivity, oxidation reduction potential (ORP), and dissolved oxygen (DO). In order to

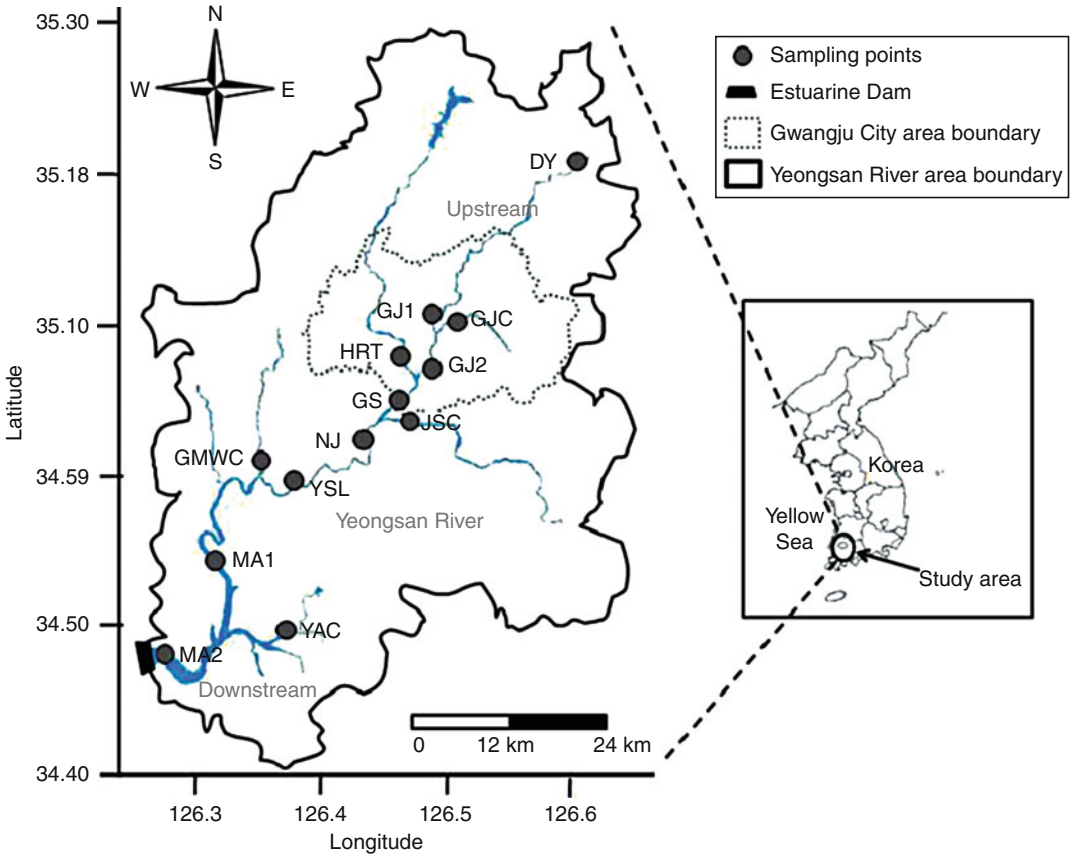

Wastewater Treatment Plant: Anthropogenic Micropollutant Indicators for Sustainable River Management. Figure 1 Map of sampling sites in Yeongsan River area, Korea (*DY* Damyang, *GJ1* Gwangju 1, *GJC* Gwangju Creek, *GJ2* Gwangju 2, *GS* Gwangsan, *HRT* Hwangrong tributary, *JSC* Jiseok Creek, *NJ* Naju, *YSL* Yeongsan Lake, *GMWC* Gomakweon Creek, *MA1* Muan 1, *YAC* Youngam Creek, *MA2* Muan2)

investigate the relationship between water characteristics and micropollutants, the characteristics of the water samples without sodium azide were examined in terms of dissolved organic carbon (DOC), ultraviolet absorbance (UVA), specific UVA (SUVA), and total nitrogen (TN) after pretreatment using 0.7 μm glass macro-fiber filters (GFF, Whatman, Maidsone, England). The level of DOC was measured using a total carbon analyzer (Sievers, Boulder, CO, USA), equipped with an auto sampler, by employing both chemical and UV oxidation methods. DOC for brackish water, that is, non-purgable organic carbon (NPOC), was measured using the TOC V_{CPH} (Shimadzu, Kyoto, Japan), by employing the combustion catalytic oxidation method simultaneously with a nondispersive infrared (NDIR) gas analyzer TN, which was measured in TN unit (TNM-1, Shimadzu, Japan), equipped with the Shimadzu TOC analyzer. UV absorption at 254 nm was analyzed using a UV-1601 UV spectrophotometer (Shimadzu, Japan). SUVA was obtained by calculating the ratio of UVA to DOC. The fundamental water characteristics of the tested samples are shown in Fig. 3. DOC and TN were used as indicators of discharged contaminants from both point and nonpoint sources. SUVA was used as an indicator of the aromaticity of natural and effluent organic matter.

Target Compounds

Various micropollutant compounds, including 13 pharmaceuticals, four selected metabolites, and one

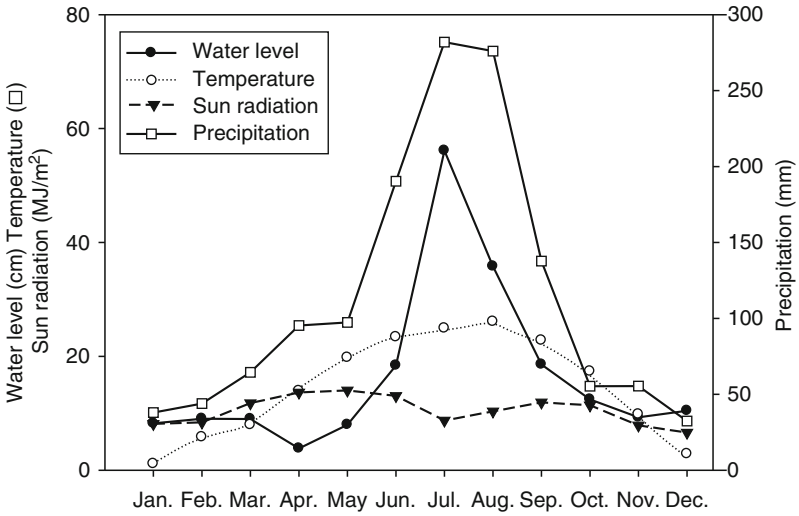

Wastewater Treatment Plant: Anthropogenic Micropollutant Indicators for Sustainable River Management. Figure 2 The 2009 monthly averaged temperature, sun radiation, water levels of Yeongsan River, and a 10-year average of precipitations in Gwangju, Korea

personal care product, were selected as listed in Table 1. Acetaminophen (ACT), atenolol (ATN), carbamazepine (CBZ), clopigogrel (CPG), diclofenac (DCF), dilantin (DLT), florfenicol (FFC), glimepiride (GMP), ibuprofen (IBU), naproxen (NPX), *O*-desmethyl-naproxen (*O*-desmethyl-NPX), sulfamethoxazole (SMX), and tri(2-chloroethyl) phosphate (TCEP) were obtained from Sigma-Aldrich (St. Louis, MO). Caffeine (CAF) was purchased via Fluka Chemie GmbH (Buchs, Switzerland). 2-hydroxyl-ibuprofen (IBU-2OH), ibuprofen carboxylic acid (IBU-CA), iopromide (IOP), and *N*-acetyl-sulfamethoxazole (N-acetyl-SMX) were purchased via Tronto Research Inc (Tronto, Canada). Carbamazepine-d_{10} and $^{13}C_1$-naproxen-d_3 were purchased from Cambridge Isotope Laboratories (Andover, MA, US). Atenolol-d_7, diclofenac-d_4, and dilantin-d_{10} were obtained from C/D/N Isotopes (Pointe-Claire, Canada). Florfenicol-d_3, ibuprofen-d_3, N^4-acetylsulfamethoxazole-d_4, and sulfamethoxazole-d_4 were obtained from Tronto Research Inc (Tronto, Canada). HPLC grade methanol was obtained from J.T Baker (Philipsburg, NJ, USA). Methyl *tert*-butyl ether (MTBE) and formic acid were obtained from Sigma-Aldrich (St. Louis, MO, USA).

These selected compounds have different aromaticity and hydrophobicity, in terms of both $\log K_{ow}$ and logD values at pH 7, and contain ionizable functional groups, which can be measured through pK_a values (Table 1). The relative degree of biodegradability (or persistency) of the tested compounds can be determined by considering both the $\log K_{ow}$ and logD values. Compounds with $\log K_{ow}$ and logD values higher than 2.0 (i.e., carbamazepine, TCEP) are highly persistent through biologically active systems, such as wastewater treatment plants and free surface constructed wetlands. Even with relatively high $\log K_{ow}$ values, compounds with lowered logD (i.e., $\log K_{ow}$ at pH 7) values, have higher removal efficiencies from biologically active ecosystems.

Solid Phase Extraction

The tested micropollutants were extracted using an AutoTrace automated solid phase extraction (SPE) system (Caliper Corporation, Hopkington, MA), equipped with 6 mL, 500 mg hydrophilic-lipophilic balance (HLB) glass cartridges (Waters Corporation, Milford, MA). The procedure used for SPE was described in a previous study by Vanderford et al. [1]. Briefly, the cartridges were preconditioned in the following order: 5 mL of MTBE, 5 mL of methanol, and 5 mL of deionized water. Five hundred milliliters

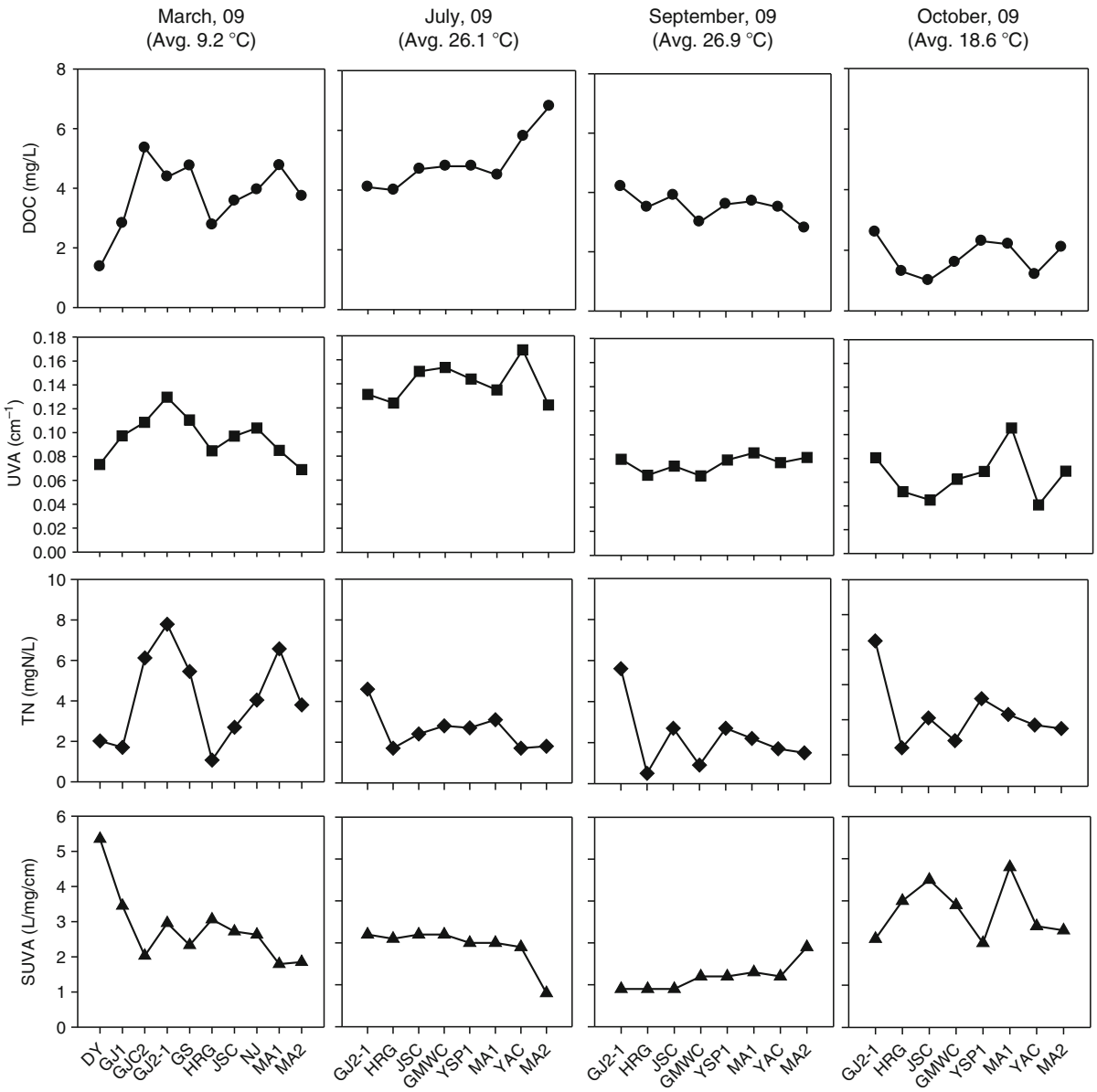

Wastewater Treatment Plant: Anthropogenic Micropollutant Indicators for Sustainable River Management. Figure 3 Characteristics of Yeongsan River waters, Korea

of samples, spiked with the addition of standards for internal calibration, were loaded onto the cartridges at 15 mL/min in duplicate, after which the cartridges were rinsed with 5 mL of deionized pure water, and then dried with a steam of air for 50 min. The cartridges were eluted with 5 mL of methanol, followed by 5 mL of 1/9 (v/v) methanol/MTBE. The eluted solution was concentrated in a water bath at 40°C with a gentle stream of air to a final volume of 500 μL, which was a concentration factor of 1,000.

Liquid Chromatography and Electrospray Tandem Mass Spectrometry

Whole analytes were measured using a Water 2,695 Separations Module (Waters, Milford, MA) coupled

Wastewater Treatment Plant: Anthropogenic Micropollutant Indicators for Sustainable River Management. Table 1
Selected target pharmaceuticals and personal care product

Analyts	Uses	Structure	pKa[a]	$logK_{ow}$[a]	logD[a] at pH7
Atenolol	Beta-blocker	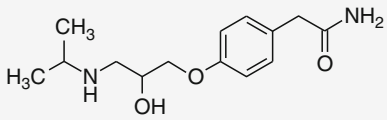	NE[b]	0.43	−2.14
Clopigdogrel	Antiplatelet agent	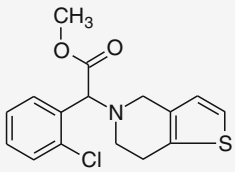	NE	4.03	3.97
Carbamazepine	Anticonvulsant	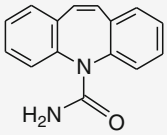	NE	2.77	2.77
Dilantin	Anticonvulsant	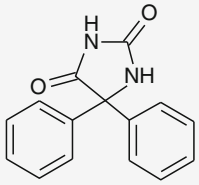	8.46	2.15	2.13
Sulfamethoxazole	Antibiotic	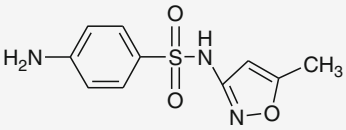	6.16	0.79	0.14
N^4-acetylsulfamethoxazole	Sulfamethoxazole metabolite	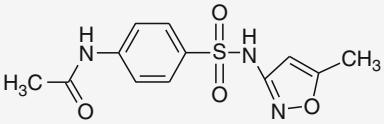	5.88	0.86	0.1
Florfenicol	Antibiotic	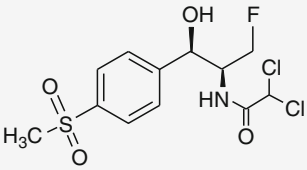	9.03	0.67	0.67

Wastewater Treatment Plant: Anthropogenic Micropollutant Indicators for Sustainable River Management. Table 1 (Continued)

Analyts	Uses	Structure	pKa[a]	$logK_{ow}$[a]	logD[a] at pH7
Diclofenac	Analgesic	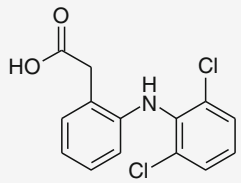	4.00	4.26	0.96
Acetaminophen	Analgesic	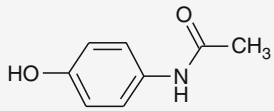	9.46	0.91	0.91
Naproxen	Analgesic	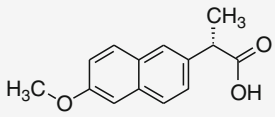	4.19	2.99	0.25
O-desmethyl-naproxen	Naproxen metabolite	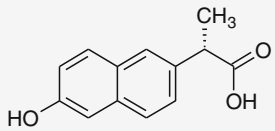	4.34, 9.78	3.9	0.23
Ibuprofen	Analgesic	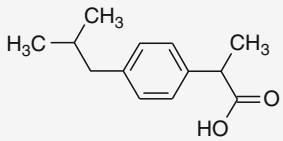	4.85	3.84	1.71
2-hydroxyl-ibuprofen	Ibuprofen metabolite	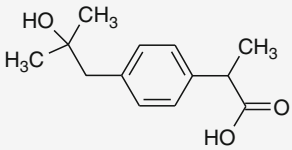	4.63	2.08	0.03
Ibuprofen carboxylic acid	Ibuprofen metabolite	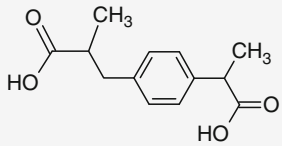	3.97, 4.77	2.78	−2.36
Glimepiride	Anticholesterol	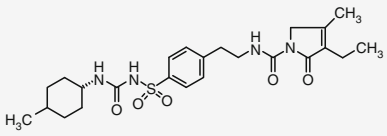	4.32	3.12	2.18

Wastewater Treatment Plant: Anthropogenic Micropollutant Indicators for Sustainable River Management. Table 1 (Continued)

Analyts	Uses	Structure	pKa[a]	$logK_{ow}$[a]	logD[a] at pH7
Caffeine	Stimulant	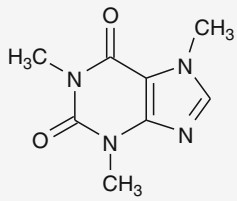	NE	−0.55	−0.55
Iopromide	X-ray contrast media	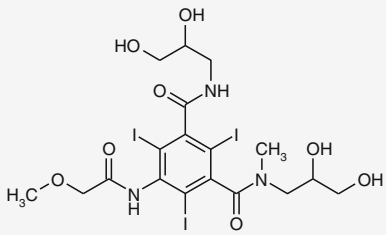	NE	−1.49	−1.54
tri(2-chloroethyl) phosphate (TCEP)	Flame retardant	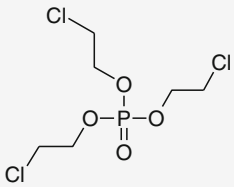	NE	2.11	2.11

[a]$logK_{ow}$, log D, pK_a value was calculated from the Software Calculator Plugins
[b]NE not exist at pH range 1–14

with a Micromass Quattro Micro triple-quadrupole tandem mass spectrometer (Micromass, Manchester, UK) in electrospray ionization mode (ESI). A 20-μL sample loop and 150 × 2.1-mm SunFire C18 column with a particle size of 3.5 μm (Waters, Milford, MA) was employed for analyte separation. A binary gradient consisting of 0.1% formic acid (eluent A) and 100% acetonitrile (eluent B) at a flow rate of 0.2 mL/min was equally applied in both ESI positive and negative modes. For target micropollutants analyses, the gradient was as follows: gradient with 10% of B was held for 0.5 min, stepped up to 50% at 0.51 min, and linearly increased to 100% for 10 min, then held at 100% for 5 min.

The triple-quadrupole tandem mass spectrometer was operated in the multiple reaction monitoring (MRM) mode to identify the analytes. Details on the MRM data of target compounds are listed in Table 2. The operation conditions were: capillary voltage, 3.0 kV; the source temperature, 150°C; desolvation temperature, 350°C; cone gas, 30 L/h; desolvation gas, 500 L/h; and collision cell pressure, 3×10^{-3} mbar.

Limit of Detection and Calibration

Method detection limit (MDL) was determined using seven different deionized water samples, fortified with unlabeled standards at 5 and 10 ng/L through the same extraction procedure used for the river-water samples. Statistical MDL was calculated by multiplying the appropriate student's T value (degree of freedom is 2.764 for $n - 1 = 10$) by the standard deviation of the replicate measurements [22]. The range of the spiked levels for MDL determination should be included

Wastewater Treatment Plant: Anthropogenic Micropollutant Indicators for Sustainable River Management. Table 2
Optimized parameters of selected micropollutants

compound	Cone voltage (v)	Collision energy (eV)	Parent ion (m/z)	Daughter ion (m/z)	Retention time (min)
ESI positive					
Atenolol	35	23	267	145	2.25
Atenolol-d_7	35	25	274	145	2.24
Caffeine	35	20	195.	138	6.11
Sulfamethoxazole	30	18	254	156	7.83
Sulfamethoxazole-d_4	25	15	258	160	7.80
Dilantin	35	13	253	182	8.68
Dilantin-d_{10}	30	12	263	192	8.63
Carbamazepine	35	18	237	194	8.70
Carbamazepine-d_{10}	35	18	247	204	8.74
TCEP	30	16	285	161	9.12
Glimepiride	28	13	491	352	11.34
Clopidogrel	25	20	322	184	12.05
Acetaminophen	28	17	152	109.9	3.98
ESI negative					
Iopromide	20	14	790	127	2.13
Naproxen	10	8	229	185	9.84
Naproxen-d_3	10	6	233	189	9.83
O-desmethyl-naproxen	15	12	215	171	8.10
Diclofenac	15	10	294	249	11.27
Diclofenac-d_4	15	12	298	254	11.23
Ibuprofen	15	8	205	161	11.63
Ibuprofen-d_3	15	8	208	164	11.63
2-hydroxyl-ibuprofen	17	7	221	177	8.17
Ibuprofen carboxylic acid	12	5	235	191	8.04
N-acetyl-sulfamethoxazole	30	13	294	198	7.71
N-acetyl-sulfamethoxazole-d_4	35	14	298	202	7.65
Florfenicol	11	25	356	336	7.84

between calculated MDL and ten times of calculated MDL. In this entry, the limits of detection (Table 3) were calculated by multiplying the MDL by 3. All analytes were quantified using a 7–8 point calibration graph at 0.5, 1.0, 5.0, 10, 50, 100, 150, and 200 μg/L, and the concentration of the isotopically labeled compounds was 100 μg/L. Recovery of the labeled internal standards was measured and used for comparison with

Wastewater Treatment Plant: Anthropogenic Micropollutant Indicators for Sustainable River Management. Table 3 Method detection limits (MDL), reporting limits (RL) for target compound, and ranges in concentrations of PPCPs and their metabolites along Yeongsan River (n = 33 for PPCPs, n = 23 for metabolites)

	MDL (ng/L)	RL (ng/L)	Min. (ng/L)	25th percentile (ng/L)	Median (ng/L)	75th percentile (ng/L)	Max. (ng/L)	Frequency (%)
Atenolol	1.2	3.4	3.4	5.1	9.5	38.8	217.5	93.9
Clopidogrel	0.6	1.9	2.2	2.8	6.3	8.6	10.4	81.8
Dilantin	1.2	3.7	5.4	8.1	16.4	23.8	31.3	78.8
Carbamazepine	0.7	2.1	2.1	10.6	26.2	77.3	180.4	97.0
Sulfamethoxazole	0.6	1.7	3.2	10.6	24.9	52.1	101.1	100.0
Florfenicol	0.7	2.0	2.5	3.6	8.9	18.7	175.6	30.3
Naproxen	3.3	10.0	11.7	16.1	38.3	84.0	265.9	60.6
Ibuprofen	1.2	3.6	5.0	9.9	25.3	69.3	521.4	66.7
Diclofenac	1.3	3.8	5.9	19.2	35.7	66.5	125.0	39.4
Acetaminophen	0.5	1.5	6.7	15.0	29.4	64.2	148.7	100.0
Glimepiride	1.5	4.6	8.0	10.2	31.5	39.4	52.6	69.7
Caffeine	1.5	4.6	12.5	27.3	74.9	209.3	1506.9	100.0
Iopromide	2.1	6.3	11.9	43.5	109.5	255.1	665.3	93.9
N-acetylsulfamethoxazole	0.9	2.7	3.0	6.5	13.0	16.0	22.3	56.5
O-desmethyl-naproxen	1.2	3.5	4.3	22.1	40.0	131.6	205.0	30.4
2-hydroxyl-ibuprofen	0.9	2.7	5.0	24.2	40.8	50.4	197.4	69.6
Ibuprofen carboxylic acid	2.3	6.8	19.6	13.2	19.8	19.9	19.9	8.7
Tri(2-chloroethyl) phosphate	7.9	23.8	29.5	89.7	136.4	253.9	799.6	97.0

the relative response ratio. The final sample concentrations were obtained after modification using the recoveries of both isotopes and inserted standards.

Statistics: Linear Regression and Correlation Coefficient Analysis

All experimental data were used to create a normal distribution after log-transformation for further statistical analyzes. The data were verified using linear regression analysis between PPCPs and water quality parameters. In addition, correlation analysis between water quality and target compounds was performed by the Pearson correlation. Whole statistical analyses were conducted using SPSS (Statistics Package for Social Sciences, version 15.0 for windows; SPSS Inc. Chicago, IL, US).

Results and Discussion

Spatial and Temporal Occurrence of Micropollutants During the Sampling Period

The levels of selected PPCPs in the Yeongsan River in Korea were investigated. The spatial distribution of PPCPs and their metabolites in the Yeongsan River are described in Fig. 4 and the concentration ranges of PPCPs and their metabolites are summarized in Table 3. As shown in Fig. 4, significantly higher

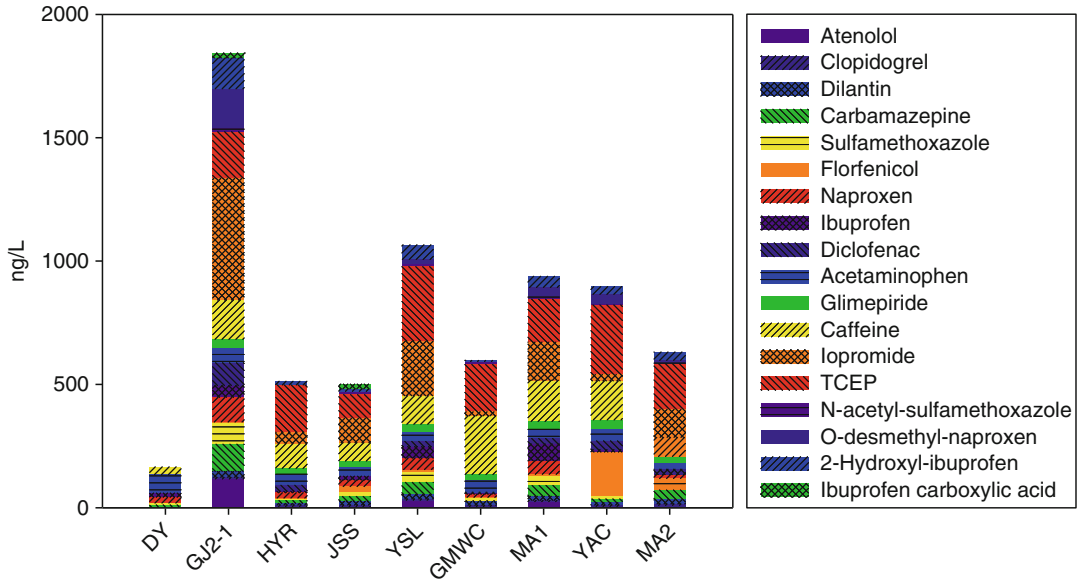

Wastewater Treatment Plant: Anthropogenic Micropollutant Indicators for Sustainable River Management. Figure 4 Spatial distribution of PPCPs and their metabolites in Yeongsan River. Averaged concentrations of target compounds at each sampling point were stacked in vertical bar graph

concentrations of most target compounds were observed at sites within the Gwangju city area (GJ2-1) regardless of seasonal variations. On the other hand, at sites upstream and in tributaries of the Yeongsan River (DY, HRR, JSS, and GMWC), most PPCPs were present at relatively low concentrations compared to the concentration in the mainstream of the Yeongsan River, which includes the Gwangju area. For example, the concentration of carbamazepine and iopromide in Gwangju (GJ2-1 site) ranged from 74.2 to 180.4 ng/L and 388.6 to 665.3 ng/L, while the concentrations in samples obtained upstream and in tributaries ranged from 2.1 to 46.1 ng/L and 11.5 to 195.4 ng/L, respectively. Based on these results, Gwangju, which is the major urban center with dense populations, was the major source of anthropogenic micropollutants in the Yeongsan River system.

The occurrence of PPCPs in the river water was found to be affected by temporal variation. Among the various target compounds, caffeine, iopromide, and TCEP exhibited a seasonally dependant behavior throughout all sampling sites on the Yeongsan River (Fig. 5). High concentrations of PPCPs were observed in March, which drastically decreased in July and September and then increased again in October. These three compounds, which had the highest concentration ranges (median at 70–140 ng/L, Table 3), might be affected by environmental conditions, such as the dilution effect of rainfall [23] in the summer season in Korea (Fig. 2).

Concentrations of Target Compounds in River Water

Most target compounds were successfully detected and their levels were consistent with previous studies [2, 9, 10]. Frequently observed compounds (frequency >90% in Table 3) included atenolol, carbamazepine, sulfamethoxazole, acetaminophen, caffeine, iopromide, and tri(2-chloroethyl) phosphate (TCEP). Among them, only three pharmaceuticals, sulfamethoxazole, caffeine and acetaminophen, were detected at all sampling dates and sites with a frequency of 100% as shown in Table 3. The median (interquartile range) concentration of these three compounds was 24.9 (10.6–52.1) ng/L, 74.9 (27.3–209.3) ng/L, and 29.4 (15.0–64.2) ng/L, respectively. The high level of

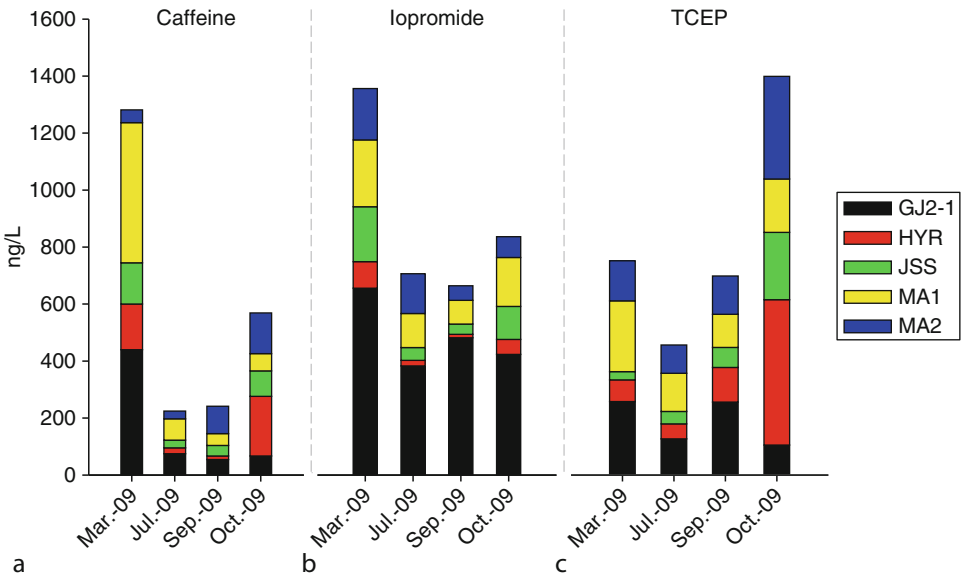

Wastewater Treatment Plant: Anthropogenic Micropollutant Indicators for Sustainable River Management. Figure 5 Temporal distribution of (**a**) caffeine, (**b**) iopromide, and (**c**) TCEP in Yeongsan River

frequency of these compounds was also reported in previous studies [2, 24].

Compounds with relatively high concentrations based on the median values included caffeine, iopromide, and TCEP. The presence of caffeine, which had a median concentration of 74.9 ng/L, has been examined in other surface waters that contain effluents from wastewater treatment plants, such as lakes and rivers, to assess the potential of using it as a chemical anthropogenic marker [17] even though the degradability of caffeine from wastewater treatment plants and surface water systems is high (81.0–99.9% removal in wastewater treatment plants in Swiss).

The X-ray contrast media, iopromide, was also found at significantly higher concentrations than other compounds ranging from 11.9 to 665.3 ng/L (median at 109.5 ng/L). Iopromide has frequently been detected at concentrations of up to 11 μg/L in WWTP effluents and 0.9 μg/L in surface waters due to its persistence and heavy loads [2, 10]. Metabolically stable iopromide, which is known to have a poor inherent biodegradability, exhibited low sorption ability, due to its low logD value of −1.54 at pH 7 (Table 1). Nevertheless, effective biotransformation of iopromide has been reported using a wastewater treatment system and bank filtration [25].

The flame retardant, TCEP was shown to have the highest median concentration (136.4 ng/L) in the broad concentration ranges of 29.5–799.6 ng/L in the Yeongsan River. Kim et al. [2] reported that TCEP was barely removed during wastewater treatment processes, including membrane bioreactor (MBR), nano-filtration (NF), and even reverse osmosis (RO) filtration system. TCEP was also detected after drinking water treatment processes, which is consistent with their recalcitrant behaviors to chlorine oxidation or ozonation [13]. Therefore, the low removal efficiency of TCEP might be due to its symmetric structure, which may increase its overall stability (Table 1).

Four different anti-inflammatories, including ibuprofen, acetaminophen, diclofenac, and naproxen had concentrations ranging from 20 to 40 ng/L (median) in the Yeongsan River. The concentration range of ibuprofen, acetaminophen, naproxen, and diclofenac was 5.0–521.4 ng/L, 6.7–148.7 ng/L, 11.7–265.9 ng/L, and 5.9–125.0 ng/L, respectively (Table 3). These values were consistent with the combined findings of worldwide studies on surface waters conducted by Fono et al. [8], Herberer [26], Winkler et al. [27], and

Tixier et al. [28]. One of the most popular painkillers in Korea is acetaminophen and this compound has been known to be easily degraded and removed by WWTPs [26]. According to Kolpin et al. [6], acetaminophen was detected at a median concentration of 110 ng/L with a frequency of 23% in US streams. However, in Yeongsan River, acetaminophen was observed at all sampling sites and dates with a frequency of 100%. Diclofenac has been reported to be rapidly and extensively eliminated by photodegradation [29]. Diclofenac was rarely detected in the Yeongsan River, presumably due to photodegradation by sunlight, except in the Gwangju city area, where relatively high concentrations (12.4–100.7 ng/L) of diclofenac were observed due to the dense population and heavy loads from WWTPs. Ibuprofen (median at 25.3 ng/L) and naproxen (median at 38.3 ng/L) were also frequently observed in the Yeongsan River with detection frequencies of 67% and 61%, respectively. Ibuprofen has been known to be relatively persistent in aquatic system [10]. According to Zwiener et al. [30], since ibuprofen, which contains carboxyl groups, had a low removal efficiency by adsorption on activated carbon due to its negative charge in neutral surface water, it is believed to rarely adsorb to suspended particles in river water. However, Tixier et al. [28] reported that ibuprofen can be readily eliminated through biodegradation and sedimentation, and naproxen can be efficiently eliminated through biodegradation and phototransformation in surface waters.

Carbamazepine and sulfamethoxazole were detected in Yeongsan River at concentration ranges of 2.1–180.4 ng/L (median at 26.2 ng/L) and 3.2–101.1 ng/L (median at 24.9 ng/L), respectively. Both compounds have frequently been reported as resistant compounds in surface water, groundwater, and estuarine water [4, 7, 11, 12].

The other compounds that were present at relatively low concentrations were dilantin, atenolol, florfenicol, and clopidogrel, which had median concentrations ranging from 6.3 to 16.4 ng/L (as median). The veterinary antibiotic, florfenicol, has been reported to be rapidly metabolized into florfenicol amine [31], supporting the low concentration of florfenicol detected in this study. Similar to the low concentration range of clopidogrel detected in this study, Huerta-Fontela et al. [32] also found that clopidogrel was rarely detected in WWTP influent and effluent samples in Spain. The concentrations of dilnatin and atenolol were in good agreement with the results reported by Kim et al. [2] and Yoon et al. [10].

Occurrence of Pharmaceutical Metabolites in the River Water

As shown in Fig. 6, the occurrence of pharmaceutical metabolites was investigated along the Yeongsan River. A higher concentration of degradation products was observed in samples obtained from the GJ2-1 sampling site in Gwangju city (9.5–22.3 ng/L for *N*-acetylsulfamethoxazole, 119.4–205.0 ng/L for *O*-desmethyl-naproxen, and 47.1–197.4 ng/L for 2-hydroxyl-ibuprofen), whereas further downstream, the concentration of metabolites decreased, presumably due to dilution from natural attenuation. The prominent occurrence of pharmaceutical metabolites at the GJ2-1 sites is likely due to the effluent-dominated water source located in the Gwangju, which indicates that a high proportion of metabolites originated from human excretion in the WWTP influent and/or transformation of parent compounds into degradation products during WWTP processes mainly by activated sludge treatments. According to previous studies [33, 34], human excretion was believed to be the main source of ibuprofen metabolites. They also found that hydroxyl-ibuprofen was stable through WWTP processes and could be produced during activated sludge treatment, meanwhile carboxy-ibuprofen readily disappeared. This is in good agreement with the distribution of ibuprofen metabolites found in the Yeongsan River.

In previous studies [14, 35], a demethylated degradation product of naproxen, *O*-desmethyl-naproxen, was found in a lab-scale wastewater treatment unit. In this study, the ether cleavage and demethylation of naproxen were reported to be an initial step in bacterial degradation under aerobic conditions, as occurs in mammals. The naproxen metabolite observed in this study was also presumably transformed during both human metabolism and wastewater treatment processes.

In the case of the human metabolites of sulfamethoxazole, *N*-acetyl-sulfamethoxazole was found in surface water receiving WWTP effluent at a concentration range less than 50 ng/L [36], while the median concentration of this compound was 13 ng/L in this study. Another concern related to acetylsulfamethoxazole is

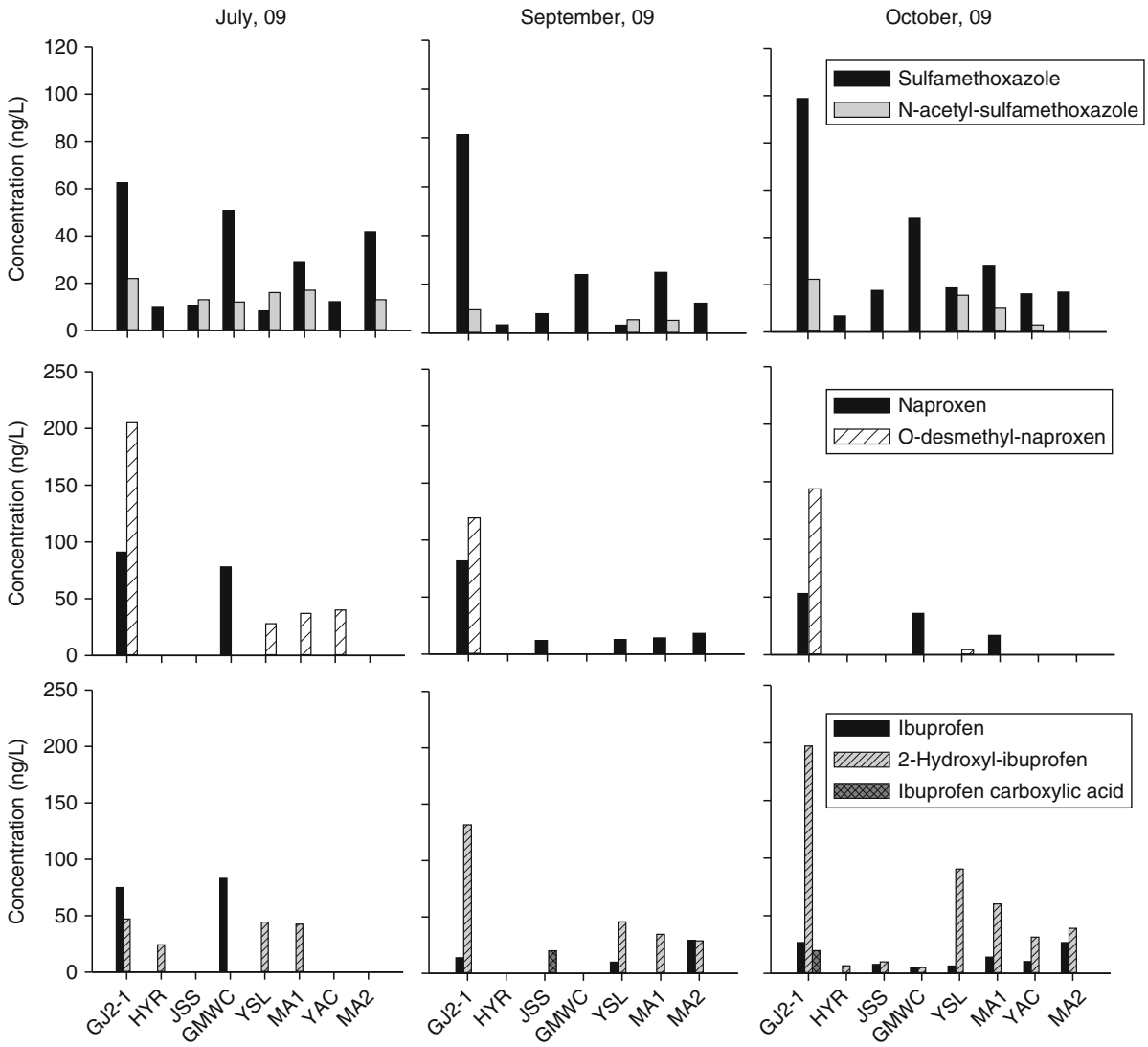

Wastewater Treatment Plant: Anthropogenic Micropollutant Indicators for Sustainable River Management. Figure 6 Spatial and seasonal concentrations (n = 2) of selected pharmaceutical metabolites and their parent compounds in the Yeongsan River, Korea

the retransformation back to the parent compound, sulfamethoxazole [37], implying reactivation of acetylsulfamethoxazole as an antibiotic compound during wastewater treatment, and/or after discharge into natural water.

Correlation Analysis Between Selected Water Quality Parameters and PPCPS

Correlation analysis was employed to evaluate the relationship between selected water quality parameters (TN, DOC, UVA_{254nm}, SUVA) and 17 different target PPCP compounds, as shown in Table 4. TN, a representative wastewater characterization parameter, had the highest correlation with PPCPs; however, DOC, UVA_{254}, and SUVA were poorly correlated with PPCPs. This is inconsistent with previous studies [10, 20] that reported significant correlations between pharmaceuticals and organic matter parameters (TSS, DOC, COD, and BOD), which presumably resulted from the association between pharmaceuticals and

dissolved organic matter. In contrast to their explanation, the behavior of PPCPs in the Yeongsan River was not likely associated with dissolved organic matter.

Seven out of the 17 target compounds were found to be strongly correlated ($r > 7.0$) to TN, implying that these compounds could be potentially used as anthropogenic molecular tracers. The correlations were in the following order as determined from the regression coefficients obtained from the Pearson correlation at 95% confidence level (two-tailed); 2-hydroxyl-ibuprofen ($r = 0.87$) > atenolol ($r = 0.85$) > carbamazepine ($r = 0.81$) > sulfamethoxazole ($r = 0.79$) > dilantin ($r = 0.78$) > naproxen ($r = 0.76$) > iopromide ($r = 0.74$) (significant value <0.000 for all). All seven compounds exhibited positive correlations with TN.

2-hydroxyl-ibuprofen was the highest correlated compound with TN, which indicates that hydroxyl-ibuprofen was much more stable and persistent in the wastewater effluent than its parent compound, ibuprofen, and the other wastewater-derived contaminants. According to Zwiener et al. [38], hydroxyl-ibuprofen was degraded much more slowly than ibuprofen in a biofilm reactor. This explanation is consistent with the results obtained and supports the notion that hydroxyl-ibuprofen is highly stable.

Atenolol, which was the second most highly correlated compound with TN, has been reported by Kasprzyk-Hordern et al. [16] as an anthropogenic indicator based on its persistent and ubiquitous occurrence. However, they also mentioned that atenolol could be susceptible to biodegradation through trickling filter and activated sludge treatments, indicating that it may be a suboptimal chemical indicator.

Carbamazepine has often been suggested as a conservative anthropogenic marker in aquatic environments [4, 7, 12, 16, 18]. The persistent behavior of carbamazepine corresponds to its low biodegradability (half-lives, $t_{1/2} > 100$ days) [3] and resistance to photodegradation. In this study, carbamazepine was highly correlated to TN with a regression coefficient of 0.81, which was consistent with other studies.

Another resistant compound in aquatic environments, sulfamethoxazole [11], had a relatively high correlation to TN ($r = 0.79$). Sulfamethoxazole has been described to be resistant to biotransformation with a half-life of >100 days [3]. Since sulfamethoxazole is widely used as both a human and veterinary antibiotic, it is difficult to determine if the presence of sulfamethoxazole at relatively high levels was caused by only human fecal contamination.

The anticonvulsant, dilantin, had a relatively high correlation with TN ($r = 0.78$), indicating that it may be a potential molecular marker. In a previous study [10], dilantin was shown to have a relatively high correlation ($r > 0.8$) with selected water quality parameters, including BOD_5, DOC, and UVA_{254}. In contrast, a negligible correlation between dilantin and selected water quality parameters, including DOC and UVA_{254}, was observed in the case of the Yeongsan River.

Anti-inflammatory, naproxen, which was highly correlated to TN with a regression coefficient of 0.76, has been regarded as a labile marker due to its photodegradability [4]. Other analgesics, such as ibuprofen and diclofenac, have been recommended as potential labile markers due to their susceptibility to biodegradation and photodegradation. Ibuprofen and diclofenac exhibited a lower correlation than the conservative markers such as carbamazepine and sulfamethoxazole, which had regression coefficients of 0.66 (p-value = 0.001) and 0.65 (p-value = 0.021), respectively. These results are in good agreement with previous studies [4, 16]. Kasprzyk-Hordern et al. [16] suggested that ibuprofen may be a potential indicator for non- or poorly treated wastewater, such as stormwater discharges, due to its readily biodegradable property in wastewater treatment.

X-ray contrast media, iopromide, can mainly be excreted without metabolization in the human body, and is rarely degraded in municipal WWTP [24]. With respect to its ubiquitous occurrence and high loads in surface water, and resistance to biodegradation, iopromide can serve as a potential tracer, which is supported by its high correlation coefficient to TN (0.74) (Table 4).

However, no significant correlations between caffeine, which has been previously considered a potential labile marker, and all the water quality parameters were observed in this study. Caffeine has been recommended as a labile chemical marker [17] with regard to its relatively high biodegradability (half-lives = 3.5–5.2 days) [3]. However, Young et al. [39] reported that caffeine was an inferior chemical indicator of sewage-derived microbes in surface waters with significantly low R^2 values between chemical and bacteriological indicators that ranged from 0.16 to 0.37, which was consistent

Wastewater Treatment Plant: Anthropogenic Micropollutant Indicators for Sustainable River Management. Table 4 Linear regression analysis between selected water quality parameters and PPCPs

Target micropollutants	n[a]	TN			DOC			UVA			SUVA		
		r[b]	*F*[c]	*p*[d]	*r*	*F*	*p*	*r*	*F*	*p*	*r*	*F*	*p*
ATN	30	0.85	72.3	0.000	0.34	3.76	0.063	0.22	1.42	0.244	−0.30	2.82	0.104
CPG	27	−0.34	3.29	0.082	−0.80	47.5	0.000	−0.89	91.5	0.000	0.27	1.96	0.174
DLT	25	0.78	36.0	0.000	0.59	12.3	0.002	0.67	18.7	0.000	−0.28	1.92	0.179
CBZ	31	0.81	53.8	0.000	0.44	6.98	0.013	0.39	5.19	0.030	−0.25	1.97	0.171
SMZ	32	0.79	49.7	0.000	0.29	2.72	0.109	0.24	1.88	0.181	−0.18	0.96	0.335
FFC	10	−0.47	2.28	0.170	−0.16	0.21	0.660	−0.11	0.10	0.760	0.13	0.14	0.720
NPX	19	0.76	23.0	0.000	0.62	10.6	0.005	0.71	17.5	0.001	−0.11	0.21	0.650
IBP	21	0.66	14.2	0.001	0.62	11.5	0.003	0.66	14.8	0.001	−0.31	2.00	0.174
DCF	12	0.65	7.45	0.021	0.40	1.91	0.197	0.33	1.19	0.302	−0.21	0.44	0.523
ACT	32	0.13	0.51	0.482	−0.26	2.20	0.149	−0.02	0.01	0.919	0.47	8.31	0.007
GMP	23	0.27	1.61	0.218	−0.08	0.14	0.715	0.33	2.60	0.122	0.60	11.9	0.002
CAF	32	0.22	1.54	0.224	−0.17	0.91	0.348	−0.14	0.56	0.461	0.22	1.48	0.234
IOP	30	0.74	33.3	0.000	0.18	0.89	0.353	0.05	0.08	0.780	−0.21	1.23	0.277
TCEP	31	0.001	0.0	0.996	−0.4	6.26	0.018	−0.47	8.23	0.008	0.19	1.09	0.304
N-acetyl-SMX	13	0.56	4.51	0.060	0.51	3.49	0.091	0.56	4.52	0.059	0.17	0.28	0.606
O-desmethyl-NPX	7	0.55	2.15	0.203	0.29	0.46	0.526	0.18	0.17	0.701	0.18	0.16	0.705
IBU-2OH	16	0.87	41.8	0.000	0.54	5.79	0.031	0.38	2.34	0.149	0.56	6.32	0.025

[a]Number of detected target compounds by LC-MS/MS
[b]Regression coefficient
[c]F-ratio
[d]Significant value. Correlations higher than 0.7 are significant at $p < 0.05$ (shown in bold)

with the results. The poorly correlated patterns of caffeine could be explained by its high biodegradability and ubiquitous discharge, resulting in distinct detections at high levels even further upstream and in tributaries, regardless of sampling dates and sites [7].

Although TCEP had the highest median concentration and was broadly distributed throughout the Yeongsan River, it was poorly correlated with all the water quality parameters. This could be caused by its sporadic occurrence, irrespective of the wastewater effluent sources.

Correlation Among the Target PPCP Compounds

Correlation among the target PPCP compounds were evaluated as summarized in Table 5. The group of

Wastewater Treatment Plant: Anthropogenic Micropollutant Indicators for Sustainable River Management. Table 5
Correlation matrix among investigated target PPCP compounds

	ATN	CPG	DLT	CBZ	SMZ	FFC	NPX	IBP	
ATN	1.00	−0.14	0.59[a]	0.84[a]	0.82[a]	−0.32	0.81[a]	0.69[a]	
CPG		1.00	−0.68[a]	−0.28	−0.10	0.17	−0.71[a]	−0.83[a]	
DLT			1.00	0.71[a]	0.65[a]	−0.52	0.54[a]	0.56[a]	
CBZ				1.00	0.92[a]	−0.18	0.77[a]	0.61[a]	
SMZ					1.00	−0.18	0.69[a]	0.52[a]	
FFC						1.00	−1.00	−1.00	
NPX							1.00	0.80[a]	
								1.00	
	DCF	ACT	GMP	CAF	IOP	TCEP	N-acetyl-SMZ	*O*-desmethyl-NPX	IBU-2OH
ATN	0.57[a]	0.24	0.12	0.49[a]	0.81[a]	0.48[a]	0.43	0.56	0.77[a]
CPG	−0.01	0.17	−0.29	0.06	0.01	0.36	−0.36	0.05	−0.10
DLT	0.67[a]	−0.06	0.55[a]	−0.06	0.61[a]	−0.02	0.80[a]	0.71	0.81[a]
CBZ	0.45	0.12	0.33	0.48[a]	0.89[a]	0.19	0.38	0.58	0.84[a]
SMZ	0.40	0.19	0.37	0.48[a]	0.88[a]	0.26	0.30	0.38	0.79[a]
FFC	−0.02	0.20	0.08	0.01	−0.14	0.26	−0.40	−0.36	−0.71
NPX	0.43	0.36	0.43	0.81[a]	0.62[a]	0.51[a]	0.35	0.91	0.53
IBP	−0.08	0.06	0.45	0.59[a]	0.53[a]	0.31	0.80[a]	−0.25	0.48
DCF	1.00	0.42	−0.13	0.00	0.41	0.01	0.25	0.99[a]	0.26
ACT		1.00	0.38	0.43[a]	0.20	0.27	0.09	0.22	−0.26
GMP			1.00	0.31	0.21	0.03	0.53	−0.26	0.06
CAF				1.00	0.39[a]	0.61[a]	−0.25	−0.12	−0.53[a]
IOP					1.00	0.30	0.46	0.24	0.75[a]
TCEP						1.00	−0.46	−0.19	−0.37
N-acetyl-SMZ							1.00	0.19	0.45
O-desmethyl-NPX								1.00	0.18
IBU-2OH									1.00

Correlation higher than 0.70 are significant at $p < 0.05$ (shown in bold)
[a]Correlation is significant at the 0.05 level (two-tailed)

compounds with relatively high correlations to TN, including atenolol, carbamazepine, sulfamethoxazole, iopromide, and 2-hydroxyl-ibuprofen, was found to have significant correlations to each other with regression coefficients higher than 0.70 and p-values <0.05. This result indicates that these compounds may have similar behaviors in river water due to their conservative properties. Glassmeyer et al. [7] reported that carbamazepine and sulfamethoxazole were highly correlated due to their recalcitrant behaviors.

Naproxen exhibited high correlations with labile tracers, such as caffeine and ibuprofen. The high correlations among these compounds implied that they displayed an analogous mobility pattern in river water and hold promise for use as labile anthropogenic markers.

Some compounds, such as florfenicol, acetaminophen, glimepiride, and TCEP, were not correlated to other PPCPs, presumably due to their high biodegradability (for florfenicol and acetaminophen) and/or sporadic distribution (for TCEP and glimepiride). No distinct correlations between the parent compound and its metabolites were observed. Among the metabolites, 2-hydroxyl-ibuprofen showed higher correlation to other PPCPs than *N*-acetylsulfamethoxazole and *O*-desmethyl-naproxen, which was most likely due to the relatively high stability of 2-hydroxyl-ibuprofen compared to the other two metabolites.

Relationship Between Regression Coefficient (*R*) and Chemical Properties of Compounds

The pharmaceutical behavior was evaluated with respect to chemical properties (Fig. 7), such as acidity constant (pK_a) and octanol-water partitioning coefficient ($logK_{ow}$ and logD, i.e., $logK_{ow}$ at pH7), by comparing the regression coefficient (r) obtained from the linear regression analysis between TN and target compounds (Table 4). As a result, $logK_{ow}$ had no noticeable correlation to the regression coefficient (r), whereas logD had a slightly negative correlation to the regression coefficient (r). In general, $logK_{ow}$ has been used to evaluate the pharmaceutical removal mechanism especially by sorption on activated carbon [40]. Lee et al. [21] used the logD parameter to elucidate the removal mechanism in a constructed wetland connected to wastewater treatment effluent, and found that logD was more suitable to predict the behavior of micropollutants than $logK_{ow}$, which was consistent with the results obtained. The r^2 value obtained from the r-logD plot was too low to verify a linear relationship between r and logD. However, by considering the complex removal mechanism including not only sorption but also biodegradation, oxidation, and photodegradation in river water, this low r^2 value indicates that sorption was not the main mechanism of

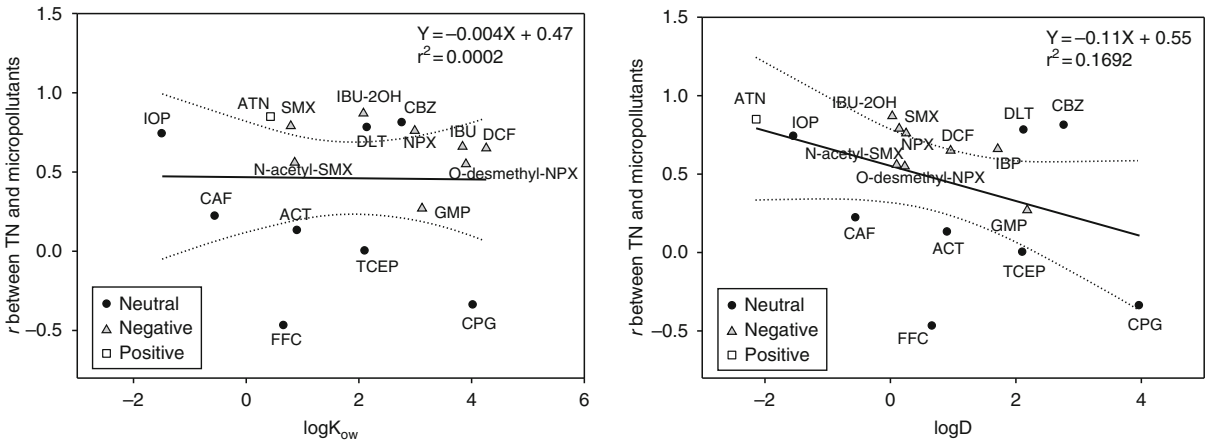

Wastewater Treatment Plant: Anthropogenic Micropollutant Indicators for Sustainable River Management. Figure 7 Relationship between regression coefficient (r) and octanol-water partitioning coefficient ($logK_{ow}$ and logD)

removal in the Yeongsan River. Despite this, the adverse proportional relationship between *r* and logD provides some information on the behavior of micropollutants in river water. Hydrophilic compounds with relatively low logD values had higher correlations to TN than hydrophobic compounds, indicating relatively low removal efficiencies for hydrophilic compounds. In addition, these results suggest that removal of hydrophobic compounds in river water occurs through sorption on organic matter. On the other hand, based on the pK_a values of target micropollutants, with respect to the functional groups of micropollutants at neutral pH, negatively charged micropollutants exhibited relatively high correlation to TN compared to the neutral charged compounds (Fig. 7). In summary, relatively hydrophilic and/or charged compounds, such as 2-hydroxyl-ibuprofen, sulfamethoxazole, naproxen, atenolol, and iopromide, play important roles as labile anthropogenic molecular markers in river water, with relatively low sorption tendencies and a relatively high biodegradation potential.

Conclusion

Eighteen different micropollutants including pharmaceuticals and their metabolites were investigated to evaluate their potential as anthropogenic molecular markers in Yeongsan River in Korea. Based on the spatial and temporal evaluation, most of the target compounds were frequently detected, exhibiting concentrations between 2 and 1,500 ng/L. In addition, these compounds were mainly discharged from the Gwangju metropolitan city, which was found to be the main source of the anthropogenic wastewater contaminants in the Yeongsan River ecosystem. The relationships between water quality parameters (TN, DOC, UVA, and SUVA) and micropollutants were examined by means of linear regression analysis. TN exhibited a strong correlation with seven compounds in the following order: 2-hydroxyl-ibuprofen, atenolol, carbamazepine, sulfamethoxazole, dilantin, naproxen, and iopromide. Through correlation analysis, the behavior of selected micropollutants was evaluated in terms of their use as conservative anthropogenic indicators (carbamazepine, sulfamethoxazole, iopromide, atenolol, and 2-hydroxyl-ibuprofen) and as labile wastewater indicators (naproxen, ibuprofen, caffeine, and diclofenac). The logD and pK_a of each compound was then used to elucidate the chemicophysical behavior of target micropollutants as anthropogenic indicators in surface water. This analysis demonstrated that the logD and pK_a values could be used to assess the suitability of potential labile molecular indicators in river water. Even though there are still some limitations in understanding the detailed behavior of candidate indicators, the chemicals suggested as potential wastewater indicators in this study are expected to be helpful in analyzing sewage contamination in river ecosystems.

Future Directions

As growing concerns of the global climate change, the need for the development of technology for water treatment is also increasing to prepare for the water scarcity. Among various technologies, water reclamation and reuse is recommended for the alternative water treatments with high sustainability. In the sustainable water treatment, however, the existence of micropollutants is another concern. Even though there is no specific regulation related to the micropollutants yet, the removal of micropollutants in aquatic environment is considered to be important for reliable water sources in the manner of sustainability. Enhancement of water quality managements system in terms of micropollutant control is a key step in the sustainable water treatment.

In addition, understanding the degradation pathway of micropollutants is also an important approach to effectively control the micropollutants in water bodies. Micropollutants are differently degraded into metabolites depending on their different physicochemical properties. Thus, removal efficiencies of micropollutants are differently affected by various removal mechanisms in terms of biodegrdation, photodegradation, and oxidation/reduction. Research of micropollutants degradation pathway in aquatic environment would be helpful to understand behaviors of micropollutants and their metabolite and provide further research directions related to the removal of micropollutants.

Natural organic matter (NOM) is believed as a promising factor for evaluating behavior of micropollutants in surface waters. In previous study [41], NOM has been known to play an important role in photodegradation processes in surface waters. As radical scavenger and as precursor of reactive species such as singlet oxygen,

hydroxyl radicals, and others, NOM can promote the photochemical transformation of micropollutants. However, most of the role of NOM in the degradation of micropollutants is still unknown. Understanding the complex interactions between NOM and micropollutants is believed to provide interdisciplinary perspectives for sustainable water quality management.

Acknowledgments

This research was supported by the Yeongsan and Seomjin River Watershed Management Committee, Ministry of Environment, Republic of Korea.

Bibliography

Primary Literature

1. Vanderford BJ, Snyder SA (2006) Analysis of pharmaceuticals in water by isotope dilution liquid chromatography/tandem mass spectrometry. Environ Sci Technol 40:7312–7320
2. Kim SD, Cho J, Kim IS, Vanderford BJ, Snyder SA (2007) Occurrence and removal of pharmaceuticals and endocrine disruptors in South Korean surface, drinking, and waste waters. Water Res 41:1013–1021
3. Benotti MJ, Brownawell BJ (2009) Microbial degradation of pharmaceuticals in estuarine and coastal seawater. Environ Pollut 157:994–1002
4. Nakada N, Kiri K, Shinohara H, Harada A, Kuroda K, Takizawa S, Takada H (2008) Evaluation of pharmaceuticals and personal care products as water-soluble molecular markers of sewage. Environ Sci Technol 42:6347–6353
5. Ternes TA (1998) Occurrence of drugs in German sewage treatment plants and rivers. Water Res 32:3245–3260
6. Kolpin DW, Furlong ET, Meyer MT, Thurman EM, Zaugg SD, Barber LB, Buxton HT (2002) Pharmaceuticals, hormones, and other organic wastewater contaminants in U.S. streams, 1999–2000: a national reconnaissance. Environ Sci Technol 36:1202–1211
7. Glassmeyer ST, Furlong ET, Kolpin DW, Cahill JD, Zaugg SD, Werner SL, Meyer MT, Kryak DD (2005) Transport of chemical and microbial compounds from known wastewater discharges: potential for use as indicators of human fecal contamination. Environ Sci Technol 39:5157–5169
8. Fono LJ, Kolodziej EP, Sedlak DL (2006) Attenuation of wastewater-derived contaminants in an effluent-dominated river. Environ Sci Technol 40:7257–7262
9. Wiegel S, Aulinger A, Brockmeyer R, Harms H, Löffler J, Reincke H, Schmidt R, Stachel B, von Tümpling W, Wanke A (2004) Pharmaceuticals in the river Elbe and its tributaries. Chemosphere 57:107–126
10. Yoon Y, Ryu J, Oh J, Choi BG, Snyder SA (2010) Occurrence of endocrine disrupting compounds, pharmaceuticals, and personal care products in the Han River (Seoul, South Korea). Sci Total Environ 408:636–643
11. Godfrey E, Woessner WW, Benotti MJ (2007) Pharmaceuticals in on-site sewage effluent and ground water, western Montana. Ground Water 45:263–271
12. Benotti MJ, Brownawell BJ (2007) Distributions of pharmaceuticals in an urban estuary during both dry- and wet-weather conditions. Environ Sci Technol 41:5795–5802
13. Benotti MJ, Trenholm RA, Vanderford BJ, Holady JC, Stanford BD, Snyder SA (2009) Pharmaceuticals and endocrine disrupting compounds in U.S. drinking water. Environ Sci Technol 43:597–603
14. Kosjek T, Heath E, Kompare B (2007) Removal of pharmaceutical residues in a pilot wastewater treatment plant. Anal Bioanal Chem 387:1379–1387
15. Onesios KM, Yu JT, Bouwer EJ (2009) Biodegradation and removal of pharmaceuticals and personal care products in treatment systems: a review. Biodegradation 20:441–466
16. Kasprzyk-Hordern B, Dinsdale RM, Guwy AJ (2009) Illicit drugs and pharmaceuticals in the environment – Forensic applications of environmental data, Part 2: pharmaceuticals as chemical markers of faecal water contamination. Environ Pollut 157:1778–1786
17. Buerge IJ, Poiger T, Müller MD, Buser H-R (2003) Caffeine, an anthropogenic marker for wastewater contamination of surface waters. Environ Sci Technol 37:691–700
18. Clara M, Strenn B, Kreuzinger N (2004) Carbamazepine as a possible anthropogenic marker in the aquatic environment: investigations on the behaviour of Carbamazepine in wastewater treatment and during groundwater infiltration. Water Res 38:947–954
19. Seiler RL, Zaugg SD, Thomas JM, Howcroft DL (1999) Caffeine and pharmaceuticals as indicators of waste water contamination in wells. Ground Water 37:405–410
20. Santos JL, Aparicio I, Callejon M, Alonso E (2009) Occurrence of pharmaceutically active compounds during 1-year period in wastewaters from four wastewater treatment plants in Seville (Spain). J Hazard Mater 164:1509–1516
21. Lee S, Kang SI, Lim JL, Huh YJ, Cho J (2010, submitted) Evaluating controllability of pharmaceuticals and metabolites, in biologically-engineered processes, using corresponding octanol-water partitioning coefficient with consideration of ionizable functional groups
22. USEPA (1999) Protocol for EPA approval of new methods for organic and inorganic analytes in wastewater and drinking water. U.S. Environmental Protection Agency, Washington, DC
23. Fernández C, González-Doncel M, Pro J, Carbonell G, Tarazona JV (2010) Occurrence of pharmaceutically active compounds in surface waters of the henares-jarama-tajo river system (madrid, spain) and a potential risk characterization. Sci Total Environ 408:543–551
24. Ternes TA, Hirsch R (2000) Occurrence and behavior of X-ray contrast media in sewage facilities and the aquatic environment. Environ Sci Technol 34:2741–2748

25. Schulz M, Löffler D, Wagner M, Ternes TA (2008) Transformation of the x-ray contrast medium iopromide in soil and biological wastewater treatment. Environ Sci Technol 42:7207–7217
26. Herber T (2002) Occurrence, fate, and removal of pharmaceutical residues in the aquatic environment: a review of recent research data. Toxicol Lett 131:5–17
27. Winkler M, Lawrence JR, Neu TR (2001) Selective degradation of ibuprofen and clofibric acid in two model river biofilm systems. Water Res 35:3197–3205
28. Tixier C, Singer HP, Oellers S, Müller SR (2003) Occurrence and fate of carbamazepine, clofibric acid, diclofenac, ibuprofen, ketoprofen, and naproxen in surface waters. Environ Sci Technol 37:1061–1068
29. Buser H-R, Poiger T, Müller MD (1998) Occurrence and fate of the pharmaceutical drug diclofenac in surface waters: rapid photodegradation in a lake. Environ Sci Technol 32:3449–3456
30. Zwiener C (2007) Occurrence and analysis of pharmaceuticals and their transformation products in drinking water treatment. Anal Bioanal Chem 387:1159–1162
31. Halling-Sørensen B, Nielsen SN, Lanzky PF, Ingerslev F, Holten Lützhøfl HC, Jørgensen SE (1998) Occurrence, fate and effects of pharmaceutical substances in the environment- a review. Chemosphere 36:357–393
32. Huerta-Fontela M, Galceran MT, Ventura F (2010) Fast liquid chromatography–quadrupole-linear ion trap mass spectrometry for the analysis of pharmaceuticals and hormones in water resources. J Chromatogr A 1217(25):4212–4222
33. Stumpf M, Ternes TA, Haberer K, Baumann W (1998) Isolation of ibuprofen-metabolites and their importance as pollutants of the aquatic environment. Vom Wasser 91:291–303
34. Weigel S, Berger U, Jensen E, Kallenborn R, Thoresen H, Hühnerfuss H (2004) Determination of selected pharmaceuticals and caffeine in sewage and seawater from Tromsø/Norway with emphasis on ibuprofen and its metabolites. Chemosphere 56:583–592
35. Quintana JB, Weiss S, Reemtsma T (2005) Pathways and metabolites of microbial degradation of selected acidic pharmaceutical and their occurrence in municipal wastewater treated by a membrane bioreactor. Water Res 39:2654–2664
36. Roberts PH, Thomas KV (2006) The occurrence of selected pharmaceuticals in wastewater effluent and surface waters of the lower Tyne catchment. Sci Total Environ 356:143–153
37. Göbel A, Thomsen A, McArdell CA, Joss A, Giger W (2005) Occurrence and sorption behavior of sulfonamides, macrolides, and trimethoprim in activated sludge treatment. Environ Sci Technol 39:3981–3989
38. Zwiener C, Seeger S, Glauner T, Frimmel FH (2002) Metabolites from the biodegradation of pharmaceutical residues of ibuprofen in biofilm reactors and batch experiments. Anal Bioanal Chem 372:569–575
39. Young TA, Heidler J, Matos-Pérez CR, Sapkota A, Toler T, Gibson KE, Schwab KJ, Halden RU (2008) Ab Initio and in Situ comparison of caffeine, triclosan, and triclocarban as indicators of sewage-derived microbes in surface waters. Environ Sci Technol 42:3335–3340
40. Westerhoff P, Yoon Y, Snyder S, Wert E (2005) Fate of endocrine-disruptor, pharmaceutical, and personal care product chemicals during simulated drinking water treatment processes. Environ Sci Technol 39:6649–6663
41. Doll TE, Frimmel FH (2003) Fate of pharmaceuticals-photodegradation by simulated solar UV-light. Chemosphere 52:1757–1769

Books and Reviews

Asano T, Burton FL, Leverenz HL, Tsuchihashi R, Tchobanoglous G (2007) Water reuse: issues, technologies, and applications. McGraw-Hill, New York

Niessen WMA (2006) Liquid chromatography-mass spectrometry, 3rd edn. Taylor & Francis, Boca Raton

Snyder SA, Wert EC, Lei H, Westerhoff P, Yoon Y (2007) Removal of EDCs and pharmaceuticals in drinking and reuse treatment processes. Awwa Research Foundation, Denver

Water and Energy Nexus

Gustaf Olsson
Industrial Electrical Engineering and Automation (IEA), Lund University, Lund, Sweden

Article Outline

Glossary
Definition of the Subject
Introduction
Water and Energy Interdependencies
Energy Use in Water and Wastewater Operations
Energy on the Demand Side
Energy Recovery from Wastewater
Monitoring and Control for Better Efficiency
Water Use and Impacts on the Aquatic Environment from Energy Production
Conclusions
Future Issues
Bibliography

Glossary

Anaerobic Conditions in a biological treatments system characterized by the absence of oxygen in any of its forms.

Anoxic No oxygen present – nitrate instead of oxygen is used by the organisms.

Aquifer A natural underground layer that contains water.

BOD Biochemical oxygen demand, a measure of the organic carbon content in the wastewater.

Brackish water Water that is neither fresh nor salt.

Denitrification The conversion of nitrate-nitrogen to gaseous nitrogen through anoxic cell growth.

Desalination The changing of salt or brackish water into fresh water.

Eutrophication A significant increase in the concentration of chemical nutrients in an ecosystem.

Evaporation The process of liquid water becoming water vapour.

Fresh water Water that contains only small amounts of dissolved solids.

Groundwater Water that is pumped from aquifers.

Nitrification The conversion of ammonia-nitrogen to nitrite and nitrate-nitrogen through cell growth.

Renewable resources Total resources offered by the average annual natural inflow and runoff that feed a catchment area or aquifer natural resources that, after exploitation, can return to their previous stock levels by the natural processes of growth or replenishment.

Salt water Water that contains significant amounts of dissolved solids.

Surface water Water pumped from sources open to the atmosphere, such as rivers, lakes, and reservoirs.

Definition of the Subject

Water and energy are inextricably linked. Water is needed to generate energy and energy is needed to extract, treat, and distribute water and to clean the used and polluted water. This is the water–energy nexus and as a consequence, both challenges must be addressed together. Energy, water, and environmental sustainability are closely interrelated and are vital not only to the economy but to the health and welfare of all humans.

As a consequence of the close interrelationship between water and energy, the design and operation of water and wastewater systems should take the energy aspect into consideration. Similarly, energy production cannot be planned without taking water resources and water quality into consideration. Water availability is often undervalued and taken for granted. Population growth, climate change, urbanization, and rising health and environmental standards increasingly call for an integrated approach. The design of our cities, suburbs, homes, and appliances has enormous implication for water and energy consumption. As a result, we cannot continue to utilize the critical resources water and energy in an inefficient and wasteful manner.

In this chapter, after an introductory section, we will focus on the following main issues:

- Section 2: How the interrelationships between water and energy look like
- Section 3: Efficient design and operation of water and wastewater facilities
- Section 4: Attention to the water-related energy use at the end user
- Section 5: Energy recovery from wastewater, such as biogas production
- Section 6: The use of monitoring and control to make operations more efficient
- Section 7: Water requirements for energy production

In the last two sections, Conclusion and Future Issues, we summarize some of the findings and look for some future directions to deal with the water and energy nexus.

Introduction

Water has always been mankind's most precious resource – there are no substitutes. The struggle to control water resources has shaped human political and economic history. Population growth and economic development are driving a steadily increasing demand for new clean water supplies and it is well documented that lack of access to clean water has major health implications. Many see the water security as the key environmental issue of the twenty-first century.

Water and energy are the critical elements of sustainable economic development – without access to both of them, economies cannot grow, jobs cannot be created, and poor people cannot move out of poverty. On a global basis, neither water nor energy are in short supply. What is in short supply is energy and water at a price that people can afford to buy. We have to find better ways to use the water wisely, in our homes, in agriculture, and in industry. Using the water wisely includes producing the potable water and cleaning the wastewater using less energy. Pumping water, pressurizing water distribution systems, and pumping

wastewater are major energy consumers. Aeration of activated sludge systems is another major energy consumer.

Control and automation in water and wastewater operations can contribute to improve the sustainability by smart monitoring systems, disturbance attenuation, using energy wisely, and to maximize energy production.

Water and Energy Interdependencies

The interdependence between water and energy has been recognized during the last few years. Allan Hoffman wrote, in 2004 [1], on the topic: "The energy security of the United States is closely linked to the state of its water resources. No longer can water resources be taken for granted if the U.S. is to achieve energy security in the years and decades ahead. At the same time, U.S. water security cannot be guaranteed without careful attention to related energy issues. The two issues are inextricably linked." In the USA, the energy–water nexus initiative was initiated in 2004 as an informal DOE National Laboratory initiative to develop a better understanding of the link between the nation's energy and water supplies. The laboratories conducted preliminary assessments that indicated that the interdependence between energy and water supplies was much broader and much deeper than initially thought [1].

The increasing scarcity of water has been given much attention on the World Water Forums (1997 and every 3 years), UN Millenium Summit (2000), and now we are in the middle of the UN Decade of Water (2005–2015). Special workshops and conferences have been arranged, such as [2–4] and an interesting overview is found in [5].

Increasingly, there is a risk that water and energy interests are in conflict. Some examples can illustrate this:

- Between 1% and 18% of the electrical energy in urban areas is used to treat and transport water and wastewater. Furthermore, the energy related to water use – mostly heating the water in households and industries – requires about ten times more energy compared to the energy needed to deliver the clean and cold water and to treat the wastewater.
- To treat impaired water to drinking standards requires more energy. Most water treatment plants today are gravity draining through sand with some chlorine added. But as contaminants grow, old technology does not work. Either membrane or thermal water treatment is more energy intensive than traditional methods.
- Thermal power plants require huge amounts of cooling water. For example, around 39% of all freshwater withdrawals in the USA are used for thermoelectric energy production. This is roughly the same amount of water as for irrigation [6]. Most of the cooling water is returned but around 3% is actually consumed, mostly by evaporation. Water availability has become a contentious siting issue for thermoelectric power plants and must compete with demands from municipalities, agriculture, and other industries.
- Climate change and increasing drought in many regions will decrease the flow in many rivers. Consequently, the cooling water may become insufficient for the need of the thermal power plants along the river.
- Energy exploration and production requires a lot of water and consequently will generate a lot of wastewater. Pure water is injected down a hole for oil or gas production, fracturing the shale formation to release oil or gas. Then, the water is brought back up with the oil or gas. The water is then severely contaminated. Today that water is injected thousands of meters down where it evaporates and is out of the water cycle.
- It is apparent that hydropower generation depends on water. A hydropower dam can be a serious environmental problem. The dam itself often serves as a gigantic sedimentation basin, and the solid material that earlier served as fertilizers downstream now are trapped in the dam. Obviously, the water flow downstream is affected. This has implications for the agriculture, water fauna, for recreations, and many other human activities. Increasing water shortage in combination with increased water use in many regions is now causing lack of water in the dams. With lower water levels, the generation of electricity is decreasing.

It is critical to understand the key roles and responsibilities associated with the management, operation, and use of the water and energy resources. This includes government agencies, private industry, as well as individual users. The interdependencies

between water and energy should force us to conduct planning and operation in such a way that both the water and energy flows are tracked. Such a systems analysis should recognize the inputs and outputs for each aspect of the system as well as the storage reservoirs for the entire system.

The Supply of Water

Considering the importance of the topic, it is interesting to examine how much resources have been spent on water resources research. The situation in the U.S. is interesting. Since 1973, the population of the United States has increased by 26%, the GDP and federal budget outlays have more than doubled, and federal funding for all research and development has almost doubled, while funding for water resources research has remained stagnant [7]. Still, the pressure on water resources increases with population and economic growth. There is an increase in the number of conflicts over water, so there are strong incentives to focus much more on the water and energy issues, both in many parts of the industrialized world and in the developing world.

The economy of water and energy behaves in a particular way [8]. When the supply is scarce, there is a high price inelasticity of demand. A small reduction of supply leads to a huge increase in price. As a result, the total value (price quantity) rapidly increases as total quantity declines [9]. This is true for any resource that is essential and non-substitutable. As there is less water or energy available, their price quickly increases. This can create havoc in markets and stress the whole economic system. Diminished water supplies may lead to direct conflict and violence.

When energy and water supplies are abundant, their value is low. It may seem that we have an infinite supply and there is no need to worry. However, as we approach depletion, even small perturbations due to unforeseen climatic events, sharp increases in demand, or technical malfunction result in disproportionate changes in their values and prices, if the market is allowed to work.

When energy supply of nonrenewable fossil fuels is depleted, we are looking for renewable sources. Similarly, we are over-utilizing fresh water resources in many places. This is compensated by increasing the energy use to import water from other basins (such as S. California, Table 1), desalinate salt water, or reuse wastewater. Furthermore, nonrenewable water is depleted by over-pumping from fossil aquifers. These practices are not sustainable and will leave our children with fewer options. We need to think much more in terms of increased efficiency and conservation.

Water and Energy Nexus. Table 1 Energy requirements to pump 1 m^3 to the water treatment in some different places (Data from [10, 11])

Location	kWh
Sweden (average)	0,22
Sweden lowest	0.04
Sweden highest	0.64
N. California, USA	0,04
S. California, USA	2,3
Melbourne, Australia	0,09
Adelaide, Australia	1,9

Energy Use in Water and Wastewater Operations

Energy is needed to extract water from underground aquifers, transport water through canals and pipes, manage and treat wastewater for reuse, and desalinate brackish and sea water to provide new fresh water sources. To get the energy data is not always easy. Statistics for water abstraction, treatment, and distributions are maintained by OECD and Eurostat and also by UN for different sectors. However, the corresponding energy consumption is usually not recorded in the water statistics, so it is not easy to recognize the interconnection.

Using the water wisely includes producing the potable water and cleaning the wastewater using less energy. Pumping water, treating the water to drinking quality, pressurizing water distribution systems, pumping and treating wastewater is a major energy consumer. In the USA and in the UK, this amounts to about 3% of the nation's electrical energy use. In Sweden, the corresponding number is 1%, while in Israel it is around 10%. This also means that water extraction and cleaning will have an impact on the greenhouse gas (GHG) emission. On a global basis, the water/wastewater

sector contributes with 1.5% of the CO_2 and about 5–7% of the GHG emissions. With increasing population and demand growth, the GHG emissions will most likely exceed 7% [9].

Some national water utility associations maintain statistics on energy consumption by the water sector. The power consumption follows typically a daily, weekly, and sometimes, seasonal use pattern. There is a potential for compensating some of the daily-use pattern by pumping to water storage reservoirs during low load hours for the power plants and vice versa for the high load hours.

Drinking water production is increasingly crucial, in particular in dry countries. The use of desalination is growing at a significant rate in many industrialized countries, and this development further emphasizes the close coupling between water and energy. At the same time, billions of people in developing countries have not yet turned on the first electrical light. This means that the structure of electrical energy generation and distribution has to be carefully considered. There is a wide variation of the electrical energy needed to produce drinking water. The large differences reflect both the different efforts needed to obtain the clean water and the water consumption. Table 1 shows some examples to illustrate the energy requirements to produce clean water.

S. California and Adelaide are dry places, and the water has to be pumped long distances. This is reflected in the very high energy costs for these places. The energy can be compared with the energy requirement to desalinate seawater, which is typically 4 kWh/m^3. If there were unlimited energy, we would never have a problem with obtaining water for use. For example, there are vast resources of saline water that could be desalinized to provide for all the imaginable demands for water if there is energy to run those operations and then pump water to wherever it is needed. That is certainly not the case.

Wastewater collection, treatment and discharge, sludge treatment, and disposal require electrical power for pumping and aeration in biological treatment processes. Again, statistics for wastewater generation, collection, and treatment as well as sludge generation and disposal are maintained by OECD and Eurostat and also by UN for different sectors. As for water supply, the corresponding energy consumption is seldom recorded in the water statistics. Some national water utility associations maintain statistics on energy consumption by the water sector.

Primary treatment of wastewater is sometimes called mechanical treatment. Pollutants are removed by sedimentation or filters and the solids are removed by scrapers. Biological nutrient removal (BNR) is a term used to describe plants that employ biological processes to remove organic matter (C) as well as nitrogen (N) and phosphorous (P). The activated sludge process was developed in the early 1900s with the purpose to remove components that consume oxygen. When the effect of eutrophication became known, the next important step involved the development of processes that could remove nitrogen and phosphorous.

The most important process for removing organic matter is biological oxidation, which involves microorganisms feeding on the carbon and the oxygen in the water. Some of the carbon is used for the growth of the microorganisms and the remainder is converted into carbon dioxide. In the microorganisms, around half of the organic matter is used to increase the body mass and half is converted into carbon dioxide.

Nitrogen principally arrives at the plant as ammonium (60–80%). Most nitrogen removal plants will transform the ammonium into free nitrogen that will escape via the water surface. The removal of nitrogen is a slower process than the removal of organic carbon and takes place in two principal stages, nitrification and denitrification. In the first process, ammonium is transformed into nitrate (an oxidation process) and in the second process, the nitrate is reduced to nitrogen gas.

The concentration of dissolved oxygen governs carbon removal, nitrification, as well as denitrification. In the carbon removal and nitrification, the process rate will increase with the oxygen concentration. However, there is a limit to the process rate, and higher dissolved oxygen concentrations will not help the biology but only waste energy for the compressors that aerate the biological reactor. On the other hand, with too little oxygen, the microorganisms (like humans!) will suffocate and the process rate will be significantly reduced. In the extreme case, the organisms will die. The opposite applies to the denitrification: the higher the level of dissolved oxygen the lower the rate.

To aerate the biological reactors is an energy-consuming process. This means that the aerator has to be controlled so that it balances between the biological need for oxygen and the energy cost to supply the air. Table 2 gives some Australian figures to illustrate the variability.

As a comparison, the UK water industry uses 0.63 kWh to treat 1 m^3 of sewage and 0.59 kWh to treat 1 m^3 of water [12].

The two major energy consumers in wastewater treatment are pumping of the influent wastewater, and aeration. The difference between the primary treatment and the biological and advanced treatment is mainly due to the aeration energy. Typically, aeration in the biological treatment systems represent around 50% of the wastewater operating costs, while pumping represents around 60% of water treatment operating costs.

To relate the energy use to the volume of water only tells part of the truth. In order to get adequate key performance indicators, it is important to relate the energy consumption both to the amount of organic components, nitrogen and phosphorus removed.

There is a significant difference between the energy requirements for different wastewater treatment plants. The differences are due to plant size, the type of load (e.g., industrial or mainly domestic), and the type of operation. For example, in Sweden, the energy requirement for wastewater operations varies from 1.5 to 40 kWh/kg BOD (organic carbon removal), with a median value of 4.5 kWh [11].

In some countries, there is already a demand to decrease the energy requirement for water and wastewater operations. In California, a 20% increase in energy efficiency will be required according to the California Water Plan Update 2009. In China, the central government will require at least a 20% decrease in energy use [13] and in Sweden, a new energy savings program is being implemented where the goal is to save at least 20–30% in electrical energy requirement for wastewater treatment operations [11]. In Germany, the Ruhrverband has managed an ambitious energy savings program [14].

Water and Energy Nexus. Table 2 Energy requirement for wastewater treatment in Australia (Data from [10] and from Sydney Water and Brisbane Water)

Type of operation	kWh/m^3 (min, max)	kWh/m^3 average
Primary	0.1–0.37	0.22
Biological C removal (incl. primary)	0.26–0.82	0.46
Advanced C, N, and P removal	0.39–11	0.90

According to [2], it is quite feasible to obtain an energy consumption reduction by 20% by optimization and innovation. The existing systems in the water and wastewater industry have not reached the limits of improvement of its energy efficiency yet [15], [16]. It was also stated at the workshop [2] that a further reduction of the energy consumption with another 80% should be possible, but this requires a paradigm shift. The current water infrastructures have been designed and constructed on the basis of views, requirements, conditions, and technologies of decades ago. It is recognized that in the present systems, wastewater treatment, water treatment, and distribution are very energy intensive. New concepts could include topics like alternative sanitation approaches (vacuum system, separation at the source), from waste toward resource (P and N recovery; wastewater as nutrient for algal-based biofuel), microbial fuels cells, tailored water quality, and use of alternative resources, etc. The water and wastewater sector could benefit for technology developments and breakthrough in related areas like energy production, sensor development, nanotechnology, etc. Many research efforts have already been done in this direction [17].

Some of the important areas where energy efficiency needs to be addressed are:

- Water and wastewater pumping efficiency, including primary pumping, recirculations, and sludge pumping
- Motor controls, including soft start
- Aeration in biological treatment systems
- Mixing
- Water losses
- Demand side management – consumer behavior
- Operation of anaerobic digesters

Every energy efficiency improvement has to be tested from two angles: (1) How is the process affected,

and (2) what is the cost of the efficiency improvement. Every wastewater treatment operator is responsible for the effluent water quality. Therefore, the regulatory requirements are always the primary goal and the energy efficiency becomes secondary. At the same time, it has been shown that sometimes a better efficiency will also create a better process performance.

There are two principal possibilities for better process efficiency, retrofitting the equipment and using control and automation. In the latter case, one also has to consider the investment in instrumentation, actuators (such as controllable pumps and compressors), and computer control systems.

Here, we will give a couple of examples of efficiency improvements by retrofitting or control. By designing pumps for adequate flows, operating at dynamically changing pressures and using variable speed pumping, there is a great potential for energy savings [18]. It is well-known that variable speed operation will save a lot of energy. Figure 1 illustrates the fact that the power requirement for pumping is proportional to n^3, where n is the speed of the pump. At the same time, the flow rate is proportional to n. In other words, as the speed of the pump is halved, the flow rate will be halved while the power requirement decreases to 1/8. This is the very basic motivation to use variable speed drives in order to save energy.

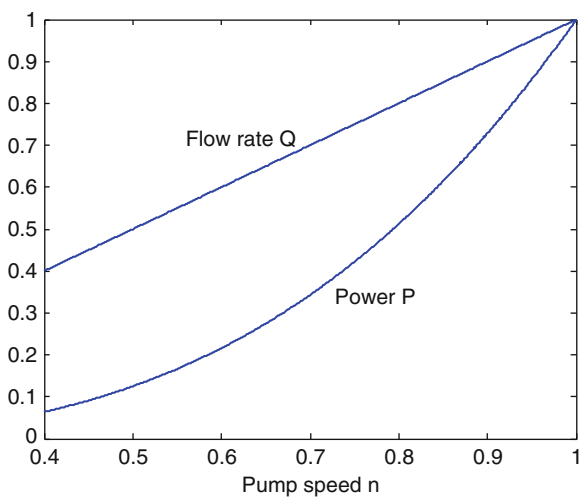

Water and Energy Nexus. Figure 1
The relationship between the flow rate Q and the pump speed (n) (*the upper curve*) and the power P and the speed (*the lower curve*) according to the affinity laws

It is not sufficient, however, to introduce variable speed pumping to save energy. The pump has to be designed so that its efficiency is at a maximum at the most common flow rate. This is a fact that is often overlooked in pumping of both water and wastewater systems.

Aeration of activated sludge systems is another major energy consumer. By automatic control of dissolved oxygen adjusted for variable wastewater loading, more energy savings are possible, and as a bonus, the biological activity is favored. There is a wealth of literature of dissolved oxygen control and a state-of-the art is given in [19], while [20–22] gives further experiences and evidence. In another chapter of this book [23], more details will be explained.

Often, the mixing of wastewater consumes too much energy. According to German experiences, 2–3 W/m^3 is sufficient [14].

Energy savings can be obtained both by selecting the adequate equipment and by feedback control. Efficient pumping requires not only the proper pumps but also a control system that can adapt the pumping to the process needs. Likewise, energy efficient aeration requires not only sensors for dissolved oxygen and air flow rate but also controllable compressors and adequate air valves.

Water saving is directly related to energy saving, also in water industry operations. Leakage reduction, metering, recycling, and demand reduction all contribute to less waste of water.

Energy on the Demand Side

A lot of efforts are today spent on the supply side instead of on the conservation and efficiency side. For example, in Nevada, USA, the Southern Nevada Water Authority states [8]: "One of the main objectives of the Authority is to obtain additional water from Colorado River to support urban growth of its member agencies." In general, hardly any water utility or water company has direct responsibility to reduce demand. At the same time, problems with energy and water supply are looming.

A lot of energy is used for bottled water. Only in the USA, the bottled water industry is a $15 billion

industry and this industry consumes a lot of energy to manufacture, package, and transport bottled water over huge distances [8]. The average American in 1976 drank 6 l of bottled water a year, according to Beverage Marketing Corp. In 2009, the consumption was 108 l, more than 2 l/week. According to [24], "we are moving one billion bottles of water around a week in ships, trains, and trucks in the United States alone. That's a weekly convoy equivalent to 37,800 18-wheelers delivering water." Actually, 24% of the bottled water the Americans buy is tap water repackaged by Coke and Pepsi. Every year, 50 billion water bottles are used in the USA – 167 for each person – and 38 billion of them are pitched into landfills in the USA. This is more than $1 billion worth of plastic that represents a lot of wasted energy. Actually, only 23% of the recyclable polyethylene terephthalate (PET) plastic bottles are actually recycled.

There is an interesting and strange attitude toward water. In a country like Sweden, the tap water quality is excellent, and from a quality point of view, bottled water will never be needed to replace the tap water. Still the Swedes consume around 30 l of bottled water per person and year. They pay 3–4 times the price for gasoline for the water, which is around 3,000 times the price for the tap water. In a recent examination (2009) of bottled water, only 2 out of 15 brands of bottled would be accepted as tap water according to the drinking quality standards.

Water usage has an energy cost. Both energy use and water use have to be sustainable. The use of suitable energy sources is discussed elsewhere and is outside the scope of this chapter. However, also the consumption of water has to be sustainable. Recent droughts have put the focus on the water consumption in some countries. It is apparent that the water consumption is quite different in different countries. Looking at individual cities (100 cities compared), the specific water consumption varies globally from 0.34 to 650 l/capita/day [25], while the total charge for drinking water varies from $0,015/m^3 to $3.13/m^3. Some national comparisons are given in Table 3.

The Water Poverty Index has been developed in [27]. Canada, Norway, and Iceland are the countries with the highest index. No country has higher than 78. The index gives an assessment of the national water management and includes resources (water available), access to water supply and sanitation, economic standard, water use, and water environment.

It is true that the natural conditions are quite different. Still these figures often reflect the habits and sometimes misuse of water. Naturally, the price of water has a role to play here (see section "Water and Energy Interdependies"). In general, the price paid by the consumer has a direct influence on the amount that is used. In the USA, the average household spends 0,006% of the income on water. The corresponding numbers for UK are 0,013%, for Pakistan 1.1%, and for Tanzania 5.7% [26]. It is most often true that the poor people pay more. While the average U.S. household pays around $0.5/m^3, and a German pays $1.9, poor people often depend on informal vendors.

Water and Energy Nexus. Table 3 Water consumption in some countries [8, 26]

Country	Water use (l/capita/day)			Water poverty index (scale 0–100)
	Domestic	Agriculture	Industry	
USA	600	1,900	2,100	65
Australia	500	2,600	340	62
Canada	800	480	2,800	78
China	85	910	345	51
Germany	190	310	1,060	65
The Netherlands	80	460	820	69
India	140	1,500	95	53

A typical water price in Dhaka, Bangladesh is \$0.4/m^3, in Phnom Penh, Cambodia \$1.6, and in Manila, Philippines \$4.7/m^3 [26].

Curbing demand is cheaper, faster, and ultimately more beneficial to individuals than increasing supply. Conservation of energy saves both energy and water. Optimal water use saves both water and energy.

It should be realized that more than 90% of the water-related energy use is spend in the home. This is true for many industrialized countries. This fact is easy to realize just from a simple theoretical calculation. Usually, only a fraction of a kWh is needed to produce 1 m^3 of drinking water. To heat this water from 15°C to 60°C requires 52 kWh, with no losses taken into consideration. Now, imagine how much warm water can be saved by using the showers, washing machines, dishwashers, etc. in a more economic way. Earlier it was stated that some 20–30% of the energy consumption for water and wastewater operations should be required. This saving should be profitable under most circumstances. Still, the same greenhouse gas emission savings could be achieved by only some 2–3% savings of warm water. Most water companies do not wish to take the responsibility for the domestic use of the water. Still, they usually have a good contact with the customers and should be able to easily influence the greenhouse gas emissions.

Energy Recovery from Wastewater

Energy recovery from sludge treatment is quite common and the biogas may be used for power generation, fuel for transport, or heating. In some cases, installation of heat pumps in wastewater treatment plant effluents has provided energy in terms of heat recovery. The power consumption in wastewater treatment and transportation follows typically a daily, weekly and sometimes, seasonal use pattern. Stormwater handling occasionally adds to the energy requirement. There is a potential for compensating some of the daily-use pattern by conducting certain treatment processes during low load hours for the power plants and vice versa for the high load hours.

A wastewater treatment plant is not only an "end-of-pipe" solution to clean wastewater. It can also serve as an energy producer. The interest in biogas is increasing and there is a large unused potential in maximizing the production of biogas, used for both heating and as a replacement of gasoline in transportation, [28–31]. Recent data show that anaerobic digestion uses only some 20% of the energy content of the sewage. By-products from sewage treatment in combination with organic solid waste can provide a valuable source of energy if managed and utilized effectively. About one third of the chemical energy in the biogas can be transformed into mechanical energy The rest of the energy becomes heat, but this can, of course, be recycled and used for heating. In order to use the biogas for engine fuel, the gas has to be further upgraded by removing carbon dioxide and hydrogen sulfide.

The biogas is produced in an anaerobic process where microorganisms break down the organic content of the sludge in the absence of oxygen. The process produces a methane and carbon dioxide-rich biogas. Furthermore, the nutrient-rich digestate can be used as fertilizer. The first part of the process is a so-called bacterial hydrolysis where organic polymers in the input material break down to become available as food for other organisms. Acidogenic bacteria then convert the sugars and amino acids into carbon dioxide, hydrogen, ammonia, and organic acids. These organic acids are then converted into acetic acid by Acetogenic bacteria, and additional ammonia, hydrogen, and carbon dioxide are generated. Finally, the products are converted to methane and carbon dioxide by the Methanogenic bacteria.

There are several factors that can influence the energy balance in the sludge handling in a wastewater treatment plant:

- *Primary sedimentation*: It may be possible to separate more sludge in the primary sedimentation. As a result, less organic carbon will be brought into the biological treatment step, so less aeration energy will be needed. In this choice, the organic carbon is chosen to produce biogas. However, organic carbon is also needed in the nitrogen removal process and insufficient carbon may limit the nitrogen removal capability.
- *Sludge thickening*: One way to increase the biogas production is to improve the thickening of sludge before the anaerobic digester. With a more efficient removal of water from the sludge, the sludge volume will decrease. Consequently, the retention time

of the digester can be increased. Also, less energy will be needed to heat the sludge before the digester.
- *Sludge heating*: The heat content of digested sludge can be used to heat the incoming sludge.

In cold countries, the heat content of the effluent water can provide significant heating not only to the plant facilities but also to city buildings via district heating systems [32]. In fact, most wastewater treatment plants can be net producers of energy.

There are other optimization aspects to consider. From an energy perspective, it looks straightforward to maximize the biogas production. However, from the digester, there will be reject water that has to be recycled to the wastewater treatment process. This water normally contains high concentrations of ammonium nitrogen. Therefore, the water that is recycled from the digester will significantly increase the load to the wastewater treatment plant, and thus to the energy requirement to operate the nitrification. This demonstrates that an energy balance has to be calculated in an integrated way and must consider the complete plant.

Monitoring and Control for Better Efficiency

Monitoring

To track the process operational state via the instrumentation is called *monitoring*. For the clean water supply, online monitoring will be required throughout the system, including at the tap. The availability of low-cost instrumentation will encourage better leakage detection [33, 34] and water quality monitoring [19]. In wastewater treatment systems, the use of instrumentation, control, and automation has proven to significantly reduce the costs for operation and detection, and early warning systems are key components in a sustainable water system. The development of reliable, affordable, and robust online instrumentation systems has been significant. Computing power no longer is a constraint, which means that the combination of measurements and model prediction can serve successfully in many systems.

Leakage detection in water distribution systems is becoming increasingly important as energy prices are raised. Leakages can appear as sudden bursts or they can appear as losses that will only gradually grow in size. Today, there are powerful automatic methods not only to detect that a leakage or burst appears, but also to locate the position with great accuracy. This can be obtained both in single pipe systems and in pipe networks. The idea of early warning and problem detection is fundamental. The losses caused by late detection can be significant. Leakages cause not only losses to the various damages of the leaking water. The extra energy to pump leaking water is significant, and it is not unusual to find 30–40% water losses in water distribution system. This power loss is intolerable, but still surprisingly accepted.

Similarly, early warning systems composed by arrays of sensors in drinking water intakes can prevent severe quality disturbances into the system.

Automatic monitoring is also crucial in wastewater treatment operation. Of course, it should be related to the influent flow rate, concentration, and composition. Furthermore, monitoring equipment operation makes it possible to early detect malfunctions, so that major process faults can be avoided. Several examples of this are given in [19, 35–37].

Control

The fundamental principle of control is feedback. The process (e.g., an aerator, a chemical dosage system, or an anaerobic reactor) is all the time subject to disturbances. The current state of the process has to be measured by some sensor and this is the basis for a decision. In order to make a decision, the goal or purpose of has to be expressed. The controller calculates a decision that appears as an output signal from the controller. Via an actuator, which is typically a pump, a valve, or a compressor it will manipulate the process. In other words: *control is about how to operate the plant or process toward a defined goal, despite disturbances* [38].

Traditional wastewater treatment plant control is still unit process oriented to a great extent. Some examples of state-of-the-art control that will influence the energy efficiency are [19, 39]:

- Aeration control has the purpose to supply the microorganisms with adequate dissolved oxygen while saving maximum energy. Dissolved oxygen control will save a lot of electrical energy compared to no control at all. A time-varying setpoint of the dissolved oxygen concentration will further reduce the energy consumption.

- In a sequential batch reactor, the length of the different phases should be controlled. During the ammonia nitrogen oxidation time, the aeration is controlled until all the ammonia nitrogen has been consumed;
- The control of anaerobic processes aims at regulating the biogas flow, at stabilizing the process, and at maximizing its productivity. Still current state-of-the-art focuses on unit process operation;
- In section "Energy Recovery from Wastewater", some examples of integrated control for biogas production were presented.

Water Use and Impacts on the Aquatic Environment from Energy Production

The demand for water is growing. The world water demand has more than tripled over the past half century. In the year 2000, the global water use was estimated to be about 30% of the world's total accessible fresh water supply. That fraction may reach 70% by 2025 [1].

This means that there will be more competition for the water needed for energy production. As a consequence, more water-intensive energy producers will be forced to look for more efficient alternatives. A key indicator may be "energy return on water invested" [8, 40].

Hydropower is often considered as "green" energy in the sense that the electric power production does not generate any emissions of greenhouse gases. Hydropower now generates about 19% of the world's electrical power. However, there are many signs of serious ecological impacts of hydropower generation. Dams do not only influence downstream transport of sediments, which has consequences for agriculture; they also serve as giant sedimentation basins. Fertilizers from the river no longer reach downstream agriculture. The sediments are instead collected on the bottom of the basin. Eutrophication in dams is another serious problem and evaporation from water dams in warm countries has not been sufficiently addressed as a great threat to freshwater availability. Dams can also act as physical barriers, restricting migration of aquatic wildlife.

On a global basis, only about one third of available hydropower potential has been used. However, the environmental and social costs for large dams will probably prevent much further development of large hydropower systems. Still there is a potential for small hydropower plants – less than 10 MW – that could be adequate for remote rural areas. The reservoirs needed for large hydropower plants globally cover a surface area of around 500,000 km^2 – roughly the size of Spain. With a lot of hydropower in warm countries, there is a huge loss of water due to evaporation. The social cost is also significant. Around 80 million people have been forced to move due to dam constructions.

Thermal power plant operations – both coal fired and nuclear – require large amounts of cooling water. For example, in the USA almost 40% of the withdrawn freshwater is used for cooling in thermoelectric plants; however, only about 3% is actually consumed, mostly by evaporation. Heating of the water and the risk of radioactive contamination present great environmental challenges. Addition of chemicals, for example inhibitors, anti-scaling agents, and biocides in cooling towers, may represent high environmental loads of hazardous substances. Although these are at relatively low concentrations, accumulation of chemicals can be harmful in the long term. A wide variety of processes are already employed in power plants to recover, recycle, and reuse water. An overview of these technologies is found in [41].

Climate change will add to the risks of conflict between water and energy. The efficiency of the cooling process depends on the temperature difference between the cooling water and the temperature related to the plant. Consequently, there are strict requirements on the temperature of water that is used. With a higher cooling water temperature, more water is needed to provide the same cooling effect. Most plants have regulations or other constraints that limit their ability to adjust their withdrawal rates. In the short run, this means that they will get less cooling, a corresponding decrease in turbine backpressure, less efficient generation, and less electric energy for the same amount of raw energy input. Also, many nuclear plants have safety limits on intake temperature that could trigger complete shutdowns more frequently in altered climate scenarios. In addition, environmental concerns usually impose limitations on the temperature of water discharged back into the streams and reservoirs.

Water and energy industries are competing for the same resource. For instance, availability of cooling

water is a key issue for many power plants. If a river's flow is reduced, as they can do seasonally, power plants may find there isn't enough water available for cooling. This issue will only become more critical with climate change. It is quite apparent that the water quantity and quality aspects are not always placed sufficiently high on the agenda of many power companies. It will be increasingly important to establish networks of water and energy professionals to deal with the close relationship between water and energy.

It is obvious that energy savings in households and in industry will have a large impact on the need for electrical energy and consequently on water consumption and ecology. Technology development, for example, using more efficient pumps, refrigerators, air conditioners and heating systems, and power electronic motor control will offer a most significant impact on the total electrical energy use.

As an ironic consequence of technological development in developing countries, low-cost asynchronous motors and pumps have increased the water extraction for agriculture. One reason for the non-sustainable groundwater pumping is that the surface water is too contaminated. In some cases, this has had catastrophic consequences for groundwater levels and salinity of the soil. More efficient use of water for agriculture is therefore of paramount interest. This requires education, better equipment, probably economic support, and also some new legislation.

The "environmental friendly" zeal for ethanol has not considered the extensive irrigation required for the grain that supply ethanol. The situation in Midwestern USA can illustrate the problem. If irrigation is used, at least 1 m^3 of water is needed for every 10 km travelled by an ethanol-powered vehicle [42]. According to [42], in case of ethanol-fuelled vehicles, there is a need to move from our old way of thinking – gasoline used per kilometer – to water used per kilometer. This water is often extracted from aquifers in a non-sustainable way. Fossil water is used and will not be replaced for generations.

It should also be noted that various portions of the ethanol production cycle have different water requirements. For example, in biofuel production irrigation requires orders of magnitude more water than ethanol biorefineries, as shown in Table 4. However, the intensity of water consumption can be much higher for refineries, where thousands of cubic meters of water are to be withdrawn on the spot, significantly changing local hydrology and requiring additional infrastructure to provide that water.

Water and Energy Nexus. Table 4 Estimated use of water for various technologies of biofuel production (From [8])

	Irrigation use (l water/l ethanol)	Refinery use
Oil		0.5–1 l water/l gasoline
Corn	0–1,900 l water	2–5 l water/l ethanol
Cellulose (sorghum) sugar	0–400 l water	6 l water/l ethanol

According to estimates from U. S. Department of Energy (DOE), more than 4 l of water are needed for every liter of transportation fuel produced, threatening the limited water supplies (DOE Report 2006:80). China announced that it needs to curb coal-to-liquid production, because of concerns over pollution and the volumes of water consumed. Nevertheless, more recently, it was announced that the facility "will start operating later this year and is expected to convert 3.5 million tons of coal per year into 1 million tons of oil products such as diesel for cars." [8]. They will use groundwater and recycled water from coal mines to supply the 8 million tons it will need each year. In some parts of China, 30 years ago, the water table was 5 m below the ground. Today, it is 35–40 m below the ground because the groundwater is used in an unsustainable way.

Conclusions

Water and energy are the two most fundamental ingredients of modern civilization. Without water, people will die. Without energy, we cannot produce food or run our homes or industries. Considering the close relationship between water and energy, it is obvious that the challenges have to be treated in an integrated manner and single issues cannot be treated in isolation. An integrated approach means that the whole system has to be considered, including pure water resources, energy consumption, water usage, wastewater treatment, water

reuse, receiving water, and possible energy production. Integrated systems can only be considered by cooperation between several specialists. The interdisciplinary view has to be recognized, which also means that we have to exercise much more communication between engineers and scientists of different disciplines, but also between technology people and professionals in social sciences, behavior sciences, economy, and political decisions.

Saving energy and water is not just a technical challenge. Maybe the most important factor is our consumer attitudes and behavior. This includes how we use hot and cold water for showers, dishwashers, and washing machines. What kind of machinery is used? How do we consume water for gardening, etc.? As an example, the long drought in Queensland, Australia has forced the authorities in Brisbane to enforce a decreasing consumption. In 2005, the consumption was 300 L/day/person and in 2007, this had decreased to 130 [43]. This included restrictions for external water use and recommendations for internal water consumption.

As the world population grows, the demands for both water and energy increases faster than ever. It looks as if the world has become aware of the era of peak oil, seeing the fluctuations of the oil price. It seems that we are approaching an era of peak water – there will be lack of cheap water. The situation should already be considered a crisis, but the public in many developed countries has not grasped the urgency. Water is ultimately more important than oil, because it is more immediately crucial for life. We have government departments of energy. As Webber [42] points out, we should have a Department of Water that would ensure the effective use of water. Water is certainly a human right, but it should not be free or cheap. If we think that water is important, we should put a realistic price on it. The attitude toward water consumption may be the crucial ingredient. Furthermore, new approaches to financing, managing, and maintaining systems must be developed, as well as approaches to involve local communities.

The energy and water nexus has to be recognized by decision makers, researchers, and engineers as a vital one. It will not only determine the way to extract, treat, and distribute water, but also collect and treat wastewater. The role of water has to be fully recognized in the production of energy, both for electricity and for transportation. For individuals, there are many ways to influence both the water and energy consumption in their daily lives, for example at home and when making transport choices. Creating the right pricing, policy, and regulatory environment is critical to encouraging behavioral changes, and ensuring a sustainable use of water and energy.

Conservation of energy saves both energy and water. Optimal water use saves both water and energy.

Future Issues

In the future, water supplies and treatment will probably become more energy intensive. Readily accessible freshwater supplies are limited or have been fully allocated in some areas. The new alternative water resources considered are sea water, brackish water, produced water, or impaired water. This means increased energy consumption for pumping at deeper depths and longer distances. New technologies to access and treat nontraditional water resources will require increased energy consumption per cubic meters of water.

Many new technologies offer interesting solutions. Wave energy offers sustainable solutions for energy generation, and the combination of desalination plants and wave energy generation is likely to be a very interesting area for research and development for water professionals in cooperation with power systems researchers. Microbial fuel cells (MFC) offer another interesting combination of water and energy issues. MFCs present an interesting energy challenge and also offer sustainable treatment of biological substances as a by-product [43].

Heat production from groundwater or effluent water in treatment plants is technologically possible, and application rates should increase along with investment in relevant infrastructure, for example, district heating systems could be applied at large scales.

Regulatory aspects of balancing the competing interests of water and energy needs by several sectors and industries is a multidisciplinary task. There is an emerging need to create professional platforms where such issues can be discussed and further developed on "neutral ground." A focus should be on the development of concepts and motivating incentives rather than case-specific matters. For example, water pricing represents an issue not only affecting water and wastewater

utilities but also energy and agricultural sectors. It is obvious that new incentives and attitudes have to be developed in order to save water and save energy.

There is an urgent need for a paradigm shift from promoting growth to sustainability. Sustainable growth is impossible on a finite planet; we can only talk about sustainable development. We have created a global system that is closely coupled, and crises in one location send waves of disruption throughout the system. The fact that we live in a globalized system creates new opportunities, but also increases our risks, since there may be no place to go in case of a collapse. It will be unlikely that one developed country or region will be able to maintain its high quality of life if the rest of the world will be in substantial crisis. We have become very interdependent worldwide.

Bibliography

1. Hoffman A (2004) The connection: water and energy security, Institute for the analysis of global security. http://www.iags.org, Aug 2004
2. Water and energy (2008) Report of the GWRC research strategy workshop (www.globalwaterresearchcoalition.net), London
3. IWA (2008) Water and energy workshop, IWA World Water Congress, Vienna, Austria. Presentations published on http://www.iwahq.org/Home/Themes/Water,_climate_and_energy/
4. IWA (2009) Water & energy – mitigation in the water sector & potential synergies with the energy sector. In: International conference, international water association, Copenhagen, Denmark, 29–30 Oct 2009
5. Pate R, Hightower M, Cameron C, Einfeld W (2007) Overview of energy-water interdependencies and the emerging energy demands on water resources. Sandia National Laboratories, Albuquerque, New Mexico, SAND 2007-1349 C. See also www.sandia.gov/energy-water
6. Energy demands on water resources: report to congress on the Interdependencies of Energy and Water, DOE Report to congress, Jan 2007, http://www.sandia.gov/energy-water/docs/121-RptToCongress-EWwEIAcomments-FINAL.pdf. Accessed Feb 2010
7. Webb EK, Johnson J (2009) Federal engagement in water resource technology development: current programs and the future. J Contemp Water Res Educ 143:3–16
8. Voinov A, Cardwell H (2009) The energy-water nexus: why should we care? J Contemp Water Res Educ 143:17–29
9. Farley J, Gaddis E (2007) An ecological economic assessment of restoration. In: Aronson J, Milton S, Blignaut J (eds) Restoring natural capital: science, business and practice. Island Press, Washington, DC
10. Kenway SJ, Priestley A, Cook S, Seo S, Inman M, Gregory A, Hall M (2008) Energy use in the provision and consumption of urban water in Australia and New Zealand, CSIRO: Water for a Healthy Country National Research Flagship, CSIRO Australia and Water Services Association of Australia
11. Lingsten A, Lundkvist M (2008) Description of the current energy use in water and wastewater systems in Sweden (in Swedish). The Swedish Water & Wastewater Association, SWWA, www.svensktvatten.se
12. University of Oxford, Department of Earth Sciences, Environmental KTN, www.environmental-ktn.com. Accessed 9 Feb 2010
13. Chen J (2008) Personal communication. TsingHua University, Beijing
14. Thöle D (2008) Ways to identify possibilities of energy saving at wastewater treatment plants. In: IWA (2008) Water and energy workshop, IWA World Water Congress, Vienna, Austria. Presentations published on http://www.iwahq.org/Home/Themes/Water,_climate_and_energy/
15. Nowak O (2000) Expenditure on the operation of municipal wastewater treatment plants for nutrient removal. Water Sci Technol 41(9):281–289
16. Alegre H, Baptista JM, Cabrera E Jr, Cubillo F, Duarte P, Hirner W, Merkel W, Parena R (2006) Performance indicators for water supply services, 2nd edn. IWA, London. ISBN 1843390515
17. Urbanwater (2008) A Swedish research programme on "Sustainable Urban Water Management." http://www.urbanwater.org
18. Yates MA, Weybourne I (2001) Improving the energy efficiency of pumping systems. J Water SRT Aqua 50:101–111
19. Olsson G, Nielsen MK, Yuan Z, Lynggaard-Jensen A, Steyer JP (2005) Instrumentation, control and automation in wastewater treatment systems. Scientific and Technical Report No.15, IWA, London, UK
20. Serralta J, Ribes J, Seco A, Ferrer J (2002) A supervisory control system for optimising nitrogen removal and aeration energy consumption in wastewater treatment plants. Water Sci Technol 45(4–5):309–316
21. Watts JB, Cavenor-Shaw AR (2008) Process audit and asset assessment using on-line instrumentation. Water Sci Technol 37(12):55–61
22. Rosso D, Stenstrom MK, Larson LE (2008) Aeration of large-scale municipal wastewater treatment plants: state of the art. Water Sci Technol 57(7):973–978
23. Olsson G (2010) Instrumentation, monitoring, control and automation in water and wastewater systems. IWA Publishers, London
24. Fishman C (2007) Message in a bottle. Fastcompany. Dec 2007, http://www.fastcompany.com/magazine/117/features-message-in-a-bottle.html. Accessed Feb 2010
25. International statistics for water services, International Water Association (IWA) Specialist group on statistics and Economics, IWA Biennial Conference, Vienna 2008
26. Clarke R, King J (2006) The atlas of water. Earthscan, London
27. Lawrence P, Meigh J, Sullivan C (2003) The water poverty index: an international comparison. Keele Economic Research Papers 2002/19, March 2003

28. Börjesson P (2008) Biogas from waste materials as transportation fuel–benefits from an environmental point of view. Water Sci Technol 57(2):271–275
29. Wiese J, Kujawski O (2008) Operational results of an agricultural biogas plant equipped with modern instrumentation and automation. Water Sci Technol 57(6):803–808
30. Siegrist H, Salzgeber D, Eugster J, Joss A (2008) Anammox brings WWTP closer to energy autarky due to increased biogas production and reduced aeration energy for N-removal. Water Sci Technol 57(3):383–388
31. Tilche A, Galatola M (2008) The potential of bio-methane as bio-fuel/bio-energy for reducing greenhouse gas emissions: a qualitative assessment for Europe in a life cycle perspective. Water Sci Technol 57(11):1683–1692
32. Fred, T. (2008). Large scale heat transfer from wastewater to city heating and cooling systems. In: IWA (2008) Water and energy workshop, IWA World Water Congress, Vienna, Austria. Presentations published on http://www.iwahq.org/Home/Themes/Water,_climate_and_energy/
33. Misiunas D, Lambert MF, Simpson AR, Olsson G (2005) Burst detection and Location in water distribution networks. Water Sci Technol/Water Supply 5(3–4):71–80
34. Misiunas D, Vitkovsky J, Olsson G, Simpson AR, Lambert MF (2005) Pipeline break detection using the transient monitoring. J Water Resour Plann Manag ASCE 131(4):316–325
35. Olsson G (2008) Process control. In: Henze M, van Loosdrecht M, Ekama G, Brdjanovic D (eds) Biological wastewater treatment – principles, modelling and design. IWA Publishers, London
36. Kaelin D, Rieger L, Eugster J, Rottermann K, Bänninger C, Siegrist H (2008) Potential of in-situ sensors with ion-selective electrodes for aeration control at wastewater treatment plants. Water Sci Technol 58(3):629–637
37. Shao-Yuan L, Rosso D, Jiang P, Larson LE, Stenstrom MK (2008) Real-time efficiency monitoring for wastewater aeration systems. Water Pract Technol 3:3
38. Olsson G, Newell B (1999) Wastewater treatment systems. Modelling diagnosis and control. IWA Publishers, London
39. Ingildsen P (2002). Realising full-scale control in wastewater treatment systems using in situ nutrient sensors. PhD thesis, Department of Industrial Automation, Lund University, Lund, Sweden (Access via www.iea.lth.se)
40. Spreng DT (1988) Net energy requirements and the energy requirements of energy systems. Praeger Press, New York
41. Wolfe JR, Goldstein RA, Maulbetsch JS, McGowin CR (2003) An electric power industry perspective on water use efficiency. J Contemp Water Res Educ 143:30–34
42. Webber M (2008) Catch-22: water versus energy, Scientific American Earth 3.0, pp 34–41
43. Keller J (2008) From microbial fuel cells to bio-electromechanical systems: how to convert organic pollutants to electric energy and more. In: IWA (2008) Water and energy workshop, IWA World Water Congress, Vienna, Austria. Presentations published on http://www.iwahq.org/Home/Themes/Water,_climate_and_energy/

Water and Wastewater Operation: Instrumentation, Monitoring, Control and Automation

Gustaf Olsson
Industrial Electrical Engineering and Automation (IEA), Lund University, Lund, Sweden

Article Outline

Glossary
Definition of the Subject
Introduction
Incentives for Control
Basic Control Actions
Control of Biological Oxidation
Control of Denitrification
Monitoring
Plant Wide Control
Future Directions
Bibliography

Glossary

Actuator A transducer that reacts to a control signal and performs the desired action.

Anaerobic Conditions in a biological treatments system characterized by the absence of oxygen in any of its forms.

Anoxic Nitrate serves as terminal electron acceptor.

Closed loop control System where the controlled variable is measured and the result of the measurement used to manipulate one of the process variables. Also called feedback control.

Denitrification The conversion of nitrate nitrogen to gaseous nitrogen through anoxic heterotrophic cell growth.

DO Dissolved oxygen.

Nitrification The conversion of ammonia nitrogen to nitrite and nitrate nitrogen through autotrophic cell growth.

Online estimation Estimation of model parameters during the operation of the system.

Open loop control System where information about the controlled variable is not used to manipulate any of the system inputs to compensate for variations in the process variables. Also called sequencing.

ORP Oxidation-reduction potential or redox.

OUR Oxygen uptake rate is the rate at which oxygen is utilized by microorganisms, typically expressed in mg/L/h.

PID controller Three mode controller combining the actions of proportional (gain), integral (reset), and derivative (rate) elements into a single unit.

Redox Oxidation-reduction potential or ORP.

Setpoint The desired value for a control system, that is a temperature, flow rate, pressure, or level at which a process should operate.

WWTP Wastewater treatment plant.

Definition of the Subject

Instrumentation, control and automation (ICA) are now essential in all water and wastewater operations. While wastewater treatment plants (WWTPs) have been upgraded from relatively simple mechanical/biological plants for organic removal, the plants of today are increasingly complex and include not only biological nutrient removal but also the requirement to interact on both a plant wide level and with the sewer systems.

The ideal ICA system contains four functional components:

- A quality team of people who feel a deep sense of ownership of the system and the treatment plant and who are committed to the continuous improvement ethics.
- An instrumentation system to gather adequate process variable information.
- A monitoring system to acquire data, process and display the data, detect and isolate abnormal situations, assist in diagnosis and advice, and finally simulate the consequences of operational adjustments. A proper data acquisition and reporting is crucial.
- A control system to meet the goals of the operation. This can take place both locally within the treatment process by low-level control system or by coordination of the various processes within the plant as well as with the sewer system.

Automation in wastewater treatment systems have to include several disciplines:

- Process engineering: The focus of the ICA efforts always has to be the process. Therefore process knowledge, including the equipment to operate the process, is essential for a successful control. Dynamic modeling and simulation is used as an important tool.
- Instrumentation technology: Measurements of the states and parameters of the process requires instrumentation knowledge.
- Signal processing: Handling the measurement data has the purpose to remove inadequate data and extract essential information from the sensors and instruments.
- Monitoring: Based on the measurement information, a monitoring and detection function has to help to make the operation reliable.
- Operator guidance: Based on measurements and monitoring, the computer system should support the operator to make the adequate decisions.
- Automatic control: The controller makes the decision how to change the control variables (liquid and airflow rates, dosages, reaction times, etc.).
- Actuator technology: The design and operation of pumps, compressors, and valves.
- Production planning: This includes planning how to operate the plant to prepare for future disturbances and external changes. This can include planning for a coming rain event, extreme loads (like a tourist season), or temperature due to seasonal variations.

The concept of control is further described in the Introduction. There are several incentives for control of wastewater treatment systems, and they are illustrated in Incentives for Control. Disturbances to the plant motivate feedback control and this requires that the goal for the control is clearly defined. Basic Control Actions presents the basic ideas of control concepts and some of the basic control actions that have to take place to just keep the plant running. In Control of Biological Oxidation, some specific control systems are described for the biological oxidation processes, where dissolved oxygen (DO) control is a key operation. Control of Denitrification describes how control can make the

reduction process denitrification more efficient and economical. Monitoring is to keep track of the current process operational state via the instrumentation. This is further described in Monitoring. In order to satisfy increasing demands on effluent quality and ecological standards, it is needed to apply an integrated view of the whole plant operation and its connection upstream to the sewer network and downstream to the receiving water. These aspects are discussed in Plant Wide Control. In Future Directions, finally, some future perspectives are discussed.

Introduction

Advanced control is getting increasingly demanded in water and wastewater treatment systems and has been subject to a lot of applications in other parts of the process industry. Various case studies have shown significant savings in operating costs and remarkably short payback times. Process control in wastewater treatment systems is today well recognized as an integrated part of the plant operation. Still, however, the industry has a lot to learn from other process industries, like the chemical or paper-pulp process industries. It is the process knowledge, the sensor technology, and the way the plants have been designed and built that may limit what can be achieved today. Wastewater processes do have some unique features: the flow rates, the disturbances, the small concentrations, the organisms, the separation, and the fact that all the "raw material" has to be accepted and treated.

During many years, the incentives to apply automatic control were missing. Operators and organizations did not have the incentives to develop operation based on instrumentation, control and automation (ICA). Economic incentives are of course essential and today many organizations have created such economic driving forces that have accelerated the application of ICA.

There are several technical driving forces that have contributed to make ICA being applied much more:

- *Instrumentation development*: Today online instrumentation for some key components are available and getting both reliable and profitable to use. This includes sensors for ammonia, nitrite/nitrate, and phosphate.
- *Actuators*: Variable speed technology is well proven for electrical motors. This means that both pumps and compressors can be operated flexibly, which will have a significant impact on the quality of the operations.
- *Computer systems*: Distributed computer systems, including PLCs (programmable logical controllers) are available in modules and can be adjusted to the size of the plant.
- *Automatic control*: The control technology and engineering is sufficient for most needs and is often packaged in the real-time computer systems.
- *Process knowledge*: This has increased tremendously over the last decades. Dynamic models of the treatment systems are available in commercial simulators and this can be of help not only for the design but also for operator guidance.
- *Education*: The level of education of operators is often high and increasing. However, unfortunately the education of process designers most often does not include anything about dynamics and control. This was recognized already in 1974 at a conference at Clemson University, South Carolina, USA. Professor John Andrews recognized the need for education at all levels and he noted: "A course in *Process Dynamics and Control* is commonly found in most chemical engineering curricula. We would be well advised to include a course in *Dynamics and Control of Wastewater Treatment Systems* in environmental engineering curricula." Today there are such courses at a few universities, and it has taken a long time to make this vision come true.

Demands from the regulatory agencies are also important driving forces and give incentives for control. Demands on organic matter content, nitrogen, and phosphorous components in the effluent require good operation consistently, around the clock. The only reasonable solution to this challenge is online measurements and automatic control.

Economic incentives are today much more apparent, and the requirement for economic operation are expressed clearly at many plants.

It is generally acknowledged that the introduction of ICA during the last decades has increased the capacity of biological nutrient removal (BNR) wastewater treatment plants by 10% to 30%. If these possibilities

are further exploited by intelligent use of measurements and information technology, the improvements due to ICA will have a significant impact during the next decade. It has the potential to reduce operating costs – such as electrical energy, chemicals, sludge disposal, and in some countries green taxes – and to keep the effluent quality consistently acceptable, despite load variability and plant disturbances. Furthermore, ICA can make the plant meet increasing load demands. For apparent reasons, ICA has to be integrated already in the plant design process.

As the complexity of the plants and processes has grown, the electrical and real-time computer systems have developed even faster. It is expected that ICA will have an even larger impact on both the performance and economy of wastewater treatment systems in the coming decade.

More detailed descriptions of the state of the art of ICA in wastewater treatment systems are given in the books [1–3].

Incentives for Control

Control is about how to operate the plant or process toward a defined goal, despite disturbances.

Disturbances

Disturbances are the main reason why control is needed. They are present all the time and will affect the process, so they cannot be neglected. The load varies every minute, hour, day, and month with respect to its flow rate, its concentrations, and its composition. Under all these varying load conditions, the plant has to operate in such a way that it satisfies the effluent requirements. A wastewater treatment process is quite unique in the process industry. The "raw material" cannot be controlled and simply has to be accepted. Despite this lack of quality control of the input the "product," the effluent water, has to satisfy a sufficiently good standard all around the clock.

Disturbances related to the influent can be described as in Fig. 1, which represents a municipal treatment plant in a suburb with no industrial plant connected to the wastewater treatment plant. Diurnal variations are apparent and the flow rate varies at least by a factor of 10. The concentration variations are almost in phase with the flow rate variation, so the total load varies significantly. Under all these conditions, the plant has to be operated satisfactorily. Traditional design usually solves the variability problem by increasing the tank

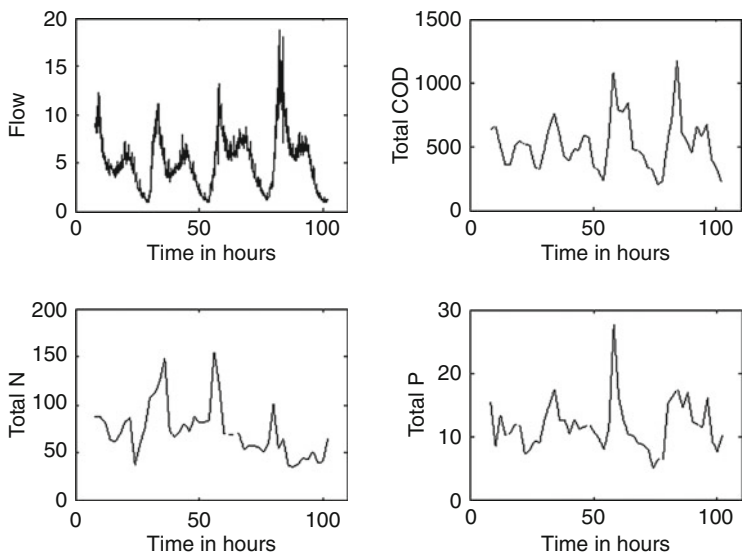

Water and Wastewater Operation: Instrumentation, Monitoring, Control and Automation. Figure 1
Diurnal variations from Thursday through Sunday in a municipality without any industry. There is no rain during this period

volumes. In this way, the variations are smoothed and the plant can produce a satisfactory effluent. However, the price of such an overdesign is high. Also, at low loads the plant may be "underloaded" and the retention time in the system will simply be too long.

Many treatment plants have to receive stormwater from rain. This causes two types of disturbances. One is of course the higher flow rate, which will decrease the retention time in the process. Furthermore, it may risk the performance of the settler, which will result in loss of sludge into the effluent. Thus, the effluent quality will deteriorate while the process will lose sludge-containing microorganisms that serve in the waste removal process. The other rain disturbance is due to the rate of change of the flow rate. A sudden rate of change will again cause problems in the settler unit. Any sedimentation has to guarantee a smooth laminar flow, but the sudden flow increase will propagate to the settler and cause hydraulic upsets and some turbulence. This is of course detrimental for the settler performance.

In many plants, there are unintentional disturbances caused by the equipment. If the plant is supplied with only on/off control of the influent pumps, any pump start will cause a sudden flow increase into the plant. The result is again an upset of the settler performance. Consequently, a good control and operation of the plant will assume smooth pumping using variable speed control of the pumps.

A wastewater treatment plant consists of many unit operations that are connected serially or via recirculations. As a result, a disturbance in one of the units will propagate to some other unit. These kinds of disturbances are less obvious, but may significantly influence the plant operation. One example can illustrate this. Reject water (supernatant) from an anaerobic digester is usually recirculated to the influent of the wastewater treatment plant. The supernatant has often a high concentration of nitrogen components and will consequently increase the load to the plant quite significantly. This can be illustrated by Fig. 2.

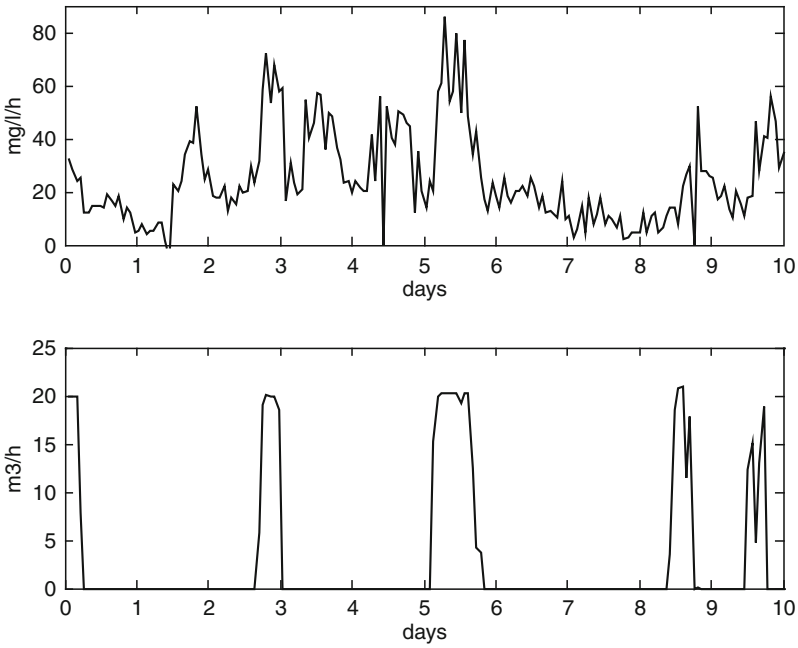

Water and Wastewater Operation: Instrumentation, Monitoring, Control and Automation. Figure 2
The consequence of recirculation of reject water (supernatant) from an anaerobic digester back to the treatment plant during a 10-day period. The lower curve shows the supernatant flow rate. The concentration is very high, so the impact on the wastewater treatment is significant. The upper curve shows the oxygen uptake rate in the aerator, which is a sign of the biological activity as well as the load (M.K. Nielsen, Denmark, personal communication, 2006)

If the supernatant is recirculated at a high load situation, the operation of the biological reactor will suffer. Therefore, it is important not only to control each one of the unit processes but also their interaction. This recirculation should be activated only at the low load periods.

The Control Goals

The ultimate goal of the operation of a wastewater treatment plant is to satisfy the effluent criteria. They can be expressed in terms of organic material content, total nitrogen, total phosphorus, and suspended solids. However, given the many steps of the operations from the influent to the effluent it is most often almost impossible to base any control action on measurements of the effluent quality. Instead, a number of intermediate goals have to be formulated in order to synthesize some control action. Examples of such goals are:

- Grow the right biomass population
- Maintain adequate mixing
- Keep the level of dissolved oxygen at the right level
- Maintain an adequate airflow rate while minimizing the pressure
- Keep the sludge blanket level in the settler between given limits
- Avoid overload of the clarifier
- Avoid too long retention time of the sludge in the settler

Another goal is to *minimize the operational costs*. Here a control system can make a significant contribution to savings. The two major energy consumers in wastewater treatment are pumping of the influent wastewater and aeration. Typically, aeration in the biological treatment systems represents over 80% of the energy costs for biological treatment (Olsson G, ►Water and Energy Nexus, this volume). Depending on the geographical conditions pumping costs can be quite different in different plants, but pumping together with aeration represents most of the energy cost.

Aeration can be controlled so that the microorganisms will receive just enough air to function, but not more. Any excess of air flow will cost money. Likewise, the pumps have to be designed in such a way that they have a maximum efficiency at the most common flow rates. On top of this it is important to control the flow rates smoothly, so variable speed drives are important for good control.

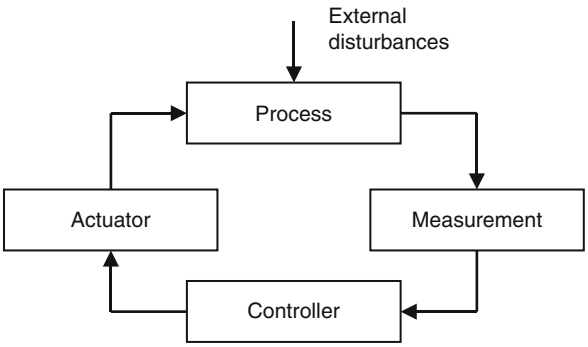

Water and Wastewater Operation: Instrumentation, Monitoring, Control and Automation. Figure 3 Illustration of the feedback principle

Basic Control Actions

The fundamental principle of control is feedback, illustrated by Fig. 3. The state of the process is measured by some online sensor (or a human observer). Based on the measurement a decision is made how to correct the process in order to reach the goal. The decision is made in the controller that will send a command to some actuator that will make the correction of the process. The reason that measurements and corrections have to be made all the time is that disturbances will influence the process behavior in some way.

One is faced with feedback systems all the time in one's daily life. The human body would not function without a huge number of feedback loops. For example, to stand up requires feedback. The balance system in the ears and the vision will measure if the body is straight. The brain calculates how to change the feet in order to keep the balance and the muscles (the "actuators") will make the change happen.

While driving a car the driver all the time applies feedback. The eyes watch the speedometer and the road, etc., and the brain will compose all that

information and make a decision what to do in the next moment. This is translated to the muscles to turn the steering wheel, to brake, or to accelerate. The reason all the time for the feedback is that the scene is changing continuously. In other words, the "process" is subject to disturbances that force one to use feedback.

Open Loop Control

It is important to understand the difference between feedback control (also called closed loop control) and open loop control. In open loop control, the control action is simply triggered by a timer. No measurement of the result is made. Some common examples of open loop control are:

- A pump that is switched on certain time intervals and switched off the rest of the time. No flow rate measurement is made.
- A sequential batch reactor (SBR), where the phase length is only determined by a timer. For example, in nitrogen removal the reactor is aerated a given time and then not aerated in the next time interval. Again no measurement is made of the ammonium or nitrate concentrations at the end of each phase. More of this is discussed in Control of Biological Oxidation and Control of Denitrification.
- A sludge scraper is operated every *n*th minute. The sludge level is not measured, so sometimes the scraper will remove only small amounts of sludge and at other times too much sludge.
- Two compressors may provide aeration for the biological reactor. One of them may be switched on during the day and switched off during the night. No confirmation of the resulting dissolved oxygen concentration is made.

It is obvious, that measurements and feedback control are necessary to truly compensate for variable loads and other disturbances. Open loop control may seem to have a lower cost, since it does not require measurements. However, if operating costs are calculated, then the open loop control is mostly inferior. Furthermore, if the effluent quality is to be maintained, then feedback is superior.

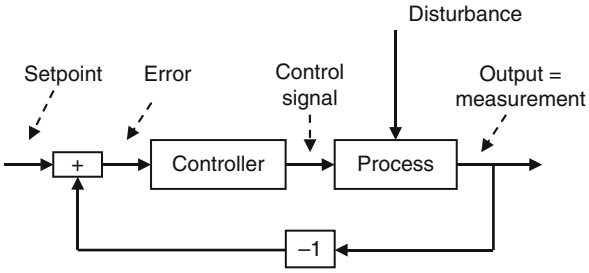

Water and Wastewater Operation: Instrumentation, Monitoring, Control and Automation. Figure 4
A simple control loop

Control of the Equipment

The top priority for any operation is to keep the plant running. This means that all the equipment, such as pumps, valves, motors, compressors, sludge scrapers, etc., simply have to work as intended. Many of these operations are not directly influencing the effluent quality, but without a proper operation of the equipment the effluent quality will suffer sooner or later.

Figure 4 is a control engineering block diagram and illustrates the principle of a simple control loop for the local controllers. Assume that one wishes to control the airflow rate in an aerator. The desired value (setpoint) may be provided in two different ways. The operator can manually set the desired airflow rate or another controller can send a signal that the airflow rate has to be changed. The desired value is compared with the measured airflow rate that can be measured for example by a differential pressure sensor. The controller acts on the difference between the desired and the measured values, the error. The controller tries to bring the error to zero in the best possible way. The controller will send its control signal to a valve and some motor or pneumatic device may open or close the air valve. The external disturbance in this case may be the varying oxygen demand from the microorganisms in the aerator.

Opening or closing an airflow valve means that the pressure in the air pipe will change. A pressure controller is used to keep the pressure constant, despite the disturbances. Again, the structure of the pressure controller looks like Fig. 4. The controller calculates the

difference between the desired pressure and the measured pressure and produces a control signal that will influence the airflow production from a compressor. This means that the pressure controller provides a new setpoint to the compressor.

It is assumed that the compressor has a variable speed drive system. Then the pressure controller has given the setpoint of the speed. The pressure controller will send a signal "increase the speed" in order to increase the pressure and this implicates that the speed controller setpoint is increased. The speed controller of a motor again looks similar to Fig. 4. Basically, the speed controller compares the actual motor speed with the desired speed and attempts to make the difference (error) equal to zero. Still, if the pressure sensor is not satisfied, then the speed setpoint will be further changed until the speed of the compressor is such that the pressure setpoint has been reached.

It is obvious that any wastewater treatment plant contains a large number of local controllers for physical variables like pressures, speeds, levels, liquid flow rates, and airflow rates. It is not at all apparent how each one of them will influence the final product, but all of them have to work satisfactorily in a well-functioning plant.

The control problems at the equipment level are very similar in any process industry, and a wastewater treatment plant is no exception. Almost all these controllers are of PI (proportional + integral) type, that is, the control signal is proportional to the error signal and to its time integral. Such a controller has the form:

$$u = u_0 + K\left(e + \frac{1}{T}\int e\, dt\right)$$

where u is the control signal, u_0 an offset signal, e the error, K the proportional gain, and T the integral time. In a local controller, the tuning of the two parameters K and T is the primary task. A too small K will make the controller response slow while a too large K will make the controller react too quickly. It may also cause instability of the system. The integral part of the controller has one purpose, to finally make the error equal to zero.

The design of feedback controllers has attracted considerable attention in the control literature. Many advanced control algorithms based on for example dynamic models, neural networks, and fuzzy logics have been proposed. However, no convincing evidence has been made available suggesting that these advanced algorithms produce better control performance in wastewater treatment systems than the conventional PID (proportional-integral-derivative) algorithms, which have been used in most practical process control applications (more than 95% of the controllers in a typical paper and pulp industry are PID controllers). Control systems based on simple rules (rule-based control) have also found successful applications.

All measurements on the equipment level are physical measurements, such as levels, pressures, air and liquid flow rates, so the sensor technology is well established [4]. There are literally hundreds of textbooks in control, so just two are selected for the bibliography. The textbooks [5], [6] give a good introduction into control theory applied for process control.

Control of Biological Oxidation

The control actions in the various unit processes will influence the quality of the water more directly. Some examples of important control actions that are of great importance for the quality of the operation of the plant, and thus the effluent water quality are provided. The interested reader may refer to [7] for a detailed description of the biological processes in wastewater treatment.

The Aeration Process

In the biological reactor, *organic matter* is removed by biological oxidation. Microorganisms feed on the carbon and the oxygen in the water. Some of the organic matter is used to maintain the organisms, while the rest is converted into carbon dioxide. The process is very similar to the way in which humans use food (organic matter) to generate energy. The energy is released when the organic matter is converted into carbon dioxide during respiration. Approximately half of the organic matter is used to increase the body mass of the microorganisms, and the rest is converted into carbon dioxide.

Most of the *nitrogen* that arrives at the wastewater treatment plant comes as ammonium (60–80%).

The remainder is predominantly bound to both soluble and particulate organic matter. The nitrogen bound to organic matter is released as ammonium. The particulate material is hydrolyzed and produces soluble organic matter and nitrogen.

The removal of ammonium takes place in two principal stages: nitrification and denitrification. The nitrification process oxidizes ammonium into nitrate, while denitrification reduces nitrate into free nitrogen. The nitrification process is performed by a group of microorganisms called nitrifiers. Nitrifiers are autotrophs, that is, they can use carbon dioxide (which the water contains) to grow, as opposed to the heterotrophic microorganisms, which feed on easily degradable organic matter. Oxygen is a prerequisite for this process. Conditions in which dissolved oxygen is present are called "aerobic conditions."

Dissolved Oxygen Control

It is obvious that the concentration of dissolved oxygen (DO) is crucial for the oxidation of both organic matter and of ammonium. Both these processes take place in the same reactor. If the DO concentration in the aerator is too low, then the growth rate of the organisms will be limited, as illustrated in Fig. 5. If the DO level is very high then the increase of the growth rate is only marginal. Therefore, a too high DO level will make the operating costs too high.

To begin with, it is assumed that the desired DO concentration is constant. The microorganism growth rates will increase for an increasing organic or ammonium load. This can be noticed as an increasing oxygen uptake rate (OUR). In other words, if the load increases, then the DO concentration will decrease due to the increase of the oxygen uptake rate.

The control of aeration has been the subject to considerable research since 1970s, when the dissolved oxygen (DO) sensors reached a level of robustness and precision suitable for feedback control [2]. Today, the control of DO to a setpoint is considered a mature technology from the methodological point of view. Remember, that the actuators are crucial. Thus, the compressor has to allow a variable airflow that is required by the control system. Still there may be

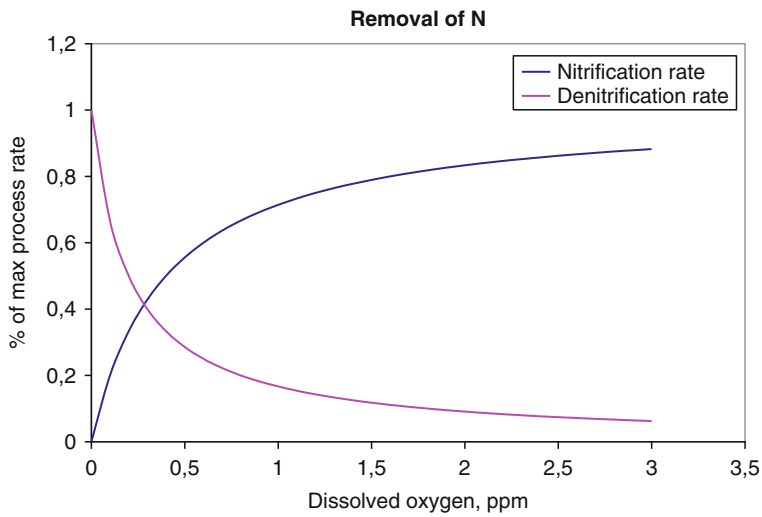

Water and Wastewater Operation: Instrumentation, Monitoring, Control and Automation. Figure 5
The principal behavior of the growth rate of microorganisms as a function of the DO concentration. For aerobic microorganisms the growth rate will increase with the DO concentration, while for anoxic organisms the growth rate is highest for an oxygen-free environment

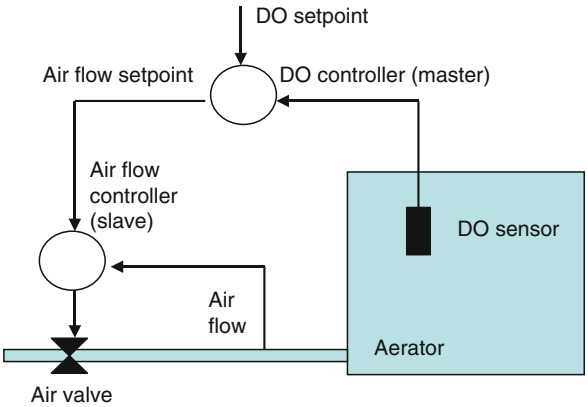

Water and Wastewater Operation: Instrumentation, Monitoring, Control and Automation. Figure 6 Structure of a standard dissolved oxygen (DO) cascade control loop

inadequate capacity of the blowers for very high loads. From a control point of view, this is a common problem: The control variable most often has a lower and upper bound.

Figure 6 illustrates the structure of a typical DO control system.

A DO controller is based on the measurement of the DO concentration in the reactor. It is, for simplicity, assumed that the reactor is a completely mixed aerator. Then the DO sensor will represent the concentration in the whole aerator. A too low DO concentration has to be compensated by an increase in the airflow rate. Consequently, a too high DO concentration will be decreased by decreasing the airflow rate. In the control system, the DO concentration is compared with the DO setpoint and the DO controller (the master) will calculate the necessary airflow change required to change the DO concentration toward the desired value. However, the DO controller does not directly manipulate the air valve. Instead, the desired airflow is given as a setpoint to a second controller, the airflow controller (the slave). This controller receives the airflow rate measurement and compares it with the desired airflow. This difference will then make the actuator (a compressor or a valve) change the airflow to the desired value. The loop is called a *cascaded control loop* and is the standard configuration in most DO control systems.

Dissolved Oxygen Control Based on Ammonia Measurements

The oxidation of ammonia via the nitrifiers is a slower process than the oxidation of the organic matter. This means that the organic matter will disappear faster than the ammonia. Therefore, the decrease of the ammonia concentration is of primary interest. With the development of nutrient sensors it has been possible to extend the dissolved oxygen control to allow for an online adjustment of the level of oxygen supply. It means that the appropriate DO setpoint can be determined by online ammonia measurements. For details, [1], [2], [3] should be referred to.

If the aerator is designed like a plug flow reactor then the ammonia concentration is high at the inlet and will gradually decrease toward the outlet. If the ammonia concentration approaches zero well before the outlet, then the operation has been too ambitious and the last part of the reactor is not needed for the oxidation process. This behavior can be corrected with DO control. If the DO setpoint is lowered, then the growth rate of the nitrifiers will be slightly smaller. Thus, the DO setpoint should be decreased so much that the ammonia will approach zero close to the inlet. As a consequence, the energy consumption will decrease.

Conversely, if the ammonia does not approach zero at the outlet there may be several reasons. The first one to be tested is if the DO setpoint has been too low. Then the setpoint can be increased (but only to a maximum value) to ensure that the growth rate of the organisms has been sufficient. If the ammonia still does not approach zero, then the aerator is overloaded at that time and the nitrification capacity is insufficient.

A DO setpoint controller can be a simple PI controller. The setpoint of the controller is the desired ammonia value at the outlet of the aerator. The controller produces a control signal, which will serve as the desired DO setpoint. This signal is then sent to the DO control system (Fig. 6). Now the DO setpoint becomes a time-varying value and no longer a fixed value given by the operator. The resulting controller has become a hierarchical

structure of three controllers working in cascade by the master–slave principle.

This kind of ammonia controller DO setpoint has been introduced in many plants. The energy savings can be significant, especially during low load periods. In the experiments reported in [8], the savings were 28% compared to the parallel line where a constant DO setpoint was applied. This corresponds to a significant part of the operating costs and can motivate the extra cost of an ammonia analyzer.

Phase Length Control in Sequential Batch Reactors

Sequential batch reactors (SBRs) are quite popular in many places and they offer interesting control opportunities. During the biological oxidation phase, there is no influent to the reactor. As a result the organic matter content will decrease with time. Likewise the ammonia concentration will decrease as a function of time, but slower than the organic matter. The ammonia concentration as a function of time looks like the ammonia concentration as function of the reactor length in a plug flow reactor. Ammonia is oxidized to nitrite and then to nitrate, so the decrease in ammonia corresponds to an increase in nitrate concentration.

A great advantage with an SBR compared to a continuous flow reactor is that the ammonia concentration change can be measured online with just one sensor. The oxidation process is completed when the ammonia concentration approaches zero.

From a control point of view, there is an even more attractive way to determine the phase length of the oxidation in the reactor. A DO control system will serve the same purpose in an SBR as in a continuous flow reactor. Now it is assumed that the DO is to be kept constant during the oxidation phase. In the beginning, the oxygen uptake rate is high. Consequently, the required airflow rate is high. As the reaction goes toward completion the required airflow rate will decrease gradually and when the ammonia has been oxidized then the air flow demand will no longer decrease but will approach a constant low value. This behavior can determine the end of the oxidation phase.

If the phase length of an SBR is controlled by a timer, as in open loop control, then the completion of the reaction cannot be guaranteed. As a result, many SBR operations are made with a safety margin. This means that the ammonia level approaches zero well before the end of the oxidation phase. This of course will cost money, both in terms of energy and – more important – in terms of lower plant capacity.

Control of Denitrification

In the denitrification process nitrate is converted into free nitrogen gas. The denitrification process is a reduction process and is performed by heterotrophic microorganisms, denitrifiers. They are the same type of organisms that use oxygen to oxidize organic matter when oxygen is present. Conditions in which oxygen is not present are called anoxic. Under such conditions the heterotrophic organisms can convert organic matter and nitrate into free nitrogen, carbon dioxide, and increased body mass.

Nitrification and denitrification cannot take place at the same time, since the former is aerobic and the latter is anoxic. Treatment plants are therefore designed to allow these processes to occur either in different places (as in a continuous flow system) or at different times (as in a sequential batch reactor).

The concentration of dissolved oxygen also governs the denitrification process, and the denitrification rate will be hindered by any oxygen present, as illustrated in Fig. 5. Therefore, it is extremely important to prevent oxygen from entering the anoxic process. Oxygen can accidentally enter such an environment via the surface of water, via recirculated water from the aerobic process tanks or from filter backwashing.

The denitrification requires not only nitrate but also easily degradable organic matter. Therefore, it must take place where the organic matter is

present. Since the inlet water contains a high concentration of organic matter the denitrification can paradoxically be placed before the nitrification. From the outlet of the nitrification process, nitrate-rich water is recirculated into the anoxic reactor.

First, consider a plug flow like anoxic process with continuous flow. The concentration of nitrate will decrease along the reactor and should approach zero toward the end of the anoxic reactor. The outlet concentration can be measured with a nitrate sensor. As in the aerobic system, if the concentration approaches zero well before the outlet, then there is an overcapacity. In this case, the control action is different than for the aerator.

If the nitrate concentration in the anoxic reactor has approached zero before the outlet, then the recirculation flow rate of nitrate-rich water can be increased until the nitrate concentration approaches zero close to the anoxic reactor outlet. In this way, the capacity of the anoxic reactor can be increased. Similarly, if the nitrate concentration is too high at the outlet of the anoxic zone then too much nitrate-rich water has been recirculated and the recirculation flow rate must be decreased. More details are found in [8].

Nitrate sensors are commercially available today, so a control system using this information can be readily installed. The setpoint of the controller is simply the desired nitrate concentration value close to the anoxic reactor outlet. The control signal is connected to the speed controller of the recirculation pump.

In a sequential batch reactor, the phase length of the denitrification can be readily controlled. A single nitrate sensor can measure the nitrate concentration. When it approaches zero the anoxic phase is completed. More results on phase length control in SBR systems are found in [9].

The redox potential (oxidation-reduction potential, ORP) contains certain distinctive features that can be used for denitrification control. Denitrifying activity has been found to decrease with an increased redox potential that corresponds to an increased oxygen concentration. The relationship between denitrifying activity and the redox potential has been found to be more or less linear. However, during transient conditions the relationship may be far from linear. There can be a distinct change in the slope of the redox when the nitrate has been consumed, but there is much debate about the efficiency of this measurement, especially under transient conditions. However, a lot of results have been reported, see [10].

Monitoring

To track the current process operational state via the instrumentation is called *monitoring*. Monitoring has to start with the validation of measurement data. Even reliable instrumentation can fail during operation, which can have serious consequences if the instrumentation is used in closed loop control. There are many data screening methods that should be applied, see [1, 2]. Missing data have to be detected, limits of the signal amplitude and its rate of change should be tested, and outliers should be identified. If a signal is expected to be constant then the variability of the signal can give information. Deviations of the signals larger than $\pm 2\sigma$ and $\pm 3\sigma$ from the mean should be noted. It is obvious that deviations large than 3σ ought to be observed carefully and suitable operations have to be implemented.

In some cases, it is possible to perform cross-validation on measurements from more instruments if any correlation is expected, [1, 11]. If the confidence in a measurement decreases, it may be possible (on a short-term basis) to use an estimated value, but eventually control must be set to a default scheme until confidence in the measurement has been restored.

In a sophisticated treatment plant there is a huge data flow from the process. More instrumentation and new instrumentation development will further provide more data. Unlike humans, computers are infinitely attentive and can detect abnormal patterns in plant data. The capability of computers to extract patterns (useful information) is rarely utilized beyond simple graphing. Information technology is not commonly

used to encapsulate process knowledge, that is, knowledge about how the process works and how to best operate it. Process knowledge is typically built up from the experience of operators and engineers but all too often disappears with them when they leave. If process knowledge can be encapsulated, then not only is it retained but the computer can also assist decision-making in plant operation. The potential of substantial operator support for diagnosis and for corrective actions is there and has been demonstrated, but it needs to be adopted by the water and wastewater industry.

The early detection and isolation of faults in the biological process are very effective because they allow corrective action to be taken well before the situation becomes unfavorable. Some changes are not very obvious and may gradually grow until they become a serious operational problem.

Most signals are corrupted by noise, coming either from the instrument itself or from the process. Such noise should be eliminated and signal processing offers many methods, both simple and sophisticated. A simple moving average is often used, but more sophisticated methods can offer much better possibilities to extract information from a noisy signal.

There are many variables that are not directly measured but still of great interest. Here two examples, oxygen uptake rate and nitrification rate, are discussed.

The oxygen uptake rate (OUR) is a function of the biological oxidation of both organic matter and of ammonia nitrogen. It is obvious that the OUR has a major influence on the DO mass balance in the water, and an increase of the OUR must be compensated by an increase in the airflow rate. From a simple mass balance of DO the OUR can be calculated from the airflow rate, the oxygen transfer rate (from gaseous to dissolved oxygen), and from the DO concentration. This makes it possible to track the activity of the organisms in the biological reactor [2].

The reaction rate can be readily calculated in an SBR. Having just one ammonia analyzer makes it possible to track the ammonia concentration as function of time. From this information, it is possible to calculate the rate of change of ammonium. This in turn can inform the operator about the performance of the nitrification. Full-scale experiences are reported in [12].

Plant Wide Control

There are several driving forces that motivate the challenge to integrate all wastewater operations in a drainage area. From a European perspective the need for integrated modeling and control has increased dramatically by the EU-Water Framework Directive, which forms a basis for water policy for the EU and associated countries. It focuses strongly on ecological criteria and strategic integrated management. The system boundaries are extended to include river management at a basin scale as well as point-source and diffuse-source pollutions. A new set of integrated and harmonized tools supporting the intention of the WFD is required.

Instrumentation, control and automation (ICA) play an important role for the integration and concepts like *integrated* control, *system-wide* control, and *plant-wide* control are often mentioned. Both the sewer system and the wastewater treatment plant (WWTP) have an impact on the receiving water. Combined sewer overflows (CSOs) as well as the wastewater treatment effluent will influence the quality of the receiving water, the former at discontinuous events and the latter on a continuous basis. Here the concept of plant-wide control is defined as the combined sewer and WWTP control and operation. The objective is to make maximum use of the system capacity in order to meet large disturbances, where the ultimate purpose is to minimize the combined load to the receiving water.

For the sewer the goal is to minimize the amount of CSO. The aim of the control of the WWTP is to satisfy the effluent requirements while minimizing the operational costs [2]. During storm conditions, these goals may be difficult to reach. It is obvious that the control of the sewer system – isolated from the WWTP operation – will lead to suboptimal solutions. If the goal of the sewer operation is to minimize the CSO, the WWTP may soon be overloaded. The result of such an overload is firstly a short-term impact due to the increased effluent

pollution. Then a possible washout of organisms may cause a long-term impact by making the WWTP operation less efficient during an extended period of time.

In order to implement plant wide control, the interactions between the system parts and their dynamic characteristics have to be understood. This includes choosing the best locations of sensors and actuators, which is the basis for the control structure. ICA has a large impact on integrated operation and compromises have to be made when integration of different unit operations is getting realized. Modern plant computer systems allow a wide distribution of control but this is not always met by corresponding control structures.

Integration aims at minimizing the impact on the receiving water, while ensuring a better resource utilization. The system resilience is an important factor. This includes its ability to attenuate disturbances, but should also reflect its sensitivity to major disturbances or even purposeful and harmful attacks. In the integrated approach, the ultimate goal is to formulate some criterion for the receiving water and its ecological quality while satisfying various economic and technical constraints. There is a great challenge to relate this performance to the plant effluent and possible sewer overflow. Performance measures of the plant operation that relate effluent quality to the resources that are needed to obtain it, such as energy, chemicals, and other material and operating costs, are needed. This is not yet solved satisfactorily, but promising research is in progress, such as [13]. Models are getting developed to find strategies to dynamically find maximum WWTP loading according to continuous monitoring and prediction of the operational state. Another aspect is storage management (in the sewer system and in retention tanks), not only during storms but also during normal operations. By mixing different types of wastewater to compensate, for example, for nutrient deficit or overload the capacity of the plant can be maximized.

All integration means some kind of compromise. This is apparent and integrations at various levels have been applied for a long time. If there were no interactions, then the individual optimization of each subprocess would be the best strategy. Having couplings in reality means that an integrated approach is better than if each one of the processes were controlled separately. Another way to phrase the compromise is to call it a multi-criterion index: Various performances have to be weighted and compared with each other. This is a common approach in integrated water management [14]. The idea is illustrated with some examples:

- The interaction between the aerator and the settler is a classical integration problem, reflected in the compromise that has to be done in return sludge flow rate control.
- The anoxic zone in a pre-denitrifying plant interacts closely with the nitrifying aerator. Oxygen-rich water is recirculated from the aerator to the anoxic zone. The DO level has to be a compromise between sufficiently good nitrification and denitrification. This has been discussed in Control of Biological Oxidation and Control of Denitrification.
- Recycle streams interconnect various parts of a treatment plant. As noted in Incentives for Control, supernatants from the sludge treatment are most often highly concentrated in nutrients and have to be synchronized in time with the plant influent load.
- The target for the sludge production is not the same in different plants. Sometimes the target is to maximize the biogas production, at other plants the sludge production needs to be minimized.
- In the combined sewer and WWTP operation, the individual system operations are sometimes in conflict, so the overall goal of minimizing the load to the receiving water has to overrule the individual goals [14].

Future Directions

ICA will play an increasing role in wastewater treatment systems. It has been noted that the introduction of ICA can increase the capacity of a treatment plant, both a continuous flow system and a sequential batch reactor system. To meet future environmental and efficiency demands it is needed to increase the integration of plant design

and operation. Today, most often the ICA is added to an already existing design, which often leads to insufficient performance.

The instrumentation development will favor more implementations of control systems and lead to more consistent and economical operation of the treatment plants. Furthermore, the actuator equipment has to get more attention. Variable speed control is a proven technology today, but often not observed by the designers. Furthermore, efficient design of pumps and compressors is a prerequisite for economic operation of the plants.

Today most design is based on safety factors for the operations and the disturbances to the plant. There is a clear ambition to gradually make the design more model based, where various risk factors can be taken into consideration. This will result in a better coupling between design and operation.

Plant wide control still needs to be developed. More stringent energy consumption requirements will be one driving force for this development. In Plant Wide Control, the compromise of sludge production was mentioned. A wastewater treatment plant not only consumes electrical energy. It can also produce energy as biogas in the anaerobic digestion. This will immediately require a compromise between the biological oxidation and the anaerobic digestion. The organic matter in the influent is needed to some extent for the nitrification and the denitrification. However, in order to maximize the biogas production as much organic matter as possible should bypass the aerobic oxidation and be forwarded to the digester. Thus, a plant size production planning will be required.

Today many of the unit processes in the wastewater treatment plant can be controlled, but methods and criteria need to be further developed to achieve the integration of unit processes within the plant and to further integrate the plant into an urban water treatment system.

Bibliography

1. Olsson G, Nielsen MK, Yuan Z, Lynggaard-Jensen A, Steyer JP (2005) Instrumentation, control and automation in wastewater treatment systems. Scientific and technical report No.15, IWA Publishing, London, UK, ISBN 1-900222-83-3
2. Olsson G, Newell B (1999) Wastewater treatment systems. Modelling, diagnosis and control. IWA Publishing, London, ISBN 1-900222-15-9
3. Olsson G (2008) Process control. In: Henze M, van Loosdrecht M, Ekama GA, Brdjanovic D (eds) Biological wastewater treatment – principles, modelling and design. UNESCO, IWA Publishing, London. ISBN 9781843391883
4. Vanrolleghem PA, Lee DS (2003) On-line monitoring equipment for wastewater treatment processes: state of the art. Water Sci Technol 47(2):1–34
5. Marlin TE (2000) Process control. Designing processes and control systems for dynamic performance, 2nd edn. McGraw-Hill, New York. ISBN 0-07-039362-1
6. Wilkie J, Johnson M, Katebi R (2002) Control engineering. An introductory course. Palgrave, New York. ISBN 0-333-77129-X
7. Henze M, van Loosdrecht M, Ekama G, Brdjanovic D (eds) (2008) Biological wastewater treatment – principles, modelling and design. UNESCO, IWA Publishing, London, ISBN 1843391880
8. Ingildsen P (2002) Realising full-scale control in wastewater treatment systems using in situ nutrient sensors. Ph.D. thesis, Dept of Industrial Automation, Lund University, Lund, Sweden (access via www.iea.lth.se)
9. Rönner-Holm SGE, Holm NC (2009) Special automation and regulation strategies for enhancing sequencing batch reactor (SBR) performances. Water Sci Technol 60(5):1161–1172
10. Cecil D (2008) The control of denitrification time in full scale by the automatic detection of the low nitrate bend in the redox curve. Water Sci Technol 57(7):1095–1101
11. Lynggaard-Jensen A, Frey M (2002) Use and reporting of data – data handling and validation. In On-line monitoring for drinking water utilities. American Water Works Association Research Foundation, Denver, Colorado (2002). ISBN 1-58321-183-7
12. Rosen C, Ingildsen P, Guildal T, Nielsen MK, Jacobsen BN, Ønnerth T (2004) On-line estimation of nitrification and denitrification capacity at Avedøre wastewater treatment plant. In: Proceedings of the international conference upgrading of wastewater treatment plants (AquaTech2004). Amsterdam, September 30–October 1 2004
13. Benedetti L, Prat P, Nopens I, Poch M, Turon C, De Baets B, Comas J (2009) A new rule generation method to develop a decision support system for integrated management at river basin scale. Water Sci Technol 60(8):2035–2040
14. Vanrolleghem P, Fronteau C, Bauwens W (1996) Evaluation of design and operation of the sewage transport and treatment system by an EQO/EQS based analysis of the receiving water imission characteristics. In: Proceedings of WEF conference urban wet weather pollution. Québec, 16–19 June 1996, pp 14.35–14.46

Water Reclamation System and Micropollutants

Jiang Yong Hu, Se-Keun Park
Division of Environmental Science and Engineering, National University of Singapore, Singapore

Article Outline

Glossary
Definition of the Subject
Introduction
Endocrine Disrupting Compounds
Removal of Endocrine Disrupting Compounds in Membrane Bioreactor Systems
Future Directions
Bibliography

Glossary

Activated sludge process A biological method of wastewater treatment that is performed by a variable and mixed community of microorganisms in an aerobic aquatic environment.

Biodegradation The reaction processes mediated by microbial activity.

Endocrine disrupting compounds (EDCs) An exogenous agent that interferes with the synthesis, secretion, transport, binding, action, or elimination of natural hormones in the body, which are responsible for the maintenance of homeostasis, reproduction, development, and/or behavior.

Hydrophobicity The physical property of a molecule that is repelled from a mass of water.

Membrane bioreactor (MBR) The combination of a membrane process like microfiltration or ultrafiltration with a suspended growth bioreactor.

Micropollutant Pollutant, which exists in very small traces in water.

Sludge retention time (SRT) An operational parameter, which measures how long the sludge can remain in a reactor.

Sorption The action of absorption or adsorption.

Water reclamation The various treatment systems and their process trains, which further treat the used water for different reuse purposes.

Definition of the Subject

Endocrine disrupting compounds (EDCs), sometimes known as "hormonally active agents" or "endocrine modulators," are micropollutants with the potential to elicit negative effects on the endocrine systems of humans and wildlife and are emerging as a major concern for water quality. In the past few decades, more and more chemicals were monitored as the source of estrogenic activity in wastewater and the primary sources of estrogenic activity in wastewater were found to be natural estrogens such as estrone, 17β-estradiol and estriol, and synthetic compounds like 17α-ethinylestradiol, alkylphenols, and alklphenol ethoxylates. EDCs are either partially retained in the sludge, or metabolized to a more hydrophilic but still persistent form, and discharged consistently from the wastewater treatment plant into the receiving waters, thereby causing endocrine disrupting effects to aquatic organisms even at very low concentrations (ng/L). As conventional processes are not able to fully and systematically eliminate EDCs to a satisfactory level, membrane bioreactor (MBR) is considered as a promising technology in water reclamation to achieve further removal of EDCs due to specific design characteristics (such as high sludge age, high biomass concentration, and complete particle and microorganism retention). The MBR, which integrates biological process with membrane filtration, is an effective water reclamation process developed for recent decades and surpasses the limitations of the conventional activated sludge process. Therefore, with respect to the wastewater reclamation and reuse, elimination of EDCs in wastewater is typical state-of-the-art application of the MBR technology.

Introduction

There is a growing concern worldwide for the potential effects of endocrine disrupting compounds (EDCs). These EDCs can mimic or modulate the action of a particular natural hormone in human and wildlife. They can also attach onto receptors intended for a particular hormone, interfering and altering the normal binding of the hormone to its receptors.

Many adverse health and environmental problems are found to be linked to EDCs. Colborn et al. [1] observed various disturbing consequences relating to

the alteration and interference of endocrine functions in humans and wildlife. These effects of EDCs depend on several factors such as its type, dosage, and exposure duration. The adverse effects caused by EDCs have raised concerns pertaining to the levels of EDCs present in the environment. To facilitate the excretion of urine, the female body primarily excretes estrogens in a biologically inactive form as sulfate and glucoronide conjugates, which may exist in the influents and effluents of sewage treatment plants (STPs) [2]. Others have also reported that estrogenic activities are present in sewage and treated effluents [3, 4]. These treated effluents are often discharged into surface water bodies such as rivers, seas, or lakes, to which humans and wildlife are often exposed.

EDC concentrations in treated effluents are sufficient to induce vitellogenin biosynthesis in male fish [5], alterations of endocrine reproductive systems, decreased fertility and growth, poor hatching, egg shell thinning and abnormal thyroid function for birds, reptiles, and mammals [6, 7], and malformations of newborns, undescended testicles, abnormal sperm, low sperm counts, abnormal thyroid function, breast cancer, testicular prostate cancer for humans [8–10]. A classic example is the feminization of male fish like trout downstream of sewage treatment plant in some areas of England and the USA [5, 11].

The EDCs present in the sewage can be categorized into two main groups, namely, estrogens and alkylphenols. The predominant estrogens can be subdivided into natural estrogens and synthetic estrogens. Natural estrogens such as estrone (E1), 17β-estradiol (E2), and estriol (E3) are present in the human excreta whereas synthetic estrogens such as 17α-ethinylestradiol (EE2) can be found in contraceptives. Alkylphenols like bisphenol A (BPA) and nonylphenol (NP) are released from manufacturing industries. Natural estrogens, i.e., E2 and E1, are effective at the nanogram per liter level [12, 13], while most other EDCs are biologically active at the microgram per liter level. For example, levels reported to affect fish were in the range of 1–4 ng/L for EE2 [14, 15], 1–10 ng/L for E2, and 1–10 μg/L for alkylphenol in vitro [16], and in vivo [13].

To investigate whether the effluent of most STPs contains EDCs and whether these EDCs lead to the above effects, several investigators have attempted to quantify the concentrations of those compounds in the effluent of municipal or industrial STPs. The steroid estrogens reportedly ranged from 3 to 9 ng/L for E1 [4, 17], 0.1 to 5 ng/L for E2 [18, 19], and 0.1 to 9 ng/L for EE2 [4, 17, 20], and 4-NP and BPA were detected in the effluent at levels from 0.16 to 0.36 μg/L [21].

It is clear that STPs are not able to treat the wastewater to a satisfactory level. As a result, methods to improve their removal efficiency should be explored. Membrane bioreactor (MBR) is an attractive option mainly due to its improved effluent quality. Holbrook et al. [22] studied a membrane bioreactor pilot plant and a STP receiving the same domestic wastewater. The influent 17β-estradiol equivalent concentration (EEQ) was 16.25 ng/L, while the effluent EEQ was 4.5 ng/L for MBR and 7 ng/L for STP, on average. It showed that the MBR achieved a higher reduction in EEQ concentrations than the conventional treatment system.

MBR system is a biological treatment process that combines with membrane separation process in order to biologically treat wastewater and physically separate solid and liquid in an integrated step. The integration of biological water treatment with its filtration across porous membranes, driven by a pressure difference, was first applied for the separation of activated sludge by a membrane and its recycling to the aeration tank [23]. Its technological and economical efficiency (including the decrease in the membrane cost) have improved steadily since, allowing for more practical applications. Subsequently, MBR has been extensively adopted from the mid-1990s for the treatment and reclamation of municipal and industrial wastewaters.

Application of membrane separation techniques for biosolid separation can overcome the disadvantages of the sedimentation tank and biological treatment steps. The membrane offers a complete barrier to suspended solids and yields higher quality effluent. The outstanding merits of MBR over the conventional activated sludge systems include excellent quality of treated water, small footprints, complete solid–liquid separation, high biomass concentration, prolonged sludge ages, less sludge production, and better process reliability in the bioreactor [24, 25]. The main advantage of MBR system is a complete retention of the biomass within the bioreactor as separation is achieved via membrane filtration. Thus, MBR can be operated

at much higher biomass concentrations providing a higher biological activity per volume. A very long sludge retention time (SRT) can also be maintained, allowing for the establishment of a more diverse community with broader physiological capabilities. This feature is of particular importance for EDCs, which usually need high biomass and long periods for their complete biological degradation/transformation to harmless products.

It is generally agreed that MBR performs better than conventional STP for biological removal of bulk organic matter. Yet, the fate of EDCs during MBR treatment and the mechanisms relevant for their removal are much less documented. This article reviews the removal of EDCs during wastewater reclamation applying MBR and STP, as well. Biodegradation of EDCs is discussed as a major mechanism, as well as their removal by sorption onto sludge.

Endocrine Disrupting Compounds

General Characteristics of EDCs

Natural estrogens E1, E2, and E3 have an aromatic A ring, basic C18 skeleton estrane and no carbon side-chain at C17 (Table 1). These are composed of the four rings: a phenol, two cyclohexanes, and a cyclopentane. The difference in the compounds within the C18 group lies in the configuration of the cyclopentane ring (ring D) at positions C16 and C17. For example, E1 has a carbonyl group on C17, E2 has a hydroxyl group on C17, and E3 has two hydroxyl groups on C16 and C17. Hydroxyl and carbonyl functional groups make them capable of participating in hydrogen bonding as a proton donor or proton acceptor species. Table 1 shows the physical and chemical properties and the biological potency of estrogens. From the octanol–water partition coefficient (log K_{OW}) values, E1 and E2 are considered to be more hydrophobic than E3. The estrogenic activity of E2 is much stronger than E1 and E3 as revealed by the results of yeast assay [27] and feminization of male fishes [28].

The synthetic estrogen EE2, which is used for estrogenic deficiencies treatment and oral contraceptive pill, has lower solubility and is somewhat more hydrophobic than the other steroid estrogens (log K_{OW} values shown in Table 1). The major difference between EE2 and the natural estrogens is the long persistence in the environment with a dissipation time in the order of 20–40 days in river systems [29]. Also, EE2 is known as an extremely potent estrogen, and its strong estrogenicity was shown in both in vitro and in vivo studies [15].

Estrogens are usually released from conjugated forms with glucuronide (G) and/or sulfate (S) groups linked to the H in the –OH group of the steroid ring. It is known that most of estrogen conjugates exist in influent and effluent of STP with high frequency for both glucuronide and sulfate estrogens. However, the conjugated estrogens have low estrogenic potency compared with the parent compounds [30].

BPA and NP are widely used in a variety of industrial and residential applications and stimulate production of the biomarker of estrogenic activity, vitellogenin, in male fish [31–33]. BPA and NP usually possess similar endocrine disrupting activities due to phenyl ring in their chemical structures.

BPA is a monomer utilized to manufacture polycarbonate plastic and epoxy resins. It is a moderately water-soluble compound (300 mg/L at 20°C) and dissociates in an alkaline environment (p*K*a 9.9–11.3). Numerous toxicological and biochemical studies have confirmed that BPA has estrogenic properties and an agonistic effect toward the estrogenic receptor. Estrogenicity of BPA was first reported in 1936 by Dodds and Lawson and subsequently identified as a result of studies on the release of estrogenic material from autoclaved polycarbonate flasks [34]. The estrogenic activity of BPA is less potent than that of E2 in in vitro assays [34–36]. However, the results of in vivo studies on the estrogenicity of BPA are conflicting in terms of the effective dose.

NP is a chemical substance with a phenolic ring and an attached lipophilic linear nonyl chain or, more usually, branched nonyl group. 4-NP, in which the side chain is attached to the carbon directly opposite the hydroxyl group, is the most common member of NP family. NP is a hydrophobic compound with a log K_{OW} of 4.5 and low solubility in water. This exhibits minor estrogenic potency. In stimulating estrogenic activity, NP was 1,000–100,000 times less potent than E2. In vitro studies showed that NP could activate the estrogen receptor with a potency of 5,000–7,000 times lower than that of E2 [37].

Water Reclamation System and Micropollutants. Table 1 Physicochemical properties and estrogenic activity of estrogens

EDCs	Chemical structure	Molecular weight (g/mol)	Water solubility at 20°C (mg/L)	Log K_{ow}	E2 relative potency (YES)	E2 relative potency (E-screen)
Estrone (E1)	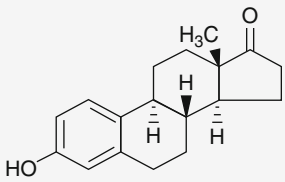	270.4	13	3.43	0.38	0.01–0.096
17β-Estradiol (E2)	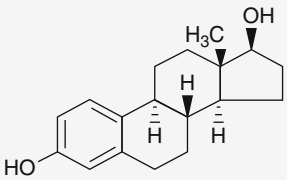	272.4	13	3.94	1.0	1.0
Estriol (E3)	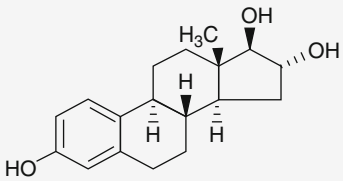	288.4	13	2.81	0.024	0.1–0.25
17α-Ethinylestradiol (EE2)	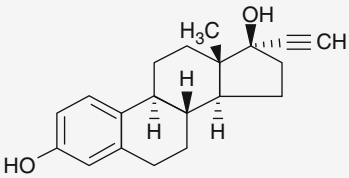	296.4	4.8	4.15	1.19	0.91–1.0
Bisphenol A (BPA)	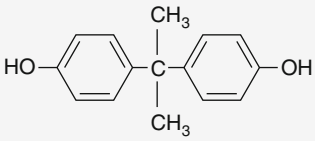	228.0	300	3.40	1.0×10^{-5}	1.26×10^{-5}
Nonylphenol (NP)	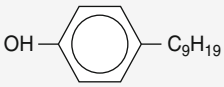	220.0	5.43	4.48	1.7×10^{-4}	7.8×10^{-5}

Source: Teske and Arnold [26]

Estrogenic potencies from yeast estrogen screen (YES) bioassay data and/or the E-Screen bioassay

Occurrence of EDCs and Their Conjugates in Aquatic Environment

The presence of EDCs in the environment has become a concern because they may interfere with the reproduction of man, livestock, and wildlife. So far, a number of studies have reported the occurrence of EDCs in measurable concentrations (ng/L or μg/L) in wastewater, surface water, groundwater, and even drinking water. Various reported concentrations for major EDCs in these different aquatic environments are listed in Table 2. The highest concentrations of EDCs have been observed in wastewaters. Some studies showed a very wide distribution of EDCs with some sporadic occurrence [17, 44, 45, 54, 65]. The levels of natural EDCs appear to be much higher than those of synthetic estrogen EE2. In the studies, E1 was detected frequently with high concentrations in effluent of STPs [17, 55, 68, 69]. In some cases, EE2 has been reported to more frequently occur in the effluents of STPs with concentrations ranging from <5 to 178 ng/L [54]. Obviously, alkylphenol chemicals are present at much greater concentrations than estrogens in aqueous environmental samples. Some research exceptionally showed that natural and synthetic estrogens as well as alkylphenols can be detected in drinking water samples at pg/L or ng/L levels [40].

From Table 2, it can be seen that the EDCs pass through STPS without being completely removed and remain with fluctuating concentrations in effluent. These discharges from STPs may be the main reason for the wide distribution and occurrence of EDCs in surface waters, ground waters, and even in drinking waters. In particular, concentrations of some EDCs such as E1 are higher in effluent than in influent [17, 68, 69], probably due to microorganism-induced transformation (e.g., from E2 to E1). Incomplete removal and degradation of EDCs by existing STPs not only results from the fluctuation of EDC levels in the influent, but the processes of the STPs, and as well as operational conditions [70].

A number of past studies have shown the estrogenic activity in STP effluents using fish or other biological assay systems [12, 71]. In the study carried out by Purdom et al. [12], EE2 could induce vitellogenin (VTG) in male rainbow trout at concentration as low as 0.1 ng/L. In addition, Routledge et al. [13] concluded from the dose–response curves in male rainbow trout that the threshold response for VTG production probably occurred between 1 and 10 ng/L for E2, and between 25 and 50 ng/L for E1, respectively. Indeed, alkylphenols can have estrogenic effects in fish at concentrations from 1 to 10 μg/L [13, 14]. Jobling and colleagues [14] showed that these chemicals were also estrogenic in fish, and therefore might be partially responsible for the estrogenic effects (e.g., intersexuality) observed in wild fish. Recent report on VTG induction by 4-NP demonstrates the presence, in different fish species, of a lowest observed effect concentration identifiable by the range of 10–20 μg/L NP [72]. From these findings, it is emphasized that EDCs that are present in sufficient quantity in treated as well as raw wastewater may be discharged with effluents into receiving waters to produce estrogenic effects.

Treatment of EDCs in Conventional Sewage Treatment Plants

Since EDCs have been identified and quantified in a wide variety of environments associated with municipal or industrial STPs effluents, the removal of these substances in these treatment plants is becoming an increasingly important environmental issue worldwide. The activated sludge process is commonly used to treat wastewater in the world. There are many research data suggesting that the activated sludge STPs can remove EDCs during treatment, although its conventional purposes are the removal of bulk organic substances from wastewater. The removal performances for EDCs in activated sludge STPs are in a wide range. The removal occurs mainly through sorption by sludge and subsequent biodegradation [73]. Johnson et al. [74] reported that the activated sludge processes could remove 74% of E1 and 88% of E2. Baronti et al. [17] also reported that the removal rates of E1, E2, E3, and EE2 from wastewater in activated sludge STPs were 61%, 87%, 95%, and 85%, respectively. In the Brazilian activated sludge STPs, E1, E2, and EE2 were eliminated up to 83%, 99.9%, and 78%, respectively [75]. Moreover, efficiencies over 90% have been reported for E1, E2, and EE2 in activated sludge STPs [68, 76]. Johnson and Sumpter [73] have reviewed the literature on the fate of EDCs in activated sludge STPs. They suggested that the activated sludge

Water Reclamation System and Micropollutants. Table 2 Occurrence of EDCs in various aquatic environments at levels of ng/L

EDCs	Wastewater		Surface water	Ground water	Drinking water
	Raw	Treated			
E1	25–132 [17]	2.5–82 [17]	<0.1–3.4 [38]	ND[a]–120 [39]	0.2–0.6 [40]
	44 [41]	17 [41]	0.2–6.6 [42]	ND–4.5 [43]	
	29–670 [44]	Nd–72 [44]	<0.3–7.2 [45]	ND–1.6 [46]	
	19–78 [47]	1–96 [47]	5–12 [48]		
	20–130 [45]	<0.3–11 [45]	1.4–12.9 [49]		
	ND–18.3 [50]	ND–6.7 [50]	<17–38 [51]		
	57.8–83.3 [52]	6.3–49.1 [52]	ND–7.4 [53]		
	4–33 [54]	0–147 [54]	ND–4.6 [46]		
	230–510 [55]	ND[55]	1.1–3.0 [56]		
E2	4.0–25 [17]	0.35–3.5 [17]	<0.3–5.5 [38]	ND–45 [39]	0.2–2.1 [40]
	11 [41]	1.6 [41]	0.6–1.0 [42]	6–66 [57]	2.6 [58, 59]
	35–125 [44]	ND–30 [44]	<0.8–1.0 [45]	13–80 [60, 61]	ND–2.6 [53]
	2.4–26 [47]	0.2–14.7 [47]	2–6 [48]	ND–0.79 [46]	
	17–150 [45]	<0.8 [45]	ND–8.8 [49]		
	22.0 [62]	0.95 [62]	<0.7–1.7 [51]		
	ND–161.6 [52]	ND–5.4 [52]	1.6–15.5 [63]		
	0–11 [54]	0–158 [54]	ND–3.8 [53]		
E3	24–188 [17]	0.43–18 [17]	2–5 [48]	ND–0.16 [46]	
	72 [41]	2.3 [41]	ND–3.3 [49]		
	23–48 [48]	ND–1 [48]	ND–3.1 [64]		
	23–660 [44]	ND–275 [44]	ND–1.7 [53]		
	138–381 [65]	<1–4.9 [65]	ND–1.9 [46]		
	2–22 [54]	0–29 [54]	1.0–2.5 [56]		
EE2	0.40–13 [17]	ND–1.7 [17]	<0.1–4.3 [38]	ND–0.94 [46]	0.15–0.5 [40]
	4.9–7.1 [56]	2.7–4.5 [56]	<0.3–0.4 [45]		
	<0.3–5.9 [45]	<0.3–2.6 [45]	ND–1 [48]		
	3–70 [44]	ND–5 [44]	5.7–30.8 [63]		
	<0.7–14.4 [65]	<0.7–4.1 [65]	0.1–5.1 [40]		
	ND–1.2 [52]	ND–0.6 [52]	ND–4.6 [53]		
	0–2 [54]	0–178 [54]	1.1–2.9 [56]		

Water Reclamation System and Micropollutants. Table 2 (Continued)

EDCs	Wastewater		Surface water	Ground water	Drinking water
	Raw	Treated			
BPA	332–339 [48]	13–16 [48]	<8.8–1,000 [45]	ND–7 [48]	0.5–2.0 [40]
	250–5,620 [45]	<43–4,090 [45]	0.5–14 [40]	ND–930 [46]	5 [66]
	720–2,376 [44]	16–1,840 [44]	ND–600 [46]		
	281–3,642 [65]	6–50 [65]	15–29 [48]		
	88–438 [54]	11–1,054 [54]	65–295 [66]		
	450–3,300 [55]	610–710 [55]	ND–5.7 [67]		
NP	4,194–8,768 [48]	1,120–2,235 [48]	<110–4,100 [45]	ND–3,100,000 [39]	2.5–16 [40]
	240–19,000 [45]	550–1,500 [45]	6.7–134 [40]	ND–1,500 [46]	
	1,570–27,411 [65]	426–4,926 [65]	ND–890 [46]		
	14,728–41,207 [54]	ND–90,043 [54]	1,289–1,466 [48]		
	2,100–4,500 [55]	300–400 [55]	1.3–21.3 [67]		

[a]Not detected

process can consistently remove over 85% of E2, E3, and EE2, but the removal performance for E1 appears to be less and is more variable. Slightly lower removal of E1 is probably due to the conversion E2 to E1 during the treatment and the cleavage of estrogen glucuronides and sulfates (e.g., E1-3G and E1-3S) [41, 77, 78]. In addition to estrogens, removal of BPA and NP by activated sludge STPs has been reported at different degrees in the literature [45, 48, 50, 65, 79]. In particular, a very wide range of the removal efficiency, from 10% to 99% for BPA and 33–93% for NP, is found in the references by Drewes et al. [65] and Clara et al. [79]. Their removal rates in activated sludge process were reported to be dependent on the applied sludge retention time or the mass load to plant.

It is known that natural estrogens initially excreted by humans are mainly in sulfate or glucuronide conjugates (e.g., E1-3S, E2-3G, E3-17G, etc.), and then they are changed to free estrogens. Glucuronide estrogens were reported easily changed to their free estrogens while sulfate estrogens were more recalcitrant to biotransformation [65, 77, 80]. D'Ascenzo et al. [65] reported that estrogen glucuronides spiked into wastewater from a septic tank at 25 μg/L were lost with half-lives of ~6 h and the loss of estrogen sulfates proceeded much slower with half-lives of 2.5 days. Although estrogen conjugates are biologically less active, they are potential sources of active estrogens due to dissociation in STPs or as a result of the input of untreated wastewater directly into surface water. D'Ascenzo et al. [65] examined the fate of estrogen conjugates in activated sludge STPs and observed that E2-3G, E3-16G, and E2-3S were completely removed while a fraction of E1-3G (0.7 ng/L), E1-3S (9 ng/L), and E3-3S (2.2 ng/L) with relatively lower removal rate passed through the treatment system. Lower elimination of E1-3S in activated sludge STPs was also reported in a study by Reddy et al. [2].

In the literature on the fate of EDCs in activated sludge STPs, reported removal percentages for EDCs most often exceed 80%. However, in spite of the considerable removal rates, the low levels of EDCs that are being discharged in the final effluents of activated sludge STPs may still provoke estrogenic effects in fish and other aquatic organisms. It is generally agreed that, in most cases, the estrogens and alkylphenols will not be completely eliminated in activated sludge STPs. So, there is a need for further investigation on treatment processes to achieve EDC concentrations in effluent below estrogenic limits.

Removal of Endocrine Disrupting Compounds in Membrane Bioreactor Systems

General Aspects of MBRs

Membrane processes are regarded as key elements of advanced wastewater reclamation and reuse schemes. MBR is a promising process combination of activated sludge treatment and membrane separation. The bioreactor is operated similar to a conventional activated sludge process but without the need for secondary clarification and tertiary steps like sand filtration. MBR process is generally performed using low-pressure membranes such as microfiltration (MF) or ultrafiltration (UF) that are capable of displaying a barrier effect based on size exclusion, with pore size ranging between 50 and 10,000 nm (MF) and 1–100 nm (UF) [81]. MF and UF membranes assist activated sludge process in MBR. Suspended solids and microorganisms responsible for biodegradation are separated from the treated water by a membrane filtration. Although direct physical sieving effect of micropollutants generally of molecular weight lower than 400 g/mol is of minor importance due to the relatively large pore sizes of MF and UF membranes, hydrophobic substances tend to accumulate onto the sludge, and therefore, they are removed from the effluent.

The membranes can be placed in the external circuit of the bioreactor (known as external MBR) or they can be submerged directly into the bioreactor (known as submerged MBR). The membranes are usually of flat sheet or hollow fiber configuration if placed inside the bioreactor, or multi-tube if placed outside it. In case of the external MBR configuration, the mixed liquor is circulated to a membrane module that is outside the bioreactor, where pressure drives the separation of water from the sludge. The concentrated sludge is then recycled back into the reactor. For the submerged MBR configuration, a suction force is applied to draw the water through the membrane, while the sludge is retained on the membrane surface. Membranes act in the aeration basin as filter and improve the biological treatment of the effluent. A manifold at the base of the reactor diffuses compressed air within the reactor, providing oxygen to maintain aerobic conditions. The air bubbles also function to scour the membrane surface and clean the exterior of the membrane as they rise in the reactor. The submerged configuration is more commonly used for wastewater reclamation than the external configuration because it is less energy consuming and less detrimental for the biomass [82].

MBR treatment of municipal wastewater yields high-quality water with reported removal percentages of 95%, 98%, and 99% (or greater) for chemical oxygen demand (COD), biochemical oxygen demand (BOD), and suspended solids (SS), respectively [83]. This is primarily ascribed to the absolute barrier provided by the membrane but can also be improved by the microbiology. Factors such as high biomass concentration and long sludge ages or SRT could be correlated with the high performance of wastewater treatment. Generally, due to the complete retention of biomass via membrane filtration, MBR is operated at much higher mixed liquor suspended solids (MLSS) concentrations, ranging from 8 to 25 g/L or even more [24, 84, 85], which provide a high biological activity per unit volume. A longer SRT can also be maintained. The sludge age in MBRs is mostly in range of 20–50 days and occasionally more than 100 days in small MBRs where almost no sludge removal may occur [86]. The prolonged SRT operation favors the growth of slowly growing specialized microorganisms, which are able to remove slowly degradable components in the reactor [87]. In a MBR, SRT can be controlled independently from hydraulic retention time (HRT), enabling MBR operation at high SRT and low HRT. The lower HRT allowable for MBR treatment may be a benefit of the higher biomass concentrations and be further supported by the fact that most of the biomass in an MBR occurs in freely suspended form [88]. This provides easier access for substrates as compared to bacteria aggregated into flocs that prevail in conventional activated sludge [89]. Due to the higher MLSS concentrations at a constant volume load, food to microorganism (F/M) ratio is usually lower in MBR. Stephenson et al. [24] reported that F/M ratio of MBR is in the range of 0.05–0.15 kg COD/kg MLSS·d. A lower F/M ratio results in substrate limitation and may force microorganisms to metabolize poorly degradable compounds [88]. This is one explanation why removal of poorly degradable pollutants may be superior in MBR systems and why this can be achieved at lower HRT. Studies on MBR note less sludge production. Bouhabila et al. [90] reported less sludge production ranging of 0.2–0.34 kg MLSS/kg $COD_{removed}$ in MBR as compared with 0.3–0.5 kg

MLSS/kg $COD_{removed}$ in conventional activated sludge process. It has been shown that sludge production is greatly decreased as sludge age increases [89, 91]. Lower F/M ratio and longer sludge age in the MBR are generally used to explain this lower production rate.

It is likely that biomass composition and structure in an MBR is considerably different from a conventional activated sludge. In the literature, the floc size distribution of MBR sludge and conventional activated sludge is reported to be 10–100 μm in membrane bioreactors and 100–500 μm for conventional sludge [92, 93]. Ng and Hermanowicz [94] recently showed that the MBR biomass was composed of smaller, weaker, and more uniform-sized flocs and higher fraction of dispersed microorganisms compared to the conventional activated sludge. The smaller flocs from MBRs could stimulate a higher oxygen and/or carbon substrate mass transfer and thus higher activity levels in the system. The presence of much higher amount of non-flocculating microorganisms could contribute to poorer sludge settling but better organics removal in the MBR. Zhang and coworkers [92] also found that nitrification activities in MBR processes averaged 2.28 g NH_4–N/kg MLSS·h, which was greater than in conventional processes (0.95 g NH_4–N/kg MLSS·h). Many studies have proven that MBR can operate as a high-rate nitrifying technology that can be applied in the nitrification of wastewater containing a high concentration of ammonia nitrogen [95].

MBR process has obvious advantages over the conventional activated sludge processes, e.g., excellent effluent quality, small footprint, less sludge production, and flexibility of operation, and becomes a promising alternative for wastewater treatment. Drawbacks of MBR operation under high MLSS concentration include limitations in oxygen diffusion leading to increased aeration cost, mass transfer limitation, and membrane fouling, which may require frequent membrane cleaning [96]. High solid concentrations may have an influence on sludge viscosity, so affecting the circulation of bulk sludge and the shear stress at the filtration cake surface [97].

MBR Performance in Removal of EDCs

It is clear that conventional processes in STPs are not able to eliminate EDCs to a satisfactory level. As a result, methods to minimize the discharge of those compounds should be explored. MBR is an attractive option due to the potential for increased endocrine disruptor removal. Holbrook et al. [22] studied the EEQ (which is the total concentration of estrogenic active compounds in an environmental sample normalized to that of natural estrogen E2, determined by yeast estrogen screen bioassay) in one pilot-scale MBR and two full-scale STPs receiving the same domestic wastewater and showed that MBR removes estrogenic activity more effectively than STPs. The MBR showed a 73% removal of estrogenic activity from domestic wastewater, which was 10–15% greater than the two STPs examined [22]. A recent study also reported that the MBR has relatively good performance in the removal of estrogenic activity compared to STP [98]. The overall estrogenic activity of MBR effluents was in the range of 0.75 ± 0.44 to 1.24 ± 0.22 ng EEQ/L for pilot-scale plant and 1.60 ± 0.93 to 1.70 ± 0.56 ng EEQ/L for lab-scale system. Those are comparable to those of other effluents, e.g., 2.9 ng EEQ/L from the STP located in Cobis, Italy [17] and 2.5 ng EEQ/L from Penha, Rio de Janeiro [75], especially lower than the values of 10.5 ng EEQ/L from the STP in Frankfurt/Main, Germany [75], and the 6 ng EEQ/L reported by Körner et al. [21]. The observed decrease in overall estrogenicity in MBR may be caused by its process intensification through high biomass concentration.

Estrogenic activity is removed with degradation and/or transformation of the parent estrogen compound. There have been some studies on the fate and removal efficiency of EDCs in MBR systems. Reports on EDCs removal by MBRs are listed in Table 3. The literature data suggest that MBR has good removal capacities for EDCs, although removal efficiencies differ from different reports. In a study by Joss et al. [68] on removal of E1, E2, and EE2 in various municipal STP and MBR, the results show comparable removal of EDCs in the MBR (96% for E1, >98% for E2, and >75% for EE2) and in three conventional activated sludge systems (49–99% for E1, 88–98% for E2, and 71–94% for EE2). For E1 and E2, degradation activity was seen to be higher in the MBR sludge than in the conventional activated sludge by a factor of 2–3. They explained this difference in activity by the longer sludge age (30 days in MBR vs. 12 days in STP) and smaller floc size (10–100 μm in MBR vs. 100–500 μm in STP).

Water Reclamation System and Micropollutants. Table 3 Summary of some studies on fate and removal efficiencies of EDCs in MBR systems

EDCs	MBR	Operating factor conditions	Removal (%)	Effluent concentration (ng/L)	References
E1	Submerged; MF-UF	SRT = 30 days; MLSS = 0.22–0.29 g/L	96	2.4 ± 0.5	[68]
	External; UF	SRT at 10°C = 22, 40, 82 days; HRT = 0.5–4 d; MLSS = 6.3–11.8 g/L	27.6–100	ND[a]–21	[44]
	Submerged; UF	SRT = 40 day; MLSS = 10–15 g/L	NA[b]	ND–1.2	[99]
E2	Submerged; MF-UF	SRT = 30 day; MLSS = 0.22–0.29 g/L	>98	<0.5	[68]
	External; UF	SRT at 10°C = 22, 40, 82 days; HRT = 0.5–4 d; MLSS = 6.3–11.8 g/L	95.2–100	ND–6	[44]
	Submerged; MF	MLSS = 2.7–3.5 g/L; pH = 4.3–8.0	98–100		[100]
	Submerged; UF	SRT = 40 days; MLSS = 10–15 g/L	NA	ND–1.1	[99]
E3	External; UF	SRT at 10°C = 22, 40, 82 days; HRT = 0.5–4 d; MLSS = 6.3–11.8 g/L	99.7–100	ND–1	[44]
EE2	Submerged; MF-UF	SRT = 30 day; MLSS = 0.22–0.29 g/L	>75	<0.5	[68]
	External; UF	SRT at 20°C = 11, 20, 40 days	60–70	1–3	[101]
	External; UF	SRT at 20°C = 11, 20, 40 days	25–80	NA	[102]
	External; UF	SRT at 10°C = 22, 40, 82 days; HRT = 0.5–4 d; MLSS = 6.3–11.8 g/L	33.3–100	ND–4	[44]
	Submerged; MF	MLSS = 2.7–3.5 g/L; pH = 4.3–8.0	60–70	NA	[100]
	Submerged; UF	SRT = 40 day; MLSS = 10–15 g/L		0.9–1.6	[99]
BPA	External, UF	SRT at 20°C = 11, 20, 40 days	97–99	NA	[102]
	External; UF	SRT at 10°C = 22, 40, 82 days; HRT = 0.5–4 d; MLSS = 6.3–11.8 g/L	92.7–99.3	16–158	[44, 79]
	Submerged; MF	MLSS = 2.7–3.5 g/L; pH = 4.3–8.0	50–100	NA	[100]
	Submerged; MF	HRT = 6 h; MLSS = 13.6 g/L	97.5	1.22	[103]
	Submerged; UF	SRT = 40 day; MLSS = 10–15 g/L	NA	2.5–12.6	[99]
	Submerged; MF	SRT = 350 d; HRT = 4–8 h; MLSS = 5–13 g/L	>93.7	<0.08	[104]
NP	External, UF	SRT = 10, 27, 55 days; HRT = 0.5–4 d; MLSS = 6.3–11.8 g/L	85–91	297–482	[79]
	Submerged; MF	HRT = 6 h; MLSS = 13.6 g/L	>98	<0.88 ng/L	[103]
	Submerged; MF	HRT = 10 h; MLSS = 11–20 g/L	96	<2 ng/L	[104]

[a]Not detected
[b]Not available

In their study, MBR sludge is characterized by higher specific surfaces. Clara et al. [44] also showed that high removal rates (80–100%) could be achieved for E1, E2, E3, EE2, and BPA in MBR systems operating at different SRTs. They noted that although high removal rates could be achieved in conventional STP operating at high SRT, the MBR allows achieving high SRT within a compact reactor, resulting in higher volumetric

reaction rates as compared to the conventional STP. Zuehlke et al. [105] studied the performance of two MBR pilot plants (hollow fiber polyvinylidene fluoride membrane modules with pore size of 0.2 μm and membrane area of 9 m^2) operated in parallel to a full-scale STP fed with the same raw municipal sewage. More than 90% of E1 and E2 and about 80% of EE2 were removed by the conventional STP, respectively. Removal rates could further be improved by MBR; E1 and E2 were removed up to 99% and EE2 up to 95%. Especially for EE2, in most cases, its concentrations in MBR effluents were reported to be below or approximately 1 ng/L. Using a pilot-scale MBR, Spring et al. [99] found that MBR was more efficient at removing E1, EE2, and BPA to low ng/L levels than STP receiving the same wastewater. Concentrations found in the MBR effluents ranged between ND–1.2 ng/L (0.6 ng/L) for E1, 0.9–1.6 ng/L (1.1 ng/L) for EE2, and 2.5–12.6 ng/L (5.6 ng/L) for BPA, while those in STP effluents were 0.9–2.9 ng/L (1.6 ng/L) for E1, 1.0–2.7 ng/L (1.6 ng/L) for EE2, and 3.5–15.8 ng/L (8.7 ng/L) for BPA, respectively.

Some studies focused on the removal of BPA and NP from wastewater during MBR treatment [103–105, 107]. Both substances were reported to be removed to a large extent by MBR treatment. In a study of Schröder [103], the elimination BPA and NP in MBR treatment was 97.8% and >98%, respectively. Concentrations of BPA and NP observed in the MBR effluents were 1.22 ± 0.10 μg/L and below the detection limit of 0.88 ng/L, while those in the conventional STP effluents were 4.63 ± 1.51 μg/L and 0.92 ± 0.11 μg/L, respectively. Chen et al. [104] studied the removal efficiencies of BPA at different BPA sludge loadings. The results showed BPA removal efficiency in MBR higher than 94% and that MBR could effectively remove BPA despite the changes in sludge loadings of BPA ranging from 0.046 to 10.2 g/kg·day. Using a lab-scale MBR, González et al. [105] found that MBR treatment could eliminate nonylphenolic compounds with an overall efficiency of 94%, which represented significant improvement in comparison to the STP treatment where only 54% of the total nonylphenolic compounds were removed. Cirja et al. [108] performed a study aimed at giving a better insight into the possible fate of NP during wastewater treatment by using a lab-scale MBR designed and optimized for fate studies carried out with radiolabeled compounds. The mass balance of NP residues at the end of the study showed that 42% of the applied radioactivity was recovered in the effluent as degradation products of NP, 21% was removed with the daily excess sludge from the MBR, and 34% was recovered as adsorbed in the component parts of the MBR. A high amount of NP was associated to the sludge during the test period, while degradation compounds were mainly found in the effluent.

Recently, the fate of EDCs and their conjugates was investigated in 3 pilot-scale and 2 lab-scale MBR systems [98]. Pilot-scale MBRs, where the membranes were submerged directly into anoxic and aerobic bioreactors, were at SRT of 21 days and HRT of 6 h. Lab-scale MBRs were operated at different SRTs (17 and 33 days) with schematic diagrams similar to the pilot-scale MBR. The concentrations of estrogens and conjugates, as well as their removal efficiencies, in the various MBR systems are shown in Table 4. The high removal rate of E1 (80.2–91.4%) in MBR systems, compared to 61 ± 38% [17] and around −80% [78] in STPs reported in literature, means that E1 could be eliminated very fast, even though E1 can be produced in the MBR systems by oxidation of E2 or deconjugation of estrogen conjugates. While compared with the removal rate of E2 of 64% [75] and 85% [41] by STPs, E2 removal efficiency in this study (49.3–63.1%) was relatively low. The low concentration of conjugates in the MBR effluents, which had a maximum concentration of 27 ng/L, suggested that a majority of steroid conjugates was removed in the MBR process by various bacteria stains in the activated sludge. The fecal bacteria *Escherichia coli*, which exists in large quantities in the feces, is able to synthesize large amounts of the β-glucuronidase enzymes [109], and it has been suggested to be responsible for the removal of estrogen glucuronides after treatment. Furthermore, Johnson and Sumpter [73] suggested that the activated sludge containing arylsulfatase enzyme could achieve desulfation. It is however clear that substantial amounts of E1, E1-3S, E1-3G, and E2-G still passed through the treatment system and entered the aquatic environment. Therefore, it is inadequate to be concerned with only free estrogens in the effluent of treatment plants, as conjugates can be converted to free estrogens further downstream in the receiving water.

Water Reclamation System and Micropollutants. Table 4 Concentrations and removal efficiencies of natural estrogens and conjugates in MBR systems

	E1	E2	E1-3G	E1-3S	E2-G (3G+17G)	E2-3S	E2-3,17S	BPA	4-NP
Influent (ng/L)									
Pilot	16.50–44.05 (27.81)	ND[a]–5.74 (ND)	ND–43.4 (24.7)	24.78–39.03 (29.85)	82.50–97.50 (92.05)	10.68–13.14 (12.03)	ND–99.4 (30.21)	0.01–2.05 (0.18)	ND–1.21 (0.16)
Lab	16.63–49.95 (32.11)	ND–6.21 (ND)	ND–30.10 (20.95)	20.49–25.56 (22.02)	41.02–99.50 (50.00)	8.82–17.70 (13.62)	ND	ND–1.20 (0.15)	ND–9.07 (0.41)
Effluent (ng/L)									
Pilot-A	1.81–11.21 (4.24)	ND–2.06 (ND)	ND–11.02 (6.60)	9.03–17.97 (15.30)	12.23–24.34 (18.05)	ND–5.13 (ND)	ND	ND–0.16 (0.05)	0.002–4.34 (0.64)
Pilot-B	1.71–12.12 (3.25)	ND–2.07 (ND)	ND–11.15 (8.05)	9.15–18.39 (16.41)	17.85–35.25 (27.00)	ND–4.68 (ND)	ND	ND–0.60 (0.07)	0.01–5.93 (0.42)
Pilot-C	1.82–7.21 (4.51)	ND–2.83 (ND)	ND–20.21 (16.30)	10.53–26.25 (23.13)	14.32–28.47 (24.05)	ND–5.46 (ND)	ND	ND–0.07 (0.04)	0.07–6.70 (0.72)
Lab-17d	2.70–3.78 (2.96)	ND	2.50–4.95 (3.10)	17.61–19.71 (17.79)	15.58–26.25 (19.88)	ND–8.22 (ND)	ND	ND–0.25 (0.03)	ND–1.88 (1.12)
Lab-33d	ND–2.83 (2.76)	ND	2.73–4.60 (3.70)	13.53–24.51 (17.80)	13.50–23.33 (17.25)	ND	ND	ND–0.14 (ND)	ND–2.12 (1.41)
Removal (%)									
Pilot-A	80.3	63.1	84.9	38.3	80.4	85.2	100	73.7	−417.6
Pilot-B	82.3	62.9	77.0	48.3	73.5	91.1	100	68.9	−161.1
Pilot-C	80.2	49.3	62.4	10.1	73.9	80.2	100	77.9	−439.5
Lab-17d	84.0	60.0	81.2	21.5	55.1	84.5	–	82.2	−269.3
Lab-33d	91.4	66.5	83.5	32.2	67.2	100	–	90.1	−313.4

Source: Hu et al. [98]

[a]Not detected; Figures in brackets indicate median value

It is clear that the removal rates of E1-3G (62.4–84.9%), E2-G (55.1–80.4%), E1-3S (10.1–48.3%), and E2-3S (80.2–100%) were lower than those reported by D'Ascenzo et al. [41], which were 84%, 100%, 64%, and 100%, respectively, in STPs (Table 4). The low removal rates of estrogen conjugates may be caused by two reasons. First, the relatively short HRT of the MBR systems (6 h) compared with STPs did not allow enzymes sufficient time to degrade conjugates in the MBR process, as both glucuronides and sulfates are difficult to convert. Reported half-lives are 6 h for estrogen glucuronides and 2.5 days for estrogen sulfates [41]. Second, all MBRs were operated with pre-denitrification zones, which may have decreased the biodegradation rate of the compounds of concern. Moreover, the extremely low removal rate of E1-3S could be caused by its slow biotransformation and conversion from E2-3S or other parent conjugates.

As shown in Table 4, for alkylphenol compounds, BPA was removed well with a removal efficiency of 68.9–90.1%, but 4-NP concentration was amplified (removal efficiency of −439.5% to −161.1%) in almost all MBR systems, as compared with that of influents. This indicates that 4-NP could be produced from parent compounds in the MBR systems.

In general, an enhanced degree of EDCs removal has been discoverable for MBRs. However, in the comparative study on removal of EDCs by MBR and conventional STP, no significant differences between the removal efficiencies in the conventional STP and the MBR have also been observed. In a study of Lesjean et al. [110], for instance, high removal rates (>80%) could be achieved for less polar EDCs (E1, E2 and EE2), which represents only a slight improvement since the STP treatment commonly yields elimination of 75–95%. The comparative study of Clara et al. [101] also showed similar elimination of EE2 in MBR and STP systems, with removal rates of 60–70%. The EE2 degradation is more likely linked to the activity of nitrifying bacteria present in biological treatment process [111–113]. In a study of Urase et al. [100], the removal of E2 by MBR was always recorded to be high (∼100%) regardless of pH, while the removal of BPA was low (∼50%) in the acidic pH condition (4.3–5.0). A considerable part of E2 was converted to E1 and a part of converted E1 remained in the MBR effluent. Weber et al. [114] report that E2 turnover rates to E1 did not differ greatly between conventional STP and MBR sludge. For BPA and NP, high elimination rates (>90%) could be achieved in both STP and MBR [79]. Especially in STP, degradation of alkylphenolic compounds appears to be a function of the operated SRT. Clara et al. [79] observed no removal of BPA and NP in the high-loaded STP operating at SRT between 1 and 2 days. The removal rate can vary depending on the operating characteristics of STP (i.e., plant size, SRT, HRT, temperature, influent concentration, and adaptation time), although high removal rate can be achieved in a well-operated STP. On the other hand, despite achieving a better elimination, operating problems such as bad sludge characteristics and foam formation in MBR systems can affect the variation in effluent concentrations of EDCs [115]. However, MBR processes could cope much better with the fluctuations in the influent concentrations of EDCs, despite the low sludge age [106]. Furthermore, due to the higher diversity of microorganisms in MBR, the acclimating procedure of sludge to EDCs such as BPA in MBR would require less time than in conventional STP [104].

MBR is generally shown to be more effective in removing EDCs than conventional STP, although contradictory results are documented in literature. Therefore, the MBR gives room for expectation that with this alternative wastewater reclamation, the environmental risk associated with EDCs can be reduced. This is probably because, first, MBR is operated under longer SRT that may facilitate additional biological transformation of EDCs. Second, because of the higher biomass concentrations, MBR is operated under the low F/M ratio, which could result in more complete mineralization of poorly degradable organic compounds. Third, the membrane (MF or UF) serves as a complete barrier to the estrogen-bound solids or colloids. Finally, an additional removal of hydrophobic compounds by membranes can be expected, because they are sorbed onto the particles that form a deposition layer on the membrane surface. These characteristics are generally not provided in STPs.

Mechanisms of EDCs Removal

The mechanisms of EDCs removal is currently one important focus of research, because several mechanisms may exist through which MBRs achieve a better

elimination of EDCs than STP. Considering low values of vapor pressure of most of the EDCs, stripped fraction removed by volatilization can be neglected [85]. Since MF and UF membranes applied in MBR have a pore size between 100 and 10,000 times larger than the physical size of EDCs (molecular weight lower than 300 g/mol), direct physical retention by the membranes is of minor for EDCs. In MBR, EDCs can sorb to solids and subsequently be separated from the treated water by MF or UF. In addition, EDCs can be biodegraded after an association with the biomass in the MBR. Therefore, the removal of EDCs in MBR system is commonly achieved by sorption on solids, biodegradation, or a combination of both.

Sorption Estrogens and their conjugates can be sorbed to biomass before appreciable degradation occurs. Andersen et al. [116] reported that the sum of sorbed E1 and E2 to sludge ranged from 7.8 to 13 μg/kg. Ternes et al. [117] also reported that up to 37 μg/kg of E1 and 49 μg/kg of E2 sorbed onto sludge. In a study for the evaluation of EDCs on MBR sludge [98], the levels of sorbed E1, E1-3S, E2-3S, BPA, and 4-NP were up to 10.42, 18.32, 2.52, 34,350, and 68,800 μg/kg, respectively (Table 5). However, no estrogen glucuronides could be detected on MBR sludge. Although natural estrogen sulfates are relatively hydrophilic, the sorbed amounts are comparable to that of E1. It can be seen that generally the amount of 4-NP sorbed onto the sludge solids is more than that of BPA sorbed onto the sludge solids (Table 5). This may be due to the fact that 4-NP has a higher log K_{OW} and lower aqueous solubility, so 4-NP is more likely to be adsorbed onto sludge solids.

Sorption of organic micropollutants to the sludge in treatment plants depends on two main mechanisms [118]: absorption and adsorption. Absorption is the hydrophobic interactions of the aliphatic and aromatic groups of a compound with the lipophilic cell membrane of the microorganisms and with the lipid fraction of the sludge. Adsorption is the electrostatic interactions of positively charged groups of the chemicals with the negatively charged surfaces of the biomass. Absorption is related to the substance's lipophilicity, characterized by the K_{OW}. Adsorption is related to the tendency of a substance to be ionized or dissociated in aqueous phase, which is characterized by the dissociation constant (p*K*a).

Water Reclamation System and Micropollutants. Table 5 Amounts of natural estrogens and conjugates sorbed to the sludge in MBR systems

	E1	E1-3S	E2-3S	BPA	4-NP
Anoxic (μg/kg)					
Pilot-A	ND[a]–9.70 (6.80)	ND–11.91 (3.44)	ND–0.31 (0.22)	0.47–14,460 (2,070)	7,245–13,600 (10,220)
Pilot-B	ND–6.40 (5.64)	ND–14.68 (4.36)	ND–1.92 (0.97)	0.55–34,350 (2,620)	ND–4,610 (3,010)
Pilot-C	ND–8.11 (5.62)	ND–11.21 (3.48)	ND–0.23 (0.16)	0.01–8,480 (4,250)	ND–4,600 (3,627)
Lab-17d	ND–7.66 (4.98)	ND–2.48 (1.11)	ND–0.28 (0.12)	1.04–8,460 (1,570)	ND–6,660 (2,800)
Lab-33d	ND–8.40 (7.38)	ND–5.78 (2.35)	ND–1.22 (0.42)	1.47–10,560 (2,080)	ND–11,400 (4,000)
Aerobic (μg/kg)					
Pilot-A	ND–2.04 (1.40)	ND–6.21 (4.52)	ND–0.75 (0.38)	2.24–1,820 (353.38)	3020–15,630 (13,380)
Pilot-B	ND–3.73 (1.56)	ND–8.36 (5.16)	ND–2.52 (1.13)	0.89–2,000 (221.13)	278.15–68,800 (16,960)
Pilot-C	ND–4.42 (2.24)	ND–8.21 (4.84)	ND–0.34 (0.18)	0.03–1,360 (273.22)	290.16–56,700 (10,490)
Lab-17d	ND–2.42 (1.22)	ND–5.32 (2.77)	ND–0.22 (0.12)	ND–1,190 (157.23)	ND–9,300 (5,160)
Lab-33d	ND–10.42 (7.98)	ND–10.96 (6.21)	ND–1.96 (0.82)	ND–1,250 (189.19)	134.02–18,130 (10,060)

Source: Hu et al. [98]

[a]Not detected; Figures in brackets indicate median value

The K_{OW} value reflects the equilibrium of partitioning the organic solute between the organic phase, i.e., octanol and water phases. High K_{OW} is characteristic for hydrophobic compounds, poor hydrosolubility, and high tendency to sorb on organic material of the sludge matrix [85]. Based on the log *Kow*, sorption to sludge is predicted to play an important role in the removal of hydrophobic compounds from the liquid phase. The following may be used as a general guide [85]: (1) log $K_{OW} < 2.5$ results in low sorption potential; (2) $2.5 < \log K_{OW} < 4.0$ yields medium sorption potential; (3) log $K_{OW} > 4.0$ leads to high sorption potential. Generally, the more hydrophobic a chemical substance, the greater the amount accumulated in the solid phase, whereas the more hydrophilic the chemical, the greater its concentration in the aqueous phase. The estrogenic compounds are generally characterized by relatively medium hydrophobicity with typical K_{OW} values between 3 and 5 (Table 1). The synthetic estrogens, due to their higher K_{OW} can be more easily removed from the water phase than the natural estrogens that are characterized by lower hydrophobicites. Apart from this, the presence of other hydrophobic chemicals present in different environments may compete with the estrogens for available binding sites in the sorbent [119].

A common approach to determine the fraction of EDCs sorbed onto sludge is the use of the solid-water distribution coefficient (K_D, in L/kg), defined as the ratio between the concentrations in the solid and liquid phases at equilibrium conditions (Eq. 1).

$$K_D = \frac{C_{sorbed}}{SS \cdot C_{soluble}} \quad (1)$$

where C_{sorbed} is the sorbed estrogen concentration onto sludge (μg/L), $C_{soluble}$ is the soluble concentration in equilibrium with the sorbed concentration, and *SS* is the sludge concentration (kg/L). Other characteristic parameters used to describe the adsorption capacity of solids are K_{OM} and K_{OC} values. The K_{OM} (L/kg) relates the K_D value to the organic matter of the sorbent (Eq. 2), whereas the K_{OC} (L/kg) refers to the organic carbon content of the sorbent (Eq. 3).

$$K_{OM} = K_D \cdot \frac{SS}{VSS} \quad (2)$$

where *VSS* is the volatile sludge concentration (kg/L).

$$K_D = K_{OC} \cdot f_{OC} \quad (3)$$

where f_{OC} is the fraction of organic carbon in the solids.

With mainly hydrophobic interactions, the K_D can be estimated from the K_{OW} (or even better from K_{OC}), whereas by electrostatic interactions, K_D is found empirically. The log K_D (or log K_{OC}) values of several EDCs appear to be independent of log K_{OW}, indicating that hydrophobic interaction is not the predominant sorption mechanism for EDCs [120]. Besides hydrophobic processes that are taking place, a number of other reactions like complex formations with metal ions, ion exchange, and hydrogen bindings decide about the partition of the organic compound between the solid and the liquid phase [121]. Since the organic fraction of the sludge (i.e., VSS) is relevant for adsorption processes [122], MBR sludge can be expected to have higher sorption potential as the organic matter content is higher compared to the sludge of conventional activated sludge process (CASP). On the other hand, both electrostatic and hydrophobic interactions can govern estrogens and their conjugate adsorption, depending on the properties of the adsorbate such as the surface charge and the existence of hydrophobic domains [123, 124].

Clara et al. [122] investigated sorption behavior of E2, EE2, and BPA to sludge. High adsorption potential to sewage sludge could be observed for these substances, with no saturation levels detected. Substances with log K_D values lower than 2 are negligible for adsorption. For substances with log K_D values higher than 4, sorption to the sludge is a major removal process. In the work by Clara et al. [122], all investigated substances show K_D values between these boundaries and proof to be relevant for this removal pathway. Authors also found that the sorption isotherm is linear over a concentration range of several orders of magnitude. Andersen et al. [125] determined the sorption of E1, E2, and EE2 to activated sludge. The experimentally obtained log K_D values were 2.60 (2.44–2.72, 2.68 (2.45–2.83), and 2.77 (2.65–2.86) L/kg for E1, E2, and EE2, respectively. Using the experimental f_{OC} (27.7 ± 0.1%) and K_D for the sludge, log K_{OC} were also determined to be 3.16, 3.24, and 3.32 L/kg for E1, E2, and EE2, respectively. The results for log K_{OC} by Andersen et al. [125] are consistent with the data determined by Clara et al. [122]. In the work by Ternes et al. [126],

log K_D for EE2 was determined to be 2.54 (2.49–2.58) L/kg. This corresponds to log K_{OC} of 2.93 (2.86–3.00) L/kg for EE2. In another study, the specific sorption coefficients K_D, K_{OM}, and K_{OC} of activated sludge for E1, E2, and their conjugates were determined [127]. The mean values of log K_D were 2.78, 2.61, 1.67, and 1.94 L/kg; log K_{OM} were 2.96, 2.79, 1.77, and 2.04 L/kg, and those of K_{OC} were 3.31, 3.12, 2.21, and 2.46 L/kg for E1, E2, E1-3S, and E2-3S, respectively. The sorption potential of sludge for a certain estrogen in MBR appears to be similar to that of conventional activated sludge. In a study of Chen et al. [104], the range of log K_D for BPA in MBR sludge was from 2.00 to 2.75 L/kg, which was similar to the reported value between 1.89 and 2.41 [122]. Authors also concluded that that although BPA is hydrophobic, the sorption process contributed very little to the BPA removal.

The solution pH affects the solution chemistry of the estrogens and estrogen conjugates, the activity of the functional groups (carboxylate, phosphate, and amino groups) in the biomass as well as the competition of compounds for the binding site. The effect of pH on adsorption of natural estrogens and their conjugates by the activated sludge is shown in Table 6 [127]. The adsorption isotherm of steroid estrogens and their conjugates by the activated sludge can be described by the Freundlich isotherm. The pH value appears to be an important parameter, which affects the adsorption capacity. In the work by Chen and Hu [127], the sorption capacities of E1 and E2 to activated sludge were the highest at neutral pH, but decreased while pH decreased or increased. For both E1-3S and E2-3S, sorption capacities were highest at pH 2, while lowest at pH 11.5. The lower capacities of E1 and E2 at pH 2 and 11.5 could be due to the competition of sludge adsorption sites by cations or electrostatic repulsion from particles of similar charges. The lowest adsorption capacity of estrogen conjugates at pH 11.5 could by caused by electrostatic repulsion, and the highest capacity at pH 2 might be due to the increased sulfate adsorbability. In another study, pH conditions irrelevant for the sorption of E1, E2, EE2, and BPA were found [128]. The change in pH from 7.0 to 4.4 has no effect on their K_D [128] On the other hand, at high pH values, a release of the adsorbed fraction to the liquid phase was observed for E2, EE2, and BPA in a study of Clara et al. [122]. Desorption occurred at pH values in the range of the pKa values (10.4 for E2, 10.7 for EE2, and 10.3 for BPA of the investigated compounds.

Experimental data on the sorption behavior of EDCs to MBR sludge are very scarce, probably due to the difficulties of solid samples analysis. To overcome this problem, the use of K_D values appears to be a useful tool to predict distribution between both phases. However, an accurate determination of this coefficient is required to avoid misunderstandings in the establishment of the mechanism responsible for the elimination of a particular compound.

Biodegradation Biodegradation is an important estrogen removal mechanism in both STP and MBR systems. Though the degradation pathways are still incomplete, estrogenic activity is removed with

Water Reclamation System and Micropollutants. Table 6 Effect of pH on isothermal constants (K_F[$mg^{1-1/n}$ $(m^3)^{1/n}$ g TSS^{-1}] and 1/n) of Freundlich model for steroid estrogens and their conjugates

	E1		E2		E1-3S		E2-3S	
pH	K_F	1/n	K_F	1/n	K_F	1/n	K_F	1/n
2	0.23	0.94	0.11	1.04	0.189	0.863	0.347	0.881
5	0.26	1.08	0.22	0.96	0.032	0.857	0.064	0.830
7	0.36	1.05	0.60	0.99	0.022	0.739	0.052	0.736
9	0.29	0.92	0.26	0.95	0.032	0.810	0.056	0.807
11.5	0.05	1.00	0.04	1.08	0.006	0.742	0.012	0.887

Source: Chen and Hu [127]

biotransformation of the parent estrogen compound. This deserves further attention when considering the fact that sorption only involves a phase shift of the pollutants and no degradation or even transformation. For nonpolar trace organics, in general, sorption to the biomass and subsequent retention of the solids by the membranes will be a major removal mechanism. For polar compounds, sorption will be limited and elimination can only be achieved through biodegradation.

The biodegradation of micropollutants such as EDCs in the sludge phase is described by pseudo-first-order kinetic model as given below [68, 129]:

$$\frac{dC_T}{dt} = -k_b X_{SS} C \quad (3)$$

where dC_T/dt is the reaction rate (ng/L·day), C_T is the total estrogen concentration (ng/L), k_b (L/g·day) is the pseudo-first-order rate coefficient for estrogen biodegradation, X_{SS} is the concentration of suspended solids (g/L), and C is the soluble estrogen concentration (ng/L). The term "first order" refers to the direct proportionality of the transformation rate to the soluble substance concentration and the term "pseudo" refers to its proportionality to the sludge concentration [129].

Joss et al. [129] have determined biodegradation kinetic constants (k_b) for a large number of compounds with the sludge from CASP and MBR. Based on the k_b values, three groups of compounds were defined according to their susceptibility to biological degradation: (1) hardly biodegradable with $k_b < 0.1$ L/g·day; (2) moderate biodegradable with $0.1 < k_b < 10$ L/g·day; and (3) highly biodegradable compounds with $k_b > 10$ L/g·day. The reported k_b values of E1, E2, and EE2 are in the range of 200–300, 300–800, and 7–9 L/g·day, respectively [129, 130]. From the classification scheme, E1 and E2 are expected to be highly biodegraded, whereas partial biodegradation is predicted for EE2.

In general, trace organic removal is better in MBR than in STP. Yet, the most effective treatment option depends strongly on the target compounds present in wastewater. In treatment process with a combination of different mechanisms (sorption and biodegradation) for removal of compounds, the following considerations can be taken into account according to the k_b and K_D (or K_{OC}) values of a particular compound [130]:

- Compounds with high k_b and low K_D (or K_{OC}) values are very well transformed independently of SRT and HRT.
- Compounds with low k_b and high K_D (or K_{OC}) values are retained in the aerobic reactor by sorption and significantly transformed when the SRT is long enough to accomplish biological degradation.
- Compounds with high k_b and medium K_D (or K_{OC}) values are moderately transformed independently of HRT and slightly dependant on SRT.
- Compounds with low k_b and K_D (or K_{OC}) values are not removed nor biotransformed regardless of HRT and SRT.

For instance, E1 and E2 belong to compounds with high k_b and medium K_{OC}, while EE2 has low k_b and high K_{OC} values [68, 131]. Clara et al. [44] showed a dependency of the removal of E1 and E2 on SRT in STP and MBR, high removal rates at the prolonged SRT. EE2 could be removed at significant rate under aerobic conditions at sufficient SRT [68]. Therefore, this information would be useful for selection of the treatment option for EDCs removal from wastewaters.

The sludge characteristics are an important factor for biodegradation. There are important sludge characteristics that are to be considered for biological transformation of estrogens [129]: (1) diversity of the activity of the biomass due to either differences in microbial population or the expressed enzymatic activity, (2) floc size of the sludge for compounds being well degraded, and (3) the fraction of active biomass within the total suspended solids. Significant differences in sludge characteristics have been observed between CASP and MBR sludges [44, 47, 68, 93, 94, 129].

In the case of MBR, the bioreactor and membrane units cannot be regarded as individual unit operations because they interact with respect to both biological reactions and membrane filtration. High SRT and full retention of solid particles on membranes enable biological adaptation to less biodegradable compounds and can promote a wider diversity of the microbiological communities, resulting in changes in removal rates and efficiencies. Possible changes in the activated sludge composition can be used for the establishment of "specialized" microorganisms [65]. The membrane

not only retains all biomass but also prevents the escape of exocellular enzymes and soluble oxidants creating a more active biological mixture capable of degrading a wider range of organic compounds [132]. In a study by Cicek et al. [132], enzymatic activity tests showed that (1) overall activity was consistently higher in the MBR, (2) both systems produced enzymes specific for the degradation of feed chemicals, (3) no enzymes were detected in the MBR effluent compared to significant amounts in the CASP, and (4) the MBR contained more enzymes in the soluble phase than the CASP. Data from literature show that higher sludge age, often reached in MBRs, may significantly improve the removal of specific compounds [133, 134]. For compounds like trimethoprim, and macrolide antibiotics azithromycin, erithromycin, and clarithromycin, a clear increase in transformation was found at sludge ages of 60–80 days [134].

A high SRT in a biological process positively affects the overall activity of slow growing microorganisms (e.g., nitrification). Baek and Pagilla [135] found that the high SRT (103 ± 9 days) of MBR system retained more active nitrifying bacteria than CASP (SRT of 10–15 days). Furthermore, MBR enables nitrifying bacteria to develop and persist in the system even under short SRTs (2–10 days) [96]. Complete nitrification was demonstrated in MBRs at sludge ages of 5–72 days [136]. The treatment process configuration may affect the removal of estrogens as has been shown by significant higher removal rates with nitrifying activated sludge [76]. Estrogens removal rates of greater than 90% were achieved in MBRs with nitrification and denitrification [68]. Vader et al. [111] demonstrated the degradation of EE2 by a nitrifying sludge with a high ammonium (NH_4^+) oxidizing activity. Shi et al. [137] and Yi and Harper [138] used nitrifying mixed cultures to degrade EE2 and suggested that the key enzyme for nitrification, i.e., ammonium monooxygenase, could mediate an EE2/NH_4^+ cometabolism. These authors brought forward the concept that nitrifiers initially degrade EE2 into intermediates that subsequently serve as a substrate for heterotrophic organisms. On the other hand, some authors suggested that the primary mechanism for EE2 degradation is more likely linked to the activity of heterotrophic bacteria [139]. They suggested that the EE2 removal by axenic cultures of ammonia-oxidizing bacteria is only due to the abiotic nitration reaction with EE2, governed by the high NO_2^--N levels after oxidation of the high NH_4^+-N concentrations in batch tests.

The biomass developed in MBR systems can be characterized by smaller floc size with respect to the removal efficiency of micropollutants. In CASP, flocs may reach several 100 μm in size [140]. This means that the substrate can reach the active sites inside these flocs only by diffusion, which causes an additional resistance and limits the overall reaction rate. Hydrodynamic stress in MBRs reduces floc size to approximately 30–60 μm in immersed systems [92, 141] and 3.5 μm in side-stream MBRs [94], and thereby, indirectly increases the apparent reaction rate. Smaller flocs can explain enhanced mass transfer for both oxygen and carbon, thus enabling a higher removal rate and more adaptability to changes in the influent quality and quantity [142]. In another study, it was demonstrated that the flocs were more active and displayed greater species diversity [132]. Furthermore, some enzymatic activities increase proportionally to the higher specific surface area of MLSS, which is directly related to the floc structure [85].

SRT has been reported as determinative for biodegradation of micropollutants. Clara et al. [44] suggested that a critical value for the sludge age can be determined. With regard to natural estrogens, a strong correlation between achievable effluent concentrations and the $SRT_{10°C}$ (temperature corrected SRT) was observed [44]. For these substances, a critical value was identifiable for the $SRT_{10°C}$ amounting to approximately 10 days, but for EE2, contradictory results were obtained and beside the SRT, other influences seem to be of importance [44]. These authors concluded that for STPs operated at $SRTs_{10°C}$ higher than 10 days, low effluent concentrations can be achieved for many biodegradable micropollutants, which corresponds to an SRT required for efficient nitrogen removal. On the other hand, at long SRT, the accumulation of dead or inactive microorganisms occurs in the MBR, and thus affects the sludge activity [93, 143]. Joss et al. [129] noted that the slightly lower transformation rate constants found in MBR operated at 30–40 days of SRT as compared to CASP sludge with 10–12 days of SRT operation, may be, caused by the higher inert matter accumulation in the MBR sludge. Baek and Pagilla [135] suggested that the biomass in the MBR system

with longer SRT of 103 ± 9 days was not in a physiological state characteristic for growth due to low substrate per unit biomass. Increasing the SRT beyond 30 days does not seem to improve the removal for micropollutants [130]. An explanation could be in the fact that biodegradation of micropollutants is most likely performed in a cometabolic manner as the low concentrations do not likely sustain growth for specific microorganisms, because in this case, the SRT necessary for an efficient biodegradation of the primary substrate is the relevant parameter [144].

Several researchers have studied the influence of initial concentration of EDCs and MLSS concentration on EDCs biodegradation performance. Ternes et al. [77] reported the behavior and occurrence of E2 and E2 glucuronides in aerobic batch experiments with activated sludge, and they found that E2 and E2 glucuronides in the ng/mL range were cleaved and eliminated even faster than in the experiments spiked with higher concentrations (mg/mL range). More recently, Li et al. [145] studied the degradation kinetics of E2 under different operating parameters in aerobic batch experiments by activated sludge, and they found comparably that the degradation rate with higher initial concentration was faster by making use of first-order model. In another study, it was demonstrated that the biodegradation of E2 and its conjugates depends on the initial concentration and MLSS concentration of activated sludge [127]. There was a clear trend that the degradation rates of E2, E2-3G, and E2-3S generally increased with the increase of initial concentration range from 10 to 200 μg/L at MLSS of 4 g/L. It suggests that the higher initial substrate concentration has more stimulatory effect on the microorganisms in activated sludge. This could be explained by the reason that the degradation intermediates of E2 or its conjugates did not compete for the degradation by relatively high biomass concentration (4 g/L) with studied compound itself, and the inhibitory effect was unnoticeable. The same tendency was also reported by Li et al. [145], in which they used sludge (MLVSS of 1.75 g/L) to degrade E2 with initial concentration of 10, 30, and 50 μg/L. Chen and Hu [127] also found that MLSS concentration has a great effect on the degradation rates of E2 and its conjugates. Results showed that the biodegradation rates of E2 in the initial concentration of 50 μg/L increased with the increase of MLSS concentration of activated sludge from 4 to 12.5 g/L. This could be explained by more microorganisms and bacterial population in activated sludge at higher MLSS concentration that would carry out the degradation of E2 and its conjugates more effectively.

Future Directions

The reclamation and reuse of treated water imposes as the most adequate solution for the future sustainable water management. One of the key issues in water recycling is the emerging problem of micropollutants such as EDCs. Conventional wastewater treatment plants are not effective in the complete elimination of EDCs and their discharges have a great potential to affect the aquatic environment. So far, several studies have proved that MBR is able to achieve an enhanced degree of EDCs removal from wastewater compared to conventional wastewater treatment. However, most of research data are still incomplete or inconclusive on: (1) the predominant removal mechanism reponsible for the respective EDC removal under real MBR process conditions, and (2) the understanding of biotransformation pathways of EDCs and their metabolites with estrogenic activity during MBR treatment. Within these areas, several research topics can be defined. An emerging task in MBR process treating EDCs present in wastewater is the complete mineralization associated to negligible effluent concentrations. It can be achieved through the optimization of determinative parameters (e.g., SRT, HRT, organic loading, sludge concentration, redox conditions, and reactor configuration, etc.) for EDCs removal.

Research into identification of microbial species and strains that can degrade estrogens with the possible application to wastewater treatment has led researchers to explore other areas. For instance, using strains of *Rhodococcus* isolated in activated sludge from wastewater treatment plants, Yoshimoto et al. [146] found rapid degradation of high concentration (100 mg/L) of natural and synthetic steroid estrogens (E1, E2, E3, and EE2). Therefore, search for specific microorganisms with high estrogen-degrading activity and their use in wastewater treatment deserves further research. Introducing estrogen-degrading strains into MBR is an interesting option in a way that would provide a flexible and efficient degradation.

Bibliography

1. Colborn T, Dumanoski D, Myers JP (1996) Our stolen future: Are we threatening our fertility, intelligence, and survival? –A scientific detective story. Dutton, New York
2. Reddy S, Iden CR, Brownawell BJ (2005) Analysis of steroid conjugates in sewage influent and effluent by liquid chromatography–tandem mass spectrometry. Anal Chem 77:7032–7038
3. Harris CA, Henttu P, Parker MG, Sumpter JP (1997) The estrogenic activity of phthalate esters *in vitro*. Environ Health Perspect 105:802–811
4. Desbrow C, Routledge EJ, Brighty GC, Sumpter JP, Waldock M (1998) Identification of estrogenic chemicals in STW effluent 1. Chemical fractionation and in vitro biological screening. Environ Sci Technol 32:1549–1558
5. Jobling S, Nolan M, Tyler CR, Brighty G, Sumpter JP (1998) Widespread sexual disruption in wild fish. Environ Sci Technol 32:2498–2506
6. Preziosi P (1998) Natural and anthropogenic environmental oestrogens: the scientific basis for risk assessment endocrine disrupters as environmental signalers: An introduction. Pure Appl Chem 70:1617–1631
7. Holm L, Berg C, Brunstrom B, Ridderstrale Y, Brandt I (2001) Disrupted carbonic anhydrase distribution in the avian shell gland following in ovo exposure to estrogen. Arch Toxicol 75:362–368
8. Chilvers C, Pike MC, Forman D, Fogelman K, Wadsworth ME (1984) Apparent doubling of frequency of undescended testicles in England and Wales 1962–81. Lancet 2:330–332
9. Kimmel CA (1993) Approaches to evaluating reproductive hazards and risks. Environ Health Perspect 101:137–143
10. Rajpert-De Meyts E, Skakkeboek NE (1993) The possible role of sex hormones in the development of testicular cancer. Eur Urol 23:54–61
11. UK Environment Agency (1997) The identification and assessment of oestrogenic substances in sewage treatment works effluents. Bristol, UK
12. Purdom CE, Hardiman PA, Bye VJ, Eno NC, Tyler CR, Sumpter JP (1994) Oestrogenic effects of effluents from sewage treatment works. Chem Ecol 8:275–285
13. Routledge EJ, Sheahan D, Desbrow C, Brighty GC, Waldock M, Sumpter JP (1998) Identification of estrogenic chemicals in STW effluent. 2. *In vivo* responses in trout and roach. Environ Sci Technol 32:1559–1565
14. Jobling S, Sheahan D, Osborne JA, Matthiessen P, Sumpter JP (1996) Inhibition of testicular growth in rainbow trout (*Oncorhynchus mykiss*) exposed to estrogenic alkylphenolic chemicals. Environ Toxicol Chem 15:194–202
15. Länge R, Hutchinson TH, Croudace C, Siegmund F, Schweinfurth H, Hampe P, Panter GH, Sumpter JP (2001) Effects of the synthetic estrogen 17α-ethinylestradiol on the life-cycle of the fathead minnow (*Pimephales promelas*). Environ Toxicol Chem 20:1216–1227
16. Jobling S, Sumpter JP (1993) (1993) Detergent components in sewage effluent are weakly oestrogenic to fish: An *in vitro* study using rainbow trout (*Oncorhynchus mykiss*) hepatocytes. Aquat Toxicol 27:361–372
17. Baronti C, Curini R, D'Ascenzo G, Di Corcia A, Gentili A, Samperi R (2000) Monitoring natural and synthetic estrogens at activated sludge sewage treatment plants and in a receiving river water. Environ Sci Technol 34:5059–5066
18. Huang CH, Sedlak DL (2001) Analysis of estrogenic hormones in municipal wastewater effluent and surface water using enzyme-linked immunosorbent assay and gas chromatography/tandem mass spectrometry. Environ Toxicol Chem 20:133–139
19. Snyder S, Villeneuve DL, Snyder E, Giesy JP (2001) Identification and quantification of estrogen receptor agonists in wastewater effluents. Environ Sci Technol 35:3620–3625
20. Spengler P, Körner W, Metzger JW (2001) Substances with estrogenic activity in effluents of sewage treatment plants in southwestern Germany. 1. Chemical analysis. Environ Toxicol Chem 20:2133–2141
21. Körner W, Bolz U, Submuth W, Hiller G, Schuller W, Hanf V, Hagenmaier H (2000) Input/output balance of estrogenic active compounds in a major municipal sewage plant in Germany. Chemosphere 40:1131–1142
22. Holbrook RD, Novak JT, Grizzard TJ, Love NG (2002) Estrogen receptor agonist fate during wastewater and biosolids treatment process: a mass balance analysis. Environ Sci Technol 36:4533–4539
23. Smith CW, Di Gregorio D, Talcott RM (1969) The use of ultrafiltration membrane for activated sludge separation. In: Proceedings of the 24th annual Purdue industrial waste conference. Purdue University, West Lafayette, pp 1300–1310
24. Stephenson T, Judd S, Jefferson B, Brindle K (2000) Membrane bioreactors for wastewater treatment. IWA, London, UK
25. Visvanathan C, Ben Aim R, Parameshwaran K (2000) Membrane separation bioreactors for wastewater treatment. Crit Rev Environ Sci Technol 30(1):1–48
26. Teske SS, Arnold RG (2008) Removal of natural and xenoestrogens during conventional wastewater treatment. Rev Environ Sci Biotechnol 7:107–124
27. Matsui S, Takigami H, Matsuda T, Taniguchi N, Adachi J, Kawami H, Shimizu Y (2000) Estrogen and estrogens mimics contamination in water and the role of sewage treatment. Water Sci Technol 42(12):173–179
28. Chistianshen BL, Winther-Nielsen M, Helweg C (2002) Feminization of fish: the effect of estrogenic compounds and their fate in sewage treatment plants and nature. Environmental project no. 729, Danish Environmental Protection Agency, Denmark, 184 pp
29. Jürgens MD, Holthaus KIE, Johnson AC, Smith JJL, Hetheridge M, Williams RJ (2002) The potential for estradiol and ethinylestradiol degradation in English rivers. Environ Toxicol Chem 21:480–488
30. López de Alda MJ, Barceló D (2001) Review of analytical methods for the determination of estrogens and progestogens in wastewaters. Fresenius J Anal Chem 371:437–447

31. Li MH, Wang ZR (2005) Effect of nonylphenol on plasma vitellogenin of male adult guppies (*Poecilia reticulata*). Environ Toxicol 20:53–59
32. Nozaka T, Abe T, Matsuura T, Sakamoto T, Nakano N, Maeda M, Kobayashi K (2004) Development of vitellogenin assay for endocrine disrupters using medaka (*Oryzias latipes*). Environ Sci 11:99–121
33. Paulozzi LJ (1999) International trends in rates of hypospadias and cryptorchidism. Environ Health Perspect 107:297–302
34. Krishnan AV, Stathis P, Permuth SF, Tokes L, Feldman D (1993) Bisphenol A: An estrogenic substance is released from polycarbonate flasks during autoclaving. Endocrinology 132: 2279–2286
35. Gaido KW, Leonard LS, Lovell S, Gould JC, Babai D, Portier CJ, McDonnell DP (1997) Evaluation of chemicals with endocrine modulating activity in a yeast-based steroid hormone receptor gene transcription assay. Toxicol Appl Pharmacol 143: 205–212
36. Kuiper G, Carlson B, Grandien K, Enmark E, Haggblad J, Nilsson S, Gustafsson JA (1997) Comparison of the ligand binding specificity and transcript tissue distribution of estrogen receptor α and β. Endocrinology 132:2279–2286
37. Routledge EJ, Sumpter JP (1996) Estrogenic activity of surfactants and some of their degradation products assessed using a recombinant yeast screen. Environ Toxicol Chem 15:241–248
38. Belfroid AC, Van der Horst A, Vethaak AD, Schäfer AJ, Rijs GBJ, Wegener J (1999) Analysis and occurrence of estrogenic hormones and their glucuronides in surface water and waste water in The Netherlands. Sci Total Environ 225:101–108
39. Swartz CH, Reddy S, Benotti SJ, Yin H, Barber LB, Brownawell BJ, Rudel RA (2006) Steroid estrogens, nonylphenol ethoxylate metabolites and other wastewater contaminants in ground water affected by a residential septic system on Cape Cod, MA. Environ Sci Technol 40:4894–4902
40. Kuch HM, Ballschmiter K (2001) Determination of endocrine-disrupting phenolic compounds and estrogens in surface and drinking water by HRGC-(NCI)-MS in the pictogram per liter range. Environ Sci Technol 35:3201–3206
41. D'Ascenzo G, Corcia AD, Gentili A, Mancini R, Nazzari RMM, Samperi R (2003) Fate of natural estrogen conjugates in municipal sewage transport and treatment facilities. Sci Total Environ 302:199–209
42. Isobe T, Shiraishi H, Yasuda M, Shinoda A, Suzuki H, Morita M (2003) Determination of estrogens and their conjugates in water using solid-phase extraction followed by liquid chromatography-tandem mass spectrometry. J Chromatogr A 984:195–202
43. Fine DD, Breidenbach GP, Price TL, Hutchins SR (2003) Quantitation of estrogens in ground water and swine lagoon samples using solid-phase extraction, pentafluorobenzyl/trimethylsilyl derivatizations and gas chromatography–negative ion chemical ionization tandem mass spectrometry. J Chromatogr A 1017:167–185
44. Clara M, Kreuzinger N, Strenn B, Gans O, Kroiss H (2005) The solids retention time–a suitable design parameter to evaluate the capacity of wastewater treatment plants to remove micropollutants. Water Res 39:97–106
45. Vethaak AD, Lahr J, Schrap SM, Belfroid AC, Rijs GB, Gerritsen A (2005) An integrated assessment of estrogenic contamination and biological effects in the aquatic environment of the Netherlands. Chemosphere 59:511–524
46. Hohenblum P, Gans O, Moche W, Scharf S, Lorbeer G (2004) Monitoring of selected estrogenic hormones and industrial chemicals in groundwaters and surface waters in Austria. Sci Total Environ 333:185–193
47. Servos MR, Bennie DT, Burnison BK, Jurkovic A, McInnis R, Neheli T, Schnell A, Seto P, Smyth SA, Ternes TA (2005) Distribution of estrogens, 17β-estradiol and estrone, in Canadian municipal wastewater treatment plants. Sci Total Environ 336:155–170
48. Laganà A, Bacaloni A, Leva ID, Faberi A, Fago G, Marino A (2004) Analytical methodologies for determining the occurrence of endocrine disrupting chemicals in sewage treatment plants and natural waters. Anal Chim Acta 501:79–88
49. Kolok AS, Snow DD, Kohno S, Sellin MK, Guillette JLJ (2007) Occurrence and biological effect of exogenous steroids in the Elkhorn river, Nebraska, USA. Sci Total Environ 388:104–115
50. Tan BL (2006) Chemical and biological analyses of selected endocrine disruptors in wastewater treatment plants in south east Queensland, Australia. Doctor dissertation. Griffith University, Queensland
51. Kolodziej EP, Sedlak DL (2007) Rangeland grazing as a source of steroid hormones to surface waters. Environ Sci Technol 41:3514–3520
52. Robert FC, Rominder PSS, Fu HX (2007) Free synthetic and natural estrogen hormones in influent and effluent of three municipal wastewater treatment plants. Water Environ Res 79:969–974
53. Morteani G, Moller P, Fuganti A, Paces T (2006) Input and fate of anthropogenic estrogens and gadolinium in surface water and sewage plants in the hydrological basin of Prague (Czech Republic). Environ Geochem Health 28:257–264
54. Fernandez MP, Ikonomou MG, Buchanan I (2007) An assessment of estrogenic organic contaminant in Canadian wastewaters. Sci Total Environ 373:250–269
55. Liu ZH, Ito M, Kanjo Y, Yamamoto A (2009) Profile and removal of endocrine disrupting chemicals by using an ER/AR competitive ligand binding assay and chemical analyses. J Environ Sci 21:900–906
56. Cargouet M, Perdiz D, Asmaa MS, Sara TK, Levi Y (2004) Assessment of river contamination by estrogenic compounds in Paris area (France). Sci Total Environ 334:55–66
57. Peterson EW, Davis PK, Orndorff HA (2000) 17β-estradiol as an indicator of animal waste contamination in mantled karst aquifers. J Environ Qual 29:826–834
58. Roefer P, Snyder S, Zegers RE, Rexing DJ, Fronk JL (2000) Endocrine-disrupting chemicals in a source water. J Am Water Works Assoc 92(8):52–58
59. Nghiem LD, Manis A, Soldenhoff K, Schäfer AI (2004) Estrogenic hormone removal from wastewater using NF/RO membranes. J Membr Sci 242:37–45

60. Wicks C, Kelley C, Peterson E (2004) Estrogen in a karstic aquifer ground water. Ground Water 42:384–389
61. Campbell CG, Borglin SE, Green FB, Grason A, Wozei E, Stringfellow WT (2006) Biologically directed environmental monitoring, fate, and transport of estrogenic endocrine disrupting compounds in water: a review. Chemosphere 65:1265–1280
62. Braga O, Smythe GA, Schäfer AI, Feitz AJ (2005) Fate of steroid estrogens in Australian inland and coastal wastewater treatment plants. Environ Sci Technol 39:3351–3359
63. Shen JH, Gutendorf B, Vahl HH, Shen L, Westendorf J (2001) Toxicological profile of pollutants in surface water from an area in Taihu Lake, Yangtze Delta. Toxicology 166:71–78
64. Xiao XY, McCalley DV, McEvoy J (2001) Analysis of estrogens in river water and effluents using solid-phase extraction and gas chromatography–negative chemical ionisation mass spectrometry of the pentafluorobenzoyl derivatives. J Chromatogr A 923:195–204
65. Drewes JE, Hemming J, Ladenburger SJ, Schaauer J, Sonzogni W (2005) An assessment of endocrine disrupting activity changes during wastewater treatment through the use of bioassays and chemical measurements. Water Environ Res 77:12–23
66. Rodriguez-Mozaz S, López de Alda MJ, Barceló D (2004) Monitoring of estrogens, pesticides and bisphenol A in natural waters and drinking water treatment plants by solid-phase extraction–liquid chromatography mass spectrometry. J Chromatogr A 1045:85–92
67. Beck IC, Bruhn R, Gandrass J, Ruck W (2005) Liquid chromatography-tandem mass spectrometry analysis of estrogenic compounds in coastal surface water of the Baltic Sea. J Chromatogr A 1090:98–106
68. Joss A, Andersen H, Ternes T, Richle PR, Siegrist H (2004) Removal of estrogens in municipal wastewater treatment under aerobic and anaerobic conditions: consequences for plant optimization. Environ Sci Technol 38:3047–3055
69. Johnson AC, Williams RJ, Simpson P, Kanda R (2007) What difference might sewage treatment performance make to endocrine disruption in rivers? Environ Pollut 147:194–202
70. Liu ZH, Kanjo Y, Mizutani S (2009) Removal mechanisms for endocrine disrupting compounds (EDCs) in wastewater treatment – physical means, biodegradation, and chemical advanced oxidation: a review. Sci Total Environ 407:731–748
71. Körner W, Hanf V, Schuller W, Kempter C, Metzger J, Hagenmaier H (1999) Development of a sensitive E-screen assay for quantitative analysis of estrogenic activity in municipal sewage effluents. Sci Total Environ 225:33–48
72. Isidori M, Cangiano M, Palermo FA, Parrella A (2010) E-screen and vitellogenin assay for the detection of the estrogenic activity of alkylphenols and trace elements. Comp Biochem Physiol C Toxicol Pharmacol 152:51–56
73. Johnson AC, Sumpter JP (2001) Removal of endocrine disrupting chemicals in activated sludge treatment works. Environ Sci Technol 35:4697–4703
74. Johnson AC, Belfroid A, Di Corcia A (2000) Estimating steroid estrogen input into activated sludge treatment works and observation on their removal from the effluent. Sci Total Environ 256:163–173
75. Ternes TA, Stumpf M, Mueller J, Haberer K, Wilken R-D, Servos M (1999) Behavior and occurrence of estrogens in municipal sewage treatment plants–I. Investigations in Germany, Canada and Brazil. Sci Total Environ 225:81–90
76. Andersen H, Segrist H, Hlling-Sorensen B, Trnes TA (2003) Fate of estrogens in a municipal sewage treatment plant. Environ Sci Technol 37:4021–4026
77. Ternes TA, Kreckel P, Mueller J (1999) Behaviour and occurrence of estrogens in municipal sewage treatment plants–II. Aerobic batch experiments with activated sludge. Sci Total Environ 225:91–99
78. Carballa M, Omil F, Lema JM, Llompart M, Garcia-Jares C, Rodriguez I, Gomez M, Ternes T (2004) Behaviour of pharmaceuticals, cosmetics and hormones in a sewage treatment plant. Water Res 38:2918–2926
79. Clara M, Strenn B, Gans O, Martinez E, Kreuzinger N, Kroiss H (2005) Removal of selected pharmaceuticals, fragrances and endocrine disrupting compounds in membrane bioreactor and conventional wastewater treatment plants. Water Res 39:4797–4807
80. Panter GH, Thompson RS, Beresford N, Sumpter JP (1999) Transformation of a non-oestrogenic steroid metabolite to an oestrogenically active substance by minimal bacterial activity. Chemosphere 38:3579–3596
81. Semião AJC, Schäfer AI (2010) Xenobiotics removal by membrane technology: an overview. In: Fatta-Kassinos D, Bester K, Kümmerer K (eds) Environmental pollution, vol 16. Springer, Netherlands, pp 307–338
82. Ben Aim RM, Semmens MJ (2002) Membrane bioreactors for wastewater treatment and reuse: a success story. Water Sci Technol 47(1):1–5
83. Manem J, Sanderson R (1996) Membrane bioreactors. In: Malleviale J, Odendaal PE, Wiesner MR (eds) Water treatment membrane processes. McGraw-Hill, New York, pp 17.1–17.31
84. Galil NI, Sheidorf Ch, Stahl N, Tenenbaum A, Levinsky Y (2003) Membrane bioreactors for final treatment of wastewater. Water Sci Technol 48(8):103–110
85. Cirja M, Ivashechkin P, Schäffer A, Corvini PFX (2008) Factors affecting the removal of organic micropollutants from wastewater in conventional treatment plants (CTP) and membrane bioreactors (MBR). Rev Environ Sci Biotechnol 7:61–78
86. Abegglen C, Joss A, McArdell CS, Fink G, Schlüsener MP, Ternes TA, Siegrist H (2009) The fate of selected micropollutants in a single-house MBR. Water Res 43:2036–2046
87. Rosenberger S, Kruger U, Witzig R, Manz W, Szewzyk U, Kraume M (2002) Performance of a bioreactor with submerged membranes for aerobic treatment of municipal waste water. Water Res 36:413–420

88. Weiss S, Reemtsma T (2008) Membrane bioreactors for municipal wastewater treatment – a viable option to reduce the amount of polar pollutants discharged into surface waters? Water Res 42:3837–3847
89. Massé A, Spérantio M, Cabassud C (2006) Comparison of sludge characteristics and performance of a submerged membrane bioreactor and an activated sludge process at high solids retention time. Water Res 40:2405–2415
90. Bouhabila EH, Ben Aïm R, Buisson H (1998) Microfiltration of activated sludge using submerged membrane with air bubbling (application to wastewater treatment). Desalination 118:315–322
91. Bouhabia EH, Ben Aïm R, Buisson H (2001) Fouling characterisation in membrane bioreactors. Sep Purif Technol 22–23:123–132
92. Zhang B, Yamamoto K, Ohgaki S, Kamiko N (1997) Floc size distribution and bacterial activities in membrane separation activated sludge processes for small-scale wastewater treatment/reclamation. Water Sci Technol 35(6):37–44
93. Huang X, Gui P, Qian Y (2001) Effect of sludge retention time on microbial behaviour in a submerged membrane bioreactor. Proc Biochem 36:1001–1006
94. Ng HY, Hermanowicz SW (2005) Membrane bioreactor operation at short solids retention times: performance and biomass characteristics. Water Res 39:981–992
95. Gao M, Yang M, Li H, Wang Y, Pan F (2004) Nitrification and sludge characteristics in a submerged membrane bioreactor on synthetic inorganic wastewater. Desalination 170:177–185
96. Cicek N, Macomer J, Davel J, Suidan MT, Audic J, Genestet P (2001) Effect of solids retention time on the performances and biological characteristics of a membrane bioreactor. Water Sci Technol 43(11):43–50
97. Pollice A, Giordano C, Laera G, Saturno D, Mininni G (2006) Rheology of sludge in a complete retention membrane bioreactor. Environ Technol 27:723–732
98. Hu JY, Chen X, Tao G, Kekred K (2007) Fate of endocrine disrupting compounds in membrane bioreactors systems. Environ Sci Technol 41:4097–4102
99. Spring AJ, Bagley DM, Andrews RC, Lemanik S, Yang P (2007) Removal of endocrine disrupting compounds using a membrane bioreactor and disinfection. J Environ Eng Sci 6:131–137
100. Urase T, Kagawa C, Kikuta T (2005) Factors affecting removal of pharmaceutical substances and estrogens in membrane separation bioreactors. Desalination 178:107–113
101. Clara M, Strenn B, Ausserleitner M, Kreuzinger N (2004) Comparison of the behaviour of selected micropollutants in a membrane bioreactor and a conventional wastewater treatment plant. Water Sci Technol 50(5):29–36
102. Kreuzinger N, Clara M, Strenn B, Kroiss H (2004) Relevance of the sludge retention time (SRT) as design criteria for wastewater treatment plants for the removal of endocrine disruptors and pharmaceuticals from wastewater. Water Sci Technol 50(5):149–156
103. Schröder H.Fr. (2006) The elimination of the endocrine disrupters 4-nonylphenol and bisphenol A during wastewater treatment – comparison of conventional and membrane assisted biological wastewater treatment followed by an ozone treatment. Water Pract Technol 1(3):0060(1–9)
104. Chen J, Hwang X, Lee D (2008) Bisphenol A removal by a membrane bioreactor. Process Biochem 43:451–456
105. González S, Petrovic M, Barceló D (2007) Removal of a broad range of surfactants from municipal wastewater – Comparison between membrane bioreactor and conventional activated sludge treatment. Chemosphere 67:335–343
106. Zuehlke S, Duennbier U, Lesjean B, Gnirss R, Buisson H (2006) Long-term comparison of trace organics removal performances between conventional and membrane activated sludge processes. Water Environ Res 78:2480–2486
107. Wintgens T, Gallenkemper M, Melin T (2002) Endocrine disrupting removal from wastewater using membrane bioreactor and nanofiltration technology. Desalination 146:387–391
108. Cirja M, Zühlke S, Ivashechkin P, Schäffer A, Corvini PFX (2006) Fate of a 14C-labeled nonylphenol isomer in a laboratory-scale membrane bioreactor. Environ Sci Technol 40:6131–6136
109. Dray J, Tillier F, Dray F, Ullmann A (1972) Hydrolysis of urine metabolites of different steroid hormones by β-glucuronidase from *Escherichia coli*. Ann Inst Pasteur 123:853–857
110. Lesjean B, Gnirss R, Buisson H, Keller S, Tazi-Pain A, Luck F (2005) Outcomes of a 2-year investigation on enhanced biological nutrients removal and trace organics elimination in membrane bioreactor (MBR). Water Sci Technol 52(10–11):453–460
111. Vader JS, van Ginkel CG, Sperling FM, de Jong J, de Boer W, de Graaf JS, van der Most M, Stokman PG (2000) Degradation of ethinyl estradiol by nitrifying activated sludge. Chemosphere 41:1239–1243
112. De Gusseme B, Pycke B, Hennebel T, Marcoen A, Vlaeminck SE, Noppe H, Boon N, Verstraete W (2009) Biological removal of 17α-ethinylestradiol by a nitrifier enrichment culture in a membrane bioreactor. Water Res 43:2493–2503
113. Koh YK, Chiu TY, Boobis AR, Scrimshaw MD, Bagnall JP, Soares A, Pollard S, Cartmell E, Lester JN (2009) Influence of operating parameters on the biodegradation of steroid estrogens and nonylphenolic compounds during biological wastewater treatment processes. Environ Sci Technol 43:6646–6654
114. Weber S, Leuschner P, Kämpfer P, Dott W, Hollender J (2005) Degradation of estradiol and ethinyl estradiol by activated sludge and by a defined mixed culture. Appl Microb Biotechnol 67:106–112
115. González S, Petrovic M, Barceló D (2008) Evaluation of two pilot scale membrane bioreactors for the elimination of selected surfactants from municipal wastewaters. J Hydro 356:46–55
116. Andersen HR, Andersen AM, Arnold SF (1999) Comparison of short-term estrogenicity tests for identification of hormone-disrupting chemicals. Environ Health Perspect 107:89–108

117. Ternes TA, Andersen H, Gilberg D, Bonerz M (2002) Determination of estrogens in sludge and sediments by liquid extraction and GC/MS/MS. Anal Chem 74:3498–3504
118. Larsen TA, Lienert J, Joss A, Siegrist H (2004) How to avoid pharmaceuticals in the aquatic environment. J Biotechnol 113:295–304
119. Lai KM, Johnson KL, Scrimshaw MD, Lester JN (2000) Binding of waterborne steroid phases in river and estuarine systems. Environ Sci Technol 34:3890–3894
120. Yamamoto H, Liljestrand HM, Shimizu Y, Morita M (2003) Effects of physical-chemical characteristics on the sorption of selected endocrine disruptors by dissolved organic matter surrogates. Environ Sci Technol 37:2646–2657
121. Boxall ABA, Blackwell P, Cavallo R, Kay P, Tolls J (2002) The sorption and transport of a sulphonamide antibiotic in soil systems. Toxicol Lett 131:19–28
122. Clara M, Strenn B, Saracevic E, Kreuzinger N (2004) Adsorption of bisphenol-A, 17β-estradiole and 17α-ethinylestradiole to sewage sludge. Chemosphere 56:843–851
123. Mikkelsen LH (2003) Applications and limitations of the colloid titration method for measuring activated sludge surface charges. Water Res 37:2458–2466
124. Ganaye VA, Keiding K, Vogel TM, Viriot ML, Block JC (1997) Evaluation of soil organic matter polarity by pyrene fluorescence spectrum variations. Environ Sci Technol 31:2701–2706
125. Andersen HR, Hansen M, Kjolholt J, Stuer-Lauridsen F, Ternes T, Halling-Sorensen B (2005) Assessment of the importance of sorption for steroid estrogens removal during activated sludge treatment. Chemosphere 61:139–146
126. Ternes T, Joss A, Siegrist H (2004) Scrutinizing pharmaceuticals and personal care products in wastewater treatment. Environ Sci Technol 38:392–399
127. Chen X, Hu J (2009) Degradation of 17β-estradiol and its conjugates: Effects of initial concentration and MLSS concentration. Process Biochem 44:1330–1334
128. Urase T, Kikuta T (2005) Separate estimation of adsorption and degradation of pharmaceutical substances and estrogens in the activated sludge process. Water Res 39: 1289–1300
129. Joss A, Zabczynski S, Göbel A, Hoffmann B, Löffler D, McArdell CS, Ternes TA, Thomsen A, Siegrist H (2006) Biological degradation of pharmaceuticals in municipal wastewater treatment: Proposing a classification scheme. Water Res 40:1686–1696
130. Suárez S, Carballa M, Omil F, Lema JM (2008) How are pharmaceutical and personal care products (PPCPs) removed from urban wastewaters? Rev Environ Sci Biotechnol 7:125–138
131. Ying GG, Kookana RS, Kumar A, Mortimer M (2009) Occurrence and implications of estrogens and xenoestrogens in sewage effluents and receiving waters from South East Queensland. Sci Total Environ 407:5147–5155
132. Cicek N, Franco J, Suidan M, Urbain V, Manem J (1999) Characterization and comparison of a membrane bioreactor and a conventional activated sludge system in the treatment of wastewater containing high molecular weight compounds. Water Environ Res 71:64–70
133. Joss A, Keller E, Alder AC, Goebel A, McArdell CS, Ternes T, Siegrist H (2005) Removal of pharmaceuticals and fragrances in biological wastewater treatment. Water Res 39: 3139–3152
134. Göbel A, McArdell CS, Joss A, Siegrist H, Giger W (2007) Fate of sulfonamides, macrolides, and trimethoprim in different wastewater treatment technologies. Sci Total Environ 372:361–371
135. Baek SH, Pagilla K (2009) Microbial community structures in conventional activated sludge system and membrane bioreactor (MBR). Biotechnol Bioprocess Eng 14:848–853
136. Fan XJ, Urbain V, Qian Y, Manem J, Ng WJ, Ong SL (2000) Nitrification in a membrane bioreactor (MBR) for wastewater treatment. Water Sci Technol 42(3–4):289–294
137. Shi J, Fujisawa S, Nakai S, Hosomi M (2004) Biodegradation of natural and synthetic estrogens by nitrifying activated sludge and ammonia-oxidizing bacterium *Nitrosomonas europaea*. Water Res 38:2323–2330
138. Yi T, Harper WF (2007) The link between nitrification and biotransformation of 17 alpha-ethinylestradiol. Environ Sci Technol 41(12):4311–4316
139. Gaulke LS, Strand SE, Kalhorn TF, David Stensel H (2009) Estrogen biodegradation kinetics and estrogenic activity reduction for two biological wastewater treatment methods. Environ Sci Technol 43:7111–7116
140. Wisniewski C, Leon Cruz A, Grasmick A (1999) Kinetics of organic carbon removal by a mixed culture in a membrane bioreactor. Biochem Eng J 3:61–69
141. Song KG, Choung YK, Ahn KH, Yun H (2003) Performance of membrane bioreactor systems with sludge ozonation process for minimization of excess sludge production. Desalination 157:353–359
142. Radjenović J, Matošić M, Mijatović I, Petrović M, Barceló D (2008) Membrane bioreactor (MBR) as an advanced wastewater treatment technology. Hdb Env Chem 5S:37–101
143. Han SS, Bae TH, Jang GG, Tak TM (2005) Influence of sludge retention time on membrane fouling and bioactivities in membrane bioreactor system. Process Biochem 40:2393–2400
144. Sipma J, Osuna B, Collado N, Monclús H, Ferrero G, Comas J, Rodriguez-Roda I (2010) Comparison of removal of pharmaceuticals in MBR and activated sludge systems. Desalination 250:653–659
145. Li F, Yuasa A, Obara A, Mathews AP (2005) Aerobic batch degradation of 17-β estradiol (E2) by activated sludge: effects of spiking E2 concentrations, MLVSS and temperatures. Water Res 39:2065–2075
146. Yoshimoto T, Nagai F, Fujimoto J, Watanabe K, Mizukoshi H, Makino T, Kimura K, Saino H, Sawada H, Omura H (2004) Degradation of estrogens by *Rhodococcus zopfii* and *Rhodococcus equi* isolates from activated sludge in wastewater treatment plants. Appl Environ Microbiol 70:5283–5289

Waterborne Diseases of the Ocean, Enteric Viruses

Jacquelina W. Woods
US Food and Drug Administration, Center for Food Safety and Applied Nutrition, Gulf Coast Seafood Lab, Dauphin Island, AL, USA

Article Outline

Glossary
Definition of the Subject
Introduction
Enteric Viruses Found in the Environment
Detection of Enteric Viruses
Future Directions
Bibliography

Glossary

Attenuate To reduce or weaken a pathogen.

Cultivate The ability of viruses to replicate under ideal conditions.

Enteric virus Viral particle associated with human feces. Enteric viruses range in size of 20–80 nm and contain RNA or DNA enclosed by a protein capsid.

Environmental stability (microorganism) The ability of an organism to withstand degradation when exposed to environmental factors, such as temperature and sunlight.

Epidemiology The study of the causes, distribution, and patterns of health and illness in a population.

Gastroenteritis Inflammation of the stomach and large and small intestines.

Genogroup Related viruses within a genus.

Icosahedral Having a geometric structure that contains 20 identical equilateral triangular faces, 30 edges, and 12 vertices.

Open reading frame (ORF) A DNA sequence that does not contain a stop codon. ORFs are presumptive genes.

Serotype Distinct antigenic variations within a subgroup or subspecies of bacteria or viruses.

Viremia The presence of viruses in the blood spread through primary and secondary transmission.

Definition of the Subject

Human *enteric viruses* pose a significant health threat in the aquatic environment since they are transmitted via the fecal-oral route. Human activities such as faulty septic systems, agricultural runoff, urban runoff, sewage outfall, and wastewater discharge from vessels are ways enteric viruses are introduced into the environment. There are approximately 140 enteric viruses found in humans, and approximately one billion per gram of feces where at least 10% of the population can shed these viruses at any given time [1]. Enteric viruses can be transferred throughout the environment by attaching to particulates in groundwater, estuarine water, seawater and rivers, estuaries, shellfish grown in contaminated waters, and by aerosols emitted from sewage treatment plants [2]. The fate of these enteric viruses can take many routes, such as rivers, lakes, sewage, land runoff, estuaries, and groundwater. Humans can be exposed to enteric viruses through various routes: crops grown in land irrigated with wastewater or fertilized with sewage, shellfish grown in contaminated water, sewage-polluted recreational waters, and contaminated drinking water. In a waterborne disease outbreak study between 1946 and 1980, water system deficiencies that contributed to these outbreaks were categorized under five major headings: (1) use of contaminated untreated surface water, (2) use of contaminated untreated groundwater, (3) inadequate or interrupted treatment, (4) distribution network problems, and (5) miscellaneous [3]. Deficiencies in treatment and distribution of water contributed to more than 80% of the outbreaks.

Introduction

The most commonly studied enteric viruses belong to the families of single-stranded RNA viruses (ssRNA) [*Picornaviridae* (enteroviruses, polioviruses, coxsackieviruses, hepatitis A virus, and echoviruses), *Caliciviridae* (noroviruses, caliciviruses, and astroviruses)], double-stranded DNA (dsDNA) [*Adenoviridae* (adenoviruses)], and double-stranded RNA (dsRNA) [*Reoviridae* (reoviruses and rotaviruses)]. These enteric viruses have cellular and molecular structures that make them resistant to current water treatment processes. Emerging enteric viral pathogens like Aichi virus (ssRNA), sapovirus (ssRNA), and

picobirnaviridae (bi-segmented dsDNA) have properties similar to currently studied enteric viral pathogens in that they are non-enveloped, resistant to heat inactivation, stable at low pH, resistant to chlorination, or resistant to UV light inactivation [1]. Parvoviruses (the smallest known enteric viruses with ssRNA and high heat resistance) and polyomaviruses (include JC virus, BK virus, and simian virus 40 which are non-enveloped dsDNA viruses) can also be considered emerging viruses but do not cause acute *gastroenteritis* as do the most commonly studied enteric viruses [4–6].

Although enteric virus infections are associated primarily with self-limiting gastroenteritis in humans, they may also cause respiratory infections, conjunctivitis, hepatitis, and diseases that have high mortality rates, such as aseptic meningitis, encephalitis, and paralysis in immunocompromised individuals [7]. In addition, some enteric viruses have been linked to chronic diseases, such as myocarditis and insulin-dependent diabetes [1].

Human enteric viruses can be transmitted by water, food, fomites, and by human contact. They typically have a low infectious dose which makes them an immediate public health concern. In some instances, e.g., norovirus infections, the infectious dose can be as little as one to ten virions with a secondary attack rate of 50% [7]. The risk for infection when consuming viral contaminated water is at least tenfold greater than that for pathogenic bacteria with similar exposures [8]. The World Health Organization (WHO) estimates that the most common waterborne disease, diarrhea, is responsible for 4.6 billion episodes of diarrhea and causes 2.2 million deaths worldwide [9]. Enteric viruses in water are of particular concern because of the potential for contamination from a variety of sources. Because significant advances have been made in the area of environmental virology, enteric viruses have now been recognized as the causative agents in many nonbacterial gastroenteritis cases and outbreaks identified in the past as of unknown etiological origin [2]. Enteric viruses have been detected and linked to many outbreaks from contaminated waters and foodstuff [10–12].

Enteric Viruses Found in the Environment

Norovirus

An outbreak of acute gastroenteritis occurred among students and teachers in a school in Norwalk, Ohio, in 1968 [13]. The initial attack rate had a morbidity of 50%, and a secondary attack produced a higher rate of 82% [14]. Nausea and vomiting occurred in >90% of those affected, while diarrhea occurred in 38% of those affected. The clinical onset of the illness was typically 12–24 h with duration of 12–60 h. Upon subsequent transmission of stool filtrates to human volunteers in 1972, a small round-structured virus (SRSVs) ~27-nm was identified by electron microscopy [15]. Later studies revealed that other SRSVs morphologically similar to NoV caused gastroenteritis, but Norwalk virus remained the prototype of these fecal viruses [14]. Before the discovery of NoV, most cases of gastroenteritis not attributed to bacteria were thought to be caused by nonbacterial gastroenteritis [16]. In 1981, Greenberg et al. published data proposing that NoV might be a calicivirus. In 1993, Jiang et al. provided molecular evidence that NoV was a calicivirus with a 7.6-kilobase (kb) viral genome consisting of a positive sense, single-stranded, polyadenylated RNA. The genome consists of three *open reading frames* (ORFs), which code for the nonstructural proteins including the RNA polymerase (ORF1), capsid protein (ORF2), and a minor structural protein (ORF3). Noroviruses can be separated into five *genogroups* (GI, GII, GII, GIV, and GV) based on the sequence comparison of the RNA polymerase and capsid regions [17, 18]. Genogroup I infects humans only, genogroup II infects humans and swine, and genogroup IV infects humans and canine. Genogroup III infects bovine animals, and genogroups V infects mice. Of the five genogroups, the classification scheme for the different clusters and strains identifies NoV GI containing 8 clusters, GII containing 17 clusters, and GIV containing 1 cluster (Table 1). Noroviruses have an assigned nomenclature where strains are named after the geographic location of the outbreak from which they are first described. The genogroups and genotypes were characterized and classified based on the RNA polymerase region and the complete capsid gene sequences [17, 18]. To date, the most common genogroup implicated in gastrointestinal infections is genogroup II.

Noroviruses are transmitted primarily through the fecal-oral route, consumption of fecally contaminated food or water, or by person-to-person contact. There is a high rate of secondary infection, and this can occur by airborne transmission. Outbreaks commonly occur in

Waterborne Diseases of the Ocean, Enteric Viruses. Table 1 Genogroups, clusters, and strains of human norovirus

GI		GII		GIV	
Cluster	Strain	Cluster	Strain	Cluster	Strain
4	ChibaJPN00	15	J23-USA02	1	Alpha-NLD99
5	MusgroveGBR00	4	Bristol-GB93		
2	SOV-GBR93	12	Wortley-GB00		
6	Hesse-DEU98	1	Hawaii-US94		
1	NY-USA93	16	Tiffin-US03		
3	DSV-USA93	5	Hillingd-GB00		
7	Wnchest-GBR00	2	Msham-GB95		
8	Boxer-USA02	10	Erfurt-DEU01		
		13	Faytvil-US02		
		17	CSE1-US03		
		6	Seacrof-GB00		
		8	Amstdam-NLD99		
		9	VAbeach-US01		
		14	M7-US03		
		7	Leeds-GB00		
		3	Toronto-CAN93		
		11	SW918-JPN01		

schools, nursing homes, hospitals, camps, daycare centers, cruise ships, and any other close community situation. Because norovirus is not listed as a reportable disease to health officials, estimates of the level of infection may not be accurate.

To date, the ability to *cultivate* norovirus has been futile, although several attempts have been made. A Duizer et al. study [19] utilized 27 different cell lines in an unsuccessful attempt to cultivate norovirus. Straub et al. [20] utilized human embryonic intestinal epithelial cells (INT-407) with 3-D tissue culture. The use of INT-407 cells with 3-D tissue culture appeared to be promising as this method provided the closest attempt at mimicking the structure of in vivo cells. The difficulty with cultivation of norovirus may be explained by its specific requirements or receptors needed for attachment to cells in order for replication to occur. Experiments with recombinant norovirus particles and human gastrointestinal biopsies showed preferential binding to epithelial cells of the pyloric region of the stomach and to enterocytes on duodenal villi [19]. Human-specific blood group antigen H1–type expression was shown to be necessary for norovirus attachment to the cells, and most routine cell cultures lack the characteristics of these specialized human intestinal epithelial cells.

The majority of background information on the biological properties of norovirus has been obtained through humans who volunteer for human feeding studies [21, 22]. Infectivity can only be assessed in human dose–response experiments, and the infectious dose had been determined to be around ten virus genomes [22]. This is very critical when considering norovirus survival. Norovirus remains infectious under refrigeration and freezing conditions, it survives well in the environment, and it is resistant to heat and drying conditions. This was demonstrated in an outbreak at a long-term care facility where norovirus survived on fomites and continued to cause infection 2 weeks after the initial peak of illnesses [23]. Norovirus will

continue to be a significant health threat worldwide as this virus continues to evolve. The lack of a tissue culture cell line for effective propagation of norovirus will hinder complete understanding of how this virus causes infection in addition to decreased progression on the development of a productive vaccine.

Hepatitis A Virus

Hepatitis A is a non-enveloped RNA virus 27–32 nm in diameter. It has an *icosahedral* symmetry and belongs to the genus *Hepatovirus* of the *Picornaviridae* family. HAV has a positive-polarity single-stranded 7.5-kb genome with a single ORF with three distinct regions (P1, P2, and P3) [24]. Region P1 consists of four capsid proteins VP1–VP4. Region P2 consists of nonstructural proteins 2A–2C, and region P3 consists of nonstructural proteins and virus-specific proteins (VPg) [24]. HAV demonstrates a high degree of antigenic (amino acid) and genetic (nucleotide) conservation throughout the genome [24, 25]. Although this high propensity for conservation exists, there is still enough diversity to define HAV genotypes and subgenogroups [26]. The genomic regions commonly used to define HAV genogroups include (1) the C terminus of the VP3 region, (2) the N terminus of the VP1 region, (3) the 168-bp junction of the VP1/P2A regions, (4) the 390-bp region of the VP1/P2B regions, and (5) the entire VP1 region [26, 27]. A total of six genotypes have been identified: genotype 1A, 1B, II, III, IV, V, and VI. Genotypes I, II, and III are of human origin, and IV, V, and VI genotypes are of nonhuman primate origin. Genotype I and III are the most prevalent genotypes isolated from humans [28]. Because there is only one *serotype* of HAV, individuals infected by HAV in one part of the world are protected from reinfection by HAV in another part of the world.

Infections with HAV can produce effects that range in severity from asymptomatic to death from fulminant hepatitis. Infections with HAV are typically self-limiting and do not result in chronic liver disease. The virus shed in the feces and peak fecal excretion, hence infectivity, occurs prior to the onset of symptoms [29]. Clinical manifestations can increase with age, and with older children and adults, symptoms are typically present with jaundice occurring in 70% of those infected [29]. An average incubation period is 28 days with a range of 15–50 days. Symptoms include gastroenteritis, fever, malaise, anorexia, nausea, abdominal discomfort, dark urine, and jaundice, all which may last up to 2 months. Chronic liver disease has not been shown to persist, although 15–20% of those infected may have prolonged or relapsing disease lasting up to 6 months [30]. Fulminant hepatitis is a rare complication in HAV infections, only occurring in $<1\%$ of those infected, with the highest rates occurring in young children and elderly adults who may have underlying liver conditions [28]. Among those with fulminant disease, reported findings demonstrate nucleotide and/or amino acid substitutions in the 5′ untranslated region, P2 region, and the P3 region of the HAV genome [28, 31].

Cell culture propagation of human and nonhuman HAV has occurred in African green monkey kidney and fetal rhesus monkey kidney cells [32, 33]. Propagation of HAV of human origin is quite different than propagation of other picornaviruses of human origin. HAV of human origin requires an extensive adaptation period or serial passages before it grows in cell culture, and once it has adapted, HAV becomes *attenuated* as demonstrated by not producing disease in experimentally inoculated nonhuman primates [34]. Mutations causing attenuation in viral nucleic acid could play a significant role in the adaptation of HAV in cell culture [24, 33]. The attenuated strain HM-175 was adapted in cell culture, and this strain is currently used as vaccination agent for HAV [24].

HAV is a major cause of acute hepatitis in developed countries, while in developing countries, it can be considered endemic [35]. HAV is transmitted primarily by the fecal-oral route, via person-to-person contact, and by contaminated food or water, while the other common hepatitis viruses (hepatitis B and hepatitis C) are typically transmitted by blood or body fluids. HAV is stable in the environment when associated with organic material, and it is resistant to low pH and heating [36]. The name "hepatitis" is derived from the fact that HAV replicates in the liver and affects the liver. The source of the infectious agent, however, cannot be identified in approximately 50% of reported hepatitis A cases in the U.S., partly because of the long incubation before the appearance of symptoms [28]. Because outbreaks of HAV can cause considerable morbidity and even mortality, it is imperative that HAV be isolated and identified as the implicated pathogen.

Enterovirus

Human enteroviruses are members of Picornaviridae family and *Enterovirus* genus. They are icosahedral, non-enveloped, with a diameter of 27–30 nm. The genome is 7.5–8.5 kb and is composed of single-stranded positive polarity RNA. Enteroviruses are further divided into the subgenera/species of poliovirus, coxsackieviruses, echoviruses, and enteroviruses, and they are marked according to their serotypes. The poliovirus group consists of three different serotypes. Types 1 and 3 are recognized as epidemic, while type 2 is endemic [37]. Coxsackieviruses consist of groups A and B, where the A group contains 24 serotypes, and the B group contains six serotypes. In 2003, the International Committee on Taxonomy of Viruses classified *Enteroviruses* into four groups of species based on their molecular properties [38] (Table 2).

Infections due to enteroviruses are common, causing a range of disease including pharyngitis and poliomyelitis. In the United States, it is estimated that 30–50 million enterovirus infections occur a year, of which only 5–15 million are symptomatic [37]. The virus is spread by the fecal-oral route and person to person through direct contact with secretions of an infected individual. The incubation period is usually 3–7 days with virus transmission lasting 3–10 days after symptoms appear. Replication occurs in the gastrointestinal track, but can occur in other tissues, such as nerve and muscle [37, 39]. Polioviruses typically infect their host by attacking the central nervous system, causing paralysis (poliomyelitis) in infected individuals. The spread of poliovirus has been limited by the development and use of vaccines. The Sabin trivalent oral live attenuated vaccine (OPV) consists of three live attenuated strains of 1, 2, and 3 serotypes grown in cell culture. The Salk vaccine is a trivalent inactivated polio vaccine (IPV) given by injection. The Sabin vaccine has an advantage over the Salk vaccine in that it elicits secretory IgA antibody production in addition to IgA, IgM, and IgG serum antibody production [40]. Coxsackieviruses have been associated with respiratory infections, gastroenteritis, insulin-dependent diabetes, myocarditis, and pericarditis [1]. Echoviruses are typically less infectious and are usually associated with the common cold and other respiratory diseases. The numbered enteroviruses have not been widely studied, but they are generally associated with bronchiolitis, conjunctivitis, meningitis, and paralysis [7, 41]. Also, enteroviruses are one of few enteric viruses which produce *viremia* in infected patients.

Enteroviruses are resistant to most concentrations of chlorine used in sewage treatment, and they are tolerant to cold and warm temperatures. This makes them ideally suited for survival in the environment. Stability of enteroviruses in the environment is dependent on temperature, humidity, and UV radiation. In order to inactivate 90% of poliovirus in salt water environment, 671 days at 4°C is required; on the other hand, an increase in the temperature to 25°C reduces the inactivation time by 25 days [37]. Symonds et al. [81] collected sewage influent and effluent from several wastewater treatment plants (WWTP) across the United States and revealed that 75% of the sewage influent and 8.3% of the effluent contained enteroviruses. In 2003, the largest European outbreak of enterovirus-related infection occurred in Belarus [42]. Over 1,300 people became ill, and water contaminated with echovirus and coxsackievirus was identified as the source of the infection. Aside from water and sewage samples, enteroviruses have been detected in food samples. In 1914, the first described food-borne outbreak was linked to milk contaminated with poliovirus [43]. After pasteurization of milk was adopted, transmission of enterovirus by contaminated milk decreased dramatically. Despite its demonstrated presence in the

Waterborne Diseases of the Ocean, Enteric Viruses. Classification of human enteroviruses

Groups of enteroviruses	Species of enteroviruses
Enterovirus-A	Coxsackievirus A2–8, 10, 12, 14, 16
	Enterovirus 71, 76, 89, 90, 91
Enterovirus-B	Coxsackievirus A9
	Coxsackievirus B1–6
	Echovirus 1–7, 9, 11–21, 24–27, 29–33
	Enterovirus 69, 73–75, 77–78, 79–88, 100–101
Enterovirus-C	Coxsackievirus A1, 11, 13, 17–22, 24
	Poliovirus 1–3
Enterovirus-D	Enterovirus 68, 70

environment and sewage, there have been very few food-borne-related outbreaks due to enterovirus.

Adenovirus

Adenoviruses are members of the *Adenoviridae* family and the *Mastadenovirus* genus, which comprises five genera and infects hosts across the extended spectrum of vertebrates [44, 45]. Human adenoviruses are a double-stranded DNA virus containing a non-enveloped icosahedral shell with fingerlike projections forming each of the 12 vertices [46]. Its DNA is linear, about 35 kb in size, and it encodes for more than 30 structural and nonstructural proteins [47]. In 1953, the first adenovirus was isolated from human adenoid tissue [48]. There are 51 serotypes of adenovirus, and they are divided into six species, A–F, based on their hemagglutination properties, their oncogenic potential in rodents, and DNA homology or GC content [44].

Infections with adenoviruses can result in a wide range of clinical symptoms. Subgroups A, D, and F are sites for gastrointestinal infections. Subgroup B is responsible for lung and urinary tract infections. Subgroups C and E are responsible for respiratory tract infections. Serotypes 40 and 41 are the cause of most adenovirus associated–gastroenteritis, and serotypes 4 and 7 are associated with most cases of ARD (acute respiratory disease) in the United States [49]. Most adenovirus infections are self-limiting except cases where the infected individual is immunocompromised. However, in 2007, there were cases of a new emerging strain of adenovirus 14 that caused fatal respiratory disease in healthy individuals [50]. After the primary infection, immunity is conferred to the causative adenovirus serotype.

Human adenoviruses are specific to humans even though adenoviruses infect a range of animals. In 2005, Cox et al. reported no viable human adenovirus detection in feces of cattle, valve, pig, sheep, horse, dog, poultry, wombat, cat, kangaroo, possum, wood duck, rat, wild pig, fox, rabbit, ferry cat, goat, carp, and deer. In domestic sewage worldwide, human adenoviruses have been detected in high concentrations and their detection in sewage seems to have little seasonal variability [2, 44, 51]. As with most enteric viruses, adenovirus survives better in the environment and sewage treatment than the current indicator bacteria. Adenoviruses have increased resistance to UV light, and this increased resistant could be due to the DNA repair mechanism of the host cell. Because of the *environmental stability* of adenovirus, they have been suggested as an indicator of viral pollution [52]. In current literature, adenovirus has been associated with waterborne outbreaks. Foodborne outbreaks have been suspected but not confirmed [49, 53].

Rotavirus

Rotaviruses are a significant cause of infantile viral gastroenteritis, with 114 million annual cases of diarrhea and up to 352,000–592,000 deaths in children younger than five worldwide [54]. Rotavirus' increased activity occurs during peak respiratory virus activity, rising in the winter and peaking in the spring.

Rotaviruses are members of the family *Reoviridae* and are double-stranded RNA with 11 segments and a triple capsid structure. Classification of rotavirus into P and G genotypes/serotypes are based on the outer capsid proteins, VP4 (P protein) and VP7 (G protein). Only 14 G and 15 P genotypes have been identified in humans [55]. There are seven different serogroups of rotavirus (A–G). Although individuals may have multiple rotavirus infections over time, group A rotaviruses cause the greatest numbers of cases of acute gastroenteritis (AGE) in children under 2.

The primary route of transmission of rotavirus is the fecal-oral route; additionally, the persistence of rotaviruses in aquatic environments and their resistance to water treatment and disinfection processes may facilitate their transmission to humans. Rotavirus has been implicated in many waterborne epidemics, and these viruses have been isolated in sewage, river water, groundwater, and drinking water [56–58]. Rotaviruses are resistant to most disinfectants, heat, proteolytic enzymes, and pH with ranges of 3–10. Their ability to survive in various environmental conditions for long periods of time contributes to their high rate of infection.

The burden of rotavirus disease has prompted a need for an effective vaccine. In 1998, FDA-approved RotaShield, a tetravalent human-rhesus genetic reassortant vaccine. RotaShield was withdrawn from the US market after it was shown to be associated with intussusceptions in infants. Vaccine development

continued with the license of a monovalent human rotavirus vaccine Rotarix™ and the pentavalent bovine-human reassortant vaccine RotaTeq™. To date, neither of the later derived vaccines have been associated with intussusceptions.

Hepatitis E Virus

Hepatitis E virus infections are a major cause of acute enterically transmitted non-A, non-B (ET-NANB) hepatitis in many developing countries throughout Middle East, Asia, and Africa [59]. This disease is associated with >50% of sporadic acute hepatitis which is a cause for great public health concern [60]. HEV can be both endemic and epidemic with outbreaks generally associated with fecal contamination of drinking water. North America and Europe have generally been considered non-endemic with documented cases from individuals who had previously traveled to endemic areas. It has been implied that HEV disease may be zoonotic in endemic regions and regions where HEV disease is non-endemic [61]. Domestic animals such as cattle, sheep, and pigs all appear to be reservoirs of the virus, which may explain the presence of anti-HEV antibodies in individuals with no obvious or known contact with human strains of the virus.

Hepatitis E is a single-stranded non-enveloped positive-sense RNA virus approximately 27–30 nm in diameter with a genome of about 7.2 kb [62]. HEV is currently classified as the only member of the genus *Hepevirus* in the family *Hepeviridae* [63]. Phylogenetic analysis has identified four significant genotypes of HEV [62]. Genotype 1 (G1) was isolated from Africa and Asia, genotype 2 (G2) from Mexico, and genotype 3 (G3) and genotype 4 (G4) from the United States, China, Japan, Europe, and Vietnam [62]. Genotype 3, which differs from genotypes 1, 2, and 4 by 25.6–26.3%, 25.3–25.5%, and 23.7–24.7%, respectively, is the first animal strain of HEV to be characterized [61]. Additional HEV genotypes may be present as other new strains have not been completely sequenced and therefore cannot be prominently assigned to a genotype at present time.

Recognition of Hepatitis E as a distinctly unique agent of human disease did not occur until the 1980s [64] with the development of serological laboratory tests. Prior to the development of these tests, clinical HEV infection was determined to be the etiological agent by process of elimination. Since the *epidemiology* of hepatitis A had been well characterized, assumptions were plausible that >90% of the adult population in most Asian and Indian countries had previous exposure to HAV and were therefore immune to HAV infection [65]. This statement was proven when serologic tests for the diagnosis of hepatitis A and hepatitis E were applied to stored clinical samples collected during a waterborne epidemic of viral hepatitis in India [65]. Among these stored samples were those of the epidemic that occurred in Delhi, India, in 1955–1956 where in a population of 1.6 million, approximately 29,300 jaundice cases occurred, with an estimated 67,700 non-icteric infections. This was the first reported outbreak of disease where ET-NANB hepatitis was determined to be the etiological agent and virtually 100% of stored serum samples from such epidemics were found to contain IgG anti-HAV but not IgM anti-HAV. This can be considered definitive evidence for the existence of a previously unrecognized hepatitis as the etiological agent in past epidemics [65]. Application of current HEV immunological tests on these epidemic samples can further strengthen the evidence for ET-NANB as the causative agent in these waterborne outbreaks occurring decades ago.

The epidemiology and virology of hepatitis E suggest that HEV is less readily transmitted than HAV [64]. In South Asia, HEV incidence has been characterized by marked seasonality, with outbreaks occurring during the rainy or monsoon seasons [65]. Outbreak investigations often reveal fecally contaminated drinking water as the source of HEV infections. It appears that rain-induced flooding allows sewage to contaminate water supplies which explains the seasonal associations. Communities with inadequate sewage disposal are prone to recurrent HEV outbreaks. Low levels of community sanitation are also strongly associated with both epidemic and endemic HEV. An example of this occurred in Indonesia where the use of river water for cooking and drinking, improper disposal of human waste, and poor personal hygiene were significantly associated with increased anti-HEV IgG seroprevalence. More recent interactions between changing human culture and HEV are seen in epidemics of hepatitis E that occur among refugee camps

under substandard living conditions in Ethiopia and Somalia [66]. These findings highlight the risk of HEV to aid workers and military installations stationed in countries where HEV is epidemic. Therefore, prevention and control of HEV in epidemic areas will entail improvements in community sanitation, management of sewage distribution, and treatment of drinking water.

Enterically transmitted Hepatitis E has a secondary attack rate around 2% and a relatively low infectivity compared to hepatitis A, which has a 10–20% secondary attack rate among household contacts. It is not clear why HEV has a lower secondary attack rate than HAV. The lowered environmental stability of HEV may contribute to its lower secondary attack rate [63]. Also, studies of HEV have shown an association between the severity of the disease and inoculum size, where a larger infectious dose of HEV may be required to cause overt disease. There has been no recognizable difference in attack rates or infection rates by sex where there was documented exposure to HEV [65]. However, some studies have shown that adult men in some instances may have a greater risk of developing clinical illness. This could be due to infectious dose since men could have higher exposure rates than women. In addition, societal restrictions placed on women in some cultures may minimize their exposure to HEV [64].

Transmission of hepatitis E from mother to child has been reported with associated morbidity and mortality. A small study was conducted among ten pregnant women who were infected with HEV in their third trimester. Of those who had successful delivery, six transmitted HEV to their child. HEV antigen was found in five of the six infants, and anti-IgM was found in three of six infants [65]. Other studies have also shown a twofold increased risk of clinical HEV disease among pregnant women compared with non-pregnant women of reproductive age [65]. Both epidemic and clinical studies have shown that pregnant women have an increased likelihood of developing acute hepatitis and even fulminant hepatic failure after HEV infection. Since hepatitis infections involve the liver, it is reasonable to assume that the increased complications of pregnancy due to hepatitis can lead to increased adverse outcomes with risks of neonatal icterus. These reported findings of vertical transmission pose difficulty in accessing the risk of fecal-oral infections in newborns.

Despite our discovery of the hepatitis E, this virus continues to pose a global public health problem. There have been many advances in understanding the clinical, virological, and epidemiological characteristics of HEV, but there are still many unanswered questions. Development of an effective vaccine is currently not possible because a cell culture system that efficiently grows the virus has not been discovered, although there have been different vaccine candidates purposed. As future research of HEV continues, the epidemiologic features of this important virus will be clarified further and a protective vaccine will be developed. Perhaps then we can resolve the reasons for increased morbidity and mortality in pregnant women and determine factors which lead the persistence of protective antibodies. Once these questions have been answered, we will have better control and understanding of hepatitis E.

Detection of Enteric Viruses

In the past, detection of enteric viruses in environmental samples largely depended on whether the agent grew in cell culture. For those types that do, such as enteroviruses and adenoviruses, detection by virus replication in cell culture demonstrated infectivity as well as their presence. The ability to detect viruses by cell culture is a clear advantage when assessing whether environmental samples or foods are microbiologically hazardous. The capacity to do quantitative assays is also a bonus of cell culture. Cytopathic effect or virus-specific killing or lysing of cells is visible by ordinary light microscopy. Cell culture assays were the most widely used protocol for detection of enteric viruses until the 1990s [53, 67, 68]. While cell culture offers quantitative analysis and infectivity, the high cost, long turnaround time, and labor-intensive efforts are drawbacks. There are many cell lines suitable for growing enteric viruses. Buffalo green monkey (BGM) cell line has been shown to give higher plaques forming units per milliliter (PFU/ml) and faster CPE for coxsackieviruses and polioviruses [69].

There are a host of enteric viruses that are capable of growth utilizing cell culture, but two significant enteric viruses, human noroviruses and wild-type HAV, are difficult or unable to propagate in cell culture. Cell culture would apparently not be a proactive monitoring protocol given the length of time required to complete most assays and difficulties of propagation.

However, cell culture used in conjunction with detection emerging assays can be used to address the issue of viability while comparing the sensitivity of each representative assay.

Detection of enteric viral pathogens with molecular-based PCR assays has successfully been utilized for a number of years [17, 70–72]. Conventional PCR methodology utilizes a pair of oligonucleotides or primers, each hybridizing to one strand of double-stranded DNA (dsDNA) target. The types of primers used can be (1) random primers – short single-stranded DNA fragments with all possible combinations of bases, (2) polythymine primers – 16-base-long thymine primers that will hybridize with the polyadenine end of the mRNA, and (3) specific primers – only the targeted region specific to the primers will be amplified. The primers act as a substrate for DNA polymerase which creates a complementary strand by the way of sequential addition of deoxynucleotides. The process of PCR can be summarized into three steps: (1) denaturation – dsDNA is separated by an increase in temperature, (2) annealing – the temperature is decreased to allow the primers to anneal to the separated DNA, and (3) extension – the extension of the DNA fragment with the primers attached by addition of deoxynucleotides. For RNA viruses such as enteroviruses, NoV, and HAV, RT-PCR, or the conversion of RNA to cDNA, is necessary. During reverse transcription, a primer is required for the reverse transcriptase (RNA-dependent DNA polymerase) to initiate the synthesis of cDNA from the viral RNA. For DNA viruses, reverse transcription is not a necessary step. The final PCR product is analyzed by electrophoresis in the presence of ethidium bromide in which the correct size of the product can be examined visually by ultraviolet light. Hybridization with digoxigenin-labeled probes or genetic sequencing can be used to further identify PCR products. If the products examined are from environmental samples, cloning of the PCR products may also be required as there can be multiple strains of individual viruses present.

Real-time quantitative PCR or qPCR is used to quantitatively determine the amount of original target present in the sample [73, 74]. During a qPCR assay, the amplicon produced during each cycle can be quantified using SYBR Green (nonspecific attachment to dsDNA), or by using a fluorescent internal probe (specific hybridization) [74]. For SYBR green assays, melt curve analysis is important to ensure that the desired DNA fragment is detected as different DNA fragments have different T_m (melting temperature). For fluorescent internal probes, fluorescence is measured during each cycle, and when the amount of fluorescence exceeds the background level (threshold level), the sample is scored as positive. The number of cycles required to reach the threshold level, commonly referred to as the cycle threshold value (C_t), correlates with the amount of target in the sample prior to amplification [73]. Real-time PCR is an excellent tool for detection of enteric viruses in environmental samples and has been used successfully to determine the concentrations of viral genomes [75, 76].

Multiplex PCR, which utilizes multiple primer sets within a single PCR reaction, can be used to simultaneously detect different groups of viruses. However, this multiple viral detection can be difficult to optimize because of the different annealing temperature requirements of dissimilar primer sets and because of the properties of the viral nucleic acids found between viral groups [41]. Real-time PCR (qPCR) has been quite successful for detection of multiple enteric viruses, because it can analyze each target independently in the same assay by using specific internal probes binding to different fluorochromes that the real-time PCR equipment can analyze independently [77, 78]. Furthermore, the PCR products can be of a similar size, providing better amplification efficiency. For viruses that grow poorly in cell culture, the detection by PCR integrated with cell culture (i.e., ICC-PCR) drastically reduces the time needed for detection [79]. The detection of enteroviruses in water can be between 3 and 14 days using cell culture, 5 days using integrated cell culture, and less than a day using direct real-time PCR. Because viruses are normally present in very low concentrations in environmental samples, the level of sensitivity of most PCR is advantageous for detection of low copy number. While the sensitivity of PCR is beneficial, the presence of inhibitory substances (i.e., humic acid or heavy metals) in concentrated environmental samples is of concern. Internal controls for real-time PCR have been developed to determine the presence of inhibitors in a sample and ensure that reaction conditions are optimal [80].

While there has been tremendous progress in molecular detection assays, complications remain. Even though most molecular-based assays are specific, sensitive, rapid, and cost efficient, there has been no development of a universal method or standardization. Perhaps future development of molecular-based assays that can establish infectivity will combine best of cell culture and PCR when it comes to the detection of enteric viruses in the environment.

Future Directions

Enteric viruses in the aquatic environment have been thoroughly studied over the years. Their persistence and distribution in the environment continues to cause threats to public health. Development of molecular techniques has allowed detection of these viral pathogens, especially those that cannot be readily propagated utilizing cell culture techniques. As we continue to make advances in understanding the pathogenic nature of these viruses, we can be instrumental in preventing disease outbreaks and improve public health.

Bibliography

Primary Literature

1. Griffin DW, Donaldson KA, Paul JH, Rose JB (2003) Pathogenic human viruses in coastal waters. Clin Microbial Rev 16:129–143
2. Bosch A (1998) Human enteric viruses in the water environment: a minireview. Int Microbial 1:191–196
3. Lippy EC, Waltrip SL (1984) Waterborne disease outbreaks 1946–1980: a thirty-five year prospective. J Am Water Works Assoc 76:60–67
4. Bofill-Mas S, Pina S, Girones R (2000) Documenting the epidemiologic patterns of polyomaviruses in human populations by studying their presence in urban sewage. Appl Environ Microbiol 66:238–245
5. Brauniger S, Peters J, Borchers U, Kao M, Borchers U (2000) Further studies of thermal resistance of bovine parvovirus against moist and dry heat. Int J Hyg Environ Health 203:71–75
6. Engelbrecht RS, Weber MJ, Salter BL, Schmidt CA (1980) Comparative inactivation of viruses by chlorine. Appl Environ Microbiol 40:249–256
7. Kocwa-Haluch R (2001) Waterborne enteroviruses as a hazard for human health. Pol J Environ Stud 10:485–487
8. Haas CN, Rose JB, Gerba CP, Regli R (1993) Risk assessment of viruses in drinking water. Risk Anal 13:545–552
9. World Health Organization (2010) Guidelines for drinking-water quality. Recommendations, 3rd edn. World Health Organization, Geneva
10. Beuret C, Kohler D, Baumgartner A, Luthi TM (2002) Norwalk-like virus sequences in mineral waters: one year monitoring of three brands. Appl Environ Microbiol 68:1925–1931
11. Daniels NA, Bergmire-Sweat DA, Schwab KJ, Hendricks KA, Reddy S, Monroe SA, Fankhauser RL, Monroe SS, Atmar RL, Glass RI, Mead P (2000) A foodborne outbreak of gastroenteritis associated with Norwalk-like viruses: first molecular traceback to deli sandwiches contaminated during preparation. J Infect Dis 181:1467–1470
12. Munnoch S, Ashbolt R, Coleman DJ, Walton N, Beers-Debble MY, Taylor R (2004) A multi-jurisdictional outbreak of hepatitis A related to a youth camp-implications for catering operations and mass gatherings. Commun Dis Intell 28:521–527
13. Adler J, Zickl R (1969) Winter vomiting disease. J Infect Dis 119:668–673
14. Atmar R, Estes MK (2001) Diagnosis of noncultivatable gastroenteritis viruses, the human caliciviruses. Clin Microbiol Rev 14:15–37
15. Kapikian AZ, Wyatt RG, Dolin R, Thornhill TS, Kalica AR, Chanock RM (1972) Visualization by immune electron microscopy of a 27-nm particle associated with acute gastroenteritis. J Virol 10:1075–1081
16. Rippey SR (1994) Infectious disease associated with molluscan shellfish consumption. Clin Microbiol Rev 7:419–425
17. Ando T, Monron SS, Gentsch JR, Jin Q, Lewis DC, Glass RI (1995) Detection and differentiation of antigenically distinct small round structured viruses (Norwalk-like viruses) by reverse transcription-PCR and southern hybridization. J Clin Microbiol 33:64–71
18. Zheng D, Ando T, Fankhauser RL, Beard RS, Glass RI, Monroe SS (2006) Norovirus classification and proposed strain nomenclature. Virology 346:312–323
19. Duizer E, Schwab KJ, Neil FH, Atmar RL, Koopmans MPG, Estes MK (2004) Laboratory efforts to cultivate noroviruses. J Gen Virol 85:79–87
20. Straub TM, Honer zu Bentrup K, Orosz-Coghlan P, Dohnalkova A, Mayer BK, Bartholomew A, Valdez CO, Bruckner-Lea CJ, Gerba C, Abbazadegan CM, Nickerson CA (2007) In vitro cell culture infectivity assay for human noroviruses. Emerg Infect Dis 13:396–403
21. Dolin R, Blacklow NR, Dupont H, Formal S, Buscho RF, Kasel JA, Buscho RF, Kasel JA, Chames RP, Hornick R, Channock RM (1971) Transmission of acute infectious nonbacterial gastroenteritis to volunteers by oral administration of stool filtrates. J Infect Dis 123:307–312
22. Teunis PF, Moe CL, Liu P, Miller SE, Lindesmith L, Baric RS, Le Pendu J, Calderone RL (2008) Norwalk virus: how infectious is it? J Med Virol 80:1468–1476
23. Wu HM, Fornek M, Schwab K, Chapin AR, Gibson K, Schwab E, Spencer C, Henning K (2005) A norovirus outbreak of a long-term-care facility: the role of environmental surface contamination. Infect Control Hosp Epidemiol 26: 802–810
24. Cohen JL, Rosenblum B, Ticehurst JR, Daemer RJ, Feinstone SM, Purcell RH (1987) Complete nucleotide sequence of an

attenuated hepatitis A virus: comparison with wild-type virus. Proc Natl Acad Sci USA 84:2497–2501
25. Lemon SM, Jansen RW, Brown EA (1992) Genetic, antigenic, and biological differences between strains of hepatitis A virus. Vaccine 10(suppl 1):S40–S44
26. Robertson BH, Janson RW, Khanna B, Totsuka A, Nainan OY, Siegl G, Widell A, Margolis HS, Isomura S, Ito K, Ishizu T, Moritsugu Y, Lemon SM (1992) Genetic relatedness of hepatitis A virus strains recovered from different geographical regions. J Gen Virol 73:1365–1377
27. Hutin YJ, Pool E, Cramer EH, Nainan OV, Weth J, Williams LT, Goldstein ST, Gensheimer KF, Bell BP, Shapiro CN, Alter MJ, Margolis HS (1999) A multistate, foodborne outbreak of hepatitis A. National hepatitis A investigation team. N Engl J Med 340:595–602
28. Nainan OV, Armstrong GL, Han X, Williams I, Bell BP, Margolis HS (2005) Hepatitis A molecular epidemiology in the United States, 1996–1997: sources of infection and implications of vaccination policy. J Infect Dis 191:957–963
29. Lednar WM, Lemon SM, Kirkpatrick JW, Redfield RR, Fields ML, Kelly PW (1985) Frequency of illness associated with epidemic hepatitis A virus infections in adults. Am J Epidemiol 122: 226–233
30. Glikson M, Galum E, Owen R, Tur-Kaspa R, Shouval D (1992) Relapsing hepatitis A: a review of 14 cases and literature survey. Medicine (Baltimore) 71:14–23
31. Fujiwara K, Yokosuka O, Fukai K, Imazeki F, Saisho H, Omata M (2001) Analysis of full-length hepatitis A virus genome in sera from patients with fulminant and self-limited acute type hepatitis A. J Hepatol 35:112–119
32. Flehmig B (1980) Hepatitis A-virus in cell culture I. Propagation of different hepatitis A-virus isolates in a fetal rhesus monkey kidney cell line (FRhK-4). Med Microbiol Immunol 168:239–248
33. Daemer RJ, Feinstone SM, Gust LL, Purcell RH (1981) Propagation of human hepatitis A virus in African green monkey kidney cell culture: primary isolation and serial passage. Infect Immun 32:388–393
34. Feinstone SM, Kapikian AZ, Purcell RH (1973) Hepatitis A detection by immune electron microscopy of a virus-like antigen associated with acute illness. Science 182: 1026–1028
35. Jothikumar N, Cromeans TL, Sobsey MD, Robertson B (2005) Development and evaluation of a broadly reactive Taqman assay for rapid detection of hepatitis A virus. Appl Environ Microbiol 71:3359–3363
36. Hollinger FB, Emerson SU (2001) Hepatitis A virus. In: Knipe DM, Howley PM (eds) Fields virology, 4th edn. Lippincott Williams & Wilkins, New York, pp 799–840
37. Rajtar B, Majek M, Polanski L, Polz-Dacewicz M (2008) Enteroviruses in water environment – a potential threat to public health. Ann Agric Environ Med 15:199–203
38. Khetsuriani N, Lamonte-Fowlkes A, Oberst S, Pallansch MA (2006) Centers for disease control and prevention: enterovirus surveillance-United States, 1970–2005. Morb Mortal Wkly Rep 55:1–20
39. Colbere-Garapin F, Christodoulou C, Crainic R, Pelletier I (1989) Persistent poliovirus infection of human neuroblastoma cells. Proc Natl Acad Sci USA 86:7590–7594
40. Howard RS (2005) Poliomyelitis and the postpolio syndrome. Br Med J 330:1314–1318
41. Fong T, Lipp EK (2005) Enteric viruses of human and animals in aquatic environments: health risks, detection, and potential water quality assessment tools. Microbiol Mol Biol Rev 69: 357–371
42. Amvrosieva TV, Paklonskaya NV, Biazruchka AA, Kazinetz ON, Bohush ZF, Fisenko EG (2006) Enteroviral infection outbreak in the Republic of Belarus: principal characteristics and phylogenetic analysis of etiological agents. Cent Eur J Public Health 14:67–73
43. Jubb G (1915) The third outbreak of epidemic poliomyelitis at West Kirby. Lancet 1:67
44. Jiang X, Wang M, Wang K, Estes MK (1993) Sequence and genomic organization of Norwalk virus. Virology 195:51–61
45. Wigand R, Adrian T (1986) Classification and epidemiology of adenoviruses. In: Doerfler W (ed) Adenovirus DNA. Martinus Nijhoff, Boston
46. Stewart PL, Fuller SD, Burnett RM (1993) Difference imaging of adenovirus – bridging the resolution gap between X-ray crystallography and electron-microscopy. EMBO J 12: 2589–2599
47. Friefeld BR, Lichy J, Field J, Gronostajski RM, Guggenheimer RA, Krevolin MD, Nagata K, Hutwitz J, Horowitz MS (1984) The in-vitro replication of adenovirus DNA in the molecular biology of adenoviruses. In: Doerfler W (ed) Current topics in microbiology and immunology. Springer, Berlin, pp 221–225
48. Rowe WP, Huebner RJ, Gilmore LK, Parrot RH, Ward TG (1953) Isolation of a cytopathogenic agent from human adenoids undergoing spontaneous degeneration in tissue culture. Proc Soc Exp Biol Med 84:570–573
49. Center for Disease Control and Prevention (2005) Adenoviruses. CDC, Atlanta [Ref Type: Pamphlet]
50. Center for Disease Control and Prevention (2007) Acute respiratory disease associated with adenovirus serotype 14 – four states, 2006–2007. Morb Mortal Wkly Rep 56:1181–1184
51. Carter MJ (2005) Enterically infecting viruses: pathogenicity, transmission and significance for food and waterborne infection. J Appl Microbiol 98:1354–1380
52. Pina S, Puig M, Lucena F, Jofre J, Girones R (1998) Viral pollution in the environment and in shellfish human adenovirus detection by PCR as an index of human viruses. Appl Environ Microbiol 64:3376–3382
53. Goyal SM (2006) Viruses in food. Springer, New York
54. Grimwood K, Buttery JP (2007) Clinical update: rotavirus gastroenteritis and its prevention. Lancet 370:302–304
55. Martinez-Laso J, Roman A, Head J, Cervera I, Rodrigues M, Rodrigues-Avial I, Picazo J (2009) Phylogeny of G9 rotavirus genotype: a possible explanation of its origin and evolution. J Clin Virol 44:52–57
56. Grassi T, Bagordo F, Idolo A, Lugoli F, Gabutti G, De Donno A (2010) Rotavirus detection in environmental water samples by

tangential flow ultrafiltration and RT-nested PCR. Environ Monit Assess 164:199–205
57. Abad FX, Pinto RM, Bosch A (1994) Survival of enteric viruses on environmental fomites. Appl Environ Microbiol 60:3704–3710
58. Gratacap-Cavallier B, Genoulza O, Brengel-Pese K, Soule H, Innocenti-Francillard R, Bost M, Gofit L, Zmirou D, Seigneurin M (2000) Detection of human and animal rotavirus sequences in drinking water. Appl Environ Microbiol 66: 2690–2692
59. Ooi W, Gawoski JM, Yarbough PO, Pankey GA (1999) Hepatitis E seroconversion in United States travelers abroad. Am J Trop Med Hyg 61:822–824
60. Casares-Clemente P, Pina S, Buti M, Jardi R, Martin M, Bofill-Mass S, Girones R (2003) Hepatitis E virus epidemiology in industrialized countries. Emerg Infect Dis 9:448–454
61. Engle RE, Yu C, Emerson SU, Meng XJ, Purell RH (2002) Hepatitis E virus (HEV) capsid antigens derived from viruses of human and swine origin are equally efficient for detecting anti-HEV by enzyme immunoassay. J Clin Microbiol 40: 4576–4580
62. Li T-C, Saito M, Ogura G, Ishibashi O, Miyamura T, Takeda N (2006) Serological evidence for hepatitis E virus infection in mongoose. Am J Trop Med Hyg 74:932–936
63. Emerson SU, Purcell RH (2003) Hepatitis E virus. Rev Med Virol 13:145–154
64. Purcell RH (1994) Hepatitis virus: changing patterns of human disease. Proc Natl Acad Sci USA 91:2401–2406
65. Labrique AB, Thomas DL, Stoszek SK, Nelson KE (1999) Hepatitis E: an emerging infectious disease. Epidemiol Rev 21:162–179
66. Isaacson M, Frean J, He J, Seriwatana J, Innis BL (2000) An outbreak of hepatitis E in northern Namibia, 1983. Am J Trop Med Hyg 62:619–625
67. Farrah SR, Goyal SM, Gerba CP, Wallis C, Melnick JL (1977) Concentration of enteroviruses from estuarine water. Appl Environ Microbiol 33:1192–1196
68. Rao VC, Seidel KM, Goyal SM, Metcalf TG, Melnick JL (1984) Isolation of enteroviruses from water, suspended solids, and sediments from Galveston Bay; survival of poliovirus and rotavirus adsorbed to sediments. Appl Environ Microbiol 48: 404–409
69. Chonmaitree T, Ford C, Sanders C, Lucia H (1985) Comparison of cell cultures for rapid isolation of enteroviruses. J Clin Microbiol 26:2576–2580
70. Caro V, Guillot S, Delpeyroux F, Crainic R (2001) Molecular strategy for 'serotyping' of human enteroviruses. J Gen Virol 82:79–91
71. Croci L, Medici DD, Morace G, Fiore A, Scalfaro C, Beneduce F, Toti L (1999) Detection of hepatitis A virus in shellfish by nested reverse transcription-PCR. Int J Food Microbiol 48: 67–71
72. Chapron CD, Ballester NA, Fontaine JH, Frades CN, Margolin AB (2000) Detection of astroviruses, enteroviruses, and adenovirus types 40 and 41 in surface waters collected and evaluated by the information collection rule and an integrated cell culture-nested PCR procedure. Appl Environ Microbiol 66:2520–2525
73. Gibson UE, Heid CA, Williams PM (1996) A novel method for real time quantitative RT-PCR. Genome Res 6:995–1001
74. Mackay IM, Arden KE, Nitsche A (2002) Real-time PCR in virology. Nucleic Acids Res 30:1292–1305
75. Donaldson KA, Griffin DW, Paul JH (2002) Detection, quantitation of enteroviruses from surface waters and sponge tissue from the Florida Keys using real-time RT-PCR. Water Res 36:2505–2514
76. Heim A, Ebnet C, Harste G, Pring-Akerblom R (2003) Rapid and quantitative detection of human adenovirus DNA by real-time PCR. J Med Virol 70:228–239
77. Kageyama T, Kojima S, Shinohara M, Uchida K, Fukushi S, Hoshino FB, Takeda N, Katayama K (2003) Broadly reactive and highly sensitive assay for Norwalk-like viruses based on real-time quantitative reverse transcription PCR. J Clin Microbiol 41:1548–1557
78. Logan C, Leary JJ, O'Sullivan N (2006) Real-time reverse transcription PCR detection of norovirus, sapovirus and astrovirus as causative agents of acute viral gastroenteritis. J Clin Microbiol 44:3189–3195
79. Reynolds KA, Gerba CP, Abbaszadegan M, Pepper LL (2001) ICC/PCR detection of enteroviruses and hepatitis A in environmental samples. Can J Microbiol 47:153–157
80. Burkhardt W, Woods JW, Calci KR (2005) Evaluation of wastewater treatment plants' efficiency to reduce viral loading using real-time RT-PCR. In: 105 general meeting (ASM Abstract)
81. Symonds EM, Griffin DW, Breitbart M (2009) Eukaryotic viruses in wastewater samples from the United States. Appl Environ Microbiol 75:1402–1409

Books and Reviews

Berg G (1983) Viral pollution of the environment. CRC Press Boca Raton, FL, New York

Cox P, Griffith M, Angles M, Derre D, Ferguson C (2005) Concentration of pathogens and indicators in animal feces in the Sydney watershed. Appl Environ Microbiol 71:5929–5934

Gerba CP, Smith JE Jr (2005) Sources of pathogenic microorganisms and their fate during land application of wastes. J Environ Qual 34:42–49

Greenberg HB, Valdesuso JR, Kalica AR, Wright RG, McAuliffe VJ, Kapikian AZ, Chanock RM (1981) Proteins of Norwalk virus. J Virol 37:994–999

Hurst CJ (2000) Viral ecology. Academic, California

Jiang SC (2006) Human adenoviruses in water: occurrence and health implications: a critical review. Environ Sci Technol 40:7132–7140

Koopmans M (2005) Outbreaks of viral gastroenteritis: what's new in 2004? Curr Opin Infect Dis 18:295–299

Koopmans M, Duizer E (2004) Foodborne viruses: an emerging problem. Int J Food Microbiol 90:23–41

Leclerc H, Schwartzbrod L, Dei-Cas E (2002) Microbial agents associated with waterborne diseases. Crit Rev Microbiol 28: 371–409
Lund E (1982) Waterborne virus disease. Ecol Dis 1:27–35
Rheinheimer G (1992) Aquatic microbiology, 4th edn. Wiley, Chichester
Varnam AH, Evans MG (2000) Environmental microbiology. ASM Press, Washington, DC

Waterborne Infectious Diseases, Approaches to Control

Alan Fenwick[1], Albis Francesco Gabrielli[2], Michael French[1], Lorenzo Savioli[2]
[1]Department of Infectious Disease Epidemiology, Schistosomiasis Control Initiative, Imperial College London, London, UK
[2]Department of Control of Neglected Tropical Diseases, World Health Organization, Geneva, Switzerland

Article Outline

Glossary
Definition of the Subject
Introduction
Malaria
Schistosomiasis
STH (*Ascaris*, *Trichuris*, and Hookworm Infections)
Onchocerciasis (River Blindness)
Lymphatic Filariasis
Trachoma
Guinea Worm: A Worm on Its Own
Cholera and Typhoid
Dengue and Dengue Hemorrhagic Fever (DHF)
Future Directions
Bibliography

Glossary

Neglected tropical diseases A group of poverty-promoting and disfiguring diseases disproportionately affecting the poorest populations in developing countries. They are termed neglected because they lack the visibility, research support, and funding of other, more high profile, infections, such as malaria, HIV/AIDS, and tuberculosis. Several can be treated with inexpensive, effective treatment, while for others new drugs are needed.

Waterborne infectious diseases Those diseases that rely on, or are heavily associated with, water for at least one stage of their life cycle or transmission, or affect populations closely related to areas of water.

Definition of the Subject

Waterborne diseases represent a significant and substantial burden on human health that disproportionately affects those living in the developing world. Human populations are attracted to live near surface water, particularly in areas such as sub-Saharan Africa (SSA) where it may represent a scarce resource. The development of water resources to exploit their potential has undoubtedly been of great benefit to some human populations via, for example, an increase in the amount of land suitable for agriculture provided by irrigation schemes, or the provision of hydroelectric power following the construction of dams and reservoirs. However, as an unintentional consequence such development may have unwittingly increased the extent of human waterborne infections by increasing the areas of suitable habitat for disease vectors and/or intermediate hosts, as well as attracting human populations to congregate, thereby aiding the life cycles of many infectious organisms [1–3].

The tools to treat, control and, in some cases, eliminate and eradicate some of these diseases already exist and there are examples of considerable, but not complete, success. Redoubling of efforts against such infections is advocated. In this entry, the major waterborne diseases that impact on human health, their extent, and the current position with regard to control are examined.

Introduction

Water- and Sanitation-Related Diseases Considered (in alphabetical order)

- Cholera
- Dengue and dengue hemorrhagic fever
- Guinea worm disease (Dracunculiasis)
- Lymphatic filariasis (Elephantiasis)
- Malaria
- Onchocerciasis (River blindness)

- Schistosomiasis (Bilharzia)
- Soil-transmitted helminthiasis (STH – ascariasis, trichuriasis, and hookworm)
- Trachoma
- Typhoid and paratyphoid enteric fevers

These diseases represent a diverse taxonomic group of infections stretching from viruses to multicellular macro-parasitic helminth infections. A brief description of the main infectious organisms is presented in Table 1.

While malaria has (rightly) long had strong visibility and powerful political advocacy behind its control, many of the other diseases have not traditionally benefitted from such a profile. However, in the last decade, a number of individuals advocating on behalf of each of these diseases have changed the perception of them internationally. The World Health Organization has endorsed these increases in recognition and by establishing a "Department of Neglected Tropical Diseases" within the organization, it has encouraged a growing realization that each of the hitherto

Waterborne Infectious Diseases, Approaches to Control. Table 1 Classification of major waterborne diseases affecting human health. MDA: suitable for control via mass drug administration. *STH* soil-transmitted helminthiasis, *M* million, *DALYs* disability adjusted life years

Family	Disease	Type and species	DALYs	Infected globally
Protozoa	Malaria	Cerebral (*Plasmodium falciparum*)	46.5M [12]	515M clinical cases of *P. falciparum* malaria [13]
		Others (*P. vivax; P. ovale; P. malariae*)		
Helminth (MDA)	Schistosomiasis (Bilharzia)	Intestinal (*Schistosoma mansoni, S. japonicum*)	13–15M [14]	207M [2]
		Urogenital (*S. haematobium*)		
	STH (Worms)	Roundworm (*Ascaris lumbricoides*)	10.5M [15]	807M [15]
		Whipworm (*Trichuris trichiura*)	6.4M [15]	604M [15]
		Hookworm (*Necator americanus*; *Ancylostoma duodenale*)	22.1M [15]	576M [15]
	Onchocerciasis (River blindness)	*Onchocerca volvulus*	0.5M [16]	37M [16]
	Lymphatic filariasis (Elephantiasis)	*Wuchereria bancrofti*; *Brugia malayi*	5.8M [17]	120M [17]
Helminth (non-MDA but eradicable)	Guinea worm	*Dracunculus medinensis*	<0.1M [18]	<1,800 [18]
Bacteria (MDA)	Trachoma	*Chlamydia trachomatis*	2.3M [19]	84M [19]
Bacteria (non-MDA)	Cholera	*Vibrio cholera*		3–5 M cases annually [20, 21]
	Typhoid and paratyphoid enteric fever	*Salmonella enterica*		27.1M [22]
Virus	Dengue and dengue hemorrhagic fever	*Flavivirus*	528,000 [23]	50M [23]

under-recognized diseases requires specific expertise, targets, and interventions in order to effectively control them. However, it has also been recognized that where overlaps in control approaches exist between infections, not least with regard to the targeted populations, and the frequency and mode of treatment, then an integrated approach to control can be employed which should be more cost-effective than the separate, individual, vertical control programs which have previously been employed. Indeed, there is a growing momentum behind such an approach [4–10]. The progress made in the control of each of these waterborne diseases to date is outlined in Table 2; alongside the aim of control (i.e., whether it be morbidity control, local elimination, global eradication [see [11] for definitions of these terms]) and the control strategies employed.

Malaria

Malaria is without doubt the world's most feared and important parasitic disease as measured by the extent of its distribution, the annual number of cases, and the death toll it exerts, particularly in infants [35–36]. It is estimated that 300–500 million cases of malaria occur each year, leading to over one million deaths [35–36], of which 75% occur in children under the age of 5 [37] (Fig. 1). The symptoms of malaria vary by parasite species and by individual human host. Fever, chills, headache, muscle aches, tiredness, nausea, and vomiting are common symptoms, but infection can also result in anemia and jaundice [25]. In the absence of effective treatment, convulsions, coma, severe anemia, and kidney failure can also occur. In the case of *Plasmodium falciparum,* the most common species of malaria in Africa, the severe cerebral form can develop which will lead to death without treatment. As a result, cerebral malaria is one of the leading causes of death in under-5-year-old children in Africa. Fortunately, many people living in areas with regular malaria transmission survive malaria and develop some protective immunity after repeated infections. Recently the field of malaria control has been challenged by Bill and Melinda Gates to begin aiming for global elimination of the infection, a target that has not been seriously attempted for decades [24, 38].

Input Photo of Malaria Effects

Four species of the protozoan genus *Plasmodium* infect man (*Plasmodium falciparum, P. vivax, P. ovale,* and *P. malariae*). All four are transmitted by the bite from an infected mosquito of the genus *Anopheles* and all four undergo similar life cycles. When a mosquito bites an infected person, it ingests blood, and takes up any malaria parasites in that blood meal. The parasite then develops in the mosquito passing through a number of stages until after between 9 and 30 days, the parasite is ready to pass back to another human. The form infective to humans (the sporozoite) is to be found in the mosquito's salivary glands from where it will be injected into the next human host when the mosquito takes future blood meals.

Once back in the human host, the sporozoites migrate to the liver where they multiply and spread into the bloodstream. The liver phase can last between 8 days and several months, depending on the malaria species. Further growth and multiplication then takes place inside red blood cells, and it is the regular destruction of these red blood cells which causes the characteristic intermittent fevers. The released parasites then invade new blood cells, and the cycle of multiplication and fever continues, with most people suffering their first fever 10 days to 4 weeks following infection. Malaria kills when the *P. falciparum* parasite invades the brain and causes cerebral malaria.

Malaria occurs mostly in tropical and subtropical countries, particularly in sub-Saharan Africa (90% of morbidity), Southeast Asia (India, Sri Lanka, Vietnam, and the Solomon Islands are endemic), and the forest fringe zones in South America (Brazil and Colombia are endemic), but its distribution is heavily dependent on the availability of suitable water bodies which support the mosquito larvae. The mosquito species vary considerably in their water and ecological requirements, in regard to levels of sunlight, aquatic vegetation, water flow, brackishness, and turbidity in a particular microhabitat. Several human factors have changed the distribution of the mosquito, for example (relatively) clean and dry urban cities may no longer support mosquitoes and therefore reduce transmission, while climate change may allow malaria to thrive in higher altitude areas than previously. The construction of irrigation systems and reservoirs, particularly in Africa, and

Waterborne Infectious Diseases, Approaches to Control. Table 2 A summary of the current status of the major waterborne infectious diseases, aims and approaches to control. *ACT* artemisinin combination therapy, *DEC* diethylcarbamazine, *APOC* African Program for Onchocerciasis Control, *MDA* mass drug administration

Disease	Current status (2011)	Control aim	Control strategy
(1) Malaria	300–500 million cases per year and up to one million deaths [13]. *Plasmodium falciparum* in Africa causes the most fatalities	Transmission control and, recently, eradication [24]	Preventing mosquito bites using long-lasting insecticide-impregnated bed nets. Presumptive treatment, speedy home-based treatment, ACTs, vector control [25]
(2a) Schistosomiasis (Bilharzia)	Over 200 million people infected; over 85% in Africa [2]. Irrigation projects and dams exacerbate the problem – treatment coverage needs to be expanded from current level of 10–20%	Morbidity control and, recently, local elimination [26]	Annual or biannual treatment with praziquantel protects children from future consequences [27]. Improved socioeconomic status, water supplies, and sanitation are necessary for elimination
(2b) Soil-transmitted helminthiasis (STH)	Over one billion of the poorest children and adults infected globally. Annual treatment coverage is now approaching 50%	Morbidity control	Six-monthly or annual deworming treatment of preschool and school-age children with albendazole or mebendazole [28]
(2c) Onchocerciasis (River Blindness)	Great progress in recent decades. 19 countries treated by APOC. Still 50 million infections in Africa because hypo-endemic areas are not treated. Elimination in some foci in Africa thought possible. Elimination being approached in Central and South America [29, 30]	Interruption of transmission (Americas)/ Morbidity control (elsewhere)	Multiple annual MDA rounds with ivermectin (Mectizan®)
(2d) Lymphatic filariasis (Elephantiasis)	120 million infected globally. A serious economic problem in Africa and the Indian subcontinent, but progress is being made toward elimination. 500 million people treated annually [31]	Global elimination as a public health problem	Multiple annual MDA rounds with albendazole and ivermectin (Mectizan®) (in Africa) or albendazole and DEC (elsewhere)
(3) Guinea worm	Rapidly approaching eradication. Fewer than 400 cases reported during the first quarter of 2011. Sudan, Ethiopia, Mali, and Chad are the countries with most residual infections (www.cartercenter.org)	Global eradication	Individual case finding and case containment, clean water provision and filtration, vector control (abate). Regular surveillance of endemic villages
(4) Trachoma (preventable blindness)	80 million infected, 8 million visually impaired [19]. Treatment expansion satisfactory: 70 million due to be treated in 2011 [32]. Has been eliminated from Morocco	Global elimination as a public health problem	Annual treatment (for 3–5 years) with azithromycin (Zithromax®), as part of a "SAFE" strategy (*S*urgery, *A*ntibiotics, *F*ace washing, and *E*nvironmental improvement) [33]
(5) Cholera	3–5 million cases and 120,000 deaths annually. A disease which follows disruption of services, clean water and sanitation after natural disasters [20]	Minimization and control of outbreaks	Up to 80% of cases can be successfully treated with oral rehydration salts. Effective control measures rely on prevention via provision of safe water and sanitation. Oral cholera vaccines can be used for control, but should not replace conventional control measures

Waterborne Infectious Diseases, Approaches to Control. Table 2 (Continued)

Disease	Current status (2011)	Control aim	Control strategy
(6) Typhoid and paratyphoid enteric fever	Conservatively estimated at 27 million infection and 215,000 deaths annually, mostly in SSA and Southeast Asia	Minimization and control of outbreaks	Improving sanitation, identification and treatment of carriers, and use of typhoid vaccines to reduce susceptibility to infection [34]
(7) Dengue and dengue hemorrhagic fever	250 million at risk and 50 million cases annually in over 100 countries, and increasing. Can be fatal [23]	Transmission and morbidity control	Effective clinical management. Replacement of fluids and sometimes blood transfusions. Vector control also required

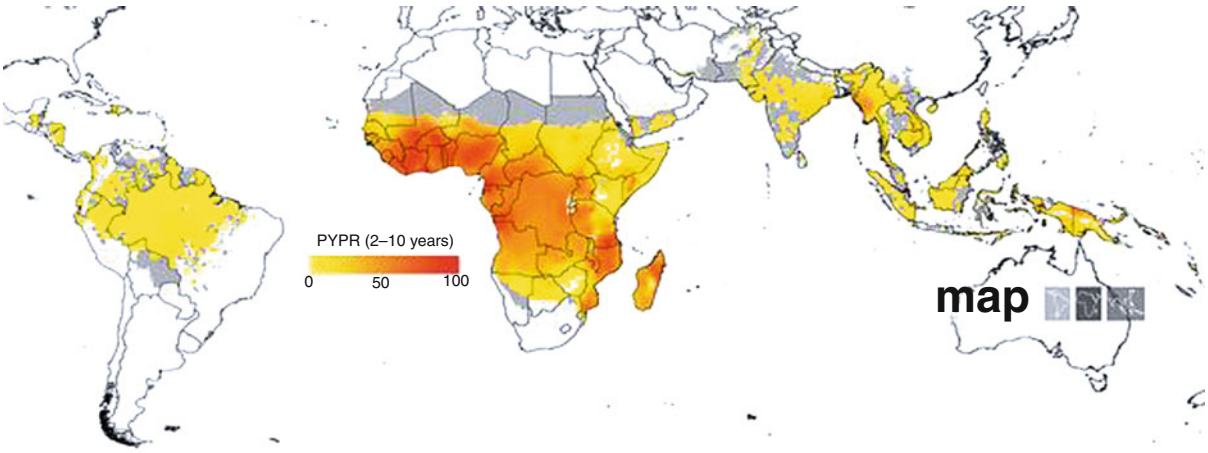

Waterborne Infectious Diseases, Approaches to Control. Figure 1
The spatial distribution of *P. falciparum* malaria endemicity. Reproduced from work carried out by the Malaria Atlas Project [40]. *Pf*PR (2–10) corresponds to the *P. falciparum* parasite rate in 2–10-year olds

changes in rice cultivation can lead to dramatic increases in the extent of areas suitable for malaria transmission. Indeed, malaria, once thought to have been eliminated in some countries, has returned as a result of the poor maintenance of water facilities and irrigation systems.

The Control of Malaria

In the 1960s, malaria was thought close to elimination after the widespread and effective use of DDT (dichlorodiphenyltrichloroethane) to control mosquito populations and chloroquine to treat infections in humans [39]. Neither of these interventions is as effective in the twenty-first century; the use of DDT has stopped due to environmental concerns and the development of resistance [39]. Equally, the parasite has developed resistance to chloroquine, and to a succession of antimalarial drugs which followed it.

In 2011, the WHO strategy for malaria comprises four main interventions, and is implemented through the Global Malaria Program (GMP) and the Roll Back Malaria (RBM) partnership:

- Reducing mortality, particularly among children, by early case-detection and prompt treatment with effective antimalarial drugs
- Promoting the use of insecticide-treated bed nets, especially by children and pregnant women
- Prevention of malaria in pregnancy by applying intermittent preventive therapy
- Ensuring early detection and control of malaria epidemics, especially in emergency situations

In addition, vector control can be an effective control tool; mosquito breeding sites can be removed by filling in and/or draining suitable water bodies and through other environmental management schemes, while the vectors can be controlled using chemical (IRS - Indoor Residual Spraying) and biological control in certain circumstances.

Current Drugs: Artemisinin-Based Combination Therapies (ACTs)

Widespread parasite resistance has arisen to the majority of antimalarials and the management of resistance presents a key battle in the fight for malaria control and eventual eradication. The newest class of drugs, artemisinins, has a very different mode of action to conventional antimalarials, which makes them particularly useful in the treatment of resistant infections [41]. However, in order to control the development of resistance to this drug, its use is only recommended in combination with another nonartemisinin-based therapy. Artemisinin produces a very rapid amelioration of clinical symptoms and is known to cause a reduction in the transmission of gametocytes, which may help decrease the potential for the spread of resistant alleles. To date there have been very few reported side effects to drug usage, however, one great worry is that resistance to Artemisinin may develop and indeed some resistant strains may be emerging [42].

All the treatment combinations outlined below have been recommended by WHO for treatment of *P. falciparum* [43].

Artesunate and amodiaquine (*Coarsucam* and ASAQ). This combination has been tested and proved to be efficacious in many areas where amodiaquine retains some efficacy.

Artesunate and mefloquine (*Artequin* and *ASMQ*) has been used as an efficacious first-line treatment regimen in areas of Thailand for many years. Mefloquine adverse reactions seem to be reduced when the drug is combined with artesunate possibly due to a delayed onset of action of mefloquine. This is not likely to be an option for long-term use in Africa due to the long half-life of mefloquine, which potentially could exert a high selection pressure on parasites.

Artemether and lumefantrine (*Coartem Riamet*, *Faverid*, *Amatem* and *Lonart*). This combination has been extensively tested and is effective in children under 5. It has been shown to be better tolerated than artesunate plus mefloquine combinations. There are no serious side effects documented but the drug is not recommended in pregnant or lactating women due to limited safety testing in these groups. This is the most viable option for widespread use and is available in fixed-dose formulae, which should increase compliance and adherence.

Artesunate and sulfadoxine/pyrimethamine (*Ariplus* and *Amalar plus*). This is a well-tolerated combination but the overall level of efficacy still depends on the level of resistance to sulfadoxine and pyrimethamine thus limiting its usage.

Dihydroartemisinin-piperaquine (*Duo-Cotecxin*, *Artekin*). Has been studied mainly in China, Vietnam, and other countries in Southeast Asia. The drug has been shown to be highly efficacious (greater than 90% clinical response rate).

Pyronaridine and artesunate (*Pyramax*). Manufactured by Shin Poong Pharmaceutical. Has been tested and demonstrated a clinical response rate of 100% in one trial in Hainan (an area with high levels of *P. falciparum* resistance to Pyronaridine). A multicenter phase III trial conducted in Africa found a 99.5% response rate [44].

Current Prophylactics

For travelers to malaria endemic areas who have never been exposed to malaria before, a course of prophylactics is recommended as a protection. Several options exist, as detailed in Table 3.

Waterborne Infectious Diseases, Approaches to Control. Table 3 Current prophylactic malaria tablets available for exposure-naïve individuals

Proganil	100 mg tablets are supplied as **Paludrine**
Chloroquine	150 mg tablets are supplied as **Nivaquine** or **Avloclor**
Mefloquine	250 mg tablets are supplied as **Larium**
Malarone	A combination of **Atovaquone** 250 mg and **Proguanil** 100 mg
Doxycycline	100 mg capsules or tablets

Bed Nets

Insecticide-treated nets (ITNs) were developed in the 1980s to combat malaria by preventing the mosquito from biting humans while they sleep. More recently, longer lasting insecticide nets (LLINs) have been developed which are impregnated with insecticides such as permethrin or deltamethrin. The latest production technologies (e.g., Olyset or DawaPlus) allow for a new generation of LLINs, which release insecticide for approximately 5 years. Such ITNs have been shown to be an extremely effective and cost-effective method of malaria prevention [45], aiding the drive toward Millennium Development Goal 6, which specifically calls for reduced malaria infection. These nets, which are typically available for $2.50–$3.50 (€2–€3) are generally purchased by donor groups like the Bill and Melinda Gates Foundation (BMGF), the President's Malaria Initiative (PMI) and the Global Fund and distributed through in-country distribution networks. One debate that has been ongoing for several years is whether or not international organizations should distribute ITNs and LLINs to people for free in order to maximize coverage and reduce price barriers. Some argue that cost-sharing between the international organization and recipients would lead to greater usage of the net because people will value them if they pay for them. Irrespective of the specifics of the approach, the main target has to be in assisting people, who most need the bed nets, to receive them and use them correctly.

Current Insecticides

Insecticides against malaria are used in two main ways: First, to kill the larvae breeding in water bodies close to human habitation; second, to kill the adult mosquitoes to prevent them biting humans inside a house. Fogging machines can be used to safely distribute insecticide in community-wide spraying in towns and tourist resorts. Unfortunately, sprayed insecticides are often expensive and the effects are only transitory, allowing mosquitoes to reinvade. There are two currently used insecticides: (1) **Malathion** – an organophosphate often used to treat crops against a wide array of insects. It can be sprayed directly onto vegetation, such as the bushes where mosquitoes like to rest, or used in a 5% solution to fog open areas. In the small amounts used for mosquito control, it poses no threat to humans or wildlife. (2) **Permethrin** is a synthetic form of a natural insecticide (pyrethroid) which can be mixed with oil or water and applied as a mist. Both malathion and permethrin are also available in sprays for use for Indoor Residual Spraying (IRS). IRS kills adult mosquitoes that land on sprayed surfaces. Its two primary effects are to reduce the life span of vector mosquitoes so that they can no longer transmit malaria, and to reduce the density of the vector mosquitoes [46]. IRS is currently being funded by the PMI and the Global Fund. Historical and programmatic documentation has clearly established the impact of IRS [47] and expansion of coverage is likely to continue.

DDT has long been the cheapest insecticide and the one with the longest residual efficacy against malaria vectors (6–12 months depending on dosage and substrate), although environmental and resistance problems have largely curtailed its use. Other insecticides have relatively shorter residual effect (pyrethroids: 4–6 months; organophosphates and carbamates: 2–6 months).

Schistosomiasis

Three major species of schistosome worms infect humans [48]:

- *Schistosoma japonicum* (intestinal schistosomiasis) is found only in China and the Far East and infects humans and domestic animals. The intermediate host are amphibian snails of the genus *Onchomelania*.
- *S. mansoni* (intestinal schistosomiasis) originated in Africa, but was carried by humans to South America and the Caribbean where a suitable snail host was able to support transmission. Primates may also become infected. The intermediate hosts are snail species of the genus *Biomphalaria*.
- *S. haematobium* (urogenital schistosomiasis) is found only in Africa and the Middle East and there is no animal reservoir. The snail intermediate hosts are certain species of the genus *Bulinus*.

The worms of each species live in the blood vessels of humans and the female worm lays eggs which either escape through the urine (*S. haematobium*) or feces (*S. mansoni/S. japoncium*) to continue the life cycle or remain in the body trapped in the intestine wall,

bladder wall, or liver tissues. In female hosts, the worms and eggs can invade the genital system and cause damage [49]. Once the eggs have exited the body they will hatch only when they reach freshwater. The emerging free swimming larvae (miracidia) need to find and invade the correct snail intermediate host species in order to survive. Once there, they undergo asexual reproduction in their host snail over a period of a month developing through the "sporocyst" and "daughter sporocyst" intermediate stages. Eventually the next free living larval stage (cercariae) emerges from the snail into water as swimming organisms with a body and a tail. They have a short life during which time they are attracted to any human skin immersed in the water. They will attach to and penetrate unbroken skin, shedding the tail in the process. The body (now a schistosomulum) migrates to the lungs and passes through the diaphragm to reach the liver. About 6 weeks after initially penetrating the host, the worm in the liver will reach maturity – and about one centimeter in length. The male and female adult worms pair and the male carries the female to their selected blood vessels where they can live and produce eggs, typically for a period between 2 and 10 years [50]. *S. haematobium* worms reside around the bladder, and hence the eggs pass out in the urine. *S. japonicum* and *S. mansoni* worms reside in the blood vessels in the mesentery and hence their eggs breaking into the intestine and being voided with the feces [51–53] (Figs. 2 and 3).

An estimated 207 million people are infected globally with schistosomiasis [2] with almost 90% of those infected found in Africa [54]. The first symptom of infection is irritation at the site of penetration and is rarely noticed. A classic symptom of heavy infection is caused by the passage of schistosomula through the lungs 5–10 days after infection, but this is only seen

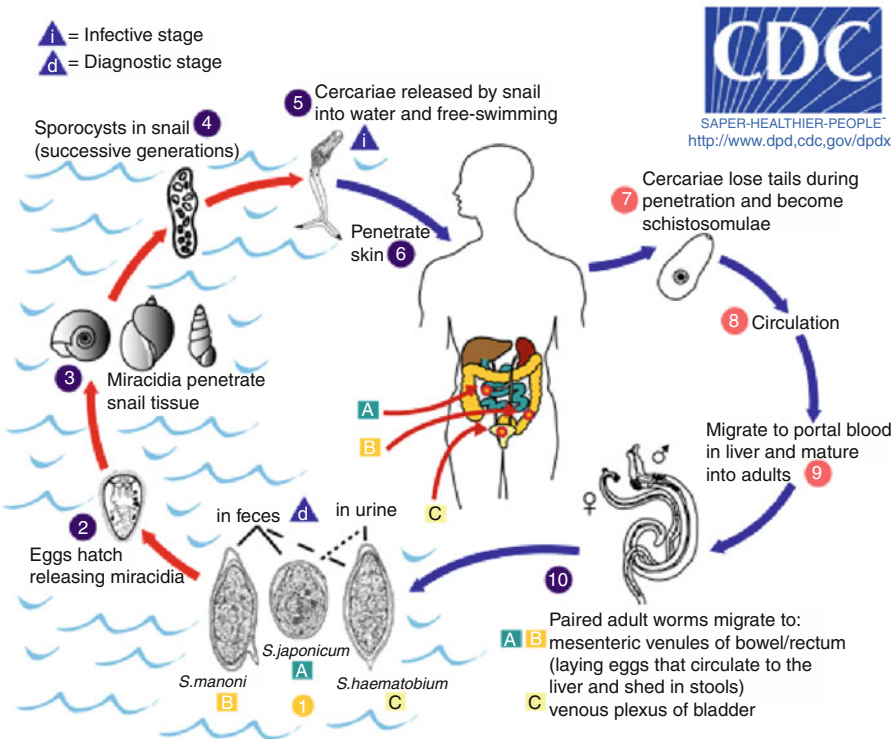

Waterborne Infectious Diseases, Approaches to Control. Figure 2
Life cycle of the three major schistosome species that infect humans (Taken from http://www.dpd.cdc.gov/dpdx/html/schistosomiasis.htm, Centers for Disease Control)

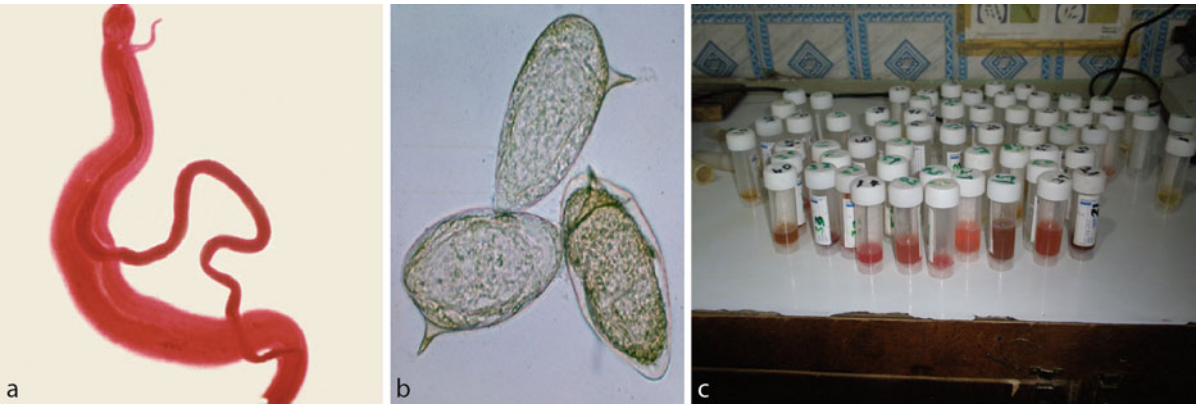

Waterborne Infectious Diseases, Approaches to Control. Figure 3
(**a**) A pair of schistosome adult worms, showing the female (thin worm) present in the male's gonotrophic canal, (**b**) Schistosome eggs, and (**c**) the characteristic sign of urogenital impact, blood in the urine

when many worms are passing through concurrently, as in the case of a single heavy exposure. Subsequent symptoms occur as the worms mature and start laying eggs. This can lead to blood in the urine in *S. haematobium* cases (a finding that is also used as a major diagnostic feature). *S. japonicum* and *S. mansoni* eggs breaking into the intestine can cause diarrhea and blood in the stool but this is less obvious and therefore, not a definitive diagnostic feature [48, 51–52].

Schistosomiasis is a multifaceted disease. The worms can live for up to 30 years [55, 56] and the eggs that collect in the body cause increasing organ damage over time. Heavy infections lead to severe symptoms and death from bladder cancer in *S. haematobium* infections and from portal hypertension in *S. japonicum* and *S. mansoni* infections. Uninfected people exposed to an initial heavy infection by swimming in a water body containing many infected snails can suffer extreme early symptoms, while light infections may never be detected. The norm for people residing in endemic areas is for chronic infection lasting years to occur before serious consequences are recognized. This happens because the chronic infection stage can cause significant but often undiagnosed subtle morbidity, including anemia, stunting, urinary and intestinal problems, lassitude and reduced growth, poorer school attendance and performance. Meanwhile, overt and severe organ damage can gradually occur over the course of this worsening process [48, 51, 52, 57–58] (Fig. 4).

Waterborne Infectious Diseases, Approaches to Control. Figure 4
Late stages of schistosomiasis infection, showing severe morbidity

Treatment

Currently there seems to be little chance of elimination of schistosomiasis in its transmission heartland of rural Africa because to date, elimination has only been possible in countries that have undergone significant socioeconomic development, such as Japan and Puerto Rico. Substantial improvements in water and sanitation conditions in rural African areas are required in order to permanently interrupt transmission. On a wider scale, sustained economic development is needed to eventually rid the world of this disease. Until then, the currently followed strategy is to focus on morbidity control via the large-scale administration of the drug praziquantel to at-risk groups (although recently this has been shown to also have an effect on transmission [59–60]) [61]. An annual round of treatment reaching school-age children would have a substantial effect on improving the quality of life of treated children, and protecting them from the serious consequences of their infections in later life [7].

Schistosomiasis can be treated with the generic drug praziquantel [62] (administered at 40 mg/kg body weight) which kills the adult worms. Praziquantel is currently available off-patent at a cost of about 8 USD cents (5 GBP pence) per tablet from a number of manufacturers, most of which are in India, South Korea, and China. On average 2.5 tablets are needed to treat a child and 4 tablets per adult, equating to 20 cents for the tablets needed to treat a child and 32 cents for an adult. The pharmaceutical company Merck Serono has recently committed to a drug donation program that pledges 200 million tablets over 10 years, enough to treat eight million children per year in high-prevalence areas in Cameroon, Malawi, Mozambique, Nigeria, and Senegal. It is hoped that further donations may be forthcoming in future; however, the situation is complicated as the active ingredient for the tablets is the constraining factor in the supply chain due to uncertainty in market demand. WHO is working with the drug companies to attempt to stabilize the market over the medium- to long-term, because Africa is desperately short of praziquantel ([63] and website www.schisto.org).

Improved Funding

During the 1980s several schistosomiasis control programs were started in Africa using donated drugs (by the German developmental organization GTZ) but once the drug donations ended, the programs proved to be unsustainable and ceased. In the 1990s, three countries (Egypt, Brazil, and China) applied to the World Bank for funding and as a result they all reduced their schistosomiasis burden to below what constituted a public health problem, using a combination of drug treatment and molluscicides. The cost of molluscicides, however, proved a barrier to any expansion of their use.

At the start of this century, the Bill and Melinda Gates Foundation (BMGF) made significant funds available for treatment (from 2003 to 2006) through the Schistosomiasis Control Initiative (SCI; www.schisto.org). Six countries (Burkina Faso, Mali, Niger, Tanzania, Uganda, and Zambia) benefited from this donation and led the way in Africa for the development and implementation of national schistosomiasis programs. Thanks to the UK's Department for International Development (DFID) (2008–2013) and the United States Agency for International Development (USAID) (2006–2013), more resources have been made available (primarily through the Schistosomiasis Control Initiative [SCI] and Research Triangle International [RTI]) to expand coverage of schistosomiasis treatment throughout Africa. By working together several countries will receive the support they need to reach national coverage. Other countries plan to start implementation programs in 2011 (Côte d'Ivoire, Liberia, Malawi, and Mozambique). However, even given this expansion, many countries in need of national control programs have yet to start.

Although elimination of infection is not a target in mainland Africa, Zanzibar is aiming for elimination in 5 years from 2011; thanks to a project supported by the Gates Foundation, DFID and WHO which aims to identify the approaches (chemotherapy, water and sanitation improvement, health behaviors) needed to achieve this end point [26]. The chances of success are thought to be high because of many years of control interventions and the insular island biogeography that contributes to preventing importation of cases. Implementation will be organized by the Zanzibar government with assistance from the Ivo de Carneri Foundation on Pemba Island, The WHO, The University of Athens-Georgia, the London Natural History Museum, SCI Imperial College, and the Swiss Tropical Institute.

STH (*Ascaris, Trichuris*, and Hookworm Infections)

There are three separate worms which together constitute the soil-transmitted helminths (STH), so named because their life cycles do not involve an intermediate host. They are the roundworm (*Ascaris lumbricoides*), the whipworm (*Trichuris trichiura*), and the hookworm (*Necator* and *Ancylostoma* spp.). These worms inhabit the human intestine, with their eggs passed out in the feces [15–51, 52, 64].

Roundworm and whipworm cause infections associated with poor hygiene: good sanitation would prevent eggs from contaminating the environment, and regular hand washing when preparing or eating food would prevent the eggs from being ingested. Unfortunately in poor rural areas devoid of toilets, feces tend to be deposited anywhere and the roundworm and whipworm eggs are able to develop on the soil and be ready to reinfect a human host by ingestion, usually on food. Heavy infections lead to malnutrition and growth stunting in children, reduced educational achievement, and loss of future earning power [15, 65–68].

The life cycle of hookworm differs because the eggs that are passed in the feces hatch and the larvae need to pass through some developmental stages before they are ready to reinfect a human host. Infection is acquired when the free-living larvae attach themselves to the feet and ankles of passers-by. They then penetrate the skin, migrate around the body, and end up in the intestine where they attach and gorge on blood. Those individual hosts who have very heavy infections will almost certainly develop anemia as the major result, which has a serious effect on young children but also on women of childbearing age because anemia is the major cause of poor birth outcomes, and infant and maternal mortality [52, 69–71].

The nationwide elimination of these worm infections goes hand in glove with socioeconomic development, for example, these three worms used to be common in Europe and the USA, but with widespread access to safe water and sanitation, they have been eliminated from the majority of developed countries. In South Korea and Japan, infection rates were over 80% following the Second World War but during a period of 15 years this rate was reduced to less than 0.5% [72].

It is estimated that globally over a billion people in 2011 do not have the water and sanitation levels needed to eliminate these STH and are infected with one or more worms in developing countries.

Treatment

The intestinal worms can be expelled from the body with a single 400 mg tablet of albendazole (or a 500 mg tablet of mebendazole) [62, 73]. In endemic areas where prevalence of infection is above 20%, an annual dose (or two doses when prevalence is $\geq$50%) of deworming tablets throughout a child's life (from the age of 1 to 14) will have an amazingly positive effect on their growth and nutritional status, their school attendance, and cognitive ability [61].

While for many years STH deworming for preschool-age children has been included into immunization interventions throughout the world [73], school-age children are usually targeted through school-based treatment interventions. A boost to STH deworming coverage has been "unintentionally" provided by the lymphatic filariasis (LF) elimination program (see LF below) because one of the drugs which has been delivered in ever increasing numbers since 2000 to eliminate LF is albendazole [74]. Approximately two billion albendazole tablets have been delivered globally since the program began [46], which means that the ancillary effect on these worms can be assumed to be significant.

Two pharmaceutical companies have pledged drug donations specifically to reduce the prevalence of STH (for a summary of these, and other drug donations, see Table 4). Johnson & Johnson has been donating 50 million tablets a year through the nongovernmental development organization (NGDO) "Children Without Worms" since 2005 and in 2010 they pledged to increase their donation of mebendazole to 200 million tablets a year, which will be mainly used in Asia and the Americas. "Feed the Children International" also donate several million mebendazole tablets through another organization, "Deworm the World," which directs the drug to where it is needed mostly through Ministries of Education.

For Africa, GSK announced in October 2010 that from 2012 they will donate an additional 400 million albendazole tablets a year to target school-age children throughout the world. Over the next 5 years this will make a huge difference to the health and quality of life of the world's children.

Waterborne Infectious Diseases, Approaches to Control. Table 4 The contribution of the pharmaceutical industry to the control of waterborne infectious diseases

Company	Commitment
MERCK	Merck has reconfirmed their commitment (now already over 25 years) to donate ivermectin (Mectizan®) for as long as needed against both onchocerciasis and lymphatic filariasis in Africa
gsk GlaxoSmithKline	GSK has already donated almost two billion tablets of albendazole against lymphatic filariasis and will continue until elimination is achieved. In October 2010, GSK committed an additional 400 million tablets a year for 5 years to deworm school-age children worldwide
Johnson & Johnson	Johnson & Johnson has, for several years, donated 50 million tablets of mebendazole per year for intestinal worms – from 2012 this will be increased to 200 million tablets per year
Pfizer	Pfizer committed to provide doses of azithromycin (Zithromax®) for trachoma In 2009 alone they donated 50 million tablets; in 2011 that number will reach 70 million
Eisai	In October 2010, EISAI committed to provide two billion tablets of DEC against lymphatic filariasis which is used with albendazole outside of Africa
MEDPHARM	Medpharm (a generic manufacturer) has contributed praziquantel against schistosomiasis in the years 2004–2006
MERCK	Merck Serono has agreed to donate 200 million tablets of praziquantel over 10 years

Meanwhile, both DFID and USAID support these donations by providing essential logistical and financial support for the distribution of the tablets. DFID currently funds delivery in eight African countries (Côte d'Ivoire, Liberia, Malawi, Mozambique, Niger, Tanzania [including Zanzibar], Uganda, and Zambia), and USAID in ten countries (see Fig. 5) and coverage is likely to expand during 2012–2015.

Onchocerciasis (River Blindness)

Onchocerciasis is a "filarial" worm that is endemic mainly in Africa and the Americas near fast-flowing rivers or streams where the host fly breeds. The adult

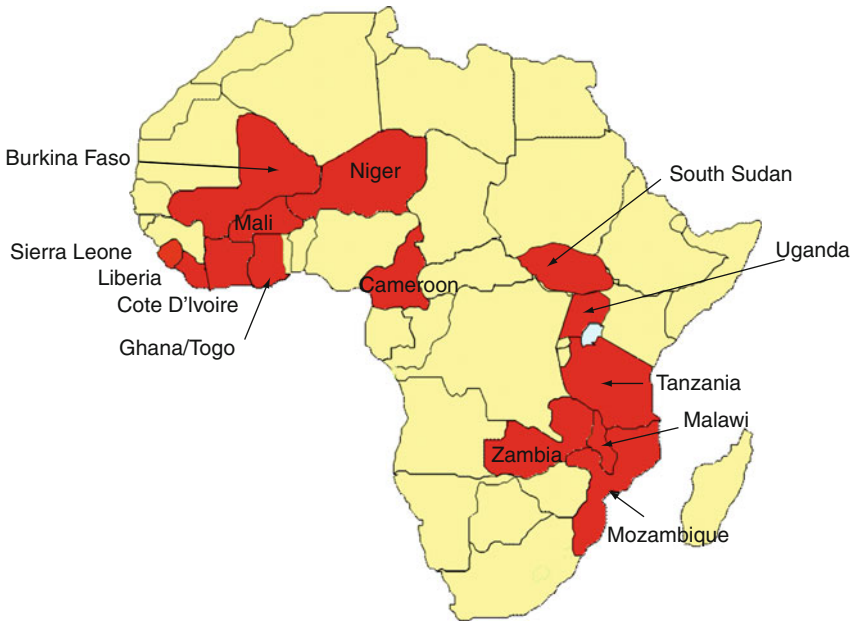

Waterborne Infectious Diseases, Approaches to Control. Figure 5
Countries in sub-Saharan Africa currently operating national or subnational schistosomiasis control programs

worm lives in nodules in the human body and gives birth to larvae (microfilariae) which migrate around the skin waiting to be picked up when a black fly (*Simulium* species) bites. The larvae develop in the black fly and are then transmitted back to another human host when the fly next bites [51, 52].

Prior to the 1970s this parasite was devastating to African populations. The larvae were responsible for great discomfort due to the itching they caused. However, much worse was the widespread blindness caused by the infection near the great rivers in Africa because the larvae produced by the adult worms in the human body migrate across the eye. As recently as 1970, up to 50% of adult populations living on the banks of fast moving rivers suffered impaired vision due to the persistent biting of the black fly [75–78].

The control of river blindness represents a major success in disease control, perhaps, matched only by smallpox eradication in 1979–1980 and latterly the progress toward the elimination of LF (see below). Three major programs (OCP, APOC, and OEPA), an insecticide (DDT), a pharmaceutical company (Merck), and a drug (ivermectin, Mectizan®) contributed to this success which is commemorated by a statue in front of the WHO headquarters in Geneva [79] (Fig. 6).

The OCP (Onchocerciasis Control Program) was initiated in the 1970s in West Africa to control onchocerciasis and provided DDT to be sprayed into rivers to kill the black fly larvae which breed in these fast-moving waters and therefore, to eliminate disease transmission. Nine countries implemented control as part of the OCP and as a result their endemic onchocerciasis was controlled and over a 20-year-period infection rates and blindness were reduced to very low levels [80–81].

Sadly the widespread use of DDT was shown to be environmentally unacceptable, but a major breakthrough saved the program when the drug ivermectin (Mectizan®) was found to have the effect of destroying microfilariae for a year after a single annual dose [82]. The drug manufacturer, Merck and Co., Inc., recognized that poor people in Africa would never be able to afford to purchase this drug, and so agreed to donate the drug to all those who live in endemic areas "for as long as needed" [29]. Today, some 25 years later, this donation continues, and in October 2010 the Merck commitment was renewed. Since 1986 Mectizan® has been distributed widely in OCP countries (and subsequently in 19 African Program for Onchocerciasis Control [APOC] countries) reaching over 50 million

Waterborne Infectious Diseases, Approaches to Control. Figure 6
Statue at the World Health Organization headquarters in Geneva, of a child leading an adult blinded by onchocerciasis through the village (Taken from http://www.cdc.gov/globalhealth/ntd/diseases/oncho_burden.html, Photo Credit: Carter Center)

people annually, and thereby saving millions of people from losing their sight [83].

The OCP closed down when its objectives had been met by the year 1996 but the APOC was then launched to oversee the distribution of Mectizan® in 19 additional African countries with the help of a number of NGOs (The Carter Center, Sightsavers, CBM, Helen Keller International, World Vision) [84]. The APOC mandate has recently been renewed to continue treatment until 2020, and during that time will look at the possibility of a changed strategy (doubling the dosage) to bring about elimination in some foci instead of merely control.

APOC and its partners have not managed complete coverage in Africa due to a complication to what should be a simple control program. Another parasitic filarial worm, *Loa loa,* which also produces live larvae that circulate in the body, coexists with onchocerciasis in some areas in Central Africa. Some patients with *Loa loa* when treated with Mectizan® can suffer disastrous consequences, such as encephalopathy [85]. Thus in parts of Central Africa where *Loa loa* is endemic, it is not safe to control onchocerciasis (nor LF) using MDA because of the possible dangerous complications. This is a matter yet to be resolved and further discussion is advocated [86].

The Onchocerciasis Elimination Program for the Americas (OEPA) is a regional initiative in the Americas with the goal of eliminating morbidity of river blindness and interrupting transmission in six endemic countries: Brazil, Colombia, Ecuador, Guatemala, Mexico, and Venezuela. The OEPA strategy is to encourage the endemic countries to provide sustained Mectizan® mass treatment every 6 months with the aim of reaching at least 85% of 500,000 persons estimated to be at risk of the disease [87]. All six endemic countries have established effective national programs and there are no new cases of blindness attributable to onchocerciasis in the American region. As of 2011, transmission is continuing in only two countries, Brazil and Venezuela, with surveillance in place in the remaining four [88].

In Africa, the plan for the future is continuation with the successful control program and annual Mectizan® treatments, but for the first time WHO are considering with selected governments the idea of intensifying the strategy with the aim of interrupting transmission permanently. It is thought that in many countries that have been offering annual Mectizan® for many years, the worms are beginning to die out and so by increasing frequency of treatment for a short period elimination may be achievable [89].

Lymphatic Filariasis

Two filarial worms *Brugia malayi* and *Wuchereria bancrofti* infect 120 million people globally with lymphatic filariasis (LF), with a further 600 million at risk of infection. The intermediate host of these worms are mosquitoes of several genera, and the global distribution is very extensive – Africa, the Indian subcontinent, many Pacific Islands, the Caribbean, and tropical America [90]. The deformity and misery caused by this disease are horrific. The adult worms live in and block the lymphatic system, which prevents the drainage of lymph fluid. This causes swelling of lower limbs, secondary infections, and, in the case of some men, the scrotum becomes grotesquely swollen [91]. Meanwhile, the millions of larvae which the females produce circulate in the bloodstream to be picked up by a mosquito for the transmission cycle to be completed.

The Global Alliance for the Elimination of Lymphatic Filariasis (GAELF) is supported by many partners (see http://www.filariasis.org/who_we_are/partners.html) and is housed at the Centre for Neglected Tropical Diseases (CNTD) in Liverpool. This alliance is probably the most successful disease control alliance ever formed as evidenced by the expansion of treatment coverage against this terrible affliction (see [31, 90] and website www.filariasis.org). The principle is that an annual combined dose of albendazole with Mectizan® in Africa and albendazole with DEC outside of Africa given to the whole community will effectively prevent transmission for a year. This is because the concentration of microfilariae in the blood will be so reduced that the biting mosquitoes will not pick them up [74]. Since the filarial adult worms live for an average of just 6 years elimination can be a reality if transmission can be interrupted for six consecutive years [92–94], resulting in huge health and economic benefits [95–97].

The elimination program is being underpinned by the donation pledges of pharmaceutical companies, dating back to the late 1990s. GSK made a commitment to donate albendazole, and Merck & Co. Inc. extended their onchocerciasis donation of Mectizan® to include LF in Africa [98]. Elsewhere DEC was purchased until 2010 when EISAI made their donation for the future. Currently, approximately 600 million people receive treatment annually against LF [46]. Delivery is being funded by individual governments with assistance from the BMGF, USAID and DFID. This emphasizes the capacity of major pharmaceutical companies to work together on a major global health problem.

One unfortunate note is that many people in Africa who need treatment for LF are not yet receiving it as some governments are yet to embrace the value that the LF program provides. Approximately 80 million people are currently being treated annually with free drugs in Africa but because of the *Loa loa* complication [99] and because of the civil unrest in many parts of Africa poor coverage in some areas has not yet been resolved.

Nevertheless, the LF elimination program has achieved some fantastic results: Egypt and Zanzibar [100], and most recently Costa Rica, Suriname and Trinidad and Tobago have stopped MDA because they have successfully achieved their elimination targets [31, 90, 101]. The new donation from EISAI in Japan, amounting to two billion tablets a year, will be sufficient to treat at least the Indian subcontinent (and possibly the four countries in the American continent that are still endemic), and raising hopes of elimination of LF by 2020.

However, the drug treatments do not reverse the disfiguring morbidity that has already developed. For these cases, an individual care approach is needed based on hygiene and surgery, where appropriate (Fig. 7).

Case management of such patients has expanded and improved, and leg washing has increased the care of elephantiasis patients and has led to reductions in leg swellings by preventing secondary infections. Hydrocele surgery is slowly becoming more widespread as "surgery camps" are being established in different countries [102]. For example, in Niger, SCI supported over 600 hydrocele operations in 2010. These have been extremely successful and hundreds of men have come forward requesting the free-of-charge 20-min surgical intervention, performed under local anesthetic. The cost of each intervention at one of SCI's camps averages less than $200, which includes pre- and postoperative treatment (www.schisto.org).

Trachoma

Blindness due to trachoma is caused by the after effects of conjunctivitis due to *Chlamydia trachomatis* infections carried by flies. Trachoma is simply a disease of

poor hygiene, combined with dry and dusty conditions, and poverty. After severe conjunctivitis the eyelids become affected by scarring, and eyelashes are turned inward toward the eye and damage, and eventually destroy the cornea over time, leading to irreversible blindness. Improved water and sanitation would soon lead to elimination of trachoma. Meanwhile, treatment with Zithromax® and regular hand and face washing is all that is needed for prevention of new cases [19, 103] (Fig. 8).

For existing trichiasis cases simple surgery can correct the problem. Face washing and improved water and sanitation are essential components in a trachoma elimination strategy. The World Health Organization

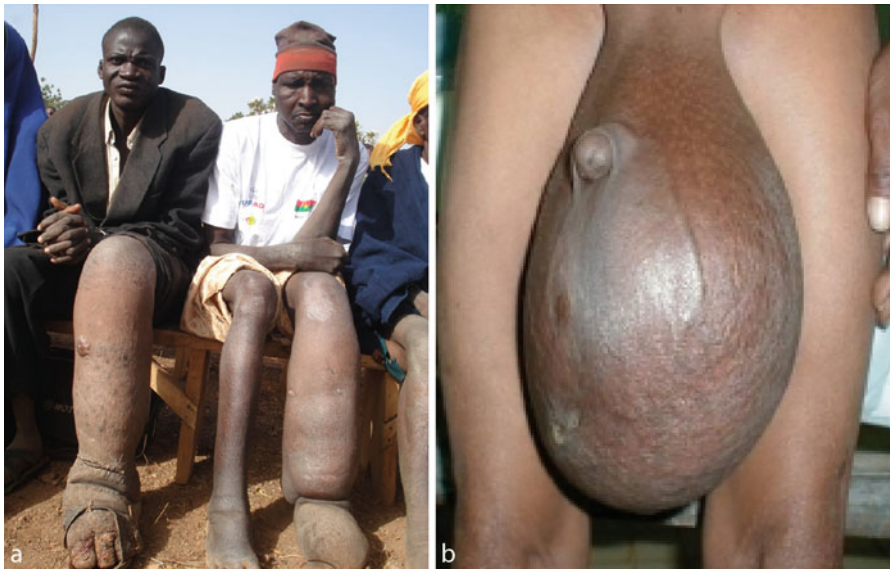

Waterborne Infectious Diseases, Approaches to Control. Figure 7
Morbidity caused by long-term lymphatic filariasis to the (**a**) legs, lymphedema and (**b**) scrotum, hydrocele

Waterborne Infectious Diseases, Approaches to Control. Figure 8
(**a**) Trachoma is caused by the bacteria *Chlamydia trachomatis* which is often spread by flies in areas of poor sanitation; (**b**) Trachoma's major effects include corneal damage and irreversible blindness

promotes the global elimination of blinding trachoma by 2020 (GET 2020) through an integrated approach named the SAFE strategy – S for surgery, A for Antibiotics, F for face washing, and E for environmental improvements to reduce the infestation of flies. The International Trachoma Initiative (ITI), established in 1999, and a number of other NGDOs are very active in promoting eye care and control of trachoma, possibly combined with that of onchocerciasis where relevant. Excellent progress has been made in some countries, and ITI's flagship program has contributed to eliminating trachoma from Morocco [103].

Early treatment is effective: azithromycin – Zithromax®, an antibiotic for active infection, which is currently donated by Pfizer needs to be administered annually. In 2011, it is estimated that approximately 70 million doses of Zithromax® will be distributed. A new website www.trachoma.org has been developed to provide information about trachoma and the treatments provided by ITI. The target for reaching elimination of blinding trachoma globally remains as "2020." As of this year:

- About 41 million people have active trachoma needing treatment.
- About 8.2 million people are estimated to have an advanced stage infection and therefore are blind or at risk of blindness.
- Fifty-seven countries are endemic, with up to 1.2 billion people living in at-risk areas.
- Since 1999, Pfizer has donated 225 million doses of Zithromax®.

Guinea Worm: A Worm on Its Own

Imagine having a worm a meter in length crawling around your body just under your skin. When the female adult worm is ready to lay her eggs, she emerges through the skin around the ankle. This subsequent burning sensation causes the victim to bathe the leg in water to cool it down. This is exactly what not to do because the worm emerges and deposits thousands of larvae into the water. These larvae infect water fleas where they develop and subsequently reinfect humans when the fleas are ingested when water is directly used for drinking. This is Guinea worm (Fig. 9).

The life-cycle of Guinea worm involves no animal host, thereby reducing the number of possible control targets. The control strategy is therefore based on identification of infected individuals, reporting and containment of cases, on behavioral change so those infected individuals do not contaminate the water, and on improved water supplies. Such combined efforts could and should lead to the eradication of Guinea worm disease. People can only get infected by swallowing infected water fleas. This happens only when people are forced to drink water from open ponds which contain these fleas, and this only happens when the water they drink has not been filtered.

Waterborne Infectious Diseases, Approaches to Control. Figure 9
A photograph of the adult Guinea worm (dracunculiasis) slowly being extracted from its emergence point, here on the top of the foot (Taken from http://www.maximsnews.com/news20081209guineawormeradication10812090803.htm, Photo Credit: Photo © The Carter Center/Louise Gubb, Ghana, 2007)

Thus eradication of this unique worm was recognized to be possible some 20 years ago, and WHO and the Carter Center have been working toward this end ever since. However, there is no drug treatment for Guinea worm; the only course open to an infected person is the slow extraction of the very long worm from the skin by gently winding the worm around a stick and pulling it out over several days.

The Guinea Worm program is now moving toward eradication. The number of annual cases has been dramatically reduced from over one million in 1988 to fewer than 2,000 in 2010; and the disease remains endemic in just four countries – Chad, Ethiopia, Mali, and Sudan (www.cartercenter.org; [104]). A number of countries have been certified as free of transmission,

and there are several more countries which have not reported cases during the previous year (Burkina Faso, Cote d'Ivoire, Ghana, Kenya, Niger, Nigeria, Togo) and are considered to be in precertification phase. Once a country has been certified, there is a continued need for surveillance – in order to prevent reestablishment of transmission until global eradication is achieved.

Cholera and Typhoid

The bacterial infections cholera (caused by *Vibio cholerae*) and typhoid (caused by *Salmonella typhi*) are endemic in countries where poor water and sanitation prevail. However, they cause their greatest damage when they reach epidemic outbreaks during times of crisis such as after natural disasters: flood, earthquakes, and tsunamis. During these periods many displaced persons congregate in temporary camps with poor sanitation, and where drinking water sources are contaminated. These really are diseases that thrive when basic services have broken down, and can quickly overwhelm public health services in such locations [105]. Cholera bacteria are most often associated with waterborne transmission, but can also be transmitted by contaminated food [105]. The classic symptoms of cholera are profuse, watery diarrhea, and vomiting, which can rapidly lead to severe dehydration and death in hours if left untreated. In addition to these severe sequelae of infection, there will likely be many, unreported cases that are asymptomatic or result in nonspecific mild symptoms [106]. Treatment of cholera via oral and intravenous rehydration therapy has resulted in reductions in fatality rates, but it still remains a dreaded disease [20]. The consequences of infection are vomiting and diarrhea, and treatment is patient care and rehydration. In epidemics about 5% of those infected will die, but if rehydration can be provided, recovery is usually achieved. Typhoid fever is caused by the bacterium *Salmonella enterica* serotype Typhi (*S. typhi*). Improvements in water and sanitation virtually eliminated typhoid from the majority of the developed world, yet it still exerts a significant public health burden in the developing world [107]. The most common mode of transport is through contaminated water, or food that has come into contact with contaminated water, and thus is heavily associated with poor water and sanitation. The burden of disease is thought to be highest in children under the age of 5 who suffer the most serious sequelae of infection [108]. The emergence of drug resistance to a succession of antibiotics, most recently to quinolones, has put great pressure on public health systems in resource-poor settings [107].

Dengue and Dengue Hemorrhagic Fever (DHF)

These are acute febrile diseases, found in the tropics, and caused by four closely related virus serotypes, transmitted by the *Aedes* mosquito which bites during the day. The disease is now endemic in more than 100 countries in Africa, the Americas, the Eastern Mediterranean, Southeast Asia, and the Western Pacific [109]. Southeast Asia and the Western Pacific are the most seriously affected. Before 1970 only nine countries had experienced DHF epidemics, a number that had increased more than fourfold by 1995. Not only is the number of cases increasing as the disease is spreading to new areas, but explosive outbreaks are also occurring. In 2007, Venezuela reported over 80,000 cases, including more than 6,000 cases of DHF [110].

- During epidemics of dengue, infection rates among those who have not been previously exposed to the virus are often 40–50%, but can reach 80–90%.
- An estimated 500,000 people with DHF require hospitalization each year, a very large proportion of whom are children. About 2.5% of those affected die.
- Without proper treatment, DHF fatality rates can exceed 20%. Wider access to medical care from health providers with knowledge about DHF – physicians and nurses who recognize its symptoms and know how to treat its effects – can reduce death rates to less than 1%.

Early treatment with therapy to tackle shock due to hemoconcentration reductions and bleeding is crucial. Increased oral fluid intake is recommended to prevent dehydration. In extreme cases, internal gastrointestinal bleeding may occur requiring a transfusion.

Unfortunately, progress on control of this infection has been poor. Dengue fever is becoming more prevalent in some areas, which is cause for great concern. The spread of dengue is attributed to expanding geographic distribution of the four dengue viruses and their mosquito vectors, the most important of which is the

predominantly urban species *Aedes aegypti*. A rapid rise in urban mosquito populations is bringing ever greater numbers of people into contact with this vector, especially in areas that are favorable for mosquito breeding, for example, where household water storage is common and where solid waste disposal services are inadequate.

Future Directions

Great progress has been made in some areas of the battle against waterborne diseases. Control of malaria has long captured the scientific community's attention and with the recent Bill and Melinda Gates call to aim for eradication hopefully significant further progress will be accomplished. Control and elimination of some of the other waterborne diseases, such as some of the NTDs (schistosomiasis, STH, onchocerciasis, LF, trachoma), can be achieved through inexpensive (or even donated), effective, and easily administered drugs. Even more promisingly, Guinea worm is on the verge of becoming the world's second major human infectious disease to be eradicated from the globe (following smallpox [111]). This has been achieved with no available drug; but purely through health education and behavior change. For other diseases, like dengue, cholera, and typhoid, the picture is bleaker; increases in the number of cases and their distribution demand that further tools be developed and greater effort is expended in their control.

Clearly, for all these waterborne diseases discussed here, permanent change will be aided hugely by improvements in water and sanitation, particularly in the transmission heartlands of sub-Saharan Africa and Southeast Asia. Naturally, people will continue to be drawn to areas providing sources of water, and the exploitation of such resources will play a crucial role in socioeconomic development of less-developed countries. A multisectorial approach to disease control is advocated, for example, when carrying out the development of water resources (drinking water, sanitation, dams, hydroelectric power), a greater integration between engineering and health sectors is required to effectively combat these waterborne diseases permanently. In the mean time, it is advocated to use whatever tools are currently available to reduce infection and transmission and ease the burden of these diseases.

Bibliography

1. Fenwick A (2006) Waterborne infectious diseases – could they be consigned to history? Science 313:1077–1081
2. Steinmann P et al (2006) Schistosomiasis and water resources development: systematic review, meta-analysis, and estimates of people at risk. Lancet Infect Dis 6:411–425
3. Keiser J, Singer BH, Utzinger J (2005) Reducing the burden of malaria in different eco-epidemiological settings with environmental management: a systematic review. Lancet Infect Dis 5:695–708
4. Fenwick A et al (2009) The Schistosomiasis Control Initiative (SCI): rationale, development and implementation from 2002–2008. Parasitology 136:1719–1730
5. Hotez PJ et al (2009) Rescuing the bottom billion through control of neglected tropical diseases. Lancet 373:1570–1575
6. Hotez PJ et al (2006) Incorporating a rapid-impact package for neglected tropical diseases with programs for HIV/AIDS, tuberculosis, and malaria. PLoS Med 3:e102
7. Lammie PJ, Fenwick A, Utzinger J (2006) A blueprint for success: integration of neglected tropical disease control programmes. Trends Parasitol 22:313–321
8. Zhang Y et al (2010) Control of neglected tropical diseases needs a long-term commitment. BMC Med 8:67–75
9. Kolaczinski JH et al (2007) Neglected tropical diseases in Uganda: the prospect and challenge of integrated control. Trends Parasitol 23:485–493
10. Linehan M et al (2011) Integrated implementation of programs targeting neglected tropical diseases through preventive chemotherapy: proving the feasibility at national scale. Am J Trop Med Hyg 84:5–14
11. Molyneux D, Hopkins DR, Zagaria N (2004) Disease eradication, elimination and control: the need for accurate and consistent usage. Trends Parasitol 20:347–351
12. WHO (2004) World health report 2004: changing history. World Health Organization, Geneva. http://www.who.int/whr/2004/en
13. Snow RW et al (2005) The global distribution of clinical episodesk of *Plasmodium falciparum* malaria. Nature 10:214–217
14. King C (2010) Parasites and poverty: the case of schistosomiasis. Acta Trop 113:95–104
15. de Silva NR et al (2003) Soil-transmitted helminth infections: updating the global picture. Trends Parasitol 19: 547–551
16. Dadzie Y, Neira M, Hopkins D (2003) Final report of the conference on the eradicability of onchocerciasis. Filaria J 2:2
17. Zagaria N, Savioli L (2002) Elimination of lymphatic filariasis: a public health challenge. Ann Trop Med Parasitol 96:S3–S13
18. Centre C (2011) Dracunculiasis eradication: the final inch. http://www.cartercenter.org/news/documents/doc2229.html
19. Kumaresan JA, Mecaskey JW (2003) The global elimination of blinding trachoma: progress and promise. Am J Trop Med Hyg 69:S24–S28
20. WHO (2006) Cholera, 2005. Wkly Epidemiol Rec 81:297–308

21. WHO (2003) Cholera unveiled. Global Task Force on Cholera Control, Editor, Geneva. http://whqlibdoc.who.int/hq/2003/WHO_CDS_CPE_ZFK_2003.3.pdf
22. Crump JA, Luby SP, Mintz ED (2004) The global burden of typhoid fever. Bull World Health Organ 82:346–353
23. Suaya JA, Shepard DS, Beatty ME (2006) Dengue: burden of disease and cost of illness. Working paper for the scientific working group on dengue research, convened by the special programme for research and training in tropical diseases, Geneva, 1–5 October 2006
24. Roberts L, Enserink M (2007) Did they really say. . .eradication? Science 318:1544–1555
25. WHO (2008) Global malaria control and elimination: report of a technical review. World Health Organization, Geneva
26. Knopp S et al (in press) From morbidity control to transmission control: time to change tactics against helminths on Unguja Island, Zanzibar. Acta Trop. doi: 10.1016/j.actatropica.2011.04.010
27. Richter J (2003) The impact of chemotherapy on morbidity due to schistosomiasis. Acta Trop 86:161–183
28. WHO (2002) Prevention and control of schistosomiasis and soil-transmitted helminthiasis. In: World health organization technical report. World Health Organization, Geneva, pp I–v1
29. Thylefors B (2008) The Mectizan donation program (MDP). Ann Trop Med Parasitol 102(S1):S39–S44
30. Basáñez MG et al (2006) River blindness: a success story under threat? PLoS Med 3:e371
31. GAELF (2010) Half-time in LF elimination: teaming up with NTDs. In: Sixth meeting of the global alliance to eliminate lymphatic filariasis, Seoul, 1–3 June 2010
32. Mariotti SP, Pascolini D, Rose-Nussbaumer J (2009) Trachoma: global magnitude of a preventable cause of blindness. Br J Ophthalmol 93:563–568
33. West S (2003) Blinding trachoma: prevention with the SAFE strategy. Am J Trop Med Hyg 69:S18–S23
34. Crump JA, Mintz ED (2010) Global trends in typhoid and paratyphoid fever. Clin Infect Dis 50:241–246
35. Breman JG (2001) The ears of the hippopotamus: manifestations, determinants, and estimates of the malaria burden. Am J Trop Med Hyg 64S:1–11
36. Snow RW et al (1999) Estimating mortality, morbidity, and disability due to malaria among Africa's non-pregnant population. Bull World Health Organ 77:627–640
37. Brooker S et al (2008) Malaria in African schoolchildren: options for control. Trans R Soc Trop Med Hyg 102:304–305
38. Greenwood B (2009) Can malaria be eliminated? Trans R Soc Trop Med Hyg 103(S1):S2–S5
39. Kapp C (2000) WHO wins reprieve for DDT against malaria. Lancet 356:2076
40. Hay SI et al (2009) A world malaria map: *Plasmodium falciparum* endemicity in 2007. PLoS Med 6(3):e1000048
41. Chawira AN et al (1987) The effect of combinations of qinghaosu (artemisinin) with standard antimalarial drugs in the suppressive treatment of malaria in mice. Trans R Soc Trop Med Hyg 8:554–558
42. Lim P et al (2009) Pfmdr1 copy number and artemisinin derivatives combination therapy failure in falciparum malaria in Cambodia. Malar J 8:11
43. WHO (2006) Guidelines for the treatment of malaria. World Health Organization, Geneva
44. Tshefu AK et al (2010) Efficacy and safety of a fixed-dose oral combination of pyronaridine-artesunate compared with artemether-lumefantrine in children and adults with uncomplicated *Plasmodium falciparum* malaria: a randomised non-inferiority trial. Lancet 375:1457–1467
45. Maxwell CA et al (2002) Effect of community-wide use of insecticide-treated nets for 3–4 years on malarial morbidity in Tanzania. Trop Med Int Health 7:1003–1008
46. WHO (2011) Malaria: Indoor residual spraying. http://www.who.int/malaria/vector_control/irs/en/index.html
47. Pluess B et al (2010) Indoor residual spraying for preventing malaria (review). The Cochrane Libr 4:CD006657
48. Gryseels B et al (2006) Human schistosomiasis. Lancet 368:1106–1118
49. Poggensee G, Feldmeier H (2001) Female genital schistosomiasis: facts and hypotheses. Acta Trop 79:193–210
50. Fulford AJ et al (1995) A statistical approach to schistosome population dynamics and estimation of the life-span of *Schistosoma mansoni* in man. Parasitology 110:307–316
51. Crompton DW, Savioli L (2007) Handbook of helminthiasis for public health. Taylor and Francis, Boca Raton
52. Cook G, Zumla A (eds) (2008) Manson's tropical diseases, 22nd edn. W.B. Saunders, London
53. Mahmoud AAF (2001) Schistosomiasis. Imperial College Press, London
54. Fenwick A (2006) New initiatives against Africa's worms. Trans R Soc Trop Med Hyg 100:200–207
55. Warren KS et al (1974) *Schistosomiasis mansoni* in Yemeni in California: duration of infection, presence of disease, therapeutic management. Am J Trop Med Hyg 23:902–909
56. Harris ARC, Russell RJ, Charters AD (1984) A review of schistosomiasis in immigrants in western Australia, demonstrating the unusual longevity of *Schistosoma mansoni*. Trans R Soc Trop Med Hyg 78:385–388
57. de Clerq D et al (1998) The relationship between *Schistosoma haematobium* infection and school performance and attendance in Bamako, Mali. Ann Trop Med Parasitol 92:851–858
58. Vennerveld BJ, Dunne DW (2004) Morbidity in schsistosomiasis: an update. Curr Opin Infect Dis 17:439–447
59. Miguel E, Kremer M (2004) Worms: identifying impacts on education and health in the presence of treatment externalities. Econometrica 72:159–217
60. French MD et al (2010) Observed reductions in *Schistosoma mansoni* transmission from large scale administration of praziquantel in Uganda: a mathematical modelling study. PLoS Negl Trop Dis 4:e897
61. WHO (2006) Preventive chemotherapy in human helminthiasis. Coordinated use of anthelminthic drugs to control interventions: a manual for health professionals and programme managers. World Health Organization, Geneva

62. WHO (2009) WHO model formulary. Based on the 15th model list of essential medicines 2007. World Health Organization, Geneva
63. Hotez P et al (2010) Africa is desperate for praziquantel. Lancet 376:496–498
64. Bethony J et al (2006) Soil-transmitted helminth infections: ascariasis, trichuriasis, and hookworm. Lancet 367:1521–1532
65. Nokes C et al (1991) Geohelminth infections and academic assessment in Jamaican children. Trans R Soc Trop Med Hyg 85:272–273
66. Nokes C et al (1992) Parasitic helminth infection and cognitive function in school children. Proc R Soc Lond B 247:77–81
67. Simeon D et al (1994) School performance, nutritional status and trichuriasis in Jamaican schoolchildren. Acta Paediatr 83:1188–1193
68. Hutchinson SE et al (1997) Nutrition, anaemia, geohelminth infection and school achievement in rural Jamaican primary school children. Eur J Clin Nutr 51:729–735
69. Albonico M et al (2006) Intervention for the control of soil-transmitted helminthiasis in the community. Adv Parasitol 61:311–348
70. Brooker S, Hotez PJ, Bundy DAP (2008) Hookworm-related anaemia among pregnant women: a systematic review. PLoS Negl Trop Dis 2:9
71. Smith JL, Brooker S (2010) Impact of hookworm infection and deworming on anaemia in non-pregnant populations: a systematic review. Trop Med Int Health 15:776–7959
72. Yokogawa M (1985) JOICFP's experience in the control of ascariasis within an integrated programme. In: Crompton DW, Nesheim MC, Pawlowski ZS (eds) Ascaris and its public health significance. Taylor and Francis, London, pp 265–278.
73. Albonico M et al (2008) Controlling soil-transmitted helminthiasis in pre-school-age children through preventive chemotherapy. PLoS Negl Trop Dis 2:e126
74. Ottesen EA (2006) Lymphatic filariasis: treatment, control and elimination. Adv Parasitol 61:395–441
75. Kirkwood B et al (1983) Relationships between mortality, visual acuity and microfilarial load in the area of the onchocerciasis control programme. Trans R Soc Trop Med Hyg 77:862–868
76. Prost A (1986) The burden of blindness in adult males in the Savanna villages of West Africa exposed to onchocerciasis. Trans R Soc Trop Med Hyg 80:525–527
77. Murdoch ME et al (2002) Onchocerciasis: the clinical and epidemiological burden of skin disease in Africa. Ann Trop Med Parasitol 96:283–296
78. Little MP et al (2004) Incidence of blindness during the onchocerciasis control programme in western Africa, 1971–2002. J Infect Dis 189:1932–1941
79. Boatin BA, Richards FO (2006) Control of onchocerciasis. Adv Parasitol 61:349–394
80. Hougard J-M et al (1997) Twenty-two years of blackfly control in the onchocerciasis control programme in West Africa. Parasitol Today 13:425–431
81. Boatin B (2008) The onchocerciasis control programme in West Africa (OCP). Ann Trop Med Parasitol 102(S1): S13–S17
82. Dadzie KY et al (1991) Onchocerciasis control by large-scale ivermectin treatment. Lancet 337:1358–1359
83. Tielsch JM, Beeche A (2004) Impact of ivermectin on illness and disability associated with onchocerciasis. Trop Med Int Health 9:A45–A56
84. Amazigo U (2008) The African programme for onchocerciasis control (APOC). Ann Trop Med Parasitol 102(S1):19–22
85. Gardon J et al (1997) Serious reactions after mass treatment of onchocerciasis with ivermectin in an area endemic for *Loa loa* infection. Lancet 350:18–22
86. Padgett JJ, Jacobsen KH (2008) Loiasis: African eye worm. Trans R Soc Trop Med Hyg 102:983–989
87. Sauerbrey M (2008) The onchocerciasis elimination program for the Americas. Ann Trop Med Parasitol 102(S1):S25–S29
88. Onchocerciasis Elimination Program for the Americas (OEPA) (2011) Distribución geográfica de la oncocercosis y situación de la transmisión en las Américas. http://www.oepa.net/epidemiologia.html
89. Cupp EW, Sauerbrey M, Richards FO Elimination of human onchocerciasis: history of progress and current feasibility using ivermectin (Mectizan®) monotherapy. Acta Trop 120 S1:S100–S108
90. GAELF (2011) Global programme to eliminate lymphatic filariasis: progress report on mass drug administration, 2010. Wkly Epidemiol Rec 86:377–388
91. Nienga SM et al (2007) Chronic clinical manifestations related to *Wuchereria bancrofti* infection in a highly endemic area in Kenya. Trans R Soc Trop Med Hyg 101:439–444
92. Gyapong JO et al (2005) Treatment strategies underpinning the global programme to eliminate lymphatic filariasis. Expert Opin Pharmacother 6:179–200
93. Gambhir M et al (2010) Geographic and ecologic heterogeneity in elimination thresholds for the major vector-borne helminthic disease, lymphatic filariasis. BMC Biol 8:22
94. Michael E et al (2006) Mathematical models and lymphatic filariasis control: endpoints and optimal interventions. Trends Parasitol 22:226–233
95. Ottesen EA et al (2008) The global programme to eliminate lymphatic filariasis: health impact after 8 years. PLoS Negl Trop Dis 2:e317
96. Hooper PJ et al (2009) The global programme to eliminate lymphatic filariasis: health impact during its first 8 years (2000–2007). Ann Trop Med Parasitol 103(S1):S17–S21
97. Chu BK et al (2010) The economic benefits resulting from the first 8 years of the global programme to eliminate lymphatic filariasis. PLoS Negl Trop Dis 4:e708
98. Hopkins AD, Molyneux DH (2009) A decade of ivermectin-albendazole donation for lymphatic filariasis. Ann Trop Med Parasitol 103(S1):S3
99. Molyneux DH (2009) Filaria control and elimination: diagnostic, monitoring and surveillance needs. Trans R Soc Trop Med Hyg 103:338–341

100. Mohammed KA et al (2006) Progress towards elimination lymphatic filariasis in Zanzibar: a model programme. Trends Parasitol 22:340–344
101. Rawlins SC et al (2004) Evidence for the interruption of transmission of lymphatic filariasis among schoolchildren in Trinidad and Tobago. Trans R Soc Trop Med Hyg 98:473–477
102. Brantus P (2009) Ten years of managing the clinical manifestations and disabilities of lymphatic filariasis. Ann Trop Med Parasitol 103(S1):S5–S10
103. Knirsch C (2007) Trachoma: ancient scourge, disease elimination, and future research. Curr Infect Dis Rep 9:21–28
104. Barry M (2007) The tail end of guinea worm – global eradication without a drug or a vaccine. N Engl J Med 356:2561–2564
105. Sack DA et al (2004) Cholera. Lancet 363:223–233
106. Glass RI et al (1982) Endemic cholera in rural Bangladesh. Am J Epidemiol 116:959–970
107. Bhutta Z (2006) Endemic cholera in rural Bangladesh, 1966–1980. Br Med J 333:78–82
108. Sinha A et al (1999) Typhoid fever in children aged less than 5 years. Lancet 354:734–737
109. WHO (1997) Dengue haemorrhagic fever: diagnosis, treatment prevention and control. World Health Organization, Geneva
110. San Martin JL et al (2010) The epidemiology of dengue in the Americas over the last three decades: a worrisome reality. Am J Trop Med Hyg 82:128–135
111. Henderson DA (1976) The eradication of smallpox. Sci Am 235:25–33

Waterborne Parasitic Diseases in Ocean

Robin M. Overstreet
Department of Coastal Sciences, Gulf Coast Research Laboratory, University of Southern Mississippi, Ocean Springs, MS, USA

Article Outline

Glossary
Definition of the Subject and Its Importance
Introduction
Parasites Acquired When People Eat Infected Seafood Products
Parasites Acquired When People Have Direct or Indirect Contact with Them
Parasites That Produce Excretions or Secretions That Result in an Immunological Response in People
Management, Control, and Treatment of Parasites Affecting People
Future Directions
Acknowledgments
Bibliography

Glossary

Autoinfection Reinfection of a host by the progeny of a parasite already present in the same host individual without exposure to the external environment.

Cyst/Encapsulation A cyst is a structure to aid dissemination or protection of a parasitic stage derived from the parasite and in some cases additionally from the host. A capsule differs by being derived from the host, often as a cellular response.

Erythema Abnormal redness of the skin due to local congestion as in inflammation, caused by irritation or injury to the tissue.

Hermaphrodite parasite An individual containing both male and female gametes that can be functional concurrently or with one following the other; some able to form zygotes.

Hypersensitivity reaction A damaging and sometimes fatal reaction produced by the normal immune system, which requires a pre-sensitized, immune state of the host.

Life cycle of parasite The orderly sequence of distinct stages through which the agent progresses in the course of development to maturity or sexual stage.

Life history of parasite The life cycle of an agent including facultative paratenic hosts, feedback strategies, interaction with the environment, and other ecological influences.

Paratenic host A specific host, also termed "transport host," which acquires a stage of an agent that does not develop to the subsequent stage and can be either acquired by another paratenic host or by a final host; that host can be critical in completing a life cycle.

Pathogenesis The production or development of a disease, specifically the cellular reactions and other pathologic mechanisms occurring in the progression of the disease.

Reservoir host A definitive host that serves as an alternant relative to the host of interest for an agent that disseminates infective stages.

Salinity An expression of concentration of salts dissolved in water, including primarily chloride,

sodium, magnesium, sulfur, calcium, and potassium but with other elements in low concentrations. It is usually expressed as parts per thousand (ppt) or parts per million (ppm) and usually based on the electrical conductivity ratio of the sample to "Copenhagen water," an artificial seawater manufactured to serve as a world "standard" or more recently in practical salinity units (psu) as the conductivity ratio of a seawater sample to a standard KCl solution. Full strength seawater is considered 35 ppt, or 35 g of salt per liter of solution; salinity in estuaries can fluctuate from 0 to over 35 ppt daily, seasonally, or yearly, depending on winds, rain, currents, temperature, and geography.

Urticaria An allergic reaction comprising pale, pink, focal swellings, or wheals, on the skin that itch, burn, or sting; also referred to as "hives."

Zoonosis An animal disease transmissible to humans under natural conditions or a human disease transmissible to animals.

Definition of the Subject and Its Importance

Several parasites that infect marine and coastal animals or contaminate the marine and coastal waters can infect humans and present a significant public health risk. Historically, parasites from the marine environment were ignored as representing a risk. More recently, more researchers have investigated actual or potential human marine infections; easily observable worms and other metazoans have been experimentally studied to determine if they can infect model mammals; some humans are now more likely to come into contact with infective parasites; immunocompromised people are more susceptible to parasitic infections; molecular methods have been used to differentiate known or potential infective parasitic species; improved molecular and serological methods have been developed to detect known protozoan and metazoan parasites; and infectious parasites have been investigated in detail. As discussed in this chapter, some parasites involved with marine waters and seafood products can kill large numbers of people, other fatal ones are rare, many cause human illness, and infections or the possibility of infections keeps people from eating seafood or entering marine waters. Moreover, the economic loss of seafood products from actual or perceived problems involving parasites in seafood caused by media exposure can be significant [1, 2] just as it is when involving perceived contamination of seafood by oil or other toxicants (gulfseagrant.tamu.edu/oilspill/pdfs/latourismPerception_BPOilWave1.pdf).

Introduction

Textbooks once considered parasites of marine origin or those in the marine environment as posing no public health risk. Over the last few decades, more and more parasites in different groups have been determined to be zoonotic agents that either are known to infect humans or can serve as a potential public health risk based on experimental infections in nonhuman mammalian hosts or are closely related to known human-infecting agents. These parasites include metazoans and "protozoans" that occur in water or in seafood products. Protozoa occurs in quotation marks because its historic higher taxonomic groups are not necessarily closely related [3] and some include stages with more than one cell. For example, a single myxosporidian spore may develop from a stage consisting of 13 cells, and molecular data demonstrate no relationship between Myxosporea and any group consisting of members with single cells and recognized as a protozoan. At least one metazoan taxonomic group, ascaridoid nematodes, has members that produce excretions and secretions (ES) that are potentially harmful to susceptible people.

Numerous factors are involved with risk of infection. For example, the likelihood of a visitor or traveler getting infected by eating raw seafood in well-known urban Japanese or other Asian restaurants is relatively low, but dining in rural local restaurants or street shops has a higher risk of infection with a variety of parasites [4]. The highest worldwide risk for a helminth infection is from preparation of raw or inadequately cooked seafood at home. This is usually because restaurants typically use products historically known not to be infected in the region from which they were collected or the products were frozen and then thawed. Public health risk also occurs for personal contact with parasites for people using coastal and marine water for either occupation or recreation.

An apparent increase in human infections has occurred because of increased opportunities to get

infected. (1) A global spread and increased popularity of "exotic cuisines" at least partially relates to increased human infections because of the increase in various media such as television and magazines. This has led to an increase in homemade raw seafood products, which are much more likely to contain infective parasites than products served in restaurants. (2) The increased popularity of raw products also relates to an increase and translocation of people throughout the world. People that move or visit abroad take their cuisines with them. They may eat infected products in their new surroundings that are similar to the uninfected products they ate in their native country. They can also spread their diseases as they travel, allowing new intermediate hosts and reservoirs to become established. (3) Much of the world's population is becoming more affluent, and with that more people are able to try new cuisines. Also, there is more opportunity to partake of established cuisines. For example, in Vietnam the improved economy has increased the traditional social activities that are conducive to eating more raw seafood and, consequently, acquiring more parasites. (4) With the resulting increase in people and demand for healthy fishery products, there has been increased utilization of different fishing grounds, species, and stocks. Even though some stocks are overfished, methods are now available for ships to go farther to sea or deeper to catch replacement products, possibly with improved transportation and storage systems. When a specific fish is assumed to be free from parasites harmful to humans, when the same species is caught in a different location, when it is maintained on a vessel longer, or when it is produced on fish farms, that resulting fish product may have or it may acquire harmful parasites. Also, fishing a previously underutilized species may result in obtaining an infected stock. (5) Regulations such as those protecting specific animals may result in an increased public health risk. For example, protecting seal pups and reducing seal fashions increases the final host population for *Pseudoterranova* spp., which results in a heavily infected cod intermediate host population. Also, the need to discharge fisheries wastes from commercial and subsistence vessels results in increased infections in fishes and marine mammals that feed on the wastes. Alternatively, regulations in some countries are lacking in regard to fishery products or for imported fishery products but not necessarily all meats, leaving consumers with the false impression that the products are safe. (6) Climatic and environmental health conditions are always changing, and, with those changes, infection dynamics of parasites quickly change. For example, during the El Niño of 1997–1998, the junction of the warmwater Kuroshio Current from the south with the cool Oyashio Current from the north moved 3,000 km northward from Kyushu to Hokkaido, Japan. This migration of the current's junction and its temperature elevation of 3.4°C caused an increase in abundance of krill, the intermediate host of *Pseudoterranova azarasi* and members of the *Anisakis simplex* complex. The sea lion final host of *P. azarasi* occurred in Hokkaido but not Kyushu, and, in addition, protected cetaceans that are the final hosts of *A. simplex* sensu lato migrated north so as to feed heavily on krill or on fish that ate the krill, acquiring the juvenile nematodes from them. Consequently, the Japanese used to eating nearly parasite-free seafood from Hokkaido began acquiring infections. In contrast, pollution from Southeast Asia kept some fish intermediate hosts of *A. simplex* sensu lato from migrating to Japan, especially to southern Kyushu, reducing the number of anisakiasis cases there [5]. Each few years, climate in some regions worldwide changes enough to influence the seafood production and the parasitic infections. (7) Reduced resistance in some people because of disease, organ transplants, or immunosuppressive drug therapy relate to an increased susceptibility to various parasites, especially parasites that can replicate in or on humans with being challenged by an additional dose of parasites.

Increased documentation of human infections results from increased technical abilities. (1) Improved media coverage allows people to know when an epidemic occurs. It also stimulates potentially infected people to get examined, sometimes unnecessarily and to the detriment of the seafood industry. (2) Diagnostic tests are becoming better and more available both because of research plus technical advancements and because various funds are made available to survey regions or satisfy needs. (3) The same can be said for accurate identifications. Molecular means make it easy to detect parasites that cannot be seen grossly or a juvenile that cannot be morphologically associated with an adult, upon which the species has been named

and described. (4) With good identifications and detection methods, more critical examinations can be obtained and compiled, allowing for useful epidemiological assessments.

The organization involves five sections. The first treats parasites that people acquire from the marine environment by eating seafood. The second treats those where people get infected with parasites by contact with them, either directly by active penetration by the parasites or indirectly by passive association with the agents. In the third, people get disease from allergens from parasites or parasite products. This is followed by a section on management, control, and treatment of the infectious parasites. The final section briefly examines what is required in the future to reduce, eliminate, or keep infections under control. In the first section on acquisition of parasites by eating inadequately prepared food, examples are divided into those that mature in humans and those that do not. The reason for this is that worms that mature in humans are voided or produce eggs that can be detected in fecal examinations. Those parasites that do not mature in the patient or produce cyst dispersal stages are more difficult to detect without immunological or invasive techniques. Moreover, the consumer not able to provide proof of a parasitic infection is less likely to find medical help, and the medical community is less likely to specifically diagnose, report the condition, or show a follow-up interest in the case. Several of these agents that have not yet been reported are treated as potential public health risks. The first two sections are each divided by taxonomic groups. In some cases the same parasites or members of the same parasitic group fit into more than one section, and the possible confusion is discussed in the different cases.

Parasites Acquired When People Eat Infected Seafood Products

Zoonotic parasitic diseases acquired by eating inadequately prepared infected seafood products include most of those treated by disease researchers and reported in recent literature. Some of the responsible agents are seen grossly, such as 5–10 m of senile cestode strobilae protruding out of the anus of alarmed seafood consumers or a 4-cm-long ascaridoid nematode being vomited or passing out through the nose of someone recently eating uncooked cod. Most zoonotic diseases are recognized by the signs of a disease or fortuitous findings of diagnostic features. Not all infections are diseases. A few hundred small marine heterophyids probably can line the human intestine without apparent symptoms, but more may cause pathological alterations and result in disease. A lot of factors involving the patient and the history of the infection can influence the alterations. Perhaps easier to envision would be a non-marine example of the hookworm *Necator americanus*. A barefoot boy can pick up a few dozen juveniles penetrating his feet from the warm, moist soil. There may be a slight itching and rash where the juveniles enter, but as they are carried to the lungs, pass up the respiratory tract to the mouth, are swallowed, and ultimately attach to the intestine as 7- to 11-cm-long adults, they produce no symptom. On the other hand, increase the number, say above 50, and pathological changes can occur during all the phases. Most important, once attached, the blood loss becomes enough to produce anemia and protein deficiency, and the resulting loss of iron and protein may retard growth and mental development. This will be associated with abdominal pain, diarrhea, loss of appetite and weight, and "disease." Numbers of worms alone can shift an "infection" without disease to a "disease."

Parasites That Mature in Humans

Helminths (Worms in General) Most agents that mature in humans are helminths. Helminth diseases consist largely of those acquired by eating inadequately prepared seafood products usually infected with platyhelminths and nematodes, but occasionally with other agents. Some agents are freshwater parasites that, because of their complicated life cycles, have one or more stages that enter the coastal or marine environment. Presently, several of these are treated as freshwater cases because of the epidemiological aspects of the case. As more cases are studied, more human infections that involve strictly marine parasites will be demonstrated.

Many more cases of marine helminth infections probably exist than are reported or recognized by physicians. Surveys involving fecal examinations

exhibit adult worms or their eggs, but, for a variety of reasons, the samples are difficult to acquire and the corresponding infections are difficult to correctly diagnose or get reported. Most medical attention is not likely to culminate in confirmed reports of identified agents because physicians or technicians not familiar with proper techniques, means to correctly identify the agents, or people to consult are interested in treatments and not the specifics of a parasitic infection. Even when treated, the patient never knows what was causing the signs of disease because the agents are killed and digested or degenerate. On the other hand, in some countries where considerable raw or insufficiently prepared seafood is consumed, attention by researchers and the medical community results in an abundance of case reports. The Japanese and Koreans provide good examples of documented cases of infections by marine parasites.

Platyhelminths consist mostly of hermaphroditic soft-bodied worms. Those hermaphrodites of medical marine significance are cestodes (tapeworms) and trematodes (flukes), and most of those that mature in humans were consumed as larval stages. For many, the taxonomic identification is confused and the life cycle is partially or fully unknown. Moreover, infections are often undiagnosed because fecal examinations are not always conducted or are conducted by those without parasitological training. Moreover, the eggs of many species are similar in appearance.

Cestodes Cestodes infective to humans from marine hosts are members of the family Diphyllobothridiidae in the Diphyllobothriidea, previously classified in the artificial assemblage Pseudophyllidea, now represented as comprising two unrelated clades, "Bothriocephalidea" and "Diphyllobothriidea" [6]. *Diphyllobothrium latum* is the best known member of the group, and it is considered a freshwater member with a cyclopoid-freshwater fish-bear/human/vertebrate cycle. Unpublished studies attempting to infect Mississippi marine fishes with the agent were unsuccessful; most copepod species developed a strong cellular response to the larva, and a mixture of "infected" copepods did not produce an infection in the Atlantic croaker. However, five human infections reported from eating the estuarine mullet *Liza haematocheila* in Korea were identified as *D. latum* on the basis of morphological characteristics [7]. Molecular tools should be able to confirm that identification as those tools have confirmed or corrected identifications of other species mentioned later.

Many human case reports have been identified as *Diphyllobothrium pacificum*, which typically matures in the pinnipeds. A recent taxonomic assessment of *D. pacificum* [8] involved numerous available specimens of variously misidentified species, including *D. latum* and *D. pacificum*. As it turned out, the classic publication [9] reporting human infections by *D. pacificum* in Peru was actually dealing with *Diphyllobothrium arctocephalinum*. Both *D. pacificum* and *D. arctocephalinum* occur along the South American Pacific coast in fur seals and secondarily in humans, with *D. pacificum* ranging north into Alaska and Japan and *D. arctocephalinum* restricted to the Southern Hemisphere, ranging south to South Australia and South Africa [8]. In one review, there are ten reported species of *Diphyllobothrium* from humans [10], including 6 from Japan [11], and in another there are 15 species [12]. Of the latter 15, not including *D. arctocephalinum*, there are eight nominal species in marine final hosts that also have been reported from humans: *Diphyllobothrium cameroni* (Hawaiian monk seal), *Diphyllobothrium cordatum* (Arctic seals, walruses), *Diphyllobothrium hians* (Arctic seals), *Diphyllobothrium orcini* (killer whale), *D. pacificum* (sea lions, eared seals), *Diphyllobothrium scoticum* (leopard seal, southern sea lion), and *Diphyllobothrium stemmacephalum* (harbor porpoise, bottlenose dolphin).

The species commonly infecting humans in Japan and previously referred to there as *D. latum* has been confirmed as *Diphyllobothrium nihonkaiense* ([8, 12], and others) (Fig. 1). The brown bear (*Ursus arctos*) is its natural definitive host, but it commonly infects humans, with some preserved worms measured as long as 8.8 m. Since infections are acquired from Pacific salmons (mainly cherry, pink, and chum salmons plus the Japanese huchen), either from the sea or just leaving the sea, it is considered a marine infection. Molecular studies have shown that human infections in Far East Russia up to the Kamchatka Peninsula reported as *Diphyllobothrium klebanovskii* are conspecific, identical to *D. nihonkaiense*. Molecular sequences also suggest the existence of two genotypes, biologically homogeneous populations not defined by locality [13]. Infections also involve consumers in Canada [14].

Waterborne Parasitic Diseases in Ocean. Figure 1 Author in Meguro Parasitological Museum, Tokyo, Japan, standing next to an 8.8-m-long specimen (> 10 m before fixation) of the tapeworm *Diphyllobothrium nihonkaiense* and the curators, the late Shunya Kamegai on *right* and Jun Araki on *left*

Moreover, salmon are exported to many countries, resulting in genetically confirmed infections in consumers in France and Switzerland [15] as well as New Zealand [16]. Another "freshwater" species, *Diphyllobothrium ursi*, also infects salmons and both brown and black bears as well as humans and dogs that feed on salmon or eat salmon-liver paste [17]. Cestodes and other parasites maturing in terrestrial definitive hosts that infect anadromous fishes such as Pacific salmonids or their freshwater fish or invertebrate hosts can be eaten by marine fishes, which in turn, serve as paratenic hosts. On the other hand, freshwater fishes can become paratenic hosts of helminths of marine origin. They can feed on infected marine fishes entering brackish river mouths or lower reaches of the rivers, or they can feed on anadromous fishes migrating upstream. A confirmed example is the plerocercoid of *Diphyllobothrium alascense* of dogs and rarely humans from the anadromous boreal smelt (*Osmerus mordax*) being transferred to the paratenic freshwater burbot (*Lota lota*) [18].

Members of *Diplogonoporus* have been reported from over 200 people in the twentieth century. Most cases have been identified as *D. balaenopterae*, or the names are probably synonyms of that species, a species that infects consumers in Japan but also Korea [12, 19]. A case from Spain probably represents infection from fish imported from the Far East [20]. Genetic analyses of 18S rDNA, ITS1, and cox1 nucleotide sequences of isolates were obtained from five Japanese cases [21]. The phylogenetic analysis of that material revealed little divergence and a close relationship to *Diphyllobothrium stemmacephalum*, a species maturing in the harbor porpoise and bottlenose dolphin rather than in whales as in *D. balaenopterae*. Data suggest that not only is *Diplogonoporus* paraphyletic, but those genetic data show that so are *Spirometra folium* and *Spirometra decipiens* [22].

Coastal Peruvians of ancient times had infections of *Diphyllobothrium* sp. as determined from coprolites [23], but infections of *D. pacificum* recently seem to be less prevalent in the northern Pacific Ocean, resulting from decreasing numbers of marine mammals and commercially important fishes like the pollack [8].

Not only have diphyllobothriid species been misidentified in the past, but human infections have been and will probably continue to be missed in many cases. They are most easily detected when a human expels lengthy portions of senile strobilae. Signs are variable but usually not severe [11, 24]. Most cases are probably not reported. The author did not experience any symptoms from an infection of four long specimens of *D. latum* other than mild discomfort several hours prior to periodic release of senile strobilae. The treatment of choice for the adult tapeworm infections in humans is a single dose of praziquantel (10–20 mg/kg) plus 30 g of magnesium sulfate as a purgative, if specimens are to be adequately studied.

Trematoda (Digenea, Flukes) Trematodes have a molluscan first intermediate host from which free-living cercariae are shed. The cercaria of most groups encysts or becomes encapsulated as a metacercaria in a second intermediate host, and this metacercaria matures as a hermaphroditic individual in a vertebrate final host when the second intermediate host is eaten. Because there are so many trematode taxonomic groups and species, there are numerous exceptions to the basic life cycle, and some of these involve species that can infect humans. For example, the well-known freshwater sheep liver fluke, *Fasciola hepatica*, encysts as small white spherules (metacercariae) on vegetation. Most people

that get infected do so by eating raw watercress on which the metacercariae have encysted. Schistosomes do not encyst but develop through the juvenile stage (schistosomula) in the final host where they ultimately mature in a blood vessel as separate male and female worms.

Depending on the taxon, the larval stage in the egg (miracidium) either hatches and penetrates its molluscan host or hatches after being eaten by a specific mollusk. The germ cells develop through a series of two or more asexual phases before shedding a continual production of hundreds to millions of infective cercariae. Some species have broad specificity in the molluscan, second intermediate host, or final host. Second intermediate hosts differ by family of trematode, but those discussed below include fishes, crustaceans, insects, mollusks, and none. Most of those marine/estuarine species reported from humans have a broad specificity of mammal or avian hosts. Most are rather small intestinal worms that necessitate a microscope to detect them unless hundreds are present, and each of these produces a continuous flow of a large number of small (25–30 μm long) eggs in the human feces for weeks or years. Most species are difficult to obtain in a healthy condition after medicinal treatment, are not transferred from the medical community to taxonomic parasitologists, are difficult to distinguish from one another, and produce minimal symptoms in light infections. Consequently, the number of human-infecting species and the prevalence and intensity of infections with marine trematodes are most certainly underestimated. Most of what is known has come from parasitologists within the medical community of Japan and Korea, where consumers eat an abundance of raw and "inadequately" prepared seafood products.

According to recent literature [25], an estimated 18 million people are infected with fish-borne intestinal trematodes. This was considered an underestimate, and it included some freshwater species. In the Republic of Korea, 17 species represent five families (Heterophyidae, Echinostomatidae, Plagiorchiidae, Neodiplostomidae, and Gymnophallidae) [26]. Of those, ten are heterophyids and, of those, seven are prevalent among residents who consume raw flesh from estuarine fishes in south and west coastal areas [25–27]. Those are *Heterophyes nocens*, *Heterophyopsis continua*, *Pygidiopsis summa*, *Stellantchasmus falcatus*, *Stictodora fuscata*, *Stictodora lari*, and *Acanthotrema felis*. Documentation of all food-borne trematodes in humans includes 70 species in 14 families [25], but several are not from marine hosts and presently infected people are estimated to surpass 50 million.

Heterophyidae (Opisthorchioidea). As with zoonotic infections from eating fishes in Japan, Korea, China, and Thailand, such infections from Vietnam are now being recognized as a food safety risk in a country whose people have a strong tradition of eating raw fish [28]. The heterophyids use a snail first intermediate host, a fish second intermediate host, and either a bird or mammal definitive host. A prevalence of heterophyid infections with *Haplorchis pumilio* (100%), *Haplorchis taichui* (70%), *Haplorchis yokogawai* (6%), and *S. falcatus* (3%) was determined from expelled (25 mg/kg praziquantel, followed by a saturated solution of magnesium sulfate) adult worms in a survey of residents from coastal Nam Dinh Province south of Hanoi in 2005. The recent finding of those parasites in Vietnam suggested to the surveyors [28] that some may be introduced rather than endemic, increased in magnitude with intensification of aquaculture, or increased because of increased consumption and importation of raw fish. Difficulty presently exists in determining from which fishes the infections are acquired in people throughout Vietnam as well as the rest of the world where people eat raw fishes. Human-infecting species are beginning to be recognized in food fishes as those fishes are examined for parasites. For example, examination of wild and cultured grouper (*Epinephelus bleekeri*, duskytail grouper, and *Epinephelus coioides*, orange-spotted grouper, both marine species) have revealed *Heterophyopsis continua* and *Procerovum varium* (recognized as a freshwater parasite), and examination of mullet (*Mugil cephalus*) have revealed *Pygidiopsis summa* and *H. continua* from brackish water in Khanh Hoa Province in central coastal Vietnam [29]. The long tradition of eating raw fish has intensified with increasing affluence; a higher prevalence between men (69%) and women (23%) can be explained because the social gatherings where consumption of raw or pickled fish occurs have historically been male-oriented [28]. Concern exists

for the exportation of infected fresh fishes, some freshwater species, because aquaculture in rural Vietnam is increasing in economic importance [30].

Human infections have been known from Japan for decades even though most are freshwater species [25]. All three species of *Metagonimus* are freshwater species in regard to the snail host, but, in Korea, one, *Metagonimus yokogawai*, infects a marine fish, which consumers eat raw. Actually, an amphidromous fish, the sweetfish, *Plecoglossus altivelis*, spawns in rivers near the sea. Then, the fish fry feed on plankton at sea until 5–7 cm TL at which time they enter into the river mouths. Infections can be acquired from the fish in estuarine habitats. Sequence data readily separate the three species [31].

In the Western Hemisphere, there are several heterophyids that present a human health risk. For example, in the USA, species of *Phagicola* represent one of several potential infectious genera (not accepting *Phagicola* as a junior synonym of *Ascocotyle*). Knowledge about human infections from the Southeast US has not progressed much beyond anecdotal mention [1], but *Phagicola nana* (Fig. 2) from several fishes [32], *Phagicola longa* [33] from mullets (Fig. 3), and several other species (Fig. 4) probably occur in many consumers who eat inadequately prepared fish.

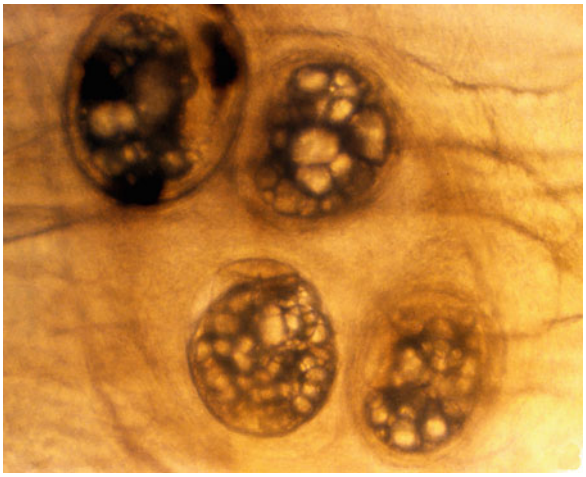

Waterborne Parasitic Diseases in Ocean. Figure 2 Living encysted metacercariae of the heterophyid *Phagicola nana* in fillet of largemouth bass, *Micropterus salmoides*, from Mississippi estuary. The cysts average 0.30 mm across

Heterophyes heterophyes, a heterophyid from the Middle East has been reported from fish-eating patients in Florida never having left the USA [34, 35]; these infections were most likely species of *Phagicola*. Actually, even capillarid eggs get misidentified as those of *H. heterophyes* in Egypt, where the trematode is common [36]. Unlike many heterophyids in the USA that exhibit a high "site specificity" in the second intermediate fish hosts, meaning found in one or few specific organs or tissues, *P. nana* occurs in many

Waterborne Parasitic Diseases in Ocean. Figure 3 Mounted and stained adult specimen of the heterophyid *Phagicola longa* from an experimental infection originating from a metacercaria in *Mugil cephalus* from Mississippi

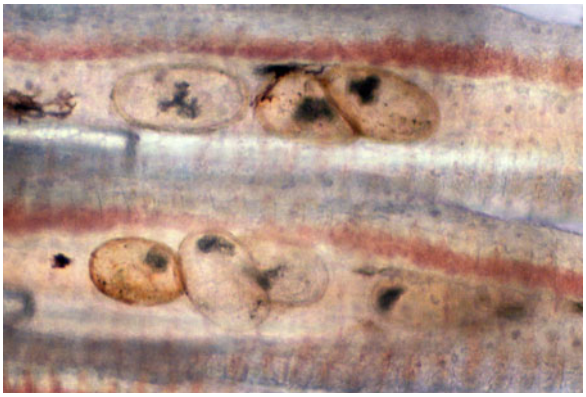

Waterborne Parasitic Diseases in Ocean. Figure 4 Living encysted metacercariae of the heterophyid *Phagicola diminuta* in gills of Gulf killifish, *Fundulus grandis*, a bite-sized fish from Mississippi estuary

tissues such as the muscular fillets in addition to the viscera, gills, and other sites [32]. Moreover, *P. nana* infects a few different fishes such as the largemouth bass (*Micropterus salmoides*) and several sunfishes (Centrarchidae), popular recreational fishes in estuaries of the Southern US that are consumed in a variety of cuisines. Most heterophyid species infect specific organs in specific small fishes that are eaten raw in their entirety by specific groups of people, if eaten at all. As with several different parasites, some heterophyids that constitute public health risks constitute species complexes that are difficult to distinguish by morphological features. For example, what is commonly reported as *Centrocestus formosanus* is a mixture of morphologically similar species. Members of this complex are common in the Far and Middle East, but some apparently have been introduced into Hawaii, USA mainland, and Mexico through introduced infected snails (*Melanoides tuberculatus*) in the aquarium trade on vegetation and with fishes [37]. Members of this basically freshwater heterophyid complex infect a large number of fish hosts, including some estuarine species.

The reason for stressing heterophyids is because, even though most species measure 1 mm long or less, they often occur in large numbers, influence public health, and can result in severe pathological changes in humans. A series of studies in the 1930s based on human infections in the Philippines was summarized in 1940 [38]. Five heterophyids were identified from 33 of 297 autopsy cases, not all randomly chosen: *H. yokogawai* (16 cases, 13 alone), *H. taichui* [5], *Haplorchis calderoni* [2], *Haplorchis vanissima* [1], and *Diorchitrema pseudocirrata* [6]. These occurred either singly or with other species. The other species consisted of the microphallid *Microphallus brevicaecum*, which was originally identified as a heterophyid (*Heterophyes brevicaeca* but later recognized as *Spelotrema brevicaeca*) (in 11 cases), an echinostomid identified as *Euparyphium ilocanum* [2], and an unidentified plagiorchiid (*Plagiorchis* sp.) [1], plus the common heterophyids already listed. All the trematodes occur normally in the intestine, where lesions were not found to be severe. More important, eggs of the heterophyids *H. yokogawai* and *H. taichui* and the microphallid *M. brevicaecum* were also associated with acute and chronic lesions in the heart and other visceral organs such as liver, spleen, kidneys, brain, spinal cord, and lungs. *Diorchitrema pseudocirrata* also occurred in some of those lesions in mixed infections but never by itself. Worm eggs, especially from degenerated adults, enter into the blood and lymphatic streams and are carried to different visceral tissues where they provoke the cellular reactions. Adhesions and hemorrhaging were common complications. Of 34 positive cases (1 did not exhibit an intestinal infection), 15 (44%) had visceral complications (1 in brain with fatal hemorrhaging, 1 in spinal cord, and 13 in heart). Of 89 enlarged hearts in these charity patients in the Philippines, the 13 (15%) with myocardial or valvular lesions associated with worm eggs were assumed to have caused the heart dysfunction, a value attributed to heterophyid-caused fatal heart disease [39]. Adult worms (Fig. 5) identified as *Heterophyes heterophyes* also encapsulate in the human brain [40].

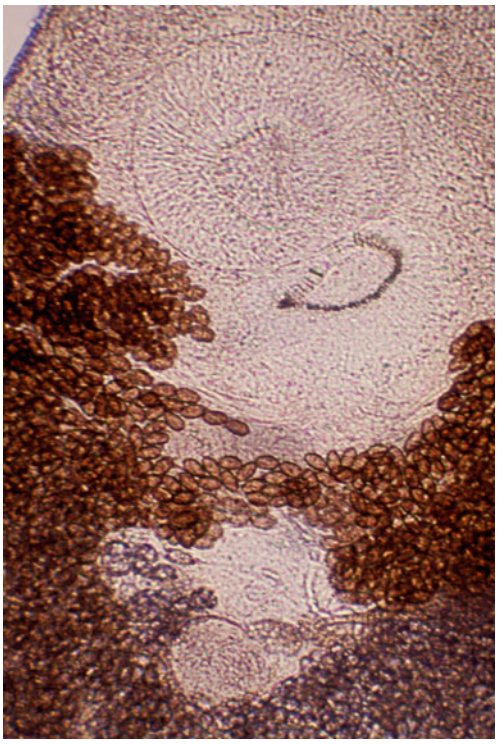

Waterborne Parasitic Diseases in Ocean. Figure 5 Close-up of living 0.8-mm-long adult specimen of the trematode *Heterophyes* sp. from Bardawil Lagoon, Northern Sinai, Egypt, showing diagnostic sclerites in the modified genital sinus, often misstated as a "gonotyl," below the ventral sucker

An enormous number of infective metacercariae can occur in some habitats. To appreciate the life cycle, each adult out of the thousands that can be present in the intestine of a human or in that of a domestic dog or cat produces thousands of eggs, with several hundred laid daily for several weeks or months. One dog was reported to host 13,000 specimens of *H. heterophyes*. Each egg produces a miracidia that can infect a snail. In the lakes along the Nile Delta and in the Bardawil Lagoon, over 90% of the host snail population can be infected (Figs. 6, 7). Just short of 500 cercariae can be released from each of the abundant snails daily for a year, but with decreasing cercarial production over time. Each cercaria survives 1–2 days, and mullets are common hosts. Eleven emaciated specimens of *Liza ramada* contained 1,730–6,000 metacercariae per gram for an estimated 582,000 metacercarial cysts in one 255-mm-long fish. A specimen of *Mugil cephalus* from the same location had 1,136 metacercariae per gram [41]. Fishermen, seafood dealers, children of those people, and those who taste fish being prepared commonly become infected because the rules established for protection of the consumers buying the products are not always followed by the handlers. Moreover, fishermen do not always completely cook their fish.

Waterborne Parasitic Diseases in Ocean. Figure 6
Street vendors selling fresh fish in El Arish, Northern Sinai, Egypt

Waterborne Parasitic Diseases in Ocean. Figure 7
Close-up of activities in Fig. 6, showing vendor displaying salted mullet. A regulation at the time was to keep fish salted for 8 days before selling them to the public. Eight days was necessary for the heavy infections of heterophyid metacercariae to lose their infectivity

Microphallidae (Microphalloidea). Members of small intestinal trematode complexes other than Heterophyidae also have been misidentified. Microphallidae constitutes one of those families. One or more microphallid members also have a relatively broad specificity of the final host and can also cause severe potentially fatal pathologic lesions [38, 42]. As mentioned above, *Microphallus brevicaecum* from shrimp has been determined to be the cause of human mortalities in the Philippines. Microphallids are superficially similar to heterophyids and also infect birds and mammals and occasionally fishes, reptiles, and amphibians, but the microphallids have entirely different cercariae, differ phylogenetically, and use crustaceans such as crabs and palaemonid and peneid shrimps as second intermediate hosts rather than fishes.

Troglotrematidae (Gorgoderoidea). Nanophyetus salmincola is another small, about 1-mm-long, trematode that infects the intestine of numerous mammals, including humans. In fact it is probably unknowingly the most common helminth in people of the North American Pacific Northwest. It produces gastrointestinal distress, fatigue, loss of weight, and peripheral eosinophilia when numerous specimens occur in humans, and can be diagnosed easily from its relatively large, 0.090–0.100-mm-long, diagnostic eggs that appear in stools about a week after eating infected fish. No symptom occurs in most light infections. Basically a freshwater parasite, cercariae form metacercariae in several salmons and steelhead trout (*Oncorhynchus mykiss*, also known as sea-run

rainbow trout) as well as freshwater fish and amphibians that do not make oceanic migrations. Infections in the Pacific Northwest are attributed to eating raw, incompletely cooked, cold-smoked salmon and steelhead trout and their eggs [43]. A second species, *Nanophyetus schikhobalowi*, needs to be studied molecularly to determine if it is conspecific with *N. salmincola*. It had been demonstrated to infect as many as 98% of the people in some eastern Siberian villages.

The trematode in the Pacific Northwest serves as host for the rickettsial agent, *Neorickettsia helminthoeca*, which in turn causes "salmon poisoning disease" of canines. Dogs that are fed infected salmon may die, but humans and other non-canines are not known to be affected. Nevertheless, the loss of dogs in the Arctic can be a serious problem.

Gymnophallidae (Gymnophalloidea). Gymnophallids mature in shore birds, gulls, and diving ducks. However, members of Gymnophalloides also infect mammals. Human infections with *Gymnophalloides seoi* are known only from Korea, but most are tiny, <1 mm, and it and other species all use a variety of mollusks as first and second intermediate hosts and probably infect people throughout the world where mollusks are consumed raw. *Gymnophalloides seoi* is acquired primarily from eating the raw oyster, *Crassostrea gigas*, known as the Japanese oyster, Miyagi oyster, giant oyster, immigrant oyster, and giant Pacific oyster, and infects the intestine and possibly pancreatic duct of human consumers [25, 27]. Nevertheless, like *G. seoi*, which infects the Palearctic oystercatcher, *Haematopus ostralegus*, most members of this genus can be experimentally administered into a variety of birds and mammals, suggesting the human health risk. Studies with mice demonstrate that *G. seoi* produces focal responses for 2–3 weeks, at which time the mucosal integrity is restored. If provided with immunosuppressive treatment, the mice underwent minimal goblet cell hyperplasia, extended retention of worms, and invasion of the submucosa. Even though genetics of hosts also play a role in this sequence, immunosuppressed humans are at risk for transference of eggs and worms to remote organs as with heterophyid infections. With a relatively low production of eggs relative to heterophyids, a total of 100 specimens would be necessary to produce 8,400 eggs per day, considerably fewer than most heterophyids [25].

Echinostomatidae (Echinostomatoidea). Members of some other trematode families also infect the small or large intestine but grow slowly and reach larger size (roughly 3–7 mm) compared with those mentioned above (0.5–2.0 mm); a few marine members are known to infect humans. A total of 21 members of Echinostomatidae are listed as causing human infections, some resulting in gastroenteritis [25]. Of those, all were from freshwater mollusks except two. One, *Acanthoparyphium tyosenense*, can be acquired in Korea from eating at least the raw bivalves *Mactra veneriformis* and *Solen grandis* and the gastropod *Neverita bicolor* available at a coastal village seafood market [44]. The gastropod first intermediate hosts *Lunatia fortuni* and *Glassaulax didyma* shed cercariae that infect the gills of the popularly eaten bivalves. Ducks serve as the natural definitive host, but experimental infections in chick and seagull have confirmed the adult infection [25]. Related species, and there are several, such as what was identified as *Acanthoparyphium spinulosum* in the oyster *Crassostrea virginica* from Texas, USA, are probably also commonly infective to humans, but such infections are limited only by the infrequency with which the molluscan second intermediate hosts are eaten raw [45].

Plagiorchiidae (Plagiorchioidea). Human infections with *Plagiorchis* spp. are uncommon, but 12 cases have been reported. *Plagiorchis vespertilionis* occurred in a man from coastal Republic of Korea who often ate raw mullet and gobies and was not known to eat caddisfly larvae, mayfly larvae, or dragonfly nymphs. The insects were suggested as possible intermediate hosts and are known hosts for many other species of *Plagiorchis*. The patient also contained *Heterophyes nocens*, acquired from fish [46]. Nevertheless, fish were suggested intermediate hosts, and perhaps the infection was transmitted by eating raw estuarine fish that had recently fed on infected dragonflies or some infected insect larva, joining the freshwater parasite with the coastal habitat. Members of *Plagiorchis* and related genera mature in birds and mammals plus accidentally in amphibians and reptiles. They are

relatively large (3–5 mm) and usually occur in low numbers in the final hosts.

Didymozoidae (Hemiuroidea). Humans do not get infected by didymozoids! These trematodes of fishes are unusual in that they occur usually in pairs of either hermaphroditic individuals or as separate sexes like mammalian schistosomes and occur encysted in the flesh, encysted in other tissues, or even free in body spaces other than the lumen of the alimentary tract like most trematodes. The group is mentioned because people eat infected fish products and diagnosticians find the small reniform didymozoid eggs (roughly 0.015–0.030 mm long but in some species up to 0.040 mm) of the worms in human stool samples, leading those diagnosticians to assume either an active trematode or protozoan infection. Such misidentifications have been reported from people eating marine fishes in Japan, Taiwan, and the Philippines, but cases could occur throughout the world where infected fish are abundant, especially in pelagic tropical and subtropical fishes [47].

Nematoda (Roundworms) Nematodes, or roundworms, comprise both free-living and parasitic groups. Parasitic groups that have marine members exhibiting a public health risk also fit into different groups: those that mature in humans, those that have larvae that can infect humans eating inadequately prepared seafood, those that produce excretions or secretions that result in an immunological response in humans, and those that can be acquired by being in the water with free-living stages or handling infected products. When consumers think of parasites in seafood, they typically think of anisakiasis involving grossly apparent nematode juveniles. Of the many nematode groups, each may have a different strategy in completing a life cycle. An example cycle will be mentioned for each major group of worms.

Trichinellidae (Dorylaimia, Trichinellida). Trichinellosis has received considerable attention over the last 150 years of control efforts, but in the past 20–30 years, there has been a dramatic reemergence as an emerging zoonosis [48]. The reasons are severalfold involving changing agricultural, marketing, environmental, and economic practices and conditions, but basically prior attentions involved *Trichinella spiralis* in domestic pork. In the 1940s and 1950s, a large number of marine and terrestrial mammals in Alaska were examined for what was then known as *T. spiralis*, and most had infections [49]. A total of 320 native individuals from three Alaskan areas given intradermal tests showed that 28% from Wainwright, Alaska, tested positive. There are now at least ten recognized species or genotypes, and the involvement of the sylvatic cycle of some of those is responsible for new human cases. For purposes of this review, *Trichinella nativa* and to a lesser degree *Trichinella britovi* play a role. *Trichinella nativa* infects the carnivores that inhabit the marine environs: polar bear (*Ursus maritimus*), walrus (*Odobenus rosmarus*), Arctic fox (*Alopex lagopus*), and wolf (*Canis lupus*), but it is even known from China in domestic pigs. This species differs from the others in that it can survive the freezing process, the process that keeps domestic pork safe to eat. Uncertainty exists in how long the frozen juveniles remain infective, but, when juveniles from walrus meat were stored at −20°C for up to 20 months, some remained infective to experimental guinea pigs [50]. There was a gradual degradation process that rendered some noninfective. The freezing resistance appears to be related to the parasite-nurse cell-host complex, and the nurse cells yield a cryoprotectant when occurring in carnivore muscle tissue but not when in rodents [51]. Outbreaks are common in the Canadian Arctic where uncooked walrus meat is eaten raw, frozen, and aged by Native Americans as "igunaq" [52], but some that get infected also eat the products cooked [53]. This product is produced by placing meat and fat tissues into skin bags, which are sewn shut and aged about a meter under a cache of rocks or gravel along a beach. When meat from experimentally infected seal was prepared as igunaq and allowed to ferment, as air-dried meat (nikku), and as both raw and partially cooked sausage (core temperature less than 50°C), it remained infective for at least 5 months under laboratory conditions. The food product was fed to cats and the extracted juveniles were orally inoculated into mice [54]. Whale is usually eaten as muktuk, a preparation of fermented skin and blubber containing no muscle [53].

Trichinella britovi also occurs in temperate areas of the Palearctic region where people obtain infections primarily from eating wildlife. Apparently, it cannot resist freezing for a long period; the juveniles of

T. spiralis, which have been reported from a variety of marine mammals, die after 4 days at −10°C. The status of infections from marine mammals requires additional research. The cycles of all the species are similar to each other but different from other nematodes in this chapter. The definitive host, including human, eats uncooked infected meat from another definitive host, and the juveniles are released when the cyst is digested in the stomach. The juveniles invade the mucosa of the upper intestine and develop into mature adults within 2 days. After 4 days, the mated female starts depositing motile juveniles, a process that continues for 4–16 weeks and produces up to 1,500 juveniles in the nonimmune host. These juveniles pass within the lymphatic system or mesenteric venules to muscles, usually striated ones, where it encysts. Striated muscle tissue stimulates development of nurse cells and capsule formation within 2–3 weeks (Fig. 8). The coiled juveniles can survive in human muscle for years, even though calcification may occur within 6–9 months. Infections can be fatal with as few as five juveniles per gram of muscle, but infections can be much higher, especially if the initial dose in an immunologically naïve consumer contains hundreds of cysts in striated muscle. A low initial dose establishes a protective immunity to challenge doses.

Paracapillaria philippinensis (until recently [55], a trichinellid that was and still is referred to by some as *Capillaria philippinensis*) seems to be spreading geographically. This small intestinal nematode produces mortality in humans. More than 2,000 human cases have been reported from the Philippines and Thailand, with several of those from more recent cases in Korea, Japan, Taiwan, India, Iran, United Arab Emirates, Egypt, Italy, Spain, and the United Kingdom [56], but with some of those acquired from eating freshwater fishes or imported fishes. The number of human cases is being reduced in Thailand, but infections probably contribute significantly to mortality there [57]. The life cycle probably includes a bird definitive host as shown by experimental infections in a fish-eating rail and heron, even though many mammals can host transient infections, and humans and the Mongolian gerbil can die from infections in less than 2 months [58]. Eggs passed by the definitive host hatch in a variety of freshwater and estuarine fish species. At least when the gerbil or human eat the infected fish, the juveniles develop into males and females that release a first-stage juvenile from a thin-shelled egg, which in turn can autoinfect the host and produce adults, with a female that produces the typical capillarid thick-walled eggs that are released in the feces. Even though most second generation females are oviparous, a few females still produce juveniles that can progress to autoinfection and hyperinfection, a condition in which the produced juveniles penetrate the intestinal mucosa and proceed with migration. At autopsy, 1 l of bowel fluid contained an estimated 200,000 specimens in all stages [58].

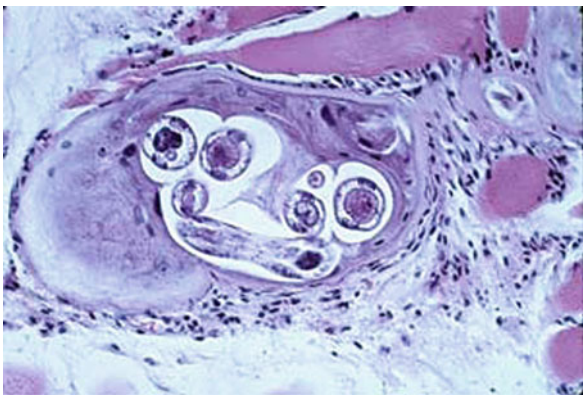

Waterborne Parasitic Diseases in Ocean. Figure 8 Section of coiled specimen of juvenile *Trichinella spiralis* encapsulated in striated muscle tissue

Signs of infection in humans are varied: they can include abdominal pain, diarrhea, vomiting, heart irregularities, edema, and weight loss, with the blood exhibiting low protein, calcium, potassium, and sodium, and with high immunoglobulin E (IgE) with diminished levels of IgG, IgM, and IgA for several months after treatment with albendazole. Albendazole seems more effective than thiabendazole and mebendazole because there is no relapse, presumably because only albendazole affects the larval stages [58].

Epidemiological studies are lacking in most reports, but where infections are common, elderly aboriginal groups with infections in Taiwan prefer Chou-Bao, which includes soaking raw, small entire fish in fermented millet [56], and infected Filipinos consume Kinilaw, which consists primarily of raw pilchards, or other small fishes from coastal lagoons, marinated in vinegar, garlic, onions, ginger, tomato, and various

peppers. The small fishes throughout SE Asia also are eaten whole as raw products, and some native groups (Ilocanos of Northern Luzon, Philippines) use animal organs and intestinal juices to season rice and other foodstuffs [58]. Most human cases have been traced to consumers that eat small, raw entire fish, but exact causes are not known. When diagnosis is delayed, the disease can be severe, with up to 30% fatality in some localities in the Philippines.

Dioctophymatidae (Dorylaimia, Dioctophymatida). The giant kidney worm, *Dioctophyme renale*, rarely infects humans, but the potential because of aquaculture and new cuisines is increasing. Even though usually considered a freshwater parasite, it also is common in the estuarine environment [1]. Its life cycle involves an oligochaete and a fish, amphibian, or reptilian paratenic host. Its counterpart *Eustrongylides* will be discussed later because it does not mature in humans. *Dioctophyme renale* matures in and completely devours the kidneys of its definitive host. The site is usually restricted to the right kidney, probably because of migratory behavior of the acquired juvenile. If it does not encounter the right kidney, it can mature in the peritoneal cavity, where it also causes harm (Fig. 9); it can also become encapsulated and form a subcutaneous nodule [59]. Human infections are usually diagnosed by the worm eggs in urine, followed up by radiological exams to detect enlarged or calcified kidneys. The worm has a cosmopolitan occurrence, but most human infections are from Iran and from freshwater habitats. In fact, human coprolites dated about 3,375 YBC from an archeological site in Switzerland suggest that human infections were more prevalent in the Neolithic than now [60]. In the USA, sylvatic infections are common in the mink (*Mustela vison*) in brackish marshes of southern Louisiana [1].

Acanthocephalans (Spiny-Headed Worms) Acanthocephalans from marine products are not known to mature in humans. However, a few from terrestrial arthropods such as cockroaches do produce eggs in humans. In fact, eggs were found in human coprolites from a cave in Utah dated about 1869 BC ± 160 years and 20 AD ± 240 years [61]. On the other hand, juveniles can attach in the lumen of the intestine without maturing, and, because they are in the lumen and can be voided in the feces, they are treated here.

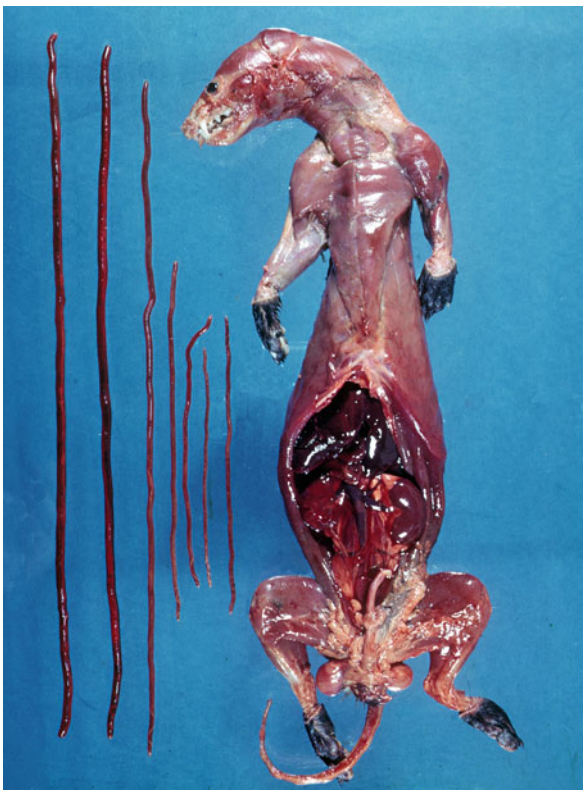

Waterborne Parasitic Diseases in Ocean. Figure 9 Specimens of the giant kidney worm, *Dioctophyme renale*, removed from a mink's abdominal cavity in Louisiana. This species usually devours all the parenchyma in the right kidney of the mink and other fish-eating carnivores, but these specimens ended up in the cavity and matured without killing the host

This seems to be the case for *Corynosoma strumosum* in a person from Alaska [62] and *Bolbosoma* sp. from a Japanese fisherman [63]. The first case was noticed when the infected male was treated with Atabrine. The worm matures in seals but is known as a juvenile in dogs, otters, birds, and other fish-eating birds. When fresh marine fish were fed to mink, some mink died [64]. Even though not routinely detected in people, *C. strumosum*, common as adults in pinnipeds and as juveniles from birds and other mammals in the Holarctic, was considered probably to be common in humans but for a short duration [18, 62]. The second case was detected because the worm had penetrated the intestine and was surgically removed because the disease was initially diagnosed as appendicitis.

Acanthocephalans are like nematodes because they both have separate males and females. However, all species are parasitic, and molecular data place them with rotifers. The life cycle includes an arthropod or crustacean and a vertebrate. In the case of the two palaeacanthocephalans mentioned above, the crustacean is unknown, but it could be small or large. The life history is typically completed by seal, whale, or sea otter by feeding on a paratenic fish host containing an encysted or encapsulated larva or juvenile. Most acanthocephalans have a rather specific crustacean and final host and a larger but still rather specific range of paratenic hosts. Even though the definitive host is quite specific, the worm may attach in the intestine of non-closely-related hosts. For example, two palaeacanthocephalan species that mature in a few teleost fishes can be acquired by local dasyatid stingrays as juveniles from amphipods and attach to the spiral valve without developing further or without migrating to the viscera or muscles as paratenic parasites [65]. Stingrays are not typical final hosts for any acanthocephalan.

Information on additional juvenile acanthocephalans that penetrate through the alimentary tract and cause a host response, sometimes severe, appears later in the next section of this chapter.

Parasites with Larvae That Can Infect Humans Eating Inadequately Prepared Seafood

The best-studied parasitic infections in humans eating raw marine seafood are caused by members of the ascaridoid genus *Anisakis* and first recognized in the 1960s in the Netherlands, Japan, and the USA, even though Native Americans in Alaska passed specimens of both *Anisakis* sp. and *Pseudoterranova decipiens* sensu lato in feces [66]. There is now confusion in the names given the human disease because ascaridoids other than species of *Anisakis* also induce similar infections. These agents plus infections and potential infections by non-ascaridoid members of a variety of classes, based on the ability of such species to cause disease in nonhuman mammals, are also discussed in this chapter. In 1988, a group interested in standardizing nomenclature of ascaridoid diseases recommended calling disease involving a member of *Anisakis* as "anisakiasis" and disease caused by any member of the family Anisakidae as "anisakidosis," even though some authors use a name referring to the responsible generic agent or the host response, such as "eosinophilic granuloma." DNA-based techniques have allowed accurate diagnosis, species differentiation, and phylogenetic relationships. Diseases caused by members of other higher taxa also create some confusion with terminology of the names.

Anisakidae (Spirurina, Ascaridomorpha). Species of *Anisakis* are the most widespread cause of notable and severe human disease. Until recently, human infections were divided into two types of juveniles, *Anisakis* type I and type II [67] based on the presence of a caudal spine and the length of the ventriculus, a glandular structure separating the muscular esophagus and the intestine. A group of 21 species based on adults were divided into three primary species [68], including *Anisakis simplex* with ten junior synonyms, *Anisakis typica* with one synonym, and *Anisakis physeteris* with three synonyms. With improved molecular tools, some of those junior synonyms have been accepted, and additional species have been recognized. *Anisakis* type I juveniles comprise the *Anisakis simplex* complex: *Anisakis simplex* sensu stricto, *Anisakis pegreffii*, *Anisakis simplex* C [69], *Anisakis ziphidarum*, and *A. typica*. *Anisakis* type II juveniles comprise *A. physeteris*, *Anisakis brevispiculata*, and *Anisakis paggiae*. All of these can be differentiated and are considered human pathogens. The differences in pathogenesis and location in the human probably reflects the different species, at least in part. Recent polymerase chain reaction amplification (PCR) methods show that *A. pegreffii* comprises the source of most infections in consumers in Italy but that *A. simplex* sensu stricto is the most common species in people in Japan (Figs. 10 and 11) even though fish in the Sea of Japan are known to be infected with *A. pegreffii* [70]. Also, *A. pegreffii* seems to cause gastric distress in humans and *A. simplex* seems to mostly affect the intestine. Exceptions involve the abdominal cavity, mesentery, and oral cavity [71]. Juveniles typically measure 1–3 cm in length.

The different species can be differentiated by cetacean host and geographical locality. *Anisakis schupakovi* infects the Caspian seal, *Pusa caspica*, and belongs in the genus as do a couple other species from delphiniids in South America rivers and other isolated habitats. Tabularized reviews list which species of *Anisakis* have

Waterborne Parasitic Diseases in Ocean. Figure 10 Section of *Anisakis simplex* in ileum of human patient in Japan. Note the characteristic eosinophilic response, referred to as "eosinophilic granuloma," surrounding the diagnostic section of the worm

been confirmed molecularly from different cetaceans, cephalopods, and fishes [70]. The life cycle of *Anisakis* spp. includes a cetacean final host, from which worm eggs (Fig. 12) are deposited in feces and embryonate in seawater; the active, hatched third-stage juvenile (the same as for *Pseudoterranova decipiens*), also referred to as a larva, is eaten by a crustacean [72]. The juvenile hatching from most nematode groups is a second-stage juvenile. Euphausids are known to host the infective third-stage juvenile. A variety of paratenic hosts, including specific fishes, squids, and crustaceans can acquire and maintain the infective juveniles by feeding on the euphausid or some undetermined crustacean hosts. The appropriate cetacean feeds on any appropriate animal with an infective juvenile. In some cases, there can be a large cluster of these worms, involving third-, fourth-, and fifth-stage juveniles and adults attached within a stomach ulcer. As with several ascaridoids in a variety of genera and host groups, individuals not embedded in the ulcerated tissue will leave the ulcer and forage among the digesting prey in the stomach only to return at a later time.

Cultured fish usually do not exhibit ascaridoid infections present in their wild counterparts because they are fed a diet that does not contain infective

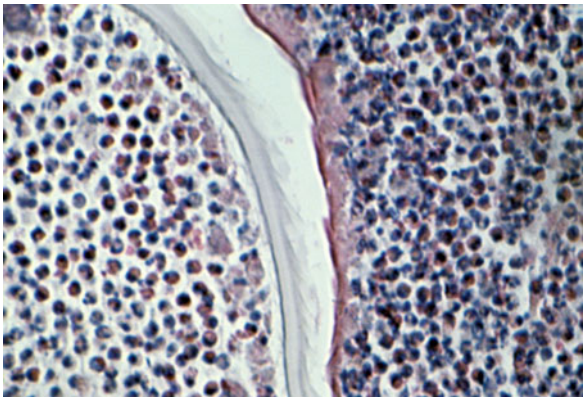

Waterborne Parasitic Diseases in Ocean. Figure 11 Section through degenerating specimen of *Anisakis* sp. in stomach of experimentally infected miniature pig showing juvenile with infiltrated eosinophils and surrounding infiltrate consisting almost exclusively of eosinophils

Waterborne Parasitic Diseases in Ocean. Figure 12 Egg of *Hysterothylacium reliquens* showing infective third-stage juvenile representative of ascaridoids infective to humans. In this species, the juvenile hatches and the free juvenile is eaten by an appropriate copepod, which in turn is eaten by an appropriate fish. That fish or the copepod is eaten by a paratenic host or by the definitive fish host

juvenile worms. Such is not always the case. Infected prey can enter a sea pen or be fed to the cultured fish in fish farms or cages. When juvenile specimens of the greater amberjack, *Seriola dumerilli*, and three-line grunt, *Parapristipoma trilineatum*, were imported into Japan from China for grow-out in fish farms, they were determined to be heavily infected with *Anisakis pegreffii* [73]. The Japanese Ministry suggested the fish were fed wild infected fish before being exported. In any event, it required that the products, originally grown for sashimi (raw fish), be frozen prior to taking them to market, considerably reducing their value.

Humans become infected with juveniles of *Anisakis* when they eat uncooked or inadequately prepared seafood containing an infective third- or fourth-stage juvenile. Symptoms and signs of infection probably vary by species of *Anisakis*, condition of worm, and condition and genetics of patient. Some patient complaints include sudden epigastric pain, nausea, diarrhea, and urticaria occurring within an hour but usually at about hour 6. Because infections are difficult to diagnose, the acute infection caused by a migrating or encapsulated juvenile develops into a chronic case with intermittent abdominal pain lasting from weeks to several years. There may be a slight fever and moderate leukocytosis up to 15,000 leukocytes per cubic milliliter. Peripheral eosinophilia can vary from 4% to 41% and will be discussed later in the chapter. The condition presenting other vague symptoms cannot be diagnosed with various immunologic assays because the sera cross-reacts with related nematodes or even with human sera [74], but more specific serological tests are being perfected and various molecular tools are being developed [75, 76]. Most prior cases have been identified morphologically after misdiagnoses of appendicitis, ileitis, cholecystitis, Crohn's disease, and tuberculosis peritonitis, and a variety of neoplasms resulted in resection of the corresponding lesions. In most cases, the worms penetrate or embed in the ileum or duodenum but occasionally penetrate the stomach as for *A. pegreffii*. Anisakiasis occurs in the Netherlands and other European countries, Japan, the USA, and Chile, and cases are remaining high. When the estimated prevalence of *A. simplex (A. pegreffii?)*-specific IgE assay in the population of Madrid, Spain, was tested by enzyme-linked immunosorbent assay (ELISA) as well as for cross-reactivity, 12% of the healthy population tested positive compared with 22% in southern Spain determined with a somewhat different technique [76] and without any indication of cross-reactivity. Those testing positive in Madrid were more likely to admit to being habitual consumers of fresh (Fig. 13) or undercooked fish as opposed to eating frozen and cooked products like reported for the negative population.

As with "*Anisakis simplex*," "*Pseudoterranova decipiens*" also was recognized as a single species. It infected fishes and humans and could be identified by a morphological diagnostic juvenile and a variable adult, but the adult matured in pinnipeds rather than cetaceans. Recently, however, this agent of human infections that was supposed to occur worldwide has been shown to include several species, most in specific

Waterborne Parasitic Diseases in Ocean. Figure 13 Italian fisherman aboard fishing boat with catch including sardines infected with *Anisakis pegreffii*. Fresh fish from boats in the Port of Civitavécchia, Italy, are boxed, iced, and sold to restaurants, seafood dealers, and others

pinnipeds and consequently in specific geographic regions. Molecular and biochemical tools, backed with morphological features, have shown this species to represent a complex of at least six species: *Pseudoterranova decipiens* sensu stricto, *Pseudoterranova krabbei*, *Pseudoterranova bulbosa*, *Pseudoterranova azarasi*, *Pseudoterranova cattani*, and *Pseudoterranova decipiens* E. There are also exceptions to the strict host specificity within this genus: *Pseudoterranova ceticola* and *Pseudoterranova kogiae* both infect the cetaceans *Kogia simus* and *Kogia breviceps* (dwarf and pigmy sperm whales, respectively) [70].

When consumers eat infective juveniles of *Pseudoterranova* spp., the condition is usually not serious. Specimens are typically longer than those of *Anisakis* spp., roughly 4 cm versus 2 cm but dependent on age and development of worm, species, and temperature, and they usually have a more reddish or darker coloration. Whether they occur in the flesh or viscera of the fish depends on the species of worm and species of fish for both *Anisakis* spp. and *Pseudoterranova* spp. Specimens are often noninvasive and void in the feces or vomited; they tickle the throats of those eating inadequately prepared seafood when they migrate from the stomach back up the esophagus into the oropharynx, or they are coughed up into the mouth. *Pseudoterranova* spp. that cause disease usually involve the mucosal or submucosal tissues of the stomach. The common name of *P. decipiens* from the harbor seal had been "codworm" because the species was so abundant in cod, the second intermediate/paratenic host, especially during strict protection of harbor seal pups, which contained heavy infections. Actually, the "sealworm" consists of *P. decipiens* sensu stricto and *P. krabbei*, which can occur in mixed infections in *Phoca vitulina* and *Halichoerus grypus*, and both infect the cod, *Gadus morhua* [70]. Infections of large, 2–4-mm-long, unidentified fourth-stage juveniles of species of *Pseudoterranova* have become more prevalent and better recognized in Chile during recent years. Of 15 patients, all but one appeared to lose the infection through the mouth after irritation; one was voided through the anus with intense diarrhea. The patients all enjoyed seviche or fried fish [77]. Differing clinical signs between human infections in the USA and Japan may be different because the cause is from separate species. These may be *P. bulbosa* and *P. azarasi* in Japan and *P. decipiens* sensu stricto and *P. bulbosa* in the USA (Fig. 14) [70].

The life history of *Pseudoterranova decipiens* sensu lato is more studied than that of known species of *Anisakis* sp. [78]. The life cycle differs slightly from that of known species of *Anisakis* sp. The first intermediate host is a small crustacean such as several mycidacean species that spend part of their life in the benthos [79]. The hatched third-stage juveniles are not active. The agent in the crustacean appears to require a fish or large invertebrate paratenic host to complete the history in the pinniped.

Members of *Contracaecum* have been reported from both pinnipeds and fish-eating birds. Even though morphologically they appear similar, those from the pinnipeds and birds are molecularly separated, perhaps with those species from seals representing *Phocascaris*, which is paraphyletic within *Contracaecum* [70]. Like for *Pseudoterranova decipiens, Contracaecum osculatum* from phocid seals consists of a complex of at least five genetically recognized, but not all named, species. There are 11 mammalian species that have been sequenced. Because they are from temperate and polar areas, there is less known about human infections, but they are discussed based on known genetic information [70]. Two human cases of *C. osculatum* sensu lato have been reported from Hokkaido, Japan [80].

Species of *Contracaecum* from birds appear to be phylogenetically separate from the seal species and confused taxonomically. Each of the well-known

Waterborne Parasitic Diseases in Ocean. Figure 14 Commercial fillet with conspicuous specimens of *Pseudoterranova decipiens* sensu lato

species actually comprises a separate complex [81]. Members of the genus were not originally thought to infect humans, but at least two human cases of unidentified species from a bird or seal have been reported [82], and at least fourth-stage juveniles of a member of the *Contracaecum multipapillatum* complex (Fig. 15) can infect and mature in experimentally infected kittens but not rats, ducks, and chickens [83]. The worms, some attached, were in the intestine, causing hemorrhaging and associated with small ulcers.

Because members of *Hysterothylacium*, many of which were originally placed into the genus *Contracaecum*, mature in fishes, no one expected them to infect humans. Juveniles of *Hysterothylacium aduncum* have been suspected as the cause for eosinophilic granuloma in humans [84, 85], and *Hysterothylacium* type MB larva can produce pathological alterations, including eosinophilic granuloma, consistently in rodents (mice and rats) and rhesus monkey (*Macaca mulatta*) (Figs. 16 and 17) and probably humans [86]. The juvenile is small (1.4–3.1 mm long) but occurs in large numbers in some of its several secondary intermediate or paratenic fish and invertebrate hosts [87]. Worms penetrated the stomach or duodenum within an hour or so, with the attraction of an abundance of eosinophils accompanied by an apparent decrease of those leukocytes in the peripheral blood. Not all species of *Hysterothylacium* will penetrate the alimentary tract or cause lesions in mammals [87, 88], and juveniles of some species approach 3 cm long. A Japanese male passed a living young adult female specimen of *H. aduncum* after suffering chronic abdominal pain and diarrhea for a month. Whether the worm was acquired as a juvenile or an adult was not clear, but he had eaten raw fish, *Gadus macrocephalus* fillet pressed against kelp (Tara no kobujime) a month before onset of symptoms and *Oncorhynchus nerka* sliced and quick frozen (Ruibe), a week before onset [89]; both the cod and salmon host *H. aduncum*. The symptoms cleared following excretion of the worm. Whether *Terranova* type HA juveniles from Hawaiian

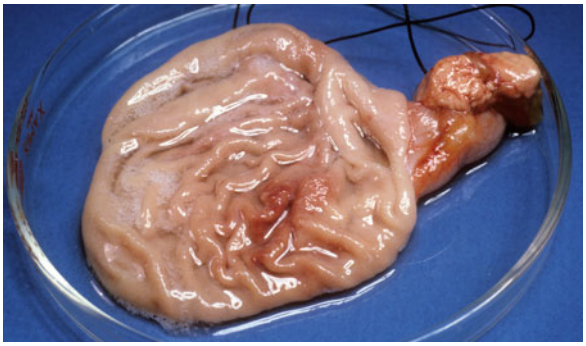

Waterborne Parasitic Diseases in Ocean. Figure 16 Stomach of rhesus monkey, *Macaca mulatta*, 5 h post-feeding with juveniles of *Hysterothylacium* type MB showing hemorrhagic lesions where juveniles penetrated

Waterborne Parasitic Diseases in Ocean. Figure 15 Red drum, *Sciaenops ocellatus*, exhibiting infective juveniles of *Contracaecum multipapillatum* sensu lato in mesentery. The same species is also common in fillets or viscera of other fish species in coastal Mississippi

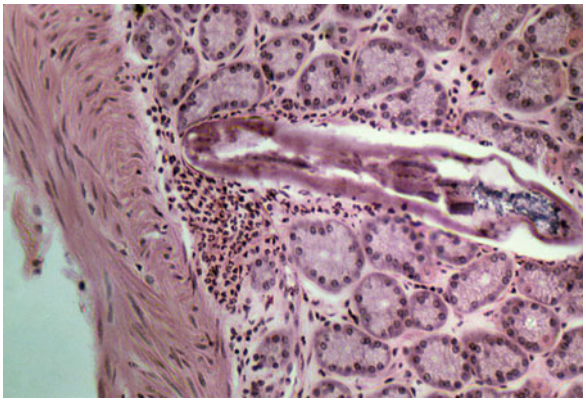

Waterborne Parasitic Diseases in Ocean. Figure 17 Section showing juvenile of *Hysterothylacium* type MB penetrating near muscularis mucosae of rhesus monkey stomach surrounded by eosinophils at 1.5 h post-feeding

bony fishes mature in sharks or in a marine mammal is not known, but, when gavaged into the laboratory rat, it migrates into the submucosa and forms a granuloma but does not pass through muscularis mucosae [90].

Other Nematodes Gnathostomatidae (Spirurina, Gnathostomatomorpha). Gnathostome nematodes are easily recognized by their spiny anterior swelling in both juveniles and adults. They are best known as public health risks of freshwater species but are mentioned here because the fishes that host the infective juveniles move into estuarine and marine habitats where they infect mammals and humans in coastal areas. *Gnathostoma spinigerum* occurs throughout Asia with infected humans primarily in Thailand and Japan, but *Gnathostoma hispidum, Gnathostoma doloresi*, and *Gnathostoma nipponicum* have all been identified from human cases in Japan [4, 91]. *Gnathostoma binucleatum* infects humans eating seviche made with estuarine fish in Sinaloa, Mexico [92], as do other species. With infections of *G. spinigerum* and *G. binucleatum*, the juveniles usually produce a migrating erythema (larval migrans) on the peripheral portions of the body for a few days to several years. Juveniles of the three other species usually migrate into surface skin, forming a serpiginous eruption on the trunk before disappearing spontaneously within 3 months. The juvenile can migrate into the central nervous system (CNS) and other vital organs such as lungs, intestine, genital organs, ear, and nose, occasionally producing a fatal disease, especially when involving the CNS [93, 94].

The typical life cycle starts with adults within a tumor-like mass in the stomach wall and serosa (Fig. 18) of the mammal host. Eggs extrude into the stomach and pass out with the feces. First-stage juveniles hatch within 12 days and develop when eaten by *Cyclops* sp. or presumably some other cyclopoid copepods. Development progresses in the copepod hemocoel to the third-stage juvenile and are infective to a variety of fishes, amphibians, reptiles, birds, and mammals, including humans. Perhaps in some species, a specific fish serves as a second intermediate host, but fish serve as a primary paratenic host (Fig. 19), allowing the juvenile to migrate or encapsulate in any of the previously indicted paratenic hosts necessary to maintain the population until eaten by the proper definitive host. Human infections can come from any of the paratenic hosts and probably from drinking freshwater containing infective copepods. The importance of marine or estuarine hosts depends on the area, since infections can occur in freshwater or estuaries and freshwater hosts can migrate into estuarine or marine habitats.

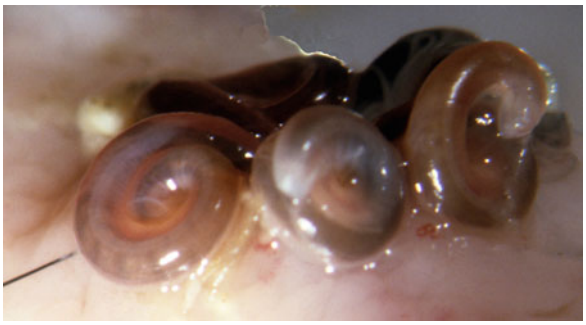

Waterborne Parasitic Diseases in Ocean. Figure 18 Tumor-like mass containing a few adult individuals of *Gnathostoma* sp. in the serosa of the stomach of the raccoon in Mississippi

Waterborne Parasitic Diseases in Ocean. Figure 19 Infective third-stage juvenile of *Gnathostoma* sp. in mesentery of the Gulf killifish, *Fundulus grandis*, in open marine lagoon of offshore barrier island, Horn Island, Mississippi

The true marine counterpart of *Gnathostoma* is *Echinocephalus*, and at least *Echinocephalus sinensis* can probably infect humans. It matures in rays and sharks in the South Pacific and is transmitted by at

least the oyster *Crassostrea gigas* and scallops. It was observed throughout the year in Hong Kong, but juveniles administered to kittens, monkeys, and puppies were infective to those mammals from August through October only [95]. When a dose of 600 worms was given to a kitten, most were apparently vomited, but the host died at 16 h. A total of 134 worms were recovered in various visceral organs. All but one of nine other kittens administered with fewer juvenile worms, 130–350, survived, but exhibited visceral larval migrans during the first 40 h. Kittens examined at days 3, 4, and 9 revealed no juvenile worm. The two different monkey species given 80 or 200 juveniles and dogs given larger doses each showed similar results of worms located throughout various visceral organs for the first 40 h post-feeding and no worm after 3 days. Substantial infections were also achieved at 18 h in kittens when fed additional worms acclimated in oysters at 28°C and 33°C [96]. Humans are potentially at risk, especially if eating heavily infected mollusks and any worms enter the CNS. There are several other species of *Echinocephalus*, and some may also have the ability to penetrate the alimentary tract of mammals and undergo a visceral or cutaneous migration. Gnathostomes cause both cutaneous and visceral migration, and human cases are probably much more common than diagnosed because specimens of the fast-moving worms are difficult to collect or biopsy; a refined serological method should be able to determine the presence of gnathostomes, and specific diagnoses should allow for a better understanding of marine associations.

A related unidentified juvenile spiruroid nematode known as suborder Spirurina type X has been known to cause creeping eruption in at least 28 Japanese [97]. The juvenile is acquired by eating raw tiny squid (*Watasenia scintillans*) as sashimi in Japan; the serpiginous erythematous eruption along the abdomen took 4 weeks to become apparent. All infections were confirmed with an indirect immunofluorescence test.

Metastrongyloidea (Rhabditina, Strongyloidea). *Angiostrongylus cantonensis* is usually considered a freshwater or terrestrial disease, even though it was originally thought to be acquired from improperly prepared marine fishes. There are several ways that this rat metastrongyle nematode can infect humans that involve estuarine or fully marine situations, and they have been reviewed [98]. The species matures in the pulmonary arteries of rats (Fig. 20) and has a rather complicated life cycle. Eggs lodge in the arteries and capillaries of the rat lung where they hatch (Fig. 21); the first-stage juvenile migrates through the alveoli and up the trachea before being swallowed and ultimately passed out in the feces. The juvenile develops to a third stage in a molluscan intermediate host. When the juvenile in the mollusk, its slime trail, or a paratenic host feeding on the host or the free juvenile is eaten by the rat, it migrates to the subarachnoid space adjacent to the brain (Fig. 22). After a couple of weeks, it forces its way into the venous system to be carried to the pulmonary arteries. Humans are accidental hosts, and the infective juvenile still goes into the brain cavity, but it remains there and often enters the brain tissue (Fig. 23) and causes behavior problems and even death in the patient. Because of abnormal behavior in infected humans, many never receive medical attention. Even though the infective juveniles do not necessarily survive as long in marine waters or in marine invertebrate or vertebrate hosts as freshwater counterparts, they survive long enough to transmit the infections. The eastern oyster, *Crassostrea virginica*, and northern quahog, *Mercenaria mercenaria*, can serve as intermediate hosts in 15 ppt, and large amounts of the

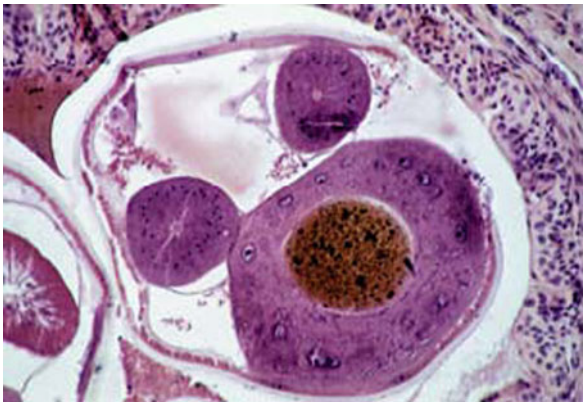

Waterborne Parasitic Diseases in Ocean. Figure 20 Section of adult female of *Angiostrongylus cantonensis* associated with other males and females in pulmonary artery of rat definitive host. The paired creamy-white uterine branches spiral around the hematin-filled intestine giving a diagnostic barber-pole appearance to this 20–30-mm-long worm when alive

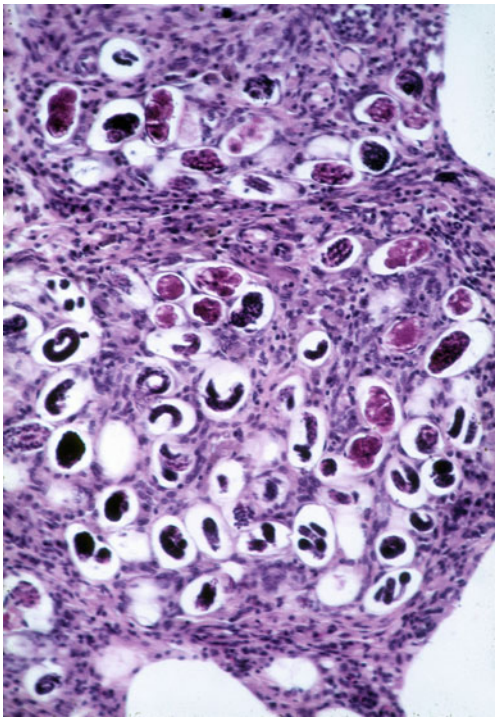

Waterborne Parasitic Diseases in Ocean. Figure 21 Section of rat lung showing deposited eggs and hatching juveniles of *Angiostrongylus cantonensis* infective to mollusks

Waterborne Parasitic Diseases in Ocean. Figure 22 Section of fourth-stage juvenile of *Angiostrongylus cantonensis* developing normally in meninges of brain of rat after 29 days without any apparent inflammatory response

oyster are eaten raw. There are many possible ways for humans to acquire the infection, but it is difficult to discern individual cases. In Tahiti, special dishes involve a sauce prepared from uncooked shrimp hepatopancreas (liver/digestive gland) often containing infective juveniles mixed with grated coconut and "coconut milk." Infections originated in the Indo-Pacific, but have spread by rats aboard ships to the Northern Hemisphere. Infections have become recognized in Hawaii, Cuba, Puerto Rico, and the USA through Louisiana.

Dioctophymatidae (Dorylaimia, Dioctophymatida). Juveniles of *Eustrongylides* spp., like those of *Dioctophyme renale*, are relatively large and red, making ingestion seem unlikely. However, when fish intermediate or paratenic hosts are eaten alive whole, a severe peritoneal infection can occur. In the USA, eating live fish is usually a behavior to gain attention or a hazing ritual. Consequently, fishermen eating their bait, tavern clientele taking a wager, and students being initiated as well as unaware consumers eating homemade sushi are likely victims [99]. Unlike *D. renale*, which matures in mammals, all species of *Eustrongylides* mature in birds. Three well-known species are recognized, *Eustrongylides ignotus* from North and South America plus New Zealand, usually infecting herons and egrets; *Eustrongylides tubifex* from North and South America, Europe, and into Asia in ducks, loons, and cormorants; and *Eustrongylides excisus* from Europe, Asia, and Australia in ducks, cormorants, and herons [100]. Juveniles of all should be regarded as a health risk, and all occur in both freshwater and estuaries. In Mississippi, *E. ignotus* occurs mostly in estuarine conditions and commonly spreads to its second intermediate mosquito fish and *Fundulus* hosts by a variety of tubificid and other oligochaete first intermediate hosts. Because paratenic hosts such as largemouth bass and striped bass commonly eat mosquito fish and fundulids and are preferred seafood products, humans dining on these and

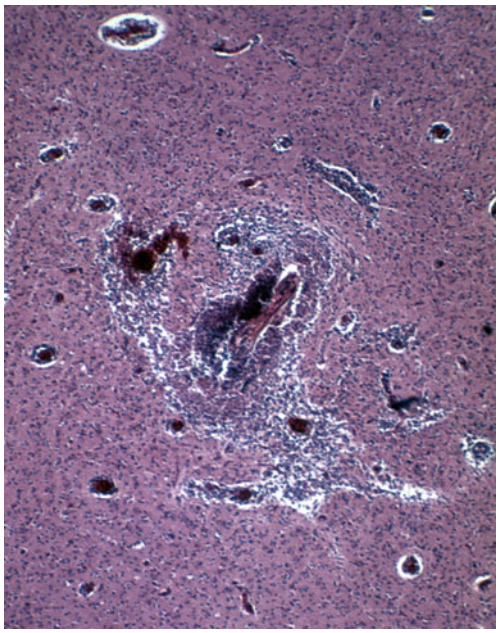

Waterborne Parasitic Diseases in Ocean. Figure 23 Section of juvenile of *Angiostrongylus cantonensis* after abnormal migration into brain of a Thai, showing atypical inflammatory response in human brain

other fishes wild or in culture [101] in an uncooked state are at a high risk for infection.

Dracunculidae (Spirurina, Spiruromorpha, Dracunculoidea). *Dracunculus insignis*, once thought to be a synonym of *Dracunculus medinensis*, the "fiery serpent" of the Bible and possibly the "snakes" in the caduceus of the American Medical Association and many other medically related societies, constitutes a public health risk. It occurs in the hind legs of the raccoon in the brackish marshes of the northern Gulf of Mexico [1] as well as freshwater habitats throughout North America and presumably is transmitted by paratenic fish and frog hosts. Consequently, *D. insignis* could be acquired by someone eating raw fish, not presently the habit of most persons living in a region abundant in seafood typically eaten in a cooked state.

Other Parasites

Acanthocephala (Spiny-Headed Worms) Acanthocephalans, especially those that mature in the alimentary tract of marine mammals, pose a threat to those who eat raw fishes. Two palaecanthocephalans were discussed above as species that occur in the intestine of humans, even though they did not mature in the patients. They also did not penetrate the human digestive tract. Another case of what was tentatively identified as *Bolbosoma* sp., presumably the same marine mammal parasite species mentioned earlier [63], penetrated through the intestine and became encapsulated in a granulomatous mass on the serosa of the ileum in the peritoneal cavity of a 16-year-old boy in Japan [102]. Another species, one that matures in a fish, *Acanthocephalus rauschi*, was discovered in the peritoneum of a native in Alaska. The frequency of acanthocephalan infections in humans, especially native groups from the Arctic where fishes containing infective juveniles are eaten raw, is difficult to discern but is probably substantial [18, 62].

The spiny-headed worm with hooks on the everting proboscis can produce severe lesions if it penetrates through the intestine or occurs in large numbers. An experimental study feeding rats with *Centrorhynchus* sp. from a paratenic host resulted in the worms penetrating the intestine on day 1, entering the muscles by day 5, and producing granulomas on day 20 [103]. When captive primates feed on intermediate hosts or are fed paratenic hosts, they can die when the worms invade beyond the serosa but otherwise produce a focal inflammatory response without harming the host [104]; when large die-offs occur, the invading worms are usually associated with secondary bacterial involvement.

Members of the Archiacanthocephala, *Moniliformis moniliformis* from rats and *Macracanthorhynchus hirudinaceus* from pig have been reported from man throughout much of the world, sometimes with serious complications. They are acquired from terrestrial arthropods such as roaches or paratenic hosts. Nine specimens of the relatively large related *Macracanthorhynchus ingens*, known from the raccoon, *Procyon lotor*, and a few other carnivores, was reported from the intestine of a 1-year-old child in Texas [105]. The worm is common in coastal areas, so it could be transmitted to humans in estuarine, freshwater, or terrestrial paratenic hosts as well as from wood roaches and millipedes, if eaten raw.

Sebekidae (Crustacea, Pentastomida, Porocephalida). Nymphs of pentastomes, a crustacean group perhaps derived from and of equal status as Branchiura (argulid parasites of fish and amphibians) also can migrate in and

become encapsulated in human visceral organs. A marine threat would be *Sebekia mississippiensis*, a parasite from the lungs of the American alligator. Nymphs are abundant in the western mosquito fish (*Gambusia affinis*) (Figs. 24 and 25) and present in the Atlantic croaker and gulf killifish, which may or may not have acquired the infection from the mosquito fish from estuarine and marine habitats, like its alligator final host. When any of the intermediate or paratenic fish, snake, or turtle hosts and possibly eggs is eaten by a mammal, the nymphs migrate and usually become encapsulated by the mammal. The opossum and river otter were infected in Mississippi, suggesting a human potential host [106], since humans are known to host nymphs of other pentastomes. This and related species infect other crocodilians. At least one case report for a related species of *Sebekia* involved skin dermatitis in a woman in Costa Rica [107]. An autopsy of a woman from Georgia, USA, with presumptive acquired immunodeficiency syndrome (AIDS) revealed the cuticle of an unidentifiable pentastome in her pericardial sac and epicardium associated with tuberculous pericarditis [108]. Non-marine-inhabiting pentastome species of several genera present an equal risk to infect people.

Protozoans Sarcocystidae (Alveolata, Apicomplexa). The coccidian *Toxoplasma gondii* has final hosts that contain a sexual, coccidian-like phase, restricted to cats and other felines, all terrestrial mammals. Human infection results from shed oocysts in feline feces, by ingesting tissue cysts in warm-blooded mammals and birds, by eating passive vector hosts, and by congenital transmission. Infected humans, predominantly immunocompromised patients or transplant recipients on immunosuppressive therapy, can develop encephalitis, mental retardation, and blindness. If infection occurs for the first time during pregnancy, the parasite can cross the placenta into the brain or eye, and possibly cause miscarriage. The reason for the large number of human infections, perhaps a significant portion in some geographic regions, in the marine environment, may be the low number of oocysts necessary to establish a human infection. As an example, a pet cat sheds oocysts for only a few days during its lifetime, and it produces about 25 g of feces per day. However, in each fecal

Waterborne Parasitic Diseases in Ocean. Figure 24 Nymphs of *Sebekia mississippiensis* partially pulled from body cavity of intermediate host, the western mosquito fish, *Gambusia affinis*, which is infective to paratenic fish, turtle, and mammalian hosts, including humans, or to the alligator definitive host

Waterborne Parasitic Diseases in Ocean. Figure 25 Anterior end of *Sebekia mississippiensis*, a pentastome from the lung of the American alligator in Mississippi

deposit, tens of millions of oocysts may be produced, and as few as one oocyst can infect a mouse or pig [109]. The small floating oocyst can sporulate into the infectious agent at 15 or 32 ppt and remain infectious for long periods, up to 6 months at 15 ppt [110]. These oocysts, resistant to most disinfectants, however, have not been reported from coastal waters even though present in marine and coastal animals [111, 112]. When experimentally exposed to the eastern oyster, the agent in oyster tissue was infectious to mice for 6 days [113], but, even though experimentally exposed mussels (*Mytilus galloprovincialis*) tested positive by PCR assay, mice fed with various PCR-positive tissues as old as 21 days demonstrated infections for at least 3 days only when fed digestive gland tissue [114]. At least 13 marine mammals, including dolphins, have shown a positive reaction by agglutinations and indirect fluorescent antibody tests [111, 115]. The California sea otter (*Enhydra lutris nereis*) has been studied most extensively because *T. gondii* has been associated with meningoencephalitis and extensive mortalities in the California population. There are three dominant genotypes, two of which have been identified from human infections; the otter had two genotype isolates in the brain and heart, and one of those was one that was known from humans and the other a rare one [111]. The otter feeds on mollusks, and evidence indicates land-based runoff as the source of the otter infections, suggesting "potent implications for human health" [116]. Perhaps crustaceans also serve as vectors. Additional epidemiological evidence deals with Inuit women of childbearing age in Northern Quebec, Canada, where seals are infected [117]. About half were seropositive to *T. gondii*, and seropositive women were at least four times more likely to have eaten dried seal meat or seal liver than seronegative counterparts. Seronegative women during pregnancy are now instructed to avoid all uncooked or dried meat, particularly seal and caribou, and to refrain from skinning animals.

Microspora. Microspora is a large phylum with obligate intracellular members that infect and obtain their energy from primarily invertebrates and lower vertebrates, cold-blooded vertebrates. The life cycles of microsporidans include several patterns including a direct cycle, a cycle that needs a true intermediate host, a transovarian cycle, and a cycle that passes through a vector without undergoing any development. Members of few genera infect mammals, with *Encephalitozoon cuniculi* being the best known. A few species have been reported from humans, and most of those represent immunologically incompetent individuals [118]. These include *Encephalitozoon intestinalis* and *Encephalitozoon hellem*. Others, such as *Pleistophora ronneafiei*, *Trachipleistophora hominis*, and *Anncaliia vesicularium*, involve species with fish or other cold-blooded hosts. These species are named for material taken from human AIDS or otherwise immunologically incompetent patients, and they may have already been named earlier from a cold-blooded host, even a marine one. *Pleistophora ronneafiei* was suspected to have been injected into a prisoner in Florida with a syringe containing infective material from a fish [1, 118]. A study conducted on other microsporidans to determine human risk from spores reaching coastal and marine waters tested the viability of the three indicated species of *Encephalitozoon* [119]. As expected for spores of species that can infect humans, the viability decreased as temperature increased from 10°C to 20°C. More proliferation of the parasites tested at 0, 10, 20, and 30 ppt occurred at the lower salinity concentrations, with *E. hellem* and *E. intestinalis* surviving better than *E. cuniculi*, in which survival lasted 1–2 weeks at 10 ppt. Those former two still proliferated at 4 weeks, with some proliferation of *E. intestinalis* at 10 ppt at 12 weeks. Consequently, all three species could infect humans and marine mammals or contaminate shellfishes. At least *E. hellem* and *E. intestinalis* can contaminate water with spores passed by aquatic birds [120]. *Enterocytozoon bieneusi* may be the most common microsporan of man. A total of 81 different genotypes with 111 different genotype names have been identified, with 26 exclusively in humans, but with none from marine animals [121]. The species without a characterized genotype was identified with PCR from an ill bottlenose dolphin (*Tursiops truncatus*) [122].

Myxozoa. Myxozoans, actually multicellular parasites that get placed in most textbooks as protozoans, seem to be bilaterian metazoans, possibly in a sister group to the Nematoda [123], or a trachylinan Cnidaria; members are not thought to infect humans. Spores occur primarily in fishes and amphibians, but atypical species have been reported from a variety of

other hosts. Sexual development takes place in oligochaetes and a variety of other invertebrates. Because people often eat fish infected by myxosporidians, they can exhibit spores from the product passed in their feces. There is no indication that any myxosporan has actually infected healthy humans and undergone vegetative reproduction. Two patients were reported to exhibit spores and diarrhea, but at least one of those was an immunosuppressed, HIV-positive patient infected with the human coccidian *Isospora belli* and the other had human helminths *Strongyloides stercoralis, Hymenolepis nana*, and *Ascaris lumbricoides* [124]. Other case reports, such as some in Australia involving eating fish that had been frozen, exist but probably do not represent human infections [125]. Spores of *Henneguya salminicola* also have been reported from human diarrheic feces [126, 127]. Patients had been eating salmon, and, in one case, the spores were misdiagnosed as human sperm, resulting in scandalous consequences [126].

Parasites Acquired When People Have Direct or Indirect Contact with Them

Parasites acquired by contact consist of both helminths and protozoans, but helminths usually actively enter humans by direct contact. In some cases, difficulty exists distinguishing between active and passive contact. Also diseases acquired from agents in marine water fit into different groups. Some originate from estuaries and marine habitats, but most seem to have a freshwater origin but can tolerate marine or estuarine conditions.

Direct (Active) Contact with Disease-Causing Agents

Trematoda Schistosomatidae. Members of the Schistosomatidae exhibit atypical features among trematodes such as having separate male and female individuals rather than being hermaphroditic and living in blood. They also do not have a distinctive second intermediate host, but there occurs a juvenile stage, schistosomula, that develops from the cercaria after it penetrates the definitive host. Those species that mature in humans use as their first intermediate host freshwater snails only, but some members in marine snails occurring throughout much of the world that infect birds and mammals produce cercariae that accidentally penetrate humans and establish a hypersensitivity dermatitis.

Dermatitis, known as "swimmer's itch," "clam digger's itch," and other terms, results when humans are challenged by epithelial penetration of the cercariae of some specific schistosome species occurring in the mesenteric blood vessels of the avian and mammalian marine and freshwater hosts. Swimmer's itch is best known for freshwater species; however, several marine species result in similar human responses. Some freshwater cercariae can survive well in low-salinity conditions, but salt usually kills the snail hosts. For example, the cercariae of *Bolbophorus damnificus* can tolerate 2.5 ppt sodium chloride, a concentration toxic for the freshwater snail host *Planorbella trivolvis* that sheds it [128].

For cases of most dermatitis caused by schistosome cercariae, the cercaria hangs in or near the surface of the water where it comes into contact with the appropriate bird or mammalian (such as raccoon) host. Consequently, a pruritic maculopapular rash occurs on the human body in contact with the surface, often around the knees or ankles for those occurring in shallow water. Typically, when the cercaria penetrates human skin that it had previously penetrated with no or limited discernment by the patient, it produces a more apparent prickling sensation for several minutes. Depending on the number of cercariae and the host immune system, this condition may be associated with "macular eruption" (color change in 5–10 mm focal area without elevation or depression) with diffuse erythema or urticaria. Later in the day an itchy "macropapular eruption" (elevated colored area, 5–10 mm) develops and the papules "progress" to fluid-filled vesicles that may become secondarily infected because of the tendency to scratch them. Over the next week to month, the lesions become pigmented and apparent. The "hypersensitivity" reaction is not a true allergic one, and, when the same cercarial species or one with cross-reactivity penetrates the skin in the future, it produces a more severe dermatitis. Occasionally, systemic signs such as fever lymphadenopathy and edema develop [129].

A large number of marine schistosome species probably produce human dermatitis. The number of reported species, however, has remained low because of the inability until now with molecular tools to identify the species, the paucity of studies associating specific species with dermatitis, and the lower likelihood of human contact with cercariae in the marine

environment when compared with infective species in freshwater. Swimmers in several freshwater lakes are more prone to continual visits to cercarial/snail-laden portions of the lake. Moreover, the fact that a variety of agents in marine habitats can produce a rash, apparently including non-schistosome cercariae, makes diagnosis of the cause of the rash difficult.

Austrobilharzia variglandis is probably the best known marine cause of the dermatitis, but what is identified as *A. variglandis* probably consists of a complex of several species from California [130], Hawaii [131], Australia [129], and elsewhere as well as the clam beds of Rhode Island [132] and Connecticut [133] where it is transmitted by *Ilyanassa obsoleta* to a variety of gulls plus the double-crested cormorant and Canada goose. At least *Austrobilharzia terrigalensis* in the silver gull *Larus novaehollandiae* and *Batillaria australis* (as *Pyrazus australis*) in South Australia and Western Australia [134] has been distinguished from misidentified Australian *A. variglandis*. The snail *I. obsoleta* ranges along the Atlantic coast to Florida. *Austrobilharzia variglandis* was reported from the migratory American white pelican in Mississippi [135]. A second species from the northern Gulf of Mexico, *Austrobilharzia penneri*, occurs in *Cerithidea scalariformis*. Gulls are important definitive hosts of marine schistosomes, especially species of *Austrobilharzia*, and since gulls and shorebirds commonly occur in close association with humans, there is a tendency for infections in Hawaii, Australia, and China [129, 136]. There is need to accurately differentiate species worldwide because most or all produce dermatitis.

Members of other blood fluke genera also produce dermatitis. *Gigantobilharzia huttoni* in both the brown pelican and American white pelican and the Antilles glassy-bubble, *Haminoea antillarum* (Cephalaspidea), occurs in Florida [135, 137, 138]; *Gigantobilharzia acotylea* caused dermatitis in the Venice Canal, Italy [139]; *Ornithobilharzia* cf. *canalicula* infects terns, and *Batillaria minima* from the Gulf of Mexico in Florida, USA [140, 141], although the dermatitis attributed to this cercariae was rightfully questioned [138]. Unidentified species producing dermatitis were reported from southern California in *Littorina keehae* (as *L. planaxis*) [142], from eastern Australia in the limpet *Siphonaria denticulate* on rocky shores [143], and from other regions such as Japan [144]. One from California occurs in the Japanese bubble snail (*Haminoea japonica*), which was introduced into San Francisco Bay in about 1999 [136]. Comparative sequence data did not allow information on whether the blood fluke was native to California, introduced from Asia in the snail, or a species from Asia acquired from migrating birds.

As indicated above, most schistosome species responsible for dermatitis are shed from freshwater snails in freshwater. Ten genera contain these species and are cited [145] compared with just three genera from salt or brackish waters. Studies on species of *Trichobilharzia* have provided some information that may relate to human infections. When bird species are experimentally exposed to a mouse, rather than mammalian skin trapping and eliminating the cercariae, it allows some to produce schistosomula. In the case of *Trichobilharzia regenti*, the agent typically penetrates the skin of the bird host and migrates to and becomes established in nasal tissues after passage through the peripheral and central nervous system [146]. When in a mouse, even a small number of the agent in the CNS can produce severe responses [147]. Members of *Trichobilharzia* as well as of *Gigantobilharzia* and *Ornithobilharzia*, especially on the initial exposure to experimental mammals, can progress to the lungs and CNS where they can produce severe pathological alterations [145].

Nematoda Strongyloididae (Rhabditina, Rhabditoidea). Some members of the nematode genus *Strongyloides* cause a creeping eruption (larval migrans) or rash in people exposed to juveniles and then challenged at a later date. Two species proven to cause the dermatitis in man are *Strongyloides myopotami* from the nutria (*Myocastor coypus*) and *Strongyloides procyonis* from the raccoon (*Procyon lotor*). These are probably the principal agents of what trappers, hunters, fishermen, and oil workers in the northern Gulf of Mexico call "marsh itch." A human volunteer was exposed in his arm to a relatively small number of third-stage juveniles of *S. myopotami* on seven occasions over 11 months before a minor rash (pruritus with small papules) erupted and lasted about 5 days [148]. Following that time, the volunteer was sensitized and juveniles of both species produced a reaction.

Those from the raccoon allowed to penetrate the opposite arm produced more extensive reaction at the site of penetration for a few days, but, after disappearing for several days, it reappeared 5 cm from the site. Future exposures responded similarly but the recurrence resulted in a sinuous creeping eruption that spread from the arm to the chest. The juveniles migrating near the surface differs from the reaction by the larvae of blood flukes mentioned earlier. The species from the raccoon is morphologically similar to the human species, *Strongyloides stercoralis* (Fig. 26), which can undergo autoinfection. When a challenge dose of 185 juveniles of the raccoon species were exposed, at least one was able to mature and produce juveniles for a few days. The normal life cycle of species of *Stronglyloides* differs from that of most nematodes. The threadlike parasitic female in the mucosa of the intestine deposits eggs passed in the feces as either eggs or first-stage juveniles. In the external environment, the juvenile develops into a feeding rhabditiform juvenile, which in turn develops into an infective third-stage filariform juvenile. The non-feeding filariform can invade the definitive host or develop further into a single free-living generation of both males and females. These mate and produce infective juveniles, even though under optimal conditions, the offspring may develop into a second free-living generation. Infective juveniles penetrate the skin and pass by the cutaneous blood vessels to the lungs, where they break out of the alveoli and migrate by the respiratory tree to the pharynx and intestine, maturing in mucosal epithelium in about 2 weeks. The parasitic female produces juveniles without being fertilized and is parthenogenic. Most species of *Stronglyloides* infect one or few related amphibian, reptile, mammal, and bird hosts. Probably few species would be capable of producing creeping eruption in humans, but at least two from mammals in the Southern US do. Unpublished research in Mississippi showed that the free-living infective filariform juveniles of *S. myopotami* and *S. procyonis* can tolerate seawater well.

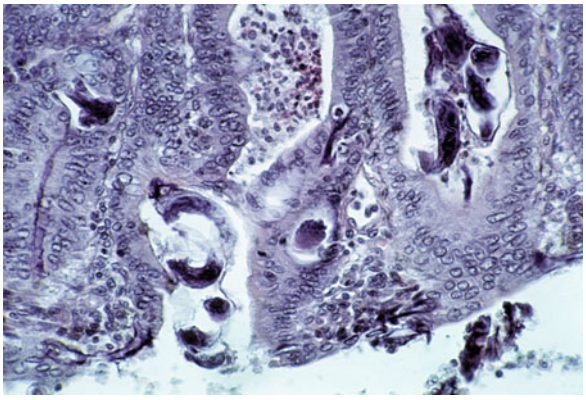

Waterborne Parasitic Diseases in Ocean. Figure 26 Juveniles of *Strongyloides stercoralis* passing from human intestinal crypts and representing zoonotic species, some released as eggs and others as hatched juveniles

Miscellaneous agents. Unusual circumstances can result in involvement by a parasite not expected to affect humans. For example, a diving accident resulted in such a case with an adult philometrid (Dracunculoidea) nematode, a parasite that matures in non-intestinal sites in fishes. A scuba diver in Hawaii accidently stabbed himself when reloading a spear gun and then later cleaned a fish to eat. He noticed some parasites and discarded the fish, but 3 h later he sensed a 1-cm portion of a red worm protruding from the stab wound. He tried to kill and remove this firmly still-attached worm with vinegar, rubbing alcohol, and forceps. Because of the pain, he had the worm surgically removed by a physician [149]. Other parasites or free-living marine invertebrates can also take advantage of wounds or create their own. Isopods (Crustacea, Peracarida) in the Aegidae, Cymothoidae, Cirolanidae, and other flabelliferan families can produce lesions and urticaria, and are especially annoying. Even an amphipod has produced acute urticaria in a diver in Hawaii [1].

Protozoans Acanthamoebidae (Amoebozoa). A few different free-living amoebae can cause severe disease if they can enter a human. Best known is *Naegleria fowleri* (Excavata, Heterolobosea, Vahlkampfiidae), which causes fatal "primary amoebic meningoencephalitis (PAM)," but it is restricted to freshwater habitats and moist soil throughout the world. Several species of *Acanthamoeba*, however, occur in marine waters or along marine beaches as well as in freshwater habitats. Species are known to cause chronic granulomatous amoebic encephalitis (GAE), granulomatous skin and lung lesions, and amoebic keratitis. The life cycle of *N. fowleri* consists of an amoeboid, feeding, and replicating trophozoite. During periods of low nutrients or desiccation, the motile amoeboid stage forms either

a biflagellated, non-feeding, non-replicating trophozoite or a cyst until conditions improve. Human tissues contain only the amoeboid stage. The trophozoite apparently enters through the nasal cavity and migrates into the brain and central nervous system (CNS) along the olfactory nerve. The PAM typically progresses rapidly from a sudden headache and fever to coma and death, without much possibility of diagnosis before death. Species of *Acanthamoeba* do not have a flagellated trophozoite, the amoeboid trophozoite has spike-like pseudopodia and is more sluggish, and three-layered cysts can occur in human tissues. The portal of entry may differ for different species. Invasion appears to be from a primary focus in the skin, lower respiratory tract, or nasopharynx, with dissemination of the trophozoite reaching the CNS through the circulatory system and possibly by crawling along the outside of blood vessels [150]. Signs of GAE progress much slower and initially are less severe than for PAM; they take weeks or months to result in death, and infections are difficult to diagnose. In contrast with PAM, which affects healthy people, GAE is usually associated with chronically ill, immunocompromised, or otherwise debilitated patients. Predisposing factors for infections include broad-spectrum antibiotics, steroid or antineoplastic therapy, radiation therapy, alcoholism, pregnancy, and bone marrow or renal transplantation. Many of the earlier diagnosed infections, especially in non-compromised patients, were associated with *Balamuthis mandrillaris*, a morphologically similar free-living but genetically different species that has been considered a soil-inhabiting species.

Which species of *Acanthamoeba* infect humans in the marine environment and how they infect the people have not been established. Several isolates of the *Acanthamoeba* complex have been cultured from marine waters or beaches [151–153], and eight strains are pathogenic to mice and potentially to humans. Of 17 species of free-living amoeba cultured from salt water in Northwest Spain, only *Acanthamoeba polyphaga* was pathogenic to mice [154]. Seven species have been associated with human disease, and of these, *Acanthamoeba castellanii, Acanthamoeba culbertsoni, Acanthamoeba hatchetti, Acanthamoeba rhysodes, A. polyphaga*, and *Acanthamoeba griffini* have been identified from amoebic keratitis, a hard-to-treat disease of the cornea [155]. This disease causes severe ocular pain, photophobia, recurrent epithelial breakdown, and edema, and confirmed by trophozoites and cysts in a corneal scrape or biopsy. It was recognized in 1973 and not common until 1985 when contact lenses became popular. Lenses are maintained in a saline or tap water solution in a reusable storage case that can get contaminated.

Members of *Acanthamoeba* also have the ability to harbor viruses and bacteria, perhaps serving as vectors or reservoir hosts for a variety of agents. Isolates of *Acanthamoeba* from water sources in the Canary Islands revealed four different serotypes of adenoviruses, one related to ocular disease and the others unknown, probably respiratory, gastroenteritis, or neurologic [156]. A large DNA mimivirus was identified from *A. polyphaga*. Experimental studies [157] have shown that coxsackie B3 viruses can be adsorbed on the surface and accumulated within *A. castellanii*. The same marine amoeba can also host the bacteria *Chlamydia pneumoniae* and *Legionella pneumophila*. It did not prey on *Vibrio parahaemolyticus*, but it secreted a factor that promoted survival of the bacterium in coculture, suggesting the amoeba provides a survival to the extracellular pathogen in the environment [158]. These and other facultative parasites probably contribute greatly to transmission of microbial disease agents as can obligate parasites [159].

Nonparasitic: But Confused with Parasites In the marine environment, there are, in addition to schistosome cercariae, a variety of nonparasitic agents that cause similar appearing rashes. The stinging nematocysts of several members of the phylum Cnidaria (previously called Coelenterata) have been held responsible for "seabather's rash" or "seabather's eruption." Members usually go through an alteration of generations with asexual polyploidy and sexual medusoid generations, but there are variations of this life cycle. Divers can brush against the nematocysts of fire corals (Hydrozoa, Anthomedusae, *Millepora* spp.) with their encrusting calcareous coral-like skeletons, while bathers can become entwined in expandable fishing tentacles lined by batteries of nematocysts of the "man-of-war" (Hydrozoa, Siphonophora, *Physalia* spp.) hanging from the gastrozooid, maintained on the surface by a gas-filled float. This floating colony appears like a medusa but is actually a highly modified polyp.

When the long, up to 13 m, tentacle of the Atlantic *Physalia physalis* washes onto sandy beaches, it gets ground up in the surf, leaving minute pieces with undischarged batteries of nematocysts to get into bathing suits or work gear. Medusa of several jellyfishes (Scyphozoa) have been associated with stings and rashes. Moreover, some sea wasps and box jellyfishes (Cubozoa), exhibiting square cross sections of their medusa, have been shown to cause human fatalities. The planula larvae of true jellyfishes, such as the thimble jelly, *Linuche unguiculata*, get under swimsuits, and challenge exposures produce a hypersensitive rash reaction (Fig. 27). Cases are common along the Southeastern Atlantic US, Mexico, and the Caribbean Sea, but exact identifications and prevalence of these and other cases worldwide require study. Systemic symptoms from the planulae are considered more common than with schistosome dermatitis [129]. The sting from the planula larva of the burrowing anemone (e.g., Anthozoa, *Edwardsia lineata* as *E. leidyi*), appearing as a "tiny pink egg" [160] attached to the inner lining of bathing suits, has been associated with seabather's eruption in Long Island, New York, from mid-August through early September. The planula also parasitizes ctenophores, which can get caught in swimming apparel and transmit the condition. Not all rashes attributed to blood flukes or cnidarians come from those agents. Many cases also result not from ejected toxins but from rubbing between the bathing suits and human skin of molluscan opisthobranch gastropod shells, sponge spicules, and spines of zoea and megalops larvae of crabs and shrimps, swarms of which can occur seasonally in heavy concentrations. Rashes attributed to "sea lice" are misleading; the term "sea lice" is a common name usually attributed to a variety of parasitic copepods but primarily *Lepeophtheirus salmonis* infesting salmon. None of these copepods produces human rashes, but some marine dermatitis caused by cnidarians has been referred to as caused by sea lice. Some polychaetes (Annelida) produce an irritating rash as does contact with the excrement of some sea cucumbers (Holothuroidea) or eating some inadequately cooked species. Contact with Cyanobacteria (previously referred to as blue-green algae), such as *Lyngbya majuscula* growing on sea grasses in Hawaiian waters, has been identified as causing "swimmer's itch" or "seaweed dermatitis." The agent is called fireweed in Australia. Rashes also result from some "harmful algal blooms" (red tide) throughout the world. The Internet includes some incorrect or misleading information, but researchers are tackling some of the cases, especially since they have a large impact on recreational and occupational activities in the marine and coastal environments.

Waterborne Parasitic Diseases in Ocean. Figure 27 Visiting, teaching marine biologist at San Salvador, The Bahamas, exhibiting back with hypersensitive rash developed after and presumably caused by exposure to challenge dose of planula larvae of the thimble jelly, *Linuche unguiculata*

Indirect (Passive) Contact with Disease-Causing Agents

Eating products contaminated with an agent or drinking contaminated water are herein considered differently than eating infected products because the food or water contaminated with the organism serves as a mechanical or passive vector of the agent rather than as a host that the organism requires for its survival. Also, the agent does not actively penetrate the skin as achieved by an agent of swimmer's itch or marsh itch.

Trematodes Humans occasionally get infected with trematodes in a passive process. A person does not knowingly eat a product, and the parasite does not actively penetrate a host. For example, a seafood handler who came in contact with an abundance of fresh

killed coho salmon (*Oncorhynchus kisutch*) known to be heavily infected with the trematode *Nanophyetus salmincola* developed an infection exhibiting acute clinical signs. He denied eating raw or cold-smoked fish and rarely ate any seafood products. Alternatively, he could have transferred the minute metacercariae on his hand to his mouth while smoking [1, 43].

Protozoans Giardiinae (Excavata, Diplomonadida). Species of the flagellate *Giardia* have long been associated with severe diarrheal disease in humans. They are typically considered as freshwater or terrestrial species acquired when people drink contaminated water, but they have recently been found to be abundant in marine waters. The agents were thought to be confined to those discharged in raw sewage disposal and from recreational swimmers throughout the world, both raising public health risks. Consequently, infectious cysts or the trophozoites of the flagellates have been detected along some marine beaches near sewage outfall and canals influenced by runoff, where bathing is common in Hawaii [161], as well as in Panama and Hong Kong [111]. The trophozoite is a microscopic pear-shaped organism with four pairs of flagella. Two of these occur within the resistant cyst, and when the vertebrate host acquires the cyst, it excysts, releasing the trophozoites which reproduce asexually by binary fission and remain in the lumen or attach to the mucosa of the small intestine. Under the appropriate conditions, encystment occurs and both the cysts and trophozoites pass out with the feces. The taxonomic classification of members in the genus is not well established, but there are five recognized species (e.g., [162]), and the genetic characterization of *Giardia duodenalis*, also referred to as *Giardia intestinalis* or *Giardia lamblia* and the species with the widest host-specificity, groups at least seven genetic assemblages (genotypes) including Assemblage A, the one most commonly found in humans [163]. *Giardia* sp. occurs widespread in the river otter (*Lontra canadensis*) from the marine waters of Puget Sound Georgia Basin of Washington [164], but species also occur abundantly in the feces of a variety of temperate and Arctic marine mammals such as the right whale (*Eubalaena glacialis*, 71% prevalence), bowhead whale (*Balaena mysticetus*), ringed seal (*Phoca hispida*, 65%), California sea lion (*Zalophus californianus*), and harbor seal (*Phoca vitulina*) but not the beluga whale (*Delphinapterus leucas*) or bearded seal. Assemblage A occurred in the harp seal (*Phoca groenlandica*), gray seal (*Halichoerus grypus*), and harbor seal (*Phoca vitulina*) but not the beluga whale [165]. Moreover, despite the common occurrence of infections in adult seals and cyst contamination on ice floes, cysts were not encountered in seal pups less than 1 year of age. However, the epidemiology and potential for zoonotic transmission in marine systems remains virtually unknown [164], but the genotypes of *G. duodenalis* in the harbor seal in Puget Sound, Washington, were the same as from a canine, from other sites, and were mostly novel genotypes [166]. Cysts remain infective for about 56 days in relatively deep freshwater cool lake water, but at least those of *Giardia muris* become inactivated by the combination of salinity and sunlight in warm Hawaiian marine beach water within 3–6 h [167]. In the Netherlands where the salinity remains stable at 28–31 ppt, *Giardia* cysts were detected in what was considered to be a low estimate of 12% of oysters, where viability was presumed to be preserved, representing some public health risk to those consumers who ate the oysters raw [168]. Cysts have also been filtered out of the water and concentrated by the blue mussel, *Mytilus edulis*, and other bivalves, and this tool has been used to monitor *G. lamblia* in Ireland [169] and for that and other species or genotypes elsewhere [112, 170]. Depending on the size and species of bivalve, it can filter as much as 20–100 l of water per day. Much information on human health risks from beaches and marine waters, animal health, source of agents, dispersal of agents, and primary vectors can be established by a variety of surveillance programs. For example, a survey of live and dead, stranded and bycatch, birds, dolphins, seals, and fishes was conducted in the Northwest Atlantic using PCR techniques [171]. With the exception of infections in seals, those of *Giardia* spp. were more frequent than those of *Cryptosporidium* spp., to be discussed next.

Coccidiasina (Chromalveolata, [Alveolata, Apicomplexan]). Coccidian species in the genus *Cryptosporidium* pose a stronger human risk for infections than those in *Giardia* [112], especially species in estuaries compared with freshwater [169]. Typically, marine mammals, invertebrates, and marine water are examined for the agents concurrently with *Giardia*

because the agents are transmitted by the fecal-oral route from humans and other mammals. Thick-walled oocysts are passed in the feces as a resting cyst, each with four sporozoites infective to the vertebrate host, where development occurs. Additionally, there is a thin-walled cyst that cannot survive long in a harsh environment, but it may lead to endogenous autoinfection. This seems to be especially true for persistent infections in immunocompromised patients. A total of 14–15 species are accepted [172, 173], and several are known to infect humans: *Cryptosporidium hominis* (previously *Cryptosporidium parvum* genotype 1), *C. parvum*, *Cryptosporidium meleagridis*, *Cryptosporidium felis*, *Cryptosporidium canis*, and *Cryptosporidium muris*, with most human infections from *C. hominis* and *C. parvum*. Human agents have been detected in more marine recreational areas than *Giardia*. They occurred in Hawaii, Panama, Puerto Rico, Australia (tidal area of Georges River), and Hong Kong [111]. In fresh deionized water, oocysts of *C. parvum* can survive for at least 6 months at 0–20°C, 3 months at 25–30°C, 1 week at 35°C [172]. As many as 10^9 to 10^{10} can be excreted from bovine calves or non-compromised humans per week, and as few as 30 oocysts have been known to infect a human volunteer [174]. Bioassays in mice show that oocysts of *C. parvum* can survive 12 weeks in 30 ppt at 10°C and at 20°C for 12 at 10 ppt, 8 weeks at 20 ppt, and 4 weeks at 30 ppt, which was long enough for the oocysts to be removed by filter feeding bivalves such as the eastern oyster (*Crassostrea virginica*) [170]. Literature reports consist of a variety of bivalve mollusks from seven countries that contained *Cryptosporidium* as detected by immunofluorescence microscopy, bioassay in mice, or molecular methods [111]. In North America, oocysts have been detected from New Brunswick to Texas. Gill washings from the oyster near a large cattle farm and septic tanks were positive for the oocysts and infective to mice [170]. The agents occur in hematocytes as well as on gill surfaces, and they were more abundant after rainfall events, with two of the four identified species (*C. hominis* and *C. parvum*) infective to humans [111]. The same two species plus *C. meleagridis* also occurred in North American commercial products [111]. Species have also accumulated in hard clams, bent mussels, and zebra mussels [175]. To date, no human cryptosporidiosis cases have been linked to eating raw shellfish [111], even though some human genotypes have been concentrated in various bivalves. There is a higher prevalence of infection of both *Cryptosporidium* spp. and *Giardia* spp. in the ringed seal and right whale than in reported terrestrial mammals, and those infections might result from ingestion of contaminated water or from prey that had concentrated oocysts [176]. Other hosts of *Cryptosporidium* spp. include the California sea lion, bowhead whale, dugong (*Dugong dugon* in Australia), and marine foraging river otter but not the bearded seal and beluga whale [164, 176]. Isolates from the ringed seal from Nunavik, Quebec, were genetically characterized using two gene fragments and actin loci as *C. murus* plus two novel genotypes that were distantly related [177]. The risk for recreational bathers to come into contact with *C. parvum* was significantly greater on weekends than on weekdays, when the number of bathers was lower. The same was true in that Chesapeake Bay marine beach for *G. duodenalis* and *Enterocytozoon bieneusi*, a microsporidian to be discussed below [178]. The proportion of water containing the agents also correlated significantly with enterococci counts. The study suggested using those counts to indicate the presence of the parasites and recommended preventing diapered children from entering the water, restricting the number of bathers in the recreational areas, advising those with gastroenteritis to avoid bathing, and using showers prior to and after bathing.

Birds contract cryptosporidiosis with at least five avian species and numerous avian genotypes, and some of these have been investigated in regard to infecting mammals. They can also serve as vectors of *Cryptosporidium* spp., *Giardia* spp., and microsporidians infective to humans. In fact, aquatic birds seem to play a substantial role in contaminating water around the world, and managing water resources could benefit by incorporating protection measures for pathogens linked to these birds [120, 179]. In contrast, little research has been conducted to evaluate the public health threat of species of *Cryptosporidium* and related genera described from marine and freshwater fishes and from amphibians and reptiles. The various taxa and isolates have been reviewed [180].

Entamoebidae (Amoebozoa). Some strains or species of amoeba *Entamoeba histolytica* complex also are

zoonotic threats. Poorly documented records of infections in the bottlenose dolphin (*Tursiops truncatus*) from Cuba, Mexico, and other locations suggest a relationship among the marine mammals, sewage, recreational beaches, and human infections. Researchers at the Gulf Coast Research Laboratory and the American Type Culture Collection have seen cysts but were unable to culture material from the bottlenose dolphin (*Tursiops truncatus*) from Mexico. Because there were slight morphological differences between it and *E. histolytica* sensu stricto, this subject deserves a critical investigation to determine if the dolphin form is restricted to marine mammals and whether it can cause fulminating dysentery, bloody diarrhea, fatigue, and abdominal pain in humans. Possibly, the agent was acquired by the dolphin from humans during associated recreational activities or from human sewage.

Parasites That Produce Excretions or Secretions That Result in an Immunological Response in People

Ascaridoid juvenile nematodes produce excretions and secretions (ES products) that elicit immunological responses. These responses include both the allergic response by the host to living worms migrating into or through tissues and true anaphylactic reactions triggered by dead or living worms by food-borne, airborne, and skin contact routes [75]. Ascaridoids are unusual among nematodes to produce such reactions. Most concerning is that some sensitized individuals respond to infected cooked seafood products and even chicken that has been fed fish meal made from infected fish products [181].

The tissue migration by ascaridoids is made possible by potent proteolytic enzymes released from the esophageal gland and excretory cell through separate anterior openings. These contain hyaluronidase, serine proteases, anticoagulants, and numerous other identified and unidentified substances, but only specific ones probably produce the well-defined, erosive, hemorrhagic lesions in the gastric mucosa and these and others produce other effects in the human accidental host. Metabolic products released by the migrating juvenile also produce humeral and cellular responses, especially involving the acute lesions. These products, also including surface and somatic components of the juvenile, form insoluble immune responses with antibody. Some also cause direct IgE-independent degranulation of mast cells, at least in sensitized mice, and chemotaxis of eosinophils associated with thermolabile factors from the parasite, and produce the characteristic local response in the digestive tract but not systemically like in most other helminth infections [75]. When either living or dead individuals of *A. simplex* are ingested, cholinergic hyperactivity and adrenergic blockade can be rapidly induced, resulting in focal reactions associated with living worms but widespread along the entire bowel if the worm becomes ruptured or disintegrated. These activities may explain why 70% of the symptoms in *A. simplex*-induced anaphylactic reactions involve the digestive tract.

Anaphylaxis appears to be complex. Rodent studies demonstrate a mixed Th1/Th2 pattern of cytokines when the host is sensitized and challenged intravenously with certain parasites, but not when challenged orally. When the antigen is an extract of *A. simplex* proteins or a live worm, a strong Th2 response occurs, resulting in scratching, irritability, diarrhea, and puffiness around the eyes within 1 h. The multifaceted immune hypersensitivity reactions after induction by members of the *Anisakis simplex* complex have been investigated in terms of a wide range of parasite products and host cells; a concise helpful review treats all the known facets [75]. Hypersensitivity is usually diagnosed by skin prick tests and in vitro confirmation (specific IgE, histamine release, and basophil activation test). The skin prick test for *A. simplex* was first used in 1995 and now is used by physicians as an important test for cases of urticaria and anaphylaxis [75, 182, 183].

Recognition of allergic signs has been emphasized because of cases in Spain and South Africa. In Spain where fish is consumed abundantly, what was referred to as *A. simplex* is the most important hidden food allergen in the adult population suffering acute urticaria and anaphylaxis. It comprises as much as 10% of the anaphylaxis previously diagnosed as idiopathic [75], if the specific immunoglobulin E (IgE) detection by ImmunoCAP assay did not overestimate the number of sensitized subjects. Anisakiasis in Spain is caused primarily by eating pickled anchovy (*Engraulis encrasicholus*). That fish plus European hake (*Merluccius merluccius*) and cod (*Gadus morhua*,

just in Atlantic Ocean rather than in both the Mediterranean Sea and Atlantic Ocean) are eaten by allergic patients. Half the 64 allergic patients in one report required emergency treatment [184]. Half of the patients presenting signs of infection said they ingested raw fish, but the remainder ate cooked fish or, in rare cases, canned fish. Allergic cases requiring hospitalization demonstrated respiratory arrest, severe shock, and persistent angioedema.

In Spain, the matter of allergic responses in "gastroallergic anisakiasis" remains complicated and seems to be reported primarily from some regions in Spain. Patients entering the hospital emergency room with a severe acute epigastric pain and positive *Anisakis* prick tests plus total and specific IgE assays were divided into two groups. One group was diagnosed by the presence of at least one worm in the stomach, and the other group which had no worm seen in the stomach. Most patients had just eaten raw or pickled anchovies. Both groups averaged about 5 h, but up to 26 h, between intake of raw fish and onset of hypersensitivity symptoms, and no significant difference occurred between the two in their allergic symptoms of urticaria, angioedema, erythema, bronchospasm, and anaphylaxis, suggesting a borderline condition between a food allergy and parasitic disease supporting quick removal of the worm from the stomach. Moreover, only 26 of 40 patients required drug therapy to manage the allergic reaction, with only three requiring it for more than 1 day, suggesting an acute, self-limiting disease. In contrast, anaphylaxis can be life threatening, but abdominal symptoms disappeared within a few hours after removal of the worm [185]. When a portion of the *Anisakis*-sensitized groups with gastric worms, without gastric worms, and with no gastroscopy conducted (when symptoms did not persist for more than 8 h) were challenged with frozen worms from the blue whiting (*Micromesistius poutassou*, from either Atlantic or Mediterranean sources) and later from undocumented hosts on multiple occasions, there was no patient who suffered a reaction. This lack of a response to the thermostable proteins suggested that live worms had to be present for the allergic symptoms to occur [186]. Because the specimens from the Mediterranean Sea were from the anchovy, they were *A. pegreffii* [70] and not *A. simplex* as reported, even though if some material came from the Atlantic Ocean, both species could have been present. However, human infections with *A. pegreffii* are typically gastric in nature, and those of *A. simplex* are usually intestinal, based on findings from Japan, where 10% of healthy adults were seropositive against the *Anisakis* antigen [187]. The fact that some individuals exhibit allergic episodes when no viable nematode is present may express a difference between the effects of *A. pegreffii* and some other species of *Anisakis* or may be variation in responses by individual patients.

The cases in Western Cape Province, South Africa, involved workers in fish-processing plants. An epidemiological study of 578 workers from two large-scale plants reported 30 workers (5%), who said they had allergic symptoms to seafood. A total of 87% said symptoms occurred after eating fish, 40% after handling them, and 17% after smelling them. A prevalence of sensitization was tested as 6% with a higher value of 8% sensitive to *Anisakis* [188, 189]. *Anisakis*-specific IgE reactivity in the workers was determined to be associated with bronchial hyperreactivity and dermatitis. In corresponding mice studies, the juvenile worm induced a striking Th2/type 2 response. The investigation suggested that consumers acquiring an infection most likely can acquire sensitization to anaphylaxis, but that exposure to *Anisakis* proteins alone may be enough to elicit allergic reactions in sensitized individuals. In other words, occupational exposure to infected fish or fish meal constitutes a risk factor for developing sensitization to *Anisakis* or other ascaridoid-related allergic disease.

Historically, eating fish fillets infected with the plerocercoids of trypanorhynchean cestodes has been considered harmless with rare exception. All members of the group mature in elasmobranchs. In fact, some infected intermediate host products are preferred over noninfected counterparts; one example is the flesh of the Atlantic pomfret, *Brama brama*, also known by a variety of other common names, infected with plerocercoids of *Gymnorhynchus gigas* and preferred by some Portuguese [99]. Recently, the rat and mouse were orally inoculated with plerocercoids of *G. gigas* to test for anti-worm IgG, M, and A (H + L) levels in intestinal fluids and serum as well as specific serum IgE levels by enzyme-linked immunosorbent assay (ELISA) [190]. Levels of all increased in the challenged mouse, producing distress. The rat had an increased expression of

heat shock proteins in the intestine and spleen. Repeated exposure to the worm in the rodents produced clinical signs appearing progressively more rapid and lasting longer, suggesting that feeding on infected fish triggered production of anaphylactic-type antibodies in rat, mouse, and, by implication, human.

Management, Control, and Treatment of Parasites Affecting People

Management

Management starts with education about parasites. Parasites are or may be involved with a recognized or unrecognized problem but are not necessarily harmful or bad, if certain practices are recognized or followed by regulating agencies, funding agencies, the seafood industry, consumers, and those using marine waters for occupation or recreation. Harm can be done if partial data deludes people not to eat seafood or not to enter the water.

Being alerted to public health risks allows people to make choices about what product to eat, how it should be prepared, when to avoid a product, when not to enter specific bodies of water, and when to visit a physician. If the industry provides a safe and sanitary product to its customers, the number of customers will increase.

Control

The best way for processors and restaurants to control infections with most helminths and most protozoans is to freeze or heat the product. Some restaurants flash-freeze products sold as fresh to avoid infective products, and apparently few customers can detect the difference from the never frozen products. If products with few or no parasites can be provided to these groups by fishermen or fish farmers, that product will be in higher demand, able to meet regulations, and more valuable. Controlling infections by interrupting a parasite life history link and harvesting from a noninfected region are easy ways to avoid future problems.

Heating and Freezing

Historically, the US Food and Drug Administration (FDA) [191] has recommended food-service industries to cook fish products to an internal temperature of at least 63°C by conventional methods or to an internal temperature of 74°C by a microwave process rotated midway through the process and allowed to stand for 2 min afterward. Any process sufficient to kill bacterial pathogens also will kill parasites.

However, the FDA, under the seafood Hazard Analysis and Critical Control Point (HACCP) regulations, will allow for a facility to submit to it an alternative proposal with justification to modify the recommendations. When ten specimens of *Anisakis simplex* sensu lato were embedded into an approximate 1.8-cm-thick portion of a fillet of the arrowtooth flounder (*Atheresthes stomias*) and microwaved, the viability of the worms was assessed. Survival was determined as 31% at 60°C, 11% at 65°C, 3% at 74°C, and 0% at 77°C [192]. Thick salmon fillets with *Diphyllobothrium* spp. and *Anisakis* spp. require additional cooking. Microwaving pork chops with *Trichinella spiralis* still had active juveniles at 82°C, and microwaving can produce temperatures differing by 20°C when measured just 1 cm apart. The purpose of HACCP Regulation, as implemented in 1997, is for processors of fish and fisheries products to develop and implement reasonable plans for safe and sanitary procedures. Recommendations are established at each point that specific parasites can be detected, eliminated, or treated, and FDA will guide and work with those people and facilities in the industry to provide their specific appropriate plans and systems (www.fda.gov/Food/FoodSafety).

Freezing infected fisheries products is also not clear because the effectiveness depends on the temperature of the process, the length of time undergoing freezing, the length of time held frozen, the fat content of the product, and the species and stage of the parasite. For example, most cestode plerocercoids are more susceptible to freezing than nematode juveniles, which in turn are more susceptible than encysted trematode metacercariae. FDA recommends the following: freezing and storing at −20°C or below for 7 days, freezing at −31°C or below until solid and then storing at that temperature for 15 h, or at −4°C for 24 h. The fishing industry has used a process called "blast freezing," which rapidly reduces the temperature to −40°C, and it has shown to effectively kill parasites and not have much influence on flavor or texture of the product. Also, most US sushi bars freeze their fish [1].

Other communities have different recommendations or regulations. The European Food Safety Authority presented a scientific opinion on food safety related to parasites in fishery products [193]. The presence of *Anisakis* was of major concern for products intended for marinating, salting, and eating fresh. Treatments should provide an equivalent level of protection as freezing at −20°C for ≥24 h, at −35°C for ≥15 h, or −15°C for ≥96 h at the product's core; heat treatment should be >60°C for at least 1 min. These are less rigorous than those in the USA but more than some other regulations. Emphasis focused on the insufficiency of many traditional marinating and cold-smoking methods to kill the juvenile worms. Some metacercariae can tolerate more-harsh temperatures and treatments than other parasites.

Detection of Parasites and Culling

Large parasites and those that contrast well with the infected seafood product are those most easy to detect. Many of these are not harmful to consumers, but they will have an influence on whether consumers will purchase the products or eat them in a "raw" state. Some, such as *Anisakis* spp. and *Pseudoterranova* spp., constitute a public health risk, and these have attracted research in detection methodology. The efficiency of successively more accurate methods for detecting these nematodes range from (1) gross visual inspection, (2) candling on a light table, (3) candling of belly flaps (ventral portion of fish), (4) ultraviolet illumination (UV) of frozen fillets, (5) pepsin/hydrochloric acid degradation, and (6) UV illumination of frozen remains [194]. Candling or passing a product over a light table, either sandwiched between two glass or plastic plates, sliced fillet, or whole fillet, has been a popular method for several decades and usually the recommended method during industrial processing of marine fish intended for human consumption. European Union regulation 91/493/EEC and Norwegian fish quality regulations require removal of any visible parasites seen in gross inspection of commercial products by spot checking [194]. The more efficient methods indicated above are occasionally used for scientific purposes, and in one article [194] examining Norwegian spawning herring, mackerel, and blue whiting from the Northeast Atlantic Ocean for nematode juveniles in fillets, the detection efficiency for candling was 10% or less. After testing with the other listed methods, the highest values were obtained with UV illumination of remains after enzymatic digestion. Size and thickness of fillet as well as texture and color of flesh influence the efficiency. Pressing 2–3 mm layers of fillet with a hydraulic and manual press between 12-mm-thick acryl glass sheets, deep-freezing the removed cake in a plastic bag, and examining the sample in the bag with UV light at 366 nm more than doubles the recovery rate of candling at 1,500 lx; this method is rapid and good for surveys [195]. Imaging spectroscopy provides a promising method to detect spectral and spatial information from nematodes in cod as deep as 0.8 cm below the surface of the fillet. That is deeper than can be determined by manual inspection, but the instrumentation has not been perfected enough for commercial use [196].

Fish Farming Practices

In Europe, apart from farmed Atlantic salmon, sufficient monitoring data on marine products are not available [193]. A wealth of information occurs in the literature and on Internet sites about how to detect and treat parasites and control infections, usually with focus on health of the cultured product rather than on a human consuming or coming into contact with the product. This chapter does not recommend or discuss the numerous specific methods for use in fish farms and other aquaculture operations, but parasites are best managed in those facilities by breaking the link in the life cycle that can disrupt or eliminate the infections. Fish in culture can have more or fewer parasites than wild products, and the degree relates to several factors [1].

Treatment

This chapter mentions a few chemotherapeutic treatments for infected patients but purposely does not attempt to provide compounds for all taxa. People are becoming resistant to some compounds, some compounds have serious side effects, the Internet contains both good and poor or misleading advice, and new compounds are continually being tested or made available. Because a reader should use or recommend the

most reliable treatment for the agent or strain, the reader should seek professional advice. Recent information has been compiled such as that found in the most recent edition by Garcia listed in the "Books and Reviews" or some other recent source. The Centers for Disease Control and Prevention (CDC) has a website with much helpful information and a willingness to respond to individuals that contact it. On the other hand, methods to avoid infections by properly freezing or cooking a product occur above. Of course, because of well-entrenched customs, the wonderful flavor of raw or specially prepared seafood, and the lack of knowledge about most parasites, inadequately prepared and uncooked products will always pose a risk of infection.

Future Directions

As seen already in this chapter, a wealth of information has been acquired in the last few decades regarding parasites that pose a public health risk. Many questions remain unanswered and lifetimes of research will be required to answer these and additional questions regarding the risks and what to do about them. Some of the suggested paths for future research occur below in five overlapping categories:

1. Harmful parasites presently unknown or unrecognized still need to be discovered. Because of new cuisines, opportunities to get infected, methods to characterize agents, and methods to detect agents as well as variability in human responses to parasites, those parasites need to be determined that are capable of infecting humans. As seafood products are overfished or the consumers increase in number, seafood products need to come from new areas or new products. Consequently, the risk for acquiring an infection from a product historically recognized as safe increases without the consumer's knowledge. Protozoans cannot be seen without a microscope, and infections by marine species and freshwater species flushed into the marine environment are being recognized as important agents affecting human health, and the marine environment probably contains many more of these than recognized.
2. An improvement in taxonomy of many parasitic groups will allow the scientific community and public to know what species or genotypes are involved with diseases in different areas resulting from different parasite life histories. Morphologically similar species can elicit entirely different responses, and the knowledge of what specific agents are where and what signs of disease result from which of those agents comprises a fundamental cornerstone of biology and research. Taxonomic research will involve morphological treatment of quality specimens from both humans and natural hosts backed up with corresponding molecular characteristics. Molecular tools (PCR, quantitative PCR, sequence analysis, and other techniques) allow better detection and diagnosis of some of these parasites and consequently improve our understanding of the epidemiology of human infections, the geographic range of the agents, the hosts of the agents, and the longevity of the parasites. Taxonomic studies matching genetic sequences with corresponding morphological data help identify or establish sister and cryptic (closely related) species or strains. This is true for helminths as well as protozoan groups as indicated in the discussion of specific taxa. In addition to needing supplemental molecular research on taxonomy, identifications, and diagnoses, molecular tools will help determine/confirm life cycles, life histories, mechanisms of pathogenesis of infections, and approaches to manage, control, and treat the specific agents.
3. Once specific agents are characterized, methods to detect and diagnose them need improvement, especially by noninvasive means. This is especially important because many parasites do not mature in humans, thereby not allowing the detection of diagnostic eggs, cysts, and spores in the feces or blood. Even when parasites do mature in patients, they cannot always be specifically identified. For example, most heterophyids have very similar eggs, and biological variation occurs for each species. Cross-reactivity occurs in many of the present serological and molecular assays. In the case of *Paracapillaria philippinensis*, there is a need to identify juvenile stages as well as serologic or other diagnostic methods to assess infections when eggs and adult specimens are not apparent in fecal examinations. Improved molecular assays could also

detect specific infected fishes in specific locations that are responsible for most of the resulting human infections. More sensitive methods are necessary to detect general and specific isolates of *Cryptosporidium*, *Giardia*, and *T. gondii* in bivalves, where some unknown and nonremovable components inhibit the presently used PCR reactions [168]. As indicated above, many more protozoans probably infect humans, and new methods will allow their detection.

4. Surveillance methods of known agents require improvement so that infections can be reduced, and causes can be detected. In Europe, the EFSA recommends coordinated studies to improve and implement surveillance and diagnostic awareness of allergic reactions to parasites in fishery products and encourages epidemiological studies throughout Europe to assess the impact of *Anisakis* on human-associated disease, including all allergic forms [193]. All surveillance programs in the marine environment are in an early stage of research, and many could be implemented in conjunction with microbiological studies involved with maintaining healthy waters.
5. There is a need to create ways to avoid parasitic infections without having to reduce seafood consumption or reduce time spent in the water for recreation or occupation. The spread of information in a subtle manner should definitely reduce parasite infections in most countries today. On the other hand, this can be difficult when an improved economy in areas such as Vietnam have increased the social activities that are conducive to eating more raw seafood because it is "healthier when eaten raw" and acquiring more parasites. Also, global climate changes can affect infections as exemplified earlier for the peoples of Hokkaido Island, Japan, who understood parasitic infections and depended on their seafood products.

A few causes for human infection by zoonotic parasites that seem correctable by means other than spreading knowledge about specific parasites include unsanitary defecation habits, use of human excreta as fertilizer, inadequate sewerage systems, and inadequate aquaculture practices. New ideas associated with acquired knowledge about infective parasites and their life histories can contribute to modifications in sources of products and methods of complex food consumption and cooking habits. The latter include economic and sociocultural factors such as beliefs and tradition. Examples of traditional dishes in addition to those already mentioned include raw or partially cooked aquatic products such as raw crab soaked in soy sauce (ke-jang, Korea), raw drunken crabs and raw grass carp in China, and raw fish in Thailand (Koi-pla [raw fish with chopped garlic, lemon juice, chili, rice, and vegetables] and pla som). In contrast, in some industrialized countries like Japan, where eating raw fish is widespread, infections can be coupled with foreign travel and with eating imported foods or exotic delicacies.

Acknowledgments

I thank Janet Wright for help with organization of the literature and Kim Overstreet and Jean Jovonovich for reading the draft. Some of the figured histological sections are from the author's old photographs taken of slides in the collection of the late Paul C. Beaver at Tulane Medical School. The review is based on work supported by USDC, NOAA, award no. NA08NOS4730322 and subaward no. NA17FU2841, the NSF under grant no. 0529684, and US Wildlife, Fisheries, and Parks, CIAP, award M10AF2015, MS.R. 798.

Bibliography

Primary Literature

1. Deardorff TL, Overstreet RM (1991) Seafood-transmitted zoonoses in the United States: the fishes, the dishes, and the worms. In: Ward DR, Hackney CR (eds) Microbiology of marine food products. Van Nostrand Reinhold, New York, pp 211–265
2. Fischler C (2002) Food selection and risk perception. In: Anderson GH, Blundell J, Chiva M (eds) Proceedings from the symposium food selection, from genes to culture. Danone Inst., Paris, France, pp 135–151
3. Adl SM, Simpson AGB, Farmer MA, Andersen RA, Anderson OR, Barta JR, Taylor FJR (2005) The new higher level classification of Eukaryotes with emphasis on the taxonomy of protists. J Eukaryot Microbiol 52:399–451
4. Nawa Y, Hatz C, Blum J (2005) Sushi delights and parasites: the risk of fishborne and foodborne parasitic zoonoses in Asia. Clin Infect Dis 41:1297–1303
5. Ishikura H, Takahashi S, Yagi K, Nakamura K, Kon S, Matsuura A, Sato N, Kikuchi K (1998) Epidemiology: global aspects of

anisakidosis. In: Tada I, Kojima S, Tsuje M (eds), ICOPA IX 9th International Congress of Parasitology, Bologna, Italy, pp 379–382
6. Kuchta R, Scholz T, Brabec J, Bray RA (2008) Suppression of the tapeworm Order Pseudophyllidea (Platyhelminthes: Eucestoda) and the proposal of two new orders, Bothriocephalidea and Diphyllobothriidea. Int J Parasitol 38:49–55
7. Chung PR, Wm S, Jung Y, Pai SH, Nam MS (1997) Five human cases of *Diphyllobothrium latum* infection through eating raw flesh of redlip mullet, *Liza haematocheila*. Korean J Parasitol 35:283–289, Article in Korean
8. Rausch RL, Adams AM, Margolis L (2010) Identity of *Diphyllobothrium* spp. (Cestoda: Diphyllobothriidae) from sea lions and people along the Pacific coast of South America. J Parasitol 96:359–365
9. Baer KG (1969) *Diphyllobothrium pacificum*, a tapeworm from sea lions endemic in man along the coastal area of Peru. J Fish Res Board Can 126:717–723
10. Adams AM, Rausch RL (1997) Diphyllobothriasis. In: Connor DH, Chandler FW, Schwartz DA, Manz HF (eds) Pathology of infectious diseases, vol II, Appleton and Lange. Stamford, Connecticut, pp 1377–1389
11. Yamane Y, Shiwaku K (2003) *Diphyllobothrium nihonkaiense* and other marine-origin cestodes. Prog Med Parasitol Jpn 8:245–259, Meguro Parasitological Museum (Tokyo)
12. Scholz T, Garcia HH, Kuchta R, Wicht B (2009) Update on the human broad tapeworm (Genus *Diphyllobothrium*), including clinical relevance. Clin Microbiol Rev 22:146–160
13. Arizono N, Yamada M, Fukumoto S, Nakamura-Uchiyama F, Ohnishi K (2009) Diphyllobothriasis associated with eating raw pacific salmon. Emerg Infect Dis 15:866–870
14. Wicht B, Scholz T, Peduzzi R, Kuchta R (2008) First record of human infection with the tapeworm *Diphyllobothrium nihonkaiense* in North America. Am J Trop Med Hyg 78: 235–238
15. Wicht B, de Marval F, Peduzzi R (2007) *Diphyllobothrium nihonkaiense* (Yamane et al., 1986) in Switzerland: first molecular evidence and case reports. Parasitol Int 56: 195–199
16. Yamasaki H, Kuramochi T (2009) A case of *Diphyllobothrium nihonkaiense* infection possibly linked to salmon consumption in New Zealand. Parasitol Res 105:583–586
17. Margolis L, Rausch RL, Robertson E (1973) *Diphyllobothrium ursi* from man in British Columbia – first report of this tapeworm in Canada. Canadian J Public Health 64:588–589
18. Rausch RL, Adams AM (2000) Natural transfer of helminths of marine origin to freshwater fishes, with observations on the development of *Diphyllobothrium alascense*. J Parasitol 86:319–327
19. Chung DI, Kong HH, Moon CH, Choi DW, Kim TH, Lee DW, Park JJ (1995) The first human case of *Diplogonoporus balaenopterae* (Cestoda: Diphyllobothriidae) infection in Korea. Korean J Parasitol 33:225–230
20. Clavel A, Bargues MD, Castillo JF, Rubio MD, Mas-Coma S (1997) Diplogonoporiasis presumably introduced into Spain: first confirmed case of human infection acquired outside the Far East. Am J Trop Med Hyg 57:317–320
21. Arizono N, Fukumoto S, Tademoto S, Yamada M, Uchikawa R, Tegoshi T, Kuramochi T (2008) Diplogonoporiasis in Japan: genetic analyses of five clinical isolates. Parasitol Int 57: 212–216
22. Skeríková A, Brabec J, Kuchta R, Jiménez J, García HH, Scholz T (2006) Is the human-infecting *Diphyllobothrium pacificum* a valid species or just a South American population of the holarctic fish broad tapeworm, *D. latum*? Am J Trop Med Hyg 75:307–310
23. Holiday DM, Guillin S, Richardson DJ (2003) Diphyllobothriasis of the Chiribaya culture (700–1476 AD) of southern Peru. Comp Parasitol 70:167–171
24. Kamo H (1981) Present situation of human diphyllobothriasis in Japan. Yonago Acta Med 25:144–155
25. Chai J-Y (2007) Intestinal flukes. In: Murrell KD, Fried B (eds) Food-borne parasitic zoonoses: fish and plant-borne parasites. Springer, New York, pp 53–115
26. Chai JY, Lee SH (2002) Food-borne intestinal trematode infections in the Republic of Korea. Parasitol Int 51:129–154
27. Cho S-H, Cho P-Y, Lee D-M, Kim T-S, Kim I-S, Hwang E-J, Na B-K, Sohn W-M (2010) Epidemiological survey on the infection of intestinal flukes in residents of Muan-gun, Jeollanam-do, the Republic of Korea. Korean J Parasitol 48:133–138
28. Dung DT, De NV, Waikagul J, Dalsgaard A, Chai JY, Sohn WM, Murrell KD (2007) Fishborne intestinal zoonotic trematodiasis, Vietnam. Emerg Infect Dis 13:1828–1833
29. Vo DT, Murrell D, Dalsgaard A, Bristow G, Nguyen DH, Bui TN, Vo DT (2008) Prevalence of zoonotic metacercariae in two species of grouper, *Epinephelus coioides* and *Epinephelus bleekeri*, and flathead mullet, *Mugil cephalus*, in Vietnam. Korean J Parasitol 46:77–82
30. Perry B, Sones K (2007) Poverty reduction through animal health. Science 315:333–334
31. Yang J-J, Guk S-M, Han E-T, Chai J-Y (2000) Molecular differentiation of three species of *Metagonimus* by simple sequence repeat anchored polymerase chain reaction (SSR-PCR) amplification. J Parasitol 86:1170–1172
32. Font WF, Overstreet RM, Heard RW (1984) Taxonomy and biology of *Phagicola nana* (Digenea: Heterophyidae). Trans Am Microscop Soc 103:408–422
33. Overstreet RM (1978) Marine maladies? Worms, germs, and other symbionts from the northern Gulf of Mexico. Mississippi-Alabama sea grant consortium, MASGP-78-021, Blossman Printing, Ocean Springs, MS, 140p
34. Welberry AE, Pacetti W (1954) Intestinal fluke infestation in a native Negro child. Bull Dade County Med Assoc 24(34):45
35. Adams KO, Jungkind JL, Bergquist EJ, Wirts CW (1986) Intestinal fluke infection as a result of eating sushi. Am J Clin Pathol 86:688–689
36. Youssef FG, Mikhail EM, Mansour NS (1989) Intestinal capillariasis in Egypt: a case report. Am J Trop Med Hyg 40:195–196

37. Mitchell AJ, Overstreet RM, Goodwin AE, Brandt TM (2005) Spread of an exotic fish-gill trematode: a far-reaching and complex problem. Fisheries 30(8):11–15
38. Africa CM, de Leon W, Garcia EY (1940) Visceral complications of intestinal heterophyidiasis of man. Monographic series no. 1, University of the Philippines, Manila
39. Kean BH, Breslau RC (1964) Cardiac heterophyidiasis. In: Parasites of the Human Heart. Grune and Stratton, New York, pp 95–103
40. Deschiens R, Collomb H, Demarchi J (1958) Distomastose cerebrale a *Heterophyes heterophyes*. In: Abstracts of the sixth international congress of tropical medicine and malaria. Lisbon
41. Paperna I, Overstreet RM (1981) Parasites and diseases of mullets (Mugilidae). In: Oren OH (ed) Aquaculture of grey mullets. Cambridge University Press, Cambridge, pp 411–493
42. Heard RW, Overstreet RM (1983) Taxonomy and life histories of two North American species of "*Carneophallus*" (= *Microphallus*) (Digenea: Microphallidae). Proc Helminthol Soc Wash 50:170–174
43. Eastburn RL, Fritsche TR, Terhune CA Jr (1987) Human intestinal infection with *Nanophyetus salmincola* from salmonid fishes. Am J Trop Med Hyg 36:586–591
44. Chai J-Y, Han E-T, Park Y-K, Guk S-M, Lee S-H (2001) *Acanthoparyphium tyosenense*: the discovery of human infection and identification of its source. J Parasitol 87:794–800
45. Little JW, Hopkins SH, Schlicht FG (1966) *Acanthoparyphium spinulosum* (Trematoda Echinostomatidae) in oysters at Port Isabel. Texas J Parasitol 52:663
46. Guk S-M, Kim J-L, Park J-H, Chai J-Y (2007) A human case of *Plagiorchis vespertilionis* (Digenea: Plagiorchiidae) infection in the Republic of Korea. J Parasitol 93:1225–1227
47. Justo MCN, Tortelly R, Menezes RC, Kohn A (2008) First record in South America of *Didymosulcus palati* and *Didymosulcus philbranchiarca* (Digenea, Didymozoidae) with new hosts records and pathological alterations. Mem Inst Oswaldo Cruz 103:207–210
48. Murrell KD, Pozio E (2000) Trichinellosis: the zoonosis that won't go quietly. Int J Parasitol 30:1339–1349
49. Rausch R, Babero BB, Rausch RV, Schiller EL (1956) Studies on the helminth fauna of Alaska. XXVII. The occurrence of larvae of *Trichinella spiralis* in Alaskan mammals. J Parasitol 42:259–271
50. Leclair D, Forbes LB, Suppa S, Proulx J-F, Gajadhar AA (2004) A preliminary investigation on the infectivity of *Trichinella* larvae in traditional preparations of walrus meat. Parasitol Res 93:507–509
51. Pozio E, La Rosa G, Rossi P, Fico R (1989) Survival of *Trichinella* muscle larvae in frozen wolf tissue in Italy. J Parasitol 75:472–473
52. Proulx J-F, MacLean JD, Gyorkos TW, Leclair D, Richter AK, Serhir B, Forbes L, Gajadhar AA (2002) Novel prevention program for trichinellosis in Inuit communities. Clin Infect Dis 34:1508–1514
53. Margolis HS, Middaugh JP, Burgess RD (1979) Arctic trichinosis: two Alaskan outbreaks from walrus meat. J Infect Dis 139:102–105
54. Forbes LB, Measures L, Gajadhar A, Kapel C (2003) Infectivity of *Trichinella nativa* in traditional northern (country) foods prepared with meat from experimentally infected seals. J Food Prot 66:1857–1863
55. Moravec F (2001) Redescription and systematic status of *Capillaria philippinensis*, an intestinal parasite of human beings. J Parasitol 87:161–164
56. Lu L-H, Lin M-R, Choi W-M, Hwang K-P, Hsu Y-S, Bair M-J, Liu J-D, Want T-E, Liu T-P, Chung W-C (2006) Human intestinal capillariasis (*Capillaria philippinensis*) in Taiwan. Am J Trop Med Hyg 74:810–813
57. Saichua P, Nithikathkul C, Kaewpitoon N (2008) Human intestinal capillariasis in Thailand. World J Gastroenterol 14:506–510
58. Cross JH (1992) Intestinal capillariasis. Clin Microbiol Rev 5:120–129
59. Beaver PC, Theis JH (1979) Dioctophymatid larval nematode in a subcutaneous module from man in California. Am J Trop Med Hyg 28:206–212
60. Le Bailly M, Leuzinger U, Bouchet F (2003) Dioctophymidae eggs in coprolites from Neolithic site of Arbon-Bleiche 3 (Switzerland). J Parasitol 89:1073–1076
61. Moore JG, Fry GF, Englert E Jr (1969) Thorny-headed worm infection in North American prehistoric man. Science 163:1324–1325
62. Schmidt GD (1971) Acanthocephalan infections of man, with two new records. J Parasitol 57:582–584
63. Tada I, Otsuji Y, Kamiya H, Mimori T, Sakaguchi Y, Makizumi S (1983) The first case of a human infected with an acanthocephalan parasite, *Bolbosoma* sp. J Parasitol 69: 205–208
64. Nuorteva P (1966) *Corynosoma strumosusm* (Rudolphi) and *C. semerne* (Forssell) (Acanthocephala) as pathogenic parasites of farmed minks in Finland. J Helminthol 40:77–80
65. Buckner RL, Overstreet RM, Heard RW (1978) Intermediate hosts for *Tegorhynchus furcatus* and *Dollfusentis chandleri* (Acanthocephala). Proc Helminthol Soc Wash 45:195–201
66. Hitchcock DJ (1950) Parasitological study on the Eskimos in the Bethel area of Alaska. J Parasitol 36:232–234
67. Berland B (1961) Nematodes from some Norwegian marine fishes. Sarsia 2:1–50
68. Davey JT (1971) A revision of the genus *Anisakis* Dujardin, 1845 (Nematodes: Ascaridata). J Helminthol 45:51–72
69. Mattiucci S, Nascetti G, Cianchi R, Paggi L, Arduino P, Margolis L, Brattey J, Webb SC, D'Amelio S, Orecchia P, Bullini L (1997) Genetic and ecological data on the *Anisakis simplex* complex with evidence for a new species (Nematoda, Ascaridoidea, Anisakidae). J Parasitol 83:401–416
70. Mattiucci S, Nascetti G (2008) Advances and trends in the molecular systematics of anisakid nematodes, with implications for their evolutionary ecology and host-parasite co-evolutionary processes. Adv Parasitol 66:47–148

71. Yoshimura H, Akao N, Kondo K, Ohnishi Y (1979) Clinicopathological studies on larval anisakiasis, with special reference to the report of extra-gastrointestinal anisakiasis. Jap J Parasitol 28:347–354
72. Køie M, Berland B, Burt MDB (1995) Development to third-stage larvae occurs in the eggs of *Anisakis simplex* and *Pseudoterranova decipiens* (Nematoda, Ascaridoidea, Anisakidae). Can J Fish Aquat Sci 52:134–139
73. Yoshinaga T, Kinami R, Hall KA, Ogawa K (2006) A preliminary study on the infection of anisakid larvae in juvenile greater amberjack *Seriola dumerili* imported from China to Japan as Mariculture seedlings. Fish Pathol 41:123–126
74. Sakanari JA, McKerrow JH (1989) Anisakiasis. Clin Microbiol Rev 2:278–284
75. Audicana MT, Kennedy MW (2008) *Anisakis simplex*: from obscure infectious worm to inducer of immune hypersensitivity. Clin Microbiol Rev 21:360–379
76. Puente P, Anadón AM, Rodero M, Romarís F, Ubeira FM, Cuéllar C (2008) *Anisakis simplex*: the high prevalence in Madrid (Spain) and its relation with fish consumption. Exp Parasitol 118:271–174
77. Torres P, Jercic MI, Weitz JC, Dobrew EK, Mercado RA (2007) Human pseudoterranovosis, an emerging infection in Chile. J Parasitol 93:440–443
78. Bowen WD (1990) Population biology of sealworm (*Pseudoterranova decipiens*) in relation to its intermediate and seal hosts. Canadian Bulletin of Fisheries and Aquatic Sciences 222. Canadian Government Publishing, Canada
79. Jackson CJ, Marcogliese DJ, Burt MDB (1997) Role of hyperbenthic crustaceans in the transmission of marine helminth parasites. Can J Fish Aquat Sci 54:815–820
80. Ishikura H, Takahashi S, Sato N, Matsuura A, Nitto H, Tsunokawa M, Kikuchi K (1996) Epidemiology of anisakidiosis and related human diseases and studies on parasites infecting marine mammals, fishes and squids. Bull Mar Biomed Inst Sapporo Med Univ 3:23–37
81. Fagerholm H-P, Overstreet RM (2008) Ascaridoid nematodes: *Contracaecum, Porrocaecum*, and *Baylisascaris*. In: Atkinson CT, Thomas JN, Hunter DB (eds) Parasitic diseases of wild birds. Wiley-Blackwell, Ames, pp 413–433
82. Im KI, Shin HJ, Yoag TS (1989) Twenty cases of gastric anisakiasis. Korean J Parasitol 27:323 (Abstract, in Korean)
83. Vidal-Martinez VM, Osorio-Sarabia D, Overstreet RM (1994) Experimental infection of *Contracaecum multipapillatum* (Nematoda: Anisakinae) from Mexico in the domestic cat. J Parasitol 80:576–579
84. Petter AJ (1969) Enquête sur les nématodes des sardines pêchées dans la région nantaise. Rapport possible avec les granulomes éosinophiles observés chez l'homme dans la région. Ann Parasitol Hum Comp 44:25–35
85. Petter AJ (1969) Enquête sur les nematodes des sardines pêchées dans la région nantaise. Identification des larves d'ascarides parasitant les sardines (en rapport avec les granulomes éosinophiles observes chez l'homme dans la région). Ann Parasitol Hum Comp 44:559–579
86. Overstreet RM, Meyer GW (1981) Hemorrhagic lesions in stomach of rhesus monkey caused by a piscine ascaridoid nematode. J Parasitol 67:226–235
87. Deardorff TL, Overstreet RM (1981) Larval *Hysterothylacium* (=*Thynnascaris*) (Nematoda: Anisakidae) from fishes and invertebrates in the Gulf of Mexico. Proc Helminthol Soc Wash 48:113–126
88. Gonzales L (1998) Experimental infection of mice with *Hysterothylacium aduncum* (Nematoda: Anisakidae) larvae from marine-farmed trout in Chile. Arch Med Vet 30:139–142
89. Yagi K, Nagasawa K, Ishikura H, Nakagawa A, Sato N, Kikuchi K, Ishikura H (1996) Female worm *Hysterothylacium aduncum* excreted from human: a case report. Jpn J Parasitol 45:12–23
90. Deardorff TL, Kliks MM, Desowitz RS (1983) Histopathology induced by larval *Terranova* (Type HA) (Nematoda: Anisakinae) in experimentally infected rats. J Parasitol 69:191–195
91. Nawa Y (1991) Historical review and current status of gnathostomiasis in Asia. Southeast Asian J Trop Med Public Health 22(Suppl):217–219
92. Diaz Camacho SP, Zazueta-Ramos M, Ponce-Torrecillas E, Osuna Ramirez I, Castro Velazquez R, Flores Gaxiola A, Baquera Heredia J, Willms K, Akahane H, Ogata K, Nawa Y (1998) Clinical manifestations and immunodiagnosis of gnathostomiasis in Culiacan, Mexico. Am J Trop Med Hyg 59:908–915
93. Schmutzhard E, Boongird P, Vejjajiva A (1988) Eosinophilic meningitis and radiculomyelitis in Thailand, cause by CNS invasion of *Gnathostoma spinigerum* and *Angiostrongylus cantonensis*. J Neurol Neurosurg Psychiatry 51:80–87
94. Elzi L, Decker M, Battegay M, Rutishauser J, Blum J (2004) Chest pain after travel to the tropics. Lancet 363:1198
95. Ko R (1976) Experimental infection of mammals with larval *Echinocephalus sinensis* (Nematoda: Gnathostomatidae) from oysters (*Crassostrea gigas*). Can J Zool 54:597–609
96. Ko R (1977) Effects of temperature acclimation on infection of *Echinocephalus sinensis* (Nematoda: Gnathostomatidae) from oysters to kittens. Can J Zool 55:1129–1132
97. Goto Y, Tamura A, Ishikawa O, Miyachi Y, Ishii T, Akao N (1998) Creeping eruption caused by a larva of the suborder Spirurina type x. Br J Dermatol 139:315–318
98. Overstreet RM (2005) Medical importance: Infection by the rat lungworm, *Angiostrongylus cantonensis*. In: Rohde K (ed) Marine parasitology. CSIRO Publishing, Collingwood, Victoria, Australia, pp 442–446, 556–557
99. Overstreet R (2003) Flavor buds and other delights. J Parasitol 89:1093–1107
100. Measures LN (1988) Revision of the genus *Eustrongylides* Jägerskiöld, 1909 (Nematoda: Dioctophymatoidea) of piscivorous birds. Can J Zool 66:885–895
101. Mitchell AJ, Overstreet RM, Goodwin AE (2009) *Eustrongylides ignotus* infecting commercial bass, *Morone chrysops* female X *Morone saxatilis* male, and other fish in the southeastern USA. J Fish Dis 32:795–799
102. Beaver PC, Otsuji T, Otsuji A, Yoshimura H, Uchikawa R, Sato A (1983) Acanthocephalan, probably *Bolbosoma*, from

the peritoneal cavity of man in Japan. Am J Trop Med Hyg 32:1016–1018
103. Choi C-J, Lee H-J, Go J-H, Park Y-K, Chia J-Y, Seo M (2010) Extraintestinal migration of *Centrorhynchus* sp. (Acanthocephala: Centrorhynchidae) in experimentally infected rats. Korean J Parasitol 48:139–143
104. Schmidt GD (1972) Acanthocephala of captive primates. In: Fiennes TW, Karker S (eds) Pathology of simian primates part II. Karger, Basel, pp 144–156
105. Dingley D, Beaver PC (1985) *Macracanthorhynchus ingens* from a child in Texas. Am J Trop Med Hyg 34:918–920
106. Overstreet RM, Self JT, Vliet KA (1985) The pentastomid *Sebekia mississippiensis* sp. n. in the American alligator and other hosts. Proc Helminthol Soc Wash 52:266–277
107. Mairena H, Solano M, Venegas W (1989) Human dermatitis caused by a nymph of *Sebekia*. Am J Trop Med Hyg 41:352–564
108. Abadi MA, Stephney G, Factor SM (1996) Cardiac pentastomiasis and tuberculosis: the worm-eaten heart. Cardiovasc Pathol 5:169–174
109. Dubey JP, Lunney JK, Shen SK, Kwok OCH, Ashford DA, Thulliez P (1996) Infectivity of low numbers of *Toxoplasma gondii* oocysts to pigs. J Parasitol 82:438–443
110. Lindsay DS, Collins MV, Mitchell SM, Cole RA, Flick GJ, Wetch CN, Lindquist A, Dubey JP (2003) Sporulation and survival of *Toxoplasma gondii* oocysts in sea water. J Eukaryot Microbiol 50:S687–S688
111. Fayer R, Dubey J, Lindsay D (2004) Zoonotic protozoa: from land to sea. Trends Parasitol 20:531–536
112. Robertson LJ (2007) The potential for marine bivalve shellfish to act as transmission vehicles for outbreaks of protozoan infections in humans: a review. Int J Food Microbiol 120:201–216
113. Lindsay DS, Phelps KK, Smith SA, Flick G, Summer SS, Dubey JP (2001) Removal of *Toxoplasma gondii* oocysts from sea water by eastern oysters (*Crassostrea virginica*). J Eukaryot Microbiol 48:S197–S198
114. Arkush KD, Miller MA, Leutenegger CM, Gardner IA, Packham AE, Heckeroth AR, Tenter AM, Barr BC, Contad PA (2003) Molecular and bioassay-based detection of *Toxoplasma gondii* oocyst uptake by mussels (*Mytilus galloprovincialis*). Int J Parasitol 33:1087–1097
115. Dubey JP, Zarnke R, Thomas JN, Wong SK, Van Bonn W, Briggs M, Davis JW, Ewing R, Mense M, Kwok OCH, Romand S, Thulliez P (2003) *Toxoplasma gondii*, *Neospora caninum*, *Sarcocystis neurona*, and *Sarcocystis canis*-like infection in marine mammals. Vet Parasitol 116:275–296
116. Miller M, Conrad P, Gardner I, Kreuder C, Mazet J, Jessup D, Dodd E, Harris M, Ames J, Worcester K, Paradies D, Grigg M (2004) An update on *Toxoplasma gondii* infections in California sea otters. Vet Parasitol 125:133–134
117. McDonald JC, Gyorkos TW, Alberton B, Maclean JD, Richer G, Juranek D (1990) An outbreak of toxoplasmosis in pregnant women in northern Quebec. J Infect Dis 161: 769–774
118. Cali A, Takvorian PM (2003) Ultrastructure and development of *Pleistophora ronneafiei* n. sp., a Microsporidium (Protista) in the skeletal muscle of an immune-compromised individual. J Eukaryot Microbiol 50:77–85
119. Fayer R (2004) Infectivity of microsporidia spores stored in seawater at environmental temperatures. J Parasitol 90:654–657
120. Slodkowicz-Kowalska A, Graczyk TK, Tamang L, Jedrzejewski S, Nowosad A, Zduniak P, Solarczyk P, Girouard AS, Majewska AC (2006) Microsporidian species known to infect humans are present in aquatic birds: implications for transmission via water? Appl Environ Microbiol 72:4540–4544
121. Santín M, Fayer R (2009) *Enterocytozoon bieneusi* genotype nomenclature based on the internal transcribed spacer sequence: a consensus. J Eukaryot Microbiol 56:34–38
122. Rhinehart HL, Townsend FI, Overstreet RM, Visvesvara GS, da Silva A, Pieniazek NJ (1996) First report of microsporidiosis in the bottlenose dolphin, *Tursiops truncatus*. Annual Conference of International Association for Aquatic Animal Medicine 27:13–14
123. Canning EU, Okamura B (2004) Biodiversity and evolution of the Myxozoa. Adv Parasitol 56:43–131
124. Moncada L, López M, Murcia M, Nicholls S, León F, Guío O, Corredor A (2001) *Myxobolus* sp., another opportunistic parasite in immunosuppressed patients? J Clin Microbiol 39: 1938–1940
125. Boreham R, Hendrick S, O'Donoghue P, Stenzel D (1998) Incidental finding of *Myxobolus* spores (Protozoa: Myxozoa) in stool samples from patients with gastrointestinal symptoms. J Clin Microbiol 36:3728–3730
126. McClelland R, Murphy D, Cone D (1997) Report of spores of *Henneguya salminicola* (Myxozoa) in human stool specimens: possible source of confusion with human spermatozoa. J Clin Microbiol 35:2815–2818
127. Lebbad M, Wilcox M (1998) Spores of *Henneguya salminicola* in human stool specimens. J Clin Microbiol 36:1820
128. Venable DL, Gaudé AP III, Klerks PL (2000) Control of the trematode *Bolbophorus confusus* in channel catfish *Ictalurus punctatus* ponds using salinity manipulation and polyculture with black carp *Mylopharyngodon piceus*. J World Aquacult Soc 31:158–166
129. Walker J (2005) Medical importance: marine schistosome dermatitis. In: Rhode K (ed) Marine parasitology. CABI, Wallingford, pp 439–442, 555–556
130. Grodhaus G, Keh B (1958) The Marine dermatitis-producing cercaria of *Austrobilharzia variglandis* in California (Trematoda: Schistosomatidae). J Parasitol 44:633–638
131. Chu GWTC, Cutress CE (1954) *Austrobilharzia variglandis* (Miller and Northup, 1926) Penner, 1953, (Trematoda: Schistosomatidae) in Hawaii with notes on its biology. J Parasitol 40:515–552
132. Stunkard HW, Hinchliffe MC (1952) The morphology and life-history of *Microbilharzia variglandis* (Miller and Northup, 1926) Stunkard and Hinchliffe, 1951, avian blood-flukes whose larvae cause "swimmer's itch" of ocean beaches. J Parasitol 38:248–265

133. Barber KE, Caira JN (1995) Investigation of the life cycle and adult morphology of the avian blood fluke *Austrobilharzia variglandis* (Trematoda: Schistosomatidae) form Connecticut. J Parasitol 81:584–592
134. Bearup AJ (1955) A schistosome larva from the marine snail *Pyrazus australis* as a cause of cercarial dermatitis in man. Med J Aust 1:955–958
135. Overstreet RM, Curran SS (2005) Parasites of the American white pelican. Gulf Caribbean Res 17:31–48
136. Brant SV, Cohen AN, James D, Hui L, Hom A, Loker ES (2010) Cercarial dermatitis transmitted by exotic marine snail. Emerg Infect Dis 16:1357–1365
137. Leigh WH (1953) *Cercaria huttoni*, sp. nov., a dermatitis-producing schistosome larva from the marine snail, *Haminoea antillarium guadalupensis* Sowerby. J Parasitol 39:625–629
138. Leigh WH (1955) The Morphology of *Gigantobilharzia huttoni* (Leigh, 1953) an avian schistosome with marine dermatitis-producing larvae. J Parasitol 41:262–269
139. Nobile L, Fioravanti ML, Pampiglione S, Calderan M, Marchese G (1996) Report of *Gigantobilharzia acotylea* (Digenea: Schistosomatidae) in silver gulls (*Larus argentatus*) of the Venice Lagoon: considerations on its possible etiological role in the human dermatitis observed in the same area. Parassitologia 38:267
140. Penner L (1953) The biology of a marine dermatitis producing schistosome cercaria from *Batillaria minima*. J Parasitol 39:19–20
141. Malek EA, Chang TC (1974) Medical and economic malacology. Academic, New York
142. Penner L (1950) *Cercaria littorinalinae* sp. nov., a dermatitis-producing schistosome larva from the marine snail, *Littorina planaxis* Philippi. J Parasitol 36:466–472
143. Ewers WH (1961) A new intermediate host of schistosome trematodes from New South Wales. Nature 190:283–284
144. Komiya Y, Ito J (1952) The morphology of *Cercaria sturniae* Tanabe, 1948 (cercaria of *Gigantobilharzia sturniae* Tanabe, 1951), a cause of cercaria dermatitis in Japan. Jpn J Med Sci Biol 5:215–220
145. Kolárová L (2007) Schistosomes causing cercarial dermatitis: a mini-review of current trends in systematics and of host specificity and pathogenicity. Folia Parasitol 54:81–87
146. Hrádková K, Horák P (2002) Neurotopic behaviour of *Trichobilharzia regenti* in ducks and mice. J Helminthol 76:137–141
147. Kolárová L, Horák P, Cada F (2001) Histopathology of the CNS and nasal infections caused by *Trichobilharzia regenti* in vertebrates. Parasitol Res 87:644–650
148. Little MD (1965) Dermatitis in a human volunteer infected with *Strongyloides* of nutria and raccoon. Am J Trop Med Hyg 14:1007–1009
149. Deardorff TL, Overstreet RM, Okihiro M, Tam R (1986) Piscine adult nematode invading an open lesion in a human hand. Am J Trop Med Hyg 35:827–830
150. Recavarren-Arce S, Velarde C, Gotuzzo E, Cabrera J (1999) Amoeba angeitic lesions of the central nervous system in *Balamuthia mandrilaris* amoebiasis. Hum Pathol 30:269–273
151. Sawyer TK, Visvesvara GS, Harke BA (1977) Pathogenic amoebas from brackish water and ocean sediments with a description of *Acanthamoeba hatchetti*, n. sp. Science 196: 1324–1325
152. Daggett P-M (1982) Protozoa from polluted waters; potential human pathogens. In: Colwell RR (ed) Microbial hazards of diving in polluted waters: a proceedings. Maryland Sea Grant Publication UM-SG-TS-82-01. University of Maryland, College Park, pp 39–42
153. Lorenzo-Morales J, Monteverde-Miranda CA, Jiménez C, Tejedor ML, Valladares B, Ortega-Rivas A (2005) Evaluation of *Acanthamoeba* isolates from environmental sources in Tenerife, Canary Islands, Spain. Ann Agric Environ Med 12:233–236
154. Fernandez M-CA, Crespo EP, Mallen MM, Ares MPMP, Casas MC (1989) Marine amoebae from waters of northwest Spain, with comments on a potentially pathogenic euryhaline species. J Eukaryot Microbiol 36:239–241
155. Ledee DR, Hay J, Byers TJ, Seal DV, Kirkness CM (1996) *Acanthamoeba griffini*: molecular characterization of a new corneal pathogen. Invest Ophthalmol Vis Sci 37:544–550
156. Lorenzo-Morales J, Coronado-Álvarez N, Martínez-Carretero E, Maciver SK, Valladares B (2007) Detection of four adenovirus serotypes within water-isolated strains of *Acanthamoeba* in the Canary Islands, Spain. Am J Trop Hyg 77:753–756
157. Mattana A, Serra C, Mariotti E, Delogu G, Fiori PL, Cappuccinelli P (2006) *Acanthamoeba castellanii* promotion of in vitro survival and transmission of coxsackie B3 viruses. Eukaryot Cell 5:665–671
158. Laskowske-Arce MA, Orth K (2008) *Acanthamoeba castellanii* promotes the survival of *Vibrio parahaemolyticus*. Appl Environ Microbiol 74:7183–7188
159. Overstreet RM, Jovonovich J, Ma H (2009) Parasitic crustaceans as vectors of viruses, with an emphasis on three penaeid viruses. Integr Comp Biol 49:127–141
160. Nuzzi R, Zaki MH (1982) Unusual health effects associated with surface waters. New York State J Med 82:1347–1349
161. Johnson D, Reynolds K, Gerba C, Pepper I, Rose J (1995) Detection of *Giardia* and *Cryptosporidium* in marine waters. Water Sci Technol 31:439–442
162. Thompson R (2004) The zoonotic significance and molecular epidemiology of *Giardia* and giardiasis. Vet Parasitol 126:15–35
163. Monis P, Andrews R, Mayrhofer G, Ey P (2003) Genetic diversity within the morphological species *Giardia intestinalis* and its relationship to host origin. Infect Genet Evol 3:29–38
164. Gaydos J, Miller W, Gilardi K, Melli A, Schwantje H, Engelstoft C, Fritz H, Conrad P (2007) *Cryptosporidium* and *Giardia* in marine-foraging river otters (*Lontra canadensis*) from the Puget Sound Georgia Basin ecosystem. J Parasitol 93:198–202

165. Olson M, Appelbee A, Measures L (2004) *Giardia duodenalis* and *Cryptosporidium parvum* infections in pinnipeds. Vet Parasitol 125:131–132
166. Gaydos J, Miller W, Jognson C, Zornetzer H, Melli A, Packham A, Jeffries S, Lance M, Conrad P (2008) Novel and canine genotypes of *Giardia duodenalis* in Harbor Seals (*Phoca vitulina richardsi*). J Parasitol 94:1264–1268
167. Johnson D, Enriquez C, Pepper I, Davis T, Gerba C, Rose J (1997) Survival of *Giardia*, *Cryptosporidium*, Poliovirus and *Salmonella* in marine waters. Water Sci Technol 35:261–268
168. Schets F, Van den Berg H, Engels G, Lodder W, de Roda HA (2007) *Cryptosporidium* and *Giardia* in commercial and non-commercial oysters (*Crassostrea gigas*) and water from the Oosterschelde, the Netherlands. Int J Food Microbiol 113:189–194
169. Lucy FE, Graczyk TK, Tamang L, Miraflor A, Minchin D (2008) Biomonitoring of surface and coastal water for *Cryptosporidium*, *Giardia*, and human-virulent microsporidia using molluscan shellfish. Parasitol Res 103:1369–1375
170. Fayer R, Graczyk T, Lewis E, Trout J, Farley C (1998) Survival of infectious *Cryptosporidium parvum* oocysts in seawater and eastern oysters (*Crassostrea virginica*) in the Chesapeake Bay. Appl Environ Microbiol 64:1070–1074
171. Bogomolni AL, Gast RJ, Ellis JC, Dennett M, Pugliares KR, Lentell BJ, Moore MJ (2008) Victims or vectors: a survey of marine vertebrate zoonoses from coastal waters of the Northwest Atlantic. Dis Aquat Org 81:13–38
172. Fayer R (2004) *Cryptosporidium*: a water-borne zoonotic parasite. Vet Parasitol 126:37–56
173. Appelbee A, Thompson R, Olson M (2005) *Giardia* and *Cryptosporidium* in mammalian wildlife – current status and future needs. Trends Parasitol 21:370–376
174. Dupont HL, Chappell CL, Sterling CR, Okhuysen PC, Rose JB, Jakubowski W (1995) The infectivity of *Cryptosporidium parvum* in healthy volunteers. N Engl J Med 332:855–859
175. Graczyk T, Marcogliese D, de LaFontaine Y, Da Sliva A, Mhangami-Ruwende B, Pieniazek N (2001) *Cryptosporidium parvum* oocysts in zebra mussels (*Dreissena polymorpha*): evidence from the St Lawrence River. Parasitol Res 87:231–234
176. Hughes-Hanks J, Rickard L, Panuska C, Saucier J, O'Hara T, Dehn L, Rolland R (2005) Prevalence of *Cryptosporidium* spp. and *Giardia* spp. in five marine mammal species. J Parasitol 91:1225–1228
177. Santín M, Dixon B, Fayer R (2005) Genetic characterization of *Cryptosporidium* isolates from ringed seals (*Phoca hispida*) in Northern Quebec, Canada. J Parasitol 91:712–716
178. Graczyk TK, Sunderland D, Awantang GN, Mashinski Y, Lucy FE, Graczyk Z, Chomicz L, Breysse PN (2010) Relationships among bather density, levels of human waterborne pathogens, and fecal coliform counts in marine recreational beach water. Parasitol Res 106:1103–1108
179. Graczyk TK, Majewska AC, Schwab KJ (2008) The role of birds in dissemination of human waterborne enteropathogens. Trends Parasitol 24:55–59
180. Ryan U (2010) *Cryptosporidium* in birds, fish and amphibians. Exp Parasitol 124:113–120
181. Armentia A, Martín-Gil FJ, Pascual C, Martín-Esteban M, Callejo A, Martínez C (2006) *Anisakis simplex* allergy after eating chicken meat. J Investig Allergol Clin Immunol 16:258–263
182. Del Pozo MD, Moneo I, Fernández de Corres L, Audicana MT, Munoz D, Fernandez E, Navarro JA, Garcia M (1996) Laboratory determinations in *Anisakis simplex* allergy. J Allergy Clin Immunol 97:977–984
183. Del Pozo MD, Audicana MT, Diez J, Muñoz I, Ansotegui IJ, Fernández E, García M, Etxenaguisa M, Monio I, Fernández de Corres L (1997) *Anisakis simplex*, a relevant etiologic factor in acute urticaria. Allergy 52:576–576
184. Audicana MT, Ansotegui IJ, Fernández de Corres L, Kennedy MW (2002) *Anisakis simplex*: dangerous – dead and alive? Trends Parasitol 18:20–25
185. Daschner A, Alonso-Gómez A, Cabañas R, Suarez-d-Parga J-M, López-Serrano M-C (2000) Gastroallergic anisakiasis: borderline between food allergy and parasitic disease – Clinical and allergologic evaluation of 20 patients with confirmed acute parasitism by *Anisakis simplex*. J Allergy Clin Immunol 105:176–181
186. Alonso-Gómez A, Moreno-Ancillo A, López-Serrano MC, Suarez-de-Parga JM, Daschner A, Caballero MT, Barranco P, Cabañas R (2004) *Anisakis simplex* only provokes allergic symptoms when the worm parasitizes the gastrointestinal tract. Parasitol Res 93:378–384
187. Takahashi S, Ishikura H, Sato M, Iwasa K (1993) Seroimmunodiagnostics of anisakiosis. Ann Rev Immunol Cyugai-Medical, Tokyo, 211–217 (in Japanese)
188. Nieuwenhuizen N, Lopata AL, Jeebhay MF, Herbert DR, Robins TG, Brombacher F (2006) Exposure to the fish parasite *Anisakis* causes allergic airway hyperreactivity and dermatitis. J Allergy Clin Immunol 117:1098–1105
189. Jeebhay MF, Robins TG, Miller ME, Bateman E, Smuts M, Baatjies R, Lopata AL (2008) Occupational allergy and asthma among salt water fish processing workers. Am J Ind Med 51:899–910
190. Vázquez-López C, de Armas-Serra C, Bernardina W, Rodríguez-Caabeiro F (2001) Oral inoculation with *Gymnorhynchus gigas* induces anti-parasite anaphylactic [sic] antibody production in both mice and rats and adverse reactions in challenge mice. Int J Food Microbiol 64:307–315
191. U.S. Food and Drug Administration (1997) Food code, sections 3–401.11 (A1) and 3–401.12. In: 1997 Recommendations of the United States Public Health Administration. U.S. Food and Drug Administration, Washington, D.C.
192. Adams AM, Miller KS, Wekell MM, Dong FM (1999) Survival of *Anisakis simplex* in microwave-processed arrowtooth flounder (*Atheresthes stomias*). J Food Prot 62:403–409
193. EFSA Panel on Biological Hazards (BIOHAZ) (2010) Scientific opinion on risk assessment of parasites in fishery products. EFSA Journal 8:1543 (91 pp)

194. Levsen A, Lunestad BT, Berland B (2005) Low detection efficiency of candling as a commonly recommended inspection method for nematode larvae in the flesh of pelagic fish. J Food Protect 68:828–832
195. Karl H, Leinemann M (1993) A fast and quantitative detection method for nematodes in fish fillets and fishery products. Arch Lebensmittelhyg 44:124–125
196. Heia K, Sivertsen AH, Stormo SK, Wold JP, Nilsen H (2007) Detection of nematodes in cod (*Gadus morhua*) fillets by imaging spectroscopy. J Food Sci 72:E11–E15

Books and Reviews

Anderson RC (2000) Nematode parasites of vertebrates: their development and transmission, 2nd edn. CABI, New York
Beaver PC, Jung RC, Cupp EW (1984) Clinical parasitology, 9th edn. Lea and Febiger, Philadelphia
Brusca RC, Brusca GJ (2002) Invertebrates, 2nd edn. Sinauer, Sunderland, MA
Coombs I, Crompton DWT (1991) A guide to human helminths. Taylor & Francis, London
Crompton DWT, Saviolo L (2007) Handbook of helminthiasis for public health. CRC Press, Boca Raton, FL
Eiras JC, Segner H, Wahli T, Kapoor BG (eds) (2008) Fish diseases, volumes 1 and 2. Science Publishers, Enfield, NH
Fayer R (2010) Taxonomy and species delimitation in *Cryptosporidium*. Exp Parasitol 124:90–97
Garcia LS (2007) Diagnostic medical parasitology, 5th edn. ASM Press, Washington, DC
Grabda J (1991) Marine fish parasitology: an outline. VCH, New York
Horák P, Kolárová L, Adema CM (2002) Biology of the schistosome genus *Trichobilharzia*. Adv Parasitol 52:155–233
Krauss H, Weber A, Appel M, Enders B, Isenbert HD, Schiefer HG, Slenczka W, von Graevenitz A, Zahner H (2003) Zoonoses: infections diseases transmissible from animals to humans, 3rd edn. ASM Press, Washington, DC
Murrell KD, Fried B (2007) World class parasites: volume 11, Foodborne parasitic zoonoses, fish and plant-borne parasites. Springer, New York
Nawa Y, Nakamura-Uchiyama F (2004) An overview of gnathostomiasis in the world. Southeast Asian J Trop Med Public Health 35(Suppl 1):87–91
Orihel TC, Ash LR (1995) Parasites in human tissues. American Society of Clinical Pathologists, Chicago
Rhode K (ed) (2005) Marine parasitology. CABI, New York
Roberts LS, Janovy J (2008) Foundations of parasitology, 8th edn. McGraw-Hill, New York
Williams H, Jones A (1994) Parasitic worms of fish. Taylor & Francis, London
Woo PTK (ed) (2006) Fish diseases and disorders vol 1: Protozoan and metazoan infections, 2nd edn. CABI, Cambridge, MA
Zhou X-N, Lv S, Yang G-J, Kristensen TK, Bergquist NR, Utzinger J, Maline JB (2009) Spatial epidemiology in zoonotic parasitic diseases: insights gained at the 1st International Symposium on Geospatial Health in Lijiang, China, 2007. Parasit Vectors 2:10–25

Weather Prediction Models

Julio T. Bacmeister
NCAR Earth System Laboratory, National Center for Atmospheric Research, Boulder, CO, USA

Article Outline

Glossary
Definition of the Problem
Introduction: Direct Simulation of Atmospheric Flows
Development of Modern NWP Models
How Are NWP Models (Versus Climate Models) Evaluated?
Initialization and Data Assimilation
Future Directions
Bibliography

Glossary

Assimilation The process of combining observations of the atmosphere with a "first guess" (usually a model forecast) to define the atmospheric state on a forecast model grid.

Geostrophic balance A possible state of rotating fluids in which flow is directed along pressure gradients rather than across them.

Gravity waves Rapidly moving atmospheric disturbances driven by gravity acting on vertical density gradients. Often arise as a consequence of spurious geostrophic imbalance in initial conditions.

Hydrostatic balance State in which the vertical pressure gradient force cancels the downward accleration of gravity. Approximately obeyed in atmospheric flows with horizontal scales larger than several km.

Instabilities (or unstable modes) Spatial patterns in a flow that are able to extract energy from the background flow and grow in amplitude.

Primitive equations Complete set of equations describing flow of a thin envelope of fluid or gas surrounding a sphere.

Resolution Separation in space of notional points at which quantities are defined in a numerical model.

Definition of the Problem

Awareness of weather and concern about weather in the proximate future certainly must have accompanied the

emergence of human self-consciousness. Although weather is a basic idea in human existence, it is difficult to define precisely. Weather intuitively refers to a set of atmospheric conditions prevailing over a relatively small area, and even more emphatically, over a relatively short time. The immediacy contained in our notion of weather may be reflected in the fact that in many languages the same root appears in the words for time and weather, for example, Spanish (*tiempo*) or Hungarian (*idö*). Thus, weather is to be distinguished from the notion of climate, or more subtly from the notion of "spells" which imply a time window anywhere from a week to several years. Our experience of weather does involve quantities which can be defined with reasonable precision. These include air temperature, wind speed, precipitation rates and types, cloud cover, and also humidity, air-quality, and barometric pressure. Numerical weather prediction (NWP) is the attempt to predict the evolution of such quantities by solving a set of partial differential equations which describe the dynamics of a fluid like the atmosphere [1, 2]. These equations must be solved using approximate or "numerical" techniques using computers. They are integrated forward in time from a set of initial conditions, which are derived from an optimized combination of observations and previous model forecasts. This bootstrapped procedure is known as the analysis cycle and is an integral part of the activities at all modern forecasting centers.

NWP and global climate simulation are closely related problems. The models used in both endeavors are essentially the same. A key difference between NWP and the climate problem is the role of atmospheric initial conditions. Initialization of the atmosphere is of secondary importance in multiyear climate simulations. However, good initialization of the atmospheric state is at the heart of the forecasting problem. Initialization must give an accurate and comprehensive representation of the state of the atmosphere that is compatible with numerical forecast model being used. The initial state must also satisfy a number of "balance constraints" to avoid spurious initial variability.

Lewis Fry Richardson (1881–1953) reported the first numerical weather forecast, performed using hand calculations, in 1922 [3]. His attempt did not succeed for reasons that are summarized below, and discussed in detail in the book by Lynch [2], but Richardson's effort marks the beginning of NWP as a field of inquiry.

Introduction: Direct Simulation of Atmospheric Flows

In order to appreciate the challenges faced by numerical models of the global atmosphere it is useful to have a sense of the complex nature of the motions which must be represented. A brief account of some of the dynamical processes that play a part in weather is given below. For more details, the reader is referred to the excellent, comprehensive introduction to the dynamics of the atmosphere and ocean by A.E. Gill (1937–1986) [4].

A Zoology of Atmospheric Motion

The atmospheric flows which are responsible for creating weather span a wide range of space and time scales and are driven by rich variety of dynamical and thermodynamic processes. Atmospheric flows may be forced by features at the Earth's surface. Mountainous terrain forces atmospheric circulations with spatial scales ranging from several kilometers to several thousand kilometers. Surface temperature contrasts, most pronounced between land and ocean but also created by variations in ground cover, force sea-breeze circulations with scales of tens of kilometers, [5] as well as continental-scale monsoonal circulations (Table 1) [6–8].

External forcing can produce wave-like motions in the atmosphere. Gravity waves, or buoyancy waves, exist because of density stratification in the atmosphere, and are analogs to waves on the surface of water. These waves are typically one to hundreds of kilometers in scale, and have periods of minutes to hours, although in the tropics both spatial and temporal scales may be longer [4]. Gravity waves may play a role in triggering convection [9–11], as well as in organizing convection in the mesoscale [10, 12, 13]. Mountain waves are large, nonlinear, gravity waves generated by flow over mountains with horizontal scales from less than ten kilometers to several hundred kilometers. Such waves are responsible for a number of local but intense winds [14]. Gravity waves are also notorious for contaminating forecasts when errors in initial conditions are present.

Weather Prediction Models. Table 1 Motions in atmosphere

Phenomenon	Spatial scale	Temporal scale	Role in weather
Acoustic waves	Meters	Seconds	None
Gravity waves	1–1,000 km	15 min to days	Initiating and organizing convection. Mountain flows, e.g., chinooks, Foehns . . .
Eastery waves	500–2,000 km	Days	Organizing tropical convection, tropical cyclogenesis
Baroclinic instability	Thousands of km	Days	Midlatitude cyclogenesis
Madden–Julian oscillation	10,000 km	20–60 days	Possible modulation of tropical and midlatitude weather

Rossby waves [4, 15–17] named after the Swedish meteorologist Carl Gustav Rossby exist because of the change in the effective rotation rate experienced by a fluid parcel as it moves from equator to pole. The effective rotation rate at the Equator is zero, since all of the effects of Earth's rotation are directed in the vertical and are felt as a slight reduction in the pull of gravity. At the poles, the effective rotation rate is as intuitively expected – one cycle or 2π radians per day. In between equator and pole, this rate varies as the sine of latitude. Rossby waves which exploit this gradient have scales of thousands to ten thousands of kilometers and periods of days to weeks. Immense planetary-scale Rossby waves or "planetary waves" generated by topographic features such as the Himalayas and Rockies, as well as, by continental-scale land-sea contrasts, dominate the tropospheric flow and are responsible for the mean position of the jet-streams, and for the mean paths of storms.

Probably more important in the overall problem of weather, and certainly more difficult to predict, is another class of flows driven by internal exchanges of energy in the atmosphere. These instabilities or unstable modes are essentially flow patterns that are able to extract energy from their surroundings and grow in amplitude. Initial growth of unstable modes is typically exponential. Familiar examples of such behavior in fluids include the growth of wind driven waves on the surface of water. The convective instability of a fluid heated from below is another example that is both familiar in everyday experience and also important in the atmosphere.

In the atmosphere, a particularly important mode of unstable growth is through baroclinic instability [18, 19]. This instability arises from a combination of thermal and inertial effects in a rotating fluid with a horizontal temperature along the lower boundary. Baroclinic instability is characterized by length scales of 1,000 km and growth times of days – making it a key factor in weather. It is fair to say that the problem of weather forecasting in midlatitudes is essentially that of predicting the evolution of baroclinically unstable modes in the atmosphere.

The tropics possess another as yet poorly understood class of motions, in which moist heating plays a key role in energizing and modifying wave motions in the atmosphere [20]. Tropical easterly waves [21] have periods of several days and scales of hundreds to thousands of kilometers and play an important role in the genesis of tropical cyclones [22–24]. The Madden–Julian oscillation or "MJO" [25, 26] is an eastward traveling disturbance in the tropics with a length scale close to 10,000 km and a period of weeks. It is thought to play a role in modulating tropical cyclone frequency in various basins [27–31] and possibly midlatitude disturbances as well [32, 33]. The dynamics behind the MJO are not yet understood. Successful forecasting of the MJO could improve prospects for accurate forecasts out to lead times of weeks [34].

Early History

Weather prediction, not climate simulation, was the original motivation for developing numerical models that describe the time evolution of the atmosphere. Richardson's 1922 attempt at NWP predates initial attempts to study climate numerical models by at least four decades. The first attempts at simulating the longer-term equilibrium state of the atmosphere did not occur until the 1960s [35].

The notion of predicting weather systematically using equations to describe the evolution of systems can probably be traced to the Norwegian meteorologist Vilhelm Bjerknes (1862–1951) [1, 2] who founded the famous "Bergen School" of meteorology [36, 37]. Bjerknes considered graphical methods to predict the motion of fronts and other features in the atmosphere, as well as numerical techniques to solve the equations themselves. However, it was L. F. Richardson who finally conceived and implemented a concrete plan to use a numerical solution of the partial differential equations describing the atmosphere (see section on "primitive equations") to make forecasts. His approach was remarkably prescient both in concept and in detail. He employed a finite-difference technique on a regularly spaced grid of points over central Europe and attempted to predict the tendency of surface pressure over 6 h. Richardson's forecast was a famous failure or "bust" (see the book by Lynch [2] for a detailed and readable account of Richardson's attempt, as well as for a comprehensive account of the development of NWP). However, the reasons for Richardson's failure lay in the initial conditions used in the forecast not in his method as Richardson himself suspected [2].

The potential for numerical prediction was clear. The major obstacle beside the question of initialization, was the sheer amount of calculation required to produce even a short forecast over a limited area. Richardson imagined computational "factories" employing thousands of people to produce weather forecasts [2]. The appearance of electronic computers soon after World War II made numerical prediction plausible. The potential application to the problem of weather prediction was recognized by one of the main intellects behind the development of electronic computers John von Neumann (1903–1957) [1]. In the first successful attempts at NWP using electronic computers so-called filtered equation sets were used [2]. Filtered equations describe a limited set of atmospheric motions, but allow large time steps to be taken in numerical integration and side step the need for well-balanced initial conditions (see sections on "Numerics and Initialization").

Development of Modern NWP Models

It was recognized early on by Jule Charney and others that models using filtered equations were not a promising long-term path for NWP [2]. As computer power increased, the limitations on the time-step length allowed by more complete equations became less important. The problem of initialization was not solved, but its tractability became apparent [38]. Development work on NWP models using the primitive equations began in the late 1950s and eventually led to the adoption of primitive equation models at all major forecasting centers by the mid 1960s [2].

The Primitive Equations

The primitive equations are essentially the complete Navier–Stokes or Euler equations for fluid motion with the hydrostatic approximation invoked. As long as the horizontal scales of interest are much larger than 10 km, the hydrostatic approximation is well satisfied. However, at the time of writing, major NWP models are reaching horizontal resolutions that test the limits of this approximation. The Euler equations using a generalized vertical coordinate η, including connections between the fully nonhydrostatic system and the hydrostatic system currently used in NWP models, are nicely described by Laprise [39].

The hydrostatic primitive equations include an equation describing the evolution of horizontal momentum or velocity V:

$$\frac{d}{dt}V + f\mathrm{k} \times V = -\alpha\nabla_\eta p - \nabla_\eta \phi + F_{phys}$$

where f is the Coriolis parameter or local apparent rotation rate and k is the unit vector in vertical direction. The symbol ∇_η denotes a gradient along surfaces of fixed η. As is common in the meteorological literature φ denotes the geopotential height or potential energy density of a fluid parcel along constant η. The remaining symbols α and p denote specific volume and pressure. This equation is simply the fluid dynamical form of Newton's law $F = ma$, where the right-hand side contains forces accelerating fluid parcels in the horizontal. In current meteorological literature, the individual velocity components are usually designated as u for the eastward or "zonal" component, and υ for the northward or "merdional" component.

Another equation restates the first law of thermodynamics $dE = dQ + dW$ in fluid form:

$$C_p \frac{d}{dt}T - \alpha\frac{d}{dt}p = H_{phys}$$

where T is the absolute temperature and C_p is the heat capacity of air at constant pressure. In both the momentum and energy equations the symbol $\frac{d}{dt}$ is used to denote:

$$\left(\frac{\partial}{\partial t}\right)_\eta + V \cdot \nabla_\eta + \dot{\eta}\frac{\partial}{\partial \eta}$$

the Lagrangian derivative that tracks changes in a quantity following a fluid parcel.

A prognostic equation for mass continuity is also required:

$$\left[\frac{\partial}{\partial t}\left(\frac{\partial p}{\partial \eta}\right)\right]_\eta + \nabla_\eta \cdot \left(V\frac{\partial p}{\partial \eta}\right) + \frac{\partial}{\partial \eta}\left(\dot{\eta}\frac{\partial p}{\partial \eta}\right) = 0$$

where $g^{-1}\frac{\partial p}{\partial \eta}$ is the mass per unit area in a column between surfaces of constant η.

Three diagnostic relationships are needed to complete the system. The equation of state for a gas:

$$p\alpha = RT$$

and a relationship that determines the geopotential height of η-surfaces:

$$\phi = \phi_s + \int_\eta^{\eta_s} \alpha \frac{\partial p}{\partial \eta'}\, d\eta$$

This relationship uses the surface geopotential height φ_s as well as the integral of the hydrostatic relationship:

$$\frac{\partial p}{\partial \eta} = \frac{1}{\alpha}\frac{\partial \phi}{\partial \eta}$$

between pressure and specific volume.

The right-hand sides of the momentum and energy equations also contain the terms F_{phys} and H_{phys}. These represent the effects of physical parameterizations on the grid scale variables, and include effects from radiative heating, friction, and other processes which will be described in more detail in the section on parameterization. The use of the generalized vertical coordinate η gives the equations a somewhat unfamiliar look. However, replacing η with the geometric height z, and noting that $\nabla_z \varphi = 0$ reduces them to a more familiar form.

Due to the complex shape of Earth's topography most NWP models do not use geometric height as their vertical coordinate. Most use a version of the so-called σ-coordinate defined by:

$$\sigma = \frac{p - p_t}{p_s(x, y, t) - p_t}$$

where $p_s(x, y, t)$ is the surface pressure and p_t is the pressure at the model top, typically a constant value. The coordinate surface $\sigma = 1$ follows the bottom of the model domain while $\sigma = 0$ follows the top. Boundary conditions on "vertical" velocity become simply $\dot{\sigma}(1) = \dot{\sigma}(0) = 0$. Thus, the difficulties of representing flow boundaries in and around topographic obstacles are replaced by the need for a prognostic equation describing π_s. This is obtained by integrating the mass continuity equation in the vertical.

The primitive equations can describe all of the motions discussed in the introduction except for fully three dimensional acoustic waves. They do allow a horizontal acoustic mode known as the Lamb wave [4] which can produce difficulties for numerical integrations. Gravity waves and convective instabilities with horizontal scales much smaller than 100 km are not well represented, and this may become a significant handicap for models in the next 10 years (see section on "Future Directions").

In addition to the equations describing the dynamics and thermodynamics of the atmosphere, modern NWP models include equations that describe the evolution of trace gases and trace species in the atmosphere. Each additional species results in an additional prognostic equation of the form:

$$\frac{d}{dt} q_i = C_{i,phys}$$

where q_i is the mixing ratio of the ith species and $C_{i,phys}$ are the sources and losses of the species. The most important of these trace quantities is water vapor. Water vapor was included in primitive equation NWP models early on [40]. As NWP model domains were extended into the tropics during the 1970s [41] strong condensational heating associated with high tropical humidities presented problems for NWP that spurred the development of deep convection parameterizations [42] (see section on "Parameterization"). More recently, NWP models have incorporated prognostic treatment of condensed water species known as prognostic cloud schemes [43, 44].

Numerics

Closed form solutions of the primitive equations do not exist. Approximate numerical techniques must be used. An illustration of how this proceeds is given here using a simple equation that describes one dimensional advection of a constituent C by a constant flow u:

$$\partial_t C + u\partial_x C = S$$

Figure 1 shows three time steps from a numerical integration of this equation. Finite-difference approximations of the partial derivatives in both space and time are calculated as shown in the figure. The approach illustrated is known as a "centered difference" since the approximation uses a symmetric stencil of equally weighted points. With these approximations to the derivatives in time and space, a solution for the tracer distribution at $\tau + 1$ can be obtained:

$$C(i, \tau + 1) \approx C(i, \tau - 1) - u2\Delta t\left(\frac{C(i+1, \tau) - C(i-1, \tau)}{2\Delta x}\right)$$

As a technical detail, notice that to start (or initialize) this calculation two time levels of data must be given. In practice, these can be set equal to each other. Once initial values are given, the arithmetic equation above can be repeated, or iterated, many times to give the time evolution of C.

The algorithm described above is a simple but stable scheme that was employed in early numerical models. However, it has many undesirable properties, which are described in [45]. Nevertheless, the basic concepts illustrated by this method hold for all explicit finite-difference approaches. In implicit methods, the terms in the approximation of $\partial_x C$ above are replaced by their values at time $\tau + 1$. In the case above, this leads to a tridiagonal matrix problem that can be easily solved using standard techniques [45].

The most natural coordinate system for a global atmospheric model is spherical, with latitude and longitude as the horizontal coordinates. Unfortunately, as either pole is approached, equally spaced longitude lines come arbitrarily close together. This presents problems for most finite-difference numerical schemes, which become inaccurate or unstable when information travels across multiple grid lengths in a single time step. For example, in the simple case described in Fig. 1 the time step must be chosen such that $\frac{u\Delta t}{\Delta x} < 1$ to avoid numerical instability. Versions of this limit, known as the Courant-Friedrichs–Levy (CFL) limit, exist for

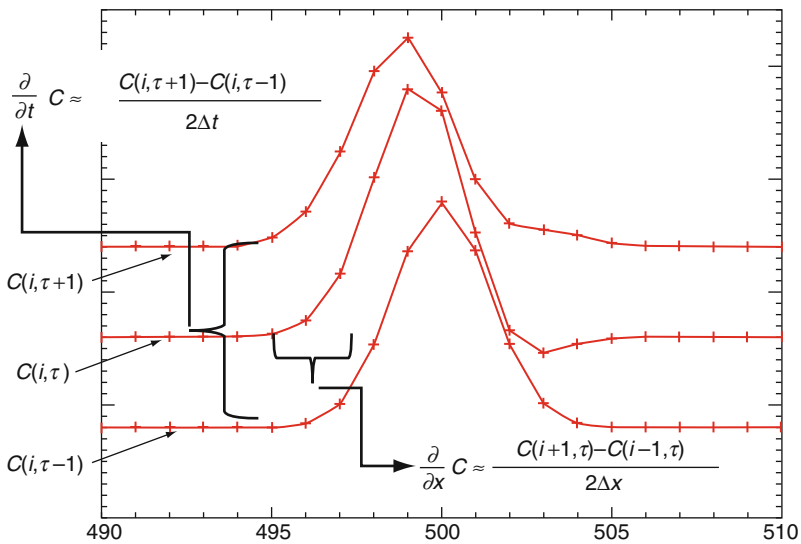

Weather Prediction Models. Figure 1

Three time steps from numerical advection of a Gaussian tracer pulse using a second-order, space-centered, time-centered finite-difference scheme. The +'s indicate grid-point locations. A constant velocity of $u = -0.5$ is used with grid spacing $\Delta x = 1$ and time step $\Delta t = 1$

most explicit finite-difference schemes. In systems of equations that support propagating waves, as the primitive equations do, the relevant velocity in the CFL limit is typically the sum of the wave propagation speeds and the advective speed. Thus, the stability of explicit calculations is limited by the fastest wave modes in the system, which are often of little interest, for example, Lamb waves or deep gravity waves. Global models whose numerics are based on finite differences ("grid-point models") address this issue by introducing polar filters which are designed to suppress small-scale motions in the polar regions of the model.

A revolutionary innovation occurred in the late 1960s with the introduction of spectral techniques for solving the primitive equations [46]. Spectral models decompose the atmosphere into a finite sequence of spherical harmonic functions, rather than onto a grid of points. For example, the wind u is approximated by:

$$u(\lambda, \theta, z, t) = \sum_{n=0}^{N} \sum_{m=-n}^{n} U_n^m(z, t) Y_n^m(\lambda, \theta)$$

where λ is longitude and θ is latitude. The time evolution of the atmospheric flow is then represented as the time evolution of the amplitudes $U_n^m(z, t)$. Nonlinear advection terms arising in the primitive equations may be dealt with directly in spectral space, as interactions of spherical harmonics or in physical space with transformation of the tendencies back to spectral space [45].

The resolution of spectral models is determined by the truncation parameter N. The form of the finite sum used above is referred to as a triangular truncation. A model with $N = 799$ in this kind of decomposition is referred as a "T799" model. Lynch [2] gives a useful rule-of-thumb for estimating the spatial resolution Δ corresponding a particular value of N. He uses $\Delta \approx (2\pi a_e)/2\ N$ or $\Delta \approx (20{,}000\ km)/N$ where the circumference of the Earth $2\pi a_e$ has been approximated by 40,000 km.

Spectral techniques are not only highly accurate, but also nicely sidestep the pole problem faced by grid-point models formulated in terms of latitude and longitude on the sphere. Discretization into spherical harmonics produces no special difficulties at the poles.

A disadvantage of spectral schemes is that fields with strong variation across small-spatial scales, such as most trace gas concentrations (including water vapor), precipitation, or topography cannot be represented without introducing significant spurious nonlocal oscillations in these fields. This behavior, known as the Gibbs phenomenon is a simple consequence of attempting to represent highly localized features with global basis functions. The nature of these truncation errors is such that the amplitude of spurious oscillations decreases slowly with resolution. The presence of Gibbs oscillations can lead to serious problems in global simulations, such as the formation of negative trace gas concentrations.

Due to the difficulties in spectrally representing fields with intense spatial variability, grid-point models have not been abandoned. In addition, grid-point models can be made more efficient than spectral models at very high resolution. So, while most operational forecasting centers currently use some form of spectral dynamical core in their NWP models, this may change in the next decade. Current research is focused on developing grid-point or finite element approaches on nonstandard grids such as the icosahedral, that is, "bucky-ball" or "soccer-ball," grid to bypass the pole problem encountered in latitude-longitude discretizations (see section on "Future Directions") (Table 2).

Parameterizations

Representation of physical processes such as radiation, turbulence, gravity wave drag, convection, and precipitation also became more sophisticated in NWP models as they evolved. The earliest successes in NWP using a filtered barotropic model did not even formally incorporate temperature as a prognostic variable. Today, NWP models may track several condensed water species, as well radiatively active trace gases such as ozone. It was the incorporation of radiative transfer schemes and simple moist convective adjustment schemes into NWP models in the 1960s [35] that led to the first climate models capable of self-consistently representing the basic feature of Earth's atmospheric general circulation.

Parameterization development for NWP models has followed that for climate models. The suite of parameterizations currently used in global NWP models is identical to that used for climate simulations. It is arguable whether most physics parameterizations

Weather Prediction Models. Table 2 Parameterizations in Weather Forecasting models. The first column gives the usual designation used in the meteorological community. The second column summarizes the effects of the parameterization. The third column indicates the primitive equation forcing term in which tendencies from the parameterization appear

Parameterization	Effects	Included in
Deep convection	Transports heat, moisture and momentum vertically. Damps convergence	H_{phys}, $\mathbf{F}_{phys}$, $C_{i,phys}$
Orographic gravity wave drag	Decelerates flow over mountains	$\mathbf{F}_{phys}$
Planetary boundary layer (PBL) turbulence	Transports heat, moisture and momentum vertically	H_{phys}, $\mathbf{F}_{phys}$, $C_{i,phys}$
Radiation (Solar and IR)	Calculates heating due radiative flux convergence	H_{phys}
Diagnostic cloud	Estimates cloud cover and thickness	
Prognostic cloud	Calculates cloud condensate concentrations and estimates cloud optical properties	H_{phys}, $C_{i,phys}$

exert an appreciable effect on short-term (1–3 day) forecasts. Deep convection and orographic wave drag parameterizations have been shown to exert a significant short-term effect [47–49]. At medium range (3 days to 2 weeks), physical parameterizations are thought to have an important effect on forecast skill (Bengtsson 2000). In addition climate biases resulting from deficient parameterizations can have a negative impact on data assimilation schemes (see section on "Data Assimilation Systems"). This can indirectly affect short-term forecasts by introducing errors in the initial conditions.

How Are NWP Models (Versus Climate Models) Evaluated?

Perhaps the most significant differences between global climate models and NWP models arise from the different jobs they are expected to perform. Ideally, a solver for the primitive equations, coupled to set of physically realistic parameterizations of processes like convection, should perform both long-term and short-term simulations of the atmospheric flow with equal accuracy. However, this is not the case. Even when run at comparable resolutions, models developed for NWP and climate do not perform each other's tasks with comparable skill. The likely cause of this discordance is the process of model tuning. The need for "tuning" is widely recognized in both the NWP community and the climate modeling community as an inevitable consequence of using imperfect models [41]. The bulk of model tuning occurs in choosing empirical factors that regulate physical parameterizations. Some of this can be explained (or excused) as an attempt to represent unknown sub-grid distributions of quantities such as water vapor, temperature, or topographic roughness. Unfortunately, the process of selecting these empirical factors can be ad hoc, and parochial in character. Even if optimal tunings exist that combine high accuracy in short-term forecasting as well as unbiased climate simulations, they are unlikely to be found. Groups involved in developing climate models rarely have the computational resources to perform extensive testing of their models at high resolution in forecast mode, while NWP groups are typically under intense operational pressures, and have little time or incentive to examine their models in free-running climate simulations.

There is as yet no set of universally accepted metrics for climate models, although developments in this direction are taking place [50]. Metrics typically targeted by climate modelers include seasonal mean distributions of precipitation and seasonal mean planetary wave patterns. Other, functional, constraints exist for atmospheric models used in climate research. For example, when used in coupled climate simulations, that is, connected through boundary fluxes to ocean and land surface models, obtaining correct global budgets of energy and momentum in an atmospheric model is critical. Thus, intensive tuning of cloud parameterizations is usually conducted to ensure that seasonal and annual-mean radiation budgets at the top of the atmosphere are realistic, to minimize spurious long-term drift in extended simulations. Generally speaking, exact conservation of energy and momentum is a key concern in the design of atmospheric models

for climate, while being of secondary importance in the design of NWP models.

On the other hand, operational NWP models are regularly subjected to a number of rigorous, and more-or-less universally accepted tests at each step in their development. Not surprisingly, these tests emphasize short-term simulation accuracy rather seasonal or annual-mean performance.

500 hPa Height Anomaly Correlation

At many centers including the European Center for Medium Range Weather Forecasting (ECMWF), the most important measure of global forecast model performance or skill is the 500 hPa height anomaly correlation. This measure is essentially the pattern correlation of two maps of geopotential height anomalies φ' interpolated to a pressure level of 500 hPa (corresponding to altitude close to 5 km). A height anomaly is defined the deviation in height from its average value along a latitude circle. One map is an analysis of height anomaly at 500 hPa $\phi'_{ana}(x, y, p_{500}, t_a)$ (see section on "Initialization and Data Assimilation") and the second is a map of forecast height anomaly valid at the same time $\phi'_f(x, y, p_{500}, t_a)$ where $t_a = t_i + \Delta t_f$. Here Δt_f is the forecast lead time and t_i is the initiation time. These two height fields are then used to form a correlation.

$$r_{500}(\Delta t_f) = \frac{\left\langle \phi'_f(t_i + \Delta t_f), \phi'_{ana} \right\rangle}{\sqrt{\left\langle \phi'_f, \phi'_f \right\rangle \left\langle \phi'_{ana}, \phi'_{ana} \right\rangle}}$$

where <> represents the spatial covariance over some region, typically the southern hemisphere or the northern hemisphere.

Figure 2 shows the average evolution of r_{500} in two major global forecast models for the period January 1 through March 31, 2009. The plots illustrate the state-of-the-art in NWP as of this writing. As expected the pattern correlations decrease with time, but remain quite high, above 0.8, out to a forecast lead of 5 days. Northern hemisphere correlations are higher in both systems, probably reflecting the higher density of in situ measurements available there. Many operational forecasting centers do not allow changes to their systems that degrade this measure of performance.

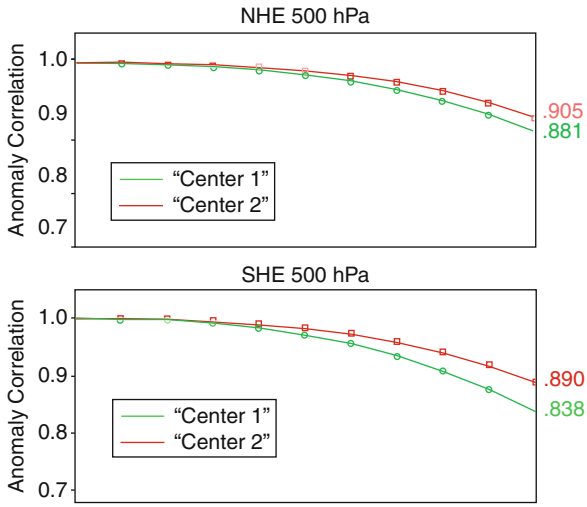

Weather Prediction Models. Figure 2
Mean evolution of 500 hPa anomaly height correlation in two major global NWP models for the January through March

Although using r_{500} as *the* single measure of forecast accuracy may seem somewhat restrictive, it should noted that that the geopotential height φ at 500 hPa is an integrated measure of the temperature in a deep layer, form the surface to around 5,000 m. So, r_{500} is a concise summary of model performance in a horizontally extensive and deep atmospheric slab.

Skill Scores

The S1 skill score [51, 52] has been used since the 1950s by forecasters at the National Meteorological Center (NMC), and after 1995 the National Center for Environmental Prediction (NCEP), to evaluate forecast performance. An S1 score can be defined for any quantity. It is calculated:

$$S1(\chi) = 100 \times \frac{\int_A |\nabla(\chi_f - \chi_o)| dA}{\int_A \max(|\nabla\chi_f|, |\nabla\chi_o|) dA}$$

where χ_f is forecast χ and χ_o is the observed value for verification. $S1$ then is the ratio of the integrated absolute gradient in forecast error, normalized by the integrated absolute gradient of the quantity itself, where at each location the larger of the forecast or observed values is used. A value of $S1 = 0$ represents a perfect forecast. The quantity χ used to calculate $S1$ is typically sea-level pressure or geopotential height.

The $S1$ skill score was selected by NMC from many measures of forecast quality with guidance from practicing forecasters. Forecasters in 1950s noted that values of $S1$ around 20 corresponded to very good forecasts, while values of 70 or more represented nearly worthless forecasts. As a result, it became common practice to express "skill" as $2(70 - S1)$, so that now a very good forecast $S1 = 20$ has a skill score of 100, while useless forecasts have a skill score of 0 [52].

Equitable Threat Scores

Evaluation of precipitation forecasts is difficult for a number of reasons. Precipitation is a field with high variance and sharp boundaries. In many circumstances, the important forecast parameter is whether rain or precipitation (above a certain threshold) has occurred. Such categorical forecasts are evaluated using various methods based on matrices of possible outcomes, for example, **YY** – rain is forecast and occurs, **YN** – rain is forecast but does not occur, **NY** – rain is not forecast but occurs, and **NN** – rain is not forecast and does not occur. The most commonly used method is that of Equitable Threat Scores (ETS) [53] which attempts to account for the long-term statistical probability of each category.

Initialization and Data Assimilation

A moment's reflection shows that establishing initial conditions for a global model of the atmosphere is a nontrivial task. First of all, there may be instrumental errors in the measurements of wind, temperature, humidity, or other quantities needed to specify the initial state of the atmosphere. While perhaps the most obvious problem, instrumental error may also be the least important problem faced in initialization. A more serious problem is hinted at in Fig. 3 which shows the current global distribution of radiosonde balloon launch sights. Radiosondes provide very accurate and reliable measurements of winds, temperatures, and humidities from the surface to around 10 km altitude. Launches are made by international agreement at either 0Z or 12Z ("Z" refers to Greenwich mean time) or at both times, depending on the station. However, as the figure shows, radiosonde launch sites are distributed in a completely unstructured way across the globe. High concentrations occur in the developed world, with sparse or no coverage over oceans and over less-developed land areas. Even in the developed world the location of sites is determined by human factors – and is more-or-less spatially random. Numerical models of the atmosphere, both spectral and grid point, require a spatially structured set of numbers to begin their integrations. Satellite data presents similar challenges. While it is structured – along orbital tracks – the structure does not conform to the needs of NWP models. In addition, satellite data is asynchronous, that is, sampling occurs continuously as the satellite travels, not at a specified time as with radiosonde data.

Thus a major challenge faced in NWP is to derive a complete model state on a structured set of points at a single instant in time, from data that may be neither spatially structured nor representative of a single point in time. Naive interpolation in space and/or time is inadequate. The model state derived from the data must not only cover the globe, it must do so while also satisfying a number of other dynamical and physical constraints.

Fluid flows, and vector fields in general, can be decomposed into a sum of divergent ($\nabla \cdot \mathbf{u_1} \neq 0$) and nondivergent ($\nabla \cdot \mathbf{u_2} = 0$) components. Generally speaking, the atmospheric motions of most significance in 1–5 day forecasts are characterized by "small" horizontal convergence and divergence in a relative sense. In these flows, two or three of the terms in the momentum equation form a dominant steady-state balance that describes the flow to first-order. These balanced flows are *almost* nondivergent. However, their time evolution can be profoundly affected by the small divergent component. The earliest and most basic balance identified by meteorologists is the so-called geostrophic balance, described below. The subtleties of the divergent wind field in geostrophically balanced flow are what doomed L. F. Richardson's pioneering NWP experiment.

Geostrophically Balanced Flow

The origin of geostrophic balance is most easily seen by performing a scale analysis of the momentum equation in the primitive equation system. Scale analysis is a common procedure in fluid mechanics to

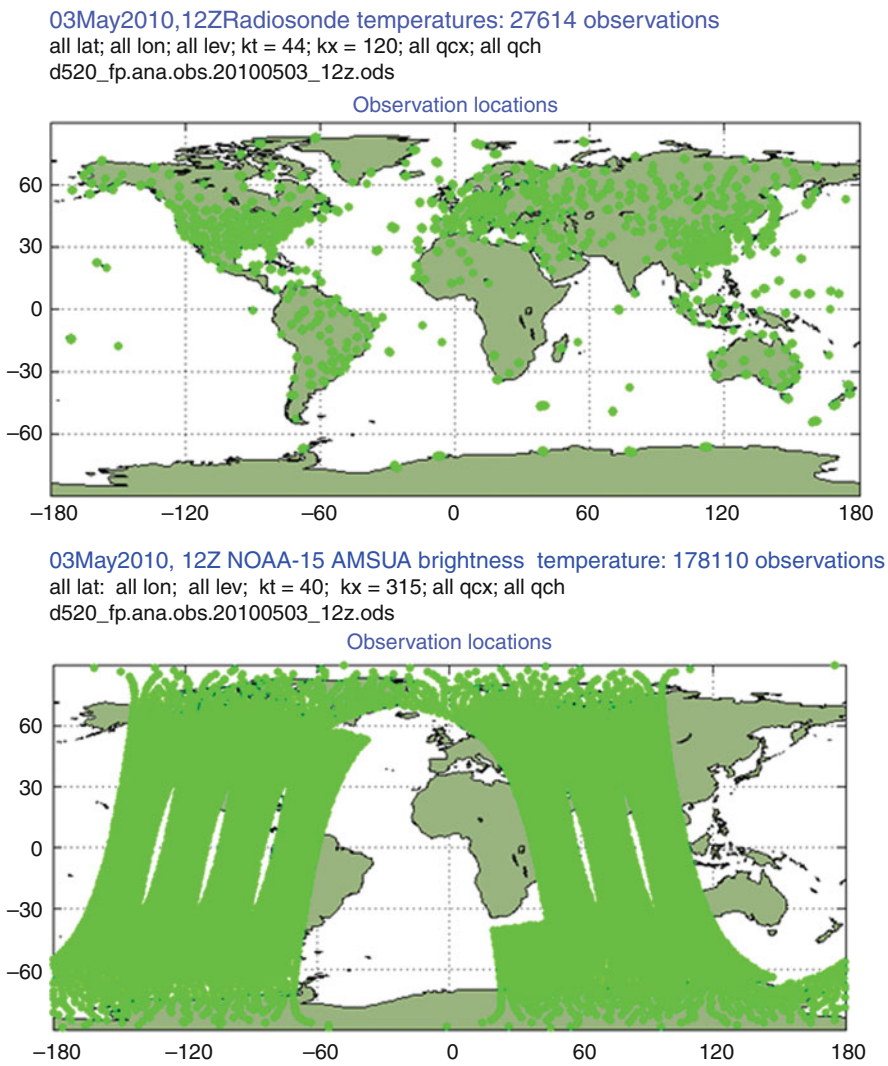

Weather Prediction Models. Figure 3

Locations of radiosonde observations (*top*) and satellite temperature observations (*bottom*) for May 12, 2008 from NASA's GEOS-5 DAS

systematically identify the most important terms in the complicated equations describing fluid flow [4]. It begins by identifying scales of motion for the phenomenon of interest. For midlatitude weather systems, especially after considering the spacing and resolution of radiosonde and satellite data, a reasonable choice of spatial scale L is around 1,000 km. Other reasonable choices of scales are for horizontal wind $U \sim 10\ \mathrm{ms}^{-1}$, and for pressure disturbance $P \sim 10$ hPa or 1,000 Pa. These scales along with local apparent rotation rate f with values $\sim 10^{-4}\ \mathrm{s}^{-1}$ in midlatitudes are used to estimate the sizes of the terms in the equation. For example, $\frac{d}{dt}V$ will be $\sim U^2/L$ where the horizontal advective time scale has been used as the relevant time scale. It is easy to see that the ratio of this term to the Coriolis term $f\mathbf{k} \times V$ will scale as U/fL, which is a key nondimensional parameter in dynamic meteorology known as the Rossby number or *Ro*. For the scales of motion typical for midlatitude systems, *Ro* is close to 0.1. So the advective term is likely to small compared to the Coriolis term and also, it turns out, compared to the pressure gradient.

Thus, the "leading order" balance in midlatitude systems is left as:

$$f\mathrm{k} \times V = -\alpha \nabla_z p$$

where we have used height as the vertical coordinate. Equivalent expressions exist for other vertical coordinates. In component form this balance is written as:

$$-fv = -\alpha \partial_x p; \; fu = -\alpha \partial_y p$$

This balance is the dominant feature of midlatitude flow. It is also responsible for one of the most counter-intuitive aspects of weather maps in midlatitudes – that the wind blows along pressure contours rather than from high pressure to low pressure. It is also the reason air flows in a counterclockwise sense around low-pressure centers in the northern hemisphere. A perplexing aspect of this balance is that it is a steady-state relation. In other words, the largest forces in the system give no information about its time evolution.

It is easy to see that this leading-order geostrophic flow is horizontally nondivergent. However, spurious divergent flow features can easily appear when constructing initial conditions from observations of horizontal. An idea of the difficulty of this challenge can be obtained by considering the following argument. The relative vorticity of the horizontal wind is determined from:

$$\zeta = \partial_x v - \partial_y u$$

and, further scale analysis of the equations of motion in midlatitudes (see [45]) shows that the ratio $\nabla \cdot V$ to ζ will typically be close to Ro or ~ 0.1. The individual horizontal derivative terms in the expressions for vorticity and divergence are of the same order. The small relative magnitude of $\nabla \cdot V$ is only possible through near cancelation of its much larger component terms. It is not trivial to maintain this cancelation during the data assimilation process. Errors in the divergence can have large effects on surface pressure tendencies since

$$\partial_t p_s \sim p_s \nabla \cdot V.$$

More complete and correct balance relationships than geostrophic balance can be derived [54]. Balanced initial conditions have been sought in a number of ways during the history of NWP. The most successful of these was perhaps nonlinear normal mode initialization introduced in the 1970s [55–57]. In this technique, fast and slow normal modes of the nonlinear equations of motion are found through an iterative procedure.

Data Assimilation Systems

Modern operational centers handle the problem of initializing their forecasts by using a data assimilation system (DAS). A central feature of a DAS is the forecast model itself (or a linearized version thereof). Analyses at operational forecasting centers are typically performed four times daily at 00Z, 06Z, 12Z, and 18Z. The analysis procedure combines measurements with a short model forecast, typically 6 h initialized with the previous analysis. This forecast is often referred to as the "first guess" or "background." The job of the analysis algorithm, denoted by the yellow diamond in Fig. 4, is to blend the myriad sources of data, which includes radiosonde observations satellite measurements, pilot reports, surface station reports, ship buoy measurements, and more, with the forecast to produce an optimal estimate of the state of the atmosphere on the model grid. The process illustrated in Fig. 4 depicts a "3D-Var" system. In 3D-Var, data gathered within an analysis time window, typically 3 h before and after the standard analysis times, is assumed to be synchronous. The analysis then consists of an optimal blending of measurements and forecast background in space.

This optimal blending can be expressed as a "cost function minimization." The cost function is written in matrix form [2, 54, 58]:

$$J(\mathrm{x}) = (\mathrm{x} - \mathrm{x}_b)T\ \mathrm{B}^{-1}(\mathrm{x} - \mathrm{x}_b) + [\mathrm{y} - H(\mathrm{x})]^T \mathrm{R}^{-1}[\mathrm{y} - H(\mathrm{x})] + J_b(\mathrm{x})$$

where $\mathbf{x}$ is a model "state vector," that is V, T, q and possibly other analyzed species on the model's numerical grid (or spectral decomposition). The quantity $\mathbf{x}_b$ is the model state from a forecast, that is, the first guess or background, and the matrix $\mathbf{B}$ is the background, or forecast, error covariance matrix. This matrix is a key piece of the analysis algorithm, and is estimated by examining differences between forecasts radiosonde observations [59] or more recently by calculating the covariance of different short forecasts, for example, 24 h and 48 h, valid at the same time [60, 61].

The second term in the cost function contains the observation error covariance matrix $\mathbf{R}$, the observation

vector **y** and a vector $H(\mathbf{x})$ which is the result of the "observation operator" H acting on the model state **x**. In the case of an observation taken by a thermometer placed at a model grid-point, the observation operator would simply select the appropriate element of **x**. However, in the case of remote satellite observations, which directly measure radiances (photons) from the atmosphere, H could represent a complex radiative transfer calculation using for example T and q from the model state to estimate the radiance measured by a particular instrument. The approach of transforming model quantities into a form that is directly comparable with observations, sometimes referred to as "radiance assimilation," led to dramatic increases in the positive impact of satellite measurements on forecasting [62].

The third term in the cost function represents balance constraints on the flow, such as those discussed in the section on "Geostrophically Balanced Flows". Inclusion of such a term at NCEP has eliminated the need for a separate initialization procedure for forecasts [60].

The task of the analysis algorithm is to find the model state $\mathbf{x}_a$ that minimizes the cost function $J(\mathbf{x})$. For more details on how this solution is actually accomplished the reader is referred to discussion in Chap. 5 of Kalnay (2003) [54]. 3D-var as described here is used by NCEP as well as in slightly modified version by NASA's Global Modeling and Assimilation Office (GMAO) in their GEOS-5 DAS [63]. A somewhat different approach known as 4D-Var is used at ECMWF. This approach takes into account the possibly asynchronous nature of data when formulating the cost function. For more details, see the discussion in Kalnay (2003).

Ensemble Forecasting

The early thinking of researchers in NWP was that the central problem of forecast initialization was to correctly filter out rapid divergent motions, and, that once this was accomplished no fundamental limits on atmospheric predictability existed. A series of seminal papers by Edward N. Lorenz proved this to be incorrect [64–66]. Lorenz showed that simple analogs to atmospheric equations of motion possess a sensitive dependence to

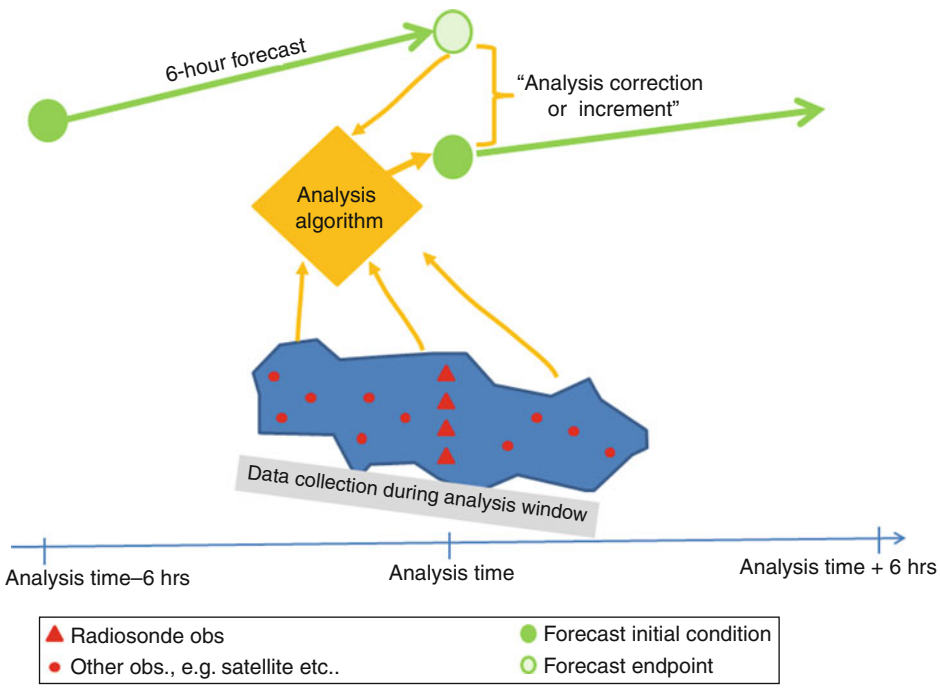

Weather Prediction Models. Figure 4
Schematic diagram of 3D-var analysis

initial conditions. In other words, small differences in even well-balanced initial conditions will cause forecasts to become uncorrelated after a finite time.

Modern operational forecasting centers typically perform ensembles of many runs with slightly different initial conditions, as well as a single higher-resolution "deterministic" run to produce forecasts for a given time [54, 67]. The generation of ensemble members is a nontrivial task. Ideally, the members of the ensemble should vary in special directions in phase space that are related to the most rapidly growing instabilities in the flow [54, 68].

Future Directions

Weather forecasts have improved demonstrably during the 50 year history of NWP. This is illustrated in Fig. 5, which shows the evolution of r_{500} at 3, 5, and 7 days over the last 30 years in the ECMWF system [69]. Part of the improvement is traceable to the explosion in the amount of satellite data over the last 30 years. However, a large part of the improvement in skill is due to improvements in the forecast and analysis "system," such as increased forecast model resolution, improved analysis algorithms etc. This is nicely demonstrated in the bottom panel of Fig. 5, which shows the evolution of skill in retrospective forecasts, using the *current* ECMWF system on the historical data base. The skill of retrospective forecasts is significantly higher, indicating that the improved forecast and analysis system makes a significant, perhaps the dominant, contribution to the overall increase in skill seen in the last 30 years. One aspect of improvement that is clearly due to improved data sources (satellites) is the convergence of skill in southern and northern hemispheres.

Scalable Dynamical Cores

As computing power increases NWP model resolution also continues to increase. In the last several years, the increase in computer power has appeared primarily in the form of massively parallel machines with larger and larger numbers of processors, rather than in the form of faster individual processors. This means that "time-to-solution" has not decreased dramatically in recent years, but the size of feasible calculations has increased dramatically. This has stimulated the development of scalable models. Scalability means that model speed increases more-or-less linearly with the number of processors used. A trivial example of perfectly scalable problem is the addition of 1,000 pairs of numbers a + b = c. If one processor is available then the calculation will take 1,000 CPU time units. If 1,000 processors are available the entire calculation can take place in 1 CPU time unit. However, communication between processors also costs time. In any real numerical model of the atmosphere processors eventually need information residing in other processors. This prevents numerical models of the atmosphere from scaling perfectly.

The amount of cross-processor communication required can vary widely depending on model design. Ideally decomposition will maximize the ratio of area to perimeter in computational subdomains to minimize the need for cross-processor communication. The scalability of grid-point models on latitude-longitude grids is severely hampered by the need to apply polar filters to overcome numerical instabilities that arise due to the convergence of longitude lines at both poles. These filters typically require knowledge of atmospheric fields all the way around latitude circles. Thus, modelers must either decompose the globe into thin computational domains circling the globe, which will lead to large communication requirements in the north–south direction, or they must pay the cost of frequent "gathers" to obtain the necessary inputs for polar filters. Transforms in spectral models likewise require knowledge of fields around latitude circles.

Recent efforts in numerical techniques for global atmospheric models have focused on the development of grid-point or finite element models on nonstandard grids [70–73]. Several examples of such grids are shown in Fig. 6. These grids have fairly uniform grid cell sizes over the entire globe. Polar filters are therefore not required.

Nonhydrostatic Dynamics

Once horizontal resolution becomes much finer than 10 km, nonhydrostatic effects must be taken into account. This will require models based on a different set of equations. One option is to simply use the full Euler or Navier Stokes equations [39, 74] and pay the costs associated with the short time-steps required by the presence of acoustic waves. Another approach is to

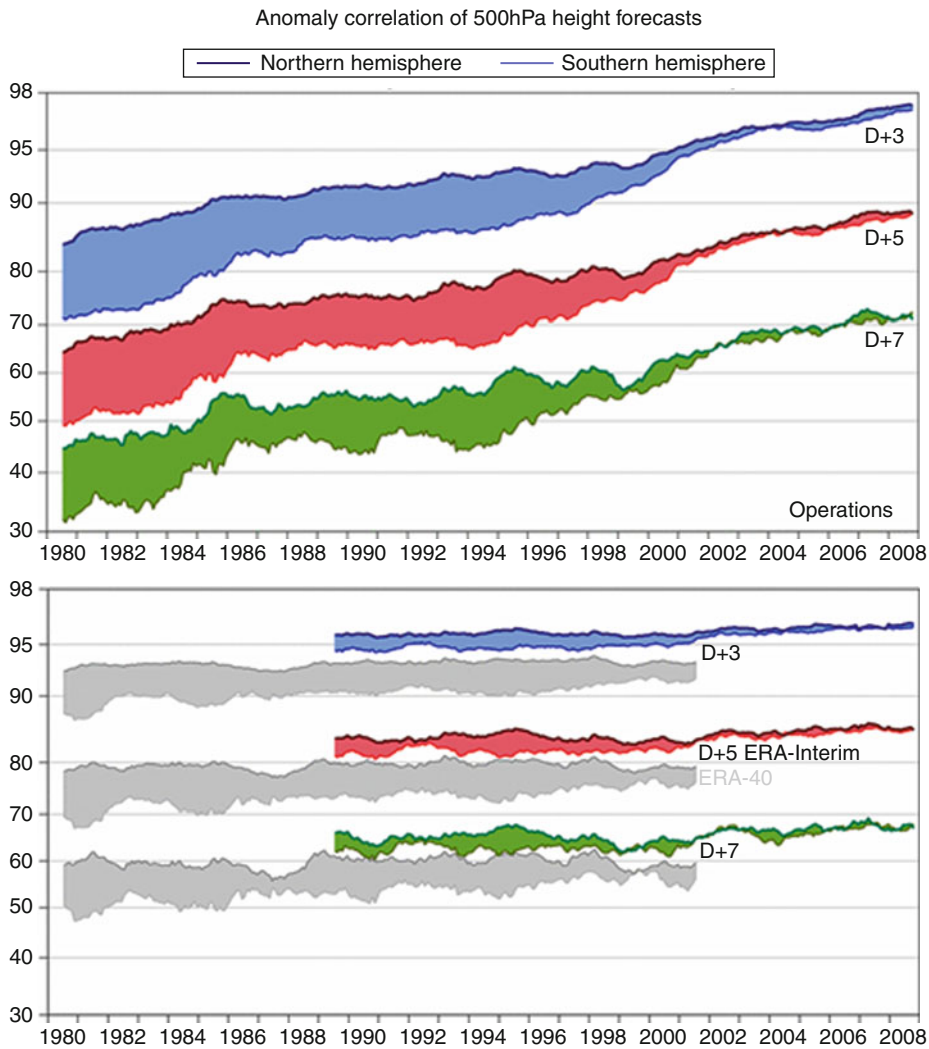

Weather Prediction Models. Figure 5

Evolution of forecast skill at ECMWF, adapted and extended from the study of Simmons and Hollingsworth (2002). The *top panel* shows a history of r_{500} at 3, 5, and 7 days from the ECMWF operational forecast beginning in 1980. The *colored* and *shaded areas* are bounded by southern hemisphere skill below and northern hemisphere skill above. The *lower panel* shows retrospective forecasts produced using two versions of current ECMWF analysis and forecast systems. In these cases, the "system" is fixed in time, while data inputs evolve in actual historical fashion

use an inelastic equations system [75], but this requires solution of an elliptic equation which is an intrinsically nonlocal procedure and again raises cross-processor communication costs.

Seamless Models for Climate and Weather

Modern global NWP and climate models are essentially the same. Both use the same set of dynamical equations (see section on "Primitive Equations"). Both also use the same set of physical parameterization schemes (see section on "Parameterization"). In practice, differences do exist between global models of the atmosphere intended for climate simulation and those intended for forecasting. Operational global NWP models have typically used resolutions that are a factor of 8–16 times higher than those used in long climate simulations. Other differences arise, more-or-less unintentionally,

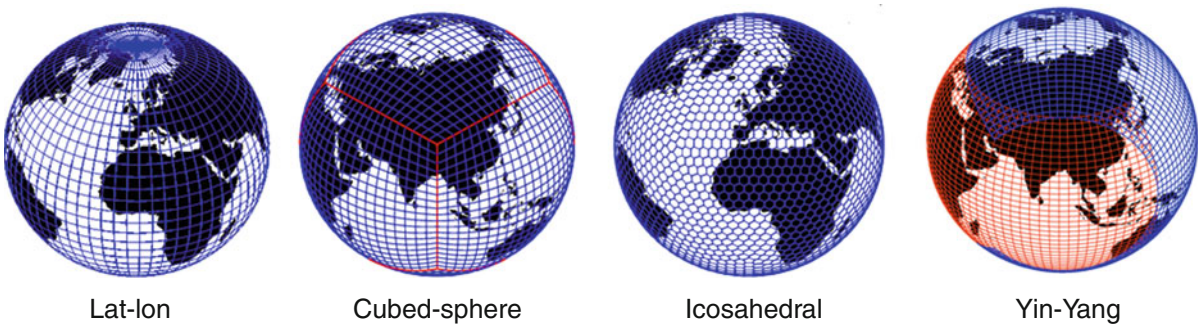

Weather Prediction Models. Figure 6
The standard latitude-longitude "lat-lon" grid (*leftmost globe*) compared with newer, non-traditional grids for global atmospheric models

in the tuning process as a consequence of the different metrics used in the evaluation of NWP and climate models (see section on How are NWP models (versus climate models) evaluated?).

Climate researchers understand that atmospheric phenomena such as squall lines and tropical cyclones may play a role in establishing climate on both regional and global scales. Such "mesoscale" features are not resolved in climate models with resolutions of 100 km or coarser. However, the continued increase in computer power, and the recent emphasis on massively parallel architecture, will allow decadal or even century-long simulations at resolutions close to 10 km in the near future. At these resolutions, mesoscale circulations should be well represented. These resolutions will also present novel challenges to the sub-grid parameterizations used in climate models, as assumptions about scale-separation and statistical equilibrium become questionable.

Bibliography

1. Tribbia J, Anthes R (1987) Scientific basis of modern weather prediction. Science 237:493–499
2. Lynch P (2006) The emergence of numerical weather prediction: Richardson's dream. Cambridge University Press, Cambridge, MA
3. Richardson L (1922) Weather prediction by numerical process. Cambridge University Press, Cambridge
4. Gill A (1982) Atmosphere–ocean dynamics. Academic, London
5. Simpson J (1994) Sea breeze and local winds. Cambridge University Press, New York
6. Lau K, Li M (1984) The monsoon of East Asia and its global associations_survey. Bull Amer Meteor Soc 65:114–125
7. Webster P, Tomas R (1998) Monsoons- processes, predictability, and the prospects for prediction. J Geophys Res 103(C7): 14451–14510
8. Douglas M, Maddox R, Howard K, Reyes S (1993) The Mexican monsoon. J Clim 6(8):1665–1677
9. Koch S, Handley C (1997) Operational forecasting and detection of mesoscale gravity waves. Weather Forecast 12(2)
10. Moncrieff M, Liu C (1999) Convection initiation by density currents: role of convergence, shear, and dynamical organization. Mon Weather Rev 127(10):2455–2464
11. Lac C, Lafore J, Redelsperger J (2002) Role of gravity waves in triggering deep convection during TOGA COARE. J Atmos Sci 59(8)
12. Houze R Jr (2004) Mesoscale convective systems. Rev Geophys 42. doi:10.1029/2004RG000150
13. Grabowski W, Moncrieff M (2006) Large-scale organization of tropical convection in two-dimensional explicit numerical simulations. Q J Roy Meteor Soc 127(572):445–468
14. Smith R (1979) The influence of mountains on the atmosphere. Adv Geophys 21:87–230
15. Longuet-Higgins M (1964) Planetary waves on a rotating sphere. Proc R Soc Lond A Math Phys Sci 279(1379):446–473
16. Andrews D, McIntyre M (1976) Planetary waves in horizontal and vertical shear: the generalized Eliassen-palm relation and the mean zonal acceleration. J Atmos Sci 33:2031–2048
17. Hoskins B, Ambrizzi T (1993) Rossby wave propagation on a realistic longitudinally varying flow. J Atmos Sci 50: 1661–1671
18. Charney J (1947) The dynamics of long waves in a baroclinic westerly current. J Meteor 4(5):135–162
19. Eady E (1949) Long waves and cyclone waves. Tellus 1(3):33–52
20. Kiladis G, Wheeler M, Haertel P, Straub K, Roundy P (2009) Convectively coupled equatorial waves. Rev Geophys 47. doi:10.1029/2008RG000266
21. Burpee R (1972) The origin and structure of easterly waves in the lower troposphere of North Africa. J Atmos Sci 29(1):77–90
22. Landsea C et al (1993) A climatology of intense (or major) Atlantic hurricanes. Mon Weather Rev 121(6):1703–1713

23. Pytharoulis I, Thorncroft C (1999) The low-level structure of African easterly waves in 1995. Mon Weather Rev 127(10)
24. Thorncroft C, Hodges K (2001) African easterly wave variability and its relationship to Atlantic tropical cyclone activity. J Clim 14(6):1166–1179
25. Madden R, Julian P (1994) Observations of the 40–50-day tropical oscillation: a review. Mon Weather Rev 122(5):814–837
26. Zhang C (2005) Madden-Julian oscillation. Rev Geophys 43(2). doi:10.1029/2004RG000158
27. Liebmann B, Hendon H, Glick J (1994) The relationship between tropical cyclones of the western Pacific and Indian Oceans and the Madden–Julian oscillation. J Meteor Soc Japan 72(41):1–412
28. Maloney E, Hartmann D (2000) Modulation of hurricane activity in the Gulf of Mexico by the Madden-Julian oscillation. Science 287(5460):2002
29. Maloney E, Hartmann D (2000) Modulation of eastern North Pacific hurricanes by the Madden-Julian oscillation. J Clim 13(9)
30. Elsner J, Jagger T, Niu X et al (2000) Changes in the rates of North Atlantic major hurricane activity during the 20th century. Geophys Res Lett 27(12):1743–1746
31. Hall J, Matthews A, Karoly D (2001) The modulation of tropical cyclone activity in the Australian region by the Madden–Julian oscillation. Mon Weather Rev 129:12
32. Bond N, Vecchi G (2003) The influence of the Madden–Julian oscillation on precipitation in Oregon and Washington. Weather Forecast 18(4):600–613
33. Jones C, Waliser D, Lau K, Stern W (2004) The Madden–Julian oscillation and its impact on northern hemisphere weather predictability. Mon Weather Rev 132(6)
34. Waliser DE, Lau KM, Stern W, Jones C (2003) Potential predictability of the Madden–Julian oscillation. Bull Amer Meteor Soc 84:33–50
35. Manabe S, Smagorinsky J, Strickler R (1965) Simulated climatology of a general circulation model with a hydrologic cycle. Mon Weather Rev 93(12):769–798
36. Namias J (1980) The early influence of the Bergen School on synoptic meteorology in the United States. Pure App Geophys 119(3):491–500
37. Grenas S (2005) Vilhelm Bjerknes' vision for scientific weather prediction. In: The Nordic seas: an integrated perspective: oceanography, climatology, biogeochemistry, and modeling. American Geophysical Union, Washington, DC, p 357
38. Hinkelmann K (1951) Der Mechanismus des meteorologischen Lärmes. Tellus 3:285–296
39. Laprise R (1992) The Euler equations of motion with hydrostatic pressure as an independent variable. Mon Weather Rev 120(1):197–207
40. Shuman F, Hovermale J (1968) An operational six-layer primitive equation model. J Appl Meteor 7(4):525–547
41. Bengtsson L (2001) The development of medium range forecasts. In: 50th anniversary of numerical weather prediction, commemorative symposium, Potsdam
42. Kasahara A (2000) On the origin of cumulus parameterization for numerical prediction models. Gen Circ Model Dev 70:199–224
43. Tiedtke M (1993) Representation of clouds in large-scale models. Mon Weather Rev 121:3040–3061
44. Del Genio A, Yao M, Kovari W, Lo K (1996) A prognostic cloud water parameterization for global climate models. J Clim 9:270–304
45. Haltiner G, Williams R (1983) Numerical prediction and dynamic meteorology, 2nd edn. Wiley, New York
46. Leith C (1965) Numerical simulation of the earth's atmosphere. In: Methods in computational physics, vol 4. Academic, New York
47. Webster S, Brown A, Cameron D, Jones C (2006) Improvements to the representation of orography in the Met Office Unified Model. Q J Roy Meteor Soc 129(591):1989–2010
48. Clark A, Gallus W Jr, Xue M, Kong F (2009) A comparison of precipitation forecast skill between small convection-allowing and large convection-parameterizing ensembles. Weather Forecast 24(4):1121–1140
49. Bhanu Kumar O, Ramalingeswara Rao S, Muni Krishna K (2009) Role of cumulus parameterization schemes in simulating heavy rainfall episodes off the coast of Maharashtra state during 28 June–4 July 2007. Meteorol Atmos Phys 105(3): 167–179
50. Gleckler P, Taylor K, Doutriaux C (2008) Performance metrics for climate models. J Geophys Res 113:D06104
51. Teweles S, Wobus H (1954) Verification of prognostic charts. Bull Amer Meteor Soc 35:455–463
52. Shuman F (1989) History of numerical weather prediction at the National Meteorological Center. Weather Forecast 4:286–296
53. Gandin L, Murphy A (1992) Equitable skill scores for categorical forecasts. Mon Weather Rev 120:361–370
54. Kalnay E (2003) Atmospheric modeling, data assimilation, and predictability. Cambridge University Press, Cambridge, MA
55. Machenhauer B (1977) On the dynamics of gravity oscillations in a shallow water model, with applications to normal mode initialization. Beitr Phys Atmos 50:253–271
56. Baer F, Tribbia J (1977) On complete filtering of gravity modes through nonlinear initialization. Mon Weather Rev 105(12): 1536–1539
57. Tribbia J (1984) A simple scheme for high-order nonlinear normal mode initialization. Mon Weather Rev 112:278–284
58. Daley R (1993) Atmospheric data analysis. Cambridge University Press, New York
59. Thiebaux HJ, Pedder MA (1987) Spatial objective analysis with applications in atmospheric science. Academic, London/Orlando, p 308
60. Parrish D, Derber J (1992) The National Meteorological Center's spectral statistical-interpolation analysis system. Mon Weather Rev 120(8):1747–1763
61. Buehner M, Gauthier P, Liu Z (2005) Evaluation of new estimates of background-and observation-error covariances for variational assimilation. Q J Roy Meteor Soc 131(613):3373–3384
62. Derber J, Wu W (1998) The use of TOVS cloud-cleared radiances in the NCEP SSI analysis system. Mon Weather Rev 126(8): 2287–2299
63. Rienecker M, Suarez M, Todling R, Bacmeister J, Takacs L, Liu H, Gu W, Sienkiewicz M, Koster R, Gelaro R et al (2008) The GEOS-5

data assimilation system-documentation of versions 5.0.1, 5.1.0. NASA Technical Memorandum, NASA/TM-2007, 104606
64. Lorenz E (1965) A study of the predictability of a 28-variable atmospheric model. Tellus 17(3):321–333
65. Lorenz E (1969) The predictability of a flow which possesses many scales of motion. Tellus 21(3):289–307
66. Lorenz E (1969) Atmospheric predictability as revealed by naturally occurring analogues. J Atmos Sci 26(4):636–646
67. Lewis J (2005) Roots of ensemble forecasting. Mon Weather Rev 133(7):1865–1885
68. Toth Z, Kalnay E (1993) Ensemble forecasting at NMC: the generation of perturbations. Bull Amer Meteor Soc 74:2317–2330
69. Simmons A, Hollingsworth A (2002) Some aspects of the improvement in skill of numerical weather prediction. Q J Roy Meteor Soc 128(580):647–678
70. Ringler T, Heikes R, Randall D (2000) Modeling the atmospheric general circulation using a spherical geodesic grid: a new class of dynamical cores. Mon Weather Rev 128(7):2471–2490
71. Skamarock W, Klemp J, Ringler T, Thuburn J (2008) A hexagonal C-grid atmospheric core formulation for multiscale simulation on the sphere. AGU fall meeting abstracts, San Francisco, CA, p 01
72. Putman W, Lin S (2009) A finite-volume dynamical core on the cubed-sphere grid. Astron Soc Pac Conf Ser 406:268
73. Taylor M, Fournier A (2010) A compatible and conservative spectral element method on unstructured grids. J Comput Phys 229:5879–5895
74. Klemp J, Skamarock W, Dudhia J (2007) Conservative split-explicit time integration methods for the compressible nonhydrostatic equations. Mon Weather Rev 135(8):2897–2913
75. Grabowski W, Smolarkiewicz P (2002) A multiscale anelastic model for meteorological research. Mon Weather Rev 130(4)

Wide Area Monitoring, Protection and Control

James S. Thorp, Arun G. Phadke
Bradley Department of Electrical and Computer Engineering, Virginia Polytechnic Institute and State University, Blacksburg, VA, USA

Article Outline

Glossary
Definition of the Subject
Power System Monitoring
Protection
Power System Control
Future Directions
Bibliography

Glossary

Adaptive protection A protection philosophy which permits and seeks to make adjustments automatically in various protection functions in order to make them more attuned to prevailing system conditions.

Fault A short circuit in the power system.

GPS Global Positioning System.

Hidden failure A defect or error in relay that does not manifest itself immediately but which can cause a miss-operation when the system is stressed.

NERC North American Electric Reliability Corporation.

Phasor A complex number describing a sinusoidal signal.

PMU Phasor Measurement Unit.

RTU Remote Terminal Unit.

SCADA Supervisory Control and Data Acquisition.

Synchrophasor A phasor measurement with a precise time tag.

WAMS Wide Area Measurement System.

Definition of the Subject

The Electric Power Infrastructure

A power system consists of generators which convert energy from some primary form – such as coal, wind, gas, sunlight, or water flow – into electric power. Most generators in modern power systems produce alternating currents and voltages (AC) which are then transmitted over appropriate distances to supply loads. It is economical to transmit power at higher voltages in order to limit losses in the transmission lines. Voltages of desired values are obtained with the help of transformers which let through most of the power (small amount of losses are incurred in the transformers), only changing voltages and currents from one side of the transformer to the other. The "power" handled by the transformers is the product of currents and voltages, so that higher voltages have accompanying smaller currents. In general, the longer the distance for transmission, the greater is the economical voltage at which to transmit the power. Most power transmission is through overground transmission lines, while in special circumstances (such as crossing a large body of water or in congested urban areas) underground cables

are used. There is a range of voltages in use for transmission: 800 (kilovolts – thousands of volts), 500, 400 kV, etc. The household voltages in most countries are 120 V or 240 V which are obtained through stages of transformations as power is passed through transmission, sub-transmission, and distribution systems. For technical reasons, sometimes it is advantageous to convert AC power to DC (direct current) power by high-power electronic converters, transmit it as DC power, and convert it back to AC at the receiving end. The power-handling capacity of total system generation is expected to be some 10–20% greater than the expected load in order to provide a margin of security. Similarly, the transmission system is planned with sufficient number of alternative paths connecting loads to generators so that should some lines get disconnected due to faults, the loads continue to be served. In North America and many countries, the frequency of the AC system is nominally set at 60 Hz, while in some other countries, it is 50 Hz. The actual frequency of the system stays close to the nominal values, and in well-regulated power systems, the variations from nominal frequency are less than 0.1 Hz. The North American power system has approximately 900 gigawatts (900,000,000,000 W) of power generation capacity – consisting of about 70% thermal power generators, 14% hydroelectric generators, 13% nuclear, and small amounts of wind, solar, and other renewable power sources. The continent is crisscrossed by about 200,000 circuit miles of high-voltage transmission lines, further supplemented by lower-voltage distribution circuits serving customers at lower voltages at the load centers. The generation capacity in North America is sufficient to meet load demands with adequate margins overall, although in spot locations, the available margins or transmission capacity may not be sufficient.

Operating the Power Grid Reliably

In order to provide electric power reliably to consumers, it becomes necessary to manage the generation, transmission, and consumption of electric power in an efficient manner. Since the load demand is controlled by the consumers and may change randomly depending upon consumers' wishes, and since the generation must match this demand (and losses) instant by instant, an elaborate system of controls is put in place at generators and at Energy Management Centers on the power grid. Such controls must take into account the possibility of faults in the system due to natural disasters (floods, hurricanes, and fires), equipment failure, or man-made disasters. These events are contingency events, and the power grid must continue to meet the demands of consumers with minimum interruptions when faced with such contingencies. In addition, the power system must maintain its operating frequency within a narrow band around the nominal value (60 Hz in North America), and the operating voltage at the consumers' locations within a narrow band around its nominal value. To be prepared to deal with a reasonable set of contingencies adequately, it is necessary that the system operators are made aware of the condition of the power infrastructure accurately at all times. This is achieved through a system of measurements made on the power grid at frequent intervals, from which the network flows and voltages are estimated. The technical term for this process is "state estimation" of the power system. The ability of the power system to meet its loads in the presence of contingencies is much enhanced if the state of the system is known precisely and with sufficient frequency so that as the transmission system, loads, and generation change during the day, the changes are tracked accurately by the measurement process. A measurement technique made possible by the advent of digital computer-based measurements and the Global Positioning System (GPS) is the highly precise and effective "synchrophasors" technology.

Sine Waves, Phasors, and Synchrophasors

Alternating currents and voltages vary as sinusoids with a period determined by the frequency of the system. Thus, in North America where the frequency is 60 Hz, a nominal voltage or current will vary with time as shown in Fig. 1. Note that the sinusoid is shown to be a pure sine wave, whereas in practice, the waveform could have some noise in it. A *phasor* is a mathematical way of representing this sinusoid. It is a complex number with its magnitude equal to the RMS (root mean square) value of the sinusoid, and its phase angle is the angle measured with respect to the start of the time axis and the peak of the sinusoid. One period is equivalent to 2π radians or $360°$. Angles measured to the left of $t = 0$ are positive angles, and angles measured to the

right are negative angles. Thus, the phasor representing the sinusoid in Fig. 1 is given by:

$$\text{Phasor} = X\varepsilon^{j\theta} = X\cos\ \theta + j\,X\sin\theta$$

where X is the RMS value of the sinusoid. Phasors are generally calculated from samples taken from a sinusoid over a time span known as data window, which is usually of the order of one period of the sinusoid.

The GPS satellite system transmits (among other data) a 1-pulse-per-second (1 pps) which can be received by GPS receivers. A characteristic of the GPS system is that a 1 pps received by any receiver placed anywhere on earth is within 1 μs of the pulse received by another GPS receiver. Consider a power system shown in Fig. 2 in which different power facilities (substations) are separated by large distances. The sinusoids of voltages and currents in the two substations would in general be different from each other in magnitudes and phase angles of the sinusoids. A sinusoid at the substation shown in red in Fig. 2 is measured from the instant shown as t = 0, which is identified with the 1 pps received from the satellite, while the measurement at the substation shown in green has the t = 0 time marker at the same instant, and measures the phasor at that location. The two synchrophasors can now be placed on the same phasor diagram and show correctly the relative magnitudes and phase angles of the two signals as they exist at that instant. Synchrophasors can be measured at all network buses and assembled at the system control center to form a coherent picture of the

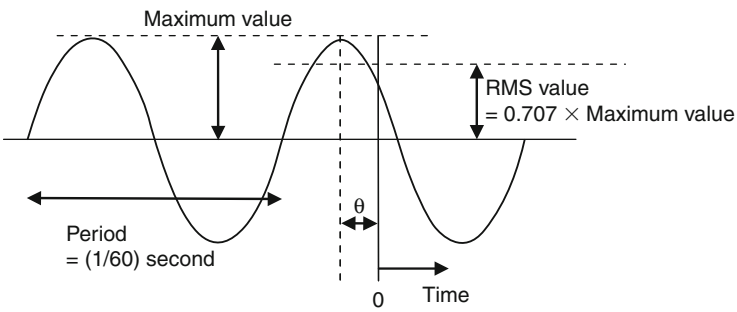

Wide Area Monitoring, Protection and Control. Figure 1
A sinusoidal voltage or current and its phasor representation

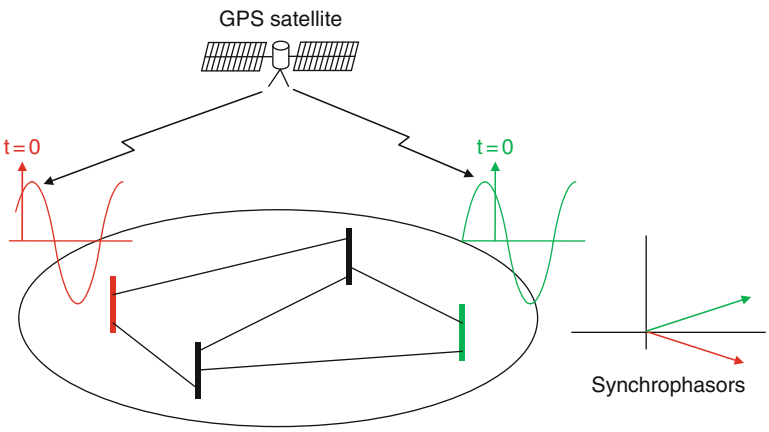

Wide Area Monitoring, Protection and Control. Figure 2
Voltages and currents in substation at different locations

state of the power system. Such a picture can be refreshed as frequently as once per cycle of the power system frequency and is thus able to track the behavior of the power system as it goes through normal or abnormal changes brought about by daily load variations or major disturbance. This ability to monitor the power system continuously with precise simultaneous measurements is made possible by the technology of the synchrophasors.

Importance of Positive Sequence Measurements

The entire AC power system is made up of three-phase sources and loads. (Three-phase system makes the most economical use of the capability of large generators and motors.) The three phases are considered to be balanced in most normal operating conditions. When faults or unusual disturbances occur, the system may become severely unbalanced, but such unbalances last only for a short time, and the system soon returns to a balanced state. It is well to provide a more precise definition of balanced operation.

When the voltages and currents in a three-phase AC system are of equal magnitude and differ in phase from each other by equal amounts (360°/3 = 120°), the system is said to be balanced. This is illustrated in Fig. 3, where the three signals (voltages or currents) of the three phases are illustrated by red, green, and blue colors. The three phases are usually labeled.

"a," "b," and "c" in most power systems, although in some countries, they are referred to by three different colors (red, yellow, and blue). If the power system is balanced, it turns out that it is not necessary to consider it to be a three-phase system in most computational tasks; all analyses can be performed in a single-phase mode, and from the single-phase results, the conditions in the three phases can be inferred. This leads to much simpler computational procedures for all power system problems. Technically, this single-phase representation is known as the "*positive sequence*" representation. In general, a three-phase parameter (voltage, current, or impedance) can be represented by three "sequence" components: positive, negative, and zero. Under balanced conditions, only the positive sequence component exists, and the negative and zero sequences are zero. When severe unbalances occur (e.g., when there is a line to ground fault), negative and zero sequence components become significant. Even in normal operation, there may be a small amount of unbalance present in the power system; thus, small amounts of negative and zero sequence components may exist on the power system during normal operating conditions. However, for most analyses, it is assumed that the unbalance can be neglected, and the power system may be assumed to be balanced; hence, only a single-phase representation using positive sequence voltages, currents, and impedances is appropriate.

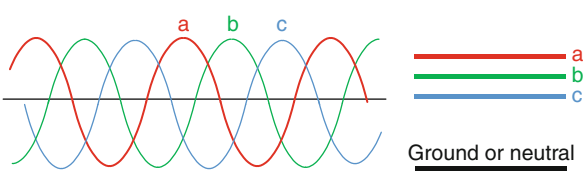

Wide Area Monitoring, Protection and Control. Figure 3 Balanced voltages and currents in a three-phase power system

Since most power system problems are handled with positive sequence quantities, it is most advantageous to measure synchrophasors of positive sequence voltages and currents. This is accomplished by measuring synchrophasors of individual phase voltages and currents (X_a, X_b, and X_c) and calculating positive sequence synchrophasors (X_1) from them:

$$X_1 = 1/3\left[X_a + \left(-1/2 + j\sqrt{3/2}\right)X_b + \left(-1/2 - j\sqrt{3/2}\right)X_c\right]$$

Phasor Measurement Unit (PMU)

Synchrophasors are measured by Phasor Measurement Units (PMU) installed in power system substations. A simplified schematic diagram of the PMU is shown in Fig. 4.

Currents and voltages from the power system are transformed to measurement levels by instrument transformers, which are then supplied to the filter stage of the PMU which removes destructive induced voltages and currents as well as higher frequencies in order to avoid aliasing errors in the sampled data. The GPS receiver provides the 1 pps from the GPS satellites and is divided into desired sampling rates by a phase-locked clock. Typical sampling rates may vary between

12 samples per cycle of the power frequency to higher sampling rates measured in kilohertz. The phasor processor converts samples of each phase into a synchrophasor and finally into a positive sequence synchrophasor measurement which is assigned a time stamp before the measurements are transmitted over a suitable communication network to provide a stream of synchrophasor measurements. Typical reporting rates for the synchrophasors are of the order of once every cycle to once every few cycles depending upon the user's requirements.

WAMS Architecture Overview

WAMS (Wide Area Measurement System) consists of Phasor Measurement Units (PMU) installed in power system substations and connected to one or more layers of Phasor Data Concentrators (PDC) so that system-wide phasor data can be made available at various regional or central locations for engineering applications (see Fig. 5). The PMUs are placed in substations, where they collect voltage and current data. If multiple PMUs exist within one substation, their outputs are streamed to a PDC within the substation – shown in yellow color – over a local area network (LAN). Where there is one PMU per substation, the data from those PMUs and the substation PDC is connected to a regional PDC – shown in green color – over a wide area network (WAN). Regional PDCs in turn can be connected to a central PDC – shown in blue color – over another WAN. Each PDC basically collates data from the lower-level devices and by matching their time stamps creates a data stream as though it was a PMU with many inputs. The PDC may also remove faulty data, deselect some data, or alter the phasor reporting rate as required by specific applications.

The LAN and WAN are likely to be private wired or fiber-optic communication networks on which high communication rates can be achieved. It is not expected that public WAN would be used for this purpose, as the questions of security and communication delays may rule this option out. In many cases where fiber-optic options are not available, digital microwave, leased phone lines, or any other available communication channels may be utilized by the WAMS system. Of course, the throughput rate as well

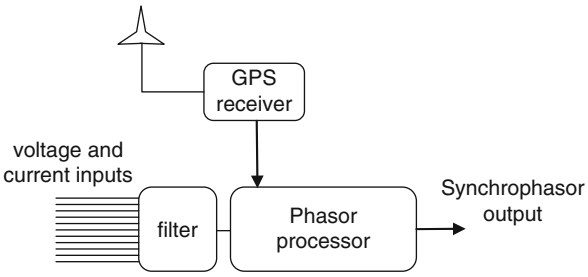

Wide Area Monitoring, Protection and Control. Figure 4
A simplified block diagram of a generic PMU

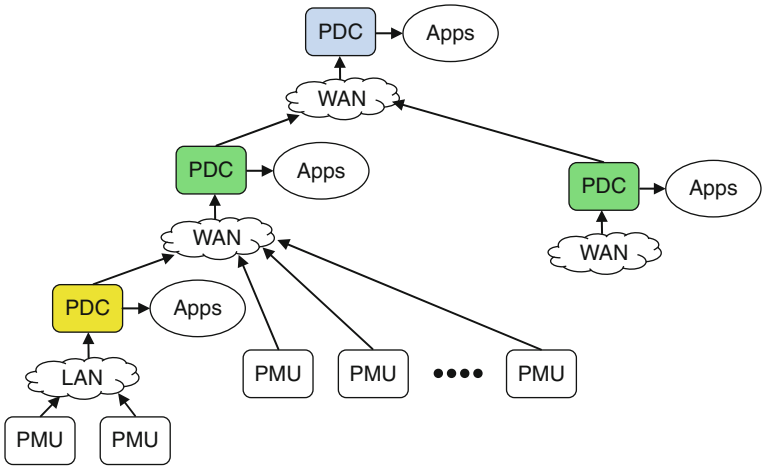

Wide Area Monitoring, Protection and Control. Figure 5
Wide area measurement system architecture

as data latency of communication media dictates which of the WAMS applications can be successfully implemented in such systems.

Suitable application tasks may be implemented at each PDC. Clearly, the data available at each PDC covers differing regions of the power system. Applications of WAMS for power system monitoring, protection, and control will be described in the following sections, where the amount of data needed by a specific application and the region of the power system which must be visible to the application will be discussed. As a general rule, the applications at lower levels of PDC require lesser amounts of data and respond more quickly than those at higher-level PDCs. In general, it has been found that the fast-responding applications can tolerate measurement latencies in the order of 50–100 ms.

Power System Monitoring

Reconstruction of Events

The job of reconstructing the events involved in a major disturbance is a daunting one. Months and immense effort is involved. It is typically difficult even to determine the sequence of events. Phasor measurements with precise time tags were not numerous in 2003, but the few that did exist stood out among the unsynchronized data. From the simple function of fault recorders to complicated reconstructions involving thousands of buses, time-synchronized measurements are vital.

State Estimation

One of the conclusions of the report on the 1965 Northeast blackout was that, at that point, power system operators had insufficient information about the system they were controlling. State estimation and the modern energy management system were created to deal with these problems. Early state estimation "polled" SCADA systems connected to Remote Terminal Units in substation by moving systematically from substation to substation covering the entire system is the total scan. The measurements were power flows on lines, power inputs (injections) into buses, and occasional voltage magnitudes. It was necessary to assume that the system was *static* during the scan, i.e., the system did not change during the scan. Another view of the resulting estimate of the state is that it is the state of a hypothetical system which could support the complete set of measurements. Depending on how long the scan takes and the changes in the system that took place during the scan, the hypothetical system may not exist or may be quite different from the real system. The state of the power system was taken as the positive sequence voltages at the buses which could not be measured directly. The measurements and the estimated state were all complex numbers, magnitudes and angles, or real and imaginary parts. The calculation had to solve large numbers of nonlinear equations and was iterative. That combined with the data scan made the process slow with new estimates available every few minutes [1]. The result was a picture of the state of the system presented to operators and to the software that did the energy management (contingency analysis, for example). Faster computers and improved communication have reduced minutes to seconds over the decades.

The complex voltage at bus k with angle θ_k and magnitude V_k is given by

$$E_k = V_k e^{j\theta_k}$$

The measurements are complex flows and injections. The real power flow from bus r to bus r with a series impedance z_{rs} between r and s and a shunt admittance at bus r of y_r is

$$P_{rs} = V_r^2[|Y_{rs}|\cos(\beta_{rs}) + |y_r|\cos(\alpha_r)] - V_r V_s \cos(\theta_r - \theta_s - \beta_{rs})$$

where α_r and β_{rs} are the angles of the admittance of the series and shunt branch respectively:

$$\frac{1}{z_{rs}} = |Y_{rs}|e^{-j\beta_{rs}} \quad y_r = |y_r|e^{j\alpha_r}$$

In general, the measurements depend on the states which are complex voltages $\mathbf{V}$ at angle $\boldsymbol{\theta}$.

$$\mathbf{z} = \mathbf{g}(\mathbf{V}, \boldsymbol{\theta}) + \boldsymbol{\varepsilon}$$

Usually, the measurement errors are assumed to have zero mean and are independent, with a diagonal covariance matrix $\mathbf{W}$:

$$\mathrm{E}\{\varepsilon\} = 0, \quad \mathrm{E}\{\boldsymbol{\varepsilon}\boldsymbol{\varepsilon}^{\mathrm{T}}\} = \mathbf{W}, \quad \mathrm{w_{ij}} = 0, \quad \mathrm{w_{ii}} = \sigma_{\mathrm{i}}^2$$

The estimate is formed by minimizing the weighted differences between the actual measurements and the

computed measurement as a function of **V** and **θ.** The weights are the inverse of the covariances giving more weight to better measurements and less to low-quality measurements:

$$J(\mathbf{V},\boldsymbol{\theta}) = [\mathbf{z} - \mathbf{g}(\mathbf{V},\boldsymbol{\theta})]^{\mathbf{T}}\mathbf{W}^{-1}[\mathbf{z} - \mathbf{g}(\mathbf{V},\boldsymbol{\theta})] = \sum_{i=1}^{m} \frac{(z_i - g_i(V,\theta))^2}{\sigma_i^2}$$

Writing a Taylor expansion about the last iterate $\mathbf{V}^{\mathbf{k}}$, $\boldsymbol{\theta}^{\mathbf{k}}$:

$$\mathbf{g}(\mathbf{V},\boldsymbol{\theta}) = \mathbf{g}(\mathbf{V}^{\mathbf{k}},\boldsymbol{\theta}^{\mathbf{k}}) + \mathbf{G}\begin{bmatrix} \mathbf{V} - \mathbf{V}^{\mathbf{k}} \\ \boldsymbol{\theta} - \boldsymbol{\theta}^{\mathbf{k}} \end{bmatrix}$$

where **G** is a matrix of first partial derivatives of the elements of **g** with respect to the components of **x** evaluated at x^k. If

$$\begin{bmatrix} \Delta\mathbf{V} \\ \Delta\boldsymbol{\theta} \end{bmatrix} = \begin{bmatrix} \mathbf{V} - \mathbf{V}^{\mathbf{k}} \\ \boldsymbol{\theta} - \boldsymbol{\theta}^{\mathbf{k}} \end{bmatrix}, \quad \Delta\mathbf{z} = \mathbf{z} - \mathbf{g}(\mathbf{V}^{\mathbf{k}},\boldsymbol{\theta}^{\mathbf{k}})$$

then one step in the iteration is given by

$$\mathbf{G}^{\mathbf{T}}\mathbf{W}^{-1}\mathbf{G}\begin{bmatrix} \Delta\mathbf{V} \\ \Delta\boldsymbol{\theta} \end{bmatrix} = \mathbf{G}^{\mathbf{T}}\mathbf{W}^{-1}\Delta\mathbf{z}$$

$$\mathbf{H}\begin{bmatrix} \Delta\mathbf{V} \\ \Delta\boldsymbol{\theta} \end{bmatrix} = \mathbf{G}^{\mathbf{T}}\mathbf{W}^{-1}\Delta\mathbf{z}$$

The gain matrix **H** is large and sparse, and the equation is usually solved with Gaussian elimination. The matrix **G** is sparse much like the load flow Jacobian. By organizing the measurements into active and reactive power, the equivalent of the fast decoupled load flow can be used to simplify the expression further. With real or active power measurements (sub A) first followed by reactive power (sub R):

$$\mathbf{z} = \begin{bmatrix} \mathbf{z_A} \\ \mathbf{z_R} \end{bmatrix}, \quad \mathbf{z_A} = \begin{bmatrix} \mathbf{P_{km}} \\ \mathbf{P_k} \end{bmatrix}, \quad \mathbf{z_R} = \begin{bmatrix} \mathbf{Q_{km}} \\ \mathbf{Q_k} \\ \mathbf{V_k} \end{bmatrix}$$

and states as angles followed by voltage magnitudes to form

$$\begin{bmatrix} \mathbf{H_{AA}} & \mathbf{0} \\ \mathbf{0} & \mathbf{H_{RR}} \end{bmatrix}\begin{bmatrix} \Delta\boldsymbol{\theta} \\ \Delta\mathbf{v} \end{bmatrix} = \mathbf{G}^{\mathbf{T}}\mathbf{W}^{-1}\begin{bmatrix} \Delta\mathbf{z_A} \\ \Delta\mathbf{z_R} \end{bmatrix}$$

Using the assumptions from the fast decoupled load flow (small angle difference, voltage magnitudes near 1, and large X/R for the lines), the off diagonal blocks of **H** are zero. An approximate **H** can even be computed with angles set equal to zero and voltage magnitudes set equal to one at the cost of more iterations.

The addition of even a few direct measurements of angle to the previous formulation has a number of advantages and creates symmetry in the problem statement. When angle measurements are included, z_A and z_R both have three entries [2, 3]:

$$\mathbf{z} = \begin{bmatrix} \mathbf{z_A} \\ \mathbf{z_R} \end{bmatrix}, \quad \mathbf{z_A} = \begin{bmatrix} \mathbf{P_{km}} \\ \mathbf{P_k} \\ \boldsymbol{\theta}_\mathbf{k} \end{bmatrix}, \quad \mathbf{z_R} = \begin{bmatrix} \mathbf{Q_{km}} \\ \mathbf{Q_k} \\ \mathbf{V_k} \end{bmatrix}$$

The matrix **G** is modified in an obvious manner, but otherwise, the previous development applies. In order to use the PMU measurements in the conventional SCADA-based system, it is also necessary to put those measurements on the same reference as the convention estimate which has a reference bus. This generally requires the addition of a PMU at the reference bus.

PMUs can also measure the currents in lines connected to the bus. The addition of line currents measurements can be used to compute the bus voltages on adjacent buses if the line model is known. The PMU measurements of both voltage and current have time tags and are different in nature from the SCADA measurements but can improve the conventional estimates even if the time tag is not used and the PMU data is simply treated as additional SCADA data.

PMU-Only Estimators

A modest number of PMUs will permit a PMU-only measurement system for selected parts of the system. For example, a PMU-only estimator for the 500-kV portion of a utility is quite possible. Phasor measurements of the bus voltages and line currents at some 500-kV buses can form the basis of a linear estimate for the 500-kV system that can be updated as often as once a cycle. There have been studies of the number of PMUs required, their location, the phasing in of such systems, and their reliability [4–6]. While the results of these papers are interesting, the actual sequence of installation of PMUs and the locations of the PMUs are frequently far from optimal. Many other issues influence these decisions in the real world.

Even recognizing the practical side of the problem, the theoretical results are that fewer PMU are required

than might have been imagined. If we assume that any PMU can measure the bus voltage and all of the line currents at that bus (for a large number of lines, this may not be true for some PMUs, and more than one PMU must be installed in a substation), then the problem of the minimum number of substations required to measure the state of the system can be solved. The most direct solution technique uses the node-node incidence matrix for the system. The matrix A has only 0s and 1s with $A_{ii} = 1$ and $A_{ij} = 1$ if there is a line from bus i to bus j. Using a vector x which has a one in position j if substation j is equipped with PMUs, then for any x the product y = Ax can be formed. Then, y_k is the number of times the voltage at bus k is seen by the various PMUs. If x = [1 0 0 1 0 0 1 0 0 1 0 0 1 0]' indicating PMUs at bus 1, 4, 7, 10, and 13 in the IEEE 14 bus system with A matrix below, then y = [1 2 1 2 2 1 2 1 3 1 1 1 1 1]', indicating that monitoring these five buses can completely observe the system. Nine of the buses are seen by only one PMU, however.

Assuming that only some PMU measurements of bus voltages and line currents are used in the estimate, consider the pi equivalent for a transmission line in Fig. 6. The state of the system is the set of complex bus voltages. The measured currents are linear function of the state, assuming the line parameters are known.

The measurements at both ends of the line are

$$\begin{bmatrix} E_p \\ E_q \\ I_{pq} \\ I_{qp} \end{bmatrix} = \begin{bmatrix} 1 & 0 \\ 0 & 1 \\ y_{pq} + y_{p0} & -y_{pq} \\ -y_{pq} & y_{pq} + y_{q0} \end{bmatrix} \begin{bmatrix} E_p \\ E_q \end{bmatrix}$$

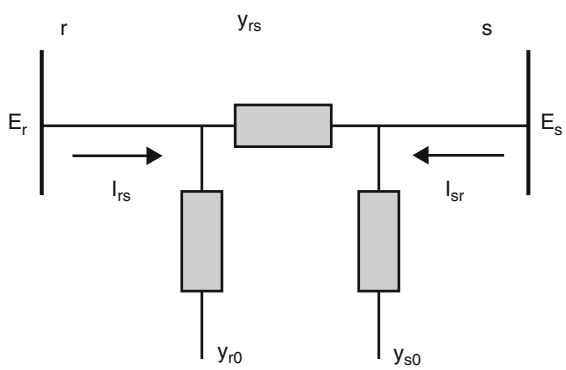

Wide Area Monitoring, Protection and Control. Figure 6 Pi equivalent of a transmission line

For a more complex network, the measurements can be written as

$$\mathbf{z} = \begin{bmatrix} \mathbf{II} \\ \mathbf{YA} + \mathbf{Y_s} \end{bmatrix} [\mathbf{E_b}] = \mathbf{BE_B}$$

where **II** is related to a unit matrix with diagonal entries equal to one where a voltages is measured and zero otherwise. The second set of measurements are the currents expressed as flows in the shunt elements through y_s and in the series branches. **A** is an incidence matrix, and y is a matrix of series impedances. The matrices **Y** and $\mathbf{Y_s}$ are complex while the entries in **II** and **A** are only zeros and 1. With **Y = G + jB** and **Ys = Gs + jBs**, both the measurements and states can be written as real and imaginary, and the real products are (real*real-imag*imag) and the imaginary product as (real*imag + imag*real) to form

$$\begin{bmatrix} \mathbf{z_r} \\ \mathbf{z_x} \end{bmatrix} = \begin{bmatrix} \begin{bmatrix} \mathbf{II} \\ \mathbf{GA} + \mathbf{G_s} \end{bmatrix} & \begin{bmatrix} \mathbf{0} \\ -\mathbf{BA} - \mathbf{B_s} \end{bmatrix} \\ \begin{bmatrix} \mathbf{0} \\ \mathbf{BA} + \mathbf{B_s} \end{bmatrix} & \begin{bmatrix} \mathbf{II} \\ \mathbf{GA} + \mathbf{G_s} \end{bmatrix} \end{bmatrix} \begin{bmatrix} \mathbf{E_r} \\ \mathbf{E_x} \end{bmatrix} + \boldsymbol{\varepsilon}$$

$$\hat{\mathbf{x}} = (\mathbf{B}^T\mathbf{W}^{-1}\mathbf{B})^{-1}\mathbf{B}^T\mathbf{W}^{-1}\mathbf{z} = \mathbf{Mz}$$

The estimate is then given by the least squares solution where **W** is the covariance of the measurement errors. Note that the matrix **M** is constant, can be computed off-line, and only changes when there is a change in topology (a breaker opening). The resulting estimate is free of the static assumptions and truly dynamic.

Instrument Transformer Calibration for All-PMU Estimators

The network in Fig. 7 shows CTs and CVTs. A precision PT is shown in red. All CTs and CVTs are assumed to have a ratio correction factor: k_i. The true voltages and currents satisfy network equation: $E_t = ZI_t$. The actual measurements are related to true values by the ratio correction factors: $I_m = k_iI_t$. and $E_m = k_eE_t$. A set of E_m and I_m is obtained over several points during daily load variation. With sufficient number of such measurements, a WLS solution for the ratio correction factors can be formed [7]. Large numbers of simulations have shown that the k's can be determined with high accuracy (equal to that of the good PT).

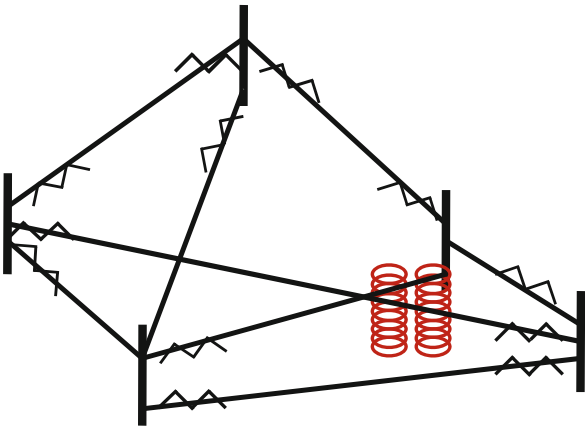

Wide Area Monitoring, Protection and Control. Figure 7 Three-phase CTs and CVTs with a precision PT

With the notation of the PMU-only estimator, the calibration problem can be written as

$$\mathbf{z} = \mathbf{KBx}$$

where K is a diagonal matrix of ratio correction factors, and x is the set of complex bus voltages. Both the k's and the x's are to be estimated. It is clear that with a k for every measurement that there are too many unknowns in that if **K** and **x** are solutions the α**K** and **x**/α are also solutions. For this reason, one ratio correction factor is taken as 1 (the voltage measurement is taken as being correct); the k is removed from the set of unknowns. A precision PT or a new high-quality CVT can be used for this purpose.

The estimation of all the k's and all the x's from one set of measurements is not possible. It is also necessary for the states to be sufficiently different to estimate all the ratio correction factors. A possible approach is to perform the calibration place over a 12-h period with measurements at a 1-h interval used for the calibration. The calibration is a batch solution for all the states (12* the dimension of the state) and the ratio correction factors. It is also assumed that:

1. The transformer ratio correction factors are constant over the simulation period.
2. At least one PT is perfect, which can be used as reference to calibrate other current and voltage transformers.
3. The system model (network impedance matrix) is accurate.
4. The 12 cases are used to get 12 different operating conditions which are sufficiently redundant to estimate the ratio correction factors of transformers.

Each PTs and CTs have a ratio error of the form:

Measurement = M* True

where M is the ratio correction factor M = |M| $\angle\theta$, where both M and θ are randomly distributed with zero mean. If the precision PT is not perfect but has a known accuracy η, then all the CTs and PTs will have essentially that accuracy.

Seams

Creating a single state estimator for the connection of two large independent systems each with large state estimators is a challenging task. The individual estimators may each involve tens of thousands of buses and represent many years of effort. The estimators may be of different types, come from different vendors, involve different rates, etc. The proposal that two 30,000 bus estimators be merged into one 60,000 estimator is liable to fall on deaf ears. At the simplest level, the problem can be solved by recognizing that the only problem is that the estimators have different references and place two PMUs to measure the difference in the references. A PMU at the reference bus for system 1 and a PMU at the reference bus for system 2 would be sufficient.

A slightly more elaborate solution is to include some buses near the boundary in both systems. This could be done by considering tie lines to be in both systems as shown in Fig. 8.

If ϕ is the angle between the references for the two systems and there are nb boundary buses, a more refined estimate of V can be obtained by averaging over the boundary buses as

$$\hat{\varphi} = \frac{1}{\mathrm{nb}} \sum_{\mathrm{i}}^{\mathrm{nb}} (\hat{\theta}_{1\mathrm{i}} - \hat{\theta}_{2\mathrm{i}})$$

where the terms in the sum are the difference between the estimated angles at bus I in the two systems. A further refinement, [8], can be made by forming a performance index including the differences between the measured and calculated real and reactive flows in the tie lines that can be minimized by choice of the angle difference ϕ.

Protection

Several areas of application of synchrophasors to protection are "adaptive" (sections "Adaptive Security/Dependability," "Adaptive Out-of-Step," and "Adaptive Loss-of-Field"). Traditionally, relays were set, and the setting could only be changed by a visit to the substation. Microprocessor relays allowed the relay engineer to change setting remotely, and the concept of adaptive protection introduced the possibility of automatic response to system conditions. "Adaptive protection is a protection philosophy which permits and seeks to make adjustments automatically in various protection functions in order to make them more attuned to prevailing system conditions" [9]. PMUs have made adaptive protection possible. There is an extensive literature on a variety of adaptive protection applications [9–15].

Adaptive Security/Dependability

Traditionally, relays have been biased toward dependability where dependability is defined as the "degree of certainty that a relay or relay system will operate correctly." There is an inevitable trade-off between dependability and security, "the degree of certainty that a relay or relay system will not operate incorrectly," that is, incorrect relay operations are either failure to trip in situations in which they should trip or trips in situations when they should not trip. With multiple primary relays (as many as three) and multiple backup relays (both zone 2 and zone 3), the existing system is heavily biased toward dependability. Examination of NERC data indicates that incorrect relay operations are involved in two third of major disturbances, not necessarily as the initiating event but as a contributing factor to cascading outages. The mechanism of "hidden failures" in relays underlies relay involvement in major disturbances. A hidden failure is "a defect or error in relay that does not manifest itself immediately but which can cause a miss-operation when the system is stressed." The largest cause of hidden failures is thought to be maintenance. The Internet and Chemical plants also have maintenance-related hidden failures.

The solution to at least some relay involvement in cascading outages is to adjust the security/dependability balance when the system is stressed. One simple way to accomplish this is to require that two of the three relays see the fault before tripping the breaker. This voting procedure only requires altering the way the outputs of the primary relays are combined. The relay logic itself is left unchanged. The PMU contribution to process is to determine if the system is in a stressed condition. Figure 9 shows a voting scheme.

In a specific application, the location of the relays that will vote has to be identified. Important paths or tie lines whose loss would have a serious impact are obvious choices. Then, the location of the phasor measurement and the logic of translating measurements into a decision to vote have to be determined. One successful approach to these two problems is the use

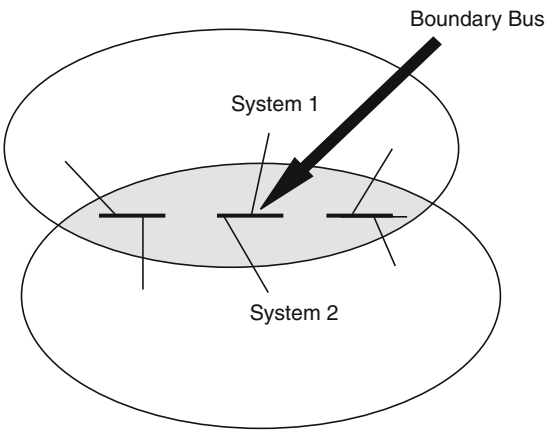

Wide Area Monitoring, Protection and Control. Figure 8 Boundary buses between two systems

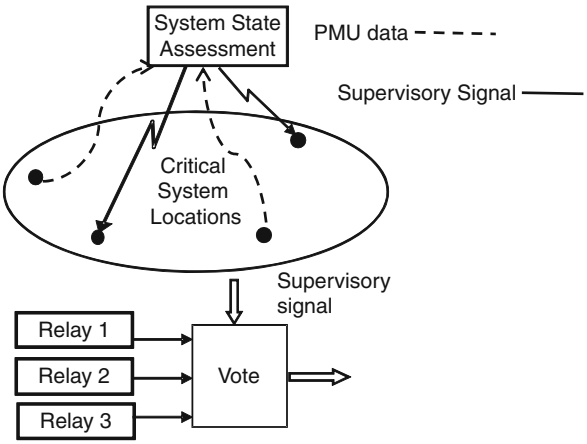

Wide Area Monitoring, Protection and Control. Figure 9 An adaptive security/dependability protection scheme

of decision trees. The tree is trained with a selection of a large number of scenarios where it can be determined that a vote would be beneficial combined with a similar set of scenarios in which voting is not necessary. For example, if the path included parallel lines, the loss of an additional line due to a hidden failure can have serious consequences. Many transient stability simulations have to be performed to determine conditions where voting is indicated. The tree is selected with data mining software from an array which has a row for each events and a column for every measurement that might possibly be used. All bus voltages and line currents in the area could be included in the matrix, for example. The last column has a 1 for voting and a 0 for not voting. The data mining software selects the measurements to be used to form a tree.

A tree is shown in Fig. 10. The grey boxes are splitting nodes while the white and textured boxes are terminal nodes. The first splitting node selects one measurement and tests that measurement value against a threshold. The remaining splitting nodes also use only one variable, and it is possible that the same variable can be reused in other splitting nodes with different γ's. The tree finds both the measurement m_k and the threshold γ. Typically, the initial splitting nodes for these power system problems are quite effective, and the splitting nodes lower in the tree are making fine corrections: $m_k \leq \gamma$ *or* $m_k > \gamma$ splitting logic.

Monitoring Approach of Apparent Impedances Toward Relay Characteristics

Relay settings are made at the time of commissioning of the substation and the protection system. Once made, these settings are generally not subjected to periodical review. Although this is not a universal practice, more and more power companies have limited manpower available for such tasks, and it is usually the case that the relay settings are seldom if ever revisited.

It is a fact that many of the relay settings are based upon certain assumptions made about the power system configuration and load levels. This is particularly true about the slower protection functions such as backup zones of distance relays, loss-of-field relays, etc. As years go by, the relay settings which depend upon system conditions may no longer be appropriate for the prevailing power system conditions because of the natural evolution of the power system. As the relay settings become inappropriate, the possibility of false trip of such relays becomes likely. One of the watershed blackout events is the 1965 blackout in North Eastern United States. The settings of some relays involved in this event were made 9 years before the event and had become inappropriate for the system conditions existing in 1965. Misoperation of these relays was a main contributing factor of this blackout.

PMUs employed for WAMS can be programmed to track the behavior of apparent impedance continuously and provide an alarm to the relay engineers that the apparent impedance trajectory recently (on recorded date and time) came within a prescribed distance of the trip characteristic. This is particularly effective when distance relays are used for the protection function. The concept is illustrated in Fig. 11.

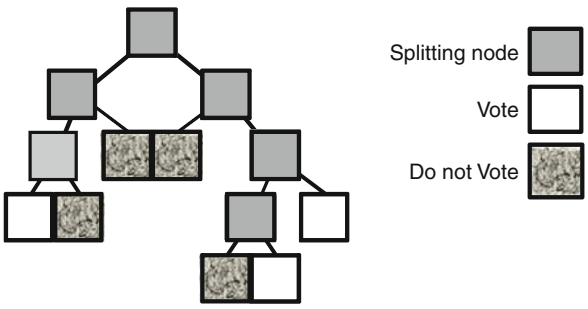

Wide Area Monitoring, Protection and Control. Figure 10
A decision tree with five splitting nodes

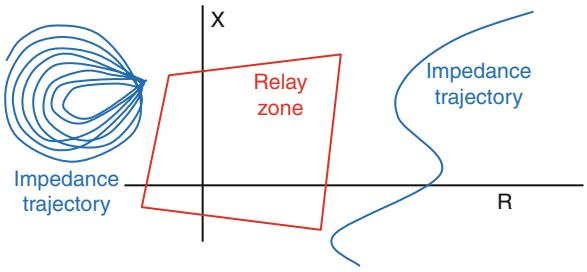

Wide Area Monitoring, Protection and Control. Figure 11
Zone setting of the relay in question is shown in *red*. Impedance trajectories are shown in *blue*, and two types of trajectories – one corresponding to stability swing and the other to load changes – are shown

The figure shows that load changes as well as stability swings did indeed come close to the relay zone, and a message to this effect is sent to the relay engineer responsible for this setting. After reviewing the incident, the relay engineer may decide to review and modify the relay setting, or ignore the alarm confirming that the setting is in fact appropriate for the prevailing power system state.

Adaptive Out-of-Step

Out-of-step (OOS) relaying is used to determine if a major power system disturbance is likely to result in loss of synchronization between groups of generators in the system and lead to island formation of portions of the power system. The present practice is to use distance relays at the terminals of generators or on transmission lines which lie at the electrical center of expected system disturbances. The traditional OOS has a characteristic as shown in Fig. 12 with an inner zone and an outer zone in the relay impedance plane. Using large number of transient simulations performed on the power system, the settings of these relay zones are determined. The inner zone is such that no stable power swing crosses into it, while unstable swings are expected to cross the outer and inner zones in sequence. A timer is set somewhat greater than the largest dwell time of the unstable impedance trajectory between the two zones. The zone boundaries and the timer are then used to detect whether or not a prevailing disturbance will lead to instability.

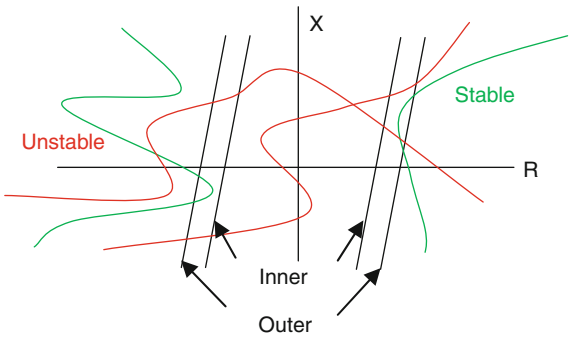

Wide Area Monitoring, Protection and Control. Figure 12
Traditional out-of-step relay characteristic. All stable swings remain outside the inner zone while the unstable swings cross the outer and the inner zones in time which is shorter than the timer setting of the relay. Stable swings are shown in *green*, while unstable swings are shown in *red*

The traditional out-of-step relays are often inadequate when the power system changes or when unanticipated outages occur. In such cases, the relay settings may not be appropriate to the prevailing system conditions, and the OOS relay is likely to misoperate.

Adaptive out-of-step relaying principle proposes to use real-time measurements to determine whether or not an evolving disturbance is going to lead to instability. The most promising real-time measurements to achieve this goal are the phasor measurements provided by the PMUs. In this approach, the first step is to detect the formation of coherent groups of generators and, once the coherent groups have been determined, to predict the likely outcome of power swings between the coherent groups. In order to determine coherency between generators, it is necessary to track the rotor angles of generators in time as the disturbance evolves. The rotor angles are determined from phasor measurements performed at the terminals of the generators and then using the generator equivalent circuit to determine rotor angles. In many cases, it is sufficient to track the behavior of the positive sequence voltage angle at the generator terminals. Figure 13 illustrates the concept of this type of adaptive out-of-step relaying.

It is of course possible that there are some unusual disturbances whereby it is not possible to identify the coherent groups or make a successful prediction based upon an observation window. However, a success rate of around 90% seems to be possible in most power systems and should be considered to be a good outcome of the adaptive out-of-step relaying principle.

Supervision of Backup Zones

Distance relays are used to protect transmission lines. It is common practice to use three zones of distance relays to cover the complete transmission line (with zones 1 and 2) and provide a backup protection for neighboring transmission lines with zone 3. The three zones are given different operating times – zone 1 being the fastest, zone 2 having an operating time of about 300 ms, and zone 3 operating in about 1 s, thus giving

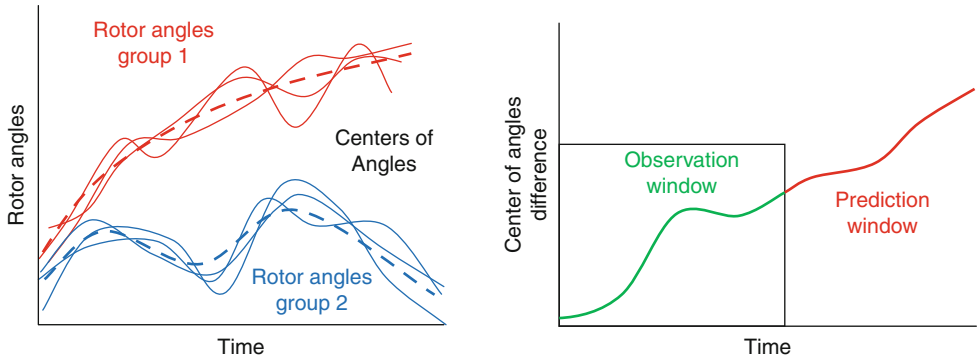

Wide Area Monitoring, Protection and Control. Figure 13
Adaptive out-of-step relaying principle. Generator rotor angles are monitored to determine whether coherent groups are being formed. Once the coherent groups are formed, a prediction regarding the outcome of the swing can be made

enough time for relays of the neighboring lines to operate if there is a fault on those lines. Backup zones of protective relays – in particular the third zone of distance relays – are known to be encroached upon by load swings during system disturbances. As load excursions in the relay protective zones lead to incorrect trips, this usually leads to a worsening situation and accelerates the approach to cascading system failures. Some engineers have recommended getting rid of these overreaching zones completely in order to avoid false trips of this type. However, there are documented cases [16] where it is found to be essential to have zone-3 protections in order to back up neighboring circuits when their primary protection fails for some reason [16]. It then becomes necessary to consider ways in which the overreaching zones of distance relays can be made secure against false trips due to load excursions.

Consider a portion of a power system shown in Fig. 14. Zone 3 of the distance relay at station A (shown in red) is assumed to be picked up because of load excursion during a power system contingency. The decision to be made is whether the zone-3 pickup is due to a fault on lines BC or BD or is in fact caused by a load excursion. If it is a fault on lines BC or BD, at least one of the PMUs located at stations B, C, or D (shown in blue) will indicate a zone-1 fault. If none of the PMUs confirm the existence of such a fault, then zone 3 of the relay at A must be blocked. As zone-3 operating times are of the order of 1 s, there is ample time to get the information from stations B, C, and D to the relay at station A. It should be noted that if an

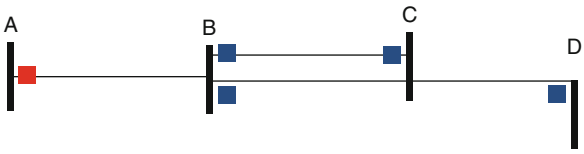

Wide Area Monitoring, Protection and Control. Figure 14
Supervising zone 3 of the distance relay at station A. It is assumed that PMUs exist at stations B, C, and D

unbalanced condition is detected at station A, an unbalanced zone-3 fault is indicated, and the blocking of its operation is not appropriate. As load excursions are balanced phenomena, the blocking logic based upon inputs from B, C, or D is appropriate only under balanced network flow conditions.

Adaptive Loss-of-Field

Large generators in power systems are generally protected against operating with reduced field current. The problem faced by these generators is instability when the field current is suddenly reduced due to some problem in the excitation circuit. The traditional protection against loss-of-field (LOF) uses offset impedance relays connected at the terminals of the generator. The relay settings are determined by the impedance of the generator and the equivalent impedance (Thévénin impedance) of the power system to which the generator is connected. A typical loss-of-field characteristic is shown in Fig. 15.

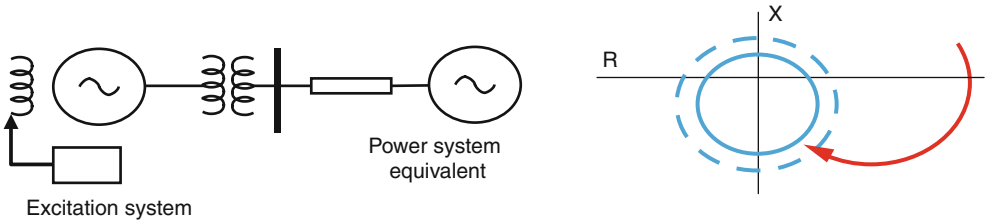

Wide Area Monitoring, Protection and Control. Figure 15
Generator with its excitation system connected to power system. Characteristic of the LOF relay connected to generator terminal is shown on the right

The LOF relay setting consists of two concentric offset impedance circles as shown in the figure in blue color. The inner circle is the actual stability limit, whereas the outer circle shown by dotted line provides an alarm to the operator to take some corrective action before stability limit is reached. The center and radius of the circles are determined by the machine impedance (including the step-up transformer impedance) and the Thévénin impedance of the power system equivalent. A typical impedance trajectory indicating a loss-of-field condition is shown in red: the start of the trajectory is in the first quadrant where the pre-disturbance load is assumed to exist, and as the field current decreases, the impedance trajectory moves in the fourth quadrant and may enter one of the zones of the relay.

During a major disturbance on the power system as transmission lines are lost due to faults or other contingencies, the power system Thévénin impedance may undergo significant changes. These changes should be taken into account and the relay characteristics modified accordingly. If this is not done, it is likely that instability of the generator could result even though the impedance trajectory has not entered the zones set according to "system normal" conditions. An adaptive LOF relay would track the behavior of the power system as it undergoes changes during system disturbances and correct the relay settings automatically to reflect the prevailing state of the Thévénin impedance. In general, the network changes remote from the generator do not affect the Thévénin impedance significantly, and there may be just a few network configurations for which the relay characteristic needs to be changed. The possible contingencies and their corresponding relay settings could be pre-stored as various setting groups in the LOF relay, and when one of these contingencies actually occurs on the system, the relay setting changes to the appropriate group.

Intelligent Islanding

When subjected to catastrophic events, generators in the power system may lose synchronism with each other so that they can no longer continue to operate as components of a single power system. Usually, generators tend to maintain synchronism within individual groups, which could get separated from the rest of the power system. Several islands may be formed in this fashion, each island stabilizing as a separate power system with its own generation, transmission system, and load. If the formation of islands is allowed to happen in an uncontrolled fashion, it is possible that unsustainable islands would be formed, and some islands or the entire power system may be subjected to a blackout. This is the motivation for implementing an intelligent islanding scheme.

The first step in such a scheme is to identify groups of generators which remain coherent as a precursor to forming an island. This concept is illustrated in Fig. 16.

Consider the power system in Fig. 16, which has been subjected to a significant contingency, and as a result, groups of generators shown in red and blue develop rotor movements as illustrated in the swing curves shown on the right. Based upon this movement of rotors, it can be concluded that the group of blue generators is a coherent group, and the red generators form another coherent group. The next step is to match the capacity of blue generators with loads shown in blue, thus making up the structure of the proposed island. The red loads are then teamed with red generators, which are also approximately matched in generated power and load. Having identified load and

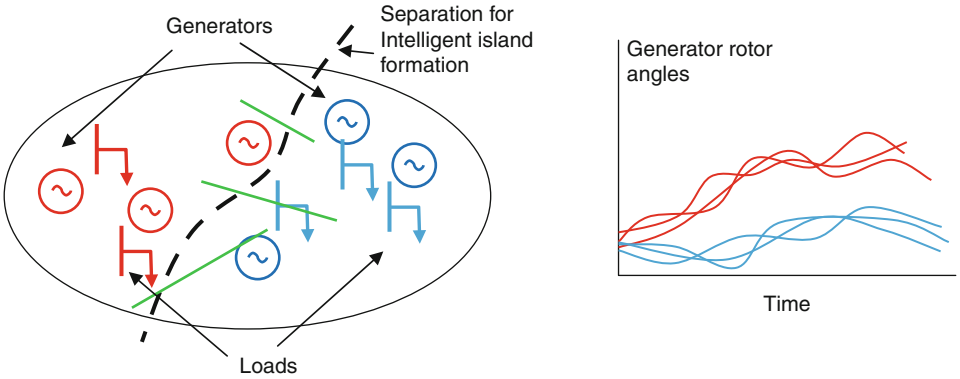

Wide Area Monitoring, Protection and Control. Figure 16
Intelligent islanding principle. Coherency of groups of generators is established, and then possible island with those generators is identified

generation match, the next step is to identify the least number of lines (shown in green) which when opened will create two islands which have the potential to survive as two independent power systems, which can be re-synchronized into a single power system at a later stage.

Intelligent Load Shedding

Most modern power systems are equipped with an underfrequency load shedding scheme by which certain amount of load is shed in order to match available generation with load it can serve. This may become necessary when a block of generation is lost due to faults or other causes, or when the power system has broken up into islands with unequal generation and load. In this scheme, the load shedding is accomplished only after the frequency of the system changes because of the load-generation mismatch. A more intelligent approach to load shedding would be to anticipate the possibility of a load-generation mismatch developing, which may (if unchecked) lead to system islanding. Such an approach requires that an estimate of the load-generation mismatch be formed as soon as it takes place and then shed an appropriate amount of load without waiting for the system to break up into islands and the island frequency to change.

Consider a generic power system shown in Fig. 17. It is a part of an interconnected power system, and it has several tie lines (shown in green) connecting it to the rest of the grid. As the system undergoes a change – such as a loss of some generation – a potential for load-generation imbalance within the boundary of the power system occurs. If changes in the tie line flows are monitored by the Wide Area Monitoring System, it reflects the contributions made by the rest of the grid to aid the power system in riding through this disturbance. From the changes in the tie line flows, an estimate of the impending load-generation imbalance in the system can be made. If it is determined that the potential imbalance is significant, and that if not corrected immediately may lead to islanding of the power system, load shedding could be initiated by supervisory control without waiting for the frequency to decay.

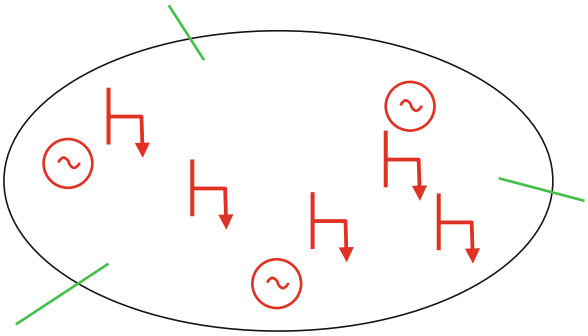

Wide Area Monitoring, Protection and Control. Figure 17
Intelligent load shedding principle. Changes in tie line flows are used to determine load shedding requirements to balance load and generation within the system

A number of simulation studies need to be performed on the complete grid with various scenarios of generation loss. For the cases which lead to islanding in the simulation studies, different amounts of loads to be shed to prevent the formation of island can be established. The results of these studies can then be used as an aid in determining the load shedding required in actual cases of generation loss.

Power System Control

Prior to synchrophasor measurements, essentially all control in the interconnected power system was based on local measurements. Control that responded to the power system frequency was a possible exception since frequency is a global quantity viewed on a long time scale. Many techniques were developed to deal with the limitation of local measurements. A variety of equivalents, coherent groups, and reduced order models were use to develop control strategies. The existence of wide area measurements with time tags opened up the possibility of control based on some remote measurements. Full state feedback as employed in smaller systems is still impossible, but feedback of important variables can be considered. The choice of the control strategy and placement of remote measurements are problem dependent and are current research topics. Concerns with latency in the signals, the performance of data concentrators, and the design of communication networks have delayed control applications more than some other areas.

Control of Sustained Oscillations

Very low frequency lightly damped low-frequency oscillation has been observed in large power systems for decades. The interactions between groups of machines displaced by large distances tend to be at frequencies less than 1 Hz. The analysis of such modes is based on small signal linear models found by linearizing about an operating point. Such Inter-area oscillations are tolerated when they have sufficient damping but can become a serious threat when the damping starts decreasing. The evolution of a 0.27-Hz mode in the WECC disturbance in 1996 is representative. The oscillation began as 0.27 Hz with 7% damping. The tripping of a significant line altered the mode to 0.254 Hz with 3.46% damping which over the course of about 200 s became 0.252 Hz with 1.2% damping. Shortly thereafter, another line tripped, a generator was dropped, and the mode became unstable [17]. In China, in 2008, two system-wide low-frequency-oscillation events occurred respectively in the South China and Central China grids [18]. A 0.4-Hz oscillation was a precursor to the 2003 Eastern China disturbance [18, 19]. The conventional approach to damping such oscillations is to employ a power system stabilizer (PSS). PSSs use local information such as accelerating power, the generator rotor speed deviation, or frequency deviation as input to the regulator to damp oscillations.

Modern digital power system stabilizers [20] still use local measurements of power and frequency and are aimed at single inter-area oscillations. There have also been studies including remote measurements in a coordinated multi-input environment [21, 22]. The number of remote measurements considered in these studies has been small compared to the number of such measurements that are possible. In rapidly growing systems such as the Chinese power system, the limitation of PSSs that are designed for specific modes is more apparent. The need to retune PSSs has prompted investigation of techniques to adapt PSS operation to changing system conditions [23, 24]. The most ambitious approach is to coordinate PSSs, FACTS devices, and DC lines in stabilizing inter-area oscillations [25–28]. Linear feedback based on various robust control techniques have been employed to deal with power system nonlinearity and uncertainty. Time delays have been modeled as uncertain parameters [25], unmeasured portion of the system was represented by unmodeled dynamics [27], and LMI techniques used to design robust H_2/H_∞ controllers [28–33].

Control of Large Oscillations

Faults that remain on the system longer than a "critical fault clearing time" can cause oscillations large enough that the nonlinear nature of the system is exposed. The oscillations are described by a coupled set of nonlinear differential equations. Depending on the complexity of the representation of the generators, each machine can be described from 2 to 20 or more state variables. At the simplest level, the "classical" machine model involves the rotor angle and speed (the derivative of the angle).

If the rotor angle is denoted by δ, the "swing" equation for a single machine in a per-unit system takes the form:

$$M\ddot{\delta} + D\dot{\delta} = P_m - P_e$$

where M is the inertia of the machine, D is the damping, P_m is the mechanical input power, and P_e is the electrical output power. The equation is nonlinear since the electrical power is a function of angle differences, i.e., P_e depends trigonometrically on δ. In equilibrium, $P_m = P_e$, and δ is constant. The equal area criterion in section "Adaptive Out-of-Step" is developed from examination of the swing equation for a single machine. Even in using reduced order modeling in large systems, there are hundreds of coupled nonlinear differential equations to be solved in order to study the transient stability problem. The equations are coupled by the P_e term because every machine connected to machine n has an electrical power contribution to P_e. If the fault duration is too long, the system is moved away from equilibrium on the "fault on trajectory" and begins to oscillate or swings when the fault is cleared. In large systems, the time for one period of a transient swing is a second or more, suggesting that time is available for PMU measurements to be used in control of these oscillations. The means available for control are somewhat limited. Fast valving of steam turbines; insertion of a dynamic brake; generator, reactor, and line switching; control of DC line flow; and FACTS devices are possible. Specific applications of PMU inputs to some of these controls have been reported [34–40]. The use of PMU measurements in these control schemes should improve their performance.

In one study, the control involved the DC lines and was discrete in nature. The PMU measurements were mapped into regions where specific discrete control actions were taken [41]. Many off-line simulations were used to generate the mapping, but no time was involved in real-time computing a control action.

Remedial Action Schemes

Remedial Action Schemes (also known as Special Protection Schemes or System Integrity Protection Schemes – SIPS) are designed to address a problem caused by a relaying action. For example, the loss of one of three parallel lines could overload the remaining two lines. The scheme might not always be enabled but could be armed based on system conditions. If the flow in the lines was large enough, the control scheme could drop load and/or generation when a relaying action removed any of the parallel lines. In some cases, operators arm the RAS scheme. All SIPS are essentially specially designed control and protection systems and can be enhanced with PMU input [42]. The addition of PMU information for SIPS could be managed using the decision tree approach used for adaptive security/dependability in section "Adaptive Security/Dependability" The proper coordination of large numbers of these schemes is an even more challenging problem.

System Restoration

Synch check relays are used to ensure that two AC systems are synchronized. For a system to be synchronized, the frequency, phase angle, and voltage must be within preset limits. Wide area measurements could be used to perform these same functions across breakers used to close tie lines between islands reclosing when the angle differences are within acceptable bounds. If the angles exceed acceptable limits, a generation-load rescheduling within the islands could bring the quantities within limits. The large number of unsuccessful attempts to reclose in Europe in November 2006 gives testimony to the need for real-time angle measurements in restoration [33]. Restoration could only be achieved after the phase angles of separated areas become acceptable.

Artificial Neural Networks (ANN) have been proposed to aid in system restoration [45]. The ANNs can be trained to determine island boundaries for restoration and to determine a sequence of switching operations which would lead to restoration, taking into account overvoltages due to light load conditions and problem caused by cold-load pickup.

Future Directions

Wide Area Measurement Systems utilizing Phasor Measurement Units have become the power system sensors of choice. These systems deliver precise simultaneous measurements of key power system variables from which reliable real-time models of power systems can be created and intelligent monitoring, protection, and control decisions could be implemented.

These measurements also offer one of the most reliable tools for postmortem analyses of catastrophic events taking place on the power systems. From such analyses follows an understanding of realistic models of power system elements and more realistic simulation tools.

The future of this technology holds the promise that power systems of the future will be made more secure – that is, they will be less immune to catastrophic failures – and in rare cases when such failures do occur, their impact will be considerably reduced in its physical extent and duration. This will be made possible through protection and control tasks which take into account precise knowledge of the current state of the system and take actions which are best suited to the prevailing power system conditions.

It is already clear that the technology is making an impact on all major power producers throughout the world. As the world brings into the mainstream of electric power establishment greater number of alternative energy sources, dependence on this technology is going to be even greater as engineers face the challenge of integrating these newer-generation systems which behave in unpredictable and intermittent fashion. Application of this technology in coming years will usher in an era of cleaner, abundant, and reliable supply of electricity to future generations.

Bibliography

Primary Literature

1. Dopazo JF et al (1975) Implementation of the AEP real-time monitoring system. IEEE Trans Power Apparatus Syst 95:1618–1629
2. Thorp JS, Phadke AG, Karimi KJ (1985) Real-time voltage phasor measurements for static state estimation. IEEE Trans Power Apparatus Syst 104:3098–3107
3. Phadke AG, Thorp JS, Karimi KJ (1986) State estimation with phasor measurements. IEEE Trans Power Syst 1:233–241
4. Nuki RF, Phadke AG (2005) Phasor measurement placement techniques for complete and incomplete observability. IEEE Trans Power Deliv 20:2381–2388
5. Gou B, Abur A (2001) An improved measurement placement algorithm for network observability. IEEE Trans Power Syst 16:819–824
6. Abur A (2005) Optimal placement of phasor measurements units for state estimation. PSERC Publication 06–58, Oct 2005
7. Zhou M (2008) Phasor measurement unit calibration and applications in state estimation. Ph.D. dissertation, Virginia Tech
8. Jeffers R (2007) Wide area state estimation techniques using phasor measurement data. Virginia Tech Report prepared for Tennessee Valley Authority
9. Centeno V, De La Ree J, Phadke AG, Michel G, Murphy RJ, Burnett R (1993) Adaptive out-of-step relaying using phasor measurement techniques. IEEE Comput Appl Power 6:2–17
10. Horowitz SH, Phadke AG, Thorp JS (1988) Adaptive transmission system relaying. IEEE Trans Power Deliv 3:1436–1445
11. Rockefeller GD, Wagner CL, Linders JR, Hicks KL, Rizi DT (1988) Adaptive transmission relaying concepts for improved performance. IEEE Trans Power Deliv 3:1446–1458
12. Hedding RA, Mekic F (2007) Advanced multi-terminal line current differential relaying and applications. In: Protective Relay Engineers, 60th annual conference, College Station, 27–29 Mar 2007, pp 102–109
13. Lien K-P, Liu C-W, Jiang J-A, Chen C, Yu C-S (2005) A novel fault location algorithm for multi-terminal lines using phasor measurement units. In: Proceedings of the 37th annual North American power symposium, Ames, Iowa, 23–25 Oct 2005, pp 576–581
14. Lin Y-H, Liu C-W, Jiang J-A (2000) An adaptive fault locator for transmission lines tapped with a source of generation-using synchronized voltage and current phasors, pp 1379–1383
15. Yu C-S, Liu C-W, Yu S-L, Jiang J-A (2002) A novel adaptive PMU-based transmission-line relay-design and EMTP simulation results. IEEE Trans Power Deliv 17:33–46
16. Horowitz SH, Phadke AG (2006) Third zone revisited. IEEE Tran Power Deliv 21:23–29
17. Hauer AJF, Trudnowski DJ, DeSteese JG (2007) A perspective on WAMS analysis tools for tracking of oscillatory dynamics. In: IEEE Power Engineering General meeting, Tampa, 24–28 June 2007, pp 1–10
18. Dong M, Yang D, Huang Y (2008) Analysis on the low frequency oscillation incidents measured by WAMS of central China power grid during the 2008 ice hazard. Cen China Electr Power 21:22–25
19. Zhu F, Liu ZH, Chu L (2004) Achievement and experience of improving power system stability by PSS/excitation control in China. In: IEEE Power Engineering Society general meeting, Denver, 10 June 2004, pp 1767–1771
20. Kamwa I, Grondin R, Trudel G (2005) IEEE PSS 2B versus PSS4B: the limits of performance of modern power system stabilizers. IEEE Trans Power Syst 20:903–915
21. Kamwa I, Gerin-Lajoie L (2000) State-space system identification-towards MIMO models for modal analysis and optimization of bulk power systems. IEEE Trans Power Syst 15:326–335
22. Zhang Y, Bose A (2008) Design of wide–area damping controls for interarea oscillations. IEEE Trans Power Syst 23:1136–1143
23. Yu GL, Zhang H, Xie H, Wang CG (2007) Wide-area measurement-based robust control of power system considering signal's delay and incompleteness. In: Power Engineering Society general meeting, Tampa, 24–28 June 2007
24. Hu G, He R, Yang H, Wang P, Ma R (2005) Iterative Prony method based power system low frequency oscillation mode

analysis and PSS design. In: Transmission and distribution conference and exhibition: Asia and Pacific, Dalian, 2005, pp 1–6
25. Gibbard MJ, Vowles DJ, Pourbeik P (2000) Interactions between, and effectiveness of, power system stabilizers, and FACTs device stabilizers in multimachine systems. IEEE Trans Power Syst 15:748–755
26. Yu Gl, Zhang BH, Xie H, Wang GC (2007) Wide-area measurement-based nonlinear robust control of power system considering signal's delay and incompleteness. In: Power Engineering Society general meeting, Tampa, 24–28 June 2007
27. Li X, Yan Q, Hu Y (2008) Decentralized coordinated robust adaptive control for AC/DC interconnected power system based on WAMS. IEEE Asia-Pacific Conf Circuits Syst 2008: 1896–1899
28. Dou C, Jin S, Bo Z, Jia Q, Xue H (2007) Decentralized stabilizer design for model-based uncertain large interconnected power systems based on WAMS. In: IPES, Singapore, 3–6 Dec 2007, pp 799–806
29. Rao PS, Sen I (2000) Robust pole placement stablizer design using linear matrix inequalities. IEEE Trans Power Syst 15:313–319
30. Soliman M, Emara H, Elshafei A, Bahga, A, Malik OP (2008) Robust output feedback power system stabilizer design: an LMI approach. In: IEEE Power and Energy Society general meeting conversion and delivery of electrical energy in the 21st century, Pittsburgh, 20–24 Jul 2008, pp 1–8
31. De Campos VAF, Da Cruz JJ, Zanetta LC (2006) Pole placement and robust adjustment of power systems stabilizers through linear matrix inequalities. In: Power systems conference and exposition, Atlanta, 29 Oct–1 Nov 2006, pp 2180–2187
32. Bensenouci A, Abdel Ghamy AM (2007) Mixed H∞/H2 with pole placement design of robust LMI-based put feedback controllers for multi-area load frequency control. In: EUROCON, Warsaw, 9–12 Sept 2007, pp 1561–1566
33. Jabr RA, Pal BC, Martin N (2010) A sequential conic programming approach for the coordinated and robust design of power system stabilizers. IEEE Trans Power Syst 25:1627–1636
34. Rostamkolai N (1986) Adaptive optimal control of AC/DC systems. Ph.D. dissertation, Virginia Tech
35. Manansala EC (1989) Adaptive power system control. Ph.D. dissertation, Virginia Tech, Aug 1989
36. Rostamkolai N, Phadke AG, Thorp JS, Long WF (1988) Measurement based optimal control of high voltage AC/DC systems. IEEE Trans Power Syst 3:1139–1145
37. Manansala EC, Phadke AG (1991) An optimal centralized controller with nonlinear voltage control. Electr Mach Power Syst 19:139–156
38. Mili L, Baldwin T, Phadke AG (1991) Phasor measurements for voltage and transient stability monitoring and control. Workshop on application of advanced mathematics to power systems, San Francisco, 4–6 Sept 1991
39. Snyder AF et al (1988) Inter-area oscillation damping with power system stabilizers and synchronized phasor measurements. In: PowerCon 1988, China
40. Smith MA (1994) Improved dynamic stability using FACTS devices with phasor measurement feedback. MS thesis, Virginia Tech
41. Rovnyak S, Taylor CW, Thorp JS (1995) Real-time transient stability prediction–possibilities for on-line automatic database generation and classifier training. In: 2nd IFAC symposium on control of power plants and power systems, Cancun
42. Madani V, Taylor E, Erwin D, Meklin A, Adamik M (2007) High speed control scheme to prevent instability of a large multi-unit power plant. In: Protective Relay Engineers, 2007: 60th annual conference, Clemson power system conference, pp 271–282
43. Sattinger W (2005) Developments in UCTE and Switzerland WAMC course at ETH Zürich, 30 Aug–1 Sept 2005
44. ENTSOE (2003) European network of transmission system operators for electricity. Final Report of the Investigation Committee, 28 Sept 2003 Blackout in Italy. https://www.entsoe.eu/index.php?id=59
45. Bretas AS, Phadke AG (2003) Artificial neural networks in power system restoration. IEEE Trans Power Deliv 18: 1181–1186

Books and Reviews

Horowitz SH, Phadke AG (2008) Power system relaying, 3rd edn. Wiley, Chichester/Hoboken
IEEE Standard C37.118-2005 (Revision of IEEE Std 1344–1995) IEEE standard for synchrophasors for power systems
Kundur P (1994) Power system stability and control. McGraw-Hill, New York
Phadke AG, Thorp JS (2008) Synchronized phasor measurements and their applications. Springer, New York
Phadke AG, Thorp JS (2009) Computer relaying for power systems, 2nd edn. Wiley, Chichester
Rogers G (2000) Power system oscillations. Kluwer, Norwell

Wind Power Balancing

Lennart Söder[1], Hannele Holttinen[2]
[1]Royal Institute of Technology, Electric Power Systems, Stockholm, Sweden
[2]Technical Research Centre of Finland VTT, VTT, Finland

W

Article Outline

Glossary
Definition of the Subject
Introduction

Physical Balancing
Electricity Markets and Production Planning
How Wind Power Changes the Balancing of Systems
Results from Integration Studies
Conclusions and Future Directions
Bibliography

Glossary

Primary control The instant reaction in a power system to keep the continuous balance between production and consumption.

Secondary control Normally automatic changes in the production system in order to release used primary controlled units.

Control area A change in production or consumption in a certain control area will cause an automatic response from the secondary controlled units in the same control area.

Regulating capacity The power plants and consumers which can change their production or consumption when requested in order to keep the balance.

Balancing market A market where regulating capacity can be bid in and the best offers are then used when balancing is needed.

Balancing reserves Regulating capacity that is bid into a balancing market.

Balancing area A change in production or consumption in a certain balancing area will cause an automatic or manual response from the regulating capacity in the same balancing area.

Definition of the Subject

Wind power balancing considers the challenge to keep a continuous balance between total production and total consumption in a power system. The varying wind speed introduces special considerations concerning how to keep this balance in an efficient way. This article is mainly focused on wind power as a part of a larger power system.

Introduction

In a power system there is always a challenge to keep the balance between total production and total consumption. This challenge has existed ever since the first power systems were installed more than 100 years ago. Since 1970 the amount of wind power has grown from a marginal source to levels of more than 50% during some situations in certain parts of some systems. This increase is expected to continue, which means new challenges and requirement of new methods to keep the requested balance in an efficient way.

This chapter provides an overview about the challenges that are faced with the integration of large-scale wind power into the power system. There are always changes in production and consumption in all power systems since the load changes continuously and there are sometimes sudden outages in power plants and/or power lines. Despite these changes, the continuous balance between production and consumption is always kept. With larger amounts of wind power, the net changes in the controllable part of the production and consumption system will increase since wind power changes will increase the overall changes seen by the rest of the system. The challenges include balancing of changes and keeping enough margins for reacting to changes depending on uncertain forecasts. Also, methods for estimation of the size of the increased challenges need to be addressed, as well as efficient market rules for an economic operation.

This chapter first describes the challenge of how to keep the physical balance between production and consumption in any power system, Physical Balancing. This is followed by a section concerning how the planning of the balancing can be organized in an electricity market, Electricity Markets and Production Planning. The next section includes a description of how a power system is affected when the share of wind power increases. Finally results from several larg-scale integration studies and conclusions from the chapter are presented, "Results from Integration Studies" to "Conclusions and Future Directions."

Physical Balancing

The starting point is that electricity cannot be stored. Today, some electricity storage technologies exist but are still not cost effective to be used in large power systems. This means that as soon as electricity is consumed it has to be generated and vice versa, that is, as soon as electricity is generated it has to be consumed. This applies always and is a physical law that cannot be changed. In practice, this means that as soon as a lamp

is switched on, the corresponding electricity has to be produced somewhere else. The other way around it is true that – when a wind or coal power station (or any other power station) generates power – at exactly the same time, the electricity has to be consumed somewhere else. This means electricity cannot "disappear"! There are of course always losses in the power system but these are usually only a few percent (in, e.g., Sweden ca. 10%) of the consumption if the entire chain from the generation feed-in via power lines all the way to the consumer is considered. Losses are caused by power lines and transformers that get warmer when a current flows through them. In practice, this means that total production (= what generators feed into the power system) is always larger than what consumers take out of the power system. Sometime, the words "power shortage" or "excess power" are used in this context. These terms, however, rather refer to economic issues. From a physical perspective, there is no "excess power" or "power shortage." "Power shortage" means that somebody *would like* to consume electricity, but that there is no power available at the consumer's location or for the price the consumer is willing to pay. As opposed to this, "excess power" refers to a situation where there are power stations that *could* produce power if consumers were willing to consume more and to pay the price for this power.

It is naturally a challenge for the power system to maintain an exact balance between production and total consumption including power system losses. The biggest challenge for a power system is often a situation where – for some reason – there is a sudden unplanned stop in a large power station. In that case a production capacity of, for example, about 1,000 MW of power generation can be lost, which corresponds to the amount of power generated in a larger nuclear power station. In the exact moment when such an incident occurs, the design rule is normally that all consumers continue to be supplied with power as usually, that is, as the failed power station cannot supply them any longer, the electricity has to come from another power source. A power source that is always available as "reserve" power are all the spinning parts of the generators, generators that are on-line producing electricity (in hydro-power stations, nuclear power stations, coal and gas power stations, and others) of the entire power system, such as, for example, the whole Nordic power system, the Central European EU UCTE System etc. The spinning parts include the rotor, the shaft, and the turbine. At the very moment a large power station comes to a sudden stop, the power is supplied from the energy stored in all these spinning parts, and then reserves start to operate in different time scales. A bicycle can be used to illustrate how the balance in a power system is maintained. This is shown in Fig. 1.

Regulating Capacity and Reserves in Power Systems

In power systems it is, as discussed above, crucial to maintain both the flexibility and reserves necessary to keep the system operating under a range of conditions. These conditions include possible unscheduled plant outages, as well as predictable and uncertain variations in load and in primary generation resources including wind. Day-ahead scheduling for unit commitment is done according to the load (and wind) forecast and real-time load following is accomplished with operational reserves.

Continuous Balancing: Load Following Capacity

Since production always has to equal consumption a power system needs to be *flexible*. As consumption varies, even production has to vary accordingly. Here, power stations that are available for continuously following power consumption are defined as *load following capacity*. This group comprises a large number of power stations as the difference in consumption between day and night can amount to several thousand MW. *Power consumption* refers here to the net consumption that has to be supplied by power stations whose production is controlled specifically with that goal. In a first step, wind power is considered as "negative power consumption," that is, the other power stations have to supply the net consumption = difference between actual power consumption and wind power production.

Figure 2 shows a continuous curve that describes the power consumption that has to be continuously supplied where the *load changes* are met by controllable power production, that is, *load following capacity*. Most of the load following in the figure is scheduled day ahead. In the figure the hydro power is used for daily regulation, while nuclear power during this week is

used for weekly regulation (to help to follow the lower consumption during weekend).

The figure shows an example of the continuous variations of net consumption. It always exactly equals production that, therefore, also has to vary. There are some phenomena to consider:

- When net consumption is at its lowest level it can only increase. This is due to that consumption increases and/or wind power decreases. At this level, also controllable production is at a low level, resulting in that there are several power stations with margins to increase their production. In practice, it is not possible to say when the lowest production level is reached; therefore, it is necessary to have standby capacity to decrease production even then.
- Challenge for following an increasing power consumption. There are often some power plants on-line that can increase their production level and this can be done at short notice. In addition it is possible to start up power plants that are not on-line. For many power plants this can take 4–12 h. The challenge is to keep enough power plants on-line to be able to follow the changes needed in short notice. Some power systems may have limitations as to how fast production can be increased. This is a particularly big challenge in systems with thermal power plants, for example, coal-fired power stations, as these need time to heat up and may have limitations regarding the ramping speed in MW/min. Hydro power often can move from zero to full production in a short time, 5–10 min, but how short this time is depends on a number of different factors, such as water supply, conditions due to water legislation, current operational mode and technical solutions of the individual plant. It is also possible to use demand response – lowering consumption in these cases.
- Challenge for following a decreasing power consumption. Technically it is possible to *decrease* production of the power plants on-line to the desired level in most cases, but this can in some cases result in energy losses when, for instance, steam has to be dumped or water has to be spilled. Most power plants have a minimum operation limit before they have to be shut down, and shutting down can be a lengthy process. It is also possible to use demand response – increasing consumption in these cases.

Continuous Balancing: Operational Reserves Day-ahead scheduling can cover most of the load following. However, one challenge when operating a power system is that there are no perfect forecasts. A lot of things may occur, for instance, power line interruptions, unpredicted changes in consumption and unpredicted changes in wind power or other generation. Independent of what happens, controllable power stations have to change production in that case because total production has to equal total consumption at all times. This means, there have to be reserves, that is, margins to change production level in case of such events. The assumption is to have reserves in power stations, but it is also possible to have reserves in the form of changed consumption and/or changed transmission on controllable power lines to power systems in neighboring countries. However, if you change the transmission on controllable lines you move the balancing requirement to the other side of the line and the production (or consumption) has to be changed there instead.

On the bicycle in Fig. 1, another cyclist has to pedal if somebody stops pedaling. The cyclist that now pedals more was not able to pedal to the maximum before. The *margin* this cyclist has can thus be called a *reserve* that this person has in case somebody else stops pedaling or somebody else breaks stronger. The same occurs in a power system. If a power station stops working, if wind power plants decrease production, or if somebody increases power consumption, there has to be some other power station that can increase production. If a nuclear power station with a usual production of 1,000 MW suddenly stops, other power stations have to have margins to directly increase production by 1,000 MW. If wind power production decreases by 200 MW, there have to be other power stations that take over that production to supply power consumption if at the same time there are no changes in consumption as production always is equal to consumption.

It is important, though, to take into account, that "reserve" means that a power station stands by to produce more. On the bicycle, there is one person

Bicycle	Power system
	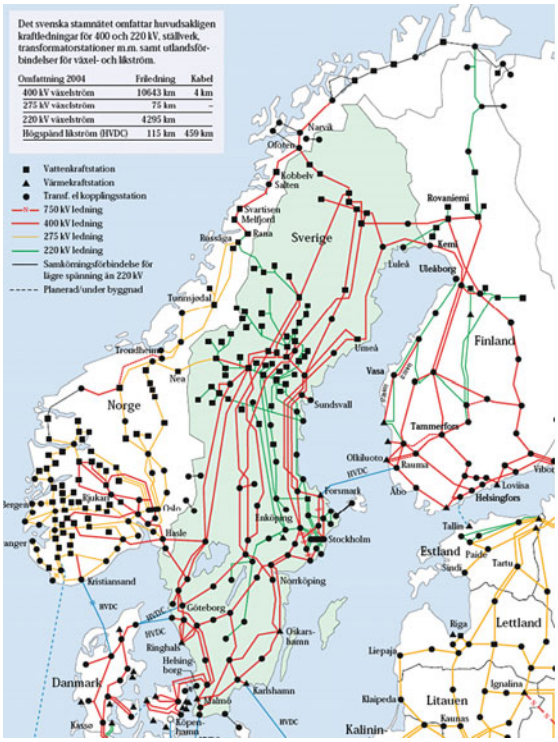
It is assumed that some people on the bicycle pedal and others break. Air resistance and wheel resistance are “losses” and are part of the breaking process. If cyclists pedal the whole time exactly as much as they break, the bicycle will move at a constant speed.	This corresponds to a situation where total production equals total consumption in the power system (e.g., the Scandinavian power system shown in this figure). This balance means that all large generators (with so-called synchronous generators where the electrical frequency is directly related to how fast the generator spins) spin with the same frequency and you get a constant frequency in the entire power system. It is normally 50 Hz, that is, the alternating voltage changes polarity between plus and minus exactly 50 times per second.
If somebody stops pedalling because his leg suddenly hurts, the bike slows down. It does not directly stop because it has a certain inertia due to the weight of the people on the bike and of the bike itself.	This corresponds to a situation where a power station suddenly stops production. The power system starts to slow down and the frequency slightly decreases. It starts decreasing in the same way the bike starts slowing down. However, the frequency does not directly drop as there is a large amount of kinetic energy in the turbines, etc. that drive the generators.
When the bike’s speed (the same speed across the entire bicycle) decreases, there are some cyclists who pedal and have a speedometer. If they notice that the speed goes down they can pedal stronger in order to compensate for the cyclist whose leg hurts. The remaining cyclists increase their power on the pedal to a level that keeps the speed constant. Again there is a balance between pedallers and breakers.	This corresponds to a situation where there are frequency meters installed in several Scandinavian power stations, mainly hydropower stations, that continuously measure the electric frequency (which is the same in the entire Scandinavian power system). When the frequency decreases, the power production in these power stations increase in order to compensate for the reduced production in one of the other power stations. After that the frequency is stable again. All this happens automatically, independent of who has caused the imbalance: whether a power station fails, the wind speed drops in a wind power plant, somebody increases power consumption, or somebody starts-up a power station, etc. After that, suitable power stations are started up by manual regulation in order to restore the automatic reserve.
In a large power system such as, for example, the Scandinavian one, it is important to take into account limitations in the transmission capacity in order to not overload the lines when variations in one area are compensated with changes in another area. On the bike, the chain can jump off if everybody in the front pedals and everybody else breaks.	

Wind Power Balancing. Figure 1

Illustration of how to keep the balance in a power system [1]

that *stands by* to pedal more in case this is needed, that is, no effort is involved in *standing by*. The same occurs in the power system; the power station that maintains *margins=reserves* does not produce any power, but *would be able* to do so if required. Sometime there is a misconception of those power stations that are kept as a reserve increase emissions continuously or use water unnecessarily. However, there might be a certain effect if you operate a power station at a lower efficiency. In order to create fast reserves, coal-fired power stations are sometimes operated at low levels (with lower efficiency), even though production costs may be higher than optimal (the person on the bicycle cannot be at home and sleep). A power station (or part of a power station) that works as a *reserve* cannot produce any power; as the actual goal is *not* to produce any power, but just to *stand by* to do so if required. It is mainly power production that causes, for instance, coal-fired power stations to emit carbon dioxide and water from hydro-power station dams to flow through the turbines. It is also important that there are steady reserves for down-regulation if load decreases or wind power increases. To do this cost efficiently this should be done without this down-regulation causing unnecessary spill in hydro power, for example.

It is a big challenge to design a system that keeps reserves in a way that is economically efficient. Some power stations (e.g., hydropower stations that are operated at optimum efficiency or gas turbines on hold) hardly incur any costs for *keeping reserves*, but there will be costs *if they are used*. In other power stations (e.g., coal-fired power stations that operate at a low level), there are costs for keeping reserves (energy losses due to less efficiency), but efficiency increases if the reserves are used, that is, the production increases. An efficient approach to handling reserves must therefore take into account the costs of keeping them, the costs of using them as well as an estimate of the probability of being used. An efficient way of handling reserves has to include efficient market signals that give correct incentives.

The examples refer to reserves for production increase, but there are also corresponding examples for reserves regarding the decrease of production. Figure 3 shows an example of a (wrong) forecast at the beginning of a time period for hours 5–24, and an updated forecast for hours 15–24.

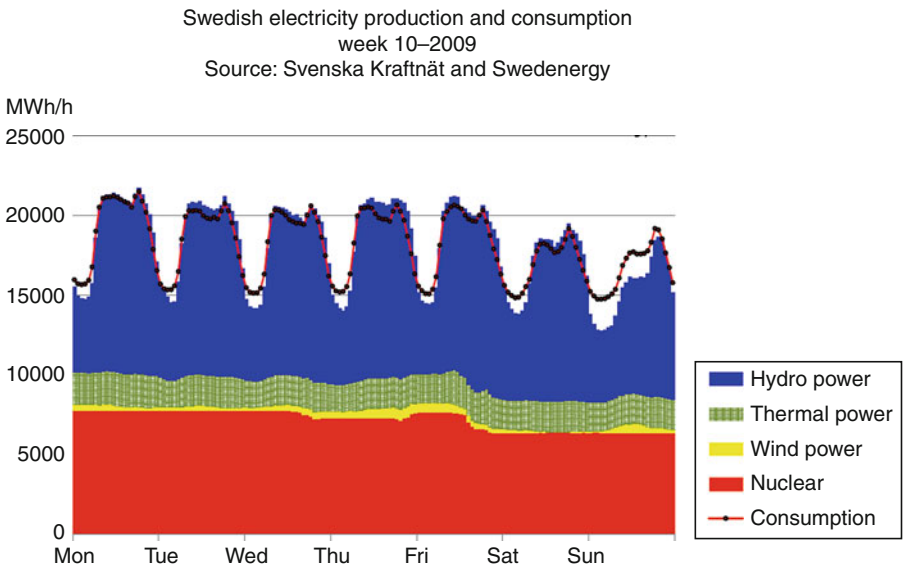

Wind Power Balancing. Figure 2
Power production and consumption in Sweden during week 10, 2009. The difference between production and consumption corresponds to the power traded with neighboring countries. Power consumption changes continuously during the week and has to be supplied by controllable production

The *reserves* that have to be kept depend on how fast they are available and how large the demand is for different time horizons, that is, what are the dimensioning events. Here the time horizon is of key importance: It may happen, for instance, that it will get very cold (very high power consumption in a system with large amounts of electric heating) within a few days. But if all available resources can be started within 4 h, a decision has to be taken only 4 h before the high power consumption will occur. However, it may be necessary for the respective power station to call in employees and this may require a notice of 24 h.

If you continuously update the forecast, this means that you also can continuously decrease the uncertainty of the forecast for a certain hour. Figure 4 shows the needed production increase in relation to the forecasts in Fig. 3. It shows that for the forecast for the hours 5–24, the forecast error for hour 20 is 1,800 MW; but in the updated forecast for hour 15–24, the forecast error for the same hour has decreased to 600 MW. If the power stations need a start-up time of 15 h, a reserve capacity of 1,800 MW is required at hour 5; but if 5 h are sufficient for the start-up, the required reserve capacity is only 600 MW based on the forecast error at hour 15.

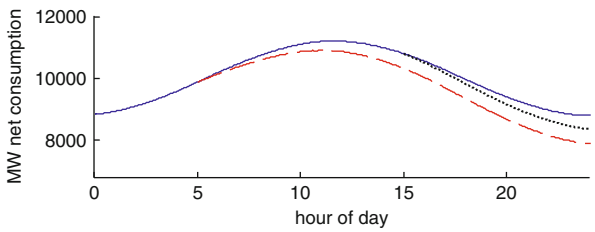

Wind Power Balancing. Figure 3
Actual power consumption = production in other than wind power plants (*blue solid line*) and forecasts from time $t = 5$ (*red dashed line*) and time $t = 15$ (*black dotted line*)

In the following, the reserves are grouped according to how fast they are needed, which also is connected to the forecast certainty for the same time horizon.

Reserve Categories Reserves can be divided into different categories according to the time scale within which they are operating. There are different practices and terminology in different power systems, but generally speaking there is first an instantaneous reserve that is maintained in power plants operating on-line and is activated automatically to correct for frequency fluctuations. These can be further divided to working at several time scales (from some seconds to a minute). Then there is a somewhat slower reserve that is activated 10–15 min after the occurrence of frequency deviation from nominal frequency. It replaces the instantaneous reserve. This reserve consists mostly of rapidly starting gas turbine power plants, hydro (pump) storage plants, unloaded generation already online, and load shedding can also be used.

There is wide agreement on the type of reserves that must be carried and the time frames that are relevant, but there is no universal agreement on nomenclature. Here the following terminology is adopted:

- Contingency reserve (also called disturbance reserve): capacity that is online and synchronized to guard against unforeseen equipment failure.

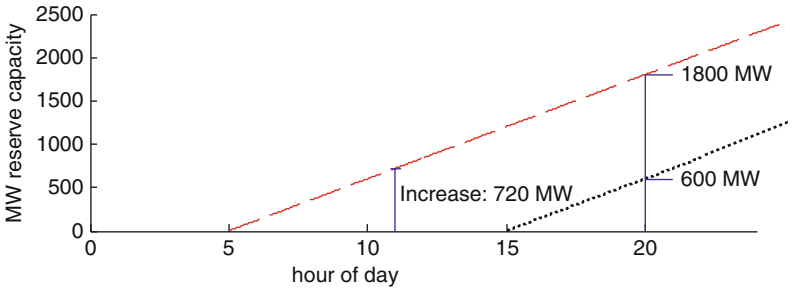

Wind Power Balancing. Figure 4
Forecast errors from the first forecast for hour 5–24 (*red dashed line*) and for the updated one for hour 15–24 (*black dotted line*). This corresponds to the production increase required within the respective time interval. At hour 5, there have to be reserves of 720 MW that can be started up within 6 h

The amount of contingency reserve is typically based on the largest potential source of failure, either the largest generator or tie line in the system. Contingency reserve is held independently of the variability of loads, and is typically shared among participants within the balancing area, reducing the overall contingency requirements for the individual entities. Some portion of the contingency reserve can be non-spinning, but must be capable of responding quickly if needed. This reserve includes both primary (automatic) and secondary/tertiary (manual) reserves.

- Primary/secondary control (also called regulating reserve, response, instantaneous/momentary reserve, primary/secondary reserve): fast fluctuations in system load require fast generation response. Regulation consists of flexible generation that is responding with a speed/droop characteristic to frequency changes (primary control, timescale several seconds) or connected to automatic generation control (AGC) systems trying to adjust the production to certain frequency targets (secondary control, timescale several seconds to minutes). The AGC will send control signals to the participating regulating units as needed to offload used primary reserves so that the aggregate load is balanced with generation. Units that provide primary/secondary reserve are usually run near the mid-point of the operating range. When a regulating unit is required to deviate from that preferred operating point for a longer period of time, adjustments are made to the units on economic dispatch so that the regulating unit can return to its mid-point operating setting.
- Tertiary control (also called load-following reserve tertiary reserve, minute reserve): This consists of generation that may be called on to increase or decrease output over slower time frames than regulating units. The units that are available for load following must be committed in advance, or capable of quickly starting and synchronizing with the grid, typically within 10 min. Depending on the resource mix that is available to the power system operator, load-following reserve can be either spinning or non-spinning, or as is most common, will be a combination of both. Slow-start generation must be committed prior to becoming available for dispatch or to supply reserves.
- Planning reserve (also called long-term reserve): This type of reserve covers not only operating requirements, but recognizes that not all of the installed capacity may be available when needed. Planning reserve is usually found to be in the range of 12–20% of peak load, depending on the system and the planning criteria in use at the locale in question.

An example of how the reserves operate is illustrated in Fig. 5. It shows the frequency of the system and activation of reserves as a function of time when a large power plant is disconnected from the power system. Activation of reserves divides the reserves into primary reserve (also called instantaneous or automatic reserve), secondary reserve (also called fast reserve) and long-term reserve (also called slow or tertiary reserve). Primary/secondary reserve is activated automatically by frequency fluctuations. Tertiary reserve is activated manually or automatically in 10–15 min after the occurrence of frequency deviation from nominal frequency. It replaces the primary reserve and it will be in operation until long-term reserves substitute it as seen from Fig. 5. The tertiary reserve consists of spinning reserve (hydro or thermal plants in part load operation) and standing reserve (rapidly starting gas turbine power plants and load shedding).

It is fairly straightforward to determine contingency reserve required because the largest contingency is a known specific event. Primary/secondary/tertiary control performance and reserve allocation is more difficult to specify. It is not practical and it is not necessary for any single balancing area within an interconnection to continuously perfectly match generation and load. For example, the Control Performance Standard 1 (CPS1) in the USA recognizes this and places an annual statistical limit on the 1-min product of balancing area imbalance and system frequency deviation. Note that this is a performance metric, not reserve requirement. A balancing authority must have "enough" reserves to meet the statistical performance standards, however much that is.

The key aspect of load/frequency control on interconnected systems mainly addresses three time frames and these are generally considered as Primary Control (or governor response, designed to arrest

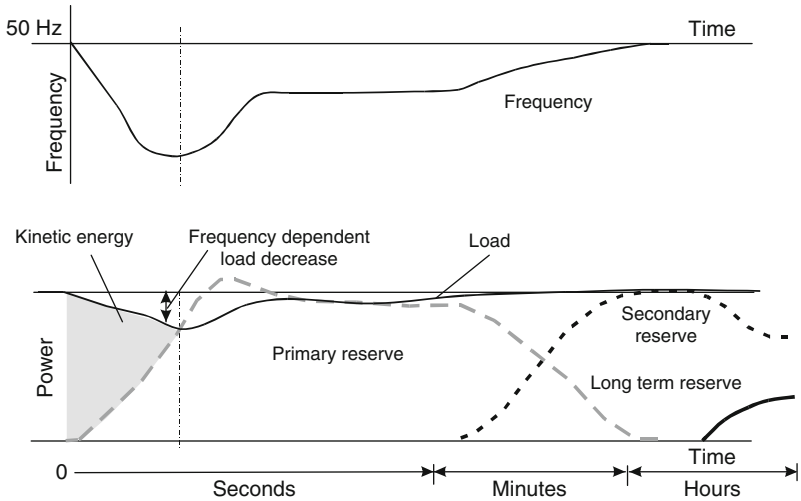

Wind Power Balancing. Figure 5
Activation of power reserves and frequency of power system as a function of time when a large power plant is disconnected from the power system [2]

frequency decay), Secondary Control (designed to reset the primary control response as well as to balance supply and demand) and Tertiary Control.

Primary Control

The primary control considers the capability of the system to meet sudden load and/or generation changes. The primary control is separate for each synchronous power system. A synchronous power system is a power system where all producers and consumers are connected to each other through transformers and AC transmission and distribution lines. Anything from a diesel generator set supplying a single load to a multinational grid as the Nordel system (which connect Norway, Sweden, Finland and the eastern part of Denmark), or the central European UCTE grid can constitute a synchronous grid. An AC line has to have the same electric frequency at both ends of the line. If there were different frequencies at the ends then the voltage angle shift would increase until it reaches 180°, resulting in unacceptable large currents on the line. The same is valid for transformers. The conclusion is that in a synchronous grid the average electric frequency must be the same. For short periods the frequency can be slightly different, but that will cause large power oscillations in the grid, which can result in serious disturbances.

In a synchronous grid there has to be some kind of primary control. A short description of this type of control, cf. Fig. 1, is given here:

- Assume that a power system is in balance, that is, electricity generation and consumption are equal.
- At a certain time the consumption increases, while the generation remains the same.
- There is rotational energy stored in all synchronous machines connected to the system, more exactly in the rotors and the connected turbine shafts. Since the generation and consumption always have to be in balance the load increase is compensated using the rotational energy, which causes the rotor speed to decrease in the synchronous machines.
- In synchronous machines, there is a strong connection between rotor speed and electric frequency. This means that all synchronous machines in a synchronous grid, in principle, rotate at the same speed. The reduced rotor speed therefore results in a frequency decrease in the grid.
- In some power plants there is frequency sensitive equipment, which sends a signal so the generation increases when the frequency decreases. These power plants are referred to as primary controlled units.
- As long as the frequency keeps falling the primary controlled units will increase their generation.

Finally, the balance between generation and consumption will be restored and the frequency will be stable again. It should be noted that the new stable frequency will be lower than the original frequency!

In the description above it is assumed that it was a load increase that triggered the primary control. A corresponding course of events will come up if there is a failure in a generating unit – if a generating unit is stopped and the load is constant then the remaining units in the system will have to increase their generation. A load decrease and/or a generation increase also causes similar courses of events. The only difference is that the frequency is increasing, which results in generation decreases in some power plants.

Permissible Frequency Range In each power system there is a nominal frequency – North and South America usually 60 Hz, whereas most of the remaining world uses 50 Hz – and it is not possible to allow too large deviations from the nominal frequency, because there is then a risk that important components in the power system are damaged. If, for example, the electric frequency would coincide with the harmonic oscillation frequency of turbine blades or shafts, then these power plants have to be shut down to avoid expensive repairs. Another problem is that generators and transformers are designed for the nominal frequency and a deviating frequency can cause heating of the windings, resulting in damages. Finally, there might be certain kinds of loads that do not work satisfactory if the frequency deviates too much from the nominal.

Speed-Droop Characteristics As explained above there are some power plants which automatically adjust their generation whenever the frequency of the system changes. The speed-droop characteristic is a measure of how large the change in generation is for a certain change in frequency

Definition The speed-droop characteristic, R, indicates how the generation in a power plant is changed when the frequency changes. It is measured in MW/Hz. If G_0 is the generation at nominal frequency, $f_0 = 50$ Hz, it holds that $G = G_0 - R(f - f_0)$.

The notion of speed-droop characteristics is illustrated in Fig. 6. In practice it is often inconvenient to use the formula given in the definition. It is easier to just calculate how the changes in generation and frequency relate to each other:

$$\Delta G = R \cdot \Delta f.$$

Then it is simple to conclude whether a certain change corresponds to an increase or a decrease; there must be a shortage of generation if the frequency is falling and therefore the primary control must result in an increase of generation, etc.

When calculating frequency changes, it is necessary to also consider the reserves available in the primary controlled power plants; it is impossible to increase the generation of a power plant operating at maximal capacity regardless of the speed-droop characteristic. This means that when primary control is considered, both the total speed droop and the total available primary reserves are to be defined. The total speed-droop is in, for example, the Nordic

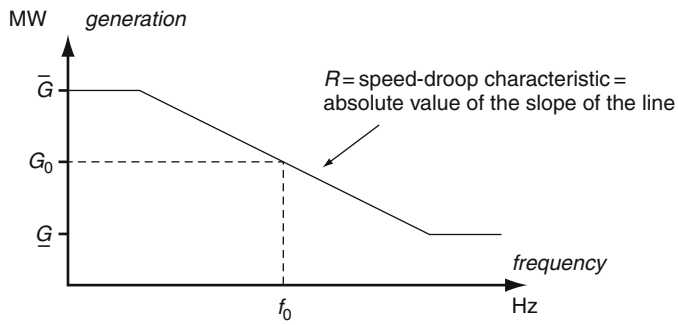

Wind Power Balancing. Figure 6
The relation between frequency and generation in a power plant participating in the primary control

synchronous system divided between the different areas such as Sweden often keeps around 2,500 MW/Hz, Norway 2,000 MW/Hz, Finland 1,250 MW/Hz, and Eastern Denmark 250 MW/Hz at nominal frequency, 50 Hz. This means a total speed droop of 6,000 MW/Hz. This implies, for example, that a sudden outage in Sweden of 600 MW decreases the frequency with 0,1 Hz which causes a compensation of 250 MW in Sweden, 200 MW in Norway, 125 MW in Finland, and 25 MW in Eastern Denmark. This example illustrates the important issue that when many regions or countries are interconnected, then an outage in one part of the system will affect the generation in other parts of the system, which means that margins also have to be kept on the transmission lines between the different parts. The overall aim of the primary control is to balance all sudden changes, so the same process is valid also for changes in, for example, load or wind power production. In some systems the contingency reserve will be activated at a lower frequency than the normal frequency range, to keep the two reserve categories separate.

Secondary and Tertiary Control

The ability of the power system to maintain the balance between production and consumption starts from automatic frequency regulation of the primary regulation and continues with secondary and tertiary control. A consequence of primary regulation is that there still is a frequency deviation, even if the frequency drop or increase has been stopped. The use of primary regulation also means that reserve margins are utilized. A consequence is also that the transmission between different areas will change as shown above. Note that if you have a *constant* frequency – independent of whether it is 50.0 or 49.95 Hz – production and consumption are balanced, similar to the bicycle that moves at constant speed. However, the system is designed to operate within a range of $50 \pm \varepsilon$ Hz (ε is often in the range 0.01–0.5 Hz); and outside these limits, there are smaller margins as part of the margins have already been used. If the frequency approaches the limits, it is desirable to move the system back to the middle of this range. The only way to do this is to start-up new power stations (or disconnect consumption) for frequencies that are below 50.0 Hz or disconnect power stations for frequencies above 50.0 Hz. This has to be done quite often, several times per hour, as consumption – and subsequently the frequency – varies continuously.

Secondary Control is often under, so-called, automatic generator control, AGC, such that a control block/area that is in imbalance following a disturbance autonomously restores the frequency to the target frequency and the power interchanges with adjacent control blocks to their preset levels. Thus, there is a continuous interaction of the primary and secondary regulation. Secondary control timescale of operation is several, for example, 5–10 min.

The function of a control area is essential for the operation of a power system. The result of the AGC is often that all changes within the control area will within around 5–10 min be automatically balanced within the same control area. If the area contains, for instance, wind power and the wind power decreases with 100 MW when consumption remains constant, then the AGC can control the other power stations in the same area so they automatically increase their production with 100 MW. It is of course technically necessary to increase the power production somewhere to compensate for the decreased wind power production. But if the control areas are very small, then margins have to be kept in each area and the balancing is automatically performed internally in each area although it may be a better economic solution to balance outside the control area. The term *balancing area* can be used to define the areas which have a common balancing. Assume that there are two control areas, but one have an overall (manual) system that studies the economic operation of the system and changes the set value of the transmission between the areas (used for the AGC in each area) if this is to prefer for an economic operation of the two areas. In this example there are then two control areas but only one balancing area.

The Scandinavian Nordel system is not divided into control areas, although the size of the system is about a circle with the diameter of around 1,500 km. In this system there is no automatic AGC, but a system is implemented where all producers provide bids where they offer to increase or decrease their power production within 5–10 min for a certain cost. When an increase of power production is needed (=secondary–tertiary control) then the cheapest bid is accepted that

fulfils the transmission constraints. This means for instance that if wind power decrease in Eastern Denmark is causing an imbalance for the system, then the decrease is first compensated with the primary control, and then the primary control could be replaced with an increase in Finnish hydro power 1,500 km away if they provide the lowest cost bid for their up-regulation and the transmission grid operators find it suitable to change the transmission in this way. In a congested transmission situation a bid which is closer to the imbalance source has to be accepted.

Electricity Markets and Production Planning

A power system always has to have a balance between production, G_i and consumption, D_i, that is, for a power system consisting of i load points in the transmission and distribution systems.

$$\sum_i G_i = \sum_i D_i + \text{losses}$$

This equation is valid independent of the length of the period, that is, if G_i and D_i are measured as MWh/h, MWs/s or MW. The aim of the market is to keep the continuous balance between production and consumption in an efficient and reliable way. First the general structure of operation planning will be presented.

The planning (i.e., before a specific hour) and operation (i.e., within the specific hour) of a power system can be illustrated as in Fig. 7. The overall aim of any market design is to obtain a reliable power supply and an efficient use of available resources.

Failure to keep the electricity system running has serious and costly consequences, thus the reliability of the system has to be kept at a very high level. Security of supply needs to be maintained in both the short and the long term. This means maintaining both the flexibility and reserves necessary to keep the power system operating under a range of conditions, including peak load situations. These conditions include credible plant outages (disturbance reserves) as well as predictable and uncertain variations in load and in primary generation resources, including wind (operational reserves). In the above presented general process, this means that in all stages A–E enough margins have to be taken into account in order to maintain the security.

Load following is performed partly beforehand (stage A–D) as scheduling and dispatch of power plants according to the load forecast and partly by operational reserves to balance the load forecast errors. Scheduling includes planning the start-ups and shut downs of slower power plants, called unit commitment, in the time scale of 3–12 h (stage C–D). Optimizing the use of the water stored in hydro power reservoirs, the hydro power plants take into account an even longer scheduling horizon. The scheduling can be based on electricity market operation, where bids for production and bids for consumption based on forecasts are made. Figure 8 shows an example of the actual load in the power system over 3 h compared to hourly forecasted load, denoting forecast errors and short-term load deviations in the system.

In addition to frequency control, the voltage level is managed to prevent under- and over-voltages in the power system and to minimize grid losses. Frequency is a wide area quantity. Measures can be taken anywhere in the system to maintain the balance, as long as transmission capacity is available. Voltage is a local quantity, and voltage management should be taken care of in the vicinity of imbalances. In order to manage the voltage level during disturbances, reactive reserves in power

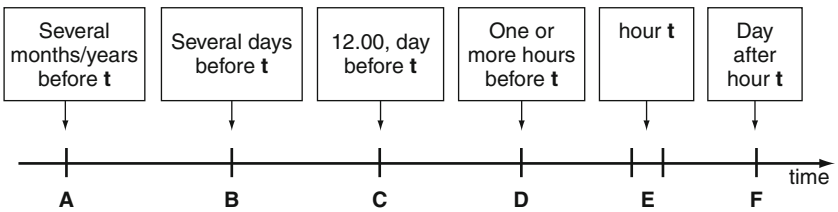

Wind Power Balancing. Figure 7
Planning and operation of a power system

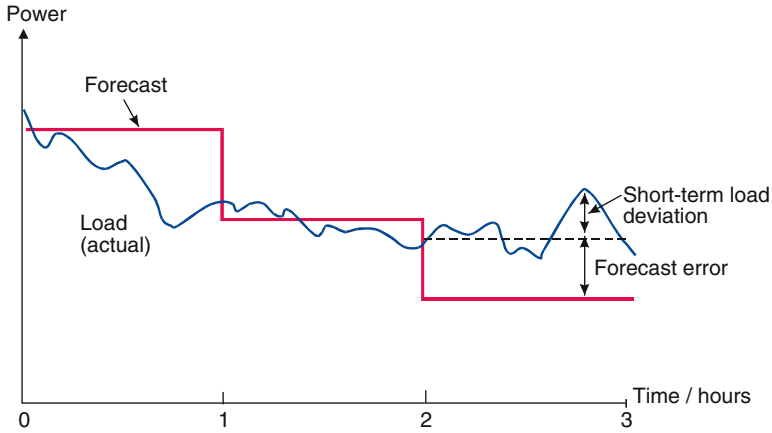

Wind Power Balancing. Figure 8
Example of actual load in the system over 3 h compared to forecasted load

plants are allocated to the system. These reserves are mainly used as primary reserves in order to guarantee that the voltage level of the power system remains stable during disturbances. Power plants and special equipment, for example, capacitors and reactors, control the reactive power. The voltage ratio of different voltage levels can be adjusted by tap-changers in power transformers. This requires a reactive power flow between different voltage levels.

Seasonal/Yearly Planning

Physical aim: This is especially important for a hydro-based system, where the aim of this planning is to decide how much water (in reservoirs and inflow) should be stored for future use. Too much water stored for months ahead, or next year could lead to future spillage, while too little stored water could lead to lack of energy which could cause water deficit in the future. In a thermal power system, the seasonal planning includes scheduling and coordination of unit maintenance.

Market process: In a hydro power system the tool for optimal storage is the *water value* which is an evaluation of the water for different reservoir levels and different time periods. Different water value in different periods is an indication that it is profitable to change the storage plan. In a liberalized market each hydropower company makes its own estimation of its water value and the result is used internally for planning and externally for trading. For thermal unit maintenance the aim is normally to schedule maintenance to low load periods.

Weekly Planning

Physical aim: The aim of this planning in a hydro system with reservoirs is to decide how the available water for the week in the specific region (available from inflow and storage where the use for the storage is planned in stage A) should be distributed between the days of the week. In a thermal power system there may be some planning concerning amount of staff needed for operation of units needed to supply forecasted load, cf. Fig. 2 where the nuclear power is downregulated during the weekend.

Market process: The tool for optimal storage in a hydro system is also here the water value, which is estimated by each actor on the market.

Daily Planning: Day-Ahead Market

Physical aim: The aim of this planning is to decide for each plant how it should be operated, that is, how much power that should be produced in each power plant during each hour in the coming day. In a hydro power system the available water at different price levels for the whole day is a result from the weekly planning. In the planning, the consumption level, production in other sources, and transmission limits have to be considered. In a thermal power system there are

two parts: the *unit commitment*, which includes which units have to be on line for production and/or reserve keeping, and the *economic scheduling*, which includes the planned production level in each unit.

Market process: In this description it is assumed that the day is divided into whole hours. This is the case in, for example, the Nordic power market, but there may also be other time steps as, for example, ½ h. One challenging part is that the power plants have to be operated in an economical way at the same time as the transmission limits have to be considered. This is done slightly different in different systems, depending on if congestion management is handled with implicit auction, explicit auction, counter trading, or another method [3]. The description below is based on implicit auction = market splitting which is used in the Nordic system. There are then four stages here:

C1. First the transmission limits for each hour and each bottleneck are decided. These limits are calculated by the organization responsible for the transmission system, for example, TSO:s. It is based on an assumed production and consumption level in each area or each node together with a dimensioning rule including the N–1 criterion (= the system has to stand an outage even if the largest unit or the heaviest loaded transmission line fails) and margins considering uncertainties. The margins have to consider that the limits consider MW limits, but in stage C3, these limits are used as hourly limits considering MWh/h. This description is based as an assumption of the so-called *market splitting* method, also denoted *implicit auction*. There are other versions, for example, *market coupling*, but in any system there must be an interaction between transmission operation and margins and plant scheduling. The more close in time the transmission and production scheduling are performed, the more economic efficient the whole system is operated.

C2. The second stage in a liberalized market with several producers is the production/consumption bidding process where the aim is to put bids to a spot market (Nordpool in the Nordic market) concerning how much power in total could be produced during each hour in each company at which price. The bids concerning each hour have to be delivered the day before the real trading day. This is the day-ahead market: in Nordic system the bids have to be delivered before noon a certain day for all hours during the coming day.

C3. The third stage is the calculation of which bids that should be accepted considering transmission limits between bidding areas (Nordic system is based on areas), or limits between nodes where a node-based system (based on DC load flow) is used. This means that as many cheap bids as possible from stage 2 are accepted regarding the transmission limits from stage 1. This calculation is made by the exchange (Nordpool in the Nordic market).

C4. The fourth stage is the operation planning which is performed individually by the owners of the different production sources after the result of the bids. This means that the accepted amount of production bids for each hour have to be met with produced power in some way (combination of own production in each company and bilateral trade with other companies). This stage includes production planning with the physical aim as above.

Intraday Market

Physical aim: To get an economical operation of all power plants for each specific hour during the day. Here better forecasts for each hour can be used, since the decisions are taken closer to the hour. Especially in a power system with wind power, this phase is important since the 2–3 h wind power forecasts are much better than the 24 h forecasts. Any larger deviations to plans made previous day can be corrected in intraday market.

Market process: It is performed after the spot market for each hour has been closed, that is, when the day-ahead planning is finished. This includes in the Nordic power market the Elbas Market and other bilateral trade. The main aim is to cover forecast errors concerning load levels, wind power production levels, production costs and/or outages for each hour. Bids on the Elbas market are distributed electronically and accepted when they are found economical (is there an English term for this kind of market?). There are the same stages here as concerning the daily market:

D1. The transmission limits for each bottleneck are set by transmission system operator. This means that they can be updated compared to what is previously set for the daily market.
D2. Bids concerning production in a certain area can be delivered.
D3. For each geographical area only bids that can be used in that area (considering transmission limits and prescheduled trading) can be accepted.
D4. When a bid is accepted, both the seller and buyer have to consider this in their planning.

Hourly Operation

Physical aim: Within each hour the system balance between production and consumption has to be kept continuously in an economical and reliable way, considering production and transmission limits.

Market process: Final schedules are given to the TSOs 30–90 min before the operating hour and the balancing after that is the responsibility of TSOs. This is to avoid cross regulation where each actor regulates their schedules as only the system net imbalances need to be regulated, resulting in a more efficient use of regulation capacity. The continuous balance is kept with primary control (frequency controlled power plants that keep enough margins for this), which is distributed between different power plants in different regions. Used primary reserves are off-loaded using secondary/tertiary reserves, which in the market mean acceptation of bids from the so-called regulating market, or balancing market. These bids can also be used for offloading of bottlenecks (if the amount of power flowing on lines between two areas is too close to physical limits) in order to keep enough margins also on these bottlenecks. There may also be an automatic system (Automatic Generation Control – AGC) which changes the production in some selected units in order to keep the balance and offload units activated by the primary control. The stages in the operation are:

E1. The transmission limits for each bottleneck are estimated by the transmission system operator. Here the MW limits (not MWh/h) are considered.
E2. Bids concerning production increase and decrease in each area or in each node are delivered before each hour.
E3. When bids are needed (for total system needs and/or for offloading of bottlenecks) they are accepted by the operator. If an AGC system is active, then some power plants are activated automatically.
E4. When a bid is accepted the company that put the bid has to activate it directly, or to be more specific, start the procedure of activation. It may take several minutes until the full bid is activated.

Post-trading

Aim: The hour has now passed which means that the physical balance has already been kept, as described for step E above. But what happened in step E was that the system operator, for example, bought power from one producer to supply the system since some consumers that perhaps had a contract with another producer increased their consumption. The aim of the post-trading is to arrange economical balance so it matches the contracts on physical delivery on the market.

Market process: This is mainly relevant in liberalized markets. The contracts for each actor must have been reported to the system operator. All actors connected to the grid must have a contract concerning the economical responsibility for the production and/or consumption. This is denoted *balance responsibility*. If, for example, retailer R1 has a contract to deliver all power to consumer D1 (i.e., retailer R1 is *balance responsible* for consumer D1) then this information has to be reported to the system operator. Then retailer R1 can write contracts concerning production with producer P1 and P2. The aim of steps A-D for retailer R1 is then to try to buy the expected consumption of consumer D1 for hour h from producer P1 and P2 or some other producers. These contracts then have to be reported to the system operator. The basic market tool, the *balance responsibility*, means that there is an *economic incentive* for the market actors to keep an hourly balance between production and consumption. The physical intra-hour balance is kept by the system operators. If, for example, R1 has not bought enough from P1 or P2, then some other producer have delivered the power needed for D1, and the post-trading then implies that R1 has to pay for this extra power. The post-trading, balance settlement, can have several rules. For example, there can be extra penalties for all deviations or then the imbalance pricing can reflect the real

cost for imbalances, as €/MWh, for each hour. Furthermore, even following a price signal from the balancing market, the imbalance pricing can be a one-price system or two-price system. In one-price system there is a cost for those that have been causing the imbalance with a deviation to the same direction up/down as balancing market demand and a revenue for those that have had their deviation to the opposite side. In two-price system, the producers get the spot price during the hours when the deviation has been to the opposite side of system imbalance (balancing market demand) and the balancing price is only used when the deviation is to the same side as balancing market demand.

It can be noted that all the steps above, Planning, A–D, and real-time operation, E, also exist in not liberalized markets, but step F is mainly interesting when there are several actors, which is not the case in many vertically integrated markets.

How Wind Power Changes the Balancing of Systems

The varying production patterns of wind generation changes the scheduling and unit commitment of the other production plants and use of transmission between regions. These changes will be made according to wind power production forecasts 2–40 h ahead and either losses or benefits are introduced to the system, compared with the situation without wind. Most of the energy produced by wind power will impact the scheduling process, but there is a crucial impact on the operating reserves as well. Depending on the prediction accuracy, parts of the wind power production variations remain unpredicted or are predicted incorrectly, and there will also remain subhourly changes in output. This is what has to be handled by load following reserve or the balancing market.

When speaking about the impacts of wind, it is important to know just how variable and predictable the resource is. Wind power production is characterized by variations on all time scales: seconds, minutes, hours, days, months and years. Predictability increases in shorter time scales, but even the short-term variations are to some extent unpredictable. There are means to reduce the variability of wind power production. Staggered starts and stops from full power as well as reduced (positive) ramp rates can reduce the most extreme fluctuations, in both magnitude and frequency, over short time scales [4]. This reduction is at the expense of production losses, so any frequent use of these options should be weighed against other measures (in other production units) in cost effectiveness.

Power systems usually cover larger areas. It is then relevant to look at the aggregated wind power production from the whole system or balancing area. Large geographical spreading of installed wind power will reduce the variability and increase the predictability of the aggregate wind power production. The variability and predictability can differ in different regions of the world. When assessing the amount of variability it is also important to know how concentrated or distributed the wind power is built in the power system area.

To estimate the impact of wind power on power system balancing, it has to be studied on a power system or balancing area basis. Every change in wind output does not need to be matched one-for-one by a change in another generating unit moving in the opposite direction. Rather, it is the total system aggregation of the variations in all loads and generators that has to be balanced. The relative increase in system fluctuations due to wind power depends on the wind penetration level – what portion of consumption is covered by wind power production. Also, each system is different: the levels of load variability, as well as the flexibility in the system, differ from region to region and from country to country. This means that even for systems with the same wind penetration level the challenge of wind integration and any costs related to that will be different [5, 6].

Also the operational routines of the power system are relevant – how often the forecasts of load and wind are updated, for example. If a re-dispatch based on forecast update is done in 4–6 h, this would lower the costs of integrating wind compared with scheduling based on only day-ahead forecasts. Emerging intraday markets reflect this, giving the opportunity for hourly updates. The costs will depend on the marginal costs for providing regulation or mitigation methods used in the power system as well as on the market rules. The way the power system is operated regarding the time lapse between forecast schedules and delivery will impact the degree of uncertainty wind power will bring about.

There are already several power systems and control areas coping with large amounts of wind power [7]. The experience from Denmark, Spain, Portugal and Ireland that have integrated 9–20% of wind energy (of yearly electricity demand) show that wind power production will only have to be curtailed at some rare instances, and that TSOs need on-line information of both the production and demand levels as well as respective forecasts in their control rooms. Spain and Portugal have launched centers for distributed energy that convey data to TSOs and even can react to control needs [8].

How Variable and Uncertain is Wind Power Production?

When estimating the system impacts of wind power, it is crucial to describe the variability and uncertainty of wind power in the right way for the aggregated wind power production of the relevant area. Relevant questions are: how much is the variability on average and in extreme situations? How much are the forecast errors for different times ahead, on average and in extreme situation? As there is considerable smoothing effect when combining the output of individual turbines and wind farms, especially in the minute and hourly time scale, it is important to know how large the area in question is and how dispersed or concentrated the wind power capacity will be distributed in the area.

Variability of Distributed Wind Power Production

The variability of wind has been widely studied. Recently also measured large-scale wind power production data has become available to give insight on the variability that is relevant for power system operation (Fig. 9). In-depth information about the variability can be found in [9–15].

Generally, the variability of wind decreases as there are more turbines and wind power plants distributed over the area. Larger areas also decrease the number of hours of zero output – one wind power plant can have zero output for more than 1,000 h during a year, whereas the output of aggregated wind power in a very large area is always above 0 (Fig. 10). The variability also decreases as the time scale decreases – the second and minute variability of large-scale wind power is generally small, whereas the variability over several hours can be large even for distributed wind power. For time scales from several hours to day ahead, forecasting of wind power production is crucial.

Even if some general conclusions can be drawn from the variability of large-scale wind power, however, it should be noted that the size of the area and the way wind power plants are distributed is crucial. Also, the landscape can have influence. Offshore, the wind resource has been found to be more coherent, thus increasing the variability compared to similarly distributed wind power onshore. For power system operation, it is important to know how often there are higher

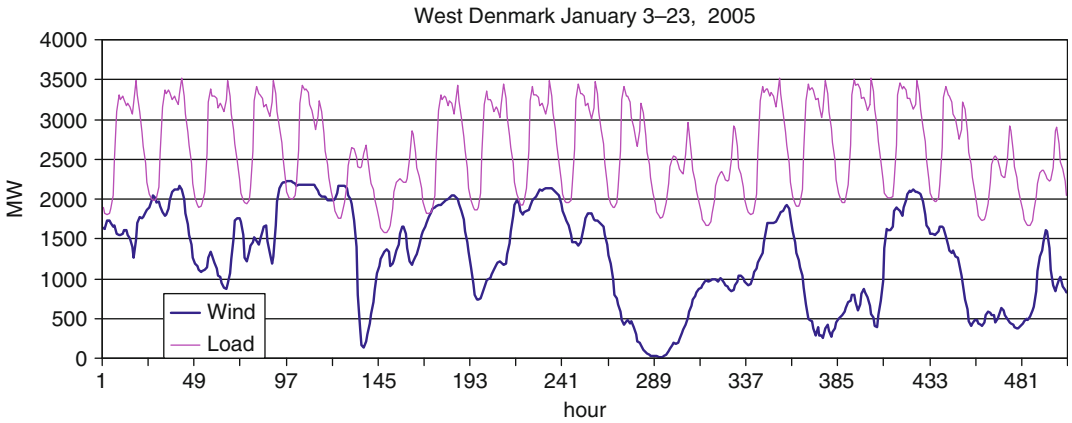

Wind Power Balancing. Figure 9
Wind power production (2,400 MW wind power) and load in Western Denmark. The worst storm event so far, of 8th January 2005, can be seen in hours 128–139 (Data source http://www.energinet.dk)

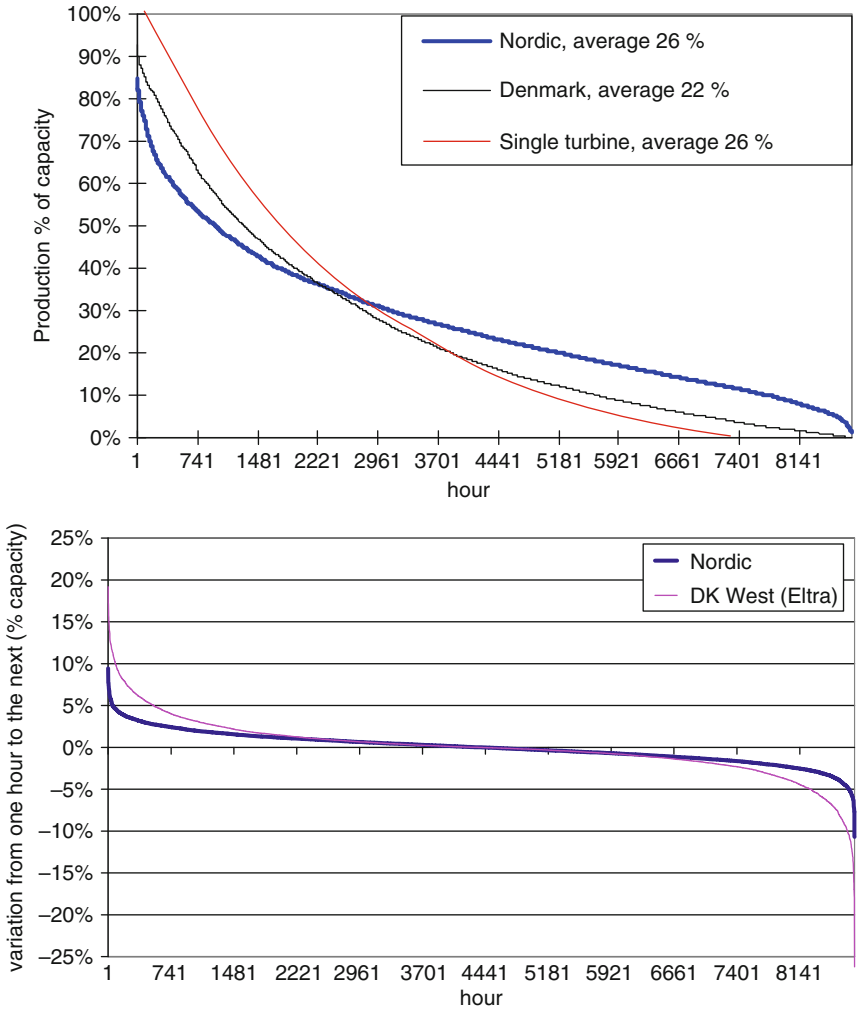

Wind Power Balancing. Figure 10

Wind power production and hourly variability as duration curves showing the smoothing effect from a larger area aggregated wind power [11]

variations in output, and also an estimation of the extreme event is important. For large-scale wind power where there are a high number of individual turbines and wind farms, the intermittency that may be seen in a single turbine output will become a more smooth variability visible in the hourly time scale.

General findings on large-scale variability can be summarized as [16]:

Very fast variations of distributed wind power are low (second–minute level). Even for a single wind power plant, the standard deviation of 1 s variations is only 0.1% of installed capacity. The 1 min variations (step changes) has the standard deviation from 2.1% to 0.6% of nominal capacity for a smaller and larger (250 turbines) wind farm [12]. There is increase in variability from the 10 min to the hourly time scale. The hourly variations do not smooth out very much inside one wind power plant.

The largest hourly step changes recorded from regional distributed wind power range from ±10% to ±35% depending on region size and how dispersed the wind power plants are. These are extreme values. Most of the time the hourly variations will be within ±5% of installed capacity [8]. The German example illustrates this: wind power changes are inside ±1% of the installed power 84% of time for 15 min

intervals and 70% of the time for 1 h time intervals (Fig. 11) [17].

Storm events can cause the most dramatic ramps – in West Denmark, for example, 80% of wind power production was lost during 6 h when wind speeds exceeded the cut-out limit of the turbines. Developing the forecasts for storm events is important.

For large offshore wind power plants ramp rates can be more dramatic and this should be taken into account if most of the wind power capacity in the region is concentrated on one offshore site.

Forecast Errors of Distributed Wind Power Production The short-term forecasting of wind power production is still a recent power system tool when compared to load forecasting. For wind power, the level of accuracy will not be as high as for load. The experience so far shows that the overall shape of the production can be predicted most of the time. However, large deviations can occur both in the level and in the timing of the winds [18, 19]. For power system operation, it is also relevant to know the uncertainty of the forecast. At times of low uncertainty, there is not so much need for short-term reserve allocation and at times of high uncertainty reserve allocation and potentially also measures of controlling wind power output can be used in system operation.

Level of accuracy improves when combining predictions for larger areas. For a single wind power plant the mean error for day-ahead forecasts is between 10% and 20% (as root-mean-square-error RMSE, % of nominal capacity). For a single balancing area this error will be below 10%. The latest results from West Denmark day-ahead forecasts show an average prediction error MAE (mean absolute error) of 6.0% of installed capacity, as an RMSE (root-mean-square-error) the error is 8.9%. In these numbers the relative forecast errors are to nominal capacity of wind power. When looking at the relative errors to average power (which give errors in terms of energy) the 6.0% for West Denmark corresponds to an error of 24% of yearly energy. The forecasts refer to day ahead, that is, $t + 13 \ldots t + 37$ h and are based on a wind power capacity of 1,512 MW [8].

Further reductions can be expected from combining different forecasting models: The first results from Germany show the best model performing at 5.1% RMSE, a "simple" combination 4.2% and "intelligent" combination 3.9% [20]. An important issue is that when wind power is spread over large areas, the actual

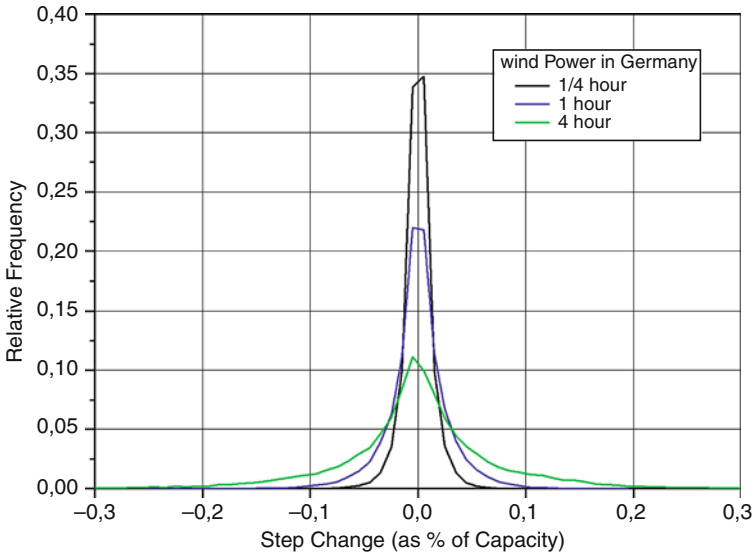

Wind Power Balancing. Figure 11
Short-term changes within an hour of total wind power production [17]. A positive value reflects an increase in power and a negative value a decrease

production of other wind power plants in the up-wind direction can be used as one input for the forecast of the production in other wind power plants and thus for example a storm front crossing an area can be better forecasted some hours in advance.

While the total balancing energy needed for the integration of wind power stems from the mean forecast error, the need for reserve power is closely connected to the largest forecast errors, that is, the tail in the probability density function (pdf) of forecast errors. Large wind power forecast errors are mainly caused by errors in the underlying weather prediction. Due to the chaotic nature of the weather, the pdf of the forecast error is not Gaussian [20]. Figure 12 shows as an example the probability density distribution of errors for a day-ahead wind power forecast for Germany; also shown is a fitted Gaussian distribution. It can be seen that large errors occur much more frequently than expected by a Gaussian distribution, causing a need for large reserve power in comparison to the balancing energy.

Main Challenges for Balancing for Power System Integrating Wind Power

There are several challenges regarding the handling of large amounts of wind power in power systems. The overall general challenge is to maintain a continuous balance, in an economical and reliable way with minimum environmental effects. Within this context, there are two important special cases that are often discussed: low wind and high load situation and high wind in low load situation. The main challenge C1 and the two important special cases C2–C3 are described as following:

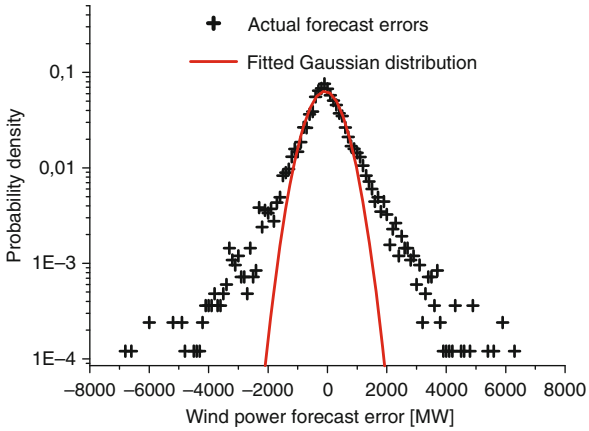

Wind Power Balancing. Figure 12
Probability density distribution of errors for the day-ahead wind power forecast for Germany; also shown is a fitted Gaussian distribution [21]

C1. *Handling the continuous balancing*. The challenge for the continuous balancing process is that controllable production and consumption have to maintain the balance on all time scales. With larger amounts of wind power, there is a larger uncertainty because wind power forecasts are not as exact as the corresponding power consumption forecasts. For economic calculations the efficiency of power stations operating on part-load in order to compensate changes in production levels has to be taken into account. The continuous balancing process applies to both the technical capacity available for increasing other generation when the net load increases (wind power will make this harder if it decreases while the consumption is increasing) and for decreasing other generation in an economically feasible way when the net load decreases (wind power will make this harder during the instants when wind power increases while consumption is decreasing). This issue is further explained in the subsequent part of this section.

C2. *Low wind and high load*. Situations with high power consumption are the basis for dimensioning the power generation capacity that has to be installed in a power system, often called as "capacity adequacy issue." This challenging situation occurs comparatively seldom; every 5–10 years electricity consumption is very high. And power consumption may be high in the neighboring countries/regions, too, which reduces the possibilities of importing power. With large-scale wind power, this situation will persist, but not only on a consumption level, but also regarding variable wind power production. Looking at past situations of high power consumption in Sweden and Finland [22], there are situations both with high wind power production and with small amounts of wind power. When dimensioning the power system, wind power production both in the balancing area and in its neighboring areas have

to be taken into account regarding high power consumption levels. There is no power station with a 100% certain availability during times of high power consumption. Similarly to the fact that there is no guarantee that a thermal power station will work exactly at the time when power consumption peaks, you cannot assume that there are strong winds when power consumption is high. In order to arrive at an assessment whether the number of other power stations can be reduced due to wind power plants, the capacity value of wind power has to be estimated. This is done exactly the same way it is done for all other types of power stations, independent of whether they are wind, coal-fired, nuclear or hydro-power stations. The capacity value of wind power is often in the order of 10–20% of the installed wind power capacity. This issue is further discussed in chapter Wind Power: Economy, Market, Subsidies, Payment Mechanisms, and Capacity Credit.

C3. *High wind power and low load.* If you add large amounts of wind power to a certain area without changing anything else, this may result in very low prices and/or that not all wind power can be used and/or that thermal power stations often are used at low efficiency and/or that water has to be spilled past the turbines. If such situations occur often, it becomes economically beneficial to (a) increase transmission capacity from the area, (b) invest in pump storage in rivers (low price for pumping up to higher reservoirs and the water can be used when prices are higher), (c) have a flexible power consumption (e.g., power storage in district heating or charge electric vehicles during such situations). (d) further develop the low load production possibilities of other power plants. Some power plants cannot operate at lower than, for example, 60% of rated capacity but have to shut down. This is one example that Denmark has done to ease the wind power integration – decreasing the lowest possible generation level of thermal plants to be able to stay on line (and produce ancillary services). The key point here is that an appropriate dimensioning is an economic issue as low prices promote investment in suggestions (a)–(d); at the same time, large investments will increase electricity prices. It is difficult to actually dimension the system "correctly" as lead times for investments cause an uncertainty regarding the investment planning. The "correct" dimensioning means in the practice that further investment (pump storage, transmission system, flexible power consumption) has a higher cost than the value it adds. It is important to remember that even a "correctly" dimensioned power system may include spill as it is not rational to dimension a power system without any spill. The conclusion is that – independent of whether the dimensioning is "correct" or not – it is very valuable that there is flexibility in both production and consumption, for example, that other production than wind power can produce at the lowest level possible.

How Wind Changes the Load Following on a Day-Ahead Time Scale

The scheduling process in power systems are made usually day ahead, as described in the previous section. Wind power forecasts are used in this process, in a similar way as load forecasts. The varying production patterns of wind generation changes the scheduling and unit commitment of the other production plants and use of transmission between regions. Either losses or benefits are introduced to the system, compared with the situation without wind. Most of the energy produced by wind power will impact the scheduling process, but there is a significant impact on the operating reserves as well, as the forecast errors of wind power can be large.

As there can be a large difference on the wind power production levels in daily time scale, there will be a large impact on how the conventional power plants are run in a power system with more than 10% wind power penetration (of yearly energy). Low wind and high wind days can mean a difference on conventional power production almost as much as the installed capacity of wind power. This is illustrated in Fig. 13 by the West Denmark data from January, 2005 (wind penetration is about 24% of total gross demand and installed wind power capacity about 2,400 MW).

Large variations in wind power output can result in operating conventional power plants less efficiently. Optimized unit commitment, that is, planning the starts and shutdowns of slow-start units, is more

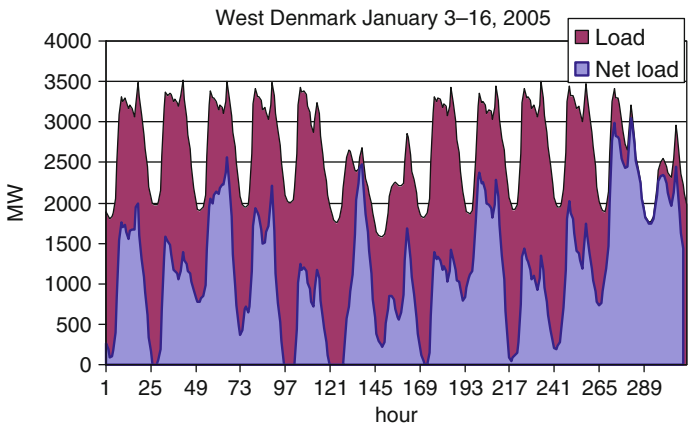

Wind Power Balancing. Figure 13
There will be a large impact of wind power on how the conventional power plants are run with a high wind penetration level (2 weeks from West Denmark, where wind power produces 24% of yearly electrical energy). Net load is electricity consumption (load) minus wind power generation

complicated when the variable and uncertain output from wind power is included. There will be more part load operation of conventional power plants. Start-ups and shut-downs of conventional power plants may also increase, especially to make room for the difference of low wind and high wind days. At higher penetration levels it has been noted that start-ups will decrease and more and more part-load operation at low levels is seen instead of shutting them down [11].

An important issue is also that the wind power forecasts are not perfect. This is illustrated in Fig. 14, where a real forecast is shown together with the real outcome.

It must though be noted that the large deviation considers a 24–32 h forecast since the drawn forecast is performed the day before at 11.00. For the actual scheduling of all hours, the flexibility of the existing system is essential. If, for example, all units can start up in 6 h, then the actual operation of the power plants in hour 13 can be planned at hour 7 which is illustrated with a circle in Fig. 11. This means that the 26 h forecast can be replaced with a 6 h forecast which is normally significantly better.

When wind power is added to the system, increase in costs due to increase in losses (increased operation in reduced efficiency) and wear and tear can be seen. This is however a moderate extra cost at least with penetration levels of 10–20% of wind power in the system.

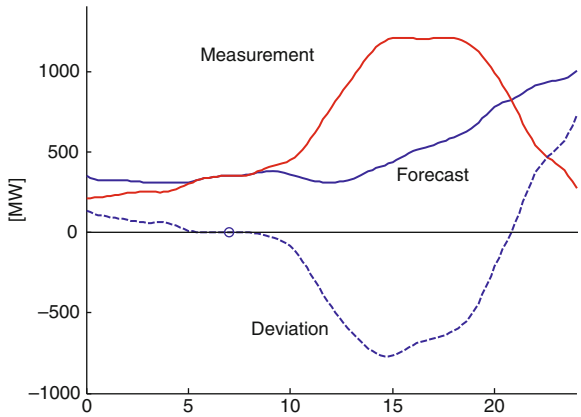

Wind Power Balancing. Figure 14
Forecast, real production, and deviation for a day with large forecast error in the West Danish system

If wind power production exceeds the amount that can be absorbed while maintaining adequate reserve and dynamic control of the system, a part of the wind energy produced may need to be cut off (curtailed/spilled). It can though be noted that if 1% of wind power is spilled, then this increases the cost of the wind power with 1%. For a significant impact on the cost of wind power, the spillage has to be high. It can be noted that for, for example, hydro power investments, it is common to accept spillage in different situations, since this is found to be an economic solution.

For efficiency of production, the interest is on how the conventional capacity is run and how the variations and prediction errors of wind power change the unit commitment: both the time of operation and the way the units are operated (ramp rates, partial operation, starts/stops). These effects are in most cases analyzed by making simulations of system operation. In simulation models the reserve requirement is often taken into account, too, based on a simple rule how much reserves of moving up and down needs to be allocated to generation units in the simulation.

Wind power may influence the hydro power reservoir contents and reservoir management. When the wind production is large compared to the reservoir size in the area, there is a clear effect on reservoir management [11]. Wind power may also influence the losses of hydro power production. For example, a large wind power production in the spring flood time can result in the loss of some hydro production.

The impact of wind power on the power transmission depends on the location of wind power plants relative to the load, and the correlation between wind power production and load consumption. Wind power, like any load or generation, affects the power flow in the network and may even change the power flow direction in parts of the network. The changes in use of the power lines can bring about power losses or benefits. Increasing wind power production can affect bottleneck situations.

Modeling Wind Power in Dispatch The simulation results give insight into the technical impacts that wind power has, and also the (technical) costs involved. Analyses on how current market mechanisms affect wind power producers is also important. For wind power impact on the operation of power systems, modeling on an hourly level would be needed to catch the variability of wind. The models used in integration studies are often not specifically designed for dealing with high shares of wind power.

There are two critical challenges in energy system simulations: how the export possibilities to areas outside the simulated region are taken into account and how the wind power uncertainty at different time scales is taken into account in the model.

The effects of wind power on a power system are spread over the total control area (synchronously operated area), balancing area or electricity market, with constraints on transmission capacities between the areas. Effects of wind power are first seen as an increase in exchange of electricity between the areas. The results will, however, show only increase in transmission unless boundary conditions are set, to be able to see the limits to the transfer of wind power variability to the neighboring areas. Contingencies, which have an impact on dynamic phenomena in the time scale of seconds, cannot be modeled with an hourly time scale model. Due to this, the low transmission possibility scenario is often used, and this can underestimate the exchange possibilities during most of the time.

In real life some corrections to schedules after day ahead are possible. Developing methods of incorporating wind power uncertainties into existing planning tools and models is of crucial importance. Modeling the effect of prediction errors is complicated by the uncertainties to different time scales of unit commitment (starting and shutting down slow thermal units) and dispatch (production levels of thermal units). Problems can also emerge from the simulation logic in itself: optimization of the system can be fundamentally different if taking into account the different nature of wind power production. Also, regulation requirements are often not modeled directly, but based on years of operating experience, so the effect of wind power cannot be modeled either [23]. Electricity market interactions and price levels should also be looked at when simulating wind power in the system.

Also the simulation case set up and comparison, to catch the effects of wind power, is of importance. Usually wind is added to the system and any effects are analyzed comparing the production and costs of the system with and without wind. For assessing the cost of variability of wind, the comparison can be made by adding wind as a flat production block over 24 h, or with a foreseeable diurnal pattern.

Which Power Production Will Wind Power Replace? As has been explained above, production and consumption always balance. This means that all power that is fed into the power system at some point will always be used. If a wind power plant produces power, the need for other power production decreases accordingly. For each kilowatt hour of wind power, 1 kWh less is needed from another power plant (if the losses remain the same).

The question is which power stations will be replaced. Both in regulated and deregulated electricity systems, the use of the production form with highest marginal cost will be lowered by wind energy. But this may be different during different hours of the year. For most systems with some coal fired production plants, it is mostly coal power production that will be replaced by wind power. This is true when wind energy provides a minor amount of the total electricity consumption. This is also valid for large amounts of wind, for the countries where electricity production is based on coal. For other conditions, wind energy may replace gas fired production (with lower CO_2 emissions), or even CO_2 free production forms such as hydro, biomass or nuclear power. Even if the hydro production is reduced by wind energy, the hydro power stored in the reservoirs may be used later, possibly reducing fossil fuel fired production. Interconnected systems can also respond in such a way that wind power is partly replacing coal fired production in a neighboring country [11].

The exact result depends on the amount of wind power in the power system, and on the amount and costs of coal and gas fired production in the system.

In the following, some reasoning regarding the different power generation types and their role in power systems with large-scale wind power is provided:

Hydro-power: When wind power increases, it is often reasonable to decrease hydro-power production as it is comparatively easy to control. In practice, the amount of water passing through the power station is reduced and the water is stored in the dam instead. You have to keep in mind, though, that there will be more water in the reservoir that can be used later. In principle, you can say that for each kilowatt hour of wind power, it is possible to store 1 kWh of hydro-power in the dam. That means that wind power does *not* replace hydro-power, but shifts hydro-power production between hours. The amount of energy that hydro-power produces is mainly dependent on how much it rains. It is important, though, to remember that this only describes the general issue. There are many important details that have to be taken into account for an exact assessment of the opportunities. These include:

- During spring flood, the storage capacity of the dams may be limited.
- Different dropping heights and storage levels result in different efficiencies of hydro-power stations, that is, different amounts of energy per cubic meter of water.
- Forecast security requires certain margins as water that is dropped through the turbine of a power station will take, for instance, an hour to arrive at the next reservoir, and the conditions may have already changed by then.
- Water legislation sets clear limits to how reservoirs may be filled/emptied and how the plants may be operated. Similarly, power companies may even have self-imposed restrictions, that is, they do not make full use of the water legislation as this would lead, for instance, to inconveniences for local residents or tourists.
- It is a combination of water inflow, physical control options and water legislation that limits the control options in hydro-power stations.

Nuclear power: Nuclear power has an operating cost (cent per kilowatt hour) that is almost always lower than the electricity price. Therefore, they always try to produce as much as possible in these power stations. If wind power production increases, there are other power stations than nuclear that will decrease production instead. Nuclear generation can be reduced at times when there is a limited export options to countries with more expensive power production and in a situation where there is high wind power production and low load and all other generation is already cut-off. Nuclear power plants often have their yearly maintenance scheduled at times of spring floods when reduction of hydro power generation would result in spillage.

Coal/gas/oil power: There is coal power in the Scandinavian and Northern European power system that can be replaced by other power production. If it rains heavily in Sweden and/or there is a lot of wind power, it is mainly coal power that will reduce production in these countries because Sweden either exports power to these countries or reduces imports. The reason for reducing just coal power is that it has most often the highest operating costs. Sometimes, there are also other power stations, such as gas or oil-fired power plants, with operating costs that are even higher than that of coal power; and consequently, their production will be

decreased instead. It should be added that the green certificate trading leads to a situation where coal power prices increase the most (most carbon dioxide per kWh of produced power) which results in an increased interest in reducing just that production. One special case is combined heat and power production (CHP) where heat demand is setting the level of electricity production from the plants. However, in many cases there is a heat storage and thus also the electricity generation from these plants can technically be operated in a flexible way.

Conclusions: Wind power production results in that other power stations are operated at a lower capacity in comparison to a situation without wind power. If there are large amounts of hydro-power, then wind power will lead to the rescheduling of hydro-power to later points in time. Therefore wind power production at one point in time can indirectly lead to a reduced thermal power production at a later point in time. Wind power production mainly results in a reduced production in coal-fired power plants either in the area or in the neighboring areas. That requires a sufficient transmission capacity to countries with coal power, though, and that the actual pricing makes coal power the power with the highest operating costs.

How Wind Impacts the Balancing During the Operating Hour, Operating Reserves

Depending on the prediction accuracy, parts of the wind power production variations remain unpredicted or are predicted incorrectly, and there will also remain subhourly changes in output. This is what has to be handled by load following reserve or the balancing market.

During the hour of operation, the balance is first secured by means of primary reserve (automatic frequency control). In the event of major frequency deviation, the TSOs adjust the production or the consumption manually, using secondary/tertiary reserve. The reserve can be allocated by contracts between some producers (and consumers) and system operators or through a common regulating power market, where the players submit their bids for upward and downward regulation of production or consumption.

To estimate the impact of wind power on power system operating reserves, it has to be studied on a control area basis. Every change in wind output does not need to be matched one-for-one by a change in another generating unit moving in the opposite direction. It is the total system aggregation, from all production units and consumption, which has to be balanced. A producer with flexible production could in principle counteract changes in its own wind power production also during the operational hour. Self regulation is discouraged, however, as it is more cost effective for both the system and the individual players to bid all regulating power to a joint pool for the system operator to use the cheapest options first. Otherwise there is a risk that, for example, wind power changes for one actor that physically are balanced out by changes in other wind power stations owned by another actor instead are balanced by each actor, which is not rational.

The increase in short-term reserve requirement is mostly estimated by statistical methods combining the variability or forecast errors of wind power to that of load and investigating the increase in the largest variations seen by the system [6]. Usually margins for "possible" extreme situations are kept. The term "possible" then normally includes a certain percentage of what in reality could happen. A straightforward method to define "possible" is the commonly used "$N - 1$ criterion," that is, it is necessary to keep reserves for an outage of the largest production unit or interconnector, which could be a challenge during both, import and export situations. This is a common dimensioning criterion for disturbance (contingency) reserve. In addition to that, some operational reserve is carried on top of that to cover variability and forecast errors, but there are no commonly used criteria to dimension this part of reserve. Some TSOs begin to use probabilistic approaches to define a suitable level of reserves.

Although wind power plants can at times create large "ramps" (i.e., large swings in production level), at current wind penetrations in most parts of the world these are not big enough or fast enough to be considered contingency events [5, 24].

Primary control is performed on a time scale of seconds/min. On this time scale, variations are already smoothed by different gusts for the individual turbines, inertia of the large rotors as well as variable speed turbines absorbing the variations, and there is no correlation between the variations of geographically dispersed wind farms. This is why the effect of wind power

on the system operation in the primary control time scale is very small even at considerable penetration [9, 25, 26].

For operational reserves, the unforeseen variations induced from wind power are relevant on the time scale of 10 min^{-1} h, where impacts of wind power can be clearly seen.

Methods to Estimate Allocation of Reserves Effects of wind power on reserve requirements, on a time scale of minutes, are often estimated based on statistical methods. The statistical approach for estimating the increase in reserve requirements is based on looking at the variability as a probability density. Combining the variability of wind with load variations, and looking at the increase in the net load variations is often referred to as the "3σ method" [27, 28]. This means that three times the standard deviation can be taken as a confidence level for how much of the variations should be covered by reserves (values of 2–7 have been used instead of 3; [6]).

It is of central importance to separate need of flexibility in longer time scales of several hours to a day (power plants that can follow net load variation) and need of reserves that can be activated in seconds or minutes time scale (power plants that can follow unforecasted net load variations). To illustrate the need of flexibility, Fig. 15 shows the needed power increase divided in scheduled production and reserves.

3 Sigma Methodology A widely used method for estimating the incremental increase of variability that the power system must balance when adding wind power is the consideration of the difference between the distribution of variations before and after wind power. As an estimate of the increase in variability, the standard deviation (σ) of the distribution can be used as a confidence level. Even if this is not the method by which the operating reserves are allocated in real power systems, this method is fairly easy to use and produces a value that is related to the degree by which wind power increases the variability in the power system [29].

Also the risk of forced outages can be included when estimating the increase in reserve requirements, which means combining the uncertainty of load, wind and other production. Because of spatial variations of

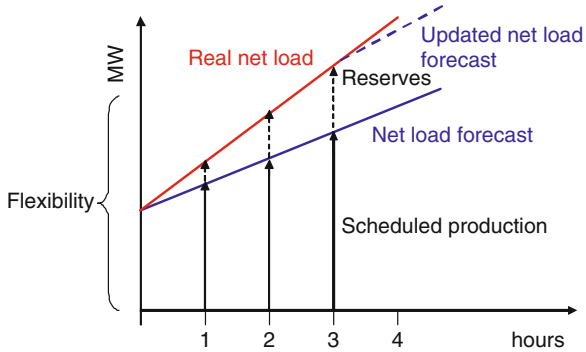

Wind Power Balancing. Figure 15
Flexibility in the power system to follow varying load and wind power production (the net load) consists of scheduled production and reserves. The need of flexibility is not the same as need of reserves, since a part of the net load variation can be forecasted

wind from turbine to turbine in a wind plant – and to a greater degree from plant to plant – a sudden loss of all wind power on a system simultaneously due to a loss of wind is not a dimensioning event. This is an important consideration for first contingency evaluation (disturbance/contingency reserves).

The reserve issue can be approached by noting that the system operator must balance the aggregate loads and generation. It is then possible to study the variability of load and wind power with time series of variations of wind power (P) and load (L):

$$\Delta P_i = P_i - P_{i-1} \tag{1}$$

$$\Delta L_i = L_i - L_{i-1} \tag{2}$$

where i denotes the hour (from 2 to 8,760 in 1 non-leap year). The increase of variability that wind power brings to the power system can be seen when comparing their combination (net load) with the original load time series. Net load is the load minus the wind power production for each hour. The net load hourly variations are calculated like the hourly variations (1), but now for the net load time series (NL), where wind power production is subtracted from load:

$$\begin{aligned}\Delta NL_i = & NL_i - NL_{i-1} = (L_i - P_i) \\ & - (L_{i-1} - P_{i-1}) = \Delta L_i - \Delta P_i\end{aligned} \tag{3}$$

In Fig. 16, the amount of hourly variations that the system sees is depicted showing 1 year of data in

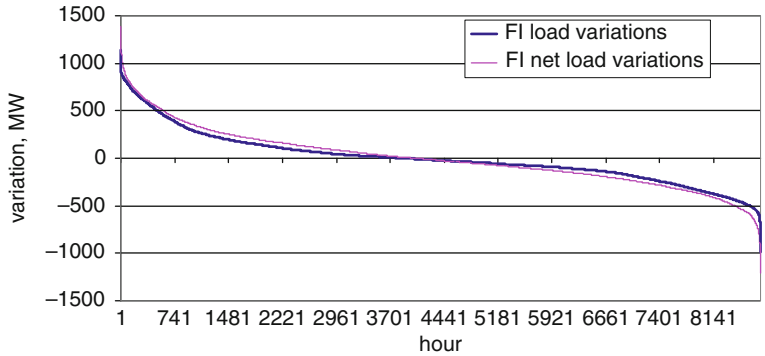

Wind Power Balancing. Figure 16
Duration curves of annual load variations without wind power and net load variations with wind power. The case is for Finland in the year 2000 with hypothetical 6,000 MW wind (17% of gross demand) [11]

decreasing order (duration curve). There are two curves, the load variations without wind and load variations together with wind (the hourly variations of net load). The difference in the maximum values of MW of variations with and without wind indicates the amount that the operating reserve capacity must be increased. The difference in overall MW variations shown in the duration curves indicates the increased amount of existing reserve capacity operating, when wind power is added. The same capacity can in principle be used for both up and down regulation, and the variations as well as the increase should essentially be symmetrical. Either up or down (positive or negative) variations can determine a need for an increase in the reserves.

Planning and operating a power system is based on probabilities and risk. Reserves in the power system – with or without wind power – are generally determined so that variability within a certain probability are covered, for example 99.99% of the variability.

Standard deviation σ tells about the variability of the time series, it is the average deviation from mean value μ:

$$\sigma = \sqrt{\frac{\sum_{i=1}^{n}(x_i - \mu)^2}{n}} \tag{4}$$

For a normally distributed probability distribution, the standard deviation σ is a measure indicating that about 68% of the data is inside ±σ of the mean value. Taking a range of ±3σ will cover 99%, and ±4σ will cover 99.99% of all variability. For hourly variations, the mean value is 0 by definition.

If the variability of load and wind power production can be assumed to be uncorrelated, the standard deviation of net load time series (σ_{NL}) can be determined by a simple square root sum of the standard deviations of load (σ_L) and wind power (σ_W) time series:

$$\sigma_{NL} = \sqrt{\sigma_L{}^2 + \sigma_W{}^2} \tag{5}$$

The hourly variability of wind power production and load do experience some correlation in the data of some regions. Also, the distribution of the variations is not usually strictly a normal distribution. However, formula (5) has been checked for several sets of data and it has produced accurate results for the standard deviation of the net load [30].

Finally, the increase, *I*, in the variability due to the wind can be formulated as the increase in some multiple of σ, calculating the increase from σ_L to σ_{NL} using for example 4σ as the confidence level covering most of the variability:

$$I = 4(\sigma_{NL} - \sigma_L) \tag{6}$$

In Fig. 17 the distribution curves for the variations in load and net load are depicted, showing also how far 2σ, 3σ, and 4σ reach to cover the variability of the dataset.

Exceedence Level A related approach to calculating load following reserve requirements for wind is to work the previous example backward. Instead of calculating some multiple of σ, which corresponds to a

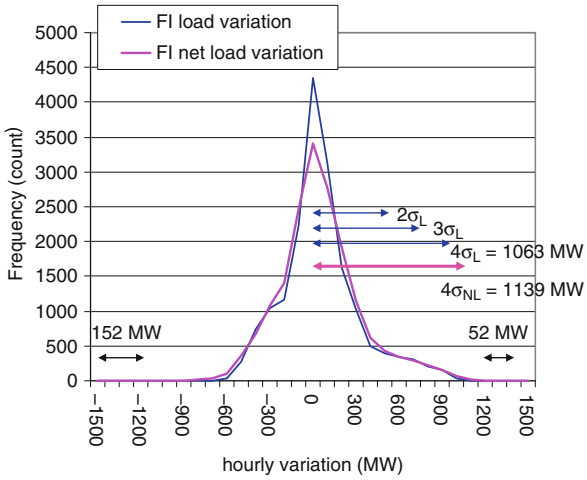

Wind Power Balancing. Figure 17
An example of estimating the increase in hourly variability seen by the system ([31] Finland 2000–2001 data). If only maximum variation is looked at, the increase is determined at the tails of the distribution (52 MW increase in positive up-variation and 152 MW increase in negative down-variation). Looking at the standard deviation of the distributions, there is a difference of 76 MW in the 4σ coverage of the variability (1,139–1,063 MW)

given (low) probability that load will exceed generation, the probability level is chosen based on a priori risk tolerance. For example, if the chosen exceedence level is 99%, then the load (or load minus wind) can be sorted and the entry for the 99th percentile can be extracted. In a normal distribution, this would correspond to 3σ. However, if the underlying distribution is not normal, using an exceedence level can provide an alternative approach that provides the same level of risk.

To examine the reserve impact of wind, this approach can be easily done by (1) calculating a given exceedence level (percentile) for load alone, (2) calculate the same exceedence level (percentile) for the load net wind, and (3) comparing the incremental capacity of the two calculations.

Different Time Scale Reserves There are different requirements for different time scales in operational reserves, and this can be reflected in the amount of sigmas needed as a confidence level.

Regulating reserve must be available through the automatic generation control (AGC) scheme and responds over time periods of up to several minutes. It is not uncommon for the system operator to carry regulating reserves equal to ±5σ or ±6σ, where σ is the system variability measured as standard deviation of the load variability.

However, over longer time scales it may be possible to obtain generator responses from other sources, including non-AGC units that are spinning and synchronized, market participants, or quick-start generation that is not spinning. In systems with significant run-of-river hydro, the overall system variability will also be a function of the hydro variability over the time scale of 10–60 min, in addition to load and wind forecast errors and sub-hourly ramping. Some studies in the USA, for example, [31–33], have used 2σ as the preferred metric to calculate load following requirements for wind. This is based on the requirement (imposed by the North American Electricity Reliability Corporation, NERC) that the minimum required score for control performance standard 2 (CPS2) is 90%, which approximately corresponds to the normal probability value for 2σ. Other US studies have used ±3σ as the appropriate confidence interval [24, 29, 34]. Another study undertaken by GE Energy of the Ontario system used ±3σ and used a corresponding exceedence analysis as a supplement [35].

Combining the Impacts of Different Time Scales

When estimating the changes in balancing and any increase in reserve requirements this is usually done for different time scales. However, there are many time-based interrelations. Primary regulation and – to a certain degree – secondary regulation maintain the continuous balance. In order for that to work, it is necessary to continuously plan und re-plan so that there will be sufficient margins for maintaining the balance between production and consumption in a reliable and economic way. It is not possible to simply add up several types of reserves as they are interrelated. The events that occur during a certain hour, for instance, are a part of what can happen during the 24 h-period, cf. Fig. 18.

The difference between flexibility $P_k n(t)$ and reserves $P_k r(t)$ is that $P_k n(t)$ sets the total flexible capacity that has to be available, while $P_k r(t)$ only includes the part of the flexible capacity that must be available

within the time t without being prescheduled. Prescheduling means that power plants with longer start-up times are included in flexibility $P_k n(t)$, because it is assumed that their start-up process is initiated before the actual operation hour such that they are online in time period k+t. The capability of both $P_k n(t)$ and $P_k r(t)$ are strongly connected to the ramp rates of available power plants and in the case of $P_k n(t)$ start-up times of available power plants. The examples in Fig. 18 are mainly on hourly bases, but common reserve categories are, for example, "primary reserves" $= P_k r$(around 1 min) and "secondary reserves" $= P_k r$ (around 1–5 min).

The examples in Fig. 18 show a case where production needs to be increased to follow the net load. There is also a need to decrease production when net load decreases. It is generally easier to decrease generation than to increase it, for example, by disconnection of generating plants (including wind power).

It can be noted that:

- Wind power can only decrease when there is a production level and only decrease largely when there is a large production. In a situation with no wind power, there is no need to include wind power when determining downward reserves or flexibility in the power system.
- In a situation with high wind power production, that is, a situation with possible decrease of wind power production, other units are not in operation (since some of the load is met with wind power). This means that these units can increase their production if wind power decreases and/or load increases. This is based on the assumption that $P_k n(t)$ and $P_k r(t)$ can increase their production fast enough. This means that *flexibility* and *reserve keeping* in a system with wind power is often more *an issue of ramp rates and start-up times*, than a need of more capacity – more fast ramping and starting capacity can be needed, if the forecast errors are large enough that the slow units cannot follow.
- In many real systems (here called system A), there are connections to neighboring systems (system B). In system A a common approach is then to use a probabilistic (= statistical) approach concerning the need of reserves and flexibility, assuming that during a certain percent of the time the needed flexibility/reserves are imported from system B. But then the needed reserves in system A also have to consider possible outages in the transmission to system B. This means that one can estimate $P_k n(t)$ and $P_k r(t)$ from a probabilistic density function of possible changes (i.e., *variability* for $P_k n$) or *forecast error* (for $P_k r$) and a certain percentage of accepted need for import of power. This method can also be used when one wants to make a rough estimate of needed $P_k n(t)$ or $P_k r(t)$ for a future system based on knowledge of $P_k n(t)$ and $P_k r(t)$ in the current

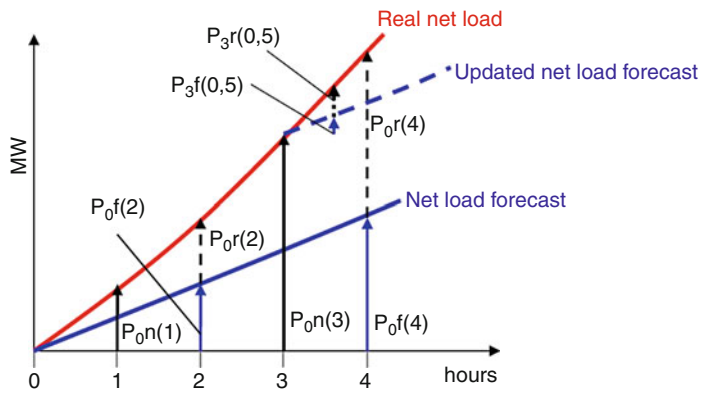

Wind Power Balancing. Figure 18

Need of "Flexibility" is the need for some units to follow the "net load variability," marked $P_k n(t)$. This can be partly done by units scheduled beforehand, to follow the "net load forecast," marked $P_k f(t)$, while "reserves" is the need for some units to follow the "net load forecast errors," marked $P_k r(t)$

system. Also in systems without interconnections there are some dimensioning criteria which means that one only keep margins for "possible" situations. The term "possible" then normally includes a certain percentage of what in reality could happen. Also in these systems it is possible to use a probabilistic approach. A straightforward method to define "possible" is the commonly used "N–1 criterion," that is, it is necessary to keep reserves for an outage in the largest unit.

- The different time frames for both $P_k n(t)$ and $P_k r(t)$ are strongly interconnected. If one, for example, have enough $P_k n(4\ \text{h})$, then this in general *includes* that during this period there must be enough $P_k n(1\ \text{h})$. This means, in this case, that there is no meaning in calculating $P_k n(4\ \text{h}) + P_k n(1\ \text{h})$ since they overlap significantly. Such additions are only valid when they contain different units. In reality there is also an overlap between $P_k n(t)$ and $P_k r(t)$. Assume, for example, that $P_k n(t)$ is available, but the forecasted net load only increases $P_k f(t)$ (where $P_k f(t) < P_k n(t)$). This means that $P_k n(t) - P_k f(t)$ is available to be included in $P_k r(t)$. This is based on that this volume has a ramp rate that is high enough so it does not have to be prescheduled. It can also be noted that if the most extreme increase of net load that have ever happened is $P3(t)$, then this means that in this situation the highest requirement of *available flexibility* will be that $P_k n(t) = P3(t)$. It is then important to note that this includes $P_k r(t)$ so there is *not* a need for the system to cover both $P_k n(t) = P3(t)$ *and* a maximum $P_k r(t)$ to meet uncertainties *at the same time*.
- There is an interaction between "reserves" and market arrangements. If the net load forecasts are relatively accurate for a certain time frame (e.g., 24 h) then only a 24 h market is needed. If, on the other hand, the 24 h forecasts have low quality, then there has to be a market for changed production within that period. It is not the *variability* that requires updated markets but more the *net load forecast errors*. It must also be noted that, for example, "24 h reserves" is not a physical but mainly a market need. Most power plants need maximum 4–6 h to start up so they do not need this information 24 h in advance.

Wind Power in Electricity Markets

Wind power can take part in the electricity markets, where the energy can be traded according to wind power forecasts. As the accuracy of the forecasts is not as high as for other generation, or electricity consumption, there are almost always deviations from the traded amounts. If the imbalance prices are high, then intraday trading will considerably help the individual producers in the market to help lower the costs by better forecasts closer to delivery hour. Also aggregating wind power helps the actors in the market, as there is considerable decrease of (relative) forecast errors from dispersed production, just as is the case for load forecasts.

Balance settlement rules have a bit impact on the wind power producer. In systems where the imbalance prices are transparent and reflect the real system imbalance cost, wind power imbalance costs have been moderate [Holttinen et al., Neimane et al.]. In these systems wind power producers only pay extra costs during the hours when their imbalance has been to the same direction than system imbalance: for example need for upregulation when the whole system has used upregulation. When the imbalance costs are low, at low wind penetration levels, intraday trading is not always profitable for the actors. If the imbalance prices contain penalties for all deviations, no matter to which direction the system imbalance has been, then operating with shorter forecasts, intraday, is crucial.

Results from Integration Studies

An Integration study of wind power is often performed in order to obtain the possibilities to integrate a certain amount of wind power in a certain system and/or to estimate needed changes in the system set up in order to make it possible to integrate the wind power. "Integration cost" is then defined as the additional costs that are required in the system (except the costs for installing the new power plants) to keep customer requirement at an acceptable reliability, cf. Fig. 19. [36].

First two terms have to be defined:

- *The replaced system* = The power system consisting of other power sources in the system that will be replaced by the new power source

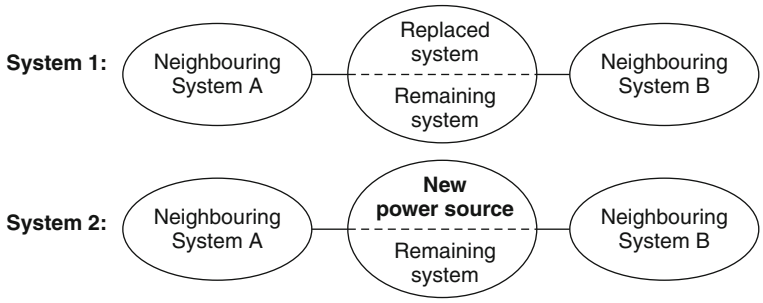

Wind Power Balancing. Figure 19
Integration cost = [costs in system 2] – [costs in system 1]

- *The remaining system* = The power system consisting of the other power sources, that are the same in both alternative systems

It is important to note that how the *replaced system* is selected is essential for the result. If the alternative to wind power (i.e., the *replaced system*) is nuclear power that is not taking part in regulation (as the amount of production changes should be kept small) the consequence of having wind power is also smaller compared to if wind power would replace easily regulated gas-fired generation.

Also the selection of the *remaining system* is essential. If wind power is to be integrated in a system with a large share of nuclear power (i.e., the *remaining system*) this will then cause a much larger "integration cost" compared to a study where the *remaining system* consists of easily regulated gas-fired generation.

Integration cost can be divided into different components arising from the increase in the operational balancing cost and grid expansion cost. The value of the capacity credit of wind power can also be stated. Here only the results on "balancing" are summarized.

Many wind integration studies give estimated impacts as increase in reserve requirements (MW) and integration costs ($/MWh, €/MWh). Many studies give the results in less comparable ways, like impacts on the scheduling of other power plants and exports.

Different metrics for the results have been used in the studies: Results as monetary value per MWh of wind or per MWh of total consumption (reflecting the increase in consumer price). There are also results as % of more wind power production needed to cover extra losses.

For increased balancing it is important to note whether a market cost has been estimated or whether the results refer to technical cost for the power system. There is also benefit when adding wind power to power systems: it reduces the total operating costs and emissions as wind replaces fossil fuels. The trade-off between curtailing wind output in critical times and providing new transmission or production capacity would be needed in some cases 37.

In the following graphs only the cost component has been analyzed. The case studies summarized are not easy to compare due to different methodology and data used, as well as different assumptions on the interconnection capacity available.

Determining what is "high" penetration of wind power is not straightforward. Often either energy or capacity metrics are used: wind power production as % of gross demand (energy) and wind power as % of peak load (capacity). To determine high penetration for a power system also interconnecting capacity needs to be looked at. This is because critical moments of high wind and low load can be relieved by using interconnector capacity.

Results for Increase in Reserve Requirements

Wind generation may require system operators to carry additional operating reserves. From both the experience and results from studies performed, a significant challenge is the variability of wind power within 1–6 h. Frequency control (time scale of seconds) and inertial response are not crucial problems when integrating wind power into large systems at the present time, but may be a challenge for small systems (like Ireland)

and will become more of a challenge for systems with high penetration in the future.

The results presented in Fig. 20 for increase in reserve requirements due to wind power are from following studies: Finland and Nordic [11], Sweden [37], Ireland [38], the UK [39], Germany [40]; Minnesota 2006 [32] and California [41].

The estimated increase in short-term reserve requirements in the studies has a large range: 1–15% of installed wind power capacity at 10% penetration (of gross demand) and 4–18% of installed wind power capacity at 20% penetration. Time scales used in the estimation explain much of the differences in results:

- If only hourly variability of wind is taken into account when estimating the increase in short-term reserve requirement, the results are 0.5–4% of installed wind capacity or less, with penetrations below 10% of gross demand.
- When 4 h forecast errors of wind power are taken into account, an increase in short-term reserve requirement of 4–5% of installed wind capacity has been reported, with penetration levels of 5–10% of gross demand.

The highest results in Fig. 20 are from a study where 4 h variability of wind (not forecast error), combined with load forecast error, results in 15% reserve requirement at 10% penetration and 18% reserve requirement at 20% penetration of gross demand [39]. The latest achievements in wind forecasting show a considerable improvement of predictions also in short time scales, so using updated forecasts would reduce this estimate. If day-ahead forecast errors are left to be balanced with the short-term reserves, the increase in short-term reserve requirement is nearly 10% (two points for Germany reflect difference in up- and down-regulation requirements) [40]. In this German study, the reserve requirement is taken as the average impact of day-ahead forecast errors of wind power. The maximum values would result in an increase that is 15–20% of installed wind capacity.

In most studies, reserve requirements for different time frames are summed up – for example, increase in regulating reserves + increase in load following reserves. There are some studies showing larger increase in reserve requirement than shown here. Swedish TSO published estimates that are 35–48% of installed wind capacity [42]. This is due to adding up several cases and time frames of reserves. However, the different time

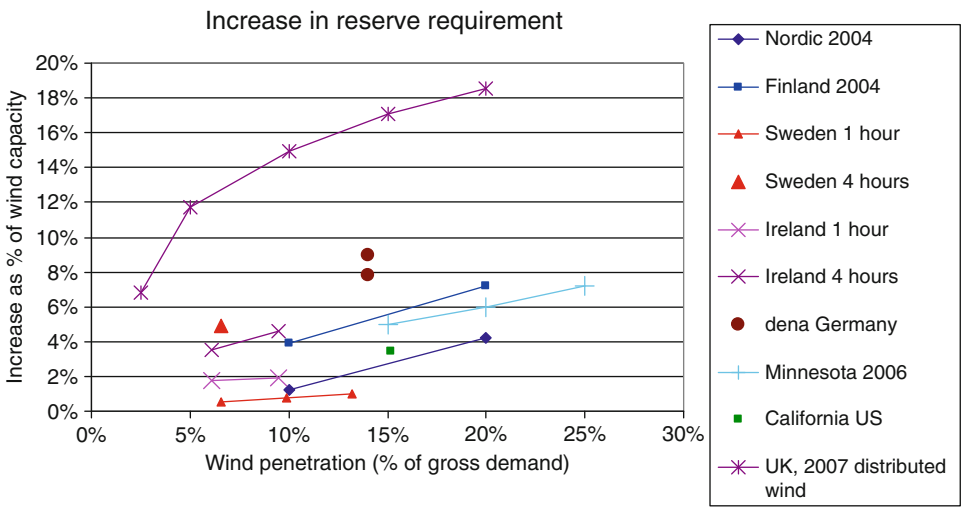

Wind Power Balancing. Figure 20
Results for the increase in reserve requirement due to wind power. German Dena estimates are taking into account the day-ahead uncertainty (for up and down reserves separately) and UK the variability of wind 4 h ahead. In Minnesota and California, day-ahead uncertainty has been included in the estimate. For the others the effect of variations during the operating hour is considered. For Ireland and Sweden the 4 h-ahead uncertainty has been evaluated separately

frames, for example, 1 h ahead and 4 h ahead, are strongly overlapping. If one has enough flexibility for 4 h, then this in general implies that during this period there is enough flexibility for 1 h ahead. In this case there is no meaning in summing up these reserve requirements since they overlap significantly. Such additions are only valid when they contain different units.

An important issue is that "increase in reserve requirements" does not necessarily mean need of new investments. The amount of wind-caused reserves is at highest when wind power is on a high production level. In these situations the other power stations are operated on a low level, which means that they can act as reserves and increase the generation if wind power decreases. This means that flexibility and reserve keeping in a system with wind power is an issue of ramp rates and start-up times, together with a need of more capacity – more fast ramping and starting capacity can be needed, if the forecast errors are large enough that the slow units cannot follow. This must be considered when "increased reserve margins" are to be estimated.

Balancing Cost

Wind power impacts on power system balancing can be seen in several time scales, from minutes to hours, up to the day-ahead time scale. General conclusions on increase in balancing requirement will depend on region size relevant for balancing, initial load variations and how distributed wind power is sited. Here also, the operational routines of the power system are relevant – how often the forecasts of load and wind are updated, for example.

To arrive at estimates for balancing cost, the operating reserve impact is one issue (increase in reserve requirement from statistical methods) and impact on efficiency of conventional power plants for day-ahead operation is another issue (simulations). For the simulations most results are based on comparing costs of system operation without wind and adding different amounts of wind. The costs of variability are also addressed by comparing simulations with flat wind energy to varying wind energy, for example in Minnesota, USA [32] and Greennet Nordic+Germany [43].

It is important to pay attention to the representativeness of wind input data (how well does the wind data represent the geospread of the power system, how is wind power simulated, what time scale effects on variability and predictability have been taken into account) and also how the main setup for the assessment or simulation is made (wind power replacing other production or capacity and to what extent is the power system operation optimized when wind power production is added). The level of detail of the simulation model (time resolution, level of detail in simulating conventional generation and transmission, pricing) and how the uncertainty in the wind plant output forecast is handled with respect to the load forecast uncertainty are also important.

The check-list developed in [35] can be used to find out whether the simulation approach has been conservative or whether some important aspects have been omitted, producing either high or low estimates for the impacts. The most general finding comparing the study setups is the use of interconnection capacity – this is crucial when estimating the impacts of wind power.

The results presented in Fig. 21 for increase in balancing costs due to wind power are from the following studies: Finland and Nordic countries [11], the UK [44, 39], Ireland [45], Colorado [45], Minnesota [46, 32], California [47, 48]; Nordic countries and Germany [43].

From the cost estimates presented in investigated studies it follows that at wind penetrations of up to 20% of gross demand (energy), system operating cost increases arising from wind variability and uncertainty amounted to about 1–4 €/MWh wind power produced (Fig. 21). This is 10% or less of the wholesale value of the wind energy. The actual impact of adding wind generation in different balancing areas can vary depending on local factors. Important factors identified to reduce integration costs are aggregating wind plant output over large geographical regions, larger balancing areas, and operating the power system closer to the delivery hour with accurate forecast systems.

The highest estimates of reserve requirements from Germany and the UK are not reflected in balancing costs, as from both studies it was concluded that this amount of reserve can be handled with the current conventional power plants. From the UK, only the increased cost of operating existing reserves has been estimated.

In addition to estimates, there is some experience from Denmark for the actual balancing costs for the existing wind power. For West Denmark, the balancing cost from the Nordic day-ahead market has been 1.4–2.6 €/MWh for a 24% wind penetration (of gross demand). These numbers are quite in the middle of theoretically estimated results from studies in Fig. 21. The balancing cost paid by the wind power producers is not the same as increase in technical cost of balancing for the amount of wind power. However the market costs from Denmark and Spain reflect the cost incurred to the system. In Denmark the cost is low compared to the penetration level, as the cost comes from Nordic market where wind power penetration is still small.

The interconnection capacity to neighboring systems is often significant. For the balancing costs, it is then essential to note in the study setup whether the interconnection capacity can be used for balancing purposes or not. A general conclusion is that if interconnection capacity is allowed to be used also for balancing purposes, then the balancing costs are lower compared to the case where they are not allowed to be used.

Balancing Cost from Electricity Markets In Finland and Sweden, the balancing costs as payments for wind power producers have been estimated from the balancing market (Nordic Regulating market) prices to be 0.3–1.4 €/MWh depending on how distributed the wind power is and on the market price level for balancing [49, 50]. In Sweden, the use of 15 min operating reserves has been estimated to increase by 18–56% of current amounts due to wind power forecast errors 1 or 4 h ahead for 4,000 MW wind power (8% of gross demand) [51]. The increased cost of system imbalances of Finland due to future wind power prediction errors was estimated to be 0.2–1 €/MWh for penetration levels of 1–10% of gross demand, assuming the Nordic balancing market was available (no bottlenecks) [52].

The use of an intraday market to help reduce the imbalance costs of wind power has been examined in Germany [53] and for the Nordic market in Finland [54] and Sweden [51] have shown that for the current price assumptions there is not a straightforward benefit to use an intraday market. This is because trading at an intraday market would mean correcting all imbalances, whereas the imbalance payments only apply to the imbalances that affect the power system net imbalances, thus not 100% of time (at low wind penetrations only 50% of time).

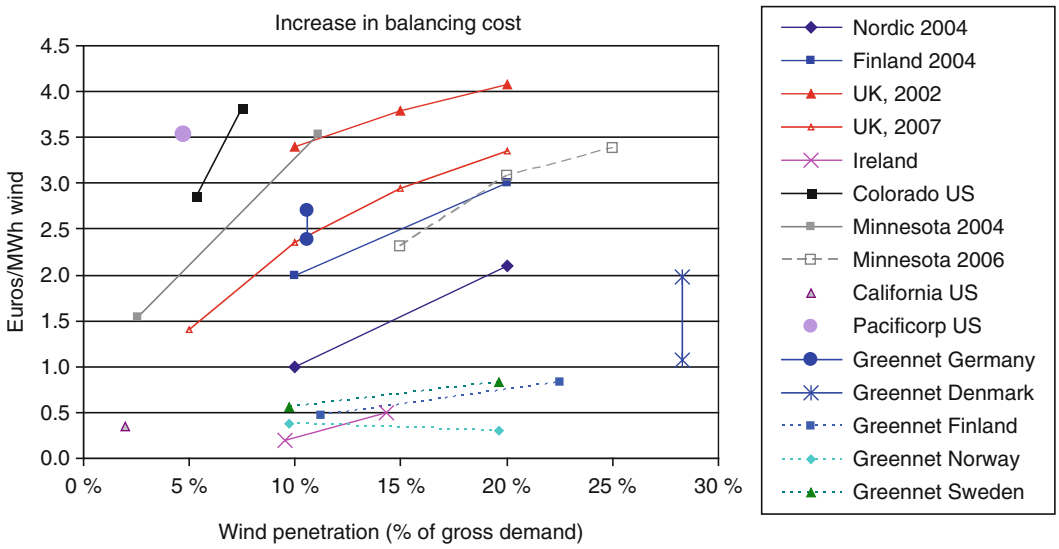

Wind Power Balancing. Figure 21
Results from estimates for the increase in balancing and operating costs due to wind power. The currency conversion used here is 1 € = 0.7 £ and 1 € = 1.3 US$. For UK, 2007 study the average cost is presented here, the range in the last point for 20% penetration level is from 2.6 to 4.7 €/MWh

Other Balancing Related Results

Not all case studies presented results quantified as MW of increase in reserve requirements or monetary values for increase in balancing costs.

In Denmark the TSO has estimated the impacts of increasing the wind penetration level from 20% to 50% (of gross demand) and concluded that further large-scale integration of wind power calls for exploiting both, domestic flexibility and international power markets with measures on the market side, production side, transmission side, and demand side [55, 56].

For the Netherlands, the simulations show the benefit of international trade of electricity and postponing market gate closure for wind integration. Wind power worsens the business case for thermal generation: CCGT during peak demand and base-load coal during low demand [57].

The Irish All Island Grid Study shows that going from 2 to 6 GW wind, the operational costs of the electricity system fall by €13/MWh when compared to the base case – due to cost benefit approach in the study, the cost component was not published as such [58].

For New York, 10% penetration of capacity, incremental regulation due to wind was found to be 36 MW. No additional spinning reserve was needed. Incremental intra-hour load following burden increased 1–2 MW/5 min. Hourly ramp increased from 858 MW to 910 MW. All increased needs can be met by existing NY resources and market processes. System cost savings of $335–$455 million for assumed 2008 natural gas prices of $6.50–$6.80/MMBTU were found. Day-ahead unit-commitment forecast error σ increased from 700–800 to 859–950 MW. Total system variable cost savings increases from $335 million to $430 million when state-of-the-art forecasting is considered in unit commitment ($10.70/MWh of wind) [59].

Storage The value of storage in the power system operation in the UK was estimated to be 252–970 £/kW [37]. For Germany a 27 M€/year revenue could be foreseen for 400 MW CAES (250 M€ investment) [54]. In the NL international exchange was seen as a more promising alternative to storage in the system [58]. In Ireland adding storage did not bring additional value in the All Island Grid Study results [59].

For wind penetration levels of 10–20% of gross demand in power systems, the cost effectiveness of building new electricity storage is still low (excluding hydro power with large reservoirs or pumped hydro). With higher wind penetration levels the extra flexibility that also storages can provide will be beneficial for the power system operation, provided they are economically competitive with other forms of flexibility. It is important to notice, however, that any storage should be operated according to the needs of aggregated system balancing. It is not cost effective to provide dedicated back-up for wind power in large power systems where the variability of all loads and generators are effectively reduced by aggregating, in the same way as it is not effective to have dedicated storage for outages in a certain thermal power plant, or having specific plants following the variation of a certain load.

Conclusions and Future Directions

Wind power impacts on power system balancing can be seen in several time scales, from minutes to hours, up to the day-ahead time scale. General conclusions on increase in balancing requirement will depend on region size relevant for balancing, initial load variations and how concentrated/distributed wind power is sited.

Several issues that impact on the amount of wind power that can be integrated have been identified. Aggregation benefits of large areas help in reducing the variability and forecast errors of wind power as well as help in pooling more cost effective balancing resources. An alternative to large balancing areas is to allow and promote intraday and intra-hour trading between different balancing areas in order to obtain low-cost balancing services. System scheduling and operating electricity markets at less than day-ahead time scales help reduce the forecast errors of wind power that affect operating reserves. Transmission is the key to aggregation benefits, electricity markets and larger balancing areas.

Wind integration has mainly been studied to wind penetration levels of 10–20% of gross demand (up to 50% of peak load), with some first efforts to study higher penetration levels of 40–50% of gross demand [56, 57, 59]. What happens in larger penetration levels, where wind becomes a more dominating part of power system, is not completely clear. Studies will have to

cover larger areas to take the cross border transmission into account properly [60]. The future power systems may also provide different options for flexibility in demand side that do not exist today. Future integration studies should take into account the foreseen high penetration of PV or ocean power. This will help smoothing the variability of individual technologies.

Recommendations for integration studies:

It is very important to take the variability of wind into account in a right way in power system studies. The variability will smooth out to some extent if there is geospread wind power, and part of the variability can be forecast. Because of spatial variations of wind from turbine to turbine in a wind power plant – and to a greater degree from wind power plant to wind power plant – a sudden loss of all wind power on a system simultaneously due to a loss of wind is not a credible event. Sudden loss of large amounts of wind power due to voltage dips in the grid can be prevented by requiring fault-ride-through from the turbines. Recommendations for wind integration studies include:

- Capturing the smoothed out variability of wind power production time series for the geographic diversity assumed and utilizing wind forecasting best practice for the uncertainty of wind power production
- Examining wind variation in combination with load variations, coupled with actual historic utility load and load forecasts
- Capturing system characteristics and response through operational simulations and modeling
- Examining actual costs independent of tariff design structure
- Comparing the costs and benefits of wind power

In most cases the question is whether extra investments to power systems are economically profitable or not in the new system with larger amount of wind power – not only stating that a certain amount of extra reserve capacity and/or new transmission lines, etc., are a prerequisite in order to build any wind power.

For high penetration levels of wind power, the optimization of the integrated system should be explored. Modifications to system configuration and operation practices to accommodate high wind penetration may be required. Not all current system operation techniques are designed to correctly incorporate the characteristics of wind generation and surely were not developed with that objective in mind. Increasing power system flexibility through such means as transmission to neighboring areas, generation flexibility, demand side management and optimal use of storage (e.g., pumping hydro or thermal) in combination with market aggregation and operation closer to real time will impact the amount of wind that can be integrated cost effectively.

Bibliography

Primary Literature

1. Söder L (2002) Explaining power system operation to nonengineers. Power Eng Rev, April 2002
2. Hirvonen R (2000) Material for course S-18.113 Sähköenergiajärjestelmät. Helsinki University of Technology Power systems laboratory, 2000 (in Finnish)
3. ETSO-2006 (2006) An overview of current cross-border congestion management methods in Europe, European Transmission System Operators, May 2006, available from http://www.entsoe.eu/
4. Kristoffersen JR (2005) The horns rev wind farm and the operational experience with the wind farm main controller. In: Proceedings of Copenhagen Offshore Wind, October 2005, Copenhagen, Denmark
5. Holttinen H, Milligan M, Kirby B, Acker T, Neimane V, Molinski T (2008) Using standard deviation as a measure of increased operational reserve requirement for wind power. Wind Eng 32(4):355–377
6. Milligan M, Porter K, DeMeo E, Denholm P, Holttinen H, Kirby B, Miller N, Mills A, O'Malley M, Schuerger M, Soder L (2009) Wind power myths debunked. IEEE Power Energy Mag 7(6):89–99
7. Soder L, Hofmann L, Orths A, Holttinen H, Wan Y, Tuohy A (2007) Experience from wind integration in some high penetration areas. IEEE T Energy Conver 22(1):4–12
8. Holttinen H, Meibom P, Orths A, van Hulle F, Lange B, O'Malley M, Pierik J, Ummels B, Tande JO, Estanqueiro A, Matos M, Gomez E, Söder L, Strbac G, Shakoor A, Ricardo J, Smith JC, Milligan M, Ela E (2009) Design and operation of power systems with large amounts of wind power. Final report, IEA WIND Task 25, Phase one 2006–2008. Espoo, VTT. 200 p. + app. 29 p. VTT Tiedotteita – Research Notes 2493. http://www.vtt.fi/inf/pdf/tiedotteet/2009/T2493.pdf
9. Ernst B (1999) Analysis of wind power ancillary services characteristics with German 250 MW wind data. NREL Report No. TP-500-26969. 38 p. http://www.nrel.gov/publications/
10. Focken U, Lange M, Waldl H-P (2001) Previento – a wind power prediction system with an innovative upscaling algorithm. In: Proceedings of EWEC'01, 2nd–6th July, 2001, Copenhagen, pp 826–829
11. Holttinen H (2004) The impact of large scale wind power production on the Nordic electricity system. PhD dissertation.

VTT Publications 554. Espoo, VTT Processes. 82 p. + app. 111 p. http://www.vtt.fi/inf/pdf/publications/2004/P554.pdf
12. Wan Y (2005) Fluctuation and ramping characteristics of large wind power plants. Windpower 2005 (Windpower 05) Conference and Exhibition (CD-ROM), 15–18 May 2005, Denver, Colorado. Washington, DC: American Wind Energy Association; Content Management Corp. NREL Report No. CP-500-38057. 13 p
13. EWEA (2005) Large scale integration of wind energy in the European power supply: analysis, issues and recommendations (December 2005). http://www.ewea.org/
14. IEA (2005) Variability of wind power and other renewables. Management options and strategies. http://www.iea.org/Textbase/publications/free_new_Desc.asp? PUBS_ID=1572
15. Giebel G (2007) A variance analysis of the capacity displaced by wind energy in Europe. Wind Energy 10:69–79
16. Holttinen H, Meibom P, Orths A, Lange B, O'Malley M, Tande JO, Estanqueiro A, Gomez E, Söder L, Strbac G, Smith JC, van Hulle, F. (2010) Impacts of large amounts of wind power on design and operation of power systems, results of IEA collaboration. Submitted and accepted to Wind Energy journal
17. ISET (2005) Wind energy report Germany 2005. ISET, Kassel
18. Giebel G, Brownsword R, Kariniotakis G (2003) The state-of-the-art in short-term prediction of wind power. A literature overview. EU project ANEMOS (ENK5-CT-2002-00665). http://anemos.cma.fr
19. Kariniotakis G et al (2006) Next generation forecasting tools for the optimal management of wind generation. In: Proceedings PMAPS Conference, Probabilistic Methods Applied to Power Systems, KTH, Stockholm, Sweden, June 2006
20. Focken U (2007) Optimal combination of European weather models for improved wind power predictions. In: Proceedings of EWEC'07, 7th–10th May, 2007, Milan, Italy
21. Lange B, Cali Ü, Jursa R, Mackensen R, Rohrig K, Schlögl F (2006) Strategies for balancing wind power in Germany. In: German Wind Energy Conference DEWEK 2006, Bremen, November 2006
22. Holttinen H, Stenberg A (2008) Tuulivoiman tuotantotilastot. Vuosiraportti 2008. Espoo, VTT. 47 s. + liitt. 8 s. VTT Working Papers; 132. http://www.vtt.fi/inf/pdf/workingpapers/2009/W132.pdf
23. Dragoon K, Milligan M (2003) Assessing wind integration costs with dispatch models: A case study. Windpower, Austin
24. Milligan M, Kirby B (2007) The impact of balancing areas size, obligation sharing, and ramping capability. In: Proceedings of the WindPower 2007 Conference, June 3–5, 2007. Los Angeles, CA, USA. NREL-CP-500-41809. http://www.nrel.gov/docs/fy07osti/41809.pdf
25. Kirby B, Milligan M, Makarov Y, Hawkins D, Jackson K, Shiu H (2003) California Renewables Portfolio Standard. Renewable generation integration cost analysis. Phase I: One year analysis of existing resources. Results and recommendations. California Energy Commission/California Public Utilities Commission. http://cwec.ucdavis.edu/rpsintegration/
26. Dany G (2001) Power reserve in interconnected systems with high wind power production. In: IEEE Power Tech Conference, 10–15th September, 2001, Porto, Portugal
27. Soder L (1993) Reserve margin planning in a wind-hydro-thermal power system. IEEE Trans Power Syst 8(2):564–571
28. Milligan M (2003) Wind power plants and system operation in the hourly time domain. In: Proceedings of Windpower 2003 Conference. May 18–21, 2003 Austin, Texas, USA. NREL/CP-500-33955. http://www.nrel.gov/publications/
29. Kirby B, Hirst E (2000) Customer-specific metrics for the regulation and load following ancillary services. ORNL/CON-474, Oak Ridge National Laboratory, Oak Ridge TN, January 2000
30. Holttinen H (2005) Impact of hourly wind power variations on the system operation in the Nordic countries. Wind Energy 8(2):197–218
31. EnerNex/WindLogics (2006) Minnesota Wind Integration Study Final Report. vol I, prepared for Minnesota Public Utilities Commission, November 2006. http://www.puc.state.mn.us/portal/groups/public/documents/pdf_files/000664.pdf
32. EnerNex Corporation (2007) Final Report – Avista Corporation Wind Integration Study. Avista Utilities. http://www.uwig.org/AvistaWindIntegrationStudy.pdf
33. Idaho Power Corporation (2007) Operational impacts of integrating wind generation into idaho power's existing resource portfolio. http://www.idahopower.com/pdfs/energycenter/wind/windIntegrationstudy.pdf
34. GE Energy (2007) Californian intermittency analysis. http://www.uwig.org/CEC-500-2007-081-APA.pdf
35. GE (2006) Ontario Wind Integration Study. Final Report to: Ontario Power Authority (OPA), Independent Electricity System Operator (IESO) and Canadian Wind Energy Association (CanWEA). http://www.uwig.org/OPA-Report-200610-1.pdf
36. Soder L (2008) On methodology for modelling wind power impact on power systems (R. Inst. Technol., Stockholm, Sweden); Holttinen H (2008) International Journal of Global Energy Issues, 29(1–2):181–198
37. Axelsson U, Murray R, Neimane V (2005) 4000 MW wind power in Sweden – Impact on regulation and reserve requirements. Elforsk Report 05:19, Stockholm, 2005. http://www.elforsk.se
38. Ilex, UMIST, UCD and QUB (2004) Operating reserve requirements as wind power penetration increases in the Irish electricity system. Sustainable Energy Ireland, 2004
39. Strbac G, Shakoor A, Black M, Pudjianto D, Bopp T (2007) Impact of wind generation on the operation and development of the UK electricity systems. Electr Power Syst Res 77(9):1143–1238, Elsevier
40. Planning of the grid integration of wind energy in Germany onshore and offshore up to the year 2020 (Dena Grid study). Deutsche Energie-Agentur Dena, March 2005. English summary and full German version http://www.dena.de/themen/thema-reg/projektarchiv/
41. Porter et al (2007) Intermittency analysis Final report. July, 2007. http://www.uwig.org/CEC-500-2007-081.pdf
42. Kraftnät S (2008) Large scale expansion of wind power – consequences for the transmission grid and need of

regulation power. http://www.svk.se/Global/01_Om_oss/Pdf/Rapporter/ 080601_Bilaga_vindkraftrapport_2008.pdf (In Swedish)
43. Meibom P, Weber C, Barth R, Brand H (2009) Operational costs induced by fluctuating wind power production in Germany and Scandinavia. IET Renew Energy Gener 3(1):75–83, March 2009
44. Strbac G (2002) Ilex Energy. Quantifying the system costs of additional renewables in 2020. DTI, 2002. http://www.dti.gov.uk/energy/developep/080scar_report_v2_0.pdf
45. Zavadil R (2006) Wind Integration Study for Public Service Company of Colorado. May 22, 2006. http://www.xcelenergy.com/XLWEB/CDA/0,3080,1-1-1_1875_15056_15473-13518-2_171_258-0,00.html
46. EnerNex/WindLogics (2004) Xcel North study (Minnesota Department of Commerce). http://www.state.mn.us/cgi-bin/portal/mn/jsp/content.do?contentid=536904447&contenttype=EDITORIAL&hpage=true&agency=Commerce
47. Shiu H, Milligan M, Kirby B, Jackson K (2006) California Renewables Portfolio Standard Renewable Generation Integration Cost Analysis. California Energy Commission, PIER Public Interest Energy Research Programme. http://www. energy.ca.gov/pier/final_project_reports/CEC-500-2006-064.html
48. PacifiCorp (2005) Integrated Resource Planning. http://www.pacificorp.com/Navigation/Navigation23807.html
49. Holttinen H, Saarikivi P, Repo S, Ikäheimo J, Koreneff G (2006) Prediction errors and balancing costs for wind power production in finland. In: Proceedings of 6th workshop on Offshore and Large Scale Integration of Wind Power, 25–26th October, 2006, Delft, The Netherlands
50. Neimane V, Carlsson F (2008) A massive introduction of wind power. Changed market conditions? Elforsk report 08:41. http://www.vindenergi.org/Vindforskrapporter/v_132.pdf
51. Brandberg M, Broman N (2007) Future trading with regulating power, Magnus Brandberg and Niclas Broman, Master's Thesis, Uppsala Universitet. An updated version, together with Nilsson, in Minerals and Energy – Raw Materials Report, vol 23(1): March 2008, pp 1–11
52. Helander A, Holttinen H, Paatero J (2010) Impact of wind power on the power system imbalances in Finland. Accepted to IET Renewable Power Generation Journal
53. FGE/FGH/ISET: Bewertung der Optimierungspotenziale zur Integration der Stromerzeugung aus Windenergie in das Übertragungsnetz (2007) http://www.erneuerbare-energien.de/inhalt/42024/4591/
54. Holttinen H, Koreneff G (2007) Imbalance costs of wind power for a hydro power producer in Finland. In: Proceedings. European Wind Energy Conference EWEC2007. Milan, Italy, 7–10 May, 2007. European Wind Energy Association, EWEA
55. Energinet.dk: System Plan (2007) www.energinet.dk
56. Eriksen PB, Orths A (2008) Challenges and Solutions of Increasing from 20 to 50 Percent of Wind Energy Coverage in the Danish Power System until 2025; Invited Keynote Paper. In: Proceedings of the 7th international Workshop on Large Scale Integration of Wind Power and on Transmission Networks for Offshore Wind Farms; 26–28 May 2008, Madrid, Spain
57. Ummels BC (2009) Power system operation with large-scale wind power in liberalised environments. PhD thesis, Delft University of Technology, The Netherlands, 192 p
58. All Island Grid Study (2008) http://www.dcenr.gov.ie/Energy/North-South+Co-operation+in+the+Energy+Sector/All+Island+Electricity+Grid+Study.htm
59. The Effects of Integrating Wind Power on Transmission System Planning, Reliability, and Operations. Report on Phase 2, GE Energy. Prepared for The New York State Energy Research and Development Authority, City, State, March 2005. http://www.nyiso.com/public/services/planning/special_studies.jsp
60. Van Hulle F, Tande JO, Uhlen K, Warland L, Korpås M, Meibom P, Sørensen P, Morthorst PE, Cutululis N, Larsen H, Woyte A, Verheij F, Kleinschmidt C, Moldovan N, Holttinen H, Lemström B, Uski-Joutsenvuo S, Gardner P, Purchala K, Tiedemann A, Kreutzkamp P (2009) Final Report TradeWind. http://www.trade-wind.eu
61. Matevosyan J (RigaTechnical Univ., Riga, Latvia) (2004) Estimation of potential wind energy curtailment for wind power plants in power systems with bottleneck problems; Soder L (2004) EPE-PEMC 2004 11th International Power Electronics and Motion Control Conference, vol 5, pp 5–502

Books and Reviews

Söder L (2004) On limits for wind power generation. Int J Global Energy Issues 21(3):243–254

Söder L (2005) The value of wind power. In: Ackermann T (ed) Wind power in power systems. Wiley, ISBN 0-470-85508-8

Wind Power Generator Systems and Local Power System Interconnection

Torbjörn Thiringer
Department of Energy and Environment, Division of Electric Power Engineering, Chalmers University of Technology, Göteborg, Sweden

Article Outline

Glossary
Definition of the Subject
Introduction
Operational Requirements on a Wind Turbine Generator System: General
Wind Turbine System Electrical Components
Power Electronics
Wind Turbine Generating Systems
Power Quality Impact

Fixed-Speed Wind Turbines
DFIG and Full Converter Turbines
Behavior During Network Faults
Future Directions
Abbreviations
List of Commonly Used Variables
Bibliography

Glossary

Converter Electronic object that can change a voltage and current form into another form.

Doubly fed induction generator system (DFIG) A common electrical system for wind turbines that has a converter in the rotor circuit.

Fault-Ride-Through – FRT The ability of a wind turbine to be immune against voltage dips in the connected network.

Fixed-speed system Simplest wind turbine electrical system consisting of mainly an induction machine and capacitors.

Full-power systems Wind turbine electrical system which has a converter between the stator of the wind turbine generator and the grid transmitting the whole power from the turbine.

Power quality An expression for how close the voltage is to its ideal waveform, and the quality of the current injected by an object into the grid.

Reactive power Oscillating power that only causes losses and do not provide an active power transfer.

Definition of the Subject

The electrical system of a wind turbine could be referred to as the heart of the wind turbine. The main purpose of the electrical system is of course to convert the incoming mechanical energy on the shaft to electrical energy that is fed into the connected power grid. This conversion should naturally be done with a minimum of losses as well as with the smallest component size possible.

In addition, the electrical system has the ability to influence the power quality impact that a wind turbine has on the power grid and also the ability to control the speed and torque on the machine shaft (if it is equipped with a power electronic converter) and in this way maximize the energy capture as well as to keep the stresses on the structure to a minimum.

These requirements (high energy capture, good power quality impact, low stresses on the structure in order to minimize the material needed) have in combination with the technical development led to an evolution of wind turbines and definitely regarding the electrical systems of wind turbines. This development is continuously ongoing and is the reason to why we have several different concepts of electrical generating systems for wind turbines.

This entry explains the commonly used technologies for generating systems for wind turbines today, their design, function, and properties. In addition, it also presents how turbines made up of the various technologies influence the grid to which they are attached.

Introduction

Wind turbines, or rather wind mills, have existed for millenniums, mainly for crop grinding and water pumping purposes. In 1887 the first electricity-generating wind turbine was erected and used for battery charging. During the years the sizes of the wind turbines increased and became more and more connected to the grid for conventional power infeed generation. 1931 a 100 kW wind turbine was erected in the USSR. The first megawatt (MW) machine was erected in the USA in 1941 [1].

However, due to the enormous amounts of available fossil fuels, the more expensive wind energy electricity was no greater success during the greater part of the twentieth century. However, with the oil crises in the beginning of the 1970s the interest awoke and the modern era of wind energy started. In many countries, for instance in Denmark and in the USA, more modern wind turbines started to be built and erected. By the beginning of the 1980s, the standard maximum size was around 50 kW and at the end of the 1980s 200 kW. Ten years later, the maximum size was up to around 2 MW and 10 years further 6 MW turbines existed. The most economical size has typically been a bit smaller than the maximum size. Another important shift happened in the 1990s, the variable-speed operation was introduced into commercial turbines after having mainly been a research topic.

In short, the development of electrical systems for wind turbines has moved from being small isolated grid disturber to being large grid-friendly and even

grid-reinforcing production units. This development has to a great extent been built on the development of power electronics. Today (2011) there is a lot of focus on large wind farms connected to the transmission networks, but local integration of wind turbines will also continue to be an important issue.

Operational Requirements on a Wind Turbine Generator System: General

Stationary Requirements

As partly mentioned in the previous section, a wind turbine generator system shall have a low weight, low maintenance need, as well as a high efficiency. The resulting goal is of course, that it shall be as cheap as possible in relation to the produced electrical energy. It shall also be able to convert the maximum power without becoming overheated. The sizing of the electrical system of course follows the maximum rating of the wind turbine, in which it is going to be inserted, and the electrical system must be able to handle this power as well as some overload. The efficiency should preferably not be the best for the rated operation, instead it is more important that the efficiency is as highest for medium speeds. In Fig. 1 the wind distribution for a site with an average wind speed of 7 m/s is presented, as well as the available energy for each specific wind speed, which demonstrates the focus area for having a high efficiency of the electrical system.

From Fig. 1 it is very clear that high efficiency around 1–2 times the mean wind speed is a key issue for the electric generating system. Moreover, it can be noted that below 3 m/s and above 20 m/s there is hardly any energy at all.

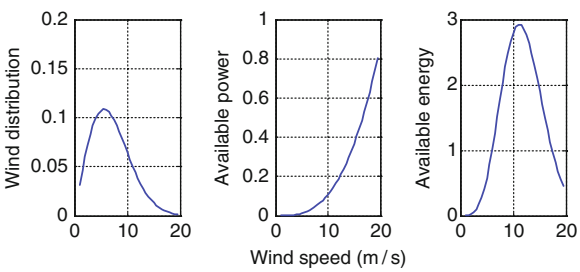

Wind Power Generator Systems and Local Power System Interconnection. Figure 1
Using 7 m/s as average wind speed. Wind speed distribution, available power in the wind and available energy as a function of wind speed

The system must have the ability to be overloaded for short times, without losing its functionality. Electrical machines have in this regard a highly desirable property, they can be overloaded for a short time, since the magnetic ability of the generators are usually much higher than the steady-state thermal limitation. However, this is not the case with the power electronic converters; they usually cannot even handle a few seconds of higher power compared to their rating.

Dynamic Requirements

In this section, there appear a number of terms which will be declared in the upcoming section. The main purpose of this section is to underline the great benefit of having an electrical generating system that can control the speed and torque of a wind turbine in a broad range.

Apart from the pure stationary demands on proper rating and high efficiency, a very important issue is that the electrical system of the wind turbine must provide a sufficient smoothness regarding the electric power flow in order not to cause stresses either on the structure or on the power quality of the grid.

For a traditional fixed-speed wind turbine, there is a trade-off between softness and efficiency. It is the rotor resistance in the induction generator used in this system that is the key variable. This together with the input torque determines that a fixed-speed system should be stall controlled. The key equation here is

$$J\frac{d\omega}{dt} = T_{\mathrm{w}} - T_{\mathrm{e}}$$

where J is the inertia of the system, T_{e} is the electrodynamical torque, and T_{w} is the torque from the wind acting on the rotor. In the case that the rotor speed cannot change, the electrodynamical torque will be equal to the shaft torque created through the aerodynamic power conversion by the rotor, which means that all unevenness in the incoming torque is transmitted further in the system. This causes both mechanical wear and a poor power quality impact. However, for fixed-speed systems, the speed can change a little bit, and even more if the induction generator has a high rotor resistance, which unfortunately gives a lower efficiency. Anyway, the speed variations for a

fixed-speed wind turbine system are low. In Fig. 2 the power versus wind speed for some different pitch angles are presented. Pitch angle is a quantity that tells how "turned" the blade is toward the rotational plane.

From the figure it can be noted that a wind increase around 20 m/s will lead to a very large power variation if a pitch angle of 20° is used, which will lead to stresses on the mechanical construction as well as a power output that varies substantially. Accordingly stall control must be used for a fixed-speed turbine, where the power variations are much lower. This can be noted by observing the 2° and 25° pitch angle curves at 20 m/s, where the turbine is producing rated power. An increase in 2 m/s, leads to a reduction of the power by 10% for the 2° angle while it for a 25° angle leads to an increase of 50%, which would strongly stress the turbine.

Another observation from the figure is that it can be noted that a fixed pitch angle at 0° would be the safe choice for this turbine. A drawback is then that some energy is lost in the high wind speed region. If some overpower can be accepted a slightly higher pitch angle could be possible to use. Important to point out is also that with changing air pressure, the power production will vary.

Power Versus Wind Speed Relation

The equations used to obtain the static power versus wind speed presented in Figs. 1 and 2 can be easily found in literature, for instance in [2], and the key equations for doing these calculations are

$$P_{\text{wind}} = \frac{1}{2}\rho A W S^3$$

$$P_{\text{mech}} = \frac{1}{2}\rho A W S^3 C_{\text{p}}(\lambda)$$

$$\lambda = \frac{\omega_r R}{WS}$$

where P_{wind} is the available power in the wind, P_{mech} is the power that can be converted from P_{wind}, R is the rotor diameter, A is the area swept by the rotor, ρ is the air density, λ is the tip-speed ratio, C_{p} is the power coefficient determining the ratio between P_{mech} and P_{wind}.

C_{p} is a function of λ. For a specific λ, C_{p} has it highest value, about 0.45–0.5. This means that if the rotor speed can vary proportionally with the wind speed, the power capture can be maximized. In order to vary the rotor speed, a variable-speed turbine is needed. For higher wind speeds, the available power in the wind becomes far too high, so C_{p} must go down in order to limit the power. This reduction can be done in two ways, either the blades lose their aerodynamic efficiency, "stall control," or the blades are turned out of the wind, "pitch control."

If the rotor speed was allowed to vary, as for a variable-speed turbine, it can be noted from the earlier presented speed equation that there is a term, $Jd\omega/dt$, that can take up the incoming power variations and give a smooth power output (Power is directly related to T_{e}). By selecting a proper power electronic control, the electrodynamical torque can be controlled and then also the stresses on the mechanical structure as well as and the power fluctuations going out to the grid, can be reduced. For a variable-speed turbine, pitch control is generally used, since pitch control gives less stresses on the wind turbine. In this case, the turbine can speed up in case of a gust (keeping the shaft torque constant through the generator system) and during the acceleration, the additional energy is stored in the rotational energy and then the turbine can pitch the blades to return to a suitable aerodynamic power conversion. This gives a requirement on the torque control ability of the generating system; it must have a bandwidth of at least 10 Hz. This is no

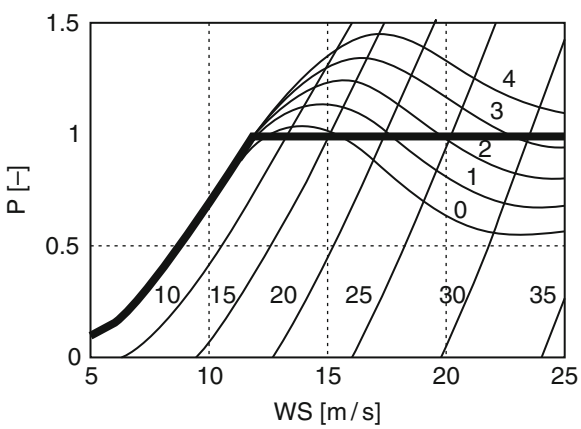

Wind Power Generator Systems and Local Power System Interconnection. Figure 2
Wind speed versus power (1 corresponds to full power) for various pitch angles for one given pressure

problem for electrical generating systems in general, where torque demands can be realized in a matter of less than 10 ms.

In addition, the energy capture by the rotor can be increased since an optimal speed can be used for each wind speed. However, this is a cost issue. Today, the fixed speed systems often comprises two fixed speeds, and in this way, modern fixed-speed systems have about the same energy production as variable speed systems.

Wind Turbine System Electrical Components

Electrical Fundamentals

Voltage, Currents, Power, Energy, and Loss In electrotechnology, the intensity source is voltage and resulting flow is current. The units are Volts [V] for the voltage and Ampere [A] for current. There are three basic electrical properties related to passive elements in electrotechnology, namely, the resistance, the inductance, and the capacitance. The relation between currents and voltages are for these three elements:

$$u(t) = Ri(t)$$

$$u(t) = L\frac{di(t)}{dt} \text{ or } i(t) = i(t_0) + \frac{1}{L}\int_0^t u(t)dt$$

$$i(t) = C\frac{du(t)}{dt} \text{ or } u(t) = u(t_0) + \frac{1}{C}\int_0^t i(t)dt$$

In Fig. 3 below, a resistor, a capacitor, and an inductor are shown.

The power flowing in an electrical system is

$$p(t) = u(t)i(t).$$

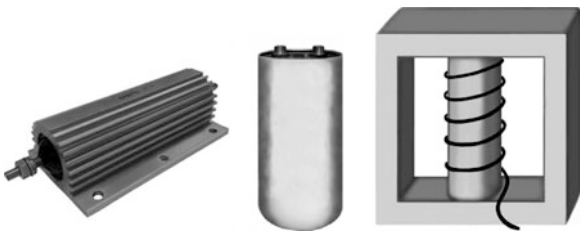

Wind Power Generator Systems and Local Power System Interconnection. Figure 3
Resistor, capacitor, and inductor

By integrating the instantaneous power, the energy can be determined as

$$W(t) = \int_0^t p(t)dt.$$

The losses in electrical systems are typically related to resistances in the systems and can directly be found as

$$p_{\text{loss}}(t) = Ri^2(t)$$

or

$$p_{\text{loss}}(t) = \frac{u^2(t)}{R}.$$

where i is the current flowing through the resistive element and u is the voltage over it.

It is possible to use constant voltage and current levels as well as an alternating voltage and current in an electrical system; these are referred to as Direct Current = DC and Alternating Current = AC. HVDC accordingly means High Voltage Direct Current. The frequency of the alterations is typically 50 or 60 Hz in grids around the world. In Fig. 4 below both DC-quantities as well as AC-quantities (50 Hz) are depicted.

This type of AC-supply is referred to a single-phase supply, more about the commonly used three-phase supply will soon follow. Here some observations can be performed. The average power in both cases in Fig. 4 are 3 W. In the case of the AC-system the instantaneous power however oscillates with twice the frequency of the voltage and current, which is a drawback when using

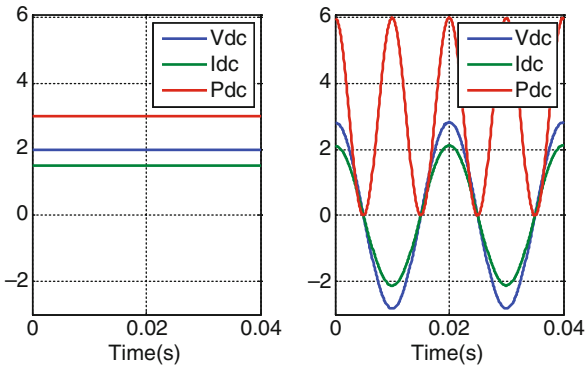

Wind Power Generator Systems and Local Power System Interconnection. Figure 4
Left: DC-quantities. *Right*: AC-quantities

single-phase AC-system for power electronic equipments, where this power variation needs to be tackled.

Moreover it can be observed that the peak values of the currents and voltages are higher that the quantities in the DC-system. Due to the constant changing of the level of current and voltage, it is in an AC-system necessary to have a peak value that is $\sqrt{2}$ higher than the so-called rms-value:

$$\hat{U} = \sqrt{2}U_{\mathrm{RMS}}$$

The RMS-value approximately/exactly corresponds to the DC-level, in this example exactly. For further information, the reader is encouraged to look in a textbook on the subject, for instance [3].

In the case treated in Fig. 4, the voltage and currents were exactly in phase. However, when applying AC-voltage on a circuit consisting of inductances and capacitances, there will be a phase shift. In Fig. 5 an R-L circuit subjected to an alternating voltage, v, and the resulting quantities are displayed.

One obvious observation is that the current now is lagging the voltage and that the power level is lowered, although the peak voltage and peak current are the same. This gives rise to three different powers.

The active and reactive power is defined as

$$P = UI\cos(\phi)$$

and

$$Q = UI\sin(\phi).$$

The active and reactive power are related as

$$S = \sqrt{P^2 + Q^2}$$

where S is the apparent power.

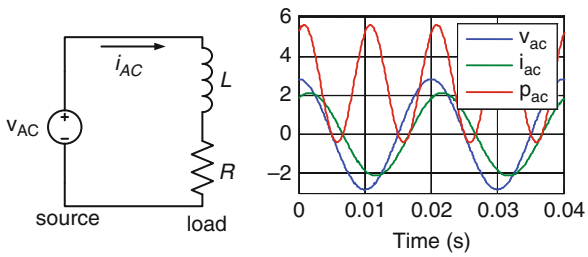

Wind Power Generator Systems and Local Power System Interconnection. Figure 5
A voltage source acting on an R-L load

It is the apparent power that is important for the electrical dimensioning of a component since it composes the peak value of the current and voltages. The active power is the desired one and the reactive power is usually undesired. An important quantity that tells how much of the transmitted power that is useful is the power factor:

$$PF = \cos(\phi)$$

These four equations above are only valid in the absence of harmonics. In the presence of harmonic voltages, there is a need for more definitions. Here the reader is encouraged to consult power electronic literature, for instance, [3].

Three-Phase System It is possible to use three single-phase systems where the AC-voltages are separated with one-third period apart to form a three-phase system. This corresponds to an angle displacement of 120° between each of the single-phase systems.

$$u_{\mathrm{R}}(t) = \sqrt{2}U_{\mathrm{RMS}}\sin(\omega t)$$

$$u_{\mathrm{S}}(t) = \sqrt{2}U_{\mathrm{RMS}}\sin(\omega t + \frac{2\pi}{3})$$

$$u_{\mathrm{T}}(t) = \sqrt{2}U_{\mathrm{RMS}}\sin(\omega t + \frac{4\pi}{3})$$

$$i_{\mathrm{R}}(t) = \sqrt{2}U_{\mathrm{RMS}}\sin(\omega t + \varphi)$$

$$i_{\mathrm{S}}(t) = \sqrt{2}U_{\mathrm{RMS}}\sin(\omega t + \frac{2\pi}{3} + \varphi)$$

$$i_{\mathrm{T}}(t) = \sqrt{2}U_{\mathrm{RMS}}\sin(\omega t + \frac{4\pi}{3} + \varphi)$$

In Fig. 6, three-phase currents and voltages are shown for a case with $U_{\mathrm{RMS}} = 230\mathrm{V}$, $I_{\mathrm{RMS}} = 150\mathrm{A}$ and $\phi = 30°$.

An advantage is that the instantaneous power

$$p(t) = u_{\mathrm{R}}(t)i_{\mathrm{R}}(t) + u_{\mathrm{S}}(t)i_{\mathrm{S}}(t) + u_{\mathrm{T}}(t)i_{\mathrm{T}}(t)$$

now is continuously constant, so that in power electronic systems using a three-phase supply, there is less need of filtering capacitors in order to obtain stiff voltages after the in power electronic equipment very common rectification. Moreover,

$$i_{\mathrm{R}}(t) + i_{\mathrm{S}}(t) + i_{\mathrm{T}}(t) = 0$$

and

$$u_R(t) + u_S(t) + u_T(t) = 0$$

which means that there is no need for a return conductor, so more power can be transmitted per conductor. This is illustrated in Fig. 7.

These nice properties together with the invention of the three-phase induction machine (see coming section) have led to a condition where three-phase systems completely dominate the electric power transmission as well as power supply today.

***Jω*-Method** A convenient mathematical method that can be used to calculate the currents and voltages if the quantities are in steady state and oscillating with one frequency only, is the $j\omega$-method, [2]. The sinusoidally varying quantity is represented with a complex number where the magnitude and phase shift are represented. The representation can be done either in Cartesian coordinates or in polar coordinates.

$$A + jB = \sqrt{A^2 + B^2}\, e^{j\,\mathrm{atan}\left(\frac{B}{A}\right)}$$

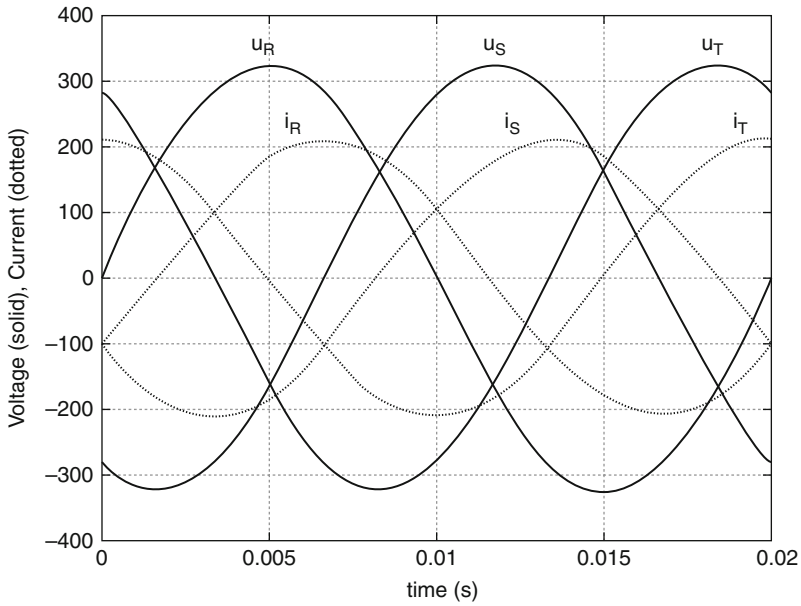

Wind Power Generator Systems and Local Power System Interconnection. Figure 6
Three-phase currents and voltages

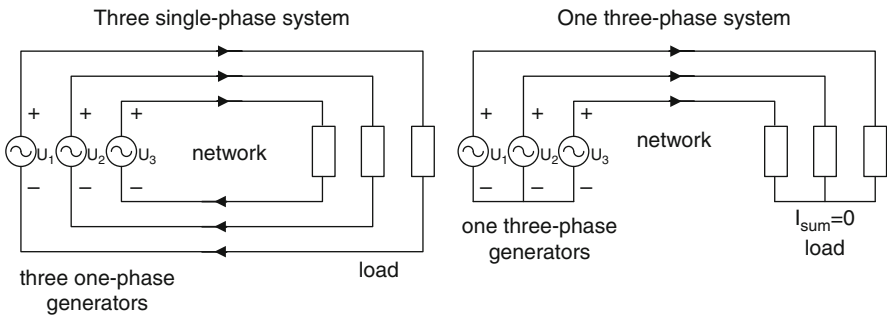

Wind Power Generator Systems and Local Power System Interconnection. Figure 7
Three single-phase systems as well as a three-phase system

When a polar coordinate system is used, the magnitude in combination with the angle is referred to as a phasor.

Due to the steady-state assumption and a single oscillating frequency, the derivative d/dt can be replaced with $j\omega$, and then calculations can be performed, see the example when determining the currents in an RL-circuit. In Fig. 8, an example of an RL-circuit supplied by an alternating voltage source is shown.

The equation for the circuit is

$$u(t) = Ri(t) + L\frac{di(t)}{dt}.$$

or using the jω-method,

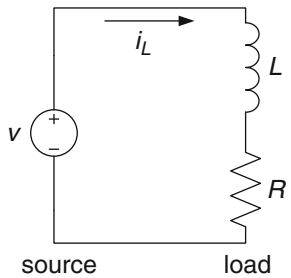

Wind Power Generator Systems and Local Power System Interconnection. Figure 8
A voltage source acting on an RL load

$$\underline{U} = R\underline{I} + j\omega L\underline{I}.$$

The resulting waveforms are shown in Fig. 9.

The Transformer Power is voltage times current. In order to have a convenient end-usage a lower voltage level is needed, while for transportation a higher voltage is needed to keep the losses, that is, the currents down.

Due to the simplicity with which voltage could be changed into different voltage levels, alternating-current systems (AC-systems) became the dominating ones for higher power already around year 1900. The object that transforms voltage from one voltage level to another one is called a transformer, see Fig. 10 where two photos of a large as well as a small transformer are shown together with the symbol of a three-phase transformer.

The equations governing the voltage and current relations (Observe: a bit idealized) between the primary and secondary side are the following:

$$\frac{U_1}{N_1} = \frac{U_2}{N_2}$$

$$I_1 N_1 = I_2 N_2$$

Electric Machines (Generators and Motors)

Electric machines can generally both convert rotational energy into electrical energy (generator operation) and the opposite (motor operation). When an electric

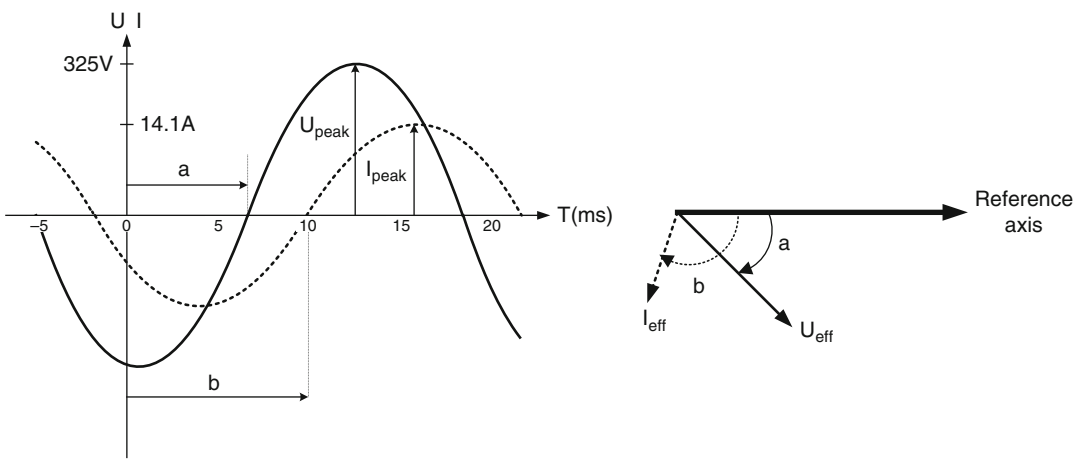

Wind Power Generator Systems and Local Power System Interconnection. Figure 9
Voltages and currents as time traces as well as in phasor representations

machine is designated to produce electrical energy from another source, the term "generator" is typically used. Here the more general term "machine" will frequently be used.

There are three main types of electrical machines. These are the DC-machine, the induction machine (asynchronous machine), and the synchronous machine. They all consist of a rotor that rotates, and usually is located in the inside of the machine and a stator, which is standing still.

There are three fundamental principles that are used in an electrical machine, which gives rise to a conversion between electrical and mechanical energy.

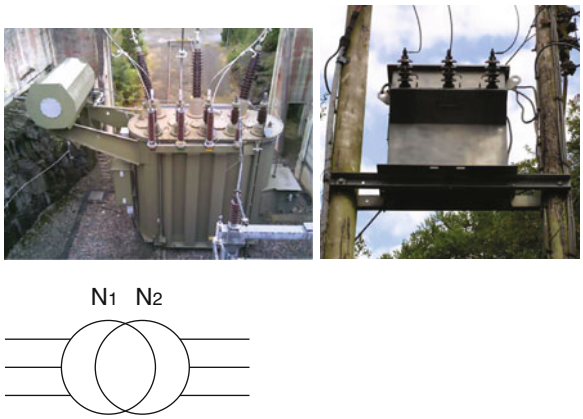

Wind Power Generator Systems and Local Power System Interconnection. Figure 10
Transformer, photo and circuit description, N_1 is the number of windings on the primary side and N_2 is the number of windings on the secondary side

- A force is produced by the cross product of a current flowing in magnetic field $F = B \times I$. If this force is applied at a certain distance, r, from the axis of the rotor, a torque will be formed according to $T = F \times r$. Force can also be looked upon as being created by two interacting magnetic fields, more about this follows below.
- A magnetic field is created by a permanent magnet or an electromagnet.
- A flux change through a coil leads to an induced voltage in this coil. $e = \frac{d\psi}{dt}$

Figure 11 illustrates in a simple fashion the three physical fundamentals, for a more thorough description, [4] is recommended.

There is an alternative way of looking into the force creation, which is illustrated in Fig. 12.

By having a magnetic vector in the rotor and one in the stator, the rotor will be exposed to a force

$$T = |\psi_S||\psi_r| \sin(\delta)$$

and the result will be that the rotor would like to align itself with the magnetic vector of the stator. If the magnetic vector (flux vector) now rotates, the rotor will also rotate. Some recommended textbooks for further information are [4–7].

DC-Machine Although the primary interest here is to use the machines as generators, the more general term "DC-machine" will frequently be used in this section.

In order to create the varying flux through a coil, either the coil must move (as in a DC-machine) or the flux through the coil must vary (AC-machine).

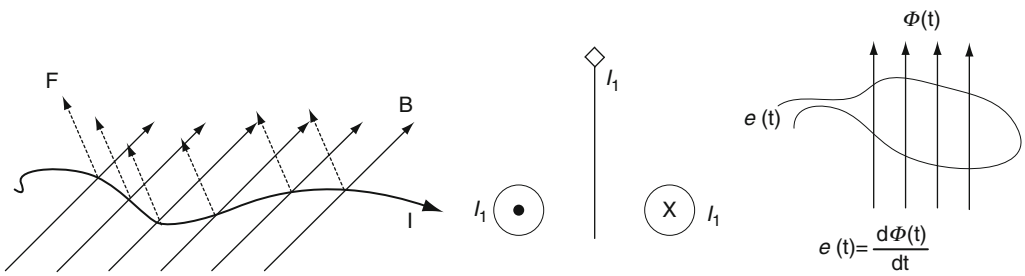

Wind Power Generator Systems and Local Power System Interconnection. Figure 11
Three electromagnetic fundamentals making up key factors for the operation of an electrical machine. Same order as the bullets above. See [4] for more details

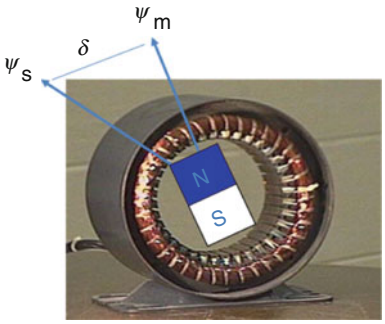

Wind Power Generator Systems and Local Power System Interconnection. Figure 12
Illustration of one magnetic vector in the rotor and one imposed in the stator giving an alignment force, making the machine to rotate

Wind Power Generator Systems and Local Power System Interconnection. Figure 13
Left: Stator with field winding. *Right*: Rotor with armature winding

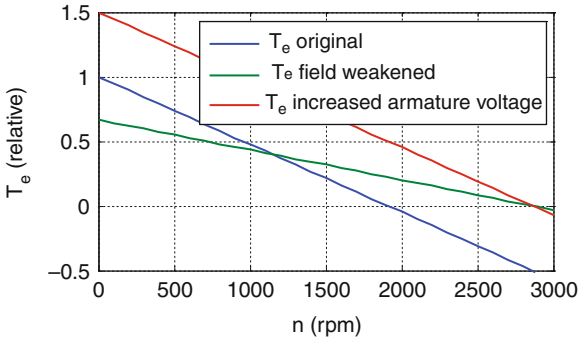

Wind Power Generator Systems and Local Power System Interconnection. Figure 14
Torque–speed characteristics of the separately magnetized DC-machine

In the DC-machine, this "fluxtaking coil" is located in the rotor and accordingly there is a need for a mechanical shifting of the current. This is done in something called the commutator. Due to practical reasons, such as that the machine becomes expensive, the commutator has reliability problems and that the power level is close to the maximum for this machine, the DC-machine is nowadays hardly not used for wind energy applications, and in this case limited to very small turbines.

In Fig. 13 the stator and the rotor of a DC-machine is presented. The field winding creates the field, and when the rotor is inserted and the rotor conductors are carrying a current in the magnetic field originating from the field winding, forces are formed which will create a rotation of the DC-machine.

The separately magnetized DC-machine has the torque–speed characteristic presented in Fig. 14. The torque presented is the electrodynamical torque, T_e, which is the torque that the machine sets up based on the electrical conditions. The blue curve corresponds to an original setting. By adjusting the field voltage or the armature voltage, it is possible to alter the torque–speed characteristic and in this way obtain a torque or speed control. Earlier, before converters for AC-machines became useful, it was the DC-machine that was used for variable-speed drive applications.

In the figure, a negative torque corresponds to generator operation. For instance, note the blue curve for speeds above 1,900 rpm. This means that if a driving wind torque is applied, the turbine will speed up until the incoming torque is balanced by the electrodynamical torque set up by the DC-machine.

Rotating Flux Vector Before continuing with the alternating current machines, there is a need to tackle the issue that an AC-machine will not have a "room-fixed" flux, instead it will rotate. Accordingly, this section tries to explain how a rotating flux vector is built up from the voltages applied to the machine and from the resulting currents.

By feeding a coil with an AC-voltage, an AC-current will result and a pulsating magnetic flux will be created. The direction of the magnetic flux follows the magnetic axis of the coil which is perpendicular toward the coil. The direction can be determined using the right hand, with the fingers in the direction of the current in the coil, and then the magnetic flux direction is in

the direction of the thumb. In Fig. 15, the magnetic vector is depicted for one time instant.

If several coils are acting on the same magnetic path, there will be a total magnetic vector composed of all coils that act on this magnetic path. By using three coils that are displaced 120° "roomwise" and feeding them with voltages displaced 120° in angle (time), a rotating magnetic vector will be created, see illustration in Fig. 16. In the figure, three time instants are presented, where it can be noted how the gray arrow representing the total magnetic vector rotates with a constant speed and constant magnitude.

Depending on the rotor design, a flux vector will be created in the rotor and the angle between the applied magnetic vector from the stator and the rotor flux vector will give rise to a driving torque and a rotation that has the same speed as the rotating magnetic flux vector originating from the stator (synchronous machine), or slightly lower (induction machine).

By placing the magnetic vector in the stator before the magnetic vector from the rotor, the machine will operate in motor operation, and by putting the magnetic vector from the stator behind the magnetic flux from the rotor (and thus braking the rotor) the machine will operate as a generator.

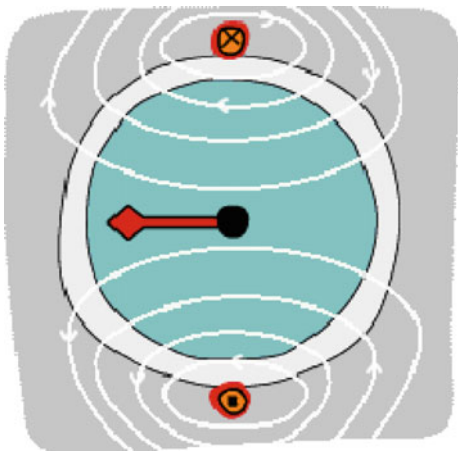

Wind Power Generator Systems and Local Power System Interconnection. Figure 15
Magnetic flux created by current flowing in a single-phase coil

Synchronous Machines The synchronous machine has its name since the rotor will rotate synchronously with the stator flux vector. The machine can have (1) permanent magnets, (2) an electrical winding, or (3) just a magnetically uneven rotor shape. In Fig. 17, a simplified figure of a permanent-magnet synchronous machine is presented.

As earlier mentioned, a machine with a magnetic vector created in the rotor by permanent magnets or a field winding are made to rotate as motors by applying a rotating magnetic vector created from the stator, before the magnetic vector of the rotor. In this way, the stator magnetic vector is "pulling" the rotor behind itself. In generator operation, it is the load (wind/water/steam) that makes the rotor to rotate, and then, in order to brake the machine so it does not overspeed, a rotating magnetic vector created by the stator, currents must exist. Usually this magnetic vector is created by applying voltages to the stator, but it is also possible to allow voltages to be generated in the stator by the field vector from the rotating rotor, and then

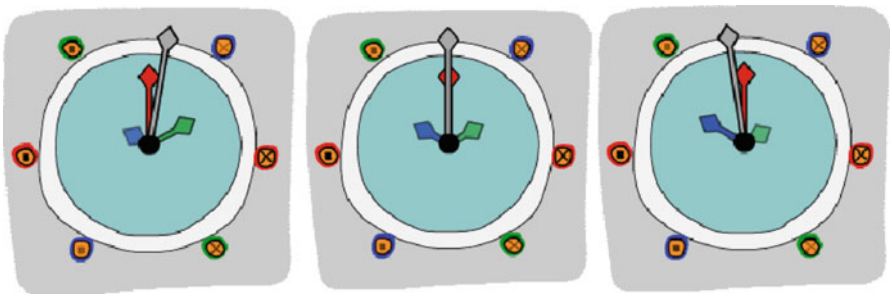

Wind Power Generator Systems and Local Power System Interconnection. Figure 16
Magnetic flux created by a three-phase coil, forcing the machine to rotate counterclockwise

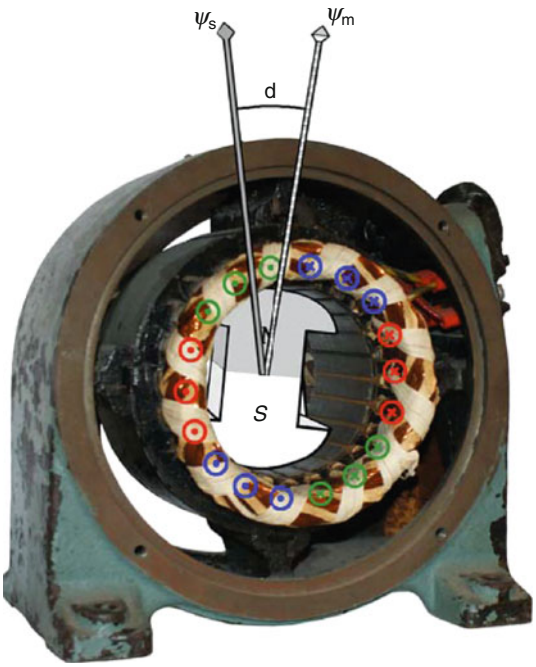

Wind Power Generator Systems and Local Power System Interconnection. Figure 17
Simplified picture of permanent magnet machine, with stator flux (*gray arrow*) and magnet flux (*gray-white arrow*).

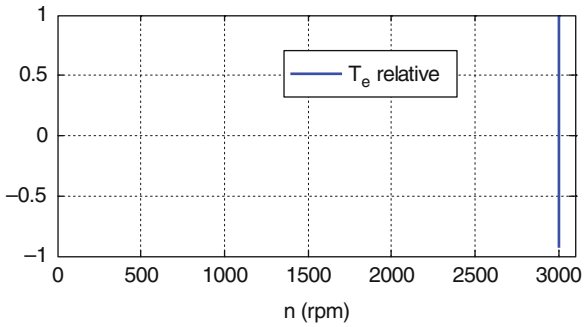

Wind Power Generator Systems and Local Power System Interconnection. Figure 18
Speed–torque characteristics of a synchronous machine

Wind Power Generator Systems and Local Power System Interconnection. Figure 19
Photo of an "opened" three-phase induction machine as well as a rotor originating from another machine

connect the stator windings to a passive load (a load that can be represented by an RLC-circuit).

The torque–speed characteristics for a two-pole synchronous machine is presented in Fig. 18 for a frequency of 50 Hz. If the rotor has more poles, it will rotate slower; a four-pole machine would with 50 Hz rotate with 1,500 rpm. If a voltage having a 60 Hz frequency is applied, the machine would rotate a bit quicker; more about this will come below in the pole-pair section.

Induction (Asynchronous) Machines A photo of an opened three-phase induction machine is presented in Fig. 19 together with a rotor.

From the figure, the stator windings can be observed, located around the rotor with their magnetic axes directed in to the rotor. By using the right hand, and pointing the thumb inward from the stator in to the rotor, the other fingers on the right hand, depicts how the windings in the stator are placed with the fingers showing the current direction. Larger machines are in principle almost always three-phase, and accordingly, as described above, there are three magnetic axes pointing inward, displaced 120° from each other around the rotor.

Further, the rotor can also be observed in the photos. The rotor consists of laminated iron sheets/plates, which can be assumed to be isolating toward currents. In these laminations, however, there are cast aluminum slots, where a current can flow. If the stator of the induction machine is supplied by a three-phase power source, a rotating magnetic flux will be created. As this magnetic wave rotates through the rotor, the short-circuited current paths (that can be observed in the figure) try to put up currents that counteract this imposed magnetic field. These currents form together with the imposed flux vector a driving torque. The process with which the currents are created in the rotor is called induction, and hence the name induction motor. If the machine rotates exactly with the speed of the magnetic flux vector set up by the stator,

there will be no induced currents and the torque will be zero. However, the larger the differences between the speed of the rotor and the speed of the magnetic field, the larger the torque will be. However, a too large speed difference will cause a reduction of the torque and the machine will lose its thought functionality. The point where the torque is at its maximum is referred to as the stall point. In Fig. 20, the flux vector (white) together with the current vector in the rotor (gray) is presented for a lightly loaded motor point as well as for operation at full speed as a generator.

In the figure it can be noted that, exactly as for the DC-machine that the speed increases in generator operation. If the induction machine is driven by a wind turbine rotor, it is the torque formed from the wind that increases the speed.

The fact that the induction machine operates asynchronously with the frequency of the supply gives it its alternative name, the asynchronous machine.

The machine presented in Fig. 20 has a rated slip of 5% (slip is the relative speed change that the machine has within its normal operating region). Larger machines have a rated slip of below 1%. In [8], page 124, a figure presents typical slip values for induction generators as a function of size and pole-pair number. The slip increases with higher rotor resistance, which gives a smoother operation, since the speed is allowed to vary more. However, the higher the rotor resistance, the higher the losses. The efficiency of a modern induction generator for wind turbine applications is above 95% once the loading is between one-third of full load and full load.

Of special interest for wind energy applications is an induction machine where the rotor instead has windings and these windings are connected to slip rings at the end of the machine. In Fig. 21, slip rings that are connected to the rotor windings can be observed on a 22 kW induction machine.

To the rotor slip rings it is possible to connect a converter. The advantage is that such a converter becomes fairly small in comparison with attaching a converter in the "normal way," that is, to the stator,

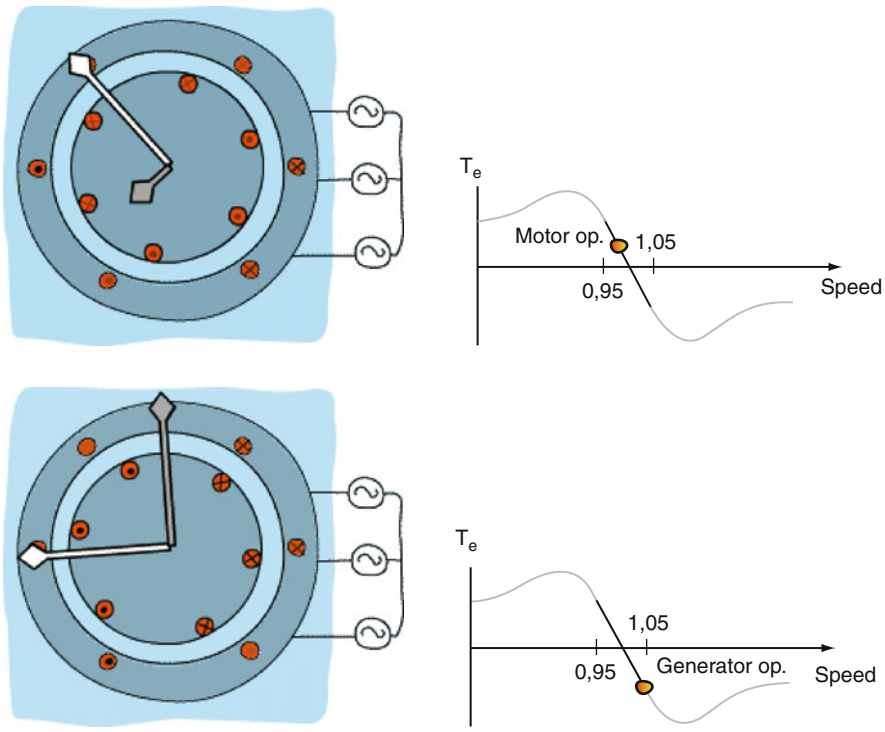

Wind Power Generator Systems and Local Power System Interconnection. Figure 20
Upper picture, operation of the induction machine as a motor with a moderate torque. Lower picture, operation as a generator with full torque. White vector is the resulting magnetic vector, and the current vector is depicted in gray

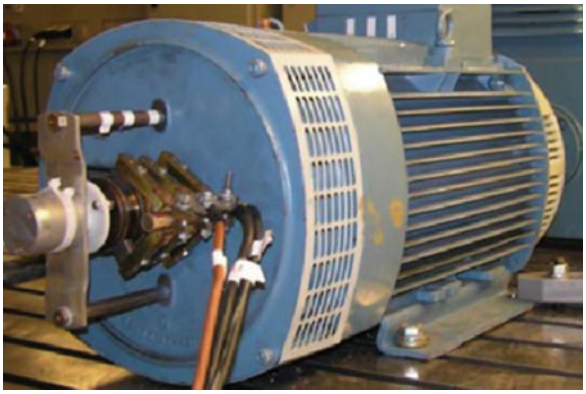

Wind Power Generator Systems and Local Power System Interconnection. Figure 21
Slip rings connected to the rotor windings of a 22 kW induction machine

giving low cost and low losses in the generating system of the wind turbine since only a fraction of the total produced power goes through the converter. More about this will follow in the descriptions of the wind energy generating systems.

Pole-Pair Number If there only is a north and a south pole in the stator and the rotor, the synchronous machine will rotate with the same frequency as the applied electrical frequency

$$\Omega_m = \omega_{\mathrm{el}}.$$

The induction (asynchronous) machine will, as mentioned before, deviate maximum a few percent from the speed determined by the equation above.

The rotational speed in rpm (round per minute) can be found using the relation

$$n = \Omega_{\mathrm{m}} \frac{60}{2\pi}.$$

Often, an electrical machine consists of more than a south pole and a north pole (referred to as 1 pole-pair, with the notation $p = 1$). In Fig. 22, an example of a two- and a four-pole machine is depicted.

The relation now becomes for the synchronous machine,

$$p\Omega_m = \omega_{\mathrm{el}}.$$

Here, the magnetic flux per pole-pair changes with the same speed as the applied frequency. However,

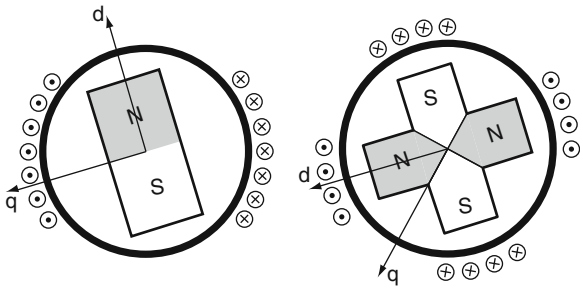

Wind Power Generator Systems and Local Power System Interconnection. Figure 22
Two- and four-pole synchronous machine

since there are several pole-pairs involved, this means that the speed of the rotating flux vector is shifted down with the number of pole-pairs, seen from the stationary reference system. Apart from giving the possibility to change the rotational speed, the use of a higher number of pole-pairs can also give a possibility to optimize the machine for certain applications.

Again, for the induction machine there is a slight speed difference between the physical rotor speed and the speed of the magnetic vector, but the same reasoning holds for a no-loaded induction machine.

Power Electronics

Converter

The rotational speed of an AC-machine is governed by the number of pole-pairs as well as the frequency of the electric supply it is connected to. This is the reason why traditional (also called Danish concept) turbines are called fixed-speed turbines. This type of machine is put in generator operation by the driving wind, but the speed is governed by the grid frequency 50/60 Hz, the number of pole-pairs, and the gearbox ratio.

In order to control the speed of an AC-machine, it is a necessity to be able to alter the frequency of the voltage applied to the electric machine. In this way, the magnetic flux vector will alter its speed. For this purpose a converter is used. The converter has an AC-side connected toward the generator and a DC-side that sends the electrical power toward the grid, via another converter. This second converter has its AC-side toward the grid.

The needed varying frequency is created by switching transistors quickly (a couple of kHz) and in

this way a switched voltage pattern is formed, that in average (for a switching period, i.e., 0.5–1 ms) has a desired average that has a "main fundamental waveform" that corresponds to the desired applied frequency. In Fig. 23, a simplified sketch of a converter is depicted together with a 200 A power module making up a so-called phase leg, which builds up the phase voltages, in this case phase *c*. The transistor is either on or off, and in a phase leg, the upper or lower is always on and the other off. This means that the voltage potential in point *c* jumps between $+V_d/2$ or $-V_d/2$. Once the voltages are created by the transistors, the current will then flow out from the generator and towards the DC-link. Also in the figure, bottom right, a complete conversion from the variable generator frequency to the 50/60 Hz grid frequency is depicted.

Since there are three-phase voltages created, the phase potentials will contain also another level. The resulting phase voltage and the resulting current for one phase is presented in Fig. 24.

In the switching pattern, it can be observed that there is a more low-frequency wave that is imposed on the machine, in this case having a frequency of slightly lower than 50 Hz. Due to that the machine windings contain inductance, it means that the high-frequency switching of the voltage will only lead to fairly small current ripple (added on the desired fundamental waveform) as can be observed in the figure. Since it is the current that forms the torque in an electrical machine, the torque produced by the generator will in principle only be based on this desired low-frequency signal. The higher switching frequency is filtered away.

The same power converter can also be connected towards the power grid, as shown in Fig. 23, however into the power grid it is not allowed to inject to much current harmonics. A problem is that the grid does not have enough inductance and accordingly a filter is needed in order to bring down the current harmonics to reasonable values.

The losses are fairly low in a power converter and can be down to 2% for a DC/AC-conversion in a wind turbine converter. However, there is also a need to convert the voltages and currents from DC to the grid AC-quantities, and accordingly around 3–4% is what can be achieved regarding converter efficiency. At low load, the efficiency is, of course, lower.

STATCOM and SVC

A STATCOM is in principle the same object as the converter presented in Fig. 24. However, on the DC-side there is only a capacitor. The AC-side is connected

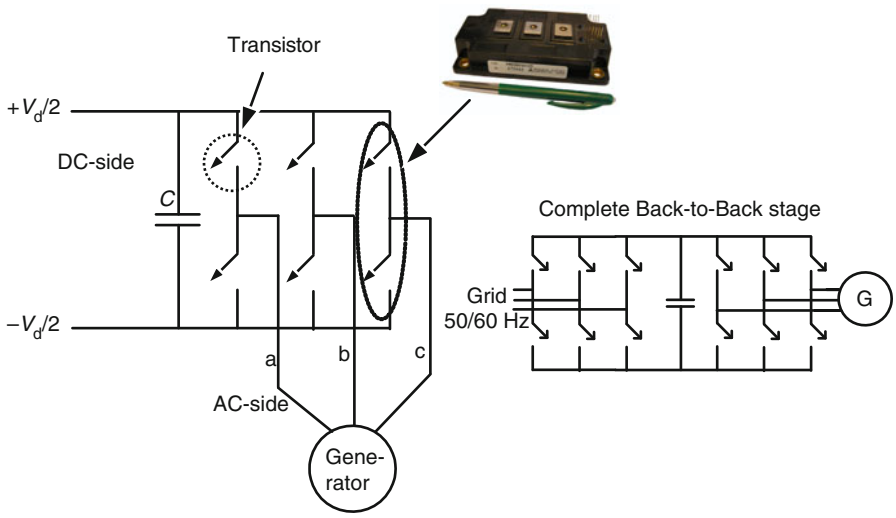

Wind Power Generator Systems and Local Power System Interconnection. Figure 23
Left: Principle sketch of switching converter. *Upper right*: 200 A power module consisting of two transistors, making up the phase voltage *c*. *Lower left*: A complete B2B-stage, making the conversion form the generator voltage to the 50/60 Hz AC-voltage of the grid

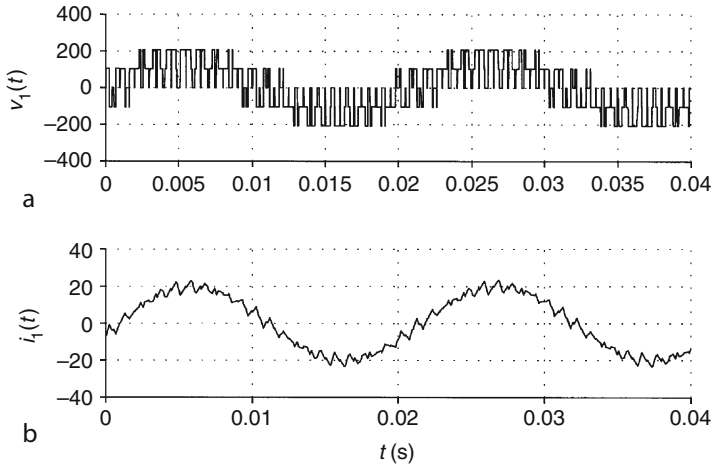

Wind Power Generator Systems and Local Power System Interconnection. Figure 24
A phase voltage created by a three-phase converter as well as one resulting machine phase current

to the grid. It can be used to adjust the reactive power that is exchanged with the power grid. Typically it can be used to compensate a shortage of reactive power, either due to long inductive lines between the wind installation and a strong grid connection point, or due to that traditional fixed-speed wind turbines with insufficient reactive power compensation is used. Moreover, it can be used to stabilize the network in case of grid disturbances.

An SVC is a simpler and cheaper variant, which usually has a sufficient operational performance for performing the phase compensation.

Wind Turbine Generating Systems

A frequently asked question is: Which electrical generating system is the best, and this question is not possible to answer. The systems all have good performance and the differences in performance versus cost do not give a clear answer. However, it is obvious that there has been a shift from traditional fixed-speed turbines toward variable-speed turbines.

When it comes to produced energy per swept area given a certain average wind speed, all the concepts produce a similar amount of yearly energy [9], if really old-fashioned fixed-speed turbines, (which were not equipped with the two-speed facility as will be explained below) are disregarded.

Typical stator voltages are 690 V. However, the voltage levels are slowly moving upward as the power increases further above 2–3 MW. A benefit of being below 1,000 V is that there are more available service technicians.

Fixed-Speed System

The fixed-speed wind turbine system was the wind turbine system that dominated the market until the millennium shift (2000). It is still used today in power levels up to 2 MW and is a well-proven design. Often this system is referred to as the "Danish concept."

This type of wind turbine system is equipped with an induction generator which is directly connected to the grid. It is not a good solution to have a synchronous generator directly connected to the grid in this application since it will be too stiff, and cause large stresses on the drive train of the turbine (shafts, gearbox). The small slip that the induction generator has (0.5–1% at rated operation) will give sufficient smoothness.

Larger turbines of this type (>1 MW) are always equipped with the possibility to operate at two specific speeds. Either they are equipped with pole-changing generators which provides a lower generator output with a lower fixed speed and a larger generator rated power with a higher, fixed rotor speed. The turbine can also be equipped with two separate generators. In this way, the energy efficiency is as good for this turbine, given a certain rotor swept area and maximum shaft torque, as that of a variable-speed wind turbine. Of course, a variable-speed turbine is able to convert

more of the energy in the wind into shaft power, since it can exactly match the rotor speed to the wind conditions, [9], and in this way more of the power available in the wind can be converted into mechanical power. However, since no power electronics is used, there are no losses in a converter system. In addition, the two-speed facility still has a very high energy capture from the wind. Finally, the fact that the low speed generator has a lower flux level gives lower no-load losses, which is perfect for low wind speed operation. The turbines are as mentioned earlier, stall-controlled (the blades are mounted fixed into the hub, and cannot turn around their axes), more modern ones with active stall control (meaning that the blades turn slightly in order to be able to adjust the power level at high wind speeds, also adapting to temperature changes and different pressure conditions).

These types of turbines are robust and cheap, since the electrical system in principle only consists of an induction generator with shunt capacitors connected directly toward the grid as presented in Fig. 25. The pole-pairs of the generators are either 2 and 3 or 3 and 4 depending on the preferred speed range of the turbine. The first combination gives that the lower rotor speed is 67% of the higher one, and the second combination that the lower rotor speed is 75% of the higher one.

A slight drawback is that the starting of an induction machine requires large currents to magnetize the machine. In order to overcome this problem to some extent, the turbine is equipped with a soft-starter (consisting of antiparallel thyristors) in order to keep the currents below rated, when the turbine is being connected to the utility grid.

Phase-compensating capacitors are used to compensate for the no-load reactive power consumption of the generator, or in some cases also for full-load operation. In order to obtain a better controllability, an SVC or a STATCOM can be added in shunt with the wind energy unit.

Smaller units have the transformer connected outside the turbine while larger ones have the transformer either at the bottom of the tower or up in the nacelle. An advantage of having the transformer up in the nacelle is that it helps as counterweight towards the turbine rotor.

Fixed-Speed Systems with Variable Rotor Resistance

The fixed-speed turbine with a variable rotor resistance is in principle the same as the previous one, with reactive power compensation by capacitors and a soft-starter used to keep the currents below rated during the process of connecting the turbine to the grid, see Fig. 26. The difference is that the rotor resistance can be controlled which gives this turbine a limited rotor speed controllability and also fault current control

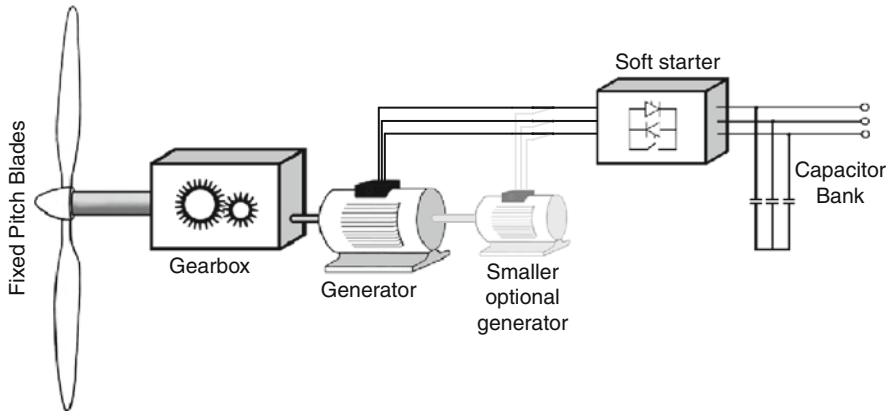

Wind Power Generator Systems and Local Power System Interconnection. Figure 25
Simplified electrical scheme of a fixed-speed wind turbine system. Here a two-generator system is presented, one larger with a higher rotational speed and higher power and one with lower speed and lower power. It is also possible to have so-called pole-shifting generators which can have these two generators in one generator

capability. The rotor speed can now be controlled in a speed range of about −2% to +5% from the nominal one. A difference toward the previously described fixed-speed wind turbines is that the fixed-speed wind turbine with a variable rotor resistance usually is pitch controlled.

The fixed-speed turbine with a variable rotor resistance was manufactured by Vestas in the 1990s, but the production continued for many years for delivery to the US market.

Full-Power Converter Systems

The full-power converter system gives the highest degree of freedom regarding the control of the electrical quantities as well as the mechanical ones. The name "full-power converter system" comes from the fact that all the produced wind power has to go through the converters, which is not the case for the DFIG system, which will be explained in a coming section. In this concept, the generator is completely decoupled from the grid by a power electronic AC/AC-converter between the stator of the generator and the grid. This means that from a grid point of view, it is irrelevant what type of generator is used, or if a gearbox is used or not. Siemens uses a cage-bar induction generator while General Electric uses a permanent-magnet generator. Both these systems are with an ordinary gearbox. Recently, more and more manufacturers are taking up this concept. Also, the full-power converter turbine is pitch controlled.

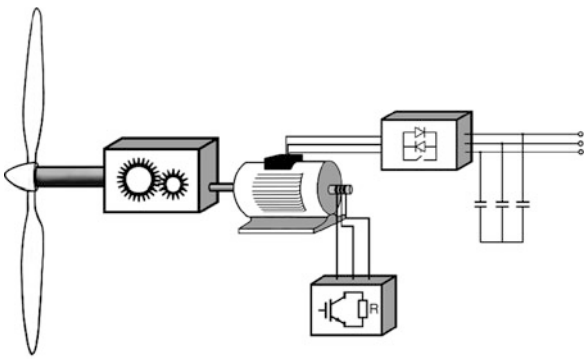

Wind Power Generator Systems and Local Power System Interconnection. Figure 26
Electrical scheme of fixed-speed system with a variable rotor resistance

In this system, all the power is flowing through a DC-link in the converter. The converter consists of two sets of DC/AC-converters as the ones presented in Fig. 23. The reactive power is completely decoupled between the machine and grid side of the DC-link and can be produced or consumed separately on each of the DC-link sides. In fact, the grid side converter can be programmed to work as a STATCOM, in addition to its original task of feeding active power from the turbine into the grid, with very little additional cost. The amount of reactive power that can be supported to the grid is determined by the size of the grid side converter. This concept is presented in Fig. 27.

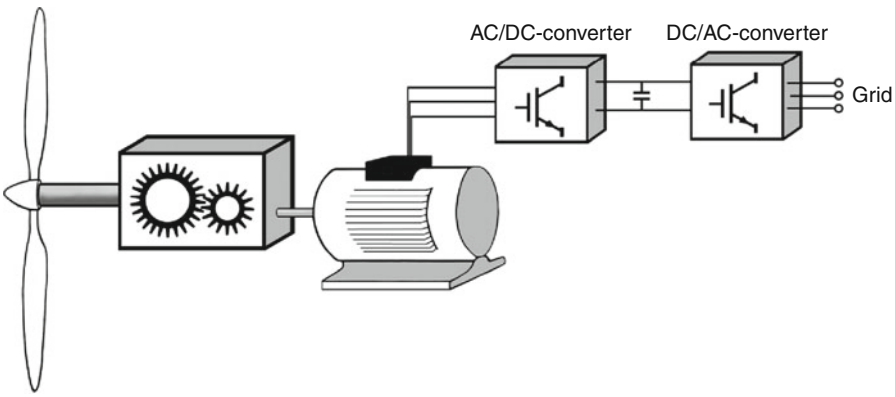

Wind Power Generator Systems and Local Power System Interconnection. Figure 27
Simple scheme of full-power system

Slowly Rotating Generators Which Operate Without Gearbox

The objective of using a slowly rotating electrical generator, although this will be a much larger generator for the same power rating, is that the gearbox can be eliminated (or made smaller, since the gear ratio can go down), thus saving the cost of the gearbox and saving the gearbox losses, in addition to the increased reliability. As for many other aspects of wind energy, there is no clear answer if it is worth to use a slowly rotating generator and removing the gearbox or not.

An AC-machine operates at a frequency governed by the frequency of the voltage applied to the generator (for the synchronous machine exactly the same, for the induction machine, almost the same, just the slip must be considered). However, as mentioned before, there is an additional design parameter that can give a certain ratio between the applied voltage frequency and the rotational speed of the machine and that is the pole-pair number. The relation between the applied electrical frequency and the mechanical speed as a function of pole-pair number is

$$\Omega_{\mathrm{m}} = \frac{\omega_{\mathrm{el}}}{p}$$

where Ω_{mech} is the mechanical rotational speed and ω_{el} is the electrical angular frequency. The drawback is that the large number of poles will make the machine to have a very high diameter. In order to reduce the needed number of pole-pairs and in this way keep the radius down, the supply frequency can be lowered to some extent in these systems. In Fig. 28, a sketch comparing the difference between the geared system and the non-geared system is presented. There is no difference in grid interface equipment (converters, etc.) between the two systems.

The directly driven machines can typically be supplied with a slightly lower electrical frequency, for instance 20 Hz, corresponding to 120 rad/s giving a needed number of pole-pairs of 100–200. For more information, the interested reader can in [10] find a comparison that is done based on a 500 kW system.

The largest manufacturer of this type of system is Enercon that uses electrically magnetized field windings. The consequence is that the rotor diameter and thus the whole generator diameter become very large. A possibility to have a rotor with a lower diameter is to use permanent magnets instead of the electrically magnetized rotor poles. In addition, the efficiency can be increased in this way.

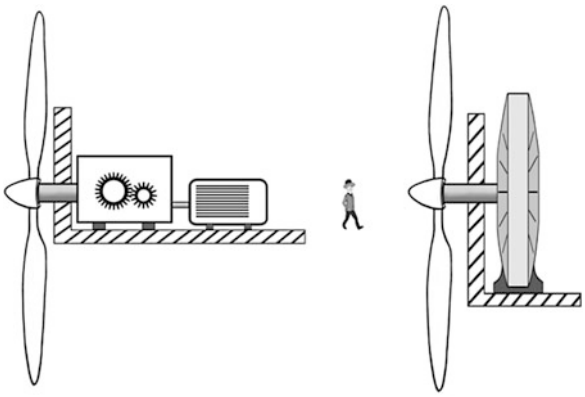

Wind Power Generator Systems and Local Power System Interconnection. Figure 28
Principle sketch of conventional (geared) and directly driven generator, interface with converters to the grid has been omitted, but is the same for both systems

Doubly Fed Induction Generator Systems

During the last years (2005–2010), this has been the dominating wind turbine type. The converter in this turbine is located in the rotor circuit path giving a cheap and energy-efficient solution for variable-speed operation. The reason is that the converter rating only has to handle 20–30% of the turbine rating which both gives a lower investment cost and lower losses in the power electronic converter. A simplified electrical scheme of the system is presented in Fig. 29.

In the doubly fed induction generator, the currents in the rotor are formed by the rotor converter instead of only being induced from the stator. Of course, the induction from the stator must be considered when the rotor currents are being controlled. The rotor currents can now be controlled with a slip much larger than what is possible with a cage-bar induction machine. However, in order to handle the induction from the stator, the rotor voltage must exceed the slip (s) times the stator voltage

$$U_{\mathrm{r}} > sU_{\mathrm{s}}.$$

If this criteria is fulfilled, the rotor converter can feed in a current having a suitable frequency and in this

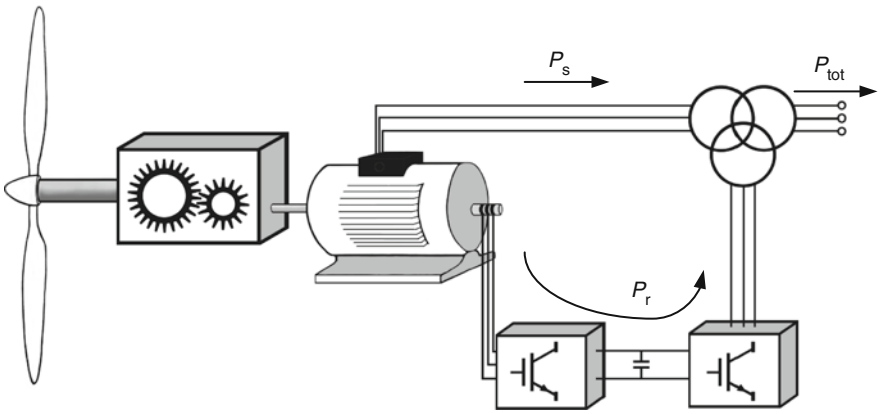

Wind Power Generator Systems and Local Power System Interconnection. Figure 29
Electrical scheme of DFIG system

way obtain a variable-speed operation. The power direction is actually from the grid into the rotor at low wind speeds, but at high wind speeds, the power flows from the rotor toward the grid.

It can actually be discussed if this is an induction machine. It is also possible to feed in DC-currents into the rotor, and then it is an electrically magnetized synchronous generator.

For a DFIG system, it is a trade-off between speed span and dimensioning of the rotor converter and rotor windings. The closer to the synchronous speed of the system that the turbine can be operated at, the lower the voltage applied to the rotor windings will be and also the lower the power transfer, in the rotor circuit including converter, in relation to the whole power can be.

Initially it can be thought that it would be favorable to have the synchronous speed of the system in the middle of the rotor speed interval. However, it is more favorable to have the synchronous speed a bit higher. The power that goes through the rotor in relation to the total power is proportional toward the slip in the machine.

$$P_r = sP_{tot}$$

It is accordingly important to keep the slip low at the highest power level. At lower power levels, it is OK with a higher slip since the transferred power anyway is fairly low. The fact that a variable speed wind turbine shall have a low rotational speed at low wind speeds in order to follow the optimal power coefficient, C_p, and an upper speed limit gives a speed–torque operation region as presented in Fig. 30.

From the figure, it can be observed that a rating of 20% of the full power is sufficient for this turbine and the speed span is in principle 50–100%. A full-power converter system can operate a turbine at 0–100% of the speed; however, 40–100% is what typically is used, which means that the rotor speed range of the DFIG turbine is almost "full-speed range." The investment cost and the converter losses are thus lower compared to the case if the whole energy flow would have had to be coped by a full-power converter. However, it should be mentioned that the rotor voltage is also proportional toward the slip and the stator voltage

$$U_R = s|U_S|$$

where

$$s = \frac{\omega_S - \omega}{\omega_S}$$

and where ω_S is the synchronous speed.

From the figure, with the location of the synchronous speed it can from the equations above be deducted that the highest rotor voltage will occur at the lowest rotor speed. Had the synchronous speed been in the middle of the speed span, the maximum rotor voltage could have been lower. However, a suitable trade-off is to select a bit higher synchronous speed as presented in Fig. 30.

Worth mentioning is about voltage levels of the rotor converter. It is beneficial to go up a bit in voltage,

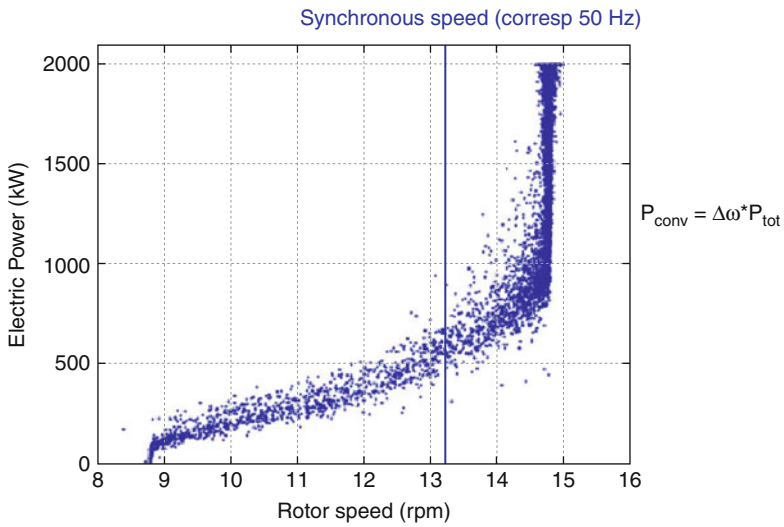

Wind Power Generator Systems and Local Power System Interconnection. Figure 30
Rotor speed versus power relation for DFIG wind turbine. The rotational speed 13.2 rpm corresponds to the electrical frequency of 50 Hz, accounting for pole-pairs in the generator as well as the gearbox ratio. $P_{conv}=P_r$

for the used power level for the converter, since the currents then come down. The way that this is done is that the number of turns in the rotor typically is higher than in the rotor. In this way, the voltage level of the rotor is still in the same vicinity as for the stator.

The energy efficiency of this system can be slightly improved by operating the generator in Y for low wind speeds and Delta for higher wind speeds [9]. For Δ-Y connections of an electric machine, please consult one of the electric machine textbooks.

The reactive power can easily be controlled to unity power factor using the DFIG system. The fact that the turbine is of variable-speed type, gives a smooth active power output. Since it is a variable-speed turbine, pitch control is used, as mentioned earlier.

A drawback with this system was earlier that it was difficult to have a good immunity toward severe voltage dips [11]. This is due to the fact that faults in the supply network creates large over-currents in the rotor for which the power electronic converter is not designed. Today (2011) solutions to handle these severe grid disturbances are provided by the manufacturers.

Power Quality Impact

The voltage in the grid should ideally consist of one sinusoidal component 50 or 60 Hz and nothing else. The magnitude of this voltage shall always be the same and in the three-phase system the voltages shall be separated 120° apart. In this case, the power quality is excellent. Any deviation, such as harmonics, voltage level variations, deviations in frequency, etc., is a negative power quality impact. In case the deviations become too large, then there is a risk for having power quality problem [7].

Traditionally, there has been a fear for negative power quality impact from wind turbines. However, this fear has more been based on uncertainties rather than on facts, in particular there has been a fear about flicker problems, but hardly any has been reported.

Anyway, in the beginning, the wind turbines did not have the best power quality impact, so they could be said to be passive grid disturbers. However, today modern turbines have a very good power quality impact, and they can even reinforce the grid. So, it can be said that wind energy converters have gone from being passive grid disturbers to being active grid-reinforcing units.

Power Quality Aspects

Definition of Equivalent Network A power system consists of a large amount of nodes connected together by power lines, as the one presented in Fig. 31.

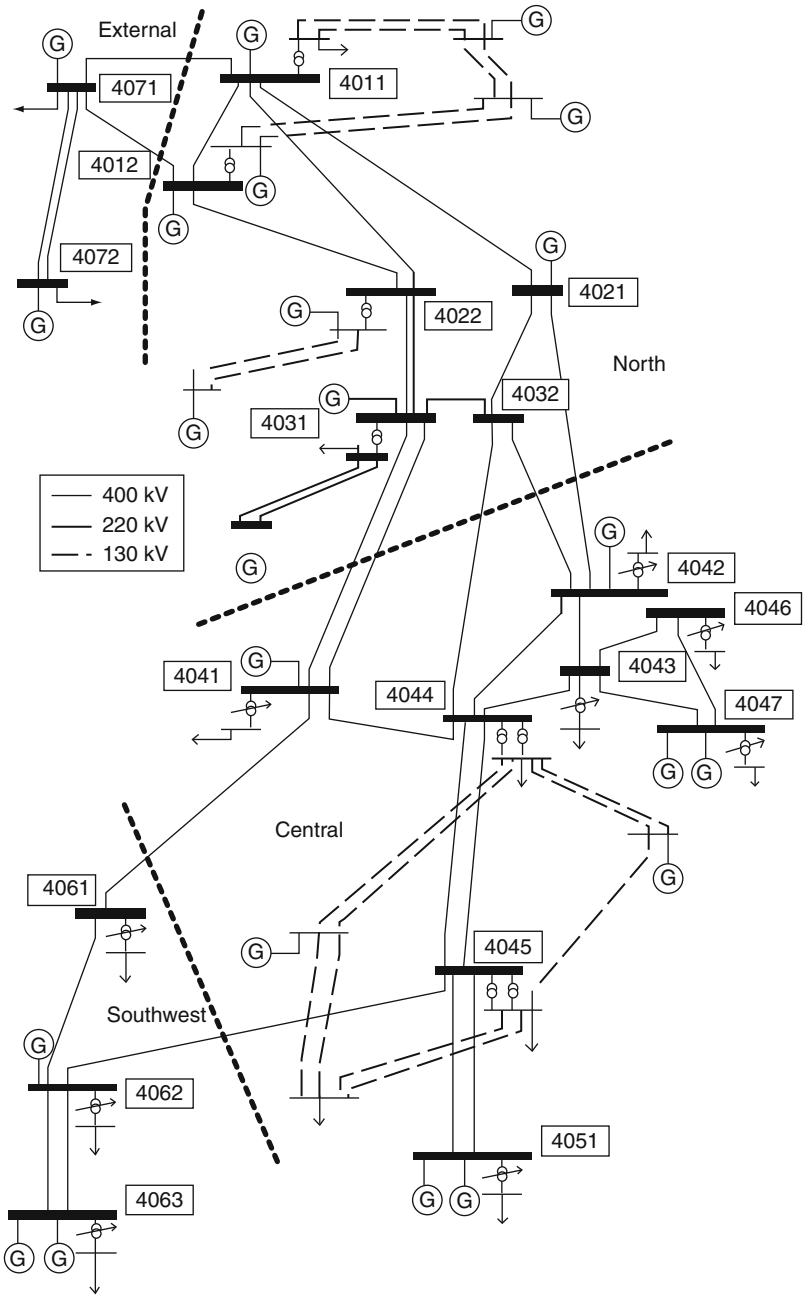

Wind Power Generator Systems and Local Power System Interconnection. Figure 31
Meshed network, in this case based on the Cigre Nordic 32-bus system

In order to perform calculations on the voltage level influence that a new power unit would have on the grid, as well as to determine possible fault currents, a network equivalent is constructed, consisting of an infinitely strong voltage source, and an impedance, according to Fig. 32.

An infinitely strong voltage source is used, in the picture it is here represented by a nuclear power station, but consists in principle of all objects connected to grid. From this infinitely strong voltage point, an impedance is defined to a grid connection point called PCC, Point of Common Connection. In case that there

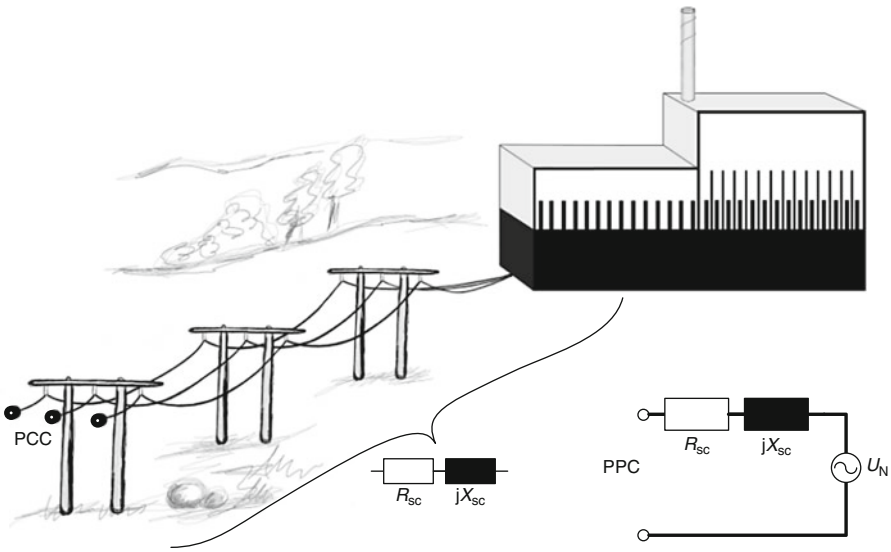

Wind Power Generator Systems and Local Power System Interconnection. Figure 32
Definition of network impedance, that is, a line with an equivalent impedance and an infinitely strong voltage source behind the impedance, making up the PCC calculation point

would be a short-circuit in the PCC, a short-circuit current would appear with a value of

$$I_{sc} = \frac{U_N}{\sqrt{3}Z_{sc}}.$$

A commonly used term is the grid strength, and it is defined as

$$S_{sc} = \sqrt{3}U_N I_{sc}$$

often called short-circuit capacity of the grid, $\sqrt{3}$ is a factor originating from the calculations used for a three-phase system, but is not needed to comprehend in order to follow the calculation setup.

When a new power source, for instance a wind turbine installation is going to be connected to the grid, a grid strength and information of the grid impedance is obtained from the responsible utility, from which the equivalent resistance and reactance can be determined. The relations are

$$R_{sc} = Z_{sc}\cos(\psi_{sc})$$

$$X_{sc} = Z_{sc}\sin(\psi_{sc})$$

where Ψ_{sc} is the grid short-circuit impedance angle, R_{sc}, X_{sc}, and Z_{sc} are the grid short-circuit resistance, reactance, and impedance, respectively.

Voltage Level Influence in PCC Now, if an energy production is connected to the PCC the voltage increase would be

$$\Delta U = R_{sc}I_{active} + X_{sc}I_{reactive}$$

where I_{active} and $I_{reactive}$ are the active and reactive powers coming from the energy production unit, for instance a wind farm.

The active and reactive current components can be found as

$$I_{active} = \frac{P}{U_N}$$

and

$$I_{reactive} = \frac{Q}{U_N}.$$

Worth noting is that the reactive power, Q, can be altered for variable-speed wind turbines and the voltage influence can then be controlled. Keeping Q to 0, gives lowest line losses and is what today (2011) typically is done, meaning the power factor, PF = 1.

The utility has to keep the voltage levels within certain limits. In Sweden, EN50160 states ±10% on lower voltage levels. Since other loads are connected to the lines as well as the fact that there is a need for

safety margins, a wind turbine installation could be allowed to vary the voltage level within a few percent. As can be noted from the equation above, the voltage level will increase as the power production increases. As mentioned above, the reactive power exchange with the grid can be used to control the voltage level. Today (2011) this option is rarely used, since the overall control of the power network could become more complicated if a lot of distributed generation tried to control the voltage levels in their vicinity.

Voltage Level Influence at the Turbine The wind energy installation could also have a certain distance to the PCC and then there will of course also be a voltage difference between the wind turbine installation and the PCC, see Fig. 33. The line resistance, reactance, and impedance are denoted as R_L, X_L, and Z_L.

The resulting voltage variation at the turbine compared to PCC then becomes

$$\Delta U = R_L I_{active} + X_L I_{reactive}.$$

Voltage Fluctuations and Flicker Emission

The varying wind speed and also the mechanical design of a wind turbine cause a varying output power. This varying output power then causes voltage variations on the grid to which the turbine is connected to. The observation from customers on a quickly varying voltage disturbance is that light bulbs start to blink. In [12], it is stated how the flicker evaluation should be conducted, based on experiments made more than half a century ago on when people started to detect a flickering light from an incandescent light. The result of using the flicker algorithm is the flicker severity index values, one 10 min value and one 2 h value, P_{st} and P_{lt}. If these values reach 1, most people start to get annoyed and some persons already can note a flicker level of 0.7. National regulations state how much flicker a wind turbine may contribute with to the grid. A typical value is 0.25 in P_{lt}. The sensitivity for a flickering lamp is as most sensitive for a frequency of 1000 changes per minute giving a frequency of 9 Hz, where only a 0.3% variation in the voltage magnitude can be observed. In Fig. 34, the sensitivity limit as a function of frequency is given.

The standard IEC 61400–21 gives a guideline of how the flicker originating from a wind turbine shall be determined. The current coming from the wind turbine shall be recorded and fed into a fictitious network using various grid angles. The strength of the fictitious network ($S_{k,fic}$) shall be 50 times the rating of the wind turbine

$$S_{sc,fic} = 50 S_n$$

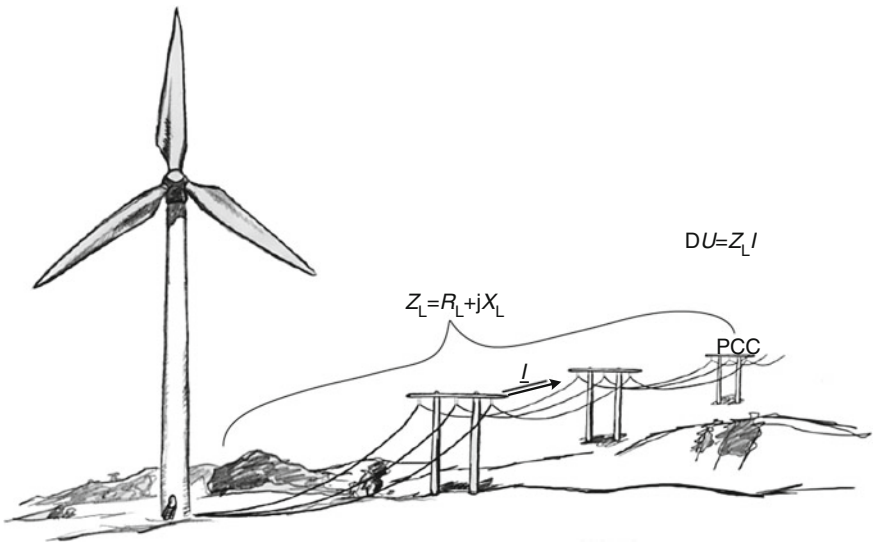

Wind Power Generator Systems and Local Power System Interconnection. Figure 33
Wind turbine attached to the grid as well as calculation of voltage level influence

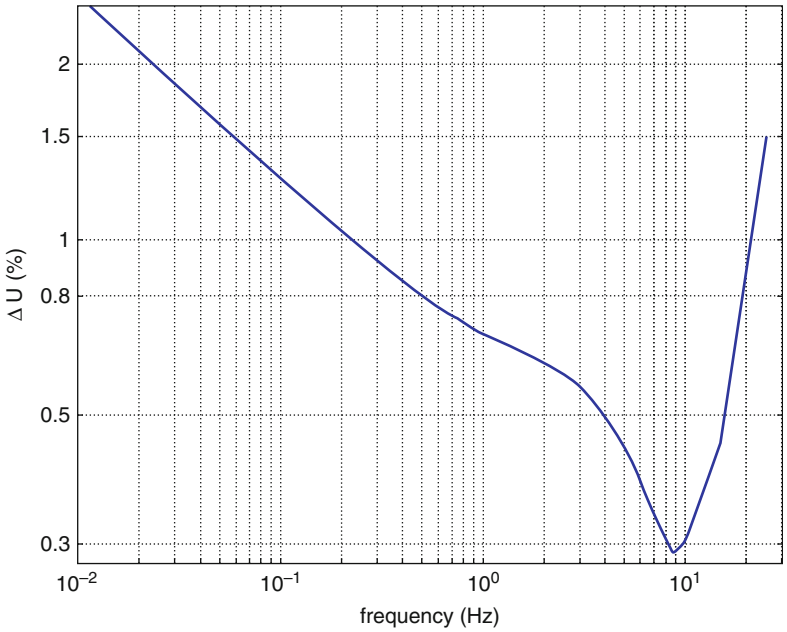

Wind Power Generator Systems and Local Power System Interconnection. Figure 34
Limit for when a voltage variation can be detected by the eye

according to [13]. After having determined the fictitious flicker emission, $P_{st,fic}$ on this fictitious network, a dimensionless flicker coefficient c_f is formed as

$$c_f = 50P_{st,fic}$$

which then can be used to determine what flicker contribution a turbine will create on a grid to which it is being connected. The flicker coefficient shall be determined for four different grid short-circuit impedance angles, Ψ_{sc}, 30°, 50°, 70°, and 85°.

The development of modern variable-speed wind turbines has led to a situation where the flicker emission is not a problem today. In addition, when several turbines are connected in a group, these have a tendency to even out the power pulsations, and accordingly giving an even lower flicker emission. IEC 61400–21 states

$$P_{st} = \sqrt{N}P_{st,ind}$$

where $P_{st,ind}$ is the flicker emission from one single turbine and N is the number of turbines. However, according to [14, 15] the equation above underestimates the flicker emission from a whole wind park, in particular if traditional fixed-speed wind turbines are used. The reason is that the flicker emission does not only originate from the wind turbines, also the grid itself imposes voltage disturbances on the turbines, which they reflect back as flicker emission. These reflected disturbances all come in the same phase from all wind turbines, and that is the reason why the equation above might give a bit too optimistic results.

A final comment is also that incandescent lights will slowly be outshifted due to their poor energy efficiency and in Europe this is driven by a legislative process that already is ongoing.

Harmonics Any period waveform can be composed by a number of sinusoidal components, according to

$$f(t) = \frac{a_0}{2} + \sum_{n=1}^{\infty} a_n \cos(n\omega t) + b_n \sin(n\omega t)$$

where

$$a_n = \frac{2}{T}\int_{t_0}^{t_o+T} f(t)\cos(n\omega t)dt$$

and

$$b_n = \frac{2}{T}\int_{t_0}^{t_o+T} f(t)\sin(n\omega t)dt.$$

In Fig. 35, an example of a square wave and its decomposition into Fourier components is shown.

Harmonics can occur both in voltage and in current. A wind turbine (or other components attached to the grid) can inject current harmonics into the grid. Depending on how strong the grid is, this will result in harmonics in the voltage. A strong grid will be less affected while a weak grid will be more substantially affected.

The voltage in the grid can never in reality be without harmonics, and these harmonics could disturb attached equipment, such as wind turbines. It is the responsibility of the grid owner to ensure that there are not too much harmonics in the grid.

The wind turbine in itself seldom gives rise to problems with harmonics. However, wind turbines connected to a local grid with cables, transformers, and inductors may as a combination amplify harmonics. Examples from literature [15] show that individual harmonics can be amplified at least three times. These local resonances is one concern regarding the failing transformers and generators in certain sea-based wind farms, so care has to be taken regarding PWM-patterns of switching converters and the operation of breakers, in particular vacuum breakers. For more details regarding PWM patterns, see Sect. Power Electronics – Converter. It should be pointed out that single wind turbines with PWM-converters provide sufficient filtering so without a local resonance there will not be a problem with harmonics.

Fixed-Speed Wind Turbines

Steady-State Influence

Earlier, fixed-speed systems did not have a real reactive control ability. They had a capacitor connected to the stator terminal compensating for the no-load consumption of the turbine, which gave a voltage profile, depending on the network type, according to Fig. 36.

In a network with a grid strength (S_{sc}) of 20 times the strength of the connected network, the voltage level influence for three different network angles is presented in Fig. 37. In this figure, the reactive power at no-load that the induction generator needs, has been compensated for using capacitors. That is why the voltage change is zero for zero power. Otherwise, the produced power-voltage relation would be different.

Another point that needs to be addressed regarding Fig. 37 is that today capacitor banks are often connected in stages, which are used to keep the power factor close to unity for various operating conditions. This would mean that the voltages in Fig. 37 would increase somewhat. In principle, more capacitors could be connected and used for reactive power control and such solutions are offered by manufacturers of this type of turbine. Full-power converter systems and well as DFIG systems have an inherent possibility to control the reactive power and in the base case, the reactive power is kept as close to zero as possible. The result from a voltage level point of view is actually negative, since the reactive current no longer brings the voltage

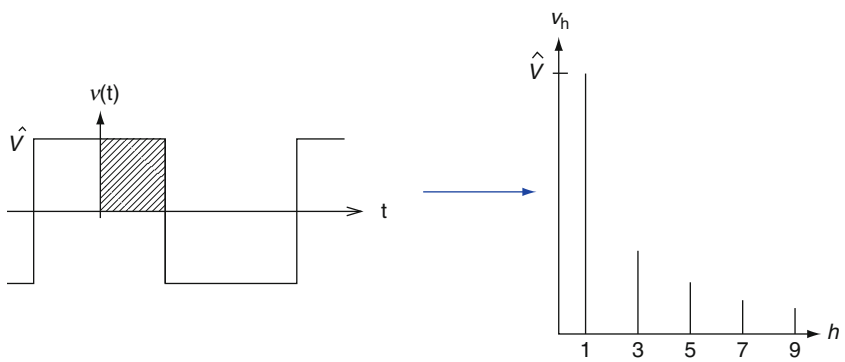

Wind Power Generator Systems and Local Power System Interconnection. Figure 35
Square wave and its decomposition into Fourier components

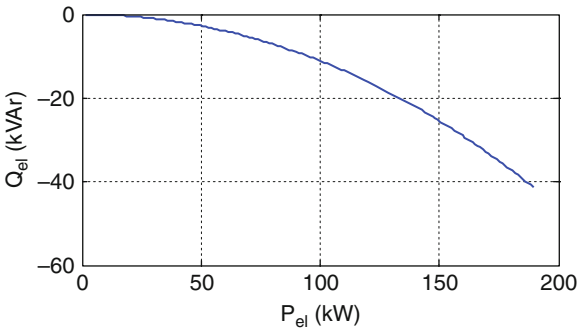

Wind Power Generator Systems and Local Power System Interconnection. Figure 36
Reactive power consumption as a function of active power for a traditional 180 kW wind turbine generator. Phase-compensating capacitors are installed compensating for the no-load consumption of reactive power by the wind turbine induction generator

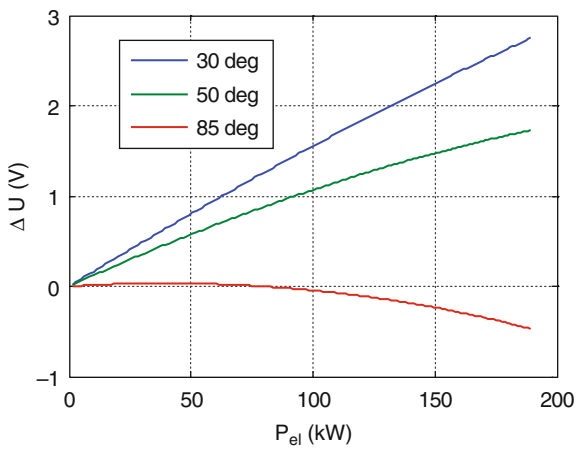

Wind Power Generator Systems and Local Power System Interconnection. Figure 37
Voltage level influence of a traditional fixed-speed wind turbine on a network with a grid strength of 20 times the rating of the wind turbines. Three different grid angles, Ψ_{sc}

level down, the voltage level will now be slightly higher given the same active power production.

Flicker Emission

Due to the inability of the fixed-speed systems to take up an incoming increase in the torque to the generator

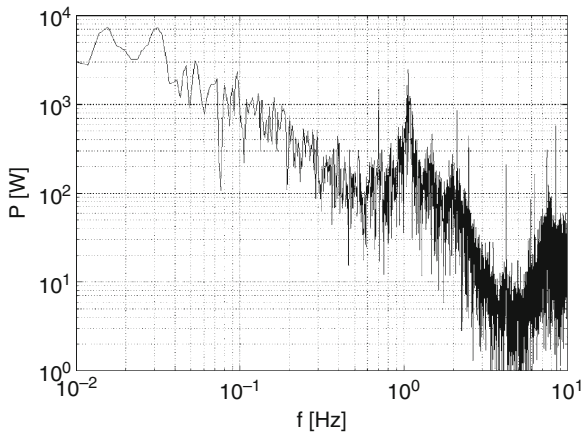

Wind Power Generator Systems and Local Power System Interconnection. Figure 38
Output power spectrum of a fixed-speed wind turbine

by adjusting the rotor speed, these torque variations go through the system. In Fig. 38, the power spectrum from a fixed-speed turbine is presented.

The reactive power will also vary and the consequence is of course that the voltage level on the adjacent network will vary. In Fig. 39, such a variation is presented close to a wind park consisting of three 180 kW turbines in a rural area.

In order to validate the severity of this pulsation, it is decomposed into its frequency components and presented as a function of fluctuation frequency together with the flicker limit line in Fig. 40.

There are several reasons for the unevenness of the power. The major reason is that the wind speed changes and thus the power production. In addition, the wind speed over the rotor disc is not constant, instead the wind speed across the rotor disc varies, and when the rotor rotates in this wind field, power pulsations are created. Figure 41 tries to illustrate this behavior.

Apart from the variations that originate from the fluctuations that come from the wind, the turbine in itself as well as the generator also contribute to the output power spectrum.

Important to mention is that not only the turbine itself creates a flicker impact, the adjacent grid will also contain variations that through the turbine becomes flicker. Typically, this is the case for higher frequencies, [14].

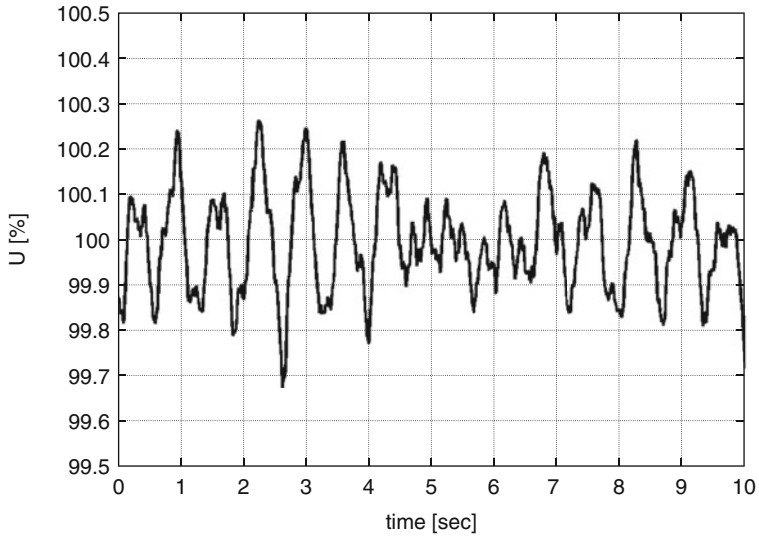

Wind Power Generator Systems and Local Power System Interconnection. Figure 39
Voltage level variations close to an older fixed-speed wind turbine

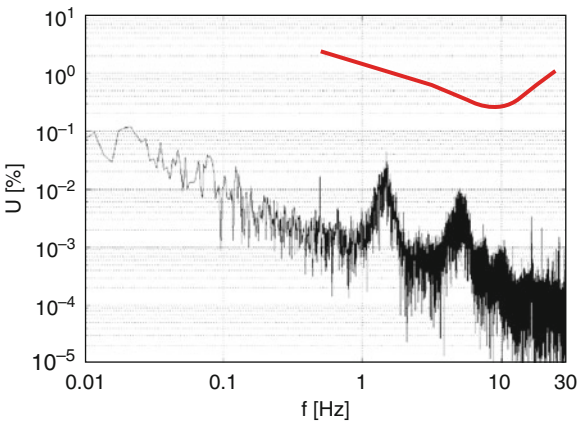

Wind Power Generator Systems and Local Power System Interconnection. Figure 40
Voltage spectrum close to a fixed-speed turbine and in red the flicker limit

The flicker coefficients were earlier up to about 8 for fixed-speed turbines, but today the flicker coefficients are usually lower.

For a variable-speed turbine, the incoming mechanical power has the same behavior. However, a very important aspect is that for the variable-speed turbines, this torque/power variation is taken up by small rotor speed adjustments, and the power pulsations do not come out to the grid. Accordingly, these "rotational-formed oscillations" are not visible in the output power from variable-speed turbines.

Special Considerations for the Start-up of a Fixed-Speed System

When a fixed-speed wind turbine is to be connected to the grid, the generator needs to be magnetized, which gives rise to a high current, seen in Fig. 42 below between 1 and 2 s.

Thanks to the soft-starter, the current is limited to a value below the rated current which in this case was a peak value of 400 A. Between 2 and 3 s the no-load-current of the generator can be observed. Then at the time instants 3.3 and 4.2 s two capacitor stages are connected and the current finally almost become zero. The consequence on the voltage level during the connection then becomes as presented in Fig. 43.

In IEC-61400-21 it is stated that a voltage change factor and a flicker step factor shall be determined. For variable-speed turbines, these coefficients become rather unimportant; however, for fixed-speed turbines they can be a limiting factor regarding the installation of such a turbine on a weak network.

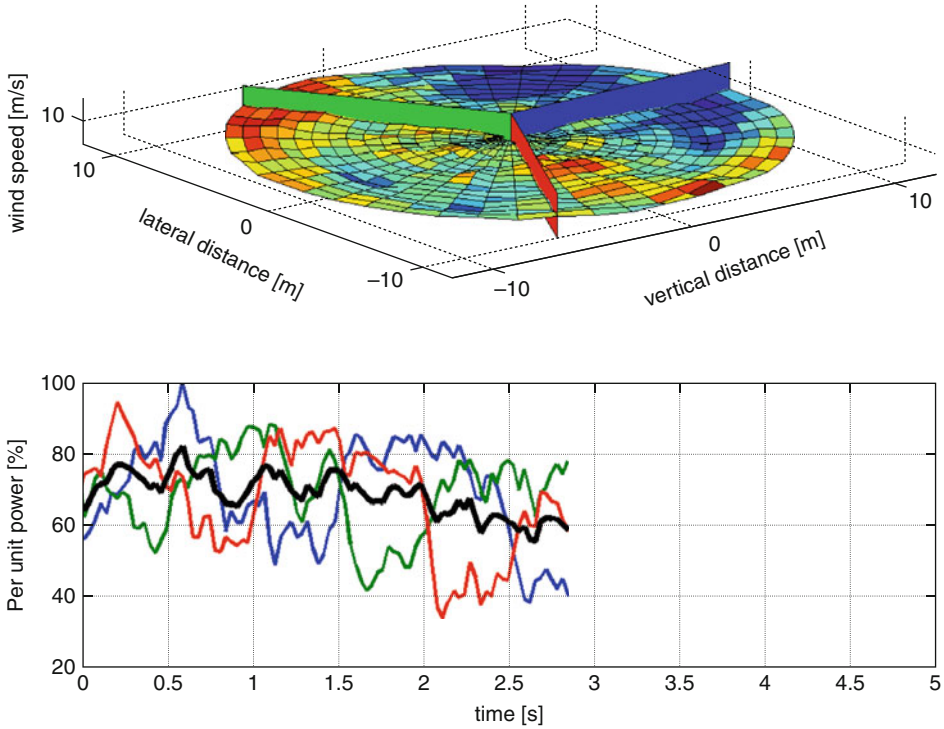

Wind Power Generator Systems and Local Power System Interconnection. Figure 41
Blade rotation and resulting torque forming on the individual blades as well as the average torque formation

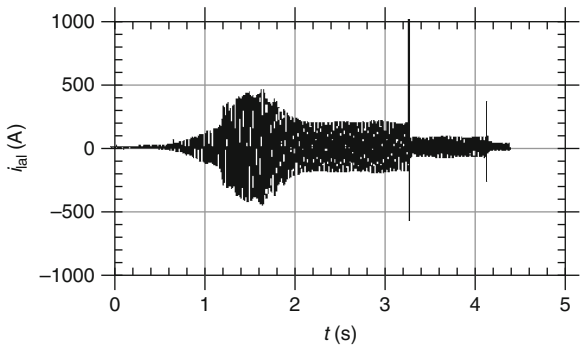

Wind Power Generator Systems and Local Power System Interconnection. Figure 42
Inrush current when connecting a traditional fixed-speed wind turbine

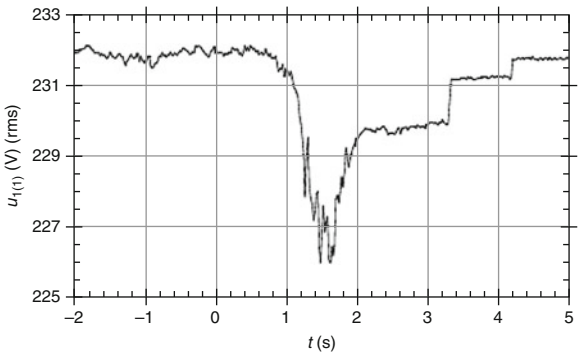

Wind Power Generator Systems and Local Power System Interconnection. Figure 43
Voltage level during the connection of a traditional fixed-speed turbine, ratio between Pn/Ssc is around 40

DFIG and Full Converter Turbines

Steady-State Influence

The variable-speed systems have an excellent reactive power control ability which can be used for voltage control, but it is seldom utilized today. Using a power factor (PF) of one, the voltage level influence then becomes as presented in Fig. 44, using a grid strength 20 times the rating of the wind turbine. However, by using a variable power factor, as the traditional

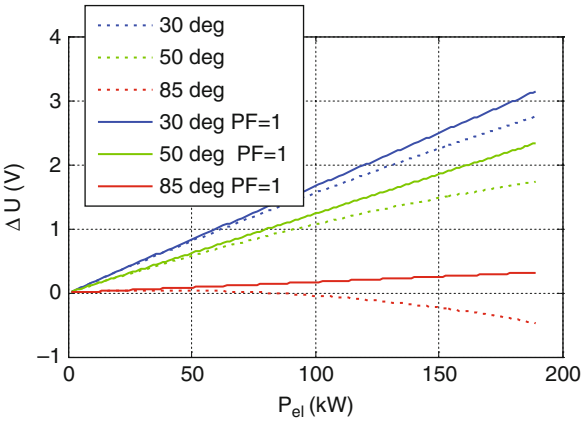

Wind Power Generator Systems and Local Power System Interconnection. Figure 44
Voltage level influence by a fixed-speed (*dashed*) and variable-speed (or modern fixed-speed) wind turbine (*solid*). The fixed-speed turbine is assumed to have a variable power factor while the variable-speed turbine is assumed to have a constant power factor of 1

fixed-speed turbines, at least the older ones do, the voltage variations are actually lower, as seen in the figure. As long as the maximum current level of the turbine or line is reached, it is possible to completely eliminate the voltage variations due to the varying power production, by an appropriately selected reactive power injection.

If a system is designed to have an extra reactive power ability, apart from the voltage level control, this can also be useful during fault situations, and the electrical system must in some parts be rated to handle a higher current.

In the DFIG system, reactive current and thus reactive power can easily be generated through the generator, while the full-power system needs a larger grid side converter to produce reactive power for the grid. This is especially true when the wind turbine is operating at full power, then there is in the original design no room for reactive power production. For a full-power converter system an over dimensioning of the grid side converter by 8% gives a possibility to produce or consume more than 40% reactive power also at rated power operation. One large manufacturer of full-power converter wind turbines has a grid side converter that has a 40% over current capacity. For the DFIG it is also possible to generate reactive power, however, not as easily using the grid side converter as for the full-power converter system.

At lower wind speeds, the turbine can consume or produce reactive power without an over-dimensioned grid side converter.

An interesting possibility is thus that a DFIG or full-power converter wind turbine system can act as a STATCOM when the wind turbine is standing still due to low wind.

Flicker Emission

Variable-speed turbines have the ability to control the rotor speed. In this way, the disturbances that originate from the wind as well as from the mechanical design of the turbine can be taken up as speed variations. In case the speed variations become too large (in particular that the rotor speed becomes too high at high wind speeds), the pitch control can be used to take the turbine back to proper rotor speeds. In addition, the converter also makes it possible to reduce the wind generating system's response to disturbances that are already existing in the grid. The result is that variable-speed turbines have flicker coefficients, c_f, of between 1.5 and 4, define depending on the grid impedance angle and average wind speed.

Active Power Control for Wind Turbines

Normally wind turbines are not used for load leveling, since this would mean loss of produced energy. However, with the exception of fixed-speed turbines without pitch control mechanism, wind turbines can be used for this purpose (as spinning reserve), but, this requires that the turbines are not operating at their maximum power production point, but instead with a reduced value. In the case that the network needs more power, the production can now be increased to the maximum one.

Already, grid codes, for instance that of ELTRA, suggest that this feature should be included in the control of a wind turbine, at least if it is a part of a large wind farm.

Harmonic Current Emission from Wind Turbines

Fixed-speed turbines emit harmonic currents mainly because voltage harmonics exist in the grid and these

are "mirrowed" in the current coming out of the generating system. In addition, the electric generator in itself also contributes with harmonic currents, since the design cannot be completely sinusoidal. However, these harmonic current emission levels are usually very low.

Converter-operated wind turbines, of course emit harmonics, since they are equipped with power electronic converters.

Full-power converter systems typically inject harmonic currents having a frequency of one or a couple of kHz. The turbines are equipped with harmonic filters, so that the current emissions are below the ones stipulated in the standards. Figure 45 depicts the harmonic current emission from a wind farm consisting of seven variable-speed wind turbines.

From the figure, it can be noted that generally the total harmonic current distortion is below 1.3% for this wind farm, which is a level far below usual limits.

Behavior During Network Faults

Fault Behavior and Requirement on Fault Behavior

Also during deviations in voltage and frequency, the wind turbines should continue to stay on line. For various regions, the valid grid code put requirements of the immunity level toward voltage and frequency deviation that the wind energy installation should be able to cope with. One example, however valid for a whole wind farm connected to a high voltage level from E.ON Netz is shown in Fig. 46.

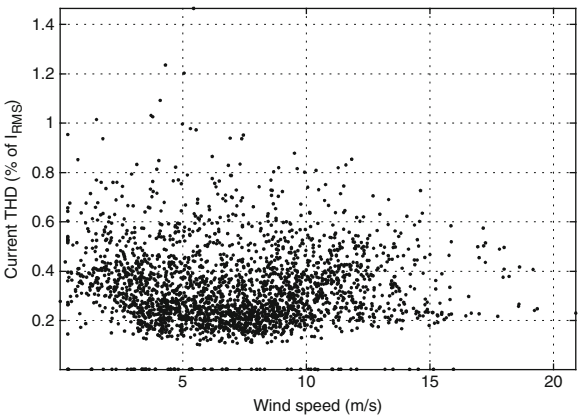

Wind Power Generator Systems and Local Power System Interconnection. Figure 45
Total harmonic current distortion (THD_i) from a wind farm consisting of seven variable-speed wind turbines

Although this requirement is for a large wind farm, at the end it still puts the demands on the individual wind turbines.

For each country, there is a specific grid code that states a reference voltage dip curve which future wind energy installations must be able to handle (Ride Through). Some grid codes specify the voltage curve at the PCC (Point of Common Connection, which means where the wind turbine installation is connected to the grid) while others, for example, the Swedish, states certain points in the main national network, in the Swedish system, the meshed 400 kV-system. If the grid codes specify the voltage behavior immunity level at PCC, it means that potential wind energy installation installers accordingly must do more advanced calculations (dynamic simulations) to check that their installation will meet this requirement. Depending on the various regions, there are different demands that shall be fulfilled. In Fig. 47, some examples are given.

Fixed-Speed System

The response of a fixed-speed wind turbine is much dominated by the direct connection between drive train, generator, and grid. As induction generators in general, a reduced grid voltage may lead to excessive reactive power consumption by the turbine if the wind speed is somewhat high. In addition, there is a risk that a fixed-speed turbine can overspeed in case of a too low voltage, due to the fact that the electromagnetic ability of an induction generator deteriorates quickly at lower grid voltages.

Whenever there is a quicker change in the supplying voltage, the generating system of the wind turbine reacts strongly. The fixed-speed system contributes with a fault current according to an induction motor, but driven with a negative load. Again, the system has a limited ability to control the fault currents. In Fig. 48, the measured response to a fairly small voltage disturbance for a fixed-speed wind turbine is presented. As can be noted in the figure, the resulting electric output power oscillations range up to rated power, although the voltage dip is not unusually large, only about 10%. The real consequence is if the voltage adjacent to the

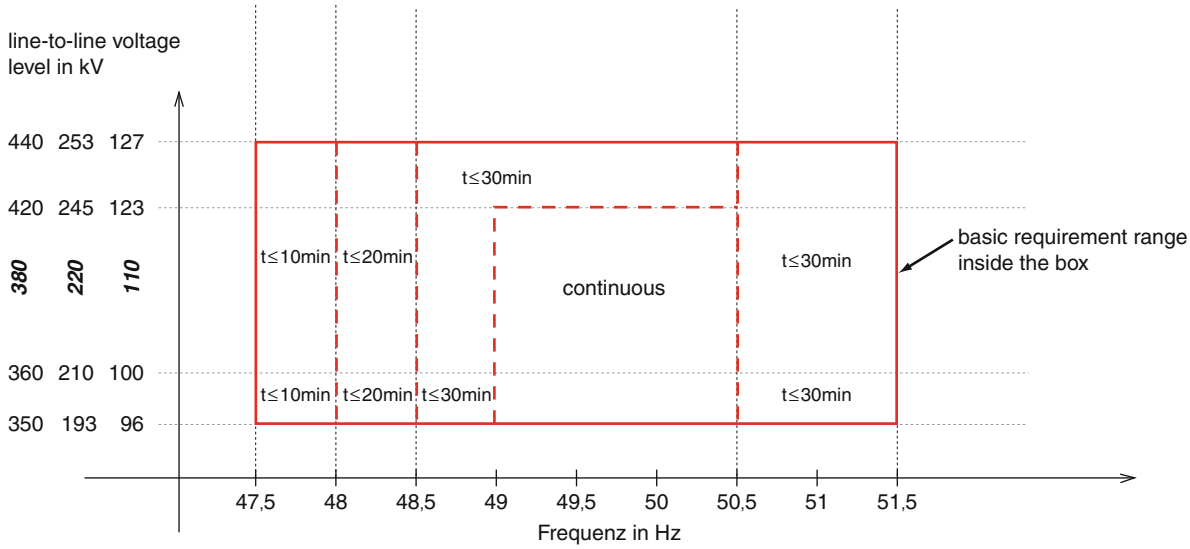

Wind Power Generator Systems and Local Power System Interconnection. Figure 46
Operational requirements regarding staying on line as a function of voltage level and frequency

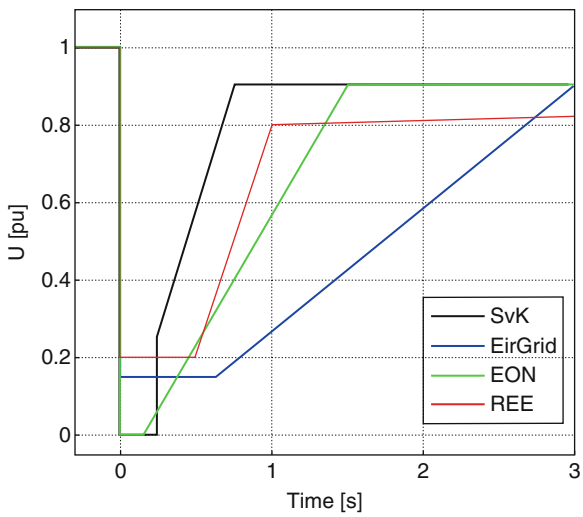

Wind Power Generator Systems and Local Power System Interconnection. Figure 47
Examples of required under-voltage immunity for wind energy installations

turbine is influenced in such a way that it would disturb customers. And, in the example presented in Fig. 48, the turbine response would NOT cause any noticeable problems for nearby customers.

No recording of a short-circuit for fixed-speed wind turbine was available. In Fig. 49, the result from a 15 kW machine exposed to a three-phase short-circuit is presented. In the figure, the currents are presented instead of the power. The peak currents are about seven times the rated ones. In this case, the voltage on the adjacent grid is anyway very severely disturbed, so the currents taken by the induction machine do not deteriorate the voltage quality for the nearby customers further. However, the wind turbine would be severely disturbed and would have to be disconnected from the electrical network. Overspeeding and overcurrent could damage the fixed-speed turbine. However, newer regulations today about under-voltage immunity, put harder restrictions on the wind turbines, also fix-speed ones, regarding whether the turbine is allowed to disconnect or not.

Earlier fixed-speed systems could not ride-through voltage disturbances. However, today a large manufacturer of a fixed-speed system provides a ride-through facility that is sufficient for the whole of Europe.

Fixed-Speed System with Active Pitch Mechanism

The fixed-speed systems with active pitching mechanism can to some extent use the pitch controller to provide a varying output that can be used to counteract a need from the grid. It is possible to change from 100% to 20% production within a couple of seconds. Till date, the turbines have not been designed for power/frequency control.

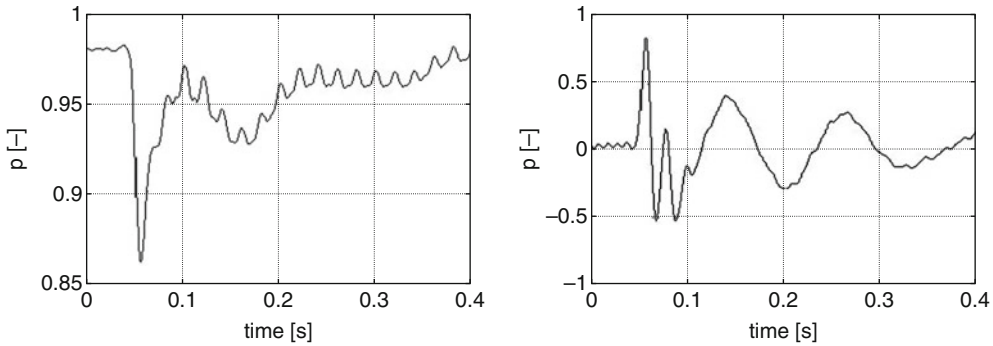

Wind Power Generator Systems and Local Power System Interconnection. Figure 48
Voltage magnitude and resulting electric power response for a fixed-speed turbine

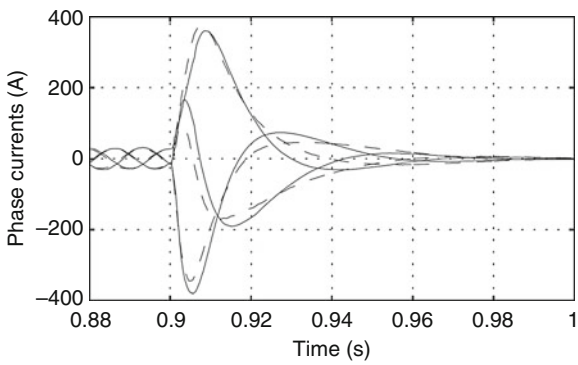

Wind Power Generator Systems and Local Power System Interconnection. Figure 49
Currents from a 15 kW machine following on a three-phase short-circuit, solid lines are measurements and dashed lines are simulated values

DFIG System

The immunity toward grid disturbance is for the standard DFIG turbine low, due to the small rotor converter used in this system. At a larger voltage dip, the rotor currents become too large. Only dips with a remaining voltage higher than 75–85% could be handled. In the original DFIG system the fault currents were similar or worse than for a fixed-speed system. When a larger fault occurred, this turbine had to quickly (within about 40 ms) be disconnected from the network. In Fig. 50, the response to a smaller voltage dip is presented and in Fig. 51 the response to a short-circuit. The smaller voltage dip is as noted, very well handled by the DFIG system, while the short-circuit, the turbine cannot handle.

In order to improve the immunity level to deal with the new grid codes, additional equipment must be added.

When the turbine is not allowed to be disconnected due to a disturbance, there is a surplus of power that will lead to overvoltages in the power electronics. The surplus of power is caused by the fact that when the voltage is low, the power that can be fed out into the electrical network is limited, since the current cannot be higher that the rated one. If the voltage is 0, no power can be fed out to the network. Then two things can be done. One is that the turbine is allowed to speed up a bit while the pitch goes into action and reduces the incoming power. When the voltage returns, the turbine can be pitched back to its pre-fault operating condition. However, this takes a while which is undesirable since from a power network stability point of view, it is desirable to have the pre-fault power production immediately when the voltage returns. Instead an alternative approach can be used. If the incoming power is kept constant, then the difference toward the power that can be fed out into the network can instead be dissipated by the turbine. For this purpose, typically power-electronic controlled resistors "breaking choppers" can be used.

Changes that can achieve this functionality are the insertion of power-electronic controlled resistors in the power electronic circuits, as mentioned above, or by using over-dimensioned power semiconductors. In Fig. 52 below a crude scheme for a ride-through system for a DFIG turbine is presented. A key component in the ride-through systems is the "breaking chopper" where the power that cannot be supplied into the grid

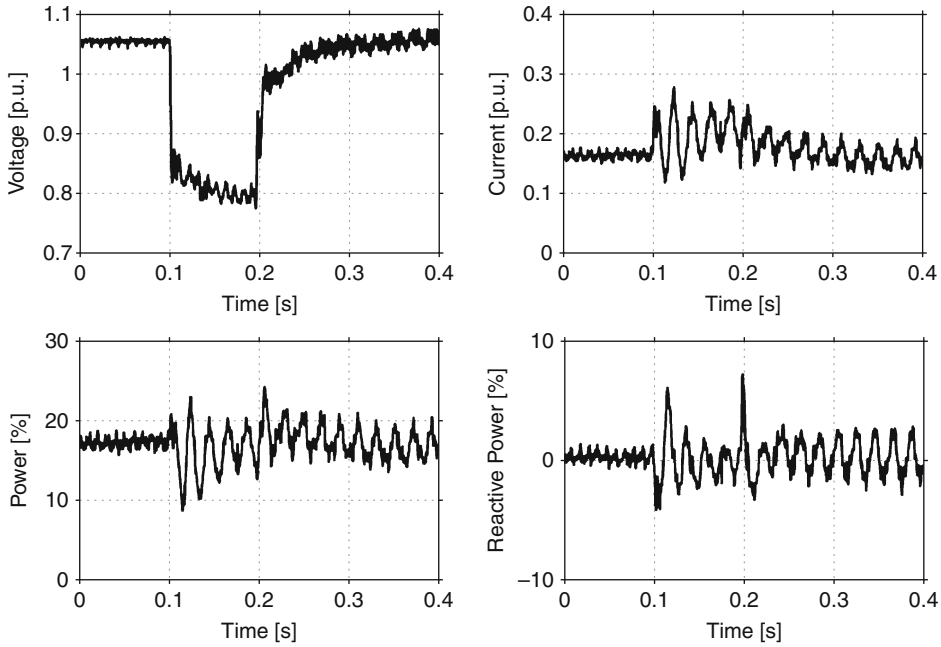

Wind Power Generator Systems and Local Power System Interconnection. Figure 50
Measured response to a minor voltage dip by a DFIG system

during the disturbance is dissipated. The breaking chopper can also be located on the AC-side.

In Fig. 53, a photo of the DC-link chopper is presented for such a system.

A photo of the AC-side crowbar for a wind turbine equipped with under-voltage immunity functionality is presented in Fig. 54.

These additions can nowadays (2011) be considered as state of the art. In Fig. 55, a recorded voltage waveform on a 2 MW DFIG system with a ride-through ability function is presented.

The current through the breaking chopper has the appearance as presented in Fig. 56 during the fault.

The resulting active and reactive power response is depicted in Fig. 57.

From the figure, it can be noted that the turbine very well manages to handle this voltage disturbance.

Full-Power Converter System

Any suitable fault current can be provided as long as the current rating of the converter valves is not exceeded. Observe that the contribution to the short-circuit power of the grid usually is much lower for a variable-speed wind turbine than for a conventional synchronous generator connected directly toward the grid. This means that since a modern wind turbine with full-power converter has a very low fault current, it will be required to perform a review of the protection settings if such turbines are to be installed into a system in great numbers.

Comparison of Systems

Comparisons of the various systems can be found in literature, so they will not be repeated here, and also the fact that in order to improve the grid performance several improvements have been made during the years, blending the properties of the system, leads to the fact that no such comparison is shown here.

The most important question is "What is the cost for each produced kWh for a unit that fulfills the grid codes," and all systems can be made to fulfill the requirements, so it is mainly an issue of cost. For all systems there exist technical solutions, often using power electronics to obtain the desired performance.

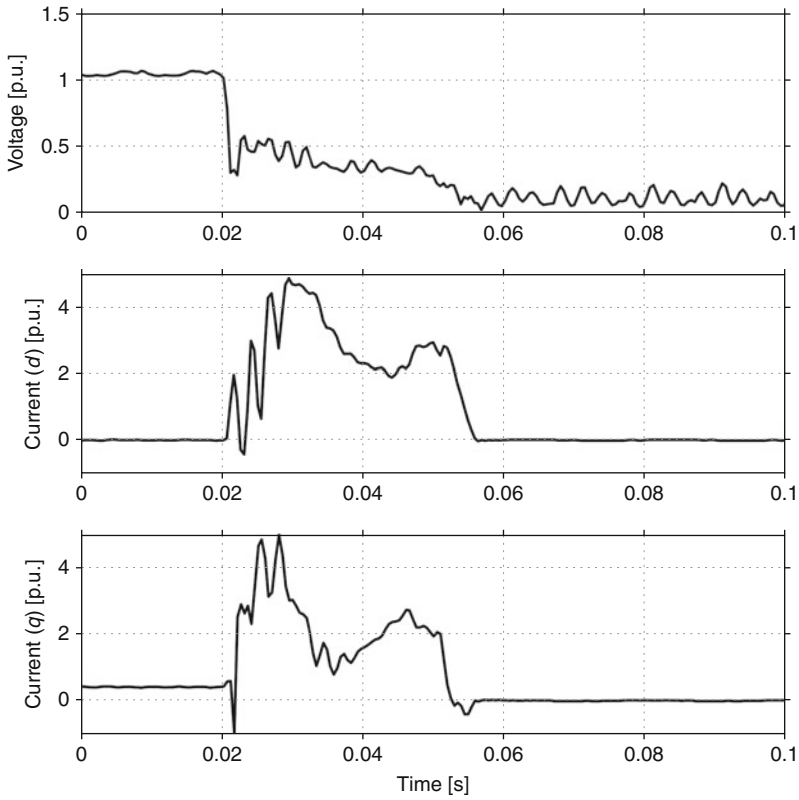

Wind Power Generator Systems and Local Power System Interconnection. Figure 51
Measured response to a larger voltage dip (a short-circuit in the feeder) by a DFIG system

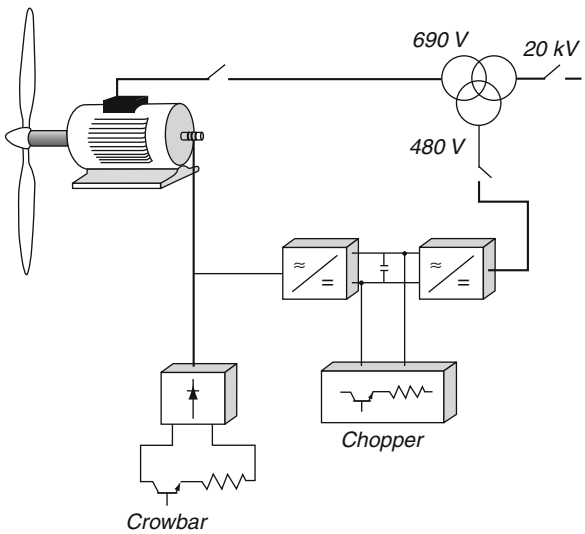

Wind Power Generator Systems and Local Power System Interconnection. Figure 52
Example of a ride-through system of a DFIG wind turbine system

Future Directions

It is never easy to predict what will happen in the future, but some qualified guesses are possible to make. For sure the wind turbines will continue to increase in sizes, but where the upper economical size will be in the future, is not easy to predict. Moreover, the trend that more and more wind turbines will be power electronic driven seems also to be continuing. The reduction of losses in power electronic components could lead to the condition that the full-power converter system could be more favorable compared to the DFIG system. The permanent-magnet multipole generators seem from a research point of view to have a great potential; however, they today (2011) seem not yet to have reached industrial readiness at full scale.

Today (2011) there exist usually generating systems with a full-range gearbox (around three gearing stages) or no gearbox with a machine with a high number of poles. A possible development in the future is

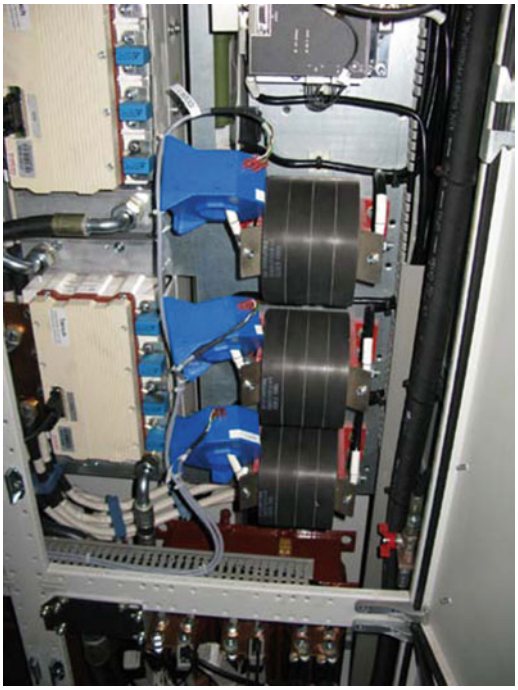

Wind Power Generator Systems and Local Power System Interconnection. Figure 53
Breaking resistors on the DC-link, black round "cans" in the left part of the picture. Blue objects are current sensors and the white plastic covers contain the transistors used to control the current through the breaking resistors

Wind Power Generator Systems and Local Power System Interconnection. Figure 54
AC-crowbar, at the bottom of the picture

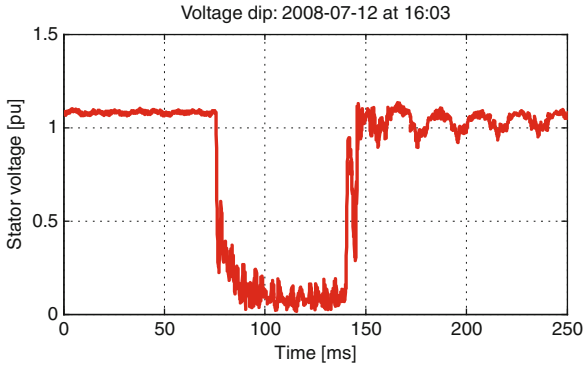

Wind Power Generator Systems and Local Power System Interconnection. Figure 55
Voltage waveform on July 3, 2008, on a DFIG turbine

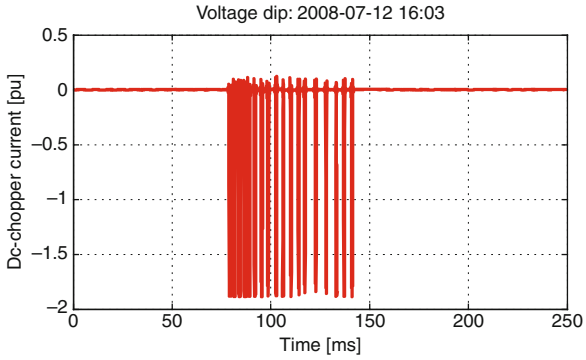

Wind Power Generator Systems and Local Power System Interconnection. Figure 56
Current through the breaking chopper

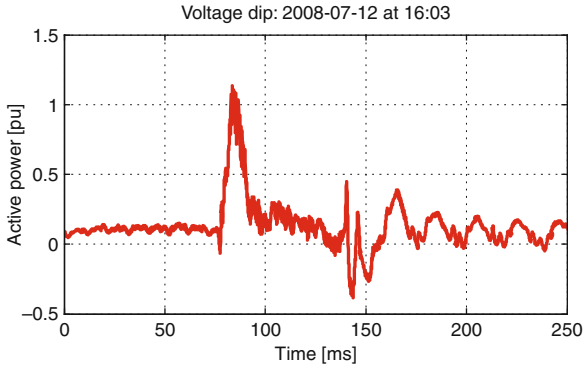

Wind Power Generator Systems and Local Power System Interconnection. Figure 57
Active and reactive power response due to a voltage dip down to almost 0% remaining voltage

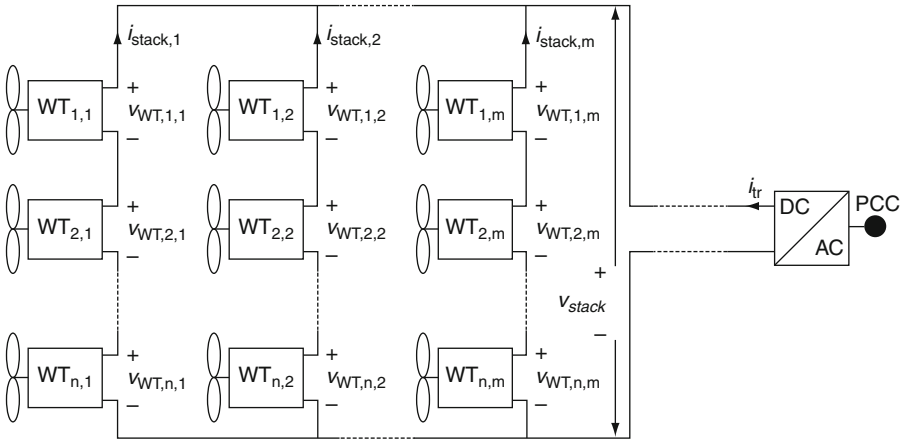

Wind Power Generator Systems and Local Power System Interconnection. Figure 58
Series DC wind park

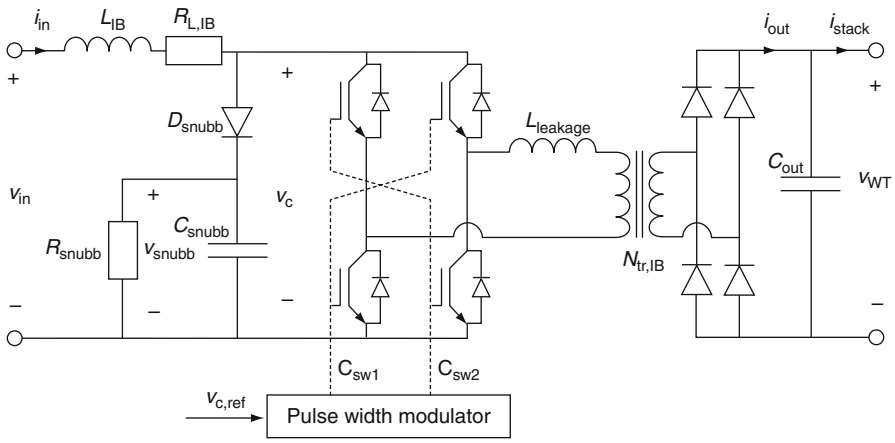

Wind Power Generator Systems and Local Power System Interconnection. Figure 59
Full bridge isolated boost converter suitable for a wind turbine with DC as output

that machines and gearboxes could become more integrated, and also perhaps one or two gearing stages could be combined with machines having an intermediate number of poles.

A possible future that means greater changes compared to the ones that have been mentioned above, is that HVDC-networks might be a reality in future sea-based wind farms. In such a case, the generating systems should be designed in such a way that they feed out DC in an appropriate way. In [16] a system based on wind turbines connected in series on their DC-outputs is presented according to Fig. 58.

In Fig. 59, an example of how the converter system for such a "DC wind turbine" could look like is presented.

Abbreviations

AC	Alternating current
DC	Direct current
IM	Induction machine
PE	Power electronics
PF	Power factor
THD	Total harmonic distortion

$\mathbf{THD_i}$	Total harmonic distortion for the current
$\mathbf{X(n)}$	Harmonic number

List of Commonly Used Variables

A	Area [m^2] real quantity
B	Magnetic flux [T] imaginary quantity
C	Capacitance [F]
F	Force [Nm]
C_p	Aerodynamic power coefficient
I	Current [A]
I	Complex current vector [A]
I_{active} $I_{reactive}$ $= I_q$ I_d	Active (quadrature axis) and reactive (direct axis) current [A]
J	Inertia [kgm^2]
L	Inductance [H]
N	Number of turbines
N_1, N_2	Number of turns in a transformer
P_{conv}	Power transmitted by a converter [W]
P_e P	Electric power [W]
P_{st}	Short-term flicker severity index
$P_{st,ind}$	Short-term flicker severity index individual turbine
P_{lt}	Long-term flicker severity index
P_{loss}	Power loss [W]
P_{mech}	Mechanical power [W]
P_R, P_S, P_{total}	Rotor, stator, and total power [W]
P_w	Available power in the wind [W]
Q_e Q	Reactive current [VA]
R	Resistance [Ω] radius [m]
R_L	Line resistance [Ω]
R_{sc}	Short-circuit resistance [Ω]
S	Slip
S	Apparent power [kVA]
S_{sc}	Short-circuit capacity [VA]
$S_{sc\ fic}$	Fictitious short-circuit capacity [VA]
S_n	Rating of wind energy installation [VA]
T	Torque [Nm]
T_e	Electrodynamical torque [Nm]
T_s	Shaft torque [Nm]
T_w	Wind torque [Nm]
U	Voltage [V]
U	Complex voltage vector [V]
U_1, U_2	Primary and secondary voltage [V]
U_N	Rated voltage [V]
U_R, U_S	Rotor and stator voltage [V]
$\hat{U}$ U_{rms}	Peak and rms-value of voltage [V]
V_{dc}	DC-link voltage [V]
W	Energy [Ws]
WS	Wind speed [m/s]
X	Reactance [Ω]
X_L	Line reactance [Ω]
X_{sc}	Short-circuit reactance [Ω]
Z_L	Line impedance [Ω]
Z_{sc}	Short-circuit impedance [Ω]
c_f	Flicker coefficient
e	Induced voltage [V]
i_r i_s i_t	Phase currents [A]
n	Rotational speed [rpm]
p	Instantaneous power [W] pole-pair number
r	Distance [m]
t *time*	Time [s]
u_r u_s u_t	Phase voltages [V]
ΔU	Voltage variation [V]
Φ	Phase angle between voltage and current [Degree]
Ψ	Flux [Wb]
Ψ_{sc}	Short-circuit angle [Degree]
Ψ_s, Ψ_r, Ψ_m	Stator rotor, magnetizing flux linkage ("flux") [Wb]
Ω_m	Rotor speed [rad/s]
δ	Load angle [deg]
λ	Tip-speed ratio
ω	Speed [rad/s]
ω_{el}	Electrical speed [rad/s]
ω_s	Synchronous speed [rad/s]

Bibliography

Primary Literature

1. Vestergaaard J, Brnadstrup L, Goddard RD (2004) A brief history of the wind turbine industries in Denmark and the United States. In: Academy of International Business (Southeast USA Chapter) conference proceedings, November 2004, pp 322–327
2. Dorf RC, Svoboda JA (2004) Introduction to electric circuits, 6th edn. Wiley, New York. ISBN 0-471-44795-1
3. Mohan N, Undeland T, Robbins W (2003) Power electronics. Wiley, New York. ISBN 0-471-22693-9
4. Cheng DK (1993) Fundamentals of engineering electromagnetics. Prentice Hall, Upper Saddle River. ISBN 0-201-56611-7
5. Hughes A (2009) Motors and drives-fundamentals, types and applications. Elsevier. ISBN-13: 978-0-7506-4718-2
6. Mohan N (2003) Electric drives – An integrative approach. MNPERE. ISBN 0-9715292-1-3

7. Krishnan R (2001) Electric motor drives-modelling, analysis and control. Prentice-Hall. ISBN: 0-13-0910147
8. Heier S (1998) Wind energy conversion systems. Wiley, New York. ISBN: 0 471 97143 X
9. Petersson A (2003) Modeling and control of doubly-fed induction generators for wind turbines. Licentiate thesis, Department of electric power engineering, Chalmers University of Technology, Göteborg, Sweden
10. Grauers A (1996) Design of directly driven permanent magnet generators for wind turbines. Doctoral thesis, Chalmers University of Technology, Gothenburg, Sweden
11. Petersson A et al (2005) Modeling and experimental verification of grid interaction of a DFIG wind turbine. IEEE Trans Energy Conver 20(4):878–886
12. IEC 61000-4-15, Testing and measurement techniques – Flickermeter – Functional and design specifications. Advanced Test Equipment Corp, San Diego, CA
13. IEC Standard 61400–21 (2001) Wind turbines measurement and assessment of power quality characteristics of grid connected wind turbines, 1st edn. Bureau Central de la IEC/CEI, Genéve
14. Thiringer T, Petru T, Lundberg S (2004) Flicker contribution from wind turbine installations. IEEE Trans Energy Conver 19(1):157–163
15. Thiringer T (1996) Power quality measurements performed on a low-voltage grid equipped with two wind turbines. IEEE Trans Energy Conver 11(3):601–606
16. Lundberg S, Thiringer T (2009) Design considerations for a power electronic converter for series connection of wind turbines. In: Second EPE – Wind energy chapter seminar, April 23–24, 2009, Royal Institute of Technology, Stockholm, Sweden
17. Thiringer T (2007) Experimental experiences of the summation of flicker contribution from individual wind turbines in a wind park. In: 9th international conference on energy and power systems, IASTED 2007, Clearwater, Florida, USA. January 3–5

Books and Reviews

Abdulahovic T (2009) Analysis of high-frequency electrical transients in offshore wind parks. Thesis, Department of electric power engineering, Chalmers University of Technology, Göteborg, Sweden

Ackermann T (2005) Wind power in power systems. Wiley, Chichester

Akhmatov V, Eriksen PB (2007) A large wind power system in almost island operation – A Danish case study. IEEE Trans Power Syst 22(3):937–943

Bollen MHJ, Gu IYH (2006) Signal processing of power quality disturbances. Wiley, Canada

Bongiorno M, Petersson A (2009) Development of a method for evaluation of wind turbines ability to fulfil Swedish grid codes. Elforsk report 09:25, Elforsk, Frederiksberg

Burton T et al (2001) Wind energy handbook. Wiley, Chichester

Cardell JB, Anderson CL (2009) Estimating the system costs of wind power forecast uncertainty. In: IEEE power & energy society general meeting, 2009. PES '09, 26–30 July 2009

Chen Y, He Y, Bao Y, Shen J (2008) Present situation and future development of wind power in China. In: 3rd IEEE conference on industrial electronics and applications, 2008. ICIEA 2008, 3–5 June 2008

Dell RM, Rand AJ (2004) Clean energy. Royal Society of Chemistry, Cambridge

Elkington K (2009) Modelling and control of doubly fed induction generators in power systems. Royal Institute of Technology, Stockholm, Sweden

Evans J, Shawwash Z (2009) Assessing the benefits of wind power curtailment in a hydro-dominated power system. In: CIGRE/IEEE PES joint symposium on integration of wide-scale renewable resources into the power delivery system, 2009, 29–31 July 2009

Fadaeinedjad R, Moallem M, Moschopoulos G, Bassan S (2007) Flicker contribution of a wind power plant with single and multiple turbine representations. In: IEEE electrical power conference, 2007. EPC 2007, Canada, 25–26 Oct. 2007

Fang C (2009) Practical problems and coping strategies of wind power industry in China. In: World non-grid-connected wind power and energy conference, 2009. WNWEC, Nanjing, 24–26 Sep 2009

Fang C, Bao C, Qi W (2009) The construction goals and spatial layout project of the offshore three Green Gorges in China. In: World non-grid-connected wind power and energy conference, 2009. WNWEC, Nanjing, 24–26 Sep 2009

Fuchs E, Masoum M (2008) Power quality in power systems and electrical machines. Academic Press, Burlington, MA

Gasch R, Twele J (2004) Wind power plants: fundamentals, design, construction and operation. Earthscan Publications, London

Gipe P (2002) Wind power in view wind turbines, aesthetics, and public acceptance. Academic Press, San Diego, CA

Gipe P (2004) Wind power: renewable energy for home, farm, and business. James & James, UK

Gu M (2009) Research on strategic importance of non-grid-connected wind power for U.S. energy development. In: World non-grid-connected wind power and energy conference, 2009. WNWEC, Nanjing, 24–26 Sep 2009

Gu L, Jin C (2009) Performance evaluation of non-grid-connected wind, power industry cluster. In: World non-grid-connected wind power and energy conference, 2009. WNWEC, Nanjing, 24–26 Sep 2009

Hau E (2006) Wind turbines – fundamentals, technologies, application, economics. Springer, New York

He A, Yan Z, Gu W (2009) Research on non-grid-connected wind power systems used for hydrogen production from water-electrolytic. In: World non-grid-connected wind power and energy conference, 2009. WNWEC, Nanjing, 24–26 Sep 2009

Heier S (2009) Grid integration of wind energy conversion systems, Wiley, New York

Hoffman DL, Molinski TS (2009) How new technology developments will lower wind energy costs. In: CIGRE/IEEE PES Joint

symposium on integration of wide-scale renewable resources into the power delivery system, 2009, 29–31 July 2009

Holmgren M, Haarla L, Matilainen J, Holttinen H (2009) Power regulation resources required by wind power in Finland and regulation characteristics of power plants. In: CIGRE/IEEE PES joint symposium on integration of wide-scale renewable resources into the power delivery system, 2009, 29–31 July 2009

Holttinen H et al (2009) Design and operation of power systems with large amounts of wind power. Final report, IEA WIND Task 25. VTT technical research centre, Finland

Jin J, Chen Q, Ma Y, Gong C (2009) Non-grid-connected wind power system and its high power DC-DC converter. In: World non-grid-connected wind power and energy conference, 2009. WNWEC, 24–26 Sept 2009

Kai T, Tanaka A (2008) A new smooth scheme for power fluctuation using inverter of wind power generation with doubly fed induction generator. In: International conference on electrical machines and systems, 2008. ICEMS 2008. Wuhan, China

Keeley G (2009) Spain's wind turbines supply half of the national power grid. *The Times*, 10 November 2009

Kundur P (1993) Power system stability and control. McGraw-Hill, New York

Li M (2009) A study on the exploitation of wind energy and the development of the non-grid-connected wind power industry in central China. In: World non-grid-connected wind power and energy conference, 2009. WNWEC, Nanjing, 24–26 Sep 2009

Li M, Fang C (2009) Information system of on-grid and non-grid-connected wind power industry based on SuperMap. In: World non-grid-connected wind power and energy conference, 2009. WNWEC, Nanjing, 24–26 Sep 2009

Li DD, Niu LQ (2008) Reliability analysis of electric distribution system integrated with wind power. In: 3rd IEEE conference on industrial electronics and applications, 2008. ICIEA 2008, 3–5 June 2008

Ming L, Xiong F, Yue W, Leqiang Z, Zhaoan W, Gang L, Weizheng Y (2009) Overvoltage protection of high power IGBTs in wind power converters under short circuit. In: IEEE 6th international power electronics and motion control conference, 2009. IPEMC '09, 17–20 May 2009

Lin HC (2006) On line web-based maximum wind power monitoring and control system. In: IEEE international conference on systems, man and cybernetics, 2006. SMC '06, vol 5, 8–11 Oct 2006

Liu J, Schweizer D, Seiler K (2009) Wind power interconnection and integration roadmap: An RTO's perspective. In: IEEE power & energy society general meeting, 2009. PES '09, Calgary, 26–30 July 2009

Lobo MG, Sanchez I (2009) Aggregated wind power prediction methods based on distances between weather forecasting vectors. In: International conference on clean electrical power, 2009, 9–11 June 2009

Luickx PJ, Delarue ED, D'haeseleer WD (2009) Effect of the generation mix on wind power introduction. IET Renew Power Gener 3(3):267–278

Manwell et al (2002) Wind energy explained – theory, design and application. Wiley, Chichester (Recent years have seen a growth in the implementation and economic viability of wind energy technology. This safe and abundant source of clean, renewable energy is now making a significant contribution to electricity supplies worldwide. Addressing the growing requirement for information on the theory and practical application of wind technology, Wind Energy Explained provides a through introduction to this multi-disciplinary field)

Max L (2009) Design and control of a DC collection grid for a wind farm. Thesis, Department of electric power engineering, Chalmers University of Technology, Göteborg, Sweden

Meei-Song K (2007) Generation cost assessment of an isolated power system with a fuzzy wind power generation model. IEEE Trans Energy Conversion 22(2):397–404

Meibom P, Weber C, Barth R, Brand H (2009) Operational costs induced by fluctuating wind power production in Germany and Scandinavia. IET Renew Power Gener 3(1):75–83

Meier S (2009) System aspects and modulation strategies of an HVDC-based converter system for wind farms. Royal Institute of Technology, Stockholm, Sweden

Mohan N et al (2003) Power electronics – converters, applications and design. Wiley, New York

Muljadi E, Butterfield CP, Chacon J, Romanowitz H (2006) Power quality aspects in a wind power plant. In: IEEE power engineering society general meeting, 2006, Montreal, Canada

Muljadi E, Mills Z, Foster R, Conto J, Ellis A (2008) FAULT analysis at a wind power plant for one year of observation. In: IEEE power and energy society general meeting – conversion and delivery of electrical energy in the 21st century, 2008, 20–24 July 2008

Muljadi E, Nguyen TB, Pai MA (2009) Transient stability of the grid with a wind power plant. In: IEEE/PES power systems conference and exposition, 2009. PSCE '09, Seattle, 15–18 March 2009

Obersteiner C, Saguan M (2009) On the market value of wind power. In: 6th international conference on the European energy market, 2009. EEM 2009, 27–29 May 2009

Paensuwan N, Yokoyama A (2009) Risk-based dynamic TTC calculation in a deregulated power system with a large penetration of wind power generation. In: CIGRE/IEEE PES joint symposium on integration of wide-scale renewable resources into the power delivery system, 2009, 29–31 July 2009

Ravn HF (2006) Short term wind power prognosis with different success criteria. In: International conference on probabilistic methods applied to power systems, 2006. PMAPS 2006, 11–15 June 2006

Shinde SM, Patil KD, Gandhare WZ (2009) Dynamic compensation of reactive power for integration of wind power in a weak distribution network. In: 2009 international conference on control, automation, communication and energy conservation, 2009. INCACEC 2009, 4–6 June 2009

Tanabe T, Sato T, Tanikawa R, Aoki I, Funabashi T, Yokoyama R (2008) Generation scheduling for wind power generation by

storage battery system and meteorological forecast. In: IEEE power and energy society general meeting – conversion and delivery of electrical energy in the 21st century, 2008, 20–24 July 2008

Thakur T, Goyal S, Gambhir J, Kaur I (2008) Optimisation of imbalance cost for wind power marketability using hydrogen storage. In: Joint international conference on power system technology and IEEE power India conference, 2008. POWERCON 2008, 12–15 Oct 2008

Tsikalakis AG, Katsigiannis YA, Georgilakis PS, Hatziargyriou ND (2006) Determining and exploiting the distribution function of wind power forecasting error for the economic operation of autonomous power systems. In: IEEE power engineering society general meeting, 2006

Ummels BC, Pelgrum E, Kling WL (2008) Integration of large-scale wind power and use of energy storage in the Netherlands' electricity supply. IET Renew Power Gener 2(1):34–36

Wämundson M, Hassan F (2009) Optimum DC-link solution in HVDC wind park actively interfaced to the grid. Elforsk report 08:45, Elforsk, Frederiksberg

Wang J, Shahidehpour M, Zuyi Li (2009) Security-constrained unit commitment with volatile wind power generation. In: IEEE power & energy society general meeting, 2009. PES '09, 26–30 July 2009

Wang L, Wei J, Wang X, Zhang X (2009) Wind power interconnection and integration roadmap: An RTO's perspective. In: IEEE power & energy society general meeting, 2009. PES '09, 26–30 July 2009

Wang L, Wei J, Wang X, Zhang X (2009) The development and prospect of offshore wind power technology in the world. In: World non-grid-connected wind power and energy conference, 2009. WNWEC, Nanjing, 24–26 Sep 2009

Wang L, Dong L, Hao Y, Liao X (2009) Wind power prediction using wavelet transform and chaotic characteristics. In: World non-grid-connected wind power and energy conference, 2009. WNWEC, Nanjing, 24–26 Sep 2009

Watson R (2001) Large scale integration of wind power in an island utility-an assessment of the likely variability of wind power production in Ireland. In: IEEE porto power tech proceedings, 2001, vol 4. Portugal

Xing-wei X, Gang M, Guang-hui S, Hong-peng Z, Kai-yuan H, De-bin G, Jia-qi T, Xin M, Yong X (2009) The problems and solutions for large-scale concentrated integration of wind power to partially weak regional power grid. In: International conference on sustainable power generation and supply, 2009. SUPERGEN '09, 6–7 April 2009

Yan Z, Gu W (2009) Research on integrated process of large-scale non-grid-connected wind power and coal-to-ethylene glycol. In: World non-grid-connected wind power and energy conference, 2009. WNWEC, Nanjing, 24–26 Sep 2009

Zha L, Song J, Liu H (2007) Simulation study of wind power with continuously variable transmission. In: 2nd IEEE conference on industrial electronics and applications, 2007. ICIEA 2007, 23–25 May 2007

Wind Power Grid Integration: Transmission Planning

Dale Osborn
Midwest ISO, Columbus, OH, USA

Article Outline

Adjustment of Economic Simulation Model Transmission Line Ratings
Economic Studies
Value-Based Long Range Planning Method
Wind Integration Studies
Other Information to Answer Questions
Conclusion
Bibliography

How is transmission planning done? In as many ways as there are different goals of many organizations influenced by regulation. The discussion will relate to entities connected to a large interconnected grid.

Three types of organizations of utilities exist in the USA:

1. The utilities who participate in a Regional Transmission Organization (RTO). RTOs may consist of utilities from several states or one state as in the case of the New York Independent System Operator or California System Operator. RTOs have planning processes that incorporate the entire footprint of the RTO. Most of the RTOs operate markets.
2. Utilities who do not participate in a RTO. The individual utilities have their own planning processes. Some of the utilities have relationships with other utilities for joint planning.
3. Merchant transmission that plans transmission and seeks participants to help fund the transmission project.

The National Electric Reliability Corporation (NERC) has the responsibility of enforcing power system reliability operating and planning standards in the USA and coordinating with Canada. Every utility in the USA and Canada participates in the NERC reliability assessments to assure that the transmission system will meet standards and is expected to perform reliably.

Most of the criteria for planning of transmission are based on the NERC standards.

There are three large areas or interconnections that operate as interconnected systems in the lower 48 states of the USA. The three interconnections are weakly tied with HVDC back to back transmission. Hydro Quebec is also tied to the USA and Canada with HVDC ties. ERCOT (TEXAS) is an interconnection on its own. Alaska has its own systems.

Transmission is planned to serve the native load plus purchases and sales transactions. Models are built on the interconnection level so that the interaction of all native load and transactions in the USA and Canada can be studied simultaneously with a major transmission line model. NERC coordinates the model building process.

The transmission models are obtained by a utility or an RTO and then the detailed transmission in their areas and sometimes sub-transmission (below 100 kV) are added. Thus, any utility or RTO has a detailed model of their footprint and a good representation of how they will react with the transmission system adjacent to them.

Energy markets, larger footprints of the RTOs compared to utilities, the insertion of significant quantities of wind and solar generation, and the federal government funding of coordinated planning at the interconnection level has recently initiated integrated studies on a much larger scale than has previously been done in the USA. One primary driver for the studies is to plan transmission for the use of wind, solar, and other renewable resources. Wind, solar, and other renewable resources are not located near the major loads. Transmission will have to be constructed to take advantage of renewable resources. The transmission needed for renewable resource is for energy that provides an optional fuel source and is not necessarily needed for reliability purposes. Economic criteria for building transmission are entering the transmission planning processes.

The present US transmission system is similar to a net with weak points between the geographic boundaries of organizational and former organization zones. State boundaries, country boundaries, RTO boundaries, former utility boundaries, and geographic restrictions such as lakes and national parks are usually the location of the weak links in the net that create holes. There are strong ropes that reinforce the net in some areas.

There are three basic philosophies concerning transmission design:

1. Do only what is needed. This is the present reliability process for transmission planning. This has worked for years, but does not address the characteristics and economics of renewable energy very well.
2. Plan for reliability and reinforce the system at the constraint locations. This looks like a good approach until one analyzes the large power transfers that renewable energy resources, such as wind energy, would require for efficient energy markets. Rebuilding all the AC underlying system to transfer high power transfers and the control of loop flow is a formidable task. There are over 300 constraints in the EWITS [1] study. Fixing one constraint does not mean that the constraint just moves over to another area. The area that the constraint moved would then need to be fixed also with a transmission expansion. Separating which fixes are needed for reliability and how much of the fix is related to the market is a quagmire that may not be possible to be resolved.
3. Design a transmission overlay that would produce an efficient system of markets including the effects of renewable energy without impacting the underlying AC system significantly. Reliability would be mainly addressed in the transmission planning of the underlying AC system. The overlay would be designed to be self-contingent, economical, and not create reliability problems either in the overlay or the underlying system. One advantage of the overlay philosophy is that the transmission design and the cost of the overlay can be separately identified and not comingled with the reliability upgrades. The transmission planning process to make the markets efficient can be addressed separately from the existing transmission planning processes that design the underlying AC system.

The most likely choice of the three philosophies is that all of the above will be used. A transmission system design with a top layer overlay that delivers bulk energy to the energy market, a second layer that consists of RTOs and large utilities, and a third layer of utilities not in a RTO, public power, and possibly

federal power agencies may be envisioned for the Eastern Interconnection. ERCOT may or may not be further interconnected with HVDCties. The Western Interconnection may have another organization based on coordination without energy markets.

The following is a simplistic explanation of the levels or layers of transmission planning.

Municipals and small utilities probably can do most of their planning with power flow studies to check for overloaded lines and to maintain voltages within acceptable limits. Contingency studies are run to confirm that the system will not be adversely affected for probable events. Generally the NERC planning standards are used as criteria. Short circuit and relay coordination studies are done to assure that the equipment is within ratings and properly protected for faults. The outside transmission system adequacy is usually studied by a NERC region or a RTO in their area. The engineers may participate in the NERC regional studies or the RTO meetings for coordination of plans. Reliability is the focus of the studies. Engineers at this level are very specific about the details of the design of the transmission system. Economic and technical evaluation of multiple alternatives is usually performed for each prospective project. Larger utilities may have a division that studies individual areas on their system in a similar manner. The NERC region or the RTO usually does not study their system to the detail that they do.

Larger utilities have complete planning staffs with specialists in areas such as dynamics. They perform their own studies for the generation interconnection, transmission expansion, dynamics, possibly equipment specification transient studies and transmission service requests.

Providing testimony to support proposed plans is a transmission planning function.

Very large utilities may break the transmission system into voltages or regions and have multiple sections of transmission planners. These utilities may have a research department.

There is usually a separate department for protection studies and short circuit studies. There are usually separate departments for generation expansion, production cost simulations, market use studies, resource adequacy, and load forecasting outside the planning department.

If a larger utility is in an RTO, the generation interconnection studies may be performed by the RTO or under contract with them. The larger utility would probably participate in RTO planning meetings and on task forces. Regional transmission expansion studies involving multiple utilities are probably performed by the RTO. The larger utilities usually run their own version of the RTO studies for verification of results and to test their own concepts.

The processes for expansion planning vary greatly from RTO to RTO.

Some of the common processes are as follows:

1. Studies to determine the ability of a generator to deliver to a utility load or to the RTO as a whole.
2. Generation Interconnection and expansion studies.
3. Longer-term, larger power transfer transmission service studies to shorter-term transmission service studies are approved or denied by a tariff administrator using a program to evaluate the current status service available. There are too many transmission service requests for a study to be done for each request and the time is not sufficient many times to do a study.
4. Available Transmission Capacity (ATC) studies are the link from planning to operations and tariff administration for transmission service requests. ATC is published multiple times per day.
5. Shorter-term transmission expansion planning up to 10 years in advance. The transmission that is approved for construction comes from these plans. These are bottom-up plans. Bottom-up planning starts with the system today and sequentially determines the best set of alternatives to provide reliable service in the future. Power flow, power transfer sensitivity, voltage stability, dynamics, economic evaluation of the alternatives, small signal stability, and large amounts of contingency analysis are studies performed annually. The plan is approved by the Board of Directors for construction by the Transmission Owners. RTOs do not own transmission.
6. Constraint mitigation is also evaluated by the RTOs.

The part where the RTO planning methods depart from each other and large utilities is in the long range transmission expansion planning.

Most of the RTOs use a multi-scenario AC study analysis followed by an economic analysis in a bottom-up process to determine the long range transmission expansion plans. The methods used are very similar to their short-term transmission expansion plans.

The Midwest ISO uses a bottom-up short-term transmission expansion process similar to the other RTOs. A mid-range Midwest ISO plan that will accommodate the present 23,000 MW of Renewable Portfolio Standard requirements (wind) for the Midwest ISO footprint is being developed to specify the sequence of transmission expansion from the short-term to the long-term expansion plan. The long-term expansion plan would be some future expansion similar to the EWITS or the EIPC [2].

The Midwest ISO uses a top-down value–based approach with an end year of 15 years out for the long range plan. Multiple scenarios or futures are studied that determine the probable outcomes of the conditions that the power system may be expanded. Economic simulations are run to provide economic and power flow performance data from a simulated energy market for 8,760 h in a year. Generation forecasts are optimized for each future. Differences between the economic simulations produce rough budget information that can be used to determine if and what transmission might be considered. Transmission plans are developed from the differences of economic and power flow information. Graphical outputs and tables are used to determine the location of conceptual transmission expansion and their size.

Multi-RTO and large utility studies on for the Eastern Interconnection have been made completed. A study for the Western USA is expected this year. ERCOT does its own studies. Canada is doing its own Pan-Canadian study. DOE/NREL is sponsoring an all US Renewable Energy Future Study for the year 2050 for up to 80% renewable generation of all types which should be out later in 2010. DOE funded coordinated transmission studies for the Eastern Interconnection and the Western Interconnection that are just starting.

One major limitation to coordinated studies is time-synchronized data for renewable generation. The Eastern Wind Integration Study produced a publicly available data set for each 10 min for the parts of the Eastern Interconnection having wind. Having time-synchronized data enables the value of geographic diversity and the availability of wind generation to serve the peak load, capacity credit. Time-synchronized data allows the location of wind resources in different areas such as onshore and offshore. The Western Wind and Solar Integration Study also has wind data similar to the EWITS wind, but the two databases are not time-synchronized due to different vendors producing the data. Solar data lags wind data in development, but progress is being made. The data from Canada is not synchronized with the US data. Political borders affect data generation as well as transmission planning.

Figure 1 shows the capacity factors of wind units for the eastern USA in the area covered by the EWITS database for wind production.

Figure 2 shows the output from the EWITS wind output database for the maximum wind output for the years. Red and orange colors show high wind energy production. Blue represents poor production. Some areas that traditionally have excellent wind outputs are not on peak.

Figure 3 shows the worst day of a year. Almost all the wind over the eastern USA is off. Arguments about wind not being a reliable resource often refer to plots like Fig. 3. The focus of studies is to find out what can be done with the wind resource. The overall system is designed to fill the gaps left by wind energy to produce a reliable and economical system.

The diversity of wind is greater in the north–south direction in the eastern USA than for the west–east direction. The plot in Fig. 4 shows that long distances are required to reduce the correlation of wind energy production.

Figure 5 shows the reduction in variability from the EWITS study as the wind resource is expanded over the eastern USA and tied together with transmission.

The variation of wind is reduced by a factor of 4. Transmission can link the geographically diverse regions of the eastern USA together to produce a better energy product that would require fewer reserves to manage. Note there is a level of saturation as the wind resource exceeds 5,000 MW.

Not only does wind vary from minute to minute, the yearly output can vary by up to 26% from the maximum output year to the minimum output year. A study by WindLogics reported this result for an examination of a 12-year time span using forecasted information. Variations of this magnitude produce

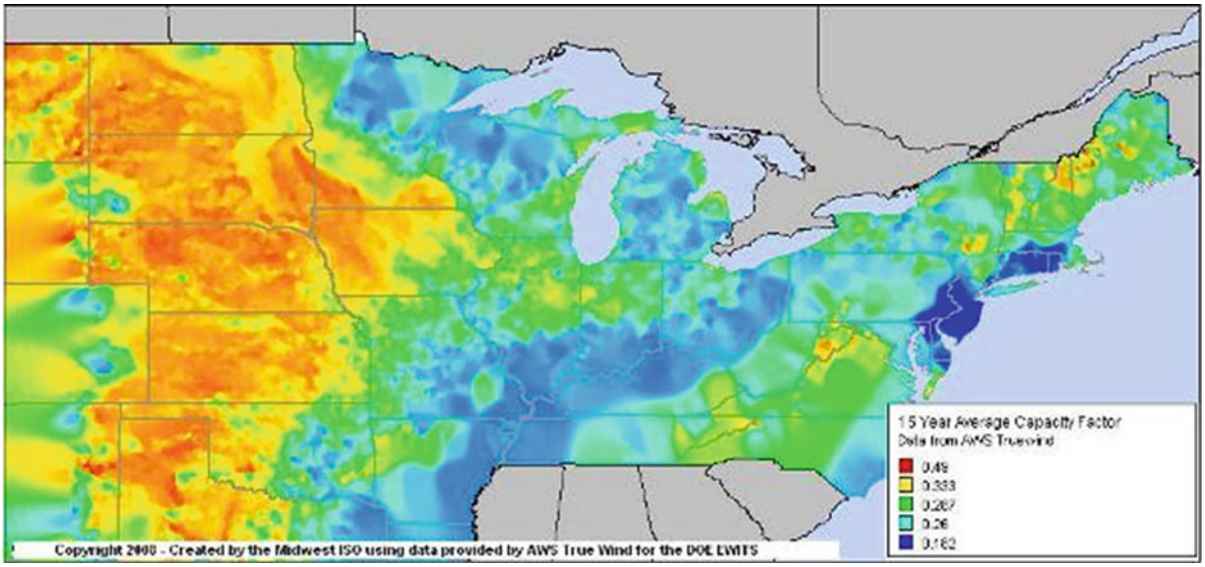

Wind Power Grid Integration: Transmission Planning. Figure 1
Capacity factors of wind units for the eastern USA

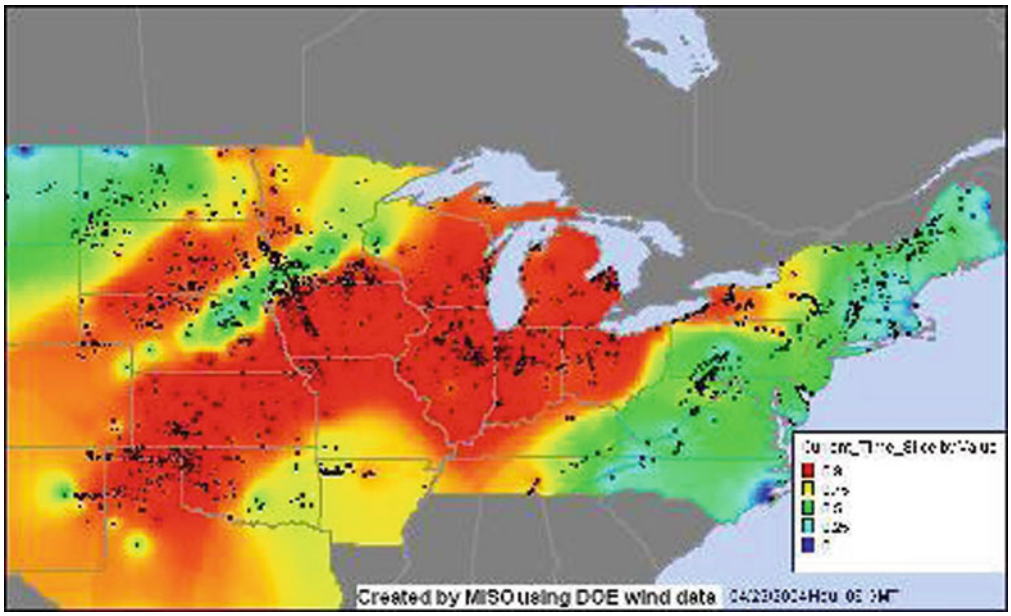

Wind Power Grid Integration: Transmission Planning. Figure 2
Maximum wind output for the years. *Red* and *orange* colors show high wind energy production. *Blue* represents poor production

different generation patterns that must be included in the design of transmission systems. Multiple years of study data are run through the economic simulations to determine annual variability patterns. Unfortunately, only 3 years of hourly data exist for the EWITS database.

The aggregation of wind energy also increases the probability that the wind generation would be available

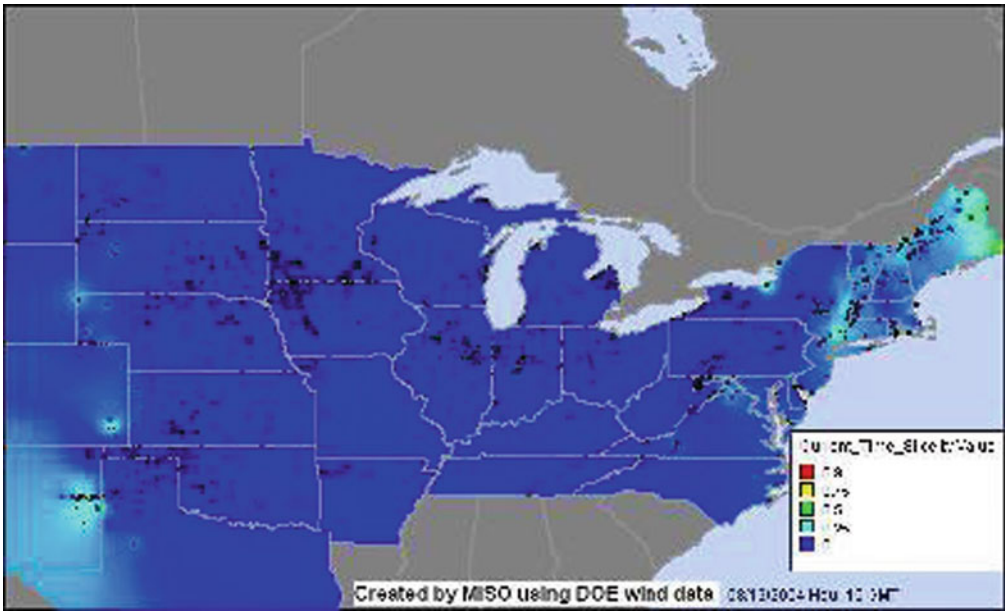

Wind Power Grid Integration: Transmission Planning. Figure 3
Worst day of a year. Almost all the wind over the eastern USA is off

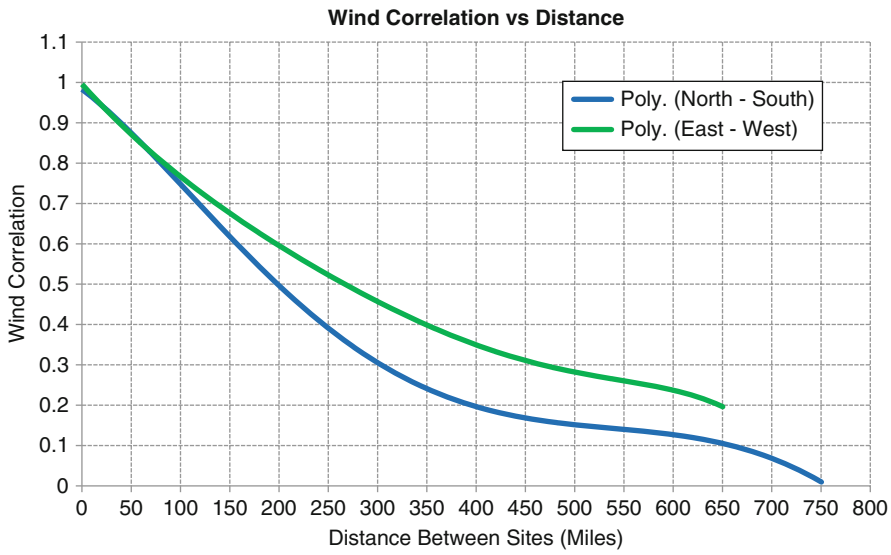

Wind Power Grid Integration: Transmission Planning. Figure 4
Long distances are required to reduce the correlation of wind energy production

on peak. A loss of load probability expectation calculation is performed that shows the component due to aggregation of resources and the component due to the transmission overlay for 3 years. The transmission overlay has a large impact when the wind is located primarily in the western (Scenario 1) part of the Eastern Interconnection than in the eastern part (Scenario 3).

The EWITS study, Fig. 6, shows that the capacity credit of wind for a large aggregated area can be in the range of 24%. This is three times higher than the

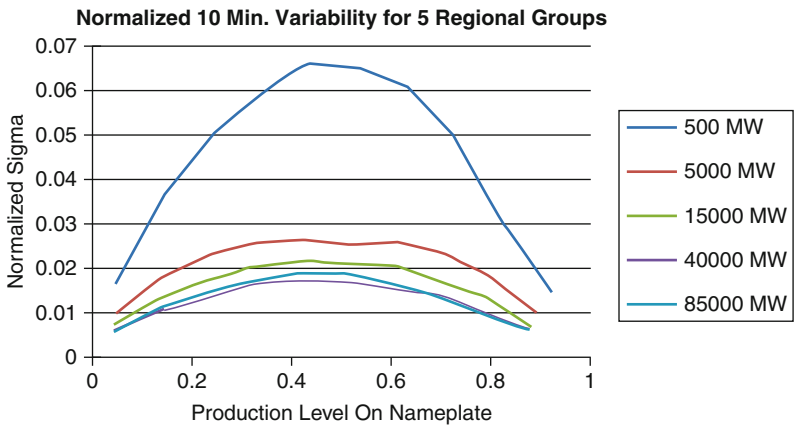

Wind Power Grid Integration: Transmission Planning. Figure 5

Reduction in variability from the EWITS study as the wind resource is expanded over the eastern USA and tied together with transmission

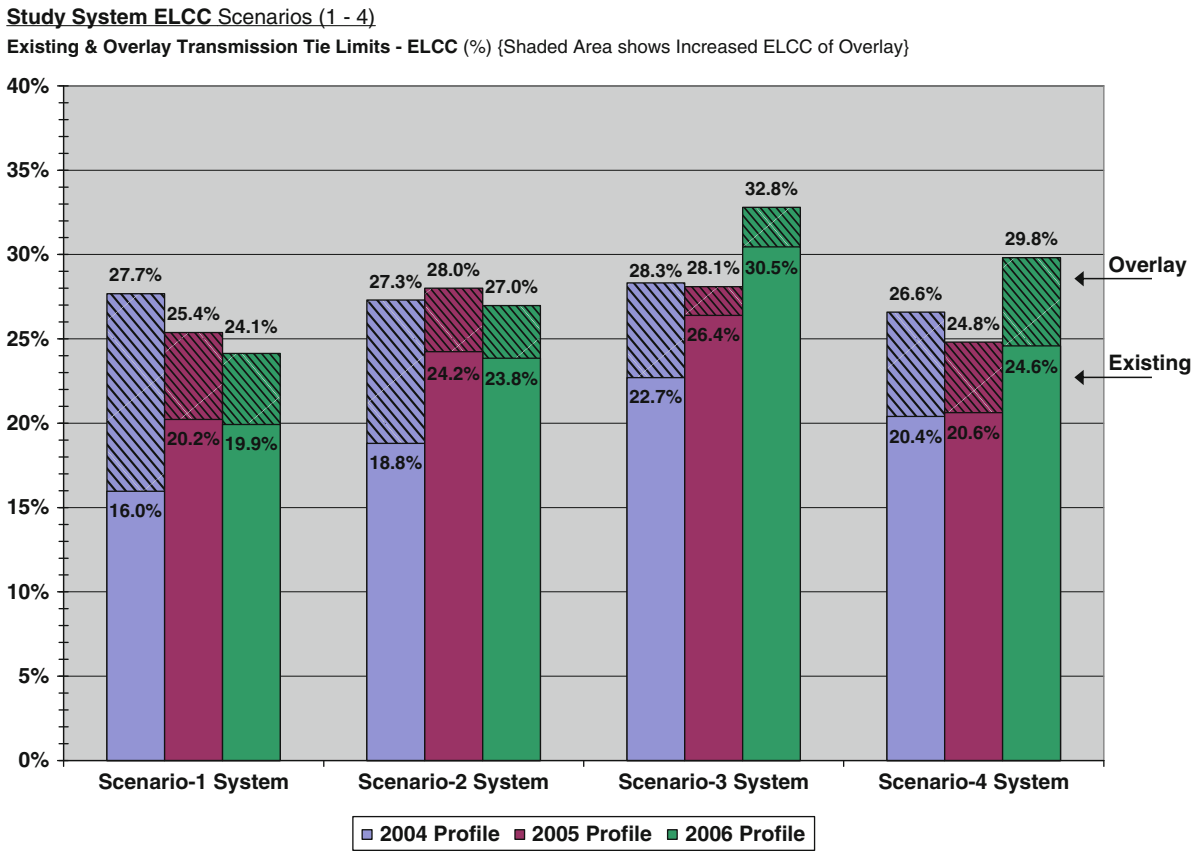

Wind Power Grid Integration: Transmission Planning. Figure 6

The EWITS study shows that the capacity credit of wind for a large aggregated area can be in the range of 24%

present Midwest ISO wind capacity credit of 8%. Less conventional generation is needed for the generation forecast with a higher wind capacity credit. The amount of wind generation is not reduced as the wind generation resource has to be large enough to produce the RPS requirements. Transmission helps the process, but the geographic diversity of the wind resource is the primary factor in improving the wind capacity credit.

Figure 7 is a representation of wind energy production hourly for a year normalized to the output of load in the area. Curve fits through the highly variable plots enable one to see trends. The load curve has a summer peak with minimum load during the spring and fall. The wind has a minimum output during the peak period for the load and maximum outputs during the spring and fall when the load least needs generation. Wind is also more variable than the load during the spring and fall periods.

If the load and the corresponding wind energy output are sorted in descending order by load, a load duration curve is produced which shows the amount of time in which the load level is achieved (Fig. 8). The peak load occurs only for 1 h of the year. The trend curves show that wind generation has an average base load characteristic off-peak and a reduced capability on peak. Thus, the wind generation would offset base load generation production during the off-peak periods. Base load generation needs to have about a 60% capacity factor (average output divided by maximum output over the year). Wind decreases the base load capacity factor to the point that a combustion turbine or low capacity factor combined cycle plant may be the best selection for the generation forecast when combined with wind energy.

The mix of generation types to serve the load is a combination of the capital costs to construct a generator and the energy costs to operate the generator. Base load generation has higher capital costs and lower fuel costs. Gas fired generation has lower capital costs and higher fuel costs. Generation forecasting programs are run to determine the optimal mix of generation that is needed to reliably serve the load. When operating generation with low costs operating costs are run first. The higher cost operating cost generation is run next until the generation is stacked in merit order. Figure 9 shows a simplified generation merit order stack. The area under the load duration curve to the left is the energy supplied for the load. The area above the load duration curve and to the right is energy that may be bid into the energy market for sale. The area between the purple line and the yellow line depict the

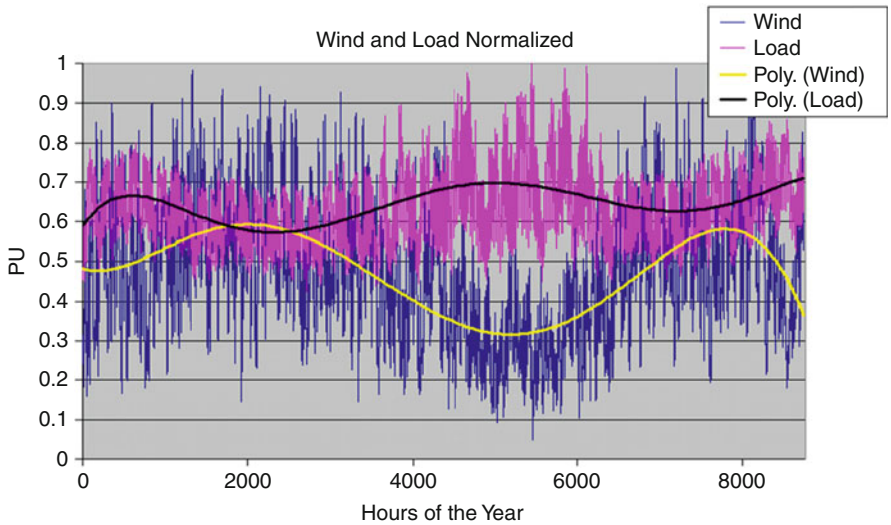

Wind Power Grid Integration: Transmission Planning. Figure 7
Hourly wind energy production for a year normalized to the output of load in the area

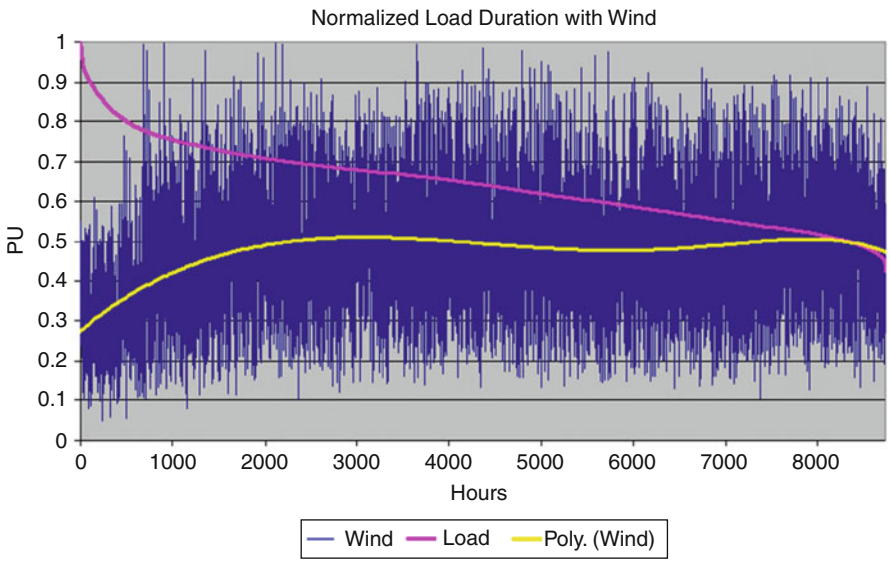

Wind Power Grid Integration: Transmission Planning. Figure 8
Load duration *curve* (*magenta*), which shows the amount of time in which the load level is achieved. The peak load occurs only for 1 h of the year

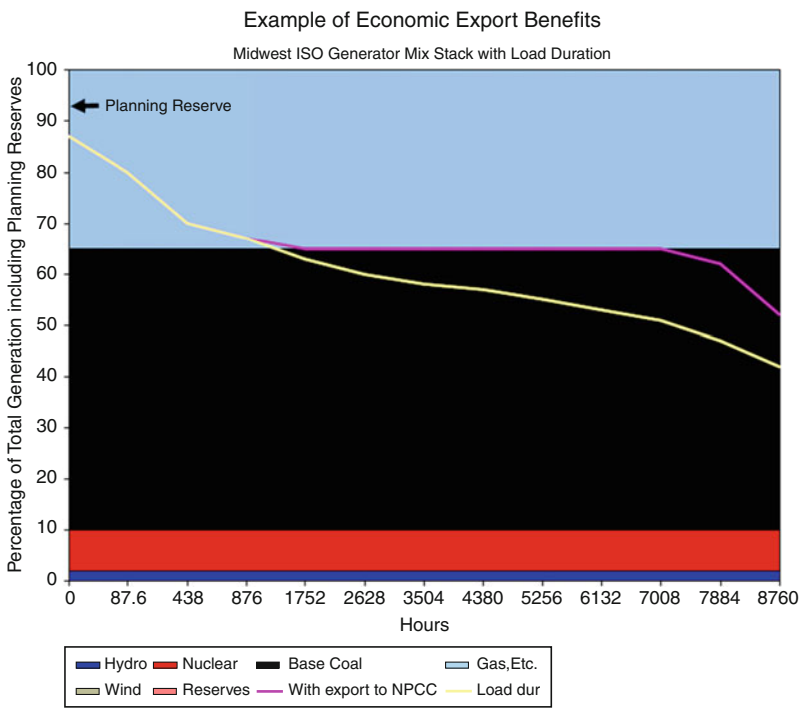

Wind Power Grid Integration: Transmission Planning. Figure 9
All generation is used to meet the peak load. Generation that can be used to meet load has a 100% capacity credit for this example

energy that might be sold on the energy market. The purchasing party has limitations on how much energy it can accept.

All generation shown in Fig. 9 is used to meet the peak load. Generation that can be used to meet load has a 100% capacity credit for this example.

Figure 10 shows the result of injecting wind generation into the generation mix. Coal generation is forced upward on the stack. Coal is forced into an area usually occupied by gas generation in an optimal generation mix. The capacity factor of coal is reduced. More coal generation is available for sale. The area between the purple line and the yellow line is energy that might be sold on the energy market. The purchasing area cannot receive all the available energy. The coal generator must be reduced in output to match the load plus purchase chart. Even with sales, the coal capacity factor is reduced compared to Fig. 9, and this is a benefit for global warming. For the purchaser, the use of coal energy may be against their green commitment. Is the goal global warming or local contribution to global warming?

For this example wind has a capacity credit of about 5%. If peak load and energy grow at the same rate, the vertical axis will increase and the graph will be proportional to Fig. 10. If the average load factor (load energy divided by the peak load times 8,760 h per year) is 60% and the average wind generator capacity factor is 30%, then 2 MW of wind generation has to be added for each MWH of energy growth. If the RPS wind growth requirement is 20% of the load energy, then the wind generation to be added would be 0.4 MW. Assume the generator reserves are about 12%. Reserves provide some extra generation if something would happen to a generator at the peak period to replace the generator with the outage. Gas generation would be added for 1.10 MW (1.12 minus 2% credit for the wind). For each MW of load added, 1.5 MW of gas and wind generation would be added. The mix of coal would be very gradually reduced. At the present rates of load growth it would require 15 years to adjust the generation mix to an economically optimal mix.

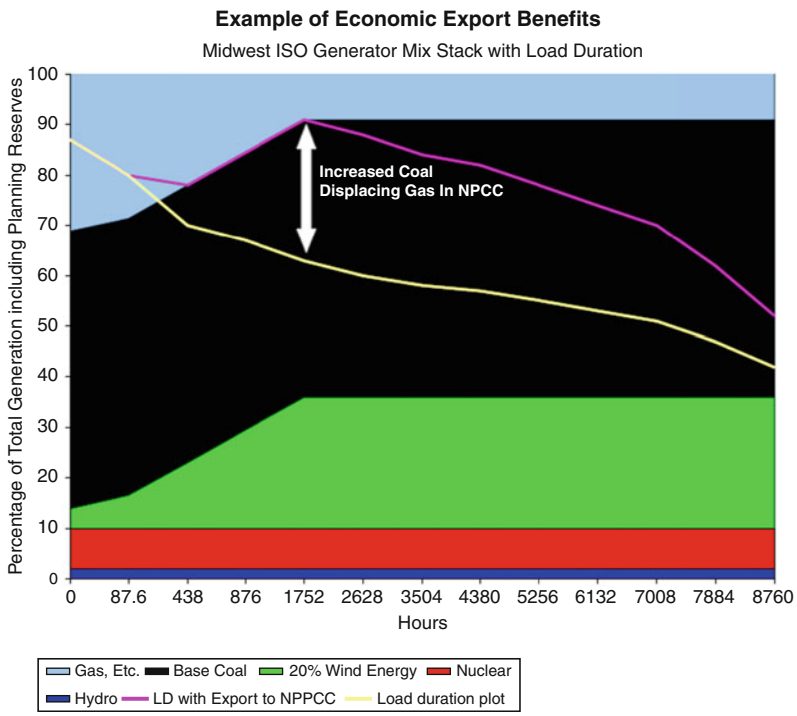

Wind Power Grid Integration: Transmission Planning. Figure 10
Example of economic benefits

Adjustment of Economic Simulation Model Transmission Line Ratings

Economic models use linear or "DC" representation of transmission lines that do not have distance considerations considered. A linear line is modeled as having a MW rating and an impedance. There are no voltage drop, dynamic rating considerations, and distance considerations. AC power flows and dynamic studies automatically consider all the factors due to the mathematical representation of the lines. The power flow models used by economic simulation programs use power flow data that may have a thermal rating that is higher than what can actually be carried on the transmission line. To resolve this issue, the economic simulation models have lines rated according the St. Clair curve shown in Fig. 11 that accounts for the decreasing power transfer capability of a transmission line with distance. Lines in the power flow case that is an input to the economic simulation case have ratings that are adjusted by the length of the transmission line and the voltage of the line. For 765 kV a 1.2 times multiplier to the St. Clair curve is used. For a 345 kV line a 1.5 times multiplier is used. The multiplier is chosen to reflect power flow values that are achieved during contingency operation. Adjusting the ratings of transmission lines produces more realistic line loadings for the economic simulation than that produced using the ratings from a power flow case. The surge impedance loading (SIL) of a 345 kV line is approximately 400 MW. The surge impedance loading a 765 kV line is about 2,260 MW. The rating of an 800 kV HVDC line is about 6,400 MW.

Figure 12 shows the relative cost of constructing a transmission line to transmit 1 MW 1 mile. The 765 kV and HVDC appear to be the best options. However, the line choice has to consider distance and loading.

AC versus HVDC is also an option that must be considered in transmission overlay design. HVDC lines cost less than overhead AC lines of the same voltage. HVDC convertor stations cost more than AC substations. Figure 13 shows the distance to consider an 800 kV HVDC line rather than a 765 kV line to is about 600 miles. The overlays for JCSP [3] and EWITS used this guideline for the two and three terminal HVDC lines included in the design.

The HVDC lines need to be loaded to be chosen for the overlay design. The steps on the plot in Fig. 14 represent a transmission line of either AC or HVDC. The plot shows that at least two 800 kV lines with a power transfer of 4,300 MW are needed before HVDC is considered to be an option. If the AC system had a 1,500 MW contingency level, the loading level on three HVDC lines to form a self-contingent system for

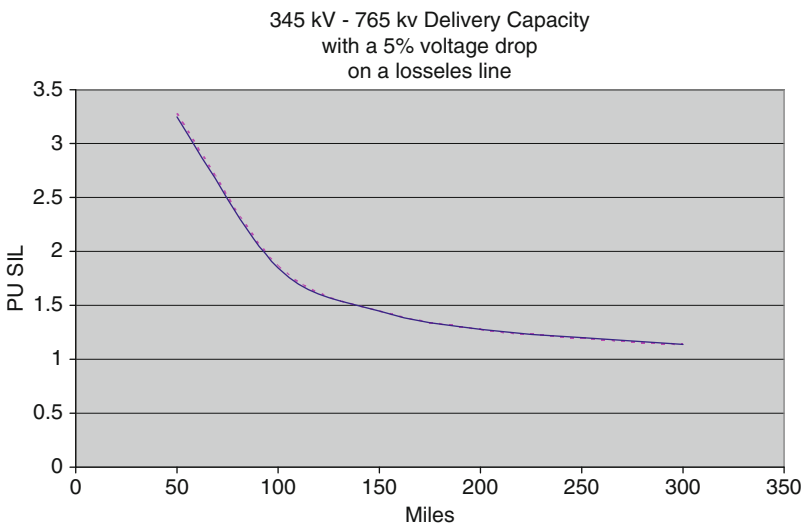

Wind Power Grid Integration: Transmission Planning. Figure 11
Decreasing power transfer capability of a transmission line with distance

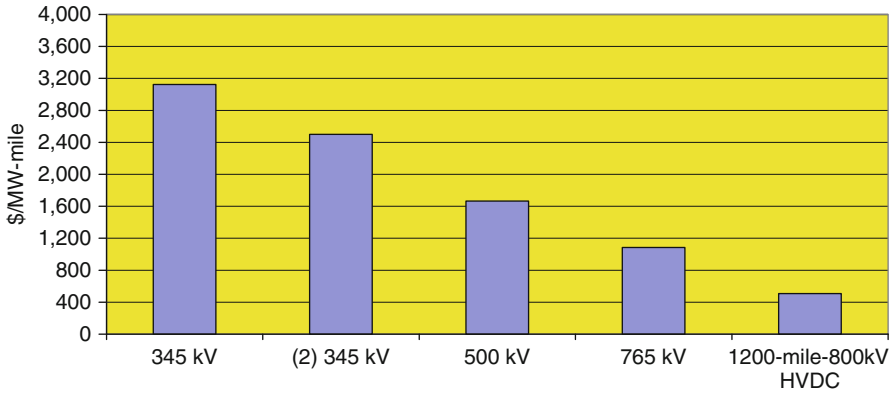

Wind Power Grid Integration: Transmission Planning. Figure 12
Relative cost of constructing a transmission line to transmit 1 MW 1 mile

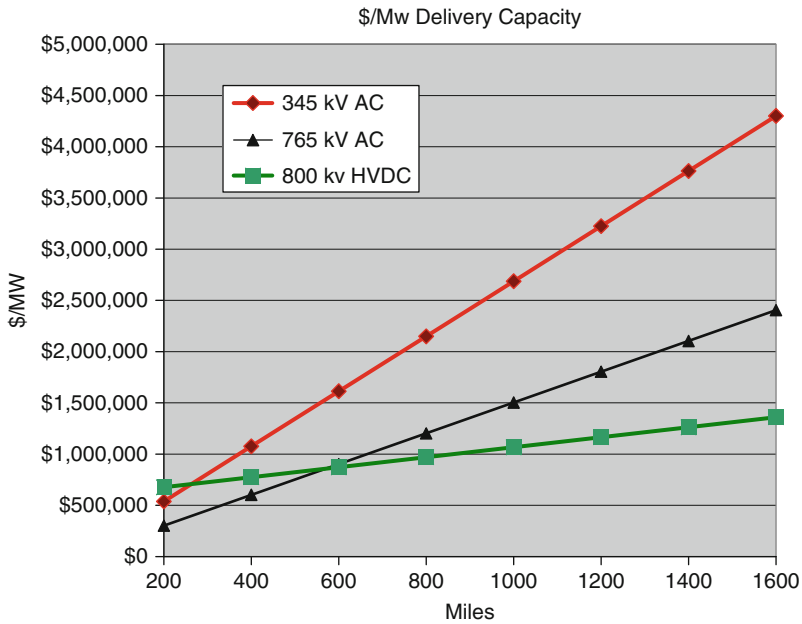

Wind Power Grid Integration: Transmission Planning. Figure 13
Transmission line cost as a function of distance for three voltage levels

the loss of one HVDC line would be 7,900. The HVDC maximum schedule per line would be about 3,950 MW. This may work and have to be tested, but the value is below the threshold. For a three-line HVDC system the HVDC line schedule would be 14,300 MW. Each HVDC line would be scheduled at 4,766 MW, which is above the threshold. The economic simulations for the JCSP and the EWITS showed that this loading would occur about 80% of the time on the HVDC lines. This roughly validates the Rule of Three. The HVDC overlay would carry only energy and not capacity. This allows the overlay to be loaded heavier than if it had to deliver the full power schedule after a contingency under a security constrained criteria. The generation forecast for each region has enough generation to serve the load. Each area is not dependent

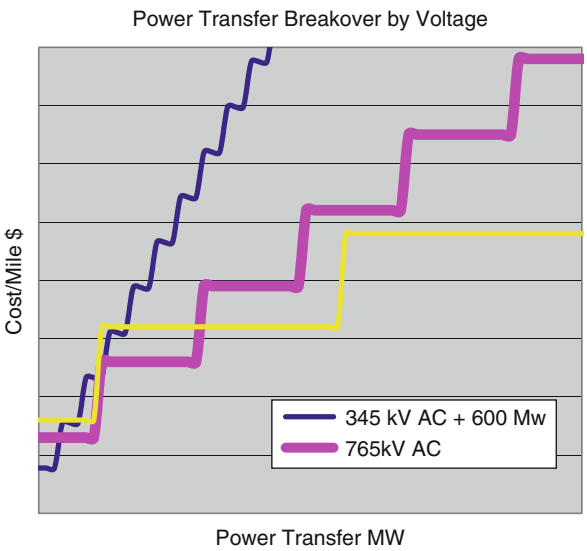

Wind Power Grid Integration: Transmission Planning. Figure 14
Power transfer breakover by voltage

upon imported capacity. The HVDC lines would run at rated load for no more than 30 min. With a 5-min dispatch interval in the energy market, it is highly possible that the security constrained schedule would be reached in 5–10 min.

A recent short investigation into underground HVDC delivery includes:

1. Superconducting plus and minus 200 kV HVDC at about 10,000 MW with a spare pole to create a self-contingent system using Voltage Source Converters of about 750 MW each. The higher converter count would be able to link more market segments into one HVDC line. The spare pole decreases the number of lines needed to construct a self-contingent system.
2. Gas insulated transmission has the capacity to deliver 800 kV HVDC with a similar spare pole configuration or a metallic return for a self-contingent system. The fewer number of larger converters maybe a problem to locate. While gas insulated transmission has been used for years in some form, the long distance aspects have not been addressed.
3. Electric pipe is a XPLE nanoparticle insulated heavy conductor in a pipe. The increased cross-sectional area of the conductor reduces the heat losses to values that can be dissipated through the pipe. Higher currents than cable are possible.

While HVDC breakers and networks have been discussed with the underground options, it may be possible to link separate HVDC lines with AC backup transmission to transfer power to healthy poles similar to the overhead HVDC design used in the JCSP and EWITS. The AC backup design may be possible to have the initial HVDC lines constructed without having to wait for the development, testing, design modifications, and retesting of HVDC breakers and networks.

The high level of activity with the submarine HVDC cables indicates that larger HVDC links may be possible. A constrained and a "copper sheet" difference case may provide insight into the scope of the problem. The difficulty is the construction of a European model for the production cost simulation including transmission such as that used in PROMOD [4], GE MAPS [5], or GRIDVIEW (ABB) [6].

Economic Studies

There are many questions that need to be answered when considering a transmission expansion study including wind. Most of the questions focus on economic impacts, carbon reduction, impact on other generation, wind curtailment, and total cost of different futures. There are few questions about the voltage levels or the power flow on transmission lines. Many different factions are involved in the political and economic processes influencing the design of the transmission system. The studies need to be able to address the questions.

Economic drivers that create value from having transmission are as follows:

1. The energy markets in the Eastern Interconnection of the USA and elsewhere have areas with lower cost resources and loads with higher priced energy. Connecting a lower cost resource to a higher priced load area with a transmission line displaces the local high-priced generation with the low-cost resource and lowers the price to the load. The low-cost generation resource may receive more revenue than it would have without the transmission. HVDC transmission produces

higher revenue for the generating resource compared to an AC transmission system. Revenue from an HVDC overlay is not distributed among the intervening generation and diluted by transmission constraints as is the case with AC transmission designs.

2. Wind generation creates large surpluses of energy production capability during the off-peak period. Wind generation has a very low marginal cost. Wind pushes coal generation upward in the merit order stack of generation so that less energy is by coal for the local use that took the wind energy. The coal energy is considerably lower priced than natural gas fired and oil fired generation. If transmission capacity is available, the coal energy replaces the natural gas energy at the higher priced area. The capacity factor of wind generation in good wind areas can be in the 40% capacity factor range. The gas generation displaced by coal has lower capacity factors. Natural gas produces about 60% of the carbon dioxide as coal per MWH. The carbon savings based on fuel usage is not enough to offset the difference in capacity factor reductions. Thus, the total carbon dioxide production is reduced (see JCSP example).
3. Generation capital and fixed operation costs are paid for by the utility or RTO purchasing the generation capacity. Only the marginal cost of energy (fuel and variable operation and maintenance costs) is used to determine the cost of the energy in a market. With wind energy there is no fuel cost, and the operational and maintenance cost is small. If wind energy is placed into the energy market it is usually bid as a price taker. This happens when wind is to be curtailed because of minimum generation requirements. Coal generation is difficult to start after a shutdown. Therefore, coal generation has to be left on line at minimum generation levels to meet the next day's load. If the load is less than the sum of all the minimum generation in an area, wind may have to be curtailed. A price taker has a very good chance of being a successful bidder in an energy market as this is a bottom price. A price taker receives the clearing price of the energy market. Gas generation usually sets the clearing price on the east coast of the USA. For a natural gas price of $8/MBTU the cost of energy from a combined cycle may be in the $60/MWH range. Coal would be in the $20–$40/MWH range depending on the location. Wind would have a cost in the $4/MWH range. Thus, if the market clearing price was based on natural gas generation and there was sufficient transmission to deliver the wind energy, the wind generator revenue would be $60/MWH minus losses and transmission costs. Assume the cost of transmission and losses is about $50/MWH. Thus, the wind generator would have a net income of $6/MWH. The alternative may be curtailment of generator output. Transmission provides larger markets for wind energy that allow the full output of the wind generators.
4. Transmission decreases the variability of wind by aggregating the variation of wind generation over a large geographic area by a factor of about 4. Having less variation of the wind generation reduces the reserve capacity that must be online and spinning or held as a fast start reserve generator if the wind would quit.
5. Onshore wind generation has a poor contribution to the peak capacity of a system. The lowest output of the wind generation in a year is the summer season. The wind primarily is present at night and not during the peak period of the day. The capacity credit for the Midwest ISO is about 8%. The capacity credit from the EWITS study with aggregated wind generation is about 25%. If the wind generation for a 20% US Eastern Interconnection case is 230,000 MW, then 39,000 MW less of some type of generation would be needed to serve the load. If the cost were about $600,000 per MW, the aggregation of wind with the transmission overlay would be worth about $24B. This will not pay for all the transmission, but it would help.
6. Load aggregation would reduce the generation requirement of the US interconnection by about 6%. If the load of the US Eastern Interconnection were 600,000 MW, the reduction would be 36,000 MW. For a savings similar to the wind aggregation number above this will not pay for all the transmission, but it would help.
7. Demand resources can bid to a relatively small area since their contribution is limited by their

small shift factors that contribute to correcting a problem. An overlay transmission system would increase the marketing area for a demand resource to a good part of the US Eastern Interconnection. The probability of being accepted as a bid in the energy or ancillary services market is increased with a transmission system.

8. Reliability is difficult to price. An overlay could provide a means of solving many of the frequency regulation and high impact disturbances that occur today or are expected to occur in the future. Performance improvements may be a choice.
9. Nuclear generation may be an option in a low carbon generation scenario. Nuclear plants are large and are difficult to assimilate into a single utility in a short period of time. A large transmission overlay would allow full assimilation of the output of a large nuclear plant at market prices corrected for transmission and losses.
10. The transmission overlay may also make it possible to use the present brown field sights that nuclear sites presently exist to add additional nuclear generation. The present transmission would have to be expanded greatly for this to be done. Short circuit capacity may be a limitation. If the transmission overlay interconnection were several sections of HVDC, the short circuit capacity could be managed by connecting a generator to an HVDC converter that adds little short circuit capacity and designs the AC connections accordingly. The high-capacity contingency rating of the HVDC overlay could accommodate the loss of a nuclear generator and be stable.

The EWITS and JCSP studies only used the production cost savings from the energy market to justify transmission with a benefit greater than the cost for a 20% wind energy requirement. Typical AC transmission expansions justified for reliability criteria have a benefit to cost ratio of about 0.3–0.6 to 1. Grouping lines together that have synergistic affects can raise the benefit to cost ratio near one to slightly greater than one. Designing a system of transmission lines in a time frame that can load the lines produces a better result for studies with high wind energy.

The evaluation period and method may determine the outcome as much as the study. Wind and other renewable resources have costs that do not escalate significantly with time. The fuel and operation and maintenance costs for conventional generation escalate with time. Thus, a short-term evaluation tends to minimize the value of renewable resources.

In the USA, most wind generation Renewable Portfolio Standards will not reach their maximum percentages until 2025. Multiple HVDC transmission lines are included in the designs to transfer the power associated with the RPS. The Midwest ISO alone has a 23,000 MW RPS level by 2025. The minimum self-contingent design for a three 800 kV HVDC line system is 14,300 MW. A transmission overlay would be possible with the Midwest ISO generation alone. If shorter times are chosen for the study, the generation to justify a transmission overlay is not available.

The seven step transmission planning method used by the Midwest ISO, EWITS, and the JCSP uses a top-down method of planning (see Fig. 15). The end result is calculated first for the entire system. This is often referred to as "holistic" planning. The transmission overlay is planned as a system and not as a series of lines with this method. The generation necessary to load the entire system is evaluated. The sequence of getting to the end state is calculated next. Experience has shown that the larger the area studied the better the results. The largest studied is the Eastern Interconnection with a focus on the US Eastern Interconnection. The end result cannot be constructed as the sum of smaller area solutions in the large area. The Midwest ISO performed Midwest ISO only studies. Very little transmission was required as the entire area has about the same type of choices for generation with just a small change in fuel prices from the east side of the system to the west. Benefits less than the cost of transmission were obtained from the study. If such a transmission expansion were constructed, the higher cost of the Midwest ISO component would just raise the cost of the whole project and reduce the benefit to cost ratio of the transmission overlay.

Bottom-up processes start at the present and add lines sequentially in time. The bottom-up process is an extreme case of sub-optimization. Short times are used that limit the possibility of choice of higher efficiency multiple line systems. More money in total is spent on the sequential expansion than a coordinated expansion. Transmission funds are used to mitigate

constraints with limited value as the constraint just moves to another location unless multiple lines are constructed. The main argument in supporting the bottom-up method is that this is the way it has always been done and will be done as the state regulatory processes also approve one line at a time.

The Rule of Three explains the difference in the results in sequential bottom-up study processes and a top-down system design.

The Rule of Three is a very simple economic concept that applies to most transmission choices.

1. If one line is to be constructed, then the voltage probably should be of the highest existing voltage if the line can be loaded. The reason for this is that the present transmission lines limit the loading on a higher voltage line well below the capability of the line. Bottom-up sequential processes are always in this mode. Some organizations like the status quo and argue for bottom-up sequential processes.
2. If two lines are to be constructed, the difference between a higher voltage overlay and an existing voltage is about breakeven. The second higher voltage overlay increases the load that both higher voltage lines can carry. There seems to be an exception of this with long HVDC lines. Two lines are enough to be more economical. The problems with loop flow spreading benefits over the AC system, even to entities that probably would not care to participate in the transmission expansion. Free ridership is a problem with long distance AC lines. HVDC lines strategically can place the collection of low-cost energy at a high-priced area.
3. If three lines are to be constructed and are able to be loaded, then the higher voltage lines will be a superior economic choice. Wind generation produces conditions that load lines economically if studied near the full development of the wind resource.

In the USA, there is typically a higher rate of return for generation than for transmission. Utilities have focused on generation and usually supplied the minimum transmission necessary based on reliability and need. The state regulatory mind-set reinforced this decision mode. The higher rates of return for FERC-approved (interstate) transmission have changed the decision mind-set of the utilities. Independent transmission companies are willing to address multi-line transmission expansions if they can obtain tariff cost recovery from an RTO.

Europe with the difference of hydro generation in the Nordic area, coal in Germany, the nuclear in France, the solar potential in Spain, and the distributed wind may also have the potential for a similar high-voltage transmission overlay.

At the power levels being identified and the high cost of overhead transmission it may be justified to the underground HVDC overlay or at least major portions of it. Socially, underground HVDC may be an acceptable solution while overhead may be very difficult to impossible.

Value-Based Long Range Planning Method

The Midwest ISO planning method starts with an economic analysis to develop the conceptual transmission expansion for each future or scenario. An optimum generation expansion plan or forecast is produced for each future. Generation mixes and locations affect the transmission design. A transmission plan is developed for each future based on the economic information from studies. The conceptual plan will be economical. Since there are multiple futures and multiple conceptual transmission plans one looks for transmission lines that are common to every plan or could be modified to fit the other plans. The transmission is the "no regrets" transmission. No matter which future actually happens, the transmission will still be needed. The common plan is tested for robustness with about four other futures to determine the transmission that would be added to the "no regrets" plan to work well with that future.

Figure 15 is a process diagram of the value-based transmission planning method.

The futures are coordinated with the Planning Advisory Committee (PAC). The PAC consists of sector representatives from the transmission owners, independent transmission companies, generators, environmental, large customers, regulators, etc. A future is a set of assumptions that describes a possible outcome. A future has its own generation forecast. A 20% wind energy future may be one future. An all-gas conventional generation may be a second future. Delayed transmission may be a third future. Nuclear forced in

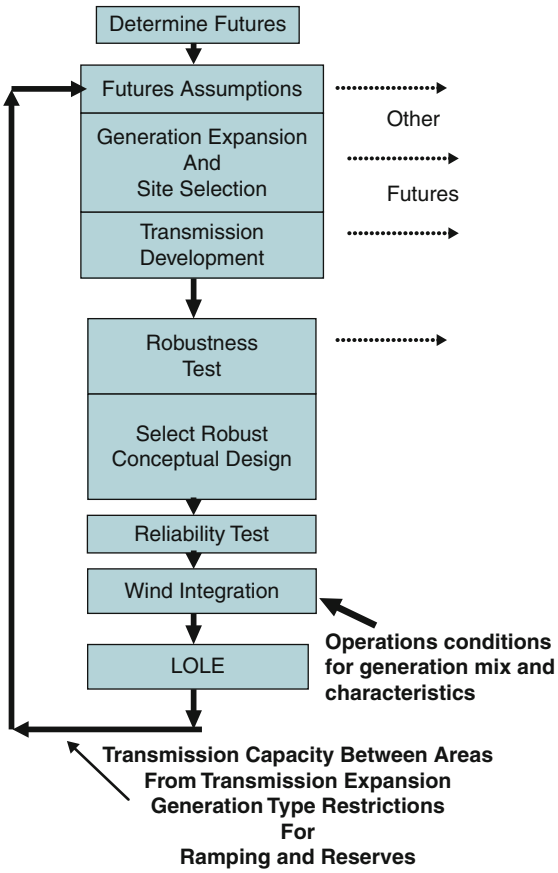

Wind Power Grid Integration: Transmission Planning. Figure 15
The seven step transmission planning method used by the Midwest ISO, EWITS, and the JCSP

at a given level may be a fourth future. A Reference future usually is the most economic generation forecast without future constraints.

Generation forecasts have an excess of transmission capacity due to the fact that wind generation does not produce energy at the peak periods reliably. Wind generation in the Midwest ISO footprint presently is given an 8% capacity credit to apply to the peak load period. The other 92% is excess generation capacity that may produce energy off-peak.

Sensitivity studies are run on futures. A sensitivity study may be a carbon tax. A carbon tax could also be a future with its own generation expansion. Different wind site locations may be sensitivity. Different wind sites may require a unique transmission expansion plan per sensitivity.

Figure 16 shows the generation forecasts for the EWITS futures. Scenario 1 is a 20% wind energy future with generation located strongly in the western part of the Eastern Interconnection. Scenario 3 is a 20% wind energy future with wind generation strongly located offshore of the east coast of the USA. Scenario 2 is a mixture of Scenarios 1, 3. The 20% futures have about 225,000 MW of wind generation. Scenario 4 is a 30% wind energy future, with 330,000 MW of wind generation. The capacity factor of the wind changes the generation that is needed to produce 20% wind energy.

Figure 17 shows the location of the generation by type for Scenario 2 of EWITS. The location of the generation affects the transmission system design.

Information to design a transmission expansion is determined from differences in the 8,760 h per simulated year of market operation runs. A simulation includes the economic modeling of every generator in the Eastern Interconnection, the existing transmission, and load data. A Reference future can be run with its own transmission expansion or without the transmission expansion. The with transmission expansion would be used in the "no regrets" robust transmission selection process. The without transmission expansion would be used as a starting point for each of the other scenarios. The without transmission expansion run uses the present transmission with a future generation forecast. The without transmission expansion is referred to as the constrained case. A second case is run that is called a "copper sheet." A copper sheet has no constraints to power flow. Energy flows to where it would in a perfect energy market. Existing transmission line ratings are placed at very high values. No resistance is modeled for the transmission lines. No interchange flow is modeled. No hurdle rates (the pancake transmission service rates between areas or the inefficiencies in the energy markets) are modeled.

The wholesale energy price differences with the expansion forecast generation without transmission expansion is shown in the left plot of Fig. 18. The right-hand plots are the whole sale with the transmission expansion (Fig. 19). There is just a little congestion remaining with the transmission. Some congestion must remain to produce a value for the transmission.

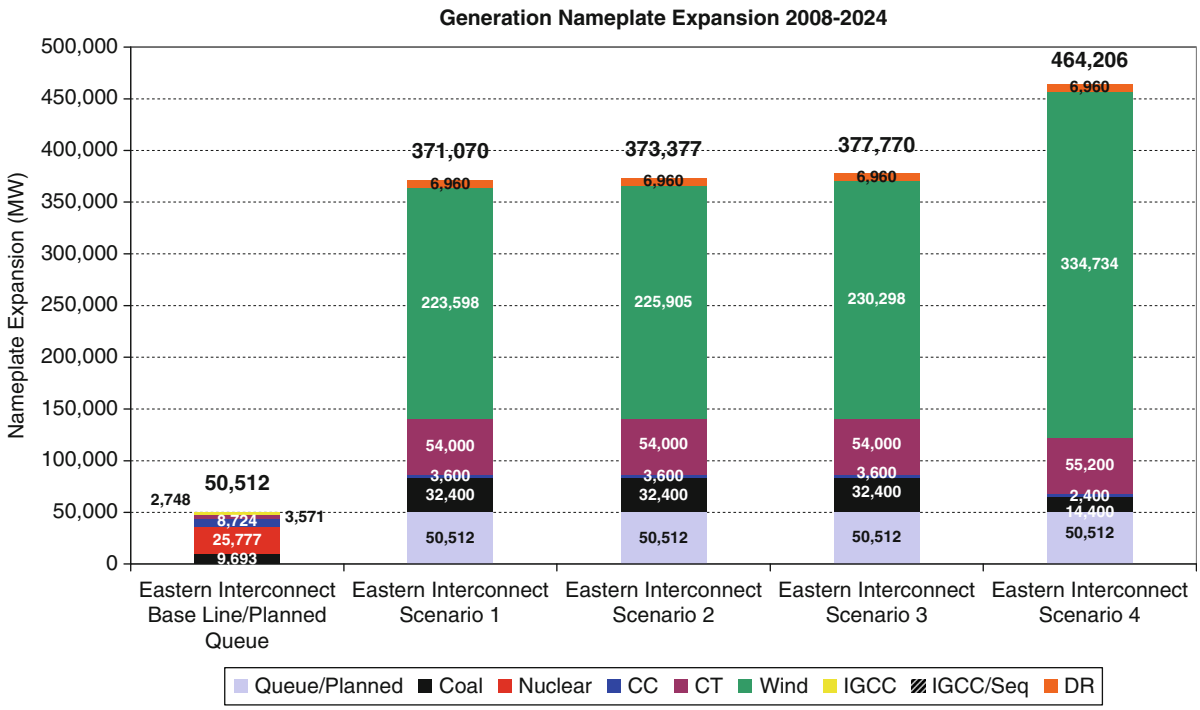

Wind Power Grid Integration: Transmission Planning. Figure 16
Generation forecasts for the EWITS futures

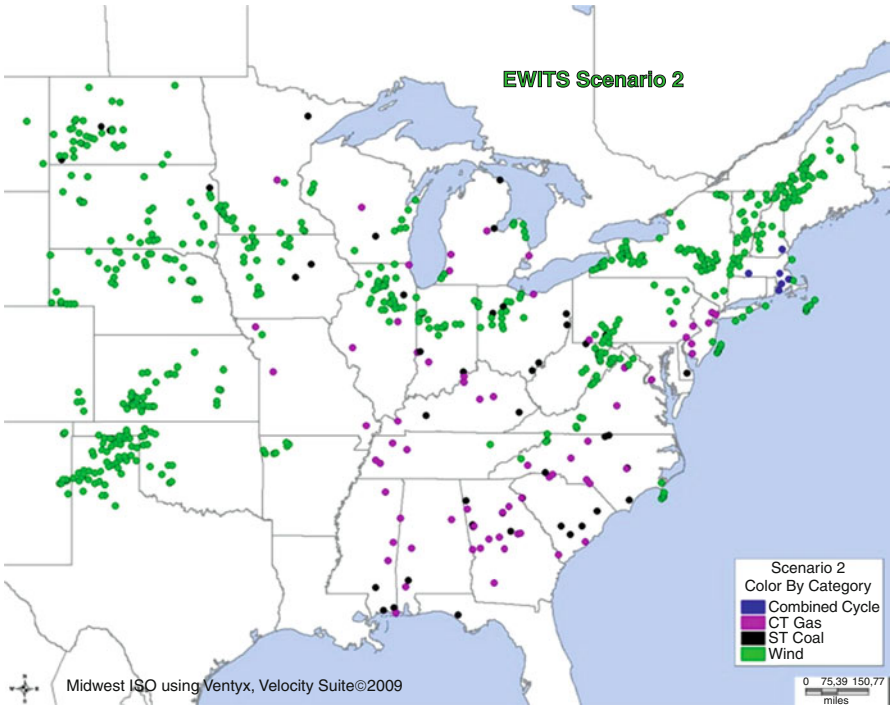

Wind Power Grid Integration: Transmission Planning. Figure 17
The location of the generation by type for Scenario 2 of EWITS

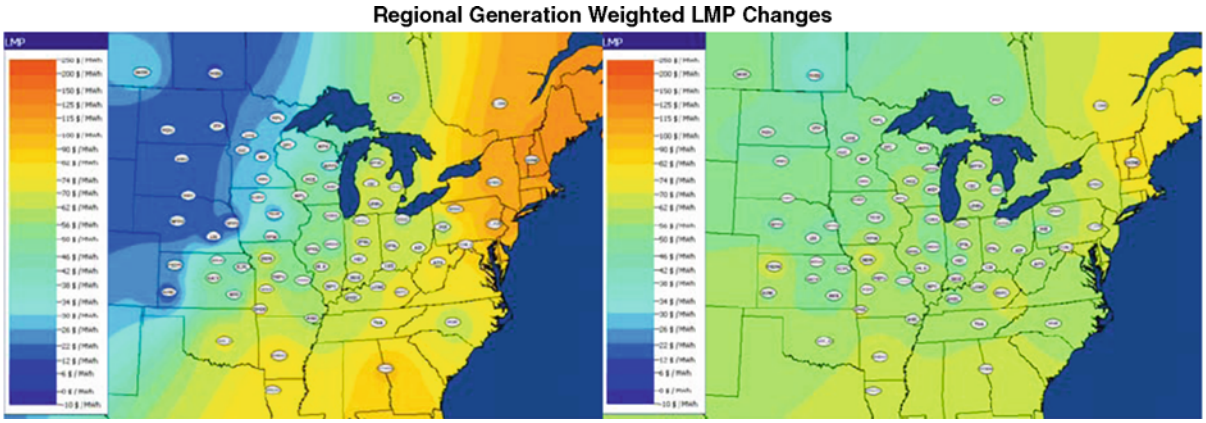

Wind Power Grid Integration: Transmission Planning. Figure 18
Scenario 1 annual generation weighted LMP comparison

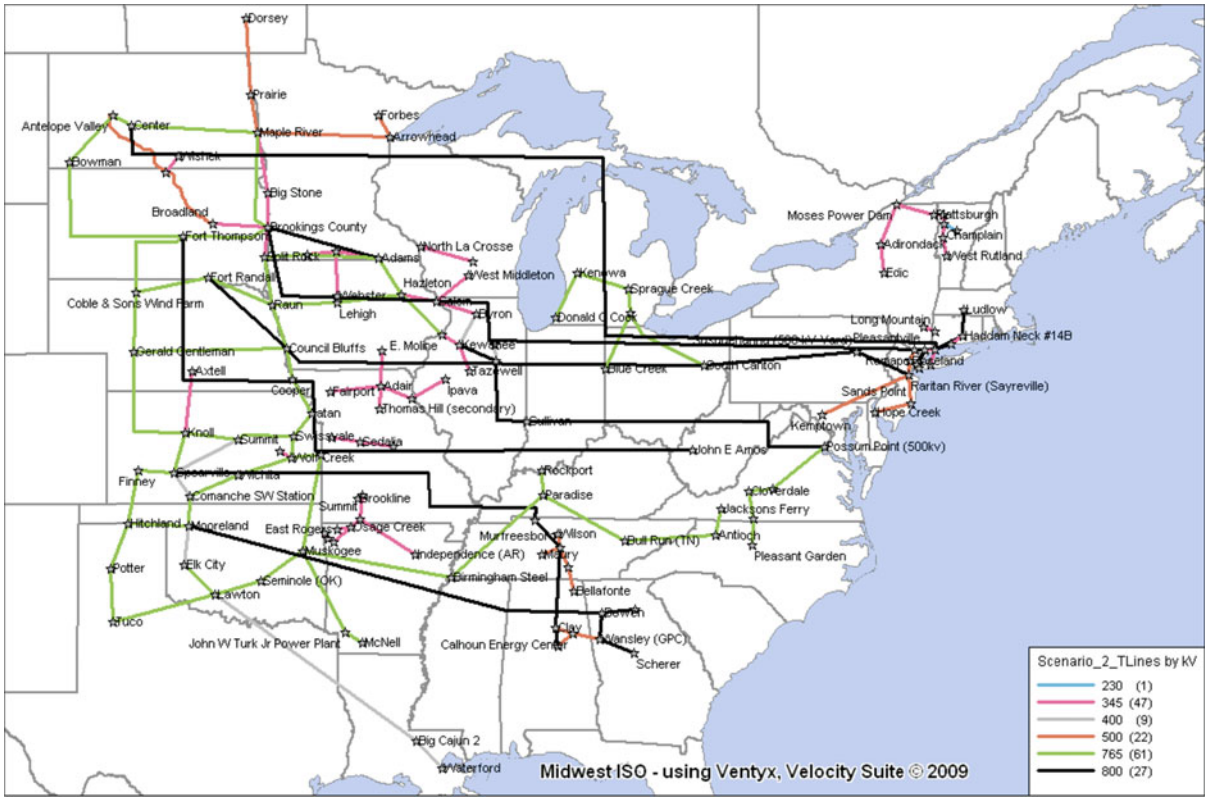

Wind Power Grid Integration: Transmission Planning. Figure 19
Resulting transmission expansion

The constrained price as shown in Fig. 18 on the left shows the price difference that may exist before the transmission overlay is constructed. Generator pockets (blue) and Load pockets (orange) can be easily found. The changes in the color represent areas of constraints called congestion. Congestion is a measure of the inefficiency of an energy market. Quebec is not modeled and the chart uses New England's prices. Price is one

tool to use to determine the transmission, but a better indicator is where energy is sourced and where energy is sunk from the economic models. Sources and sinks include both price and the quantity of energy which are needed to determine value. A price differential for a volume of energy produces revenue that can help pay for the transmission expansion. A high price with a low volume of energy associated with it may have a lower value than a lower price with a high volume. While price is a market signal for the energy markets, it is not a good signal for transmission planning.

The difference in the production cost, the Constrained versus the Copper Sheet, adjusted for sales and purchases provides an estimate of the total potential budget for transmission. Experience has shown that a practical budget may be 70% of the maximum potential budget. Figure 13 is an example of the maximum potential budget for transmission expansion broken down by area. Geographical areas in the USA could be geographical areas in another large country or countries such as in Europe.

The pie chart shows the benefits to the loads. There are also benefits to the generators. Depending on the regulation agreement, sometimes the total benefit to an area is a sum of the load price changes and the generator revenues. If an area is a low-cost producer, the generation can be self-scheduled to serve your own load to prevent increases in the price of energy to the load. The generation schedule does not change the self-scheduling if an area is a low-cost producer is just an accounting process. The results of the study do not change. These are real-time details that cannot be modeled 15 years in advance, but they should be considered when reading a result Fig. 20.

Price differences, while indicative, cannot pay for transmission lines. A volume of energy at a good price difference is needed. The location of where a transmission line would collect low-cost energy and where the transmission line would deliver the low-cost energy to a high-priced area can be determined by looking at the increased energy supplied from an area's generation. Figure 21 is a plot of sources (dark red) and sinks (dark blue) that represent the direction of major transmission expansions as indicated by the arrows.

Figure 22 is a bubble diagram or interchange flow diagram that shows the difference in the flow of energy

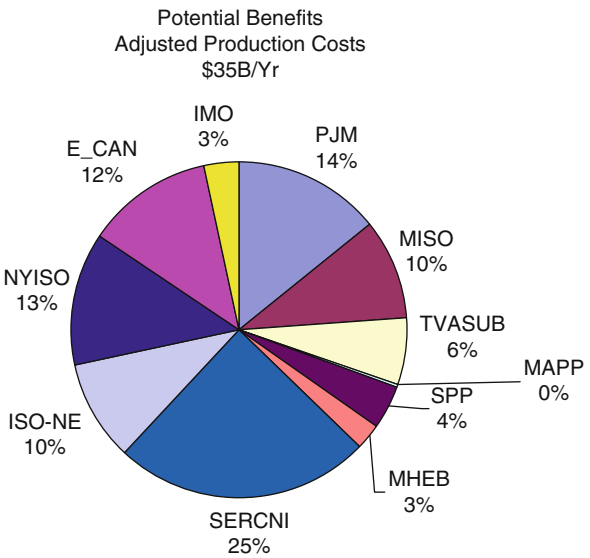

Wind Power Grid Integration: Transmission Planning. Figure 20
From the EWITS study

in the Copper Sheet case versus the Constrained case. The general direction of transmission and a relative size can be determined from this diagram. The diagram on the right is a difference with the Copper Sheet and the Overlay. The remaining transmission and direction is indicated by the lines. Most of the incremental power flow has been delivered directly by the Overlay. The areas that may use more transmission are in *orange*. The blue color indicates little need for additional transmission capacity between the areas. The blue also indicates the lack of loop flow through the underlying transmission system. The underlying transmission system would probably require few expansions due to the delivery of the wind energy. The underlying system will not be burned down due to the Overlay as some suggest. The use of a self-contingent HVDC and AC Overlay allows the control of the loop flow by using the scheduling ability of the HVDC lines.

The hourly economic simulations produce the hourly power flow on transmission lines for a year. The black heavy line on the left interchange diagram shows an interface which is the sum of flows on lines crossing a geographic border. Interfaces are defined perpendicular to major flows at areas of change of

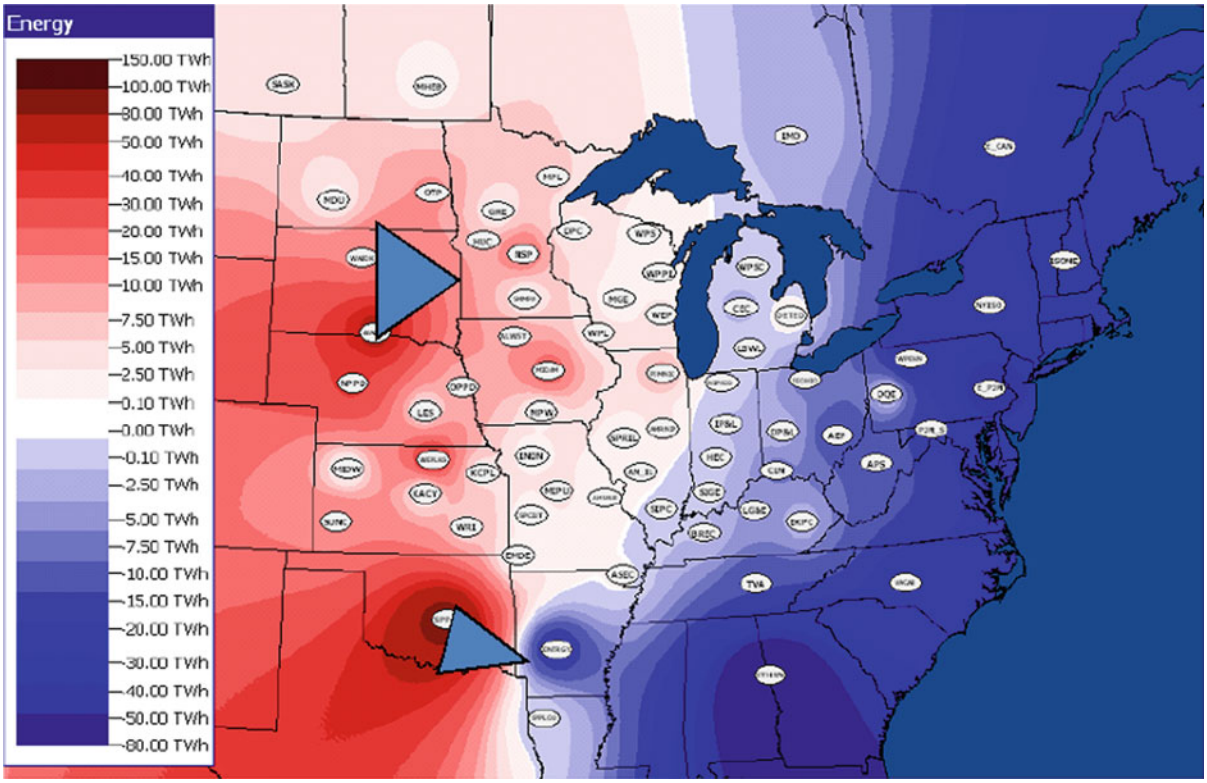

Wind Power Grid Integration: Transmission Planning. Figure 21
Scenario 2 generation difference between unconstrained case and constrair

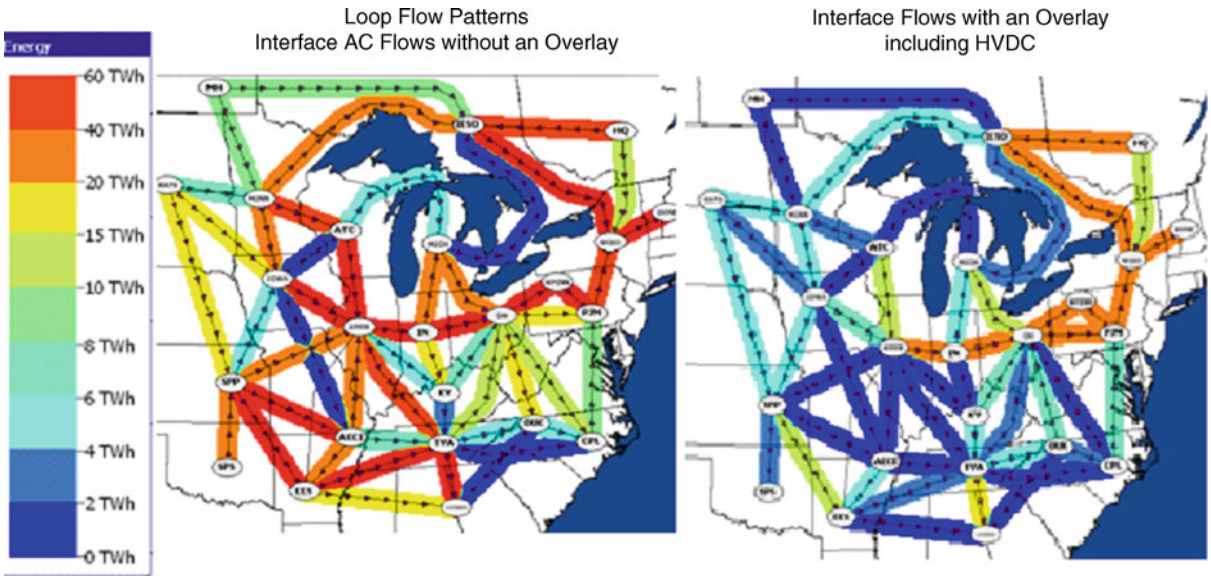

Wind Power Grid Integration: Transmission Planning. Figure 22
Bubble diagram or interchange flow diagram that shows the difference in the flow of energy in the copper sheet case versus the constrained case

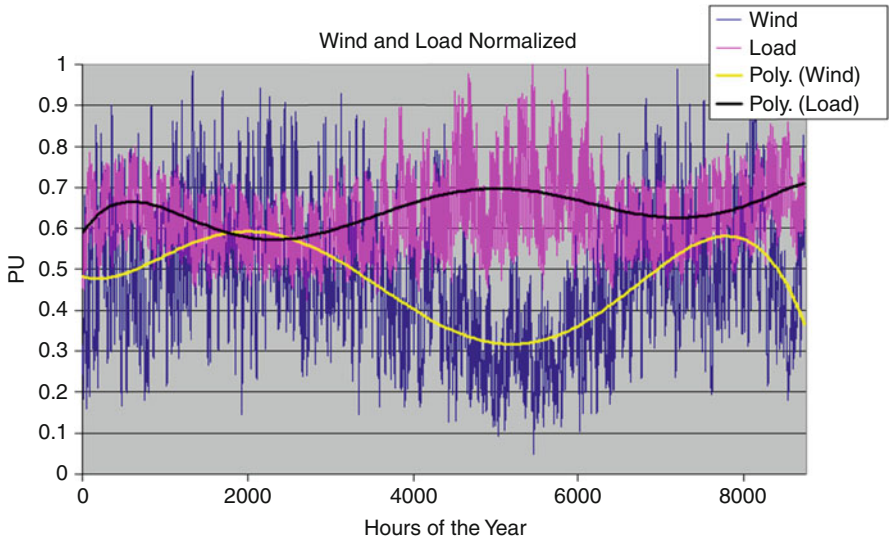

Wind Power Grid Integration: Transmission Planning. Figure 23
Wind generation output versus the load

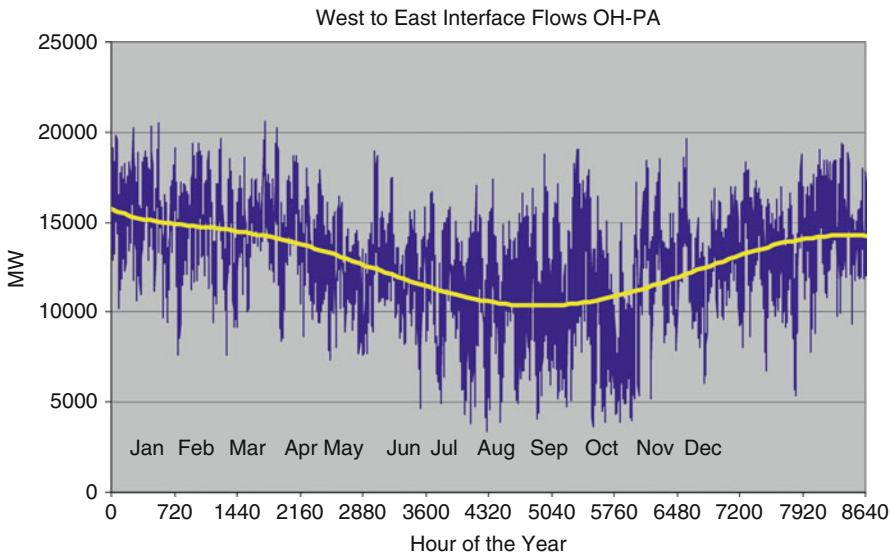

Wind Power Grid Integration: Transmission Planning. Figure 24
Load versus interchange

flow. Locations can be estimated by the places that colors change on the price plot (Fig. 18) or the source sink diagram (Fig. 21). The heaviest loading of the transmission is off-peak in the spring, fall, and winter. The lightest loading of the transmission system is during the summer peak. The plot of wind generation output versus the load is shown in Fig. 23. The trend lines through the plots show that wind energy production is about to counter when it is needed most. The interchange plot in Fig. 24 shows a similar pattern. The interchange plot shows that the heaviest transmission flows occur off-peak. The spare

transmission capacity on peak adds to the generation reliability. Generation can use the spare transmission on peak to transfer power into an area that would need it. The amount of transmission that is needed can be estimated by inspection, but a more formal method is used.

Loop flow data can be sorted from ascending to descending values and then a load duration curve of the power flow across an interface can be plotted. Based on this curve one can estimate how often a certain transmission level is exceeded, and then a selected level of transmission capacity can be selected. The energy flow at the maximum power level would be very small and create little value. Experience has shown that if a transmission line that would transmit 80% of the energy, not 80% of the peak value, then the line would have good potential for being an economical expansion, c.f. Fig. 25. The load duration and 80% energy process converts energy flow to power transfer (MW) quantities. Transmission lines are rated in MW of power transfer capability. Once the power transfer level is known, the number and voltage of transmission lines can be estimated for each interface.

An examination of the flow that transfers power through multiple interfaces provides an estimate of the distance that power flows through areas and may be a candidate for a longer AC line or may qualify for a DC line if the distance is more than 600 miles in the examples given previously. Table 1 shows the power transfers through multiple interfaces for the EWITS futures.

Power transfers between multiple interface locations can be used to estimate the transmission that would be included in the overlay.

Table 1 shows the interface numbers using this process for the EWITS study. Scenarios 1–3 had a 20% wind energy level with about 225,000 MW of wind generation. Scenario 2 had a mixture of wind generation using onshore and offshore wind. Scenario 1 used primarily high-capacity factor wind located in the high plains in the western part of the Eastern Interconnection. Scenario 3 had a high proportion of the wind offshore of the east coast. Scenario 4 had a 30% wind generation scenario with strong wind both offshore and onshore in the west as well as in the middle for about 330,000 MW of wind generation. Energy is converted to power transfer capability in MW which is what transmission lines are rated. The Ohio-Eastern PJM (OH-EPJM) Scenario 2 or compared to a three-line HVDC system rating of 14,300 MW one can see it is about a match. The distance across the system is greater than 600 miles. So the HVDC lines terminals are selected using the information in the source-sink diagram in Fig. 21. The choice of the least expensive option in Fig. 12 further validates the choice. Another simulation is chosen to simulate your choices. The examination of the constraints and the information

Transmission Capacity designed to deliver 80% of desired energy flow

Wind Power Grid Integration: Transmission Planning. Figure 25
The 80% energy process

Wind Power Grid Integration: Transmission Planning. Table 1 Top 24 interfaces with the largest annual energy difference

Interface	EWITS Scenario 2 Additional transfer needs (MW)	EWITS Scenario 1 Additional transfer needs (MW)	EWITS Scenario 3 Additional transfer needs (MW)	EWITS Scenario 4 Additional transfer needs (MW)
AMRN – IN	22,901	28856	13223	24,609
IN – OH	16,594	20843	9633	17,081
OH – EPJM	14,378	18662	8715	12,928
SPS – SPP	13,983	13482	7743	13,399
SPP – EES	11,598	12551	6417	12,160

specific to the new case with the transmission expansion allows the design to be refined to that in Fig. 19. It takes four to five iterations to refine a design. Computer simulations require 6 days to run. Information to design the system is derived from the economic computer simulations and the differences between simulations. It would be very difficult to formulate a set of alternatives using power flow to design a system such as that in Fig. 19.

A short visual examination can identify the potential common elements in the four scenarios. A rigorous ranking produces a lot more computer work and does little better to identify a robust transmission plan of "least regrets." The black lines are the HVDC lines. Green lines are 765 kV lines. Red lines are 345 kV. Orange lines are 500 kV (Figs. 26–29).

EWITS skipped the Robustness Test, The Robust "least regrets" transmission selection, and the Reliability test. The Reliability section of the study is passing through the least regrets plan developed using economic techniques with the best estimate of the generation, usually a conservative forecast, to determine if the plan could pass the tests that the Midwest ISO subjects all the reliability-based plans. The Midwest ISO added a lot of dynamic reactive devices to the EWITS Scenario 2 transmission plan and loaded the HVDC to maximum generation with wind generation schedules to obtain a solved power flow. General Electric set up a rough dynamics case and ran a few tests of AC and HVDC outages without showing any great concern. Although this process was very rough and would have to be run with many more contingencies, the study gives one faith that it may work with a large wind resource. The Midwest ISO is not about to finance a study to do a definitive dynamics study without the assistance of others for the Eastern Interconnection.

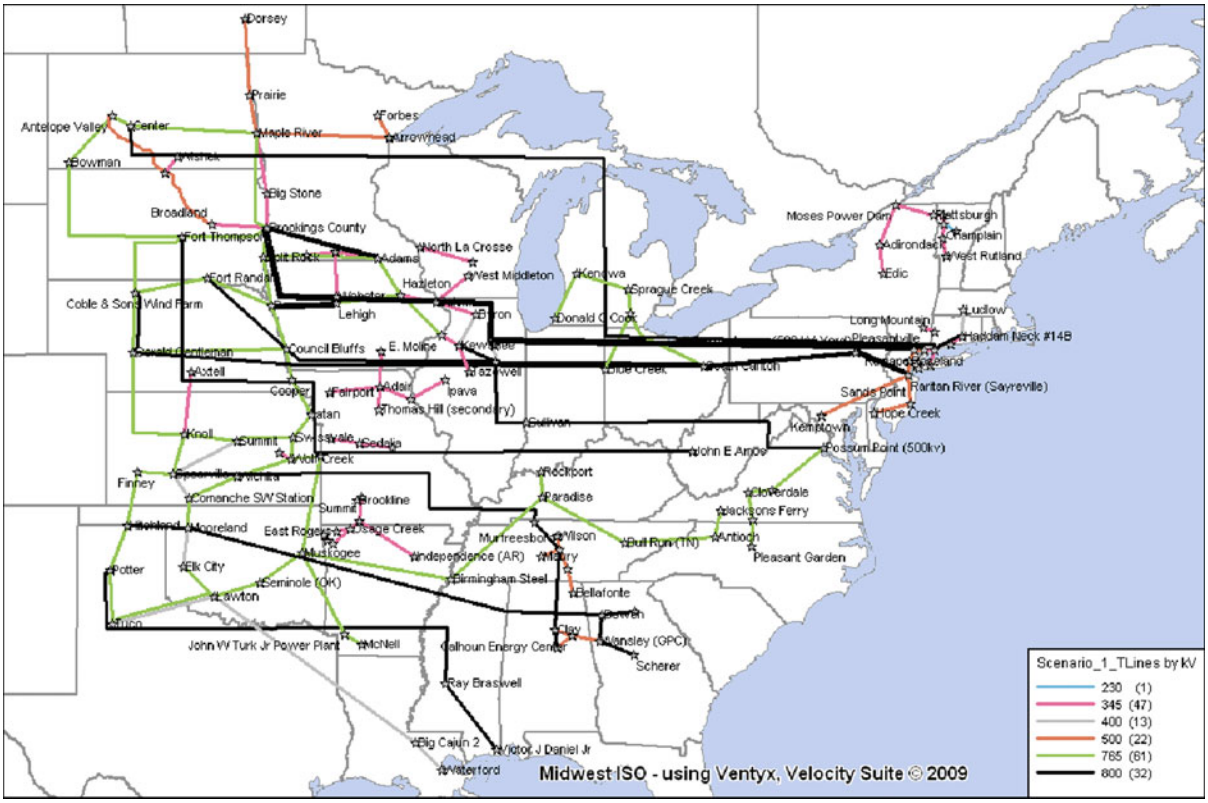

Wind Power Grid Integration: Transmission Planning. Figure 26
EWITS Scenario 1–20% strong western wind generation locations

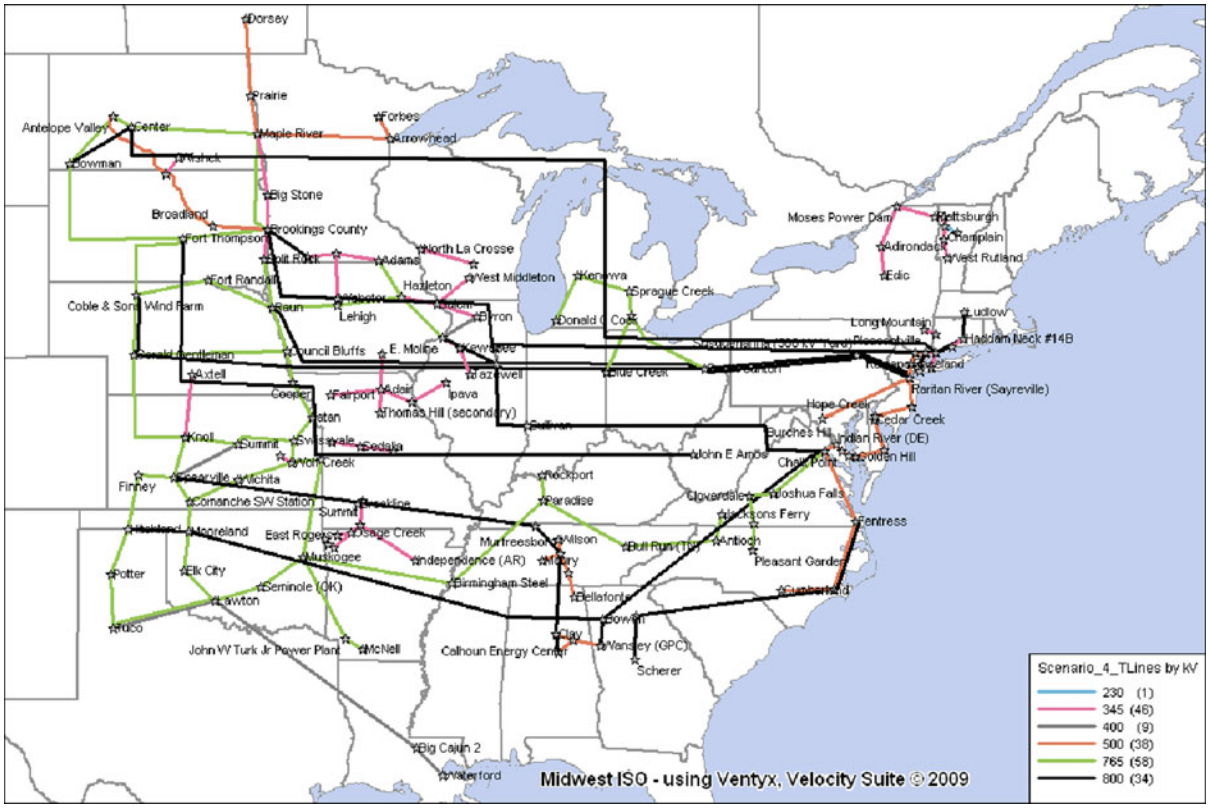

Wind Power Grid Integration: Transmission Planning. Figure 27
EWITS Scenario 2–20% mixed wind generation locations

The Eastern Interconnection Planning Collaborative will have to do one if it is to be done. If it were done, the wind generation levels would be far less than a 20% energy level.

Figure 30 shows the total cost of the four EWITS futures. The wind capital cost contributes to most of the variation between the futures. Wind integration costs that people obsess about are a small portion of the total cost, even less than the projected variable operation and maintenance cost on the wind machines. Transmission is a distant third in the ranking of components behind Wind Capital Cost and Production Cost (Fuel& VOM).

Wind Integration Studies

Statistical distributions of the rate of change of power or ramping requirements were produced. Tails of the distributions were examined for the maximum rates of change. Generator spinning and fast start reserves were estimated to manage the tail events. The reserves in the economic simulations were changed in the dispatch algorithm to model the system operation with the higher reserves. The cost of operation with a perfect wind forecast and a forecast with forecasting errors were compared to determine the cost of wind integration.

The output of the wind integration section of the study can be used to modify the assumptions to be used in the next iteration of the study. Spinning reserve, fast start requirements, and the capacity credit for wind are three key factors that modify the generation forecast assumptions list and available generation lists.

Probabilistic or statistical planning techniques with multiple year runs are needed to assess the cost of variability and the effects on transmission system

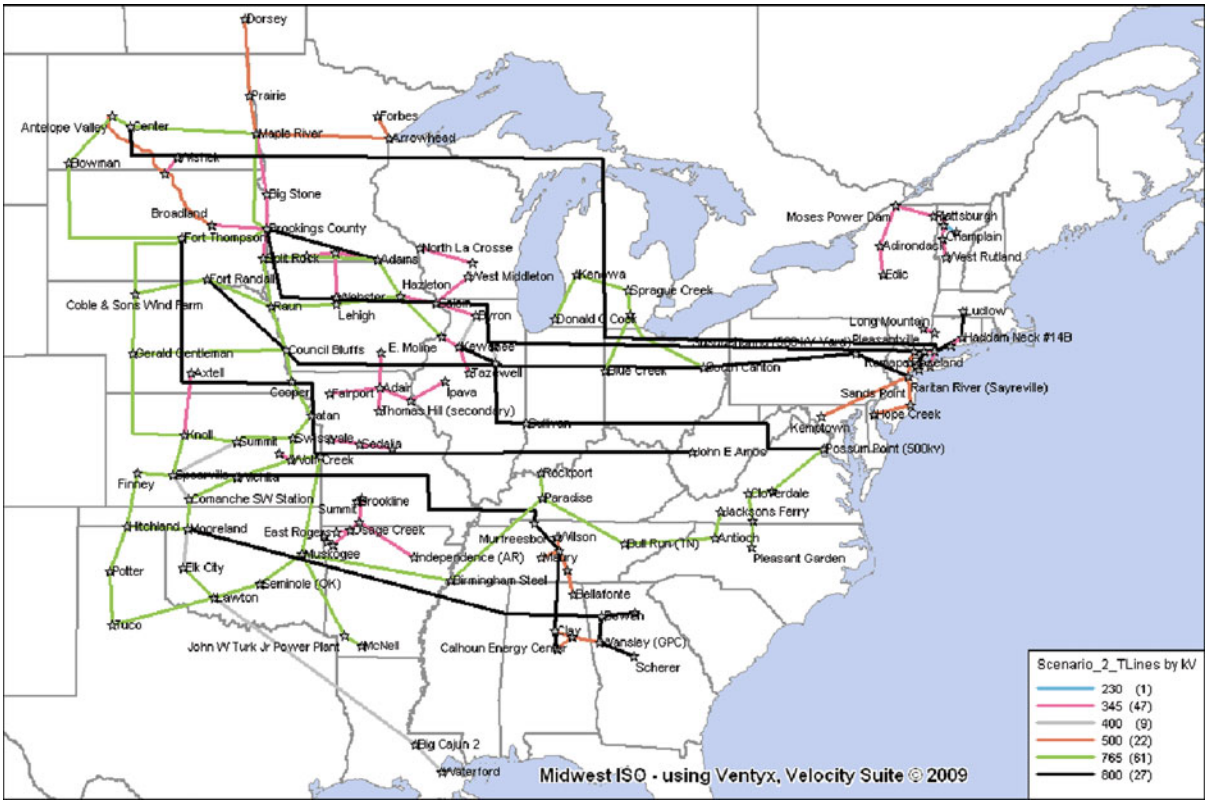

Wind Power Grid Integration: Transmission Planning. Figure 28
EWITS Scenario 3–20% heavy offshore east coast wind generation locations

design. Should one design a transmission system for the best wind year? It may be lower in total cost to curtail the extreme wind and build transmission more toward a value that would handle less wind. The economic studies allow one to determine the choice of the level to design transmission for wind energy variability.

If one must meet 20% energy each year, for example, then there has to be more wind generation added and the associated transmission to deliver a good portion of the wind energy to account for low wind energy years.

The wind energy variations are quite high when taken at the turbine or wind plant level. Geographic diversity of wind resources can be summed by a transmission overlay to produce a less variable wind energy resource than any of the individual plants. The EWITS study produced the graph in Fig. 5 that shows the reduction in variation of wind as the wind is aggregated. The variation of wind is reduced by a factor of 4 just by aggregation.

One must remember that the weather affects load levels just as it does wind levels. Wind and load patterns must be matched using the same year for studies. Future years must be matched also. Multiple years of wind and load patterns are scaled to future load levels to produce hourly models for economic studies. If statistical models of wind were used, both the wind model and the load model would need to be matched.

Less generation is needed in reserve to manage the wind variation if there is a transmission system that can aggregate wind generation. The transmission lines that aggregate wind energy would have much higher variable loading that would be the case with conventional generation. The reactive power variations would produce voltage variations on the AC power system if the wind were aggregated on the AC system. Dynamic

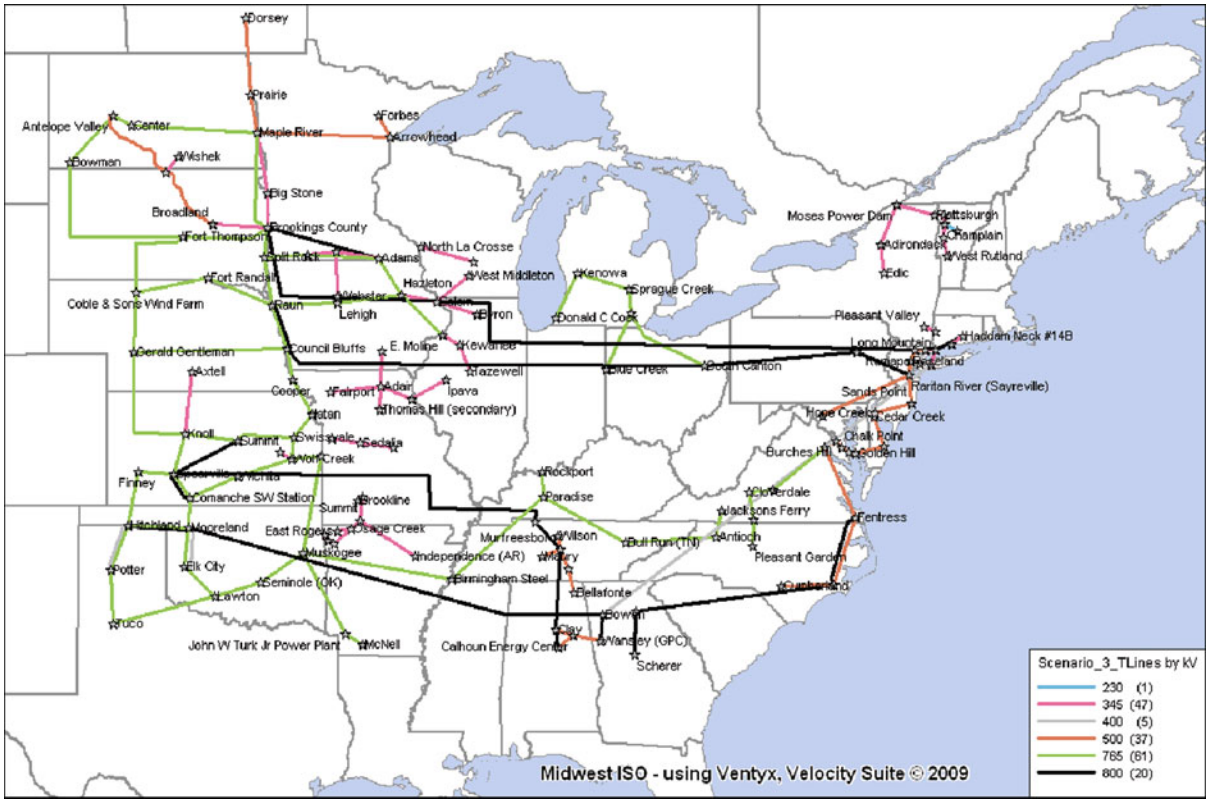

Wind Power Grid Integration: Transmission Planning. Figure 29
EWITS Scenario 4–30% wind energy, heavy everywhere wind generation locations

reactive power support would have to be distributed across an AC transmission system to manage the voltage in an all AC design. An HVDC transmission overlay would restrict voltage regulation to be at the terminals of the HVDC converters. This would simplify the AC system design. If the HVDC system is scheduled to transmit variability, the areas receiving the variability in energy flow would have to provide dynamic reactive power support. Having the HVDC lines have varying schedules could relieve the AC system from having to have reserve generation close to the wind generation to control frequency and power interchange schedules. Probably gas fired generation would have reduced loading if the HVDC lines were delivering energy to an area. The gas generation on the receiving end could provide the regulation. Ancillary Services revenues would be increased for the generators on the receiving end. Less total generation would have to be constructed to serve wind. More wind generation could be placed in areas with an HVDC convertor than could be accomplished without the HVDC convertor. The wind generation system would require fewer AC transmission ties to manage the wind variability.

Other Information to Answer Questions

Figure 31 provides information on the carbon dioxide reduction Scenario 2 sensitivity test for various carbon tax prices. The 30% wind energy level reduces carbon dioxide about the same as a $70/ton tax and costs less. This type of analysis is performed to answer questions about the carbon performance. Other information on the curtailment of wind, conventional generation capacity factors and the time running a minimum generation, the number of starts on generation, the revenue changes on generation, all emissions, etc., can be produced from the economic simulations.

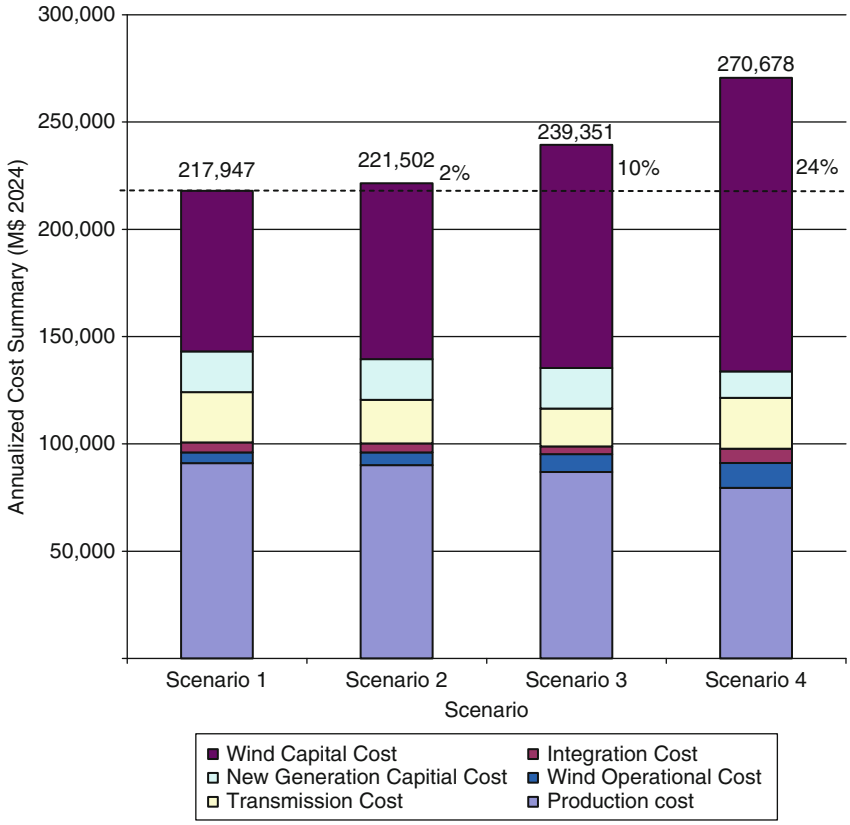

Wind Power Grid Integration: Transmission Planning. Figure 30
Total cost of the four EWITS futures

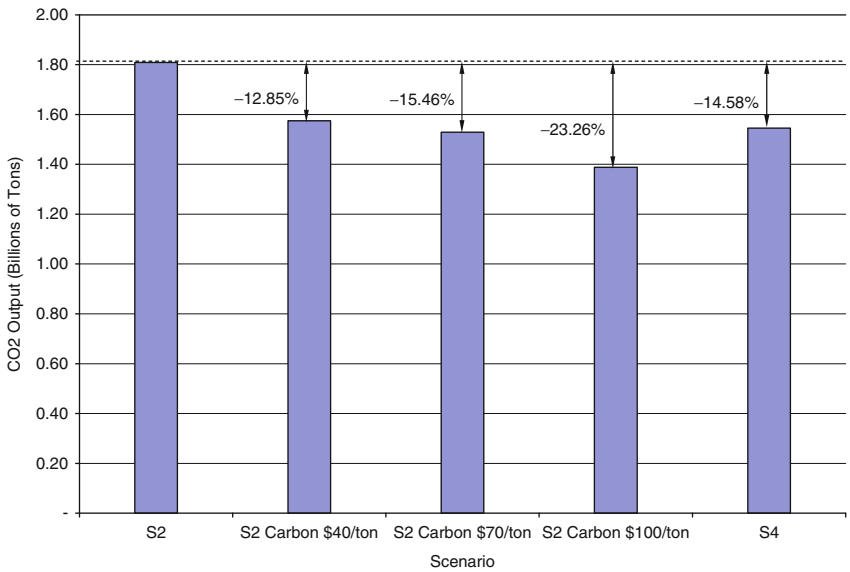

Wind Power Grid Integration: Transmission Planning. Figure 31
Carbon dioxide reduction Scenario 2: sensitivity test for various carbon tax prices

Conclusion

Overlay transmission systems can be designed to economically and reliably serve load and deliver renewable energy.

Overlays are a layer of transmission which spans the underlying transmission systems. Overlays require different planning techniques than those of the underlying systems.

The criteria and degree of study of the underlying and the overlay vary considerably. The underlying studies are more detailed concerning the design of the transmission facilities. Level of involvement in a number of departments of specialists may occur at a large utility. For a small utility one or a few people may perform many tasks to get the details necessary to construct a transmission expansion.

The involvement of many different people with widely varying backgrounds and interests have driven the transmission planning processes to provide more information than has been required in the past. Larger transmission expansions have attracted more stakeholders in the process.

The creation of the RTO and the insertion of large amounts of wind energy and solar in some areas has changed the way transmission is being planned. Energy resources, such as wind, require probabilistic evaluations that exceed the conventional generation need for such analysis.

Bibliography

1. EWITS – Eastern Wind Integration and Transmission Study. The National Renewable Energy Laboratory, US. http://www.nrel.gov/wind/systemsintegration/pdfs/2010/ewits_executive_summary.pdf
2. EIPC – Eastern Interconnection Planning Collaborative. http://www.eipconline.com/
3. JCSP – Joint Coordinated System Plan (JCSP) 2018 summer reliability study Report. https://www.midwestiso.org/Library/Repository/Study/JCSP/JCSP_Report_Volume_2.pdf
4. PROMOD. http://www.ventyx.com/analytics/promod.asp
5. GE MAPS – GE Multi-Area Production Simulation Software. http://crai.com/consultingexpertise/content.aspx?tID=828&subtID=842&terTID=896
6. GRIDVIEW. http://www.ferc.gov/eventcalendar/Files/20100608140700-Zhu,%20ABB%20-%206-9-10.pdf

Wind Power, Aerodynamics and Blade Technology

Martin O. L. Hansen
DTU Mechanical Engineering, Technical University of Denmark, Lyngby, Denmark

Article Outline

Glossary
Definition of the Subject and Its Importance
Introduction
Where Does the Energy Come From
How Is the Energy Harvested
How Much Energy Can Be Harvested
Environmental Conditions
Blade Element Momentum Theory, BEM
Computational Fluid Mechanics
Rotor Blades
Future Directions
Bibliography

Glossary

A Rotor area
a Axial induction factor
a' Tangential induction factor
B Number of blades
C_d Drag coefficient
C_l Lift coefficient
C_p Power coefficient
C_T Thrust coefficient
C_θ Tangential velocity in far wake
D Aerodynamic drag
L Aerodynamic lift
M_R Rotor shaft torque
M Bending moment, torque
P Power
p Load
R Blade radius
r Local radius on blade
T Thrust
u Axial velocity in the rotor plane
u_1 Axial velocity in far wake
V_o Wind speed

$\boldsymbol{V}_{\mathbf{rel}}$ Relative velocity to blade
$\mathbf{W}$ Induced velocity
$\boldsymbol{\alpha}$ Angle of attack
$\boldsymbol{\theta}$ Local blade angle with rotor plane
$\boldsymbol{\rho}$ Air density
$\boldsymbol{\sigma}$ Solidity, material stress
Φ Flow angle
$\boldsymbol{\omega}$ Angular velocity

Definition of the Subject and Its Importance

Wind energy has been used for thousands of years to drive sailboats, for grinding grains, and for pumping water. For approximately 100 years, wind energy has also been used to produce electricity by connecting the rotor shaft to a generator and thus transforming wind mills into wind turbines. With the growing awareness to find alternatives to fossil fuels in order to reduce the CO_2 emission and to become less dependent on oil-producing regions, wind energy has reached a new age, where wind turbines are no longer produced by local black smiths but by very large companies using advanced design tools similar to the aeronautical industry. It is the purpose of this entry to give an introduction to wind turbine aerodynamics and describe the aerodynamic design tools presently used and what tools may be used in the future.

Introduction

Wind turbines are becoming a bigger and bigger contribution to the production of electricity, with global annual growth rates of more than 20%. In windy regions as, e.g., Denmark, 20% of the total electrical energy produced already stems from wind turbines, and this number is even higher in the western part, where the wind resources are larger. In the 1980s, where the commercial wind turbines were introduced to the market, they were considered a nightmare for the utility companies since the electricity production from wind turbines is strongly correlated with the wind speed and thus variable in nature. The utility companies preferred a few large power plants (often coal, gas, or nuclear) that could easily be controlled to balance the consumption. Today they have realized that in windy areas, the price of electricity measured in \$/kWh is actually competitive with the more conventional means of power production, and some of them have actually become developers that build and operate large wind farms. The production price from wind turbines has not always been as low as today, and the technological developments done over the 30 years have helped. In the beginning, the fatigue loads from the turbulent wind approaching the rotor were not very well known, and therefore, the structures were built excessively strong using a lot of unnecessary material. Research on wind turbine aerodynamics has helped a lot to reduce the uncertainties of the loads, and thus, it has become possible to reduce the weight measured in kg/kW and thus also the price of the wind turbines. Most of the theories are quite old and stem from propeller theory (ship and airplanes) [1], but have in recent years been extended with empirical models specifically dedicated to wind turbines. A very important contribution to this were two EU projects [2, 3], where most of the available design tools were tested against real measurements and the so-called engineering models calibrated against these full scale experiments. The first part of entry describes very basically the origin of the energy contained in the wind and next some very classical theory is presented as, e.g., described in [1, 4] defining many of the important parameters and non-dimensional numbers used in wind turbine aerodynamics. Next, the classical Blade Element Momentum method (BEM), as derived in [1] but with the necessary engineering models derived in, e.g., [2, 3] is shown. The BEM model is still by far the most used tool in wind turbine design and load calculations, since it is very fast and in most cases quite reliable. Finally, some more advanced numerical tools based on Computational Fluid Dynamics will be addressed.

Where Does the Energy Come From

The energy extracted from a wind turbine comes from extracting some of the kinetic energy contained in the wind. In Fig. 1, A denotes an area perpendicular to the wind velocity.

The mass flow, $\dot{m}$ [kg/s], that travels through this area with a speed of V_o is

$$\Delta m = \rho A L = \rho A V_o \Delta t \Rightarrow \dot{m} = \frac{\Delta m}{\Delta t} = \rho A V_o \quad (1)$$

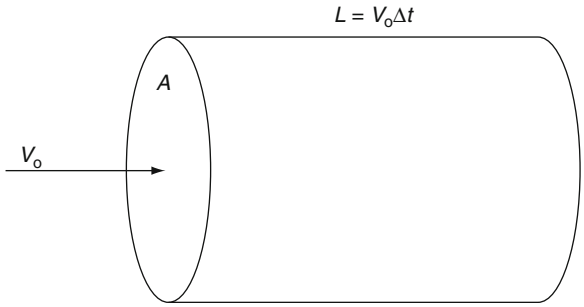

Wind Power, Aerodynamics and Blade Technology. Figure 1
Volume of air that has traveled through the area, A, with a speed of V_o in time Δt

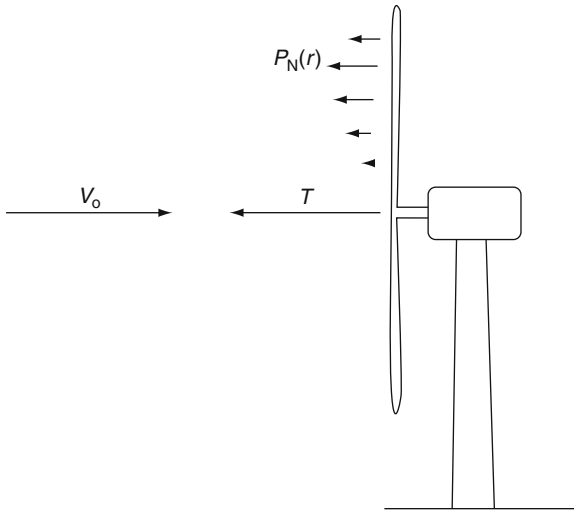

Wind Power, Aerodynamics and Blade Technology. Figure 2
Thrust force stemming from normal load distribution to slow down the wind speed

where ρ denotes the air density slightly depending on temperature and atmospheric pressure but approximately 1.2 kg/m^3. For a wind turbine rotor with a diameter of 90 m and wind speed of 10 m/s, the mass flow is around 76 t/s. The kinetic energy, ΔE_{kin}, contained in the air volume shown in Fig. 1 is

$$\Delta E_{\text{kin}} = \frac{1}{2}\Delta m V_o^2 = \frac{1}{2}\rho A V_o^3 \Delta t \tag{2}$$

and thus the available power (provided that the wind speed could be reduced to 0 m/s)

$$P_{\text{avail}} = \frac{\Delta E_{\text{kin}}}{\Delta t} = \frac{1}{2}\rho A V_o^3 \tag{3}$$

In order to extract kinetic energy from the wind, it is necessary to create a force opposite to the wind velocity and thus reducing the wind speed to something less behind the rotor. This force is denoted the thrust, T [N], and is a result of the loading normal to the rotor disc, $p_N(r)$ [N/m], $T = \int_0^R p_N(r)\, dr$, see Fig. 2.

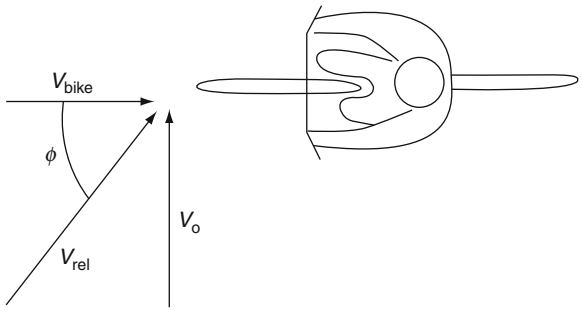

Wind Power, Aerodynamics and Blade Technology. Figure 3
Man cycling with the wind speed coming 90° to his heading

How Is the Energy Harvested

The thrust force is created by the local flow past the rotor, which resembles a man cycling with the wind coming 90° to his heading, see Fig. 3.

In Fig. 4 is shown a similar situation, where the velocity of the bike is replaced by the rotational speed of the rotor, $\omega \cdot r$.

Comparing Figs. 3 and 4, it is seen that the only difference is an extra velocity, **W**, appearing on the blade section. This velocity is denoted the induced velocity and is caused by the aerodynamic forces created by the flow past the blades. The relative wind, $\mathbf{V_{rel}}$, seen by a blade section is thus the vector sum of the wind speed, $\mathbf{V_o}$, the induced wind, **W**, and the rotational velocity due to blade rotation, $\omega \cdot r$. If the blade section shown in Fig. 4 is mounted at an angle to the rotor plane, θ, then the flow past the blade section is similar to the flow past an airfoil with an angle of attack of α as shown in Fig. 5. Φ is denoted the flow angle, and the angle of attack is the difference between the flow angle, Φ, and θ.

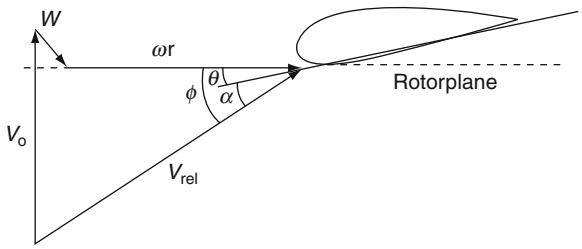

Wind Power, Aerodynamics and Blade Technology. Figure 4
Flow seen on a local section of the blade. The situation resembles the cycling man seen in Fig. 3, except for the induced velocity **W**

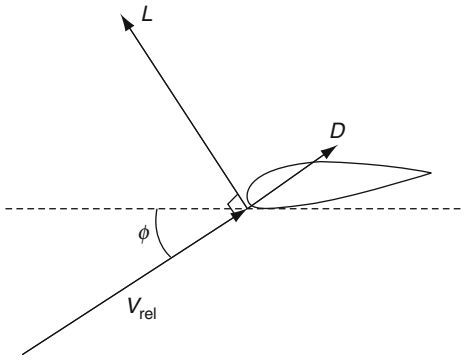

Wind Power, Aerodynamics and Blade Technology. Figure 5
Aerodynamic forces on an airfoil with an angle of attack of α with the incoming wind

From Fig. 5, it is directly seen that the normal load stems from the lift and drag projected normal to the rotor plane as

$$p_N = L\cos\phi + D\sin\phi \tag{4}$$

Also there is a tangential load, which can be found as the lift and drag projected into the rotor plane as

$$p_T = L\sin\phi - D\cos\phi \tag{5}$$

The induced velocity shown in Fig. 4 is a direct result of the aerodynamic load that also influences the incoming air. To conclude, the thrust needed for extracting kinetic energy from the air is created by the normal component of the aerodynamic loads and the tangential loads yield a torque on the rotor shaft, M_R, that can be used to drive a generator as

$$M_R = \int r p_T dr \tag{6}$$

From Fig. 4, it is seen that the angle of attack, α, is increased with increasing wind speed provided that the angular velocity is kept constant. The lift force is for small angles of attack increasing almost linearly with the attack α, since the airflow following the aerodynamic profile is more and more bent requiring larger pressure forces. For these low angles of attack, the drag force is small and relatively constant. There is, however, a limit on how much the flow can be bent, and at a certain angle of attack, the flow will no longer be able to follow the surface of the airfoil but will separate and large vortices are formed on the downwind side of the wind turbine blade. In this situation, the flow is said to stall and the lift is decreased and the drag is quickly increased, reducing the tangential load, see Eq. 5. When the tangential load is decreased also the rotor torque is reduced, according to Eq. 6, and thus also the power. This is exploited on so-called stall-regulated wind turbines where the blades are rigidly clamped to the hub and the angle with the rotor plane is thus constant. If the angular velocity at the same time is constant, then the wind turbine will stall at a certain wind speed and thus passively reducing the power at high wind speeds.

How Much Energy Can Be Harvested

To answer this question, one must consider an ideal rotor without losses. Figure 6 shows a streamtube intersecting the rotor plane at radius, r.

The conservation of linear momentum on the control volume comprised by the streamtube and neglecting the axial component of the pressure forces yields the local contribution, dT, to the total thrust

$$dT = \rho \cdot u \cdot dA(V_o - u_1) = 2\pi r \rho u (V_o - u_1) dr \tag{7}$$

where $\rho u dA = 2\pi r \rho u dr = d\dot{m}$ denotes the mass flow through the rotor. dA is area of the strip in the rotor plane, u the velocity in the rotor plane, and u_1 the velocity in the far wake. Further, the Bernoulli equation can be used from point 1 to 2 and again from point 3 to 4 in Fig. 6, yielding that the pressure jump across the rotor can be expressed as

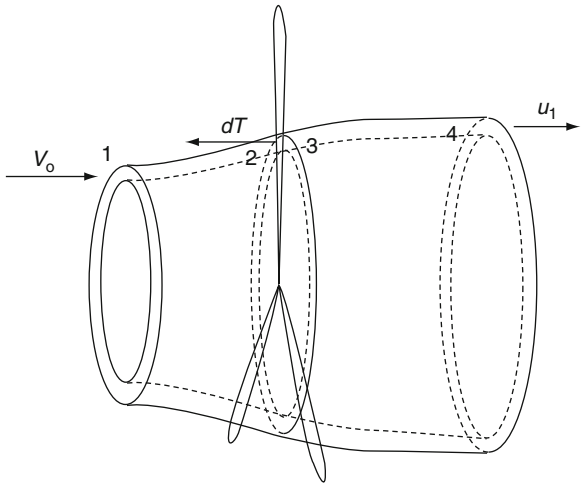

Wind Power, Aerodynamics and Blade Technology. Figure 6
Streamtube of the flow through the rotor

$$\Delta p = \frac{1}{2}\rho\left(V_o^2 - u_1^2\right) \tag{8}$$

Utilizing that the thrust force stems from the pressure jump across the rotor as $dT = dA \cdot \Delta p$ Eqs. 7 and 8 give that the velocity in the rotor plane is the mean of the undisturbed wind speed and the speed in the far wake

$$u = \frac{1}{2}\left(V_o + u_1\right) \tag{9}$$

For more details about the derivations of Eqs. 7–9, see [5]. Due to the tangential loads, Eq. 5, the wake is set into rotation and the relationship between local torque, dM, and tangential velocity in the far wake, C_θ, can be estimated using the conservation of angular momentum and since the power is the torque multiplied with angular velocity, the local contribution to the power becomes

$$dP = \omega dM = \omega \cdot d\dot{m} \cdot r \cdot C_\theta = 2\pi r^2 \omega \rho u C_\theta dr \tag{10}$$

The axial, a, and tangential, a', interference factors are introduced as the non-dimensional axial and tangential induced velocities in the wake just behind the rotor as

$$a = \frac{W_{\text{axial}}}{V_o}$$
$$a' = \frac{W_{\text{tangent}}}{\omega r}$$

The induced velocity, $\mathbf{W} = (W_{\text{axial}}, W_{\text{tangent}})$, is drawn in Fig. 4. Equations 7 and 10 are derived as if the loads, tangential and normal, are distributed evenly on the annulus at the rotor plane sketched in Fig. 6. This situation corresponds to a wind turbine with an infinite number of blades, and since this is in practice, it is not the case Prandtl derived a correction to the momentum equations by introducing the so-called Prandtl tip loss factor

$$F = \frac{2}{\pi} cos^{-1}\left(\exp\left[-\frac{B}{2}\frac{R-r}{r\sin\phi}\right]\right) \tag{11}$$

where B is the number of blades, R the rotor radius, r the local radius, and ϕ the flow angle at radial position r. The correction is applied by multiplying the right hand sides of Eqs. 7 and 10 by F. More information on the derivation of Prandtl's tip loss correction can be found in [1].

Utilizing this correction and applying expression (9) for the axial velocity at the rotor plane together with the definitions of the axial and tangential induction factors yields an expression for the available power. Note the induced velocity in the far wake is twice that of the one in the rotor plane, i.e., $C_\theta = 2a'\omega r$

$$dP = 4\pi\rho\omega^2 V_o a' F(1-a) r^3 dr \tag{12}$$

Equation 12 can be integrated to

$$P = 4\pi\rho\omega^2 V_o \int_0^R a' F(1-a) r^3 dr \tag{13}$$

Now introducing the power coefficient, C_p, as the ratio between the shaft power and the maximum available power

$$C_p = \frac{P}{\frac{1}{2}\rho V_o^3 A} \tag{14}$$

and the tip speed ratio, λ, as the ratio between the rotational speed of the tip and the free wind speed

$$\lambda = \frac{\omega R}{V_o} \tag{15}$$

Eq. 13 can be expressed in terms of the power coefficient and the tip speed ratio as

$$C_p = \frac{8}{\lambda^2}\int_0^\lambda a' F(1-a) x^3 dx. \tag{16}$$

So to optimize the power coefficient, the expression $f(x) = a'F(1-a)x^3$ should be maximized for each radial position $x = \omega r/V_o$

Doing this, one utilizes following relationship between a and a', which can be derived geometrically from Figs. 4 and 5 and assuming the induced velocity to be in the same direction as the lift

$$x^2 a'(1+a') = a(1-a) \tag{17}$$

Assuming zero drag and optimizing $f(x)$ and integrating Eq. 16 numerically yield the following curves shown in Fig. 7a for the power coefficient as a function of the tip speed ratio and the number of blades. These curves show the theoretical maximum of C_p when all losses are neglected. It is also seen for a fixed tip speed ratio how the power depends on the number of blades. The asymptotic value for an infinite number of blades and an infinite tip speed ratio can be shown to be $C_{p,max} = 16/27 \approx 60\%$ and is denoted the Betz limit and is considered the highest possible ratio of the available power that can be harvested from the wind. This occurs at a thrust coefficient, $C_T = 8/9 \approx 0.89$, where C_T is defined as

$$C_T = \frac{T}{\frac{1}{2}\rho V_o^2 A} \tag{18}$$

If one reduces the thrust force, T, below this value, the slowing down of the wind speed is reduced and thus also the decrease in kinetic energy that can be harvested into shaft power. If, on the other hand, the thrust is increased above the optimum value, then air is flowing around the wind turbine instead of through the rotor disc and thus reducing the effective mass flow through the rotor and again reducing the decrease in kinetic energy from upstream to downstream of the wind turbine. In Fig. 7b, it is shown how the power coefficient depends on the tip speed ratio when drag is taken into account and it is seen that to maximize C_p, one should increase the lift to drag ratio.

Environmental Conditions

A wind turbine rotor is not facing a constant wind but a wind field that is continuously changing in time and space due to atmospheric turbulence, wind shear, and influence of the tower. The wind shear is created by the friction between the wind and the ground, and the atmospheric turbulence is produced mechanically and thermally. The thermal contribution comes from an uneven heating of the surface, and if the temperature of the air close to the surface becomes high compared to air above, a plume of air may rise creating a mixing of the flow. The mechanical mechanism is mainly driven by the unstable boundary layer developed by the friction with the surface, where the wind speed becomes zero. Also the flow past obstacles and complex

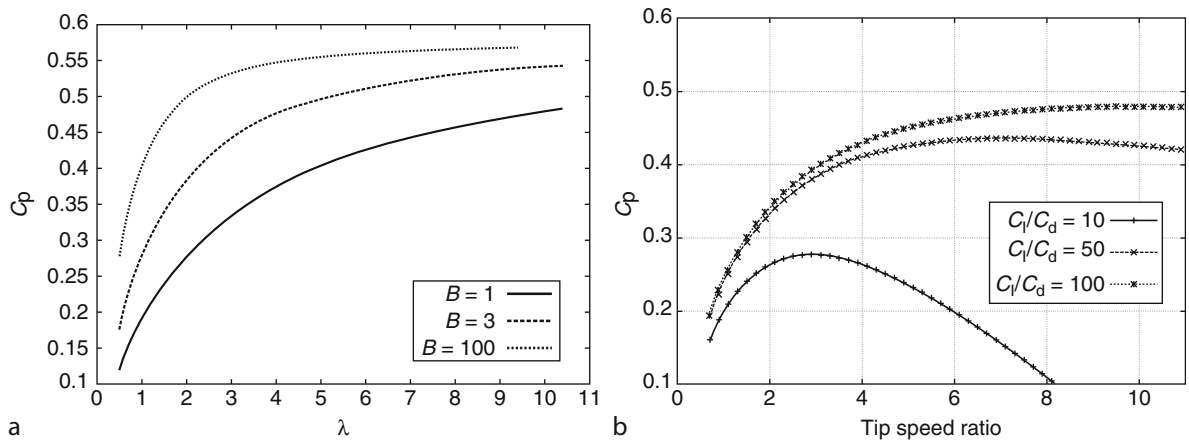

Wind Power, Aerodynamics and Blade Technology. Figure 7
(**a**) The theoretical maximum power coefficient, neglecting all losses, as a function of the tip speed ratio and number of blades. (**b**) The theoretical maximum power coefficient, when the drag is also taken into account, as a function of the tip speed ratio for a fixed number of blades of 3

terrain will cause mechanically generated turbulence. Figure 8 shows a snapshot of such an inflow to a wind turbine. The wind shear is drawn by the dashed line that represents the time-averaged velocity at a given height. Another very severe example is when a wind turbine is placed behind one or more wind turbines in a wind farm. In this case, the turbine will experience higher turbulence due to the extra turbulence created by the wake of the upstream turbines.

Since the inflow varies in time and space, a local segment on one of the blades will experience a constantly changing wind speed, and thus the angle of attack and thereby also the aerodynamic loads as indicated in Fig. 4 will constantly change in time and will thus contribute to fatigue damage. So before the loads and thus the output of a wind turbine are calculated, one needs to generate a realistic time and space history of the wind field. Realistic in the sense that it has the same statistical properties as the free wind, both with respect to the power spectrum and spatial correlations as e.g., described in the IEC norm [6]. Some of the most used methods to create a 3D time-varying wind field are described in [7, 8].

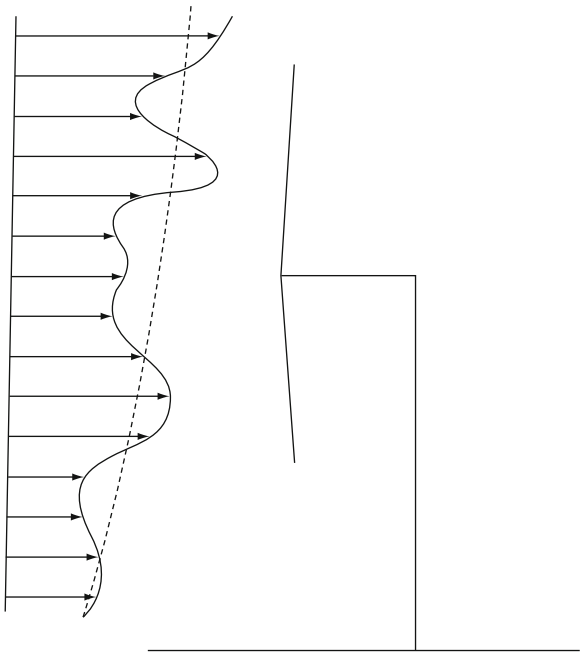

Wind Power, Aerodynamics and Blade Technology. Figure 8
A snapshot of a typical inflow to a wind turbine

Blade Element Momentum Theory, BEM

The most used tool for predicting aerodynamic loads on a wind turbine is the so-called BEM method (Blade Element Momentum method). The BEM model is very popular since it is extremely fast compared to more sophisticated methods such as Computational Fluid Dynamics. A fast method is needed since the loads on a wind turbine are by nature time dependent mostly due to the time-varying incoming wind. Often time series of 600 s are required and a typical time increment, Δt, could be 0.02 s. That is the loads have, for each time series, to be calculated approximately 30.000 times. To do a full design calculation following, e.g., the IEC norm [6] would require in the order of 1,000 such time series. It is therefore in the next many years completely unrealistic to do CFD for a complete design verification.

The BEM model is basically a steady model that computes the flow state where the airflow through the rotor is in equilibrium with the aerodynamic loads along the rotor blades. In order to calculate the unsteady loads, several so-called engineering models must be added. They are called engineering models, since they do not solve directly the physics behind the various phenomena but merely models their effects. The most important one is called dynamic wake or dynamic inflow since it introduces a time delay to the change in the air velocities whenever the aerodynamic loads are changed by, e.g., pitching the blades, see e.g., [2, 3]. The time constant for dynamic inflow/wake is for large wind turbines in the order of 10 s and very important, especially for pitch-regulated wind turbines. Another time delay model called unsteady airfoil data or dynamic stall is also added. A section on a wind turbine blade is constantly experiencing a time-varying angle of attack at a relatively high frequency mainly due to not only turbulence but also wind shear, yaw misalignment, and tower passage. The flow over this airfoil section is thus never in equilibrium with the instantaneous angle of attack, but is lagging behind in time but always chasing the instantaneous equilibrium. The time constant for the unsteady aerodynamics is much lower than the dynamic wake/inflow and in the order of 0.01 s, but including the model is important since depending on the mean angle attack, the amplitude, and frequency, it may enhance stability,

see e.g., [9–11]. Also a model is included that redistributes the induced velocities azimuthally whenever the rotor is not perfectly aligned with the wind. This redistribution yields a restoring yaw moment and is thus important for floating wind turbines with very low torsion stiffness in the tower. The BEM method relies on 2-D airfoil data, $C_l(\alpha)$ and $C_d(\alpha)$, to calculate the lift and drag. ρ denotes the air density and c is the width of the local airfoil and denoted the chord.

$$L = \frac{1}{2}\rho V_{\text{rel}}^2 c C_l(\alpha) \tag{19}$$

and

$$D = \frac{1}{2}\rho V_{\text{rel}}^2 c C_d(\alpha) \tag{20}$$

The relative velocity, $V_{\text{rel}} = \left|\vec{V}_{\text{rel}}\right|$, and the angle of attack, α, is computed from Fig. 4 as

$$\alpha = \phi - \theta \tag{21}$$

and

$$\vec{V}_{\text{rel}} = \vec{V}_{\text{o}} + \vec{W} - \vec{V}_{\text{rot}} \tag{22}$$

where $\vec{V}_{\text{rot}}$ is the rotational speed of the blade section and $\vec{W}$ the induced velocity as defined by $\vec{W} = \left(W_{\text{axial}}, W_{\text{tangent}}\right)$. If the induced velocity is known then the relative velocity and thus the flow angle can be calculated by Eq. 22 and then the angle of attack is given by Eq. 21 and finally the aerodynamic loads from Eqs. 19 and 20. The induced velocity is a direct result of the aerodynamic loads on the incoming air. If one puts up the balance between the local thrust force expressed by the momentum deficit in the wake as given by Eq. 7 and expressed directly from the aerodynamic loads Eq. 4, utilizing that $dT = Bp_{\text{N}}dr$, then an expression for the axial induction factor, Eq. 23, can be derived. Similarly an equation for the tangential induction factor, Eq. 24, can be derived through the conservation of angular momentum and the local torque from the blades $dM = Brp_T dr$.

$$a = \frac{1}{\frac{4F\sin^2\phi}{\sigma C_n} + 1} \tag{23}$$

$$a = \frac{1}{\frac{4F\sin\phi\cos\phi}{\sigma C_t} - 1} \tag{24}$$

ϕ is the flow angle, F is Prandtl's tip loss correction, $\sigma = Bc/2\pi r$ is called the solidity, and $C_n = p_{\text{N}}/\frac{1}{2}\rho V_{\text{rel}}^2 c$ and $C_t = p_T/\frac{1}{2}\rho V_{\text{rel}}^2 c$ are the normal and tangential force coefficients, respectively. 23 and Equations 24 yield the induced velocity in non-dimensional form and they must in principle be solved iteratively since a and a' depend on ϕ, C_{n}, and C_{t} that again depend on a and a'. Equations 23 and 24 express the situation where the induced velocity is in equilibrium with aerodynamic loads. However, the induced velocities change very slowly in time due to the inertia of the mass of air affected by the rotor loads. This phenomenon is denoted dynamic inflow or dynamic wake and a typical time constant is in the order of 10 s. In an unsteady BEM calculation where the time step is in the order of 0.01–0.05 s, the induced velocity changes very little in one time step and one can thus simply use the value from the previous time step on the right hand side of Eqs. 23 and 24 when updating a new set of quasi steady values of a and a'. Having done this, one puts these quasi steady values through a dynamic wake filter to simulate the inertia as, e.g., shown in [2] to determine the final induced velocity at the new time step. Knowing this, one can now compute at this new time the aerodynamic loads as described above and one can then proceed to the next time step. If the thrust coefficient, C_T, as defined in Eq. 18 is large, that is, the force responsible to slow down the wind speed becomes big compared to the momentum of the incoming flow, then the flow through the rotor is no longer comprised by nice streamlines as sketched in Fig. 6 but is much more complicated. This case is denoted the turbulent wake state and is characterized by large zones in the wake containing reversed flow. Here the momentum theory simply breaks down and Eq. 23 is replaced by an empirical relationship between the thrust coefficient and the axial induction factor as

$$C_T = \begin{cases} 4a(1-a)F & a \le \frac{1}{3} \\ 4a\left(1 - \frac{1}{4}(5-3a)a\right)F & a > \frac{1}{3} \end{cases} \tag{25}$$

The BEM is so fast that it on a fast computer can calculate the dynamic behavior of a wind turbine in real time, also taking the structural response of the wind turbine into account. Doing this, the structural velocities are included when estimating the angle of attack, and the strong coupling between the aerodynamic loads and the structural response is denoted aeroelasticity.

Computational Fluid Mechanics

Instead of solving the global momentum equations as in the BEM model one could alternatively solve the Navier-Stokes equations, which are also momentum equations but in differential form. This has the advantage that none of the so-called engineering models are needed, since all the physics modeled through time delays as, e.g., the response of induced velocities on a change in loads is directly contained in the governing flow equations. Also if a full Navier-Stokes simulation is performed, then the uncertainty in the 2-D airfoil data, $C_l(\alpha)$ and $C_d(\alpha)$, is in principle removed. This is of course provided that it is possible to calculate correctly the flow on the blades including the transition from laminar to turbulent boundary layer and the correct separation lines. Full 3-D CFD calculations are made since the 80th about fixed wings for airplanes and helicopter rotors using unsteady Euler solvers [12–15]. The first full Navier-Stokes solutions of wind turbine rotor aerodynamics were published in the 1990s [16–21], where [16] is considered the first complete wind turbine rotor calculation using the 3-D Navier-Stokes equations. However, the first viscous 3-D calculation of a rotating wind turbine blade was made using a viscous-inviscid interaction technique [22], where the potential flow applying a panel method was coupled with the 3-D boundary layer equations. With this model, it is possible to calculate the flow up to a moderate separation. The breakthrough of CFD for wind turbines came with the blind test organized by the National Renewable Energy Laboratory, NREL, after a controlled measurement campaign of a real wind turbine in the NASA Ames 80 × 120 ft wind tunnel [23, 24]. CFD computations made by Risø National Laboratory [25] fitted very well the measured flow and pressure distributions even at high angles of attack and have later inspired other research groups and industry to apply CFD in their aerodynamic research.

Doing CFD one has first to create a computational grid resolving the blades and the outer flow domain (in and outflow). This grid should in principle be fine enough to capture all the scales of the vortices comprised in the flow. It is not possible to resolve the smallest turbulent eddies since this would require an enormous number of gridpoints. Therefore one often solves the Reynolds Averaged Navier-Stokes, RANS, equations where the equations have been time averaged. To solve these, one needs to model the Reynolds stresses coming from the unsteady perturbations from the turbulent eddies. Most of the recent RANS simulations for wind turbines were done using the k-ω, SST model [26] or Spalart-Allmaras [27]. The RANS models do, however, have some problems computing accurately the flow and thus blade loads in massive stall. It seems that more modern methods like the so-called Detached Eddy Simulation, DES [28, 29], give better results in stall, but at a much higher computational cost. In a DES model, the dynamics of the larger vortices bigger than the computational mesh is directly simulated, whereas the influence of the smaller vortices is modeled similar to RANS. There is hope that when a DES model is used together with a 3-D transition model, very good results can be obtained also at massive stall. But even then there is no way that this type of CFD models can replace the BEM method in design validation calculations were up to thousand time series of 600 s needs to be calculated. But CFD is used to validate the airfoil data used in the BEM calculations for new designs and they are used together with measurements to check and calibrate the engineering models needed by the BEM method.

There exist some hybrid methods that sometimes are used in the design calculations and where CFD replaces the calculation of induced velocities, but where the actual boundary layers on the blades is replaced by volume forces determined from airfoil data in a similar way as in the BEM method. One such model is the Actuator Line model, AL model [30], where the kinematics of the wake is determined directly by Navier-Stokes equations but the aerodynamic loads calculated using tabulated airfoil data and estimating the local angle of attack in the computational grid at the position of the blades. These methods are very well suited to use when calculating the flow within a wind park, where turbines are placed behind other turbines.

Another type of CFD model used for wind turbines is the vortex methods, where vorticity is shed into the wake depending on the time variation of the lift (bound circulation). One such method is the GENUVP code [31].

Rotor Blades

Having determined the outer geometrical blade shape (airfoils, twist, and planform) using, e.g., a BEM code together with some optimization algorithm, one has to build a blade that can withstand the ultimate and fatigue loads. Most wind turbine blades are built from glass fiber mats glued together by epoxy or polyester. To carry the shear forces, so-called shear webs connect the suction side of the blade with the pressure side. These shear webs also ensure the thickness of the blade, that is, that the blade is not squeezed together, when the blade is bent by the aerodynamic loads. When building a blade, one often makes a shell of the pressure and suction side, respectively, and glues the two parts and the shear webs together as sketched in Fig. 9. One has to prove by applying all the load cases described in the norms [6] that the structure will not fail during its design lifetime of typically 20 years.

When a blade is geometrically upscaled from one radius, R_1, to a larger radius, R_2, all lengths are scaled with the ratio R_2/R_1, see Fig. 10. By operating the new blade at the same tip speed ratio as the old smaller blade, one ensures that the local blade sections at similar non-dimensional positions, r/R, experience the same flow angle and thus the same angle of attack.

Also the rotational speed is the same at similar non-dimensional positions, r/R, along the blade and thereby also the relative velocity. The only thing changing for the aerodynamic loads, Eqs. 19 and 20, is the chord, which increases as R_2/R_1. That is the aerodynamic loads increase linearly with the radius, and the blade bending moments, $M = \int rp(r)dr$, thus increase as the third power of the upscaling. The material stress is calculated about the principal axes, see Fig. 9, as

$$\sigma = \frac{M_1}{I_1}x_2 - \frac{M_2}{I_2}x_1 \tag{26}$$

and since the moment of inertia, I, increases with the fourth power of the length, the material stress from the aerodynamic loads is unchanged when upscaling a blade. The minus sign on the second term on the right hand side of Eq. 26 is because compression stress is considered positive and tension negative. For gravity loads, the upscaling causes problems, since the mass per length, m [kg/m], increases with the power of two of the radius, i.e., the bending moments from gravitational loads, $p = mg$, increases as the fourth power with the radius and finally the material stress will increase linearly with the radius according to Eq. 26. This puts a limit to how much one can do a simple upscaling of a wind turbine blade, because at some point, the stress from the gravitational loads will exceed the ultimate stress that the material can carry before failure. So when

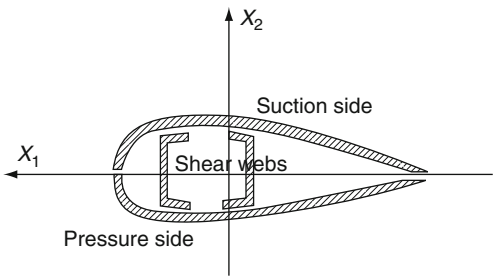

Wind Power, Aerodynamics and Blade Technology. Figure 9
Sketch of a cross section in a typical wind turbine blade

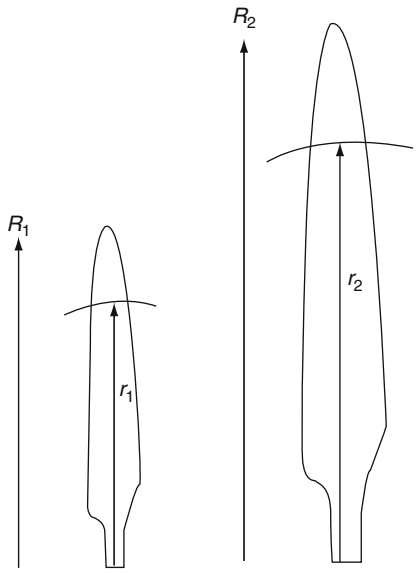

Wind Power, Aerodynamics and Blade Technology. Figure 10
Geometrically upscaling of a blade multiplying all lengths by R_2/R_1. Keeping the same tip speed ratio, $\lambda = \omega R/V_o$, the angles of attack at the non-dimensional positions, r/R, are the same

building bigger and bigger blades, one has to make the blades relatively lighter by using less material or at some places changing to a stronger and lighter material, e.g., carbon fiber.

Future Directions

In the future, one will still rely on the BEM method, when calculating all the design cases required by the norms. Probably also the BEM method will be used in optimizations, since this normally requires many calculations of the design which is changing during the optimization process. However, the final design will be checked using full 3-D CFD to see if there is some unexpected flow taking place. Further, CFD will be used to estimate the local lift and drag coefficients along the blade needed as input to the BEM method. In many years to come, the CFD tools will be sharpened with respect to transition models, turbulence models, and computational efficiency/resolution, that is, the affordable number of gridpoints.

Finally, hybrid methods such as the Actuator Line method will be applied when investigating the aeroelastic behavior of wind turbines placed in large wind farms, where the inflow is heavily altered from the upstream turbines compared to the turbines in the first row seeing the undisturbed wind.

Bibliography

1. Glauert H (1935) Airplane propellers, Division L. In: Durand WF (ed) Aerodynamic theory, vol 4. Springer, Berlin, pp 169–360
2. Snel H, Schepers JG (1995) Joint investigation of dynamic inflow effects and implementation of an engineering method. ECN-C-94-107
3. Schepers JG, Snel H (1995) Dynamic inflow: yawed conditions and partial span pitch control. ECN-C-95-056
4. Betz A (1926) Wind energy and its use by windmills. Ökobuch, Staufen
5. Hansen MOL (2008) Aerodynamics of wind turbine, 2nd edn. Earthscan, London
6. IEC 61400–1 Ed.3 CD. 2. revision (2004) 'Wind Turbines. Part 1: Design requirements,' edited by IEC TC88-MT1
7. Veers P (1988) 'Three-dimensional wind simulation' SANDIA report. SAND88-0152 UC-261
8. Mann J (1998) Wind field simulation. Probl Eng Mech 13: 269–282
9. Øye S (1991) Dynamic stall, simulated as a time lag of separation. In: McAnulty KF (ed) Proceedings of the 4th IEA symposium on the aerodynamics of wind turbines, Rome, ETSU-N-118
10. Leishman JG, Beddoes TS (1989) A semi-empirical model for dynamic stall. J Am Helicopter Soc 34(3):3–17
11. Hansen MH, Gaunaa M, Madsen HA (2004) A Beddoes-Leishman type dynamic stall model in state-space and indicial formulations. Risoe-R-1354(EN)
12. Sankar NL, Wake BE, Lekoudis SG (1986) Solution of the unsteady Euler equations for fixed and rotor wind configurations. J Aircr 23(4):283–289
13. Jameson A, Baker TJ (1983) Solution of the Euler equations for complex configurations. AIAA Paper 83–1919
14. Pulliam TH (1984) Euler and thin layer Navier-Stokes codes: ARC2D, ARC3D, notes for computational fluid dynamics users workshop, The University of Tennessee Space Institute, 12–16 March 1984
15. Agarwal RK, Deese JE (1997) Euler calculations for flowfield of a helicopter rotor in hover. J Aircr 24(4):231–238
16. Hansen MOL, Michelsen JA, Sørensen NN (1994) Navier-Stokes solver for rotating wing. In: European wind energy conference, Thessaloniki, pp 557–561
17. Hansen MOL, Sørensen JN, Michelsen JA, Sørensen NN (1997) A Global Navier-Stokes Rotor prediction Model. AIAA 97–097
18. Sørensen NN, Hansen MOL (1998) Rotor performance predictions using a Navier-Stokes method. AIAA 98–0025
19. Xu G, Sankar LN (1999) Computational study of horizontal axis wind turbines. AIAA 99–0042, Reno, January 1999
20. Duque EPN, van Dam CP, Hughes S (1999) Navier-Stokes simulations of the NREL combined experiment phase II rotor. In: Proceedings 1999, ASME wind energy symposium, 37th AIAA aerospace science meeting and exhibit, AIAA 99–0037, Reno, January 1999
21. Sørensen NN, Michelsen JA (2000) Aerodynamic predictions for the unsteady aerodynamics experiment phase-II rotor at the National Renewable Energy Laboratory. AIAA-2000-0037
22. Sørensen JN (1986) Three-level viscous-inviscid interaction technique for the prediction of separated flow past rotating wing. PhD thesis, AFM-83-03, Technical University of Denmark
23. Fingersh LJ, Simms D, Hand M, Jager D, Contrell J, Robinson M, Schreck S, Larwood S (2001) Wind tunnel testing of NREL's unsteady aerodynamics experiment. AIAA-2001-0035 Paper, 39th Aerospace sciences meeting & exhibit, Reno
24. Simms D, Schreck S, Hand M, Fingersh LJ (2001) NREL unsteady aerodynamics experiment in the NASA-Ames wind tunnel: a comparison of predictions to measurements. NREL/TP-500-29494, June 2001
25. Sørensen NN, Michelsen JA, Schreck S (2002) Navier-Stokes predictions of the NREL Phase VI rotor in the NASA Ames 80-by-120 wind tunnel. AIAA-2002-0032
26. Menter FM (1993) Zonal two equation k-ω turbulence models for aerodynamic flows. AIAA-paper-932906
27. Spalart PR, Allmaras SR (1992) A one-equation turbulence model for aerodynamic flows. AIAA-92-0439
28. Travin A, Shur M, Strelets M (1999) Detached-eddy simulation past a circular cylinder. Flow Turbul Combust 63:293–313

29. Strelets M (2001) Detached eddy simulations of massively separated flows. AIAA-2001-0879
30. Sørensen JN, Shen WZ (2002) Numerical modelling of wind turbine wakes. J Fluids Eng 124(2):393–399
31. Voutsinas S, Belessis M, Huberson S (1993) Dynamic inflow effects and vortex particle methods. In: Proceedings of the European community wind energy conference, Germany, pp 428–431

Wind Power, Introduction

Lennart Söder
Royal Institute of Technology, Electric Power Systems, Stockholm, Sweden

Article Outline

Meteorology and Wind Power
Aerodynamics and Blade Technology for Wind Power
Wind Power Grid Integration: Local Grid, Power Quality and Wind Power Generator Systems
Offshore Wind Power, Including Connection to Shore
Wind Power, Balancing of All Sustaining Factors
Wind Power: Economy, Market, Subsidies, Payment Mechanisms, and Capacity Credit
Wind Power: Transmission Planning
Wind Power Systems, Small Scale
Wind Power – Environmental Impact: Noise Emissions
Wind Power: Basic Challenge Concerning Social Acceptance
Wind Power Installations, Global
Bibliography

Windmills have existed for at least 3,000 years, mainly for grinding grain or pumping water. The use of windmills to generate electricity is a twentieth-century development and in the early 1970s started the development toward modern wind turbine technology. Wind power has increased significantly during the last decade and there are currently many power systems, or subsystems, with comparatively large amounts of wind power. In 2009, Spain covered 14% [1] of their electric energy demand with wind power. The corresponding figures were for Portugal 15% [2], Ireland 11% [3], and Western Denmark 25% [4].

This means that wind power has developed from a marginal source to a source with important impact on national power system balances. But in many countries, wind power still only contributes to a small part of the electric supply. The total installed capacity at the end of 2009 reached 158,000 MW including 37,000 MW installed during 2009. A third of these additions were made in China, which experienced yet another year of over 100% growth [5]. From 1996 to 2009 the mean increase of the amount of wind power was 28% per year.

There are several reasons why wind power increases so fast. They include (a) more cost-efficient technology, (b) higher energy prices depending on high demand and decreasing oil resources, and (c) increasing interest in energy sources with low emissions of CO_2 and other gases.

To be able to develop this type of system it is necessary to combine knowledge from several areas such as meteorology, aerodynamics, mechanics, electric machinery, and power systems. In order to obtain a cost-efficient wind power system with low environmental impact, all these parts have to be integrated together with a power system which can balance and transfer the produced power from the wind power plants to the power consumers.

Figure 1 shows the basic energy flow from the wind to electricity for the final consumer.

The basic energy flow starts with the wind. Winds are movements of air masses in relation to the ground surface. The winds are caused by pressure forces and sometimes also by the gravitation. The main origin of winds is temperature differences. The horizontal component is dominating. The energy in the wind comes from the mass, that is, the air, which is in motion. This is called the kinetic energy of the wind. To "use wind energy" is the same as transferring this kinetic energy into, for example, electric energy. Thereby the kinetic energy is decreased, that is, the wind speed is decreased. A wind turbine transfers the energy in the wind into a turning torque on the turbine shaft. A basic understanding of how this works can be obtained from aerodynamics and classic theory concerning forces when an airfoil moves in a flow. The turning torque of the turbine shaft then drives the generator and the output is then electric energy, that is, the generator transfers the mechanical energy in the rotating shaft into electric energy out from the

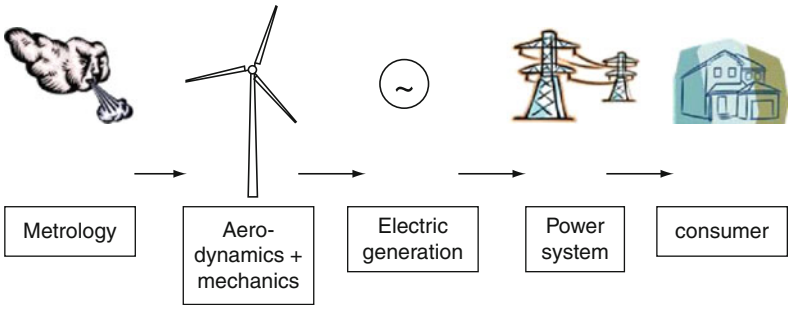

Wind Power, Introduction. Figure 1
Energy transfer from the wind resource to the final consumer

generator. The electric energy is then transferred to the consumers on electric wires and consumers finally use the energy for lightning, heating and cooling or for appliances such as computers or other electric machines. There must also be a system solution in order to supply the consumers with electricity exactly when they need it, which may not be the same situation as when the wind blows.

This section on Wind Power is comprised of 12 detailed entries which present the technology basis of this important source of electric power. The chapter on "Meteorology and Wind Power" describes the development in Wind Power Meteorology followed by "Aerodynamics and Blade Technology for Wind Power," which contains a description of the function and efficiency of a blade. The generation of electricity is then described in "Wind Power Grid Integration: Local Grid and Power Quality and Wind Power Generator Systems" and the specific challenges of offshore installations are shown in "Offshore Wind Power, Including Connection to Shore." Since wind power is changing in intensity, the balancing of this source is crucial which is described in "Wind Power, Balancing of all Sustaining Factors" while in "Wind Power: Economy, Market, Subsidies, Payment Mechanisms, and Capacity Credit," the economics of wind power is handled. Transmission issue of wind power grid integration is discussed in an interesting contribution called "Wind Power: Transmission Planning." Another interesting and increasing possibility is small-scale wind power which is treated in "Wind Power Systems, Small Scale." The environmental impact and acceptance are handled in "Wind Power – Environmental Impact: Noise Emissions" concerning noise emission and in "Wind Power: Basic Challenge Concerning Social Acceptance" with the issue of public acceptance. The technology, economy, and acceptance have led to a global fast increase of wind power which is finally summarized in "Wind Power Installations, Global." Key aspects of each of the above listed entries are presented below.

Meteorology and Wind Power

The availability of a suitable wind resource at a turbine site and the ability to accurately calculate it over the 20−year life span of the turbine are essential preconditions for the developments of wind energy as a major global provider of electricity. Therefore, the objective for research on wind conditions for wind energy resource and design purposes is to be able to determine the wind conditions with a high accuracy at any place on the Earth which could be a potential site for wind energy exploitation. The wind conditions at a specific site are basically dependent on two factors: the regional climatology and the local topography. The current fast development in Wind Power Meteorology can be termed "From Global to Local" which is synonymous with the process that goes from catching the relevant information from Global dataset, applying the data in meteorological models from global to mesoscale, which in turn produces spatial and temporal information to be used by microscale models to produce the relevant information on the wind conditions for design and for power production at a specific site for specific wind turbines. Therefore, most studies of wind conditions for wind power still rely on the use of local measurements in combination with microscale models.

Aerodynamics and Blade Technology for Wind Power

The energy extracted from a wind turbine comes from extracting some of the kinetic energy contained in the wind. Assume that the wind speed is constant, and that the wind turbine is rotating at a constant speed. This implies that each part of the blade is hit by a constant wind speed, but not the same total wind speed since this is the vector sum of the wind speed and the turning speed, which increases depending on the distance from the center of rotation, since the rotational speed increases proportional to the radius. The wind speed and the turning speed are about perpendicular since the wind turbine is turned toward the wind. The airfoil has an angle of attack of α to the air stream. This angle is the angle between the chord, c, and the direction of the flow, V. This angle then changes if only wind speed changes, only rotational speed changes, or if the blade is pitched.

The aerodynamic efficiency is connected to the ratio between the tip speed and the wind speed. From efficiency point of view, the blades should move faster, that is, higher speed of the shaft, when the wind speed is higher, and this has an impact on the requirements of the electric generation system.

Since the wind speed varies in time and space, a local segment on one of the blades will experience a constantly changing wind speed, and thus, the angle of attack and, thereby, also the aerodynamic loads will constantly change in time and will thus contribute to fatigue damage. This means that the amount of turbulence in the wind has to be considered when blades are designed. Having determined the outer geometrical blade shape (airfoils, twist, and platform) using, for example, the Blade Element Momentum theory (BEM), together with some optimization algorithm one has to build a rotor blade that can withstand the ultimate and fatigue loads. Most wind turbine blades are today built from glass fiber mats glued together by epoxy or polyester.

Wind Power Grid Integration: Local Grid, Power Quality and Wind Power Generator Systems

The electrical system of a wind turbine could be referred to as the heart of the wind turbine. The main purpose of the electrical system is to convert the incoming mechanical energy on the shaft to electrical energy that is fed into the connected power grid. This conversion should be done with a minimum of losses as well as with the smallest size possible.

In addition, the electrical system has the ability to influence the power quality impact that a wind turbine has on the power grid and also the ability to control the speed and torque on the machine shaft (if it is equipped with a power electronic converter) and, in this way, to maximize the energy capture as well as to keep the stresses on the structure to a minimum.

These requirements (high energy capture, good power quality impact, low stresses on the structure in order to minimize the material needed) have in combination with the technical development led to an evolution of wind turbines and definitely regarding the electrical systems of wind turbines. This development is continuously ongoing and is the reason to why there are several different concepts of electrical generating systems for wind turbines.

Offshore Wind Power, Including Connection to Shore

Offshore Wind Power is defined as construction of wind farms, located in the water, generating electricity from wind. Land-based wind power will remain dominant in the immediate future but installations at sea will become increasingly important. There are already today, 2010, several installations in Denmark, Sweden, UK, and Germany.

Compared to onshore wind, offshore wind is more complex and costly to install and maintain but also has a number of key advantages. Winds are typically stronger and more stable at sea than on land, resulting in significantly higher production per unit installed. At sea, wind turbines can be bigger than on land because of the logistical difficulties of transporting very large turbine components from the place of manufacturing by road to installation sites on land.

Wind Power, Balancing of All Sustaining Factors

Wind power balancing considers the challenge to keep a continuous balance between total production and total consumption in a power system. The varying wind speed introduces special considerations

concerning how to keep this balance in an efficient way. In a power system, there is always a challenge to keep the balance between total production and total consumption. This challenge has existed ever since the first power systems were installed more than 100 years ago. With the increasing amount of wind power new challenges arise.

There are always changes in production and consumption in all power systems since the load changes continuously and there are sometimes sudden outages in power plants and/or power lines. Despite these changes, the continuous balance between production and consumption is always kept. With larger amounts of wind power, the net changes in the controllable part of the production and consumption system will increase since wind power changes will increase the overall changes seen by the rest of the system. The challenges include balancing of changes, and keeping enough margins for reacting to changes depending on uncertain forecasts. Also, methods for estimation of the size of the increased challenges need to be addressed, as well as efficient market rules for an economic operation. When the share of wind power increases or is expected to increase it is common that so-called "integration studies" have been performed and the setup of these ones can be essential for a realistic estimation of the consequence of more wind power.

Wind Power: Economy, Market, Subsidies, Payment Mechanisms, and Capacity Credit

With increasing concern regarding climate change and emissions from conventional power plants, new markets have developed that allow for the trading of the clean energy attributes of wind and other renewable energy sources. Two examples are green power markets and renewable energy standards. Wind energy can also be bought and sold in wholesale energy markets including bulk power exchanges. In some areas, capacity markets exist that provide payment for installed capacity that is available when needed. Capacity markets are generally based on the capacity contribution that a power plant or responsive load can make toward planning reserves, which is called the capacity credit or capacity value. The general motivation behind a capacity market is to ensure sufficient revenue for the generator and ensure sufficient installed capacity.

In some countries, government incentives exist that encourage the development and use of wind energy (or other renewable energy sources). These include, for example, renewable energy standards, wind energy tax credits, or green power markets. Because of its variable and uncertain characteristic, wind energy can increase overall operating reserves that are needed to manage uncertainty. Specific methods to measure this cost have evolved, and today, there is some controversy surrounding the topic and its precise definition. Integration impacts and costs are not unique to wind. Nuclear power, for example, typically requires larger contingency reserves and increases cycling of other base-load generation. All investments in the power system impact system operations and costs.

Wind Power: Transmission Planning

The transmission grid is essential for an efficient use of large-scale introduction of wind power. With the transmission grid it is possible to, to some extent, even out the variation of wind power in large areas and to coordinate the balancing resources in the different interconnected areas. Transmission planning includes both the internal planning in each subregion and the overall planning for the whole interconnected system. Overlay transmission systems can be designed to economically and reliably serve load and deliver renewable energy. Overlays are a layer of transmission which spans the underlying transmission systems. Overlays require different planning techniques than those of the underlying systems. The involvement of many different people with widely varying backgrounds and interests have driven the transmission planning processes to provide more information than has been required in the past. Larger transmission expansions have attracted more stakeholders in the process.

Wind Power Systems, Small Scale

There is a growing interest for the use of small wind systems. Small wind systems can be seen in autonomous operation for pumping water, desalinization, and

battery charging. A growing amount of small wind turbines is connected to the grid, most of them behind the meter. Electricity production with wind turbines on buildings is a fairly new development with an interesting potential. Safe and reliable operation of small wind turbines is technically challenging since they usually operate in more turbulent flows than large-scale wind turbines. For an efficient application of small-scale wind power systems it is important to have knowledge of working principles of various type of the technology, their safety and control system, noise and vibration as well as investments costs and the cost of energy.

Wind Power – Environmental Impact: Noise Emissions

Wind turbines generate sound. Mainly this sound source is of aeroacoustic origin as improved sound insulation of the nacelles has reduced the mechanical sound sources. Unwanted sound is called noise and is a major factor when assessing nuisance caused by wind turbines. The increasing height of wind turbines has led to better possibilities to harvest wind at higher altitudes but has also contributed to increased noise levels in stable atmospheric conditions when the sound is easily transmitted due to a high wind speed gradient. Rapid development of large wind farms in rural, earlier unexploited, areas could cause large acceptance problems for nearby residents if noise is not properly considered in the development process.

Wind Power: Basic Challenge Concerning Social Acceptance

Successful implementation of new technologies requires social acceptance. Historically, for the implementation of wind energy this was considered a relatively simple issue that could be addressed by applying effective communication strategies. Without much study, social acceptance of wind power was considered a matter of merely public acceptance, and any problems with public acceptance were viewed as issues of education. Furthermore, public acceptance was primarily negatively defined, under the heading of "nontechnical factors." Three distinguishing dimensions of the social acceptance of renewable energy innovations have been recognized, all with its own character and dynamics: sociopolitical acceptance, with a focus on decisions that create favorable conditions for the other two forms of acceptance; community acceptance that concerns the decisions about the integration of wind power scheme at a certain location; and market acceptance, which is about willingness to invest among all different kinds of actors, including willingness to pay for wind-generated power among consumers.

Wind Power Installations, Global

Wind power has been utilized for over 3,000 years to aid with human activities. Although it was predominantly used as mechanical power at the beginning, gradually, with industrialization, the focus shifted to the use as electrical power. With the arrival of the oil price shock in the early 1970s, the use of wind energy as electrical power started to gain more focus, and since the end of the twentieth century, wind energy has become one of the most important sustainable energy resources. The installation of wind power production capacity is growing at a rapid pace, doubling every 3 years, and is expected to continue growing in the future, providing around 20% of the worlds' power needs by 2030. With strong growth in onshore and offshore developments in Europe, and rapid market expansions in the rest of the world, it is imperative that the knowledge which is currently concentrated in a few countries be spread, as implications on research, education, and electric utilities all around the globe are significant.

Bibliography

1. Spain: http://www.ree.es/ingles/sistema_electrico/pdf/infosis/sintesis_REE_2009_eng.pdf
2. Portugal: http://www.centrodeinformacao.ren.pt/EN/InformacaoTecnica/TechnicalData/2009.pdf
3. Ireland: http://www.eirgrid.com/media/Annual%20Report%202009.pdf and http://www.ieawind.org/AnnualReports_PDF/2009/Ireland.pdf
4. Denmark: http://www.danskenergi.dk/~/media/Energi_i_tal/Dansk_Elforsyning_Statistik_2009.pdf.ashx
5. Global Wind Energy Council (2008/2009) Global installed wind power capacity (MW). http://www.ewea.org

Wind Power: Basic Challenge Concerning Social Acceptance

Maarten Wolsink
Department of Geography, Planning and International Development Studies, University of Amsterdam, Amsterdam, The Netherlands

Article Outline

Glossary
Definition of the Subject
Introduction: Four Starting Points
Dimensions of Social Acceptance of Energy Innovation
Actors
Subjects of Acceptance
Sociopolitical Acceptance
Community Acceptance
Market Acceptance
Significant Attributes Connected to Identity
Future Directions
Bibliography

Glossary

Attitude Disposition to evaluate a psychological object – the attitude object –, representing a summary evaluation of this object captured in such attribute dimensions as good–bad, harmful–beneficial, pleasant–unpleasant, and likable–dislikable.

Attribute Character ascribed to an attitude object about which an actor may hold a belief (expectancy) and an evaluation (value).

Collaborative planning Planning with delegated responsibility to stakeholders who engage in interest-based negotiation about a plan or a project.

Community A body of people viewed collectively, e.g., the local community surrounding a wind farm location or a community holding a collective interest.

Discourse A shared way of apprehending the world; in this case, reflecting how the environment (including wind power implementation) is interpreted and given meaning.

Framing The way an issue (or an attribute) is defined and presented by actors – biased by their own perspective – in order to affect the perception of the issue by others: to encourage certain interpretations and to discourage others.

Innovation A change of ideas, that becomes manifest in products, processes, or organizations, that are applied successfully in practice.

Institutions Existing patterns of behavior, determined by existing societal rules "the rules of the game in a society."

Landscape The part of the environment that is the human habitat as it is perceived and understood through the medium of our perceptions.

NIMBY Depreciative interpretation and characterization of opposition to a facility: an attitude of objection to the siting of a facility in the proximity ("backyard"), while by implication raising no such objections to similar developments elsewhere; acronym of "not-in-my-back-yard."

Place identity Human binding to the physical environment at a certain place or area associated concepts: place attachment, sense of place.

Public acceptance The degree to which a phenomenon is taken by the general public, the degree to which the phenomenon is liked by individual citizens.

REFIT Renewable energy feed-in tariff, a class of financial procurement systems creating a priority market for renewable generated electricity by guaranteed access to the grid with a long-term fixed price per kilowatt-hour.

RPS Renewable Portfolio Standards, a class of financial procurement systems based on certificates issued for renewable generated electricity – "green certificates" – with a legal quote for renewables creating a market for trading certificates.

Smart grid Power grid consisting of a network of integrated microgrids that can monitor and heal itself.

Social acceptance The degree of which a phenomenon (e.g., wind power implementation) is taken by relevant social actors, based on the degree how the phenomenon is (dis-)liked by these actors.

Socio-technical system A system be made up of scientific and technological, as well as socio-economic and organizational components.

Definition of the Subject

Successful implementation of new technologies requires social acceptance. Historically, for the implementation

of wind energy this was considered a relatively simple issue that could be addressed by applying effective communication strategies. Without much study, social acceptance of wind power was considered a matter of merely public acceptance and any problems with public acceptance were viewed as issues of education. Furthermore, public acceptance was primarily negatively defined, under the heading of "nontechnical factors" [1].

However, innovation must be considered a much broader concept, as there is nothing inevitable about how new technology is developed and implemented. The willingness to accept phenomena related to innovation of different parts of society, including all realms beyond "the public," can be subdivided in two broad categories:

- Acceptance of the creation of new socioeconomic conditions needed for implementation.
- Acceptance of the consequences of the implementation: implementation will affect current practices in society and forcing some to change.

The very limited number of first studies on acceptance in the 1980s indeed focused upon public attitudes [1–4]. One of the first observations also was that social acceptance studies should look at the conditions that determine the effective support that applications of wind power would get at all different levels of decision making. This is already a very important conclusion. Actors involved in developers tend to perceive the issue from their own perspective: they only see the resistance they are confronted with against their projects, and they tend to frame this phenomenon as resistance against wind power per se. This is certainly not a phenomenon restricted to wind power, it can be found in almost any domain of infrastructure decision making (roads, waste facilities, power transmission lines, nuclear power facilities, prisons, etc, but also new housing districts or schools). However, if this kind of framing becomes persistent, it might become an even stronger impediment for positive decision about wind power developments, as it obstructs collaborative ways of decision making (see sections "Mind the "Gap"" and "The Backyard").

The initial studies immediately showed that neither public support, nor support from crucial stakeholders at varying scale levels could be taken for granted. The pioneer of social acceptance studies, Carlman, observed that building wind turbines was "a matter of public, political, and regulatory acceptance," and therefore she carried out a study on the acceptance of wind power among decision makers [5, p. 339]. Her study suggested that there were several constraints for social acceptance beyond public acceptance.

Soon in the 1980s, other academics joined this approach and specified the definition and analysis of the problematic issues for implementation [4, 6]. These studies focused on issues such as the lack of support among key stakeholders – including the limited commitment of energy utilities – reluctance among policy makers to dedicate themselves to convincing policies, and the lack of understanding of the roots of attitudes toward wind power schemes among local residents and local communities.

Because implementation issues are much broader than public opinion with regards the application of the energy source "wind," the nature of the studies has changed. The number of studies remained limited during the nineties, but a significant increase took place during the last decade. Many of these studies focused upon the level of decision making about building wind farms, which is the crucial factor in the success rate of a country's wind power development. As the character of all these cases of building wind farms shows a wide variety, most of these studies are designed as single case studies. Beside those studies, some comparative case studies have been carried out to compare the differences between countries, and single cases that analyzed the development of policies within a country.

The intensive study of social acceptance has a rather short history, and because the concept is complex our understanding of the issue is still limited [7]. Only recently, a first effort to elaborate the concept of social acceptance of renewable energy innovation was made [8]. Three distinguishing dimensions of the social acceptance of renewable energy innovations are now recognized, all with it's own character and dynamics: sociopolitical acceptance, with a focus on decisions that create favorable conditions for the other two forms of acceptance; community acceptance that concerns the decisions about the integration of wind power scheme at a certain location; and market acceptance, which is about willingness to invest among all different kinds of actors, including wiliness to pay for wind-generated power among consumers.

Introduction: Four Starting Points

Socio-technical Systems

Successful implementation of new technologies requires sociopolitical acceptance. The implementation of wind power is a form of innovation, as it implies the application a relatively new form of energy supply. By definition, innovation is the successful application of new ideas, transferred into products, processes, or organizations. The integration of new technologies such as wind power in society is not a matter of simply applying science; also there is a series of factors in the social environment that co-determine it: social, economic, cultural, and different technological factors [9]. Regarding wind power, these include the integration of this new way of generating power in the existing energy supply and consumption, as well as the appearance of modern wind turbines in our landscapes and as part of communities and local or regional economies.

In addition to technological concerns, the application of wind energy carries a strong socioeconomic component. Significant scientific and technological challenges need to be overcome, but as history shows, well-developed science and technology are not sufficient to foster application of technologies. Making it affordable does not address the entire challenge; the society may fail to allot acceptable locations for the facilities or fail to deliver the required social and financial investments. This observation leads to *basic assumption I*:

- An energy system containing a substantial part of wind-generated power and also a substantial part of wind-generated energy consumption, should be considered a new socio-technical system (STS).

Acceptance of Distinguishable Aspects

A STS is a system with new scientific and technological as well as socioeconomic and organizational components, which is reflecting new ideas and concepts on the proffered design of such new systems [10]. Other related examples of innovations are, for example, the introduction of a new production process in a factory, (an STS combining new techniques with a different organization of the process) limiting the amount of emissions and final waste after consumption. Or the development and introduction of an ecological certificate (including the organization and techniques needed to generate reliable information, monitoring producers in all phases, and effectively informing potential consumers) aiming to affect consumer choices that would put pressure on producers and distributors in the production–consumption chain. The introduction of electric vehicles also heavily depends upon the organization and implementation of infrastructure to load these cars, including the question who will provide this infrastructure. In fact, the latter example will soon be very relevant for further implementation of renewable energy as well (see section "Future Directions").

Any STS pays attention to the linkages between these two components, links that are necessary to fulfil societal functions [11]. Such functions can be – among others – support of regional economies, provision of energy, reduction of environmental impact, etc. The development of distinguishable sub-functions of the new crucial technologies requires favorable institutional conditions and extensive social learning. This also holds for wind power [12, 13]. Hence, the second *basic assumption (II)* states two things:

- All aspects of a new STS featuring a substantial amount of wind power are subject to social acceptance.
- An actor may accept certain aspects, while simultaneously rejecting other aspects, as a result of social, economic, and/or political learning processes.

In all domains, to-be-implemented innovations require institutional changes and careful strategic governance, especially when such innovations concern fundamental shifts in ways of thinking about the way the system is designed and how it should work [10].

Institutional Change

For wind power, it is not only the technical novelties that are subject of acceptance, but rather the new ways of organizing the STS and how to take decisions about it that are required to build the turbines and to integrate their variable energy production into the system of energy supply and demand. In particular, those new ways of organizing require new ways of thinking, which only emerge though processes of organizational and policy learning. Developing an

STS requires the understanding of and the will to change crucial "rules of the game in a society," the short definition of *institutions* [14]. Institutions are defined as mutually reinforcing patterns of behavior and thinking (of actors of all levels), as reflected in formal and informal rules, norms, and procedures. These patterns of thinking and behavior can be recognized within all realms of society, including governance systems.

The way existing supply and demand of electrical power are shaped is full of patterns of behavior of all kinds of actors. These behavioral patterns are based on formal and informal rules that have emerged over time. These rules are not necessarily defined to further the integration of new energy sources, as they have emerged in the past under different conditions, serving different ends. The most essential changes in ways of thinking concern modes of thought that are historically rooted in the competent organizations. This phenomenon is called "path dependency" and reflects the historical roots of existing institutions [14, 15]. The process "by which actions are repeated and given similar meaning by others" is *institutionalization* [16, p. 117]. The existing ways of things are done and how they are organized all result from past institutionalization processes. That includes, for example, how infrastructure is built and how supply of electricity is organized in the power supply sector. However, at that time, these institutions were framed to serve societal needs that did not include the implementation of a resource like wind, and within a context of a different socioeconomic environment. The existing patterns were not designed with the new STS in mind and therefore path dependency in an existing STS is often responsible for unfavorable conditions that forestall the introduction of a new STS, such as wind power implementation. This may eventually lead to a deadlock in the development of the new system, known as institutional "lock-in." This is an important source of nonacceptance among different actors with regard numerous elements of wind power implementation. Therefore, the third *basic assumption III* is:

- Existing institutions (existing patterns of behavior as determined by existing societal rules) often impede the development and implementation of new views, approaches, techniques, and practices required for the implementation of wind power.

The social acceptance of wind power is a complex issue due to a combination of two factors: an STS that includes wind power may induce different reactions from an actor (assumption II) and there are many different types of actors who are involved at various scale levels, all with their own institutionally embedded behavioral patterns (assumption III). This complexity provides for many opportunities for misunderstandings. These have emerged in "common sense" approaches with regards learning and acceptance. What is considered "common sense" is often no more than a habitual pattern of thinking that is mutually copied by actors and reinforced by frequent use. This manner of institutionalization, the tendency to copy or follow others in the organization of an actors' own behavior – known as "mimetic" repetition [17] –, is a strategy used by social actors to address uncertainty as well as to mask the appearance of their own uncertainty. Existing ideas about how to implement wind power and how to integrate it in society are full of such institutionalized ways of thinking, which are often classified as "knowledge." However, this is often unjustified as they are in fact no more than institutionalized commonsense ideas that may become barriers to actual implementation.

Generalizing, we can recognize the three major commonsense approaches to wind power implementation. These can be found among many different actors at all scale levels, but most relevant is that they belong to policy beliefs of actors (public agencies, governmental, but also stakeholders) that often hold dominant positions in policy. These three commons sense approaches are:

- The so-called "technological fix": a tendency to focus on technology while not recognizing the social components of the STS. An example with regards wind is the focus on the technological potential of wind power.
- The simplification and reduction of the issue of social acceptance to mere public acceptance. In many policy documents, public acceptance is simply used as a proxy for social acceptance, but without any justification. This is tempting, as it reduced a very complex phenomenon to simple figures of public opinion, but it also reduces the validity of these figures to approximately zero.

– The one-sided focus on the objectors of wind development. In most documents about social acceptance the support for wind power and wind power projects among all different kinds of actors is taken for granted. As a result, it is hardly investigated, hardly valued, and not well understood.

Beyond Common Sense

The first commonsense approach is to simply neglect the issue of social acceptance or to handle it as a secondary aspect of residual questions. From the beginning of modern wind energy development, social acceptance issues were considered elusive and hard to calculate ("soft factors") and usually negatively defined as "nontechnical factors" [1]. Moreover, these factors were narrowly defined as the term public acceptance was considered synonym to social acceptance. The institutionally determined approach of society's abilities to implement wind power tends to focus on the so-called "technical potential," sometimes combined with assessments of the financial feasibility of that potential [18]. Even if social constraints are included in the assessment of the potential, they remain limited to "planning" consideration, based on a uniform criterion for the possibility of land use for the construction of wind turbines [19]. The concept of the technical potential of renewable energy options implies that technology need only be developed and applied to solve all of a country's energy problems. A study conducted in the USA found that this has become somewhat of a mantra in discussions about both electricity and energy policy more broadly [20, p. 4511]. However, much of the technically and meteorologically available possibilities cannot be utilized without violating generally applied social norms or without challenging existing interests. The social potential is ultimately the potential that really indicates what capacity can be implemented. The main bias in the approach of the technical potential is that it narrowly frames the concept of social acceptance as a collection of "barriers" to achieving our potential.

The combination of the second and third general commonsense approaches has prevented the understanding of social acceptance of wind energy innovation for a long time. Unfortunately, from the viewpoint of wind power implementation, they are still widespread among developers and policy makers alike [21, 22]. The second commonsense bias is the simplified idea that social acceptance is equal to public acceptance. The reduction of acceptance to public opinion is a strong bias, because it completely ignores the position of all societal actors beyond the level of the individual. The perspectives of these other actors, companies, public bodies, organizations, etc. are certainly not mere translations of personal attitudes, and particularly not of ordinary citizens, and in many cases their influence on decision making and eventually on actual implementation rates is much stronger than that of the public [23].

The third commonsense bias is the one-sided focus on the potential objectors of wind energy development and neglect of the supporting side that accepts such development. Still many studies only focus upon why people oppose and why stakeholders object (e.g., [20]), whereas it is equally important why wind power is supported in the first place [7, 8]. How much support is there – also for wind power schemes, as is in most cases supporters outnumber objectors – and what are the reasons for actors to be in favor? Acceptance is, by definition, taking what is offered, whether by favor or reception. Of course, this definition also implies the inclusion of the side of refusal in the concept. Social acceptance is a bipolar phenomenon. Following definitions from psychology on the social acceptance of individuals [24], the social acceptance of a phenomenon like the implementation of wind power is the degree to which people like or dislike the phenomenon. The concept includes all degrees, from full refusal to total adoption. Therefore, the narrow focus on the opposing forces to wind power developments neglects the essential side of acceptance issues. The bias is that the position of support is apparently taken for granted and considered as the "natural" position. Consequently, the supportive position does not seem to need an explanation, whereas the position of refusal becomes deviant. Understanding social acceptance requires both positions to be analyzed as equally legitimate in principal [7, 23].

Hence, the fourth fundamental proposition for understanding social acceptance is – *basic assumption IV* –:

- The objection to any wind power development must be considered as a potentially legitimate, rational, and

informed position: All positive, active support as well as passive supporting attitudes, are equally important for obtaining a good understanding of the acceptance of wind power.

Dimensions of Social Acceptance of Energy Innovation

Although used often, the term social acceptance is seldom properly defined. Here a systematic elaboration is provided, starting from three distinguishing dimensions of the social acceptance of renewable energy innovations [8]. These are presented in Fig. 1, along with the main issues that should be addressed within those dimensions. Sociopolitical acceptance is related to the support or resistance toward policies that affectively promote the implementation of wind power. This is not only related to government. Today "governance" is the preferred concept, which implies that the drafting and implementation of policy is not restricted to actors within the realm of government, but rather it includes many social actors. These so-called "stakeholders" include all social actors who are involved in negotiating, influencing, and lobbying, because they perceive a specific policy as affecting their (vested) interests. The recognition that policy is in fact shaped within a broader arena that includes both private and public actors is referred to as "governance" [25].

Policies tend to focus primarily on the economic investments in new STS. Policy instruments are usually designed (or perceived as designed) to create incentives for positive investment decisions. They are determined to affect the market decisions of actors. These actors primarily are incumbent energy companies, but they may also include newly emerging actors who are entering the market, or existing actors in other domains who discover wind power as a new and promising investment area. The supporting side of "market acceptance," which is a willingness to support or take part in investment, is not the only required and favorable position, however. The nature of wind power installations is fundamentally that they are part of the phenomenon of "distributed generation," in which the power scale, the power delivery (directly to the consumer or to the grid), the mode of operation, ownership, the purpose, and the location of the power generation are as essential as the generated power itself [26]. All these elements are subject to the acceptance within the community in which the generation takes place.

In the commonsense approaches, community acceptance is seen as the bottleneck of wind power development. Indeed, the most problematic issues with regard to acceptance manifest themselves in the discussions about establishing wind farms. By definition, this is a discussion at the level of community acceptance, but the idea that the roots of problematic acceptance lie within the community only emerges because of the combination of two commonsense views: the dominant narrow interpretation of social acceptance as public acceptance and the focus upon objectors while neglecting positive support. The three-dimensions model of acceptance of renewable energy innovation (Fig. 1) shows that social acceptance is much more than simple public opposition on the local level. Before discussing these three

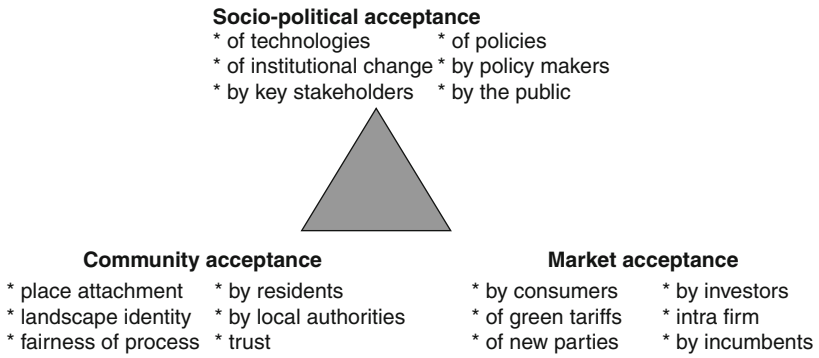

Wind Power: Basic Challenge Concerning Social Acceptance. Figure 1
Three dimensions of social acceptance of renewable energy. Adapted from [8, p. 2684]

dimensions, we focus upon two basic features determining the construction of social acceptance within all three dimensions:

- The different actors: who is taking a favorable or opposing position?
- The different subjects: to what attitude object are those actors defining their position?

Actors

As the first component in the social dimension of the socio-technical system, all relevant social actors involved in the process of acceptance must be considered. Table 1 shows broad categories of social actors relevant to the acceptance of the new STS. All actors will exhibit different degrees of support or opposition toward any of the socioeconomic and technologic aspects of the STS of energy provision that includes wind. For example, the acceptance of wind power by an existing power distributor may be highly determined by the value it places on the variability of wind power. For such a company, acceptance concerns the specific wind-related pattern of energy production, which they perceive as complicating reliable provision. Their perception of variability is different, and discussing this attribute they are "framing" it differently: they tend to define this variability as "intermittency" [27]. Their acceptance also concerns completely different aspects, such as their attitude toward newly emerging energy producers like farmers, corporations of civilians investing in wind power, or newly emerging companies that focus on the development of renewables' installations. During the discussion of the three dimensions of social acceptance, the question "who is accepting?" and the actors presented in Table 1 will repeatedly be referred to. In addition to the question "who is accepting," the other main question "what" is to be accepted will be elaborated.

Subjects of Acceptance

Attitude Objects and Attributes

Acceptance is an act of decision making, based on a trade-off between pros and cons. It is a behavior based on considerations of several aspects regarding the subject. These considerations eventually manifest themselves in a positive or negative disposition (attitude) toward the intention to take action and to say either "yes" or "no" to a certain phenomenon – the attitude object. In psychology, a particularly influential framework on the relation between attitudes and behavior is the Theory of Planned Behavior (TPB) [28, 29]. This model has proven as successful in explaining various types of environmentally relevant behavior, such as choice of travel mode, household-waste composting and recycling, energy saving, water consumption, etc. The model is also applicable to attitudes regarding decisions about implementing renewable energy solutions [30].

Figure 2 illustrates how attitudes and their relation with behavior are constructed according to the TPB. Central is the attitude-object relationship, which in this case is the concrete action of supporting or rejecting a particular decision regarding wind power implementation. Attitudes are constructed according to a model of expectancies and values. The attitude is based on several "beliefs" about the object. Each belief associates the object with a certain attribute; a person's overall attitude toward the object is determined by the subjective evaluation of those attributes. Although people can form many different beliefs about an object (many potential attributes are presented in Table 2), it is assumed that only beliefs that are readily accessible in memory – "salient beliefs" – influence attitudes. There are many possible actions regarding the application of wind power and all these actions are different attitude objects. From a theoretical starting point, it is fundamental that there can only be clear empirical relations established between attitudes and behavior as both are related to the same object.

The process illustrated in Fig. 1 particularly holds true for attitudes held by individuals. The act of social actors and their underlying positions will generally be based on the same kind of attributes, but the way they are processed in organizations is different from the processing that takes place in the mind of an individual. However, for both types of actors, individual as well as collective, the significance of the existence of attitude-objects relation and several underlying attributes related to that object remains the same. Although it is not possible to simply apply attitude theory and behavior on groups of individuals that together constitute a social actor, the principle remains the same: the actions and positions of social actors also focus on an object, similar to the attitude-object relation for an

Wind Power: Basic Challenge Concerning Social Acceptance. Table 1 Actor categories with relevant acceptance to one or more aspects of wind power implementation

Stakeholders in development	• Incumbents in the existing energy supply sector	– Existing power production companies
		– Power distributing companies
		– Grid managing organizations/ companies
	• Wind power developers	– Existing companies investing in wind as a new activity
		– New emerging organizations or companies, specialized in renewables
	• Wind turbine industry-related actors	
	• Actors with vested interests in domains relevant to establishing wind farms (e.g., R&D, consultancy, engineering, construction, etc.)	
	• Actors representing energy consumers' interests	
	• All actors with secondary interest in investments in wind power (e.g., financial)	
Authorities and public bodies	• National government	– Ministries in policy domains relevant to wind power implementation
		– Energy market regulator(s)
		– Government agencies
	• Regional governments	– Spatial planning officers
		– Regional economic development officers
	• Local governments	– Spatial planning officers
		– Local economic development officers
Stakeholders in related domains	• Landscape-protection organizations	
	• Environment- and nature-protection organizations	
	• All actors with interests in competing spatial functions	
	• Actors with interests in economic sectors potentially affected by wind power	
Public	• General public (electorate, public opinion)	
	• Individuals with any perceived interest in wind developments	
	• Communities (geographically or socially defined)	
	• Civil society organizations representing affected interests	
	• Civil society organizations established because of wind power implementation issues	– Organizations established for private investment in wind developments
		– Organizations established to counteract proposed wind developments

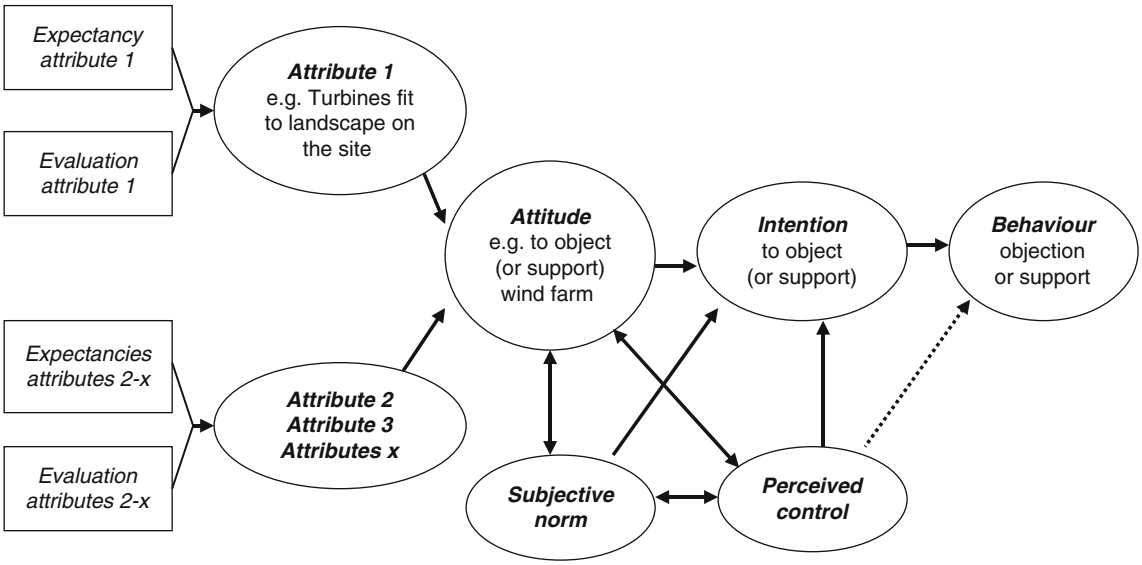

Wind Power: Basic Challenge Concerning Social Acceptance. Figure 2
Formation of attitudes based on expectancies and values about attributes of the object of behavior, in relation to intention and behavior, according to the Theory of Planned Behavior [29, p. 182]. Subjective norm: perceived expectancies of important "others" Perceived control: control of the individual over behavior and its aims

individual. Hence, the question is what are the attitude objects in the case of wind power implementation and which potential attributes exist in those cases?

Two Types of Objects

Within the social acceptance of wind power, many attitude objects exist, because there is a wide range of different kinds of decisions connected to wind power development. For example, an energy company may decide to invest – or not to invest – in a particular wind farm. For consumers, it can also be a decision to invest in a wind farm or to subscribe to a "green power" scheme that includes wind-generated power. For a government actor, it may be a decision to take on a share in the investment in a wind farm [31], to grant a subsidy to investors, to implement a certain financial procurement instrument, etc. Eventually, these decisions seem to converge on the fundamental attitude of the actor toward the implementation of wind power: does an actor have a clear positive, supporting attitude or a negative, opposing attitude toward wind power. However, this is an oversimplification, as for all types of decisions the beliefs and evaluations with regard to wind power are only one of many possible attributes at play.

According to the above-described expectation that there would be strong really existing relations between the attitudes, the intention, and subsequently the decision (Fig. 2), a fundamental requirement is that the objects of attitude and decision fully correspond. However, the attitudes toward a general support of wind power policy and the attitudes toward the construction of a particular wind farm have two completely different attitude objects. As a result, the relationship between the general support for wind power and a decision to support a particular wind farm will be weak. The unfounded expectation that this relation should be strong, reinforced by the commonsense approaches to social acceptance (section "Beyond Common Sense"), has led to strong and persistent misunderstandings about the nature of social acceptance. The two most important misunderstandings concern the fact that public support for wind energy, as expressed in opinion surveys, is high in most countries; however, in many of these countries, the success rates in establishing wind power developments are actually rather low. The two misconceptions are:

– Objections that result from the so-called individual attitude–behaviour "gap": people are generally in

Wind Power: Basic Challenge Concerning Social Acceptance. Table 2 Attributes of attitudes toward wind power and toward wind power schemes

Attitude object: socio-technical system (power supply with a substantial amount of wind power)		Attitude object: project (wind power scheme)	
Essential characteristics	Associated attributes	Essential characteristics	Associated attributes
Environmentally benign, renewable character	Alternative to fossil	Wind power	Clean character
	Alternative to nuclear		Supply characteristics
	Source cannot run out		Visibility
Supply characteristics	Variability	Location and site	Landscape identity
	Reliability		Nature wildlife
	Capacity credit		Annoyance (noise)
	Domestic source		Wind farm design
			Competing spatial functions
Visibility	Visual: landscape impact of turbines	Investor and/or (co-)ownership	Community in/outsider initiative
	Nature/wildlife: impact on particularly birds		Local economy (benefits/ employment)
			Local shareholders
			Community identity
Economics	Price compared to alternatives	Decision-making process	Open/closed
	Economics related to supply characteristics		Participation of public
	Impact on industry and employment		Participation of stakeholders
			Spatial planning procedure Legitimate / "fair"
			Spatial planning procedure
Organizational aspects energy sector	Distributed		
	Decentralized		
	Small scale		
	Options third parties		

favor of wind power, but they change their mind as soon as they are confronted with a proposal;

– The idea that objections to wind developments are simply manifestations of the so-called "not in my backyard" (NIMBY) syndrome.

By dividing the wide range of decisions about wind power implementation into two categories, Table 2 shows the potential objects that are related to (1) decisions concerning the general application of wind power and the integration of wind-generated energy in our society (on the left), and (2) decisions about establishing concrete wind developments (on the right).

Attitude Object: Energy Source

The idea that wind power as a renewable energy source is a clear climate change mitigation measure seems the

most obvious attribute of the attitude object "wind power." For this attitude object, the attributes are connected to the characteristics of a new socio-technical system of energy supply that includes substantial portion of wind power. Of course, a prominent characteristic of wind power is its more environmentally benign character compared to alternatives. This attribute is currently dominated by the wish to avoid greenhouse gas emissions, but this immediately shows the dynamic nature of the phenomenon of social acceptance. In the seventies, when several developed countries in Western Europe and some USA states introduced wind power developing policies, climate change was not an argument used to support wind power, neither in public opinion nor among the actors involved in energy supply or policy. There were some environmental arguments, as fossil fuels were clearly associated with air pollution, and also other considerations, as in several countries the public and also some governments were eager to develop alternatives to nuclear power. Clearly, the environmentally benign character of renewable source energy is still a significant attribute for the attitude object "wind power," but the argument has only recently shifted toward mitigating climate change.

Several studies involving various stakeholders, policy makers, developers, and the public, demonstrated that attributes other than the renewable character of wind are significant for acceptance by all of the relevant actors in these categories [21, 22]. These characteristics and the associated attributes summarized in Table 2 are not only related to the energy source (such as the variability, often framed as "intermittency") but also to the institutional aspects of implementation of wind energy, such as new options and consequences for incumbents in the energy sector and for national economic and industrial development. Similarly, the price to pay for wind-generated power is obviously important for all types of actors, but for different actors we are dealing with different prices. Their significance is very different in the three dimensions of acceptance (Fig. 1) and they will be discussed in more detail in sections "Sociopolitical Acceptance," "Community Acceptance," and "Market Acceptance."

Attitude Object: Wind Development Project

The object of attitudes toward concrete projects of wind power application concerns two kinds of decisions: decisions about investing in such development and decisions about building a wind farm at a certain site in a particular community. The character of such decisions is entirely different from general decisions to promote or to restrain further wind power development. As a matter of fact, only one characteristic of these decisions concerns the source of energy. The other characteristics of the decisions are all related to details of the specific proposal. It is important to note that these attributes are only remotely related to the character of the energy source itself, but nevertheless they are at least equally important and often more important than the attributes directly related to wind power as the source of energy.

Some of the attributes in Table 2 of decisions about projects seem to correspond with attributes associated with the object of wind power in general. For example, in both types of decisions, economic arguments play a significant role. However, the economic arguments for applying wind power and its impact on general welfare and industrial development are very different from the economic valuation by potential investors in a wind power project, or from the local community's beliefs about the existence and valuation of the project's contribution to the local economy. Similarly, at the general level, landscape issues are certainly very important for determining the attitudes toward wind power development. Here it concerns a general belief that large-scale wind power implementation will result in a myriad of wind turbines popping up in the landscape and the valuation of this phenomenon. Usually, this aspect is neutrally referred to in terms like "visual impact" [32], but in most studies any impact in terms of visibility is generalized and considered beforehand as "intrusive" or "disturbing," as if this valuation applies to all types of landscapes and also to all individuals. The landscape evaluation discussed in section "Landscape/Seascape" shows that the visual impact of wind turbines varies significantly among both individuals as well as cases, and that it is not only evaluated negatively. In decisions about a particular project, the general assessment is translated into "landscape identity," which is something very different as it is not primarily determined by the common denominator "wind turbines" but rather by the landscape characteristics of the site of that particular project as they are perceived by the people that feel attached to that site. As these

landscapes vary widely among different project cases, they cannot be considered as principally determined by the general landscape assessment of wind power.

A similar "translation" takes place in the organization of energy supply. For wind power in general, as is discussed in section "Sociopolitical Acceptance" on sociopolitical acceptance, the option for third parties and new actors to invest in wind power is a relevant attribute (Table 2). In the translation into a particular project, this becomes a question of wind farm ownership and community involvement, or the acceptance of investments and ownership of a wind power development by companies from outside the community [33].

The large differences between the relevant actors and attributes in the decisions about applying the energy source and the decisions about building wind farms result in only a weak correlation between support for wind power and support for wind farm proposals. The limits of this correlation may be the origin of what is usually referred to as the "gap" between general high acceptance of wind power and the perception that a large number of decisions about building wind farms are failing [34]. The latter perception is problematic, as it is hard to define a basis to establish number of failing and successful projects. It fully depends on when an idea to build a wind farm is considered as a "project" that can either become a success or a failure. Official numbers can be derived from planning consent and building permits, but the success rate becomes high for countries with a planning system in which permit applications start after – unofficial – negotiations, whereas in other countries an application is the start of the process. Example figures from the UK during a 5 year period showed that 60% of applications were eventually refused, while 40% were approved [35].

Again, such figures are highly depending on the context of the country and its planning system and practice, but at least they show that it is far from self-evident that a wind scheme will be realized. However, it is questionable whether this phenomenon indicates that "gap" between general high acceptance of wind power and refusal to support local developments really exists. In fact, the limited correlation between support for wind power and support for wind farm proposals is poorly recognized and understood by wind power advocates and policy makers alike. The fundamental question regarding this "gap" is why decisions about a particular project, which are taken by local actors and the interested investors, would be highly affected by the fact that national public opinion shows high positive responses to wind power. A clear correlation between general national public opinion and local decision making is theoretically not supported. Even within a single actor, there is a distinction between the attitude with an attitude object (wind energy) that is entirely different from the object of behavior (taking decisions about investing in a wind farm and siting it). Table 2 shows that both objects have many different attributes; therefore, the fundamental condition that the objects of attitude and behavior must be the same to find a clear relation between attitude and behavior ([28]; Fig. 2) is not fulfilled. The commonsense idea that a decision regarding building a wind farm is primarily informed by general attitudes on wind power, is unfounded by what is known about the relationship between attitudes and decision behavior. Speaking in terms of attitude-behavior theory, the objects of attitude and behavior simply do not correspond.

Mind the "Gap"

With regards the assumed "gap" between general acceptance of wind power and still a low number of positive decisions to build wind farms, Bell et al. [34] distinguish between a possible "social gap" and an "individual gap." The "social gap" refers to the high-level public support for wind energy expressed in opinion surveys and the low success rate achieved in planning applications for wind power developments.

The individual "gap" emerges from the idea that many of the failures to establish wind developments arise from the fact that individuals, in particular local residents, have a positive attitude to wind power in general, but actively oppose a particular wind power development when confronted with a proposal. The most popular commonsense explanation for this assumption is the claim that NIMBY-ism is responsible for this gap, but Bell et al. already explain the weaknesses of the NIMBY claim in explaining an attitude-behavior gap [34, p. 465]. This popular label is briefly discussed in section "The Backyard," as it is currently still prominent in commonsense thinking about acceptance of wind power.

However, the terminology of an existing "gap" may also be considered disputable. Table 2 shows the different potential attributes that can be connected to those objects. The comparison of these two categories already reveals a large divergence between the objects in the two columns. The attitude object "wind power" (left) is only one of four main characteristics of the object "wind power project" (right). Attitudes toward a concrete proposal for the construction of a wind farm at a specific location and toward investing in a wind farm include many potential attributes all related to variables that show a wide variety among cases. The fact that this proposal is an attempt to implement wind power is only one of these many attributes; some of the other attributes are often more important for key actors than the implementation of wind power. Examples of potentially more important attributes include the type of the developer – from a large energy company to a nonprofit community associated initiative –, the landscape of the chosen location, the connection of the wind farm to the local economy, the potential environmental impact, etc.

From a developers' point of view, the struggle to site a wind power development is easily interpreted as a problem of local inhabitants trying to safeguard their environs against turbines [2, 36]. The number of documents reproducing the common perception that any resistance these developers face is an indication of a so-called NIMBY-syndrome is overwhelming and this commonsense view is continuously reproducing itself. It is prominent among the strong proponents of wind power and presented as a "fact" [36, p. 299]. As this idea is engrained, some discussion is required, above all because it is a perfect example of institutionalized thinking patterns that eventually become barriers to the acceptance of wind development schemes.

The Backyard

Many proposed wind developments indeed do encounter resistance, but this cannot be considered evidence for the existence of a NIMBY syndrome. Stronger evidence is needed that the individual's motivation to resist is as selfish as the use of the term NIMBY suggests [36]. The problem is that such evidence has seldom been found, but still the interpretation of any opposition in terms of the backyard is repeated over and over again [37, 38]. Any reference to an alleged "not-in-my-back-yard" syndrome suggests a degree of selfishness, conservatism, unwillingness to cooperate, or ignorance of environmental issues. For example, with regard to renewable energy facilities, Kahn [39, p. 26] gives a fairly clear characterization. A NIMBY opponent would be

- *Democratic* with a small "d," since his/her political right of self-determination is exercised to the fullest
- *Parochial* because he/she is unconcerned with broad impacts
- *Reactive* in that he/she is not generally concerned with planning or siting issues per se
- The NIMBY – opponent is *not an environmentalist*

Although this view is still very prominent among developers and policy makers, with the start of public and social acceptance studies in the 1980s, researchers started to question the relevance of this rather normative NIMBY label. The first notion to be reluctant with the use of this label suggested that it is dangerous for authorities or utilities to use this acronym. It tends to offend the public and will generate stronger opposition and the use of the qualification may easily become counterproductive [40]. The indolent use of the NIMBY label has become a tool to question the legitimacy of the opposition and the actors who represent it. This is a violation of basic assumption IV about the legitimacy of all views on wind power implementation. Meanwhile all efforts of authorities and developers to narrow local concerns about schemes that often have been developed without involving them have become an indication of sociopolitical nonacceptance. If policies really want positive local decisions on wind power schemes, the acceptance in implementation in policy of assumption IV is crucial.

The last two decades, the "theory" of the backyard-motivated resistance to wind developments has increasingly become discredited by researchers: "The NIMBY concept that has been most frequently used to describe negative perceptions of wind farms has failed to receive empirical support" [38, p. 136]. In fact, all researchers investigating the motives for resistance to wind developments, in light of the general public support for the technology, reached a consensus on NIMBY [34, 38, 41–43], which is succinctly summarized as follows: use of this term does not explain the opposition. There are three general reasons against the use of

this term. "First, it is generally used as a pejorative implying selfishness as an underlying cause; second, it appears to incorrectly describe much of the local opposition to wind projects; and third, the actual causes of opposition are obscured, not explained, by the label" [44, p. 124]. Currently the most comprehensive overview of research of community acceptance of on- and offshore wind power — also including other cases of energy innovation infrastructure such as tidal, wave, marine, hydrogen, and bioenergy – discards it as follows: "Fundamentally, the backyard concept is built upon an impoverished view of the 'home' (. . . . . .), local concerns about the impact of renewable energy projects clearly transcending the boundaries of specific properties, or implicating wider spatial domains such as publicly owned landscapes and seascapes" [45, p. 62]. The alternative put forward in that study to think beyond the backyard is place identity, a concept that emphasises the enormous variety of geographical identities of places that can be used for wind power development, which includes landscape as well as community identity variables (section "Identity of Place").

The erosion of the assumed relevance of NIMBY-ism is not only due to studies on wind power. For example, a study on the acceptance of nuclear waste storage facilities also questioned its applicability, as it observed that the users of the NIMBY label do not apply a clear definition and hence, do not make clear what they really mean when they use the label. A clear definition is needed, because if all opposition to facilities were NIMBY-ism, then the concept would be both quite empty and unnecessary [46]. However, when it is clearly defined what motives are distinctive for NIMBY-ism, there is hardly anyone found to whom the definition applies [46, 47]. The most distinctive definition of NIMBY is "an attitude ascribed to persons who object to the siting of something they regard as detrimental or hazardous in their own neighbourhood, while by implication raising no such objections to similar developments elsewhere" [48]. The second part of this definition is crucial, because it distinguishes NIMBY from opposition motivated by other factors as it explicitly relates the opposition to merely the fact that it is situated in the backyard. Most of the manifold critical stands are related to this aspect, because that people support similar development elsewhere is not supported by empirical evidence. The assumption implies that close means opposition, far away is support. The most comprehensive effort to formulate a theory of NIMBY postulates as the most fundamental hypothesis that the universal factor is geographical proximity. "The rule is simple: The closer residents are to an unwanted facility, the more likely they are to oppose it." [49, p. 290]. This idea is circulating in policies and publications so frequently, that some researchers seem really surprised to find exactly the opposite. The general truth is that, in some cases, this relation between opposition and distance is actually found – though even these studies emphasise that his should not be considered a result validating the backyard these [50] – but more often researchers find that people close to the wind developments are on average more in favor of them (e.g., [69, 93]), and the proximity hypothesis must be considered falsified.

Developers and policy makers, in particular those in countries that have not been successful in establishing institutional frames that facilitate rapid implementation rates, are still inclined to think in terms of "backyard" attitudes of the local public [21, 39]. The persistence of this inclination is probably due to the fact that ultimately the local level is the level where the real decisions about investments and building concrete wind power farms are taken. The institutional factors that affect decision making on that level are summarized in Fig. 3 [51]. It is good to note that factors such as "population density" and "geographical potential," including the geographical distribution of wind resources, are clearly informing the possibilities for establishing wind farms. As described in the section "Institutional Change," the focus here is on the institutional factors that are found in the upper part of Fig. 3. The key question is how decision making on the local level is organized and how social networks, operating on either the same or other levels, are influencing those decisions. Market acceptance and community acceptance are mainly connected to this level, whereas essential factors that are framing those decisions are located at the level of general sociopolitical acceptance.

Sociopolitical Acceptance

The three keys elements to securing to positive decisions about establishing wind farms are:

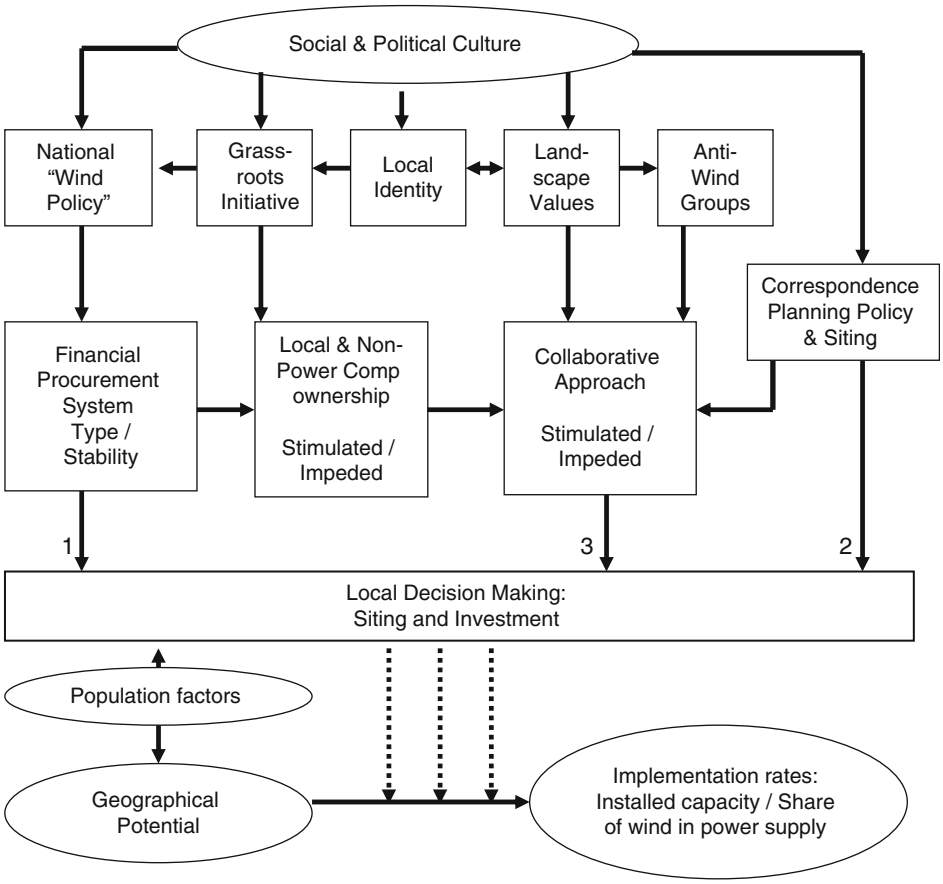

Wind Power: Basic Challenge Concerning Social Acceptance. Figure 3
Overview of institutional factors affecting the decisions about wind power implementation (Adapted from [51, 52])

1. The shape and the reliability of the financial procurement system (Fig. 3: 1), which is of overwhelming importance for the utilization of the potentially significant willingness to invest in wind developments;
2. The type and amount of effective support generated within the national and regional planning system for policies that develop wind power capacity (Fig. 3: 2);
3. The degree to which collaborative decision making on the level of communities is allowed and stimulated by the sociopolitical framework (Fig. 3: 3).

The third factor is closest to the central question in sociopolitical acceptance, as this factor is partly determined by the two others, the financial procurement system and the planning regime. Collaborative planning and decision making [53] is the favorable condition for reaching positive decisions about wind farm construction, but the conditions that determine whether or not collaborative approaches prevail at the community level largely depend on sociopolitical acceptance. The willingness to establish effective support regimes in these domains varies greatly. Clearly visible in Europe (Fig. 3 is the result of an analysis of six EU cases) [51, 54], it has also been equally significant in the comparison of the effectiveness of policy frameworks among states in the US [55, 56].

There are four institutional variables which concern decision making above the community level: the institutional and financial support system; the planning regime that should be in line with the support system [57]; the value attached to landscape preservation; and the framework determining the degree of local ownership of wind power schemes. Of these four,

landscape values are connected to history and largely culturally determined, and exercise great influence on decision making regarding wind power schemes (see section "Landscape/Seascape"). It is one of the reasons why a collaborative approach in decision making is so important. The other three factors are mainly informed by the institutional developments in the dimension of sociopolitical acceptance. These three constitute the institutional capacity that can foster and exploit the high average support for wind as a power source (Table 2, left). Some countries have shown limited learning to develop this institutional capacity [58]. Most still rely upon the assumed high level of acceptance among the public. This support is very strong in most countries, but it is important to notice that in all countries there is a minority that does not support wind power and, furthermore, support is almost always conditional [34]. In order to meet the conditions for that support, serious institutional change is needed, but those changes are subject to sociopolitical acceptance.

Institutional Conditions

The main problem with sociopolitical acceptance is that it is hard for policy makers to recognise basic assumption II of social acceptance, the institutional nature of WP implementation, especially the sociocultural side of the STS. Within policy, there is a strong rooted institutional tendency to look at energy issues and at environmental issues in general primarily – may be even solely – as technical problems. Also experts see the "energy problem" as a chiefly technical issue, and policymakers tend to continue to overly rely on technology for providing solutions to issues that it cannot address, namely, deeper social, political, and cultural problems [59, 60]. If one assumes that policymakers are willing to promote wind power, this inappropriate focus remains an obstacle to looking at the technologies to be socio-technical and consequently policymakers continue to promote renewables ineffectively [20]. Although many developed countries have been promoting wind power for more than two decades and also have instituted policies in support of wind power, there are enormous differences in the effectiveness of these policies.

The comparative assessments of countries and state-specific sociopolitical contexts provide some understanding of the policies and processes that affect wind deployment. For example, a comparison of four US states established that although the state of Massachusetts implements supportive policies, this support has been insufficient to trigger deployment as deployment costs remained very high. On the other hand, Texas' targeted policy and spatial planning fostered policy that was in line with the energy policy objectives, and facilitated deployment. Furthermore, the positive aspects of community-based wind development have been shown, also with regard public acceptance, in particular in Minnesota [60] and Texas [50].

Related to the factors in Fig. 3 (discussed in the next sections in greater detail), it is important to emphasize that the existing discourses on all aspects of sociopolitical acceptance among all important key stakeholders show fundamental differences, for example in Europe [21], the UK, and Australia [22]. Also in the US, the nature of wind energy discourses differs significantly within states [60]. These contrasting discourses reveal strong deviating beliefs about the necessity of wind-generated power as well as fundamentally deviating beliefs about how to implement wind power. These differences reflect separately operating and usually competing advocacy coalitions within the domain of policies that are relevant to wind power. Within the conflicting policy belief systems of these advocacy coalitions [61], the problematic nature of sociopolitical acceptance is reflected [21]. Within different discourses, actors usually also use different terminology for basically the same attributes, phenomena, and issues. All actors have vested interests, and almost any actor has inherent tendencies to use specific terminology to create a certain perspective that fits to their views. This process is called "framing" and this has proven to be effective, because individuals perceive losses and gains differently, depending on how a phenomenon or issues is presented to them [62]. Some examples: some may define financial procurement as "financial support," whereas others prefer to frame it as "subsidies"; the fact that wind power supply is not following demand but the presence of wind may be called "variability," but it is also presented as "intermittency" [27]; the continuous power supply of large-scale power from nuclear may be presented as "reliable," but it can also be framed as "inflexible."

The strong differences in policy beliefs reflect the level of acceptance for the change of essential institutions, for example the willingness to support the choice for and the implementation of effective regulatory regimes and the willingness to establish planning regimes that create the necessary environment for collaborative decision making at the local level. Besides overcoming the resistance from strong stakeholders, in particular in the energy sector, it is not easy to introduce supportive regulatory systems. Supportive regulation is complex: changing a single element of a current system, for example only the financial support system, or only the planning regime, will not overcome barriers at deeper political, cultural, and social levels.

Public Opinion

What is usually seen as most problematic, general public acceptance of the energy source, is in fact least problematic [23]. Several indicators show, from the beginning in the 1980s and 1990s onward [63] that public acceptance of renewable energy technologies and policies is high in many countries. General public opinion polls in Europe show that the majority agrees with public support for renewables, also in countries where the government provides relatively little support [64]. In the US, a majority also supports building wind facilities. In a study on different power-generating facilities, it was found that attitudes about plant siting depend heavily on perceptions of environmental harm and costs of the particular facilities, but the effects of these attributes are similar across different types of fuel sources [65]. This suggests that people view all power sources in the same framework and differentiate them on perceived endowments, environmental harm being the most important. Thus, both solar and wind power enjoy high public rating compared to other sources [64, p. 27]. This positive overall picture of public support for the wind power as energy source for a long time misled policy makers to believe that social acceptance is not an issue. This is a mistake, for three reasons:

1. General public support is only based on attributes with regard to the energy source in general and not connected to attributes that are cases specific (Table 2).
2. Public support is based on fairly low information levels [66]. As a result, when the public becomes better informed, their views become more balanced, for example when there is a wind power proposal and a public discussion about it within their community [67]. In fact, because of the very high level of positive attitude in the poorly informed initial condition, the average shift as a result of becoming informed shows the pattern of a regression to the mean (see the end of this section).
3. Public support may be averagely high, but this average still contains a minority of people that generally do object to wind energy. In all studies on discourses, the objectors to wind energy appear as a distinguished class of actors, not only among the public but also among the key actors in wind power decision making at all levels [21, 68]. In concrete cases of wind farms proposals, the part of the public and the actors that represent this objectors' discourse will almost certainly participate. Because of the strong emotional component in landscape valuation, their involvement in decision making is usually very intense, because landscape is the main attribute for attitudes toward wind power projects (see section "Landscape/Seascape").

The commonsense focus on opposition as a barrier to wind power development implies a "taken for granted" view on the willingness among the public to take positive decisions about wind power. While the willingness to invest (positive investment decisions) and the willingness to integrate wind power applications in the community (positive construction and application decisions) are conceptually very different. In practice, these two are sometimes treated in a similar way within existing institutional arrangements. For example, willingness to pay for "green power" [69, 70] is by no means similar to willingness to invest in a wind farm and even less similar to a positive attitude toward a particular wind power scheme. Therefore, a positive attitude toward "green power" or "green tariffs" is not a proxy for public attitudes toward renewables in general and even less for attitudes regarding wind power (see section "Market Acceptance").

A particular feature of public acceptance is its time dimension. The typical pattern of acceptance before,

during, and after a project follows a U-curve, falling from high average general acceptance to more critical levels of acceptance during the siting phase (usually still positive on average) and back up to a higher level of acceptance once a project is up and running [41, 67]. Remarkably, this effect is due to the low levels of public knowledge in the first stage, when people are not yet confronted with any wind development in their environs. Information and discussion about a concrete project in the community is increasing knowledge. This is making attitudes more nuanced and therefore averagely less extremely positive in cases where no high emotional attributes prevail. In other cases, it may also result in more polarization, which also means a lower average positive attitude, when strong emotional attributes – community and landscape identification related – are at stake [68]. Again, this attenuation effect on the generally positive attitudes as a result of increased information levels runs contrary to common sense, as developers and authorities often expect that increasing knowledge will help to reduce objections against wind power projects [71]. However, this expectation is based on an illusion, as there is no study that provides any evidence of a positive relationship between the level of knowledge about wind energy and attitudes toward wind energy or toward a particular wind power project.

Whereas the general public support does not imply strong impediments for wind power implementation, the following set of institutional domains in policy development and energy provision are the distinguishing determinants for the level of sociopolitical acceptance.

Economic Conditions and Financial Support

Support regimes and their stability provide the basic premise for successful wind power programs, and their perceived stability has a positive effect on investment decisions. The support regimes are primarily financial, and obviously the substantial incentives provide a stronger support than small incentives. However, the institutional conditions of the support systems are even more important: do they subsidize capacity or generated energy?; do they support existing incumbents or do they attract new market actors?; are the subsidies ultimately paid by tax payers or are they guaranteed rates ultimately paid by energy consumers? These essential characteristics affect the effectiveness of the support as well as all three sorts of social acceptance.

In most countries, the dominant approach has been to stimulate investments with the introduction of government subsidy or by deploying a tax credit. However, the renewable energy feed-in tariff (REFIT) system, as a financial procurement system, has become a cornerstone for the deployment of wind power in successful countries [72, 73]. The effectiveness is due to the fact that this system is not only favoring investments – market acceptance – in wind schemes, but it is favoring investments by new actors in energy production, which is also supportive to collaborative planning of wind power schemes because those actors often have strong connections or are rooted in the community (Fig. 3).

The clear example of the promotional role of this key instrument in fostering social acceptance is the innovation of wind and solar technologies in Germany, which is linked to the rapid diffusion that resulted from the nature of the policy instruments employed. However, the application of a clearly effective policy instrument like REFIT is everything but easy; most countries did not implement it and in fact its implementation is subject to sociopolitical acceptance. Analysis of the sociopolitical process that led to the adoption of these instruments in Germany demonstrates how the regulatory framework is formed in a "battle over institutions": "The German parliament, informed and supported by an advocacy coalition of growing strength, backed support policies for renewables-sourced electricity against often-reluctant governments and the opposition from nuclear and coal interests" [74, p. 256]. On the one hand, this example illustrates high acceptance as the instruments that were implemented were very effective indeed, but, on the other hand, the example also reveals that there are strong forces that provide sound resistance in the policy process. Such resisting stakeholders exist in all four categories of actors (Table 1), but with regards the financial procurement system and the guaranteed access to the grid, the strongest resistance is often found among the incumbents in the energy sector itself [51, 75]. This feature of access of new market actors in fact reflects the choice to prioritize power generated

with renewable sources over conventional power generation, and the appearance of new actors on the market is a key in innovation processes [8, 12]. The incumbents in the power sector prefer a system based on Renewable Portfolio Standards (RPS) with a claim that such systems are market based. Although they do not create an electricity market (unlike REFIT, which creates this marked based on fixed prices) and only offer certificates, RPS supporters claim that it is more market based and more cost effective [74, 76]. However, several studies have shown that REFIT is at least far more effective, and some also claim more cost effective [77, 78]. The RPS systems actually limit the market to a few large energy companies [75, 79].

National policy defines the objectives, conditions, and instruments of the financial support systems. Most significant is the fact that REFIT grants grid access to all and it provides financial risk reduction for new investors [76], and therefore it supports new, more inventive, and renewable-friendly players, thus enhancing market competition. Furthermore, the emergence of such market competition puts pressure on the incumbents. This is a crucial positive reinforcement for any civil society initiative that seeks to promote renewable energy. In order to exploit the large potential of supportive attitudes in the society, favorable conditions and institutional change are needed. The introduction of REFIT systems was a major effective institutional change in some countries, but many countries still refrain from introducing such systems. Moreover, despite its undeniable effectiveness, the REFIT is continuously under attack from energy companies and several EU member state governments. The new regulatory regime in Germany has gained widespread support, but resistance still exists and has sought to influence European regulation in order to replace the regulatory regime adopted in Germany [79, 80].

The most significant institutional changes – changes of the "rules of the game" – are achieved by political decisions, so the roots of the huge differences in success rates of wind power implementation can be found in primarily problematic sociopolitical acceptance. In some countries, sociopolitical acceptance of effective new regulatory regimes has been high and accompanied by policy changes, in many other countries it has enjoyed only rhetorical support. Expressed preference is not always evidently followed by action among policymakers and structural measures – institutional change – are yet to materialize.

The Impact of the Spatial Planning and of Location Decision Making

A persistent line of explanation for the implementation deficit that several countries experience with regards their performance achieving substantial wind power capacity is the existence of a "planning problem" [71]. This implies that spatial planning would constitute a "barrier" to the expansion of wind energy. Most of the attention in social acceptance studies has been focused on studying the continued deficit in implementation as a result of problematic local decision making [8]. From the developer's perspective, the planning problem is usually interpreted as an attitude-behavior "gap" between general public support for wind power and local opposition to wind power schemes (section "Mind the "Gap""). The reaction to these problems is often a request for more perseverant planning instruments that would enable authorities to overrule local opposition. However, the nature of the planning problem is strongly contingent on the discourse that the actor supports, and the most prominent followers of the "planning as a barrier" line are found among developers and authorities in countries that have not been very successful in implementation [21]. Actors in more successful countries have learned that collaborative planning approaches that foster civil society initiatives and involve local stakeholders generally produce an increase in positive decisions about investing and siting wind farms.

The request for a more powerful, in fact top-down planning regime produces a uniform, inflexible system. Motivations for adopting such approaches may also reflect centralizing planning cultures. A clear example of this is the Welsh approach to the planning problem, as a reflection of the UK's centralizing tendency in planning. The Welsh 2005 planning guidance on renewable energy superimposed centrally determined "Strategic Search Areas" for large-scale, onshore wind farm development onto local decision-making processes [81]. It is doubtful whether such increased centralization will help accelerate wind power implementation. In a comparison of UK and Australian policies, it was concluded that such policies did not

ease conflict over wind energy projects. On the contrary, they have been criticized as endorsing wind energy while neglecting concerns about landscape and place [22]. Another example is Sweden, where the main purpose of the national planning instruments is to strengthen wind power as a public interest in local land-use planning processes. According to Bergek [82], this purpose is not well served because civil servants became more inclined to treat wind power as a private interest when the country targets are achieved.

If national planning uniformly superimposes the locations and site selection, it can only apply the general attributes of wind energy (Table 2; left column). In decision making regarding projects, these constitute only a part of the attributes (Table 2; right column) that are significant to the actors involved in the process. In the practice of such decision making, another UK study showed how the attitudes of people in the immediate vicinity of proposed wind farms exercised the most important influence on the decisions made by local authorities [83]. This not only includes the perception of the appropriate match between the wind farm and the character of the landscape (section "Landscape/Seascape") but also concerns the perceived local economic benefits. Interestingly, the study also concluded that there is a lot that wind power developers can do to improve the prospects of successful planning. This is where the endorsement of national policies through top-down planning may easily become a factor creating mistrust (see section "Community Acceptance"). In addition to landscape concerns, negative attitudes also emerge in response to the dissatisfaction with the planning and decision-making processes [84]. The opposition to wind power developments may even be shaped largely by the manner in which planning and decision making on wind schemes takes place [67, 85], for example the manner of organizing public consultations [86]. The issue is that all local cases of wind power implementation show a wide variety of place identification factors, because both the landscapes as well as the social structure of the host communities differ greatly. Hence, the attributes of wind power developments as listed in Table 1 will be assessed differently in all cases. Uniform policies cannot address this diversity. Studies of the underlying reasons for opposition show that the objections are very heterogeneous [68]. As wind power is already a contested realm, also the legitimacy of national policy is problematic, in particular when hierarchical power is used overtly to site turbines.

In case planning is actually organized with a focus on local decisions and not primarily based on national uniform policy regulation, the consequence is that the planning context may vary between different municipalities, as community acceptance levels may be different and may also vary in time. This poses a particular difficulty for larger, nationally or even internationally operating companies. It is also not congruent with national uniform systems that claim to support wind power in a cost-effective way. As was noted in an analysis of Swedish wind power planning, municipal planning tends to undermine the cost-efficiency goal of the "green certificates" trading systems [87]. In Germany, the feed-in support system – REFIT – has positively affected the involvement of the civil society and local initiatives to wind farms and correspondingly. The implemented planning system did not endorse the selection of sites by higher authorities; instead it only set a priority for wind developments *("Priviligierung")* and then left the actual planning of the local wind development and site selection to local governance [88].

There are huge differences in national planning systems. In general, it can be concluded that planning systems are not creating the problems of social acceptance. Planning is not the source of the problems, but in many cases may become the carrier as the planning process is framing how local decisions are taken, and most issues related to acceptance manifest themselves in the planning process. Therefore, supportive planning systems are generally those that effectively foster and enhance market and community acceptance, i.e., a system that stimulates collaborative decision making at the level where crucial decisions about establishing wind farms are taken. Substantial evidence points to the many benefits of the early, sustained, and reciprocal engagement of host communities. Such strategies have been linked with improved chances of planning success and are seen as offering developers the opportunity to gain the trust of host communities and among actors that invest in wind power projects, to identify and address their concerns and to effectively communicate the potential risks and benefits. This does not happen on the national level but rather mostly on the local, with the notable exception of Spain [31].

Community Acceptance

Two Dimensions of Community Involvement

Historically, the focus within this issue of social acceptance of renewable energy innovation has been on public acceptance as the cornerstone of community acceptance. Community acceptance refers to the specific acceptance of siting decisions and renewable energy projects by local stakeholders, particularly residents and local authorities. In the commonsense approach of "nontechnical factors" (see section "Beyond Common Sense"), it was soon recognized that energy companies trying to develop pilot projects faced problems with the communities. Because they were usually incapable to handle these problems, about the local resistance in the communities where they wanted to establish those developments, the debate around NIMBY-ism unfolded. Section "The Backyard" describes that this classification of local nonacceptance is not fruitful as it violates Basic Assumption IV by questioning the legitimacy of the actors' positions and because it fully neglects the high potential of positive acceptance at the community level of initiatives that originate within the local community itself and in civil society more broadly. The utilization of such labels denigrates opposition to proposed wind development as cynical and selfish.

Most case studies that analyze the motives and beliefs of local actors reveal a wide range of considerations, ranging from strong support for local initiatives to rejection of wind developments in principle. The essence of the difference between the positions that people take regarding specific wind development projects and the support for application of wind power in principle is that the latter general support is qualified [23, 34, p. 463]. All actors in society may be prepared to support any wind development that meets certain criteria, and they will tend to oppose developments that do not meet those criteria. From the developers' point of view, their main concern is the construction of the wind turbines, but other actors have other concerns: the selection of a site out of many alternatives, different options for who is the investor and owner of the turbines, and considerations on who will decide about the project and how. For the developer, these aspects are not variables but self-evident constants. They are inclined to present the proposal in a way that creates a narrow frame for the community. The developer is not inclined to look at himself as a variable, as just one out of many alternatives. Usually, the proposal is a wind farm at a chosen location with an already selected site. For the community, this manner of planning a wind power scheme ("decide – announce – defend") is seen as "framing" the decision-making process: it presents the most significant aspects of the project as already decided upon, without their participation [67].

This "framing" of decisions of wind power is rooted in several institutions, such as rules and procedures in spatial planning systems, and existing preferences in energy policies that favor developments initiated by the incumbents in the energy sector. The process of altering these types of institutions is part of sociopolitical acceptance (section "Sociopolitical Acceptance"). Moreover, these kinds of problems do not remain restricted to wind power. Local acceptance of all types of infrastructure facilities is steeped in local conflict [89] and infrastructures that aim to further environmental policy targets, such as environmentally benign waste management, and climate change adaptation or mitigation are no exceptions [90]. The roots of these conflicts are complex as they always combine opposing interests regarding the use of the facility and the burden of the facility in terms of local social or environmental impact. Considering wind power, four different types of conflicts of interest may be recognized, which are based on two dimensions:

1. Application of wind power as a public interest versus wind power as a private interest of the owner of the wind farm
2. Wind power in conflict with various private interests versus wind power in conflict with public interests of the community [82, p. 2360]

Actors of all four categories listed in Table 1 are attached to any of the four types of conflict. By definition, developers represent private interests, except when local or regional authorities participate in wind farms, as occurs in Spain [31]. Nevertheless, developers often claim that their project is an application of an environmentally benign energy source and represents a public interest: "The benefits of wind power are felt by the masses in improved environmental quality, diversity of energy resources, and compliance of

international agreements [..but] the costs are borne locally." [91, p. 505]. In case the developer is a community outsider, such as an incumbent energy company, the local perception will assign the developer as representing private interest, whereas the impact is perceived as a burden to the community's public interest [33]. When developers emerge from within the community, their interest may be private (e.g., a farmer) but it may be public when the developer is a cooperative rooted in the community, as frequently has been the practice in success stories like Denmark and Germany. In addition to these interests, there is the second dimension of community involvement: the decision-making process that may vary from closed and institutionally constrained to open and participatory. On both dimensions of "community renewable energy," the utility wind farm scores low, with severe consequences for its acceptability from the community's viewpoint [33, p. 498].

An illustration is given in a recent study in Germany, showing clear differences in acceptance between two fairly similar communities, including the visual impact and concern over environmental protection and high energy use. A community energy initiative in a village called Zschadraß, changed the perception of the local people toward renewable energy compared to a control community – village called Nossen – without such an initiative. The residents of Zschadraß had become consistently more positive about renewable energy: "Community co-ownership of wind energy leads in fact to a higher level of local acceptance toward the nearby installed wind turbines than ownership of a wind farm by a commercial company" [92, p. 7]. Some significant figures: the statement "There are already enough wind mills in the area" was supported by 39% in Nossen, and only 8% in Zschadraß, and comparable figures on the statement " '. . .and that causes a disturbance of the landscape" were 18% and 4% respectively.

Identity of Place

Related to the local acceptance of wind power projects is the question whether institutional settings foster the community's identification with the project, such as locally organized or publicly owned wind power. This can obviously be the result of community involvement in the outcome of the project, which can take the form of ownership or shareholder participation. However, the identification can also be more symbolic "sense of ownership" [93], as a result of effective involvement and influence in the siting process.

Moreover, all the forms of involvement are part of or are supporting collaborative decision making at the level of wind power scheme (Fig. 3: 3). How decision making is organized and how social networks at this level are involved in projects strongly shapes the possibilities for identification with the project by all actors at the community level [94].

The most frequently mentioned commonsense interpretation of identification is the proximity of the selected wind farm site; this proximity hypothesis is closely associated with the "backyard" explanation of rejection of wind farm development, i.e., local attitudes to wind power would be negatively correlated with proximity to wind turbines. However, studies have failed to find evidence for the presumed negative effect of spatial proximity on public attitudes. Although some studies did indeed find more negative attitudes at closer distance [50], several studies found – sometimes to the researcher's surprise – that attitudes to wind power as well as to the existing project became more positive at shorter distances [69, 93]. These results also seem to be independent of the national policy context. For example, a recent study in New Zealand found similar results to the previous studies in Europe: neither was there a clear relationship between the proximity of the submitters of appeals to the proposed wind farm and their appeals, nor did proximity increase the likelihood of them having negative perception of the proposal [95].

If it is not proximity, then the question is what really motivates local actors (i.e., residents, their civil society organizations, and the representatives in public administration). An alternative proposed for proximity or the narrow interpretation of backyard-protective reactions is "*identity of place*" or "*place attachment*" [96–98]. These are both concepts in which the focus of explanation shifts away from the physical aspects of the development toward the socially constructed, symbolic attributes of places. It is essential how the identity of a place is interpreted by members of the community (not primarily restricted to residents) in order to "fit" with development proposals. Several empirical findings support the significance of the link between responses to

facilities and place attachment and community commitment. A well-known example is hydropower [99], but recent studies on wind power have also confirmed the importance of this relationship, among residents and local communities [57]. Empirical support for the significance of place identity is presented in a study in two coastal communities in Wales that are confronted with the same nearshore wind developments (North Hoyle and Gwynt y Mor). In one community, clear correlations between place attachment and landscape-identity evaluations about the wind farms were found, and in the other there was not such a relation ("Fence in the bay": $r = 0.20$). Accordingly, in the community where people saw this relation between their place attachment and the landscape impact of the wind farm, there also was a correlation with oppositional behavior ($r = 0.20$) and none in the other community [98, p. 276].

In the concept of place attachment, there is a prominence of social and physical elements, whereby the latter are connected to landscape characteristics in particular [100]. This follows the general finding that landscape quality is by far the most important attribute of attitudes toward wind power projects. In environmental conflicts about siting wind power schemes, in the commonsense approach, the wind turbines are the object of the conflict; however, in fact, the physical space is the object of the conflict and not only the location of the conflict (section "Landscape/Seascape").

The meaning of the concept of "community" can also be based on the feeling attached to the physical as well as the social attributes of a place. For example, place attachment can be high among tourists coming to the community, whereas in the community itself people care for this identity because the attraction is considered economic valuable. Another important group combining physical and social characteristics of the community are the members of organizations that work on the preservation and conservation of certain areas. The conflict over renewable energy facilities has often a character what has been labelled as "green on green" [42], with organizations that belong to the environmental movement at both sides of the conflicts. This may be related to the time scope of the environmental issues: some impacts become immediately manifest, in particular any visual change in the landscape, whereas other have a long-term risk character, among these most effects of climate change. As many environmental organizations have primarily emerged because of landscape and nature protection values, their natural reaction to wind farms also concerns the potential threat to these values. Their identification will usually be strong because of values of landscape and ecology, but the identification will also be rooted in historic links to a place or in general ideas about the character of areas, e.g., in terms of "rural" [101, 102]. Studies also showed that this identification with places does not necessarily reflect negatively on the development of wind power (see section "Landscape/Seascape") and the clearest example of this is the fact that farmers often have positive connotation with "harvesting" the wind on their land because they are used to associating their land with production. On the other hand, in some cases, proposed wind developments are the origin of new emerging landscape protection organizations [103].

Benefits

The most problematic aspect of community acceptance is caused by the fact that in many countries the framework of sociopolitical acceptance leads to projects that are initiated by actors who are outsiders to the community. First, this model neglects the potential of support for wind power initiatives that originates from within the community. Second, the community and the places valued by the community are used for interventions that do not create benefits for the community. Some studies suggest that local financial benefits "are critical to the acceptance of new turbines" [91, p. 507], or, put in a more prudent way, "renewable energy projects can become more locally divisive and controversial if benefits are not generally shared among local people" [33, p. 499]. Clearly, the benefits are shared when community members are shareholders in the wind farm, and the conflict of private vs. public interest is effectively mitigated.

Thus, in all cases of wind farms initiated by developers outside of the community, securing benefits for the community represent a significant problem. Nevertheless, community benefits can also be defined more broadly than direct financial gain, such as benefits-in-kind (provision of assets by the developer, e.g., parking facilities, children's playground, educational material for schools, footpath, etc.) or investments

in environmental mitigation or enhancement [104]. As long as community members perceive the local benefits as valuable, they can be considered substantial, for example when they concern involvement of local small companies and employees in construction, maintenance, and management of the wind farms. Contribution of renewables is often suggested to positively affect local sustainability in a general sense. In the same way that usually the environmental dimension of sustainability is emphasized [105], the local dimensions of the social – inclusion, governance – and economical dimension – development, efficiency, employment – may also be promoted by a wind farm [106]. Several studies have shown indications that wind farm developments have indeed furthered local employment and the local or regional economy. However, these results remain ambiguous: the effects cannot be considered substantial [107] or the benefits are not experienced in the community but more dispersed, so general employment benefits are found at the national scale [108]. Special cases of community economies that may benefit from wind power projects can be found on islands, where wind power may help to reinforce the sustainability of the community [78, 109]. The general picture of local sustainability through wind energy is ambiguous, without any notable general tendency. This is reflected in the discourses around decision making on wind projects in the community. A clear objector's discourse has been recognized in a discourse study focussing on presumed negative local economic impact [68]. A general framework to analyze the contribution of renewable energy deployment to local sustainability has been proposed by Del Rio and Burguillo [106].

Some aspects should still be mentioned, as in certain cases they affect the acceptance of communities. These are farming and tourism, both economic sectors that may be considered land uses that compete with wind power deployment. Concerning the contribution of wind power to local sustainability, there is some evidence that rural areas may benefit because farmers are able to continue their business with a new resource to harvest from their land. As a matter of fact, this kind of positive acceptance is clear in most countries as many private investments in wind have been made by farmers on their own land. The picture for tourism is generally less positive. Community acceptance is adversely affected by the perceptions that clients, the tourists, would not like turbines. Communities that heavily dependent on tourism, and in particular the stakeholders with interest in those activities, tend to be reluctant to allow renewable energy infrastructure – including wind turbines in the landscape – because it may easily affect the character of the area that is considered the primary attraction for tourists [110]. Several studies on the cost and benefits of wind power for tourism show ambiguous results, highly determined by the kind of landscape and the kind of tourism [111, 112]. An interesting topic is in particular the relation between wind power and tourism on island communities and also of nearshore wind power and tourism in coastal areas generally [113]. It is not always clear whether the tourists really do not like the turbines or that this is primarily untested fear of the actors in the tourist sector. In some cases, there is evidence that wind turbines may add to the tourist value of remote communities as they are seen as emphasizing the character of the location [93].

Fairness and Trust

Having local benefits that balance the burden that the community has to bear – at least in their own view – is a question of equity and fairness that is typical of environmental conflict and decision making on infrastructure [89, 90]. These are questions related to distributional justice (How are costs and benefits shared?), fairness of process (Is there a fair decision-making process that provides all relevant stakeholders with an opportunity to participate?), and trust (Are the information and the intentions of the investors and actors from outside the community trusted?) [52, 114].

These questions are strongly affected by the degree of collaborative decision making (Fig. 3: 3). In cases where the wind farm project clearly generates community benefits, the problems with community acceptance will remain limited. This often holds for different sorts of community ownership, but this will not be sufficient, in particular when the benefits are unequally distributed among the members of the community. Furthermore, the dimension of community involvement may also create feelings of (un)fairness if community members feel that the project is imposed on the community.

The "utility wind farm," or any other project initiated outside the community, is clearly the model with

the greatest probability of meeting distrust [115]. In particular in policies that favor developments by large companies, there is a tendency to include some prescribed compensation to generate community benefits. However, this is a dangerous strategy, as the intrinsic motivation of the community members with a positive acceptance can easily be undermined [116]. Some practices of compensation in wind power cases show that the introduction of community benefits in case of a wind farm built by a community outsider may reinforce feelings of mistrust and it can easily be interpreted as an effort to bribe the opposition. Although community benefits, financial or otherwise, are presented as means of creating greater equity, experiences with this kind of compensation of local burden to the community show that "even the most well intentioned developers may have a hard time earning the trust of local communities" [117].

Market Acceptance

Social acceptance can also be interpreted as market acceptance or as the process of market adoption of an innovative STS. The literature on diffusion of innovation explains that the adoption of innovative products by consumers takes place through a communication and negotiation process between individual adopters and their environment [118]. A technology like wind power is bound to infrastructure, such as the power grid, which makes it inherently more complex to diffuse this innovation than other products. However, using the insights from this literature, it is helpful to study market acceptance at the consumer level.

Consumers can, and in successful examples of implementation do, play a role as investors. They have participated in cooperatives or other civil initiatives – "*Bürgerinitiative*" in German – to establish wind farms and thus became shareholders. There is a wide range of motives for such initiatives, but a strong driving force behind this development were various grassroots initiatives (Fig. 3) based on environmental concern and the willingness to be involved in the development of alternatives to conventional and nuclear power generation [88, 119]. In the meantime, such civil initiatives have evolved into new energy companies with an inherent high degree of acceptance of renewables energy.

The alternative to investments by civilians in wind power is the choice in their role as consumers to subscribe to any kind of "green power" [120]. Such labels are in fact a type of marketing strategy used by energy companies, generating power through a mixture of sustainable energy generation [30, 121]. Most of these schemes include wind power, and consumers have the opportunity to switch to renewable energy supply without being actually involved in the physical generation. The "green power" schemes are probably the area where market adoption is rather isolated from the broader social acceptance picture. A study from Sweden shows that rejection or acceptance of green power does not correlate with proximity to renewable power facilities [69]. Nevertheless, if consumers would demand increased amounts of green power, wind farms would still need to be sited to supply this demand. The separation between (physical) supply and demand is inherent in the concept of green power marketing and trading, and it is a continuation of existing institutions in the power sector. The model is strongly favored by the incumbents in the energy sector, similar to the support they provide to RPS systems. This might aggravate the problem of social acceptance, for example if there is high green power demand, but the energy companies are not able to generate sufficient sociopolitical and community acceptance for building the corresponding wind power production infrastructure. Extensive international green power trade, that might also be favored by an internationally (e.g., EU wide) operating green certificates system, something that is strongly supported by Eurelectric – the European umbrella organization of the power supply sector – would reinforce such problems [79]. It seems questionable whether residents of a country with large wind resources, such as Scotland, would be willing to bear the burden of the export of green power generated by many large wind farms. It would become a market model that would provide a "free rider" escape for countries that scale-up the original "backyard" concept to their entire nation [122, p. 209] in which they do not opt to produce a sufficient amount of renewable energy within their own country needed for making the transition to a sustainable energy supply.

In a wider understanding of market acceptance, the focus is not just on consumers but also on investors and the structure of the economy. Examples of studies on

market acceptance are, for example, the "translation" of market stimulation and the effect of policy instruments as applied in Europe, in different markets such as the US. Bolinger [123] emphasizes the importance of the use of instruments that rapidly develop the domestic market for wind technology, in combination with incentives for using power technology that is manufactured locally. As the studies comparing the policies applied by different US states show, the sociopolitical acceptance of such measures is very different [49–51]. Equally important is the acceptance on new but rapidly developing markets like China. There the relation between the development of a domestic market and the development of a wind turbine industry has been reversed. The market is working under a strong centrally directed development regime, including the obligation to use wind turbines built in China, and moreover strong institutional impediments exist with regards the effective inclusion of regional and local identity in the wind developments. Together with the fact that the general market is determined by set prices in cases of noncompetitive contract wind farms, or in underbidding in cases of competitive concession projects, many wind farms are not embedded in the regional or local economy and they are often qualitatively low developments suffering from poor economic performance [124].

With all kinds of market systems, there is also the issue of intra-firm acceptance of renewable energy innovation. Numerous examples show that large firms are subject to path dependency when it comes to their investment behavior. For the general picture of social acceptance, early market formation is an essential contribution to building the legitimacy of renewable energy innovation as a whole [125, 126]. The issue of wind power implementation is also connected with the development of a wind power technology industry, as the existence and progressive development of a domestic market for application is the key to the development of this new branch of industry [127].

The success story countries developed a strong domestic market without large investments from existing energy companies. How social acceptance is constructed within existing energy companies would be an issue well worth studying. This could very well be linked to some of the research on cognitive barriers within firms with regard to taking up environmental and sustainability issues [128]. Many of the energy companies still own and manage significant parts of the grid; even though in some countries, the grid management is subdivided in regional monopolies and is separated from power generation. The role, position, and objectives of existing energy companies are a strong manifestation of market acceptance. In the Netherlands, the energy companies held a gatekeeper role and decided about the remuneration and grid access for more than a decade, whereas the German government forced power companies to accept competition from third parties [88]. The latter factor is an essential feature of the success of the German "feed-in" legislation and the Renewable Energies Act which effectively stimulated third parties to invest in wind turbines [119]. It is clear, particularly from the position of the energy companies toward the REFIT and RPS support schemes, that they prefer systems that enhance their position in the market over the introduction of systems that stimulate third-party investments in small-scale renewable power generation [73, 78]. Moreover, there is a link with sociopolitical acceptance, because the incumbent energy companies are influential stakeholders in the development of energy policies and they try to use their influence in the crucial political decisions about the design of financial procurement systems, the access to the grid for other investors in renewable energy systems, and the introduction of green certificates trading systems [79].

Significant Attributes Connected to Place Identity

Numerous potential attributes of wind power application are shown in Table 2. Most of these with high relevance for sociopolitical acceptance are connected to issues concerning governance and institutional change, or they are general attributes of the wind power technology, such as its variable supply character. Some attributes come to the fore on the level of general application of wind power as well as in any specific case of building a wind farm. The way they show up in these cases, however, is very different. These attributes concern the impact that building wind turbines has on the environment, and these impacts are not primarily determined by the wind turbines itself or by the wind farm design. The impact is primarily determined by the existing local environment before establishing the

development. Three categories of impact can be distinguished that are discussed in almost any case: landscape, wildlife, and annoyance.

Landscape/Seascape

The attribute "landscape" is by far the most significant in social acceptance. Attitude studies in the 1980s and 1990s already indicated that the discussions on the desirability of large-scale application of wind power focus upon the degree to which wind turbines can be integrated in the landscape [3, 4, 41]. In most policy documents and in approaches of developers, this weak spot is recognized, but the issue is poorly understood. In the realms of policy and developers, it is usually narrowed down to "visual impact" [39, 129]. Two approaches can be recognized. In the first approach, studies try to develop instruments for visual impact assessment, and these tend to focus only on the visibility as the determining factor [130]. The second approach tries to include assessments of landscape by the public, but this approach is also meant to find generally applicable parameters of visual impact in order to quantify the corresponding impact [131].

With regards the issue of social acceptance, both approaches fail to address the essence of the landscape issue. The inevitability of the highly visual character of wind power is reason of the importance of the landscape issue, but the visibility is not the problematic impact itself. The visibility is making the landscape the most important – salient – attribute of wind power acceptance because it unifies three kinds of strongly varying elements. Landscape assessment of wind power varies, because:

1. The landscape impact varies widely among cases, as the character of the landscape is very different at the locations.
2. Within each landscape, there are many distinguishable elements that may differently be affected.
3. The valuation of the impact shows a wide variety among individuals: some can positively value landscape elements, whereas other individuals value the same element negatively.

Furthermore, the third factor of subjective valuation is also connected to the geography of the case, as local communities may differently assess similar landscapes because the identity of their community, including the landscape surrounding it, is historically and culturally determined. This is what is making the landscape issue highly subjective, and impossible to quantify objectively.

The notion of "visual impact" almost automatically classifies the impact on the landscape as negative. This strong simplification can also be found among the minorities that oppose to wind power in general. In individual attitudes, the beliefs and valuation concerning landscape are the strongest determinants of attitudes toward the energy source wind power [41, 52]. A clear example of this is the sociocultural approach by Brittan [132] who uses a terminology that classifies wind turbines as "alien" to the landscape, determining their unacceptability. He compares wind turbines to weeds, "invaders" offending aesthetic values in a field of native flora: "To the extent that standardized machines are plunked down in a standardized way, then no matter who owns them, the local character of the community is thereby weakened if not also destroyed" [132, p. 178]. This is clearly the philosophy of a strong general opponent of wind power, but the quote also underlines the significance of landscape and place identity for this attitude (see section "Public Opinion").

In the late 1980s, the first studies that tried to establish the significance of arguments that inform attitudes to wind energy already showed that these attitudes primarily root in values concerning landscape [4, 41]. Ever since, public perception studies as well as acceptability case studies show that attitudes mainly reflect the assessment of the acceptability of turbines in terms of congruency between turbines and the type of landscape in which they are sited [133–135]. Despite the enormous variation that already exists between "typical" national or regional landscapes, studies in different countries have shown that it is the type of landscape in which the turbines are sited that is the most determining factor in acceptance of wind power. This holds for onshore as well as offshore [136, 137]. The idea that acceptability offshore will be higher and easier to achieve assumes that offshore wind power schemes would avoid the issue of destroying the landscape, which is again based on the simplistic idea that visibility determines landscape impact. Several recent studies show that the idea that building wind farms "over the sea and far away" would solve the social

acceptance issue is naïve [138]. Landscapes may also be "seascapes" and these are also determining public acceptability, in particular since most offshore schemes are still nearshore.

Several studies of nearshore wind power have shown evidence that social acceptance is inevitably a topic, and the crucial factor of the impact on the seascape has indeed come to the fore [139, 140]. Table 3 shows the impact of visual factors of a large proposed nearshore wind farm on the attitudes toward wind power development in the region. The variance in the acceptability could largely be explained by these visual factors, but in fact there were only two variables that described the character of the landscape that were important. Landscapes with ecological value are clearly negatively associated with siting wind turbines, but it is important to see that they are very positively associated with areas already in use for economic activities. All visual factors concerning the turbines and the way the wind farm would be designed did not significantly add explained variance. Hence, it is the qualification of the landscape that is the key to visual impact. Some cases show that the identification to seascapes with high iconic value – e.g., Nantucket Sound MA in the US and the WaddenSea in the Netherlands – has produced strong oppositional movements and eventually failing large wind farm proposals [44, 141, 142]. These studies also show the significance of the concept of "place identity," as the values attached to those seascapes are strongly associated with cultural heritage and ecological values, giving these conflicts a typical "green on green" character [42].

Wind Power: Basic Challenge Concerning Social Acceptance. Table 3 Support for wind power development in the entire region, explained by landscape type factors and design factors [52]; standardized regression coefficients (β)

Landscape/design factor	β	t	$p < 0.01$
Landscape I character: economically applied area	0.45	10.5	+
Landscape II character: nature, ecological value	−0.28	−7.9	+
Landscape III character: residential use	0.06	1.53	$p > 0.1$
Landscape IV character: offshore (North Sea)	−0.03	−0.14	$p > 0.1$
Wind farm design I large/small wind farms	0.01	0.33	$p > 0.1$
Wind farm design II small/tall turbines	0.01	0.23	$p > 0.1$
Wind farm design III small/large numbers	0.04	1.10	$p > 0.1$

$N = 535$; $R = 0.66$; $R^2 = 0.44$

The question that remains is how to handle the landscape/seascape issue. Any assessment of the congruence between local landscapes and a wind power scheme may be very subjective indeed, but nevertheless it is the number one issue that should be addressed in decision making. There are two strategies to handle this issue that usually enhance the conflict, but that are frequently applied by developers and authorities. The first strategy is trying to "objectify" the assessments by efforts to develop instruments for the objective assessment of visual impact, which was, for example, tried with an instrument of "viewshed simulations" applied in the Nantucket Sound case ("Cape Wind") [141]. A second strategy is to hire one of more "experts" to finally decide what the visual impact is and this strategy was applied in the WaddenSea case by calling in the official state's architect [142]. In both cases, the strategies failed because these methods try to abstract the essence of the identity of the landscape, which is that it is primarily the values that determine this place identity.

For any decision that addresses the identity of the landscape, it is crucial to apply a method that assesses landscape quality interaction with the new elements – the wind turbine – as it is actually perceived by the relevant viewers. By definition, landscape is the part of the environment that is the human habitat as it is perceived and understood through the medium of our perceptions [143]. Apparently, most developers and authorities alike do not like it, but these perceptions of landscapes are rooted in community values and history, and the only way to deal with them is to deal with the people holding these values. It is crucial to apply methods that assess landscape quality interaction as it is actually perceived by the viewers, because the value of the landscape is "in the eye of the beholder" [144, 145]. Together with the strong influence of the landscape issue on people's acceptability judgments, these observations all underline why collaborative planning strategies – see Fig. 3 – including cooperative and participatory decision making are crucial.

This applies to onshore wind, but also to offshore [140] although the communities that are involved will often be different. For offshore wind farms a new practice of spatial planning at sea is emerging, and similar to planning on land, the involvement of crucial stakeholders is essential [146, 147]. Most of these are representing competitive uses of space at sea and coastal land uses that can be affected by near-shore wind development. To name a few: tourism, nature wildlife, shipping tracks, fisheries, oil and gas exploitation, national defence, etc. Some experimental involvements of vested interests at sea are currently investigated, in particular the co-development of wind power with new ways of marine culture and commercial fisheries [148].

Wildlife

Nature and landscape are strongly connected in perceptions. The strong commitment and tacit knowledge about the ecological qualities of the landscape are also shaping landscape perceptions within communities. This results in the "green-on-green" character of many conflicts about wind power schemes as organizations founded for the protection of natural values and wildlife are often involved in questioning wind power developments [42].

Similar to the attribute "landscape," the fundamental factors that determine the actor's assessment of the attribute "nature and wildlife" are the visibility and the identity of the location in the eyes of the community members. The fact that the casualties of birds are so visible is making the phenomenon inevitable for policy makers, developers, and local decision makers. In terms of attitudes, with regards bird casualties, we are dealing with beliefs about a "salient" attribute ([28]; see section "Attitude Objects and Attributes"). Efforts to assess the factual impact on avian wildlife are still not definitive. The impact is heavily dependent on what kind of species of birds (and similarly also bats) could be affected. Furthermore, the acceptability is as always not only depending on the factual impact of wind turbines on wildlife but it is also depending on similar impact of the alternatives to wind power [149]. Hence, there is no doubt that there is some impact on avian wildlife, and even serious adverse consequence on some species, but in fact the impact of alternatives, in particular coal and nuclear power on wildlife (including the impact of power lines) is probably much stronger. The impact of hydropower is not primarily on avian wildlife, but its impact on fish and river ecosystems, in general, seems very high, but how should this be compared to the impact of wind turbines on some species? Because of the high visibility, wind power is vulnerable to a more negative profile than hydropower has in regard to its impact on fish. The high visibility of wind turbines and of eventual casualties is making this impact a serous problem with regard to the acceptance of wind turbines at certain locations.

The impact on birds is mainly connected to the location. The presence of birds is obviously geographically determined – due to breeding grounds, migration routes, etc. – and these are fairly objective factors, but the social valuation of the impact depends heavily on how the affected species are valued. These are species that are already rare and endangered, but also species that enjoy a valued status as icons of certain places, for example the sea eagle, a bird with high iconic value that has spurred discussion about the closing of an existing wind farm in Norway [150]. The strongest valuation is again connected to the characteristic presence of certain species or of entire ecosystems in which these species are essential elements. The presence of such species can add much to the identity of certain locations and then it will strongly affect the acceptability in the eyes of the communities that strongly identify with the place, such as nature-protection organizations.

In the collaborative decision making, the discussion may be focused upon accepting the building of the wind turbines at the site or to select another site. It may also concern the way of siting the wind farm, whereby specific characteristics of the living patterns of the birds can be used to redesign the wind farm [151]. The impact on wildlife is not the strongest factor in determining attitudes to wind farm developments, but the issue is closely linked to question of place identity and in particular landscape identity (section "Identity of Place"). Hence, for social acceptance it is very important that the issue is addressed in the collaborative decision-making process by means of participation of the organizations representing the interest of nature and wildlife.

Annoyance: Noise

The local impact of wind turbines is often described in terms of annoyance. For example, the visibility of the turbines is sometimes referred to as visual annoyance or intrusion. As described in section "Landscape/Seascape," this description is mainly determined by valuation. The most serious sources of annoyance are shadow flicker and the sound produced by wind turbines. The valuation of that sound is usually referred to as "noise," a term with a clearly negative connotation. Shadow flicker is very severe indeed, but it can be avoided because the places where the moving shadows appear can easily be calculated [152]. The perception and experience of noise, however, is a very complicated matter.

Noise has been addressed from the early 1980s onward as a serious issue concerning wind turbines. Technology development has reduced the production of sound by wind turbines, but simultaneously the size of the turbines has increased. In decision making about the siting of turbines, noise can play a significant role. In the collaborative process, the issue of sound produced by the turbines should be taken seriously. However, this does not mean that the expectations about noise annoyance are primarily determined by the sound of the turbines. The first study on the relation between the actual sound pressure produced by wind turbines and annoyance was carried out in the early 1990s when the number of people living close enough to wind turbines to be seriously affected was rather limited. This study in three countries found that the level of annoyance among surrounding residents was stronger affected by attitudes to the wind turbines than by the factual sound pressure [153].

This phenomenon has been replicated in a more sophisticated noise annoyance study. It combined on-site physical measurements of sound pressure with adequate measurements of all relevant variables to annoyance among residents on several locations in Sweden. In that study, the strongest influence on annoyance was from two attitude variables concerning wind turbines in general and to the visual impact of the wind turbines [154, p. 484]. In a second study, these relations were specified in a model and tested, and the result is shown in Fig. 4 [155]. The figure shows that there is a positive correlation between dB(A) sound pressure levels and annoyance, but noise annoyance is much stronger related to the visual attitude. This visual attitude has been measured with indicators as the impact on the landscape, a judgment in terms of beautiful or ugly, and a judgment about natural versus unnatural. As usual, this attitude is in turn strongly related to the general attitude to wind turbines, measured in terms of general opinion, efficient power generation, and necessity. Figure 4 presents the results for those residents that could see at least one wind turbine. There were no differences between rural and built-up areas, but the relations became weaker on locations with hilly or rocky terrain and among people that could not see any of the wind turbines. The study shows that even for noise annoyance, which is about the sound that is produced by the turbines, the landscape issue is still a more important attribute than the sound itself. This finding reinforces the overall dominant significance of landscape for acceptance of wind turbines.

Future Directions

The issue of social acceptance of wind power will come to the fore even more prominent in the coming decades, but the character of acceptance issues in the three dimensions will probably change. In the coming decades, the problems concerning the institutional constraints for the emergence of a new STS in its early adoption phase will gradually shift toward the social

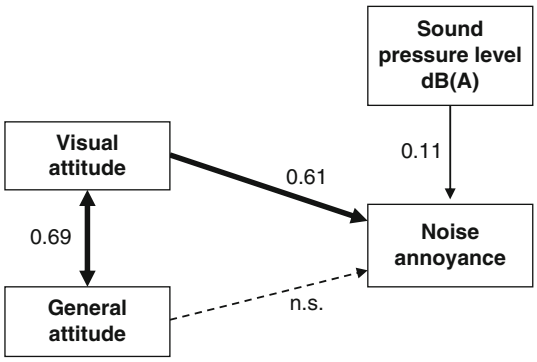

Wind Power: Basic Challenge Concerning Social Acceptance. Figure 4
Structural equation model [155, p. 384] presenting strength of paths explaining noise annoyance for residents who could see at least one turbine (N = 843)

acceptance of interconnected sustainable energy systems in which wind power is only one of the substantial components. It will no longer be an issue of introducing a new kind of energy supply, but of implementation of sufficient capacity of renewable sources required to establish a full transition toward sustainable energy supply. In all three dimensions of social acceptance, new problematic issues will emerge because of the enormous requirements in the amount of space needed to establish that capacity. This is considerably underestimated in policy – as well as the rest of the society – in particular with regards the power–space ratio in relation to the energy consumption in developed countries. This ratio shows the impressive amounts of land-use change needed [122].

The current awareness of the required space for sustainable energy supply is still limited and, hence, the consequences in terms of landscape occupation and potential environmental conflicts are neither fully recognized. One of the major changes that is recognized though, is the potential rapid development offshore. This constitutes a major new challenge, but as indicated – section "Landscape/Seascape" – the issue of social acceptance may be different there because of other competing spatial claims and key stakeholders, but this definitely does not result in less complexity in decision making. Again, a collaborative approach to decision making is needed to handle these complexities in a way that furthers acceptance among the crucial actors.

The essential role for collaborative planning approaches to wind power emphasizes the role of communities. This line of practice will only become more important because of the number of wind power projects and therefore the number of communities that need to be involved. There should be no misunderstanding though, that the complexities of the realities of community can easily be underestimated. Although most acceptance studies reveal that the role of communities is essential, there should be no presumptions about communities that they are always benign toward sustainability [156] and their willingness to further the development of renewable and sustainable energy cannot be taken for granted. A comparison of different cases of community energy has shown that community support for wind power projects, even if they are rooted in parts of the community, is definitely not self-evident. This analysis concludes that "trust between local people and groups that take projects forward is part of the package of conditions which can help projects work and for local people to feel positive about getting involved and about process of project development" [157, p. 2662]. However, there are no simplistic prescriptions of "what works" and community wind power projects cannot simply be replicated from place to place. Again, the essence of the implementation of a new STS in a community is that understanding the social context of innovation and technology diffusion is just as important as its technical dimensions. Studies that enhance our understanding of how to embed renewable energy supply in communities still have a short history, and the understanding is still limited.

The most significant aspect of collaborative decision making about and community acceptance of wind power projects is the fit to the identity of the landscape in the eyes of the community members. Within the sociopolitical acceptance dimension, there is a persistent preference for efforts to try to avoid the far-reaching subjectivity of "the eyes of the beholder" [144]. The efforts to develop technological instruments to objectively assess the "visual impact" will not enhance trust, as they are not helpful to address the valuation of landscape identity. A more fruitful direction for the analysis of the landscape issue with newly developed technological instruments is where such techniques are applied to support the collaborative planning process of wind power schemes. Recently, some studies have shown considerable progress in that direction [158, 159].

The main question of social acceptance will remain how to build sociopolitical and market acceptance for the collaborative way of planning and decision making that is needed. This key to the large number of positive investment and space-making decisions will even become more important because wind power is becoming increasingly part of an all-embracing STS of integrated sustainable energy supply. The new power supply system will have to integrate growing numbers of distributed generation units [26, 160]. This STS may include several components, such as solar PV, small-scale CHP, tidal, geothermal, and hydropower, and all of these are subject to questions with regard social acceptance [161]. Furthermore, the increasing amount of capacity with a variable supply character is adding

new challenges to the power grid, which in the current situation is considered storage capacity for sources like wind power [162]. For sociopolitical acceptance, this development asks for willingness to invest in the development of a new STS based on a power grid that can handle the increasing tendency of distributed generation and decentralized optimization [163].

The integration of all the components of sustainable power generation, including the mutual fine-tuning and optimization of local supply and demand and possibly with the introduction of local storage capacity – e.g., electric vehicles [164]– must be embedded in a "smart grid" [165]. All the new technologies needed for this integration will become subject to acceptance decisions, as incumbents in the existing power sector should institutionally support them in policy, and they need willingness to investments by many market actors, including the acceptance by consumers. The issue of community acceptance will come to the fore more prominent as well, as we are dealing with more distributed generation that by nature depends largely on decisions on that level. The future "smart grid" will probably be something like "a network of integrated micro-grids that can monitor and heal itself" [165, p. 570] in which the micro-grids are in fact connecting communities of consumers that partly have become producers themselves – or coproducers – and mutual suppliers. All questions of (co-)ownership and involvement in decision making that have come to the fore as crucial in wind power development will become more complex. They become embedded in questions about ownership and about who will be in control of all the facilities that are part of the new supply system, which in particular includes the smart meters and smart regulating devices that will be the hubs of the smart micro-grids. The social acceptance of wind power will become embedded in the acceptance of all kinds of decisions about this future STS of sustainable energy supply and demand.

Bibliography

Primary Literature

1. Carlman I (1982) Wind energy potential in Sweden: the importance of non-technical factors. In: Fourth international symposium wind energy systems, Stockholm, pp 335–348, 21–24 Sept 1982
2. Bosley P, Bosley K (1988) Public acceptability of California's wind energy development: three studies. Wind Eng 12:311–318
3. Wolsink M (1986) Public acceptance of large WECS in the Netherlands. In: European wind energy conference, 1986, vol II. Raguzzi, Rome, pp 587–592
4. Thayer RL, Freeman C (1987) Public perceptions of a wind energy landscape. Landscape Urban Plan 14:379–398
5. Carlman I (1984) The views of politicians and decision-makers on planning for the use of wind power in Sweden. In: European wind energy conference, Hamburg, pp 339–343, 22–36 Oct 1984
6. Wolsink M (1987) Wind power for the electricity supply of houses. Neth J House Environ Res 2:95–214
7. Aitken M (2010) Why we still don't understand the social aspects of wind power: a critique of key assumptions within the literature. Energ Policy 38:1134–1841
8. Wüstenhagen R, Wolsink M, Bürer MJ (2007) Social acceptance of renewable energy innovation: an introduction to the concept. Energ Policy 35:2683–2691
9. Bijker WE, Law J (eds) (1992) Shaping technology/building society: studies in sociotechnical change. MIT Press, Cambridge, MA
10. Geels FW (2004) From sectoral systems of innovation to socio-technical systems – insights about dynamics and change from sociology and institutional theory. Res Policy 33:897–920
11. Hekkert M, Suurs RAA, Negro SO, Kuhlmann S, Smits REHM (2007) Functions of innovation systems: a new approach for analysing technological change. Technol Forecast Soc 74:413–432
12. Jacobsson S, Johnson A (2000) The diffusion of renewable energy technology: an analytical framework and key issues for research. Energ Policy 28:625–640
13. Kamp LM, Smit REHM, Andriesse CD (2004) Notions on learning applied to wind turbine development in the Netherlands and Denmark. Energ Policy 32:1625–1637
14. North D (1990) Institutions, institutional change and economic performance. Cambridge University Press, Cambridge
15. Thelen K (1999) Historical institutionalism in comparative politics. Annu Rev Polit Sci 2:369–404
16. Scott WR (1987) The adolescence of institutional theory. Admin Sci Quart 32: 117, 493–511
17. Powell WW, DiMaggio PJ (eds) (1991) The new institutionalism in organizational analysis. Chicago University Press, Chicago
18. Hoogwijk M, de Vries B, Turkenburg W (2004) Assessment of the global and regional geographical technical and economic potential of on-shore of wind energy. Energ Econ 26:889–919
19. Yue C-D, Min-How Y (2009) Exploring the potential of wind energy for a coastal state. Energ Policy 37:3925–3940
20. Sovacool BK (2009) Rejecting renewables: the socio-technical impediments to renewable electricity in the United States. Energ Policy 37:4500–4513
21. Wolsink M, Breukers S (2010) Contrasting the core beliefs regarding the effective implementation of wind power

international study stakeholder perspectives. J Environ Plann Man 53:535–558
22. Jessup B (2010) Plural and hybrid environmental values: a discourse analysis of the wind energy conflict in Australia and the United Kingdom. Environ Polit 19:21–44
23. Wolsink M (2000) Wind power and the NIMBY-myth: institutional capacity and the limited significance of public support. Renew Energ 21:49–64
24. Baumeister RF, Leary MR (1995) The need to belong – desire for interpersonal attachments as a fundamental human motivation. Psychol Bull 117:497–529
25. Rhodes RAW (1996) The new governance: governing without government. Polit Stud 44:652–667
26. Ackermann T, Andersson G, Söder L (2001) Distributed generation: a definition. Electr Pow Syst Res 57:105–204
27. Devine-Wright P, Devine-Wright H (2006) Social representations of intermittency and the shaping of public support for wind energy in the UK. Int J Glob Energ 25:243–256
28. Ajzen I (1991) The theory of planned behaviour. Organ Behav Hum Dec 50:179–211
29. Ajzen I (2001) Nature and operation of attitudes. Annu Rev Psychol 52:27–58
30. Bang HK, Ellinger AE, Hadjimarcou J, Traichal PA (2000) Consumer concern, knowledge, belief, and attitudes toward renewable energy: an application of the reasoned action theory. Psychol Market 17:449–468
31. Dinica V (2008) Initiating a sustained diffusion of wind power: the role of public-private partnerships in Spain. Energ Policy 36:3562–3571
32. Möller B (2006) Changing wind-power landscapes: regional assessment of visual impact on land use and population in Northern Jutland, Denmark. Appl Energ 83:477–494
33. Walker G, Devine-Wright P (2008) Community renewable energy: what should it mean? Energ Policy 36:497–450
34. Bell D, Gray T, Haggett C (2005) The 'social gap' in wind farm siting decisions: explanations and policy responses. Environ Polit 14:460–477
35. Toke D (2005) Explaining wind power planning outcomes: some findings from a study in England and Wales. Energ Policy 33:1527–1539
36. European Wind Energy Association (EWEA) (2009) Wind energy: the facts. A guide to the technology, economics and future of wind power. Earthscan, London/Sterling
37. Freudenburg WR, Pastor SK (1992) Nimbys and lulus: stalking the syndromes. J Soc Issues 48:39–61
38. Devine-Wright P (2005) Beyond NIMBYism: towards an integrated framework for understanding public perceptions of wind energy. Wind Energ 8:125–139
39. Kahn RD (2000) Siting struggles: the unique challenge of permitting renewable energy power plants. Electr J 13:21–33
40. Wolsink M (2006) Invalid theory impedes our understanding: a critique on the persistence of the language of NIMBY. T I Brit Geogr 31:85–91
41. Wolsink M (1989) Attitudes and expectancies about wind turbines and wind farms. Wind Eng 13:196–206
42. Warren CR, Lumsden C, O'Dowd S, Birnie RV (2005) 'Green on green': public perceptions of wind power in Scotland and Ireland. J Environ Plann Man 48:853–875
43. Jones CR, Eiser JR (2009) Identifying predictors of attitudes towards local onshore wind development with reference to an English case study. Energ Policy 37:4604–4614
44. Kempton W, Firestone J, Lilley J, Rouleau T, Whitaker P (2005) The off-shore wind power debate. Views Cape Cod. Coast Manage 33:119–149
45. Devine-Wright P (2011) From backyards to places: public engagement and the emplacement of renewable energy technologies. In: Devine-Wright P (ed) Renewable energy and the public: from NIMBY to participation. Earthscan, London
46. Sjöberg L, Drottz-Sjöberg B (2001) Fairness, risk and risk tolerance in the siting of a nuclear waste repository. J Risk Res 4:75–101
47. Wolsink M, Devilee J (2009) The motives for accepting or rejecting waste infrastructure facilities. Shifting the focus from the planners' perspective to fairness and community commitment. J Environ Plann Man 52:217–236
48. Oxford English Dictionary (2010) http://dictionary.oed.com/entrance.dtl. Accessed 15 Apr 2010
49. Dear M (1992) Understanding and overcoming the NIMBY syndrome. J Am Plann Assoc 58:288–300
50. Swofford J, Slattery M (2010) Public attitudes of wind energy in Texas: local communities in close proximity to wind farms and their effect on decision-making. Energ Policy 38:2508–2519
51. Toke D, Breukers S, Wolsink M (2008) Wind power deployment outcomes: how can we account for the differences? Ren Sust Energ Rev 12:1129–1147
52. Wolsink M (2007) Planning of renewables schemes. Deliberative and fair decision-making on landscape issues instead of reproachful accusations of non-cooperation. Energ Policy 35:2692–2704
53. Healey P (1997) Collaborative planning: shaping places in fragmented societies. Macmillan, London
54. Marques AC, Fuinhas JA (2011) Drivers promoting renewable energy: a dynamic panel approach. Ren Sust Energ Rev 15:1601–1608
55. Bohn C, Lant C (2009) Welcoming the wind? Determinants of wind power development among U.S. states. Prof Geogr 61:87–100
56. Menz FC, Vachon S (2006) The effectiveness of different policy regimes for promoting wind power: experiences from the states. Energ Policy 34:1786–1796
57. Ohl C, Eichhorn M (2010) The mismatch between regional spatial planning for wind power development in Germany and national eligibility criteria for feed-in tariffs – a case study in West Saxony. Land Use Policy 27:243–254
58. Breukers S, Wolsink M (2007) Wind energy policies in the Netherlands: institutional capacity-building for ecological modernisation. Environ Polit 16:92–112
59. Heiman MK, Solomon BD (2004) Power to the people: electric utility restructuring and the commitment to renewable energy. Ann Assoc Am Geogr 94:94–116

60. Wilson EJ, Stephens J (2009) Wind deployment in the United States: states, resources, policy, and discourse. Environ Sci Technol 43:9063–9070
61. Sabatier PA (1998) The advocacy coalition framework: revisions and relevance for Europe. J Eur Publ Pol 5:98–130
62. Tversky A, Kahneman D (1981) The framing of decisions and the psychology of choice. Science 211:453–458
63. Walker G (1995) Renewable energy and the public. Land Use Policy 12:49–59
64. Eurobarometer (2007) Energy technologies: knowledge, perception measures. European Commission, Brussels
65. Ansolabehere S, Konisky DM (2009) Public attitudes toward construction of new power plants. Public Opin Quart 73:566–577
66. Klick H, Smith ERAN (2010) Public understanding of and support for wind power in the United States. Renew Energy 35:1585–1591
67. Wolsink M (2007) Wind power implementation: the nature of public attitudes: equity and fairness instead of "backyard motives". Ren Sust Energ Rev 11:1188–1207
68. Ellis G, Barry J, Robinson C (2007) Many ways to say 'no', different ways to say 'yes': applying q-methodology to understand public acceptance of wind farm proposals. J Environ Plann Man 50:517–551
69. Ek K (2005) Public and private attitudes towards "green" electricity: the case of Swedish wind power. Energ Policy 33:1677–1689
70. Clark CF, Kotchen MJ, Moore MR (2003) Internal and external influences on pro-environmental behavior: participation in a green electricity program. J Environ Psychol 23:237–246
71. Ellis G, Cowell R, Warren C, Strachan P, Szarka J (2009) Expanding wind power: a problem of planning or of perception? Plann Theory Pract 10:523–532
72. Muñoz M, Oschmann V, Tabara JD (2007) Harmonization of renewable electricity feed-in laws in the European Union. Energ Policy 35:3104–3114
73. Lauber V (2004) REFIT and RPS: options for a harmonised community framework. Energ Policy 32:1405–1414
74. Toke D (2007) Renewable financial support systems and cost-effectiveness. J Cleaner Prod 15:280–287
75. Jacobsson S, Lauber V (2006) The politics and policy of energy system transformation – explaining the German diffusion of renewable energy technology. Energ Policy 34:256–276
76. Mitchell C, Bauknecht D, Connor PM (2006) Effectiveness through risk reduction: a comparison of the renewable obligation in England and Wales and the feed-in system in Germany. Energ Policy 34:297–305
77. Krewitt W, Nitsch J (2003) The German Renewable Energy Sources Act. An investment into the future pays off already today. Renew Energy 28:533–542
78. Toke D (2005) Are green certificates the way forward for renewable energy? An evaluation of the UK's Renewable obligation in the context of international comparisons. Environ Plann C 23:361–375
79. Jacobsson S, Bergek A, Finon D, Lauber V, Mitchell C, Toke D, Verbruggen A (2009) EU renewable energy support policy: faith or facts? Energ Policy 37:2143–2146
80. Toke D (2008) The EU renewables directive – what is the fuss about trading? Energ Policy 36:3001–3008
81. Cowell R (2007) Wind power and "the planning problem": the experience of Wales. Eur Environ 17:291–306
82. Bergek A (2010) Levelling the playing field? The influence of national wind power planning instruments on conflicts of interests in a Swedish county. Energ Policy 38:2357–2369
83. Toke D (2005) Explaining wind power planning outcomes: some findings from a study in England and Wales. Energ Policy 33:1527–1539
84. Dimitropoulos A, Kontoleon A (2009) Assessing the determinants of local acceptability of wind-farm investment: a choice experiment in the Greek Aegean Islands. Energ Policy 37:1842–1854
85. Loring J MacLaren (2007) Wind energy planning in England, Wales and Denmark: factors influencing project success. Energ Policy 35:2648–2660
86. Aitken M, McDonald S, Strachan P (2008) Locating 'power' in wind power planning processes: the (not so) influential role of local objectors. J Environ Plann Man 51:777–799
87. Söderholm P, Ek K, Petterson M (2007) Wind power development in Sweden: global policies and local obstacles. Ren Sust Energ Rev 11:365–400
88. Agterbosch S, Breukers S (2008) Socio-political embedding of onshore wind power in the Netherlands and North Rhine-Westphalia. Technol Anal Strateg Man 20:633–648
89. Mannarini T, Roccato M, Fedi A, Rovere A (2009) Six factors fostering protest: predicting participation in locally unwanted land uses movements. Polit Psychol 30:895–920
90. Wolsink M (2010) Contested environmental policy infrastructure: socio-political acceptance of renewable energy, water, and waste facilities. Environ Impact Asses 30:302–311
91. Devlin E (2005) Factors affecting public acceptance of wind turbines in Sweden. Wind Eng 29:503–511
92. Musall FD, Kuik O (2011) Local acceptance of renewable energy – A case study from southeast Germany. Energ Policy 39:3252–3260
93. Warren CR, McFadyen M (2010) Does community ownership affect public attitudes to wind energy? A case study from south-west Scotland. Land Use Policy 27:204–313
94. Hindmarsh R, Matthews C (2008) Deliberative speak at the turbine face: community engagement, wind farms, and renewable energy transitions. J Environ Pol Plann 10:217–232
95. Graham JB, Stephenson JR, Smith IJ (2009) Public perceptions of wind energy developments: case studies from New Zealand. Energ Policy 37:3348–3357
96. Wester-Herber M (2004) Underlying concerns in land-use conflicts – the role of place-identity in risk perception. Environ Sci Pol 7:109–116
97. Jackson JB (1994) A sense of place, a sense of time. Yale University Press, New Haven

98. Devine-Wright P, Howes Y (2010) Disruption to place attachment and the protection of restorative environments: a wind energy case study. J Environ Psychol 30:271–280
99. Vorkinn M, Riese H (2001) Environmental concern in a local context. The significance of place attachment. Environ Behav 33:249–263
100. Stedman RC (2002) Is it really just a social construction? The contribution of the physical environment to sense of place. Soc Nat Res 16:671–685
101. Woods M (2003) Conflicting environmental visions of the rural: windfarm development in Mid Wales. Sociol Ruralis 43:171–288
102. Bergmann A, Colombo S, Hanley N (2008) Rural versus urban preferences for renewable energy developments. Ecol Econ 65:616–625
103. Moragues-Faus AM, Ortiz-Miranda D (2010) Local mobilization against wind farm developments in Spanish rural areas: new actors in the regulation arena. Energ Policy 38:4232–4240
104. Cowell R, Bristow G, Munday M (2011) Acceptance, acceptability and environmental justice: the role of community benefits in wind energy development. J Environ Plann Man 54:539–557
105. Dincer I (2000) Renewable energy and sustainable development: a crucial review. Ren Sust Energ Rev 4:157–175
106. delRio P, Burguillo M (2008) Assessing the impact of renewable energy deployment on local sustainability: towards a theoretical framework. Ren Sust Energ Rev 12:1325–1344
107. Faulin J, Lera F, Pintor JM, García J (2006) The outlook for renewable energy in Navarre: an economic profile. Energ Policy 34:2201–2216
108. Hillebrand B, Buttermann H, Behringer J, Bleuerl M (2006) The expansion of renewable energies and employment effects in Germany. Energ Policy 34:3484–3494
109. Kaldellis JK, Zafirakis D (2007) Present situation and future prospects of electricity generation in Aegean Archipelago islands. Energ Policy 35:4623–4639
110. Dalton GJ, Lockington DA, Baldock TE (2008) A survey of tourist attitudes to renewable energy supply in Australian hotel accommodation. Renew Energy 33:2174–2185
111. Frantál B, Kunc J (2011) Wind turbines in tourism landscapes: Czech experience. Ann Tourism Res 38:499–519
112. Riddington G, McArthur D, Harrison T, Gibson H (2010) Assessing the economic impact of wind farms on tourism in Scotland: GIS, surveys and policy outcomes. Int J Tourism Res 12:237–252
113. Lilley MB, Firestone J, Kempton W (2010) The effect of wind power installations on coastal tourism. Energies 3:1–22
114. Gross C (2007) Community perspectives of wind energy in Australia. The application of a justice and community fairness framework to increase social acceptance. Energ Policy 35:2727–2736
115. Mumford J, Gray D (2010) Consumer engagement in alternative energy – can the regulators and suppliers be trusted? Energ Policy 38:2664–2671
116. Frey BS, Oberholzer-Gee F (1997) The cost of price-incentives: an empirical analysis of motivation crowding out. Am Econ Rev 87:746–755
117. Aitken M (2010) Wind power and community benefits: challenges and opportunities. Energ Policy 38:6066–6075
118. Rogers EM (1995) Diffusion of innovations, 4th edn. The Free Press, New York
119. Breukers S, Wolsink M (2007) Wind power in changing institutional landscapes: an international comparison. Energ Policy 35:2737–2750
120. Zarnikau J (2003) Consumer demand for 'green' power and energy efficiency. Energ Policy 31:1661–1672
121. Wüstenhagen R, Bilharz M (2006) Green energy market development in Germany: effective public policy and emerging customer demand. Energ Policy 34:1681–1696
122. MacKay DJC (2008) Sustainable energy – without the hot air. UIT, Cambridge
123. Bolinger MA (2005) Making European-style community wind power development work in the US. Ren Sust Energ Rev 8:556–575
124. Han JY, Mol APJ, Lu YL, Zhang L (2009) Onshore wind power development in China: challenges behind a successful story. Energ Policy 37:2941–2951
125. Bergek A, Jacobsson S, Sanden BA (2008) 'Legitimation' and 'development of positive externalities': two key processes in the formation phase of technological innovation systems. Technol Anal Strateg 20:575–592
126. Bird L, Bolinger M, Gagliano T, Wiser R, Brown M, Parsons B (2005) Policies and market factors driving wind power development in the United States. Energ Policy 33: 1397–1407
127. Lewis JI, Wiser RH (2007) Fostering a renewable energy technology industry: an international comparison of wind industry support mechanisms. Energ Policy 35:1844–1857
128. Bansal P, Roth K (2000) Why companies go green: a model of ecological responsiveness. Acad Manage J 43:717–736
129. Kaldellis JK, Kavadias KA, Paliatsos AG (2004) Environmental impacts of wind energy applications: "Myth or reality?". Fresen Environ Bull 13:413–423
130. Bishop I (2002) Determination of thresholds of visual impact: the case of wind turbines. Environ Plann B 29: 707–718
131. Kaldellis JK (2006) Evaluation of Greek wind parks visual impact "public attitude and experts' opinion". Fresen Environ Bull 15:1419–1426
132. Brittan GG (2001) Wind, energy, landscape: reconciling nature and technology. Philos Geogr 4:169–184
133. Mercer D (2003) The great Australian wind rush and the devaluation of landscape amenity. Austral Geogr 34:91–121
134. Johansson M, Laike T (2007) Intention to respond to local wind turbines: the role of attitudes and visual perception. Wind Energy 10:435–451
135. Zografos C, Martinez-Allier J (2009) The politics of landscape value: a case study of wind farm conflict in rural Catalonia. Environ Plann A 41:1726–1744

136. Bishop ID, Miller DR (2007) Visual assessment of off-shore wind turbines: the influence of distance, contrast, movement and social variables. Renew Energ 32:814–831
137. Ladenburg J, Dubgaard A (2009) Preferences of coastal zone user groups regarding the siting of offshore wind farms. Ocean Coast Manage 52:233–242
138. Haggett C (2008) Over the sea and far away? A consideration of the planning, politics and public perception of offshore wind farms. J Environ Pol Plann 10:289–306
139. Ladenburg J (2009) Visual impact assessment of offshore wind farms and prior experience. Appl Energ 86:380–387
140. Gonzalez MI, Estevez B (2005) Participation, communication and negotiation in environmental conflicts: offshore wind energy in the Trafalgar Sea area. Arbor-Ciencia Pensamiento y Cultura 181:377–392
141. Phadke R (2010) Steel forests or smoke stacks: the politics of visualisation in the Cape Wind controversy. Environ Polit 19:1–20
142. Wolsink M (2010) Near-shore wind power – protected seascapes, environmentalists' attitudes, and the technocratic planning perspective. Land Use Policy 27:195–203
143. Bell S (1999) Landscape: pattern, perception and process. Routledge, New York
144. Lothian A (1999) Landscape and the philosophy of aesthetics: is landscape quality inherent in the landscape or in the eye of the beholder? Landscape Urban Plan 44:177–198
145. Parsons R, Daniel TC (2002) Good looking: in defense of scenic landscape aesthetics. Landscape Urban Plan 60:43–56
146. Jay S (2010) Planners to the rescue: spatial planning facilitating the development of offshore wind energy. Mar Pollut Bull 60:493–499
147. Gray T, Haggett C, Bell D (2005) Offshore windfarms and commercial fisheries in the UK: a study in stakeholder consultation. Ethics Place Environ 8:127–140
148. Michler-Cieluch T, Krause G, Buck BH (2009) Reflections on integrating operation and maintenance activities of offshore wind farms and mariculture. Ocean Coast Manage 52:57–68
149. Sovacool BK (2009) Contextualizing avian mortality: a preliminary appraisal of bird and bat fatalities from wind, fossil-fuel and nuclear electricity. Energ Policy 37:2241–2248
150. Solli J (2010) Where the eagles dare? Enacting resistance to wind farms through hybrid collectives. Environ Polit 19:45–60
151. Nadaï A, Labussière O (2010) Birds, wind and the making of wind power landscapes in Aude, Southern France. Landscape Res 35:209–233
152. Verkuijlen E, Westra CA (1984) Shadow hindrance by wind turbines. In: European wind energy conference, Hamburg, pp 356–361
153. Wolsink M, Sprengers M (1993) Windturbine noise: a new environmental threat? In: Vallet M (ed) Noise as a public health problem, vol 2. INRETS, Bron, pp 235–238
154. Pedersen E, Persson-Waye K (2007) Wind turbine noise, annoyance and self-reported health and well-being in different living environments. Occup Environ Med 2007:480–486
155. Pedersen E, Larsman P (2008) The impact of visual factors on noise annoyance among people living in the vicinity of wind turbines. J Environ Psychol 28:379–389
156. Dalby S, Mackenzie F (1997) Re-conceptualising local community: environment, identity and threat. Area 29: 99–108
157. Walker G, Devine-Wright P, Hunter S, High H, Evans B (2010) Trust and community: exploring the meanings, contexts and dynamics of community renewable energy. Energ Policy 38:2655–2663
158. Higgs G, Berry R, Kidner D, Langford M (2008) Using IT approaches to promote public participation in renewable energy planning: prospects and challenges. Land Use Policy 25:596–607
159. Bishop ID, Stock C (2010) Using collaborative virtual environments to plan wind energy installations. Renew Energ 35:2348–2355
160. Chicco G, Mancarefla P (2009) Distributed multi-generation: a comprehensive view. Ren Sust Energ Rev 13:535–551
161. Gardner J, Car-Cornish SG, Ashworth PN (2008) Exploring the acceptance of a domestic distributed energy market in Australia. Australasian J Environ Man 15:93–103
162. Charles D (2009) Renewables test IQ of the grid. Science 324:172–175
163. Stadler I (2008) Power grid balancing of energy systems with high renewable energy penetration by demand response. Utilit Policy 16:90–98
164. Green RC, Wang L, Alam M (2011) The impact of plug-in hybrid electric vehicles on distributed networks: a review and outlook. Ren Sust Energ Rev 15:544–553
165. Marris E (2008) Upgrading the grid. Nature 454:570–573

Books and Reviews

Agterbosch S (2006) Empowering wind power. On social and institutional conditions affecting the performance of entrepreneurs in the wind power supply market in the Netherlands. Netherland Geographical Studies 351, KNAG, Utrecht

Breukers SC (2007) Institutional capacity building for wind power, a geographical comparison. Vossius Pers/Amsterdam University Press, Amsterdam, http://dare.uva.nl/record/209600 [Open access]

Devine-Wright P (ed) (2011) Renewable energy and the public: from NIMBY to participation. Earthscan, London

Ellis G, Cowell R, Warren C, Strachan P, Szarka J, Hadwin R, Miner P, Wolsink M, Nadai A (2009) Interface. Wind power: is there a "planning problem"? Plann Theory Pract 10:521–547

Jay SA (2008) At the margins of planning. Offshore wind farms in the United Kingdom. Ashgate, Aldershot

Kahn J (2004) Local politics of renewable energy. Project planning, siting conficts and citizen participation. Lund University, PhD thesis

MacKay DJC (2008). Sustainable energy – without the hot air. www.withouthotair.com [Open access]

Nadaï A, van der Horst D (eds) (2010) Wind power planning, landscapes and publics. Land Use Policy 27(Special Issue):181–254
Scheer H (2002) The solar economy: renewable energy for a sustainable global future. Earthscan, London
Sovacool B (2008) The dirty energy dilemma: what's blocking clean power in the Unitied States? Springer, Dordrecht
Szarka J (2007) Wind power in Europe: politics, business and society. Macmillan Palgrave, Basingstoke
Wüstenhagen R, Wolsink M, Bürer MJ (eds) (2007) Social acceptance of renewable energy innovation. Energ Policy 35(Special Issue):2683–2810

Wind Power: Economy, Market, Subsidies, Payment Mechanisms, and Capacity Credit

Michael Milligan[1], Lori Bird[1], Suzanne Tegen[1], Kevin Porter[2], Sari Fink[2], Brendan Kirby[1]
[1]National Renewable Energy Laboratory, Golden, CO, USA
[2]Exeter Associates, Columbia, Maryland, USA

Article Outline

Glossary
Definition of Subject
Introduction
Wind Energy in Wholesale Markets
Wind Energy and Energy Markets in the United States
Wind Energy and Energy Markets in Europe
Wind Energy and Capacity Markets
Wind Energy Tax Credits
Green Power Markets
Capacity Credit
Wind Integration Costs
Cost Trajectory for Wind Energy Technology
Wind Energy and Economic Development
Future Directions
Bibliography

Glossary

Ancillary services Additional services that are required to manage the delivery of energy. Examples include reactive power support, balancing and regulation, and operating reserves.

Balancing area The collection of generation, transmission, and loads within a metered boundary where a power system operator maintains the load-resource balance.

Capacity markets Market-based method of procuring sufficient generation and demand response to assure that future load and reserve requirements will be met.

Day-ahead market Hourly wholesale electricity market that is cleared the day before the operating day.

Real-time market Hourly or sub-hourly wholesale market that is cleared shortly before the operating interval.

Reserves (operating) Additional generating capacity that is available in real time or near real time if needed to compensate for unanticipated generator failures (contingency reserves) or unanticipated changes in load or wind generation (load-following reserve).

Reserves (planning) Generating capacity that is built in excess of predicted load in a future time period. This excess reserve margin is calculated to account for unexpected failures of power plants, ensuring an adequate supply of electricity at all times.

Self-schedule Decision by a generator operator to operate at a specific time regardless of price.

Unit commitment The process of determining the optimal mix of generators that must be started or otherwise made available one or more days in advance of need.

Wind energy penetration Percentage of wind relative to the rest of the system. This is typically calculated using energy on an annual basis; the percentage of total energy demand for a year that wind energy provides.

Wholesale electricity markets Wholesale bulk power market that facilitates the exchange of energy among buyers and sellers.

Definition of Subject

With increasing concern regarding climate change and emissions from conventional power plants, new markets have developed that allow for the trading of the clean energy attributes of wind and other renewable energy sources. We discuss these green power markets and their role in demonstrating compliance with renewable energy

standards. Wind energy can also be bought and sold in wholesale energy markets, exchanges where bulk energy is bought and sold. In some areas, capacity markets exist that provide payment for installed capacity that is available when needed. Capacity markets are generally based on the capacity contribution that a power plant or responsive load can make toward planning reserves, which is called the capacity credit or capacity value. The general motivation behind a capacity market is to ensure sufficient revenue for the generator and sufficient installed capacity.

In some countries, government incentives exist that encourage the development and use of wind energy (or other renewable energy sources). These may include the following:

1. Renewable energy standards, sometimes called renewable portfolio standards: These standards specify some percentage of all energy or capacity that must be provided by renewable energy resources.
2. Wind energy tax credits: reduction in tax liability to encourage development and use of wind energy. The tax credits can be based on the amount of energy production from the wind plant, or can be based on investment or other economic attribute.
3. Green power markets: a market where the "green" attributes of renewable energy can be traded. The objectives of these markets can be to help in satisfying compliance rules for renewable energy standards, or could be alternatives to policies that limit the emissions (including carbon) from conventional power plants.

Because of its variable and uncertain characteristic, wind energy can increase overall operating reserves that are needed to manage uncertainty. The costs associated with this increase in reserves and changes in the way the system is dispatched are called wind integration costs. Specific methods to measure this cost have evolved, and today there is some controversy surrounding the topic and its precise definition. Integration impacts and costs are not unique to wind. Nuclear power, for example, typically requires larger contingency reserves and increases cycling of other base-load generation. All investments in the power system impact system operations and costs.

With the recent increase in actual and planned wind-generated electricity, there has been an accompanying increase in estimating the economic development impacts of wind. These impacts result from expenditure on the construction and operation of wind turbines or plants. Much of the focus of economic development impact studies is on jobs related to the wind plant, and the change in spending that occurs as a result.

All of these issues are potentially important as decision makers evaluate policies that may influence the development of wind energy.

Introduction

Wind energy has seen significant growth in the past several years. As a result, it has become more visible to power system planners and operators, electricity wholesale market designers, and to policy makers. During the same period, there have been substantial changes in the way that electricity systems are operated. The single major change has been the movement toward large coordinated wholesale electricity markets. The confluence of these two development trends has resulted in a substantial body of analysis and development of market mechanisms that are intended to promote economically efficient exchange of electricity, taking into account the characteristics of the many generating technologies that are used today, and in the near future.

Wind energy is integrated, bought, and sold using a variety of markets and mechanisms. In this entry we examine several key wind energy issues related to economic development, wholesale electricity markets, subsidies, and capacity value. Because wind energy is integrated into a large complex power system, wind issues often must be analyzed in that context. Electricity markets, for example, apply to all buyers and sellers in a particular region. Because there are other generation technologies in use on the grid, markets must be designed and operated in such a way that the characteristics of all technologies can be recognized that result in economically efficient power system operation, achieving appropriate reliability targets.

This entry examines the characteristics of the wholesale electricity markets in which wind energy operates, discusses the capacity value and implication for the acquisition of other generation to ensure generation adequacy, the role of tax credits, integration cost impacts, and the economic development impacts

of wind energy development. The entry concludes with a brief assessment of future directions.

Wind Energy in Wholesale Markets

The way wind energy participates in wholesale energy markets can vary significantly. In this section we describe some of the key approaches used in the United States and in Europe. We note that wholesale electricity markets in many parts of the world are currently undergoing changes that may alter some of the discussion contained in this entry. Market characteristics discussed herein were in place at the time of this writing. Common elements in international comparisons include the basic operation of wholesale electricity markets. These markets help manage the bulk power system (combination of large generators and high-voltage transmission) balance, which requires total generation to equal total load at all times. When operated on short time steps, such as 5 or 10 min, these markets can provide the power system operator with access to generation on a sub-hourly basis, subject to generator economics. If electricity demand is increasing, generating units that have offered to increment their output can be chosen to do so, based on generation price bids. In some regions (e.g., much of the Western portion of the United States) energy markets are based more on bilateral contracts (private contracts between any two parties on their own terms for their own reasons), and operate on hourly time steps across balancing areas that are sometimes only weakly interconnected. Hourly scheduling and dispatch restricts access to the physically available generation, which may be capable of responding but cannot be accessed by the power system operator. Generators that may be physically capable of responding, but that are not economic, will not be called upon in favor of other less expensive generation.

Well-functioning markets provide for economically efficient exchanges between buyers and sellers, with transparent information available for all parties. Economic efficiency is attained when markets provide the goods and services that are most desired by consumers and society, at lowest possible cost. Markets can also help efficiently integrate wind energy [1].

In some market areas there are ancillary products that are also exchanged. These can include capacity markets, and various types of reserve products, such as grid-synchronized fast response reserves, nonsynchronized slow response, contingency reserves, and regulating reserves. The terminology in Europe differs from that in the United States, but the general properties are similar.

In addition to providing an institutional mechanism to tap into existing energy supplies or ancillary services, markets provide signals to investors about relative scarcity and value. In perfectly competitive markets, these prices and all other information are fully transparent, and investment occurs in an economically efficient manner. If wholesale electricity markets function in this way, prices would induce developers to ensure that appropriate generating resources and transmission are available at future dates when needed. Typically, the relatively small number of sellers results in varying degrees of imperfect competition in wholesale electricity markets, resulting in at least some loss of economic efficiency. When energy markets are unable to provide sufficient generation capability to provide needed services such as ramping or minimum generation levels that may be needed to complement wind energy at high penetrations, other supplementary markets may need to be developed.

Wind Energy and Energy Markets in the United States

There are seven regional transmission organizations (RTOs) and independent system operators (ISOs) managing parts of the electric grid in the United States – PJM Interconnection (PJM), Midwest ISO, New York ISO (NYISO), ISO New England (ISO-NE), California ISO (CAISO), Electric Reliability Council of Texas (ERCOT), and the Southwest Power Pool (SPP). These entities operate the grid for approximately 65% of total US electricity demand [2]. PJM, the NYISO, the CAISO, the Midwest ISO, and ISO-NE, all operate wholesale energy markets, based on location-specific prices know as locational marginal prices (LMPs) that are for both day-ahead and real-time markets, with generation dispatched in real time at 5-min intervals. SPP and ERCOT are currently in the process of implementing LMP-based markets with plans to have fully functioning wholesale markets in place within the next few years. Three of the RTOs/ISOs (PJM, NYISO,

ISO-NE) also administer capacity markets or capacity auctions. Another ISO, the Midwest ISO, conducts a residual capacity auction where load-serving entities (LSEs) can make up shortfalls. The vast majority of capacity however, is obtained via bilateral contracts and the Midwest ISO's auctions are not used to any significant extent.

Other regions, particularly the West and Southeast, are not in RTOs nor do they have RTO-administered energy or capacity markets. Instead, they have hourly bilateral markets and utilities are responsible for meeting their own capacity obligations. Wind energy generation is variable and uncertain, and therefore not dispatchable in the traditional sense like conventional generation has been operated. In non-RTO markets, any variations in output from day-ahead schedules and real-time output are subject to the energy imbalance provisions of Order 890 that was issued by the Federal Energy Regulatory Commission (FERC) in 2007. Imbalances are differences between the scheduled and actual flows from generators or to loads. Imbalances of less than or equal to 1.5% of scheduled energy, or up to 2 MW (whichever is greater), would be netted monthly and settled at the power system operator's incremental or decremental costs. Imbalances of between 1.5% and 7.5% of schedule energy, or between 2 and 10 MW (whichever is larger), would be settled at 90% of decremental costs and 110% of incremental costs. ISO and RTOs have different methods of handling energy imbalances from wind power – these are outlined in Table 1.

As wind penetration increases, some power system operators are taking steps to more actively incorporate wind in their dispatch. The NYISO, for instance, has integrated wind plants into its economic dispatch system and treats wind resources like all other generation. In the NYISO markets, generators indicate their willingness to redispatch through their economic offers. Wind facilities, like all generators, are required to submit economic price curves into the real-time market, due 75 min before each operating hour (optional for day-ahead market). The wind energy price curves consist of price–quantity pairs that indicate the LMPs at which each wind facility is willing to operate. The price curve can include up to 11 price–quantity pairs, which can be changed with each bid, and can also include negative prices. Wind facilities that receive a production tax credit (PTC) may be willing to continue providing energy even when wholesale prices drop below zero because payments such as the PTC are received by wind plants any time they produce energy; thus, the wind plant can earn revenue when price is negative as long as price exceeds the negative of the PTC. The NYISO's Security Constrained Economic Dispatch software (SCED) recognizes that wind facilities cannot increase production on demand, and therefore, the offers from wind plants are taken as the prices below

Wind Power: Economy, Market, Subsidies, Payment Mechanisms, and Capacity Credit. Table 1 Energy imbalance settlement

Entity	Imbalance settlement
PJM	For wind resources that are self-scheduled, operating reserve deviation charges apply on differential between day-ahead and real-time levels exceeding a dead band; differentials less than 5% or 5 MW incur no deviation charges. Wind resources that are not self-scheduled are assessed deviation charges based on how closely they follow PJM dispatch signals.
NYISO	If scheduling day-ahead, buy out shortfalls at real-time LMPs. Up to 3,300 MW exempt from under-generation penalties during unconstrained operations.
ISO-NE	If scheduling day-ahead, deviations are settled at real-time LMP.
Midwest ISO	Settled at real-time price with no deviation penalties.
SPP	Wind is not subject to uninstructed deviation charges.
CAISO	If participating in wind forecasting, then hourly deviations are accumulated for monthly average of energy imbalances and settled at a monthly weighted market-clearing price and. If not participating in wind forecasting, then subject to 10-min imbalance energy charges.
ERCOT	Any imbalances are settled at zonal market clearing prices. No take back of payment for over generation if within ±50% of scheduled capacity. Wind-only scheduling entities are exempt from deviation charges.

Source: Utility Wind Interest Group. *Wind power and electricity markets*. August 2009. http://www.uwig.org/WindinMarketsTableSept09.pdf

which each wind facility no longer wishes to produce energy. The NYISO has also implemented a centralized wind forecasting system. All wind plants must meet the technical requirements for participating in wind forecasts and are required to provide NYSIO with meteorological data. The wind forecasts are used to determine day-ahead generator commitments and are integrated into the SCED. The NYISO evaluates all generator offers, the wind forecast, and the load forecast to produce a least-cost dispatch solution every 5 min, then sends automatic dispatch signals to all generators.

Wind resources in PJM, ISO-NE, and the Midwest ISO can submit bid curves into the day-ahead and real-time markets.

1. In PJM, if a wind facility has cleared as a capacity resource through the forward capacity market the facility must offer into the day-ahead market. In early 2009, PJM reprogrammed its dispatch software to allow for negative price offers and implemented a centralized wind forecasting system with plans to integrate the forecasts into their market operations.
2. In the Midwest ISO, if a wind facility has a capacity obligation it must offer or self-schedule into the day-ahead market. The Midwest ISO has a centralized wind forecasting system that is used for reliability, outage coordination, and analysis, but not for market operations.
3. In ISO-NE wind facilities that have cleared as a capacity resource in the forward capacity market must bid or self-schedule into the real-time market. ISO-NE does not currently utilize wind forecasting.

Noncapacity designated wind facilities participating only in the real-time markets receive real-time LMP for the energy provided. Wind plants that do not qualify or do not want to receive capacity payments do not participate in the day-ahead market. Instead, they accept payment based on the LMP clearing price for each market interval.

CAISO implemented day-ahead and real-time markets in 2009 but wind facilities are still considered price takers, which can if they wish, sell energy into the real-time markets at real-time LMP. SPP and ERCOT are in the process of creating wholesale LMP-based markets but at current, energy transactions are conducted bilaterally by the relevant entities. CAISO and ERCOT both have centralized wind forecasting systems while SPP requires balancing authorities or wind generators to provide forecasts. How energy from wind facilities is treated in CAISO, SPP, and ERCOT may change in the future as their wholesale electricity markets evolve.

Because wind energy has a near-zero marginal cost, it is nearly always economically efficient to accommodate the wind energy whenever it is available, backing down other generation sources that require fuel. We note that exceptions may exist in cases that involve a constrained transmission interface that causes wind to be curtailed. Curtailment need not be for the full amount of wind generation during the critical time period. Energy prices in the market are often set by the cost to generate one additional MWh of energy, and can vary by location depending on grid congestion, load, wind, and mix of other generation. At high wind energy penetrations, the energy price tends to be driven down (as it would be with the addition of any low-marginal-cost energy provider such as nuclear), reducing the output, and therefore the annual capacity factors, of conventional generators. This can reduce the realized revenue stream, and depending on the level of load and wind, energy prices can be very low or even negative in extreme cases. It is unclear whether the resulting price volatility will induce economically efficient levels of different types of generation in the long run. This is a general concern with electricity pricing issues and not unique to wind.

Wind Energy and Energy Markets in Europe

Just as in the North America, there is a great deal of diversity in the structural details of European electricity markets with some reasonably consistent characteristics. Day-ahead markets are working in most countries. Intra-day hourly markets exist in some countries. Fifteen-minute balancing markets exist in a few countries. While half of the US load is served in regions with 5-min markets, no 5-min markets exist in Europe. The European Network of Transmission System Operators for Electricity (ENTSO-E) is working to harmonize markets throughout Europe with long-term, day-ahead, intra-day and balancing markets. The ENTSO-E took over all operational tasks of the six existing TSO associations in Europe in July 2009 and now encompasses 42 TSOs from 34 countries [3].

Comparing North American and European power systems, or discussing them in the same paper, is complicated by differences in the terminology used in each location. "Regulation" in North America, for example, refers to the minute-to-minute balancing ancillary service that is procured through hourly markets in ISO/RTO regions and obtained from dedicated generation capacity in all regions. In Europe, Transmission System Operators (TSOs) operate hourly energy markets that are often referred to as "regulation" balancing markets. North American "regulation" is obtained from secondary reserves in Europe. Secondary reserves (centralized power system operator control of generation through automatic generator control) are typically obtained through mandatory requirements in Europe rather than through day-ahead hourly regulation markets as is done in much of North America. Wind "regulation" requirements and costs in European studies typically refer to intra-day energy scheduling costs. Wind advocates in Europe recognize the benefits of shorter gate closure times, faster market clearing, and larger geographic market scope, and are encouraging market harmonization [4].

The Nordic countries, Germany, France, and the Netherlands provide an example of typical European electricity markets structure. As in North America, a series of markets clear successively as real time is approached [5]:

1. Bilateral over the counter electricity trading: trading takes place between individuals outside of the public markets.
2. Day-ahead hourly market (spot market), which close between 10 am and noon of the day-ahead.
3. Intra-day hourly market is another hourly market that operates within the day. Markets typically clear 2 h ahead (75 min ahead in Germany). Some countries have 2-h intervals rather than hourly.
4. Intra-hour market(s). This is in fact two linked markets operating at 15-min intervals. The TSO acts as the sole buyer in the first and the sole seller in the second and facilitates the sub-hourly transactions.
   (a) "Regulating power market" (RPM). A real-time market for the TSO to purchase energy to counter imbalances from the day-ahead schedules. Both generators and loads can be sold into the market. Typically, all suppliers get the market clearing price but in Denmark each supplier gets its bid price. Settlements are typically determined after the fact.
   (b) "Balancing market." A real-time market that is linked to the RPM. The TSO is the sole supplier in this market and both generators and loads are price takers to settle imbalances from day-ahead schedules.

In Denmark, the RMP is subdivided according to the different service response times (secondary and tertiary reserves). In the Netherlands, TenneT (the TSO) contracts annually for reserves and obtains 15 min balancing energy (regulating power) through least-cost bids. Spain assigns primary reserve requirements to all generators and can adjust the amount annually. Secondary reserves are obtained day-ahead through a bidding process. Tertiary reserves are obtained through 15 min energy scheduling. In Belgium, the Access Responsible Parties are responsible for balancing portfolios in the day-ahead and hourly time frame. The TSO is responsible for balancing the aggregate system with secondary and tertiary reserves [6].

Cross-border trading typically has, depending on applied methods, less scheduling flexibility than that provided by within-country markets, effectively limiting wind and load aggregation benefits. An exception is in the Nordic market in Northern Europe where there is a common regulating market between four countries where the cheapest bids in the four countries is used if there is physical room on the transmission. This means, for example, that wind power changes within 15 min in Denmark can be balanced in Finland if the cheapest bid is in Finland and there is transmission capacity available through Sweden.

There are also differences in how wind is treated within each national market. Wind is outside the markets in France, which uses a feed-in tariff. In Germany, the four TSOs are required to convert variable wind into flat profiles equal to the long-term average wind generation. Wind is balanced as a separate balancing group. The costs for balancing wind are socialized in Germany. Wind plants in the Netherlands are always combined with other loads and generation as a part of a balanced portfolio from a Program Responsible Party.

Wind Energy and Capacity Markets

It is common practice in the electric power industry to maintain additional generating capacity (or to be able to call upon customers to reduce demand) to ensure that demand for electricity is met in case demand is higher than expected, or a generating or transmission project is unexpectedly out of service. Such additional generating capacity or demand reduction capability is collectively known as reserve capacity. How much more reserve capacity is maintained varies by power system operator, but 10–15% is a common rule of thumb for planning reserves, whereas lesser amounts are used in the operation time frame.

Reserve requirements are managed differently throughout the United States, whereas Europe generally does not have capacity markets. In some cases, a state regulatory entity or regional reliability entity sets the reserve requirement and utilities are responsible for meeting that requirement through their own generating or demand resources, or through bilateral contracts with other utilities, generators, power marketers, or demand response providers. In the northeastern United States (but not including New York), annual capacity auctions are deployed to solicit needed capacity 3 years in advance of identified need, with incremental auctions if additional capacity is needed. The following are some examples of how reserve capacity is acquired:

1. California ISO

   California is an example of a jurisdiction that requires load-serving entities (LSEs) to self-supply capacity through with their own generation ownership of facilities or through bilateral contracts. The California Public Utilities Commission (CPUC), along with the California ISO, sets an annual reserve requirement and also a forward resource adequacy requirement for the next operating year. LSEs must demonstrate they have sufficient capacity reserves 1 year in advance. Historical wind generation during the peak period is used to determine wind's contribution to resource adequacy.
2. New York ISO

   The New York ISO (NYISO) is an example of a jurisdiction that provides a capacity market which acts as a backstop procurement mechanism in addition to generation ownership by LSEs and bilateral contracting. The majority of LSEs opt to procure capacity outside the centralized ISO market. The NYISO capacity requirement also includes a locational element, and LSEs are required to make up capacity shortfalls for each zone through purchases in the twice-yearly backstop capacity auctions. New York uses historical wind production data and reliability-based techniques to assess wind's contribution to resource adequacy.
3. PJM Interconnection and ISO New England

   PJM and ISO New England (ISO-NE) administer energy markets and have both implemented 3-year forward capacity requirements through centralized forward markets. LSEs are required to obtain adequate capacity to meet reserve requirements 3 years in advance through the forward capacity markets. LSEs can opt to self-supply capacity through ownership or bilateral contracts for capacity via a special arrangement, but must commit to doing so for a set period. The vast majority of LSEs opt to obtain capacity through the forward markets. Under the PJM's Reliability Pricing Model (RPM) capacity market and the ISO-NE's Forward Capacity Market (FCM), auctions are held 3 years in advance of the delivery year, with supplemental annual incremental auctions where LSEs can purchase capacity to make up shortfalls or sell excess reserves. Wind facilities can bid their capacity into the PJM and ISO-NE capacity auctions and receive the per-MW market clearing price. Prices for capacity can vary greatly from region to region and from auction to auction. Table 2 shows the capacity prices for the four major zones for PJMs base-year RPM auctions that have been held as of May 2010.

   PJM partitions the region into zones based on individual utility territories (see Fig. 1 for the 2012/2013 zonal results) and calculates the capacity reserve requirements by zone. The zonal capacity price differentials are mainly due to transmission capacity constraints. Depending on where the constraints are located, the zonal groupings can vary from auction to auction. For example, in the 2012/2013 auction, DPLS was a constrained utility area and received an individual zonal clearing price, while in other auctions the price has been the same as in EMAAC. The majority of the low-cost generation capacity is located within RTO MCP

Wind Power: Economy, Market, Subsidies, Payment Mechanisms, and Capacity Credit. Table 2 Capacity prices for PJMs base-year RPM auctions (as of May 2010)

Delivery year	RTO	MAAC	SWMAAC	EMAAC
June 2007–May 2008	$40.80/MW-day	$40.80/MW-day	$188.54/MW-day	$197.67/MW-day
June 2008–May 2009	$111.92	$111.92	$148.80	$210.11
June 2009–May 2010	$102.04	$191.32	$191.32	$237.33
June 2010–May 2011	$174.29	$174.29	$174.29	$174.29
June 2011–May 2012	$110.00	$110.00	$110.00	$110.00
June 2012–May 2013	$16.46	$133.37	$133.37	$139.73
June 2013–May 2014	$27.73	$226.15	$226.15	$245.00

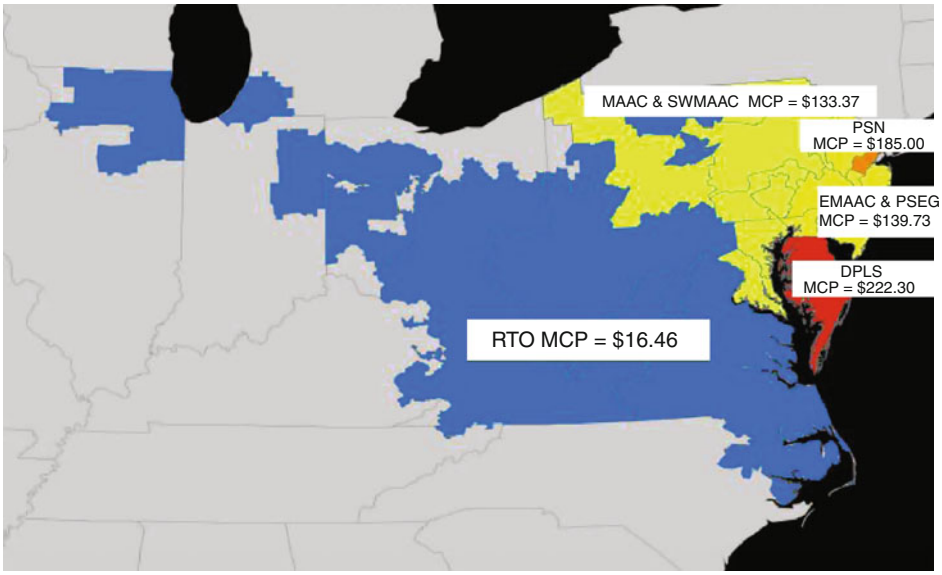

Wind Power: Economy, Market, Subsidies, Payment Mechanisms, and Capacity Credit. Figure 1 PJM RPM auction zones and clearing prices for 2012/2013 auction (Source: PJM 2012/2013 BRA clearing price map, May 27, 2009)

zone, while the majority of PJM load is in the east. PJM reported that 323 MW of wind capacity cleared in the 2012/2013 auction, representing 13% of PJM's total nameplate wind capacity. PJM sets a wind capacity factor limit at 13% of nameplate unless a wind facility can provide historical date proving a higher capacity factor is warranted. PJM's 13% capacity factor limit for wind plants that do not yet have historical experience is based on PJM analysis of PJM's past experience with wind at that time. Therefore, wind facilities can only bid 13% of nameplate capacity into the RPM markets.

The ISO-NE FCM contains two zones, Maine and Rest of Pool, and has held three auctions as of the end of 2009. These auctions all yielded the same clearing price for both zones. The clearing prices and the amount of

wind capacity that cleared in each FCM auction are outlined in Table 3. We note that ISO-NE reports clearing prices in kW-months (the price of a kW of generation or demand response capacity available for a month). The table therefore contains approximate conversions to MW-days (the price of a MW of generation or demand response capacity available for a day).

Wind Energy Tax Credits

Several tax incentives have served to boost utility-scale wind energy development in the United States. This discussion focuses on wind energy but the tax credits detailed here were/are also available for other eligible resources. Investment tax credits (ITCs) were the first federally enacted incentive utilized for promoting wind energy development. The ITC for wind was introduced in the Energy Tax Act of 1978, and provided a 10% federal tax credit on new investment in wind generation technologies. ITCs are tax credits equal to a percentage of the value of qualifying tangible, depreciable property. Such credits directly offset the investing taxpayer's federal income tax liability and are claimed on the tax return for the year a wind turbine and related equipment is first placed in service. In 1981, Congress shortened the depreciation period for wind technologies from 18 years to 5 years (which are still in effect today). Combined with state incentives and favorable power purchase rates, the ITC and the accelerated depreciation helped kick-start the modern wind industry, particularly in California. Total installed wind capacity increased from 10 MW in 1981 to 1,039 NW in 1985. However, the ITC expired in 1985, and a sharp decrease in fossil fuel prices in 1986 led to a drop in power purchase prices to levels that were uneconomic for new wind projects. As a result, and after installing over 1,000 MW in 5 years, US wind capacity installations plummeted, with only 500 MW of wind capacity installed between 1987 and 1998.

Wind Power: Economy, Market, Subsidies, Payment Mechanisms, and Capacity Credit. Table 3 Clearing prices and wind capacity in FCM auctions

Delivery year	Capacity clearing price	Wind capacity (MW)
June 2010–May 2011	$148/MW-day[a]	10
June 2011–May 2012	$118	81
June 2012–May 2013	$97	93

The wind industry received a new tax incentive when Congress approved a PTC as part of the Energy Policy Act of 1992. The PTC is tied to energy production and provides a per-kWh tax credit for energy produced from a qualifying renewable facility. The PTC is currently (2010) set at 2.1¢/kWh over the first 10 years of operation for wind energy and is adjusted annually for inflation. The PTC has been renewed several times and was allowed to lapse a few times. The latest renewal was in 2009 as part of the American Recovery and Reinvestment Act (ARRA) for wind projects that go into service by the end of 2012. Table 4 shows the history and duration of the PTC.

The ARRA also extended a 50% depreciation bonus that was first made available in 2008, which allows a project developer to deduct half the cost of a project when it is first placed in service. This depreciation bonus is a limited-time offer available only for projects completed and placed in-service by the end of 2009.

The availability (or lack thereof) of tax credits has affected US wind project development over the last 3 decades. Wind energy development activity seems to correlate with the availability of the ITC in the early 1980s and the PTC, which lapsed in 2002 and 2004 (see Fig. 2).

In addition to extending the PTC through 2012, the ARRA also created an option to choose an Investment Tax Credit (ITC) or a cash grant instead of the PTC. PTC-qualified wind facilities can opt to receive a 30% ITC in lieu of the PTC but the depreciable basis of property must be reduced by half of the ITC amount. The cash grant option is available for projects placed in service in 2009 or 2010 or that started construction by the end of 2010 and are in service by the end of 2012. The grant can be up to 30% of the total cost of the project and applications must be submitted by October 1, 2011. The grant is excluded from gross income and, as with the ITC, the depreciable basis of the property must be reduced by half the amount. On September 1, 2009, the Treasury and the DOE announced the first round of grants in lieu of the PTC/ITC through the ARRA was being distributed to two solar projects and

Wind Power: Economy, Market, Subsidies, Payment Mechanisms, and Capacity Credit. Table 4 PTC history and duration

Legislation	Date enacted	PTC eligibility window (for wind)	PTC lapse duration	Effective duration of PTC window (considering lapses)
Energy Policy Act of 1992	01/24/92	1994-June 1999	n/a	80 months
Ticket to Work and Work Incentive Improvement Act of 1999	12/19/99	July 1999–2001	6 months	24 months
Job Creation and Worker Assistance Act	03/09/02	2002–2003	2 months	22 months
The Working Families Tax Relief Act	10/04/04	2004–2005	9 months	15 months
Energy Policy Act of 2005	08/08/05	2006–2007	None	24 months
Tax Relief and Health Care Act of 2006	12/20/06	2008	None	12 months
Emergency Economic Stabilization Act of 2008	10/03/08	2009	None	12 months
American Recovery & Reinvestment Act of 2009	02/13/09	2010–2012	None	36 months

Source for original table: [2]. Modified to include EESA 2008 and ARRA 2009.

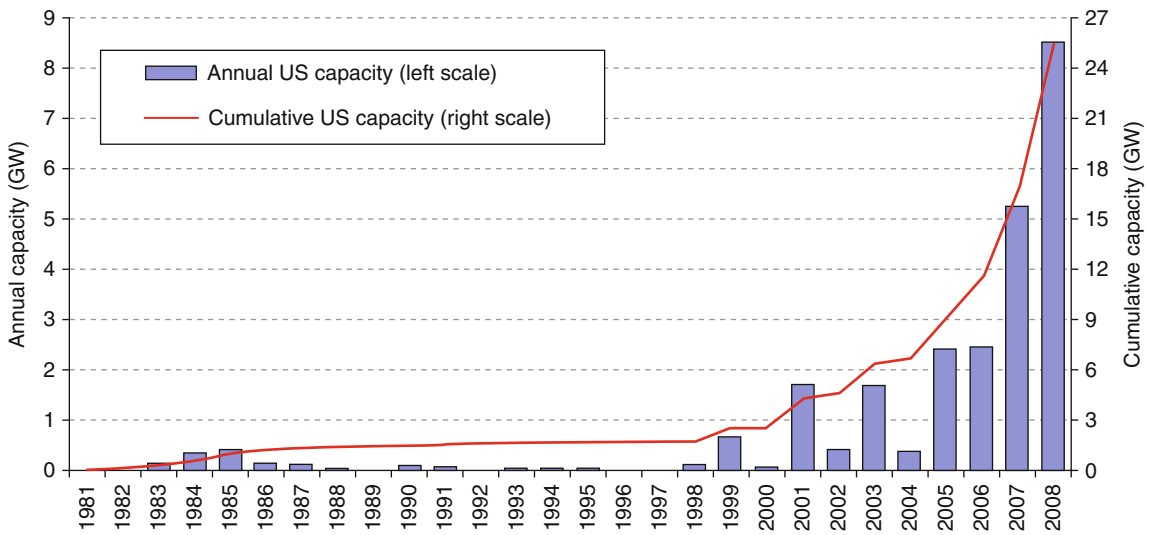

Wind Power: Economy, Market, Subsidies, Payment Mechanisms, and Capacity Credit. Figure 2 Wind development and the PTC [11]

ten wind projects. Table 5 shows the amounts that were awarded to wind projects.

As shown in Table 6, European countries favor two mechanisms to facilitate renewable generation: the feed-in tariff (FIT) system and quota regulation in combination with a Tradable Green Certificates (TGC) market. Other policy instruments, such as tender schemes, are no longer used as the main policy scheme in any European country. However, there are instruments, such as production tax incentives and investment incentives, which are frequently used as supplementary instruments [4]. FIT rates range from

Wind Power: Economy, Market, Subsidies, Payment Mechanisms, and Capacity Credit. Table 5 ARRA wind project grants

Wind project awards	Location	Amount
Evergreen Wind Power V, LLC	Danforth, Maine	$40,441,471
Moraine II Wind Farm	Woodstock, Minnesota	$28,019,520
Canadaigua Power Partners, LLC	Cohocton, New York	$52,352,334
Canadaigua Power Partners II, LLC	Cohocton, New York	$22,296,494
Wheat Field Wind Farm	Arlington, Oregon	$47,717,155
Hay Canyon Wind Farm	Moro, Oregon	$47,092,555
Pebble Springs Wind Farm	Arlington, Oregon	$46,543,219
Highland Wind Farm	Salix, Pennsylvania	$42,204,562
Locust Ridge II, LLC	Shenandoah, Pennsylvania	$59,162,064
Penascal Wind Farm	Sarita, Texas	$114,071,646
Total awarded to wind plants		*$499,901,020*

Source: DOE Press Release. *Treasury, Energy Announce $500 Million in Awards for Clean Energy Projects*. September 1, 2009. http://www.energy.gov/news2009/7851.htm

€52 to €114/MWh for on shore wind plants and up to €130/MWh for off shore.

Green Power Markets

Green power markets can be classified as compliance and voluntary market. Compliance markets exist because of policy decisions, primarily state Renewable Portfolio Standards (RPS) that require electric service providers within the state to have a minimum amount of renewable energy in their electricity supply. RPSs also often define the specific types of renewable resources that are eligible for RPS compliance and include set-asides that direct suppliers to obtain a portion from a specific resource, most often solar power. For example, suppliers in New Jersey must meet a portion of their RPS from in-state solar generation; thus there is an internal

Wind Power: Economy, Market, Subsidies, Payment Mechanisms, and Capacity Credit. Table 6 Primary wind mechanisms in Europe

Primary mechanism for wind	European countries
Feed-in tariffs	Austria, Cyprus, Czech Republic, Estonia, France, Germany, Greece, Hungary, Ireland, Latvia, Lithuania, Luxembourg, Portugal, Slovakia, Slovenia, Spain, Switzerland
Quota obligation with TGC	Belgium, Italy, Poland, Romania, Sweden
Investment subsidies and tax incentives	Finland, Malta
Other	Bulgaria: mandatory purchase obligation
	Denmark: market price premium for on-shore and tendering system for off-shore
	The Netherlands – premium price tariff

New Jersey solar Renewable Energy Credit (REC) market for RPS purposes.

Voluntary markets are consumer driven and allow consumers to choose to do more than policy decisions require, that is, voluntarily purchase green power or RECs above and beyond their particular utilities RPS requirements. Voluntary consumer decisions to buy electricity supplied from renewable energy sources represent a powerful market support mechanism for renewable energy development. While the compliance market represents a larger portion of renewable energy and REC sales, the voluntary market helps develop nationwide renewable energy capacity that exceeds what mandatory markets contribute alone (see Fig. 3).

In the early 1990s, a small number of US utilities began offering "green power" options to their customers. Since then, these products have become more prevalent, both from traditional utilities and from renewable energy marketers operating in states that have introduced competition into their retail electricity markets or are offering RECs online. Today, more than half of all US electricity customers have an option to

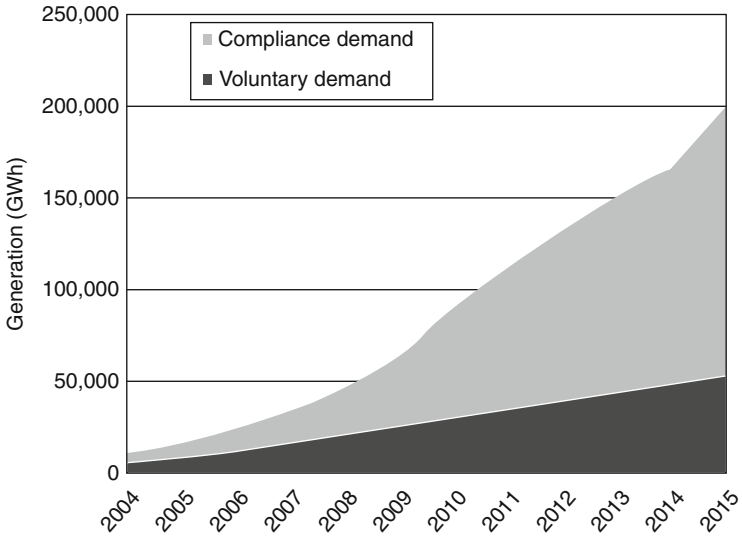

Wind Power: Economy, Market, Subsidies, Payment Mechanisms, and Capacity Credit. Figure 3
Historic and projected demand for renewable energy [12]

voluntarily purchase some type of green power product directly from a retail electricity provider, while all consumers have the option to purchase RECs.

More than 850 utilities, or about 25% of utilities nationally in the United States, offer some type of green power programs to customers. These programs allow customers to purchase a green power product, which can include receiving some portion of their power supply as renewable energy (almost always at a higher price), offset a portion of their power supply with RECs, or contribute funds for the utility to invest in renewable energy development. The term "green power" generally refers to electricity supplied in whole or in part from renewable energy sources, such as wind and solar power, geothermal, hydropower (typically low-impact or small hydro), and various forms of biomass. Many utilities or alternative energy suppliers often do have access to local renewable energy resources but will offer a bundled green power product to consumers. A bundled green power product consists of the local electricity supply resource bundled with supplier purchased RECs.

In states with competitive (or restructured) retail electricity markets, electricity customers can buy electricity generated from renewable sources or bundled with RECs, by switching to an alternative electricity supplier that offers a green power product. In some of these states, default utility electricity suppliers offer green power product options to their customers in conjunction with competitive green power marketers that do not require customers to switch. Nearly a dozen states that have opened their markets to retail competition have experienced some green power marketing activity.

Finally, regardless of whether they have access to a green power product from their retail power provider, any consumer can purchase green power by buying RECs in the voluntary markets, which represent the "environmental attributes" of electricity generated from renewable energy-based projects. This provides a way for consumers to support renewable energy development (through REC purchases) without having to switch to an alternative electricity supplier. Today, several dozen companies actively market RECs to residential or business customers throughout the United States. Many REC marketers also sell greenhouse gas emissions offsets sourced from renewable energy projects.

In 2008, approximately one million consumers and businesses purchased more than 24 billion kilowatt-hours (kWh) worth of green power products from their power suppliers or in the form of RECs (0.6% of total US 2008 electricity consumption). Of the total green power purchased, 71% was supplied from wind

energy, followed by biomass energy sources, including landfill gas (17%); hydropower (primarily low impact or small hydro) (9%); geothermal (2%); and solar (<1%). At the end of 2008, kilowatt-hour sales of renewable energy in voluntary markets represented a generating capacity equivalent of about 7,300 MW of renewable energy sources (1% of the peak US 2008 demand). The estimated market value of green power product sales in 2008 is between $110 and $190 million.

Green power product purchases have grown steadily in recent years, although preliminary data for 2009 suggest a slowing in the market presumably due to the economic downturn. In 2008, purchases increased by 34% (in kilowatt-hours) from the previous year, with annual average growth of 41% since 2004 (Table 7). REC purchases, primarily by businesses and institutional customers, have been driving much of the market growth, increasing 47% in 2008.

Purchases by nonresidential customers have outpaced those by residential consumers in recent years, with businesses and organizations now representing more than three-quarters of all green power product purchases. According to the US Environmental Protection Agency's Green Power Partnership, a program that works with businesses and organizations that purchase green power, some of the leading purchasers of green power, mainly in the form of RECs, in the United States include Intel, Kohl's, PepsiCo, Whole Foods, the City of Houston, and Dell. EPA maintains a list of the top purchasers on its Web site.

While full market data are not yet available for 2009, the EPA Green Power Partnership saw its partner purchases increase by 5% in 2009. This represents considerable slowing in partner purchases compared to the increases of 44% and 68% during the two previous years. Therefore, the economy is likely having some dampening effect on the market. In contrast, EPA also reported that it had about 300 companies or organizations join its Green Power Partnership in 2009, a large number based on historic standards, bringing the total Partners to 1,200.

Although renewable energy policies are now increasingly driving renewable energy development, voluntary markets can continue to play a role going forward. Today, more than half of US states have renewable energy standards requiring utilities or power suppliers to obtain a certain fraction of their generation from renewable sources (e.g., 20% renewable by 2020). However, consumers who want to purchase a greater share of renewable energy (100%) or support technologies that might not be incentivized by policies may want to continue to participate in these markets and support the development of new renewable energy resources.

Capacity Credit

Power system planners work to ensure that sufficient generating capacity is installed to meet projected demand for electricity. Although in some cases this

Wind Power: Economy, Market, Subsidies, Payment Mechanisms, and Capacity Credit. Table 7 Estimated annual green power purchases by market sector, 2005–2008[a]

Market sector	(Millions of kWh)							
	2005	2006	2007	2008	% Change 2004/2005	% Change 2005/2006	% Change 2006/2007	% Change 2007/2008
Utility green pricing	2,500	3,400	4,300	4,800	33%	39%	25%	12%
Competitive markets	2,200	1,700[b]	3,200	3,900	−19%	−20%[b]	88%[b]	22%
REC markets[c]	3,900	6,800	10,600	15,600	126%	75%	55%	47%
Retail total	*8,500*	*11,900*	*18,100*	*24,300*	*37%*	*41%*	*53%*	*34%*

[a]Includes sales of new and existing renewable energy. Totals and growth rates may not calculate due to rounding.
[b]2006 sales figures may be underestimated because of data gaps.
[c]Includes only RECs sold to end-use customers separate from electricity.

function is performed by markets, the fundamental issue of acquiring or otherwise procuring capacity is important to ensure long-term generation resource adequacy. To assess resource adequacy, a reliability-based analysis is usually performed that utilizes the forecast load demand, along with the generation fleets' reliability characteristics to determine whether there are sufficient generation resources at some future date. This typically uses probabilistic analysis so that the risk of having insufficient generation can be quantified. What is important is the overall system assessment, but it is often useful to assess the contribution that any individual power plant, or group of plants, makes toward overall resource adequacy. This contribution is known as the capacity credit, or capacity value, of the resource, and is typically measured either in MW of capacity or as a percentage of the rated capacity of the plant.

Calculating the capacity contribution of wind power plants requires detailed load data, data for the balance of generation, and wind production estimates, hourly or daily, that are time-synchronized with the load. The capacity value as measured by effective load-carrying capability is based on a reliability metric such as loss of load expectation (LOLE), which is often measured in units of days/year. A common reliability target is an LOLE of 0.1 day/year, or1-day-in-10-years, and is illustrated in the following figure as the area (magnified) under the left tail of the probability distribution in Fig. 4.

The basic principle underlying capacity value, called effective load-carrying capability (ELCC), is that the generation system should achieve the same reliability with wind as it does without wind. Using the above figure as an example, the generation fleet without the wind plant has an LOLE of 0.1 day/year. When the wind generation is added, the curve shifts to the right, indicating a high level of planning reserve during many, but not all, hours. This shift causes a reduction in the area under the curve, which was originally at 0.1 day/year, but is now less than that. To bring the system reliability back to its original value, the loads are increased incrementally until the area under the left tail of the curve is restored to its original value of 0.1 day/year. The amount of load increase that holds reliability constant is the ELCC of the wind plant.

The portfolio of generation needed to complement wind, especially at high penetration rates, is different than without wind. Typical capacity values for wind plants range from 5% to 40% of nameplate capacity, depending on the wind characteristics and correlation with load (values outside this range are possible, although somewhat unlikely). A conventional power plant can have an ELCC in the range of 50–95%,

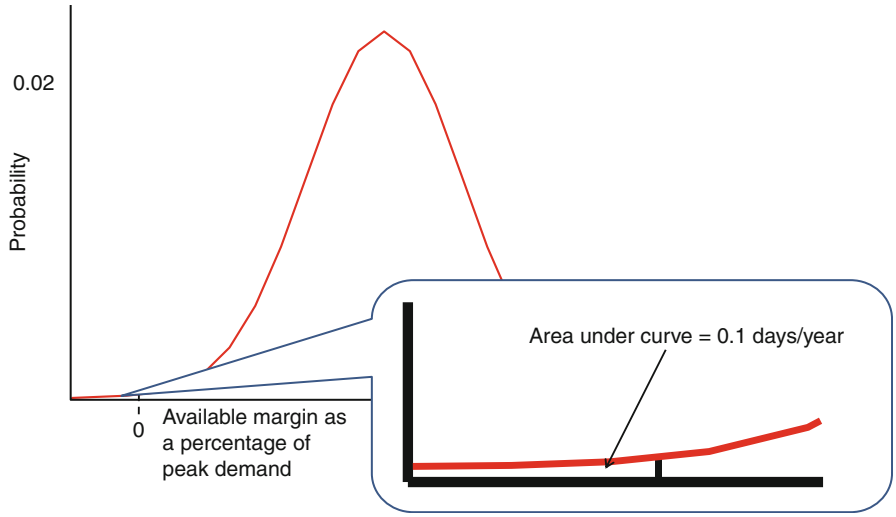

Wind Power: Economy, Market, Subsidies, Payment Mechanisms, and Capacity Credit. Figure 4
Common reliability target: An LOLE of 0.1 day/year, or 1-day-in-10-years

whereas wind plants are significantly below this. Because of this, wind is primarily an energy resource that has limited capacity value. This implies that the generation portfolio that complements a high wind penetration scenario will need to provide a higher ratio of ELCC per unit of energy than would be the case without wind. For example, with a high wind penetration, instead of requiring a baseload capacity penetration of 50% of the peak demand (example only), the ratio of baseload generation would decline, and some baseload generation would be replaced by cycling generation with faster ramp rates (MW/min) and lower turndown levels (minimum sustained generation level, in MW).

Wind Integration Costs

Over the last several years, various entities have conducted wind integration studies in an effort to assess what is needed to accommodate larger amounts of wind energy on the electric grid, and how much this might cost. Integration studies generally simulate power systems under a certain penetration of wind energy and evaluate the impacts on the grid and estimate the incremental operating costs incurred due to the added variability and uncertainty of wind energy.

Two general approaches have been employed to determine wind integration impacts in the United States. The first approach estimates the cost of increased operating reserves in the regulation, load-following and unit commitment time frames that are required to balance the increased net load variability introduced by wind generation. These studies generally focus on wind's impact on ancillary services and compare wind with an energy-equivalent flat block of energy. The flat block will have no variability or uncertainty associated with it so that the operational differences can explicitly show the impacts of wind energy. Although the flat block is a useful construct because of its inherent certainty and constant energy delivery, recent work has identified some weaknesses in this approach [7]. Because the flat energy block is calculated to be energy-equivalent to the wind, large inter-day ramps in this artificial benchmark unit can occur as a result of significant differences in day-to-day production between the wind energy and the flat block. This effect can be significant at high wind penetrations. In addition, the flat block schedule tends to have more on-peak energy and less off-peak energy than wind generation. As a result, the daily flat block is worth \$1.50–\$2.00/MWh more than the wind generation, and the resulting estimated wind integration costs may be overstated.

The second approach does not directly determine the cost of wind integration, but examines the impact that wind has on system commitment and dispatch, and calculates the net value of wind power between a base case and a case (or cases) with wind. The net value of wind represents cost savings from wind displacing more costly units, minus any additional costs that may be incurred from the need for additional ancillary services. Using this technique, the wind case is compared with that of an identical system without wind power, and all impacts are compared and considered from higher penetrations of wind power. Although this does not separate the impacts of wind on various levels of reserves, those impacts are captured implicitly in the modeling framework and results.

The technique most often employed is to estimate these costs as the difference in overall electric system production costs between a base case scenario and one that incorporates a certain level of variable and unpredictable wind energy penetration. Integration costs vary primarily due to the size of the balancing area being modeled, the accuracy of the wind forecasting (if used), the use (or not) of sub-hourly scheduling, the flexibility of the existing resource fleet, the type of ancillary services being employed, and the geographic diversity (or lack thereof) of the wind energy. The following table (Table 8) lists the main findings of the major US wind integration cost studies conducted between 2003 and 2007, most of which utilized some form of the flat block approach. The average cost of integrating wind energy was found to be about \$5.00/MWh. Recent work has raised the issue of whether existing methods for calculating integration costs are indeed measuring these costs accurately, and whether there may be integration costs for integrating other generating technologies that have not been addressed [8].

In 2008, the National Renewable Energy Laboratory (NREL), under the sponsorship of the U.S. Department of Energy, initiated the largest, most ambitious and comprehensive regional-level wind power integration studies conducted so far, in the United States.

Wind Power: Economy, Market, Subsidies, Payment Mechanisms, and Capacity Credit. Table 8 Main results from major US wind integration cost studies

Date	Study	Wind capacity penetration	Integration cost ($/MWh)				
			Regulation	Load following	Unit commitment	Gas supply	Total
2003	Xcel-UWIG	3.5%	0	0.41	1.44	–	1.85
2003	We energies	29%	1.02	0.15	1.75	–	2.92
2004	Xcel-MNDOC	15%	0.23	–	4.37	–	4.60
2005	PacifiCorp-2004	11%	0	1.48	3.16	–	4.64
2006	Calif. (multi-year)[a]	4%	0.45	Trace	Trace	–	0.45
2006	Xcel-PSCo	15%	0.20	–	3.32	1.45	4.97
2006	MN-MISO[b]	31%	–	–	–	–	4.41
2007	Puget sound energy	12%	–	–	–	–	6.94
2007	Arizona Pub. Service	15%	0.37	2.65	1.06	–	4.08
2007	Avista utilities	30%	1.43	4.40	3.00	–	8.84
2007	Idaho Power	20%	–	–	–	–	7.92
2007	PacifiCorp-2007	18%	–	1.10	4.00	–	5.10
2008	Xcel-PSCo[c]	20%	–	–	–	–	8.56
Average cost							*5.02*

Source: U.S. Department of Energy, *2008 Wind technologies market report*, July 2009.
Note: not all types of costs were evaluated in all studies.
[a]Regulation costs represent 3-year average.
[b]Highest over 3-year evaluation period.
[c]This integration cost reflects a $10/MMBtu natural gas price scenario. This cost is much higher than the integration cost calculated for Xcel-PSCo in 2006, in large measure due to the higher natural gas price: had the gas price from the 2006 study been used in the 2008 study, the integration cost would drop to $5.13/MWh.

Western Wind and Solar Integration Study (WWSIS)

The Western Wind and Solar Integration Study (WWSIS) [9] examined up to 30% wind and 5% solar penetration scenarios in the WestConnect area, which includes Wyoming, Colorado, New Mexico, Arizona, and Nevada. This study evaluated system costs with and without wind energy, and also examined the implication of this high level of variable generation on reserves. Wind events occur much more slowly than contingency events. However, wind may increase the level of flexible reserves (ramping capability) that must be available, either as part of the unit commitment process or as quick-start capability that can be activated as needed. The International Energy Agency Task 25, Design of Power Systems with Large Amounts of Wind Energy, is examining this issue, as is the National Renewable Energy Laboratory in the United States in collaboration with University College, Dublin's Electricity Research Center. This study did not attempt to estimate the integration cost per se of wind or solar, in part given the difficulty of properly establishing a robust benchmark case (Milligan and Kirby Integration Cost vs. value paper). However, the study did examine the economic impact of balancing area cooperation (joint unit commitment and economic dispatch) and found that the study footprint would experience savings of about $2 billion/year (based on $42 billion/year production cost) by utilizing this form of cooperation.

Eastern Wind Integration and Transmission Study (EWITS)

The Eastern Wind Integration and Transmission Study (EWITS) study [10] area includes most of the

Eastern Interconnection and is examining a 20% wind penetration scenario along with a transmission expansion component. The study includes the Midwest ISO, PJM, ISO New England, the New York ISO, the Southwest Power Pool, the Tennessee Valley Authority, the Mid-Continent Area Power Pool, and various other interested parties.

The EWITS study pushed the state of the art for wind integration cost forward. This study found that severe inter-day ramps, imposed by the flat-block proxy resource (which is only a fictitious benchmark unit) significantly distorted production costs. Instead, the EWITS approach estimated the cost based on adding wind into the system with no additional reserves as the "base case," then determining the delta value by adding reserves to cover the additional variability and uncertainty of wind at the various penetration rates and geographic dispersion. In 2009 dollars, the integration costs ranged from about $3.80 to $5.40/MWh of wind generation.

Cost Trajectory for Wind Energy Technology

Historically, the busbar cost of wind energy has declined significantly, though it has increased in recent years. Although there are a number of factors behind this reduction in cost, the primary driver has been the adoption of new technologies that allow for lighter components and taller towers. This results in the capture of more energetic winds that tend to be higher from the earth's surface. Today's typical wind turbine has a tower height of 80–100 m. The historical cost decline has been driven not only by higher towers, but also by larger rotors that increase energy capture. However, it is likely that wind turbines will not continue to grow indefinitely because of the so-called square-cubed law. This relationship says that as rotors increase in size, the energy capture will increase as the square of the swept area. At the same time, the volume of material required increases as the cube of the rotor size. Thus, cost increases faster than energy capture, holding constant all other factors. The square-cube law has been overcome by the introduction of advanced materials and other strategies that can reduce the per unit weight, but delivering the required volume, of material. As wind turbines become larger, there are also increases in logistical issues such as transporting large blade or tower components across the land. For these reasons, it seems unlikely that the historical cost decline can continue, and that more modest incremental improvements will occur instead.

The logistical limitations of on-shore wind technology, transportation, are not as much of an issue with off-shore technology because ships can easily transport larger blade and tower units. However, the installation and operation/maintenance cost of off-shore turbines are higher because of the harsher sea-based environment, and the difficulty of accessing turbines for maintenance. Cost trajectories are uncertain, and will be driven in large part by the reliability of off-shore turbines. This issue, critical for all wind turbines, is especially significant because harsh weather conditions can limit access to off-shore turbines; therefore to mitigate the need for on-site maintenance a reliable turbine is necessary.

Table 9 is taken from Thresher et al., which is the source of much of this discussion, and shows results from the U.S. Department of Energy's WindPACT Project. The table shows the likely ranges of cost and energy capture for future wind technology. Using 2002 as a base, the most likely outcome is a substantial increase in capacity factor with a small drop in capital cost, although the latter appears to be in doubt given the recent surges in commodity prices.

Wind Energy and Economic Development

Installing new wind power generation not only creates electricity, but also supports new manufacturing, construction, maintenance, and other jobs, as well as contributing to the economy. Depending on the local workforce and resources, a new wind project can provide many construction jobs for the local area, increase sales for local manufacturers and retailers, and support jobs and increased economic activity at local hotels, restaurants, grocery stores, and other suppliers of goods and services.

How much the new wind projects will impact their local community depends on many factors:

1. Are the developers using local labor for siting, legal assistance, road building, and turbine erection?
2. Will any of the project supplies or turbine components come from the local area (e.g., local blade production)?

Wind Power: Economy, Market, Subsidies, Payment Mechanisms, and Capacity Credit. Table 9 Areas of potential technology improvement

Areas of potential technology improvement			
		Cost increments (best/expected/least, percent)	
Technical area	Potential advances	Annual energy production	Turbine capital cost
Advanced tower concepts	* Taller towers in difficult locations	+11/+11/+11	+8/+12/+20
	* New materials and/or processes		
	* Advanced structures/foundations		
	* Self-erecting, initial or for service		
Advanced (enlarged) rotors	* Advanced materials	+35/+25/+10	−6/−3/+3
	* Improved structural-aero design		
	* Active controls		
	* Passive controls		
	* Higher tip speed/lower acoustics		
Reduced energy losses and improved availability	* Reduced blade soiling losses	+7/+5/0	0/0/0
	* Damage tolerant sensors		
	* Robust control systems		
	* Prognostic maintenance		
Drivetrain (gearboxes and generators and power electronics)	* Fewer gear stages or direct drive	+8/+4/0	−11/+6/+1
	* Medium/low speed generators		
	* Distributed gearbox topologies		
	* Permanent-magnet generators		
	* Medium voltage equipment		
	* Advanced gear tooth profiles		
	* New circuit topologies		
	* New semiconductor devices		
	* New materials (GaAs, SiC)		
Manufacturing and learning curve	* Sustained, incremental design and process improvements	0/0/0	−27/−13/−3
	* Large-scale manufacturing		
	* Reduced design loads		
Totals		+61/+45/+21	−36/−10/+21

3. When the project is operational, will the owners hire local workers to maintain and repair turbines?
4. What type of payments will landowners receive for allowing the turbines on their land?
5. How are property taxes determined for the wind project owners?

Some of these questions are specific to the United States where typically, wind power developers will lease

land from private citizens, and pay taxes to local counties, or negotiate with local governments for payments in lieu of taxes. However, the basic principles of economic development impacts apply everywhere. The net impact that wind energy has on jobs can be calculated by tracing the spending patterns and jobs created that are caused by the spending on the wind plant, and deducting the spending and jobs that would have been developed in the absence of wind. Approaches that can be applied include econometric analysis and input–output analysis, both of which are well-established methods. Input–output analysis can easily be adapted to alternative industries or locations and can be based on economic coefficients that describe the interaction between related sectors of the economy.

The JEDI Model

The U.S. Department of Energy's National Renewable Energy Laboratory (NREL) has an input–output model that estimates the jobs and economic impacts associated with new wind power. The Jobs and Economic Development Impacts (JEDI) model requires very little user input, and is used by local officials, wind power developers, and other interested parties to estimate local jobs, salaries, and economic development impacts associated with new wind projects. JEDI is based on project-specific inputs from the model user (the more information about the project, the more accurate the results will be) and on default inputs derived from industry averages and interviews. Below is a sample listing of jobs included in the JEDI output (Fig. 5).

JEDI is a free tool that provides the user with default information on land lease and property tax revenues for wind. Various ownership and financing structures can be incorporated by the user if they do not want to use the defaults. JEDI presents gross project-specific results. It does not consider potential electricity price impact or alternative investment options. JEDI results are reported on a statewide scale; however, JEDI can be used on a county, regional, or national basis by incorporating additional data (not included in the model). JEDI model defaults are based on interviews with industry experts and project developers. Economic multipliers contained within the model are US-specific and derived from a company called the Minnesota IMPLAN Group who uses data from many sources including the US Census and Bureau of Economic Analysis. You can learn more at www.implan.com

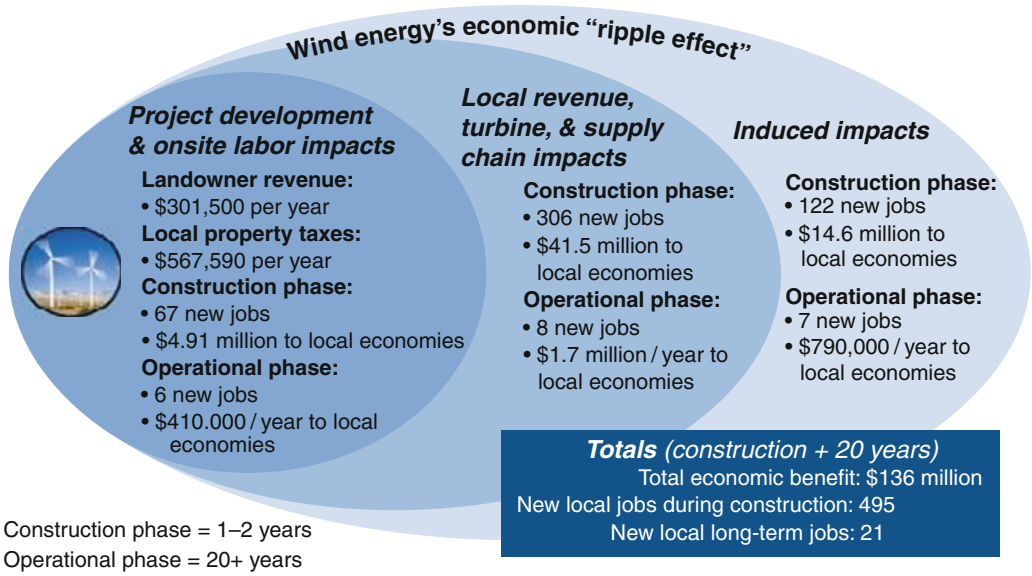

Wind Power: Economy, Market, Subsidies, Payment Mechanisms, and Capacity Credit. Figure 5
Wind energy's economic ripple effect

In addition to the JEDI wind model, there are also models for other technologies such as concentrating solar power and natural gas. These US-based models can be found at http://www.nrel.gov/analysis/jedi/

What Is the Difference with Local Components? Typical US wind projects do not have locally made major components (blades, towers, and gear boxes). However, if any of the major components can be manufactured in the local region, the benefit to the local economy is much greater. This table shows the results of jobs and economic impacts from two almost identical projects. However, the first one has no locally made components and the second one has locally manufactured blades. This example is for the state of Colorado, where wind turbine blade manufacturing facilities are located.

Figure 6 displays results from the JEDI model, and shows that there will be approximately 140 more local jobs supported by the same new wind project if locally manufactured blades are used. Not only will the number of jobs increase but the economic impact to the (usually rural) community where the wind farm is placed will experience temporary economic growth during construction and permanent increases in operations jobs, land lease payments, property tax revenues, and local service jobs.

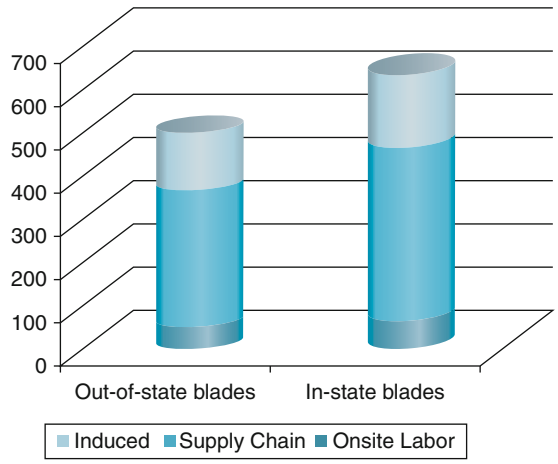

Wind Power: Economy, Market, Subsidies, Payment Mechanisms, and Capacity Credit. Figure 6
Jobs supported by new wind project: local vs. out-of-state blades

Future Directions

As the penetration of wind energy increases on power systems around the world, there remain questions regarding the interaction of wind energy with wholesale electricity markets. Wind energy has a near-zero marginal cost, which provides it with a high degree of economic merit in economic dispatch decisions that rank generation by marginal cost. At high penetration rates, wind may significantly reduce the spot price for electricity, which will reduce payments to conventional generation owners. In more extreme cases, the revenue shortfall for other generators may make it impossible for owners to meet capital cost payments. This may discourage base-load generation that cannot be easily or quickly cycled offline, instead encouraging more flexible generators that can economically operate at lower capacity factors. However, it is not clear, nor has it been conclusively demonstrated, that an economically efficient outcome can be attained in the long run. It is possible that capacity, along with other ancillary services, may be required in the short run to ensure reliable and economic operation of the power system; and in the long run to elicit the required level of flexibility in the balance of the power system. Power systems with high levels of wind generation will generally need more flexible generation (increased ramping and lower turn-down capability), access to this flexibility through market or other institutional mechanisms, and operational practice that can make best possible use of the technologies and institutions involved.

Various types of subsidies or requirements for minimum levels of renewable energy are attempts to incorporate all costs (private costs plus external costs) into decision making and implementation. Because pollution cost falls on a third party, these attempts at market adjustment, if done correctly, can elicit the economically efficient level of renewable energy. However, experience in the United States shows that tax credits (and other nonmarket incentives) can play havoc with development if wind energy if the credits longevity are in question.

Future areas of research will likely cover several broad themes: technology development, analytic tools and metrics for integration, and electricity market development.

Land-based turbine developments include advanced tower concepts, advanced rotors, reduced energy losses,

drive-train/gear-box reliability improvements, and increased efficiency and lower costs in manufacturing. Each of these evolutionary directions is expected to lower the bus-bar cost of wind energy, thus improving the economics. Off-shore turbine technology developments will also include more advances in platform designs and costs, improving the economics of this variation in wind energy technology.

There is increasing interest in wind plants that can provide reserves to the power system. Much of the required technology exists, although institutional constraints and lack of general awareness of this capability has hindered its use. With increasing wind penetrations, better institutional/operating rules, and modest changes in control algorithms, wind turbines could soon provide much of the reserves that are now required from conventional generation to help support wind energy.

At high wind penetrations there are questions about whether the existing markets will induce the required levels of flexibility from the remainder of the generation fleet. Research and analysis, including advanced power system market modeling will help answer these questions, and suggest potential future enhancements to markets that may include more robust capacity markets, metrics to assess flexibility need and supply, and relevant market products over the key time scales most relevant to wind energy integration. At the same time, advanced methods for unit commitment that involved stochastic optimization, although promising, will not be easily integrated into power markets without significant development.

Bibliography

Primary Literature

1. Milligan M, Kirby B, Gramlich R, Goggin M (2009) Impact of electric industry structure on high wind penetration potential. NREL/TP-550-46273. National Renewable Energy Laboratory, Golden. http://www.nrel.gov/docs/fy09osti/46273.pdf
2. ISO/RTO Council (2007) Increasing renewable resources, how ISOs and RTOs are helping meet this public policy objective. ISO/RTO Council, 16 Oct 2007
3. ENTSO (2009) The harmonized electricity market role model Version 2009–01. http://www.entsoe.eu/. Accessed 26 July 2009
4. Kjaer C et al (2009) Wind energy – the facts. European Wind Energy Association, Brussels
5. Morthorst P-E, Awerbuch S (2009) The economics of wind energy. European Wind Energy Association, Brussels
6. Morthorst PE (April 2007) TradeWind: further developing Europe's power market for large scale integration of wind power. Risø National Laboratory, Technical University of Denmark
7. Milligan M, Kirby B (2009) Calculating wind integration costs: separating wind energy value from integration cost impacts. NREL Report No. TP-550-46275. National Renewable Energy Laboratory, Golden, p 28. www.nrel.gov/publications
8. Milligan M, Ela E, Lew D, Corbus D (2010) Advancing wind integration study methodologies: implications of higher levels of wind. NREL technical report (to appear)
9. http://www.nrel.gov/wind/systemsintegration/wwsis.html
10. http://www.nrel.gov/wind/systemsintegration/ewits.html
11. Wiser R, Bolinger M (2008) Wind technologies market report. NREL Report No. TP-6A2-46026. DOE/GO-102009-2868. Department of Energy, Energy Efficiency & Renewable Energy Office. Golden, July 2009
12. Bird et al (June 2010) An examination of the regional supply and demand balance for renewable electricity in the United States through 2015. National Renewable Energy Laboratory, Golden
13. Wiser R, Bolinger M, Barbose G (November 2007) Using the federal production tax credit to build a durable market for wind power in the United States. Ernest Orlando Lawrence Berkeley National Laboratory, Berkeley

Books and Reviews

Bird L, Kreycik C, Friedman B (2009) Green power marketing in the United States: a status report (2008 Data). NREL/TP-6A2-46581. National Renewable Energy Laboratory, Golden http://www.nrel.gov/docs/fy09osti/46581.pdf. Accessed Sep 2009

U.S. DOE Green Power Network Web site: http://apps3.eere.energy.gov/greenpower/ U.S. EPA Green Power Partnership http://www.epa.gov/greenpower/

Wind Turbine Noise Emissions

Karl Bolin, Mats Åbom

KTH Royal Institute of Technology, KTH-The Marcus Wallenberg Laboratory for Sound and Vibration Research, Stockholm, Sweden

Article Outline (Table of Contents)

Glossary

Definition of the Subject and Its Importance

Introduction

Basic Concepts
Noise Sources
Sound Propagation
Human Impact
Conclusions
Future Directions
Bibliography

Glossary

Sound pressure *(p)* The amplitude of the fluid's pressure disturbances around the steady state pressure which in air is perceived as sound, see Fig. 1.

Noise Is unwanted sound.

Sound pressure level (SPL, L_p) A logarithmic function of the sound pressure with the unit decibel [dB], see (7)

Sound level *(L_A, L_B, L_c)* Filtered sound pressure level with different filters (A, B, C) resembling the human hearing system at different loudness, see Fig. 6.

Acoustic power level *(L_W)* A measure of the radiated sound power in dB from acoustic sources, see (8).

Sound speed *(c)* The propagation speed of sound in different media.

Audible sound Defined as pressure fluctuations between 20 Hz and 20 kHz.

Amplitude modulation Sound with a periodically varying level (amplitude).

Masking The change of loudness of one sound due to another.

Low-frequency sound Is normally defined as audible sound between 20 Hz and 100 Hz or 200 Hz.

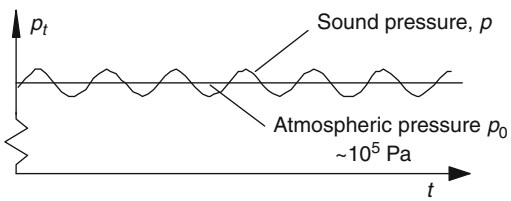

Wind Turbine Noise Emissions. Figure 1
An acoustic pressure field $p(\mathbf{r},t)$ ordinarily implies only small disturbances. Normal speech at a distance of several meters, for example, gives a sound pressure p of the order 0.01 Pa superimposed upon atmospheric pressure p_0, which is about 10^5 Pa

Directivity The variation of sound pressure level in different directions from a source

Definition of the Subject and Its Importance

Wind turbines generate sound. Mainly this sound source is of aeroacoustic origin as improved sound insulation of the nacelles has reduced the mechanical sound sources. Unwanted sound is called noise and is a major factor when assessing nuisance caused by wind turbines. The increasing height of wind turbines has led to better possibilities to harvest wind at higher altitudes but has also contributed to increased noise levels in stable atmospheric conditions when the sound is easily transmitted due to a high wind speed gradient. Rapid development of large wind farms in rural, earlier unexploited, areas could cause large acceptance problems for nearby residents if noise is not properly considered in the development process. Several epidemiological studies have shown noise is the most prominent annoyance and show strong interdependence to visibility and lack of economic incentive from wind power.

Introduction

Wind turbines symbolize the hopes of a brighter future and solutions to serious problems such as global warming and energy shortage. Today's rapid expansion of wind turbines, both in quantity and size, can have a dramatic impact on the landscape in rural areas throughout the world. Although greenhouse gas emissions of wind turbines are low, the local scenery is often altered when wind farms are constructed. This often leads to concerned neighbors forming pressure groups opposing the projects. Transparent and unbiased information from contractors can often reduce the negative reactions from neighbors. The nearby residents are also usually protected by noise guidelines from authorities that developers have to comply with.

Naturally, not all wind energy is transformed into electricity at wind turbines. Inevitably some power is lost, for instance, in the generator or due to friction-induced forces in the mechanical system. Some of these losses generate sound. Early reports on wind turbine noise originate from the 1980s [1, 2]. Today's wind turbines mainly emit sound from the blades as they move through the air [3]. The amount of sound transmitted through the atmosphere is governed by not only

the acoustic reflection at the ground but also by the atmospheric conditions [4, 5]. Sound from wind turbines regularly causes annoyance to people nearby and should therefore be perceived as noise or unwanted sound. Noise from wind turbines is the main cause of concern to nearby residents [6–8] and should therefore be considered when determining the environmental impact of wind turbines.

Basic Concepts

Sound can be seen as an elastic wave motion where pressure disturbances propagate in a gas or a fluid with a sound speed c. At a certain point in space **r** and time t, an acoustic wave can be described by the sound pressure $p(\mathbf{r},t)$ [Pa]. Sound pressure variations are normally very small deviations of the ambient pressure as illustrated in Fig. 1.

Omitting the effects of humidity and atmospheric pressure, the speed of sound in still air is given by

$$c = 331\sqrt{\frac{273+T}{273}} \quad [\mathrm{m/s}], \tag{1}$$

where T is the temperature in degrees Celsius. If there is wind present, the propagation is affected and the effective sound speed becomes: $c_{eff} = c + U$, where U is the flow speed in the direction of the sound propagation. For outdoor sound propagation, the temperature and wind speed variations in the atmosphere will cause sound speed variations. These variations will have an effect on long distance sound propagation since it will cause the sound waves to refract and propagate along curved paths, see section "Sound Propagation."

The *root mean square* or *RMS value* is marked by $\tilde{p}$ and is defined according to

$$\tilde{p} = \sqrt{\frac{1}{T}\int_0^T p^2(t)dt}, \tag{2}$$

where T is the integration time. The rms-value is very important since it gives information about the time average of the power in the acoustic wave.

Plane waves are characterized by the condition that points with the same acoustical state form parallel planes. Figure 2 shows how a pure plane wave is excited in a duct by a harmonically oscillating piston at one end.

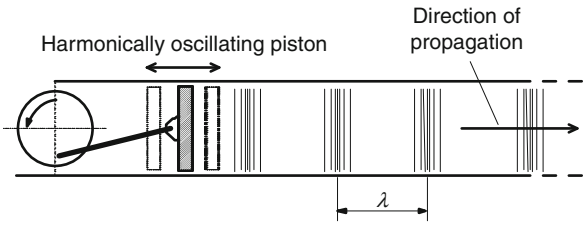

Wind Turbine Noise Emissions. Figure 2
A harmonically oscillating piston in an infinitely long duct gives rise to a plane longitudinal acoustic wave that propagates in the duct. The frequency f of the wave is the same as the piston oscillating frequency. The wavelength λ, i.e., the distance between two pressure maxima or minima, is related to f and the sound speed via: $c = f\lambda$

For outdoor sound propagation, plane waves are useful, since at large distance from a source (*far field*), all sound fields can be approximated as plane waves. In order to characterize the strength of an acoustic source, such as wind turbines or fans, its (time-averaged) acoustic power W is measured for a certain operating condition. For a plane wave, the (time-averaged) acoustic power per unit area or intensity I is given by

$$I = \tilde{p}^2/\rho_0 c, \tag{3}$$

where ρ_0 is the density and c the speed of sound (for air at 20 C and normal pressure $\rho_0 c$ is around 400 [Pa s/m]).

Spherical and Cylindrical Sound Waves

When modeling outdoor sound sources, two simple models are spherical and cylindrical waves. A spherical model is useful at large distances from any source and implies that the (time-averaged) sound power W is preading equally over a large spherical surface, see Fig. 3.

This implies that intensity for a spherical source is given by

$$I = \frac{W}{4\pi r^2}, \tag{4}$$

where r is the radial distance. In this equation, the intensity for a plane wave can be used at large distances from the source which leads to

$$\tilde{p}^2 = \frac{\rho_0 c W}{4\pi r^2}. \tag{5}$$

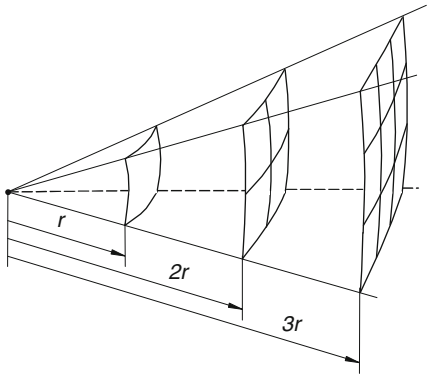

Wind Turbine Noise Emissions. Figure 3
In spherical wave propagation, sound power is divided over an ever-increasing area. The intensity decreases to one fourth of its original value for a doubling of the distance to the source, and to one ninth when the distance is tripled

This last equation can be used to compute the sound pressure from a source with a given power at a certain distance. Alternatively, it can be used to determine the sound power by measuring the sound pressure and this is actually the method used for wind turbines. In practice, an outdoor source is normally on a reflecting ground, and to compensate for this, propagation over a half sphere is assumed. This means that the factor 4π is changed to 2π in (4) and (5). Another modification of (5) is to allow that the sound or acoustic intensity emitted in different directions varies. This variation of the sound intensity is called *source directivity*.

Similarly by assuming propagation over a cylindrical surface with height (or width) H, one can derive the formula

$$\tilde{p}^2 = \frac{\rho_0 c W}{2\pi r H}. \tag{6}$$

This equation applies at large distances for outdoor sound sources which can be seen as a line source (a road) or at some distance for a source located between two reflecting surfaces. An example would be a sea-based wind turbine, where the sea surface represents a totally reflecting surface and where, for certain atmospheric conditions, sound propagating upward is also reflected below a certain maximum height H [9]. When used for large distance, the effect of dissipation during the propagation must also be considered in (5) and (6), see section "Attenuation and Geometrical Spreading." This will introduce an exponential factor $[\exp(-\alpha r)]$ in these equations, where the frequency-dependent damping constant α can be obtained from ISO 9613.

Levels and Decibels

At the beginning of the 1920s, it had become possible to carry out routine sound measurements. An acoustic group at Bell Systems in the USA introduced a measurement quantity that they called a "sensation unit," which was based on a logarithmic scale with base 10. The unit *Bel* (after Alexander Graham Bell), defined as the base-10 logarithm ($\log_{10}$) of the quotient between two acoustic power values, eventually proved to be impractically large. Today, the unit commonly used is, instead, a tenth of a Bel. One decibel (1 dB) corresponds both to the measurement precision that can typically be obtained in acoustic measurements and to the amount of change that a human can discern in ideal circumstances.

The *Sound Pressure Level* L_p (or *SPL*) is defined as

$$L_p = 10 \cdot \log_{10} \frac{\tilde{p}^2}{p_{ref}^2} \tag{7}$$

where $\tilde{p}$ is the rms-amplitude of the sound pressure and $p_{ref} = 2 \cdot 10^{-5}$ Pa is the *reference value of sound pressure*. The reference value of sound pressure approximately corresponds to the lowest sound pressure that a young person with normal hearing can perceive at 1,000 Hz. As an example, ordinary speech corresponds to a sound pressure level of around 60 dB.

The *Sound Power Level* L_W indicates the acoustic power with respect to an internationally accepted reference as

$$L_W = 10 \cdot \log_{10} \frac{W}{W_{ref}} \tag{8}$$

where W is the time-averaged sound power and $W_{ref} = 10^{-12}$ [W] is the *reference value of sound power*.

Sound power is used to define the strength of various sources and from a known sound power and an assumption of the radiation, e.g., spherical waves, the sound pressure at a certain distance can be computed.

As an example for a source emitting spherical waves (5), one obtains the following relation between sound power and sound pressure levels

$$L_p = L_W - 10\log_{10}(4\pi r^2) \approx L_W - 11 - 20 \cdot \log_{10} r, \tag{9}$$

where it is assumed that $\rho_0 c = 400$ [Pa s/m] and r is the distance in m.

Examples of sound powers and sound power levels from different objects can be seen in Fig. 4. From (9), it follows that at 1 m, the sound pressure level is 11 dB less than the sound power level and for each increase in distance with a factor 10, the level will decrease with 20 dB.

Addition of Sound Fields

For sound pressure, the principle of superposition applies; so, the total sound pressure $p_{tot}(t)$ is the sum of the individual waves sound pressures $p_n(t)$, i.e.,

$$p_{tot}(t) = \sum_{n=1}^{N} p_n(t). \tag{10}$$

In order to determine the SPL of the resulting total sound pressure, the RMS sound pressure must be used in accordance with (7). Assuming the most common case that the individual waves originate from N independent sources, the total RMS value is simply

$$\tilde{p}_{tot}^2 = \sum_{n=1}^{N} \tilde{p}_n^2 \tag{11}$$

The corresponding rule for the total SPL from N sources becomes

$$L_{p_{tot}} = 10 \cdot \log_{10} \sum_{n=1}^{N} 10^{L_{pn}/10}. \tag{12}$$

As an example, if two sources of equal strength are added:

$$\begin{aligned} L_{p_{tot}} &= 10 \cdot \log_{10}(10^{L_{p_1}/10} + 10^{L_{p_1}/10}) \\ &= 10 \cdot \log_{10}(10^{L_{p_1}/10} \cdot 2) \\ &= L_{p_1} + 10 \cdot \log_{10} 2 = L_{p_1} + 3\text{dB}, \end{aligned}$$

that is an increase of 3 dB in the SPL.

Characterization of Sound According to Frequency

Sound can be characterized by its frequency content. For mankind, *audible sound* is normally defined as the range 20–20,000 Hz. Frequencies lower than 20 Hz are called *infrasound*, and over 20,000 Hz are called *ultrasound*. Most acoustic phenomena are frequency-dependent,

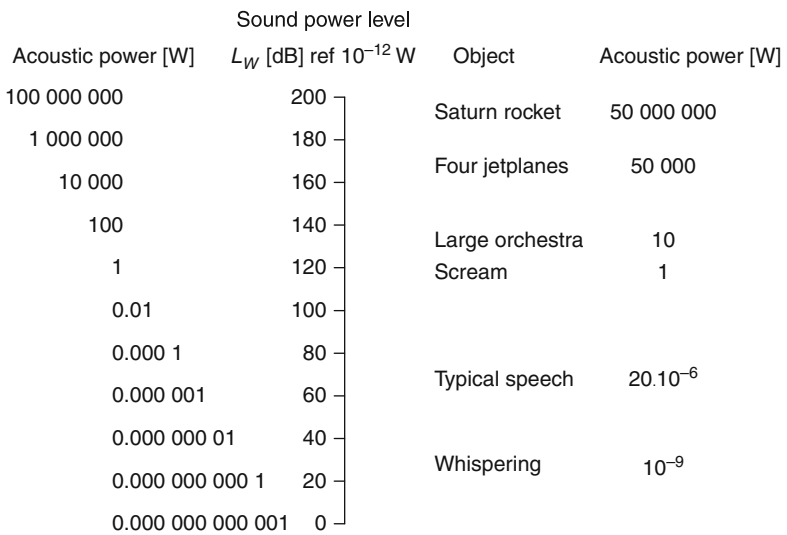

Wind Turbine Noise Emissions. Figure 4
The sound power and Sound Power Level for a number of typical sound sources

and it is well known that different sound sources have different characters, see Fig. 5.

Mathematically, each time signal, for instance, an acoustic pressure p(t), can be seen as sum (integral) of harmonic signal. This is called Fourier analysis and means that an acoustic signal can be represented as a function of frequency or a spectrum. Normally spectra are expressed; so, they represent power which implies that for sound pressure, they are based on the RMS values. The total power in a spectrum can be obtained by applying (11) and sum over all the frequencies since different frequencies can be regarded as independent sources.

In practice, the frequency resolution in a Fourier analysis is related to the measurement time T, giving a resolution of $\Delta f = 1/T$. For noise control purposes and especially when studying sources with a broadband character, i.e., no distinct tones, it is convenient to present the data in broader frequency bands. Often one-third or octave bands are used for this purpose. The standardized octave bands covering the audible range are: 31.5, 63, 125, 250, 500, 1 k, 2 k, 4 k, 8 k, 16 kHz. Each of these octave bands can be split into 3 one-third octaves.

Measures of Noise

The strength of sound is measured by a sound level meter that, in its simplest form, gives the SPL in dB. The SPL does not, however, take account of the nonlinearity of our perception with respect to frequency, as reflected in the concept of loudness [10]. To better reflect the human perception of sound, sound level meters contain filters, so-called *weighting filters*, that amplify the microphone signal in different amounts at different frequencies; see Fig. 6.

Today A-weighting is the common measure for characterizing outdoor sound and most regulations refer to A-weighted dB values, sometimes denoted dB (A) or dBA. A sound pressure level which is A-weighted is called *sound level* and can be denoted L_A. If the spectrum of sound is known

$$L_A = 10 \cdot \log_{10} \sum_{n=1}^{N} 10^{(L_{pn} + \Delta A_n)/10} \quad [\text{dB}] \tag{13}$$

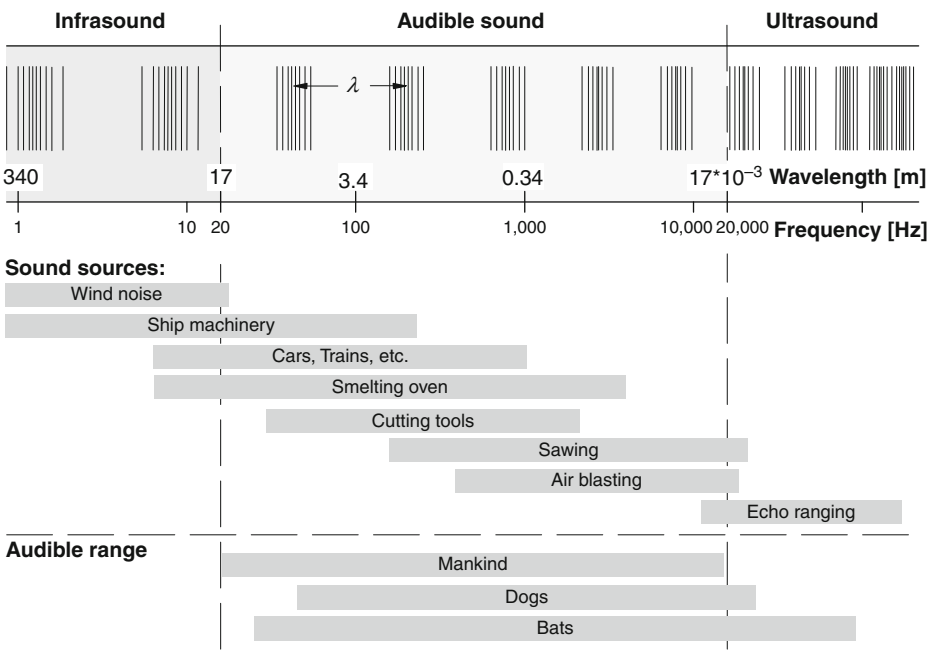

Wind Turbine Noise Emissions. Figure 5
Classification of sound according to frequency, and the relation between frequency and wavelength in air with a sound speed $c = 340$ m/s. Frequency ranges of various sound generation mechanisms

where L_{pn} [dB] is the third-octave or octave band level in band n and ΔA_n [dB] is A-weighting in band n.

Determination of Wind Turbine Source Data

To characterize a wind turbine, the acoustic power or sound power level L_w (8) is estimated using a standard procedure, which in most countries comply with the IEC 61400-11 [11]. This procedure stipulates that the measurements are done at a reference position on the ground at different wind speeds. The wind speed data used should preferably be taken at the center of the turbine (the hub). The measured data is then interpolated to correspond to a reference wind speed of 8 m/s at 10 m height, assuming a standard atmospheric wind profile. Normally manufacturers present the data for a wind turbine as an A-weighted sound power plus the octave band spectrum for the power. Given the A-weighted power, the sound level from a turbine up to a distance of 1,000 m can be estimated from [12]

$$L_A = L_{W_A} - 8 - 20 \cdot \log_{10} r - 0.005 \cdot r \quad [\text{dB}], \qquad (14)$$

where L_{W_A} is the A-weighted sound power level, r the distance in m, and the last term represents atmospheric damping. Equation 14 is based on (9) modified for a half spherical wave, i.e., assuming a reflecting ground. A typical value for the sound power level for 1 MW machines is around 100 dB(A). It can be noted that in terms of acoustic power output, this only corresponds to 0.01 W, i.e., a single wind turbine is not a powerful sound source. As a comparison, a large passenger aircraft at takeoff creates acoustic powers in the range 1,000–10,000 W.

Noise Sources

Most modern wind turbines are of the type shown in Fig. 7, i.e., consist of a rotor attached to a horizontal axis which via a gearbox drives a generator. The rotor+gearbox and generator are enclosed in a housing which is mounted on a tower. Other less common types are based on a vertical rotor and axis where the gearbox and generator can be put on the ground. Here the discussion will focus on the first most common type of turbines.

The noise sources on a wind turbine can be split into two types: mechanical and aerodynamic.

Mechanical Noise

The mechanical noise is normally dominated by the gearbox and generator, the strongest source being the gearbox, which transmits its vibrations to surfaces that can radiate sound to the surrounding, i.e., the housing, the rotor blades, and the tower. For modern well-designed machines, the mechanical noise can be considered to be of secondary importance compared to the

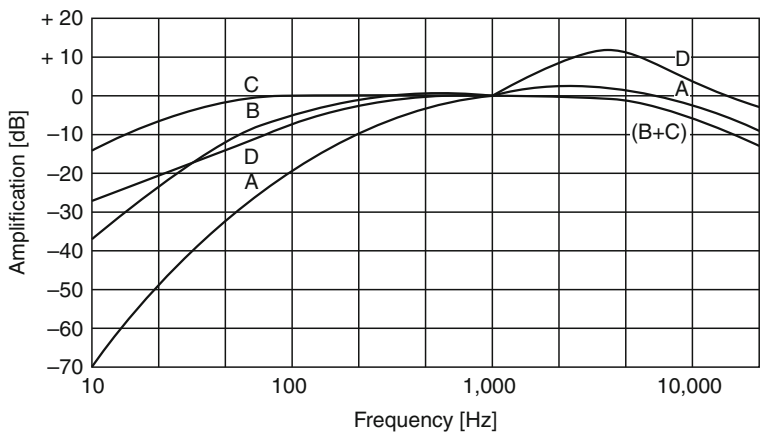

Wind Turbine Noise Emissions. Figure 6
A-, B-, C-, and D-weighting curves. A-weighting is the most common. For low and high frequencies, the amplification is negative, implying that these frequencies are damped to compensate for the lower sensitivity of humans to low- and high-frequency sound

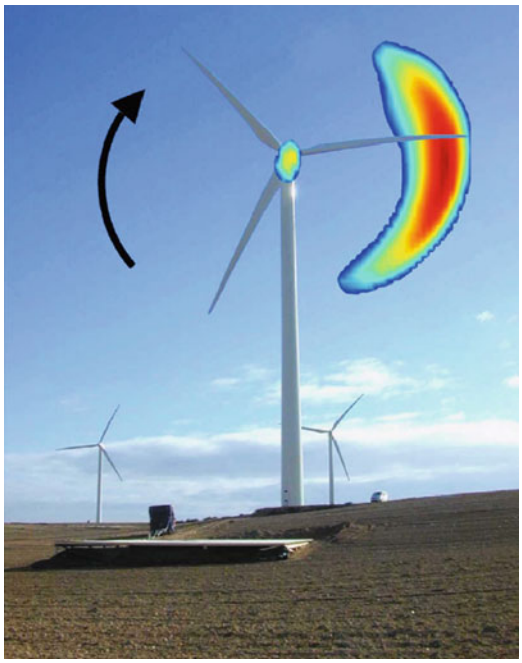

Wind Turbine Noise Emissions. Figure 7
Example of modern 2.3 MW wind turbine with rotor diameter 94 m and hub height 100 m [13, 14].
In front (upwind) of the turbine is an acoustic antenna which produced the source image plot shown in the picture. The more "hot" a region is the stronger the acoustic source in the rotor plane

aerodynamic noise [13–15]. However, since gearbox noise can produce tones which are more annoying than the aerodynamic broadband noise, mechanical defects in a machine can lead to temporary noise problems.

Aerodynamic or Aeroacoustic Noise

Sound production by a flow can be explained by Lighthills equation [16]

$$\left(\frac{1}{c^2}\frac{\partial^2}{\partial t^2} - \nabla^2\right)p = \frac{\partial^2 \rho_0 u_i u_j}{\partial x_i \partial x_j}, \tag{15}$$

where u represents a flow velocity component, ∇^2 is the Laplace-operator, x is a Cartesian coordinate axis, $i,j = 1,2,3$ and a summation over i,j is assumed. The left hand side of (15) represents the classical wave equation and the right hand side is the flow-driven source distribution creating the sound field. The source term represents an unsteady transport of momentum in the flow and is related to turbulence. When solid surfaces are present, the source term will be modified and can be amplified in particular at sharp edges [17]. Motion of the surface will also modify the resulting sound generation and cause Doppler (frequency) shift as well as change the directivity [16].

The aerodynamic noise can be split into three parts: low frequency, inflow-turbulence noise, and airfoil self-noise [13–15]. The low-frequency noise is related to interaction between the blades and tower wakes or large vortex structures from nearby rotors. The problem with tower wakes is uncommon nowadays when most rotors are operated upstream of the tower. The effect or vortex structures from nearby rotors can be a problem in wind turbine parks with too closely spaced machines. The inflow-turbulence noise is, for low frequencies, related to the modulation of the lifting force of the blade by the incoming turbulence which changes the flow speed and angle of attack. For higher frequencies, it can be seen as an interaction between the turbulence and the leading edge. The incoming turbulence will depend on the meteorological conditions as well as the surrounding terrain, i.e., one can expect quite different conditions for a turbine in open terrain as compared to one placed in a forest area.

The self-noise is the minimum sound a rotor will produce when placed in an ideal undisturbed inflow with minimum turbulence. The most important self-noise mechanism for large rotors is turbulent boundary layer trailing edge noise (TBL). Other possible sources are trailing edge bluntness noise and blade tip noise. But both these mechanisms are normally small for modern well-designed turbines and can be disregarded.

In conclusion, the turbulence-inflow and the TBL noise are the dominating aerodynamic sources. A typical example of the spectra produced by these mechanisms is shown in Fig. 8. The turbulence-inflow noise tends to be dominating at low frequencies less than 100–200 Hz for large wind turbines. The TBL noise has a distinct peak and dominates the midfrequency range which is important for the overall A-weighted sound pressure. The total (A-weighted) sound level is therefore normally dominated by TBL contribution but one cannot say that the turbulence-inflow part can be completely neglected [15]. An interesting note in this context is that for long range

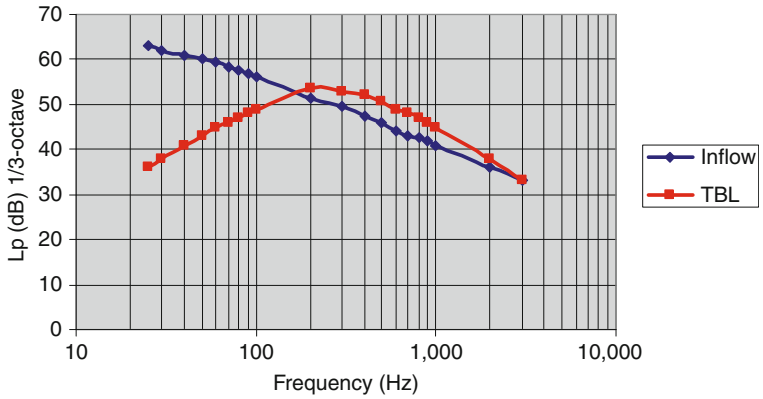

Wind Turbine Noise Emissions. Figure 8
Example of computed inflow-turbulence and TBL noise spectra for a wind turbine with 61 m hub height and a rotor diameter of 91 m. The wind speed is 10.3 m/s at the hub and the rotor RPM 17.5. The model used is based on Lowson [18] where more details can be found

propagation (>5 km), the atmospheric damping will remove the mid- and frequency spectrum, which could make the inflow-noise contribution the dominating source.

Efforts to design silent blades and in particular to reduce the TBL noise have been made, for instance, in the EU-project DATA [19]. The result obtained by noise-optimized blade designs was an overall reduction of 4 dB. In addition, the idea [20] to modify a (straight) trailing edge, e.g., into use a saw tooth shape, to reduce the interaction between the turbulence and the edge was tested and gave an additional 2–3 dB reduction [19].

Source Directivity and Modulation Figure 7 shows a measured source distribution for a large wind turbine. It is clear from this picture that almost all sound radiated (to the ground) is emitted during the downward motion of the blades. The explanation for this unsymmetrical source distribution is associated with the directivity of the TBL noise and the effect of motion on this directivity [13, 14]. This directivity will cause a pulsating sound described by an amplitude modulation of the TBL noise with the blade passing frequency and is responsible for the characteristic "swish" sound close to wind turbines, see Fig. 9. As seen in the figure, the modulation amplitude just in front and behind a large wind turbine is around 2 dB(A). Positions in the rotor plane generate much larger modulations or close to 6 dB(A).

For a group of wind turbines which are running independently, modulation effects will tend to average out at larger distances. Also the fact the transmission through the atmosphere is affected by stochastic and time-varying conditions will tend to reduce the modulation.

Concerning the directivity in the ground plane, there is significant variation as shown in Fig. 10. As seen from the figure, there is an 8 dB(A) drop in level between the position right in front of the turbine and in the rotor plane.

Sound Propagation

The perceived wind turbine noise is not only depending on the source but the transmission also plays an essential role. From a brief examination of the propagation problem, one might believe that sound is spherically dispersed and that the ground either absorb or reflect the sound rays. However, the nature of sound propagation is much more complex than this. Sound is a wave motion and consequently refracts when moving through regions with changing wave speed just like light when moving through a prism. Furthermore, ground reflections are altered both by the irregularities in the terrain as well as different amounts of reflection. Therefore, the sound propagation from wind turbines is varying with place and time. A turbine that is easily heard downwind of the plant in stable atmospheric conditions could be

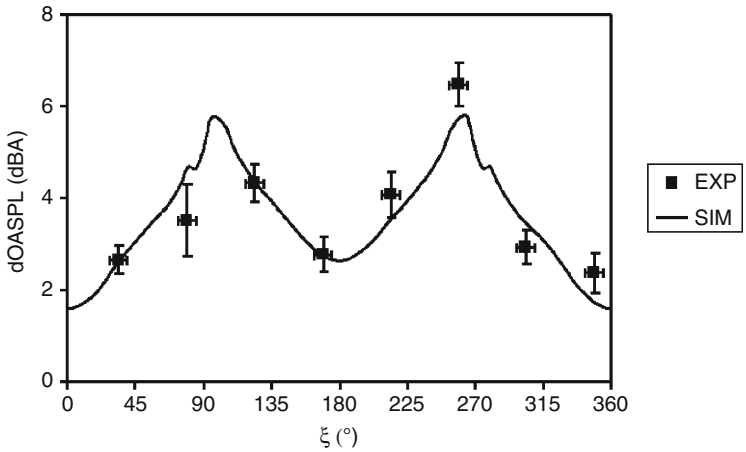

Wind Turbine Noise Emissions. Figure 9
Far-field modulation amplitudes for TBL noise for the wind turbine in Fig. 7. The position 0° corresponds to right behind (downwind) and 180° right in front of the wind turbine (upwind). (From Ref. [14])

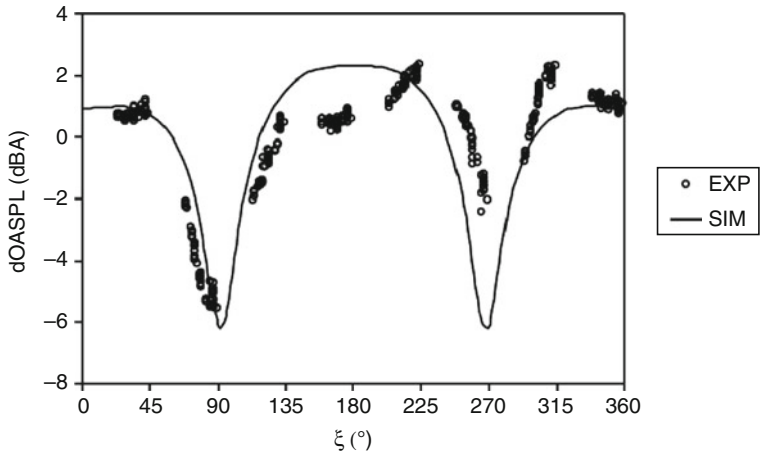

Wind Turbine Noise Emissions. Figure 10
Directivity in the far field for the wind turbine in Fig. 7. The position 0° corresponds to right behind (downwind) and 180° right in front of the wind turbine (upwind). (From Ref. [14])

impossible to perceive when the wind shift direction and the atmosphere changes to an unstable state.

Attenuation and Geometrical Spreading

The intensity of the sound decrease as it propagates. This reduction is caused by geometrical spreading, see Sect. "Spherical and Cylindrical Sound Waves," and by attenuation of the sound pressure.

Attenuation of sound is due to thermal and viscous effects as well as molecular relaxation when the sound wave propagates. The amount of attenuation is dependent on sound frequency, air temperature, atmospheric pressure, and humidity. The attenuation increases with frequency, atmospheric pressure, and humidity but decreases with temperature. A standardized calculation procedure, ISO 9613 [21], exists for frequencies from 20 Hz to 20 kHz.

Sounds are also geometrically dispersed as described in Sect. "Spherical and Cylindrical Sound Waves." Close to the source, in the near field, this spreading is spherical and is proportional to r^2. However, at longer distances, this rule of thumb could not be used as sound rays reflect at the ground and refract when traveling through air with different acoustic sound speeds. Examples of refracting sound waves can be seen in Figs. 11 and 12. As can be seen in the former figure, the sound is refracted downward and a channel of high sound intensity is observed below 200 m altitude. If instead the sound is refracted upward, as shown in Fig. 12, a sound shadow is observed on the ground after 2 km range. To further complicate the matter, wind turbulence scatters sound which causes the pronounced shadow zone in Fig. 12 to be diminished when taking the fluctuations of wind into account as can be seen in Fig. 13.

Ground reflections are also an important factor to take into account for sound propagation. In some conditions, the ground is absorbing sound, for example, when covered by snow or with leaves. On the other hand, at water surfaces or concrete ground, the sound is almost totally reflected. Measurements and models of

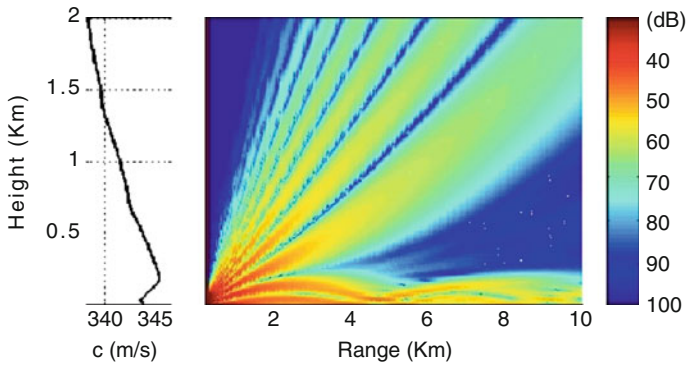

Wind Turbine Noise Emissions. Figure 11
Sound speed profile (*left*) and sound field (*right*). Computed sound transmission in a downward refracting atmosphere (increasing wind speed up to 200 m altitude) is shown. (Reprint from Bolin et al. [5])

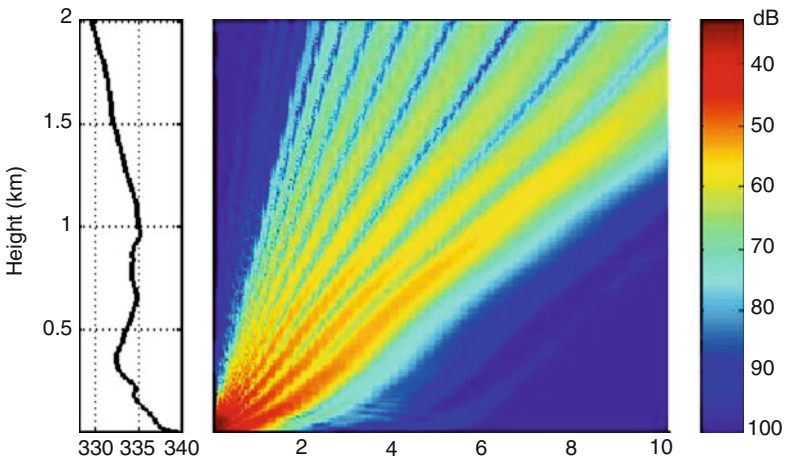

Wind Turbine Noise Emissions. Figure 12
Sound speed profile (*left*) and sound field (*right*). Computed sound transmission in a laminar upward refracting atmosphere (decreasing wind speed) is shown. (Reprint from Bolin et al. [5])

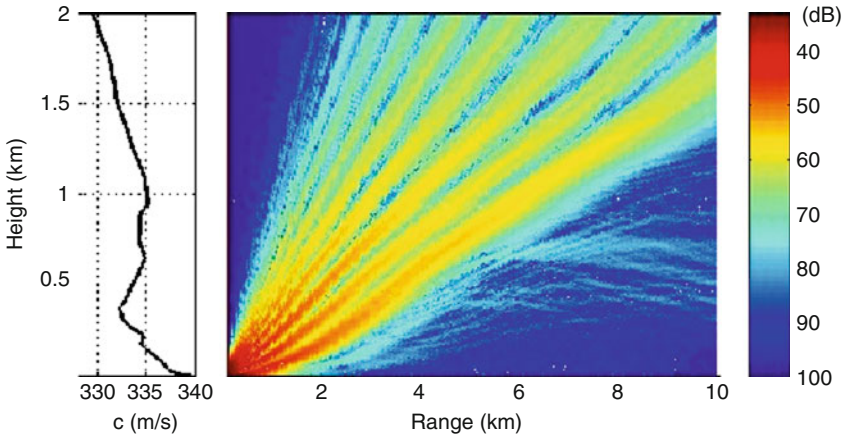

Wind Turbine Noise Emissions. Figure 13
Sound speed profile (*left*) and sound field (*right*). Computed sound transmission in a turbulent upward refracting atmosphere (decreasing wind speed) is shown. (Reprint from Bolin et al. [5])

ground reflections from sound have been conducted by Delany and Bazley [22] and Attenborough [23] among others. Often, the terrain is irregular. In such conditions, the sound rays are not reflected with the same incidence angle as reflected angle in the horizontal plane as seen in Fig. 14. Periodical perturbations of the ground, for example sea waves, can under certain conditions be modeled according to Boss theory [24]. Furthermore, complex terrain such as hills and forests influences the atmospheric conditions [25] and consequently the sound propagation. For propagation through vegetation, an extra attenuation of the sound should be added as described in ISO9613 [21].

Sound can be seen as a longitudinal wave spreading from the source. The basic equation for the propagation of sound is consequently the wave equation without a source term (RHS of (16) equals zero) seen below

$$\nabla^2 p - \frac{1}{c^2}\frac{\partial^2 p}{\partial \tau^2} = 0 \tag{16}$$

The sound wave can be considered harmonic if the time dependence of the sound pressure can be described by

$$p(r,t) = \mathrm{Re}\left(p_c e^{-i\omega t}\right) \tag{17}$$

where p_c is the amplitude, ωt is the phase where ω is the angular frequency (f = $2\pi\omega$). Thus, the wave equation (16) can be rewritten into the Helmholtz equation

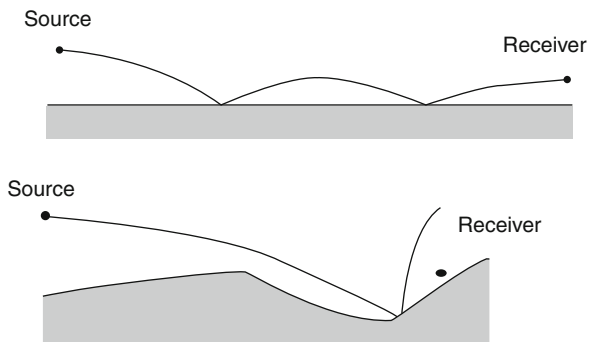

Wind Turbine Noise Emissions. Figure 14
Top: Sound ray in a downward refracting atmosphere reaching the receiver in two reflections. *Bottom*: Sound ray in irregular terrain not reaching the receiver

$$\nabla^2 p_c - k^2 p_c = 0 \tag{18}$$

where $k = \omega/c$ is the wave number. The field of computing sound propagation consequently largely deals with techniques to solve this equation.

Computational Atmospheric Acoustics

The field of computational atmospheric acoustics has many similarities to the fields of underwater acoustics as well as seismology. Although boundary conditions and input parameters differ depending on the field of

research, the governing equations are essentially the same. Therefore, numerical algorithms developed in one area are often also useful at other applications.

Methods of calculating atmospheric sound propagation can be divided into several subgroups. Here these different techniques are only covered briefly by comments on some of their advantages and disadvantages respectively. For an excellent overview of the field of atmospheric sound propagation, the interested reader is referred to Salomons [26]. Several different approaches exist to estimate sound propagation. Some of these methods are based on the Helmholtz equation (18), and is either direct solutions to this or using variable substitutions to solve the problem. On the other hand, other methods are based on ray tracing algorithms and Snell's law.

- *ISO9613* [21] is an engineering method to estimate sound propagation outdoors under "favorable" sound transmission conditions. These situations are characterized by downwind and moderately downward refracting atmospheric states. Furthermore, the method is stated to be used for ground-based noise sources. However, wind turbines nowadays emit sound at much higher altitudes than the method was intended to cover. Although the algorithm can be considered coarse and somewhat inappropriate to be used for wind turbine applications, it is widely implemented in noise mapping, probably because of the simplicity and computational speed of the estimations or maybe because of the credibility due to being an ISO-standard.
- *Ray tracing* methods, also known as geometrical acoustics, are based on viewing the sound as refracting beams propagating from the source to the receiver. An example of a downward refracting sound speed profile can be seen in the upper subfigure of Fig. 15. The sound is in this case

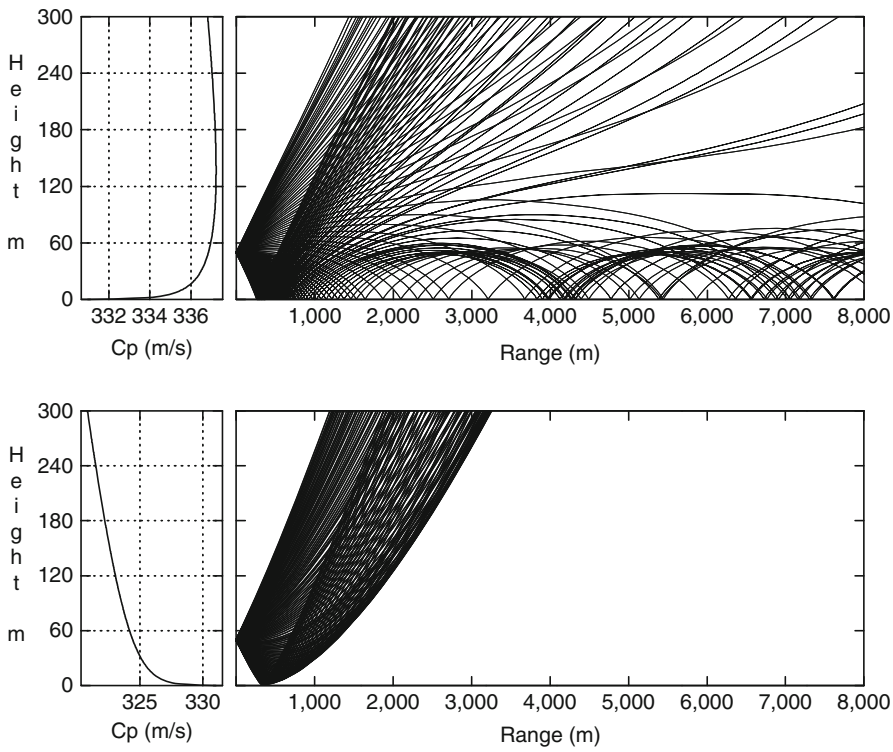

Wind Turbine Noise Emissions. Figure 15
Upper: Sound speed profiles for increasing (*upper figure*) with height and decreasing (*lower figure*) with height. *Lower*: Pictures of the sound rays propagating from a source to 8 km distance

bent downward and the intensity is higher than for spherical spreading. This simulation can be compared to upward refracting conditions shown in the lower subfigure of Fig. 15. As can be seen, the sound energy is bent upward and an acoustic shadow zone occurs at the ground after 0.5 km. Apart from illustrative examples of ray tracing calculations, Fig. 15 also shows the two most important shortcomings of ray tracing methods. In the upper figure, points where sound rays converge can be observed. At these positions, ray tracing algorithms predict infinitive sound pressures which is incorrect. In the lower figure, a shadow zone, a region without rays, is seen after 0.5 km at ground level. This prognosis is also erroneous and gives the false impression that no sound reaches this area while in fact sound propagates into this region. Methods, for instance, caustic diffraction fields [27, 28], deal with these two incorrect states but the ray tracing is still considered unsuitable for accurate sound propagation calculations at complicated sound speed profiles [26].

- *Fast field programs* were originally developed for underwater acoustic applications. This method is the numerical solution of the inhomogeneous Helmholtz equation for a monopole sound source

$$k^2 \frac{\partial}{\partial z}\left(k^{-2}\frac{\partial P}{\partial z}\right) + k^2 P = -4\pi\delta(z - z_s) \qquad (19)$$

Where k is the wave number, P is the Fourier transform of p in the horizontal wave number domain, δ is the Dirac delta function, z_s is the source height. This algorithm can be used in both two and three dimensions but requires assumptions of constant ground conditions and wave numbers in (19) within each layer. As the reality often deviates strongly from the assumptions mentioned above, especially for long propagation distances, Fast field programs are suitable to deal with the sound propagation at short ranges. Analytical solutions of (19) are possible for very simple sound speed profiles and are referred to as normal mode solutions.

- *Parabolic equation solutions* are another family of useful computational methods for estimating sound propagation. If the Helmholtz equation (18) is assumed axisymmetric, it is reduced from three to two dimensions. It can be shown [26] that by using the variable substitution $p = c^{-1/2}\psi^* exp\,(ikr)$, the two-dimensional Helmholtz equation may be rewritten as

$$\frac{\partial^2\psi}{\partial r^2} + 2ik(z)\frac{\partial\psi}{\partial r} + \frac{\partial^2\psi}{\partial z^2} + (k(z) - k_0(z))\psi = 0 \qquad (20)$$

neglecting $\partial^2\psi/\partial r^2$ is possible if ψ varies slowly with range which is the case for narrow propagation angles which gives

$$2ik(z)\frac{\partial\psi}{\partial r} + \frac{\partial^2\psi}{\partial z^2} + (k(z) - k_0(z))\psi = 0 \qquad (21)$$

which has the shape of a parabolic equation. Several different numerical methods to solve this equation exist, for instance, Crank-Nicholson and Green's function solutions. These methods can use an arbitrary varying sound speed profile and changing ground conditions but are unsuitable for computations of the near field as the pressure field is not slowly varying in that region. However, at long ranges, such methods combined with local meteorological measurement have been shown to give accurate predictions of sound transmission at offshore wind turbines [5].

Concerning sound propagation calculations of wind turbine noise, these usually use the ISO 9613 [21] standard, and the acoustic source power for the turbine is acquired from the manufacturer at certain wind speeds according to the different national standards. This yields estimations of sound levels at reception points indifferent to ground irregularities and meteorological conditions. The current trend in assessing the sound propagation issue is to use more advanced prediction methods than ISO9613. One example is the Nord2000 software based on ray tracing algorithms which take into account different meteorological classes, and therefore, weather-dependent estimations of the sound levels at reception points can be calculated. This can be considered a natural development as databases with meteorological and ground conditions exist in many countries. Using these databases in softwares such as NORD2000, computing sound propagation gives improved quality of the noise mapping at wind turbine sites.

Human Impact

Sound from wind turbine is per definition not noise until someone hears it and is annoyed by it. Then the reactions differ from person to person. In today's society, noise pollution is a serious issue affecting a large part of the population. Noise can, apart from causing annoyance, also lead to other adverse effects such as sleep disturbance, tinnitus, and hearing loss [29]. Weak evidence also points toward an increased risk for myocardial infarction when exposed to traffic noise [30]. The noise levels for wind turbines are far too low to evoke tinnitus and hearing loss. Sleep disturbance caused by wind turbines has been investigated by Pedersen & Persson-Waye [6] where 16% of respondents reported interrupted sleep at exposure levels above 35 dBA.

Noise and the Auditory System

In the field of acoustics, noise is defined as unwanted sound. The perception of sound sources consequently determines if they are perceived as wanted or unwanted. It has been shown that persons with economic incentive in nearby wind farms are less annoyed by the sound than people not benefiting from the turbines [8]. The owner enjoys the gentle hum while his neighbor is distressed by the eternal swoosh and the interrupted scenery. Before the 1970s and the oil crisis, wind turbine farms were relatively small and thus noise seldom spread to neighbors. This might be one reason that noise annoyance was not a severe issue before the development of larger wind turbines in the 1980s when the adverse effects from noise were first observed by staff at NASA [1].

The auditory system in humans is a complicated and much investigated sensory organ. It starts at the ear lobe working as an antenna and then the sound propagates into the ear canal and reaches the eardrum. Here the pressure fluctuations are transmitted to the inner ear via the middle ear bones malleus, incus, and stapes, the smallest bones in the human body, to the inner ear and the cochlea where the organ of Corti transforms the movements in the fluid to nerve impulses. These are transmitted to the brain where they are processed and the sensation of hearing is produced. All this is indeed a remarkable system with an exceptional sensitivity, recognizing pressure fluctuations down to 20 μPa and still robust enough to withstand amplitudes up to 400 Pa. It is partly due to this enormous flexibility the logarithmic dB scale is used in acoustics.

Dose–Response Relationships

It has been shown that increased wind turbine noise levels cause increasing annoyance to nearby residents. This correlation has been established in three different epidemiological studies by Pedersen and coauthors [6–8] performed in the Netherlands and in Sweden. Two studies have been conducted in flat farmland areas mainly of rural character [6, 8]. In the third paper [7] noise annoyance in both rural and suburban areas as well as hilly terrain was investigated. Apart from the statistically significant dose–response relationship, the studies also suggested that intrusive sound characteristics or visual impact influences the perceived annoyance [6]. It was also confirmed from an earlier study by Wolsink [31] that a negative opinion of the impact of wind turbines on the landscape has strong correlation to annoyance [8]. It should however be emphasized that it is not clear when negative opinions precede the annoyance or vice versa. Anyway, the results from the research performed by Pedersen and coauthors give extremely valuable insight when noise from wind turbines annoys nearby residents and should definitely be considered when developing wind turbine sites.

Comparisons between dose–response relationships of different community noise sources are seen in Fig. 16. As can be observed, wind turbine noise is considered more annoying than traffic noise at the same doses (dBA). This has many times been seen as a proof that wind turbine noise is much more annoying than most conventional noise sources. However, a problematic issue with these comparisons is the differing dose calculation between the sources. For most environmental noises, e.g., road traffic noise and aircraft noise, the noise dose for the affected people is estimated by traffic intensity and distance to source. However, for wind turbine noise, this is not the case. Rather than using the actual noise dose, the sound level at a specific wind speed (8 m/s at 10 m height) is used, thereby not knowing the actual noise dose of the subjects. This could give large differences in actual noise

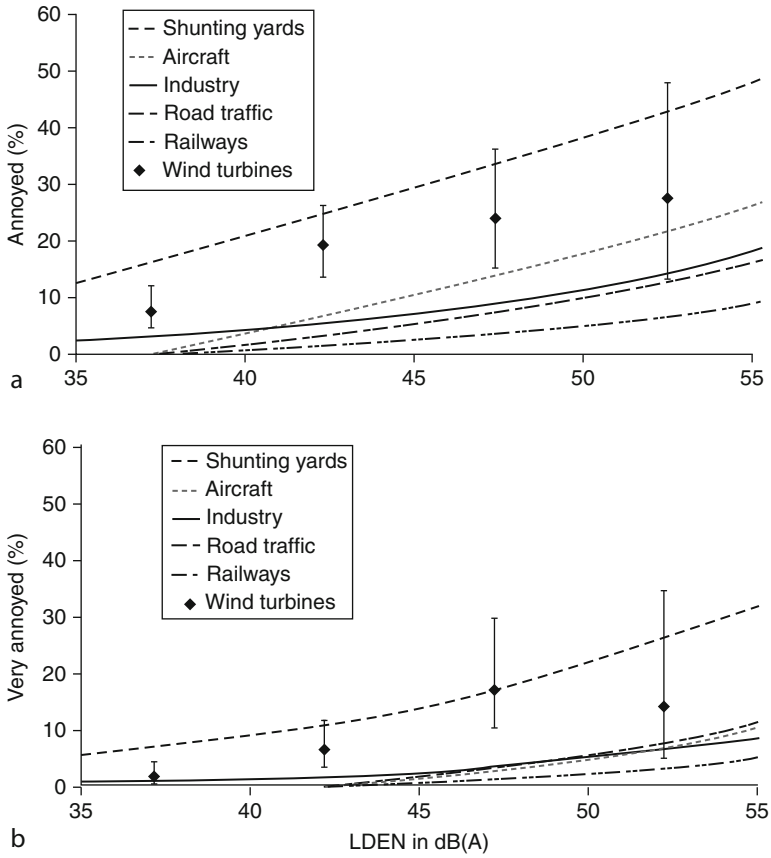

Wind Turbine Noise Emissions. Figure 16

Comparison between dose–response relationship for other noise sources and wind turbine noise. Proportion of annoyed shown in (**a**) and highly annoyed in (**b**). (Reprint from [8])

exposure, for instance, old stalled regulated turbines increase their noise emission significantly from wind speeds at 8 m/s to maximum noise levels at cutoff wind speed as discussed in section "Determination of Wind Turbine Source Data." Consequently, at a site with high wind speeds, the dose for persons living close to such a turbine could be much higher than for others living at sites with lower wind speeds although both have the same nominal noise exposure at wind speed of 8 m/s at 10 m height.

Masking

When two sounds are heard simultaneously, the perception is altered as when heard alone. Therefore, the loudness of a sound is not only dependent on its sound level but also on the context in which it is presented. This auditory phenomenon is called masking and will influence the perceived loudness of wind turbine noise.

For example, a turbine close to a busy highway will be less audible than the same turbine in a tranquil farmland.

Modern turbines usually have noise with broadband character without tonal components. As a result, ideal maskers are sources of similar character as spectral overlap between the sounds increases the masking effect. A laboratory study concerning if natural sounds could mask wind turbine noise has shown that inaudibility of wind turbine noise requires

10 dB higher background sounds than turbine noise [32]. Results from the same paper show that when the wind turbine and background have the same sound levels, the turbine is perceived as 5 dB quieter than if heard alone. In an epidemiological study, road traffic noise had to exceed the sound level of the turbines by 20 dB in order to show a statistically significant masking effect [8]. The British wind turbine noise guidelines [33] considers masking when setting emission levels by allowing a 5 dB higher equivalent sound level compared to the background noise exceeded 90% of the time. However, several factors influence the turbine noise and background sound. For example, traffic noise decreases in off-peak hours which often correspond to times when the turbine noise is loud. The increasing turbine heights give dramatic differences between the wind speed at hub height and at the ground [4]. This is especially pronounced in stable atmospheric conditions when the wind gradient increases. Thus, temporal variations, both of the wind turbine noise and the background sound, have to be considered if masking is to be evaluated correctly. For instance, wind-induced background sounds have to take fluctuations due to turbulence and different wind speed profiles into account [34]. Thus, although masking is probably commonly occurring, it remains to be evaluated in field conditions to what degree this has an effect in practice.

Low-Frequency Noise

When discussing low frequencies, acousticians define this as the lower range of the audible scale, often between 20 and 100 or 200 Hz. The growing size of wind turbines has generated fears that the low-frequency part has increased. Investigations of the impact at these frequencies suggest that the low-frequency levels have not increased significantly at newer turbines and it does not appear to be a source of concern [35, 36].

Guidelines

Different evaluation methods to regulate wind turbine noise are present all over the world. To give a full description of each of these is naturally impossible within this book and therefore the principles governing these guidelines and some examples are treated in this section. The guidelines have been divided into three categories: the first based on absolute sound level limits, the second sort founded on relative sound level compared to background sounds, and the third kind with limits as a function of wind speed.

Sound level limits are the main method to base guidelines upon. This is the most obvious choice of limit and is practical and straightforward to comply with. Often these rules constrain the sound levels outside nearby residential buildings at specific meteorological conditions. For instance, the Danish guidelines are set to 45 dBA in residential areas at a wind speed of 8 m/s at 10 m height.

Limit values are often calculated in equivalent levels over a duration time T, denoted $L_{eq,T}$, which is an average of the sound pressure (normally A-weighted) expressed in dB. T is normally set to between 5 min and 1 h for wind turbine noise. It is often usual to have specific night time limits lower than day time values (see, for example, the German and State of Washington guidelines).

This sort of rule is simple and the relation between emission levels and noise annoyance has been established in epidemiological studies [6–8]. However, criticism of this kind of guidelines claims that the sensation of hearing is not only based on the level of the noise source but should be viewed in a wider context in order to get a more complete picture of the noise problem. Moreover, as discussed in section "Dose–Response Relationships," the noise dose at wind speeds of 8 m/s at 10 m height could deviate considerably from actual noise exposure.

Limits relative to background sound levels use the fact that masking of wind turbine noise by other sound sources influences the loudness. Background noise is usually wind generated, for instance, vegetation sounds [32]. Therefore, the allowed turbine noise depends on wind speed as in the British and French standards. Measurements of background sounds have to be performed at neighboring properties to apply this method. This kind of procedure can thus be time consuming as statistically reliable data should be gathered for different wind conditions and seasons.

Furthermore, a noise-polluted area, say from road traffic, will obtain more noise and this could be considered unfair. One way of circumventing both these objections is to use models for wind-generated noise, which exist for vegetation and sea wave sounds [34, 37]. However, the accuracy of these models is not yet verified by long measurement campaigns, and therefore, predictions can presently be seen as a complement to measurements rather than an independent base of information.

Levels as a function of wind speed can be considered equivalent to assuming uniform background levels at all locations. This is an intermediate between the two earlier described methods as sound level limits are set and masking assumed by increasing allowed limits with wind speed. From many points of view, this solution offers several positive aspects as masking is taken into account in a simple way. However, different locations have varying background sound and this is not taken into account. In this context, it is not surprising that the Netherlands has guidelines according to this principle as the country has a reasonably uniform terrain and therefore suitable to the required generalization.

Conclusions

Wind turbine noise has to be considered in the planning process when building wind farms. Sound is mainly described in the unit decibel (dB) which is a logarithmic function of the sound pressure. Noise is mainly generated by unsteady aerodynamic flows at the blades trailing edge, as improvements have reduced the mechanical noise sources and consequently tonal sounds are no longer a problem in current wind turbines (as of year 2011) when properly working. Today pitch-regulated wind turbines can also be run in silent modes where less noise generation is preferred rather than optimal power output. Sound transmission from source to receiver is dependent on the amount of ground reflections and also by the meteorological conditions. Acoustically hard ground, such as water, and atmospheric conditions of downward refracting sound increase the proportion of sound transmitted to receivers. Models dealing with sound propagation vary from relatively simple algorithms mainly valid at shorter distances to more complicated methods at longer distances and complex terrain. The wind turbine noise effects on humans are mainly sleep disturbance and nuisance. Correlation between visibility and lack of economic incentive and annoyance has been reported from epidemiological studies. Different noise emission guidelines exist. Some of these specify a limit at certain wind speeds while others have limits depending on the background sound level. However, the context governs which approach and specific limits that are appropriate. To preserve the scenic beauty of landscapes and not add unnecessary noise to pristine environments, concern of the environmental impact in general and noise in particular is strongly advised when planning new wind farms. Noise emissions from wind turbines will persist, and with a large expansion of the number as well as size, the problem could increase drastically if proper measures are not taken in the planning stage. Therefore, noise should be considered at an early phase in the development process and an open dialogue between wind contractors and the public is strongly advised.

Future Directions

The rapid development of wind turbines will probably continue in the forthcoming years. The average size of wind turbines has increased tremendously over the last decades. If and when this growth will be halted is difficult to foresee. As not only the size but also the number of wind turbines is increasing, large populations, mainly in rural areas, will be affected by wind turbine noise. The potential for reducing the dominating aerodynamic noise by optimized blades is in the range 4–6 dB, which is not sufficient to solve the problem. Improvements of the noise mapping by advanced noise propagation algorithms are therefore important to minimize the noise emission in critical areas and to warn when noise annoyance issues are likely to arise. Furthermore, sleep disturbance tests would also be an interesting research subject as higher emission levels often occur at nighttime. Field studies regarding masking that would validate results from laboratory studies would also give interesting results. As a conclusion, the need for further studies regarding the noise problem is important as noise is the most common source of concern for residents near wind turbines.

Bibliography

1. Stephens DG, Shepherd KP, Hubbard HH, Grosveld FW (1982) Guide to the evaluation of human exposure to noise from large wind turbines. NASA TM 83288, Langley Research Center, Hampton, Virginia, USA
2. Sutherland LC, Mantey R, Brown R (1987) Environmental and cumulative impact of noise from major wind turbine generator developments in Alameda and Riverside Counties- Literature review and measurement procedure development, Wyle Research Report WR87-8
3. Guidati G, Ostertag J, Wagner S (2000) Prediction and reduction of wind turbine noise: an overview of research activities in Europe, AIAA paper 2000-0042
4. van den Berg GP (2004) Effects of the wind profile at night on wind turbine sound. J Sound Vib 277:955–970
5. Bolin K, Boué M, Karasalo I (2009) Long range sound propagation over a sea surface. J Acoust Soc Am 126: 2191–2197
6. Pedersen E, Persson-Waye K (2004) Perception and annoyance due to wind turbine noise. A dose-response relationship. J Acoust Soc Am 116:3460–3470
7. Pedersen E, Persson-Waye K (2007) Wind turbine noise, annoyance and self-reported health and well-being in different living environments. Occup Environ Med 64(7): 480–486
8. Pedersen E, van den Berg GP, Bakker R, Bouma J (2009) Response to noise from modern wind farms in the Netherlands. J Acoust Soc Am 126:634–643
9. Åbom M, Boue M (2007) Long range sound propagation over the sea with application to wind turbine sound
10. Zwicker E, Fastl H (2001) Psychoacoustics: facts and models. Springer, Berlin
11. International Electrotechnical Commission (2001) IEC 61400-11 standard: wind turbine generator systems C part 11: acoustic noise measurement techniques
12. Ljunggren S (2001) Ljud från vindkraftverk (sound from wind turbines). Technical report 6241, Boverket, Energimyndigheten & Naturvårdsverket, Sweden (in Swedish)
13. Oerlemans S, Sijtsma P, López BM (2007) Location and quantification of noise sources on a wind turbine. J Sound Vib 299:869–883
14. Oerlemans S, Schepers JG (2009) Prediction of wind turbine noise and validation against experiment. Report National Aerospace Laboratory NLR-TP-2009-402
15. Guidati G, Ostertag J, Wagner S (2000) Prediction and reduction of wind turbine noise: an overview of research activities in Europe. American Institute of Aeronautics and Astronautics Paper 200-0042
16. Howe M (2008) Acoustics of fluid-structure interactions. Cambridge University Press, Cambridge
17. Williams JEF, Hall LH (1970) Aerodynamic sound generation by turbulent flow in the vicinity of a scattering half plane. J Fluid Machanics 40:657–670
18. Lowson MV (1994) Design prediction model for wind turbine noise. Flow Solutions Report 94/06, ETSU W/13/00317/REP
19. Oerlemans S, Schepers JG, Guidati G, Wagner S (2001) Experimental demonstration of wind turbine noise reduction through optimized airfoil shape and trailing-edge serrations. Report National Aerospace Laboratory NLR-TP-2001-324
20. Hove MS (1991) Noise produced by a sawtooth trailing edge. J Acoust Soc Am 90:482–487
21. ISO9613 (1995) Attenuation of sound during propagation outdoors. International Organization for Standardization, Geneva, Switzerland
22. Delany ME, Bazley EN (1970) Acoustical properties of fibrous absorbent materials. Appl Acoust 3:105–116
23. Attenborough K (1985) Acoustical impedance models for outdoor sound surfaces. J Sound Vib 99:521–544
24. Boulanger P, Attenborough K, Taherzadeh S, Waters-Fuller T, Li KM (1998) Ground effect over hard rough surfaces. J Acoust Soc Am 104:1474–1482
25. Kaimal JC, Finnigan JJ (1994) Atmospheric boundary layer flows. Oxford University Press, New York
26. Salomons E (2002) Computational atmospheric acoustics. Kluwer, Dordrecht
27. Ludwig D (1966) Uniform asymptotic expansion at a caustic. Common Pure Appl Math 19:215–250
28. Kratsov YA (1968) Two new wave asymptotic methods in the theory of wave propagation in inhomogeneous media. Sov Phys Acoust 14:1–17
29. Berglund B, Lindvall T, Schwela DH (2000) Guidelines for community noise. World Health Organisation, Geneva
30. Selander J, Nilsson ME, Bluhm G, Rosenlund M, Lindqvist M, Nise G, Pershagen G (2009) Long-term exposure to road traffic noise and myocardial infarction. Epidemiology 20: 272–279
31. Wolsink M, Sprengers M (1993) Wind turbine noise: a new environmental threat? vol 2. ICBEN, Nice, France, pp 235–238
32. Bolin K, Nilsson ME, Khan S (2010) The potential of natural sounds to mask wind turbine noise. Acta Acustica united Acustica 96:131–137
33. Meir R et al. (1996) The assessment and rating of noise from wind farms. Technical report ETSU-R-97, Department of Trade and Industry, Harwell, UK
34. Bolin K (2009) Prediction method for wind-induced vegetation noise. Acta Acustica united Acustica 75:607–619
35. Pedersen T, Madsen KD (2010) Low frequency noise from large wind turbines, summary and conclusions on measurements and methods, Technical report Delta acoustics, AV1272/10
36. O'Neal R, Hellweg RD, Lampeter RM (2011) Low frequency noise and infrasound from wind turbines. Noise Control Eng J 59(2):135–157
37. Bolin K, Åbom M (2010) Air-borne sound generated by sea waves. J Acoust Soc Am 127:2771–2779

X

Xenobiotic Protection/Resistance Mechanisms in Organisms

Christopher J. Kennedy[1], Keith B. Tierney[2]
[1]Department of Biological Sciences, Simon Fraser University, Burnaby, BC, Canada
[2]Department of Bi'ological Sciences, University of Alberta, Edmonton, AB, Canada

Article Outline

Glossary
Definition of the Subject
Introduction
Mechanisms of Resistance
Conclusions and Future Directions
Bibliography

Glossary

Absorption In living organisms, the process by which environmental molecules move across biological membranes.

Adaptation The intergenerational genetically based selection of individuals for specific traits at the population level.

Avoidance The act of keeping away from or withdrawing from an undesirable environmental chemical.

Biotransformation The enzymatic conversion of a foreign or endogenous chemical to another form (metabolite) in living organisms.

Contaminant Any substance that enters a system where it is not normally found.

Defense A strategy or mechanism by which an organism protects itself or maintains its function in the face of a xenobiotic challenge.

Hydrophilicity Hydrophilicity refers to a physical property of a molecule that can transiently bond with water (H_2O) (dissolve in it) through hydrogen bonding.

Hydrophobicity Hydrophobicity (Gr. *Water fearing*) is the physical property of a molecule that is repelled from a mass of water.

K_{ow} Octanol water partition coefficient, which generally describes the degree of hydrophobicity of a chemical. High Log K_{ow} values >4 are typical of hydrophobic chemicals.

Lipophilicity Lipophilicity (Gr. *fat-liking*) refers to the ability of a chemical compound to dissolve in fats, oils, lipids, and nonpolar solvents.

Phase I reactions Also called asynthetic or functionalization reactions and include oxidation, reduction, and hydrolysis reactions. In these reactions, a hydrophobic xenobiotic is usually converted to more water soluble metabolite.

Phase II reactions Also called synthetic or conjugation reactions in which a xenobiotic is covalently bound to an endogenous molecule forming a water soluble metabolite.

Phase III transport The products of Phase I or II biotransformation reactions and some parent xenobiotics are transported out of cells by various protein transport families collectively termed Phase III transport. In some cases, these transporters prevent the cellular entry of xenobiotics.

Pollutant A contaminant that adversely alters properties of the environment.

Resistance The capacity of a population of organisms to withstand the effects of a harmful environmental agent through genetic selection of less susceptible individuals.

Tolerance Reduced sensitivity of an individual organism, tissue, or cell to a foreign chemical and its toxic effects through acclimatory processes.

Toxicodynamics The process of the interaction of chemical substances with target sites (molecules, cells, tissues, or organs) leading to adverse effects.

Robert A. Meyers (ed.), *Encyclopedia of Sustainability Science and Technology*, DOI 10.1007/978-1-4419-0851-3,
© Springer Science+Business Media, LLC 2012

Toxicokinetics Processes of the uptake of potentially toxic substances, their biotransformation, distribution, and elimination.

Xenobiotic Chemicals that are foreign to biological systems.

Definition of Subject

Organisms have always been exposed to chemicals that are foreign to them. Evolution has produced protective mechanisms against natural chemicals, mechanisms that are currently used against exposures to anthropogenically sourced chemical contaminants. Protection can occur at the individual level, often called tolerance, or at the population level, which is called resistance. The earliest studies on tolerance and resistance mechanisms come from the insect/pesticide literature; however recent environmental and health research is providing a wealth of information on these mechanisms in other organisms including humans. There are two major categories of protective mechanisms: (1) toxicokinetically derived mechanisms, which alter the way in which organisms absorb, biotransform, and excrete chemicals; and (2) toxicodynamically derived mechanisms, in which target sites are modified to reduce sensitivity. In both of these categories, protection can occur at the molecular and genetic level, through the cellular/tissue and organ levels, and up to and including whole organism responses including changes in behavior.

Introduction

Organisms have been exposed to foreign chemicals, or xenobiotics, through evolutionary history. The challenge of this chemical affront is to maintain appropriate concentrations of particular molecules to function, while excluding xenobiotics that will interact with cellular constituents. This is problematic, as organisms must remain open to a chemically dynamic environment for essential life processes. Chemical homeostasis employs cellular, physiological, and behavioral regulatory processes in response to the accumulation of xenobiotics that may cause departures from a state of dynamic equilibrium with the environment and reduce performance (e.g., reduced growth, reproduction) or cause death. The early evolution of systems capable of reducing overall xenobiotic accumulation and their susceptibility to them, point to the evolutionary significance of xenobiotic protection mechanisms and their survival advantages.

Organisms have always been exposed to xenobiotics of natural origin. For example, host-plant resistance strategies often employ defensive secondary metabolites, known as allelochemicals (e.g., alkaloids such as nicotine, caffeine, morphine, colchicines, strychnine, and phenolics such as the cannabinoids), to influence the behavior, growth, or survival of herbivores. Herbivorous insects and mammals have evolved common protective defenses against the ingestion of allelochemicals. For example, Australian marsupials are constantly exposed to a diverse array of toxic xenobiotics that come from a wide variety of plant sources, such as Eucalyptus terpenes [1]. Marsupials display several significant xenobiotic processing mechanisms at the biochemical level for enhanced terpene detoxification, which is critically important for surviving on their unique Eucalyptus diet.

Organisms have adapted (to various degrees) to xenobiotic exposure of natural origin by evolving chemical defense/protective/resistance mechanisms. The relatively recent phenomenon of industrial pollution and the release of novel synthetic compounds into the environment at high concentrations and relatively short durations has not allowed for much evolutionary adaptation (although some) to synthetics. Most organisms rely on constituent chemical defense mechanisms for protection against this new chemical arsenal. The dramatic and catastrophic effects of pollution on many species points to the inadequacy of such defenses; however, in some cases the protection afforded by such mechanisms works equally well for anthropogenic chemicals. For example, the Great Lakes and Puget Sound, WA, have accumulated tons of PCBs, PCDDs, and PCDFs; yet despite chronic exposures to such compounds at concentrations that elicit toxicity in mammals and birds, populations of fish can flourish at very polluted locations. Although species diversity at these contaminated sites is reduced, signs of overt toxicity, with the exception of carcinogenesis, are rare. It is believed that

populations chronically exposed to high or even moderate levels of these contaminants have evolved or developed resistance mechanisms to these compounds [2].

There are two main possible means by which organisms can reduce their sensitivity to xenobiotics; those that occur at the level of the individual through acclimatory processes (often termed tolerance) and those that occur on populations of organisms in which the genetic constitution of a population is changed in response to the chemical, so that a greater number of individuals are able to resist it compared to the unexposed population (often termed resistance). Acclimation occurs at the level of the individual, where organisms become more tolerant as a consequence of a prior exposure through genetic or epigenetic mechanisms. Tolerance brought about through acclimation is not transmitted across multiple generations, therefore it is believed to wane if exposure is removed, for example, in remediated environments.

Adaptation is the intergenerational genetically based selection of more resistant individuals at the population level that results in individuals contributing relatively more offspring to subsequent generations. In order for adaptation to occur, resistant phenotypes must be present in sensitive populations before exposure, albeit at low frequencies. After remediation, adaptations may also disappear from populations because the selective pressure has been removed, but this occurs slower than for the acclimation process. Examples of heavy metal tolerance in plants are common and demonstrate dramatic changes in susceptibilities over a few generations. The evolution of industrial melanism in moths is an example of resistance that is widely cited as an example of contamination as a selective pressure for evolution.

Insect resistance to pesticides has been a well-studied area in this regard due to its scientific, economic, ecological, and health significance; pesticide resistance is a significant cause of failures in agricultural and pest management programs. Resistance to insecticides was first documented in 1914 by A. L. Melander for scale insects to an inorganic insecticide. Between 1914 and 1946, 11 additional cases of resistance to inorganic insecticides were recorded. Since 1945, it has been estimated that between 500 and 1,000 species of pests have developed a resistance to a pesticide. It was believed that the development of organic insecticides such as DDT would prevent insecticide resistance; however, by 1947 DDT resistance was exhibited by houseflies. With the introduction of every new insecticide class – cyclodienes, carbamates, formamidines, organophosphates, pyrethroids, even *Bacillus thuringiensis* – cases of resistance surfaced within 2–20 years [3].

Xenobiotic resistance is also significant in the area of human health. It is a major cause of failure of human therapies and has implications in antibacterial, anticancer, antipaludic, and antihuman immunodeficiency virus-1 (HIV-1) therapies. The mechanisms behind this resistance are conserved among bacteria, eukaryotic cells, parasites, and viruses [4].

Mechanisms of Resistance

Organisms use a variety of mechanisms to avoid the effects of toxic substances. These strategies range from the molecular to the behavioral level. Several different mechanisms have been proposed whereby resistance to chemical contaminants can develop in animal populations. The literature cites several classification schemes; however, here they are organized according to:

1. Mechanisms of decreased exposure through toxicokinetically derived resistance. Specific mechanisms in this category include reduced uptake or increased elimination of toxicants, thereby decreasing body burdens. Increased metabolic transformations of xenobiotics to less toxic or persistent forms can contribute to resistant phenotypes. Also, the sequestration of contaminants within cellular organelles or binding to proteins are means by which toxicants are unable to exert their toxic effects despite their accumulation.
2. Mechanisms of decreased sensitivity through toxicodynamically derived resistance. Mechanisms here include: increases in target receptor insensitivity (target site resistance) through changes in receptor structure, up- or down-regulation of target receptors, or decreases in the responsiveness of signal transduction pathways. Circumvention is the

bypassing of an inhibited pathway through an alternate route; limited opportunities for this mechanism exist, however it can occur.

Toxicokinetically Derived Resistance Mechanisms

Reductions in Xenobiotic Uptake

Limits to Exposure: Avoidable Exposures Ideally, organisms act to limit their exposures to harmful substances by sensing the substance and moving into a cleaner environment (Fig. 1). For this to occur, four conditions are necessary: (1) the substance must exist in the environment in a gradient, (2) the organism must be able to perceive the substance's presence, (3) the organism must identify the substance as harmful, and (4) the organism must be able to move itself away from exposure. When met, these conditions provide a means of behavioral avoidance.

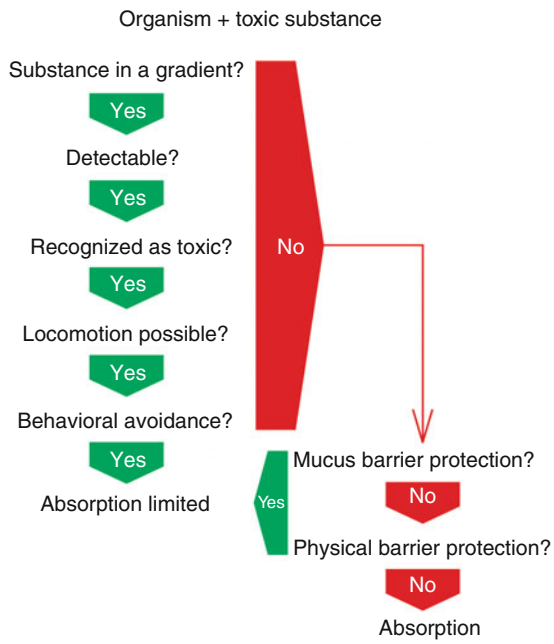

Xenobiotic Protection/Resistance Mechanisms in Organisms. Figure 1
There are many factors that determine whether an organism existing in a contaminated environment will end up absorbing any given contaminant. These factors include sensory and behavioral responses (e.g., the ability to detect a contaminant and move away from it), as well as the characteristics of the outermost structures (e.g., the permeability of keratin of skin and the chitin of arthropod cuticle)

Environmental gradients – In aerial and aquatic environments of the past and present world, the first condition (a substance varying in concentration over space) is satisfied over small to large scales for innumerable toxic substances of natural and human origin. In the past, substances that organisms sought to avoid included hydrocarbons, toxins from plants and algae, and some arising from volcanic activity. Today, there is an ever increasing array of synthetics including pesticides, flame retardants, surfactants, and pharmaceuticals. Many of these synthetics are based on substances of natural origin, for example, pyrethroid insecticides are structurally similar to compounds of the chrysanthemum flower, and ethinylestradiol used in birth control pills is a more potent form of estrogen. Overall, there are few organisms that do not experience gradients of substances of both natural and synthetic origin.

Perception of environmental gradients – To meet the second condition of behavioral avoidance, organisms possess exteroceptive sensory mechanisms to gather environmental chemical and/or conditional information. Such mechanisms utilize intensity receptors, regardless of species. Intensity receptors can be relatively simple and exist at the molecular level in single-celled organisms such as in *Euglena* spp. [5], or more complex, such as those relying on multisensory neuron integration. The majority of our knowledge comes from the second category, for organisms with few sensory neurons (e.g., ~32 in *Caenorhabditis elegans*) [6] to millions (e.g., humans have ~six million olfactory sensory neurons alone) [7]. These sensory neurons rely on a diverse array of G-protein coupled receptors (GPCRs) that transduce molecular signals from the outside of the organism to the inside. The array of receptors in any given organism can be enormous – mice, for example, have 1,000–1,200 distinct olfactory receptors [8]. All intensity receptors have evolved to detect "natural" substances, and not novel compounds of human origin. Nevertheless, given the fact that many synthetic toxic compounds are based on naturally produced compounds, it is not unreasonable to expect "historic" sensory machinery to be able to function to some degree in the current environment.

Perceiving a substance as harmful – There are two routes by which a substance may be identified as

harmful: through innately (genetically) recognizing it as so, or through acquiring (learning) its harmful nature. The former constitutes the most basic form of avoidance, that is, instinctive and not learned responses, which include reflexes and fixed action patterns (FAPs; a series of contiguous responses that continue until completion, e.g., sneezing). The latter involves memory and cognition, and so is restricted to organisms capable of these functions.

With innate avoidance responses, organisms respond aversively to unconditioned stimuli – stimuli that need not have been previously encountered. Reflexes, for example, do not even involve the brain (e.g., nociceptive withdrawal reflex to painful stimuli). Other innate responses may involve higher order neurological signal integration, such as in fishes that instinctively avoid sulfur dioxide and chlorine, which presumably helps maintain acidic and ionic balance [9]. Similarly, *Drosophila* instinctively avoids CO_2, apparently because CO_2 is associated with stressed conspecifics [10]. While these example substances can be increased in the environment as a result of human activities, their avoidance response is based on receptors and neural circuits. With synthetic, perceptible substances, there is no guarantee that an organism will identify them as harmful and so move down a concentration gradient. In fact, the opposite can occur – fishes are known to swim up concentration gradients of various pesticides, including bentazone, dalapon, and prochloraz [11]. Furthermore, innate responses may change over time, becoming reduced or enhanced in magnitude. Reduced responses can occur following successive exposures through neurological habituation (also referred to as "non-associative learning"). Decreased gill withdrawal response to painful stimuli is well documented in sea slugs (*Aplysia* spp.) [12]. Conversely, enhanced responses can occur with neurological sensitization. Drug seeking behaviors to amphetamine and cocaine are good examples [13]. What these innate response modifying mechanisms suggest is that over time, desirable avoidance responses may be lost or attenuated, and undesirable attraction responses may be enhanced.

In the absence of an innate response, organisms may limit future exposures to toxic substances by learning to avoid them. A mechanism by which this occurs is through associative learning, which occurs when an organism learns to associate a conditioned stimulus (e.g., certain tastes or smells) with an unconditioned unpleasant or otherwise undesirable stimulus (e.g., pain). Through their pairing, the organism may even learn to respond aversively to the conditioned stimulus alone. This process is widely employed by organisms, using not only exteroceptive sensors, but also interoceptive sensors (i.e., those responding to internal stimuli). A well-known natural example of exteroceptive-based associative learning is the avoidance animals will show to skunks following an unfortunate interaction. Presumably this could occur for a toxic substance if an organism learned to pair it and its effects with a location or odor, although experimental examples are absent. A more tested form of learned avoidance is based on interoceptive responses. Ingestional aversive learning, for example, occurs when an organism ingests a specific food item, later experiences internally based pain or distress, and subsequently chooses to avoid that food in the future. Interoceptive avoidance learning is used by many organisms with naturally occurring toxins, from grasshoppers [14] to humans [15]. Furthermore, while associative learning was previously thought only to occur in organisms that posses neurological systems, recent evidence suggests the contrary: gene-regulatory networks appear to impart this ability in single-celled organisms [16]. Interoception is also the basis for the well-used conditioned taste aversion (CTA) assay. For CTA, a novel taste (conditioned stimulus) is typically paired with an injected toxin, and the rate at which the organism develops CTA is determined. This rate can be rapid in mice, just one pairing of the insecticide metabolite paraoxon with a novel taste was sufficient for development of CTA [17]. Clearly, should an animal survive an initial exposure to a toxic substance and associate a stimulus with that substance, future exposures have the potential to be avoided.

Innate and acquired avoidance responses may be adversely affected when an exposure is unavoidable and toxic substances are taken up (e.g., ingested) by the organism, especially if the substances are neurotoxic. Most of the studies of this type of impairment have focused on how natural avoidance responses are lost following contaminant exposure (e.g., the common toad (*Bufo bufo*) failed to behaviorally respond to chemical cues released by Turkish crayfish (*Astacus*

leptodactylus) following exposure to the herbicide amitrole [18]. However, at least one study noted that contaminant exposure will modify future contaminant avoidance. Specifically, vendace (*Coregonus albula*) given weeklong exposures to bleached kraft mill effluent (BKME) and then subsequently given the choice to select clean versus contaminated water chose (preferred) BKME-contaminated water [19]. Predicting whether an organism will make the right choice when given the option to avoid exposure almost certainly requires empirical evidence.

Aversive locomotion – Those organisms with physical means to move in response to stimuli can do so by means of one of two sensory routes, and these are based on the complexity of their sensory mechanism(s). At the most simple extreme, the input from a single sensor can be used to guide locomotion. The resulting movement, referred to as klinotaxis, is evident in a behavioral phenotype characterized by "side-to-side" searching. This oscillatory motion is necessary for the organism to establish a gradient over the receptor, and therefore over the environment itself. Klinotaxis is generally understood to refer to positive motion, that is, up a gradient; however, the reverse is also possible. For more complex organisms, that is, those with paired intensity receptors, tropotaxis can occur. This motion is behaviorally evident in more linear movement, since the paired receptors can provide information of a concentration gradient across the location of the receptors, not just the environment. As for structures that enable movement, even single-celled spp. have the means, for example, *Euglena* spp. and its flagellum. A consideration is that locomotory ability is known to be highly sensitive to impairment by toxic substances, such as to the numerous anticholinesterase (anti-AChE) organophosphorus insecticides [20, 21].

Limits to Absorption: Unavoidable Exposures Arguably all organisms today receive exposure to synthetic substances. Toxic effects may ensue if any one or more of the four necessary avoidance conditions are not met and the substance passes into or through the external and internal coverings, that is, protective barriers, and into the tissues of the organism. Barriers include secretions, secretion clearance mechanisms, the epithelium, and other physical barriers to uptake.

Across phyla, organisms produce mucous to cover external and internal surfaces and cavities with an environmental interface. With vertebrates such as fish and mammals, goblet cells within mucous membranes are responsible for the production of mucus and are found in places such as the mouth, stomach, nose, and genitals. With invertebrates, including those in marine (e.g., *Polychaeta* worms) and terrestrial (e.g., slugs) [22, 23] environments, mucous is produced in mucous cells (mucocytes), which are in similarly sensitive areas of environmental exposure such as the malpighian tubules of arthropods [24]. Mucus fulfills multiple roles and contains constituents such as mineral salts, antibacterial enzymes, agglutinating glycoproteins (mucins), immunoglobulins, and other specialized proteins. These substances together form a mucous matrix, which serves as a potential "trap" for environmental substances, such as with tetracycline [25]. For vertebrates, proteins can be secreted into the mucous to achieve an additional function, namely, detoxification (i.e., biotransformation). Specifically, Phase II (conjugation) enzymes (e.g., glutathione *S*-transferases [GSTs]) can be found in mucus [26]. In sensory neurons, the presence of defensive biotransformation enzymes is critical not only for protection, but also to "inactivate" odorants and facilitate their removal [27]. Currently the presence of biotransformation enzymes in insect mucus remains to be explored, although biotransformation enzymes are known to be found in sensory organs (e.g., in the antennae of the moth *Mamestra brassicae*) [28]. Whether biotransformation occurs or not, for organisms with cilia, mucus (and any trapped substances) may be removed by mucociliary clearance, that is, propulsion of mucous away from cavities.

The outermost physical barrier of many organisms is covered with skin or epithelium, and fibrous protein or sugar-based coverings. Epithelium functions as a permeability barrier to toxic substances, limiting percutaneous absorption (cutaneous permeation), such as can occur with organophosphorus insecticides [29]. The resistance of skin is largely due to the stratum corneum, which contains dead cells rich in fibrous proteins known as keratin [30]. These dead cells are continuously sloughed off and replaced, sending any trapped substances with them. In many organisms, keratin is also found in more rigid and resistant

structures such as beaks, hooves, (reptilian) shells, and scales. In invertebrates and fungi, a barrier of polysaccharide termed chitin exists, and it has a similar strength to keratin. Chitin can be so formidable a barrier that numerous synthetic agents exist to inhibit its formation [31]. Nevertheless, outer barriers are not always uniform in strength; in fact there can be features that limit protective function. In mammals, for example, the pilosebaceous unit, which is composed of hair, its follicle, and the sebaceous gland, can provide an avenue of uptake [32]. Ultimately, the ability of outer physical barriers to prevent the uptake of foreign substances is a function of exposure concentration, duration, and the physicochemical properties of the substance.

Increases in Xenobiotic Elimination and Reductions in Accumulation

Biotransformation Biotransformation is defined as the conversion of a substance from one form to another by the actions of enzymes within an organism and is distinguished from physical-chemical processes that can also effect chemical conversions (e.g., photolysis). Biotransformation usually refers to the combined transformations, reflecting the reality that a particular chemical may undergo a number of chemical changes. A molecule or its biotransformational product, its metabolite, may be modified at a number of different positions with a variety of modifications, possibly resulting in several metabolites.

Xenobiotic metabolism is basically a process that introduces hydrophilic functionalities onto the foreign molecule to facilitate excretion. The availability of xenobiotics for biotransformation reactions and the rates of metabolism therefore have important implications on the tissue levels of toxicants, metabolite patterns, and xenobiotic half-life, all of which affect the bioaccumulation, persistence, and the severity and duration of a toxic response. For example, it has been shown that the four order of magnitude difference in the bioaccumulation of two structurally related compounds, DDT (2-bis(*p*-chlorophenyl)-1,1,1-trichloroethane) and 2-bis(*p*-methylthiophenyl)-1,1,1-trichloroethane, with similar lipophilic characteristics, was due to the latter compound's ability to be biotransformed by the mosquitofish (*Gambusia affinis*) [33].

Hydrophobic (high log K_{ow} [octanol:water partition coefficients] value) and lipophilic chemicals (e.g., PCBs, cyclosporine A) are not easily excreted, as they partition back into cells and tissues from excretory media (e.g., urine, bile). Water-soluble chemicals are not reabsorbed because lipid membranes of cells lining excretory routes act as barriers to their reuptake. This is why many lipophilic compounds tend to accumulate: they are easily absorbed and poorly excreted. For example, southern resident Killer Whales in the Pacific Northwest contain PCB concentrations as high as 146 mg/kg lipid weight, placing them among the most PCB-contaminated marine mammals in the world [34]. Therefore, the general scheme of biotransformation processes is the conversion of lipophilic compounds to more polar hydrophilic metabolites.

All organisms have the ability to metabolize foreign compounds that are taken up; however, their evolved abilities in this regard vary widely. The highest biotransformation ability is usually found in mammals and birds, followed by fish and reptiles, and invertebrates. Major sites of biotransformation include respiratory tissues, nasal mucosa, and the skin and gastrointestinal tract (all sites of potential entry of xenobiotics). The major site of biotransformation in organisms is the liver or functional equivalent. This organ has a high lipid content (to enhance lipophilic chemical accumulation), a high blood flow (increased delivery), and high titers of biotransformation enzymes.

Biotransformation generally occurs through a sequence of reactions termed phase I and phase II reactions (Fig. 2). In phase I reactions a nucleophilic functional group (e.g., –OH, –SH, –NH_2, –COOH) is

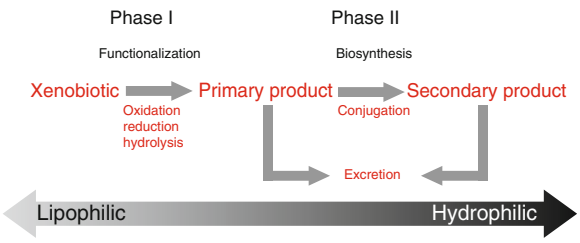

Xenobiotic Protection/Resistance Mechanisms in Organisms. Figure 2
The general biotransformation scheme for xenobiotics in organisms through phase I and phase II reactions. The general trend is to convert lipophilic compounds to more hydrophilic metabolites, which are more easily excreted

introduced or exposed in the parent molecule. In phase II reactions, the phase I metabolite or parent molecule already containing a functional group is conjugated to an endogenous molecule (e.g., sugar, amino acid, sulfate). Phase I metabolites are more polar than the parent molecule, increasing excretion potential, as well as rendering them suitable for phase II enzymatic reactions. Phase II reactions form exceptionally water-soluble products that undergo significant ionization at physiological pH. The endogenous conjugating moieties are also substrates for secretion proteins in transport epithelia. Phase I reaction products can be less toxic than the parent compound or may be bioactivated to more toxic metabolites (see below in oxidation reactions), a significant process in the toxicity of many environmental contaminants (e.g., dibrominated diphenyls) and drugs (e.g., acetominophen).

Phase I Reactions (Asynthetic, Functionalization Reactions) Phase I reactions are the predominant biotransformation pathway for most xenobiotics and include microsomal monooxygenations, cytosolic and mitochondrial oxidations, co-oxidations in the prostaglandin sythetase reaction hydrolysis reactions, epoxide hydration, and reduction reactions. The common definition of Phase I reactions includes oxidation, reduction, and hydrolysis reactions, a grouping that lacks any mechanistic coherence. The modern systematic classification of enzymes (Enzyme Commission numbering system) groups together oxidations and reductions (catalyzed by oxidoreductases, EC class 1) but places hydrolysis reactions in a completely separate class (class 3). Not uncommonly, the term "phase I metabolism" continues to be used, mainly as an outdated synonym for P450-dependent oxidations. Regardless of nomenclature, the common theme to these reactions is to either unmask or introduce a polar functional group in or onto the parent xenobiotic.

Oxidation The cytochrome P-450 (CYP)-dependent mixed function oxidase (MFO) system of eukaryotes consisting of membrane lipids (e.g., mostly localized to the endoplasmic reticulum [ER], but also present in mitochondrial inner membranes), the enzyme cytochrome P450 (P450s), and an electron transfer chain (NADPH-cytochrome P450 reductase in the ER, and redoxin reductase/redoxin in mitochondria) is crucial for oxidative, peroxidative, and reductive metabolism. P450s have two functions in general: (1) a protective role in the degradation or provision of polar handles for the solubilization of xenobiotics in preparation for excretion, and (2) a broad functional role in the biosynthesis of critical signaling molecules used for the control of development and homeostasis.

P450s constitute a superfamily of heme enzymes present in every living species on Earth from archaebacteria to humans. Despite their occasionally minimal sequence similarity, all CYPs have a similar structural fold with a highly conserved core. Due to its high diversity, a systematic classification of individual CYP forms into families and subfamilies has emerged. The protein sequences within a given gene family are at least 40% identical (e.g., CYP2A6 and CYP2B6), and the sequences within a given subfamily are >55% identical (e.g., CYP2A6 and CYP2A7). Individual members of a family or subfamily are labeled again by Arabic numerals (e.g., CYP3A4, CYP3A7). There are 17 different families and 59 functional P450 genes currently known in humans. In this respect, hepatic drug oxidation is a major source of interindividual variation in pharmacokinetics and therapeutic response. The expression of individual P450 proteins in the liver is influenced by a number of factors, such as genetic make-up, disease, ageing, and environmental factors (e.g., smoking, alcohol, nutrition, pollutants) [35].

Early P450 research, suggested that only a few types of organic compounds served as P450 substrates, but it is now known that P450 substrates are an enormous and diverse group of compounds, including endobiotics and xenobiotics, and the list continues to grow. P450s do not conform to the typical textbook definition of an enzyme as a highly specific biological catalyst, and it has been predicted that the substrate base could be a million or more compounds [35]. Endobiotic substrates include such compounds as steroids, bile acids, fatty acids, prostaglandins, fat-soluble vitamins, amino acids, eicosanoids and retinoids, lipid hydroperoxides, and leukotrienes. Xenobiotic substrates include most of the therapeutic drugs and environmental contaminants, antioxidants, dyes, and plant products such as flavorants and odorants. The enzymes in the families 1–3 are mostly active in the metabolism of xenobiotics, whereas the other families have

important endogenous functions. Interestingly, mutations that inactivate CYP enzymes with physiological functions often lead to serious diseases, whereas similar mutations in xenobiotic-metabolizing CYPs rarely do.

It should also be noted that P450 cytochromes occur in a variety of tissues other than liver. For example, P450 has been found in olfactory and respiratory nasal mucosa of animals, including fish.

Nature has found many ways to utilize atmospheric dioxygen to functionalize molecules for their degradation or synthesis through the use of a diverse set of cofactors. P450 is a heme (Fe at the active site) containing oxygenase, conscripted to metabolize atmospheric dioxygen in an oxygenase catalytic cycle (Fig. 3), resulting in the incorporation of one oxygen atom into a substrate. This hydroxylation reaction has the following overall stoichiometry:

$$RH + O_2 + NADPH + H^+ \rightarrow ROH + H_2O + NADP^+,$$

where RH represents a xenobiotic or endogenous substrate and ROH is the product. The most important property of all known P450s is their ability to bind and activate two atoms of oxygen. A second characteristic property of P450s is that their active site is a heme macrocycle with the central atom, the heme iron, being bound to the protein structure through the anionic, thiolate sulfur of a cysteine residue. The mode by which the heme is bound to apoprotein enables the ability of all P450s to activate the Fe–O–O moiety. The third common property of all P450 enzymes is their similar overall structure and shape, in which most of the secondary-structure elements, as well as the overall folding pattern, are conserved. NADPH-cytochrome P450 reductase uses NADPH as a cofactor that, after binding of the substrate to oxidized CYP P450, transfers electrons to CYP P450, thereby reducing it, allowing for several steps whereby one atom of oxygen from O_2 is transferred onto the xenobiotic and the other oxygen is used to form water. The oxygenation and other alterations of the very diverse number of substrates by P450s may seem indiscriminate, but in many instances the modification is positionally and even stereochemically specific. Some examples of reactions catalyzed by the microsomal cytochrome P450 system are given in Fig. 4.

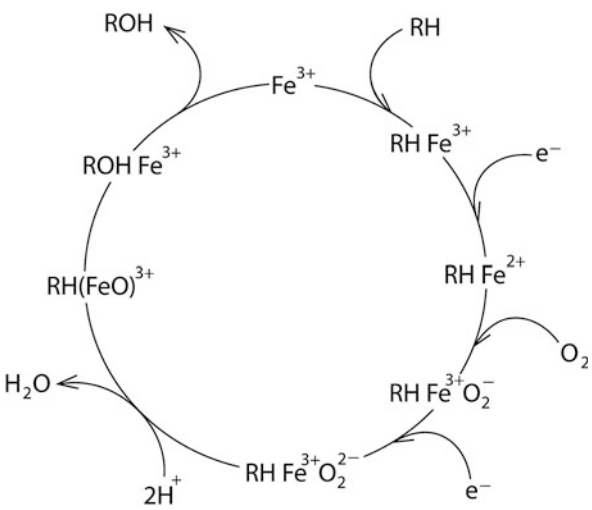

Xenobiotic Protection/Resistance Mechanisms in Organisms. Figure 3
The cytochrome P450 catalytic cycle

Biotransformation generally results in reduced toxicity through the genesis of less toxic metabolites, although bioactivation to more toxic products (bioactivation) is a significant process in the toxicity of many compounds. Reactive intermediates can be formed directly through either phase I (oxidative or reductive reactions) or phase II reactions (less common), or by a rearrangement of a metabolite to an unstable form. Reactive intermediates are usually electrophilic and can react with nucleophilic sites on molecules such as the sulfhydryl group of glutathione and cysteine, or the guanine base in DNA. For example, the addition of oxygen to PAH C=C can produce an epoxide that can nonenzymatically react with macromolecular nucleophiles, resulting in covalent bond formation. Benzo[*a*]pyrene is a procarcinogen, and via a series of oxidation and hydrolysis reactions, a highly reactive metabolite (+)-benzo[*a*]pyrene-7,8-diol-9,10-epoxide is formed, which can react with cellular DNA and initiate the carcinogenic process [36].

Other important Phase I oxidative enzymes include flavin-containing monooxygenase, which catalyzes the oxygenation of nitrogen and sulfur compounds, and the epoxide hydrolases, which hydrolyze various epoxides to diols. The cytochrome P-450 and flavin-containing monooxygenase enzymes are localized in the microsomes, while epoxide hydrolases occur in both the microsomal and cytosolic fractions of the cell.

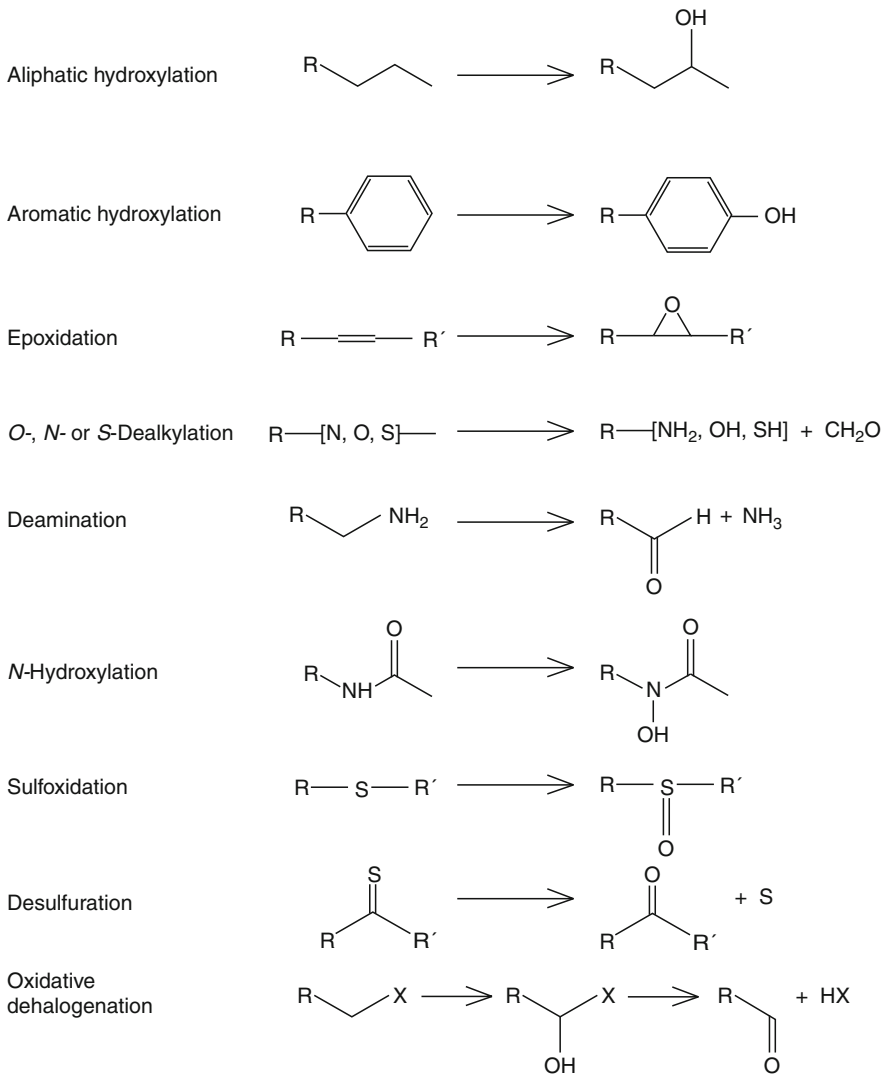

Xenobiotic Protection/Resistance Mechanisms in Organisms. Figure 4
Typical oxidation reactions catalyzed by cytochrome P450 monooxygenases

Reduction Reduction reactions are also catalyzed by P450, owing to the transfer of reducing equivalents of P450 reactions to the xenobiotic substrate, rather than molecular oxygen. Reductions are most likely to occur with xenobiotics in which oxygen tension is low. Reductions can occur across nitrogen–nitrogen double bonds (*azo reduction*) or on nitro groups (NO_2). Frequently, the resulting amino compounds are oxidized forming toxic metabolites. Some chemicals can be reduced to free radicals, which are reactive with biological tissues.

Hydrolysis Hydrolysis reactions are typically not carried out by the P450 system. Grouping hydrolysis together with oxidation (as in phase I reaction) means separating hydrolysis from glutathione conjugation (phase II reaction), however, both hydrolysis and glutathione conjugation are reactions of an abundant cellular nucleophile (water or GSH) with a xenobiotic electrophile. In most cases, hydrolysis and glutathione conjugation are competing pathways for the disposition of xenobiotics (e.g., PAH dihydrodiol epoxides,

alkylating agents, *O*-acetoxy esters of aromatic amines, etc.) but they are certainly not sequential. The most significant hydrolyzing enzymes are carboxylesterases, arylesterases, cholinesterases, and serine endopeptidases. The hydrolysis of xenobiotic esters and amides generate carboxylic acids, alcohols, and amines. Such metabolites are all susceptible to phase II conjugation and excretion.

Phase II Reactions (Biosynthetic, Conjugation Reactions) Phase II reactions involve the biosynthetic union or coupling (conjugation) of xenobiotics or functionalized intermediates from phase I reactions with endogenous molecules generating hydrophilic conjugated metabolites that are devoid of toxicological activity and easily eliminated. Various endogenous molecules that are ionizable at physiological pH such as carbohydrates, proteins or amino acids, sulfur or phosphate components, or intermediates in lipid metabolism, are used in these reactions. Conjugated metabolites are substrates for specific transport proteins in epithelial tissues and are secreted with great efficiency. Conjugation reactions have a dual purpose; they have a role in intermediary metabolism of endogenous compounds as well as in the biotransformation of xenobiotics.

These reactions can be categorized by the mechanism of interaction between the conjugating agent and the xenobiotic. In type I reactions (e.g., glycosides, sulfates, methylated, and acetylated conjugates), ATP is used to form an activated "high-energy" intermediate. This activated coenzyme is conjugated to the substrate at the site of one of the functional groups. In type II conjugation reactions, the substrate itself is activated and then combines with an unactivated coenzyme (e.g., an amino acid), forming the phase II metabolite. In type III reactions, the xenobiotic or its metabolite already possesses the intrinsic reactivity to enzymatically react with a conjugating agent without the preformation of a high-energy intermediate (e.g., formation of glutathione conjugates). The enzymes that catalyze the reaction between the substrate and activated coenzyme are collectively called transferases. These reactions are usually considered as detoxication reactions, but in certain cases, bioactivation occurs (e.g., N-glucuronides of N-hydroxyarylamines are transported to the bladder, where β-glucuronidase hydrolysis in the acidic urine produces hydroxylarylamines, which spontaneously form electrophilic arylnitrenium ions and cause bladder cancer [37]). Major phase II reactions include glucuronidation, sulfation, acetylation, and conjugation with glutathione or amino acids.

Glucuronidation Glucuronidation represents the major route of sugar conjugation, and qualitatively and quantitatively, glucuronide formation is the most important form of conjugation of both xenobiotics and endogenous compounds in most organisms. Four general categories of O-, N-, S-, and C-glycosides are formed and increase the compounds' polarity and ultimately their excretion in urine or bile. In glucuronidation, the high-energy nucleotide uridine diphosphate (UDP)-glucuronic acid (UDPGA; Fig. 5) interacts with the functional group on the acceptor molecule (the substrate or aglycone) forming a conjugate with D-glucuronic acid. The transfer of glucuronic acid from UDPGA to the aglycone is catalyzed by a family of enzymes called UDP-glucuronosyltransferases (UGTs). There are multiple forms of UGTs that have different substrate specificities in the same species and in different species. For example, the domestic cat, *Felis catus*, can form glucuronide conjugates of thyroxin and bilirubin, but is unable to form other glucuronide conjugates. UGTs are localized to the ER of all tissues, but the majority of activity is found in the liver. Location in the ER is a strategy whereby it has direct access to products (including reactive intermediates) generated by microsomal P450, an excellent example of the integration of the sequestration of lipophilic xenobiotics in the lipids of the ER, the addition or unmasking of a functional group, and the conjugation of this functional group with the highly polar D-glucuronic acid.

Sulfation As with glucuronidation, these conjugation reactions are found in most organisms and are important to both endogenous (e.g., thyroid and steroid hormones, catecholamine neurotransmitters, the tyrosinyl group of peptides and proteins, and bile acids) and xenobiotic compounds, particularly those chemicals with hydroxyl groups, but also contributes to the biotransformation of 1°, 2°, and 3° alcohols,

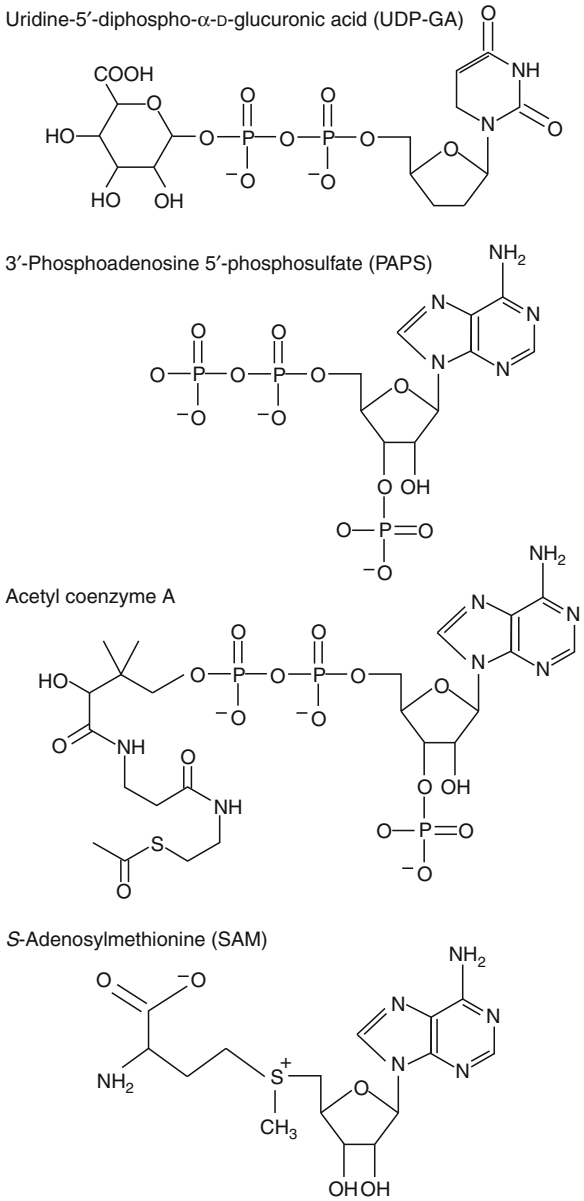

Xenobiotic Protection/Resistance Mechanisms in Organisms. Figure 5
Phase II high energy cofactors

amines, and to a lesser extent, thiols. The resulting compounds are generally less toxicologically active and more polar, thus more readily excreted in the urine, with little in bile (this however, is species dependent). However, a number of compounds are converted to highly labile sulfate conjugates that form reactive intermediates that have been implicated in carcinogenesis and other toxicities. Sulfate conjugation is a multistep process, comprising activation of inorganic sulfate, first, by converting it via ATP to adenosine-5′-phosphosulfate (APS), and further to the activated form, 3′-phosphoadenosine-5′-phosphosulfate (PAPS; Fig. 5) by ATP sulfurylase and APS kinase. PAPS is synthesized in all cells, but the highest concentrations are found in the liver or functional homologue in organisms without livers. Interestingly, the cat has very high levels of this conjugating enzyme system, perhaps compensating for the lack of glucuronidation as a primary conjugation mechanism. Sulfotransferases catalyze the reaction, whereby the SO_3^- group of PAPS is readily transferred in a reaction involving nucleophilic attack of the phenolic oxygen or the amine nitrogen on the sulfur atom with the subsequent displacement of adensine-3′,5′-diphosphate. Interestingly, sulfation is a high affinity, low capacity conjugation reaction, which is opposite to glucuronidation. At low phenol concentrations, sulfation predominates; at high concentrations, glucuronidation is the most important pathway. The major classes of sulfotransferases that metabolize xenobiotics are aryl sulfotransferases, alcohol sulfotransferases, tyrosine-ester sulfotransferases, and amine N-sulfotransferases.

Methylation Methylation involves the transfer of methyl groups from one of two methyl donor substrates, *S*-adenosylmethione (SAM (Fig. 5)) or N^5-methyltetrahydrofolic acid. Methylation is a common biochemical reaction of endogenous compounds (e.g., proteins, nucleic acids, phospholipids), but is not usually of quantitative significance in the biotransformation of xenobiotics. Methylation differs from most other conjugation reactions in that it masks functional groups, which may reduce water solubility and/or impair its ability to be excreted or participate in other conjugation reactions. N-methylation is an important reaction in metabolizing 1°, 2°, and 3° amines. Methyl groups from SAM are also transferred to the thiol-containing xenobiotics (e.g., thiopyrimidine drugs).

Acylation There are two types of acylation reactions based on the activated component. Acylation reactions involve foreign carboxylic acids and amines to form amide conjugates. In the first type, an activated

conjugating intermediate acetyl CoA (Fig. 5) reacts with a xenobiotic through acetyl CoA: amine N-acetyl transferases (mostly cytosolic enzymes) in a reaction called acetylation. Acetylation reactions require a specific cofactor, acetyl-CoA, which is obtained mainly from the glycolysis pathway via direct interaction of acetate and coenzyme A, or from the catabolism of fatty acids or amino acids. The primary site of acetylation is the liver, although extrahepatic sites have been identified as well (e.g., spleen, lung, and gut). This reaction has been studied extensively in humans because of its important consequences in drug therapy and in the carcinogenicity of certain xenobiotics.

In the second type of acylation reaction, amino acids are conjugated to carboxylic acid containing xenobiotics following activation of the foreign compound to form an acyl CoA derivative catalyzed by the enzyme acid:CoA ligase (a mostly cytosolic enzyme). The acyl CoA subsequently reacts with an amino acid (most frequently glycine, glutamine, alanine and histidine, and ornithine in birds, and taurine in fish) to form an acylated amino acid conjugate, catalyzed by N-acyltransferase. The reaction is categorized as a high affinity, low-medium capacity system, and given that it has only a relatively small substrate base such as aromatic, heteroaromatic and arylacetic acids, it is not considered as effective as the main conjugation reactions (glucuronidation, sulfate, GSH-conjugation).

Glutathione Conjugation and Mercapturic Acid Formation Glutathione (GSH) is a tripeptide that contains cysteine, glutamic acid, and glycine. In its reduced form, it acts as an antioxidant due to its nucleophilic nature at the sulfur group, and as such, it is essential in protecting cells from reactive oxygen species (ROS). GSH is found almost exclusively in its reduced form since the enzyme that reverts it from its oxidized form, GSH reductase, is constitutively active, and is present in high concentrations in all tissues, particularly the liver.

The glutathione *S*-transferases (GSTs) are a family of mainly cytosolic enzymes (microsomal and mitochondrial forms do exist) that play an important role in xenobiotic resistance by several distinct mechanisms: increased detoxication, sequestration of the xenobiotic, and decreased xenobiotic activation. Arguably the most important function is to catalyze the initial reaction in the formation of N-acetylcysteine (mercapturic acid) derivatives of a diverse group of xenobiotics with the following characteristics in common: some degree of hydrophobicity, presence of an electrophilic carbon atom, and some tendency to react with glutathione nonenzymatically (e.g., electrophilic substrates including herbicides, insecticides, pharmaceuticals and anesthetics, anticancer agents, carcinogens, antibiotics, etc.) GSTs are found ubiquitously in all tissues, with the highest levels in the testes, liver, intestine, kidney, and adrenal glands of humans. They have also been found in every organism examined.

The initial step in mercapturic acid formation (Fig. 6, with example) involves the formation of a glutathione conjugate. GSH conjugation involves the formation of a thioether link between the GSH and electrophilic compounds. The reaction can be considered as the result of nucleophilic attack by GSH on electrophilic carbon atoms; thus conjugation with glutathione usually results in detoxication of electrophilic compounds by preventing their reaction with nucleophilic centers in other biomolecules. The enzyme γ-glutamyltranspeptidase, a membrane-associated enzyme found in high concentrations in cells that provide absorptive or excretory functions, removes glutamic acid from the GSH-conjugate, forming a cysteinyl glycine conjugate. Glycine is then removed from this metabolite by the enzyme cysteinyl glycine dipeptidase or aminopeptidase M, to form the cysteine S-conjugate (pre-mercapturic acid), which is acylated by N-acetyltransferases, resulting in the formation of the N-acetyl derivative, mercapturic acid.

Modifiers of Biotransformation The dramatic significance of biotransformation and the mechanisms to achieve the protection and resistance of organisms from the effects of xenobiotic exposure have been discussed. There are a number of endogenous (physiological) and environmental factors that affect the abilities of different organisms to use biotransformation in a protective role, factors which can modify their susceptibility to toxicants. Some of the more important intrinsic factors include the following:

- Species, strain, and other genetic variations (particularly interesting with individual sensitivities to either drugs or environmental contaminants from a health perspective)

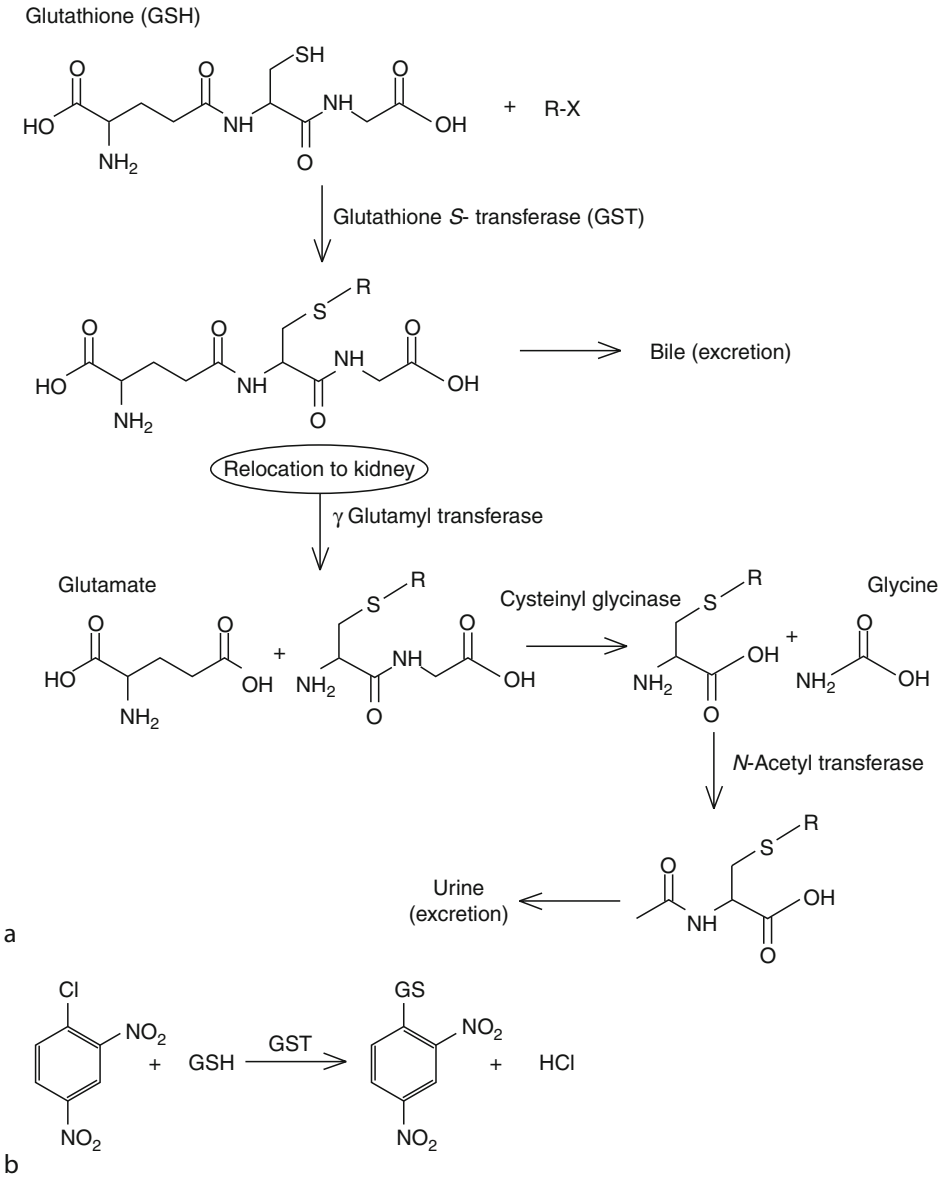

Xenobiotic Protection/Resistance Mechanisms in Organisms. Figure 6
(**a**) Glutathione conjugation and mercapturic acid formation. (**b**) An example of glutathione conjugation

- Development (under complex ontogenic control)
- Sex (males typically > females)
- Age (low in fetus and infants, increasing in age and declines with old age)
- Hormones (complex interrelationship: antagonistic, additive, and synergistic relationships)
- Pregnancy (decrease in maternal enzymes)
- Disease (tissue and organ-specific as to magnitude, but generally decreases with hepatic disease, infections, cancer)
- Diurnal and seasonal cycles (direction with circadian rhythms depends mostly on the endogenous function of enzymes; season in wildlife usually reflects hormonal fluctuations)

- Nutritional effects (deficiencies generally decrease enzymes) [38]

Extrinsic factors that can modify biotransformation include: pre-exposure to xenobiotics, resulting in either inhibition of biotransformation enzyme systems or induction (increases) in enzyme concentrations following exposure. In ectothermic organisms, environmental temperature and the rate of temperature change can play a large role in altering xenobiotic metabolism.

Prior exposure to some contaminants can increase the biotransformation capability of organisms by a process called *induction*. For example, P450 isoforms in the 1A (CYP1A) subfamily are inducible by planar PAH and HAH, including chlorinated biphenyls, dibenzo-*p*-dioxins, and dibenzofurans, as well as several drugs including the classic (well studied pharmacologically) inducers phenobarbital and 3-methylcolanthrene. The Ah receptor (AhR), a soluble protein with a high binding affinity for planar PAH and HAH, controls the induction of cytochrome CYP1A. The aryl hydrocarbon receptor nuclear translocator (ARNT) and the AhR together form a transcription factor complex through which altered gene expression and toxicity occurs [39]. Their dimerization is dependent upon high affinity binding of planar PAH and HAH to the AhR. The AhR:ARNT complex then binds specific genomic recognition sites (xenobiotic response elements, XRE) on DNA. This alters the transcription of target genes that include both phase I and phase II biotransforming enzymes. Other nuclear receptors are involved in the induction of biotransformation enzymes, and considerable current research effort is focused in this area. Like AhR, orphan nuclear receptors (e.g., constitutive androstane receptor [CAR], pregnane X receptor [PXR], and retinoid X receptor [RXR]) comprise a gene superfamily that encodes the transcription factors that sense endogenous (e.g., small lipophilic hormones) and exogenous (e.g., drugs, xenobiotics) compounds, and transfer this information into cellular processes by regulating the expression of their target genes [40]. The regulation and induction of phase II enzymes is less well understood, and recent research has revealed the existence of several *cis*-acting regulatory elements including the antioxidant response element (ARE/electrophile response element [EpRE]), xenobiotic responsive element (XRE/aromatic hydrocarbon responsive element [AhRE]), activator protein-1 (AP-1), and nuclear factor-kappa B (NF-kB) binding sites. In the case of ARE, xenobiotics induce stress responses leading to potential sulfhydryl modification of Keap1-Nrf2 and other signaling pathways, which leads to the activation of the transcription factors such as Nrf2/Maf and increases ARE-mediated gene expression including phase II enzymes [41]. Maximum induction with chemicals is dependent on species, inducer (variation exists in inducer strength), route of administration, and dose; however, induction can occur quite rapidly (within hours in in vitro assays, days in vivo), and enzyme activities can remain elevated for weeks upon withdrawal of the inducer.

Unlike induction (a physiologically regulated and evolved process for protection), the inhibition of biotransformation enzymes can include a multitude of mechanisms including competition for active sites or cofactors of enzymes, decreased biosynthesis, increased degradation of enzymes or cofactors, allosteric changes in enzyme conformation, loss of functional tissue, etc.

Phase III Transport In many cases, these transporters act as a first line of defense, preventing toxic chemicals from entering the cell. However, if a compound is not recognized by these transporters and enters the cytoplasm, detoxifying enzymes in the cell may modify the chemical to a more hydrophilic form. In this case, related cellular transporters can again come into play, effluxing the modified products out of the cell. There are two main types of these: *ATP-binding cassette* (ABC) and *solute carrier* (SLC) proteins (Fig. 7).

ABC Proteins ABC transporters are evolutionarily ancient, and three ABC subfamilies of efflux (multidrug) transporters involved in the biochemical defense against toxicants have both health and environmental significance [42]. ABC drug efflux transporters have a wide phylogenetic distribution and are found in vertebrates as well as in deuterostome invertebrates, protostome invertebrates, fruitflies, protozoans, and yeast. Homologous proteins are also present in plants, though their roles in multidrug efflux have not been firmly established. ABC transporters include members of the P-glycoprotein (P-gp [ABCB]) family, the multidrug resistance protein

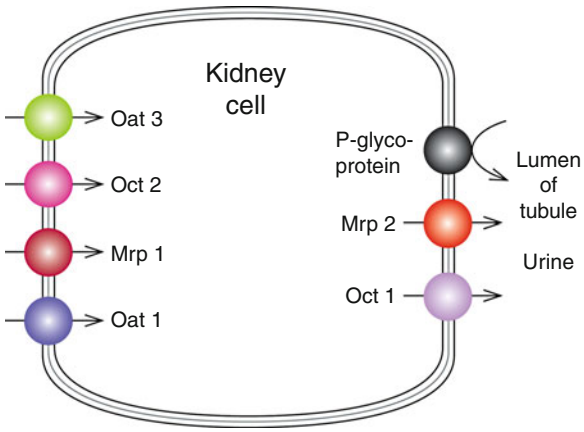

Xenobiotic Protection/Resistance Mechanisms in Organisms. Figure 7
Vectorial transport of xenobiotics and their metabolites is accomplished by efflux transporters as pictured in this kidney cell. *Oat* Organic anion transporter, *Oct* Organic cation transporter, *Mrp* multidrug resistance-associated protein

(MRP [ABCC]) family and the breast cancer resistance protein (BCRP or MXR [ABCG]) family. These ABC proteins are membrane-bound transporters coupling ATP hydrolysis to the translocation of substrates across biological membranes. These efflux pumps provide important protection to internal tissues (e.g., blood–brain barrier, liver, kidney, and placenta) and to sites of entry of environmental contaminants (e.g., gills, gastrointestinal tract).

P-Glycoprotein (ABCB Family) The multidrug resistance (MDR due to its remarkably nonspecific substrate base) protein, P-glycoprotein (P-gp for "permeability glycoprotein," [ABCB1]), transports both endogenous and exogenous substrates and is found in a broad range of taxa [43]. It is a transmembrane energy-dependent pump that mediates the efflux of a large number of moderately hydrophobic compounds. P-gps confer MDR to tumor cell lines [44] and tumors of human patients [45], and have been described in many aquatic wildlife species [46]. It appears that, in addition to normal cell function, P-gp activity contributes to the relative hardiness of fish living in contaminated environments, providing multixenobiotic resistance (MXR).

Although the high resolution structures of ABC proteins and the structure–function relationships of mammalian P-gp have been characterized in recent years, how it works as an efflux pump or its role in normal physiology is still unknown. A role for P-gp certainly exists in altering the pharmacokinetics of natural endogenous compounds and xenobiotics, although the full range of substrates for P-gp has not yet been explored. The factors that regulate P-gp are also not yet fully understood, and understanding the regulation of these efflux pumps is essential in determining their role in normal physiology. Limited evidence suggests P-gp is up-regulated (induced) in response to a number of signals, including specific substrates, toxicants, heat stress, and nuclear factors [47].

P-glycoproteins are expressed in many of the same tissues as biotransformation enzymes (e.g., cytochromes P450); however, biotransformation is not a prerequisite for efflux. Compounds are transported as parent molecules, and among P-gp substrates, no consensus structure has been defined, although within each class of chemicals certain chemical features have been defined that seem to be essential for functional interaction (moderate hydrophobicity, small size, and positively charged domains). Their interaction with biotransformation systems, or other transporters (e.g., multidrug resistance protein [MRP]) are unclear. Although it is now clear that the induction of CYP enzymes and P-gp are not co-regulated, they may interact through CYP-mediated production of P-gp substrates or CYP-mediated- or glutathione (GSH) depletion-mediated increases in intracellular reactive oxygen species (iROS) [48]. As a first line of cellular defense against xenobiotic influx, P-gp may be overwhelmed by high concentrations, or may not recognize certain classes of compound, which enter cells and are acted on by biotransformation enzymes such as P450, followed by the conjugation of the metabolite. The conjugated metabolite can then be eliminated by another ABCC family of efflux transporters, which recognize the conjugated moiety (e.g., MRP).

Multidrug Resistance-Associated Protein (ABCC Family) Conjugates require export across cell membranes, and conjugated metabolites may be subject to further metabolism (e.g., the pathway of mercapturic acid formation) or transported without

further modification out of cells. The use of the term "Phase III metabolism" to describe membrane transport of drug conjugates [49] is also potentially misleading, since proteins such as MRP1 effect transport of some drugs in their parent form, without any prior biotransformation, and actually prevent cellular uptake. Some members of the multidrug resistance-associated protein (MRP, ABCC) family also contribute to multidrug efflux by acting like P-gp to efflux unmodified xenobiotics. However, members of this family also act on endogenous substrates that are normal products of metabolism, or act on xenobiotics that have been modified as a part of the above mentioned phase I and phase II biotransformation processes. The resulting conjugated, negatively charged molecules are recognized by various ABCC transporters and then exported from the cell [48].

Multixenobiotic Resistance Protein (ABCG Family) ABCG2, a member of the ABCG family commonly referred to as breast cancer resistance protein (BCRP), also causes significant resistance to a limited group of chemotherapeutic treatments (substrate specificity is less broad than for ABCB and ABCC [50]) as well as effluxing dietary toxicants [51]. A difference from the aforementioned transporter types, which are so-called full transporters (the gene product constitutes one structural unit), is that ABCG2 is a half transporter, in which two protein molecules are assembled to form a structural unit active as a homodimer. ABCG2 also plays a role in the translocation of essential compounds, such as riboflavin, into breast milk and may also transport certain toxicants into milk. In fact, in an environmental sense, transfer of milk to offspring of top predators such as whales, puts calves at a higher trophic level than the mothers, making young the highest risk group [52].

Multixenobiotic Resistance (MXR) MXR is a phenomenon that increases the potential for survival of aquatic organisms in polluted environments through enhanced expression of one or more MDR-like transport mechanisms (e.g., P-gp or MRP) that restrict xenobiotic uptake [53]. As mentioned earlier, these transporters act as first lines of defense against xenobiotics and are found in tissues where exchange with the environment can ensue. Such transport systems are present at some basal level in animals maintained in unpolluted environments, and they appear to be up-regulated on exposure to pollutants.

Mixtures of xenobiotics can compromise this defense because competitive binding of different chemicals to the transporters can sabotage the activity of transporter binding sites or saturate them. In addition, some of the chemicals in the mixture might be direct inhibitors of the transporter activity. The resultant competition or inhibition, termed chemosensitization, can decrease transporter activity of chemicals in a mixture such that toxic substances normally excluded from the cell can now enter.

Solute Carrier Proteins Elimination in most organisms occurs via the kidneys and hepatobiliary route or functional equivalent. In kidney tubules and in hepatocytes, as well as other tissues, there exist a number of other xenobiotic (or metabolite) export pumps that mediate the vectorial transport of substrates from the basolateral extracellular fluid into the cells on the basolateral sides of cells and export them to excretory media on the luminal side of cells (e.g., facing canaliculi or lumen) (Fig. 7). Some of these transporters include the aforementioned ABC proteins. At the basolateral membrane are members of the SLC superfamily of proteins, the organic anion transporters (Oat1, Oat3), and organic cation transporters (Oct2). Oat1 exhibits a broad substrate specificity and is responsible for the cellular uptake of most amphiphilic organic anions. High levels of expression of organic cation/carnitine transporter (OCTN1) are seen in barrier and excretory tissues as well [54].

Regulation of Efflux Transporters Pregnane X receptor (PXR), constitutive androstane receptor (CAR), peroxisome proliferators activated receptors (PPAR), liver X receptor (LXR), and farnesoid X receptor (FXR) are all nuclear receptors that bind to specific DNA response elements that produce effects on phase III efflux transporters, although which specific transporters and the mechanisms are still unclear [41]. PXR appears to regulate several efflux transporters including P-gp, MRPs, and Oats. Common mechanisms exist between phase I and phase II xenobiotic metabolizing enzymes through AhR/ARNT, and binding to AhR-xenobiotic

response elements and subsequent induction of mRNA suggesting coordinate regulation. Moreover, several types of phase II enzyme inducers have been empirically shown to increase the excretion of phase II metabolites. Since phase II metabolites are transported out of cells by P-gp, MRPs, and OatP2, phase III transport processes may be coordinately regulated; however, the precise mechanisms are not clear.

Storage The distribution of organic xenobiotics to sites of storage are in most cases not directed, but are the results of simple chemical partitioning. Storage sites may be the target sites (e.g., paraquat in lung), or sites of noninteraction. Therefore, storage can only be considered a protective mechanism in the latter case. Major storage sites can include the following: plasma proteins (e.g., Cu is stored by ceruloplasmin [55]), liver and kidney (e.g., organic acids bid to Y protein/ligandin in liver), fat (e.g., chlordane, DDT, PCBs, dioxins), and bone (e.g., Pb). Xenobiotic sequestration inside the cell appears to be an uncommon protective mechanism. Doxorubicin (chemotherapy drug) was shown to be sequestrated into small cellular vesicles whose concentration was correlated to the cellular resistance level to the drug [56]. This storage mechanism could participate in exocytosis and elimination. Glutathione *S*-transferase and other transferases contain lipophilic domains that can serve as binding sites for a number of exogenous compounds that are not substrates for reactions [57]. Organisms have few mechanisms for protection against metal contaminants. Metallothioneins (MTs) are ubiquitous low molecular weight proteins rich in cysteines with a high affinity for specific metals. They function in metal homeostasis by binding essential metals (e.g., Zn) and in defense by sequestering nonessential metals (e.g., cadmium). MTs have been identified in most tissues, and can be greatly induced in tissues that are active in metal uptake, storage, and excretion [58].

Toxicodynamically Derived Resistance Mechanisms

Toxicodynamically derived resistance refers to alterations in xenobiotic-receptor interactions. This can be manifest by alterations in target site, increased or decreased concentrations of target molecules, or circumvention of target function. Whether any of these resistance mechanisms arises and is retained in a population depends on a number of factors, most importantly its presence in the population and the physiological cost of the mechanism to the organism. Variable resistance mechanisms will come into play on different time scales; for example, a single major resistance mechanism should arise first with some associated cost, a cost that can potentially be corrected by epistasis with subsequent less costly mechanisms.

Cellular Detoxification Many xenobiotics have similar modes of action, and the evolutionary chemical history of organisms has equipped them with various mechanisms in dealing with toxic effects they are likely to encounter. Many xenobiotics or their metabolites are electrophilic and highly reactive. For example, alkylating agents and drugs have lethal activity that is linked to electrophilic (quinines, cations) or radical species. The structure of GSH and its chemical characteristics have been described previously. The GSH thiol group performs a nucleophilic attack on the target electrophile and forms a stable conjugate that is nonreactive.

Target Site Alterations

Structural Modification In contrast to the above example, many xenobiotics (particularly therapeutic drugs) are targeted to a specific molecule or cellular component. An organism may resist the action of a xenobiotic due to target site modification that affords it an efficient resistance mechanism. Non-silent point mutations within structural genes are the most common cause of target-site resistance [59]. These changes can be brought about by alterations in amino acid sequences, the distances between critical amino acid residues, and protein topography. These mechanisms can be rapidly acquired when the xenobiotic has a unique cellular receptor or when the xenobiotic resembles the target's endogenous substrate. Structural mutations (non-silent) that give rise to this type of resistance to the effects of a given xenobiotic can incur costs to the organism; altered binding/catalysis by structural changes can lead to biological effects from reduced functionality of the target in its normal physiological roles. For selection of the mutations to occur, the resultant amino acid change

must reduce the binding of the xenobiotic without causing a significant loss of the primary function of the target site. The number of possible amino acid substitutions, therefore, can be very limited. It is not surprising that identical resistance-associated mutations are commonly found across highly diverged taxa [59]. The degree to which function is impaired by the resistance mutation is reflected in the fitness of resistant individuals in the absence of xenobiotic selection and the persistence of resistance in the field.

There are several classic examples of structural target site modification as a mechanism in insecticide resistance; resistance to organophosphates (OPs) and carbamates, legacy organochlorine insecticides, and the naturally derived insecticides (pyrethrins) are discussed as targets to components of the insect nervous system.

Acetylcholinesterase-based resistance has been well documented in numerous strains of mites, ticks, houseflies, and mosquitoes. The OPs and carbamates target acetylcholinesterase (AChE), an enzyme localized in the synapse that hydrolyzes the neurotransmitter acetylcholine once it has excited postsynaptic nerve membranes. The OP insecticides are converted to their oxon analogues via the action of monooxygenases before acting as AChE inhibitors. Alterations in AChE in OP-and carbamate-resistant insects result in a decreased sensitivity to inhibition of the enzyme by these insecticides [60]. The determination of kinetic constants of inhibition of AChE indicated that the binding affinities between AChE and the oxon metabolites of OPs or carbamates were lower in more resistant insect strains.

GABA receptors belong to a superfamily of neurotransmitter receptors that include nicotinic acetylcholine receptors. These receptors are formed by the oligomerization of five subunits around a central transmitter-gated ion channel. The GABA receptor in insects is a heteromultimeric gated chloride-ion channel, a widespread inhibitory neurotransmission channel in the insect's central nervous system and in neuromuscular junctions. The $GABA_A$ receptor-chloride channel complex is known to be the target of cyclodiene insecticides. Dieldrin first enhances and then suppresses γ-aminobutyric acid (GABA)-induced chloride currents. An alanine-to-serine substitution in the putative channel-lining domain of the GABA receptor confers resistance to cyclodienes such as dieldrin in a broad range of dieldrin-resistant insects [61]. The only variation in resistant insects is that glycine rather than serine can sometimes be the substituted amino acid residue. Despite the widespread switch away from the use of cyclodiene insecticides for agricultural and public health use the resistance allele is still found at relatively high frequencies in insect field populations. The insect GABA receptor is implicated as a site of action for some pyrethroids and avermectins as well as cyclodienes.

DDT and pyrethroids cause persistent activation of Na^+ channels by delaying the normal voltage-dependent mechanism of inactivation. Insensitivity of Na^+ channels to insecticide inhibition, also called knockdown or *kdr-like resistance*, was inferred from cross-resistance between DDT and pyrethroids, which act on the same site within the Na^+ channel. Several mechanisms of resistance have been proposed and involve a reduction in the number of Na^+ channels, changes in the fluidity of nerve membranes, or alterations in the binding characteristics between Na^+ channels and insecticides. Changes associated with resistance are more variable than those seen in with GABA receptors but are still limited to a small number of regions on this large channel protein. The first mutation to be characterized in *kdr* insects was in the housefly. The Na^+ channel of housefly contains 2,108 amino acids, which fold into 4 hydrophobic repeat domains. A leucine to phenylalanine point mutation in the S6 transmembrane segment of domain II produced 10- to 20-fold resistance to DDT and pyrethroids [62]. More than 500-fold resistance is found in "*super-kdr*" houseflies, which possess a mutation in a second methionine to threonine substitution further upstream in the same domain.

Overexpression of Target The up-regulation of target is also be a resistance mechanism by which the target is allowed to fulfill its biological function even in the presence of the xenobiotic at physiological concentrations and resultant toxicity. This is a compensatory mechanism for the portion of the target that is occupied. Thymidilate synthase (TS) is the major cellular target of 5-fluorouracyl (5-FU), a chemotherapy agent. 5-FU is activated to 5′-monophosphate-5-fluorouridine, which interrupts the action of TS, blocking the synthesis of the pyrimidine thymidine, a nucleotide required for DNA

replication, resulting in a thymidine deficiency and cell death in replicating cells. Resistant tumor cells show increased TS activity through increases in the amount of target per cell [63].

Down-regulation (Including Gene Disruption or Silencing) Finally, decreasing target site sensitivities can be achieved by down-regulation of receptor levels or responsiveness of signal transduction pathways. This can be problematic, as down-regulation of an important physiological process can lead to reduced function. Down-regulation can also occur for repressors; for example, AhR repressor mutations in regulatory factors causing disruption in silencer elements can result in overexpression of AhR and may carry a high cost due to dominant expression in the wrong tissues; like structural mutations, these types of mutations may arise early in resistance, but disappear when less deleterious alternatives come about. One example of down-regulation occurs in resistance to cancer chemotherapy. Topoisomerase II is a homodimeric enzyme that is essential for DNA replication since it modifies DNA topology by transient breakage of DNA and religation. During this process, an intermediate complex between the enzyme and DNA forms and is susceptible to several cytotoxic chemotherapy drugs (e.g., mitoxanthrone) that stabilize the complex leading to DNA fragmentation and chromosomal aberrations and rearrangements. In resistant tumor cells, topoisomerase II is down-regulated to levels just required for cell division, thereby reducing the amount of DNA damage caused by these drugs [63, 64].

Circumvention of Target This is a rare phenomenon of resistance but has been documented very early in organisms that have alternative mechanisms to bypass the affected site of action. An example of circumvention occurs in citrus-scale insects resistant to hydrogen cyanide. Widespread application of hydrocyanic acid (HCN formulation) was initially limited to the fumigation of valuable tree crops such as citrus fruits, which led to the development of other HCN-based insect and rodent control products for the fumigation of ships, stores, factories, and even residential buildings. The target molecule is cytochrome oxidase, in the fourth complex of the electron transport chain. HCN binds to Fe within this protein, preventing it from transferring electrons to oxygen, resulting in an inability to aerobically produce ATP. Citrus-scale mites utilize an HCN-insensitive flavoprotein as an alternate electron carrier in the place of cytochrome oxidase, enabling electron transport [65].

Conclusions and Future Directions

Understanding the role of protection (tolerance and resistance) has numerous significant implications for the quality of life and the environment. It impacts the area of human health in disease treatment (e.g., chemotherapy), pharmacology (e.g., new drugs, individual susceptibilities, safety), and public health protection programs (disease and vector control). It is also crucial for many areas of the environment in determining sensitive and sentinal species, biomarker development, establishment of water quality guidelines, new chemical development, and risk assessment. As well, it has considerable economic ramifications (e.g., modern agriculture and pest resistance, cross-resistance, genetically modified food, biological control, integrated pest management programs). Few real tools for delaying or preventing the onset of resistance to chemicals such as pesticides and chemotherapeutic agents have yet to be put into practical use. Furthering basic scientific understanding of biological relationships (e.g., herbivory and allelochemicals), biological toxins and antidotes, development theories for resistance evolution, etc. are also of value.

Imagining future directions for a subject area as broad and multidisciplinary is fraught with potential omissions. Directions for more research are as diverse as the applications that would be supported. One thing is clear, however: With the enormous advances being made in molecular biology (e.g., toxicogenomics, bioinformatics, metabolomics) and its sophisticated tools, insights into the mechanisms and manipulations of protection against xenobiotics are fast approaching. These new tools and information will be transforming, and if researchers make a conscious effort to link molecular data to population or ecological levels, gains in this sphere of study will be vast.

Bibliography

1. Ngo NT, Stupans I, McKinnon RA (2009) Xenobiotic detoxification in Australian marsupials – an overview. Comp Biochem Physiol Part A 154:S5
2. Wirgin I, Waldman JR (2004) Resistance to contaminants in North American fish populations. Mut Res 552:73–100

3. Mallet J (1989) The evolution of insecticide resistance: have the insects won? Tree 4:336–340
4. Saves I, Masson J-M (1998) Mechanisms of resistance to xenobiotics in human therapy. Cell Mol Life Sci 54:405–426
5. Ray K, Levandowsky M (2001) Effects of ionic blocking agents on shape, motility and chemosensory responses in Euglena. Abstracts of the General Meeting of the American Society for Microbiology 101:734
6. Bargmann CI (2006) Chemosensation in *C. elegans*. In: WormBook (ed) The *C. elegans* Research Community, WormBook, 29 pp. doi:10.1895/wormbook.1.123.1, http://www.wormbook.org
7. Doty RL (2001) Olfaction. Ann Rev Psychol 52:423–452
8. Rouquier S, Giorgi D (2007) Olfactory receptor gene repertoires in mammals. Mut Res/Fund Mol Mech Mutagenesis 616:95–102
9. Hall LW, Burton DT, Graves WC, Margrey SL (1984) Behavioral modification of estuarine fish exposed to sulfur dioxide. J Toxicol Environ Health 13:969–978
10. Suh GSB, Wong AM, Hergarden AC, Wang JW, Simon AF, Benzer S, Axel R, Anderson DJ (2004) A single population of olfactory sensory neurons mediates an innate avoidance behaviour in Drosophila. Nature 431:854–859
11. Tierney KB, Baldwin DB, Hara TJ, Ross PS, NScholz NL, Kennedy CJ (2009) Review: olfactory toxicity in fishes. Aquat Toxicol 96:2–26
12. Kandel ER (2009) The biology of memory: a forty-year perspective. J Neurosci 29:12748–12756
13. Pierce RC, Kalivas PW (1997) A circuitry model of the expression of behavioral sensitization to amphetamine-like psychostimulants. Brain Res Rev 25:192–216
14. Lee JC, Bernays EA (1990) Food tastes and toxic effects: associative learning by the polyphagous grasshopper *Schistocerca americana* (Drury) (Orthoptera: Acrididae). Animal Behav 39:163–173
15. Craig AD (2002) How do you feel? Interoception: the sense of the physiological condition of the body. Nat Rev Neurosci 3:655–666
16. Fernando CT, Liekens AML, Bingle LEH, Beck C, Lenser T, Stekel DJ, Rowe JE (2009) Molecular circuits for associative learning in single-celled organisms. J R Soc Interface 6:463–469
17. Lopez-Grancha M, Sanchez-Amate C, Navarro M, Carvajal F, Sanchez-Santed F, Cubero I (2006) Lateral parabrachial lesions disrupt paraoxon-induced conditioned flavor avoidance. Toxicol Sci 91:210–217
18. Mandrillon A-L, Saglio P (2007) Herbicide exposure affects the chemical recognition of a non native predator in common toad tadpoles (*Bufo bufo*). Chemoecology 17:31–36
19. Myllyvirta TP, Vuorinen PJ (1989) Avoidance of bleached kraft mill effluent by pre-exposed *Coregonus albula* L. Water Res 23:1219–1227
20. Patil VK, David M (2010) Behavioral and morphological endpoints: as an early response to sublethal malathion intoxication in the freshwater fish, *Labeo rohita*. Drug Chem Toxicol 33:160–165
21. Tierney KB, Casselman M, Takeda S, Farrell AP, Kennedy CJ (2007) The relationship between cholinesterase inhibition and two types of swimming performance in chlorpyrifos-exposed coho salmon (*Oncorhynchus kisutch*). Environ Toxicol Chem 26:998–1004
22. Martin GG (1978) Ciliary gliding in lower invertebrates. Zoomorphology 91:249–261
23. Storch V, Welsch U (1972) The ultrastructure of epidermal mucous cells in marine invertebrates (Nemertini, Polychaeta, Prosobranchia, Opisthobranchia). Mar Biol 13: 167–175
24. Taylor HH (1971) The fine structure of the type 2 cells in the Malpighian tubules of the stick insect, Carausius morosus. Cell Tissue Res 122:411–424
25. Khanvilkar K, Donovan MD, Flanagan DR (2001) Drug transfer through mucus. Adv Drug Delivery Rev 48:173–193
26. Debat H, Eloit C, Blon F, Sarazin B, Henry C, Huet J-C, Trotier D, Pernollet J-C (2007) Identification of human olfactory cleft mucus proteins using proteomic analysis. J Proteome Res 6:1985–1996
27. Starcevic SL, Zielinski BS (1995) Immunohistochemical localization of glutathione S-transferase pi in rainbow trout olfactory receptor neurons. Neurosci Lett 183:175–178
28. Maïbèche-Coisne M, Jacquin-Joly E, François MC, Nagnan-Le Meillour P (2002) cDNA cloning of biotransformation enzymes belonging to the cytochrome P450 family in the antennae of the noctuid moth *Mamestra brassicae*. Insect Mol Biol 11:273–281
29. Boutsiouki P, Thompson J, Clough G (2001) Effects of local blood flow on the percutaneous absorption of the organophosphorus compound malathion: a microdialysis study in man. Arch Toxicol 75:321–328
30. Moon KC, Maibach HI (1991) Percutaneous absorption in diseased skin: relationship to the exogenous. In: Menne T, Maibach HI (eds) Exogenous dermatoses: environmental dermatitis. CRC Press, Boca Raton, pp 217–226
31. Matsumura F (2010) Studies on the action mechanism of benzoylurea insecticides to inhibit the process of chitin synthesis in insects: a review on the status of research activities in the past, the present and the future prospects. Pesticide Biochem Physiol 97:133–139
32. Singh P, Sihorkar V, Jaitely V, Kanaujia P, Vyas SP (2000) Pilosebaceous unit: anatomical considerations and drug delivery opportunities. Indian J Pharmacol 32:269–281
33. Kapoor IP, Metcalf RL, Herwe AS, Coats JR, Khalsa MS (1973) Structure-activity correlations of biodegradability of DDT analogs. J Agric Food Chem 21:310–315
34. Ross PS, Ellis GM, Ikonomu MG, Barrett-Lennard LG, Addison RF (2000) High PCB concentrations in free-ranging Pacific killer whales, *Orcinus orca*: effects of age, sex and dietary preference. Mar Poll Bull 40:504–515
35. Coon MJ (2005) Cytochrome P450: nature's most versatile biological catalyst. Ann Rev Pharmacol Toxicol 45:1–25
36. Kennedy CJ, Tierney KB (2008) Energy intake affects the biotransformation rate, scope for induction, and metabolite

profile of benzo[a]pyrene in rainbow trout. Aquat Toxicol 90:172–181
37. Cui L, Sun H, Wishnok JS, Tannenbaum SR, Skipper PL (2007) Identification of adducts formed by reaction of N-acetoxy-3, 5-dimethylaniline with DNA. Chem Res Toxicol 20:1730–1736
38. Hodgson E, Levi PE (1994) Biochemical toxicology, 2nd edn. Appleton & Lange, Norwalk
39. Denison MS, Pandini A, Nagy SR, Baldwin EP, Bonati L (2002) Ligand binding and activation of the Ah receptor. Chem Biol Interact 141:3–24
40. Levine SL, Perdew GH (2001) Aryl hydrocarbon receptor (AhR)/AhR nuclear translocator (ARNT) activity is unaltered by phosphorylation of a periodicity/ARNT/single-minded (PAS)-region serine residue. Mol Pharmacol 59:557–566
41. Xu C, Li CY-T, Kong A-NT (2005) Induction of Phase I, II and III drug metabolism/transport by xenobiotics. Arch Pharm Res 28:249–268
42. Epel D, Luckenbach T, Stevenson CN, MacManus-Spencer LA, Hamdoun A, Smital T (2008) Efflux transporters: newly appreciated roles in protection against pollutants. Environ Sci Technol 42:3914–3920
43. Cooper P, Vogelbein W, Van Veld W (1996) Immunohistochemical and immunoblot detection of P-glycoprotein in normal and neoplastic fish liver. In: Ostrander G (ed) Techniques in aquatic toxicology. CRC Press, Boca Raton, pp 307–325
44. Juliano RL, Ling V (1976) A surface glycoprotein modulating drug permeability in Chinese hamster ovary cell mutants. Biochim Biophys Acta 455:152–162
45. Gerlach JH, Kartner N, Bell DR, Ling V (1986) Multidrug resistance. Cancer Surv 5:25–46
46. Kurelec B, Krca S, Lucic D (1996) Expression of multixenobiotic resistance mechanism in a marine mussel *Mytilus galloprovincialis* as a biomarker of exposure to polluted environments. Comp Biochem Physiol 113:283–289
47. Bard S (2000) Multixenobiotic resistance as a cellular defense mechanism in aquatic organisms. Aquat Toxicol 48:357–389
48. Felix R, Barrand A (2002) P-glycoprotein expression in rat brain endothelial cells: evidence for regulation by transient oxidative stress. J Neurochem 80:64–72
49. Ishikawa T (1992) The ATP-dependent glutathione S-conjugate export pump. Trends Biochem Sci 17:463–468
50. Litman T, Druley TE, Stein WD, Bates SE (2001) From MDR to MXR: new understanding of multidrug resistance systems, their properties and clinical significance. Cell Mol Life Sci 58:931–959
51. van Herwaarden AE, Jonker JW, Wagenaar E, Brinkhuis RF, Schellens JHM, Beijnen JH, Schinkel AH (2003) The breast cancer resistance protein (BCRP1/ABCG2) restricts exposure to the dietary carcinogen 2-amino-1-methyl-6-phenylimidazo [4, 5-b]pyridine. Cancer Res 63:6447–6452
52. Ross PS (2006) Fireproof killer whales (*Orcinus orca*): flame-retardant chemicals and the conservation imperative in the charismatic icon of British Columbia, Canada. Can J Fish Aquat Sci 63:224–234
53. Kurelec B (2002) The multixenobiotic resistance mechanism in aquatic organisms. Crit Rev Toxicol 22:23–43
54. Miller DS (2002) Xenobiotic export pumps, endothelin signaling, and tubular nephrotoxicants – a case of molecular hijacking. J Biochem Mol Toxicol 16:122–127
55. Twomey PJ, Viljoen A, House IM, Reynolds TM, Wierzbicki AS (2005) Relationship between serum copper, ceruloplasmin, and non–ceruloplasmin-bound copper in routine clinical practice. Clin Chem 51:1558–1559
56. Cornwell MM, Safa AR, Felsted RL, Gottesman MM, Pastan I (1986) Membrane vesicles from multidrug resistant human cancer cells contain a specific 150- to 170-kDa protein detected by photoaffinty labelling. Proc Natl Acad Sci USA 83:3847–3850
57. Kaplowitz N (1980) Physiological significance of glutathione S-transferases. Am J Physiol 239 (Gastrointest Liver Physiol 2): G439–G444
58. Sigel A, Sigel H, Sigel RKO (2009) Metallothioneins and related chelators. Metal ions in life sciences, vol 5. RSC Publishing, Cambridge
59. Taylor M, Feyereisen R (1996) Molecular biology and evolution of resistance to toxicants. Mol Biol Evol 13:719–734
60. Skouras PJ, Margaritopoulos JT, Seraphides NA, Ioannides IM, Kakani EG, Mathiopoulos KD, Tsitsipis JA (2007) Organophosphate resistance in olive fruit fly, *Bactrocera oleae*, populations in Greece and Cyprus. Pest Manage Sci 63:42–48
61. Gao J, Kozaki T, Leichter CA, Rinkevich FD, Shono T, Scott JG (2007) The A302S mutation in Rdl that confers resistance to cyclodienes and limited cross-resistance to fipronil is undetectable in field populations of house flies from the USA. Pesticide Biochem Physiol 88:66–70
62. Soderlund DM (2008) Pyrethroids, knockdown resistance and sodium channels. Pest Manage Sci 64:610–616
63. Skovsgaard T, Nielson D, Maare C, Wassermann K (2004) Cellular resistance to cancer chemotherapy. Int Rev Cytol 156:77–157
64. Vassetzky YS, Alghisi GC, Gasser SM (1995) DNA topoisomerase II mutations and resistance to anti-tumour drugs. Bioessays 17:767–774
65. Hoskins WM, Gordon HT (1956) Arthropod resistance to chemicals. Ann Rev Entomol 1:89–122

Glossary Terms

€ 1584
α 7181, 12203
α-γ Transformation 6938
ρ 7181
β 7181
β-β Transformation 6938
δ 7181
η 1584
η_c 5499
η_f 5499
$\eta_{f,b}$ 5499
$\eta_{f,i,}$ 5499
η_m 5499
η_{th} 5499
$\eta_{th,Carnot}$ 5499
$\eta_{th,Otto}$ 5499
η_v 5499
Φ 12203
γ 5499
γ_b 5499
λ_{max}^{abs} 5174
λ_{max}^{em} 5174
μ_1, First molecular weight moment 4617
ω 12203
φ 5500
Φ 5174
Φ^{em} 5174
ρ 12203
$\rho_{a,i}$ 5500
σ 12203
τ 5500
θ 12203
${}_1Q_2$ 5500
${}_1W_2$ 5501
${}_2W_3$ 5501
3 Phase boundary 8328
3D Pose estimation 10590
$3D^{pol}$ 8126
${}_3W_4$ 5501
3'UTR 8126
${}_4W_5$ 5501
${}_5W_6$ 5501
5'UTR 8126
${}_6Q_1$ 5500
${}_6W_1$ 5501
a 12202
A 12202
AAV 10815
Abandoned mines 6646
Abiotic factor 148
Abiotic 10139, 11375
Abiotic stress 1, 10732
Ablation 2761
ABR 1145
Abscisic acid 9145
Absolute humidity 893
Absorbed dose 3022, 4905, 8387, 8448, 8559, 11026
Absorber 2349
Absorber tube 9562
Absorption, $a(\lambda)$ 8952
Absorption coefficient 309
Absorption 309, 4774, 10139, 12293
Absorptivity or absorptance (α) 9449
Abstract community 3278
Abuse 6098
AC motor 11523
AC 9432
ACC 6449, 6951
Acceleration method 9851
Acceptable limit 3515
Access time 1854
Accessible ecosystem 10796
Accident 3515
Acclimation 3253, 7229
Acclimatization 10732
Accretion 2761
Accumulation 2761
Acetosyringone 2583
Acid deposition 167
Acid drainage 6665
Acid neutralizing capacity (ANC) 167
Acid (rock or mine) drainage 6646

Acidity constant 11912
Acidophile 6646
Acoustic power level *(L_W)* 12275
ACPE 8123
Acquired immunodeficiency syndrome (AIDS) 4997, 11129
ACS 4957
ACT 11068
Actinides 7142, 8598
Action level 3515
Action levels 9079
Action spectrum 9649
Activated carbon 3426
Activated sludge process 11961
Activation energy 4094
Activation overpotential 6720
Active material 6122
Active region 9469
Active remote sensing 309
Activity concentration 8387
Activity 3705, 8559
Actuator 11946
Acute dose 5573
Acute toxicity test 11220
AD 5296
AdaBoost 6951
Adaptation 148, 2929, 3253, 7229, 10732, 12293
Adaptation (with respect to climate change) 4673
Adaptive capacity 167
Adaptive control 46
Adaptive governance 3342
Adaptive management 565, 3342
Adaptive protection 12079
Adaptive response 5573
ADAS 64
ADB 1145
Additive genetic variance 473, 10732
ADG 7866
Adiabatic process 5216
Adjuvant 6291
ADP 1583
Adsorption 4774, 7006, 10139, 10962
Adult 3620
Advanced biofuel 5461
Advanced driver assistance system 3067
Advanced natural ventilation system (ANV) 6865
Advection 9049, 10139
Adverse effect 3620
Adverse health effect 206
AEM 372
AER 1426, 8112
Aerobic 10139
Aerodynamic diameter 167, 206
Aerodynamic resistance 3211
Aerosol extinction 309
Aerosol optical depth 111, 168, 9673
Aerosol 111, 167, 206, 309, 606, 6740
Aerosols 622
Aesthetics 10360
AF 1145
AFC 372, 3872
AFP 8123
AFP surveillance 8123
African easterly jet (AEJ) 5070
African easterly waves (AEWs) 5070
After shocks 2424
Aggregated transfer parameter ($T_{ag}m^2\ kg^{-1}$) 8425
AGM 5881
Agribusiness applications 4353
Agricultural practices 2740
Agricultural residues 1487
Agricultural waste 10000
Agricultural water 11873
Agriculturally marginal land 1268
Agriculture 2740
Agrobacterium tumefaciens 10732
Agrobacterium tumefaciens 8058
Agrobacterium-mediated transformation 2583
Agroecology 149
Agroecosystem, agrosystem – agricultural ecosystem 5428
Agroecosystem 149, 2740
Agroforestry 149
Agronomic crops 2740
Agronomic performance/trait 10732
Agronomy 2740
AGT 7777
Ah Ampere hour 6938
Ah 5881
AIA (The American Institute of Architects) 5332
AIC 652
Air changes per hour (ACH) 6865
Air equivalence ratio 5235
Air mass 9673, 9705

Air pollutants 11291
Air pollution monitoring 168
Air pollution policy 168
Air pollution 11291
Air quality 168, 11291
Air quality guidelines 206
Air quality index 11291
Air quality monitoring 168, 206
Air sparging 10139
Air toxic 298
Air-conditioning 9509
Airline emission index 652
Airtight construction 7629
Albedo 8537, 9619, 9696, 9705
Alcohol 987, 1025
Aldolase 10732
Algae 346, 7006, 9109
Algorithm 10192
Aliphatic 10139
Alkalinity 7006
Alkaloid 10636
Allele frequency 10733
Allele 2781, 7972, 10733
All-electric range (AER) 10502
Allelic exclusion 10733
Allelopathy 149
Allocative efficiency 2720
Allochthonous 5047, 7006
Allogenic 10733
Allometric scaling 8387
Allopolyploid Plants 10733
Allopolyploid 10733
Allosteric Regulation 10733
Allothermal gasification 1426
Alpha particle 5560, 8559
Alpha radiation 5573, 8448
Alternate daily cover (ADC) 5706
Alternating current (AC) 671
Alternative energy 10317
Alternative fecal indicators 6319
Alternative fuel 5461
Alternatives analysis 1833
Alternator 5083
AM1.5 6566
Ambient air 206, 11291
Ambient and task lighting 3675
Ambient concentration-response function 206
Ambient 4235, 5047
AMFC 372
AMMA 5070
Ammonification 6646
Amorphous 6646, 9240
Amphoteric 8598
Amp-hour (Ah) 671
Amplification 2424
Amplitude modulation 12275
Amplitude 2424
An outbreak 9079
Anabolic 10733
Anadromous 6386
Anaerobic digestion 1607
Anaerobic 10139, 11932, 11946
Analgesic 10636
Analogue radionuclide 8387
Analysis 11737
Analyte 1646
Analytical pipeline 6692
Anchor grouting 4201
Anchorage failure moment 6201
Ancillary services 12254
Ancillary services 8980
Andesite 11613
Aneuploid 6150, 10733
Aneuploidy 10733
Animal bioreactor 10864
Animal breeding 406, 9358
Animal cloning 10895
Animal genetic resources 406
Animal model (AM) 1795
Animal welfare 406
Annual efficiency 1351
Annualized operating cost 1855
Anode – (negative electrode) 708
Anode 3886, 6498, 6720, 7731, 9885
Anomaly 9795
Anoxic 11932, 11946
Anoxic sediment 7006
Antarctic bottom water 5856
Anthracite 2173, 8347
Anthropocene 7229
Anthropogenic indicator 11911
Anthropogenic 206, 7328, 8467, 8879
Anthropogenic radionuclides 8655
Anthropogenic source 298

Anthroposphere 3450
Antibiotic 498, 10733
Antibiotic resistance 498, 2259
Antibody 10733, 10864
Antilock braking system (ABS) 8848
Antimicrobial 10852
Antinutrients 1676, 10733
Antioxidant 3655
Antireflection coating layer (ARC) 9196
Antisense RNA 10733
Antiserum 10733
AP 1583
APAR 7902
APC 90
APC residues 11838
APCS 5909
Aperture 9588
APM 7777
Apoptosis 10636
Apparent competition 10062
Apparent optical properties (AOP) 8952
Application efficiency 5619
a' 12202
APTS 90
APU 9904
Aquaculture 511, 5893, 9109, 10317
Aquiclude 4201, 4414
Aquicludes 5706
Aquifer 4201, 4414, 9000, 11933
Aquifer unit 4806, 5712
Aquifers 5706
Aquitard 5712
Arabinoxylan 10839
Arc plasma 8097
Arc plasma torch 8097
Archaea 5047
Architecture 3367
Arctic oscillation 10117
Area of focus 565
Area source 298
Argo floats 5856
Armature winding 11523
Articulated bus 1855
Artisanal fisheries 581
ASCC 5909
ASF 1426
Ash 2173, 2194, 2271, 4866, 8347
Ash residue 11737
a-Si 9432
Assessment process 8702
Assimilation 12062
Assisted reproduction 10815
Association mapping 2528
Associative effect 9358
ASTER 8939
At-grade BRT 1855
Atmophilic 10577
Atmosphere Model Intercomparison Project 2510
Atmosphere 8467, 11291
Atmospheric boundary layer (ABL) 6583
Atmospheric boundary layer 309
Atmospheric rivers 7245
Atmospheric surface layer 6584
(Atmospheric) Wind stress 7366
Atoll 8468
Atom economy 4584, 4616
ATRA 7777
Attainable yield 2720
Attenuate 11985
Attenuation 2424
Attenuation depth 8919
Attitude 12218
Attribute 12218
Audible sound 12275
AUSC 2163
Austenitic stainless steel 7193
Autochthonous 5047, 7006
Autocorrelation 9744
Autoinfection 12018
Automated guided transit (AGT) 1855
Automotive night vision 11097
Automotive PEMFC 8231
Autothermal gasification 1426
Autothermal reforming (ATR) 3955
Autotrophic 1476, 6372
aVDPV 8123
Average operating speed 1855
Average recurrence interval (ARI) or return period 10095
Average speed 5971
AVHRR 8939
Aviation 652
Avirulent 10733
AVL 90

Avoidance 12293
Azoic conditions 9174
B 12202
Bacillus thuringiensis (Bt) 10733
Back cross (BC) 2528
Backcross 2689, 6425
Background level 168
Background levels 206
Backscattering, $b_b(\lambda)$ 8953
Bacteria 5047
Bacterial pathogens 8758
Bacteriolytic 10852
Bacteriostatic 10852
Bacterium 10694
Bactofection 2583
Baghouse 8347
Balance of plant (BOP) 3860
Balanced mechanical ventilation with heat recovery 7629
Balancing area 8980, 12098, 12254
Balancing market 12098
Balancing reserves 12098
Balneology 4162, 4353
Band gap 7881
Baroclinic 5856
Barotropic 5856
Barrage 10613
Barrel 4380
Basalt 11613
Base bending moment 6201
Base temperature 2540
Baseline 4201, 6951, 9000
Base-load demand 4190
Baseload plant 7296
Baseload plants 4235
Baseload 4235, 7296
Basic reproductive number 5347
Basicity 6720
Basin 4806
Bathymetry 7365
Battery efficiency 739
Battery electric vehicle 11502
Battery management system (BMS) 671
Battery pack 671
Battery 671, 708, 3471, 3847, 11502
Battery state of charge 5083
Battery string 671
Battery/battery pack 6122
Battery-powered electric vehicle (BEV) 10502
Bayes classifier 6951
Bayes' Theorem 2098
Bayesian inference 415
bbl 3955
BCMS 11068
Beacon, traffic pylon, guiding reflector post 3067
Beauty 10360
Becquerel (Bq) 5573, 8448
Bedstead barrier 5934
Beef Improvement Federation (BIF) accuracy 1723
Behavioral model 10192
BEMS 6865
Benchmark 4201
Beneficial insects – arthropods 149
Beneficial use 3029, 11737
Beneficiation 6665
Benthic boundary layer 9128
Benthic 1959
Benthos 7006, 8201
Best available technology (BAT) 168, 11838
Best linear unbiased prediction (BLUP) 389, 1795
Best management practice (BMP) 10095, 10139, 9174
Beta particle 5560
Beta particles 11026
Beta radiation 5573, 8448
Beta-diversity 3357
BEV 7847
bf 1583
BGF 11552
BHA (bottom-hole assembly) 4380
BIBAC 2583
BIDS™ 10261
Bike lane 806
Bike locker 806
Bike rack 806
Bike station 806
BIM model 10299
Binary power plant 4162
Binary vector 2583
Binary-cycle power station 4235
Bio energy 1531
Bioaccumulation factor (BAF) 3265
Bioaccumulation 822, 4819, 7006, 9156, 10657
Bioassay (BIOlogical ASSAY) 6354

Bioavailability 1676, 8387
Bioavailable 9156
Bio-based products 1268
Biobased vs. biodegradable 9025
Biocenosis 8468
Biochar 845
Biochemical conversion 1198
Biocoal 1067
Bioconcentration factor (BCF) 3265
Bioconcentration 822, 10657
Bioconversion 10733
Biodegradable 10733
Biodegradation 9049, 10139, 11961
Biodegradation/biomineralization 1627
Biodeposition 9174
Biodiesel 921, 1607, 11429
Biodiscovery 3150
Biodiversity 939, 1531, 5047, 6216, 10085, 10765
Bio-economic index 1723
Bioenergy crops 1476
Bioenergy 1174, 1198, 1268, 1476, 1487, 1607, 2271
Bioethanol 961, 988, 1607
Bioextraction 9109
Biofloc 533
Biofortification 1676
Biofouling 581
Biofuel 347, 1002, 1025, 1198, 1231, 1268, 1426, 1487, 1531, 1607
Biofuel program 1002
Biofuels 10503
Biogas cleaning 1089
Biogas 1025, 1089, 1174, 1231, 1607, 1618
Biogas substrate 1174
Biogas upgradation 1618
Biogenic 168, 206, 8879
Biogeochemical cycle 7365
Biogeochemical cycling 7328
Biogeochemistry 6372
Biohydrogen 5116
Bioindicator 8387
Bioinformatics 10733
Biokinetic model 11026
Biokinetic studies 8387
Bioleaching 6646
Bioliquid 1025
Biological biohydrogen generation 5116
Biological contaminants 9079
Biological control 5428
Biological half-life ($t_{\frac{1}{2}}^{bio}$) 8598
Biological half-life 7006, 8387, 11026
Biological invasion 5548
Biological modeling 1
Biological pump 6372, 7229
Biological survey 3265
Biologically effective UV radiation 11375
Biomagnification 822, 9156, 10657
Biomarker 1184
Biomarkers 3265
Biomass ash 9821
Biomass gasification 1661
Biomass 149, 347, 1002, 1025, 1174, 1198, 1231, 1269, 1298, 1476, 1487, 1531, 1607, 2271, 5116, 7006, 10733, 11429
Biomass residues 1174, 1487
Biomethane 1174, 1618
Biomimicry 8856, 10332
Biomineralization 10403
Biomining 6646
Biomitigative services provided by extractive aquaculture 542
Bio-oil 11429
Biopharmaceuticals 8058
Biophilia 3675, 10261
Bioprocess 10733
Bioreactor 6519
Bioremediation 1627
Bio-SNG 1607, 1661
Biosphere 168
Biosynthesis 822, 10734
Biosynthetic 10734
Biota 6633, 7006, 7229
Biotechnology 10734
Biotic factor 149
Biotic ligand model (BLM) 10051
Biotic 10139, 11375
Biotic Stress 10734
Biotransformation 12293
Biotroph 2559
Bioturbation 7006, 8387
Bioturbation transport 9128
Bioventing 10139
Bi-phase expander 4235
Bipolar plate 5881, 7694
Bitumen 7457, 7798

Bituminous coal 2173, 8347
BL 5173
Black body 2349
Black carbon 845
Black liquor 1174
Blackbody (BB) radiation 9412
Blackbody radiator 9795
Blade 7393
Blanket 7086
Blastocyst 6150
Bleed 4201
Blocking, blocking losses 2349
Blood stage 6291
Blow out 4380
BLUP (best linear unbiased prediction) 7972
BLUP 473, 9358
B/M 4616
BMEP 5500
BMGF 11068
BOD 1145, 5909, 11933
BOE 3955
Bogie or truck (United States) 1855
Boiler ash 11720
Boiler efficiency 1351
Boiler 1351
Bone morphogenetic proteins (BMPs) 10886
BOP (blow-out preventer) 4380
BOP 7866
BoP 9934
bOPV 8123
BORDA 1145
BOS 9432
Bottom ash 11720, 11737
Boundary layer 11311
Boundary layer pressurized balloon (BLPB) 5070
Boussinesq approximation 7366
bpy 5173
Brackish water 11933
Brackling 6201
Brake controller 8848
Brake-by-wire 8848
Braking energy 8848
Braking forces 11481
Braking performance 11481
Braking system 11481
Branding 1833
Brayton cycle 6804, 7086
Breakdown 11158
Breakthrough time 3501
BREEAM 6865
Breed 389
Breeder 7086
Breeding nuclei 8307
Breeding ratio 4050
Breeding value (BV) 1795
Breeding value 415, 473, 2781, 8307, 9359
BREF 11838
Brightening 9731
Brightness contrast/glare 2846
Brine 2897, 4235
Briquetting 1067
Broadband radiation 9673
Broken arrow 8387
Brownfield 11362
BRT 90, 1890
Brushless DC motor 11523
BSL 8123
BTDF 2804
Bt-expressing transgenic crops 10713
BtL fuels 921
BtL 1039, 1584
Btu 2163, 3955
Bubble pressure 7866
Bubbly jet 10975
Building and street scales 11263
Building Environmental Assessment Method (system or scheme) 8702
Building information model 10192
Building information modeling (BIM) 10299
Building life cycle 10192
Building performance 10192
Build-operate-transfer (BOT) 1855
Buildup factor 8537
Bulk coefficients 594
Bulk heterojunction 7553
Buoyant jet 10975
Buried tritium 10997
Burnup 7193
Bus corridor 1833
Bus lane 1833, 1855
Bus 806
Bus priority 1833
Bus rapid transit (BRT) or Bus transit with high level of service (BHLS) 1855

Bus rapid transit (BRT) 1810
Bus rapid transit 5971, 10923
Bus rapid transit vehicle 1810
Bus transit system (BTS) 1855
Buses 4945
Busway 1833
Butanol 1607
Buy America 1811
By-catch 6179
By-product of a reaction 4616
By-product 11699
°C 2163
c 7181
C Rate 7546
C3 Grasses 6020
C_3 photosynthetic system 10390
C3 2615
C3-plants 1476
C4 Grasses 6020
C_4 photosynthetic system 10390
C4 2615
C4-plants 1476
CAA 5909
Cable system 11158
Cadmium telluride (CdTe) solar cells 7932
Calcification 7229
Calcium carbonate saturation horizon 7229
Caldera 4162, 11633
Calibration 11455
Callus 10734
Calorie 4162
Calorific value 2173, 8348
Calorimetry 7201
Calvin Cycle 10734
Calving 10886
CAMARTEC 1145
CAN 6951
Cancer 5573
Candidate gene 473, 6425
Cap rock 4162
Capacity building 565, 6692
Capacity factor 2349, 4191, 4235
Capacity, installed (or Nameplate) 4235
Capacity markets 12254
Capacity 708, 4235, 6122, 7546, 11503
CAPEX 1584
Capital assistance/expenditures 1811
Capital cost 4340
Capsid 8123
Capsomere 8123
Carbon abatement (CA) 845
Carbon capture and sequestration (CCS) 2149
Carbon Credit 845
Carbon cycle 2510
Carbon dioxide capture and storage (CCS) 4119
Carbon dioxide (CO_2) 4754, 8348
Carbon (dioxide) equivalent 845
Carbon dioxide equivalents ($CO_{2,eq}$) 4755
Carbon dioxide 4235
Carbon dioxide removal (CDR) 10117
Carbon geoengineering 4104
Carbon leakages 1487
Carbon monoxide (CO) 8348
Carbon monoxide 206
Carbon nanotube 3426
Carbon neutral net-zero and the 2030 challenge 3675
Carbon selectivity 3933
Carbon sequestration 161, 7267
Carbon stability factor (CSF) 845
Carbon structure and texture 6769
Carbonate rocks 5645
Carboniferous 2173
Carbonization 7866
Carbon-rich soils 1488
Carcinogen 3620, 11026
Carnot cycle 6805
Carnot efficiency 9588
Carpools 4945
Carrying capacity 565, 1959
Cartagena protocol on biosafety (CPB) 2286
Cascading 6098
Casein micelle 10852
Cassette 2583
CAT 5173
Catabolic 10734
Catadromous 6386
Catalyst 921, 1025, 7585, 10734
Catalytic membrane reactor (CMR) 3955
Catalytic oxidizer 10139
Catchment (or river basin) 5817
Catchment 7006, 8634, 8688
Cathode – (positive electrode) 708
Cathode 3886, 6498, 6720, 7527, 7731, 9885
Cathode processor 7142

Cave 5645
CB (carbon black) 9588
CBA 4784, 11759
CBD 5971
CCR-5 4997
CCS 2163, 4957
CCV 11158
CD 8112
CD155 or PVr 8123
CD4+ 4997
CD4+ T cell 4997
CDC 8123
cDNA 2689, 10815
CDR 8112
CdS 9432
CdTe 1977, 9432
CEA 4784
CED 1584
Cell cycle 6150, 7217
Cell 671, 708, 6122
Cellulose 6020
Celsius temperature (°C) 893
Cementitious 3821
CEMS 4957
Cenospheres 3821
Centerline 5645
Central receiver system, concentrating receiver system (CRS) 2349
Centrifugal contactors 7142
Ceramic glass 8794
Ceramic waste 7142
CERCLA 2005
Cereal crops 1488
Cereals 4550
Certification 8702
Certification system 1488
Cetane number 1025
CFAR 6951
CFBC 2163
CFD models 6584
CFD 4957, 5296
Cfm (cubic feet per minute) 5332
CFR 11068
CH_4 1039, 1584, 7866
Chalcopyrite compounds 9394
Chalcopyrite solar cells 7932
Challenge trial 6291
Channelization device 5934
Chaotic system 2510
Charcoal 846
Charge depleting (CD) 10503
Charge reserve 6938
Charge sustaining (CS) 10503
Chemical contaminants 9079
Chemical flux 9129
Chemical inputs 7328
Chemical mobility 9129
Chemical oxygen demand (COD) 1174
Chemical sinks 7328
Chemical structure of carbon dioxide 10169
Chemical transport model 10129
Chemisorption 4584, 10139
Chemometrics 5382
Chemotherapeutants 6354
Chernobyl 10403
Chimera 7217
Chimeric animal 10895
Chimeric 2583
Chimerism 10815
Chlorofluorocarbon (CFC) 10130
Chlorofluorocarbons (CFCs) 168
Chloroplast 1476, 10734, 11375
CHP 1426, 4235, 5296, 7866, 9934, 11759
CHP unit 1089
CHP/DHC 5296
CHP-F 1584
Chromatin 6150, 7217
Chromophore 11375
Chromosomal recombination 2689
Chromosome aberrations 11026
Chromosome 11026
Chromosphere 9795
Chronic dose 5573
Chronic exposure 11026
Chronic toxicity test 11220
Chronosequence 3278
CIGS 9432
Circadian rhythm 10852
Circular jet 10975
CIS 9432
Cistern 8688
Cistron 10734
City 11325
Classification 3170, 8794

Clausius–Clapeyron equation 7245
Clay 4584
Clean development mechanism 4474
Clean gas 1445
Clearness index 9744
Clear-sky index 9744
Clear-sky radiation 10621
Clementsian succession 3278
Climate change 168, 1488, 2078
Climate forecast 2510
Climate model 2510
Climate policy (greenhouse gas mitigation policy) 5398
Climate 111, 622, 5358
Climate projection 2510
Climate sensitivity 622, 2098
Climate-based daylight modeling 2804
Climatology 2119, 6584
Climax community 3278
Clone 7217, 10734
Cloning 10864
Cloning vector 2689
Closed dumps 5706
Closed fuel cycle (full recycle) 4050
Closed loop control 11946
Closed loop system 4133
Closure plan 5733
Cloud condensation nuclei 9696, 9795
Cloud droplet activation 111
Cloud tower 7866
CMIP-3 2098
CML 1584
CMOS image sensor 11097
CMOS 6951
CO 1039
Co 1039, 1584
CO_2 capture 1909, 2149
CO_2 enhanced oil recovery (EOR) 2149
CO_2 equivalent 1488
CO_2 1039, 1584, 2061, 2163
Coal bed methane (CBM) 7446
Coal combustion by-products (CCPs) 3821
Coal mineral matter 3821
Coal 3821, 8348
Coal preparation 2174
Coal washing 6665
Coalification 2174
Coal-to-liquids (CTL) 2222
Coarse particles 11291
Coastal and marine spatial planning 2259
Co-combustion 2271
COD 1145, 5909
Coding sequence 4013
Codon bias 8123
Codon 8123, 10734
COE 2163, 3397, 7156
Coefficient of performance (COP) 9509
Coenzyme 10734
COEX™ 7142
Cofactor 10734
Cogeneration 1400, 6805, 8081
Cognitive vehicle 2463
Cohort study 8879
Cold seep 6405
Cold turkey 10636
Cold-water coral reef 6405
Collaborative planning 12218
Collapse 5645
Collection 11655
Collection vehicle 11655
Collector area: Aperture, absorber, and gross area 9449
Collector loop (PTC) 7619
Collector mean temperature (T_m) 9449
Colloid 8387
Colored or chromophoric dissolved organic material (CDOM) 8953
Combined cycle power plant 6805
Combined heat and power (CHP) 6805, 8174
Combined heat and power generation (CHP) 4755
Combined heat and power plant (CHP Plant) 8081
Combined heat and power 1232
Combustion efficiency 1351
Combustion (of biomass) 1607
Combustion 1231, 2271, 5501, 11851
Combustion residues 5235
Combustor 6805
Comfort 1833
Command and control 168
Commensal organism 5047
Commensal 6319
Commercial solid wastes (CSW) 5707
Commercial speed 1834
Commingled operation 5950

Comminution 8795
Committed dose 8559
Commodity chemicals 7585
Common relevant picture 2463
Community 6646, 12218
Community-owned water resources 2319
Commuter rail 5971
Commuter rail service 1811
Compacted clay liner (CCL) 5747
Companion animal 8073
Comparative genomics 10734
Compartment 7006
Compartment model 7006
Competition 149, 10035, 10062
Complementary DNA (cDNA) 10734
Complementation 2689
Complex dose 3596
Complex hybrid vehicles 5083
Composite materials 6896
Composite 1723
Composition analysis 10734
Composting 9979
Compressibility 5712
Compressible gas 3933
Compressor 6805
Computer vision 11455
Concatemer 2583
Concentrate (also called retentate) 11873
Concentration factor 8387
Concentration polarization 2897
Concentration 10954
Concentration ratio (CR) 8425, 11220
Concentration ratio 2349
Concentration-response functions (CRFs) 168
Concordiasi 5071
Concrete community 3278
Concrete 3821
Condensate 4235
Conduction band 7881
Conduction 4162
Conduction-dominated systems 4191
Conductivity 7006
Confidence interval 7006
Confined aquifer 10139
Confined disposal facility (CDF) 3029
Confinement 10796
Confounding factor 9156
Congestion pricing 5021
Conjugated molecule 7553
Conjugation 2583
Connectance 3299
Connectivity 939
Consequence 4119
Conservation agriculture (CA) 5619
Conservation medicine 6179
Consist 1855
Consolidated sustainability metrics 168
Constructed wetland (CW) 11891
Construction and Demolition Debris 11699
Construction and demolition waste 10000
Consumer 149, 3306
Contaminant 2430, 3029, 12293
Contaminant fate and transport 4774
Contaminant or pollutant 2005
Contaminants 11737
Contaminated land/water 6646
Contaminated sediment or contaminated dredged material 3029
Contaminated soil 2430
Contamination 1174, 3515
Contemporary groups 436
Contextual map 3170
Contrails 652
Contrast sensitivity 3135
Control and safety systems 3397
Control area 12098
Control (power split) strategy 3471
Control simulation 2510
Convection 2016, 2031, 4163, 10955, 10962
Convection-dominated systems 4191
Convention on biological diversity (CBD) 2286
Conventional breeding 1, 1676, 10734
Conventional imbibing 8174
Conventional oil and gas 7446
Conventional treatment 11873
Conventional vehicle 10482
Convention/protocol/treaty 2286
Conversion efficiency 1977
Conversion route 1199
Converter 5083, 7086, 12135
Conveyor belt 2510
Coolant 7086
Cooling 9509
Cooling tower 4235

Cooperative group (CG) 2463
Coprocessing (of coal) 2222
Co-product allocation 5893
Coral reef 2489
Core plate 7193
Core 4179, 7086
Coreceptor (CCR-5 or CXCR-4) 4997
Coriolis force 6584
Corn stover 1269
Cornell medical index 10261
Corridors and stepping stones 939
Corticosteroids 7973
Cosmogenic 8468
Cost of greenhouse gas mitigation (economic cost) 5398
Cost of saved primary energy 9509
Cost 4235
Cost-benefit analysis 3515, 10448
Coulomb force 8559
Coulombic efficiency 671, 9293
Coumarins 10734
Counter-footprint 9025
Countermeasure 3515
Counterselectable marker 2583
Coupled chemistry-climate model (CCM) 10130
Cover 5747
CPC (compound parabolic concentrator) 9588
CPC 9562
CPE 8123
CPOx 3955
Cr poisoning 9851
Cradle to Cradle® 8856, 9026
Crassulacean acid metabolism (CAM) plants 1476
C-rate 671
CRE/*loxP* 10671
Cretaceous 2174
Critical crop N uptake 2661
Critical group 8468
Critical load 168
Critical natural capital 168
Critical period 3620
Critical plant N concentration 2661
Critical 3787, 7086
Critical toxicity value (CTV) 11220
Crop management 6201
Crop resistance to pests 5428
Crop rotation 1098
Crop structure 10035
Crop trait 2689
Cross section 11201
Crossbreeding 10734
Cross-linked polyethylene (XLPE) 11158
Cross-subsidization 1855
Crust 4179
Cryoconservation 7973
Cryosphere 280
Crystalline 6646
Crystallization 11582
CS 8112
CSE 11325
CSES 1145
c-Si 9432
CSP (concentrating solar power) 9588
CSP 9758
C_d 12202
C_l 12202
C_p 12202
$C_{p,b}$ 5500
C_θ 12202
C_T 12202
$C_{v,b}$ 5500
CTD (conductivity-temperature-depth) 4909
CTD 10390
CtL 1584
CTL 3955
CTRV 6951
Cullet 8795
Cultivate 11985
Curbside collection 11655
Current collector 6122
Cut point 2194
Cut size 2194
Cut-in wind speed 7393
Cut-off-wall 10403
Cut-out wind speed 7393
CV 1426, 5296
CVD 9293
cVDPV 8123
CVT 11523
CW with free water surface 11891
CW with horizontal subsurface flow 11891
CW with vertical flow 11891
CWP 7296
CXCR-4 4997

Cyanobacteria 4819, 6372
Cyberinfrastructure (CI) 6692
Cyclability 7546
Cycle life 6122
Cycle 6122
Cycling 3306
Cyst/Encapsulation 12018
Cyto- 10734
Cytokines 10734
Cytoplasm 7217
Cytoplast 6150
D 12202
Dacite 11613
Daily soil cover (DSC) 5707
DALY 1298
Dam failure 2788
Dam 2788
Damage caused by a pest 5428
Damage 3233
Dangerous situation 2463
Darrieus rotors 3397
DART 10403
Data alignment 3170
DAWT 3397
Day-ahead market 12254
Daylight autonomy 2846
Daylight factor 2804
Daylight metric 2804
Daylight 2804
DC motor 11523
DC 9432
DCS 4957
DDGS 988, 1039
DDT 11068
De novo synthesis of PCDD/F 6975
DE 1039, 1039, 1584
Dead zones 6354
Deadheading 1855
Debris avalanche 11613
Decay chain 8468
Decision support system (DSS) 9316
Decision support systems (DSS) 5619
Decommissioning 3515, 6633, 7055
Decomposer 149
Deconstruction 2391
Decontamination 3515, 7056
Dedicated energy crops 1269
Dedicated lines 4929
Deep liquid level 4202, 9000
Deep liquid zone 4202, 9000
Deep water formation 2510
Deep western boundary current 5856
Default value 7006
Defects 9394
Defense 12293
Deficit irrigation (DI) 5619
Defined use 9026
Deforestation 1531
DEFRA 5296
Degradation 7694
Degree of asymmetry 4616
Degree of convergence 4616
Dehydration avoidance 2638
Dehydration tolerance 2639
Dehydroxylation 4584
De-inking 8795
Deliberate release 10765
Demand 4235
Demand response 2977, 10448
Demographic change 5835
Demonstration project 9509
Denitrification 6646, 11933, 11946
Dense medium 2194
Density dependence 10062
Density 10035, 10955
Density, urban density 5786
Deoxyribonucleic acid (DNA) 5573
Depleted uranium (DU) 11220
Depletion 9026
Depolarization ratio 309
Deposit 8634
Deposition 10997
Depth of discharge (DoD) 671
Depth of discharge 11503
Depuration 822, 4819
Derivatized 3150
Desalination 9758, 11933
Desertification 2929
Design flow 10095
Design for environment (DfE) 3443
Design-build model 1855
Design-build-operate-maintain (DBOM) model 1855
Desorption 10962

Destination vector 2583
Destructive assay 7201
Detailed balance 9412
Detection and attribution 2098
Detection time 7201
Detention 8688
Deterministic effect 5573
Deterministic effects 11026
Detritivores 6309
Developer 4202
Development plan 5785
Developmental disorders/effects 3620
Devonian 2174
Dewar 4380
DEWATS 1145
Dew-point temperature (DPT) 893
DG 9904, 9934
DHC 5296
Diafiltration 8024
Diagnostic test 11158
DIAL 309
Diametrical line (or route) 1855
Diapycnal mixing 7366
Diatom 6372
Diatoms 4819
Di-benzo-furan 10577
Dicotyledonous 1477
Dielectric loss 11158
Diesel gallon equivalent (DGE) 5462
Diesel IC engine 5083
Diet 10734
Differentiation 7217
Diffraction 6067, 8953
Diffuse attenuation coefficient, K(λ) 8953
Diffuse attenuation coefficient 8919
Diffuse fraction 9795
Diffuse hemispherical radiation 9673
Diffuse sources of air pollutants 11291
Diffuser 10975
Diffusion coefficient 2016, 2031, 2048, 10955, 10962
Diffusion 2016, 2031, 2048, 7006, 7527, 10403, 10955, 10962
Diffusivity 2016
Digital elevation model (DEM) 10621
Digital map 6951
Dilution 10955
Dimictic lake 5673
Dimictic 7006
Dimming 9731
DIMS 3108
Dinoflagellates 4819
Dioxin 10577
Dioxins (PCDD/F) 11720
Diploid 6150, 10734
Dirac delta 2031, 2048, 10962
Direct coal liquefaction (DCL) 2222
Direct current (DC) 671
Direct DNA transfer 2583
Direct effects (or impacts) 10796
Direct farm income benefit 4433
Direct gain 7640
Direct normal irradiance, beam irradiance 7619
Direct normal irradiation (DNI) 2349
Direct normal radiation 9673
Direct normal solar irradiance 9589
Direct potable reuse 11873
Direct retorting 7457
Direct spectral irradiance $E_{\lambda,D}$ 9649
Direct use 4179, 4235
Direct/diffuse light 2846
Directional drilling 4380
Directivity 12275
Direct-use material 7201
Disaster waste 10000
Discharge 4221
Discourse 12218
Disease resistance/susceptibility 2963
Dish 6031
Dislocations 9196
Disparity 6951
Dispatch 4235
Dispatchability, dispatchable 2349
Dispatchable electricity 4191
Dispersal 939
Dispersion coefficient 2031
Dispersion 2016, 2031, 9049
Dissimilatory reduction 6646
Distraction 3108
Distributed energy resources (DER) 5134
Distributed generation (DG) 5134
Distributed generation 2977, 10448
Distribution coefficient (K_d) 8387
Distribution grid 2977
Distribution management system 2977

Distribution substation 2977
Distribution system 2977
Distribution uniformity 5619
District heating (DH) 11768
District heating 4353
Disturbance 149, 3326, 6216
Disulfide 3655
Ditchline 5645
Diurnal 8879
Divergence-with-gene-flow model of speciation 3357
Diversion 7201
Diversity 149
DM 1145
DME 1039, 1426, 1584, 3955
DMFC 372
$dmgBF_2$ 5173
dmgH 5173
DM/oDM – (organic) dry matter 1098
DNA adduct 3596
DNA (deoxyribonucleic acid) 4997
DNA 11026
DNA sequencing 10734
DNI 9432, 9744
DO 11946
DoD 8112
DOE 2163, 2222, 3955, 10935
Domain 4013
Domestication 149, 2689
Dominant species 149
Dominant-negative molecule 10852
Donor cell 6150
Dopamine 10636
Dopant 7881
Doping 7881
Doppler 6951
Dormancy 9145
Dose and dose rate effectiveness factor (DDREF) 11026
Dose conversion coefficient 8387
Dose equivalent 8560
Dose (exposure)–response relationship 3620
Dose mean lineal energies 11026
Dose 3515, 8537, 10997, 11026
Dose rate 11026
Dose-response assessment 6605
Dosimeter 3022, 4905
Dosimetric model 11026
Dosimetry 4905, 11026
Double envelope 3675
Doubly fed induction generator system (DFIG) 12135
Downdraft combustion 1351
Downflow 4414
Downscaling 8903
Downscaling methods 6584
dpb 5173
DPF 244
$dpgBF_2$ 5173
dpp 5173
dpq 5173
Drag 3397
Draught (Draft) 7296
Dredged material 3029
Dredging collections 3151
Dredging 3029
Drift eliminator 4235
Drift 4235
Driftsonde 5071
Drill collars 4380
Drive cycle 5083, 10542
Drive (PTC) 7619
Driver Assistance System (DAS) 2464, 3099, 10590, 11098
Driver Behavior Questionnaire (DBQ) 3099
Driver biological 3108
Driver Characteristics 3099
Driver mutation 3596
Driver physical 3108
Driving performance 3108
Driving simulator 3082
Drop-off center 11655
Drought 2929
Dry deposition 606, 8879
Dry FGD 8348
Dry process 8715
Dry steam 4235
Dry-bulb temperature (DBT) 893
Drylands 2929
Dryout 4202
DSM 7847
DTC 11523
Dual-mode buses 1818
Dual-mode 7777
Dual-use technology 7201

Dunite 1909
Durability 7694, 11582
DVC 5296
Dye sensitization 7881
Dye sensitized solar cells (DSSC) 7932
Dynamic downscaling 6584
Dynamic envelope 5934
Dynamic mapping 3171
Dynamic model 7006
Dynamic models 1927
Dynamic range 11098
Dynamic statistical downscaling 6584
Dystrophic 7006
EA 5173
Early brightening 9731
Earth Observing One (EO-1) 8939
Earth system model 2510
Earthquake fault 3233
Earthquake 2424
Earth's orbit 9619
Earth's revolution 9619
EAST 7156
$E_{auxiliaries}$ 4617
Ebb tide 10613
EBD (evidence-based design) 5332
EC framework program 7936
EC 3872
E_c 7181
ECA 7866
Eco-efficiency analysis 6633
Ecoliteracy 8856
Ecological aesthetics 10361
Ecological aquaculture 9174
Ecological footprint 6853, 9026
Ecological forecasting 2259
Ecological goal function 3306
Ecological half-life ($t_{\frac{1}{2}}^{eco}$) 8598
Ecological half-life 7006
Ecological sustainability 8856
Ecology 6216, 8856, 11325
Economic biomass potential 1174
Economic injury level of a pest 5428
Economic potential 1532
Economic threshold of a pest 5428
Economy of scale 1855
Ecosystem approach to aquaculture (EAA) 1959
Ecosystem concept 8856
Ecosystem dynamics 6216
Ecosystem engineer 3299
Ecosystem functioning 3300
Ecosystem goods and services 2929
Ecosystem 149, 168, 533, 1531, 2740, 5817, 6216, 7006, 8388, 8856, 9109, 10085, 10765, 11325
Ecosystem service 10085
Ecosystem services 3201, 3313, 4673, 5835, 10765
Ecosystem-based management (EBM) 1959
Ecotherm 11375
Ecotilling 2720
Ecotone effect 3358
Ecotone 3326, 3358
ECRH or ECH 7156
ECS 4957
Ectotherm 5047
EC_x 11220
Ecycling 3443
ED 5173
Eddy 5856
Edge city 5971
Edge effect 3358
Edible vaccines 8073
E_{excess} 4617
E-factor 4584
E-factor with respect to mass (E_m) 4617
E-factor with respect to molecular weight (E_{mw}) 4617
EFDA 7156
Effective dose 8560
Effective half-life 7006
Effective MWCO 10530
Effective population size (N_e) 1795
Effective population size (N_e) 473
Effective population size 406, 7973
Effective root zone 1098
Effective stress 5712
Effective surface albedo 11149
Efficiency of daylight 2846
Efficiency of energy generation 8097
Efficiency 4235, 6805, 7619, 7866
Efficiency (PTC) 7619
Effluent 4235
Effusive 11633
EfW 4957, 5296, 11759
EGS 3501, 4235
EGSB 1145
EGU 5909

EIA 2163
eIPV 8123
EJ 1039, 1489
E_{kernel} 4617
Ekman transport 5856
El Nino-Southern Oscillation 2510
El Niño and Southern Oscillation (ENSO) 6740
El Niño-Southern Oscillation (ENSO) 5358, 7366, 9795
Elasticity of demand 1855
Electric coupling 3367
Electric double layer capacitor 6769
Electric load 5103
Electric storage cookers 9486
Electric vehicle (EV) 3860
Electric vehicle 3367, 9293, 10482, 11503
Electrical conductivity 2934
Electrical trees 11158
Electricity generation efficiency 8081
Electricity generation 1232
Electrocatalyst 7731, 8204, 8231
Electrocatalytic reaction 2934
Electrochemical capacitor (EDLC) 3426
Electrochemical capacitor 3847
Electrochemical remediation 10403
Electrode-active material 7546
Electrokinetic screens 10403
Electrolyte 3886, 6122, 6498, 6720, 6938, 7546, 9886
Electrolyte membrane 8328
Electrolyte window 739
Electromagnetic spectrum, visible (VIS) and near-infrared (NIR) 11098
Electromigration 10403
Electromobility 3847
Electromotive force (emf) 7546
Electron acceptor 7553
Electron donor 7553
Electron volt (eV) 5560, 7086
Electron/hole 9562
Electronic fare payment 90
Electronic waste, e-waste and waste electrical and electronic equipment (WEEE) 3443
Electroosmosis 10403
Electrophile (or electrophilic chemical) 3655
Electrophoresis 10403
Electrorefiner 7142
Electrostatic precipitator (ESP) 8348
Electrowinning 6646
ELISA 1646
ELP 8073
ELPylation 8073
Embodied energy 2391
Embryonic development 6790
Embryonic germ cell 10864
Embryonic period 3620
Embryonic stem cell 10864
Emergence 8123
Emergency 3515
Emerging contaminants 2078
Emerging disease 5358
Emergy analysis 6853
emf 11523
e^- 5881
Emission standard 244
Emission trading 652
Emissions 206, 5235, 6805, 7822, 11291
Emissions standard 4236
Emissivity (ε) 9449
Emittance (M) 9449
Empirical model 2098
EMS 10935
Endemic 8123
Endemic stability 5358
Endocrine disrupting compounds 2078
Endocrine disrupting compounds (EDCs) 11961
Endogenous 10852
Endopeptidase 10852
Endothermic 9588
Endotoxin 5047
Energy and power 8373
Energy balance 1002, 10886
Energy capacity 11503
Energy conversion efficiency 8081
Energy Conversion technology 9000
Energy crops 1174, 1488, 1607, 6020
Energy density or specific energy 708
Energy density 3426, 9293, 9821
Energy efficiency 1488, 4236
Energy equivalence factors 11838
Energy forest trees 1488
Energy from ocean currents 6345
Energy from waste (EfW) 11681
Energy grasses 6020
Energy 1488, 4236

Energy source 4236
Energy storage 5103
Energy sustainability 4050
Enforcement 168
Engineered (or enhanced) geothermal systems (EGS) 4191
Engineering structures 3233
Enhanced electrochemical remediation 10403
Enhanced (engineered) geothermal systems (EGS) 4163
Enhanced geothermal system (EGS) 4414
Enhanced geothermal systems 4179
Enhanced weathering 1909
Enrichment 11201
Enrichment tails (also depleted uranium) 11202
Ensemble simulations 2510
Enteric virus 11985
Enterococci 6319
Enteroviruses 8123
Enthalpy 5216
Entry clone 2583
Envirocats™ 4584
Environment 1231, 2004, 2740, 8468
Environmental conditions 7425
Environmental control 7822
Environmental education 10014
Environmental effects (or impacts) 10797
Environmental effects 6759, 7822
Environmental exposures and environmental hazards 3620
Environmental harm 10765
Environmental impact 10713
Environmental monitoring 4880
Environmental (or green) assessment 8702
Environmental perception 3067
Environmental pollutants 9079
Environmental stability (microorganism) 11985
Environmental surveillance (as related to polioviruses) 8123
Enzymatic hydrolysis 961
Enzyme 1476, 10734
$E_{overall}$ (or E_m) 4617
EP 1584
EPA 9110
EPBT 9432
Ephemeral region 9469
EPI 8124
Epicenter 2424, 4202, 4414
Epidemic 5047, 7383, 8124
Epidemiological case studies 10261
Epidemiological 2259
Epidemiology 8758, 9156, 11985
Epigenetic effects 8058
Epigenetic 3253
Epigenetic regulation 7217
Epigenetics 1, 2540, 10734
Epilation 4905
Epilimnion 7006
Epipolar line 6951
Episodic 6216
Episomal 2583
Epistasis 6425
Epitaxy 9412
Epitopes 8124
EPRI 2163
EPT index 3265
eq 1039, 1584
Equilibrium climate sensitivity 2510
Equinox 9619
Equivalence ratio 11429
Equivalent dose 3022, 4905, 8448
Equivalent water thickness 4563
Equivalent weight 8328
Eradication 5548, 8124
Erosion 3705
Erythema 4905, 12018
Erythemal UV radiation 11149
Erythemally weighted irradiance E_{CIE} 9650
Escapees 533
Escherichia coli (*E. coli*) 6319
ESP 9432
Essential nutrients 3769
EST 2689
Esterification 921
Estimated breeding value (EBV) 1795
Estimated breeding value 436
Estimated-no-effect value (ENEV) 11220
Estrus 10886
et 5173
Ethanol fermentation 961
Ethanol 988
Ethylene propylene rubber (EPR) 11158
Etiological agent 9079
ETU 7866

EU 1039, 1584
E.U. 5296, 6951
Eukarya 5047
Euphotic zone 6372, 7296
EUR 1039
EURT 10403
Eutrophic 7006
Eutrophication 4819, 10839, 11933
EV 8112
Evacuated tube collector (ETC) 9449
Evacuation 3515
Evaporation 11933
Evaporation (of water) 5817
Evapotranspiration coefficient (TC/ETC) 1098
Evapotranspiration (ET) 5619
Evapotranspiration 3211, 4673, 7006, 7245, 10997
EVD cells 9851
Event mean concentration (EMC) 10095
Event 10735
Evidenced-based design 10261
Evolution 8124
Ex situ retorting 7457
Ex situ treatment technologies 2430
Exceedance 8879
Excess risk 206
Exchange current density (i_o) 6720
Exciton 7554
Exclusion 5315
Exclusive economic zone 7383
Exemption level 3515
Exergy efficiency (for a solar thermochemical process) 9589
Exfiltration/infiltration 6865
Exothermic 9588
Exotic species 6354
Exotoxin 5048
Expected progeny difference 1723
Experimental Breeder Reactor-II 7142
Explant 2583
Exploitation 6633
Exploration 2174, 6633, 7798
Exposure assessment 6605, 10735
Exposure pathway 3515, 7056
Exposure 168, 206, 3022, 3515, 3620, 4905, 6605, 9156, 9650
Express bus 5971
Express lane 5021
Express toll lanes (ETL) 5021
Expressway 5021
Extended constant power range 10542
Extended producer responsibility (EPR) 3443, 11673
Extensive green roofs (EGR) 4698, 4730
External conditions 7393
External conditions (wind turbines) 7425
External forcing 2119
Externalities 1834, 7296
Extinction coefficient 309
Extinction 9673
Extra high voltage (EHV) 11158
Extractant 6646
Extraction well 10139
Extraterrestrial solar radiation 9673
Extruded dielectrics 11158
Eye damage 11375
°F 2163
f 5500
F_1 bird 639
(*F/A*) 5500
Fabric filter 8348
Facade enclosure envelope 3675
FACE 10390
Facilitation 10035
Facility 2005, 4236
Factor Analysis 3099
FACTS 10935
Facula 9469
Facultative organism 5048
Fahrenheit temperature (F) 893
Failure wind speed 6201
Fallout radionuclides 3706
False alarm rate 6951
FAME 1039
fAPAR 7902
Faraday efficiency (Coulomb efficiency) 7546
Fare collection 1834
Far-field effects 9174
Farm yield 2720
Farming system 9316
Farmyard manure 7667
Fast approximate model (FAM) 11263
Fast neutrons 7086
Fast pyrolysis 1518
Fate and transport 10139
Fatigue 3108

Fault 4163, 4236, 12079
Fault-Ride-Through – FRT 12135
FB 1145
FBB 4697, 4730
FBR 9432
FC 1039, 3872
FCR (feed conversion ratio) 6354
FE 1039
Feasibility study 10139
Fecal indicator bacteria (FIB) 7667
Fecal indicator 6319
Federal Transit Administration 1811
Feed conversion ratio 8307
Feedback loop 10062
Feedback mechanisms 7245
Feedback 622, 8879
Feed-in tariff, FiT or FIT 8373
Feed-in tariff 7936
Feed-in tariffs 10449
Feedstock 1026, 10735
Feedstocks 921
f^* 4617
Fe-N-C catalyst 8265
FEP 7866
FERC 10935
Fermentation 988, 1607
Fermi energy 739
Ferrous metal 8795
Fertile fuel 7193
Fertile 3787, 7086
Fertility 10886
Fertilizer efficiency 3769
Fetch 7425
Fetus 3620
FFA 1040
FFV 1040
FG 5296
FG-DVC 5296
FGT 4957
Fibrous root system 9062
Field capacity 1098
Field winding 11523
Field-failure 6098
Field-oriented control 18
Fill factor of the cell 6566
Filled insulation 11158
Filler DNA 2583
Filter ash 11720
Finally, CERLA brought into being a new federal agency 2006
Financial assurance 7056
Fine particles 11291
Finite resources 3201
fIPAR 7902
FIR (far-infrared) 6951
Firing temperature 6805
First flush 8688
First flush effect 8688
First-generation cells 9852
First-service conception rate 10886
Fischer-Tropsch diesel 6020
Fischer–Tropsch (FT) process 1607
Fischer–Tropsch reaction 2222, 3955
Fish 4380
Fish sighting 6405
Fissile fuel 7193
Fissile 3787, 7086
Fission 7086, 8589
Fissionable 7086
Fissionable fuel 7193
Fitness constraint 7973
Fitness 1741, 8307
Fixed carbon 1488
Fixed-route bus service 1811
Fixed-speed system 12135
Flame-arresting vent 6938
Flash steam 4163, 4236
Flash tank 4236
Flashing light signal assembly 5934
Flat plate collector (FPC) 9449
Flat world assumption 6951
Flavonoids 10735, 11375
Fleet management 90
Flexible AC transmission system (FACTS) 9333
FLL 4697, 4730
Float V 5881
Floc 7866
Flood tide 10613
Flooded cell 5881
Flooding 8328
Flotation 8795
Flow 3306
Flow systems 4806
Flow-sheet design 961

Flue gas desulfurization (FGD) 8348
Fluff 8795
Fluidized bed 11851
Fluvial system 3706
Flux 2016, 8537
Fly ash 4236, 11737
FMEP 5500
f(nb) 4617
FOC 11523
Focus 2424
Food additive 10735
Food chain 822, 7006
Food intoxication 5048, 7384
Food safety hazards 9079
Food security 10713
Food web 822, 7007
Foodborne disease 5048, 7384
Foodweb 8388
Forbush decrease 9796
Forecast 2119
Forest 1488, 1531
Forward genetics 2689, 6426
Forward osmosis 2897
Fossil fuel 4163
Fouling 2897
Foundation 7393
Founder bird (F_0) 639
Fourier-transform infrared spectroscopy (FTIR) 5382
FOW 1584
Fractionation 11202
Fragmentation 939
Framework 8702
Framing 12218
FRC 7156
FRCC 5909
Free ion activity model (FIAM) 10051
Free-drifting sediment traps 7268
Frequency 1855, 2424
Fresh water 11933
Friction velocity 594
FRT 7777
Fructan 10735
Fruit biomass 1174
f(sac) 4617
$f_{\text{final}-1}$ 5500
f_{final} 5500
FT 1040, 1426, 1584
Fuel cell durability 8231
Fuel cell electric vehicle 11503
Fuel cell electrocatalyst 8328
Fuel cell performance 8231
Fuel cell 3847, 3860, 5084, 6720, 9589
Fuel cell stack 9886
Fuel cell system (FCS) 8204
Fuel cell vehicle 3367
Fuel cells (FC) 8204
Fuel consumption 11481
Fuel flexibility 3886
Fuel oriented 1426
Fuel 1174, 1488
Fuel-cell vehicle (FCV) 10503
Full-power systems 12135
Fully computational model (FCM) 11263
Fumarole 4163, 11633
Functional foods 10735
Functional genomics 10735
Functional traits 8307
Functional unit 5893
Fundamental period 2424
Fungus 10694
Fusion of virus and cell membranes 4997
Fusion/entry inhibitors 4997
FV 7181
G2V 7847
G6PD 11068
GaAs 9432
Gabion basket 5645
Galactic cosmic rays (GCRs) 9796
Gamma radiation 5560, 5573, 8448
Gamma spectrometry 3706
GAP I 8124
GAP II 8124
GAP III 8124
Gap 6241
GAP 8124
Gap states 9240
Gas diffusion layer (GDL) 8204
Gas diffusion layer 8328
Gas hydrates 7446
Gas to liquids (GTL) 3955
Gas turbine 6805
Gas-expanded liquids 3933
Gas-Heated reforming (GHR) 3955

Gasification (of coal) 2222
Gasification 1231, 1445, 1608, 3997, 5235
Gasifier 1445
Gasohol 11429
Gasoline gallon equivalent (GGE) 5462
Gastroenteritis 11985
Gastrointestinal 10852
GATE 1145
Gateway 2583
GAVI 8124
GCM 2061, 8903
GDE 3872
GDL 3872, 7866, 7866
GE 4070
Gearbox 7393
Gel cell 5881
Gene copy number 10864
Gene expression 10735, 10864
Gene flow 10713, 10735
Gene mapping 10735
Gene pool 10735
Gene 2689, 6692, 10735
Gene pyramiding 2528
Gene sequencing 10735
Gene silencing 1676, 10735
Gene stacking 10345
Gene targeting 2583, 2964, 10864
Gene transfer 10735
General circulation model (GCM) 2098, 6740
General purpose lanes (GP) 5021
Generalist 149
Generation (electricity) 4236
Generation interval (*L*) 1795
Generation interval 2781
Generation 11655
Generator 4236, 5084, 6805, 11523
Generic model 7007
Genetic correlation 415
Genetic damage 11375
Genetic engineering 1, 347, 2964, 4013, 10735, 10815
Genetic improvement 347
Genetic map 10735
Genetic marker 473
Genetic parameters 9359
Genetic recombination (of polioviruses) 8124
Genetic resource 1741
Genetic selection/selective breeding 10886
Genetic trends 406
Genetic variation 8307
Genetically modified (GM) crop, transgenic crop 5428
Genetically modified plant 5315
Genetically modified/genetically engineered/transgenic organisms 2287
Genetically modified/transgenic organisms 10765
Genogroup 11985
Genome 10735, 10852
Genome-wide selection or genomic selection (GS) 2528
Genome-wide selection 2781
Genomic selection 415
Genomics 1741, 10735
Genomics-assisted breeding (GAB) 2528
Genotoxic 3596
Genotype × environment interaction 4550
Genotype by environment interaction 463
Genotype 1676, 8124, 10735
Genotypes 436
Geochemical modeling 10051
Geocomposites 5747
Geodesic 581
Geoengineering 4104, 10161
Geographic information system (GIS) 9705, 10621
Geographic information systems (GIS) 3358
Geographical routing 11552
Geologic carbon sequestration (GCS) = geologic CO_2 storage (GCS) 4119
Geologic repository 7142
Geological sequestration 2149
Geology 4236
Geomembrane 5645
Geomembranes or flexible membrane liners (FML) 5747
Geomembranes 5707
Geonets 5748
Geopressured 4163
Geostrophic approximation 7366
Geostrophic balance 12062
Geostrophic flow 5856
Geostrophic wind 6584
Geosynthetic clay liners (GCL) 5707, 5748
Geosynthetics 5748
Geotextiles 5748
Geothermal combined cycle 4236

Geothermal direct use 4133
Geothermal energy 4163, 4191, 4236
Geothermal fluid 4236
Geothermal heat pump 4133
Geothermal heat pumps 4236
Geothermal power station 4236
Geothermal 4221, 4237
Geothermal reservoir engineering 5217
Geothermal resource 5217
Geothermal steam 4237
Geothermal system 4202, 9000
Germ cell 10864
Germ cells 10815
Germ line chimera 639
Germplasm 10735
Gestation 3620
Gettering process 9196
Geyser 4163, 4237
Geysers, The 4237
GFATM 11068
GFR 4050
GHG 1040, 2061, 9432
GHI 9744
GIF 4050
Gigawatt (GW) 4237
Gigawatt-hour (GWh) 4237
GIS 1298
GIZ 1145
GJ 1489, 5296
Glacial isostatic adjustment (GIA) 4564
Glacier 2455, 2761
Glaciers 280
Glass 11582
Glass-ceramic 11582
Gleasonian succession theory 3278
Glider 5856
Global albedo (A) 9796
Global circulation model (GCM) 9796
Global data archive 6584
Global fallout 8388, 8655
Global hemispherical radiation 9673
Global Mean Air Surface Temperature (GMAST) 9796
Global Navigation Satellite System (GNSS) 3067
Global PAR 7902
Global positioning system (GPS) 1855, 9705
Global spectral irradiance $E_{\lambda,G}$ 9650
Global toxification 6179
Global warming factor (GWF) 4755
Global warming potential (GWP) 7268
Global warming 6805, 9486
β-Glucan 10839
Glycanase 10839
Glycoalkaloid toxins 10736
Glycomacropeptide 10852
Glycosylation 8058
GMEC 11068
GMP 11068
GMT 8124
GNP 2163
GOARN 8124
Go-devil 4202
GOES 8939
Golden rice 10736
Governance 1531, 4104, 5835
gp120 4997
GPEI or GEI 8124
GPLN 8124
GPS (global positioning system) 6951
GPS 10935, 12079
GPSR 11552
Grain boundaries 9394
Grain boundary (GB) 9196
Grain development 4550
Grain growth 4550
Grain quality 4550
Graminicide 10345
Granite 3501
Graphitization 7866
Gravity waves 12062
Gray (Gy) 5573, 8448, 11027
Green and sustainable remediation 10139
Green belt 5786
Green building 10332
Green certificates 8373
Green chemistry 4642, 7585
Green house gas (GHG) savings 921
Green infrastructure 4673, 4698, 4730, 11344
Green solvent 10169
Greenfield development 5786
Greenhouse effect 4237, 6805
Greenhouse gas (GHG) 4755
Greenhouse gas 168
Greenhouse gases (GHG) 11681

Greenhouse gases (GHGs) 1488, 10503
Greenhouse 9766
Grid 4237
Grid route structure 5972
Gross erosion 3706
Gross power 7296
Ground albedo 9744
Ground motion 2424
Ground motions 3233
Ground source heat pumps 4191
Grounding line 2761
Groundwater 2430, 4202, 4414, 4774, 5645, 9000, 11933
Groundwater treatment technologies 2430
Groundwater vulnerability to contamination 4806
Grout 5645
Growing media 4698, 4730
Growth management 5786
GRT 7777
GS 5173
GtL 1584
GTP 652
Guaranty ecological flow 2788
Guidelines 206
Guideway 1855, 6241
Guild 10062
Gurley 8715
GW 2163
GWP 652, 1040, 1298, 1584, 9432
Gypsum 6646
H_2 1040, 1584, 7866
H_2S (hydrogen sulfide) 4380
H_2SO_4 5881
H_3PO_4 7866
Haar wavelets 6951
HAB 9156
Habitat network 939
Habitat patch 939
Habitat 149, 939, 3029
HACCP: Hazard Analysis Critical Control Point 6605
Hadley cell 7245
Hadley circulation 9619
Hadron 8560
Hagberg falling number (HFN) 6201
Half-life 3706, 7194, 8448, 8468, 8589, 10139
Halophyte 6309
Haploid 6150, 10736
Haplotype 2528, 6426
Hapten 1646
Hardness (water) 7007
Harm 10797
Harmful algae 4819
Harmful algal bloom 6179
Harmful algal blooms 2259
Harvest index (HI) 2661
Harvest index 1477, 2639, 2720, 10345, 10390
HAWT 3397
Hazard characterization 10736
Hazard identification 6605, 10736
Hazard 4120, 4866, 6605, 10657, 10736, 10797
Hazard traits 4846
Hazardous agent 9156
Hazardous air pollutants (HAPs) 168
Hazardous event 6605
Hazardous materials assessment 4846
Hazardous materials characterization 4846
Hazardous 206
Hazardous substance 2005
Hazardous waste (HW) 4880
Hazardous waste 5733, 5748, 9995, 11582
HBRA 8468
HCPV 9432
HDL 9110
HDPE 5909
Headway 1834, 1855
Health effects 6605, 11376
Health 5332
Health risk assessment 8688
Heap leaching 6646, 6665
Heat content 4909
Heat exchange reforming (HER) 3955
Heat exchanger 4163, 4237, 4353
Heat flow 4163, 4179
Heat gain from daylight versus electric light 2846
Heat generation efficiency 8081
Heat pipe 9449
Heat pump 4163, 4179, 4353
Heat rate 6805
Heat recovery steam generator (HRSG) 2349, 6805
Heat resistance 10390
Heat storage cookers 9486
Heat tolerance 10390
Heat transfer fluid (HTF) in a CRS 2349
Heat transfer fluid ("HTF") 7619

Heating value 6805
Heavy metals 11737
Heavy rail 5972
Heliosphere 9796
Heliostat field 2349
Heliostat 2349, 6031
Helper plasmid 2583
Hematopoietic 11027
Hemicellulose 6020
Hemizygous 10864
HEMM 9293
Hemolysin 5048
Henry's law 9049, 10139
Herbaceous biomass 1174
Herbaceous fuels 9821
Herbaceous 149, 1269
Herbicide hypersensitivity 10345
Herbicide resistance 10345
Herbicide tolerance 4433
Herbicide-tolerant transgenic crops 10713
Herbivore 149
Hereditary effect 11027
Hereditary 10736
Heritability (h^2) 1795
Heritability (narrow sense) 415
Heritability 2781, 6426, 8307, 9359
Hermaphrodite parasite 12018
Hermatypic 2489
Hermetic seal 6498
Heterogeneous 4584
Heterojunction 1977
Heterojunctions 9394
Heteromorphic life histories 9110
Heterosis 473
Heterostructure 9886
Heterotrophic 1476, 6372
Heterozygote 10736
Heterozygous 10864, 10886
HEV 5881, 7847, 8112
Hg 2163
HHV 1298, 2163, 4957
HICC 5909
Hidden failure 12079
High efficiency 9394
High occupancy vehicle (HOV) Lane 1856
High pressure fluid filled (pipe type or HPOF) 11158
High rate treatment 10095
High throughput 6790
High voltage (HV) 11159
Higher heating value (HHV) 5235
High-level radioactive waste (HLW) 8589
Highly enriched uranium (HEU) 7201, 11202
High-occupancy toll (HOT) lanes 4945
High-occupancy vehicle (HOV) lanes 4945
High-temperature fuel cells (HTFC) 5134
High-temperature proton exchange membrane fuel cell (HT-PEMFC) 3860
High-temperature system 4202, 4414, 9000
HIV 1145
HIV-1 subtypes or clades 4998
HIV-2 4998
HLNRA 8468
HM 7181
HMI (human–machine interface/interaction) 3082
Holdup 7201
Holism 168
Holocene 2490, 11613
Homing endonuclease 2583
HOMO 739, 5173
Homogeneous 4584
Homogeneous catalysis 3933
Homogeneous nucleation 111
Homogenization 939
Homojunction (heterojunction) 9196
Homologous 10736
Homologous recombination 2583, 10736, 10852, 10864
Homoplasmy 8073
Homozygote 10736
Homozygous 10864, 10886
HOR 3872
Horizontal gene transfer 10736
Horizontal grate 6449
Hormesis 3253
Hormone 10736
Horticultural residues 1174
Host 149, 5347, 10736
Hot carrier solar cell 7932
Hot dry rock (HDR) 4237
HOT Lane 5021
Hot sedimentary aquifers 4191
Hot Spring 4163
Hot-water process 7798
HOV 5021

HPS 4957
HRSG 2163
HRT 1145
h_1 5500
h_2 5500
h_3 5500
h_{3a} 5500
h_5 5500
h_6 5500
h_e 5500
h_i 5500
HT-PEFC 3872
HT-PEM 7866
H-type VAWT 3397
Hub height 6584
Human Factors 3099
Human health risk assessment 4880
Human immunodeficiency virus (HIV) 4997, 11129
Human-centered design 3082
Humidified fuel 2934
Humidity 893
Hurricane 5071
HVAC (heating, ventilation, and air-conditioning system) 5332
HVAC 10333
HVO 1040
Hyb 1040
Hybrid (asymmetric) capacitor 3426
Hybrid brake system 8848
Hybrid electric vehicle (HEV) 5084, 10503
Hybrid electric vehicle (HEV) 3860
Hybrid electric vehicle 3367, 11503
Hybrid energy storage 5103
Hybrid geothermal cycles 4237
Hybrid geothermal power stations 4237
Hybrid 3108, 5103, 10736, 10895
Hybrid solar cookers 9486
Hybrid solar system 7641
Hybrid system 2349
Hybrid vehicle 1856, 10482
Hybrid vehicles 4945
Hybrid ventilation 6865, 10333
Hybrid-electric vehicle (HEV) 3471
Hybridization 10736
Hydraulic conductivity 4806, 5712
Hydraulic head 5712
Hydraulic residence time 7007
Hydrocarbon ionomers 6538
Hydrocarbons 10139, 10482
Hydrodynamic dispersion 10139
Hydrodynamics 10139
Hydrogen oxidation reaction (HOR) 7757, 8328
Hydrogen 7881
Hydrogen production 7881
Hydrogen separation 5135
Hydrogeology 10139
Hydrograph 9049
Hydrographic sections 5856
Hydrological connectivity 7667
Hydrological cycle 8688
Hydrology 4179
Hydrolysis 9049, 10139
Hydrophilic/hydrophobic phase separation 6538
Hydrophilicity 12293
Hydrophobic 10139
Hydrophobic pocket factors 8124
Hydrophobic pocket 8124
Hydrophobicity 11961, 12293
Hydrostatic approximation 7366
Hydrostatic balance 12062
Hydrothermal carbonization 1067
Hydrothermal eruption 4414
Hydrothermal 4163
Hydrothermal resource 4237
Hydrotreating 1608
Hygroscopicity 111
HyMeX 5071
Hyperion 8939
Hypersensitivity reaction 12018
Hyperspectral 8919
Hypocenter 4202, 4415
Hypolimnion 7007
Hyporheic flow 5673
Hypoxia 6179
Hypsicity index 4617
I 4617
I_a 5173
IADB 1145
IAM 6031
IAQ (indoor air quality) 5332
IC 1145
ic 5173
ICE 5909
Ice sheet 280, 2761

Ice sheets 2455
Ice shelf 2761
Iceberg ploughmark 6405
Icefield 2761
ICF 7156
Icosahedral 11985
ICRH or ICH 7156
ICS 1298
ICSI 10815
IC_x 11220
i.d. 8124
Ideal PAR energy sensor 7902
Ideal PAR quantum sensor 7902
Identity preservation 10736
Ideotype 1477
IEA 1040, 1298, 2163
IEC 61400–1 6584
IEQ (indoor environmental quality) 5332
IFAD 1145
IFMIF 7156
IGCC 1426, 2163
Igneous rocks 3501
III-V Solar cells 7932
Illegitimate recombination 2584
Illuminance 2804
Illuminance (lux/lumen/candela) 2847
ILUC 1488
i.m. 8124
$IMEP_g$ 5500
$IMEP_n$ 5500
Immission 5235
Immobilized catalyst 9562
Immortal stranding 3596
Immunoassay 10736
Immunodeficient 8124
Immunogen 10736
Immunogenicity 6291, 8124
Immunoglobulin (Ig) 8058
Immunostimulants 6354
Impact ionization 9412
Impact on beneficial insects 10713
Impact 5548
Implantable defibrillator 6498
Impurity poisoning 3887
IMTA 6309, 9110
In planta transformation 2584
i.n. 8124
In situ conversion 7798
In situ 310
In situ retorting 7457
In situ stress 3501
In situ treatment technologies 2430
In vitro 10736, 10852, 11027
In vivo 10736, 11027
Inattention 3108
Inbred 1676, 10736
Inbreeding coefficient (F) 1795
Inbreeding coefficients 436
Incidence angle 9673
Incidence 4998, 11129
Incident angle modifier (IAM) 9449
Incineration 4880, 11720
Incinerator 9979
Inconel 7194
Independent system operator 8980
Index of refraction (real), n 8953
Index selection 8307
Indicator species 3278
Indicator trait 2781
Indirect coal liquefaction (ICL) 2222
Indirect effects (or impacts) 10797
Indirect gain 7640
Indirect potable reuse 11873
Indirect retorting 7457
Indoor air quality (IAQ) 6865
Indoor environmental quality (IEQ) 10333
Indoor solar cooking 9486
Induced subsidence 2788
Induced traffic/demand 4929
Inducer 10736
Induction machine (IM) 18
Industrial enzymes 8024
Industrial Materials 11699
Industrial solid wastes (ISW) 5707
Industrial waste 10000
Infant 3620
Infection 5358, 6605, 8124
Infectious agent 5347
Infectious disease 5358, 6605
Infinitesimal genetic model 415, 436
Infinitesimal Model 473
Information system (IS) 6692
Infrared spectroscopy 5382
Infrasound 11633

Inherent optical properties (IOP) 8953
Initial condition ensemble 2098
Initiation 3596
Injection aquifer 4202
Injection 4237
Injection (reinjection) 4415
Injection (syn. reinjection) 4202
Injection well 10139
Injection zone 9000
Inline system 10095
Innovation 12218
Inorganic 10139
In-place 330
INS 6951
Insect orders 4013
Insect resistance crops 10713
Insect resistance 4433
Inserted DNA 10736
Insertion compound 739
Insolation 9619
Instabilities (or unstable modes) 12062
Installed capacity 4474
Institutional controls 7056
Institutions 12218
Instrumented vehicle 3082
Integrase inhibitors 4998
Integrase 4998
Integrated assessment model (IAM) 5398
Integrated assessment 1531
Integrated breeding platform (IBP) 6692
Integrated coastal zone management (ICZM) 1959
Integrated Coastal Zone Management (ICZM) 511, 9174
Integrated earth system model (iESM) 5398
Integrated multi-trophic aquaculture (IMTA) 543, 1927, 10317
Integrated pest management (IPM) 5428
Integrated pest management 149
Integrated project delivery (IPD) 10299
Integrated waste management 11682
Integration 2584
Intelligent materials pooling (IMP) 9026
Intelligent transport system (ITS) 1834
Intelligent transportation system (ITS) 1856, 11455
Intelligent transportation systems 1818
Intensity 2424
Intensive green roofs (IGR) 4698, 4730
Inter tropical convergence zone 7245, 9619
Interaction coefficient 8537
Intercalation compound (host material, insertion compound) 709
Intercept factor 7619
Intercepted photosynthetic active radiation (IPAR) 2661
Interception loss 5817
Intercrop 1098
Intercropping 149
Interface 9129
Interfacial impedance 6037
Interfacial tension 10139
Interferogram 11633
Interferometric synthetic aperture radar (InSAR) 8939
Interim remedial action 10139
Interior permanent magnet (IPM) 18
Interlining 1856
Intermediate host 5358
Intermediate pyrolysis 1518
Internal combustion engine (ICE) 3860, 5084
Internal combustion engine vehicle (ICEV) 10503
Internal emitter 11027
Internal resistance 6720
Internal variability 2119
Interoperability 10192
Intertropical convergence zone (ITCZ) 6741
Interurban 5972
Intervention 3515
Introgressed 10736
Introgression library lines (ILLs) 6426
Introgression 1676, 10797
Inulins 10736
Invasibility 5548
Invasion ecology 5548
Invasional meltdown 5548
Invasive species 5548, 6179
Inventory 3706
Invertase activity 10737
Inverted T-DNA repeat 10671
Inverter 5084
Inverters 8373
Invisible present 6216
Ion exchange capacity 6538
Ion exchange 4584
Ionic channels 6539

Ionic liquid electrolyte 6037
Ionic liquids 10169
Ionic resistance 7866
Ionic stress 5315
Ionization 3022, 4905
Ionizing radiation 5560, 8448
Ionomer 8328
Ionomers 6538
Ionosphere 4564
i.p. 8124
IPAR 7902
IPCC 2061
IPCE 6566
iPS cells 10815
IPV 8124
IR camera 6449
IRES 8124
Irradiance (downward planar), $E_d(\lambda)$ 8953
Irradiance 8919, 9705, 11149
Irradiance reflectance, $R(\lambda)$ 8953
Irrigation 8688
Irrigation return flows 5619
IRS 11068
isc 5173
ISG 11523
ISO 10935
Isoflavones 10737
Isolated gain 7641
Isomorphic life histories 9110
Isopycnal coordinate 7366
Isoseismal map 2424
Isotope 3022, 4905, 5634, 8468, 10997
Isotopes 7086, 7194
Isotopic effects 10997
Isotropic effect 11027
i.t. 8124
ITD 8124
ITER 7156
Iterative closest point (ICP) algorithm 10590
ITN 11068
ITR 11552
ITS (intelligent transport systems) 3082
ITS 90
iVDPV 8124
IVF 10815
Jacket 11159
Jahn–Teller effect 709
JCO 8468
Jet in coflow 10975
Jet in crossflow 10975
Jet 10975
Jet stream 9796
Joint development 10923
Joint network 3501
Joint 11159
Joule (J) 4163, 4353
J_{th} 11202
Jurassic 2174
Justification (for intervention) 3515
Karst 2788, 5645, 6633
Karyoplast 6150
KBR 4564
Kernel mass of waste 4617
Kernel reaction mass efficiency 4617
Kerogen 7457
Keystone species 3300
KfW 1145
kg 7181
Kilowatt (kW) 4237
Kilowatt-hour (kWh) 4237
Kinematic viscosity 2048, 10955, 10962
km 1040
Knock in 10737
Knock out 10737
Knockdown 2964, 10852, 10895
Knockin 10852, 10886, 10895
Knockout 10852, 10864, 10886, 10895
Knockout/knockin 2964
Known geothermal resource area 4237
K_{ow} 12293
k_x 5173
KVA 5881
kW 7181, 7866
kWh 3955, 5296, 7181
kW_h 5296
kWh(e) 7181
L 12202
LA 5173
Lahar 8940, 11613, 11633
LAI 3211
Lake/river ice 2761
Lambda 1299
Laminar flow 2031, 2048, 10962
Laminated dielectrics 11159

Land consumption 5786
Land cover 5786
Land degradation 2929
Land disposal 5707
Land surface processes 3211
Land use (land-use emissions) 5399
Land use pattern 5786
Land use plan 5786
Land use planning 5786
Land use 1532, 5786, 5836
Land-based and offshore mariculture systems 6309
Landfill bioreactor 5720
Landfill cap 5707
Landfill gas (LFG) 5707
Landfill gas 1089, 1618
Landfill 5720, 5733, 9979
Landfilling 11737
Landscape assessment 10361
Landscape capacity 10361
Landscape character 10361
Landscape connectivity 5772
Landscape design 10361
Landscape dynamics 5772
Landscape ecology 939, 5772, 5817
Landscape fragmentation 5772
Landscape function 5772
Landscape management residues 1174, 1488
Landscape pattern 5772
Landscape perception and preference 10361
Landscape planning 5818, 5836
Landscape 5772, 5817, 10361, 12218
Landscape sensitivity 10361
Landscape structure, function, and pattern structure 5818
Landscape structure 5772
Landscape sustainability 5772
Landscape value 10361
Landscape water balance 5818
Langley plot 9705
Lanthanides 8598
Lapse rate 622
Large dams 2788
Large scale 1426
Laschamp event 9796
Laser fluorosensor 7491
Laser range finder (LIDAR) 11455
Laser scanner 65, 3067
Last glacial maximum (LGM) 2098
Latent heat storage 10551
Latent tuberculosis infection (LTBI) 11129
Lateral flow assay 1646
Lateral roots 9062
Lateral tire forces 3052, 11187
Laterite 1909
Lava 4163
LC_{50} 3265
LCA 1040, 1584, 5909, 9432, 9934, 11759
LCI 1040, 1584, 5909, 9432, 9934
LCIA 1040, 1584
LCM (lost-circulation material) 4380
LD_{50} 5573, 11220
LDL 9110
Leachate 5707, 5733, 5748
Leachate recirculation 5720
Leaching 4237, 7667, 10139, 11720, 11737
Leaching requirements 5619
Lead 206
Lead time 2098
Leadership in Energy and Environmental Design (LEED) 4698, 4730
Leaf area index (LAI) 2661
Lean 5501
Lean thinking 10299
LEED™, BREEAM™, Greenstar™, CASBEE™ 10261
Legacy 3326
Legume 149
Lentic 5673
Lentiviral vector 10895
Lentiviruses 10864
Level of service (LOS) 1856
Levelized electricity cost (LEC) 9766
Levelized power cost 4340
LFG 5909
LFGTE 5909
LFR 4050
LHCD or LH 7156
LHV 1299, 4957
Lib files 6584
Lidar 280, 310, 6584
Life cycle analysis (LCA) 7932, 10140
Life cycle analysis 921
Life cycle assessment (LCA) 3450, 5893
Life cycle of parasite 12018

Life cycle 9934
Life history of parasite 12018
$LiFePO_4$ 7527
Lifetime 606, 7694
Lift 3397
Light distillate 2222, 3955
Light distribution curves (LDC) 2847
Light nonaqueous phase liquid (LNAPL) 10140
Light rail 806, 5972
Light rail transit (LRT) 1811, 1856, 5935
Light rail transit 5950
Light rail vehicle (LRV) 1856
Light rail vehicles (LRVs) 5935
Light saturation constant 347
Lignin 6020, 6896
Lignite 8348
Lignocellulose 1269, 11429
Lignocellulosic ethanol 1608
Lignocellulosic material 961
Li-ion battery 9293
Likelihood 4120
Limnology 5673
Line capacity 1856
Lineages 8124
Linear energy transfer (LET) 5573
Linear energy transfer 11027
Lined ditch 5645
Lining 5748
Linkage disequilibrium (LD) 2528, 6426
Linkage disequilibrium 415, 473
Linkage drag 6426
Linkage 10737
Linke turbidity factor 10621
Linked trip 1856
Lipid peroxidation 3656
Lipophilicity 12293
Liquefaction 988
Liquefied natural gas (LNG) 3956
Liquid density 10140
Liquid viscosity 10140
Liquid-dominated system 4202, 4415
Lithium-ion battery (LIB) 7527
Lithium-ion capacitor 3426
Lithosphere 6633
Livestock animal 8073
Livestock 10886
Living building 10333
Living modified organism (LMO) 2287
Living modified organism 10766
Living systems thinking 8856
LN 6449
Load (electric) 4237
Load factor or coefficient of utilization 1856
Load (internal/primary) 7007
Load (secondary) 7007
Local flow system 4806
Local minimum 11552
Locally preferred alternative 1856
Locational patterns 8856
Locus (Plural loci) 10737
Locus 1676, 7217
Lodging 6201
Lodging-proof ideotype 6201
LOEC 3265
Logarithm of the odds ratio (LOD) 6426
Log-normal distribution 11202
Longitudinal IAM 6031
Longitudinal 6031
Longitudinal tire forces 3052, 11187
Long-term effect 6633
Longwave 9705
Low impact development (LID) 4731
*LA 5173
Low-emission and energy-efficient vehicles 4945
Low-enriched uranium (LEU) 11202
Lower explosive limit 10140
Lower heating value(LHV) 4755
Lowest observed adverse effect level (LOAEL) 3620
Lowest-observed-effect level (LOEL) 11220
Low-Exergy System 4133
Low-frequency sound 12275
Low-impact development (LID) 3450, 4698
Low-level jet 7245
Low-level radioactive waste (LLW) 8589
Low-NO_X burners (LNB) 8348
Low-temperature PEM fuel cell (LT-PEMFC) 3860
LPG 1299
LPS 4957
L-pyr 5173
LRD 4957
LRT 1890
LUC 1488
LULUCF 1489
Luminance 2804

Luminosity 9619
Luminous efficacy 9705
LUMO 739, 5173
Lysogenic conversion 5048
$\dot{m}_a$ 5500
$\dot{m}_f$ 5500
M 4617, 12202
m 5500
Maar 11613
Macerals 2174
Macroalgae 9110
Macrocycle 8265
Macronutrient 1676, 10737
Macronutrients 3769
Macrophyte 6646
Macrophytes 7007, 11891
MACT (Maximum Achievable Control Technology) 298
Madden–Julian oscillation (MJO) 6741
Mafic 11202
Maglev (magnetic levitation) 6241
Magma chamber 5217
Magma 4163, 4179, 4237
Magnetic Induction 6241
Magnetic shear 7156
Magnets, electromagnetic 6241
Magnets, permanent 6241
Magnets, superconducting 6241
Magnitude 2424
Main shock 2424
Major disease 8124
Major drainage flow paths 10095
Major ions and nutrients 7328
Major source 298
Makeup well 9000
Make-up well cost 4340
Make-up well 4202
Malaria 498, 11068
Malnutrition 1676
Managed lanes 5021
Manned submersible 3151
Manning equation 9049
Mantle 4179
MAPREC 8124
Marginal cost 1856
Marginal value 3313
Mariculture 511, 9110
Marine and hydrokinetic energy 6345
Marine aquaculture 7384
Marine fisheries enhancement 6386
Marine 6386
Marine protected areas 6354
Marker assisted selection or marker aided selection (MAS) 10737
Marker 2689, 10737
Marker-assisted selection (MAS) 1476, 2528
Marker-assisted selection 473, 10864
Markers 389
Market potential 1532
Martensitic or ferritic steels 7194
Mascons 4564
Masking 12275
Mass Balance Model 10657
Mass balance 2761
Mass boundary layer 595
Mass impregnated non-draining Cable (MIND) 11159
Mass intensity 4617
Mass selection 8308
Mass spectrometry 10737
Mass transfer coefficient 2016
Mass transfer 2016, 4774, 6720
Mass transfer rate 9129
Mass transport 4094
Mass-burn incineration 11787
Material flow analysis (MFA) 3450, 11708
Material life cycle 4847
Material recovery facility 11655
Material recovery parameter 4617
Materials bank 9026
Materials security 9026
Materials selection 4847
Matrix flow 7667
Matrix 6720
Maximum electrical stress 11159
Maximum load section (MLS) 1856
MBT 5296
MCFC 3872
MCL 6951
mc-Si 9432
MDCV 11159
MDG 1299
Me_2bpy 5173
Me_2phen 5173

MEA 372, 7694
Mean free path 5634
Mean or average electrical stress 11159
Mean residence time (MRT) 846
Mean residence time 161
Mean sea level 2455
Measures 3108
Mechanical coupling 3367
Mechanism of action 3620
MED 9758
Medicinal plants 6519
Medium voltage (MV) 11159
Megacity 8879
Megagram (Mg) 1269
Meganuclease 10895
Megawatt (MW) 4237
Megawatt-hour (MWh) 4237
Meiosis 6150
Membrane bioreactor (MBR) 11873, 11961
Membrane distillation 2897
Membrane electrode assembly (MEA) 7757, 8174, 8204, 8328
Membrane/PEM 8231
Memory effect 672
Mendelian sampling 2781
MeOH 1040, 1584
MEP 5500
Meridional overturning circulation (MOC) 7366
Meridional overturning circulation 5856
Meridional 5856
Mesohumic 7007
Meson 8560
Mesophile 6646
Mesoscale convective system (MCS) 5071
Mesoscale model 6584
Mesoscale 8903, 11263
Mesoscopic 6566
Messenger RNA (mRNA) 10737
MET 4070
Metabolic engineering 6519
Metabolic heat and water 8308
Metabolism 10737
Metabolite 10737
Metabolites 11911
Metabolome 1184
Metabolomics 1184, 10737
Metal waste 7142
Metallic shield 11159
Metalloid 7328
Metal-support cells 9852
Metanalysis 6426
Metaphase II (MII) 6150
Metaphase 7217
Metapopulation 939, 5428, 5772
Metastability 9240
Methanation 1661
Methanogenesis 6647
Metrics 8879
Metro 806
Metro rail 1890
Metropolitan planning organization (MPO) 1856
MF 1584
MHD 7156
MICC 6449
Microaerophilic 10140
Microarray 8124, 10737
Microbial pollution 8758
micro-CHP 9904
Microclimate 149
Microcrystalline 9240
Microemulsion 10169
Microgrid 5084
Micronutrient 1676, 10737
Micronutrients and trace elements 7328
Micronutrients 3769
Microorganism 497
Micropollutant 11911, 11961
Microsatellite 7973
Microscale model 6584
Microscopic cross section 3787
Microstructure 9240
Microwave sensor 7491
Microwaves 4642
Middle distillate 2222, 3956
Mie scattering 9705
mill 7181
Mineral carbonation 1909
Mineral 1676
Mineralization 9049, 9562
Mini-chromosome 10737
Minichromosome 2584
Minimal cassette 2584
Minimal erythemal dose (MED) 11376
Minimum electrical stress 11159

Mining life cycle 6647
Minor actinides 7142
Minor disease 8124
Minor drainage flow paths 10095
Minority carrier diffusion length L 9197
Minority carrier lifetime τ and diffusion length L 9196
Mirror, mirror panel (PTC) 7619
MISC 1584
Misch metal 6938
Miscibility gap 7527
MIT 2163
Mitigation 1627, 2424
Mitigation (with respect to climate change) 4674
Mitochondria 11376
Mixed ionic electronic conductor 3887
Mixed layer 4909
Mixed mode or hybrid HVAC 10261
Mixed model equations 436, 473
Mixed models 415
Mixed waste (MW) 5748
Mixed-mode or Hybrid HVAC 3675
Mixed-mode ventilation 6865
Mixer-settler 7142
Mixing ratio 11311
Mixture calorific value 5462
MJ 1040, 1584
MLCT 5173
MMCT 5173
mmf 11523
MMV 11068
mn 1040
MNVT 8124
Mo 1040
Mobile source 298
Mobile sources 206, 8879
Mobilization 7667
Modal split 1811, 1856
Mode 5972
Model 1959, 9000, 9316
Modeling framework 1928
Modeling 10095
Models 1532
Moderator 7086
Modern biotechnology 2287, 10766
MODIS 8939, 9696
Module (PTC) 7619
Moist static energy (MSE) 6741
Molecular breeding (MB) 6693
Molecular breeding platform (MBP) 6693
Molecular breeding value 1723
Molecular farming (also pharming) 8059
Molecular flow 5634
Molecular growth 6975
Molecular marker 1476
Molecular markers 2720
Molecular pharming 8073
Molecular weight cutoff (MWCO) of a membrane (absolute MWCO) 10530
Monitoring 7056
Monoaromatic hydrocarbons (MAHs) 10140
Monoclimax 3278
Monoclonal antibody 8059
Monocotyledonous plants 1477
Monogenetic field 11613
Monomer 11376
Monomitic 7007
Monopolar cell 5881
Monorail 1856
mono-Si 9432
Monsoon 7245
Monte Carlo 7007
Monte Carlo code 9705
Montreal protocol 10130
mOPV 8124
Morbidity 206
Morgan 473
Morphogenesis 11376
Morphometric 7007
Mortality 168, 206, 11130
Mosaicism 10815
Motion planning 2464
Motivation 10865
Motor 11523
MOX 7181, 11202
Mpa 2163
MRF 5296
mRNA 10737
MRO 5909
MSDS 5881
MSF 9758
MSR 4050
m_1 5500
m_2 5500

m_3 5500
m_4 5500
m_6 5500
m_a 5500
M_b 5500
m_f 5500
M_R 12202
m_r 5500
m_{total} 5500
MSW incineration 11838
MSW 3997, 5296, 5909, 8097, 10577, 11759
MSWI 4866
MSWU 11202
MTF 7156
Muffler 4237
Multicrystalline silicon 9197
Multidestination transit route networks 5972
Multieffect distillation 2897
Multifocal vision system 46
Multigene transfer 2584
Multigenic 10737
Multijunction 9412
Multijunction solar cell 7932
Multi-laser sensing system 3171
Multimodal 1819
Multi-model ensemble (MME) 2098
Multiphase catalysis 3933
Multiplication factor 7086
Multipollutant monitoring 168
Multipurpose cookers 9486
Multi-scale analysis 3326
Multistage flash distillation 2897
Multi-trophic relationships 149
Multivoltage solar-electric cooker 9487
Municipal solid waste (MSW) 4755, 5235, 5748, 8795, 9995, 11787, 11838
Municipal solid waste 10000, 10014
Municipal solid wastes (MSWs) 5707
Mutagenesis 4013
Mutant 10737
Mutation Breeding 10738
Mutation 2689, 10738, 10886
MW 2163, 5296
MWD/MTU (mega watt days of energy produced per metric ton of uranium contained) 6688
MWh 2163
MWh(e) 7181
Mycobacterium tuberculosis 11130
Mycorrhizae 149
Mycotoxin 1098
N dilution 2661
N 4617, 5500
n 7181
Nacelle 7393
Nachhaltigkeit 6633
Nanocarbon 6769
Nanocrystalline 9240
Nanofiltration (NF) membrane 10530
Nanohybrid capacitor 3427
Nanoparticle 1646
Nanotechnology 6790
Nanowire 9293
Narrow genetic base 2528
National Ambient Air Quality Standards 206
National REAP in the EU 8373
National Transit Database (NTD) 1856
Natural attenuation (NA) 10403
Natural attenuation 5748
Natural capital 168, 3314
Natural enemy 10062
Natural gas liquids (NGL) 3956
Natural monopoly 10449
Natural organic matter (NOM) 10051
Natural resource management 3342
Natural ventilation 6865, 10333
Naturalistic driving behavior 3082
NBI 7156
NCCs 8125
Neap tide 10613
Near isogenic lines (NILs) 6426
Necking 6201
Negative electrode 6122
Negative feedback 2510
Neglected tropical diseases 11997
Neighborhood scale 11263
NEON 3201
Neonate 3620
NERC 5909, 10935, 12079
Nested systems of governance 564
Net erosion 3706
Net power 7296
Net primary productivity (NPP) 846
NETL 2163
Network analysis 3306

Network 9469
Network system 7778
Net-zero buildings 10333
Neurostimulation or neuromodulation 6498
Neurovirulence attenuation sites 8124
Neurovirulence 8124
Neutralizing antigenic sites 8124
Neutron capture cross section 7194
Neutron 8537
New urbanism 1890
Newton's law of gravitation 4564
Next-generation sequencing (NGS) technologies 2528
NG 7866
NGO 1145
NGOs 8125
Ni 1040
Niche overlap 10062
Niche 8201
Nickel cadmium fiber plate 6938
NID 8124
NIDs 8125
Night cooling 6865
Night ventilation 3675
NIL 2689
NIMBY 12218
NIMBYism 6354
Ni-MH 6938
n-i-p solar cell 9241
NIR 65, 6951
NIRWARN 6951
Nitric oxide (NO) 8348
Nitrification 11933, 11946
Nitrogen absorption efficiency (NAE) 2661
Nitrogen conversion efficiency (NCE) 2661
Nitrogen dioxide (NO_2) 8348
Nitrogen fixation 10738
Nitrogen nutrition index (NNI) 2661
Nitrogen oxides 206
Nitrogen use efficiency (NUE) 2661
Nitrous oxide (N_2O) 4755
NMHC 1299
NMVOC 1299, 1584
NNMC 8265
NO 5296
No tillage agriculture 4433
NO_2 244
NOAEL 3253
Noble metals 7142
No-build scenario 1856
NOEC 3265
Noise 12275
Nonaqueous phase liquid (NAPL) 10140
Nonaqueous phase liquids (NAPLs) 2430
Noncondensable gases (NCG) 4237
Non-condensible gas 4415
Nondestructive assay 7201
Non-ferrous metal 8795
Non-flame incineration 6976
Nonnative species (synonyms: alien, exotic, foreign, nonindigenous) 5548
Nonpecuniary benefit 4433
Nonpoint source pollution 7667, 8688
Nonpoint SOURCE 9049
Non-potable water 2319
Nonpotable water 8688
Nonstructural genes 8125
Non-traction load 5103
Non-transferred arc plasma torch 8097
Nonvolatile dissolved organic carbon (NVDOC) 5748
Nonwoven separators 8715
No-observed-effect level (NOEL) 11220
NORM 8388, 8468
Normal hydrogen electrode (NHE) 7731
North Atlantic deep water 5856
North Atlantic Oscillation (NAO) 9796
Northern annular mode (NAM) 9796
North/south 11068
Nosocomial 5048
Novel mechanisms for insect resistance 10713
Novel trait 10797
NO_x limited 11311
NO_x 2163, 5296, 11311
NO_X 8348
NPCC 5909
NPEV 8125
nr 5174
NRC 2163
NSL 8124
n_R 5500
Nuclear fission 8448
Nuclear fuel clad or cladding 7194
Nuclear fuel cycle 7056

Nuclear magnetic resonance (NMR) 6068
Nuclear material (NM) 7201
Nucleic acid 10738
Nucleotides 10738
Nucleus 4998, 10738
Nuclide 3023, 4905, 5560, 7086, 8560
Nudging 8903
NUR 11552
Nutraceutical 10738
Nutrient certificates 9026
Nutrient 6372
Nutritionally improved 10738
O_2 7866
O_3 244
O-Bahn 1856
Objective analysis 4909
OBR 1040
Observer or estimator 3052, 11187
OCC 5909
Ocean acidification 7229
Ocean color 8919
Ocean conveyor belt 5856
Ocean current 8655
Ocean fertilization 7267
Ocean gyre 7366, 8655
Ocean observatory 7282
Ocean ranching 10317
Ocean thermal energy conversion 6345
Ocean thermal resource 7296
(Oceanic) Mesoscale eddy 7366
OCP 2934
Octanol-water partitioning coefficient 11912
OCV 372
ODM 1145
OE 1040
OECD 1040, 2163
Off-line stations 7778
Off-line system 10095
Off-quadrant 5935
Off-road vehicle 5084
Offset 9026
Offshore aquaculture 511
Offshore co-management 511
Offshore 4474
Offshore wind developments 4474
Offshore wind farms 512
Offshore wind turbine 7394
Off-site impacts 3706
OH 7156
OHI 6404
Ohmic loss (η_{IR}) 6720
Oil mining 7798
Oil sands 7446
Oil shale 7446, 7457
Oilseeds 4551
Oleaginous microorganisms 11429
Oligohumic 7007
Oligomerization 4013
Oligonucleotide 8125
Oligotrophic 6354, 7007
Olivine 1909, 7527
O&M 4957
OM 7847
Omics 1184
Oncogenic process 3596
One health 2259
One-electron reduction 6038
Online estimation 11946
ONP 5909
Onshore wind developments 4474
On-site impacts 3706
Ontology 10192
Oocyte 11027
Oogenesis 11027
Oomycetes 2559
Open circuit voltage (E_{OCV}) 6720
Open circuit voltage 11503
Open dumps 5707
Open fuel cycle (once-through cycle) 4050
Open loop control 11946
Open Loop System 4133
Open magnetic field 9469
Open ocean aquaculture 512, 581
Open ocean farming 6759
Open reading frame (ORF) 11985
Open solar flux 9796
Open-ocean mariculture 3556
Open-pit excavation 6633
Open-water disposal 3029
Operating assistance/expenditures 1811
Operating reserve 8980
Operating speed 1856
Operating temperature difference 9449
Operating window 7694

Operation mode 3367
Operational crop management 9316
Operations and maintenance (O&M) Cost 4340
Operon 10738
OPEX 1584
Opioid 10636
Opportunistic pathogen 5048
Opportunity cost 1856
Optical depth, ζ 8953
Optical depth 9705
Optical enhancement 9241
Optical flow 10590
Optical mass 9706
Optical sensor 7491
Optically shallow waters 8953
Optimal power flow (OPF) 9333
OPV 8125
ORC power station 4237
ORC 1426
Order-of-operations thinking 10333
Ordovician 2174
Ore 6647
ORF 2689
Organic chemicals 7329
Organic efficiency 2194
Organic liquid electrolyte 6038
Organic matter 149
Organic 10140
Organic Rankine cycle (ORC) 1608, 4237
Organic solar cells 7932
Organically bound tritium (OBT) 10997
Organism 10766
Organoleptic 10738
Ormat energy converter (OEC) 4237
Ornamental fisheries 6179
Orography 6584
ORP 11947
ORR 3872, 8265
ORT 5021
Orthotopic tumor 3151
Orthovoltage x-rays 11027
Osmotic energy 6345
Osmotic pressure 2897
Osmotic stress 5315
Osmotic tolerance 5315
OSPAR 8388
OTEC 7296
OTEC transfer function 7296
OUR 11947
Outage 4237
Outbreaks 8125
Outbreeding depression 6386
Output variables 7007
Ovarian follicle 10886
Overall mass transfer coefficient 2016
Overcharge 6122
Overfire air (OFA) 8348
Overpotential (η) 6720
Overpotential 2934
Overturning circulation 5856
Ovulation 10886
Oxidation 6372, 7585, 10140
Oxidative stability 6038
Oxidative stress 3656
Oxy 2163
Oxy/FGR 2163
Oxyfired combustion 2149
Oxygen ionic conductor 3887
Oxygen reduction reaction (ORR) 7731, 7757, 8328
Oxygen stoichiometry 2934
Oxythermal parameter 5673
Ozone hole 10130
Ozone layer 168
Ozone 206, 10130
Ozone-depleting substance (ODS) 10130
P 12202
P 1584
p 5500, 12202
P3HT poly(3-hexyl thiophene) 7554
Pacemaker 6498
PAFC 3872, 7866
PAH 9156
Paleoclimatology 9796
PAN 7866
Pandemic 5048, 7384
Pantograph 1856
Paper insulated lead covered (PILC) 11159
PAQ 6865
PAR irradiance 7902
PAR 2615
PAR waveband 7902
Parabolic trough collector ("PTC") 7619
Parallel hybrid vehicles 5084
Paramagnetic 1646

Parameter space 2098
Parameterization 622, 3211
Parasite 149
Parasitic loads 5135
Parasitic power, parasitic losses 2349
Parasitism 149
Parasitoid 149
Paratenic host 12018
Paratransit 1834, 1856
Parthenote 6150
Partial discharge 11159
Partial oxidation (POx) 3956
Participation 565
Participation rate 11655
Particle bombardment 2584
Particle Filter 6951
Particulate 5673
Particulate matter, 10 μm 206
Particulate matter, 2.5 μm 206
Particulate matter (PM) 4237
Particulate matter 168, 206
Particulates 11291
Partition coefficient (K_d) 7007, 11220
Partitioning 10140
Passenger capacity 1834
Passivating layer 7194
Passivation 9197
Passive house building 7629
Passive microwave sensor 7491
Passive 7640
Passive remote sensing 310
Passive survivability 3675
PassivHaus™ 3675
Patch dynamics 5772
Patchiness 149
Patchy landscape 150
Pathogen 498, 5347, 6319, 6605, 10694, 10738
Pathogenesis 5048, 7384, 12018
Pathogenic 5048
Pathogenicity factors 10694
Pathogenicity island 5048
Pathogenicity 9157, 10694
Pathogen/pathogenic 10852
Pathogens 2259, 7667, 8688, 11873
Pattern analysis 5773
Pattern literacy 8856
Pattern 3326
Pavement markings 5935
Pay back time 7932
Pb 5881
PbO_2 5881
$PbSO_4$ 5881
PC 2163
PCBM ([6,6]-phenyl C_{61}-butyric acid methyl ester) 7554
PCBs 9157
PCC Streetcar 5973
PCDD/Fs 5296
PCR 2689
PC/SC 2163
PC/USC 2163
PDC 10935
Peak section load 1834
PE-based 11159
Pedagogy 3201
Pedestrian automatic gate 5935
Pedestrian 5935
Pedestrian-light rail at-grade crossing 5935
Pedestrian-oriented development 169
PEFC 3872
Pegmatite 11202
Pelagic 1959, 7007
Pelletizing 1067
Pellets 9821
PEM (polymer electrolyte membrane) fuel cell 9589
PEM 372
PEMFC 372, 7694
Pentose fermentation 961
People mover 1857
Peptide 498, 10738
Perched aquifer 4202
Perennial 1269
Perfluorinated sulfonic acid containing polymer (PFSA) 8328
Perfluoro sulfonic acid ionomers 6539
Perfluorosulfonic acid (PFSA) 7757
Perforated city 11362
Perforation 5836
Performance decay 7866
Performance standards 9174
Perinatal stage 3621
Period 2424
Periphyton 7007
Permaculture 8856

Permafrost 280, 330, 2761, 9696
Permanent magnet material 18
Permanent magnet synchronous machine (PMSM) 17
Permeability 3501, 4163, 4179, 4202, 4415, 7007, 9001, 10140
Permeable reactive barriers 10403
Permeate water 2897
Permian 2174
Persistence 10657
Persistent and bioaccumulative toxins (PBT) 3443
Persistent organic pollutants (POPs) 7329, 10140
Persistent poliovirus infection 8125
Personal care products 11911
Personal construct theory 10361
Perturbed physics ensemble 2098
Pest 5428
Pesticide 10738
PET 3997, 5909
Petrol-diesel 1026
Petrophysical 330
PF 7156
pH 4237, 7229
Pharmaceuticals 11911
Pharmacognosy 8024
Phase diagram 7527
Phase I reactions 12293
Phase II reactions 12293
Phase III transport 12293
Phasor 12079
phen 5174
Phenology 2540
Phenome 1
Phenotype 1, 150, 1676, 1741, 9359, 10738
Phenotype/phenotypic 10852, 10886
Phenotypes 436
Phenotypic selection 6426
Phenotyping 1, 8013
Phenylketonuria 10852
Phenylpropanoids 10738
Pheromones 5428
PHEV 7847, 8112, 9293
Photoassimilates 2639, 4551
Photoautotrophy 347
Photocatalysis 7881, 9563
Photocatalyst 7881
Photocatalytic water splitting 7881
Photochemical smog 11291
Photoelectron 6068
Photo-Fenton 9563
Photoinhibition 347
Photolysis 9049
Photon cutting 9412
Photon 8537, 8560
Photoperiod sensitivity 2540
Photoreactor 9563
Photorespiration 1476
Photosphere 9469, 9796
Photostationary steady state 11311
Photosynthesis 347, 6372, 10738
Photosynthetic action spectrum 7902
Photosynthetic active radiation (PAR) 2661
Photosynthetic efficiency 1476
Photosynthetic photon flux density (PPFD) 7902
Photosynthetically active radiation (PAR) 7902
Photosynthetically available radiation (PAR) 8953
Photosystem 347
Phototaxis 11376
Photovoltaic capacity 7935
Photovoltaic (effect) 1977
Photovoltaic electricity generation 7935
Photovoltaic module and photovoltaic system 7935
Photovoltaic (PV) energy system 7936
Photovoltaics 7932, 9706
Photovoltaics (PV) 7935
Phreatic 11633
Phreatomagmatic 11613
Phthalocyanines 7554
Phycotoxins 4819
Phyllochron 2540
Phylogenetic tree 8125
Physical signal extraction 3108
Physical-mechanical properties 9821
Physicochemical conversion 1199
Physisorption 4584
Phytase 10839
Phytate (phytic acid) 1676, 10738
Phytic Acid 10839
Phytoalexin 2559
Phytochemicals 10738
Phytomer 2540
Phytoplankton 6372, 7007, 8201
Phytoremediation 10403
PIC 1299

Picornaviridae 8125
PID controller 11947
p-i-n solar cell 9241
Piscivorous 7007
Pitchblende 6688
PJ 1489
pkm 1584
Place attachment 10361
Place identity 12218
Place 8856, 10361
Placer 11202
Placing on the market 10766
Plage 9469
Planar device 9886
Plane jet 10975
Plankton 7007, 8201
Plant breeding 6693
Plant cell culture 6519
Plant growth 11376
Plant growth regulators – (PGRs) 6201
Plant molecular pharming 8024
Plant oil fuel 8081
Plant operating mode 1400
Plant productivity 1
Plant stress 4551
Plant-based expression 8073
Plantibodies 8073
Plantship 7296
Plasma-enhanced chemical vapor deposition (PECVD) 9241
Plasmid 498, 5048, 10738
Plasticity 463, 10739
Plastid 8059, 10739
Plate 6938
Plate tectonics 4179
Platform 6405
Pleiotropic 10739
Pleiotropic effects 8308, 10852
Pleiotropy 6426
Pleistocene 11613
Plug-in hybrid electric vehicle (PHEV) 3471, 10503
Plug-in hybrid 5083
Plume 10975
Pluripotent 7217
Pluripotent cell 10895
Plus-energy buildings 8373
Plutonium (Pu) 7194
PM 2164
PM_{10} 244, 11291, 11311
$PM_{2.5}$ 244, 11291
PMEP 5500
PMU 10935, 12079
pn-junction 1977
Pocket plate electrodes 6938
POCP 1584
Point mutation 10886
Point source 4238, 5048, 9049
Point sources 169
Point (stationary) sources of air pollutants 11292
Point-to-point 7778
Polarization, $\eta = V_{OC} - V(q, I.....)$ 740
Polarization 310, 6720
Polarization resistance 2934
Policulture (also intercrop) 10036
Poliomyelitis 8125
Poliovirus 8125
Polisilicon or polycrystalline silicon 7936
Pollutant 12293
Pollution prevention 8771
Polybenzimidazoles (PBIs) 8173
Polychlorinated biphenyls (PCBs) 10140
Polychlorinated dibenzo-*p*-dioxins and dibenzofurans (PCDD/Fs) 4880
Polyclimax 3278
Polyclonal 10739
Polycrystalline thin films 9394
Polyculture 150, 533, 6309, 10317
Polycyclic aromatic hydrocarbons (PAHs) 1628, 10140
Polyethylene (PE) 11159
Polygeneration 1426
Poly-generation 5135
Polygenes 2528
Polyketide 498
Polymer electrolyte membrane (PEM) 8174, 8204
Polymer 10739
Polymerase chain reaction (PCR) 5382, 6319
Polypeptide 8125, 10739
Polyploid 2689
Polysaccharides 9110
Ponor 5645
POPs 9157
Population exposure 169
Population genetics 415

Population 10085
Porosity 10140, 11263
Position effect 10671
Positional cloning 2689, 6426
Positive control device 5935
Positive electrode 6122
Positive feedback 2510, 9696
Positron 8560
Post-closure plan 5733
Post-combustion capture 2149
Posterior probability 2098
Postpolio syndrome 8125
Posttranscriptional gene silencing (PTGS) 10671
Posttranscriptional modification 10739
Posttranslational modification 8059
Posttranslational processing 8125
Potable water 2078, 2319, 8688, 11873
Potential 1532
Potential temperature 4909
Potential vorticity 5856
Potential yield 2720, 10036
Potential yield water limited 2720
Potentially responsible party or PRP 2005
Pour point 1026
Power capacity 4221, 4340
Power collection system (wind turbines) 7425
Power conversion efficiency (PCE) 6566
Power curve 6584
Power density and specific power 709
Power density 3427
Power electronic converter 10542
Power electronics 5084
Power frequency 11159
Power plant 4238
Power plants 11481
Power 4238
Power purchase agreement (PPA) 7936
Power quality 12135
Power station 4238
Power-to-heat ratio 8081
Pozzolan 3821
PPA process 8174
ppy 5173
PR 9432
Practical energy density or specific energy 709
Prandtl's mixing length 2048
Prebiotics 6354
Precautionary principle 566, 10261
Precipitable water 9706
Precipitates 9197
Precipitation 4238, 10140
Precision agriculture 5428
Precombustion capture 2149
Precursor pathway of PCDD/F formation 6976
Predation 150
Predator 150, 7007, 10062
Prediction 2119, 2464
Pre-erythrocytic 6291
Preferential flow 7667, 10140
Pregnancy 3621
Preharvest sprouting 9145
Preimplantation embryo 10815
Preparatory behavior 3082
Pre-reforming 3956
Presentation 11655
Pressure-retarded osmosis 2897
Preterm birth 3621
Pretreatment 961
Prevalence 4998, 11130
PReVENT 6951
Price elasticity of demand 1532
Price 4238
Primary battery 672
Primary breeders 8308
Primary cell 6498
Primary control 12098
Primary energy saving 9509
Primary particles 244
Primary pollutants 169, 11311
Primary producer 3306
Primary production 150
Primary productivity 7007
Primary roots 9062
Primary standards or guidelines 206
Primary standards 169
Primary trace atmospheric gas or particles 310
Primitive equations 12062
Primordial germ cells 639
Primordial 8468
Prion 10852
Prior probability (marginal probability) 2098
Privatization 1811
Probiont 6354
Process integration 961

Processed refuse fuel (PRF) 11787
Processing 11655
Produced energy 11839
Producer gas 1426
Product gas 1445
Product gas treatment 1445
Product gas utilization 1445
Production trait 10886
Production traits 8308
Production zone 4202, 9001
Productivity 150
Products 5501
Profiling 10739
ProFusion 6951
Promoter 1676, 2584, 10739, 10852, 10886
Promoter trap 7217
Promotion 3596
Pronuclei 7217
Pronucleus 10865
Proof-of-payment (POP) Fare Collection System 5973
Proofreading 8125
Prooxidant 3656
Propagule pressure 5548
Proportional-integral (PI) controller 672
Protease inhibitors 4998
Protease 4998
Proteasome inhibitor 3151
Protective action 3516
Protein 10739
Proteolysis 4013
Proteomics 10739
Protista 6354
Protocrystalline silicon 9241
Proton conductivity 8174
Proton exchange membrane (PEM) 3860, 7757
Proton exchange membranes 6539
Proton-exchange membrane fuel cells (PEMFC) 7731
Protonic conductor 3887
Proto-oncogene 3596
Protoplast fusion 10739
Protoplast 10739
Protozoan pathogens 8758
Provoked poliomyelitis 8125
PRT 7778
Pseudo-capacitor 6769
Pseudofeces 6759
psi 2164
P_1 5500
P_2 5500
P_3 5500
P_{3a} 5500
P_4 5500
P_5 5500
P_6 5500
P_7 5500
P_b 5500
P_e 5500
P_i 5500
P_{in} 5500
P_{limit} 5500
Pt mass activity 7731
p(t) 7181
PT 9001
PTFE® 7866
Pt-specific activity 7731
Pu 7181
Public acceptance 12218
Public good 10449
Public involvement 10014
Public perception 2319
Public transport 1834
Public transport service 1811
Public transportation (also called transit, public transit, or mass transit) 5935
Public transportation 10923
Public transport/transit 806
Public–private partnership 1834
Public–private partnership (PPP) 1857
Public–private partnerships/models 1811
Pulse power efficiency 3471
Pulsed columns 7142
Pump-to-wheels (PTW) 10503
Purchased transportation services 1811
PUREX 7142
Purifier 4238
PV cells, modules, systems 8373
PV: photovoltaics 8373
PV 7181, 9432
PVC 1145, 3997, 10577
PVR 8125
PVR Tg21 transgenic mouse 8125
py 5173

Pylon (PTC) 7619
Pyranometer 9673, 9731
Pyrheliometer 9673
Pyrochelates 8265
Pyroclastic 11633
Pyroclastic flow or pyroclastic density current 11613
Pyrocumulus 10117
Pyrolysis (of coal) 2222
Pyrolysis 1518, 1608, 3997, 5235, 7457
Pyrolysis-biochar system (PBS) 846
Pyrophoric 8468
Pyroprocessing 4050, 7142
Q 5174
q 5174, 7156
QA 372
QMRA 6605
Q_{HV} 5500
$Q_{HV,f}$ 5500
$Q_{HV,i}$ 5500
QTL 4070
QTLxE 4070
Quad 11202
Quality assurance for daylight control 2847
Quality of life 10361
Quality of service 1819
Quality protein maize (QPM) 1676
Quantitative genetics 415
Quantitative microbial risk assessment 8758
Quantitative PCR 6319
Quantitative trait loci 10739
Quantitative trait loci (QTL) 2964
Quantitative trait loci (QTLs) 2528
Quantitative trait locus 2689, 6426
Quantitative trait locus (QTL) 1, 389, 473, 6693
Quantum yield 9563
Quasispecies 8125
Quaternion 10590
Quench 9589
Quorum sensing 5048
$\overline{R}$ 5500
R 12202
r 5500, 12202
r 7181
R1 energy efficiency factor 11839
R1 formula 11839
R1/D10 11759
Radar 280
RADAR 6951
Radarsat 7491
Radial hexagon 4617
Radial line (or route) 1857
Radial pentagon 4617
Radial transit route systems 5973
Radiance, $L(\lambda)$ 8953
Radiance 8919, 9706
Radiation dose 5573, 11149
Radiation 2349, 3023, 4905
Radiation use efficiency 2720
Radiation use efficiency (RUE) 2661
Radiation weighting factor 8388
Radiative balance 169
Radiative forcing 111, 622, 652, 8879, 9796
Radiative transfer 9706
Radiative transfer theory (RTT) 7902
Radical (or free radical) 3656
Radioactive 5560, 8468
Radioactive half-life ($t_{1/2}$) 8598
Radioactive Waste 4774
Radioactivity 8448
Radioisotope 8468
Radiological survey 7056
Radiometer 7491
Radiometers 280
Radiometry 9706
Radionuclide deposition 8634
Radionuclide or radioisotope 10403
Radionuclide 3023, 4905, 8448, 8468
Radionuclide washout 8634
Ragone plot 709, 3847
Rainscreen 3676
Rainwater harvesting 2319, 8688
Rainwater 8688
Rainwater storage tank 8688
Raman spectroscopy 5382
Range image 3171
Rankine cycle 6805
Rapeseed oil fuel 8081
Rapid transit 1834, 5973
RAS 6309, 10935
Raster 10621
Rate law 4094
Rate of charge/discharge, nC 740
Rated wind speed 7394
Rating (labeling) 8702

Raw gas 1445
Raw material cost 4617
Rayleigh scattering 9706
RCC 8125
RCM 8903
RCT 8125
R&D 1145, 2164, 11069
R&D&D 1040, 1427, 1584
RD&D 2164
RDD 8468
RDF 3997, 5296, 11759
RDT 11069
Reactants 5501
Reaction kinetics 6720
Reaction norms 463
Reaction step 4617
Reaction yield 4617
Reactive oxygen species (ROS), sometimes reactive oxygen intermediates (ROI) 3656
Reactive power 9334, 12135
Reactive transport model 4775
Reactivity 3787, 7086
Reactor 7086
Realizable biomass potential 1174
Real-sky radiation 10621
Real-time market 12254
Real-time passenger information (RTPI) 1857
Reanalysis dataset (Global Data) 6584
Rearrangement (in relation to polioviruses) 8125
Reburning 8348
Recalcitrant carbon 846
Receiver efficiency 2349
Receiver 6031
Receiver (PTC) 7619
Receiver, solar receiver 2349
Receptors 6345
Recharge 4221, 5645
Rechargeable (secondary) battery 7546
Reclaimed asphalt pavement (RAP) 2391
Reclaimed water 2319, 8688, 11873
Reclamation 6647, 6665
Recognition element 1646
Recombinant DNA 10739
Recombinant inbred lines 6426
Recombinant protein 10865
Recombinant proteins 639
Recombinase 10815
Recombination 9412
Recovery 7798
Recreational waterborne illness 8758
Recruitment 6386
Rectangularity 10036
Rectifier 5084
Recultivation 6633
Recycled aggregate (RA) 2391
Recycled concrete aggregate (RCA) 2391
Recycled vs. recyclable 9026
Recycling 8771, 9026, 9979, 10014, 11699
Redox couple 740
Redox cycling 3656
Redox 10140, 11947
Redox signaling 3656
Redox stability 9852
Reduction 6372, 10140
Reemergence 8125
Re-entrainment 7296
Reference level 3516
Reference wind 6584
Refining 7822
REFIT 12218
Reflection 8953
Reflector 6031
Reflectors – contoured prismatic, mirror and diffusing blinds 2847
Reforestation 1532
Reformate 3860
Refraction 8953
Refuse-derived fuel (RDF) 5235, 11787
Regenerate 8856
Regeneration 10739
Regenerative braking 8848, 10542
Regenerative design 8856, 10333
Regenerative development 8856
Regional flow System 4806
Regional resource assessment 6584
Regolith 5645
Regular 1857
Regulating capacity 12098
Regulation 4238
Regulations 7822
Regulatory gene 10739
Regulatory sequence 10739
Regulon biotechnology 1
Rehabilitation 6633, 11699

Reinforced concrete 5645
Reintroduction 6386
Relative biological effectiveness (RBE) 5573, 11027
Relative humidity 310, 9696
Relative humidity (RH) 894
Relaxation 6068
Release 2005
Reliability 1834, 2781, 3099, 4238
Reliability versus cost reduction 9852
Relocation 3516
Remedial action 3516, 10140
Remediation 3516, 6633, 6647, 10140, 10435
Remedy or remedial action 2005
Remobilization 8388
Remote sensing 3358
Remote sensing reflectance, $R_{rs}(\lambda)$ 8953
Remotely operated vehicle (ROV) 3151
Removal 2005
Renaturation 11362
Renewable electricity standard 10449
Renewable energy certificates 10449
Renewable energy 1231, 2977, 4238, 11787
Renewable feedstock 3933
Renewable fuel 5462
Renewable 4221
Renewable resources 1269, 4238, 11933
Renewable water resources 11873
Repletion 9027
Replication 1002, 10739
Reporter gene 2584
Representative concentration pathways (RCPs) 5399
Reproductive performance 10886
Reproductive/breeding efficiency 10886
Reprogramming 7217
Research models 1928
Reserved lane 5021
Reserves (operating) 12254
Reserves (planning) 12254
Reserves 2174, 7446
Reservoir host 12018
Reservoir 3501, 4202, 4238, 4415, 9001
Reservoir-triggered seismicity 2788
Residence time 5673, 9049
Residential solid wastes (RSW) 5707
Residual (liquid) saturation 4202, 9001
Residual radioactivity 7056
Residual time series 9744
Residual waste 11655
Resilience 169, 533, 2929, 3342, 3450, 4674
Resistance 10694, 12293
Resolution 12062
Resonance 2424
Resource complementarity 10036
Resources 330, 2174, 7446
Response to selection 389, 9359
Responsivity 9673
Restocking 6386
Restoration 6647
Restorative design 8857
Resuspension 7007
Retardation factor 10962
Retention 8689
Retort gas 7457
Retort water 7457
Retorting 7457
Retorting residue or spent shale 7457
Retrofit 2424
Retrovirus 639
Retroviruses 10815
Return period 2424
Reuse 2319, 8771, 9979
Revenue 4238
Reverse genetics 2689, 6426
Reverse osmosis 2897
Reverse transcriptase 4998
Reverse transcriptase (RT) inhibitors 4998
Reverse-acting grate 6449
Reversible hydrogen electrode (RHE) 7731
Reynolds number 2048, 10962
RF, rf 7156
RFC 5909
RFLP 2689
RG-AEM 372
Rhizobium 10740
Rhizomes 6020
Rhizosphere 9063
Rhyolite 11614
Ribonucleic acid (RNA) 10740
Ribosome 10740
Ribozyme 10740
Rich 5501
Riding horse 1795
Right-of-way (ROW) 1857
Right-of-way (r-o-w) 5935

Right-sizing systems 10333
Risk analysis 10740
Risk assessment 207, 3516, 3621, 6605, 10140, 10435, 10713, 10740, 10766
Risk characterization 6606, 10740
Risk communication 10740
Risk management 10740
Risk 207, 3516, 4120, 4866, 6606, 10435, 10657, 10740, 10797
Risk-based policy 169
River energy 6345
River 9049
RNA interference 10852
RNA interference (RNAi) 2964
RNA (ribonucleic acid) 4998
RNA-dependent RNA polymerase 8125
RNAi 10740
RO 9758
Road construction site 3067
Road marking 3067
Roadway alignment 5645
Robustness 7694
ROC 5296, 6952
Rock pad 5646
ROI 6951
Rolling stock 1811
Rooftop 8689
Root architecture 9063
Root cap 9063
Root distribution 9063
Root hair 9063
Root lodging 6201
Root mean square (RMS) 672
Root morphology 9063
RORSAT 8468
ROS 9145
Rossby radius (of deformation) 7366
Rotor 7394
Rotor–nacelle assembly (RNA) 7394
Roughness length 6585
Route of exposure 3621
ROV 6405
RPS 12218
R(R)DE 8265
RRL 8125
R_5 5500
R_6 5500
r_c 5500
R_e 5500
RTG 8468
RTU 12079
RuBPc-o 2661
RUE 2615
Runoff 8634
Runoff water 2320
Rural electrification 1445
$r(x_i,x_j)$ 7181
rxn 5174
Saccade 46
Saccharification 988, 11429
Sacrificial reactions 4617
Safe Zone 6098
Safeguards 7201
Safety barrier 3067
SAFOTEST 10740
SAGE 8125
Saharan air layer (SAL) 5071
Saline soil 5315
Salinity 7366, 12018
Salt tolerant plant 5315
Salt water 11933
Sanitary landfill 9979
Sanitary landfills 5708
Sankey diagram 11839
Saprophyte 2559
Satellite altimetry 2455
Satellite 4564
Saturated zone 10140
Saturation 4238
Saturation state of calcium carbonate (Ω) 7229
Savonius rotors 3397
SC 7156
SCADA 10935, 12079
Scale 3326, 5773, 5818, 6216
Scale-up 10740
Scaling 4238, 5773
Scarcity 9027
Scattering coefficient 310
Scattering 310
Scatterometer 7491
Scavenging 8388
SCC 4957
Scenario 1532
Scene flow 10590

Scene understanding 3171
scf 3956
Scheduled speed 5973
Schmidt and Prandtl numbers, Sc and Pr 595
Scintillator 5560
Scleractinia 2490
SCNT 10815
Scour 7425
SCR 245, 4957
Screenable marker 2584
Screening models 1928
Screw expander 4238
Scrubber 4238
Scrubbing 11720
SCWR 4050
SD 7181
SDR 11553
Sea ice 280, 2761
Sea level rise 2455
SEA 10577
Sea ranching 6386
Sea state 7394
Seabed 7394
Seafood 9079
Seafood-associated toxins 9079
Seasonal reproduction 10886
Seasonal snow 280
Sea-vegetables 9110
Seaweed 9110
Second crop 1098
Second crop soybeans 4433
Secondary battery 672
Secondary control 12098
Secondary effect 8308
Secondary metabolites 3151, 6520, 10740
Secondary or rechargeable cell 6498
Secondary particles 245
Secondary pollutants 169, 11311
Secondary roots 9063
Secondary standards or guidelines 207
Secondary standards 169
Secondary treatment 11873
Second-generation bioethanol 961
Second-generation cells 9852
Secondhand smoke 10636
Sediment budget 3706
Sediment delivery ratio 3706
Sediment mixing 8388
Sediment 3029, 3706, 7007
Sediment source fingerprinting 3706
Sediment source 3706
Sediment surface layers 9129
Sedimentation 3706, 5673
Sedimentation rate 7007
Seed bank 150
Segmentation 3171
Segregated biomass 1174
SEI layer 740, 6038
SEI 1145
Seismic 4163
Seismic wave 2424
Seismic zoning 2424
Seismicity 2424
Seismology 2424
Selectable marker 2584, 10740
Selection intensity (i) 1795
Selection 1741, 1795, 9359
Selective attention 46
Selective breeding 5315, 10740
Selective catalytic reduction (SCR) 4755, 8348
Selective medium 10740
Selective noncatalytic reduction (SNCR) 8348
Selectivity 10345
Self selection 10923
Self-contained fluid filled (FF or LPOF or PILC) 11159
Self-discharge 6938, 7546
Self-discharge rate 672
Self-oxidation 7585
Self-schedule 12254
Semantics 10192
Semiconductor 7881, 9563
Sensible heat storage 10551
Sensitivity analysis 7007
Sensitizer 6566
Sensor calibration 3171
Sentinel 5048
Sentinel species 6179
Separation capability 5634
Separation factor 5634
Separation 8795, 11655
Separator 740, 4238, 6122, 7547, 8715
Sequence homology 10740
Sequences 5048

Sera-binding tests 10740
SERC 5909
Series hybrid vehicles 5084
Seroconversion index 8125
Seroconversion 8125
Serotype 8125, 11985
Service operation plan 1834
Sessile organism 3151
Seston 6759
Set-out rate 11655
Setpoint 11947
Sewage sludge gas 1089, 1618
Sexual maturation 3621
Sexual stage 6291
SF 7181
SFR 4050
Shading for passive cooling balanced by passive solar heating 2847
Shadowband 9706
Shale gas 7446
Shale oil 7457
Shallow water collections 3151
Shallowness approximation 7366
Shared corridor 5950
Shared right-of-way 5950
Shared track 5950
Shattering 10345
Shear failure 3501
Shielded cable 11159
Shifting agriculture 150
Shikimate pathway 10741
Shinkansen 4929
Ship discharge 7491
Shockley–Queisser limit (SQ limit) 9412
Shoot apex 2540
Short rotation coppice (SRC) 6020
Short rotation plants 1489
Short turning 1857
Shortwave 9706
Shrinkage 5836
Shrinking city 11362
Shutdown separator 8715
Shuttle 1857
SIA 8125
SiC 7866
Side product of a reaction 4617
Sideslip angle 3052, 11187
SIDO 1145
Sievert (Sv) 8448
SIGMATIST 3278
Signal Priority 90
Signal sequence 10741
Signal transduction 10741
Significant quantity (SQ) 7201
Significant wave height 7425
SiH_4 9432
$SiHCl_3$ 9432
Siicon solar cells 7932
Silent circulation 8125
Silent infection 8125
Silent presence 8125
Silurian 2174
Simulation 90, 9316
Single nucleotide polymorphism 10886
Single nucleotide polymorphism (SNP) 473, 2964
Single-copy transformant 10671
Sinkhole 5646, 6633
Sinter plate cells 6938
SIPS 10935
siRNA 10816, 10895
Site density (S_D) 8265
Site evaluation 3516
Site selection 6759
Site-specific recombination 10741
Siting 6585
Skin damage 11376
Skyshine 8537
SL 8125
Slag 3997, 6633
SLI batteries 672
SLI 5881
Slow pyrolysis 1518
Sludge 1174, 6309
Sludge retention time (SRT) 11961
Slug lines 5021
Slurry jet 10976
Slurry 7667
Small interfering RNA (siRNA) 10741
Small scale 1445
Small-scale cogeneration unit 1400
Smart grid 2977, 12218
Smart growth 10923
Smog 8879, 11292
Smooth-pursuit movement 46

SNAP 8468
SNCR 4957, 6449
SNG 1040, 1427, 1584
SNIDS 8125
Snow 2761
SNP (single nucleotide polymorphism) 7973
SNV 1145
SO_2 2164
SOC 8112
Social acceptance 12218
Social interactions 9359
Socio-ecological justice 169
Socio-technical system 12218
SOEC 9904
SOFC 2934, 3872, 9904, 9934
Soil ice 2761
Soil microbial processes 3769
Soil 2430
Soil quality 161
Soil remediation 2431
Soil texture 1097
Soil water balance 5619
Solar air system 7641
Solar architecture 7640
Solar cavity receiver 9589
Solar cell conversion efficiency η 9197
Solar cell 1977
Solar cell production capacities 7936
Solar cells 7932
Solar chemical heat pipe 9589
Solar concentration ratio 9589
Solar constant 9470, 9696
Solar cookers 9487
Solar cycle 9469
Solar dryer 9487
Solar energetic particles (SEPs) 9796
Solar energy utilization 9766
Solar field 7619
Solar fraction (F_{sav}) 9449
Solar fuels 9589
Solar geoengineering 4104
(Solar) Irradiance (G) 9449
Solar irradiance 9619
Solar module 1977
Solar photochemistry 9563
Solar radiation database 10621
Solar radiation management 10161
Solar radiation management (SRM) 10117
Solar radiation 9673
Solar spectral irradiance (SSI) 9706
Solar spectrum AM 1.5 9449
Solar thermochemical process 9589
Solar updraft tower (SUT) 9766
Solar wind 9797
Solar zenith angle 11149
Solid Biofuel 2271
Solid electrolyte interface (SEI) 709
Solid electrolyte interphase (SEI) 6068
Solid oxide fuel cell (SOFC) 9886
Solid polymer electrolyte 6038
Solid polymer fuel cell (SPFC) 3860
Solid waste 5733, 9979, 9995
Solid waste composition* 9995
Solid waste discarding* 9995
Solid waste disposal* 9995
Solid waste generation rate* 9995
Solid waste generation* 9995
Solid waste management system* 9995
Solid waste management* 9995
Solid waste recycling* 9995
Solid waste reuse* 9995
Solubility 4239, 10140
Solubility product 4094
Solute 5673
Solution 5646
Solvent engineering 3933
Solvent extraction 7142
Somaclonal selection 10741
Somatic cell count 10852
Somatic cell nuclear transfer (SCNT) 2964
Somatic cell 7217
Somatic nuclear cell transfer 10865
Sorption 9509, 11961
Sorption (verb: to sorb) 10140
Sorption/desorption 4775
Sorting 8795
Sound level *(L_A, L_B, L_c)* 12275
Sound pressure level (SPL, L_p) 12275
Sound pressure *(p)* 12275
Sound speed *(c)* 12275
Source activities 11655
Source apportionment 169
Source material 7201
Source reduction 8771, 9979, 10014

Source to sink 8857
Source treatment technologies 2431
Source–sink balance 4551
South Pacific convergence zone 7245
Southern blot (DNA blot) 2584
SOx 9432
SP 1584
Spa 4163, 4354
Space charge 11159
Space-averaged load factor 1857
Spallation 8468
Spatial arrangement 10036
Spatial autocorrelation 3326
Spatial heterogeneity 5773
Spatial planning 5786
Spatially explicit models 5773
Special fissionable material 7201
Special nuclear material (SNM) 7201
Speciality chemicals 7585
Speciation 8388, 10051, 10140
Species average fitness 10062
Species (biological species concept) 10085
Species 4094
Species richness 150
Specific activity 10997
Specific and wide adaptation 4070
Specific capacity (in mAh/g or Ah/kg) 7547
Specific capacity 709, 9293
Specific energy 9293
Specific heat 4221, 4909
Specific storage 5712
Spectral error 7902
Spectral radiance $L_{\lambda,}$ 9650
Spectral solar irradiance (SSI) 9797
Spectral weighting function 11376
Spectral-selective coating 9449
Spectroradiometer 11149
Spectroradiometry 9706
Spectroscopy 5560
Spent fuel 7142
Spherical harmonics 4564
Spillage, spillage losses 2349
Spin state 740
Splash zone 7426
Splice 11159
SPP 5909
Sprawl 5836
Spring tide 10613
SR 3997
SRC 1040, 1584
SRF 5296
SRT 1145
SS 1584
s_1 5500
s_2 5500
s_3 5500
s_4 5500
s_5 5500
S&T 11069
Stability 4239
Stabilized efficiency 9241
Stable coexistence 10062
Stable transformation 2584
Stack 8205, 9934
Stakeholders 406, 1819, 8125
Stand 4380
Stand-alone furnaces 1351
Standard test conditions (STC) 1977
Standards 207
Starch 988
State Director 5733
State of charge 740
State of charge (SoC) 672
State of health (SoH) 672
State 5733
Stationarity 3326
Stationary sources 207, 8879
Statistical entropy analysis (SEA) 11708
Statistical entropy 11708
Status of development 1400
Steam cycle 7086
Steam methane reformation (SMR) 5135
Steam methane reforming (SMR) 3956
Steam Rankine cycle 4239
Steam turbine 6806
Steam zone 4202, 9001
Stem failure moment 6201
Stem lodging 6201
STEM 3201
Stereo camera system 6952
Stereo vision 10590
Stereotypy 7973
Steric sea level 2455
Stewardship 533, 564

Stilbenes 10741
Stirling engine 1608
Stochastic effect 5573
Stochastic effects 11027
Stochastic model 10192
Stock enhancement 6386
Stoichiometric coefficient 4618
Stoichiometric factor (SF) 4618
Stoichiometric 5501
Stomata 1476
Stomatal resistance 3211
Storage 11655
Storage Reserve (capacity) 4120
Storage Resource (capacity) 4120
Storm water runoff 4730
Stormwater havesting 10095
Stormwater 8689
Stormwater runoff 4698
STR 1584
Strategic crop management 9316
Stratification 5673, 7007
Stratification thermal time index 9145
Stratosphere 310, 2510, 9619, 9706, 9797, 10130, 11149
Stratospheric aerosols 10117
Street canyon 11312
Streetcar 1857, 5973
Stress caused by volume changes 9852
Stress 1184
Stressor 1184
Stressors 6345
Stripping ratio 2174, 6665
Strombolian 11614
Structural gene 10741
Structural genes (in relation to polio) 8125
Structure activity relationships (SARS) 6790
Structured decision making 3342
Structured (regular)/unstructured (irregular) grid 7366
STS marker 2689
Sub 4380
Subbituminous coal 8348
Subgrid heterogeneity 3211
Subgrid scale 623
Subjective experience 10865
Subjective report 3108
Submerged longline 6759
Subsea template 6405
Subsidence 4163
Substantial equivalence 10741
Substrate 10741
Sub-structure 7394
Subsurface 10141
Subtropical zones 10390
Subunit vaccine 6291
Suburb 11325
Suburban rail 806
Suburbanization 5786
Successional stages 150
Sulfur dioxide 207
Sulfur dioxide (SO_2) 8348
Sulfur oxides 8348
Sulfur poisoning 9852
Summer solstice 9619
Sun 9469
Sun sensor 7619
Sunphotometry 9706
Sunshade 10161
Sunspot number 9469
Sunspot 9469
Super-Alfvénic 9797
Superbinary vector 2584
Supercapacitor or electrochemical capacitor 6769
Superconductors 6241
Supercritical fluid 3933, 10169
Superinsulation 7630
Supervirulent 2584
Supplementary cementing material 3821
Supplementation 6386
Support structure 7394
Support/supported 4584
Surface freshwater flux 7245
Surface functionality 6769
Surface jet 10976
Surface longline 6759
Surface mixed layer 7268
Surface runoff 7667, 8689
Surface solar radiation 9731
Surface water 11933
Surface-enhanced Raman spectroscopy (SERS) 5382
Surface-mounted PMSM (SM-PMSM) 18
Surtseyan type 11614
Susceptibility 3621
Suspended matter 7007

Suspended solids 3029
Suspension culture 6758, 8059
Sustainability assessment 8702
Sustainability 1002, 1489, 1741, 2061, 3201, 3450, 3556, 3933, 4643, 5733, 5836, 8024, 8689, 10317, 10435, 10713, 11069, 11699
Sustainable 4221, 10482
Sustainable agriculture 2528
Sustainable battery 7547
Sustainable building 10333
Sustainable design 10299
Sustainable development potential 1532
Sustainable development 566, 1002, 1857, 2529, 5733, 11699
Sustainable energy 11787
Sustainable mining 6633
Sustainable 1269
Sustainable remediation 1628, 10435
Sustainable urban drainage systems 4674
Sustainable water use 2320
Sverdrup 5856
SW 7181
Swing gate 5935
Switched reluctance motor 10542
Synchrophasor 12079
SYNCOM 6449
Synergy 5135
Syngas 1608, 9589
Syngas (synthesis gas) 1427
Synonymous nucleotide substitutions 8126
Synteny 6426, 10742
Synthesis gas 11429
Synthesis gas (syngas) 2222, 3956
Synthesis 6216
Synthesis tree 4618
Synthetic aperture radar 280
Synthetic aperture radar (SAR) 8939
Synthetic biofuel 1427
Synthetic 1427
System boundary 5893
System (electric) 4239
System 4239, 9316
Systematic error 2098
Systemic acquired resistance (SAR) 10694
Systemic herbicide 10345
Systems biology 10742
Systems thinking 8857
T 12202
t 7181, 11202
T3 6449
Tactical crop management 9316
TAG 8126
Tailings dams 6665
Tailings ponds 6665
Tailings 6647, 6665
Tan δ (TD) 11159
Tandem 9412
Tangential route (or Line) 1857
Tannins 10742
Tap density 740
Taproot 9063
Taproot system 9063
Tar sand mining 7798
Target bond forming reactions 4618
Target bond map 4618
Target load 169
Target site 10345
Tariff and non-tariff barriers 1002
Taurine 6179
Taxonomy 10192
TCI 1040, 1584
TCR 2164
TD 8126
T-DNA 2584, 8059, 10742
TEC 2934
Technical biomass potential 1174
Technical efficiency 2720
Technical potential 1532
Technology push/market pull 1819
Tectonic plates 2424
TED 1145
Teleconnection 9619
Teleconnections 2119, 7245
Temperate zones 10390
Temperature inversion 8879, 11312
Temperature polarization 2897
Temporal 8879
Temporal separation 5950
TEN 4929
TENORM 8468
Tensile failure 3502
TeO_2 9432
TEQ 5296
Teratogenic 10636, 11027

Terminal 6938
Termination 11159
Terminator 2584
Terra preta 846
Terrestrial 8468
Tertiary 2174
Testing 11737
Tetraploid 6150
TEV 4784
Texturization 9197
TF 7156
TGA 5296
TGV 4929
th 1040
The department of energy 6688
The El Niño–Southern Oscillation (ENSO) 7245
The National Priority List or NPL 2006
The southern ocean 8656
The sublime 10361
The Superfund 2005
The United States Nuclear Regulatory Commission 6688
The wind atlas method 6585
Theoretical biomass potential 1174
Theoretical energy density, specific energy, capacity 709
Theoretical potential 1532
Thermal anomaly 4222
Thermal Bridge free 7630
Thermal bridge 3675
Thermal comfort 6865
Thermal conductivity 4222, 7194
Thermal drawdown 3502
Thermal expansion 2455
Thermal fuel power 8081
Thermal infrared radiation (TIR) 8919
Thermal mass 10333
Thermal neutrons 7087
Thermal pollution 4239
Thermal runaway 6098, 6123
Thermal stability index 6976
Thermal time 2540
Thermalization 9412
Thermistor 4909
Thermobitumen 7457
Thermochemical biohydrogen generation 5116
Thermochemical conversion 1199, 1518, 2271
Thermochemical heat storage 10551
Thermocline 2349, 4909, 7007, 7245, 7366, 8655
Thermodynamic system 3306
Thermohaline circulation 2510, 5856, 7366, 8655
Thickness sensor 7491
Thin film 1977
Thin stillage 988
Thin-film cells, a-silicon (a-Si), mc-silicon (mc-Si) 8373
Thin-film solar cells 9394
Thiol 3656
Third-generation cells 9852
Thorium 6688
Thorium (Th) 7194
THORPEX 5071
Three-phase boundary 6720
Threshold dose 3253
Threshold energy 6098
Threshold power 6098
Ti Plasmid 10742
Tidal basin 10613
Tidal currents 10613
Tidal energy 6345
Tidal stream 10613
Tides 10613
Tiered approach 6790
Tight gas 7446
Tight ultrafiltration (UF) membrane 10530
Tile method 3211
Timed-transfer system (TTS) 1857
Timeform handicap ratings 1796
Time-for-space substitution 3278
Time-of-use pricing 10449
Tipping point 10118
Tire forces 3052, 11187
Tissue culture 10742
Tissue tolerance 5315
TJ 1489
TL 5173
T-lymphotropic 4998
T-NAWDEX 5071
TNT 8468
TOC 4957
TOD 1890
Tolerance 12293
Tolerance threshold 9079
Toll 5021

Top of atmosphere 9619
Topographic index 3211
Topography 6585, 10621
Topology 9063
Topotactic transformation 709
TOPV 8126
Torch thermal efficiency 8097
Torrefaction 1067, 1608
Total material requirement (TMR) 10403
Total (overall) mass of waste 4618
Total (overall) reaction mass efficiency 4618
Total solar energy transmission (g/SHGC) 2847
Total solar irradiance (TSI) 9706, 9797
Tower 6031, 7394
Toxic pollutant 3029
Toxicity characteristic leaching procedure (TCLP) 3444
Toxicity 1184, 3029, 10658
Toxicity test 3265
Toxicodynamics 12293
Toxicogenomics 3265
Toxicokinetics 3621, 12294
Toxicology testing 6790
T-PARC 5071
tpy 5174
Trace organics 8689, 11874
Track 5573
Tracking (PTC) 7619
Traction load 5103
Traction 5973
Tractive effort 11481
Traditional breeding 10742
Traffic control devices 5935
Traffic signal 1834
Trait 1, 1476, 8013
Tramway 1857
Transactivation domain 2584
Transboundary pollution 11312
Transcription activator–like effector nucleases (TALENs) 10742
Transcription 7217, 10742
Transcriptional gene silencing (TGS) 10671
Transcriptome 10742
Transdisciplinarity (TD) 6179
Transdisciplinary 566
Transesterification 921, 1026, 1608
Transfection 2584, 7217
Transfer coefficient (F_f d $kg^{-1}F_m$ d L^{-1}) 8425
Transfer coefficient k_{Xi} 10577
Transfer coefficient (TC) 11220
Transfer DNA (T-DNA) 10671
Transfer function 8634
Transfer 7668, 11655
Transfer station 11655
Transfer velocity 595
Transferred arc 8097
Transformant 2584
Transformation 2584, 8059, 10742
Transformative research 6216
Transgene expression variability 10671
Transgene 1676, 6520, 8059, 10742, 10797, 10852, 10886
Transgenesis 10895
Transgenic bird lines 639
Transgenic bird 639
Transgenic organism 10742
Transgenic plant 1676, 10671, 10694, 10742
Transgenic plants 8024, 8073
Transgenic 2584, 4013, 10852, 10886
Transient expression 2584, 8059, 8073
Transit choice riders 1819
Transit 5974
Transit ridership 1890
Transit signal priority (TSP) 1857
Transit value capture 1890, 10923
Transition metal chalcogenides 8265
Transition 8126
Transit-oriented development, or TOD 5973
Transit-oriented development 169, 1811
Transit-oriented development (TOD) 1819, 1834
Translation 10742
Translocation 10997
Transmissible spongiform encephalopathy 10742
Transmission 4239
Transmissions 11481
Transparent conductive oxide (TCO) 9241
Transpiration 5818
Transplastomic plants 8073
Transplastomic 2584
Transport equation 8537
Transport mechanisms 10141
Transport model 9129
Transport 11655
Transport vehicle 11655

Transportation demand management 90
Transportation Equity Act for the 21st Century 1811
Transportation 10482
Transposon 2690, 10345, 10742, 10815
Transuranic waste (TRU) 8589
Transuranics 8598
Transversal 6031
Transversal IAM 6031
Transversions 8126
Travel time savings 1812
Traveler information 90
TRE 5909
Treatable flow 10095
Treatment measures 10095
Treatment 11737
Treatment train 10095
Tremor 11633
Triacylglycerol (TAG) 11429
Triassic 2174
Tributary 7007
Trickle charging 6938
Tri-generation 1661
Trigger for thermal runaway 6098
Trigger point 4202
Triglyceride 6896
Trip 4380
Triple bottom line 10261
Triple phase boundary (TPB) 8205
Tritiated water (HTO) 10997
Tritium 10997, 11027
Trolley bus 5974
Trophic level 822, 3300, 7007
Trophic transfer 4819
Tropical biennial oscillation (TBO) 6741
Tropical health 11069
Tropical zones 10390
Tropopause 623
Troposphere 169, 310, 2510, 9620, 9706, 9797
Trotter 1796
Trough 6031
Truck 1857
Trunk pipeline 6405
Trypsin inhibitors 10742
TSO 10935
T_1 5500
T_4 5500
T_5 5500
T_6 5500
$T_{cv,adiabatic}$ 5500
T_e 5500
T_H 5500
T_i 5500
T_L 5500
T_r 5500
T-Test 3099
Tuberculosis 498, 4998, 11130
Tubular plate electrodes 6938
Tumor suppressor gene 3596
Tunneling Effects 4929
Turbidity 3029, 8919
Turbine generator 4239
Turbine 4239, 10613
Turbulence intensity 6585
Turbulence 6585
Turbulent diffusion coefficient 2031, 2048
Turbulent diffusion 2031, 2048, 10955
Turnover frequency (TOF) 3933, 8265
Twist-off 4380
Two (2)-phase zone 4202, 9001
Two-class problem 6952
Two-electron reduction 6038
Twomey effect 9696
u 12202
U 7181
UASB 1145
UCTE 9432, 10935
$|UD|$ 4618
Ultracapacitor (electrochemical capacitor) 3471
Ultracapacitor 5084
Ultrafine particles 245, 11292
Umbilical 6405
Uncertainty 6606
Uncertainty analysis 7007
Unconformity 11202
Unconventional oil and gas 7446
Underground Thermal Energy Storage (UTES) 4133
Under-pressured 4380
Undifferentiated 7217
UNICEF 8126
Unintended effect 10742
Unit commitment and economic dispatch 8980
Unit commitment 12254
Unlinked trip 1857
Unsaturated (saturated) fatty acids 10852

Unsaturated/vadose zone 10141
UOX 7181
Up, down conversion 7932
Upconversion 9412
Upcycling 9027
Updraft combustion 1351
Upgraded solid biofuel 1067
UPS 5881
Uranium dioxide (UO_2) 6688, 7194
Uranium 6688
Uranium (U) 7194
Uranium utilization 4050
Urban air quality 11263
Urban design plan 5786
Urban ecology 6853
Urban forest 11344
Urban forestry 11344
Urban form 169
Urban green space 11344
Urban greening 11344
Urban growth boundary (UGB) 5786
Urban heat-island effect 3450, 4674
Urban Mass Transportation Act 1812
Urban metabolism 6853
Urban meteorology 11263
Urban mining 6853
Urban 11292, 11325
Urban Redevelopment Program "Stadtumbau Ost" ("Urban Redevelopment East") 11362
Urban smog 11292
Urban sprawl 4806, 5786
Urban sustainability 3450
Urban system 5787
Urban wildlife 939
Urban woodland 11344
Urbanization 5786
UREX 7142
Urticaria 12019
US EPA 5909
US 1040
Used nuclear fuel or spent nuclear fuel (SNF) 8589
USTB 1145
U_1 5500
u_1 5500, 12202
u_2 5500
U_2 5501
u_3 5500
U_3 5501
u_{3a} 5500
u_4 5500
U_4 5501
Utility 4239
Utilization ratio 8081
UTM 6952
UV index 9650
UV Radiation 11149
UV (ultraviolet) radiation 11376
UV-A radiation 9650
UV-B radiation 9650
V 5501
V2B 7847
V2G 7847
Vaccine 8059
Vaccine resistance 6291
Vaccine strains 8126
Vadose zone 4202
Valence band 7882
Validation (model) 7007
Validity 3099
Value pricing 5021
VANET 11553
Vanpools 4945
Vapor pressure 10141
Vapor(or steam)-dominated resources 4239
VAPP 8126
Variability 6606
Variable generation 8980
Variant 5347
Variety 10742
Variography 3326
VAWT 3397
V-blender 7142
VCV 11159
VDPV 8126
Vector competence 5358
Vector 5358
Vehicle control systems 3052, 11187
Vehicle detection 11455
Vehicle dynamics 3052, 11187
Vehicle energy source 11503
Vehicle maintenance 1812
Vehicle miles traveled (VMT) 5974
Vehicle operations 1812
Vehicle performance 11481

Vehicle resistance 11481
Vehicle simulations 3471
Vehicle tracking 11455
Ventilation 5856, 6865
Ventilation effectiveness 6865
Ventilation flow rate 6865
Verkehrsverbund or federation of transit operators 5974
Vernalization 1098
Vernalization sensitivity 2540
Vertical flow 4806
Vertical (normal) tire forces 3052, 11188
Very short-lived species (VSLS) 10130
Vestibulo-ocular reflex 46
VGA 6952
VHLW 7181
VHTR 4050
Vibrational (molecular) spectroscopy 5382
Viewshed 10621
vir Gene 2584
Viral pathogens 8758
Viral vector 8059, 10865
Viremia 8126, 11985
Virion 4999
Virtual technology for aquaculture 1928
Virtual versus real 3201
Virulence 2559, 5048, 10742
Virus 10694, 10743
Viscous boundary layer 595
Visible, near infrared, and short-wave infrared (VIS, NIR, and SWIR) 8919
Visual capacity 10361
Visual odometry 46
Visual sensitivity 10361
Vitamin D 9650
Vitamin 1676
Vitrification 8097, 11582
VMT 1890, 5021
VO 1040
VOC limited 11312
VOC 4957, 11312
Void ratio 5712
Volatile matter 2174, 8348
Volatile organic compounds (VOC) 5748
Volatiles 11633
Volatility 10141
Volatilization 9049
Volcano 4163
Volume development 7007
Volunteer weed 10345
VOR 5021
VOT 5021
VP1 8126
VP2 8126
VP3 8126
VP4 8126
VPg 8126
VRLA cell 5881
v_1 5501
V_1 5501
V_2 5501
v_2 5501
v_3 5501
V_3 5501
v_{3a} 5501
v_4 5501
V_5 5501
V_6 5501
V_d 5501
V_{max} 5501
V_{min} 5501
V_o 12202
V_{rel} 12203
VTD 9432
Vulcanian 11614
Vulnerability 2929, 3621
Vulnerability (with respect to climate change) 4674
W 12203
W 5501
Wafer 9197
Walker circulation 7245
Wall jet 10976
WAMPAC 10935
WAMS 12079
WASAZA 1145
Washability 2194
Washout 4380
WAsP 6585
Waste characterization 10000
Waste disposal 9979
Waste diversion 11673
Waste dumps 6665
Waste incineration 11839
Waste management 3516, 5720, 11673

Waste 10000, 11851
Waste prevention (aka Source reduction) 11673
Waste rock 6647
Waste water 4202, 4415
Waste* 9996
Waste-to-energy 9979
Waste-to-energy (WTE) 11682, 11708, 11768
Waste-to-energy (WtE) 5235
Wastewater effluent 11912
Wastewater 8689, 11874
Wastewater reclamation 11874
Wastewater reuse 11874
Water balance 4806
Water gas shift reaction 2222
Water gas shift reaction (WGSR) 3956
Water mass formation 5856
Water mass 5856
Water quality change 4806
Water quality objectives (WQOs) 10095
Water quality 2078
Water reclamation 11961
Water reuse 2078, 8689
Water Safety Plan (WSP) 6606
Water tree retardant cross-linked polyethylene (WTRXLPE) 11159
Water trees 11160
Water use efficiency 1269
Water use efficiency (WUE) 1098, 1477, 5619
Water vapor pressure (P_v) 894
Waterborne disease 5048, 7384
Waterborne infectious diseases 11997
Water-dominated resource 4239
Water–gas shift (WGS) 5136
Water-leaving radiance, $L_w(\lambda)$ 8954
Watershed 533
Water-use efficiency (WUE) 2639
Watt 4239
Watt (W) 4163, 4354
Watt-hour (Wh) 672, 4239
Wave Energy 6346
WBT 1299
WC – Whole crop 1098
Weather modification 4104
Weather 623
Weathering 1909
WECC 5909, 10935
Weibull probability density function 6585
Weighting 8702
Well-being 6865
Wellhead protection area 4806
Well-to-pump (WTP) 10503
Well-to-tank (WTT) efficiency 5136
Well-to-wheels (WTW) 10503
WENE-048 predictions 6585
West African monsoon 5071
Wet cake 988
Wet deposition 606, 8880
Wet FGD 8348
Wet process 8715
Wet weight (ww) 4755
Wet-bulb temperature (WBT) 894
Wetland 11891
WH 6938
WHA 8126
Whey 10852
WHO 8126, 11069
WHO (World Health Organization) 5332
Whole systems thinking 10333
Whole-organism vaccine 6292
Wholesale electricity markets 12254
WID 5296
Wide dynamic range (WDR) 11098
Wildlife 8425
Wildtype 10743
Wind energy penetration 12254
Wind profile 6585
Wind shear 7426
Wind turbine 7394
Winter smog 11292
Winter solstice 9620
Wireless vehicular communication 2464
WOA05 7296
Woody fuels 9821
Working ion 740
WPV or wild poliovirus 8126
WRAIR 11069
W_b 5501
W_f 5501
W_{gross} 5501
W_{ig} 5501
W_{in} 5501
W_{ip} 5501
W_{net} 5501
WSUD 10095

WTE incinerator 4866
WTE 5296, 5909, 8097, 11759
WTW 1040
WWTP 11947
X factor 10542
XBT (eXpendable BathyThermograph) 4909
Xenobiotic 3657, 12294
Xenolith 11614
x_i 7181
X-ray 11027
x_i 5501
Yaw angle 10590
Yaw rate 10590
Yeast 988
Yellowcake 11202
Yield gap 2720
Yield 2194, 11376
y_i 5501
Z-crossing 5935
Zenith angle 9673
Zeolite 4584
Zinc finger 2584
Zinc finger nuclease 10815
Zinc finger nuclease (ZFN) 10895
Zinc finger nucleases (ZFNs) 10886
Zinc-finger nucleases 8059
Zircaloy 7194
Zircar 6938
ZLD 9758
ZnO 1040, 1584
Zonal 5856
Zonal service 1857
Zone theory of PIC formation 6976
Zoning 5787
Zoonosis 5048, 5358, 12019
Zoonotic diseases 8073
Zoonotic infection 2964
Zoonotic pathogen 9157
Zoonotic 2259
Zooplankton 7007, 8201
Zooxanthellae 2490
Zygote 6150, 7217

Index

A

abandoned mine
– methane (AMM) 6807
– tunnel/cavity systems 4152
ABA, see abscisic acid
Abaqus 6108
abate pollution 2507
ABC protein 12307
abiotic elicitor 6528
abiotic stress 1, 2712, 9065, 10748, 10751
ablative pyrolysis 1521
abortive poliomyelitis 8142
AB-PBI, see poly(2,5-polybenzimidazoleI)
abrasion 253
abscisic acid (ABA) 6, 9068, 9150, 10750
– biosynthesis 9150
– embryonic content 9150
– in dormancy maintenance 9150
absolute cavity radiometer 9679
absorbed glass mat battery 775
– gel cell 775
absorption 9512, 9628, 11974
– chillers 9520–9521, 9524
– heat pumps 4140
– of organic micropollutants 11974
– refrigeration cycles 4318
– spectroscopy 6075
absorptive air dehumidifier 9531
absorptive glass mat 11512
abstract community 3278
abuse tolerance 6139
– lithium ion cell 6139
abyssal
– changes 4922
– temperature 4923, 4924
– abyssal temperatures 4923
– warming 5872
Acanthamoeba 12045, 12046
Acanthocephalans 12031–12032, 12040
Acari 5438
accelerating rate calorimetry (ARC) 6108
accelerator mass spectrometry (AMS) 8657
accelerometer 3060, 4567, 4569, 11196
accident 72, 3131
– drowsiness-related 3131
– involving children 67
– pedestrian-related 72
acclimation 3257
accumulator 741, 5102
– bladder-type 5102
acetaldehyde 306, 835, 3610, 10641
acetaminophen 1189, 11922
acetate 11020
– tritium-labeled 11020
acetic acid 3942, 3989
Acetobacter diazotrophicus 1274
acetogenesis 1149
acetone 1466
acetonitrile (AN) 3424, 3497, 3935, 3941, 6775
– electrolytes 3430
acetosyringone 2588–2589
acetyl CoA carboxylase (ACCase) 360
acetylation 3604
acetylcholinesterase (AChE) 3260, 12311
– inhibition 3260
acid aerosol 8892
acid base accounting (ABA) 6663
acid catalysis 3944, 4586
acid degradation 11445
– products 11439
acid deposition 175
acid gas 4987, 5239
– neutralization 5239
– removal (AGR) 2236
acid mine drainage (AMD) 6639, 6653, 6658, 6661–6663, 6673
– bioremediation 6661
– heavy metals 6673
– lime-treated 6658
– value extraction process (AMD VEP) 6662
– water quality 6663
acid neutralizing capacity (ANC) 175
acid rain 171, 175, 188, 6809, 7843, 8349
– mass balance 11749
acid rock drainage (ARD) 6653
acid water 2252
acidic drainage 6663
acidic fuel cell 3880
acidic polymerase 2971
acidic protogenic hydrogen 8337
acidification 548, 1150, 1598, 8883
acidogenesis 1149
Acinetobacter 1630
acoustic Doppler current profiler (ADCP) 6761
acoustic quality in indoor environments 10276
acoustic signal 12279
– Fourier analysis 12279
acoustic thermometry 4916, 4924
acoustic wave 12066
acquired immunodeficiency syndrome (AIDS) 4996, 4999–5000, 5011–5012
– definition of the problem 4999
– global epidemic 4996
– T-lymphotropic retrovirus (HTLV) 5000
– treatment 5011
– vaccine 5012
Acrolein 2058, 2060
acrylated epoxidized soybean oil (AESO) 6900, 6908
acrylic acid 6917
acrylonitrile-butadiene-styrene (ABS) 4852
acrylonitrile 6917
ACS study 226
actinides 4053, 4777, 8621
– recycling 4053
– reprocessing 4053
Actinidia 1709
actinon 8478
action by galvanism 6500
action spectra 9651
activated carbon (AC) 797, 3430, 4992, 6771, 6785
– properties 6770
– nanoporous texture 6785
activation neutron 8569
activation photon 8572
active bumper 73
active cavity radiometer 9471
active design guidelines 10279
active Doppler wind lidar (DWL) 324
active geothermal conditioning 4133
active oxidation 1344–1345
active pedestrian protection system (APPS) 72
active perception 48

active safety vehicles (ASV) 71
active solar hot water collector 3695
active vision 48
active volcano 11617, 11622
acute flaccid paralysis (AFP) 8142, 8153
acute lymphoblastic leukemia (ALL) 3642
acute respiratory syndrome (SARS) 10860
acylalanine fungicides 2568
ad hoc on-demand distance vector 11553
AdaBoost (adaptive boosting) 83, 6960, 6968
– algorithm 83
– cascade 83
– classifier 11460, 11468, 11476
– training process 83
adamantaneacetic acid (AAA) 7747
adamantanecarboxylic acid (ACA) 7747
adaptation 3365
– systems 2931
adaptive cruise control (ACC) 71, 76, 3068
adaptive governance 3352–3353
adaptive loss-of-field 12091
adaptive management 3342, 3345, 3347, 3349–3352, 3354–3355
– alternatives 3349
– elucidate consequences 3350
– identifying and evaluating tradeoffs 3351
– implementation 3351
– law 3354
– objectives 3349
– participatory active 3351
– structured decision making 3347, 3355
adaptive neuro-fuzzy inference system (ANFIS) 3125
adaptive out-of-step relaying 12090
additive genetic effect 418
additive genetic variance 475
additive main effects and multiplicative interaction (AMMI) model 4082
adenine arabinoside (Ara-A) 3153
adeno-associated virus (AAV) 10827, 10917
adenosine diphosphate (ADP) 1479
adenosine triphosphate (ATP) 1478–1479, 1682, 3428, 6374
Adenoviridae 11990
adenovirus 8760, 8765, 11990
– infections 11990
adiabatic combustion process 5514
adiabatic cooling 4738
adiabatic steam separation 5230
adipic acid 11830
– synthesis 7592
– technologies 7593
ADMA, see automotive dynamic motion analyzer
ADP-glucose 2709
– pyrophosphorylase 2709
– synthetase 2709
adsorption 9512, 9522, 11975–11976
– chiller 2383, 9524
– cooling systems 9521, 9524
– isotherm 11976
advanced backcross QTL (AB-QTL) 2532
– analysis 6440
advanced breeding line 8015
advanced burner reactor (ABR) 4060
advanced combustion control (ACC) 6473
advanced driver assistance systems (ADAS) 71
advanced glazing systems or materials (AGSM) 2836, 2839
– evaluation 2839
advanced greedy forwarding (AGF) 11560, 11572, 11574
advanced high-temperature reactor (AHTR) 4057
advanced informed agreement (AIA) procedure 2305, 10769
advanced land imager (ALI) 8943, 8949
advanced lead–acid battery consortium (ALABC) 774
advanced liquid metal reactor (ALMR) 4057
advanced metering infrastructure (AMI) technology 10451
advanced natural ventilation (ANV) 6884
advanced oxidation process (AOP) 7607, 7609, 9563
– non-Fenton 7609
advanced pre-crash safety system 3114
advanced public transportation systems (APTS) 91–92, 95, 99
– control strategies 99
– measures of effectiveness (MOE) 95
– simulation-based modeling 92
advanced spectroscopic portal monitor (ASP) 7213
advanced thermal system (ATS) 2355
advanced traffic management system (ATMS) 96
advanced traveler information system (ATIS) 96
advanced water treatment plant (AWTPs) 2090
advection-dispersion-reaction (ADR) mass transport equations 4099
Aedes mosquito 12014
AEM, see alkaline (anion) exchange membrane
aeolian soil 2432
aeration 11670, 11938
– of activated sludge systems 11938
aerial feeders 3012
aerial photography of ice 282
aerobic bacteria 3845
aerobic batch experiments 11979
aerobic bioremediation 10151–10152
aerobic oxidation 10174
– of alcohols 10174
aerobic oxygen concentration 1934
AEROCOM model 137
aeroderivative gas turbine 6831, 6833, 6847
aerodynamic 12213
– diameter 11302, 11320
– efficiency 12137
– flow 12291
– load 12205, 12208–12209, 12211
– dynamic inflow 12209
– dynamic wake 12209
– engineering models 12208
– power conversion 12137
– roughness length 11267, 11269
aerodyne aerosol mass spectrometer 122
aerofoil 4486
Aeromonas 5055–5056, 5064
– hydrophila 5056
aerosol 111–114, 117, 119–120, 123–124, 127, 130–132, 135, 139, 141, 171, 316, 610, 623, 630, 1254, 1316, 1335, 1338, 2108, 2116, 4108, 8961, 10623, 11153, 11314
– accumulation mode 127
– aerosol–climate interactions 141, 6747
– aerosol–cloud interaction 119, 6756
– aerosol–cloud–precipitation interactions 139
– air pollution 141
– atmospheric correction 8961
– backscattering ratio 316
– backscatter 127
– climatology 9636
– cloud droplet activation 132
– emissions 2100
– formation 113
– global budgets 124
– global burdens 124
– homogeneous nucleation 117
– hygroscopicity 132
– in climate models 630
– in the atmosphere 11153
– information 9644
– iron supply 7269
– layer 135
– mass distribution function 135
– mass spectrometry 122
– model 9723

– optical depth (AOD) 135, 196, 9635, 9735, 11155
– global distribution 135
– particle 113
– pollutants 8887
– population 112
– radiative effect 2108
– reflectance 8961
– size distribution 114, 127
– stratospheric 130, 4108, 10119
– submicron-sized 120
– sulfate 119
– vertical distribution 127
– water uptake 131
aerostat 5082
AESO-styrene
– copolymers 6922
– polymers 6919
– viscoelastic and mechanical properties 6919
afforestation 2117, 5823
aflatoxin 3596
– B1 (AFB1) 3643
AFLP, see amplified fragment length polymorphism
African easterly jet (AEJ) 5072
African easterly wave$_s$ (AEW) 5072
African horse sickness (AHS) 5361
African monsoon 5074
– multidisciplinary analysis (AMMA) program 5072
afterburner 6976
Agency for Toxic Substances (ATSDR) 2010
agglomeration 1068
aggregate breeding value 424, 2786
Agreement on Agriculture (AoA) 1021
agribiotechnology 4511
agribusiness 2746, 4362
– geothermal energy 4362
agriculture/agricultural 430, 577–578, 1446, 1534, 1537, 1567, 1573, 2324, 2329, 2529, 2687, 2742, 2744–2746, 3635, 4496, 4515, 5429, 5431, 5438, 6361, 7675, 7677, 9145, 10366, 10713, 10724, 10745
– benefits 2746
– biotechnology 4504, 4528, 10745
– by-products 1567
– collectivization 10366
– contaminants 7675
– cultivation 1490
– dormancy 9145
– economics 1549
– ecosystems 5429
– entomology 5438
– environmental impacts 2745
– evapotranspiration 1544
– food chain 3525
– countermeasure 3525
– remedial actions 3525
– genetic engineering 4515
– genetic improvement 430
– impact on biodiversity 10724
– innovation 4496
– inputs 1565
– insect pests 5429, 5431
– intensification 10371
– irrigation 2687, 11878
– water quality 11878
– land 1508, 1775, 3707
– accelerated erosion 3707
– energy crop production 1508
– in South Africa 1775
– land use 5828
– nitrogen loads 5828
– planning 9327
– landscapes 945
– management 1564
– improvement 1564
– maximum residue limit (MRL) regulation 6361
– nutrients 2746
– pesticide 300
– pesticide-based 3635
– plants 5608
– radiation-induced effects 5608
– pollutants 7677
– population 9360
– genetic improvement 9360
– practices 2741, 2748
– fallow 2748
– footprint 2744
– monoculture 2748
– tillage 2748
– production 150, 1133, 9316–9317
– agro-technical possibilities 9317
– decision making 9317
– socio-economic conditions 9317
– sustainability 1133
– system 152
– productivity 5429
– rationalization 1534
– reclaimed water use 2329
– reduced-till 10745
– research 1766, 2757, 4515
– residues 1292, 1537, 1573
– science 577, 2529, 2746, 2753
– soils 161, 7667
– nutrient transfer 7667
– pathogen transfer 7667
– street landfill 2012, 2014
– sustainability 2529, 2742, 5438
– systems 7671, 7673, 7676
– contaminants 7676
– dangerous microorganisms 7671
– fecal microorganism 7673
– nutrient sources 7673
– nutrients 7671
– wastes 6806, 10004, 10007
– characterization 10007
– generation 10007
– water usage 2324
agriculturalists 2932
agrifood systems analysis 3209
agro forestry 1579
Agrobacterium 2589, 2594, 2601, 2606, 6523, 8044
– *Agrobacterium*-mediated transformation 2588
– *Agrobacterium tumefaciens* 8060, 10672
agro-biodiversity 1542–1543
agro-biotechnology 2293
agrochemicals 10695
agroecology 150, 566, 2688
agroecosystem 150–151, 153, 162, 2553, 2687, 2742, 2746, 2752, 5429, 5431, 9317
– sequestration of CO_2 162
– strategic management 9317
– sustainability 151
– time-specific management 2752
agro-food biotechnology 10766–10767
agroforestry 151, 1564, 1571
agrofuel 1381
agro-industrial wastewater pretreatment 1172
agro-infection 8077
agro-infiltration 8077
agronomic interactions with CO_2 sequestration 161
agronomic technique 2728, 2731, 2734
– yield-positive 2734
agronomic trait 10748
agronomy 2734
agrosystem 5448
agro-technology system 1122
Agulhas leakage 8661
ahermatypic colonial scleractinian 6413
air bleed 8221
air chemistry 11323
air circulation 912
air collector 9488
air conditioning 3677, 4737, 4745, 10269
air contaminant 7714
– mitigation 7714
air core reactor 9345
air dehumidification 9532
air density difference 9791

air drilling 4383, 4428
– noise reduction 4428
air flow 11263, 11264, 11266–11267, 11279, 11281
– characteristic regions 11263
– in urban areas 11274–11275
– computational models 11274
– mesoscale models 11275
– isolated street canyons 11281
– mesoscale 11266
– modelling calculations 11279
– neighborhood scale 11267
– wind tunnel experiments 11279
– windows 3692
air gap membrane distillation 2920
air leakage 896
air molecules 11152
air movement in rooms 6873
air poisoning 7530
air pollution 112, 141, 167, 169–170, 172, 175–177, 179, 181–182, 185–188, 190, 192–195, 203–205, 207–209, 224, 245, 247–248, 261, 272, 298, 307, 1010, 1506, 2030, 3640–3641, 4012, 4111, 7852, 8880–8882, 8889, 8891, 9737, 10482, 10585, 11292–11293, 11300, 11313, 11347
– acid deposition 175
– acidification 179
– adverse effects 224
– air pollutant 170, 204, 224, 3648, 8349, 8895, 11312
– childhood cancer 3648
– coal combustion 8349
– health effects 224
– aircraft 209
– best available technology (BAT) 185
– climate change 177, 179, 194
– combustion of hydrocarbons 209
– control (APC) 9986
– devices (APCDs) 4881, 10584, 10585
– residues 4867, 4868, 11597, 11742, 11752
– system (APCS) 272, 4012, 4958, 4992, 5910, 5911, 11738, 11752, 11788
– technology 11696
– designing urban areas 192
– economic damages 179
– ecosystem effects 8891
– electricity 208
– exacerbation of asthma 3641
– from transport 261
– global problems 177
– health effects 172, 205, 8891
– healthcare costs 176
– history 11313
– hot spots 11300
– impacts on ecosystems 176
– institutional changes 195
– legislation 8881
– management 199
– mass transfer 2030
– mitigation 188, 190
– monitoring 167, 169, 177, 180, 185, 189, 192, 196–198, 8889
– benefits 177
– computer modeling 197
– design methodologies 197
– oversimplifications 198
– satellite observations 196
– sustainability 189
– no-effect threshold 204
– optimally cost-effective solutions 187
– ozone depletion 179
– particulate matter 204
– pathways 248
– policy 185
– policy-making 186
– precipitation chemistry monitoring 181
– problems 9655
– public involvement 194
– regional problems 175
– satellite remote sensing 182
– science 194
– socioeconomic distribution 193
– sugarcane ethanol production 1010
– surface transport 245
– sustainability 167
– transportation-based 7852
– transport-related 247
– visibility problems 176
air quality (AQ) 112, 141, 180, 182–183, 186, 204–205, 207, 209, 211, 213, 224, 234, 239, 244, 261–262, 271, 299, 310, 630, 943, 8880, 8882, 8889–8891, 8894–8897, 11292, 11294–11295, 11299–11301, 11303–11304, 11314, 11347
– air treatment 271
– city air 943
– climate change 8897
– computer modeling 182
– decision-making for policy 8894
– gaseous pollutants 8882
– guidelines and standards 204–205, 8895
– health effects 11295
– impacts 211
– of geography 11299
– of meteorology 11299
– of particle pollution 11301
– of topography 11299
– improvement 11347
– index (AQI) 11292, 11296
– legislation 262, 8895
– management (AQM) 209, 261, 11293
– management policy 205
– measurement 8889, 11304
– locations 11303
– metrics 11321
– models 261
– monitoring 8890, 11314
– stations 180
– no-effect threshold 205
– numerical modeling 183
– origins 11294
– planting of vegetation 271
– pollutants 8882
– pollution haven 186
– regional context 8896
– regulations 2185
– regulators 239
– satellite observation 182
– standards and guidelines 224, 234, 8895
– surface transportation 244
– US legal framework 213
– warnings 178
– WHO process 224
air ratio 2166
air receiver 2365
air sparging 2449, 10148, 10152
air temperature 10391, 10392
air toxic 298, 299–302, 306
– carcinogens 299
– health effects 301, 306
– maximum achievable control technology 301
– mobile sources 302
– pathways 300
– sampling 302
– source categories 299
– toxic cycle 302
air traffic 652–654, 658, 663
– carbon dioxide emissions 658
– changes of air chemistry 663
– control 2470
– emissions 654
– influence on climate 653
– Kyoto Protocol 658
– lighting system 4994
– transport system 658
air treatment 271
air-blown autothermal reforming 3967
air-blown gasifiers 1434
airborne
– brake particle 253
– contaminants 5334

– dust particle 115, 10581
– material 208
– microorganisms 11389–11390
– ozone 313
– DIAL 313
– photo-reconnaissance 282
– radar 284
– radioactivity 8583
– radionuclides 8455
– remote sensing 8922
– sensors 8923
– toxic chemicals 298
– water vapor 317
– DIAL 317
air-conditioning 2814, 4690, 9509, 9529
– desiccants 9529
air-cooled condenser 4981
aircraft 209, 309–310, 313, 652, 665
– atmospheric research 313
– differential absorption lidar (DIAL) 310
– emission standards 665
– radiation environment 8473
– reactor experiment (ARE) 4058
– sensors 8929
air-electrode batteries 3495
air-heating solar collector 9466, 9467
airline emission index 665
airline–HST cooperation 4940
airport 11298
air–sea
– heat transfers 4921
– interaction 7254
– interface 2512, 7268
airtight construction 7635
air-to-liquid sample collectors 1651
air–water
– gas exchange 595, 604
– gas transfer 597, 602
– oxygen transfer 10958
airy waves 7402
Aitken mode 114
ALARA principle 4906
Alaska gas hydrate research 330
albedo control 9701
albendazole 12030
Albizia 1290
alcohol/alcoholic 1028, 3610, 3912, 10641
– abuse 3590
– alcohol/diesel blends 5493
– as SOFC fuels 3912
– carcinogenic mechanisms 3610
– consumption 10637, 10641, 10654
– fermentation 1046, 1222–1223
– fuel 5468, 5477, 5479
– route 11451
– use 3598
alcoholism 10642
alcoholysis reaction 927
aldehyde 300, 2242
Alexandrium 4821–4824, 6762
– description 4821
– detection 4823
– economics 4822
– mouse bioassay 4823
– nutrient interactions 4824
– origins 4824
– toxicity 4821
algae/algal 346–352, 359–365, 523, 534, 1925, 2084, 2494, 4820, 11439
– algal–coral atolls 2490
– as human/animal food source 347
– biomass 361
– productivity 350
– biotechnology 352
– blooms 2086, 2322, 4820, 4835, 7388
– chloroplast transformation 365
– cultivation 348
– domestication 351
– fertilization 349
– for biofuel production 348, 364
– large-scale cultivation 364
– life cycle 349
– lipid metabolism 360
– mass culture 363
– molecular farming 362
– natural biodiversity 351
– nuclear genetic transformation 365
– phenotypes 347
– photosynthesis 2494
– production 6359
– refinery 361
– triacylglycerols 359
alien gene 4497
aliphatic radical polymers 7550
alkaline 372–374, 378–379, 969, 1318
– anion-exchange membranes (AEMs) 372, 374–377, 379–382, 8260
– as potential electrolytes in fuel cells 381
– ion-exchange capacity (IEC) 377
– metal-cation-containing 377, 381
– patents 382
– polysulfone-based 380
– polysulfone 379, 380
– properties 375
– pyridinium- or phosphonium-based 376
– QA-containing radiation-grafted 375
– research challenges 382
– synthetic routes 377
– earths 2948
– electrolytes 8269
– membrane 373
– fuel cell (AFC) 373, 3388, 3851, 3867, 3880, 3884, 8233
– ionomer 373, 374, 378–379
– membrane fuel cells (AMFCs) 372, 379, 382
– research challenges 382
– with H_2 as fuel 379
– metal chlorides 1345
– phosphatase 4019
– polymer electrolyte membranes 8216
– solution 7738
– transesterification 929
– zinc–air battery 748
alkalinity 120
alkali 1668
– alkali–silica reaction (ASR) 2405, 2409
alkaloid 6522
alkane 10663
– thiols 1648
Alkene 10663
alkylate 7835
alkylation 7837
alkylphenol chemicals 11965
all-black detector thermal offset 9682
all-bus system 1885
allelochemical 2749, 10350, 12294
alleviating poverty 2737
allocation procedure 934
allochthonous pathogen 5059, 8760
allometry 8436
allothermal gasification 1429
alloy system 9300
– high-energy mechanical milling (HEMM) 9300
allozyme 3363
– diversity 3363
alluvial soil 2432
allyltoluidine 7595
AlNiCo alloys 25
alpha amylase 991
alpha decay 8564
alpha radiation 5575, 5579, 8464
alpha-neutron sources 8569
alternating current (AC)
– electricity 2977
– generator 6815
– power 7309

alternative energy sources 8174
alternative fuel 268, 921, 5463–5464, 5466, 5488, 5495, 5542
– classification 5463
– for compression-ignition (CI) engines 5488
– ignition characteristics 5542
– legislation 5463
– market share 5464
– on engine performance 5463
– properties 5466
– technical implications 5463
– well-to-wheel analysis 5495
alternative oxidase (AOX) 5
alternative water source 8691
altimeter radar sensors 8931
alumina 2249
– catalyst 3965
aluminol 8604, 8614
aluminophosphate 7593
aluminosilicate 8606
– clays 7812
aluminum 715, 2405, 7195, 8778, 8815
– automotive scraps 8815
– chloride 4606
– recycling 8778
– tolerance 2713
Alzheimer's disease 3155
amaranth 1694, 2640
Amax 2631
ambient temperature lithium battery 11518
ambient urban air pollutant emission 11316
ameliorating soil 2408
American monsoon system (AMS) 7256
American National Standards Institute (ANSI) 3007
americium 8388, 8391–8392, 8582, 8620–8621, 8667
– americium–241 3761
– oxidation states 8392
– speciation 8391
AMFC, see alkaline membrane fuel cell
amikacin 11140
amines 2152, 4652
– selective transformation 4652
amino acid 836, 839, 1681–1682, 1694, 10842, 11409
– mycosporine-like 11409
– sulfur-containing 839
β-aminobutyric acid (BABA) 2574
δ-aminolaevulinic acid dehydratase 10651
aminopeptidase N 4017, 4019
ammonia 118, 127, 268, 382, 610, 1136, 1334, 3770, 3773, 3777, 3782, 3989–3990, 7314, 8367, 10638, 10653
– ammonia-containing gas 4986
– emissions 1136
– fiber explosion (AFEX) 969
– general process description 3990
– Haber-Bosch process 3770
– reaction pathway 3990
– synthesis 3990–3992
– catalysis 3991
– commercial activities 3992
– reactors 3991
– volatilization 3773, 3777, 11894
ammonium 850, 1103, 3772, 3781, 7673
– ammonium-oxalate (AO) 8606
– phosphates 3772
amnesic shellfish poisoning (ASP) 9085
Amoebozoa 12049
amorphous hydrogenated silicon 9256
– materials 9254–9256, 9259–9260
– doped material properties 9259
– light-induced degradation 9260
– optoelectronic properties 9256
– semiconductor properties 9254
– undoped 9255
– microstructure 9256
– thin film 9261
– photoconductivity 9261
amorphous silicon 9221, 9296, 9436
– photovoltaic devices 9247
amorphous solar cell 7955
amphibians 9165, 10089
– as sentinels 9165
amphiphilic molecule 7567
amphitropical distribution 2492
amplified fragment length polymorphism (AFLP) 5390, 6696
AMULETT 74
amylase
– inhibitors 4031–4032
– promoters 2596
amylopectin 989, 4555
amylose 4555
anaerobic baffled reactor (ABR) 1153
anaerobic digestion 978, 980, 1089, 1098, 1105, 1130, 1134, 1149, 1174, 1224–1225, 1612–1613, 1619, 2417
– anaerobic digester gas (ADG) 7867
– conversion processes 1098
– digester gas (ADG) 7867
– of excrements 1134
– raw material 1105
anaerobic fermentation 1050, 1140, 1174, 1177, 1179
anaerobic filter 1153
anaerobic microorganism 11901
Anagros epos 156
Anatoxin-a 4832, 4834
anchor marker 6432
anchovies 3577–3578
Anderson-Schultz-Flory (ASF) distribution 2242
andesitic water 5228
anellovirus 8131
aneuploidy 3603, 3606
angiotensin II 1188
angular-rate sensor 56
anhydrosugar 965
aniline 7595
animal 392, 406, 413, 431, 440, 445, 446, 453, 455, 458, 473, 485, 490, 495, 823, 949, 8002–8003, 9123, 11398
– additive genetic effects 455, 458
– agriculture 1783
– aquaculture 9123
– base population 440
– biodiversity 150, 1749
– biomass 823
– biotechnology 10865, 10870
– ethical limits 10865
– breeding 386, 388–389, 391, 393–399, 405, 407–410, 413, 415–416, 420, 426, 428, 436–438, 441, 457, 473–474, 1778, 1796, 1807, 2787, 2964, 7973, 7990, 7996, 7998, 8000, 8308, 9358–9359, 9362–9368, 9370–9371, 9373–9381, 9383–9387, 9389, 10814
– accounting for variation in group size 9385
– additive genetic variance 9363
– artificial insemination 389
– artificial selection 9389
– associative common-litter effects 9386
– associative heritability 9381
– associative-effect models 9389
– Bayesian techniques 391, 398, 436
– behavioral traits 9373
– best linear unbiased prediction (BLUP) 391, 436, 474, 9375–9377
– biometrical methods of selection 8308
– breeding schemes 9359
– categorical data 457
– data recording 7990
– degree of dilution 9386
– deoxyribonucleic acid (DNA)-level diagnostic procedures 8308

– developing countries 388
– dominance 416
– economic indexes 457
– epistasis 416
– estimation of genetic parameters 9380
– expected progeny differences (EPD) 428
– foundations 415
– frozen semen 389
– genetic drift 409
– genetic improvement 410, 9359
– genetic progress 1807
– genetic trends 441
– genetic variance 393, 9370
– genetics 386, 389
– genome-wide selection 2787
– genomics 2787
– Griffing's associative effects 9377, 9383
– group heritability 9370
– group selection 8000, 9368, 9370, 9380
– hard-to-measure traits 7998
– heritable competition 9365
– heritable effects 9363
– heritable variance 9364
– identifiability of the associative genetic variance 9387
– individual selection 9368
– industry 495
– infinitesimal model 398, 437, 474
– linear statistical model 438
– long-term challenges 405
– major genes 474
– marker-assisted selection 2964
– mass selection 9368
– maternal genetic effects 9383
– maternally affected traits 9378
– mating 416
– methods of estimation 441
– methods 389, 395
– mixed model equations (MME) 398, 441
– mixed models 398
– modeling 436
– molecular genetics 399
– Monte Carlo Markov chains 391
– multilevel selection 9371
– multiple traits 9359
– neuroendocrinology 7996
– non-genetic associative effects 9384, 9386
– non-heritable genetic effects 9363
– nucleus-multiplier scheme 396
– objective 409
– optimum designs 9387
– optimum index selection 9371
– phenotype 9371
– phenotype-driven 2964
– phenotypic value 9374
– polymorphic markers 8308
– predicted transmitting abilities (PTA) 428
– prediction accuracy 420
– prediction reliability 420
– pseudo-BLUP selection index 9378
– quantitative genetics 415, 9362
– quantitative trait loci (QTLs) 2964
– quantomics approach 7998
– random effects 426
– reliabilities 441
– reproductive technology 7990
– residual or restricted maximum likelihood (REML) 391
– response to selection 9366–9367
– schemes 407
– selection criterion 9367
– selection 408–409, 416
– single record per animal 441
– social behavior traits 8000
– social interactions 9374
– social model 9363
– social selection experiments 9379
– socially affected traits 9358, 9383
– square root of heritability 9374
– stakeholders 408
– standard errors (SE) of estimated parameters 9387
– statistical methods 397, 9380
– statistical power 9387
– sustainability 389, 391, 407, 413, 7973
– sustainable systems 394
– technology 1778, 7983
– theoretical developments 416
– traditional BLUP model 9376
– traits 436
– transgenesis 399
– domestication 152, 207
– genetic resources 1762, 1771, 7975
  – for food and agriculture (AnGR) 406
– genetic value 473
– genotyped 431, 485, 490
– hybrids 392
– identification 2783
– improved feeding and management 406
– integrity 10879
– manure 1147, 1152
– missing parents 440
– models (AM) 428–430, 437, 439, 444, 446, 448–450, 454–455, 459–461, 1796, 3264
  – assumptions 439
  – binomial traits 459
  – count data 461
  – culling 455
  – extensions and variations 429
  – genetic relationships 439
  – heterogeneous variances 461
  – hierarchical models 461
  – inbreeding coefficients 439
  – infinitely dimensional trait 448
  – international comparisons 461
  – Legendre polynomials 449, 450
  – limitations 439
  – low heritability traits 455
  – maternal effects 446
  – model comparisons 461
  – models for survival data 459
  – multiple trait models 454–455
  – plotting curves 454
  – proportional hazard model (PHM) 460
  – random regression models 448, 449, 450, 454
  – reduced animal model 430
  – regression functions 449
  – repeated records 444
  – robust estimation 461
  – scaling time variables 449
  – sire model 430
  – survival analyses 460
  – threshold model 459
  – traits 455
  – Weibull baseline hazard function 460
– molecular genetics 473
– most probable producing ability 446
– pedigree 440
– permanent environmental effects 446
– pests 5431
– production 406, 473, 494, 1741, 1759, 1761, 7991, 10840
  – genomic selection 1761
  – heat stress 1759
  – infinitesimal model 494
  – intensification 7991
  – water requirements 1759
– product 1744, 8001
– purchasing 413
– pure lines 392
– ranking 453

– records 1778
– analysis 1778
– data capturing 1778
– dissemination 1778
– repeated records 445
– residual error effect 458
– resources 1746
– management 1768
– welfare 413, 1785, 7990, 8003, 10814, 10877–10878
– problems 8002
anion
– exchange capacity (AEC) 8610
– mobility 6053
anionomer 373, 374
anisakiasis 12032, 12034, 12050
anisakidosis 12032
Anisakis 12032, 12034, 12051, 12053
– *simplex* 12050, 12052
Annelida 12047
anode 740, 752, 3873, 6068–6069, 6091, 6105, 6116, 6127–6128, 6142, 6737, 9907
– anode–electrolyte interface 6042
– deposition of nickel 6105
– hydrogen oxidation reaction 7731
– materials 6091, 6116
– overpotential 6737
– silicon-based 6142
– tail gas 5170
– with Li^+-ion liquid electrolytes 752
anolyte 749
anomaly initialization 2129
Anopheles mosquito 6293, 6295
anopheline
– mosquito 11072
– vectors 11078
anorthite 11603
anorthosites 1910
ANOVA $model_s$ 4080, 4083
– reference 4083
anoxic limestone drain 6661
anoxic methane oxidizer 6411
anoxic water 7347
antagonistic microorganism 2570
Antarctica/Antarctic 287
– AVHRR mosaic 287
– bottom water (AABW) 5860, 5871–5872, 8677
– ice mass loss 4576
– intermediate water (AAIW) 8677
– ozone hole 10132, 10135
– peninsula 282
– radar image mosaic 287
antenna protein 355
Anthozoa 2495
anthracite 2178
anthracnose 1277
anthranilate 1695
anthrax 5361, 5369
anthropocene 579, 607, 614, 2095, 7230, 7270
anthropogenic
– air pollution 9737
– carbon dioxide 7268
– climate change 2115, 2119, 10118
– emissions 10296
– greenhouse gases 10118
– metals 7350
– anthropogenic micropollutants 11912, 11922
– particulate matter 8887
– radioactive material 8498, 8514
– radioactivity 8488
– monitoring 8670
– radionuclides 8409, 8527, 8656, 8658, 8666, 8673, 8681
– Atlantic ocean 8666
– in the marine environment 8658
– Indian ocean 8666
– wastewater contaminants 11930
anthroposphere 3450, 10578
anti-air pollution action plans 1396
antibiosis 499, 5442
antibiotic 497
– emerging pathogens 497
– molecules 500
– resistance 499
antibody
– plant-based production 8074
– receptor molecules 1649
antibody-based diagnostics 5384
anti-brake system (ABS) 3861
anticancer gene 3607
anticarcinogen 3613
antifreeze protein genes 10798
anti-infective agent 3164
anti-lock brake system (ABS) 76, 3053, 8852, 11188, 11497, 11500
antimalarial(s) 11084
– activity 11082
– drug 6292, 11080
antimicrobial peptide (AMP) 2965
antimicrobial protein 10854
anti-mycobacterial antibiotics 11141
antioxidant 578, 3589, 3660, 3662, 3667
antiparallel thyristors 12150
antiparasitic agent 3164
– from marine sources 3164
antireflective coating (ARC) 9216
antiretroviral therapy (ART) 4999, 11137
– drugs 5010
antithrombin 640
anti-tuberculosis
– drugs 11136, 11141
– therapy 11131
antitumor agent 3153, 3156, 3160
– in clinical trials 3160
antitumor compound 3153
– marine-sourced 3153
antiviral agent 3164
– from marine sources 3164
Apatite 3895
Aphis maidis 1275
aplidine 3160
Aplidium albicans 3160
aplysiatoxin 4832
apoptosis 3628
apostatic selection 10076
apparent competition 10065
aquaculture 511–512, 514, 527, 533–536, 538–540, 542–544, 546, 555–557, 559, 561, 564, 566–568, 570, 572–574, 576–577, 581–582, 1769, 1927–1928, 1930, 1932, 1941, 1944, 1948, 1950, 1952–1953, 1955, 1960, 1969, 1971, 3320, 3557, 3560, 3574, 5894, 5897, 5899, 5902–5906, 6182–6183, 6354, 6356–6357, 6361–6362, 6759, 6767, 7263–7264, 7267, 8201–8202, 9175, 9183, 9187, 9390, 10318, 10798
– agency 572
– alternative farming methods 5899
– aquaculture-derived food products 9180
– food safety 9180
– Aquapod systems 581
– biomass 543
– carrying capacity 1928, 1948
– certification schemes 9183
– communities 534
– competition for feed 9390
– culture of shellfish 9175
– development 555, 561, 573, 5894
– disease 1932
– modeling 1953
– diversification 546
– ecological 533
– ecosystem 533, 535, 568, 7264
– approach 1950
– effects on biodiversity 6183
– effects on fisheries 6183
– environment 5894
– concerns 3560
– impacts 8202
– management 5906
– European 527
– FAO ecological approach 535

– farming technologies 5894
– farm 536, 543, 556
– feed conversion ratio (FCR) 5899
– feeds 3574
– for the poor 577
– improved governance 572
– in the Mediterranean 6354
– industrial 538
– industry 1952
– integrated multi-trophic (IMTA) 542
– life cycle assessment (LCA) 5893, 5897–5899, 5902
  – allocation 5897
  – impact assessment 5898
  – impact categories 5898
  – in food production 5898
  – system boundaries 5897
– macroeconomic factors 7264
– management 555, 570, 1971
– maximum residue limit (MRL) regulation 6361
– monoculture 544
– nearshore 559, 582
– nutrient extractive 557
– offshore 514
– open ocean 514
– polyculture 7264
– pond heating 4365
– production 5893, 6182, 6362, 9174, 10318
  – of finfish and shellfish 9174
  – of mussels 6759, 6767
  – systems 572
– public perception 6357
– real-time applications 1955
– reduction of variability 9390
– regulations 1969
– research models 1941
– resilience capacity 535
– restoration of ecosystems 576
– rich internet applications (RIA) 1955
– scale 536
– science 577
– screening models 1941
– service industries 540
– social acceptance 1944, 6357
– social ecology 538, 573
– social equity 6356
– solar energy inputs 5903
– stewardship council 9183
– sustainability 564, 566–567, 574, 1930, 7267, 9187
  – tools 5894
– toolbox 7263
  – transmission of disease and parasites 5904
  – triple bottom line 539
  – true carbon emissions 5906
  – virtual tools 1952
  – wastewater 5897
  – water quality 5905
aquafeeds 5899
aquaplanet 624
Aquapod™ 582–586, 588, 592, 593, 3580
  – artisanal fish farming 592, 593
  – bolt tests 586
  – cage system 7265
  – compression tests 586
  – containment 583
  – cost 584
  – engineering 584
  – experience 588
  – installations 588
  – mooring 584
  – net pens 586
  – structural exoskeleton 583
  – submersibility 582
  – technology 584
  – waste management 584
  – wire mesh 585
aquaponic 544, 548, 8202
aquasol 9135
aquatic
  – animal code 1946
  – ecosystems 537, 573, 576, 2340, 3526, 3533, 5603, 5674, 10958, 11254, 11892
    – contaminated sediments 3526
    – countermeasures 3526
    – radiosensitivity 5603
    – remedial actions 3526
    – remediation strategy 3533
    – restoring 576
    – sediment-associated contaminants 11254
  – environment 6189, 9143, 11912, 11965
    – antibiotics 6189
    – interface compartment (IC) concept 9143
    – micropollutants
    – occurrence of endocrine disrupting compounds 11965
  – farming ecosystems 533
  – food 513, 7264, 7267, 8408, 10331
    – radioactivity 8408
    – sustainability 10331
  – habitats degradation 3706
  – invasive species 6184, 6363
  – landscape 6190
    – climate change 6190
  – organisms 2260, 11233–11234
    – adsorption of radionuclides 11234
  – plankton 11408
    – UV sensitivity 11408
  – products 1951, 9175
  – radioecology 7008, 7030
  – systems 1938, 1940, 1953, 5674, 7009, 8962, 10051–10052
    – optical classification 8962
    – pathogens 1953
    – speciation 10051
    – sustainability 5674
    – toxicity of metals 10052
    – uptake of radionuclides 7009
aqueous batteries 8746
  – separator 8746
aqueous complexation 4777
aqueous environment 7386
aqueous potassium hydroxide 780
aquifer 342, 4785, 4798, 4815
  – contamination 4798
  – geothermal system with surface discharge 4153
  – mineralogy 4127
  – pumping tests 4815
  – remediating polluted 4785
  – remediation 4803
  – store 10556
  – tests 4816
  – thermal energy storage (ATES) 4133, 4152, 4154
Arabidopsis 3, 6, 8, 1695, 1697, 1707–1708, 1714–1715, 2553, 2591, 2690, 4035–4036, 4038, 5324–5325, 6432, 6528, 9071–9072, 10676, 10679, 10682, 10687, 10698, 10750
  – genome 10679
  – genome program 4035
  – ribulose bisphosphate carboxylase (RuBisCO) 4038
  – salinity tolerance 5325
  – salt stress 5325
  – *thaliana* 2550, 2626, 9146, 10671, 10673
  – transformants 10682
arabinose fermentation 974
arabinoxylanases 10845
arable land biotic community constraints 155
arachidonic acid (ARA) 1697
Arachnida 5438
aragonite 7236
arboriculture 11355
arbuscular michorrhiza 155
  – fungi (AMF) 3779

arc volcano 11639
archaeological landscape 10378
Archiacanthocephala 12040
architecture 3677, 10196, 10300
– of indigenous cultures 10300
– unplugged 3677
Arctic
– food chains 8459
– ice dynamics joint experiment (AIDJEX) 2763
– ice loss 9702
– lichens 8454
– monitoring and assessment programme (AMAP) 8457
– oscillation (AO) 2137, 2513, 10124
– polar vortex 10133
– sea ice 282, 2521
– warming 3219
arenesulfonylation 4598
Arenicola maritima 1921
Arge process 2244
Argentine biosafety system 2289
ARGO float 2524, 4915, 4924
argon 5226
arid ecosystem 2930
aromatic hydrocarbon
– degradation 1634
– ionomers 6562
Arrhenius
– behavior 6083
– equation 3899
– expression 1518
– function 9053
– temperature 2025
arsenic 172, 3647, 4887, 10638
arsenobetaine 7356
ARTEMIS project 258
artemisinin 11080, 11084
Arteria thaliana 359
arterial median busway 1819
artesunate 11080
Arthrobacter 8028
Arthropod 5457
– identification 5457
artificial
– chromosome 2585, 2607
– insemination (AI) 391, 397, 421, 433, 466, 1724, 1737, 2782, 2785, 9367, 10868
– lagoons 10616
– lighting 2808, 2827, 2831, 10392
– artificial neural network (ANN) 2911, 3116, 3123, 12095
– photosynthesis 5174, 7611
– radioactivity 8389
– radionuclide 8452
– in the environment of caribou/reindeer 8452
– selection 416
– sky 2820
– mirror box design 2820
artisanal fishery 592
aryl hydrocarbon receptor (Ahr) 4884, 4886, 6793
Whole Foods Markets (WFM) 3574
asbestos 1924, 2417, 3606
– fibers 3596
– in construction 2417
ascaridoid 12050
– infections 12033
ASCCUE project 4691
ascorbate biosynthesis 1709
ascorbic acid 1685, 1708
asexual reproduction 6150
ash 1252, 1255–1256, 4003, 4866, 4869
– as a fertilizer 1256
– behavior 1252
– characteristics 1252
– management 11749–11750, 11755
– around the world 11755
– regulatory aspects 11750
– melting 1236, 1340
– behavior 1315
– mixture 1256
– residue 2195, 11738, 11741–11744, 11747–11754
– asphaltic mixtures 11753
– building blocks 11754
– codisposal with MSW in landfills 11748
– containment 11748
– density 11741
– disposal 11738
– extraction leaching procedures 11750
– for construction 11753
– from waste combustion systems 11738
– handling 11743–11744
– landfill disposal 11747
– leachate disposal 11748
– liners 11748
– metal separation 11744
– moisture content 11741
– monofills 11747
– permeability 11742
– Portland cement treatment 11754
– processing 11744
– risk assessments 11752
– salinity of leachate 11748
– samples 11752
– state regulations 11751
– storage 11744
– testing 11751
– treatment 11744, 11752
– vitrification 11754
– scraper 1383
– utilization 1255
– vitrification 4003
ashfill 11747
ash-melting furnace 4001, 4005
ash-melting system 3998
Asian aerosol 6753
Asian monsoon 6747, 7258
– impacts of aerosols 6747
ASK-FORCE organization 4531
asphalt 2406, 2413
– concrete 4871
– mixtures 2406, 2413
– pavement 11703
– production 11701
aspheric nanoparticle 7891
aspiration toxicity 4849
assessment of estuarine trophic status (ASSETS) model 1937
assimilable organic carbon (AOC) 10537
assimilative capacity 1933–1934
associated natural gas 7803
association mapping (AM) 2532, 6430, 6432
associative breeding value 9365, 9370
associative genetic variance 9381
asteracea 1115
asthma 3641
astronaut 8561
– solar-flare radiation exposures 8561
asymmetric hybrid capacitor 3430
asymmetric hydrogenation 10172
asynchronous machine 12142
asynchronous tillage 157
ataxia 2970
atenolol 11926
at-grade busway 1872, 1874
Atlantic
– meridional overturning circulation (AMOC) 2136, 7379
– multi-decadal oscillation (AMO) 2136
– salmon 10799–10800, 11411–11412
– tropical cyclones 5073
– warm pool (AWP) 7255
atmophilic heavy metal 10583, 10588
atmosfair airline index (AAI) 665

atmosphere/atmospheric 310, 595, 607, 609–612, 614, 616, 623, 628, 637, 653, 2512, 9627
– aerosol 111, 191, 311
– air traffic 653
– as an integrator 614
– backscattering 311
– biogeochemistry 606–607, 617, 3296
– hydrologic cycle 607
– inverse modeling 617
– biogeochemical cycles 614
– biota 614
– boundary layer (ABL) 6592, 6594
– brown cloud (ABC) 1308
– bulk plume model 628
– carbon 1559
– cycle 607
– dioxide 595, 3297, 7231, 7268, 9697, 9703
– chemistry 310
– chemistry transport models 8893
– Eulerian models 8893
– Lagrangian models 8893
– circulation 2125–2126
– corrosion 4251
– dioxygen 12301
– flows 11277, 12063
– direct simulation 12063
– gases 310, 10623
– general circulation modeling (AGCM) 622, 623, 634, 6743
– calibration (tuning) 634
– evaluation 634
– halogens 10135
– iron cycle 612
– irradiance 9638
– lidar (ATLID) 325
– modeling 637, 2510, 12069
– modeling intercomparison project (AMIP) 2511, 6743, 6745, 8910
– nitrogen 170, 8353
– cycle 609
– nuclear testing 8491
– nuclear weapons test 8585, 8638, 8656, 8662
– global fallout 8662
– numerical model simulation 2512
– oscillations 9639
– oxygen 11316
– cycle 612
– ozone 9652, 11149, 11152
– phosphorus cycle 610
– pollutants 3591
– pollution 328
– radiation measurement program 9720
– reanalyses 2517
– rivers 7249
– sulfur cycle 611
– testing fallout 8493
– total heating 7253
– transport 607, 616
– tritium 11002
– turbulence 12207
– water vapor 317
– weapons testing 8620
– winds 7398
atmosphere-ocean climate model 10162, 10164
atmosphere-ocean coupling process 7374
atmosphere-ocean general circulation model 6748
atmosphere-water exchange 594, 596–597, 600–603
– description of transport 597
– eddy correlation flux measurements 602
– empiric parameterization 603
– geochemical tracer techniques 602
– influence of surface films 601
– influence of waves 600
– laboratory facilities 602
– mass boundary layer 596
– thermography 602
– tracer injection 602
– turbulent and molecular transport 596
– viscous boundary layer 597
atoll 2491
atom economy (AE) 4586, 4615, 4619, 4621, 4624, 4635
atomic age 8488
atomic bomb test 8426
atomic electron 3788
atomic energy commission (AEC) 8539
atomic hydrogen flux 9251
atomic mass 3792
– measurements 3792
atomic vapor laser isotope separation (AVLIS) 5642
atovaquone 11084
atovaquone-proguanil 11083
ATP/NADPH stoichiometry 358
ATP-sulfurylase (APS) 1714
atrazine 10959–10960
– pesticide 2042
atrium 902, 905, 912
– temperature 912
Attacin 10700
attainable yield (AY) 2722
attention assist system 3114
attenuated total reflectance infrared (ATR-IR) spectroscopy 3937
audible sound 12278
Auger electron 8574
Auger kiln reactor 1524
Aujeszky disease 10914
Auristatin PE 3155–3156
austenitic stainless steels 7197
Australian monsoon 6752
– impacts of aerosols 6752
authorization agreement 11368
auto mobilization 1858
autochthonous pathogens 5049, 8759
autoclaved aerated concrete (AAC) 3831
autogamous crop 6440
autogas 5470
auto-highway expansion 1861
automated
– guideway transit (AGT) 1876, 7778, 7780
– lighting control system 2842
– parking facility 7795
– passenger counters (APC) 101
– people mover 7778, 7780, 7792
– shading system 2837
– transit technologies 7787, 7794
– vehicle 7795
– location (AVL) 91, 98, 1835, 1852
– monitoring (AVM) 91
automatic
– braking 84
– cab signaling (ACS) 5967
– driver assistance systems 11126
– machine-vision-based 11126
– emergency break 3068
– generation control (AGC) 12104, 12111, 12107, 12124
– heat exchanger cleaning system 1343
– identification system (AIS) 259
– mapping 3077
– opening vents (AOVs) 6881
– passenger counter (APC) 91, 98, 103
– pedestrian gate 5949
– photocontrol 2842
– snow detection 289
– train control (ATC) 5967
– train protection (ATO) 1869
– train stop (ATS) 5967
– vehicle detection 11478
– water pasteurization indicator 9505
– weather station (AWS) 9323
automation sequence 2980
automobile 7587
– catalytic converter 7587
– propulsion technologies 268
automobile-centric land use 10264

automotive
– catalytic converters 8249
– dynamic motion analyzer (ADMA) 3071
– drive cycles 8243
– electronic technologies 3053
– fuel cell 8235
– cooperation (AFCC) 8239
– history 8235
– imaging application 11099
– imaging environment 11100, 11103
– human perception 11100
– industry 6954
– sensor fusion 6954
– night vision systems 6952
– pedestrian recognition system 6953
– polymer electrolyte membrane (PEM) fuel cells 8241, 8243, 8247–8248
– cold temperatures 8247
– commercialization 8248
– electrode degradation 8247
– operational modes 8241
– stacks in vehicles 8243
– shredder residue (ASR) 5244, 8811, 8819
– transportation 8193
– automotive vision environment 11106
autonomous road vehicle 2464
autonomous underwater vehicle (AUV) 7291
auto-regressive moving average (ARMA) 3119
autothermal gasification 1429
autothermal reforming (ATR) 3862, 3883, 3964, 8193
autunite 10413
auxiliary solution cell (ASC) 10428
available transmission capacity (ATC) 12176
available vehicle-occupancy (AVO) 4953
avalanche photo detectors (APDs) 327
average breeding value 420
average eye closure speed (AECS) 3128
average social breeding value 9390
avian
– breeding 648
– germ cell lineage 646–647
– propagation 647
– influenza 641, 648, 1759, 10860
– virus 2971
– leukosis virus 2968, 10904
– livestock 1747, 1749
– malaria 5369
– retrovirus 642
– transgenesis 638, 641, 647
– methods 641
– technologies 10813
aviation 205, 652, 656, 658
– and atmosphere 652
– CO_2 658
– fuel 658, 921
– net warming 656
aviation-induced cloudiness (AIC) 662
avidin 4038
avirulence (Avr) gene 2700
Avogadro's number 6079, 6083
awareness model 3110
axial flow reactor design 3992
AZaspiracid shellfish poisoning (AZP) 9086
azeotrope 995, 11434, 11448
azeotropic ethanol 11434, 11448
azidothymidine 3153
azithromycin 506
azole 500
azooxanthellate 2493

B

bacillary dysentery 5060
bacillus 2570
Bacillus sphaericus 4021
Bacillus thuringiensis (Bt) 4013, 4014, 4024, 4037, 5451, 10715
– brinja 4527
– cotton 2311, 4507, 4526
– endotoxins 4516
– insecticidal toxins 4014, 4024
– maize 4530
– pest resistance 4024
– toxin 4026, 4028
– first-generation crops 4026
– mutagenesis experiments 4028
back pressure turbines 11776
backcross procedure 6436
back-emf 25, 35
background radiation 5586
background sound levels 12290
back-pressure steam turbine 4311
backscatter
– coefficient 311
– lidar 325
back-to-back converter 9347
backup compression chiller 9539
bacteria/bacterial 498, 1093, 5049, 5054, 7671, 7684, 9088
– antibody 1653
– artificial chromosome (BAC) 2607, 2691, 2701, 2704–2705, 2713, 10909–10910
– biodiversity 5049
– biofilters 6313
– blight 2576
– disease 10700
– from ocean 5063
– from seawater or seafood 5048
– enzyme β-glucuronidase (GUS) 8049
– fish pathogens 6360
– hydrolysis 11940
– infections 10854
– in the ocean 5049
– pathogens 9086, 9088, 9102
– seafood-associated 9086
– shrimp-associated 9102
– proteins 8049
– secretion systems 5054
– sulfur-reducing 1093
bactericides 2567
– peptides 10700
bacteriophages 11389
bacterioplankton 11390, 11408
bacterium 4016
– *Bacterium coli* 5059
– spore-forming process 4016
Bacteroides 6326
– *phages* 6329
– *thetaiotaomicron* 6328
bactofection 2585
baffling effect 9178
bagasse 1006–1007, 1011, 1276, 1292–1293, 11448
– lignocellulosic-rich 1292
baghouse 8357, 11807
– filter (BHF) 1250, 1340, 5239, 11711
– fines 11701
balance of plant (BOP) 6561, 6828, 8206
balanced intermodal transportation 1862, 1875
balancing area cooperation 8990
balneology 4164, 4170, 4354, 4359
bark combustion 1342
barley 1111, 1122, 2705
– grain 9149
– dormancy 9149
– inflorescence 2705
– yellow dwarf luteovirus 1281
barnase gene 2593
barotropic flow 5870
barracuda 827, 832
barrage 10613, 10614
barrier 2447
– reefs 2491
barrow gas field 340
basal cell carcinoma (BCC) 9661, 11398
basalt 1910
basaltic tuff 1910
baseline surface radiation network (BSRN) 7910, 7914

baseload electricity 4765
baseload plant 8982
basic
– daylighting strategy 2810
– diffusion 2017
– energy flow 12213
– oxygen furnace (BOF) 8810, 11594
– reproductive number 5347
Bastnäsite 9948
batch combustion 1354
batch reactor 3936
bathymetry 5870, 6761, 8679
bathythermograph 4911
battery 671–687, 689, 692, 694–696, 698–700, 702, 704, 706, 708, 710, 711, 740, 741, 747, 748, 765–772, 774–777, 779, 785, 793, 2935, 3392, 3427, 3472, 3479, 3480, 3847, 3852, 5107, 5882–5884, 5888–5890, 6146, 6499, 6940, 7547, 7548, 8112, 8113, 8121, 8715–8718, 8741, 8751, 11510
– absorptive glass mat (AGM) 5887
– active materials 740
– anode 740
– assembled characteristic charging 684
– assembled constant-current charging 684
– assembled taper characteristic charging 684
– bulk charge 673
– cage egg production 10877
– capacitive contactless charger 696
– capacity 741
– cathode 708, 740
– materials 711
– cells 675
– balancing 700
– construction 772
– cathode- and anode-active materials 7547
– charger configurations 687
– charge-sustaining (CS) mode 8113
– charging circuits 698, 704
– electromagnetic compatibility (EMC) 698
– electromagnetic interference (EMI) 698
– for photovoltaic (PV) systems 685
– with AC sources 687
– charging efficiency 769
– charging protocols 695
– charging techniques 671, 680
– chemistries 674, 768, 8716
– choosing 775
– constant-current charging 681
– constant-voltage charging 681
– contactless charging 694
– current 689
– current-based SoC estimation 699
– designs 5882, 5884, 5885, 5887
– discharge
– current I 741
– efficiency 769
– rates 5889
– reactions 5888–5889
– dry 775
– dual Li-ion intercalation system 710
– effect of temperature 5890
– efficiency 770
– electric vehicle (BEV) 3475, 7847–7849, 7853–7858, 10495, 10502, 11509
– demand side management (DSM) 7848, 7857
– economic feasibility 7856
– human behavior modeling 7855
– mobile decentralized storage 7849
– modeling 7854
– new markets 7853
– outage management (OM) 7848, 7858
– policy strategies 7854
– power system planning 7855
– electrical energy storage 767
– electrical modeling 770
– electrochemical cells 741
– electrochemistry 772
– electrolyte 5890
– electromagnetic interference (EMI) 696
– energy capacity 775
– energy density 741, 3479
– energy management 11505
– depth of discharge (DoD) 11505
– state of charge (SoC) 11505
– energy loss 5107
– energy/power ratio 8121
– energy storage systems (BESS) 692, 704
– characteristics 3472
– equalization charge 673
– failure 673
– flat and tubular electrodes 5885
– float charging 673
– for vehicle applications 11510
– gel batteries 5887
– gravity measurement 699
– health measurement 699
– hermetic seals 6499
– industry 706, 8715
– interface electronics 3480
– internal resistance 771
– Kalman filter technique 700
– layered transition lead acid 771
– layered transition metal oxides 711
– lead
– acid 673, 674
– antimony 774
– calcium 774
– life 776, 5890
– lithium
– air 766
– ion 677, 785
– iron sulfide 678
– metal salt 766
– maintenance 5890
– management 671, 677, 698, 3392
– management system (BMS) 699, 701, 703, 3371, 6146
– cell charge equalization 701
– flying capacitor 701
– passive balancing 701
– standby batteries 699
– switched capacitor charge equalization method 701
– DC-DC converter methods 703
– materials 6514
– material safety data sheets (MSDS) 5884
– maximum power output 769
– medical devices 6499
– metal air 679, 793
– mixed constant-current and constant-voltage charging 682
– monopolar and bipolar electrodes 5884
– multi-output transformer 702
– nail penetration test 8741
– negative terminal 741
– nickel systems 8751
– nickel-cadmium 676, 777
– nickel-metal hydride 676, 779
– nickel-zinc 679
– organic functional polymers 7548
– overcharge reactions 5889
– positive terminal 741
– power 775
– capability 741
– power split strategies 3480
– pulse-charging technique 682
– pulse-width modulation charge regulators 686
– rapid charge 674
– rechargeable 741, 769
– redox-flow 766
– separator 8717, 8726, 8728, 8730, 8731, 8733–8734, 8736–8737, 8751–8753
– characterization 8728
– classification 8718

– electrical resistance 8728
– Gurley number 8728
– mathematical modeling 8751
– melt integrity 8736
– mix penetration strength 8734
– pore size 8731
– porosimetry 8731
– porosity 8730
– properties 8728
– puncture strength 8733
– requirements 8726
– shrinkage 8734
– shutdown 8734
– tensile strength 8734
– tortuosity 8731, 8752
– wettability 8736
– wetting speed 8736
– series charge regulators 685
– shunt charge regulators 686
– silver–zinc 748
– single-phase, phase-controlled rectifiers 687
– sodium-beta 680
– sodium sulfur 678, 765
– solar energy storage 5883
– stacked cells 8717
– starting-lighting-ignition 674
– starved electrolyte 775
– state of charge (SoC) 699, 5888, 8112
– string 673
– sustainability 706
– taper characteristic charging 683
– technologies 303, 768, 3392
– temperature effect 770, 776
– tender 673
– thermal management 5107
– thermal runaway 8741
– three-phase, phase-controlled rectifiers 689
– trickle charge 673
– valve-regulated lead-acid (VRLA) 675
– voltage 681–682, 689, 3374–3375
– measurement 699
– waste processing 7548
– zinc–air 748
– zinc bromine 680, 793
– zinc–manganese 747
battery-powered electric vehicle (BEV) 10524
– wheel-to wheel results 10524
battery/ultracapacitor system 5111–5112
– active interconnection 5112
– passive interconnection 5111
Baumann rule 4257
bauxite 11597, 11832
bay area rapid transit (BART) 811
Bayesian
– classifier 3073
– decision networks 2484
– decision rule 11460
– method 391, 398
– model 432
– networks (BNs) 3117, 3120
– statistics 6697
– theorem 2110
B-dot equation 4096
beacon 3076–3077, 11572
– beacon-assist geographic forwarding (BGF) 11552, 11554, 11555
– interval 11556
beam radiation 10625
beam therapy 8561
Beavis effect 490
bedrock 5649
– aquifer 4796
– geologic character 5649
beef cattle 388, 1723–1738, 1772
– accuracy 1730
– birth weight 1728
– breeding 1770
– average 1727
– complementarity 1735
– selection 1732
– pyramid 1724
– value (BV) 1726
– calving ease 1728
– composites 1735
– crossbreeding 1732–1734, 1736
– economic index 1731
– expected progeny difference (EPD) 1724, 1729
– genetic defects 1725
– genetic improvement 1724
– heterosis 1734
– independent culling levels 1731
– industry 1723
– maintenance energy (ME) 1729
– marbling (MARB) score 1729
– Mendelian sampling 1727, 1730
– milking potential 1733
– molecular breeding values 1738
– molecular information 1737
– multiple-trait selection 1731
– percentile ranks 1727
– phenotype 1724
– of horns 1725
– rebreeding 1733
– retained heterosis 1734
– tandem selection 1731
– trait types 1725
– transmitting ability (TA) 1726
– weaning weights 1728
Beer-Lambert Law 6074
Beer–Lambert–Bouguer's law 7917
Beer's law 2620, 2766, 3215, 7914, 7917, 7924–7925
beet 1113
behavior of organisms 10075
benchmark dose (BMD) 3255
beneficial footprint 9032
beneficial insects 10717
beneficial resource repletion 9036
– application tools 9036
benefit cost ratio (BCR) 4789
benign tertian malaria 11075
Benson–Calvin cycle 2645
bent-axis hydraulic motor 5101
bentazon 10352
benthic
– animals 3042
– ecosystems 6194
– environment 1972
– habitat 1965
– life 6410
– macroinvertebrates 3273
– effects of contaminants 3273
– models 1935
– organisms 11234
– spot photography 6409
benzene 302, 306, 857, 7593, 10440, 10638
benzenesulfonic acid 6557
benzimidazole fungicide 2568
benzo(a)pyrene 3612, 10638
benzofuran 4873
benzoic acid metabolism 1193
benzothiazole 253
Bergen School of meteorology 12065
Bernoulli equation 12205
beryllium 172, 3716, 3731–3733, 3740, 3743, 4888, 8582
– activity 3743
– depth distribution 3732
– extraction 11597
– fallout 3717, 3732
– fluorides 4059
– for documenting soil redistribution rates 3732
– neasurements 3731–3733, 3740
– production 3716
beta decay 8564
beta radiation energy 11058
– Monte Carlo simulation 11058
beta zeolite 4592
beta-amylase 992
Betts-Miller scheme 629

beverage manufacturing 2072
bias correction spatial disaggregation (BCSD) 8916
biaxial incident angle modifier (IAM) 6035
bicarbonate 1909, 1915, 2899, 7330
bicycle, see bike
bicycling 806
bi-directional energy- and light transmission value 2889
bi-directional transmission distribution function 2839
Bifidobacterium 6326
Big Brother experiment 8907
bike 808
– parking 806, 820
– at train stations 806
– metro stations 806
– parking spaces 808
– rack 813, 816
– routes 811
– sharing program 815
– station 806, 811, 815
– transport 6498
bike-and-ride 812
– facilities 806, 808
– parking 813
bike-bus integration 816
bike-rail integration 820
bike-transit
– coordination 810
– integration 807–809, 811–815
– case studies 809
– Chicago 813
– Minneapolis 813
– New York/New Jersey 815
– Portland 812
– San Francisco 811
– Toronto 814
– Vancouver 812
– Washington 815
Bikini atoll test site 3540
binary closed-loop power plant 4193
binary copper compound 6088
binary Cry toxin 4020
binary ionic liquid electrolyte 6054
binary vectors 2592
binding energy 3792
bioaccumulation 822, 826, 831, 3270, 8404, 10662
– factors (BAFs) 3587
– toxins (PBTs) 3444
bioactivation pathway 3629
bioaerosol 115, 3640
bio-alcohol 10752
bioassay 1650, 1652, 2337
– detection strategies 1652
– immunomagnetic particle purification 1652
– referencing 1650
bioassessment protocols 3273
bioaugmentation 1632, 1638, 2444–2445
bioavailable metal 10054
– uptake 10054
biobarrier 10415
bio-based product 1269, 9031
biobecoming 8865
bio-butanol 10752
biocatalysis 7597–7598, 7612
– sulfur oxidation 7597
biocell 5723
biocentric design 8861
biochar 845, 846, 850, 851, 853, 855–857, 861, 870, 873, 875–877, 879–883, 885–888, 1518, 1528, 2117
– agri-environmental policies 886
– agronomic value 885
– carbon 879, 880
– abatement 861
– stability factor (CSF) 857
– storage value 885
– carbon-to-nitrogen ratio 883
– cation exchange capacity 853
– contaminants 855, 880
– dioxins 856
– emission of nitrous oxide and methane from soil 883
– engineered 886
– fractions 881
– heavy metals 855
– in grassland systems 887
– key functions 875
– loss 881
– microbial activity 876
– polycyclic aromatic hydrocarbons (PAHs) 855
– predictability 887
– production 851
– cost 873
– renewable energy incentives 886
– soil nutrient dynamics 882
– specific surface area 853
– stability 857, 880
– stable carbon 875
– sustainability 888
– waste management 886
biochemical
– composition 2410
– conversion 1222
– oxygen demand (BOD) 2066, 5688, 11968
biochemical–molecular level 11396
biocide 155, 2721
bioclimatic
– analysis 897
– architecture 9741
– design 893–895, 899, 902, 912
– atriums 902
– large-scale applications 912
– practices 899
– resources 895
– strategies 894
– wintergardens 902
bioclogging 7684
biocoal 1082, 1084–1085
– applications 1085
– properties 1084
bioconcentration 822, 3270
– factor (BCF) 4850, 4860, 7020, 7029, 10662
bioconduit 1632, 1638
biodegradable
– compounds 11977
– micropollutants 11978
– organic carbon (BDOC) 10537
– organic matter 11895
– wastes 9984
– composting 9984
biodegradation 1628, 1629, 1635, 2433, 9053, 10151, 10440, 10660, 11976, 11977, 11979
– of micropollutants 11979
– of vinyl chloride (VC) 2433
– sludge characteristics 11977
biodeposition 1967, 9176
biodetritus 832
biodiesel 359, 360, 921–925, 927, 930, 931, 933, 1002, 1028, 1035, 1040, 1042–1045, 1054, 1062, 1232, 1490, 1561, 1592, 1613, 1614, 1616, 1670, 3460, 5463, 5466, 5471, 5472, 5474, 5475, 5488, 8978, 10507, 10511, 10512, 10756, 11434, 11446
– advanced 1045, 1054
– algae-based 360
– cetane number 5475
– conventional 1044
– emissions 1035
– engine emissions 931
– environmental issues 931
– history 922
– iodine number 5474
– microalgae 927

– nonedible oils 925
– production 923–924, 5466
– lipase-catalyzed 929
– quality 930
– rapeseed oil 924
– soybean oil 924
– soybean-based 10512
– specifications 930
– sustainability 933
– tar-loaded 1670
– utilization 923
– viscosity 5472, 5474
biodiffusion 9141
– transport 9135
– coefficient 9137
biodigester 1923
biodiminution of metals 8407
biodiversity 940, 948, 1138, 1140, 1490, 1509, 1533, 1536, 1542, 1543, 1557–1559, 1561, 1567, 1572, 1574, 1575, 1749, 1773, 2267, 2300, 2309, 2742, 2749, 2756, 3299, 3358–3359, 3361, 4749, 5553, 7974, 9030, 9035, 10031, 10086, 10090, 10357, 10358, 10726, 11333, 11348
– as reflected by breed 1749
– assessment 10086
– climate change effects 1575
– consequences 1558
– conservation 948, 956, 1557, 1572, 1574
– at business sites 956
– ecotones 3358
– green roofs 4701
– history of research 3359
– in farm animal genetic 1773
– in the city 938, 10357
– invasive species 5553
– local 1543, 1559
– loss 940, 1493, 1509, 1543, 1559, 2749, 2756, 9028, 10358
– policy 2309
– protection 1533
– reduction 1138
– shaping 3361
– value 1567
bioelectricity 862, 871
bioenergy 861–862, 867, 871, 926, 1009, 1041, 1203, 1270, 1477–1478, 1485, 1489, 1493–1494, 1505, 1533–1534, 1542, 1548, 1551, 1557–1558, 1565, 1609, 2681, 5410–5411, 8976
– agricultural residues 1270
– carbon-neutral system 860
– conversion 1557
– routes 1494
– costs 1558
– crops 1477, 1485
– cultivation 1542
– demand 1565
– from waste products 5410
– globalization 1534
– plants 1478
– potentials 1542, 1551
– process chain 1493
– production 1544, 1557
– costs 1493
– water use 1544
– purpose-grown 5411
– routes 1609
– sources 1494
– supply 1565
– sustainability requirements 1505
– technical restrictions 1505
– transport costs 1557
– transportation 1494
– use 1490, 1497, 1551
– land use change (LUC) 1497
– sustainability 1490
bioethanol 189, 867, 921, 935, 961, 987, 1001, 1040, 1042, 1046–1047, 1199, 1222–1223, 1232, 1477, 1499, 1502, 1561, 1616, 8978–8979, 10752
– conventional 1046
– from celluloses 961, 8979
– from starch 987, 991
– grinding process 991
– from sugar 1001, 8979
– lignocellulosic 1047
– plants 1502
– production 1477
biofilm 2029
– toxin diffusion 2029
biofilter 555, 10108–10109
biofloc 535
– aquaculture 8203
biofortification 1690, 2536, 4525
biofouling 1624, 3564, 7304, 7314, 10539
biofuel 268, 347, 348, 352, 363, 549, 553, 861, 868, 921, 922, 934–936, 962, 997, 1002, 1006, 1019, 1021, 1025–1027, 1030, 1032, 1034, 1035, 1040, 1047, 1054–1055, 1057–1059, 1061, 1063–1064, 1067, 1073, 1200, 1216, 1237, 1269, 1314, 1315, 1352, 1420, 1427, 1496–1497, 1499, 1500, 1549, 1554, 1562, 1574, 1587, 1593, 1616, 1925, 2271, 2685, 2737, 2756, 3393, 5126, 6245, 8977, 9832, 9846, 10503, 10506–10508, 10513, 10515, 10527, 10743, 10744, 10752, 11316, 11430, 11431
– advanced 1500
– algae-based 10527
– ashes 1497
– ash-related problems 1315
– blends 11431
– calorific value 9832
– capital investment requirements 1054
– carbon 10506
– neutrality 1035
– characteristics 1314
– chemical composition 1314
– collection 1496
– crops 1554, 2756
– cultivation 1496
– economic feasibility 1549
– emissions 1034
– energy density. 9846
– environmental impacts 1057–1058
– European directive 935
– feedstock 5905
– fish processing co-products 5905
– first-generation 1006, 1500, 1549, 1562
– food prices 1500
– food vs. fuel debate 1499
– for micro cogeneration 1420
– from siliceous algae 1925
– fuel
– orientation 1427
– delivery and storage 1030
– future-generation 1063
– global warming 1064
– green house gas emissions 934
– growth 1027
– industry 1030, 2756
– land use 1496
– life-cycle analysis (LCA) 10506, 10513, 10514
– coproduct treatment 10514
– boundary 10507
– life cycle impact assessment 1059
– logistical structure 1019
– net calorific value 1200
– non-advanced 1500
– of the next generation 1216
– pathways 10506, 10508
– pellets 1073
– polygeneration 1427
– production costs 1054–1055, 1593
– production 1442, 1495, 1500, 1591–1592, 10515
– capital-related costs 1591
– consumption-related costs 1591
– economic assessment 1591
– negative impacts 1495
– process chain 1442

– total capital investment 1592
– wheel-to-wheel (WTW) life cycle assessment (LCA) 1500
– second-generation 1574
– supply chains 1587
– use 1032
– well-to-wheel costs 1055
– refining 1027
– residues 1497
– second-generation 936, 1006, 1500, 1549
– supply chain 1030, 1058
– sustainability 1057
– sustainable buildings 1025
– synthetic 1047
– technical combustion properties 9832
– transportation 1061
– upgraded new solids 1067
– World Trade Organization (WTO) 1021
biofumigation 2577
biogas 978, 980, 982, 997, 1026, 1029, 1031, 1043, 1050, 1081, 1089, 1091, 1093–1097, 1107, 1123, 1130, 1140, 1149, 1151, 1153, 1169–1171, 1174, 1176, 1179, 1199, 1225–1227, 1263, 1267, 1613, 1619–1620, 1622, 1624–1625, 3859, 3914, 4772, 6806, 8977, 9940, 11451, 11833–11834, 11940
– as a fuel 1227
– bottles 1031
– carbon footprint 1263
– chemical scrubbing 1625
– cryogenic upgrading 1625
– digester 1149, 1153
– economic and financial sustainability 1170
– electricity
– economics 1096
– generation 1267
– production 1093
– energy crops 1097
– energy plants 1140
– environmental sustainability 1170
– fermenters 1093
– for electricity generation 1089
– for sanitation 1171
– formation mechanisms 6806
– gas-otto engine 1094
– history 1620
– Hi-tech applications 1089
– ignition-oil engines 1094
– internal methane enrichment 1624
– lower heating value (LHV) 1225
– membrane technologies 1625
– micro-gas turbines 1094
– plant 1107, 1123, 1130, 1153, 1226
– Chinese model 1153
– pressure swing adsorption 1625
– process 1149
– production 1090, 1091, 1095, 1097, 1100, 1145, 1623
– developing countries 1145
– energy crops 1100
– history 1090
– technologies 1090, 1623
– upgradation 1623
– reactor 1149, 1226
– recovery 9988
– settler (BS) 1153
– social and cultural sustainability 1169
– sources 1089
– substrates
– from industries 1174, 1179
– from municipalities 1174, 1176
– sustainability 1170
– systems 1151, 1152
– hydraulic retention time (HRT) 1152
– sludge retention time (SRT) 1152
– upgradation to biomethane 1624
– upgrading plant 1622
– use 1154, 1156, 1158–1160, 1162–1169
– Africa 1162
– Algeria 1163
– Bangladesh 1154
– Belize 1166
– Bolivia 1167
– Burundi 1163
– China 1156
– Columbia 1167
– Cuba 1168
– Ethiopia 1164
– India 1156
– Jamaica 1168
– Kenya 1164
– Lesotho 1164
– Morocco 1165
– Nepal 1158
– Nicaragua 1169
– Pakistan 1158
– Philippines 1159
– Rwanda 1166
– Tanzania 1165
– Thailand 1160
– Tunisia 1165
– Vietnam 1160
– utilization 6806
– yields 1107
biogasification 11665
biogas-sanitation 1148, 1151, 1169
biogenic
– carbon 4759
– gas 7449
– uranium 4778
– volatile organic carbon (BVOC) 3225
biogeochemical
– cycles 6383–6384, 10658
– role of modeling 6384
– ecosystem 11332
– processes 11328
– reaction path modeling 4099
biogeochemistry 606, 3297, 4099, 6372
– of the atmosphere 3297
bioherm 6411
biohydrogen 362, 1051, 8979
– production 5116–5117, 5119–5120, 5122
– by dark fermentation 5120
– combined dark and methane fermentation 5122
– continuous stirred-tank reactor (CSTR) 5119
– dark fermentation 5117
– hydraulic retention times (HRT) 5119
– photofermentation 5120
– photolysis 5117
– process principles 5117
bio-indicator 8402
bioinformatics 2530
bioinsecticide 5457
biokinetic models 8404, 11058
bioleaching 6660–6661
bioliquid 1028, 3912, 5161
biolistics 8044
biological
– community 3280
– control 5449, 5453
– agent (BCA) 2570
– integrated pest management 5449, 5453
– degradation process 1226
– diversity 6180, 10766
– global loss 6180
– ecology 11325
– effective irradiance 11377
– invasion 5548
– pattern 5548
– process 5548
– invasions 3298
– literacy 3204

– monitoring 4893
– nutrient 9035
– removal (BNR) systems 11889
– organization 3268
– oxidation 11936, 11953, 11958
– oxygen uptake rate (OUR) 11958
– pest control 5447
– processing 1933
– assimilative capacity 1933
– reactor 11953
– redox signaling 3657
– research 10812, 10869
– spatial structure 3328
– species concept 10086
– surveys 3267
– traits 8437
– allometric functions 8437
– water treatments 11912
biolytic tank 1148
biomagnification 822, 826, 828, 831, 8406, 10662
– ciguatera fish poisoning 828
biomarker 1184–1185, 3254, 3258, 3274, 4893
– diagnostic 1185
– predictive 1185
– prognostic 1185
biomass 348–349, 359, 364, 551, 561, 577, 823–824, 846, 848, 852–853, 862, 867, 872, 921, 958, 1026–1027, 1030, 1035, 1038, 1041, 1043, 1048, 1064, 1068–1069, 1072, 1074–1076, 1089, 1091, 1098, 1146, 1176–1177, 1198–1200, 1203–1206, 1214, 1222–1223, 1228, 1231–1234, 1237–1238, 1243, 1245, 1255, 1263, 1268, 1270, 1299, 1301, 1305, 1308–1309, 1313, 1347, 1404, 1424, 1445–1448, 1476–1478, 1483, 1487, 1489, 1493–1496, 1503, 1505–1507, 1509–1510, 1512, 1517, 1528, 1531, 1533, 1536–1537, 1539, 1547–1548, 1570, 1583, 1585, 1590, 1594, 1600–1601, 1607, 1609–1611, 1665, 2117, 2271–2273, 2280, 3945, 5116, 5121, 5123–5124, 5126, 5163–5164, 6020, 8975–8979, 9031, 11435, 11437, 11440–11442, 11447, 11451
– 4F dilemma 1505
– accumulation of neutral lipid 359
– agglomeration 1069
– algal 348–349
– as building material 1548
– as energy carrier 1233
– as renewable source of energy 1198
– availability 1205, 1494
– billion ton study 1270
– biochemical conversion 1206
– biological processing 11447
– boilers 1243, 1528
– briquetting 1068
– burning 120–121
– organic aerosol (BBOA) 122
– carbon footprint 1263
– chains 1568
– GHG balances 1568
– coal-fired power plants 2272
– co-combustion 1611, 2271
– co-firing 872, 1245, 1255, 8978
– combustion 862, 867, 872, 1231, 1232, 1250–1252, 1313, 1346, 1347, 1610, 5304
– ash 1252
– control systems 1346
– for electricity generation 8978
– NO_x control systems 1250
– particle control systems 1250
– SO_2 control systems 1251
– sources 1308
– to electricity 1232
– combustor 11442
– containing celluloses 1223
– containing starch 1223
– containing sugar 1222
– conversion 1041, 1496, 1600, 3945
– into hydrogen 5121
– plant 1204
– processes 11440
– routes 1203
– technologies 1228, 5163
– cookstove 1299, 1305, 1309
– costs 1594
– crop 1270–1272
– annual 1272
– economic issues 1271
– farmer involvement 1270
– impact on soil fertility 1270
– logistics 1271
– perennial 1272
– crops for biofuels and bio-based products 1268
– cultivation 561
– demand for energy 1547
– dual fluidized bed steam gasification 5124
– energy 1298, 1312, 1351, 1400, 2625, 9030
– conversion technology 1146
– crops 2117
– heat provision 1298, 1312, 1351
– in developing countries 1298
– unintended consequences 9030
– entrained flow gasification 5124
– feedstock (BTL) 853, 5164, 5490
– flexibility 1590
– fisheries 577
– fluidized bed gasification 5124
– for energy production 1510, 9031
– for micro-cogeneration 1424
– from landscape management measures 1176
– from municipal waste 1177
– fuel 1265, 9821, 9824, 9835, 9838, 9848
– moisture content 9838
– molecular Composition 9824
– price 1265
– gasification 846, 1214, 1426, 1446–1447, 1449–1451, 1665, 5124, 5128, 5163, 89789608
– adsorption-enhanced reforming 5128
– chemical basics 1449
– for electricity and fuels 1426
– for rural electrification 1445
– Güssing model 5128
– plants 5126
– reaction 5123
– reactor principles 1451
– system 1030
– technical basics 1450
– generation 1478
– of electricity 1447
– greenhouse gas balance 1263
– growth 1483
– harvesting 364
– herbaceous 1074
– hydrogen 5116
– in developing countries 1232
– in plants and animals 1478
– incineration facilities 9031
– integrated gasification combined cycle (BIGCC) 1612
– lignocellulosic 5123
– main sources 1570
– biomass materials 10580
– metabolism 1483
– micro-cogeneration 1404
– non-lignified 1098
– nutrients 1601
– pelletizing 1069
– physicochemical conversion 1206
– plant-based 3945
– post-combustion 2280
– potential 1506–1507, 1536, 1539, 1570
– power plant 1251, 1257, 1261, 1264
– carbon emissions 1261
– chimneys 1251
– cost analysis 1264
– environmental impacts 1257

– gaseous emissions 1257
– investment cost 1264
– preprocessing 1237
– pretreatment 1448
– for gasification 1048, 1585
– processing 2273, 11437
– production 823, 1476, 1507, 1535, 1565–1566, 2616, 8976
– competition for water 1566
– fertilizers 1535
– food and feed production 1535
– land use 1535
– pest control techniques 1535
– protected areas expansion 1566
– use of degraded land 1565
– water resources 1535
– provision 1487
– pathways 1509
– pyrolysis 848, 852, 1517, 5163, 8979
– raw material 1072
– residues 1493, 1536–1537
– resources 1228, 1531, 1533, 8976–8977
– for biogas 1091
– impacts 1301
– sources 1043, 1089, 1200
– storage 1238
– supply 1567
– costs 1567
– sustainability 1064, 1503, 1512, 8977
– requirements 1495
– thermal decomposition 1076
– thermochemical conversion 1205, 11441
– to hydrocarbons 11451
– to hydrogen systems 5126, 8979
– to liquid (BtL) 1583, 1593–1594, 1601, 1603–1604
– comparison with fossil fuels 1601
– comparison with other biofuels 1603
– environmental assessment 1594
– fuel 1494
– learning curve effect 1594
– life cycle assessment (LCA) 1594
– process 2255
– production costs 1593, 1604
– sensitivity analyses 1593
– technical assessment 1604
– torrefaction 1075
– upgrading technologies 1609
– use 1487, 1489, 1496, 1615–1616
– for heat and electricity 1615
– for transport fuels 1616
– in stoves 1301
– on a global scale 1607
– vegetal and animal mass 1234
– wastes 1537
biomass–solar energy system 1372
biomass-to-electricity plants 1238, 1240
biomaterial 1549, 1568
biomedicine 10812, 10869, 10875
biomes 1560
biomethane 348, 362, 1043, 1050, 1062, 1174, 1616, 1618–1620, 1622–1623, 1625–1626, 1662, 1674, 5121, 8979
– anaerobic digestion 1619
– as green gaseous vehicle fuel 1622
– economics 1625
– feed-in-tariffs 1623
– gas grid distribution 1626
– gasification 1619
– production 1620, 1623
– technologies 1623
– utilization 1620
– via biogas 1062
biomimetic 8863
– catalysts 7599
– chemistry 7598
bio-mimicry 7598, 8871, 8874, 9033, 10316
– architecture 4732
biomineralization 10415
biomining 6660
– engineering approaches 6660
biomitigation 543, 557
BioMOBY project 6701
biomolecule 1647
biomonitoring 4893–4894, 9163
– adipose tissues 4894
– human milk 4894
– marine mammals 9163
– urine 4894
Bio-Mos 6361
bio-oil 851–852, 1213–1214, 1614, 5164, 11439, 11445
bio-optical algorithm 8926
biopesticide 5451
biopharmaceutical 926, 8059–8060, 8064–8065, 8074
– downstream processing 8065
– for human clinical trials 8065
– glycan structure 8064
– proteins 648
biopharming 639
biophilia 3677, 8864, 11333
bio-phillic architecture 4732
biopile 1632
bioplug 1632, 1638, 1639
biopolymer 1524, 6778, 9824, 10418
– seaweed-based 6778
– thermal cracking 1524
– trenching 10418
bioprecipitation 10415
bioreactor 639, 1635, 1639, 3595, 6525, 10869
– animal-based 639
– landfilling 5730, 9986, 9991, 9992
– wave-mixed 6525
bioreduction 4778
biorefinery 958, 978, 1064, 1272, 1610
– infrastructure 1272
– plants 1043
bioregional design 914
bioremediation 349, 1627–1632, 1639, 1642–1643, 2300, 2444, 3595, 4099, 6661, 7077, 10151, 10155, 10438, 10440
– advantages 1629
– as a mitigation tool 1629
– candidate contaminants 1629
– disadvantages 1630
– economics 1631
– ex situ or in situ processes 1631
– for sustainable mitigation 1632
– mitigation
– programs 1642
– strategies 1643
biosafety 2292–2293, 2295, 2297–2298, 2305, 2309–2311, 4500–4501, 4503, 4506, 4509–4510, 4514, 4517, 4519, 4524, 4529, 10747, 10758, 10769, 10917
– advisory commissions and committees 2311
– assessment 4517, 4519
– Brazilian legislation 4510
– clearing-house 2305, 10769
– education 4503
– European legislation 4510
– framework 2288, 2290, 2292, 2295, 2299–2300, 2302, 2304
– Argentina 2288
– Canada 2290
– China 2292
– India 2295
– International Obligations 2304
– South Africa 2300
– The Philippines 2299
– United States of America (USA) 2302
– policymaking 4524
– policy 2309
– regulation 2293, 2297, 2311, 10769
– in agriculture 4509
– science debate 4514
– regulatory process 10769
– regulatory systems 2310, 2313
– process-based 2313

– reserve level trials 2298
– system 2305
biosensor 1646–1648, 1650, 1654, 1659
– bench-top SPR systems 1647
– detection limit by analyte type 1654
– sample acquisition 1650
– self assembling monolayers (SAMs) 1648
– sensor surface preparation 1648
– small molecule detection 1654
– storage and preservation 1650
– surface
– passivation with blocking proteins 1650
– plasmon resonance (SPR)-based 1646
bioslurry 1149, 1155, 1632
bio-SNG 1051, 1062, 1444, 1612, 1663–1665
– biomass
– pretreatment 1664
– resources 1663
– supply 1663
– conversion technology 1664
– from biomass 1612
– gasification 1665
– mechanical pretreatment 1665
– SPREETA 1659
– thermal pretreatment 1665
– thermochemical pretreatment 1665
– thermochemical production pathway 1664
biosolids 2417, 7673
– co-digesting 2417
biosparging 2445, 10152
biosphere 189, 191, 635, 8635, 10165
– accidental introduction of pollutants 8635
– net primary productivity (NPP) 10165
– nutrient certificates 9041
– reserves 11353
biostimulation 4099
biosurfactant 5458
biosynthesis 822
biosynthetics 2685, 10743
– enzymes 4035, 6531
– metabolic channeling 6531
– fuels 1064
– natural gas (Bio-SNG) 1661, 1662, 1667–1672, 1674, 8979
– carbon dioxide removal 1669
– cold gas efficiency 1671
– distribution infrastructure 1669
– entrained-flow concept 1674
– gas cleaning 1667
– greenhouse gas emissions 1672
– methanation 1668
– pathway 6528
– production 1662
– production costs 1671
– production pathways 1669
– raw-SNG upgrading 1668
– reference concepts 1669
– technical assessment 1670
biotech crop 4433, 4435, 4463, 4466, 4468, 4470, 10715, 10745, 10759
– economic effects 4468
– economic impact 4435
– global economic impact 4433
– nonpecuniary benefits 4466
– total cost 4470
biotechnology 1677, 1692, 2287, 2291, 2294, 2685, 4433, 4471, 4496, 4500–4501, 4506, 4509, 4511, 4522, 4534, 5456, 8027, 10706, 10743, 10758, 10880–10882
– benefit-cost ratios 2287
– Brazil 4511
– commercial agriculture 4533
– deficit model 4501
– economics 4506
– education 4500
– ethical dialogues 10882
– food-safety management 2294
– for nutritional improvement 1677
– information systems 4522
– monological dialogue 10881
– nutritional improvement 1692
– policies 4509
– public discussions 10880
– public participation 10880
– regulatory framework 2291
– respect for autonomy 10880
– safety net 2291
– strategies 1692
– wicked problems 4534
biotic
– diversity 3287
– ecosystem 3287
– elicitors 6527
– homogenization 951, 11337
– index 3267, 3273, 3587
– invasion 154
– ligand model (BLM) 3585, 10052, 10053, 10055, 10058, 10059
– bioaccumulation 10058
– physiologically based approach 10058
– predicting toxicity in algae 10059
– toxicity-based approach 10058
– limitation 154
– resistance 5550
– stress 2725, 10725, 10744
– stress tolerance 10748
biotin 1684
biotope 944–945, 952, 10368
– area factor 4711, 4736
biotoxicity test 4868
biotoxin detection 9093
biotransformation 3256, 10660, 12299, 12301, 12305
– modifiers 12305
bioturbation 7026, 8397, 8399, 9136
– transport 9135
bioventing 1632, 2448, 10151
biowaste 3914, 11663, 11665
biparental linkage mapping 6429
bipolar
– batteries 5892
– cell ctacks 11514
– bipolar plate 7708, 7877, 11514
bird 10089
birth defect 3638–3639
bisphenol A (BPA) 2090, 3258, 3261, 3586, 3636, 3637, 4861, 4862, 6902
– hazard assessment 4861
– low-dose effects 3261
bis-sulfonyl imide acid 8338
bitumen 2407, 7451, 7461, 7465, 7467, 7470, 7478, 7809, 7812, 7814, 7819
– foamed 2407
– mining 7812
– recovery 7811–7814, 7816–7817
– direct heating of the tar sand 7813
– hot-water process 7811
– non-mining methods 7814
– oleophilic sieve process 7813
– SAGD (steam-assisted gravity drainage) 7817
– solvent extraction process 7813
– thermal methods 7814
– separation 7812
– cold-water process 7812
– sand-reduction process 7812
– spherical agglomeration process 7812
– upgrading 7819
bituminous coal 2169, 2177, 2229, 2233, 3835, 8350
bitumoid 7465
bivalent cations 8608
bivalve 518, 1967
– aquaculture 1959–1961
– carrying capacity 1959
– harvesting 1961

– ongrowing 1961
– processing 1961
– seed collection 1960
– biodeposits 1967
– culture 1935, 1970
– social carrying capacity 1970
– molluscs 9176
– production 1960
– shellfish 9176, 9178
– filtering seston 9176
– filtration capacity 9178
– releasing nutrients 9176
Bjerknes feedback mechanism 2126
black carbon 124, 631, 10123
– aerosol 190, 1308, 10120, 10124
black coal 2177
black hole 11102
black redstart 4722
black roofers 4736
black water event 8926
blackbird 946
blackbody
– radiation 11115
– temperature 9708
– Planck distribution 9708
blackout 10935, 10940–10941, 10945–10950, 10953
– disturbance propagation 10945
– pre-outage conditions 10940
– prevention 10946
– quick restoration 10950
– real-time system monitoring 10947
– risks 10940
– symptoms 10941
– system integrity protection schemes 10948
– system restoration 10949
blade element momentum theory 12208
blast furnace (BF) 8810, 11594
– slag 11594, 11701
blastocyst 6151, 6162, 6170, 7218
– injection 10821
blastoderm 641, 646
blastomere 6151, 6166, 6167
blend morphology 7570
blind spot detection (BSD) 71
blinds 2868, 2876
block copolymer 6548, 6550
blood fluke genera 12044
blood lead concentration 3259
bloom 2085
– ecology 2260
blowout prevention equipment (BOPE) 4402
blue carbon 553
blue mussel 518, 522, 544, 548, 4822, 6764
blue revolution 539, 562
blue tongue 5370–5371, 5374
– influence of climate change 5371
blue water 1544
– irrigation 1544
blue-baby syndrome 3783
blue-green algae 4820, 4830
blue-water spearfishing 3572
bluff surface jets 10983
– non-buoyant 10983
bluff wall jet 10981
body clock 2828
body mass index (BMI) 10264, 10646
Bohr magneton 6079
boiler 1243–1245, 1368, 1370, 1386, 1390, 1398, 1462, 1615
– ash 1336, 11731, 11732, 11738
– characterization 11731
– disposal practice 11731
– stabilization processes 11732
– thermal treatment 11732
– efficiency 1386
– emissions 1390
– exit gas temperature 2166
– firewood–charged 1370
– fixed bed combustion systems 1243
– fluidized bed combustion systems 1244
– gas-fired 1462
– heat losses 1244, 1398
– pulverized fuel combustion systems 1245
– slag 11702
– wood–fueled 1368
boiling liquid expanding vapor explosions (BLEVEs) 5256
boiling water reactor (BWR) 4063, 4906, 7198
bolometer 5571
Boltzmann
– constant 2023, 3800, 6083
– equation 3806
– transport theory 7176
bomb test 3712–3713, 3761
bone morphogenetic protein (BMP) 10890
Bonferroni correction 483
Bonner sphere spectrometers 5569
Boorola gene 399
boosting technology 3117, 5536, 5537
borehole system 4148
borehole thermal energy storage (BTES) 4147, 4148, 4150
boron 7199
borosilicate glass (BSG) 1980, 9583
Bos indicus 1738
Bos taurus 1738
Boss theory 12285
Bothriocephalidea 12022
Botryococcus braunii 359
bottled water 11938–11939
– energy cost 11939
bottom ash 1336, 1341, 3828, 3834, 4868, 5250, 6460, 6487–6488, 8352, 10583, 10585, 11720–11721, 11727, 11738, 11740, 11742, 11746, 11800
– burnout 11723
– characterization 11723
– chemical composition 11740
– discharger 6460
– disposal 11722
– dry discharge 6488
– effect of aging 11727
– extractor 4971
– final destination 11724
– leaching properties 11725
– metals 11740
– organic ingredients 11723
– particle (grain) size distribution 11742
– post-combustion treatment 11724
– quality improvement by sintering 11729
– quality 11729
– toxic metals 11742
– utilization 11729
– potential 11727
– regulations 11722
– vitrification 11746
– washing 11746
bottom fishing 3557
bottom pressure recorder (BPR) 4577
Boudouard reaction 1450, 2244
Bouguer–Lambert–Beer law 9717, 9721
boundary growth 3307
boundary layer
– meteorology 6592
– theory 6732
Boussinesq
– approximation 2053, 7370, 7372, 7379
– assumption 2060
– eddy 2051
– diffusion coefficient 2051
bovine
– genome 1779
– Johne's disease 1758
– leukocyte adhesion deficiency 494
– semen 1771
– spongiform encephalopathy (BSE) 1759, 2969, 4867, 8029, 10859

– tracheal antimicrobial peptide (bTAP) 2967
– trypsin 4030
– tuberculosis 1758, 5367
– viral diarrhea virus (BVDV) 2970
Brachypodium 6429
brachytherapy 8520, 8561, 8581
Bradford-Hill criteria 3266
bradycardia 6501
Bragg's law 6071
brain damage 10641
brain development 3633
brake
– actuator 8852
– design regulation 11501
– fuel conversion efficiency 5520
– mean effective pressure (BMEP) 5477
– specific energy consumption (BSEC) 5490
– system design 11499
braking 11497, 11499–11500
– energy 8116, 8848–8851
– distribution over braking power 8851
– distribution over vehicle speeds 8849, 8850
– force 8851, 8855, 10544, 11494, 11499
– distribution 8855, 11497
– stability 11500
– strength 11497, 11499
– torque 8854
brassicas 1699
BRAVO accident 8492
Brayton
– cycle 4055, 6816–6817, 6824, 7136
– efficiency 6824
– helium turbine 4053
– thermodynamic 7102
– topping cycle (BTC) 6824
Brayton–Rankine cycle 6825, 9603, 9605
– power plan 6826
Brazil 1007, 1014, 1016
– country profile 1007
– ethanol production 1007
– ethanol program 1002
– Eucalyptus potential productivity project (BEPP) 1291
– rural workers 1016
– social governmental program 1014
bread wheat 5321
break crop effect 2734
breaking chopper 12166
breaking waves 7404
breeder's equation 420–421
breeding/breed, see also animal breeding 11, 386–389, 392–394, 396–397, 399–401, 408–412, 417–418, 422–425, 428, 430, 463, 471, 478, 1116, 1484, 1723, 1740, 1765, 1782, 1795, 2527, 2530, 2536, 2650–2651, 2686, 2784, 4071, 4074, 4518, 6425, 6434, 6439–6440, 6706–6708, 8017, 9361, 10395
– additive genetic deviation 418
– animals 1796
– best linear unbiased predictions (BLUP) 1796
– backcross 399
– basic genetic model 417
– birds in town 949
– capacity development 6707
– colchicination 4518
– companies 395
– conservation 393
– conventional 2650
– definition 392
– environmental sensitivity 411–412
– fertility 478
– for heat resistance 10395
– for sustainable agriculture 2527
– genomic selection 387
– genomics-assisted 2530, 2536
– germplasm strategy 4074
– globalization 471
– horses 388
– hypothalamic-pituitary-adrenocortical axis 1782
– in beef cattle 1723
– in developing countries 1740
– in horses 1795
– local 394
– major genes 399
– marker-assisted 2686, 6425, 6439
– marker-assisted selection (MAS) 430, 2530, 2651
– methods 1484
– mixed model methodology 425
– multiplication 396
– multi-trait selection 424
– nucleus 412
– objective 408, 410, 424
– of agricultural crops 1116
– of superior animals 417
– organizations 409, 478
– permanent environmental effects 422
– phenotypic selection 418
– plan development 6708
– principles of selection 417
– programs 409, 463, 471, 1763, 4071, 4073, 6440, 7977, 8014, 8015
– quantitative trait loci (QTLs) 430, 2651
– recording scheme 411
– scheme 410, 412, 2784
– consumers 412
– of selection 401
– risks 410
– selection index 422
– selection of the survivors 9361
– services 6706
– social interactions 9361
– stock 1777
– strategy 1765
– support services 6707
– sustainable systems 394
– synthetic 393
– training population 400
– trait-based 8017
– transgenes 8060
– tropics 1740
– value 387, 397, 401, 408, 418, 425, 426, 428, 441, 470, 474, 490–492, 1796, 1798, 2785, 2786, 6439, 9362, 9364, 9376
– Bayesian methods 491
– best linear unbiased predictions (BLUP) 426, 491, 492
– effective population size 492
– estimation model 474
– mixed model equations (MME) 490, 9376
– workbench tools 6706
– workflows 6706
Bremsstrahlung 8575
– angular distribution 8575
– energy distribution 8575
brevetoxin 4825, 9164
– in mollusks 9095
bright pupil effect 3129
brightening 9731, 9733, 9735, 9737
brightness
– contrast control 2864
– temperature 286
– difference method 11640
brine 4269, 5220
– chemistry 4404
– cooling curve 4269
– extraction 4129
– holding tank (BHT) 4312
– piping 4291
briquetting 1067–1068, 1070, 1085, 2186
brise-soleil 2814
Brønsted–Evans–Polanyi
– postulate 3416
– relationship 3417

broadband
– filter radiometer 11150
– irradiance 9716
broccoli 3613
broiler 8312, 8320, 8323–8324
– avoidable distress 8324
– breeder females 8311
– breeding 8308–8322, 8325
– ascites syndrome 8316
– delayed entry into lay 8315
– deleterious secondary effects 8322
– egg weight 8312
– erratic oviposition defective egg syndrome (EODES) 8311
– feed conversion ratio (FCR) 8314
– framework of population genetics 8322
– hatchability problems 8312, 8318
– heat distress 8316
– heat stress 8318
– increased water consumption 8315
– industry 8309, 8325
– biological costs 8325
– Chicken of Tomorrow contests 8309
– Cornish breed males 8309
– management 8325
– juvenile weight for age (JWfA) 8310
– male overfeeding 8316
– methods for genetic improvement 8320
– modern commercial broiler 8319
– multistage incubator 8313
– nipple drinkers 8315
– production traits 8309, 8320
– proportion of breast meat (PBM) 8309, 8317
– pulmonary hypertension syndrome 8316
– quantitative trait loci 8321
– quasi-EODES at entry to lay 8318
– reduced locomotor activity 8319
– resource allocation model 8310, 8325
– selection-induced genetic variation (SIGV) 8322
– single-stage incubators 8319
– skeletal problems 8314
– sources of genetic variation 8321
– stimulatory lighting 8315
– sudden death syndrome 8316
– target weight 8310
– from farm to market 8324
– heat sensitivity 8320
– metabolic deficiency 8312
– production 8308
– traits 8323
– society 8324
– stocking density 8324
– toxicity disorders 8312
– unavoidable distress 8323
– welfare 8323–8324
broken arrow 8506
bromate 2907
bromine 794, 10135
bronchitis 3641
Bronsted acidity 4588, 4598, 4603–4604
brook 9049
brown roof 4701, 4711
Brownfields 5852
– interim use 5852
– Revitalization Act 2011
Brownian
– diffusion 9135
– motion 2017
brownmillerite-type oxide 3894
Brucella 5056
Bruggeman exponent 8752
Brunauer-Emmett-Teller model 7766
Bruntland Commission 1491, 11683
brush border membrane vesicle (BBMV) 4017
brushed DC machine 18
brushless DC machines (BLDC) 18, 23
– motor drives 23
brushless motor 11528
bryolog 3155
Bryopsis 3161
bryostatin 3155
Bt, see *Bacillus thuringiensis*
BTEX 1633
bubble plume 10992
bubbling fluidized bed (BFB) 5124
– combustion (BFB) furnaces 1326
– gasifier (BFB) 1456
bubbly jet 10990–10992
buck converter 690
bucket ladder dredge 3033
Bugula neritina 3153, 3155
building an ocean 7284
– observing network 7284
building industry 9027
building 895, 1030, 1038, 1424, 2428, 2808, 2881, 3675–3677, 3679–3680, 3683, 3692, 3693, 3695, 3697, 3700, 4147, 4158, 4718, 4743, 5332, 5335, 5336, 5338, 5344, 6866, 6870, 7634–7635, 7637, 8375, 8703–8704, 8707–8709, 8711, 8712, 9028, 9030, 9032, 9034, 9043, 10193, 10197, 10205, 10245–10251, 10255, 10257, 10269, 10286, 10296–10297, 10342, 10554
– acoustical problems 5336
– airtight construction 7635
– automation 1424
– behavior prediction 10248
– biological materials 9030
– carbon
– footprint 6866
– neutrality 3676, 3677
– climatization 10554
– conditioning 4158
– construction 2861, 11705
– applications of waste materials 11705
– daylight 2861
– contemporary information technology 10257
– control 10197, 10246, 10249
– design 10247
– video cameras 10249
– costs 10205
– Cradle to Cradle® principles 9034
– cross-scale assessment 8709
– daylighting 2808, 5335
– design 3680
– day-night load balancing strategies 3693
– daytime cooling 3693
– day-to-day operations 1030
– delivery process 10245
– design 914, 918, 2812, 5336, 10192, 10205, 10261
– application of energy modeling tools 10205
– climate-adapted 2812
– for change 3700
– for disassembly 3700
– for sustainability 3680
– performance-based 10205
– prescriptive-based 10205
– simulation tools 10192
– ecological footprint 4743
– embodied energy 10342
– enclosures 3676, 3697, 10287
– sustainability 3697, 10287
– energy
– balance 4718, 7637, 8375
– consumption 10246, 10251
– efficiency 10297
– saving 10255
– simulation tools 10205
– energy-optimized 2881

– environmental assessment 8703–8705
  – proliferation 8705
– environmental control 3679
– environmental impact 2428
– environmental performance 8712
– evidence-based design (EBD) 5332, 5338, 5344
– facades 2888, 3677
– footprint 4147, 9028
– foundation
  – heat exchangers 4146
  – piles 4149
– ground-coupling 3693
– healthcare facility design 5332
– ice storage cooling strategy 3693
– implementing nutrient certificates 9043
– information modeling 10199, 10308, 10310–10312, 10314
  – computer-aided drafting (CAD) 10308
  – computer-aided facilities management (CAFM) 10312
  – construction phase 10310
  – design phase 10308
  – manufacturing phase 10311
  – materials life-cycle cost analysis (LCA) 10311
  – parametric data 10314
  – software 10314
– integrated control 10251
– internal heat gains 3692
– internal load dominated 895
– management system 10246
– mechanical systems 10290
  – sustainability 10290
– mechanically ventilated 10269
– natural cooling 3683
– natural ventilation 3683, 6866
– net-zero energy 8708
– nighttime ventilation 3693
– occupancy detection 10248
– operations 1038
– passive infrared (PIR) motion detectors 10249
– performance 10197, 10199–10201
  – architectural zones 10201
  – data sharing 10199
  – energy modeling tools 10208
  – graphical-user interfaces (GUI) 10194
  – interoperability 10199
  – modeling 10197, 10200, 10208
  – occupancy schedule 10200
  – simulation 10193, 10194, 10197, 10200, 10311
  – simulation tools 10193
  – surrounding ecological and environmental conditions 10201
  – thermal control zoning 10201
– perimeter conditioning systems 3679
– photovoltaic solar (PV) elements 3695
– project's life cycle 10205
– protection 3700
– research establishment environmental assessment method (BREEAM) 8703
– scale 11269
– simulation 10193, 10257
– space heating 4365
– structural mass 3693
– superefficient 3676
– sustainability 3675, 10286
  – assessment 8707, 8708
  – design strategies 5338
– technologies 6870
– thermal comfort 7634
– thermal conditioning 5344
– topsoil 9032
– total energy demand 3677
– valuation 8711
– vapor migration 3697
– ventilation system design 5335
built environment 10264, 10281, 10285–10286, 10292, 10302, 10359
– environmental statistics 10286
– human health 10264, 10281
– sustainability 10285, 10302
– water 10292
built-in roofing 7955
bulbar poliomyelitis 8142
bulk
– atmospheric composition 11314
– chemicals 7590
  – catalysts 7590
– heterojunction 7566
– mean velocity 2032
– silicon anode 9296
  – failure mechanisms 9296
bulk-shielding facilities 8539
bulky waste 5244
bulldozer 5092
bullet train 4932
Bulmer effect 421
Bunsen–Roscoe law 9651
buoyancy/buoyant
– buoyancy-driven (stack) ventilation 6871
– effect 6872
– flux 10979
– jet 10979
– surface jets 10983
buprenorphine 3275, 10646
buried tritium 11003, 11021, 11060
Burkitts lymphoma 3644
burnable poison 3806
burnable waste 11861
bus 1879, 1889, 2999
– air pollution 1879
– assignment 97
– automation 1821
– configuration 2999
– fuel consumption 1879
– lane 1821–1822, 1850, 1861, 4946
– light rail service coordination 5988
– line capacity 1884
– network 5996
– operator driving behavior 97
– preferential treatments 1871
– protection 3011
– route duplication 5995
– service 1870
– stops 95
– transit model 96
– transit routes 1885
– transit system 1870, 1873, 1893, 1895, 1900, 5982, 5995
  – capacity 1895
  – cost characteristics 1893
  – land-use densities 1900
– transit-oriented development 1889
bus rapid transit (BRT) 93, 1810, 1812–1814, 1816, 1818–1831, 1833, 1835–1837, 1839–1840, 1845–1846, 1854, 1870, 1873, 1881, 1891, 1894, 6496, 10924–10925
– Africa 1846
– Asia 1846
– Australia 1846
– buses in tunnels 1870
– Canada 1840
– capital costs 1836
– characteristics 1835
– components 1835
– corridors 10925
– decision-makers 1826
– definition 1873
– design studies 1820
– developments 1813
– dual-mode systems 1820
– early busways 1821
– educating the public 1831
– Europe 1845
– exclusive right-of-way 1822
– finance 1827
– funding 1827, 1837

– guided buses 1870
– guideway cost 1894
– impacts 1835
– infrastructure 1824
– in the developing world 1839
– institutional issues 1818, 1822
– integrated transit systems 1837
– intergovernmental issues 1823
– international experience 1821
– interorganizational issues 1823
– intra-agency 1825
– key systems 1833
– labor and human factors 1827
– land use 1828
– Latin America 1840
– liability 1828
– long-term funding commitments 1830
– managing perceptions 1831
– marketing 1827
– network supplements 1814
– New Zealand 1846
– operating cost 1894
– origins 1820
– physical environment 1829
– planning 1828
– policy issues 1833
– political will 1826
– private participation 1837
– public relations 1827
– public transit agency 1824
– rail-ready 1816
– roadway-related issues 1830
– running ways 1816, 1819
– stakeholders 1823
– safety 1828
– stakeholder experience 1829
– status around the world 1836
– technological developments 1839
– transit-oriented development 1831
– United States 1840
– worldwide history of development 1833
busbars 2999
business district 955
BusMEZZO 103
bus-only roadway 1819
bus-only transit system 5998
busway 1816, 1821, 1874, 10926
– facilities 6005
butane 3969
butanol 5481, 5494
– *n*-butanol 5482
Butler–Volmer equation 3876
Butler–Volmer model 3420
butterfly bush 954
butyrated kraft lignin 6928
by-product 10001
– materials 11701
bystander effect 11030

C

cable 11165, 11167–11175
– cleanliness 11168
– components 11167
– conductors 11167
– contaminants 11172
– designs 11180
– recoverable 11180
– recyclable 11180
– dry design type 11169
– electrical stresses 11165
– electrical treeing 11174
– extrinsic defects 11172
– failure processes 11170
– insulation 11168
– breakdown 11171
– interaction between moisture and temperature 11175
– manufacture 11169
– metal sheath 11168
– oversheath (jacket) 11169
– partial discharges 11174
– power transmission grid 11170
– protrusions 11172
– screens 11168
– semiconductive screening materials 11167
– systems 11160–11162, 11164, 11178–11179, 11183, 11184
– alternating current (AC) 11162
– commissioning 11183
– diagnostic testing 11183, 11184
– diagnostic trends 11183
– direct current (DC) 11162
– electrical stresses 11162
– life expectancy 11178
– motorformer 11164
– powerformer 11164
– real-time control 11183
– reliability 11183
– submarine connections 11164
– total lifetime cost 11179
– uses 11164
– voltage rating 11161
– types 11165
– voids 11173
– voltage classes 11171
– water trees 11175
– wet aging 11175
– insulation breakdown 11171
– voltage classes 11171
Cabtrack program 7786
cadmium 3630, 4888, 6943, 10588, 10638, 11713
– cadmium–nickel cell 750
– telluride 9436
Caenorhabditis elegans 10856
Caephalosporium caerulens 501
caffeine 11922, 11926
calcareous phytoplankton 7237
calcification 7234
calciotropic hormone 9654
calcite 4127, 8624
calcium 1104, 2563, 7330, 9829, 11856
– aluminate phosphate (CaP) cement 4404
– carbonate ($CaCO_3$) 6375, 7231
– silicates 1915
– sulfite 8360
caldera 11621–11622, 11634
– geophysical observations 11634
calibration procedure 11464
californium 8582
CALIPSO
– lidar system 325
– satellite 323
calorific value adjustment 4975
calorimetric bomb 9833
CalTOX model 4859
Calvin–Benson cycle 349, 357, 362, 1479, 2624, 2626
Calvin-cycle 1478
calving law 2771
camera
– calibration 49
– motion estimation (CME) 57, 58
– camera motion estimation 58
– platform 48
Campylobacter 5061, 6625, 6628, 7684
Canadian-Deuterium-Uranium (CANDU) reactor 7198
CAN-bus signal 3124
– properties 3600
– evaluation 3259
– susceptible individuals 3608
– childhood 3642
– disinfection by-products (DBPs) 3647
– endocrine disruptors 3648
– geographical distribution 3642
– pesticides 3646
cancer 3589, 3642, 3646–3648, 9656
– cells 3600
– properties 3600
– childhood 3642
– disinfection by-products (DBPs) 3647

– endocrine disruptors 3648
– etiological causes 3589
– geographical distribution 3642
– pesticides 3646
– risk 3259, 3599, 3608
– evaluation 3259
– susceptible individuals 3608
cancer-causing agent 221
candidate gene 488–489
Candidatus endobugula sertula 3155
Candidatus endoecteinascidia frumentensis 3157
cannibalism 10067
Canny filter 3078
canola 4450
– glyphosate-tolerant 4450
canopy 2615, 2621–2623, 2628, 2634, 2671, 2735
– development 2623
– canopy height 11269
– photosynthesis 2621, 2628, 2671, 2673
– properties 2621
– reflectance under irrigation 2735
– temperature depression 2634
Canter's theory of place 10373
cap grouting 5656
capacitor 795, 796, 802, 3430
– banks 3004
– electrochemical double layer 796
– energy density 802, 3430
– electrochemical double layer 796
– energy density 3430
capacity for aquaculture 1931
cap-and-trade program 5418
CAPEX deferral 3013
capillary flow porometry 8731
caprolactam 301
capsid protein 8133
capture
– fisheries 543, 578, 591, 7387, 10798
– gamma photons 8572
captured radiation 2624
– photosynthetic mechanisms 2624
capuramycin 503
car
– accident 66
– batteries 9990
– following 3137–3139
– age-related changes 3137
– low visibility condition 3138
– time headway (THW) 3139
– shredding residues 8837
– speed 67
carbamazepine 2339, 11924, 11926
carbenicillin 2589
carbide 3972
carbohydrate 965, 1482, 1678, 3574, 4552, 4560
– intolerant 3574
– Protic Ionic Liquids 6787
carbon 164–165, 721, 797, 846–848, 851, 857–858, 861–862, 870, 874, 877, 879, 1235, 2149–2150, 2251, 2254, 3427, 5412, 6133, 6374, 6773, 6775–6776, 6781, 6783, 6785
– abatement efficiency (CAE) 862
– abatement strategy 847
– abatement 851, 857, 861, 870, 874
– efficiency (CAE) 862
– strategy 847
– activated 797
– aerogels 797
– biogeochemical cycle 6374
– black 9604
– budgets 3223
– capture 2150, 2165
– and reuse (CCR) 9036
– and sequestration (CCS) 2149, 3846
– and storage 6839, 6847
– catalysts 7696
– charcoal-derived 879
– corrosion 7719, 8225
– cycle 607
– debt 858, 1498, 1504, 2756
– deposition 3907–3908
– dioxide (CO_2), see there
– drawdown 7268
– efficiency 4586
– electrodes 3427
– footprint 548, 1026, 1233, 1263, 2848
– of buildings 1026, 2848
– for electrical double-layer capacitors 6773
– for pseudo-capacitors 6775
– geoengineering 4108
– heteroatom-enriched 6776, 6781
– hidden C cost (HCC) 164
– host plant 877
– intensity 1550
– in terrestrial systems 5412
– isotope
– composition, mass spectrometry 8017
– discrimination (CID) 2650, 8017
– techniques 4756
– life cycle analysis (LCA) 164
– long-term storage 848
– materials 6128
– mitigation 848, 857, 862
– monofluoride (CF_x) 6503
– monoxide (CO) 170, 235, 609, 1043, 1389, 2240, 2277, 3970, 4968, 5488, 7594, 8350, 8882, 10483, 10639, 11293, 11316
– oligomerization 2240, 3970
– polymerization 2240, 3970
– nanofibers 9302
– nanotubes 797, 9301, 9610, 10181
– neutrality 857, 3677, 8710
– nitrogen-rich 6781
– oxidation 8293
– plant-captured 848
– price 5418
– rental rate 5412
– ribbon 9206
– sequestration 165, 2251, 2254, 4095, 4119, 7268, 7271, 7279, 9605, 9697, 10745, 10961
– seaweed-based 6783
– taxes 1570
– thermo programmed desorption (TPD) analyses 6785
– carbon trading credit (CTC) 551, 552
– for electrical double-layer capacitors 6773
– for pseudo-capacitors 6775
– heteroatom-enriched 6776, 6781
– nitrogen-rich 6781
– seaweed-based 6783
– capture and storage (CCS) 4120, 4122
– post-combustion capture 4120
– costs 1921
– environmental costs 1922
– social costs 1922
carbon-based pseudo-capacitors 6787
– protic ionic liquids 6787
carbon dioxide 161, 207, 245, 608–609, 823, 848, 851, 857, 933, 1150, 1152, 1784, 1909, 2149, 2156, 2163, 2166, 2169, 2501, 2757, 3458, 3599, 4120–4122, 4171, 4772, 5297, 6375, 7304, 7329, 8350, 10169, 10482, 10484, 12102
– atmospheric fluxes 6375
– capture 2169
– and sequestration (CCS) 2172
– and storage (CCS) 4120–4122
– CO_2-enhanced oil recovery (CO2-EOR) 2157
– coal-based 2163
– compression in PC and IGCC plant 2169

– concentration 10391
– costs 1921
– environmental costs 1922
– social costs 1922
– emission 608, 654, 933, 1504, 1784, 2166, 2172, 3458, 4121, 5911
– factor (CEF) 857
– fertilization effect 609, 2757
– in the atmosphere 608
– long-term isolation 2149
– migration 2156
– monitoring and verification (M&V) 2158
– post-combustion capture 4120
– price 5413
– stabilization 5413
– reduction 2163
– removal 2115–2117, 4108, 10119
– sequestration 162, 1909, 1921, 1922
– and storage 4689
– splitting thermochemical cycles 9602
– storage 4125
– mechanisms 2156
– supercritical 10169
– transport 1912
carbon-negative energy 860
carbon-sequestering systems 9032
carbon-support corrosion 7763
carbon-to-nitrogen (C/N) ratio 1152
carbonaceous waste 9608
carbonate 1316
– aquifer 4796
– chemistry 7231
– electrolytes 6724
– ion 6721, 7234, 7236
– carbonate ions 6721, 7236
– minerals 2157
– molecules 6061
– rock 1913, 1915, 5646, 5661
– salts 7897
– weathering 2118
carbonate-containing liquid electrolytes 6085
carbonation 374, 1910, 1919
– materials 1910
– modes of application 1910
– Protic Ionic Liquids 6787
carbonic acid 2118, 7234
carbonization 1449, 1527, 2416, 6770
carbonized rice husks (CRHs) 874
carbonyl
– oxygen atom 6063
– sulfide 8353
carbonylation 3946
carbothermal reduction of metal oxides 9596
carboxylate 11440
– platform 11450
carboxylation 3224
carboxylic acid 2242
carboxymethylcellulose (CMC) 6092, 6133
carcinogen 3254, 3258–3259, 3589, 3596, 3600, 3605, 3608, 3610–3612
– DNA
– adduct 3259
– mutations 3600
– exogenous 3610
– low-dose effects 3254
– methylating 3608
– risk assessment 3258
carcinogenesis 3255, 3596, 3600, 3644
carcinogenic agents 3648
– during puberty 3648
carcinogenicity 4849
– DNA adduct 3259
– DNA mutations 3600
– exogenous 3610
– low-dose effects 3254
– methylating 3608
– risk assessment 3258
cardiac pacemakers 6501, 6514
cardiac resynchronization therapy defibrillator device (CRT-D) 6507
cardiovascular disease 9656
Caribbean reefs 2492
caribou 8448, 8450, 8457, 8462
– radiation doses 8462
car-like vehicle 2477
carnivore 823–825, 827, 831
Carnot
– cycle 3385, 3849, 3854, 3927, 4252, 4296, 6817
– efficiency 5142, 5511, 5538, 6818, 9513, 9592, 9594, 9905
– heat engine 5519
– law 1241
– process 1248, 9413
Carnot-equivalent cycle 6818
carotene 7915
– β-carotene 1699, 1705, 1716, 10758
carotenoid 1699
carpet recycling 8827, 8830
– comminution 8830
– fiber identification 8830
– separation 8830
– sorting 8830
carpools 92, 4952, 5024, 5029
carp 547
carragenophyte 9120
carrying capacity 1931–1932, 1941, 1959, 1961–1962, 1964–1965, 1968, 1970, 1972
– assimilative capacity 1932
– decision framework 1970
– ecological 1962, 1965
– functional categories 1962
– management tools 1972
– modeling 1964
– physical 1961
– production 1962
– social 1962, 1968
– sustainable bivalve aquaculture 1959
carsharing 92
Cartagena Protocol on Biosafety (CPB) 2288, 2304, 4496, 4519, 4520, 4521, 10768
Cartesian
– coordinate system 3811
– radar coordinates 6967
caryopsis 2542
– allele 2706
CASAC ozone panel 233–234
cascade catalysis 7612
casein 10855
cash crops 1228, 1563
casinghead gasoline 7803
cassava 990
– vein mosaic virus 10687
cast iron 10555
– stoves 1362
– mechanical properties 6935
– thermomechanical properties 6934
castor oil 6907–6908
– alcoholysis products 6907
– bisphenol A propoxylate glyceride maleates 6908
– maleates 6908
– monoglyceride maleates 6908
– oil-based polymers 6934–6935
– mechanical properties 6935
– thermomechanical properties 6934
– pentaerythritol glyceride maleates 6907
cataclysmic eruption 11624
catalase (CAT) 4, 3662
catalysis/catalytic 4609, 7586, 7613
– chain transfer polymerizations 3945
– computer-aided molecular design 7613
– converters 1396
– cracking 4588, 7832–7833
– sour wastewater 7833
– spent process catalysts 7833
– graphite formation 2942
– high-throughput experimentation (HTE) 7613

– in chemistry 4609
– membrane reactors (CMR) 3969
– oxidation 7588, 7590, 7594
– of hydrocarbons 7594
– propylene to propylene oxide 7590
– ozone loss 10131
– partial oxidation (CPOx) 3968
– reforming 3967
– post-combustor 5271
– reactions 10563
– reformer gases 7842
– steam reformer (CSR) 7879
– transformations 4585
– two-stage liquefaction (CTSL) 2230
– wet air oxidation (CWAO) 7608
catalyst 8213
– dust 7833
– electrokinetics 373
– whiskerettes 8213
– sour wastewater 7833
– spent process catalysts 7833
– of hydrocarbons 7594
– propylene to propylene oxide 7590
cataract 11412
catchment 8634–8635, 8637, 8642, 8648
– contaminants 8635
– inland water 8642
– land-surface model (CLSM) 4575
– migration of radioactive substances 8642
– radioactive pollution 8635
– radionuclide concentration 8637
– storage compartments 8648
– studies 5823
catchment-to-tap systems 6624
catechol 10667
cathode 709, 729, 740, 752, 3873, 6039, 6068–6069, 6086, 6105, 6127, 6129, 6505, 6733–6734, 9907
– gas-phase mass transfer 6734
– Li-ion liquid electrolytes 752
– materials 6086, 6144
– nickel metal particle 6105
– overpotential 6733–6734
– oxygen reduction reaction 7731
– ray tube (CRT) 3444
cathode/electrolyte interface 6060
– Li-ion liquid electrolytes 752
cation/cationic
– exchange capacity (CEC) 875
– exchange reactions 8608
– geothermometry 5220, 5222
– composition geothermometer (CCG) 5221
cattle 1747, 1752
– breeding 7973
cause-effect relationship 3266
cave 5646, 5661
– biota 5663
– mapping 5661
cavitating fluid (CF) 2763
cavity
– receiver 2364
– thermal energy storage (CTES) systems 4153
– flexible 1982
– CdTe solar cell production 1984
CdTe solar cell 1976–1979, 1981–1983, 1985–1989, 1991–1993, 1995–1998
– annealing treatment methods 1988
– As-deposited CdTe layers 1989
– bifacial 1996
– buffer layers 1995
– $CdCl_2$ treatment 1989
– CdS buffer 1985
– CdTe absorber layer 1986
– CdTe bandgap 1991
– CdTe deposition techniques 1987
– CdTe thickness reduction 1992
– close space sublimation (CSS) 1987
– electrical back contact 1993
– electrodeposition 1988
– environmental, health, and safety issues 1997
– flexible modules 1982
– high vacuum evaporation (HVE) 1987
– industrial production 1981
– influence of polycrystallinity 1992
– metal organic chemical vapor deposition (MOCVD) 1987
– performance stability problem 1996
– pn-heterojunction 1983
– processing technology 1979, 1983
– production 1984
– highly resistive and transparent layer 1984
– properties 1983
– p-type 1978, 1981, 1985
– resources of raw materials 1998
– screen printing 1988
– spray deposition 1988
– sputtering 1987
– state-of-the-art 1978
– superstrate configuration 1996
– transparent conductive oxide layer 1983
– vapor transport deposition (VTD) 1987
– window layer 1983
celestite 9950
Celgard
– membranes 8730
– separators 8725
cell/cellular
– clones 6525, 10828
– cultures 6519
– secondary metabolites 6519
– death from high-LET radiation 5579
– fusion 10770
– genome 10904
– glasses 11604
– membrane thermostability 10396
– metabolic pathways 9656
– performance and safety 8737
– effect on cell performance and safety 8737
– physiology 6532
– prion protein 2969
– sorting 647
– fluorescence-activated 647
– magnetic-activated 647
– transfection 10899
– turnover 3605
– voltage 742
– overvoltage 742
– polarization 742
– wall biosynthesis 502
cellobiose 973
cellulase 972, 973, 8048
cellulolytic enzyme 8052
cellulose/cellulosic 963, 1042, 1075–1076, 1105, 1519, 6020, 9824, 11435
– ethanol 1269, 8048, 10508–10509, 10514–10515, 10752, 11429
– switchgrass-based 10515
– fibers 8725
cement 4872
– hydration process 2408
– kilns 5286, 5288
– production 4871
cenosphere 3825, 3828
Central American volcanic belt (CAVB) 11619
central electricity generation 9935
central heating
– boilers 1367
– kitchen stoves 1365
– systems 1387–1388
– efficiency 1387
– wood-burning 1388
central limit theorem 398

central receiver system (CSR) 2350
central-city redevelopment 10931
centralized generation 3012
centralized traffic control (CTC) 5967
centrifugal collectors 1393
centrosome 6168–6169
– inheritance 6168
Cephalopholis argus 831
– biomass 831
– ciguatoxicity 831
ceptometer 7923
ceramic brick 3833
ceramization 11601
cercariae 12043
CERCLA, see also Comprehensive Environmental Response, Compensation, and Liability Act
– grain quality 4550
– color 2707
– quality 2707
– amylose content 2708
– ethylene-releasing compound 6210
– inhibitors of gibberellic acid biosynthesis 6210
cereal 1111, 2708, 6210, 4552, 6201–6202, 8018, 9151
– amylose content 2708
– endosperm 4552
– ethylene-releasing compound 6210
– grains 10842
– crops 1130, 4550
– grain quality 4550
– inhibitors of gibberellic acid biosynthesis 6210
– lodging 6202
– resistance 6201
– preharvest sprouting 9151
– seed 2707
– color 2707
– quality 2707
– water soluble carbohydrates (WSC) 8018
cerebellar neurodegeneration 2970
cerebral malaria 11088
ceria sulfide 2945
Cerulenin 500
cesium 8452, 8621
– cesium–134 3714
– cesium–137 3712, 3728–3730, 3733–3734, 3738, 3743
– activity 3728, 3743
– chronology 3738
– depth distribution 3729, 3734
– estimating 3733
– fallout 3729
– measurements 3730, 3734
– post-fallout redistribution 3729
– redistribution 3728
– waste 4776
cestode 12022, 12052
Cestodes 12022
cetane number 11430
chalcopyrite 7968, 9397
– compounds 9395
– phase diagram 9397
– semiconductors 9396
chamber 4975
CHAMP (CHAllenging MiniPayload)
– satellite 4566
– mission 4565
channel
– erosion 3742
– siltation 3758
– tunnel 4940
chaos theory 2523
chaotic system 2523
char 851, 884, 5305, 5313
– burnout time 5313
– from solid wastes 5305
– char gasification 5312, 5314
– irrigation 884
– mobility 884
– soil-water dynamics 884
charcoal 847–848, 874, 876–877, 879, 1213, 1300, 1322, 1324, 1327, 1352, 1518, 2117, 3427
– adsorption of phosphorus 876
– combustion 1322, 1327, 1335
– environmental 879
charge-sustaining hybrid 3484
– burnout time 5313
– from solid wastes 5305
– irrigation 884
– mobility 884
– soil-water dynamics 884
checkerboard 11462, 11465
– plane 11462
chelation therapy 3260
chemical/chemicals 2037, 10956–10957, 10955
– batteries 3367–3368, 5105–5106, 5114
– energy density 3368
– practical specific energy 5105
– specific power 5106
– theoretical specific energy 5105
– composition 2410, 11740
– carbon–nitrogen (C/N) ratio 2410
– contamination 2259
– diffusion 10955
– engineering 4614
– fate 10956
– fuel conversion 9937
– hazard evaluation for management strategies (CHEMS–1) 4860
– heat storage 10561
– hydrophobicity 10662
– importance of mixing 10957
– in the environment 2016, 2030, 2048, 10954, 10975
– dispersive transport 2030
– fate 10954
– transport 10954
– transport with jets and plumes 10975
– turbulent transport 2048
– interfacial transfer 10956
– mass 10964
– rate of accumulation 10964
– mass balance (CMB) modeling 8889, 8894
– multiphase transport 10956
– nitrogen 6771
– oxidants 3658
– oxidation catalyst 7587
– oxygen demand (COD) 9569, 11968
– pollution 191
– recycling 8826
– retardation coefficient 2037
– reverse osmosis 10955
– tracers 4209
– transformation 4644–4645, 4647
– oxidation reactions 4645
– protection–deprotection reactions 4644
– reduction reactions 4647
– surface-mediated 4644
– transport 10958, 10962
– processes 10955
– resistance 10958
– turbulent diffusion 10955
– wastes 4585
– weathering 1910, 1913
– weed control with herbicides 10345
cheminee 1361
chemisorption 1648
chemistry-climate model (CCM) 10137
chemoautotroph 823, 6414
chemotherapy of malaria 11081
chernikovite 10413
Chernobyl accident 3534, 3536–3537, 3585, 3710, 3712, 5592–5593, 5601, 5606, 7008, 7012, 7020, 7029, 7053, 8388, 8409, 8457, 8465, 8498, 8500, 8638, 8667, 10426

– agriculture 3534
– aquatic ecosystems 3536
– cooling pond 5598
– decontamination of settlements 3537
– effects of remediation 3537
– effects of radiation 5593
– exclusion zone 8500
– experimental results 8638
– fallout 3713, 3718, 3734, 7005, 8465
– in Scandinavian watersheds 7005
– map 7029
– forest 3536
– radiocesium 7012
– concentrations 7029
– in lakes 7020
– radiostrontium 7012
– remediation strategies 3537
– transport of radionuclides 7008
– urban ecosystems 3537
– in Scandinavian Watersheds 7005
Chernobyl Forum 3528
– exclusion zone 8500
– fallout 8465
chicken 639, 640–642, 645
– blastoderm 645
– embryonic stem cells 645
– growth rate 8314
– oocyte 642
– production 1778
– retroviruses 642
– transgenesis 639, 640
– zygote 641
childhood 3646–3648
– cancer 3642, 3646, 3648
– leukemia 3647–3648
children 3621, 3623–3627, 3629, 3631–3635, 3649
– absorption of chemicals 3626
– behavioral patterns 3625
– biotransformation 3629
– cellular metabolism 3629
– development phases 3624
– disease prevention 3624
– disinfection by-products (DBPs) 3632
– effects of passive smoking 3632
– environmental exposures 3649
– environmental health threats 3622
– environmental threats 3621, 3622, 3649
– environmental toxicants 3622
– exposure patterns 3623
– hand-to-mouth behavior 3631
– indoor air pollutants 3626
– ingestion
– of nonfood items 3625
– of pesticides 3631
– life expectancy 3621
– mercury-associated effects 3634
– metabolic pathways 3624
– metabolic rate 3625
– microenvironment 3626
– nervous system 3632
– neurobehavioral deficits 3635
– neuropsychological effects 3634
– neuropsychological testing 3635
– neurotoxic effects of lead 3633
– oral exposures to chemicals 3625
– pollutants 3629
– rate of oxygen consumption 3625
– special risks 3622
– susceptibility 3627
– to environmental toxicants 3623
– toxicokinetics 3626
– vulnerable life stages 3623
chimney 1251
– effect 9766
– stoves 1362, 1366
chitinase 4034
– genes 10697
chitosan 2576
Chlamydia trachomatis infection 12011
Chlamydomonas reinhardtii 353, 356, 358, 360, 365
Chlo 2405
chloracne 5267
chloraquine 5379
Chlorella
– *ellipsoidea* 365
– *vulgaris* 348, 360
– *zofingiensis* 356
chloride 1316, 2041, 7330
– fertilization 2563
– residence time 2041
chlorinate 10407
– abiotic reductive dehalogenation 10407
chlorinated
– aliphatic hydrocarbons 10142
– dioxin 4873
– chlorinated hydrocarbon 7002
– hydrocarbons (CHCs) 6990, 7002, 10153–10155
– biodegradation 10154
– enhanced bioremediation 10154
– enhanced biostimulation 10155
– in situ chemical oxidation 10155
– molecular growth 7002
– monitored natural attenuation 10154
– multiphase extraction 10154
– soil vapor extraction (SVE) 10154
– polycyclic aromatic hydrocarbons (ClPAH) 6995
– VOCs 10153
– waste 5244
chlorination 4885, 10535
chlorine 3911, 4009, 4881, 6996, 9564, 9830, 10135, 11597
– corrosion 1346
– dosing 6625
– gas 5252, 10653
– isomerizations 7002
– poisoning 3911
chlormequat 6210
chloroacetomide herbicide 10350
chloroalkylation 378
chlorobenzene 6999
chloroethene 2435, 2443
chlorofluorocarbon (CFC) 177, 613, 5860, 7343, 8670, 9710, 10130, 10131
– chlorofluorocarbon–11 2523
chloroperoxidase enzyme 7597
chlorophenol (CLPs) 4883, 4887, 6999
chlorophyll 352–355, 359, 1478–1479, 1949, 2618, 2621, 2624, 2670, 7274, 7915, 7917, 8922, 8925, 8963, 8965–8966, 11381, 11387
– antenna size 355
– biosynthesis 354
– empirical algorithms 8963
– fluorescence 354–355, 359, 2634, 8925
– primary productivity algorithms 8965
– satellite-derived 8966
– semi-analytical algorithms 8965
chloroplast 354, 358, 366, 1479, 2624, 2644, 2664, 8044, 8047, 8077, 11395
– genome 2606, 4024
– respiration pathway 358
– thylakoid membrane 356
– transformation 365, 2606
chloroquine 6292, 11077, 11082
chlororespiration 358, 2444
Chlorpyrifos 3260, 3586
choice-set generation 105
– in coastal and estuarine waters 8927
– lysogenic conversion 5052
cholera 5052, 5063, 5361, 7385, 12014
– antimicrobial treatment 5063
– outbreak 8927
– in coastal and estuarine waters 8927
– toxin (CTX) 5052
– lysogenic conversion 5052
– vaccine 7385
Cholesky factorization 2473
cholesterol 1681, 4037
– oxidase 4037
cholinergic syndrome 3260

chromate 10410
– poisoning 3904
chromatin 2553, 3604, 3608, 6154, 6158, 6171, 10908, 10911
– modifications 3608, 6158
– relaxation 6171
– remodeling treatments 6171
chrominance 11122
chromium 4889, 9953, 10410
– chromium–iron battery 3853
– oxide 3962
– poisoning 9872, 9894
chromophore 7559, 11380–11381
chromophoric dissolved organic material (CDOM) 8955
chromosome/chromosomal 478, 483, 488
– aberrations 3602, 5581
– instability (CIN) 3606
– mutations 3606
– segment homozygosity (CSH) 7979
– transfer 6156
chronic alcohol consumption 3589, 3590, 3610
chronic irradiation 5588
chronic myeloblastic leukemia (CML) 3602
chronic obstructive pulmonary disease (COPD) 213
chrysotile 1924
chunk rock backfill 5656
chytridiomycosis 5370
– in amphibians 5370
– influence of climate change 5370
cigar burner 1324
cigarette smoke 228, 3612, 10638, 10640
– toxic compounds 10640
ciguatera 9104
– fish poisoning (CFP) 827, 828–829, 3592, 7389, 9083
– biomagnification 829
– cardiovascular symptoms 828
– gastrointestinal symptoms 828
– neurological symptoms 828
ciguatoxin 827–828, 830, 831, 3592, 3594, 9082
– biotransformation 830
CIMMYT wheat genotypes 4074
cinnabaramide 3163
circadian efficiency 2829
circadian rhythm 2828, 10275
circuit breaker 3001–3002
– sulfur hexafluoride (SF_6) gas-insulated 3002
circular jet 10976, 10980
circular plume 10988
– crossflow 10988
circulating fluidized bed (CFB) 1456, 5124
– gasifiers 5127
– incinerators 5278
circulation model 2098
circumpolar
– bottom waters (CBW) 8658
– deep water (CDW) 5860, 8677
cirrus cloud 661, 663
cisgenetic 4497
cistron 10913
– co-expression 10913
– mosaic of biotopes 944
– producing energy 958
citrate-dithionite-bicarbonate (CDB) 8606
– sustainability 6854
city 942, 944, 953, 958
– as ecosystems 6856
– as landscape 942
– development 6853–6854
– sustainability 6854
– environments 942
– gas 3910, 3916
– growth 5718
– intervention programs 5844
– of biotopes 944
– planning 952
– producing energy 958
– topography 11313
– transportation 7779
– water management 4735
– water structure 953
city-branding strategy 4689
city-suburban-exurban systems 11337
civil aviation 653
civilian aircraft 6813
clam digger's itch 12043
clamshell dredge 3032
clarithromycin 506
– waste-to-energy plant 11846
clathrate hydrates 330
clathrate 334, 7453
– hydrates 330
Claude cycle 7306
Claus plant 2237
Clausius Rankine cycle 1241
Clausius–Clapeyron equation 132, 7248
Clausthal test facility 6466
– limitations 4600
clay 4593–4598, 4600
– acidic properties 4594
– aldol condensation 4598
– alkylation 4598
– catalysis 4596, 4600
– limitations 4600
– dioctahedral 4594
– esterification 4596
– etherification 4597
– interlayer 4594
– montmorillonite 4598
– Na^+ exchange 4596
– pillaring 4595
– structure 4593
– sulfonylations 4598
– supporting materials 4600
– trioctahedral 4594
clayzic 4605
Clean Air Act (CAA) 213, 215, 298, 1392, 7825, 11738
Clean Air Interstate Rule (CAIR) 10525
Clean Air Scientific Advisory Committee (CASAC) 217
clean burning natural gas 331
clean energy 9743
Clean Water Act (CWA) 5674, 5827, 6334, 7825
cleanup dredging 3048
clear ocean water 11387, 11390
clear sky option 2826
Clearfield hybrid 4450
clear-sky
– diffuse radiation 10626
– index 10627
– values 9751
– radiation 10624
– computing 10624
Clementsian succession 3288
– sustainability science 3288
clerestory window 2811, 2823
– atmospheric aerosol 144
– change 636
– consultant 899
– direct aerosol influence 141
– dynamics 3212
– effects of air traffic 653
– erosivity 163
– forcing 632
– models 624, 637
– of a region 8906
– problems 626
– random variability 3345
– response 632
– seamless models 12076
– sensitivity 633
– top-down solar forcing 9808
climate 141, 144, 163, 624, 626, 632–633, 636–637, 653, 899, 2062, 3212, 3345, 8906, 9808, 12076
– anomalies 2128
– atmospheric aerosol 144

– change 112, 310, 348, 636, 849, 1489, 1506–1507, 1545, 1558–1560, 1567, 1784, 2061–2064, 2066–2071, 2078, 2084, 2095, 2097, 2099, 2114, 2118, 2149, 2319–2320, 2324, 2345, 2455, 2502, 2633, 2756, 2932, 3207, 3209, 3707, 4110, 4121, 4673–4674, 4676–4678, 4680, 4689, 4722, 5358, 5366–5367, 5369, 5398, 5419, 8013, 8880, 10391, 10749, 11354, 11692
  – adaptation of cities 4678
  – agricultural productivity 10749
  – anthropogenic-related 2502
  – ASCCUE project 4680
  – assessment 5419
  – business perspective 2070
  – CO_2-induced 2099
  – crop growth 2633
  – definition 2062
  – disease in wildlife 5367
  – earth system 2509
  – ecosystems 2068
  – effect on water resources 2324
  – effects on crop plants 10391
  – effects on epidemiological dynamics 5367
  – effects on infectious diseases 5358
  – emergence of new diseases 5367
  – future effects 2064
  – geoengineering 2118, 4110
  – global water sustainability 2061, 2067
  – green infrastructure 4673
  – greenhouse gases 2068
  – harmful algal blooms 2084
  – human activities 2320
  – human-induced 2149
  – impact on industrial sectors 2071
  – impact on marine animals 5369
  – impact on water quality 2066
  – impacts on emerging contaminants 2078
  – indicators 2068
  – indicators by USEPA 2063
  – integrated assessment model (IAM) 5398
  – intergovernmental panel 4677
  – mitigation 4689
  – modeling methodology 2095
  – observational records 2320
  – oceans 2068
  – ocean acidity 2069
  – plant breeding 8013
  – projections 2097
  – remediation 2114
  – response 1559
  – science 3209
  – sea level rise 2069
  – sea surface temperature 2069
  – signal 8914
  – snow and ice 2068
  – society 2068
  – urban areas 4676
  – urban vulnerability 4676
  – urbanization 4674
  – weather and climate 2068
– CO_2-induced 2099
– consultant 899
– convention 1542, 1544
– direct aerosol influence 141
– dynamics 3212
– effects 9795
  – of air traffic 653
  – solar-induced 9795
– engineering 4105, 4112
– erosivity 163
– forcing 632, 5415
– forecasts 2067, 2120, 2129, 2523
  – tercile classes 2129
– gas balances 1134
– gas emissions 1135
– intervention research 4113
– intervention technology 4112, 4113
– model 623, 624, 637, 2102, 2106, 2109–2112, 2140, 2510, 2513–2517, 2520, 5419, 5865, 7367, 9735, 10125, 10162, 12069
  – coupling socioeconomic models 2112
  – ensemble Kalman filter 2111
  – European modeling centers 2140
  – fully coupled simulations 2515
  – globally averaged surface temperature 2520
  – independence 2106
  – interactive carbon cycles 2513
  – model emulator 2109
  – model equality 2109
  – model error 2111
  – model tuning 2109
  – model validation 2517
  – multi-model ensembles 2106, 2109, 2112
  – parameterizations 2102
  – perturbed physics ensemble 2110, 2112
  – representative concentration pathway (RCP) 5419
  – simulation 2112, 2514
  – tuning 2106
  – validation 2106
– globally averaged surface temperature 2520
– independence 2106
– interactive carbon cycles 2513
– multi-model mean 2106
– tuning 2106
– validation 2106
– monitoring 4925
– of a region 8906
– prediction 2104, 2119, 2123, 2128, 2130–2135
  – Brier skill score 2133
  – climate variability 2132
  – data assimilation 2128
  – decadal 2135
  – dominant drivers 2135
  – forecast skill 2132
  – internationally coordinated efforts 2134
  – limit of predictability 2133
  – multi-model ensembling 2131
  – one-tier forecasts 2128
  – systems 2128
  – recalibration 2131
  – reliability diagram 2130
  – seasonal-to-decadal 2119
  – super-ensemble 2104
  – two-tier forecasting 2128
– decadal 2135
– dominant drivers 2135
– super-ensemble 2104
– problems 626
– quality 9035
– random variability 3345
– regime 4110
– response 632
– risks 2067
  – for water infrastructure 2067
– science 623, 2096, 2099
– sensitivity 633, 1560, 2107, 2111, 5859, 5871
– seamless models 12076
– simulations 2101, 2103, 12064
  – multi-model ensembles (MMEs) 2103
  – perturbed physics ensemble (PPE) 2103
– system 2129
  – butterfly effect 2129

– top-down solar forcing 9808
– variability 2120–2121, 2123, 2125–2126, 2128, 2145
– decadal prediction 2120
– seasonal-to-interannual 2125–2126, 2128
– zones 9647
climate-based daylight modeling 2832, 2841
climate–soil interaction 153
climate-species matrix 11355
climatology 8911
– simulations 8911
climax
– community 3281–3282
– vegetation 3279, 3282
clindamycin 502
clinical trials in humans 8066
clinoptilolite 8622
cloned animals 6170
– perinatal/neonatal care 6170
cloned embryo 6171–6172
– aggregation 6172
– chromosomal abnormalities 6171
– community effect 6172
– epigenetic embryo complementation 6172
– RNA interference 6172
cloning 2691, 2965, 6150, 6157, 6167, 6173, 6525, 7218, 10820, 10865, 10908, 10910, 10918
– definition 6150
– efficiencies 6167, 6172, 6173
– RNA interference 6172
– insulators 10910
– map-based 2691
– problems 6157
close-coupled integrated two-stage liquefaction (CC-ITSL) 2232
closed absorption systems 9516
– in refrigeration 9516
closed cooling tower 9534
closed cycle heat-driven chiller 9515
closed landfill 5743, 5744
– energy generation 5743
– solar energy 5743
– wind energy 5744
closed loop system 4144, 4150–4152
– aquifer-based system 4151
– recycling 2400
– surface water system 4152
– water-based systems 4150
closed population 410
closed reproduction 396
Clostridium perfringens 6323, 6326
cloud 629–630, 634, 661, 667, 9630, 9633, 9697, 9699, 9701–9702, 9716, 9718, 9809, 11152
– aircraft-induced 667
– albedo 9633
– control 9702
– effect 9809
– enhancement 9696
– aviation-induced 661
– cirrus-type 9718
– climatologies 8910
– condensation nucleus (CCN) 630, 6747, 8899, 9697
– cosmic ray modulation 9809
– coverage 9699
– droplets 138
– activation 132
– formation 661
– drops 9701
– earth's radiant energy system (CERES) 8910
– feedback 634
– glaciation 139
– in climate models 630
– information 9633
– nuclei 134, 138
– optical depth (COD) 9633, 9718
– parameterization 629
– patterns 9754
– seeding 4106
– super-parameterization 629
cloud-aerosol lidar and infrared pathfinder satellite observation (CALIPSO) 322
cloudiness 659, 9749
– aviation-induced 659
– albedo effect 9809
– cirrus-type 9718
– condensation nucleus 9697
– cosmic ray modulation 9809
– in climate models 630
– super-parameterization 629
clupeiform fisheries 3577
Cnidaria 12046
CO emission 1390, 1397
coaction 3281
coagulase-negative staphylococci (CoNS) 5061
coal 1356, 2164–2166, 2168, 2173–2174, 2176–2177, 2179–2191, 2194–2198, 2200–2204, 2206–2207, 2217, 2223–2224, 2226, 2235, 2237, 2283, 3824, 3846, 5162, 6649, 8350
– ash 3822–3823, 3837
– potential health issues 3837
– as an energy source 2164
– bed methane (CBM) 6807, 7451
– boilers 2283
– bottom ash 11702
– burning steam turbine 6806
– carbon-to-hydrogen ratio 8350
– centrifugal dewatering 2203
– char 8352, 8354
– combustion 2172, 5304, 8349–8350
– air pollutant emissions 8350
– air pollution 8349
– by-products (CCPs) 3822
– products 11705
– cleaning 2200
– characteristics 2195
– coal workers' pneumoconiosis (CWP) 6652
– consumption 6649
– coprocessing 2235
– dense medium separators 2200
– dewatering 2203
– dust 6652
– particles 2283
– excavation 6649
– filtration dewatering 2204
– float–sink analysis 2195
– fly ash 3837, 11702
– for electricity generation 3824
– formation 2176
– froth flotation separators 2202
– fuel 2218
– future production 2188
– future supply 2173
– gas 3915
– gasification 2168, 2224, 2237, 5162, 5280, 6681, 6722, 6838
– combined cycle 2172
– gasifiers 1457
– generation 12183
– global resources 2173, 2176
– grinding 2166
– liquefaction 2226
– mechanized mining operations 2197
– mine/mining 2181, 2187, 6649–6652, 6654, 6671
– air pollutants 6654
– gas 6807
– impacts of dust 6652
– methane (CMM) 6651, 6807, 7451
– methane emissions 6654
– methods 2188
– pollution of air 6651
– pollution of water 6652

– pollution 6650
– wastes 6669
– occurrences 2177
– plants 9445
– power production 12120
– power station 1436, 2208, 12099
– co-firing 1436
– fine particulate emissions 2208
– postcombustion technologies 2208
– preparation 2194, 2200, 2205–2206, 2208–2217
– air quality 2216
– air toxics 2209–2210
– beneficial impacts 2206
– clarification 2205
– cleaning of fine particles 2211
– control 2214
– conversion processes 2217
– dewatering of fine particles 2212
– dry processing 2217
– dust 2216
– greenhouse gas emissions 2211
– on-line analysis 2214
– pollution abatement 2208
– process water quality 2215
– sizing of fine particles 2213
– slurry disposal 2214
– solid–liquid separation 2213
– storage 2205, 2214
– sulfur 2209
– technical issues 2211
– thickening 2205
– waste disposal 2205
– processing
– operations 2196
– technologies 2194
– production 2186, 2190, 2191, 2207
– curve 2189
– economics 2207
– forecast perturbations 2190
– limitations 2190
– pyrolysis 5162, 7475
– quality 2195
– recoverability 2180, 2185, 2191
– recovery 2195
– reserve 2180–2181, 2183, 2185, 2206
– classifications 2179
– resources 2180–2181, 2191, 2223, 3846
– seam gas (CSG) 7451
– sizing 2198
– smoke 207
– spiral concentrator 2201
– storage 2217
– stripping ratio 2184
– thermal dewatering 2204
– tonnage estimates 2179
– transportation 2207
– transporting 2195
– utilization 2165
– washability 2195, 2206
– washing 2217
– water-based separators 2201
– water slurry 2238
– world production 2182
coal-char stabilization 2218
coal-fired boiler 8352
– flue gas 8352
coal-fired power plant 3824, 8354, 8356, 8359, 8361–8367, 8485, 12102
– air pollutant emissions 8367
– combustion modification technologies 8362
– dry flue gas desulfurization 8361
– electrostatic precipitator 8354
– fabric filter baghouse 8356
– low-NO_x burners 8363
– NO_x emissions control technologies 8362
– overfire air 8363
– postcombustion technologies 8362
– radioactivity 8485
– reburning 8364
– selective catalytic reduction 8366
– selective noncatalytic reduction 8365
– SO_2 emissions control technologies 8359
– wet flue gas desulfurization 8359
coalification process 1213
coal-to-chemical plant 2153
coal-to-diesel (CRD) plant 2244
– carbon dioxide 2250
– environmental factors 2250
coal-to-liquids (CTL) technology 1585, 2223, 2250, 3971
– carbon dioxide 2250
– commercialization 2253
– environmental factors 2250
– life cycle analyses 2254
– utility water 2252
– commercialization 2253
coastal
– aquaculture production 10319
– sustainability issues 10319
– area 7034, 7036, 7038, 7039
– A-sediments 7039
– digital elevation model 7034
– radiocesium 7038
– ranking of fluxes 7036
– water exchange 7034
– A-sediments 7039
– climate 2081
– community 2264
– ecosystem 540, 1967, 2258–2259, 7231
– sustainable management 2258
– environments 2263
– degradation 2263
– eutrophication 9117
– finfish aquaculture 7265
– fish farming 514
– marine spatial planning (CMSP) 7265
– model 7034, 7036, 7043
– mass-balance model 7043
– morphometry 7033
– radioecology 7032
– remote sensing 8932
– resources 592
– overexploitation 592
– security 2264
– storm 3316
– tourism 7391
– upwelling 7238
– waters 8759, 8761, 8763
– fecal contamination 8763
– indicator bacteria 8761
– pathogens 8759
cobalamin 1684
cobaloxime 5203, 5212
cobalt 172, 712, 715, 757, 2242, 3774, 3975–3976, 4888
– catalysts 3975
– oxide 7548
– sulfate 6941
Cobb–Douglas production function 1557
cobia 588
cocaine 3590, 10643–10644
– addiction 10644
Coccidiasina 12048
coccolithophore 7235–7237
coccolithophorid 6375
– phytoplankton 8956
co-combustion 1609, 2270, 2272–2274, 2276–2283, 11793
– ash formation 2279, 2282
– Berlin case study 2282
– corrosion 2276, 2281
– emissions 2277, 2282
– erosion 2276, 2281
– flue gas
– denitrification 2278
– desulfurization 2278
– fouling 2276, 2281
– in dust-fired systems 2273
– in fluidized bed systems 2280
– of biomass 2272
– in coal-fired systems 2274

– of sewage sludge 2278–2279, 2282
– of straw 2281
– of wood 2270, 2283, 2284
– economic efficiency 2284
– slagging 2276, 2281
– utilization 2282
– with lignite 2280
cocultivation 558, 1928
cocurrent gasifier 1453, 1454
Codex Alimentarius 2314
codworm 12035
Cody-Collins optical gap 9252
coercive field intensity 25, 27
COEX™ process 7147
coexistence mechanisms 10071
– competition-based 10071
– predation-based 10071
co-fermentation 977
co-firing 1245, 1284, 1609, 2272
– in coal plants 1284
cogeneration 1403, 6833
– directive 8082
– efficiency 6833
– installation 1403
– cogeneration plant 6831, 6833, 8095
– heat-to-power ratio 6833
– system 1033, 1402
cogging torque 45
cognition network technology (CNT) 6800
cognitive ability 3136
– age-related declines 3136
cognitive distraction 3112
cognitive vehicle 2467–2469, 2476
– cooperative decision making 2476
– cooperative driving 2476
– distributed negotiation protocol 2469
– warning systems 2476
coke 1352
coking 7832
cold crucible induction melting (CCIM) 11586
cold fusion 7170
cold heavy oil production with sand (CHOPS) 7818
cold production 9510, 9512, 9517, 9534
– buffer storage 9534
– evaporator 9517
– mechanical vapor compression 9510
– thermally driven 9512
cold seawater 7314
cold storage 10559
cold water
– coral reefs 6413, 6415
– threats 6415
– fish 5698
– oxythermal habitat 5698
cold-crucible induction melter 11589
coleoptera 4016, 4030, 4033
coleoptile 8020
coliform bacteria 6324
coliphage 8765
collapse 5650
– of highways 5650
collector 2202
Colletotrichum graminicola 1277
collision
– avoidance (CA) 71, 2471, 2483
– detection 3140–3142
– in fog 3140
– sensitivity 3142
– simulated foggy effect 3141
– mitigation system 84
– collision sensor 66
– warning (CW) 71, 2476
collision-coalescence efficiency 139
colloid/colloidal
– filtration theory 7683
– material 7679
– organic carbon (COC) 8395
– organic matter (COM) 10539
colon cancer 1189
color filter material 11116
color image 11120
– sensor 11116, 11117
– light sensitivity 11117
– signal saturation 11120
colored dissolved organic matter (CDOM) 8924, 8926, 8962, 8964
colorimetric calibration 11119
comb-branch
– copolymer 6052
– polymer 6052
– polyethers 6051
combinatorial biochemistry 6520
combined ash 11738
combined cycle gas turbine (CCGT) plant 3849
combined cycle power plant (CCPP) 3849
combined heat and power (CHP) 1400, 1494, 1662, 3462, 4312, 7867, 7876, 8081, 9886, 9916, 9973, 11768
– cycle 9528
– generation 1436, 4763, 9936
– producer gas 1436
– process 1210
– production 1427, 1446, 12121
– system 1033, 1404–1405, 1407–1412, 1415, 1417, 1420, 1422–1423, 1609, 1611, 3873, 5301, 6831, 7711, 9520
– electrical efficiency 1420
– engine-driven 1404
– hot-air turbine 1410
– internal combustion engines 1404
– inverse gas turbine 1411
– market-ready plants 1415
– micro gas turbines 1412
– pilot plants 1417
– private household sector 1422
– small business and community facilities 1423
– steam piston engines 1405
– steam screw-type engine 1407
– steam turbine 1409
– stirling engine 1408
combined heat and power (CHP) plant 1200, 1234, 2271, 4154, 8082–8083, 11781
– electricity output 11781
– internal combustion engine 8083
– oil–fuelled 8082–8083, 8087, 8089–8094
– asynchronous generators 8092
– combustion engine 8089
– economic efficiency 8093
– electrical connection 8091
– emissions 8093
– emission reduction 8090
– exhaust gas pipe 8091
– exhaust gas recirculation 8090
– fuel system 8089
– generator 8091
– heat exchanger 8092
– heat generation costs 8094
– operation 8092
– peak load boilers 8092
– planning 8092
– synchronous generators 8092
– technical fundamentals 8087
combined single- and double-flash station 4299
combined solar dryer 9488
combined thermal epithermal neutron (CTEN) method 7209
combustible liquid wastes 5246
combustion 1210, 1234, 1240–1242, 1254–1255, 1260–1261, 1302, 1304, 1313, 1318–1320, 1325, 1332, 1335, 1352–1356, 1358, 1380, 1383, 1386, 1389, 1396, 1404, 1446, 1448, 1610, 2153, 2171, 2275, 2279, 4960, 5237, 5241, 5246, 5254–5255, 5262, 5282, 5302, 5308, 5312, 5514, 6461–6463, 6467, 6474, 6841, 6848–6849, 10482–10483, 11442, 11787, 11852
– adjustment of fuels 1383
– aerosol formation 1335

– air 1412, 2166, 5237, 5249, 5254, 5272, 5275–5276, 6462, 6838, 8364, 11711, 11856
  – flow 6474
  – preheating 5254
  – requirements 11825
  – system 4966, 6461
– air-blown 2171
– annual efficiency 1389
– ash utilization 2279
– ash-forming elements 1318, 1335
– ash-related problems 1332
– biomass-fueled 1396
– boilers 1242
– chamber 1319, 1320, 1380, 4963, 5258, 5262, 5265, 5271, 5273, 5275
  – air supply 5275
  – corrosion problems 5265
  – flow patterns 5258
  – residence time 5262
  – rotary kiln incinerators 5273
  – shaft furnaces 5273
  – stationary furnaces 5271
  – underfeed stoker units 1320
– char burnout 5308
– closed-looped steam cooling 6848
– control 4958, 4972, 6467, 6468
– cooling down effect 1353
– devolatilization 5308, 5312
– efficiency 1354, 1386, 5510
– engine 1224, 3856, 9909
– engineering 11795
– firing temperatures 6841
– FLIC code 5302
– FLUENT code 5302
– fluidized bed combustors 1254
– furnace types 1355
– gas 1356, 1358, 6838
– gaseous emissions 1332
– grate 4964–4966, 6454, 11771
  – air-cooled block 4965
  – block rows 4965
  – module 4965
  – water-cooled blocks 4966
– grate-fired combustors 1254
– heat transfer 1304
– industrial technologies 1319
– internal 1404
– kinetic modeling 5514
– mathematical modeling 5302
– medium and large-scale industrial 1320
– modification technology 8363–8364
  – low-NO_x burners 8363
  – overfire air 8363
– nitrogen oxides 5241
– of flammable gas 5246
– of hydrocarbon fuels 10482
– of municipal refuse 11787
– of solid biomass 1313
– of solid waste 5236
– of sulfur 10483
– of volatiles in the porous bed 5308
– oxyfired 2153
– oxygen-enriched air (SYNCOM) 6463
– plant 1337
– process control optimization 1260
– products 5262
– combustion profile 4973
– pulverized fuel combustors 1255
– re-burning 1261
– recirculation of flue gas 6462
– requirements 1352
– residues 5237, 11787
– science 5246
– small-scale (domestic) 1320
– staged-air 1261
– submerged 5282
– system 1352, 6450
  – biomass-fueled 1352
– technology 1260, 1320, 1325, 6461
  – dust combustion 1320
  – fixed-bed combustion 1320
  – fluidized bed combustion 1325
  – fluidized bed furnace 1320
  – pretreatment systems 1320
– temperature 1304
– thermal cycles 1241
– time 1304
– train 4960
– turbulence 1304
– underfeed rotating grate 1325
– volumetric heat release rate 5255
combustion-generated particles 6999
commercial
  – air traffic 653
  – fisheries 3576
  – gas diffusion 8187
  – livestock industry 1774
  – nuclear power 8482
  – recycling 3445
    – techniques 9613
  – satellites 8928
  – solar thermal power 10567
commercialisation of GM crops 2286
communications network 2984
communication-based train technology (CBTC) 1897
community 3278
  – atmosphere model (CAM) 624
  – climate system model (CCSM) 2512
  – dynamics 3278
  – earth system model (CESM) 5424
  – ecology 3298
    – competition 3298
    – predation 3298
  – forest program 11351
  – of practice (CoP) 6704
    – crop-based 6704
commuter rail 1900, 6006
  – line 5983
  – services 5963
commuter railroad 1812
compact city 4675, 5789, 5840
compact reforming 3963
compactness index 11269
competition 10063–10064, 10068–10069, 10077, 10079–10080
  – chemical interference 10079
  – equalizing mechanisms 10069
  – exclusion principle 10068, 10069
  – feedback loops 10064
  – interspecific 10064
  – intraspecific 10064
  – relative nonlinearity 10077
  – spatial partitioning 10077
  – stabilizing mechanisms 10069
  – temporal partitioning 10077
competition–colonization trade-off hypothesis 10078
complete combustion 1397
complex urban junction 11285
composite electrode capacitors 798
composite sustainability indices 9187
compost bioreactor 6662
composting 1238, 1632, 4958, 8772, 9980, 9984, 10031, 11657–11658, 11833
compound
  – fertilizers 3772
  – nucleus 3801, 3802
  – parabolic concentrators (CPCs) 9583
comprehensive environmental response and liability information system (CERCLIS) 2009
comprehensive environmental response, compensation, and liability act (CERCLA) 2004, 2007–2014, 7826
  – agriculture street landfill project 2012
  – applicable or relevant and appropriate recommendations (ARARs) 2010
  – basic elements 2007
  – Brownfields revitalization act 2014
  – citizen roles 2008
  – criticisms 2013
  – defenses against liability 2011
  – enforcement tools 2012

– environmental health 2004
– liability scheme 2010
– original CERCLA 2007
– priority list of hazardous substances 2010
– remediation priorities 2009
– SARA revisions 2008
– small business liability relief 2014
– states and local governments 2012
– sustainability 2004
compressed natural gas (CNG) 268, 1881, 5462, 5470, 5484
compression ignition combustion 5525
– glow plug 5525
compression ignition engine 931, 5488, 5503, 5526–5527, 5531, 5539, 6809
– catalyst 5531
– diffusion heat release 5527
– fuel injection 5526
– multi-injection strategies 5527
– net soot release 5531
– non-petroleum fuel 5488
Compton scattering 3804, 5561, 8542
computational atmospheric acoustics 12285
computational fluid dynamics (CFD) 6479–6480, 6884, 8211
– simulation 6480
computer 3446, 3447
– life cycle 3447
– monitor 3444
– take-back programs 3446
– vision sensors 11456
– vision system 11459–11460
– three-dimensional (3D) LIDAR-based calibration 11459
– two-dimensional (2D) planar-based calibration 11460
concatemerization of plasmids 2603
concentrated acid hydrolysis 966
concentrating cooker 9493
concentrating photovoltaics (CPV) 7938, 7942, 7947, 9419
concentrating receiver system (CRS) 2349, 2352, 2366, 2369–2372, 2377, 2381–2384, 2387
– absorption cooling 2383
– commercial 2377
– desalination 2382
– ecological balance 2352
– examples 2372
– future cost development 2384
– high flux receiver 2387
– hybridization 2371
– investment costs 2383
– LEC 2384
– power production 2352
– regenerators 2370
– research facilities 2372
– secondary uses 2381
– storage 2369
– tower constructions 2366
– under construction 2381
– under development 2381
concentrating solar power (CSP) 7620, 9740
concentration polarization 2916
– equation 10532
concentration unit 2026
conceptual knowledge 4535
concrete 3830, 8550
– blocks 3834
– community 3278
– mix 2404
– shield material 8550
condensate pump 4289
condensation nucleus 9699
condensation system 1395
condensed phase composition process 11320
condenser 4981
– analysis 4263
condensing boiler technology 1388
conditioning strategy 4133
conditioning system 3685
– mixed-mode 3685
conducting polymer 797
conductivity-temperature-depth (CTD) sensor 4913
cone
– penetration test 7429
– snail toxin 3165
– spring ecosystem 3311
congenital rubella syndrome 5349
congestion pricing 5022
coniferous forest 5822
conjugation 2584
conjunctivitis 12012
connectivity-aware routing (CAR) 11572
Conrad recycling process 1524
conservation
– agriculture 162, 5625
– biology 3203, 3359, 10078, 10080
– hatcheries 6387
conserved orthologous set (COS) marker 6429
consolidated bioprocessing (CBP) 977
constant current (CC) 678
constant flux, constant sedimentation rate (CFCS) model 3737
constant initial concentration (CIC) model 3738
constant rate of supply (CRS) 3738
constructed wetland 1633, 10102, 10190, 11892–11893, 11895–11898, 11901, 11903, 11906, 11929
– for various types of wastewater 11903
– for wastewater treatment 11893
– phosphorus removal 11906
– with emergent macrophytes 11896
– with floating mats of emergent macrophytes 11897
– with floating-leaved macrophytes 11895
– with free water surface 11893
– with free-floating macrophytes 11893
– with horizontal subsurface flow 11898
– with submerged macrophytes 11895
– with subsurface flow 11897
– with vertical subsurface Flow 11901
construction 2391–2392
– planning 2423
– process 2392
– waste 2391, 2395–2397, 2399–2400, 2402, 2412, 2414, 2417–2418, 10007–10008
– accidental waste 2395
– asbestos 2417
– characterization 10008
– classifications 2396
– composition 2396
– dust 2417
– energy recovery 2414
– environmental hazards 2417
– generation 10007
– leaching 2418
– managing 2397
– metallic materials 2396
– mineral fraction 2397
– organic materials 2397
– polymer components 2412
– predictable waste 2395
– recycling 2400
– reduction 2399
– reuse 2399
– separation process 2402
– sustainability issues 2417
– sustainable management 2418
– wastewater 2418
– work 11700
– wasted materials 11700
construction and demolition (C&D) materials 8795, 11700, 11705
consumer–resource relationship 10063
consumption footprint 9029
consumption waste 10004
containment technology 2450

contaminant 2437–2438, 3045, 3266, 3269, 3274, 3518, 3708, 8636, 8645, 9080, 9136, 10143, 11229
– biological degradation 10143
– biomarkers 3274
– chemical form 2438, 9080
– cloud deposition 8636
– control of upstream sources 3045
– dry deposition 8636
– effects on organisms 3266
– exposure route 3269
– exposure time 3269
– in the environment 3518
– mass balance equation 8645
– organismal characteristics 3269
– seafood-associated biological 9080
– speciation 2438
– toxicokinetic models 3274
– transfer 7680, 7681, 7683
– rapid pathways 7680
– slow pathways 7683
– transport
– in groundwater 2437
– models 9136
contaminated
– areas 3545
– decision-aiding techniques 3545
– ecosystem remediation 8532
– groundwater 7077
– sediment 3031, 3038
– dredging 3038
– soil 2430–2431, 2437
– soil remediation 2431, 2437, 2450
– emerging trends 2450
– surface water 7077
– water 3587, 9566
– consumption 3587
contamination 2439–2440, 3516–3517, 3522, 3525–3526
– countermeasures 3517
– in trees 3526
– international terminology 3517
– of drinking water 1639, 7045
– of the environment 3516
– optimized remediation strategy 3522
– pathways 3525
– remediation 2440
– risk assessment 2439
contingency reserve 12104
continuous emission monitoring system (CEMS) 183, 259, 4960, 11696
continuous stirred tank reactor (CSTR) 3938
continuous variable transmission (CVT) 11546
contrail cirrus 662–663, 668
contrast sensitivity 3143
– Pelli Robson test 3143
control law 52
controllable network transformer 9353
controlled cooking test (CCT) 1306
controlled flux technique (CFT) 603
convection
– dispersion equation (CDE) 8620
– transport 2060
convective
– available potential energy (CAPE) 140
– flux rate 10964, 10965
– hydrothermal resources 4165
– transport terms 10967
convector 4375
Convention on Biological Diversity (CBD) 4519, 4522, 5555, 10768
conventional breeding 1691, 2650, 2734
– new tools 2734
conventional fuels 11430
conventional spark ignition engine 5540
– homogeneous mixture 5540
convergence criterion 2110
conversion 1240, 1247–1248
– chemical into thermal energy 1240
– combustion boiler 1369
– electrode 729
– from mechanical to electrical energy 1248
– from thermal to mechanical energy 1247
– plant 1588
– CHP-F method 1588
– overall efficiency 1588
– technologies 1205, 1609
conveyor 4970
conveyor belt 2514, 5867, 5868
cook kit model 9502
cooker 9490–9491
– concentrating-type 9491
– hot-box type 9490
– hybrid 9491
– vapor-type 9491
cooking 1301, 9490
– combustion chamber 1364
– energy 9490
– firewood 9490
– of food 9489
– plate 1364
– temperature 9490
cookstove 1299–1300, 1302, 1305–1307
– biomass-fueled 1299, 1302, 1307
– efficiency 1302, 1305
– impact on global warming 1307
– indoor air pollution 1307
– percent heat utilized (PHU) 1306
– wood-fired 1306
cool roofs 3693, 4718
cooling 9509, 9512, 9521
– closed adsorption systems 9521
– coil 9528
– effect 139, 908, 2116, 4680
– energy 4690
– facility 1249
– heat-driven 9512
– magma bodies 4184
– networks 4763
– system 9525, 9529, 9532, 9536, 9549
– experiences 9549
– open liquid desiccant systems 9529
– open solid desiccant systems 9525
– solar-assisted 9532
– useful solar heat 9536
– tower 9546
cooperation among cognitive vehicles 2464
cooperative driving 2476
cooperative motion planning 2480, 2482–2483
– elastic bands 2483
– mixed-integer linear programming 2482
coordinator vehicles 2469
copepod fecal pellets 8396
COPERMA monomer 6932
COPERMA-styrene polymers 6931
Copernicus' heliocentric model 2100
copper 4889
– chromium arsenate 3631
– deficiency 1687
– indium
– diselenide 8381
– gallium diselenide 9436
– phthalocyanine 7574
– sheet 12193
copper-ceria 2942–2945
– catalysis 2944
– conductivity 2943
– poisoning 2945
– stability 2945
coprocessing with coal 2235
co-pyrolysis 2415
coral 2493, 2504–2506
– host cell 2493
– physiology 2505
– polyp 2492
– population dynamics 2504
– restoration 2505–2506
– transplants 2506
– triangle 2496, 2500

coral reef 2489, 2490, 2492–2498, 2502–2504, 2507, 3151, 3231, 3563, 6188, 6410
– biodiversity 2495
– biology 2492
– communities 2507
– destruction 6188
– distribution 2490
– diversity 2498
– ecological goods 2498
– ecology 2492
– ecosystem 2489, 2496, 2502, 2503, 3231, 6232
– fisheries 2496
– geology 2490
– management 2503
– optimal environmental requirements 2494
– physical connectivity 2497
– services 2498
– threats 6188
– water quality 2504
coral-alga symbiotic complex 2494
coral-zooxanthellae complex 2490
co-refining 1221
Coriolis
– effects 6593, 7341, 11264, 11266, 11276
– flowmeter 4205
– force 2774
– parameter 11265
– term 12072
corn 351, 4463
– ethanol 10508, 10514
– production belt 4444
– rootworm resistance 4463
corn-boring pest 4452, 4454
– insecticide 4454
coronal mass ejection (CME) 8577
corporate imaging 8777
corrosion 1344, 1462
cosmic ray (CR) 8472, 8473, 8561, 8565, 8622, 8577
– flux 3716
– ray-cloud connection 9809
cosmogenic
– environment 8473
– isotopes 9803, 9811
– solar-induced variations 9811
– radiation 8470
– radionuclides 8565, 8656
cost
– of electricity (COE) 6845
– of solar electricity 9412
cost–benefit analysis (CBA) 4789
cost–effectiveness analysis (CEA) 4789
CO_2, see carbon dioxide
cotton plant 10397
cotton 2301, 4446, 4457
– insect-resistant 4457
cottonwood 1285
cotyledon cells 4554
Coulomb
– collisions 7161
– effects 7558
– forces 3793
– scattering 5561
countercurrent gasifier 1452, 1470
countercurrent recycle cascade 5639
counter-footprint 9033
countermeasure 3517, 3522, 3544
– decision-aiding tools 3544
– different environments 3522
countryside biogeography 3363
coupled model intercomparison project–5 (CMIP5) 2144
Courant number 2035
Courant-Friedrichs–Levy (CFL) limit 12067
courtyard 6866
covered lagoon digester 1153
Cowper regenerator 10553
Coxsackie virus 11989
– Coxsackie A (CAV) 8138
cracking temperature 1464
crack 10644
Cradle to Cradle® 9033
– energy 9036
crash barrier 3071
Crassulacean acid metabolism 1481
Cre/*lox*P system 2608
Creutzfeldt-Jakob disease 2969
criteria pollutant 218, 222, 2165
critical crop mass (Wc) 2665
critical solvent de-ashing (CSD) 2232
Cromadur 6821
crop/cropping 1–2, 151, 1567, 1676, 2527, 2541, 2544, 2558–2560, 2562, 2567–2568, 2615, 2627, 2638–2639, 2641, 2661, 2665–2666, 2671, 2674, 2676, 2681, 2686–2688, 2690, 2698, 2720, 2723, 2731, 2735, 2742, 2749–2750, 2755, 4013, 4039, 4465, 4471, 4075–4076, 4088–4089, 4492, 5315, 5320, 6820, 8018, 10037–10043, 10347, 10694, 10749
– abiotic stress-tolerant 2
– adaptation to environmental stress 10749
– agronomy 2686
– assimilate sinks 2627
– biomass 2676
– accumulation rate 2666
– biotechnology 1676, 4471
– branching 10040
– breeding 2530, 2690
– plant genomics technologies 2530
– Bt-expressing 4039
– canopies 2617, 2620, 2623
– digitization 2623
– components 2742
– density 2562
– design 2742
– development 2540, 2541, 2547, 2552, 2556
– regulation 2547, 2552
– related to temperature and photoperiod 2540
– diseases 2558, 2560, 2567, 2574, 2577, 2688
– biofumigation 2577
– controlling 2560
– host eradication 2560
– induced resistance 2574
– sanitation 2560
– soil solarization 2577
– use of chemicals 2567
– diversification 151, 2750
– domestication 2698, 10345
– dry-matter production 10037
– efficiency 6820
– epicuticular waxiness 8018
– evapotranspiration 9321, 9323
– for insect resistance 4013
– genetic ability to capture 10039
– genetically engineered 4013
– genetically modified 2742, 2755, 4492
– genotype 10036, 10043
– growth model 4089
– growth rates 10038
– growth simulation model 9316, 9321, 9322, 9326
– nutrient management 9322
– operational management 9322
– pest management 9322
– water management 9321
– herbicide-resistant 10347
– herbicide-tolerant 4465
– high density 10041
– improvement 2698
– light interception (LI) 2627
– insect-resistant 4039, 4465
– irrigation 6628
– loss 10694

– management 2627, 2686, 2731, 6208, 9316–9318, 9323, 9326
  – decision support systems (DSSs) 9318
  – integrated pest management 9326
  – simulation models 9316, 9318
  – water management 9323
– marker-based genome selection 2735
– mass accumulation 2671
– models 9317, 9319
  – simulation tools 9319
  – strategic management 9319
  – tactical management 9319
  – technical coefficient generators (TCGs) 9319
– monocultures 10037
– nitrogen content 9325
– nitrogen use efficiency (NUE) 2674
– nutritional improvement 1676
– pest 151, 156
– phenology 2544, 4075–4076
– phenotypic plasticity 10041
– physiology 2686, 4088
– planting arrangement 10042
– plants 2583, 2690, 10391, 10395, 10744
  – increased temperature effects 10391
  – mitigating effects of global warming 10395
  – modifications 10744
  – transformation methods 2583
– polycultures 10037
– practice 154
– production 1122, 2564, 2639, 2662, 6658, 9063, 9069
  – irrigation with coal-mine water 6658
  – irrigation 2564
  – nitrogen 2662
  – rotation of crops 1122
  – water 9063
– productivity 2559, 2681, 2687, 5621, 11452
– protectant fungicides 2567
– protection 2559, 9325, 9328
  – disease management 9325
  – pest management 9325
– radiation use effeciency (RUE) 2615, 2627
– rectangularity 10043
– residues 2749
– resistance 5442–5443
  – insect–plant relationships 5442
  – integrated pest management 5443
  – plant characteristics 5442
– resource use 10037
– responses
  – to available soil water 2638
  – to nitrogen 2661
– root systems 9065, 9068, 9070
– rotation 151, 1122, 1125, 1136, 2560, 2750, 5455
– salinity tolerance 5315
– salt tolerant 5320
– science 2681
– silking 10039
– simulation models 2553, 2555, 2735, 8014, 9320
– size effect 2672
– species 6441–6442
  – DNA-based markers 6442
  – wild relatives 6441
– structure 10036, 10039, 10041–10043, 10045, 10047
  – density 10043
  – effect of plant arrangement 10042
  – effect of soil resources 10041
  – plant yield 10043
  – responses in monocultures 10041
  – responses in polycultures 10045
– system (CS) 155, 1122, 1137, 2740, 2741, 2743–2745, 2749, 2751–2753, 10758
  – biodiversity 2753
  – biological synergism 2749
  – classification 2741
  – dynamic 2752
  – environmental damages 2745
  – flexibility 2744
  – humus balances 1137
  – new technologies 2753
  – plurispecific 2751
  – resilience 2743
  – shaping nature 2740
  – sustainability 1129
  – technical synchronization 2752
– tillering 10040
– trait 2689, 2692, 2714
  – gene isolation 2689, 2692
– transpirational cooling 8018
– under water scarcity 2641
– water depletion 1544
– water productivity (CWP) 1544
– water stress index (CWSI) 5626
– water usage 5623
– water use efficiency 1567
– yield 2720, 2723, 10036
  – potential 2641

crop–livestock pairing 2751
crop-soil simulation models 9328
crop-to-residue ratio 1538
crop–weed interactions 10048
cross ventilation 6876, 6881
crossbreeding 487, 1732, 1734, 1765, 1772, 1777, 1782, 2785, 7974, 7984
  – schemes 9391
  – systems 1736
crosscurrent gasifier 1455
cross-fertilization 10778
crown gall 10701
  – disease 2587
crude oil 7446, 7801–7802, 7806, 7822
  – extraction 7801
  – multilateral wells 7801
  – production methods 7802
  – secondary wells 7801
  – thermal recovery methods 7806
Cry protein 4017, 4019–4023
  – coding sequence 4023
  – insertion into the cell membrane 4020
  – interactions with receptors 4017
  – oligomerization 4019
  – promoters 4022
  – protein coding sequence 4022
  – toxicity 4019
Cry protoxin 4016
Cry toxin 4028
cryocooler 6256
cryogenic air separation process 2171
cryosphere 280, 284, 635, 2761, 2764, 3231
  – airborne and space-borne remote sensing technologies 280
  – conservation of energy 2764
  – modeling 2761
  – remote sensing 282, 284
  – thermodynamics 2764
cryptorchidism 3639, 3648
cryptosporidiosis 6615, 12049
Cryptosporidium 6326, 6333, 6613, 6615, 6628, 7677, 7683, 7686, 12049
crystal lattice 7561
crystal silicon photovoltaic cells 9674
crystalline
  – ribbons 9205
  – silicon 8381, 9254, 9259, 9296
    – anode 9295
    – cells 9436
    – photovoltaic module 9434
    – solar cell 9198, 9265

– technology 7933, 7938
– wafers 9215, 9241
– solar cells 9241, 9267
– Quasi Femi level splitting 9267
CSS-CdTe solar cells 1989
Cubozoa 12047
cullet 8802–8804, 8806, 8839
– contaminants 8802
– cross-contamination 8803
– recycling technologies 8803
– sorting 8806
culling of animals 455
cultivated crop 10705
– disease management 10705
cultivated plant resources 1757
cultivated soil 3728
cultural eutrophication 5673
cultural geography 10369
cultural identity 10370
cultural landscape 10371, 10375
culture medium 6526
– optimization 6526
culture-based diagnostics 5383
cultured fish 10799, 12033
cumulative internal illuminance 2825
cumulus-oocyte complex (COC) 6154
cup plant 1115
curbside recycling 8784
Curie-Weiss behavior 6086, 6090
current 7406
– ambient air quality 185
– data collection 7406
– interruption 6728
– transformers (CTs) 3009
cut corner 1690
cutterhead pipeline dredges 3035
cyanide 2502
cyanobacteria/cyanobacterial 356, 2084, 2089, 4830–4831, 4833–4835, 7388, 7669
– bloom 2086
– formation 4835
– description 4830
– detection 4834
– economics 4833
– nutrient interactions 4834
– origins 4834
– toxicity 4831
– toxins 4832
cyanobloom 4833–4835
cyanogenic glycoside 4035
cyanosafracin B 3157
cyanotoxin 2085, 4831, 4833–4834
cyber taxi 7792
cycled-spheres reactor 1525
cycle 2455
cyclic siloxane 10668
cyclin-dependent kinase inhibitor 6 gene 10687
cycloalkane 10664–10665
cyclobutane pyrimidine dimers (CPD) 3611, 9664
cyclohexanedicarboxylic anhydride (CDCA) 6902, 6910, 6922
cyclohexanol 7592
cyclohexanone 4590
– oxime 4590
cyclohexene 7593
cyclone burners 1327
cyclone/cyclonic 1250, 1339, 1667, 2199, 5239, 7402
– classifying 2199
– furnaces 5281
– melters 11586
– separator 1339
Cyclotella 350, 353
– *cryptica* 360, 365
cyclotrimerization of alkynes 10175
cylinder parabola 7620
cylindrical dams 2800
cylindrospermopsin 2086, 4832
Cylindrospermopsis raciborskii 2089
cypermethrin 10718
Cyprinus carpio 1939
cystathionine γ-synthase (CGS) 1695
cysteine 836–837
– protease inhibitor 10718
– residues 3667
cysteine-rich antifungal proteins 10697
Cyt toxins 4021
cytochrome
– oxidase 3594
– P450 (CYP) 3593, 3662, 7588, 7598
cytomegalovirus (CMV) 5000
cytoplasmic reprogramming 6164
cytoplast 6150
cytosine
– arabinoside 3153
– methylation 10909
cytotoxicity 3605
Czochralski-Grown monocrystal 9202

D

daily mean irradiance 9750
– probability function 9750
dairy 388
– cattle 395, 402, 407, 411, 1770, 1774, 2781–2787
– artificial insemination 2785
– breeding 2781–2782, 2786, 2787
– fertility 411
– genetic evaluation 2784, 2786
– genetic improvement 2783
– health trait 2784
– heritability of milk production 402
– mastitis 411
– population 2785
– production 2781
– progeny testing scheme 2785
– cows 1784
– methane production 1784
– farm 2782
– genetics 2782
– milk 10855
– products 1754
– semen market 2782
dam 2788–2791, 2793, 2795–2798, 2800–2801, 3555
– collapse 2797
– construction 2755, 2788, 2795
– cylindrical 2800
– disaster 2791
– ecosystems 2795
– engineering 2788
– environmental problems 2790
– environmental protection 2801
– failures 2789–2791
– heritage protection 2793
– induced subsidence 2797
– in karst 2798
– microclimate 2796
– reservoir fluctuations 2795
– spring submergence 2797
damage 3608
daptomycin 504
Darcy's law 3222
dark fermentation 5117, 5121, 5165
– combination with photofermentation 5121
dark ocean surfaces 8958
DARPA urban challenge 66
Darrieus wind turbine (DWT) 3401, 3411, 3412, 4486
d-axis 25
day vision 11100
daylight/daylighting 908, 913, 2804–2806, 2810, 2817, 2819, 2821, 2824–2825, 2827–2828, 2830–2834, 2836, 2838, 2841–2843, 2846, 2848, 2850, 2853, 2856, 2858–2860, 2863, 2865–2867, 2870, 2872, 2876, 2881, 2887, 2892, 3681–3682, 3688, 5336, 6876, 10290, 11115

– advanced glazing systems and materials 2836
– autonomy (DA) 2834, 2881
– benefit 2842, 2854
– challenges 2859
– climate-based 2832
– conditions 2825
– contribution of sun 2819
– controls 2846
– cost-effectiveness 2843
– definition 2848
– design 2850, 2866, 2885
  – design flexibility 2858
  – quality assurance 2885
– distribution 2806, 2863, 2872, 3681
– dynamic control 2838
– effectiveness 2866, 3682
– energy 2842
– energy saving potential 2854
– evaluation 2816, 2831
– exposure 2805
– factor (DF) 2817–2823, 2825, 2833, 2843
  – absolute values 2823
  – clear sky options 2833
  – graphical, tabular, and analytical methods 2820
  – influence of building properties 2818
  – physical modeling 2820
  – prediction by computer simulation 2821
  – standards 2822
  – uniformity 2819, 2823
  – value 2805
  – Waldram diagram 2820
– fixture 3681
– from perimeter glazing 2836
– glare index (DGI) 2828
– guidelines 2816, 2824
– health 2828, 2856
– hours 9622
– human factors 2827
– Hunt model 2830
– illuminance 2830
– illumination 2836
  – indoors 2806
– in buildings 2804, 2831
– in special-purpose buildings 2810
– louver geometry 2866
– louver surface qualities 2867
– management systems 2848
– measures 2816
– metrics 2833
– natural variability 2828
– nonvisual effects 2828
– nutrient ingestion 2856
– optimization 2850
– optimized mirror geometries 2867
– prediction techniques 2817
– productivity 2828
– redirection
  – blinds 2870
  – louvers 2876
  – systems patents 2892
– redistribution 2865
– responsive systems 2841
– saving energy 2841
– simulation 2821
– snapshot evaluations 2825
– strategy 2810
– sustainability 10290
– technology 2850, 2887
– transmission 2853, 2860, 3688
– user operation of lights and shades 2830
– visual comfort 2827
– with effective shading 2859
daylit environment 2815, 2829–2830, 2840
  – measuring 2840
  – performance 2829
  – productivity 2829
  – well-tempered 2815
DC motor 11526
DC-DC converter 690
DDGS 996
De Micromis Party Exception 2012
Deacon process 5252
deacylation 4644
debenzylation 4644
  – of carboxylic esters 4644
Debye–Hückel equation 4096
decadal climate variability 2123
decadal forecast 2525
decadal prediction 2137–2138, 2140, 2143–2145
  – data assimilation 2145
  – internationally coordinated efforts 2143
  – model fidelity 2137
  – observations 2140
  – prediction experiments 2138
decarbonator 2899
decarboxylation 2218, 4653
  – of cinnamic acids 4653
deceleration
  – area 84, 87
  – control interface (DCI) 76
decentralized generation 2977
dechlorination 2445, 4006
decommissioning 7079
  – of facilities 3542
    – remediation 3542
decomposer 11229
deconstruction 2395
decontamination 3525, 3532, 7075
  – factor (DF) 3527
  – of land 3532
  – of water 9563
Dee-Geo-Woo gen 2697
deep aquifer remediation tool (DART) 10415, 10416
deep circulation theory 5863
deep ocean 5857, 5860, 5866, 5871, 5873–5874, 5876, 7347
  – circulation 5857, 5860
  – climate variability 5866
  – hydrography program 5876
  – hydrothermal activity 7347
  – observations of change 5871
  – observing system 5873–5874
  – overturning circulation 5873
  – sediments 7359
  – waters 7347
    – scavenged elements 7347
deep sea drilling project (DSDP) 6417
deep water 5859, 6414
  – circulation 5859
  – ecosystem 6414
  – formation 2514
  – masses 5859
deep western boundary current (DWBC) 5857
deep-cycle battery 5883
deep-dose equivalent 3026
defense meteorological satellite program (DMSP) 8932
deferent 2100
defibrillator 6510
deficiency syndrome 2856
deficit irrigation 5630–5631
deflocculant 4416
deforestation 549, 608, 1009, 2499, 3307, 3833, 4746, 4751, 5823
degasification 11852–11853
degassing 1449
deglaciation 2456, 2460
degraded soil 1571
Degussa process 1526
Dehalococcoides 2437, 2445
dehumidification enthalpy 9531
dehydration 5, 1021, 2641, 2643
  – avoidance 2641
  – catalyst 2250
  – plants 1021

dehydration-responsive element binding protein 10750
dehydrodidemnin B 3160
deindustrialization 11362, 11363
delayed coking 7831
delayed neutron 8567
delayed oscillator mechanism 2127
Delft ladder 2399
delithiation 712, 724, 726
deltamethrin 12003
demagnetization 28
demand surface 197
demand-response (DR) interconnection engineering 3015
demographic decline 11364
demolition waste 2391, 2395–2397, 2399–2400, 2402, 2412, 2414, 2417–2418, 10007
– classifications 2396
– composition 2396
– energy recovery 2414
– environmental hazards 2417
– generation 10007
– managing 2397
– metallic materials 2396
– mineral fraction 2397
– organic materials 2397
– processing requirements 2402
– recycling 2400
– reduction 2399
– reuse 2399
– separation process 2402
– sustainability issues 2417
– sustainable management 2418
– wastewater 2418
dendrite 786, 790
dendrogram 5390, 7975, 7976
– Raman-based 5390
Dengue hemorrhagic fever (DHF) 12014
denitrification 163, 884, 1136, 2278, 3781, 11894, 11901, 11936, 11956
DENOX system 2278
dense medium cyclone (DMC) 2200
densification 4684
density dependence 10065
density functional theory (DFT) 376, 3982, 6040, 6084, 6773, 7734, 8212
– Gibbs free energy 7734
deontic knowledge 4535
deoxyribose nucleic acid (DNA) 11393
– strands 5581
dephlogisticated air 3660
depleted uranium 11216
– munitions 8513
deposit formation 1340, 1342
deposited sediment 3728–3729, 3741
depositional sinks 3733
– establishing chronologies 3733
depression 9666
depth sounding radar 284
derived air concentration (DAC) 11055
dermatitis 12043
dermatotoxin 2085
desalinated water 7298, 7305, 7321, 11887–11888
– energy comparison 11888
– energy cost 11887
desalination 2079, 2324, 2897–2903, 2904, 2905, 2907–2912, 2915, 9758, 11886
– cost analysis models 2912
– energy consumption 11886
– for sustainable water resource 2897
– forward osmosis (FO) 2915
– granular media filter 2910
– industry 2898
– microfiltration 2910
– multieffect distillation (MED) 2901
– multistage flash (MSF) distillation 2898
– of seawater 2082
– plants 9759, 11944
– multi-effect distillation (MED) 9759
– multi-stage flash (MSF) 9759
– renewable energy–powered 9759
– posttreatment processes 2907
– pretreatment processes 2905, 2910
– reverse osmosis (RO) 2902
– solar-driven 9758
– desalination systems 2382
– ultrafiltration 2910
desert ecosystem 1552, 2933
desertification 2929, 3364
– impact on human systems 2929
desiccant
– air-conditioning systems 9525
– cooling system 9558
– evaporative cooling (DEC) systems 9515
design for the environment (DfE) 3446, 3447
desilylation 4645
De-Soete model 5309
desulfurization 1093, 2224, 2278–2279
detection 3076, 3078
– of beacons and traffic pylons 3076
– of road markings 3078
dethioacetalization 4645
detoxification of organic wastes 1629
detoxifying enzyme 4
detritivore 823, 824
detritus 824, 826, 1963–1964
– food chain 824, 826
developing country 1146, 1154, 1563, 1741, 1744, 1749, 1767, 1768, 1783, 1863
– agricultural growth 1563
– animal resource management 1768
– avian livestock 1749
– biogas production 1146
– brain-drain 1783
– breeding 1741
– development of biogas use 1154
– education 1767
– food-importing 1563
– inadequate sanitation 1146
– meat production 1744
– public transport investments 1863
– rural development 1563
developing region 1755
– livestock production 1755
developing world 1772, 1774, 1779–1781, 1786
– animal agriculture 1780
– animal breeding 1774
– breeding objectives 1779
– farming systems 1772
– livestock industries 1786
– multifunctional role of livestock 1781
developmental disorder 3638
devolatilization 1428
Dewar 4406
dewaxing 7839
DFIG turbine 12166
DGAT1 gene 488
dhurrin 4035–4036
diabetes mellitus 9656, 11135
diacylglycerol acyltransferase 488
diagnostic nuclear medicine 8580
diagnostic X-ray 8580
DIAL, see differential absorption lidar
diarrhea 5063
diarrheic shellfish poisoning (DSP) 9085
diatomateous earth 3958
diatom 4826, 6380, 7273, 7348, 11408
dibenzofuran 4880
dichlorobenzene 10972, 10974
– total concentration (TDCB(z)) 10974
dichlorodiphenyltrichloroethane (DDT) 3631, 3635, 6292, 11078
diclofenac 11924
dicot 1484
Dictyonema shale 7467
didemnin 3160
Didymozoidae 12029
Diels–Alder reaction 10174

diesel 267, 1002, 1218, 3860, 3956, 3978, 5493
– blends 5493
– buses 1881, 5981
– electric locomotives 5095
– electric system 5096
– engine 932, 1460, 5088, 5525, 5531, 5532, 5534, 5536
– boosting 5536
– fuel conversion efficiencies 5534
– soot-NO_x tradeoff 5531
– fuel 2246, 5494, 6246, 11430
– filter smoke number (FSN) 5494
– hydrotreatment 2246
– multiple unit cars (DMUs) 5959, 5966
– particulate filter (DPF) 267, 11322
– sulfur-free 3956
diethyl
– carbonate (DEC) 6127
– phthalate (DEP) 10667
diethylhexyl phthalate (DEHP) 3638
diethylstilbestrol (DES) 3628, 3629, 3636, 3638
differential absorption lidar (DIAL) 309–311, 313, 317, 320, 325, 3231
– airborne ozone 313
– airborne water vapor 317
– equation 311
– space-based 320, 325
differential global positioning system 3070
differential scanning calorimetry (DSC) 6108
differential thermal analysis (DTA) 11601
differentiation-associated gene 6162
diffraction method 6070
diffuse double layer model (DDLM) 8614
diffuse
– irradiance 9628, 9630
– light 2806
– radiation 7920, 9682, 9716, 10625, 10633
– sky illuminance 2824
– sky irradiance/radiation 9682, 9720, 11382
diffuse-radiation fertilization 7921
diffusion 2017–2022, 2025, 2047, 2049, 2051
– across a thin film 2017
– across interfaces 2025
– boiling flux 2021
– coefficient 596, 2018, 2021–2024, 2049
– in gases 2023
– in liquids 2024
– in solids 2024
– concentrated 2020
– dispersion 2021
– equation 2020, 2051, 10956, 10962, 10963, 10969
– development 10963
– flux doubles 2018
– Gaussian concentration profiles 2022
– mathematical description 2017
– permeance 2018
– unsteady 2019
diffusive flux rate 10963–10964, 10966
diffusive transport with convection 2034
Digenea 12023
digestive proteinase 4029
digital elevation map (DEM) 8940, 10622
digital map 6955, 6974
digital signal processor (DSP) 11542
digital solar atlas 10629
dihydrodipicolinate synthase (DHPS) 1694
dihydropyrimidinone 4654
dilantin 11926
dilithium ethylene dicarbonate 6042
dilute-acid hydrolysis 967
dimethyl
– phthalate (DMP) 10667
– sulfate 3985
– sulfide 120, 611, 2116, 7272
– sulfoniopropionate 7272
dimethylether (DME) synthesis 1043, 1049, 1062, 1428, 2225, 2235, 2247, 3985–3987, 5468, 5473, 5488, 5492
– commercial activities 3986
– dehydration reaction 3985
– fixed bed reactors 3986
– gas phase production 3986
– pathway 3985
– slurry phase production 3987
dimethylsulfoxide 3424, 10906
α,α-dimethyltricarballylic acid 123
dimming effect 141, 6748
dinitrogen monoxide 1598
dinoflagellate 829, 832, 2493, 4821, 9086
Dioctophymatidae 12031, 12039
dioxin 172, 856, 3634, 4883–4884, 4904, 4992, 5237, 5240, 5263, 5267–5268, 5289, 7000, 8110, 10666, 11720, 11869
– chlorination 10666
– diets 5289
– emission 11697
– formation 4881
– non-chlorinated 10666
– salient factors 5267
diphenyl ether (DPE) 7747
Diphyllobothriidea 12022
diploid animal genome 478
dipole magnet 6261
dipstick assay 5383
Dipteran pests 4025
Dirac function 2020, 2043, 8648
direct aerosol radiative forcing effect 135
direct air capture (DAC) 2151, 2154, 4108
direct alcohol fuel cell (DAFC) 10501
direct beam 9691
– radiation 11382
direct breeding value (DBV) 9363, 9367
direct capture of high-purity streams 2151
direct carbon fuel cell (DCFC) 10501
direct coal liquefaction (DCL) 2223, 2229
– block flow diagram (BFD) 2229
direct contact membrane distillation 2920
direct current (DC)
– electricity 3873
– power transmission 11181
direct DNA transfer 2590, 2594, 2603, 2606
– chemical methods 2590
– integrity 2603
– minimal expression cassettes 2594
– physical methods 2590
– transgene structure 2603
direct field-oriented control 42
direct gene transfer 2594
direct irradiance 9630
direct land use change (DLUC) 934, 1497, 10513
direct light 2806
direct liquefaction 2228, 2253
direct methanol fuel cell (DMFC) 373, 3389, 3850, 3858, 3866, 6539, 8266, 8269, 10501
direct normal irradiance (DNI) 9591, 9630, 9635, 9718, 9748
direct radiation 9716
direct solar dryer 9487
direct solar radiation 7911, 9573
direct-alcohol fuel cell 3916
direct-beam radiation 9692
direct-injection engine 5482
directional drilling 4397
directionally solidified (DS) superalloy 6848
direct-methanol fuel cell 3912
dirty air 239
dirty bomb 8529
disaster 2265
– waste 10010–10011
– characterization 10011
– generation 10010
discarded computer 3444
discarded solid waste 5708
disclimax 3282, 3285
discounting 7184

disease-resistant transgenic animals 2963
disease 11997
– epidemics 411
– water- and sanitation-related 11997
disinfection 11391
– by-products (DBPs) 2084, 2907, 3632, 3638, 3647, 3649, 7587
disperse city 5840
dispersion 2021, 2031–2033, 2035, 2037–2038, 2047, 10956
– coefficient 2021, 2032, 2033, 2037, 2041, 8617
– longitudinal 2033
– tracer determination 2041
– in groundwater flow 2035
– in laminar flow 2032
– in rivers 2038
– in turbulent flow 2033
– of pollutants 259
– Peclet number 2037
– plug flow 2032
dissolved
– gas drive 7803
– inorganic carbon (DIC) 8668
– metal 10051
– organic carbon (DOC) 6372, 8395, 8396, 10533, 11386
– organic matter (DOM) 9111, 10052, 11231
– organic nitrogen (DON) 6372
– oxygen 5673, 5688, 11954
– control 11947
distance relay 12089–12090
distillation 977, 981, 994, 996, 1006, 1047
– plant 981
distillers' dried grain with solubles (DDGS) 989
distraction 3112, 3114, 3121, 3124–3125
– ANFIS model 3125
– detection 3121, 3124
– algorithms 3112
distributed
– energy resources (DER) 3012, 3019
– generation 2977, 3012, 3014, 3016–3017, 3019, 3395, 3465, 9935
– impact on system protection 3019
– machine-based 3019
– impact
– on ferroresonance 3019
– on power quality 3017
– on voltage regulation 3016
– technology landscape 3014
– vehicular environment 2469
– wind power production 12113, 12115
– forecast errors 12115
– variability 12113
distribution 2978–2981, 2984–2985, 2987, 2989, 2995, 3003, 3011
– arrester housings 3003
– automation functionality 2985
– breakers 2978
– capacitor 2979, 2989
– devices 2978
– ethernet-based 2984
– feeders 2987
– circuits 2978
– protection 3011
– fuses 2979
– network protocol (DNP) 2984
– point-to-point protocol (PPP) 2984
– reclosers 2978
– safety 2981
– substations 2995, 2998–2999, 3005, 3008–3010
– automation 3008
– bus protection 3010
– busbars 2999
– design 3005
– incoming sub-transmission supply line 3009
– physical appearance 3008
– primary feeder 2995
– protection 3008
– transformers 2998
– transformer protection 3010
– switches 2978
– system 2976, 2978, 2984, 2988, 2989, 3019
– communications system 2984
– integrated volt/VAR control (IVVC) 2988
– intelligent electronic devices (IEDs) 2984
– microgrid operation 3019
– volt/VAR control (VVC) 2987, 2989
district heating 4359
– pipework 11783
– pumps 11776
disturbance model 51
disurbanization process 11364
diurnal temperature range (DTR) 9735
divergence-with-gene-flow model 3362
diversification 2742
diversity
– indexes 3299, 10085
– of plant and animal life 939
DNA 641–642, 644, 648, 3599–3600, 3603, 3605, 3607–3608, 3643, 10824
– coding sequence 3603
– damage 3599–3600
– encoding 641
– markers 462, 480
– methylation 2606, 6159–6160, 6171, 10686
– reprogramming 6159
– methyltransferases 3603
– microinjection 7219, 10902–10903, 10917
– molecule 639
– exogenous 639
– mutations 3599, 3600, 3605
– polymerases 3599, 5384
– polymorphism 476
– repair 3599, 3643
– sequencing 2690
– technology 474
– topoisomerases 3607
– transfer into the cell 10824
– transgenic constructs 642
– transposon 644, 648
– vaccines 6300
Dobson spectrophotometer 9723
docosahexaenoic acid (DHA) 1697, 9080
dog 11400
Dolabella auricularia 3153
dolastatin 3155
dolomite 1913, 5646
dolphin 3569
domestic
– biotechnology 2288
– energy
– carrier 8976
– supply system 1370
– fuel emissions 11316
– heating 1615, 11295
– waste 4903
– wastewater 11962
– membrane bioreactor 11962
domestication/domesticated 386, 390, 416, 1746, 2690, 2744, 9151, 10813, 10867
– crop 351
– genetic analysis 2690
– molecular isolation 2690
– molecular techniques 390
– nature 2744
– of animals 10852
– syndrome 8045
– through artificial selection 8002

domoic acid 4826, 4829
– detection 4829
– in shellfish 4829
– quantitation 4829
donor cell 6167
– reprogrammability 6167
donor chromatin 6171, 6173
dopamine 10644
dopant 3024
Doppler pellet sensor 6359
dormancy 9145–9149, 9151–9153
– breakage 9153
– classifications 9146
– definitions 9146
– genes 9148
– implications
– in agriculture 9147
– in weed control 9152
– in cultivated species 9148
– in natural seed banks 9152
– lack of 9151
– malting barley 9149
– persistence 9148
– sunflower 9148
Dorno radiation 11149
dose–response curve 3254
dose–response relationship 3253–3256, 11378
– cellular responses 3256
– epidemiological studies 3256
– exposure to mixtures 3255
– for biomarkers 3254
– nonmonotonic 3255
– sigmoidal curve 3253
dosimeter 3022, 3027, 3028
– electronic 3028
– of record 3027
double fire gasifier 1457
double perovskite 2952–2954
– catalysis 2953
– conductivity 2953
– stability 2954
double rotary kiln pyrolysis 1525
double strand break (DSB) 10822
double-compartment solar oven 9501
double-cropping system 1123, 1139
double-flash
– power station 4298
– steam power station 4280
– turbine 4257
double-stranded
– DNA (dsDNA) 11985
– RNA (dsRNA) 11985
doubly fed induction generator systems 12152
doubly salient permanent magnet machine 11528
Douglas-fir 3290
– individual-based model 3290
Dow membrane 6541
downdraft combustion 1357, 1385
– vertical or lateral 1357
downdraft gasifier 11443
downhill simplex algorithm 10607
downhole
– heat exchangers 4372
– monitoring techniques 4204
– pumps 4367
downwind 11267
doxorubicin 3157
doxycycline 643, 10915, 10919, 11083
Dracunculidae 12040
drag bit 4394
dragline bucket dredge 3034
drainage 5668
– basin 8634
– problems 5666
draw solution 2916, 2920
DREB/CBF protein 7
dredged material 3032, 3038–3039, 3041–3042, 3047–3048
– beneficial use 3041
– confined disposal facilities 3039
– disposal 3038, 3048
– management 3047
– placement 3038
– transportation methods 3038
– treatment 3042
dredge/dredging 3028–3029, 3031–3035, 3038, 3042, 3044–3045, 3047–3048
– construction 3031
– dredged material management 3031
– electric powered 3048
– environmental cleanup 3038
– environmental considerations 3028
– environmental enhancement 3031
– environmental regulation 3045
– equipment 3032
– for environmental cleanup 3033
– hydraulic 3031, 3034
– mechanical 3031, 3032
– mining 3031
– navigation 3031, 3048
– of contaminated sediments 3038
– of navigation channels 3045
– reclamation 3031
– regulatory authorities 3047
– removal of surface-dwelling biota 3042
– resuspension of sediments 3044
– ships 3035
– sponsors 3047
– sustainable 3047
– technological innovations 3048
drift 492
driftsonde 3231, 5073–5074
– ballooning systems 5073
– miniature in situ sounding technology 5073
– observations 5073
– system 5072, 5081
– test-campaign 5081
– trajectories 5074
drillable straddle packer (DSP) 4401
driller 4382
drilling/drill 4382–4383, 4385, 4388, 4390–4397, 4399–4400, 4403, 4405–4408, 4416, 4427–4428, 7800
– acoustic telemetry 4406
– bits 4394
– blowouts 4427
– bottom-hole assembly (BHA) 4393–4394, 4396
– casing 4383
– designs 4390
– cementing 4403
– collars 4396
– commercial planning software 4388
– contractor 4405
– core rig 4391, 4395
– cuttings 4382
– dewars 4406
– directional 4383, 4396
– disposal of waste 4416
– downhole measurements 4406
– environmental impacts 4416
– expandable tubulars 4408
– fluids 4397, 4398, 4399, 4401–4402
– blowout 4402
– blowout preventer (BOP) 4402
– circulating system 4398
– kick 4402
– mud program 4399
– mud systems 4398
– properties 4398
– well control 4401
– hole stability 4383
– instrumentation 4405
– lost circulation 4399
– mud 4397
– mud-pulse telemetry 4406
– noise 4428
– pipe 4395, 4409
– platforms 6638
– rate of penetration (ROP) 4385
– rig 4392, 4405
– rotary rigs 4391

– slimhole 4390
– string 4382, 4392, 4396–4397
– surface measurements 4405
– system 4381
– basic functions 4381
– selection criteria 4390
– trouble 4385
– waste materials 6638
– well
– completion 4403
– cost 4385
– design 4385
– wellbore sealing 4400
– with casing (DWC) 4407
drinking water 2089, 2755, 3454, 3639, 6607–6611, 6615, 6621, 6623, 9564, 10537, 11936
– chlorination by-products 3639
– consumption 6611
– cryptosporidium 6615
– disinfection 9564
– exposure assessment 6611
– *Giardia* concentration 6623
– hazard identification 6609
– health risks 6608
– of hazardous events 6623
– health targets 6607
– microbial risk assessment 6623
– odor control 10537
– pathogenic microorganisms 6607
– pollution 2043
– public health status 6608
– quality 11387
– risk assessment 6608–6609
– safety 6608, 6621
– taste control 10537
– treatments 10537
driver 3083, 3085, 3099–3100, 3103, 3105, 3107–3110, 3112–3114, 3118, 3120–3122, 3126, 3129–3131, 3135
– alert control 3114
– anger scale 3100
– assistance system 3052, 3067, 3107, 11098, 11099, 11126, 11456, 11468
– automatic detection 3067
– biologically inspired 3052
– camera-based vision systems 11098
– site mapping 3067
– requirements of vision systems 11099
– vision-based 11099, 11126
– attention warning system 3114
– commercial products 3114
– behavior 3082, 3099, 3100
– at intersections 3082
– patterns 3112
– self-reported survey 3100
– behavior questionnaire (DBQ) 3100, 3102–3104, 3107
– factor analysis theory 3107
– participants 3100
– Cronbach's alpha reliability coefficient method 3102
– data statistical analysis 3104
– method 3100
– Pearson correlation coefficient 3103
– quantification analysis 3104
– reliability 3102
– validity 3102
– biological measures 3118, 3129
– characteristics 3099, 3103
– quantification 3105
– distraction 3109, 3124, 3127, 3131
– bright pupil effect 3127
– detection 3121
– road geometry 3124
– template matching method 3127
– drowsiness 3114
– estimate system 3120
– eyelid features 3120
– fatigue 3109, 3113
– detection 3120
– inattention 3108, 3115, 3126, 3130–3132
– biomathematical models 3130
– detection 3116–3117
– driver fatigue monitor (DFM) 3115
– face segmentation 3126
– hybrid measures 3132
– monitoring 3131
– systematical design consideration 3131
– intentions 3122
– mental state 3120
– mistake 3100
– driver monitoring system 3114
– navigational error 3085
– older population 3135
– physical measures 3120, 3122
– physical parameters 3130
– physical signal extraction 3126
– posture dynamics 3126
– preparatory behavior 3083, 3085, 3088, 3091, 3093, 3095
– influence of road structure 3091
– influence of traffic conditions 3088
– influence of vehicle velocity 3088
– prediction of onset location 3095
– structural equation modeling 3093
– self-evaluation 3107
– skill 3100
– sleepiness 3110
– state monitor (DSM) 3115
– state sensor (DSS) 3116
– visual behavior 3112
– visual distraction 3122
drivers-pressures-state-impact response 10377
driving 3085–3086, 3100, 3104, 3107, 3112, 3122, 3130, 3135–3137, 3143
– age-related functional deteriorations 3135
– behavior 96, 3135
– data collection 3085
– older drivers' 3135
– research 3100
– cognitive distraction 3112
– corridor 80, 88
– inattention 3110
– monitoring system (DIMS) 3110
– dynamics 256
– lane keeping 3136
– older adults 3135
– performance measures 3122, 3130
– recorder system 3086
– safety 3052, 3082, 3136–3137, 3140
– age-related changes 3136
– car following in fog 3137
– collision detection 3140
– simulators 3086
– skill 3104, 3105
– inventory 3100
– self-evaluations 3105
– speeds 3088
– steering control 3137, 3143
– style 3107
– tasks 3083
– time-to-contact (TTC) 3136
– under reduced visibility conditions 3135
drop collision 9700
drop-in fuel 10527
dropsonde 5073
– data 5081
Drosophila 10679
drought 2090, 2646, 2652, 2789, 8905
– frequency 2321
– stress 2649
drowsiness 3121
– detection 3121
– eye movement 3121
– level 3120

drug 3152
– abuse 10642, 10654
– delivery 11080
– discovery in ocean 3150
– discovery 1188
– marine-derived 3152
– overdoses 3590
dry air cooling tower 9513
dry ash 6488, 11743
dry combustible 11830
dry fuel 9834
– calorific value 9834
dry matter production 11396
dry recooling 9534
dryland 2755, 2930, 2932, 3315
– productivity 2930
dry-steam
– dry-steam gathering 4290
– power station 4278
dry-tomb sanitary landfills 5721, 5732
dual carbon cell 3430
dual clutch transmission 3489
dual combustion boiler 1369
dual fluidized bed gasifier 1432
dual fuel engine 1528
dual mechanical port (DMP) machine 11546
dual-fluid organic rankine cycle 4315
dual-pressure cycle 4267
duct burner 4986
Dugoff tire model 3056, 11191
Dulong equation 5245
dulse 522
Dunaliella bardawil 359
Dunaliella salina 350, 358, 360, 365
dung 1538
dunite 1910, 1912, 1917–1918, 1922
– intrusion 1918
Dunne runoff 3222
durum wheat 5321
dust/dusty 124
– collection 5239
– combustion 1320, 1327
– fuel quality 1327
– firing 2273
– gas model 2922
– suppressant 270
dustpan dredge 3038
Dutch tank leaching test 11726
dwarfing gene 2697, 2692, 6202, 6211
dye sensitized solar cell (DSSC) 7934
dye tracing 5664
dye-sensitized solar cells (DSSCs) 3855, 6567, 6576, 7940
dynamic(s) 2766
– building simulation 6884
– capacitor 9353
– cropping systems 2742
– downscaling 6597
– *dq0* modeling 33
– environment 3195
– contextual map 3195
– link library 11197
– mechanical behavior 6920
– plasticization 6920
– pressure oscillation 6841
– range extension 11110
– experimental observations 11110
– range 11106–11107
– definition 11106
– reliability criterion 11107
– roughness 2054, 2060
– source routing 11553
– traffic assignment (DTA) models 7854
– vegetation models 3292
dynamometer 5505
dynamometric wheel 3061, 11196
dynode 5565
DyNOR®
– process 4960
– system 4985

E

E. coli, see *Escherichia coli*
Earnshaw's theorem 6247
earth 4180, 4568
– atmosphere 9804
– berming 4146
– crust 3239
– ecosystems 9740
– energy balance 5415
– gravitational potential 4568
– gravity field 4568
– heat balance 4917
– heat sources 4180
– integration 4146
– magnetic field 8577
– pipes 4146
– radiation budget (ERB) sensors 9627
– sheltering 900, 4146
– solar effects 9804
– surface 9731, 9749
– energy balance 9731
– irradiance 9749
– system 2099–2100, 3201, 3211–3212, 3230
– carbon cycle 2100
– environmental literacy 3201
– model (ESM) 623, 2112, 2511, 2513, 3212, 7367, 10137, 10167
– modeling the land component 3211
– monitoring 3230
– total magnetic field 8471
– tubes 4146, 4148
– water cycle 11874
EarthCARE satellite 324
earthquake 2423–2425, 2427, 2429, 3233–3235, 3240, 3242, 3243, 3245–3249, 3508, 3553, 4128, 4422, 4570, 11633, 11635, 11642, 11646
– associated with volcanoes 11635
– bridges and viaducts 3240
– buildings 3248
– building codes 2429
– characteristics 3234
– construction planning 2427
– dams 3242
– deformation 3234
– early warning systems 2429
– engineering 3234
– epicenter 2424
– faulting 3233, 3249
– ground and structure interaction 2425
– ground condition considerations 2425
– ground motion 3234
– considerations 2425
– landslides 3248
– line-like and tubular structures 3247
– mitigation 2427
– monitoring 2429, 11635
– power transmission lines 3246
– risk 2427
– roadways and railways 3240
– rockfalls 3248
– strong-motion station 3235
– subways 3245
– surface breaks 3234
– tunnels 3243
– waves 2427
earth–sun geometry 9711
earth-to-air heat exchangers 4146
earth-to-sun distance 11152
east urals radioactive trace (EURT) 3531
eastern wind integration and transmission study (EWITS) 12269
Ebara TwinRec process 3998
– recovery 3998
– recycling 3998
ebb generation 10614
eccesis 3281
Echinostomatidae 12028
echovirus 11989
eco-certification 10318
eco-design 3447, 10318
eco-driving 268

eco-efficiency 9028
– unintended consequences 9028
EcoFuel 11796
eco-imperialism 4524
eco-indicator 99 196
ecolabeling 556–557, 575, 10318
ecoliteracy 8860, 8869
ecological/ecology 3291, 3583
– aquaculture 533, 537, 540, 566
– development model 540
– base flow 2795
– carrying capacity 1965
– certification standards 1963
– communities 3303
– computational power 3291
– education 3203, 3205
– energetics 3285
– epidemiology 3267
– food webs 3451
– footprint 2746, 3450, 6861, 9028
– forecasting 2265
– gradients 3357–3358
– in the city 11327
– lung 1624
– network 6216
– of species 10092
– processes 6219–6220
– invisible place 6220
– invisible present 6219
– pyramid 824
– risk assessment 3264, 3268
– biological organization 3268
– choosing the appropriate organisms 3268
– succession 3278–3280, 3292, 3297
– historical development 3280
– sustainability 8858, 8861–8862, 8876, 10369
– systems 3296
– toxicity 4855
– transition 3359
economic
– feasibility 3469
– injury level (EIL) 5432
– input–output life cycle assessment (EIO-LCA) 1501
– scheduling 12110
– sustainability 8708
– assessment (EESA) 4785
– threshold (ET) 5432, 5433
– limitations 5433
– valuation methods 4789
– value 9042
Ecopath 1967–1968
eco-region 1557, 1560
eco-roof 4732, 10359
Ecosim 1967
ecosystem 156, 158, 536, 547, 568, 2176, 2490, 3279, 3281, 3284, 3286, 3287, 3297, 3299–3303, 3306–3309, 3311–3313, 3317, 3318, 3326–3327, 3329, 3331–3335, 3338, 3342, 3351, 3354, 3358, 3547, 4495, 5553, 8857, 10078, 10090
– adaptive management 3342
– anthropogenic disruption 3317
– approach to aquaculture (EAA) 1960, 1969
– autocorrelation 3333
– compartment models 3286
– concept 3283
– cone spring model 3309, 3311
– contamination 3547
– coral reef 2490
– definition 3284
– development 3312
– diversity 10090
– dynamics 3326
– ecological energetics 3286
– ecotonal interfaces 3338
– ecotones 3358
– engineers 3303
– usefulness for management 3303
– flow analysis 3297, 3306, 3312
– flow matrix 3308
– food-chains 3312
– functioning 3301–3302, 3318, 10078, 10782
– geostatistics 3335
– goal functions 3311
– health 536, 547, 1932
– integrity 536
– invasive species 5553
– keystone species 3300
– limits 536
– management 3354
– mathematical optimization models 3312
– modelling 3309, 7009–7010
– multiple spatial scales 3331
– network flow model 3308
– panarchy 3351
– peat-forming 2176
– point pattern analysis 3333
– science 529
– service 3297, 3306, 3313–3324, 10359, 10362, 10369, 10723, 10782
– across systems 3315
– classification 3314
– definition 3314
– distributional effects 3323
– dynamic effects 3323
– economic valuation methods 3318
– global policy 3321
– history 3317
– human health 3323
– in China 3320
– initial development 3317
– institutional design 3324
– InVEST 3322
– mapping 3321–3322
– marine spatial 3320
– modeling 3320
– monetary valuation 3323
– NatCap 3322
– research efforts 3321
– resource decisions 3319
– supply chain 3316
– synergies 3323
– trade-offs 3323
– water funds 3319
– sources of heterogeneity 3329
– spatial analyses 3332, 3333
– spatial autocorrelation 3334
– spatial patterns 3297, 3326–3327
– spatial processes 3331
– spatial scale 3335
– structure 3307
– sustainability 3326
– total system throughflow (TST) 3308
– traits 3303
ecosystem-based management (EBM) 1968
ecotilling 2734, 4497
ecotone 3298, 3357–3359, 3361–3365
– agricultural 3363
– biodiversity 3364
– characterizing 3359
– conceptual Framework 3358
– conservation 3364
– effects on biodiversity 3359
– environmental transitions 3365
– evolutionary processes 3361
– history of research 3359
– human-generated 3358
– human-related 3363
– measuring 3359
– patterns of biodiversity 3361
– planning 3364
– populations 3358, 3363
– sustainability 3361, 3364
– urban 3363
ecotope 11338
ecotoxicity 4856, 7605

ecotoxicology 3266
– of radioactive substances 3583
EcoTrends Project 6232
Ecteinascidia turbinata 3157
ectotherm 5058
edaphoclimatic resources 2749
eddy
– correlation 602
– diffusion coefficient 2055
– diffusivity 2033
– velocity 2052
eddy-permitting model 7368
edge effect 3364
edible solid waste 9980
edible vaccine 8077
E-diesel 5493, 11434
Edmonton transit system 5994
education recycling 10033
Edwardsiella 5056
E-factor 4615, 4619, 4623
– values 4623
effective delayed neutron fraction 3814
effective disinfection time (EDT) 9581
effective skin dose 11381
– transmission 11381
effective surface albedo 11156
effective UV protection 11385
E-gas gasifier 2239
egomotion 6971
ego-vehicle 10590, 10592
eicosapentaenoic acid (EPA) 1697, 9080, 9114
Einstein diffusive motion 8209
Ekman divergence flow 8672
El Niño Southern Oscillation (ENSO) 2123, 2125, 2455, 2515, 4573, 6742, 7253, 7259, 7374, 9320, 9639, 9805, 10164
– events 2122, 2123, 2125, 2130, 2144, 5898, 8927
– index 7259
– phenomenon 2122, 4565
– teleconnections 2123
elastic collision 3789
elastic scattering 3802
elastic-band method 2483
elastic-viscous-plastic (EVP) material – 2763
elastin-like polypeptide (ELPs) 8065, 8078
elastomeric binder 9307
elected fusion 6954
electric arc furnace (EAF) 8810, 11588
– dust (EAFD) 9613, 11597
electric
– braking system 10544
– car 303, 6247
– conductivity 2947
– coupling 3372–3377
– backward boosting 3377
– backward bucking 3376
– devices 3374
– forward boosting 3376
– forward bucking 3375
– double-layer 3428
– capacitor (EDLC) 3427–3428
– energy 2886, 3368, 3370, 3394, 12213
– conductor 3394
– distribution 3394
– efficient transmission 3394
– measurement 2886
– transformation 1249
– generating unit (EGU) 5915
– grid 7850, 10522, 10563
– reliability 7850
– stability 7850
– heating 12103
– lighting 909, 2810, 2854, 2863, 2881
– energy consumption 2854
– machine 5110, 12141
– flywheel system 5110
– motor 3370, 10543
– electric motor drives 11524
– torque-speed characteristic 10543
– pipe 12186
– power 1331, 2164
– generation 4168, 6808
– industry 2072, 10475
– infrastructure 10450, 12079
– network 7849
– production 1330
– utilities 11160
– rail technology 1881
– reliability 10946
– road vehicle 268
– stress 11162
– substation 3394
– traction system 1816
– trolley bus 5980
– utility industry 2977
– vehicle (EV) 710, 719, 768, 795, 3367, 3368, 3391, 3392, 3458, 3857, 6147, 8112, 10498, 10542, 11503, 11509, 11523, 11524, 11539, 11541
– architectures 3368
– battery management 6147
– battery-powered 3368, 8112
– electric motor drive 11524
– electronic interface 3391
– onboard energy source 795
– power converters 11539
– soft-switching converters 11541
– traction motor 11523
electrical/electrically
– blackouts 10935
– calibrated radiometers 9471
– compensation radiometers 9676
– conductivity 8356
– back corona 8356
– resistivity 8356
– double-layer (EDL) 742, 6788
– capacitors (EDLC) 6773
– energy 3873, 7848
– mobile decentralized storage (MDS) 7848
– demand 9334
– storage 7851
– generating system 12149
– generation 2991
– substations 2991
– grids 10943
– heating 776
– machine 12142–12143, 12148
– AC-machine 12142
– DC-Machine 12142
– rotating flux vector 12143
– power generation 2935
– power system 672, 10937
– powertrain 11504
– stress 11172
– submersible pump (ESP) 7804
– system 9338, 12135
– distributed control techniques 9338
– dynamic granular control (DGC) 9338
– optimal power flow (OPF) 9338
– transmission systems 3393
– transnational infrastructures 10936
– tree 11174
electricity 208, 1040, 1095, 1200, 1266, 1547, 2164, 3395, 3397, 3846, 4475, 4481, 5137, 5539, 6500, 6829, 7192, 8981, 10453, 10938
– as medicine 6500
– blackouts 10938
– daily patterns 8981
– demand 2164
– requirements 7192
– distribution 2977, 3395
– fossil-based 1040
– from biomass 1200
– from natural gas 6829
– generation 1547, 2163, 3396
– with small wind turbines 3396
– grid 8986
– generator modeling 8986
– interconnection 8986

– market 7853, 9334, 12109–12111, 12131, 12255
  – daily planning 12109
  – day-ahead market 12109
  – hourly operation 12111
  – intraday market 12110
  – post-trading 12111
  – seasonal/yearly planning 12109
  – weekly planning 12109
– mix factor 4764
– mono- and co-combustion 1266
– network 3013, 7863, 10449
  – outage management 7863
  – smart grids 3013
– pathways 10520
  – battery-powered electric vehicle (BEV) 10520
  – plug-in hybrid electric vehicle (PHEV) 10520
– Peltier effect 5539
– physiological effects 6500
– poly-generation 5137
– price 10456
  – critical peak pricing (CPP) 10456
  – real-time pricing (RTP) 10456
  – time-of-use pricing (TOU) 10456
– production 1095, 1435, 2384, 3397, 7185, 10450, 11768, 11772
  – energy discount rate 7185
  – estimated costs 2384
  – life-cycle cost 7185
  – Rankine steam cycle 11768
  – steam turbine 11772
  – via gasification 1435
– reliability 10453
– seasonal patterns 8981
– Seebeck effect 5539
– storage 8995, 12098
  – chemical storage 8995
  – compressed air 8995
  – pumped hydroelectricity storage 8995
– supply 1089
  – based on biogas 1089
– system 8981
  – background 8981
– transmission 3395
– value chain 10946
– wind-generated 4475
electricity-to-heat ratio 11786
electroactive catalyst layers (ECLs) 3874
electrocardiogram 6501
electrocatalysis 3880
electrocatalyst 3883, 7611, 7732, 8212
electrocatalytic fuel oxidation 2940
electrocatalytic oxidation 2939
electrochemical
– active surface area values (ECSA) 7706
– battery 11504–11505
  – calendar life 11505
  – cycle life 11505
  – electrical efficiency 11505
  – energy capacity (EC) 11505
  – energy density 11505
  – power density 11505
  – specific energy 11505
  – specific power 11505
– capacitors (EC) 3427, 3429, 3852, 6772
  – operation voltage 3429
– cell 741, 769, 7741
  – electrolyte 741
  – separator 741
– double layer capacitors (EDLC) 3852
– energy storage 706
– etching (voltammetric dealloying) 7740
– hydrogen
  – production 3414
  – pump 8196
  – separation (EHS) 5143
– mass transfer processes 10422
– Ostwald ripening 8187
– photovoltaics 3854
– remediation 10420
  – electromigration 10420
  – electroosmosis 10420
  – electrophoresis 10420
– supercapacitors 3426
– surface area (ECSA) 7746
– vapor deposition (EVD) 9853–9855
electrochromic glazing 2843
electro-conductivity 3434
electrode 757, 3873, 3880, 3899, 3905, 6068, 6127
– anode materials 3905
– cathode materials 3899
– fabrication 6133
  – winding process 6133
– interface 3880
– kinetics 6729
  – AC impedance 6729
– reactions 746
– surfaces 6045
  – decomposition 6045
– tap density 757
electrode-active material 7550
– organic radical polymers 7550
electrode–electrolyte contact 742
electrode-electrolyte interface 6038, 6058
– molecular dynamics simulations 6058
electrodynamical torque 12143
electrokinetic remediation 10428, 10430
electrokinetic-permeable reactive barriers 10429
electrolysis 3414, 5163
– of water 5163
electrolyte 743, 750, 3879, 3387, 3878, 3880, 3885, 3888, 6038–6042, 6045, 6054, 6060, 6068, 6084, 6127, 6131–6132, 6144, 9907
– additives 6132, 6144
– EC-based 6042
– electrochemical stability 6064
– electrode surfaces 6084
– fluorite-type materials 3888
– interface 3880
– ion conduction 3878
– ionic liquid–based 6060
– materials 6127
– membranes 8331
– modeling of reductive decomposition 6041
– molecular dynamics simulations 6045
– non-aqueous 743, 750, 6068
– Ohmic losses 3885
– oxidative stability 6039
– quasi-aqueous 3879
– single-ion conductor 6054
– solvents 6040, 6060
– stability 6038
– electrolyte systems 5887
– window 742
electrolyte/electrode interactions 6064
electrolytic copper refining 1998
electromagnetic
– co-energy 22
– compatibility (EMC) 696
– disturbance 697
  – capacitive coupling 697
  – conductive noise 697
  – inductive coupling 697
– force (EMF) 8851
– interference (EMI) 696, 9683
– photon 11376
– radiation 2615, 3787, 4566, 7902, 8560–8561, 8577, 8929, 9651, 9706, 9713, 9803
  – radiometers 9713
– torque 22, 29, 33, 41
– waves 9620, 9628
electromagnetism 3789
electromagnet 6242, 6257, 6268
electromechanical energy conversion 18
electromigration 10421
electro-mobility 1064, 3855, 3857, 3873

electron 357, 3024, 3788, 8468
– antineutrinos 11208
– beam evaporation 9200
– capture 8564, 8574
– energy loss spectroscopy (EELS) 723
– impact emission spectroscopy (EEIS) 9402
– mediator 3662
– microprobe analysis (EPMA) 2439
– relay 5177
– transfer 5211, 7559
– reactions 3657
– transport pathways 357
electron-beam irradiation 9101
– antibacterial effects 9101
electron-positron pair 8582
electronic
– brake distribution (EBD) 76
– conductivity 2941, 2943, 2947, 3438, 3894, 3900
– for direct hydrocarbon anodes 2941
– control unit (ECU) 3861
– dosimeters 3027
– fare payment 91–92
– fuel injection (EFI System) 1016
– horizon method 2467
– insulator 741
– knowledge 4503
– stability control (ESC) 76, 3053, 11188
– stability program 3070
– toll collection (ETC) 4946, 5023
– waste 3443–3445
– consumer-based 3445
– producer responsibility (EPR) regulations 3445
– regulation 3443
electroosmosis 10421
electrooxidation 8267
electrophile 3660
electrophoresis 10422
electroporation 10797, 10869, 10899
electrorefiner 7152
electrostatic energy 8614
electrostatic precipitator (ESP) 272, 1336, 1339, 1134, 1393, 1394, 1437, 1467, 2209, 3822, 3837, 5239, 8355–8356, 11711, 11800
– specific collection area (SCA) 8356
electrostatic repulsive energy 756
electrotechnology 3007, 12138
electrothermal reduction of metal oxides 9595
electrowinning 6661
elemental iron 10411
elemental tritium 11055
– gas 11048
– inhalation 11055
element-sensitive electron energy loss spectroscopy (EELS) 7744
elephantiasis 12011
elevated heat pump effect (EHP) 6748
ELISA analysis 1653
ELPylation 8078
Elsbett engine 8089
ELSY project 4056
Elysia grandifolia 3161
Elysia rufesens 3161
embryo/embryonic
– dormancy 9149
– cells 6160
– pluripotency 6160
– gonad cells 10908
– stem cell 6161, 6166, 6794, 7219, 10817, 10820, 10827, 10907
– for the zebrafish 6794
– zebrafish model 6793
embryo-derived stem cells 10821
– pluripotency 10821
emerging contaminant 2079, 2082–2083, 9567
– transport 2082
emerging infectious disease 6184
emission 247, 251, 253–254, 257–259, 264, 266, 271, 273, 9907
– abrasion 253
– cold-start 251, 257
– control 251, 4960
– evaporative 253
– from transport 254, 273
– mitigation measures 271
– monitoring 183
– legislation 264
– of primary particles 259
– process 250
– combustion 250
– reduction 161, 192, 266
– program 185
– restrictions 9907
– resuspension 254
– shipping 258
– trading schemes 9031
– transport-related 247
e-motion 4580
empirical partitioning isotherm 8611
empirical valence bond model (EVBM) 3419
enantiomer drug 8028
enantioselective catalyst 7605
encephalitis 5360, 8154
enclosed fireplace 1361
enclosure design 3699
– human safety 3699
– longevity 3699
Encoal 2217
endangered species act (ESA) 3354
endemic
– gill disorder 549
– infectious disease 11090
– malaria 11070
– Southern malaria 11089
endobiotics 12300
endo-cellulase 8048
endochitinase gene 10697
endocrine
– disrupting compound (EDC) 2084, 3260, 10534, 10668, 11961, 11963, 11965, 11973
– characteristics 11963
– removal 11973
– treatment 11965
– wastewater reclamation 11963
– disruptors 3637
– modulators 11961
– system 3635–3636
endocytosis 10899
endogenous plant protein 8064
– O-glycosylation 8064
endoplasmic reticulum (ER) 3669, 8063
endo-polygalacturonase 10699
endoproteinase 4031
endosperm 4555, 4560
endothermic chemical transformation 9590
enemy release hypothesis 5551
energetic electron 8472
energetic neutron 8582
energetics 10156
energization current 3010
energy 672, 804, 867, 1122, 1199, 1478, 1570, 1574, 1584, 2349, 2847, 3457, 3502, 3848–3849, 11789, 11944
– balance 2762, 4718, 4910, 10506, 11848
– balancing models 7638
– boundary limits 11848
– charge system 3370
– consumption 1026, 1477, 8115
– in typical driving cycles 8115
– conversion 1257, 1478, 3849, 5102
– for auxiliary power 5102
– losses 1257
– path 1232
– processes 3848, 4251
– systems 2847, 4298, 4295, 9934
– technology 1236
– cost 2184

– crop 1098, 1109, 1225, 1506, 1536, 1538, 1545, 1565, 2632, 6020
  – grasses 6020
  – lignocellulosic 6020
  – production 1109, 1508
  – trees 6020
– debt 3307
– demand 1570, 4690
  – reduction 4690
– density 744, 3852, 3877, 5105
– discounting 7185
– efficiency 1584, 11537
  – factor 11848
  – products 3463
– energy-plus buildings 10333
– exchange stations 7853
– exploration 11934
– farming 1539
– flows 1299
– food-related 1299
– for transportation 3457
– fossil fuel–derived 867
– from processed refuse 11789
– from waste (EfW) 4958, 11690, 11841
– global demand 3502
– grasses 6024
– information administration (EIA) 2181
– innovation 12223
  – social acceptance 12223
  – stakeholders 12223
– maize (EM) 1117–1120
  – breeding 1116, 1120
  – cold tolerance 1118
  – German–Mexican inbred lines 1120
  – late maturity 1118
  – Southern European lines 1119
– management 3848
– market 12175, 12188, 12255
– mining 6681
– mix factor 4764
– modeling 10239
  – geometric acquisition 10239
  – tools 10245
– payback time (EPBT) 9432–9433, 9440, 9441
– performance 2073
– plants 1099, 1122
  – production 1138
– prices 7968
  – escalation 10453
– production 9906
  – renewable-based power production increase 9906
  – significant structural investments 9906
– recovery 2907, 5298–5300, 10584, 11846
  – by thermal treatment of wastes 5299
  – from MSW by incineration 5300
  – from waste 5298, 11846
– renewable sources 1199
– resources 2175, 3502
  – hydrocarbon-based 3502
– saving 11944
– security 1574, 7852, 10503
– solar-thermal 2349
– storage 672, 707, 3427, 3471, 3472, 3476, 3495, 3849
  – bill 10462
  – cookers 9492
  – policy 10457
  – requirements 3476
  – sector 804
  – systems (ESS) 6125
  – technologies 3472, 5102
– supply 1489, 1572
  – cost-efficient 1572
  – security 1489
– systems language 8858
– transformation 5408
– transmission 2867
– usage 7876
  – in a supermarket 7876
– yield 867
energy–climate crisis 4121, 4129
energy-from-waste (EfW) 5297
  – industry 5298
  – plant 5300, 5302
    – grate combustion systems 5302
energy-generation technology 9432
  – environmental impacts 9432
enforcement cost 5025
engine
  – fuel efficiency 10493
  – multi-gear transmission 3382
  – power split hybrid drive train 3384
  – torque 5477, 8119, 11482
engineered
  – geothermal system (EGS) 3501–3511, 4191, 4192, 4197, 4295, 5231
    – commercial acceptance 3505
    – definition 3501, 3502
    – development 3504, 3508
    – economic models 3506
    – global potential 3504
    – parasitic losses 3506–3507
    – possible road map 3511
    – power output 3507
    – power plant 3510
    – productivity index 3507
    – reservoir creation mechanism 3506
    – reservoir 3507, 3511
    – Soultz project 3505
    – stimulated deep reservoir 3503
    – sustainability 3509
    – technology 3504
    – water losses 3511
  – landfills 4904
  – osmosis 2915
  – models 12210
  – plastics 6541
engineering–procurement–construction (EPC) 2924
enhanced
  – actinide removal plant (EARP) 8408
  – bioremediation 1632
  – bus transit service 1872
  – geothermal system (EGS) 4187, 4233, 4246, 4323, 4331, 4350, 4407, 4422–4423, 11649
    – induced seismicity 4422
    – power stations 4323
  – gravity concentrators 2212
  – masonry stoves 1366
  – natural attenuation (ENA) 10430
  – oil recovery (EOR) 2251, 2254, 7802, 7806, 7808, 7814, 7827
    – chemicals 7827
    – cyclic steam injection 7808
    – thermal methods 7808
  – stoves 1365
  – water recovery 2160
  – weathering 1909, 1916
enhancing human health 2262
ensemble Kalman filter 2111
Entamoebidae 12049
enteric virus 11876, 11985–11986, 11992
  – detection 11992
  – found in the environment 11986
Enterobacteriaceae 6324
enterococcal surface protein (*esp*) gene 6328
Enterococcus 5057, 5064, 6319, 6323, 6325, 6331
  – *faecalis* 500
  – *faecium* 6328
  – treatment 5064
enterotoxin 5062, 6328
enterovirus 11989
  – infections 11989
entomopathogen 5444, 5450–5451
  – for insect control 5451
entrained flow
  – gasification/gasifier 1432, 1441, 1666, 5126
  – reactor 1457
entrained solids 4249

entrainment 10613
entropy 9938
environment/environmental 3267, 4070, 4415, 4534, 10075
– adaptation 4070
– assessment methods 8704
– biosensing 1646, 1651, 1657
– filter sampling 1651
– liquid samples 1651
– multiplex detection 1657
– solid surface samples 1651
– subtractive inhibition assays for large molecules 1657
– carcinogenesis 3596
– carcinogens 3610
– careers 10033
– contaminants 3519, 9567
– solar photocatalytic degradation 9567
– countermeasures 3515
– damage 3445
– decision support systems (EDSS) 3517, 3545
– definition 4415
– deviation 464
– economic analysis 4788
– economic sustainability assessment 4789
– education 10019–10020, 10024–10025
– awareness 10020
– field trip 10025
– public's awareness 10024
– sensitivity 10020
– E-factor 4619
– engineering 2019, 10438
– flow requirements 2795
– fluid dynamics code (EFDC) model 9059
– geology 3553
– health 299, 6606
– risk assessment 6606
– impact assessment (EIA) 261, 6367
– indicators 9186
– information 10019
– injustice 193
– interaction 4070
– journalism 10026
– justice 191, 10028, 11339
– law 3354
– literacy 3203, 3207, 10033
– management 3353, 5827
– decision-making support systems (DSS) 5827
– map 3184
– medicine 225
– modeling for radiation safety (EMRAS) program 8439
– models 7010
– collective parameters 7010
– monitoring 1646
– trends 3267
– negotiations skills seminars 10027
– outreach 10019
– partitioning 10075
– performance index (EPI) 196
– policy 187, 3288
– pollutants 4893
– product declarations (EPD) 9038
– life cycle assessment (LCA) 9038
– protection 191, 2687
– protection agency (EPA) 1500
– radioactivity 3583
– regulation 7824
– remediation 10436, 10438–10439, 10441, 10446
– advances in science 10439
– risk assessment 10441, 10446
– scientific measurements 10446
– sustainability principles 10438
– restoration 3516, 3584
– risk factor 67
– sensitivity 412, 463
– site assessments (ESA) 2438
– stewardship 10019, 10024
– sustainability 566, 10321, 10503
– tobacco smoke (ETS) 3632, 3640, 3645
– toxicants in children 3627
– effects during gestation 3627
– effects on germ cells 3627
– toxicants 3633
– toxicity 3663, 3665
– non-radical mechanisms 3665
– toxicology 3586, 3595, 3620, 3655, 3670
– carcinogenesis 3595
– children at risk 3620
– oxidative stress 3655, 3670
– transport models 11019
– water requirements (EWR) 1545
– wicked problems 4534
enzymatic engineering 10830
enzymatic hydrolysis 967, 972, 976
enzyme 8024, 8052
– classification (EC) number 8025
– storage 8052
enzyme-linked immunosorbent assay (ELISA) 5383
eosinophilic granuloma 12032
epicycle 2100
epidemiological model 5352
– within-host dynamics 5352
epigenetics 2971
– instability (EIS) 3607
epigenome 6166
epilancin 504
episomal
– transgenesis 10821
– vectors 10906
epistasis 494
epoxidation catalyst 7602–7603
– Jacobsen-type 7603
epoxide
– hydrase 1634
– hydrolases 12301
Epstein-Barr virus (EBV) 5000
equal temperature split 4275, 4278
equation 5675
– of motion 627
equatorial belt 9637–9638
equilibrium
– climate sensitivity (ECS) 2516
– tidal theory 10614
equine infectious anemia virus 10905
equipment grounding 3004
equivalent
– network 12154
– water thickness 4568
Equus ferus caballus 1797
ErbB3 3161
ergonomic design 10278
Ergun equations 5306, 5308
Eribulin 3158–3159
erosion 1918, 3705, 3707, 3710, 3723
– on agricultural land 3707
– use of fallout radionuclides 3710
erucic acid 4557
erythema 4906, 11378
erythromycin 500, 505
Erythroneura elegantula 156
erythropoietin 8064
Escherichia coli 5059, 6319, 6325, 6328, 6622, 7332, 7669, 8077, 8761
– isotherm 7678–7679
– toxin genes 6328
essential amino acid 1692
– availability 1692
essential fatty acid 1696
ester-carbonate compound 6043–6044
esterification 928
ester 10667

estimated breeding value (EBV) 419, 422, 443, 446, 459, 2786, 9368, 9373, 9375, 9378
– selection 9375
– accuracies 9368
estradiol 6154
estrogen 11963, 11974, 11976, 11978
– glucuronides 11971
– biodegradation 11976
– receptor (ESR) 10892
– sorption 11974
estuarine ecosystems 11913
estuary/estuarial 7338
– effect 2796
– phytoplankton productivity 7338
– redox processes 7338
ethane 3994
ethanol 303, 359, 962, 978, 980, 982, 996, 999, 1005, 1006, 1012, 1016, 1018–1020, 1022, 1028, 1222–1224, 1477, 1504, 2242, 3633, 3859, 5463, 5466, 5473, 5478–5480, 5493, 8175, 10507–10508, 10510, 10527, 10641, 11316, 11430–11431, 11449
– blends 5493
– Brazilian 1005
– experience 1018
– taxes 1012
– consumption 10641
– health problems 10641
– corn-based 1504, 10527
– dehydration 996, 999
– engine fleets 1016
– first-generation 980
– from sugarcane 982, 1005
– agrochemicals 1010
– air pollution 1010
– soil quality 1010
– plant 978, 10510
– price 1012
– production 1222
– cycle 11943
– programs 1019
– second-generation technologies 1022
– transportation 1019
– use 1224
– of agricultural land 1020
ethephon 6210
ether 10666, 11445
ethyl
– acetate 3935
– alcohol, see ethanol
– methanesulfonate mutagenesis 2704
– methyl carbonate (EMC) 6127
ethylbenzene 4590
ethylendiamine 8291
ethylene 3961, 3994
– carbonate (EC) 6040, 6042, 6044, 6070, 6127
– electrolytes 6085
– one-electron reduction 6042
– two-electron reduction 6044
– epoxidation 3943
– glycol 381
– diacetate 11830
– propylene diene monomer [M-class] rubber 3003
– refrigeration 3961
– response factor (ERF) 2706, 2713
ethylene-expanded liquid 3943
ethylene-propylene-diene (EPDM)
– copolymer 8744
– monomer 7724
ethylnitrosourea (ENU) 6794
ethyl-tertiary-butyl-ether (ETBE) 1042
Eucalyptus 1288–1289, 1293, 1539
– species 1289
euchromatin 2553
Euclidean distance 2465–2466, 2470–2471, 10598
– metric 10610
eukaryotic organisms 1654
Euler equation 12065, 12075
Eulerian model 261, 11284
Eulerian-integral model 10990
euphausids 12033
eurobarometer 10872
European
– food safety authority 10773
– landscape convention 10387
– lead-cooled system (ELSY) 4056
– list of waste 11592
– soil moisture and ocean salinity satellite (SMOS) 8931
– waste incineration plants 11734
– wind atlas 6600
– workplace regulations 2879
europlasma gasification process 8109
eutrophication 943, 1598, 1620, 1935, 1942, 1950, 2502, 3044, 3783
– in dams 11942
evaluated nuclear data files (ENDF) 8587
evaluated nuclear structure data files (ENSDF) 8587
evaporation 253, 257, 2899
– cooling 897, 4709, 9526, 9528
evapotranspiration 1545, 3213, 4690, 4718, 4740, 5621, 7246
– coefficient (ETC) 1102
evidence-based building design 5340–5341, 5343
– economic performance 5340
– hospitals 5340
– office buildings 5343
– schools 5341
evolution/evolutionary 10081
– biology 4529, 9371, 9389
– scientific controversy 4529
– genetics 468, 9380
E-waste, see electronic waste
EWITS study 12179
excavating machine 3032
excess air factor 2166
excessive lead–210 3715, 3730, 3733, 3737
– depth distributions 3737
– measurements 3730, 3737
– sedimentation rates 3733
excitation energy 3794, 3801
exciton-blocking layer (EBL) 7574
exclusive economic zone (EEZ) 7321, 7384
exergy 5518, 5520–5521, 11766
– destruction 5521
– system efficiency 9592, 9594
exhaust gas 6816
– recirculation (EGR) 267, 6849
– stream 8091
– thermal energy 6816
exo-cellulase 8048
exogenous carcinogen exposure 3610
exotic germplasm 8017, 8019
exotic oils 6897
expanded natural graphite (ENG) 9613
expansion–intensification agricultural model 153
expendable bathythermograph (XBT) 2500
experimental
– breeder reactor II (EBR-II) 4060
– car 11196–11197
– observer performances 11196
– test conditions 11197
– validation of observers 11197
– technology demonstration reactor (ETDR) 4054
– vehicle 3060
explanatory knowledge 4535
exploration drilling 4417, 6417
explosives 10156
export 1489
exposome 3658
express
– bus 6005, 6006
– corridors 6006
– services 1872

– lane 5023, 5028, 5031, 5042
– earned credits 5042
– users 5029
expressway 5032
extended Kalman filter 2472, 3059, 11194
extended producer responsibility 3445
extended X-ray absorption fine structure (EXAFS) 6076
extended-range electric vehicle (EREV) 11509
extending dynamic range 11109
– reliably 11110
– technologies 11109
extensive ecosystem 3526
– countermeasures 3526
– remedial actions 3526
extensive marine aquaculture 514
exterior shading devices 3689
external dosimetry 3023
external quantum efficiency (EQE) 6575
extraction boreholes 4809
extraterrestrial irradiance/radiation 10625, 10627
extraterrestrial spectrum (ETS) 9707
extreme ultraviolet (EUV) 9708
extreme wave 7404
extreme wind 7402
extruded cable 11170
– core manufacture 11170
eye closure 3121
– duration 3121
– frequency 3121
eye-dose equivalent 3026

F

FabH 500
fabric filter 4960, 4990, 8357–8358, 11807, 11815
– filtration media 8357
facade 3675, 3677, 3680, 3683, 3686–3687, 3690, 3692, 3694, 3697, 3699, 3702
– climate-responsive 3687
– daylighting as dominant source of lighting 3680
– designed to manage water 3697
– double envelope 3690
– effective maintainability 3699
– glare control 3687
– individual access to the natural environment 3677
– innovation through systems integration 3702
– load balancing 3692
– mean radiant temperature control 3690
– minimizing excessive heat losses or heat gains 3686
– natural ventilation 3683
– natural weathering 3699
– passive solar heating 3694
– rain screens 3690, 3697
– shading 3687
– temperature control 3687
facial action coding system (FACS) 3121
facilitation 3281
factorial regression model 4082, 4086
factual knowledge 4534
faculae 9800
Faecalibacterium 6327
falciparum malaria 6295, 11076–11077, 11083
– resistance to chloroquine 11083
Falkenmark's water crowding indicator 2326
fallout radionuclide 3705–3706, 3709, 3711, 3720–3721, 3723, 3742, 3744–3746, 3749, 3755, 3758, 3760
– activity 3749
– as tracers 3723
– biological 3721
– corers 3746
– depth distribution 3721
– diffusion-like processes 3721
– field techniques 3745
– for sediment source fingerprinting 3755, 3758
– for tracing suspended sediment sources 3742
– in soil erosion and sedimentation 3749, 3760
– in the soil 3718
– inputs 3711
– inventory 3749
– measurements 3748
– Germanium detectors 3748
– uncertainty considerations 3748
– laboratory techniques 3745, 3746
– sediment source 3744
– sources 3711
– storage in soil 3720
– techniques 3746
fallow 2748
FAME 1466
– scrubber 1466
family biotic index 3273
FAO ecosystem 534
Faradaic materials 3499
Faraday constant 745, 3875, 3927, 5105, 5139, 5157
fare collection system 92
far-infrared (FIR) cameras can 11115
farm/farming 2728, 2729
– animal 476, 478, 482–483, 486, 1757, 1773, 1783, 1785, 8001, 11402
– biodiversity 1773
– economic traits 478
– fine mapping 486
– genetic resources 1783
– genetic variation 1785
– production 7973
– QTL mapping 486
– random breeding population 482
– UV hazards 11402
– welfare 1785
– aquaculture resource management (FARM) 552
– bivalves 1960, 1963
– carbon 165
– fit with nature 540
– income 4435
– multiplication unit 396
– new technologies 2728
– productivity 10714
– system 151, 394, 2741, 2750
– diversification 151, 2750
– terminal sires 396
– traditional 2729
farmer 4507
– farmers' association 395
– suicides in India 4507
FARMSCAPE tools 9327
farnesyl transferase 7
fasciolosis 5361
fast breeder
– reactor (FBR) 7104, 7135, 11216
– test reactor (FBTR) 4060
fast bus 5989
fast flux test facility (FFTF) 4060
fast ignition 7171
fast neutron 7090
fast pyrolysis 1520, 1522, 11445
fast-neutron-spectrum breeder reactor (FBR) 7103
fatigue 3112, 3120, 3123, 3129
– detection 3120, 3129, 3123
– algorithms 3112
– quantifying 3129
fatigue-related accident 3109
fat 1678
fatty acid 927–928, 1681
– biosynthesis 360, 500
– ethyl esters (FAEE) 927, 5488
– methyl esters (FAME) 928, 1042, 1044, 1206, 1219, 1443, 3945, 5488, 8083
faulting 3250
favorable free 9596

feasibility study (FS) 2009
feature-level fusion 6954
fecal
– bacteria 6329, 7679, 7682
– coliform 6324, 6325, 11877, 11879
– contamination 6624, 8763
– indicator 6319, 6322–6323, 6333–6334
– applications 6333
– bacteria (FIB) 7671, 9164
– detection 6323
– important attributes 6322
– rapid methods 6334
– risk of pathogen exposure 6333
– microbes 7674
– microorganisms 7670
– pollution 6319–6320, 6323, 6326, 6329–6331, 6333, 8761
– host-associated marker 6331
– impact on coastal waters 6320
– microbial source identification 6330
– quantification of bacterial indicators 6329
– sources 6326
– viral indicators 6329
– waterborne disease 6320
– source identification (FSI) 6330
feces composting 9980
fed aquaculture 540, 544, 577, 7264
federal facility compliance act 10018
feed 2682
– chute 4962
– hopper 4962
– pump analysis 4263
– security 2682
– slurry 2204
feedback control 51
feedback loop 10068
feeder
– circuits 2980
– protections 3011
– voltage 2978
feed-in tariff (FIT) system 1099, 10340, 12263
feedstock 1270
– availability 1270
– suitability 869
fenestration industry 2838
Fenton
– chemistry 7607, 9575
– reaction 6542
– reagent 7607, 9575
Fenton-like reagent 9575
fermentation/fermenter 962, 973, 975, 988, 993–994, 999, 1091, 1093, 1132, 1137, 1181, 1223, 1613, 2117, 3914, 9940
– energy savings 999
– gas 9940
– residues 1137
– utilization 1132
Fermi
– constant 6079
– contact shifts 6080
– energy 754
ferredoxin 1479
ferric
– citrate 9577
– iron 9576
– photoreduction 9576
– iron–water complexes 9576
– oxalate 9577
– oxyhydroxide 10414
ferrierite 4590
ferrite magnet 28
ferromagnet 6247
ferromagnetic circuit 6248
ferroresonance 3019
ferrous contaminants 8805
ferrous metals 8811
– recycling 8811
fertility 10889
fertilization management 2663
fertilizer/fertilizing 1103, 1135, 2578, 2742, 3768–3770, 3772–3776, 3778–3784
– additives 3773
– ammonia emissions 3781
– ammonia-based 3782
– cost of nutrients 3775
– decision support 3779
– distribution 3770
– effects on agricultural productivity 3774
– emissions 1135
– energy cost 3783
– environmental benefits 3781
– industry 2747
– greenhouse gas emissions 3781
– human health 3783
– in organic farming 3780
– inorganic 3769
– macronutrients 3769
– management 3776, 3778, 3784
– marketing 3770, 3773
– mining 3770
– nutrients 3769
– optical sensor 3780
– phosphorus 3778
– potassium 3778
– precision agriculture 3779
– prices 3770, 3773
– recommendations 3779, 9328
– resource availability 3783
– science 3768
– soil
– acidification 3782
– tests 3775
– subsidies 3774
– sustainability 3769–3770
– technology 3768
– transport costs 3772
– use 2687
– sustainability 2687
– water pollution 3781
– yield maps 3779
fetus 3626
– exposure to toxicants 3626
fiber 1678, 8827
– dietary 1678
– fiber filter 10107
– insoluble 1678
– recycling 8827
– soluble 1678
fiberboard 2410
fiber-optic communication networks 12083
fibroblast 10827
fibropapillomatosis 6193
Fick's law 2017–2018, 2021, 3810, 3812, 9134, 10963, 10991
field
– crops 11398
– orientation
– algorithm 42
– principle 36
– reconstruction method (FRM) 44
– relevant for driving (FRD) 3122
field-oriented control 36
field-reversed configuration (FRC) 7167
filamentous algae 3563
filter ash 11731–11734
– Bamberg model 11732
– characterization 11731
– disposal practice 11731
– Ferrox process 11733
– stabilization processes 11732
– thermal treatment 11732
filter cake 1006
filter-feeding fouling organisms 1965
filtration collectors 1393
final renewable fuel standard 1500
final sink 10581
fine coal 2213
– dewatering 2213
fine mapping 487, 2712

fine particulate pollution 229
finfish 7265
– aquaculture 1935, 6365
– cage culture 1967
– culture 6762
– production 7265
finite impulse response 56
fire code requirement 1031
fire corals 12046
fire tube boiler 1343
fired brick 3833, 3834
– manufacturing 3834
fireplace 1360
fireweed 12047
firewood 1232, 1368
– boiler 1356
Fischer–Tropsch (F-T)
– diesel 935, 1054
– fuels 1049, 1062, 1584
– hydrocarbon production 1589
– process 2224, 3971, 5472, 5473, 5491
– reaction pathway 3971
– reaction 936, 2240, 2252, 3975, 5225, 5226
– Anderson–Schultz–Flory (ASF) distribution 3975
– catalysts 3975
– product water 2252
– stoichiometry 3963
– synthesis 922, 1428, 1442, 1585, 2236, 3845, 3958, 3964, 3970, 3972, 3976–3977
– catalyst beds 3976
– chain initiation and propagation 3972
– chain termination 3972
– commercial activities 3977
– formation of C_1 species 3972
– kinetics 3976
– product upgrading 3977
– reactors 3976
fish 9165, 10089, 11408
– aggregation devices 3566
– aquaculture 558, 1942
– as sentinels 9165
– cages 1949
– culture systems 10799
– diversity 6181
– farm/farming 522, 583, 591, 1930, 1942, 1947, 3557, 3560, 3576, 3580, 3581
– ecological footprint 3581
– farm escapees 3567
– net pens 3580
– open-ocean 3581
– worker safety 583
– habitat projections 5697
– under future climate scenarios 5697
– habitat simulation program 5696
– health management 3580
– mariculture 9120
– meal 3574
– oil usage 3574
– UV hazards 11408
fishery 535, 540, 546, 550, 592, 6182–6183, 6387–6389, 6391, 6393, 6395, 7390, 11408
– artisanal 592
– ecosystems 540, 2266
– governance 6393
– habitat destruction 6182
– hatchery-based 6388
– interactions 6183
– management 546, 6387, 6389, 6391
– science 6388
– scientists 6395
– stocks 6387
– enhancement 6388
– UV hazards 11408
– wastes 12020
fish-hunting cone snail 3165
fish-in to fish-out ratio 5899
fishing 2504
– down the food chain 3576
– regulation 2504
– technology 512
fissile
– fuel 7179
– isotope 3791, 3819, 7178
– nucleus 3791
– nuclides 7089
– plutonium 7104
fission 3791, 3793–3796, 3799, 3803, 3806–3807, 3809, 3813, 3818, 7088–7090, 8560
– activation energy 3793
– chain reaction 7089
– energy 7090
– fissionable materials 7089
– fragments 3799
– neutron-induced 3794
– neutrons 3809, 8567
– production 7089
– product 3791, 3818, 7152, 8600
– decay heat 7152
– nucleus 3795
– poisons 3807
– reactor 3790, 3799, 8567
– cooling system 3799
– design 3796, 3799, 3803
– development 3818
– fuel reprocessing plant 7179
– heavy elements 3790
– performance 3813
– physics 3787
– source 3806
fission-product photon 8570
fitness ratio 10067, 10072
fixed bed reactor (FBR) technology 2243
fixed gear ratio single gear box 3370
fixed bed gasifier 1430, 1451
fixed-gearing transmission 11535
fixed-speed turbine 12150, 12160, 12161, 12164, 12165
– start-up 12161
– with a variable rotor resistance 12150
– with active Pitch Mechanism 12165
flagella 5050
flared natural gas 6811
flash distillation 2899
flash flood 1561
flash power station 4309
– bottoming organic rankine cycle 4309
flash pyrolysis 1213
flash steam rankine cycle 4276
flat toll 5030
flatfish 519
flat-plate collector 9524
flatworm 3152
flavin adenine dinucleotide (FAD) 1684
flavin mononucleotide (FMN) 1684
flavonoid 6522
flax gene 10699
fleet management 91
flexible AC transmission system (FACTS) 8987
flexible bus 1861
flexible paratransit 1858
flexible-fuel vehicle (FFV) 1004, 1616, 5465, 10491, 10507, 10527, 11432
flicker 3004
– emission 12160
– severity index 12157
float/floating
– drum digesters 1153
– ice 2765, 2772, 2774
– offshore wind turbine (FOWT) 7395, 7416
– technology 3231
– voltage 5883
float-zone-grown monocrystal 9201
flood/flooding 917, 2789–2790, 2792, 7699, 8943, 10751
– basalts 1912
– control 2790
– control dam 3744
– deposits 3760

– emergency alarm systems 2792
– frequency 2321
– generation 10615
– inundation 3736, 3754
– management 4687
– prevention 5827
– regulation 2790
– remote sensing 8943
– risk 11334
– tide 10615
flooded electrolyte lead acid 8747
floodplain 3735–3737, 3740–3741, 3753–3754
– CIRCAUS model 3740
– cultivated 3737
– deposits 3754
– microtopography 3736
– profile 3723
– sedimentation rates 3753
– surface 3736, 3741
floral initiation 2646
floral pre-meiotic differentiation 2646
floral sterility 10394
– heat-induced 10394
floret 2542
flotation
– collectors 2216
– machines 2202
flour fortification initiative (FFI) 1688
flow cytometry 6527
flow matrix 3308
flow modelling 11277
– individual buildings 11277
– surrounding streets 11277
flower initiation 2647
flowering 2552, 2646
– plants 1140
– time 2556, 2697, 4076
flowing property 9844
flue gas 171, 1254, 1323, 1336, 1345, 1386, 1389, 1393, 1395, 1468, 2152, 2272–2274, 2278, 3822, 3966, 4960, 4975, 4987, 4990, 4993, 5266, 6451, 6463, 6998, 8354, 8359, 8361, 8365, 11784, 11809
– aerosol concentration 1254
– cleaning 1448, 1610, 5238, 5249, 5269, 5289
– equipment 2273
– composition 5266
– condensation 1395
– installation 11784
– desulfurization 171, 2278, 3822, 8359, 11702
– scrubber material 11702
– emissions 1389
– fly-ash concentration 1254
– of full-scale combustors 6998
– quality 4993
– recirculation 2171, 2272, 4968, 4984, 6463
– treatment 1249, 1393, 1468
– volume flow 2274
fluid bed combustor 11804
fluid catalytic cracking 7832
fluid density interface 2052
fluid enthalpy 9008
fluidization 1432
fluidized bed
– combustion plants 1244
– reactors 7956
– gasification 3998, 5127
– gasifiers 1431, 1456, 1666, 11443
– gasifying melting systems 11586
– incinerators 5278, 5280
– systems 2273, 11855, 11861
– limitations 11855
– reference projects 11861
– selected concepts 11861
– technical features 11855
fluidized catalytic cracking 2246
fluke 12023
FLUMAGIS project 5828
fluorenylidene biphenylene 6551
fluorescein 4209
fluorescence/fluorescent 11377
– in situ hybridization (FISH) 2602, 5384
– radiation 8574
– yield 8575
fluoride 786
fluorinated polymer 6539
fluorine 6504
fluorite anode 2958
fluoroelastomer 7724, 7872
fluorophosphate 727
fluoropolymer 9582
fluorous solvent 7601
fluquinconazole 6209
fluridone 9148
flux
– angle 42
– correction 2512
– equations 2027
– linkage equation 40
– weakening 35
fluxomics 6532
flux-reversal/switching permanent magnet machine 11529, 11530
fly ash 1322, 1336, 1363, 2195, 3820–3825, 3827–3828, 3830–3831, 3834–3836, 3838, 4001, 4867–4868, 4872, 5237, 5253, 6489, 8352, 8354, 10583, 11583, 11720, 11739–11740, 11742, 11746, 11800
– applications 3827–3828
– bricks 3835
– chemical composition 11740
– classification 3825
– collection systems 3822, 3825, 3830
– construction products 3823
– environmental impacts 3836
– heavy metals concentrate 11800
– in concrete 3830
– management 3824
– metals 11740
– chlorides 4872
– particle (grain) size distribution 11742
– production 3821
– properties 3825
– in concrete applications 3831
– rate of utilization 3821
– soluble salts 11742
– toxic metals 11742
– toxic trace elements 3838
– utilization 3824
– vitrification 11583, 11746
– washing 11746
flyback converter 692
flying capacitor method 703
flywheel 5107–5110, 5114
– brushless DC motor (BLDC) 5110
– energy capacity 5108
– induction motor 5110
– permanent magnet (PM) 5110
– power capability 5110
– switched reluctance motor (SRM) 5110
– system 5110
– efficiency 5110
– theoretical specific energy 5109
flywheel/ultracapacitor system 5114
foam cement 4403
focused identification of germplasm strategy (FIGS) 2734
fodder beet 1112
fodder cropping 1127
foehn wind 11299
fog 3138–3140, 3142
– collision
– detection 3140
– risk 3140
– contrast sensitivity 3142
– density
– condition 3139
– values 3138

– investigation and dispersal operation (FIDO) 4106
– reduced visibility 3138, 3140
folate 1710
folding bike 814
folic acid 1684, 1710
follicle maturation 10891
follicular stimulating hormone 6154
food 576–577, 837, 1746, 2289, 2682, 2685, 2687, 2721, 2736–2737, 2743–2744, 2754
– animals 10858
– health status 10858
– chain 822–825, 949, 3576
– biomagnifications 822
– contamination 7668
– in town 949
– magnification principles 824
– magnification 825
– modeling 824, 8427
– theory 822
– waste 824
– contamination 4897
– crops 1545, 2649, 8044
– effect of drought 2649
– generally regarded as safe (GRAS) status 8044
– non-food crops 8044
– demands 1566
– food and feed regulation 10775
– GMO-derived 2289
– industry 1180
– insecurity 1676, 1746, 2685, 2737
– methylmercury-containing 837
– processing 9487
– production 577, 1546, 1741, 2536, 2744, 2754, 10853
– from farm animals 1741
– safety 6614, 10769
– safety hazard 9082
– seafood-associated 9082
– security 1750, 2529, 2682, 2687, 2721, 2736, 2743, 10714
– traceability 576
– warmer 9493
– waste 11657, 11833
– food web 3301, 11408
food and feed regulation 10775
food-feed-fuel 1566
– market mechanism 1566
foot-and-mouth disease (FMD) 411, 1759, 5351, 5360, 10860
– mathematical models of the spread 5351
– virus (FMDV) 2970, 8075
footprint on the oceans 3558
footrot 1758
forage
– cropping 1127
– harvesters 1130
– mixture 1114
forced-draft cooling towers 9533
forecast 2119, 2131, 2132, 2523
– models 8921
– overconfident 2131
– probabilities 2129
– monsoon rainfall 6741
– reliability 2131
– retrospective 2131
– seasonal-to-interannual 2132
– skill 2125
– uncertainty 2131
foreign breed 392, 394
foreign DNA 10901, 10906
forest 1538, 3315, 3328–3331, 3533
– change 3290
– disturbance 3326, 3329
– ecosystem 3328–3330
– fire 8944, 8945
– remote sensing 8944, 8945
– gap models 3292
– management 3289, 3329
– modeling concept 3289
– models 3290
– individual-tree-based 3290
– regeneration processes 3329
– remediation strategy 3533
– residues 1538
– spatial heterogeneity 3329
– succession 3329, 3331
forestry 1567, 1573, 3289–3291
– by-products 1567
– JABOWA model 3291
– management 1539
– models 3291
– gap model 3291
– residues 1573
– site index 3289
formaldehyde 303, 3989, 10639
formaniferans tube worms 3151
forward converter 692
forward looking infrared radiometer (FLIR) 11640
forward osmosis (FO) 2915, 10540
– bioreactors (FO-MBR) 11890
fosmidomycin 502
fossil 3844
– biofuel 552
– carbon 4759
– dioxide 1598
– diesel 1601
– energy mix factors 4764
– energy 3844, 9620
– fuel 161, 164, 170, 348, 608, 668, 867, 870, 872, 930, 1040, 1099, 1217, 1584, 1601, 1608, 2175, 2191, 3462, 3928, 3929, 3934, 4120, 4121, 4225, 4376, 4762, 5174, 5462, 6566, 6806, 8174, 8348
– combustion 8887, 8895
– emission 116
– energy 1351
– price fluctuations 1584
– heat mix 4770
– hydrocarbon 1300
– primary energy sources 9935
– resource 2222, 3844
fouling index 10540
foundation pile 4147
founder animal 10876
foundry sand 11702
Fourier transform infrared (FTIR) spectroscopy 5386, 10539
Fourier transformation 6073, 10972
Fourier transform-ion cyclotron resonance MS (FT-ICR MS) 1186
four-pole induction motor 5091
four-wheel vehicle model (FWVM) 3055, 11189–11190
fowl cholera 641
fraction of absorbed photosynthetically active radiation (fAPAR) 7902, 7925
– satellite observations 7925
fractional interception 2618
fractionated aquaculture system 544
fractured aquifer 4795, 4796, 4798
– coal tar contamination 4798
fragmented infrastructure 10303
Francisella 1932
free energy 3875
free estrogen 11967
free fatty acids (FFA) 1045
free ion activity model (FIAM) 10052
free oxide 2432
free radical chain reactions 3663
free radical polymerization 2945
free sugar 11435
free water surface 11893
free-air controlled enhancement (FACE) 3225
free-driving condition level 3094–3095
free-rolling buildings 3677
freeway busway 1858, 1875
freeway traffic surveillance applications 11457
freezing nuclei 659
freezing point 2766
Freidel-crafts reaction 4606

freight railroad 5964
– vehicle 5957
freight rapid transit 7792
freight train 5965
frequency control 8987
– interconnection queue process 8987
fresh-air ventilation 7631
freshwater 1546, 6318, 7669, 10292
– availability 10292
– ecosystems 2065, 3316
– fecal indicators 6318
– fish 10089
– freshwater fish farming 525
– microbial contamination 7669
– ornamental fisheries 6187
– resources 2320, 2322, 2332
– impact of climate change 2320
– shrimp 8202
– supply 2078
– system 2064
Fresnel
– approximation 2353
– collector 2351, 6031
– surface 2868, 2870
Freundlich
– isotherm 7678, 8612, 8618, 10968
– partition coefficient 8612
Friedel–Crafts alkylation 4590, 4598, 4625, 4631
fringing reef 2491
FROG (free ranging on grid) technology 7792
froth flotation 2202, 2212, 2216, 2412
frother 2202, 2216
Froude number 10993
frozen semen 396
frozen soil 3214, 3220–3221
fructose 1278
fruit maturity 2649
fruit tree 2652
F_0 founder bird 645
fuel 1037, 1254, 1287, 1303, 1319, 1327, 2255, 2381, 3907, 3911, 3915, 5139, 5245, 5251, 5284, 5520, 6721, 9822
– assemblies 8590
– batteries 3429
– carbon deposition 3907
– characterization 9822
– chemical energy 6721
– clad 7196
– combustion 251
– consumption rate 11493
– conversion efficiency 5510, 5520
– cycle 10503
– pump-to-wheels (PTW) stage 10503
– well-to-pump (WTP) stage 10503
– well-to-wheels (WTW) metric 10503
– economy 3483, 3500
– of a vehicle 10492
– simulation 3486
– efficiency 10482
– elementary analysis 5251
– exergy 5520
– flexibility 1037, 3907
– from solar energy 9589
– gas 1462, 2171, 3998
– tar removal 1462
– treatment 1462
– gasification 1327
– heat energy 6833
– heating value 1303
– higher heating value (HHV) 5245
– impurity 3911, 3915
– incomplete oxidation 1319
– infrastructure 2255
– injection units 3861
– knock 5532
– legislation 267
– nitrogen 5309
– oil 4378
– carbon pollution 4378
– oxidation 2939, 2946
– particles 1254
– processing 5139, 5141, 5144–5145, 5157, 7879
– accidents 8502
– endothermic reforming reactions 5139
– endothermicity 5141
– exothermic fuel cell reactions 5139
– steam methane reforming 5144
– steam reformation (SMR) 5157
– water–gas shift (WGS) 5144, 5157
– water–gas-shift (WGS) reaction 5144
– procurement 2282
– refuse-derived 5284
– savings 6016
– light rail transit (LRT) 6016
– solar thermal production 2381
– specification 9822
– storage 1030
– utilizations 5156
– electrochemical efficiency 5156
– factors 5139
– reaction loss 5156
– washing 1260
– waste 6449
– wood-derived 1287
fuel–air
– cycle analysis 5513, 5515
– mass flow ratio 6819
fuel cell 1032, 1413, 1462, 2935, 3385, 3495–3496, 3847, 3849, 3858, 3861–3863, 3868, 3870, 3872–3873, 3877, 3880–3881, 3883, 3886, 3926, 3928, 3930, 5141, 5161, 6721–6722, 6725, 6832, 7694, 7695, 7700, 7703, 7706, 7713–7714, 7717–7719, 7732, 7740, 7741, 7867, 7876, 8206, 8207, 8210–8211, 8217–8219, 8223–8226 8228, 8240, 8245, 8266, 8290, 8292, 8329, 8344, 10516
– accelerated stress tests 7719
– activation losses 7706
– air
– bleeds 7718
– contaminants 7713
– alternative approaches 3886
– architecture 8218
– as a power system 3863
– carbon 3858
– corrosion 7718
– catalytic activity 8292
– cathode catalyst 7740
– classification 3880
– commonly used fuels 3861
– CO poisoning 8226
– comparison to alternate technologies 3847
– contaminants for catalysts 7717
– costs 7700
– critical parameters 8210
– critical specifications 8210
– current–voltage characteristics 3495, 8210
– definition 3873
– efficiency 9600
– electric vehicles 11509
– electrical efficiency 7703
– electrochemistry 3872
– electrodes 6725, 7762, 8344
– gas-transport properties 7762
– energy
– conversion 3930
– end game 8228
– families 3881
– for hybridization 3868
– forklift applications 8228
– freezing 8223
– gas diffusion layer 8207
– Gibbs free energy 8206

– H_2-air front 8245
– high temperature 6722
– hybrid architecture 3870
– hybrid vehicles (FCHV) 3371, 8239
  – drive train 3390
– industry 6561, 8206
– life cycle assessment (LCA) 3928
– load following 8225
– load-leveled control strategy 3496
– low temperature 6721
– market requirements 7867
– mass flow 3877
– materials 7703
– measurements 8290
– medium-temperature 7867
– methanol-fed 3883
– nanoscale materials 8211
– non-noble metal catalysts (NNMC) 8266
– Ohmic losses 7706
– operating temperature 7732
– platform strategy 8217
– poisoning 7714
– power assist control strategy 3496
– power plants 7879
  – balance of plant (BOP) 7879
– process of designing 8217
– product
  – development process 8219
  – strategy 8217
– proton exchange membrane (PEM) technology 10516
– Pt metal dissolution 7741
– quality function deployment (QFD) process 8217
– reliability 8226
– source of fuels 3862
– stability of alloys 7717
– stack 10500
– start/stops 8224
– sustainability 8228
– system 3385, 3390, 7762, 8207
  – cost 8226
  – efficiency 5141
  – engineering 8219
  – hybridization 3390
  – propulsion battery 7762
– technical readiness 8223
– technologies 3385, 3872
– triple phase boundary 8211
– types 3872
– vehicle (FCV) 3367, 3371, 3385, 3484, 3389, 3495, 3496, 5161, 7695, 8253, 10500, 10515
  – architectures 3385
  – hydrogen pathways 10515
  – power split strategies 3495
  – powertrain configurations 3495
  – recent progress 8253
  – simulation results 3496
  – simulations using ultracapacitors 3495
  – ultracapacitors 3484
– V-flow stack configuration 8240
– voice of the customer (VOC) 8217
– water management 8329
fuelwood 1289, 1300
fugacity of oxygen 2939
Fukushima accident 8389
full converter turbine 12162
  – steady-state influence 12162
full facility tolling 5043
full hybrid electric vehicles 11508
full-bridge converter 692
full-power converter system 12151, 12164, 12167
fumarole 4426, 11617, 11630, 11639
functional food 10751–10752
fungal agent 3164–3165
  – from marine sources 3164
fungal disease 2731
fungal pathogen 10696
Fungia 2493
fungicide 2567, 2578, 5440
  – protection 2721
  – resistance 2569
furan 172, 4883–4884, 4992, 8110, 10666
furnace 1351, 1354, 1355, 1370, 1373, 1377, 1379, 1380, 1383, 1384, 1417, 5255
  – automatically charged 1373
  – drop-down feeding
    – with cup burner 1375
    – with tilting grate 1377
  – for bulk material 1383
  – for herbaceous fuels 1381
  – for whole bales 1384
  – heat storage 1370
  – horizontally fed burners 1380
  – manually charged 1355
  – pellet-fueled 1375
  – small-scale 1351
  – underfed burners 1379
  – wood burning 1355, 1370, 1417
Fusarium 1281
fuse 3001, 3012
fusion
  – neutrons 8568
  – power plants 7177
  – reactor blanket 7179
  – techniques 6954
    – grid-based 6954
fusion–fission hybrid 7178, 7179
future climate 2099, 2101, 2104, 2109–2111
  – Bayesian methodology 2109, 2110
  – best-guess simulation 2104
  – discrete probability distribution 2111
  – probabilistic statement 2109
FutureGen project 2159
fuzzy
  – inference system (FIS) 3116
  – logic 1346

G

Gabon reactor 3793
gain-of-functions strategy 2970
galactic cosmic radiation/rays (GCR) 8541, 8472, 8560, 8577, 8586, 9477, 9797
β-galactosidase reporter genes 644
gallium arsenide (GaAs) 7935
galvanic cell 740
Gambierdiscus 831–832
  – *toxicus* 829
gambiertoxin 829
gametocytocide 11086
gametogenesis 6153
gamma
  – decay 8564
  – photon 8568, 8570
    – sources 8570
  – radiation 5574, 5584, 5587, 5589, 5608, 5611
    – effects on life span 5589
  – ray 3026, 5561, 5574, 8537, 8552, 8553, 8600
    – dose, albedo approximations 8551
    – MicroSkyshine 8553
    – photon 7207
    – shielding methods 8540
    – Skyshine 8553
    – spectra 7207
    – streaming 8552
    – tracking spectrometers 5572
  – spectrometry 3747
    – analyzing soil and sediment samples 3747
Gammaproteobacteria 5055
garbage 10014
garden atrium 909
garden city movement 8857
gas/gaseous 1590, 3947, 7449–7450, 7453, 7455
  – anhydrous ammonia 3772
  – batteries 3849, 8232

– biofuels 1215
– biomass 1415
  – use of biogas 1415
– burnout 4969
– cap 7801
  – drive 7803
– capture system 5925
– centrifugation 5634, 5636
– chromatography-MS (GC-MS) 1186
– clathrates 6846
– cleaning 1442, 1589, 1590, 1662, 11733
  – residues 11720, 11733
  – strategy 1437
– collection systems 4772, 5741
– compression cables 11180
– conditioning 1442, 1589, 1590
– deepwater exploration 7450
– diffusion 5634–5635, 5637, 5641
  – electrode (GDE) 3874, 8292
  – ideal cascade 5641
  – layer (GDL) 3874, 7697, 7701, 7759
  – media (GDM) 7697, 7699, 7701, 7708, 7758
  – overpotential 7759
– diffusivity 2938
– distributor 11854
– energy carrier 1662
– engine 1460, 1469, 1470, 1528
  – cocurrent gasifier 1469
  – countercurrent gasifier 1469–1470
– entry act 1623
– exchange 597, 600
  – smooth water surfaces 600
– flood 7804
– flow modeling 5302
– flux 11630
– from coal beds 7455
– from tight sandstones 7455
– fuel 5470, 5484, 6838
– generation 1447
– geologic occurrence 7449
– geothermometry 5225
– hydrate 330, 331, 333–335, 337–339, 341, 342, 344, 3845, 6846, 7453
  – Canada 337
  – China 335
  – commercialization 333
  – depressurization 344
  – Eileen trend 338
  – exploration in Alaska 338
  – field programs 335
  – field scale reservoir simulation study 342
  – global distribution 331
  – history 330
  – Hot Ice No.1 well 339
  – India 337
  – inhibitors 344
  – Japan 335
  – material balance study 342
  – Mt. Elbert–01 Hydrate Test well 339
  – New Zealand 338
  – production 333
  – resource potential 334, 338
  – South Korea 335
  – stability modeling for BGF pools 341
  – tarn trend 338
  – thermal methods 344
  – United States 337
– in conventional fields 7449
– insulated transmission 12186
– mobility 7808
– multiplication 5564
– organic (hydrocarbon) air pollutants 11316
– phase oxidation 1352
– pipeline 6419
– plumes 11639
– pollutants 11322
– production 344
– remaining resources 7453
– shales 7455
– solubility 3947, 6724
– starvation 4614
– tar 1463
– transfer 603
– tritium light sources (GTLS) 8525
– turbine 1032, 1461, 2372, 6806, 6808, 6811, 6812, 6814–6817, 6820–6824, 6843, 9936
  – basic thermodynamics 6815
  – Brayton cycle 6816
  – combined cycle (GTCC) power plant 6807
  – combustor 6808
  – cooling 6822
  – development 6812
  – externally heated 1461
  – F-class 6811
  – firing temperature 6817
  – generator 6843
  – history 6812
  – intercooling 6823
  – modular helium reactor (GT-MHR) 4053
  – natural gas burning 6806
  – power plants 6814, 12103
  – recuperation 6823
  – steam cycle 2168
– voltaic battery 3929
– wells 4332
gas-cooled fast reactor system 4053
gas-expanded liquid (GXL) 3933, 3935–3936, 3947
  – catalytic reactors 3936
  – for sustainable catalysis 3933, 3947
  – thermodynamic and physical properties 3935
gas-to-liquids (GtL) 1585, 3956
  – technologies 3955
gas-expanded liquid (GXL) 3934, 4613
gas-fired boiler 1462
gas-heated reforming 3965
gasification 847–848, 867, 872, 878, 1206, 1208, 1214, 1240, 1319, 1322, 1327, 1380, 1416, 1427–1429, 1433–1435, 1439, 1441, 1446, 1448–1450, 1456, 1459, 1528, 1585, 1589–1590, 1611, 2169, 2237–2238, 3967, 3997–3998, 4012, 5126, 5162, 5164, 5236, 5289, 5300, 6465–6466, 8102, 11442–11443, 11833, 11837, 11852–11853
  – agent 1446, 1448, 1450
  – allothermal 1429
  – autothermal 1429
  – biochar system 861
  – biomass pretreatment 1439
  – entrained flow gasifiers 2238
  – FICFB process 1459
  – fluidized bed gasifiers 2237
  – for rural electricity 1446
  – gas conditioning 1441
  – grate-based 6466
  – hydrocarbon reforming 1441
  – moving bed gasifiers 2237
  – of black carbon 11853
  – of straw 1528
  – of waste 5236
  – plasma-assisted 8102
  – power production 1435
  – principles 1428
  – reactions 1449, 1456
  – reactor 1434
    – for syngas generation 1439
  – small-scale 1427
  – synthesis
    – applications 1439
    – reactions 1441
  – thermal-chemical 1433
  – with post-combustion 6465

gasifier/gasifying 1215, 1430–1431, 1448, 1451, 1528, 1586, 2237
– waste 1430
gas-insulated Lines (GIL) 11185
gas–liquid interface 9129
gasohol 1007, 11431
gasoil 2229
gasoline 299, 302, 307, 1002, 1004, 1224, 1302, 5479, 5483, 11430
– combustion 3591
– air pollution 3591
– engines 5532, 5536
– boosting 5536
– gallon equivalent (GGE) 5468
– hybrid electric vehicles 10520
– lead 10649
– plug-in hybrids 8232
gas-phase
– mass-transfer control process 6732
– molecular growth reactions 6995
– oxidation 1353
– 3-T-Rule 1353
– processes 11317
– in urban environments 11317
gas–solid dissociation reaction 10561
gas-to-particle conversion 1336
gastroallergic anisakiasis 12051
gastroenteritis 5053–5055, 5064, 9087, 11986
– *Aeromonas* 5055
– food poisoning 5064
– seafood-borne 9087
– V. parahaemolyticus 5053
– V. vulnificus 5054
gate turnoff thyristor (GTO) 11539
gateway technology 2589
Gaussian
– dispersion theory 261
– distribution 10977
– mixture model classifier 11460
– noise filter 3072
– probability distribution 10971
– theorem 3805, 3814
Gauss–Newton algorithm 10601
gaze stabilization 58
gaze-world mapping 3125
gear ratio design 11486
gearbox 11486, 12152
geary corridor 1817
Geiger–Mueller counter 3023, 5564
gel battery 5887, 11514
geldanamycin 506
gel-type polymer electrolyte 8743
Gemini program 8233
gene 2690, 3609, 10398
– activity 10812
– cloning 10895
– cloning 2690
– construction 10908
– random integration 10908
– deletion 2609, 10915
– discovery 2, 6528
– encoding 645
– gene expression 10682, 10868
– control 10682
– reprogramming 6173
– single-copy T-DNA transformants 10682
– flow 3365, 10724
– gun method 10797
– heat-tolerant 10398
– hypermethylation 3603
– imprinting 6161
– inactivation 10913
– interfering RNAs 10913
– integration 10900, 10902
– random integration 10900
– targeted integration 10902
– isolation 2690
– knocking 10889, 10912
– knockout 10912, 10919
– animals 7226
– ontology (GO) initiative 6701
– polymorphisms 3609
– revolution 6693
– silencing 2605, 6530, 10677
– mutants 10687
– splicing 4517
– targeting 645, 2608, 2972, 8061, 10817, 10822, 10831, 10918
– therapy 10918
– in humans 10918
– transcription 7221
– transfer 2586, 2590, 2748, 2972, 4513, 10672, 10696, 10816, 10869, 10897, 10899–10900, 10916
– into animals and plants 10897
– into cells 10899
– into embryo 10900
– methods 10899
– microinjecting 10916
– to plants 2586
– transmission 398
– trapping 10916
– vectors 10916
genealogy
– database 6705
– management system (GMS) 6699
general circulation model (GCM) 10162, 11416
general food law 10773
general systems theory (GST) 8858
generation
– forecast 12185, 12190
– interconnection 12176
generation-IV reactors (GEN-IV reactor) 4050
generator operation 12141
generic power system 12093
genesis and rapid intensification process (GRIP) 320
gene-therapy protocols 10821
genetic(s) 394, 476–478, 1758
– aberrations 7222
– ablation 10914
– applications 10869
– control of traits 6428
– correlation 493, 4085
– distance 6428
– distinctiveness 7975
– drift 1803
– engineering (GE) 2, 8, 2529, 2536, 2685, 2731, 4013, 4493, 4501, 4510–4511, 4518, 6531, 10695–10696, 10744, 10812, 10821, 10841, 11450
– conjectural risks 4518
– European law 4511
– limitations 8
– natural mutation 4518
– of crops for insect resistance 4013
– techniques 10821
– evaluation 440, 1776, 1782
– mixed model equations (MME) 440
– heterogeneity of residual variation (GHRV) 470
– improvement 411, 7983, 9390, 10798, 11396
– rograms 1769, 7983
– target traits 7983
– via transgenesis 10798
– introgression from other populations 477
– lag 412
– major genes 476
– manipulation (GM) 2566
– maps 6428, 6431
– marker 400, 411, 462
– marker-assisted selection 476–477
– modification 4536–4537, 10770, 10812, 10821, 10865, 10867
– debate 4537
– to livestock 10869
– mutations 10816

– of trait complexes 1769
– pest control 5453
– QTL mapping 478
– resource 1769
– management 7984
– support service 6707
– selection 1800, 10396, 10897
– in horse populations 1800
– transformation 2584
– trends 444
– variability 393
– variance 9382
genetically engineered food 10760
genetically engineered (GE) product 10816
genetically engineered microorganism (GEM) 1631
genetically modified crop 2755, 4505, 4521, 4532–4534, 10745, 10766–10768, 10772, 10774, 10777–10779, 10785–10789, 10791
– agronomic characterization 10787
– approval procedures 10774
– case-by-case principle 10788
– coexistence
– measures 10779
– policy 10778
– comparative safety assessment 10786
– compositional analysis 10787
– contained use 10772
– costs 4521
– decision-making processes 4532
– deliberate release directives 10772
– deployment 10788
– environmental risk assessment 10786
– food and feed regulation 10774
– global cropping area 10767
– GM-free labeling 10777
– labelling thresholds 10779
– legal conditions 10767
– lost benefits of overregulation 4521
– molecular characterization 10787
– new management 4533
– objectification 4534
– phenotypic characterization 10787
– regulatory oversight 10768
– revised deliberate release directive 10772
– risk
– assessment 10766
– assessment concepts 10785
– communication 10766
– handling 4505
– management 10766
– science-based assessment 10786
– sustainability assessment 10791
– tiered approach 10789
– wicked problems 4533
genetically modified organism (GMO) 2287–2288, 2290, 2293, 2295, 2298–2299, 2301–2303, 10771, 10775, 10777, 10780–10784, 10791
– analysis plan 10784
– assessment endpoints 10783
– biosafety framework 2288
– characterization 10782
– commercialization 2298, 2301, 2303
– conceptual model 10783
– environmental pathways 10783
– global use 2287
– hazard identification 10782
– labeling
– provisions 10777
– thresholds 10777
– levels of exposure 10783
– measurement endpoints 10784
– problem formulation 10781
– protection goals 10782
– regulatory framework 10771, 10791
– regulatory oversight
– in Argentina 2288
– in Canada 2290
– in China 2293
– in India 2295
– in South Africa 2301
– in the Philippines 2299
– in the USA 2302
– risk
– assessment 10780
– assessors 10782
– communication 10780
– management 10780
– traceability regulation 10775
– technologies 2288
GEN-IV
– nuclear systems 4052
– reactors 4050, 7055
genome/genomic 391, 396, 478–479, 489, 1185, 3275, 3588, 3605, 4518, 6436
– backcrossing 6436
– estimated breeding values (GEBV) 2535
– fingerprinting techniques 8016
– information 1779, 6701
– in mammals 479
– instability 3606, 3608
– intrinsic integrity 4518
– misconception 4496, 4503, 4517
– network 4511
– pre-selection 492
– profiling techniques 8016
– recombination 8137
– relationship matrix 491
– revolution 489, 10814
– sequence/sequencing 1739, 2690, 2714, 10823, 10895
– selection 387, 399–401, 413, 494, 1779, 1786, 2530, 2535, 4089, 6427, 6435, 6438, 9359, 9390
– computer support systems 1779
– technologies 2535
genome-wide
– association (GWA) studies 2965
– marker-assisted selection (GWMAS) 431
– selection (GWS) 6694
genotype/genotyping 463–464, 466, 489, 1737, 2686, 4070, 4072, 6711
– by environment 4080, 4082–4083, 4085–4088
– additive main effects and multiplicative interaction (AMMI) model 4083
– bilinear models 4082
– characterization 4080
– computer software for GE analyses 4088
– factorial regression models 4085–4086
– interaction 463–464, 4070
– interaction term 4080
– mixed model framework 4087
– regression-on-the-mean analysis 4080
– statistical tools in the interpretation 4082
– variance-covariance model 4087
– by locations (GL) 4072
– by years (GLY) 4072
– by years (GY) 4072
– canalization 466
– database 6705
– homeostasis 466
– identification 4072
– information 4086
– support service (GSS) 6708
– value 464
genotype–environment interaction 411
genotype–phenotype information 6695
GenStat 6698
gentle combustion 11721
gentrification of the countryside 10363
geochemical
– modeling/models 3554, 4094–4099
– computer programs 4096
– definition 4095

– reaction path modeling 4098
– speciation–solubility modeling 4097
– coupled reactive mass transport modeling 4099
– reaction network 4096, 4099
– speciation 10053
geochemistry 3511, 4096, 4098, 5217, 9004
geodesy in volcano monitoring 11644
geodetic surveying techniques 11636
geodimeter 4211
geoengineering 850, 1924, 2115, 2118, 4104–4107, 4109–4116, 7271, 7278, 9703, 10137, 10163
– acceptability 4111
– climate change 4110
– ethics 4111
– governance
– frameworks 4105
– issues 4104
– government funding 4112
– informed consent 4111
– international frameworks 4116
– national and minilateral frameworks 4115
– nonstate frameworks 4114
– numerical model study 10163
– policy 4104
– regulation 4116
– research
– projects 4113
– stages 4109
– simulation 10163
– sociopolitical linkages 4109
– technologies 4107
– weather modification 4106
geographic information system (GIS) 1962, 5434, 5824, 6191, 6884, 7034, 8859, 9319, 10622
geohazard map 5662
geologic/geological 4095
– carbon sequestration (GCS) 4123–4124
– capacity 4123
– opportunity 4123
– potential impacts 4124
– carbon sequestration 2149–2150, 2152, 2154, 2165, 4119
– CO_2 storage 4122
– hazards 5661
– heat source 4192
– mapping 11634
– repositories (CCS) 5409
– reservoirs (CCS) 5412
– sequestration 4121
– storage deployment 2157
– structure map 9004
geomagnetic activity 9800, 9803
geomaterial 3234
– fracturing 3234
– slippage 3234
geomembrane 5657, 5752, 10412
geometric hedged field 10366
geometrical acoustics 12286
geometry turbocharger 5536–5537
geoneutrino 11208, 11209
geophysical mapping 6413
geophysics 7799
geopotential height 12070
geopressured
– geothermal systems 4320
– reservoirs 4246
– resources 4165, 4181
geo-reference 3196
GEOS-Chem model 230
GEOSECS
– data 8675
– project 8663
geosphere 10356
geospread wind power 12132
geostationary
– earth radiation budget (GERB) sensor 9627
– ocean color imager (GOCI) 8960
– satellites 7286, 9620, 9627
geostatistics 3335, 9753
– kriging 9753
geostrophic
– balance 6592, 12071
– wind 6592, 6600, 7398, 11266, 11276
geotextile 4732, 5752
geothermal
– binary station 4269, 4270
– turbine size 4270
– blowout 4427
– brines 4247–4248
– characterization 4248
– cascading 4376
– cement 4403, 4404
– conceptual model 9005
– conditioning 4133, 4139–4140, 4142, 4150–4152, 4155, 4158
– annual energy use 4155
– approaches 4139
– aquifer thermal energy storage (ATES) 4152
– aquifer-based systems 4151
– energy carrier 4140
– heat pumps 4142
– infrastructure 4158
– installed capacity 4155
– principles 4139
– rock systems 4142
– subsurface soil 4142
– surface water system 4152
– water-based systems 4150
– development 4335
– drilling 4351, 4381, 4384, 4399–4400, 4407, 4409
– downhole measurements 4409
– dual-tube reverse circulation 4400
– lightweight fluids 4400
– lost circulation 4399
– lost-circulation materials (LCM) 4400
– lost-circulation treatment 4384
– mud-pulse telemetry 4409
– solid expandable tubulars 4409
– wellbore sealing 4400
– electric power plants 4194
– electricity generation 4193
geothermal 4195, 4206, 4225
– energy 1477, 4134, 4163–4165, 4167, 4169, 4173, 4176–4177, 4179, 4190–4191, 4196–4199, 4222, 4226, 4240, 4330–4332, 4350, 4354, 4359, 4361, 4363, 4375, 4377, 4381, 4416, 4418, 4422, 4429, 9001, 11210, 11649
– accessibility 4197
– agribusiness applications 4361
– agricultural drying 4363
– bonds 4429
– conversion systems 4295
– definition 4163, 4191
– direct utilization 4173
– district heating 4359
– drilling 4381
– economic considerations 4375
– environmental considerations 4176
– environmental footprint 4191
– environmental impacts 4416
– excessive production 4222
– expectations 4190
– extraction 4128
– flux 11208
– for electric power production 4164
– future 4330
– geology 4179
– global resource assessments 4198
– ground temperature changes 4418
– hydrology 4179
– industrial applications 4363
– magma body 4332

– nature 4190
– renewability 4226
– reserves 4331
– resources 4165
– savings 4177, 4377
– space heating 4359
– sustainability 4226
– sustainable production 4222
– technologies 4196
– use 4190
– utilization 4162, 4167, 4199, 4354
– waste liquid disposal 4422
– worldwide installed capacity 4354
– environment 4415
– field 4204–4205, 4210, 4215, 4216, 4217, 4226–4227, 4229, 4231, 4292, 4352, 4415, 4423, 4426, 9000, 9002, 9012, 9018, 9020, 9021, 9023, 11619
– casing integrity 4205
– changes in fluid pressure 4204
– changes in fluid temperature 4204
– electrical resistivity 4215
– fluid flow rates 4210
– fluid mass 4205
– forecast simulation 9020
– ground surface movements 4210
– heat flow studies 4229
– hydrothermal eruptions 4426
– induced seismicity 4215
– liquid-dominated 4226
– lumped-parameter model 4229
– micro-earthquakes 4216
– geothermal field monitoring 4201
– natural thermal features 4415
– numerical simulation 4229
– piping system 4292
– reservoir engineering 9000, 9002
– reservoir simulation 9021, 9023
– sodium fluorescein 9012
– surface monitoring 4210
– sustainability 4352
– sustainable capacity 4227, 4231
– thermal features 4217
– volumetric flow rate 4205
– wellbore simulator 9021
– fluid 4197, 4206, 4207, 4245–4248, 4253, 4267, 4273, 4302, 4362, 4416–4417, 4426, 9003
– calcium carbonate ($CaCO_3$) 4207
– carbon dioxide 4426
– chemistry 4246
– dissolved solids 4248
– flashing process 4273
– heat content 9003
– mass withdrawal 4416
– production 4247
– pumps 4288
– reinjection temperature 4253
– separation processes 4273
– heat pumps (GHP) 4140, 4151, 4173, 4178, 4193, 4199, 4331, 4354, 4373, 4378
– coefficient of performance (COP) 4373
– energy efficiency ratio (EER) 4373
– monitoring 4203–4204
– basic principles 4203
– down-hole techniques 4204
– interpretation of the results 4204
– program planning 4203
– purposes 4203
– plants 4427–4428
– footprint 4428
– good engineering practices 4428
– good management practices 4428
– land use 4427
– visual impacts 4427
– power 4245, 4340–4342, 4345–4346, 4348–4349
– capacity 4221, 4222, 4340
– capital cost 4342
– capital expenditure 4345
– conversion technology 4234, 4239
– cost calculations 4340
– definition 4340
– economics 4340
– economy of scale 4341
– expansion 4334
– generation 4184
– history of operation 4346
– industry 4223
– industry system 4279
– levelized cost 4245, 4342, 4349
– plant 4193, 4353, 4376
– plant capacity 4348
– production 4159, 4182
– well productivity 4341–4342
– power station 4243, 4249, 4251, 4254, 4285–4286, 4288, 4295, 4297, 4300–4302, 4304–4305, 4310, 4315, 4317, 4321, 4327–4328, 4330, 4332, 4350, 4426
– air-cooled condensers 4285
– binary station 4315
– combined cycle 4310
– cooling tower 4286
– cost estimates for installed kilowatt (kW) 4243
– cost estimates for megawatt-hour (MWh) 4243
– Costs 4243
– CO_2 emission 4426
– dry-steam reservoir 4254
– dry-steam power station 4297
– energy conversion process 4251
– experimental 4315
– first and second law of thermodynamics 4251
– flash-crystallizer/reactor-clarifier (FCRC) systems 4300
– geopressured systems 4332
– helical screw expander 4330
– hybrid 4321
– material selection 4249
– metallic materials 4249
– optimization 4295
– organic Rankine cycle configurations 4302
– pH modification (pH-Mod) systems 4301
– pumps 4288
– rotary separator turbine 4330
– steam Rankine cycle 4254
– supercritical cycle 4317
– sustainability 4295
– total-flow systems 4328
– trilateral flash cycle (TFC) 4327
– two-phase 4304
– two-phase heat source 4305
– using hyper saline brines 4300
– project 4241, 4244
– aggregate risk 4241
– comparison with other technologies 4244
– design 4241
– implementation 4241
– recooling 9534
– reserves 4195
– reservoir 4212, 4223, 4233, 9002–9003, 9005–9007, 9010, 9014, 9016, 9021, 9022
– capillary tubing system 9010
– discharge characteristics 9006
– evaluation 9002, 9022
– fluid enthalpy 9014
– groundwater 4212
– injectivity index 9006
– interference among wells 9010
– lip pressure method 9007
– mass production and reinjection 9014
– monitoring 4201
– natural-state simulation 9016
– numerical model 9016

– numerical simulation 9014
– permeability 9006
– permeable zone 9005
– power capacity 4233
– pressure 9003, 9014
– sensitivity study 9021
– simulation model 4228
– temperature 9003, 9014
– wellbore simulation 9010
– resource 3502, 4165, 4170, 4183, 4188, 4194, 4197, 4214, 4240, 4245, 4350, 4351, 4353, 4376, 4380, 4414, 4428–4429, 5217
– characteristics 4245
– direct heat utilization 4353
– direct utilization 4170
– distribution 4351
– drilling 4380
– economic measures 4429
– energy conversion systems 4240
– environmental aspects 4414
– ground movements 4429
– injection 4428
– microgravity 4214
– non-power producing applications 4188
– plant design 4429
– regulations 4429
– rock formations 4384
– steam 4322
– turbine 4250
– supplies 4194
– system 4153, 4187, 4192, 4203, 4364, 4418
– conduction-dominated systems 4192
– convection-dominated systems 4192
– depletion of groundwater 4418
– design 4138
– direct-use temperature requirements 4364
– for electrical power generation 4203
– ground deformation 4418
– hot sedimentary aquifer systems 4192
– hybrid systems 4192
– permeability 4187
– water-based 4153
– transmission lines 4369
– waste water 4424
– water 4357, 4362, 4365–4367, 4415
– balneology 4357
– bathing 4357
– cultural uses 4415
– drops 4252
– swimming 4357
– temperature 4367
– well 4192, 4206, 4351, 4368, 4385, 4387, 4389, 4427, 5220, 5226
– casing program 4389
– corrosion 4206
– cost 4385
– designing 4387
– downhole pumps 4368
– landslides 4427
– lineshaft pumps 4368
– planning 4387
– wellbore geometry 4389
geothermic
– plant 11596
– waste 11606
– vitrification 11606
geothermometry 5219, 5220
germ cell 3628, 10900
– environmental damage 3628
– mutagenicity 4849
– purification 646
German energy scenario 4770
germinal vesicle (GV) 6164
germinate 6701
germination 9146
germplasm 10395
– heat-tolerant 10395
gestation 3629
geyser 4217, 4358
giant kidney worm 12031
giant pumices 11622
Giardia 12048–12049
Giardiinae 12048
gibberellin (GA) plant hormones 2693
Gibbs
– free energy 117, 743, 745, 3873, 3879, 3927, 5139, 5156
– of solvation 3424
– oscillations 12068
– sampling 468
Gibbs–Donnan effect 2904
Gibbs-Thomson effect 7762
Gibbsite 8606
gill site interaction model (GSIM) 10052
gill-type atmosphere 7376
glacier/glacial 281, 286–288, 292, 2061, 2065, 2069, 2455, 2458, 2460, 2513, 2762, 2766, 2768, 2769, 2771, 2776
– airborne radar ice sounding 292
– dynamics 2767
– governing equations 2767
– geometry 2768
– glacier ice 2769
– basal flow 2769
– glaciological data 2771
– InSAR Measurements 287
– isostatic adjustment (GIA) 2456, 4570, 4575, 4579
– mass loss 288
– melting 2458, 2460
– modeling 2769
– regional image mapping 286
– soil 2432
– surface elevation 288
– velocity 288
glaciology 283
glare control 3688
glare filter 2837
Glaser coupling 10175
GLASOD database 1555
glass 8801, 11605, 11607
– ceramics 11601–11602, 11604–11606
– matrix composites 11606
– open-celled 11605
– by direct sintering 11604
– by nucleation 11601
– by sinter-crystallization 11602
– by the petrurgic method 11604
– ferromagnetic behavior 11602
– fibers 11604
– cullet 11584, 11598, 11607
– fibers 11604
– foams 11604
– network 11582
– powders 11602
– recycling 8779, 8801, 9991
– plants 8839
– waste-derived 11605, 11607
– windows 2808
glasshouse
– studies 10393
– trials 10718
Gleasonian succession 3290
Glen's flow law 2768, 2770
gliadin 4555
global
– aerosol population 112
– agriculture 10743
– air pollution 11314
– aquaculture alliance (GAA) 9183
– atmospheric models 8905
– biodiversity 10092
– carbon cycle 3707

– change assessment model (GCAM) 5403, 5406, 5409–5410
  – agriculture 5409
  – agriculture-land-use component (AgLU) 5410
  – architecture 5406
  – bioenergy 5410
  – energy system 5406
  – land use 5409–5410
  – partial equilibrium framework 5406
– chemical transport model 230
– circulation model (GCM) 2119, 6597, 9804
  – mesoscale models 6597
  – microscale model 6597
– climate 8903
– climate change 7245, 8659, 9686, 11930
  – general circulation models 9686
– climate forecast 2131
global
– climate model/modeling (GCMs) 2761, 3213, 6743, 6755, 8903
  – biosphere-atmosphere transfer scheme (BATS) 3213
  – bucket model 3213
  – downscaling modeling 6755
  – Simple Biosphere Model (SiB) 3213
  – simulations 3291
– climate simulations 8908, 8916
– climate system 6741
– demand for energy 9905
– dimming 141, 9731, 9733
– earth observation system of systems (GEOSS) 8921
– emission
  – inventory 663
  – model for integrated systems (GEMIS) 4761
– energy 2186
  – challenge 9905
  – global energy and water-cycle experiment (GEWEX) 9623
  – supply 2191
– environmental change 6190
– fallout radionuclides 8862, 8663, 8665, 8675
  – deposition density 8675
  – GEOSECS project 8663
  – monitoring 8663
  – Pacific Ocean 8665
– fishing crisis 3556
– food
  – production 1742
  – security 1745, 2687, 6427
  – supply 7386
– freshwater 7685
  – resources 2345, 8689
– genetic resource management 7975, 7982
– greenhouse gas emissions 10505
– horizontal irradiance (GHI) 9674, 9691, 9745
  – estimating diffuse hemispherical radiation 9691
  – estimating direct beam (DNI) 9691
– hydrate resource 333
– hydrological cycle 8013
– Interagency IPY Polar Snapshot Year (GIIPSY) 292
– irradiance 9628
– land use 5788
– laser enrichment (GLE) 5643
– malaria program (GMP) 12001
– mean air surface temperature (GMAST) 9799
– mean temperatures 2143
– meteoric water line (GMWL) 5228
– momentum equations 12210
– nuclear energy partnership (GNEP) 4060
– nuclear weapons testing 8491
– ocean circulation 8661, 8669, 8672
– ocean hydrography 7287
– ocean networks 7287
  – drifters 7287
  – floats 7287
  – gliders 7287
  – moorings 7287
  – seafloor cables 7287
– ocean observations 5873
– ocean observing network 7282
– ocean ship-based hydrographic investigations program (GO-SHIP) 5875
– polio
  – eradication initiative 8149
  – laboratory network (GPLN) 8151
– population 1507, 1553, 1742
– positioning system (GPS) 74, 1852, 4565–4567, 6962, 12080
  – occultation 4565
  – receivers 4566
– spectral irradiance 9716
– system for mobile communication (GSM) 74
– temperature 2105
  – change potential 654
– thermohaline circulation 8658–8659, 8662
– tilted irradiance (GTI) 9755
– toxification 6188
– transport energy 9335
– urbanization 10358
– warming factors (GWF) 4760, 4763
– warming 1, 112, 141, 144, 162, 348, 548, 850, 2062, 2080, 2455, 3233, 3451, 3707, 3845, 4104, 4738, 7844, 8690, 8775, 9741, 10161, 10391, 10441, 10483, 10486
  – costs 10486
  – gas 10296
  – impacts on water resources 2080
  – potential (GWP) 654, 1307, 858, 1501, 5415, 5911, 7272
  – sunshade 10161
– water 2061, 2070
  – balance 7251
  – cycle 3222, 9736
  – resources management 2061
  – sustainability 2061, 2062, 2064, 2070
– weather 2081
globalization 4533
globally harmonized system of classification and labeling of chemicals 4848
glucanase 10845
  – genes 10697
glucan 991, 999
glucoamylase 992
glucose 1278, 11020
glucosidase 8048
glucosinolate 1192
glucosuria 11240
β-glucuronidase (GUS) 2598
glucuronidation 3643, 12303
glucuronide estrogen 11967
glufosinate 4472, 10352
glutamic acid 550
glutathione 4666, 12305
  – peroxidase 3662
    – selenium-dependent 3662
  – S-transferases (GSTs) 3643
glycan modifications 8063
glycerine 1045, 1219
glycerol 362, 926, 929, 3935, 6913, 11447
glycerolysis 6904
glycomacropeptide 10855
glycopeptide antibiotics 504
glycophytes 5318
glycoprotein 4828, 8068, 8074
  – plant-produced 8068
glycosylation 8068
  – N-glycosylation 8063
  – O-glycosylation 8064
glycosylphosphatidyl-inositol (GPI) 4017

glyphosate 2598, 4435, 4444, 4472, 4530, 10348, 10352, 10716, 10723
– resistance 4530
Gnathostoma 12037
goat 1765
– breeding 1763
– genetic resource management 1765
– meat (chevron) production 1752
Goddard Earth Observing System chemical transport model (GEOS-chem) 196
goethite 8606, 8610, 8622–8623
Goiânia accident 3538–3539, 8528
– mechanical decontamination 3539
– remediation actions 3539
gold
– catalysts 7585
– mine tailings 6674
– surface 1647, 1648
gold-binding peptide (GBP) 1648
golden Rice project 4525
Goldschmidt factor 2940
gonadotropin 10819, 10891
gonocyte 5577
good agricultural practice 1133
Google Earth 3171
Google StreetView 3171
Gorgoderoidea 12027
gossypol 4039, 4509
GRACE 4568–4569
– data 4569, 4571, 4573, 4575, 4577–4579
– analysis 4568
– accuracy 4571
– cryospheric studies 4575
– earthquakes 4579
– ocean information 4569
– ocean studies 4577
– solid earth studies 4579
– satellite 285, 3232, 4567
– accelerometers 4567
– microwave K-band ranging instrument 4567
– orbit-control thrusters 4567
– pair 4564
– ultra-stable oscillator 4567
– science data system 4569
gradient wind 7398
grain 4551, 4553, 4555, 4558, 4560, 9149
– components 4555
– crops 2673
– dormancy 9149
– germination 9149
– growth 4553, 4555
– hardness 4560
– production 1743
– quality 4550–4551, 4557–4559, 6203
– concept and importance 4551
– environmental effects 4558
– genotypic effects 4557
– impact of lodging 6203
– management strategies 4559
– segregation 10724
– source–sink balance 4553
– structure 4551, 4553
– weight 4558
– yield 6203, 8018
– impact of lodging 6203
– production 10040
graminaceous plant 1712
Graminae 1279
gram-positive organism 5064
– treatment 5064
granular activated carbon (GAC) 10148
granular media filter 2910
graphene nanosheet 6779
graphite 752, 6133
– bipolar plates 8252
– intercalation compound (GIC) 710, 6140
– staging phenomenon 6140
– interface 6058
– lithium anode 707
– nitrogen atoms 8275
grass roof 4701
grass weed 10348
grassland 3315
grate
– combustion 4960–4961, 11836
– furnaces 1322, 1324
– siftings/riddlings 4970
gravel siltation 3755
gravimeters 4570
gravimetric energy 741
gravimetric power density 8237
gravitational acceleration 3055
gravitational driving stress 2770
gravity 4214, 4565, 4570, 4580, 7799
– changes 4580
– data 4570
– drive 7803
– measurement 4565
– field 4564, 4569
– mascons 4569
– of earth 3232
– recovery and climate experiment (GRACE) 4563
– waves 12066, 12068
grazing food chain 824
great ocean conveyor belt 5859, 8661
greedy perimeter coordinator routing (GPCR) 11566
greedy routing model 11569
green aerated concrete 3831
green algae 353, 356, 360, 362, 365, 553, 927, 2543
– hydrogenases 362
green architecture 4691, 4703, 10933
green belt 5806
– policies 11350
green biotechnology 4492, 4504, 10749
green brick 3833
green building 5332, 5334, 5336, 5341, 6891, 8705, 8711, 8861, 10192, 10194, 10302
– acoustics 5336
– assessment systems 9031
– noise control 5336
– sustainable design principles 5341
green business sites 956
green catalyst 7584, 7592, 7598
– E-factor 7592
green catalytic transformation 4584
green certificate 8380
green chemistry 4585, 4614–4616, 4619–4620, 4634, 4642–4643, 4847, 4855, 6790, 6796, 7584, 7586, 7589, 7610, 10169, 10658
– 12 principles 4620, 4643
– catalysis 7586
– hazardous materials assessment methods 4855
– metrics 4586, 4616
– oxidation catalysts 4615, 7584
– principles 7589
– with microwave energy 4642
– zebrafish model 6796
green city 958
green design guidelines 5343
green diesel 5473, 5488–5489
green electricity 4481, 4485
green energy 1287
green engineering 4847, 4855, 7586, 7611, 7612
– hazardous materials assessment methods 4855
green envelope 4709
green facade 4748
green fluorescent protein (GFP) 640, 2600, 8063
– encoding gene 10677
green infrastructure 4673–4674, 4678, 4683, 4691, 4693, 10359–10360, 11347
– climate change 4673
– vulnerability 4691
green metrics 4615, 4618–4619, 4637
– algorithms 4619
– calculations 4619
– definition 4618

green nanoscience 6790, 6792, 6796
green oxidation catalyst 7884, 7585, 7605, 7612
green power 12242, 12265
– markets 12216, 12254, 12264
green procurement 11676
green revolution 152, 562, 2529, 2541, 2550, 2634, 2692, 2741, 2748, 4073, 10345, 10744
green roof 3462, 4698, 4701–4706, 4716, 4708, 4710–4711, 4714, 4717–4719, 4721, 4723, 4725, 4727, 4728, 4730–4732, 4735, 4742–4746, 4748–4750, 6876, 10359, 10356
– as ecosystems 4732
– audit 4725
– benefits to urban areas 4714, 4717
– biodiversity 4721, 4738, 4748
– building code 4727
– cooling effect 4746, 4750
– ecological functions 4730
– ecological synergy 4750
– energy performance 4744
– energy savings 4719
– evaporative cooling
– capacity 4742
– consumption 4738
– evaporation of water 4746
– extensive 4717
– flash floods 4719
– growing media 4710, 4731
– infrastructures 4697
– in Germany 4703
– in urban areas 4716
– incentive programs 4704
– intensive 4717
– London audit 4723
– longevity 4708, 4731
– lysimeter 4742
– modern technology 4704
– photovoltaic solar panels 4719
– planting techniques 4711
– policy
– in European countries 4705
– programs 4710
– pollution removal 4719, 4721
– quantifying 4727
– rainwater management 4735, 4743
– reduced air conditioning requirements 4745
– reducing energy requirements 4737
– retrofitting 4725
– role in Urban Planning 4721
– Sedum 4749
– simple intensive 4701
– stormwater runoff 4719, 4735
– surface temperatures 4745
– technology 4721, 4731
– thermal insulation 4735, 4738
– thermal lag effect 4737
– thermal performance 4744
– toolkit 4723
– urban heat island effect 4718
– urban planning tool 4728
– water management 4739
– weed control 4739
– wildlife potential 4727
– worldwide historic roots 4702
– worldwide distribution 4706
green school 5342
green screen 4862
– for safer chemicals 4860
green sea turtle 3568
green solvent 7601, 10183
green space 11356
– plan 4728
green sustainable building 9028
green synthesis 7606
– for bisnoraldehyde (BNA) 7606
green technology 4743, 10341
green tide 553
green urbanism 10933
green wall 3687, 3689, 4723, 4733
– energy saving 3689
green waste 5244
green water 1544
green wedge 952
greenhouse 911, 4365
– distillery 9759
– effect 131, 348, 634, 1200, 2499, 2757, 7844, 9766
– heating 4365
– trapping 9809
– warming 9647, 9734
– whitefly 5435
greenhouse gas 144, 162, 177, 204, 245, 299, 613, 632, 653, 769, 851, 921, 1057, 1134, 1261, 1308, 1533, 1552, 1602, 1784, 1909, 8775, 8898, 9742, 10586, 11694
– balances 1261, 1533, 1535
– emissions 1134, 1308, 1504, 1533, 1535, 1575, 2068, 3224, 4675, 4754, 4765, 4769, 5462, 9441, 10296, 11665, 11668, 11692
– by landfilling 4765
– by waste incineration 4769
– from solid waste management 11665
– impacts 1552
– mitigation strategy 11694
– reduction 10586
greening program 11351
Greenland ice sheet 10165
Greenpeace 4526–4527
Green's function 11636
greenshell mussel 6764
greenwash 562
grey infrastructure 4678
grid 10944
– development 10936
– history 10936
– splitting 10944
grid-enabled vehicles (GEVs) 9334, 9337
– Policy Drivers 9337
Griffithsin 3164
Grignard reaction 4623
gross calorific value (GCV) 1234, 1303, 1315, 9833
gross collector efficiency 9543
gross domestic product (GDP) 1765
Grotthus
– motion 743
– shuttling 8209
Grotthus–Draper law 11377
ground 3235, 3237, 3239, 3249–3250
– acceleration 3235
– breaks 3239
– deformation 3239
– deformations 3237, 3249
– heat flux 3217
– motion 2425, 3233, 3234
– shaking 3250
– source heat pumps (GSHP) 4191, 4193, 4351
– stores 10556
– surface 3185
– elevation 5712
– segmentation 3185
– temperature distribution 4134
grounding 3003
ground-level ozone 176, 245
ground-reflected radiation 10626
ground-source heat pumps 4356
groundwater 1545, 1635, 1638, 2327, 2336, 2433, 3221, 3455, 3595, 4126–4127, 4212–4213, 4424, 4687, 4775, 4777, 4784, 4786, 4806–4813, 4815–4816, 5646, 5648, 5654, 7669, 7685–7686, 7812, 10142, 10146, 10149–10150, 10153, 10190, 10409–10410, 10414, 10436, 10445, 10970, 11001, 11944
– aquifers 4127, 4212, 5648
– behavior 4815
– chlorinated aliphatic compounds 10445
– chlorinated aliphatic hydrocarbons 10153
– chromium-contaminated 10410

– climate framework 4812
– concentrations 10436
– contamination 1638, 4424, 4775, 4786, 4794, 5654, 7685, 7812, 10142, 10970
– ex situ approaches 1635
– extraction 4806, 4812
– flow system theory 4816
– flow systems 4808–4809
– functioning 4807
– geochemical changes 4126
– geological framework 4811
– heat production 11944
– impacts of radioactive wastes 4775
– importance for urban development 4809
– in situ remediation approaches 1638
– management 5827
  – policies 4807
– microbial and nutrient transport 7685
– microbial pollutants 7686
– movement 5646
– multiphase extraction 10149
– nitrate 3781
– pathogen-contaminated 7669
– piezometric surface 4213
– pollution 4687
– potable 4127
– pumping 10146, 10150, 11943
– quality response 4810
– quality 4126, 4807, 4816
– recharge 6626
  – program 2083
– redox conditions 4777
– remediation 3595, 4784, 4790, 4804, 10407
  – benefits 4804
  – economic analysis 4790
  – using permeable reactive barriers (PRBs) 10407
– removal of metals 10409
– reservoirs 4418
– resources 2324
– salinity 4804
  – due to urban growth 4804
– storage 3221
  – capacity 4809
– tritiated water 11001
– uranium removal 10414
– vertical flow control 4813
– vulnerability to contamination 4808
groundwater–surface water interactions 7686–7687
group on earth observations (GEO) 8921
GROWSCREEN 10
growth
  – chamber studies 10393
  – differentiation factor (GDF) 10890
  – hormone (GH) genes 10798
  – respiration 3224
guanosine triphosphate (GTP) 1710
guaranty ecological flow 2795
guided rapid transit 1816
guiding reflector posts 3076
Guinea worm 12013
Gurley value 8733
guttation fluid production 8046
Gymnophallidae 12028
gypsiferous mine water 6658
gypsum 2408, 6653, 6658, 8360, 11712
  – closed-loop recycling 2408
Gyrodactylus salaris 1940
gyrometer 3060, 11196

H

Haar features 83, 86
Haar-wavelet filters 6968
Haber–Bosch process 850, 2662, 2741
habitat 951
  – availability in cities 951
  – birds directive 9181
  – destruction 6180
  – for biodiversity 11354
  – loss 1542
  – management 156
  – quality 3332
  – suitability models 1962
Hadley cell 7251, 8968
Hadley Center Atmosphere Model (HadAM3) 3291
Hadley circulation 6745, 9637–9639
Hagberg falling number [HFN] 6203
Hahn-echo pulse 6083
Haldane mapping function 479
Haldor Topsøe's Integrated Gasoline Synthesis (TIGAS) process 3988
half-bridge converter 692
halichondrin B 3158
Hall effect 42, 700
haloacetic acid (HAA) 10537
halocarbon 8885, 9741
  – source gases 10135
Haloclean pyrolysis 1528
Haloclean-gas tight rotary kiln 1525
halogen 8583
halophyte 5318, 6313–6314
halothane gene mutation 476
Hamiltonian term 6081
handmade cloning (HMC) 6154
haplotype 487, 6431, 6435
  – diversity 6431
  – profiling 6435
harbor 11298
hard carbon 6140
Hardy–Weinberg proportion 7980
harmful algal bloom (HAB) 1953, 2259, 2260, 2264, 2265, 4819, 4820, 6180, 6762, 7332, 7388, 7389, 7671, 8926, 9117
  – research plan 2260
  – total cost 7389
  – warning systems 2265
harmful parasite 12054
harmonic voltage 12139
harmony of water 10189
harvest 1130–1131, 1484
  – index 1484, 2639–2640, 2652, 2676, 2736, 8019
  – simulation model 3331
  – storage 1130–1131
  – transport 1130
Harvie–Moller–Weare (HMW) formulation 4097
hatchery
  – fish 6391, 6394, 6398
  – reform project 6399
Haun stage 2542
H-axis 25
hazard ranking system (HRS) 2009
hazardous
  – air pollutant (HAP) 170, 172, 298, 2209, 5480, 8350, 11306
    – emissions 4883
    – hydrocarbon-based 5480
  – compounds 6976
    – thermal destruction 6976
  – incinerator emission 4891
    – scientific publications 4891
  – material 4846–4848, 4856, 4862, 4904
    – assessment frameworks 4862
    – assessment 4846, 4856
    – characterization 4846, 4848
    – flammable substances 4848
    – governance 4847
    – management 4847–4848
    – misuse 4847
    – oxidizing substances 4848
    – pyrophoric substance 4848
    – vitrification 4904
  – organic substances 4871, 10581
    – life cycle release 4871
  – solid residues 4866

hazardous waste (HW) 4881, 4903–4904, 5244, 5256, 9980, 10018, 11583, 11589, 11592, 11598, 11830
– ashes 4904
– dioxins 4904
– disposal 5733
– gaseous emissions 4904
– incineration ashes 4866, 4869, 4874, 4903
– application in or as building and geotechnical materials 4869
– before utilization 4869
– treatment 4869
– uses as adsorbent 4874
– utilization 4869
– incinerator 4880–4882, 4898
– best available technologies (BAT) 4881
– biokinetics 4898
– biological monitoring 4898
– dioxin emissions 4898
– emissions 4880
– heavy metals emissions 4882
– non-incineration methods 4903
– potential contents 4903
– variances 4903
– landfill 5753, 5762
– sites 10441
– risk assessment process 10441
hazardous and solid waste amendment 10017
haze factor 9274
H-coal 2230
heading date 2697
headway-based control 106
health/healthy
– buildings 5332, 5333
– indoor environmental quality (IEQ) 5333
– built environment 10260
– indoor air 10271
– effects of air pollution 174
– hazards 4862, 9091, 9167
– seafood-associated 9091
– sentinels for early warning 9167
– physics 4905–4906
– definition 4905
– development 4906
– history 4906
healthcare facility 5339
– evidence-based design 5339
heap leach dump 6677–6678
– detoxification 6678
hearing aid battery 6513
hearing loss 6513
heart failure devices 6507
hearth 1305
heat 1199
– buffer storage 1370
– conduction equation 5686
– convectors 4375
– diffusivity 10553
– energy 3502, 4770
– substitution 4770
– engines 3848, 5142
– for electricity production 5142
– exchange reforming 3965
– exchanger 4264, 4371, 10568
– evaporator 4264
– preheater 4264
– extraction equipment 4172
– flux 4746
– from biomass 1199
– island effect 10359
– mix factors 4764
– of combustion 5245
– of fusion 10557
– of melting 10557
– production 1611
– gasifiers 1611
– pump efficiency 4141
– seasonal performance factor (SPF) 4141
– pumps 4193, 4334, 4373
– performance (COP) 4193
– system design 4142
– radiation 1361
– recovery steam generator (HRSG) 2168, 2367, 2371, 6828
– rejection system 2814, 9539
– sources 4184
– storage 1372, 2370, 4134, 10552
– stress 10400
– supply 1372
– combined systems 1372
– tolerance during reproductive development 10399
– transfer 4140, 4364, 5519, 10555, 10557, 10561
– transfer effect 5509
– transfer fluid (HTF) 2364, 2366, 2368, 2369, 7628, 9452, 9453, 10564, 10568, 10576
– air 2369
– parabolic trough collectors 7628
– salt 2368
– sodium 2369
– water/steam 2369
– transfer rate 2900
– composites 10561
– concepts 10561
– transmission 2850
– coefficient 2850
heater 1362
heating
– boilers 1365
– of domestic water 9450
– oil burner 1377
– place 1361
– value 1234, 9832
heating, ventilating, and air-conditioning (HVAC) 10246, 10333, 10552
– environmental footprint 10333
heat-island effect 4678–4679
heat-resistant
– cowpea cultivars 10396
– rice cultivars 10397
– wheat cultivars 10398
heat-shock protein 5, 10399
heavy metal 3629–3630, 3783, 4887, 9089, 10409, 10418, 10423, 11306, 11308
– combined chemical and phytoremediation 10418
– contamination 10409
– electrochemical removal 10423
– exposure 3630
– in seafood 9089
– in the urban atmosphere 11306
– precipitation 10409
– trace elements 11306
– urban areas 11306
heavy oil 7809, 7819
– production 7817
– horizontal wells 7817
– inert gas injection (IGI) 7817
– upgrading 7819
heavy rail 1812
heavy-duty vehicle 3069
Heck coupling reaction 10175
– of phenyl iodide 10175
Heisenberg uncertainty principle 3801
Helgeson–Kirkham–Flowers (HKF) equation 4096
heliostat 2353–2354, 2356–2365, 2373, 2387, 2388, 6034, 6036, 9590
– aiming strategies 2361
– air Receiver 2365
– blocking 2358
– canted-glass mirror 2353
– cavity receiver 2364
– components 2353
– direct absorption receiver 2363

– field 2352, 2360–2361, 2373, 2383, 6031, 9614
– design 2356
– investment costs 2383
– overall efficiency 2360
– receiver types 2361
– flat-type single mirror heliostats 2354
– ideal shape 6034
– manufacturability 2388
– non-focused 2354
– one-dimensional aiming 2361, 2362
– optical loss 2360
– radiant power 2357
– shadowing 2358
– shapes 2353
– single aim point 2361
– size 2354, 2387
– small-mirror systems 2356
– spillage. 2359
– stretched-membrane focused 2354
– sub-mirror 2353
– theoretical consideration 2357
– tube receiver 2364
– two-dimensional aiming 2361
– types 2353
– user-defined aiming strategy 2363
Heliothis pest 4467
heliotron 7163
Helmholtz-Smoluchowski law 10421
Helminthosporium turcicum 1277
helminths 11877, 11879, 12021, 12054
hematite 8623, 11602
hematopoietic stem cell (HSC) 10826
hemicellulase 973
hemicellulose 964, 974, 1075–1076, 1519, 6020, 9824–9825, 11436–11437
– sugar 970
hemikryptophyte 1139
Hemiptera 4026
hemispherical camera 7924
hemispherical radiation 9690–9692
– on a tilt 9691
hemolytic-uremic syndrome 5063
Henry's law 2027–2028, 9053
– constants 6722, 6726, 10143, 10958, 10959
hepatitis 10645, 11988, 11991
– A 11988
– cell culture propagation 11988
– genogroups 11988
– infections 11988
– B (HBV) 5000
– E 11991, 11992
– transmission 11992
– epidemiology 11991
– virology 11991
hepatoblastoma 3644–3645
hepatocellular carcinoma 3609–3610
hepatotoxic shellfish poisoning (HSP) 4832
hepatotoxins 2085, 4831
Hepeviridae 11991
herbaceous
– biomass 1075, 1176, 1202, 2275
– fuels 9838
– plants 11398
herbicides 1286, 2092, 2748, 2751, 4435, 4439, 4472, 5440, 10345, 10349, 10352, 10723, 10748
– glyphosate 10346, 10351
– hypersensitivity 10352
– resistance 10346, 10716
– resistances 10351
– mitigating gene flow 10351
– stacking 10351
herbicide-resistant
– crops 10347
– genes 10349
herbicide-tolerant
– canola 4447, 4449–4451
– Australia 4450
– Canada 4447
– global economic impact 4451
– USA 4449
– cotton 4446–4447
– global economic impact 4447
– USA 4446
– maize 4444–4445
– Argentina 4444
– Canada 4444
– global economic impact 4445
– Philippines 4445
– South Africa 4445
– USA 4444
– soybeans 4435, 4438–4439, 4442
– Argentina 4435–4436
– Bolivia 4442
– Brazil 4438–4439
– Canada 4439
– global economic impact 4443
– Mexico 4442
– Paraguay 4439
– Romania 4439–4440
– South Africa 4439
– Uruguay 4439
– USA 4435
– weeds 4530
herbivore/herbivorous 823, 2504, 5442
– antibiotic mechanisms 5442
– antixenotic mechanisms 5442
– clupeiforms 3577
– insects 5438
– species 513
hereditary nonpolyposis colorectal cancer (HNPCC) syndrome 3607
heritability 467, 489
heritable variance 9365
– effect of group size 9365
hermatypic coral 2494
heroin 3590, 10643–10645
herpes viral vectors 10907
herpes virus 10906
heteroatom 5251, 6771
heterochromatin 2553, 10911
heterocycle 4653
heterocyclic hydrazones 4656
heterogeneous catalyst 4585, 4614
heterogeneous photocatalysis 9564, 9566
heterojunction solar cells 7939
heterologous gene sequence 8046
heterologous protein production 8030, 8046
Heterophyidae 12024
heterophyid 12025–12026
heteroplasmy 6169
heteropoly acid (HPA) 7600, 8339
heterosis 475, 493–494, 1734, 2736
heterotroph 823
heterozygote 479
– excess method 7980
hexachlorobenzene (HCB) 4883, 4887, 6995
hexachlorocyclohexane 10659
hexaferrite 25
hexafluorpropylene 6511
hexane 3935
hexavalent uranium 11223
hexavalent uranyl ion 11235
hexazinone 2092
hexose 982
– sugar 974
Heyrovsky reaction 3415, 3420, 3422, 3876
Heyrovsky–Volmer mechanism 3416
hidden hunger 1683
hidden Markov model (HMM) 3117, 3120
hidden semi-Markov model 10249
hierarchical fuzzy partitioning (HFP) method 3120
hierarchical hidden Markov model 10250
hierarchical location service (HLS) 11562
high density polyethylene 1635
high electric conversion efficiency 3851
high entropy materials 11708
high nitrate low chlorophyll water 7268
high resolution transmission electron microscopy (HRTEM) 7739

high-angle annular dark-field (HAADF) 7739
high-capacity bus 1896
– corridors 1902
high-concentration photovoltaics 9437
high-density polyethylene (HDPE) 8722, 9983
higher mixed liquor suspended solids (MLSS) 11968
highest occupied molecular orbital (HOMO) calculations 6040
high-level nuclear waste repositories (HLNWR) 8605
high-level radioactive waste (HLW) 7067, 8589, 11582, 11585
– treatment 11585
– vitrification 11585
highly enriched uranium (HEU) 11203
high-occupancy toll (HOT) lane 4945, 5021–5032, 5034–5037, 5039, 5041–5044, 6497
– all lanes priced uniformly 5039
– average variable cost (AVC) 5034
– congested drive cycles 5037
– congestion pricing model 5037
– cost of infrastructure 5026
– demand 5028
– demonstration Effect 5043
– diversion 5029
– dynamic demand schedule 5035
– eligibility requirements 5025
– enforcement cost 5025
– equity 5041
– exemptions 5030
– features of priced lanes 5023
– hypercongestion 5028
– inefficiency 5034
– land use impacts 5042
– lexus lanes 5041
– loss of capacity 5026
– management 5022
– marginal cost (MC) 5034
– microeconomic theory 5025
– monopoly 5030
– multiclass networks 5032, 5043
– multiclass service 5024, 5039
– network effects 5037
– nonoptimal pricing 5036
– number of priced lanes 5032
– performance objectives 5025
– price volatility 5031
– pricing alternatives 5032
– public–private partnerships 5044
– related markets 5037
– revenues 5030
– safety 5025
– cost 5025
– some lanes priced 5039
– travel time reliability 5030
– utilization 5028
– value
– of travel time savings 5029
– of travel time (VOT) 5027
– pricing 5021
high-occupancy vehicle (HOV) 5022, 5032
– discounts 5032
high-occupancy vehicle (HOV) lane 1865, 4945–4954, 5024–5025, 6005, 6496
– access treatments 4947
– allowed vehicles 4947
– case studies 4951
– concurrrent flow lane 4946
– design 4948
– dynamic pricing 4954
– effectiveness 5025
– enforcement 4948
– exclusive lanes 4946
– facilities 1821
– marketing 4950
– microeconomic theory 5025
– operating Hours 4947
– park-and-ride lot 4952, 4953
– peer-enforcement 4949
– planning 4948
– precursor 5024
– public information 4950
– routine enforcement 4949
– selective enforcement 4949
– special enforcement 4949
– supporting facilities and services 4947
– transit stations 4952
– travel-time savings 4953
– types of lanes 4946
– vehicle-occupancy requirements 4947
high-performance building 10195, 10261, 10308
– integrated design 10308
high-quality energy storage system 5104
high-resolution mapping 2697–2698
high-speed
– motors 11544
– rail systems 4929, 6247, 6258, 6271, 6497
– development 4929
– technology 4929
– train 4930–4934, 4936–4942
– cooperation with airlines 4939
– development 4930, 4942
– economic costs 4937
– energy source 4942
– environmental sustainability 4941
– financing strategies 4937, 4938
– infrastructure capabilities 4931
– inter-city express 4936
– MAGLEV 4934
– main planning principles 4936
– network 4930
– number of stations 4937
– route capacity 4938
– Shinkansen Model 4932
– socio-economic impacts 4940
– spatial development 4934
– spatial imbalance 4940
– station location 4936
– sustainability 4931
– TGV 4933
– tilting trains 4933
– transport impacts 4938
– tunneling effects 4940
high-temperature
– chlorine corrosion 9829
– electrolysis 9938
– Fischer–Tropsch (HTFT) technology 2225
– fuel cell (HTFC) 5138, 5140–5142, 5145, 5154, 5157
– electrochemical and catalytic processes 5141
– external reformation configurations 5145
– fuel flexibility 5138
– fuel processing relationship 5138
– internal reformation (IR) 5140, 5145
– representative performance characteristics 5145
– subsystem 5142
– polymer electrolyte membrane fuel cells (HT-PEMFC) 7867
– superconducting (HTS) 6254, 6257, 6290, 11185
high-voltage DC transmission 9347
highway 5657, 5658
– drainage systems 5657
– relocation 5658
– flooding 5653
– trucks 6284
histamine-producing bacteria (HPB) 9104
histone 8, 3604, 6159–6160
– acetylation 6159
– methylation 6160
– phosphorylation 3604
– sumoylation 3604
– ubiquitinylation 3604

Hitachi Zosen Inova 4987
– energy-from-waste 4960
– navigator 4975
– semidry FGT process 4987
– steam boiler 4976
– technology 4994
Hittorf number 3878
HIV infection 11137
H-metasomatism 5218
Hoffmann analyte 10638
Hofmann elimination
– degradation 379
– reaction 375
holding strategy 104, 106
holistic system 190
holobiont 2493
Holocene 9803
– reefs 2492
hologram 2866
Holothuroidea 12047
Holstein cattle 1759
HO/MA polymers 6924
– dynamic mechanical properties 6924
home composting 11657
homogeneous
– catalysis 3938
– charge compression ignition (HCCI) 5541
– engines 5540
– ignition control 5541
– nucleation 117–118
– photo-Fenton 9564
homography 10601
homologous recombination (HR) 10902
– pathway 10822
Homopteran plant pest 4033
homoserine 10843
homozygosis 10891
homozygote 479
hookworm 12007
Hopper dredge 3035, 3037, 3044
horizon/horizontal
– axis wind turbines (HAWTs) 3399
– deformation 4211
– grate 6457, 6459
– luminance 2818
hormesis 3255–3256, 3666
hormonally active agents 11961
horse 388, 1806
– breeding 1796–1801, 1803–1805, 1807
– autochthonous breed 1797
– Bayesian animal model method 1800
– Bayesian Thurstonian models 1807
– effective population Size 1801
– estimated breeding values (EBVs) 1798
– genetic drift 1803
– genetic evaluations 1798
– genetic parameters 1797
– genetic progress 1800, 1804
– genomic breeding values (GEBVs) 1807
– goals 1797
– heritability of racing performance traits 1798
– important traits 1799
– inbreeding 1801, 1804
– international genetic evaluations 1800
– Interstallion project 1800
– multiple trait (MT) AM-BLUP procedures 1799
– multistage selection 1801
– pedigree file 1799
– registration of pedigree files 1797
– selection 1798
– thoroughbred population 1805
– Thurstonian model 1800
– timeform ratings 1805
– culture 1807
– populations 1801–1802
– estimates of genetic trend 1802
– genetic Progress 1801
– racing performance 1806
horsehead pump 7804
horticulture 2186
Horton runoff 3222
hospital waste 5244
host cell proteins 8065
host coral 2493
host DNA 10901
host eradication 2560
host resistance 2566
hot box oven 9495
hot carrier solar cell 9427, 9428
hot dry rock (HDR) 3504, 4352
– resources 4166
hot gas cleaning 1438
hot ice
– gas hydrate research 337
– No. 1 well 339
hot mix asphalt baghouse fines 11701
hot pool 4218
hot spot 4183
hot spring 4218, 4358
hot water boiler 1345
hot-air heating system 1402
hot-air turbine 1410, 1419
hourly clearness index value 9751
– probability distribution 9751
household
– cooking 1300
– furnaces 10586
– voltages 12080
– waste 8819, 10009
HSI-based technology 8844
Hubbert curve 7448–7449
human biology 2262, 4893
human diet 1566
human earth system 5403, 5418
human ecosystem 3286, 11329
human enteric virus 11986
human eukaryotic cell 498
human eye 47
human fish 2799
human footprint 2745
human genome 3608
human health 2263, 8919, 9156
– hazards 4860
– remote sensing applications 8919
– sentinel species 9156
– well-being 2263
human immunodeficiency virus (HIV) 4996, 5000–5008, 5010, 5012–5014, 5352, 10905
– basic virology 5000
– candidate vaccines 5012
– cause of AIDS 5002
– clinical management 5012
– cytotoxic T cell (CTL) response 5352
– epidemiology 5003
– of the global pandemic 5003
– genetic diversity 5008
– genome 5002
– global epidemic 4996
– heterosexual transmission 5007, 5010
– high-risk populations 5005
– homosexual transmission 5010
– immunogenicity 5012
– incidence 5004
– injecting drug use 5006
– mathematical models 5352
– mother-to-child transmission 5003, 5007, 5014
– phylogenetic analyses 5008
– postexposure prophylaxis (PEP) 5007
– preexposure prophylaxis (PrEP) 5007
– prevention 5006
– public health efforts 5013
– recombinant viruses 5010
– replication cycle 5001
– safe sex 5007
– sexual transmission 5003, 5007

– subtypes 5010
– treatment 5010
– type 1 (HIV–1) 4999
– vaccine 5006
human lysozyme (hLZ) 2967
human metabolome database (HMDB) 1186
human milk 10879
human pathogen 2263
human polyomavirus 6329
human society 940
– global urbanization 940
– urban growth 940
human toxicity potentials (HTPs) 4856
human visual sense 47
human visual system (HVS) 11098, 11101
human waterborne infection 11997
human-scale landscape 5774
humanure 1151
Humboldt ecosystem 540, 578
humid air
– distillation (HAD) 9760
– turbine (HAT) 6823, 6849
humidification 3866
humidity 132
humpback whales 3570
humus
– balance 1137, 1509
– formation 1137
– repro-method 1137
– site-adapted Balancing Method 1137
– VDLUFA-Method 1137
hunger 1741
hurricane 5070, 7402
– synoptic flow 5072
– tracking with driftsondes 5070
hybrid
– braking system 8848, 8851
– breeder 390
– capacitor system 3439, 3440
– carbon ultracapacitors 3486
– constructed wetlands 11903
– cooker 9494–9495
– electric storage models 9495
– cookers 9491, 9495
– drive train 3380, 3383
– speed coupler 3383
– torque coupler 3380, 3383
– electric buses 11509
– electric vehicle (HEV) 710, 768, 3367, 3860, 3368, 3870, 3392–3393, 3855, 5082–5087, 5089–5091, 7847, 8112, 8232, 10542, 11503, 11504, 11506
– architecture 5085, 5087, 5091
– battery 5087, 5090
– configuration 11506
– diesel HEV 5089
– electric propulsion 5089
– energy management 11506
– energy storage 5089
– four-pole induction motor 5091
– fuel cell powered 3860
– gasoline-powered 8232
– off-road 5089
– parallel HEV 5087
– plug-in 3393
– power boost 11504
– series HEV (SHEV) 5085, 5086
– track-type tractor 5091
– ultracapacitor 5087
– vehicular propulsion 5085
– energy storage 3392, 5103, 5104, 5110
– vehicle applications 5103
– food processor 9500
– geothermal biomass power station 4323
– geothermal cycles 4309
– geothermal fossil fuel power station 4322
– geothermal power station 4321, 4323, 4329
– two-phase turbine 4329
– hydraulic vehicle 5097–5098
– energy storage 5097
– high-pressure (HP) accumulator 5098
– hydraulic vehicles (HHV) 5097, 5100, 5101
– energy storage accumulator 5100
– regenerative braking 5100
– imaging 8587
– membranes 6561
– poplar 1286, 1294
– propulsion 268
– recooling 9534
– rice 8019
– systems 3426
– technology 3868
– VAR systems 9344
– vehicle 3486, 3371–3372, 3377, 3379, 3390, 3472, 3477, 5104, 5107
– architecture 3371, 3372
– charge-sustaining 3477
– concept 3371
– electric coupling 3377
– electric load 5104
– flywheel 5107
– fuel cell–powered 3390
– mechanical coupling 3379
– ultracapacitor 5107
– ventilation 6873, 10269, 10334
hybrid-electric
– passenger car applications 3482
– vehicle (HEV) 3496, 3499, 3472, 10490, 10488, 10495
– architecture 10495
hybridization 2371
hybrid 392–393
hydrasun 9666
hydrate 330, 7453
hydraulic
– accumulator 5099
– dredging 3034, 3041
– fracturing 6846, 7804
– hopper dredge 3037
– hybrid vehicles (HHV) 3371
– motor 5098
– stress 2080
– technology 3031
– theory 6413
hydrazine 6780
hydride 3417
hydrocarbon 209, 331, 1174, 1394, 1441, 1586, 2156, 2241, 2434, 2945, 3502, 3907, 3958, 5162, 5531, 6406, 6416–6417, 6551, 7594, 10482, 10483, 11444–11445, 11452
– from alcohols 11452
– from carboxylates 11452
– from lignocellulose 11452
– from sugar 11452
– fuel 2153, 2936, 2939, 5154, 5531
– burning 2153
– oxidation 2936
– gasification 5162
– industry 3504
– ionomers 6541, 8336–8337
– membranes 6544, 6548, 6551
– membrane 3930, 7705, 7771–7772, 8251
– micro-seepage 6416
– oxidation 2946, 2950
– pollution 769, 1633
– polyaromatic 5531
– polymers 6557
– with superacid groups 6557
– proton exchange membrane 8334
– non-fluorinated 8334
– refining 2154
– reformation 5140
– endothermicity 5140
– process 5161
– resources 6406
– synthesis 3958
– thermal stability 2945
– unburned 10483
– utilization 2938

hydrocele 12011
hydrochloric acid 4010
hydrochlorofluorocabon 10132
hydroconversion process 2246
hydrocoral 2498
hydrocracker gas 7842
hydrocracking 2246, 3978–3979, 7834
– heavy paraffins (Wax) 3978
hydrocyclone 8825
hydrodynamic 9060
– tidal model 4579
hydrodynamism 1949
hydroelectric
– generators 12080
– plant 8985
– power plant 2795
hydroelectricity 3464, 8981
hydrofiner 1221
hydrofluoric acid (HF) 786, 791
– alkylation 7836–7837
hydroformylation 3939, 3940, 3946–3947, 3949, 3950, 10175
– CXL-based 3949
– of higher olefins 3947
– of olefins 10175
hydrofracturing 4188
hydrogen 668, 1043, 1051, 2228, 2382, 2385, 3387, 3414–3415, 3417–3418, 3420–3422, 3425, 3500, 3858, 3927–3928, 4067, 5116, 5118, 5135–5138, 5141–5143, 5147, 5149, 5152–5154, 5158, 5160, 5165, 5167, 5170–5171, 5173–5174, 5189, 5203, 5210, 5226–5227, 5484, 5486–5487, 7882, 8195, 8205, 8208, 8221, 8232, 8235–8236, 8239, 10506, 10515–10519, 10997, 11000
– adsorption 3421
– autothermal reforming (ATR) 8221
– binding strength 3418
– biological production 5116
– catalytic partial oxidation (CPO) 8221
– cation 8208
– chlorine (HCl) 5252, 7843, 8350, 9831, 11712
– emissions 2282
– consumption 3500, 5118
– by fuel cell vehicles 10517
– coproduction system 5158
– cryo-adsorbed 8235
– cyanide 10639
– delivery 10517
– direct injection 5487
– dilution 9244
– economy 5174
– efficiency 5152
– electrochemical
– production 3414, 3425
– pumping 8195
– electrode 5888, 6949
– electronic coupling 3418
– engine efficiency 5487
– evolution 3418, 3421
– at metal electrodes 3420
– catalysts 3422
– reaction (HER) 3414
– fluoride (HF) 8350
– food production 5160
– for fossil fuel refining 4067
– for oil refining 5160
– from biomass 5116, 5131
– market implementation 5131
– from fossil fuels 5137
– fuel 2939, 5195, 5210, 6246, 7088, 7757
– fuel cell 8219, 8329
– fuel initiative (HFI) 8236
– fueling station 8194, 8236
– fuel-cycle pathways 10516
– gas 7593, 8175
– cleanup system 5170
– ions 5165
– isotope 11027
– life-cycle analysis 10519
– liquefaction 10517
– low energy density 5171
– metabolism 362
– molar concentration 5149
– molecules 3418, 7896
– nucleus 3800
– oxidation 3418, 5138
– reaction (HOR) 3414, 7732, 7757, 8208, 8232, 8340
– peroxide 3565, 3662, 8215, 8242, 8278, 8340, 9575
– propylene oxide 7591
– photocatalysis 5189, 5203, 5210
– pipelines 8235
– plasma 9242
– poly-generation 5138
– producing ammonia for fertilizer 5160
– production 363, 3862, 5119, 5123, 5131, 5133, 5137, 5147–5148, 5150–5151, 5158–5160, 5162, 5164–5167, 5170–5171, 5178, 5181, 5187, 5189–5190, 5194–5197, 5200, 5206, 5209, 7883, 7888, 7895–7896, 7898, 10516–10517
– addition of iodide 7898
– bifunctional Pt-based system 5209
– biochemical pathways 5131
– biological production methods 5164
– bulk stack 5147
– by dark fermentation 5119
– by solid biomass gasification 5123
– CO loss 5181
– cobaloxime system 5200
– cobalt complexes 5197
– comparative efficiency analyses 5150
– compression 10517
– costs 2385, 5171
– dissolved additives 7896
– electrochemical 5187
– electrolysis cells 5167
– enteric-type mixed-acid fermentation 5166
– external reforming 5148
– from algae 5167
– from high-temperature fuel cells 5133
– fuel cell coproduction 5170
– methods 5160
– microbial electrolysis 5167
– multiphotonic system (Z-Scheme) 7895
– nanophotocatalytic 7883
– pathways 10518
– photobiological 5165
– photocatalyst 5190, 5194, 5195, 5206, 7883, 7888
– photochemical 5187, 5189, 5196
– photochemical water reduction 5178
– photofermentation 5167
– photoinitiated charge separation 5178
– photoinitiated electron collection (PEC) 5178
– photolytic process 5164
– pressure swing adsorption (PSA) 5158
– Rh-based supramolecular and multicomponent systems 5189
– Rh-based multicomponent photocatalysis 5197
– science 5159
– steam methane reformers 5137
– Strickland reactions 5166
– supplemental input method 5151
– technology 5159
– thermal efficiency 5151

– thermochemical sulfur–iodine cycle 5162
– thermochemical Westinghouse cycle 5162
– via electrolysis 10516
– via steam methane reforming 10516
– via wind energy 10516
– water electrolysis method 3862
– pump 8196
– purification 5143, 8195
– radioactive isotope 10997
– reforming process 8221
– separation 5135, 5136, 5141, 5143, 5149, 5152, 5170
– parasitic loads 5149
– pressure swing adsorption (PSA) 5143, 5170
– stable isotopes 5227
– starvation 7766
– steam reforming (SR) 8221
– storage 5486
– in fuel cell vehicles 10517
– sulfide 2025, 4171, 4176, 4247, 4426, 6381–6382, 6660, 8353
– supply chains 5153
– thermochemical biomass processes 5116
– thermodynamic theory 3414
– transport impacts 5152
– underpotential deposition (UPD) 3415, 3420
– vehicle 268, 5136, 8239
– via direct solar production 5173
– vibration 3417
– well-to-tank efficiencies 5142
– well-to-tank (WTT) efficiencies 5142, 5153
– yield 5119, 5147
hydrogen-air fuel cells 8225
hydrogen-containing fuels 3887
hydrogen-dilution gas flow ratio 9245
hydrogen-oxygen fuel cell 7695
hydrogen-powered vehicles 5465
hydrogenase 362, 3422, 3423, 5211, 11004
– iron-based 5211
– enzyme 10999
– organometallic nature 3423
hydrogenated silicon 9251–9254, 9256–9258, 9272
– amorphous 9251, 9254
– to microcrystalline Si:H properties 9257
– bandgap 9252
– Collins-Cody gaps 9252
– defects in the μc-Si:H material 9272
– electron and hole transport properties in μc-Si:H 9258
– films 9256
– germanium alloys 9247
– materials 9243, 9245, 9258
– Fermi level 9258
– Si:H-based materials 9243
– microcrystalline 9241
– nanocrystalline 9241
– Tauc's gap 9252
– Urbach edge 9253
– Urbach tails 9253
hydrogenated vegetable oil (HVO) 1206, 1220, 5489
hydrogenation 3938, 3945, 3950, 3979, 10171–10172
– asymmetric 10172
– of isophorone 10172
– of nitro compounds 10172
– of phenol 10172
hydrogenolysis 2228
hydrography 5875–5876, 8658
hydrolases 10845
– in the gastrointestinal tract 10845
hydrologic/hydrological 2455
– cycle 2108, 2320–2321, 3317, 7245, 8643, 8689, 9804
– restoration 8692
– evaluation of landfill performance 5725
– models 3212, 5824
– three-dimensional (3D) 3212
– process 8635
– systems 9011
– tracer test 9011
hydrology 1546, 3585, 4574, 11334
hydrolysate 974, 977
hydrolysis 966–968, 972, 1149–1150, 9052
– concentrated acid 966
– dilute-acid 967
– enzymatic 967, 972
– fermentation (SHF) 993
– pretreatment 968
hydroperoxide 3662, 6543
hydrophilic compounds 11930
hydrophobic
– compound 10967, 10969
– membranes 10537
– organic matter 10537
– pocket 8135
hydroponics 8202–8203
hydro-power 3456, 8976, 11934, 11942, 12118, 12120, 12240, 12246
– investments 12118
– reservoir 12119
– station 12102
– system 12109
– market process 12109
hydrosphere 595
hydrostatic pressure 4128
hydrostatic primitive equation 7370
hydrotalcite 4600
hydrothermal
– brine 5231
– carbonization 1068, 1080, 1082–1083, 9849
– commercialization 1083
– energy balance 1082
– flue gas 1083
– wastewater 1082
– convective systems 4331
– eruptions 4426
– fluid 5223, 5227
– concentration of silica 5223
– geochemical modeling 5227
– liquid 5224
– reservoir 4192, 4227
– resource 3512, 4330, 4351
– system 3509, 3511, 5216–5217, 5219–5220
– cap rock 5217
– geochemistry 5216
– geothermometers 5220
– upgrading (HTU) 1081, 1085, 1614
– vents 11389
hydrothermolysis 969
hydrotransport 7810
hydrotreating 1221, 1613, 2247, 3979, 7834
– light paraffins 3979
hydroxide 2432, 8606
– apatite 3895
– ions 3898
hydroxyl
– functional triglycerides 6898
– radicals 9563, 9568
hydroxyl-ibuprofen 11926
hydroxyl-interlayered smectites (HIS) 8605
hydroxyl-interlayered vermiculites (HIV) 8605
hydroxylamine 381
hydroxyproline-rich glycoproteins (HRGPs) 8064
hyflon 7704
hygromycin phosphotransferase 2597
hygroscopic inorganic oxide 8339
hygroscopicity 6747, 10571
hyoscyamine–6β-hydroxylase 6531

hyperbolic equations 8907
hyperion 8944
– sensor 8928
hypermethylation 3257, 3607
hyperparasitemia 11076
hyperspectral
– imaging (HSI) 8806, 8817
– for the coastal ocean (HICO) 8960
– satellite sensors 8928
hypertension 9657
hypertensive lung syndrome 8317
hypnozoitocide 11086
hypomethylation 3608
hyponatremia 3253
hypospadia 3648
hypovigilance 3120
hypovitaminosis 9654
hypoxic water 7347
hypsicity 4623
hysteresis 3225
Hysterothylacium 12036

I

ibuprofen 2092, 2339, 4592, 11924
ICE, see internal combustion engine
ice 2761–2762, 2765, 2767–2768, 2771, 2774
– ablation 2765
– accretion 2765
– accumulation 2765
– modeling 2762
– rheology 2768, 2774
– stress tensor 2767
– warm-based 2771
– cloud 661
– Ice Cloud and land Evaluation Satellite (ICESat) 320
– dynamics 2770
– ice mass loss 2459, 4563, 4575
– dynamic thinning 2459
– nuclei (IN) 134, 630, 6747
– sheet 286–288, 292, 2458, 2460, 2513, 2762, 2763, 2769, 2771, 2775–2776
– airborne radar ice sounding 292
– computational considerations 2771
– geometry 2776
– Huybrechts model 2763
– InSAR measurements 287
– mass changes 4570
– mass loss 288
– modeling 2769
– regional image mapping 286
– simulations 2775
– sounding radar 283, 294
– strength 2775
– thickness distribution (ITD) 2763
– velocity 2772
– volume 2773
ice-albedo feedback 2762
ice-atmosphere interface 2766
iceberg calving 2766
IceBridge program 284, 293
icefield 2762
icelandic horse 1798, 1803
– breeding goal 1803
ice-ocean interface 2775
ice-rafted debris (IRD) 9803
ice-thickness distribution 2772
icosahedron 586
ICSI-mediated gene transfer (ICSI-MGT) 10826
icy surface 281
ideal gas law 8905
identity preservation measures 10779
idiotype 8066
– breeding 6434
– vaccines 8067
igloo 6869
ignition 1303, 5254
– air preheating 5254
illegal dumping 10028
illicit radiological material trafficking 7212
– border and port monitoring 7212
illuminance 2807–2808, 2816, 2823, 2826–2827, 2829, 2832
– availability 2823
– visualization 2826
illumination 2806–2808, 2831
– direct components 2807
– indirect components 2808
– of the building 2831
imager response model 11111
Imhoff tank 1148
imidazole 8344
immobilized microbe bioreactor (IMBR) 1635
immune-reconstitution syndrome (IRIS) 11138
immunoassay 5384
immunochromatography 5383
immunosuppression 9663
– UV-induced 9663
implantable cardiac defibrillator (ICD) 6087, 6507, 6510
– batteries 6507
implantable cardiac pacemaker 6501, 6502, 6506
– batteries 6502
imprinted gene 6161
improved cookstove (ICS) 1302
in situ
– chemical oxidation 10152
– mining 6680
– vitrification 11591
in trans silencing capacity 10681
in vitro
– fertilization (IVF) 10819, 10906
– maturation (IVM) 6154, 10819
inactivated polio vaccine (IPV) 8148, 11989
inbreeding 400, 410, 413, 418, 440, 442, 474–475, 492, 1734, 1803, 6440, 7978, 9390
– coefficients 442
– depression 1801, 2785
– horse populations 1803
incident photon to current conversion efficiency (IPCE) 6575
incident radiation 7910
– spectral composition 7910
incinerability ranking 6977, 6988, 7001
– thermal stability-based 6977, 7001
incineration 2449, 3997, 4869, 4903, 5235, 5237, 5241–5242, 5249–5253, 5256, 5267, 5270, 5282, 5288, 5290, 5300–5301, 5303–5304, 6976, 6989–6990, 10578, 10582, 11852–11853, 11858
– alternatives 3997
– ashes 4867
– carbon dioxide concentration 5250
– chlorinated compounds 5252
– combustion air 5237
– cool zone 6990
– corrosion problems 5301
– cost 5242
– dioxins 5267, 5288
– energy balance 5303
– environmental pollution 5288
– facility 11841
– projected energy losses 11841
– flame zone 6989
– FLIC code 5304
– flue gases 5300
– formation of pollutants 5251
– hazardous waste 5256
– heat content of waste 5253
– heat recovery 5241
– high-temperature, non-flame thermal zone 6989
– in a molten salt bath 5282
– incomplete combustion 5250
– mass balance 5303
– modeling equations 5304

– non-flame 6976
– plants 4763
– availability 5242
– potential by-products 6989
– pre-flame zone 6989
– products 5249
– public acceptance 5242
– public image 5288
– safety aspects 5256
– simple, small-scale forms 5270
– slagging operation 5290
– surface catalysis zone 6990
– technologies 5235
– thermogravimetric analysis (TGA) 5304
– train 4972
– with combined heat and power (CHP) 5301
incinerator 4000, 5247, 5248, 5253, 5255, 5257, 5259, 5260, 5264, 5268, 5272, 5276, 5289, 5296, 5309
– boilers 5257
– design 5264
– computer fluid dynamics (CFD) 5259
– design aspects 5259
– draft 5248, 5260
– emissions 5289
– furnace 5237, 5257, 5258, 5270
– air supply 5258
– ash extraction 5257
– capacity 5255
– duties 5257
– feeding equipment 5257
– flow patterns 5258
– types 5270
– selection criteria 5270
– grate
– combustion 5296
– type 4000
– heat recovery 5264
– load factor 5255
– mechanical grate stokers 5272
– mechanical drives 5260
– NO formation 5309
– operating factors 5268
– plants without heat recovery 5264
– reciprocating grates 5272
– regulation and controls 5260
– residence time 5248
– residues 5253
– rotary kiln plant 5276
– stoichiometry 5248
income 213
– environmental factors 213
incomplete combustion 6989
– zone theory of formation of products 6989
Inconel 4979
in-core radiolysis 4065
increased livestock fertility 10885
incubator 8313
Indel mutation 3603
index of refraction 8956
Indian ocean dipole (IOD) phenomena 4573
Indian summer monsoon 6753
indicator organism 3588
indigenous architecture 10300
indigenous plants 3462
indirect aerosol radiative effect 137
indirect coal liquefaction (ICL) 2224, 2235
– Fischer–Tropsch process 2224
indirect field-oriented control (IFOC) 42
indirect land use change (ILUC) 934, 1010, 1497, 1502, 10513
– economic input–output models 1502
indirect radiative forcing effect 135
indirect solar drier 9488
indirect solar gain 7661
indirect storage concepts 10567
indium 1978
individual attitude–behaviour gap 12226
individual sustainable mobility 7787
indoor
– air pollution 1492, 3640, 11293
– air quality (IAQ) 5334, 6875, 7630, 11296
– natural ventilation 6875
– air temperature 10257
– environment 5335, 6865
– environmental control 5335
– ventilation system design 5335
– environmental quality (IEQ) 5332–5333, 10278, 10335
– illumination 2804, 2827
– pollution 1301
– smoke 213, 239
induced pluripotent stem cells (iPS cells) 2972, 7223, 10820, 10827, 10828, 10907
induced seismicity 4127–4128, 4215, 4422
– Mohr–Coulomb criterion 4128
induced systemic resistance (ISR) 2574
induced-draft cooling tower 9533
inductance matrix 38
induction
– machine (IM) 18, 35, 37, 3392, 12145, 12153
– fundamental equations 37
– motor (IM) 44, 11527
– fault-tolerant control 44
inductively coupled plasma mass spectrometry (ICPMS) 8657
industrial
– boiler 1304
– bulk 7589
– catalysts 7589
– ecology 3454, 8790
– enzyme 8024–8029, 8051
– bioconversion of grain to ethanol 8027
– current uses 8025
– development of applications 8025
– global market 8027
– historical background 8025
– microbial producer 8029
– plant-based production 8024
– plants as sustainable sources 8051
– production 8028
– sustainable production 8024
– facility 7184
– cost analysis 7184
– gas turbine 6833
– gasification 2240
– hazardous 4903
– metabolism 6858
– mineral mine wastes 6669
– oxidation catalysis 7590
– plants 8085
– oil processing 8085
– pollution 10441
– proteins 8032
– production 8044
– radiography 8523, 8561
– residues 1180
– revolution 207
– stormwaters 11897
– waste 1179, 1493, 10003, 10004
– characterization 10004
– generation 10003
– wastewater 9564, 9568
inelastic collision 3789
inelastic scattering 3801
– photons 8572
inert gas 6733
– step addition (ISA) 6722, 6728, 6730
inertial confinement fusion (ICF) 7173
– laser development 7173
inertial flowmeter 4205
infant 3625
– metabolic rate 3625
– mortality 3621
– rate of oxygen consumption 3625
infection kernel 5351
infectious disease 507, 5347–5349, 5352–5355, 5378, 5362, 5364, 5380–5387, 5392, 6606

– antibody-based diagnostics 5383
– basic reproductive number 5347
– classical culture-based diagnostics 5383
– climate change 5358, 5359–5362, 5364, 5366, 5370–5372, 5380
– bluetongue 5371
– chytridiomycosis 5370
– effects on hosts 5364
– effects on vectors 5364
– extreme weather events 5366
– genetic resistance 5364
– intensity or severity 5361
– malaria 5372
– spatial associations 5360
– temporal-interannual associations 5361
– temporal-seasonal associations 5360
– disease control 5381
– endemic stability 5364
– host heterogeneity 5349
– importance of rapid diagnosis 5382
– influence of climate 5362
– infrared spectroscopy 5386
– mathematical epidemiology 5348
– modeling 5347, 5355
– molecular diagnostics 5384
– multilevel models 5353
– Raman spectroscopy 5387
– SI model 5354
– SIR Model 5348
– spectroscopy-based diagnostics 5385
– surface-enhanced Raman spectroscopy 5392
– weather 5359
– within-host evolution of HIV 5352
– within-host models 5347
infectious pancreatic necrosis virus (IPNV) 548
infectious parasites 12021
infectious salmon anemia virus (ISAV) 548
infective metacercariae 12027
infiltration fields 11901
infinite couple 2025
inflorescence 2703
– architecture 2703
influenza virus infection 5379
– influenza A virus 2970
information entropy 7542
infrared (IR) 11114
– absorption spectroscopy 5385
– effects 9665
– radiation 2321, 9666
– reflection methods (NIR) 9837
– sensing 11114
– spectroscopy 5386
– thermography 10
infrasound 12278
infrastructure 3468
– maps 3080
– planning 3468
infrastructure-to-vehicle communication 3080
ingestible medical devices 6517
inhabited area 3527
– countermeasures 3527
– remedial actions 3527
initialization shock 2129
injection
– engines 932
– pump 4289
inland waterbody 5674
inner cell mass (ICM) 6151, 6157
inner-city brownfield sites 11368
inorganic
– arsenic 3647
– chemicals 10144
– physicochemical properties 10144
– materials 10560
– thermal stability 10560
– photovoltaic (PV) 7554
– pollutants 2434, 7607
– pollution 2502
– semiconductors 7575
– triple superphosphate 7685
– waste 11583
InSAR technique 288
insect 5438, 5444, 5454, 5457
– amylases 4031
– for pollination 10723
– genetics 4039
– double-stranded RNA (dsRNA) 4039
– herbivores 4026, 4030
– identification 5438
– natural enemies 5444
– pathogens 5450–5451
– bacteria 5451
– for microbial control 5450
– fungi 5451
– nematodes 5451
– viruses 5451
– insect pests 4013, 5433, 5452
– mass trapping 5452
– introduction of traits 5457
– population 5436, 5437, 5450
– aggregated distributions 5436
– distribution patterns 5437
– entomopathogenic organisms 5450
– densities 5435
– random distributions 5436
– uniform distributions 5436
– resistance 4013
– sterilizing 5454
insecticidal
– genes 4029
– protein 4014, 4037, 4038
– avidin 4038
– *Photorhabdus luminescens* 4037
insecticide 2747, 3594, 4035, 4454, 4457, 4467, 5440, 5459, 10748, 11078–11079, 12003
– against malaria 12003
– resistance 5457
– detection 5457
– monitoring 5457
insect–plant interactions 5442
insect-resistant
– cotton 4457–4458
– Argentina 4458
– Australia 4457
– Brazil 4461
– China 4457
– global impact 4462
– India 4460
– Mexico 4459
– South Africa 4460
– USA 4457
– maize 4453–4454, 4456
– Argentina 4453
– Canada 4453
– economic impact 4457
– South Africa 4454
– Spain 4454
– potatoes 4464
– transgenic crops 4039
– sustainability 4039
instantaneous clearness index 9751
Institute of Electrical and Electronics Engineers (IEEE) 3007
institutionalization 12221
instrumental knowledge 4535
instrumented vehicle 3086, 3088
insulation 2998, 7634
– comfort principle 7634
– materials choices 7634
insulin 8027, 8067
insurance nitrogen 3777
integral fast reactor (IFR 4057, 7150
integral line-beam skyshine method 8553
integral shading devices 3688
integrated aquaculture 6366
integrated assessment modeling (IAM) 5398–5402, 5412, 5414, 5416–5417
– economic costs 5417

– higher resolution 5400, 5402, 5422, 5424
– climate impacts 5422
– integrated Earth System Models (iESMs) 5424
– highly aggregated 5400, 5401
– in mitigation policy analysis 5412
– multiple greenhouse gases 5414
– stabilization studies 5416
integrated breeding 6695, 6702, 6703, 6705, 6708
– helpdesk 6703
– hubs 6708
– portal 6703
– platform 6702
– workbench 6705
integrated building design 10245
integrated coastal zone management (ICZM) 513, 554, 1968, 9189
integrated combined cycle gasification (IGCC) 2240
integrated delivery process 10294
integrated design
– practice methodologies 10315
– process 10308
integrated Earth System Model (iESM) 5424
integrated electrokinetic remediation technology 10429
integrated gasification 6847
– combined cycle (IGCC) 1216, 1438, 8105, 8350
– fuel cell plant (IGFC) 9930
integrated gross oil refining (IGOR^{+}) 2232
integrated hydro-economic modeling 5828
integrated mariculture 9117
integrated marine biogeochemistry and ecosystem research (IMBER) project 6383
integrated multi-trophic aquaculture (IMTA) 543–544, 1928, 1937, 3581, 6309–6311, 6313–6314, 6316, 9111, 9117, 10322, 10324
– biological and chemical processes 6313
– biological aspects 6316
– economical aspects 6316
– engineering aspects 6316
– history 6311
– land-based 6310, 6312
– nutrient budget 6312
– nutrient composition 6314
– pilot scale systems 6314
– variations 544
integrated nutrient management (INM) 162
integrated ocean drilling program (IODP) 6408
integrated pest management 153, 5428, 5429, 5432, 5434, 5443, 5447–5450, 5452–5453, 5455–5456, 5458
– behavioral control 5452
– biological control 5443, 5447–5448, 5450
– biotechnology 5456
– compatibility of pheromones 5453
– crop diversification 5449
– cultural control 5455
– economic threshold 5432
– genetic control 5453
– genetically modified (GM) crops 5456
– host-plant resistance 5456
– implementation 5458
– microbial control 5450
– pheromones 5452
– precision agriculture 5434
– strategy 5432
– sustainability 5432
– tools 5434
integrated project delivery (IPD) 10307
integrated satellite tracking of pollution (ISTOP) 7517
integrated sequential bio-refinery (ISBR) 561
integrated starter-generator (ISG) systems 11548
integrated two-stage liquefaction (ITSL) 2231
integrated waste management 11682–11683, 11688, 11691, 11828
integrated water resources management 5827
– decision-making support systems (DSS) 5827
integrated water vapor (IWV) 9724
integrated wind plants 12257
intelligence quotient (IQ) 3633
intelligent
– energy 8206
– islanding 12092
– load shedding 12093
– transportation system (ITS) 91, 1820, 1835, 1852, 3082, 4955, 5967, 11455
– vehicle (IV) 3080, 3108, 3170, 3172, 3176, 5460, 6950, 11097, 11187
– driver inattention monitoring system 3108
– dynamic environment sensing 3170
– laser scanners for perception 3176
– night vision pedestrian warning 6950
– safety system (IVSS) 73
– technologies 2464, 5460
– true color night vision video systems 11097
– unscented Kalman filter 11187
inter-tropical convergence zone (ITCZ) 7251
interacting ecosystem 1954
interagency ocean research plan 2261
Interbull 396
intercalation electrode 6123
intercity highway truck 6284
interconnected power system 12093
intercooled recuperated engine (ICR) 6849
intercrop 151, 156, 1123, 1579, 2741, 2751, 5449, 10046
intercrystallite ionic transport 724
interdigitated back contact solar cells 7939
interface/interfacial
– compartment model 9129
– electronics 3495
– infrastructure 7856
– mass transfer 2026
– transformer 3018
interference competition 10075
interferometer 288
interferometric synthetic aperture radar (InSAR) 4575
intergovernmental panel on climate change (IPCC) 2099
interior energy input 4138
interior permanent magnet (IPM) 23
interior shading 3690
interior systems 10290
– sustainability 10290
intermediate 11439
– cells 10907
– heat exchanger (IHX) 4060, 4068
– level semiconductors (ILSC) 9424
– pyrolysis 1518, 1524
– principles 1524
– process technology 1524
internal combustion engine 250, 1404, 3371, 3860, 3868, 5461, 5463, 5499, 5502, 5501, 5505–5512, 5515, 5518–5519, 5521, 5522, 5525, 5528, 5529, 5535, 5537, 5538, 5542, 7694, 10482, 10488, 10490, 11485, 10502
– advanced engine controls 5537
– alternative fuels 5461, 5463, 5542
– basic operating cycle 5502
– boosting 5535
– charge heating 5509
– combustion duration 5528
– combustion efficiency 5510
– compression ignition engines 5525
– developments 5499
– diesel cycles 5511

– cycle analysis 5519
– emissions formation 5529
– engine downsizing 5535
– engine-out emissions 5535
– exergy 5518
– destruction 5521
– exhaust pollution 5529
– friction 5507
– fuel conversion efficiency 5507
– fuel–air cycle analysis 5512, 5515
– fuel–air equivalence ratio 5518
– gross work 5506
– in-cylinder work 5505–5506
– Otto cycle 5511
– power/torque/speed curve 5507
– pressure–crankangle diagram 5505
– pump work 5506
– quasi-static effects 5509
– ram effect 5509
– spark ignition combustion 5522
– thermal efficiency 5510
– thermodynamic analysis 5510
– torque-speed characteristic 11485
– tuning 5509
– variable geometry engine designs 5537
– variable valve timing 5538
– internal combustion engine vehicles 11316, 11503
– volumetric efficiency 5507
– curve 5508
internal concentration polarization 2918
internal dosimetry 3023
internal heat transfer 10572
– Sandwich concept 10572
internal ribosome entry site (IRES) 10848
internalin 5058
International Atomic Energy Agency (IAEA) 8486, 8612
International Building Performance Simulation Association (IBPSA) 10194
International Commission on Radiological Protection (ICRP) 3519, 11046
International Electrotechnical Commission (IEC) 3007
International Geosphere-Biosphere Program (IGBP) 8920
International Lead Association (ILA) 5884
International Nuclear and Radiological Event Scale (INES) 8504
International Nuclear Event Scale (INES) scale 10426
International Organization for Standardization (ISO) 3008
International Panel on Climate Change (IPCC) 8894
international plant protection convention 2314
international polar year (IPY) 292
international pyrheliometer comparison (IPC) 9677
International Satellite Cloud Climatology Project (ISCCP) 8910, 10629
International Telecommunication Union (ITU) 3008
International Thermonuclear Experimental Reactor (ITER) Joint Project 7162
International Trachoma Initiative (ITI) 12013
international transboundary breeds (ITB) 7974
International Waste Generation Comparison Rates 8772
Internet-accessible materials exchanges 8792
internet 4502–4503
– science education 4503
interoception 12297
interpenetrating networks (IPNs) 6897
interplanetary field (IMF) 9477
interplanting crop 156
interplate 3237
intersection 3083, 3091, 3095
– after curves 3095
– control systems 2476
– road structures 3091
interspecific density dependence 10065
intertropical convergence zone (ITCZ) 6742, 9634, 9646
inter-vehicle distances 2467
intracellular calcium homeostasis 9654
intracellular signaling pathways 3589
intracytoplasmic sperm injection (ICSI) 10817, 10819, 10906
intragenics 4497
intraguild predation 10067
intra-scene dynamic range 11106
intraspecific density dependence 10065
introgression library line (ILL) 6433
introgression 477
– of transgenes into wild populations 10801
intron trap 7223
intrusion 1918
inulin 1115
invasion
– biology 10078–10079
– ecology 5548, 5556
invasive species 5547, 5549–5551, 5554–5556
– biological control 5556
– colonization pressure 5549
– ecological impacts 5551
– eradication 5555
– factors affecting establishment success 5550
– maintenance control 5556
– management of invasions 5554
– niche breadth-invasion success hypothesis 5550
– prevention 5555
– propagule pressure 5549
– risk assessment 5554
– socioeconomic impacts 5554
invasive treatment 7999
in-vehicle information systems (IVIS) 3124
in-vehicle navigation 3082–3083, 11457
inverse electrolysis 3929
inverse gas, turbine 1411, 1420
invertebrate 9165, 10087
– sentinels 9165
inverted roof 4702
inverted terminal repeat regions (ITR) 10903
investigational new animal drug (INAD) 3565
investment tax credit (ITC) 12262
involuntary smoking 3632
iodine 1686, 1689, 4209, 8393, 8484, 8622
– deficiency 1686
– fortification of salt 1689
– iodine oxide 119
– toxicity 1686
iodobenzene diacetate (IBD) 4646
ion/ionic
– association theory 4097
– conduction 3878
– conductivity 742, 2949, 2951, 3892, 3896
– correlation 6047
– molecular dynamics simulation 6047
– diffusion 3439
– dynamic correlation 6048
– exchange 4588
– liquid 970, 3936, 3939, 4647, 4648, 6085, 10177
– chemical reactions 10177
– electrolytes 6054
– MW-assisted synthesis 4647
– solvent-free synthesis 4648
– synthetic application 4648
– transfer 742
– transport protein 5

– liquid–based electrolyte (ILE) 6060, 6063
– solid salt 3939
– stress 5317
– tolerance 5319
– exclusion 5319
– tissue tolerance 5319
ion-aerosol clear-air mechanism 9810
ion-exchange membrane 8719
ion-exchange reactions 4098
ionization chamber 5562, 5563
ionizing radiation 3023, 3629, 3644, 4907–4908, 5560, 5562, 5572, 5574, 5578, 5581–5582, 8433, 8537, 8560–8562, 8587, 9661, 11041
– adaptive response 5578
– assessment of the environment 8433
– chromatid aberrations 5581
– dose fractionation 5578
– dosimetry 3023
– environmental protection 5582
– gas-filled detectors 5562
– low dose exposure 5578
– on nonhuman biota 5572
– origins 8562
– repair of DNA 5581
– single- and double-strand breaks (DSBs) 5581
– sources 8560, 8587
– tritium beta particle 11041
ionizing radioactivity 8426
ionomer 7760, 8332, 8344, 8337
– chemical modification 8337
– degradation 6543
– ion transport 7760
– membranes 6557, 6559–6560
– inorganic nanoparticles 6560
– superacid-containing 6559
– water transport 7760
iopromide 11923
iridium oxide nanoparticles 7611
iron 612, 1685, 1689, 1713, 6379–6380
– acetate 8285
– biogeochemical cycle 6379
– catalysts 2245, 3975
– concentration 9577
– deficiency 1685
– fertilization 2117, 4113, 6380
– fortification 1689
– hydrogenase 5180, 5187
– multicomponent systems 5187
– in ocean surface waters 6379
– nitrate 721
– oxalate 8285
– phthalocyanine 8273, 8277
– source 9577
– stoves 1362
– sulfide 8352
– toxicity 1685
– uptake 1713
iron-III fluoride 6088
iron-lift configuration 6289
iron-nickel battery system 6940
iron-stimulated bloom 7274
irradiance 7906, 9755
– distributions 9751
– geometry 7922
– long-term variability 9755
– maps 9750
– satellite-based 9750
– reflectance 8957
irradiation tests 4068
irradiator 8523, 8524
irrigated agriculture 5620–5623, 5627, 5631, 9324
– control of salinity 5621, 5623, 5627
– economic viability 5622
– efficiency of water use 5631
– quality of return flows 5627
irrigated crop production 5624
– optimal use of rainfall 5624
– soil water storage 5624
irrigation 2790, 5620–5626, 5628–5631
– advisory services 5629
– decision support systems 5628
– efficiency 5622
– food production 5620
– groundwater use 5630
– management 5619, 5622, 5625, 9321
– for efficient crop production 5619
– improvement of sustainability 5622
– plant water sensors 5625
– under water scarcity 5629
– methods 5623
– networks 5631
– on demand 5625
– pressurized systems 5626
– process 5621
– scheduling 5626, 5628, 9323
– simulation models 5628
– sustainability 5620
– systems 2324
– timing 5626
– uniformity of water distribution 5626
– water 5621
– requirements 5624
ischemic heart disease 213
isentrope 616–617, 6817
isentropic enthalpy 4274
isentropic turbine 4257, 4262
– efficiency 4262
island
– biogeography 947, 5775, 11328
– networks 10937
iSNR hole 11113
iso-butanol 5466, 5469, 5482
isoflavene 8135
isomeric transition 8564
isomerization 2246
isoniazid 11139
iso-octane 5469, 5478, 5516
isoparaffin 3979
isopentenyltransferase 10750
isoprene 3225, 8897
isoprenoid 502, 6522
– biosynthesis inhibition 502
isoseismic map 2428
isotherm 6817
isothiocyanate 3613
isotope/isotopic 3286, 3788, 3789, 3792, 8468, 8599
– activity ratios 8413
– dilution mass spectrometers (IDMS) 7206
– fractionation 5229
– of plutonium 3789
– separation 5634–5635, 5637, 5639–5641
– cascade theory 5637
– countercurrent recycle cascade 5639
– factor 5635
– ideal cascade 5639
– McCabe–Thiele diagram 5640
– potential 5641
– separative work unit 5641
– shift 5642
iteration 440
iterative closest point algorithm (ICP) 10608

J

Jahn–Teller effect 714, 717, 726
– distortion of the Mn^{3+} ion 726
– Mn^{3+} ions 714
JANAF thermochemical table 5515
Janzen-Connell hypothesis 10078
Japanese recycling law 4010
Jarvis-type stomatal resistance 3217
Jatropha 2632
– *curcas* 922, 925
– oil 8087
jellyfish 12047
Jersey barrier 3073, 3074

Jerusalem artichoke 1115
jet 10976, 10980, 10984, 10987, 10990
– coflow 10984
– crossflow 10987
– deflection 10987
– effect of boundaries 10980
– engine 6260
– exhaust condensation trail 659
– fuel 11430
– velocity 10990
JFE process 4001–4003
– commercial operation experience 4003
– direct melting 4003
johnsongrass 10346, 10349
JoinMap 6698
Joint Global Ocean Flux Study (JGOFS) 6383
joint regression analysis 4080
jorumycin 3161
joule heating 776
joule-heated ceramic melter (JHCM) 11585
jumping genes 10830

K

kahalalide 3160
Kalina cycle 4296, 4318–4319
– process 1267
Kalman filter 50–51, 57, 700, 3054, 3058, 3065, 3078, 11189
– algorithms 3059, 11194
– unscented 57
kanamycin 11140
kaolinite 8622
Kaposi's sarcoma 3644, 4999
Karenia brevis 4824–4826
– description 4824
– detection 4825
– economics 4825
– nutrient interactions 4826
– origins 4826
– toxicity 4825
karlotoxin 9086
Karman's constant 11267
Karolinska sleepiness scale (KSS) 3117
karst 2798, 5646, 5648–5650, 5654, 5658, 5661, 5664–5665, 5669
– aquifer 2798, 5669
– areas 5649–5650, 5652, 5658, 5666
– by transportation facilities 5658
– cave development 5649
– filtration system 5666
– untreated ditches 5652
– character 5649
– dye tracing 5664
– features 5649, 5653
– drainage issues 5653
– flooding of highways 5653
– geohazard study 5661, 5665
– geotechnical information 5658
– groundwater 5646, 5654
– haystack-type 5646
– human modification 5646
– map 5660
– problems 5648
– sinkholes 5650
– soils 7686
– oocyst transport 7686
– terrane 5645, 5649
– issues 5645
– transportation issues 5645, 5649
karst-related drainage 5666
karst-related subsidence 5655
– remedial treatment techniques 5655
karyoplast 6150
Kasalath allele 2698
Kashin–Beck disease 1686
katabatic winds 11299
K-band ranging system 4567
Keeling curve 9703
Keggin ion 4596
kelp 544, 550
Kelvin
– effect 134
– equation 117
keratinocyte 3611
kernel E-factor 4629
kerogen 7459–7465, 7469–7470, 7474–7476
– changes in the macromolecular structure 7476
– composition 7462
– decomposition 7470, 7476
– kinetics 7476
– mechanisms 7476
– rates 7469
– degradative analysis 7464
– functionalities 7464
– isolation 7463
– macromolecular structure 7462
– nondestructive analysis 7465
– pyrolysis 7475
– pyrolytic behavior 7464
kerosene 658, 666, 1218, 1302, 3978, 7446, 11430
Keshan disease 1686
ketone 3945, 11451
– CO_2-expanded 3945
keyhole limpet hemocyanin (KLH) 8066
key-population 947
keystone
– predation 10081
– predator 10072, 10073
– species 3300, 3302–3303
– ecosystem engineering 3302
– usefulness for management 3303
K-fuel 2217, 2218
Kőhler curve 132
kiln dust 11702
kimberlite 1924
kinematic viscosity 2048
kinetic energy 3788, 3790, 3793, 3799, 8562, 8849, 10543–10544, 10619, 11489, 12204
– flux density 10619
– from the wind 12204
kinetic hydrate inhibitor (KHI) 344
kinetic nucleation 119
kinetic occlusion 3146
– information 3147
– age-related decrements 3147
Kirchhoff's law 9417
– circuit law 6146
– current law 39
– voltage law 39
kitchen
– conditions 1310
– stove 1364
klarite 5393
Kölbel–Schulze methodology 1055
Klebsiella 6324
klinotaxis 12298
K-metasomatism 5218
knight shift 6081, 6091
knockin 10902
Knoevenagel reaction 4608
knowledge
– accumulation 4502
– deficit model 10881
Knudsen
– diffusion 2024
– flow 2921
Koi herpesvirus 1940
Kolmogorov complexity 3120
Komatsu mining truck 5102
Kona Blue Water Farm 3558–3560, 3562, 3564, 3567, 3570–3572, 3574
– benthic impacts 3562
– biofouling on the farm structures 3564
– cultural resources 3572
– environmental concerns 3560
– farm operations 3558–3559
– fish meal 3574
– fish oil usage 3574

– marine mammal monitoring plan (MMMP) 3570
– offshore farm site 3558
– pest management strategy 3564
– recreational use impacts 3571
– shark management plan 3567
– viewplane aesthetics 3572
– water quality 3562
– wildlife interactions 3567
Kosambi mapping function 479
Koutecky–Levich equation 7750
Kozeny–Carmen equation 4187
KPT (kitchen performance test) 1306
kraft lignin 6928
Kröger–Vink notation 2941, 3898
kriging 197
– of differences 9754
Kronecker delta 3811
krypton 8484, 8583
K-shell electron 8564
Kyoto protocol 515, 654, 664, 3858
Kyshtym accident 5592, 5601

L

La Niña event 2126, 2130
laboratory car 3061–3062
– dynamic link library 3062
– estimation process algorithm 3062
– test conditions 3061
Lachnospiraceae 6327
lactation 1777
lactic acid fermentation 1131
lactobacilli 994
lactoferrin 10874, 10900
lactose 10855
lacustrine
– biology 291
– deposits 11620
lacZ gene 2589
lagoon 2491
Lagrange equation 11463
Lagrangian
– coordinate system 2034
– derivative 2765
– trajectory analysis 8672–8673
– trajectory model 261
lahar 11642
– flows 8942
lake 5673, 5674, 5676, 5678–5681, 5683–5685, 5688–5690, 5692–5698, 5700
– acid rain 5678
– aging process 5673
– atmospheric input 5678
– biological processes 5679
– biology 5676
– biomanipulation 5700
– bottom 5689
– diffusive oxygen flux 5689
– chemical kinetics 5680
– chemistry 5676
– density- or wind-driven currents 5683
– dissolved oxygen 5693
– eutrophication 5673, 5681, 5684
– external material inputs 5676
– geometry ratios 5682, 5698
– hydraulic residence time 5680
– hypolimnia 5698
– ice 291
– ice-cover model 5684
– internal nutrient loading 5679
– lethal temperature (LT) isotherm 5695
– liming 7046
– management 5700
– manipulation of water quality 5680
– model simulations 5692
– nutrients from watersheds 5678
– particle settling 5678
– phytoplankton concentration 5689
– radiation attenuation 5690
– resuspension 5678
– sediment 5680, 5686
– air bubble plume 5680
– heat fluxes 5686
– simulation
– of Cisco habitat 5694, 5696
– of water quality 5683
– stratification 5681
– sustainability 5674
– sustainable cold-water fish habitat 5697
– sustaining fish habitat 5692
– vertical mixing 5681
– water temperature 5685, 5693
– year-round dissolved oxygen model 5688
– year-round water temperature 5684
Lamb wave 12066, 12068
Lambertian scattering 7919
Lambert's cosine law 9676
Laminaria 9122
land 1506, 1555
– abandonment 10371
– allocations 5410
– availability for energy crop production 1506
– consumption 5787–5789, 5791, 5793–5795, 5799–5800, 5804, 5807–5809
– compensation systems 5804
– drivers 5791
– minimization 5808, 5809
– models 5793
– motorized transport demand 5799
– policy responses 5800
– spatial planning 5799, 5807, 5809
– supply-driven factors 5794
– systematization 5795
– undesirable effects 5788, 5795
– unintended social outcomes 5799
– cover change 5778
– degradation 1555
– disposal 5706, 5709
– finding sites 5709
– of solid waste 5709
– efficiency 1504
– ice 2766
– management 1511, 3279, 4677
– successional recovery 3279
– mosaic 10369
– subsidence 5712–5713, 5715–5718
– causes 5713
– economics 5718
– environmental Effects 5717
– fluid withdrawal 5716
– geology study 5715
– groundwater extraction 5715
– hydrogeology 5715
– in urban environment 5712
– monitoring 5718
– problems 5713
– properties of the soils 5715
– properties variation in time 5716
– solid extraction 5717
– tunneling 5717
– underground construction 5717
– treatment 1635
land surface 3212–3213, 9636
– catchments 8700
– model 3212–3217, 3219–3220, 3222
– bucket models 3213, 3220
– bulk-layer models 3219
– force-restore method 3217
– Monin-Obukhov similarity theory 3216
– net shortwave radiation 3215
– Stefan-Boltzmann constant 3216
– subgrid heterogeneity 3214
– surface data 3214
– topography-based runoff models 3222
– variable infiltration capacity (VIC) model 3214
– warming 204
land use 1550, 3553, 5778, 5787, 5793–5795, 5800–5801, 5803–5805, 5807, 5820–5821,

5825–5826, 5836, 5839–5840, 5847, 5849, 10264, 10294, 10923
– and land cover (LULC) 5827
– carbon-and-nitrogen-dynamics models (CANDY) 5826
– catchment models 5825
– change 1497, 1498, 1501, 1502, 1560, 5825
– satellite data 1502
– comprehensive planning 5800
– controlling factor for water and nutrient dynamics 5825
– decentralized governance 5794
– eco-hydrological models 5820
– effect on hydrological cycle 5821
– efficiency 1504
– environmental problems 5820
– evapotranspiration 5849
– global dimension 5787
– governance 5794
– impacts 5795
– management 1550, 3207
– natural processes 5820
– negative planning 5803, 5807
– perforation 5839–5840, 5847
– planning 1561, 3553, 4677, 5801, 5805, 5818, 10264, 11344
– analysis system (LUPAS) 9327
– blue-print-planning 5805
– legally binding 5801
– legislation 5803
– persuasion 5805
– regulations 5803
– sequential test 5805
– water resources management 5818
– positive planning 5803
– public planning 5801
– runoff generation model 5826
– sector-specific planning 5800
– spatial planning 5805, 5807, 5836
– sustainability 5820, 10294
– tradable permit schemes 5804
– whole-farm simulation model 5826
– zoning 5793
land-atmosphere interaction 8911
land-based culture 1935
land-consuming human activity 5791
land-water storage 2459
landfarming 1632, 2444
landfill/landfilling 4765, 4772, 4799, 4904, 5709–5711, 5720–5721, 5723, 5732–5734, 5736–5739, 5743, 5745, 5747, 5749–5753, 5755, 5757, 5760–5763, 5910, 5918, 5928, 5930, 5932, 8773, 9984–9987, 9992, 9996, 9999, 10003, 10581, 10584, 11585, 11665, 11675, 11697, 11747, 11828, 11834, 11835, 11852
– bioreactor 5720–5724, 5726–5730, 5763
– aerobic 5723
– alternative daily cover materials (ADCs) 5728
– anaerobic 5723
– biocell 5723, 5730
– biochemical oxygen demand (BOD) 5722
– cell configuration 5724
– final cover 5728
– gas collection systems 5727
– gas production 5728, 5730
– historical evolution 5721
– horizontal infiltration trenches 5726
– hybrid 5723, 5730
– infiltration ponds 5726
– leachate management 5724
– pre-wetting of waste 5727
– spray infiltrators 5727
– types 5722
– uneven moisture distw Wells 5726
– waste degradation 5728
– waste settlement 5729
– cell capacity 5711
– cell construction sequence 5711
– classification 5750
– closure 5732–5733, 5736–5738
– compacted clay liners (CCL) 5752
– controls 9992
– covers 5755
– design 5710, 5749
– directive 11684
– disposal 5733
– program flexibility act 10019
– diversion 11674
– drainage layers 5753
– dry-tomb 5721
– emissions 11697
– factors 5932
– external costs 4799
– facility property 5739
– finding sites 5709
– flexible membrane liners (FML) 5752
– gas (LFG) 4767, 5722, 11835
– collection 5910, 11690
– gas to energy (LFGTE) 5910, 5918
– gas 5743, 9986
– capture for energy recovery 11675
– collection efficiency 5932
– energy 5745
– management 5723
– geological mapping 5751
– geomembranes 5752
– geosynthetic clay liners (GCL) 5750, 5752
– greenhouse gas emissions (GHG) 9987
– groundwater composition 5751
– leachate 5720, 5755
– collection system 9985
– containment 5711
– control 5747, 5751, 5763
– disposal 5761
– management 5723
– monitoring 5757, 5762
– treatment 5760
– life cycle inventory 5928
– liners 5752
– monitoring 5757
– of untreated ash 11747
– post-closure
– control 5761
– development 5745
– plan 5736
– requirements 5734
– reuse 5737–5740, 5746
– economics 5740
– infrastructure 5739
– master plan 5738
– of land 5732
– permitting 5738
– sustainability 5740
– runoff/infiltration control 5757
– semi-aerobic 9992
– simulators 10003
– sites 5733
– selection 5751
– sustainable reuse 5733
– SO_2 emissions 5930
– sustainability 5741–5742
– economic aspects 5742
– environmental aspects 5741
– gases 5741
– sociopolitical aspects 5742
– total LCI emissions 5918
– viability for reuse 5737
– waste input management 5749
landscape 3329, 3359, 5772–5774, 5777–5778, 5780, 5783, 5808, 5818–5821, 5830, 5835, 10356, 10358–10359, 10363, 10367–10368, 10371–10372, 10375–10378, 10380–10381, 11876
– aesthetic quality 10368
– aesthetic value 10371
– architecture 10367
– as art 10376
– assessment 10372
– balance 5820

– change 10382, 10384
  – monitoring 10382
  – quality of life 10384
– character 10372
  – assessment (LCA) 10372
– complexity 5778
– components 5774
– conservation 5783
– cultural heritage 10376
– definition 10367
– designs 11332
– diversity 10363
– ecology 947, 3298, 3359, 5772–5775, 5777, 5780, 5783, 5819
  – accuracy assessment 5783
  – data acquisition 5783
  – definition 5774, 5775
  – European perspective 5773
  – evolving concepts 5775
  – goal 5777
  – nature–society interactions 5783
  – North American perspective 5773
  – research topics 5777
  – spatial heterogeneity 5775
  – spatial scaling 5780
– extensive agricultural use 10356
– functions 5821
– human-dominated 5778
– human-scale 5774
– irrigation 11876
– management residues 1176
– mosaics 5777
– pattern
  – analysis 5780
  – optimization 5783
– planning 5830, 5835, 5785, 5817, 10358, 10372
  – for minimizing land consumption 5785
  – for sustainable water usage 5817
– preservation 5808
– project 10386
– quality interaction 12245
– sensitivity 10378
– shrinking 5835
– spatial signature 3329
– structure 5818
– sustainability 5783, 10356, 10359, 10377, 12293
– sustainable water use 5830
– time 10375
– value 10378
– visual capacity 10381
– visual impact assessment 10380
  – visual sensitivity 10380
  – water balance 5819
landslide 3248, 3553
land-surface hydrology model (LSM) 4570, 4573, 4575
lane departure warning (LDW) 71
lane-keeping assist (LKA) 3068
lane-tracking system 3126
Langevin recombination rate 7561
Langley plot technique 9714
Langmuir
  – adsorption 9574
  – isotherm 8612, 8618
Langmuir–Hinshelwood mechanism 9572
lanthanide 2944, 3902, 7889, 8621
lanthanum 9860, 9949
  – chromate 2946–2947, 2949, 2951
    – catalysis 2949
    – conductivity 2947
    – stability 2951
  – chromites 9853
  – ferrites 3907
  – manganite–based cathode 9860
    – chromium poisoning 9860
  – strontium manganite (LSM) 9853, 9872, 9955, 9963
lantibiotics 504
Laplace field 11163
Laplace transform 10972
Laplace equation 4570
large eddy simulation (LES) 11278
large Hadron collider (LHC) 6242, 6253
large offspring syndrome (LOS) 6157, 10819
large-scale combustion plants 1313
Larix spp. 3292
Larmor time scale 6081
laser
  – atmospheric sensing experiment (LASE) 317
  – fluorosensor 7501, 7519
  – in-space technology experiment (LITE) 320
  – isotope separation (LIS) 5642
  – measurements 3197
    – geo-referencing 3197
  – range finder (LIDAR) 11457
  – scanner 70, 75, 3176, 3179–3180, 3185
    – horizontal matching 3179
    – LIDAR 3176
    – mirror range 3180
    – segmentation 3185
    – vertical matching 3179
  – ultrasonic remote sensing of oil thickness (LURSOT) sensor 7513
laser-induced breakdown spectroscopy (LIBS) 8817
LASSO methodology 432
late blight 2578, 2701
latent heat energy storage 10565
latent heat storage 10557
lateral tire forces 3056
laterite 1918
  – nickel 9953
lattice nitrogen 6771
Laurentide ice sheet 2770
lava flow 11615, 11620, 11641
Lavoisier mass balance 9138
law
  – of blackbody radiation 9417
  – of diminishing returns 2991
  – of mass conservation 5249
  – of thermodynamics 6815, 6816, 10001, 11852
Lawesson's reagent 4645
leachate 5724–5726, 5748–5750, 5757–5758, 5760–5763
  – composition 5749
  – containment 5711
  – contamination 5748
  – controlling 5749
  – control 5762
  – disposal requirements 5761
  – management 5723
  – measuring 5757
  – monitoring 5750, 5758
  – production rate 5725
  – quality 5763
  – recirculation 5724–5726
  – sampling 5757
  – treatment methods 5760
lead 172, 189, 235, 773, 3630, 4055, 4890, 8462, 8481, 10409, 10648, 10650, 10654
  – alloys 5885
  – batteries 10649
  – dioxide 773
  – exposure 3260
    – low-dose effects 3260
  – grids 5885
  – health effects 10650
  – intoxication 3591, 10650
  – lead–210 3715
    – annual fallout 3715
    – from volcanic eruptions 3715
  – poisoning 10649
  – production 10404
  – sulfide 10648
lead-acid battery 674, 685, 699, 706, 749, 771, 773, 774, 776, 777, 3478, 3483,

5881–5883, 5887, 8746, 8749, 10404, 11503, 11511, 11512
– advanced 774
– by construction 774
– by electrode material 774
– circuit model 777
– commercial designs 5882
– cost 776
– electrodes 5887
– flooded 774
– for sustainable energy 5881
– gravity measurement 699
– hybrid electric vehicle 5883
– markets 5882
– recycling 10404
– separators 8746
– uninterruptible power systems (UPS) 5882
– valve-regulated 774, 11512
– vented 774
lead-antimony battery 774
lead-based paint 10651
lead-battery electrode 5885
lead–bismuth 4055
lead-calcium battery 774
lead-contaminated dust 10651
lead-cooled fast reactor 4055
leaded gasoline 10649
leaf 2630
– area index (LAI) 2667
– measurements 7921
– values 10038
– area ratio (LAR) 2668, 2670, 2672
– color chart (LCC) 2670
– elongation rate (LER) 2672
– nitrogen 2632
– photosynthesis 2632, 2672
– photosynthetic capacity 2626, 2630
leaf-electrolyte-leakage 10396, 10398
leaking water 11941
lean construction 10305
lean design 10305, 10311
lean production 10304, 10306
– integrated delivery processes 10306
lean tissue growth rate (LTGR) 7987
LEA-type protein 5
Leclanché cell 747
lectin 4033, 4034, 4828
– insecticidal activity 4033
– toxicity 4033, 4034
legacy 6229
– training 6229
Legendre polynomial 469, 3811
Leghorn hen 392
Legionnaires' disease 7385
legume lectin 4031
LemnaTec 10
lentic waterbody 5676
lentiviral vector 644, 10904, 10919
lentivirus 5000, 10826
Leontief's input–output methodology 3308
lepidopteran 4030, 4033, 4035, 4038
– pests 4038
lepidoptera 4016
lettuce 1709
Leucena 1290
leukemia 3603, 3644
– of the blood 302
– radiation-related 3644
levelized electricity generation cost (LEC) 1265
Levenberg–Marquardt algorithm 10606, 11464
Lewis acid 4605, 4591, 4603, 4606
– aluminum chloride 4606
– in acylation 4606
Lewis–Whitman laws 9137
LFP 713
Li-air battery 703
lichen–caribou food chain 8461
lid tank shielding facility (LTSF) 8539
LIDAR, see also light detection and ranging 322, 3172, 6592, 6594, 11459
– calibration 11464
– computer vision calibration 11459
– coordinates 11462
– equation 312
– range gating 6592
– sensors 5460, 11456–11457
– space-based 322
– technology 310, 6589
life cycle
– analysis (LCA) 4856
– life cycle impact assessment tools 4856
– assessment (LCA) 196, 1594, 1597, 3453, 5893, 5895, 5909, 5910
– aquaculture production systems 5893
– ecologically based 3453
– economic input-output 3453
– history 5895
– software tools 5895
– solid waste management (SWM) 5910
– hazard profile of a material 4851
– impact assessment (LCIA) 1597, 5896
– inventory 5910, 5925, 9435
– analysis (LCI) 1597, 5896
– emission factors 5925
life-enhancing device 6499
life-sustaining device 6499
Li-Fraumeni cancer family syndrome 3609
light 2876, 2885
– capture 2663
– contaminants removal 8805
– detection and ranging (LIDAR) 8958, 8970
– direction ceiling 2876
– distribution 2886
– energy 349, 1478
– conversion into chemically bound energy 1478
– flows 2885
– harvesting 352, 2623, 2663, 6571, 6573, 6578
– by advanced 6578
– complexes 2624
– infrastructure rapid transit 5985
– light-to-biomass conversion 355
– meters 2830
– non-aqueous phase liquids 4795
– oils 7844
– pipe 2811, 2840
– reactions 1479
– redirection
– ceilings 2876
– systems 2867
– shelf 2811
– sources 11105
– spectral distribution 11105
– to solar gain ratio (LSGR) 2887
– transmission 2840, 2850
– treatments 2856
– tube 2811
– water reactor (LWR) 4063, 7095
– well 2811
light rail
– investments 6016
– lines 1886
– carrying capacity 1886
– revolution 5982
– transit (LRT) 1810, 1812, 1814, 1817, 1840, 1854, 1865, 1868–1870, 1881, 1891, 5934–5936, 5939–5940, 5950–5952, 5955, 5957–5959, 5961–5964, 5966, 5968, 5971, 5974–5976, 5989, 5997, 6005, 6010, 6013–6014, 6016, 6497
– adoption in North America 5989
– applications 1868
– capital investment 6005
– characteristics 1869
– collision safety 5955
– commingled operation 5963, 5968

– control and communication systems 5959
– crossing warning sign 5940
– current operating scenarios 5961
– definition 5955, 5974
– developments 1814, 1865
– high-floor vehicles 5962
– historical background 5952, 5976
– innovations 5976
– insurance 5963
– intra-suburban transit usage 5975
– investments 5997
– investments on land use patterns 6013
– land use 6014
– liability insurance 5966
– liability issues 5963
– low-floor designs 5961
– network supplements 1814
– passenger-carrying capacity 5974
– pedestrian conflicts 5939
– pedestrians 5936
– platform access level 5961
– pollution reductions 6016
– right-of-way 5936, 5950, 5964
– risk assessment 5959
– soles and impacts 1870
– safety 5968
– scheduled speeds 5975
– shared corridor 5951
– shared infrastructural issues 5950
– shared right-of-way 5951
– shared track 5951
– shared-track operations 5958
– shared-track practice 5964
– shared-use operations 5957
– systemic viability 5971
– technology 1817
– traction power system 1817
– traffic density 6010
– viability 5975
– vehicle (LRV) 5935, 5937–5938, 5942, 5945, 5952, 5955
– collisions with pedestrians 5938
– motor vehicle collision 5937
– pedestrian-LRV crossings 5942
– positive control devices 5945
light-beam induced current (LBIC) 9214
light-emitting diodes (LEDs) 7908
light-sensitive photodiode 11109
lighting 2841, 2880, 10290
– control models 2841
– design 2880
– power densities (LPDs) 2842
– simulation programs 2821
– sustainability 10290
lignin 964–965, 1042, 1075–1076, 1105, 1519, 6020, 9824–9825, 10752, 11437
lignite 1084, 2171, 2177–2178, 2183, 2272, 4399, 4770
– combustion 1084
– resources 2183
lignocellulose/lignocellulosic 1043, 1485, 1494, 6020, 11437, 11450, 11453
– biomass 1234, 1273, 1562, 1579, 6027, 8048
– from perennial grasses 6027
– resources 1534
– crops 1609, 6029
– energy crops 1565, 6019
– ethanol 983, 1053, 1064, 11450
– fuels 9836
– material 962, 972, 1518
– substrate 988
lignocellulose-to-ethanol process 966
Li-ion battery, see also lithium-ion battery 709, 713, 7548, 8253, 9293
– configuration 713
– silicon-based anodes 9293
Li-ion capacitor (LIC) 3441
lime 1383, 7046
– kilns 5286
limestone 1383, 1913, 5646, 8360
– reservoir rock 7802
limnology 5674
limonium 2626
linalool 4036
Lindal diagram 4355, 4363
lindane 3631, 10664
linear concentrating collector 6031
linear energy transfer (LET) 11044
linear Fresnel collector 6031–6032, 6035–6037
– benefits 6036
– disadvantages 6036
– main features 6036
– receiver design 6035
– target markets 6037
linear Fresnel reflector 6033, 6034–6035
– design 6033
– optical losses 6035
– reference area 6035
linear induction motor (LIM) 6260
linear isotherm 8613, 8618
– equation 8611
linear non-threshold radiation response 3258
linear partitioning coefficient 8612
linear synchronous motor (LSM) 6260
– propulsion system 6273
lineshaft pump system 4367
linkage
– disequilibrium (LD) 481, 487, 489, 7979
– drag 6428
Linke turbidity coefficient 10629, 10632
Liouville equation 3817
lipases 929
lipid
– biosynthesis 360
– hydroperoxides 3663
– metabolism 6
– peroxidation 3662–3664
– chain reactions 3664
– transfer proteins (LTPs) 10698
lipidomics 1193
lipophilic
– pesticides 3275
– toxins 3593
lipopolysaccharide 4832
liquefaction 989, 991, 2224, 3250, 3959, 3997
liquefied
– fuels 5469, 5482
– natural gas (LNG) 1622, 3957, 3959–3960, 5462, 5468, 5470, 5484, 6847, 7448
– refrigeration system 3960
– thermal efficiency 3959
– petroleum gas (LPG) 268, 2223, 5462, 5468, 5470, 5482, 5484
– refrigerant 9522
liquid aluminum 8779
liquid 2028, 6917
– biofuels 1414, 1543, 1562, 1563, 1608, 8083, 8978, 10527
– biomass 1416
– chromatography 11916
– desiccant 9558
– air-conditioning (LDAC) systems 9515
– electrolyte 741, 6068, 6131, 7878, 8716
– separators 8716
– energy storage 10569
– fertilizer 3771–3772
– for combined heat and power (CHP) 8978
– fuels 1267, 5469, 11430
– electricity generation 1267
– hydrogen 7299
– kinematic viscosity 2028
– natural gas (LNG) 1881
– phase dimethyl ether process (LPDME^{TM}) 2248

– phase methanol 2248
– polymers 3936
– solids contact (LSC) reactors 1632
– solvent extraction (LSE) 2224
– storage materials 10555, 10557
– surface tension 6917
– ternary aerosol (LTA) 130
– waste storage 8504
– working fluid 10565
– direct storage 10565
liquid-metal-cooled fast reactors 4062
LISICON 762
Listeria 5058, 5064
– in fish 9102
– treatment 5064
listeriosis 5058
lithiated graphite 6068, 6091
lithiation 716
lithium 709, 712, 714, 716–717, 719–722, 725–726, 728–729, 748–749, 751, 753, 760, 764, 771, 785–786, 791, 4059, 6058–6059, 6084, 6086, 6089, 6634, 7540–7542, 7544, 9293–9294
– anisotropic thermal vibrations 7541
– anode 716, 749, 753
– battery 703, 3473, 3481, 3499, 5883, 6037–6038, 6502, 8719
– electrode/electrolyte interfaces 6038
– electrolyte 6038
– electrolyte stability 6037
– medical devices 6502
– power capability 3473
– bis(oxalato)borate (LiBOB) 719, 9310
– bromide 4375, 9517
– cell technologies 6502
– chloride 6505
– cobalt oxide (LCO) 6142, 7548, 11519
– composition 7532
– compounds 6069
– desolvation 6058–6059
– electrochemical alloys 9294
– $FePO_4$ 722
– fluoride (LiF) 6504
– free-energy profile 6058
– hexafluorophosphate ($LiPF_6$) 786, 791
– in nanoparticles 729
– ion 6510
– iron oxides 6089
– iron phosphate ($LiFePO_4$) 6060
– $LiFePO_4$ 721, 722, 725, 729, 764, 771
– $LiMnPO_4/MnPO_4$ system 725
– $LiNiO_2$ 712
– $LiNi_{0.5}Mn_{0.5}O_2$ 714
– $LiNi_{1/2}Mn_{3/2}O_4$ 720
– Li_2CoSiO_4 728
– Li_2FeSiO_4 728
– Li_2MnO_3 714
– Li_2MnSiO_4 728
– Li_2NiSiO_4 728
– Li_xCoO_2 712
– manganese
– oxide ($LiMn_2O_4$) 713, 791
– spinels 719
– maximum entropy method (MEM) 7542
– metal oxides 6068
– metal polymer batteries 11519
– nanoparticulate $LiMnPO_4$ 725
– neutron diffraction 7540
– nickel oxide 6143
– non-stoichiometry 722
– nuclear distribution 7544
– phosphates 726
– phosphorus oxynitride 9310
– polymers 786, 8742
– Separator 8742
– primary batteries 748
– salts 751, 6046, 6069
– shifts 6090
– spinel framework 760
– tetrafluoroborate ($LiBF_4$) 6504
– thionyl chloride 6504
– titanate anode 6142
– transference number 6084
– transition metal-containing poly-anionic compounds 726
– transport 6055, 6086
lithium-air battery 766
lithium-carbon monofluoride 6503
– monofluoride-silver vanadium oxide 6510
lithium-iodine 6502
lithium-ion battery 707, 717, 727, 730, 768, 785–788, 790–791, 3428, 3429, 3857, 6060, 6067, 6068, 6069, 6097–6099, 6100, 6103, 6104–6106, 6108, 6109, 6111–6114, 6116–6118, 6119, 6122–6126, 6132, 6133, 6137–6138, 6141, 6145, 6146, 7528, 8720, 8739, 11519
– abuse safety tests 6099, 6118
– abuse tolerance 6117
– anode 9299
– decomposition reactions 6111
– materials 6141
– capacity fading (CF) 790
– cell
– balancing 6146
– components 6126
– level safety 6138
– cell-operating voltage 6125
– chemistry 785
– commercial success 6124
– cost 791
– cylindrical cell 6116
– dynamic stress test (DST) 788
– efficiency 787
– electrochemical reactions 6067
– electrochemistry 6069
– energy storage capability 6124
– field-failures 6099, 6103, 6117
– graphite-free 727
– heat release 6100
– history 6123
– internal shorts 6119
– circuits 6103
– formation in a field-failure 6105
– $LiMn_2O_4$ 717
– manufacturing
– process 6133
– quality 6104
– market survey reports 6125
– mechanisms of internal shorting 6106
– prismatic cell 6116
– reliability 788
– safety 6097–6098, 6100, 6119, 6137
– safety testing procedures 8739
– development 8721
– safe zone 6113
– concept 6114
– self-heating of the cell 6111
– separators 6132, 6145, 8720, 8721
– short initiation 6104
– system level safety 6138
– technology 6122
– thermal runaway (TR) 790, 6099, 6138
– from internal shorts 6108, 6109
– threshold energy 6112
– transportation applications 6119
– working mechanism 6123
lithium-ion capacitor (LIC) 3431
lithium-ion cell 677, 6099, 6101, 6102, 6120, 6127, 6129, 6131, 6132, 6134–6135, 6137, 8716
– autoignition 6101
– cell balance 6131
– cyclability 6129
– exothermal reactions 6101
– external abuses 6099
– triggers 6102
– fabrication process 6134
– field-failures 6120
– flat plate pouch configuration 6135
– formation and aging 6137
– hot box test 6102

– ideal electrolyte solute 6132
– liquid electrolytes 6131
– mechanism 6127
– safety failures 6099
– solid electrolyte interface (SEI) 6129
– thermal runaway 6101, 6102, 6120
lithium-ion gel polymer batteries 8743
– separator 8743
lithium-iron monosulfide 678
lithium-manganese dioxide 6508
lithium-silicon alloy 9294, 9296
lithium-silver vanadium oxide 6507
lithium-sulfur battery 765
lithostatic pressure 4128
litter 9990, 10009
liver damage 10641
livestock 1747, 1750, 1754, 1764, 1766, 1772, 1780, 1782, 2964, 9360, 10848, 10853, 10858, 10888, 10890
– biodiversity 1772
– breed 7974, 7979, 7984
– improvement 7983
– maintenance 7984
– breeding 1764, 1766, 1779
– development 407
– objectives (LDOs) 407
– strategies (LDS) 407
– distribution 1747
– domestication 1747
– environmental footprint 10848
– excreta 7986
– fertility 10890
– transgenic improvement 10890
– for human food production 10853
– for meat production 1754
– genetic improvement 1782, 9359, 9360, 9364, 10853
– genetic resource management 7979
– genome 10828
– infectious diseases 2964
– industries 10887
– sustainability 10887
– poor management 10888
– production 1757
– disease 1757
– productivity 1754
– products for ensuring food security 1750
– reproduction 1780
– robustness 7991
– somatic cell nuclear transfer 6149
– species 8002
– genetic adaptation 8002
– survivability 1780
– with enhanced health characteristics 10858
living building challenge (LBC) 8708
living modified organism (LMO) 2287
living nutrient bridge 8873
living ocean 6178, 6180
living planet index 940, 10088
living roof 4701, 4718
living wall 4714
Loa loa 12010–12011
load Love number 4568
local breed 394
local bus route 1885
local material 9031
local meat production 1744
local traffic emission 263
localized hydrogen starvation 7766
location-allocation method 197
locomotive 5095
– diesel engine–based 5095
– propulsion system 5095
lodging 6204–6206, 6210–6211, 6213
– anchorage failure moment 6205
– base-bending moment 6205
– crop management effects 6210
– mechanisms 6204
– models 6204
– plant breeding 6210
– plant growth regulators 6210
– resistance 6202, 6211
– risk 6206, 6208, 6210, 6213
– methods for controlling 6208
– stem failure moment 6206
logarithm of the Odds ratio 6430
logarithmic velocity profile 2054
London smog 143, 245
long-lived greenhouse gases (LLGHG) 145
long-range atmospheric transport (LRAT) 4884
long-term climate change 10081
long-term ecological research (LTER) network 6216, 6222, 6224–6225, 6227–6230, 6234, 6236
– achievements 6229
– augmented LTER sites 6225
– decadal plan 6236
– education 6234
– evaluation of LTER sites 6224
– formal vision 6216
– formation 6222
– global positioning systems (GPS) 6224
– governance structure 6227
– information
– dissemination 6228
– management 6236
– infrastructure 6230
– legacies 6229
– major milestones 6222
– mission 6227
– research 6230
– programs 6222
long-term intersite decomposition experiment team (LIDET) 6233
longwave radiation 9741
Lophelia pertusa 6414, 6416
Lorenz force equation 41
Los Alamos Sea Ice model 2775
loss-of-field relay 12089
Lotic Intersite Nitrogen Experiment (LINX) 6233
Lotka–Volterra competition equations 10065, 10075
Lotka–Volterra equations 10065, 10068, 10075
louver 2871, 2872, 2874, 2875
– adjustability 2875
– daylight-optimized 2872
– light-redirecting 2874
– sunlight-reflective 2871
– W-shaped 2872
low doses 3256
– physiological response 3256
low emission furnace 1397
low emission zone (LEZs) 270
low energy building 7642
low NO_x technology 6481
low-ash fuel 1382
low-cal house 7630
low-carbon
– economy 2756
– energy sources 9697
low-density lipoprotein (LDL) 1685
low-dose effect 3262
low-dose treatment 3256
– adaptation 3256
– compensation 3256
low-earth orbit (LEO) 8471
low-emission vehicle (LEV) 5025
low-entropy material 11708
low-frequency noise 12290
low-input farming 155
low-level radioactive waste (LLW) 8390, 8589, 8594, 8595
– disposal 8595
low-maintenance battery 5886
low-tech biogas 1146, 1153, 1172
low-temperature
– carburization process (LTC) 1525
– combustion (LTC) 5541
– Fischer–Tropsch (LTFT) technology 2225
– storage 10559

– low-volatility gas 113
– water gas shift (LTWGS) 2248
lower heating value (LHV) 9936
lowest observed adverse effects level (LOAEL) 3255, 3630
loxP sequence 10682
luciferase (LUC) 2598
lugworm 1921
Lujo virus 5353
Lumbrineris brevicirra 3152
luminaire 2827
– potential glare effect 2827
luminance 2832
– range 11108
luminance–chrominance color space 11122
luminosity 9621
luminous efficacy model 2826
lump oil shale 7485
lung 3639
– cancer 213, 3609, 3612
– development 3639
– function 3642
Lurgi methanol synthesis 3984
luteinizing hormone 6154
lux–flood acid-base theory 6723
Lyapunov function 53
lymphatic filariasis 12011
– elimination program 12011
lymphocyte 5577
lymphoma 3603
lyngbyatoxin-a 4832
lysine 1693–1694
– biosynthesis 1694
lysostaphin 2967, 10858
lyzozyme 10700, 10854

M

maar 11627
Macbeth color checker chart 11121
machine learning 6960
– AdaBoost algorithm 6960
MacMullin number 8726, 8730, 8733
macroalgae 518, 553, 832, 1192, 2502, 4820, 6313, 7388, 9111
– ponds 6313
macroalgal culture 3581
macrobenthos fauna 6416
macrocycle 8272, 8274
– carbon-supported 8274
Macrocystis pyrifera 362
macro-environmental sensitivity 470
macromineral 1682
macromolecule 1105, 1213
macronutrient 1677–1678, 1683, 1691, 3769, 7268, 7278
– deficiencies 1683
– disorders 1683
– in fertilizer 3769
macroparasite 523
macrophyte 11894, 11900
– free-floating 11894
macropore 855, 7681–7682
– flow 7674
mad cow disease 10859
Madden Julian oscillation (MJO) 2144, 5074, 12064
Madelung ionic electrostatic energy 760
Maedi-visna virus 2968
magic angle–spinning (MAS) spectra 6078
MAGIC (multiparent advanced generation intercross) 4075
Maglev (magnetic levitation) 6241, 6242, 6246–6249, 6251, 6254, 6256, 6263, 6273, 6279, 6281, 6286, 6288–6289
– applications 6281
– development programs 6263
– electric transport 6246
– electrodynamic 6249
– electromagnetic 6242
– energy storage 6288
– engineering 6256
– factory 6279
– magnets 6254
– passenger system 6242
– physics 6247
– power storage (MAPS) 6288
– system 6263, 6266, 6271, 6284
– construction costs 6284
– first-generation 6263
– passenger-only transport 6266
– second-generation 6271
– technology development 6241
– train 4934
– transport system 6248
– vehicle 6241, 6251, 6256, 6261, 6262, 6273
– loads 6286
– quadrupole magnets 6261
– water transport 6289
magma 4182, 5217, 11614, 11616
– degassing 5217
– fluids 5228
– primary neutralization 5228
– resources 4167
magmatic activity 11634, 11636
Magneplane 6258
magnesite 1912, 1914, 1919
magnesium 1104, 7236, 7330, 7338, 9829
– oxides 11856
– silicate 1919
magnetic
– field 20–21, 7160, 7161
– rotating 21
– rotational transform 7161
– stationary 21
– levitation 6243
– mirror 7160
– nanoparticles 4662
– reflections 6071
– resonance imaging 10
– resonance spectroscopy (NMR) 1186
– saliency 24
– scattering 6071
– stiffness 6260
magnetic-geared PM brushless drive 11547
magnetism (magnetometer) 7799
magnetite 8623, 11602
magnetization 20
magnetosphere 8471–8472, 8579
main chains 6539
maintenance respiration 3224
maize 1109, 1119, 1122, 1276, 1499, 2703, 2707–2708, 4039, 4444, 4452, 4463, 8044
– allele 2703
– domestication 2703
– traits 2703
– exotic breeds 1119
– herbicide-tolerant 4444
– inbred 2703
– insect-resistant 4452
– lysine content 2707
– rootworm resistance 4463
– transgenic avidin-expressing 4039
– waxy locus 2708
major gene 476
major marine ecological disturbance (MMED) investigation 6191
malaria 502, 5369, 5372–5374, 5380, 6291–6293, 6295–6297, 6299–6302, 11070–11071, 11073–11079, 11081–11082, 11084, 11086–11090, 11998–11999, 12001–12003
– artemisinin-based combination therapies (ACTs) 12002
– atlas project (MAP) 11074
– blood-stage vaccines 6300
– chemotherapeutics 11082
– chemotherapy 11081, 11084
– control 11073, 11086, 12001
– current insecticides 12003
– current prophylactics 12002
– diagnostics 11074, 11077
– disease 6293
– drug-resistant 6292
– effects 11999

– endemic areas 12002
– endemic zones 11074
– epidemiology 6295
– eradication 6292
– gametocytocidal therapy 11086
– global burden 11076
– health costs 11079
– hypnozoites 11086
– immunity 6296
– influence of climate change 5372
– insecticides 11079
– insecticide-treated nets (ITNs) 12003
– life cycle 6293
– longer lasting insecticide nets (LLINs) 12003
– morbidity 11074
– mortality rates 11075
– multistage, multi-antigen vaccines 6301
– parasite 6292, 6293, 6296
– pathogenesis 6293
– pre-erythrocytic Vaccines 6299
– prevention 2790
– transmission 5372, 6295, 6302, 11078
– transmission-blocking vaccines 6301
– uncomplicated 6295
– vaccines 6291, 6292, 6296, 6298, 11073, 11087, 11088, 11090
– development 6297, 11089
– obstacles 6298
– whole-organism vaccines 6302
malate-oxaloacetate 358
maleate 6916, 6924
– functionality 6924
– half-esters 6916
maleinized
– hydroxylated oil 6904
– soybean oil monoglyceride 6902, 6912
– resin synthesis 6912
– triolein oil 6925
malignant melanoma (MM) 9661
malignant tertian malaria 11076
malinated hydroxylated oil polymer synthesis 6914
malnutrition 1677, 1683, 1687–1688, 1690–1691, 2754, 4525
– agronomic approaches 1690
– biofortification 1690, 4525
– conventional breeding 1691
– emergency measures 1687
– fortification programs 1688
– long-term measures 1688, 1690
– supplementation programs 1687
mammal/mammalian 3270, 3599, 10088
– livestock 1747
– metabolomes 1186
– oxidative damage 3599
– toxicity tests 6797
– uptake of contaminants 3270
managed pressure drilling 4403
mandatory renewable energy target (MRET) 4485
manganese 717, 791, 2418, 4889, 9951
– leaching 2418
– oxide spinel 716, 717, 725
Mangrove ecosystem 570
Manhattan project 3789, 3817
man-made
– aquifers 10556
– ecosystems 8859
– metabolism 10579
Manning equation 9054–9055
mannopine synthase promoter (pMAS) 10677
manure-borne bacteria 7682
Manzamine A 3164
maple syrup urine disease (MSUD) 1683
mapping 3071, 3078, 3171–3172, 6598
– karst areas 5659
– of road markings 3078
– of safety barriers 3071
– robot-centric 3172
– safety barriers 3072
– satellite-based 3171
MapQTL 6698
Maralinga test site 3541
Marcus model 3418
Marek's disease 641
mariculture 526, 528, 558, 570, 6309, 6356, 6389, 7323, 9183
– best management practices 9183
– in the Mediterranean 6356
– OTEC-based 7323
marine
– agronomy 546, 557, 576, 9116
– and hydrokinetic (MHK) energy 6345–6349, 6351–6352
– development 6349
– environmental effects 6349
– exclusion of aquatic receptors 6352
– installations 6347
– mitigation strategies 6351
– ocean currents 6348
– regulatory drivers 6351
– risk evaluation 6352
– river turbines 6348
– salinity gradients 6348
– technology 6347
– temperature gradients 6348
– tidal devices 6348
– wave energy converters 6348
– animals 9157
– as sentinels 9157
– aquaculture 513, 525, 582, 6760, 7386–7387
– small-scale 7387
– biodiversity 2496, 3152
– biogeochemical cycles 7230
– biogeochemistry 6372–6373
– cycles 6373
– biology 558
– biota 7230, 8411
– radioactivity 8411
– biotoxins 9086
– cage culture 8202
– carbon cycle 6375, 7232
– biogeochemical considerations 7232
– carbonates 7236
– polymorph mineralogy 7236
– disturbance 6191
– ecological disturbances (MMEDs) 6191
– ecosystem 822, 3302, 3316, 6184, 6191, 6192, 6194, 11408
– biomagnification 822
– disease tracking 6191
– distress 6194
– ecosystem health 6180
– emerging and reemerging diseases 6184
– health of marine vertebrates 6192
– sentinels of ocean health 6192
– energy technology 10618
– environment 3151, 6383, 7386, 8388, 8407, 8656, 9089
– anoxic zones 6383
– anthropogenic activities 9089
– as a source of medicaments 3151
– environmental radionuclides 8656
– hypoxic zones 6383
– radioactive substances 8388
– radiological implications 8407
– finfish 6398
– fish 6311, 10090
– integrated land-based cultures 6311
– fisheries 6386, 6388, 7263
– fisheries enhancement 6386, 6388, 6389–6391, 6394–6395, 6398–6399, 7263

– active adaptive management 6399
– effectiveness of stocking 6398
– legacy from the past 6395
– progress 6395
– responsible approach 6391
– scientific and strategic development 6389
– technological and tactical constraints 6390
– food web 829, 6182
– habitats 9168
– sentinels 9168
– helminth infections 12021
– heterophyids 12021
– life 6405
– OHI-related installations 6405
– litter 6194
– macroalgae 9111
– mammals 9166, 10089
– as sentinels 9166
– mining 6634
– natural products 7385
– organisms 2264, 7237
– antibiotic resistance 2264
– photosynthesis 553
– phytoplankton 7344
– carbonic anhydrase 7344
– polar air 127
– pollution 8920–8921, 8927, 8931
– remote sensing 8921
– wind speed 8931
– protected area (MPA) 525, 561, 2504, 6355
– recruitment subsidy 2504
– radioactivity 8658
– radioecology 8388, 8412
– radionuclide 8662
– reef ecosystem 829
– reserves 2504
– schistosome species 12043
– sentinel 9159
– alternative use 9158
– applications for monitoring exposure 9159
– biomagnification 9158
– chemical contaminants 9159
– desirable characteristics 9158
– sensitivity for bioaccumulation 9158
– snow 8396, 9135
– spatial planning (MPS) 561
– species hatchery 10330
– stratocumulus clouds 9699
– systems 1943
– toxin 827, 9157
– vegetable 9122
– vegetation 553
mariner transposon 645
maritime aerosol 9635
marker gene 2597–2598
– negative selectable 2598
– screenable 2598
marker haplotype 6431
marker-assisted
– backcross (MABC) 2532, 6435, 6694
– breeding (MAB) 6427, 6434
– improvement of crop performance 6434
– recurrent selection (MARS) 2530, 2535, 6435, 6438
– selection (MAS) 2530, 6429, 6435, 6437, 6694, 10868
– in a segregating population 6437
Markov Chain Monte Carlo (MCMC), 398
– algorithms 6697
– method 432
– procedure 3184
– techniques 2110
Markov
– decision process 94
– model 3117
– networks 3184
marsh itch 12044
Mars-van Krevelen-type (MvK) mechanism 2949
MARTIN
– grate technology 6477
– infrared combustion control (MICC) 6468
– technology 6451, 6491
– waste-to-energy technology 6448
mascon 4569
mash 993
masking 12289
Maslow's hierarchy of needs 10361
masonry
– convection heaters 1364
– stoves 1362
– tiled stoves 1390
mass balance 5249, 5675, 10965–10966
– control volume 10966
– equation 8892
mass burn facility 9997
mass concentration of particles 11302
mass conservation
– equation 10962
– law 8637, 8645
mass flow controller (MFC) 6730
mass phenotyping 8014
mass spectrometry (MS) 1186, 5574
mass transfer 2025–2030, 2918, 2922
– coefficients 2026–2027, 2030
– of ammonia 2029
– of oxygen 2028–2029
– interfacial 2026
mass transit 6496
mass transport 2034, 2050
– equation 2034, 2050, 10970
mass transportation 7786
mass-burn
– facilities 11711, 11817
– incineration 11788
– incinerators 11789, 11817
mass–energy relationship 3789
massive artificial graphite (MAG) 6141
– battery application 6141
mass-transfer control processes 6735
mastadenovirus 11990
mastitis 1758, 2784, 2967, 10858
materials 9031, 11709, 11789
– balances 11709
– biobased 9031
– certificate 9038
– entropy evaluation 11709
– from processed refuse 11789
– flow analysis (MFA) 3453
– hazards 4850
– life cycle contributions 4850
– life cycle 4851
– recovery facilities (MRF) 4758, 5298, 8778, 8785, 8786, 11832
– safety data sheets (MSDS) 9027, 9029
– to recycle 8797
maternal
– genetic effects 9361, 9378
– genetic model 448
– heterosis 1735
– smoking 3640
– to zygotic transition (MZT) 6151
MatLab 8226
matrix attachment region (MAR) 10678
maturation promoting factor (MPF) 6162, 6164, 6169
Maunder minimum 9801, 9806
maximum brake torque (MBT) 5524
maximum entropy method (MEM) 9896
maximum ground acceleration 3235
maximum ground velocity 3235
Maxwell–Boltzmann velocity distribution 3800
Maxwell's equations 3787, 3789, 7176
meadow of constitution square 4701
mean-headway strategy 107

measurement vehicle 3070
– laser scanner 3070
– sensors 3070
meat 10853, 10856
– consumption 1754, 1757
– with enhanced nutritional qualities 10856
mechanical
– battery 5107
– braking 8854
– coupling 3372, 3379
– device 3379
– speed couplers 3379
– torque coupler 3379
– recycling 8821
– vapor compression (MVC) 9759, 9761
mechanically switched capacitor 9341, 9345
mechanically switched reactor 9341, 9344
mechanics of motion 10614
medaka 11411
MEDEA program 283
medical device battery 6498, 6499
– design 6499
medicinal plant 6519–6520, 6529–6531
– controlling the expression of transgenes 6529
– genetic engineering 6530
– metabolic pathways 6531
– transgenic plants 6531
Mediterranean aquaculture 6355–6367, 7265
– benthic impacts 6358
– disease outbreaks 6360
– ecosystem effects 6364
– escapes 6362
– fish farming 6358
– herbivorous fish 6367
– history 6355
– indicators for sustainability 6367
– integrated aquaculture 6366
– introduced exotic species 6363
– market 6363
– parasites 6365
– policy issues 6365
– seagrasses 6364
– sustainability 6356
– use of probiotics 6361
– water quality 6359
– zoning 6366
Mediterranean mussels 6764
Mediterranean Sea environment 6355
medium density fiber board (MDF) 1536
mega-ammonia technology 3993
mega-ampere spherical torus (MAST) 7162
megaciy 1887
megafaunal species 6409
mega-landfills 11828
mega-methanol production process 3984
meganucleases 4498, 10912
Megaron House 7644
MegaSyn process 3984
Mehler-peroxidase reaction 2644
meiosis 6165, 6431
Meishan pig 1772
melanocytic tumor 9663
melanogenesis 9661
melanoma 11400, 11404
melatonin 2829–2830, 10267
melting ice 282
membrane
– bioreactor (MBR) 9564, 10191, 11889, 11961–11962, 11968, 11969, 11975, 11978
– biomass 11978
– conventional activated sludge process (CASP) 11975
– microfiltration 11968
– removal of endocrine disrupting compounds 11968, 11969
– treatment of municipal wastewater 11968
– ultrafiltration 11968
– technology 11889
– distillation (MD) 2916, 2920, 9760, 10540
– bioreactor (MDBR) 11890
– electrode assembly (MEA) 3883, 7695, 7758, 8174, 8186, 8189, 8208, 8330, 8341
– area-specific resistance (ASR) 8341
– design concepts 7758
– PPA-processed *p*-PBI 8189
– processes 7758
– electrolytes 6538
– filtration 10108, 10531–10532
– fouling 2905, 11889
– hydration 8210
memory
– brushless Machine 11548
– effect 6945
menaquinone 1685
Mendel/Mendelian
– defects 494
– laws 390, 10896, 10903
– resistance 6437
– sampling effect 1727
– sampling variance 418
menhaden 3577
meningitis 8154
mercury 172, 300, 304–306, 833–839, 2195, 2210, 3592–3593, 3630, 3634, 4890, 4904, 4992, 6514
– bioaccumulation 834, 837
– biomagnifications 837
– concentrations 838, 6189
– cycling 833
– distribution 833
– in the oceanic ecosystem 837
– intoxication 835–836
– metallic 834
– methylation 834
– poisoning 305, 834–835
– pollution 836
– selenide 839
– sources 833
– tests 5205
– toxicity 839
– volatilization 833
meridional overturning circulation (MOC) 5859
Merino sheep 1758
– blowfly 1758
meristem activity 2666
mesenchymal stem cell (MSC) 7223
– as nuclear donors 7223
mesocosm 3269
mesophile 5050
mesophyll 2625, 2643
mesopic vision 11101
mesoscale 11265, 11275
– convective systems (MCS) 5071, 5072, 5074, 5078
– iron fertilization 6379
mesoscopic solar cells 6566, 6568, 7934
– dye-sensitized 6568
mesoscopic traffic simulation model 95
– BusMEZZO 103
metabolic
– diseases 8312
– engineering 6531
– syndrome 8312
metabolite 1189, 1484
metabolome 6441
metabolomics 1184–1186, 1189–1190, 1192–1193, 3588, 3658, 4496, 6532
– bacterial 1193
– environmental 1189
– in animal sciences 1186
– in microbiology 1192
– in plant sciences 1190
– with aquatic plants or algae 1192
metabonomics 1185
metagenomics 6328
metagonimus 12025

metal 4854–4855, 10051, 10053, 10055, 10158–10159, 10403–10404
– bioaccumulation 10055
– bioavailable form 10053
– bipolar plates 7709
– contaminants 10157
– geochemical fixation 10157
– stabilization 10157
– excavation 10159
– global production 10404
– hazard characterization 4854
– hazardous waste output 4855
– hydride alloy (MH) 6945
– hydride–nickel cell 750
– hydroxide 8609
– interconnects 9858, 9860
– mine wastes 6669
– monitored natural attenuation 10159
– ores 10406
– organic chemical vapor deposition (MOCVD) 9402
– oxide 798, 8603, 8606
– cathodes 6100
– phthalocyanines 8272
– phytoextraction 10158
– phytoremediation 10158
– phytostabilization 10159
– phytovolatilization 10159
– pump-and-treat method 10404
– recovery 6662
– recycling 8810
– remediation methods 10404
– speciation 10051, 10052
– stabilization in soils 10158
– sustainable remediation methods 10403
– toxicity 10055
– predictions 10059
– valence state 4854
– working fluids (MWFs) 7610
metal-air battery 679, 793, 3853, 3856, 11517
metal-insulator-metal (MIM) model 7563
metalloids in marine systems 7356
metallomacrocycle 8272
metalloporphyrin 5176
metallothionein 3257
metallurgical
– coke 2195, 8104
– grade silicon (MGS) 9610
– industry 9608
– silicon 9198
– purification 9198
metamorphic rock 4186
metaplast 7478
metapopulation
– ecology 5437
– theory 947
Metastrongyloidea 12038
metavanadate 4891
metazoan 12019, 12042
meteoric waters 5230
meteorology/meteorological 6583, 11274, 12214
– computational models 11274
– flows 11276
– perturbation modelling 11276
– processes in urban areas 11263
– wind power 12214
– in urban areas 11263
methacrylated
– glycerides 6918
– soybean oil monoglycerides 6916
methadone 10646
– programs 5006
methanation 1149, 1450, 1662, 2416
– synthesis 1442
methane 245, 281, 330, 337, 344, 609, 663, 666, 668, 849, 851, 1029, 1107, 1134, 1147–1148, 1152, 2211, 2241, 2243, 2746, 3845, 3957, 3964, 3970, 3994, 4123, 5119, 5471, 6651–6652, 6722, 7446, 7843, 8175, 8885, 9697, 9703, 10483, 11835
– bacteria 5119
– cold flame oxidation 3994
– coupling reaction 3994
– fermentation 5121
– bacteria 1148
– gas 4767
– hydrate 334, 341, 344
– replacement of CO_2 344
– reforming for methanol/DME synthesis 3970
– steam reforming 3964
– methane synthesis reactor 1443
– markets program 6652
methane-to-gasoline (MTG) process 2225
methanization 1150
methanogenesis 163, 4127
– microbes 5167
methanogen 1151, 6328
methanol 381, 928–929, 1049, 1429, 2225, 2247, 2249, 3389, 3866, 3883, 3935, 3938, 3958, 3980–3983, 3988–3989, 3994, 5466, 5477, 7594, 8175, 8237, 11444
– chemical processes 3989
– commercial synthesis 3983
– dehydration reaction 2249
– distillation plant 3981
– MOGD process 3988
– synthesis 2248, 3981–3983
– activities 3983
– catalysis 3982
– reaction pathway 3981
– reactors 3982
– to gasoline (MTG) process 3988
methanol-to-gasoline technology 2250
methanolysis 928–929
– lipase-catalyzed 929
methanotrophic bacteria 6411
methanotroph 6414
methemoglobinemia 3783
methicillin-resistant *Staphylococcus aureus* (MRSA) 5061, 5383
methionine 836–837, 1189, 10843
– adenosyltransferase 3608
– sulfoxide reductases (MSR) 3666
methoxyfenozide 2597
methoxyl 1519
methylation 3257, 3604
methyl chloride 10131
methyl-diethanolamine (MDEA) 2238, 3964, 3993
methylester 1045
methylmercury 305, 825, 833–836, 839, 3593, 3629–3630, 3634, 8350
– poisoning 835
– pollution 836
methyl-tertiary butyl ether (MTBE) 189, 303, 3989, 4590, 5477
methyltrioxorhenium 3943
metro systems 1821, 1863, 1871
Michael addition 4608
Michaelis–Menten
– enzymatic kinetics 5206
– formula 2668, 9053
micro anaerobic digestion 1424
micro cogeneration 1402, 1415, 1421
– global importance 1402
– potential fields of application 1421
micro engines 5502
micro gas turbine 1412, 1416, 1421, 6832
micro gasification 1424
micro hybrid vehicle 11506
micro porous layer (MPL) 7697, 7699
micro turbine 6833
microalgae 350, 352–353, 362, 553, 559, 561, 927, 1192, 4820, 5117, 6310, 6313, 11439
– hydrogen production 5117
– ponds 6313
microarray technology 6795
microbacteria 10957
microbe 498, 6190, 7671

microbial
– contaminants 7673
– electrolysis 5167
– fatty acid biosynthesis pathway 500
– fuel cells (MFC) 11944
– phytase 10842
– pollutants 7670, 7675, 7688
– pollution 1630, 6331, 11901
– resistance 499, 507
– source tracking (MST) 6330
– transfer 7681
microbial-enhanced oil recovery (MEOR) 7819–7820
microbisporicin 504
microcalorimetry 7538
microcin C7 507
microclimate 2832
microclimatic design 914
microclimatology 6639
micro-combined heat and power (micro-CHP) 9913
microcrystalline
– material deposition 9249
– silicon photovoltaic modules 9436
– solar cells 9269
microcystin 4831, 4834, 4835
micro-earthquake 4215, 4422–4423
microelectricalmechanical (MEM) systems 8195
microelectronics 11542
microenvironment/microenvironmental 249
– effect 464
– sensitivity 470
microfiber glass separator 8750
microfibril 963
microfiltration 11885
micro-gas turbine (MGT) 1331, 1332
microglass separator 8750
microgrids 3019
microhomology 2601
micro-hybrid 3485, 3487
microirrigation 5628
micro-light shelf 2837
microminerals 1687
micronutrient 1677, 1682, 1690, 3775
microorganism 498, 1628, 11389–11392
– biological effects 11389
– effects of UV radiation 11390
– UV environment 11389
microparasite 523
Microphallidae 12027
micropollutant 2090, 10191, 10534, 11912, 11915, 11921, 11930, 11968, 11977
– biodegradation 11977
– micropollutant target compounds 11914
– degradation pathway 11930
– in river water 11930
– solid phase extraction 11915
– spatial and temporal occurrence 11921
microporous polyolefin separator 8721
microporous separator 8719
microprocessor 11542
– relays 12088
micro-RNAs 10911
microsatellite 480, 486, 493
– instability (MSI) 3607
microscale wave breaking 601
microscopic phytoplankton 8954
microscopic simulation model 95
– MITSIMLab 95
microscopic traffic simulation model 93
microseismicity 4129, 4216
Microsoft Virtual Earth 3171
microspora 12042
microspore 2647
microsporidial gill disease of salmon (MGDS) 549
micro-topography 2764, 3753
microtubule 3159
microwave 4643, 4615, 4644, 4660, 4663
– for nano-catalyzed aqueous protocols 4663
– for chemical synthesis 4644
– irradiation 4650–4654, 4657
– coupling reactions 4650
– Heck coupling reaction 4651
– Hiyama cross-coupling reaction 4652
– nitrogen heterocycles 4654
– reactions in near-critical water 4653
– Sonogashira coupling reaction 4652
– Stille reaction 4652
– Suzuki reaction 4650
– synthesis of nanomaterials 4657
– nanoparticles 4660
– scatterometer 7511
– sensors 8930
midazolam 3275
Mie scattering 135, 325, 9630
migration 3281
mild hybrid electric vehicle 11507
milk 2783, 10853–10854
– composition 10854
– consumption 1755
– goats 1755
– marketing systems 2783
– powder
– consumption 1755
– production 1755
– production 2782, 2784
– traits 2784
– productivity 10888
– with enhanced nutritional qualities 10854
– yield 2782
milled-tooth bits 4394
millennium ecosystem assessment (MA) 3314
Minamata disease 835, 839, 4890
mine/mining 6633–6634, 6636, 6638–6643, 6645, 6647–6649, 6651, 6653, 6655–6658, 6660, 6663, 6665–6667, 6671–6672, 6675–6676, 6678, 7810, 10405
– acid rock drainage 6666
– acidic drainage 6663
– air pollution 6639
– backfilling 6675
– bioprocessing 6660
– biosphere 6640
– companies 2188
– cryosphere 6640
– drainage waters 11899
– decommissioning 6641
– design optimization 6657
– eco-efficiency analysis 6643
– engineering 6657
– environmental impact 6633, 6636, 6648, 10405
– excavations 7810
– exploitation phase 6638
– exploration 6638, 6648
– extraction 6649
– heap leach dumps 6676
– history 6634, 6671
– hydrosphere 6639
– industry 6634, 6645
– influenced water (MIW) 6653
– life cycle 6648
– lithosphere 6641
– loss of biodiversity 6647
– miner's rule 7413
– natural resources 10405
– pedosphere 6640
– phytotechnology 6658
– planning 6676
– production 6679
– reclamation 6671, 6678
– plan 6649
– recultivation phase 6641
– remediation 6675
– restoration process 6653

– revegetation 6678
– sites 6659
– phytotechnology 6659
– small-scale 6641
– solid waste 6665, 6666
– subsidence 6651
– sustainability 6633, 6636, 6642, 6647, 6655
– opportunity 6657
– tailings 6667
– disposal 6672
– threat analysis 6657
– waste 6643, 6648, 6666
– water 6658, 6661
– irrigation 6658
mineral 1712, 1715, 6647, 6648
– ash 5253
– chemical analysis 5253
– bioavailability 1715
– carbonation 1909–1910
– density in cereal grains 1715
– deposit 6637, 6655
– progressive exploitation 6655
– exploration 4391
– extraction 6647
– fertilizer 1133
– paragenesis 4098
– processing wastes 11702
– resources 6640
– solubility 4097
– storage in sink tissues 1715
– sulfides 6639
– transport 1712
– trapping 4123
– uptake 1712
miniature suns 7157
minibus 1860
minichromosome 2585
minimal erythema dose (MED) 11379
MINLAKE numerical simulation model 5684
mirror box skies 2820
Miscanthus 1107, 1279–1280, 1282, 1293, 1486, 1539, 1579, 2275, 2632, 6024–6025, 6027
– as a biomass crop 1282
miscellaneous agent 12045
MISR (multiangle imaging spectrometer) 196
missense mutation 488
mite 5438
– identification 5438
mitigation 1633, 2115
– goals 1642
– hydrocarbons 1633
– petroleum 1633
– strategy 1628
– bioremediation 1628
mitochondria 357
mitochondrial gene flow 3362
mitochondrion 6168
– inheritance 6168
mitotic cell cycle 6165
MITSIMLab 96
mixed alcohols 11444
mixed ash 11739
mixed carbide fuel 4062
mixed crops 10045
mixed function oxidase (MFO) system 12300
mixed ionic-electronic conducting (MIEC) 2938
mixed metal montaminants 10428
– electrochemical remediation 10428
mixed oxide (MOX)
– cathodes 6143
– fuel 4062, 7145, 7188
mixed traffic 1862
mixed-mode ventilation 6889
mixing length theory 2055
mobile ad hoc network (MANET) 11553
mobile mapping system (MMS) 3171
mobile oxyanion 4872
mobile phone 8716
mobile robotics 3171, 3172
– exteroceptive sensor 3172
mobility 666, 3068
mock urban setting test (MUST) 11273
model atmosphere 9723
model output statistics (MOS) 9645
modeled solar radiation 9687
modeling in animal breeding 436
moderate resolution imaging spectroradiometer (MODIS) 196, 6762
– satellite data 3215
modern breeding method 4529
– negative effects 4529
modification 4107
– weaponization 4107
modified Mercalli intensity scale 2425
modulation transfer function (MTF) 11107
Mohr–Coulomb equation 4128
molasses 1275
molecular beam epitaxy (MBE) 9402
molecular biology 2530, 6708, 10875
molecular breeding (MB) 2682, 2683, 4517, 6692, 6693
– hubs 6709
– platforms (MBP) 2683, 6692, 6693, 6695, 6709, 6711–6714
– communities of practice 6713
– data management 6712
– demand-driven 6712
– human capacity 6711
– impact on crop breeding 6714
– markers services 6711
– potential 6709
– potential economic impact 6713
– precise phenotyping 6711
– scope 6709
– sustainability 6713
– technology-push 6712
– utilization 6711
molecular clock 8139
molecular diagnostics 5385
molecular diffusion
– coefficient 596
– flow 2922
molecular dynamics (MD) simulation 6038, 6046
molecular flow 5635
molecular genetics 6694, 10695
– technology 7978
molecular ideotype 6434
molecular laser isotope separation (MLIS) 5642
molecular marker (MM) 430, 2530, 2683, 6696
molecular oxygen 612
molecular pharming 8073
molecular photovoltaic cells 6581
molecular scattering 9718
molecular weight cutoff (MWCO) 10532
molecule 498
Mollier chart 4277
Mollier diagram 4255, 4274
molluscan
– mariculture 9180
– best management practices (BMPs) 9180
– certification standards 9180
– integrated multi-trophic aquaculture (IMTA) 9180
– regulatory standards 9180
– shellfish 9099–9100, 9176
– associated pathogens 9099
– safety 9100
mollusk culture 6760, 6766
Moloney murine leukemia virus (MMLV) 643
molten 2367
– carbonate fuel cell (MCFC) 3388, 3851, 3867, 3879, 3881, 3884, 5134, 5138, 5142, 5170, 6720, 6722, 6724–6725, 6727–6728, 6730–6731, 6811, 7866, 9853

– analysis of Cell Behavior 6731
– anode 6725
– cathode electrode 6725
– components 6722
– electrochemical resistance 6727
– electrolytes 6721, 6722
– electrolyte loss in the cell 6724
– inert gas step addition (ISA) method 6730
– ohmic loss 6727
– open circuit voltage 6727
– oxygen reduction 6725
– performance analysis 6727
– reaction characteristics 6728
– rock resources 4167
– salt 2369, 2373, 2380, 2387, 3879, 6054, 10556, 10566
– corrosion 5265
– electrolyte 6056
– liquid film receiver 2363
– reactor experiment (MSRE) 4057, 4058
– storage 10569–10570
– silicon 9206
molybdate 11727
molybdenum nitrides 8267
momentum transfer 11268
monazite 9948
Monin-Obukhov similarity theory 3216, 6594
monitored natural attenuation (MNA) 1632, 2445, 10430
monk seal 3569
mono-aromatics 10665
mono-centric city 1821
monochrome image 11125
monoclimax 3284
monocot 1484, 2593, 2596
monocotyledon 9066
monocrystalline
– silicon 9207
– transfer layer 9207
– solar cell 9197
monoculture 154, 547, 2749, 6311, 10045
monoethanolamine 3993
monofill 11747
monogenetic volcano 11617
– cones 11628
monoglyceride 6898, 6904
monomer 6897
– triglyceride-based 6897
monorail guideway 6272
monosaccharide 1105, 1678
monoterpene 3225
monounsaturated fatty acid 4557
monovalent cation 8608
Monsi–Saeki equation 2620
monsoon 2126, 5070, 6740–6744, 6747, 6749–6750, 6753–6755, 7256, 8905
– circulation 6741, 6749, 6755, 7258
– climate change 6753
– climate system 6754
– direct radiative forcing (DRF) 6747
– dynamics 6742, 6750
– evolution 6754
– forecast 6742
– high-resolution global models 6744
– impacts of aerosols 6747
– modeling 6740, 6743, 6755
– precipitation regimes 7256
– regions 6741
– retrospective modeling 6744
– seasonal characteristics 7256
– tracking with driftsondes 5070
monsoon-intraseasonal oscillations (MISO) 6743
Monte Carlo
– analysis 6612
– computer programs 3809
– method of simulating radiation 8540
– simulation 3810, 6615
– statistics 3819
– transport 8555
– calculations 8552
montmorillonite 4594
Montreal Protocol 177, 4116, 10134, 10137
mooring 587, 593
– single-point 593
Moran's eigenvector map (MEM) 3337
Moran's *I* 3334
Morex allele 4078
Morganella morganii 5060
Morgan 478
morphine 10644
morpholinoethanesulfonic acid 5209
morpholino 6794
Mortality 9657
MOSFET 702
moss bioreactor 8077
motional narrowing 6082
motive fluid pump 4290
motor
– design 11533
– drive 11504, 11543
– battery 11504
– control strategies 11543
– operation 12141
– torque 3369, 3372
– vehicle traffic 5982
mountain glaciers 2776
mouse epiblast stem cells 10821
movement
– prediction–based routing 11560
– protein 2702
movement-based routing algorithm (MORA) 11561
moving boundary method 2765
moving grate furnaces 1321
moving vehicle detection system 11472
Mt. Elbert–01 hydrate well 339
mud
– drilling 4383, 4428
– noise reduction 4428
– logging 4405
– instrumentation 4405
mulch farming 162
mulching 2562
multi-angle imaging spectroradiometer (MISR) 8943
multiblock copolymer membrane 6552
multicarrier generation 9425
multicellular macro-parasitic helminth infection 11998
multichannel image data 11122
multiclass highway service 5040
multicrystalline silicon 9201, 9203
– industry 9218
– solar cells 7952
– wafer 9208, 9210–9214
– extended crystallographic defects 9208
– grain boundaries (GBs) 9208
– hydrogenation 9210
– improvement 9212
– impurity 9208
– impurity gettering treatments 9211
– interstitial iron 9213
– material improvement techniques 9210
– n-type 9213
– p-type 9214
multicrystalline solar cell 9197
multicyclone 1250, 1339
multidestination
– bus 5999
– transit 5988
– transit networks 6011
– transit systems 6001
– travel capability 6005
multidrug resistance protein (MRP) 12308
multi-effect
– desalination 9761
– distillation (MED) 2901
– humidification 9760
multielectron chemistry 5210

multi-environment trials (METs) 4071
multifaceted disease 12005
multifocal camera 48
multifocal vision system 47, 54, 61
multi-gear transmission 3369, 3381, 10496, 10544, 11485
multi-gene expression 10847
multi-gene traits 10840
multigenerational learning 10304
multi-junction solar cell 9253, 9278, 9418–9420, 9429
– lattice parameters 9420
– optoelectronic properties 9420
multi-laser sensor system calibration 3197
multilateral initiative on malaria (MIM) 11072
multimedia compartment (MMC) model 9137
multimodal transportation system 1829
multinary chalcopyrite compounds 9396
– as photovoltaic materials 9396
multi-nozzle quiet combustion" or MNQC system 6841
multiphase
– catalysis 3945
– extraction (MPE) 2447
– jets 10990
multiphoton conversion 9424
multiphysics finite element (FEA) analysis 44
multi-planar LIDAR system 11457, 11460
multiple
– cropping 2741
– exciton generation 9425
– gene transfer (MGT) 2593
– hearth furnaces (MHF) 5277
– jets 10989
– T-DNA repeats 10681
– trait index 6440
– vehicles 2478
– path planning 2478
multiple-stage steam separation 5230
multiple-use marine area 515
multipollutant monitoring 195
multipotent mesenchymal stem cells (MSCs) 7224
multipurpose pyroprocessing complex (MPC) 7154
multi-robot motion planning 2479
multi-sensor pedestrian recognition 6953
multi-species pond cultivation 9110
multi-stage desalination (MSD) 9760
– with heat recovery 9760
multi-stage flash (MSF) distillation process 2898
multi-stage gasifier 1457
multi-temperature generation 9427
multi-trophic aquaculture 9182
– environmental benefits 9182
multi-vehicle motion planning 2476, 2478
– decoupled planning 2478
multiwall carbon nanotubes (MWCNT) 3853, 8294
multixenobiotic resistance protein 12309
municipal
– incinerator fly ash 4874
– piped water supply 6629
– plastic waste 4008
– composition of raw material 4008
– properties of reclaimed products 4008
– sewage treatment 11903
municipal solid waste (MSW) 1538, 3997, 4755–4758, 4769, 4958, 5236, 5238, 5244, 5298, 5720, 5765, 5909, 5932–5933, 6450, 6465, 8097–8102, 8797, 8818, 9980, 9982, 9991, 10009, 10014, 10578, 10588, 11596, 11703, 11721, 11739, 11824, 11830–11832, 11836, 11841–11842
– air required for combustion 11824
– boiler efficiency 11841
– calorific value (CV) 5298
– carbon content 4756
– carbonaceous materials 8098
– characterization 10009
– chemical heat content 8098
– chlorine concentration 11831
– collection 11831
– combustion 6450
– combustor ash 11703
– composition 8098, 11830
– composting 11832
– decision support tool (MSW-DST) 11688
– discarded in landfills 5933
– flue gas temperature after boiler 11841
– fossil carbon content 4758
– gasification 6465, 8098, 8101
– generation 5765, 10009
– grate combustion facility 8099
– heating value 11830
– incineration 4870, 5238, 10588, 11596
– incinerator 4866, 5298, 11721
– in Japan 3997
– inorganic materials 8098
– low heating value 11842
– management (MSWM) 9984
– net calorific value 11842
– non-transferred arc plasma torch 8100
– organic compounds 8099
– plasma-assisted gasification 8100
– plasma-assisted processes 8102
– post-recycling 5932, 11836
– processing 11831
– recycling 9991, 11831
– reuse 9982
– thermal treatment 8097
– transferred plasma arc 8100
– vitrification 11583
municipal waste 1177, 4903, 11818, 11821, 11860
– aluminum content 11860
– heating value 11821
– landfills 5762
– properties 11818
– plastics 4011
municipal wastewater 2335, 9564
– discharge 2084
– treatment 11874
muon decay 8578
murine hepatitis virus 2969, 10859
murine *Mx1* gene 2965
musculoskeletal disease 9655
mushroom corals 2493
mussels 520, 521, 523, 549, 552, 1965, 6759, 6763, 6746
– cultivation 6764
– culture 6758
– droppers 6763
– filter-feeding 552
– ropes 6763
– species 6764
– in open ocean cultivation 6764
mutagenesis
– breeding 4493
– of the nuclear genome 366
mutant allele 2709
mutation 402, 488, 3258, 3600–3601, 3603
– accumulation 3600
– causative 488
– epigenetic 3603
– in somatic cells 3258
– oncogenic 3600
– radiation-induced 3258
– single-base substitution (SBS) 3601
– underlying QTL 488
mutual inductance matrix 38
mycobacterial infection 11135
Mycobacterium 503, 5058
– *bovis* 11130
– *marinum* 5058, 5064
– treatment 5064
– *smegmatis* 503

– *tuberculosis* 500, 503, 11130, 11132–11133, 11139
– infection 11132
– transmission 11133
mycobiota 2561
Mycoplasma hyopneumoniae 1651
mycorrhizae 1283
mycorrhizal fungi 877
mycotoxin 10705, 10746
myostatin 10892
– gene (*MSTN*) 488, 10857
Myxobolus cerebralis 6195
– parasite detection 6195
Myxosporea 12019
Myxozoa 12042

N

N-acetylhexosaminidase 4035
Nachhaltigkeit 3289
Naeglaria fowleri 8759
Nafion 6554, 6559–6560, 7760, 7771–7772, 8183, 8189, 8209, 8214, 8332, 8337, 8343, 8725
– composites 6560
– membrane 6551
naloxone 10646
nanocarbon 6769, 6788
– for supercapacitors 6769
nano-catalyst 4643, 4662–4665, 4667
– as susceptors 4663
– MW-assisted 4662
– ruthenium hydroxide 4665
– stability 4664
nanocomposite concept 9299
nanocrystalline materials 9302
nanocrystal 7748, 7749, 9250
nanoengineering 8211
nano-environmental and human safety (nanoEHS) 6791
nano-ferrite 4661
nanofiltration 2904, 10530, 10532, 11884
nanogate capacitor 3430
nanohybrid capacitor (NHC) 3432, 3434, 3441
nano-immunomagnetic particle 1656
nanoimprint technology 11118
nanolayer 7892
nanomaterial 4657, 4659, 6790, 6792, 6800
– greener synthesis 4659
– toxicity 6800
nano-optical filter 11118
nano-organocatalyst 4666
nanoparticle 4667, 10588
nanoporous carbon 6778
– electrodes 6776
nanorod 6579
nanoscroll 7892
nanosheet 7892
nanosized photocatalyst 7890
nano-sizing cathode powder 730
nanostorage capacitor 3430
nanostructure 7891–7892
– electrodes 8212
– one-dimensional (1D) 7891
– two-dimensional (2D) 7892
nanostructured
– silicon 9298
– anodes 9305
– thin film (NSTF) 7707
– catalyst 7744, 8343
– electrodes 8213
nanosynthesis process 6800
nanotechnology 6790
nanotoxicity 6790, 6792–6793, 6795–6797
– assay 6796
– high-throughout testing 6795
– tests 6792, 6793
– embryonic zebrafish 6793, 6797
nanotoxicology 4615, 6790, 6792, 6797
– in green nanoscience 6790
– mammalian models 6792
– models 6792
– role in green nanoscience 6792
– zebrafish model 6797
nanowire 9304
– silicon-based 9304
naphtha 2243, 2247, 3978, 3980, 4010
– slurry phase distillate (SPD) 3980
naphthene 7844
naproxen 11926
narrowband multifilter radiometers 11150
Nasicon 726, 730, 762, 727
– framework 762
National Air Pollution Control Administration (NAPCA) 215
National Cattle Evaluation (NCE) 1727, 1738
National Ecological Observatory Network (NEON) 3205
National Electrical Manufacturers Association (NEMA) 3007
National Emission Standards for Hazardous Air Pollutants (NESHAP) 4882
National Environmental Policy Act (NEPA) 3354, 10016
National Fire Protection Association (NFPA) 3007
National Immunization Day (NID) 8146
National Maglev Network 6282–6284
– private financing 6284
National Morbidity and Mortality Air Pollution Studies (NMMAPS) 226
National Oil and Hazardous Substances Pollution Contingency Plan (NCP) 2008
National Pollutant Discharge Elimination System (NPDES) 1937, 2076
National Priority List (NPL) 2008
National Spherical Torus Experiment (NSTX) 7162
National Toxicology Program (NTP) 3636
native fluid 4124
natural attenuation 1632, 1638, 10429
natural capital 190
– Natural Capital Project (NatCap) 3321
natural cooling 908, 3683
natural disaster 916, 3232, 3234, 3553, 8940, 10484
– remote sensing 8940
natural draft furnace 1354
natural draft operation 1357
natural earth systems 5403, 5418
natural earthquake 2424
natural ecosystem 534
natural enemy partitioning 10076
natural estrogen 11962–11963, 11967, 11978
natural fission reactor 8476
natural gas 1038, 1438, 1662, 1674, 2165, 2254, 3844, 3846, 3859, 3928–3929, 3956–3957, 3959, 3964, 3968, 3987, 3993–3994, 4770, 5470, 5485–5486, 6679, 6806, 6811, 6836, 6846, 7087, 7446–7447, 7449, 7454, 7802, 7843, 9337, 9604
– combustion 6836
– condensation boiler 9546
– consumption 3968
– conversion to syngas 3957
– coproduction of methanol 3987
– desulfurized 3964
– direct conversion to liquids 3993
– direct injection (DI) 5485
– discoveries 6679
– drilling technologies 6846
– emissions 6836
– exhaust gas recirculation (EGR) 5485
– fuel 6738
– gasoline 7803
– global reserves 7454
– global resources 7446
– history 6811
– hydrates 330
– in conventional fields 7449
– in electricity generation 6846
– liquefaction 3959
– liquids (NGL) 3957, 7449
– methane content 3957

– oxidative coupling to light hydrocarbons 3994
– pipelines 9337, 9354
– power 6804
– selective oxidation to methanol 3994
– system 1227
– thermal decomposition 9604
– utilization 6811
– vehicles 5465, 5485
natural gas–fired gas turbine 6843
– economics 6843
natural gasoline 7803
natural genetic engineering 4518
natural graphite 6141
natural grassland 1554
natural green roof 4732, 4739, 4752
– total phyto-mass 4732
natural heat recharge 4226
natural heating 905
natural hot springs 5220
natural illumination 2804, 2809, 9742
natural image 11123
– traffic-relevant color information 11123
natural light 6891
– sources 11115
natural mutation 4518
natural oil 6897
natural opiate 10644
natural organic matter (NOM) 7331, 10058, 10659, 11930
natural radiation 3583, 8470, 8479
– sources 3521
natural radionuclide 8453, 8462, 8600
– in the environment of caribou/reindeer 8453
natural resources 3344, 6655
– adaptive management 3344
– flows 6853
– management 3342, 3346, 3355
– overexploitation 6655
natural sandwich material (LNS) 1281
natural selection 10071
natural terrestrial plants 11397
natural triglyceride 6898
natural ventilation 902, 3684–3685, 6865, 6870–6871, 6873, 6876, 6880–6882, 6884, 10269, 10334
– airflow rate 6871
– benefits 6882
– computer-aided prediction 6884
– condensation management 6880
– design
– elements 6884
– guidelines 6881
– requirements 6873
– effectiveness 6880
– fire safety 6880
– for cooling 6876
– fresh air 6873
– health 6884
– humidity 6880
– in-built environment 6865
– models 6884
– noise 6876
– principles 6870
– productivity 6884
– urban pollution 6876
– with mixed-mode mechanical conditioning 3685
natural wetlands 11892
naturally occurring radioactive material (NORM) 3519, 5561, 8469, 8479, 8564, 8601
naturalness 1543
nature deficit disorder 11349
Nature Research Center (NRC) 3206
nature 2744
– domestication 2744
– reserves 1557
nature-deficit disorder 3205
Navier–Stokes equations 2767, 8905, 10977, 10979, 12065, 12075, 12210
– Reynolds-averaged 10977, 10979
navigation 3175
– channel 3031, 3048
– dredging 3031, 3042, 3045, 3048
– environmental effects 3042
– GPS/IMU based 3175
– maps 3068
– satellite 8515
– systems 3083–3084
– in-vehicle 3084
NCA 713
NdFeB magnet 25, 27, 30
Nd:YAG laser 311
near isogenic line (NIL) 6433
near-edge X-ray absorption fine structure (NEXAFS) 6076
near-infrared (NIR)
– sensitivity 11126
– spectrum 9723
nearshore
– marine 6759
– wind power 12245
near-surface temperature 4910
neat fuel 11434
necessary water 10189
NEDOL process 2233
negative electrode material 6128, 6140, 6941, 6511
– lithium ion cell 6140
neighbor-awareness position update (NAU) 11554
neighborhood scale model 11276
Nellore breed 1760
nematicide 2567, 5440
nematocyst 12046
nematode 12029, 12037, 12042, 12044
Neobenedenia sp. 3565
neodymium magnet 26
neoendemics 3362
neomycin phosphotransferase 2597
neonate 3626–3627
– elimination rates 3627
– hydration of the skin 3626
– metabolic pathways 3627
neopentyl glycol (NPG) 6902
nepheline 1924
nereistoxin 3152
Nernst equation 2935, 5139
Nernst potential 6570
Nernst-Einstein equation 6083, 6548
Nernst-Einstein-Townsend equation 10421
Nernstian loss 5155
– voltage drop 5155
Nernst-Masse 3929
Nernst's law 3875
nerolidol 4036
nervous system 3632
nesquehonite 1919
nested association mapping (NAM) 4075
nested regional climate model 8905
nested-association mapping (NAM) 6443
net calorific value (NCV) 1200, 1234, 1331, 9832, 9838, 11842
net carbon assimilation 3223
net collector efficiency 9543
net energy
– analysis 2184
– efficiency 868
– metering (NEM) 10454, 10463, 10460, 10466, 10476
– tariffs 10460
net pen culture 590
net present value (NPV) 4789
net primary productivity (NPP) 161
net solar gain 7644
net solar radiation 10626
network and information growth 3308
net-zero building 3676, 7643, 7665, 10342
net-zero energy performance 8710
neurodegenerative prion disease 10859

neuromodulation 6510
– batteries 6510
neuronal migration 3628
neurostimulator 6510
neurosyphilis 11075–11076
neurotoxic shellfish poisoning (NSP) 9085
neurotoxicity 3634
– PCB-related 3634
neurotoxin 834, 2085, 3586, 3593, 3635, 4832, 7272, 7277
neutrino 3794, 8537, 8561, 11206, 11208
neutron 3788, 3794–3795, 3800–3803, 3805–3812, 3814, 3815, 3817–3818, 7208, 7209, 7213, 8468, 8552–8554, 8567, 8569, 11206
– balance 3795, 3800, 3803, 3807
– Broglie wavelength 3802
– capture 3801
– chain reaction 7114
– channeling 3810
– density 3805, 3807, 3814, 3817
– detection 5567
– detectors 5569, 7209
– deterministic transport theory 8554
– diffraction 6070–6072, 7542, 9896
– diffusion equation 3810, 3812
– distributions 3805
– dosimetry 3026–3027, 8551
– albedo technique 3027, 8551
– energy 7089, 7099
– distributions 8569
– fluctuations 3818
– kinetic energy 3794
– loss 3808
– measurement 7208
– momentum 3802
– Monte Carlo simulation 3809, 3815
– multiplication factor 3808
– poisons 7094
– production 3808
– reaction 3806
– scattering 3801
– shielding 8540, 8549–8550
– capture gamma photons 8549
– with concrete 8550
– skyshine 8553
– sources 7213, 8567
– spectroscopy 5568
– streaming 8552
– transport equation 3805, 3807, 3809, 3811, 3818
new climate proof crop 2640
"New Deal" legislation 3288
new drug entity (NDE) 6521
new greenery 11372
new open space 11372
new transport equation 3806
new urban landscape 11365
Newcastle disease virus (NDV) 641, 8075
Newtonian gravitation 2100
Newton–Raphson iteration method 4096
Newton's law 12065
Newton's theories of gravitation 10614
next-generation sequencing (NGS) technology 6428, 6529
Niacin 1684
niche opportunity 10079
nickel 172, 4861–4862, 4890, 9952
– active materials 6939
– batteries 6938–6939
– cadmium 6943–6944
– cadmium batteries 676, 777, 6943
– fiber plate batteries 6944
– pocket and tubular plate cells 6943
– sealed sinter plate cells 6944
– cobalt manganese oxide 6144
– electrode 6939–6940
– construction 6940
– reaction 6939
– hazard assessment 4861
– metal hydride (NiMH) battery 707, 775, 779–782, 3479, 3483, 6946, 8717
– cylindrical 781
– overcharge 780
– over-discharge reactions 780
– prismatic 782
– types 780
– metal hydride (MH) electrode 6945
– oxyhydroxide (NiOOH) 779, 11515
– sintering 9873
nickel-based battery 6938, 11515
nickel-hydrogen battery 707, 6940, 6948
nickel-iron battery (Ni-Fe) 6940, 6942
– fabrication process 6942
– performance 6942
nickel-metal hydride cell 676
nickelous hydroxide (NiOOH) 777
nickel-zinc battery 679, 6947
Nicotiana tabacum 10671
Nicotiana 10704
nicotinamide adenine dinucleotide (NAD) 1684
nicotine 10639
night ventilation 3684, 3693
night vision 11100
– cameras 11098
– environment 11104
– images 11102
– systems 11103, 11126
– camera-to-display 11126
nighttime driving 11099
nikkomycin 503
Nile red 361
NIMBY (Not in My Back Yard) syndrome 5721
nino3 SST 2519
niobate oxide 7889
niobium oxynitride 8271
niobium-titanium (NbTi) 6251
Nipponbare protein 2698
NIR
– illuminator 82, 87
– spectra 75
Nisin 504
nitrapyrin 3773
nitrate 1103, 2088, 3770, 3781, 3783, 7671
– concentrations 2088
– radical 11317
– reductase 1192
nitric acid 119, 134, 11317
– trihydrate (NAT) 130
nitric oxide (NO) 250, 4968, 5488
nitride fuel 4062
nitrification 884, 1136, 3455, 3773, 3781, 11894, 11901, 11936, 11956
nitrification–denitrification process 10961
nitrile 7579
nitrite salt 10569
nitrogen 552, 849, 1000, 1103–1104, 1109, 1308, 1433, 1668, 2169, 2632, 2641, 2662–2665, 2667–2668, 2670, 2672, 2674–2677, 2687, 2747, 3592, 3776–3777, 4558–4560, 6377–6378, 7671, 7989, 8350, 9827, 10041, 11894, 11896, 11936
– absorption efficiency (NAE) 2674, 2677
– assimilation 6378
– availability 2641, 2664, 2676, 4559–4560
– biogeochemical cycles 6377
– concentration 2664
– conversion efficiency 2675, 2677
– critical plant concentration 2665
– crop responses 2662
– nitrogen cycle 6378
– deficiency 2670, 2672, 2673
– effects on harvest index and components of grain yield 2673
– effects on leaf and canopy photosynthesis 2672
– demand 2663, 2665
– denitrification 11896

– dilution effect 2668, 2670
– dioxide pollution in urban areas 11301
– distribution 2676
– emission 7989
– shadow price 7989
– fertilization 4559
– fertilizer 1104, 2562, 2616, 2662, 2663, 2676, 3776, 4560, 9325, 10749, 11332
– fuel bound 1308
– gas 10959–10960
– harvested index (NHI) 2676
– heterocycles 4654
– in plants 2663
– in soils 2662
– nitrification 11896
– nutrition index (NNI) 2662, 2668
– oxide (NO_x) 170, 230, 666, 2277, 2282, 2746, 3641, 6806, 8349, 11585, 11855
– emissions 666
– low NO_x technologies 6483
– molecule 666
– supply conditions 2677
– taxation 7989
– nitrogen trichloride 10653
– uptake 2667, 2676
– use efficiency 2674, 2677, 3777
– volatilization 11896
nitrogen-rich nanocarbon 6781
nitrophenol 1636
nitrophosphate 2747
nitrous oxide 245, 849, 883, 1134, 1136, 5241
– emissions 1136
nitroxyl radical organocatalyst 7606
no observed adverse effect levels (NOAEL) 3254, 3586
no observed transcriptional effect levels (NOTEL) 3275
nodal method 3813
nodularin 4832
noise 12279, 12288
– auditory system 12288
– dose–response relationships 12288
– measures 12279
– pollution 12288
nonadditive genetic deviation 418
nonaqueous clathrate 330
nonaqueous phase liquid 10962
non-condensable gase (NCG) 4247, 4311, 4326, 4425
non-CO_2 emission 1504
nondestructive assay (NDA) technique 7207
non-enzyme protein 8032
non-ferrous slag 11703
non-flame incineration 6975–6976
nonfood aquaculture 576
non-fossilized organic material 1608
nonground vehicle 5088
nonhazardous waste materials 4867, 5734
non-Hodgkin's lymphoma (NHL) 3646, 8066
non-homologous end joining (NHEJ) pathway 10822
nonhuman biota 8409, 8463
– radiation dose 8463
– radiological protection 8409
nonintegrated two-stage liquefaction (NTSL) 2231
nonionizing radiation 5574
non-methane hydrocarbon (NMHC) 609, 5488
nonnative species 5549, 5551, 5556
– Allee effects 5556
– biological control 5556
– maintenance control 5556
non-noble metal catalyst (NNMC) 8285, 8286, 8297
– activity 8286
– Fe-N-C catalysts 8297
nonnucleoside reverse transcriptase inhibitors (NNRTI) 5011
nonparasitic agent 12046
non-pharmaceutical proteins 8078
– plant-derived 8078
non-photochemical quenching (NPQ) 355
non-photosynthetic sinks 2628
non-platinum-group metals (non-PGM) 373
nonpolar carbon dioxide 10170
non-polio enterovirus 8149
– genomes 8138, 8141
nonreactive radionuclide 11231
non-renewable
– energy resources 1602
– generation 3014
– resource depletion 548
nonribosomal peptide synthases (NRPS) 504
non-Sabin-like virus 8153
non-target arthropod 10718
non-woody biomass fuels 9827
non-wovens 8719
– materials 8725
nopaline synthase gene (pNOS) 10672
nopaline 10677
Nordic power market 12110
norhalichondrin B 3159
normal hydrogen electrode (NHE) 6570
normalized difference vegetation index (NDVI) 2618, 6221
Norovirus 7385, 9105, 11986–11987
– biological properties 11987
– cultivation 11987
– genogroups 11986
North American monsoon (NAM) 7256
North Atlantic
– deep water (NADW) 5859, 8677
– oscillation (NAO) 2137, 2455, 5873, 9805–9806
– temperature predictions 2143
North Pacific
– gyre oscillation (NPGO) 6231
– pressure index (NPPI) 2135
Norwalk virus 11986
NO_X emission 273, 1333, 1348, 1391
– from biomass combustion 1333
no-tillage 2748
– agriculture 3592
– cultivation 1270
not-in-my-back-yard syndrome 12227, 12230
novel food regulation 10772, 10774
novel gene products 10845
novel protein foods (NPF) 1547
novel $trait_s$ 4521
noxious photochemical smog 245
n-type silicon 9213
nuclear accident 3585, 5592, 7005, 7016–7019, 7023–7025, 7030, 7047, 8389, 8602
– areas
– of accumulation 7025
– of erosion 7024
– of transportation 7024
– biouptake rates 7019
– catchment area 7016
– countermeasures 7047
– erosion–transportation accumulation 7024
– fallout
– curves 7018
– on the catchment 7023
– modelling coastal marine systems 7030
– rivers fluxes 7017
– sediment transport 7018
– suspended particulate matter 7024
nuclear clad material 7196
nuclear decommissioning 7056, 7065, 7069–7070, 7072–7076, 7079–7080
– cost estimates 7072
– decontamination methods 7074
– dismantling and removing buildings 7075
– equipment 7074
– final inspections 7079
– general methodologies 7069
– groundwater restoration 7070
– performance assessment 7073

– reclaiming disturbed land 7080
– remediating residual radioactivity 7076
– safety 7073
– site characterization 7070
– status of decontamination 7080
– surveys 7079
– total costs 7073
– waste management and disposal 7065
nuclear design calculation 3810
nuclear disaster 3862
nuclear donor cell 6166
– sources 6166
nuclear energy 3555, 4050–4052, 7051, 7087, 8598, 8601
– electric generation 7087
– GEN-IV 4052
nuclear envelope breakdown (NEBD) 6165
nuclear explosive 7087, 8585
nuclear facility 7055, 7057–7058, 7070–7071
– decommissioning 7055, 7058, 7070, 7071
– decontamination 7058, 7070
– dismantlement 7058, 7070
– types 7058
nuclear fission 7087, 8603, 11202
– power plants 7054, 7086, 7087
– process 7197
– nuclear fission reactor 7052, 8515
nuclear forensics 7213
nuclear fuel 5633, 6691, 7054–7055, 7063–7064, 7142, 7196, 8584, 8593, 8667, 11204
– back end fuel cycle facilities 7064
– clad materials 7196
– cycle 3583, 5574, 6688, 6689, 7054, 7056–7057, 7059–7060, 7064, 7082, 7146, 8426, 8484, 8584, 9443, 11222
– facilities 7080
– front end facilities 7060
– waste storage and disposal 8584
– disposal 6691
– enrichment 7062
– gaseous diffusion 7062
– fabrication 6691
– facilities 7063
– isotope separation methods 5633, 7054
– management 11203
– materials 7194
– operation 6691
– recycling 7088, 8593
– reprocessing 7055, 7142, 8584
– facility 7064, 8667
– plant 8503
– resources 11204
nuclear fusion 7055, 7156–7158, 7162, 7164–7165, 7167–7170, 7175–7177, 7179
– cold fusion 7170
– compact toroids 7165
– confinement systems 7168
– electrostatically plugged cusps 7168
– field-reversed configuration 7167
– hypervelocity impact fusion 7175
– inertial confinement fusion (ICF) 7170
– inertial electrostatic confinement (IEC) 7169
– levitated dipole experiment 7169
– magnetized target fusion (MTF) 7168
– muon-catalyzed fusion 7170
– of hydrogen isotopes 7157
– open magnetic confinement 7168
– plasma focus 7168
– plasma physics theory 7176
– polywell 7169
– pulsed, high-density fusion 7168
– reaction 7157
– reactor
– design 7177, 7179
– requirements 7158
– reversed field pinch 7164
– RF plasma confinement 7169
– rotating plasmas 7168
– stellarators 7164
– tandem mirror 7168
– technology issues 7176
– tokamak 7162
nuclear gauge 8523
nuclear generation 12188
nuclear genome transformation 365
nuclear industry 7053, 11221
– uranium 11221
nuclear magnetic resonance (NMR) spectroscopy 6078
nuclear material 7202–7206, 8497
– accidents 8497
– accounting 7204
– control measure 7202
– destructive analysis 7205
– key measurement points (KMP) 7205
– mass spectrometry 7206
– material balance areas (MBA) 7205
– measurement technology 7204, 7205
– nondestructive assay 7206
– technologies for safeguarding 7203
nuclear maturation 6163
nuclear medicine 4908, 7052, 8561, 8580, 8587
– radionuclide 8523
nuclear power 209, 4770, 7138–7139, 7180–7181, 8585, 8981, 12120
– economics 7055, 7180
– facilities 7184
– levelized costs 7184
– financial viability 7181
– future 7138
– generation 8482
– industry 8583, 8598
– new nuclear installations 7139
– occupational exposure 8585
– plant 7052, 7063, 7080, 7182–7183, 7186–7191, 7195, 8484, 8587, 11223–11224
– buying nuclear fuel 7187
– cooling water 7187
– cost comparisons 7191
– costs and their uncertainties 7189
– decommission costs 7186
– discount 7190
– enrichment 7187
– estimating uncertainties 7188
– external costs 7191
– financial risk 7182
– fuel fabrication 7187
– interest rates 7190
– interim spent fuel storage 7188
– life-cycle cost 7183
– operating costs 7186
– power facility construction 7186
– routine operational releases 8484
– spent fuel disposal 7188
– spent fuel recycle 7188
– waste management 11224
– production 7186
– capital costs 7186
– cost calculations 7186
– reactor 7087–7090, 7094–7097, 7099, 7101–7103, 7107, 7109, 7111–7112, 7114, 7120–7123, 7125–7131, 7133–7136, 8583, 10998
– advanced boiling-water reactors (ABWR) 7131
– advanced CANDU reactor (ACR) 7133
– advanced heavy water reactor (AHWR) 7134
– advanced light-water reactor 7127
– advanced reactors 7127
– boiling-water reactor 7096, 7109
– CANDU reactors 7109
– classifications 7089
– control 7094
– design 7090
– design-basis accidents 7121

– emergency core cooling systems (ECCS) 7122, 7128
– energy sources 7121
– European pressurized-water reactor (EPR) 7133
– fast breeder reactors 7103
– fast-neutron reactors 7135
– gas-cooled fast breeder reactor (GCFBR) 7109
– gas-cooled fast reactors (GFR) 7136
– gas-cooled reactors 7101, 7129
– generation IV nuclear reactors 7135
– generation-III reactors 7131
– heavy-water reactors 7099, 7133
– high-temperature gas-cooled reactors 7134
– lead-cooled fast reactors (LFR) 7136
– light-water graphite reactors 7102
– light-water reactors 7095, 7131
– liquid-metal reactor 7130
– maintenance 7114
– molten-salt breeder reactor (MSBR) 7109
– molten-salt reactors (MSR) 7136
– operation 7090, 7109
– operation features 7112
– plant control systems 7120
– postaccident radioactivity removal 7123
– power reactor inherently safe module (PRISM) 7130
– pressurized-water reactor 7097, 7111
– quality assurance (QA) requirements 7126
– refueling outages 7112
– safety 7094, 7121, 7125
– safety systems 7122
– shutdown 7111
– sodium-cooled fast reactors (SFR) 7136
– supercritical water-cooled reactors (SWCR) 7136
– systems 7095
– thermal design 7094
– very high-temperature gas reactors (VHTR) 7136
– worldwide perspective 7107
– stations 9766
nuclear proliferation 7210
nuclear radiation 5561
nuclear reaction 3790, 3796, 5567
– neutron-induced 5567
nuclear reactor 209, 7054, 7056, 7057, 7149, 7150, 7193–7194, 7199, 8539
– accident 8465, 8498, 8616
– for propulsion 8539
– fuel 7054, 7193–7194
– materials 7054, 7193–7194, 7199
– coolant materials 7198
– moderator materials 7197
– structural materials 7199
– neutron poison materials 7199
– operations 8482
nuclear regulatory commission 8592
nuclear reprocessing 7143–7144, 7146–7147, 7149–7150, 7160
– advanced aqueous separations process 7146
– aqueous reprocessing 7143
– equipment 7147
– aqueous separation technology 7144
– centrifugal contactors 7149
– COEX™ process 7147
– columns 7147
– liquid–liquid extraction 7143
– magnetic confinement 7160
– process technology 7150
– PUREX process 7144, 7146
– pyroprocessing 7150
nuclear reprogramming 6158, 6170, 6172
nuclear safeguards 7054, 7201–7203, 7215
– historical development 7202
– nondestructive measurement technology 7203
– nonproliferation policy 7202
nuclear safety 3543, 7053
nuclear security programs 7203
nuclear smuggling 7212–7213
nuclear spectroscopy 3803
nuclear steam-supply system (NSSS) 7099
nuclear submarine accidents 8512
nuclear technology 4906, 7202, 8388, 8426
nuclear terrorism 7203, 7212, 7214
nuclear test/testing 3540, 3541, 7202
– grounds 8492
– potassium fertilizer treatment 3541
– remediation 3540
nuclear transfer (NT) 6150–6152, 6154, 6155, 6165, 7217–7222, 7226, 10820
– basics 7221
– cell-cycle coordination 6165
– cell-mediated transgenesis 7220
– cloning animals 7218
– direct transgenesis 7220
– efficiency 7226
– embryo development 6151
– enucleation methods 6155
– experiments 7218
– from somatic cells 7220–7221
– gene targeting 7222
– in mammals 6152
– maturation-promoting factor (MPF) 7221
– microinjection 7219
– micromanipulator 6154, 7221
– production of transgenic animals 7218
– techniques 6154
– with differentiated cells 7222
nuclear transformation 2600
– consequences 2600
nuclear transgene 2600
nuclear transgenic plants 8062
nuclear waste 4775, 7071, 7139, 8592, 8602, 10423, 11608
– disposal 8591
– long-term management 7139
– repository 8592
– storage tanks 8602
– environmental contamination 8637
nuclear weapon 3531, 3803, 7051, 7054, 7087, 7182, 7201, 7210–7211, 8452, 8488–8490, 8529, 8531, 8601, 8625, 8585–8586
– accidents 3533, 8505
– broken arrow 8505
– characteristics 8488
– detonations 8496
– atmospheric 8490
– exoatmospheric 8490
– underground 8490
– underwater 8490
– explosions 8637
– environmental contamination 8637
– fallout 8541
– structure shielding 8541
– fission-based 8489
– fission yield 8585
– fusion yield 8585
– hydroacoustic monitoring 7211
– materials 7201
– open source information 7210
– physical designs 8490
– radioactive wastes 8586
– reduction 8531
– satellite imagery 7210
– seismic monitoring 7211
– technology 7202
– terrorist weapon 8529
– test/testing (NWT) 3547, 7018, 8389, 8469, 8488, 8492–8493, 8598, 8635, 8662,
– anthropogenic disturbances for biodiversity 8492

– thermonuclear fusion based 8489
– uranium 8625
nuclear-powered vessel accidents 8509
nucleating agents 11601
nucleation 117
– scavenging 630
– theorem 119
nucleic acid 1653, 8065
nucleophile 3660
nucleoprotein (NP) 2971
nucleoside 7385
– reverse transcriptase inhibitor (NRTI) 5010
nucleosome 3604
nucleotide instability (NIS) 3607
nucleus mass number 3790
nuclide 5560
Nud gene 2706
nudation 3281
nuisance effect 426
null allele 2552
null flux
– configuration 6250, 6258
– loop geometries 6250
numerical weather prediction/forecast 5071, 5081, 12063, 12068, 12074–12075
– ensemble forecasting 12074
– models 12069
– nonhydrostatic dynamics 12075
– parameterizations 12068
– remote satellite observations 12074
– scalable dynamical cores 12075
nutrient 1103, 1677, 1682, 1683, 1690, 3708, 3769, 3774, 3776, 3782, 4554, 7678
– adsorption isotherms 7678
– bioavailability 1690
– calculations 9042
– modeling 9042
– certificate 9027, 9038–9040, 9041, 9045, 9046
– authentication 9039
– bankable and trading value 9046
– buildings 9045
– categories 9041
– contents 9040
– industry labeling 9041
– material composition 9040
– material functions 9041
– material-defined pathways 9041
– proprietary information 9041
– risk management features 9046
– security of supply 9039
– transition mechanism 9039
– value partnerships 9039
– deficiencies 1683
– facultative 1682
– from the soil 3769
– humic substances 1103
– in plant tissue 3774
– law of the minimum 3776
– leaching 5828
– movement 3782
– phloem-delivered 4554
– recovery 557
– trading credits (NTC) 551, 9118
– transfer 3782
– through animals 3782
nutrition 10752, 10888–10889
nylon 8829, 8831
– depolymerization 8831
– recycling 8829
– solvent extraction 8831

O

oarweed 518
obesity 3591, 10646, 10654
object tracking 61
objective sleepiness scoring (OSS) 3119, 3129
observability matrix 3059
obstacle 78–79
– fixed 79
– L-shaped 78
– moving 79
– new 79
– unknown 79
obstruction of the sky 11383
occidental building 3693
occupational exposure to chemicals 222
Occupational Safety and Health Administration (OSHA) 7826
ocean/oceanic 2458–2459, 2501, 2514, 2523, 3232, 3296, 3316, 3575, 3579, 4569, 4909, 4920, 5047, 5856–5858, 5865, 5871–5872, 5874–5875, 6179–6180, 6184, 6186, 6188–6189, 6196–6197, 6346–6347, 6372, 6372, 6375, 6378–6379, 7229–7230, 7232, 7233, 7239, 7243–7244, 7246, 7249, 7260, 7263, 7267, 7279, 7282–7284, 7293, 7296–7299, 7302, 7328, 7329, 7333, 7337–7341, 7343–7344, 7347, 7348, 7349, 7354, 7356, 7360–7361, 7367–7368, 7371, 7378–7379, 7382, 7384, 7396, 8389, 8919, 9156
– acidification 2501, 6180, 6375, 7229–7230, 7279
– biological effects 7234
– calcifiers 7236
– chemical changes 7233
– elevated CO_2 7235
– geographic variability in pH 7237
– metabolic considerations 7235
– upwelling 7238
– altered circulation 7233
– anthropogenic forcing 7283
– anthropogenic inputs 7347, 7354
– anthropogenic transgressions 6197
– atmospheric input 7333, 7339, 7348
– atmospheric particulate concentrations 7360
– basins 5869
– near-rectangular geometry 5869
– basin-wide monitoring 5875
– biodiversity 6196
– biogeochemical considerations 7232
– biogeochemical cycle 7367
– biogeochemical processes 7367
– biogeochemical signatures 7279
– biogeochemistry 3296, 6372, 7271, 7279
– bloom 2776
– bottom pressure (OBP) 4568, 4577
– carbon dioxide concentrations 6373
– carbon model 7378
– chemical distributions 7343
– chemicals 7361
– chemistry 7329
– circulation 4565, 7343, 7373, 10662
– isopycnal coordinate system 7373
– topographic effects 7373
– tracers 7343
– color 3232, 8923–8924, 8958, 8962
– algorithms 8962
– sensors 8924
– color remote sensing 8954, 8960, 8962, 8966, 8968–8969
– atmospheric correction 8960
– biological oceanography 8966
– chemical oceanography 8969
– environmental monitoring 8969
– harmful algal blooms (HABs) 8969
– ocean physics 8968
– concentration of CO_2 7230
– contaminated with PCBs 6189
– conveyor 5859, 8680
– currents 6347
– cycling
– of chemicals 7340
– of organic chemicals 7356
– deep circulation 5856
– deep conveyor belt circulation 7344
– deep water 5857
– denitrification 6378
– distribution of evaporation 7249
– drilling program (ODP) 6417
– dynamic topography 4577

– ecological stresses 6179
– economy 7384
– ecosystems 2068, 3579
– energy 6346, 7242–7244
  – technologies 7244
– engineering 7298, 7396
– evaporation 3232, 7244, 7256, 7260
  – precipitation regimes 7256
– exclusive economic zones (EEZs) 7243
– export of particulate material 7337
– farm technologies (OFT) 585, 588
– farming 7263
– fate 7328
– fertilization 4108, 4113, 7267
– floor 6410
  – "cold seep" locations 6410
– forecast models 7293
– general circulation models (OGCM) 4916, 7365, 7367, 7371–7373, 7379
  – horizontal grid system 7371
  – simulation of marine ecosystem 7379
  – sub-grid scale parameterization 7373
  – vertical coordinate systems 7372
– geochemical cycling 7361
– global overturning circulation 5865
– global thermostat 6180
– health 2264, 2267, 6193, 8922
  – early warning systems (OHEWS) 2264
  – habitat destruction 6193
  – sentinels 6193
  – warning systems 2267
– heat content 2523, 4909, 4920, 4924, 5872, 5874
  – monitoring 4924
– heat reservoirs 7252
– heat transports 4921
– heating term 7371
– human bacterial diseases 5047
– hybrid coordinate ocean model 7301
– hydrocarbon investigation (OHI) 3554
– hydrological cycle 7246
– information 7282
– infrastructure 7284
– input
  – from the sediments 7339
  – from hydrothermal vents 7338
  – from the terrestrial environment 7337
– invasive species 6184
– iron fertilization (OIF) 7270–7271, 7276, 7277, 7279
  – as a geoengineering tool 7276
  – dissolved oxygen 7279
  – efficiency 7276
  – potential side effects 7277
– kinetic energy 7368
– mankind's global footprint 3575
– man-made radioactivity 8389
– mass gains 4563
– mass redistribution 4569
– meridional overturning 5856
– mesoscale eddies 7368
– model 3212, 7369, 7370, 7371, 7373–7375, 7377
  – atmosphere model 7369, 7374
  – biogeochemical cycle modeling 7377
  – Bjerknes–Wyrtki model 7374
  – boundary conditions 7370
  – Cane–Zebiak model 7374
  – computational fluid dynamics (CFD) methods 7369
  – equations of motions 7370, 7373
  – Gill-type model 7375
  – hydrostatic primitive equations 7369
  – sea surface temperature (SST) 7371
– mooring 7287, 7302
– nitrogen 612
  – fixation 6378
– observation data 7368
– observatories 3232, 7282, 7291, 7293
  – data-centric cyberinfrastructure strategy 7291
  – information systems 7291
  – micro electro-mechanical systems (MEMS) chip technologies 7293
  – Ocean Observatory Initiative (OOI) 7291
– observing network 7282, 7285, 7286, 7289
  – high frequency radar 7286
  – platforms available 7285
  – propeller-driven AUVs 7289
  – satellites 7285
– oceans and human health (OHH) 2259, 7383
  – economic impacts 7383
  – programs 2259
  – social impacts 7383
– organic chemicals 7337, 7340
– organic contaminants 7360
– osmotic gradients 6347
– overturning circulation 5857–5858
– pollutant elements 7361
– pollution 6188
– precipitation 7244
– predatory species 6186
– radiocarbon data 8657
– remote sensing applications 8919
– research plan 2262
– riverine inputs 7339, 7348
– role of iron 6379
– salinity 2140, 2514, 5872
  – anomalies 2140
– science community 7293
– sea-level change 7379
– sentinel species 9156
– sequestration 4121
– simulations 7379
– sinking particles 7343
– surface mixed layer 7371
– sustainable aquaculture 7263
– temperature 2459, 4909, 4911, 4916, 4917, 4922, 4924, 6180
  – abyssal 4922
  – acoustic measurements 4924
  – Argo system 4913, 4924
  – changes 4917, 4922
  – decadal changes 4922
  – fields 4911
  – geothermal heat flux 4922
  – gradients 6347
  – interpolation methods 4916
  – satellite altimetry 4924
  – surface mixed layer 4911
  – thermometers 4911
– thermal energy conversion (OTEC) 7296, 7297–7298, 7300, 7302–7303, 7305, 7310, 7312–7313, 7315–7316, 7318–7320, 7323–7324
  – capital costs 7324
  – challenges 7302
  – closed-cycle OTEC (CC-OTEC) 7297, 7310, 7311
  – closed-cycle 7310
  – cold water pipe 7318
  – control parameters 7312
  – design environment 7313
  – economics 7323
  – electrical interface 7315
  – environmental impact 7303
  – experimental apparatus 7300
  – history 7297
  – hybrid cycle 7298
  – inspection, maintenance, and repair (IM&R) 7319
  – log-mean-temperature-difference (LMTD) 7312
  – moored OTEC configurations 7312
  – open-cycle 7305, 7306–7307, 7309–7310

– plants 7302
– power cycle 7313
– seawater components 7316
– site selection criteria 7319
– submarine power cable 7319
– technical limitations 7302
– thermal resource 7243, 7297, 7299, 7320
– thermohaline circulation 7341
– uptake
– of anthropogenic CO_2 7239
– of carbon dioxide 5871
– warming 2458
– water 6181, 7341, 7348–7350, 8963
– aluminium cycling 7348
– bio-optical modeling 8963
– cadmium cycling 7349
– column distributions 7360
– iron cycling 7348
– lead cycling 7350
– manganese cycling 7348
– measurement of salinity 6181
– mercury cycling 7350
– quality 8928
– silver cycling 7350
– sinking 7341
– upwelling 7341
– zinc cycling 7349
– wind-driven circulation 7341
– wind-driven Ekman transport 5874
– zonal flows 5865
ocean–atmosphere
– composition model 9804
– coupling 7258–7259, 9808
– interactions 3213
– system 2127, 2129
ocean-ranching 10326
oceanographic
– data 1944
– modeling community 8670
– satellite sensors 8932
oceanography 2457, 4911, 4916, 8966
– GCM codes 4916
– ocean color remote sensing 8966
OceanSITES network 5876
octahedral lithium 7539
octanol 7357, 10659, 10969
octanol-water partitioning coefficient 4850, 10969
octocoral 2498
octopine 10677
ocular neoplasms 11402
odd oxygen 10130
OECD-baseline scenario 1557, 1559
O.E.T. Calusco process 1527
off-bottom offshore cultivation 517
off-road vehicle 3393, 5083, 5085, 5088, 5089, 5092
– application 5092
– heavy-duty applications 5088
– HEV architectures 5085
– hybrid electric technology 5083
– hydraulic systems 5089
– hydraulic technology 5083
– military 5092
– scraper/bulldozer 5092
offshore
– aquaculture 514, 522–523, 528, 559, 7265
– biological studies 522
– feasibility study 528
– one-step cultivation 522
– physical and technical studies 523
– collector 521, 7437
– internal electricity grid 7437
– co-management 527
– drilling 6404, 6406
– electricity system 7439
– farming 523, 3558, 6760, 6765
– hydrocarbon industry (OHI) 6405–6406, 6408, 6411, 6413, 6415–6416, 6418, 6420–6421
– drilling 6418
– fish protection by pipelines 6420
– geophysical data 6413
– history 6406
– impact of platforms 6421
– mapping 6416
– marine fauna 6408
– observations along pipelines 6418
– pipeline routes 6416
– platforms 6415
– pollution 6416
– predrilling 6411
– production drilling 6418
– seafloor processes 6411
– macroalgae growout 6764
– oil platform 6765, 7396
– polyculture 8203
– ring 521
– substation (OSS) 7437
– wave 7406
– wind data collection 7400
– wind energy 7243, 7265, 7393–7394, 7422
– capital costs 7422
– economics 7422
– wind farm 521, 514, 6594, 6765, 7397
– wind parks 7440
– wind power 7425–7426, 12215
– connection to shore 12215
– wind power plant 4478, 7423, 7429–7433, 7435–7437, 7439–7442, 7444
– availability 7441
– average cost 7423
– barriers of water flow 7432
– benthic fauna and flora 7432
– connection to Shore and Offshore Substation 7439
– current 7431
– economy 7444
– environmental conditions 7442
– environmental Impact 7432
– external conditions 7429
– feed-in tariffs 7423
– fish 7432
– fixed charge rate (FCR) 7423
– floating foundations 7437
– foundations 7435
– gravity-based foundations 7435
– high voltage direct current technology 7439
– impact of electromagnetic fields 7432
– installation 7440
– jacket structures 7436
– levelized production costs (LPC) 7444
– line commuted converter 7439
– magnetometric investigations 7429
– marine Spatial Planning 7431
– monopile foundations 7436
– reliability 7441
– renewable energy certificates (RECs) 7423
– renewable portfolio standard (RPS) 7423
– sea ice 7431
– sea mammals 7433
– soil conditions 7429
– tidal effects 7431
– tripod foundations 7437
– visual impact 7432
– water depths 7430
– waves 7431
– wind conditions 7430
– wind resource 7397, 7400
– land/sea breezes 7400
– wind turbine 7243, 7394, 7400, 7402, 7404, 7406, 7413–7415, 7417–7418, 7420, 7427, 7433
– ancillary components 7415
– breaking waves 7404

– components 7413
– currents 7406
– design 7420
– doubly fed induction generator (DFIG) 7415
– drivetrain 7414
– electrical transmission system 7418
– environmental aspects 7420
– external design conditions 7400
– extreme waves 7404
– floating support structure 7417
– gearbox 7414
– high-voltage direct current (HVDC) 7420
– installation 7420
– main components 7394
– materials 7418
– rotor–nacelle assembly (RNA) 7413
– safety regulations 7427
– soils 7406
– support structure 7415
– technology 7433
– tension leg platform (TLP) 7417
– waves 7402
– wave forces 7406
– wind/wave correlations 7404
– wound rotor induction generators (WRIG) 7414
Ohmic polarization 744
Ohmic resistance 2944
Ohm–Kirchhoff law 9129, 9136
Ohm's law 9136
OIF 7276
– evaluation 7276
oikosteges 4701, 4705, 4737, 4742, 4751
oil 3845, 4550, 6245, 7446, 7448–7450, 7453, 7474, 7493–7494, 7497, 7798, 7802, 7805, 8085
– circuit breakers 3002
– competition" crisis 6245
– consumption 1022, 10487
– crisis 6245
– crops 11438
– deepwater exploration 7450
– field 5220
– geologic occurrence 7449
– global resources 7446
– grain quality 4550
– in conventional fields 7449
– interaction with light and electronic waves 7493
– mining 7809
– mobility 7805
– pipelines 6418
– pollution 7516
– Oil Pollution Act 7826
– satellite monitoring systems 7516
– purification 8085
– price 1563
– production 1218, 7818
– pressure pulsing technologies (PPT) 7818
– recovery 7798, 7807, 7815, 7819, 7827
– by retorting 7474
– chemical flood recovery methods 7807
– combustion processes 7815
– gas flood recovery methods 7807
– microbial technology 7819
– process wastes 7827
– processes 7827
– steam-based processes 7815
– reflectance 7494
– remaining resources 7453
– reserves 10487
– reservoir 7802
– beam pumps 7802
– underground pressure 7802
– resources 10487
– sand 7451, 7797, 7804, 7809
– exploration 7797, 7809
– production 7797, 7809
– seed 1218
– shale 7452, 7457–7462, 7464, 7467–7476, 7481–7483, 7485–7486
– assay methods 7471
– bitumen 7470
– classification 7459
– combustion 7468
– composition 7460
– conversion 7458, 7467
– direct combustion 7467
– ex situ technologies 7483
– Fischer assay method 7472
– galoter process 7483
– gasification 7468
– heat carrier 7482
– heat transfer 7481, 7486
– high-temperature pyrolysis 7468
– in situ technologies 7486
– kerogen 7461, 7462
– kerogen material 7458
– low-temperature pyrolysis 7468
– mineral matter 7460, 7470
– mining 7481
– oil recovery 7458
– organic matter 7461
– particles 7485
– processing 7457, 7481
– production 7469
– pyrolysis 7474–7476
– pyrolysis products 7464
– research 7486
– resources 7467
– retorting oil yields 7473
– Rock-Eval analysis 7472
– thermal dissolution 7469
– thermal effects during retorting 7471
– thermal efficiency 7483
– thermochemical-based conversion 7469
– shortages 7448
– spectra 7497
– spill 3232, 7491, 7492, 7511, 8929, 8930
– countermeasures 7511
– infrared imagery 8930
– scene analysis system (OSSAS) 7514
– spill remote sensing 7491–7494, 7497–7498, 7500–7502, 7504, 7506–7507, 7510–7518
– atmospheric properties 7493
– digital photography 7497
– from satellites 7492
– GIS databases 7510
– infrared camera 7492
– infrared sensing 7498
– integrated airborne sensor systems 7514
– interferometric radar 7511
– laser fluorosensors 7501
– microwave scatterometers 7511
– microwave sensors 7502
– near-IR wavelengths 7498
– optical sensors 7494
– radar 7504
– radar satellites 7516
– radiometers 7502
– Raman signal 7502
– real-time displays and printers 7518
– routine surveillance 7518
– satellite remote sensing 7515
– satellite scatterometers 7510
– scanners 7497
– shipborne radar 7507
– side-looking airborne radar (SLAR) 7506
– slick thickness determination 7511
– slick thickness relationships 7512
– small remote-controlled aircraft 7518
– specific thickness sensors 7513
– still cameras 7497
– surface wave radars 7511
– synthetic aperture radar (SAR) 7506

– tracking 7517
– ultraviolet sensors 7500
– underwater detection 7517
– video cameras 7497
– video photography 7492
– thickness measuring 7513
– oil thickness 7513
– thermal mapping 7513
– under ice detection 7517
– visible indications 7494
– weathering 7493
– well 4332
– yield 7474
oil-fired power plant 12120
oil-in-water 7497
– measurement 7497
oil-on-water slick thickness 7511
oilseed 4551, 4556, 4557
– fatty acid profile 4557
oily sour wastewater 7831
old corrugated container (OCC) recycling 8786
older driver 3135, 3140, 3143, 3145
– collision risk 3143
– increased crash risk 3135
– optical flow information 3145
– RMS speed error 3140
oleaginous algae 362
oleaginous microorganisms 11452
olefin 3934, 3980, 3988, 7594, 7603, 7605, 7835, 10175
– enantioselective electrocatalytic epoxidation 7603
– metathesis 10175
oleic acid 4557
oleosome 4556
OLGA scrubber 1467
oligoether 6051
oligomeric perfluorosulfonic acid dispersion 378
oligomerization 4019
oligonucleotide-mediated mutagenesis 10771
oligosaccharides 991
oligotrophic sea 8925
olive fruit 2649
olivine 1912, 1914–1917, 1919–1920, 1922–1923, 1925, 2118, 5131, 6086, 6129, 6143, 7527
– geopolitical implications 1925
– grains 1920
– in biodigesters 1923
– mine 1916, 1917, 1922
– phosphate 7530, 7532–7533, 7535–7536, 7538–7539, 7544
– cathode materials 7527
– data 7536
– diffractograms 7530
– electrochemical and structural 7536
– electrode material 7544
– lattice parameters 7535
– lithium compositions 7533
– miscibility gap 7538
– verification of lithium diffusion 7539
– verification of phase diagram 7532
– reactor 1919
– sand 1923
– weathering 1915
omega–3 oils 3577
omega–3 polyunsaturated fatty acids (PUFAs) 838
omics 3587
– platforms 11
omnivores 823
onchocerciasis 12008
– control program 12009
– elimination program for the Americas (OEPA) 12010
oncogenesis/oncogenic 3258
– genetic errors 3596
– mutations 3606
oncogenes 2588
oncosis 3161
One Health Initiative 2263, 9169
one ocean-one health paradigm 9157
one-electron transfer 3658
Online
– bioreactor systems 1633
– Mendelian inheritance in man (OMIM) 3609
onshore wind 12187, 12246
oocyte 5577, 6162, 7221, 10819, 11033
– maturation 6154, 7221
oogenesis 6162, 11033
ooplasmic reprogramming factor 6164
opaque2 corn mutant 1693
open building 6878
open circuit voltage 7563
open cooling cycles 9558–9559
open fireplaces 1360
open legs search 82
open net-cage aquaculture 10320
open ocean 7296, 7333–7334, 7336
– anthropogenic metals 7334
– aquaculture 581, 588
– crustal metals 7336
– farming sites 6761, 6764
– characterization 6761
– selection 6761
– mariculture 3555–3557, 3566, 3575, 3579
– alternative feedstuffs 3575
– mussel farming 6762, 6765–6766
– environmental considerations 6766
– methods 6762
– multiuse facilities 6765
– technologies 6762
– transport of chemicals 7333
– vertical temperature distribution 7296
– waters 6760
– farming 6760
open office 5333
open reading frame (ORF) 2698, 2701, 2703, 10832
open solar flux (OSF) 9800
open sorptive cooling cycle 9525
open space 11361
– development 11366
– clearance of redundant sites 11366
– simple clearance 11366
– planning 11372
open water
– cultivation 1935, 9110
– fish farm 547
open wet cooling tower 9533
open-circuit
– photovoltage 6568, 6571, 6576
– voltage 742
open-end drill pipe (OEDP) 4400
open loop 4150
– error 57
– gaze stabilization 56
– methane refrigeration 3960
– recycling 2399
open-pit mine/mining 6634, 6667
open-pollinated crops 8045, 10725
open-road tolling (ORT) 5024
open-top gasifier 1453
operational cloud observation 9633
operational farm management 9328
operational nutrient management system 9328
operational street pollution model (OSPM) 261
opiates 10642
opioid
– analgesics 10642–10643
– methadone 10643
– receptors 10643
Opisthorchioidea 12024
opium alkaloid morphine 6522
optical/optically
– air mass 9712, 9721
– depth 9715

– flow field 3144
– flow information 3145
– visual processing 3145
– oceanography 8957
– radiation 9674
– stimulated luminescence (OSL) 3027
optimal power flow (OPF) 9338
ORACLE system 325
oral polio vaccine 8146
oral vaccine 8066
orange carotenoid protein (OCP) 356
orbitography 2457
ordinary polynomials 469
ore 6667
organic
– aerosols 637
– batteries 4615, 7546–7547, 7549, 7552
– conjugated polymers 7549
– definition 7547
– radical polymers 7552
– redox polymers 7549
– carbon (OC) 1913, 10659
– emissions 11868
– carbonyl sulfide 130
– chemicals 10658
– compounds 2418, 2435, 6987, 11320
– appendix VIII list 6987
– leaching 2418
– nitrogen-containing 2435
– contaminants 2446, 10143
– properties 10143
– crops 10759
– production 4013
– electrode-active materials 7549
– electroluminescence devices (OLED) 7934
– farming 3780
– fertilizer 1132
– fouling 10538
– index 10540
– liquid electrolyte (OLE) 6045, 6060, 6063
– metal species 10052
– molecule 7556
– photovoltaics (OPV) 7554, 7556, 7565–7566, 7572, 7576–7579, 7940
– bulk heterojunction (BHJ) 7566, 7578
– cell 7563
– degradation 7577
– fabrication 7576
– flexible plastic substrates 7565
– low band gap polymers 7579
– operating principles 7556
– operational stability 7577
– solution-processed 7566
– transparent conductive oxide (TCO) 7565
– vaccum-depositied 7566
– vacuum-processed 7572
– pollution/pollutant 2502
– oxidative degradation 7607
– photomineralization 9572
– Rankine cycle (ORC) 1241, 1267, 1313, 1331, 1332, 1439, 1610, 1611, 4260, 4265–4268, 4271, 4276, 4296, 4303–4304, 4309, 4327, 4353, 8978
– dual-fluid 4268
– dual-pressure 4266
– fluid 4275
– process 1409
– recuperated 4265, 4304
– supercritical 4267
– temperature cascading 4265, 4303
– working fluid selection 4268
– semiconductors 7556–7557, 7564
– photoinduced charge transfer 7557
– solar cell 7553, 7555, 7560, 7564, 7576, 7580, 7934
– building 7564
– efficiency 7560
– photovoltaic power generation 7580
– tandem cell 7576
– solids 7558
– photoconduction 7558
– sulfur 2209
– waste 1538, 1579, 2416, 11583, 11675, 11872
– compound 4958
– gasification 2416
– zinc 253
organically bound tritium (OBT) 10998, 11002, 11021, 11028, 11029, 11036, 11046, 11056
– adverse health effects 11036
– current ICRP models 11046
– definition 11021
– formation in plants 11002
– ingestion 11056
organism 3269, 12294–12299, 12310, 12312
– aversive locomotion 12298
– biotransformation 12299
– circumvention of Target 12312
– ecological function 3269
– interoceptive sensors 12297
– mechanisms of resistance 12295
– mobility 3269
– monitoring after contamination 3269
– perception of environmental gradients 12296
– resistance mechanisms
– toxicodynamically derived 12310
– toxicokinetically derived 12296
– sensory mechanism 12298
– sensory neurons 12296
– target site alterations 12310
– unavoidable exposures 12298
– xenobiotics 12294–12295
organism-radionuclide combination 8438
organization of the petroleum exporting countries (OPEC) 7447
organocatalysis 4665, 7604, 7612
organochlorine (OC) 10667
organodisulfide 7549
organogenesis 2606
organohalogen 1629, 3634
organophosphate 3631
– fungicides 2569
– pesticides (OP) 3260
organophosphorus contaminants 9568
Organosolv lignin 1519
original oil-in-place (OOIP) 7802
oritavancin 504
ornamental fisheries 6187
orographic clouds 9639
orography 2106, 2352, 11276
orphan poliovirus 8155
orthophosphoric acid 3879
oryzacystatin 4031
osmoprotectant 5
osmotic
– adjustment (OA) 2641
– pressure 2905, 2916
– stress 5, 5316–5317
– effects on crop plants 5317
– tolerance 5319
Osmyb4 gene 2652
osteodystrophy 11414
osteomalacia 9655
Ostwald ripening 7716, 7761
o-toluidine 7595
Otto cycle 5503, 5512, 11430
– efficiency 5512
Otto engine 1460, 5522
outbreeding 418
outdoor air pollution 3641
outdoor pollution 1301
out-of-step (OOS) relaying 12090
outside ventilation 10271
ovary development 2647
overall thermal efficiency 4260
overbank sedimentation 3741, 3753

overcast irradiance 10627
overfertilization 3774, 3777
overfire air 6451, 6462, 6465, 8363–8364
overfishing 2502, 6182, 6195
overhead
– track 7784
– transmission 12189
overlay transmission 12202
overliming 974
overturning circulation 5866, 5868, 5873
– conceptual models 5866
– observations 5868
– observing system 5873
overvoltage 3002
ovine lentivirus 2968
ovum 6151
oxalate 10699
oxalic acid 1919
oxanthiins 2568
oxic groundwater 4777
oxidant 5139
– gases 3641
oxidation/oxidative 111, 1240, 3906, 3940–3942, 3946, 3950, 4645–4646, 7588, 10173, 10177
– catalysts 7588, 7594, 7596, 7606, 7611, 8090
– for synthesis gas production 7594
– for the environment 7607
– inspired by biology 7596–7597
– polyoxometalates 7612
– chemistry 7587
– wastewater treatment 7587
– definition 7588
– dehydrogenation (ODH) 7594
– enzymes 4034
– H_2O_2-based oxidations 3942
– O_2-based 3940
– of alcohols 4645
– of aromatic alcohol 10177
– of cyclohexane 10173
– of cyclooctane 10173
– of dihydropyridines 4646
– of hydrogen 3906
– of methylbenzenes 3941
– of styrene to acetophenone 10173
– of sulfides 4646
– quenching 5203
– reaction 7588
– selective 3946
– stress 4, 3589–3590, 3657–3658, 3660, 3662–3667
– biomarkers 3664
– definition 3663
– environmental sustainability 3667
– free radical 3660
– hypothesis 3666
– non-radical 3666
– radical-free biology 3665
oxidation–reduction reaction 3657
oxide 3889, 3892–3895, 3897, 3906
– apatite-type 3895
– $Ba_2In_2O_5$-based 3894
– brownmillerite-type 3894
– CeO_2-based 3892
– fuels 8584
– interconnection 9858
– $LaGaO_3$-based 3893
– nanoparticles 6574
– of nitrogen (NO_x) 11293
– perovskite-related 3893
– perovskite-type 3897, 3906
– proton-conducting 3897
– ZrO_2-based 3889
oxidizing nickelic hydroxide ($Ni(OH)_2$) 777
oxone 7605
oxyanion from mortars 4872
oxycodone 10642
oxy-combustion 9603
oxyfiring combustion 2151, 2153
oxygen 207, 612, 1235, 2029, 2953, 3893, 3901, 3905, 3927, 3968, 5227, 6383, 7590, 8232
– anions 2937
– biogeochemical cycle 6383
– concentration in water 2029
– consumption 3968
– cycle 5886
– gasification 5123
– gas 6383
– ion transport 2941
– ionic conductivity 3888, 3893
– non-stoichiometry 2953
– overstoichiometry 3905
– partial pressure 7735
– production 11348
– reduction reaction (ORR) 6543, 7701, 7732, 7734, 7736, 7750, 7757, 8208, 8212, 8232, 8269, 8271–8274, 8279, 8282–8283, 8285, 8294, 8340
– arc-plasma gun technique 8271
– carbon-based materials 8274
– face-to-face dicobalt-porphyrins 8273
– heat treatment 8283
– heterocycles 4655
– in acidic media 7734
– in alkaline electrolyte 8269
– kinetics 7736
– measurements 7750
– metal-containing macrocycles 8279
– metal-free macrocycles 8279
– niobium oxide 8271
– non-noble metal catalysts with molecular centers 8272
– non-pyrolyzed Macrocycles 8272, 8282
– oxalate-supported pyrolysis 8282
– pore-filling method (PFM) 8285, 8294
– Pt size effect 7736
– rate-determining step (RDS) 7734
– rotating disk electrode (RDE) 7734
– thermodynamics 8212
– separation from air 2154
– stable isotopes 5227
– stoichiometry 2941, 2950
– transport membrane 3969
– vacancy 2947
– concentration 3901
oxygenated fuel 5492
oxygenated organic aerosol (OOA) 122
oxygen-evolving complex (OEC) 7611
oxygenic photoautotroph 347
oxygenic photosynthesis 349, 355
oxynitride 7890, 8270
oxysulfide 2945
oxysulfide 7890
oyster 518, 522, 6765
– culture 1969
ozonation 10537
ozone 176, 180–181, 187, 209, 221, 223, 226, 230–231, 233–235, 261, 300, 310, 313, 613, 624, 653, 663, 668, 3641, 3944–3945, 8349, 8882, 8885, 8897, 9628, 9658, 9661, 9723, 9741, 9810, 10130, 10132, 10135, 10137, 10483, 11152, 11301, 11318–11319
– atmospheric profile 313
– chemistry–climate interactions 10135
– contact tanks 6624
– depletion 10132, 10133
– effects 10133
– middle latitudes 10133
– potential (ODP) 4271, 5415
– tropics 10133
– health effects 226, 230
– hole 613, 2513, 11416
– layer 188, 10130–10131, 10134, 11376
– Chapman mechanism 10131
– destruction 177
– Montreal Protocol 10134

– monitoring
– instrument (OMI) 11151
– stations 181
– mortality 231
– NAAQS 230, 233
– pollution 11319, 11322
– recovery 10135, 10137
– standard 234
– stratospheric 10130
ozone-depleting substances (ODSs) 10130
ozone-destroying radicals 10132
ozonesondes 9723
ozonolysis 3944, 3950

P

Paal–Knorr reaction 4666
Pacejka's "Magic Formula" 3056
pacemaker 6501
Pacific decadal oscillation (PDO) 2135, 2455
Pacific decadal variability (PDV) 2135
packed bed combustion 5305
packet delivery ratio (PDR) 11562
paclitaxel 3155, 6525
pair distribution function (PDF) analysis 6073
pair production 5561
paleoclimate 624, 6754, 7276
– information 2074
– studies 9803
palladium 7600
palmitic acid 4557, 9114
paludification 2176
pamaquine 11081–11082
p-aminobenzoate (PABA) 1710
panarchy 3351–3352
panchromatic
– image information 11121
– luminance channel 11119
Panicoideae 1114
Panicum virgatum 1282
pantothenate 1711
papaya 4464
– ringspot-resistant 4464
– ringspot virus (PRSV) 2566
paper
– cables 11167, 11169, 11175
– recycling 8780
– sludge ash 4874
papermaking 8797
parabola 6033
parabolic mirror 9590
parabolic trough 2351, 2385, 7619–7620
– collector (PTC) 7619–7621, 7622, 7624–7625, 7628
– absorber (receiver) 7621
– drive Mechanism 7625
– foundation 7628
– heat transfer fluid 7628
– mirror 7621
– optical efficiency 7624
– performance properties of receivers 7622
– pylons 7628
– solar power plants 7620
– solar technologies 4244
– support structure 7625
– technology description 7621
– tracking 7625
– concentrators 9583
paraffin 7844, 10559
paralytic
– poliomyelitis 8142, 8151
– shellfish
– poisoning (PSP) 4822, 9083
– toxins (PSTs) 4821
parameter-elevation regressions on independent slopes model (PRISM) 8909
parasite 548, 9089, 12019, 12021, 12040, 12043, 12052–12054
– acquired by contact 12043
– control 12052
– culling 12053
– detection 12053
– fish farming practices 12053
– freezing 12052
– heating 12052
– infected seafood products 12021
– management 12052
– of marine origin 12019
– seafood-associated 9089
– taxonomic research 12054
– treatment 12053
parasitic disease 11999
parasitic infection 12020
parasitoid 5444
paratransit 1876
park 11356
– design 11356
– trees 11345
park-and-ride lot 4952
parking
– demand 10930
– garages 7858
– policies 10928, 10930
– space 10929
Park's transformation 21, 33
parrotfish 832
partial differential equation (PDE) 10968
partial oxidation (POX) 3862, 3883, 3967, 5162
partial root-zone drying (PRD) technique 9068
particle
– accelerators 8581
– emission 273
– mass concentrations 11302
– number concentrations 11303
– pollution 11304
particulate
– inorganic carbon (PIC) 8969
– organic carbon (POC) 7275
– organic matter 172, 223, 226, 235, 245, 1391, 8887, 9111, 11293, 11295, 11308, 11320
– Emission 1391
– health effects 226
partitioned aquaculture system 544
passenger demand 99
passive cooling 6876, 6882
passive earth sheltering 4133
passive geothermal conditioning 4142
passive geothermal heating-and-cooling system 7631
passive house 7629–7630, 7632–7633, 7635–7640, 7648
– air flow 7636
– airtight construction 7635
– building energy standard 7631
– carbon footprint 7639
– climate-changing opportunity 7632
– construction methods 7630, 7633
– cooling 7638
– dehumidification 7638
– design 7630, 7633
– economic sustainability 7639
– eliminating thermal bridges 7635
– energy
– balancing 7638
– calculation 7632
– consumption 7638
– recovery ventilation 7636
– standard 7630
– heat recovery ventilators (HRVs) 7636
– high-performance windows and doors 7637
– internal heat gain 7637
– legislative programs 7639
– monitoring programs 7640
– planning package (PHPP) 7631, 7638
– Smith house 7632
– superinsulation 7633
– ventilation system 7636
passive irradiation 8530
passive smoking 3632

passive solar architecture 9741
passive solar building 7641, 7642, 7665
– concepts 7642
passive solar design 894
passive solar facade 3694
passive solar heating 7640–7644, 7649, 7651–7662, 7664–7665
– annual heating energy 7655
– applications by building types 7649
– architectural integration 7651
– building 7650
– applications by climate 7650
– inappropriate building types 7650
– new construction 7650
– renovation 7650
– types 7643
– climates 7643
– design advice 7656, 7660
– direct gain 7642, 7652
– fixed shading 7654
– glazing spacers 7653
– history 7644
– in built environment 7640
– indirect gain 7642, 7656
– insulation 7649
– isolated gain passive 7642
– isolated gain/hybrid 7661
– mass roof 7658
– mass solar air systems 7662
– mass walls 7657
– no-mass solar air systems 7662
– principles 7649
– solar air systems 7662
– solar insulation 7659
– sunspaces 7664
– transparent insulation 7658
– vacuum glazing 7653
– windows 7652
– frames 7653
passive solar house 7645, 7647, 7648
– computer models 7647
– New England salt box 7645
– reference houses 7647
– sunspaces 7648
– Swiss Appenzell House 7645
– windows 7648
Passivhaus 7631
pastoralists 2932
paternal heterosis 1735
path choice model 105
pathogen 3594, 5363, 6605
– climate warming 5363
– detection 6614, 8766
– uncertainty analysis 6614
– high hydrostatic pressure (HHP) treatment 3594
– in water 6605
pathogenesis-related proteins 10697
pathogen-inducible promoters 10707
path-velocity decomposition 2478
pattern harmony 8870
Pauli exclusion principle 3793
pavement material 11700
– recycling 11700
payback time 1498
peak
– ground acceleration (PGA) 3236
– phosphorus 3783
– streamflow 2065
peaking plants 7192, 8982
peat 2173–2174, 2176–2177, 2179, 2181, 2183, 2186, 2188, 2191, 3846
– formation 2176
– future production 2188
– future supply 2173
– global resources 2173, 2176
– occurrences 2177
– production 2186
– recoverability 2191
– reserves 2183
– classifications 2179
– resources 2181
pebble bed modular reactor (PBMR) 4053
pebble bed versus prismatic 4068
Pechiney process 1079
Peclet number 2035
pedestrian 66, 68, 72–73, 5940–5942, 5948, 6953, 6971
– automatic gates 5948
– collision detection system 66
– crossing regulatory and warning devices 5940
– crosswalk signals 5941
– detection 65, 68–69, 74, 6952, 6957, 6967, 6973, 11104
– automotive millimeter wave radar 74
– boosted feature-level sensor fusion 6957
– communication-based 74
– experiments 6967
– scenario-driven search 68
– thermal infrared camera-based 74
– visible camera-based 74
– delineation markings 5942
– movements 5945, 5947
– fixed barriers 5945
– moveable barriers 5947
– protection
– airbag 73
– system 72
– recognition system 6953, 6956–6957, 6961–6962, 6964–6966, 6968
– constant turn rate and velocity (CTRV) motion model 6964
– egomotion estimation 6964
– evaluation of position hypotheses 6965
– image features 6961
– Monte Carlo localization (MCL) 6962
– multi-sensor hypotheses 6962
– radar features 6961
– radar preprocessing 6965
– road course estimation 6968
– sensor alignment 6957
– sensor Configuration 6956
– threat analysis 6966
– universal transverse mercator (UTM) coordinates 6964
– threat analysis 6971
– traffic signal 5940
– vehicle separation 72
– visibility 68, 72
– warning application 6955
– camera sensor 6955
– radar sensor 6955
– warning system 6966, 6972
pedestrian-light rail at-grade crossing 5939
pedestrian-only street 7785
pedestrian–vehicle collision 73
pedigree-based marker-assisted selection system (PBMASS) 6699
pedosphere 1103
pellet 1026, 1070, 1072, 1355, 1365, 1373, 1375, 1397, 1564, 1610, 11791
– clad interaction (PCI) 7200
– furnaces 1375
– machines 1070
– mill 1070, 1074
– quality 1072
– stoves 1376
– with water jackets 1367
pellet-chimney stove 1375
pelletization 1609, 9849
pelletizing 1067–1068, 1070, 1073–1075, 1085
– energy consumption 1075
– pellet mills 1074
– raw material 1073–1074
Peltier
– cooling 9511
– effect 9511
Pelton wheel 4321
pendant sulfonic acid group 6555

penicillin 499–500
Penicillium notatum 499
pentachlorophenol (PCP) 1636, 4887
pentaerythritol 6904
pentaglyme 6049
pentosane 991
pentosan 999
pentoses 982
peptidic antimicrobial 503
PERC, see perchloroethylene
percentage road center (PRC) 3125
Perchlorate 3637, 10439
Perchloroethylene 303, 3591
PERCLOS 3113, 3115, 3129
PERC 306
Perdew–Burke–Ernzerhof (PBE) functional 6045
Perdix perdix 945
perennial
– cropping 1579
– crops 1139, 1539
– forage grass 1114
– grass 1279, 6026–6027
– nitrogen fertilization 6027
– rhizomes 6026
– ice 2762
– lignocellulosic biomass 1571
– lignocellulosic crops 1572
perfluorinated sulfonic acid (PFSA) 6542, 7702, 7757, 8189, 8196, 8209, 8215, 8232
– containing polymers (PFSA) 8332, 8333
– equivalent weight (EW) 8332
– relative humidity 8333
– durability 6542
– ionomer membrane 6541
– membrane 3930
– proton-conducting 8232
perfluorovinylether 7704
perforated city 5840, 5852
pericentriolar material (PCM) 6168
peripheralization of the periphery 4941
periphyton 3272
– effects of contaminants 3272
peri-urban agriculture 11370
peri-urban area 952
permaculture 8871, 8874
permafrost 281, 291, 337, 2762, 2764, 2776, 3845, 4577
– gas hydrates 337
permanent downzoning 11370
permanent environmental effect 444
permanent green space 11366
permanent magnet 21
– brushless motors (PMBM) 11528
– hybrid motor 11531
– synchronous machine (PMSM) 18, 23, 3392
– motor drives 23
– surface-mounted (SM) 23
– transverse flux machine (TFM) 11549
permanganate 2447
permasoft 2764
– models 2764
permeable reactive barrier (PRB) 2447, 10407–10409, 10415, 10416, 10418, 10441, 10445
– application 10418
– biobarriers 10418
– combined PRB–phytoremediation systems 10418
– construction methods 10415
– cut-off walls 10416
– deep soil mixing 10416
– drilling 10416
– funnel-and-gate system 10408
– gate structures 10416
– hydraulic fracturing 10418
– injected systems 10418
– jet technology 10416
– reactive thin walls 10416
– sustainability 10441
permeate recovery 2905
permethrin 10667, 12003
perovskite 2952, 3893, 3897, 3900, 3902
– oxides 3900, 3902
– cathodes 9865
– structure 3900
peroxidase activity 4034
peroxidation 2412
peroxide 8332
peroxiredoxin–6 3664
peroxisome 8047
peroxy acetyl nitrate (PAN) 11299, 11320
peroxycarbonate 7897
peroxycarbonic acid 3942
peroxynitrite 3665
persistent bioaccumulative and toxic (PBT) 10658
persistent contrail cover 662
persistent organic pollutant 3658, 4883, 7330, 8890, 10155, 10156, 10658, 10661, 10663, 11583
– chemical classes 10663
– incineration 10156
– Stockholm convention 10663
– vitrification 10156
personal care products 11912
personal construct theory 10374
personal digital assistant (PDA) 8716
personal rapid transit (PRT) system 1876, 6497, 7777–7780, 7782–7784, 7787–7788, 7791
– architectural design 7791
– development 7777, 7780
– expositions 7784
– Heathrow airport system 7780, 7788
– history 7779
– hospital setting 7791
– international conferences 7784
– Morgantown system 7780, 7783
– programmed modules 7787
– test tracks 7783
– US Government participation 7782
– versus existing transportation 7788
pertechnetate 8624
perturbed physics ensemble (PPE) 2102
pervaporation 995
pervious pavement 3462
pest 5438, 5441
– control 5429, 5431, 5441, 5454
– sterile insect technique 5454
– crop resistance 5441
– density 5435
– herbivore 157
– insects 4025
– invasion 5431
– numbers 5433
– populations 5443
– predator–prey relationships 5443
– taxonomic adscription 5438
Peste des petits ruminants (PPR) 5360
pesticide 1188, 1190, 1192, 2560, 2569, 2578, 2742, 2745, 2750, 3631, 3646, 3270, 5438, 5441, 5448, 10155, 10667, 10758, 12295
– exposure 3270
– insect resistance 12295
– metabolomic investigations 1192
– problems associated 5441
– registration 2304
– resistance 5441
petrol 267, 5532
– engine 5522
– sulfur-free 267
petroleum 1633–1634, 2176, 2189, 2434, 3844, 7242, 7296, 7797–7800, 7803, 7820, 7827, 7829, 7831, 7844–7845, 10483–10484, 10487, 10526
– atmospheric distillation 7829
– coking 7831
– consumption 7845, 10487
– dehydration 7829
– desalting 7829

– diesel fuel 5471, 5473
– energy savings 10526
– exception 3595
– exploration 7797–7799
  – geophysical borehole logging 7799
– gas 7842
– hydrocarbon (PHC) 1629, 1633, 1638, 2434, 10146, 10150, 10151
  – biodegradation 10150
  – bioventing 10151
  – components 7844
  – enhanced bioremediation 10151
  – monitored natural attenuation (MNA) 10150
– industry 7825–7826
  – Clean Air Act Amendments 7825
  – Comprehensive Environmental Response, Compensation, and Liability Act 7826
  – Occupational Safety and Health Act 7826
  – Oil Pollution Act 7826
  – Resource Conservation and Recovery Act 7825
  – Safe Drinking Water Act 7825
  – Toxic Substances Control Act 7826
  – Water Pollution Control Act 7825
– liquid effluents 7844
– pipelines 9337
– production 7797, 7800, 7804, 7822
  – chemical waste 7822
  – hazardous waste 7822
– recovery 7803
– refining 7822, 7827, 7832–7833, 7835, 7838–7839, 7841–7842, 7845
  – alkylation 7835
  – catalyst disposal 7845
  – catalytic cracking 7842
  – catalytic reforming 7838
  – chemical waste 7822
  – coking 7845
  – deasphalting 7839
  – dewaxing 7839
  – environmental control 7822
  – environmental effects 7822
  – fluid catalytic cracking 7832
  – gaseous emissions 7841
  – hazardous waste 7822
  – hydrocracking 7833
  – hydrotreating 7833, 7835
  – isomerization 7838
  – polymerization 7835
  – solid effluents 7845
– reservoirs 4418, 7820
– resources 7242, 7296, 10484
  – toxic component 1634
  – transportation 7827
  – vacuum distillation 7829
  – visbreaking 7831
  – waste 1634
Pfeiffer complex 8272
Pfotzer maximum 8474
P-glycoprotein 3159, 12308
Phaeodactylum tricornutum 350, 365
phagocyte 3664
phanerozoic 2495
pharma crops 8045
pharmaceutical 8032, 8067, 8078, 10534, 11912
  – for animal health 8078
  – industry 6520
  – plant-derived 8067
  – proteins 8050, 8059–8060, 8073
pharmacology 3253
phase change direct storage 10566
phase change material (PCM) 10557, 10560, 10570, 10572
  – high-temperature storage 10560
  – indirect storage 10570
  – macro-encapsulation 10572
phaseolotoxin 10701
phaseolus 4032
  – α–amylase inhibitor gene 4032
phase-pure perovskite 2948
phase-shifting transformer (PST) 9346
phasor 12080, 12081
  – data concentrators (PDC) 12083
  – measurement unit (PMU) 10951, 12082, 12084–12087, 12095
    – instrument transformer calibration 12086
    – PMU-only estimator 12085, 12087
phenanthroline 8277, 8285
phenodyn 10
phenol formaldehyde resin 9958
phenological scale 2545
phenology 2541, 2544, 2548, 2554, 11395
  – developmental response to temperature 2548
  – sub-models 2554
phenol 857, 1636, 10667
phenopsis 10
phenotype/phenotypic 436, 465–468, 486, 1780
  – interaction term model 466
  – multiple-trait model 467
  – plasticity 463, 466
  – reaction norm model 468
  – selection 418, 6694
phenotyping 9–10, 2686, 4088, 6437, 6695
  – platforms 10
  – techniques 4088
phenoxyl radical 7000
phenylacetaldehyde glycerol acetal 4592
phenylketonuria (PKU) 1683, 10855
phenylpropanoid 6522
pheophytin 1479
pheromone 5452
phlogopite 1924
phononic engineering 9427
phosphate 4873, 6527, 9027
phosphate-olivine 7529
  – miscibility gap 7529
phosphine gas 611
phosphoenolpyruvate carboxylase promoter 4023
phosphoenolpyruvate (PEP) carboxylase 1481
  – promoter 4023
phosphogypsum 3517
phospholipase D1 gene 2647
phospholipid 578, 1681
phosphonic acid 7773
phospho-olivine 721, 726, 7528
  – binary phase diagram 7528
  – crystal chemistry 7528
  – Gibbs phase rule 7528
phosphoric acid 7738, 7773, 8188, 8207, 8331–8332
phosphoric acid fuel cell (PAFC) 3388, 3851, 3867, 3881, 3884, 3930, 7866–7875, 9853
  – anode catalyst layer 7870
  – applications 7875
  – bipolar plates 7871, 7875
  – catalyst decay 7872
  – cathode catalyst layer 7870
  – cell stack assembly
    – components 7869
    – life 7872
  – coolers 7871
  – edge seals 7871
  – electrolyte management 7873
  – electrolyte matrix 7869
  – gas diffusion layer (GDL) 7869
  – movement of acid 7874
  – non-repeat components 7872
  – power plants 7868
  – stationary applications 7866
  – water management 7874
phosphorus 610, 875, 1601, 3592, 3778, 3911, 6377, 7671, 7677, 7684, 7686, 9829, 10842, 11607, 11894, 11901
  – biogeochemical cycles 6377
  – loading model 1929

– fertilization 2562
– poisoning 3911
phosphorylation 3604
photo-allergenic reaction 11405
photoanode 5165, 7882, 7884
photoassimilate 2645, 4552
photoautotroph 823
photobiological algae system 5117
– for biohydrogen production 5117
photobiological effect 11387, 11378
photobioreactor 350, 363, 5122
photobleaching 4661
photocatalysis/photocatalytic 5210, 7882, 9567
– disinfection 9579
– fuel generation 7898
– hydrogen production 7881, 7884–7887, 7890
– absorption of photons 7885
– development 7890
– evaluation 7886
– experimental setup 7887
– modification 7890
– photonic efficiency 7887
– quantitative measurements 7886
– uantum yield 7887
– mineralization 9571
– process 9565
– systems 9572
– true activation energy 9572
– water
– purification 9572
– splitting 7898
photocatalyst 7882, 7884, 7890, 7891
– for H_2 production 7884
– low-dimensional nanostructure 7891
– nanosize effect 7890
– porous materials 7891
photocathode 3025, 5565
photocell 2826
photochemical
– oxidant 209
– ozone creation potentials 11320
– pollutants 11307
– smog 143, 245
– water splitting 5175
photochemistry 2644
photoconductors in electrophotography 7574
photocurrent 9197
photodimerization 9662
photodiode 7907
photoelectric effect 3804, 5561
photoelectrochemical water-splitting process 5160, 5164
photoelectrochemistry 3854
photo-electrolysis 3414
photoelectron 5565
photoemission 4661
photoexcitation 4661, 6571
photo-Fenton process 9765, 9575–9576, 9584
– acidification 9576
photofermentation 5117, 5119
photogenerated electrons 7884
photogrammetry 3171
photographic image quality 11109
photography 2618
photoinhibition 353, 356
photoinitiated electron collector 5179
photoluminescence 9397
photolyase 11396
photolysis 5194, 9053
– of acetonitrile solutions 5194
photometer/photometry 2840, 9713
photomineralization 9570, 9574
photomorphogenesis 1705
photomultiplier tube 3024–3025
photon/photonic 349, 1977, 1983, 5386, 7554, 8554
– activation 9572
– addition 9424
– cutting 9426
– deterministic transport theory 8554
– efficiency 9573
– pholtovoltaic stock index 7937
– radiation 8542
– shielding 8547
– buildup-factor concept 8547
photoneutrons 8568
photooxidation of polymers 7577
photooxidative stress 2627
photoperiod 2548, 2550, 2552, 2556
– insensitivity 2550, 2552
– responsive gene 4076
– sensitivity 2551
– genetic regulation 2551
photopic luminous efficiency function 11101
photopic vision 3138, 11100
photo-processing software 8920
photoprotection 353, 2627, 2650
photoreactivation 11393
photoreactor 9570, 9585
– irradiation way 9585
photo-realistic rendering program 2821
photoreceptor 2829
photorepair 11378
photorespiration 2624–2625, 2633, 2645
Photorhabdus luminescens 4037
photosensitive ganglion cell 2829
photosensitivity 11405
photospace in automotive vision 11104
photosphere 9800
photostationary state (PSS) 8885
photosynthate 2626
photosynthesis and evapotranspiration model (PnET) 6221
photosynthesis/photosynthetic(ally) 161, 347–348, 350, 353, 559, 1100, 1105, 1263, 1477–1479, 1482–1483, 2084, 2117, 2495, 2547, 2615–2616, 2618, 2621, 2624, 2643, 2663, 2666, 2687, 3223, 3583, 5174, 5187, 5690, 6373–6374, 6376, 7232, 7234, 7903, 7914, 7916, 7932, 8954, 9714, 9740, 10391, 11002, 11019
– action spectrum 7903
– active radiation (PAR) 1482, 2616, 7902, 7904–7906, 7909–7915, 7917, 7919, 7921, 7924–7925, 7927, 9714
– absorbed by canopies 7921
– absorption by leaves 7915
– aerosol loading 7912
– below the atmosphere 7911
– calibration 7909
– definition 7902
– clouds 7912
– global shortwave irradiation 7912
– in water 7913
– irradiance 7906
– measurement errors 7910
– measurement stations and networks 7914
– measurement 7902, 7904, 7927
– modeling 7902
– multidirectional transmission instruments 7924
– quantifying 7904
– radiation field inside a vegetation canopy 7919
– radiation interception 7917
– radiative transfer in plant canopies 7917
– relationships between fAPAR and LAI 7925
– scattering inside the canopy 7919
– spectral corrections 7909
– spectral errors 7909
– techniques for measuring 7906
– vegetation canopies 7915
– waveband 7905, 7914
– activity 10
– available radiation 8956
– canopy 2628
– efficiency 1100
– in water 7914
– land-based 2117

– light harvesting 356
– photon flux density (PPFD) 7902, 9714
– process 7555
– radiation (PAR) 2671
– radiation 7903
– tritium 3583, 11002
photosystem 352, 354, 1479
– antenna systems 354
phototoxic reaction 11405
phototrophic octocoral 2501
photovoltage 7564, 9197
photovoltaic (PV) 685, 1977, 1978, 3464, 3695, 5165, 7554, 7932–7933, 7935, 7939–7944, 7959, 7960, 7965, 7968–7969, 8372–8378, 8380–8383, 8985, 9197, 9241, 9394, 9396, 9415, 9432–9434, 9437–9439, 9441–9443, 9446, 9743, 9744
– annual capacities 8374
– average cost 7948
– balance of system 8380
– carbon footprint 9443
– CdTe solar cells 7939
– cell 3855, 6566, 6571–6572
– conventional p–n junction 6572
– chalcopyrite compounds 9396
– chalcopyrite-type compounds 9394
– commercial thin-film technologies 7939
– conversion 6572, 9414
– collection losses 9414
– losses in semiconductor-based devices 9414
– net absorption losses 9414
– converters 6571
– copper indium gallium sulfur selenide material 7939
– costs 8381
– domestic electricity markets 7960
– downstream processes 9434
– effect 7936
– efficiency 9418
– emerging markets 7965
– emerging technologies 7940
– energy 7932
– payback time (EPBT) 9432, 9439, 9446
– environmental sustainability 7942
– feed-in tariff 8377, 8383
– financial support 8376
– generators 3466
– global markets 8374
– greenhouse gas emissions 9439, 9441
– harmonization process 9442
– high-concentration PV system 9437
– high-efficiency solar cells 7940
– historical political development 8383
– industry 7946
– technology mix 7946
– life cycle assessments (LCAs) 7933, 9442, 9443
– market 7933, 7959, 8372
– economics 8382
– material science 7968
– microelectronics 7969
– modules 9438, 9510
– balance of system (BOS) 9438
– national policies 8376
– operation and maintenance 9434
– panels 4719
– policies 7933, 8372
– power
– generation 7943
– plants 8375
– prices 8381
– trends 7948
– products 8381
– quality assurance 7943
– recycling 7943
– research activities 7941, 7943
– role in general electricity supply 8376
– rooftop
– application 9443
– mounting systems 9438
– sensors 7907
– SET-Plan 7944
– status 7933
– storage system 7969, 8378
– system 3697, 7938, 7941, 9549
– crystalline silicon modules 7938
– grid 8380
– thermalization 9415
– thin-film materials 9394
– toxic gas emissions 9443
– upstream processes 9433
photowatt 9204
phreatomagmatic eruption 11627
phthalate 3636, 3638
– acid esters (PAEs) 10667
phycocolloid 9112
phycotoxin 4821, 7388
phyllochron 2542–2543, 2549
phylloquinone 1479, 1685
phyllosecretion technology 8046
phyllosilicate 4593, 8603, 8606
– clays 8604, 8614, 8621, 8623
phylogenetic
– signal 8438
– trees 7975
phylum 2496
Physcomitrella patens 356
physical balancing 12098
physicochemical conversion 1217
physiological
– breeding 8020
– traits 4075
physiologically-based pharmacokinetic (PBPK) modeling 3266
phytase 10747, 10798, 10845
– pigs 10842
phytate 1716, 10752
phytoalexins 10698
– synthesis gene 10705
phytochelatin 1190
phytodegradation 6658
phytoene 1699, 1716
– desaturase 1699
– synthase 1699
phytoextraction 6658
phytohormone 2588, 6527
phytohydraulic 6658
phytomass 1175
phytomer 2541, 2542, 2556
phyto-mining 6642
phytopathogen 157, 9564
Phytophthora infestans 2559
phytoplankton 1935, 1937, 1963–1964, 2501, 3232, 4830, 5690, 6311, 6375–6376, 6380, 7235, 7268, 7272–7275, 7348, 7913, 8203, 8402, 8922, 8954, 8959, 8964–8965, 11408
– as biofilter 6311
– bloom-forming 8964
– blooms 7272, 7275
– iron-stimulated 7275
– carbon 7275
– fixation 8965
– growth rate 7274
– net primary production (NPP) 1937
– pigment absorption features 8959
– radionuclide cycling 8402
– stocks 7275
– UV sensitivity 11408
– waveband of radiation 7913
phytoremediation 1633, 2448, 10152, 10155
phytosequestration 6658
phytosiderophore 1712, 1713
– biosynthesis 1713
phytotechnology 6658, 6660
phytovolatilization 6658, 10155
pica behavior 3625
picornaviral infection 8142
Picornaviridae 8131, 8133, 11988–11989
picornavirus 8133, 8137
pig 1764, 7992, 7994, 7996, 7999

– breeding 1764, 7972, 7978–7979, 7981–7986, 7988–7989, 7991, 7994, 8001–8004
– advanced feeding strategies 7988
– artificial selection 8002
– balanced feeding 7986
– breeding goals 8004
– co-ancestry management 7984
– commercial product evaluation 7981
– deprivation 7994
– ethical aspects 8001
– expected conserved diversity 7982
– genetic improvement 7983, 7991
– group selection 8001
– inbreeding 7984
– indiscriminate crossbreeding 7984
– integrity 8003
– marginal diversity 7982
– mate selection 7984
– pollution 7985
– population size 7979
– production traits 7981
– reduction of nitrogen emission 7986, 7989
– relative utility 7981
– robustness traits 7981
– selection for robustness traits 7991
– cells 10896, 10917
– coping strategy 7996
– dominance aggression 7999
– effects of chronic stress 7996
– environmental sensitivity 7992
– fibroblasts 10829
– harmful social behavior 7999
– instinctive behavior patterns 7994
– production 1785, 10869
– ecological footprint 10869
piglet castration 7999
pigmentation 11404
pillared clays 4596
pilot injection engine 1460
pinene oxidation 122
Pinus spp 3292
pipeline 3451, 4369, 6404, 6406, 6420
– drifts of dead fish 6420
– dredge 3035
– installations 4370
piping
– installation 4369
– material 4369
piscicide 547
piston
– engine 5502–5504
– crankshaft 5504
– four-stroke cycle 5503
– reciprocating motion 5501, 5504
– two-stoke cycle 5503
– velocity 597
pitch
– axis camera 49
– rate sensor 86
pitchblende 6690
pitched roof 4740
Pitzer's model 4097
pixel-level noise reduction 11113
place dependence 10374
place identity 10374
placentomegaly 6157
Plagiorchiidae 12028
plague 5361
Planck's
– constant 3801
– feedback 633
– law 7905
plane 10984
– jets 10976
– plume 10978
plane-of-array irradiance 9722
planetary albedo 9710
planetary boundary layer 5078
plankton 826, 1964, 3272
– effects of contaminants 3272
– fecal pellets 8396
planning advisory committee (PAC) 12189
plant 9, 392, 1103, 1129, 1191, 1479, 1484, 1486, 2351, 2540, 2542, 2544, 2564–2566, 2624, 2625, 2574, 2682–2683, 2688, 2691, 2700, 2703, 2725, 2757, 4040, 5317–5319, 5324, 6521, 6523, 6525, 6528, 6530, 6532, 6696, 8024, 9063, 10036, 10042, 10044, 10393–10394, 10671, 10672, 10745, 11395
– architecture 2703, 11395
– available nutrients 875
– available water-holding capacity (PAWC) 9320
– biodiversity 150
– biomass 848, 1269, 1486, 9826
– biotechnology 5456, 6696, 10679
– breeders 2725
– breeding 1484, 1691, 2529, 2536, 2677, 4492, 4496–4499, 6700, 8013–8014, 8021
– alien gene transfer 4497
– climate change 8013
– cyberinfrastructure 6700
– data management 6700
– eco-tilling 4497
– improved crop varieties 8021
– in a changing environment 8014
– meganucleases 4498
– new biotechnology approaches 4496
– synthetic biology 4499
– tilling 4497
– tools 10745
– transformation 4498
– under a changing climate 8013
– C3 plants 2624
– C4 plants 2625
– canopy 2617
– cells 8060
– applications 6525
– cultures 6527
– carbon source 6527
– cell culture 6523
– cloning 2691
– community 3285
– defense 4035
– secondary metabolism 4035
– density 10044
– development 2540
– of resistance 2566
– developmental stages 2544
– disease 2559, 2561–2562, 2570, 2577, 2688, 2750, 10695–10696, 10705
– biological control 2570
– crop-rotation effects 2750
– integrated control 2577
– disease resistance 2700
– soil amendments 2562
– sowing practices 2561
– domestication 152, 207
– dry matter 10038
– elevated atmospheric carbon dioxide concentration effects 10393
– fertilization 392
– for pharmacognosy 8024
– functional types (PFTs) 3215
– genetic engineering 6530
– genome 2682, 2691, 10672
– genomics 2529, 2530, 6427, 6532
– glycosylation 8050
– growth 1102, 5316
– effects of salt stress 5316
– regulators (PGRs) 6202, 6210
– system 8045
– temperature 1102
– water usage 1102
– growth–promoting rhizobacteria (PGPR) 2574
– hairy root 6523
– cultures 6523
– improvement 2
– insect-resistant 4040

– interactive effects of increases in temperature 10394
– investment 9066
  – resource acquisition (RLD) 9066
– ionic stress 5317
– ionic tolerance 5319
– macronutrients 7278
– material 2586
– metabolic engineering 6528
– minichromosomes 2607
– molecular biology 2757, 6523
– molecular pharming 2683
  – pharmaceuticals for human health 8058
  – veterinary applications 8073
– morphology 11395
– naming plant parts 2542
– nonhost resistance 2564
– nutrients 1103
– oil 8081–8082, 8084–8085, 8087, 8095
  – biodegradability 8095
  – ecotoxicity 8095
  – extraction 8085
  – fuels 8080, 8083
  – fuel-relevant properties 8085
  – processing 8085
  – purification 8085
  – resins 6919
– osmotic tolerance 5319
– pathogenic bacteria 10700
– pathogens 2559
– pesticide" 2304
– phases 2544
– phenology 3224
– phenomics 9, 2634
– phenotyping 2683
– photosynthetic strategies 1479
– promoters 2596
– protection 1129
– protein supplements 10842
– rectangularity 10044
– research 9
– roots 9063
– salinity tolerance 5318
– salt stress 5324
– secondary metabolism 6521, 6522
  – biotechnological production 6522
– selection 1484
  – of high-producing lines 6525
– self-fertilization 392
– spatial arrangement 10036, 10042
– species for transformation 8044
– systematic phenotyping 9
– taxonomy 3282
– transformation 2585–2586, 2591–2592, 2595, 2682, 8032, 8060, 10695
  – binary vectors 2592
  – promoters 2595
  – vectors 2591
– transgene expression 10671
– tumor 2587
– types of resistance 2565
– under salt stress 1191
– under water stress 1191
– virus infection 2566
– waste 8051
– with novel traits 4521
plant-based expression systems 8074
plant-made pharmaceuticals 8067
plant-produced biologics 8030
plant–soil ecosystem model 1502
plasma
  – jet 8099
  – theory 7161, 7176
  – torches 8099, 8103, 8105–8107, 8110
    – furnaces 11588
    – thermal energy 8106
    – water-cooling system 8107
  – treatment 9200
plasma-enhanced chemical vapor deposition (PECVD) 9242
plasma-processed hydrogenated amorphous silicon 9248
plasmasphere 8472
plasmochin 11081
plasmodia 11075
Plasmodium 6293
  – *falciparum* 501–502, 6299, 11999
    – circumsporozoite protein (CSP) 6299
plasmonic resonators 9424
plasterboard 2409
plastic 2410, 2414, 2416, 8819, 8821
  – calorific value 2414
  – co-gasification 2416
  – deformation 3250
  – lithium-ion battery 6091, 8744
  – litter 9991
  – macro-sorting 8821
  – manufacturing 4852
  – materials 4852
    – hazard characterization 4852
  – near-infrared spectroscopy (NIR) 8821
  – polyethylene terephthalate (PET) 9580
  – recycling 8780, 8819, 8822, 8824–8826
    – air classification 8824
    – centrifuges 8825
    – chemical recycling 8826
    – density separation processes 8824
    – electrostatic separation 8825
    – energy recovery 8826
    – flotation 8826
    – hydrocyclones 8825
    – jigging 8825
    – laser aid identification 8822
    – magnetic and eddy current separations 8824
    – micro-sorting 8822
    – selective dissolution 8826
    – sink and float process 8824
    – X-rays analysis 8822
  – solid waste (PSW) 8818
  – waste 2414, 4005, 4008, 4011, 9983
    – combustion 2414
    – liquefaction 4005
plasticity 464, 467
plastid transformation 2606, 4024, 8062
plastochron 2542–2544
plastoquinone 358–359, 1479
  – state1–2 transition 358
plate heat exchangers 4371–4372
plate tectonics 4181–4182, 11614
  – spreading centers 4182
  – subduction zones 4182
platensimycin 500
platforms 6404, 6406
platinum 3882, 3979, 7696, 7742–7744, 7746, 8265
  – alloy 7747, 8212, 8265
    – nanocrystal electrocatalysts 7747
  – catalyst 8266, 8295, 8329
  – d-band center energies 7742
  – film electrode 3421
  – loading 7751
  – monolayer catalyst 7742, 7743
  – nanoparticles 3880, 7743
  – nanotubes 7746
    – electrocatalysts 7744
  – nanowire 7744
  – surfaces 7734
    – oxygen reduction reaction 7734
platinum-based catalyst 7761
  – degradation 7761
platinum-group metal (PGM) 373, 7757
platooning of buses 1876
platyhelminth 12022
pleconaryl 8135
pleiotropy 493
pleistocene calderas 11617
Plinian eruption 11614
plow layer 3727
plowed soil 155

plowing 3532
plug flow
– biogas digester 1153
– reactor model 2032
plug-in hybrid electric vehicle (PHEV) 692, 710, 768, 779, 3487, 7847–7849, 7853–7858, 8112, 8113–8115, 8117, 8121, 9293, 10496, 10520–10527, 11508
– all-electric range (AER) 3479, 8115, 8121
– blended control atrategy 8117
– charge-depletion range (CDR) 8121
– daily driving distance 8113
– demand side management (DSM) 7848, 7857
– economic feasibility 7856
– electric demand (load) profiles 10522
– electricity
– consumption 10521, 10525
– generation mix 10525
– fuel consumption 10521, 10525
– fuel-cycle pathways 10521
– generation mix 10523
– greenhouse gas effects 10520
– human behavior modeling 7855
– load profile 10523, 10527
– mobile decentralized storage 7849
– modeling 7854
– motor and battery power 8114
– new markets 7853
– operation strategies 8115
– outage management (OM) 7848, 7858
– policy strategies 7854
– power density requirements 3479
– power system planning 7855
– share of miles electrified 10526
– wheel-to wheel results 10524
plum pox virus (PPV) 10704
plumbemycin 507
plume 10976, 10978, 10980, 10984, 10987, 10988, 10990
– coflow 10984
– crossflow 10987
– density 10978
– effect of boundaries 10980
– in stagnant environment 10976
pluripotent cell 10900, 10907
pluripotent gene 6160
plus energy building 8375
plutonium 209, 239, 3534, 3541, 3761, 6689, 7063, 7145, 7195–7196, 7207, 7209, 8388, 8390–8392, 8394, 8398, 8496, 8509, 8539, 8582, 8590, 8593, 8623, 8667
– chemical forms 8394
– contamination in soils 8509
– decontamination 8509
– in seawater 8392
– in the sediments 8398
– measurement 7209
– oxidation states 8391
– oxide 3534
– reprocessing methods 8593
– speciation 8391
– use in sediment tracing investigations 3761
PMSM 34
– field-oriented control 34
Pneumocystis carinii pneumonia 4999
Poaceae 1109, 1114
pod car 1876
poikilotherms 5595
point kinetics equation 3813–3815
Poiseuille flow 2922
poison 3256, 7122, 10636
– control rods 7122
– distribution 461, 479
– potential 6062
polar
– amplification 2762
– circle 9622
– ecosystems 7236
– ice mass 282
– orbiting satellites 8970, 9627, 9749
– ozone loss 10132
– satellite constellation 294
– stratospheric clouds (PSCs) 130, 10132
– stratospheric ozone 9797
pole tide 4569
pole-to-pole observation 284
polio 8123, 8126, 8128, 8130, 8140, 8149, 8151, 8156, 8162
– definition 8126
– disease transmission 8128
– endgame vaccination strategies 8162
– epidemiology 8123, 8130
– eradication 8126, 8151, 8156
– infections 8128
– laboratory manual 8151
– passive immunization 8149
– vaccine 8126, 8140
poliomyelitis 8126, 8128–8129, 8141, 8145, 8150, 8157, 11989
– endemic countries 8150
– global eradication 8145
– importation countries 8150
– mass vaccination trials 8145
– polio-free countries 8150
– vaccine failure 8157
polioviral RNA 8137
poliovirus 5380, 8126, 8129–8131, 8133, 8135, 8137–8139, 8144–8145, 8148, 8153–8155, 8157, 8161, 11989
– capsid proteins 8131
– country-to-country transmission 8154
– culturing 8130
– endogenous transmission 8153
– environmental samples 8155
– genome 8131
– immunodeficient patients 8157
– inactivated 8144, 8148
– infection 8129, 8136, 8142–8143, 8145, 8149, 8151
– at the level of the host cell 8136
– at the level of the individual host 8142
– effectiveness of vaccination 8151
– fecal–oral transmission 8143
– immunization history 8143
– immunoglobulin 8149
– in cells, individuals, and populations 8136
– in populations 8149
– macrophage migration inhibition (MIF) technique 8145
– intratypic differentiation 8153
– mass immunization campaigns 8148
– misincorporation rate 8139
– molecular evolution 8141
– natural infections 8144
– neurovirulence 8131
– noncapsid regions 8138
– non-vaccine 8155
– person-to-person transmission 8157
– polyprotein 8133
– receptor 8135, 8136
– cloning 8136
– identification 8136
– serotypes 8130, 8141
– transmission 8145
– vaccine failure 8161
– vaccine-derived 8135, 8141, 8155
Polix 9204
pollen
– development 2646
– drift 10724
– fertility 2646
– sterility 8018
pollination 958
pollinator 10723
– diversity 157
pollock fishery 3575

pollutant 170, 223, 249, 259, 221, 4883, 4894, 4897, 5529, 7822, 7824, 10096, 10979, 11292
– average exposure 249
– biokinetics 4894
– biological monitoring 4893
– coal-related 2211
– combustion-generated 5529
– dietary intake 4897
– dispersion 259
– in urban streets 11300
– emitted by incinerators 4883
– emissions 11295
– environmental monitoring 4893
– environmental regulations 7824
– excess morbidity 223
– in the atmosphere 11292
– mass flux 10979
– mortality effects 223
– stormwater 10096
– transfer 7687, 7688
– flooding 7688
– transformation 259
polluter pays principle 2419, 3445, 4785
pollution 388, 535, 7852, 9907, 10486
– biological 535
– control 3461
– best management practices (BMPs) 3461
– costs 10486
– pollution effect 221
– pigs 388
– prevention act 10018
– redistribution 7852
– restrictions 9907
– transport 11295
poloidal magnetic field 7162, 7166
polonium 8462, 8481
PolScope 6155
poly(2,2'-(1,4-Phenylene)5,5'-Bibenzimidazole) 8180
poly(2,2'-(dihydroxy–1,4-phenylene)5,5'-bibenzimidazole) 8185
poly(2,5-Polybenzimidazole) 8180
polyA trap selection 7223
polyacrylonitril 6781, 8283
polyamide imide (PAI) 9308
polyaniline 7549
polyannaline 764
polyaromatic hydrocarbon (PAHs) 5531, 10665
polyazine bridging ligand 5177
polybenzamidazole (PBI) 374, 7767, 7870, 8176–8178, 8183–8184, 8186, 8188–8190, 8209, 8215, 8331
– acid-doped membrane 8176
– "direct acid casting" (DAC) technique 8177
– dynamic durability tests 8189
– fuel cell 8173, 8191
– combined heat and power (CHP) devices 8191
– hexafluoroisopropylidene-containing 8184
– membrane 3861
– electrode assembly durability 8186
– electrode assembly manufacturing 8190
– *m*-PBI 8178
– PBI-inorganic composites 8184
– PBI-PA fuel cell systems 8188
– poly(2,5-polybenzimidazole) 8180
– segmented PBI block copolymers 8186
– sulfonated 8183
– synthesis 8177
– synthetically modified 8178
– *m*-PBI 8178
polybrominated diphenyl ether (PBDE) 3275, 10666
polycarbonate plastic 3261
polychlorinated
– biphenyl (PCB) 3632, 4883, 4885, 6189, 6988, 9157, 9167, 10142, 10662, 10665, 10957, 11583
– in the marine food chain 9157
– dibenzofurans (PCDFs) 6990
– dibenzo-*p*-dioxin 4880, 6977, 6990, 6998
– diphenyl 5289
– naphthalene (PCN) 4883, 4886
polyclimax 3284
polycrystalline
– CdTe solar cells 1992–1993
– materials 9197
– platinum surfaces 3883
– semiconductor 1980
– polycrystalline silicon 7959
– solar cell 9395
– solar cells 7946, 7951
polyculture 546–547, 8201, 8203, 9182–9183, 10045
– cover crop 151
– successes 8203
– systems 3581, 6310
polycyclic aromatic hydrocarbon (PAH) 855, 880, 1397, 1463, 1636, 1639, 3257–3258, 3594, 3609, 5237, 6987, 8886, 10008, 10662, 11303–11304, 11308, 11321
– emissions 11304
– long-range transport 11304
– sampling artifacts 11304
– sources 11304
polyetherketone (PEK) 7870
polyethylene (PE) 2411, 2413, 7209, 8748, 9582, 9773
– oxide (PEO) 751, 6070, 8745
– PEO-based polymers 6048
– separators 8748
– terephthalate (PET) 3453, 4008, 8820, 8842, 9983
polyfurfuryl alcohol resin (PFA) 6140
polygalacturonase inhibiting protein (PGIP) 10699
poly-generating fuel cell 5140
polygeneration 1444
– plants 2153
polygene 6429
polygonum 1116
polyhydroxy complex 8395
poly-β-hydroxybutyric acid (PHB) 5387
polyimide 1980
– ionomer membranes 6555
polyketide 6522
– antibiotics 505
polyline 78
polymer
– cables 11169
– concrete 6278
– electrolyte 6070, 6811, 8224, 8720
– nanoscale channels 8224
– electrolyte fuel cell (PEFC) 3881, 3916, 9853
– electrolyte membrane (PEM) 374, 8205, 8207, 8209, 8214–8216, 8224, 8229, 8231
– alkaline-based 8216
– automotive applications 8231
– freezing point 8224
– fuel cell 8205
– high-temperature 8215
– proton-conducting 8209
– temperature proton 8214
– electrolyte membrane fuel cell (PEMFC) 1414, 3850, 7866, 8174, 8204, 8240, 8249–8252, 8255–8256, 8258–8260, 8265, 8566
– alloy catalysts 8256
– automotive 8240
– bipolar plate targets 8252
– cost breakdown 8249
– durability 8251

– graphite-based bipolar plates 8260
– highly electron-poor poly (phenylene) backbones 8259
– high-surface-area carbon 8258
– incremental engineering modification of membranes 8259
– membrane targets 8250
– metal separators 8260
– nanoparticles 8256
– non-noble metal catalysts for oxygen reduction 8265
– non-precious metal catalysts 8258
– platinum catalysts 8266
– Pt-alloy 8256
– Pt-based electrocatalysts 8255
– targets of performance and durability 8249
– engineering 7580
– properties 6930
– castor oil-based 6930
polymerase chain reaction (PCR) 5384
polymer/polymeric 377, 2397, 6050–6051, 6550, 6897, 6908, 6924, 6926–6927
– architectures 6051
– binders 9308
– cable 11168
– composite materials 6897
– electrolytes 6048
– in construction and demolition waste 2397
– from plant oils 6908
– petroleum-based 6926
– relaxation 6050
– SOPERMA-styrene 6927
– triglyceride-based 6924
– with sulfonic acid clusters 6550
polymerization 3945
polymorphic molecular markers 6693
polymorphism information content (PIC) 479
polymorphous silicon 9244
polymorph 728
polyolefin 2411, 5247, 8727, 8731, 8746, 8841, 8842
– recognition-separation 8841
– recovery 8842
– resin 8721, 8724
– separator 8735
polyose 9825
polyoxometalate (POM) catalyst 7600
polyphenol oxidase (PPO) 4034
poly(phenylene)s 6544
– ether sulfone 6557
– ionomers 6546
– sulfide 8357
polyphosphoric acid (PPA) 8174, 8177
polypropylene 523, 8722, 8735, 9582
– microporous films 8723
– oxidation 7593
– separators 8727
polypyrrole 764, 7549
polysaccharide 989, 1105, 1678, 9113, 11002
– extraction 9124
polysilicate 8395
polysilicon 7956–7959, 9198–9199, 9201, 9435
– filaments 7957
– hyper-pure 7958
– manufacturers 7957
– production 7957
– fluidized bed process 7957
polystyrene (PS) 3946, 4852, 6927, 8231
polysulfide 6660
polysulfone 380
poly(tetrafluoroethylene) (PTFE) 6539, 7696, 8186, 8209, 8357
polythionate 6660
polythiophene 6567, 7567, 7572
poly(trifluoroethylene) 6539
polyunsaturated fatty acid (PUFA) 1681, 1696, 4557, 9080
polyvinyl chloride (PVC) 836, 4006, 4852, 8748, 8820, 8842
– separators 8748
polyvinylidene difluoride (PVdF) 6133, 8259
polyvinylidene fluoride (PVDF) 6511, 9306
poly(vinylphosphonic acid) (PVPA) 6557
polyvinylpyridine 6781
polyvinyltoluene (PVT) 5566
Polywell 7169
pond aquaculture management and development (POND) model 1936
Pontryagin's minimum principle 52
Pooideae 1114
pool heating 4365
poor air quality 11307
poplar 1285, 1287, 1293, 1539, 6021
– as a source of biofuels 1287
population
– decline 5839, 5844, 5850, 10357
– effects on infrastructure 5844
– growth 2079
population-level genetic resource management 7983
Populus 1285, 6021
porcine endogenous retrovirus (PERV) 10832
porcine insulin 8027
pore water 2766
– biodiffusion 9141
– influence of salts 2766
pork 1751
porosity 4186
– matrix-dominated 4186
– porosity 4186
porous concrete 3831
porous silicon (PS) 9207, 9216
Porphyra 9114–9116
– aquaculture 9116
– genome 9115
Porphyridium cruentum 350
porphyrin molecule 7559
portable 12-VDC cooker 9496
portable fuel cells 3916
portable industrial radiography sources 8519
Portland cement 2406, 3827, 3830
position-based routing protocols 11560
positive breeding values 9365
positive electrode material 6129, 6142, 6506, 6510
positive nickel electrode material 6941
positive train control (PTC) 5967
positron
– annihilation photons 8572
– decay 8564
possession-tracking mechanism 9043
post-anthesis water stress 2649
post-combustion 2210, 4975, 5262–5263, 5273, 6465–6466
– capture (PCC) 2151, 2152
– of mercury 2210
– chamber 4975
– control technologies 2209
– of the gas product of volatilization 6466
postglacial rebound 4579
postpolio
– eradication 8160
– sustainability 8160
– syndrome 8144
post-recycling residues 11833
posttranscriptional gene silencing (PTGS) 2605, 8061, 10673, 10757
posttranscriptional regulation 7
potable groundwater 4126
potable water 2090
potassium 1104, 3778, 4165, 4180, 7330, 8461, 9829, 11607
– chloride fertilizer 2563
– fluoride 4608
– supported on alumina 4608
potatoe 4464
– insect-resistant 4464
– leafroll virus 10704

potential coal reserve 2181
potential energy 8849
potential of mean force (POMF) 6062
potential organic fouling index 10539
potential yield (PY) 2721, 2722, 2733, 2736
– future progress 2736
– lifting 2733
– water-limited 2722
poultry 401, 407, 413, 1764
– breeding 407, 1769, 7973, 8307
– genetics 401 8307
– meat production 1751, 8309
– *Salmonella pullorum* 8309
– production 641
poverty 1677, 1741
– abatement 1489
– alleviation 535, 578
powder metal fuel (PMF) 11591
powder neutron diffraction 6072
powder X-ray diffraction (PXRD) 6070
power cable system 11164, 11170
power consumption 12099–12100
power conversion/converter 3372, 4240, 12148
– efficiency 7563
power decentralizing distribution 3464
power density 3852
power electronics 12147, 12150, 12166
– controlled resistors 12166
– converter 12147
– equipments 12139
– inverter 39
power flow 9340, 9341, 9351–9352
– angle control 9341
– as an enabler for improved energy markets 9354
– between two AC buses 9340
– DC control 9341
– dynamic granular control (DGC) 9341
– emerging technologies 9351
– impedance control 9340
– model 12184
– smart wires (SW) 9352
– thin AC converters 9352
– VAR control 9339, 9341
– voltage control 9341
power generation 2166, 2172
– coal-based 2166
– power generation cycle 1330
– efficiency 2172
power grid 10943, 10951, 12080, 12135
– wide area monitoring, protection, and control (WAMPAC) systems 10951
power plant 2270, 2349, 2796, 4065
– coal-fired 2270
– fossil-fired 4065
– solar-thermal 2349
power production 1313–1314, 1438
– combustion-based technologies 1314
– with IGCC Processes 1438
power quality 3017
power rating 2998
power shortage 12099
power station 2207
– thermal efficiency 2207
power supply quality 3004
power switchgear 2999
power system 2999–3000, 8987, 10940, 10942–10943, 10946, 10953, 12082, 12084, 12090, 12092, 12094–12095, 12099, 12105–12108, 12116, 12123, 12266
– analysis 10943
– blackouts 10935
– busbars 2999
– capacity credit 12266
– contingency reserve 12103
– continuous balancing 12099, 12100
– control 12094
– of large oscillations 12094
– of sustained oscillations 12094
– disturbance 10940, 10946, 12090
– electricity markets 12108
– frequency
– control 8987
– instability 10942
– grounding 3003
– integrating wind power 12116
– islanding 10942
– load following 12108
– modeling 7855, 7861, 10943
– monitoring 12084
– operational reserves 12100
– permissible frequency range 12106
– positive sequence measurements 12082
– primary control 12105
– production planning 12108
– reconstruction of events 12084
– regulating capacity 12099
– regulation 707
– reserves 12099, 12103, 12123
– secondary control 12107
– speed-droop characteristics 12106
– state estimation 12084
– substations 12082
– switchgear 3000
– switching apparatus 3000
– system restoration 12095
– tertiary control 12107
– Thévénin impedance 12092
– voltage control 8987
power tower 2371
– hybridization 2371
power train system architecture 802
power transfer 12196
power transportation 11429
pozzolan 3825, 3827
Prandtl tip loss factor 12206
Prandtl's mixing length 2054, 2060
precipitable water (PW) 9724
precipitation 2106
– forecasts 12071
– parameterizations 2106
precision
– agriculture 3779, 5434
– irrigation 5627
precombustion capture 2151, 2153
precrash
– safety (PCS) 71, 73, 76
– warnings 3114
predation 10063–10064, 10072–10073, 10076, 10080
– feedback loops 10064, 10072
– frequency-dependent 10076, 10080
– partitioning 10073
predation–competition trade-offs 10080
predator partitioning 10076
predator 5444, 10075
– feedback loops 10075
predator–prey interactions 5450
prediction experiment 2140, 2143
predictive emissions monitoring system 183
pre-erythrocytic 6300
– vaccines 6301
preferential oxidation (PROX) 3883
pregermination 9151
pregnancy 3628, 3639
– embryonic and fetal development 3628
– maternal smoking 3639
preharvest sprouting (PHS) 9151
preliminary site assessment 2438
premature chromosome condensation (PCC) 6165
prenatal irradiation 5577
prepared fuel 11802
presenteeism 10280
pressure agglomeration 1070
pressure swing adsorption (PSA) 1052
pressure-retarded osmosis (PRO) 2916
pressurized combustion (PC) plant 9930
pressurized water reactor (PWR) 4906, 7198
primaquine 11077, 11082, 11084–11085
primary aerosol formation 111, 115
primary air distribution system 4960
primary air flow 4967

primary battery 741, 746–747
– solution-precipitation reaction 746
primary energy consumption in the EU 1314
primary neutralization 5217
primary pollutant 248, 7823
prime power 9916
primordial germ cell 646, 648, 10907, 10908
– gene targeting 648
primordial radionuclide 8656
principal component analysis (PCA) 8894
principal nutrient metabolic (PNM) model 11059
principal organic hazardous constituents (POHC) 6976
– destruction efficiency 6976
principal organic pollutant (POP) 5237
prion disease 2969
priority strategy 102
private allele 7976
proalcohol 1002–1003
Proalcool program 1007
probenazole 2576
procarcinogen 3256
process gas 7841
process gas-heated reforming 3966
processed refuse fuel (PRF) 11793, 11796, 11818, 11821, 11825
– heating value 11821
– power production 11825
– properties 11818
processing ash 11754
processing reactions 5154
– internal reformation 5154
producer gas 1214, 1433–1435, 1437–1438, 1441, 1443, 1446
– cleaning 1441
– scrubbing 1437
product
– branding 8777
– gas 1459, 1465, 1468
– application 1459
– dust removal 1468
– fuel gas cooling 1468
– hydrogenation 1465
– water removal 1468
– recycling solutions (PRS) 3446
– of incomplete combustion (PIC) 5237, 5240, 6976, 6992–6993, 7001
– emissions from full-scale facilities 6992
– zone theory 6993
production 5167, 5169
– costs 5169
– energy flow 3308
– nuclear-energy-based 5167
– of meat 10840
– thermochemical methods 5169
– well 4247, 4360
– calcite scaling 4247
– in sedimentary basins 4360
production-carrying capacity 1962, 1964, 1971
– modeling 1964
progeny 444
– testing 400, 401, 476, 2785
program crop 2743
programmable logic controller (PLC) 2214
programmable multispectral imager (PMI) 8929
progressive harmonization 8867, 8870
project to intercompare regional climate simulations (PIRCS) 8910
prokaryotic cyanobacteria 4820
prokaryotic microorganisms 498
prolactin receptor (PPLR) 10892
promoter
– methylation 2605
– trap 7223
prompt fission
– gamma photons 8571
– photons 8570
prompt neutron 8567
– lifetime 3814, 3815
pronuclear microinjection 10822, 10824, 10869
proof-of-payment (POP) fare system 5984, 5987, 5994
prooxidant 3589, 3667
propane 334, 3960, 3969
– deasphalting 7839
– prechilling 3960
propanol 4600
propargyl methanesulfonate (PMS) 6040
propelling energy 8848
propene 7590
propulsion 10543
– extended constant power range 10543
propylene
– carbonate (PC) 3430, 3497, 9309
– epoxidation 3943
– oxide (PO) 3942, 7590
propylene-expanded liquid 3943
prostate cancer 3637
proteasome inhibitor 10827
protectant 2304
– fungicides 2567
– plant-incorporated 2304
protected lithium electrode (PLE) 730
protegin–1 (PG–1) 2968
protein 577, 639, 1681, 4033, 4559, 11437
– analytes 1655
– direct detection 1655
– biopharmaceutical 639
– carbohydrate-binding 4033
– chains 1567
– disulfide isomerase (PDI) 3669
– inhibitors 4031
– mammalian amylases 4031
– production 8050
– environmental impact 8050
– proteinase inhibitors (PIs) 4029
– quality 4559
– synthesis 4559
proteolysis 4016
proteome 6441
proteomics 1185, 3588, 3658, 4496
protic ionic liquids (PILs) 6787, 6788
protocrystalline 9242
– amorphous hydrogenated silicon film 9263
protocrystallinity 9247
proton 3788, 3861, 8208, 8468
– accelerators 8582
– concentration effect 8339
– conductivity 6547, 7702, 7759–7760, 7767, 8216, 8224
– of the ionomeric membrane 7759
– exchange membranes (PEMs) 3871, 6539, 7757, 8207
– exchange membrane fuel cell 373, 3385, 3863, 3871, 6539, 7694–7695, 7697, 7699, 7702, 7704–7705, 7707–7715, 7719–7720, 7722–7724, 7731, 7732, 7737, 7741, 7756, 7757, 7760, 7766, 7770, 7772, 7774, 8174, 8328, 8330, 8334
– air starvation 7712
– bipolar plates 7708, 7723
– catalyst durability 7732
– cell voltage variations 7711
– chemical instability of membranes 7720
– choice of the protogenic group 7772
– component costs 7699
– components 7702
– concomitant reduction of relative humidity 7713
– cost of components 7704
– cost reduction 7724
– costs 7695
– design development 7756
– durability 7707, 7710
– durability improvement 7724
– edge protection 7709
– electrodes 7705

– electrolyte 7695
– for transportation 6539
– formation of peroxide 7720
– freezing 7715
– freezing conditions 7722
– fuel starvation 7712
– gas diffusion 7705, 7719
– impact of air contaminants 7713
– impact of hydrogen contaminants 7714
– ionomer 7760
– lifetime 7710
– loss of activity 7710
– materials 7695, 7756
– materials degradation 7715
– mechanical degradation of membranes 7722
– membranes 7704
– membrane contamination by ionic species 7723
– membrane development 7766
– microporous layers 7719
– morphology 7770
– operating temperature 7732
– operating window 7697
– performance 7697
– performance breakdown 7699
– platinum catalyst loading 7732
– platinum-based electrocatalysts 7731
– Pt monolayer electrocatalysts 7741
– Pt-alloy electrocatalysts 7737
– real-life conditions 7711
– sealing materials 7724
– seals 7709
– seals degradation 7723
– silicone seals 7724
– stack 7774
– temperature overshoots 7713
– transport losses 7708
– wear of cell 7715
– recoil scintillation detector 5568
– transfer 3419
– transporting medium 8340
– transport 7770
– trapping 8472
proton-beam accelerator 8586
protonic conductor 3897, 3899
proto-oncogene 3601, 3643
protoporphyrinogen oxidase 10350
protoporphyrin 10651
prototype fast breeder reactor (PFBR) 4061
protoxin activation 4016
protozoan 12019, 12041–12042, 12045, 12048
protozoa 7671, 7684, 8764
proven bull 2784
prymnesiophyte 7272–7273
pseudo-capacitance 3499, 6776, 6778, 6781–6782, 6784
– due to nitrogenated functionalities 6781
– in basic and acidic media 6778
– in neutral medium 6782
– related with reversible hydrogen electrosorption in nanoporous carbons 6784
pseudocapacitor 795, 797, 3427, 3852
– electrode materials 797
pseudo-faradic effect 6776
pseudo-faradic reactions 6782
pseudomonad 501
Pseudomonas 8028
– *aeruginosa* 5061
– *fluorescens* 3157
– marine-derived 3157
pseudo-nitzschia 1655, 4826–4828, 4830
– description 4826
– detection 4828
– economics 4827
– nutrient interactions 4830
– origins 4830
– species identification 4828
– toxicity 4826
pseudorabies virus (PRV) infection 2968, 10859
psychology of place 10373
pterin 1710
p-toluidine 7595
p-type silicon 9213
public breeding program 2536
public ecology 539
public green 953
public health 217, 220
public parking garages 7858
Public Research and Regulation Initiative (PRRI) 4530, 4531
public transit 1821
– agency 1824
– travel 1819
public transportation 91, 94, 806–807, 809, 811, 816, 1812, 1815, 1835, 1863–1865, 3459–3460, 6496, 10924, 10933
– bicycling 806–807, 816
– captive riders 1863
– choice riders 1863
– cycling 811
– developing countries 1863
– effectiveness 1864
– financing capacity 1864
– improvements 1815
– industrialized countries 1863
– land use 10933
– modal integration 1865
– organizational capacity 1864
– public participation 1864
– rail-based 1815
– road-based 1815
– right-of-way acquisition 1864
– traffic enforcement 1865
puffer fish poisoning 9085
pulmonary hypertension syndrome (PHS) 8317
pulpwood 1287
pulse detonation combustion (PDC) 6849
pulse width modulation (PWM) method 3375
pulverized coal combustion 2169, 2172, 8350
– particulate emissions 8350
pulverized coal
– coal-fired boilers 8347
– coal-fired generating stations 3821
– in ultra-supercritical steam cycle (PC/USC) 2166
– plants 2167
pulverized fuel ash (PFA) 3821
pulverized fuel combustion 1245
pumice fall deposit 11621
pump-and-treat system 2447
pure alcohol 1223
pure breed(ing) 392, 2785
pure ethanol 1003, 1028
pure gasoline 1007
pure methane 341
PUREX process 7145–7146
– waste treatment 7146
purifying protein 8078
purine 8137
push-pull converter 692
putative gene 488
pylon 3076–3077
pyramiding 2566, 4027
– alleles 6438
– of resistance transgenes 4027
pyranometer 9677, 9679, 9683, 9685, 9732, 9746
– calibration 9679
– responsivity functions 9683
pyrazine 7579
pyrex glass powder 11604
pyrgeometer 9732
pyrheliometer 7908, 9676–9677, 9685
– calibration 9677
– uncertainties 9685
pyridine 6906
– polybenzimidazoles 8182
pyridinic nitrogen atom 8274, 8279, 8295
pyridoxal 1684

pyridoxamine 1684
pyridoxine 1684
pyrimidine 2569, 8137, 8138
– cyclobutane dimers 11396
pyrite 6653, 6668, 8352
pyritic sulfur 2209, 2211
pyrochemical separation technologies 4059
pyrochlore 3893
– fluorite-type 3893
– structured oxides 2957
pyroclastic flow 11621, 11641
pyroforce gasification concept 1469
pyroformer 1526
pyrogenic aerosol 116
pyrolysis/pyrolytic 846–848, 851–853, 858, 869, 878, 1075–1076, 1206, 1212, 1214, 1428, 1448, 1518–1524, 1526–1529, 1585, 1609, 1614, 2226, 2414, 3958, 4006, 4008, 5126, 5164, 5236, 5247, 5289, 5298, 5300, 5307, 6996, 8281, 11442, 11445, 11833, 11852
– biochar systems (PBS) 851, 857, 871, 873, 885, 888
– sustainability 885
– bitumen 7478
– bubbling fluid bed reactor 1521
– char 882, 1529
– circulating fluid bed reactor 1521
– decomposition 1208, 1213, 1240, 1302, 1352, 1380, 1449
– degradation mechanisms 1518
– depolymerization-vaporization-cross-linking (DVC) model 5307
– devolatilization 5307
– energy balance 853
– evaporation of moisture 5307
– fast 1520
– feedstocks 852
– gases 1527
– gas 1529
– intermediate 1521, 1524
– kinetic parameters 1518
– liquid 1529
– pyrolyzed macrocycles 8269
– mechanical fluidized 1522
– of straw 1528
– of wood waste 869
– oil 1214
– oxalate-supported 8281
– permanent gas formation 1519
– principles 1521
– process technology 1521
– pyroformer 1526
– rotating cone reactor 1523
– slow 1526
– techniques 1527
– temperature control 852
– twin screw reactor 1522
pyromorphite 2442
pyrophoric metallic plutonium 3534
pyroprocessing 7150, 7153
pyroxene 11603
pyrrhotite 9953
pyrrole 7579

Q

Q allele 2704
Q gene 2704
q-axis 24
QC calculation 6039
Qi standard 704
quadrupole magnetic levitation 6275
quadrupole magnets 6261–6262
quadrupole mass spectrometer (QMA) 9402
quality protein maize (QPM) 1693
quality wheat region 1125
quantative
– microbial risk assessment (QMRA) 3587–3588, 6606, 6609, 6625, 6630, 8758, 8763
– improving the technique 6630
– improving the utility 6630
– wastewater reuse 6625
– genetics theory 7977
– of traits 9389
– trait loci (QTL) 2, 387, 400, 480, 2675, 4073, 4558, 5321, 6427, 6429, 6697
– alleles 6433
– by environment interaction (QEI) 6697
– cloning 6433, 6442
– mapping 6429, 6432, 6439, 6694, 6697
– QTL-based modeling 6434
quantum
– chemistry 6038
– dots 4661
– theory of light 7554
quarry by-products 11703
quartz sand 1923, 9434
quench reactor 3992
queue jumping green signals 1872
queuing 103
quick scatterometer 8944
quinine 7595
quinoa 2640
quinolone 5379
quinone 6778
quinone/hydroquinone pair 6776
quorum sensing 11889

R

rachitis 11414
radar altimeter/altimetry 2456, 4577, 8931
radar sensor 6957
radial all-bus category 5999
radial pentagon analysis 4621–4622, 4638
radiance 2821, 2839
radiant cooling 897
radiant exposure 11380
radiant Flux 9573
radiant water-based cooling systems 2858
radiation 135, 3023, 3258, 3518–3519, 3583–3585, 3787, 4906–4908, 5561–5562, 5573–5580, 5582–5591, 5594–5597, 5600–5604, 5606–5609, 7054, 7067, 7213, 7904, 8426, 8448, 8463–8464, 8467, 8471–8472, 8478, 8481–8482, 8490, 8531–8532, 8536–8538, 8544–8546, 8552–8554, 8556, 8561, 8965, 9710, 11152, 11155
– absorbers 5569
– accidents 3517, 3531, 3547
– Kyshtym accident 3531
– acute doses 5574, 5585
– anthropomorphic phantom 8545
– assessment 8425
– transfer parameters 8425
– atmospherically reflected 8553
– biological damage 8561
– biological effects 4906
– biological response 5575
– biology 11041
– bremsstrahlung 8545
– cancer 5575
– treatment 5582
– capture 2620
– by crop canopies 2620
– cell death 5575
– characteristics 5561, 5574
– chromosomal aberrations 5587, 5603, 5607
– chromosomal damage 5588
– chronic doses 5585
– conversion
– efficiency 2617
– factor 2617
– damage 5575
– to DNA 3585
– detection 5561, 5564–5572
– advancements in detection methods 5570

– advancements in detector materials 5569
– advancements in signal measurement 5572
– Compton-suppressed germanium detector 5571
– devices 7054
– equipment 8481
– fast neutron detectors 5568
– Geiger-Müller counters 5564
– moderating detectors 5569
– neutron detectors 5567
– proportional counters 5564
– scintillation detectors 5565
– semiconductor detectors 5566
– slow neutron detectors 5568
– detectors 3023, 5562
– disturbance 698
– dose 5576, 8410
– dose-to-biota assessment 8410
– linear-quadratic model 5576
– screening dose rate 8410
– dose–effect relationships in animals 8463
– dose–response relationship 5576
– dosimetry 7054
– effectiveness factor (REF) 11043
– effects 5590
– at elevated background concentrations 5586
– hibernating animals 5590
– on amphibians and reptiles 5595
– on animals 5584
– on aquatic invertebrates 5602
– on aquatic organisms 5596
– on aquatic plants 5609
– on biota 5573
– on birds 5594
– on caribou and reindeer 8448
– on fish 5600
– on life span 5589
– on mammals 5585, 5587
– on pine trees 5606
– on terrestrial invertebrates 5601
– on terrestrial plants 5604
– pocket mouse 5590
– poikilotherms 5590
– energy 3028, 4643, 8462
– measurement 3028
– environmental protection 5582
– equivalent dose 3023
– exoatmospheric burst 8490
– expanded and aligned field 8545
– exposure 4907–4908
– field irradiator studies 5590, 5608
– fission reactor physics 7054
– fluence-to-dose conversion factors 8544
– flux 7906
– density 7908
– from solar and galactic sources 8561
– genetic effects 5573
– in nonhuman species 5586
– genotoxic effect 5603
– harmful effects 4906
– health physics 7054
– high background areas 8478
– highly enriched uranium (HEU) 7213
– impacts on human populations 8464
– in the environment 8467
– intensity characterization 8544
– isotropic point detector 8546
– legacy 3518, 3584
– sites 3518
– low-dose effects 3258
– morphological effects 5608
– mortality in fish 5597
– nonhuman biota 5580
– orphan sources 8532
– output (factor) 8549
– photosynthetically available 8965
– point kernel for uncollided Dose 8546
– Poisson distribution 5603
– possible effects in reindeer 8464
– protection 3519, 4905, 4907, 7054, 7067, 11392
– guidelines 5583
– of individuals 5583
– principles 8531
– radiometric quantity 7904
– relative biological effectiveness (RBE) 5578, 5579
– reflection 8550
– albedo methods 8550
– resistance 8556
– risk assessment 8532
– safety culture 3518
– selected geometries 8546
– shielding 7054, 8536–8538, 8542–8543, 8548, 8556
– broad-beam attenuation 8548
– design 8542
– geometric progression formula 8542
– history 8538
– Monte Carlo calculations 8542
– of buildup factors 8542
– point-kernel computer codes 8548
– practice 8543
– source characterization 8543
– skyshine dose 8553
– smoking 8482
– source 7054, 8520–8524, 8526–8528, 8559, 8563, 8579, 8581–8582
– accelerators 8581
– brachytherapy sources 8520
– calibration sources 8521
– commercial Sources 8524
– consumer products 8521
– industrial isotope 8582
– industrial sources 8520, 8523
– in medicine 8579
– irradiators 8523
– lost source 8526
– medical sources 8522
– moisture/density devices 8521
– occupational medical exposure 8581
– orphan source 8527, 8528
– physical characterization 8563
– research sources 8526
– specific source incidents 8527
– used in human activities 8579
– well logging sources 8520
– spectrometers 8586
– therapy 8580
– transfer theory 7905
– transport 8540–8541
– streaming through ducts 8552
– surface reflectivity 135, 9710, 11155
– use efficiency (RUE) 2615–2617, 2629, 2631–2632, 2671
– determination 2617
– environmental factors 2632
– improvement 2629
– sources of variation 2631
– species variation 2631
– stage of crop development 2632
– technically enhanced naturally occurring radioactive material (TENORM) 5591
– tissue sensitivity 5577
– transfer parameters 8426
– transiting 8472
– transmission of beams 8556
– transport 8556
– equation 8538
– theory 8554
– trapped particle 8471
– uncollided radiation doses 8545
– wavelengths 11152
radiation-induced cancer 11034
radiation-producing reaction 8562
– binary reactions 8562
– energetics 8562
– radioactive decay 8562

radiative
– forcing 631, 10122
– input data 9722
– three-dimensional 11156
– transfer models (RTMs) 9707, 9722, 11149–11150, 11156
– transfer model simulations 7926, 9715–9716
– Monte Carlo modeling 9716
– theory (RTT) 7906, 7911
– three-dimensional 9716
– transfer 9688, 11397
radical battery 7552
radical chain reaction 3664
radical polymer 7551
radio communication 2984
radioactive 3517, 3790, 7065
– aerosols 8449
– contaminant 4778–4779
– environmental modeling assessment 4778
– isotherm-based transport modeling 4779
– multi-component reactive transport modeling 4779
– contamination 3518, 3522, 3524, 3528, 3530–3531, 3540
– environmental behavior 3522
– EURANOS project 3531
– in food products 3524
– inhabited area 3528
– management options 3524, 3528
– mobility 3522
– nuclear testing sites 3540
– radiological impact 3524
– STRATEGY project 3530
– waste disposal options 3528
– decay 8562–8564, 8570, 8599
– constant 3790
– law 3737
– types 8564
– doses 7044
– aquatic pathways 7044
– fission 8583
– products 8623
– iodine 3286, 8523
– isotope 11027
– of hydrogen 11027
– material 4209, 7057, 7076, 8470, 8500, 8508, 8518, 8589
– categories 8518
– ground deposition 8500
– tracer test 4209
– nuclides 5561
– pollution 5594
– radium 8538
– seawater 7390
– thorium 11205
– tracers 8594
– transmutations 8562
– disposal 7077
– groundwater impacts 4774
– groundwater restoration 7067
– hazardous and mixed wastes 7068
– high-level waste 7067
– intermediate-level waste 7068
– land disposal 8486
– low-level waste 7068
– management 7055, 7077, 8477, 8531, 8588
– materials 8512
– ocean disposal 8486
– ocean dumping 8487
– offsite disposal 7079
– onsite waste management 7079
– phyllosilicate clays 8603
– reactive soil components 8603
– repository 8603
– soil environment 8598
– spent nuclear fuel 7067
– uncontaminated wastes 7069
radioactivity 3024, 4907, 5560, 6688, 7044, 7047, 7059, 7114, 7800, 8387, 8397, 8434, 8448–8449, 8470, 8485, 8487, 8532
– aquatic food chain 7044
– Chernobyl-derived 8397
– coal-fired power plants 8485
– concentrations 7048
– in drinking water 7048
– in rivers and reservoirs 7048
– ratio in Models 8434
– detectors 5560
– in caribou and reindeer 8448
– in the marine environment 8387
– in the surface seawater 8487
– methods of food preparation 7047
– sources in the environment 8470
– sources 8449
– transport 8532
radiobiology 3583
radiocarbon 8668
radioc(a)esium 3534–3535, 3710, 3721, 7009, 7012, 7018, 7024, 7029, 7045, 8388, 8393–8394, 8397, 8399, 8429–8430, 8441, 8454, 8457, 8465, 8644, 8647
– contamination 3536
– countermeasure 3536
– fallout 8457
– lake model 7029
– migration from lake catchments 8644
– model 7024
– speciation 8393
– transfer coefficient 8429
radiochemistry 8599
radioecological data 8435
radioecology 3583, 7010, 7031, 7048, 8413, 8653
– coastal models 7031
radiogenic heat 4138
radiogenic resource 4166
radioimmunoassay 8580
radioimmunoimaging 8581
radioimmunotherapy 8581
radioiodine 3534, 7045, 8430
– transfer to milk 8430
radioisotope/radioisotopic 3511, 8468–8469, 8542, 8569
– decay data for shielding design 8542
– identification devices (RIIDs) 7214
– in the environment 8469
– transport 3286
– thermoelectric generators (RTGs) 8515
radiolabeling 8522
radiological
– assessments 8441
– transfer parameters 8441
– dispersal device (RDD) 8529, 8530
– environmental assessment models 8439
– modeling 8653
– protection 8426
– toxicity 8514
radiometer 9473, 9474, 9676, 9681
– calibration sources of uncertainty 9681
– long-term behavior 9474
radiometry/radiometric 9713
– from space 9470
– measurements 2886, 9645
– power units 11103
– stations 10623
radionuclide 2435, 3023, 3516–3517, 3519, 3524, 3527, 3535, 3547, 3555, 3583, 3585, 3706, 3711, 3719, 3722, 3725, 3730, 3761, 3762, 4778, 5586, 5610, 7008, 7010, 7013, 7026–7028, 7039, 7045, 7046, 7048, 7074, 7211, 8388, 8390, 8396–8399, 8400–8402, 8404–8406, 8411, 8412, 8426–8433,

8435–8437, 8441, 8454, 8456, 8468, 8524, 8531, 8543, 8563, 8597, 8599–8600, 8607, 8611, 8615–8618, 8620, 8626, 8634–8639, 8642, 8647–8651, 8653, 8655, 8656, 8663, 8664, 8668, 10403, 10423–10425, 11051, 11220, 11232
– activity concentration 3535, 8427
– activity 3725
– aggregated transfer parameter 8432
– allometric relationships 8437
– allometry 8405
– alpha-emitting 5586
– analytical techniques 8668
– as tracers 3719
  – of ocean currents 8655
– balance in the catchment 8647
– behavior
  – in estuaries 8401
  – in the marine environment 8412, 8663
– bio-accumulated 8404
– bioavailability 11232
– bioconcentration factor (BCF) 7027
– biological half-life 8405, 8436
– biological recycling 8402
– biomagnification 8406
– bioreduction 4778
– biouptake in fish 7026
– Carlsson–Yamagata model 8649
– chemical speciation 8607
– cleaning of soil 10425
– concentrations 7033, 7042, 7044, 8674–8675
  – factors 8402
  – in coastal areas? 7033
  – in human foodstuff 8426, 8441
  – in runoff water 8650
  – in surface water 7044, 8675
  – in water 7042
  – Indian ocean 8674
– contaminants 4775, 4777, 4780
  – adsorption 4777
  – desorption 4777
  – mass transfer processes 4780
– contamination 5598, 7038
  – of coastal areas 7038
  – of surface waters 7045
– convection dispersion equation (CDE) 8617
– cycling in the foodweb 8402
– decays 8563, 8599
– depth distribution 3722
– dissolution 8611
– dose–response models 8531
– downward movement 3722
– drinking Water 7045
– electrokinetic cleaning of soil 10428
– electrokinetic localization 10424
– entrainment properties 8651
– environmental behavior 3547, 8401
– environmental surveillance 7211
– exposure pathway 8441
– fallout 3706
– fate 8597
– food chain transfer 8406
– freshwater pathway 7048
– geographical distribution 8412
– global fallout 8635, 8637, 8656
– half-life 3730
– important soil processes 8607
– in fish 7028
– in lichens 8454
– in marine systems 8411
– in maternal milk 11051
– in *Rangifer tarandus* 8456
– in seawater 3585, 8668
  – distribution 8668
  – transport 8668
– in sediments 8397
  – active A-sediments 7039
– in water 7027
– influence of bioturbation 8399
– intake at equilibrium 8430
– interactions 8393, 8395
  – in the water column 8393
  – with colloids 8395
  – with suspended particulates 8393
– internally ingested 5610
– inventories in sediments 8398
– linear non-threshold (LNT) model 8531
– long-lived 7074
– marine environment 8390
– measurements 3762
– migration 8617, 8644, 8646, 8649, 8651
  – aggregated models 8646, 8649
  – from catchments 8634, 8642, 8651, 8653
  – in the soil 8620
  – model 8648
  – reductionistic models 8644, 8646
  – velocities 7010
– mobility in soils 8428
– modeling 7013, 8400
– monitoring 7211
– natural sources 8600
– partitioning 8607, 8617, 8626
– precipitation 8611
– primordial 3583
– redissolution from sediments 8398
– redox-sensitive 8616
– release 7074
– remediation 10425
– remobilization 8399
– removal 10423
– sampling 8668
– scaling factor 8639
– scavenging from the water column 8396
– soil-borne 8616
– solid–liquid distribution coefficient 8428
– sorption 8611, 8618
– sources 8543, 8662
  – in the marine environment 8662
– speciation 3585
  – in seawater 8390
– storage compartment 8649
– sustainable remediation methods 10403
– toxicity 11232
– trace nutrients 8616
– tracers 8524, 8658, 8681
  – in the world ocean 8664
– tracing 8678
  – of ocean currents 8678
– transfer
  – coefficient 8428, 8429
  – coefficient equation 8431
  – data 8435
  – function 8648
  – function per unit deposition 8638
  – to farm animals 8428
– transport 4780
  – by runoff waters 8636
  – in terrestrial environments 8597
  – processes 7008
– transuranic 10427
– uptake by fish and aquatic foodstuffs 7046
– use in sediment tracing investigations 3761
– vegetation transfer factors 8615
– wastes 4775
radiopharmaceutical 8522, 8580, 8594
radiosensitivity 5578, 5584
radiosonde 9724
radiostrontium 3534, 7009, 7012, 7033, 7045, 7047–7048, 8388, 8429, 8647
  – in runoff water 8647
  – lake liming 7048
radiotoxic nuclide 8481
radiotoxicity 7146
radiotracer 8413

radium 7059, 7061, 8538, 8623
– radium–226 3715
radon 8475, 8478, 8531, 8623
– gas 8478, 8481
– radon–222 3715
raft culture 6761
Ragone plot 3852
rail 1889
– corridors 10927
– interoperability directives 4943
– mass transit 1893
– cost characteristics 1893
– public transportation 5974
– rights-of-way 5974
– technologies 1883
– transit 1877, 1894–1895, 1897, 1900
– capacity 1895
– electrically powered 1877
– impacts on property values 1897
– land-use densities 1900
– operating cost 1894
– transit investments 5998
– criticisms 5998
– transit line 5966
– transit-oriented development 1889
– transport 246, 258
– activity data 258
– models 257
railway
– signal systems 5967
– technology 4929
rain
– screens 3697
– water 3460
rainfall 8690, 8692
rainforest 2745
rainstorm event 4685
rainwater 2324, 2327, 2330, 2332, 2334, 4746, 8688–8695, 8697–8700, 10190, 11874, 11875
– boiling 8698
– contaminants 8697
– contamination 8694
– filtration 8698
– guidelines 2332
– harvesting 2330, 4746, 10190, 11875
– alternative water supply 8691
– catchment 8690
– infiltration 8691
– maintenance 8700
– nonpoint source pollution 8692
– operation 8700
– storage 8690, 8694
– system design 8699
– technologies 8693
– treatment 8691
– infiltration 8695, 8696
– capillary action 8696
– gravity 8696
– types of systems 8696
– limitation 2332
– management 4743
– microbial contamination 8698
– nonpoint source pollution 8692
– operation 8700
– public perception 2334
– quality 8697
– roof catchment systems 8690
– samples 8697
– standards 2332
– storage 8690, 8694, 8699
– treatment 8697, 8699
– chlorination 8699
– chlorine tablets 8699
– ozone 8699
– ultraviolet (UV) light water disinfection 8699
– urban runoff control 8692
ram feeder 4963
Raman
– chemical imaging spectroscopy (RCIS) 5390
– crystalline fraction 9249
– crystallinity 9250
– fingerprints 5393
– scattering 7501
– spectroscopy 5385
– signal 7502
– spectroscopy 5387, 5389–5390, 9899
– acinetobacter 5390
– pathogen detection 5389
random
– bred population 485
– breeding population 482
– linkage disequilibrium 482
– waves 7403
Rangifer
– *tarandus* 8462
– *terandus* 8450
Rankine cycle 1330, 3819, 4055, 4061, 4169, 4260, 4296, 6824, 11762
– bottoming cycle (RBC) 6824, 6829
– efficiency 2167
– plant 2385
– steam cycle 2167
– steam plant 2172
Raoult effect 134
rapeseed oil 924, 4557, 8085–8086
– methyl esters (RME) 923
– viscosity 8086
rapid bioassessment protocols (RBPs) 3274, 3587
rapid diagnostic tests 5383
rapid transit
– lines 5989, 6014
– subway lines 5997
– technology 1879
rapidity 3452
rare earth
– element (REE) 6634, 9925, 11024
– materials 5102
– oxides (REO) 9948
raw gas
– cleaning 1586
– upgrading 1662
raw marine seafood 12032
raw material 6896, 8771, 9027, 9043, 11437
– cascading 9043
– extraction 9027
– production 2072
– scarcity 9027
raw product gas 1464
raw seafood product 12020
raw spectral pixel response 11118
rawinsondes 9724
ray effect 8555
ray tracing method 12286
Rayleigh scattering 135, 311, 325, 8960–8961, 9628, 9652, 11155
Rayleigh-Taylor instability 7171
reactant gas
– addition (RA) 6722, 6728, 6735
– permeability 7769
reaction energy 3423
– DFT-calculated 3423
reaction mass efficiency (RME) 4586, 4615, 4619, 4636
reaction norm 464
reaction torque 22
reactive nitrogen species (RNS) 3601, 3665
reactive oxygen species (ROS) 4, 350, 2644, 2651, 3599, 3662, 5317, 6168
– detoxification 2651
reactor 3805, 3808, 3813, 3814, 3816
– application 3804
– Doppler broadening 3804
– control elements 3808
– perturbations 3816
– physics 3798
– power changes 3816
– primary nuclear design 3808
– principle design process 3813
– reactivity 3814

– shielding 8539
– theory 3810
– trial configuration 3808
real time kinematic GPS 3071
real-sky irradiation 10626, 10629, 10632, 10634
real-time
– seismology 2429
– spectroscopic ellipsometry (RTSE) 9245, 9247
reanalysis climate 2108
ReaxFF 6039, 6043–6044
– simulations 6044
rebranding 11353
reburning 8364
recharge oscillator 2127
rechargeable battery 8715
– separator membranes 8715
recipient oocyte 6162–6163
– enucleation 6163
– sources 6162
reciprocating engines 1032
reciprocation combustion engine 1459
recirculated flue gas 4968, 4985, 6465
recirculating aquaculture system (RAS) 6313
recirculation system 548
reclaimed concrete material 11703
reclaimed (recycled) asphalt pavement (RAP) 11703
reclaimed water 2327–2328, 2331–2332, 2334, 11875–11876
– applications 11875
– guidelines 2332
– microbial pathogens 11876
– public perception 2334
– road runoff 2331
– roof runoff 2331
– standards 2332
– water qualities 11875
recognition
– algorithm 3117
– elements 1647, 1649, 1653, 1656, 3588
– attachment of "adapter molecules." 1649
– physical adsorption 1649
recombinant
– antibodies 8078
– biopharmaceuticals 8068
– DNA technology 8060, 8075, 10816
– insulin 8027, 8067, 10816
– nucleic acid techniques 10770
– protein 639, 640, 8024, 8052
– chicken 640
– plant-derived 8030, 8052
– storage proteins 1693
recombinase gene 10685, 10899
recombinase-mediated cassette exchange (RMCE) 10831, 10913
reconfigured integrated two-stage liquefaction (RITSL) 2232
reconnaissance satellite photograph 283
reconstructed embryos 6169–6170
– activation 6169
– culture 6170
recooling 9534, 9536
– by natural water resources 9534
recoverable coal 2197
recreation vehicle (RV) 3868
recreational waterborne illness (RWI) 8758
recreational water 3588, 6320, 6626, 6629, 8758, 8760, 8766
– fecal indicator 8766
– health data 8766
– microbial risk assessments 8758
– monitoring 8760
– risk 8758
– fecal indicators 8758
– pathogens 8758
recrystallisation 4586
rectification 994
rectisol 1590, 2153, 2239
recursive least square 50, 57
recyclability 3445
recycled aggregate 2404
recycled asphalt 11705
– planings (RAP) 2406
recycled concrete aggregate (RCA) 2404
recycled content 9029, 9037
– unintended consequences 9029
recycled material 11701, 11705
– current specification 11705
recycled wastewater 6628
recycled water 2333, 11887–11888
– energy comparison 11888
– energy cost 11887
recycling 569, 2398, 2400, 2404, 2407, 2409–2410, 2413, 2419, 3445–3447, 4958, 8771–8773, 8776–8782, 8784–8787, 8789, 8792, 8794–8795, 8797, 8801–8802, 8808–8810, 8812–8815, 8817–8818, 8827–8829, 8833, 8835–8837, 8844, 9027, 9037, 9589, 9979, 9997, 10031, 10580–10581, 11658, 11674, 11684, 11689, 11699–11700, 11737, 11852, 11870
– aluminum 8778, 8787, 8814
– as a rehabilitation alternative 11700
– automated collection 8784
– awareness 10027
– cardboard 8786
– carpets 8829
– ceramic glass recognition 8808
– collection 8771, 8784
– common hindrances 8782
– common problems 8781
– concept 8795
– containers 8782
– control actions 8833
– cycle 9983
– definition 8771
– drop-off centers 8784
– dual energy X-ray transmission (DE-XRT) 8836
– dual-stream collection 8785
– economy 11710
– environment 8481
– environmental benefits 8773
– ferrous metals 8810
– fibers 8827
– financial analysis 8787
– fresh concrete 2407
– glass 8779, 8787, 8801
– goals 8789
– human factors 8781
– hyperspectral imaging (HSI) 8836
– applications 8837
– in hot mix asphalt 2407
– incentive programs 8785
– industry 8776–8777
– innovative sensing technologies 8835
– laser-induced breakdown spectroscopy (LIBS) 8836
– material
– integrity 9037
– misplacement 8781
– recovery facility (MRF) 8785
– metal 8809
– metallic waste 2413
– methods 8784
– mineral waste 2404
– newspaper collection 8786
– non-ferrous metals 8814–8815
– non-glass materials 8802
– of energy-intensive materials 9589
– of glass 2409
– on-line recognition 8808
– organic waste 2409
– paper 8780, 8797
– plant 8832, 8834
– scale control 8834
– plastics 2410, 8780, 8817, 8818
– polluting agents 8812
– processes 8777
– ratio 10012

– program 11660
– rotating drums (RD) 8812
– separation 8771, 8813
– shredding 8812
– single equipment control 8835
– single-stream collection 8785
– sorting 8814
– steel (tin) cans 8787
– technologies 8794, 8797
– textile 8828
– timber 2419
– X-ray fluorescence spectroscopy (XRF) 8836
red algae 356, 365
red angus breed 1724
red list index (RLI) 10087
Red Maasai
– breed 1772
– sheep 1758
red mark syndrome 1932
red oil 8503
red tide 1925, 4820, 4825, 7388, 7390
redox 786
– circuits 3666
– cycling 3660
– electrolyte 3855
– energy 762
– flow batteries 3853
– proteomics 3667, 3669
– reactions 3657, 3852, 4099, 4622–4623, 6782, 8610
– pseudo-faradic 6782
– reduction-oxidation reaction 6069
redox-active metals 10157
redox-flow battery 750, 766
reduced height (*Rht*) alleles 6210
reduction fishery 550
reductionism 8643
reductive dechlorination (RD) 2444
reductive stress 3658
redundancy 3452
reed canary grass 6024–6025
reef 2490, 2493, 2498, 2506
– accretion 2493
– fish 2498
– invertebrates 2506
reef-associated organism 2502
reef-building coral 2493–2494
reference animals and plants (RAPS) 8434
reference diffuse irradiance 9679
reference wind speed 6604
reference-frame theory 39
refinery gas 7841, 7842
reflected radiation 10633
reflector 6031
reforestation 1571, 2513, 4746
refractive index (RI) 1647, 3587
refrigerant 9517
– compression 9522
– cycle 9518
– vapor 9517–9518
refrigeration 4375, 9509, 10559
refuse-derived fuel (RDF) 5284, 5289, 9997, 11761, 11791, 11793, 11795–11796, 11803, 11805, 11810, 11812–11815, 11821, 11825, 11836, 11837
– advanced resource recovery facilities 11796
– air-classified 11791
– air quality control equipment 11814
– baghouse 11815
– co-firingwith coal 11793
– operations 11795
– combustion 11836
– conveyors for movement of materials 11812
– electrostatic precipitator (ESP) 11814
– emission control 11805
– equipment description 11803
– heating value 11821
– higher heating value (HHV) 11821
– low-sulfur RDF 11793
– magnets for ferrous recovery 11812
– mechanical biological treatment (MBT) 11837
– power production 11825
– processing equipment 11810
– screens used in resource recovery 11812
– scrubber 11815
– shredders for size reduction 11810
– steel pan conveyors 11813
regasification 6847
regenerative
– braking 3393, 3496, 8848–8849, 8853, 10542–10544, 10548, 11504, 11537, 11540
– capacity 8868
– design 8866
– development 8855, 8860, 8866
– selective catalytic reduction (RSCR) system 11807
– thermal oxidizer 10574
regenerator 2370
region of no escape (RONE) 84
regional air quality 8879–8880
– definition 8880
– legislation 8880
– monitoring 8880
regional bus system 5995
regional climate modeling 8902, 8903, 8905, 8909–8910, 8912
– Dynamical Downscaling 8912
– Evaluating 8909
regional climate simulation 8908, 8916
regional earth system model 8905
regional rapid transit development 5996
regional transit network 5988
regional transmission organization (RTO) 12174, 12176
– planning methods 12176
regression-on-the-mean models 4080
regulatory impact analyses (RIA) 235
regulon biotechnology 6, 11
reheat combustor 6822
Reichardt's hypothesis 10990
reindeer 8448, 8450, 8457, 8462
– radiation doses 8462
relative biological effectiveness (RBE) 11028
relative positive acceleration (RPA) 256
relative statistical entropy (RSE) 11709
relay setting 12089
reliability diagrams 2130
reliably extending dynamic range 11113
reluctance torque 22, 24, 34
remanent magnetism 25
remanufacturing 3447
remedial
– investigation (RI) 2009
– objective 4785–4786
– strategy 4786–4787
– technologies 4786, 4787
remediation 2439–2440, 3517, 3520–3522, 3530, 3542, 3544–3546, 3584, 4788, 4790–4791, 4795–4797, 4799, 4803, 10190, 10414, 10435, 10439
– benefits 4791, 4796
– blight reduction 4795
– by biomineralization 10414
– by objectives 3544
– cost-effectiveness analysis 3545
– decision-aiding tools 3544
– decommissioning 3542
– different environments 3522
– economics 4788
– sustainability analysis 4797
– ethical acceptability 3530
– external costs 4790
– financial costs 4790
– indicative remedial costs 4799
– industry 10439–10441
– risk assessment process 10441
– sustainability 10441
– justification 3520, 3546

– multi-attribute-utility analysis (MAUA) 3546
– removal of disamenity 4795
– site evaluation 3521
– strategy 3520
– sustainability 4803
– principles 10435
– technologies 2440, 2443, 2447
– chemical treatment 2446
– classification 2440
– electrokinetic separation 2449
– microcosm studies 2443
– multiphase extraction 2447
– permeable reactive barriers 2447
– selection 2439, 2440
– thermal treatment 2448
– unplanned external costs 4791
REML (restricted or residual maximum likelihood) 398
remote sensing 285, 3171, 8920–8922, 8930, 8939–8941, 8943, 8948, 8952, 8957
– active sensors 8940
– data 8923
– measurement of electromagnetic radiation 8921
– of natural disasters 8939, 8948
– of ocean color 8952
– of sea surface salinity 8930
– passive sensors 8940
– reflectance 8957
– shipboard observations 8922
– study of volcanic activity 8941
– techniques 8929
– telemetering 8922
– tracking flooding 8943
renaturation 11366, 11373
renewability 9037
renewable cooling 9451
renewable diesel 10511
– from soybeans 10511
renewable electricity generation 8980
renewable energy 511, 514, 672, 1146, 1313, 1347, 1446, 1477, 1478, 1489, 1533, 1609, 2150, 2995, 4226, 4334, 5116, 7968, 8975, 9035, 10937
– certificates (RECs) 10457
– from biomass 8975
– from plants 1478
– in developing countries 1146
– portfolio standards 4226
– certificates (RECs) 10457
– credit (REC) market 10463, 10476, 12264
– entry act 1623
– innovation 12223, 12238, 12243
– community acceptance 12238
– community involvement 12238
– intra-firm acceptance 12243
– policies 12266
– power plant 11809
– powered desalination 9761
– resources 3395
– sources 1574, 3394, 3464, 7852, 7962
– standards 12216
– strategy 8384
– systems 9673
renewable fuel 5463, 5489
– hydrogenated-derived 5489
– standards (RFS) 1499
renewable generation 3014, 8980, 8989, 8992–8995, 8997, 9335
– curtailment 8997
– demand response 8994
– electricity storage 8995
– flexible generation 8997
– forecasting techniques 8993
– locational marginal prices 8992
– markets 8989, 8994
– new loads 8997
– operating tools 8994
– policy drivers 9335
– stochastic planning 8994
– thermal unit cycling 8989
renewable generator 8991
– ancillary service markets 8991
– capacity markets 8991
renewable heating 9451
renewable penetration 8992
renewable portfolio standards (RPS) 12264
renewable resources 6896, 7848, 8983
– characteristics 8983
renewable-energy-powered vehicles 8329
renieramycin 3161
Reoviridae 11990
reproduction/reproductive 10817–10818, 10889
– female germ line 10818
– male germ cells 10817
– sinks 2628
– system 3637
– development 3637
– technologies 10826, 10867
– toxicity 4849
reprogramming 6159–6160
– of DNA methylation 6159
– of gene expression 6160
– of histone modifications 6159
reptiles 9165, 10090
– as sentinels 9165
research program (WCRP) 8921
reserve sharing agreements 8990
reservoir 2788, 2792, 2797, 2800, 2801, 5674–5676, 5678–5681, 5683, 5692, 5700, 7799, 9022
– biological processes 5679
– biomanipulation 5700
– construction 2788
– density- or wind-driven currents 5683
– engineering 9001
– environmental protection 2801
– eutrophication 5681
– external material inputs 5676
– fluctuation 2792
– forecast simulation 9022
– geological variability 7799
– hydraulic residence time 5680
– in karst 2800
– internal nutrient loading 5679
– limnology 5675
– management 5700
– manipulation of water quality 5680
– monitoring 4219
– nutrients from watersheds 5678
– particle settling 5678
– sediment bed 5679
– flux of solutes 5679
– sediment transport 5675
– sedimentation 3708
– simulation of water quality 5683
– slope instability 2792
– stimulation 3503
– sustainability 5674
– sustaining fish habitat 5692
residual
– camera motion 58
– feed intake (RFI) 1738
– gas trapping 4122
– nutrients 3780
– oil solvent extraction 2232
– radioactivity 7076
– soil 2432
residues 1180–1182
– from beer production 1181
– from cereal processing 1180
– from meat processing 1182
– from milk production 1182
– from pulp and paper production 1182
– from sugar production 1181
– from the manufacturing of fruits, vegetables, and potatoes 1180
– from vegetable oil production 1181

– from wine production 1182
– in distilleries 1182
resilience theory 3344, 3452
resistance allele 6437
– pyramiding 6437
resistance thermometer 9681
resonance effect 7556
resonance ionization mass spectrometry (RIMS) 8657
resource 3347, 4225, 10063
– allocation theory 410
– behavior 3345
– biological species 10063
– certificate 9038
– competition 10075
– conservation 8774, 10581, 10584
– conservation and recovery act (RCRA) 7825, 10016
– conservation efficiency (RCE) 11692
– consumption 10063
– dynamics 3345
– exploitation 4225
– flows 6853–6855
– sustainable management 6854
– urban planning 6855
– management decisions 3347
– monitoring 3345
– of plants 10063
– partitioning 10073, 10076
– productivity 1503
– recovery 10588
– recovery act (RRA) 10016
– repletion 9025
– shortages 11700
resourcefulness 3452
resource-use efficiency 155
respiration energy flow 3308
respiration 2645
respiratory infection 5360
respiratory syndrome virus (PRRSV) 1651
respiratory toxicant 3640
restocking 6388
restricted feeding 9366
restricted greedy routing 11566
restricting germination 9146
restriction fragment length polymorphism (RFLP) 6696
resuspension of material 254
resveratrol 10698
retardation
– coefficient 2041
– factor 8618
retinol-binding protein (RBP) genes 10892
retrospective forecasts 2138, 2143
retroviral
– infections 8139
– vectors 642
retrovirus 642, 643, 4999, 5001, 10797, 10826, 10904, 10905
– replication-competent 643
– replication-defective 643
return to nature 4737
reusability 3445
reuse 3447, 8792
– of materials 9029
reused water 2327, 2328
reverse airflow baghouse 8357
reverse Monte Carlo (RMC) technique 6073
reverse osmosis (RO) 2382, 2902, 7323, 9759, 9761, 10530, 10532, 11884
– with photovoltaic 9761
reverse transcriptase 5002
– chain reaction (RT-PCR) 2699
reverse transcription (RT)-Southern blotting 2699
reverse-acting grate 6454–6456
– siftings 6455
– Vario 6456
reversed field pinch (RFP) 7164
reversible hydrogen electrode (RHE) 7763, 8208
Reynolds
– averaged Navier-Stokes (RANS) equations 12210
– averaging 2060
– equations 10980
– number 2028, 2048, 10991
– stress closure 11277
– stress model (RSM) 11281
rhenium 3975
rhinovirus 8131
rhizobacteria 155
rhizocticin 507
rhizoctonia 6209
rhizodegradation 6658, 10152, 10155
rhizome 1280, 1282, 11898
rhizosheath 6206
rhizosphere 8615
rhodium 3947–3948
– catalyst 3939, 3947, 3948
ribavirin 8139, 8149
ribbon-silicon technologies 9435
riboflavin 1684
ribosomal DNA (rDNA) gene 2691
ribosome inactivation protein 2647, 4034
ribulose–1,5-bisphosphate (RuBP) 1100
rice 2706, 2710–2711, 8018–8019, 10347
– blast disease 2576
– C_4 photosynthesis pathway 8019
– elite inbred lines 8019
– new plant type 8019
– plant architecture 2706
– production 8018
– seed
– color 2710
– shattering 2711
– selective herbicides 10347
– yield potential 8018
rice–fish farming 8201
rice-water stool 5052
Richards equation 3220
Richardson number 10983
riddling 4970
rides 2405
Rietveld refinement 7530, 7540
rifampicin 11139
rifamycin 506
Rift Valley Fever (RVF) 1759, 5361
rill erosion 3709, 3744
Ripley's *K* statistic 3334
risk assessment 3265–3266, 3273, 3274, 3275, 6606
– animal models 3275
– basic framework 3266
– biological surveys 3273
– biomarkers 3274
– genomics 3275
– physiologically-based pharmacokinetic (PBPK) models 3274
– toxicokinetic models 3274
risk of disease burden 6629
– disability adjusted life years (DALYs) 6629
risk-screening environmental indicators (RSEI) 4859
river 9049, 9050, 9051, 9054–9055, 9057–9059, 9061
– advection 9055
– basin 9049
– management 5825
– blindness 12008, 12009
– control 12009
– catchments 8638
– contamination 8638
– channel regulation 5828
– characteristics 9049
– contaminants 9050, 9061
– dispersion 9055
– dissolved oxygen 9057
– ecosystem 4689
– fate 9049
– flood management 4688

– floodplain 3723, 3738, 3741, 3753, 8652
– radionuclide removal 8652
– flow 6347, 9054, 9056
– impacts on water quality 9056
– hydrodynamic model 9055
– ice 291
– Manning equation 9054
– mathematical formulations 9051
– modeling 9058, 9061
– pathogen pollution 9050
– point source pollution 9050
– pollutant loadings 9057
– quality 9055
– residence time 9057
– sediment siltation 9050
– transport 9049, 9054, 9059
– water 11922, 11924
– concentrations of target compounds 11922
– occurrence of pharmaceutical metabolites 11924
– waterbody 9051
rms-error 60
RNA
– interference (RNAi) 4039, 10757, 10761, 10771, 10854
– Double-Stranded RNA 4039
– technology 355
– molecules 4513
– silencing 10699, 10701–10702
RNA virus 642, 8140
RNA-silencing mutants 10706
road 3068–3069
– markings 3069
– work zones 3068
– congestion pricing 5022
– construction sites 3067–3068, 3071
– safety barriers 3071
– course estimation 6962, 6973
– crossing 68
– markings 3078–3079
– in work zones 3078
– network 2465
– pricing 5033
– basic theory 5033
– recognition systems 6952
– safety 65, 67, 70, 88
– sweeping and washing 269
– topology 2470
– traffic 205, 258, 664
– activity data 258
– transport model 254–256
– average-speed models 254
– combustion 254
– COPERT 255
– instantaneous models 256
– modal models 256
– multiple-regression models 256
– traffic situation models 256
– transport 245–246
– pollution 248
– source of pollution 246
– work map 3068–3069, 3071, 3075, 3077
– beacon 3077
– pylon 3077
– wireless communication 3075
– work zone 3070
road-traffic conditions 3084
road-traffic environment 3082, 3085
roadway network 7851
– efficiency 7851
Roault effect 132
robot/robotics 2477, 2479, 3172
– configuration 2477
– mapping 3172
– path-velocity decomposition 2479
robustness 3452
rock 4186, 4192
– geothermal systems 4148
– insulating capacity 4192
– permeability 4186
– systems 4142
– rock and reed systems 1633
rockfalls 3248
rocking-chair battery 11519
rogue bore 4427
roll back malaria (RBM) partnership 12001
roller-cone bit 4394
Roman house 903
roof
– catchments 8693
– water quality 8693
– gardens 4700, 4702, 4703, 4717, 4731, 4748, 10359
– technology 4703
– greening 4690, 4734
– in Germany 4734
– vegetation 4751
– water collection systems 8699
roofing shingle scrap 11704
rooflights 2809, 2812
rooftop water harvesting 8690, 8694
room temperature ionic liquid (RTIL) electrolyte 6054
root 9062, 9063, 9065–9066, 9068–9072
– abiotic stress 9066, 9071
– anatomy 9065
– biomass 9066
– chemical signals 9068
– development 9066, 9068
– field phenotyping 9071, 9072
– fraction 9063
– length density (RLD) 9066
– lodging 6203, 6205, 6207
– longevity 9070
– marker-assisted selection (MAS) 9072
– mean square deviation (RMSD) 9642
– morphology 9065
– nutrients 9068
– capture 9070
– penetration ability 9070
– resource capture 9069
– topology 9065
– traits 9065, 9069
– uptake of water and nutrients 9062
– water capture 9069
root-knot nematode 2702
root–shoot signaling 2643
Rossby
– length scale 11265
– number 12072
– wave 2136
Ross–Nilson G-function 7918
rotary kiln 1525, 1528, 5275, 5276
– incineration 5273, 6976
rotating magnetic flux 12145
rotating magnetic vector 12144
rotating ring disk electrode (RRDE) method 7739, 7745
– electrode stability 7745
rotavirus 11990
– route of transmission 11990
rotor 19
– inlet temperature (RIT) 6820
roundworm 12007, 12029
route guidance 3082–3084, 3093
– presentation timing 3093
routing
– error 11573
– in straight way 11578
– overhead ratio (ROR) 11565
– protocol 11553, 11556, 11575
– position-based 11553, 11575
rubber separator 8748
rubble 4722
Rubella 5349, 5351
– host heterogeneity 5349
– vaccination 5349, 5351
rubidium 4180
rubisco 2624–2625, 2634, 2644
rumex 1116
run definition 97

runoff waters 2336, 8635
run-of-mine coal 3846
rural areas 10364
– intensification 10364
– marginalization 10364
rural development 1564
rural electrification 1445
rural land use 5787
Russian Global Navigation Satellite System (GNSS) 3071
ruthenium 3975, 5176, 5191, 6571, 8266
– catalyst 8266
– complexes 6575, 6579
– oxide 798
rye 1111, 1122

S

Sabatier principle 3415, 3421
Sabin vaccine 8144
Sabin-like virus 8153
saccade 47, 49, 52, 54
– controller 52
saccharification 977, 989, 992, 11449
Saccharina 9122
Saccharomyces cerevisiae 973, 975, 1193, 6299
Saccharum 1273
S-adenosylmethionine (SAM) 1695
safe drinking water 7825, 9564
safe water framework 6607
safety barrier 3072, 3075
– detection 3075
saframycin 3157
Saharan air layer (SAL) 5072
Salicaceae 6021
salicylic acid 8024
saline
– formations 2155, 2160
– groundwater 4127, 4129
– soils 5315, 5318, 5327
Salinispora tropica 3163
salinity 2154, 2712, 4248
– stress tolerance 2712
– minimum water (SSM) 8659
– tolerance 5321–5323, 5326
– crops 5327
– gene combinations 5326
– proteins 5326
– traits 5322
salinization 5316
salinosporamide A 3162, 3164
salmon 519, 544, 575
– aquaculture industry 10319
– farming 3575
– production 1946
– stocks 6389
Salmonella 5051, 5060, 8765
– *enterica* 12014
– *pullorum* 8309
salmonellosis 5060, 5360, 5381
salmonid
– aquaculture 6391
– spawning gravels 3755
salt 2367
– accumulation 2755
– hydrates 10557, 10559
– iodization 1692
– overly sensitive (SOS) pathway 5324
– passage rates 2905
– sensitivity assay 5321
– sequestration 5326
– stress 2712, 5324
– tolerance 5319
– mechanisms 5319
– of dicotyledonous crop species 5319
– tolerant crop 5320, 5322, 5323
– breeding programs 5322
– transgenic approaches 5323
– varieties 5320
salting procedure 7047
– centrifugation 7047
– rotation 7047
samarium strontium cobaltite (SSC) cathode 9863
samarium–cobalt (SmCo magnets) 26
sand dune 3283
sand-lime bricks 3833
sandstone 7801
sandwich assay 1656
sanitary city 11340
sanitary landfill 4767, 5721, 5731, 5736, 11340, 11835
– alternative daily cover (ADC) 11835
– dry-tomb type 5731
sanitation 2560
sanitizing wastewater 1171
saprophytic microbiota 2561
Sarcocystidae 12041
sasol slurry phase distillate (SSPD) process 2225
satellite 4566, 4567, 4569, 4576, 7515, 8490, 8950, 9197, 9627
– aerosol index 6748
– altimetry 2456
– colonies 5550
– equations of motion 4569
– laser altimetry 4576
– mascons 4569
– multi-angle imaging spectroradiometer (MISR) sensors 7515
– observation 182, 197, 7285
– ocean color
– data 8970
– imagery 8955
– sensors 8926
– orbit
– control 4567
– perturbations 4565
– orientation 4567
– photography 283
– rainfall observations 8950
– remote sensing 8920, 8947
– for oil spills 7515
– of forest fires 8947
– safe mode 4567
– sensors 8921, 8923, 9627, 9741
– silicon solar cells 9197
– Stokes coefficients 4569
– system-generated electromagnetic pulse (SGEMP) 8490
saturation ratio 132
saturnism 10483
Savonius rotor 3402
sawtooth signal 55
saxitoxin 4821, 4823, 4832, 9083
scalar control 35
scalded skin syndrome 5062
scallop culture 7266
scallops 4829
scan line 3188, 3190
– classification 3188, 3190
– segmentation 3190
– super-segmentation 3190
scanning transmission electron microscopy (STEM) 7739, 7744
scattering
– effect 9628
– law 3800
scene photometry 11103
Scenedesmus communis 356
schedule 104
– coordination 104
– definition 97
schedule-based strategies 106
Schiff-base epoxidation catalysis 7602
Schistosomatidae 12043
schistosome worms 12003
schistosomiasis 12003, 12005–12006
– control programs 12006
– improved funding 12006
– treatment 12006
schistosomosis 5360

Schizochytrium limacinum 362
Schlumberger's modular formation dynamics tester 331
Schmidt number 596, 600, 604
school pond project 954
school yard 954
Schottky diode 1993
Schultz-Flory distribution factor 2242
Schwarze Pumpe 1430, 1440
Science education 3202
scientific
– drilling 6417
– information 4502
– knowledge 4502
scientification of planning 4535
scientometric 4502, 4515
scintillation detector 5565
scleractinian corals 2503
Scleractinia 2493, 2505
Scofield factor 6075
scombrotoxin 9082, 9101, 9104
– fish poisoning 9083
scotopic vision 11101
scrap tires 11704
scraper 5092
scrapie disease 2969
screen printing 9960
screenable marker gene 2598
screen 2198
screw-type engine 1407
scrubber 1340
– reaction products 11739
Scyphozoa 12047
sea
– clutter 7504
– floor 3151
– ice 280–281, 286, 2514, 2518, 2761–2763, 2766, 2775
– brine-pocket physics 2766
– computational considerations 2775
– global climate models 2763
– models 2763
– seasonal 2762
– level 2455, 2457, 2459–2460, 2492
– change 2455, 2492
– present-day 2457
– regional variability 2459
– rise 2460
– variability 4910
– variations 2455
– ranching 6388, 6398
– spray 124
– state 7402
– vegetables 9112
– water 8390
– radionuclides 8390
sea surface 7246
– height (SSH) 4577
– saturation specific humidity 7246
– temperature 2134, 2138, 2500, 2517, 3213, 4915, 4917–4920, 5866, 6742, 7248, 7304, 9701
– anomalies 2138, 7304, 8930
– Argo system 4918
– climate forecasts 4918
– long-term warming 4919
– satellite radiometers 4915
– satellite sensors 4917
– spatial mean temperature 4920
– subsurface thermal information 4915
seabass 519
seabed pockmarks 6412
seabirds 3569
seabream 519
SEAfarm 10325–10327
seafloor 5863, 5865, 6408–6410, 6412, 6419, 6423
– bathymetry 5865
– documentation 6410
– electro-optic cables 7287
– life 6408
– macrofauna 6409
– mapping 6423
– remote sensing 6412
– temporary anoxic conditions 6419
seafood 513–514, 534, 540, 543, 550, 560, 574, 838, 3579, 5050, 5893–5894, 5896, 5898, 6400, 6759–6760, 7386–7387, 9080–9081, 9086, 9089–9093, 9095–9096, 9099, 9101–9102, 9104–9105, 10317–10318, 12020, 12032
– alternative sources 3579
– antimicrobial drug contaminants 9090
– aquaculture-derived 9081
– bacterial pathogens 9086
– bio-preservation 9101
– biotoxins 9102
– detection 9095
– commodities 5896
– constitutes 9080
– consumers protection 9102
– consumption 838
– contamination 5050, 9081
– crisis 3556
– detection
– of biotoxins 9093
– of microbial pathogens 9096
– of norovirus 9105
– drug residues 9096
– food safety hazards 9081
– foreign imports 7387
– heat cold pasteurization 9104
– high hydrostatic pressure 9104
– histamine-producing bacteria 9101
– inadequately prepared 12032
– individually quick frozen 9104
– industry 543, 9092
– organochlorine compounds 9090
– parasite-free 12020
– parasite-infected 9089
– post-harvest-processing (PHP) 9104
– production 5898, 6400, 10328
– public safety 9091
– regulatory agencies 9091
– regulatory authorities 9099
– safety 2266–2267, 9079, 9093, 9099
– scombrotoxin 9101
– storage 9086
– supply 6760, 7387
– sustainability 534, 5893, 10324
– consumer demand 10324
– system 10323–10324, 10327–10330
– business model 10327
– economic sustainability 10327
– economy of scale 10330
– hatchery capacity 10330
– infrastructure 10329
– operational efficiencies 10328
– sustainable energy alternatives 10327
– toxic heavy metals 9089
– toxin detection 9093, 9104
– trade 540
– value chain planning 574
– *Vibrio* 9099, 9102
– watch cards 574
seafood-associated health hazards 9104
– detection methods 9104
seafood-borne disease/illness 7384, 9080, 9086, 9104
– biotoxin-linked 9104
seafood-borne pathogen 9099
seafood-borne poisoning 9083
sealed lead acid (SLA) battery 774
sea-level change 3233
sealless tubular cell 9857
seam 12087
seamless prediction 635, 2524
sea-salt 115, 125
Seasat-A Satellite Scatterometer (SASS) 8932
seascape 560

seasonal
– affective disorder (SAD) 9620, 9666
– climate 2120, 2134
– forecasting 9320
– forecasting 2119, 2122
– prediction 2144
– snow 289, 2762
sea-vegetable 9111
seawater 2899, 2904, 2919, 3455, 5050, 7230, 7233, 8668, 11874, 11887
– carbonate system 7233
– concentration of CO_2 7230
– contamination 5050
– desalination 2324, 2897, 3455, 11874
– direct cooling 4153
– dissolution of CO_2 7233
– osmotic pressure 2919
– radiocarbon samples 8668
– reverse osmosis (SWRO) 2904, 2910, 2911
– filtration process 2910
– network model 2911
– operational models 2910
– temperature 4910, 7307
– measurements 4910
– monitoring 4910
seaweed 518, 520, 547, 549, 551, 555, 559, 6312, 9109–9112, 9114–9116, 9118–9120, 9122–9123, 10326
– air-agitated tank culture system 9120
– aquaculture 7266, 9109, 9115, 9119
– biotechnology applications 9115
– crop 9116
– cultivation 555, 9116
– dermatitis 12047
– ecosystems services 9118
– exploitation 9123
– feed stocks 9123
– forced cultivation 9116
– genetic transformation 9123
– land-based aquaculture 9110–9111
– land-based cultivation 9118, 9122
– morphology 9111
– nutritional value 9112
– past and present uses 9112
– physiology 9119
– porphyra 9114
– production 9110, 9118
– successful on-land cultivation 9120
– taxonomy 9115
– undaria 9114
sebaceous gland adenocarcinoma 11404
Sebekidae 12040
secondary aerosol formation 111
secondary air injection 4960
secondary battery 741, 743, 745, 749, 759, 766
– cathode 759
– cost 745
– cycle life 741
– efficiency 741
– insertion compounds 743
– lithium–metal salt 766
– with aqueous electrolytes 749
secondary combustion chamber (SCC) 4969
secondary electron 5564
secondary energy carrier 1205
secondary ionizing radiation 8472
secondary lithium batteries 8720
secondary organic aerosol (SOA) 120, 8882, 8888
secondary pollutant 7823
sediment/sedimentary 1638, 3044, 3045, 3047, 3709, 3723, 3742, 3744, 3753–3754, 3757–3758, 3760, 3762, 10967, 10968
– adsorption 10967
– basins 4165, 4186, 4331
– budget 3762
– contamination 3044
– control
– measures 3753
– of upstream sources 3045
– strategy 3742
– deposition 3758
– desorption 10967
– in situ remediation approaches 1638
– isotope tomography (SITS) model 3739
– management 3047
– output 3744
– overloading 3045
– oxygen demand (SOD) 5679, 5688
– redistribution 3723
– resuspension 3044
– rock 7046
– shortage 3047
– source 3742
– fingerprinting techniques 3742, 3760
– types 3742
– storage 3709
– transfer 3742
– to the channel network 3757
– transport 2058, 9136
– by a river 3754
– dynamics 3744
– rates 10968
– trap 3741, 3753
sedimentation rate 3734
– overestimation 3734
sedimentation 1965, 3705, 3708, 3710, 3724, 3739–3740, 7033
– from surface water (SW) to deep water (DW) 7033
– in depositional sinks 3724
– quasi-continuous 3740
– soil erosion 3708
– traps 3739
– use of fallout radionuclides 3710
– water erosion 3708
sediment–water interface 3738, 9128, 9129, 9133–9141, 9144
– biodiffusion coefficient 9139
– Brownian transport 9139
– calculated fluxes 9140
– chemical transport 9129
– colloid Brownian diffusivity 9139
– color images 9129
– compartment 9133
– concentration 9137
– model 9144
– Darcian water advection 9139
– environmental models 9137
– flux
– behavior 9141
– equation 9135, 9136
– interface compartment (IC) model 9140
– Lavoisier mass balance 9138
– molecular diffusive transport process 9134
– multimedia compartment (MMC)
– flux equation 9138
– model 9140
– net flux 9133
– resistance-in-series (RIS) model 9140
– simulation methods 9138
– transport process theories 9133
sedum 4711, 4732, 4749
see green roof 4705
Seebeck effect 1415, 5539
seed 2710, 4553–4554, 4558, 9147, 9152, 9154
– bank dormancy 9153
– biomass 4553
– dormancy 9145, 9146, 9154
– germination 9147, 9152
– growth 4558
– inventory management system (IMS) 6699
– lots 9151
– falling number (FN) test 9151
– maturity 9147
– morphology 3291
– production regulations 10779
– quality 2649

– shattering 2710
– water concentration 4554
seedling resistance 2565
SEFABAR project 409
segmented gamma scanning (SGS) 7208
seismic
– design codes 3250
– event 3508
– liquefaction 2793
– network 11624
– path measurements 11635
– waves 2424
– zoning maps 2428
seismicity 2793, 11630, 11646
– induced 2793
– reservoir-triggered 2793
seismographic network 2429
seismological eruption 11643
seismology 11635
seismometer 4216, 11635
selectable marker gene 2597
selected water quality parameter 11925
– correlation analysis 11925
selection index 423, 425–426, 436, 1780, 2786
– drawbacks 426
selection-induced genetic variation (SIGV) 8322
selective breeding 390, 10865, 10840, 10868
selective catalytic reduction (SCR) 267, 933, 1333, 2254, 4769, 4984, 5263, 6849, 8091, 8362, 8366, 11849
selective catalytic remover 11806
selective noncatalytic reduction (SNCR) 1333, 6483, 8362, 8365
selenium 838–839, 1686, 1691, 3774
– deficiency 839, 1686
– toxicity 1686
selenocysteine 3666
– methyltransferase (SMT) 1714
selenoenzyme 1686
selenol 3666
selenomethionine 1691, 1715
selenoprotein 837, 1713, 7356
selenosis 1687
selexol 1590, 2153
selexol-washing technology 1621
self-pollinating plant 8045
Sellafield 8389, 8408
– signal 8667
semen cryopreservation 648
– in avian species 648
semiconductor 7892–7895
– alloy 7895
– cocatalyst deposited 7893
– composites 7895
– detectors 5566
– doping 7894
– dye-sensitized 7892
– semiconductor silicon 9197
semidry reactor 4960
semidwarfing gene 4073
semiempirical mass formula 3793–3794
semiochemical 5452
semivariogram 9753
semi-volatile micropollutant 5240
semivolatile organic compound (VOC) 111
sendai virus (SV) 6157
sensible heat 2370, 10557
– storage 10552, 10565, 10568
– in solid media 10568
sensor 3172, 3175–3176, 3179–3180, 8920
– alignment 11461
– architecture 3172
– calibration 3176, 3179
– coarse registration 3179
– configuration 11461
– data alignment 3176
– fine registration 3180
– fusion architecture 6957
– geometry 3175–3176
– satellite-based 8920
– technology 2484, 6954
sensorweb 8950
sentinel
– habitats 9157, 9167–9169
– coral reefs 9168
– tidal creeks 9169
– marine species 9157
– species 9163, 9165, 9169
– elucidating mechanisms for toxicity 9165
– establishing pathogenicity 9165
– harmful algal bloom (HAB) toxins 9163
– risk assessment 9169
separation of isotopes by laser excitation (SILEX) 5643
Separion separator 8725
septic tank 1148
septicemia 5054, 5063
– treatment 5063
– V. vulnificus 5054
sequence
– analysis 2699
– haplotypes 6431
– information 8
sequential batch reactor (SBR) 11956
sequential combustion 6822, 6849
sequential extraction test (SET) 2439
sequestration 1909
– science 2159
– deployment challenges 2159
serine
– acetyltransferase (SAT) 1696
– proteinase 4029–4031
Seriola rivoliana 3565
serpentine 1914
sertraline 4624
serum calcium homeostasis 9654
service reliability 104, 106
sewage
– gas 6806
– sludge 2279, 5244
– sludge ash 4873, 4874, 11704
– application in agriculture 4873
– sludge incineration 4868, 5277
– multiple hearth furnaces (MHFs) 5277
– treatment facility 5760
sewer and water treatment infrastructure system 4153
sex-specific transgenerational effect 3257
sexually transmitted disease 5354
– SI model 5354
shade leaf 2623
shading 2861, 3682, 3688–3689
– geometry 7654
– light shelves 3689
– overhangs 3689
shadow effect 9801
shaft furnace 5273
shale
– combustion 7482
– gas 7452
– oil 7452, 7454, 7474
– pyrolysis 7474
– recovery 7480
shallow combustion 1358, 1365
shallow-dose equivalent 3026
Shannon-Wiener diversity index 3273
shared climate policy assumption (SPA) 5422
shared socio-ecosystem pathway (SSP) 5422
shark 3567
sharpless epoxidation 7602
shear web 12211
sheep 1758, 1765, 1775
– body louse 1758
– breeding 1760, 1763, 1776
– diseases 1758
– genetic evaluation 1775
– genetic resource management 1765
– meat production 1752
sheet 292
– erosion 3709

shellfish 534, 1949, 4822, 4824, 6311, 9178–9179
– aquaculture 7266, 9174–9175, 9185, 9188, 9190
– best management practices 9185
– sustainability 9188, 9190
– biodiversity 9179
– culture 1943, 6766, 9176, 9180, 9182, 9189
– benthic effects 9189
– evolution of sustainability 9180
– industry-led initiatives 9182
– integrated multi-trophic aquaculture (IMTA) 9182
– interactions 9176
– pelagic effects 9189
– exotic species 9178
– filtration capacity 9178
– integrated land-based cultures 6311
– structures 9179
Sherwood relation 10538
Shiga toxin 5060
Shigella 499, 5051, 5059
shigellosis 5060
shikimate–3-phosphate 10717
shikimate 10717
Shinkansen train 4932, 4935
ship stack emission 138
ship track 138
shipping emission 246
shipping model 258
Shockley-Queisser limitation 7575, 9416
shoreline morphology 2460
short-rotation
– coppice (SRC) 6021
– forestry 1575
– wood 1603
shortwave
– global irradiance 9726
– radiation 9674, 9741
– solar spectrum 9714
SHOTS project 8681
shrimp 575
– farming 1929, 1942, 7387
– industry 6183
shrinking city 5837, 5839, 5846, 5849, 5851, 5853
– spatial planning strategies 5849
shrinking population 5839
shrinking urban region 11362
shutdown corrosion 4250
shuttle-cock battery 11519
sialic acid 8050
sick building syndrome 3679, 5335, 10268, 10267, 10272
side-caster 3038
sideromycin 507
siderophore 507, 6379
sideslip angle 3053
sieves 2198
sifting 4970
sign driver assist system 3126
signal priority 99
signal-controlled intersections 1884
signaling 3637
signum function 55
silage maize 1117–1119
– cold tolerance 1118
– late maturity 1118
– Southern European lines 1119
silanol 8604, 8614
Silceram ceramics 11604
silica
– gel 4604
– geothermometry 5223
– sand 7812
silicate 8604
– waste 11604, 11606
– weathering 2118
siliceous algae 1925
silicoaluminophosphate (SAPO) 2249
silicon 2563, 6091, 6142, 6380, 9198, 9203, 9293–9294, 9303, 9308
– anode 9294, 9297, 9306, 9309–9311
– closed-circuit voltage (CCV) 9297
– cycle life 9297
– cycling stability 9311
– delithiation 9294
– effect of electrolytes 9309
– effect of succinic anhydride 9309
– electrochemical lithiation 9294
– galvanostatic intermittent titration (GITT) 9297
– quasi-open-circuit voltage (QOCV) 9297
– salts 9310
– SEI formation additives 9309
– sodium carboxylmethylcellulose–based binder 9306
– solvents 9310
– band gap 9209
– biogeochemical cycle 6380
– carbide cladding 7197
– cell 9224, 9225, 9681
– non-concentrating 9224
– multiple photolithography steps 9225
– elastomers 7724
– electrochemical alloys 9294
– electrode 9308
– feedstock 9198
– heterojunction solar cells 9228, 9230
– gases 9435
– filaments 7957
– modules 9438
– monoxide (SiO) 9203, 9304
– nanoparticles 9293, 9303, 9304
– one-dimensional 9304
– nanostructures 9293
– nanowires 9293, 9303
– nitride 9230
– oxide 9220, 9230
– photodiode instruments 9682
– production 7956
– ribbon 9206
– rubber 3003
– sheets 9207
– solar cell 7946, 7953, 9196–9197, 9226, 9232, 9233, 9240, 9273, 9280–9283
– boron-diffused front emitter 9232
– cell designs 9282
– cell optimization 9273
– cell structures 9280
– crystallographic defects 9226
– light-induced degradation 9281
– materials 9281
– modules 9280
– monocrystalline 9233
– monocrystalline cells 9226
– multicrystalline 9233
– n-type mc-Si cells 9232
– optical enhancement 9273
– optoelectronic properties 9282
– performance issues 9280
– production technology 9283
– semiconductor properties 9282
– thin-film 9240
– wafer-based 7946
– surface texturization 9216
– wafer 7957
silicon/carbon
– composites 9300–9301
– ball milling 9300
– deposition of silicon on mesocarbon microbeads (MCMB) 9301
– high-temperature pyrolysis 9300
– nanotube composites 9301
silicosis 11135
siloxanes 1094
Silso 9204
silt density index (SDI) 10531, 10539
silver halide photography 11107
silver vanadium oxide 6087, 6508
silver–zinc battery 748

simian immunodeficiency virus (SIV) 5000, 8146
simple hot box oven 9493
simple jet 10977
simple natural ventilation (SNV) 6884
simple plume 10978
simple sequence repeat (SSR) 6696
Simpson's diversity index 3273
simultaneous saccharification and fermentation (SSF) 993
sine wave 12080
single nucleotide polymorphism (SNP) 400, 416, 480, 1737, 1779, 2965, 6696
single stage partial oxidation (PROX) 8222
single-copy transformant 10684–10685
single-copy transgene 10680
single-crystal (SC) 6848
– superalloy 6848
single-crystalline
– cell 9201
– silicon wafers 9203
single-flash power station 4279, 4298
single-ion conductor 6053
single-nozzle (diffusion flame) combustor 6840
single-nucleotide polymorphism (SNP) technology 4088
single-occupant vehicle (SOV) 1901, 4946, 5022
single-scattering albedo (SSA) 11155
single-step adiabatic steam separation 5230
single-stranded RNA virus 11985
single-vehicle tree 2481
sinkhole 3553, 5648–5650, 5652–56535668
– collapse 5648, 5650, 5652, 5653
– warning signs 5652
– development along highways 5649
– formation in roadway ditches 5652
– opening improvement/protection 5668
– rock pad 5657
– surface mapping 5662
sinorhizobium 1193
sinter-crystallization 11602, 11606
SION1 alkaline ionomer 380
SIR model 1938, 5348
– with vaccination 5348
sire 483
– heterozygous 483
– model 469
– variation 483
Sirius model 2554
site index 3290
Six-City Study 225, 226
skimmer pump 10146–10147
– sustainable features 10147
skin cancer 3611, 3645, 9661, 9663
– etiology 9663
– UV-induced 9663
skin-reddening 9658
sky
– luminance 2818
– radiance 11382
– radiation 9674, 9691
– view factor (SVF) 11269
skylight 2806, 2825
slab
– earthquakes 3237
– ocean 2514, 2516
slag/slagging 1340, 1345, 4855
– incineration 5281
– utilization 4003
slagceram 11601
slagsitall 11601–11602
sleep disturbance 2829
SLI battery 5882
sliding charge furnace 1380
sliding-mode control 52
slimhole-drilling 4387
slip angle 3057
slope failure 3250
SLOSS (single large patch or several small patches) principle 948
slow neutron 5568
slow pyrolysis 1518, 1526
– principles 1526
– process technology 1526
slowly rotating generator 12152
sludge 1177–1178, 1182, 6314
– conditioning 4874
– incineration 4875
slurry 1226, 9580
– bed reactor (SBR) 3971, 3976
– hydrogenation 2229
– jets 10992–10993
– of organic matter 1226
– SlurryCarb™-process 1080, 1082–1083
small angle X-ray (SAXS) diffraction 7771
small business liability relief 2011
small interfering RNA (siRNA) 2970, 10703
small modular reactor 7192
small secure transportable autonomous reactor (SSTAR) 4055
small solar power system (SSPS) 2369
small stock breeding 1770
small ungulates 11404
small wind turbine 3397–3399, 3403, 3405, 3406–3409, 3411, 3413
– costs 3405
– inspection and maintenance visit costs 3408
– of energy 3406
– of foundation and installation 3407
– operation and maintenance costs 3407
– replacement costs 3408
– tower costs 3407
– feasibility 3398
– generic design requirements 3413
– noise 3403
– on rooftops 3409
– operating on buildings 3411
– technology 3399
– vibrations 3403
small-bus services 1877
small-for-gestational-age effect 3639
smallpox 8126, 8150, 8160
– vaccine 8075
small-scale combustion unit 1351
small-scale heat and power system 1404
– conversion technologies 1404
smart community 10472
smart electric grids 10933
smart garage 7859
– demand 7859
– electric power capacity 7859
smart grid 3013, 3021, 3393, 3396, 9333–9334, 10449, 10451–10452, 10454, 10457–10462, 10464–10470, 10472, 10474, 10476, 10935, 10937, 10947
– barriers to the deployment 10451
– customer privacy protection law 10467
– deployment 10451, 10476
– development 10451
– distributed control 9334
– dynamic pricing 10462, 10464, 10466, 10468
– energy storage systems 10457
– European technology platform 10474
– feed-in tariffs 10457
– funding mechanisms 10470
– government agencies 10459
– initiatives 11185
– interconnection standards 10460, 10464, 10467
– international collaboration 10474
– investments 10452
– legislation 10458, 10461, 10468
– net metering 10454, 10465–10466
– policies 10449, 10454, 10458, 10459, 10472, 10476
– frameworks 10451
– in Italy and the UK 10470
– of the European Union 10468
– of the United States 10459
– proactive grid management 10449

– renewable electricity standards (RES 10457
– smart metering targets 10466, 10467
– standards 10469
– technologies 8994, 10449
– wide-area blackouts 10937
smart grip 10454, 10456
– demand response 10456
– dynamic pricing 10456
– interconnection standards 10454
– smart metering targets 10456
smart metering 10456, 10466, 10472, 10476
– commercialization 10472
– targets 10461, 10464
SmCo magnet 26, 30
Smith cycle 4328
smog 141, 208, 6808, 8349, 8881
smoke detectors 8525
– ionization-based 8525
smoking 10638
smooth-pursuit
– control 54
– movement 49, 51
– state-space control 51
snow 289, 2761, 2764–2766, 3217–3218, 9636
– ablation 2765
– accretion 2765
– accumulation 2765–2766
– blindness 11388
– cover fraction (SCF) 3219
– heat storage 3217
– interception capacity 3218
– models 2764
– water 3219
snowpack 2762
SNP marker 387
social carrying capacity 1968, 1971
social genetic effect 9361
social network analysis (SNA) 1939
social resilience model 2931
social urban infrastructure 5846
social-ecological system (SES) 1969, 3319, 3351
sociocultural information 11358
socio-ecological system 940, 3312
socioeconomic 4528
– models 2112
– status 213
– influence on health 213
socioeconomic sustainability 10320
socio-technical system (STS) 12220
sod roof 4701
soda-lime glass 11607
sodar 6594
sodium 765, 7330
– chloride 5316
– fire 2369
– fluorescein 9012
– hypochlorite 10653
– nitrate 10572
– silicate-activated slag (SSAS) cement 4404
sodium-beta battery 680, 11518
sodium-cooled fast reactor 4060
sodium-sulfur battery 678, 765
soil cultivation 155
soil decontamination technologies 10424
soil 849–850, 876, 1103, 1137, 1287, 1536, 1557, 1634, 1635, 1638, 2430–2433, 2564, 3213–3214, 3217–3218, 3220–3221, 3224, 3708–3709, 3718, 3722, 3750, 3775, 7670, 7674, 7675, 7678–7679, 7685, 8610, 9067, 10407, 10967, 10968
– adsorption 10967
– architecture 7684
– transfer of microbes 7684
– biology 151
– carbon 3224, 3707
– cavities 5649
– colloid-associated transfer 7679
– constituents 2432
– contaminants 2433, 2435, 10404
– halogenated organic compounds 2435
– metals and metalloids 2435
– radionuclides 2435
– contamination 2430–2431, 2440, 4794, 8796
– destruction technologies 2440
– extraction technologies 2440
– immobilization technologies 2440
– removal technologies 2440
– cultivation 155
– decontamination technologies 10424
– defecation 7670
– desorption 10967
– erosion 163, 3584, 3706–3708, 3724–3725, 3727, 3749, 3751–3752, 7675
– annual cost 3708
– countrywide survey 3751
– field scale investigation 3749
– quantification of soil redistribution 3725
– evaporation efficiency 3214
– ex situ approach 1634
– fallout radionuclides 3718
– fertility 1137, 7668
– flushing 2448
– gaseous phase 2433
– geochemical processes 7675
– heat storage 3217
– hydrology 3213
– in situ remediation approaches 1638
– mellowness 1103
– mineralogy 8604
– minerals 2432, 8608
– moisture 3213, 3220, 3221, 4137
– nutrient 155
– transfers 7674
– organic amendments 2564
– organic carbon sequestration 1287
– organic matter (SOM) 3782, 8606
– origin 2432
– particle associated transfer 7679
– pathogen transfer 7674
– phosphate adsorption 7685
– pH 876
– physical characteristics 876
– pore-size distribution 850
– properties 2432
– quality 1536
– redistribution 3708–3709, 3718, 3722, 3725–3726, 3745, 3750
– conversion models 3726
– qualitative information 3726
– sampling fields 3745
– remediation 2431–2432, 4797, 10407, 10429
– Based on Natural Processes 10429
– resources 9067
– restoration 1557
– saturation state 2432
– salinity 5316
– soil and water assessment tool (SWAT) model 1942, 5826
– solarization 2577
– sorption theory 7678
– structure 7668
– surface complexation modeling (SCM) 8610
– systems 7668
– temperature 3218, 3224
– testing 3775
– thermal diffusion 3217
– total petroleum hydrocarbon (TPH) levels 1635
– transfer of water 7674
– transpiration efficiency 3214
– transport rates 10968
– vapor extraction (SVE) 2446, 10147
– washing 2449
– water 3220
– freezing 3220

soil–cell interactions 7679
soil–root–microbe interactions 2734
soil:solution ratio 8618
soil–structure interaction 2427
soil-to-plant transfer factor (TF) 8615
soil-transmitted helminths (STH) 12007
– deworming 12007
– lymphatic filariasis (LF) elimination program 12007
– treatment 12007
soil–water–atmosphere–plant model (SWAP) 9324
sol particle immunoassays 5383
solar absorber 9457
solar activity 2101, 9475, 9707
solar air
– preheating 2371
– system 7662
solar aluminum processing 9609
solar beam 10625
solar cavity-receiver 9593
solar cell 1976, 6568, 6576, 6578, 7578, 7938, 7944, 7949, 9197, 9201, 9215, 9217–9218, 9220–9223, 9225, 9227–9229, 9231, 9241–9243, 9245, 9260, 9262, 9264–9265, 9271, 9273, 9276–9278, 9282, 9394, 9398, 9412, 9432
– aluminium alloyed rear emitter 9231
– alkaline etching process 9217
– a-Si:H-based 9260
– back reflectors 9276
– back surface field (BSF) 9221
– chalcopyrite-based 9394
– chalcopyrite-type compounds 9400–9402, 9405–9408
– absorber fabrication processes 9401
– coevaporation processes 9402
– efficiency 9407
– epitaxial layers 9402
– grain boundaries 9400
– junction formation 9406
– large-scale production 9406
– limitations 9407
– modification of the material system 9408
– multinary alloys 9401
– perspectives 9407
– role of sodium 9400
– single crystals 9402
– substrate configuration 9405
– surface properties 9400
– vacuum evaporation methods 9402
– collection of photocurrent 9398
– commercial development 6578
– crystalline silicon wafers 9201
– degraded steady state (DSS) 9262
– dye-sensitized 6568
– efficiency value 9278
– emitter wrap through (EWT) technique 9223
– end of life efficiency 9276
– energy payback times 9432
– environmental issues 9432
– fill factor 6576
– heterostructures 9229
– hydrogenated amorphous silicon 9241
– interdigitated back contact (IBC) 9222
– isotropic texturization 9218
– light-induced degradation 9264
– limitations on the operation 9271
– mc-Si-Based 9225
– metallization
– techniques 9221
– wrap through technique (MWT) 9223
– monocrystalline Cells 9223
– multi-junction cells 9276
– multi-junction structures 9242
– nanocoax-based 9282
– N-type silicon-based 9228
– optical enhancement 9273
– optimization 9273
– photogenerated carriers 9398
– plasma texturing 9220
– plastic-encapsulated 7578
– PLUTO technology 9227
– principles of cell operation 9265
– production companies 7949
– p-type UMG-mc-Si-based 9227
– reactive ion etching (RIE) texturization 9220
– reproducibility of cell fabrication 6578
– silicon surface 9215
– antireflection coating 9215
– texturization 9215
– single-junction p-type silicon-based 9215
– stability 6578
– Staebler–Wronski effect (SWE) 9241
– technology 7938, 7944
– thin-film material 9245
– triple junction stacked cells 9277
– very high efficiencies approaches 9412
solar central receiver plants 10573
– regenerator storage 10573
solar chemical heat pipe 9606–9607
solar chemical technologies 2381
solar collector 907, 6032, 9449–9450, 9452–9456, 9458–9460, 9464–9466, 9511, 9513, 9519, 9532, 9541, 9764, 10564–10565, 10573
– absorber 9456
– material 9458
– air-heating collectors 9466
– construction 9456
– covered liquid-heating flat-plate collectors 9464
– efficiency
– curves 9454
– factor 9459
– evacuated tube collectors 9465
– fields 6810
– fin-and-tube constructions 9459
– functioning 9452
– heat pipe 9465
– heat removal
– construction 9458
– tubes 9459
– housing elements 9460
– instantaneous efficiency 9453
– loop constructions 9466
– mean temperature 9455
– non-concentrating 9449
– optical losses 9452
– perforated absorber 9466
– Sidney tube 9465
– stagnation temperature 9454
– thermal losses 9452
– transparent cover 9459
solar combination store 10556
solar concentration 9418, 9420
– ratio 9591
solar conditioning 4133, 4142
solar constant program 9707
solar constant 9469–9470, 9621, 9676, 9697, 10163
solar cooker/cooking 9486, 9490, 9492–9494, 9498–9499, 9502, 9505, 9506
– advantages 9506
– cash saving 9505
– cum dryer 9499
– cum water heater 9498
– energy saving 9505
– environmental aspects 9505
– human health 9505
– hybrid concentrating model 9502
– social aspects 9505
solar cooling 9450, 9510, 9515, 9534, 9540, 10560
– applications 10560
– common system designs 9515
– cost performance 9534

– system 9509, 9510, 9540
– conversion chains 9510
– cost effectiveness 9540
– economical assessment 9540
– energy balancing 9540
– plants 9550
solar cosmic rays (SCR) 8472
solar cracking 9604
solar cycle 9472, 9475, 9479, 9483
– signal 9799, 9806
solar dermatosis 11400
solar desalination 9760
– using multi-stage sesalination with heat recovery 9760
solar detoxification 9562
solar dish 2351
solar disinfection 9579
– of water 9562
solar driving energy 9534
solar dryer 9486, 9487, 9759
solar electricity 1981, 1997, 8373
– cost-effective production 1997
solar electromagnetic radiation 9797
solar electromagnetic spectrum 9706
solar elevation angle 9712
solar energetic particles (SEP) 9797, 9810
solar energy applications 11391
solar energy 1233, 1370, 1477, 1977, 3306, 3466, 4691, 5174, 6566, 7641, 7661, 7936, 8976, 9412–9413, 9457, 9487, 9588, 9731, 10556
– absorptivity 9457
– applications of water storages 10556
– by photovoltaics 4691
– collection 9614
– conversion 5176, 9412
– conversion efficiency 9413–9415
– blackbody limit 9413
– Carnot limit 9413
– electrical losses 9415
– Landsberg limit 9414
– multicolor limit 9414
– nonradiative recombination 9415
– optical losses 9415
– Shockley–Queisser (SQ) limit 9413, 9415
– systems 9692
– thermal losses 9415
– thermodynamic limits 9413
– time reversibility 9414
– drying 9487
– economy 9766
– input 4135
– in thermochemical processing 9588
– limiting efficiency 9413
– management 2887
– photovoltaic conversion efficiency 9412
– potential 9646
– Shockley-Queisser model 1977
– transmission 2850–2851
solar forcing 9808
solar fraction for cooling 9537
solar fuel-cell technology 7611
solar fuel 2382, 9589–9590
solar fullerenes 9610
– synthesis 9610
solar gain 896
solar generation 8984
solar geoengineering 4108
solar geometry 915, 9711
solar glass 9459
solar heat 9511, 10564
– gains 3686
solar heating 906, 3694, 9450, 10560
– applications 10560
solar house 7641, 7646
solar hydrogen photocatalysis 5180, 5211
– iron-based system 5180
solar hydrogen production 3414, 5174–5175, 5187, 5190–5193, 5195, 5201, 5205, 5211–5212
– biomimetic iron hydrogenase 5187
– cobalt CATs 5212
– direct water reduction 5195
– light absorption 5175
– multicomponent co-based systems 5201
– photocatalysts 5190, 5212
– photocatalytic activity 5211
– Pt and Pd-based homogeneous systems 5205
– rhodium-based supramolecular photocatalysts 5190–5193
solar industry association 8384
solar insolation 10564
solar instrumentation 9692
solar irradiance/irradiation 2766, 8382, 9619–9621, 9640, 9647, 9677, 9756, 9806
– accuracy 9640
– at the top of atmosphere (TOA) 9620
– distribution 9647
– energy 2363
– flux density 9621
– global distribution 9619
– meteorological modeling 9756
– regional climate effects 9806
– uncertainty 9640
– world standard group (WSG) 9677
solar light energy 6568
– bulk heterojunction 6568
solar lime 9611
solar luminosity 9620
solar magnetic cycle 9797
solar measurement 9693
solar modules 9280
solar multivoltage cooker 9496
solar output 9799
solar oven 9507
solar particle event (SPE) 8577, 8578, 8586
solar photocatalysis/photocatalytic 9568, 9582
– detoxification process 9565
– disinfection 9564–9565, 9580
– processes 9581
– drinking water 9581
– water treatment 9582
solar photo-Fenton 9574–9575
solar photon 9712, 9716
– scattering effects 9716
solar photoreactor 9570, 9577
solar photovoltaic 4244
– generation 9335
solar physics 9483
solar pond 10556
solar power 209, 9592, 9906
– tower 2349
solar production 9594, 9603, 9608, 9612
– of fuels 9594
– of high-purity lime 9612
– of H_2 from fossil fuels 9603
– of material commodities 9608
– of metals 9594
solar radiation 350, 1100, 1140, 1234, 2351, 2372, 2619, 2625, 2814, 7273, 7564, 7621, 7643, 7653, 7913, 8560, 8577, 8924, 9197, 9396, 9428, 9470, 9493, 9649–9650, 9666, 9673–9674, 9676, 9680, 9685–9686, 9688–9690, 9693, 9696, 9705, 9707, 9709, 9711, 9731, 9740, 9743–9745, 9750, 9752–9754, 10621–10624, 10626–10630, 11406
– calculation procedure 10630
– components 9674
– cross-correlation analysis 9753
– database 10622, 10629
– digital elevation model 10623, 10624
– digital surface models (DSM) 10624
– distribution function 9750
– earth's atmosphere 9709
– energy 10118
– fluctuations 9744
– flux density 2619
– for solar energy utilization 9673
– forecasting 9743
– ground meteorological stations 10630
– ground-reflected 10626

– guide to measurement uncertainty (GUM) 9680
– history 9740
– human behavior 9666
– human health 9649
– instrumentation 9676
– management 2115, 4108, 9696, 10118–10120, 10122, 10124–10125, 10161, 10166
– aerosols in the stratosphere 10118
– climate model simulations 10120
– costs 10120
– history 10119
– risks 10119
– stratospheric 10124
– stratospheric aerosols 10125
– sunshades 10161, 10166
– volcanic eruptions 10122
– Markov chain models 9752
– measurement 9685, 9693, 11382
– scale 9676
– modeled data sets 9690
– modeling topographic effects 10623
– outside of the earth's atmosphere 9707
– parameters 10628
– penetrating a water body 7913
– period of record 9689
– physical models 9688
– rectennas 9428
– r.sun model 10627
– satellite observations 9754
– satellite-based models 9689
– satellite-derived 10629
– small-scale variability 9754
– solar energy conversion 9686
– spatial interpolation 9753
– spatial variability 9744–9745, 9752
– spectral distribution 9743
– spectrum 9705
– statistical analysis 9745
– sustainability 9743
– temporal resolution 9689
– temporal variability 9744–9745, 9750
– time series characteristics 9752
– transmission 9711
– aerosols 9711
– clouds 9711
– through the atmosphere 9711
– triangulated irregular networks (TINs) 10624
– versus climate change 9731
solar radiative power 9591
solar reactor 2382, 9599
solar receiver 2366, 9593
solar reforming 9605
solar resource 9646
– assessment 9743
solar roof programme 8383
solar silicon processing. 9609
solar spectral irradiance (SSI) 9707
solar spectrum 9725, 9727
– standard spectra 9725
solar steam
– cooking system 9503
– gasification 9607
– reforming 9605
solar storm activity 8532
solar surface irradiance 9620, 9628
solar system 2100
solar thermal collector 3695, 9461, 9462, 9468, 9518
– collector types 9461
– insulation 9461
– liquid-heating 9468
– noncovered flat plate collectors 9462
– reflector 9461
solar thermal desalination 9758, 9762
– markets 9762
solar thermal electricity generation 9591
solar thermal energy 9458, 9546, 9763–9765, 10551
– desalination 9765
solar thermal heating 9450
solar thermal power 10552
– plants 2386, 8984, 10557
– station 2369
solar thermal recycling 9612
– of hazardous waste materials 9612
solar thermal storage 10556
solar thermal system 9450
solar thermal tower 2352
– pollution 2352
solar thermochemical process 9593–9594, 9614
– economics 9614
– environmental impacts 9614
solar tower 2350–2351, 2387, 9773
– power plant 9774
– receivers 2387
– system 2367
– technology 2382
– desalination systems 2382
solar tracking device 9583
solar transformation energy 9427
solar transmittance 3689
solar ultraviolet radiation 11149–11150
solar updraft tower 9766–9768, 9771, 9773, 9775–9781, 9784, 9786, 9789, 9791–9793
– annual energy outputs 9793
– calculations 9776, 9778
– collector 9768
– roof 9771, 9786
– components 9768
– computational fluid dynamics (CFD) 9778
– custom-made thermodynamic simulation code 9789
– earthquakes 9775
– electricity generation costs 9792
– flow redirection 9778
– generator 9779
– large-scale plants 9791
– layout 9776
– output behavior 9781
– physical model 9781
– prototype 9784
– safety 9780
– settlement 9775
– storage 9771
– technical concept 9767
– temperature 9775
– tower 9773
– turbines 9777
– vertical wind velocity 9786
solar UV inactivation 9580
solar UV irradiance 9581, 9652
solar variability 9799
solar wall 7657, 7659–7660
solar water splitting 5175
solar window 900
solar wind 8579, 9803
solar zenith angle (SZA) 3215, 9628, 9630, 11152
solar zinc processing 9610
solar-assisted air-conditioning systems 9521, 9558
solar-assisted cooling system 9535
– energy balance 9535
– sensitivity analysis 9535
solar-driven heat buffer 9538
solar-electric microwave oven 9495
solar-generated electricity 9614
solar-grade
– polysilicon 7951
– silicon 7956, 7958, 9204
solar-hybrid gas turbine systems 2384
solar-hybrid micro-turbine (SHM) 2372
solaria for horses 11406
solar-produced carbon nanotubes 9610
solar-to-biomass conversion 352, 356
solgate 2372
sol-gel synthesis 4602

Solhyco 2372
solid acid catalysis 3947
solid biofuel 1067, 1072, 1085, 1199, 1207, 1209, 1210, 1241, 1492, 2271, 2273, 9821, 9824, 9827, 9831, 9834–9836, 9839–9842, 9844, 9847–9848
– ash
– content 9840
– melting properties 9840
– bridging properties 9844
– bulk density 9844
– calorific value 9834
– co-combustion 2271, 2273
– combustion 1210
– composition 9824
– deformation temperature 9841
– dimensions 9842
– estimating an amount of energy 9835
– fine matter 9842
– flow temperature 9841
– hemisphere temperature 9841
– impact of ash content 9835
– main elements 9827
– moisture content 9836
– particle density 9847
– physical-mechanical properties 9841
– resistance to abrasion 9848
– shape 9842
– shrinkage starting temperature, SST 9840
– size classes 9842
– thermochemical conversion 1207
– trace elements 9831
– volatile matter 9836
solid biomass 1352, 1416
solid electrode 745
solid electrolyte interface (SEI) 710, 6057, 6129, 6137, 9305
– model compounds 6057
solid electrolyte interphase (SEI) 6070
solid fertilizers 3772
solid fuel 239, 4009, 4769, 5246
– from waste plastics 4009
solid ion conductors 8720
solid mine waste 6666, 6668–6671, 6673, 6675, 6676, 6680
– acid 6673
– backfilling 6675
– disposal facilities 6676, 6680
– environmental problems 6666, 6673
– geochemical composition 6668
– health concerns 6673
– remediation 6675
– sources 6669
– storage/disposal 6671
– types 6668
– water contamination 6676
solid oxide electrolysis (SOEC) 9917
solid oxide fuel cell (SOFC) 1414, 2934, 2938, 2940, 2950, 2954, 3388, 3851, 3868, 3879, 3884, 3887, 5134, 5138, 5142, 5170, 6811, 7866, 9852, 9854–9855, 9858, 9861–9862, 9865–9867, 9869, 9874–9880, 9885–9889, 9891–9900, 9904, 9907–9911, 9913–9915, 9917–9919, 9922–9926, 9928–9929, 9934, 9938–9939, 9941–9942, 9944, 9947, 9949–9954, 9956, 9962–9964, 9966–9969, 9971, 9973
– accelerated materials discovery 9894
– active parts 9934
– advances in characterization 9879
– advantages 9910
– allocation between electricity and heat 9973
– anode polarization resistance 2950
– anomalous situation 9869
– area specific resistance (ASR) 9907
– auxiliary power units (APU) 9914, 9928
– balance of plant manufacturing 9969
– carbon
– deposition 9874
– footprint 9942
– reduction potential 9941
– cassette-type stack design 9962
– cell stack 9908
– CHP installation 9941
– chromium 9953
– companies 9918
– competitiveness 9928
– components 9963
– configurations 9887
– contamination 9867
– cost 9925
– in relation to applications 9878
– issues 9854, 9876
– CO_2 emission reductions 9939
– degradation 9866
– due to gaseous impurities 9876
– in cell performance 9869
– development of in situ diagnostics 9895
– devices 9887
– different types 9910
– diffraction measurements 9898
– distributed generation (DG) 9915, 9928
– dual proton-oxygen ion-conducting 9889
– durability 9854, 9865
– edge effect 9867
– effects
– of high conductive electrolyte 9879
– of minor species 9880
– of stack weight 9867
– efficiency 9886
– electrocatalysts 2940
– electrode materials 9893
– electrolyte materials 9891
– end-of-life treatment 9973
– energy demand for processing 9962
– environmental impacts 9967–9968
– equivalent annual cost (EAC) 9928
– exhaust gas 9938
– failures 9866
– in flow systems 9865
– feedstock material 9964
– field tests 9865
– flexibility 9886
– forecast the future cost 9926
– gas distribution 9867
– heterostructures 9892
– high power density (HPD) tubes 9919
– impurities 9875
– in situ materials characterization 9895
– integrated planar SOFC concept 9966
– intermediate temperatures 9886
– gaseous species 9880
– lanthanum 9949
– large central power plants 9929
– life cycle assessment 9944, 9967, 9971
– results 9968
– lifetime 9923
– lightweight 9962
– lightweight plasma-sprayed design 9963, 9964
– loan repayment factor (LRF) 9928
– long-term operation 9866
– manganese 9951
– manufacturing
– cost calculations 9925
– of components and cell 9956
– marketing issues 9904
– markets 9911
– materials 9944
– metal interconnect 9858
– metal support cells 9862
– micro-CHP units 9913, 9929
– micro-fabrication techniques 9888
– micro-planar 9888
– 3D microtomography 9899
– microtubular 9887
– mixed reactant fuel cells 9887
– mobile applications 9917
– net present value (NPV) of 9928

– neutron scattering studies 9896
– nickel 9952
– novel materials 9889
– off-grid 9917
– operation
– conditions 9869
– temperature 9862
– oxidation of hydrocarbons 2938
– oxide interconnect 9858
– PowerCore 9909, 9922
– proof of competitiveness 9922
– Raman spectroscopy 9899
– raw materials 9947
– redistribution of current flow 9869
– redox
– issues 9861
– stability 9956
– reliability 9854, 9862, 9865, 9924
– sealless tubular cells 9855, 9877
– seals 9861
– secondary power 9917
– sensitivity analysis of power density 9969
– SMMO anodes 2954
– spectroscopic techniques 9898
– stack
– behavior 9879
– manufacturing 9963
– modules 9909
– stationary stack design 9954
– steps in commercialization 9922
– strontium 9950
– sulfur contaminations 9875
– sustainability aspects 9934
– synchrotron
– diffraction 9897
– synchrotron X-ray studies 9897
– technology 9907
– test equipment 9900
– thermal cyclability 9956
– yttrium 9947
– zirconium 9947
solid petroleum coke (petcoke) particles 9607
solid polymer electrolyte (SPE) 3879, 3881, 6048, 8743
solid recovered fuel (SRF) 11837
solid solution
– geothermometry 5227
– semiconductor 7895
solid storage material 10553
– thermomechanical stability 10553
solid waste 5304, 5708, 5766, 6670, 8783, 9979, 9981–9984, 9986, 9991–9992, 9995–10000, 10013–10014, 10016, 10019, 10021, 10579, 11655, 11838
– analysis 8788
– economic benefits 8788
– aesthetic degradation 9986
– biodegradation 9999
– characterization 10000
– collecting 9996
– collection 11655
– composition 9998
– composting 9984
– discarded by humans 5708
– disposal 9979, 9987, 9995, 9997
– act (SWDA) 10016
– on land 5708
– pollution 9987
– vectors 9987
– education 10013
– energy resource 11838
– environmental education 10019
– environmental impacts 10014
– exchanges 8790
– generation 10000
– rate 9998
– incineration 9986
– land disposal 9984
– landfilling 9984, 9996
– laws and regulations 10016
– management 8772, 8789, 9981, 9998, 10579, 11656, 11695
– development 9998
– hierarchy 8772
– model 9991
– separation 11656
– source activities 11656
– stabilization wedge 11695
– storage 11656
– successful programs 10021
– system 9996
– waste hierarchy 11695
– minimization 8774, 8777, 8789, 10014
– personal and social benefits 8777
– open dumping 9996
– planning framework 10021
– public involvement 10013, 10021
– quantities 6670
– reaction models 5304
– recycling 9979, 9983, 9995, 9999
– assessments 8783
– reduction unit (SWARU) 11791
– resource depletion 9992
– reuse 9982
– source reduction 9981
– transport(ing) 9996, 11655
– treatment 5766, 8800
solid-electrolyte interphase (SEI) 742, 6041
solidification 2444
solid-recovered fuel (SRF) 5297
solid-to-energy conversion bed 5305
solubility trapping 4123
solugas 2372
solute chemical 10964
– sink rates 10964
– source 10964
solute metal 4855
solvation free energy 3424
solvent 3934
– refined coal 2231
solvent-free molten salts electrolyte 6056
somatic cells 10897
– count (SCC) 2967
– culture infection 10826
– nuclear transfer (SCNT) 6150, 6153, 6162, 10813, 10817, 10827
– agricultural application 6153
– application for livestock 6153
– factors affecting development of embryos 6162
– multiplication 6153
somatotropin 8062
soot cirrus 662
sootblower 4978
SOPERMA
– monomer 6932
– polymer properties 6926
sorghum 1110, 1127, 1272, 1276
– bicolor 1111
sorption 11974
– of organic micropollutants 11974
sound 12278–12279, 12283, 12289
– according to frequency 12278
– attenuation 12283
– fields 12278
– geometrical spreading 12283
– intensity 12277
– level limits 12290
– masking 12289
– power 12277
– level 12277
– pressure
– level 12277
– variations 12276
– propagation 12287, 12291
– calculations 12287
– waves (seismograph) 7799, 12276
– cylindrical 12276
– spherical 12276
– weighting filters 12279

sour gas 2237
sour wastewater 7834
source water 6611, 6615
– cryptosporidium 6615
– pathogen occurrence 6611
source–sink balance 4554
source 8519
– irradiator facilities 8519
– teletherapy units are 8519
South Asian monsoon (SAM) 6745
South Atlantic anomaly (SAA) 8471
Southern blot hybridization 2603
Southern hemispheric circulation 6753
Southern oscillation index (SOI) 6220, 8927
soybean 577, 1708, 1715, 4435, 4467, 4468, 4530, 5317
– cost of production 4435
– ferritin 1715
– genome 2690
– glyphosate-resistant 4530
– herbicide-tolerant 4435, 4468
– oil 924, 6901, 6904, 6906, 6910, 6925
– epoxidized 6910
– monoglyceride methacrylates (SOGLYME) 6902, 6906, 6929
– pentaerythritol alcoholysis reactions 6904
– pentaerythritol glyceride maleates 6904
– with acrylic acid 6901
– osmotic stress 5317
– production 4467
space
– absolute radiometric reference 9473
– conditioning 4359
– cooling 10559
– gravimetry 2459
– heating support 9558
– nuclear power source accidents 8514
– radiation environment 8471
– shielding 8541
space-borne camera 283
space-borne remote sensing 8940
spacecraft 4567, 8472
spallation neutron sources 8570
spark ignition
– combustion 5522
– engine 5468, 5477, 5519, 5532, 5533, 5539, 5540
– alternative fuels 5477
– direct injection 5539, 5540
– reciprocating engine 6832
spatial aerosol distribution 9629
spatial analysis 3336, 3338
– Eigenvector methods 3336
– Fourier analysis 3336
– spatial autocorrelation 3336
– spatial boundary analyses 3338
– spatial clustering 3338
– variography 3336
– wavelet analysis 3336
spatial autocorrelation 3327, 3334
spatial correlogram 3334
spatial crop structure 10035, 10037
spatial heterogeneity 3327, 3329, 3331–3332
– assumption of stationarity 3332
– data type 3332
– ecological consequences 3331
– levels of organization 3329
spatial mean velocity 2031
spatial mismatch hypothesis 5799
spatial pattern analysis 3328
spatial scale 3335
spatial statistics 3333
spawning gravels 3755
special sensor microwave/imager (SSM/I) 8932
specialty chemicals 7596
– catalysts 7595
speciation 3358, 3361, 3365
– allopatric 3361
– parapatric 3361
– sympatric 3361
species 10061, 10063, 10068, 10072, 10085–10087, 10090–10091
– breeding 1770
– coexistence 10072
– mechanisms 10068
– competition 10061
– conservation 10091
– definition 10086
– diversity 3300, 10085, 10087
– species diversity ecosystems 3299
– ecosystem function 10090
– extinction 10091
– genetic lineage 10086
– interactions 10063, 10091
– loss 6180, 10091
– niches 10068
– non-vertebrate 10087
– predation 10061
– taxonomic groups 10087
species–enemy relationships 10063
specific energy 3852, 3877
– capacity 5105
specific gamma-ray constant 8548
specific heat of a material 4136
specific leaf area (SLA) 2673
specific power 3852
spectral
– calibration 11119
– effects 9682
– efficiency of light 11379
– energy 11125
– irradiance at the surface 11387
– radiation 9713
– sensitivity 11114–11116
– of color imagers 11116
– shifting 11413
– solar irradiance (SSI) 9801
– solar radiation 9727
spectraradiometry 9725
spectroheliogram 9481
spectrophotometer 8808
spectroradiometer 9713, 9714, 9727, 11103, 11106, 11150
spectroscopic ellipsometry 9269
spectroscopic-based diagnostics 5394
spectroscopy 11381
speed 4930
– control 68, 72
– coupling device 3380
– sensor 3087
spent fuel 10423
spent nuclear fuel (SNF) 7067, 7181, 7188, 8589–8590, 8599, 8602
– interim storage facilities 7181
– radioactivity 8602
– storage 7188
spermatagonia 11033
spermatogenesis 1686, 3645, 10818
– germ-cell mutations 3645
spermatogonia 646
sperm 6151
sperm-mediated gene transfer (SMGT) 10825
spherical harmonics 4568
spherical neutron dosimeters 5569
spheromak 7165
sphingolipid 1681
spike
– fertility 2629
– index 2629
spikelets 2542
spilled radiation 2359
spinal cord stimulation 6510
spinal poliomyelitis 8142
spin-orbit coupling 6074
spiny-headed worm 12031
spirurina type X 12038
split service voltage 2978
splitter 2202
spongothymidine 3153

spongouridine 3153
spontaneous fission 8564
sporozoite 6293
SPR process 4006, 4010–4011
– by-products 4010
– description 4006
– productivity improvement 4011
– recycled products 4010
spray dryer absorber (SDA) 11807
spray irrigation 6626
sprinkler irrigation 6658
squamosa-promoter binding protein 2704
squamous cell carcinoma (SCC) 9661, 11398, 11402
squash 4464
– virus-resistant 4464
squirrel cage induction motors 5096
stabilization 2444
stable transformation 2585, 2590
stack health algorithms 8225
stack ventilation 6872, 6881, 6890
stacked elemental layer 9404
– rapid thermal process (RTP) 9404
stacking of resistance transgenes 4027
Staebler–Wronski effect (SWE) 7933, 8382, 9260
staged combustion 1319
stand-alone furnace 1386
– efficiency 1386
stand-alone furnace 1358, 1398
– operational safety 1398
– optimization of systems 1398
standard bus 1895
standard deviation of lane position (SDLP) 3112
standard hydrogen electrode (SHE) 6039
standard mean ocean water (SMOW) 5228
standardbred trotter 1803
– inbreeding 1803
standing column well (SCW) 4151
Stanford watershed model 5823
staphylococcal food poisoning 5062
Staphylococcus 500, 502, 5061
– *aureus* 500, 502, 2967, 5061
– *pneumonia* 500, 501
– treatment 5064
starch 988–989, 4555, 11435
– crops 11438
– raw materials 989
start-up burner 4969
starvation 535
STATCOM 12148
state transition equations 2474
static synchronous compensator 9342
static synchronous series compensator 9350
static VAR compensator 9342
stationary fuel cell applications 7867
– market requirements 7867
statistical downscaling method 6597
statistical entropy analysis (SEA) 11712, 11716
– environmental impact 11716
statistical mechanics 3787
– foundations 3787
stator 19
– fault 44
steady-state polarization (SSP) 6728
steam
– accumulator 2370, 10566–10567
– boiler 1345, 4977–4980, 4982, 4986
– auxiliary boiler systems 4977
– chemical dosing system 4980
– cleaning 4977
– cooling system 4982
– feed water system 4982
– preheating 4986
– rappers 4978
– sootblower 4978
– surface protection 4979
– turbine system 4980
– water shower cleaning 4977
– explosion 969
– gasification 1662, 5123, 5125
– generator 4980
– system (SGS) 2367, 2380
– line scrubbing 4284
– methane reformation (SMR) 3862, 3961, 5135–5136, 5138, 5142, 5144, 5154, 5161, 9606, 10516, 10518
steam pipe/piping 4292
– double-flash gathering system 4292
– single-flash gathering system 4292
– piston engines (SPE) 1248, 1331, 1405, 1420
– power stations 4297
– Rankine cycle systems 4297
– reforming 5125
– screw-type engine 1407
– storage systems 10560
– superheaters 5264
– traps 4284, 4291
– turbine 1247, 1330, 1409, 3849, 4250, 4278, 4282, 4284, 4311, 11773, 11775
– back-pressure 4311
– direct contact condensers 4284
– equipment 4250
– flash chambers 4284
– flash tank 4284
– hs diagram 11773
– purifiers 4282, 4284
– separators 4282
– surface condensers 4284
steam-enhanced oil recovery (SAGD) 4409
steam-generating power plant 8349
steam-methane reforming 5174
stearoyl-CoA desaturase (SCD) 10856
steel recycling 9991
steel slag 11704
steering control 3143–3144
– root means square steering error 3144
– under reduced contrast conditions 3143
Stefan condition 2765
Stefan-Boltzman
– constant 2766, 9592
– equation 633
– law 3216
stellarator 7163
stem cell 3605
– division 3605
– immortal stranding hypothesis 3605
– marker 647
stem lodging 6203–6204
steptoe allele 4078
stereoselective synthesis 7602
sterilization 11391
– by triploidy 10801
Stern-Volmer
– emission quenching 5194
– kinetics 5176
steroidogenesis 3275
sterol 14[α]-demethylase 1188
stewardship 566
stillage 996–997, 1047
stipules 1285
Stirling cycle 9512
Stirling engine 1248, 1331, 1332, 1348, 1408, 1417–1419, 1461, 1469, 1471, 1610–1611, 10495
– countercurrent gasifier 1469, 1471
stitching 6462
stochastic state-space representation 3058, 11193
stock enhancement 6387–6388, 6391, 6396
– evaluation 6396
– monitoring 6396
stoichiometric $LiNiO_2$ 712
Stokes
– coefficients 4568
– flow diagnostic equation 2768
– law 7026
– system 2771
Stokes–Einstein equation 2024
storage container 10556

storm track 2126, 2134, 2136, 5075
stormwater 3460, 4685–4686, 4692, 4717, 4720, 8690, 8692, 8696, 1009510096, 10098, 10100–10101, 1010310104, 10106–10112, 10115, 10360, 11348
– artificial neural networks (ANN) 10111
– biofilter 10108–10109
– biofiltration systems 10101
– characteristics 10096
– deep bed filtration 10107
– education 10100
– fiber filters 10107
– filtration 10103
– harvesting 10095–10096, 10104, 10111
– management 4684, 4686, 10096, 11332
– management model (SWMM) 10111
– measuring treatment effectiveness 10111
– microfiltration 10108
– monitoring of water quality 10111
– nonpoint source pollution 8690
– objectives 10106
– physiochemical treatment 10107
– pollutants 10096
– removal 10115
– pollution 10098, 10100, 10106
– pretreatment devices 10103
– quality 10098, 10106
– recycling 10104
– reuse 10095–10096, 10110
– runoff 4717, 4720, 8696, 10360, 11348
– rates 4720
– sand filtration device 10104
– taxes 4705
– treatment 10096, 10113, 10115
– biofiltration 10115
– effectiveness 10112
– measures 10098
– MUSIC model 10113
– targets 10106
– ultrafiltration 10108
– volumes 4720
stove 1310, 1352, 1358, 1389, 1492, 1615
– emissions 1389
– permanent combustion 1358
– technology 1310
strainmeter 11638
strategy metrics 4622
stratigraphic trapping 4122
stratigraphy 11629
stratosphere/stratospheric 113, 118, 2116, 2513, 9806, 10120, 10124, 10130–10131, 10135
– aerosols 130, 4108, 9628, 10117, 10120, 10121, 10123, 10125, 10137
– black carbon 10123
– solar radiation management 10117
– sulfate 10121
– types 10121
– chemistry 10131
– cooling 10135
– engineered particles 10124
– heating 10124
– ozone 613, 11157
– depletion 10130
– hole 11153
– layer 314, 653
– natural ozone layer 10130
– transport 8887
– pollution 205, 10129
– sulfate 10121
stratosphere–troposphere coupling 9808
stratovolcano 11615, 11620, 11622, 11624, 11629, 11642
straw
– combustion 1342
– fuel furnaces 1382
– gasification 5130
stream 9049
street canyon vortex flow 11300
street canyon 259, 11272
– scale 11313
– vortex flow 11300
street scale 11269
street tree 11345
street ventilation 11281
– wind tunnel experiments 11281
streetcar 1813–1815, 1890, 5978–5979, 5981, 5984, 6011
– decline 5978, 5981
– investments 6016
– lines 5983, 10931
– Presidents' Conference Committee 5979
– productivity 5984
– revolution in technology 5979
– systems 5975–5976, 5982, 6015
– capital infusion 5982
– municipalization 5982
– traffic densities 6011
streptavidin 4038
Streptococcus 503, 5057, 6325
– *iniae* 3566, 5057, 5064
– *mutans* 8075
– pneumoniae 503
Streptomyces 501, 502
– *griseus* 503
– *lavendulae* 502
– *platensis* 500
– *rubellomurinus* 502
– *tenjimariensis* 1193
streptomycin 10677
– phosphotransferase (*SPT*) 10677
stress- and maturation-induced promoter 10750
stress tolerance 3
stressor 1184, 1193
– heavy metals 1193
stress 1184, 1191
– salinity-related 1191
strip mine 6671, 6679
strobilurin 2569
Stronglyloides 12044, 12045
strontianite 8624
strontium 8452, 8459, 8623, 8639, 9950
– strontium–90 3710
– titanate (STO) 2954, 2955, 2956, 9892
– catalysis 2956
– conductivity 2955
– wastes 4776
structural equation modeling 3093, 3097
structure activity relationship (SARS) 6800
structured decision making 3347–3348
structure 4553
– endosperm 4553
styrene 5566, 6909, 6918–6919, 6928
– butadiene rubber (SBR) 253, 6133
– monomer 6919, 6928
subbituminous coal fly ash 2171, 2178, 2229, 3825, 8353
– fly ash 3825
submarine cable 7302, 7418, 7419, 11180
submerged combustion 5282
submergence tolerance 2713
subnational immunization day (SNID) campaigns 8146
subsea steel structures 6405
subsea technology 6407
subsidence bowls 4211
substance concentrating efficiency (SCE) 11715
substation 2291, 3004–3009
– automation facilities 3009
– design considerations 3005
– grounding 3004
– standardization 3006, 3007
– voltage 3004
substitute natural gas (SNG) 2251
subsurface 4183, 4185, 10138, 10141–10142, 10144, 10146, 10156, 10418
– biobarriers 10418
– contaminants 10145
– sustainable remediation 10145
– transport 10142

– energetic compounds 10156
– explosive 10156
– fate 10138
– fluid flow 4185
– heat 4183
– karst 5663
– mapping 5663
– permeability 4185
– petroleum hydrocarbons 10146
– porosity 4185
– remediation 10141, 10144
– soil 4142, 4148
– sustainable remediation 10144
– temperature distribution 4185
– transport mechanisms 10141
– transport of chemicals 10138
– water 4183
sub-transmission substations 2994
subtropical belt 9638
suburban
– bus routes 1875
– light rail stations 5993
– rail transit 10925
– transit bus 813
suburbanization 5788, 5790
subway lines 5985
subway 5996
– lines 5985
succession 3281–3283, 3285, 3288
– Clements' concept 3281
– Clementsian concept 3285
– Cowles' concept 3283
– facilitation model 3285
– Gleason's concept 3283
– individualist concept 3283
– individualistic concept 3282
– land-use policy of the United States 3288
sucrose synthase 2648
sucrose 1277–1278
– synthase 2648
sudden death syndrome (SDS) 3640, 8317
Suffolk sheep 1760
sugar
– beet 1112, 1222, 4451
– costs of production 4451
– herbicide-tolerant 4451
– crop 1272, 11438, 11447
– intermediates 11440
– kelp 518, 522
– platform 11447
sugarcane 1005, 1008, 1011, 1014, 1018, 1222, 1272–1276, 1292, 1539, 11448
– agroecological zoning 1008
– as a bioenergy crop 1275
– bagasse 1276
– cogeneration 1018
– burning 1011
– crop 1014
– cultivation 1273
– ethanol 1008, 10510, 10514
– sustainability 1008
– ethanol production 1010, 1012–1013
– costs 1012
– social aspects 1013
– soil quality 1010
– genome mapping 1018
– harvesting 1014
– manual 1014
– mechanization 1014
– industry 1009
– land availability 1009
– water pollution 1009
– mills 1016
– cogeneration 1016
– plant 982
– setts 1274
– stillage in fertirrigation 1018
sulfamethoxazole 11922, 11924, 11926
sulfate 124, 171, 1316, 3778, 6381, 7338
– aerosols 2116, 10121, 10123
– sulfur 2209
– waste 11704
sulfate-reducing bacteria (SRB) 6411
sulfhydryl 1648
sulfide 6381
sulfite compounds 6145
sulfobacter oxidants 1093
sulfonated engineering thermoplastics 8335
sulfonated perfluorovinyl monomer 6544
– new synthetic routes 6544
sulfonated poly(phthalazinone ether ketone)s 6560
sulfonated polysulfones 7774, 8336
sulfonic acid group 3882
sulfopropylated polysilsesquioxane 6561
sulfotransferase (SULT) 3643
sulfur 611, 765, 969, 1150, 1430, 1667, 2250, 2252, 2942, 2945, 3778, 3906, 3910–3911, 3979, 6381–6382, 6505, 6680, 8349, 9830, 11313
– biogeochemical cycle 6381
– deprivation 363, 365
– dioxide 170, 204, 223, 235, 611, 2025, 2195, 2277, 2282, 8350, 8352, 10483, 11293, 11320
– emissions 8883, 8891
– emission 188
– fuels 11320
– heterocycles 4657
– hexafluoride 3002, 6988
– oxide (SO_2) 208, 2278, 8352, 8366
– poisoning 3911, 9875
– tolerance 3906
sulfur-containing fuels 9875
sulfuric acid 118–119, 208, 699, 773, 1093, 2167, 5887, 8883
– alkylation 7837
– in lead-acid batteries 5887
sulphated zirconia 4603
sulphonic acids 4603
summer crop 1123
summer syndrome 11409
sumoylation 3604
sun 2807
– activity 9621
– exposure 3645
– illumination 2807
– leaf 2623
– protection factor (SPF) 11385
– shading 901
sunburn (erythema) 9657, 9658, 11409, 11411
sun–climate relation 9799
sun–earth geometry 9745
sunfleck 2620, 7920
sunflower 9148–9149
– dormancy 9148
– seeds 9149
sunflower–soybean intercrop 10046
sunlight 631, 1477, 2806, 3611, 9667
– harvesting 6574
– reflection 2115
sunphotometry 9713, 9714, 9725
sunshade 2115, 10161, 10162, 10164–10166
– efficacy 10162
– engineering considerations 10166
– geoengineering 10164, 10165
– in space 10162
– climatic effects 10162
– Lagrange point 10166
sunspace 7664
sunspots 9480, 9798
– darkening 9479
– number 9475
– observations 9480
superbinary vectors 2593
supercapacitor 794–796, 798–801, 3427–3428, 3441, 3847, 3852, 6771, 6773, 6784, 11503
– bank (SB) 795
– carbon electrodes 6771
– electrochemical double layer 796
– energy efficiency 801

– in neutral medium 6784
– in organic electrolyte 6771
– model 798
– nanoporous carbon electrodes 6770
– power availability 801
– storage bank 801
– total amount of energy 800
– working principle 796
supercharging 5536
superconducting
– energy storage 6288
– loops 6274
– magnets 6250, 6253, 6257, 6259
– winding 6251
superconductor 6278
– cost 6278
supercooling 10559
supercritical carbon dioxide 2159, 10169–10171, 10173–10174, 10176–10182
– applications 10170
– carbon–carbon bond forming reactions 10174
– catalysis of enzyme 10176
– chemical reactions 10171, 10177
– cleaning 10182
– continuous synthesis of methyl ethers 10176
– diffusion coefficient 10170
– dyeing 10182
– electro-oxidation reaction of benzyl alcohol 10177
– esterification of acetic acid and ethanol 10176
– hydrogenation reactions 10171
– inorganic nanomaterials 10179
– material preparation 10179
– oxidation reactions 10173
– painting 10182
– photo-oxidation 10174
– polymerization 10178
– preparation of polymer composites 10180
– properties 10170, 10180
– chromatography 10181
– water-in-CO_2 microemulsions 10182
supercritical fluid (SCF) 4616, 10169
– chromatography (SFC) 10181
– extraction (SFE) 10170
supercritical gas extraction (SGE) 2224
supercritical light water reactor (SCLWR) 4064
supercritical water-cooled reactor 4063
Superfund Act, see also Comprehensive Environmental Response, Compensation, and Liability Act (CERCLA) 2006, 2007
Superfund Amendments and Reauthorization Act (SARA) 2008
Superfund Comprehensive Accomplishment Plan (SCAP) 2009
superfund 2015, 3595, 10436
superheated steam 10573
superheater 1345, 1346, 4978
– corrosion 5265
super-insulation 898, 7630–7631
supernatant 11950
supernova explosion 11207
superoxide dismutases (SOD) 4
supersaturated water vapor field 119
supersaturation 118
supplemental irrigation 5630
support vector machine (SVM) 3117
supported liquid membrane 8720
supported reagent 4600–4603, 4607
– adsorption 4602
– Bronsted acid catalysis 4603
– catalysis 4602
– evaporation 4601
– loading the support 4602
– preparation 4601
– solid base catalysis 4607
– wet impregnation 4601
supramolecular photochemistry 5175
supramolecular solar hydrogen photocatalysis 5175, 5209
– palladium-based 5209
surface 2767, 3222, 3239
– air flow 11265
– air temperature 4911, 4918
– albedo 634, 2764, 2766
– complexation models (SCM) 4779, 8613
– desalination processes 2160
– drainage 5656
– energy balance 2766, 3215
– evaporation 9736
– forcing 3217
– freshwater flux 7255
– hydrology 8912
– irradiance 9627
– global distribution 9627, 9637
– irrigation 5626–5627
– jet 10982
– karst map 5665
– magnetism 9484
– melting furnaces 11586
– meltwater 2767
– mining 2185, 6666–6667, 6669, 7810
– solid wastes 6667
– plasmon resonance (SPR) technology 3587
– radiation 9732
– measurements 9732
– rail systems 5984
– reflectivity 2116
– runoff 3222
– ruptures on structures 3239
– solar dimming 9734, 9737
– solar radiation 141, 9731–9734
– impacts on the climate system 9734
– urbanization effects 9732
– variations 9733
– temperature 656, 2106, 2122, 4681
– tiles 3215
– topography 8909
– transportation 205
– ultraviolet radiation 11151
– ultraviolet variability 11152
– water balance 3218
– water body 11005
– tritium 11005
– water 3455
– temperature 7307
surface-enhanced Raman spectroscopy (SERS) 5385, 5392
– bacteria identification 5392
surgeonfish 832
surrogate species 3303
suspended sediment 2055, 2058
suspended solid (SS) 11968
sustainability/sustainable 66, 151, 189, 198, 406–407, 566–567, 1490–1491, 2006, 2062, 3201, 3278, 3287–3289, 3331, 3450, 3452, 3844, 4039, 8702, 8857, 8861, 9186–9188, 10189, 10261–10262, 10299–10300, 11341
– agriculture 2742
– aquaculture 566, 569
– biochar system 885
– breeding 1756, 1807
– building 1037, 3676, 3680, 3702, 8703, 10192, 10194, 10196, 10206, 10281, 10291, 10294
– early design phase 10206
– enclosures 3702
– energy generation 10291
– experience 10196
– knowledge 10196
– operating costs 1037
– principles 10194
– theories 10194
– building design 10197, 10209

– energy modeling tools 10209
– evaluation of selected tools 10209
– building massing 10266
– health 10266
– built environment 10285, 10295
– policy matters 10295
– principles for the design 10285
– cities 6860, 11340
– concept 10189
– of water 10189
– construction 10299, 10300
– definition 1491, 10262
– design 10262–10263, 10279, 10285, 10299, 10300, 10301, 10303, 10307
– decision making 10261
– definition of health 10263
– health 10279
– integrated delivery processes 10303
– movement 10302
– development 8866
– of indicators 9186
– ecological aquaculture (SEA) 10317–10321, 10323, 10327
– chemicals 10320
– chemotherapeutic compounds 10319
– commercialization 10323
– community design input 10323
– ecological design 10320, 10321
– energy consumption 10320
– inorganic fish wastes 10320
– operational framework 10320
– operational involvement 10323
– organic fish wastes 10320
– social sustainability 10323
– species selection 10319
– stock escapes 10319
– economic aspect 11341
– ecosystem 10437
– education 3201, 3202, 3204, 3207–3208, 10025
– for incarcerated youth 3208
– history 3202
– local-to-global connections 3208
– program 3207
– student outreach in science (SOS) 3208
– twenty-first century 3204
– enclosures 3676
– energy 5882
– evaluating 3452
– farming 1783
– heating ventilation and air conditioning 10332, 10335–10342
– architectural design 10337
– bioclimate 10338
– bioregionalism 10338
– developing engineering alternatives 10336
– engineering integration 10337
– human factor 10341
– ideal design diagram 10336
– innovation 10340
– integrated design process 10337
– leadership in energy and environmental design 10337
– optimizing high tech 10339
– order-of-operations thinking 10336
– prioritizing low tech 10339
– rating systems 10342
– replication 10341
– system solutions 10335
– tools 10340
– whole systems thinking 10338
– herbicide-resistant crops 10344
– holism 198
– in animal breeding 406
– in water 10189
– indicator 9187
– matrix 9188
– indices 9186
– indoor environments 10276
– interior systems 10275
– ergonomics 10275
– health 10275
– materials 10275
– land use 10264
– health 10264
– landscape 10357, 10360, 10382, 10385
– analytical tools 10382
– construction 10385
– design 10385
– indicators 10382
– management 10385
– planning 10385
– visualization tools 10382
– lighting 10274
– health 10274
– maintenance 10279
– mining 6634, 6642
– modern concept 1490
– of transgenic insect-resistant crops 4039
– productivity 10390
– rating systems 8702
– redefining 8861
– regenerative development 8857
– remediation 10435, 10442
– forum (SURF) 10437, 10443
– resiliency 3452
– seafoods 9186
– smart grids 10448
– spatial disturbance legacies 3331
– science 3290
– modern forestry 3290
– succession 3278, 3288
– through reintegration 10299
– trajectory 567
– transportation 10481, 10489–10490, 10543
– definition 10489
– solutions 10490
– technologies 10490
– types of vehicles 10490
– urban drainage systems (SUDS) 4686
– urbanism 10294
– vegetation dynamics 3287
– vehicle
– fuels 10502
– technologies 10482
– waste management 10577, 10581
– water production 10533
– electrostatic interaction 10533
– water resource 11875
– water supply 8689
– water treatment 10530
– water usage 10358
sustained multitrait selection 9360
sustained Spheromak Physics Experiment (SSPX) 7167
sustenance 3844
swamp gas 1147
sweep gas membrane distillation 2920
sweet corn 2709
sweet sorghum 1276–1278, 1292
– as a bioenergy crop 1278
– cultivation 1277
– seed germination 1277
swimmer's itch 12043, 12047
swine flu 10860
swine pathogen 10844
swing-hammer shredder (SHS) 8812
swirl injection 4969
switched reluctance motor (SRM) 10542, 10543, 10546, 10549, 11526, 11531
– electrical structure 10546
– mechanical structure 10546
switches 3001
switchgear 2999
switchgrass 1279, 1281–1284, 1293, 6024, 6025
– agronomy 1284
– ecotypes 1282
– farming 10510
– fertility 1283
– for bioenergy 1284
– seed germination 1283

switching 10076
sylviculture 1446
Symbiodinium 2493
symmetry of ignorance 4535
synchronous machine 12142, 12144, 12147
– pole-pair number 12147
synchronous power system 12105
synchronous reference frame 39
synchronous speed 12153
synchrophasor 12080–12082, 12088
– measurement 12094
synchrotron 8577, 8586
– photon 8577
– powder diffraction 9896
– radiation 9897
SynCoal 2217, 2218
SYNCOM process 6463, 6465
SYNCOM-Plus process 6485, 6487
syncrude 2225, 3978, 7811, 7816
synfuel 3956, 6246
synthesis gas (syngas) 848, 852, 1427–1428, 1433, 1442, 2153, 2168–2169, 2171, 2224, 2226, 2235–2236, 2248, 2250, 3938, 3947, 3957, 3961, 3966–3967, 3981, 5123, 5137, 5161, 5164, 5473, 7594, 8098, 9596, 9603, 11439, 11444, 11588, 11833
– compressed 3981
– nitrogen-diluted 3967
– platform 11451
– precombustion cleanup 2169
– production capacity 3966
– use in Fischer–Tropsch GTL 3961
synoptic weather system 5078
synthesis
– plan 4632–4633, 4638
– material efficiency 4632
– strategy efficiency 4633
– tree diagram 4621
synthesized biofue 1216
synthetic
– aperture radar (SAR) 288, 8940, 8942
– biofuel 1043, 1428
– biology 4499
– breed 393
– combustion 6463
– crude oil 7816
– diesel fuel 5471, 5473, 5490
– synthetic estrogen 11962, 11963, 11975
– fertilizers 2747
– fuel 1585, 1604, 2218, 3956
– production pathways 1585
– gasoline 6246
– gas 1034
– graphite 6141
– natural gas (SNG) 1428, 1494, 1612
– organic chemistry 7596
– pharmaceuticals 6522
– porphyrins 7600
– ligands 7599
– precipitation leaching procedure (SPLP) 2442
– procedures 4585
– synthetic pulp separators (SPG) 8748, 8750
– wheats 8020
– zeolites 4586
system average interruption
– duration index 2980
– frequency index 2980
system integrity protection scheme (SIPS) 10945, 10948
systemic acquired resistance (SAR) 2574, 10697
systemic calcium homeostasis 9653
systemic fungicide 2568
systemin 4029
system-on-chip sensor 704

T

T lymphocyte 11134
tables 5515
tachycardia 6507
tachyplesin 10701
Tafel
– equation 3880
– law 3876
– reaction 3416, 3420
– slope 3420, 8341–8342
Tafel–Heyrovsky mechanism 3417
Tafel–Volmer mechanism 3416, 3420
Tafenoquine 11085
tail gas 1442, 2236
– recovery 1589
tailings
– dam 2792, 6674
– failures 2792
– flow 2793
taliglucerase alpha 8067
TAML catalysts 7609
tandem
– catalysis 7612
– cell 7576
tank melter 11586
tanker accident 7827
tantalates 7889
tantalum oxynitride 8270
target population of environments (TPE) 8014
targeted induced local lesions in genomes (TILLING) 366, 6794
targeted transposon tagging 2700
tar 1338, 1394, 1463, 1465, 1467, 1519, 1667, 5127
– cracking 5305
– degradation 1463
– removal 1467
– sand 7811
– bitumen 7798, 7813
– non-mining methods 7813
– sand mining 7809
– separation 1465
tasidotin 3156
tax incentives 12262
taxonomic key 5438
Taxus
– *baccata* 6525
– biosynthesis 6529
– cells 6525
Taylor expansion 12085
T-DNA transfer 2607
tebufenozide 2596
technetium 8393, 8397, 8403, 8430, 8522, 8624
– generators 8522
– in seawater 8403
– Speciation 8393
– transfer to farm animals 8430
technical glass-ceramics 11601
technological fix 12221
technological sustainability 8863
technologically enhanced naturally occuring radioactive material (TENORM) 8469, 8479, 8481, 8531
– tobacco product 8481
technology 2439, 2440, 4495, 4496
– agricultural 4496
– fast-track 4495
– hype cycle 4495
– trigger 4493
technosphere 10578
– nutrient certificates 9042
tectonics 4565, 11618
– setting 11634
Teflon 6948, 7696, 7704, 8341
telecamera 46, 48, 56
telecommunication back-up power systems 5883
teleconnection 2123, 2128, 2137
– El Niño-related 2128
teletherapy 8528, 8580
– accelerators 8586
tellurium 1998, 7939
telomerase 647
Temkin adsorption conditions 8342
temperature polarization coefficient 2922

temperature 4915, 4921
– anomalies 4921
– coefficient 3804
– effect on sound speed 4915
– fluctuations 4137
– observations 4911
TEMPO 7606
temporal partitioning 10076
temporary green space 11368
temsirolimus 3155
Teosinte 351, 2703
Tephra 11641
terephthalic acid (TPA) 3934, 3941
termitary 6868
termites 6868
terpolymer 6542
terra preta 881, 883
– soil 846–847
terra-vit melter 11588
terrestrial
– agriculture 560
– biogenic 120
– ecosystems 3302, 11892
– heat flow 4195
– mammals 10088
– mass changes 4563
– permafrost 281
– proteins 577
– radiation environment 8474
– sediment sinks 3738
– water storage (TWS) 3221, 4573
– wind energy 7243
terrestrialization 2176
tertiary coals 2178
Terzaghi ultimate bearing capacity theory 7407
testicular cells 10908
testis stem cell 10907
testosterone steroidogenesis 1686
tetraalkylsilicates 7592
tetraalkyltitanates 7592
tetracyanoquinodimethane 7547
tetracycline 500, 10915, 11083
tetrafluoroethylene (TFE) 8332
tetrahydrofuran 1466
tetraploidy 6166
tetrapyrrole core 8273, 8279
tetrol 121
textiles 8829
– milling 8829
– recycling 8828
thalidomide 3163
thallium 4890
theodolite 4211
theory
– of limits of selection 403
– of mass transfer 600
– of place 10374
– of planned behavior (TPB) 12224
– of relativity 3789
– of selection limits 402
therapeutic cloning 10907
therapeutic proteins 8059
thermal
– aging 2387
– breeder reactors 11216
– bridge 3687, 7635
– coal 2178
– comfort 6873
– air movement 6873
– compressor 9516
– conductivity 4135, 10555
– conversion efficiency 1347
– cracking 1464
– cycle 1241
– decomposition 1520, 2414, 3914
– desalination plants 7306
– desalination 9760, 9761
– electrical characteristics 9761
– humid air distillation 9760
– technologies 2923
– thermodynamic characteristics 9761
– destruction facility 7001
– diffusivity 4136
– dissociation of metal oxides 9595
– dryers 2204
– drying 2213
– efficiency 1211, 2208, 4264, 4267, 4275
– work ratio 4275
– energy 1302, 1353, 3804, 4133–4134, 4140, 4164, 4191, 8081
– energy storage 10551, 10563–10564
– concepts 10564
– for concentrated solar power 10563
– envelope 899
– fatigue 2387
– forcing 7368
– heat conductivity 10568
– insulation 1370, 4370, 4709, 4732–4733
– ionization mass spectrometer (TIMS) 7206, 8657
– mechanical analysis (TMA) test 8734
– neutron 3801, 3812, 7090, 8552, 8572, 8625
– energy 3800
– Monte Carlo data 8552
– oxidation 11852
– plasma technology 8097
– plasma jet 8099
– pollution 6451
– thermal power plant 1233, 1248, 5286, 11934, 11942
– co-firing of biomass 5286
– co-firing of RDF 5286
– power station 3849
– cogeneration 3849
– power system 12109
– radiation 4745
– reactor 3816–3817, 3819
– spatial oscillations 3817
– Xenon override requirements 3816
– reactors 3800, 3812
– moderators 3800
– stability 10569
– ranking 6988
– storage 896, 1423, 2379, 10564
– capacity 4199
– classification 10564
– stratification 10555–10556
– in heat storage vessels 10556
– swing absorption 8221
– treatment 11852
– waste treatment 10581, 10585, 10587
– for environmental protection 10585
– recycling process 11730
– resource conservation 10587
– thermal wind balance 6742
thermal-enhanced oil recovery 7808, 7814
thermally-driven
– air-conditioning 9558
– chiller 9512, 9536–9537, 9546
– thermodynamic analysis 9512
– cooling cycles 9510
– cooling system 9536
– cooling techniques 9511
thermally massive construction 901
thermally-operated cooling processes 9550
thermalization rate reduction 9427
thermobitumen 7478
thermochemical conversion 1205–1209, 1518
– gasification 1208
– heating and drying 1207
– oxidation 1209
– pyrolytic decomposition 1208
thermochemical gasification 1216, 1446
thermochemical hydrogen production 5123, 5131
thermocline 4911, 8670
thermocouple 1415

thermodynamic(s) 117, 3787, 3877, 3927, 4226, 4251, 4258, 8207, 8906, 9003, 9413, 9590, 9938
– driving force 2935, 5176
– equilibrium 1340, 7159
– first law 3927, 4226
– foundations 3787
– of solar thermochemical conversion 9590
– overpotential 3415
– overvoltage 3415–3416
– potential 6062
– second law 4226
– state diagrams 4255
– system 3306
thermoelectric effect 5539
thermoelectric generator 1415, 1419
thermoelectric power generation 3456
thermograph 4911
thermography 603
thermogravimetric (TG) measurement 3437
thermohaline 5858
– circulation 2524, 5872, 7377
– box model 7377
thermoluminescence dosimetry (TLD) 3024–3025
– filters 3026
– for neutron radiations 3026
– inorganic materials 3025
thermolysis of H_2O 9597
thermonuclear test 8497
thermonuclear weapons 3712
thermo-oil 1439
thermophiles 11389
thermophilic anaerobic bacteria 5119
thermo–photo ratio 2552
thermopile 9681
– pyranometers 9732
thermoplastics 8817–8818
thermoset polymer 6926
thermoset 8818
thermosphere 9803
thermostable direct hemolysin (TDH) 9087
thermotolerant coliform 6325, 11876
thermotropic 2838
thiadiazole 7579
thiamine 1684
thin film
– solar cell production companies 7954
– silicon anodes 9303
– amorphous 9303
– nanocrystalline 9303
– silicon solar cells 9241
– solar cells 7956, 9276, 9280, 9395
– back reflectors 9276
– cell structures 9280
– modules 9280
– performance issues 9280
– technologies 9405
– large-scale processing 9405
thioether 3666
thiolactomycin 501
thiol 3666
thionation 4645
thionin 10697
thionyl chloride 6505
thiophene 7567, 7579
thioredoxin 3667
thiospinel framework 760
thiosulfate 6660
thixotropic fluid 4416
thiyl radicals 3666
thorium 3819, 4165, 4180, 5610, 6689, 7055, 7061, 7063, 7102, 7195–7196, 7275, 8453, 8475, 8480, 8565, 8624, 11201, 11204–11207, 11210, 11216
– as a nuclear fuel 11204
– average vertical distribution 11210
– decay 8565
– dioxide's 7196
– energy content 11205
– geoneutrino estimates 11207
– high-temperature reactor (THTR) 4053, 7102
– molten salt seactor (TMSR) 4058
– resources 11201, 11206
thoron 8475
three-domain Cry toxin 4015, 4024, 4025, 4027, 4028
– domain exchange 4027
– fusions 4028
– mutagenesis 4028
threshold dose 3254
threshold energy 3799, 6112, 8562, 8569
Thévénin impedance 12091–12092
thymidine 11060
thyristor 11539
– thyristor-controlled series capacitor 9345
– thyristor-switched capacitor 9341
thyroid
– adult carcinomas 3644
– hormone 3637
tick-borne disease 1757
tide/tidal 10614, 10620
– barrage 10614, 10616, 10620
– possible sites 10616
– current technology 10616
– currents 10618, 10620
– development options 10620
– energy available 10618
– energy 10613
– conversion 7244
– resources 7243
– lagoons 10616
– turbine 6351
tidewater glacier 2767
tight gas 7450
tight sand 7451
tight ultrafiltration 10530
tiled stove 1363
– insert 1363
tillage 1270, 2561, 2748
– erosion 3709, 3728
– system 1134
tiller 2542
– inhibitor gene (*Tin*) 2628
tilling 4497
tilt of the earth's rotation axis 9622
tilting furnaces 5277
tilting train 4933
tiltmeter 11638
timber 2409–2410
– composting 2410
time to flowering 4076, 4078
– controlling duration of subphases 4078
– controlling 4076
time value of money 7184
tin 4889
– tin-based amorphous composite oxide (TCO) 9299
– tin-oxide 8187
tire 3056, 3064
– behaviors 3058
– curve 3057
– nonlinear region 3057
– forces 3058
– lateral friction coefficients 3064
– load sensitivity effect 3064
– models 11191
– slip angle 3056, 11191
– velocity vector 3056
tire–road
– friction coefficient 3053
– friction estimation 3054
– interaction 3056, 3065, 11199
– Dugoff model 11199
– interface 3056, 11191
titanium 2902
– carbide 8297
– dioxide 271
– silicate 7591
– oxidation catalyst 7591
T-junction 3091, 3095

tla1 355
– mutation 367
T-lymphotropic retrovirus (HTLV) 5000
tobacco 1709, 1715, 4024, 8482, 10686
– chloroplasts 4024
– genome 10686
– virus (TMV) 2590, 8077, 10678, 10702
– plants 4030, 10677
– radioisotopes 8482
– smoke 3590, 3598, 3609, 3612, 3638, 3645, 6875, 10638
– carcinogenic components 3612
– genotoxicity 3645
– toxicants 3612
tobacco-related disease 10640
tobacco-specific N-nitrosamines 10639
tocochromanol 1705, 1707
– biosynthesis 1705
tocopherol 1705
– α-tocopherol 1707
tocotrienol 1705
– δ-tocotreinol 1707
toilet wastewater 1151
Tokamaks 7161
Tokuyama's alkaline ionomer 379
toll/tolled
– collection 4953, 5031
– express lanes 5022, 5024
– highway facilities 5022
– lane 4945
– lane users 5029
– revealed preference 5029
– payers 5041
– income levels 5041
tomato line 2702
tomato spotted wilt virus (TSWV) 10703
tomato 1705
tomographic gamma scanner (TGS) 7208
tonsillectomies 8129
tool for the reduction and assessment of chemical and other environmental impacts (TRACI) 4856
top of atmosphere albedo 9627
top of atmosphere irradiance 9621
– global distribution 9621
– obliquity of the Earth's axis 9621
– solar zenith angle (SZA) 9621
topography/topographic 153, 8909
– index 3214, 3223
– solar radiation modeling 10621, 10628, 10634
topoisomerase inhibitor 5581
torque
– calculation 29
– coupler 3380, 3382
– equation 42
– (power)-speed 11484
– production 22
– productivity 28
torrefaction 1067–1068, 1075, 1079–1080, 1085, 1585, 1609, 5126
– gases 1080
– plants 1079
torrefied biomass 1078, 1086
torsatron 7163
tortuosity 4186
TOSHIBA Process 4005
total breeding value (TBV) 9364, 9371, 9375
total building energy 10246
total building performance and diagnostics (TBPD) 10195
total column water vapor (TCWV) 7248
total economic value (TEV) 4788
total energy transmission 2850
total material requirement (TMR) 10405
total nitrogen (T-N) 2336
total organic carbon (TOC) 9569, 11868
total phenotypic value (TPV) 9375
total phosphorus (T-P) 2336
total photovoltage 7576
total radiative power 9742
– spectral distribution 9742
total solar energy transmission 2886
total solar irradiance (TSI) 9470, 9472, 9475, 9478, 9707, 9742, 9799, 9481–9482
– by multi-linear regression 9482
– construction of a composite 9472
– network 9481
– observations 9470
– photospheric faculae 9481
– spectroheliograms 9481
– three-component proxy model 9478
– variability 9475
– variations 9469
total soluble protein (TSP) 8062
total suspended solids (TSS) 8926
total tritium 11013
– activity 11015
– concentration in urine 11013
total water 10189
tourism 7390–7392
– economic impact 7391
– industry 7392
– public awareness campaigns on environmental issues 7391
tower shielding facility (TSF) 8539
town gas 851, 3910
Townsend avalanche 5564
toxic(s)
– air pollutant 203
– chemicals 10636, 10638, 10648
– in the home 10648
– lifestyle-associated exposure 10638
– equivalency factor (TEF) 4883
– fish 830
– gas 208
– in the air 299
– metals 9090
– seafood-associated 9090
– organic chemicals 10657–10658
– characteristics 10658
– properties 10658
– organic pollutants 5300
– combustion 5300
– pollutants 1628
– potential indicator (TPI) 4860
– release inventory (TRI) data 4859
– shock syndrome 5062
– substances control act 7826
– wastes 10011
toxicant 3257, 3265, 3586, 3625
– acclimation 3257
– low-dose treatments 3586
– young children 3625
toxicity 3262, 3270
– biomarker 1188
– characteristic leaching procedure (TCLP) 2439, 3444
– field studies 3270
– mechanisms 3262
– testing 3270, 3271, 3273
– aquatic tests 3271
– field tests 3271
– lowest observed effect concentration (LOEC) 3271
– no observed effect concentration (NOEC) 3271
– nonstandard tests 3271
– test medium 3271
– weights 4859, 4861
toxicogenomics 3275
toxicology 3253, 3624
– exposure 3624
toxin 832, 9082, 9083
– diffusion 2029
– in a biofilm 2029
– *Gambierdiscus*-associated 832
– seafood-associated 9082–9083
trabectedin 3156
trace
– elements in the urban atmosphere 11306
– minerals 1682

trachoma 12011–12012
track sharing 1868
tracking 11460
– reflector systems 7620
traction
– industry 5979, 5981
– lines 5977
– motor 11524, 11535–11536, 10544, 10549, 11523, 11535, 11538–11539, 11544
– design methodology 11538
– fixed- or variable-gearing transmissions 11535
– geared 11536
– gearless 11536
– power electronics 11539
– single- or multiple-motor configurations 11535
– system voltage 11536
– power 8116
tractive effort 11482
tradable green certificates (TGC) market 12263
traditional Chinese medicine (TCM) 3151
traditional sustainability 9032
traffic 2484, 3080, 4931
– assignment model 274
– assistance systems 3080
– calming 72
– congestion 1858, 1861
– control devices 5938
– densities 6011–6012
– engineering 5935
– federation 5988
– flow 93
– game theoretic methods 2484
– induced demand 4931
– injuries 66
– management 270
– policy 654
– safety 2464
– signal
– controller 100
– preemption 1872
– priority (TSP) 1872
– simulation 93
– simulator 2469
– situation 256
– surveillance 98
traffic-flow point measurement 3086
trailing edge noise (TBL) 12281
Train à Grande Vitesse (TGV) 4933
TraitMill™ 10
tram 1813
transboundary pollutant 11319
transcription activator-like
– effector nucleases (TALENs) 2972, 10761
– family of type III effectors (TALEs) 4492, 4498
transcription factor 4, 10698, 10761
transcriptional gene silencing (TGS) 2605, 8061, 10673
transcriptome 4518, 6441
– sequencing 6441
transcriptomics 8, 3658, 10895
transesterification 922, 927–928, 1028, 1219, 1592, 1613
transfection 2585, 10899
transfer 8433
– coefficient 597
– DNA (T-DNA) 2691
– points 95
– resistance 597
– to wildlife 8433
transformation 2585, 2587, 2591–2592, 2682, 2691, 10675, 10686
– *Agrobacterium*-mediated 2585, 2587, 2591, 2682, 10675, 10686
– in planta technologies 2591
– protocol 8
– vector 2592
transformer 2998, 3010
– cooling 2998
– current differential protection 3010
– windings 2998
transgene 2585, 4498, 4507, 4513, 10673, 10677–10678, 10680, 10848, 10914
– by exogenous inducers 10914
– copy number 10680
– expression variability 10677
– expression 10672, 10677, 10678, 10687, 10707, 10868, 10899
– influence of the integration position 10678
– intron-mediated enhancement 10678
– loci 10675
– rearrangements 2603–2604
– sequential introduction 10848
– silencing 643–644, 2603, 2608, 10673, 10678, 10680
– zinc finger targeted insertion 4498
transgenesis 639, 644, 4493, 4496, 4504, 4517–4518, 4520–4521, 10801, 10816, 10826, 10866–10867, 10887, 10895, 10918
– lentiviral 10826
– viral-mediated 10826
transgenic(s) 2585, 10895
– alternative gene transfer methods 10895
– animals 399–400, 2965, 2972, 6153, 7217, 7222, 10814, 10823, 10840, 10847, 10866, 10870, 10872–10875, 10877, 10882, 10897, 10914–10915, 10917
– animal welfare 10877
– as a risk 10872
– cost–benefit calculations 2972
– disease-resistant 2965
– DNA microinjection 7222
– ethical dialogues 10882
– ethical issues 10874
– expression of multiple genes 10847
– in food production 10870
– moral concerns 10873
– perceptions 10872
– productivity 400
– socio-economic changes 10875
– usefulness 10873
– chicken 640, 2971
– clones 10897
– cotton 10705
transgenic crop 2682, 2685, 4435, 4493, 4504, 4512, 5324, 10346, 10694–10695, 10704, 10713–10718, 10723, 10732, 10748, 10765
– breeding 4524
– commercialized disease resistant 10704
– disease-resistant 10695
– economic impact 4435
– environmental impact 10713, 10717
– herbicide tolerance 10716, 10723
– in Brazil 4512
– insect-resistant 10715, 10717
– next generation 10732
– regulatory framework in the European Union 10765
– risk assessment 10718, 10765
– salinity tolerance 5324
– dairy cows 2967
– enzymes 8028
– fish 10796, 10797, 10799–10802, 10804–10807, 10857
– adaptive and proactive management 10807
– as biomonitors 10807
– benefits 10806
– ecological hazards 10800
– ecological risk assessment 10800
– effective risk management 10805
– electroporation 10797
– genetic hazards 10801
– growth-enhanced 10800
– hazards 10806

– interactive decision-making framework 10805
– operations management 10805
– oversight of production 10807
– phenotypic characterization 10801
– physical confinement 10804
– potential harms 10800
– reproductive confinement 10804
– risk management 10802
– food animal 10841, 10856
– herbicide resistance 10350, 10353
– crops 10345–10347
– genetic engineering strategies 10350
– non-transgenic strategies 10350
– insect-resistant crops 4024
– plastid transformation 4024
– livestock 10812, 10814, 10817, 10839–10840, 10852, 10860, 10864, 10866, 10874, 10878
– enhanced nutritional quality 10852
– environmental impact 10840
– ethical concerns 10864, 10866
– food production 10812
– integrity 10878
– naturalness 10878
– risks to humans 10874
– technologies 10814
– maize 4519
– mammals 7216
– nuclear transfer 7216
– mice 10857, 10916
– petunia 10678
– phytase enzymes 10752
– pig 10822, 10832, 10841–10842, 10844, 10857, 10859
– growth 10841
– health status 10844
– improved digestion 10841
– plant 1716, 2311, 2586, 2601, 2684, 4022–4023, 4026–4027, 4029–4030, 4034, 4036, 5327, 6531, 8045, 8047, 8049, 8050, 10672–10673, 10697, 10748
– cotransformation 1716
– cry proteins 4023, 4027
– economics of cellulases 8047
– environmental safety 8050
– fungus-resistant 10697
– generation 10673
– insect resistance 4029, 4036
– insecticidal proteins 4022
– insect-resistant 4030
– multigene transformation 6531
– multiple toxins 4026
– peroxidase activity 4034
– product recovery 8047
– product safety 8049
– pyramiding 4026
– regulation of growth 8049
– resistance to geminiviruses 10748
– safety of Host Proteins 8050
– salinity tolerance 5327
– supertransformation 1716
– poultry 10845
– enhanced digestion 10845
– health 10845
– proteins 8051
– resistance 10696, 10700, 10702
– to bacterial pathogens 10700
– to fungal pathogens 10696
– to viral pathogens 10702
– ruminants 10844–10845
– enhanced digestion 10844
– health 10845
– seed 2294, 2297, 8030
– sheep 10857
– technologies 639, 10870, 10876, 10885
– public perceptions 10870
– risks to animal welfare 10876
– welfare assessment 10876
– tobacco 4023, 10698
– vector 10823
– virus resistance 10706
– zebrafish 6798, 10798
transient climate sensitivity (TCS) 2516
transient expression 2585
transient tracers in the oceans (TTO) 8670
transit
– adjacent developments 10924
– agencies 1825, 1862
– experience 1829
– bus 1863
– applications 3482
– technology 5980
– capacity 1885
– capacity and quality of service manual (TCQSM) 98
– capital investments 5998
– costs 5998
– diesel hydraulic bus 5980
– financing 1905
– first policy 10925
– impact development fee (TIDF) 10932
– investment 5997
– line capacities 1897
– transit modeling framework 94
– modes 1859
– selection 1859
– network 97, 104, 6008
– operations control 91, 99
– performance measurement 5975
– productivity 5995, 5997
– services 1861
– downgrading 1861
– signal priority (TSP) 100, 1825, 1852
– simulation 93
– simulation laboratory 102
– simulation model 100, 107
– measures of effectiveness (MOEs) 100
– supply 95, 104
– transit systems 816, 1893
– capital costs 1893
– simulation 96
– technologies 1891, 1900
– travel time 6001
transiting radiation 8472
transition metal
– cermets 3907
– ions 6543
transit-oriented development (TOD) 1890, 10923–10925, 10927–10932
– bus-based 10925
– environmental benefits 10927
– financing 10932
– implementation tools 10930
– mixed-use 10931
– not-in-my-backyard (NIMBY) resistance 10931
– parking 10929
– ridership at the workplace 10928
– scope 10924
– tax increment financing 10932
– transportation 10927
transitway 1822, 10926
– green connectors 10926
translational ecology 9169
transmembrane osmotic pressure difference 2916
trans-Mexican volcanic belt (TMVB) 11615
transmissible gastroenteritis virus (TGEV) 2969
transmissible spongiform encephalopathies (TSE) 2969, 10859
transmission
– blackouts 10934
– cables 11177
– electron microscopy (TEM) 723, 7568
– expansion 12190, 12193, 12197
– maximum potential budget 12193
– gear box 3369
– gear ratio design 11486
– grid 3451, 12216

– lines 12189, 12193, 12196
– price differences 12193
– rule of three 12189
– of malaria parasites 11072
– planning method 12188
– plan 12189, 12197
– reliability test 12197
– robustness test 12197
– smart grid 10953
– wide area monitoring, protection, and control (WAMPAC) 10953
– substations 2994
– system 3393, 12175
– system operators (TSOs) 10939
– transmission system 12186, 12195
– economic studies 12186
– loading 12195
transmission-blocking vaccines 6301
transmutation 3791
transparent conductive oxide 1983
transparent insulation wall (TWD) 7658
transpiration efficiency (TE) 2650
transplastomic 2585
transport 6245
– activity 247
– emission 274
– model validation 274
– equation 3815, 5306
– fossil fueled 6245
– in the environment 10962
– mass 2049
– pollution 245
– protein 5
transportation 3456–3457, 3460, 6243, 7847
– applications 6119
– field-failures 6119
– demand management 92
– energy 3457
– fuels 1200
– from biomass 1200
– costs 7847
– history 6243
– impact of new modes 6243
– improvements 4948
– infrastructure 5044, 7793
– land use 3457
– modeling 7854, 7861
– networks 7851
– policy issues 7851
– policies 1862
– sector 10504
– sustainability 7847
– system 66, 91, 7861, 11455
– policy implications 7861
– water 3460
transportation-energy markets 7856
transposase 644
transposon 644, 10830, 10903–10904, 10906, 10917
– insertion 2700
– tagging 2691
Transrapid 6242, 6248, 6251, 6257, 6263, 6268
transuranic(s) 3818–3819, 7181, 8402, 8413, 8681
– elements 3791
– isotopes 3793, 8596
– waste (TRU) 8589, 8595, 8596
– waste isolation pilot plant (WIPP) 8596
transuranium 8389, 8391
transverse diffusive transport 2033
trapped radiation 8471
– belts 8577, 8579
trash 10014
travel/traveling
– behavior 96
– grate furnaces 1323
– in high speed 4931
– models 7854
– time 101
traveler information 92
travel-time variability 102
Travis hydrolytic tank 1148
treated ash aggregate (TAA) 11752
trehalose 5326
Trematodes 12023, 12043, 12047
trenching 4146
triacylglyceride 1681
triacylglycerol 361, 927, 11437
triadimenol 6209
triazine 4450
triazoles 2569
triboelectric separation 2412
trichiasis 12012
trichinellosis 12029
trichlorobiphenyl 9136
trichloroethylene (TCE) 2043, 10439, 10962
trichloro-naphthalene 4886
trichlorosilane 9199
– gas 7957
trichlorovinyl 6996
Triclosan 500, 10652
triethylamine 374
trifluoroacetic acid (TFA) 8177
trifluoromethanesulfonic acid 6557
trifluoromethyl 6539
tri-generation 1611
triggered seismicity 2793
triglyceride 578, 930, 1045, 1681, 6897, 6900
– epoxidized 6900
– oils 6935
– transesterification 930
trihalomethane (THM) 3639, 3647, 10537
3-trihydroxysilyl–1-propanesulfonic acid (THOPS) 6561
trilateral flash cycle (TFC) 4327
trimethyl boron (TMB) 9243
trinary model 1902
trinitite 8488
trinitrotoluene (TNT) 8488
triple phase boundary (TPB) 8208
triple superphosphate 3772
triple-flash power station 4298
tritiated compounds 11047–11048, 11052
– biokinetics 11052
– dosimetry 11052
– internal dosimetry 11047–11048
tritiated DNA precursor 11059
– biokinetics 11059
tritiated gas (HT) 11028, 11029
tritiated hydrocarbon 11047, 11048
tritiated hydrogen (HT) 11004, 11009, 11011–11012, 11016
– atmospheric releases 11009, 11012, 11016
– biological activity 11004
– concentrations in water 11011
– gas 10998–10999
– nonequilibrium conditions 11011
– time-dependent concentrations 11012
tritiated oil 11049
tritiated organic compounds 10999, 11049
tritiated particulate 11047
tritiated thymidine 11059
tritiated water (HTO) 10998, 11000–11001, 11006, 11008–11010, 11015, 11017, 11028, 11029, 11046, 11048, 11052, 11054, 11060
– absorption through skin 11054
– aquatic releases 11010, 11017
– atmospheric release 11006, 11008
– bioassay monitoring 11054
– biokinetic model 11060
– biological half-life 11052
– concentration
– in animal products 11009
– in soil water 11009
– current ICRP models 11046
– cycling 11000

– evapotranspiration process 11015
– molecules 11001
– reemission from 11001
– soils 11001
– Taylor model 11060
tritium-in-urine measurements 11054
tritium 3583, 5580, 5602, 5610, 7157, 8431, 8484, 8567, 8600, 8624, 8657, 8670, 8674, 8680, 10997–11000, 11003, 11005–11007, 11012, 11014, 11018–11021, 11026–11039, 11041–11043, 11045–11046, 11050, 11055, 11057, 11060–11061
– acute releases 11012
– adverse health effects 11030
– amino acids 11037
– aquatic processes 11005
– atom 11045
– beta radiation 11030, 11035, 11041, 11046
– biokinetics 11045
– biological effects 11028, 11061
– biological half-life 11000
– biological modeling 3583
– carcinogenesis 11043
– carcinogenicity 11034
– chemical Forms 11029
– chronic intake 11057
– concentration
– in animal products 11007
– in background areas 11006
– in the plant 11007
– in water 10999
– deterministic effects 11030
– DNA-bound 11060
– dose rate effectiveness factor (DDREF) 11042
– dosimetry 11026, 11045
– dynamic release 11014
– effects in the female 11033
– effects in the male 11033
– environmental behavior 10998
– environmental concentrations 11006
– environmental models 11021
– experimental studies 11042
– gas 8525, 11055
– health effects 11026, 11038
– hereditary effects 11036
– human epidemiology 11038
– intake 11050–11051
– nursing 11051
– pregnancy 11050
– in the environment 10997, 11000
– isotopic effect 11039
– lethality 11030
– model validation 11019
– Monte Carlo sampling program 11035
– nonradiological effects 11039
– nucleosides 11037
– occupational doses 11037
– plume 11005
– prenatal dosimetry 11050
– properties 10998, 11028
– radiation 11027, 11036, 11037, 11044, 11061
– dose 11031
– electron energy 11044
– ionization path lengths 11044
– radiation-induced teratogenic effects 11032
– radioactive properties 11029
– relative biological effectiveness 11041
– release 11014
– dynamic compartment models 11014
– process-oriented models 11014
– reproductive effects 11032
– routine releases 11006
– skin absorption rates 11055
– species 10998
– specific activity 10999
– stochastic effects 11034, 11061
– teratogenic effects 11031
– transferin aquatic systems 11018
– transfer in the environment 11020
– transmutation 11039
– uncertainty 11019
– uptake by terrestrial animals 11003
tritium-gas-contaminated surfaces 11056
– skin contact 11056
Troglotrematidae 12027
Trojan horse antibiotics 506
trolley buses 5980, 5989
Trombe wall 902
trophectoderm (TE) 6157, 6157
– genes 6161
tropical atmosphere 7374
tropical biennial oscillation (TBO) 6745
tropical carbon cycling 6231
tropical climate 2144
tropical cyclone 5071, 5074, 12077
tropical diseases 11070
tropical health 11068–11069, 11089, 11092
– sustainability 11068
tropical infection 11091
tropical night 4676
tropical soil 1924
tropical storm 2082, 5077
troposphere/tropospheric 113, 118, 2116, 2513, 8586, 9805–9806, 11314
– aerosols 9629, 9635
– chemistry 317
– jet stream 9809
– perturbations 9809
– ozone 170, 189, 220, 5530
– pollution 2116
– radioactive debris 8586
– solar cycle signal 9805
– sulfate aerosols 4111
– temperature mechanism 7259
truck lane 5043
true breeding value 423
true-color night vision systems 11126
trunk pipeline 6419–6421
– damage by trawl-board impact 6421
trypansome lytic factor (TLF) 2972
tryptophan 1695
T-strand 2600
tsunami 11633
– earthquake-induced 11633
tube receiver 2364
tuberculosis 11129–11131, 11133–11136, 11138–11139, 11141–11144
– case fatality 11131
– case notifications 11144
– chronic renal failure 11135
– control 11141–11142
– corticosteroid treatment 11136
– diabetic patients 11135
– disease 11134
– drug-resistant 11139
– elimination strategy 11144
– epidemiological Indicators 11130
– epidemiology 11129
– exposure 11131
– global epidemiological situation 11143
– global treatment success 11144
– hemodialytic treatment 11135
– HIV infection 11136
– incidence 11130, 11143
– infection 11134
– annual risk 11134
– average annual 11134
– control measures 11138
– key pathogenic factor 11134
– intensified case finding 11138
– isoniazid preventive therapy 11138
– mortality 11131, 11136, 11143
– multi-drug resistant 11142
– natural history 11131
– personal protective equipment 11133
– prevalence 11131, 11143
– smoking 11136
– sputum
– culture-positive pulmonary 11131
– smear examination 11133

tubular aerosol flow reactor 9601
tubular daylight guidance system (TDGS) 2811
tubular fixed bed reactor (TFBR) 2243
tubular photoreactor 9577
tubulin 3159
tumor suppressor gene 3601, 3603,3543
tuna farming 6356
tundra 1552
– *Rangifer tarandus* 8450
tungsten 8576
– bronzes 2958
– carbide 8266
tunicate 1965
tuning 5509
tunnel effects 4940
turbid water 7680
turbine 4280, 6815, 6821, 6823, 6826, 6838
– analysis 4261
– component 6821
– cooling 6823, 6826
– for double-flash steam 4280
– hot gas path (HGP) 6821
– inlet temperature (TIT) 6821, 6838
– safety 6602
– wind conditions 6602
turbocharging 5535, 5536
turbojet 6812
– engine 6812
TurboPlasma 8109
turbosorp dry scrubbing technology 11807
turbulence/turbulent 6593, 7401
– mechanically produced 6593
– diffusion 2031, 2047, 2049, 10961
– coefficient 2050, 2051
– diffusivity 600, 2053
– dissipation rate 11275
– eddies 2049, 2051
– flow 2049, 2053
– Prandtl's mixing length hypothesis 2053
– jets 10976
– in stagnant environment 10976
– kinetic energy 11275, 11286
– Schmidt number 596
– transport in the environment 2048
– viscosity 2053
– wave dissipation term 601
turn signal activation 3091
turtle 3568
TwinRec commercial plant 4000
– commercial operational experience 4000
two-electron transfers 3658
Twomey effect 9697
two-pole machine 19
typhoid 12014
typical meteorological year (TMY) 9690
tyrosine 1683

U

ubiquitin 8047
ubiquitin–proteasome pathway 2700
ubiquitinylation 3604
U-gas technology 2238
Ullmann coupling reaction 6547
ultimate neutronic investigation code 3819
ultra battery 5891, 11514
– design 5883
ultra high voltage (UHV) transmission 10473
ultracapacitor 3392, 3427–3428, 3471–3473, 3476–3478, 3480–3482, 3484–3485, 3489, 3495, 3497–3499, 3870, 5107, 5111
– combination with batteries 3476
– current–voltage characteristics 3495
– development 3472, 3498
– economic considerations 3497
– energy
– requirement 3478
– storage 3472, 3476, 3482
– hybrid vehicle simulations 3484
– interface electronics 3480
– laboratory testing 3481
– power capability 3473
– power split strategies 3480
– powertrain control strategies 3484
– reductions in battery stress 3489
– sizing components 3477
– system control strategy 3480
– vehicle
– applications 3499
– field Experience 3481
– simulation results 3485
ultracentrifugal force (UC) nanohybridization method 3434
ultrafiltration 2904, 2905, 11885
– pretreatment processes 2905
ultrafine particle 226, 250, 11302
ultrahigh-molecular-weight polyethylene (UHMWPE) 8722, 8724
ultrasound 12278
ultra-supercritical (USC) steam 2167
ultraviolet germicidal irradiation (UVGI) 10272, 11132
ultraviolet radiation (UV) 3596, 9741, 11149–11150, 11152, 11155, 11376–11377, 11412
– aerosols 11155
– biological effectiveness 11377
– clouds 11152
– distribution 11149
– geographical distribution 11152
– instrument measuring 11150
– molecular scattering 11152
– ozone 11152
– screening compounds 11412
– surface albedo 11155
– surface reflectivity 11155
– variability 11149
– wavelength regions 11150
ultraviolet (UV) 9740
ulva 553
umami 550
unburned hydrocarbons 5530, 10483
uncultivated soils 3728
Undaria 9114
underfed furnace systems 1379
underfire air 6461–6463, 6474
underground
– cable systems 11158, 11160
– structure 11160
– gallery 3235
– gamma-spectrometry analysis 8676
– geothermal system 4241
– landfill fires 11697
– mine/mining 6634, 6668, 6669, 6675, 7810
– waste backfill 6675
– power cables 11177
– dry aging 11177
– extra high voltage (EHV) 11177
– thermoelectric aging 11177
– testing radionuclide inventories 8493
– thermal energy storage (UTES) system 4148
undernourishment 1746
underwater
– acoustic 12287
– excavation 3029
– forests 6232
UNEP-SETAC toxicity model 4859
unified glare rating (UGR) 2828
unified power flow controller 9351
uninterruptible power supply (UPS) 674
universal equine life number (UELN) system 1797
universal mobile telecommunications system (UMTS) 74
unmineable coal seams 2155
unsaturated polyester (UP) resin 6915
unscented Kalman filter (UKF) 3059, 5461, 11188, 11194, 11199
– algorithm 3059
unspoilt landscapes 10379

unstabilized camera 60
unsustainable 10301
– construction 10301
– design 10301
upconversion 9424
updraft
– combustion 1356–1357
– with grate 1356
– without grate 1357
– gasifiers 11443
up-flow anaerobic sludge blanket reactor (UASB) 1154
upgraded metallurgical silicon (UMG-Si) 7957, 9200
– feedstock 9213
upgraded solid biofuel 1067
upper atmosphere research satellite (UARS) 9708
upwelled water 7239
uraninite 10411, 11212
uranium 209, 3583, 3788–3789, 3791, 3819, 4063, 4165, 4180, 4777–4779, 5610, 5634, 5636, 6689–6690, 7052, 7054, 7059–7062, 7067, 7077, 7080, 7143, 7187, 7195, 7209, 8453, 8475, 8480, 8482–8484, 8513, 8565, 8584, 8600, 8610, 8625, 10406, 10410–10411, 11201–11207, 11209–11216, 11218–11224, 11226–11231, 11233–11235, 11237–11242, 11251–11256
– absorption by fish 11242
– accumulation 11237
– algal cells 11252
– anthropogenic releases 11221
– aquatic ecosystems 11231
– aquatic food chain 11234
– astrophysical origins 11206
– average vertical distribution 11210
– background concentrations 11224
– benthic invertebrates 11254
– bioavailability 11220, 11224
– carbide (UC) 7195
– cellular toxicity 11252
– chloride 7151
– concentrations 8476
– ratios 11229
– conversion 6690, 7062, 7080, 7187, 11223
– facilities 7062
– critical toxicity value 11235
– decay 8565
– deposit types 11212
– dioxide (UO_2) 7195, 8590
– dioxide fuel 7187
– dry deposition 11227
– effects on offspring 11241
– elimination
– through feces 11238
– through kidney 11238
– energy content 11205
– enriching 3789, 6690
– enrichment 5634, 5636, 11223
– estimated-no-effect value (ENEV) 11241
– existing enrichment tails 11213
– extraction (UREX) 7067, 7147, 11214, 11216, 11219
– in situ leaching 11214
– fabrication facilities 11223
– facilities 7060
– decommissioning 7060
– fission products 10425
– fissioned 3788
– food chain 11230
– freshwater 11224
– from seawater 11214–11215
– fuel 7058, 7181
– cycle 7082
– enrichment 7062
– fabrication 8584
– future energy needs 11216
– geochemical beneficiation processes 11211
– geoneutrino estimates 11207
– gold and phosphate tailings 11214
– hexafluoride 6690, 11233
– history 6689
– igneous processes 11210
– immobilization 4778
– in floodplain soils 11233
– in munitions 8513
– in sediment 11231
– in situ leaching (ISL) 7060, 8484
– in the environment 11220
– inhalation to lungs 11237
– isotopes 6689
– isotope separation 5634
– kidney toxicity 11239
– lethality 11240
– light water reactor 11204
– lowest observed effect concentration (LOEC) 11235
– lowest-observed-effect level (LOEL) 11241
– macrophytes 11253
– measurement 7209
– mechanisms for the concentration 11209
– metal mixtures 11256
– mill/milling 7061, 7064, 7066, 7080, 8483, 11222
– groundwater restoration 7066
– tailings 7066
– mining 3542, 3543, 7054, 7059, 7060, 7066, 7187, 8482–8483, 8584, 10406, 11222
– decommissioning 3542, 3543
– remediation 3543
– mobility 11228
– mobilization 4778
– natural organic matter 11255
– nitrate 8503
– nitride 7195
– no-observed-effect level (NOEL) 11241
– nuclear power plants 11224
– occurrence 11221
– oxidation 4778
– oxide 3962, 6690, 7063, 11212, 11215
– partitioning 11233
– phytoplankon 11252
– prices 11202
– processing 8483
– radioactivity 11210
– reactive transport models 4779
– recovery 7060
– reduction 11233
– refining 11223
– remediation technologies 7077
– reserves 7054, 11203, 11216
– resources 11201, 11206
– roll-front deposits 11212
– scarcity 11216
– seawater 11227
– sediment ingestion 11235
– silicate 11215
– soil
– ingestion 11230
– invertebrates 11237
– speciation 11224
– stabilization 4778
– tailings 11222
– terrestrial environment 11227
– pathways 11230
– thermal conductivity 7195
– toxicity 11255
– alkalinity 11255
– hardness 11255
– toxicity 11220, 11224, 11235, 11239
– benchmark values 11235
– in mammals 11237
– to phytoplankton 11252
– to terrestrial plants 11235
– transfer factors 11229
– trioxide 11223, 11240

– unconventional resources 11213
– uptake 11226
– through the digestive tract 11238
– uranium–238 3715
– water temperature 11255
– waterfowl 11242
– wet deposition 11228
– zooplankton 11251
uranyl
– acetate 11235
– fluoride metabolism 11240
– hydrolysis 11228
– ion 11233, 11239
– nitrate 11235
– phosphates 10412
– sulfate 11235
urban
– aerosol 9635
– agriculture 957, 4732
– air pollution 213, 239, 245, 955, 11292, 11294–11295, 11314
– concentrations 11295
– formation 11294
– sources 11294
– air quality 916, 11262, 11273, 11291–11292, 11296, 11307, 11312, 11316
– concentrations 11291, 11296
– indices 11296
– meteorological processes 11262
– sources 11291
– airshed 11297, 11314
– areas 6853, 11263
– airflow 11263
– meteorology 11263
– sustainability 6853
– atmosphere 11306, 11312–11313
– atmospheric composition 11311, 11313, 11317, 11322
– history 11313
– atmospheric pollutants 11312
– biodiversity 940, 4738, 5846, 10358, 11333
– biotope 944
– boundary layer 11313
– bus mode 1857
– canopy 11269
– canyons 4701, 4732
– climate 4680, 4692, 4716
– climatology 918
– decrement in ozone 11317
– densification 4683, 4685
– density 5790, 5795, 5799
– design 11338
– model 193
– projects 11331
– development 4806, 5806, 5810, 5839, 10371, 11365
– models 5806
– open space 11365
– paradigms 5806
– programs 6856
– rezoning 11365
– drainage
– modeling 4685
– systems 4687, 4692
– driving cycle 8851, 8855
– drought 8689
– ecological sustainability 6853
– ecology 3299, 3363, 6861, 11324–11326, 11328–11329, 11334, 11358
– history 11326
– human ecosystems 11329
– methodological principles 11334
– urban form 11329
– ecosystem 3527, 5847, 6856, 10032, 11333, 11336
– radioactive contamination 3527
– energy and commodity production 958
– environmental planning 6856
– environment 950–951, 5712, 5715, 5717
– alien populations 950
– exotic species 950
– geology 5715
– homogenization 951
– land subsidence 5712
– nutritional "conditions." 950
– territorial behavior 950
– tunneling 5717
– farming 3207
– flooding 8689, 11331
– flow 6862, 11273
– footprint 11340
– forest 4751, 11333, 11344, 11346, 11350, 11352, 11353, 11358
– design 11353
– information 11358
– inventory 11358
– management 11353
– plans 11350
– policies 11350
– policy-making 11352
– resources 11346
– forestry 4734, 4748, 10356, 10360
– form 11329, 11331, 11363
– fox 950
– function 11331
– governance 6854
– green 953
– planning 11344
– space 4693
– space management 11358
– greening 4674, 4690, 4705, 4717, 4733–4734, 4737, 4746, 10359, 11344, 11347
– benefits 11347
– growth 5788, 5799, 11357
– undesirable effects 5788
– boundaries 5806
– habitat 946, 11326
– connectivity 946
– fragmentation 946
– heat-island effect 943, 4716, 4718, 4732, 4736, 5795–5796, 8692, 11299, 11323, 11337
– heterogeneity 11335
– hydrological cycle 8693
– hydrology 4692
– infrastructure 3451–3452, 3454, 3469, 5846, 6859, 11355
– land cover 11330
– land use 5790, 5795
– landscape 942, 943, 5796, 5850, 11348
– design 8859
– imperviousness 5796
– mass transportation act 7782
– matrix 11332, 11341
– metabolism 6857–6859, 6861, 11326
– challenges 6861
– limitations 6861
– planning 6859
– studies 6858
– meteorology 11287
– mining 6859
– mobility 1834
– modeling 3171, 5792
– Alonso–Muth–Mills model 5792
– neoclassical monocentric 5792
– tiebout local public finance model 5792
– morphology 4681
– morphometry 11269, 11273
– nature 952–953
– night traffic scene 11123
– particle pollution 11308
– pathologies 11327
– perforation 5847
– planner 952
– planning 194, 4674, 4677, 5718, 6854, 10360, 11326, 11338
– pollution 203, 8880
– change 11346
– population 11349, 11358, 11363

– public transit 1857
– public transport 1812
– rainwater 8695
– reconstruction 5850
– redevelopment 11361, 11365, 11372
  – East 11364
– urban regeneration 5807, 5851
  – temporary use of Brownfields 5851
– resource flows 6854
– runoff 5796
– shrinkage 5837, 5839–5840, 5842, 5846–5849, 5853, 11362
  – carbon storage 5848
  – consequences for urban land use 5839
  – consequences on sustainability 5839
  – demolition 5847
  – effects on ecosystems 5846
  – effects on socio-demographic sustainability 5842
  – modes of collaboration and governance 5849
  – premises 5839
  – response 5849
– soil 943
– sprawl 192, 5788, 5796–5797, 5799, 5808–5809, 10362, 11331
  – costs 5797
  – unintended social outcomes 5799
– stop-and-go driving pattern 8849
– stormwater 10095, 10105
  – improvement conceptualization 10111
  – management 10098
  – treatment 11897
– stream syndrome 11337
– survival strategies 951
– sustainability 3451, 3454, 5838, 5846, 6855, 8871, 11339
  – challenges 6854
  – planning 6855
– topology 11576
– transformation 3554
– transit modes 1861, 1891
  – bus-based 1891
  – negative trends 1861
  – rail-based 1891
– transit systems 1886
– transport systems 807, 6497, 10489
– transportation 1858, 7781
  – policies 1859
  – system 5950, 5968
  – trees 4689
  – vegetation 11344
  – waste collection 8802
  – water 4734
    – management 4741, 10105
    – management budget 4734
    – metabolism 6859
  – waterways 10095
  – wildlife 949, 953
    – communities 949
    – cpecies 949
  – wind turbine 3398
  – woodlands 11354, 11356–11357
    – areas 11351
    – trees 11345
urbanization 90, 2079, 4674, 5787, 5790, 5793, 6853–6854, 9655, 10095, 10358, 10362, 11346
  – land-intensive forms 5793
  – sustainability 6854
  – trends 5790
urea 3772, 3776
  – ammonia-based 3776
urease 3773
urethane 6901
uridylpeptide molecule 503
urocanic acid (UCA) 9663
US Clean Air Act 190
US Environmental Protection Agency 219
used nuclear fuel 8590–8593
  – dry storage systems 8591
  – geologic repository 8592
  – monitored retrievable storage facility (MRS) 8591
  – PUREX method 8592
  – reprocessing 8592
  – transportation 8591, 8593
useful daylight illuminance (UDI) metric 2834
useful energy 9938
utility theory 2480
utility wind farm 12241
UV (ultraviolet)
  – effects 11375
  – index 9658
  – light 3611
  – photoreceptors 11413
  – radiation 9651, 9657, 9660, 9662, 9664, 9665, 11384–11385, 11393–11396, 11402, 11411
    – biological damage 9662
    – cataract 9665
    – effects on plants 11393
    – eye damage 9664
    – genetic damage 11394
    – health effects 9651, 9660
    – inhibition of photosynthesis 11395
    – photoconjunctivitis 9665
    – photokeratitis 9665
    – protection 11396
    – skin treatments 9664
    – ultrastructural cell damage 11394
    – vegetation 11384
  – signature mutations 9662
    – oncogenes 9662
    – tumor suppressor genes 9662

V

vaccination 498, 2970, 5349, 8075, 8146
  – formulation 8146
  – honeymoon period 5349
  – schedules 8146
  – SIR model 5349
vaccine 498, 6292–6293, 6296, 6300–6301, 8066, 8074–8075
  – apical membrane antigen 1 6300
  – malaria 6296
  – plant-derived 8066, 8075
vacuum
  – circuit breakers 3002
  – insulated panels (VIPs) 7634
  – membrane distillation 2920
  – tower telescope (VTT) 9480
  – tube solar collectors 9524
vadose zone 2433, 4777
value pricing 5022
valued ecosystem component (VEC) analysis 8530
valve-regulated lead-acid (VRLA) battery 5886, 8750
Van Allen belt 8579
Van der Waals
  – bond 752, 755
  – forces 7561
Van Krevelen diagram 7476
vanadate 2958
vanadia-titania catalyst 8366
vanadium 4777, 4891, 6087
  – oxides 758
vancomycin 500, 504
vanillin propylene glycol acetal 4592
vanpools 4952
Vant Hoff rule 163
vapor
  – cloud explosions (VCE) 5256
  – compression 9759
    – chiller 9544, 9546
  – permeation 995
vapor-assisted petroleum extraction (VAPEX) 7819

variable frequency transformer 9348
variable heavy-chain domain (VHH) antibodies 8074
variogram 3335
vascular endothelial growth factor (VEGF) 3160
veal production 1752
vector 10918
– backbone 10675
– control 35–36, 42
vector-borne disease 5373
– climate change 5373
vedotin 3156
Vegard's law 7531, 7534, 7536
vegetable oil 1219, 1221
– use 1221
vegetation 3280, 3282, 3285, 11371
– canopy 3218
– development 11371
– diversification 156
– dynamics 3223, 3290, 3293
– ecological models 3293
– individual-based 3290
– free succession 11371
– school 3280
– SIGMATIST school 3280
– soil conditions 3282
– working dynamics 3285
– Zurich-Montpellier 3280
vegetative growth 1117
– prolongation 1117
vegetative insecticidal protein (VIP) 10716
vegetative phytomer 2541
vegetative storage protein (VSP) 2664
vehicle 2465–2466, 2468, 2471–2472, 2477–2479, 3052–3053, 3055, 3065, 3068, 3082, 3124–3125, 3136, 3139, 3177–3178, 3389, 3392, 3472, 3476, 3483–3484, 3495, 3499, 3857, 5029, 5103–5104, 5114, 5024, 5480, 5882, 6257, 8255, 8848, 10491, 10590, 10608, 11188–11191, 11194, 11481–11482, 11487–11492, 11494, 11498, 11503–11504, 11520
– acceleration 11191, 11490, 11492
– aerodynamic drag 11488, 11498
– angular velocity 11190
– biofuels 11429
– body frame 3177
– brake system 8848
– braking 11191
– forces 11494, 11498
– performance 11494
– communication systems 3082
– control
– algorithms 3053
– signals 11098
– systems 3052, 11188
– cooperative collision warning 2465
– cooperative decision making 2465
– design considerations 3476
– detection 10591–10594, 10596–10599, 10601, 10605–10606, 11455, 11460, 11467–11469, 11471–11473, 11476–11478
– adaboost algorithm 11472
– baseline distance 10605
– calibration method 11467
– clustering 10594, 10596
– computer vision integrated system 11468
– correlation-based stereo 10594
– distance metric 10606
– downhill simplex algorithm 10597
– Euclidean distance metric 10596
– experiment results 11476
– experimental evaluation 10601
– feature-based optical flow 10594
– image training preprocessing 11471
– interacting multiple model (IMM) 10592
– iterative closest point (ICP) algorithm 10593, 10596
– Kalman filter framework 10592
– Levenberg–Marquardt algorithm 10597
– LIDAR-based subsystem 11469
– model-based scene flow 10599
– monocular images 10591
– multi-planar LIDAR sensors 11478
– polar distance metric 10598
– quaternion-based optimization procedure 10597, 10598
– sensor fusion 10591, 11460
– spacetime stereo 10593
– stereo algorithms 10605
– stereo camera systems 10591
– stereo-based 3D pose estimation 10593
– stereo-based 3D reconstruction 10592
– system 11468
– tightly coupled LIDAR 11468
– vision-based system 11471
– direct hydrogen-fuel-cell-powered 8255
– distance measure 2466
– dynamic(s) 2477–2478, 3053, 11481
– behavior 3055
– parameters 3052, 11188
– states 3053, 11189
– dynamometer testing 3483, 5480
– electric load 5103
– electrification 3857, 5104
– electromagnets 6257
– energy consumption 11492
– energy sources 11503
– energy storage 3392, 5104, 5105, 5114, 11502
– batteries 5105, 11502
– fuels 11430
– cell–powered 3389, 3472, 3499
– economy 10494, 11492
– geometry 2471, 2477
– gradeability 11491
– grading resistance 11488
– hydrogen consumption 3495
– inertia force 11489
– instrumented 3086
– Li-ion battery 11520
– longitudinal forces 3055
– evolution 11191
– magnets 6259
– maximum braking 2479
– maximum steering 2479
– miles traveled (VMT) 1890, 7851, 10928
– model 2471
– motion planning 2478
– motor drive features 11504
– navigation 3082
– observability 11194
– operating fuel economy 10491
– operation 254
– oscillations 2468
– performance 3392, 11482, 11490
– information 3125
– pose 10590
– 3D pose estimation 10590
– power train structure 11482
– recognition of dangerous situations 2471
– reference rectangle 2472
– resistance 11487
– robot 3178
– rolling resistance 11487
– rafely traveling 3136
– signals 3124
– speed 11482, 11488
– stability 3053, 3065, 11188, 11199
– lateral tire forces 11199
– sideslip angle 11199
– starting, lighting and ignition (SLI) 5882
– state description 2471
– system-model 3059
– mismatches 3059

– three-dimensional pose estimation 10608
– time headway (THW) 3139
– track acceleration tests 3484
– tracking system 11473–11475, 11477
– computer vision sensors 11473
– LIDAR tracking model 11475
– particle filter–based tracking algorithm 11477
– sensor fusion probability model 11475
– sensor model 11474
– traction motors 11522
– technology 10542
– tractive effort 11491
– traffic 11298
– trip de-generation 10927
– of travel time (VOT) 5024, 5029
– velocity 3088
vehicle-assisted data delivery (VADD) protocols 11578
vehicle-based traffic simulation 108
vehicle-occupancy requirement 4946
vehicle–road interaction 3053, 11188
vehicle-road model 3055
– estimation process 3055
vehicle-to-building (V2B) operation 7857, 7859
vehicle-to-vehicle communication 2464
vehicular ad hoc networks 11552
vehicular communication 2484
– technology 2464
vehicular network (VANET) 11553
vehicular transport 11295
velocity 2050
– coordination 2478
– fluctuating component 2050
– information 3143
Velodyne 11458
Venetian blinds 2840
ventilation 896, 902, 2858–2859, 3684–3685, 6878, 6880, 6890, 10272
– air 6866
– chimneys 6890
– cooling-dominated 2859
– effectiveness 2858, 3685, 6880, 10272
– mixed-mode HVAC systems 3684
– natural 902
– strategies 6878
ventilation system 5335, 5337, 5338
– filter changeouts 5338
– maintainability 5337
ventilation-only system 2858
Venturi
– reactor 11805
– washing 1667, 1670
vernacular architecture 6866
vernalization 2547, 2549, 2552, 4078
– genes 4076
– genetic regulation 2549
vernonia plant oil 6900
VERSIT+ model 256
vertebrate genes 10909
vertebrate species 10087
vertical axis wind turbine 3399, 3409
vertical borehole 4148
– heat exchanger 4149
– system 4147
vertical chimney effect 908
vertical ground motion 2460
vertical shear stress 2770
very low NO_x-gasification mode 6481
very-high-temperature nuclear reactors (VHTR) 4066, 9598
vestibulo-ocular reflex (VOR) 47, 49, 56
veterinary candidate vaccines 8075
vibrating grate furnaces 1324
vibrational spectroscopy 5385, 5394
Vibrio 5049, 5051, 5053–5054, 5381, 8759, 9080, 9087
– *alginolyticus* 5051
– *cholerae* 5049, 5051, 12014
– *fluvialis* 5053
– *mimicus* 5053
– *parahaemolyticus* 5053
– *vulnificus* 5054
vibriosis 5050
vibrios 5050, 5064
– sodium motive force 5050
Viking gasifier 1457
Vinasse 1006, 1009
vinylene carbonate (VC) 6144
vinylethylene carbonate (VEC) 6041
vinylnaphthalene 3940
violaxanthin 7917
Vip proteins 4021, 4027
Vip3 toxins 4021
vir gene 2588
viral
– diseases 10702
– genes 10703
– infection 499
– pseudo-typing 643
– replication 10703, 10706
– vectors 8062
Virginia Fanpetals 1116
virtual biomass combustion plant 1348
virus 9088
– diseases 10705
– infections 10695
– seafood-associated 9088
– transmission 10702
– vector-mediated 10702
virus-resistant papaya 4464
virus-resistant squash 4464
visbreaking 7831
visible beam calibration 11459
visible radiation 9665
– circadian effects 9665
– damage of the retina 9665
– health effects 9665
– spectrum 11152
visible-light photoactivity 7894
vision
– fusion 81
– systems 6953
vision-based driver assistance 11098
visual
– acuity 3135
– adaptation 11098
– attention 3112
– comfort 2827
– field 2840, 3145
– high dynamic range (HDR) 2840
– information 56
– landscape aesthetics 10371
– motor routine 49
– odometry 58
– perception 46
– processing 3146
– age-related decrements 3146
– spatial integration 3146
– system 3145
– neuronal activity 3145
– temporal integration 3145
vitamin
– A 1683, 1688, 1697
– deficiency 1683
– supplements 1688
– B complex 1684
– deficiency 1684
– C 1685, 1708
– deficiency 1685
– D 1685, 11405, 11414
– deficiency 1685, 11414
– in pets 11400
– metabolism 9652
– receptor (VDR) 9654
– E 1685, 1705
– Deficiency 1685
– K 1685
– Deficiency 1685

vitellogenin 11965
vitrification 4000, 4904, 6919, 11582, 11584, 11586, 11591, 11733, 11754–11755
– advantages 11584
– cost 11755
– melters 11586
– of residues 11754
– plants 11586
– processes 11586
– self-sustaining 11591
vivax malaria 11076–11077
– vaccine 6293
VLN gas 6482
V-notch weir 4218
volatile organic compounds (VOCs) 120, 170, 230, 253, 327, 1390, 6875, 8880, 10147, 11293
volatilization 9053
volcanic
– activity 2101, 8950
– aerosols 2516
– ash 3830
– eruption 2100, 2116, 2516, 10119–10121, 11614, 11634, 11641, 11643
– explosivity index (VEI) 11634
– fields 11627
– in Mexico 11619
– gases 11639, 11642
– plumes 8941
– systems 4183
– thermal signatures 8941
– tremor 11635, 11643, 11646
volcanism 1917, 11614, 11618, 11646
volcano 3233, 3555, 11613–11615, 11628, 11633–11636, 11641–11644, 11648–11649
– aircraft 11648
– deformation 11636
– disaster assistance program (VDAP) 11635
– earthquakes 11643
– eruption forecasting 11642, 11644
– geodesy 11644
– geological mapping 11643
– geophysical observations 11634
– geothermal energy 11649
– human population 11648
– impact 11633
– lahars 11642
– landslides 11642
– lateral blasts 11642
– lava flows 11641
– Mexican 11615
– monitoring 3233, 11633, 11636, 11638–11641, 11649
– global positioning system (GPS) 11636
– gravity measurements 11638
– infrasound observations 11641
– interferometric synthetic aperture radar (InSAR) 11636
– monitoring networks 11644
– satellite monitoring 11639
– satellite remote sensing 11640
– strainmeters 11638
– thermal remote sensing 11639
– tiltmeters 11638
– observations 11633
– of Chiapas 11628
– of Mexico 11613
– pyroclastics 11641
– relationship 3415, 3418
– seismic monitoring 11635
– seismic velocity 11636
– sustainability 11648
– tephra 11641
– tsunamis 11642
volcano-earthquake interactions 11646
volcanology 8941, 11616
– in Mexico 11616
– remote sensing 8941
Volmer reaction 3414, 3420, 3876
Volmer–Heyrovsky mechanism 3415
Volmer–Tafel mechanism 3416–3417
volt amp reactives (VARs) 2979
voltage 3004, 3006, 3489
– control systems 2989
– degradation 7765
– dynamics 3489
– equation 31, 37
– instability 10941–10942
– losses 7765
– gas-transport induced 7765
– loss 7759
– protection 3002
– rating 2998
– regulation 2998, 3006, 3016
– regulators 2988, 3004
– relaxation 6728
– rise effect 3016
– sags 3004
– source converters (VSC) 11182
– stability 10949
– transformers (VTs) 3009
voltaic cell 3852
voltaic pile 740
voltammetry 3421
voltammogram 6775, 6778, 6787
volumetric
– energy density 6778
– heat capacity 4136
– power density 741
voluntary building environmental assessment methods 8702, 8710
Volvox carteri 365
von Kármán constant 596
vorinostat 3164
vortex combustors 5280
VRLA battery 5890
Vuilleumier cycle 9512

W

Wacker reaction 10173
wafer sawing 9205
Walker circulation 7254, 8968
wall
– greening 4690
– insulation 3686
– jets 10980
warm pool 7252–7253, 7260
warm roof 4702
warm seawater 7314
warming effect 139
warming hole 8911
waste 4764, 4967, 5236, 5241, 5244–5245, 5252, 5284, 5297, 5302, 5721–5722, 5727, 5729, 6453–6454, 6474, 7065, 8790–8791, 8795, 8821, 8832–8833, 8837, 9979, 10000, 10002–10003, 10007, 10010, 10014–10015, 10303, 10577–10578, 10580–10581, 11581, 11592, 11607, 11655, 11661, 11665, 11674–11676, 11682–11683, 11722, 11762, 11765, 11781, 11833, 11839, 11843, 11852, 11856
– anaerobic digestion 11675
– analysis software tool for environmental decisions (WASTED) 11671
– assessing the energy 11765
– audit process 8783
– biodegradable 9979
– biomass 1145
– boiler 11770, 11774
– bridge breaking system 6454
– categories 10002
– characteristics 5236, 10002
– chlorinated compounds 5252
– coal applications 2215
– co-firing 5241, 5284
– collection 11655, 11658–11661, 11662–11666, 11759
– ant colony system (ACS) algorithm 11664
– constraining routes 11663

– containers 11661
– cost 11664
– door-to-door system 11666
– drop-off centers 11658
– efficiency 11662
– environmental impacts 11665
– hygiene 11759
– jointness of supply 11659
– mobile pneumatic system 11666
– multi-container system 11666
– optimization 11664
– participation 11658
– pay-as-you-throw programs 11660
– programs 11661
– recycling program 11659
– sanitation 11759
– special programs 11666
– systems on recycling 11663
– vehicle loading 11662
– combustion 5265, 5279–5281, 6491, 11788, 11793
– corrosion problems 5265
– fluidized bed incinerator 5279
– mass-burn incineration 11788
– process 5302
– slagging incineration 5281
– vortex incinerators 5280
– commodity exchanges 8790
– composition 4756–4757
– composting 11675
– consumption of natural resources 10015
– crane 4962
– dealing 8795
– definition 10000
– degasification 11856
– disposal 5720, 8796, 10580, 11852
– sites 11664
– diversion 11673–11674
– hierarchy 11674
– dumping 8796, 11852
– electrical and electronic equipment (WEEE) 8819
– energy recovery 4764, 11833
– entombment 5721
– environmental impacts 10014
– exchanges 8791, 8792
– extended producer responsibility (EPR) programs 11674
– feed streams characteristics 8832
– feeding system 6453
– flows 10003
– framework directive 11684
– fuel 11860
– gases 5245
– disposal 4424
– gasification 5314, 11856
– gasifiers 1436
– generation 10011, 10578, 11656
– forecasting 10578
– monitoring 10011
– source activities 11656
– global warming 10015
– glass
– comminution 8804
– products 8839
– heat 1439, 6830
– boiler 5241, 5264, 5270
– recovery 5264, 5538
– hierarchy 11682
– important properties 5245
– improving energy efficiency 11762
– incineration 4755–4756, 4762, 4769, 4772, 4866, 5235, 5242–5243, 5246, 5266, 5269, 5289, 10582, 11722, 11726, 11768, 11859, 11869
– ashes 4868, 4873–4874
– boiler 4977
– carbon footprint 4756
– catalytic factors 5269
– chemical factor 5269
– directive (WID) 5298, 11696
– evaluation 5243
– flue gas cleaning 5269
– flue gas composition 5266
– negative public opinion 11869
– plant 4765, 11770, 11841
– recycling 5289
– release of greenhouse gas emissions 4756
– residues 11721
– sulfatation 5266
– incinerator 4969, 11760
– index 10007
– landfill 4795
– leachate 10015
– legal classification 10002
– legislation 11839
– liquids 5245
– loss of habitat 10015
– lower heating value (LHV) 11781
– management 2398, 2405, 2418, 4755, 4757, 4958, 4961, 5242, 5910, 6449, 10023, 10578, 10581, 10582, 11657, 11667, 11669, 11676, 11681, 11684, 11688–11691, 11693, 11697, 11734, 11834–11835
– application of energy factors 11691
– complete oxidation 10582
– disinfection 10582
– drop-off programs 11667
– economics 11676
– energy 11688
– for sustainable society 11681
– greenhouse gas effects 11835
– greenhouse gas emissions 11693
– hierarchy 11834
– land management 11697
– landfills 11690
– life-cycle assessment (LCA) methodology 11688
– pozzolanic components 2405
– presentation 11657
– processing 11657
– recycling 11689
– sustainability 2398, 2418
– transfer 11667
– transport 11667
– unification 11734
– materials 1237, 4759, 11699
– in construction 11699
– minimization 5297, 8773, 8775, 8788
– economic benefits 8775, 8788
– workshop 10027
– non-biodegradable 9979
– paper 8798–8800, 11658
– characteristics 8798
– collection 8798
– pulp suspensions 8800
– recycling technologies 8799
– pay-as-you-throw (PAYT) programs 11676
– pit 4961–4962
– plastics 2411, 4011, 8817, 8819–8820
– characteristics 8819
– liquefaction 4005
– recycling 8820
– re-utilization 8817
– sources 8819
– policy 11839
– pre-wetting 5727
– recovery
– maximization 8833
– of Usable Energy 11843
– recycling 8834, 11674
– flow streams 8834
– reduction 2399, 11683, 11831
– model (WARM) 11688
– strategies 4619
– re-extrusion 8821
– regulatory framework 11683
– reuse 11683
– rock 6648
– sample set selection 8837
– settlement 5729
– slurry 2206

– solids 5245
– sources 11592
– reduction 11674
– space availability 10015
– statistics 10010
– streams of interest 5244
– thermal treatment 6474, 10577–10578
– to resources 5722
– transfer 11668
– optimization 11668
– transfer stations 11668
– transportation 11665, 11669
– vitrification 11581, 11607
– volatile components 4967
– wood 1538
waste-charging area 4964
waste-derived glass 11581, 11598
– reuse 11581
– valorization 11598
waste-derived-products (WDPs) market 8796
wastelands 11892
waste-to-energy (WTE) 4958, 5298, 5910, 5911, 5914, 6451, 6487, 10578, 10589, 11690, 11708, 11710, 11715, 11720, 11737, 11738, 11759, 11768, 11787, 11828, 11833, 11837–11838, 11851–11852, 11860, 11867–11868, 11870–11871
– ash 4871
– beneficial use 11837
– management in Europe 11720
– management in the United States 11737
– residues 11737
– basic principle 11852
– bottom ash 6487
– combustion 2398, 6451
– description 11710
– facility 5915, 5928, 5930, 11758, 11769, 11784
– air-cooled condensers 11769
– as power plants 11758
– CO_2 emissions 5928
– heat market 11784
– heat rate 5915
– NO_x emissions 5930
– SO_2 emissions 5930
– fluidized bed technology 11851, 11871
– for district heating and power generation 11768, 11870
– government support 11837
– incineration 9986
– installations 4866
– life cycle inventory 5914
– plant 1266, 3997, 4899, 6453–6454, 6457, 6460–6461, 6471, 6473–6476, 6479, 6481, 6483, 6485–6486, 6489, 6491, 10588, 11721, 11760–11761–11763, 11765–11767, 11771–11777, 11779, 11781, 11839, 11843, 11846, 11849, 11854, 11863, 11866
– advanced combustion control (ACC) 6473
– alternative efficiency evaluations 11766
– boilers 11763, 11774
– boiler arrangements 11772
– boiler dynamic program 6479
– boiler efficiency 11843
– bottom ash discharger 6460
– chemical cleaning 11760
– classification 11846
– complete electricity-only energy 11773
– conventional combustion with air 6461
– cost benefit analyses (CBA) 11767
– district cooling 11781
– district heating networks 11776
– district heating turbine 11777
– district heat-producing 11776
– dust removal 11760
– efficiency formulae 11765
– electricity-only concept 11779
– emissions 11839, 11866
– energy efficiency 6476
– energy recovery 6474
– environmental impact assessment 11866
– fluidized bed systems 11854, 11863
– fly ash treatment 6489
– grate-fired boilers 11771
– grate technologies 6453
– heating pumps 11775, 11781
– horizontal boiler 6475
– horizontal grate 6457
– increasing energy recovery 11849
– internal circulation 11854
– life cycle assessment (LCA) 11767, 11839
– MARTIN plants 6471
– nass streams 11721
– material flow 11839
– NO_x reduction 6481
– operating mode concept 6471
– optimizing energy 11781
– pollutants 11839
– process simulation 6479
– rankine cycle 11762
– reference plants 6491
– residue qualities 6485
– reverse-acting grate 6454
– selective non-catalytic reduction (SNCR) 6483
– small-to-medium amounts of heat 11774
– steam turbines 11772
– superheater 11763
– sustainability 11761
– SYNCOM process 6485
– vertical boiler 6476
– process 8097, 8108, 8110
– environmental impacts 8110
– Europlasma gasification process 8108
– flue gas 8110
– plasma-assisted 8097
– product 8827
– projects 5722
– statistical entropy analysis (SEA) 11715
– technology 4962, 4963, 4967, 4971, 4973, 4975, 4978–4979, 4982–4989, 4991–4992, 4994, 6449, 11837
– acid gas removal 4987
– additive feed system 4991
– air pollution control system 4973
– ammonia injection 4986
– automated rapper system 4979
– auxiliary control systems (ACS) 4973
– bottom ash extractor 4971
– catalyst reactor 4986
– combustion chamber 4962
– combustion control system 4963
– condensate system 4983
– continuous emission monitoring system (CEMS) 4992
– demineralized water system 4984
– emission control loop 4989
– equipment control systems (ECS) 4973
– fabric filter 4989
– feed hopper 4962
– gas–gas heat exchanger 4986
– high-pressure steam (HPS) system 4982
– hydraulic station 4971
– induced draft fan 4992
– low-pressure steam (LPS) system 4983
– nitrogen oxides 4984
– operator terminal 4973
– primary air system 4967
– reagent silo 4991

– retractable sootblower 4978
– secondary air system 4967
– selective catalytic reduction (SCR) 4985
– selective non-catalytic reduction (SNCR) 4984
– stack 4994
– steam boiler 4975
– temperature control loop 4988
– treatment system 1146
wastewater 1148, 1151, 1169, 1177, 1182, 2084, 2088, 2328, 2333, 2336, 2342, 3454–3455, 3460, 4851, 4866, 6319, 6627, 8760, 8800, 9564, 10190–10191, 10531, 10535, 10579, 11873–11876, 11891, 11912–11913, 11936, 11938, 11940, 11946, 11961, 11965, 11968–11969, 11971
– biological nutrient removal (BNR) 11936
– contaminants 2088, 11912–11913
– control through wetlands 11891
– discharge 2071, 2092
– efficient pumping 11938
– effluent 11874
– endocrine disrupting compounds 11965
– energy recovery 11940
– estrogenic activity 11961
– fecal waste 6319
– for irrigation 6627
– from municipalities 1177
– from waste paper processing 8800
– investigated area 11913
– management 10579
– mechanical treatment 11936
– membrane bioreactor treatment 11971
– nitrification 3455, 11969
– nonylphenolic compounds 11971
– operation 11935, 11946
– energy use 11935
– organically polluted 1177, 1182
– outfalls 2088
– ozonated 2342
– power consumption 11940
– quality parameters 11913
– reclamation 2084, 10190, 10531, 10535, 11873–11875, 11879, 11883–11886, 11963, 11968
– adsorption 11886
– chemical oxidation 11885
– conventional treatment practice 11879
– distillation 11885
– electrodialysis 11885
– energy consumption 11886
– high-quality reclaimed water 11883
– ion exchange 11885
– membrane bioreactor (MBR) 11883
– nanofiltration 11884
– reverse osmosis (RO) 11884
– technologies 11879
– reuse 2084, 2333, 6626, 6627, 9564, 11876, 11968
– guidelines 6627
– in agriculture 6627
– sample collection 11913
– sampling sites 11913
– treatment 2082, 3454–3455, 4851, 4866, 5760, 10191, 11891, 11892, 11898, 11919, 11923, 11937, 11940–11941, 11948–11949, 11951–11958, 11962, 11979
– advanced control 11948
– aeration 11937, 11953
– anti-inflammatories 11923
– automatic control 11948
– automatic monitoring 11941
– basic control actions 11951
– biological nutrient removal (BNR) 11948
– biological treatment process 11962
– cascaded control loop 11955
– closed loop control 11952, 11957
– combined sewer overflows (CSOs) 11958
– constructed wetlands 5760, 11898
– control 11941
– control goals 11951
– control of biological oxidation 11953
– control of denitrification 11956
– control of the equipment 11952
– control problems 11953
– dissolved oxygen control based on ammonia measurements 11955
– dissolved oxygen control 11954
– disturbances 11949
– electrical energy requirement 11937
– feedback control 11951
– incentives for control 11949
– limit of detection and calibration 11919
– membrane bioreactor treatment 11979
– monitoring 11941, 11957
– natural wetlands 11892
– open loop control 11952
– operational costs 11951
– oxygen uptake rate (OUR) 11954
– phase length control 11956
– plant wide control 11958
– sludge heating 11941
– sludge thickening 11940
– technology 1169
– treatment plant (WWTP) 2328, 11911, 11940, 11947, 11959, 11989
– anoxic zone 11959
– automation 11947
– energy balance 11940
– enteroviruses 11989
– primary sedimentation 11940
– treatment sludges 4874
– virus concentration 6627
– water quality analysis 11913
WATCH-OVER 74
water 1545–1546, 1552, 1555, 1566, 1580, 2320, 2322, 2324–2325, 2327, 2329, 2343, 2501, 2639, 2643, 2755, 3218–3220, 3414, 3455–3456, 3460–3461, 3553, 5163, 5175, 6606, 6662, 9563–9564, 10189–10190, 10292, 11932, 11934–11936, 11944, 11946, 11979
– availability 2065, 2071, 2320, 2325, 2322, 9324
– in the Future 2325
– balance 2327, 4807, 4808, 5823, 5825
– boiling test (WBT) 1305
– canopy-intercepted 3218
– cascading 10292
– clouds 9633
– column 8955
– optical properties 8955
– concepts 10189
– conservation 2082
– consumption 11939
– decontamination 9563, 9565, 9582
– solar hardware 9582
– density 4910
– impact of temperature 4910
– desalination 9759
– disinfection 9563–9564
– distribution systems 11941
– leakage detection 11941
– electrolysis 1413, 3414, 5163
– energy
– interdependencies 11934
– nexus 11932
– use 11935
– erosion 3707
– evaporation 1545
– flow 8619
– Richards' equation 8619
– footprint 2073
– for irrigation 2755

– for power generation 3456
– for transportation 3460
– framework directive 6367, 9181, 9187
– funds 3319
– gas shift reaction (WGSR) 1450, 2240, 2245, 3986, 5125, 5128, 5138, 5144, 8330
– habitat 954
– harmony concept 10190, 10191
– hyacinth plant 11893
– industry 2092
– infrastructure 2067, 3455, 8691
– intoxication 10637
– leakage 2324
– management 2075, 2077, 2327, 2643, 4735, 9321, 9323–9324
  – nutrient management 9324
  – remote sensing (RS) data 9324
– molecules 8955
  – inherent optical properties (IOPs) 8955
– mullions 3692
– multielectron splitting 5175
– operation 11946
– overuse 3553
– pathogenic microorganisms 6606
– performance 2073
– photolysis 5175
– planning 5831
  – sustainability criteria 5831
– pollution 2080, 3461, 11710
  – control act 7825
  – control system 11710
– prices 2071
– production 10191
– purification 6662, 9573
  – semiconductor photocatalysis 9573
– quality 1944, 2061, 2065, 2070, 2076, 2078, 2083, 2320, 2322, 2333–2335, 2337, 2339–2340, 2343, 2501, 2504, 3706, 4808, 4813, 5675, 5678, 6611, 6623, 7668, 8923, 9035, 9052, 9058, 10189, 11876, 11879, 11921, 11941
  – bioassays 2337
  – characterization 2340
  – chemical analysis 2337
  – correlation coefficient analysis 11921
  – degradation 3706
  – deterioration 4813
  – evaluation 2340
  – in community-owned water resources 2334
  – information platform 2335
  – labeling 2343
  – linear regression 11921
  – management 9058
  – mechanistic studies 5675
  – microbial pollution 7668
  – mineralization 9052
  – models 9052
  – monitoring 11941
  – ocean color 8923
  – parameters 2337, 11879
  – pathogen contamination 7668
  – precipitation 5678
  – scoring 2339
  – studies 5675
  – testing 6623
  – user judgment 2343
– quantity 2061, 10189
– reclamation 2079, 2082, 2090, 11961, 11979
  – micropollutants 11961
– recycling 2324
– resources 1544, 1580, 2065–2066, 2074, 2075, 2319, 2322–2323, 2327, 2334, 2343, 2345, 2801, 11348, 11874, 11876, 11933
  – climate change 2322
  – community-owned 2319, 2327, 2334, 2345
  – management 3451, 11876
  – non-stationarity 2075
  – planning under uncertainty 2066
  – sustainability 2323
– retention pavement 2332
– reuse 2082, 2083, 2329, 6625, 10190, 11979
  – emerging contaminants 2083
  – QMRA 6625
– safety plans 6607
– saving 11944
– scarcity 1546, 1552, 1555, 1566, 1573, 2070–2071, 2080, 2325, 2639, 2898, 5630, 8690, 11934
– scrubbing 1622, 1624
– sensitive urban design (WSUD) 10096, 10098, 10102–10103, 10106, 10113
  – case studies 10103
  – evaluation 10102
  – potential benefits 10102
  – treatment devices 10106
  – water quality 10113
– shortage 8689
– snowmelt 3219
– soluble carbohydrate (WSC) 8017
  – QTL mapping 8017
– splitting 7882, 7885–7886, 7897–7898
  – photocatalysts 7882, 7886
  – photoelectrochemical (PEC) 7882, 7898
– storage 3218, 3220, 10189, 11875
– stress 2325, 2648, 10750
  – indicator 1555
– supply 2061, 2082, 6608, 6612–6613, 6621, 11935
  – risk characterization 6612
  – risk management 6608
– sustainability 2063, 10189–10190
  – solutions 2063
– train 6289
  – energy cost 6289
  – iron lift configuration 6289
– transpiration 1545
– treatment 6609, 6621, 10537
  – biodegradable organic matter control 10537
  – fouling 10537
  – infrastructure 4155
  – technologies 2092
– trees 11175–11177
  – inception time 11177
– tube steam boiler 1344
– use 2326, 2342, 11942
  – efficiency (WUE) 1102, 1482, 1544–1545, 1567, 2639–2640, 2645, 2652, 2755, 9321–9322
  – ranking 2342
  – sustainability 2326
– utility associations 11936
– vapor 317, 7248, 9635, 9697, 9724
– wave propagation 2792
water–air boundary 11386
waterborne
– disease 6612, 6333, 7384, 7385, 7669, 10579, 11985, 12015
  – transmission 6606
– infectious diseases 11997
  – approaches to control 11997
– microorganisms 11390
– parasitic diseases 12018
– pathogens 6320, 6611
water–energy nexus 11933
water-filled heating systems 1402
waterflood 7805
  – mobility ratio 7805
waterfowl harvest 3346–3347
WaterGap model 1555, 1566
water-leaving radiance 8957
waterlogging 2755
water-only cyclones (WOCs) 2201
waterproofing technology 4710
water-saving activity 2323

watershed 536, 3319
water-splitting thermochemical cycles 9597
watery diarrhea 5052
Watsumaga agar 5054
wave energy 6347
– conversion system 6348, 7244
– generation 11944
wax hydrocracker 2247
waxy preprotein 2709
wayfinding 3136
weather 623–624, 635, 2101, 2120, 2510, 2523, 2755, 4107, 4678, 5071, 12063, 12075, 12076
– conditions 2755
– control 4106
– forecast(ing) 635, 3212, 5081–5082, 12064
– boundary layer pressurized balloon (BLPB) 5082
– driftsonde system 5082
– weather forecasting models 10257
– hot spells 4678
– information 1784
– models 624
– prediction model 6598, 12062, 12064, 12070–12071, 12073
– data assimilation 12071, 12073
– equitable threat scores 12071
– geostrophically balanced flow 12071
– height anomaly correlation 12070
– initialization 12071
– skill scores 12070
– observing strategy 5071
– research forecast model 6598
– seamless models 12076
– vaning 7316
weathering 1910, 1913–1914, 1916–1918, 1923, 2117
– chemical 1910
– crust 1918
– enhanced 1916
– of olivine 1913–1914, 1917
– of silicate minerals 1913
weed 4739, 10353
– control 4467, 10724
– emergence models 9153
– floras 2750
– herbicide-resistant 10353
– infestation 157
– interbreeding-related 10353
– production 10043
– resistance 10349
– transposon-bearing 10353
– WeedCast model 9153
weedy rice 10348
Weende analysis standard 1105
Weibull
– distribution 7398
– probability function 11162
weight loss 10648
welding robot 4979
well productivity 4228
wellbore 4383, 4404
– pressure 9004
– scaling 4404
– simulation 9008
wellhead 4279
– pressure 4273, 4277
– separators 4279
well 5668
well-to-tank (WTT)
– efficiencies 5154
– hydrogen 5142
well-to-wheel costs (WTW) 1054
West African Monsoon (WAM) 6751, 6755, 7258
– greenhouse gas forcing 6755
– impacts of aerosols 6751
– model evaluation (WAMME) project 6746
West Nile fever (WNF) 5360
Western hemisphere warm pool (WHWP) 7255
Western wind and solar integration study (WWSIS) 12269
Westinghouse
– cycle 5162, 5168
– corporation (WPC) 8103
wet biomass 1081, 1086, 1174, 1323, 1619
– thermochemical use 1086
wet bottom combustor 5281
wet combustible 11830
wet cooling tower 9513
wet kiln 5286
wet milling technology 999
wet powder spraying (WPS) 9960
wet process method 6146
wet recooling 9533
wet scrubber 1395
wetland 3225, 3315, 3741, 5790, 11892, 11896
– water column 11896
wetness index 3214, 3223
whale 3570
wheat 1111, 1271, 2704, 4558, 6212–6213, 8017, 8020, 10347, 10352
– breeding 8016
– quantitative trait loci (QTL) 8016
– coleoptile semidwarfs 8020
– flour 1689
– iron and folate fortification 1689
– germplasm 8017, 8020
– grain 4555
– quality 4558
– inflorescence 2704
– lodging 6212
– lodging-proof ideotype 6213
– phytomers 2543
– selective herbicides 10347
wheel braking force 11501
whipworm 12007
whirling disease 6195
white spot syndrome virus (WSSV) 1932
white sweet clover 1116
whitecap reflectance 8962
whole bale furnace 1385
whole effluent toxicity (WET) test 3565
whole foods market (WFM) 3574
whole genome selection (WGS) 1739
whole plant utilization 11452
whole-crop cereal 1111, 1129, 1139
whole-organism fingerprinting 5389
– Raman-based 5389
whole-parasite vaccine 6302
wide area
– measurement system 12083
– phasor measurement units (PMU) 12083
– monitoring 12079, 12093
– network (WAN) 12083
wild allele 6441
wild fish stock 3566
wild poliovirus 8140, 8154
– genomes 8138
wild rice 2707
wilderness in the city 11371
wildlife 941
– approaching the city 941
– conservation 956
– in sustainable city planning 956
– disease 5367–5368
– cause of endangerment 5368
– effects of climate change 5368
– source of infections for humans and livestock 5368
– habitat 941
– in cities 941
– in town 950
– infections 5358
willingness
– to accept (WTA) 4788
– to pay (WTP) 4788, 4802
willow 6021–6022
Wilms' tumor 3628, 3646
wind 7398, 7400–7401
– atlas method 6594, 6599

– break 899
– climatology 6594, 6600
– conditions 6596, 12214
  – modeling 6596
– development project 12228
– direction 6589
– energy 514, 3398, 4475–4477, 4481–4483, 4485, 6585, 6600, 7850, 12120, 12129, 12146, 12203, 12214, 12222, 12226, 12236, 12255–12256, 12258, 12260, 12262, 12270, 12273
  – Africa 4485
  – applications 12146
  – associations 4476
  – capacity markets 12260
  – conversion systems 4485
  – development 4483, 12222
  – economic development 12270
  – global status 4476
  – green energy sources 4481
  – investments 6586
  – in wholesale markets 12256
  – Latin America 4482
  – location decision making 12236
  – markets in Europe 12258
  – markets in the United States 12256
  – Middle East 4485
  – output 12181
  – penetration 12273
  – planning 9645
  – price 12257
  – public support 12226
  – reanalysis data 6600
  – spatial planning 12236
  – statistics 4476
  – tax credits 12262
  – technology 4475, 12270
  – transmission tariffs 4483
  – utilization 6585
– erosion 3707
– facilities 12257
  – production tax credit (PTC) 12257
– farm 520, 524, 528, 7243, 7394, 7426, 12231
  – sociopolitical acceptance 12231
– generation 8985, 12112, 12127, 12187–12188, 12267
  – effective load-carrying capability (ELCC) 12267
  – renewable portfolio standards 12188
  – reserve requirements 12127
– integration 12131
  – costs 12268
  – studies 12198
– mills 12135
– offshore turbulence 7401
– origin 7398
– profile 6589
– resource 6586–6587, 6589, 6598, 12181, 12199, 12231
  – analysis 6600
  – geographic diversity 12181, 12199
  – geographical distribution 12231
  – mapping 6598
  – model chain 6598
– speed 6589, 6603, 7246, 7398, 7402, 11267, 12149, 12154
  – gust 7402
  – relation 12137
  – Weibull distribution 7398
– towers 6866
– tunnel 916, 11279
  – experiments 11284
  – tests 9790, 11277
– turbulence 12284
– uncertainty costs 8988
– vector 6589
wind power 4474–4475, 4483–4484, 4489–4490, 6583, 6586, 7400, 7427, 8981, 8984, 8988, 9906, 10516, 12100, 12112–12113, 12117–12122, 12124–12126, 12128–12131, 12134, 12202, 12213, 12215–12218, 12219–12220, 12224, 12233–12235, 12237–12242, 12247, 12272
– acceptance 12229
  – individual gap 12229
  – of distinguishable aspects 12220
  – social gap 12229
– aerodynamics 12202, 12215
– Asia and Pacific 4483
– balancing 12097, 12215
  – cost 12129
  – cost from electricity markets 12130
  – of systems 12112
  – related results 12131
– benefits for the community 12240
– blade technology 12202, 12215
– capacity 3397, 12115, 12128
– collaborative decision making 12241
– community
  – acceptance 12238
  – involvement 12238
– day-ahead time scale 12117
– dispatch 12119
– economic conditions 12235
– energy potential 7427
– financial support 12235
– flexibility 12125
– forecasts 12117–12118
  – errors 12121, 12128–12129
– generation 3696
– generator systems 12134
– global wind capacity 4490
– grid integration 12174, 12215
  – transmission planning 12174
– identity of place 12239
– impacts of different time scales 12124
– implementation 12220, 12235, 12237
– in electricity markets 12126
– installations 4474, 4483, 12217
– institutional conditions 12233
– integration
  – cost 12126
  – studies 12126, 12216
– intraday market 12130
– jobs and economic development impacts (JEDI) model 12272
– load following 8988
– low load 12117
– market
  – acceptance 12242
  – forecast 4489
– meteorology 6585–6586, 12214
– model chain 6586
– national planning systems 12237
– net load
  – forecast errors 12126
  – variations 12122
– noise
  – annoyance 12247
  – emissions 12217
– onshore 12113
– place attachment 12239
– plants 4477, 4479, 12114, 12116, 12267
  – capacity contribution 12267
  – Europe 4477
  – North America 4479
  – offshore 4479
– power banking system 4484
– primary reserves 12125
– production 4475, 12110, 12113, 12121, 12123
  – exceedence level 12123
  – operating hour 12121
  – operating reserves 12121
  – variability of load 12123
– project 12230
– public opinion 12234
– public support 12234
– regulation 8988
– renewable energy feed-in tariff (REFIT) system 12235
– reserve requirements 12122

– secondary reserves 12125
– simulation 12119
– small scale systems 12216
– social acceptance 12217–12219, 12242
– social actors 12224
– sociopolitical acceptance 12233
– station 12099
– storage 12131
– system balancing 12131
– transmission planning 12216
wind turbine 515, 526, 3396–3399, 3401–3406, 3410, 4477, 4481, 4483–4488, 6603, 6585–6586, 7394, 7396, 7408, 7410–7413, 7432, 8987, 10378, 10380, 10381, 10618, 12135–12136, 12146, 12154, 12156–12159, 12163, 12164, 12203, 12205, 12207, 12210–12211, 12213, 12215, 12219, 12222, 12228, 12244, 12246, 12247, 12274–12276, 12280–12282, 12289, 12291
– active power control 12163
– aerodynamic 7408, 12203
– efficiency 3401
– lift 4486
– aerodynamic noise 12281
– airborne noise 7432
– average wind speed 3410
– behavior during network faults 12164
– Betz limit 7408
– birds and bats 7432
– blade 12205
– element momentum (BEM) theory 7408, 7410
– control systems 3402
– converter-operated 12164
– costs 3406, 4488
– deployment 3398
– developed for operation on buildings 3410
– doubly-fed induction generator (DFIG) 4487
– drag-driven 3399
– ducted 3401
– dynamics 7411
– electrical systems 12215
– environmental conditions 12207
– environmental impact 12276
– farms 6810
– fatigue 7413
– fault ride through 8987
– fixed-speed 12136, 12158, 12159, 12163, 12164
– flicker emission 12157
– flows over rooftops 3410
– generator system 7396, 12136, 12149
– dynamic requirements 12136
– fixed-speed system 12149
– operational requirements 12136
– stationary requirements 12136
– harmonics 12158
– current emission 12163
– horizontal-axis 4486
– impact on wildlife 12246
– installation 4484
– kinetic energy 12203
– landscape 12244
– lift-driven 3401, 3405
– mechanics 7411
– mechanical noise 12280
– miner's rule 7413
– modulation 12282
– noise 3403, 12247, 12289, 12290, 12291
– emissions 12274
– guidelines 12290
– sources 12280
– penetration 4488
– permanent magnet generators 4487
– power quality aspects 12154
– quirrel cage asynchronous generator (SCIG) 4487
– reactive power 8987
– rotor 7408, 7411
– aerodynamics 12210
– blades 4486, 12211
– load 7412
– motions 7412
– safety systems 3402
– seascape 12244
– social acceptance 12222, 12244
– sound
– propagation 12282
– data 12280
– source directivity 12282
– squirrel cage induction generators 4487
– stall-regulated 12205
– steady-state influence 12159
– suitable dimensions 3410
– system 12138
– electrical components 12138
– electrical fundamentals 12138
– tip speed ratios 7410
– types 4485, 4487
– variable-speed 12156
– vertical-axis 4486
– vibrations 3404
– visual impact 12228, 12244
– voltage
– fluctuations 12157
– level influence 12157
– wound rotors 4487
– induction generator (WRIG) 4487
wind-driven ventilation 6870
wind-energy farm 515
windmill 517, 519, 12213
window design 2805
window to wall ratios 3686
windscreen projection 11127
wind-to-hydrogen pathway 10519
winning genotype 4085
winter
– crops 1123
– depression 9666
– wheat 1111
wireless power consortium 704
wireless vehicular communication 2484
WISDOM 1310
Wobbe index 1620
WOCE project 8664
Wolff–Chaikoff effect 1686
wollastonite 1910, 11603
wood/woody 2283, 2416, 11355
– as a resource 2283
– alcohol 5477
– bioenergy 1554
– crops 1571
– biofuels 1553
– biomass 1202, 1267, 1285, 1288, 1521, 6023
– crops 1285
– eucalyptus 1288
– chip 1026, 1209, 1212, 1373, 1610
– combustion 1391
– combustion unit 1212
– furnaces 1378
– co-gasification 2416
– combustion 11298
– energy 11349
– fuels 1316, 9830, 9834, 11349
– calorific value 9834
– furnaces 1373
– gasifier 1419
– harvesting 1309
– logs 1209
– moisture 9836
– pelletizing 1069
– pellets 1199, 1209, 1211, 1373
– stove 1211
– pyrolysis 2416
wood-burning furnaces 1355
wooden separators 8748
wood-firing 1334

woodland 3315, 11355, 11356, 11371
– landscape 11357
– management 11357
– *Rangifer tarandus* 8451
woodstove 1308
workflow transformation 10313
working ion 741, 742
– transfer 742
working waterfront 539
work-plane illuminance 3682
workplane 2829
– illuminance 3682
world
– climate 8920
– coal resources 2182
– energy council (WEC) 2181
– energy outlook (WEO) 1547
– fisheries 7390
– food
– production 2736
– program (WFP) 1688
– ocean atlas (WOA05) 7300
– ocean circulation experiment 5865
– oil production 7447
– population 1742
– radiation reference 9676
– water demand 11942
wound infection 5051, 5054
– V. alginolyticus 5051
– V. vulnificus 5054
Wright's numerator 439

X

xanthine oxidase system 3665
xanthophyll 353, 7915, 7917
xanthosine 4036
xenobiotic 822, 825–826, 3258, 3262, 3274, 3586, 3593, 3596, 3613, 6795, 12294, 12296, 12300, 12302–12305, 12309, 12310
– acylation 12304
– biotransformation 12303
– pathway 12300
– carcinogenic 3596
– cellular detoxification 12310
– electrophile 12302
– glucuronidation 12303
– glutathione conjugation 12305
– hydrolysis reactions 12302
– mercapturic acid formation 12305
– metabolism 3256, 12299
– protection 12293
– reduction reactions 12302
– resistance 12295
– solute carrier proteins 12309
– storage 12310
– sulfation 12303
– toxic effects 3593
– uptake 12296
xenon 8484, 8583
– oscillation 3817
xenotime 9948
xenotransplantation 10834, 10866, 10869, 10873
xeric roof gardens 4711
xerography 7558
xerophthalmia 1684
X ray 3026, 5561, 5574, 8537, 8538, 8574–8576, 5860
– absorption near-edge spectroscopy (XANES) 2439, 7743
– analysis 2949
– absorption spectroscopy (XAS) 6075, 7738, 8607
– pre-edge 6075
– rising edge 6075
– diffraction (XRD) 6071, 7569, 8604
– structure factor 6071
– diffractometry 5227
– energies 8575
– fluorescence 8574
– Spectroscopy (XFS) 2439
– irradiation 9101
– seafood 9101
– machines 8576
– photoelectron spectroscopy (XPS) 6074
– ultrahigh vacuum (UHV) conditions 6074
– powder diffraction (XRPD) 2439
– shielding 8538
– sources 8574
– yields 8575
xylanase 10845
xylonite 8818
xylose 964, 971, 974, 10754
xylulokinase 974
xylulose 974

Y

yard waste 11832
yaw rate sensor 77
yeast 993, 1046, 8029
– yeast artificial chromosome (YAC) 2607, 2691, 2698, 2701
yellow cake 7061, 8484, 8584, 11223
Yersinia 5056
yield 2721–2723, 2725, 2730, 2734, 2736–2737, 2749, 8017
– conventional breeding efforts 2734
– decline 2734
– field-to-field variability 2730
– fungicide protection 2721
– gap 2722, 2725, 2726, 2728–2730
– closing 2728
– estimates 2726
– farm-level technical constraints 2729
– in the developing world 2730
– gene 10750
– genetic engineering 2736
– genetic variation 2734
– growth 2723, 2737
– increase 2721
– loss 2648
– photon flux (YPF) 7903
– physiological parameters 8017
– potential 2749
– table 3289
yield-enhancing technology 2725
young bull 2785–2786
– genomic evaluation 2786
Young's modulus 2022, 8727
yttria-stabilized zirconia (YSZ) 2936, 3889
– electrolyte film 9854
yttrium 9947
– barium copper oxide (YBCO) 6254

Z

Zalypsis 3161
Zea mays 2703
zeaxanthin 356, 7917
ZEBRA cell 765
zebrafish 6793–6796, 6798, 6800
– as a green model 6796
– assay 6800
– behavior 6795
– embryos 6795
– functional analysis 6795
– genome 6793
– genome-wide genetic screens 6794
– larvae 6798
– nanomaterial absorption 6798
– nanotoxicity studies 6793
zenith luminance 2818
zeolite 4586, 4588–4590, 4592, 7153, 8606, 8621, 8622
– acidity 4588
– catalysis 4588, 4593
– cracking 4588
– limitations 4593
– catalyst 3988
– drying 7153

– in fine synthesis of speciality chemicals 4592
– isomerization 4589
– preparation 4590
– rearrangement 4590
zero energy building 7631
zero valent iron (ZVI) 10443
zero-carbon city 7792
zero-emission vehicle (ZEV) 10527
zero-heating energy buildings 7643
zidovudine (AZT) 5010
zinc 794, 1686, 1688–1689, 1691, 1713, 3778
– deficiency 1686, 3778
– electrode 6947
– fertilization 1691
– fortification 1689
– ion 6948
– oxide cycle 5169
– supplements 1688
– toxicity 1686
zinc finger 10919
– endonucleases 2608, 8061
– nucleases (ZFN) 2972, 4498, 6794, 7225, 10680, 10831, 10887, 10912
– technology 4492
zinc-air cathode 6515
zinc-air cell 6513, 6516
zinc-bromine battery 680, 793, 794
zinc–manganese battery 747
zinc-mercuric oxide 6506
zinc-silver oxide 6516
zircaloy 7195–7196
zirconium 4602, 9892, 9947, 9955
– alloy material 7196
– calcia-stabilized 9892
– oxynitride 8270
– phosphate 6561
– phophonates 8339
– yttria-stabilized 9892
zirconium-based alloy 4065
zona pellucida (ZP) 6151
zoo animal 11414
– UV exposure 11414
zoobenthos 7025
zoology of atmospheric motion 12063
zoomass 1175
zoonosis 1759, 5049, 5353–5354, 5359, 12029
– between-host transmission 5354
– within-host evolution 5354
zoonotic
– bacteria 7684
– diseases 2263, 2972, 5380
– infections from eating fishes 12024
– parasites 12055
– parasitic diseases 12021
– pathogens 9164
– indicators 9164
zooplanktivorous fish 4822
zooplankton 1963–1964, 4822, 6314, 7273, 8203, 8396, 8402, 11408
– radionuclide cycling 8402
– UV sensitivity 11408
zooxanthellae 2493
zygote 6151, 6152, 10817

This encyclopedia includes no entries for Y and Z.